A Molecular Orbital Study on the Partial Reactivity of Hydrogen of Various Amino Acids in the Abstraction Reaction by Hydroxyl Radical

Hiroyuki SHINOHARA,* Akira IMAMURA,† Takahiro MASUDA, and Masaharu KONDO

Department of Chemistry, Faculty of Science, Tokyo Metropolitan University, Fukasawa, Setagaya-ku, Tokyo 158

†*Shiga University of Medical Science, Seta, Otsu, Shiga 520-21*

(Received May 7, 1977)

The reactivities of hydrogen atoms of aliphatic amino acids toward hydroxyl radicals in the hydrogen atom abstraction reaction have been studied in terms of the energy required for stretching the C–H bond which is attacked. The energy required for stretching the C–H bond by 0.5 Å from the equilibrium bond length has been calculated by the INDO method and compared with the partial rate constants experimentally assigned to the hydrogen atoms of aliphatic amino acids. The energy required has been correlated only with the partial rate constants of the hydrogen atoms on the β-carbon atom. For the hydrogen atoms on the α-carbon atom, although data was insufficient a similar situation has been observed. The reactivities of the hydrogen atoms on the γ and δ-carbon atom failed to correlate with the stretching energy. The reasons are discussed in terms of the effect raised by the configuration of amino acid molecules in solution. The stretching energy has also been found to be consistent with the electrophilicity observed in the hydrogen abstraction reaction by hydroxyl radical.

Reactions of hydroxyl radicals with amino acids have been investigated by a number of researchers with an interest in the radiation-induced damage of proteins. Hydroxyl radicals abstract hydrogen atoms from aliphatic amino acids and the rate constants for the reactions are available.

Recently, it has been reported[1] that the partial rate constants for the hydrogen atom abstraction by hydroxyl radicals may be estimated from the rate constants determined by the *p*-nitroso-*N*,*N*-dimethylaniline method[2,3] for primary, secondary, and tertiary hydrogen atoms bound to the α, β, γ, and δ-carbon atoms of simple aliphatic amino acids. The bimolecular rate constant for the hydrogen atom abstraction by hydroxyl radicals from an aliphatic amino acid has been interpreted by summation of the partial reactivities assigned to hydrogen atoms in the amino acid molecule. However, no theoretical basis of the partial reactivities has been presented.

In the present investigation, the energy required to stretch the C–H bond by 0.5 Å from the equilibrium bond length has been calculated, to ensure a quantum chemical basis to the assigned partial reactivity. This energy is possibly used as a measure of the reactivity of a hydrogen atom toward hydroxyl readicals, since it is approximately the same as the energy required for hydrogen abstraction calculated from a reacting system composed of a hydroxyl radical and an amino acid. The energies calculated for several kinds of aliphatic amino acids have been partly correlated with the assigned parital reactivities. The effect raised by configurational changes in solution has been discussed. The electrophilic behavior of hydroxyl radical observed in the hydrogen abstraction reaction with amino acids has been explained in terms of the stretching energy.

Method

The total energies for the isolated molecules as well as the reacting systems were calculated by the UHF method[4] in the INDO approximation.[5]

Results and Discussion

The total energies and the electron distributions were calculated for glycine, alanine, 2-aminobutyric acid, valine, isoleucine, and leucine. The assumed geometries of the amino acids and hydroxyl radicals are given in Fig. 1 and the total energies in Table 1. For alanine, 2-aminobutyric acid, valine, isoleucine, and leucine, the same bond lengths and bond angles as those of glycine were assumed. In order to find the stable form of valine, the total energies of the other forms were calculated and found to be less stable than that shown in Fig. 1.

Figure 1 shows a model of the hydrogen abstraction by hydroxyl radicals from glycine. It has been assumed that the hydroxyl radical approaches the H^9 atom of glycine along the extension of the C^1–H^9 bond maintaining the angle H^9OH at 104.45° (the bond angle of water) and abstracts the H^9 atom. In a previous paper,[6] the angular dependence of the energy of the CH_4–OH system (θ, the angle of HOH was varied from 90 to 180°) was studied, and it was confirmed that the approach with $\theta=104.45°$ is most favored.

TABLE 1. THE TOTAL ENERGY OF AMINO ACIDS AND HYDROXYL RADICALS CALCULATED BY THE INDO METHOD

Amino acid	Total energy (au)
Glycine	−63.6233
Alanine	−72.0652
2-Aminobutyric acid	−80.5059
Valine	−88.9413
Isoleucine	−97.3754
Leucine	−97.7260
Hydroxyl radical	−18.1505

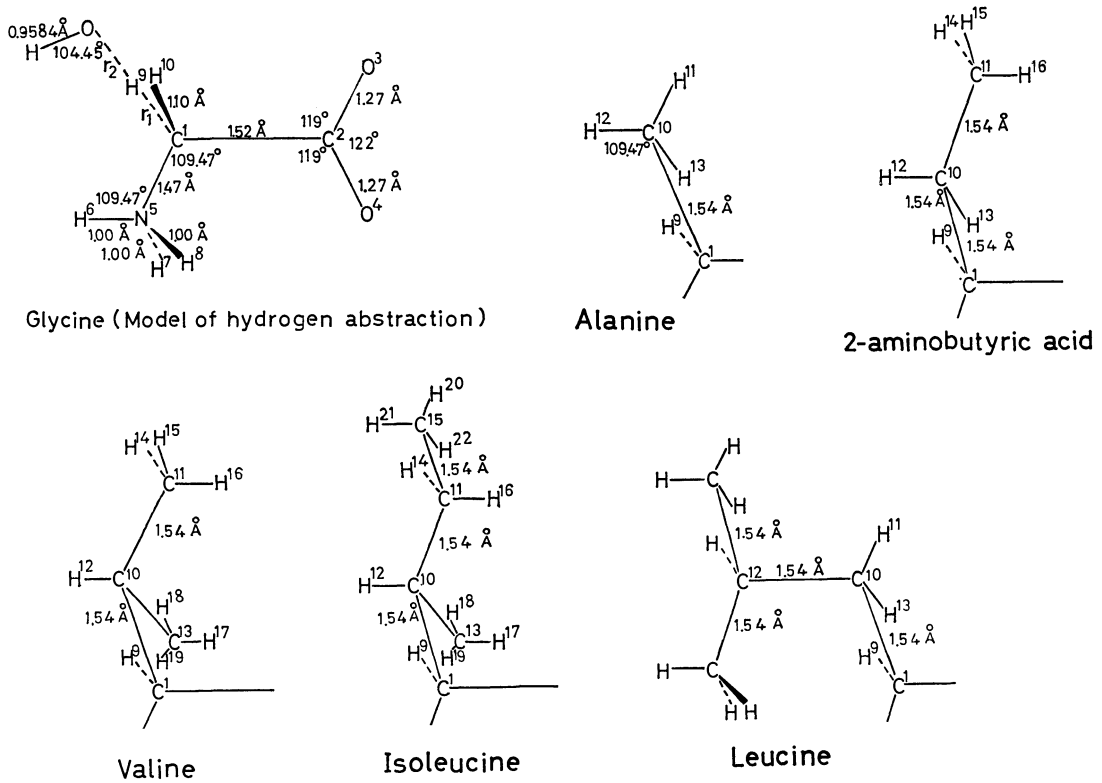

Fig 1. The geometries of amino acids and an assumed model for the abstraction by hydroxyl radical with amino acid.

Consequently, this angle has been adopted for the amino acid–OH system. The hydrogen atom of the hydroxyl radical lies in a anti-direction to the C^1–H^{10} bond with regard to the C^1–O bond. The energy dependence of the reacting system upon the intermolecular H^9–O distance, with the C^1–H^9 distance fixed at 1.10 Å was examined and the results are given in Fig. 2. The minimum quantity of energy was obtained between the intermolecular distances of 1.36 and 1.46 Å. The reacting system is more stable than the isolated state, and this is probably due to the stabilization by hydrogen-bonding between hydroxyl oxygen and the H^9 atom of glycine.

The reaction path is specified with the notation (r_1, r_2), where r_1 represents the distance in Å betweeen carbon C^1 and hydrogen H^9 which is abstracted, and r_2 that between H^9 and hydroxyl oxygen.

Figure 3 illustrates the dependence of the energy of the reacting system upon the C^1–H^9 distance r_1, when the C^1–O distance (r_1+r_2) is varied. It is conceivable that configuration interactions are important in lowering the energy for the transition state of the reacting system. However, calculation of the interactions by the UHF method is very complicated. Thus, it has been tentatively assumed that the effects of the configuration interactions are not so different, molecule to molecule in the series of aliphatic amino acid molecules, and consequently the reactivity may be compared with the energy obtained by the UHF method for the elongated C^1–H^9 bond. The following points A, B, C, and D were taken as possible reaction paths for H^9 abstraction, specified respectively by a set of r_1 and r_2 indicated in parentheses. A(1.10, 1.46), B(1.20, 1.36), C(1.30, 1.26), D(1.40, 1.16).

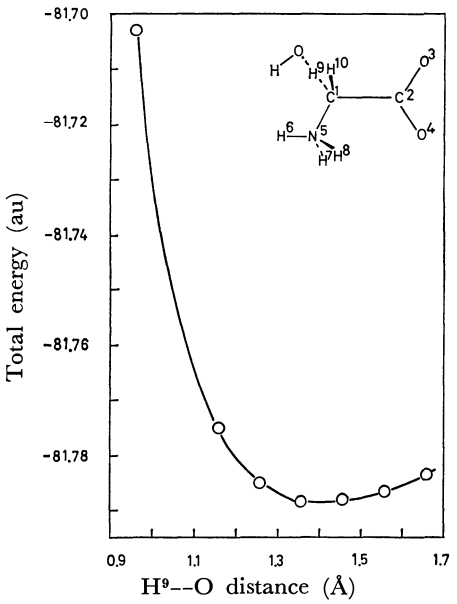

Fig. 2. Potential curve as a function of the distance between hydroxyl radical and H^9 atom in glycine-OH system.

From Fig. 3, it has been inferred that the potential curve appears to approach a maximum near D with the distance C^1–O of 2.56 Å, although the absolute value of the energy is not available. Therefore, it has been assumed that the difference in the total energy between the reacting system at D and the isolated state is an approximate measure of the reactivity of

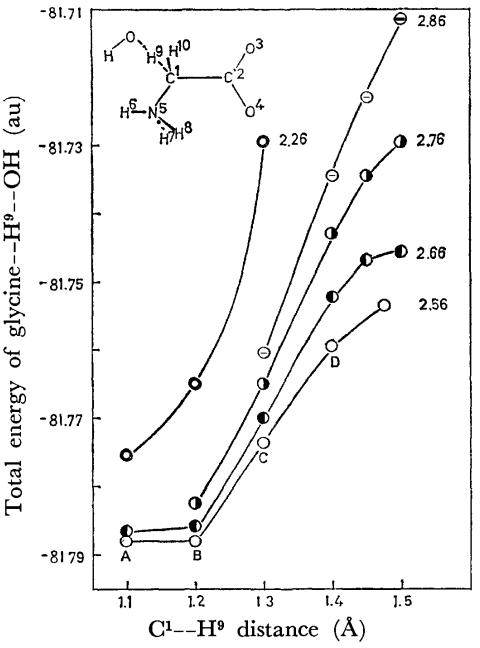

Fig. 3. Potential curves as a function of C^1–H^9 distance at various C^1–O distances in glycine–OH system. The number described near the point is C^1–O distance.

the H^9 atom (α-secondary). In order to examine the suitability of point D for other hydrogen atoms, the interaction energy between the hydroxyl radical and the H^9 atom of alanine has been calculated. As shown in Fig. 4, the favored reaction path has been found to be the same as that observed in the glycine H^9 atom. The results of Figs. 3 and 4 suggest that the path with $r_1+r_2=2.56$ Å is favored for hydrogen atoms of any type. Thus D has been taken as the reference point to compare the reactivities of hydrogen atoms bound to α, β, γ, and δ-carbon atoms.

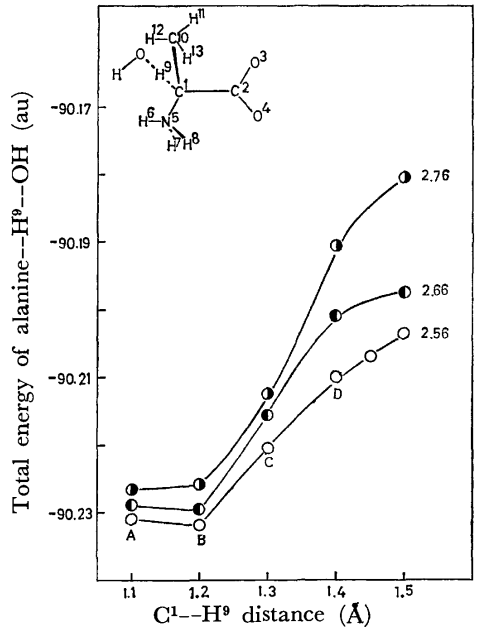

Fig. 4. Potential curves as a function of C^1–H^9 distance at various C^1–O distances in alanine–OH system. The number described near the point is C^1–O distance.

In chemical reactions, it has been recognized that the delocalization of electrons between a reactant and a reagent is a major factor in determining reactivity.[7,8] Although the potential curve should be obtained for the system including both a hydroxyl radical and an amino acid, the interaction energy could not always be obtained, because of divergence in the SCF calculation. This divergence may make the absolute values of the total energy unreliable. However, the relative values of the energy may be useful for a discussion of the relative reactivity. Thus, it has been assumed that the interaction energy could be approximated by the energy change due to the stretching of C–H bond. This model was checked in detail as follows. Several factors contribute to the abstraction reaction, for example, a) the strength of the R–H bond broken, b) the strength of forming the H–X bond, c) the stabilization energy due to delocalization of electrons, d) solvation, and so on. The relative reactivities of hydrogen atoms toward the same attacking reagent have been investigated in the present study and it appears that factors a) and c) dominate. If c) does not vary with types of C–H bonds or if a) and c) correlate linearly with each other, the reactivities of the hydrogen atoms for abstraction may be approximated to the strength of the C–H bond. The interaction energy of the glycine–OH system along the reaction path(A, B, C, D) has been compared with the total energy of glycine obtained by stretching the C^1–H^9 bond from 1.10 to 1.40 Å, in the singlet state. From a linear correlation between the total energy of the composite system and that of glycine at the same bond distance of the C^1–H^9 (Fig. 5), it has been concluded that the reactivity of the H^9 atom may be evaluated in terms of the energy required to stretch the C^1–H^9 bond by a

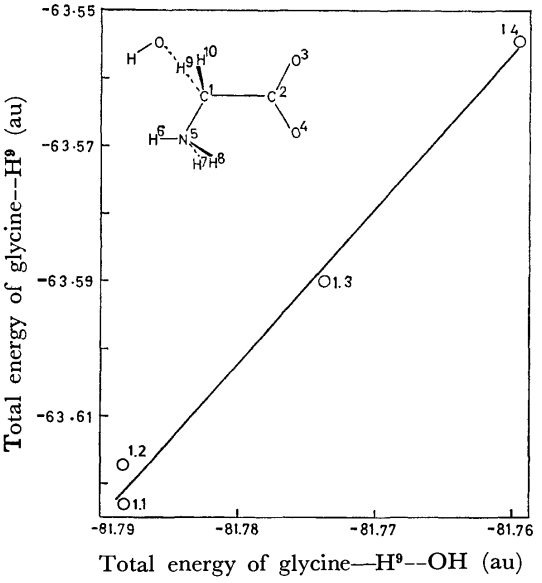

Fig. 5. The linear relationship between the energy changes by elongation of the C–H bond in question in presence and absence of OH group for glycine. The number described near the point is the bond length of the stretching C–H bond.

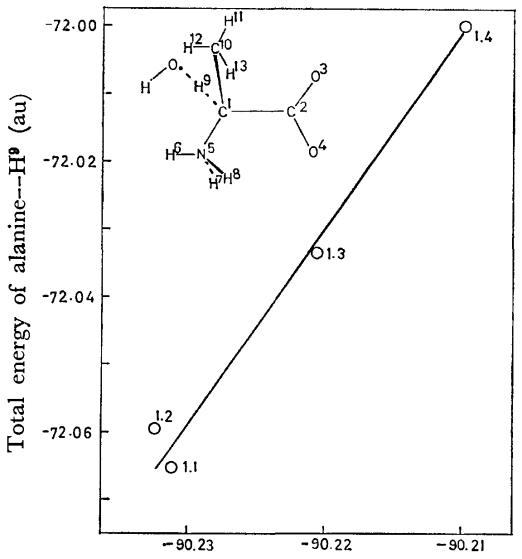

Fig. 6. The linear relationship between the energy changes by elongation of the C-H bond in question in presence and absence of OH group for alanine. The number described near the point is the bond length of the stretching C-H bond.

certain distance from the equilibrium bond length. The same argument is valid for the H^9 (α-tertiary) atom of alanine as shown in Fig. 6.

The conclusion is that the energy change due to stretching of the C-H bond interacting the hydroxyl radical may be approximated by the energy change in the absence of the hydroxyl radical. The validity of this conclusion has been examined for other types of hydrogen-atoms and the results are given in Fig. 7. ΔE_{OH} and ΔE have been difined for the reactivities of the hydrogen atoms in the following equations and have been calculated by two methods.

$$\Delta E_{OH} = E_{\text{amino acid-OH}} \text{ at D(1.40, 1.16)} - E_{\text{amino acid-OH}} \text{ at (1.10, } \infty) \quad (1)$$

$$\Delta E = E_{\text{amino acid}}(\text{C-H } 1.60) - E_{\text{amino acid}}(\text{C-H } 1.10) \quad (2)$$

Where D(1.40, 1.16) and (1.10, ∞) represent the points on the reaction path as previously defined and (C-H 1.60) and (C-H 1.10) indicate the C-H bond length. The point (C-H 1.60) has been tentatively selected in order that ΔE might approximate to ΔE_{OH}, although the absolute value of the energy may be unreliable.

The ΔE for several kinds of hydrogen atoms was found to have a close correlation with ΔE_{OH} with a few exceptions. Consequently, ΔE given by Eq. 2 has been used as an index to represent the reactivity of the hydrogen atoms of amino acids toward hydroxyl radicals in order to avoid the problem of divergency in the SCF calculation of ΔE_{OH}. Here, it should be noticed that the hydrogen atoms bound to the same carbon atom show different reactivities according to the orientation in the amino acid molecule as shown for the H^{11}, H^{12}, and H^{13} atoms of alanine in Fig. 7. This will be discussed in detail below.

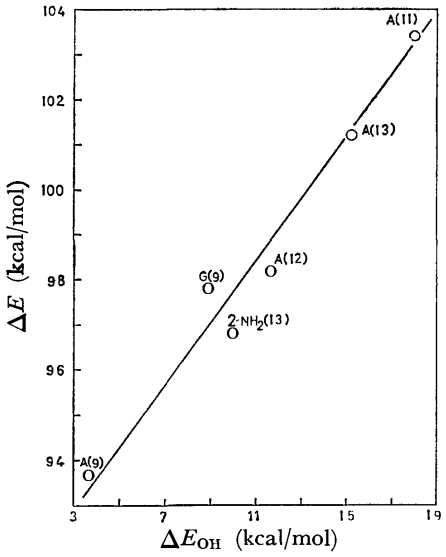

Fig. 7. Comparison of ΔE with ΔE_{OH} for different types of hydrogen atoms. G: glycine, A: alanine, 2-NH_2: 2-aminobutyric acid. The number in parenthesis indicates hydrogen atoms in Fig. 1.

TABLE 2. THE REACTIVITY OF HYDROGEN ATOMS OF AMINO ACIDS CALCULATED BY ΔE

Amino acid		Type of C-H bond	ΔE(au)[b]
Glycine	H^9	α-sec[a]	0.1560
Alanine	H^9	α-tert	0.1498
	H^{11}	β-prim	0.1468
	H^{12}	β-prim	0.1565
	H^{13}	β-prim	0.1614
2-Aminobutyric acid	H^{12}	β-sec	0.1491
	H^{13}	β-sec	0.1544
	H^{14}	γ-prim	0.1617
	H^{15}	γ-prim	0.1601
	H^{16}	γ-prim	0.1490
Valine	H^{12}	β-tert	0.1428
	H^{14}	γ-prim	0.1601
	H^{15}	γ-prim	0.1599
	H^{16}	γ-prim	0.1488
	H^{17}	γ-prim	0.1617
	H^{18}	γ-prim	0.1610
	H^{19}	γ-prim	0.1555
Isoleucine	H^{14}	γ-sec	0.1538
	H^{15}	γ-sec	0.1430
	H^{20}	δ-prim	0.1610
	H^{21}	δ-prim	0.1604
	H^{22}	δ-prim	0.1601
Leucine	H^{11}	β-sec	0.1574
	H^{13}	β-sec	0.1543
	H^{14}	γ-tert	0.1494

a) α-sec: α-secondary, α-tert: α-tertiary, β-prim: β-primary, β-sec: β-secondary, β-tert: β-tertiary. b) Atomic unit.

To compare ΔE with the experimentally assigned values of the partial reactivities of hydrogen atoms, ΔE's were calculated for various kinds of hydrogen

atoms. The calculated values of ΔE are listed in Table 2. In the case of γ-primary hydrogen atoms (H^{14}, H^{15}, H^{16}) of 2-aminobutyric acid or valine, the prediction is that H^{16} is more reactive than H^{14} or H^{15}.

The differences in the reactivities of hydrogen atoms bound to the same carbon atom have been neglected when the partial reactivities were estimated from the observed rate constants. Therefore, the reactivity of γ-primary hydrogen atoms (also, β-primary, β-secondary, and so on) has been approximated by the average reactivity of H^{14}, H^{15}, and H^{16} atoms assuming Maxwell-Boltzmann distribution among the ΔE's. The results are in Table 3.

Table 3. Comparison of ΔE with the experimentally assigned partial reactivity

Type of C–H bond	Partial reactivity $M^{-1}s^{-1}$	ΔE(kcal/mol)
α-Secondary	8.5×10^{6}	97.835
α-Tertiary	1.7×10^{7}	93.715
β-Primary	2.07×10^{7}	98.188
β-Secondary	1.77×10^{8}	93.540[a]
		96.862[b]
β-Tertiary	3.54×10^{8}	89.575
γ-Primary	4.85×10^{7}	93.465[a]
		93.343[c]
γ-Secondary	5.12×10^{8}	89.701
γ-Tertiary	1.02×10^{9}	93.715
δ-Primary	6.75×10^{7}	100.597

a) Obtained from 2-aminobutyric acid. b) From leucine. c) From valine.

The relationship between the logarithm of the experimental reactivity and ΔE is shown in Fig. 8. If the type of hydrogen atoms is not taken into consideration, no clear correlation can be found. However, when the argument is restricted to only β-hydrogen atoms, a correlation betweeen ΔE and $\ln k$ is observed, though it is not well defined. For α-hydrogen atoms, only two points are available, and consequently no conclusive statement can be inferred. However, the slope is similar to that in the $\ln k \approx \Delta E$ correlation of β-hydrogen atoms. In the case of γ-hydrogen atoms, no correlation was found. To obtain a quantitative relation between the experimentally determined rate constant and the calculated interaction energy, the configurational changes of molecules in solution needs to be taken into consideration. In the present procedure, ΔE has been calculated for the fixed geometry of the amino acid molecule. The effect of the protonated amino group on the reactivity of a given hydrogen atom may vary with the position of the atom in three-dimentional space. For γ-hydrogen atoms, the fluctuation of the reactivity due to the configurational change is probably larger than the α or β-hydrogen atoms.

With regard to the values of ΔE in Table 3, two values of ΔE are given for β-secondary and γ-primary hydrogen atoms. The ΔE of the β-secondary hydrogen atom has been evaluated to be 93.540 kcal/mol as the average for H^{12} and H^{13} atoms of 2-aminobutyric acid, whereas 96.862 kcal/mol has been obtained as the average for H^{11} and H^{13} atoms of leucine. As ΔE for the H^{13} atom of leucine is approximately the same as that for the H^{13} atom of 2-aminobutyric acid, the difference in averaged ΔE's is attributable to the difference in ΔE between the H^{11} atom of leucine and the H^{12} atom of 2-aminobutyric acid. The value for γ-primary hydrogen atoms, 93.465 kcal/mol has been obtained from H^{14}, H^{15}, and H^{16} atoms of 2-aminobutyric acid and it was approximately consistent with 93.343 kcal/mol obtained from the H^{14}, H^{15}, and H^{16} atoms of valine. This suggests that the effect of another CH_3 group (C^{13}, H^{17}, H^{18}, H^{19}) of valine upon the reactivitiy of γ-primary hydrogen atoms is not large and the same value may be used for 2-aminobutyric acid and valine. If the molecular backbone is different, the same value cannot always be applied to represent the reactivity as shown in the cases of 2-aminobutyric acid and leucine, because the reactivity of the hydrogen atom is closely related to the orientation in the molecule. As already described, there is a remarkable difference in ΔE among primary and secondary hydrogen atoms. For γ-primary hydrogen atoms of 2-aminobutyric acid, for example, the large reactivity of the H^{16} atom compared with that of the H^{14} and H^{15} atoms is ascribed to the difference in the two-center interaction energy. The two-center energy in the INDO method[5] is equal to that in the CNDO/2 method by Pople *et al.*[9,10] and consists of the three terms with different characters.

$$E_{A-B} = \sum_{\mu}^{A}\sum_{\nu}^{B} 2P_{\mu\nu}\beta_{\mu\nu} - \frac{1}{2}\sum_{\mu}^{A}\sum_{\nu}^{B} P_{\mu\nu}^{2}\gamma_{AB} + [Z_A Z_B R_{AB}^{-1} - P_{AA}V_{AB} - P_{BB}V_{BA} + P_{AA}P_{BB}\gamma_{AB}] \quad (3)$$

The first term is called the resonance term, the second the exchange term and the third the electrostatic term. The two-center energies calculated for 2-aminobutyric acid are shown in Table 4. ΔE_{C-H}, defined by the following equation, is the local energy required in stretching a C–H bond.

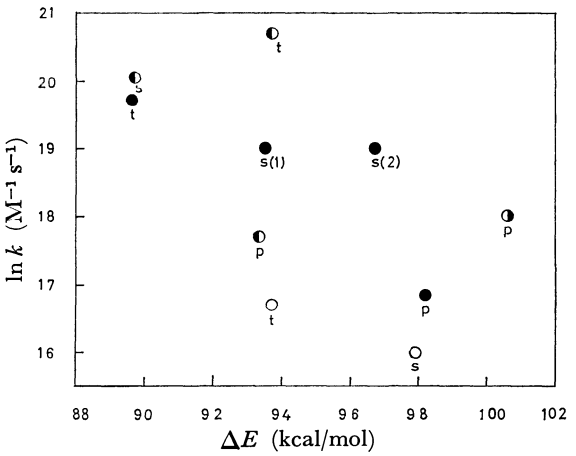

Fig. 8. Comparison of ΔE with the experimentally assigned partial reactivity. ○: α-, ●: β-, ◐: γ-, ◑: δ-, p: primary, s: secondary, t: tertiary. s(1) and s(2) are obtained from 2-aminobutyric acid and leucine respectively, see Table 3.

$$\Delta E_{C-H} = E_{C-H\ 1.60} - E_{C-H\ 1.10}, \quad (4)$$

where $E_{C-H\ 1.10}$ and $E_{C-H\ 1.60}$ are the interatomic interaction energies between carbon and hydrogen atoms at the C–H distance of 1.10 and 1.60 Å, respectively. E_{O-H} (C–H 1.10) and E_{O-H} (C–H 1.60) are the interatomic interaction energies between O^3 oxygen and hydrogen atoms (H^{14}, H^{15}, H^{16} of 2-aminobutyric acid) obtained at the C–H distance of 1.10 and 1.60 Å, respectively. ΔE, defined by Eq. 2, is the total energy required for the stretching and gives an index of the reactivity of hydrogen atoms. From the viewpoint of the energy required to stretch the C–H bond ΔE_{C-H}, the H^{16} atom is expected to the less reactive than the H^{14} and H^{15} atoms. However, ΔE gives the reverse results. For the interatomic interaction energy between O^3 and (H^{14}, H^{15}, H^{16}) atoms (E_{O-H} in Table 4), large stabilization is observed between O^3 and H^{16} atoms when the C^{11}–H^{16} bond is stretched. In the case of H^{14} and H^{15} atoms, destabilization occurred. In order to clarify the effect of the carboxyl group upon the reactivity of the H^{16} atom, a similar calculation was conducted by rotating the carboxyl group around the C^1–C^2 bond by 90°. The stabilization energy due to the interaction between O^3 and H^{16} atoms then reduces to approximately a tenth compared with the case without rotation of the carboxyl group. Accordingly, three hydrogen atoms have approximately equal reactivity as predicted from the magnitude of ΔE_{C-H}.

The interatomic interaction energy between O^3 and H^{16} atoms was further investigated by decomposing it into three components as in Eq. 3. The results given in Table 5 indicate that the resonance term is the most important and the main reason for the negative value of the O^3–H^{16} energy. Consequently it

TABLE 4. INTERATOMIC INTERACTION ENERGY OF 2-AMINOBUTYRIC ACID (au)

(A) Carboxyl group lies on the same plane with C^1, C^2, and N_5 atoms.

	C^{11}–H^{14}	C^{11}–H^{15}	C^{11}–H^{16}
E_{C-H} 1.10	−0.7536	−0.7481	−0.7470
E_{C-H} 1.60	−0.5475	−0.5433	−0.5239
ΔE_{C-H}	0.2061	0.2038	0.2231
ΔE	0.1617	0.1601	0.1490
	O^3–H^{14}	O^3–H^{15}	O^3–H^{16}
E_{O-H} (C–H 1.10)	0.0012	0.0018	−0.0179
E_{O-H} (C–H 1.60)	0.0055	0.0050	−0.0717

(B) After rotating carboxyl group by 90° around C^1–C^2 bond.

	C^{11}–H^{14}	C^{11}–H^{15}	C^{11}–H^{16}
E_{C-H} 1.10	−0.7507	−0.7496	−0.7507
E_{C-H} 1.60	−0.5476	−0.5467	−0.5461
ΔE_{C-H}	0.2031	0.2029	0.2046
ΔE	0.1615	0.1610	0.1613
	O^3–H^{14}	O^3–H^{15}	O^3–H^{16}
E_{O-H} (C–H 1.10)	0.0015	0.0011	−0.0033
E_{O-H} (C–H 1.60)	0.0046	0.0047	−0.0084

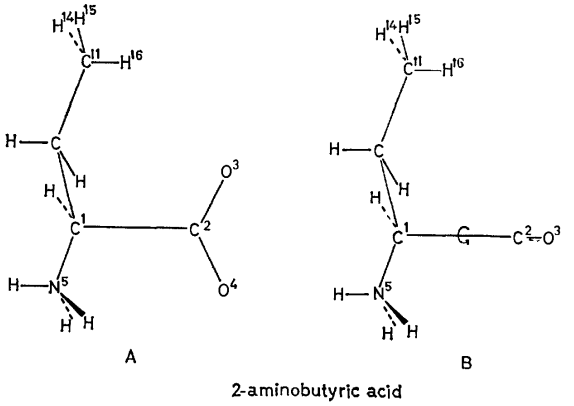

Fig. 9. Carboxyl group lies on the same plane with C^1, C^2, and N^5 atoms in A form, whereas in B form, the carboxyl group is rotated by 90° around C^1–C^2 bond.

may be concluded that the resonance interaction between O^3 and H^{16} atoms leads to an intramolecular hydrogen-bonding and this stabilization results in the large reactivity of the H^{16} atom despite the large value of ΔE_{C-H} of the C^{11}–H^{16} bond.

The reaction mechanism of the hydrogen abstraction by the hydroxyl radical from amino acids will now be discussed in terms of the electronic structure. The bond indices given by Wiberg[11] for the glycine–OH system are listed in Table 6, and the spin density and the charge transferred from glycine to the hydroxyl radical are listed in Table 7. It has been assumed that the hydroxyl readical has four valence electrons of α-spin and three valence electrons of β-spin. As shown in Tables 6 and 7, the approach of the hydroxyl radical decouples the electron pairing in the C^1–H^9 bond. The β-spin electron moves toward the H^9 atom while the α-spin electron in the opposite direction. In accordance with this spin movement, the α-spin

TABLE 5. THE DECOMPOSITION OF THE INTERATOMIC INTERACTION ENERGY BETWEEN O^3 AND H^{16} ATOMS(au)

Resonance term	−0.0617
Exchange term	−0.0101
Electrostatic term	0.0001
E_{O-H} (C–H 1.60)	−0.0716[a]

a) The interatomic interaction energy between O^3 and H^{16} atoms in Table 4 (A).

TABLE 6. BOND INDICES FOR THE GLYCINE–OH SYSTEM

Path point	C^1–H^9 bond indices		H^9–O bond indices	
	α-Spin	β-Spin	α-Spin	β-Spin
(1.10, 1.56)[a]	0.231	0.222	0.007	0.018
(A)	0.227	0.214	0.010	0.027
(B)	0.209	0.195	0.022	0.045
(C)	0.169	0.155	0.061	0.082
(D)	0.103	0.091	0.108	0.150

a) The values 1.10 and 1.56 denote the C^1–H^9 bond distance and H^9–O bond distance respectively.

Table 7. Spin density and charge transfer quantities for the glycine-OH system

Path point	Spin density			CT[b]
	C^1	H^9	O	
(1.10, 1.56)[a]	0.010	−0.044	0.015	−0.020
(A)	0.016	−0.061	0.016	−0.031
(B)	0.029	−0.120	0.015	−0.044
(C)	0.047	−0.209	0.011	−0.071
(D)	0.053	−0.239	0.006	−0.128

a) The values 1.10 and 1.56 denote the C^1–H^9 bond distance and H^9–O distance respectively. b) The charge transfer quantity from glycine to hydroxyl radical.

C^1–H^9 bond is weakened, and the β-spin H^9–O bond begins to form. This can reasonably be explained by the three-stage model proposed by Nagase *et al.*[12–14]

$$\text{Glycine } C^1\uparrow\downarrow H^9 + \uparrow OH \rightarrow \text{Gly } C^1\cdots\uparrow\downarrow\cdots H^9\cdots\uparrow OH$$
$$\rightarrow \text{Gly } C^1\uparrow + H_2O$$

References

1) T. Masuda, S. Nakano, K. Yoshihara, and M. Kondo, *J. Radiat. Res.*, **17**, 63 (1976).
2) I. Kraljić and C. N. Trumbore, *J. Am. Chem. Soc.*, **87**, 63 (1965).
3) S. Shsh, C. N. Trumbore, B. Giessner, and W. Park, "Radiation Chemistry-I," ed by R. F. Gould, Am. Chem. Soc. (1968), p. 321.
4) J. A. Pople and R. K. Nesbet, *J. Chem. Phys.*, **22**, 571 (1954).
5) J. A. Pople and D. L. Beveridge, "Approximate Molecular Orbital Theory," Mcgraw-Hill, New York (1970).
6) H. Shinohara, A. Imamura, T. Masuda, and M. Kondo, *Bull. Chem. Soc. Jpn.*, **51**, 1917 (1978).
7) K. Fukui, T. Yonezawa, and H. Shingu, *J. Chem. Phys.*, **20**, 722 (1952); K. Fukui, T. Yonezawa, and H. Shingu, *ibid.*, **22**, 1433 (1954).
8) K. Fukui, T. Yonezawa, and C. Nagata, *Bull. Chem. Soc. Jpn.*, **27**, 423 (1954); K. Fukui, T. Yonezawa, and C. Nagata, *J. Chem. Phys.*, **27**, 1247 (1957).
9) J. A. Pole, D. P. Santry, and G. A. Segal, *J. Chem. Phys.*, **43**, s129 (1965); J. A. Pople and G. A. Segal, *ibid.*, **43**, s135 (1965).
10) J. A. Pople and G. A. Segal, *J. Chem. Phys.*, **44**, 3289 (1968).
11) K. B. Wiberg, *Tetrahedron*, **24**, 1083 (1968).
12) S. Nagase and T. Fueno, *Theor. Chem. Acta (Berlin)*, **41**, 59 (1976).
13) S. Nagase, K. Takatsuka, and T. Fueno, *J. Am. Chem. Soc.*, **98**, 3838 (1976).
14) S. Nagase and T. Fueno, *Bull. Chem. Soc. Jpn.*, **49**, 2920 (1976).

A Computer Program Package for the Analysis, Creation, and Estimation of Generalized Reactions—GRACE. I. Generation of Elementary Reaction Network in Radical Reactions—A/GRACE(I)†

Yukio YONEDA

Department of Synthetic Chemistry, Faculty of Engineering, The University of Tokyo, Hongo, Bunkyo-ku, Tokyo 113

(Received February 1, 1978)

The system GRACE generates elementary reaction networks for simple reactions including free radicals, ions and even active sites in heterogeneous catalysis, and also predicts the overall reaction rates and the product distributions in radical reactions in the gas phase where the Arrhenius parameters of elementary reactions are available. In this paper, A/GRACE (part A of GRACE) is explained, which prepares elementary reaction networks for radical reactions. The reactant and the product are represented by square symmetric matrices. The off-diagonal elements represent bond multiplicity, or the number of localized electrons, between corresponding atoms, whereas the diagonal elements imply the number of unshared electrons on radical atoms. A reacting system, an ensemble of the participating molecules, is composed of atom groups, each of which consists of a center atom (usually non-hydrogen) and attached hydrogen atom(s), if any. Firstly, all the possible changes in the atom groups are selected, and the permitted combinations are preapred bearing in mind the equivalent groups in the system and the restrictions optioned. The major restriction is the complexity, *i.e.*, the number of ruptured or formed bonds. A direct sum of matrices are prepared from one of the combinations, and the elementary reaction is completed by setting the appropriate numerals, 1 or −1, to the outside elements. Secondly, the procedures are repeated until all the feasible networks are prepared. As an illustration the hydrogenation of ethylene over a heterogeneous catalyst has been cited.

In chemical research and development, both pure and applied, computers can be used for creation and estimation of chemical facts with the aid of chemical logic, as well as mere numerical calculations. Chemical facts may be divided into two groups: the static physical properties of substances and the reaction characteristics among them. The present author has already published[1] the outline of a computer program package, EROICA, for the esitimation and the retrieval of physical properties of organic molecules.

Recently several systems of chemical logic with programs for the creation, or generation, of chemical reactions have been published by Corey,[2] Ugi,[3] Wipke,[4] and Bersohn.[5] Earlier works include DENDRAL by Feigenbaum *et al.*[5a] The features and the aims of these systems are rather different, reflecting the main interests of the authors. The present author has intended to develop a system that is capable of creating all of the possible reaction routes, or an elementary reaction network, in simpler organic reactions, and estimating quantitatively the reaction rates and product distribution. The system, GRACE (*G*eneralized *R*eaction *A*nalysis for *C*reation and *E*stimation) is fundamentally similar to that of Ugi *et al.*,[3] although the systems have been developed independently, and employs square matrices for manipulation of reacting systems. The outline of our system in the earlier stage was first published in 1970 as a part of a review.[6]

This program package has the ability to create radical and ionic reactions and to accurately estimate the quantitative values of overall reaction rates and product distributions of hydrocarbon pyrolyses in gaseous phase. However, the stereochemistry is ignored. This system may be extended to find out parasitic reactions when a target reaction is given, as well as to survey all the possible reaction schemes from given raw materials to valuable products.

† CHEMOGRAM, a Computer Program Package for Chemical Logic, Part 2.

Outline of GRACE

The system of GRACE consists of three sub-systems, A/GRACE, B/GRACE, and C/GRACE, as shown in Fig. 1, and may be operated following the arrows in the flow chart. The functions of the sub-systems are as follows:

(1) A/GRACE: A given overall reaction (radical or ionic reaction) is analyzed into a network of elementary reactions, which generates the product system from the reactant system through various intermediate systems.

(2) B/GRACE: Arrhenius parameters of all the elementary reactions prepared by A/GRACE will be searched by information retrieval from a file of observed data, estimated by searching the data of resembling reactions from the file, or also estimated with the aid of empirical linear free energy relationships. However, processing is at present limited to radical reactions in gaseous phase due to the lack of observed Arrhenius parameters.

(3) C/GRACE: Simultaneous differential equations corresponding to the material balance among

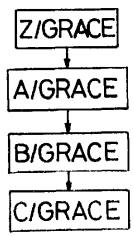

Fig. 1. Flow chart of GRACE.

species in the network are prepared automatically. Overall rate and product distribution are calculated with the given initial conditions by direct integration of the equations or assuming the stationary state. Both flow and batch reactions may be dealt with.

In addition to these three sub-systems, a minor sub-system Z/GRACE, the part Zero of GRACE, may be employed to prepare the input data for A/GRACE concerning the reactant and product from a CHEMO input, a linear input of a rational formula also proposed by the present author.[7]

Representation of Reacting System by Matrices

In this paper, a *system* is defined as an *ensemble*[3] of molecules which are employed as components of a given reaction; a *reacting system* implies all of the systems of the reactant, intermediates and the product. The representation method of reacting systems will be explained for heterogeneous hydrogenation of ethylene, as a simple example.

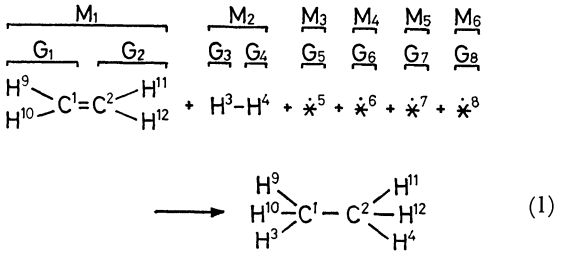

(1)

Equation 1 shows the overall reaction of hydrogenation, where the asterisks, *, represent the active sites over the solid catalyst, *e.g.*, metallic nickel, the dots over the symbols indicate radicals, and the superscripts over atomic symbols give the *atom ordinals* in this system. Symbols G and M given above in the reactant system represent *atom groups* and molecules, respectively. Here, an atom group implies the smallest ensemble of atoms, consisting of a *center atom* (usually non-hydrogen atom) and up to six *attached hydrogen* atoms, if any, although both of the hydrogen atoms in a hydrogen molecule are the center atoms; the reactant in Eq. 1 is thus composed of six molecules and eight atom groups.

Reactant and Product Matrices. A reactant matrix, symmetric and very sparse, may be prepared from Eq. 1 by appropriately assigning a row and a column to each atom. In this way the molecules and atom groups may be arranged to follow faithfully the order of chemical bonds in the system as shown in Fig. 2(a). The matrix elements represent the multiplicity of chemical bonds: 1 for a single bond, 2 for a double bond, and 3 for a triple bond. At the present stage of development, a bond with a bond order of 1.5, that is, a conjugated double bond, may not be entertained. The matrix thus prepared is termed a reactant bonding matrix, $\boldsymbol{X}_b$, where $\boldsymbol{X}$ represents the reactant system and b the bonding matrix. It can be seen that each element of the matrix represents also the number of valence electrons belonging to an

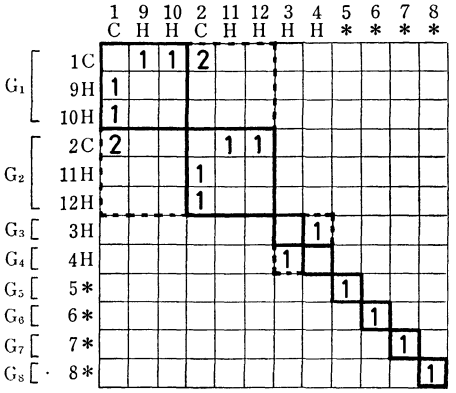

Fig. 2a. Reactant bonding matrix, $\boldsymbol{X}_b$.

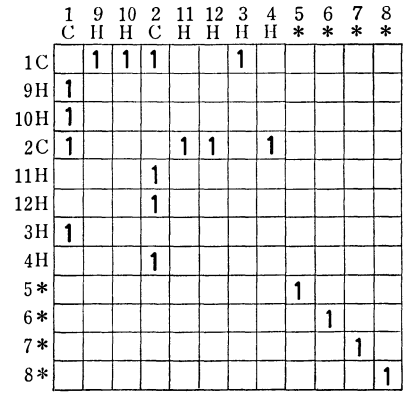

Fig. 2b. Product bonding matrix, $\boldsymbol{Y}(\boldsymbol{X}_b)$.

atom which are localized on a bond designated by the matrix. Hence, a radical atom that has at least one unshared valence electron should have valence electron(s) localized on it; *i.e.*, there is a numeral in the diagonal element.

A *product bonding matrix*, $\boldsymbol{Y}(\boldsymbol{X}_b)$ (Fig. 2(b)), may be prepared from Eq. 1 following the arrangement of the atom ordinals in $\boldsymbol{X}_b$, where $\boldsymbol{Y}$ represents a reactant and $(\boldsymbol{X}_b)$ defines the arrangement of atoms in the matrix as following the matrix $\boldsymbol{X}_b$. In the matrix $\boldsymbol{Y}$, two matrix elements having had a value of 2 in $\boldsymbol{X}_b$ are changed to 1 due to hydrogenation of the double bond.

Reaction Matrix. A reaction matrix, $\boldsymbol{R}_b$, may be defined as the difference between product $\boldsymbol{Y}$ and reactant $\boldsymbol{X}$:

$$\boldsymbol{R}_b = \boldsymbol{Y}(\boldsymbol{X}_b) - \boldsymbol{X}_b. \tag{2}$$

A reaction matrix, Fig. 2(c), is symmetric. The elements in the matrix represent the appearance or the disappearance of the localized valence electrons, and indicate bond formation and rupture, including changes in the bond multiplicity. Usually in elementary reactions, changes in the value of the matrix elements may not exceed two, since the change by two implies, for example, the sudden formation or rupture of a double bond in a single elementary step. The transformation of the double bond in ethylene to a single bond, the rupture of a single bond in a hydrogen molecule and the addition of two hydrogen atoms to ethylene may be found in Fig. 2(c). The active

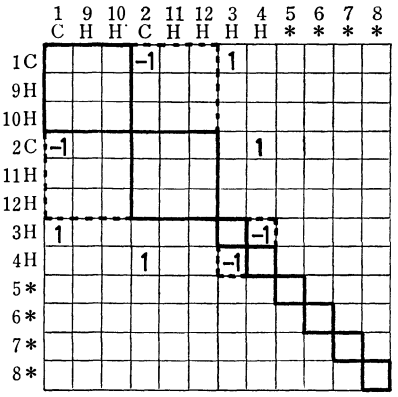

Fig. 2c. Reaction matrix, $\boldsymbol{R}_b = \boldsymbol{Y}(\boldsymbol{X}_b) - \boldsymbol{X}_b$.

sites (*) show no change in overall reaction because they are catalysts.

The sum of the matrix elements in each row as well as in each column of a reaction matrix should be zero, since the number of total valence electrons belonging to each atom does not change during reaction as far as radical reactions are concerned.

Preparation of One Step Reaction in the Elementary Reaction Network

Elementary Reaction Matrix. An elementary reaction may be defined as a simple reaction that cannot be decomposed further into simpler reactions in the sense of the transformation of the bonding. In general, only two-centered and there-centered reactions have been adopted as elementary reactions, although in some cases, such as concerted reactions, four-centered reactions may also be allowable. In a reaction matrix, the number of non-zero off-diagonal elements in the upper-right half implies the number of bonds, formed and ruptured. This number is defined as the *complexity* of a reaction (κ); complexity 1 corresponds to two-centered, complexity 2 to two- and three-centered, complexity 3 to three- and four-centered, and complexity 4 to four-centered reactions, respectively. Hereafter, an elementary reaction will be defined as a reaction with complexity not exceeding the maximum complexity (κ_{max}), for which the value of 3 or 4 is usually chosen.

An overall reaction through the r-th route will be decomposed into elementary reactions $\boldsymbol{R}^{el}{}_{rs}$ as

$$\boldsymbol{R}^{over}(r) = \sum_s \boldsymbol{R}^{el}{}_{rs}, \tag{3}$$

where $\boldsymbol{R}^{over}(r)$ represents the matrix of the above-mentioned overall reaction and s indicates the step number in the network. If the intermediate systems $\boldsymbol{I}_{r,s-1}$ and $\boldsymbol{I}_{r,s}$ are the reactant and the product of step s in route r, respectively, then

$$\boldsymbol{I}_{r,s} = \boldsymbol{R}^{el}{}_{rs} + \boldsymbol{I}_{r,s-1}. \tag{4}$$

By adding Eq. 4 recursively, Eq. 2 will be derived with Eq. 3; $\boldsymbol{R}_b$ in Eq. 2 is exactly the same as $\boldsymbol{R}^{over}(r)$ given in Eq. 3, although the latter clearly indicates the component of the network. The strategy therefore to develop a network that connects the overall reactant and the overall product is to create logically the above mentioned elementary reactions.

Preparation of an Elementary Reaction. During an elementary reaction, a change in valence electrons takes place within atom groups and between them. The change within an atom group may depend on the structure of that group, whereas the change between groups may depend on the change within groups. Thus, the following procedures will be employed as a tactics to create elementary reaction matrices.

(a) Restrictions for an elementary reaction should be given at first. The major restrictions are the maximum complexity of the elementary reaction and the maximum number of radicals involved. There may also be various minor restrictions such as the prohibition of hydrogen radicals in the gaseous phase and the prohibition of homogeneous reactions in which no active sites participate.

(b) Allowable group reaction matrices are selected for each atom group. *A group reaction matrix*, $\boldsymbol{\rho}$, is a small matrix whose order is the same as that of the atom group matrix, and represents the change within the atom group. Each group reaction matrix should satisfy the restrictions mentioned in (a).

(c) Appropriate combinations of $\boldsymbol{\rho}$'s (one $\boldsymbol{\rho}$ for each group) are selected so that these combinations again satisfy the restrictions; for example, odd number of radicals cannot be allowed in Eq. 1. In addition, the systems commonly have equivalent molecules or atom groups; (G_1 and G_2), (G_3 and G_4), and (G_5, G_6, G_7, and G_8) in Eq. 1 are equivalent atom groups, and M_3—M_6 are equivalent molecules. Such redundancy as imposing the same $\boldsymbol{\rho}$ repeatedly on equivalent atom groups should be avoided.

(d) The direct sum of a combination of $\boldsymbol{\rho}$'s are prepared along the diagonal of a blank reaction matrix. The remaining procedure is to supply the appropriate numerals, 1 or -1, in the *intergroup domain*, *i.e.*, the domain outside the atom groups, so that the filled matrix satisfies the requirement of a reaction matrix that the sum of the elements in each row should be zero. When the completed elementary reaction matrix satisfies all the restrictions, it is used to create an intermediate system, otherwise it should be discarded.

(e) Procedure (d) is repeated until all the combinations prepared in procedure (c) are exhausted. Thus all the intermediate systems which are logically allowable are created from the preceding intermediate.

Group Reaction Matrix. In general, there are several group reaction matrices which are applicable for a specified group; an example of a set of the group reaction matrices is shown in Fig. 3. This set is applicable for AH_2 groups where A designates an atomic species that has a valency not less than 2 like carbon and nitrogen; methylene groups in ethylene, dichloroethane or carbene, and an amino group in methyl amine or amino radical is represented by an AH_2 group.

In Fig. 3, $\boldsymbol{x}$ designates a group matrix representing the atom group AH_2, where n (n=0, 1, or 2) implies the number of unshared electrons localized on the

a. Atom group matrix for AH_2.

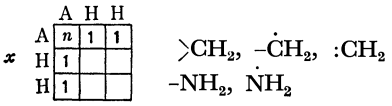

b. Group reaction matrices for AH_2.

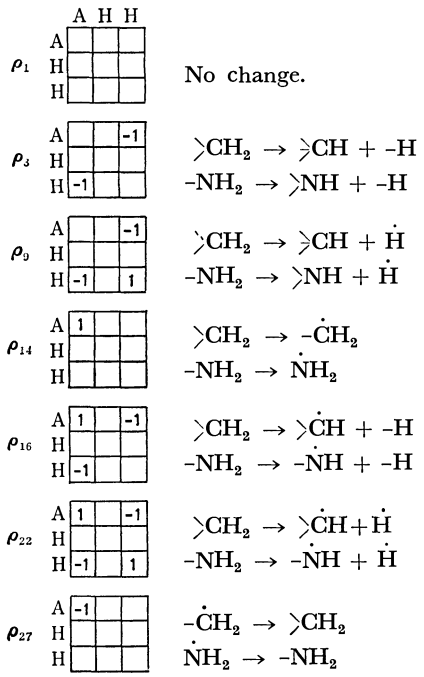

Fig. 3. Group reaction matrices for AH_2 group.

atom A. For example, carbon with $n=2$ represents a carbene molecule, and nitrogen with $n=1$ represents an amino radical.

A blank matrix $\boldsymbol{\rho}_1$ implies that no change takes place within this atom group. Matrices $\boldsymbol{\rho}_3$ to $\boldsymbol{\rho}_{27}$ represent changes illustrated in the right-hand margin, where a short bar indicates one localized electron on a bond connected to other atoms. Thus two bars implies two single bonds or a double bond and a dot indicates an unshared electron. The matrix $\boldsymbol{\rho}_{27}$ represents the disappearance of a radical atom, or an unshared electron, on the atom A, because a diagonal element, -1, on A indicates the decrease of the number of unshared electrons in the reactant. Naturally, this $\boldsymbol{\rho}_{27}$ should be applied only for $\boldsymbol{x}$ with $n \geqq 1$. All the possible changes in the atom group AH_2 are represented with these seven group reaction matrices, as far as it is assumed that only one valence electron on an atom moves from the formerly localized position to the new one.

A practical example using Eq. 1 will now be given. The following processing will be conducted under the restrictions stated in Table 1. Figure 4 shows the allowable $\boldsymbol{\rho}$'s for the methylene group in the overall reactant $\boldsymbol{X}$ under the above restrictions, where $\boldsymbol{\rho}_9$ and $\boldsymbol{\rho}_{22}$ are excluded because the hydrogen radical in the gaseous phase is prohibited, and $\boldsymbol{\rho}_{27}$ is also excluded as the methylene groups in $\boldsymbol{X}$ have no radical atom ($n=0$).

Table 1. Restrictions optioned for generation of elementary reaction network of the reaction in Eq. 1

1. Complexity of elementary reaction should not exceed 3.
2. Number of reaction centers should not exceed 4.
3. Molecularity of reaction including active sites should not exceed 3.
4. Number of radical atoms shold not exceed 4.
5. Number of uupaired electrons on an atom should not exceed 1.
6. No gaseous hydrogen radical is allowed, although hydrocarbon radicals may be allowed even in gaseous phase.
7. Number of valence electrons is 4 for carbon, and 1 for hydrogen and active sites.
8. At least one active site should participate in each elementary reaction.
9. Recombination of active sites is not allowed, as it may be impossible in actual reaction.

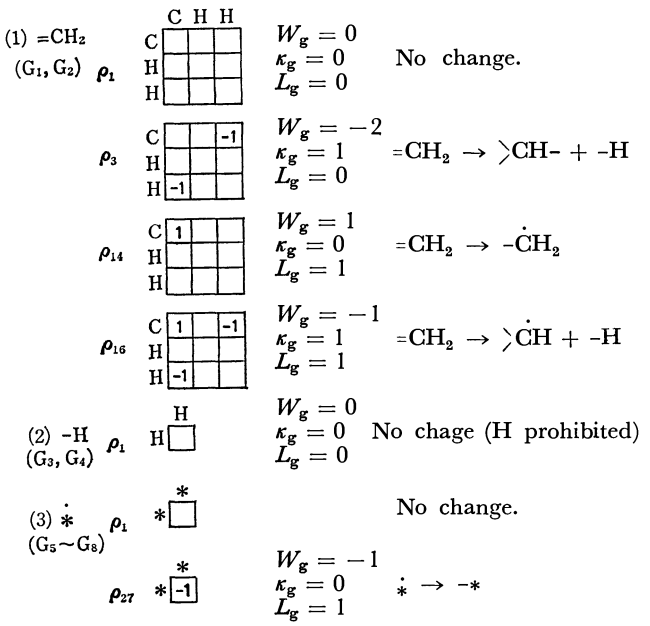

Fig. 4. Allowable group reaction matrices for methylene, hydrogen and active site groups.

For an atom group which consists of only the center atom without any attached atoms, three group reaction matrices of order 1, *i.e.*, $\boldsymbol{\rho}_1$, $\boldsymbol{\rho}_{14}$, and $\boldsymbol{\rho}_{27}$ are allowable. However, only one matrix ($\boldsymbol{\rho}_1$) will be allocated to the hydrogen atom groups in $\boldsymbol{X}$, and two ($\boldsymbol{\rho}_1$ and $\boldsymbol{\rho}_{27}$) to active sites, based on the similar reasoning as in the case of methylene.

Direct Sum of Group Reaction Matrices. The direct sum of group reaction matrices is a succession of an appropriate combination of corresponding group reaction matrices placed along the diagonal of a reaction matrix, which is shown surrounded by bold, solid lines in Fig. 5. The appropriate combination will be selected so that the elementary reaction matrix prepared satisfies both the chemical logic and given restrictions.

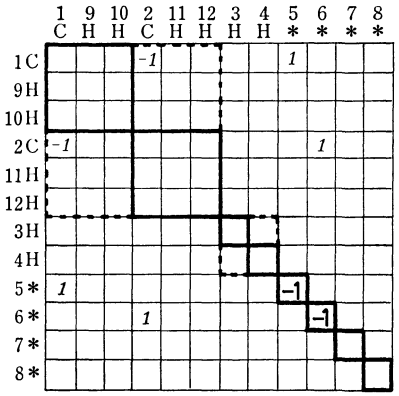

Fig. 5. An example of elementary reaction matrix.

The attributes of a group reaction matrix are defined as follows:

W_g: sum of all the elements.
κ_g: complexity.
L_g: sum of absolute values of diagonal elements.

Figure 4 illustrates the various values.

An elementary reaction matrix $\boldsymbol{R}^{el}$ may be completed by placing the appropriate numerals in the intergroup domain. Since $\boldsymbol{R}^{el}$ is symmetric, the sum of the elements in the intergroup domain is zero or even. Therefore it is a necessary condition that the sum of the elements within the direct sum should be also zero or even, because the sum of the elements of $\boldsymbol{R}^{el}$ is zero by definition. Thus,

$$\sum W_g = \text{zero or even.} \tag{5}$$

A completed direct sum matrix is a direct sum, in which the sum of the elements in every row is zero, satisfying the criteria of a completed reaction matrix. Except for this case, some changes are also necessarily expected in the intergroup domain, and their contribution to κ is not less than unity. Thus, the sum of κ_g's of ρ's should be less than or equal to $\kappa_{max}-1$. Hence,

$$\sum \kappa_g \leqq \kappa_{max} - 1. \tag{6}$$

Finally, since only a pair or pairs of unshared electrons appear or disappear as far as radical reactions are concerned, the grand sum of the absolute values of the diagonal elements should also be zero or even,

$$\sum L_g = \text{zero or even.} \tag{7}$$

The three selection rules mentioned above are still necessary conditions. Table 2 is thus derived, where all the approved combinations of ρ's are shown for each group.

Completion of Elementary Reaction Matrix. The bold lines in Fig. 5 surround the direct sum of combination No. 1 in Table 2. Then, the appropriate numerals, 1 or -1, are given to the intergroup domain so that the resulting matrix satisfies the conditions of a reaction matrix. The datails of the tactics how to allocate them will be published later. It is worthy of mention, however, that more than one set of numerals may exist for one combination of ρ's. The completed matrix should be further checked as to whether it satisfies the given restrictions such as complexity, number of reaction centers, molecularity, and so on. In the GRACE system these critical examinations are made by complex and sophisticated algorithms in the programs.

Since the elementary reaction matrix shown in Fig. 5 satisfies all the restrictions, it will be adopted as a component of the reaction network. By adding this matrix to the overall reactant matrix given in Fig. 2(a), an intermediate matrix $\boldsymbol{I}_1$ will be given as shown in Fig. 6. The change from $\boldsymbol{X}_b$ to $\boldsymbol{I}_1$ represents the reaction in the chemical formula,

$$C_2H_4 + H_2 + 4\dot{*} \rightarrow \underset{\downarrow\ *}{CH_2}\text{-}\underset{\downarrow\ *}{CH_2} + H_2 + 2\dot{*} \tag{8}$$

These procedures will be repeated on all the combinations given in Table 2 under the restriction of $\kappa \leqq 6$, and the resulting intermediates from the overall reactant are tabulated in Table 3, where No. 1a is the intermediate shown in Eq. 6. Four intermediates have

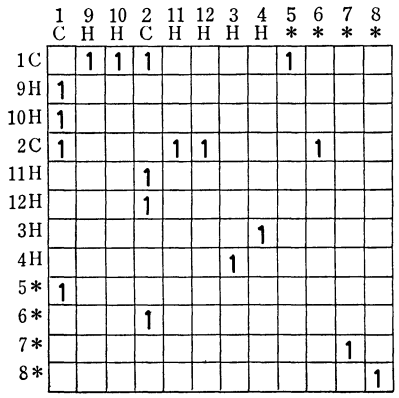

Fig. 6. An example of intermediate matrix, $\boldsymbol{I}_1$, derived from the reaction matrix in Fig. 5.

TABLE 2. ALLOWABLE COMBINATIONS OF GROUP REACTION MATRICES

Combination No.	=CH$_2$		-H		*				$\sum W_g$	$\sum \kappa_g$	$\sum L_g$
	G_1	G_2	G_3	G_4	G_5	G_6	G_7	G_8			
1	1	1	1	1	27	27	1	1	−2	0	2
2	3	1	1	1	27	27	1	1	−4	1	2
3	14	1	1	1	27	1	1	1	0	0	2
4	16	1	1	1	27	1	1	1	−2	1	2
5	3	3	1	1	27	27	1	1	−6	2	2
6	3	14	1	1	27	1	1	1	−2	1	2
7	3	16	1	1	27	1	1	1	−4	2	2

Table 3. Elementary reactions in the first step of the overall reaction

No.[a]	Created intermediate	κ	Remark
1a	$CH_2(*)-CH_2(*)+H_2+2;_*$	3	Associative mechanism (first step; adsorption of ethylene)
1b	$CH_2(*)=CH_2+2H(*)+2;_*$	3	Associative mechanism (first step; adsorption of hydrogen)
1c	$CH_2(*)-CH_3+H(*)+2;_*$	5	Associative mechanism (second step)
2	$CH(*)=CH_2+H(*)+H_2+2;_*$	3	Dissociative mechanism
3	$CH_2(*)-\dot{C}H_2+H_2+3;_*$	2	Precursor of 1a and 1c
4	$CH_2=\dot{C}H(*)+H+H_2+3;_*$	2	Precursor of 2
5	$CH\equiv CH+2H(*)+H_2+2;_*$	5	Direct dehydrogenation
6	$H^9H^3H^4C-\dot{C}H_2+H^{10}(*)+3;_*$	6	Redundant exchange of hydrogen atoms
7	$CH(*)=\dot{C}H+2H_2+3;_*$	4	Adsorptive dehydrogenation

a) Numerals indicate the combination number in Table 2, and a to c implies that plural intermediates may be created from one combination.

a κ exceeding 3 and must be abandoned at this stage. The remaining five intermediates will thus be employed as the reactants of the second step. These intermediates can be transferred to the memory of the computer in two ways. One is in the form of connectivity tables which can reproduce the matrices, and the other is in the form of canonicalized formulas. The same intermediate may be produced at different steps through varied routes, and, by these algorithms, the same intermediates may be produced even from one and the same direct sum. Therefore, always when intermediates are created, they should be identified by comparing their cannonicalized (unique and unambiguous) chemical formulas. When they are found in the storage and are judged to be the intermediates already created in other step or route, two nodes, or intermediates, must be joined. In the GRACE system, the intermediate of Fig. 6 is stored in the form of Eq. 9, which is prepared with a sub-system CANON, whose details will be reported in a forthcoming paper.

$$1*Sl'\text{-}CH2\text{-}CH2\text{-}Sl'* + 1*Sl'*+1*Sl'* + 1*H\text{-}H** \quad (9)$$

where Sl′ denotes an active site (;*), whereas * implies a delimiter for molecules and an equation.

Completion of Reaction Network

The procedures described above may be repeated step by step until no new intermediate is created from the products of the preceding elementary reactions. The overall product is also found as one of the created intermediate systems.

Figure 7 shows an example of the output format of A/GRACE for the reaction in Eq. 1 under severe restrictions. In this case, no radical has been allowed except for active sites, as usually postulated by catalytic chemists. This output has been interpreted into a more readable form in Fig. 8, where two prevailing reaction schemes can be found. The left-hand route, **1**, (**3** or **4**), **6**, **9**, and **2**, represents the associative adsorption mechanism for the hydrogenation by Horiuti and Polanyi,[8] whereas the right-hand route, **1**, **5**, **8**, and **10**, represents the dissociative adsorption mechanism for isotope exchange between ethylene and hydrogen proposed by Farkas and Farkas.[9]

The computation time to prepare the complete network amounted to 21 s on a HITAC 8800.

```
[A]REACTANT(1)    1*Sl'*+1*Sl'*+1*Sl'*+1*Sl'*+1*CH2=CH2*+1*H-H**
   PRODUCT(2)     1*Sl'*+1*Sl'*+1*Sl'*+1*Sl'*+1*CH3-CH3**
[B]INTERMEDIATES
      1           1*Sl'*+1*Sl'*+1*Sl'*+1*Sl'*+1*CH2=CH2*+1*H-H**
      2           1*Sl'*+1*Sl'*+1*Sl'*+1*Sl'*+1*CH3-CH3**
      3           1*Sl'-CH2-CH2-Sl'*+1*Sl'*+1*Sl'*+1*H-H**
      4           1*Sl'H*+1*Sl'H*+1*Sl'*+1*Sl'*+1*CH2=CH2**
      5           1*Sl'-CH=CH2*+1*Sl'H*+1*Sl'*+1*Sl'*+1*H-H**
      6           1*Sl'-CH2-CH2-Sl'*+1*Sl'H*+1*Sl'H**
      7           1*Sl'-CH=CH2*+1*Sl'H*+1*Sl'H*+1*Sl'H**
      8           1*Sl'-CH=CH-Sl'*+1*Sl'H*+1*Sl'H*+1*H-H**
      9           1*Sl'-CH2-CH3*+1*Sl'H*+1*Sl'*+1*Sl'*
     10           1*Sl'-CH=CH-Sl'*+1*Sl'*+1*Sl'*+1*H-H*+1*H-H**
   NROUTE= 5     ISTEP= 4     NRTST1= 3
[C]REACTION ROUTE
   ROUTE          STEPS IDABCK  JOINTED          STEP
                                ROUTE STEP       ( 1)( 2)( 3)( 4)(
   1 COMPLETED     4     2      0 -  0    1      3   6   9   2
   2 JOINTED       2     3      1 -  2    1      4   6   0   0
   3 JOINTED       2     3      4 -  2    1      5   7   0   0
   4 DEAD END      2     5      0 -  0           4   7   8   0
   5 DEAD END      3     5      0 -  0           5   8  10   0
```

Fig. 7. Computer output of reaction network of catalytic hydrogenation of ethylene.

[A] Intermediates **1** and **2** denote the canonicalized formulas of the overall reactant and product, respectively.

[B] Intermediates No. **3** to **10** which appear in the network.

[C] Description of the network. Captions at the right of ROUTE No. imply the sequence of elementaly reactions.

For example,

COMPLETED. Route No. 1 consists of sequence of reactant(**1**)—intermediate **3**—**6**—**9**—product(**2**) and leads the system to the overall product.

JOINED. Route No. 2(**1**—**4**—**6**) is joined to Route No. 1 at the intermediate **6** in th step **2**.

DEAD END. Route No. 4(**1**—**4**—**7**) was terminated at the intermediate **7**, because **7** cannot change further under the given restrictions.

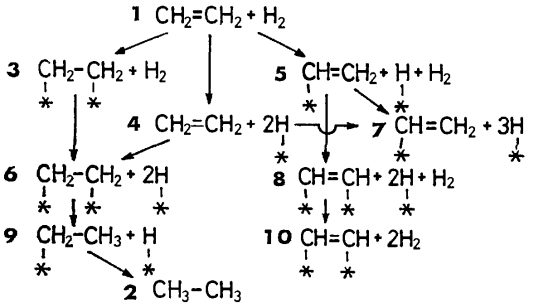

Fig. 8. Reaction routes in catalytic hydrogenation of ethylene.

Option of Restrictions in A/GRACE System. Numerous intermediates were produced even in the simplest system like that mentioned above, and hence the careful selection of restrictions is necessary to avoid the appearance of unrealistic, or thermodynamically unstable, molecules in intermediates. For example, no triple bond may be expected in the hydrogenation of ethylene, and no cyclopropene would be produced during the pyrolysis of propane. Only chemical knowledge and the experience of chemists will create a reasonable reaction network for a given reaction with the aid of the optimum selection of restrictions.

The author is grateful to Dr. Makoto Misono for his valuable discussion and to the Computer Centre of The University of Tokyo for the computation on a HITAC 8800.

References

1) Y. Yoneda, "Information Chemistry. Computer Assisted Chemical Research Design," ed by S. Fujiwara and H. B. Mark, Jr., University of Tokyo Press, Tokyo (1975), p. 239.

2) E. J. Corey and W. T. Wipke, *Science*, **166**, 178 (1969); E. J. Corey, *Quart. Rev. Chem. Soc.*, **25**, 455 (1971); D. A. Pensak and E. J. Corey, "Computer-assisted Organic Synthesis," ACS Symposium Series, No. 61, ed by W. T. Wipke and W. J. Howe, Am. Chem. Soc., Washington, D. C. (1977), p. 1.

3) I. Ugi, D. Marquarding, H. Klusacek, G. Gokel, and P. Gillespie, *Angew. Chem., Int. Ed. Eng.*, **9**, 703 (1970); I. Ugi and P. Gillespie, *ibid.*, **10**, 914 (1971); J. Blair, J. Gasteiger, C. Gillespie, and I. Ugi, "Computer Representation and Manipulation of Chemical Information," ed by W. T. Wipke, S. R. Heller, R. J. Felpmann, and E. Hyde, John Wiley, New York (1974), p. 129; J. Brandt, J. Friedrich, J. Gasteiger, C. Jochum, W. Schubert, and I. Ugi, "Computer-Assisted Organic Synthesis," ACS Symposium Series, No. 61, ed by W. T. Wipke and W. J. Howe, Am. Chem. Soc., Washington, D. C. (1977), p. 33.

4) W. T. Wipke and P. Gund, *J. Am. Chem. Soc.*, **96**, 299 (1974); W. T. Wipke and T. M. Dyott, *ibid.*, **96**, 4825, 4834 (1974).

5) M. Bersohn, *Bull. Chem. Soc. Jpn.*, **45**, 1897 (1972); M. Bersohn and A. Esack, *Chem. Rev.*, **76**, 269 (1976).

5a) *E.g.*, J. Lederberg, G. L. Sutherland, B. G. Buchanan, E. A. Feigenbaum, A. V. Robertson, A. M. Duffield, and C. Djerassi, *J. Am. Chem. Soc.*, **91**, 2973 (1969); A. M. Duffield, A. V. Robertson, C. Djerassi, B. G. Buchanan, G. L. Sutherland, E. A. Feigenbaum, and J. Lederberg, *ibid.*, **91**, 2977 (1969).

6) Y. Yoneda, "Saikin No Kagakukôgaku, 1970," ed by the Association for Chemical Engineers of Japan, Maruzen, Tokyo (1970), p. 145 (in Japanese).

7) Y. Yoneda, "Kemoguramu(CHEMOGRAM)," Maruzen, Tokyo (1972), Vol. 1 (in Japanese).

8) M. Polanyi and J. Horiuti, *Trans. Faraday Soc.*, **30**, 1164 (1934).

9) A. Farkas, L. Farkas, and E. K. Rideal, *Proc. R. Soc. London, Ser. A*, **146**, 630 (1934).

Chemiionization of Excited Mercury Atom with 253.7 nm Irradiation in the Presence of N_2 and CH_4

Akiko SIBATA, Makoto TAKAHASI,* Hitoshi MIKUNI, Hiroyuki HORIGUCHI, and Soji TSUCHIYA

Department of Pure and Applied Sciences, College of General Education, the University of Tokyo, Komaba, Meguro-ku, Tokyo 153

(Received April 1, 1978)

Chemiionization of excited mercury atom with 253.7 nm irradiation was studied. Results on the system Hg–N_2 previously reported were further confirmed. It was found that CH_4 can also induce chemiionization of Hg atoms with 253.7 nm irradiation. The dependence of ionization current on CH_4 pressure and light intensity was investigated, the ionization current being found to be proportional to the square of light intensity and to increase with increase in CH_4 pressure up to 30 Torr, reaching a constant value. N_2 and CH_4 are considered to show a similar behavior in ionization current against pressure and light intensity, and other substances such as H_2, He, CO, NO, Ar, C_2H_4, and 1-butene to give no appreciable ionization current. Thus the mechanism in which chemiionization proceeds through the collision of $Hg(^3P_1)$ with $Hg(^3P_0)$ is further confirmed.

Ionization of mercury atoms excited with 253.7 nm irradiation was first reported by Steubing in 1909,[1] the history of studies in this field being surveyed in detail by Fontijn.[2] An extensive study on this reaction was carried out by Berberet and Clark,[3] the following mechanism being proposed:

$$Hg(^3P_1) + N_2 \longrightarrow Hg(^3P_0) + N_2,$$

$$Hg(^3P_1) + Hg(^3P_0) + N_2 \longrightarrow Hg_2^* + N_2,$$

$$Hg_2^* \longrightarrow Hg_2^+ + e^-.$$

In the present study we attempted to further clarify the mechanism of the chemiionization.

Experimental

Apparatus and Procedure. Vacuum line and gas handling system are conventional ones. For irradiation of 253.7 nm light a commercial germicidal lamp (Toshiba 10 W) was used. The reaction cell and optical arrangement are schematically shown in Fig. 1. A fused quartz reaction cell was furnished with three windows of 20 mmϕ, two Pt plane electrodes (5×10 mm) for ion collection being placed inside parallel to each other 10 mm apart. Exciting light was focussed with a fused quartz condensor lens through a 5 mmϕ hole defined by Al foil in front of the reaction cell to prevent exposure of the electrodes from 253.7 nm radiation. Photoionization in the Hg–N_2 system is due to neither ejection of photoelectrons by direct irradiation nor impact of metastable mercury atoms ($Hg(^3P_0)$) on the electrode surface, provided Pt electrodes are used.[2] We have also confirmed that no appreciable ionization current thought to be caused by direct irradiation of the electrode surface was detected in the absence of N_2.

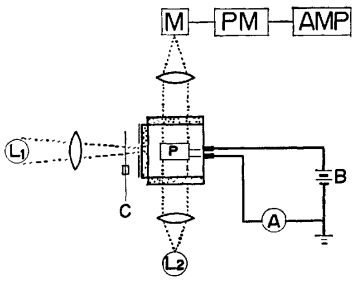

Fig. 1. Schematic view of photoionization cell.
L_1: Lamp for excitation, L_2: lamp for absorption photometry, B: battery, C: chopper, P: platinum electrode, M: monochromator, PM: photomultiplier, A: amplifier for ion current measurement, AMP: lock-in amplifier. For the ion current measurement, chopper is removed.

Ion current was measured either by a vibrating reed electrometer (Yanagimoto GCF 101) or a micro-voltmeter (Okura Denki AM 1001) as a voltage across 4.7 kΩ external resistor, no difference being observed in the values of ionization current measured by the two methods. For determination of concentration of $Hg(^3P_0)$, absorption photometry was carried out at 404.7 nm by modulation technique. The exciting light from a low pressure mercury lamp operated by DC power was chopped with a sector at 8 Hz. The light for absorption photometry was obtained from a lamp of the same type as that used for excitation. Two Vycor lenses, focal length 10 cm, were used, one to make the incident light flux parallel through the reaction cell and the other to focus the light at the position of a slit of monochromator (Fig. 1). The light at 404.7 nm was isolated from the transmitted light by a monochromator (Ritsu MC 10, grating: 600 grooves per mm). Its intensity was determined with a photomultiplier (RCA 1P 21) and a lock-in amplifier (PAR Model 186) using the chopped exciting light as time reference. Since the effective lifetime of $Hg(^3P_0)$ is in the order of ms under the present experimental condition, it can be assumed no phase delay takes place between the exciting light of 8 Hz and the transmitted light at 404.7 nm for photometry. The light for absorption photometry contains 253.7 nm DC component, but we can assume that it does not affect the modulation photometry.

Materials. Two kinds of N_2 (stated purity 99.999% from a glass bottle; stated purity 99.9% from a cylinder) were used. The latter was used after passing through a molecular sieve column cooled at liquid nitrogen temperature. Neither of these N_2 shows appreciable difference in ionization current in the experiments under comparable conditions. Other gasses (CH_4, Ar, H_2, He, CO, NO, C_2H_4, and 1-butene) were used from commercial glass bottles without further purification.

Results and Discussion

1. Collection Efficiency of Ionization Current. The relationship between photoionization current and ion collecting voltage has been studied by many workers, its main feature being summarized by von Engel.[4] At an insufficient voltage the recombination process

of the ion pair formed competes with the ion collecting process at electrodes, resulting in incomplete ion collection. With increase in voltage, the collecting efficiency of ions increases, approaching a saturated plateau value. In the plateau region, all the ions formed in the effective electric field can be collected without appreciable recombination, and the total rate of ion formation under the present experimental setup, R_{exp} (in number of ions per s) is expressed by the simple formula

$$R_{exp} = i/e,$$

where i is the total ion current in A measured at the saturated voltage, and e is elementary charge in C.

We measured the ionization current, DC voltage being varied from 10 to 150 V, keeping the pressure of N_2 constant (3.2 and 23 Torr). Saturation of current is established when 80—120 V is applied, and a higher voltage is required for a higher N_2 pressure. Under the present experimental conditions, the multiplication effect of electrons can be neglected, since the first Townsend coefficient is extremely small (approximately 7×10^{-8} at N_2 pressure of 1 Torr and applied voltage 100 V).[4]

2. Ionization Current and Concentration of Hg($^3P_0$) against N_2 Pressure and Quantum Yield of Ionization. Since it has been pointed out[2,3,5] that the ionization of Hg is closely related with the formation of Hg($^3P_0$), we attempted the determination of ionization current and concentration of Hg($^3P_0$) (denoted as N_0 hereafter) under the same experimental conditions varying the pressure of N_2. As Fig. 2 shows, the variations of ionization current and N_0 *vs.* N_2 pressure behave in a similar way. The N_2 pressure dependence of ionization current would not be expected to be completely the same as that of N_0 (Sec. 6). It was confirmed that the application of DC voltage across electrodes does not affect N_0.

Under the present conditions we can assume that all the input photons of 253.7 nm light are absorbed by mercury atoms in the reaction cell, and determine the quantum yield of ionization by actinometry. Actinometry was carried out in the system Hg–N_2O (100 Torr)–C_2H_6(60—100 Torr), the total number of input photons per s (described as Ia_{exp} hereafter) being found to be 5.0×10^{14} s^{-1}. The quantum yield of ionization ($\phi=R_{exp}/Ia_{exp}$) is thus in the range 10^{-6}—10^{-4}, depending on the pressure of N_2.

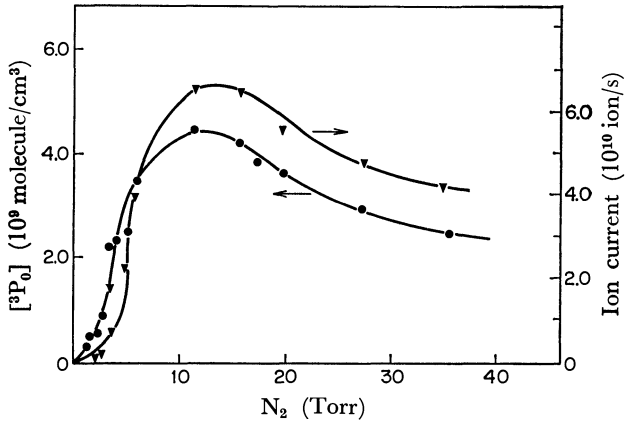

Fig. 2. Simultaneous determination of ion current and concentration of Hg($^3P_0$) *vs.* N_2 pressure in N_2-Hg system.

3. Relationship between Ionization Current and Light Intensity in the N_2–Hg System and the Effect of Hg Pressure. Ionization current was measured varying light intensity with neutral density filters of fused quartz in the range 39—100% at pressures of 1, 5, and 9 Torr of N_2. The ionization current was found to be proportional to the square of light intensity (Fig. 3), in line with the results reported by Houterman,[5] and Berberet and Clark.[3]

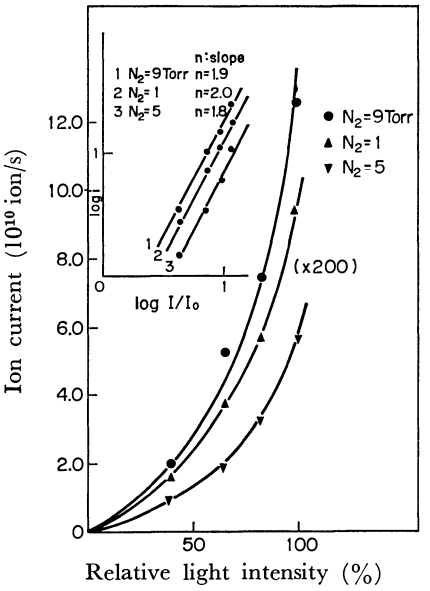

Fig. 3. Plots of ion current *vs.* light intensity in N_2–Hg system. Inserted figure is log-log plot for the same quantities.

Dependence of ionization current on Hg pressure was studied only semiquantitatively, since the actual pressure of Hg in the reaction cell was not measured. We measured the ionization current keeping the mercury reservoir at 0 °C (reported Hg pressure, 1.85×10^{-4} Torr), room temperature 24—25 °C (Hg pressure: 1.7×10^{-3} Torr at 24 °C) and N_2 pressure 10 Torr. The observed ionization current at 0 °C of mercury reservoir is about one third of that at room temperature. We may interpret this decrease of ionization current at 0 °C in terms of the decrease of radiation imprisonment due to the decrease of Hg pressure.

4. Chemiionization of Excited Mercury Atom in the System CH_4–Hg. In the proposed mechanism of chemiionization it has been assumed that the ionization takes place through the collision of Hg($^3P_1$) with Hg($^3P_0$). If this is valid, CH_4 could also induce chemiionization of mercury atom, since CH_4 has a relatively large rate constant to produce Hg($^3P_0$) from Hg($^3P_1$), and a small rate constant to quench Hg($^3P_1$) and Hg($^3P_0$) to ground state (Table 1).[6] Actually we find CH_4 gives an ionization current under 253.7 nm irradiation, the magnitude being 1/50—1/100 as com-

pared with that for N_2. Dependence of ionization current on the pressure of CH_4 has a feature similar to that for N_2(Fig. 4), its dependence on light intensity being of second order. We also investigated H_2, CO, NO, Ar, C_2H_4, and 1-butene–Hg systems. However, none of them gave any appreciable ionization current in the experimentally detectable limit (less than 10^{-11} A) under conditions similar to the cases of N_2 and CH_4.

5. Effect of $NiSO_4$ Solution Filter. The problem is whether radiation other than 253.7 nm light might participate in the chemiionization in view of the finding that the ionization current is proportional to the square of light intensity. An experiment was carried out with irradiation of 253.7 nm isolated from total radiation of the low pressure mercury lamp using a $NiSO_4$ solution filter.[7] Reduction of ionization current to 33% was observed, but it is due to the absorption of light at 253.7 nm by the filter. The pressure dependence of current is similar to that without filter. We may conclude that no direct radiation other than 253.7 nm light contributes to the chemiionization.

6. Reaction Mechanism of Chemiionization. The fact that the ionization current is proportional to the square of light intensity is a strong support for the assumption that two excited mercury atoms($Hg(^3P_0)$ and $Hg(^3P_1)$) are involved. Since only N_2 and CH_4 are known to induce chemiionization, and both have relatively large cross sections to generate $Hg(^3P_0)$ from $Hg(^3P_1)$, it is certain that one atom of $Hg(^3P_0)$ is at least involved in the ionization. The pressure dependence of ionization current is closely related to that of N_0 in the case of N_2. Simultaneous determination of ionization current and N_0 *vs.* CH_4 pressure was not possible for the case of CH_4, since N_0 is too small. However, the general feature of pressure dependence of ionization current is similar to that for Hg–N_2 system (Fig. 4).

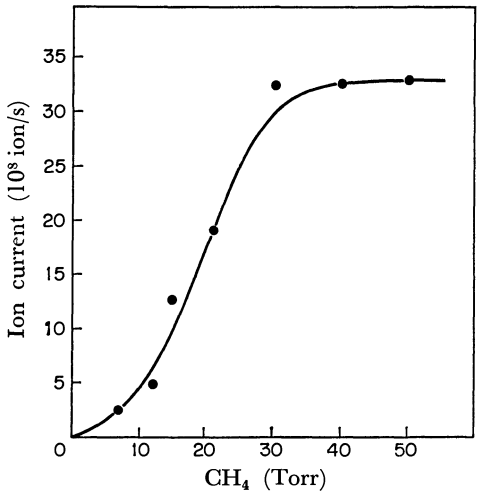

Fig. 4. Plot of ion current *vs.* CH_4 pressure in CH_4–Hg system.

The steady state concentrations of $Hg(^3P_1)$ and $Hg(^3P_0)$ are expressed in respective rate constants according to the following reaction schemes:

$$Hg(^1S_0) + h\nu(253.7\,nm) \xrightarrow{Ia} Hg(^3P_1),$$

$$Hg(^3P_1) \xrightarrow{k_f} Hg(^1S_0) + h\nu_f,$$

$$Hg(^3P_1) + M \xrightarrow{k_1} Hg(^3P_0) + M, \quad (1)$$

$$Hg(^3P_1) + M \xrightarrow{k_2} Hg(^1S_0) + M, \quad (2)$$

$$Hg(^3P_0) + M \xrightarrow{k_3} Hg(^1S_0) + M, \quad (3)$$

$$Hg(^3P_0) \xrightarrow[\text{(at wall)}]{k_4} Hg(^1S_0), \quad (4)$$

$$Hg(^3P_0) \xrightarrow[\text{(very small)}]{k_5} Hg(^1S_0), \quad (5)$$

where Ia is the number of photons absorbed per cm^3 s, k_f is effective radiative decay constant of $Hg(^3P_1)$; k_1, k_2, k_3, are quenching rate constants of excited atoms by M, k_4 is diffusion rate to wall at unit pressure (1 Torr) and k_5 is the disappearing rate of $Hg(^3P_0)$ by quenching by impurity and/or radiative decay. We can express N_1 (steady state concentration of $Hg(^3P_1)$) and N_0 by the steady state treatment as follows, neglecting the disappearance process of the excited mercury atoms by chemiionization, since the quantum yield of chemiionization is very small:

$$N_1 = Ia/(k_f + (k_1+k_2)[M]), \quad (I)$$

and

$$N_0 = N_1k_1[M]/(k_3[M]+k_4/P+k_5), \quad (II)$$

where P is the total pressure in Torr.

As Berberet and Clark[3] assumed, we may assume the following two step ionization mechanism, if the chemiionization takes place through the collision between $Hg(^3P_1)$, $Hg(^3P_0)$, and M,

$$Hg(^3P_1) + Hg(^3P_0) + M \xrightarrow{k_6} Hg_2^* + M, \quad (6)$$

$$Hg_2^* \xrightarrow{k_7} Hg_2^+ + e^-, \quad (7)$$

and the rate of ion formation, R(in number of ions $cm^{-3}\,s^{-1}$) is given by

$$R = \phi Ia = k_6N_1N_0[M]$$
$$= k_1k_6[M]^2Ia^2/(k_f+(k_1+k_2)[M])^2(k_3[M]+k_4/P+k_5). \quad (III)$$

Berberet and Clark assumed the two step mechanism, considering the fact that the lifetime of Hg_2^* is of the order of ms. The pressure dependence of i is almost similar to that of N_0 in the system N_2–Hg(Fig. 2). However, Eq. III indicates that i is proportional to N_1 and the concentration of third body as well as N_0. In the case $k_f \gg (k_1+k_2)[N_2]$, N_1 would be independent of the concentration of N_2, and the behavior of i may be similar to that of N_0.

Under the high concentration of N_2, $R \approx k_1k_6Ia^2/(k_1+k_2)^2(k_3[M]+k_4/P+k_5)$, and we may expect a linear relationship between $1/R$ and the concentration of M.

In order to evaluate the approximate ratio of the ionization current in the presence of a certain substance M to that for N_2, we derive the following equation from Eq. III, assuming $k_{6,M}$ is equal to k_{6,N_2},

$$i_M/i_{N_2} = \left(\frac{k_{1,M}[M]}{k_{1,N_2}[N_2]}\right)^2\left(\frac{k_f+(k_{1,N_2}+k_{2,N_2})[N_2]}{k_f+(k_{1,M}+k_{2,M})[M]}\right)^2 \times\left(\frac{k_{3,N_2}[N_2]+k_4/P+k_5}{k_{3,M}[M]+k_4/P+k_5}\right). \quad (IV)$$

TABLE 1. RATIOS OF IONIZATION CURRENT CALCULATED BY Eq. IV AND USED QUENCHING RATE CONSTANTS[6] OF $Hg(^3P_1)$ AND $Hg(^3P_0)$ BY SEVERAL GASES

	Ratio of ionization current,[a] i_M/i_{N_2}	Quenching rate constants (cm^3/molecule s)		
		$k_1(^3P_1 \rightarrow {}^3P_0)$	$k_2(^3P_1 \rightarrow {}^1S_0)$	$k_3(^3P_0 \rightarrow {}^1S_0)$
N_2	(1.0)	3.9×10^{-12}	$1.5\times10^{-13}>$	$1.0\times10^{-15}>$
CH_4	0.18>	1.0×10^{-13}	4.6×10^{-13}	2.7×10^{-15}
C_2H_6	0.03>	3.3×10^{-12}	2.0×10^{-12}	2.6×10^{-14}
C_3H_8	$5.0\times10^{-4}>$	1.3×10^{-11}	4.2×10^{-12}	6.3×10^{-13}
NH_3	$4.5\times10^{-4}>$	2.2×10^{-11}	1.7×10^{-11}	2.4×10^{-13}
CO_2	$7.8\times10^{-5}>$	8.0×10^{-13}	1.3×10^{-11}	3.9×10^{-13}
CO	$6.4\times10^{-6}>$	1.1×10^{-10}	1.5×10^{-11}	9.1×10^{-12}
NO	$4.6\times10^{-8}>$	3.4×10^{-11}	1.5×10^{-10}	1.7×10^{-10}
H_2	$1.9\times10^{-8}>$	$5.4\times10^{-12}>$	1.4×10^{-10}	1.1×10^{-10}
C_2H_4	$9.9\times10^{-9}>$	$8.1\times10^{-11}>$	2.4×10^{-10}	6.5×10^{-10}

a) Since k_{2,N_2} and k_{3,N_2} are given as upper limits, all the calculated ratios should be understood as upper limits.

In calculating the ratios, we used the values of the rate constants given in Table 1, 2×10^5 s^{-1} for k_f(calculated according to the Milne-Samson formula[8]), 26 Torr s^{-1} for k_4 and 100 s^{-1} for k_5. The value of k_5 is not definite, but it would not cause serious errors in calculating the ratios since the magnitude of k_5 is small as compared with that of $k_{3,M}[M]$. The calculated upper limit of the ratio, i_{CH_4}/i_{N_2} is 0.18, while the experimental value of i_{CH_4}/i_{N_2} at 10 Torr is 0.005, no measurable ionization current being observed for the other compounds(H_2, He, CO, NO, C_2H_4, Ar, and 1-butene). From Table 1 we may expect C_2H_6 to induce the chemiionization current in a measurable amount.

We observed the decrease of ionization current in the system N_2–Hg at 0 °C as compared with that at room temperature. We have estimated the ratio of ionization current at 0 °C to that at room temperature (24 °C) using Eq. III. We assume that $[N_2]$ and the rate constants defined above except k_f are almost the same at 0 °C and 24 °C, and interpret the decrease of ionization current at 0 °C in terms of the decrease of effective radiative decay lifetime($1/k_f$) of $Hg(^3P_1)$, *viz.*, the decrease of radiation imprisonment. The calculated values of k_f at 0 °C and 24 °C are 2×10^6 and 2×10^5 s^{-1} respectively. We obtain N_1 and N_0 at two temperatures as follows; N_1: 1.5×10^8 at 0 °C and 3.4×10^8 atom cm^{-3} at 24 °C, and N_0: 4.3×10^{11} at 0 °C and 9.5×10^{11} atom cm^{-3} at 24 °C. Using these values of N_1 and N_0 with Eq. III, we obtain the ratio of the ionization current at 0 °C to that at 24 °C to be 0.2, while its experimental value is 0.3. In this calculation, we assumed Ia in Eq. III to be the number of total incident photons at 253.7 nm in the reaction cell, which was determined by actimonetry carried out at room temperature.**

7. Chemiionization of N_2–CH_4–Hg System and Estimation of the Rate Constant of Excimer Formation. Since N_2 and CH_4 are the only substances known to induce chemiionization of Hg, we studied the behavior of ionization current in a mixture of N_2 and CH_4. Since N_2 has a large rate constant to produce $Hg(^3P_0)$ from $Hg(^3P_1)$ and CH_4 has a large rate constant to quench $Hg(^3P_0)$ (more than three times as large as that of N_2), we expect that N_2 mainly produces $Hg(^3P_0)$ and CH_4 quenches $Hg(^3P_0)$ in the mixture (Table 1). For the sake of confirmation we measured the ionization current in the mixture system varying the pressure of CH_4 keeping the N_2 pressure constant. The total pressure (N_2+CH_4+Ar) which may affect the absorption line profile of Hg atoms and the diffusion rate of $Hg(^3P_0)$ to wall was also kept constant. Two series of experiments were carried out, (a) N_2, 3 Torr and total pressure, 10 Torr; (b) N_2, 6 Torr and total pressure, 20 Torr. If we take reciprocals of both sides of Eq. III, we may expect a Stern-Volmer type linear relation between $1/R$ and CH_4 pressure at constant N_2 and total pressures, noting $k_{1,N_2} \gg k_{1,CH_4}$ and k_{2,CH_4}, as follows:

$$1/R = (X/k_6PIa^2)(k_{3,N_2}[N_2]+k_{3,CH_4}[CH_4]+k_4/P+k_5), \quad \text{(V)}$$

where

$$X=(k_f+(k_{1,N_2}+k_{2,N_2})[N_2]+(k_{1,CH_4}+k_{2,CH_4})[CH_4])^2/(k_{1,N_2}[N_2]+k_{1,CH_4}[CH_4])^2 \sim \text{constant}.$$

Figure 5 shows that the linear relation holds. From the empirical values of either slope or intercept, we can calculate k_6 if we substitute the values of other rate constants for N_2 and CH_4 and of Ia into Eq. V. We are aware of the accumulated large errors caused by using many rate constants (k_f, k_{1,N_2}, k_{1,CH_4}, k_{2,N_2}, k_{2,CH_4}, k_{3,N_2}, k_{3,CH_4}) in calculation. Our estimation of k_6 from slope gives the values of 9.6×10^{-29} cm^6 $molecules^{-2}$ s^{-1} (series (a)) and 8.3×10^{-29} (series (b)). The rate constant of the ternary collision (k_6) obtained here may be compared with that of an excimer formation ($Hg_2(1_u) \xleftarrow{k_{1_u}} Hg(^3P_0)+Hg(^1S_0)+N_2$). Phaneuf *et al.*[9] gave the values of the rate constant(k_{1_u}) reported by several workers. They are in the range 10^{-30}—10^{-29} cm^6 $molecule^{-2}$ s^{-1}, differing from that by McAlduff *et al.*[10] which was exceptionally large (1.33×10^{-27} cm^6 $molecule^{-2}$ s^{-1}). The value of k_6 obtained here is several times larger than k_{1_u}, but we consider it reason-

** The authors acknowledge the referee's suggestion on the interpretation of the effect of Hg pressure on the ionization current.

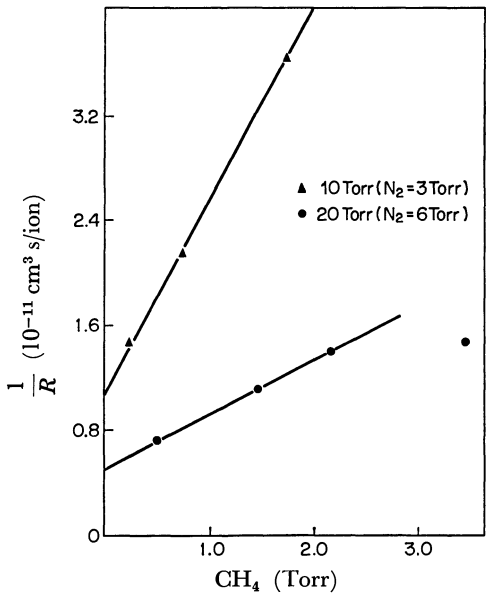

Fig. 5. Plots of reciprocals of rate of ion formation (R) *vs.* CH_4 pressure in the mixture of N_2, CH_4, and Hg for 10 Torr and 20 Torr of total pressure.

Table 2. Rate constants of ternary collision (k_6) in the systems N_2–Hg and CH_4–Hg (cm^6 molecule^{-2} s^{-1})

Pressure (Torr)	3	6	10
N_2	3.4×10^{-29}>	2.8×10^{-28}>	4.9×10^{-28}>
CH_4	1.8×10^{-29}	2.3×10^{-29}	4.0×10^{-29}

able.

The rate constant (k_6) can be also calculated by means of Eq. III instead of Eq. V using the reported rate constants and our experimental results in the system N_2–Hg or CH_4–Hg. The results, given in Table 2, increase with pressure. For the interpretation of this pressure effect and the difference of magnitudes of k_6 among N_2–Hg, CH_4–Hg, and N_2–CH_4–Hg systems we might speculate more complex mechanism in the ionization, but we feel better to refrain from further discussions on this matter, because many pressure terms are included in Eq. III. In the case of N_2, the value of k_3 which is considered to be the most important in the determination of k_6 is known only as an upper limit. Thus the values of k_6 in the system N_2–Hg should be taken as upper limits.

8. Other Possible Mechanisms of Ionization and Energetic Consideration. Since we have found that the ionization current is proportional to the square of light intensity, and that at least one atom of $Hg(^3P_0)$ is involved, the following two mechanisms might also be considered. (1) To assume the participation of one more $Hg(^3P_0)$ atom instead of $Hg(^3P_1)$. If two atoms of $Hg(^3P_0)$ are involved in chemiionization, the reciprocal of ionization current would be proportional to the square of pressure of CH_4 in the mixture experiment of N_2–CH_4. However, this is not compatible with our result (Fig. 5). In addition, the energy requirement for ionization is less favorable with the deficiency

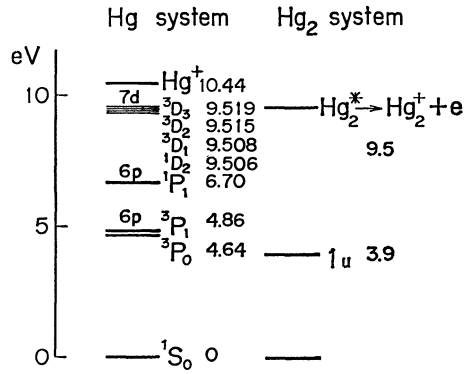

Fig. 6. Energy level diagram for Hg and Hg_2 systems.

of 0.22 eV. (2) Ionization proceeds through the absorption of another 253.7 nm photon by an excimer formed by the collision between $Hg(^3P_0)$ and ground state Hg. The formation of such an excimer (1_u) has been confirmed.[9] However, it is not probable from energetic consideration (Fig. 6) that this excimer can be ionized by absorption of another 253.7 nm photon. Furthermore, the absorption of 253.7 nm photon by the excimer is less likely, since the absorption of 253.7 nm photon by ground Hg would be much stronger.

Since the ionization potential of mercury atom is 10.44 eV, the sum of energy of $Hg(^3P_1)$ and $Hg(^3P_0)$ (4.86+4.64=9.50 eV) is not enough to give Hg atomic ion. It has been assumed[3] that the formation of molecular ion Hg_2^+ is more likely. Arnot and Milligan[11] observed mass-spectrometrically the formation of Hg_2^+ in the electron impact of dense mercury vapor, and determined its appearance potential to be 9.5 eV. They presumed that its formation proceeds through the collision of $Hg(^1D_2)$ generated by electron impact with Hg in ground state, since the energy level of $Hg(^1D_2)$ is 9.506 eV above ground state and is close to the appearance potential of Hg_2^+. In the optical excitation experiments, the formation of $Hg(^1D_2)$ is not possible, and the collision of $Hg(^3P_1)$ with $Hg(^3P_0)$ is an acceptable process for the formation of Hg_2^+ from energetic consideration. Berberet and Clark assumed the formation of an excimer Hg_2^* as a precursor of Hg_2^+, considering the decay of ionization current after switch-off of exciting light to be very slow. They estimated the lifetime of the excimer to be of the order of ms. So far we know nothing about the electronic state of the excimer. However we presume that such an excimer is in a highly excited Rydberg state, since the energy level of the excimer should be very close to its ionization level.

From energetic consideration, we should not discard the possibility of mercury ion pair formation by the collision of $Hg(^3P_1)$ with $Hg(^3P_0)$, if electron affinity of Hg is 1.53 eV exoergic.[12] If this is acceptable, the total energy balance of ion pair formation

$$Hg(^3P_1) + Hg(^3P_0) \longrightarrow Hg^+ + Hg^-$$

would be 0.59 eV exoergic. However, Makita *et al.*[13] pointed out that the value is not based on reliable experimental measurement. They estimated it to be 0.19±0.3 eV endoergic. When we adopt this value,

mercury ion pair formation by the collision of $Hg(^3P_1)$ with $Hg(^3P_0)$ is not possible.

References

1) W. Steubing, *Z. Phys.*, **10**, 787 (1909).
2) A. Fontijn, "Progress in Reaction Kinetics," ed by K. R. Jennings and R. B. Cundall, Pergamon Press, Oxford (1972), Vol. 6, p. 99.
3) J. A. Berberet and K. C. Clark, *Phys. Rev.* **100**, 506 (1955).
4) A. von Engel, "Ionized Gases," Oxford, Clarendon Press, (1965).
5) F. G. Houterman, *Z. Phys.*, **41**, 619 (1927).
6) H. Horiguchi and S. Tsuchiya, *Bull. Chem. Soc. Jpn.*, **47**, 2768 (1974).
7) J. G. Calvert and J. N. Pitts, Jr, "Photochemistry," John Wiley and Sons, (1966) p. 728.
8) E. W. Samson, *Phys. Rev.* **40**, 940 (1932).
9) Mrozowski, *Z. Phys.*, **104**, 228 (1937); R. A. Phaneuf, J. J. Skonieczny, and L. Krause, *Phys. Rev. A*, **8**, 2980 (1973); R. E. Drullinger, M. M. Hessel, and E. W. Smith, *J. Chem. Phys.*, **66**, 5656 (1977); M. Stock, E. W. Smith, R. E. Drullinger, M. M. Hessel, and J. Pourcin, *ibid.*, **68**, 1785 (1978).
10) J. E. McAlduff, D. D. Drysdale, and D. J. LeRoy, *Can. J. Chem.*, **46**, 199 (1968); J. E. McAlduff and D. J. LeRoy, *ibid.*, **43**, 2279 (1965).
11) F. L. Arnot and J. C. Milligan, *Proc. R. Soc. London, Ser. A*, **153**, 359 (1935).
12) "Kagakubinran," (Handbook of Chemistry) ed by The Chemical Society of Japan, Maruzen, Tokyo (1975), p. 1286 (original reference is not mentioned).
13) T. Makita, H. Kishi, and K. Kodera, *Mass Spectroscopy*, **21**, 293 (1973).

Kinetic Studies of Spin Trapping Reactions. II. Radiolysis of Cyclohexane

Takahisa DOBA, Shoji NODA, and Hiroshi YOSHIDA*
Faculty of Engineering, Hokkaido University, Kita-ku, Sapporo 060
(Received May 8, 1978)

In order to extend kinetic utilization of the spin-trapping techniques in radiation chemistry, γ-radiolysis of cyclohexane has been studied at room temperature using pentamethylnitrosobenzene as a spin trap. With increasing radiation dose, the cyclohexyl radical spin adduct has been found by ESR to form and then decay. Consumption of the spin trap has also been monitored by observing the optical absorption. The observed kinetic aspects indicate that the radiation-generated cyclohexyl radicals are completely trapped by 1.3×10^{-4}—6.6×10^{-4} mol dm^{-3} of the spin trap, and their G-value is 3.0. The spin-trapping rate constant has been determined to be 1.6×10^{7} mol^{-1} dm^{3} s^{-1} at 299 K based on the reported rate constant for the reaction between the cyclohexyl radical and tributylstannane. From the optical absorption study, dimeric pentamethylnitrosobenzene has been found to dissociate into the monomer, effective in the spin-trapping, with an equilibrium constant of 8×10^{-4} mol dm^{-3} in cyclohexane at 299 K. The monomer has an absorption coefficient of 48 mol^{-1} dm^{3} cm^{-1} at its absorption peak of 790 nm.

The spin-trapping technique has been developed recently[1,2] and widely used for the identification of free radical intermediates in radiation-chemical,[3-5] photochemical,[6-8] and thermal reactions.[9,10] A recent photochemical study[11] has revealed the problems inherent in this technique: the rate constant of spin-trapping reactions varies widely,[12-17] from 10^{3} to 5×10^{8} mol^{-1} dm^{3} s^{-1}, they generally compete in a complex way with other radical reactions, and spin adduct radicals subsequently react with free radicals to be spin-trapped.[11] Therefore, knowledge of the reactivities of spin traps and spin adduct radicals is needed for the quantitative utilization of the technique.

The radiolysis of cyclohexane is one of the simplest radiation-chemical reaction systems where only atomic hydrogen and cyclohexyl radicals as free radical intermediates are expected. It has been one of the most extensively studied systems.[18-22] This appears as a model reaction system where the validity of the spin-trapping technique can be tested on a quantitative base. Iwahashi *et al.*[23] have applied the technique to this system using *N*-*t*-butyl-α-phenylnitrone (phenyl-*t*-butyl nitrone, PBN) as a spin trap and concluded that "the utilization of the spin trap for the quantitative estimation of products in the radiolysis of hydrocarbons is not a very good technique." In the present study, the spin-trapping technique has been applied to the radiolysis of cyclohexane by using pentamethylnitrosobenzene (PMNB). PMNB reacts with alkyl radicals with a rate constant two orders of magnitude greater than that of PBN so that the kinetic aspects of the spin-trapping are expected to be simpler for PMNB than for PBN.

Experimental

PMNB was synthesized from pentamethylbenzene through $C_6(CH_3)_5Tl(OCOCF_3)_2$,[24,25] and purified by recrystallization from acetone solution. Spectrograde cyclohexane was used without further purification. The monomer-dimer equilibrium and optical absorption of PMNB in cyclohexane solution were studied in the manner as described before.[25] For spin-trapping experiments, solutions of PMNB in cyclohexane were degassed by the freeze-pump-thaw technique at a vacuum of 10^{-5} Torr and sealed in sample cells, which consisted of a quartz ESR tube at one end and quartz optical absorption cell at the other.

Irradiations were conducted with ^{60}Co γ-rays at a dose rate of 2.0—14 krad/min at room temperature, *ca.* 300 K. The concentration of PMNB and that of the spin adduct radicals were simultaneously monitored by a recording spectrophotometer and an X-band ESR spectrometer, respectively.

Results and Discussion

Monomer-Dimer Equilibrium of PMNB in Cyclohexane. PMNB dissolved in cyclohexane is in part present in the dimeric form. Monomeric PMNB has a weak optical absorption with a maximum at 790 nm, while dimeric PMNB has a strong absorption band with a maximum at 327 nm. According to the relationship, $c/A=1/2\varepsilon+A/K\varepsilon^{2}$ where c is the total concentration of PMNB, A is the absorbance at 790 nm, K the equilibrium constant and ε the molar absorption coefficient, K and ε for PMNB are determined to be 8×10^{-4} mol·dm^{-3} and 48 mol^{-1} dm^{3} cm^{-1} at 299 K from the observed linear dependence of c/A on A as shown in Fig. 1. Thus, 45 to 80% of PMNB is in the monomeric form and is effective in spin-trapping free radical intermediates, when dissolved in cyclohexane at the total concentration of 10^{-3} to 10^{-4} mol dm^{-3}. This behavior of PMNB is very similar to that reported previously

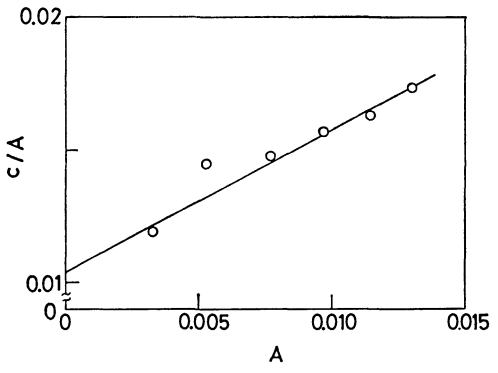

Fig. 1. The relationship between the absorbance, A, at 790 nm and the total concentration of PMNB, c, in cyclohexane at 299 K.

in benzene solution.[25,26]

Radiation-Chemical Reactions of Cyclohexane Solutions of PMNB. ESR spectra observed from the γ-irradiated solutions show a triple-doublet hyperfine structure, as shown in Fig. 2, with coupling constants of 1.40 and 0.76 mT. These have been attributed to the spin adducts of the cyclohexyl radical. Neither the spin adduct of hydrogen nor that of other free radicals could be observed by ESR. The cyclohexyl radical spin adducts decay after γ-irradiation to *ca.* 70% of the initial amount during the first hour, and then remain almost unchanged. The decay cannot be attributed to either the self-decomposition of the spin adducts or their recombination, but is probably due to reactions with some radiolytic products.

The dependence of the yield of spin adducts on the radiation dose is shown, typically in Fig. 3 for a dose rate of 14 krad/min. The yield increases at first with the initial slope independent of the PMNB concentration in the range of 6.6×10^{-4}—1.3×10^{-4} mol dm^{-3},

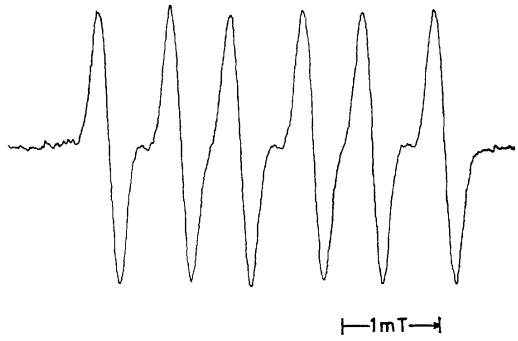

Fig. 2. ESR spectrum of pentamethylphenyl cyclohexyl nitroxide (spin adduct radical) obtained from the γ-radiolysis of cyclohexane in the presence of PMNB at room temperature.

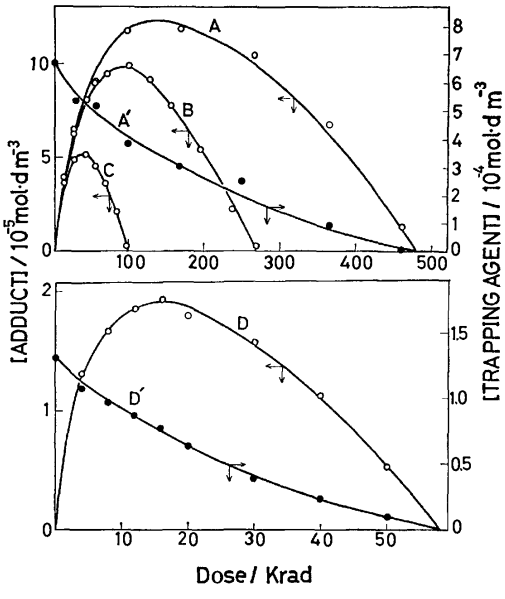

Fig. 3. The dependence of the concentration of the spin adducts (○) and that of the spin trap (●), PMNB, on the radiation dose, at the PMNB concentration (A, A') 6.6×10^{-4}, (B) 4.4×10^{-4}, (C) 2.2×10^{-4}, and (D, D') 1.3×10^{-4} mol dm^{-3}.

reaching a maximum dependent on the PMNB concentration, and then decreases to zero. The *G*-value of the spin adduct formation determined to be 3.0 from the initial slope independent of the PMNB concentration. The decrease of the dose rate to 3.3 krad/min gives no change in the *G*-value. Thus, the cyclohexyl radicals are believed to be effectively spin-trapped by PMNB, and the recombination reactions between themselves is absent at the dose rates examined.

The *G*-value of the cyclohexyl radical spin adducts has been reported to be 3 for the γ-radiolysis of cyclohexane containing PBN as a spin trap.[23] In that case, the *G*-value is slightly dependent on the PBN concentration in the range 0.1—0.01 mol dm^{-3} due to the low reactivity of PBN towards alkyl radicals.[11] It is worth noting that the *G*-values determined by the spin-trapping techniques are generally smaller than the *G*-value of 4.0 determined by using iodine as a radical scavenger.[19]

The change of the PMNB concentration with increasing radiation dose is shown in Fig. 3, representatively for the highest and the lowest initial concentrations of PMNB. The spin traps are completely consumed at the time when the spin adduct concentration reaches zero. Such an exact coincidence indicates that the same entities are responsible for both the formation and the decay of the spin adducts. Therefore, the spin adducts and the spin traps compete with each other in reacting with cyclohexyl radicals. Such a situation is very much like that previously reported for 2-methyl-2-nitrosopropane and *t*-butyl radical in a photochemical reaction system.[11]

Rate Constants and Reaction Kinetics. The change in the spin adduct concentration can essentially be expressed by the following two processes,

$$R\cdot + T \xrightarrow{k_1} A, \tag{1}$$

$$R\cdot + A \xrightarrow{k_2} \text{diamagnetic product(s)}, \tag{2}$$

where R·, T, and A represent the cyclohexyl radical, the spin trap (PMNB), and the spin adduct, respectively. Assuming that PMNB is entirely monomeric, the rate equation

$$\frac{d[A]}{d[T]} = \frac{k_2}{k_1}\cdot\frac{[A]}{[T]} - 1 \tag{3}$$

is readily derived and integrated as

$$\frac{[A]}{[T]_0} = \frac{1}{\alpha-1}\cdot\frac{[T]}{[T]_0}\left\{1-\left(\frac{[T]}{[T]_0}\right)^{\alpha-1}\right\} \tag{4}$$

with the initial condition that $[A]=0$ for $[T]=[T]_0$. α is the ratio of the rate constants, k_2/k_1. According to the above equation, the dependence of [A] on [T] is shown by the plots in Fig. 4 for several values of the variable parameter α. Figure 4 shows some of the aspects of general importance in the spin-trapping technique. As the spin-trapping reaction proceeds (the $[T]/[T]_0$ value decreases from unity to zero), the adduct radical concentration reaches a maximum value which is proportional to the initial spin trap concentration. If α is too large, the adduct radical concentration cannot be enough for the ESR detection of the adduct radical.

The dependence of [A] on [T] has been experimen-

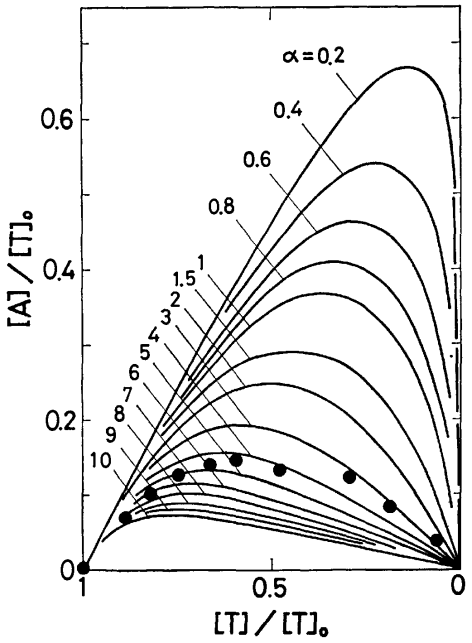

Fig. 4. The relationship between the concentration of the spin adduct and that of the spin trap, PMNB, normarlized by the initial concentration of PMNB. Theoretical curves are derived for several α values based on the Eq. 4, and experimental results (●) are obtained for the initial concentration of PMNB of 1.3×10^{-4} mol dm^{-3} at room temperature.

tally examined for the initial PMNB concentration, $[T]_0$, of 1.3×10^{-4} mol dm^{-3} and the plot is shown in Fig. 4. At this $[T]_0$ value, more than 75% of PMNB is monomeric. The plots fall in the range of $\alpha=3$ to 5. The determined value of α includes errors due to the assumptions of totally monomeric PMNB, and the disregard of the instability of the spin adduct, but it indicates undoubtedly that $k_2>k_1$. The assumed negligibility of the bimolecular recombination of the cyclohexyl radicals (important when the PMNB concentration becomes very low) and the possible effects of hydrogen atoms may also be explain the experimental plot's derivation from the single curve expected from Eq. 4.

The spin-trapping rate constant, k_1, can generally be determined by competition experiments with reactions having known rate constant, *e.g.* the reaction of the cyclohexyl radical with tributylstannane,

$$\dot{C}_6H_{11} + (C_4H_9)_3SnH \xrightarrow{k_5} C_6H_{12} + (C_4H_9)_3Sn\cdot, \qquad (5)$$

was chosen as a reference reaction, for which the rate constant has been reported to be 1.2×10^6 mol^{-1} dm^3 s^{-1} at 298 K in cyclohexane.[27] The ratio of the initial slope of spin adduct concentration *vs.* radiation dose curve in the absence and presence of tributylstannane was found to agree with the expected linear relationship,

$$\frac{d[A]}{d[A]'} = 1 + \frac{k_5[S]}{k_1[T]}, \qquad (6)$$

as shown in Fig. 5, where [A]′ represents the concentrations of the spin adducts generated in the presence

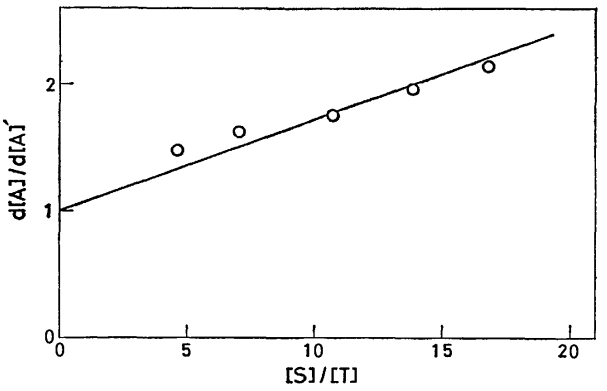

Fig. 5. The dependence of the rate of the spin adduct formation on the concentration of radical scavenger, tributylstannane, in cyclohexane at 299 K.

of tributylstannane, S. The rate constant, k_1, obtained from the slope of the straight line was found to be 1.6×10^7 mol^{-1} dm^3 s^{-1}. This value is smaller than that for the spin-trapping of *t*-butyl radicals by PMNB in benzene solution determined by using the same reference reaction, 9×10^7 mol^{-1} dm^3 s^{-1}.[11,25]

Conclusion

Simultaneous monitoring of both the spin traps and the spin adducts revealed radiation-chemical processes in the γ-radiolysis of cyclohexane solutions of PMNB. The most significant results are: (1) PMNB is an efficient spin trap such that the cyclohexyl radicals generated with *G*-value of 3.0 are thoroughly spin-trapped, (2) the cyclohexyl radical spin adducts readily disappear in the subsequent reaction with the cyclohexyl radicals. The explanation for the *G*-value of the cyclohexyl radical determined by the spin-trapping technique being smaller than the generally accepted value of ≈4 remains unknown.[28] The former results implies however that the spin-trapping technique has a future in the kinetic studies of radiation chemistry with the proper choice of the spin trap based on the rate data of the spin-trapping reactions to be accumulated further. The latter further complicates the kinetic aspects of the spin-trapping. Generally, the data on PMNB, such as the absorptivity, the monomer–dimer equilibrium, and the spin-trapping rate constant, serve as a basis to extend the spin-trapping technique to study the kinetics of free radical intermediates.

This investigation was conducted in part using the experimental facilities at the Research Reactor Institute, Kyoto University.

References

1) C. Lagercrantz, *J. Phys. Chem.*, **75**, 3466 (1971).
2) E. G. Janzen, *Acc. Chem. Res.*, **4**, 31 (1971).
3) C. Lagercrantz, *J. Am. Chem. Soc.*, **95**, 220 (1973).
4) J. R. Harbour, V. Chow, and J. Bolton, *Can. J. Chem.*, **52**, 3549 (1974).
5) F. P. Sargent and E. M. Gardy, *Can. J. Chem.*, **54**, 275 (1976).
6) K. Torssell, *Tetrahedron*, **26**, 2759 (1970).

7) T. Lin, S. H. Mastin, and N. Ohkaku, *J. Am. Chem. Soc.*, **95**, 6845 (1973).
8) K. A. Mclauchlan and R. C. Sealy, *J. Chem. Soc., Chem. Commun.*, **1976**, 115.
9) A. Ledwith, P. J. Russell, and L. H. Sutcliffe, *Proc. R. Soc. London, Ser. A*, **332**, 151 (1973).
10) T. Kunitake and S. Murakami, *J. Polym. Sci.*, **12**, 67 (1974).
11) T. Doba, T. Ichikawa, and H. Yoshida, *Bull. Chem. Soc. Jpn.*, **50**, 3158 (1977).
12) E. G. Janzen, C. A. Evans, and Y. Nishi, *J. Am. Chem. Soc.*, **94**, 8236 (1972).
13) M. J. Perkins and B. P. Roberts, *J. Chem. Soc., Chem. Commun.*, **1973**, 173.
14) E. G. Janzen and C. A. Evans, *J. Am. Chem. Soc.*, **95**, 8205 (1973).
15) E. G. Janzen and C. A. Evans, *J. Am. Chem. Soc.*, **97**, 205 (1975).
16) F. P. Sargent, *J. Phys. Chem.*, **81**, 5636 (1977).
17) S. Nigam and K. Asmus, *J. Chem. Soc., Faraday Trans. 1*, **72**, 2324 (1976).
18) R. H. Schuler, *J. Phys. Chem.*, **61**, 1472 (1957).
19) H. A. Dewhurst, *J. Phys. Chem.*, **63**, 813 (1959).
20) S. K. Ho and G. H. Freeman, *J. Phys. Chem.*, **68**, 2189 (1964).
21) P. P. Infelta and R. H. Schuler, *J. Phys. Chem.*, **76**, 987 (1972).
22) J. A. Stone and J. Esser, *Can. J. Chem.*, **52**, 1253 (1974).
23) H. Iwahashi, Y. Ishikawa, S. Sato, and K. Koyano, *Bull. Chem. Soc. Jpn.*, **50**, 1278 (1977).
24) E. C. Taylor and R. H. Danforth, *J. Org. Chem.*, **38**, 2088 (1973).
25) T. Doba, T. Ichikawa, and H. Yoshida, *Bull. Chem. Soc. Jpn.*, **50**, 3124 (1977).
26) The re-examination of the monomer equilibrium of PMNB in benzene in a wider concentration range showed that some previously reported numerical values in reference 11 should be corrected as $K=8\times10^{-4}$ mol dm^{-3} and $\varepsilon=52.6$ mol^{-1} dm^3 cm^{-1}. Accordingly, the spin-trapping rate constant of PMNB towards *t*-butyl radical should change from 1.4×10^8 to 9×10^7 mol^{-1} dm^3 s^{-1}.
27) D. J. Carlsson and K. U. Ingold, *J. Am. Chem. Soc.*, **90**, 7047 (1968).
28) R. A. Holroyd, "Fundamental Processes in Radiation Chemistry," ed by P. Ausloos, John Wiley & Sons, New York (1968), p. 413.

Proton NMR Spectra of Selectively Deuterated *p,p'*-Azoxyanisoles in the Solid State

Kikuko HAYAMIZU* and Osamu YAMAMOTO

National Chemical Laboratry for Industry, 1 Honmachi, Shibuya-ku, Tokyo 151

(Received May 12, 1978)

Selectively deuterated PAA's, PAA-d_8, and PAA-d_6 have been studied by proton NMR from 77 K to the melting point (390 K). The temperature dependences of T_1, the line width, and the second moment for these compounds are presented. It has been demonstrated that PAA is in the rigid state at 77 K on an NMR time scale, and as the temperature increases the two methyl groups begin to rotate about the C_3 axis, followed by libration about the C–O axis. There is no evidence for motions of the ring protons except self-diffusion and/or slow reorientation of the molecular axis in the higher temperature range from 286 K to the melting point.

p,p'-Azoxyanisole (PAA, 4,4'-dimethoxyazoxybenzene) is one of the most important compounds in nematic liquid crystals and has been widely studied by NMR.[1] In the proton resonance, however, it is difficult to distinguish the two different types of protons, *i.e.*, the ring and the methyl protons, although their spin-lattice relaxation times are expected to show different dependences on temperature. Thus we have synthesized the two selectively deuterated PAA's, *i.e.*, the ring-proton-deuterated PAA (PAA-d_8) and the methyl-proton-deuterated PAA (PAA-d_6), and already reported their proton relaxation times and anisotropic molecular motions in the nematic and isotropic liquid states.[2]

In this paper the spin-lattice relaxation times T_1, the line widths, and the second moments of the two selectively deuterated PAA's are presented from 77 K to the melting point. The internal motions of the methyl protons are distinguishable from the motion of the ring protons, and it is possible to discuss the effects of the internal reorientations of the side chains on T_1 of the benzene protons of the central part of the molecule.

Proton relaxation times T_1 and $T_{1\rho}$ have been studied in the solid state,[3] and the molecular motions depending on temperatures were discussed. It has been suggested that there is a question about the activation of the internal rotation around the C–O axis for PAA in the solid state. It will be shown here that such hindered rotation about this axis does not exist.

Experimental

The method of synthesis and purification of the selectively deuterated PAA's have been described in a previous paper.[2] The compounds were sealed in a 10 mm o.d. glass tube after a number of melt-solidify-pump-thaw cycles.

The proton NMR spectrum was observed by an NMR Specialities PS-60RW spectrometer operating at 55 MHz. The temperature control apparatus has been reported in the previous paper.[2] T_1 measurements were carried out by the usual 180°-τ-90° pulse sequence. The accuracy of the semilogarithmic plot was within ±10%. To obtain the cw spectrum the FID signal was digitized by a Biomation 1010 waveform recorder and then accumulated in a FACOM F-PDT-8 microcomputer. The pulse width for 90° nutation was approximately 4.5 μs. The sampling time was 0.5 to 1 μs, data points were about 200 to 600 and the accumulation was 1 to 16 times depending on the temperature. The accumulated FID signal was punched on to paper tape and Fourier-transformed by a FACOM 270/30 computer. The second moment was also calculated by the computer from the cw spectrum obtained.

Results and Discussion

The Fourier-transformed cw spectra of PAA-d_8 are shown in Fig. 1. At 77 K the methyl protons of PAA-d_8 show a triplet, which is the typical pattern for a three-spin system in the rigid lattice. The spacing between the two outer lines is 14.8 G, which agrees well with the theoretical value of 4α, where $\alpha=(3/2)\mu_H/r^3$ and $r=1.79$ Å. As the temperature increases, each line broadens, the triplet collapeses into a broad single line at about 92 K, and then the line narrows into another triplet with small splitting. The change of the spectral patttern is due to the activation of the reorientation of the methyl group about the C_3 axis and agrees well with the theoretically calculated

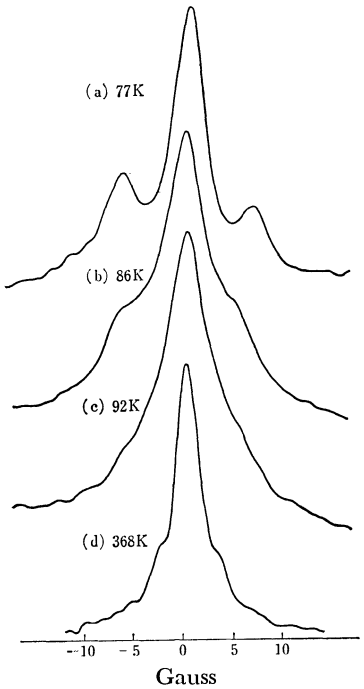

Fig. 1. Fourier transformed cw spectra of PAA-d_8 at (a) 77 K, (b) 86 K, (c) 92 K, and (d) 368 K. Throughout this paper 10^4 G = 1 T.

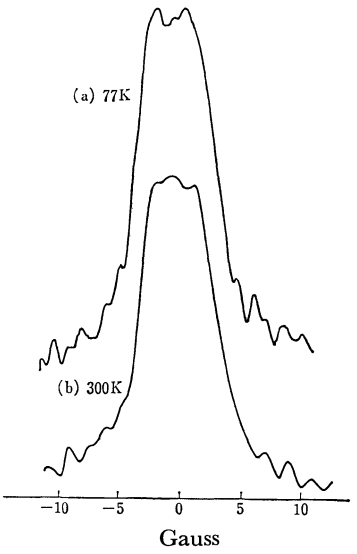

Fig. 2. Fourier transformed cw spectra of PAA-d_6 at (a) 77 K and (b) 300 K.

spectra for an isolated methyl group reported by Cobb and Johnson.[4] The spectral pattern for PAA-d_8 does not change significantly from 103 K to the melting point at 390 K (117.5 °C). The temperature dependences of the outer spacing of the triplet, the half line width of the central line, and the second moment of PAA-d_8 are shown in Fig. 3 (a), (b), and (c) respectively. Since the second moment was calculated from the Fourier-transformed spectrum, where it was difficult to draw a definite base line in the technique employed in this paper, the error was rather large, about 10 to 15% of the obtained value. This error comes directly from the uncertainty of the base line position.

The proton cw spectra of PAA-d_6 are shown in Fig. 2. As may be seen, the spectral pattern is almost unchanged from 77 K to the melting point. The line width is also constant from 77 to 285 K, and a little line narrowing is observed below the melting point, as shown in Fig. 4. The second moment of PAA-d_6 in Fig. 4 also shows a similar behavior to the line width with the change of the temperature.

In discussing the molecular motions of PAA in the solid state, interesting points are the methyl reorientation around the C_3 axis and the C–O axis, the libration of the benzene rings about the C–N axis, the molecular overall reorientation, and the self-diffusion. It has been suggested from the study of proton T_1 and $T_{1\rho}$ of PAA,[3] that the reorientation of the methyl groups about the C_3 axis is the predominant relaxation mechanism between 77 and 167 K, and that the internal rotation about the C–O axis is activated between 167 and 238 K, and in this temperature range there is also proton cross relaxation to the nitrogen. Then as the temperature increases the fast random molecular reorientation and slow self-diffusion take place. In the same paper,[3] however, it was written that as an opinion of other researchers, there is a question on the rotation about the C–O axis in the solid state.

In this study, the second moment of PAA-d_8 decreases from 22.6 to 6.0 G^2 at about 103 K, which corresponds to the change from the methyl group which is isolated in the rigid lattice to the methyl group freely rotating about the C_3 axis. If the rotation of the methyl group around the C–O axis were further activated in higher temperatures, the second moment should become about 0.56 G^2, since the second moment will decrease by a factor of $\left(\frac{3\cos^2\theta-1}{2}\right)^2$ by the additional rotation.[6] The angles COC (θ) have been determined as 118.7 and 118.1° from X-ray analysis.[5] However, at temperatures just below the melting point, the second moment is still 3.8±0.5 G^2. Thus it is concluded that the methyl groups do not rotate around the C–O axis in the solid state.

The second moment of the ring protons of PAA-d_6 is almost constant from 77 K to about 200 K, and a little narrowing is observed near below the melting point, as shown in Fig. 4. The second moment of the

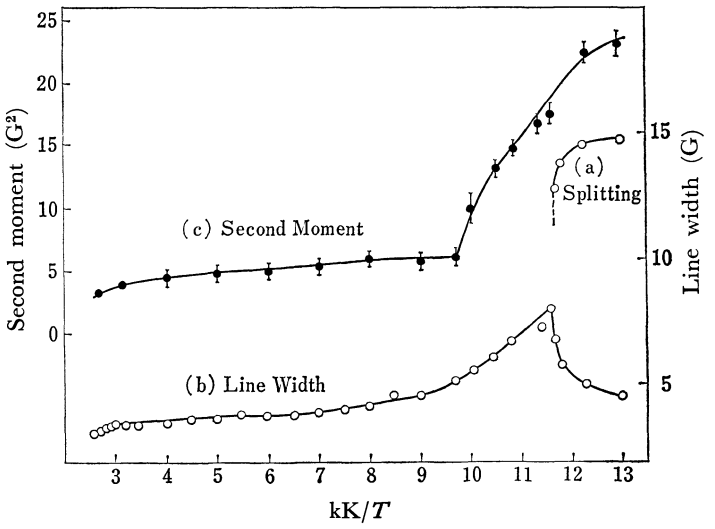

Fig. 3. The temperature dependences of (a) the spacing of the outer lines, (b) the half line width of the central line of the triplet, and (c) the second moment for PAA-d_8.

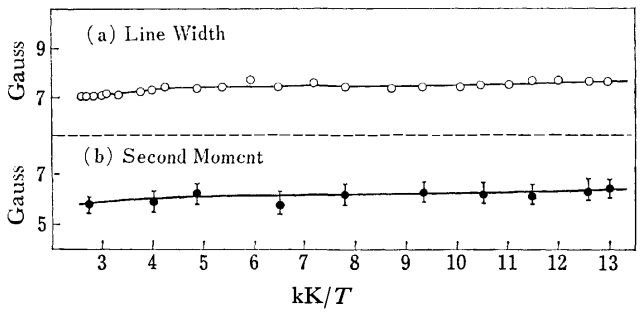

Fig. 4. The temperature dependences of (a) the half line width and (b) the second moment for PAA-d_6.

ring protons calculated for the rigid lattice is 1.67 from the protons on the same benzene ring, 0.07 from the protons of another benzene ring in the same molecule, 1.14 from the intermolecular ring protons, and 0.03 from the inter- and intramolecular CD_3 groups in the G^2 unit. The sum, 2.91 G^2 is expected for the second moment of PAA-d_6 in the rigid lattice with random orientation. However, the observed second moment is 6.2 G^2 at 77 K and 5.8 G^2 just below the melting point, both of which are larger than the calculated value. The sample used in this work was heated to melt in the nematic state for the purpose of degassing. After the rapid or slow cooling from the nematic to the solid states inside or outside the magnetic field, the second moment of PAA-d_6 observed at room temperature was almost the same value within experimental error. One possible interpretation for this disagreement between the observed and calculated second moments is that some orientation in the nematic state may still remain in the solid state. Another interpretation is the polymorphism of PAA in the solid state obtained by cooling from the nematic state as suggested by a recent study.[7] In PAA-d_8 the methyl group may be regarded as an isolated system, so that the effects of the remaining orderness or polymorphism are probably very small on the second moment of PAA-d_8.

In the calculated second moment of PAA-d_6, the intermolecular contribution is about 40%. When the molecular motion, which causes the change of the intermolecular proton-proton distance, were activated, a decreasing of the second moment should occur. Since the second moment of PAA-d_6 does not change significantly, libration about the C–N axis or the fast molecular reorientation suggested before,[3] both of which bring changes in the intermolecular ring proton distances, can not be assumed to take place below 250 K in the solid state.

The above discussion concerning the molecular motion of PAA can be applied to the T_1 behavior of PAA-d_8, PAA-d_6, and PAA. As shown in Fig. 5, the plots of T_1 *vs.* $1/T$ have minimum values at similar temperatures. This fact suggests that the motion, which gives the T_1 minimum, belongs to the same mode of molecular motion for all compounds. Considering the spectral patterns and the second moments, this motion is clearly the reorientation of the methyl groups about the C_3 axis.

T_1 of the reorientating methyl protons may be described by

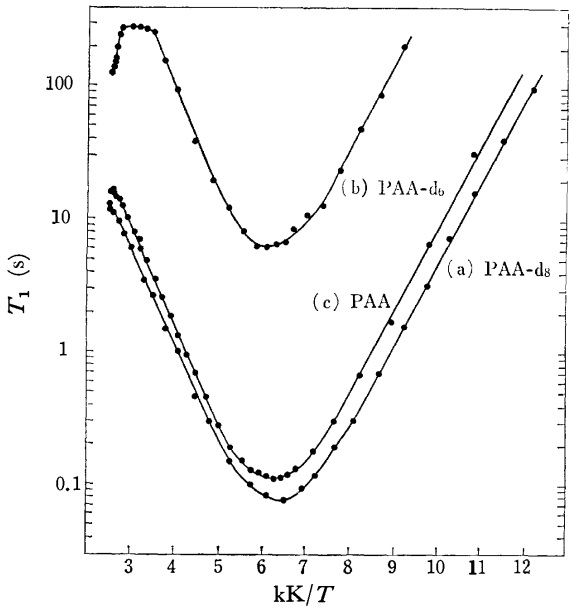

Fig. 5. The temperature dependent spin-lattice relaxations for (a) PAA-d_8, (b) PAA-d_6, and (c) PAA in the solid state observed at 55 MHz.

$$\left(\frac{1}{T_1}\right)_{\text{Methyl}} = \frac{9}{20}\frac{\gamma_H^4\hbar^2}{r^6}\left(\frac{\tau_c}{1+\omega_H^2\tau_c^2}+\frac{4\tau_c}{1+4\omega_H^2\tau_c^2}\right), \quad (1)$$

where r is the distance betweeen the protons within the methyl group, and $\omega_H=2\pi\nu_H$, ν_H being the resonance frequency of the protons (55 MHz). The condition for the T_1 minimum is $\omega_H\tau_c=0.616$. In the case of the ring protons, T_1 is very long and the contribution from the rotating CD_3 becomes important. Assuming that the ^{2}H relaxation of the CD_3 groups takes place mainly by the quadrupolar mechanism and that the correlation time for the reorientation of CD_3 is the same as that for CH_3 of PAA-d_8 at the same temperature, then the magnetic relaxation of the deutrons of the CD_3 is much faster than that of the ring protons by about 10^4 in the vicinity of the T_1 minimum. Theoretically, the non-resonant spins contribute to the relaxation of the resonant spins.[8] In this case, however, the relaxation rate of the non-resonant deuterons of CD_3 is so large that it may be assumed that the effect of the magnetization of CD_3 on the dipolar relaxation time T_1 of the ring protons may be neglected. This dipolar relaxation time T_1 directly arising from the rotating CD_3 in the weak collision limit, may be written as[8,9]

$$\left(\frac{1}{T_1}\right)_{\text{Ring}} = \frac{4}{15}\gamma_H^2\gamma_D^2\hbar^2 I_D(I_D+1)\frac{1}{N_i}\sum_{ij}\frac{1}{r_{ij}^6} \times\left(\frac{1}{2}\frac{\tau_c}{1+(\omega_H-\omega_D)^2\tau_c^2}+\frac{3}{2}\frac{\tau_c}{1+\omega_H^2\tau_c^2} +\frac{3\tau_c}{1+(\omega_H+\omega_D)^2\tau_c^2}\right), \quad (2)$$

where $\omega_D=2\pi\nu_D$ and ν_D is the ^{2}H resonance frequency, γ_D and I_D are the gyromagnetic ratio and the spin quantum number of deuteron, and r_{ij} is the distance between the ring proton i and the deuteron j of the intra- and intermolecular CD_3 groups, and N_i is the number of the ring protons. In Eq. 2, the condition of

the minimum T_1 is $\tau_c=2.7\times10^{-9}$ s ($\nu_H=55.0$ MHz). Using the proton-proton distances for PAA obtained from X-ray analysis, Eq. 2 gives $(T_{1\,min})_{Ring}=3.8$ s, and the observed value is 6.4 s, approximately 60% of the theoretical value. On the other hand, the calculated $(T_{1\,min})_{Methyl}=31$ ms, compared to the observed value of 76 ms, about 40% of the theoretical value. In both cases the observed $T_{1\,min}$ is longer than the calculated one. As described later, the agreement is considered satisfactory, and it can be said that the $T_{1\,min}$ of the ring protons is interpreted by the rotation of the neighboring CD_3 groups.

The discrepancy between the observed and the calculated $T_{1\,min}$ has already been reported for the hindered rotation of the methyl group in an isolated system, and interpreted by Johnson[10] as the following: oscillations of the methyl group, occuring in the reorientation through large angles, partially average the dipolar Hamiltonian and the efficiency of the nuclear relaxation is reduced, leading to a longer T_1 than given by the theory. Furthermore, it has been also shown that if there is cross-correlation, the relaxation is not a simple exponential decay and T_1 obtained by the half-recovery method becomes longer. In our experiments, non-exponential decay for the relaxation of all the compounds studied was not observed, but the discrepancy was a little larger, compared with the simple methyl compounds studied by Johnson. This is attributed to the coupling of the internal rotation of the methyl group about the C_3 axis with another molecular motion. In point of fact, the second moment of PAA-d_8 is smaller than the value of the isolated rotating methyl protons at this temperature.

As given in Table 1, the activation energies obtained from the slopes of log T_1 *vs.* $1/T$ plots are similar for PAA, PAA-d_8, and PAA-d_6 in both the low and high temperature sides. This is another reason why the same mode of the molecular motion affects T_1's of the ring protons as well as the methyl protons. The correlation time τ_0 was obtained from τ according to the equation $\tau=\tau_0\exp(E_a/RT)$. The values of τ_0 for PAA, PAA-d_8, and PAA-d_6 in Table 1 are reasonable for the rotation of the methyl group about the C_3 axis.[11,12] The small deviation of τ_0 for PAA-d_6 is probably due to the assumption contained in Eqs. 1 and 2.

In order to explain the value of $T_{1\,min}$ and the slight narrowing of the second moment of PAA-d_8 from about 100 K to the melting point, some additional process of molecular motion is necessary besides the reorientation of the methyl group about the C_3 axis. From the study of T_1 and $T_{1\rho}$ of PAA, it has been suggested that in the temperature region between 167 and 238 K, the slow rotation of the methyl group about the C–O axis is activated. However, there is not a clear change in the second moment of the methyl protons of PAA-d_8, corresponding to the dual reorientation of the methyl group. The second moment of PAA-d_8 decreases gradually from 6.0 to 3.8 G^2 in the temperature region betweeen 100 K and the melting point. Thus, the slow libration about the C–O axis may be considered, after the reorientation of the methyl group about the C_3 axis is activated. The effect of the libration on the second moment of the ring protons of PAA-d_6 is estimated as being negligible, although the second moment decreases from 6.2 to 5.8 G^2 near the melting point. Thus some other molecular motions are necessary to understand the narrowing.

Above 286 K ($1/T=3.5\times10^{-3}$), a large change appears in the T_1 of PAA-d_6. When the temperature increases, T_1 is nearly constant until 364 K, and then T_1 decreases sharply until the melting point. In this temperature range, however, the second moment and the line width decrease only to a small extent, and the spectral pattern does not change at all. Such change is not apparent in T_1 for the rotating methyl protons of PAA-d_8, but the line width and the second moment of this compound decrease to nearly the same extent as those of PAA-d_6. These facts suggest that motion of the whole molecule takes place at these temperatures. For such motion, the self-diffusion and the reorientation of the molecular axis have been assigned from the study of T_1 and $T_{1\rho}$ of PAA.[3] It should be noted that the motion of the whole molecule begins at temperatures about 105 K below the melting point. This wide temperature region for the self-diffusion and the molecular reorientation, even in the solid state, characterises the nematic liquid crystalline compound PAA.

Assuming that the relaxation mechanism for T_1 of PAA, PAA-d_8, and PAA-d_6 is the dipole-dipole interaction,

$$\left(\frac{1}{T_1}\right)_{PAA}=\frac{8}{14}\left(\frac{1}{T_1}\right)_{PAA\text{-}d_8}+\frac{6}{14}\left(\frac{1}{T_1}\right)_{PAA\text{-}d_8}+\left(\frac{1}{T_1'}\right) \tag{3}$$

then, $1/T_1'$ is the relaxation rate mainly due to interactions between the ring and the methyl protons and a small contribution from the interactions of the protons with deuterons. On the low temperature side of the T_1 minimum, $1/T_1'$ is negeligibly small within experimental error, while on the high temperature side, $1/T_1'$ has a value larger than the relaxation rate of PAA-d_6 at all temperatures. The gradient of the log T_1' *vs.* $1/T$ plot has almost the same as that of log T_1 *vs.* $1/T$ for PAA, PAA-d_6, and PAA-d_8 which are shown in Table 1. Then the molecular motion

TABLE 1.

Compound	$T_{1\,min}$(s)	Temp(K)	$\tau_0(10^{-13}$ s)	Activation energy(kJ/mol)	
				Low temp	High temp
PAA	0.11	159	1.9	12.1(±0.7)	14.3(±0.4)
PAA-d_8	0.076	154	1.7	11.5(±1.5)	15.0(±1.9)
PAA-d_6	6.3	165	6.4	11.8(±0.2)	13.6(±0.6)

which governs the temperature dependence of the interaction between the methyl and the ring protons in PAA is the same as that for the ring protons of PAA-d_6, which is considered to be the reorientation of the methyl groups and the motion of the whole molecule.

In conclusion, at 77 K PAA is in a rigid lattice in an NMR time scale, and as the temperature increases, the methyl groups begins to rotate around the C_3 axis, followed by slow libration about the C–O axis. The other motions which change the relative position of the ring protons do not occur until the molecular overall motions, which may be self-diffusion and slow reorientation of the molecular axis, start to take place at 286 K.

References

1) W. Wolfel, F. Noack, and M. Slohrer, *Z. Naturforsch., Teil A*, **30** 437 (1975); and literature cited therein.
2) K. Hayamizu and O. Yamamoto, *J. Chem. Phys.*, **66**, 1720 (1977).
3) R. T. Thompson, D. W. Kydon, and M. M. Pintar, *J. Chem. Phys.*, **61**, 4646 (1974).
4) T. B. Cobb and C. S. Johnson, Jr., *J. Chem. Phys.*, **52**, 6224 (1970).
5) W. R. Krigbaum, Y. Chatani, and P. G. Barber, *Acta Crystallogr., Sect. B*, **26**, 97 (1970).
6) J. G. Powles and H. S. Gutowsky, *J. Chem. Phys.*, **21**, 1704 (1953).
7) L. Bata *et al.*, *Mol. Cryst. Liq. Cryst.*, **44**, 71 (1978).
8) A. Abragam, "The Principle of Nuclear Magnetism," Clarendon Press, Oxford (1961), p. 295.
9) G. Soda and H. Chihara, *J. Phys. Soc. Jpn.*, **36**, 954 (1974).
10) C. S. Johnson, Jr., *J. Magn. Reson.*, **24**, 63 (1976).
11) H. M. Mcintyre and C. S. Johnson, Jr. *J. Chem. Phys.*, **55**, 345 (1971).
12) A. Kumar and C. S. Johnson, Jr. *J. Chem. Phys.*, **60**, 137 (1974).

Study of Metal-Polycarboxylate Complexes Employing Ion-selective Electrodes. II.[1] Stability Constants of Copper(II) Complexes with Poly(acrylic acid) and Poly(methacrylic acid)

Fumitaka YAMASHITA,* Tsuyoshi KOMATSU, and Tsurutaro NAKAGAWA
Department of Polymer Science, Faculty of Science, Hokkaido University, Sapporo 060
(Received May 26, 1978)

The copper(II) complex formation with poly(acrylic acid) and poly(methacrylic acid) in aqueous solution was studied by potentiometric titration employing glass and copper(II) ion-selective electrodes. The values of the equilibrium constants of the complex formation and the stability constants were estimated in various degree of neutralization. Since the concentration of free copper(II) ions could be determined by employing the copper(II) ion-selective electrode, the concentrations of two complex species, involving one and two carboxylato groups, were determined from stoichiometric equations. The equilibrium and stability constants of the complexes obtained were observed to pass through peaks with increase in the degree of neutralization. The order of magnitude of the equilibrium constant of the polyacrylate complex was larger than that of the polymethacrylate complex.

Studies of bivalent metal–polyelectrolyte complex formations by potentiometry have been reported by Gregor and coworkers,[2] as well as by Mandel and Leyte.[3] The formation curves, namely the average coordination numbers, of the bivalent metal–polyelectrolyte systems have a flat region in the range of higher degrees of neutralization and the value of the average coordination number is equal to 2. This result suggests that the predominant complex in the system is the bivalent metal ions chelated by two carboxylato groups.

Marinsky and coworkers[4-6] have investigated the complex formation of bivalent metal ions with polycarboxylic acid. It is concluded, though their systems are composed of gels, that two carboxylato groups of poly(methacrylic acid) coordinate to copper(II) ions in the range of higher degrees of neutralization. The stability constants of some bivalent metal complexes were also calculated.

On the other hand, it seems that the results of spectrophotometric studies have been satisfactorily interpreted. When the degree of neutralization is varied, the absorbance of copper(II) complexes with polycarboxylate passes through a maximum in the course of neutralization. This fact shows that the copper(II) complexes partially change in favor of some other form of binding, and as pointed out by Mandel and Leyte,[7] the spectrophotometric and potentiometric results show a breakdown of the chelate in the higher neutralization region.

In our previous paper,[1] it was shown that the potentiometric titration employing ion-selective electrodes was available for the investigation of complex formation of the bivalent metal ions with polycarboxylic acid, especially with poly(itaconic acid). But poly(acrylic acid) systems were studied for comparison purposes and the discussion was carried out mainly on the basis of the formation curves of complexes. In this study, then, poly(acrylic acid) (PAA) and poly(methacrylic acid) (PMA) were investigated by pH titration and potentiometry employing the ion-selective electrode, and the concentrations of the complexes formed and the formation constants were evaluated from the potentiometric data.

Experimental

Materials. The preparation of all materials used was described previously.[1,8]

Potentiometric Titration. The pH measurements were carried out in nitrogen atmosphere at 25±0.05 °C by use of a Yokogawa Model KPH-51A pH meter equipped with Toadenpa Model HG-4005 glass and HC-2005 calomel electrodes.

The activities of copper(II) ions were measured with an Orion Model 801A digital ion meter equipped with Beckman Model 39612 Cupric and Horiba Model 2010-05T calomel electrodes, and the concentrations of copper(II) ions were estimated with the calibration curve which is obtained by measurements of the systems without only polyligands. The other conditions and techniques of potentiometry were described previously.[1]

Results and Discussion

Potentiometry Employing Copper(II) Ion-Selective Electrode. In our previous paper,[1] the potentiometry employing a copper(II) ion-selective electrode applied to the copper(II) ion-polycarboxylic acid systems was discussed. In this case it was not necessary to consider the effect of pH, because the concentration of the bivalent metal ions compared with that of the polyacid is so low that all the metal ions exist essentially as chelates in the pH region where the metal hydroxides are formed in the absence of polyacid.

In the case of the present study, however, nonchelated copper(II) ions exist in the pH region where the metal hydroxides are to be formed in the absence of polyacid. Thus, all the potentiometric measurements were carried out in the pH region less than 6.00.

Concentrations of Complexes as Functions of Degree of Neutralization. Assuming that both monocarboxylato and dicarboxylato complexes are formed, and that the concentrations of the other complexes are negligible even if they are formed, the following equations hold:

$$[Cu_t] = [Cu^{2+}] + [CuA^+] + [CuA_2],$$

$$[A_t] = [A^-] + [HA] + [CuA^+] + 2[CuA_2],$$

where $[Cu_t]$ is the total concentration of copper(II)

ions and $[A_t]$ is that of carboxylato groups. In these equations, the values of $[CuA^+]$ (designating the concentration of monocarboxylato copper(II) complex), of $[CuA_2]$ (that of dicarboxylato complex), and of $[A^-]$ (that of nonchelating carboxylato groups) are unknown. In the present paper, the concentration of free copper(II) ions, $[Cu^{2+}]$, can be determined by potentiometric measurements employing the copper(II) ion-selective electrode. But these equations cannot be solved stoichiometrically without the estimation of $[A^-]$ based on some assumption.

By use of the reference plot method proposed by Mandel and Leyte,[3] the concentrations of nonchelating carboxylato groups, $[A^-]$, can be estimated. When the concentrations of free copper(II) ions have been determined by employing the copper(II) ion-selective electrode, these two stoichiometric equations make it possible to know the concentrations of the two complex species, $[CuA^+]$ and $[CuA_2]$.

In Figs. 1 and 2, the values of $[CuA^+]$ and $[CuA_2]$ obtained by the above method are plotted against the apparent degree of neutralization α'. In Fig. 1, the results for the copper(II)–PAA system (9.9×10^{-3} monomol/l PAA, 1.0×10^{-3} mol/l $Cu(NO_3)_2$, and 1.0×10^{-1} mol/l KNO_3), and in Fig. 2 those for the copper(II)–PMA system (1.0×10^{-2} monomol/l PMA, 1.0×10^{-3} mol/l $Cu(NO_3)_2$, and 1.0×10^{-1} mol/l KNO_3) are presented. As shown in these figures, the concentrations of the monocarboxylato complex are found to be significantly high, though the values of $[CuA^+]$ are relatively small compared with $[CuA_2]$. As the degree of neutralization increases, the concentrations of the two complex species, $[CuA^+]$ and $[CuA_2]$, increase and reach maxima in both systems, PAA and PMA. The values of the degree of neutralization of PAA at which the complex concentrations reach a maximum are 0.35 for $[CuA_2]$ and 0.45 for $[CuA^+]$. In the case of PMA two maxima are observed; their degree of neutralization values are 0.27 and 0.43 for $[CuA_2]$, and 0.35 and 0.60 for $[CuA^+]$.

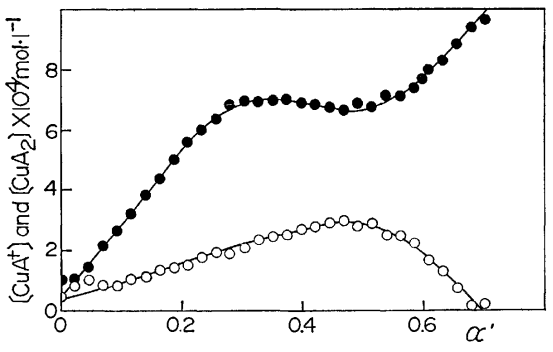

Fig. 1. Dependence of the concentrations of monocarboxylato and dicarboxylato copper(II) complexes, $[CuA^+]$ (○) and $[CuA_2]$ (●), on the apparent degree of neutralization α' for PAA system.

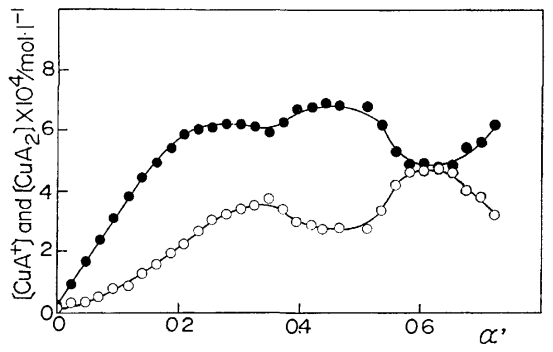

Fig. 2. Dependence of the concentrations of monocarboxylato and dicarboxylato copper(II) complexes, $[CuA^+]$ (○) and $[CuA_2]$ (●), on the apparent degree of neutralization α' for PMA system.

It is very interesting that maxima are obtained in the potentiometric measurements. In most studies[6,7,9,10] of spectrophotometric measurement it has been observed that the absorbance due to the copper(II) complex with carboxylato groups increases and passes through a maximum with increase in the degree of neutralization, and that the value of the degree of neutralization at the maximum of the absorption is about 0.3 to 0.4 for systems composed of similar concentration ratios. In the study of Mandel and Leyte,[7] it is shown that the disagreement between the spectrophotometric and the potentiometric results appears in the region of higher degree of neutralization. In such a neutralization region, the absorbance due to the complex formation begins to decrease, whereas the formation curve by potentiometry shows constant or increasing values. In the present study, however, the variations of $[CuA^+]$ and $[CuA_2]$ against the degree of neutralization show a decreasing tendency; this fact is similar to the spectrophotometric results. Therefore, potentiometric data also show that the monocarboxylato and dicarboxylato copper(II) complexes are partially broken or change in favor of some other form of binding with increase in the degree of neutralization. Since the concentration of hydroxide ions as ligands increases in the high neutralization region, some carboxylato ligands may be released and the concentrations of the complexes may decrease.

In Fig. 2, where the copper(II)–PMA system is treated, two maxima are observed. The maximum in the region of lower neutralization may be due to the conformational transition of PMA which appears in the course of potentiometric titration. Here, it is interesting that the value of the degree of neutralization at the maximum agrees with that found by the spectrophotometric measurement of the similar conditions. But it is not clear whether this maximum came from the reference plot method or the figure actually reflects the fact.

In Figs. 1 and 2, moreover, in the region of higher degree of neutralization the concentrations of dicarboxylato complex show an increasing tendency again. In such a region, the concentrations of nonchelating carboxylato groups are very high, whereas the concentrations of free bivalent metal ions are negligibly low; such an equilibrium is difficult to treat precisely. On the other hand, the estimation of the concentration of nonchelating carboxylato groups by Mandel's reference plot method may become inapplicable because of the higher charge density on the polyions. Thus,

a precise discussion is impossible in the region of such a degree of neutralization.

Stability and Equilibrium Constants of Complexes. The stability and equilibrium constants of the copper(II) complex with PAA calculated from the concentrations of the complexes obtained by the above mentioned method are shown in Table 1.

TABLE 1. STABILITY AND EQUILIBRIUM CONSTANTS OF Cu(II)–PAA COMPLEXES

α'	β_1	β_2	B_2	B_2'
0.00	9.3×10^{1}	3.8×10^{5}	6.5×10^{-4}	1.3×10^{-5}
0.05	2.0×10^{2}	3.7×10^{5}	5.1×10^{-4}	9.9×10^{-6}
0.10	1.9×10^{2}	7.2×10^{5}	7.8×10^{-4}	1.4×10^{-5}
0.15	3.0×10^{2}	9.5×10^{5}	9.5×10^{-4}	1.5×10^{-5}
0.20	4.1×10^{2}	1.4×10^{6}	1.4×10^{-3}	1.8×10^{-5}
0.25	8.2×10^{2}	2.0×10^{6}	1.3×10^{-3}	1.9×10^{-5}
0.30	1.3×10^{3}	2.8×10^{6}	1.3×10^{-3}	1.8×10^{-5}
0.35	2.5×10^{3}	3.7×10^{6}	1.1×10^{-3}	1.6×10^{-5}
0.40	4.4×10^{3}	4.7×10^{6}	9.6×10^{-4}	1.2×10^{-5}
0.45	7.3×10^{3}	5.9×10^{6}	7.9×10^{-4}	8.3×10^{-6}
0.50	1.1×10^{4}	8.0×10^{6}	7.2×10^{-4}	7.4×10^{-6}
0.55	1.5×10^{4}	1.2×10^{7}	6.7×10^{-4}	6.7×10^{-6}
0.60	1.7×10^{4}	1.7×10^{7}	6.6×10^{-4}	5.2×10^{-6}
0.65	9.7×10^{3}	2.5×10^{7}	7.0×10^{-4}	4.8×10^{-6}
0.70	3.5×10^{3}	4.0×10^{7}	7.3×10^{-4}	4.3×10^{-6}

The parameters β_1, β_2, B_2, and B_2' in the table will be discussed in some detail. When the concentration of nonchelating carboxylato groups is estimated, the effect of the change in the electrostatic potential on the polyion is considered in the reference plot method. The stability constants of the momocarboxylato and dicarboxylato complexes, β_1 and β_2, apparently vary with increase in the degree of neutralization. In the estimation of such a constant of polymer systems, therefore, it seems that the variation of the charge density on the polyion must be taken into account, as is shown in the series of these constants.

Then, consider the following equilibrium equation and constant:

$$Cu^{2+} + 2HA \rightleftharpoons CuA_2 + 2H^+, \quad B_2 = \frac{[CuA_2][H^+]^2}{[Cu^{2+}][HA]^2}.$$

Since the complex formation on the polyion is described as an exchange of copper(II) ion with two hydrogen ions, the total charge on the polyion remains unchanged by the chelate formation. Then, the B_2 without the effect of the change in the charge density may be constant. As is shown in Table 1, the sufficiently constant values of B_2 were not obtained.

On the other hand, the following equilibrium equation and constant have been proposed by Wall and Gill:[11]

$$Cu^{2+} + H_2A_2 \rightleftharpoons CuA_2 + 2H^+, \quad B_2' = \frac{[CuA_2][H^+]^2}{[Cu^{2+}][H_2A_2]}.$$

The results by this scheme with the relation of $[H_2A_2] = 1/2[HA]$ are shown in Table 1, and the values of B_2' still failed to be constant.

In all ways of evaluating the constants, no constant values independent of the degree of neutralization were obtained, but orders of magnitude of the constants may be estimated as 10^6 for β_2 and 10^{-3} for B_2 in the copper(II)–PAA system.

In Table 2, the results with the copper(II)–PMA system obtained by the same scheme of estimation are shown. Since the values of the stability and equilibrium constants of the copper(II) complex with PMA vary over a wider range, it is rather difficult to determine the order of magnitude of these constants, and the values are roughly 10^{-5} for B_2.

Comparing the values of these constants and their dependence on the degree of neutralization, it is seen that the PAA complex is relatively more stable than the PMA complex. But it is also suggested that the effect of the charge density on the polyion is not the only predominant factor in such a complicated complex formation as polyelectrolytes, and the conformational transition must be considered not only by acid dis-

TABLE 2. STABILITY AND EQUILIBRIUM CONSTANTS OF Cu(II)–PMA COMPLEXES

α'	β_1	β_2	B_2	B_2'
0.00	1.0×10^{1}	4.9×10^{5}	4.8×10^{-5}	1.0×10^{-6}
0.05	1.9×10^{2}	1.6×10^{6}	1.1×10^{-4}	2.2×10^{-6}
0.10	2.9×10^{2}	2.6×10^{6}	1.3×10^{-4}	2.5×10^{-6}
0.15	6.4×10^{2}	3.3×10^{6}	1.2×10^{-4}	2.5×10^{-6}
0.20	1.2×10^{3}	4.0×10^{6}	1.0×10^{-4}	1.6×10^{-6}
0.25	3.4×10^{3}	5.3×10^{6}	8.3×10^{-5}	1.3×10^{-6}
0.30	8.0×10^{3}	9.3×10^{6}	6.6×10^{-5}	9.5×10^{-7}
0.35	1.5×10^{4}	1.2×10^{6}	5.5×10^{-5}	7.3×10^{-7}
0.40	1.8×10^{4}	1.6×10^{7}	5.4×10^{-5}	7.0×10^{-7}
0.45	2.1×10^{4}	1.8×10^{7}	5.3×10^{-5}	6.0×10^{-7}
0.50	2.4×10^{4}	1.8×10^{7}	5.0×10^{-5}	4.8×10^{-7}
0.55	4.0×10^{4}	1.5×10^{7}	4.0×10^{-5}	3.3×10^{-7}
0.60	6.0×10^{4}	1.3×10^{7}	3.2×10^{-5}	2.8×10^{-7}
0.65	7.5×10^{4}	1.5×10^{7}	1.8×10^{-5}	1.8×10^{-7}
0.70	7.3×10^{4}	2.2×10^{7}	2.8×10^{-5}	1.7×10^{-7}

TABLE 3. COMPARISON OF STABILITY AND EQUILIBRIUM CONSTANTS WITH VALUES OBTAINED BY SOME AUTHORS

	$[A_t]$	$[Cu_t]$	μ	Constant	Ref.
Cu(II)–PAA	1×10^{-2}	1×10^{-3}	0.1(KNO_3)	$B_2=7\times10^{-4}$	by present analysis
	1×10^{-2}	1×10^{-3}	0.2($NaNO_3$)	$B_2=4.6\times10^{-3}$	2
	2.5×10^{-3}	2×10^{-4}	0.25($NaNO_3$)	$B_2=1.5\times10^{-4}$	12
	2×10^{-3}	2×10^{-4}	0.1($NaNO_3$)	$B_2=4\times10^{-2}$	13
Cu(II)–PMA	1×10^{-2}	1×10^{-3}	0.1(KNO_3)	$B_2\simeq10^{-4}$	by present analysis
	2×10^{-2}	2×10^{-3}	0.1($NaNO_3$)	$B_2=2.5\times10^{-4}$	3
	5.5×10^{-3}	4.4×10^{-4}	0.1($NaNO_3$)	$B_2=2.5\times10^{-4}$	14

sociation but also by chelation and the other steric factors.

In Table 3, the stability and equilibrium constants reported previously and estimated by the present analysis are summarized. Although it is meaningless to compare the absolute values of these constants, as was stated above, the agreement of the order of magnitude of these constants is apparent.

Thus, the conclusion is as follows. The stability and equilibrium constants of the copper(II) complexes with PAA and PMA (apparently) change with increase in the degree of neutralization; the order of magnitude of these constants can be estimated; and the B_2 values of the dicarboxylato copper(II) complex are of the order 10^{-3} for PAA and 10^{-4} for PMA, respectively.

References

1) Part 1: F. Yamashita, T. Komatsu, and T. Nakagawa, *Bull. Chem. Soc. Jpn.*, **49**, 2073 (1973).

2) H. G. Gregor, L. B. Luttinger, and E. M. Loeble, *J. Phys. Chem.*, **59**, 34(1955).

3) M. Mandel and J. C. Leyte, *J. Polym. Sci., Part A*, **2**, 2883 (1964).

4) C. Travers and J. A. Marinsky, *J. Polym. Sci., Part C*, Symposium No. 47, 285 (1974).

5) W. M. Anspach and J. A. Marinsky, *J. Phys. Chem.*, **79**, 433 (1975).

6) J. A. Marinsky and W. M. Anspach, *J. Phys. Chem.*, **79**, 439 (1975).

7) M. Mandel and J. C. Leyte, *J. Polym. Sci., Part A*, **2**, 3771 (1964).

8) M. Sakashita, T. Komatsu, and T. Nakagawa, *Nippon Kagaku Kaishi*, **1975**, 751.

9) J. C. Leyte, L. H. Zuiderwerg, and M. van Reisen, *J. Phys. Chem.*, **72**, 1127 (1968).

10) H. Nishikawa and E. Tsuchida, *Bull. Chem. Soc. Jpn.*, **49**, 1545 (1976).

11) F. T. Wall and S. T. Gill, *J. Phys. Chem.*, **58**, 1128 (1954).

12) J. V. MacLaren, J. D. Watts, and A. Gilbert, *J. Polym. Sci., Part C*, **16**, 1903 (1967).

13) P. Monjol, *Bull. Soc. Chim. Fr.*, **1972**, 1319.

14) M. Sunahara, N. Muto, T. Komatsu, and T. Nakagawa, *Nippon Kagaku Kaishi*, **1974**, 2414.

Monolayer Studies of Chiral and Racemic 12-Hydroxyoctadecanoic Acids

Taro TACHIBANA,* Tokiko YOSHIZUMI, and Kayako HORI
Department of Chemistry, Ochanomizu University, Otsuka, Bunkyo-ku, Tokyo 112
(Received June 12, 1978)

The monolayer properties of chiral and racemic 12-hydroxyoctadecanoic acids (12HOA) have been studied. Both acids showed, in each pressure-area isotherm, a pressure plateau. This was interpreted as a two-dimensional phase transition region: from the expanded monolayer composed of bent chain molecules with both the hydroxyl and carboxyl groups attached to the water surface, to the condensed monolayer composed of straight chain molecules oriented steeply to the water surface. It was suggested by measuring infrared spectra of the collapsed films and the built-up films that the condensed monolayer involves intermolecular hydrogen bonds. Differences between (*R*)- and *dl*-12HOA were found in the plateau pressure and its temperature dependence leading to the transition energy. These results were attributed to the formation of a recemic molecular compound during condensation of monolayers of *dl*-12HOA, prior to collapse, followed by a different manner of hydrogen bonding. Electron microscope observation gave strong evidence for the two-dimensional racemic compound formation. On the basis of these results and the X-ray diffraction data, molecular packing models in the condensed monolayers were proposed.

A racemic modification forms a racemic molecular compound, a solid solution, or a mixture in the crystalline solid state, while it behaves as a mixture in the liquid state and in solution. Since monolayers at the air–water interface show some different phases during compression, it is interesting to examine the formation of a racemic compound in the monolayer state. Lundquist[1] found, for 2-alkanols and certain derivatives, a monolayer behavior which was interpreted as the formation of a racemic molecular compound between enantiomer molecules. For study of this problem, 12-hydroxyoctadecanoic acid (12HOA) is especially well suited, since both enantiomers and the racemic form of this acid are readily prepared and they form stable monolayers at the air–water interface. Electron microscopic evidence was given in a recent communication from our laboratory that the racemic compound formation occurs in a monolayer state of this acid prior to collapse.[2]

The present paper has two main objects. First, monolayer studies of (*R*)-12HOA[3] are described in detail, since such studies have hitherto not been published. Next, the monolayer data for the chiral form and the racemic form are compared.

Experimental

Materials. (*R*)-12HOA was purified from commercial products as previously described.[4] The *S*-enantiomer (the *S*-acid) and the racemic acid (the *dl*-acid) were prepared by the methods described previously from the methyl ester of the *R*-enantiomer (the *R*-acid).[4] The purity estimated from gas chromatography and melting points of these samples were as follows: *R*-acid, 99.9%, 353.1 K (lit,[4] 353.6 K); *S*-acid, 99.0%, 352.7 K; *dl*-acid, 99.1%, 349.8 K (lit,[4] 352.3 K).

Methods. All films were spread from solutions in doubley-distilled benzene on a substrate of 0.01 M hydrochloric acid. The water for the substrate was twice distilled. Surface pressure was measured on a Wilhelmy-plate balance with an accuracy of ± 0.2 mN m^{-1}. Compression was done manually and, in certain cases, by a motor-driven device. The temperature of the substrate was controlled within ± 0.1 K of the desired value. The surface potential was measured by an ionization method.

Infrared spectra were recorded with a JASCO IR-A3 spectrophotometer. Powder X-ray diffraction patterns were obtained by a Rigaku Geiger-Flex 2001 diffractometer. Samples of collapsed films were transferred from the film balance to collodion-covered supports, shadow-cast with Pd-Pt alloy at an angle of 20° to the surface, and examined in a JEM-T6 electron microscope.

Results and Discussion

Monolayer Isotherms of (R)-12HOA. Molecular Conformations in Monolayers: The isotherms are shown in Fig. 1. The pressure-area curve (π-A curve) is composed of three parts: (i) a compressible region above about 95 Å^2 molecule^{-1}, a—b, (ii) a plateau, b—c, characterized by a nearly constant pressure in a range of 25 to 95 Å^2 molecule^{-1} and (iii) a highly incompressible region, c—d, with the extrapolated area at zero pressure of 24 Å^2 molecule^{-1} and a collapse at a pressure of about 35 mN m^{-1}. The a—b region appears to be a part of an expanded film, as has been seen with long chain fatty acids having *cis*-double

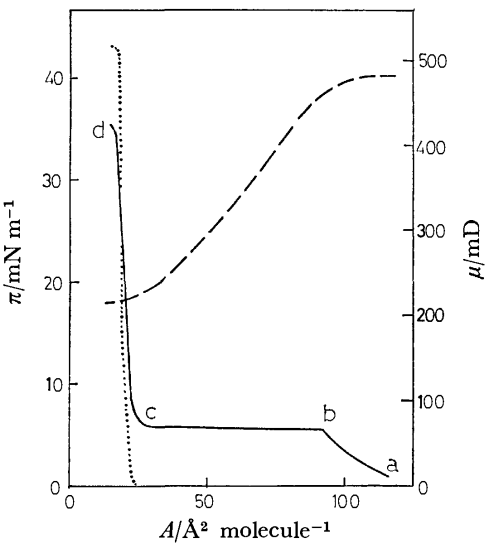

Fig. 1. Monolayer isotherms of (*R*)-12HOA and octadecanoic acid (OA). ——, π-A of (*R*)-12HOA (20 °C); ----, μ-A of (*R*)-12HOA (27 °C); ·····, π-A of OA (20 °C).

bonds or side chains. The c—d region is part of a condensed film; it is close to the isotherm of a condensed film of octadecanoic acid, represented by a dotted line in Fig. 1. Thus the isotherm shape indicates that the plateau represents not the collapse of the film, but a sharp phase transition between the expanded film and the condensed film.

The π-A curve in Fig. 1. could be interpreted in terms of an orientation and a conformation of the long chain molecule with a hydroxyl group at the 12 position, as made for isotherms of 2-(10-carboxydecyl)-2-hexyl-4,4-dimethyl-3-oxazolidinyloxyl (12-nitroxide stearic acid),[5] 9-hydroxyhexadecanoic acid,[6] and 4-hydroxyoctadecanoic acid,[7] which resemble the isotherm of 12HOA in shape. Although the 12HOA molecule can assume various conformations, it seems to be reasonable to take the following two conformations into consideration: (a) a straight chain molecule, in which the long chain is steeply oriented to the water surface with only the carboxyl group in the surface and the hydroxyl group out of the surface, and (b) a bent chain molecule, in which the long chain is bent with both the carboxyl group and the hydroxyl group attached to the surface. These forms are illustrated in Fig. 2. The packing mode of these molecules in monolayers was considered using molecular models, for which one should refer to the Appendix. The closest packing area for the straight chain molecule was 24.1 Å^2 molecule^{-1}, assuming that the straight chain molecules are steeply oriented to the interface and that intermolecular hydrogen bonds are formed between the hydroxyl groups of the adjacent molecules. This value agrees well with the limiting area, extrapolated to zero pressure, of 24.0±1.0 Å^2 molecule^{-1}. When the bent chain molecules are most closely packed with the $CH_3(CH_2)_5$— chain oriented steeply to the water surface, the minimum area calculated from the molecular model was 91 Å^2 molecule^{-1}, as

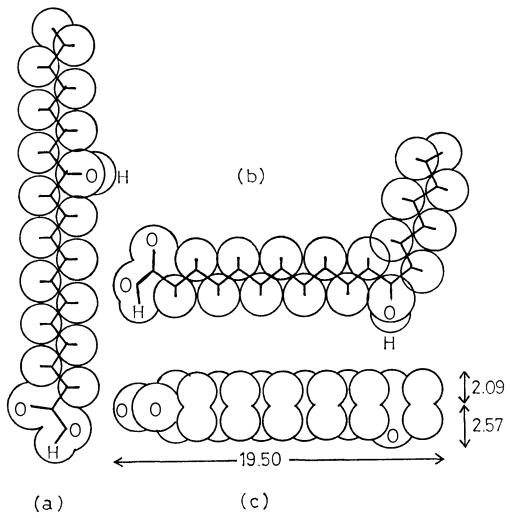

Fig. 2. Conformations of (*R*)-12HOA at the air-water interface. a) Straight chain molecule; b) bent chain molecule; c) occupation of a bent chain molecule at the water surface. The close-packed area per molecule is approximated to that of a rectangle, 19.5×4.66=91 (Å^2 molecule^{-1}).

shown in Fig. 2(c). This value is close to the observed value of the area at an inflection point, b in Fig. 1, 92—104 Å^2 molecule^{-1} (dependent on temperature), at which further compression gives the plateau. It can therefore be presumed that the a—b region in Fig. 1 exhibits an isotherm of the expanded film composed of the bent chain molecules, and that the sharp break at the point b indicates the expulsion of the hydroxyl groups from the interface. Adopting such a picture, the plateau region, b—c in Fig. 1, could be regarded as a transition state between film phases composed of the straight chain molecules and of the bent chain molecules. Thus, in this region, coexistence of the two phases under a constant pressure and temperature can be postulated from the two-dimensional phase rule.

The above-mentioned explanation was also supported by the data of surface dipole moments, μ, calculated from the surface potential. The μ-A curve is given by a broken line in Fig. 1. Here it is seen that the values of μ are little changed by compression in the same areas as the a—b region of the π-A curve, and that they decreased sharply from 490 to 220 mD in the plateau of the π-A curve. The final value, 220 mD, is comparable with the value reported for octadecanoic acid monolayer, 210 mD.[8] This result presents evidence that the molecule in the a—b region lies with a certain orientation of the polar groups on the surface and that the orientation or/and the change of conformation of the molecule occurred during compression in the pressure plateau region. Thus, the μ-A isotherm confirms the above-mentioned explanation for the π-A curve; the plateau is a transition region between a film phase composed of close-packing of the bent chain molecules and that composed of close-packing of the straight chain molecules. A gaseous film would presumably exist at pressures lower than those in the a—b region.

Recentl , Kellner and Cadenhead[6] obtained the π-A and μ-A isotherms for *dl*-9-hydroxyhexadecanoic acid. These are very similar to those for (*R*)-12HOA, and show the presence of a plateau in the π-A curve and the sharp change of μ in that region. This indicates that these two substances behave in a similar manner. They also interpreted the point of inflection corresponding to the point b in Fig. 1 as the area at which there occurs the expulsion of the hydroxyl groups from the interface. The value of the area at the point estimated from their curve is 68—74 Å^2 molecule^{-1} (28.0—8.4 °C); this is close to the value of the most closely packed area calculated from our molecular model of the bent chain molecules, 69 Å^2 molecule^{-1}.

Temperature Dependence: The temperature dependence of the π-A curves, as shown in Fig. 3, was normal; the plateau pressure rose with increasing temperature. As mentioned already, the plateau is the result of a phase transition connected with a change in the molecular conformation. On the basis of this consideration, the heat of transition, ΔH, from a film of bent chain molecules to that of straight chain molecules can be calculated from the two-dimensional Clausius-Clapeyron equation, $d\pi_t/dT=\Delta H/T\Delta A$, where π_t is

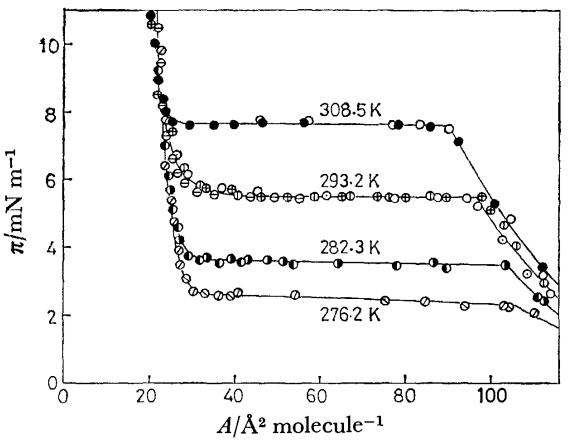

Fig. 3. Temperature dependence of π-A curves of (R)-12HOA.

the plateau pressure, ΔA is net change in molar area, and ΔH is the molar enthalpy change accompanying the transition at this temperature. The calculation was made by the same procedure as that of Glazer and Alexander,[9] who estimated the energy change involved in the phase transition of long chain urea monolayers. From the thermodynamical equation, $\Delta H=\Delta E+\pi\Delta A$, the net change in molar internal energy accompanying the transition, $\Delta E=-17.1\pm 0.3$ kJ mol^{-1} was obtained. The value is negative, indicating an energy generation during the transition from the expanded film to the condensed film. The observed value of ΔE is the sum of the energy for breaking hydrogen bonds between the hydroxyl groups on the bent chains and the water molecules, and the cohesional energy between close-packed steeply-oriented straight chains. It is interesting to investigate whether or not the cohesional energy includes hydrogen bond formation energy between the hydroxyl groups on the straight chains, in addition to van der Waals energy between the methylene groups. This will be described in the following section.

Hydrogen Bonding in Monolayers: As shown in Fig. 1, the π-A curve in the condensed film of (R)-12HOA resembles closely that of octadecanoic acid. However, differences were seen for the apparent viscosity and the collapse pressure. The condensed film of (R)-12HOA was very viscous, as compared with that of octadecanoic acid. This fact was found by blowing talc powder sprinkled on the film surface. The collapse pressure (the maximum pressure attainable) was 35 mN m^{-1} for (R)-12HOA and 42 mN m^{-1} for octadecanoic acid. These differences should be undoubtedly attributed to some effect of the hydroxyl groups on the formation of the condensed films. In bulk also, the effect of the hydroxyl groups is clearly observed; the melting point is 10 K higher for (R)-12HOA (353.6 K) than for octadecanoic acid (343.6 K).

The role of the hydroxyl groups in the molecular cohesion was investigated by measuring infrared spectra for (R)-12HOA in various states. Figure 4 shows the hydroxyl bands due to the stretching vibrations accompanied by bands due to the vibrations of the methylene and methyl groups. Two sharp bands at 3190 and 3290 cm^{-1} due to the hydrogen bonded hydroxyl

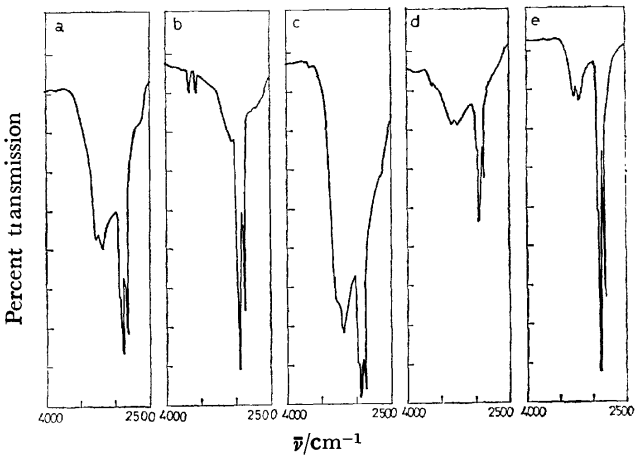

Fig. 4. IR spectra of (R)-12HOA in various states.
a) Crystalline powder in hexachlorobutadiene mull.
b) Isotropic soln. in CCl_4 (0.25% (w/v), 25 °C).
c) Jelly with CCl_4 (1.0% (w/v), 25 °C).
d) Collapsed films.
e) Built-up films on a CaF_2 plate. The angle of incidence was normal to the plate.

groups[10] are found for the crystalline powder. The spectral appearance is very similar to that of crystalline methanol,[11] in which infinite zigzag chains of hydrogen bonds are formed.[12]

On the other hand, it is particularly noteworthy that solutions of (R)-12HOA in carbon tetrachloride or aromatic solvents form jellies above a certain concentration, while octadecanoic acid separates out as crystals from the saturated solutions in the same solvents. An isotropic solution of (R)-12HOA in carbon tetrachloride exhibited the absorption bands at 3640 and 3550 cm^{-1} due to the free hydroxyl groups and the free carboxyl groups, respectively, in addition to the absorption bands at 3190 and 3290 cm^{-1} due to the hydrogen bonded hydroxyl groups. When concentration was above 0.4 percent (w/v) at 25 °C, the solutions became jellies which gave only the hydroxyl bands at 3190 and 3290 cm^{-1}. This result indicates that the jelly is held by molecular association due to intermolecular hydrogen bonding in which almost all the hydroxyl groups are taking part. Evidently, hydrogen bonding plays a prominent role in determining the intermolecular properties of (R)-12HOA in bulk.

Infrared spectra were measured also for the collapsed films obtained out of the interface, and for the built-up films transferred to a calcium fluoride plate from the condensed film at a pressure of 16 mN m^{-1} on a 0.01 M hydrochloric acid substrate by using the Blodgett technique.[13] Both the collapsed films and the built-up films gave almost the same hydroxyl absorption characteristics as did the crystals. The spectral results suggest that molecular association in the condensed monolayers at the water surface also involves intermolecular hydrogen bonding in a similar manner to that in the condensed states in bulk.

Comparison between the Chiral and Racemic Forms.

The Bulk States: Before the monolayer behavior of the chiral form is compared with that of the racemic

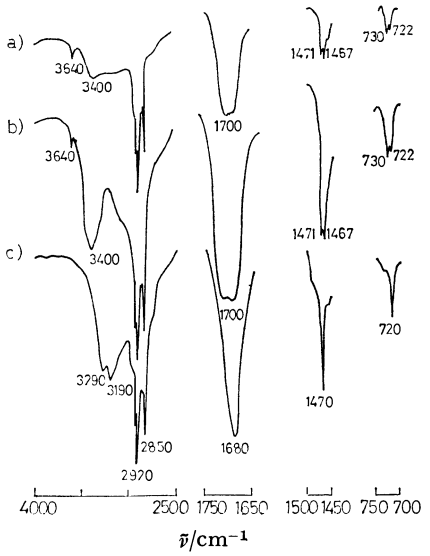

Fig. 5. IR spectra of (a) collapsed film of *dl*-12HOA, (b) crystalline powder of *dl*-12HOA, and (c) that of (*R*)-12HOA in hexachlorobutadiene mull. KBr disk method sometimes gave the spectra without 3640 cm^{-1} band of *dl*-12HOA.

form, it is necessary to elucidate differences between the two forms in the bulk behavior. The phase diagram of the *R*–*S* system for 12HOA was reported by Uzu and Sugiura,[14] who provided evidence that the *R*- and *S*-acids form a racemic compound in the crystalline state. The infrared spectra of the chiral and racemic forms in the crystalline state in Fig. 5 exhibited a difference in the absorption due to the hydroxyl groups; the *dl*-acid exhibited an absorption band at 3640 cm^{-1} due to the free hydroxyl groups in addition to that at 3400 cm^{-1} due to the hydrogen bonded hydroxyl groups, whereas the *R*-acid had no absorption band due to the free hydroxyl groups. This result revealed that appreciable numbers of free hydroxyl groups exist in the crystalline state of the racemic form, in contrast with that of the chiral form.

Furthermore, a difference was found for the location of the hydrogen-bonded hydroxyl bands; they shifted to lower frequencies for the *R*-acid than for the *dl*-acid. As is well known, the hydrogen-bonded hydroxyl band shifts to lower frequency when the hydroxyl groups form multiple hydrogen bonding. For exapmle, such a result was presented for methanol by Thiel *et al.*[15] Therefore, the present spectral results led to the following interpretations as to the arrangement of 12HOA molecules in the crystalline state.

(i) The *R*-acid molecules are favorably located in such a way that their hydroxyl groups link them by multiple hydrogen bonding, forming long sequences of hydrogen bonds.

(ii) The *dl*-acid forms a racemic compound, and the resulting steric hindrance prevents participation of all the hydroxyl groups in the formation of hydrogen bonds, leaving free a part of the hydroxyl groups and making impossible the development of the hydrogen bond sequences.

The *R*-acid sets, as described already, to a jelly in carbon tetrachloride solution above a certain concentration, whereas the *dl*-acid separates out as crystals of a racemic compound from carbon tetrachloride solution. This fact also would be explained by a difference in the mode of the hydrogen bonding between the *R*-acid and the *dl*-acid, since it is well known that a gel is composed of a network structure of polymer chains in which the solvent is trapped. The *dl*-acid behaves like octadecanoic acid in carbon tetrachloride solution in the point that both acids separate out as crystals and do not form jellies.

The miscibility of the chiral form and the racemic form with octadecanoic acid also shows a difference of the *R*-acid from the *dl*-acid in cohesional property. This was found by examining X-ray diffraction patterns for powder specimens which were prepared by fusing the *R*-acid or the *dl*-acid with octadecanoic acid. Figure 6 illustrates the typical patterns for the binary systems. It is seen from the results that the *dl*-acid forms a series of solid solutions with octadecanoic acid in a range of up to 25 mole percent of the latter, while the *R*-acid forms no solid solution with octadecanoic acid. Here again one finds a similarity of the *dl*-acid to octadecanoic acid in cohesional property. Probably, in the *R*-acid–octadecanoic acid system, formation of the solid solution is prevented by strong cohesion between the *R*-acid molecules due to the formation of the hydrogen bond sequences.

The Monolayer States: The isotherms for the *S*-acid, as one expects, agreed quite well with those of the *R*-acid. The π-*A* and μ-A isotherms for the *dl*-acid were essentially similar to those for the enantiomers, except that the *dl*-acid exhibited higher plateau pressures than did the enantiomers at the same temper-

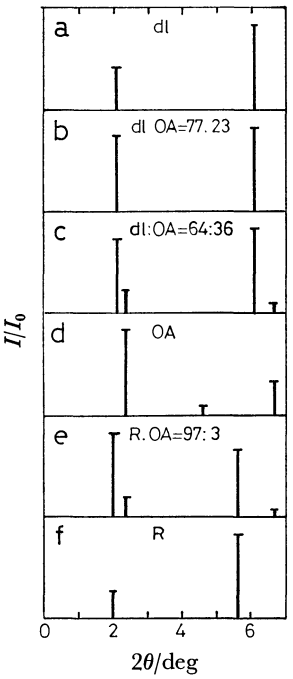

Fig. 6. X-Ray diffraction patterns (Cu *K*α).
a) *dl*-12HOA; b) *dl*-12HOA: OA=77: 23 (mol %); c) *dl*-12HOA: OA=64: 36 (mol %); d) OA; e) (*R*)-12HOA: OA=97: 3 (mol %); f) (*R*)-12HOA.

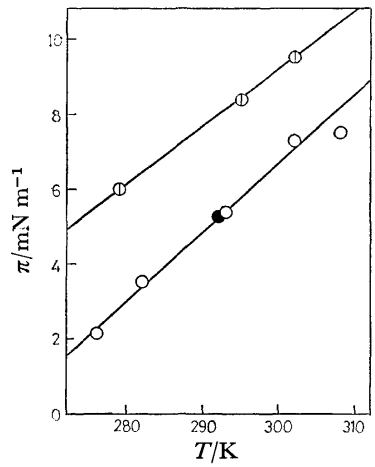

Fig. 7. Temperature dependence of a plateau pressure (at an inflection point).
○, (*R*)-12HOA; ●, (*S*)-12HOA; ◫, *dl*-12HOA.

atures. The temperature dependence of the plateau pressure revealed the difference more clearly, as seen in Fig. 7. The value of ΔE was -14.0 ± 0.3 kJ mol^{-1} for the *dl*-acid, compared with -17.1 ± 0.3 kJ mol^{-1} for the *R*-acid. Since there is no reason to believe that the chiral and racemic forms exhibit a difference in the energy which is involved when the film molecules change their conformations from the bent chain to the straight chain, detaching the hydroxyl groups from the interface, the difference of ΔE observed may be taken as that of the cohesional energy for formation of the condensed film from the expanded film. Thus, it can be seen that the condensed film of the *R*-acid is thermodynamically more stable than that of the *dl*-acid. This is consistent with the observation that the plateau pressure (*i.e.* the phase transition pressure) at the same temperature is lower for the *R*-acid than for the *dl*-acid. On the other hand, the chiral form (mp 353.6 K) has a higher melting point than the racemic form (mp 352.3 K), *i.e.*, in the crystalline state, the former has stronger cohesion than the latter. The similarity of the *dl*-acid to octadecanoic acid observed in bulk was found also for their monolayer behavior; addition of 10 mole percent of octadecanoic acid led to a pressure rise of 0.7 mN m^{-1} for the plateau pressure of the *R*-acid, while little rise was found for that of the *dl*-acid. On the basis of these facts, it is supposed that the condensed films of the *R*-acid and the *dl*-acid respectively have structures corresponding to those in bulk. Thus there is a possibility that a racemic compound of the *dl*-acid is formed in the condensed monolayer state as well as in the crystalline state. In order to investigate this problem, infrared spectral observations were made on collapsed films removed from the compressed monolayer of the *dl*-acid. The same spectra as those for the crystalline powder were obtained, as shown in Fig. 5.[16] This is taken as evidence that a racemic compound is formed in the condensed monolayers at the air–water interface. At the same time, presumably free hydroxyl groups are present in the monolayer as well as in the crystals. This explains the weaker cohesion in the monolayer of the *dl*-acid than in that of the *R*-acid.

The condensed monolayer states of the *R*-acid and the *dl*-acid respectively were examined by using two-dimensional packing models of molecules. The models demonstrate that: (i), the *R*-acid molecules are capable of forming multiple hydrogen bonds which leads to long sequences of hydrogen bonds, and (ii), when the *dl*-acid forms a racemic compound with simultaneous formation of intermolecular hydrogen bonds between *R*- and *S*-acid molecules, steric hindrance imposes restraint on the formation of multiple hydrogen bonds through the *dl*-acid molecular compounds and leaves some of the hydroxyl groups free. The details will be described in the Appendix. These models explain satisfactorily the differences between the *R*-acid and the *dl*-acid not only in the monolayer state, but also in the crystalline state, because X-ray diffraction studies showed that the crystals of both the *R*-acid and the *dl*-acid are composed of layer structures.

Electron Microscope Observation. It has been found by electron microscope observation that, when 12HOA is crystallized out from solution, the enantiomer produces helically twisted fibers, the helical sense of which is left-handed for the *R*-acid and right-handed for the *S*-acid, and that the racemic *dl*-acid separates as crystals in the form of flat platelets.[4] To study whether or not similar structures are also found for collapsed fragments of the monolayer, the monolayers were compressed continuously to a certain area at a rate of 18 Å^2 molecule^{-1} h^{-1} and immediately thereafter they were transferred to collodion supports by using the horizontal lifting method.[17] Prior to the transfer, the surface of the support had been treated with a dilute aqueous solution of Aerosol OT. This treatment made the surface hydrophilic and facilitated adhesion of the film samples to the support. Collapse structures were found to appear when the films were compressed below 21 Å^2 molecule^{-1}. Figure 8 shows electron micrographs at an apparent area of 16 Å^2 moleucle^{-1}. The micrographs for the enantiomers show twisted fibers around 800 Å in width, in addition to flat planer structures, which have been observed in the monolayer collapse of long chain fatty acids.[18] Twisting seems to occur when collapse structures are very thin ribbon-like fibers. Special attention was paid to the twisted fibers, which are characteristic of the hydroxy acid. The sense of twist is left-handed for the *R*-acid and right-handed for the *S*-acid. This chiral relationship is quite the same as that observed for the twisted fibers separated from solution. Rapid compression to areas smaller than the collapse point yielded no twisted fibers but flat structures and amorphous molecular aggregates. The twisted fibers observed here seem to result from a slow collapse process, as described by Neuman.[19]

The *dl*-acid produced not fibers but platelets, as shown in Fig. 8(c), from the monolayer as well as from solution. By comparing this result with the phase diagram of the *R*–*S* system,[14] it is reasonable to consider that the platelets are composed of a racemic molecular compound which appears in the bulk crystalline solid. Presumably the two enantiomers exist in a merely stoichiometric mixture in the monolayer at large areas

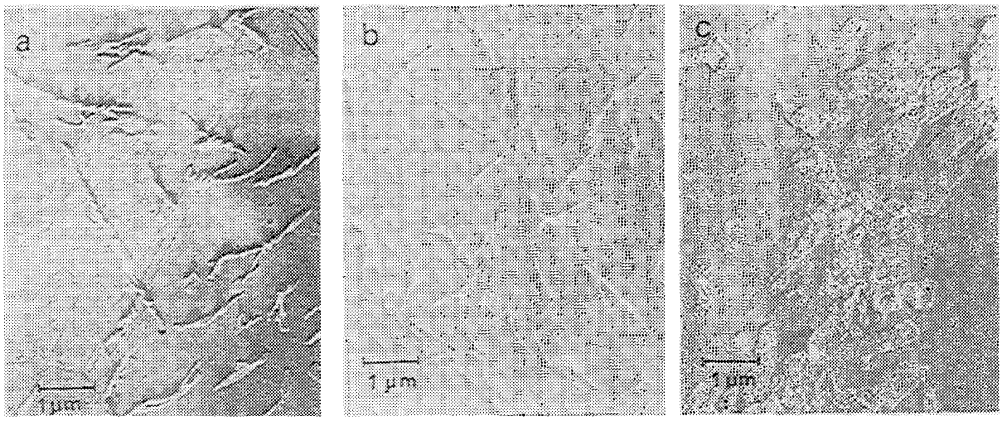

Fig. 8. Electron micrographs of collasped films of 12HOA.
a) (*R*)-12HOA, left-handed twist; b) (*S*)-12HOA, right-handed twist; c) *dl*-12HOA.
These photographs were made to show the same sense as that of the twist in the specimen.

as in the bulk liquid phase,[14] but form a racemic molecular compound during compression of the plateau region in the isotherm.

Summarizing these results, the present studies lead us to conclude that the enantiomeric mixture forms a racemic compound in the condensed monolayer state, as realized in the crystalline solid.

Appendix

Molecular Packing in Condensed Monolayers of 12HOA.
In considering the molecular packing in the condensed monolayers, the arrangement of both the carboxyl groups and the hydrogen-bonded hydroxyl groups should be taken into account at the same time. It seems reasonable to consider the packing models with reference to the bulk crystalline data, since a relationship between molecular packing in monolayer states and bulk phase structures has been recently found for long chain fatty acids[20] and phospholipids.[21] It was also found for cholesterol that the polymorphic crystalline transition was reflected in the temperature dependence of the equilibrium spreading pressure.[22] For 12HOA, the present studies revealed that various properties in the bulk crystalline phases are retained in the monolayer states. This fact implies that the monolayer structure is closely related to the crystal structure.

X-Ray analyses for single crystals of 12HOA have not been carried out on account of the difficulty of obtaining appropriate single crystals. However, the powder X-ray diffraction patterns and the infrared spectral results give considerable information about the crystal lattice, particularly for the subcell introduced by Vand[23] for packing of long hydrocarbon chains in unit cells. Powder X-ray diffraction patterns showed that side spacings of the *R*-acid and the *dl*-acid were quite different and that, therefore, the two acids belonged to different packing modes. Infrared absorption spectra for the CH_2 vibration of hydrocarbon chains showed that the splittings for CH_2 scissoring (at about 1470 cm^{-1}) and CH_2 rocking (at about 720 cm^{-1}) vibrations were found for the *dl*-acid crystals, but not for the *R*-acid (Fig. 5). If this result leads to the same relationship as that between the type of subcell and the CH_2 vibration spectra established for normal paraffins[24] and for octadecanoic acid,[25] it seems reasonable to assume that: the *R*-acid belongs to triclinic subcell, as does the A-form of octadecanoic acid; the *dl*-acid belongs to the orthorhombic subcell, as do the B- and C-forms of octadecanoic acid; and the hydrocarbon chains are, in respective cases, packed in each subcell. The main difference between the two packing modes is that every second chain plane is almost perpendicular to its neighbors in the orthorhombic subcell, while all chain planes are parallel to one another in the triclinic subcell.

The long spacing was obtained to be 46.7 Å for the *R*-acid and 43.8 Å (lit,[26] 44.3 Å) for the *dl*-acid. The latter value is close to that for the B-form of octadecanoic acid (lit,[27] 43.85 Å). Furthermore, it may be mentioned that the acute angle between the edges in rhombic plate-shaped crystallites of the *dl*-acid in Fig. 7(c) is about 70°. The B- and C-forms of octadecanoic acid are known to give rhombic plate-shaped crystals with acute angles of 74°[27] and of 56°,[28] respectively. These facts imply that the crystal structure of the *dl*-acid could be associated with that of the B-form of octadecanoic acid.

In the condensed monolayers at the water surface, molecules are two-dimensionally close-packed with the straight chain oriented steeply to the water surface. In this case, the molecular packing will be discussed with reference to that in the crystalline states described above; the concept of 'subcell' is utilized in order to predict the arrangement of hydrocarbon chains close-packed in the condensed monolayers.

Thus, packing models were constructed as follows.
(i) A projection of a straight chain molecule of the *R*-acid is illustrated in Fig. 9(a), as suggested by Vold.[29] The *S*-acid is a mirror image of it.
(ii) The extent of a carboxyl group attached to an end of the chain is neglected, when hydrocarbon chains are packed in subcells. The assumption that the lateral packing in monolayers is similar to that in the crystals leads to tilting of the chains, which facilitates packing of carboxyl groups.[30]
(iii) A hydrogen atom of a free OH group occupies the range enclosed by a dotted line in Fig. 9(a), because of free rotation of the OH bond around the C–O bond axis. On the other hand, when the chains are linked by hydrogen bonds, two oxygen atoms on the adjacent chains are brought almost into contact and the extent of a hydrogen atom, which is located between the oxygen atoms, can be neglected.
(iv) Units of CH_2CHO (represented by a thick line in Fig. 9(a)) are packed in the above-designated subcells: a triclinic subcell for the *R*-acid and an orthorhombic subcell for the *dl*-acid.

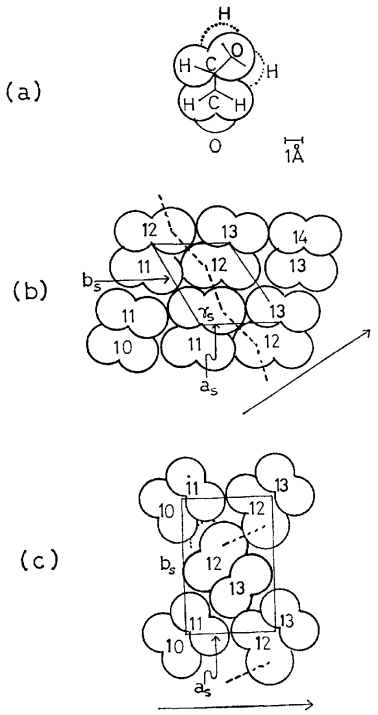

Fig. 9. Molecular models viewed from above.
a) A projection of a straight chain molecule of (*R*)-12HOA on a plane perpendicular to the chain axis; b) proposed packing model for (*R*)-12HOA in the condensed monolayer state; c) proposed packing model for the *dl*-12HOA in the condensed monolayer state. The a_sb_s planes are in the sheet of the paper, to which the molecular axis is perpendicular for *dl*-12HOA, but not for (*R*)-12HOA. The direction of a slope of the water surface is denoted by an arrow for each model.

(v) The OH direction is determined by hydrogen bond formation between adjacent molecules.
The proposed packing models for the *R*-acid and the *dl*-acid in each subcell are shown in Figs. 9(b) and (c), respectively, where the integers mean the carbon numbers on a hydrocarbon chain, and broken lines denote hydrogen bonds.

For the *R*-acid, molecules can be closely packed, with simultaneous formation of hydrogen bond sequences, in the triclinic subcell, whose dimensions (a_s, b_s, and γ_s) are 4.5 Å, 5.4 Å, and 120°. Hydrogen bond formation between adjacent chains in the triclinic subcell makes the adjacent chains shift by one CH_2 unit, as shown by the integers in Fig. 9(b). This avoids the overlapping of OH groups and leads to the tilting of the molecules to the water surface. The tilt angle of the molecules with the normal to the surface, θ, and the close-packing area per molecule in the surface, A_c, are calculated geometrically, assuming the remaining subcell dimensions, c_s, α_s, and β_s, to be 2.6 Å, 70°, and 108°, respectively, which are typical values reported for triclinic subcells.[31] The values of θ and A_c are obtained to be 21° and 24.1 Å^2 molecule^{-1},[32] respectively. The former is in good agreement with that estimated from the long spacing in the crystals, assuming that the bimolecular length is 50 Å.

For the *dl*-acid, molecules are packed in a similar manner to that in the B-form of octadecanoic acid, the structure of which was determined by von Sydow.[27] In this case, the chains in the condensed monolayer are packed in a slightly larger subcell (a_s=5.2 Å, b_s=8.0 Å) than that of octadecanoic acid, avoiding any overlapping of oxygen atoms of the OH groups. The *R*-enantiomer chain and the *S*-enantiomer chain occupy alternate positions in the subcell, forming a racemic compound with an intermolecular hydrogen bond. Steric hindrance leaves another hydrogen atom free; this is represented by a dotted line in Fig. 9(c). This model gives a packing area of 23.3 Å^2 molecule^{-1}, with a tilt angle of 27° with the normal to the surface.

The authors wish to express their thanks to Professor Makoto Hayashi of Chiba University for surface potential measurements. The present work was partially supported by a Grant-in-Aid for Scientific Research from the Ministry of Education.

References

1) M. Lundquist, *Ark. Kemi*, **17**, 183 (1960).
2) T. Tachibana and K. Hori, *J. Colloid Interface Sci.*, **61**, 398 (1977).
3) (−)-12-Hydroxyoctadecanoic acid from castor oil has been assigned the 12D-OH configuration (K. Serck-Hanssen, *Chem. Ind. (London)*, **1958**, 1554). According to the (*R-S*) system, the (−)-D-acid has the 12*R*-configuration.
4) T. Tachibana and H. Kambara, *J. Colloid Interface Sci.*, **28**, 173 (1968); *Bull. Chem. Soc. Jpn.*, **42**, 3422 (1969).
5) D. A. Cadenhead and F. Müller-Landau, *J. Colloid Interface Sci.*, **49**, 131 (1974).
6) B. M. J. Kellner and D. A. Cadenhead, *J. Colloid Interface Sci.*, **63**, 452 (1978).
7) J. T. Davies, *Trans. Faraday Soc.*, **45**, 448 (1949).
8) K. D. Dreher and D. F. Sears, *Trans. Faraday Soc.*, **62**, 741 (1966).
9) J. Glazer and A. E. Alexander, *Trans. Faraday Soc.*, **47**, 401 (1951).
10) The 3190 and 3290 cm^{-1} bands in the present work have been assumed to be due to a bonded O-H···O stretching vibration between the hydroxyl and the carboxyl groups (R. T. O'Connor, C. H. Mack, F. F. DuPré, and W. G. Bickford, *J. Org. Chem.*, **18**, 693 (1953)). Esterification or metal soap formation of the acid, however, caused a large change for the C=O stretching vibration band but only little ones for the 3190 and 3290 cm^{-1} bands, indicating that these bands are not from the carboxyl groups.
11) G. C. Pimentel and A. L. McClellan, "The Hydrogen Bond," W. H. Freeman and Co., San Francisco (1960), p. 103.
12) K. J. Tauer and W. N. Lipscomb, *Acta Crystallogr.*, **5**, 606 (1952).
13) K. Blodgett, *J. Am. Chem. Soc.*, **56**, 1007 (1935).
14) Y. Uzu and T. Sugiura, *J. Colloid Interface Sci.*, **51**, 346 (1975).
15) M. V. Thiel, E. D. Becker, and G. C. Pimentel, *J. Chem. Phys.*, **27**, 95 (1957).
16) Rapid compression sometimes gave spectra of a mixture of the enantiomers and the racemic compound.
17) K. Fukuda, H. Nakahara, and T. Kato, *J. Colloid Interface Sci.*, **54**, 430 (1976).
18) H. E. Ries, Jr., and D. C. Walker, *J. Colloid Interface Sci.* **16**, 361 (1961).
19) R. D. Neuman, *J. Colloid Interface Sci.*, **56**, 505 (1976).
20) R. E. Heikkila, C. N. Kwong, and D. G. Cornwell, *J. Lipid Res.*, **11**, 190 (1970).
21) M. C. Philips and D. Chapman, *Biochim. Biophys. Acta*, **163**, 301 (1968).
22) K. Tajima and N. L. Gershfeld, *J. Colloid Interface*

Sci., **52**, 619 (1975).
23) V. Vand, *Acta Crystallogr.*, **4**, 104 (1951).
24) R. G. Snyder, *J. Mol. Spectrosc.*, **7**, 116 (1961).
25) R. F. Holland and J. R. Nielsen, *J. Mol. Spectrosc.*, **9**, 436 (1962).
26) S. Bergström, G. Aulin-Erdtman, B. Rolander, E. Stenhagen, and S. Östling, *Acta Chem. Scand.*, **6**, 1157 (1952).
27) E. von Sydow, *Acta Crystallogr.*, **8**, 557 (1955).
28) V. Malta, G. Celotti, R. Zannetti, and A. F. Martelli, *J. Chem. Soc., B*, **1971**, 548.
29) M. Vold, *J. Colloid Sci.*, **7**, 196 (1952).
30) J. J. Kipling and A. D. Norris, *J. Colloid Sci.*, **8**, 547 (1953).
31) E. von Sydow, *Ark. Kemi*, **9**, 231 (1956).
32) The value of 23.4 Å^2 molecule^{-1} reported previously[2] is corrected to be 24.1 Å^2 molecule^{-1}.

Effects of Pressure on the Cloud Point of Nonionic Surfactant Solutions and on the Solubilization of Hydrocarbons

Shoji KANESHINA,* Osamu SHIBATA, and Makoto NAKAMURA

College of General Education, Kyushu University-01, Ropponmatsu, Chuo-ku, Fukuoka 810

(Received June 26, 1978)

Cloud points in 1.0 wt % aqueous solutions of penta- and hexa(oxyethylene) dodecyl ether increase monotonously with an increase of pressure up to 150 MPa. The elevation of the cloud-point temperature with pressure was 1.05×10^{-7} and 1.09×10^{-7} K Pa^{-1} for respective surfactant. Both volume and enthalpy changes on the separation of the surfactant-rich phase had the positive values. The rise of cloud points on compression is attributable to the enhancement of the hydrogen bonds formation between water and ether oxygens of the poly(oxyethylene) group and partly to the disruption of the "hydrophobic bonding." The cloud-point temperature at constant pressure and the cloud-point pressure at constant temperature were also examined as a function of the amount of solubilizate such as hexane and octane. There was an optimum pressure at a given temperature, as well as an optimum temperature at a given pressure, at which the solubilizing power of surfactant is maximum.

So far a few studies have been made about the effect of pressure on the properties of surfactant solutions, especially on the critical micelle concentration of ionic surfactants.[1] With respect to the nonionic surfactant, however, the effect of pressure on the cloud point has only been reported by Suzuki and Tsuchiya.[2] They found that the cloud point of aqueous solution of poly(oxyethylene) *p*-nonylphenyl ether had its maximum at about 100—200 MPa.

In this paper some results of the effect of pressure on the cloud point of aqueous poly(oxyethylene) dodecyl ether solutions are presented, and then the pressure dependence of the solubilization will be elucidated from the cloud points in the presence of hydrocarbons. No information on the pressure dependences of the solubilization is available in the literature.

Experimental

Penta(oxyethylene) dodecyl ether and hexa(oxyethylene) dodecyl ether (Tokyo Kasei Kogyo Co., Ltd.,) were used without further purification. The cloud points in 1.0 wt % aqueous solution of respective surfactant were 23.5 and 48.1 °C. Hexane and octane used as solubilizate were extra-pure grade.

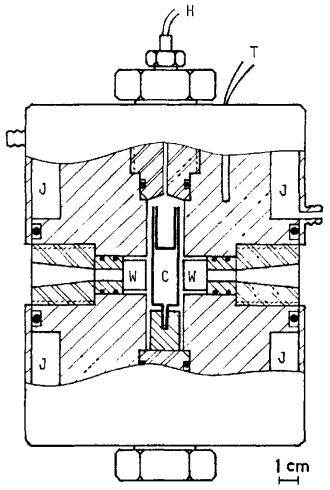

Fig. 1. Schematic diagram of the high pressure vessel equipped with optical windows. C: Syringe cell with Teflon cap in which the solution is filled, H: pressure tubing with which the pressure pump and gauge are connected, J: water jacket, T: thermocouple, W: quartz window. The pressure was sealed by means of an O-ring with a back-up ring of Teflon.

The cloud points under high pressure were determined by using the high pressure vessel with optical windows, which is shown schematically in Fig. 1. The high pressure vessel was made of stainless steel with 140 mm o.d., 20 mm i.d., and 180 mm hight. The solutions were heated or cooled slowly (0.1 °C per minute) by circulation of temperature-controlled water to the jacket. The temperature of the system was determined by the thermocouple attached to the pressure vessel. Pressures were generated by means of a screw- and hand-pump (Hikari Kikai Co.,) and measured within an accuracy of ±0.2 MPa by means of a Heise pressure gauge. Ligroin was used as pressure transmitting medium. The cloud points were decided by observing the appearence and disappearence of turbidity during the cource of heating and cooling at a given pressure. Measurements of the transmittance at 540 nm were performed with a Hitachi 139 spectrophotometer. The difference between the cloud points determined on heating and on cooling were within 1 °C.

Results and Discussion

Effect of Pressure on the Cloud Point. The cloud points in 1.0 wt % aqueous solution of nonionic surfactants are shown in Fig. 2 as a function of pressure. The cloud points for all the surfactant solutions increase monotonously with an increase of pressure up to 150 MPa. This elevation of cloud points on compression is within that caused by an increase of one oxyethylene unit in the poly(oxyethylene) chain. In other words, the alteration in the hydrophilic-lipophilic balance (HLB) of the surfactant by the compression up to 150 MPa seems to be less than that by the addition of one oxyethylene group in the poly(oxyethylene) chain. It is clear from Fig. 2 that the pressure up to 150 MPa is favorable for the dissolution of surfactant molecules in water although most of dissolved-surfactant molecules are in the micellar state. The cloud point for aqueous solutions of surfactants is generally taken to be the point where separation of the surfactant-rich phase is casued by the dehydration of ether oxygens of the poly(oxyethylene) group. Le Chatelier's principle brings about the positive volume change on separation of the sur-

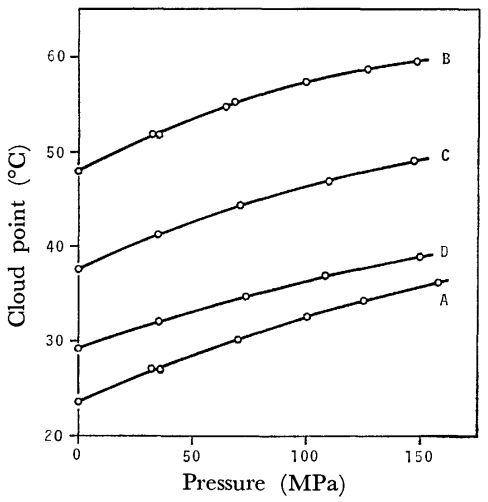

Eig. 2. Effect of pressure on the cloud point of nonionic surfactant solutions. Curve A: 1.00 wt % penta(oxyethylene) dodecyl ether solution, B: 1.00 wt % hexa(oxyethylene) dodecyl ether solution, C: 1.02 wt % hexa(oxyethylene) dodecyl ether solution containing hexane of 2.42 g/kg H_2O, D: 1.02 wt % hexa(oxyethylene) dodecyl ether containing hexane of 4.26 g/kg H_2O.

factant-rich phase. From data of apparent molal volumes of nonionic surfactants and polyethylene glycol(PEG) oligomers with various lengths of poly(oxyethylene) chain the apparent molal volume assigned for one oxyethylene group can be calculated. The values assigned for the group are 37.1 cm^3/mol for surfactant in micellar state[3] and 36.9 cm^3/mol for PEG,[4] which are found to be apparently smaller than the molal volume assigned for an oxyethylene unit in the state of pure liquids, 38.9—39.1 cm^3/mol.[4,5] That is, the volume change on formation of hydrogen-bonds between water and ether oxygens of the poly(oxyethylene) group is negative, and the increase of pressure enhances the formation of hydrogen bonds.

In the two-component, two-phase system, the Clausius-Clapeyron type equation is written as follows:[6]

$$\left(\frac{\partial T}{\partial P}\right)_{x_2} = \frac{T(y_1\Delta\bar{v}_1+y_2\Delta\bar{v}_2)}{y_1\Delta\bar{h}_1+y_2\Delta\bar{h}_2}, \quad (1)$$

where subscripts 1 and 2 refer to components 1 and 2, x and y the mole fraction in the phase α and β, respectively. $\Delta\bar{h}$ and $\Delta\bar{v}$ are the change of partial molal enthalpy and volume, respectively, on the transfer from phase α to β. In the present system, we choose surfactant as component 2 and the micellar solution as the phase α. Assuming $y_1 \ll y_2$,

$$\left(\frac{\partial T}{\partial P}\right)_{x_2} = \frac{T\Delta\bar{v}_2}{\Delta\bar{h}_2}. \quad (2)$$

As is seen from Fig. 2, $(\partial T/\partial P)_{x_2}$ is positive. That is, $\Delta\bar{h}_2$ and $\Delta\bar{v}_2$ have the same sign. The dehydration of the poly(oxyethylene) chain, *i.e.*, the hydrogen bond breaking contributes to the positive change in both $\Delta\bar{h}_2$ and $\Delta\bar{v}_2$. Further, the positive volume change is also caused by the elimination of hydrocarbon–water contact. This "hydrophobic bonding" also brings about the positive contribution to $\Delta\bar{h}_2$ because of the breakdown of ice-like structure around the hydrocarbon chain. Therefore, the rise of cloud points on compression is attributable to the enhancement of the hydrogen bonds formation and partly to the disruption of the hydrophobic bonding.

The values of $(\partial T/\partial P)_{x_2}$ are $1.05(\pm0.05)\times10^{-7}$ K Pa^{-1} for penta(oxyethylene) dodecyl ether and $1.09(\pm0.03)\times10^{-7}$ K Pa^{-1} for hexa(oxyethylene)dodecyl ether. The value for poly(oxyethylene) *p*-nonylphenyl ether is found to be $(0.8—1.3)\times10^{-7}$ K Pa^{-1} for the various compositions.[2] Assuming that the hydrophillic-lipophilic property of surfactant balances at the cloud point, the pressure of about 10 MPa is required for the temperature rise of 1 °C to keep the original HLB.

Effect of Solubilizate on the Cloud Point. The cloud points in the presence of solubilizate as hexane and octane increase monotonously with an increase of pressure. Some results are included in Fig. 2.

In Fig. 3, the cloud-point temperatures of the solutions containing 1.0 wt % hexa(oxyethylene) dodecyl ether at constant pressure are shown as a function of the amount of solubilized hexane. The solubilization end points, below which the excess hydrocarbon separates from micellar solution, are also shown only at an atmospheric pressure. As is seen from Fig. 3, the region between the cloud-point temperature isobar and solubilization curve is a homogeneous transparent phase. According to Shinoda,[7] in the region (denoted by II_{W-D}) above the cloud-point temeperature isobar the nonionic surfactant phase containing oil separates. On the other hand, the excess oil separates in the II_{W-O} region below the solubilization curve. In Fig. 4, the cloud-point temperatures of the system with solubilized octane are shown as a function of the amount of octane. The pattern of isobars is analogous in both the systems; namely, the isobars are shifted to higher

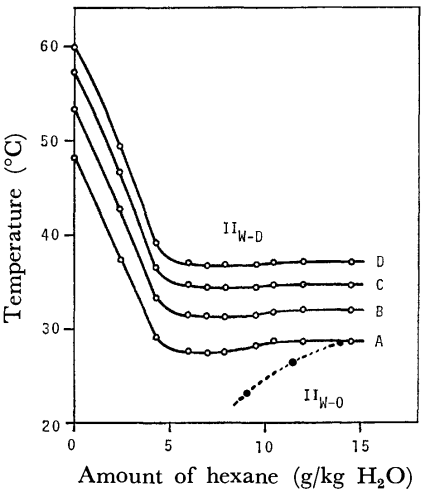

Fig. 3. The cloud-point temperature as a function of the amount of hexane solubilized at 0.1 MPa (curve A), 50 MPa (B), 100 MPa (C), and 150 MPa (D). The solubilization end points (●) are also shown only at an atmospheric pressure.

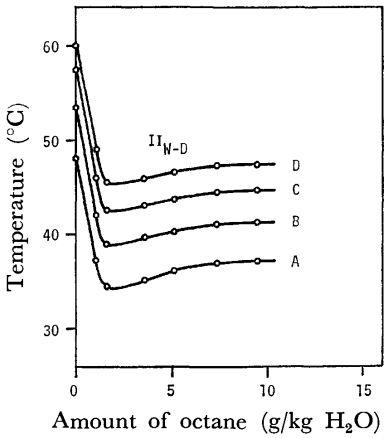

Fig. 4. The cloud-point temperature as a function of the amount of octane solubilized at 0.1 MPa (curve A), 50 MPa (B), 100 MPa (C), and 150 MPa (D).

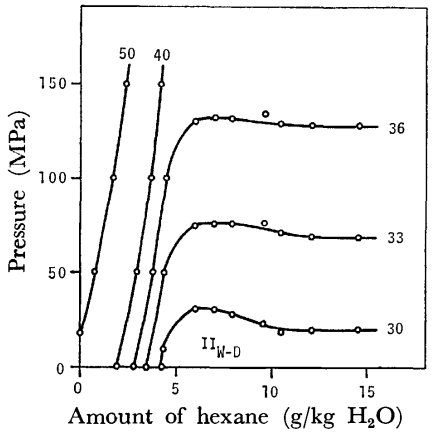

Fig. 5. The could-point pressure as a function of the amount of hexane solubilized. Numerical values refer to the temperature in °C.

temperature as the pressure increases. The cloud-point temperature is initially depressed by the addition of solubilizate and then approaches a definite temperature *via* a minimum. At the definite temperature the solubilizing power of surfactant becomes maximum. The compression up to 100 MPa elevates the optimum temperature by 6.0 and 7.6 °C for the systems with solubilized hexane and octane, respectively.

The cloud-point pressure of the solutions containing 1.0 wt % hexa(oxyethylene) dodecyl ether at constant temperature are shown in Figs. 5 and 6 as a function of the amount of solubilized hexane and octane, respectively. The cloud-point pressure isotherms for all the systems with solubilized hexane and octane are similar; the higher the pressure, the larger the area of homogeneous phase. The cloud-point pressure of the solution containing solubilized hexane more than 6 g/kg H_2O is little affected by the additional

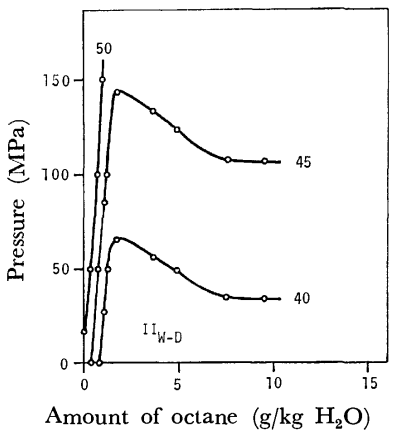

Fig. 6. The cloud-point pressure as a function of the amount of octane solubilized. Numerical values refer to the temperature in °C.

solubilization of hexane. That is, there is the optimum pressure for the maximum solubilization at a given temperature. The solubilizing power of surfactant becomes maximum at a slightly higher pressure than the pressure in the plateau region of isotherms. Also in the system with solubilized octane, there is an optimum pressure for the solubilization. The higher the temperature, the higher the optimum pressure in both systems.

The authors wish to thank Professor R. Matuura of the Department of Chemistry, Kyushu University, for useful discussion in the preparation of the manuscript.

References

1) S. D. Hamann, *J. Phys. Chem.*, **66**, 1359 (1962); R. F. Tuddenham and A. E. Alexander, *J. Phys. Chem.*, **66**, 1839 (1962); J. Osugi, M. Sato, and N. Ifuku, *Nippon Kagaku Zasshi*, **87**, 329 (1966); *Rev. Phys. Chem. Jpn.*, **35**, 32 (1965); S. Kaneshina, M. Tanaka, T. Tomida, and R. Matuura, *J. Colloid Interface Sci.*, **48**, 450 (1974); S. Rodriguez and H. Offen, *J. Phys. Chem.*, **81**, 47 (1977); T. S. Brun, H. Høiland, and E. Vikingstad, *J. Colloid Interface Sci.*, **63**, 89 (1978).

2) K. Suzuki and M. Tsuchiya, *Bull. Inst. Chem. Res., Kyoto Univ.*, **47**, 270 (1969).

3) D. I. D. El Eini, B. W. Barry, and C. T. Rhodes, *J. Colloid Interface Sci.*, **54**, 348 (1976).

4) L. S. Sandell and D. A. I. Goring, *J. Polym. Sci., Part. A2*, **9**, 115 (1971).

5) S. Kucharski, A. Sokolowski, and B. Burczyk, *Rocz. Chem.*, **47**, 2045 (1973).

6) J. G. Kirkwood and I. Oppenheim, "Chemical Thermodynamics," McGraw-Hill, New York (1962), Chap. 9.

7) K. Shinoda, "Yōcki To Yōkaido," 2nd ed, Maruzen, Tokyo (1974), Chap. 13.

Dimer and Excimer Fluorescence Spectra of Highly Polar Molecules, 3,5-Dialkyl-4-methoxybenzylidenemalononitrile

Kenji INOUE and Michiya ITOH*

Faculty of Pharmaceutical Sciences, Kanazawa University, Takara-machi, Kanazawa 920

(Received June 30, 1978)

Dual fluorescence of the ground state dimer of highly polar molecules of 3,5-dialkyl-4-methoxybenzylidenemalononitrile in 3-methylpentane solution at low temperature was investigated by steady-state and nonsecond fluorescence spectroscopies. The dimerization of these compounds was confirmed by concentration dependence of absorption and fluorescence spectra at 77 K. The dimer exhibits dual fluorescence consisting of a short-lived dimer fluorescence and a long-lived excimer fluorescence, while the monomer is almost non-fluorescent at room temperature to 77 K. The excimer formation by an orientational relaxation from the excited state of the dimer was discussed in terms of determination of the activation barrier and the fluorescence polarization.

Dual fluorescence of a highly polar molecule, *p*-dimethylaminobenzonitrile (MABN), was identified by Lippert[1] as arising from two different excited states in polar solvent. However, Rotkiewicz *et al.*[2] suggested that the dual fluorescence arose from states with the same fluorescence polarization, and that the two emitting states differed in the orientation of the dimethyl amino group with respect to the benzene ring. On the other hand, McGlynn and coworkers[3] reported that the dual fluorescence of this compound was identified as arising from a ground state dimer in a number of different solvents and suggested that the dual fluorescence consisted of the dimer and an excimer. However, Nakashima and Mataga[4] claimed that the dimer and the excimer assignment could not be correct by their concentration dependence of fluorescence spectra.

Very recently, Itoh *et al.*[5] reported dual fluorescence of a ground state dimer of a highly polar molecule, 3,5-dialkyl-4-hydroxybenzylidenemalononitrile (dialkyl-HO-BMN), in 3-methylpentane (MP) solution at low temperature. The dual fluorescence was ascribed to the short-lived dimer and to the long-lived excited species generated by the duoble proton transfer reaction in the excited state of the dimer. The excited-state proton transfer of 3,5-di-*t*-butyl-4-hydroxybenzylidenemalononitrile (*t*-Bu_2-HO-BMN) in the solid state was also reported.[6]

This paper describes the dimer formation of several dialkyl-4-methoxybenzylidenemalononitrile (dialkyl-MO-BMN) in the ground state in MP solution at low temperature, and dual fluorescence consisting a short-lived dimer fluorescence and a long-lived excimer one by the steady-state and nanosecond (ns) fluorescence spectroscopies. The structure of the dimer is proposed to be a sandwich type dimer with a center of symmetry by taking account of a crystal structure of *t*-Bu_2-HO-BMN.[6] The excimer seems to be generated by an orientational relaxation in the excited state of the dimer. The dimer and excimer fluorescence spectra are discussed in terms of an activation barrier and fluorescence polarization at low temperature.

Experimental

Materials. The preparation of the model compounds are as follows. The products were purified by colum chromatography and recrystallizations, and chracterized by IR and NMR.

4-Methoxybenzylidenemalononitrile (MO-BMN) was prepared from 4-methoxybenzaldehyde with malonitrile in benzene solution containing small amount of acetic acid and piperidine.[7] The product was recrystallized from benzene-hexane: Mp 113—116 °C.

Found: C, 71.90; H, 4.20; N, 15.09%. Calcd for $C_{11}H_8N_2O$: C, 71.74; H, 4.35; N, 15.21%.

3,5-Dimethyl-4-methoxybenzylidenemalononitrile (Me_2-MO-BMN) was prepared from 3,5-dimethyl-4-methoxybenzaldehyde by the same manner as described above. The product was recrystallized from benzene-hexane: Mp 120—122 °C.

Found: C, 73.78; H, 5.66; N, 13.01%. Calcd for $C_{13}H_{12}N_2O$: C, 73.58: H, 5.66: N, 13.20%.

3,5-Di-isopropyl-4-methoxybenzylidenemalononitrie (*i*-Pr_2-MO-BMN) was prepared by the same manner as described above. Though the product is noncrystalline syrup, the compound was identified by NMR and IR.

Measurements. Determination of the fluorescence and absorption spectra, and fluorescence polarization were described previously.[8,9] Fluorescence lifetimes and time-resolved fluorescence were determined by analysing exponential decay curves measured by an oscilloscope and by a coaxial N_2 gas-laser excitation. The decay curve was analyzed by a deconvolution method using a computer.[10]

Results and Discussion

Dimer Formation in the Ground State. The MP solution of 4-methoxybenzylidenemalononitrile (MO-BMN) shows an absorption band in the 330—360 nm region at room temperature, which shows considerable red-shift (*ca.* 10—20 nm) at low temperature (<150 K), as shown in Fig. 1. Figure 2 shows concentration dependence of absorption spectra of MP solutions of MO-BMN at 77 K. Here, a monomer dimer equilibrium of this compound in MP solution is assumed, and an association constant (K) can be written as follows:[2]

$$K = [D]/([C]-2[D]),$$

where [C] and [D] are concentrations of MO-BMN and dimer. If an absorption band at 390 nm is due almost exclusively to the dimer, an absorbance [A] at 390 nm is expressed as $A=\varepsilon[D]l$, where ε is a molar extinction coefficient of the dimer at this wavelength. The following equation is obtained:[11]

$$[C]/A = 2/\varepsilon + (1/\varepsilon K)^{1/2}(1/A)^{1/2}.$$

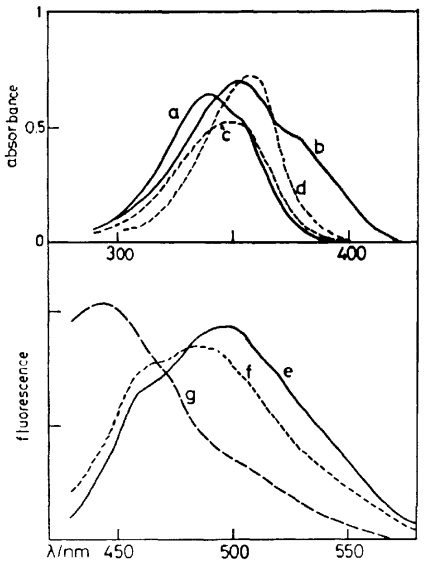

Fig. 1. Absorption spectra (a—d) of MO-BMN and fluorescence spectra (e—g) of dialkyl-MO-BMN: a) in MP solution (2.1×10^{-5} M) of MO-BMN at room temperature; b) at 77 K (2.6×10^{-5} M); c) MTHF solution (1.7×10^{-5} M) at room temperature; d) MTHF solution (1.3×10^{-5} M) at 77 K; e) fluorescence spectra of MO-BMN (1.3×10^{-5} M) at 77 K; f) of Me_2-MO-BMN in MP (2.7×10^{-5} M) at 77 K; and g) of *i*-Pr_2-MO-BMN in MP (3.3×10^{-5} M).

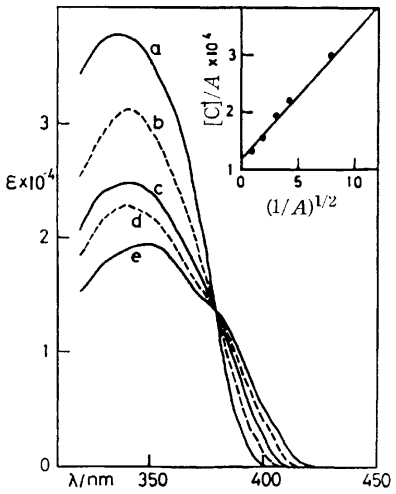

Fig. 2. Concentration dependence of absorption spectra of the MP solution of MO-BMN at 77 K and plot of $[C]/A$ *vs.* $(1/A)^2$.
a) 3.2×10^{-6} M; b) 1.0×10^{-5} M; c) 2.9×10^{-5} M; d) 4.8×10^{-5} M; e) 7.2×10^{-5} M.

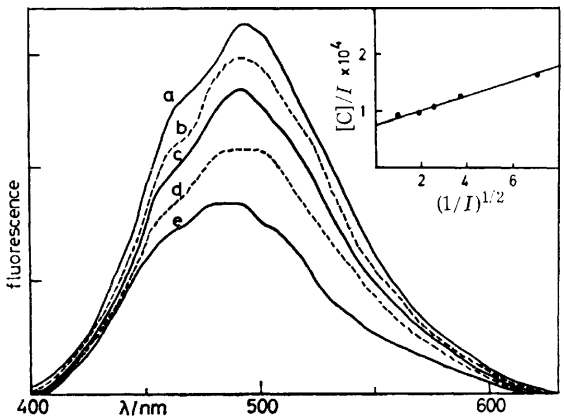

Fig. 3. Concentration dependence of fluorescence spectra of the MP solution of MO-BMN at 77 K and plot of $[C]/I$ *vs.* $(1/I)^{1/2}$.
a) 3.8×10^{-5} M; b) 2.0×10^{-5} M; c) 1.1×10^{-5} M; d) 6.2×10^{-6} M; e) 2.9×10^{-6} M. Fluorescence intensity is q unit (see in the text).

An MP solution of MO-BMN exhibits a strong green fluorescence at 77 K as shown in Fig. 1, while the solution is almost non-fluorescent at room temperature. MP solutions of 3,5-dimethyl- and 3,5-di-isopropyl-4-methoxybenzylidenemalononitrile (Me_2-MO-BMN and *i*-Pr_2-MO-BMN) also show strong fluorescence at 77 K as shown in Fig. 1. However, an MTHF solution of dialkyl-MO-BMN exhibits no significant temperature dependence of fluorescence and absorption spectra. The green fluorescence in the MP solution markedly increases in intensity with increasing concentration of MO-BMN, but the fluorescence due to the monomer does not seem to exhibit even in the dilute solution, as shown in Fig. 3. Since intensity (I) of the green fluorescence may be proportional to the concentration of the dimer [D], the following equation is obtained for the monomer dimer equilibrium;

$$[C]/I = 2/q + (1/qK)^{1/2}(1/I)^{1/2},$$

where q is a constant including several experimental factors. Plots of $[C]/A$ and $[C]/I$ exhibit linear relationship *vs.* $(1/A)^{1/2}$ and $(1/I)^{1/2}$, respectively, as shown in Figs. 2 and 3. Two straight lines confirm an assumption of the monomer dimer equilibrium, and

Table 1. Equilibrium constants (K) for the dimerization of dialkyl-MO-BMN in MP at 77 K, and fluorescence properties of the dimer (D*) and the excimer (E*), and their activation energy (E_a)

	K (M^{-1})	λ_{max} (nm) and lifetimes (ns) in bracket		E_a (kcal M^{-1})
		D*	E*	
MO-BMN	1.6×10^5	480[a] (4)	500[a] (21)	—
Me_2-MO-BMN	4.5×10^4	470—480[a] (4)	490[a] (21)	0.9
i-Pr_2-MO-BMN	2.8×10^4	450[b] (4)	470—480[a] (18)	1.1

a) The fluorescence maxima determined by time-resolved spectra (error appeoximately±5 nm) and lifetimes analyzed by a computer deconvolution (error approximately ±1 ns). b) The fluorescence maximum determined by a steady-state spectrum.

afford equilibrium constants; $K=1.6\times10^5\ M^{-1}$ from absorption spectra and $1.5\times10^5\ M^{-1}$ from fluorescence spectra. Concentration dependence of the absorption spectra of the other alkyl-MO-BMN in MP solution also shows the dimer formation at 77 K, whose K are summarized in Table 1.

Excimer Fluorescence. Nanosecond time-resolved fluorescence spectra of an MP solution of MO-BMN at 77 K shown in Fig. 4 demonstrate that the fluorescence consists of two fluorescence spectra; a short-lived fluorescence (λ_{max} 480—490 nm, $\tau=4$ ns) and a long-lived one (λ_{max} 500 nm, $\tau=21$ ns). The dual fluorescence of the dimer was also observed in the other dialkyl-MO-BMN. Figure 4 shows a fluorescence decay curve of an MP solution of MO-BMN at 77 K in comparison with a computer simulated one. Table 1 summarizes the fluorescence maxima and lifetimes in the dimers of these compounds at 77 K. The excitation spectra of the short-lived fluorescence and the long-lived one are identical each other, and are

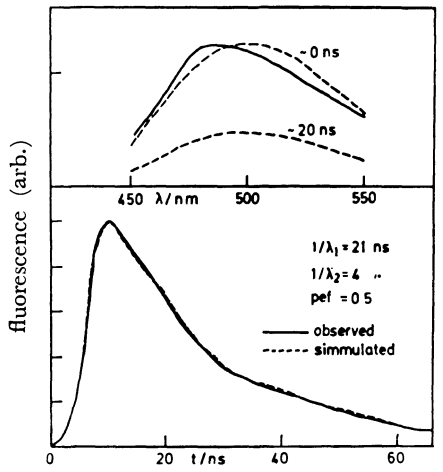

Fig. 4. Time-resolved fluorescence spectra of the MP solution of MO-BMN (3.9×10^{-5} M) at 77 K. A fluorescence decay curve monitored at 490 mn, and a simulated one; (——) and (----) are time-resolved spectra of a short-lived and a long-lived components depicted on the obtained time constants and pre-exponential factor (pef). Time indicated in the time-resolved spectra is virtually after a signal maximum of the fluorescence.

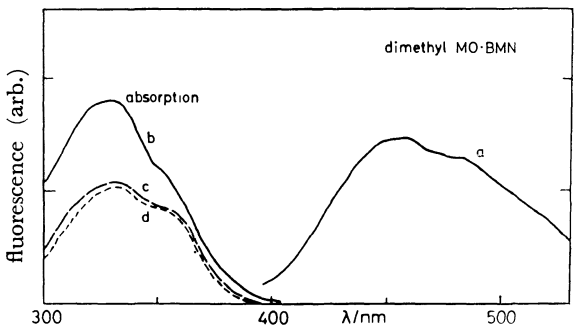

Fig. 5. Fluorescence (a) and absorption (b) spectra of an MP solution of Me_2-MO-BMN (5.1×10^{-5} M) at 77 K; fluorescence excitation spectra (c) monitored at 420 nm and (d) at 520 nm.

corresponding to the dimer absorption spectra (Fig. 5). Taking account of a large Stokes shift of the long-lived fluorescence, the fluorescence may be ascribed to the excited species (E*) generated from the excited state of the MO-BMN dimer (D*), while the short-lived one to the dimer (D*).

The photochemical reaction scheme is as follows:

$$\begin{array}{ccccc} & & h\nu & & k_3 \\ & & & & \\ D & \longrightarrow & D^* & \rightleftharpoons & E^* \\ & & & & k_4 \\ & & \swarrow^{k_1} \quad \downarrow^{k_2} & & \swarrow^{k_5} \quad \searrow^{k_6} \\ & & D+h\nu' \quad D & & D+h\nu'' \quad D \end{array}$$

Time dependent concentrations of D* and E* are expressed by the following well known equations:[12,13]

$$[D^*] = C_1 \exp(-\lambda_1 t) + C_2 \exp(-\lambda_2 t), \quad (1)$$

$$[E^*] = C_3 \exp(-\lambda_1 t) - C_3 \exp(-\lambda_2 t), \quad (2)$$

$$\lambda_1, \lambda_2 = 1/2[k_1+k_2+k_3+k_4+k_5+k_6 \mp (\{k_1+k_2+k_3 - (k_4+k_5+k_6)\}^2+4k_3k_4)^{1/2}].$$

Here, if $k_3 \gg k_4 \approx 0$, [D*] may be approximately represented by the second term of Eq. 1. The fluorescence lifetimes of D* and E* are expressed as follows:

$$\tau_D = \lambda_2^{-1} = (k_1+k_2+k_3)^{-1},$$

$$\tau_E = \lambda_1^{-1} = (k_5+k_6)^{-1}.$$

Since two fluorescence decay curves of D* and E* at a certain wavelength overlap each other, actual decay curves at several wavelengths were analyzed by the following equation:

$$[D^*] + [E^*] \propto \exp(-\lambda_1 t) + \frac{C_2-C_3}{C_3} \exp(-\lambda_2 t).$$

Fluorescence lifetimes of D* and E* of an MP solution of MO-BMN at 77 K were determined to be 4 ns and 21 ns, respectively, by computer simmulation mentioned above. Unfortunately, the fluorescence rise of E* was not detectable, because the D* fluorescence overlaps on the decay curve of E*.

Fluorescence spectra of an MP solution of *i*-Pr_2-MO-BMN at several temperatures shown in Fig. 6 reveal remarkable decrease of the short-lived fluorescence with increasing temperature (77 to 130 K). Since no significant shift of the monomer dimer equilib-

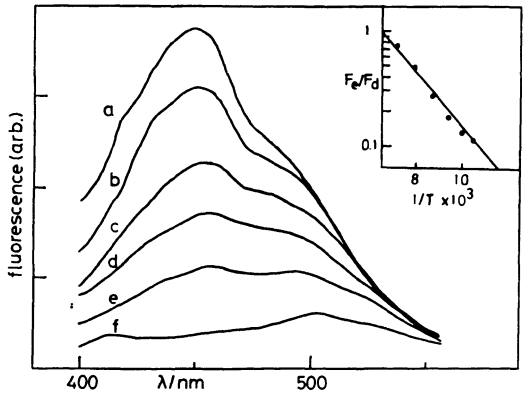

Fig. 6. Temperature dependence of fluorescence spectra of an MP solution of *i*-Pr_2-MO-BMN (3×10^{-5} M); a) 100 K; b) 108 K; c) 115 K; d) 120 K; e) 125 K; f) 132 K.

rium was detected in this temperature region, and since no monomer fluorescence was detected, the remarkable temperature dependence may be attributable to a dynamic process between D* and E* requiring a small amount of activation energy. From the fluorescence spectra shown in Fig. 6, the activation energy can be obtained to be 1.1 kcal/mol by the aid of the conventional method and assumption reported previously.[8] The activation energy in the dimer of Me_2-MO-BMN was also obtained to be 0.9 kcal/mol. However, an MP solution of MO-BMN shows no significant temperature dependence of fluorescence spectra which seems to imply a very small amount of activation energy in this photochemical process.

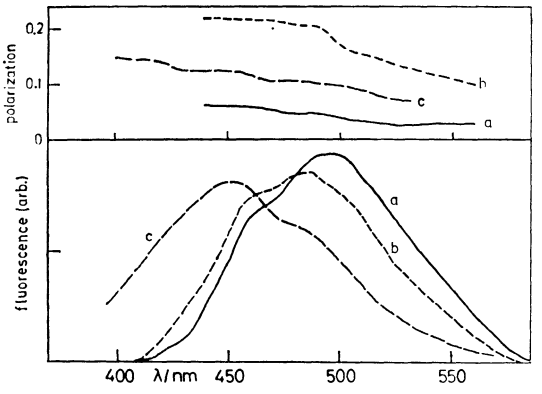

Fig. 7. Fluorescence spectra and their polarizations of MP solutions at 77 K; a) MO-BMN (4.6×10^{-5} M); b) Me_2-MO-BMN (5.9×10^{-5} M); c) i-Pr_2-MO-BMN (6.8×10^{-5} M).

Figure 7 shows the fluorescence polarizations of MP solutions of MO-BMN and dialkyl-MO-BMN at 77 K.[14] The fluorescence polarization were observed to decrease from 0.22 to 0.1 with increasing wavelength in Me_2-MO-BMN. Further, a similar behavior of the polarization was observed in i-Pr_2-MO-BMN, though no significant change of the polarization was detected in MO-BMN. The shorter wavelength (also lifetime) fluorescence and the longer wavelength (also lifetime) one were ascribed to the dimer and the excimer, respectively, as mentioned above. Therefore, the larger and the smaller polarizations may be attributable to the dimer and the excimer. The results indicate that the dimer and excimer fluorescence spectra have considerably different character of electronic transition each other. Since these compounds are highly polar molecules with strong electron donor and acceptor groups, the dimer formation may be attributable to the exciton and the charge transfer interactions between two component molecules in the sandwich dimer with a center of symmetry.[6] It seems that the photoexcitation of the dimer leads to an access of the electronic polarization of the component molecules including an orientational relaxation in the excited state, as follows:

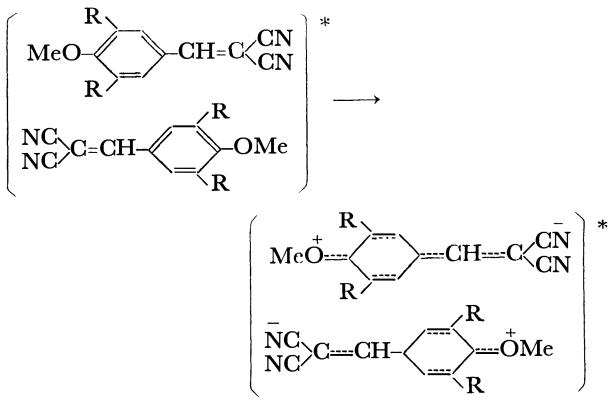

R=H, CH_3, and i-$CH(CH_3)_2$

Here, a small amount of activation energy may be required in the orientational relaxation in the excited state of the dimer. The relaxation process leading to the formation of the excimer (E*) seems to include a rotation of 4-CH_3O- group with respect to the benzene ring. The rotation of this group may be hindered by a steric effect of 3,5-dialkyl groups.[15] The argument is consistent with the activation barriers (MO-BMN<Me_2-MO-BMN<i-Pr_2-MO-BMN) as summarized in Table 1. However, it is difficult to depict the concrete structure of the dimer as well as the excimer at this stage.

References

1) E. Lippert, W. Lüder, and H. Boos, *Adv. Mol. Spectrosc.*, **1962**, 443.
2) K. Rotkiewicz, K. H. Grellmann, and Z. R. Grabowski, *Chem. Phys. Lett.*, **19**, 315 (1973).
3) O. S. Khalil, R. H. Hofeldt, and S. P. McGlynn, *Chem. Phys. Lett.*, **17**, 479 (1972).
4) N. Nakashima and N. Mataga, *Bull. Chem. Soc. Jpn.*, **46**, 3016 (1973).
5) M. Itoh, K. Inoue, T. Kuzuhara, and T. Kusui, *Bull. Chem. Soc. Jpn.*, submitted; preliminary results were presented in 26th IUPAC Congress (Tokyo) Sept. 1977.
6) M. Itoh, Y. Tanimoto, and Y. Iitaka, *J. Chem. Phys.*, in press.
7) F. Horiuchi, K. Fujimoto, T. Ozaki, and Y. Nishizawa, *Agric. Biol. Chem.*, **35**, 2003 (1971).
8) M. Itoh, T. Mimura, H. Usui, and T. Okamoto, *J. Am. Chem. Soc.*, **95**, 4388 (1973); M. Itoh, *J. Am. Chem. Soc.*, **96**, 7390 (1974).
9) T. Mimura and M. Itoh, *J. Am. Chem. Soc.*, **98**, 1095 (1976).
10) W. R. Ware, I. J. Doemeny, and T. L. Nemzek, *J. Phys. Chem.*, **77**, 2038 (1973).
11) K. C. Ingham and M. A. El-Bayoumi, *J. Am. Chem. Soc.*, **96**, 1674 (1974).
12) J. B. Birks, "Photophysics of Aromatic Molecules," Wiley-Interscience, New York, N. Y. (1970).
13) W. R. Ware, D. Watt, and J. D. Holmes, *J. Am. Chem. Soc.*, **96**, 7853 (1974).
14) T. Azumi and S. P. McGlynn, *J. Chem. Phys.*, **34**, 2413 (1962).
15) J. B. Hendrickson, D. J. Cram, and G. S. Hammond, "Organic Chemistry" McGraw Hill, New York (1970), p. 322.

Crystal Structure of 5-Bromocytosine

Masuhiro KATO, Akio TAKENAKA,* and Yoshio SASADA*

Laboratory of Chemistry for Natural Products, Tokyo Institute of Technology, Nagatsuta, Midori-ku, Yokohama 227

(Received July 14, 1978)

The crystal structure of 5-bromocytosine has been determined by X-ray analysis to investigate the bromination effect on the cytosine moiety. The space group is $P2_1/a$, with dimensions $a=16.943(2)$, $b=9.155(1)$, $c=3.846(1)$ Å, $\beta=99.89(1)°$, and $Z=4$, The structure was solved by the heavy-atom method and refined by the full-matrix least-squares method. A comparison with the cytosine structure indicates some large deviations in bond lengths and angles, which are attributed to the steric and electronic effects caused by bromination. After the VSEPR theory, the slight increase of C(2)-N(3)-C(4) angle (0.8°) is interpreted as the decrease of the effective charge of the lone pair on N(3), and this is related to the difference of pK_a values between 5-bromocytosine and cytosine.

In the course of the studies on the elementary pattern of interactions between purine-pyrimidine base and amino acid, Ohki, Takenaka, Shimanouchi, and Sasada have found that the hydrogen bond scheme between 5-bromocytosine and *N*-acylglutamic acids is quite different from that found in the complexes between cytosine and some amino acids.[1-6] To explain this in terms of molecular structure, the crystal structure of 5-bromocytosine has been determined by X-ray diffraction method.

Experimental and Structure Determination

Colourless, needle-like crystals were obtained from an aqueous solution. The crystal density was measured by flotation in a mixture of bromoform and carbon tetrachloride. Weissenberg photopraphs showed systematic absences, $h0l$ $h=2n+1$ and $0k0$ $k=2n+1$, indicating the space group $P2_1/a$. Accurate unit cell dimensions and diffraction intensities were measured on a Rigaku four-circle automated diffractometer using graphite-monochromated Mo $K\alpha$ radiation ($\lambda=0.71069$ Å). Five reference reflexions monitored periodically showed no significant intensity fluctuations during the course of data collection. The intensities collected with an $\omega/2\theta$ scanning technique were corrected for Lorentz and polarization factors. Of the 1337 independent reflexions ($2\theta\leqq55°$), 1121 had intensities greater than $3\sigma(I)$. Crystallographic data are summarized in Table 1.

The structure was solved by the heavy-atom method and refined by the full-matrix least-squares method, the minimized function being $\sum w\{|F_o|-|F_c|\}^2$. All the hydrogen atoms, found on a difference map, were included in the subsequent refinement. In the refinement, the zero-reflexions for which $|F_c|$ values were smaller than $|F_o|_{lim}$ (3.748) were omitted

Table 1. Crystal data

5-Bromocytosine	
$C_4H_4N_3OBr$	
Crystal system: monoclinic	
Systematic absences: $h0l$ $h=2n+1$, $0k0$ $k=2n+1$	
Space group: $P2_1/a$	
$a=16.943(2)$ Å	$Z=4$
$b=9.155(1)$	$D_x=2.15$ g cm^{-3}
$c=3.846(1)$	$D_m=2.14$
$\beta=99.89(1)°$	
$U=587.7(1)$ Å^3	

Table 2. Final positional and thermal parameters

Standard deviations are given in parentheses. The anisotropic thermal factor has the form $\exp[-(\beta_{11}h^2+\beta_{22}k^2+\beta_{33}l^2+\beta_{12}hk+\beta_{13}hl+\beta_{23}kl)]$.

Atom	x*	y*	z**	β_{11}*	β_{22}*	β_{33}**	β_{12}*	β_{13}**	β_{23}**
N (1)	21717(40)	39815(74)	8023(21)	169(20)	406(64)	653(53)	−162(63)	−7(16)	2(29)
C (2)	25007(47)	26816(90)	9284(26)	159(22)	622(85)	674(67)	3(70)	17(19)	−60(35)
N (3)	21061(39)	14198(72)	8226(21)	183(19)	487(61)	665(52)	−85(61)	−4(16)	49(29)
C (4)	14089(41)	14615(71)	5989(21)	165(20)	375(64)	513(47)	56(63)	47(16)	−21(29)
C (5)	10693(48)	28424(76)	4690(23)	197(22)	508(76)	523(56)	112(67)	31(18)	66(30)
C (6)	14585(45)	40758(81)	5974(23)	177(21)	513(70)	556(52)	122(69)	30(17)	33(32)
O (2)	31553(44)	26479(67)	11364(26)	285(23)	391(57)	1136(79)	−127(59)	−59(22)	−7(32)
N (4)	10440(40)	1672(75)	5129(24)	167(20)	531(70)	781(60)	−72(62)	−40(18)	5(32)
Br	242(5)	28826(9)	2023(3)	227(4)	854(12)	565(8)	62(7)	−22(2)	42(3)

Atom	x**	y***	z***	B(Å^2)
H (1)	2381(69)	457(14)	843(28)	0.0(1.8)
H (41)	1295(57)	−94(11)	603(26)	0.0(1.6)
H (42)	583(60)	1(11)	355(28)	0.0(1.6)
H (6)	1205(93)	478(18)	496(41)	2.0(2.6)

* $\times10^5$, ** $\times10^4$, *** $\times10^3$.

in each cycle of refinement. The weight functions used were: $w=1/(\sigma_p^2+q|F_o|^2)$ for $|F_o|\geqq|F_o|_{lim}$, where σ_p is the standard deviations based on counting statistics; $w=w(|F_o|_{lim})$ for $|F_o|<|F_o|_{lim}$. The coefficient q was 0.883×10^{-3}, derived from the intensity variance of the monitored reflexions.[7] The refinement was terminated when the maximum shifts of positional and thermal parameters were less than 0.16σ and 0.22σ, respectively, for non-hydrogen atoms. The final value of R is 0.069 ($R=0.056$ for the non-zero reflexions). Atomic scattering factors used were taken from "International Tables for X-Ray Crystallography."[8] Atomic parameters are given in Table 2, and observed and calculated structure factors in Table 3.[9]

Results and Discussion

Bond lengths and angles are shown in Fig. 1, and a comparison with the cytosine values[10] is given in Fig. 2. Rather large deviations from cytosine bond lengths and angles may be attributed to the steric and electronic effects caused by bromination. The lengthening of C(4)–C(5) and C(5)–C(6) bonds accompanied by the decrease of C(5)–C(4)–N(3) and C(5)–C(6)–N(1) angles are due to repulsions from Br to C(4) and C(6) atoms. The marked deviation at C(5)–C(4)–N(4) angle is obviously ascribed to the repulsion between Br and N(4). After an interpretation for benzene ring deformation[11] on the basis of the valence shell electron pair repulsion theory, the bromination at C(5) makes the C(4)–C(5)–C(6) angle enlarge, but these repulsions cause the opposite effect, so that this angle is not so large. Such steric effect of bromination may spread to the C(2)–N(3)–C(4) and C(2)–N(1)–C(6) angles, and further the N(1)–C(2)–N(3) angle, so that they slightly expand. It is plausible that the shrinkage of lone-pair lobe on N(3), which is caused by electron-withdrawing property of bromine, facilitates the release of constrain by opening of the C(2)–N(3)–C(4) angle. Therefore, the slight increase of the angle (0.8°) supports the decrease of the effective charge of lone pair on N(3), and this is related to the difference of pK_a values between 5-bromocytosine and cytosine [4.58 and 3.04, respectively[12-13]].

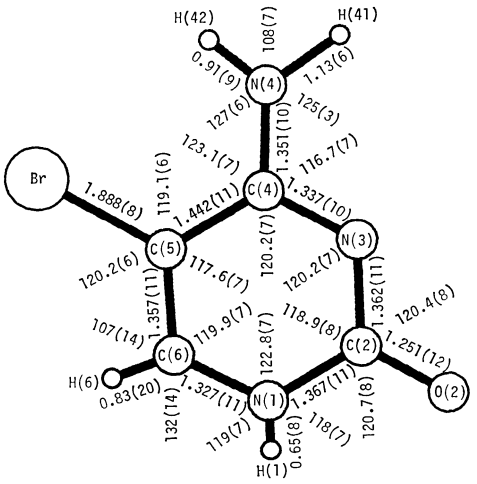

Fig. 1. Bond lengths (l/Å), angles (ϕ/°), and their standard deviations.

On the other hand, the C(4)–N(4) length is considerably short, while the C(2)–O(2) length is rather long, as compared with the average distances.[14] Such a trend which is also found in cytosine[10] indicates the contribution from the canonical formulae 2, 3, and 4 in Fig. 3, in which the amino nitrogen and carbonyl oxygen carry positive and negative charges, respectively. The shortening of C(6)–N(1) bond is due to the electronic effect of bromine as described by canonical formulae 4 and 5 in Fig. 3. This suggests the ability of proton donation of N(1)–H to be rather strong.

The least-squares plane of 5-bromocytosine together with the deviations from the plane is listed in Table 4. Although the pyrimidine ring with carbonyl oxygen O(2) and amino nitrogen N(4) is planar within 0.04 Å, the bromine atom shifts by 0.18 Å from the mean plane to relieve its steric hindrance.

As shown in Fig. 4, two hydrogen bonds between molecules related by the 2_1 axis, N(4)–H···O(2) and N(1)–H···N(3), constitute a ribbon along [010] direction. Hydrogen bond distances and angles are

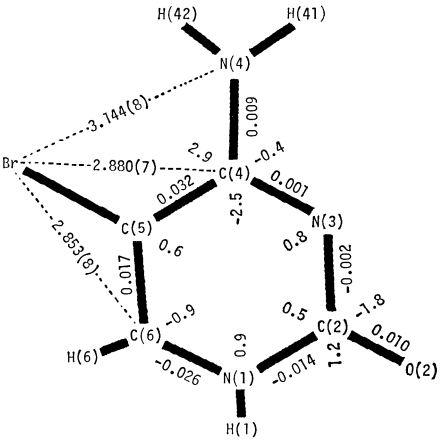

Fig. 2. Differences in bond lengths (l/Å) and angles (ϕ/°) between 5-bromocytosine and cytosine: (5-bromocytosine values) − (cytosine values).

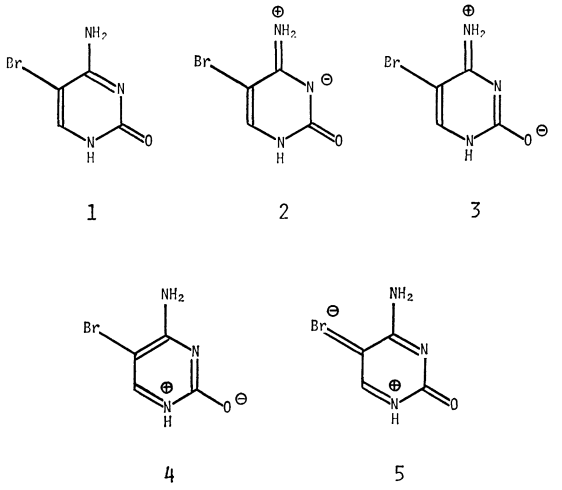

Fig. 3. Some possible canonical structures for 5-bromocytosine.

Table 4. Molecular plane

X, Y, and Z are in Å along the crystal axes, respectively
Asterisks denote atoms defining the plane.
Standard deviations are given in parentheses.

Equation to the pyrimidine ring
$-0.6242(27)X+0.0428(31)Y+0.8757(16)Z-0.587(15)=0$

Deviations (l/Å) of atoms from the plane

N(1)*	−0.025	O(2)	0.008
C(2)*	0.001	N(4)	0.043
N(3)*	0.012	Br	0.182
C(4)*	−0.002	H(1)	−0.08
C(5)*	−0.026	H(41)	0.04
C(6)*	0.043	H(42)	−0.01
		H(6)	0.00

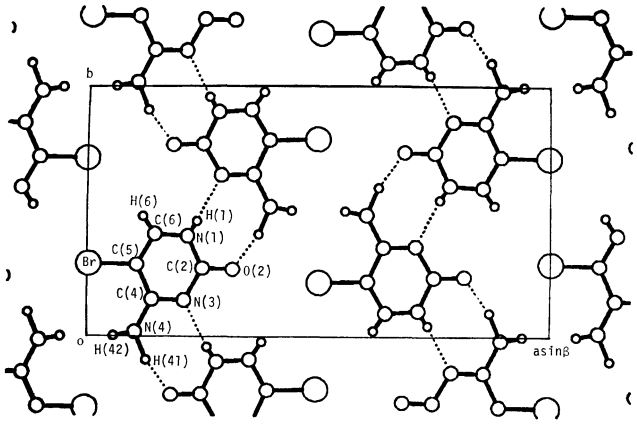

Fig. 4. The crystal structure viewed along the c axis.

Table 5. Hydrogen bond distances and angles
Standard deviations are given in parentheses.

Distance(l/Å)		Angle(ϕ/°)	
N(1)···N(3)[a]	2.820(10)	C(2)-N(1)···N(3)[a]	113.1(6)
H(1)···N(3)[a]	2.21(8)	C(6)-N(1)···N(3)[a]	121.6(6)
O(2)···N(4)[a]	2.890(11)	N(1)-H(1)···N(3)[a]	157(8)
O(2)···H(41)[b]	1.80(6)	C(2)-N(3)···N(1)[b]	111.8(6)
		C(2)-N(3)···H(1)[b]	111(2)
Symmetry codes		C(4)-N(3)···N(1)[b]	127.6(5)
(a) $\frac{1}{2}-x, \frac{1}{2}+y, 2-z$,		C(4)-N(3)···H(1)[b]	128(2)
		C(2)-O(2)···N(4)[a]	124.9(6)
(b) $\frac{1}{2}-x, \frac{1}{2}+y, 2-z$.		C(2)-O(2)···H(41)[a]	131(2)
		C(4)-N(4)···O(2)[b]	115.3(6)
		N(4)-H(41)···O(2)[b]	162(5)

listed in Table 5. The N···O and N···N distances are short as compared with the related compounds,[15] though the hydrogen bonds show poor linearity. Similar hydrogen bonding scheme is observed in the crystal structures of cytosine,[10] cytosine monohydrate,[10] and 5-bromocytosine: dioxan (2: 1) crystal.[16] Such a common feature can be interpreted by the preference of N–H···O hydrogen bond between positively charged amino group and negatively charged carbonyl group. The hydrogen donating property of the remaining N(4)–H becomes weak, so that N(1)–H is a hydrogen-donor to N(3).

The pyrimidine rings are stacked with the spacing of 3.368 Å along the c axis. There are no abnormal contacts between atoms.

Figures 1, 2, and 4 were drawn by TSD:XTAL which is a graphic display programme system for NOVA 3 mini-computer to produce crystal and molecular structures.[17] The present work was partially supported by a Grant-in-Aid for Scientific Research from the Ministry of Education.

References

1) M. Ohki, A. Takenaka, H. Shimanouchi, and Y. Sasada, *Bull. Chem. Soc. Jpn.*, **48**, 848 (1975).
2) M. Ohki, A. Takenaka, H. Shimanouchi, and Y. Sasada, *Bull. Chem. Soc. Jpn.*, **49**, 3493 (1976).
3) M. Ohki, A. Takenaka, H. Shimanouchi, and Y. Sasada, *Bull. Chem. Soc. Jpn.*, **50**, 90 (1977).
4) A. Takenaka, M. Ohki, and Y. Sasada, 36th National Meeting of the Chemical Society of Japan, Oasaka, April 1977, Abstr. I, 4M10.
5) C. Tamura, T. Hata, S. Sato, and N. Sakurai, *Bull. Chem. Soc. Jpn.*, **45**, 3254 (1972).
6) T. Hata, M. Yoshikawa, S. Sato, and C. Tamura, *Acta Crystallogr., Sect. B*, **31**, 312 (1975).
7) L. E. McCandlish and G. H. Stout, *Acta Crystallogr., Sect. A*, **31**, 245 (1975).
8) "International Tables for X-Ray Crystallography," Kynoch Press, Birmingham (1974), Vol. IV, p. 71.
9) Table 3 has been deposited as Document No. 7901, at the Office of the Bulletin of the Chemical Society of Japan.
10) R. J. McClure and B. M. Craven, *Acta Crystallogr., Sect. B*, **29**, 1234 (1973).
11) A. Domenicano, A. Vaciago, and C. A. Coulson, *Acta Crystallogr., Sect. B*, **31**, 1630 (1975).
12) A. Albert, in "Synthetic Procedures in Nucleic Acid Chemistry," ed by W. W. Zorbach and R. S. Tipson, John Wiley & Sons, Inc., New York (1973), p. 1.
13) I. Wempen and J. J. Fox, *J. Am. Chem. Soc.*, **86**, 2474 (1964).
14) "Tables of Interatomic Distances and Configuration in Molecules and Ions. Supplement 1956—1959," ed by L. E. Sutton, The Chemical Society, London (1965).
15) J. Donohue, in "Structural Chemistry and Molecular Biology", ed by A. Rich and N. Davidson, W. H. Freeman & Company, San Francisco (1968), p. 443.
16) M. Kato, A. Takenaka, and Y. Sasada, unpublished.
17) A. Takenaka and Y. Sasada, Annual Meeting of the Crystallographic Society of Japan, Hiroshima, November 1978, Abstr. p. 32.

Hydrates of Organic Compounds. IV. Clathrate Hydrates of Various Bolaform Salts

Haruo NAKAYAMA

Department of Chemistry, Faculty of Engineering, Yokohama National University, Ooka-machi, Minami-ku, Yokohama 232

(Received August 1, 1978)

The solid-liquid phase diagrams are presented for binary mixtures of water with various polymethylenebis(tributylammonium) difluorides, $[(n\text{-}C_4H_9)_3N(CH_2)_nN(n\text{-}C_4H_9)_3]F_2$ (n=4, 5, 6, 8, and 10); and with hexamethylenebis(tributylammonium) dihydroxide and its salts, $[(n\text{-}C_4H_9)_3N(CH_2)_6N(n\text{-}C_4H_9)_3](X_2$ or Y) (X=OH, Cl, and Br; Y=OOC-COO and OOC-$(CH_2)_3$-COO). It has been found that all the compounds form congruently melting hydrates which have large hydration numbers. The hydrates appear to be clathrate-like hydrates essentially similar to those formed by many tetrabutyl(or isopentyl)ammonium salts. The most stable hydrate found in this study is $[(n\text{-}C_4H_9)_3N(CH_2)_6N(n\text{-}C_4H_9)_3]F_2$ hydrate (mp 20.4 °C). The melting points of hexamethylenebis(tributylammonium) hydrates have been compared with those of the corresponding tetrabutylammonium hydrates.

Bisquaternary ammonium salts (bolaform salts) having various hydrophobic groups have been studied from several points of view; the thermodynamic and transport properties *e.g.* molal volumes,[1-3] molal heat contents and solvation enthalpies,[4,5] heat capacities,[3,6] and conductances,[7,8] colloidal properties *e.g.* micelle formation,[9] flocculating action,[10] and emulsion polymerization,[11] pharmacological properties[12] *e.g.* protein binding,[13] resistance to metabolic degradation and accumulation in the kidneys,[14] affinity to choline and its related compounds,[15] and curarelike agent action.[16]

The thermodynamic and transport properties for aqueous solutions of bolaform salts as well as numerous symmetrical tetraalkylammonium salts[17] have extensively been studied in order to examine the structural changes in the solvent in the neighborhood of the solute particles. Broadwater and Evans[1] studied the apparent (ϕ_2) and partial molal volumes of a bolaform electrolyte $[(n\text{-}C_4H_9)_3N(CH_2)_8N(n\text{-}C_4H_9)_3]Br_2$ (C_8Br_2) and found the change of ϕ_2 with concentration for C_8Br_2 was very similar to that observed for $(n\text{-}C_4H_9)_4NBr$,[18] with ϕ_2 decreasing to a minimum and increasing with concentration. The minima in the ϕ_2 *vs.* concentration curves for $(n\text{-}C_4H_9)_4NBr$ have been correlated with the formation of a stable clathrate-like hydrate.[19-21]

In the same context it is of interest to examine the ability of bolaform salts to form clathrate-like hydrates. Although only a brief note has been given concerning the formation of C_8F_2 hydrate (which melts at 5 °C and has approximately 40 water molecules),[1] no other study has been reported about the formation of clathrate hydrates of bolaform salts. It is the purpose of this paper, through the examination of the solid-liquid phase diagrams, to find the conditions for the formation of clathrate-like hydrates of bolaform salts: (1) the length of methylene chain (n) between the two nitrogen atoms in the salt having the general formula $[(C_4H_9)_3N(CH_2)_nN(C_4H_9)_3]F_2$; and (2) the kind of anions in the salt $[(C_4H_9)_3N(CH_2)_6N(C_4H_9)_3]$ (X_2 or Y) (X=OH, F, Cl, and Br; Y=OOC-COO and OOC-$(CH_2)_3$-COO). The six alkyl chains attached to the two terminal nitrogen atoms have been restricted to butyl groups since it was concluded in a previous paper[22] that either the butyl or isopentyl chain was the most suitable size for the formation of stable clathrate hydrates of tetraalkylammonium fluorides.

The clathrate-like hydrates of bolaform salts may be regarded as extended hydrates which have large guest molecules rather than tetraalkylammonium salts, although tetraalkylammonium hydrates, in a sense, may be thought of as extended hydrates compared with ordinary gas hydrates.

Experimental

Polymethylenebis(tributylammonium) dibromides $[(C_4H_9)_3N(CH_2)_nN(C_4H_9)_3]Br_2$ (n=4, 5, 6, 8, and 10; which have been denoted as C_4Br_2, C_5Br_2, C_6Br_2, C_8Br_2, and $C_{10}Br_2$ hereafter) have been prepared by refluxing an excess of tributylamine with the corresponding α,ω-dibromoalkane in ethanol.[1] The excess amine was removed by extraction with diethyl ether and recrystallizations were carried out either in an acetone/ethyl acetate mixture or an diethyl ether/methanol mixture. Since it was fairly difficult to obtain pure $C_{10}Br_2$ by recrystallization, the C_{10}-compound was obtained as the iodide, $C_{10}I_2$, by the following procedure: $C_{10}I_2$ was precipitated by adding KI solution to aqueous $C_{10}Br_2$ solution which was then extract from the reaction mixture and recrystallized from ethyl acetate.

All the salts were confirmed by IR, NMR, and elemental analysis.

Found: C, 57.41; H, 10.69; N, 4.81; Br, 27.01%. Calcd for $C_{28}H_{62}N_2Br_2$(n=4): C, 57.33; H, 10.65; N, 4.78; Br, 27.24%. Mp 157—158 °C for the bromide and 163—164 °C for the iodide.

Found: C, 58.02; H, 10.69; N, 4.62; Br, 26.90%. Calcd for $C_{29}H_{64}N_2Br_2$(n=5): C, 57.99; H, 10.74; N, 4.66; Br, 26.61%. Mp 170—171 °C.

Found: C, 58.75; H, 10.99; N, 4.36; Br; 25.22%. Calcd for $C_{30}H_{66}N_2Br_2$(n=6): C, 58.62; H, 10.82; N, 4.56; Br, 25.22%. Mp 167—168 °C.

Found: C, 59.60; H, 11.04; N, 4.27; Br, 25.32%. Calcd for $C_{32}H_{70}N_2Br_2$(n=8): C, 59.80; H, 10.98; N, 4.36; Br, 24.86%. Mp 121—123 °C (123—124 °C[1]).

Found: C, 53.41; H, 9.68; N, 3.78; I, 32.95%. Calcd for $C_{34}H_{74}N_2I_2$(n=10): C, 53.40; H, 9.75; N, 3.66; I, 33.19%. Mp 142.5—144 °C.

Fluoride solutions (C_nF_2) have been prepared by the triple decomposition of a mixture of BaF_2, Ag_2SO_4, and the corresponding bromide (or iodide) by using stoichiomet-

ric amounts of the latter two components and excess of the former.[20,22] When a small amount of bromide (or iodide) ion was found in the filtrate, an aqueous AgF solution, obtained by the neutralization of AgOH with an aqueous HF solution, was added, and the precipitated silver bromide (or iodide) was removed by either filtration (pore size 1.0 μm) or centrifuge (2000G, 30 min). Solutions of $[(C_4H_9)_3N(CH_2)_6N(C_4H_9)_3]Cl_2$ and $[(C_4H_9)_3N(CH_2)_6N(C_4H_9)_3]Y$ (Y=OOC-COO and OOC-$(CH_2)_3$-COO) (which we denote by C_6Cl_2, C_6Oxa, and C_6Glu hereafter) were prepared by neutralizing $[(C_4H_9)_3N(CH_2)_6N(C_4H_9)_3](OH)_2$ ($C_6(OH)_2$) solutions with the corresponding acids. The hydroxide $C_6(OH)_2$ was obtained by treating a solution of C_6Br_2 with freshly prepared silver hydroxide, and purified by recrystallization from water[19,20,23] in the form of a clathrate hydrate crystal (see below). Both oxalic and glutaric acids were reagent grade commercial materials and recrystallized from water. The two fluoride solutions prepared by different methods (neutralization of $C_6(OH)_2$ with HF and triple decomposition of C_6Br_2 with BaF_2 and Ag_2SO_4) showed exactly the same behavior.

The experimental procedures for determing the solid-liquid phase diagrams for the binary mixtures of these salts with water were almost the same as in previous papers.[22,23] A sample solution (about 1.0—1.5 g) was prepared by weighing out water and a concentrated sample solution obtained by dehydrating a dilute solution using a rotary evaporator and whose water content was determined by the Karl Fischer titration method. No attempt was made to remove the air dissolved in the solution.

Results

The solid-liquid phase diagrams for the binary mixtures of water with C_4F_2, C_5F_2, C_6F_2, C_8F_2, and $C_{10}F_2$ are shown in Fig. 1, indicating that all the salts form hydrates which melt congruently and have large hydration numbers. The formation of these hydrates except for C_8F_2,[1] is confirmed for the first time. Judging from the large hydration numbers, the hydrates appear to be clathrate-like hydrates. The melting points and hydration numbers of these hydrates which have been read off each phase diagram are summarized in Table 1.

Table 1. The melting points and the hydration numbers of $[(C_4H_9)_3N(CH_2)_n(C_4H_9)_3]F_2$ hydrates

n	Melting point (°C)	Hydration number
4 (stable)	2.8	39±3
4 (metastable)	−3.1	45±2
5	12.4	42±2
6	20.4	46±2
8	6.8	48±2
10	−2.2	50±2

The most appropriate methylene chain connecting the two terminal $(C_4H_9)_3N$ groups for the formation of a stable hydrate is a hexamethylene chain. The stability of the C_6F_2 hydrate (mp 20.4 °C) is comparable to that of several tetrabutyl (or isopentyl)ammonium salt hydrates.[20,22-24] The melting point and hydration number for the C_8F_2 hydrate are fairly different from those reported by Broadwater and Evans (5 °C and about 40).[1] A detailed comparison of the data is impossible because of the lack of experimental information. It has often been noticed that, for many tetraalkylammonium salt hydrates, the composition and the melting point of a hydrate which is separated from its solution phase and exposed to the atmosphere vary considerably with time.[22] Two types of hydrates (stable and metastable phases) have been found for the C_4F_2 salt. The stable phase has less water molecules (39±3) than the metastable one (45±2).

The effect of anions on the formation of clathrate-like hydrates has been examined for a series of C_6-compounds, whose cation is most suitable in size for the formation of stable hydrate as mentioned above. In Fig. 2 the solid-liquid phase diagrams for a series of C_6-compounds ($C_6(OH)_2$, C_6F_2, C_6Cl_2, C_6Br_2,

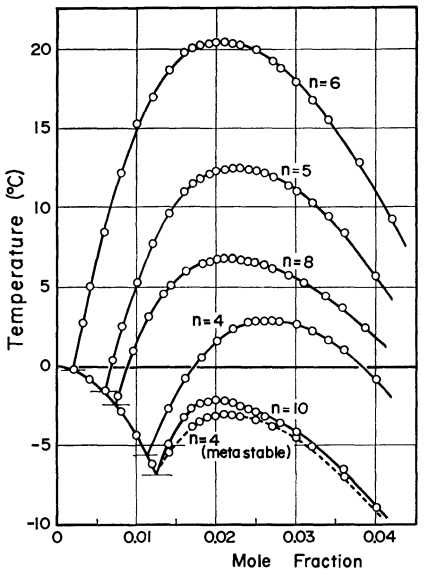

Fig. 1. The solid-liquid phase diagrams for the water + $[(C_4H_9)_3N(CH_2)_nN(C_4H_9)_3]F_2$ (n=4, 5, 6, 8, and 10) systems.

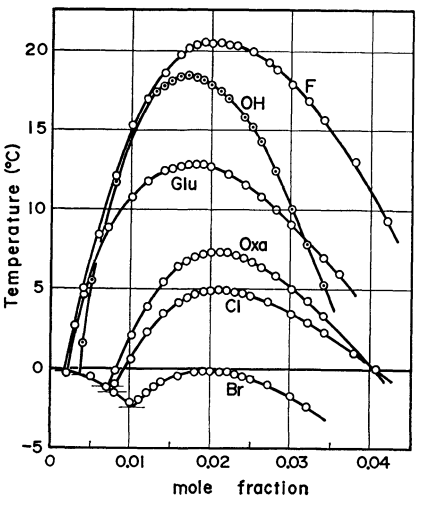

Fig. 2. The solid-liquid phase diagrams for the water + $[(C_4H_9)_3N(CH_2)_6N(C_4H_9)_3]$ (X_2 or Y) (X=OH, F, Cl, and Br; Y=OOC-COO and OOC-$(CH_2)_3$-COO) system.

TABLE 2. THE MELTING POINTS AND THE HYDRATION NUMBERS OF THE HYDRATES OF HEXAMETHYLENEBIS(TRIBUTYLAMMONIUM) AND TETRABUTYLAMMONIUM COMPOUNDS

Anion	Cation $[(C_4H_9)_3N(CH_2)_6N(C_4H_9)_3]^{2+}$		Cation $(C_4H_9)_4N^+$	
	Mp (°C)	Hydration number	Mp (°C)	Hydration number
Br^-	−0.2	48±3	12.5[a]	30.5,[a] 32.6[a]
Cl^-	4.9	47±2	15.0	28±3
			15.7[a]	32.1,[a] 33.8[a]
$(OOC-COO)^{2-}$	7.3	47±2	16.6[b]	58±1[b]
			16.8[a]	67,[a] 64[a]
$[OOC-(CH_2)_3-COO]^{2-}$	12.8	55±2	20.2[b]	55±1[b]
OH^-	18.4	58±2	28.0	33±1
F^-	20.4	46±2	28.3	31±1
			24.9[a]	32.8,[a] 34.0[a]

a) From Ref. 20. b) From Ref. 23.

C_6Oxa, and C_6Glu) are shown and indicates that all C_6-compounds examined form hydrates similar to those found in Fig. 1: characterized by their high water contents and congruent melting points. The melting points and hydration numbers obtained are summarized in Table 2, together with those of the corresponding tetrabutylammonium salts.

Discussion

The Effect of n *on the Formation of* C_nF_2 *Hydrates.* As can be seen from Fig. 1 and Table 1, C_6F_2 forms the most stable hydrate (mp 20.4 °C). From the fact that, in the clathrate hydrates of tetrabutyl(or isopentyl) ammonium salts, 7—8 water molecules are required in order to surround one butyl (or isopentyl) group, and that the C_6F_2 molecule has seven hydrophobic groups (six butyl groups and one hexamethylene chain), the hydration number of 46±2 observed for the C_6F_2 hydrate is a little bit smaller than expected. This indicates that the hydrogen-bonded water framework around the C_6F_2 molecule becomes efficient by the sharing of the common faces of adjacent polyhedra. Although the solution properties caused by the promotion of additional hydrogen bonding of the water molecules in the vicinity of the hydrocarbon groups have been studied exclusively in aqueous solutions of C_8Br_2,[1,3-5,7] the results here suggest that the structural effect in C_6-salt (and also C_5-salt) solution will be greater than that in C_8-salt solutions. The enthalpy of the $H_2O \rightarrow D_2O$ (and also $H_2O \rightarrow$propylene carbonate) transfer for C_8-cation clearly indicates that the structural effect for this ion in water is considerably smaller than that for two tetrabutylammonium ions.[5]

In Fig. 3, the melting points and hydration numbers of C_nF_2 hydrates have been plotted against n. It may be seen from the figure that both the melting points and hydration numbers vary differently with n depending upon whether n is smaller or larger than 6. When n is smaller than 6, both the melting points and the hydration numbers increase with increasing n, whereas when n is larger than 6, the melting points drastically decrease with increasing n while the hydration numbers increase in a similar manner as before but less sharply.

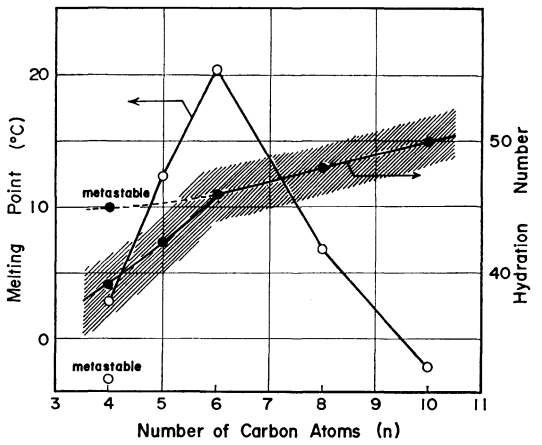

Fig. 3. The melting points and the hydration numbers of the $[(C_4H_9)_3N(CH_2)_nN(C_4H_9)_3]F_2$ hydrates as a function of n.

The hydration number of the metastable C_4F_2 hydrate lies approximately on the extention of the line for $n \geq 6$.

Although there is no evidence concerning the crystal structure of these hydrates, the following structure is consistent with the behavior shown in Fig. 3: the principal constituent of the hydrates may be considered as a clump consisting of three hydrogen-bonded water frameworks (presumably distorted tetrakaidecahedra or pentakaidecahedra) each of which surrounds one of the butyl radicals in the terminal $(C_4H_9)_3N$ group. This unit is schematically depicted in Fig. 4, with the assumption that each polyhedron is 14-hedron. The $(C_4H_9)_3N$-group sheath is denoted hereafter by 3P (P stands for polyhedron). The C_nF_2 hydrate crystal is then made up of two 3P's arranged face to face, in the interstitial space of which is accommodated a polymethylene chain, $-(CH_2)_n-$, which connects the two $(C_4H_9)_3N$-groups.

In the C_4F_2 hydrate (stable phase), the two 3P's are drawn together since they are covalently combined by a short polymethylene chain (the maximum distance between the two nitrogen atoms is 6.2—6.3 Å). The most probable configuration for this would be the

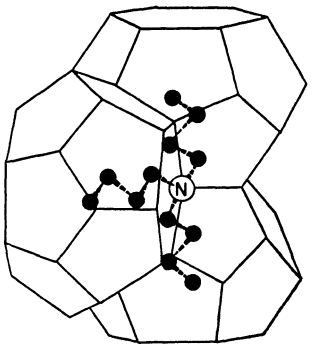

Fig. 4. The schematic representation of the water frameworks which enclathrate a $(C_4H_9)_3N$-group (3P).

twisted combination — a rotating 60° about the N–N axis as in the staggered ethane molecule conformation. The water framework within which the $-(CH_2)_4-$ chain is accommodated is automatically formed when the two 3P's approach, in agreement with the observation that the hydration number of the C_4F_2 hydrate is considerably small (39±3). The low melting point of this hydrate is presumably due to the strong distortion of the framework. The increase of both hydration number and melting point with increasing n from 4 to 6 is due to the formation of a larger and less distorted cage to accommodate a longer polymethylene chain ($-(CH_2)_5-$ and $-(CH_2)_6-$). In the compound C_6F_2, which gives the most stable hydrate, the stretched chain-length between the two nitrogen atoms, 8.8 Å, is very close to the average cage diameter of a typical polyhedron (8.7 Å for a 14-hedron and 9.4 Å for a 16-hedron[25]).

The slight increase in the hydration numbers and the drastic decrease in the melting points with increasing n from 6 to 10 reflects the situation that a few more water molecules are necessary to form a larger cage than in the case of C_6F_2 hydrate in order to accommodate the longer chain. Chain flexibility cancels this out to some extent, and furthermore the cage thus constructed is inevitably distorted compared with the most stable polyhedra such as the 14-hedron and 16-hedron. As to the structure of the metastable C_4F_2 hydrate, from the experimental results, *i.e.* a considerably low melting point and a hydration number (45±2) much larger than that in the stable phase (39±3) and position nearly on the extention of the line for $n\geq6$ as previously pointed, it appears essentially similar to the structure for $n\geq6$, but much more strained because of the short methylene chain. Presumably the two 3P's would take an eclipsed conformation in contrast to the staggered conformation which was assumed to be the stable phase as discussed earlier. Further detailed crystallographic studies of these hydrates are needed.

The Effect of Anion on the Formation of the C_6-Hydrates. The correlation between the melting points of the hydrates of C_6-compounds with various anions and those of the corresponding tetrabutylammonium compounds is shown in Fig. 5. This figure indicates two interesting facts: (1) the melting points of the C_6-compound hydrates are about 10 °C lower than those

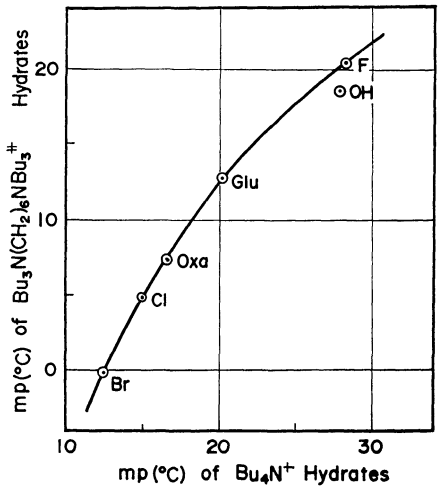

Fig. 5. The correlation between the melting points of the $[(C_4H_9)_3N(CH_2)_6N(C_4H_9)_3]^{2+}$ hydrates and those of the $(C_4H_9)_4N^+$ hydrates.

of the tetrabutylammonium compound hydrates irrespective of the type of anion; (2) there exists approximately linear relationship between the two sets of melting points. The former point emerges since the formation of the hydrogen-bonded water framework around the C_6-cation is considerably more difficult compared with the case of the tetrabutylammonium cation. The latter point indicates that the lattice distortion caused by the presence of the anion affects the stabilities of the hydrates in a similar manner in both series of salts. As may be seen from Table 2, all the C_6-compounds, except C_6Glu and $C_6(OH)_2$, have the same hydration numbers — around 47. This, suggests that they are isostructural, having a strong resemblance to the finding that the corresponding tetrabutylammonium salt hydrates are isomorphous (tetragonal).[20] The relatively large hydration number found for glutarate hydrate may be a consequence of the additional water molecules needed in order to surround the large $OOC-(CH_2)_3-COO$ anion, a striking contrast to the $[(C_4H_9)_4N]_2OOC-(CH_2)_3-COO$ hydrate which has a cosiderably small hydration number.[23] Hydroxide hydrate has also a large hydration number. A similar but less sharp trend is seen for tetrabutylammonium hydroxide hydrate and this may be due in part to the strong hydration of the hydroxide ion.

This work was supported by a Grant-in-Aid for Scientific Research from the Ministry of Education.

References

1) T. L. Broadwater and D. F. Evans, *J. Phys. Chem.*, **73**, 164 (1969).

2) J. A. Burns and R. E. Verrall, *J. Solution Chem.*, **3**, 289 (1974).

3) C. Jolicoeur and J. Boileau, *J. Solution Chem.*, **3**, 889 (1974).

4) S. Lindenbaum, *J. Phys. Chem.*, **73**, 4334 (1969).

5) C. V. Krishnan and H. L. Friedman, *J. Phys. Chem.*, **74**, 2356 (1970).

6) J. A. Burns and R. E. Verrall, *Thermochim. Acta*,

9, 277 (1974).
7) T. L. Broadwater and D. F. Evans, *J. Phys. Chem.*, **73**, 3985 (1969).
8) J. Thomas and D. F. Evans, *J. Phys. Chem.*, **74**, 3812 (1970).
9) L. A. Al'bota, V. P. Rudi, N. K. Al'bota, and M. G. Grishina, *Ukr. Khim. Zh.*, **38**, 1001 (1972); Yu. F. Deinega, Z. R. Ul'berg, L. G. Marochko, V. P. Rudi, and V. P. Denisenko, *Kolloidn. Zh.*, **36**, 649 (1974).
10) S. S. Khamraev, V. P. Rudi, T. Z. Ziyaev, and Z. S. Sidenko, *Uzb. Khim. Zh.*, **1975**, 14.
11) N. R. Amnuil, T. A. Grishina, L. I. Ershova, V. P. Denisenko, and E. I. Tishchenko, *Zh. Prikl. Khim.*, **44**, 1667 (1971).
12) G. T. Pis'ko, *Farmakol. Toksikol.*, **33**, 551 (1970).
13) O. Wassermann, *Arzneim.-Forsch.*, **22**, 1993 (1972).
14) O. Wassermann, *Naunyn-Schmiedeberg's Arch. Pharmacol.*, **275**, 251 (1972).
15) I. L. Kratskin, *Farmakol. Toksikol.*, **36**, 261 (1973); J. T. Holden, J. Rossier, J. C. Beaujouan, P. Guyenet, and J. Glowinski, *Mol. Pharmacol.*, **11**, 19 (1975), F. D. Gerlach, H. Luellmann, F. K. Ohnesorge, and O. Wassermann, *Arzneim.-Forsch.*, **20**, 751 (1970).
16) D. A. Kharkevich and A. P. Skoldinov, *Dokl. Akad. Nauk SSSR*, **219**, 762 (1974); A. P. Drozhzhin and D. N. Ibadova, *Farmakol. Toksikol.*, **39**, 21 (1976).
17) W.-Y. Wen, "Water and Aqueous Solutions," ed by R. A. Horns, Wiley-Interscience, New York (1972).
18) W.-Y. Wen and S. Saito, *J. Phys. Chem.*, **68**, 2639 (1964).
19) D. L. Fowler, W. V. Loebenstein, D. B. Pall, and C. A. Kraus, *J. Am. Chem. Soc.*, **62**, 1140 (1940).
20) R. K. McMullan and G. A. Jeffrey, *J. Chem. Phys.*, **31**, 1231 (1959).
21) Yu. A. Dyadin, I. I. Yakovlev, I. V. Bondaryuk, L. S. Aladko, and L. S. Zelenina, *Dokl. Akad. Nauk SSSR*, **203**, 1068 (1972).
22) H. Nakayama and K. Watanabe, *Bull. Chem. Soc. Jpn.*, **49**, 1254 (1976).
23) H. Nakayama and K. Watanabe, *Bull. Chem. Soc. Jpn.*, **51**, 2518 (1978).
24) R. K. McMullan, M. Bonamico, and G. A. Jeffrey, *J. Chem. Phys.*, **39**, 3295 (1963).
25) D. W. Davidson, "Water," ed by F. Franks, Plenum Press, New York (1973), Vol, 2.

Studies of the Metal Complexes of Cyclohexane Derivatives. V.[1] Copper(II) and Nickel(II) Complexes of *cis*-1,3-Cyclohexanediamine

Reiko SAITO* and Yoshinori KIDANI†

Aichi Junior College of Nursing, Kamishidanmi, Moriyama-ku, Nagoya 463

† *Faculty of Pharmaceutical Sciences, Nagoya City University, Tanabe-dori, Mizuho-ku, Nagoya 467*

(Received May 12, 1978)

A series of 1,3-chxn(*cis*-1,3-cyclohexanediamine) copper(II) and nickel(II) complexes have been prepared and studied using spectroscopic and magnetic techniques. The violet and red copper(II) complexes of 1,3-chxn were found to consist of monomeric distorted octahedra and slightly distorted square planers, respectively. The nickel(II) complexes have a square planar structure. The conformational change of the ligand from diequatorial to diaxial on coordination has been confirmed by infrared analysis.

cis-1,3-Cyclohexanediamine(abbreviated as 1,3-chxn[2]) is

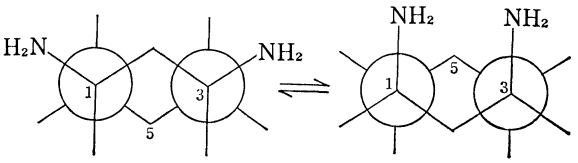

(a) diequatorial conformation (b) diaxial conformation

known to take exclusively the diequatorial conformation(a). Assuming that the transformation to the less stable diaxial form(b) occurs, this diamine is able to form metal complexes containing six membered rings as bidentate ligands. The Pd(II) and Pt(II) complexes of 1,3-chxn have been prepared and there is some evidence for the square planar structure in which the ligand exists as the diaxial conformer(b).[3] Kamisawa *et al.*[4] recently determined the molecular structure of $[Pd(1,3\text{-chxn})_2]Cl_2$ by X-ray diffraction. A similar structure for the mixed Pt(II) complex with 1,3-chxn and 2,2′-bipyridyl has been reported by Sarneski *et al.*[5]

The copper(II) and nickel(II) complexes with *cis*- and *trans*-1,2-cyclohexanediamine(abbreviated to *c*- and *t*-chxn) have been studied and it has been found that the structures of the bis complexes of nickel(II) were greatly affected by the steric configuration of these ligands.[1] In a series of studies examing the influence of the stereochemistry of the cyclohexane derivatives upon complex formation, the copper(II) and nickel(II) complexes of 1,3-chxn were prepared and studied.

Experimental

Materials. 1,3-chxn was prepared from *cis*-1,3-cyclohexanedicarboxylic acid according to the procedure in the literature.[6] *cis*-1,3-Cyclohexanedicarboxylic acid used was isolated by the method of Skita[7] from the mixed *cis*- and *trans*-diacid resulting from hydrogeneration of isophthalic acid.

Measurements. The magnetic moments were measured with a Shimadzu MB-2 magnetic balance at room temperature. Measurements of the absorption spectra were carried out using a Hitachi 124-spectrophotometer. The reflectance spectra were measured with a Shimadzu MPS-5000 spectrophotometer. The infrared spectra were recorded with a JASCO IR-2A spectrophotometer using a KBr disc.

Preparation of the Complexes. *Cu(1,3-chxn)$_2$Cl$_2$*: Copper(II) chloride dihydrate (2 mmol in 2 ml of MeOH) and 1,3-chxn (4 mmol in 2 ml of MeOH) were mixed together. The resulting violet product was recrystallized from methanol–ethanol.

Cu(1,3-chxn)$_2$ClClO$_4$: Dihydrochloride of 1,3-chxn (6 mmol) and $CuCl_2 \cdot 2H_2O$ (1.2 mmol) were dissolved in H_2O (7.5 ml) and the pH was adjusted to approximately 10 by 1 mol l^{-1} NaOH solution. To this solution $NaClO_4$ (6 mmol) was added. On warming the solution, a blue violet complex began to precipitate, and this was recrystallized from methanol.

Cu(1,3-chxn)$_2$Br$_2$ (A) and Cu(1,3-chxn)$_2$Br$_2$ (B): Copper(II) bromide (2 mmol in 15 ml of EtOH) and 1,3-chxn (4 mmol in 2 ml of EtOH) were mixed together. This method predominantly produced the violet complex, Recrystallization from ethanol gave violet crystalline powder of (A), while, recrystallization from methanol afforded the wine red needles of (B).

Cu(1,3-chxn)$_2$(NO$_3$)$_2$: Copper(II) nitrate trihydrate (1 mmol in 5 ml of H_2O) and 1,3-chxn (2 mmol in 10 ml of MeOH) were mixed and the resulting violet solution was warmed. The wine red crystals were recrystallized from methanol.

[Ni(1,3-chxn)$_2$]X$_2$ (X=Cl$^-$, Br$^-$, NO$_3^-$, and ClO$_4^-$): All the nickel(II) complexes were prepared in a similar manner as described here. To an ethanoic solution of the ligand (4—5 mmol), an ethanoic solution of the Ni(II) salt (2 mmol) was added. The yellow crystals obtained were recrystallized from methanol.

Results and Discussion

Properties of the Complexes. The results of the elemental analyses, the magnetic moments, and the colors of the complexes prepared are listed in Table 1. The copper(II) complexes are magnetically normal and are assumed to consist of monomeric species. The 1,3-chxn ligand was found to produce two forms of copper(II) complexes, a violet and a red, depending on the anion. The copper(II) complexes coordinating Br^- exist in two forms, however, the violet complex was recrystallized with some difficulty. On the other hand, this ligand afforded only diamagnetic nickel(II) complexes. The tris and bis nickel(II) complexes having octahedral or tetragonally distorted octahedral structures were not obtained.

Electronic Spectra. Some typical electronic spectra of the complexes obtained are shown in Fig. 1 and the numerical data, in Table 2. The band maxima of the red copper(II) complexes in the solid state were observed at 20400—20600 cm^{-1}, higher in energy than

TABLE 1. ELEMENTAL ANALYSES, MAGNETIC MOMENTS, AND COLORS OF THE COMPLEXES

Complex	Color[a)]	Found (Calcd) %			μ (B.M.)
		C	H	N	
$Cu(1,3\text{-chxn})_2Cl_2$	V	39.61(39.72)	7.54(7.78)	15.53(15.44)	1.84
$Cu(1,3\text{-chxn})_2ClClO_4$	BV	33.66(33.77)	6.71(6.61)	13.35(13.13)	1.86
$Cu(1,3\text{-chxn})_2Br_2$ (A)	V	32.06(31.91)	6.22(6.25)	12.31(12.40)	1.84
$Cu(1,3\text{-chxn})_2Br_2$ (B)	WR	31.63(31.91)	5.98(6.25)	12.21(12.40)	1.85
$Cu(1,3\text{-chxn})_2(NO_3)_2$	WR	34.73(34.65)	7.06(6.79)	20.52(20.20)	1.83
$[Ni(1,3\text{-chxn})_2]Cl_2$	Y	39.96(40.26)	8.15(7.88)	15.51(15.65)	dia
$[Ni(1,3\text{-chxn})_2]Br_2$	Y	32.10(32.35)	6.07(6.32)	12.72(12.54)	dia
$[Ni(1,3\text{-chxn})_2](NO_3)_2$	Y	35.08(35.06)	7.03(6.87)	20.64(20.44)	dia
$[Ni(1,3\text{-chxn})_2](ClO_4)_2$	OY	29.55(29.66)	5.77(5.81)	11.55(11.53)	dia

a) V=violet, BV=blue violet, WR=wine red, Y=yellow, OY=orange yellow.

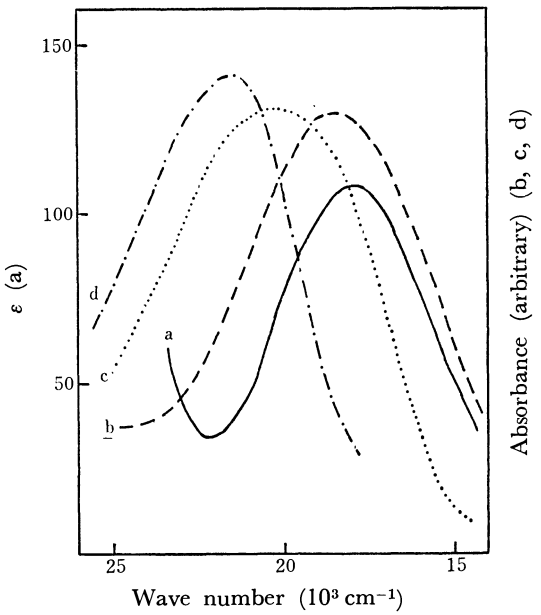

Fig. 1. Electronic spectra of (a) $Cu(1,3\text{-chxn})_2Br_2$(B) (MeOH soln.), (b) $Cu(1,3\text{-chxn})_2ClClO_4$ (Solid), (c) $Cu(1,3\text{-chxn})_2(NO_3)_2$ (Solid), and (d) $[Ni(1,3\text{-chxn})]_2$ (Solid).

those of the violet complexes which were considered to have tetragonally distorted octahedral structures. The d-d bands of the former were sufficiently high compared to the copper(II) complexes of other diamines, *e.g.*, *c*-chxn,[1] *t*-chxn,[1] and 1,3-propanediamine[8] thought to have a similar structure to 1,3-chxn. Asuming that 1,3-chxn coordinates to the copper(II) ion as a result of interconversion to the diaxial conformation(b) and that the chelate ring takes a chair conformation in the same way as $[Pd(1,3\text{-chxn})_2]Cl_2$,[4] then the considerable large steric hindrance by a H_{5a} proton

TABLE 2. ELECTRONIC SPECTRA OF THE COMPLEXES

Complex	ν 10^3 cm^{-1} (ε)	
	Solid	Solution
$Cu(1,3\text{-chxn})_2Cl_2$	19.0	18.0(106)[a)]
$Cu(1,3\text{-chxn})_2ClClO_4$	18.4	18.0(107)[a)]
$Cu(1,3\text{-chxn})_2Br_2$ (A)	18.9	18.0(107)[a)]
$Cu(1,3\text{-chx})_2Br_2$ (B)	20.6	18.0(108)[a)]
$Cu(1,3\text{-chxn})_2(NO_3)_2$	20.4	18.5(133)[b)]
$[Ni(1,3\text{-chxn})_2]Cl_2$	21.5	21.5(46.2)[a)]
$[Ni(1,3\text{-chxn})_2]Br_2$	21.5	—[c)]
$[Ni(1,3\text{-chxn})_2](NO_3)_2$	21.6	—[c)]
$[Ni(1,3\text{-chxn})_2](ClO_4)_2$	21.4	—[c)]

c) In MeOH solution. b) In DMF solution. c) The absorption spectrum could not be measured because of the low solubility of the complex.

occurs in the z-axis. Consequently, only the anionic X group which has strong bond strength would be expected to occupy tetragonal positions. As the axial field strength weakens, the in-plane field strength increases. That the structure of the red form complexes is very close to being square planar is supported and this is unusual for $Cu(diamine)_2X_2$.[9,10] In methanol solution, the copper(II) complexes of both forms, except the nitrate, have essentially the same ν_{max} and ε_{max}. It can be said that the equilibrium in the methanol solution shifts greatly towards the formation of $Cu(1,3\text{-chxn})_2(MeOH)_2^{2+}$ (Scheme 1). With the violet complexes having a distorted octahedral structure ligand-substitution reactions between the coordinated anions and solvent molecules appears to hold, while, in the case of the red complexes, the square planar structure appears to transform to the distorted octahedral structure by bonding solvent molecules.

$$\begin{array}{ccc} & & Cu(1,3\text{-chxn})_2Cl_2(\text{violet}) + 2MeOH \\ & & \uparrow\downarrow \\ Cu(1,3\text{-chxn})_2Br_2(\text{red}) + 2MeOH & \rightleftharpoons & Cu(1,3\text{-chxn})_2(MeOH)_2^{2+} + 2X^- \\ & & \uparrow\downarrow \\ & & Cu(1,3\text{-chxn})_2Br_2(\text{violet}) + 2MeOH \end{array}$$

Scheme 1.

As Table 2 shows, the visible spectrum of $[Ni(1,3\text{-chxn})_2]Cl_2$ in methanol is similar to the reflectance spectra of all the nickel(II) complexes prepared. The spectral properties of the nickel(II) complexes with 1,3-chxn suggested that only reasonable structure for these complexes is square planar. This trend has been known for the nickel(II) complexes of the bulky diamine involved.[11]

Infrared Spectra. The representative infrared spectra of the complexes in the δ_{NH_2}, ρ_{rCH_2}, ρ_{rNH_2} region are shown in Fig. 2, and the main bands are listed in Table 3. The three copper(II) complexes of the violet form exhibit a very similar infrared spectra. The characteristic bands assignable to the rocking vibration of NH_2 are observed at 600—750 cm^{-1}. For the analogue of the violet complexes, the ρ_{rNH_2} values appear due to the anionic groups bonded in the tetragonal positions. Therefore, more than four peaks corresponding to ρ_{rNH_2} appear in the spectra of $Cu(1,3\text{-chxn})_2ClClO_4$. No relationship between the frequencies of ρ_{rNH_2} and structures of the red copper(II) and nickel(II) complexes have been found.

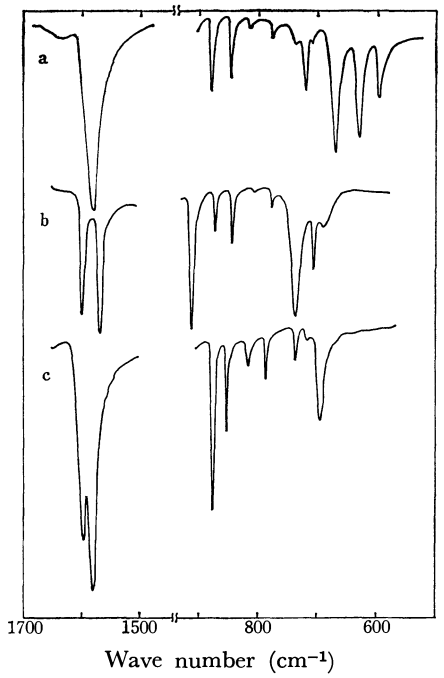

Fig. 2. Infrared spectra of (a) $Cl(1,3\text{-chxn})_2Br_2$ (A), (b) $Cu(1,3\text{-chxn})_2Br_2$ (B), and (c) $[Ni(1,3\text{-chxn})_2]Br_2$ in the δ_{NH_2}, ρ_{rCH_2}, and ρ_{rNH_2} region.

The δ_{NH_2} of the nickel(II) complexes described here show two peaks. The similar frequency separation for the red copper(II) complexes is significantly larger than that for the violet copper(II) complexes. The splitting of this band may be due to the distortion of the chelate ring or the degree of hydrogen bonding between the NH_2 groups and the anion. In the spectra of a similar type of complexes having stronger metal–N bonds, such as $[Pt(1,3\text{-chxn})_2]Cl_2$ and $[Pd(1,3\text{-chxn})_2]Cl_2$, the corresponding band shows no splitting.[3] From the δ_{NH_2} data, the structure of the red copper(II) complexes is thought very similar to the square planar complexes of nickel(II).

It is generally recognized that the degenerated stretching mode of the perchlorate ion splits into two bands on coordination.[12] As shown in Fig. 3, the infrared spectrum of $Cu(1,3\text{-chxn})_2ClClO_4$ gives evidence of the covalently bonded perchlorate group. The same band of $[Ni(1,3\text{-chxn})_2](ClO_4)_2$ appears to be single and broad, reflecting the existence of free ions. The infrared spectra of $Cu(1,3\text{-chxn})_2(NO_3)_2$ shows a broad profile of ν_{N-O} ascribable to the free ion[13] at 1300—1400 cm^{-1}, which is very similar to that of $[Ni(1,3\text{-chxn})_2](NO_3)_2$. This suggests that in the former complex the copper(II) ion is present in a planar rather than a distorted octahedral configuration.

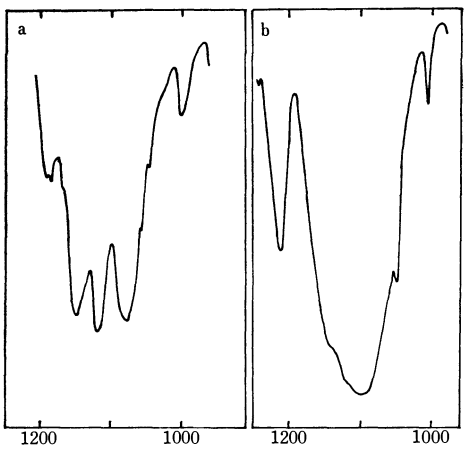

Fig. 3. Infrared spectra of (a) $Cu(1,3\text{-chxn})_2ClClO_4$ and (b) $[Ni(1,3\text{-chxn})_2](ClO_4)_2$ in the ν_{Cl-O} region.

Table 3. The main infrared bands of the complexes (cm^{-1})

Complex	ν_{NH}	δ_{NH_2}	ρ_{rCH_2}	ρ_{rNH_2}
$Cu(1,3\text{-chxn})_2Cl_2$	3230, 3110[a]	1590, 1583	817, 777	727, 678, 637, 601
$Cu(1,3\text{-chxn})_2ClClO_4$	3230, 3110[a]	1583, 1577[a]	812, 773	737, 719, 670, 632, 595[a]
$Cu(1,3\text{-chxn})_2Br_2$ (A)	3230, 3120[a]	1580	812, 775	719, 670, 630, 596[a]
$Cu(1,3\text{-chxn})_2Br_2$ (B)	3230, 3130[a]	1596, 1567	810, 777	738, 709, 690
$Cu(1,3\text{-chxn})_2(NO_3)_2$	3260, 3150[a]	1619, 1602, 1585	777	740[sh], 692, 648, 608
$[Ni(1,3\text{-chxn})_2]Cl_2$	3180, 3100	1607, 1584	810[sh], 795	715, 640
$[Ni(1,3\text{-chxn})_2]Br_2$	3170, 3100	1594, 1580	817, 787	738, 720, 695
$[Ni(1,3\text{-chxn})_2](NO_3)_2$	3280, 3140[a]	1620, 1583	810	746, 719, 645[a]
$[Ni(1,3\text{-chxn})_2](ClO_4)_2$	3300, 3260, 3200[a]	1601, 1580	778	742, 710

a) A shoulder was observed besides these bands. sh=shoulder.

As previously discussed, for coordination of the 1,3-chxn ligand to the metal ion the interconversion from the diequatorial(a) to the diaxial(b) conformer is necessary. In the infrared spectra of the cyclohexane derivatives involving axially bonded substituents, the weak rocking vibration of CH_2 appears around 800 cm^{-1}.[14] It has been found that the *c*-chxn complexes show these characteristic bands which are absent in the *t*-chxn complexes.[15] Dihydrochloride of 1,3-chxn have no bands in the region of 560—840 cm^{-1}. However, in the spectra of the complexes one or two bands were observed around 770—810 cm^{-1} as shown in Table 3 and Fig. 2. These results support the complexes involve ligands with diaxial conformation(b). Similar complex formation of 1,3,5-triaminocyclohexane taking conformational inversion have been revealed in several investigations.[16–18]

The authors would like to thank Dr. Noboru Nakayama and Dr. Haruo Matsui of the Goverment Industrial Institute, Nagoya, for the use of a Shimadzu MB-2 magnetic balance and a Shimadzu MPS-5000 spectrophotometer, respectively. Thanks are also due to Miss Masae Ishiguro and Miss Shizuko Iwauchi of the Analytical Center of Nagoya City University for the elemental analyses.

References

1) Part IV of this series: R. Saito and Y. Kidani, *Bull. Chem. Soc. Jpn.*, **51**, 159 (1978).
2) In previous paper,[3] the abbreviation, 1,3-dac was used for this ligand.
3) R. Saito and Y. Kidani, *Chem. Lett.*, **1977**, 1141.
4) K. Kamisawa, K. Matsumoto, S. Ooi, H. Kuroya, R. Saito, and Y. Kidani, *Bull. Chem. Soc. Jpn.*, **51**, 2330 (1978).
5) F. E. Sarneski, A. T. Mcphail, and K. D. Onan, *J. Am. Chem. Soc.*, **99**, 7736 (1977).
6) F. R. Hewgill and P. R. Jefferies, *J. Chem. Soc.*, **1955**, 2767.
7) A. Skita and R. Rossler, *Ber.*, **72**, 265 (1939).
8) A. Pajunen, *Suom. Kemistil. B*, **42**, 15 (1969).
9) I. M. Procter, B. J. Hathaway, and P. Nicholls, *J. Chem. Soc., A*, **1968**, 1678.
10) B. P. Lever and E. Mantovani, *Inorg. Chem.*, **10**, 817 (1971).
11) F. R. Basolo, Y. T. Chen, and R. K. Murmann, *J. Am. Chem. Soc.*, **76**, 956 (1954).
12) B. J. Hathaway and A. E. Underhill, *J. Chem. Soc.*, **1961**, 3091.
13) C. C. Addison and B. M. Gatehouse, *J. Chem. Soc.*, **1960**, 613.
14) Y. Kidani, R. Saito, and H. Koike, *Nippon Kagaku Kaishi*, **1975**, 632.
15) Y. Kidani, K. Inagaki, R. Saito, and S. Tsukagoshi, *J. Clin. Hemato. Oncol.*, **7**, 197 (1977).
16) P. A. Brauner and G. Schwarzenbach, *Helv. Chim. Acta*, **45**, 2030 (1962).
17) R. A. D. Wentworth and J. J. Felten, *J. Am. Chem. Soc.*, **90**, 621 (1968).
18) L. Fabbrizzi, M. Micheloni, and P. Paoletti, *Inorg. Chem.*, **15**, (1976).

Preparation and Isomerization of Isomers of the L- or D-Aspartato(L-histidinato)cobalt(III) Complex

Masatoshi WATABE,* Hisao YANO, and Sadao YOSHIKAWA†

General Education Department, Kogakuin University, Hachioji, Tokyo 193

† *Department of Synthetic Chemistry, Faculty of Engineering, The University of Tokyo, Hongo, Bunkyo-ku, Tokyo 113*

(Received May 16, 1978)

The six isomers of the [Co(L- or D-asp)(L-his)] complex (asp=aspartate ion and his=histidinate ion) have been prepared and the isomerization studied in the absence of any catalyst. The equilibrium mole fractions of these isomers in water has been found for L-*trans*O_5*cis*N_5, L-*cis*O_5*trans*N_5, L-*fac*, to be 0.53, 0.06, and 0.41, respectively, those for D-*cis*O_5*cis*N_5, D-*trans*O_5*trans*N_5, and D-*fac* to be 0.48, 0.01, and 0.51 respectively. The indication is that the relative positions of the six coordinated atoms around a cobalt atom cause these unequal isomer concentration ratios. The isomerisms are dealt with by means of a network of first order reversible reactions and the absolute values of the rate constants at 80 °C have been determined.

In a previous work,[1] the isomerzation of D-aspartato(L-2,4-diaminobutyrato)cobalt(III), [Co(D-asp)(L-2,4-dba)] was studied in the presence of active carbon. The relative rate constants of the isomerization and the mole fractions of the isomers at equilibrium were determined. However, those of the [Co(L-asp)(L-2,4-dba)] complex could not be determined on account of their low solubilities. In this paper, the preparation and the isomerization of the isomers of the D- or L-aspartato(L-histidinato)cobalt(III) complex are presented. All isomers are soluble in water.

Experimental

Preparation of [*Co*(L- *or* D-*asp*)(L-*his*)]. To a solution of $CoCl_2 \cdot 6H_2O$ (2.4 g) in water (20 cm^3) containing 10% H_2O_2 (5 cm^3) was added an aqueous solution containing L-aspartic acid (1.33 g), L-histidine (1.55 g), and NaOH (0.95 g). The pH of this mixed solution became *ca.* 7. The solution was stirred for 24 h at 30 °C, concentrated to about 20 cm^3 and passed through a column (30 mmϕ × 700 mm) containing a strong acid cation exchange resin (Dowex 50WX8, Na^+ form). By slowly washing the column with water, five bands were distinguished, the last three bands corresponding to the isomers of the [Co(L-asp)(L-his)] complex. The three fractions were violet (H1), brick red (H2), and red violet (H3) in that order of elution. In order to separate the bands of H1 and H2 precisely, the fractions were circulated several times in the column using a quantitative micropump. The three fractions were evaporated to dryness below 30 °C by a rotatory evaporator. The isomers of the [Co(D-asp)(L-his)] complex were similarly prepared using D-asp insted of L-asp. The three fractions were violet (I1), brick red (I2), and red violet (I3) in that order of elution. Found: (H1) C, 30.66; H, 4.95; N, 13.80%. Calcd for $CoC_{10}H_{13}O_6N_4 \cdot 3H_2O$: C, 30.21; H, 4.81; N, 14.01%. Found: (I2) C, 35.08; H, 3.87; N, 16.63%. Calcd for $CoC_{10}H_{13}O_6N_4 \cdot 0.5H_2O$: C, 34.95; H, 3.81; N, 16.31%. Found: (H2) C, 33.01; H, 3.81; N, 14.81%. (H3) C, 32.65; H, 4.15; N, 15.00%. (I1) C, 32.81; H, 4.18; N, 15.40%. (I3) C, 32.35; H, 4.25; N, 14.89%. Calcd for $CoC_{10}H_{13}O_6N_4 \cdot 1.5H_2O$: C, 32.41; H, 4.35; N, 14.89%.

The method of isomerization for the [Co(L- or D-asp)(L-his)] complex was similar to that described in a previous paper.[1] Since the H1(I1), H2(I2), and H3(I3) isomers could be easily separated by means of high speed liquid chromatography (column contained a strong cation exchange resin, TSK LS-212 Toyo Soda Ind., Na^+ form), the concentrations of these isomers were determined with a UV spectrophotometer (at 254 nm) by comparison with the peak height of a known concentration of isomer.

Results and Discussion

Characterrization. Figure 1 shows the possible isomers of the [Co(L- or D-asp)(L-his)] complex. They are denoted by L- or D-series with respect to the asp used. Both series of mixed complexes are composed of two meridional and one facial about the chromophore $[Co(N)_3(O)_3]$. The isomers are denoted by considering the 5-membered glycinato N and O atoms. The two mer isomers for the L-series are denoted by L-*trans*O_5 *cis*N_5 and L-*cis*O_5 *trans*N_5. Similarly the three isomers of [Co(D-asp)(L-his)] are designated

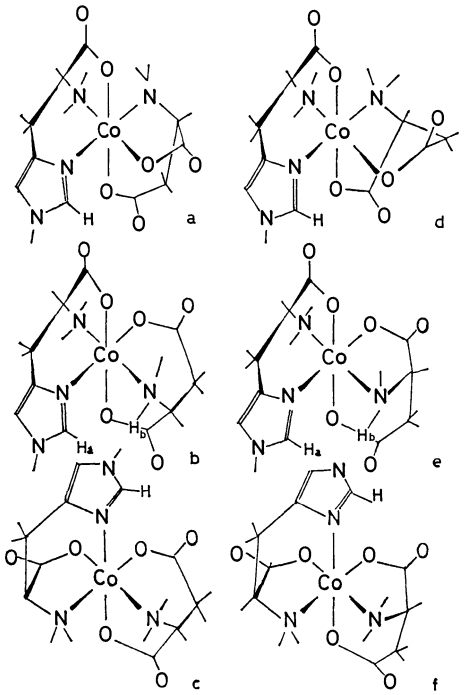

Fig. 1. The six possible geometrical isomers of the [Co(L- or D-asp)(L-his)] complex, a; *cis*O_5*cis*N_5, b; *trans*O_5*trans*N_5, c; D-*fac*, d; *trans*O_5*cis*N_5, e; *cis*O_5-*trans*N_5, and f; L-*fac*.

by D-*cisO*$_5$*cis*N_5, D-*transO*$_5$*trans*N_5, and D-*fac*. Figures 2a and 3a show the electronic absorption spectra.

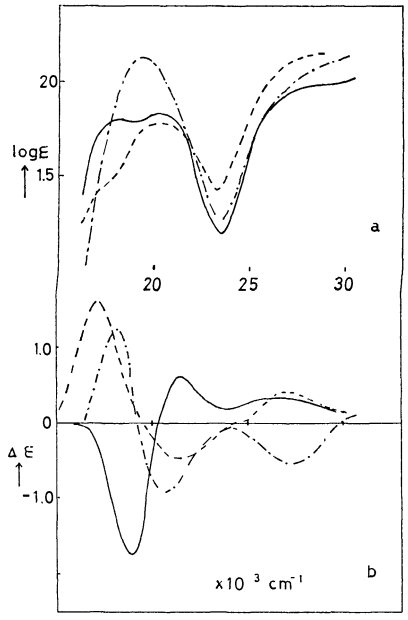

Fig. 2. Absorption (upper) and CD (lower) spectra of [Co(L-asp)(L-his)]. H1 (——), H2 (----), and H3 (— — —).

Table 1 shows the numerical data for the electronic absorption spectra of [Co(L- or D-asp)(L-his)], together with those for the isomers of [Co(L- or D-asp)(L-2,4-dba)].[1] The absorption spectra of the [Co(L- or D-asp)(L-his)] complexes were similar to those for [Co(L- or D-asp)(L-2,4-dba)]. The ligand L-2,4-dba differs from the histidine only in that it contains the NH_2–CH_2-group in the position occupied by the imidazole group in histidine. The charge transfer bands which tail into the visible region in the spectra of the [Co(L- or D-asp)(L-his)] complexes are absent in the [Co(L- or D-asp)(L-2,4-dba)] complexes. When the elution order and the similarity of the visible absorption spectra between [Co(L- or D-asp)(L-his)] and [Co(L- or D-asp)(L-2,4-dba)] are taken into account, the isomers H1, H2, and H3 are tentatively assigned as L-*transO*$_5$*cis*N_5, L-*cisO*$_5$*trans*N_5, and L-*fac*. The isomers I1, I2, and I3 are also assigned as *D*-*cisO*$_5$*cis*N_5, D-*transO*$_5$*trans*N_5, and D-*fac* in the same manner. Figures 2b and 3b show the CD spectra of the six isomers of [Co(asp)(his)]. The CD spectrum for a specific isomer *e.g.* the first eluate of the [Co(L- or D-asp)-(L-his)] complex is quite similar to that for the isomer being eluted in the same order *e.g.* the first eluate of the [Co(L- or D-asp)(L-2,4-dba)] complex. Both isomers may have the same configuration as shown in Fig. 1. However, the coordination of the L-his in place of L-2,4-dba for the [Co(L- or D-asp)(L-2,4-

TABLE 1. ABSORPTION AND CD SPECTRAL DATA OF [Co(L- OR D-asp)(L-his)]

Complex	I band				II band			
	Absorption		CD		Absorption		CD	
	$\bar{\nu}_{max}$[a]	log ε	$\bar{\nu}_{max}$	$\Delta\varepsilon$	$\bar{\nu}_{max}$	log ε	$\bar{\nu}_{max}$	$\Delta\varepsilon$
L-*transO*$_5$*cis*N_5	18.0	1.78	18.9	−1.70	27.5	1.99	27.5	0.40
	(18.2)[b]	(1.92)	(18.7)	(−2.50)	(27.2)	(2.05)	(27.2)	(0.96)
	20.2	1.83	21.5	0.60				
	(20.0)	(1.92)	(21.8)	(0.80)				
L-*cisO*$_5$*trans*N_5	17.2	1.78	17.2	1.55	*ca.* 28	2.15	27.2	0.45
	(16.7)	(1.44)	(17.5)	(2.28)	(27.2)	(1.99)	(26.8)	(0.33)
	20.4	1.78	21.5	−0.50				
	(20.4)	(1.97)	(19.8)	(−0.20)				
L-*fac*	19.5	2.12	18.2	1.20	*ca.* 27	2.05	27.6	−0.53
	(19.3)	(2.23)	(18.2)	(1.48)	(27.3)	(1.90)	(*ca.* 27)	(−0.11)
			20.6	−0.90				
			(20.6)	(−0.56)				
D-*cisO*$_5$*cis*N_5	18.2	1.85	18.4	−1.45	27.5	2.01	26.5	0.25
	(18.3)	(1.75)	(18.4)	(−2.80)	(27.3)	(1.88)	(27.8)	(0.80)
	21.2	1.65	21.2	0.95				
	(20.8)	(1.55)	(21.3)	(1.08)				
D-*transO*$_5$*trans*N_5	17.0	1.20	19.9	1.50	27.5	2.00	27.7	0.55
	(16.8)	(1.38)	(16.7)	(2.75)	(27.4)	(1.73)	(28.0)	(0.26)
	20.8	1.68	20.3	−1.55				
	(20.5)	(1.75)	(19.5)	(−2.25)			(24.8)	(0.10)
D-*fac*	19.5	2.20	18.4	0.90	27.5	2.02	27.4	−0.45
	(19.3)	(2.13)	(16.7)	(0.10)	(27.2)	(1.95)	(28.0)	(−0.20)
			20.6	−0.55				
			(19.8)	(−0.40)				

a) Wave numbers are given in 10^3 cm^{-1}.
b) The figures in the parentheses denote the data for [Co(L- or D-asp)(L-2,4-dba)].

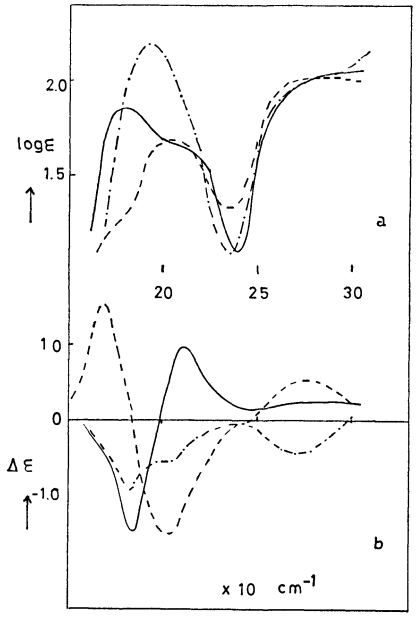

Fig. 3. Absorption (upper) and CD (lower) spectra of [Co(D-asp)(L-his)]. I1 (——), I2 (----), and I3 (———).

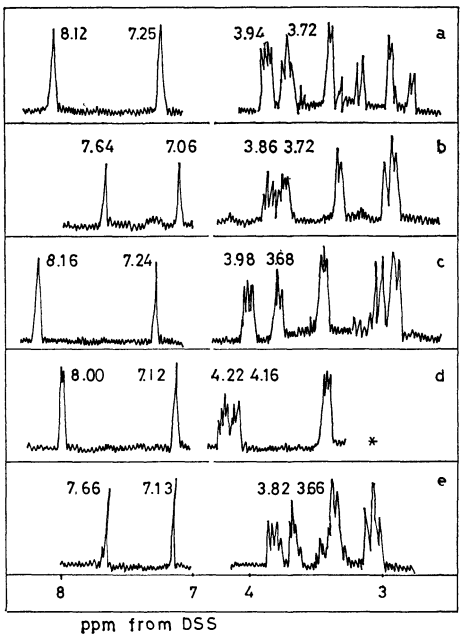

Fig. 4. PMR spectra of a; H1, b; H3, c; I1, d; I2, and e; I3.

dba)] complex decreases the magnitude of the CD peaks of the four mer isomers in the first absorption band region. It is interesting that the CD spectrum for the H1 isomer resembles that for the I1 isomer in spite of the coordination of the enantiomeric ligand.

PMR Spectra. Figure 4 shows the PMR spectra of the five isomers. The spectrum of I2 could not be obtained because of its low solubility. The L-his has the patterns of ABX and AX and the L- or D-asp that of AX only. The peaks near δ 8.0 ppm for the five PMR spectra are ascribed to the 2-protons of imidazole and the peaks near δ 7 ppm to the 5-protons of imidazole having a higher electronegativity than that for the 2-proton. The peaks at *ca.* 3.4 ppm are due to the methylene protons of asp and the peaks higher than those to the methylene protons of L-his. The peaks at *ca.* δ 4.2—3.6 ppm are assigned to those of the methine protons for L-his and L- or D-asp. The distribution of all the peaks for the five isomers agree with the prediction based on the empirical rule as developed by the authors.[2] Consequently H1, H2, and H3 were assigned as *trans*O_5*cis*N_5, *cis*O_5*trans*N_5, and L-*fac*, and I1, I2, and I3 as *cis*O_5*cis*N_5, *trans*O_5*trans*N_5, and *D-fac*, respectively.

Isomerization of the Isomers of [*Co*(L- *or* D-*asp*)(L-*his*)]. All the isomers of [Co(L- or D-asp)(L-his)] isomerized in water without any catalyst. Figure 5 shows a series of chromatograms corresponding to the change in concentration of each isomer due to the isomerization of H3. Each isomer can be separated from the mixture by high speed liquid chromatography. The TSK-212 resin is eminently suitable for the separation of the isomers of a complex with no charge. Since no concentration loss of the complex due to other reactions was found within experimental error, it was possible to treat the concentration of the complex as constant throughout the experiment and so network analysis[3] is available for this reaction. The system of differrential equations representing the behavior of the system is shown as follows:

$$da_1/dt = -(k_{12}+k_{13})a_1 + k_{21}a_2 + k_{31}a_3,$$
$$da_2/dt = k_{12}a_1 - (k_{23}+k_{21})a_2 + k_{32}a_3,$$
$$da_3/dt = k_{13}a_1 + k_{23}a_2 - (k_{31}+k_{32})a_3,$$

where a_1, a_2, and a_3 are the molar fractions of H1(I1), H2(I2), and H3(I3), respectively. The rate constant of the reaction, for which the notation of the Hi(Ii)-(i=1,2,3) isomer is transformed into Hj(Ij), is represented by k_{ij}. This analysis was applicable for obtaining the relative value of the rate constant (k_{ij}'). In order to obtain absolute values (k_{ij}), the relative rate constans are substituted in a certain differential equation, for example,

$$da_2/dt = k[k_{12}'a_1-(k_{23}'+k_{21}')a_2+k_{32}'a_3],$$

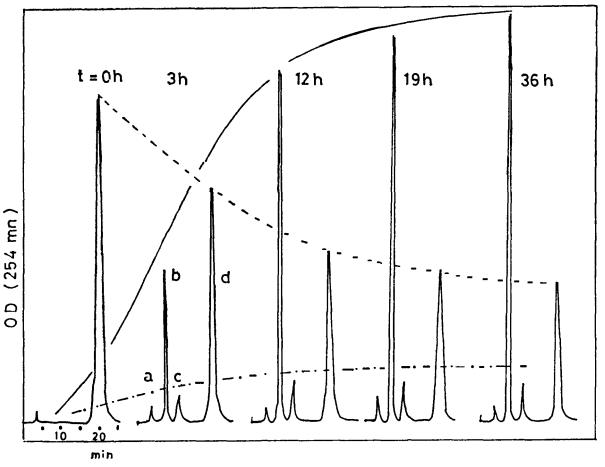

Fig. 5. High speed liquid chromatograms indicating the isomerization of the H2 isomer. a: Marker, b: H1(I1), c: H2(I1), and d: H3(I3).

where k is the ratio (k_{12}/k_{12}'). All the k_{ij} of Hi and Ii systems are shown in Fig. 6. In the case of the Hi system, the values of the rate constants decrease in the order $k_{23}>k_{31},k_{13},k_{21}>k_{12},k_{32}$. Figure 7 shows the experimentally observed compositions for isomerization. The molar fractions at equilibrium are as follows; H1(0.53), H2(0.06), and H3(0.41). The free energy differences at 25 °C are as follows: $\Delta G_{12}=G(\mathrm{H1})-G(\mathrm{H2})=-RT\ln(53/6)=-5.40$ kJ/mol and $\Delta G_{23}=RT\ln(41/6)=4.76$ kJ/mol. In case of the Ii system, the values of the rate constants decrease in the order $k_{23}\gg k_{13},k_{31}>k_{21},k_{32}>k_{12}$. This order closely resembles

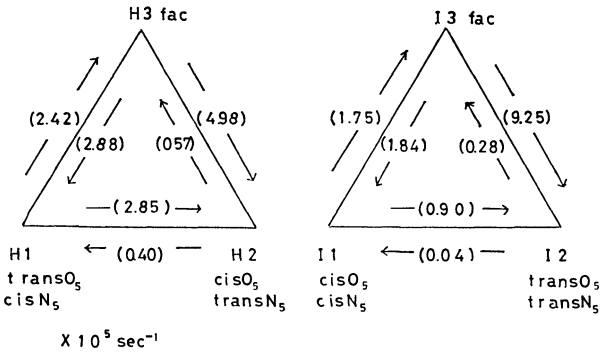

Fig. 6. Rate constants of the isomerization at 80 °C.

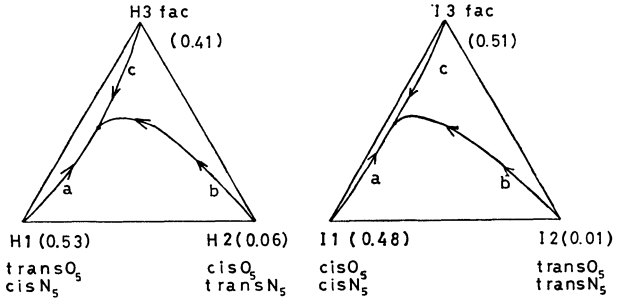

Fig. 7. Experimentally observed compositions for the isomerization at 80 °C. a: From H1(I1), b: from H2(I2), and c: from H3(I3).

the Hi system. The molar fractions at equilibrium are as follows: I1(0.48), I2(0.01), and I3(0.51). The free energy differences at 25 °C are as follows: $\Delta G_{12}'=G'(\mathrm{I1})-G'(\mathrm{I2})=-RT\ln(0.48/0.01)=-9.74$ kJ/mol and $\Delta G_{23}'=RT\ln(0.51/0.01)=9.74$ kJ/mol. In both systems each isomer may have only a little steric hindrance and hydrogen bonding between the coordinated his and asp. The fact that the molar fractions are in the order *trans*O_5*cis*N_5>L-*fac*≫*cis*O_5*trans*N_5 for [Co(L-asp)(L-his)], and D-*fac*≈*cis*O_5*cis*N_5≫*trans*O_5-*trans*N_5 for [Co(D-asp)(L-his)] suggests the existance of a common effect determing the molar fractions. Firstly the *trans*N_5 isomers must be less stable than the *cis*N_5 isomers in both systems and secondly the *trans*O_5 isomers are a little less stable than the *cis*O_5 isomers between mer isomers. In the case of the iosmerization of [Co(D-asp)(L-2,4-dba)], the molar fraction of the *trans*O_5*trans*N_5 isomer at equilibrium was the smallest of the three, although the molar distribution for the fac isomer was smaller than that for *cis*O_5*cis*N_5 (*cis*O_5*cis*N_5, *trans*O_5*trans*N_5, *fac*=0.68, 0.11, 0.21).[1] Recently, investigations of the *trans* effect for the cobalt(III) complex containing S-bonded sulfite ligands have been reported.[4] In cobalt(III) chemistry, S-bonded sulfite produces a specific and dramatic labilization of the ligands situated in the *trans* position. This electronic effect which is transmitted through the bonds may apply in this our study, *i.e.* it is suggested that the two α-nitrogen atoms avoid the *trans* position around a Co(III).

References

1) M. Watabe, S. Kawai, and S. Yoshikawa, *Bull. Chem. Soc. Jpn.*, **49**, 1845 (1976).
2) M. Watabe, K. Onuki, and S. Yoshikawa, *Bull. Chem. Soc. Jpn.*, **48**, 687 (1975).
3) M. Boudart, "Kinetics of Chemical Processes," Prentice Hall, Inc., Englewood Cliffs, New Jersey (1968).
4) a) J. E. Byrd and W. K. Wilmarch, *Inorg. Chim. Acta Rev.*, **5**, 7 (1975); b) J. M. Palmer and E. Deutsch, *Inorg. Chem.*, **14**, 17 (1975).

Chemical Ionization Mass Spectrometry of Alkyl Nitrates and Nitrites†

Rebati C. Das,†† Osamu Koga, and Shin Suzuki*

Department of Synthetic Chemistry, Faculty of Engineering, Chiba University, Yayoi-cho, Chiba 260

(Received May 23, 1978)

The mass spectrometry of alkyl nitrites and alkyl nitrates with chemical ionization using methane and isobutane as reagent gases produces quasi-molecular ions, $(M+1)^+$ and/or $(M-1)^+$. These ions have maximum abundance for lower nitrates and nitrites. The chemical ionization mass spectrometry, in conjunction with gas chromatography, can be used for quantitative estimation of alkyl nitrates and nitrites in very low amounts.

The behaviors of nitrogeneous compounds formed in the photochemical reactions of NO_x–hydrocarbon–O_2 system in the atmospheric smog as well as in the chamber model have recently gained much interest.[1-3] Unfortunately, all compounds have not been completely and unequivocally identified.[1-3] Alkyl nitrates and nitrites, present in the above system, have been analyzed in low quantities by GC method using ECD detector,[4] but many other compounds *e.g.* chloride interfere in the method. Independent confirmation is, therefore, necessary. Mass spectrometry is a very convenient method of analysis but conventional electron impact ionization (EI)method is not always suitable due to easy fragmentation of unstable compounds by electron beams producing structurally insignificant low mass fragments. Chemical ionization (CI) mass spectrometry, recently developed,[5] has been used to obtain quasi-molecular peaks [$m/e=(M+1)$ or $(M-1)$] of many organic compounds of high abundance, thus making their identification more confirmatory.

This paper reports our results on the CI mass spectrometry of alkyl nitrates and nitrites as a part of our overall program of complete identification and analysis of all the products formed in the NO_x–hydrocarbon–O_2 system.

Experimental

A Shimadzu GC-MS apparatus was used. Mostly commercially available alkyl nitrates and nitrites were used. Ethyl nitrate, pentyl and isopentyl nitrate (Tokyo Kasei Kogyo) were directly used after having checked their purity chromatographically. All other compounds were separated from the constituents present with them in the GC column consisting of PEG 400 at room temperature using helium as carrier gas (flow rate 8—11 ml/min) before introduction to the ionization chamber. Ethanolic solutions of ethyl nitrite (Wako), pentyl and isopentyl nitrite (Tokyo Kasei Kogyo) were used. Ethyl nitrite being a gas at room temperature is market as solution in ethanol. Pentyl and isopentyl nitrite are market in the mixed form. Methyl nitrate is not commercially available. It was prepared by gas phase photolysis of ethyl nitrite-O_2 system[6] and separated from other products in the above manner.

Results and Discussion

Figures 1 to 8 give the EI and CI mass spectral patterns of some common alkyl nitrates and nitrites.

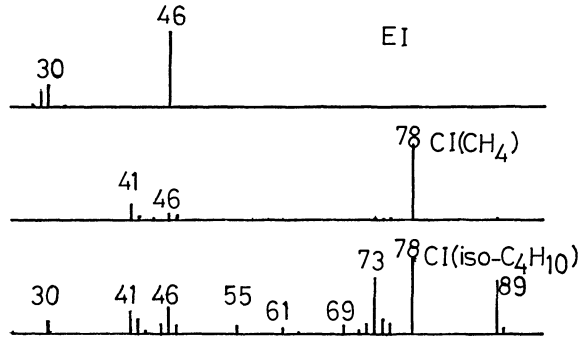

Fig. 1. Mass spectra of methyl nitrate (MW 77).

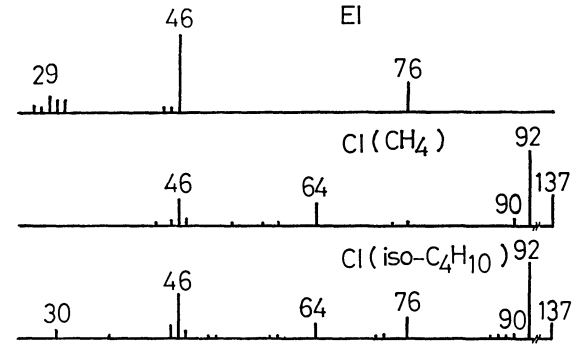

Fig. 2. Mass spectra of ethyl nitrate (MW 91).

The CI patterns are for CH_4 and i-C_4H_{10} as reagent gases. The conditions of the mass spectra presented in Figs. 1 to 8 are as follows. EI spectrum: Ion-source temperature 170 °C, Electron energy 70 eV, Pressure††† 7×10^{-7} Torr. CI(CH_4) spectrum: Ion-source temperature 170 °C, Electron energy 500 eV, Pressure††† 3×10^{-5} Torr. CI(i-C_4H_{10}) spectrum: Ion-source temperature 170 °C, Electron energy 500 eV, Pressure††† 0.75×10^{-5} Torr.

The main reactant ions are known to be CH_5^+ and $C_2H_5^+$ when methane is used as the reagent gas.[5] Similarly with i-C_4H_{10} as the reagent gas, t-$C_4H_9^+$ is the main reactant ion.[5,7] The proton and hydride transfer reactions of these ions are important for analytical purpose, because they generate the quasi-molecular $(M+1)^+$ and $(M-1)^+$ ions respectively.

† Presented at the 37th National Meeting of the Chemical Society of Japan, Yokohama, April 1978.

†† Present address: Department of Chemistry, University College of Engineering, Burla, Orissa, India.

††† Pressure is monitored between the ionization chamber and the vacuum pump in the apparatus. This pressure relates only to the reagent gas pressure.

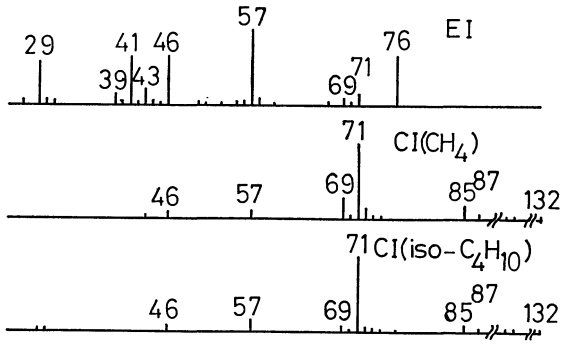

Fig. 3. Mass spectra of pentyl nitrate (MW 133).

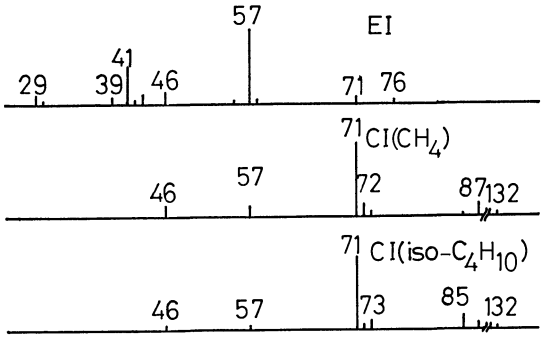

Fig. 4. Mass spectra of isopentyl nitrate (MW 133).

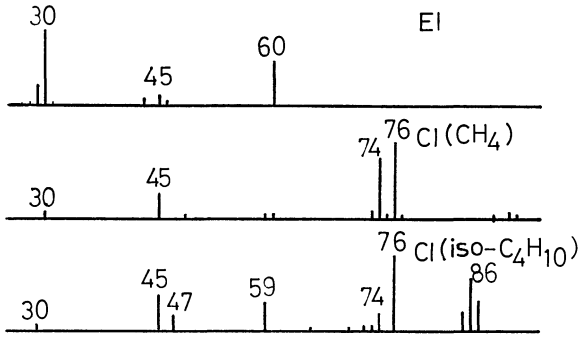

Fig. 5. Mass spectra of ethyl nitrite (MW 75).

$$RH + CH_5^+/C_2H_5^+/t\text{-}C_4H_9^+ \longrightarrow RH_2^+ + CH_4/C_2H_4/C_4H_8 \quad (1)$$

$$RH + C_2H_5^+/t\text{-}C_4H_9^+ \longrightarrow R^+ + C_2H_6/C_4H_{10} \quad (2)$$

A perusal of the figures shows that the mass spectral patterns obtained with CH_4 as the reagent gas are generally simpler (less fragments) and therefore, CH_4 is more suitable for the identification and analysis of alkyl nitrates and nitrites by CI mass spectrometry.

Almost all the compounds produce $(M+1)^+$ ion, but only in the lower homologues of nitrates and nitrites(with 1 and 2 C-atoms), it is the most abundant one. There may be two reasons for this *viz.*(i) with the increase of chain length of the molecule, the bond energy decreases causing easy fragmentation of the quasi-molecular ion and (ii) Reaction 1 producing $(M+1)^+$ ion may be sufficiently exothermic in higher homologues to exceed the bond dissociation energies. The latter explanation is more reasonable, because the decrease of bond dissociation energy from 1-C to 5-C compounds is not likely to be high.[8] Thus, the proton

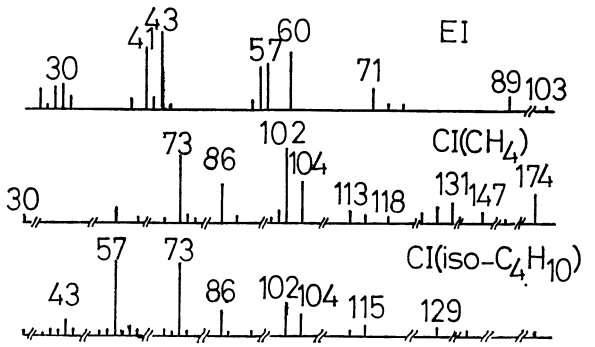

Fig. 6. Mass spectra of butyl nitrite (MW 103).

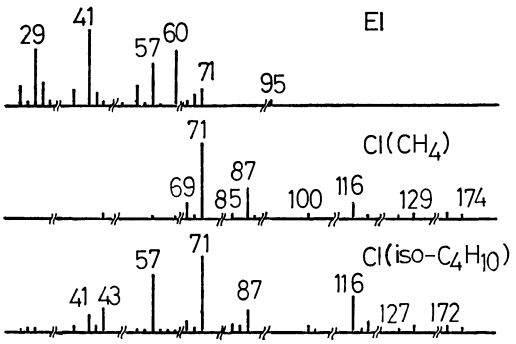

Fig. 7. Mass spectra of pentyl nitrite (MW 117).

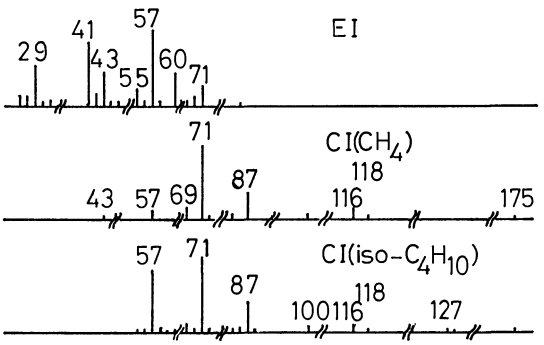

Fig. 8. Mass spectra of isopenthyl nitrite (MW 117).

affinity of ethyl nitrates and nitrites may be higher for higher homologues, because heat of Reaction 1 is given by the following equation.[7]

$$\Delta H_1 = PA(CH_4/C_2H_4/C_4H_8) - PA(RH) \quad (3)$$

(PA stands for proton affinity)

The $(M-1)^+$ ions generally do not have high abundance. It is also observed with our limited data that these ions are present in relatively greater abundance in the nitrite spectra than in the corresponding nitrate spectra with any particular reagent gas.

The EI spectra of the compounds reported in this paper are consistent with those documented in the literature.[9,10] Two characteristic ions present in the EI spectra of the nitrates are, NO_2^+ (m/e=46) and $CH_2ONO_2^+$ (m/e=76).‡[,10] The corresponding ions,

‡ Present in normal-type alkyl nitrates and nitrites except in CH_3ONO_2 and CH_3ONO.

NO^+(m/e=30) and CH_2ONO^+ (m/e=60)‡ are also present in the EI spectra of the nitrite esters. In addition to the above characteristic ions, many fragments from the alkyl carbon chain are also present. In higher homologues of the nitrate and nitrite compounds, these mass fragments from the carbon chain have relatively high abundance. Details of the EI spectra are not intended to be discussed in this paper.

Influence of Temperature and Pressure. The influence of temperature and pressure on the CI mass spectral pattern was studied in detail with ethyl nitrate as the substrate. Figure 9 shows the fraction of the relative abundance of the main ion (m/e=92) *vs.* temperature of the ionization chamber and pressure. It can be seen that the quasi-molecular ion has got maximum abundance at low temperature (170 °C) and pressure of $\approx 3\times10^{-5}$ Torr and $\approx 0.8\times10^{-5}$ Torr respectively for CH_4 and i-C_4H_{10} as reagent gases. The CI mass spectral patterns presented in this paper have, therefore, been taken at 170 °C and the above mentioned pressures.

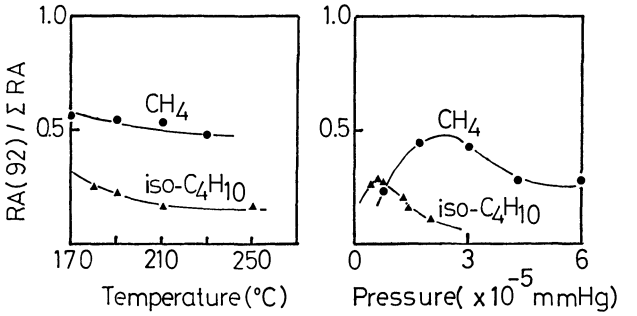

Fig. 9. Pressure and temperature dependence of mass fragments of ethyl nitrate.

Identification of Major Fragmentation Products. Complete identification of all fragments could not be made and is difficult. However, some speculations may be useful.

Methyl Nitrate (MW 77)(Fig. 1). $(M+1)^+$ is the ion with maximum abundance. Other major ions present are m/e=41, 46 (NO_2^+), and 47(NO_2H^+) for CH_4 as reagent gas and m/e=30 (NO^+), 41, 42, 45 (CH_3ON^+), 46 (NO_2^+), 47 (NO_2H^+), 55, 61 (CH_3ONO^+), 69, 72, 73 ($C_4H_9O^+$), 74, 75, and 89($C_4H_9O_2^+$) for i-C_4H_{10} as reagent gas. m/e=73 and 89 ions may be formed by the separation of CH_3ONO (m=61) and CH_3ON (m=45) groups from the cluster ion, $(RH+C_4H_9)^+$. Such cluster ions are very common in CI mass spectra with i-C_4H_{10}.[11] Unfortunately there are many unassigned ions, but only m/e=41 ion has relatively high abundance.

Ethyl Nitrate (MW 91)(Fig. 2). As in the case of methyl nitrate, the $(M+1)^+$ ion has maximum abundance. Other ions present are m/e=30 (NO^+), 45 ($C_2H_5O^+$), 46 (NO_2^+), 47 (NO_2H^+), 64 ($H_2NO_3^+$), 76 ($CH_2ONO_2^+$), and 137. The m/e=64 ion may be formed by the reaction between the reactant ions and RH or RH_2^+ by intramolecular rearrangement and fragmentation. The m/e=137 ion may also be speculated as $[(2M+1)-NO_2]^+$ ion, derived from $(2M+1)^+$ ion very often seen in the CI spectra.

Pentyl and Isopentyl Nitrate (MW 133)(Figs. 3 and 4). Quasi-molecular $(M-1)^+$ ion is present in very low abundance. $(M+1)^+$ ion has still less abundance. The base peak is due to $C_5H_{11}^+$ (m/e=71). Other ions produced in significant amounts are m/e=46 (NO_2^+), 57 ($C_4H_9^+$), 69 ($C_5H_9^+$), 72 ($C_5H_{12}^+$/$C_4H_8O^+$), 73 ($C_4H_9O^+$), 85 ($C_5H_9O^+$), and 87 ($C_5H_{11}O^+$).

Ethyl Nitrite (MW 75)(Fig. 5). As in the case of ethyl nitrate, $(M+1)^+$ ion has got maximum abundance. The $(M+1)^+$ peak is more prominent in this compound than in ethyl nitrate. The other major ions are m/e=30 (NO^+), 45 ($C_2H_5O^+$), 47 (NO_2H^+), 59 ($C_2H_5ON^+$), 85 ($C_6H_{13}^+$), 86 ($C_6H_{14}^+$), and 87 ($C_4H_9ON^+$). The last three ions are seen mainly in the i-C_4H_{10} spectrum. They may be formed by the separation of NO_2H (m=47), NO_2(m=46), and C_2H_5O (m=45) groups respectively from the cluster ion $(RH+C_4H_9)^+$.

Butyl Nitrite (MW 103)(Fig. 6). Quasi-molecular $(M-1)^+$ and $(M+1)^+$ ions are present in fairly good abundance. In the CH_4-spectrum, the former is the base peak. Other major ions present are m/e=30 (NO^+), 43 ($C_3H_7^+$), 57 ($C_4H_9^+$), 73 ($C_4H_9O^+$), 86 ($C_4H_8ON^+$), 88 ($C_3H_6ONO^+$), 113, 115, 118, 129, 131, 147, and 174. The last seven ions are obviously cluster ions whose origins are difficult to speculate. However, except m/e=131 and 174 ions, all of them are present in relatively low abundance.

Pentyl and Isopentyl Nitrite (MW 117)(Figs. 7 and 8). Both $(M+1)^+$ and $(M-1)^+$ ions are present in low abundance, but the latter ion has comparatively greater abundance. Other major ions present are, m/e=41 ($C_3H_5^+$), 43 ($C_3H_7^+$), 57 ($C_4H_9^+$), 69 ($C_5H_9^+$), 71 ($C_5H_{11}^+$), 85 ($C_5H_9O^+$), 86 ($C_4H_8ON^+$), 87 ($C_5H_{11}O^+$), and 100 ($C_5H_{10}ON^+$). Many cluster ions are also formed in very low abundance.

Quantitative Analysis by Mass Fragmentography. To study the possibility of quantitative analysis of alkyl nitrates and nitrites in trace amounts by CI mass spectrometry, mass fragmentography was attempted. This was measured at m/e=76 and 92 respectively for ethyl nitrite and ethyl nitrate using CH_4 as the reagent gas. PEG 400 at room temperature was used as the column material. It has earlier been successfully used for the separation of many organic materials, including PAN, in the atmospheric smog.[12] This

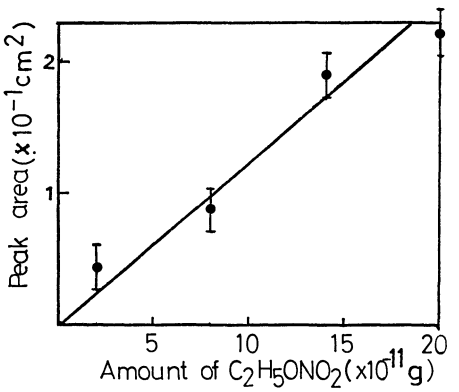

Fig. 10. Calibration curve for the analysis of ethyl nitrate by GC-CI-MF.

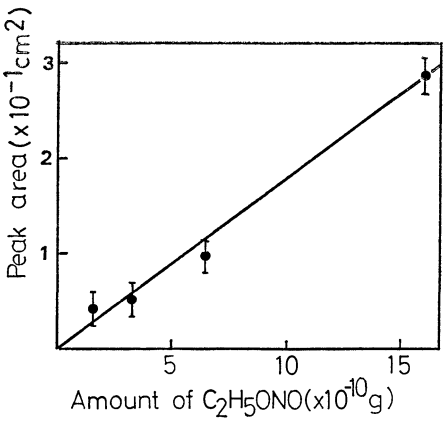

Fig. 11. Calibration curve for the analysis of ethyl nitrite by GC-CI-MF.

also has been used to separate different alkyl nitrates of low molecular weights from one another.[12] Helium was used as the carrier gas (flow rate 8—11ml/min). Standard solutions of the compounds in ethanol, in which they are stable, were injected into the column of the GC-MS apparatus and mass fragmentograms taken at appropriate GC peaks and mass numbers. The above column material could adequately separate the compounds from ethanol.

Figures 10 and 11 show the calibration curves (peak area of mass fragmentogram *vs.* amount of the compound injected into the column) at the lowest possible limits for both ethyl nitrate and ethyl nitrite respectively to give an idea about the sensitivity of the method. Qualitative detection is possible at still lower amounts of the samples (picogramme level). Quantitative analysis at picogramme level was not successful presumably due to adsorption of the samples on the glass surface of the syringe. A better sampling technique may improve the sensitivity limit.

The authors are grateful to the Japan Society for the Promotion of Science (JSPS) for award of a Senior Co-operative Fellowship to one of them (RCD). Also they wish to thank the Ministry of Education of the Government of Japan for supporting this research from the Fund for Environmental studies.

References

1) K. L. Demrjian, J. A. Kerr, and J. G. Calvert, "Advances in Environmental Science and Technology," ed by J. N. Pitts, Jr., R. I. Metcalf, and A. Leoyd., John Wiley and Sons (1974), Vol. IV, p. 1.

2) A. P. Altshuller and J. J. Bufalini, *Environ. Sci. Technol.*, **5**, 39 (1971).

3) A. P. Altshuller and J. J. Bufalini, *Photochem. Photobiol.*, **4**, 97 (1965).

4) T. Kato, "Gas-chromatographic Techniques in Air Pollution," (in Japanese), Sankyo Co., Ltd. (1975), p. 169.

5) M. S. B. Munson and F. H. Field, *J. Am. Chem. Soc.*, **88**, 2621 (1966).

6) E. R. Stephens and M. A. Price, *J. Chem. Educ.*, **50**, 351 (1973).

7) B. Munson, *Anal. Chem.*, **43**, 28A (1971).

8) S. L. Murov, 'Handbook of Photochemistry," M. Dekker Inc. (1973), p. 79.

9) "Atlas of Mass Spectral Data," ed by E. Stenhagen. S. Abrahamsson, and F. W. McLafferty, Interscience Publ, (1969), Vol. I, pp. 97, 184, 292, 443, and 646.

10) R. T. M. Fraser and N. C. Paul, *J. Chem. Soc., B*, **1969**, 659.

11) F. Field, *J. Am. Chem. Soc.*, **91**, 2827 (1969).

12) S. Izumikawa, M. Hoyahuku, K. Nakano, K. Asakuno, and T. Ohdaira, *Ann. Rep. of the Tokyo Metropolitan Res. Inst. for Environ. Protection*, **4**, 41 (1973).

The Rates of the Hydrogenation of the Coordinated Styrene and Acrylonitrile in a Rhodium-Olefin Complex [$RhClH_2(ol)(PPh_3)_2$]

Yoshimi OHTANI, Akihiko YAMAGISHI, and Masatoshi FUJIMOTO*

Department of Chemistry, Faculty of Science, Hokkaido University, Sapporo 060

(Received July 21, 1978)

Kinetics of the hydrogenation of coordinated styrene and acrylonitrile in a rhodium-olefin complex $RhClH_2(ol)(PPh_3)_2$ (ol=styrene or acrylonitrile) was studied by stopped-flow method and by the direct measurements of hydrogen-gas uptake. The equilibrium constant of the reaction $RhCl(ol)(PPh_3)_2+H_2 \rightleftharpoons RhClH_2(ol)(PPh_3)_2$, K_{34}, and the rate of the hydrogenation of the olefin in the complex $RhClH_2(ol)(PPh_3)_2$, k_{45}, were determined to be 3.2×10^3 mol^{-1} dm^3 and 2.7 s^{-1} for styrene, and 3.5×10^2 mol^{-1} dm^3 and 0.50 s^{-1} for acrylonitrile, respectively. The differences in the values for these two olefins were discussed. The data for cyclohexene were also briefly mentioned.

The catalysis of the homogeneous hydrogenation of olefins by Wilkinson's complex $RhCl(PPh_3)_3$ has been the main subject of many investigations on the homogeneous catalyses by transition metals.[1] In recent years the detailed reaction mechanism of this system has been revealed by studying independently the individual step of the complex formation processes.[2–5] However, in most investigations concerning hydrogenation of olefins, only the overall rate of the catalytic reaction has been reported.[6–8] Since the discussions based only on the observed rate constants of the overall reaction sometimes leave significant ambiguities, we need to elucidate the detailed mechanism involving the behavior of the catalytically active intermediate species by distinguishing the information on the intermediate species from those on the overall reaction.

Though no direct evidence was reported so far, the catalytic hydrogenation of olefins is believed to proceed in the molecule of an intermediate dihydrido-olefin complex, $RhClH_2(ol)(PPh_3)_2$ (ol=olefin), the rate-determining step being suggested to be the insertion of the coordinated olefin into an Rh–H bond to yield an alkyl complex (Scheme 1).[5,9] Thus the direct measurements of the step of production of an alkane from the intermediate dihydrido-olefin complex $RhClH_2(ol)(PPh_3)_2$ would be desired.

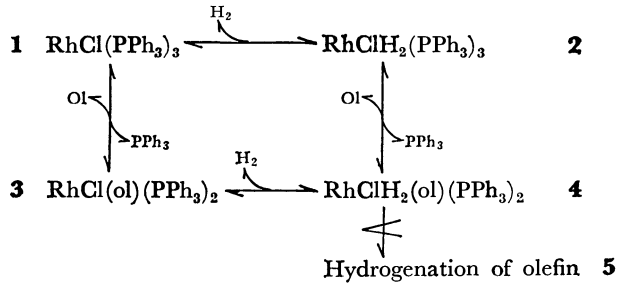

Scheme 1.

Recently Halpern *et al.* reported the value of k_{45} for cyclohexene as an olefin measured in the presence of a large excess of the free ligand PPh_3.[9,10] Since the predominant species involved under this condition are **1** and **2**, they did not observe directly the process **4**→**5**. The value estimated by them from the small intercept, however, can include a serious error. The value obtained by them ($k_{45}=0.20\pm0.04$ s^{-1}, at 25 °C) seems to be too small (*vide infra*).

In the previous paper on the catalytic hydrogenation of acrylonitrile, we confirmed the formation of $RhClH_2(ac)(PPh_3)_2$ (ac=acrylonitrile) in the absence of free PPh_3 added, and evaluated the value of k_{45}.[11,12] However, for the value of K_{34} only the lower limit could be determined by the stopped-flow measurements, giving consequently only an upper limit for the value of k_{45}.

In the present study, we adopted styrene as an olefin having a much lower coordinating ability than acrylonitrile. The values of K_{34} and k_{45} were determined by the stopped-flow method and the direct measurements of the hydrogen-gas uptake. The corresponding values for acrylonitrile, which had been estimated only from the stopped-flow method,[11] were also re-examined by the direct measurements of the uptake of hydrogen gas.

Experimental

Chlorotris(triphenylphosphine)rhodium(I) and chloro(ethylene)bis(triphenylphosphine)rhodium(I) were prepared according to Osborn *et al.*[6] Triphenylphosphine was recrystallized from ethanol. Benzene was distilled. Acrylonitrile and styrene were distilled under reduced pressure and used within a day. Commercial hydrogen and nitrogen were used without further purification. The concentration and the purity of hydrogen were determined by gas chromatography through Molecular sieve 5A.

All measurements were carried out at 20±1 °C in oxygen-free benzene. A solution of $RhCl(ol)(PPh_3)_2$ was prepared by dissolving $RhCl(C_2H_4)(PPh_3)_2$ in benzene containing styrene or acrylonitrile, and by removing the dissociated ethylene. The coordinated ethylene was easily replaced by the olefin, leaving a pure $RhCl(ol)(PPh_3)_2$ in benzene. The resultant solution was confirmed to contain no free PPh_3.[11]

The equilibria of the reaction were measured at 450 nm under an anaerobic condition with a Hitachi EPS-3T spectrophotometer or a Union Giken RA-1300 stopped-flow apparatus. The rates of the hydrogenation of olefins were measured by the uptake of hydrogen-gas as described previously.[11]

Results and Discussion

Styrene. Equilibria: The mechanism shown in Scheme 1 is proposed for the hydrogenation of olefins.[11] The steps of the complex formations are assumed to be in pre-equilibria. The hydrogenation of the

coordinated olefin is the rate-determining.[5,9] The equilibrium constant for each step of the complex formations was obtained separately from the equilibrium measurements.

The value of K_{13} was obtained from the measurements carried out by the addition of the solution of PPh_3 little by little to the solution of $RhCl(st)L_2$ (st=styrene and L=PPh_3) containing no free ligand PPh_3. Figure 1 shows the dependence of the absorbance of the solution on the concentration of added PPh_3. The solid curve reproduced with the value $K_{13}=2.4\times10^{-4}$ agrees well with the experimental values.

When a benzene solution containing hydrogen was rapidly mixed with the solution of $RhCl(st)L_2$ by stopped-flow technique under the condition of $[Rh]<[H_2]_0\ll[St]$, the stepwise changes in the absorbance at 450 nm were observed. First, a rapid exponential decrease in absorbance owing to the formation of $RhClH_2(st)L_2$ was observed. The signal terminated within 0.1 s. Then the absorbance slowly increased as the hydrogen in the solution was consumed for the hydrogenation of the styrene.[11] After 20 s the absorbance was again increased to the initial value, showing the consumption of all hydrogen molecule and the reproduction of $RhCl(st)L_2$. Figure 2 shows the dependence on the concentration of hydrogen of the decrease in absorbance in the first step. The value of K_{34} was calculated from the change in absorbance. In order to ascertain the validity of the values obtained above, we compared these values with those obtained from the direct measurements of the hydrogen-gas uptake. The curve in Fig. 2 is reproduced using the value of $K_{34}=3.2\times10^3$ mol^{-1} dm^3 evaluated from the measurements of the hydrogen-gas uptake, showing a good agreement with the results of the stopped-flow measurements.

The value of K_{12} was estimated to be 2.1×10^4 mol^{-1} dm^3.[13] Thus, from the relationship $K_{24}=K_{13}K_{34}/K_{12}$ the value of K_{24} was calculated to be 3.7×10^{-5}.

Hydrogen-gas Uptake:[11] The rate of the hydrogenation of styrene was directly measured by the hydrogen-gas uptake at 1 atm hydrogen. Figure 3 shows the rate constants observed at various concentrations of added PPh_3. From the results, the values of K_{34} and k_{45} can be estimated by the curve-fitting method.

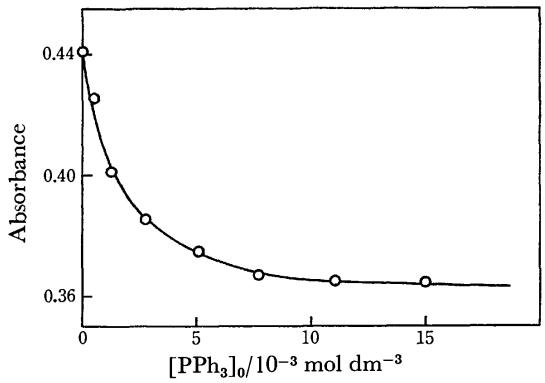

Fig. 1. The dependence of the absorbance of the $RhCl(st)(PPh_3)_2$ solution on the concentration of PPh_3 added. $[RhCl(st)(PPh_3)_2]_0=2.6\times10^{-4}$ mol dm^{-3}, at 450 nm, and 20 °C. The solid curve in the figure is reproduced with the value $K_{13}=2.4\times10^{-4}$.

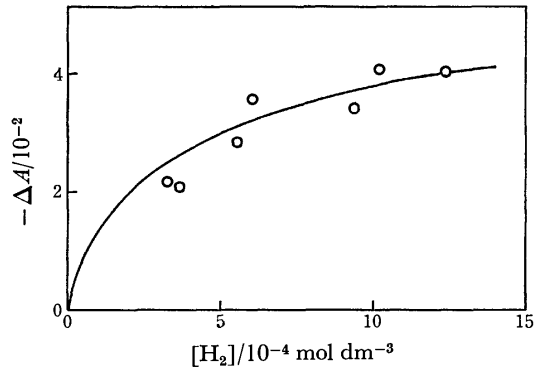

Fig. 2. The dependence of the absorbance decrease on the concentration of hydrogen in the reaction of $RhCl(st)(PPh_3)_2$ with hydrogen. The solid line in the figure is reproduced using the value $K_{34}=3.2\times10^3$ mol^{-1} dm^3, which is obtained from the measurements of hydrogen-gas uptake.

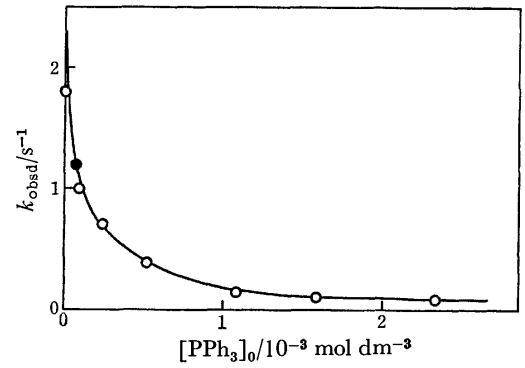

Fig. 3. The plot of the observed rate constant k_{obsd} for the hydrogenation of styrene *vs.* the concentration of PPh_3 added. The initial rates of the hydrogen-gas uptake were measured. $[Rh]_0=6.4\times10^{-5}$ (1.3×10^{-6} mol), [St]=2.6, and $[H_2]=2.8\times10^{-3}$ mol dm^{-3}. ●; $RhCl(PPh_3)_3$ without adding PPh_3. The solid line in the figure is reproduced using $K_{34}=3.2\times10^3$ mol^{-1} dm^3 and $k_{45}=2.7$ s^{-1}.

According to Scheme 1, the observed overall rate constant is expressed by

$$k_{obsd}=k_{45}\frac{[RhClH_2(st)L_2]}{[Rh]_t}, \quad (1)$$

where $[Rh]_t$ denotes the total concentration of rhodium species. Since the value of $[RhClL_3]$ is about 1/60 of $[RhClH_2L_3]$ at 1 atm hydrogen, as calculated from the value $K_{12}=[RhClH_2L_3]/[RhClL_3][H_2]=2.1\times10^4$ mol^{-1} dm^3, the contribution of $RhClL_3$ can be neglected. Therefore, $[Rh]_t$ and the total concentration of added PPh_3, $[L]_0$, are approximated as follows:

$$[Rh]_t \simeq [RhClH_2L_3]+[RhCl(st)L_2]+[RhClH_2(st)L_2] \quad (2)$$

$$[L] \simeq [L]_0-[RhClH_2L_3] \quad (3)$$

The value of equilibrium constant K_{23} is calculated by

$$K_{23} = K_{13}/K_{12} = \frac{[RhCl(st)L_2][H_2][L]}{[RhClH_2L_3][St]}$$
$$= \frac{[RhCl(st)L_2][H_2]\{[L]_0 - [RhClH_2L_3]\}}{[RhClH_2L_3][St]} \quad (4)$$
$$= 1.2 \times 10^{-8} \text{ mol dm}^{-3}.$$

The concentrations of $RhClH_2(st)L_2$ are calculated from Eqs. 2 and 4 by estimating an adequate value for $K_{34}=[RhClH_2(st)L_2]/[RhCl(st)L_2][H_2]$. The value of k_{45} can be determined by introducing the calculated value of $[RhClH_2(st)L_2]$ into Eq. 1. A set of K_{34} and k_{45} used for the calculations, which fit well with the experimental values, is evaluated to be $K_{34}=3.2\times10^3$ mol^{-1} dm^3 and $k_{45}=2.7$ s^{-1}, giving the solid line depicted in Fig. 3. Disagreement of the values obtained under the condition without PPh_3 added may be caused by the partial decomposition of the bis(triphenylphosphine) complex.

The experiments at varying concentrations of styrene were not possible, since at lower concentrations the formation of the dimeric species could not be neglected, and at higher concentrations other unidentified species were formed.

The equilibrium constant K_6 in Eq. 6 was determined to be 5.5×10^{-4} mol^{-1} dm^3 from the measurements of the reaction varying amounts of styrene with the dimer.

$$(RhClL_2)_2 + 2St \overset{K_6}{\rightleftharpoons} 2RhCl(st)L_2 \quad (6)$$

$$2RhClL_3 \overset{K_7}{\rightleftharpoons} (RhClL_2)_2 + 2L \quad (7)$$

The value of K_{13} was determined also from K_6 and K_7[14] to be 2.2×10^{-4} based on the relationship $K_{13}=K_6^{1/2}K_7^{1/2}$. The value agrees well with that obtained above.

Acrylonitrile. *Hydrogen-gas Uptake*:[8] In the previous paper we reported the values, $K_{34}\geq150$ mol^{-1} dm^3 and $k_{45}\leq0.74$ s^{-1}. In the present study, the rate of the hydrogen-gas uptake was directly measured at various concentrations of acrylonitrile and added PPh_3 (Fig. 4). The values of K_{34} and k_{45} were calculated in a similar manner to the case of styrene, to be 350 mol^{-1} dm^3 and 0.50 s^{-1}, respectively, the value $K_{23}=K_{13}/K_{12}=0.22/(2.1\times10^4)=1.0\times10^{-5}$ being used. The solid line in Fig. 4 are reproduced using these values of K_{34} and k_{45}.

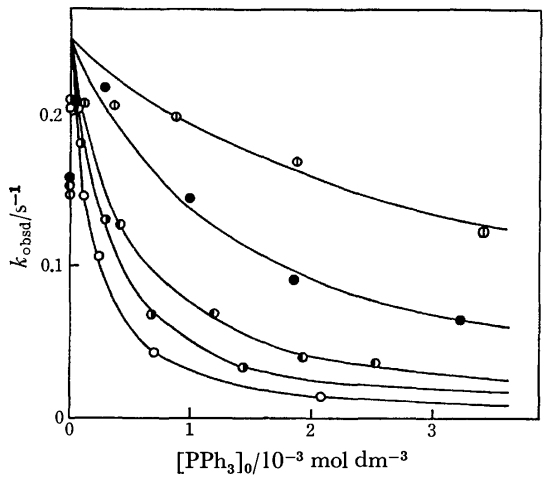

Fig. 4. The plot of the observed rate constant for the hydrogenation of acrylonitrile *vs.* the concentration of PPh_3 added. The initial rates of the hydrogen-gas uptake were measured. $[Rh]_0=1.5\times10^{-4}$ (2.9×10^{-6} mol), $[H_2]=2.8\times10^{-3}$, and [Ac]=○; 0.015, ◑; 0.031, ◐; 0.046, ●; 0.15, ⓘ; 0.46 mol dm^{-3}. The solid curves in the figure are reproduced using the values of $K_{34}=3.5\times10^2$ mol^{-1} dm^3 and $k_{45}=0.50$ s^{-1}.

Discrepancies in the data observed without PPh_3 added may be due to the dissociation of the coordinated ligand PPh_3, which causes the formation of some catalytically inactive species.

The distinct differences observed in the behavior of acrylonitrile and styrene are summarized as follows: Whereas the value of K_{13} for acrylonitrile is about 10^3 times as large as that for styrene, the values of K_{34} and k_{45} for styrene are by several times larger than those for acrylonitrile. These differences may be attributed to the difference in the coordinating properties of the two olefins having a cyano and a phenyl group as substituents. Acrylonitrile having a strong electron-withdrawal cyano group shows a large K_{13} because of the strong back-donation from the central rhodium atom. Therefore, the addition of hydrogen molecule to $RhCl(ac)L_2$ would become difficult, since the electron density on the central rhodium atom is decreased owing to the strong back-donation. The electron-releasing phenyl group in styrene would act oppositely.

Recently Halpern *et al.* reported the value of k_{45} for cyclohexene 0.20 ± 0.04 s^{-1} at 25 °C in the presence of a large excess of PPh_3. Although we intended also to obtain the value of k_{45} for cyclohexene without PPh_3 added, the measurements were not possible owing to the unfavorable precipitation of the dimeric species under the given conditions. The value of K_{13} for cyclohexene may be much smaller than that for styrene, suggesting a much lower concentration of the resultant intermediate dihydrido-olefin complex, $RhClH_2(ol)L_2$, than that for styrene. When tris(triphenylphosphine) complex, $RhClL_3$, is used as the catalyst, the observed overall rate constant for the catalytic hydrogenation of cyclohexene is about 1/3 as small as that of styrene.[7] Thus, the value of k_{45} for cyclohexene is expected not to be much smaller than that for styrene. It may be estimated to be at least larger than 0.20 s^{-1}.

References

1) B. R. James, "Homogeneous Hydrogenation," Wiley, New York (1973), pp. 204—248; G. N. Schrauzer, "Transition Metals in Homogeneous Catalysis," Marcel Dekker, New York (1971), pp. 31—36; M. M. T. Khan and A. E. Martell, "Homogeneous Catalysis by Metal Complexes," Academic Press, New York (1974), Vol. 1, pp. 46—56.

2) P. Meakin, J. P. Jesson, and C. A. Tolman, *J. Am. Chem. Soc.*, **94**, 3240 (1972).

3) J. Halpern and C. S. Wong, *J. Chem. Soc., Chem. Commun.*, **1973**, 629.

4) C. A. Tolman, P. Z. Meakin, D. L. Lindner, and J. P. Jesson, *J. Am. Chem. Soc.*, **96**, 2762 (1974).

5) Y. Ohtani, M. Fujimoto, and A. Yamagishi, *Bull.*

Chem. Soc. Jpn., **50**, 1453 (1977).
6) J. A. Osborn, F. H. Jardine, J. F. Young, and G. Wilkinson, *J. Chem. Soc., A*, **1966**, 1711.
7) F. H. Jardine, J. A. Osborn, and G. Wilkinson, *J. Chem. Soc., A*, **1967**, 1574.
8) S. Montelatici, A. van der Ent, J. A. Osborn, and G. Wilkinson, *J. Chem. Soc., A*, **1968**, 1054; J. P. Candlin and A. R. Oldham, *Discuss. Faraday Soc.*, **46**, 60 (1968); G. C. Bond and R. A. Hillyard, *ibid.*, **46**, 20 (1968).
9) J. Halpern, T. Okamoto, and A. Zakhariev, *J. Mol. Catl.*, **2**, 65 (1977).
10) So-called "hydride route" (paths **2**→**4**→**5** in Scheme 1) is predominant under the experimental conditions.
11) Y. Ohtani, A. Yamagishi, and M. Fujimoto, *Bull. Chem. Soc. Jpn.*, **51**, 2562 (1978).
12) So-called "unsaturate route" (paths **3**→**4**→**5** in Scheme 1) is predominant under the experimental condition.
13) Y. Ohtani, A. Yamagishi, and M. Fujimoto, unpublished data.
14) Y. Ohtani, M. Fujimoto, and A. Yamagishi, *Bull. Chem. Soc. Jpn.*, **49**, 1871 (1976).

The Mechanism of the Spin-Spin Coupling of Dimethyllead(IV) Complexes with ONNO Quadridentate Schiff Base Ligands and the Magnetically Non-equivalent Methyl Protons of a Dimethyllead(IV) Complex

Tetsuro MAJIMA and Yoshikane KAWASAKI*

Department of Petroleum Chemistry, Osaka University, Yamadakami, Suita, Osaka 565

(Received May 31, 1978)

Several dimethyllead(IV) complexes with ONNO quadridentate Schiff base ligands have been prepared. The spin-spin couplings between the lead nucleus and the azomethine proton of the ligands, $^3J(^{207}Pb\text{–}N{=}CH)$, as well as the lead-methyl proton couplings, $^2J(^{207}Pb\text{–}CH_3)$, have been observed in various solvents. Both J values inclease with an increase in donor strength of the solvents. The mean excitation energy, the ΔE term in the Fermi contact term plays a dominating role for the lead-proton spin-spin coupling constants. Two methyl proton signals were, for the first time, found to be magnetically non-equivalent in the dimethyllead(IV) complex of sapr.

The metal-proton spin-spin coupling constants, J(M, H), in methyl compounds of Sn, Hg, Tl, and Pb have been known to sensitively reflect changes in the configuration and electronic state around the central metal.[1] The various studies on the coupling mechanism of J(M,H), have been considered to be mainly governed by the Fermi contact interaction as approximately expressed by[2]

$$J(\mathrm{M,H}) = \mathrm{const}\cdot\alpha_M{}^2\cdot a_M(ns)\cdot a_H(1s)/\Delta E, \quad (1)$$

where $\alpha_M{}^2$ is the s character of the metal orbitals in the metal–carbon bonds, $a_M(ns)$ and $a_H(1s)$ are the hyperfine coupling constants of the ns electron in a metal atom and the 1s electron of a proton respectively. ΔE is the mean singlet-triplet excitation energy.

It has been reported that in methyltin compounds the $^2J(^{119}Sn\text{–}CH_3)$ values depend almost entirely on the s character of the tin orbitals used in the tin–carbon bonds,[1b,3] and in the methyl compounds of Hg and Tl, the effective nuclear charge is the dominating factor in addition to the s character.[4] In dimethyllead(IV) compounds changes of the $^2J(^{207}Pb\text{–}CH_3)$ values with the solvent depends largely on the ΔE term.[5]

In dimethyllead(IV) complexes, the spin-spin coupling constants between the lead nucleus and the ligand protons have, in most cases, not been observed, for example in $(CH_3)_2Pb(acac)_2$ (acac=acetylacetonato).[5a] The $^2J(^{207}Pb\text{–}CH_3)$ values have however been observed. One of the possible explanations is ligand dissociation; Eq. 2 and/or intermolecular exchange of the acac; Eq. 3 on the ^1H NMR time scale.[6]

$$(CH_3)_2Pb(acac)_2 \rightleftharpoons (CH_3)_2Pb(acac)^+ + acac^- \quad (2)$$

$$(CH_3)_2Pb(acac)_2 + (CH_3)_2Pb(acac^*)_2 \rightleftharpoons 2(CH_3)_2Pb(acac)(acac^*) \quad (3)$$

Therefore, the mechanism of the lead-proton spin-spin coupling of dimethyllead(IV) complexes has been discussed mainly on the basis of changes in the $^2J(^{207}Pb\text{–}CH_3)$ values.[1e,5a–f,7] However, observation of the lead-ligand protons spin-spin coupling constants are of importance to verify our previous assumptions that changes of the spin-spin coupling constants of dimethyllead(IV) complexes depend on changes in the ΔE term.[5]

In this work, ONNO quadridentate Schiff base ligands, shown below, were selected, since these ligands have been known to coordinate storongly to the central metal atom[8] and a spin-spin coupling constant between the lead nucleus and the azomethine proton of the ligands, $^3J(^{207}Pb\text{–}N{=}CH)$, may be predicted.

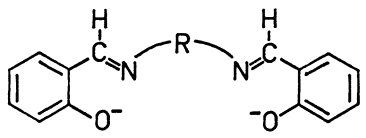

L

R=$-CH_2CH_2-$; *N,N'*-ethylenebis(salicylideneaminato): saln

R=$-CH_2CH(CH_3)-$; *N,N'*-propylenebis(salicylideneaminato): sapr

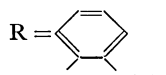

; *N,N'*-*o*-phenylenebis(salicylideneaminato): saph

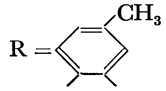

; *N,N'*-(4-methyl-1,2-phenylene)-bis(salicylideneaminato): sato

Experimental

Materials. Dimethyllead dichloride was prepared by the chlorination of tetramethyllead in ethyl acetate at −10 °C.[9] Schiff bases, *N,N'*-alkyl- or -aryl-substituted-bis(salicylideneamine)s (H_2**L**) were prepared from dehydration reactions between salicylaldehyde and the corresponding diamines by refluxing in ethanolic solution.[10] The solvents used were reagent grade and purified according to the standard method except for $CDCl_3$ which was used as supplied.

*Preparation of $(CH_3)_2Pb$**L**$\cdot S$ (**L**=saln, sapr, saph, and sato; $S=CH_3OH$ or H_2O).* Dry methanol solution (20 dm^3) of the sodium salts of an appropriate Schiff base (Na_2**L**), prepared from sodium methoxide in methanol (Na; 0.5 g, 20 mmol) and H_2**L** (10 mmol), was added dropwise under stirring to dimethyllead dichloride (2.5 g, 10 mmol) in dry methanol (30 dm^3) and the mixture was stirred for a few hours. The precipitates were filtered, washed with benzene and methanol, and recrystallized from hot methanol. The crystalline complexes obtained in this manner contained one molecule of methanol or water.[11]

Molecular Weight and Conductivity Measurements. The molecular weight of $(CH_3)_2Pb(saln)\cdot CH_3OH$ in $CHCl_3$

(0.5 wt %) was established using a Mechrolab vapor-pressure osmometer at 25 °C and was found to be 562 (504 calcd for $(CH_3)_2Pb(saln)$). This suggests that the methanol in the complex is free in solvents.[12] Molar conductances in DMSO were measured by a Yokogawa F-225A Universal bridge and a cell with a cell constant of 0.377 cm^{-1} at 25±0.1 °C. The specific conductance of DMSO used was $\kappa=4.2\times10^{-7}\,\Omega^{-1}\,cm^{-1}$. Molar conductances ($\Lambda_m$) of $(CH_3)_2PbL\cdot S$ in DMSO (10^{-3} mol dm^{-3}) were $<0.8\,\Omega^{-1}\,cm^2\,mol^{-1}$ (Table 1). All complexes were found to be non-electrolytes.

The IR, ^1H NMR, and UV Spectra. The IR spectra were recorded on a Hitachi 225 spectrophotometer. The ^1H NMR studies were conducted on a JEOL-PS-100 spectrometer operating at 100 MHz. All data were obtained in *ca.* 4 wt %. Chemical shifts were measured wih TMS as internal standard at ambient temperature. The UV spectra were recorded on a Hitachi model 356 spectrophotometer with 0.1 cm quartz cells.

Analytical data, physical properties, and IR, ^1H NMR, and UV spectral data for the dimethyllead(IV) complexes prepared in this study are summarized in Tables 1—6.

Results and Discussion

As expected, the spin-spin coupling constants between the azomethine proton and the lead nucleus, $^3J(^{207}Pb–N=CH)$, were observed for all complexes; $(CH_3)_2PbL\cdot S$ (**L**=saln, sapr, saph, and sato; S=CH_3OH or H_2O) (Tables 2—5).[13] The chemical shifts of the ligand protons, in all cases, moved to a higher magnetic field upon complex formation. In the case of the sapr complex two azomethine proton signals with different $^3J(^{207}Pb–N=CH)$ values were observed, thought due to the effect of the methyl group in the propylene unit in sapr and the difference in the strength of coordination of the two azomethine nitrogen atoms to the lead atom. One azomethine proton being closer to the methyl group (H_a) is more shielded (up-field shifts of *ca.* 0.05 ppm) and has a larger spin-spin coupling to the lead nucleus than the other (H_b). Similarly, in the sato complex two azomethine proton signals were observed, the difference in chemical shift being smaller than in the sapr complex, and the two $^3J(^{207}Pb–N=CH)$ values were equal within experimental error. Assignment of two signals is difficult to make from this result only. In IR spectra (Table 1), the stretching frequencies of the C–N double bond in CH_2Cl_2 (1608—1620 cm^{-1}) and in hexamethylphosphoric triamide (HMPA) (1608—1625 cm^{-1}) are almost the same but move to lower frequencies from those of the free Schiff bases (1618, 1620, 1628, and 1635 cm^{-1} for H_2saln, H_2sapr, H_2saph, and H_2sato in CH_2Cl_2 respectively). None of these complexes exhibited electric conductivity in DMSO (Table 1). Consequently, the ligand in these complexes may be assumed to coordinate to the lead atom as ONNO quadridentate ligands in all the solvents, according to a similar discussion in the dimethyllead complexes series.[5] In the UV spectra of $(CH_3)_2Pb(saln)\cdot CH_3OH$ (Table 6), a blue shift for the longest wavelength band was observed in the change from

TABLE 1. ANALYTICAL DATA, PHYSICAL PROPERTIES, AND IR SPECTRAL DATA OF $(CH_3)_2PbL\cdot S$

$(CH_3)_2PbL\cdot S$		Color	Mp (°C)	Found (Calcd) (%)				Λ_m[a] ($\Omega^{-1}\,cm^2\,mol^{-1}$)	Found (Calcd) mol wt[b]	ν(C=N) (cm^{-1}) in CH_2Cl_2[c] (in HMPA)[c]
L	S			C	H	N	Pb			
saln	CH_3OH	yellow	180[d]	42.42 (42.61)	4.13 (4.52)	5.30 (5.23)	38.44 (36.68)	0.75	562 (504)[e]	1620 (1625)
sapr	CH_3OH	yellow	143[d]	44.07 (43.71)	5.02 (4.77)	4.97 (5.09)	37.41 (37.69)	0.53	—[f]	1616 (1615)
saph	CH_3OH	orange-yellow	148[d]	47.12 (47.33)	4.06 (4.14)	4.73 (4.80)	35.29 (35.50)	0.50	—[f]	1607 (1605)
sato	H_2O	orange-yellow	152[d]	47.15 (47.33)	4.00 (4.14)	4.77 (4.80)	35.59 (35.50)	0.71	—[f]	1608 (1606)

a) In DMSO. b) In $CHCl_3$. c) 5 wt %. d) Decompose. e) Calcd for $(CH_3)_2Pb(saln)$. f) Not measured.

TABLE 2. THE ^1H NMR SPECTRAL DATA OF $(CH_3)_2Pb(saln)\cdot CH_3OH$

Solvent	δ(N=CH) (ppm)	δ(ring proton)[a] (ppm)				$\delta(CH_2)$ (ppm)	$\delta(OCH_3)$ (ppm)	δ(Pb–CH_3) (ppm)	$^2J(^{207}Pb–CH_3)$ (Hz)	$^3J(^{207}Pb–N=CH)$ (Hz)
		4-H[b]	6-H[c]	3-H[c]	5-H[b]					
$CDCl_3$	7.86	7.24	7.00	6.60	6.42	3.90	3.43	2.06	157.8	23.4
CH_2Cl_2	7.88	7.16	7.03	6.53	6.37	3.88	3.22	1.99	162.1	24.1
CH_3OH	8.00	7.14	7.09	6.60	6.48	3.93	—[d]	2.02	163.8	25.9
$(CH_3O)_3PO$	7.98	7.07	7.04	6.36	6.25	—[d]	—[d]	1.86	172.8	27.0
Pyridine	7.97	—[d]	—[d]	6.54	6.32	3.67	—[d]	2.03	180.0	28.1
DMSO	7.99	7.09	7.06	6.43	6.27	3.81	—[d]	1.77	178.8	29.0
HMPA	8.16	7.04	7.06	6.36	6.17	3.89	—[d]	1.78	187.5	29.3

a) 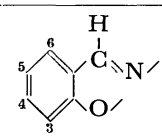 b) dd signal. c) d signal. d) Obscured by the resonance peaks of the solvents.

non-coordinating solvent to donor solvent. Other bands exhibited small changes. This, however, is quite different for $(CH_3)_2Pb(ox)_2$ (ox=8-quinolinolato) in which the red shift was obtained at the longest wavelength[5c] and this may arise from a difference in coordination to the lead atom.

The $^2J(^{207}Pb-CH_3)$ values of these complexes in $CDCl_3$ (154—158 Hz) are comparable to those of many dimethyllead(IV) complexes having a six-coordinate configuration with a linear C–Pb–C skeleton (for

Table 3. The ^1H NMR spectral data of $(CH_3)_2Pb(sapr)\cdot CH_3OH$[a]

Solvent	$\delta(N=CH_a)$ $\delta(N=CH_b)$ (ppm)	δ (ring proton) (ppm) 4-H[b]	6-H[c]	3-H[d]	5-H[e]	$\delta(-CH-)$[f] (ppm)	$\delta(CH_2)$[f] (ppm)
$CDCl_3$	7.82 7.87	7.12	7.01	6.60	6.41	7.12	3.86
CH_2Cl_2	7.82 7.87	7.14	7.02	6.56	6.40	7.14	3.85
CH_3OH	8.03 8.08	7.20	7.16	6.64	6.51	7.20	—[h]
$(CH_3O)_3PO$	7.97 8.02	7.13	6.99	6.35	6.24	7.13	—[h]
Pyridine	—[h]	—[h]	—[h]	6.62	6.53	—[h]	3.60
DMSO	7.96 8.01	7.08	7.03	6.40	6.27	7.08	—[h]
HMPA	8.04 8.09	7.05	6.98	6.33	6.14	7.05	—[h]

Solvent	$\delta(CH_3)$[g] (ppm)	$\delta(Pb-CH_3)$ (ppm)	$^2J(^{207}Pb-CH_3)$ (Hz)	$^3J(^{207}Pb-N=CH_a)$ $^3J(^{207}Pb-N=CH_b)$ (Hz)
$CDCl_3$	1.32	2.03 2.06	160.5	23.2 22.2
CH_2Cl_2	1.30	1.99 2.01	161.4	24.1 22.1
CH_3OH	1.30	1.93 1.96	164.4	24.9 23.5
$(CH_3O)_3PO$	1.27	1.84 1.85	168.6	25.1 23.7
Pyridine	1.11	1.99 2.02	177.6	—[h]
DMSO	1.18	1.75 1.76	181.4	30.0 27.8
HMPA	1.19	1.73 1.75	186.0	30.5 27.9

a) 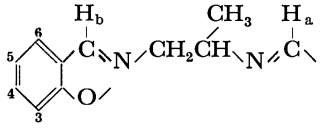

b) dt signal. c) dt signal. d) d signal. e) dd signal. f) m signal. g) d signal, coupling constant with the adjacent methine proton is 6 Hz. h) Obscured by the resonance peaks of the solvents.

Table 4. The ^1H NMR spectral data of $(CH_3)_2Pb(saph)\cdot CH_3OH$

Solvent	$\delta(N=CH)$ (ppm)	δ (ring proton)[a] (ppm) 3-H[b]	5-H[c]	Others	$\delta(Pb-CH_3)$ (ppm)	$^2J(^{207}Pb-CH_3)$ (Hz)	$^3J(^{207}Pb-N=CH)$ (Hz)
$CDCl_3$	8.23	6.69	6.50	7.4—7.1	1.93	154.7	18.8
CH_2Cl_2	8.29	6.63	6.49	7.4—7.2	1.89	158.4	19.8
CH_3OH	8.33	6.76	6.60	7.4—7.2	1.78	165.3	20.7
$(CH_3O)_3PO$	8.32	6.53	6.41	7.4—7.1	1.71	174.3	23.4
Pyridine	—[d]	6.56	6.40	—[d]	1.95	177.2	—[d]
DMSO	8.30	6.52	6.36	7.4—7.1	1.59	175.8	25.0
HMPA	8.38	6.44	6.23	7.4—7.0	1.60	190.4	27.0

a) 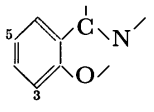

b) d signal. c) dd signal. d) Obscured by the resonance peaks of the solvents.

TABLE 5. THE ^{1}H NMR SPECTRAL DATA OF $(CH_3)_2Pb(sato)\cdot H_2O$

Solvent	δ(N=CH)	δ(ring proton)[a] (ppm)			δ(CH_3)[d]	δ(Pb–CH_3)	$^2J(^{207}Pb–CH_3)$	$^3J(^{207}Pb–N=CH)$
	(ppm)	3-H[b]	5-H[c]	Others	(ppm)	(ppm)	(Hz)	(Hz)
$CDCl_3$	8.25 8.26	6.74	6.53	7.4—7.1	2.45	1.94	154.4	18.6
CH_2Cl_2	8.25 8.26	6.61	6.48	7.4—7.1	2.43	1.88	158.7	19.1
CH_3OH	8.36 8.38	6.66	6.56	7.4—7.1	2.44	1.79	160.8	19.4
$(CH_3O)_3PO$	8.36 8.38	6.54	6.41	7.4—7.1	2.42	1.72	174.8	24.0
Pyridine	—[e]	6.56	6.40	—[e]	2.35	1.94	177.0	—[e]
DMSO	8.38 8.39	6.61	6.44	7.4—7.1	—[e]	1.63	178.7	26.3
HMPA	8.38 8.42	6.50	6.29	7.4—7.0	—[e]	1.62	189.1	28·4

a) 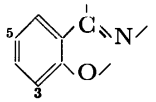 b) d signal. c) dd signal. d) Methyl proton of 4-methyl-1,2-phenylene group. e) Obscured by the resonance peaks of the solvents.

TABLE 6. THE UV SPECTRAL DATA OF $(CH_3)_2Pb(saln)\cdot CH_3OH$ IN SEVERAL SOLVENTS[a]

Solvent	λ (nm) (log ε)				
C_6H_6	—[b]	—[b]	—[b]	314(3.14)	397(3.90)
$CHCl_3$	252(4.56)	263(sh) (4.35)	278(sh) (4.02)	311(3.74)	393(3.77)
CH_2Cl_2	252(4.44)	260(sh) (4.23)	270(sh) (4.03)	316(3.93)	388(3.68)
Pyridine	—[b]	—[b]	—[b]	309(3.67)	379(4.00)
DMSO	260(4.24)	270(sh) (4.15)	278(sh) (3.97)	310(3.67)	378(3.93)
HMPA	259(4.31)	265(sh) (4.37)	275(sh) (3.93)	318(3.49)	379(3.83)

a) 5×10^{-4} mol dm^{-3}. Wavelengths (λ) and absorption coefficients (ε (mol^{-1} cm^2)) refer to band maxima and shoulders (sh). b) Obscured by absorption of the solvents.

example, 154.7 and 152.5 Hz in $(CH_3)_2Pb(acac)_2$[5a] and $(CH_3)_2Pb(ox)_2$[5c] respectively in $CDCl_3$). It is, therefore, reasonable to assume that these complexes have a six-coordinate configuration (**A**) in such non-coordinating solvents as $CDCl_3$ and CH_2Cl_2.

The proton resonances of the methyl groups attached to the lead atom, δ(Pb–CH_3), shift to a higher magnetic field and the $^2J(^{207}Pb–CH_3)$ values increase with an increase in donor strength of the solvents,[14] as in the case of other dimethyllead(IV) complexes; $(CH_3)_2PbL_2$ (L=ox, acac, $OCOC_6H_5$).[5] Therefore, the present complexes, $(CH_3)_2Pb$**L**·S, with ONNO quadridentate Schiff base ligands take a seven-coordinate configuration (**B**) in such donor solvents as DMSO and HMPA and this is supported by the $^2J(^{207}Pb–CH_3)$ values (175—190 Hz) which are comparable to or larger than those of an isolated seven-coordinated complex, $(CH_3)_2Pb(gbha)(H_2O)$ (gbha= 2,2′-(ethanediylidenediimino) diphenolato) (178—181 Hz).[15]

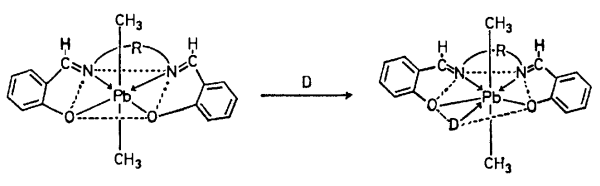

(**A**) (**B**)

D=HMPA, DMSO, pyridine, $(CH_3O)_3PO$, CH_3OH.

One of remarkable features in ^{1}H NMR spectral data shown in Tables 2—5 is that the $^3J(^{207}Pb–N=CH)$ values increase with the $^2J(^{207}Pb–CH_3)$ values. The $^3J(^{119}Sn–N=CH)$ values of $(CH_3)_2Sn(saln)$ have been reported to decrease with an increase in donor strength of the solvents, although the $^2J(^{119}Sn–CH_3)$ values increase.[16] Figures 1 and 2 show the linear relationships between the δ(Pb–CH_3) values and the $^2J(^{207}Pb–CH_3)$ and $^3J(^{207}Pb–N=CH)$ values for the dimethyllead complexes of saln and sapr respectively in various solvents. (The linear relationship was also obtained for saph and sato complexes.) In Figs. 3 and 4, the higher magnetic field shifts of the phenol ring proton resonances in these complexes with the methyl protons attached to the lead atom are shown. Interestingly, the amount of up-field shifts for 3-H and 5-H (*o*- and *p*-position to the oxygen atom respectively) are significantly larger than those for 4-H and 6-H (*m*-positions). This indicates that coordination of the solvent molecule brings about some electron donation to the lead atom and ligand, resulting in a decrease of the positive charge on the lead atom and an increase of electron density on the oxygen atom.

These results support a previous suggestion that a change of the mean excitation energy, ΔE, in the Fermi contact term plays a dominant role on the solvent dependence of the $^2J(^{207}Pb–CH_3)$ values.[5] Namely,

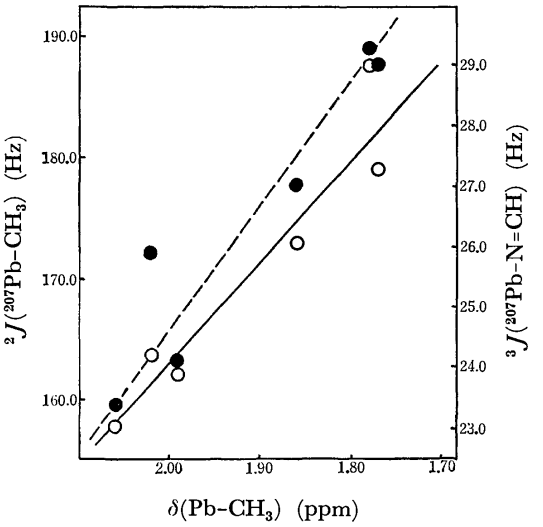

Fig. 1. Plots of the $^2J(^{207}Pb\text{-}CH_3)$ (—○—) and $^3J(^{207}Pb\text{-}N{=}CH)$ (--●--) *vs.* $\delta(Pb\text{-}CH_3)$ values for $(CH_3)_2Pb(saln)\cdot CH_3OH$ in several solvents.

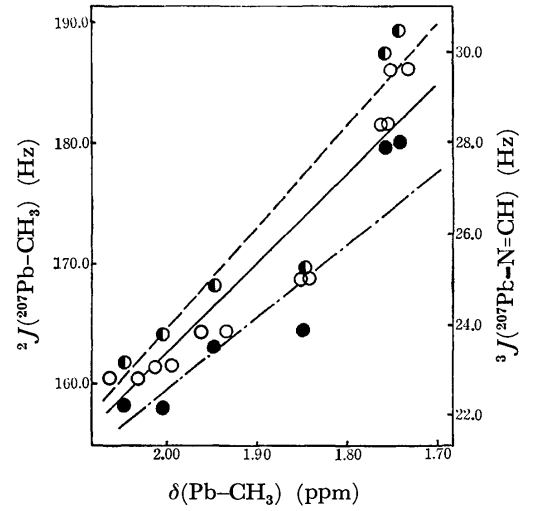

Fig. 2. Plots of the $^2J(^{207}Pb\text{-}CH_3)$ (—○—) *vs.* two $\delta(Pb\text{-}CH_3)$ values and of the $^3J(^{207}Pb\text{-}N{=}CH_a)$ --◐--) and $^3J(^{207}Pb\text{-}N{=}CH_b)$ (-·—●—·-) *vs.* the average of two $\delta(Pb\text{-}CH_3)$ values for $(CH_3)_2Pb(sapr)\cdot CH_3OH$ in several solvents. See Table 3, regarding sings of azomethine protons.

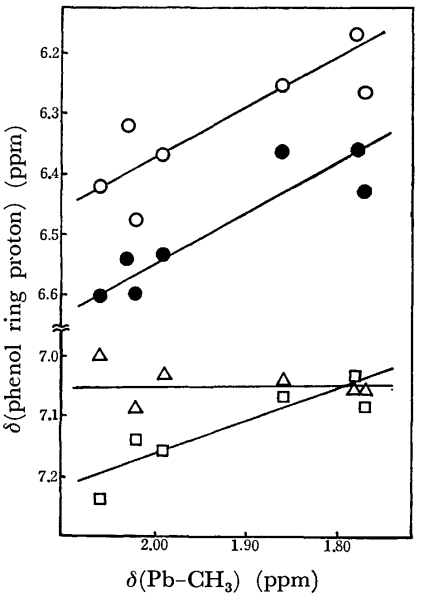

Fig. 3. Plots of the δ(phenol ring proton) *vs.* $\delta(Pb\text{-}CH_3)$ values for $(CH_3)_2Pb(saln)\cdot CH_3OH$ in several solvents; 5-H (—○—), 3-H (—●—), 6-H (—△—), and 4-H (—□—). Signs of these protons are written in Table 2.

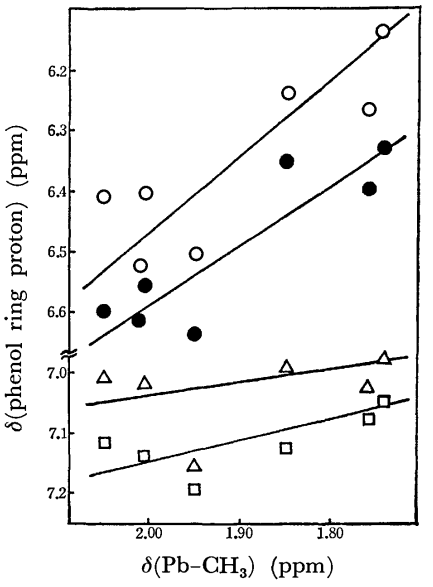

Fig. 4. Plots of the δ(phenol ring proton) *vs.* $\delta(Pb\text{-}CH_3)$ values for $(CH_3)_2Pb(sapr)\cdot CH_3OH$ in several solvents; 5-H (—○—), 3-H (—●—), 6-H (—△—), and 4-H (—□—). Signs of these protons are written in Table 3.

the increase of the $^2J(^{207}Pb\text{-}CH_3)$ values together with the $^3J(^{207}Pb\text{-}N{=}CH)$ values depend on a decrease of ΔE, which results from a decrease in the positive charge on the lead atom as a result of electron donation from the solvent molecules. It is difficult to interpret the results by the d-s mixing scheme,[1e] which has been proposed to account for the increase in the $^2J(^{205}Tl\text{-}CH_3)$ values of some dimethylthallium compounds in donor solvents. If the d-s mixing scheme were dominating, the s electron of the lead atom in the coordination plane of the ligands would transfer to the C–Pb–C bond, resulting in an increase of the s character of the lead atom for Pb–C bonds and a decrease in the coordination plane of ligands. Therefore, decrease in the $^3J(^{207}Pb\text{-}N{=}CH)$ values was expected when the $^2J(^{207}Pb\text{-}CH_3)$ values increased, and *vice versa*. This is not consistent with the results reported here. Similarly, the results can not be explained in terms of the change of $a_{Pb}(6s)$ term in Eq. 1 which decreases with decreasing positive charge on the lead atom.

From Tables 2—5, it may be seen that the δ(N=CH) values shift to a lower magnetic field with an increase in donor strength of the solvents. This change may be accounted for by two compensating factors; 1) the down-field shift due to hydrogen bonding with oxygen atom of the solvents, which grows stronger with an increase of donor strength of the solvents, (the down-

field shift of the azomethine proton for free H_2saln is as follows: 8.32, 8.53, 8.60, 8.73, 8.73, and 9.04 in $CDCl_3$, CH_2Cl_2, CH_3OH, $(CH_3O)_3PO$, DMSO, and HMPA respectively.) and 2) the up-field shift caused by the coordination of the solvent molecules to the lead atom. Indeed, the down-field shift of the N=CH proton in the saln complex from in $CDCl_3$ to in HMPA; 0.30 ppm was observed and is much smaller than that in H_2saln; 0.72 ppm. (These behaviors were observed also in sapr, saph, and sato complexes.)

It shoud be noted that the two methyl groups attached to the lead atom show different chemical shifts in the case of $(CH_3)_2$Pb(sapr)·CH_3OH, although the $^2J(^{207}Pb-CH_3)$ values were the same within experimental error. In the other three complexes only one methyl signal was observed. The magnetic non-equivalence of the methyl protons is attributed to the rigidity of the N–C–C–N skeleton of the sapr ligand and to no dissociation of the ligand attached to the lead atom. The location of the methyl group of the propylene unit outside the coordination plane, induces magnetic non-equivalence above and below the coordination plane. The sapr complex is the first example of a dimethyllead(IV) complex that has magnetically non-equivalent methyl protons, a similar observation found in the case of [$(CH_3)_2$Tl(*cis-syn-cis*-6,7,9,10,17,18,20,21-octahydrodibenzo[*b.k*][1,4,7,10,13,16]-hexaoxacyclooctadecin)]$^+$[picrato]$^-$.[17]

In conclusion, from the present work on dimethyllead(IV) complexes with ONNO quadridentate Schiff base ligands, together with a series of spectroscopic studies for several other dimethyllead(IV) complexes previously reported,[5] the ΔE term in the Fermi contact term plays a dominant role in the solvent dependence of the indirect spin-spin coupling between the lead nucleus and proton, J(M,H).

References

1) a) N. A. Matwiyoff and R. S. Drago, *Inorg. Chem.*, **3**, 377 (1964); b) T. F. Bolles and R. S. Drago, *J. Am. Chem. Soc.*, **88**, 5730 (1966); c) R. Schefford, *Helv. Chim. Acta*, **52**, 56 (1964); d) R. S. Tobias and C. F. Freidline, *Inorg. Chem.*, **4**, 215 (1965); e) G. D. Shier and R. S. Drago, *J. Organomet. Chem.*, **5**, 330 (1966), **6**, 359 (1966); f) D. P. Graddon, *ibid.*, **71**, 17 (1974); g) D. K. Dalling and H. S. Gutowsky, *J. Chem. Phys.*, **55**, 4959 (1971).

2) G. W. Smith, *J. Chem. Phys.*, **42**, 435 (1965).

3) M. M. McGrady and R. S. Tobias, *Inorg. Chem.*, **3**, 1157 (1964); G. Matsubayashi, Y. Kawasaki, T. Tanaka, and R. Okawara, *Bull. Chem. Soc. Jpn.*, **40**, 1566 (1967); Y. Kawasaki, *J. Inorg. Nucl. Chem.*, **30**, 3773 (1968); J. R. Holmes and H. D. Kaesz, *J. Am. Chem. Soc.*, **83**, 3909 (1961).

4) J. V. Hatton, W. G. Schneider, and W. Siebrand, *J. Chem. Phys.* **39**, 1330 (1963); J. V. Hatton, *J. Chem. Phys.*, **40**, 933 (1964).

5) a) M. Aritomi, Y. Kawasaki, and R. Okawara, *Inorg. Nucl. Chem. Lett.*, **8**, 69 (1972); b) M. Aritomi, Y. Kawasaki, and R. Okawara, *ibid.*, **8**, 1053 (1972); c) M. Aritomi and Y. Kawasaki, *J. Organomet. Chem.*, **81**, 363 (1974); d) M. Aritomi and Y. Kawasaki, *bid.*, **90**, 185 (1975); e) M. Aritomi, K. Hashimoto, and Y. Kawasaki, *ibid.*, **93**, 181 (1975); f) Y. Kawasaki and M. Aritomi, *ibid.*, **104**, 39 (1976); g) Y. Kawasaki and T. Majima, *Inorg. Nucl. Chem. Lett.*, **11**, 779 (1975); h) T. Majima and Y. Kawasaki, *Bull. Chem. Soc. Jpn.*, **51**, 2924 (1978).

6) In $(CH_3)_2$Pb(acac)(pan) (pan = 1-(2-pyridylazo)-2-naphtholato; ONN tridentate ligand), four bonded coupling between the lead nucleus and the acac protons (methyl and methine protons) have been observed. This suggests that dissociation of the acac ligand from the lead atom is slow in this complex with a seven-coordinate configuration: T. Sasaki and Y. Kawasaki, to be published.

7) Y. Kawasaki, *J. Organomet. Chem.*, **9**, 549 (1967); W. Kitching and V. G. Kumar Das, *Aust. J. Chem.*, **21**, 2401 (1968); V. G. Kumar Das and W. Kitching, *J. Organomet. Chem.*, **13**, 523 (1968); G. Singh, *ibid.*, **11**, 133 (1968).

8) K. Ueno and A. E. Martell, *J. Phys. Chem.*, **60**, 1270 (1956); E. J. Olzewski and D. F. Martin, *J. Inorg. Nucl. Chem.*, **26**, 1577 (1964); L. V. Interrante and J. C. Bailar, *Inorg. Chem.*, **3**, 1339 (1964); R. H. Herber and R. Barbieri, *Gazz. Chim. Ital.*, **101**, 149 (1971).

9) G. Grüttner and E. Krause, *Chem. Ber.*, **49**, 1415 (1916).

10) A. T. Mason, *Chem. Ber.*, **20**, 267 (1887).

11) The ν(O-H) stretching frequencies of $(CH_3)_2$Pb**L**·S (**L**=saln, sapr, saph; S=CH_3OH: *ca.* 3640 cm^{-1}; **L**=sato; S=H_2O: 3680 cm^{-1}) in $CDCl_3$ are comparable to those of free methanol and water in the same solvent (3640 and 3680 cm^{-1} respectively) and consequently the methanol and water in the crystals have been assumed completely free in solvents.

12) Since it is known that the addition of methanol to chloroform causes an increase of vapor pressure, the obserbed value (562) should be larger than 504 calculated for $(CH_3)_2$Pb(saln), suggesting that $(CH_3)_2$Pb**L**·S exists as a monomer and S (methanol or water in the crystals is completely free in solution: J. H. Perry, "Perry's Chemical Engineer's Handbook," 4th ed, McGraw-Hill, New York (1963), pp. 13—15.

13) Di Bianca *et al.* reported the preparation of $(CH_3)_2$-Pb(saln) by a similar procedure. However, no $^3J(^{207}Pb-N=CH)$ value was observed: F. Di Bianca, E. Rivarola, G. C. Stocco, and R. Barbieri, *Z. Anorg. Allg. Chem.*, **387**, 126 (1972).

14) V. Gutmann, "Coordination Chemistry in Nonaqueous Solutions," Springer, New York (1968).

15) T. Majima and Y. Kawasaki, *Bull. Chem. Soc. Jpn.*, **51**, 1893 (1978).

16) K. Kawakami, *J. Organomet. Chem.*, **70**, 67 (1974).

17) Y. Kawasaki and R. Kitano, *Chem. Lett.*, **1978**, 1427.

Metal Complexes of Amino Acids. XI.[1] Preparation and ^{13}C NMR Spectra of the Cobalt(III) Complexes Containing β-Alanine and Glycine

Tomoharu AMA* and Takaji YASUI

Department of Chemistry, Faculty of Science, Kochi University, Akebono-cho, Kochi 780

(Received June 17, 1978)

A series of complexes or geometrical isomers, $[Co(\beta\text{-ala or gly})(en)_2]^{2+}$, $[Co(\beta\text{-ala or gly})_2(en)]^{+}$, $[Co(\beta\text{-ala or gly})(ox)_2]^{2-}$, and $[Co(\beta\text{-ala or gly})_2(ox)]^{-}$, were prepared and their ^{13}C NMR spectra were measured. Assignments of their structures and ^{13}C NMR signals were made. The β-alaninate carbons in the complexes resonate at 33.6±0.5, 38.3±0.6, and 183.0±1.5 ppm and the glycinate carbons at 46.3±1.3 and 187.4±1.4 ppm. The ^{13}C chemical shifts of the mixed (β-alaninato)(glycinato) complexes consist of those of the corresponding isomers of bis(β-alaninato) and bis(glycinato) complexes.

^1H NMR has been widely used to study the structures and reactions of the cobalt(III) complexes containing amino carboxylate as the chelate ligands. Recently, ^{13}C NMR has been applied to the study of cobalt(III) complexes, and it has been found that the ^{13}C NMR is useful to determine the geometrical structures of the cobalt(III) complexes with organic ligands.[2-15] Determination of the geometrical structure of the complex by ^1H NMR is sometimes difficult because of the complicated signals caused by spin-spin couplings. In most case, since carbon atoms are closer to cobalt(III) atom than hydrogen atoms in the complexes, ^{13}C NMR makes it possible to obtain more useful information than ^1H NMR concerning the structures of the cobalt(III) complexes. However, ^{13}C NMR data of the cobalt(III) complexes are few for satisfactory discussion of the relation between the chemical shifts and the stereochemical structure of the complex.

In the present study, we attempted the preparation of the complexes, $[Co(\beta\text{-ala or gly})(en)_2]^{2+}$, $[Co(\beta\text{-ala or gly})_2(en)]^{+}$, $[Co(\beta\text{-ala or gly})(ox)_2]^{2-}$, and $[Co(\beta\text{-ala or gly})_2(ox)]^{-}$ (C_2- and C_1-*cis*(*O*)-$[Co(\beta\text{-ala})_2(en)]^{+}$ and *trans*(*O*)-, *cis*(*O*)*trans*(N_g,*O*)-, *cis*(*O*)*trans*(*N*)-, and *cis*(*O*)*trans*(N_β,*O*)-$[Co(\beta\text{-ala})(gly)(en)]^{+}$ are new complexes), and measured their ^{13}C NMR spectra. In this paper we report on their preparation, absorption and ^{13}C NMR spectral data, and assignments of the structures.

Experimental

Preparation of the Complexes. Isomers of Bis(β-alaninato)(ethylenediamine)cobalt(III) Chloride: An aqueous solution containing 19 g of β-alanine, 6 g of ethylenediamine, and 4 g of sodium hydroxide in 100 cm³ of water was added to an aqueous solution containing 24 g of cobalt(II) chloride hexahydrate in 80 cm³ of water. The mixed solution was oxidized with 20 g of lead dioxide at 75 °C for about 30 min with stirring, and cooled to room temperature. After removal of insoluble matter by filtration, the filtrate was poured into a column (30 mm×800 mm) containing a cation exchange resin (Dowex 50WX8, 200—400 mesh, K^+ form). After the column had been swept with 3 dm³ of water, the adsorbed band was eluted with 0.05 M aqueous solution of potassium chloride. The band separated into three bands, another violet-red band remaining at the top of the column. The eluted solution from each band was concentrated to a few milliliters in a vaccum evaporator at 30—35 °C. To the concentrated solution was added a large amount of methanol, potassium chloride deposited being filtered off. Acetone was added to the filtrate in order to deposit crude complex. Each crude complex obtained was recrystallized from aqueous solution by addition of methanol and acetone. The first eluted band was confirmed to be *trans*(O)-$[Co(\beta\text{-ala})_2(en)]Cl$ from its absorption spectrum.[16] Isomer from the second eluted band: Found: C, 27.12; H, 6.44; N, 15.89%. Calcd for $[Co(\beta\text{-ala})_2(en)]Cl\cdot 1.5H_2O$: C, 26.86; H, 6.48; N, 15.66%. Isomer from the third eluted band: Found: C, 26.22; H, 6.64; N, 15.33%. Calcd for $[Co(\beta\text{-ala})_2(en)]Cl\cdot 2H_2O$: C, 26.20; H, 6.60; N, 15.28%.

Isomer of (β-Alaninato)(glycinato)(ethylenediamine)cobalt(III) Chloride: 10 cm³ of 60% perchloric acid was gradually added to a suspension of 5.0 g of *mer*(*N*)-(carbonato)(glycinato)-(ethylenediamine)cobalt(III) monohydrate in 50 cm³ of water. After vigorous evolution of gas had subsided, the solution was adjusted to pH 9 by addition of 2 M NaOH, and then 5 g of β-alanine was added to the alkaline solution. The solution was kept at 65 °C for 3 h and then cooled to room temperature. The resulting solution was poured into a column (30 mm×800 mm) containing a cation-exchange resin (Dowex 50WX8, 200—400 mesh, K^+ form). After the column had been swept with 3 dm³ of water, the adsorbed band was eluted with 0.05 M KCl. The band separated gradually into four violet-red ones, a red-violet band remaining at the top of the column. Each eluted solution was concentrated to a few milliliters in a vacuum evaporator at 35—40 °C. A large amount of methanol was added to the concentrated solution, potassium chloride deposited being filtered off. Acetone was added to the filtrate and then crude complex deposited was collected. Each crude complex was recrystallized from aqueous solution by addition of methanol and acetone. Isomer from the first eluted band: Found: C, 24.97; H, 5.98; N, 16.56%. Calcd for $[Co(\beta\text{-ala})(gly)(en)]Cl\cdot H_2O$: C, 25.12; H, 6.02; N, 16.74%. Isomer from the second eluted band: Found: C, 25.11; H, 6.00; N, 16.61%. Calcd for $[Co(\beta\text{-ala})(gly)(en)]Cl\cdot H_2O$: C, 25.12; H, 6.02; N, 16.74%. Isomer from the third eluted band: Found: C, 27.07; H, 6.07; N, 16.87%. Calcd for $[Co(\beta\text{-ala})(gly)(en)]Cl\cdot 0.5MeOH$: C, 27.08; H, 6.06; N, 16.84% (methanol containing in this ratio was checked by ^1H NMR). Isomer from the fourth eluted band: Found: C, 26.22; H, 5.55; N, 17.67%. Calcd for $[Co(\beta\text{-ala})(gly)(en)]Cl$: C, 26.55; H, 5.73; N, 17.70%.

C_1-cis(O)-(Glycinato-2,2-d_2)(glycinato)(ethylenediamine)cobalt(III) Chloride: C_1-*cis*(*O*)-bis(glycinato)(ethylenediamine)-cobalt(III) chloride (150 mg) was dissolved in 9 cm³ of deuterium oxide, and then deuterium oxide solution of sodium carbonate (1 M, 1 cm³) was added to the solution. The solution was allowed to stand at 40 °C until the ^1H

NMR signal at 3.44 ppm, assigned to the methylene proton of I-position glycine (see Results and Discussion), disappeared (about 3 h).[17] To the solution was added 0.5 cm³ of 2 M deuteriochloric acid, and a large amount of acetone. The red crystals deposited were collected and recrystallized from deuterium oxide solution by addition of acetone.

C_1-cis(O)-, C_2-cis(O)-, and trans(O)-Bis(glycinato-2,2-d_2)-(ethylenediaamine)cobalt(III) Chloride and (Glycinato-2,2-d_2)-bis(ethylenediamine)cobalt(III) Dichloride: The complexes were prepared in a similar way to that described above. Chloride of each complex (150 mg) was dissolved in 10 cm³ of 0.1 M sodium cabonate-deuterium oxide solution. The solution was allowed to stand at 50 °C for *ca.* 3 h. To this was added 0.5 cm³ of 2 M deuteriochloric acid, followed by a large amount of acetone, and the deuterated complex deposited was collected. ^{1}H NMR spectra of the deuterated glycinato complexes are shown in Fig. 1 with those of the non-deuterated complexes.

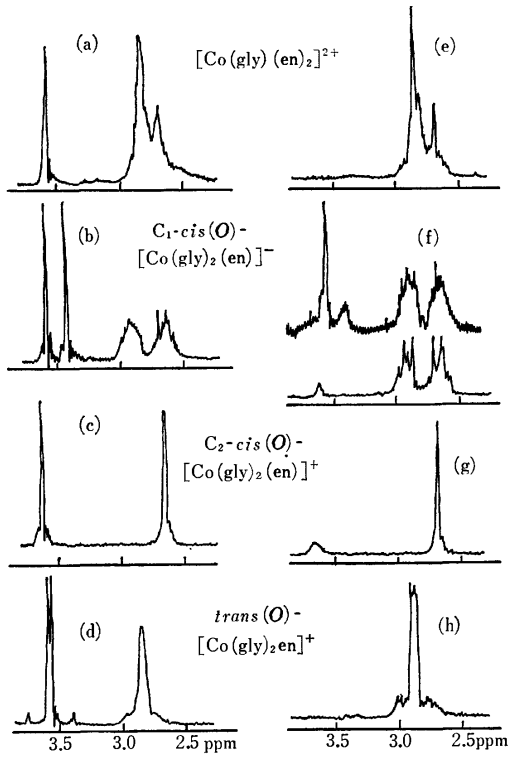

Fig. 1. ^{1}H NMR spectra of the glycinato complexes. (a), (b), (c), and (d): Non-deuterated complexes, (e), (f), (g), and (h): deuterated complexes.

The other complexes examined were prepared by the methods reported.[1,18-20]

Measurements. The electronic absorption spectra of the complexes were measured with a Hitachi EPS-3T spectrophotometer in aqueous solution. The ^{13}C NMR spectra were measured on a JEOL Model MFT-100 spectrometer in pulse Fourier transform/proton noise decoupled mode at 25.15 MHz in deuterium oxide solution. The ^{13}C chemical shifts were measured relative to benzene (in capillary) and converted into chemical shifts from TMS by means of the relation $\delta_{TMS}=\delta_{benzene}-128.5$ ppm. The errors were about $\pm$0.15 ppm. The ^{1}H NMR spectra were recorded on a JEOL Model MH-100 spectrometer with DSS as an internal standard.

Results and Discussion

Both $[Co(gly)_2(en)]^+$ and $[Co(\beta\text{-ala})_2(en)]^+$ ions provide three geometrical isomers, *trans(O)*, C_1-*cis(O)*, and C_2-*cis(O)*. On the other hand, the mixed complex ion, $[Co(\beta\text{-ala})(gly)(en)]^+$, exists in four geometrical isomers of *trans(O)*, *cis(O)trans(N_β,O)*, (N_β represents the coordinated nitrogen atom in β-alanine), *cis(O)-trans(N_g,O)* (N_g represents the coordinated nitrogen atom in glycine), and *cis(O)trans(N_β,N_g)* (Fig. 2). Absorption spectral data are given in Table 1.

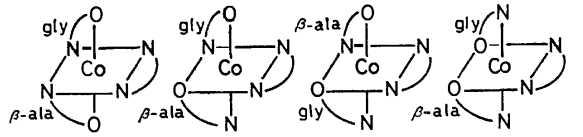

trans(O) *cis(O)trans(N$_\beta$O)* *cis(O)trans(N_gO)* *cis(O)trans(N)*

Fig. 2. The geometerical structures of possible four isomers in the $[Co(\beta\text{-ala})(gly)en)]^+$ complex ion.

Absorption Spectra. The visible absorption band at lower energy side (so-called first absorption band) of *trans(O)* isomers of $[Co(O)_2(N)_4]$ type complexes shows a marked split as compared with that of the corresponding *cis(O)* isomers. The marked split of the first absorption band was observed for the complex obtained from the first eluted band in chromatographical separation of the $[Co(\beta\text{-ala})_2(en)]^+$, the absorption spectrum of the complex quite agreeing with that of the *trans(O)*-$[Co(\beta\text{-ala})_2(en)]^+$ in the Ref. 16. Thus, we concluded that the isomer from the first eluted band takes the *trans(O)* configuration. On the other hand, the second and third eluted isomers are expected to take the *cis(O)* configuration since no marked split in the first absorption band was observed.

Matsuoka *et al.*[21] found that D_I/D_{II} value in C_2-*cis(O)* isomer of bis(amino acidato)(ethylenediamine)-cobalt(III) is smaller than that in C_1-*cis(O)* one, where D_I and D_{II} are the optical densities at the absorption maxima of the first and second absorption bands, respectively. As shown in Table 1, D_I/D_{II} value of the second eluted isomer of bis(β-alaninato)(ethylenediamine) complex is smaller than that of the third eluted isomer. Thus, we assigned the geometrical structures of the second and third eluted isomers to C_2-*cis(O)* and C_1-*cis(O)*, respectively. These assignments are in line with those from the ^{13}C NMR data.

The structure of the first eluted isomer in chromatographical separation of $[Co(\beta\text{-ala})(gly)(en)]^+$ can be assigned to *trans(O)*, since a marked split was observed in the first absorption band, which is characteristic of the complex of *trans(O)*-$[Co(O)_2(N)_4]$ type. The structure of the third eluted isomer of $[Co(\beta\text{-ala})(gly)-(en)]^+$ might be assigned to *cis(O)trans(N)* (C_2 symmetry if the chelate rings of β-ala and gly are neglected), since the D_I/D_{II} value of the third eluted isomer is smaller than that of the second and fourth eluted isomers (Table 1).

^{13}C NMR Spectra. The ^{13}C chemical shifts of carboxy carbons (C_o), α-carbons (C_α), and β-carbons (C_β) of the glycinato and β-alaninato complexes are

Table 1. Absorption spectral data of bis(amino acidato)cobalt(III) complexes

Elution order		Complex ion	I Band $10\,cm^{-1}$ (log ε)	II Band $10\,cm^{-1}$ (log ε)	Intensity ratio of I band to II band (D_I/D_{II})
GG-1	**10**	*trans*(*O*)-[Co(gly)$_2$(en)]$^+$	18.87 (1.94) *ca.* 22 (*ca.* 1.64)	27.77 (2.12)	
GG-2	**6**	C_1-*cis*(*O*)-[Co(gly)$_2$(en)]$^+$	19.97 (2.09)	27.70 (2.13)	0.91
GG-3	**3**	C_2-*cis*(*O*)-[Co(gly)$_2$(en)]$^+$	19.93 (2.04)	28.00 (2.11)	0.85
AG-1	**11**	*trans*(*O*)-[Co(β-ala)(gly)(en)]$^+$	18.61 (1.97) *ca.* 22 (*ca.* 1.68)	27.78 (2.06)	
AG-2	**8**	*cis*(*O*)*trans*(N_g,*O*)-[Co(β-ala)(gly)(en)]$^+$	19.85 (2.16)	27.71 (2.06)	1.24
AG-3	**4**	*cis*(*O*)*trans*(*N*)-[Co(β-ala)(gly)(en)]$^+$	19.88 (2.06)	27.78 (1.99)	1.17
AG-4	**7**	*cis*(*O*)*trans*(N_β,*O*)-[Co(β-ala)(gly)(en)]$^+$	19.43 (2.18)	27.68 (2.03)	1.43
AA-1	**12**	*trans*(*O*)-[Co(β-ala)$_2$(en)]$^+$	18.40 (2.00) 21.93 (1.61)	27.60 (1.94)	
AA-2	**5**	C_2-*cis*(*O*)-[Co(β-ala)$_2$(en)]$^+$	19.96 (2.10)	27.47 (1.83)	1.88
AA-3	**9**	C_1-*cis*(*O*)-[Co(β-ala)$_2$(en)]$^+$	19.47 (2.20)	27.31 (1.90)	2.02

Table 2. ^{13}C Chemical shifts of the coordinated glycinate and β-alaninate

	Complex ion	Position of the chelate ring	Carboxy carbon		Methylene carbon		
			Glycinate	β-Alaninate	Glycinate	β-Alaninate	
1	[Co(gly)(en)$_2$]$^{2+}$	—	186.7[a]	—	45.8[a]	—	—
2	[Co(β-ala)(en)$_2$]$^{2+}$	—	—	182.0	—	33.3	38.5
3	C_2-*cis*(*O*)-[Co(gly)$_2$(en)]$^+$	O	187.4[b]	—	46.5[b]	—	—
4	*cis*(*O*)*trans*(*N*)-[Co(β-ala)(gly)(en)]$^+$	O	187.4	184.2	46.0	33.3	38.4
5	C_2-*cis*(*O*)-[Co(β-ala)$_2$(en)]$^+$	O	—	184.1	—	33.1	38.0
6	C_1-*cis*(*O*)-[Co(gly)$_2$(en)]$^+$	I	186.0[b,c]	—	46.0[b,c]	—	—
		O	187.2[b]	—	46.0[b]	—	—
7	*cis*(*O*)*trans*(N_β,*O*)-[Co(β-ala)(gly)(en)]$^+$	I	—	182.0	—	33.3	37.8
		O	187.2	—	46.5	—	—
8	*cis*(*O*)*trans*(N_g,*O*)-[Co(β-ala)(gly)(en)]$^+$	I	186.0	—	45.9	—	—
		O	—	183.7	—	33.6	38.4
9	C_1-*cis*(*O*)-[Co(β-ala)$_2$(en)]$^+$	I	—	181.8	—	33.5	37.7
		O	—	184.0	—	33.3	38.2
10	*trans*(*O*)-[Co(gly)$_2$(en)]$^+$	—	187.6[b]	—	45.0[b]	—	—
11	*trans*(*O*)-[Co(β-ala)(gly)(en)]$^+$	—	187.2	181.9	45.0	33.5	38.2
12	*trans*(*O*)-[Co(β-ala)$_2$(en)]$^+$	—	—	181.5	—	33.1	38.0
13	*trans*(*N*)-[Co(gly)$_2$(ox)]$^-$	—	188.6	—	46.1	—	—
14	*trans*(*N*)-[Co(β-ala)(gly)(ox)]$^-$	—	188.7	184.4	45.9	33.7	38.1
15	*trans*(*N*)-[Co(β-ala)$_2$(ox)]$^-$	—	—	184.4	—	33.9	38.3
16	C_1-*cis*(*N*)-[Co(gly)$_2$(ox)]$^-$	I*	186.8	—	47.6	—	—
		O*	187.2	—	46.1	—	—
17	*cis*(*N*)*trans*(O_β,*N*)-[Co(β-ala)(gly)(ox)]$^-$	I*	—	184.3	—	34.1	38.8
		O*	187.2	—	46.1	—	—
18	*cis*(*N*)*trans*(O_g,*N*)-[Co(β-ala)(gly)(ox)]$^-$	I*	186.7	—	47.5	—	—
		O*	—	183.1	—	33.7	37.9
19	C_1-*cis*(*N*)-[Co(β-ala)$_2$(ox)]$^-$	I*	—	184.2	—	33.7	38.6
		O*	—	183.1	—	33.7	38.0
20	C_2-*cis*(*N*)-[Co(gly)$_2$(ox)]$^-$	O*	187.0	—	46.2	—	—
21	C_2-*cis*(*N*)-[Co(β-ala)$_2$(ox)]$^-$	O*	—	183.3	—	33.6	38.0
22	[Co(gly)(ox)$_2$]$^{2-}$	—	187.2	—	46.5	—	—
23	[Co(β-ala)(ox)$_2$]$^{2-}$	—	—	183.7	—	33.4	37.7

a) Weakened in the [Co(ND_2CD_2COO)(en)$_2$]$^{2+}$ complex ion. b) Weakened in the [Co(ND_2CD_2COO)$_2$(en)]$^+$ complex ion. c) Weakened in the C_1-*cis*(*O*)-[Co(ND_2CD_2COO)(ND_2CH_2COO)(en)]$^+$ complex ion.

summarized in Table 2. The chemical shifts of C_o, C_α, and C_β in the complexes (in which the glycinate and β-alaninate coordinate to cobalt(III) in the chelated form) are represented by $\delta_{ch}(C_o)$, $\delta_{ch}(C_\alpha)$, and $\delta_{ch}(C_\beta)$, respectively. Symbols $\delta(C_o)$, $\delta(C_\alpha)$, and $\delta(C_\beta)$ represent the chemical shifts of C_o, C_α, and C_β, respectively, of free glycine and β-alanine in acidic solutions.

The carboxy carbon resonances of the chelated glycines ($\delta_{ch}(C_o)$) were observed in the range 186.0—

188.7 ppm. On the other hand, the $\delta(C_o)$ of free glycine was 171.1 ppm. Thus, the $\Delta_{ch}(C_o)$ values ($\delta_{ch}(C_o)$ minus $\delta(C_o)$) of these glycinato complexes are found in the range 14.9—17.6 ppm. The $\delta(C_\alpha)$ of free glycine was 40.4 ppm and the $\delta_{ch}(C_\alpha)$ of glycinato complexes were observed in the range 45.0—47.6 ppm. Consequently, the $\Delta_{ch}(C_\alpha)$ values of the glycinato complexes are found in the range 4.6—7.2 ppm. The $\Delta_{ch}(C_o)$ and $\Delta_{ch}(C_\alpha)$ values of glycinato complexes are comparable to those of the other α-amino acids.[2]

The $\delta(C_o)$, $\delta(C_\alpha)$, and $\delta(C_\beta)$ values of free β-alanine are 175.9, 31.2, and 35.6 ppm, respectively. The $\delta_{ch}(C_o)$, $\delta_{ch}(C_\alpha)$, and $\delta_{ch}(C_\beta)$ values of the chelated β-alanine were observed in the ranges 181.5—184.4 ppm, 33.1—33.9 ppm, and 37.7—38.8 ppm, respectively. The $\Delta_{ch}(C_o)$ values of β-alaninato complexes are *ca.* 7 ppm, smaller than those of α-amino acidato complexes. Similarly, the $\Delta_{ch}(C_\alpha)$ values (1.9—2.7 ppm) of β-alaninato complexes are smaller than those of the α-amino acidato complexes. In this manner, the chemical shift changes caused by chelation can be used to differentiate β- and α-amino acids.[2]

In $[Co(\beta\text{-ala})_2(ox)]^-$ complex ion, one and two resonance lines of the carboxy carbons were observed for the isomers **21** and **19** (Table 2), respectively, since the chemical environments of the carboxy carbons of the two β-alaninate are equivalent in the former isomer but not in the latter one.[1] A similar relationship can be applied to the structural assignments of the two isomers of **5** and **9** in the $[Co(\beta\text{-ala})_2(en)]^+$ complex ion. The second and third eluted isomers in chromatographical separation of $[Co(\beta\text{-ala})_2(en)]^+$ show respectively one and two resonance lines arising from the carboxy carbons of β-alaninates. Thus, the structures can be assigned to C_2-*cis*(*O*) for the former (**5**) and C_1-*cis*(*O*) for the latter (**9**), respectively.

Yoneda *et al.*[22] pointed out the importance of the effect of magnetic anisotropy induced on the central cobalt(III) chromophore. Application of this magnetic anisotropy to the **6** and **3** complexes leads to the following prediction. Two chelated glycinates in the **6** complex do not occupy equivalent positions; one is present in the plane formed by the coordinated oxygen atoms of glycinates and cobalt(III) (I-position), and the other is out of plane (O-position). On the other hand, the chelated glycinates in **3** at the O-position and their steric relation to the cobalt(III) chromophore ($[Co(O)_2(N)_4]$) are identical with the O-position glycinate of **6**. The O-position glycinate in **6** is expected to show nearly equal chemical shifts of the carboxy carbon to those in **3**. A similar relation is expected between **9** and **5**. In **16**, one glycinate is in the plane formed by the nitrogen atoms of the glycinates and cobalt(III) (I*-position), and another glycinate out of the N–Co(III)–N plane (O*-position). Two glycinates in **20** present at the O*-positions and their relation to the cobalt(III) chromophore (*cis*(*N*)-$[Co(O)_4(N)_2]$) are identical with the O*-position glycinate of **16**. In this manner, the following assignments are possible. In **6**, the carbon resonances at 46.0 and 187.2 ppm are for the O-position glycinate, at 46.0 and 186.0 ppm for the I-position glycinate. In **9**, those at 33.5, 37.7, and 181.8 ppm are for the I-position β-alaninate. In **16**, those at 46.1 and 182.2 ppm are for the O*-position glycinate, at 47.8 and 186.8 ppm for the I*-position glycinate. In **19**, those at 33.7, 38.0, and 183.1 are for the O*-position β-alaninate, at 33.7, 38.6, and 184.2 ppm for the I*-position β-alaninate.

The chemical shifts of the glycinate carbons in **11** are in fair agreement with those of the glycinate carbons in **10**. The chemical shifts of the β-alaninate carbons in **11** agree with those of the β-alaninate carbons in **12**. Similar agreements in chemical shifts were observed among the same geometrical isomers of bis(β-alaninato), bis(glycinato), and (β-alaninato)(glycinato) complexes. In the case of the **17** or **18** complex ion, the following consideration, in line with the above observations, is possible. When the I*-position (O*-position) glycinate of **16** is exchanged by β-alaninate, forming **17** (**18**), the carbon resonances of the I*-position (O*-position) glycinate will disappear and those of the I*-position (O*-position) β-alaninate will appear. As we expected, the glycinate carbons in **17** resonates at 187.2 and 46.1 ppm and these chemical shifts consist of those of the O*-position glycinate in **16** (187.2 and 46.1 ppm). The chemical shifts of β-alaninate carbons in **17** are nearly equal to those of the I*-position β-alaninate in **19**. A similar relation can be expected for the *cis*(*O*) of the second eluted isomer (**8**) in chromatographical separation of $[Co(\beta\text{-ala})(gly)(en)]^+$; the resonance peaks at 186.0 and 45.9 ppm for glycinate carbons and at 33.6, 38.4, and 183.7 ppm for the β-alaninate carbons consist of those of the O-position β-alaninate in **9** and I-position glycinate in **6**, respectively. The structure of the second eluted isomer can be assigned to *cis*(*O*)*trans*(N_g,*O*). As the chemical shifts of the fourth eluted isomer (**7**), resonating at 46.5 and 187.2 ppm (glycinate), and at 33.3, 37.8, and 182.0 ppm (β-alaninate), consist of those of O-position glycinate and I-position β-alaninate. The structure of this isomer can be assigned to *cis*(*O*)-*trans*(N_β,*O*).

In the present work, the ^{13}C chemical shifts were measured in ^1H noise decoupled mode. Since the signal of the carbon bonding to hydrogen is enhanced due to the nuclear Overhauser effect from ^1H atom and no splitting resonance is observed in noise decoupled mode, the resonance peak of the methylene carbon (α-carbon) of the glycinate is expected to be fairly intense. On the other hand, the resonance of the deuterated methylene carbon of the glycine will be very weak, since the signal of the carbon bonding to deuterium is split due to the carbon-deuterium coupling, no enhancement due to the NOE from ^1H atom being expected.[8] In the chelated glycine, the resonance of the carboxy carbon (which neighbors methylene carbon) is enhanced by the NOE from the methylene protons, but the deuteration of the methylene group results in weakening of the carboxy carbon resonance. Consequently, it is possible to confirm which glycinate possesses the deuterated methylene group by comparing the ^{13}C NMR spectra of the deuterated complex with that of the non-deuterated complex.

The methylene protons in the chelated glycine are easily deuterated in basic deuterium oxide solution.[23] We succeeded in preparing five glycinato-2,2-d_2 complexes, $([Co(ND_2CD_2COO)(en)_2]^{2+}$, C_1-*cis*(*O*)-$[Co(ND_2CD_2COO)(ND_2CH_2COO)(en)]^+$, and C_1-*cis*(*O*)-, C_2-*cis*(*O*)-, and *trans*(*O*)-$[Co(ND_2CD_2COO)_2(en)]^+$, by leaving each corresponding glycinato complex in basic deuterium oxide solution to stand for an appropriate time.

It is difficult to distinguish the methylene carbon of glycinate from that of the ethylenediamine, since the chemical shifts of the methylene carbons in chelated ethylenediamine are close to those of the methylene carbon of the chelated glycinate. The ^{13}C NMR measurements of these deuterated glycinato complexes make it possible to distinguish the signals of the carbons in the deuterated glycinate ring from those of the carbons in chelated ethylenediamine.

Yoneda *et al.*[22] showed for the **6** complex that the ^{1}H NMR signal resonating at 3.44 ppm arises from the methylene protons of the I-position glycinate. It was found that the I-position methylene protons are deuterated more rapidly than the O-position methylene protons (Fig. 1 (b)).[17] Since the methylene carbon resonance at 46.0 ppm and the carboxy carbon resonance at 186.0 ppm in **6** are weakened in the C_1-*cis*(*O*)-$[Co(ND_2CD_2COO)(ND_2CH_2COO)(en)]^+$, it is concluded that these methylene and carboxy carbons belong to the I-position glycinate, and methylene carbon at 46.0 ppm and carboxy carbon at 187.2 ppm in **6** to the O-position glycinate. The assignments of the ^{13}C NMR spectra based on the deuteration method are consistent with the assignments concluded from the comparison of the bis(glycinato) complexes with (β-alaninato)(glycinato) complexes.

The ^{13}C chemical shifts of the coordinated glycinate in bis(glycinato) complexes remained unchanged by the replacement of one of the two glycinates with β-alaninate. The ^{13}C chemical shifts of the β-alaninate in bis(β-alaninato) complexes also remained unchanged by the replacement of one of the β-alaninates with glycinate. These observations suggest that the main factor which determines the chemical shifts of the coordinated glycinate or β-alaninate is the steric position of the ligands to the central cobalt(III) chromophore. This recalls the theory of the magnetic anisotropy arising from the cobalt(III) chromophore.[22] However, the Co(III) magnetic anisotropy does not account for all the behavior of the chemical shifts of the ligands. It is expected from the Co(III) magnetic anisotropy in complex **6** that the ^{13}C chemical shift of the O-position methylene carbon of glycinate is located at lower magnetic field than that of the I-position methylene carbon, but really both carbon resonances were observed at 46.0 ppm as an overlapping signal. The carboxy carbon resonances of **10** should be located at much higher magnetic field than the observed ones, according to the cobalt(III) magnetic anisotropy.

References

1) Part X of this series: T. Ama, M. Higa, N. Koine, and T. Yasui, *Bull. Chem. Soc. Jpn.*, **50**, 2632 (1977).
2) T. Ama and T. Yasui, *Bull. Chem. Soc. Jpn.*, **49**, 472 (1976).
3) T. Yasui and T. Ama, *Bull. Chem. Soc. Jpn.*, **48**, 3171 (1975).
4) T. Yasui, H. Kawaguchi, Z. Kanda, and T. Ama, *Bull. Chem. Soc. Jpn.*, **47**, 2393 (1974).
5) T. Yasui, *Bull. Chem. Soc. Jpn.*, **48**, 454 (1975).
6) O. W. Howarth, P. Moore, and N. Winterton, *J. Chem. Soc., Dalton Trans.*, **1974**, 2271; *ibid.*, **1975**, 360.
7) K. D. Gailey, K. Igi, and B. E. Douglas, *Inorg. Chem.*, **14**, 2956 (1975).
8) G. L. Blackmer and T. M. Vickrey, *J. Coord. Chem.*, **3**, 225 (1974).
9) D. A. House and J. W. Blunt, *Inorg. Nucl. Chem. Lett.*, **11**, 219 (1975).
10) R. C. Stewart and L. G. Marzilli, *Inorg. Chem.*, **16**, 424 (1977).
11) M. Kojima, M. Fujita, and J. Fujita, *Bull. Chem. Soc. Jpn.*, **50**, 898 (1977).
12) Y. Hung, L. Y. Martin, S. C. Jackels, A. M. Tait, and D. H. Busch, *J. Am. Chem. Soc.*, **99**, 4029 (1977).
13) S. Bagger and O. Bang, *Acta Chem. Scand. A*, **30**, 765 (1976).
14) F. D. Sancilio, L. F. Druding, and D. M. Lukaszewski, *Inorg. Chem.*, **15**, 1626 (1976).
15) K. D. Gailey, K. Igi, and B. E. Douglas, *J. Coord. Chem.*, **5**, 171 (1973).
16) M. Ogawa, Y. Shimura, and R. Tsuchida, *Nippon Kagaku Zasshi*, **81**, 72 (1960).
17) T. Ama, H. Kawaguchi, and T. Yasui, presented at the 37th National Meeting of the Chemical Society of Japan, 4J09 (1978).
18) K. Yamazaki, J. Hidaka, and Y. Shimura, *Bull. Chem. Soc. Jpn.*, **42**, 119 (1969).
19) J. Hidaka and Y. Shimura, *Bull. Chem. Soc. Jpn.*, **40**, 2312 (1967).
20) N. Matsuoka, J. Hidaka, and Y. Shimura, *Bull. Chem. Soc. Jpn.*, **40**, 1868 (1967).
21) N. Matsuoka, J. Hidaka, and Y. Shimura, *Bull. Chem. Soc. Jpn.*, **45**, 2491 (1972).
22) H. Yoneda, U. Sakaguchi, and Y. Nakashima, *Bull. Chem. Soc. Jpn.*, **48**, 209 (1975).
23) D. Williams and D. H. Busch, *J. Am. Chem. Soc.*, **87**, 4644 (1965).

Luminescence Spectra of Cobalt(III) Cyano Complexes

Yusuke YAMAMOTO

Department of Chemistry, Faculty of Science, Rikkyo University, Nishi-Ikebukuro, Toshima-ku, Tokyo 171

(Received July 7, 1978)

Luminescence spectra of $M_3[Co(CN)_6]$ (M=K, Rb, Cs), *cis*-$K_3Na_2[Co(CN)_4(SO_3)_2]$, and *trans*-$Na_5[Co(CN)_4(SO_3)_2]$ were measured at 20 K. Single crystal luminescence spectra of the hexacyanocobaltates(III), centered at 14100—14200 cm^{-1}, exhibited vibrational structure associated with three components, and the separation between the members of the progression was about 400 cm^{-1}. Luminescence spectra of powdered *cis*-$K_3Na_2[Co(CN)_4(SO_3)_2]$ and *trans*-$Na_5[Co(CN)_4(SO_3)_2]$ were structureless and broad centered at 13200 and 14400 cm^{-1}, respectively. Comparison of these luminescence spectra with the corresponding spin-forbidden bands indicated that the 0-0 transition lies at 18300—18600 cm^{-1} for hexacyanocobaltates(III), at 16500—17000 cm^{-1} for *cis*-$K_3Na_2[Co(CN)_4(SO_3)_2]$, and at 17700—18200 cm^{-1} for *trans*-$Na_5[Co(CN)_4(SO_3)_2]$. The vibrational structure in luminescence spectra of hexacyanocobaltates(III) can be interpreted in terms of the ν_8, ν_9, ν_{12}, and ν_{13} ungerade skeletal modes, a lattice mode, and the totally symmetric ν_2 vibrational mode. Analysis of the relative intensity of the vibrational structure in the luminescence spectra gave information about the change in the Co–C internuclear equilibrium distance from the ground state to the excited luminescent state. The relationship between luminescence and photochemical behavior of cobalt(III) complexes was also considered.

In recent years, there has been a rapidly expanding interest in the luminescence of transition-metal coordination compounds.[1] A luminescence spectrum provides a great deal of useful information not only about an excited state but also about a ground state. There have been many studies on luminescence spectra of chromium(III) complexes from the viewpoints of both their spectroscopic and photochemical aspects.[1,2] On the other hand, although there have also been extensive spectroscopic and photochemical studies of cobalt(III) complexes, there has been few papers on their luminescence.

Luminescence of cobalt(III) complex was first reported on $K_3[Co(CN)_6]$ by Porter and Mingardi[3] in 1966. They observed a broad and structureless band centered at 14400 cm^{-1}, and assigned it as $^3T_{1g}\rightarrow{}^1A_{1g}$ phosphorescence on the basis of the band position and the lifetime. Later, the luminescence spectrum of $[Co(CN)_6]^{3-}$ was studied by some workers,[4-9] but most of them have also only reported it to be structureless and broad. The author has reported vibrational structure of the luminescence spectrum of powdered $K_3[Co(CN)_6]$ at 20 K, which exhibited a progression with about 400 cm^{-1} spacing interpreted in terms of the Co–C stretching frequency for the first time.[7] Recently, Hipps and Crosby[9] have also reported vibrational structure whose spacing between the members of the progression was 420 cm^{-1} in the luminescence spectrum of $K_3[Co(CN)_6]$ at 4.2 K.

Another example of luminescence of cobalt(III) complex was *trans*-$Na_5[Co(CN)_4(SO_3)_2]$ reported by Zuloaga and Kasha.[10] They reported a broad and structureless spectrum centered at 14300 cm^{-1} at 77 K and assigned it as the $^3T_{1g}\rightarrow{}^1A_{1g}(O_h)$ phosphorescence. As mentioned above, investigations of luminescence of cobalt(III) complexes have been very limited.

This paper deals with the luminescence of cobalt(III) complexes, the luminescence of one among them, *cis*-$K_3Na_2[Co(CN)_4(SO_3)_2]$, having been observed for the first time. For single crystals of $K_3[Co(CN)_6]$, $Rb_3[Co(CN)_6]$, and $Cs_3[Co(CN)_6]$, the luminescence spectra were measured with particular care for the fine structure to make clear what kind of vibration was responsible for the intensity. Also, the position of the 0-0 transition of the $^3T_{1g}\leftrightarrow{}^1A_{1g}(O_h)$ of hexacyanocobaltates(III) and of *cis*- and *trans*-tetracyanodisulfitocobaltates(III) are presented.

Finally, the possible relationship between photochemical behavior and luminescence is discussed.

Experimental

Preparation of Materials. $K_3[Co(CN)_6]$,[11] $Rb_3[Co(CN)_6]$,[12] $Cs_3[Co(CN)_6]$,[12] *cis*-$K_3Na_2[Co(CN)_4(SO_3)_2]$,[13] *trans*-$Na_5[Co(CN)_4(SO_3)_2]$,[14] *fac*-$[Co(CN)_3(NH_3)_3]$,[15] *cis*-$[Co(CN)_2(en)_2]ClO_4$,[16] $[Co(CN)(NH_3)_5]Cl_2$,[17] and $[Co(NH_3)_6]Cl_3$[18] were prepared according to the published methods. These compounds, except for *fac*-$[Co(CN)_3(NH_3)_3]$, were recrystallized several times. Single crystals of $K_3[Co(CN)_6]$, $Rb_3[Co(CN)_6]$, and $Cs_3[Co(CN)_6]$ were obtained by slow evaporation of aqueous solutions.

Measurement of Luminescence Spectra. Excitation light from a Ushio UM-102 mercury lamp (120 W) was isolated by a Spex Micromate grating monochromator (10 cm, f 2.5, blazed at 300 nm, 1200 l/mm), then passed through a Toshiba UV-D25 filter, and projected on the sample at an incident angle of 45°. Luminescent light at right angles to the excitation light was passed through a yellow cut-off filter to reduce scattered excitation light, and was dispersed by a JASCO CT-100 grating monochromator (100 cm, f 8.6, blazed at 750 nm, 1200 l/mm). The light from the monochromator was detected by a cooled Hamamatsu R-649S (S-20) photomultiplier, a Hamamatsu C-716 preamplifier, and a Hamamatsu C-767 photon counter, and recorded by a Yokogawa 3051 recorder equipped with a Yokogawa 3053-12 DC unit. Sometimes a set of a Hamamatsu R-666 photomultiplier, with GaAs photocathode, and a JASCO L-125 lock-in amplifier was used for the detection system. The sample was cooled with an Air Products and Chemicals Cryo-Tip AC-2 for measurements at liquid hydrogen temperature and with the optical cryostat designed in our laboratory for those at liquid nitrogen temperature. The sample temperature was measured using a chromel/constantan and a chromel/Au-0.07%Fe

thermocouple.

Spectral slit width was about 8 cm^{-1} for hexacyanocobaltates(III) and *trans*-$Na_5[Co(CN)_4(SO_3)_2]$, and about 16 cm^{-1} for other compounds.

The luminescence spectra thus obtained were corrected by the standard lamp method.

Measurements of Visible and Ultraviolet Absorption, Diffuse Reflectance, Infrared, and Raman Spectra. The absorption spectra of aqueous solutions were measured with a Hitachi EPS-3T spectrophotometer. The spin-forbidden band of a single crystal of $K_3[Co(CN)_6]$ was measured with a JASCO CT-50 grating monochromator (50 cm, f 5.6, blazed at 300 nm, 1200 l/mm) equipped with a Hamamatsu R-649S photomultiplier connected with the photon counting system at liquid helium temperature. The sample was cooled with the optical cryostat.

The diffese reflectance spectra were measured with a Hitachi EPS-3T spectrophotometer, using a diffuse reflectance accessory, at room temperature.

The infrared spectra in the 200—700 cm^{-1} region were obtained with a JASCO IR-F far-infrared spectrophotometer using the Nujol mull method.

Raman spectra were measured on powdered samples with a He-Ne laser Raman spectrophotometer.[19]

Results and Discussion

Luminescence Spectra of $K_3[Co(CN)_6]$. The 20 and 77 K, 313 nm excited luminescence spectra measured on a single crystal are shown in Fig. 1. The peak position of 14200 cm^{-1} was almost the same as that of other authors,[4-9] and the half band width of the total band was about 2600 cm^{-1}. The luminescence band increased gradually in intensity with a lowering in the temperature from room temperature to about 30 K, and decreased slightly with lowering in the temperature from about 30 to 20 K. This can be explained as having been caused by the competition between non-radiative relaxation and sharpening of the each component bands; that is, from room temperature to about 30 K, the dominant effect is depression of the non-radiative process, which increases luminescence intensity, and from about 30 to 20 K, sharpening of each component band is dominant, which decreases luminescence intensity. Even at room temperature,

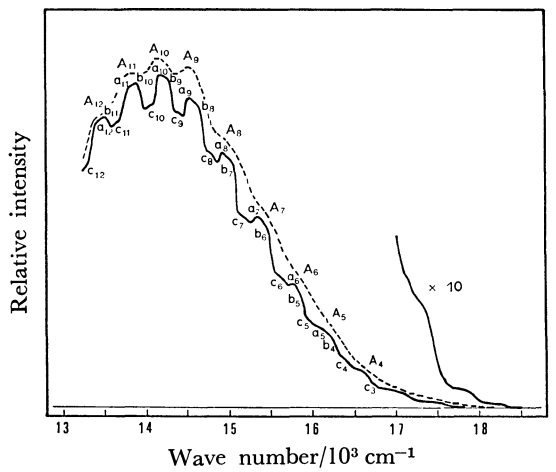

Fig. 1. Luminescence spectra of $K_3[Co(CN)_6]$.
——, 20 K; ——, 77 K.

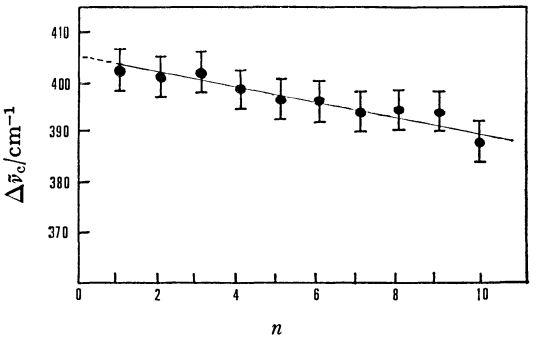

Fig. 2. Energy differences between c_n peaks, $\Delta\tilde{\nu}_c = \tilde{\nu}_{c_{n+1}} - \tilde{\nu}_{c_n}$, in $K_3[Co(CN)_6]$ at 20 K.

a structureless and very weak spectrum was observed. At 77 K, the spectrum exhibited vibrational structure with about 400 cm^{-1} spacing between the members of the progression. When the temperature was lowered from 77 to 20 K, the A_n progression at 77 K was resolved into two components, a_n and b_n progressions; moreover, a weak c_n progression appeared between the A_n progression. The average spacing of 394 cm^{-1} between the members of each progression was slightly decreased with increase in n, and the fundamental vibrational frequency was extrapolated to about 405 cm^{-1} as shown in Fig. 2.

Luminescence Spectra of $Rb_3[Co(CN)_6]$ and $Cs_3[Co(CN)_6]$. The 313 nm excited luminescence spectra of the rubidium and caesium salts were measured on single crystals at 20, 77 K, and room temperature. The spectral pattern was practically the same as that of the potassium salt. At 20 K, the maximum positions of the total bands were at 14100 and 14200 cm^{-1} for the rubidium and caesium salts, respectively. The vibrational structure, consisting of three components, was observed, but it was not so clear as in the potassium salt. The energy separation between the members of the progression was about 400 cm^{-1} as in the potassium salt. Even at 77 K, the spectra showed vibrational structure.

Position of the 0-0 Transition. Since the three salts of hexacyanocobaltates(III) showed the same vibrational pattern, the potassium salt, whose spectrum was the best resolved of the three, will be discussed.

The $^3T_{1g} \leftarrow {}^1A_{1g}$ spin-forbidden band of $K_3[Co(CN)_6]$ has been reported at different peak energy by some authors. Kida *et al.*[20] found a shoulder at 24000 cm^{-1}, while Porter and Mingardi,[3] and Jain *et al.*[21] observed weak bands at 18500 and 20833 cm^{-1}, respectively; and these three bands have been assigned as the $^3T_{1g} \rightarrow {}^1A_{1g}$ spin-forbidden transition. Recently, this spin-forbidden band was carefully reexamined by Kataoka[8] by microspectrophotometry at 77 K. A small shoulder, which was not observed at room temperature, appeared clearly at 26000 cm^{-1} when the temperature lowered to 77 K, and was assigned as the $^3T_{1g} \leftarrow {}^1A_{1g}$ spin-forbidden band.

The first component of the luminescence band, which lies at highest energy, was observed at *ca.* 18200 cm^{-1} in the 20 K sepctrum obtained. This indicates that the 0-0 transition lies at some 100 cm^{-1} higher than 18200 cm^{-1}. Comparison of the absorption peak

values with a position of the 0-0 transition obtained from the luminescence spectrum clearly shows that the positions of 18500 and 20833 cm^{-1} in absorption are too low in energy; while the peak positions observed at 24000 and 26000 cm^{-1} are consistent with the 0-0 transition obtained from this luminescence measurement. On the other hand, the calculated value for $^3T_{1g} \leftarrow {}^1A_{1g}$ spin-forbidden band is *ca.* 27000 cm^{-1}.[22] Consequently, it is more probable to assign the 26000 and/or 24000 cm^{-1} band than the 18500 and 20833 cm^{-1} bands as the $^3T_{1g} \leftarrow {}^1A_{1g}$ spin-forbidden band.

It is expected that the 0-0 transition would not obtain any appreciable intensity either in luminescence or in absorption. Thus, in order to obtain a more exact position of the 0-0 transition, vibrational structure measurement in the spin-forbidden absorption band is required. That is, comparison of the vibrational structures in both the luminescence and absorption spectra can be expected to give the 0-0 band position between their first components.

To determine the position of the 0-0 transition, the 4.2 K single crystal absorption was measured, but no vibrational structure was observed in the 17000—23000 cm^{-1} region. Consequently, the position of the 0-0 transition was not exactly determined, but would lie between 18300 and 18600 cm^{-1}.

Assignment of Vibrational Structure. To assign the vibrational structure associated with the luminescence spectrum, the normal modes of vibration of $[Co(CN)_6]^{3-}$ must be considered. Raman and infrared spectra of this complex have been studied by many workers,[23-29] but there has been some uncertainty in position and assignment, especially for low energy region skeletal vibration. The assignments of some workers are listed in Table 1.

There are five vibronic active skeletal modes, $\nu_7(t_{1u})$, $\nu_8(t_{1u})$, $\nu_9(t_{1u})$, $\nu_{12}(t_{2u})$, and $\nu_{13}(t_{2u})$; thus the fine structure of the spectrum would consist of $(\nu_7, \nu_8, \nu_9, \nu_{12}, \nu_{13})+n\nu_2(a_{1g})$ $(n=0, 1, 2, \ldots)$ peaks.[30] In these vibrational modes, it can be considered that the contribution of the deformation modes, ν_8, ν_9, ν_{12}, and ν_{13}, to the intensity would be large.[31-33] It is possible that the lattice motion would couple with the electronic level; but its contribution to the intensity, which is proportional to the degree of destruction of the center of symmetry, would be much weaker than that of the ungerade skeletal vibration.

The luminescence spectra seem to consist of three kinds of progressions, and members of each progression have about 400 cm^{-1} spacing. These progressions may be vibronic bands originated from one or more electronic levels. The ground state, $^1A_{1g}$, is not split by any perturbation, but the excited luminescent state, $^3T_{1g}$, splits into E, T_2, T_1, and A_1 by spin-orbit interaction. For $K_3[Co(CN)_6]$, the separation between the E and other upper levels, T_2, T_1, and A_1, have been reported as 30, 318, and about 500 cm^{-1}, and the lifetimes of the E, T_2, and T_1 as 463, 2615, and 28.3 μs, respectively, determined from the temperature dependence analysis of the lifetime.[9] On the basis of these separations and lifetimes, the contribution to the luminescence intensity of each level, I_l, is given by[34]

$$I_l \propto k_l \cdot g_l \cdot \exp(-\Delta E/kT) = 1/\tau_l \cdot g_l \cdot \exp(-\Delta E/kT), \quad (1)$$

where k_l is the rate constant of the luminescence process, τ_l is the lifetime, and g_l is the multiplicity. Thus the calculated intensity ratios of I_{T_2}/I_E and I_{T_1}/I_E are 2.1×10^{-2} and 2.9×10^{-9} at 20 K and 1.5×10^{-1} and 6.6×10^{-2} at 77 K. This indicates that, at 20 K, the luminescence from the T_2 and other upper levels would contribute less to the spectrum. Thus it is possible to neglect the T_2, T_1, and A_1 levels as luminescent ones.

Comparison of the energy separations betweeen adjacent components of the luminescence spectrum with those of the ungerade skeletal vibrations indicates that the most reasonable assignments are as follows. The most intense component, a_n progression, can be assigned as the transition to $(\nu_9+n\nu_2)$ or $(\nu_{13}+n\nu_2)$ level, or it may consist of two peaks corresponding to those, since the ν_9 and ν_{13} modes have nearly the same energy. Similarly, b_n progression is assigned as the transition to $(\nu_8+n\nu_2)$ or $(\nu_{12}+n\nu_2)$ level, or again it may consist of two peaks corresponding to those; while the weak component, c_n progression, cannot be assigned as any of the skeletal vibrational modes. The energy difference between the a_n and c_n progression is about 175 cm^{-1}; and the lattice modes appeared strongly at 172 and 189 cm^{-1},[26] hence the c_n progression can be assigned as the transition to the (a_n+lattice mode) level.

Calculation of the Relative Intensity of the Luminescence Band. The intensity ratio of the individual component bands from the 0-th vibrational state in the electronic state A to the n-th vibrational state in the electronic state B is given by[35]

Table 1. Raman and infrared spectra of $[Co(CN)_6]^{3-}$ ($\bar{\nu}$/cm^{-1})

	$\nu_2(a_{1g})$ νCo-C	$\nu_3(e_g)$ νCo-C	$\nu_7(t_{1u})$ νCo-C	$\nu_8(t_{1u})$ δCo-C-N	$\nu_9(t_{1u})$ δC-Co-C	$\nu_{12}(t_{2u})$ δCo-C-N	$\nu_{13}(t_{2u})$ δC-Co-C	Ref.
$K_3[Co(CN)_6]$	404	394[a]	565	414	129	380	104	26)
	408	330 (358)	564	416	90[a]	440	69[a]	23)
			562	414	128		108	27)
					92		72	28)
	408		562	415				This work
$Rb_3[Co(CN)_6]$	406		561	414		443		This work
$Cs_3[Co(CN)_6]$	413		560	415		437		This work

a) Calculated value.

$$\frac{I(B_n \leftarrow A_0)}{I(B_0 \leftarrow A_0)} = \frac{I_n}{I_0} = \left[\frac{1}{2}\alpha(\Delta r)^2\right]^n \frac{1}{n!}, \quad (2)$$

where $\alpha = 4\pi^2 m\bar{\nu}c/h$ and Δr is the difference in the equilibrium nuclear distance between the A and B states.

Setting $\frac{1}{2}\alpha(\Delta r)^2 = K$,

$$\frac{I_n}{I_0} = K^n \frac{1}{n!}. \quad (3)$$

The relative intensity of individual members of the a_n progression in the luminescence band, calculated from Eq. 3, is shown in Fig. 3 together with the observed spectrum of $K_3[Co(CN)_6]$ at 20 K. The calculated relative intensities shown by the heights of vertical lines in Fig. 3 are the one when $K=10.7$, and those of the other marks are the ones when $K=11.7$ and 12.7. When the maximum of the band occures at the n-th component, it can be seen that $n=K$ in Eq. 3, so that $K=10.7$ means that the first component of 18200 cm^{-1} in the luminescence spectrum should involve no ν_2 vibration. It is clear from Fig. 3 that the intensity ratio when $K=10.7$ is the best fit; thus it is highly probable that the 0-0 transition lies at 18300—18600 cm^{-1}.

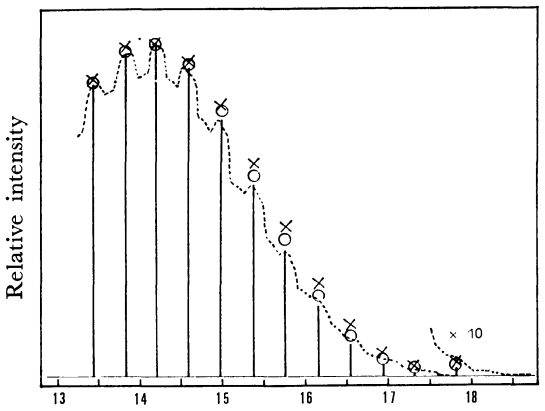

Fig. 3. Calculated relative intensity of $K_3[Co(CN)_6]$. Broken line indicates the observed spectrum. Vertical line, $K=10.7$; O, $K=11.7$; ×, $K=12.7$.

By fitting the relative intensities of the individual components in the observed luminescence band to the calculated ones, the change in the Co–C equilibrium nuclear distance, Δr, between the luminescent excited state and the ground state can be computed. The calculated change in the distance is 0.3 Å, when $K=10.7$. This value can be compared to 0.20—0.23 Å in Pt–F distance in $[PtF_6]^{2-}$.[36]

Luminescence Spectrum of cis-$K_3Na_2[Co(CN)_4(SO_3)_2]$. The 20 K, 365 nm excited luminescence spectrum is shown in Fig. 4. A broad and structureless band was observed at 13200 cm^{-1}, and its half band width was about 2000 cm^{-1}. The higher energy threshold value of the luminescence band was observed at 16500 cm^{-1}. The intensity of the luminescence was somewhat weaker than that of the hexacyanocobaltates(III).

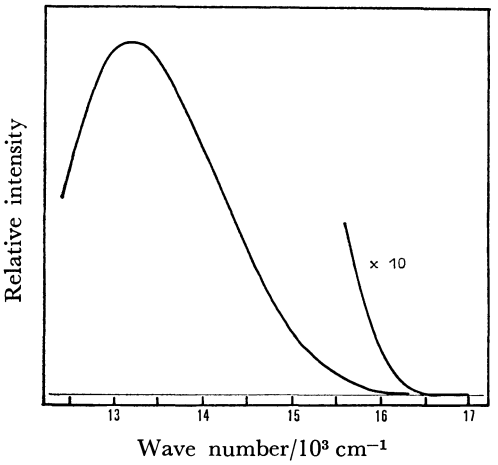

Fig. 4. Luminescence spectrum of *cis*-$K_3Na_2[Co(CN)_4(SO_3)_2]$ at 20 K.

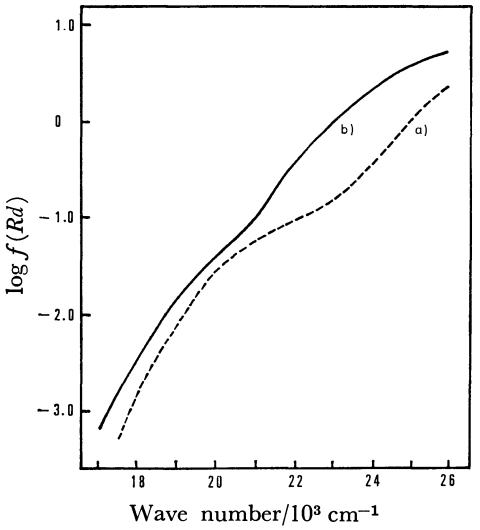

Fig. 5. Spin-forbidden bands of a) *cis*-$K_3Na_2[Co(CN)_4(SO_3)_2]$ and b) *trans*-$Na_5[Co(CN)_4(SO_3)_2]$ measured by diffuse reflectance method.

On the other hand, in the absorption spectrum obtained by the diffuse reflectance method, a weak shoulder was observed at *ca.* 20000 cm^{-1}, as shown in Fig. 5. In the figure the reflectance spectrum of *trans*-$Na_5[Co(CN)_4(SO_3)_2]$ is also shown.

The luminescence can be assigned as the transition from the lowest triplet state, $^3T_{1g}(O_h)$, to the $^1A_{1g}(O_h)$ ground state, on the basis of its position and intensity. It is consistent with the position of the luminescence band that the weak shoulder at *ca.* 20000 cm^{-1} in absorption was regarded to be the spin-forbidden band, hence it can be assigned as the $^3T_{1g} \leftarrow {}^1A_{1g}(O_h)$ spin-forbidden transition, which is the reverse process of luminescence. The 0-0 transition would lie at 16500—17000 cm^{-1} on the basis of the threshold value of the luminescence band and the maximum position of both luminescence and absorption.

Luminescence Spectrum of trans-$Na_5[Co(CN)_4(SO_3)_2]$. The 20 K, 365 nm excited luminescence spectrum is shown in Fig. 6. A broad and structureless band as in the cis salt was observed at 14400 cm^{-1}, and its

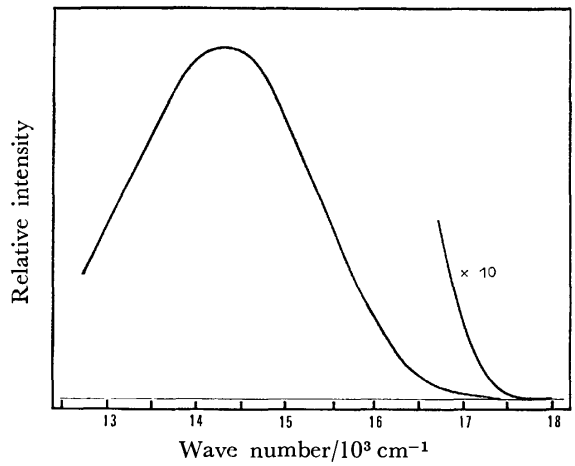

Fig. 6. Luminescence spectrum of *trans*-$Na_5[Co(CN)_4(SO_3)_2]$ at 20 K.

half band width was about 2300 cm^{-1}. The threshold value was observed at *ca.* 17700 cm^{-1}. Intensity of the luminescence was comparable to that of the hexacyanocobaltates(III). The diffuse reflectance spectrum showed a weak shoulder at *ca.* 20000 cm^{-1}, as shown in Fig. 5.

The luminescence spectrum of this complex salt has already been measured at 77 K by Zuloaga and Kasha,[10] and the spectrum obtained in the present work was essentially the same as that in this previous investigation. The luminescence can be assigned as $^3T_{1g} \rightarrow {}^1A_{1g}(O_h)$ phosphorescence and the weak shoulder observed in the absortpion spectrum can be assigned as the reverse process of the luminescence, that is the $^3T_{1g} \leftarrow {}^1A_{1g}(O_h)$ transition. The 0-0 transition would lie at 17700–18200 cm^{-1} on the basis of the threshold value of the luminescence band and the maximum position of both luminescence and absorption bands. Finally, it is interesting to note that there is some difference in ligand field strength between this complex and hexacyanocobaltates(III), but the luminescence of both appeared at almost the same position in spite of their defference in energy of the $^3T_{1g} \leftarrow {}^1A_{1g}(O_h)$ spin-forbidden band.

Luminescence of Other Cobalt(III) Complexes. Luminescence spectra of *fac*-$[Co(CN)_3(NH_3)_3]$, *cis*-$[Co(CN)_2(en)_2]ClO_4$, $[Co(CN)(NH_3)_5]Cl_2$, and $[Co(NH_3)_6]Cl_3$, excited by 365 and 313 nm light were measured in the 12000—20000 cm^{-1} region, but no luminescence was observed even at 20 K. Thus the luminescent complexes are probably restricted to those having four or more cyano ligands.

Relationship between Luminescence and Photochemical Behavior. Photochemical reaction of cobalt(III) complexes in aqueous solution have been extensively studied by many authors.[1b,1c,37] Generally, they can be classified into the following two types:

(A) Redox reaction from Co(III) to Co(II) with release of ligands,

(B) Ligand substitution reaction without reduction of central cobalt atom.

Cobalt(III) complexes almost all belong to type (A), for example, $[Co(NH_3)_6]^{3+}$,[38] $[Co(en)_3]^{3+}$,[38] $[CoCl(NH_3)_5]^{2+}$,[39,40] $[CoBr(NH_3)_5]^{2+}$,[40,41] $[CoI(NH_3)_5]^{2+}$,[42,43] $[Co(ox)_3]^{3-}$,[44] *etc.* But to date there have been reported a few that belong to type (B), for example, $[Co(CN)_6]^{3-}$,[45] $[CoCl(CN)_5]^{3-}$,[40,46] $[CoBr(CN)_5]^{3-}$,[40,46] and $[Co(CN)_5I]^{3-}$,[46] as listed in Table 2. It is interesting to note that all of them that belong to type (B) contain five or more cyano ligands.

In the photochemical reaction of type (A), the oxidation state of the cobalt atom changes from +3 to +2, hence it is considered that the reaction occurs from a ligand-to-metal charge transfer(LMCT) state. This means that the LMCT level mainly is the most populated state after irradiation of ultraviolet light and that the potential minimum of the LMCT level is lower than that of the ligand field leves, as shown in Fig. 7a). In the complexes of type (A), ligand

TABLE 2. RELATIONSHIP BETWEEN PHOTOCHEMICAL BEHAVIOR AND LUMINESCENCE OF COBALT(III) COMPLEXES

Complex	Type of photochemical reaction[a]	Phosphorescence[b]
$[Co(NH_3)_6]^{3+}$	A	−
$[Co(en)_3]^{3+}$	A	−
$[CoCl(NH_3)_5]^{2+}$	A	−
$[CoBr(NH_3)_5]^{2+}$	A	−
$[CoI(NH_3)_5]^{2+}$	A	−
$[Co(CN)(NH_3)_5]^{2+}$	×	−
cis-$[Co(CN)_2(en)_2]^+$	×	−
fac-$[Co(CN)_3(NH_3)_3]$	×	−
cis-$[Co(CN)_4(SO_3)_2]^{5-}$	×	+
trans-$[Co(CN)_4(SO_3)_2]^{5-}$	×	+
$[CoCl(CN)_5]^{3-}$	B	+[c]
$[CoBr(CN)_5]^{3-}$	B	+[c]
$[Co(CN)_5I]^{3-}$	B	+[c]
$[Co(CN)_6]^{3-}$	B	+
$[Co(ox)_3]^{3-}$	A	−

a) A, Type (A); B, Type (B); ×, Not investigated.
b) +, Phosphorescent; −, non-phosphorescent.
c) Unpublished data.

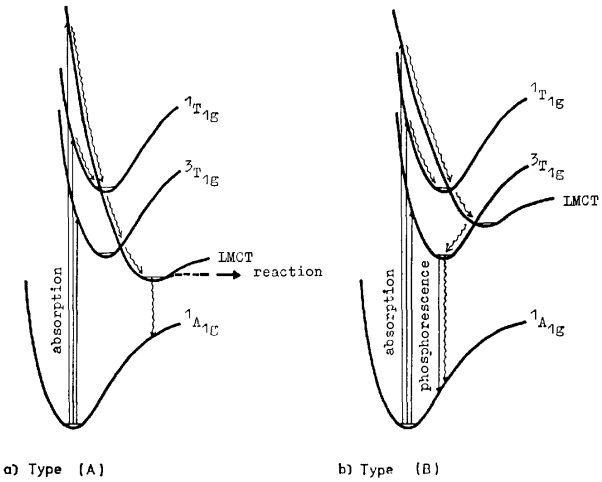

Fig. 7. Schematic diagram of potential curves of type (A) and type (B) cobalt(III) complexes.

substitution reaction also may occur, the cobalt atom maintaining its oxidation state of +3 when the complex is irradiated with a ligand field absorption band; but even in those cases when this reaction has occured, the quantum yield is lower than in the redox reaction by from 10 to 100 times. In the solid state, although there are only a few cobalt(III) complexes that undergo photochemical reaction,[47,48] the situation of electronic level of these complexes does not differ as much as in an aqueous solution. Thus in the solid state, the irradiated energy may be finally populated also to the LMCT level and would deactivate non-radiatively. Therefore, it may be concluded that the complexes of type (A) do not luminesce the $^3T_{1g} \rightarrow {}^1A_{1g}$ phosphorescence.

On the other hand, in complexes that belong to type (B), the cobalt(III) atom is not reduced, but the ligand substitution reaction does occur; hence it is considered that the energy irradiated is not populated to the LMCT level, but to the ligand field level, and a photochemical reaction occurs from this level in aqueous solution. This indicates that the lowest ligand field triplet level, $^3T_{1g}(O_h)$, would be the main populated state and lower than the LMCT level, as shown in Fig. 7b). Hence, in the solid state, the $^3T_{1g} \rightarrow {}^1A_{1g}(O_h)$ luminescence would be observed. Actually, the luminescent complexes belong to type (B), as shown in Table 2.

The author wishes to express his sincere thanks to Professors Yukio Kondo and Masayoshi Nakahara for their helpful suggestions and discussions throughout this work. He is also indebted to Mr. Hiroshi Saito of the laboratory of Physical Chemistry of Rikkyo University for making available a Raman spectrophotometer and for his help with measurements, and to Dr. Akio Urushiyama for his help with single crystal absorption measurements at liquid helium temperature.

References

1) a) P. D. Fleischauer and P. Fleischauer, *Chem. Rev.*, **70**, 199 (1970); b) V. Balzani and V. Carassiti, "Photochemistry of Coordination Compounds," Academic Press, London (1970); c) "Concepts in Inorganic Photochemistry," ed by A. W. Adamson and P. Fleischauer, Wiley, New York (1975); d) P. D. Fleischuer, A. W. Adamson, and G. Sartori, *Progr. Inorg. Chem.*, **17**, 1 (1972).

2) a) H. L. Schläfer, *Z. Chem.*, **10**, 9 (1970); b) G. B. Porter, S. N. Chen, H. L. Schläfer, and H. Gausmann, *Theor. Chim. Acta*, **20**, 81 (1971); c) I. Fischler, J. M. Kelly, P. Krisch, and G. E. Koerner, *Mol. Photochem.*, **5**, 497 (1973); d) C. D. Flint, *Coord. Chem. Rev.*, **14**, 47 (1974); L. S. Forster, *Adv. Chem. Ser.*, **150**, 172 (1976).

3) G. B. Porter and M. Mingardi, *J. Chem. Phys.*, **44**, 4354 (1966).

4) G. A. Crosby, *J. Chim. Phys.*, **64**, 160 (1967).

5) A. D. Kirk, A. Ludi, and H. L. Schläfer, *Ber. Bunsenges. Phys. Chem.*, **73**, 669 (1969).

6) A. D. Kirk, H. L. Schläfer, and A. Ludi, *Can. J. Chem.*, **48**, 1065 (1970).

7) H. Kataoka, Y. Yamamoto, M. Nakahara, and Y. Kondo, *Nippon Kagaku Zasshi*, **92**, 274 (1971).

8) H. Kataoka, *Bull. Chem. Soc. Jpn.*, **46**, 2078 (1973).

9) K. W. Hipps and G. A. Crosby, *Inorg. Chem.*, **13**, 1543 (1974).

10) F. Zuloaga and M. Kasha, *Photochem. Photobiol.*, **7**, 549 (1968).

11) *Inorg. Synth.*, Vol. II, 225 (1946).

12) $Rb_3[Co(CN)_6]$ and $Cs_3[Co(CN)_6]$ were crystallized from a $K_3[Co(CN)_6]$ aqueous solution by adding RbCl and CsCl, respectively.

13) H. Siebert, C. Siebert, and S. Thym, *Z. Anorg. Allg. Chem.*, **389**, 165 (1971).

14) H. H. Chen, M.-S. Tosao, R. W. Gaver, P. H. Tewair, and W. K. Wilmarth, *Inorg. Chem.*, **5**, 1913 (1966).

15) Y. Kondo, M. Nakahara, H, Kataoka, and Y. Yamamoto, *Nippon Kagaku Zasshi*, **92**, 272 (1971).

16) K. Kuroda, *Nippon Kagaku Zasshi*, **89**, 720 (1968).

17) H. Siebert, *Z. Anorg. Allg. Chem.*, **327**, 63 (1964).

18) *Inorg. Synth.*, Vol. II, 217 (1946).

19) The Raman spectrophotometer, with a JEOL He–Ne laser (50 mW) and a Narumi model 750Z-1200 grating double monochromator, was designed and set up by the laboratory of Physical Chemistry of Rikkyo University.

20) S. Kida, J. Fujita, K. Nakamoto, and R. Tsuchida, *Bull. Chem. Soc. Jpn.*, **31**, 79 (1958).

21) S. C. Jain, A. V. R. Warrier, and H. K. Sehgal, *J. Phys. C*, **5**, 1511 (1972).

22) J. J. Alexander and H. B. Gray, *Coord. Chem. Rev.*, **2**, 29 (1967).

23) L. H. Jones, *J. Chem. Phys.*, **36**, 1209 (1962).

24) L. H. Jones, *J. Chem. Phys.*, **41**, 856 (1964).

25) I. Nakagawa and T. Shimanouchi, *Spectrochim. Acta*, **18**, 101 (1962).

26) I. Nakagawa, *Bull. Chem. Soc. Jpn.*, **46**, 3690 (1973 .

27) J. T. R. Dunsumuir and A. P. Lane, *J. Chem. Soc., A*, **1971**, 776.

28) D. Bloor, *J. Chem. Phys.*, **41**, 2573 (1964).

29) M. Krauzman, *C. R. Acad. Sci. Ser. B*, **162**, 765 (1966).

30) F. A. Cotton, "Chemical Applications of Group Theory," 2nd ed, Wiley-Interscience (1971), p. 280.

31) S. Koide and M. H. L. Pryce, *Phil. Mag.*, **3**, 607 (1958).

32) S. Koide, *Philos. Mag.*, **4**, 243 (1959).

33) J. A. Stanko, Ph. D. Thesis, University of Illinois, U. S. A., 1966.

34) R. W. Harrigan and G. A. Crosby, *J. Chem. Phys.*, **59**, 3468 (1973).

35) C. J. Ballhausen, *Theor. Chim. Acta*, **1**, 285 (1963).

36) H. H. Patterson, W. J. DeBerry, J. E. Byrne, M. T. Hus, and J. A. LoMenzo, *Inorg. Chem.*, **16**, 1698 (1977).

37) A. W. Adamson, *Adv. Chem. Ser.*, **150**, 128 (1976).

38) M. F. Manfrini, G. Varani, L. Moggi, and V. Balzani, *Mol. Photochem.*, **1**, 387 (1968).

39) L. Moggi, N. Sabbatini, and V. Balzani, *Gazz. Chim. Ital.*, **97**, 980 (1967).

40) A. W. Adamson, *Discuss. Faraday Soc.*, **29**, 163 (1960).

41) J. F. Endicott and M. Z. Hoffman, *J. Am. Chem. Soc.* **87**, 3348 (1965).

42) N. Shinozuka and S. Kikuchi, *Nippon Kagaku Zasshi*, **87**, 413 (1966).

43) A. Haim and H. Taube, *J. Am. Chem. Soc.*, **85**, 459 (1963).

44) G. B. Porter, J. G. W. Doering, and S. Karanka, *J. Am. Chem. Soc.*, **84**, 4027 (1962).

45) L. Moggi, F. Bolletta, V. Balzani, and F. Scandola, *J. Inorg. Nucl. Chem.*, **28**, 2589 (1966).

46) A. W. Adamson and A. H. Sporer, *J. Inorg. Nucl. Chem.*, **8**, 209 (1958).

47) V. Balzani, R. Ballaradini, N. Sabatini, and L. Moggi, *Inorg. Chem.*, **7**, 1398 (1968).

48) E. L. Simmons and W. W. Wendlandt, *Coord. Chem. Rev.*, **7**, 11 (1971).

Solubility Isotherms of Reciprocal Salt-Pairs of Optically Active Cobalt(III) Complexes

Akira FUYUHIRO,* Kazuaki YAMANARI, and Yoichi SHIMURA
Department of Chemistry, Faculty of Science, Osaka University, Toyonaka, Osaka 560
(Received June 13, 1978)

Two kinds of four-component solubility isotherms consisting of (Λ-$[Co(ox)(en)_2]^+$, Δ-$[Co(ox)(en)_2]^+$)–(Cl^-, X^-)–H_2O, where X^- stands for Δ-$[Co(edta)]^-$ or (R,R)-$C_4H_5O_6^-$, have been determined experimentally at 25 °C. It has been found that neither double salt nor solid solution exists and no configurational activity is observed in these systems. The applications of these phase diagrams to the practical optical resolutions are discussed.

Several solubility isotherms of reciprocal salt-pairs which have two cations and two anions such as (Na^+, NH_4^+)–(Cl^-, HCO_3^-)–H_2O and (K^+, Mg^{2+})–(Cl^-, SO_4^{2-})–H_2O have been reported[1–3] and applied to the alkali industry. However no such isotherm has been reported for the system of metal complexes. The four-component solubility isotherms of reciprocal salt-pairs containing a pair of diastereomers are especially interesting in a viewpoint of optical resolution.

In this connection, some of the three-component solubility isotherms of chiral cobalt(III) complexes have already been reported from our laboratory.[4]

The present paper deals with the solubility isotherms (at 25 °C) of two kinds of reciprocal salt-pairs, (Λ-$[Co(ox)(en)_2]^+$, Δ-$[Co(ox)(en)_2]^+$)–(Cl^-, X^-)–H_2O, where X^- stands for Δ-$[Co(edta)]^-$ or $(+)_{589}$-(R,R)-$C_4H_5O_6^-$ (abbreviated to d-H_3tart^-). These four-component systems provide the model cases of the optical resolutions of *rac*-$[Co(ox)(en)_2]Cl$ with resolving agents containing the chiral anion X^-.

Experimental

Materials. *$[Co(ox)(en)_2]X$, $X=Cl\cdot H_2O$ and d-$H_3tart\cdot nH_2O$*: Racemic chloride monohydrate and racemic acetate were prepared and optically resolved by the methods of Dwyer *et al.*[5] and Jordan *et al.*,[6] and that improved by Koine.[7] The Δ-$[Co(ox)(en)_2]Cl\cdot H_2O$ complex was obtained from the filtrate from the less soluble diastereomer Λ-$[Co(ox)(en)_2](d\text{-}H_3tart)\cdot H_2O$ in these procedures by adding 12 M HCl, and was optically purified by repeated crystallizations from warm water. The more soluble diastereomer Δ-$[Co(ox)(en)_2](d\text{-}H_3tart)\cdot 2H_2O$ was prepared from Δ-$[Co(ox)(en)_2]Cl\cdot H_2O$, d-H_4tart, and $Ag_2(d\text{-}H_2tart)$ in the mole ratio of 2 : 1 : 1, and recrystallized from warm water. Found: C, 26.42; H, 5.56; N, 12.40%. Calcd for Δ-$[Co(ox)(en)_2](d\text{-}H_3tart)\cdot 2H_2O$: C, 26.56; H, 5.57; N, 12.39%. The Λ-$[Co(ox)(en)_2]Cl\cdot H_2O$ complex was obtained by adding 12 M HCl to a warm solution of the less soluble diastereomer.

Δ-K[Co(edta)]$\cdot 2H_2O$: This complex was resolved by the method of Jordan *et al.*[6] and optically purified by fractional crystallization after treating with a cation exchange resin K^+ form.

$[Co(ox)(en)_2]\Delta$-$[Co(edta)]\cdot nH_2O$: The less soluble diastereomer Δ-$[Co(ox)(en)_2]\Delta$-$[Co(edta)]\cdot H_2O$ was obtained by the method of Dwyer *et al.*[5] The more soluble diastereomer was prepared from Λ-$[Co(ox)(en)_2](CH_3COO)$ and Δ-$K[Co(edta)]\cdot 2H_2O$ and recrystallized from warm water. Found: C, 28.97; H, 5.11; N, 12.70%. Calcd for Λ-$[Co(ox)(en)_2]\Delta$-$[Co(edta)]\cdot 3H_2O$: C, 28.75; H, 5.13; N, 12.57%.

Measurements. Solubility was measured at 25 °C as follows: a mixed aqueous solution containing an excess of one, two, or three solid complex salt(s) in a conical flask was stirred mechanically for *ca.* 1.5 h at 25 °C in a thermostat regulated within ±0.1 °C. After the resulting saturated solution had been left to stand for a while, a portion of the supernatant solution was sucked into a weighing bottle through a cotton plug and then weighed. The amount of each ion in the saturated solution was determined as follows. The sample was diluted with water to a known volume, and its optical density and CD were measured. In the cases of containing Δ-$[Co(edta)]^-$ ion, optical densities were measured at 470.0 and 580.0 nm, and CD at 540.5 and 590.0 nm. The concentrations of {Λ-$[Co(ox)(en)_2]^+$+Δ-$[Co(ox)(en)_2]^+$} and Δ-$[Co(edta)]^-$ were derived from the observed optical densities, referring to the established values for the molar absorption coefficients of the component ions: ε(470.0 nm)=89.1 and ε(580.0 nm)=11.7 for Λ- and Δ-$[Co(ox)(en)_2]^+$, and ε(470.0 nm)=93.2 and ε(580.0 nm)=199 for Δ-$[Co(edta)]^-$. The concentrations of {Λ-$[Co(ox)(en)_2]^+$−Δ-$[Co(ox)(en)_2]^+$} and Δ-$[Co(edta)]^-$ were also derived from the observed CD values, referring to the data: $\Delta\varepsilon$(540.5 nm)=±2.31 and $\Delta\varepsilon$(590.0 nm)=±0.255 for Λ- and Δ-$[Co(ox)(en)_2]^+$ (+ and − for Λ and Δ, respectively), and $\Delta\varepsilon$(540.5 nm)=0 and $\Delta\varepsilon$(590.0 nm)=−1.66 for Δ-$[Co(edta)]^-$. The concentrations of Λ- and Δ-$[Co(ox)(en)_2]^+$ were separately calculated from those of {Λ-$[Co(ox)(en)_2]^+$+Δ-$[Co(ox)(en)_2]^+$} and {Λ-$[Co(ox)(en)_2]^+$−Δ-$[Co(ox)(en)_2]^+$}. The concentration of Δ-$[Co(edta)]^-$ was obtained from the mean values through the absorption and CD measurements. In the cases of not containing Δ-$[Co(edta)]^-$, optical densities and CD of the diluted sample solutions were measured at 497.0 and 523.0 nm, respectively, and the concentrations of Λ- and Δ-$[Co(ox)(en)_2]^+$ were separately derived, referring to the data: ε(497.0 nm)=119 and $\Delta\varepsilon$(523.0 nm)=±27.5 for Λ- and Δ-$[Co(ox)(en)_2]^+$ (+ and − for Λ and Δ, respectively). In the cases of containing d-H_3tart^- and Cl^- ions, a titration method was combined with the spectral one in order to determine the amount of d-H_3tart^-: the sample solution, which was sucked up and then weighed, was diluted to an appropriate volume and titrated with a 0.01 mol dm^{-3} NaOH solution to the end point of pH jump of the second step dissociation of the dicarboxylic acid.

In these ways, the amounts of all the cations and anions and then the amount of water in the saturated solution were obtained. Thus the concentrations of all the complex salts were calculated in molality. From a few reference experiments, it was confirmed that the optical densities and CD of the present cobalt(III) complex ions were not influenced by the coexistence of the counter ions, and that the absorption or CD value obtained for a mixed solution of several complex ions at a given wavelength was equal

to the sum of those measured for the individual complex ions.

The solid phases were identified from the elemental analyses, the absorption and CD spectra, and so on. Optical densities were measured with a JASCO UVIDEC-1 spectrophotometer and CD with a JASCO MOE-1 spectropolarimeter.

Results and Discussion

Definition of Solubility Diagrams of Reciprocal Salt-Pairs. Solubility isotherms of reciprocal salt-pairs, (A^+, B^+)–(X^-, Y^-)–solvent, can be drawn in space as shown in Fig. 1.[1] Four vectors along four axes starting from an origin O show the solubilities of AX, AY, BX, and BY in a solvent. In this definition, the mutual nearest neighbor axes are situated at an angle of 60° and have a common-ion. The angle between an axis and the opposite one becomes 90°. Any saturated solution can be expressed as a point defined by summing up the position vectors of the solubilities of the salts contained. So the points of the solubilities of the binary and ternary systems are situated on the axes and the side faces of the tetragonal pyramid, respectively, except for the two ternary systems such as AX–BY–solvent and AY–BX–solvent which have only the solid phases of $A_pB_{1-p}X_pY_{1-p}\cdot n$(solvent) and $A_qB_{1-q}X_{1-q}Y_q\cdot n'$(solvent), respectively ($0\leqq p\leqq 1$ and $0\leqq q\leqq 1$). In the four-component system, there are two ways to attribute a solution to three salts and the solvent, assuming the concentrations of all the salts to be positive; for example, the choice is possible between the sets AX+BX+AY+solvent and AX+BX+BY+solvent. However, the points of these two systems are the same in space, when each axis is graduated in molality.

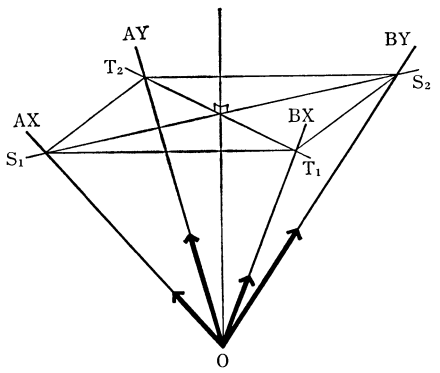

Fig. 1. Solubility diagram of reciprocal salt-pairs (A^+, B^+)-(X^-, Y^-)–solvent.

In this way, the phase diagram of reciprocal salt-pairs is strictly determined,[8] and the isotherms can be drawn by three kinds of plane figures: they are the plane projection on the horizontal base, the side elevation projected by parallel light along S_1S_2 or T_1T_2, and the clinographic projection with a light source at the origin O in Fig. 1. The clinographic projection has the property that the abscissa and ordinate indicate the mole fractions of B^+ and Y^-, respectively, to all the cations or anions (see Figs. 3 and 5).

Solubility Isotherms of (Λ-[Co(ox)(en)$_2$]$^+$, Δ-[Co(ox)(en)$_2$]$^+$–(Cl^-, X^-)–H_2O; X^-=Δ-[Co(edta)]$^-$ and d-H_3tart^-. The solubility data obtained are given in Tables 1 and 2, and in Figs. 2—5. Neither double salt including racemic compound nor solid solution

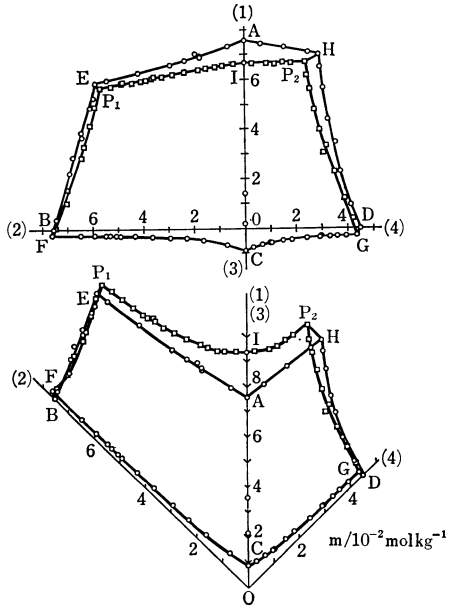

Fig. 2. The plane projection (upper) and the side elevation of the solubility isotherm of the reciprocal salt-pairs (Λ-[Co(ox)(en)$_2$]$^+$, Δ-[Co(ox)(en)$_2$]$^+$)-(Cl^-, Δ-[Co(edta)]$^-$)-H_2O at 25 °C: solubility is presented in molality m of anhydrous salt; (1) Λ-[Co(ox)(en)$_2$]Cl, (2) Δ-[Co(ox)(en)$_2$]Cl, (3) Δ-[Co(ox)(en)$_2$]Δ-[Co(edta)], (4) Λ-[Co(ox)(en)$_2$]Δ-[Co(edta)]; □, solubility of four-components; ○, solubility of two- or three-components.

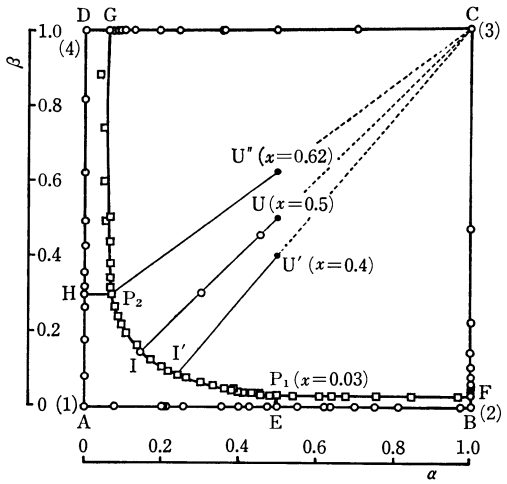

Fig. 3. The clinographic projection of the solubility isotherm of the reciprocal salt-pairs (Λ-[Co(ox)(en)$_2$]$^+$, Δ-[Co(ox)(en)$_2$]$^+$)-(Cl^-, Δ-[Co(edta)]$^-$)-H_2O at 25 °C: α, mole fraction of Δ-[Co(ox)(en)$_2$]$^+$ to all the cations; β, mole fraction of Δ-[Co(edta)]$^-$ to all the anions; (1) Λ-[Co(ox)(en)$_2$]Cl, (2) Δ-[Co(ox)(en)$_2$]Cl, (3) Δ-[Co(ox)(en)$_2$]Δ-[Co(edta)], (4) Λ-[Co(ox)-(en)$_2$]Δ-[Co(edta)]; □, solubility of four-components; ○, solubility of two- or three-components.

Table 1. Equilibrium of (Λ-[Co(ox)(en)$_2$]$^+$, Δ-[Co(ox)(en)$_2$]$^+$)-(Cl$^-$, Δ-[Co(edta)]$^-$)-H_2O system at 25 °C
In liquid phases, solubility is presented in molality m of anhydrous salt. Abbreviations are as follows: Λ-[Co(ox)(en)$_2$]Cl·H_2O=ΛCl, Δ-[Co(ox)(en)$_2$]Cl·H_2O=ΔCl, Λ-[Co(ox)(en)$_2$]Δ-[Co(edta)]·$3H_2O$=ΛR_1, Δ-[Co(ox)(en)$_2$]Δ-[Co(edta)]·H_2O=ΔR_1.

a)	b)	Liquid phase[c] $m/10^{-2}$ mol kg^{-1} ΛCl	ΔCl	ΛR_1	ΔR_1	Solid phase
A	2	7.57 (±0.09)				ΛCl
A↕E	3	7.32	0.63			ΛCl
		6.90	1.75			
		6.96	1.79			
		7.04	1.93			
		6.77	2.34			
		6.58	2.92			
		6.29	4.19			
		6.00	5.44			
B	2		7.57 (±0.09)			ΛCl
B↕E	3	0.41	7.45			ΔC
		1.60	6.98			
		2.24	6.92			
		2.88	6.78			
		3.69	6.42			
		3.90	6.44			
		4.91	6.08			
		5.30	5.96			
E	3	5.89 (±0.10)	5.89 (±0.10)			ΛCl +ΔCl
P_1	4	6.06 (±0.11)	5.68 (±0.12)		0.37 (±0.06)	ΛCl +ΔCl +ΔR_1
C	2				0.89 (±0.02)	ΔR_1
C↕G	3			0.31	0.75	ΔR_1
				0.65	0.65	
				0.96	0.55	
				1.02	0.57	
				1.47	0.48	
				1.82	0.44	
				2.42	0.36	
				2.92	0.34	
				2.96	0.32	
				3.31	0.33	
				3.59	0.32	
				3.93	0.30	
D	2			4.49 (±0.04)		ΔR_1
G	3			4.33 (±0.01)	0.28 (±0.01)	ΔR_1 +ΔR_1
G↕P_2	4	0.58		4.23	0.20	ΔR_1 +ΔR_1
		1.46		3.90	0.27	
		2.58		3.51	0.32	
		3.69		3.20	0.38	
		3.48		3.07	0.45	
		4.46		2.93	0.51	
		5.35		2.74	0.58	
		6.21		2.56	0.62	
		6.79		2.45	0.66	
P_2	4	7.38 (±0.32)		2.39 (±0.15)	0.72 (±0.15)	ΛCl +ΛR_1 +ΔR_1
D↕H	3	0.93		4.13		ΛR_1
		2.26		3.71		
		3.55		3.43		
		4.38		3.26		
		5.63		3.08		
		6.47		2.97		
A↕H	3	7.44		0.65		ΛCl
		7.28		1.56		
		7.06		2.50		
H	3	6.96 (±0.13)		2.92 (±0.04)		ΛCl +ΛR_1
C↕F	3		0.74		0.65	ΛR_1
			1.65		0.47	
			2.31		0.39	
			2.94		0.34	
			3.67		0.31	
			4.34		0.27	
			4.93		0.26	
			5.08		0.25	
			5.34		0.24	
			5.49		0.26	
			5.93		0.24	
			6.49		0.23	
F	3		7.65 (±0.07)		0.22 (±0.02)	ΔCl +ΔR_1
F↕P_1	4	0.27	7.49		0.21	ΔCl +ΔR_1
		1.31	7.04		0.23	
		2.25	6.78		0.26	
		3.18	6.44		0.28	
		3.64	6.33		0.29	
		4.50	6.08		0.31	
		5.30	5.94		0.33	
P_1↕I	4	6.13	5.27		0.37	ΛCl +ΔR_1
		6.25	4.88		0.38	
		6.33	4.80		0.42	
		6.33	4.44		0.42	
		6.39	4.06		0.44	
		6.46	3.86		0.45	
		6.57	3.65		0.54	
		6.59	3.58		0.48	
		6.63	3.25		0.51	
		6.80	2.82		0.57	
		6.95	2.35		0.64	
		7.15	1.80		0.76	
		7.26	1.51		0.81	
		7.40	1.14		0.91	
		7.57	0.86		1.02	
		7.82	0.42		1.20	
I	3	8.02 (±0.08)			1.36 (±0.02)	ΛCl +ΔR_1
I↕P_2	4	7.89		0.30	1.26	ΛCl +ΔR_1
		7.65		0.87	1.01	
		7.54		1.19	0.92	
		7.53		1.51	0.86	
		7.45		1.83	0.80	
C↕I	3	1.18			0.99	ΔR_1
		2.49			1.08	

a) Positions of the points in Figs. 2 and 3. In these expressions A↔E, for example, does not contain the points A and E. b) Number of components. c) The values in parentheses are estimated errors and were calculated from twice the standard deviations of the experimental measurements, which were repeated 3—25 times.

TABLE 2. EQUILIBRIUM OF (Λ-[Co(ox)(en)$_2$]$^+$, Δ-[Co(ox)(en)$_2$]$^+$)-(Cl$^-$, d-H$_3$tart$^-$)-H$_2$O SYSTEM at 25 °C
In liquid phases, solubility is presented in molality m of anhydrous salt. Abbreviations are as follows: Λ-[Co(ox)(en)$_2$]Cl·H$_2$O=ΛCl, Δ-[Co(ox)(en)$_2$]Cl·H$_2$O=ΔCl, Λ-[Co(ox)(en)$_2$](d-H$_3$tart)·H$_2$O=ΛR$_2$, Δ-[Co(ox)(en)$_2$](d-H$_3$tart)·2H$_2$O=ΔR$_2$. The data for A, B, E, A↔E, and B↔E are listed in Table 1.

a)	b)	Liquid phase[c] $m/10^{-2}$ mol kg^{-1} ΛCl	ΔCl	ΛR$_2$	ΔR$_2$	Solid phase
C	2				10.52 (±0.11)	ΔR$_2$
C ↕ G	3			1.13	10.19	ΔR$_2$
D	2			4.67		ΛR$_2$
D ↕ G	3			4.26	1.03	ΛR$_2$
				3.84	2.89	
				3.34	4.99	
				3.08	7.00	
				2.85	8.58	
G	3			2.89 (±0.10)	9.85 (±0.33)	ΛR$_2$ +ΔR$_2$
G ↕ P$_2$	4		0.82	2.91	9.06	ΛR$_2$ +ΔR$_2$
			0.84	2.98	9.16	
			1.73	3.07	8.63	
			2.63	3.25	8.25	
			3.30	3.33	7.98	
			3.99	3.44	7.70	
			5.03	3.48	7.51	
			5.51	3.56	7.21	
			5.90	3.71	7.05	
P$_2$	4		6.78 (±0.18)	3.89 (±0.14)	6.69 (±0.28)	ΔCl +ΛR$_2$ +ΔR$_2$
B ↕ F	3		7.22		1.10	ΔCl
			6.94		2.16	
			6.58		3.12	
			6.46		4.16	
			6.10		5.57	
			5.78		7.15	
C ↕ F	3		1.39		9.98	ΔR$_2$
			3.66		9.26	
F	3		5.70 (±0.20)		8.84 (±0.08)	ΔCl +ΔR$_2$
F ↕ P$_2$	4		6.03	0.93	8.15	ΔCl +ΔR$_2$
			6.07	1.79	7.80	
			6.39	2.77	7.26	
			6.75	3.44	6.84	
E ↕ P$_1$	4	5.49	6.23	0.74		ΔCl +ΔCl
		4.98	6.57	1.59		
		4.50	6.78	2.28		
		3.71	7.20	3.48		
		3.17	7.58	4.41		
P$_1$	4	2.97 (±0.06)	7.76 (±0.09)	4.78 (±0.05)		ΛCl +ΔCl +ΛR$_2$
A ↕ H	3	7.30		0.78		
		7.10		1.62		
		7.02		1.96		ΛCl
		6.80		2.44		
		6.80		2.65		
D ↕ H	3	1.55		4.12		
		2.75		3.74		
		3.41		3.56		ΛR$_2$
		4.45		3.33		
		5.14		3.23		
H	3	6.72 (±0.28)		2.98 (±0.04)		ΛCl +ΛR$_2$
H ↕ P$_1$	4	6.27	0.82	3.10		ΛCl +ΛR$_2$
		5.87	1.54	3.27		
		5.55	1.90	3.37		
		5.41	2.35	3.44		
		4.85	3.43	3.73		
		4.61	4.01	3.82		
		4.48	4.38	3.94		
		4.01	5.46	4.17		
		3.44	6.61	4.50		
P$_1$ ↕ P$_2$	4[d]	0.68	8.69	5.72		ΛCl +ΛR$_2$
		0.65	8.74	5.73		
			8.92	5.98	0.14	
			8.84	5.89	0.28	
			8.96	5.92	0.28	
			8.79	5.79	0.46	
			8.61	5.62	0.88	
			8.60	5.66	0.89	
			8.57	5.55	1.17	
			8.49	5.48	1.27	
			8.16	5.24	1.83	
			8.17	5.13	2.10	
			8.10	5.08	2.18	
			8.06	4.99	2.49	
			7.70	4.84	3.06	
			7.62	4.71	3.25	
			7.63	4.64	3.72	
			7.39	4.42	4.48	
			6.83	4.12	5.97	

a) Positions of the points in Figs. 4 and 5. A↔E, for example, does not contain the points A and E. b) Number of components. c) The values in parentheses mean the same in Table 1. d) The point I, where P$_1$↔P$_2$ intersects the OBD plane, has exceptionally number of components 3.

exists in these systems. In the areas of AEP$_1$P$_2$H, BFP$_1$E, CGP$_2$P$_1$F, and DHP$_2$G in Figs. 2 and 3, the saturated solutions are in equilibrium with the solids, Λ-[Co(ox)(en)$_2$]Cl·H$_2$O, Δ-[Co(ox)(en)$_2$]Cl·H$_2$O, Δ-[Co(ox)(en)$_2$]Δ-[Co(edta)]·H$_2$O, and Λ-[Co(ox)(en)$_2$]-Δ-[Co(edta)]·3H$_2$O, respectively. In the areas of AEP$_1$H, BFP$_2$P$_1$E, CGP$_2$F, and DHP$_1$P$_2$G in Figs. 4 and 5, the saturated solutions are in equilibrium with the solids, Λ-[Co(ox)(en)$_2$]Cl·H$_2$O, Δ-[Co(ox)(en)$_2$]-Cl·H$_2$O, Δ-[Co(ox)(en)$_2$](d-H$_3$tart)·2H$_2$O, and Λ-[Co-(ox)(en)$_2$](d-H$_3$tart)·H$_2$O, respectively.

In the region along the G↔P$_2$ line (Figs. 3 and 5) which has four-components containing ΛX and ΔX as solid phases (X=R$_1$ or R$_2$, and the abbreviations are the same as those in Tables 1 and 2), it was observed experimentally that the mole ratio of Λ^+ to Δ^+ in

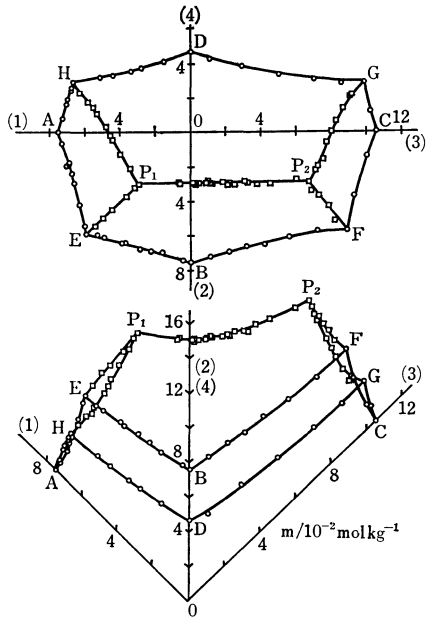

Fig. 4. The plane projection (upper) and the side elevation of the solubility isotherm of the reciprocal salt-pairs (Λ-[Co(ox)(en)$_2$]$^+$, Δ-[Co(ox)(en)$_2$]$^+$)-(Cl$^-$, d-H$_3$tart$^-$)-H$_2$O at 25 °C: solubility is presented in molality m of anhydrous salt; (1) Λ-[Co(ox)(en)$_2$]Cl, (2) Δ-[Co(ox)(en)$_2$]Cl, (3) Δ-[Co(ox)(en)$_2$](d-H$_3$tart), (4) Λ-[Co(ox)(en)$_2$](d-H$_3$tart); □, solubility of four-components; ○, solubility of two- or three-components.

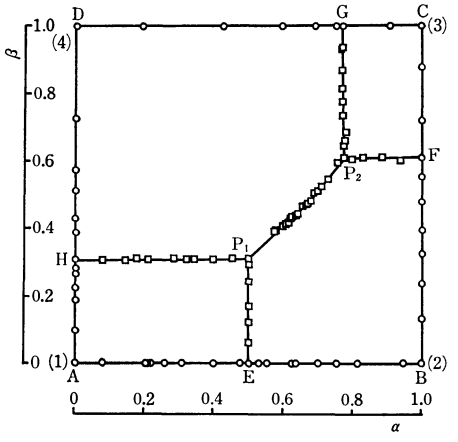

Fig. 5. The clinographic projection of the solubility isotherm of the reciprocal salt-pairs (Λ-[Co(ox)-(en)$_2$]$^+$, Δ-[Co(ox)(en)$_2$]$^+$)-(Cl$^-$, d-H$_3$tart$^-$)-H$_2$O at 25 °C: α, mole fraction of Δ-[Co(ox)(en)$_2$]$^+$ to all the cations; β, mole fraction of d-H$_3$tart$^-$ to all the anions; (1) Λ-[Co(ox)(en)$_2$]Cl, (2) Δ-[Co(ox)(en)$_2$]Cl, (3) Δ-[Co(ox)(en)$_2$](d-H$_3$tart), (4) Λ-[Co(ox)(en)$_2$](d-H$_3$tart); □, solubility of four-components; ○, solubility of two- or three-components.

the liquid phase was almost constant. The analogous situations exist in the regions of E↔P$_1$, F↔P$_1$ and H↔P$_2$ (X=R$_1$), and E↔P$_1$, H↔P$_1$ and F↔P$_2$ (X =R$_2$). In other words, when two solids having a common-ion are in equilibrium with a solution, the mole ratio between the counter ions in its solution does not change by adding the fourth ion; thus no configurational activity[9-11] was observed in the present systems.

Applications to Optical Resolution. (1) (Λ-[Co(ox)(en)$_2$]$^+$, Δ-[Co(ox)(en)$_2$]$^+$)-(Cl$^-$, Δ-[Co(edta)]$^-$)-H$_2$O System: The Δ-[Co(ox)(en)$_2$]Δ-[Co(edta)]·H$_2$O diastereomer is predominant in the solid phases (Figs. 2 and 3), and this system can be applied successfully to the practical optical resolution. One mole of *rac*-[Co(ox)(en)$_2$]Cl·H$_2$O is dissolved in an excess of water and x mol of Δ-Ag[Co(edta)] is added to it ($0 \leqq x \leqq 1$). After the resulting precipitate AgCl has been filtered off, the filtrate is concentrated at 25 °C. Ignoring the dissolved AgCl, this operation produces just the same condition as that of the above solubility isotherm (Figs. 2 and 3).

There are several cases about the values of x: in the case of $0 \leqq x < 0.03$, the situation corresponds to the region of E↔P$_1$ in Figs. 2 and 3, giving no success in the optical resolution because of the precipitation of the racemic mixture [Co(ox)(en)$_2$]Cl·H$_2$O. The value, $x=0.03$, corresponds to the point P$_1$; the optical resolution is also unsuccessful because of the simultaneous precipitations of the $\Delta+\Lambda$ mixture of [Co(ox)(en)$_2$]Cl·H$_2$O and the diastereomer Δ-[Co(ox)-(en)$_2$]Δ-Co[(edta)]·H$_2$O. In the case of $0.03 < x < 0.62$, which relates to the region of P$_1$↔P$_2$, the optical resolution is possible since the precipitation of the diastereomer Δ-[Co(ox)(en)$_2$]Δ-[Co(edta)]·H$_2$O occurs firstly and that of Λ-[Co(ox)(en)$_2$]Cl·H$_2$O later, but the yield of the pure less soluble diastereomer is not maximum. If an unsaturated solution having the composition U′ ($x=0.4$) in Fig. 3 is concentrated at the constant temperature 25 °C, the composition of the solution will remain at the point U′ so long as the solution is unsaturated. When the solution becomes saturated, the precipitation of the less soluble diastereomer will appear in this system and the point will move along the line U′→I′. At the point I′ the second precipitation Λ-[Co(ox)(en)$_2$]Cl·H$_2$O will begin to appear, and the trace of the point will proceed along I′→P$_1$. Finally at the invariant point P$_1$ the third solid Δ-[Co(ox)(en)$_2$]Cl·H$_2$O will appear. If we start from the point U ($x=0.5$), the solution composition will finally reach the point I (the invariant point in the ternary system, Δ-[Co(ox)(en)$_2$]Δ-[Co(edta)]-Λ-[Co(ox)(en)$_2$]Cl–H$_2$O), and then the composition of the liquid phase will never change. And if we start from U″ ($x=0.62$), the solution composition will finally reach the invariant point P$_2$, where the solids, Δ-[Co(ox)(en)$_2$]Δ-[Co(edta)]·H$_2$O, Λ-[Co(ox)(en)$_2$]Cl·H$_2$O, and Λ-[Co(ox)(en)$_2$]Δ-[Co(edta)]·3H$_2$O, coexist. The yield of the pure less soluble diastereomer will become maximum in the range $0.62 \leqq x \leqq 1$. From the viewpoint of saving the resolving agent, the condition, $x=0.62$, which relates to the point P$_2$ is the most desirable. The calculated yield of the pure diastereomer is 93% of Δ-[Co(ox)(en)$_2$]$^+$ (47% of the racemic one).

It has been reported that the solubility ratio of Λ-[Co(ox)(en)$_2$]Δ-[Co(edta)]·3H$_2$O to Δ-[Co(ox)-(en)$_2$]Δ-[Co(edta)]·H$_2$O in the ternary system be-

comes larger with increasing temperature.[4] Therefore, more desirable conditions of the optical resolution may be found at higher temperatures.

(2) (Λ-[Co(ox)(en)$_2$]$^+$, Δ-[Co(ox)(en)$_2$]$^+$)-(Cl$^-$, d-H$_3$tart$^-$)-H$_2$O System: In this system (Figs. 4 and 5), all the complex salts have comparable solubilities in contrast to the case (1) containing Δ-[Co(edta)]$^-$ ion. This system can be also applied in the same manner as mentioned above; the resolving agents practically used are $x/2$ mol of *d*-H$_4$tart and $x/2$ mol of Ag$_2$(*d*-H$_2$tart). The optical resolution will be successful in the range $0.31<x\leqq 1$ which correlates to the regions of $P_1 \leftrightarrow P_2$ and $P_2 \leftrightarrow G$ in Figs. 4 and 5. The yield of the pure less soluble diastereomer becomes maximum in the range $0.75\leqq x\leqq 1$ and reaches 71% of Λ-[Co(ox)(en)$_2$]$^+$ (35% of the racemic one).

References

1) R. Löwenherz, *Z. Phys. Chem. (Leipzig)*, **13**, 459 (1894).
2) W. Meyerhoffer and A. P. Saunders, *Z. Phys. Chem. (Leipzig)*, **28**, 453 (1899).
3) P. P. Fedotieff, *Z. Phys. Chem. (Leipzig)*, **49**, 162 (1904).
4) Y. Shimura and K. Tsutsui, *Bull. Chem. Soc. Jpn.*, **50**, 145 (1977).
5) F. P. Dwyer, I. K. Reid, and F. L. Garvan, *J. Am. Chem. Soc.*, **83**, 1285 (1961).
6) W. T. Jordan, B. J. Brennan, L. R. Froebe, and B. E. Douglas, *Inorg. Chem.*, **12**, 1827 (1973).
7) N. Koine, private communication.
8) A. Findlay, "The Phase Rule and Its Applications," 7th ed, Longmans, Green and Co. (1931).
9) A. Werner, *Ber.*, **47**, 2171 (1914).
10) F. P. Dwyer, E. C. Gyarfas, and M. F. O'Dwyer, *Nature*, **167**, 1036 (1951).
11) J. A. Broomhead, *Nature*, **211**, 741 (1966).

The Formation of the Oxidized Fe_3O_4-Fe_2TiO_4 Solid Solution by the Air Oxidation of the Aqueous Suspension

Takashi KATSURA,* Yutaka TAMAURA, and Gyong Sun CHYO

Department of Chemistry, Tokyo Institute of Technology, Ookayama, Meguro-ku, Tokyo 152

(Received July 14, 1978)

The oxidized Fe_3O_4-Fe_2TiO_4 solid solution with the spinel type structure was synthesized by means of ferrite methods at pH 9.0 and 65 °C. When the solid solution thus obtained was heated at 200 or 300 °C in air for 20 h, it was completely oxidized to form a ferromagnetic product, which retained the spinel type structure for Ti/Fe_{total} ratios from 0 to 0.5.

Akashi *et al.*[1] proposed a "Ferrite Method" to eliminate many kinds of heavy metal ions in waste waters with concentrations as high as 1000 ppm. It should be emphasized that the ferromagnetic sludges thus formed are completely separated from solutions by a magnet. Katsura *et al.*[2] have examined this method for treating concentrated laboratory waste waters, and have succeeded in establishing a station for eliminating the harmful heavy metal ions. Of course, the background of the ferrite method is greatly indebted to many previous fundamental studies of the formation of Fe_3O_4 by the air oxidation of a ferrous hydroxide suspension in slightly alkaline solution. During these investigations, Kiyama[3] established the stability field for the formation of Fe_3O_4 with respect to the temperature and alkalinity of the aqueous suspensions. Yasuoka *et al.*,[4] Hamamura *et al.*,[5] and Kiyama[6,7] have synthesized $MnFe_2O_4$, $ZnFe_2O_4$, $BaFe_2O_4$, and Mn- and Co-ferrites, respectively. Katsura *et al.*[2] and Kaneko and Katsura[8] have also studied the formation of a solid solution of $FeCr_2O_4$-Fe_3O_4 and the $MgFe_2O_4$-Fe_3O_4 solid solution by the ferrite method, respectively. Tamaura *et al.*[9] have studied the formation of Fe_3O_4 in the presence of a dispersing reagent. The formations of solid solutions between Fe_3O_4 and the double oxides are of much interest not only for the ferrite method, but also for the fundamental studies.

The presnet objectives are to: (1) ascertain whether or not a Fe_3O_4-Fe_2TiO_4 solid solution having the spinel type structure could be formed in its complete composition range by the ferrite method, and to (2) obtain a strongly oxidized Fe_2O_3-Fe_2TiO_5 solid solution having the ferromagnetic spinel type structure by heating the samples synthesized by the ferrite method at some higher temperatures. The latter objective is especially valuable for studying the magnetic or geomagnetic properties of highly oxidized titanomagneite found in igneous rocks.

Experimental

Reagents. The guaranteed reagent grade of $FeSO_4 \cdot 7H_2O$ and the reagent grade of $Ti(SO_4)_2 \cdot nH_2O$ were employed for preparing solutions with various Ti/Fe_{total} ratios ranging from 0 to 0.5.

Chemical Analysis. To determine Ti content in the reagent $Ti(SO_4)_2 \cdot nH_2O$ and the Ti^{4+}, Fe^{2+}, and Fe^{3+} contents in the ferrites obtained, the improved method of Iwasaki *et al.*[10] was used. But the ferrites containing various amounts of Ti^{4+} were easily dissolved by the 4 mol dm^{-3} sulfuric acid solution. Thus, there was no need to use the mixed acid solution of sulfuric acid and hydrofluoric acid.

Apparatus. The reaction vessel was a beaker with a capacity of 1 dm^3, as shown in Fig. 1. The temperature of the vessel was kept constant to 65±0.5 °C by a mantle heater controlled by an electric temperature controller. A glass tube (8) with a flat end having eight holes (0.1 cm in diameter) at equal intervals is kept in contact with the bottom of the beaker. A platinum electrode, and a calomel elctrode with a double junction are 1, 5, and 6 in Fig. 1. A thermister to control the temperature is 3 in Fig. 1, and 4 is a condenser.

Procedures. Re-distilled water (800 cm^3) was added to a separable beaker, and was flushed, using nitrogen gas free from carbon dioxide and oxygen for about 1 h. After the separable beaker was sealed, the solution was heated at 65±0.5 °C while the nitrogen gas bubbling was continued. $FeSO_4 \cdot 7H_2O$ (14.4 g) and a desired amount of the titanium(IV) sulfate solution were then added still continuing the flow of the nitrogen gas. Then, a 2 mol dm^{-3} sodium hydroxide solution free from carbon dioxide was added; the pH-stat controller was used to adjust the pH value at 9.0 or any desired value. After the solution stood for about 1 h, the pH value and the oxidation potential (ORP) became constant without further addition of the

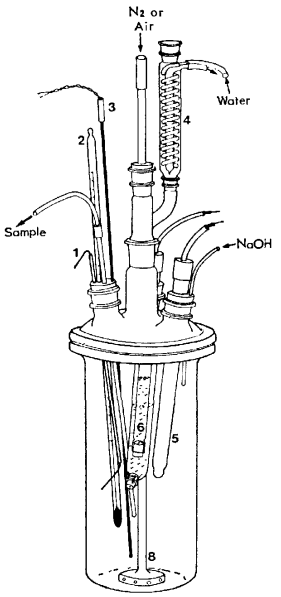

Fig. 1. The reaction vessel used in this study. The reaction vessel is separable. 1: Platinum electrode, 2: thermometer, 3: thermister, 4: condenser, 5: glass electrode, 6: calomel electrode with double junction 7, 8: glass tube with a flat end having eight holes (0.1 cm in diameter).

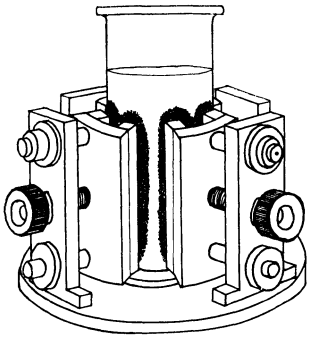

Fig. 2. Magnetic separator used in this experiment. The product is attracted by the four magnets with 1600 Oe and separated from the solution within 2—5 min.

2 mol dm^{-3} sodium hydroxide solution. Then, pre-purified air free from carbon dioxide was passed at a rate of 3 dm^3 min^{-1} through the solution in place of the nitrogen gas for a desired period of time. The temperature and the pH were kept constant during the course of the air oxidation. The end of the oxidation which completed the formation of the ferromagnetic spinel type product was easily recognized by mean of an oxidation potential measurement, as pointed out in previous studies.[8] The relationship between the ORP value and the Fe^{2+}/Fe_{total} ratio will be seen later. The oxidation product was separated from the solution in the nitrogen atmosphere by a magnetic separator devised specially for the present experiment. The magnetic separator used is illustrated in Fig. 2. The product attracted by the magnet was then washed with redistilled water several times, then with acetone to remove the water in the precipitate as completely as possible. The precipitate thus obtained was dried by the freeze-dry technique. The product was analyzed chemically to determine the contents of Fe^{2+}, Fe^{3+}, and Ti^{4+}. The dried product was examined by the powder X-ray diffraction method, infrared spectroscopy, and electron microscopy to identify the phases present in the product. The 2θ angles of the diffraction peaks were calibrated against the standard Si powder by using the Mn-filtered Fe $K\alpha$ radiation. The magnetic susceptibility and the Mössbauer spectra were also obtained for extremely oxidized Fe_2O_3-Fe_2TiO_5 solid solution having the spinel type structure. The results obtained from these magnetic and Mössbauer studies will be publised in the near future.

In order to determine the oxidation rate in the aqueous suspension, an aliquot portion of the suspended solution containing oxide and/or hydroxide was taken out by a syringe in the course of the air oxidation, as seen in Fig. 1, without any air contamination.

Results and Discussion

(1) *The Hydrolysis of Titanium in the Presence of the Fe^{2+} Ion in Aqueous Suspension.* Kaneko and Katsura[8] pointed out that the process of hydrolysis is important for producing the ferrite solid solution. In this paper, the acidic solution containing titanium(IV) and iron(II) ions (Ti/Fe ratio of 0.304) was titrated with a 2 mol dm^{-3} sodium hydroxide solution. The result is shown in Fig. 3. As seen here, the titanium(IV) ions were almost completely hydrolyzed at about pH 9. So, at pH 9.0, all ions of titanium(IV) and

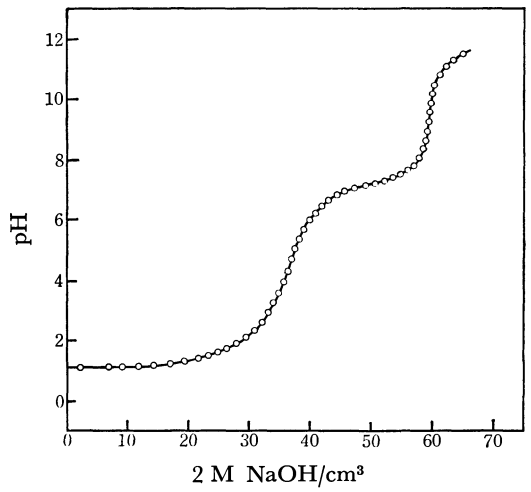

Fig. 3. The titration curve for Ti^{4+} and Fe^{2+}. The Ti/Fe_{total} ratio is 0.304, and the concentration of the NaOH solution is 2 M.

iron(II) were in the hydrous state. This suggests that the complete solid solution of Fe_2TiO_4–Fe_3O_4 could be produced by the ferrite method at a pH of 9.0 and at 65 °C, provided that the hydrolysis is one of the definite steps needed to form the ferrite, as pointed out in the previous paper.[8]

(2) *The Oxidation Rate to Form the Fe_3O_4–Fe_2TiO_4 Solid Solution.* Figure 4 shows the relationship between the Fe^{2+}/Fe_{total} ratio in the suspended solution and the reaction time(min) in the case of the ferrous hydroxide alone($Ti/Fe_{total}=0$). The measurements were performed at pH 9.0 and 11.0 at 65 °C. The ORP dependence of the Fe^{2+}/Fe_{total} ratio is also plotted in Fig. 4. As seen here, the ORP values changed abruptly from about −800 to −50 mV at pH values 9.0 and 11.0, as pointed by the letters a and b. In the early stage of the oxidation, which ranged from

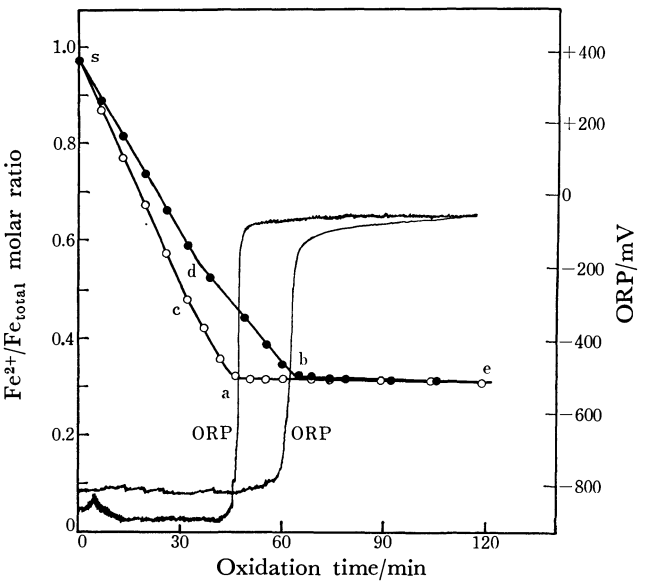

Fig. 4. The oxidation rate of the $Fe(OH)_2$ suspension by the air and the change of the oxidation potential (Pt-Calomel couple). The Ti/Fe_{total} molar ratio is 0.

point s to a or b, as is clear in Fig. 4, the oxidation rate was high, and the rate seems to be a zero order reaction. However, considering the present accuracy of chemical analysis, we may say that the oxidation rate in the early stage is constructed by two somewhat different straight lines; one is from s to d the other is from d to b at pH 9.0, and from s to c and c to a at pH 11.0. According to the results of the X-ray diffraction method and the electron microscopy, there was a large amount of ferrous hydroxide in the suspensions produced during the course from s to c or d, then gradually the amount of ferrous hydroxdie was decreased to form a large amount of ferrite in the course from d or c to b or a. At point a or b, no ferrous hydroxide crystals were found in the suspension. The oxidation rate changed greatly at just the same point as where the ORP value changed abruptly by a or b in Fig. 4. The electrochemical discussion on this phenomenon will be presented in the near future.

Figures 5 and 6 show the same relationship between the Fe^{2+}/Fe_{total} ratio in the suspended solution and the reaction time in cases of the Ti/Fe_{total} ratios of 0.071 and 0.304, respectively. As seen in Figs. 5 and 6, the great changes in the ORP values correspond to the end points of the oxidation reaction for producing the ferrite containing titanium. Because of these results, the oxidation by the air was stopped just 10 min after the abrupt change of the ORP value, and the ferromagnetic suspension was separated and dried as described before. We call the dried product thus obtained series A.

(3) *The Non-stoichiometry in Composition.* As seen in Figs. 4, 5, and 6, the compositions of the series A are not stoichiometric and the deviation from the stoichiometric composition increases with increasing the Ti/Fe_{total} ratio. For example, in the case of the Ti/Fe_{total} ratio of 0.304, the Fe^{2+}/Fe_{total} ratio should be 0.739 if the composition is stoichiometric, but as

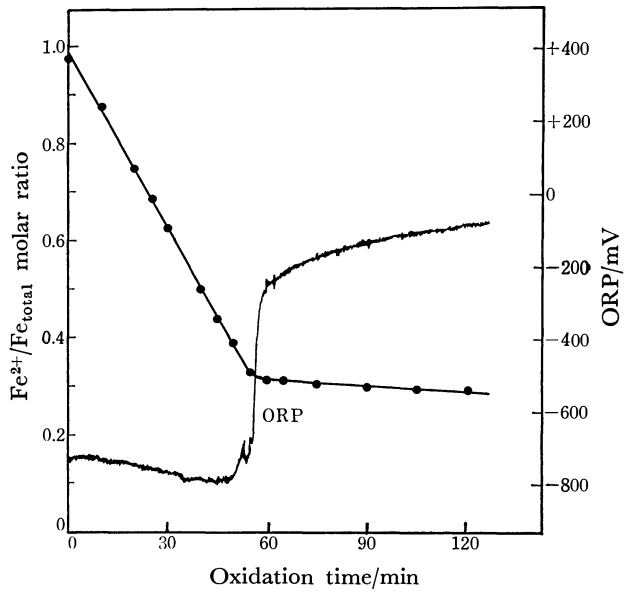

Fig. 5. The oxidation rate of the suspension by the air (Pt-Calomel couple). The Ti/Fe_{total} molar ratio is 0.071.

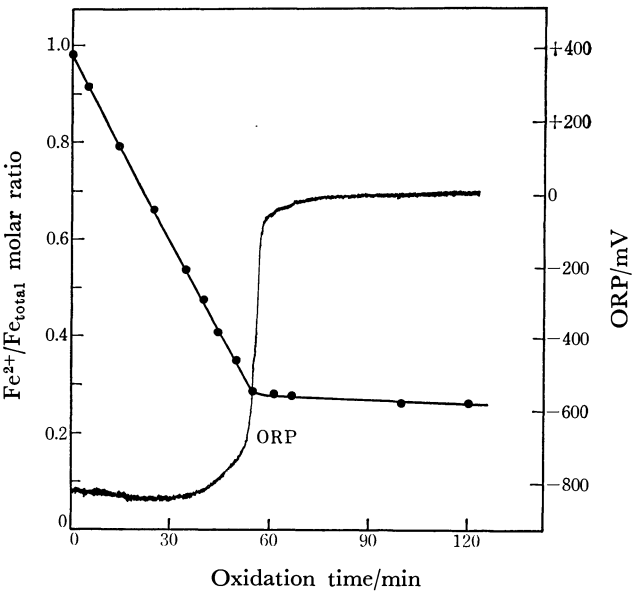

Fig. 6. The oxidation rate of the suspension by the air (Pt-Calomel couple). The Ti/Fe_{total} molar ratio is 0.304.

seen in Fig. 6, the real ratio was only 0.290. This means that the series A is oxidized. The X-ray diffraction pattern of each product showd only a typical spinel type structure.

(4) *Synthesis of the Extremely Oxidized Fe_2TiO_4–Fe_3O_4 Solid Solution.* The series A was subsequently heated at a temperature range from 80 to 400 °C in air by an electrical furnace for desired periods of time. The product thus obtained is called the series B. The series B was examined by the X-ray diffraction method, infrared spectroscopy, electron microscopy, and the Mössbauer method. Chemical analysis was also performed to determine the contents of FeO, Fe_2O_3, and TiO_2. Here we will discuss the results obtained from the chemical analysis and the X-ray diffraction method. The other results will be discussed in the near future.

It is convenient to show the chemical composition of the series B together with the series A as a ternary system: FeO, Fe_2O_3, and TiO_2. Figure 7 shows the chemical composition of the series A and B. It is well known that there exist three solid solution series in the FeO–Fe_2O_3–TiO_2 system at high temperatures: Fe_3O_4–Fe_2TiO_4(titanomagnetite with spinel type), Fe_2O_3–$FeTiO_3$(rhombohedral), and Fe_2TiO_5–$FeTi_2O_5$(orthorhombic). These are shown in Fig. 7 as straight lines. The oxygen reaction lines are also drawn by straight lines. For example, if the stoichiometric composition M in Fig. 7 is oxidized, then the composition moves along the oxygen reaction line to a point N. Some chemical compositions deviate from these oxygen reaction lines. These are due to errors in the chemical analysis. The points on the curved dotted line give the chemical compositions of the series A. The letter x means the mole fraction of Fe_2TiO_4 in the Fe_3O_4–Fe_2TiO_4 solid solution. The values of the Ti/Fe_{total} ratio of 0.071 and 0.304 which were seen in this paper

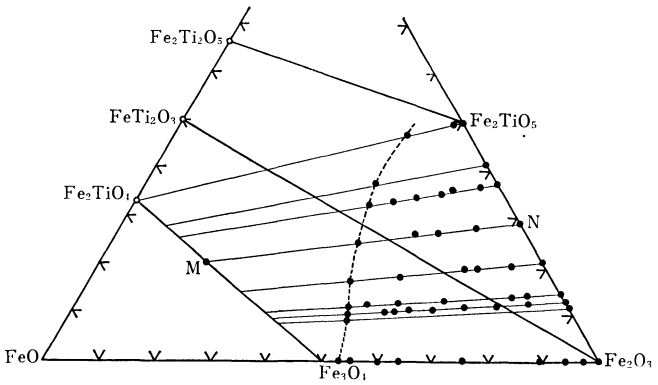

Fig. 7. The chemical composition of the series A and B expressed as FeO, Fe_2O_3, and TiO_2. Three solid solutions of Fe_3O_4-Fe_2TiO_4, Fe_2O_3-$FeTiO_3$ and Fe_2TiO_5-$FeTi_2O_5$ are given by three straight lines. The *oxygen reaction lines* are also shown by the straight lines.

correspond to the mole fractions of 0.2 and 0.7, respectively. As seen in Fig. 7, it is clear that the series A is oxidized, and the chemical composition of the series B is strongly oxidized, depending on the heating temperature and time. When we heated the series A at 200 or 300 °C for 15—20 h, then the products were completely oxidized. At high temperatures, the phase obtained by the complete oxidation of $x=1$ should be pseudobrookite (Fe_2TiO_5), and the compositions in between Fe_2TiO_5 and Fe_2O_3 should be composed of both hematite(Fe_2O_3) and pseudobrookite, if the system is in an equilibrium state.

(5) *The Identification of Phases in the Series A and B.* The X-ray powder diffraction method was adopted to identify the phases present. Infrared spectroscopy was also used to identify the presence of the α-FeOOH phase. Some examples of the diffraction patterns are shown in Fig. 8. Sample series A and B have a spinel type structure irrespective of the oxidation degree and of the Ti/Fe_{total} ratio.

Recently, Readman and O'Reilly[11] and Nishikawa *et al.*[12] have studied the magnetic properties of oxidized (cation-deficient) titanomagnetite (the Fe_3O_4-Fe_2TiO_4 solid solution which naturally occurs). They have synthesized the oxidized titanomagnetite by grinding the stoichiometric solid solution prepared at high temperatures, and have determined the relationships among the chemical composition, the magnetic susceptibility, and lattice constant of the oxidized titanomagnetite. However, it was very hard to obtain any extremely oxidized titanomagnetite with relatively large particles. Thus, the peak intensity of the powder X-ray pattern was very weak, and some people[13] do not believe in the existence of the extremely oxidized titanomagnetite. The particle size of the series A and B ranges from 1000 to 2000 Å,** and the peak intensity is strong enough to determine the precise lattice constant.

(6) *The Relationship between the Lattice Constant and the Oxidation Degree of the Spinel Type Solid Solution.* In this paper, we define the oxidation degree(OD) of each oxidized spinel type solid solution as follows:

OD=number of vacant sites/maximum number of vacant sites when completely oxidized.

Table 1 shows the relationship between the mole fraction of Fe_2TiO_4 in the solid solution and the maximum number of the vacant sites when the stoichiometric solid solution was completely oxidized. The lattice constants of completely oxidized samples are also given in Table 1. As seen here, the lattice constant is almost identical in spite of the different mole fractions of Fe_2TiO_4. This fact was suggested qualita-

** Å=0.1 nm.

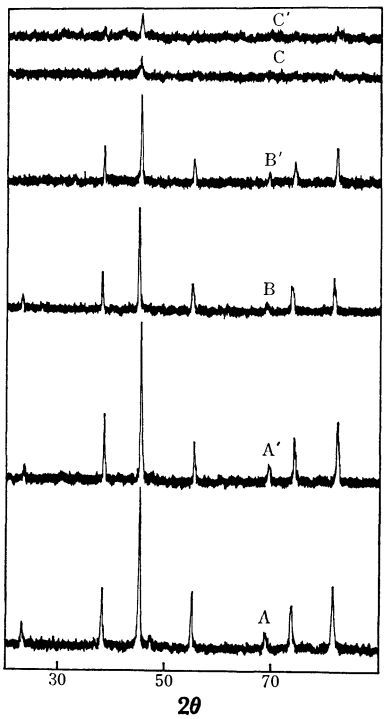

Fig. 8. The X-ray diffraction of the series A and B with radiation of Fe $K\alpha$ (Mn filtration). A: series A with $x=0$. A': Heated the sample A at 200 °C for 15 h in air, B: series A with $x=0.5$, B': Heated the sample B at 200 °C for 15 h, C: Series A with $x=1$, C': Heated the sample C at 300 °C for 15 h.

Table 1. The maximum number of the vacant sites, in the spinel type structure of the completely oxidized Fe_2TiO_4-Fe_3O_4 solid solution (based on 4 oxygen) and the lattice constants measured in this study (Å=0.1 nm)

Mole fraction of Fe_2TiO_4(=a)	Max. number of vacant site(=M)	Lattice constant/Å ±0.001
0	0.333	8.342
0.200	0.391	8.344
0.235	0.401	8.345
0.348	0.433	8.342
0.500	0.474	8.344
0.512	0.477	8.345
0.695	0.524	8.345
0.700	0.526	8.343
0.782	0.547	8.344
1.000	0.600	8.345 (±0.003)

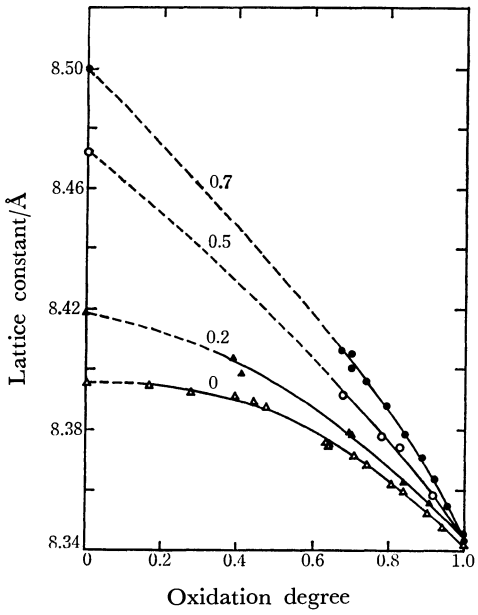

Fig. 9. The relationship between the lattice constant of the series A and B and the oxidation degree. Numbers mean the value x.

tively by Readman and O'Reilly.[10] Figure 9 shows the relationship between the oxidation degree of the series B and the lattice constant. As seen here, the lattice constant decreases gradually with increasing the oxidation degree in each sample with the same mole fraction of Fe_2TiO_4. The precise lattice constants of the stoichiometric Fe_2TiO_4–Fe_3O_4 solid solution have been determined by Katsura *et al.*[14] When we extrapolate the present results to the stoichiometric composition (OD=0), all curves fit the points for the stoichiometric solid solution.

The authers are greatly indebted to Drs. T. Nishikawa of the University of Tokyo and T. Sugihara of the Tokyo Institute of Technology for the cooperation in completing this study.

References

1) T. Akashi, I. Sugano, Y. Kenmoku, Y. Shimada, and T. Tsuji, Proc. Intern. Conf., Ferrites, p. 183, Univ. Tokyo Press (1971).
2) T. Katsura, Y. Tamaura, and H. Terada, *Koogyo Yousui*, **223**, 16 (1977).
3) M. Kiyama, *Bull. Chem. Soc. Jpn.*, **47**, 1646 (1974).
4) H. Yasuoka, A. Hirai, T. Shinjo, M. Kiyama, Y. Bando, and T. Takada, *J. Phys. Soc. Jpn.*, **22**, 174 (1967).
5) A. Hamamura, M. Kiyama, Y. Bando, and T. Takada, *J. Appl. Phys.*, **5**, 1246 (1966).
6) M. Kiyama, *Bull. Chem. Soc. Jpn.*, **49**, 1855 (1976).
7) M. Kiyama, *Bull. Chem. Soc. Jpn.*, **51**, 134 (1978).
8) K. Kaneko and T. Katsura, *Bull. Chem. Soc. Jpn.*, in press.
9) Y. Tamaura, G. S. Chyo, and T. Katsura, *Water Research.*, in press.
10) I. Iwasaki, T. Katsura, M. Yoshida, and T. Tarutani, *Bunsekikagaku*, **6**, 211 (1957).
11) P. W. Readman and O"Reilly, *J. Geomag. Geoelectr.*, **24**, 69 (1972).
12) T. Nishikawa, H. Tanaka, and T. Katsura, *Rock Magnetism Paleogeophysics*, **4**, 1 (1977).
13) For example, M. Ozima and N. Sakamoto, *J. Geophys. Res.*, **76**, 7035 (1971).
14) T. Katsura, K. Kitayama, R. Aoyagi, and S. Sasajima, *Kazan*, **21**, 31 (1976).

Bridges in Polynuclear Complexes. I. The Reaction and Reaction Products of $\mu(NH_2,O_2)$ Dicobalt Complexes with Nitrites†

Shigekazu KUBO,* Takashi SHIBAHARA,†† and Masayasu MORI

Department of Chemistry, Faculty of Science, Osaka City University, Sugimoto-cho, Sumiyoshi-ku, Osaka 558

(Received August 17, 1978)

The IR spectroscopy of the μ-amido-μ-nitro complex, $[(NH_2,NO_2)\{Co(NH_3)_4\}_2]Cl_4\cdot 2H_2O$ obtained from normal and ^{18}O-labeled $[(NH_2,O_2)\{Co(NH_3)_4\}_2](NO_3)_4$ has revealed that the O atom in the Co-N-O-Co chain comes from the O_2 bridge of the starting complex, whereas the O atom attached to the N atom from outside the chain comes from the nitrite used in the bridge conversion, $\mu O_2 \rightarrow \mu NO_2$. A reaction mechanism involving N_2O_3 as the reacting species is proposed. The reaction of $[(NH_2,O_2)\{Co(NH_3)_4\}_2]X_3$ with the nitrite in neutral solution gave a non-electrolytic μ-hyperoxo dicobalt complex, $[(NH_2,O_2)Co_2(NH_3)_4(NO_2)_4]$ (I). Treatment of I with perchloric acid gave a triple-bridged complex, $[(NH_2,NO_2,O_2)Co_2(NH_3)_4(NO_2)_2]^+$, which reproduces I when treated with sodium nitrite.

Dioxygen-bridged dicobalt complexes may be classified into two series, one of which includes brown μ-peroxo complexes, and the other green μ-hyperoxo complexes. Both react with nitrite ion but the reaction features are quite diverse depending on the nature of the starting complex and the condition of the reaction. In the case of $[O_2\{Co(NH_3)_5\}_2]^{n+}$, in an acidic solution there occurs reduction of the μ-hyperoxo complex ($n=5$) to the μ-peroxo complex ($n=4$) followed by cleavage of the O_2 bridge and formation of the mononuclear complex.[1] In the case of the ethylenediamine analog $[O_2\{Co(en)_2NH_3\}_2]^{n+}$, oxidation of the μ-peroxo complex ($n=4$) to the μ-hyperoxo complex ($n=5$) occurs in an acidic solution, whereas in a neutral solution substitution of the ammine ligands by nitro groups takes place.[2]

The double-bridged complex also reacts with the nitrite ion, and in an acidic solution, conversion of the O_2 bridge into the NO_2 bridge occurs without any change on the NH_2 bridge:[3]

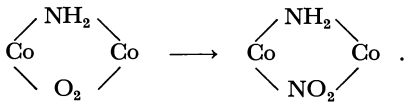

The kinetic study of the reaction of the μ-amido-μ-hyperoxo complex, $[(NH_2,O_2)\{Co(en)_2\}_2]^{4+}$, by Edwards *et al.* suggested that reduction ($\mu O_2^- \rightarrow \mu O_2^{2-}$) and bridge conversion ($\mu O_2 \rightarrow \mu NO_2$) should occur successively.[4] The first part of the present paper is concerned with the investigation into the reaction mechanism of such bridge conversion ($\mu O_2 \rightarrow \mu NO_2$) by the combined use of ^{18}O-labeling and the IR study of the reaction product.

The work on the reaction of the μ-NH_2-μ-O_2 complex with the nitrite ion in a neutral or a basic solution still seems to be meager[2] especially with the ammine complex. The remaining part of the present paper describes the study of such a reaction and some new dicobalt complexes obtained as the reaction product, one of which is a non-electrolytic μ-amido-μ-hyperoxo complex.

Experimental

Materials. $^{18}O_2$ (^{18}O atom % = 92) gas was obtained commercialy from International Chemistry and Nuclear Corp.

Analyses. Ammoniacal N was determined by titration of ammonia after distillation from aqueous sodium hydroxide with arsenic(III) oxide;[5] total N was determined similarly except for use of Devarda's alloy in place of arsenic(III) oxide; Cl in perchlorate was determined as silver chloride after decomposition of the sample with melted sodium nitrite in a nickel crucible.[6] Other elements were analysed by the standard methods.

Reaction and Preparation. 1. Preparation of ^{18}O-Substituted $[(NH_2,O_2)\{Co(NH_3)_4\}_2](NO_3)_4$: This ^{18}O-labeled dicobalt complex was prepared by the adaption of the usual method[7] by using a closed system: A 100-ml flask containing 2.5 g of cobalt(II) nitrate hexahydrate, 15 ml of water previously boiled and cooled under nitrogen, and a magnetic bar coated with Teflon was connected to a vacuum line. The flask was degassed by three freeze-pump cycles, then filled with *ca.* 1 atm ammonia gas from cylinder connected to the line. The content was stirred with a magnetic stirrer until the blue precipitate which had once appeared redissolved and the solution turned red. Although some temperature rise was observed during the absorption of ammonia, it was allowed to be, because absorption of too large excess of ammonia by cooling is unfavorable for the succeeding dioxygen-bridging reaction. After the supply of ammonia gas was stopped the reaction flask was cooled in an ice bath, and 100 ml (N. T. P.) of $^{18}O_2$ gas was introduced into it *via* a Toeplar pump, and was allowed to be absorbed by the solution for 3 h. The mercury of the pump was previously covered with liquid paraffine because it is easily oxidised in the presence of ammonia. At this stage, black crystals of $[O_2\{Co(NH_3)_5\}_2](NO_3)_4$ were precipitated. The reaction mixture was exposed again to 1 atm ammonia gas, and kept at 35 °C for 2 h to introduce the NH_2 bridge; addition of potassium hydroxide was omitted in this experiment to minimize the contamination by normal oxygen. After the reaction mixture was freezed, the flask was removed from the vacuum line, and succeeding procedures were carried out under air. Upon the freezed mixture, 3.5 g of ammonium cerium(IV) nitrate, 30 ml of nitric acid, and 50 g of ice was placed. The whole mixture was melted and stirred. The precipitate was separated from the solution,

† Presented at the 29th Annual Meeting of the Chemical Society of Japan, Hiroshima, Oct. 1973, and the 25th Symposium on Coordination Chemistry, Tokyo, Oct. 1975.

†† Present address: Department of Chemistry, Okayama University of Science, 1-1 Ridaicho, Okayama 700.

and purification *via* practically insoluble sulfate gave 380 mg of ^{18}O-substituted $[(NH_2,O_2)\{Co(NH_3)_4\}_2](NO_3)_4$; in addition, 160 mg of ^{18}O-labeled $[O_2\{Co(NH_3)_5\}_2](NO_3)_5$ was obtained as a co-product in the course of the purification of the former. The complexes were examined by the IR spectroscopy.

2. Reaction of $[(NH_2, {}^{18}O_2)\{Co(NH_3)_4\}_2](NO_3)_4$ with NO_2^- in an Acidic Solution and Isolation of Product: The procedure was modified from the method of Werner[3] owing to the scantiness of the reactant complex available for the experiment.

To a solution of 500 mg of sodium nitrite in 10 ml of water, 100 mg of the complex was added, and then 1.5 ml of 14 M nitric acid was added dropwise with stirring. The mixture was cooled in an ice bath, and the precipitated orange μ-amido-μ-nitro dicobalt complex nitrate was filtered with suction, washed with methanol, and dissolved in 1.5 ml of 12 M hydrochloric acid. After filtration, 3 ml of ethanol was added to it, and the mixture was cooled in an ice bath. The precipitate (complex chloride) was filtered, and recrystallized in the same manner. The product was washed with ethanol, and dried by aeration; yield 70 mg.

The product with normal oxygen prepared by the same procedure was submitted to chemical analysis; each product obtained in the experiments with $^{18}O_2$ and with normal oxygen respectively gave the identical X-ray diffraction pattern and IR spectrum except for the isotopic shift. Found: Co, 23.81; N(total), 28.08; N(ammoniacal), 25.23; Cl, 28.54; H, 6.02%. Calcd for $[(NH_2,NO_2)\{Co(NH_3)_4\}_2]Cl_4\cdot 2H_2O$: Co, 23.86; N(total), 28.35; N(ammoniacal), 25.52; Cl, 28.71; H, 6.21%.

3. Reaction of $\mu(NH_2,O_2)$ Complex with NH_4NO_2 in a Neutral Solution (Preparation of $[(NH_2,O_2)Co_2(NH_3)_4(NO_2)_4]$): To 750 ml of 10% ammonium nitrite, 20 g of $[(NH_2,O_2)\{Co(NH_3)_4\}_2]Na(ClO_4)_4$ (prepared by the method in Ref. 7) was added with stirring, and the mixture was allowed to stand at *ca.* 5 °C in a refrigerator. From the next day, 1 g of ammonium persulfate was added every day until the solution assumed a reddish orange color and no more precipitate increased (It took *ca.* 20 days). The green precipitate was filtered, washed with water and then with acetone, and dried by aeration; yield 8 g.

The product obtained was insoluble in any solvents so far examined, and could not be recrystallized by the usual method. For the purification, the crude product was once changed to $[(NH_2,NO_2,O_2)Co_2(NH_3)_4(NO_2)_2]ClO_4\cdot 0.5H_2O$ by the process described in the next section, and brought back to the original compound by the following procedure: To a solution of 1 g of the perchlorate dissolved in 130 ml of water was added 10 ml of 10% aqueous sodium nitrite. The mixture was allowed to stand in a refrigerator overnight. The precipitate was filtered, washed with water and then with acetone, dried by aeration, and kept over calcium chloride. Green powder; yield 0.6 g. Found: Co, 27.92; N(total), 29.66; N(ammoniacal), 16.31%. Calcd for $[(NH_2,O_2)Co_2(NH_3)_4(NO_2)_4]$: Co, 28.20; N(total), 30.16; N(ammoniacal), 16.75%.

4. Preparation of $[(NH_2,NO_2,O_2)Co_2(NH_3)_4(NO_2)_2]ClO_4\cdot 0.5H_2O$: Six grams of the crude $[(NH_2,O_2)Co_2(NH_3)_4(NO_2)_4]$ (described above) were added to 150 ml of ice-cold perchloric acid (60%) and the mixture was stirred under reduced pressure of aspirator for 2 h for dissolution. (Without reduced pressure it took longer time for dissolution and decomposition to form by-products was more pronounced.) The cold green solution was filtered with a sintered-glass filter and added in small portions to 900 ml of ether wihch had been cooled in an ice bath, care being taken to minimize the temperature rise. The flocky precipitate was filtered and washed with ether. After the ether was eliminated with aeration, the product was washed with two small portions of cold water and air dried. The green material was dissolved in 150 ml of acetone and an equal volume of ether was added to it. The mixture was allowed to stand in an ice bath for *ca.* 1 h and the precipitate was filtered, washed with ether, and air-dried. Green thin plates; yield 1.9 g. Found: Co, 24.85; N(total), 23.16; N(ammoniacal), 14.60; Cl, 7.45; H, 3.16%. Calcd for $[(NH_2,NO_2,O_2)Co_2(NH_3)_4(NO_2)_2]ClO_4\cdot 0.5H_2O$: Co, 24.53; N(total), 23.32; N(ammoniacal), 14.58; Cl, 7.38; H, 3.14%.

5. Preparation of $[(NH_2,NO_2,O_2)Co_2(NH_3)_4(NO_2)_2]Cl$: To a solution of 3 g of the perchlorate (described above) dissolved in 400 ml of water, 80 ml of 6 M hydrochloric acid was added, and the mixture was cooled in an ice bath. The precipitate was filtered, and washed with cold 2 M hydrochloric acid and then with acetone. The product was dissolved in 700 ml of cold water, and 70 ml of 6 M hydrochloric acid was added. The precipitate was filtered, washed with 0.5 M hydrochloric acid and then with acetone, and dried by aeration. Green thin prisms; yield 1.6 g. Found: Co, 29.02; N(total), 26.96; N(ammoniacal), 17.02; Cl, 8.81%. Calcd for $[(NH_2,NO_2,O_2)Co_2(NH_3)_4(NO_2)_2]Cl$: Co, 28.93, N(total), 27.50; N(ammoniacal), 17.19; Cl, 8.70%.

6. Preparation of $[(NH_2,NO_2,O_2)Co_2(NH_3)_4(NO_2)_2]Br$: To a solution of 2 g of the perchlorate (described above) dissolved in 400 ml of water, 50 ml of 24% hydrobromic acid was added, and the mixture was allowed to stand in an ice bath. The precipitate was filtered, and washed with cold water and then with acetone. The product was recrystallized from the aqueous solution by addition of hydrobromic acid and dried by aeration after filtration and washing. Green needles; yield 1.7 g. Found: Co, 26.20; N(total), 24.30; N(ammoniacal), 15.37; Br, 17.69%. Calcd for $[(NH_2,NO_2,O_2)Co_2(NH_3)_4(NO_2)_2]Br$: Co, 26.08; N(total), 24.79; N(ammoniacal), 15.50; Br, 17.68%.

Apparatus. IR spectra were recorded with samples in Nujol on a JASCO IR-E or IR-G spectrometer. Recording of absorption spectra was carried out with a Hitachi 124 spectrometer, and that of reflectance spectra with the same apparatus by use of an integration sphere attachment. ESR spectra were recorded on a JEOL JES-3B spectrometer at room temperature. Magnetic susceptibilities were determined by the Faraday technique with a Shimadzu MB-2 balance. Powder X-ray diffraction patterns were recorded on a Rigaku 2171 diffractometer with the Ni $K\alpha$ radiation.

Results and Discussion

IR Spectroscopy of ^{18}O-Labeled Complexes. 1. $\mu(NH_2,O_2)$ Complex: The IR spectra of normal and isotopically labeled $[(NH_2,O_2)\{Co(NH_3)_4\}_2](NO_3)_4$ in the region of *ca.* 700—1200 cm^{-1} are shown in Fig. 1. The fact that the labeled complex shows no peak corresponding to $^{16}O_2$ stretching vibration proves that there has been no shuffling of oxygen between O_2 and H_2O or NO_3^- in the formation process of the single-bridged complex $[O_2\{Co(NH_3)_5\}_2]^{4+}$, as well as in the transformation process to the double-bridged complex. The possibility of scrambling of oxygen atoms among the oxygen molecules and the O_2-moieties of complex ions also was excluded because a sample prepared by using a mixture of $^{18}O_2$ and $^{16}O_2$ showed no peak of ^{18}O-^{16}O stretching vibration.

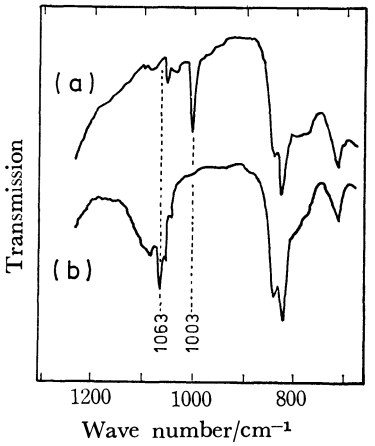

Fig. 1. IR spectra of $[(NH_2,O_2)\{Co(NH_3)_4\}_2](NO_3)_4$ (a) with ^{18}O-labeled O_2-bridge and (b) with normal O_2-bridge.

2. $\mu(NH_2,NO_2)$ Complexes: Werner[3] reported two hydrates of $[(NH_2,NO_2)\{Co(NH_3)_4\}_2]Cl_4$, one of which was monohydrate crystallized from dilute hydrochloric acid and the other tetrahydrate crystallized from aqueous solution containing some pyridine. The IR spectrum and the X-ray powder pattern of the ^{18}O-labeled complex chloride prepared as described showed that it was a third form; the chemical analysis of the corresponding normal complex conformed to the formula of dihydrate. The authors later knew that this dihydrate was reported in 1975 by Huang *et al.*[8] who crystallized it from 6 M hydrochloric acid. Not only the IR peaks due to water of crystallization the content of which is different in these three forms, but also the IR peaks due to nitro bridge and ammonia ligand showed slight differences in their frequency and intensity, such differences in some cases being of comparable magnitude to those due to isotopic effect. The variation in the IR spectrum owing to the difference in the crystal form was noticed in this laboratory, with $[(NH_2,O_2)\{Co(NH_3)_4\}_2](NO_3)_4$.[9] Thus in the detailed examination of IR spectra and especially in the discussion of their isotopic shifts, one must make sure of the identity of the number of crystal water or the crystal form of the complexes compared.

The IR spectrum of $[(NH_2, NO_2)\{Co(NH_3)_4\}_2]Cl_4$ was reported by Gatehouse[10] although it is not clear which type of the above three hydrates was examined. He assumed an asymmetric structure of the nitro bridge and assigned two strong IR peaks as shown below:

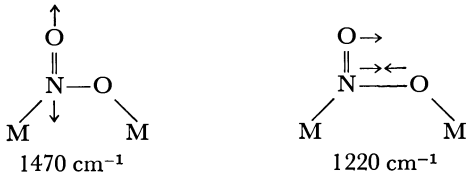

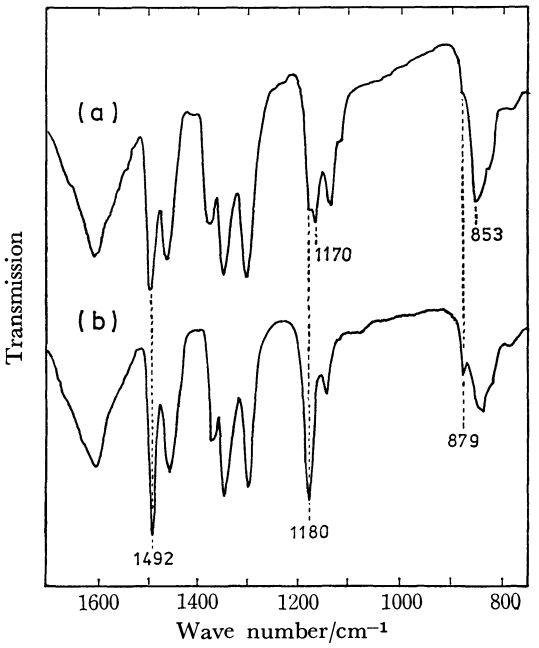

Fig. 2. IR spectra of $[(NH_2,NO_2)\{Co(NH_3)_4\}_2]Cl_4 \cdot 2H_2O$ prepared (a) from ^{18}O-labeled $\mu(NH_2,O_2)$ complex and (b) from normal complex.

Nakamoto *et al.*[11] examined a similar nitro-bridged compound $[(NO_2,OH,OH)\{Co(NH_3)_3\}_2]Cl_3$ and made the same sort of assignment.

The X-ray structural study of $[(NH_2,NO_2)\{Co(NH_3)_4\}_2]Cl_4 \cdot 4H_2O$ by Thewalt and Marsh[12] and that of $[(NH_2,NO_2)\{Co(NH_3)_4\}_2]Cl_4 \cdot 2H_2O$ by Huang *et al.*[8] both proved the correctness of the formula postulated by Gatehouse, and his assignment of the two IR bands also seems to be a sound one.

The IR spectra of two samples of $[(NH_2,NO_2)\{Co(NH_3)_4\}_2]Cl_4 \cdot 2H_2O$, one derived from ^{18}O-substituted $[(NH_2,O_2)\{Co(NH_3)_4\}_2](NO_3)_4$ and the other from the same complex with natural isotopic abundunce are shown in Fig. 2, and relevant frequencies are listed in Table 1. As the band in the normal $\mu(NH_2, NO_2)$ complex at 1180 cm^{-1} which is assigned to the vibration mainly consisting of the stretching of NO bond in the Co–N–O–Co chain shifts to 1170 cm^{-1} in the ^{18}O-labeled complex, the O atom in the Co–N–O–Co chain is concluded to have come from the O_2 bridge of the starting complex. On the other hand, the O atom attached to the N atom from outside the chain must have come from the nitrite ion since the band at 1492 cm^{-1} mainly attributable to the stretching of NO bond that makes the branch does not show appreciable shift.

The above results bear some resemblance to the case of nitrosation of aquapentaammine complex, and seems to be equally explained by assuming N_2O_3 as the

Table 1. IR frequencies of $[(NH_2,NO_2)\{Co(NH_3)_4\}_2]Cl_4 \cdot 2H_2O$ in cm^{-1}

	$\nu_{as}(NO_2)$	$\delta_s(NH_3)$		$\nu_s(NO_2)$		$\delta(NO_2)$	$\rho_r(NH_3)$
^{18}O-enriched	1493 s	1350 m	1304 m	1170 s	1138 w	853 m	843 sh
				1180 sh		879 sh	
Normal oxygen	1492 s	1351 m	1305 m	1180 s	1146 w	879 w	843 m

reacting species as[13]

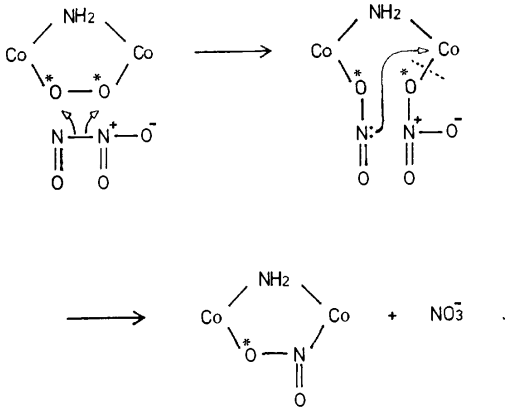

The new situation here is that the reaction seems to occur more homolytically, and that the remaining nitrite group is oxidized to a nitrate ion.

Although the $\mu(NH_2,OH)$ complex which is formed by reduction of $\mu(NH_2,O_2)$ complex is also known to react with the nitrite to form the $\mu(NH_2,NO_2)$ complex, such a reaction is reported to be very slow[14] and bridge conversion $\mu O_2 \rightarrow \mu NO_2$ through this path may be excluded.

The IR spectra of the $[(NH_2,NO_2)\{Co(en)_2\}_2]Br_4 \cdot 5H_2O$ is somewhat more complicated, but the positions and intensities of peaks assignable to NO_2 stretching vibration (1492 and 1151 cm^{-1}) are very similar to those of the corresponding ammine complex and this IR feature again is explicable only on the assumption of a nitro bridge as shown by Gatehouse and by Nakamoto *et al.* for ammine complexes. One of the reasons which led Garbett and Gillard[15] to assume a *nitrito* bridge instead of a *nitro* bridge was the high resistivity to acids, but our ^{18}O-labeled μ-amido-μ-nitro-octaammine complex also showed high stability, retaining ^{18}O in the Co-N-O-Co chain even after two cycles of recrystallization from hydrochloric acid. The other reason on which they based their conclusion was the formation of hydroxo complex ions on base hydrolysis, but nitro complexes also are known to form hydroxo complexes on base hydrolysis.

Thus the general similarity of the behavior of the ammine and the corresponding ethylenediamine complex seems to be present also in the present case of the reaction of the $\mu(NH_2,O_2)$ complex to form the $\mu(NH_2, NO_2)$ complex.

The IR absorption band due to the bending mode of the coordinated nitro group and that due to the rocking mode of ammonia ligand appears in the region of 900—750 cm^{-1}, and when both are present it is difficult to discriminate them. On the basis of ^{18}O isotope shift, the absorption at 879 cm^{-1} could be assigned to $\delta(NO_2)$ for $[(NH_2,NO_2)\{Co(NH_3)_4\}_2]Cl_4 \cdot 2H_2O$.

Reaction in Neutral or Basic Solutions. Treatment of $[(NH_2,O_2)\{Co(NH_3)_4\}_2]X_3$ with an aqueous solution of ammonium nitrite followed by oxidation with ammonium persulfate gave green powder of composition, $Co_2O_2NH_2(NH_3)_4(NO_2)_4$ (I). The ammonium nitrite was replaceable by an equimolar mixture of sodium nitrite and ammonium salt, but not by sodium nitrite alone, in which case the mixture turned red showing decomposition.

The IR spectrum of the green product (Table 2) indicated the existence of nitro ligands as well as ammine ligands and a peroxo bridge,[9] but no peaks corresponding to a nitro bridge nor those corresponding to a free nitrite ion were observable (*cf.* the preceding section). The compound is thus considered to be $[(NH_2,O_2)\{Co(NH_3)_2(NO_2)_2\}_2]$ or $[(NH_2,O_2)\{CoNH_3(NO_2)_3\}\{Co(NH_3)_3NO_2\}]$, and is the first example of non-electrolytic μ-hyperoxo dicobalt complex.

Table 2. IR absorption frequencies of $[(NH_2,O_2)Co_2(NH_3)_4(NO_2)_4]$ (I) and $[(NH_2,NO_2,O_2)Co_2(NH_3)_4(NO_2)_2]X$ (II-X) in cm^{-1}

I	II-$ClO_4 \cdot 0.5H_2O$	II-Cl	II-Br	Assignment
	3550 w			ν(OH)
3320, 3260, 3210 s	3310, 3240, 3170 s	3340, 3330, 3180 s	3290, 3240, 3160 s	ν(NH)
1630 m	1630 m	1630 m	1627 m	$\delta_{as}(NH_3)$
	1495 s	1495 s	1485 s	$\nu_{as}(\mu\text{-}NO_2)$
1410 s	1410 s	1410 s	1409 s	$\nu_{as}(NO_2)$
1328 s	1335 s	1340 s	1334 s	$\nu_s(NO_2)$
1275 s	1305 s	1317 s	1308 s	$\delta_s(NH_3)$
		1280 m		
	1180 m	1190 s	1170 s	$\nu_s(\mu\text{-}NO_2)$
1078 w		1078 m	1095 w	$\nu(\mu\text{-}O_2)$
	1089 s			$\nu(ClO_4)$
		996 w	1013 vw	
	853 w	857 w	849 w	$\delta(\mu\text{-}NO_2)$
822 m	820 s	825 s	822 m	$\rho_r(NH_3)$
		807 w		
783 vw	780 w	773, 759 w	788 w	$\delta(NO_2)$

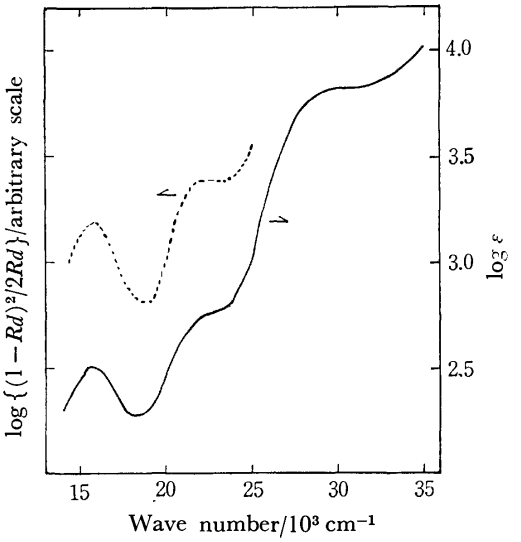

Fig. 3. Absorption spectrum of $[(NH_2,NO_2,O_2)Co_2(NH_3)_4(NO_2)_2]ClO_4$ (in 0.5 M acetic acid, ——) and diffuse reflectance spectrum of $[(NH_2,O_2)Co_2(NH_3)_4(NO_2)_4]$ (in K_2SO_4, ----).

The presence of the amido bridge was inferred from the consideration of the composition, balance of charge, and the high stability of $\mu(NH_2,O_2)$ dicobalt moiety usually observed. The possibility of the formula $[(NH_2,O_2)\{Co(NO_2)_4\}\{Co(NH_3)_4\}]$ seems to be excluded from the consideration of the reaction with perchloric acid (*cf.* next section).

The electronic spectrum obtained from diffuse reflectance measurement (Fig. 3) showed peaks of comparable intensities at $15.8\times10^3\,cm^{-1}$ ($d\pi Co^{3+}$-$\pi^*(\mu O_2^-)$) and at $22.3\times10^3\,cm^{-1}$ ("$^1A_{1g}$-$^1T_{2g}$").[16] Such intensity relation is usually encountered when the ammine complex has a second bridge such as NH_2 in addition to the hyperoxo bridge; in single-bridged μ-hyperoxo dicobalt ammine complexes the band at *ca.* $15\times10^3\,cm^{-1}$ is distinctly more intense than that at *ca.* $20\times10^3\,cm^{-1}$.

Compound I can also be obtained in a somewhat lower yield by the treatment of μ-hyperoxo complexes such as $[(NH_2,O_2)\{Co(NH_3)_4\}_2]X_4$ or $[(NH_2,OH,O_2)\{Co(NH_3)_3\}_2]X_3$ with ammonium nitrite solution. In this case oxidizing agent is unnecessary: Probably the starting μ-hyperoxo complex itself acts as an oxidizing agent as represented by the following scheme;

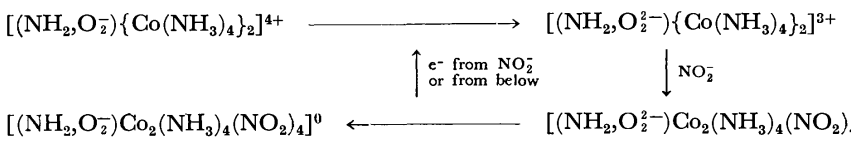

That only the terminal ammine ligands are replaced by nitro ligand and the O_2 bridge remains unattacked in the reaction of $[(NH_2,O_2)\{Co(NH_3)_4\}_2]X_3$ with the nitrite in neutral solution is in the same line as the similar reaction of $[O_2\{CoNH_3(en)_2\}_2]X_4$ which gave $[O_2\{CoNO_2(en)_2\}_2]X_2$.[2] It indicates that the bridge conversion, $\mu O_2\rightarrow\mu NO_2$ does not proceed through the reaction of the peroxo bridge with the nitrite ion but with some other chemical species present only in acidic solutions of nitrites, such as N_2O_3 as suggested in the preceding section.

Reaction of $[(NH_2,O_2)Co_2(NH_3)_4(NO_2)_4]$ with Perchloric Acid. It has not been successful to find a proper solvent of I which dissolves it without decomposition. Sixty-percent perchloric acid dissolves it with a loss of one nitrite group, the species in solution being $[(NH_2,NO_2,O_2)Co_2(NH_3)_4(NO_2)_2]^+$ (II), which can be isolated as the perchlorate by treatment with ether.

The aqueous solution of II reacts with sodium nitrite to reproduce I with a capture of one nitrite group. These reactions are very peculiar and seem to deserve closer studies. The structure of II was inferred from the chemical analysis and IR spectra (Table 2) which showed peaks assignable to a hyperoxo bridge, a nitro bridge, terminal nitro ligands, and ammine ligands. The amido bridge is considered to be present because it is usually very resistant to acids, and also because II reproduces I on treatment with sodium nitrite. The formation of nitro bridge in 60% perchloric acid in the reaction I→II again proves the stability of the nitro bridge in acids.

The absorption spectrum of II-ClO_4 solution (Fig. 3) showed peaks at $15.8\times10^3\,cm^{-1}$ ($\varepsilon=320$) ($d\pi Co^{3+}$-$\pi^*(\mu O_2^-)$), $22.8\times10^3\,cm^{-1}$ ("$^1A_{1g}$-$^1T_{2g}$"), and $29.8\times10^3\,cm^{-1}$ (specific band of nitro ligand).

Magnetic Properties. The magnetic susceptibility measurements of I, II-$ClO_4\cdot0.5H_2O$, II-Cl, and II-Br proved the existence of one unpaired electron in each complex (Table 3).

The ESR spectrum of I in powder gave $g=2.035$, and that of II-ClO_4 in solution exhibited a symmetrical pattern at $g=2.027$ with well-resolved fifteen hyperfine lines ($A_{Co}=11.8$) such as is observed with many μ-amido-μ-hyperoxo dicobalt ammine complexes.[17]

Table 3. Magnetic susceptibilities of $[(NH_2,O_2)Co_2(NH_3)_4(NO_2)_4]$ (I) and $[(NH_2,NO_2,O_2)Co_2(NH_3)_4(NO_2)_2]X$ (II-X)

Complex	μ_{eff}[a]/B. M.
I	1.60 (24.5 °C)
II-Cl	1.88 (22.6 °C)
II-Br	1.83 (24.9 °C)
II-$ClO_4\cdot0.5H_2O$	1.91 (24.5 °C)

a) Corrected for diamagnetic susceptibilities of terminal ligand, anion, and crystal water.

The authors thank Mr. Kazuyoshi Kawashima for his able assistance with some of the experimental work. They are grateful also to Dr. Hanako Kobayashi (Univ. of Kyoto) for her kind guidance on the measurements of magnetic susceptibility, to Dr. Yôzô Miura for the ESR measurements, and to Mr. Junichi Gôda for the elemental analyses.

References

1) M. Green and A. G. Sykes, *J. Chem. Soc., A*, **1970**, 3209.
2) T. Shibahara and M. Mori, *Bull. Chem. Soc. Jpn.*, **45**, 1433 (1972).
3) A. Werner, *Justus Liebigs Ann. Chem.*, **375**, 1 (1910).
4) J. D. Edwards, C.-H. Yang, and A. G. Sykes, *J. Chem. Soc., Dalton Trans.*, **1974**, 1561.
5) H. A. Horan and H. J. Eppig, *J. Am. Chem. Soc.*, **71**, 581 (1949).
6) M. Dittrich and H. Bollenbach, *Ber. Deut. Chem. Ges.*, **38**, 751 (1905).
7) M. Mori, J. A. Weil, and M. Ishiguro, *J. Am. Chem. Soc.*, **90**, 615 (1968).
8) C. Y. Huang, J. A. Weil, and B. E. Robertson, *Acta Crystallogr., Sect. B*, **31**, 914 (1975).
9) T. Shibahara and M. Mori, *Bull. Chem. Soc. Jpn.*, **51**, 1374 (1978).
10) B. M. Gatehouse, *J. Inorg. Nucl. Chem.*, **8**, 79 (1958).
11) K. Nakamoto, J. Fujita, and H. Murata, *J. Am.*

Chem. Soc., **80**, 4817 (1958).
12) U. Thewalt and R. E. Marsh, *Inorg. Chem.*, **9**, 1604 (1970).
13) R. G. Pearson, P. M. Henry, J. G. Bergmann, and F. Basolo, *J. Am. Chem. Soc.*, **76**, 5920 (1954); R. K. Murmann and H. Taube, *J. Am. Chem. Soc.*, **78**, 4886 (1956).
14) A. G. Sykes and R. D. Mast, *J. Chem. Soc., A*, **1967**, 784.
15) K. Garbett and R. D. Gillard, *J. Chem. Soc., A*, **1968**, 1725.
16) V. M. Miskowski, J. L. Robbins, I. M. Treitel, and H. B. Gray, *Inorg. Chem.*, **14**, 2318 (1975).
17) E. A. V. Ebsworth and J. A. Weil, *J. Phys. Chem.*, **63**, 1890 (1959).

Structure of 5-Hydroxy-2-hydroxymethyl-4-pyridones

Kimiaki IMAFUKU,* Makoto ISHIZAKA,† and Hisashi MATSUMURA

Department of Chemistry, Faculty of Science, Kumamoto University, Kurokami, Kumamoto 860

(Received September 8, 1977)

5-Hydroxy-2-hydroxymethyl-4-pyridone and its *N*-methyl, *N*-ethyl, and *N*-phenyl derivatives were prepared from kojic acid. The UV spectra in neutral, acid, and alkaline solutions showed that the neutral species and the conjugate acids existed in the pyridone and the pyridine form, respectively. The conjugate bases may exist in both forms. The acid dissociation constants and the halochromism have been measured and discussed.

In the protonation of the 4-pyridone (A), structure (B) represents the *O*-protonated form and (C) the *N*-protonated form.

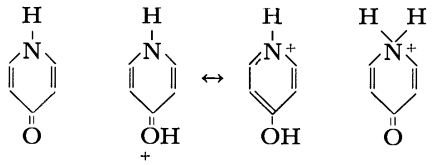

(A) (B) (B′) (C)

The theory of mesomerism predicts that the two cationic forms of B, B↔B′ should be greatly stabilized relative to type C, and their predominance has been assumed. The similarity among the ultraviolet spectra of the conjugate acids of 4-methoxypyridine, 1-methyl-4-pyridone, and 4-pyridone was taken to support such an assumption.[1] The NMR spectra also support the structure of type B↔B′.[2,3] However, the infrared and Raman spectra of these cations have been interpreted in favor of the structure of type C.[4,5]

The structure of 5-hydroxy-2-hydroxymethyl-4-pyridone in the acidic and alkaline solutions and the halochromism of its *N*-substituted derivatives are reported together with the acid dissociation constants.

Results and Discussion

Synthesis. 5-Hydroxy-2-hydroxymethyl-4-pyridone (IIa)[6] and its *N*-substituted derivatives (IIb[7] and IId) were obtained by the reaction of kojic acid (I) with the corresponding amines, while the *N*-ethyl-substituted compound (IIc) was prepared from I *via* 5-benzyloxy-2-hydroxymethyl-4-pyrone (III)[8] and 5-benzyloxy-1-ethyl-2-hydroxymethyl-4-pyridone (IV). 2-Hydroxymethyl-5-methoxy-4-pyridone (VIa)[9] and its *N*-substituted derivatives (VIb[9] and VIc) were obtained from kojic acid methyl ether (V)[9] by the reaction with the corresponding amines. The reaction of IIa with diazomethane gave 3,4-dimethoxy-6-hydroxymethylpyridine (VII) in 33% yield.

Acid Dissociation Constants. The acid dissociation constants of 5-hydroxy-2-hydroxymethyl-4-

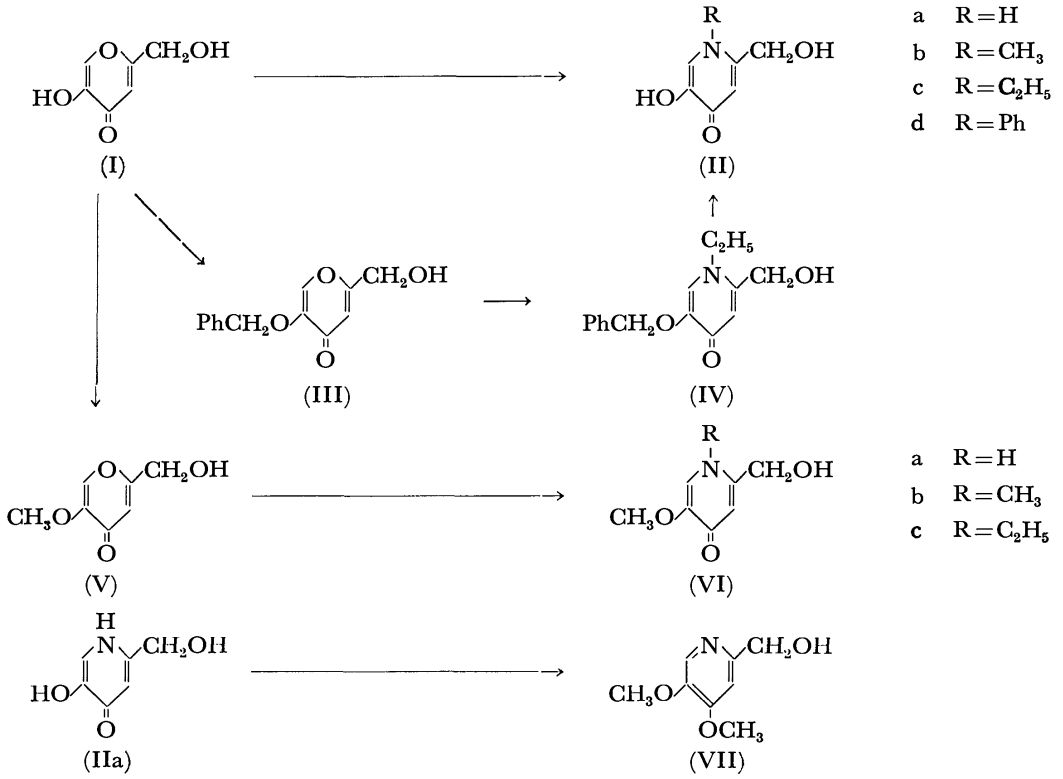

(I) (II) (III) (IV) (V) (VI) (IIa) (VII)

Scheme 1.

† Present address: Fundodai Shoyu Co., Ltd., Hokubu-machi, Houtaku-gun, Kumamoto 861-55.

pyridones IIa—d were determined spectrophotometrically in water at 25 °C. The results are summarized in Table 1, where the pK_2 and pK_1 values represent the acid dissociation exponent (pK_a) of a neutral compound and that of its conjugate acid, respectively. The pK_1 values are comparable to the pK_a values for the conjugate acids of some 4-pyridones,[10,11] and the pK_2 values to the pK_a values for some 3-hydroxy-4-pyrones.[12] These values are increased by introduction of an electron donative substitutent on the nitrogen atom, but do not give a good Hammett relationship.

UV Spectra. The UV spectral data of the conjugate acids, neutral species, conjugate bases of 5-hydroxy-2-hydroxymethyl-4-pyridone (IIa) and its *N*-substituted derivatives (IIb—d) and 2-hydroxymethyl-5-methoxy-4-pyridone (VIa) and its *N*-substituted derivatives (VIb and VIc) are summarized in Tables 2 and 3, respectively. The spectra of 5-hydroxy-2-hydroxymethyl-4-pyridone (IIa), the *N*-methyl derivative (IIb) and 3,4-dimethoxy-6-hydroxymethyl-pyridone (VII) in water and M/10 hydrochloric acid are presented in Figs. 1 and 2 as examples. The spectra of 5-methoxy derivatives VIa and VIb are also presented together with the spectra of VII in Figs. 3 and 4.

TABLE 1. pK_a VALUES OF *N*-SUBSTITUTED 5-HYDROXY-2-HYDROXYMETHYL-4-PYRIDONES

Compd	*N*-Substituent	pK_1	pK_2
IIa	H	3.26	
IIb	CH_3	3.37	9.18
IIc	C_2H_5	3.31	8.97
IId	Ph	2.64	8.82

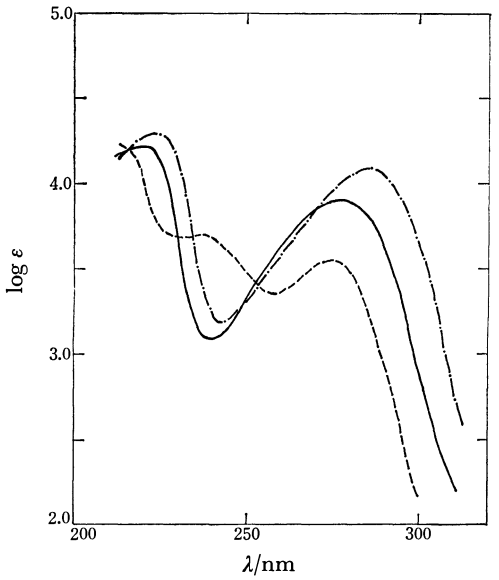

Fig. 1. The UV spectra of the neutral species.
——: IIa, —·—: IIb, ----: VII.

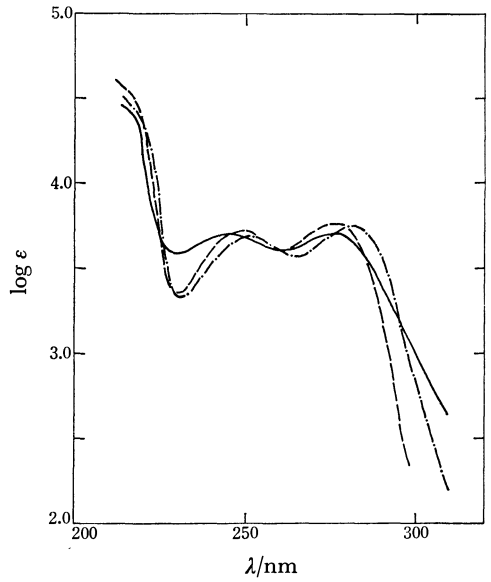

Fig. 2. The UV spectra of the cationic species.
——: IIa, —·—: IIb, ----: VII.

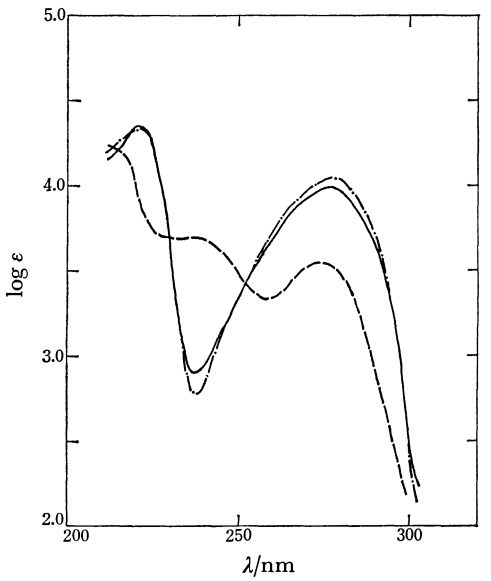

Fig. 3. The UV spectra of the neutral species.
——: VIa, —·—: VIb, ----: VII.

TABLE 2. UV SPECTRA OF *N*-SUBSTITUTED 5-HYDROXY-2HYDROXYMETHYL-4-PYRIDONES

Compd	*N*-Substituent	Conjugate acid		Neutral species		Conjugate base		$\Delta\tilde{\nu}$ / cm^{-1}
		λ_{max} / nm (log ε)	$\tilde{\nu}$ / cm^{-1}	λ_{max} / nm (log ε)	$\tilde{\nu}$ / cm^{-1}	λ_{max} / nm (log ε)	λ / cm^{-1}	
IIa	H	276 (3.70)	36230	278 (3.90)	35970	298 (3.75)	33560	−2410
IIb	CH_3	281 (3.75)	35590	285 (4.08)	35090	312 (3.96)	32050	−3040
IIc	C_2H_5	281 (3.72)	35590	286 (4.08)	34970	312 (4.00)	32050	−2920
IId	Ph	284 (3.92)	35210	290 (4.24)	34480	316 (4.10)	31650	−2830

Table 3. UV spectra of *N*-substituted 2-hydroxymethyl-5-methoxy-4-pyridones

Compd	*N*-Substituent	Conjugate acid		Neutral species	
		λ_{max} nm (log ε)	$\bar{\nu}$ cm^{-1}	λ_{max} nm (log ε)	$\bar{\nu}$ cm^{-1}
VIa	H	275 (3.63)	36360	277 (3.99)	36100
VIb	CH_3	275 (3.70)	36360	278 (4.04)	35970
VIc	C_2H_5	281 (3.72)	35590	285 (4.11)	35090

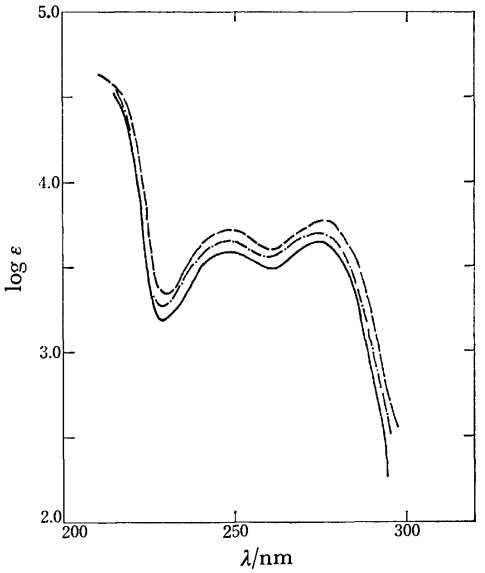

Fig. 4. The UV spectra of the cationic species.
——: VIa, —·—: VIb, ----: VII.

It may be seen from Figs. 1 and 3 that the spectra of the neutral species of IIa and VIa are similar to those of IIb and VIb, but are different from the spectrum of VII, indicating that the 4-pyridones exist predominantly in the NH-form.

As Figs. 2 and 4 illustrate, the spectra of the conjugate acids of 5-hydroxy-4-pyridones IIa and IIb and 5-methoxy-4-pyridones VIa and VIb are very similar to the spectrum of the conjugate acid of VII. This shows that the protonation of the 4-pyridones occurs at the oxygen atom at the 4-position in agreement with Katritzky and Lagowski's results.[1]

The NMR spectral data were also examined. In deuterium oxide, the positions of the peaks of the α- and β-protons of VIa (7.61 and 6.52 ppm) are considerably different from those of VII (7.93 and 7.00 ppm), while in 20% sulfuric acid those of VIa (8.72 and 7.30 ppm) are close to those of VII (8.31 and 7.57 ppm). This indicates the *O*-protonation to be in agreement with the results of Katritzky *et al.*[2,3]

The UV spectra of the conjugate bases of the 4-pyridones IIa and IIb are shown in Fig. 5 together with that of the neutral species of VII. As shown in Fig. 5 and Table 2, the maximum absorption band of IIa is shifted to a shorter wavelength from those of the *N*-substituted 4-pyridones. The spectral pattern is also different from those of the *N*-substituted derivatives, in that a broad shoulder exists at 270—280 nm.

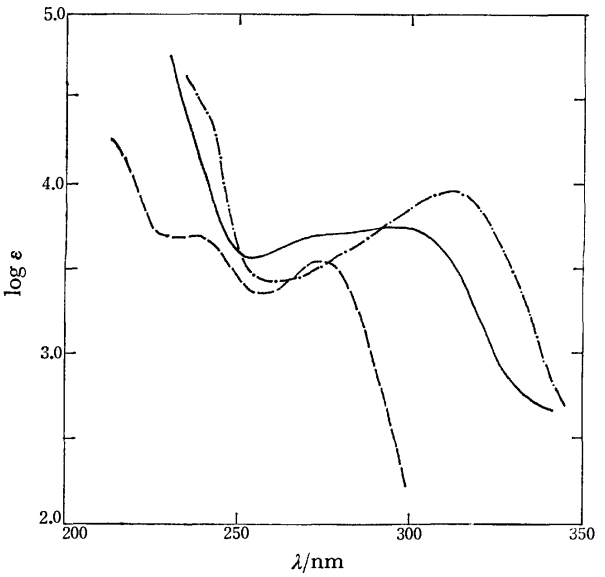

Fig. 5. The UV spectra of the anionic species.
——: IIa, —·—: IIb, ----: VII (neutral).

This shoulder closely corresponds to the maximum absorption band of the pyridine derivative VII. Thus, IIa might exist not only in the pyridone form but also in the pyridine form.

Halochromism. Rapoport *et al.*[13] measured the absorption spectra of 4-substituted 2-nitrophenols in neutral and alkaline solutions, and showed that the difference in wave number between the maxima of the longest-wavelength absorption bands in the two solutions is quantitatively related to the dissociation constant. The wave number shift is also proportional to the Hammett substituent constant. This phenomenon of halochromism is well documented and the degree of halochromism of a compound may be defined as the wave number difference ($\Delta\bar{\nu}$) between the longest-wavelength band of the neutral species and that of its conjugate acid or base.

The $\Delta\bar{\nu}$ values (Table 2) of the 4-pyridones plotted against the pK_a ($\equiv$pK_2) values, produces a straight line as shown in Fig. 6, giving the following equation by the least-square method.

$$\Delta\bar{\nu} = -583\mathrm{p}K_a - 2311 \quad (r=1.000,\ s=1)$$

The slope was comparable to that reported for the phenols.[13]

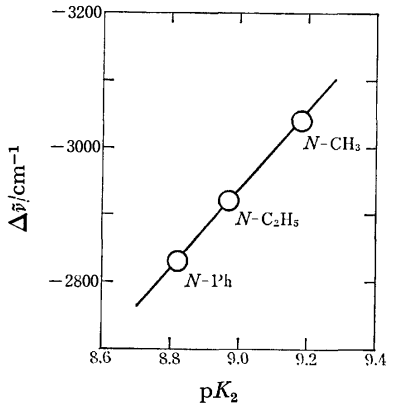

Fig. 6. The relationship between $\Delta\bar{\nu}$ and pK_2.

Experimental

All the melting points were measured on a Yanagimoto micro-melting point apparatus and are uncorrected. The IR and NMR spectra were taken on JASCO IRA-1 spectrophotometer and a Hitachi-Perkin-Elmer R-24 (60 MHz) spectrometer, respectively. The UV spectra were recorded on a Hitachi EPS-2U and EPS-3T spectrophotometer. The pH values were measured by a Hitachi-Horiba F-5 pH meter. The pK_a determination was conducted according to Albert-Serjeant's method.[14]

Materials. All the known compounds were prepared according to the methods described in the references: IIa, mp 232—234 °C (lit,[6] 237—238 °C); IIb, mp 220 °C (lit,[7] 225—227 °C); III, mp 132 °C (lit,[8] 133 °C); V, mp 165—166 °C (lit,[9] 165 °C); VIa, mp 170 °C (lit,[9] 173—175 °C); VIb, mp 203—205 °C (lit,[9] 203—204 °C).

5-Benzyloxy-1-ethyl-2-hydroxymethyl-4-pyridone (IV). A mixture of 5-benzyloxy-2-hydroxymethyl-4-pyrone (III)[8] (2 g) and 70% ethylamine solution (4 ml) was heated in a sealed tube at 130 °C for 5 h. The excess amine was evaporated off and the residue recrystallized from methanol to afford IV (1.8 g, 80.6%) as colorless needles, mp 183 °C. Found: C, 69.25; H, 6.87; N, 5.32%. Calcd for $C_{15}H_{11}NO_3$: C, 69.48; H, 6.61; N, 5.40%. IR (KBr): 1620 cm^{-1}. UV (MeOH) λ_{max}/nm (log ε): 225 (4.35), 286 (4.16).

1-Ethyl-5-hydroxy-2-hydroxymethyl-4-pyridone (IIc). A mixture of 5-benzyloxy-1-ethyl-2-hydroxymethyl-4-pyridone (IV) (2 g) and 5% palladium carbon (0.8 g) in methanol (20 ml) was stirred for 2 h at room temperature under a hydrogen atmosphere. After removal of the catalyst the solvent was evaporated off and the residue recrystallized from ethanol to afford IIc (0.9 g, 69.0%) as colorless needles, mp 187 °C. Found: C, 56.68; H, 6.67; N, 8.18%. Calcd for $C_8H_{11}NO_3$: C, 56.79; H, 6.55; N, 8.28%. IR (KBr): 1640 cm^{-1}. UV (MeOH) λ_{max}/nm (log ε): 226 (4.22), 290 (4.10).

5-Hydroxy-2-hydroxymethyl-1-phenyl-4-pyridone (IId). A mixture of kojic acid (I) (1.5 g) and aniline (2 ml) in water (5 ml) was heated on a water-bath in the presence of 12 M hydrochloric acid (0.7 ml) in a sealed tube for 3 h. Water was added to the reaction mixture, which gave a red-brown precipitate. This precipitate was recrystallized from methanol to afford IId (0.85 g, 37.1%) as colorless needles, mp 238 °C. Found: C, 66.00; H, 5.33; N, 6.44%. Calcd for $C_{12}H_{11}NO_3$: C, 66.35; H, 5.10; N, 6.45%. IR (KBr): 1645 cm^{-1}. UV (MeOH) λ_{max}/nm (log ε): 292 (4.24).

1-Ethyl-2-hydroxymethyl-5-methoxy-4-pyridone (VIc). 2-Hydroxymethyl-5-methoxy-4-pyrone (V)[9] (1.5 g) was heated with 70% ethylamine solution (3 ml) in a sealed tube at 140 °C for 4 h. After evaporation of the excess amine and water, the residue was recrystallized from methanol to give VIc (1.6 g, 90.9%) as colorless needles, mp 177 °C. Found: C, 58.93; H, 7.22; N, 7.81%. Calcd for $C_9H_{13}NO_3$: C, 59.00; H, 7.15; N, 7.65%. IR (KBr): 1635 cm^{-1}. UV (MeOH) λ_{max}/nm (log ε): 224 (4.21), 287 (4.13).

3,4-Dimethoxy-6-hydroxymethylpyridine (VII). An excess of diazomethane in ether was added to a solution of 5-hydroxy-2-hydroxymethyl-4-pyridone (IIa) (1 g) in methanol (600 ml), and the mixture allowed to stand in a refrigerator until the purple color with iron(III) chloride disappeared. After evaporation of the solvents, the residue was recrystallized from ethanol and sublimed to afford VII (0.4 g, 33%) as colorless needles, mp 121—122 °C. Found: C, 56.61; H, 6.55; N, 8.20%. Calcd for $C_8H_{11}NO_3$: C, 56.79; H, 6.55; N, 8.28%. IR (KBr): 1595 cm^{-1}. UV (MeOH) λ_{max}/nm (log ε): 234 (3.77), 274 (3.44). NMR ($CDCl_3$): 3.90 (s, 6H), 4.66 (s, 2H), 6.91 (1H), 7.97 (s, 1H).

We wish to thank Professor Satoru Yokota of Kumamoto Institute of Technology for the supply of kojic acid.

References

1) A. R. Katritzky and J. M. Lagowski, *Adv. Heterocycl. Chem.*, **1**, 352 (1963).
2) R. A. Y. Jones, A. R. Katritzky, and J. M. Lagowski, *Chem. Ind., (London)*, **1960**, 870.
3) A. R. Katritzky and R. A. Y. Jones, *Proc. Chem. Soc.*, **1960**, 313.
4) P. Sensi and G. G. Gallo, *Ann. Chim. (Rome)*, **44**, 232 (1954); *Chem. Abstr.*, **49**, 14757f (1955).
5) E. Spinner, *J. Chem. Soc.*, **1960**, 1226.
6) K. Heyns and G. Vogelsang, *Chem. Ber.*, **87**, 1377 (1954).
7) J. A. Berson, W. M. Jones, and S. L. O'Callaghan, *J. Am. Chem. Soc.*, **78**, 622 (1956).
8) S. Nonomura, H. Ueda, I. Ichimoto, and C. Tatsumi, Japan Patent, 1176 (1967); *Chem. Abstr.*, **66**, 84748y (1967).
9) J. W. Armit and T. J. Nolan, *J. Chem. Soc.*, **1931**, 3023.
10) A. Gordon and A. R. Katritzky, *J. Chem. Soc., B*, **1968**, 556.
11) H. Besso, K. Imafuku, and H. Matsumura, *Bull. Chem. Soc. Jpn.*, **50**, 710 (1977).
12) G. Choux and R. L. Benoit, *J. Org. Chem.*, **32**, 3974 (1967).
13) M. Rapoport, C. K. Hancock, and E. Meyers, *J. Am. Chem. Soc.*, **83**, 3489 (1961).
14) A. Albert, and E. P. Serjeant, "Ionization Constants of Acids and Bases," 1st ed, Methuen, London (1962), Chap. 4.

Substituent Effects on 6-Substituted 3-Hydroxy-1-methyl-4-pyridones

Kimiaki IMAFUKU,* Kumio TAKAHASHI,† and Hisashi MATSUMURA

Department of Chemistry, Faculty of Science, Kumamoto University, Kurokami, Kumamoto 860

(Received September 10, 1977)

Acid dissociation constants and UV and NMR spectra of a series of 6-substituted 3-hydroxy-1-methyl-4-pyridones have been measured. The acid dissociation constants have been analyzed in terms of the Hammett equation to give linear relationships, with $\rho=1.16$ for the conjugate acids and $\rho=1.06$ for the neutral compounds. Halochromism in the UV spectra gave the equation: $\Delta\bar{\nu}=689\,pK_a-9399$, and the Hammett plots of the chemical shifts of the 2-H, 5-H, and CH_3 protons gave linear relationships, with $\rho=1.78$, 2.56, and 1.39, respectively.

In 1967 Choux and Benoit[1] reported the substituent effects on the physical properties such as the acid dissociation constants and UV and NMR spectra of 4-pyrone derivatives. However, little is known about the 4-pyridone derivatives. The substituent effect on tautomerism of 6-substituted 3-methoxy-4-pyridones has been examined and it has been reported that the tautomeric ratios are affected by the substituents.[2]

In this paper the substituent effects on the acid dissociation constants and UV and NMR spectra of 6-substituted 3-hydroxyl-1-methyl-4-pyridones will be reported in which tautomerism does not exist.

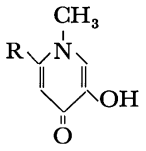

Results and Discussion

Acid Dissociation Constants. The acid dissociation constants of five 6-substituted 3-hydroxy-1-methyl-4-pyridones have been determined spectrophotometrically in water at 25 °C. The results are summarized in Table 1, where the pK_2 and pK_1 values represent the acid dissociation exponent (pK_a) of a neutral compound and that of its conjugate acid, respectively. The pK_1 values are comparable to the pK_1 values for 4-pyridone (3.37)[3] and *N*-methyl-4-pyridone (3.33).[4] The pK_2 values are slightly larger than the pK_2 values for the 3-hydroxy-4-pyrones,[1] *i.e.* the 3-hydroxy-1-methyl-4-pyridones are less acidic than the 3-hydroxy-4-pyrones.

A correlarion between pK_2 and the Hammett σ_p constants[5] has been established for the 6-substituted 3-hydroxyl-1-methyl-4-pyridones, as shown in Fig. 1,

Table 1. pK_a values

No.[a]	R	σ	pK_1	pK_2
1	CH_3	−0.170	3.43	9.29
2	H	0	3.07	9.15
3	CH_2OH	0.08[b]	3.07	9.07
4	COO^-	0.132		9.03
5	CH_2Cl	0.184	3.02	8·88

a) Numbers correspond to those in Fig. 1. b) Ref. 1.

† Present address: Prefectural Office of Hiroshima, Hiroshima 730.

and gives the following equation by the least-squares method:

$$pK_2 = 9.13 - 1.06\sigma \qquad (r=0.969,\ s=0.03)$$

The reaction constant ($\rho=1.06$) is apparently smaller than that for the proton loss of 6-substituted 3-methoxy-4-pyridones ($\rho=4.94$).[2] In the latter case tautomerism produces the 4-pyridinols but since tautomerism does not exist in the former, transmission of the substituent effect is decreased.

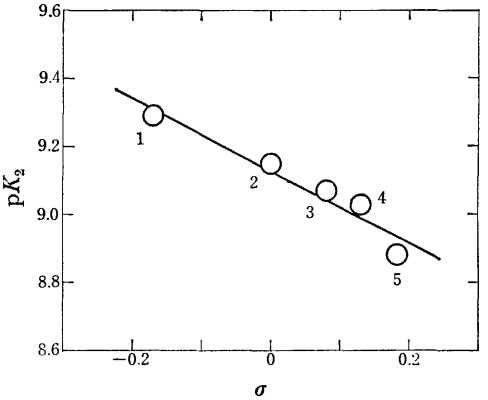

Fig. 1. The Hammett plot of pK_2 values.

The Hammett plots of the pK_1 values gave the equation:

$$pK_1 = 3.17 - 1.16\sigma \qquad (r=0.860,\ s=0.06)$$

Although the correlation is not good, the transmission of the substituent effect is enhanced by the existence of a conjugated double bond, but is considerably smaller than that in the 3-methoxy-4-pyridones ($\rho=3.01$).[2]

Halochromism in UV Spectra. The UV spectra of the 6-substituted 3-hydroxy-1-methyl-4-pyridones have been measured in neutral and alkaline solutions. The wavelengths and wave numbers are listed in Table 2 as λ_{HA} and $\bar{\nu}_{HA}$ for the neutral species and λ_{A^-} and $\bar{\nu}_{A^-}$ for the conjugate bases, respectively. The $\Delta\bar{\nu}$ values are the differences between the $\bar{\nu}_{A^-}$ and $\bar{\nu}_{HA}$ values.

A general relationship between the electronic spectra and dissociation constants has been established for 4-substituted 2-nitrophenols.[6] Plots of the $\Delta\bar{\nu}$ values against pK_a ($\equiv pK_2$) values give a linear relationship as shown in Fig. 2, which is represented by the following equation.

$$\Delta\bar{\nu} = 689\,pK_a - 9399 \qquad (r=0.959,\ s=31)$$

TABLE 2. UV SPECTRAL DATA

No.[a]	R	Neutral species			Conjugate base			$\Delta\bar{\nu}$
		λ_{HA} nm	$\bar{\nu}_{HA}$ cm^{-1}	$\log \varepsilon_{HA}$	λ_{A^-} nm	$\bar{\nu}_{A^-}$ cm^{-1}	$\log \varepsilon_{A^-}$	cm^{-1}
1	CH_3	278	35970	4.08	304	32890	3.96	−3080
2	H	282	35460	4.12	309	32360	3.97	−3100
3	CH_2OH	283	35340	4.11	311	32150	3.99	−3190
4	COO^-	284	35210	4.04	312	32050	3.90	−3160
5	CH_2Cl	283	35340	4.00	312	32050	3.89	−3290

a) Numbers correspond to those in Fig. 2.

TABLE 3. NMR SPECTRAL DATA

No.[a]	R	δ			
		2-H	5-H	1-CH_3	Others
1	CH_3	7.43 (s)	6.40 (s)	3.61 (s)	2.30 (s) for 6-CH_3
2	H	7.59 (d)[b]	6.58 (d)[c]	3.82 (s)	7.58 (dd)[d] for 6-H
3	CH_2OH	7.71 (s)	6.80 (s)	3.89 (s)	e)
4	COOH	7.88 (s)	7.13 (s)	3.98 (s)	
5	CH_2Cl	8.11 (s)	7.31 (s)	4.14 (s)	e)

a) Numbers correspond to those in Fig. 3. b) $J_{2,6}=3$ Hz. c) $J_{5,6}=7$ Hz. d) $J_{6,2}=3$ Hz and $J_{6,5}=7$ Hz. e) The δ values for 6-C**H**$_2$OH and 6-C**H**$_2$Cl could not be measured accurately because of overlapping with the signal of HOD.

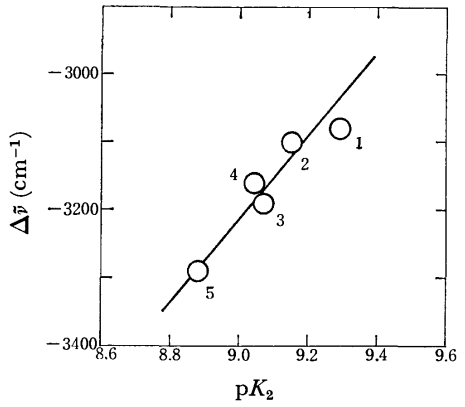

Fig. 2. The relationship between $\Delta\bar{\nu}$ and pK_2.

NMR Spectra. The ^{1}H-NMR spectral data in deuterium oxide are listed in Table 3. The chemical shifts of 3-OH could not be determined becasue of hydrogen exchange with deuterium in the solvent. The chemical shifts of 2-H, 5-H, and 1-CH_3 have been plotted against the respective σ_p constants (Fig. 3). The plots have yielded the following equations.

$$\delta_{2\text{-H}} = 1.78\sigma + 7.66 \quad (r=0.937,\ s=0.05)$$
$$\delta_{5\text{-H}} = 2.56\sigma + 6.73 \quad (r=0.939,\ s=0.11)$$
$$\delta_{CH_3} = 1.39\sigma + 3.83 \quad (r=0.977,\ s=0.03)$$

From this data the substituents have a stronger effect on the chemical shifts of the 5-H proton than on that of the 2-H proton. The chemical shifts of the 1-CH_3 are less sensitive to the substituent effects than those of the 2-H and 5-H protons. Transmission of the substituent effects was apparently larger than for the 4-pyrones.[1]

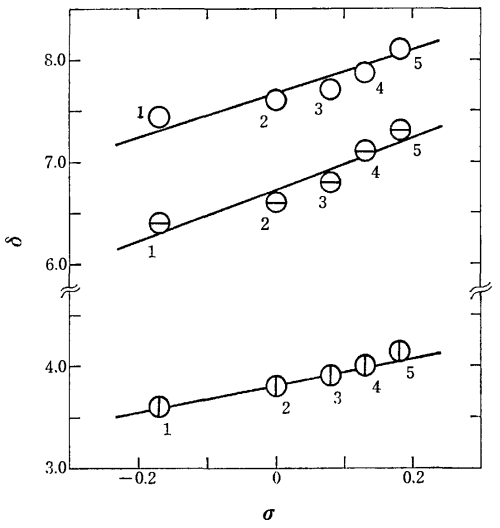

Fig. 3. The relationships of the chemical shifts with σ constants. ○: $\delta_{2\text{-H}}$, ⊖: $\delta_{5\text{-H}}$, ⏀: δ_{CH_3}.

Experimental

All the melting points were measured on a Yanagimoto micro-melting point apparatus and are uncorrected. The IR, UV, and NMR spectra were taken on JASCO IRA-1, Hitachi EPS-3T, and Hitachi-Perkin-Elmer R-24 (60 MHz) spectrometers, respectively. The pH values were measured by a Hitachi-Horiba F-5 pH meter. The pK_a values were obtained by the method of Albert and Serjeant.[7]

Materials. All the known compounds were prepared from kojic acid according to the methods in the literature: 3-hydroxy-1-methyl-4-pyridone, mp 215—217 °C (lit,[8] 212—216 °C); 1,2-dimethyl-5-hydroxy-4-pyridone, mp 270—274 °C (lit,[9] 273—274 °C); 5-hydroxy-2-hydroxymethyl-1-methyl-4-

pyridone, mp 220 °C (lit,[8] 225—227 °C).

2-Chloromethyl-5-hydroxy-1-methyl-4-pyridone was obtained by the treatment of 5-hydroxy-2-hydroxymethxl-1-methyl-4-pyridone[8] (1.0 g) with thionyl chloride (4.0 ml) at 60—70 °C for 30 min. Yield, 0.38 g (34.0%); mp 220—230 °C (from methanol-ethyl acetate); IR (KBr): 1628 cm^{-1}. Found: C, 48.36; H, 4.87; N, 8.06%. Calcd for $C_7H_8ClNO_2$: C, 48.43; H, 4.64; N, 8.07%.

2-Carboxy-5-hydroxy-1-methyl-4-pyridone was obtained by reaction of comenic acid (1.1 g) with 48% methylamine solution (2.5 g) at 60—80 °C for 4 h. Yield, 0.28 g (23.5%); mp 224—230 °C (dec) (from water); IR (KBr): 1630, 1607 cm^{-1}. Found: C, 49.68; H, 4.37; N, 8.27%. Calcd for $C_7H_7NO_4$: C, 49.71; H, 4.17; N, 8.28%.

The authors are grateful to Professor Satoru Yokota of Kumamoto Institute of Technology for the supply of kojic acid.

References

1) G. Choux and R. L. Benoit, *J. Org. Chem.*, **32**, 3974 (1967).
2) H. Besso, K. Imafuku, and H. Matsumura, *Bull. Chem. Soc. Jpn.*, **50**, 710 (1977).
3) A. Albert and J. N. Phillips, *J. Chem. Soc.* **1956**, 1924.
4) A. Gordon and A. R. Katritzky, *J. Chem. Soc., B*, **1968**, 556.
5) H. H. Jaffé, *Chem. Rev.*, **53**, 191 (1953).
6) M. Rapoport, C. K. Hancock, and E. A. Meyers, *J. Am. Chem. Soc.*, **83**, 3489 (1961).
7) A. Albert and E. P. Serjeant, "Ionization Constants of Acids and Bases," 1st ed, Methuen, London (1962), Chap. 4.
8) A. A. Berson, W. M. Jones, and S. L. F. O'Callaghan, *J. Am. Chem. Soc.*, **78**, 622 (1956).
9) J. W. Armit and T. J. Nolan, *J. Chem. Soc.*, **1931**, 3023.

Odor and Volatile Compounds in Liquid Swine Manure. III. Volatile and Odorous Components in Anaerobically or Aerobically Digested Liquid Swine Manure

Akio YASUHARA* and Keiichiro FUWA**

Chemistry and Physics Division, National Institute for Environmental Studies, Yatabe, Tsukuba, Ibaraki 300-21

***Department of Chemistry, Faculty of Science, University of Tokyo, Hongo, Bunkyo-ku, Tokyo 113*

(Received April 7, 1978)

Volatile and odorous components were isolated from anaerobically or aerobically digested liquid swine manure by direct solvent-extraction and flash-distillation under reduced pressure. The concentrations of indole, oxindole, dimethylsulfoxide, phenol, and a few carboxylic acids increased, and *o*-aminoacetophenone decreased during digestion. Alkaline components were not so important for the odor. Offensive odor was formed by mixing phenols and carboxylic acids. Complete aeration resulted in a remarkable decrease of lower carboxylic acids.

Research on malodor has attracted only few researchers in contrast to studies concerned with flavor and perfume, and therefore, it is retarded. In Japan a piggery is one of the most malodor-evolving sources. Measurements have been carried out for ammonia, trimethylamine, hydrogen sulfide, methyl mercaptan, dimethyl sulfide, *etc.* which are controlled by the Japanese law on malodor, but there are only a few studies that have investigated other compounds or have considered the nature of the malodor. In research on malodor, it is very important and difficult to isolate odorous substances from samples effectively. Broadly speaking, there are three malodor-evolving sources in a piggery, that is, pig itself, solid manure, and liquid manure. A series of past studies have been concerned with liquid manure which had accumulated, rotted, and evolved a strong malodor.[1,2]

Carboxylic acids and many other compounds have already been detected in liquid swine manure by steam distillation.[1,2] It may be true that some substances decompose thermally during steam distillation, although it is a very useful method to separate volatile compounds from nonvolatiles. In this study direct solvent-extraction and flash-distillation under reduced pressure were used for isolation of odorous compounds in order to avoid thermal decomposition.

This paper deals with the isolation and the identification of odorous compounds having a medium or high boiling point in liquid swine manure and with the change of these odorous compounds under anaerobic or aerobic digestion.

Experimental

Material and Procedure. Liquid swine manure was collcted from a drain under pigsties near Takezono, Tsukuba New Town, Ibaraki Prefecture, at an inlet of a pit.

Two experiments were carried out. In the first experiment the air-flow rate was adjusted so that liquid manure was not digested completely in order that information on intermediate changes of some components due to chemical or microbial action was obtained. An aim of the second experiment was to obtain information on the relative ratio of typical odorous components between anaerobic digestion and completely aerobic digestion. The latter experimental conditions were similar to situation of odor control for liquid manure in pigsty.

In the first experiment the liquid swine manure was divided into three parts. One part (2.5 l) was shaken with dichloromethane (400 ml) for 15 min and the lower slurry containing the organic layer was separated. The other two parts (each 2.5 l) were digested at 35 °C for a week under bubbling of nitrogen (100 ml/min) or air (100 ml/min) respectively. Then the respective digested liquid manure was shaken with dichloromethane (400 ml) for 15 min, and the lower slurry was separated. Each slurry was centrifuged at 10000 rpm for 10 min and the organic layer was separated. The extract was fractionated into three fractions as described in Fig. 1.

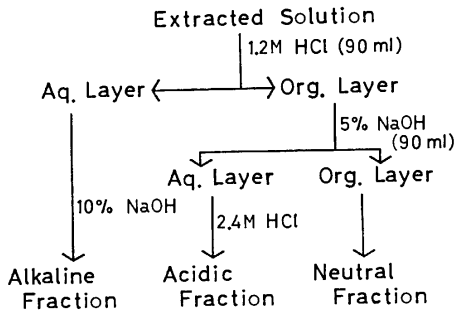

Fig. 1. Fractionation of liquid swine manure extract.

In the second experiment the liquid swine manure was divided into two parts. One part (50 l) was kept in glass bottles and digested at 20—25 °C for a week. The liquid manure became dark green and the surface was covered with a black formy film after a day, so the manure corresponded to anaerobic digestion. In the case of anaerobic digestion an inert gas such as nitrogen was not passed, when the experimental conditions approached the same situation where piggery liquid manure was stored in an anaerobic situation. The other part (each time 2 l, total 18 l) was aerobically digested by bubbling air at a rate of 2 l/min in a glass vesel at 20—25 °C for a week and then, malodor became very weak. Both parts of the rotten swine manure were flash-distilled under reduced pressure by means of the apparatus shown in Fig. 2. The receiver was chilled with ice, the two traps were cooled with Dry Ice and methanol to condense water vapor and volatiles completely, and the third trap chilled with liquid nitrogen was used

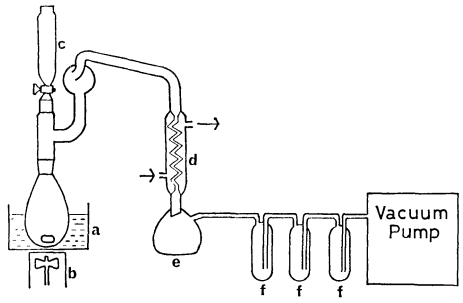

Fig. 2. Apparatus for flash-distillation under reduced prssure.
a, Water-bath; b, magnetic stirrer; c, funnel; d, Graham condenser; e, receiver; f, trap.

to prevent contamination from oil of the vacuum pump. The distillate was extracted continuously for 24 h with ethyl ether after saturation with sodium chloride. The extract was fractionated into three fractions as shown in Fig. 1.

Each fraction in both experiments was evaporated, after drying with anhydrous sodium sulfate, by means of a Kvrderna-Danish concentrator under atmospheric pressure.

Gas Chromatography. A Shimadzu Model GC-5A gas chromatograph was used. The flame detectors were operated using a hydrogen-flow rate of 50 ml/min and an air-flow rate of 0.5 l/min. Thermoconductivity detectors were used for the organoleptic tests. For the acidic fraction the gas-chromatographic conditions were as follows: injector and detector temperatures, 250 °C; column, 3 m×3 mm i.d. glass column packed with 2% DEGS+0.5% H_3PO_4 on 60- to 80-mesh, acid-washed, DMCS-treated Chromosorb W; column temperatures, 50 to 190 °C by an increase at a rate of 8 °C/min; carrier-gas (nitrogen) flow rate, 30 ml/min at 5 kg/cm^2. For alkaline and neutral fractions the gas-chromatographic conditions were as follows: injector and detector temperatures, 300 °C; column, 3 m×3 mm i.d. glass column packed with 2% OV-17 on 60- to 80-mesh, acid-washed, DMCS-treated Chromosorb W; column temperatures, 100 to 250 °C with temperature increase of 10 °C/min; carrier-gas (nitrogen) flow rate, 30 ml/min at 5 kg/cm^2.

Organoleptic Test for Odor. This test was carried out by means of smelling the odor of compounds progressively eluted from the outlet of the gas chromatograph.

Mass Spectrometry. A JEOL Model JMS-D 100 mass spectrometer was connected with a JEOL JGC-20 K gas chromatograph and a JEOL JMA-2000 mass data analysis system. The gas-chromatographic conditions were the same as above except for the size of the column. The size of the column was 3 m×2 mm i.d. The mass-spectrometric conditions were as follows: ion-source temperature, 140 °C; ion-source pressure, 1.2×10^{-6} Torr; ionizing corrent, 3×10^{-4} A; ionizing energy, 75 eV; accelerating voltage, 3 kV; mass range, *m/e* 10 to 450; scan time, 2.7 s; scan interval, 5 s. The mass data analysis procedures were subtraction of the background mass spectra, normalization by the most intense peak, and a search of mass spectra catalogue.

Results and Discussion

Digested liquid swine manure gave a pH of 8—9 regardless of anaerobic or aerobic digestion. The odors from digested liquid manure under anaerobic and aerobic conditions were very different each other. Though sulfur-containing compounds would be assumed to contribute to the difference of odor, studies on sulfur-containing components are in progress and the results will be reported at a later date. Many odorous compounds were isolated and identified from anaerobically stored piggery liquid manure by steam distillation,[1,2] but the odor of the steam-distillate has been different from the original odor. The reason for this is that some compounds are thought to decompose during steam distillation. A direct extraction has the benefit of minimizing those losses and decomposition and to keep the content ratio of many components identical to the original manure. Centrifuging above 5000 rpm was very effective for separating the organic layer of the slurry formed by shaking liquid manure with dichloromethane. The odor of the organic layer resembled that of the original manure. Typical gas chromatograms of fractions in the first experiment are shown in Fig. 3 to Fig. 5. The identification of each peak in the gas chromatogram was carried out by gas chromatography-mass spectrometry and the quantification was done by gas chromatography. The results of identification and quantification of the components related to the odor are shown in Table 1. In performing fractionation, removal of the alkaline fraction did not change the odor of the extracted solution, but removal of the neutral or acidic fraction, particularly the latter fraction, greatly altered the odor. The organoleptic test showed that the alkaline fraction did not contribute so much to the odor of swine liquid manure. Of course, ammonia and trimethylamine play an important role on the malodor,[3] but they cannot be detected by the method used in this study.

Indole and di-2-ethylhexyl phthalate decomposed easily, and skatole decomposed slowly under aerobic conditions. Indole concentration increased but for skatole the concentration hardly changed under anaerobic conditions. The results show that indole was formed from protein or its decomposed products under

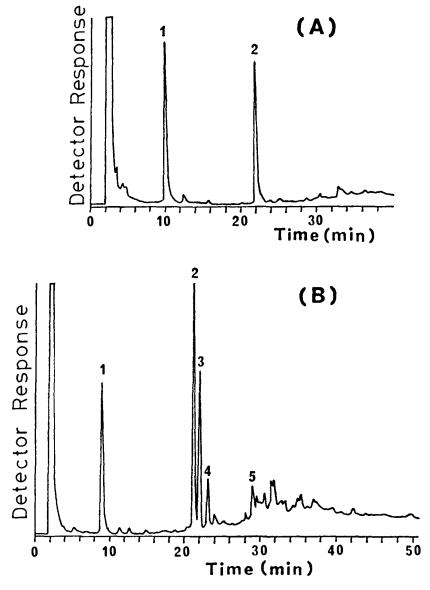

Fig. 3. Gas chromatograms of alkaline fractions.
(A), Raw liquid swine manure; (B), aerobically digested liquid swine manure.

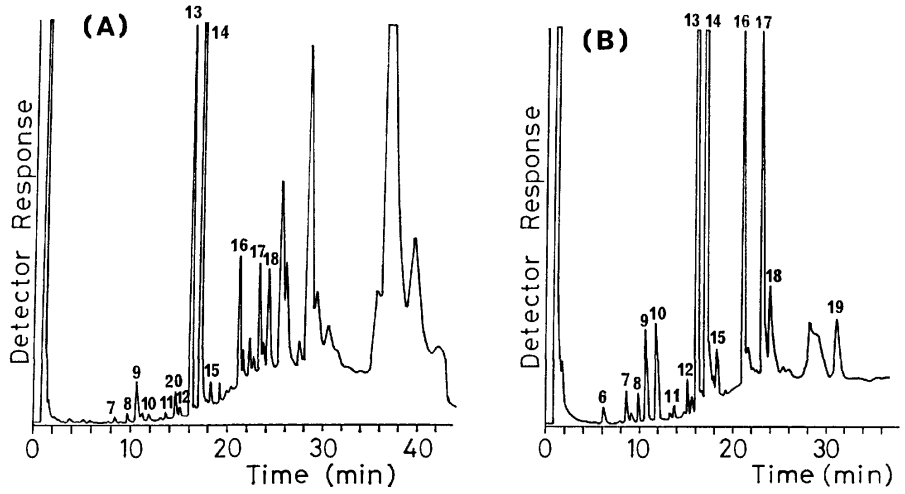

Fig. 4. Gas chromatograms of acidic fractions.
(A), Raw liquid swine manure; (B), aerobically digested liquid swine manure.

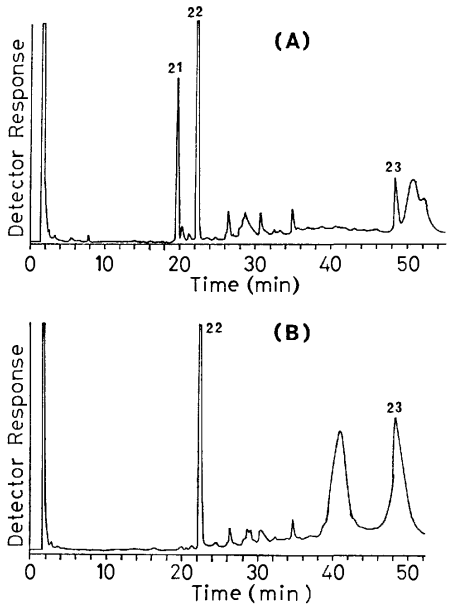

Fig. 5. Gas chromatograms of neutral fractions.
(A), Raw liquid swine manure; (B), aerobically digested liquid swine manure.

anaerobic conditions and agreed with the results reported by Spoelstra.[4] Oxindole may be supposed to be formed from indole by microbial action. Dimethylsulfide may also be supposed to change to dimethylsulfoxide. Indole, skatole, and dimethylsulfoxide were malodorous among neutral components.

In alkaline fraction, aniline, methylquinazoline, dimethyl- or ethylquinazoline, isatin, and *o*-aminoacetophenone were detected. Quinazoline derivatives and isatin were assumed to be formed during aerobic digestion. *o*-Aminoacetophenone which existed in relatively large quantities at first decreased in the same way for both digestion conditions. The odor qualities of aniline, quinazoline derivatives, and *o*-aminoacetophenone were significantly less than the odor qualities of other components.

It has been reported that concentrations of phenol, *p*-cresol, and *p*-ethylphenol have increased in anaerobically stored piggery wastes.[4] The change of phenol in this study was identical with the above result. Acetic acid, isobutyric acid, and butyric acid were not detected in raw manure, but they were found at almost the same concentrations in both anaerobically and aerobically digested manure. In this experiment there was little difference in contents of carboxylic acids among raw, anaerobically digested, and aerobically digested

Table 1. Identification and quantification of volatile and odorous components[a]

Peak No.	Compound	Raw wt/l	Anaerobic wt/l	Aerobic wt/l
1	Aniline	8.2 μg	16 μg	15 μg
2	*o*-Aminoacetophenone	294 μg	20 μg	30 μg
3	Methylquinazoline	—	trace	16 μg
4	Dimethyl- or ethylquinazoline	—	—	4.8 μg
5	Isatin	—	—	3.0 μg
6	Acetic acid	—	1.3 μg	2.6 μg
7	Isobutyric acid	—	5.2 μg	5.6 μg
8	Butyric acid	—	8.4 μg	5.2 μg
9	Isovaleric acid	28 μg	28 μg	16 μg
10	Dimethylsulfoxide	3.8 μg	32 μg	17 μg
11	Valeric acid	3.2 μg	4.8 μg	1.9 μg
12	Hexanoic acid	6.4 μg	9.2 μg	6.0 μg
13	Phenol	1.23 mg	2.5 mg	0.44 mg
14	*p*-Cresol	28.4 mg	26 mg	16 mg
15	*p*-Ethylphenol	2.22 mg	2.22 mg	2.08 mg
16	Benzoic acid	63 μg	39 μg	48 μg
17	Phenylacetic acid	50 μg	42 μg	45 μg
18	3-Phenylpropionic acid	48 μg	27 μg	10 μg
19	Oxindole	—	41 μg	7.6 μg
20	*o*-Methoxyphenol	4.1 μg	—	—
21	Indole	0.87 mg	1.63 mg	trace
22	Skatole	2.05 mg	1.89 mg	1.46 mg
23	Di-2-ethylhexyl phthalate	0.24 mg	0.14 mg	0.06 mg

a) These values are not corrected with extraction coefficients.

manures. McGill and Jackson[5] reported the content ratio of carboxylic acids in pig slurry filtrates that showed acetic acid as a major component (65.5%). This experiment gave different results, but an exact comparison was not possible since the above study[5] did not report quantitative values, but relative values. In this experiment the acidic fraction did not have an irritating odor such as acetic acid and propionic acid, but had a sweaty and putrid odor. This odor was a little different from the odor of each carboxylic acid such as butyric or isovaleric acid and phenol. The organoleptic test showed that C_4—C_6 carboxylic acids and phenylacetic acid were malodorous and that phenols had a characteristic odor. However, an offensive odor was strengthened by mixing carboxylic acids and phenols and phenols added an adhensive nature to the total odor.

Strong aeration used in the second experiment is one of the most useful methods for deodorization. Strong malodor from liquid manure almost disappeared and the odor attributed to skatole remained when air was passed at a rate of 2 l/min for a week. A complete digestion under anaerobic conditions needs more than two months.[4] Gas-chromatographic analysis is facilitated by removing nonvolatile substances from sample. Therefore, a distillation method is very convenient, but steam distillation is not so good for this purpose. Distillation under reduced pressure, although it would be expected to be a useful method, was unsuccessful because of the violent frothing of the sample. In such a case flash-distillation under reduced pressure is very valuable and it was used successfully in this experiment. This method is suitable for isolating relatively volatile compounds, although it is time consuming. Continuous extraction with ethyl ether was used in order to avoid an accumulation of impurities from the large volume of solvent.

The gas chromatograms of each fraction were essentially identical. Each peak in the gas chromatograms was assigned by gas chromatography-mass spectrometry. The quantifications of fractions were carried out by gas chromatography and their results are shown in Table 2. The quantities of alkaline components did not change so much. The odor of anaerobically stored manure was attributed to the acidic components. The odor of indole and skatole from the anaerobically stored manure was felt a little, but it was fairly strong from aerobically digested manure. The aerobically digested manure did not exhibit the odor of phenols and carboxylic acids. This fact is compatible with the result of quantification. In particular, the concentrations of lower carboxylic acids decreased or were not detected after aeration. As the concentration of the valeric acid did not decrease significantly by bubbling nitrogen gas into the aqueous solution of the acid, its disappearance during aeration would be presumed to be caused by microbial action. The function of phenols with regard to odor diminished with decreasing carboxylic acids. As indole and skatole did not decrease so much and their threshold values for odor were very low, the odor of aerobically digested manure was dominated by them.

Table 2. Quantification of odorous components in anaerobically and aerobically digested liquid swine manure[a]

Compound	Anaerobic wt/l	Aerobic wt/l
Aniline	76 μg	41 μg
o-Aminoacetophenone	248 μg	129 μg
Methylquinazoline	46 μg	29 μg
Dimethyl- or ethylquinazoline	44 μg	18 μg
Phenol	3.6 mg	0.79 mg
p-Cresol	29.2 mg	0.85 mg
p-Ethylphenol	3.8 mg	0.55 mg
Isovaleric acid	60 μg	—
Valeric acid	44 μg	—
2-Methylbutyric acid	12 μg	4 μg
4-Methylpentanoic acid	54 μg	—
Hexanoic acid	166 μg	6 μg
2-Methylpentanoic acid	18 μg	3 μg
4-Methylhexanoic acid	92 μg	9 μg
Heptanoic acid	166 μg	18 μg
Octanoic acid	166 μg	37 μg

a) These values are not corrected with recovery coefficients.

The authors wish to thank Mr. Minoru Kuriyama, a hog raiser near Tsukuba New Town, Ibaraki Prefecture, for his offer of liquid swine manure.

References

1) A. Yasuhara and K. Fuwa, *Bull. Chem. Soc. Jpn.*, **50**, 731 (1977).
2) A. Yasuhara and K. Fuwa, *Bull. Chem. Soc. Jpn.*, **50**, 3029 (1977).
3) J. R. Miner and T. E. Hazen, *Trans. Am. Soc. Agric. Eng.*, **12**, 772 (1969).
4) S. F. Spoelstra, *J. Sci. Food Agric.*, **28**, 415 (1977).
5) A. E. J. McGill and N. Jackson, *J. Sci. Food Agric.*, **28**, 424 (1977).

Pseudo-sugars. 3. Alternative Synthesis of Penta-*N,O*-acetyl-DL-validamine and Its Analogs[1]

Seiichiro OGAWA,* Isamu KASAHARA, and Tetsuo SUAMI
Department of Applied Chemistry, Faculty of Engineering, Keio University, Hiyoshi, Yokohama 223

(Received May 8, 1978)

DL-Validamine and its amino deoxy and deoxy analogs were synthesized as the acetyl derivatives from *endo*-7-oxabicyclo[2.2.1]hept-5-ene-2-carboxylic acid, the Diels-Alder adduct of acrylic acid and furan.

In a previous paper[2] a report was given on the first synthesis of penta-*N,O*-acetyl-DL-validamine starting from the Diels-Alder adduct of furan with acrylic acid, *endo*-7-oxabicyclo[2.2.1]hept-5-ene-2-carboxylic acid (**1**).[3] Acetolysis of tri-*O*-acetyl-2,3-dihydroxy-6-hydroxymethyl-7-oxabicyclo[2.2.1]heptane gave a poor yield of the desired intermediate, penta-*O*-acetyl-(1,3,5/2,4)-5-hydroxymethyl-1,2,3,4-cyclohexanetetrol (pseudo-β-D-glucopyranose),[4] since anhydro ring formation occurs simultaneously to give a dioxatricyclo compound.[5] Thus, bromination of the substituted 2-hydroxymethyl-7-oxabicyclo[2.2.1]heptane with hydrogen bromide in acetic acid has been studied in order not only to open the 1,4-anhydro ring, but also to introduce a bromine substituent into the cyclohexane ring, which can be replaced by an amino function. In the present paper, we report on the alternative synthesis of acetyl derivatives of DL-validamine and its several analogs starting from the substituted bromohydroxymethylcyclohexanes derived from **1**.

Hydrogenation of **1** with palladium black gave *endo*-7-oxabicyclo[2.2.1]heptane-2-carboxylic acid (**2**)[3] in high yield. This was reduced by lithium aluminum hydride (LAH) in tetrahydrofuran (THF) followed by acetylation with acetic anhydride in pyridine to give *endo*-2-acetoxymethyl-7-oxabicyclo[2.2.1]heptane (**3**) as a syrup in 80% yield.

Reaction of **2** with 15% hydrogen bromide in acetic acid in a sealed tube overnight at 85—90 °C resulted in cleavage of the 1,4-anhydro ring to give rise to a mixture of acetoxybromocyclohexanecarboxylic acids, from which crystalline (1,5/2)-2-acetoxy-5-bromocyclohexanecarboxylic acid (**4**) was isolated in 59% yield. In its ^{1}H NMR spectrum, a triplet of doublets at δ 5.00 having 4.5, 10, and 10 Hz-splittings could be ascribed to H-2, in line with the 1,2-trans configuration between the acetoxyl and carboxyl groups. Under similar reaction conditions, **3** afforded crystalline dibromo compound (**5**) in an isolated yield of 35%. In this case, the primary acetoxyl group was replaced by a bromide ion in addition to opening the anhydro ring. The ^{1}H NMR spectrum of **5** contained a pattern of the signals due to methine protons very similar to that of **4**. The structure of **5** was tentatively assigned to (1/2,4)-4-bromo-2-(bromomethyl)cyclohexyl acetate.

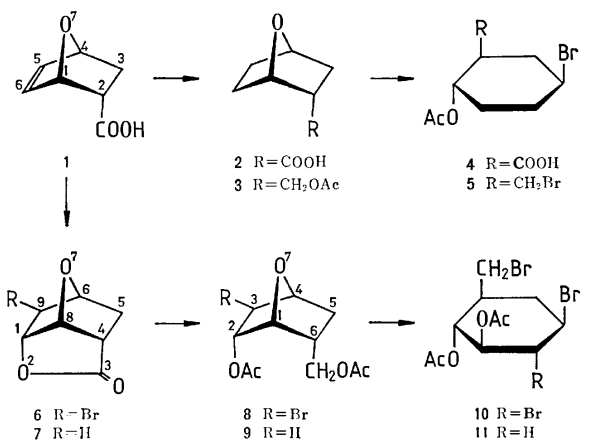

1
2 R=COOH
3 R=CH₂OAc
4 R=COOH
5 R=CH₂Br
6 R=Br
7 R=H
8 R=Br
9 R=H
10 R=Br
11 R=H

Scheme 1.

On the other hand, bromolactonization of **1** proceeded smoothly to give the bromolactone (**6**) in 91% yield. Reduction of **6** with LAH in THF followed by acetylation gave *endo*-2-acetoxy-*endo*-6-acetoxymethyl-*exo*-3-bromo-7-oxabicyclo[2.2.1]heptane (**8**) in 84% yield. Hydrogenolysis of **8** with Raney nickel in the presence of Amberlite IRA-45 (OH^-) gave the corresponding debromo compound (**9**) in 94% yield, which was also obtained analogously from the lactone (**7**) derived by hydrogenolysis of **6**.

The same treatment of **8** with hydrogen bromide in acetic acid gave selectively a single crystalline tribromide (**10**) almost quantitatively. Similarly, dibromide (**11**) was obtained from **9** in 75% yield. The structures of **10** and **11** were deduced on the basis of analytical data and ^{1}H NMR spectroscopy. Thus, the ^{1}H NMR spectrum of **10** revealed two one-proton relatively wide triplets coupled with each other at δ 4.92 and 5.22, respectively, indicating the presence of two acetoxyl groups in vicinal trans positions. These were accounted for by opening of the anhydro ring at C-4 by a bromide ion, the structure being tentatively assigned to di-*O*-acetyl-(1,3/2,4,6)-3,4-dibromo-6-bromomethyl-1,2-cyclohexanediol. In the ^{1}H NMR spectrum, **11** showed a triplet of doublets at δ 4.76 having 3.5, 8.5, and 8.5 Hz-splittings and a doublet of doublets at δ 4.96 having 8.5 and 10 Hz-splittings attributed to H-1 and H-2, respectively. Thus, **11** was assigned to di-*O*-acetyl-(1,3,5/2)-5-bromo-3-bromomethyl-1,2-cyclohexanediol.

Accordingly, the 1,4-anhydro ring was cleaved by a bromide ion regioselectively in **8** or **9** at the carbon atom adjacent to the methylene group, while, in the case of **2** and **3**, the selectivity appears to decrease, somewhat presumably, owing to the stereoelectric effects.

Dideoxyvalidamine and Its Analog. Reduction of **4** with LAH in THF followed by acetylation gave the corresponding di-*O*-acetyl-bromohydroxymethylcyclohexanol (**12**) as a syrup in 46% yield, which,

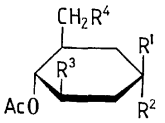

	R^1	R^2	R^3	R^4
12	Br	H	H	OAc
13	H	N_3	H	OAc
14	H	NHAc	H	OAc
15	H	N_3	H	N_3
16	H	NHAc	H	NHAc
17	Br	H	OAc	OAc
18	H	N_3	OAc	OAc
19	H	NHAc	OAc	OAc
20	H	N_3	OAc	N_3
21	H	NHAc	OAc	NHAc

Scheme 2.

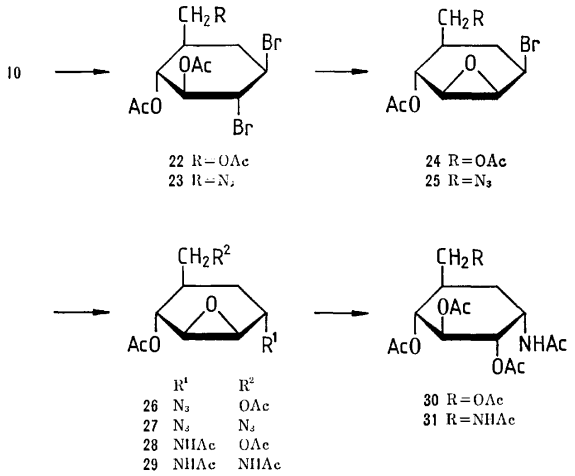

Scheme 3.

without purification, was treated with sodium azide in boiling 90% aqueous 2-methoxyethanol for 2 days to give the crude azido compound (**13**). Its ^{1}H NMR spectrum showed a relatively narrow multiplet due to the proton attached to the carbon atom bearing the azido group, suggesting that the bromine group was replaced by an azide ion with inversion of the configuration. Compound **13** was hydrogenated with Raney nickel followed by acetylation to give crystalline tri-*N,O*-acetyl-(1,4/2)-4-amino-2-hydroxymethyl-1-cyclohexanol (dideoxyvalidamine) (**14**) in 25% yield.

The similar treatment of **5** with sodium azide gave a syrupy diazido compound (**15**), which was hydrogenated and successively acetylated to give tri-*N,O*-acetyl-(1,4/2)-4-amino-2-aminomethyl-1-cyclohexanol (**16**) in 30% overall yield.

Deoxyvalidamine and Its Analog. Compound **11** was treated with 2 molar equiv. of sodium acetate in 90% aqueous 2-methoxyethanol at 90 °C overnight and then the product was acetylated to give tri-*O*-acetyl-(1,3,5/2)-5-bromo-3-hydroxymethyl-1,2-cyclohexanediol (**17**) in 78% yield. The ^{1}H NMR spectrum was compatible with the proposed structure, in which only C-7 bromine atom of **11** was replaced by an acetoxyl group. Thus, in **17**, C-7 methylene signal shifted downfield as compared with that of **11**. Reaction of **17** with an azide ion gave a syrupy azido compound (**18**) with inversion of the configuration at C-5, which was directly hydrogenated followed by acetylation to give a crystalline tetra-*N,O*-acetyl-(1,3/2,5)-5-amino-3-hydroxymethyl-1,2-cyclohexanediol (deoxyvalidamine) (**19**) in 40% yield. The structure was fully supported by the ^{1}H NMR spectrum (see Experimental).

Analogously, **11** was converted to the diazido compound (**20**) which was hydrogenated and then acetylated to give tetra-*N,O*-acetyl-(1,3/2,5)-5-amino-3-aminomethyl-1,2-cyclohexanediol (**21**) in 58% overall yield. Its ^{1}H NMR spectrum showed a pattern of ring proton signals very similar to that of **19**.

Validamine and Its Analog. Treatment of **10** with sodium acetate (2 molar equiv.) in 90% aqueous 2-methoxyethanol at 90 °C for 2 days led to the selective displacement at C-7 with an acetate ion affording tri-*O*-acetyl-(1,3/2,4,6)-3,4-dibromo-6-hydroxymethyl-1,2-cyclohexanediol (**22**) as the major product in 50% yield.[6] Similarly, on treatment with sodium azide (2 molar equiv.), **10** gave the corresponding 7-azido compound (**23**) in 91% yield. Reaction of **22** with excess methanolic sodium methoxide in chloroform followed by acetylation gave di-*O*-acetyl-1,2-anhydro-(1,2,4,6/3)-6-bromo-4-hydroxymethyl-1,2,3-cyclohexanetriol (**24**) in a quantitative yield. The ^{1}H NMR spectrum revealed a doublet due to H-3 having 9 Hz-splitting at δ 4.88, which confirmed the assigned structure of **24**, excluding the 2,3-anhydro structure resulting from an oxirane ring migration under basic conditions. Under the same conditions, **23** gave the corresponding epoxide (**25**) in 78% yield.

The reaction of **24** with 1.5 molar equiv. sodium azide in *N,N*-dimethylformamide at 90 °C was monitored by TLC.[7] After **24** had been consumed in 2.5 h, one major component was formed together with four minor components. Separation of the mixture by column chromatography gave the epoxy azide (**26**) in 30% yield as a homogeneous syrup. In its ^{1}H NMR spectrum, the signal due to proton on a carbon atom attached to the azido group appeared as a doublet of doublets having 3 and 9.5 Hz-splittings at δ 4.19. Lack of a coupling between H-1 and H-6 suggests that the azido group is located in the trans position to the adjacent anhydro ring. Hydrogenation of **26** with Raney nickel in methanol containing acetic anhydride gave the epoxy amide (**28**) which, without purification, was successively treated with boiling 80% aqueous acetic acid followed by acetylation to give a crystalline penta-*N,O*-acetyl-(1,3,4/2,6)-4-amino-6-hydroxymethyl-1,2,3-cyclohexanetriol (validamine) (**30**) in 30% yield. The compound was identical with an authentic sample[8] except for an optical activity. The anhydro ring in **28** seems to be cleaved at C-1 preferentially by an anchimeric assistance of the neighboring acetamido group, giving rise to the triol with the desired configuration.

By an analogous sequence of reactions (**27**→**29**→**31**), the 7-amino-7-deoxy analog (**31**) of validamine was prepared in an overall yield of 21%. The structure was supported by comparison of its ^{1}H NMR spectrum with that of **30**.

Experimental

Unless otherwise noted, melting points were determined on a Mitamura Riken micro hot stage and are uncorrected. Solutions were evaporated under reduced pressure at 40—50 °C. ^{1}H NMR spectra were measured at 60 MHz on a Varian A-60D spectrometer in deuteriochloroform ($CDCl_3$) or dimethyl-d_6 sulfoxide (DMSO-d_6) with reference to tetramethylsilane as an internal standard, the peak positions being given in δ-values. Values given for chemical shifts and coupling constants are of first-order. TLC was performed on silica gel (Wakogel B-10, Wako Pure Chemical Industries, Ltd.) using a mixture of butanone and toluene as an eluent. Column chromatography was carried out on Wakogel C-200.

endo-2-Acetoxymethyl-7-oxabicyclo[2.2.1]heptane (3). To a solution of the acid (**2**)[3] (6.0 g) prepared by catalytic reduction of *endo*-7-oxabicyclo[2.2.1]hept-5-ene-2-carboxylic acid (**1**)[2b] in tetrahydrofuran (THF) (100 ml) was added a slurry of lithium aluminum hydride (LAH) (2.1 g) in THF (20 ml), and the mixture was stirred at an ambient temperature for 4 h. A mixture of THF (4.2 ml) and water (4.2 ml) was added to the reaction mixture and it was left to stand overnight. A white solid was removed by filtration and washed with hot THF (20 ml). The filtrate and washings were combined and evaporated to give a colorless syrup (5.4 g), whose TLC showed a single spot in butanone–toluene (1 : 1, v/v). A 2.3 g-portion of this syrup was treated with acetic anhydride (10 ml) in pyridine (20 ml) overnight at an ambient temperature. The reaction mixture was evaporated to dryness and the residue was dissolved in ethyl acetate and washed with 0.5 M hydrochloric acid, aqueous saturated sodium hydrogencarbonate solution, and water, successively. The solution was dried over anhydrous sodium sulfate and then evaporated to give **3** (2.7 g, 89%) as a homogeneous syrup.

Found: C, 63.60; H, 8.20% Calcd for $C_9H_{14}O_3$: C, 63.51; H, 8.29%.

Treatment of the alcohol with *p*-nitrobenzoyl chloride in pyridine at 70 °C for 30 min gave a crystalline *p*-nitrobenzoate. An analytical sample was obtained by recrystallization of the crude product from ethanol, mp 104—105 °C.

Found: C, 60.79; H, 5.61; N, 5.12%. Calcd for $C_{14}H_{15}NO_5$: C, 60.65; H, 5.45; N, 5.05%.

(1,5/2)-2-Acetoxy-5-bromocyclohexanecarboxylic Acid (4). A mixture of **2**[3] (0.2 g) and 15% hydrogen bromide in acetic acid (2 ml) was heated at 80—85 °C in a sealed tube for 17 h, the reaction mixture being then poured into ice-water (40 ml). The resulting gum was collected by decantation and dissolved in chloroform. The solution was washed with water, dried, and evaporated to give a partially crystalline product. Recrystallization from ethanol–hexane gave **4** (0.23 g, 59%): mp 156—158 °C; ^{1}H NMR ($CDCl_3$) δ 1.23—2.90 (7H, m, H-1 and the six methylene protons), 2.02 (3H, s, OAc), 3.97 (1H, tt, $J_{4ax,5}=J_{5,6eq}=11$ Hz, $J_{4eq,5}=J_{5,6eq}=4.5$ Hz, H-5), 5.00 (1H, td, $J_{1,2}=J_{2,3ax}=10$ Hz, $J_{2,3eq}=4.5$ Hz, H-2), 9.35 (1H, s, COOH).

Found: C, 40.51; H, 4.77; Br, 30.45%. Calcd for $C_9H_{13}O_4Br$: C, 40.78; H, 4.94; Br, 30.14%.

(1/2,4)-4-Bromo-2-(bromomethyl)cyclohexyl Acetate (5). Compound **3** (1.6 g) was treated with hydrogen bromide in acetic acid in the same way as for **4**. The reaction mixture was poured into ice-water and extracted with chloroform, and the extracts were processed in the usual manner. The crude product was crystallized from ethanol to give **5** (1.03 g, 35%): mp 110.5—112 °C; ^{1}H NMR ($CDCl_3$) δ 1.23—2.90 (7H, m, H-2 and the six ring methylene protons), 2.05 (3H, s, OAc), 3.32—3.45 (2H, m, CH$_2$Br), 3.99 (1H, tt, $J_{3ax,4}=J_{4,5ax}=11$ Hz, $J_{3eq,4}=J_{4,5eq}=4.5$ Hz, H-4), 4.77 (1H, td, $J_{1,2}=J_{1,6ax}=10$ Hz, $J_{1,6eq}=4.5$ Hz, H-1).

Found: C, 34.37; H, 4.48; Br, 51.11%. Calcd for $C_9H_{14}O_2Br_2$: C, 34.42; H, 4.49; Br, 50.89%.

exo-*9-Bromo-2,7-dioxabicyclo[4.2.1.0^{4,8}]nonan-3-one (6).* Compound **1**[3] (10 g) was dissolved in water (300 ml) containing sodium hydrogencarbonate (7.2 g). Bromine (4 ml) was added dropwise to this solution under vigorous agitation. After completion of the addition, the mixture was stirred for 1 h, and precipitates were collected by filtration and washed with water thoroughly. Recrystallization of the crude product from ethyl acetate gave **6** (14.2 g, 91%) as prisms: mp 155—156 °C; ^{1}H NMR (DMSO-d_6) δ 2.00—2.29 (2H, m, C-5 methylene), 2.69 (1H, m, H-4), 4.37 (1H, s, H-9), 4.75 (1H, m, H-6), 4.95 (1H, d, $J_{1,8}=5$ Hz, H-1), 5.53 (1H, t, $J_{4,8}=5$ Hz, H-8).

Found: C, 38.11; H, 3.26; Br, 36.34%. Calcd for $C_7H_7O_2Br$: C, 38.39; H, 3.22; Br, 36.48%.

2,7-Dioxabicyclo[4.2.1.0^{4,8}]nonan-3-one (7). A solution of **6** (1.1 g) in ethyl acetate (20 ml) was hydrogenated in the presence of Raney nickel T-4[9] and Amberlite IR-45 (OH^-) (7.5 ml) in the initial hydrogen pressure of 3.4 kg·cm^{-2} at an ambient temperature overnight. The catalyst and resin were removed by filtration and the filtrate was evaporated. The residue was crystallized from ethyl acetate–hexane to give **7** (0.46 g, 65%) as needles: mp 85.5—87 °C; ^{1}H NMR ($CDCl_3$) δ 1.42—2.46 (4H, m, C-5 and C-9 methylene), 2.71 (1H, broad five-line peak, $J_{4,5endo}=4.5$ Hz, $J_{4,5exo}=8.5$ Hz, H-4), 4.65—4.92 (2H, m, H-1 and H-6), 5.31 (1H, t, $J_{1,8}=J_{4,8}=5$ Hz, H-8).

Found: C, 60.20; H, 5.82%. Calcd for $C_7H_8O_3$: C, 60.00; H, 5.75%.

endo-*2-Acetoxy*-endo-*6-acetoxymethyl*-exo-*3-bromo-7-oxabicyclo-[2.2.1]heptane (8).* To an ice-cooled solution of **6** (10 g) in THF (250 ml) was added dropwise a slurry of LAH (2 g) in THF (30 ml) with vigorous agitation. The reaction mixture was stirred at an ambient temperature for 3 h and worked up in the usual manner to give a syrup, which was directly acetylated by the conventional method. The product was crystallized from ethyl acetate–hexane to give **8** (11.7 g, 83.5%) as colorless needles: mp 61—62 °C; ^{1}H NMR ($CDCl_3$) δ 1.35 (1H, dd, $J_{5gem}=12.5$ Hz, $J_{5endo,6}=5.5$ Hz, H-5*endo*), 1.63—2.79 (2H, m, H-5*exo* and H-6), 2.02 (3H, s) and 2.06 (3H, s) (OAc), 3.85 (1H, d, $J_{2,3}=3$ Hz, H-3), 4.19 (1H, dd) and 4.32 (1H, dd) ($J_{6,7}=J_{6,7'}=3$ Hz, $J_{7gem}=7$ Hz, CH$_2$OAc), 4.61 (1H, d, $J_{4,5exo}=6$ Hz, H-4), 4.65 (1H, t, $J_{1,2}=5$ Hz, H-1), 5.36 (1H, broad dd, H-2).

Found: C, 42.88; H, 4.82; Br, 26.14%. Calcd for $C_{11}H_{15}O_5Br$: C, 43.12; H, 4.92; Br, 26.02%.

endo-*2-Acetoxy*-endo-*6-acetoxymethyl-7-oxabicyclo[2.2.1]heptane (9).* a) A solution of **8** (10 g) in ethyl acetate (20 ml) was hydrogenated with Raney nickel and Amberlite IR-45 (OH^-) in the same way as for **7**. The product was crystallized from ethyl acetate–hexane to give **9** (7 g, 94%) as needles: mp 48—49 °C; ^{1}H NMR ($CDCl_3$) δ 1.12—1.51 (2H, m, H-3*endo* and H-5*endo*), 2.02 (6H, s, two OAc), 1.67—2.66 (3H, m, H-3*exo*, H-5*exo*, and H-6), 4.21—4.67 (4H, m, H-1, H-4, and CH$_2$OAc), 5.04 (1H, m, H-2).

Found: C, 57.67; H, 6.91%. Calcd for $C_{11}H_{16}O_5$: C, 57.88; H, 7.06%.

b) Compound **9** was also prepared, in 52% yield, by reduction of **7** with LAH in THF as in the preparation

of **8**.

The di-*p*-nitrobenzoate was prepared by the usual method. An analytical sample crystallized from ethanol melted at 206 °C.

Found: C, 57.11; H, 4.27; N, 6.19%. Calcd for $C_{21}H_{18}N_2O_9$: C, 57.02; H, 4.10; N, 6.33%.

*Di-O-acetyl-(1,3/2,4,6)-3,4-dibromo-6-bromomethyl-1,2-cyclohexanediol (**10**).* Compound **8** (1.6 g) was treated with hydrogen bromide in acetic acid in the same way as for **4**. Recrystallization of a crude crystalline product (2.2 g) gave **10** (1.75 g, 74%) as prisms: mp 153—154 °C; ^{1}H NMR ($CDCl_3$) δ 1.79—2.85 (3H, m, C-5 methylene and H-6), 2.04 (3H, s) and 2.08 (3H, s) (OAc), 3.22 (1H, dd, $J_{6,7}$= 3.5 Hz, J_{7gem}=10 Hz, H-7), 3.45 (1H, dd, $J_{6,7'}$=1.5 Hz, H-7'), 4.02 (1H, m, H-4), 4.10 (1H, t, $J_{2,3}=J_{3,4}$=9 Hz, H-3), 4.92 (1H, t, $J_{1,2}=J_{1,6}$=9 Hz, H-1), 5.22 (1H, t, H-2).

Found: C, 29.22; H, 3.33; Br, 52.96%. Calcd for $C_{11}H_{15}O_4Br_3$: C, 29.30; H, 3.35; Br, 53.16%.

*Di-O-acetyl-(1,3,5/2)-5-bromo-3-bromomethyl-1,2-cyclohexanediol (**11**).* Compound **9** (1 g) was treated with hydrogen bromide in acetic acid in the same way as for **4**. The crude product was recrystallized from ethanol to give **11** (1.2 g, 75%): mp 136—137 °C; ^{1}H NMR ($CDCl_3$) δ 1.63—2.86 (5H, m, H-3, and C-4 and C-6 methylene), 2.01 (3H, s) and 2.05 (3H, s) (OAc), 3.26—3.40 (2H, m, CH_2Br), 4.00 (1H, nine-line peak, H-5), 4.76 (1H, td, $J_{1,2}=J_{1,6ax}$=8.5 Hz, $J_{1,6eq}$=3.5 Hz, H-1), 4.96 (1H, dd, $J_{2,3}$=10 Hz, H-2).

Found: C, 35.50; H, 4.27; Br, 43.07%. Calcd for $C_{11}H_{16}O_4Br_2$: C, 35.51; H, 4.33; Br, 42.95%.

*Tri-N,O-acetyl-(1,4/2)-4-amino-2-hydroxymethyl-1-cyclohexanol (**14**).* To a solution of **4** (0.53 g) in THF (10 ml) was added a suspension of LAH (0.09 g) in THF (6 ml) at 0 °C, and the reaction mixture was stirred at an ambient temperature for 1.5 h, and then worked up in the usual manner. The syrupy product was acetylated and purified by chromatography on silica gel with chloroform to give di-*O*-acetyl-(1/2,4)-4-bromo-2-hydroxymethyl-1-cyclohexanol (**12**) (0.27 g, 46%) as a homogeneous syrup; ^{1}H NMR ($CDCl_3$) δ 1.19—2.57 (7H, m, H-2, and C-3, C-4, and C-5 methylene), 2.03 (3H, s) and 2.06 (3H, s) (OAc), 4.00 (1H, tt, $J_{3ax,4}=J_{4,5ax}$=13 Hz, $J_{3eq,4}=J_{4,5eq}$=4.5 Hz, H-4), 4.01 (2H, d, CH_2OAc), 4.65 (1H, td, $J_{1,2}=J_{1,6eq}$= 4 Hz, H-1).

A mixture of crude **12** (0.21 g), sodium azide (0.2 g), and 90% aqueous 2-methoxyethanol (10 ml) was heated at reflux for 45 h, and then evaporated to dryness. The residue was directly acetylated in the usual manner and the product was purified by chromatography on alumina with chloroform to give di-*O*-acetyl-(1,4/2)-4-azido-2-hydroxymethyl-1-cyclohexanol (**13**) as a homogeneous syrup: ^{1}H NMR ($CDCl_3$) δ 1.45—2.41 (7H, m, H-2, and C-3, C-5, and C-6 methylene), 2.04 (6H, s, two OAc), 3.76—3.99 (1H, m, H-4), 3.96—4.11 (2H, m, CH_2OAc), 4.65 (1H, td, $J_{1,2}=J_{1,6ax}$=10 Hz, $J_{1,6eq}$=4.5 Hz, H-1).

A solution of crude **13** (0.16 g) in ethanol (6 ml) was hydrogenated with Raney nickel at an ambient temperature overnight. The product was acetylated in the usual manner. Recrystallization of the crude product from ethanol–ether gave **14** (0.043 g, 25%) as needles: mp 111—112.5 °C; ^{1}H NMR ($CDCl_3$) δ 1.19—2.21 (7H, m, H-2, and C-3, C-5, and C-6 methylene), 1.99 (3H, s, NAc), 2.05 (6H, s, two OAc), 3.88—4.26 (3H, m, H-4 and CH_2NHAc), 4.73 (1H, td, $J_{1,2}=J_{1,6ax}$=8.5 Hz, $J_{1,6eq}$=4.5 Hz, H-1), 5.73 (1H, d, J=6 Hz, NH).

Found: C, 57.23; H, 7.58; N, 5.29%. Calcd for $C_{13}H_{21}NO_5$: C, 57.55; H, 7.80; N, 5.16%.

*Tri-N,O-acetyl-(1,4/2)-4-amino-2-aminomethyl-1-cyclohexanol (**16**).* A mixture of **5** (0.47 g), sodium azide (0.59 g), and 90% aqueous 2-methoxyethanol (15 ml) was heated at 110 °C for 17 h, and then evaporated to dryness. The residue was acetylated in the usual manner and the product was purified by chromatography on alumina to give (1,4/2)-4-azido-2-(azidomethyl)cyclohexyl acetate (**15**) as a homogeneous syrup: ^{1}H NMR ($CDCl_3$) δ 1.21—2.41 (7H, m, H-2, and C-3, C-5, and C-6 methylene), 2.06 (3H, s, OAc), 3.32 (2H, d, J=4.5 Hz, CH_2N_3), 3.78—3.96 (1H, m, H-4), 4.95 (1H, td, $J_{1,2}=J_{1,6ax}$=9.5 Hz, $J_{1,6eq}$=5 Hz, H-1).

Crude **15** was hydrogenated in ethanol with Raney nickel as in the case of crude **13**. The product was acetylated in the usual manner. Recrystallization of the crude product from ethanol gave **16** (0.12 g, 30% based on **5** used) as needles: mp 189—190 °C; ^{1}H NMR ($CDCl_3$) δ 1.10—2.38 (7H, m, H-1, and C-3, C-5, and C-6 methylene), 1.97 (6H, s, two NAc), 2.06 (3H, s, OAc), 2.83—3.72 (2H, m, CH_2-NHAc).

Found: C, 57.53; H, 8.12; N, 10.12%. Calcd for $C_{13}H_{22}N_2O_4$: C, 57.76; H, 8.20; N, 10.36%.

*Tetra-N,O-acetyl-(1,3/2,5)-5-amino-3-hydroxymethyl-1,2-cyclohexanediol (**19**).* A mixture of **11** (1.86 g), anhydrous sodium acetate (1.23 g), and 90% aqueous 2-methoxyethanol (35 ml) was heated at 90 °C with stirring overnight. The reaction mixture was evaporated and the residue was extracted with hot chloroform (50 ml). The extracts were passed through a short alumina column and then evaporated to give tri-*O*-acetyl-(1,3,5/2)-5-bromo-3-hydroxymethyl-1,2-cyclohexanediol (**17**) (1.37 g, 78%) as a homogeneous syrup: ^{1}H NMR ($CDCl_3$) δ 1.62—2.87 (5H, m, H-3, and C-6 methylene), 2.01 (3H, s), 2.03 (3H, s), and 2.06 (3H, s) (OAc), 3.75—4.27 (3H, m, H-5 and CH_2OAc), 4.76 (1H, td, $J_{1,2}=J_{1,6ax}$=9.5 Hz, $J_{1,6eq}$=5 Hz, H-1), 4.96 (1H, t, $J_{2,3}$=9.5 Hz, H-2).

A mixture of crude **17** (1.05 g), sodium azide (0.6 g), and 90% aqueous 2-methoxyethanol (30 ml) was refluxed for 20 h. The reaction mixture was evaporated and acetylated in the usual manner. The product was purified by chromatography on alumina to give tri-*O*-acetyl-(1,3/2,5)-5-azido-3-hydroxymethyl-1,2-cyclohexanediol (**18**) (1.05 g) as a homogeneous syrup: ^{1}H NMR ($CDCl_3$) δ 1.52—2.57 (5H, m, H-3, and C-4 and C-6 methylene), 1.99 (3H, s) and 2.03 (6H, s) (OAc), 3.72—4.28 (3H, m, H-5 and CH_2OAc), 4.72—5.25 (2H, m, H-1 and H-2).

Compound **18** (1.0 g) was hydrogenated in ethanol (20 ml) containing acetic anhydride (0.5 ml) with Raney nickel in the same way as for **7**. The product was crystallized from ether to give **19** (0.37 g, 40% based on **17** used) as needles: mp 193—194 °C; ^{1}H NMR ($CDCl_3$) δ 1.49—2.48 (5H, m, H-3, and C-4 and C-6 methylene), 1.99 (6H, s), 2.02 (3H, s), and 2.03 (3H, s) (OAc), 3.88 (1H, dd, J_{7gem}=11.5 Hz, $J_{3,7}$=4.5 Hz, H-7), 4.15 (1H, dd, $J_{3,7'}$=4 Hz, H-7'), 4.28 (1H, m, H-5), 4.88 (1H, t, $J_{1,2}=J_{2,3}$=9 Hz, H-2), 4.97 (1H, td, $J_{1,6ax}$=9 Hz, $J_{1,6eq}$=3 Hz, H-1), 6.38 (1H, d, $J_{5,NH}$=7 Hz, NH).

Found: C, 55.00; H, 7.01; N, 4.27%. Calcd for $C_{15}H_{23}NO_7$: C, 54.70; H, 7.04; N, 4.25%.

*Tetra-N,O-acetyl-(1,3/2,5)-5-amino-3-aminomethyl-1,2-cyclohexanediol (**21**).* A mixture of **11** (0.74 g), sodium azide (0.78 g), and 90% aqueous *N,N*-dimethylformamide (20 ml) was heated at 125 °C for 20 h. The reaction mixture was processed by the usual method and the syrupy product was purified by alumina column to give di-*O*-acetyl-(1,3/2,5)-5-azido-3-azidomethyl-1,2-cyclohexanediol (**20**) (0.61 g, 97%) as a homogeneous syrup. The compound was di-

rectly hydrogenated as in the case of **18** and the product was crystallized from ethanol to give **21** (0.39 g, 59%) as needles: mp 236—237 °C (capil); ^{1}H NMR (DMSO-d_6) δ 1.36—2.46 (5H, m, H-3, and C-4 and C-6 methylene), 1.88 (3H, s) and 1.92 (3H, s) (NAc), 2.02 (3H, s) and 2.08 (3H, s) (OAc), 3.2—3.56 (2H, m, CH_2NHAc), 4.08—4.39 (1H, m, H-5), 4.85 (1H, t, $J_{1,2}=J_{2,3}=9.5$ Hz, H-2), 5.22 (1H, td, $J_{1,6ax}=9.5$ Hz, $J_{1,6eq}=5$ Hz, H-1), 7.93 (1H, t, $J_{7,NH}=J_{7',NH}=5.5$ Hz, CH_2NHAc), 8.27 (1H, d, $J_{5,NH}=6.5$ Hz, CHNHAc).

Found: C, 54.63; H, 7.28; N, 8.54%. Calcd for $C_{15}H_{24}N_2O_6$: C, 54.87; H, 7.37; N, 8.53%.

Tri-O-*acetyl-(1,3/2,4,6)-3,4-dibromo-6-hydroxymethyl-1,2-cyclohexanediol* (**22**). A mixture of **10** (9.0 g), anhydrous sodium acetate (4.9 g), and 90% aqueous 2-methoxyethanol (100 ml) was heated at 90 °C for two days. The reaction mixture was worked up by the usual method and the product was directly acetylated. TLC indicated the formation of one major and three minor components. Crystallization of the mixture from ethanol gave the main product, **22** (4.3 g, 50%) as prisms: mp 128—129 °C; ^{1}H NMR ($CDCl_3$) δ 1.77—2.71 (3H, m, H-6 and C-5 methylene), 2.01 (3H, s) and 2.06 (6H, s) (OAc), 3.74—4.26 (4H, m, H-3, H-4, and CH_2OAc), 4.91 (1H, dd, $J_{1,2}=9$ Hz, $J_{1,6}=10$ Hz, H-1), 5.20 (1H, t, $J_{2,3}=10$ Hz, H-2).

Found: C, 36.42; H, 4.17; Br, 37.65%. Calcd far $C_{13}H_{18}O_6Br_2$: C, 36.30; H, 4.22; Br, 37.16%.

Di-O-*acetyl-(1,3/2,4,6)-6-azidomethyl-3,4-dibromo-1,2-cyclohexanediol* (**23**). A mixture of **10** (4.5 g), sodium azide (1.95 g), and 90% aqueous 2-methoxyethanol (60 ml) was heated at 95 °C for 90 min. The reaction mixture was worked up by the usual method. The product was recrystallized from ethanol to give **23** (3.8 g, 91%) as needles: mp 114—115 °C; ^{1}H NMR ($CDCl_3$) δ 1.71—2.73 (3H, m, H-6 and C-5 methylene), 2.04 (3H, s) and 2.07 (3H, s) (OAc), 3.18 (1H, dd, $J_{7gem}=11$ Hz, $J_{6,7}=3.5$ Hz, H-7), 3.44 (1H, dd, $J_{6,7'}=2$ Hz, H-7'), 3.94—4.18 (2H, m, H-3 and H-4), 4.86 (1H, t, $J_{1,2}=J_{1,6}=10$ Hz, H-1), 5.19 (1H, t, $J_{2,3}=10$ Hz, H-2).

Found: C, 32.08; H, 3.68; N, 10.26; Br, 38.78%. Calcd for $C_{11}H_{15}N_3O_4Br_2$: C, 31.99; H, 3.66; N, 10.17; Br, 38.69%.

Di-O-*acetyl-1,2-anhydro-(1,2,4,6/3)-6-bromo-4-hydroxymethyl-1,2,3-cyclohexanetriol* (**24**). To a solution of **22** (2.15 g) in methanol (20 ml) was added 1 M-methanolic sodium methoxide (10 ml, 2 molar equiv.) and the mixture was stirred at an ambient temperature for 3 h. The solution was neutralized with 1 M-hydrochloric acid and then evaporated to dryness. The residue was treated with acetic anhydride (5 ml) and pyridine (10 ml) overnight. The product was purified by alumina column to give a syrup which crystallized spontaneously to give **24** (1.5 g, 98%) as prisms: mp 58—59.5 °C; ^{1}H NMR ($CDCl_3$) δ 1.54—2.19 (3H, m, H-4 and C-5 methylene), 2.05 (3H, s) and 2.11 (3H, s) (OAc), 3.26 (1H, d, $J_{1,2}=3.5$ Hz, H-2), 3.52 (1H, broad d, $J_{1,6}=2$ Hz, H-1), 3.90—4.02 (2H, m, CH_2OAc), 4.37 (1H, eight-line peak, $J_{5ax,6}=J_{5eq,6}=6$ Hz, H-6), 4.88 (1H, d, $J_{3,4}=9$ Hz, H-3).

Found: C, 42.92; H, 4.90; Br, 26.12%. Calcd for $C_{11}H_{15}O_5Br$: C, 43.02; H, 4.92; Br, 26.02%.

O-*Acetyl-1,2-anhydro-(1,2,4,6/3)-4-azidomethyl-6-bromo-1,2,3-cyclohexanetriol* (**25**). To a solution of **23** (3.3 g) in methanol (30 ml) was added 1 M-methanolic sodium methoxide (16 ml, 2 molar equiv.) and the mixture was left to stand at an ambient temperature for 5 h. The reaction mixture was processed as in the preparation of **24**. The product was chromatographed on silica gel (85 g) with butanone-toluene (1 : 12, v/v) as an eluent to give **25** (1.82 g, 78%) as a homogeneous syrup: ^{1}H NMR ($CDCl_3$) δ 1.56—2.19 (3H, m, H-4 and C-5 methylene), 2.13 (3H, s, OAc), 3.20—3.35 (3H, m, H-2 and CH_2N_3), 3.51 (1H, broad q, $J_{1,2}=4$ Hz, $J_{1,6}=2$ Hz, H-1), 4.36 (1H, eight-line peak, $J_{5ax,6}=11$ Hz, $J_{5eq,6}=6$ Hz, H-6), 4.84 (1H, broad d, $J_{3,4}=9$ Hz, H-3).

Found: C, 37.19; H, 4.14; N, 14.41; Br, 27.27%. Calcd for $C_9H_{12}N_3O_3Br$: C, 37.26; H, 4.17; N, 14.48; Br, 27.54%.

Di-O-*acetyl-1,2-anhydro-(1,2,4/3,6)-6-azido-4-hydroxymethyl-1,2,3-cyclohexanetriol* (**26**). A mixture of **24** (0.92 g), sodium azide (0.59 g), and *N,N*-dimethylformamide (15 ml) was heated at 90 °C for 2.5 h. TLC indicated the formation of one major component, together with **24** and three minor components. The reaction mixture was processed by the usual method and the product was purified in the same way as for **25** to give the main product, **26** (0.25 g, 31%) as a homogeneous syrup: ^{1}H NMR ($CDCl_3$) δ 1.51—2.55 (3H, m, H-4 and C-5 methylene), 2.05 (3H, s) and 2.12 (3H, s) (OAc), 3.10 (1H, d, $J_{1,2}=3$ Hz, H-2), 3.23 (1H, t, $J_{1,6}=3$ Hz, H-1), 3.94—4.01 (2H, m, CH_2OAc), 4.19 (1H, broad q, $J_{5ax,6}=J_{5eq,6}=3$ Hz, H-6), 4.87 (1H, d, $J_{3,4}=9.5$ Hz, H-3).

Found: C, 48.83; H, 5.56; N, 15.37%. Calcd for $C_{11}H_{15}N_3O_5$: C, 49.07; H, 5.62; N, 15.61%.

Penta-N,O-*acetyl-(1,3,4/2,6)-4-amino-6-hydroxymethyl-1,2,3-cyclohexanetriol (validamine)* (**30**). A solution of **26** (0.47 g) in methanol (14 ml) containing acetic anhydride (0.5 ml) was hydrogenated in the presence of Raney nickel as in the preparation of **7** to give a crude syrup of tri-*N,O*-acetyl-1,2-anhydro-(1,2,4/3,6)-6-amino-4-hydroxymethyl-1,2,3-cyclohexanetriol (**28**). The compound was treated with refluxing 80% aqueous acetic acid (10 ml) for 13 h and the reaction mixture was evaporated to dryness. The residue was acetylated in the usual manner and the product was crystallized from ethanol to give **30** (0.2 g, 30%) as prisms: mp 197—198 °C. The compound was identified with an authentic active sample[8] by comparison of ^{1}H NMR ($CDCl_3$) and IR spectra.

Penta-N,O-*acetyl-(1,3,4/2,6)-4-amino-6-aminomethyl-1,2,3-cyclohexanetriol* (**31**). A mixture of (0.87 g), sodium azide (0.59 g), and *N,N*-dimethylformamide (15 ml) was heated at 90 °C for 2 h. TLC indicated the formation of one major and five minor components. The products were fractionated by silica gel column (50 g) with butanone-toluene (1 : 12, v/v) as an eluent. The major fraction gave *O*-acetyl-1,2-anhydro-(1,2,4/3,6)-6-azido-4-azidomethyl-1,2,3-cyclohexanetriol (**27**) (0.37 g, 50%) as a homogeneous syrup: ^{1}H NMR ($CDCl_3$) δ 1.48—2.30 (3H, m, H-6 and C-5 methylene), 2.14 (3H, s, OAc), 3.09 (1H, d, $J_{1,2}=3.5$ Hz, H-2), 3.17—3.55 (3H, m, H-1 and CH_2N_3), 4.19 (1H, q, $J_{1,6}=J_{5ax,6}=J_{5eq,6}=2.5$ Hz, H-6), 4.83 (1H, d, $J_{3,4}=9.5$ Hz, H-3). Compound **27** decomposed on being left to stand at an ambient temperature, no satisfactory analytical data being obtained. Thus, crude **27** was directly used in the next step.

A solution of **27** (0.34 g) in methanol containing acetic anhydride (0.5 ml) was hydrogenated with Raney nickel in the same way as for **7**, and the reduction product was treated with aqueous acetic acid as in the preparation of **30**. The acetylated product was crystallized from ethanol-ether to give **31** (0.11 g, 21%) as needles: mp 246—248 °C; ^{1}H NMR ($CDCl_3$) δ 1.41—2.38 (3H, m, H-6 and C-5 methylene), 2.01 (6H, s, two NAc), 2.03 (3H, s) 2.17 (3H, s), and 2.19 (3H, s) (OAc), 2.66—3.11 (1H, m) and 3.41—3.88 (1H, m) (CH_2NHAc), 4.35—4.76 (1H, m, H-4), 4.78 (1H, t, $J_{1,2}=J_{1,6}=9.5$ Hz, H-1), 4.91 (1H, dd, $J_{2,3}=$

9.5 Hz, $J_{3,4}=4$ Hz, H-3), 5.30 (1H, t, H-2), 6.00—6.28 (2H, broad d, two NH).

Found: C, 52.52; H, 6.65; N, 7.18%. Calcd for $C_{17}H_{28}N_2O_8$: C, 52.84; H, 6.78; N, 7.25%.

The authors express their sincere thanks to Mr. Saburo Nakada for his elementary analyses.

References

1) Presented at the 26th International Congress of Pure and Applied Chemistry, Tokyo, September 8, 1977 (abstracts of papers of the meeting, p. 1099). All the compounds described in this paper are racemic. All the formulas depict one enantiomer of the respective racemates.

2) The preceding papers of this series: a) T. Suami, S. Ogawa, T. Ishibashi, and I. Kasahara, *Bull. Chem. Soc. Jpn.*, **49**, 1388 (1976); b) T. Suami, S. Ogawa, K. Nakamoto, and I. Kasahara, *Carbohydr. Res.*, **58**, 240 (1977).

3) M. P. Kunstman, D. S. Tarbell, and R. L. Autry, *J. Am. Chem. Soc.*, **84**, 4115 (1962). The facile synthesis of **1** by Diels-Alder reaction of acrylic acid with furan had been reported.[2b]

4) The nomenclature used in this paper is based on the IUPAC-IUB Tentative Cyclitol Nomenclature Rule [*J. Biol. Chem.*, **22**, 5809 (1968)]. Alternatively, according to McCasland's proposal, 5-hydroxymethyl-1,2,3,4-cyclohexanetetrols are designated pseudo-aldohexopyranoses, and their configurations are unambiguously determined by use of prefix of the corresponding true sugars (including anomers) [G. E. McCasland, S. Furuta, and L. J. Durham, *J. Org. Chem.*, **31**, 1516 (1966)].

5) In addition to penta-*O*-acetyl-pseudo-β-DL-glucopyranose, 9-*endo*-acetoxy-2,7-dioxatricyclo[4.2.1.$0^{4,8}$]nonane was isolated in 8% yield: crystals, mp 75—76 °C (lit,[3] 80—81 °C).

6) The mother liquor from crystallization of **22** was condensed and the mixture was fractionated by silica gel column to give mainly crystalline tetra-*O*-acetyl-(1,4,6/2,3)-6-bromo-4-hydroxymethyl-1,2,3-cyclohexanetriol and syrupy tetra-*O*-acetyl-(3,6/4,5)-3,4,5-trihydroxy-6-hydroxymethylcyclohex-1-ene, structures of which were tentatively assigned.

7) One of the by-products was found to be tri-*O*-acetyl-(1,2,4/3,6)-2,4-diazido-6-hydroxymethyl-1,3-cyclohexanediol, which was isolated by fractionation of the acetylated products.

8) An authentic sample was prepared by conventional acetylation of validamine hydrochloride kindly supplied by Dr. Satoshi Horii.

9) S. Nishimura, *Bull. Chem. Soc. Jpn.*, **32**, 61 (1959).

High Performance Liquid Chromatographic Analysis of Individual Bile Acids: Free, Glycine- and Taurine-conjugated Bile Acids

Sumihiko OKUYAMA,* Daisuke UEMURA,† and Yoshimasa HIRATA†

Nagoya University College of Medical Technology, Daiko-cho, Higashi-ku, Nagoya 461

†*Chemical Institute, Faculty of Science, Nagoya University, Chikusa-ku, Nagoya 464*

(Received May 8, 1978)

High performance liquid chromatographic analyses of individual bile acids (cholic, chenodeoxycholic, deoxycholic, and lithocholic acids), free and conjugated with glycine and taurine, are described. The analyses of the free and glycine-conjugated bile acids are based on the esterification of the carboxyl group of bile acids with *O*-(*p*-nitrobenzyl)-*N,N'*-diisopropylisourea (PNBDI). The bile acids in the biological samples were extracted by an Amberlite XAD-2 column, and separated by DEAE-Sepharose CL-6B into free, glycine- and taurine-conjugated bile acids. After separation, the free and glycine-conjugated bile acids were directly esterified with PNBDI. Taurine-conjugated bile acids are unable to be esterified with PNBDI, the bile acids were hydrolyzed with NaOH to produce the free bile acids, and then esterified. The *p*-nitrobenzyl ester of bile acids has a characteristic ultraviolet absorption. Consequently the compounds were separated into the individual bile acids by high performance liquid chromatography, and detected by an UV-detector. An analysis of the individual bile acids in human bile is given for an example.

Despite the progress in gas-chromatographic analysis for the estimation of free bile acids,[1,2] individual conjugated bile acids can not be separated by this method. Moreover, the preparation of samples for gas-chromatography is complicated, incurring difficulties both in precision and accuracy. A method has been developed using high performance liquid chromatography[3] to give data on conjugated as well as free bile acids in clinical medicine.

The *p*-nitrobenzyl esters of glycine-conjugated and free bile acids possess characteristic ultraviolet absorption spectra, and based on this an attempt to apply this special quality for the analysis of these bile acids has been conducted. Taurine-conjugated bile acids have been separated from free and glycine-conjugated bile acids by anion exchange column-chromatography with DEAE-Sepharose CL-6B. After collection of the taurine-conjugated bile acids, hydrolysis with NaOH at 120 °C, esterification was conducted with PNBDI as well as the free and glycine-conjugated bile acids.

Experimental

Apparatus. A Varian LC 8500 liquid chromatograph was used throughout this work and fitted with an UV detector (JASCO UVIDEC 100), and a gradient elution accessory. A μBondapak C_{18} column, commercially available from Waters Associates, was used for the analysis of the *p*-nitrobenzyl esters of bile acids.

Materials. The bile acids were obtained from Sigma, Calbiochem, and Katayama Kagaku Kogyo. PNBDI was obtained from Regis Chem. Amberlite XAD-2 and Amberlyst A-15 from Rohm and Haas. Amberlite XAD-2 was washed with methanol, acetone, and water. Amberlyst A-15 was thoroughly washed with 2 M NaOH in 70% aqueous ethanol and followed by 70% ethanol until the elutant was neutral. It was subsequently washed with 2 M HCl in 70% ethanol and followed by 70% ethanol until the elutant was again neutral. DEAE-Sepharose CL-6B was made into the acetic form with acetic acid in 70% ethanol.

Procedure. Figure 1 outlines the analytical procedure. The mixture of 12 each individual bile acids (1 mg), free, glycine and taurine-conjugated, was dissolved in 0.1 M NaOH (10 ml) in saline and the solution agitated ultrasonically for 15 min. The solution was then applied to the column of Amberlite XAD-2[4] in water (1.0 g). The sample was allowed to flow through the column (100 mm/5 mm i.d.) at a rate of about 0.2 ml/min. The column was then washed with water until neutal and the bile acids eluted with methanol (30 ml). The elutant was then evaporated to dryness *in vacuo* at 50 °C, and the residue dissolved in 72% ethanol (30 ml). This was filtered through a column of Amberlyst A-15 in the H^+ form which removed interfering cations. The effluent from the column was passed through a column of DEAE-Sepharose CL-6B in the acetate form. Free bile acids passed directly through this column and were recovered in the first fraction (A). Glycine-conjugated and a small amount of the free bile acids were eluted with 0.1 M acetic acid in 72% ethanol (B). The taurine-conjugated bile acids were eluted with 0.15 M ammonium acetate (pH 6.6) in 72% ethanol (C). The separation was quantitative with minimal overlap between groups. The fractions were taken to near dryness on a rotary evaporator.

Fractions A and B were dissolved in 0.1 M NaOH (10 ml) in saline. The mixture of fraction A and B was allowed to flow through the column XAD-2 and after elution with methanol (30 ml), the elutant was evaporated to dryness. The residue was dissolved in water (10 ml), and the solution passed over a column of CM-Cellulose (1.0 g) in order to obtain the free acid from sodium salt. The flask used in the evaporation was washed subsequently with water (10 ml), ethanol (2 ml) and water (10 ml), and then each fraction passed through the column. The final volume of collected elutant was 30 ml. The solution was evaporated to dryness *in vacuo*.

Fraction C was dissolved in 7.5% NaOH (15 ml), and then hydrolyzed in a sealed tube at 120 °C for 4 h, since taurine-conjugated bile acids are unable to be esterified with PNBDI. After the hydrolysis, the hydrolysate was directly applied to the column of XAD-2, and the bile acids extracted with methanol (30 ml). After evaporation of the extract, the residue was dissolved in water (10 ml), and passed through a column of CM-Cellulose. The elutant was collected and evaporated to dryness. The bile acids in the mixture of fraction A and B, and the bile acids in fraction C were esterified with PNBDI in *t*-butyl alcohol (1 ml) for 24 h at room-temperature, as shown in Fig. 2.

The bile acid derivatives were treated with 0.1 M HCl

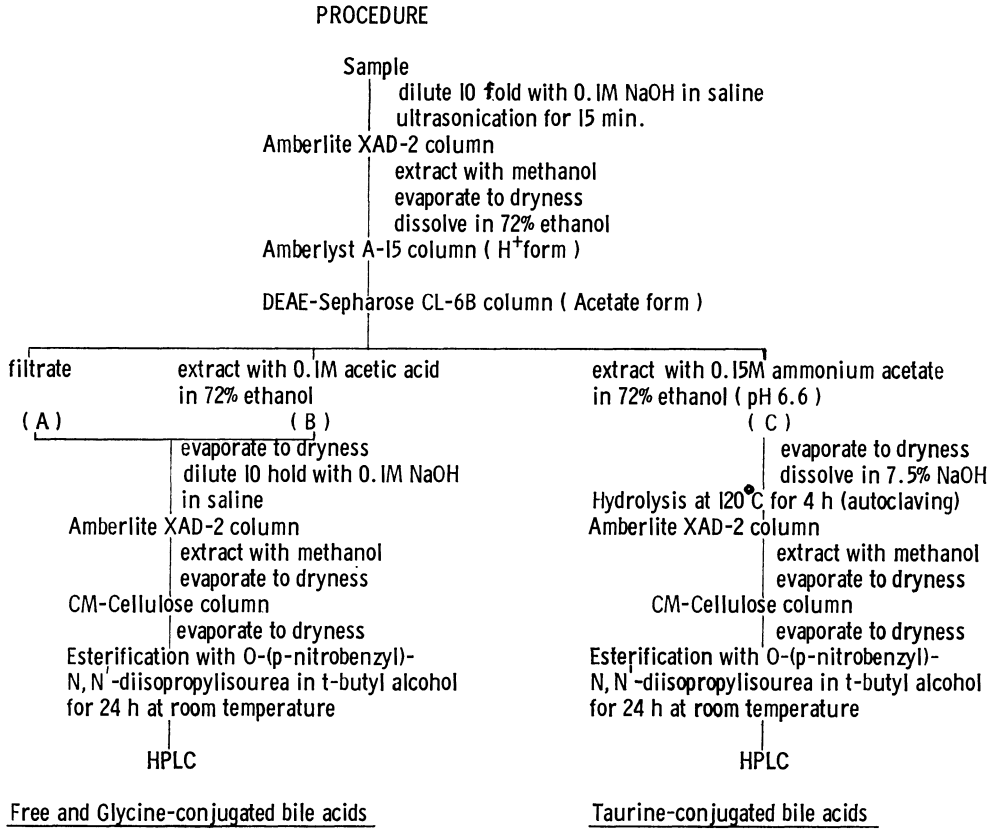

Fig. 1. The outline of analytical procedure of bile acids.

and water, and then analyzed by high performance liquid chromatography.

Operating Conditions. The conditions are shown in Table 1. The sample was injected with a microsyringe.

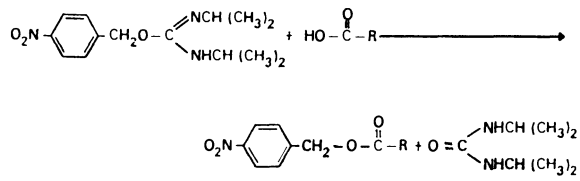

Fig. 2. The esterification reaction of bile acids with PNBDI.

Table 1. Operating conditions of high performance liquid chromatography for the determination of bile acids

Instrument	Varian LC 8500
Column	μBondapak C_{18} 30 cm×3.9 mm i.d.
Mobile phase	Solvent A KH_2PO_4 (0.01 M): Methanol 1:1
	Solvent B KH_2PO_4 (0.01 M): Methanol 1:4
Flow rate	60 ml/h
Temperature	ambient
Detector	JASCO UVIDEC 100 UV 0.02 254 nm
Pressure	1250 psi
Recorder	10 mV 2.5 mm/min
Initial b%	65% 0—80 min
Gradient b%	0.4%/min 80 min—final

Results and Discussion

High Performance Liquid Chromatographic Analysis of Bile Acids. The high performance liquid chromatographic separation of the *p*-nitrobenzyl esters of the individual free and glycine-conjugated bile acids is shown in Fig. 3. The quantity of each bile acid was

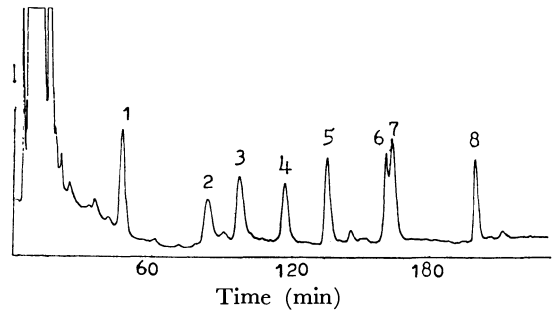

Fig. 3. High performance liquid-chromatographic separation of individual free and glycine-conjugated bile acids.

Bile acids

1.	glycocholic acid	GC
2.	glycochenodeoxycholic acid	GCDC
3.	glycodeoxycholic acid	GDC
4.	cholic acid	C
5.	glycolithocholic acid	GLC
6.	chenodeoxycholic acid	CDC
7.	deoxycholic acid	DC
8.	lithocholic acid	LC

6 μg. Each peak was identified by the addition of the *p*-nitrobenzyl ester of each authentic bile acid respectively. The separation between deoxycholic acid and chenodeoxycholic acid however was not sufficient.

High Performance Liquid Chromatographic Analysis of Bile Acids in Human Bile. Bile (1 ml), obtained by autopsy from a patient with obstructive jaundice due to cancer of pancreas head, was used in this experiment. Figure 4 shows the chromatogram of the free and glycine-conjugated bile acids in bile. The peaks were identified by the retention times. Figure 5 shows the chromatogram of taurine-conjugated bile acids in human bile. Since taurine-conjugated bile acids were hydrolyzed, each peak of the taurine-conjugated bile acid appears as the peak of the corresponding free bile acid. The concentration of individual bile acids in human bile is shown in Table 2. The total bile acid concentration in bile was 14.64 μM/ml, free 3.74 μM/ml, glycine-conjugated 8.08 μM/ml, taurine-conjugated 2.82 μM/ml. Accordingly glycine- and taurine-conjugated bile acids occupied 74% of the total bile acid in this human bile. The ratio of glycine-conjugated bile acid to taurine-conjugated bile acid (G/T) was 2.78.

The abbreviations of individual taurine-conjugated bile acids are expressed as follows:

taurcholic acid (TC)
taurochenodeoxycholic acid (TCDC)
taurodeoxycholic acid (TDC)
taurolithocholic acid (TLC)

$$\frac{C+GC+TC}{CDC+GCDC+TCDC} = 1.46$$

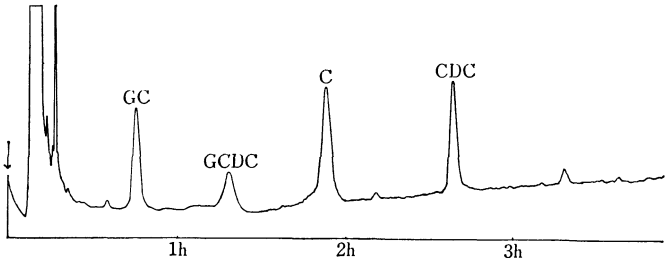

Fig. 4. High performance liquid-chromatographic analysis of free and glycine-conjugated bile acids in human bile.

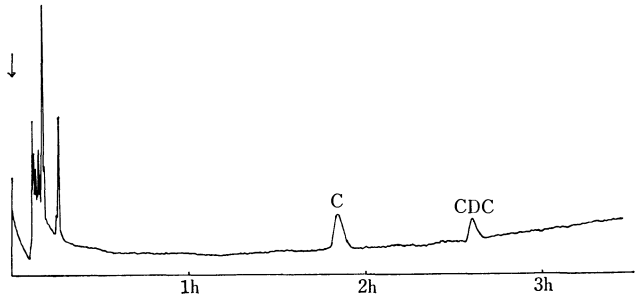

Fig. 5. High performance liquid-chromatographic analysis of taurine-conjugated bile acid in human bile.

Table 2. Bile acid in bile of a patient with obstructive jaundice due to pancreas head cancer

	Concentration in bile μM/ml
GC	4.93
GCDC	3.15
	8.08
TC	1.89
TCDC	0.93
	2.82
C	1.86
CDC	1.88
	3.74
Total	14.64

$\frac{C}{CDC}$	0.99	$\frac{GC}{GCDC}$	1.57	$\frac{TC}{TCDC}$	2.03
$\frac{GC+TC}{GCDC+TCDC}$	1.67	$\frac{C+GC+TC}{CDC+GCDC+TCDC}$			1.46
$\frac{\text{Conjugated}}{\text{Total}}$	0.74	$\frac{G}{T}$	2.78		

Significantly it means in obstructive jaundice that

$$\frac{C+GC+TC}{CDC+GCDC+TCDC}$$

is greater than 1.0.

Conclusion

The procedures described here make possible the individual separation of the conjugated and free bile acids. However, in order to complete the separation between DC and CDC in free bile acids, it is necessary to examine the conditions of the mobile phase and column. The investigation for the micro-determination of individual bile acids is in progress.

The development of the quantitative analysis of individual conjugated and free bile acids by high performance liquid chromatography may extend the value of bile acid studies in the clinical investigation of hepatobiliary disease.

References

1) D. H. Sandberg, J. Sjövall, K. Sjövall, and D. A. Turner, *J. Lipid Res.*, **6**, 182 (1965).
2) J. Roovers, E. Evrard, and H. Vanderhaeghe, *Clin. Chim. Acta*, **19**, 449 (1968).
3) S. Okuyama, D. Uemura, and Y. Hirata, *Chem. Lett.*, **1976**, 679.
4) I. Makino and J. Sjövall, *Anal. Lett.*, **5**, 341 (1972).

Synthetic Studies of Laurencin and Related Compounds. IV.[1] Synthesis of *cis*-2-Ethyl-8-formyl-3,4,7,8-dihydro-2*H*-oxocin-3-one 3-Ethylene Acetal and Related Compounds

Tadashi MASAMUNE,* Hajime MATSUE, and Hisashi MURASE
Department of Chemistry, Faculty of Science, Hokkaido University, Sapporo 060
(Received May 11, 1978)

The synthesis of *cis*-2-ethyl-8-formyl-3, 4, 7, 8-dihydro-2*H*-oxocin-3-one and its derivatives, key intermediates for synthesis of laurencin, from methyl 2-ethyl-2,5-dihydro-2-furoates is described. The structure and configuration of these compounds and the synthetic intermediates are defined clearly on the basis of the chemical and spectral evidence.

Laurencin[2] (**1**) and related compounds are a group of naturally occurring halogeno compounds with (a) medium-sized ether ring(s) as well as an enyne moiety, and the structure and configuration have been established well.[3] In recent communications[1,4] we reported the synthesis of the title compound (**2**) and its transformation into (±)-laurencin. The present paper describes details of the synthesis of the key intermediate (**2**) and related compounds.

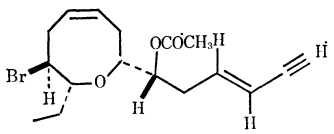

1

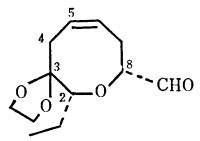

2

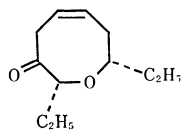

3a *cis*
3b *trans*

The synthesis of *cis*-2-ethyl-8-formylhydrooxocinone ethylene acetal (**2**) and related compounds was carried out in an analogous manner to that of the corresponding *cis*- and *trans*-2,8-diethylhydrooxocinones[5] (**3a** and **3b**), and hence required preparation of 4-ethyl-2-formyl-9-methyl-3-oxa-9-azabiocyclo[3.3.1]nonan-7-ones or their synthetic equivalents, *e.g.*, 2-acetoxymethyl-4-ethyloxaazabicyclononanones (**4**). These relevant intermediates were finally prepared by the Robinson-Schöpf condensation as described below.

The Birch reduction of 5-ethyl-2-furoic acid followed by esterification produced a 1:1 mixture of methyl *cis*- and *trans*-5-ethyl-2,5-dihydro-2-furoates[6] (**5**), which were reduced with lithium aluminium hydride to give the corresponding alcohols (**6**) in good yield. The alcohols (**6**) were submitted to ozonolysis at −70 °C in methanol, and the resulting dialdehyde mixture was immediately treated with methylamine and acetonedicarboxylic acid under the Robinson-Schöpf conditions (room temp, pH 5, 2 d). Total basic products were treated with acetic anhydride in pyridine and then purified by chromatography, giving a 3:2:1 mixture of the relevant oxaazabicyclononanones (**4a**, **4b**, and **4c**) in 7.8% yield from **6**. Further purification by column chromatography and subsequent preparative TLC effected isolation of each stereoisomer (**4a**), mp 76—78 °C, (**4b**), oil, and (**4c**), oil, in 2.2, 0.4, and 0.2% yields, respectively. In accordance with the assigned (planar) structure, each compound had the same molecular formula $C_{13}H_{21}O_4N$, and displayed ester and ketone carbonyl bands near 1730 and 1710 cm^{-1} and the same fragmentation peaks at *m/e* 225 (M^+), 196, 138, 111, and 110 in the IR and mass spectra. The configuration in question of these bicyclononanones was elucidated on the basis of the NMR spectra, which are summarized in Table 1 with those of the related compounds, 2-(acetoxymethyl)-oxaazabicyclononanones (**7a** and **7b**) (*cf.*, Experimental).

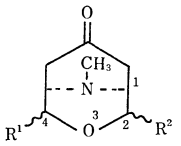

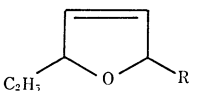

4a R^1=···C_2H_5, R^2=···CH_2OAc
4b R^1=···C_2H_5, R^2=—CH_2OAc
4c R^1=—C_2H_5, R^2=···CH_2OAc
7a R^1=H, R^2=···CH_2OAc
7a′ R^1=H, R^2=···CH_2OH
7b R^1=H, R^2=—CH_2OAc
7b′ R^1=H, R^2=—CH_2OH
8 R^1=R^2=H
9a R^1=R^3=···C_2H_5
9b R^1=···C_2H_5, R^2=—C_2H_5

5 R=$COOCH_3$ (*cis* and *trans*)
6 R=CH_2OH (*cis* and *trans*)

As shown in Table 1, all compounds (**4a**—**4c**, **7a** and **7b**) revealed the following coupling constants; $J_{1,8a}=J_{5,6a}=6$ Hz and $J_{1,8e}=J_{5,6e}\fallingdotseq 0$ Hz. These constants indicated that the dihedral angles between the proton at C_1 (C_5) and the equatorial and axial protons at C_8 (C_6) would be about 90 and 30°, respectively. Judging from these values as well as the previous result,[5,7] the piperidone ring would exist as a slightly deformed chair form. On the other hand, the coupling constants $J_{1,2e}$, $J_{1,2a}$, $J_{5,4e}$, and $J_{5,4a}$ were small for these compounds. Such constants were also observed in the NMR spectra of several 3-oxabi-

cyclo[3.3.1]nonane derivatives,[8] which also adopt a double-chair conformation. The spectral similarity between these compounds, coupled with our previous result on the conformation of 9-methyl-9-aza-3-oxabicyclo[3.3.1]nonan-7-one (**8**) and its 2,5-diethyl derivatives[5] (**9a** and **9b**), indicated that all the compounds would probably take a double-chair conformation. This assignment was confirmed by the X-ray crystallographic analysis of 2-acetoxymethyl-4-ethyloxaazabicyclononanone (**4a**),[9] one of the most important key compound; namely, in spite of the presence of 2,4-diaxial substitutents, the compound (**4a**) exists in the double-chair conformation, as illustrated in Fig. 1.

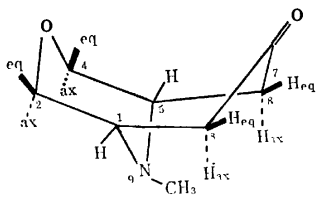

Fig. 1.

Stereochemistry of the substituent(s) at C_2 and/or C_4 in compounds **4b**, **4c**, **7a**, and **7b** was deduced from the chemical shift and signal pattern of the ethyl methylene and acetoxymethyl methylene protons. Signals due to the acetoxymethyl methylene protons of **4a**, **4b**, and **7a** were very similar each other; two double doublets (one with J=11 and 5—6 Hz and another with J=11 and 7.5—8 Hz, *cf*, Table 1) appeared at δ 4.38 and 4.18, at δ 4.69 and 4.22, and at δ 4.68 and 4.23, respectively. To the contrary, the corresponding protons of **4c** and **7b** were observed as broad singlets at higher field, δ 4.00 and 3.98, respectively. The striking difference in chemical shift and splitting pattern indicates that the acetoxymethyl methylene protons of the former three oxaazabicyclononanones (**4a**, **4b**, and **7a**) are disposed 1,3-diaxially with the nitrogen lone pair electrons[10] and free rotation of the acetoxymethyl group would be hindered. The same discussion holds for the ethyl groups of compounds **4a**—**4c**, **9a**, and **9b**; absorption peaks due to the ethyl methylene protons of **4a**, **4c**, and **9a** were observed at lower field than δ 1.58, while those of **4b** and **9b** at higher field than δ 1.40. In summary, all the compounds in Table 1 are represented by the respective assigned configurations and conformations, which would be interpreted well as the result of interaction between the ether oxygen and carbonyl carbon atoms.[11]

Treatment of *cis*-2-acetoxymethyl-4-ethyloxaazabicyclononanone (**4a**) with tosylhydrazine in acidic tetrahydrofuran under reflux and then with methyllithium in benzene and ether[12] produced olefinic alcohols (**10**), which were converted into a crystalline mixture of methiodides (**11a** and **11b**) in good yield. The methiodides, when eluted through Amberlite IRA-400 and then heated at 60—80 °C, underwent the Hofmann elimination with concurrent facile 1,5-sigmatropic hydrogen transfer to give a mixture of dienamines (**12a** and **12b**). The dienamine mixture, without isolation, was hydrolyzed in 7% fluoroboric acid under reflux to yield a mixture of keto alcohols (**13a** and **13b**), which were purified by column chromatography to give **13a** and **13b** in pure state in 32

TABLE 1. THE NMR SPECTRA OF 9-METHYL-3-OXA-9-AZABICYCLO[3.3.1]NONAN-7-ONES[a]

Proton	Chemical shifts (δ)[b] Compounds **4a**	**4b**	**4c**	**7a**	**7b**	J	Coupling constans (Hz)[c,d] Compounds **4a**	**4b**	**4c**	**7a**	**7b**
H_1	3.12 br d	3.06 br d	3.10 br d	3.08 br d	3.10 br d	$J_{1,2e}$	1.5	0.5	—	0.0	—
H_5	3.06 d	2.99 m	3.04 br d	3.08 br d	3.10 br d	$J_{5,4e}$	0.0	—	0.5	0.0	0.5
H_{2e}	3.69 br do d	3.83 br do d	—	3.80 do d	—	$J_{1,2a}$	—	—	1.0	—	0.5
H_{4e}	3.39 t	—	3.56 do d	3.51 d	3.78 br d	$J_{5,4a}$	—	1.0	—	2.0	1.0
H_{2a}	—	—	4.00 m	—	3.98 m	$J_{1,8e}$	0.0	0.5	0.0	0.0	0.0
H_{4a}	—	3.80 br m	—	4.03 br d	3.89 br d	$J_{5,6e}$	0.0	1.5	0.0	0.0	0.0
H_{6e}	2.18 d	2.23 d	2.19 d	2.20 d	2.16 br d	$J_{1,8a}$	6.0	6.0	6.0	6.0	6.0
H_{8e}	2.18 d	2.17 d	2.19 d	2.20 d	2.24 br d	$J_{5,6a}$	6.0	6.0	6.0	6.0	6.0
H_{6a}	2.80 do d	2.55 do d	2.75 do d	2.53 do d	2.72 do d	$J_{2,H}$	8	8	small	8	small
							5	6		5	
CH_3CH_2	1.70 qui	1.38 m	1.58	—	—	$J_{1,H}$	7		8		— —
							7		6		
CH_2OAc	4.38 do d	4.69 do d	4.00 br s	4.68 do d	3.98 br s						
	4.18 do d	4.22 do d		4.23 do d							

a) The spectra were measured in $CDCl_3$ at 100 MHz, and the abbreviations "H_{2e} and $J_{1,2e}$" refer to "equatorial proton at C_2 and coupling constant between H_1 and H_{2e}," respectively. b) The chemical shifts of N-CH_3 (s), acetoxyl methyl (s) and ethyl methyl protons (t, J=6.5—7.0 Hz) fell within δ 2.49—2.61, 2.02—2.05, and 0.85—0.93, respectively. c) The coupling constans were estimated by first-order approximations. d) The geminal couplings followed as: $J_{6a,6b}$ and $J_{8a,8e}$ were 15—16 Hz for all compounds, $J_{4a,4e}$ 11—11.5 Hz for **7a** and **7b**, and J_{AB} (CH_AH_BOAc) 11 Hz for **4a**, **4b**, and **7a**, respectively.

and 13% yields (from the total methiodides), respectively. The structure of these ketones was assigned on the basis of the spectral data.

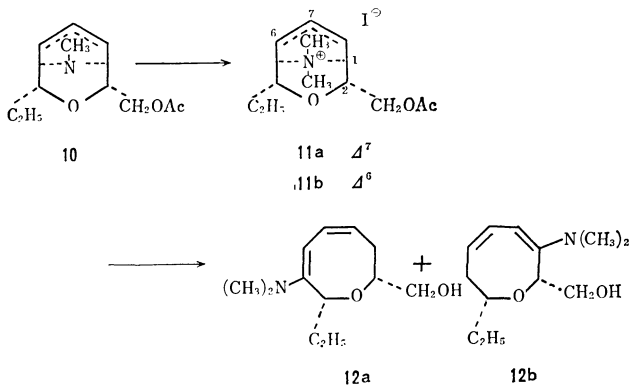

10 11a Δ^7 11b Δ^6 12a 12b

Compound **13a**, $C_{10}H_{16}O_3$ [MS, *m/e* 184 (M^+)], exhibited absorption maxima at 294 nm (ε 147, sh), 303 (173), 312 (161), and 323 (84, sh) with enhanced intensity due to the n-π^* transition, characteristic for β,γ-unsaturated carbonyl chromophores, and those at 3480 (OH), 1720 (C=O), and 1645 (C=C) cm^{-1} in the UV and IR spectra, respectively. Compound **13b** also displayed essentially the same mass, UV, and IR spectra as **13a**, indicating both the compounds to be isomers. The NMR spectra, coupled with the spin decoupling studies, provided definite evidence for disposition of the carbonyl groups in both the compounds (**13a** and **13b**). In the spectrum of **13a**, a double doublet (J=5 and 7 Hz) at δ 3.82 [C_2H_5-C<u>H</u>(O)–] was simplified to a singlet on irradiation at δ 1.70 ($CH_3C\underline{H}_2$–), but remained unchanged on that near δ 2.3 (–$C\underline{H}_2CH$=CH–). On the other hand, a double double doublet (J=2, 6, and 12 Hz) at δ 3.40 [$C_2H_5C\underline{H}$(O)–] in the spectrum of **13b** was collapsed to a broad doublet (J=6 Hz) and to a double doublet (J=6 and 12 Hz) on irradiation at δ 1.62 ($CH_3C\underline{H}_2$–) and near δ 2.3 (–$C\underline{H}_2CH$=CH–), respectively. The result reveals the presence of partial formulas $C_2H_5\underline{C}H(-O-)C(=O)-$ and $C_2H_5\underline{C}H-O-CH_2CH=CH-$ in **13a** and **13b**, respectively, confirming the assigned structures.

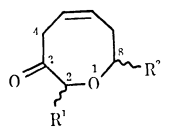

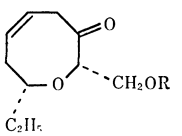

13a R^1=···C_2H_5, R^2=—CH_2OH
15a R^1=···C_2H_5, R^2=—CH_2OAc
13c R^1=—C_2H_5, R^2=···CH_2OH
14a R^1=R^2=···C_2H_5
14b R^1=···C_2H_5, R^2=—C_2H_5

13b R=H
15b R=Ac

Repetition of the aforementioned sequence on a 2:2:1 mixture of the oxaazabicyclononanones (**4a**, **4b**, and **4c**), free from pure **4a**, led to formation of a mixture of β,γ-unsaturated ketones, from which compounds **13a** and **13b** and a new compound (**13c**) were isolated in 6, 3, and 2% yields, respectively. The compound (**13c**) revealed essentially the same mass, UV, and IR spectra as **13a**, and also exhibited two characteristic double doublets (one with J=14 and 4 Hz and another with J=14 and 2 Hz) at δ 3.08 and 3.44 in the NMR spectrum. These signals are corresponding to the following peaks due to the C_4-protons of **13a**, *cis*- and *trans*-2,8-diethyltetrahydrooxocins[5] **14a** and **14b**: **13a**, δ 2.82 and 3.86 (each J=12 and 6 Hz); **14a**, δ 2.77 and 3.82 (each J=13 and 6 Hz); **14b**, δ 2.93 and 3.52 (J=16, 3 and 16, 2 Hz).[5] The spectral similarity indicated that the new compound (**13c**) would be a stereoisomer of **13a**. Indeed, compound **13c** was converted by treatment with base under mild conditions into **13a** quantitatively. The low yields of these unsaturated ketones would result from difficult separation of the products and also incomplete 1,5-hydrogen transfer in aminodienes (to dienamines corresponding to **12** derived from the *trans*-oxaazabicyclononanones (**4b** and **4c**).

Before proceeding with the synthesis, we examined the stereochemistry of reduction of the carbonyl group of the tetrahydrooxocinones. Compound **13a** was converted into the acetate (**15a**), which on treatment with sodium borohydride gave hydroxy acetate (**16**) in 60% yield as an isolable main product. The compound (**16**) showed a double doublet (J=12 and 8 Hz) at δ 2.62 in the NMR spectrum, which was attributed to one of the C_4-protons. In view of the different signal pattern due to the corresponding proton of laurencin (**1**) (δ 3.2, do do d, J=3, 7, and 13 Hz),[2] the alcohol (**16**) was suggested to possess all *cis*-configuration concerning the substituents at C_2, C_3, and C_8. In order to ascertain this assignment, the isomeric *cis*-2-hydroxymethyl-8-ethyltetrahydrooxocinone (**13b**) was likewise converted into the acetate (**15b**) and then reduced with the hydride reagent to give a 1:1 mixture of new hydroxy acetates (**17a** and **17b**), which could be isolated by column chromatography. The NMR spectrum of more polar alcohol (**17b**) revealed two characteristic peaks at δ 2.81 (do do d, J=3, 7, and 13 Hz) and 3.80 (do t, J=9, 3, and 3 Hz), which were ascribed to one of the C_4-protons and a proton on the carbon (C_3) bearing the hydroxyl group, respectively. These absorption patterns were practically the same as those of the corresponding protons (do do d, J=3, 7, and 13 Hz, and do t, J=9, 3, and 3 Hz)[2] of laurencin (**1**). On the other hand, the relevant proton at C_4 of less polar alcohol (**17a**) appeared at δ 2.64 as a double doublet (J=12 and 8 Hz) in the spectrum. All these splitting patterns, combined with the previous result [the C_4-proton in question of two reduction products, major (**18a**) and minor (**18b**), from *cis*-diethyltetrahydrooxocinone (**14a**) [δ 2.63 (do d, J=8 and 12 Hz) for **18a**, and δ 2.82 (do do d, J=3, 7, and 13 Hz) for **18b**][5] indicate that all-cis assignment to the three substituents at

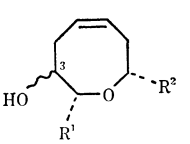

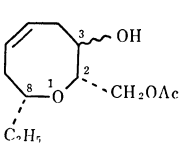

16 R^1=C_2H_5, R^2=CH_2OAc, 3α-OH
18a R^1=R^2=C_2H_5, 3α-OH
18b R^1=R^2=C_2H_5, 3β-OH

17a 3α-OH
17b 3β-OH

C_2, C_3, and C_8 of alcohol **16** is correct. The predominant formation of all-*cis*-substituted alcohol (**16**) would be convenient for substitution of the hydroxyl group to a bromine atom with the desired configuration by triphenylphosphine and carbon tetrabromide, because the bromination usually proceeds in S_N2 manner.[13]

Compound **13a** was transformed into several derivatives including the title compound (**2**). Acetalization of **13a** under usual conditions gave the ethylene acetal (**19**) in quantitative yield. The NMR spectrum revealed two double doublets (each $J=13$ and 8 Hz) due to the C_4-protons at δ 2.89, indicating that the double bond at C_5 and C_6 did not migrate during the reaction. Oxidation of **19** with chromium(VI) oxide and pyridine in dichloromethane[14] afforded crystalline aldehyde, the title compound (**2**), mp 73—74 °C, in quantitative yield, whose spectra were completely consistent with the assigned structure. On the other hand, treatment of **2** with 1 equiv of 1,2-ethanedithiol in the presence of boron trifluoride in dichloromethane resulted in thioacetalization with concomitant hydrolysis of the acetal group at C_3 to give monothioacetal (**20**), showing a β,γ-unsaturated carbonyl band at 1720 cm^{-1} in the IR spectrum. The compound (**20**) also exhibited two double doublets (each $J=13$ and 6 Hz) due to the relevant C_4-protons at δ 2.86 and 3.82, indicative of retention of the relative configuration of the substituents at C_2 and C_8.[5] The same treatment of **2** with 2 equiv of ethanedithiol led to formation of bis(dithioacetal) (**21**), while the mono(dithioacetal) (**20**) was converted into acetal dithioacetal (**22**), showing two double doublets (each, $J=13$ and 9 Hz) at δ 2.15 and 2.89 in the NMR spectrum. All these compounds (**2**, **20**—**22**) possess all functional groups convertible into those of laurencin (**1**), and hence the present result implies the synthesis of most appropriate intermediates leading to the natural product (**1**) as described in the following paper.

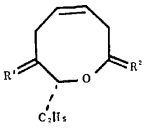

2 $R^1=OCH_2CH_2O$, $R^2=$—H, ···CHO
19 $R^1=OCH_2CH_2O$, $R^2=$—H, ···CH_2OH
20 $R^1=O$, $R^2=$—H, ···CH(S—)(S—)
21 $R^1=SCH_2CH_2S$, R=—H, ···CH(S—)(S—)
22 $R^1=OCH_2CH_2O$, $R^2=$—H, ···CH(S—)(S—)

Experimental

All the mps and bps were uncorrected. The homogeneity of each compound was always checked by TLC over silica gel (Wakogel B-5) and/or GLC (Hitachi K-53) over 10% SE-30. Column chromatography was carried out over silicic acid (Merck, Kieselgel 60, 70—230 mesh) and/or alumina (Merck, standard, Active I and II—III). The UV, IR, and NMR (100 MHz) spectra were measured in 2,2,4-trimethylpentane, in liquid state, and in chloroform-*d*, respectively, unless otherwise stated. The abbreviations "s, d, t, q, qui, m, br, do, and sh," in the NMR and IR spectra denote "singlet, doublet, triplet, quartet, quintet, multiplet, broad, double, and shoulder," respectively.

*5-Ethyl-2,5-dihydrofurfuryl Alcohols (**6**).* To a stirred slurry of lithium aluminum hydride (LAH, 6 g) in anhydrous ether (1.2 l) at 0 °C was added dropwise a solution of methyl 5-ethyl-2,5-dihydro-2-furoates[6] (**5**, 28 g) in ether (200 ml). The mixture was stirred at room temperature for 20 h, cooled, mixed with water (7.5 ml), 30% aq sodium hydroxide (7.5 ml) and then water (7.5 ml). The resulting inorganic salts were removed by filtration, and the filtrate was dried over anhydrous sodium sulfate and evaporated to leave oil, which was distilled to give **6** (11.3 g), bp 72—73 °C/15 Torr; MS, *m/e* 128 (M^+) and 99: IR (CCl_4), ν_{max} 3410, 1075, and 1030 cm^{-1}; NMR, δ 0.90 and 0.91 (total 3H, each t, $J=7$ Hz, $C\underline{H}_3CH_2$), 1.57 (2H, qui, $J=7$ Hz, $CH_3C\underline{H}_2$), 3.45 (1H, br, O$\underline{H}$), 3.57 (2H, br s, $C\underline{H}_2OH$), 4.85 (2H, m, 2$\underline{H}$ at C_2 and C_5), 5.78 and 5.91 (2H, ABq, $J=6$ Hz, 2$\underline{H}$ at C_3 and C_4). Found: C, 65.59; H, 9.47%. Calcd for $C_7H_{12}O_2$: C, 65.59; H, 9.44%.

*(2R,4R)-, (2S,4R)-, and (2R,4S)-2-Acetoxymethyl-4-ethyl-9-methyl-3-oxa-9-azabicyclo[3.3.1]nonan-7-ones (**4a**, **4b**, and **4c**).* Into a solution of **6** (29 g) in methanol (300 ml) or dichloromethane (300 ml) containing three drops of pyridine, cooled at −70 °C in a Dry Ice-ethanol bath, was passed ozonized oxygen gas, until the reaction mixture became blue. The mixture, while still at −70—−60 °C, was flushed with nitrogen for 10 min, when the blue color disappeared. After addition of dimethyl sulfide (20 ml) at the temperature, the mixture was stirred at −70—−30 °C for 30 min, then at ice-bath temperature for 2 h, and finally at room temperature for 1 h, and evaporated below 45 °C to leave oily residue containing dimethyl sulfoxide, which was treated with 25% aq acetic acid (40 ml) under reflux for 45 min and cooled to room temperature. To the solution was immediately added an aqueous solution (300 ml) containing sodium monohydrogenphosphate (4.25 g) and potassium dihydrogenphosphate (2.43 g), acetonedicarboxylic acid (36 g) and methylamine hydrochloride (16 g). The whole solution was adjusted to pH 5 with 6 M aq sodium hydroxide and stirred at room temperature for 2 d, the pH being maintained at 5.0 by occasional addition of citric acid. The solution was concentrated under reduced pressure to one-half of the volume, made acidic strongly by addition of concd hydrochloric acid and washed with ether (2×200 ml). The acidic aqueous solution was then made strongly basic with concd aq potassium hydroxide and extracted with chloroform (4×300 ml). The chloroform solutions were combined, dried and evaporated to leave oil (17.3 g). The oil was passed through a short alumina column (Merck, Active II—III, 60 g, benzene) to give oil (11.8 g), which was treated with acetic anhydride (48 g) and pyridine (120 ml). The resulting acetate mixture (14 g) was again passed through a short alumina column (45 g) to give oily basic material (12.3 g), which was purified by chromatography over silica gel (Merck, 250 g, benzene : acetone = 10 : 1) to yield a 3 : 2 : 1 mixture (3.55 g) of **4a**, **4b**, and **4c** (estimated by measurement of the NMR signals due to the C_2-protons). The mixture was further chromatographed over silica gel to give crystalline base, which was recrystallized from ether to yield **4a** (1.0 g), mp 76—78 °C. This was recrystallized from ether for analysis, mp 77—78.5 °C; mass (the text); IR (Nujol), ν_{max} 1730, 1710, 1240, 1160, and 1038 cm^{-1}; NMR (Table 1). Found: C, 60.98; H,

8.36; N, 5.51%. Calcd for $C_{13}H_{21}O_4N$: C, 61.15; H, 8.29; N, 5.49%.

A part (700 mg) of the residual oil (a 2 : 2 : 1 mixture of **4a**, **4b**, and **4c**), free from pure **4a**, was separated into two fractions by repeated preparative TLC over silica gel (benzene : acetone=9 : 1). Fractions (100 mg) with higher R_f value gave **4b** (95 mg), oil, showing a single spot; MS (the text), IR, ν_{max} 1730, 1710, 1240, 1160, and 1038 cm^{-1}; NMR (Table 1). Found: C, 61.28; H, 8.10; N, 5.31%. Calcd for $C_{13}H_{21}O_4N$: C, 61.15; H, 8.29; N, 5.49%. Fractions (520 mg) with lower R_f value were again purified by repeated preparative TLC (benzene : acetone= 9 : 1) to give **4c** (40 mg), oil, showing a single spot; MS (the text); IR, ν_{max} 1743, 1712, 1240, 1160, and 1038 cm^{-1}; NMR (Table 1). Found: C, 60.99; H, 8.32; N, 5.61%. Calcd for $C_{13}H_{21}O_4N_4$: C, 61.15; H, 8.29; N, 5.49%.

2,5-Dihydrofurfuryl Alcohol. To suspension of ether (1 l) and LAH (4.7 g) was added dropwise methyl 2,5-dihydro-2-furoate (20 g) in ether (100 ml). The mixture was allowed to stir overnight and then refluxed for 2 h. To the mixture were added water (5 ml), 30% aq sodium hydroxide (5 ml) solwly. After removal of the resulting inorganic salts by filtration, the filtrate was evaporated to leave oil, which was distilled to give the alcohol (11.3 g), bp 51—52 °C/15 Torr; MS, *m/e* 83 (M^+-CH_2OH); IR (CCl_4), ν_{max} 3400, 1090, and 1040 cm^{-1}; NMR, δ 3.12 (1H, br s, OH), 3.45 (2H, m, CH_2OH), 4.56 (2H, m, H at C_5), 4.70 (1H, m, H at C_2), 5.74 and 5.90 (2H, ABq, J=6.5 Hz, 2H at C_3 and C_4). Found: C, 59.87; H, 8.00%. Calcd for $C_5H_8O_2$: C, 59.98; H, 8.05%.

2-Acetoxymethyl-9-methyl-3-oxa-9-azabicyclo[3.3.1]nonan-7-ones (7a and 7b). Into a solution of 2,5-dihydrofurfuryl alcohol (11.3 g) and two drops of pyridine in dichloromethane (400 ml), cooled at −60—−70 °C, was passed ozonized oxygen, and the resulting blue reaction mixture was flushed with nitrogen at the temperature for 15 min. After addition of dimethyl sulfide (10 ml) at −60 °C, the mixture was stirred at −10 °C for 1 h, then at ice-bath temperature for 1 h and, finally, at room temperature for 1 h, washed with water (2×50 ml) and dried over sodium sulfate. No reaction product was obtained after removal of the dichloromethane. The aqueous washings were mixed with an aqueous solution (1.8 l) containing sodium monohydrogenphosphate (25.6 g), potassium dihydrogenphosphate (15 g), methylamine hydrochloride (26.4 g) and acetonedicarboxylic acid (53.2 g). The whole solution was adjusted to pH 5 by addition of 40% aq sodium hydroxide, and then stirred at room temperature for 2 d, the pH being maintained at 5.0 by occasional addition of citric acid. After being concentrated to one-half of the volume, the solution was made strongly acidic by addition of concd hydrochloric acid and washed with ether 2×200 ml). The aqueous solution was then made basic strongly with concd aq potassium hydroxide and extracted continuously with chloroform (1.6 l) for 48 h. The chloroform solution was washed with water, dried and evaporated to give oily residue (34.1 g), showing several spots on TLC (benzene : acetone= 3 : 1). The residue was separated into two fractions by column chromatography over alumina (500 g, benzene : methanol=60 : 5). Early fractions, eluted with benzene, gave 2-methylene-9-methyl-3-oxa-9-azabicyclo[3.3.1]nonan-7-one (**23**, 9.3 g), oil, showing a single spot on TLC; MS, *m/e* 167 (M^+), 124, and 110; IR, ν_{max} 1710, 1660, 1130, 1070, 1020, and 915 cm^{-1}; NMR, δ 2.34 and 2.40 (each 1H, br d, J=16 Hz, H_{8e} and H_{6e}), 2.60 (3H, s, NCH_3), 2.78 and 2.82 (each 1H, do d, J=16 and 6 Hz, H_{6a} and H_{8a}), 3.12 and 3.48 (each 1H, br d, J=6 Hz, H_5 and H_1), 3.80 and 4.19 (each 1H, br d, J=11 Hz, 2H at C_4), 4.25 and 4.50 (each 1H, ABq, J=9 Hz, CH_2=C_2). Rechromatography of the oil under the same conditions afforded an analytical sample of **23**. Found: C, 64.65; H, 7.84; N, 7.83%. Calcd for $C_9H_{13}O_2N$: C, 64.85; H, 8.07; N, 7.03%.

Later fractions, showing two major spots on TLC (benzene : acetone=3 : 1), gave oily substance (7.3 g), which was treated with acetic anhydride (30 ml) and pyridine (50 ml) at room temperature for 24 h. The acetates (7.8 g) were separated by chromatography over silica gel with benzene and acetone (9 : 1) to yield crystalline acetate (**7a**, 1.12 g), mp 105.5—108 °C, as an initial eluate. Recrystallization from hexane and ethanol gave an analytical sample of **7a**, mp 108—109 °C; MS, *m/e* 227 (M^+), 168, 124, and 110; IR ($CHCl_3$), ν_{max} 1730, 1710, and 1230 cm^{-1}; NMR (Table 1). Found: C, 57.83; H, 7.50; N, 6.14%. Calcd for $C_{11}H_{17}O_4N$: C, 58.13; H, 7.54; N, 6.16%. Oily acetate (**7b**), showing a single spot on TLC, was then eluted and purified by rechromatography to give an analytical sample of **7b**; MS, *m/e* 227 (M^+), 168, 124, and 110; IR ($CHCl_3$), ν_{max} 1730, 1710, and 1220 cm^{-1}; NMR (Table 1). Found: C, 57.83; H, 7.50; N, 6.14%. Calcd for $C_{11}H_{17}O_4$: C, 58.13; H, 7.54; N, 6.16%.

Acetates **7a** and **7b** were converted into the corresponding alcohols (**7a′** and **7b′**) by the method described below. To an ice-cooled solution of **7a** (280 mg) in ethanol (25 ml) was added sodium borohydride (NBH, 50 mg), and the mixture was stirred for 4 h at 0 °C. After addition of acetic acid (100 mg) and one drop of concd hydrochloric acid to decompose excess of NBH, the mixture was concentrated, made basic with aq sodium hydroxide and extracted with chloroform (2×40 ml). The chloroform solution was worked up as usual to give **7a′** (168 mg), which crystallized on trituration with ether and then recrystallized from ether to yield an analytical sample of **7a′**, mp 100—102 °C; MS, *m/e* 185 (M^+), 154, 128, and 110; IR ($CHCl_3$), ν_{max} 3330, 1710, 1100, and 1060 cm^{-1}; NMR, δ 2.26 (2H, d, J=15 Hz, H_{8e} and H_{6e}), 2.60 (3H, s, NCH_3), 2.75 and 2.80 (each 1H, do d, J=15 and 6 Hz, H_{6a} and H_{8a}), 3.58 (1H, d, J=11 Hz, H_{4e}), 3.65 (1H, do d, J=4 and 6 Hz, H_{2e}), 3.87 and 4.15 (each 1H, do d, J=4, 12 and 6, 12 Hz, CH_2OH), and 4.23 (1H, br d, J=11 Hz, H_{4a}). Found: C, 58.11; H, 8.23; N, 7.43%. Calcd for $C_9H_{15}O_3N$: C, 58.36; H, 8.16; N, 7.56%.

The isomeric acetate (**7b**, 240 mg) was converted into the alcohol (**7b′**, 130 mg), oil, in the same manner as described above, and showed the following spectra; MS, *m/e* 185 (M^+), 154, 128, and 110; IR ($CHCl_3$), ν_{max} 3330, 1710, 1100, and 1060 cm^{-1}; NMR, δ 2.22 and 2.25 (each 1H, br d, J=15 Hz, H_{6e} and H_{8e}), 2.62 (3H, s, NCH_3), 2.67 and 2.71 (each 1H, do d, J=15 and 6 Hz, H_{6a} and H_{8a}), 3.13 (2H, br d, J=6 Hz, 2H at C_1 and C_5), 3.60 (3H, m, H_{2a} and CH_2OH), 3.79 and 3.93 (each 1H, br d, J= 11 Hz, H_{4e} and H_{4a}).

2-Hydroxy-2,9-dimethyl-3-oxa-9-azabicyclo[3.3.1]nonan-7-one

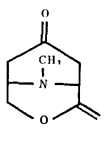

23

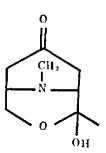

24

(24). This compound was isolated in one run of the preceding Robinson-Schöpf condensation experiments, and the structure was confirmed by the hydration of **23** described below. Compound **23** (90 mg) in chloroform (30 ml) was treated with concd hydrochloric acid (2 ml) at room temperature for 20 min. After removal of the chloroform and subsequent addition of water (5 ml), the resulting aqueous solution was made basic with 6 M aq sodium hydroxide and extracted with chloroform (2×20 ml). The chloroform solution was worked up as usual to give crystalline alcohol (**24**, 71 mg), mp 97—99 °C; MS, *m/e* 185 (M^+) and 142; IR ($CHCl_3$), ν_{max} 3420, 1715, 1070, 1020, and 915 cm^{-1}; NMR, δ 1.30, (3H, s, $C\underline{H}_3$ at C_2), 2.19 (2H, br d, J=15 Hz $\underline{H}_{8e}$ and $\underline{H}_{6e}$), 2.52 and 2.63 (each 1H, br do d, J=15 and 6 Hz, $\underline{H}_{6a}$ and $\underline{H}_{8a}$), 2.55 (3H, s, $NC\underline{H}_3$), 2.99 (1H, d, J=11 Hz, $\underline{H}_{4e}$), 4.12 (1H, do do d, J=1, 2.5, and 11 Hz, $\underline{H}_{4a}$), and 4.95 (1H, br, O$\underline{H}$). An analytical sample of **24** was prepared by recrystallization from ether and hexane, mp 100—101 °C. Found: C, 58.14; H, 8.19; N, 7.69%. Calcd for $C_9H_{15}O_3N$: C, 58.36; H, 8.16; N, 7.56%.

cis-*3-Ethyl-2-hydroxymethyl-9-methyl-3-oxa-9-azabicyclo*[*3.3.1*]-*nonenes (10)*. A solution of **4a** (2.98 g) and tosylhydrazine (3.64 g) in THF (70 ml) containing a few drops of concd hydrochloric acid was heated under reflux for 12 h in a three-necked flask, fitted with a condenser and a magnetic stirring bar. After addition of benzene (250 ml) and removal of the condenser, the solution was concentrated to 70—80 ml, when the temperature of distillates had became near 80 °C, and then cooled in an ice-bath. To the concentrated solution was slowly added a solution of methyllithium, prepared from lithium (2.0 g) and methyl iodide (13 ml), in ether (210 ml). The whole mixture was stirred at room temperature for 20 h, and then washed with water. The aqueous washings were extracted with chloroform. All the organic (ether, benzene, and chloroform) solutions were combined, dried and evaporated to leave crude olefinic alcohol (3.1 g), most of which was used for the next reaction without further purification. A part of the crude sample of **10** was purified by preparative TLC (benzene : acetone=1 : 1) to give an almost pure sample, showing the following spectra; ν_{max} 3395, 1120, 1092, 1054, and 1040 cm^{-1}; NMR, δ 0.96 (3H, t, J=7 Hz, $C\underline{H}_3CH_2$), 1.62 (2H, m, $CH_3C\underline{H}_2$), 2.40 and 2.42 (total 3H, each s, $NC\underline{H}_3$), and 5.75 (2H, br m, W_H=7 Hz, C$\underline{H}$=C$\underline{H}$).

cis-*2-Ethyl-8-hydroxymethyl- and* cis-*8-Ethyl-2-hydroxymethyl-3,4,7,8-dihydro-2*H-*oxocin-3-ones (13a and 13b), and Their Acetates (15a and 15b)*. 1) A solution of the crude olefinic alcohol (**10**, 3.0 g) in ethanol (80 ml) was refluxed with methyl iodide (62 ml) for 2 h and then evaporated to leave crystalline methiodides (3.65 g). Recrystallization from ethanol afforded a 1 : 8 mixture (crystals A, 1.33 g) of the methiodides (**11a** and **11b**), mp 213—124 °C, as the first crop; MS, *m/e* 197 (M^+-CH_3I), 142, 127, 108, and 94; IR (Nujol), ν_{max} 3330, 1200, 1172, 1140, 1108, 1045, and 995 cm^{-1}; NMR (D_2O), δ 1.28 (3H, t, J=7 Hz, $C\underline{H}_3CH_2$), 2.05 (2H, m, $CH_3C\underline{H}_2$), 3.42 and 3.76 (each 3H, s, $2NC\underline{H}_3$), and 6.3 (2H, m, W_H=7 Hz, C$\underline{H}$=C$\underline{H}$). Found: C, 42.24; H, 6.56; N, 3.29; I, 37.19%. Calcd for $C_{12}H_{25}O_2NI$: C, 42.47; H, 6.48; N, 3.13; I, 37.45%.

An aqueous solution (20 ml) of crystals A (1.30 g) was passed through a column of Amberlite IRA-400 (basic form). The eluate was collected until it was no longer alkaline and evaporated under reduced pressure below 45 °C. The residual quaternary methohydroxides were decomposed by heating at 60—80 °C under reduced pressure for 45 min to give oil, which was extracted with ether (100 ml) and chloroform (100 ml). The solutions were combined, dried and evaporated to yield a 1 : 8 oily mixture (0.86 g) of *cis*-2-ethyl-8-hydroxymethyl-3-dimethylamino- and *cis*-8-ethyl-2-hydroxymethyl-3-dimethylamino-7,8-dihydro-2*H*-oxocins (**12a** and **12b**); IR, ν_{max} 3420, 1604 (dienamine), 1140, 1115, 1103, 1078, and 1043 cm^{-1}; NMR, δ 0.96 (3H, t, J=7 Hz, $C\underline{H}_3CH_2$), 2.56 [6H, s, $N(C\underline{H}_3)_2$], 5.08 and 5.24 [total 1H (1 : 8), each d, J=4 Hz, $\underline{H}$ at C_4], 5.76 (1H, m, $\underline{H}$ at C_5), and 6.16 (1H, do d, J=4 and 10 Hz, $\underline{H}$ at C_6).

The mother liquors, obtained on removal of crystals A, were evaporated to give an 8 : 1 semi-crystalline mixture (crystals B, 2.20 g) of **11a** and **11b**, which was submitted to the same treatment as crystals A to yield an 8 : 1 oily mixtre (1.94 g) of **12a** and **12b**; IR, ν_{max} 3420, 1064 (dienamine), 1140, 1115, 1103, and 1078 cm^{-1}; NMR, δ 1.00 (3H, t, J=7 Hz, $C\underline{H}_3CH_2$), 1.72 (2H, m, $CH_3C\underline{H}_2$), 2.56 [6H, s, $2N(C\underline{H}_3)_2$], 5.08 and 5.24 [total 1H (8 : 1), each d, J=4 Hz, $\underline{H}$ at C_4], 5.70 (1H, m, $\underline{H}$ at C_5), and 6.18 (1H, do d, J=4 and 10 Hz, $\underline{H}$ at C_6).

2) An aqueous solution (7 ml) of the 1 : 8 mixture (0.85 g) of **12a** and **12b**, obtained from crystals A, was refluxed with 42% fluoroboric acid (1.5 ml) for 15 min. The reaction mixture was cooled, neutralized with saturated aq sodium hydrogencarbonate, and extracted with ether (2× 100 ml) and dichloromethene (2×200 ml). The combined organic solution was dried and evaporated to leave oil (601 mg), showing two spots on TLC (benzene : ethyl acetate=3 : 1). The oil was separated roughly into three fractions by column chromatography over silica gel (20 g, benzene : ethyl acetate=7 : 1). More mobile fractions gave **13b** (180 mg), oil, showing a single spots; MS, *m/e* 184 (M^+), 155, and 125; UV, λ_{max} 304 nm (ε 132) (sh), 312 (165), 321 (161), and 332 (95) (sh); IR; ν_{max} 3480, 1718, 1642, 1115, and 1055 cm^{-1}; NMR, δ 1.00 (3H, t, J=7 Hz, $C\underline{H}_3CH_2$), 1.62 (2H, m, $CH_3C\underline{H}_2$), 2.40 (3H, m, 2$\underline{H}$ at C_7 and O$\underline{H}$), 2.86 and 3.96 (each 1H, do d, J=12 and 6 Hz, 2$\underline{H}$ at C_4), 3.40 (1H, do do d, J=12, 6, and 2 Hz, $\underline{H}$ at C_8), 3.80 (2H, m, $C\underline{H}_2OH$), 4.00 (1H, do d, J=5 and 7 Hz, $\underline{H}$ at C_2), and 5.70 (2H, m, 2$\underline{H}$ at C_5 and C_6). An analytical sample of **13b** was obtained by rechromatography over silica gel. Found: C, 64.94; H, 8.65%. Calcd for $C_{10}H_{16}O_3$: C, 65.19; H, 8.75%. Middle fractions (99 mg) was found to be a 1 : 1 mixture of **13a** and **13b**. Less mobile fractions afforded **13a** (43 mg), showing a single spot, oil; MS, *m/e* 184 (M^+), 155, and 125; UV (the text); IR, ν_{max} 3480, 1720, 1645, 1115, 1095, and 1055 cm^{-1}; NMR, δ 1.00 (3H, t, J=7 Hz, $C\underline{H}_3CH_2$), 1.70 (2H, m, $CH_3C\underline{H}_2$), 2.30 (3H, m, 2$\underline{H}$ at C_3 and O$\underline{H}$), 2.82 and 3.86 (each 1H, do d, J=12 and 6 Hz, 2H at C_4), 3.62 (3H, m, $\underline{H}$ at C_8 and $CH_2O\underline{H}$), 3.82 (1H, do d, J=7 and 5 Hz, $\underline{H}$ at C_2), and 5.70 (2H, m, 2$\underline{H}$ at C_5 and C_6). The oil was rechromatographed over silica gel for analysis. Found: C, 65.33; H, 8.95%. Calcd for $C_{10}H_{16}O_3$: C, 65.19; H, 8.75%.

An aqueous solution (10 ml) of the 8 : 1 mixture (1.93 g), of **12a** and **12b**, obtained from crystals B, was likewise treated with 42% fluoroboric acid (2 ml) under reflux for 15 min. The reaction mixture was cooled, neutralized with saturated aq sodium hydrogencarbonate, and extracted with ether (2×200 ml) and then with chloroform (2×200 ml). The combined organic solution was worked up as usual to leave oil (954 mg), which was purified by repeated chromatography over silica gel (25 g) with benzene and ethyl acetate (8 : 1) to yield **13a** (181 mg) and **13b** (24 mg) in pure state with a 1 : 1 mixture (48 mg) of **13a** and **13b**.

3) Compound **13a** (62 mg) was treated with acetic an-

hydride (0.6 ml) and pyridine (1 ml) at room temperature overnight. The solution was poured into ice-water (5 ml) and extracted with ether (2×200 ml). The ether solutions were combined, washed with 2 M hydrochloric acid (2×10 ml) and water (2×10 ml), dried and evaporated to leave oil (15a, 69 mg), showing a single spot; IR, ν_{max} 1750, 1725, 1230, 1115, and 1040 cm^{-1}; NMR, δ 1.00 (3H, t, J=7 Hz, CH_3CH_2), 1.64 (2H, m, CH_3CH_2), 2.10 (3H, s, $OCOCH_3$), 2.30 (2H, m, 2H at C_7), 2.80 (1H, do d, J= 12 and 6 Hz, H at C_3), 3.68 (1H, m, H at C_8), 3.76 (1H, do d, J=7 and 4 Hz, H at C_2), 3.84 (1H, do d, J=12 and 6 Hz, H at C_4), 4.15 (2H, m, CH_2OCOCH_3), and 5.75 (2H, m, 2H at C_5 and C_6).

Compound **13b** (104 mg) was likewise converted into the acetate (**15b**, 110 mg); IR, ν_{max} 1750, 1725, 1225, and 1115 cm^{-1}; NMR, δ 1.00 (3H, t, J=7 Hz, CH_3CH_2), 1.56 (2H, m, CH_3CH_2), 2.05 (3H, s, $OCOCH_3$), 2.31 (2H, m, 2H at C_7), 2.84 (2H, do d, J=6 and 12 Hz, H at C_4), 3.34 (1H, m, H at C_8), 3.99 (1H, do d, J=6 and 12 Hz, H at C_4), 4.23 (3H, m, H at C_2 and CH_2OCOCH_3), and 5.78 (2H, m, 2H at C_5 and C_6).

*trans-2-Ethyl-8-hydroxymethyl-3,4,7,8-dihydro-2H-oxocin-3-one (**13c**).* The 2 : 2 : 1 mixture (16 g) of oxaazabicyclononanones **4a**, **4b**, and **4c**, described in the previous section, was transformed in almost the same manner as **4a** to give a mixture of tetrahydrooxocinones, from which **4a** (0.6 g), **4b** (0.3 g), and a new compound (**13c**, 0.2 g) were isolated by repeated chromatography. Compound **13c** showed the following spectra: MS, *m/e* 184 (M^+), 155, and 125; UV, λ_{max} 292 nm (ε 80), 303 (95), 313 (85), and 324 (40) (sh); IR, ν_{max} 3360, 1715, 1665, 1110, and 1050 cm^{-1}; NMR, δ 1.02 (3H, t, J=7 Hz, CH_3CH_2), 1.71 (2H, m, CH_3CH_2), 2.15 (3H, m, 2H at C_7 and OH), 3.08 and 3.44 (each 1H, do d, J=14, 5 and 14, 2 Hz, 2H at C_4), 3.52 and 3.76 (each 1H, do d and d, J=11, 7 and 11 Hz, CH_2OH), 3.93 (1H, m, H at C_8), 3.96 (1H, do d, J=5 and 7 Hz, H at C_2), and 5.65 (2H, m, 2H at C_5 and C_6). An analytical sample of **13c** was prepared by rechromatography over silica gel. Found: C, 64.92; H, 8.16%. Calcd for $C_{10}H_{16}O_3$: C, 65.19; H, 8.75%.

Compound **13c** (9 mg) was stirred with 5% potassium hydroxide in methanol (4 ml) at room temperature for 20 min. The solution was diluted with water (20 ml) and extracted with ether (2×30 ml). The ether solution, after being worked up as usual, afforded oil (8 mg), which was identical with **13a** in all respects (TLC, IR, and NMR).

*8-Acetoxymethyl-2-ethyl-3,4,7,8-tetrahydro-2H-oxocin-3-ol (**16**).* Compound **15a** (72 mg) in methanol (12 ml) was reduced with sodium borohydride (NBH, 50 mg) at 0 °C for 40 min. The solution was made acidic with 2 M hydrochloric acid, concentrated and extracted with ether. The ether solution, after usual work-up, left oil (65 mg), which was purified by chromatography over silica gel (2 g) with benzene and ethyl acetate (6 : 1) to give **16** (36 mg), oil, showing a single spot on TLC; MS, *m/e* 170, 168 (M^+—CH_3COOH), 125, and 116; IR, ν_{max} 3400, 1745, 2130, and 1035 cm^{-1}; NMR, δ 0.96 (3H, t, J=7 Hz, CH_3CH_2), 1.55 (2H, m, CH_3CH_2), 1.85 (1H, s, OH), 2.96 (3H, s, $OCOCH_3$), 2.29 (3H, br m, 3H at C_4 and C_7), 2.62 (1H, do d, J=12 and 8 Hz, H at C_4), 3.43 (1H, do do d, J= 8, 5, and 1.5 Hz, H at C_2), 3.67 (2H, m, 2H at C_3 and C_8), 4.08 (2H, m, CH_2OCOCH_3), and 5.78 (2H at C_5 and C_6). The sample was rechromatographed for analysis. Found: C, 63.25; H, 8.85%. Calcd for $C_{12}H_{20}O_4$: C, 63.13; H, 8.83%.

*2-Acetoxymethyl-8-ethyl-3,4,7,8-tetrahydro-2H-oxocin-3-ols (**17a** and **17b**).* Compound **15b** (120 mg) was reduced with NBH (68 mg) in methanol (15 ml) at 0 °C for 40 min. The reaction mixture was made acidic (pH 4—5) with 2 M hydrochloric acid, concentrated and extracted with ether (2×50 ml). The ether solution was worked up as usual to leave oil (114 mg), showing two spots on TLC, which was separated roughly into three fractions by column chromatography over silica gel (3 g, benzene : ethyl acetate =7 : 1). Fractions with higher R_f value gave **17b** (25 mg), oil, showing a single spot; MS, *m/e* 170, 168 (M^+—CH_3COOH), 125, and 116; IR, ν_{max} 3480, 1745, and 1235 cm^{-1}; NMR, δ 0.96 (3H, t, J=7 Hz, CH_3CH_2), 1.46 (2H, m, CH_3CH_2), 2.05 (3H, s, $OCOCH_3$), 2.06 (1H, s, OH), 2.26 (3H, br m, 3H at C_4 and C_7), 2.64 (1H, do d, J=12 and 8 Hz, H at C_4), 3.03 (1H, m, H at C_8), 3.78 (2H, m, 2H at C_2 and C_3), 4.16 (2H, m, CH_2OCOCH_3), and 5.76 (2H at C_5 and C_6). Rechromatography afforded an analytical sample of **17b**. Found: C, 62.91; H, 8.90%. Calcd for $C_{12}H_{20}O_4$: C, 63.13; H, 8.83%. Middle fractions (38 mg) were a 1 : 1 mixture of **17b** and **17a**.

Fractions (24 mg) with lower R_f value gave **17a** (24 mg), oil, showing a single spot: MS, *m/e* 170, 168 (M^+—CH_3COOH), 125, and 116; IR, ν_{max} 3480, 1740, and 1230 cm^{-1}; NMR, δ 0.96 (3H, t, J=7 Hz, CH_3CH_2), 1.47 (2H, m, CH_3CH_2), 2.07 (3H, s, $OCOCH_3$), 2.08 (1H, s, OH), 2.26 (3H, br m, 3H at C_4 and C_7), 2.81 (1H, do do d, J=3, 7, and 13 Hz, H at C_4), 3.30 (1H, m, H at C_8), 3.50 (1H, do d, J=4.5 and 9 Hz, H at C_2), 3.80 (1H, do t, J=9, 3, and 3 Hz, H at C_3), 4.24 (2H, d, J= 4.5 Hz, CH_2OCOCH_3), and 5.83 (2H, m, 2H at C_5 and C_6). An analytical sample of **17a** was prepared by rechromatography. Found: C, 63.25; H, 8.80%. Calcd for $C_{12}H_{20}O_4$: C, 63.13; H, 8.83%.

*cis-2-Ethyl-3,3-ethylenedioxy-8-hydroxymethyl-3,4,7,8-tetrahydro-2H-oxocin (**19**).* Compound **13a** (35 mg) in benzene (13 ml) was refluxed with ethylene glycol (30 mg) and *p*-toluenesulfonic acid (2 mg) for 18 h, water being removed by azeotropization. The solution was worked up as usual to give **19** (34 mg), oil; MS, *m/e* 228 (M^+), 130, and 125; IR, ν_{max} 3460, 1160, 1120, and 1022 cm^{-1}; NMR, δ 1.00 (3H, t, J=7 Hz, CH_3CH_2), 1.46 (2H, m, CH_3CH_2), 2.00 (1H, do d, J=13 and 8 Hz, H at C_4), 2.32 (3H, m, 2H at C_7 and OH), 2.89 (1H, do d, J=13 and 8 Hz, H at C_4), 3.60 (2H, br s, CH_2OH), 3.63 (2H, m, 2H at C_2 and C_8), 3.98 (4H, m, W_H=10 Hz, OCH_2CH_2O), and 5.83 (2H, m, 2H at C_5 and C_6). An analytical sample was prepared by rechromatography. Found: C, 63.35; H, 8.75%. Calcd for $C_{12}H_{20}O_4$: C, 63.13; H, 8.83%.

*cis-2-Ethyl-3,3-ethylenedioxy-3,4,7,8-tetrahydro-2H-oxocin-8-carbaldehyde (**2**).* A viscous mixture, prepared by addition of chromium(VI) oxide (1.0 g) to anhydrous pyridine (1.6 g) in dichloromethane (25 ml) under stirring, was stirred at room temperature for 15 min. To the mixture was added a solution of **19** (0.40 g) in dichloromethane (5 ml), when a tarry black deposit separated immediately. The whole mixture was further stirred for 15 min at room temperature and then decanted. The supernatant solution thus obtained, was washed with 5% aq sodium hydroxide (3×10 ml) and 5% hydrochloric acid (20 ml), dried and evaporated to yield crystalline aldehyde (**2**, 0.39 g), mp 71—73 °C, which was recrystallized from ether and hexane to give **2** (0.35 g), mp 73—74 °C: MS, *m/e* 197 (M^+—CHO) and 168; IR (Nujol), ν_{max} 2820, 1735, 1160, 1140, 1110, and 1025 cm^{-1}; NMR, δ 0.99 (3H, t, J=7 Hz, CH_3CH_2), 1.55 (2H, m, CH_3CH_2), 2.20 and 2.88 (each 1H, do d, J=13, 6 and 13, 8 Hz, 2H at C_4), 2.41 (2H, m, 2H at C_7), 3.64 (1H, do d, J=8 and 5 Hz, H at C_2), 3.70 (1H, t, J=6 Hz, H at C_8), 3.99 (4H, m, OCH_2CH_2O), 5.83 (2H, m, 2H at

C_5 and C_6), and 9.76 (1H, s, CHO). Found: C, 63.88; H, 7.99%. Calcd for $C_{12}H_{18}O_4$: C, 63.70; H, 8.02%.

*cis-2-Ethyl-8-(ethylenedioxymethyl)-3,4,7,8-tetrahydro-2H-oxocin-3-one (**20**), and Its 3,3-Ethylenedithio-(**21**) and 3,3-Ethylenedioxy-(**22**) Derivatives.* A solution of **2** (181 mg) and 1,2-ethanedithiol (74 mg, 1 equiv) in dichloromethane (30 ml) was treated with boron trifluoride etherate (74 mg) for 3 h at 0 °C, and then poured into 5% aq sodium hydrogencarbonate. The dichloromethane solution was washed with saturated brine (2×10 ml), dried and evaporated to leave oil, showing three spots on TLC. The oil was separated into three fractions by column chromatography over silica gel (5 g, benzene). Fractions with higher R_f value gave **21** (11 mg), oil, showing a single spot on TLC; MS, *m/e* 334 (M^+) and 305; IR, ν_{max} 1099, 1065, and 1025 cm^{-1}; NMR, δ 1.12 (3H, t, J=7 Hz, CH_3CH_2), 1.85 (2H, m, CH_3CH_2), 2.31 (1H, do d, J=12 and 8 Hz, H at C_4), 2.56 (2H, m, 2H at C_7), 3.24 and 3.28 (each 4H, br s, $2SCH_2CH_2S$), 3.31 (1H, do d, J=12 and 8 Hz, H at C_4), 3.51 (1H, m, H at C_8), 3.70 (1H, do d, J=9 and 2 Hz, H at C_2), 4.65 (1H, d, J=6 Hz, SCHS), and 5.88 (2H, m, 2H at C_5 and C_6). The compound was obtained from **2** in 80% yield, when 2 equiv of ethanedithiol was used.

Middle fractions gave **20** (122 mg), oil, showing a single spot on TLC; MS, *m/e* 258 (M^+) and 229; IR, ν_{max} 1720, 1645, 1100, and 1020 cm^{-1}; NMR, δ 1.00 (3H, t, J=7 Hz, CH_3CH_2), 1.70 (2H, qui, J=7 Hz, CH_3CH_2), 2.45 (2H, do d, J=7 and 4 Hz, 2H at C_7), 2.86 (1H, do d, J=13 and 6 Hz, H at C_4), 3.21 (4H, s, SCH_2CH_2S), 3.34 (1H, do d, J=7 and 4 Hz, H at C_8), 3.80 (1H, t, J=7 Hz, H at C_2), 3.82 (1H, do d, J=13 and 6 Hz, H at C_4), 4.58 (1H, d, J=8 Hz, SCHS), and 5.70 (2H, m, 2H at C_5 and C_6).

Fractions with lower R_f value afforded **22** (30 mg), oil, showing a single spot; MS, *m e* 302 (M^+) and 273; IR, ν_{max} 1159, 1130, 1103, and 1020 cm^{-1}; NMR, δ 1.04 (3H, t, J=7 Hz, CH_3CH_2), 1.54 (2H, qui, J=7 Hz, CH_3CH_2), 2.15 (1H, do d, J=13 and 6 Hz, H at C_4), 2.45 (2H, m, 2H at C_7), 2.89 (1H, do d, J=13 and 9 Hz, H at C_4), 3.20 (4H, s, SCH_2CH_2S), 3.44 (1H, do do d, J=8, 6.5, and 3 Hz, H at C_8), 3.63 (1H, t, J=7 Hz, H at C_2), 3.95 (4H, m, OCH_2CH_2O), 4.62 (1H, d, J=7 Hz, SCHS), and 5.78 (2H, m, 2H at C_5 and C_6). The compound (**22**) was obtained from **20** in 65% yield by the procedure similar to that used for the conversion of **13a** into **19**.

References

1) Part III, A. Murai, H. Murase, H. Matsue, and T. Masamune, *Tetrahedron Lett.*, **1977**, 2507.

2) T. Irie, M. Suzuki, and T. Masamune, *Tetrahedron*, **24**, 4193 (1968); *Tetrahedron Lett.*, **1965**, 1091.

3) For recent reviews, see, D. J. Faulkner, *Tetrahedron*, **33**, 1421 (1977); W. Fenical, *J. Phycology*, **11**, 245 (1975); E. Premuzic, "Progress in the Chemistry of Organic Natural Products," ed by W. Herz, H. Grisebach, and G. W. Kirby, Springer-Verlag, New York (1971), Vol. 29, p. L. Minale, G. Cimino, S. De Stefano, and G. Sodano, 417; "ibid," ed by W. Hers, H. Grisebach, and G. W. Kirby, Springer-Verlag, New York (1976), Vol. 33, p. 1.

4) T. Masamune and H. Matsue, *Chem. Lett.*, **1975**, 895.

5) T. Masamune, S. Numata, H. Matsue, and A. Matsuyuki, *Bull. Chem. Soc. Jpn.*, **48**, 2294 (1975).

6) T. Masamune, M. Ono, and H. Matsue, *Bull. Chem. Soc. Jpn.*, **48**, 491 (1975).

7) C.-Y. Chen and R. J. W. Leféver, *J. Chem. Soc., B*, **1966**, 539.

8) *Cf.*, C. Ganter, K. Wicher, W. Zwahlen, and K. Schaffner-Sabba, *Helv. Chim. Acta*, **53**, 1618 (1970); P. R. Stapp and J. C. Randall, *J. Org. Chem.*, **35**, 2948 (1970); P. Bucci, G. Lippi, and B. Macchia, *ibid.*, **35**, 913 (1970); R. J. Bishop, L. E. Sutton, M. J. T. Robinson, and N. W. J. Pumphrey, *Tetrahedron*, **25**, 1417 (1969).

9) T. Masamune, H. Matsue, S. Numata, and A. Furusaki, *Tetrahedron Lett.*, **1974**, 3933.

10) *Cf.*, a) T. A. Craff and E. R. Jones, *Tetrahedron*, **26**, 1217 (1970); D. Tabernier and M. Anteunic, *ibid.*, **27**, 1677 (1971); T. M. Moynehan, K. Schofield, R. A. Y. Jones, and A. R. Katritzky, *J. Chem. Soc.*, **1962**, 2637; M. Kotake, I. Kawasaki, T. Okamoto, S. Matsutani, S. Kusumoto, and T. Kaneko, *Bull. Chem. Soc. Jpn.*, **35**, 1335 (1962); S. Ito, J. B. Stothers, and S. M. Kupchan, *Tetrahedron*, **20**, 913 (1964). b) N. S. Bhacca and D. H. Williams, "Application of NMR Spectroscopy in Organic Chemistry," Holden-Day, Inc., San Francisco (1964), p. 21.

11) *Cf.*, N. S. Zefirov, S. V. Rogozina, E. D. Kurkutova, V. Goncharov, and N. V. Belov, *J. Chem. Soc., Chem. Commun.*, **1974**, 260; P. D. Cradwick and G. A. Sim, *J. Chem. Soc., B*, **1971**, 2218; C. Tamura and G. A. Sim, *ibid.*, **1968**, 1241; M. Dobler and J. D. Dunitz, *Helv. Chim. Acta*, **47**, 695 (1964).

12) *Cf.*, W. G. Dauben, M. E. Lorber, N. D. Vietmeyer, R. H. Shapiro, J. H. Duncan, and K. Tomer, *J. Am. Chem. Soc.*, **90**, 4762 (1968); R. H. Shapiro and M. Heath, *ibid.*, **89**, 5734 (1968).

13) R. K. Boekman, Jr. and B. Genam, *Tetrahedron Lett.*, **1974**, 913; A. K. Bose and B. Lal, *ibid.*, **1973**, 3937; J. Hooz and S. S. Gilani, *Can. J. Chem.*, **46**, 86 (1968).

14) *Cf.*, R. Ratcliffe and R. Rodehorst, *J. Org. Chem.*, **35**, 4000 (1970).

Synthetic Studies of Laurencin and Related Compounds. V.[1] Transformation of *cis*-2-Ethyl-8-formyl-3,4,7,8-dihydro-2*H*-oxocin-3-one 3-Ethylene Acetal into (±)-Laurencin

Tadashi MASAMUNE,* Hisashi MURASE, Hajime MATSUE, and Akio MURAI
Department of Chemistry, Faculty of Science, Hokkaido Uuiversity, Sapporo 060
(Received May 11, 1978)

Transformation of the title starting material into (±)-laurencin, which implies synthesis of the natural product, is described. The structure and configuration of synthetic intermediates are defined on the basis of the spectral evidence.

In the preceding paper[1] we reported the synthesis of *cis*-2-ethyl-8-formyl-7,8-dihydro-2*H*-oxocin-3(4*H*)-one 3-ethylene acetal (**1**). The present paper describes transformation of the aldehyde (**1**) into (±)-laurencin (±-**2**),[2a] which constitutes the first synthesis[2b] of a representative member of a group of naturally occurring halogeno compounds with (a) medium-sized cyclic ether skeleton(s) as well as an enyne moiety.[3]

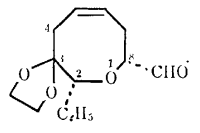

1

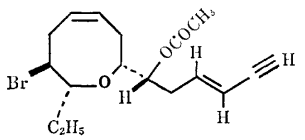

2

The transformation requires (i) conversion of the C_3-carbonyl group protected as the ethylene acetal in **1** into a bromine atom with the desired configuration (*trans* to the C_2-ethyl group), and (ii) that of the C_8-formyl into a 1-acetoxy-3-hexen-5-ynyl group (**3**). The former transformation (i) would probably proceed smoothly, apart from the yield, as had been illustrated in the synthesis of *t*-3-bromo-*r*-2,*c*-8-diethyl-3,4,7,8-tetrahydro-2*H*-oxocin[4] (**3**). On the other hand, many preparative methods for enyne units (-CH=CH-C≡CH) have recently been reported,[5] because the groups are characteristic of a number of natural products. A survey of literatures reveals that procedures applicable to the latter transformation (ii) are classified into three categories as shown in Scheme 1. The first route (iia) consists of at least two steps and involves groups of -CH(OR)CH_2CH=CHX (R=H or Ac, and X= Br, I, Cu, B, and so on) as the intermediates (**A**), which would be converted smoothly into the aimed group by various elegant methods[5a] (step 2). However, preparation of the intermediates (**A**), *e.g.*, by reaction of 3-halogeno-2-propenyl anions with the formyl group of **1** or by addition of 2-propynyl anion to the group followed by hydroboration, appeared to be considerably difficult owing to the possibility of allylic rearrangement or facile hydroboration to the *cis*-double bond in **1**.[6] This conceivable trouble led us to undertake syntheses by other routes.

The second route (iib) concerns the Grignard-type reaction of the formyl group with pentenynyl anions, obtained from 2-penten-4-ynyl halides and metals (Mg, Zn, and so on).[7] However, the reaction was reported to proceed with allylic rearrangement to give 2-ethynyl-1-hydroxy-3-butenyl groups, none of the products formed by expected addition of 2-penten-4-ynyl groups

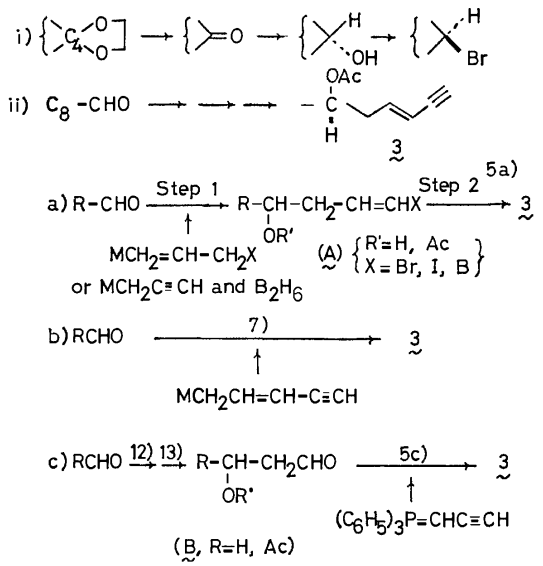

Scheme 1. Possible routes from the aldehyde (**1**) into (±)-laurencin (±**2**).

being detected.[7] Nevertheless, in view of the fact that only a small amount of the starting aldehyde (**1**) is available, the route was very attractive in the sense of one-step synthesis of the aimed group, and the following model experiments were carried out. 2-Penten-4-yn-1-ol[8] (**4**) was converted into the pentenynyl phenyl sulfide (**5**) by reaction of the corresponding bromide[8] with sodium benzenethiolate, or into the 5-trimethylsilypentenynyl phenyl sulfide (**5a**) by bromination of 5-trimethylsilyl-2-penten-4-yn-1-ol[9] (**4a**) followed by reaction with sodium thiophenolate. Treatment of butanal with trimethylsilypentenynyl anions, prepared by reaction of **5a** with butyllithium (1 mol equiv) in tetrahydrofuran (THF) at −30 °C in the presence of 1,4-diazabicyclo[2.2.2]octane (Dabco),[10] at −50 °C for 1 h and subsequent removal of the trimethylsilyl group of the resultant addition products led to formation of a 1:5 (estimated by NMR) mixture of the expected alcohol, 5-phenylthio-6-nonen-8-yn-4-ol (**6**), and its rearranged isomer (**7**) in 26% yield from **5a**. On the other hand, the same treatment of butanal with pentenynyl anions, prepared from **5** and butyllithium (2 mol equiv) under almost the same conditions, produced a 1:1 mixture of **6** and **7** in 49% yield, from which *trans*-isomer (***t*-6**) and *cis*-isomer (***c*-7**) were isolated as the main products of the respec-

tive diastereoisomers. Compound ***t*-6** exhibited the following spectra as expected: UV, λ_{max} 217 nm (ε 16000); NMR, δ 2.96 (1H, d, 2 Hz, C≡C<u>H</u>), 5.32 and 6.10 (each 1H, do d, J=16 and 2 Hz, *trans*-C<u>H</u>=C<u>H</u>). The improved yield of **6** would be caused by *dianionic* character formed from the reactant (**5**). However, attempted selective reduction of the phenylthio group, *e.g.*, the Birch reduction, catalytic hydrogenation over Raney nickel, chemical treatment with aluminium amalgam or zinc and acetic acid, and so on, all failed; the reactions resulted in reduction of the triple bond or recovery of the starting material.

R^1CH_2-CH=CH-C≡CR^2

4 R^1=OH, R^2=H

4a R^1=OH, R^2=$Si(CH_3)_3$

5 R^1=SC_6H_5, R^2=H

5a R^1=SC_6H_5, R^2=$Si(CH_3)_3$

C_3H_7-CH(OH)-CH(SC_6H_5)-CH=CH-C≡CH

6

C_3H_7-CH(OH)-CH(C≡CH)-CH=CH-SC_6H_5

7

The desired transformation was achieved by the final route (iic), a stepwise synthesis by a modification of the Corey procedure.[5c] Before proceeding with the title aldehyde (**1**), several preliminary model experiments were carried out. The route (iic) in Scheme 1 involves β-acetoxy aldehydes as the key intermediates (**B**). Reaction of 3-acetoxy-3-phenylpropanal[11] (**8**), one of the β-acetoxy aldehydes, with triphenyl(3-trimethylsilyl-2-propynylidene)phosphorane at −78 °C in THF proceeded smoothly *without elimination of acetic acid* to give a trimethylsilyl enyne compound (**9a**) in 58% yield, which on treatment with sodium hydroxide followed by acetylation afforded acetoxy *trans*-hexenyne (**9**) in 77% yield. The NMR spectrum was consistent with the structure: δ 2.80 (1H, d, J=2 Hz, C≡C<u>H</u>), 5.50 and 6.10 (each 1H, do d and do t, J=16, 2 and 16, 7, 7 Hz, *trans*-C<u>H</u>=C<u>H</u>). The route (iic) also requires extension of a formyl group to 1-acetoxy-3-oxopropyl group(s), β-acetoxy aldehyde(s) (**B**). Treatment of 3,4-dihydro-2*H*-pyran-2-carbaldehyde ("acrylaldehyde dimer") (**10**), which possesses an ether oxygen atom at β-position to the formyl group and hence is suitable for a model compound of the title aldehyde (**1**), with dimethylsulfinylmethanide in dimethyl sulfoxide (DMSO) or with dimethylsulfonium methanide in DMSO and THF,[12] produced a mixture of diastereoisomeric 2-(epoxyethyl)-dihydropyrans (**11**) in 34 or 17% yield, respectively. The low yields would result from instability of the "acrylaldehyde dimer." Hydrogenation of **11** over platinum gave 2-(epoxyethyl)tetrahydropyrans (**12**), which on further treatment with 2-lithio-1,3-dithiane in THF at −50——20 °C[11,13] followed by acetylation afforded β-acetoxy aldehyde trimethylene dithioacetals (**13**) in 62% yield from **11**. The 1,3-dithiane (**13**) was smoothly hydrolyzed with mercury(II) oxide and boron trifluoride etherate to give β-acetoxy aldehydes (**14**) in 83% yield, which in turn was converted by the same treatment as described above into the corresponding acetoxy hexenynes (**15**) in 48% yield. The NMR spectrum indicated the *trans*-configuration of the double bond in question: δ 5.52 and 6.20 (each 1H, do d and do t, J=16, 2, and 16, 7, 7 Hz). The successful result of these model experiments led us to apply these methods for construction of the relevant side chain of laurencin (**2**).

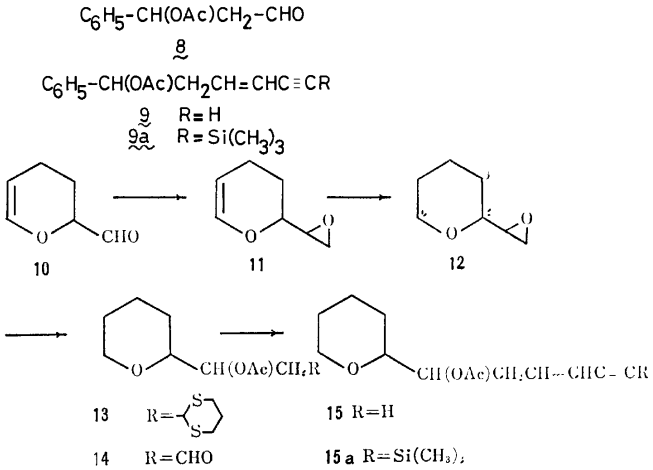

Treatment of the title tetrahydrooxocincarbaldehyde (**1**) with dimethylsulfinylmethanide in DMSO at room temperature[12] afforded epoxyethyl hydrooxocin (**16**), mp 87—88 °C, showing a single spot by GLC and TLC, in 66% yield, as a sole isolable epoxide. In the NMR spectrum the epoxy protons appeared with the C_8-proton as two multiplets at δ 2.72 and 3.25. The epoxide (**16**), when treated with 2-lithio-1,3-dithiane in THF at −70——20 °C,[13] was converted into 2-(2-hydroxyalkyl)-1,3-dithiane (**17**), which was isolated as its acetate (**17a**), mp 161—162 °C, in 80% yield. Fortunately, the acetoxymethine proton was observed at δ 5.24 with almost the same splitting pattern (do t, J=9, 4, and 4 Hz) as that (δ 4.98, do t, J=8, 5, and 5 Hz) of laurencin[2a] (**2**), indicating that the relevant acetoxymethine carbon atom possesses the same relative configuration as the corresponding carbon in the natural product (**2**). Treatment of the dithiane (**17a**) with mercury(II) oxide and boron trifluoride etherate in 15% aqueous THF at room temperature[11] effected only hydrolysis of the 1,3-dithiano-2-yl group to yield β-acetoxy aldehyde (**18**), which was immediately submitted to the Wittig reaction with triphenyl(3-trimethylsilyl-2-propynylidene) phosphorane, prepared from triphenyl(3-trimethylsiliyl-2-propynyl)-phosphonium bromide and butyllithium (1 mol equiv) in THF.[5c] The reaction took place without elimination of acetic acid as expected to give acetoxy *trans*-trimethylsilylhexenyne (**19a**), which was converted readily into acetoxy *trans*-hexenyne (**19**), oil, in 94% yield, by treatment with ammonium fluoride in *N,N*-dimethylformamide (DMF) at room temperature.[5c,14] In good accord with the assigned structure and configuration, compound **19** exhibited parent and fragmentation peaks at *m/e* 334 and 274 in the mass spect-

rum and also absorption maxima at 223 and 230 nm (ε 13000 and 10500) and at 3300, 2110, 1740, 1645, 1247, 1160, 1105, 1027, and 960 cm^{-1} in the UV and IR spectra, respectively. The NMR spectrum confirmed the structure: δ 0.98 (3H, t, J=7 Hz, $CH_2C\underline{H}_3$), 2.03 (3H, s, $OCOC\underline{H}_3$), 2.80 (1H, d, J=2 Hz, C≡C$\underline{H}$), 2.50 and 3.50 (6H and 2H, each m, $3C\underline{H}_2CH{=}CH$, and 2H at C_2 and C_8), 3.93 (4H, m, $OC\underline{H}_2C\underline{H}_2O$), 5.01 [1H, do t, J=9, 4, and 4 Hz, C$\underline{H}$(OAc)], 5.50 and 6.14 (each 1H, do d and do t, J=15, 2, and 15, 8, 8 Hz, *trans*-C$\underline{H}$=C$\underline{H}$), and 5.78 (2H, m, *cis*-C$\underline{H}$=C$\underline{H}$). A series of the reactions from the aldehyde (**1**) to the acetoxy hexenyne (**19**) *via* the epoxide (**16**) implies synthesis of the C_8-side chain (**3**) of laurencin (**2**).

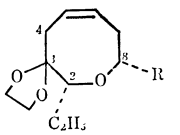

1 R=CHO

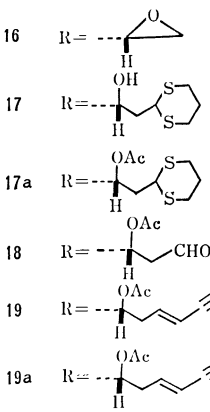

16 R= ···

17 R= ···

17a R= ···

18 R= ···

19 R= ···

19a R= ···

The final stage of laurencin synthesis consists in introduction of a bromine atom at C_3 with the *trans*-configuration to the ethyl group at C_2. Deacetalization of the tetrahydrooxocinone ethylene acetal (**19**) with *p*-toluenesulfonic acid in aqueous acetone under reflux proceeded smoothly to give ketone (**20**), oil, in 74% yield, which displayed a new absorption maximum at 1720 cm^{-1} and also a one-proton double doublet (J=11 and 8 Hz) at δ 3.86 due to one of the two C_4-protons.[1,4] Reduction of the ketone (**20**) with sodium borohydride in methanol at 0 °C[1,4] produced a mixture of alcohols, from which a major alcohol (**21**), oil, with three *cis*-oriented substituents at C_2, C_3, and C_8 of the hydrooxocin ring, and a minor alcohol (**22**), oil, a C_3-epimer of **21**, could be isolated in 50 and 30% yields, respectively. The configurations of the hydroxyl groups at C_4 in the respective compounds (**21** and **22**) were deduced by analogy of the NMR data with those of the corresponding diethyltetrahydrooxocins[4] and related compounds;[1] namely, the hydroxymethine proton in question of the former (**21**) appeared as a broad signal with half-width of 20 Hz at δ 3.64, while the corresponding proton of the latter (**22**) was observed as a clear double triplet with J= 9, 3, and 3 Hz at δ 3.72.[1,4] Contrary to the expectation that the bromination would take place easily, the major alcohol (**21**), when treated with triphenylphosphine and tetrabromomethane in dichloromethane at room temperature,[4,15] gave a complex mixture. However, an aimed bromo compound, mp 45—47 °C, could be isolated after careful chromatography in 14% yield along with the starting material (**21**, 20%). The bromo compound exhibited the following spectra: MS, *m/e* 356, 354 (M^+), 296, and 294; IR, ν_{max} 3285, 2100, 1735, 1230, 1168, 1080, 1035, and 950 cm^{-1}; NMR, δ 0.98 (3H, t, J=7 Hz, $CH_2C\underline{H}_3$), 2.03 (3H, s, $OCOC\underline{H}_3$), 2.83 (1H, d, J=2 Hz, C≡C$\underline{H}$), 4.07 (1H, do t, J=9, 3, and 3 Hz, C$\underline{H}$Br), 4.98 [1H, do t, J=8, 5, and 5 Hz, C$\underline{H}$(OAc)], 5.52 and 6.15 (each 1H, do d and do t, J=15, 2, and 15, 7, 7 Hz, *trans*-C$\underline{H}$=C$\underline{H}$), and 5.90 (2H, m, *cis*-C$\underline{H}$=C$\underline{H}$). These spectra were completely identical with those of natural laurencin (**2**), indicating completion of the synthesis of (±)-laurencin. The overall yield amounted to 1.1% from the tetrahydrooxocincarbaldehyde.

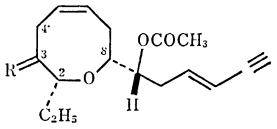

19 R=OCH_2CH_2O
20 R=O
21 R=···OH, —H
22 R=—OH, ···H
±2 R=—Br, ···H

Experimental

All the mps and bps were uncorrected. The homogeneity of each compound was always checked by TLC over silica gel (Wakogel B-5) and/or GLC (Hitachi K-53) over 10% SE-30. Column chromatography was carried out over silicic acid (Merck, Kieselgel 60, 70—230 mesh) and/or alumina (Merck, Standard, Active I and II—III). The UV, IR, and NMR (100 MHz) spectra were measured in ethanol, in liquid state, and in chloroform-*d*, respectively, unless otherwise stated. The abbreviations "s, d, t, sex, m, br, do, and sh," in the NMR and IR spectra denote "singlet, doublet, triplet, sextet, multiplet, broad, double, and shoulder," respectively.

*2-Penten-4-ynyl Phenyl Sulfides (**5**) and Their Trimethylsilyl Derivatives (**5a**).* *a)*: Into a suspension of sodium thiophenolate in THF, prepared from sodium hydride (96 mg) and benzenethiol (424 mg) in THF (5 ml), was added a 1:1 mixture of *cis*- and *trans*-2-penten-4-ynyl bromides[8] (290 mg) in THF (1 ml) at 0 °C under stirring. The mixture was stirred at room temperature for 2 h, then mixed with water (10 ml) and extracted with ether (3×10 ml). The ether solution was washed with water, 5% aq potassium hydroxide and water, dried over sodium sulfate (or magnesium sulfate) and evaporated to leave yellow oil (466 mg). The oil was purified by chromatography over silica gel (20 g) with benzene and hexane (1:4) to give *cis*- and *trans*-pentenynyl phenyl sulfides (***c*-5**, 62 mg, and ***t*-5**, 86 mg) with the mixture (82 mg), bp 85—90 °C/2 Torr: ***c*-5**, MS, *m/e* 174 (M^+), 109, 77, and 65; IR, ν_{max} 3280, 2090, 1687, and 775 cm^{-1}: NMR, δ 3.13 (1H, d, J=2 Hz, C≡C$\underline{H}$), 3.79 (2H, d, J=8 Hz, $C\underline{H}_2$), 5.50 and 6.00 (each 1H, do d and do t, J=10, 2, and 10, 8, 8 Hz, *cis*-C$\underline{H}$=C$\underline{H}$), and 7.30 (5H, m, $C_6\underline{H}_5$): ***t*-5**, MS, *m/e* 174, 109, 77, and 65;

IR, ν_{max} 3286, 2096, 1687, and 954 cm^{-1}; NMR, δ 2.84 (1H, d, J=2 Hz), 3.55 (2H, d, J=7 Hz), 5.48 and 6.22 (each 1H, do d and do t, J=15, 2 and 15, 7, 7 Hz), and 7.30 (5H, m).

b): Into an ice-cooled solution of 5-trimethylsilyl-2-penten-4-yn-1-ol alcohol[9] (**4a**) in ether (3 ml) containing pyridine (0.2 ml) was added dropwise phosphorus tribromide (1.9 g) in ether (3 ml) during a period of 15 min. The mixture was stirred at room temperature for 75 min and then mixed with ether (50 ml). The whole solution was washed with water, 5% aq sodium hydrogen carbonate and saturated brine, dried over magnesium sulfate, evaporated and then distilled to yield the corresponding bromides (2.0 g, *cis*:*trans*=1 : 2), which were used for the next reaction without further purification.

Into a suspension of sodium benzenethiolate, prepared from sodium hydride (72 mg) and thiophenol (330 mg) in THF (7 ml), was added the bromide mixture (300 mg) in THF (1 ml). The mixture was stirred at room temperature for 2 h and then worked up as described in (a) to leave oil (396 mg), which was purified by chromatography over silica gel (20 g, hexane) to give *cis*- and *trans*-isomers (***c*-5a**, 77 mg and ***t*-5a**, 177 mg) with the mixture (28 mg), bp 98—100 °C/2 Torr: ***c*-5a**, MS, *m/e* 246 (M^+), 173, 137, 109, 73, and 59; IR, ν_{max} 2146, 1690, 1250, and 760 cm^{-1}; NMR, δ 0.22 [9H, s, $Si(C\underline{H}_3)_3$], 3.80 (2H, d, J=8 Hz, $C\underline{H}_2$), 5.52 and 5.94 (each 1H, do d and do t, J=10, 2 and 10, 8, 8 Hz, *cis*-$C\underline{H}$=$C\underline{H}$), and 7.20 (5H, m, $C_6\underline{H}_5$): ***t*-5a**, MS, *m/e* 246, 173, 137, 109, 73, and 59; IR, ν_{max} 2136, 1685, 1240, and 953 cm^{-1}; NMR, δ 0.18 (9H, s), 3.55 (2H, d, J=7 Hz), 5.54 and 6.18 (each 1H, J=16, 2, and 16, 7, 7 Hz), and 7.26 (5H, m).

*5-Phenylthio-6-nonen-8-yn-4-ols (**6**) and 1-Phenylthio-3-ethynyl-1-hepten-4-ols (**7**).* *a)* Into a solution of 1:1 mixture of ***c*-5** and ***t*-5** (870 mg, 5 mmol) in THF (50 ml) containg Dabco (560 mg, 5 mmol) was added butyllithium (12 mmol) in a 15% hexane solution (6.7 ml) at −30 °C under stirring. The mixture was further stirred for 1 h at −30—−20 °C, and cooled to −50 °C. Butanal (0.45 ml, excess) was added to the cooled solution and stirred at −50—−30 °C for 30 min and then at −30—−20 °C for 30 min. The reaction mixture was poured into water (200 ml) and extracted with ether (3×100 ml). The ether solution was washed with water and saturated brine, dried and evaporated to leave oil (1.2 g), which was purified by chromatography over silica gel (40 g, benzene) to give a 1:1 mixture (452 mg) of **6** and **7** with the starting material (**5**, 220 mg). A part (60 mg) of the mixture was further separated by preparative TLC (Wakogel B-5F, benzene) to yield a *trans*-isomer (***t*-6**, 25 mg) and a *cis*-isomer (***c*-7**, 5 mg) in pure state: ***t*-6**, MS, *m/e* 246 (M^+); UV, λ_{max} 217 nm (ε 16000); IR, ν_{max} 3400, 3280, 2090, 1600, and 958 cm^{-1}; NMR, δ 0.92 (3H, br s, $C\underline{H}_3$), 1.52 (4H, m, $C\underline{H}_2C\underline{H}_2$), 2.54 (1H, s, O$\underline{H}$), 2.86 (1H, d, J=2 Hz, C≡C$\underline{H}$), 3.6 (2H, br m, $C\underline{H}$(OH) and $C\underline{H}(SC_6H_5)$], 5.32 and 6.10 (each 1H, do d, J=16, 2, and 16, 10 Hz, *trans*-$C\underline{H}$=$C\underline{H}$), and 7.30 (5H, m, $SC_6\underline{H}_5$): ***c*-7**, MS, *m/e*, 246; UV, λ_{max} 266 nm (ε 10000); IR, ν_{max} 3420, 3096, 2114, and 1678 cm^{-1}; NMR, δ 0.94 (3H, br s), 2.56 (4H, m), 2.20 (1H, J=2 Hz), 3.66 (2H, br m), 5.80 and 6.30 (each 1H, do d and d, J=10, 10, and 10 Hz, *cis*-$C\underline{H}$=$C\underline{H}$), and 7.35 (5H, m).

b): Into a solution of a 1:2 mixture of ***c*-5a** and ***t*-5a** (492 mg, 2 mmol) in THF (20 ml) containing Dabco (224 mg, 2 mmol) was added butyllithium (2.4 mmol) in 15% hexane (1.36 ml) at −30 °C. The solution was stirred for 1 h at −30—−20 °C and cooled to −50 °C. Butanal (0.45 ml, excess) in THF (0.5 ml) was added to the cooled solution and stirred as described in (a). The reaction mixture was worked up as usual to leave oil (827 mg), which was purified by chromatography over silica gel (30 mg, benzene) to give acetylene compounds (307 mg). A part (80 mg) of the mixture in methanol (2.5 ml) was treated with 5 M aq sodium hydroxide (0.13 ml) at room temperature (25 °C) for 5 min. The reaction mixture was neutralized by addition of 2 M hydrochloric acid, evaporated and extracted with ether (2×50 ml). The ether solution was worked up as usual to leave oil (51 mg), which was separated by preparative TLC over silica gel with benzene and ethyl acetate (9 : 1) to yield a 1 : 5 mixture (by NMR) of **6** and **7** (30 mg) and **5** (10 mg). The mixture was not further purified.

*trans-1-Pheny-3-hexen-5-yn-1-yl Acetate (**9**) and Its 6-Trimethylsilyl Derivative (**9a**).* Into a suspension of triphenyl-(3-trimethylsilyl-2-propynyl)phosphonium bromide[5c] (305 mg, 0.67 mmol) in THF (5 ml) cooled at −78 °C was added butyllithium (0.78 mmol) in 15% hexane (0.5 ml) under stirring. The mixture was stirred at −45—−40 °C for 30 min and cooled to −78 °C. 3-Oxo-1-phenylpropyl acetate[11] (**8**, 87 mg, 0.45 mmol) in THF (0.8 ml) was added to the cooled mixture and stirred at ice-bath temperature for 1 h. On addition of hexane (20 ml) the reaction mixture formed precipitates, which were removed by filtration. The procedure was repeated three times to give brown oil (150 mg), which was separated by chromatography (1.5 g, benzene) to yield **9a** (78 mg), oil; MS, *m/e* 280 (M^+) and 226; IR, ν_{max} 2150, 1748, 1245, 1233, 1085, 1025, and 955 cm^{-1}; NMR, δ 0.16 [9H, s, $Si(C\underline{H}_3)_3$], 2.04 (3H, s, $OCOC\underline{H}_3$), 2.62 (2H, br t, J=7 Hz, $C\underline{H}_2$), 5.52 and 6.02 (each 1H, br d and do t, J=7 and 16, 7, 7 Hz, *trans*-$C\underline{H}$=$C\underline{H}$), 5.74 (1H, t, J=7 Hz, $C\underline{H}$(OAc)], and 7.26 (5H, s, $C_6\underline{H}_5$). The sample was rechromatographed for analysis. Found: C, 71.11; H, 7.71%. Calcd for $C_{17}H_{22}O_2Si$: C, 71.28; H, 7.74%.

Compound **9a** (43 mg) in methanol (1.5 ml) was stirred with 5 M sodium hydroxide (0.75 ml) at room temperature for 10 min. The mixture was acidified with 2 M hydrochloric acid, extracted with hexane repeatedly. The hexane solution was worked up as usual to give crude alcohol (25 mg). The alcohol (22 mg) was treated with acetic anhydride (0.2 ml) and pyridine 0.5 ml to give crude acetate, which was purified by preparative TLC (benzene) to yield **9** (22 mg), oil, in pure state: MS, *m/e* 154 (M^+−CH_3COOH); IR, ν_{max} 3300, 2100, 1748, 1230, and 958 cm^{-1}; NMR, δ 2.08 (3H, s, $OCOC\underline{H}_3$), 2.66 (2H, t, J=7 Hz, $C\underline{H}_2$), 2.80 (1H, d, J=1.5 Hz, C≡C$\underline{H}$), 5.50 and 6.10 (each 1H, br d and do t, J=16 and 16, 7, 7 Hz, *trans*-$C\underline{H}$=$C\underline{H}$), 5.77 [1H, t, J=7 Hz, $C\underline{H}$(OAc)], and 7.28 (5H, s, $C_6\underline{H}_5$). Found: C, 78.47; H, 6.50%. Calcd for $C_{14}H_{14}O_2$: C, 78.48; H, 6.58%.

*2-(Epoxyethyl)-3,4-dihydropyranes (**11**).* *a)*: A suspension of sodium hydride (0.06 mol) (50% mineral oil dispersion, 2.9 g) and trimethyloxosulfonium iodide (13.2 g, 0.06 mol) in dry DMSO (60 ml) was stirred at room temperature under sitrring for 10 min, when evolution of hydrogen stopped. A solution of 3,4-dihydro-2*H*-pyran-2-carbaldehyde (**10**, 5.6 g, 0.05 mol) in DMSO (5 ml) was added to the aforementioned dimethylsufinylmethanide solution during a period of 5 min and then stirred at room temperature for 1.5 h. The reaction mixture was mixed with water (130 ml) and extracted with ether (4×100 ml). The ether solution was washed with water and saturated brine, dried, evaporated and distilled to give **11** (2.16 g), bp 68—70 °C/15 Torr; MS, *m/e* 126 (M^+), 83, and 43; IR, ν_{max} 1646, 1237, and 1070 cm^{-1}; NMR, δ 2.00 (4H, br, m, 4H at C_3

and C_4), 2.80 and 3.25 (2H and 1H, each m, 3H in epoxyethyl), 3.65 (1H, m, H at C_2), 4.70 and 6.35 (each 1H, m, CH=CH). Found: C, 66.15; H, 7.99%. Calcd for $C_6H_8O_2$: C, 66.65; H, 7.99%.

b): Into a solution of sodium methylsulfinylmethanide, prepared by treatment of DMSO (60 ml) with sodium hydride (0.06 mol) (50% mineral oil dispersion, 2.9 g) at 80 °C for 1 h, was added THF (60 ml) and then a solution of trimethylsulfonium iodide (12.4 g, 0.06 mol) in DMSO at 0 °C during a period of 5 min under stirring. To the resultant dimethylsulfonium methanide solution was added **10** (5.6 g, 0.05 mol) in DMSO (5 ml), and the whole solution was stirred at room temperature for 1 h. The reaction mixture was poured into water and extracted with ether (4×200 ml). The ether solution was worked up as usual to give **11** (1.04 g), bp 64—68 °C/15 Torr. The NMR spectrum showed complex signals similar to those of **11** obtained in (a), indicating both the samples (**11**) to be a mixture of diastereoisomers. In the following experiments were used the sample (**11**) obtained in the section (a).

*2-(Epoxyethyl)-3,4,5,6-tetrahydropyrans (**12**).* Compounds **11** (2.1 g) were hydrogenated over platinum (60 mg as $PtO_2 \cdot H_2O$) for 14.5 h, when 430 ml (1.02 mol equiv) of hydrogen had been consumed. After removal of the catalyst, the solution was evaporated and distilled to give oil (**12**, 1.7 g), bp 70—74 °C, showing a single spot on TLC; MS, *m/e* 128 (M^+) and 85; IR, ν_{max} 1255, 1110, 1094, and 1050 cm^{-1}; NMR, δ 1.60 (6H, br m, 6H at C_3, C_4 and C_5), 2.80 and 2.95 (2H and 1H, each m, 3H at C_2 and C_6). Found: C, 65.22; H, 9.64%. Calcd for $C_7H_{12}O_2$: C, 65.60; H, 9.44%.

*3-Oxo-1-(2-tetrahydropyranyl)propyl Acetate (**14**) and Its 1,3-Trimethylene Dithioacetal (**13**).* *a)*: To a solution of 2-lithio-1,3-dithiane in THF, prepared from 1,3-dithiane (1.41 g, 11.7 mmol) and butyllithium (14 mmol) in THF (45 ml) at −30——20 °C for 2 h, was added **12** (1.5 g, 11.7 mmol) in THF (2 ml) under cooling at −60 °C. The mixture was stirred at −50——30 °C for 1 h, at −30——20 °C for 1 h, and then at −20 °C for 16 h, and mixed with ether (150 ml). The ether solution was worked up as usual to leave amorphous residue (3.1 g), which was purified by chromatography over silica gel (90 g, benzene) to yield white solid (2.2 g). A part (54 mg) was further purified by preparative TLC to give solid substance (43 mg), showing a single spot on TLC. The solid (43 mg) was converted under usual conditions into the acetate (**13**), oil; MS, *m/e* 290 (M^+), 230, 119, and 85; IR, ν_{max} 1742, 1240, and 1090 cm^{-1}; NMR, δ 1.50 (6H, m, 6H at C_3, C_4, and C_5), 2.20 (2H, m, $SCH_2CH_2CH_2S$), 2.11 (3H, s, $OCOCH_3$), 2.85 (4H, m, $SCH_2CH_2CH_2S$), 3.42 and 4.00 (each 2H, m, 3H at C_2 and C_6, and SCHS), and 5.18 [1H, m, CH(OAc)].

Into a suspension of mercury(II) oxide (0.6 g) and boron trifluoride etherate (0.35 ml) in 15% aq THF (4 ml) was added **13** (0.20 g, 6.9 mmol) in THF (0.2 ml) under stirring during a period of 15 min. The mixture was stirred at room temperature for 1 h. On addition of ether (10 ml) to the mixture, precipitates were separated and removed by filtration. The filtrate was washed with 10% aq sodium carbonate and saturated brine, dried and evaporated to give oil [crude **14** (0.115 g)], which was used for the next reaction without further purification: IR, ν_{max} 2760, 1746, 1240, 1095, and 1045 cm^{-1}; NMR, δ 2.08 (3H, s, $OCOCH_3$), 2.76 (2H, m, CH_2CHO), 5.30 [1H, do t, J=3, 6 and 6 Hz, CH(OAc)], 9.66 (1H, t, J=1.5 Hz, CHO).

*1-(2-Tetrahydropyranyl)-3-hexen-5-ynyl Acetate (**15**) and Its Trimethylsilyl Derivative (**15a**).* *a)*: Into a suspension of triphenyl(3-trimethylsilyl-2-propynyl)phoshonium bromide (0.34 g, 0.75 mmol) in THF (5 ml) cooled at −70 °C was added butyllithium (0.78 mmol) (15% hexane solution, 0.5 ml) under stirring. The mixture was stirred at −40——30 °C for 30 min and again cooled to −70 °C. Aldehyde **14** (0.11 g, 0.55 mmol) in THF (0.5 ml) was added to the cooled mixture, stirred at the temperature for 5 min and then at ice-bath temperature for 1 h. On addition of hexane (20 ml), precipitates were formed and removed by filtration. The procedure was repeated three times to yield oil (0.145 g), which was purified by chromatography over silica gel (4.5 g, benzene) to give **15a** (0.124 g), colorless oil; MS, *m/e* 294 (M^+), 234, and 85; IR, ν_{max} 2170, 1748, 1248, 1235, 1090, 1050, 1040, and 960 cm^{-1}; NMR, δ 0.16 [9H, s, $Si(CH_3)_3$], 2.04 (3H, s, $OCOCH_3$), 2.44 (2H, t, J=7 Hz, CH_2CH=CH), 4.80 [1H, m, CH(OAc)], 5.52 and 6.10 (each 1H, br d and do t, J=16 and 16, 7, 7 Hz, *trans*-CH=CH). Found: C, 64.92; H, 8.82%; Calcd for $C_{16}H_{28}O_3S$: C, 65.26; H, 8.90%.

b): A solution of **15a** (60 mg, 0.2 mmol) in methanol (2 ml) was stirred with 5 M aq sodium hydroxide (1 ml) at room temperature for 5 min. The solution was made acidic by addition of 2 M hydrochloric acid and extracted with hexane (4×2 ml). The hexane solution was worked up as usual to give alcohol (35 mg), oil. The oil was acetylated under usual conditions and purified by preparative TLC over silica gel to give **15** (39 mg), oil; MS, *m/e* 222 (M^+) and 162; IR, ν_{max} 3300, 2100, 1748, 1240, 1100, 1050, and 960 cm^{-1}; NMR, δ 1.52 (6H, m, $CH_2CH_2CH_2$), 2.03 (3H, s, $OCOCH_3$), 2.48 (2H, t, J=7 Hz, CH_2CH=CH), 2.82 (1H, d, J=2 Hz, C≡CH), 3.35 and 4.00 (2H and 1H, each m, CH_2OCH), 4.86 [1H, do t, J=12, 6, and 6 Hz, CH(OAc)], 5.52 and 6.20 (each 1H, do d and do t, J=16, 2 and 16, 7, 7 Hz, *trans*-CH=CH). Found: C, 69.97; H, 8.02%. Calcd for $C_{13}H_{18}O_3$: C, 70.24; H, 8.16%.

*cis-2-Ethyl-8-epoxyethyl-3,4,7,8-dihydro-2H-oxocin-3-one 3-Ethylene Acetal (**16**).* A suspension of sodium hydride (3.12 mmol) (50% mineral oil dispersion, 0.15 ml) and trimethyloxosulfonium iodide (690 mg, 3.12 mmol) in DMSO (15 ml) was stirred at room temperature under nitrogen. A solution of **1** (593 mg, 2.6 mmol) in DMSO (5 ml) was added dropwise to the dimethylsulfinylmethanide solution and stirred at room temperature for 1 h. The reaction mixture was mixed with water (50 ml) and extracted with ether (3×20 ml) and then with ethyl acetate (2×20 ml). All the organic solutions were combined, washed with water (3×20 ml) and saturated brine, dried and evaporated to leave oil (555 mg), which was purified by chromatography over silica gel (12 g, benzene:ethyl acetate=9:1) to give **16** (418 mg), white solid. A part (145 mg) was crystallized and recrystallized from hexane and ether for analysis to give a pure sample (128 mg), mp 87—88 °C; MS, 240 (M^+) and 211; IR (Nujol), ν_{max} 1648, 1380, 1252, 1162, 1107, and 1080; NMR, δ 1.00 (3H, t, J=7 Hz, CH_2CH_3), 1.44 (2H, m, CH_2CH_3), 2.72 and 3.25 (2H and 1H, each m, 3H in epoxyethyl), 2.94 (1H, do d, J=13 and 8.5 Hz, H at C_4), 3.60 (1H, do d, J=7 and 6 Hz, H at C_2), 4.00 (4H, m, OCH_2CH_2O), and 5.82 (2H, m, *cis*-CH=CH). Found: C, 64.98; H, 8.39%. Calcd for $C_{13}H_{20}O_4$: C, 64.86; H, 8.31%.

*cis-2-Ethyl-8-[1-hydroxy-2-(1,3-dithian-2-yl)ethyl]-3,4,7,8-tetrahydro-2H-oxocin-3-one 3-Ethylene Acetal (**17**) and Its Acetate (**17a**).* To a solution of 2-lithio-1,3-dithiane in THF, prepared from 1,3-dithiane (418 mg, 3.48 mmol) and butyllithium (4.2 mmol) (15% hexane solution, 2.8 ml) at −30——20 °C for 2 h under stirring, was added dropwise **16** (418 mg, 1.74 mmol) in THF (3 ml) at −70 °C. The mix-

ture was stirred at −20 °C for 14 h, and shaken with ether (50 ml) and saturated brine (20 ml). After separation of the ether solution, the aqueous solution was extracted with chloroform (3×20 ml). All the ether and chloroform solutions were combined, washed with saturated brine, dried and evaporated to leave oil (822 mg), which was purified by chromatography over silica gel (30 g, benzene) to give **17** (564 mg), viscous oil. The oil was treated with acetic anhydride (5.6 ml) and pyridine (12 ml) at room temperature overnight and then worked up as usual to give **17a** (557 mg), mp 145—150 °C. A part (66 mg) of the sample was recrystallized from benzene and hexane for analysis to yield **17a** (45 mg), mp 161—162 °C, in pure state; MS, *m/e* 402 (M^+), 373, and 342; IR (Nujol), ν_{max} 1740, 1640, 1230, 1125, 1110, and 1090 cm^{-1}; NMR, δ 1.00 (3H, t, J=7 Hz, $CH_2C\underline{H}_3$), 1.38 (2H, m, $C\underline{H}_2CH_3$), 2.03 (3H, s, $OCOC\underline{H}_3$), 3.50 (2H, m, 2H at C_2 and C_8), 3.90 (5H, m, $OC\underline{H}_2C\underline{H}_2O$ and $SC\underline{H}S$), 5.24 [1H, do t, J=9, 4 and 4 Hz, $C\underline{H}$(OAc)], and 5.74 (2H, m, *cis*-$C\underline{H}$=$C\underline{H}$). Found: C, 56.79; H, 7.51%. Calcd for $C_{19}H_{30}O_5S_2$: C, 56.69; H, 7.51%.

cis-*8-(1-Acetoxy-3-oxopropyl)-2-ethyl-3,4,7,8-tetrahydro-2H-oxocin-3-one 3-Ethylene Acetal (**18**).* To a vigorously stirred mixture of mercury(II) oxide (387 mg, 1.79 mmol) and boron trifluoride etherate (0.22 ml, 1.79 mmol) in 15% aq THF (2.4 ml) was added **17a** (240 mg, 0.597 mmol) in THF (2 ml) at room temperature during a period of 10 min. The mixture was stirred for 15 min at room temperature and mixed with ether (10 ml). After removal of precipitates by filtration, the reaction mixture (filtrate) was washed with saturated aq sodium carbonate and then with saturated brine, dried and evaporated to leave oily substance (**20**, 111 mg), which was used for the next reaction without further purification; NMR, 2.08 (3H, s, $OCOC\underline{H}_3$), 4.00 (4H, m, $OC\underline{H}_2C\underline{H}_2O$), 5.54 [1H, do t, J=8, 4, and 4 Hz, $C\underline{H}$(OAc)], 5.86 (2H, m, *cis*-$C\underline{H}$=$C\underline{H}$), and 9.78 (1H, t, J=2 Hz, $C\underline{H}O$).

cis-*8-(1-Acetoxy-6-trimethylsilyl-3-hexen-5-ynyl)-2-ethyl-3,4,7,8-tetrahydro-2H-oxocin-3-one 3-Ethylene Acetal (**19a**).* Into a suspension of triphenyl (3-trimethylsilyl-2-propynyl)phosphonium bromide (242 mg, 0.534 mmol) in THF (2 ml) cooled at −78 °C was added butyllithium (0.543 mmol) (15% hexane solution, 0.33 ml). The mixture was stirred at −40 °C for 30 min and again cooled to −78 °C. A solution of **18** (111 mg, 0.356 mmol) in THF (1.5 ml) was added to the cooled mixture, and the whole mixture was stirred at ice-bath temperature for 1 h. After addition of ether, precipitates were formed and removed by filtration. The filtrate was evaporated to leave oil, which was separated by preparative TLC over silica gel (benzene:ethyl acetate=10:1) to give **19a** (99 mg), oil, showing a single spot on TLC; MS, *m/e* 406 (M^+), 391, 363, and 346; UV, λ_{max} 227 nm (ε 16600), 236 (22700), and 246 (17000); IR, ν_{max} 2160, 1740, 1248, and 960 cm^{-1}; NMR, δ 0.15 [9H, s, $Si(C\underline{H}_3)_3$], 2.05 (3H, s, $OCOC\underline{H}_3$), 3.50 (2H, m, 2H at C_2 and C_8), 3.94 (4H, m, $OC\underline{H}_2C\underline{H}_2O$), 5.02 [1H, do t, J=9, 4, and 4 Hz, $C\underline{H}$(OAc)], 5.45 and 6.08 (1H, br d and do t, J=15 and 15, 7, 7 Hz, *trans*-$C\underline{H}$=$C\underline{H}$), and 5.80 (2H, m, *cis*-$C\underline{H}$=$C\underline{H}$). Found: C, 64.55; H. 8.49%. Calcd for $C_{22}H_{24}O_5Si$: C, 64.98; H, 8.43%.

cis-*8-(1-Acetoxy-3-hexen-5-ynyl)-2-ethyl-3,4,7,8-tetrahydro-2H-oxocin-3-one 3-Ethylene Acetal (**19**).* A solution of **19a** (166 mg, 0.419 mmol) in DMF (17 ml) was treated with ammonium fluoride (1.7 g, excess) at room temperature under stirring. The reaction mixture was treated with water (40 ml) and extracted with ether (3×50 ml). The combined ether solution was worked up as usual to leave oil (190 mg), which was purified by preparative TLC (benzene:ethyl acetate=10:1) to give **19a** (130 mg), oil, showing a single spot on TLC; MS, UV, IR, and NMR, in the text. Found: C, 68.13; H, 7.87%. Calcd for $C_{19}H_{26}O_5$: C, 68.24; H, 7.84%.

cis-*8-(1-Acetoxy-3-hexen-5-ynyl)-2-ethyl-3,4,7,8-tetrahydro-2H-oxocin-3-one (**20**).* A solution of **19** (120 mg, 0.359 mmol) in acetone (50 ml) and water (8 ml) was heated with *p*-toluenesulfonic acid (90 mg, 0.474 mmol) under reflux for 24 h. After being cooled, the reaction mixture was treated with water (50 ml) and extracted with ethyl acetate (3×300 ml). The acetate solution was washed with 5% aq sodium hydrogencarbonate and saturated brine, dried and evaporated to leave oil (144 mg), which was purified by preparative TLC (benzene:ethyl acetate=10:1) to give **20** (31 mg), oil, and the starting acetal (**19**, 68 mg); MS, *m/e* 290 (M^+) and 230; UV, λ_{max} 322 nm (ε 194), 310 (279), 300 (300), 293 (323), 230 (sh) (11400), and 224 (14000); IR, ν_{max} 3310, 2110, 1740, 1720, 1236, and 960 cm^{-1}; NMR, δ 0.96 (3H, t, J=8 Hz, $CH_2C\underline{H}_3$), 2.06 (3H, s, $OCOC\underline{H}_3$), 2.81 (1H, d, J=2 Hz, C≡$C\underline{H}$), 3.44 (1H, m, H at C_8), 3.72 (1H, t, J=7 Hz, H at C_2), 3.86 (1H, do d, J=11 and 8 Hz, H at C_4), 5.00 [1H, do t, J=8, 5, and 5 Hz, $C\underline{H}$(OAc)], 5.52 and 6.14 (each 1H, do d and do t, J=15, 2, and 15, 7, 7 Hz, *trans*-$C\underline{H}$=$C\underline{H}$), and 5.64 (2H, m, *cis*-$C\underline{H}$=$C\underline{H}$). Found: C, 69.98; H, 7.91%. Calcd for $C_{17}H_{22}O_4$: C, 70.32; H, 7.64%.

r-*2*,c-*8-(1-Acetoxy-3-hexen-5-ynyl)-3,4,7,8-tetrahydro-2H-oxocin-3-ol and Its 3-Epimer (**22**).* Compound **20** (36 mg, 0.12 mmol) was treated with $NaBH_4$ (18 mg) in methanol (3 ml) at 0 °C for 20 min. The reaction mixture was made acidic with 2 M hydrochloric acid, concentrated and extracted with ethyl acetate (5×3 ml). The acetate solution was worked up as usual to leave oil (52 mg), showing two spots on TLC, which was separated by preparative TLC (benzene:ethyl acetate=4:1) to yield **22** (11 mg), oil, and **21** (18 mg), oil, as less and more polar fractions: **21**, MS, *m/e* 292 (M^+), 274, and 232; IR, ν_{max} 3440, 3300, 2120, 1740, 1645, 1235, 1130, 1075, 1048, 1030, and 960 cm^{-1}; NMR, δ 0.92 (3H, t, J=7 Hz, $CH_2C\underline{H}_3$), 1.86 (1H, br s, O$\underline{H}$), 2.05 (3H, s, $OCOC\underline{H}_3$), 2.82 (1H, d, J=2 Hz, C≡$C\underline{H}$), 3.40 (2H, m, 2H at C_2 and C_8), 3.64 [1H, br, W_H=20 Hz, $C\underline{H}$(OH)], 4.98 [1H, do t, J=8, 5, and 5 Hz, $C\underline{H}$(OAc)], 5.52 and 6.16 (each 1H, do d and do t, J=16, 2, and 16, 7, 7 Hz, *trans*-$C\underline{H}$=$C\underline{H}$), and 5.74 (2H, m, *cis*-$C\underline{H}$=$C\underline{H}$): **22**, MS, *m/e* 292 (M^+), 274, and 232; IR, ν_{max} 3440, 3300, 2110, 1740, 1235, 1120, 1090, 1070, 1050, 1025, and 960 cm^{-1}; NMR, δ 0.98 (3H, t, J=7.5 Hz, $CH_2C\underline{H}_3$), 2.05 (3H, s, $OCOC\underline{H}_3$), 2.80 (1H, d, J=2 Hz, C≡$C\underline{H}$), 3.10 and 3.44 (each 1H, m, 2H at C_2 and C_8), 3.72 [1H, do t, J=9, 3, and 3 Hz, $C\underline{H}$(OH)], 4.98 [1H, do t, J=8, 5, and 5 Hz, $C\underline{H}$(OAc)], 5.52 and 6.16 (each, 1H, do d and do t, J=15, 2, and 15, 7, 7 Hz, *trans*-$C\underline{H}$=$C\underline{H}$), and 5.58 (2H, m, *cis*-$C\underline{H}$=$C\underline{H}$).

r-*2*,c-*8-(1-Acetoxy-3-hexen-5-ynyl)*-t-*3-bromo-3,4,7,8-tetrahydro-2H-oxocin Acetate [(±)-**2**].* Into a solution of **21** (15 mg, 0.05 mmol) and tetrabromomethane (125 mg, 0.375 mmol) in dichloromethane (4 ml) was added dropwise triphenylphosphine (65 mg, 0.25 mmol) in dichloromethane (6 ml, dried through Molecular Sieves 4A) at room temperature under stirring during a period of 3 h, and the whole solution was stirred at room temperature for 12 h. The reaction mixture was evaporated to leave resinous material, which was purified by preparative TLC (benzene) to yield (±)-**2** (2 mg), which crystallized spontaneously and had mp 45—47 °C, with the starting alcohol (**21**, 3 mg). The spectral data (described in the text) were com-

pletely identical with natural laurencin (MS, UV, IR, NMR, and TLC).

References

1) Part IV, T. Masamune, H. Matsue, and H. Murase, *Bull. Chem. Soc. Jpn.*, **52**, 127 (1979).

2) a) T. Irie, M. Suzuki, and T. Masamune, *Tetrahedron*, **24**, 4193 (1968); *Tetrahedron Lett.*, **1965**, 1091; b) For a preliminary communication of the present paper, see; A. Murai, H. Murase, H. Matsue, and T. Masamune, *Tetrahedron Lett.*, **1977**, 2507.

3) For a recent review, see, D. J. Faulkner, *Tetrahedron*, **33**, 1421 (1977). *Cf.*, Ref. 3 in the preceding paper.

4) T. Masamune, S. Numata, H. Matsue, A. Matsuyuki, T. Sato, and H. Murase, *Bull. Chem. Soc. Jpn.*, **48**, 2294 (1975).

5) a) A. O. King, N. Okukado, and E. Negishi, *J. Chem. Soc., Chem. Commun.*, **1977**, 683; E. Negishi and A. Abramovitch, *Tetrahedron Lett.*, **1977**, 411; E. Negishi, R. M. Williams, A. Lew, and T. Yoshida, *J. Organomet. Chem.*, **92**, C4, (1975); J. F. Normant, A. Commercon, and J. Villieras, *Tetrahedron Lett.*, **1975**, 1465; E. Negishi, G. Lew, and T. Yoshida, *J. Chem. Soc., Chem. Commun.*, **1973**, 874; b) A. B. Holmes, R. A. Raphael, and N. K. Wellard, *Tetrahedron Lett.*, **1976**, 1539, J. M. Laborits, C. A. Henrick, and V. L. Corbin, *Tetrahedron Lett.*, **1975**, 4209; These procedures appear not to be applicable to the present transformation. c) E. J. Corey and R. A. Ruden, *Tetrahedron Lett.*, **1973**, 1495.

6) *Cf.* H. C. Brown and A. W. Moerikofer, *J. Am. Chem. Soc.*, **85**, 2063 (1963); **83**, 3417 (1961). G. M. L. Cragg, "Organoboranes in Organic Synthesis," M. Dekker, New York (1973), p. 73.

7) L. Migniac, Ph. Migniac, and Ch. Prevost, *Bull. Soc. Chim. Fr.*, **1965**, 3560.

8) H. B. Henbest, E. R. H. Jones, and I. M. S. Walls, *J. Chem. Soc.*, **1950**, 3650.

9) J. S. Cochrane and J. R. Hanson, *J. Chem. Soc., Perkin Trans. 1*, **1972**, 361.

10) *Cf.*, P. M. Atlani, J. F. Biellmann, S. Dube, and J. J. Vicens, *Tetrahedron Lett.*, **1974**, 2665.

11) E. Vedejs and P. L. Fuchs, *J. Org. Chem.* **36**, 366 (1971).

12) E. J. Corey and M. Chaykovsky, *J. Am. Chem. Soc.*, **87**, 1353 (1965).

13) D. Seebach and E. J. Corey, *J. Org. Chem.*, **40**, 231 (1975); E. J. Corey and D. Crouse, *ibid.*, **33**, 298 (1968); D. Seebach, N. R. Jones, and E. J. Corey, *ibid.*, **33**, 300 (1968).

14) J. Drouin, F. Leyendecker, and J. M. Conia, *Tetrahedron Lett.*, **1975**, 4053.

15) R. K. Boekman, Jr., and B. Genam, *Tetrahedron Lett.*, **1974**, 913; A. K. Bose and B. Lal, *ibid.*, **1973**, 3937; J. Hooz and S. S. Gilani, *Can. J. Chem.* **46**, 86 (1968).

The σ-Bonded Palladium(II) Complex of (Dimethylaminomethyl)ruthenocene

Shin-ichi KAMIYAMA,* Tetsuo KIMURA, Akira KASAHARA,† Taeko IZUMI,† and Mitsugi MAEMURA†

Government Industrial Research Institute, Tohoku, Nigatake, Haranomachi, Sendai 983

†*Department of Applied Chemistry, Faculty of Engineering, Yamagata University, Yonezawa 992*

(Received May 31, 1978)

The reaction between (dimethylaminomethyl)ruthenocene with lithium tetrachloropalladate(II) in the presence of sodium acetate gave di-μ-chloro-bis[2-(dimethylaminomethyl)ruthenocenyl]dipalladium(II) (**2**). The σ-bonded structure of **2** has been confirmed by IR analysis and the reactions of **2** with triphenylphosphine, thallium(I) acetylacetonate, and lithium aluminum deuteride. The reactions of chloro[2-(dimethylaminomethyl)ruthenocenyl](triphenylphosphine)palladium(II) with carbon monoxide and **2** with methyl vinyl ketone, phenyl vinyl ketone, and styrene have been examined. 1, 2-Disubstituted ruthenocene derivatives have been obtained in higher yields than those of the corresponding ferrocene derivatives.

Cope has reported the first intramolecular *ortho*-palladation of azobenzene[1] and *N,N*-dimethylbenzylamine.[2] For the regiosclective syntheses of *ortho*-substituted aromatic compounds, there has been considerable interest in the intramolecular *ortho*-metalation by transition metals of aromatic compounds containing donor ligands such as nitrogen, phosphorus and sulfur.[3] In addition, the reactions of ferrocene derivatives with palladium(II) halides have been studied.[4] Generally, there have been few synthetic investigations of the ruthenocenes in contrast to those of the ferrocenes. This paper will deal with the intramolecular *ortho*-palladation of (dimethylaminomethyl)ruthenocene and the reactions of the palladium complexes.

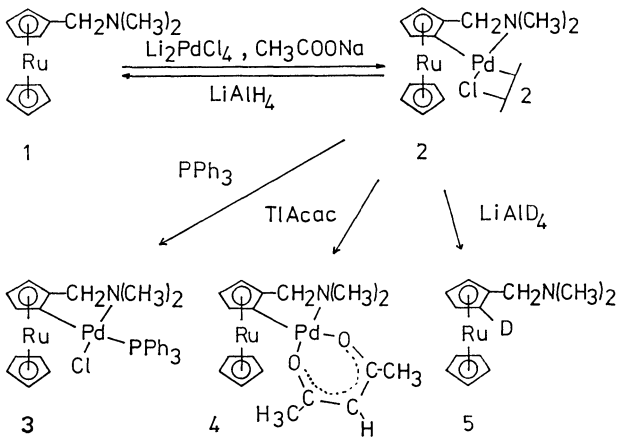

Fig. 1. Syntheses of palladium(II) complexes.

Results and Discussion

The reaction between (dimethylaminomethyl)-ruthenocene (**1**) with lithium tetrachloropalladate(II) in the presence of sodium acetate[5] gave di-μ-chloro-bis[2-(dimethylaminomethyl)ruthernocenyl]dipalladium(II) (**2**) in 78% yield. The complex **2** was shown to be an intramolecularly *ortho*-palladated complex on the basis of the reactions of **2** and the microanalytical and spectroscopic results. Measurement of the molecular weight using a vapor pressure osmometer was not conducted because of the low solubility of **2** in all common solvents. The treatment of **2** with triphenylphosphine and thallium(I) acetylacetonate afforded the monomeric triphenylphosphine (**3**) and acetylacetonate (**4**) complexes, respectively (Fig. 1). In the IR spectrum of **2**, the three bands at 323, 258, and 216 cm^{-1} have been assigned to the bridged Pd–Cl stretching absorption.[6] The single band at 357 cm^{-1} of **3** has been assigned to the terminal Pd–Cl stretching absorption. Thus, it has been confirmed that **2** is a typical chlorine-bridged binuclear complex. The low solubility of **2** in all common solvents precluded any NMR studies at room temperature. However, the ^1H NMR spectra of **3** and **4** clearly demonstrated that a palladium-carbon σ bond and a palladium-nitrogen coordinated bond existed in these complexes (Table 1). *N*-Methyl and *N*-methylene protons of **1** appear as a singlet, whereas the *N*-methyl protons appear as two broad singlets and the *N*-methylene protons as two doublets in **3** and **4**. The non-equivalence of the *N*-methyl and *N*-methylene protons in **3** and **4** can be explained in terms of a cyclic system in which the nitrogen is coordinated to the palladium and a palladium-carbon σ bond is involved.[7] To ascertain the formation of the σ-bond between pal-

Table 1. The ^1H NMR spectra of complexes **3** and **4** (δ)

Compound	-N-CH_3	Rc-CH_2-N-	Ruthenocene ring proton	Others
Pd complex (**3**)	2.97 (br s)[b]	3.74 (d)[c,e]	4.3—4.4 (m)[d]	7.2—7.7 (m) PPh_3
	3.07 (br s)	4.02 (d)[e]		
Pd complex (**4**)	2.82 (s)[a]	3.13 (d)[f]	4.3—4.7 (m)	1.91 (s) CH_3 of acac group
	3.02 (s)	3.52 (d)[f]		5.21 (s) -CH- of acac group
(Dimethylaminomethyl)-ruthenocene (**1**)	2.20 (s)	3.10 (s)	4.5—4.6 (m)	

a) Singlet. b) Broad singlet. c) Doublet. d) Multiplet. e) J=1.8 Hz. f) J=7.8 Hz.

Table 2. The ^1H NMR spectra of 1,2-disubstituted ruthenocenes (δ)

Ruthenocene	-N-CH_3	Rc-CH_2-N-	Ruthenocene ring proton	Others
1-(2-Acetylvinyl)-2-(dimethylaminomethyl)- (**6**)	2.15 (s)[a]	3.08 (d)[b] 3.37 (d) (J=14 Hz)	H_a 4.70 (m)[d] H_b 4.92 (m) H_c 4.70 (m) H_d 4.45 (s)	2.18 (s, -$COCH_3$) 6.32 (d, J=16 Hz, -C=CH-CO-) 7.40 (d, J=16 Hz, Rc-CH=C-CO-)
1-(2-Benzoylvinyl)-2-(dimethylaminomethyl)- (**7**)	2.16 (s)	3.09 (d) 3.42 (d) (J=13 Hz)	H_a 4.71 (m) H_b 4.98 (m) H_c 4.71 (m) H_d 4.45 (s)	7.16 (d, J=16 Hz, -C=CH-CO-) 7.51 (d, J=16 Hz, Rc-CH=C-CO-) 7.3—8.0 (m, Ph)
1-(Dimethylaminomethyl)-2-styryl- (**8**)	2.18 (s)	3.12 (d) 3.39 (d) (J=13 Hz)	H_a 4.60 (m) H_b 4.91 (m) H_c 4.60 (m) H_d 4.43 (s)	6.63 (d, J=16 Hz, -C=CH-Ph) 6.85 (d, J=16 Hz, Rc-CH=C-Ph) 7.1—7.3 (m, Ph)
1-(Dimethylaminomethyl)-2-(ethoxycarbonyl)- (**9**)	2.4—3.1 (m)		H_a 4.85 (m) H_b 5.18 (m) H_c 4.85 (m) H_d 4.60 (s)	1.25 (t[c], J=6 Hz, CH_3 of COOEt) 2.4—3.1 (m, -CH_2- of COOEt)

a) Singlet. b) Doublet. c) Triplet. d) Multiplet.

ladium and the cyclopentadienyl ring in **2**, **3**, and **4**, **2** was reduced with lithium aluminum deuteride to give 1-(dimethylaminomethyl)ruthenocene-2-*d* (**5**) quantitatively. Again, the starting material (**1**) was obtained by the lithium aluminum hydride reduction of **2**. The presence of deuterium in **5** was established by a comparison of the ^1H NMR and mass spectra of **5** with those of the undeuterated sample (**1**). The intramolecular palladation of α-aryl nitrogen derivatives gave the *ortho*-palladated complexes.[3,4] It appears therefore that the deuterium exists at the *ortho*-position of the dimethylaminomethyl group in **5**.

The evidence indicates a five-membered chelate-ring exists between palladium and the ruthenocene moiety in **2**, **3**, and **4**. A simple model for **2**, **3**, and **4** suggests that the chelate-ring may be five-membered rather than six-membered. This conclusion has been unambiguously supported by the reactions of **2** and **3** with various reagents (Fig. 2). The reactions of *ortho*-palladation products from numerous α-aryl nitrogen derivatives with carbon monoxide,[8] halogens,[9] alkyllithium,[10] Grignard reagents,[10] and olefins[11] have been reported. Recently, the *ortho*-palladation complexes of ferrocene derivatives have been converted into a variety of 1,2-disubstituted ferrocenes.[4,12] Complexes **2** and **3** failed to react with bromine or butyllithium. However, **2** reacted with methyl vinyl ketone, phenyl vinyl ketone and styrene in the presence of triethylamine to readily give 1-alkenyl-2-(dimethylaminomethyl)ruthenocenes (**6**, **7**, **8**) in 89—94% yields. The yields of these ruthenocene derivatives were higher than those of the corresponding ferrocene derivatives.[12] 1-(Dimethylaminomethyl)-2-(ethoxycarbonyl)ruthenocene (**9**) was obtained by the carbonylation of **3** in ethanol; the carbonylation of **2** was unsuccessful. The ^1H NMR, IR, and mass spectra of these products were all consistent with those of the proposed structures.

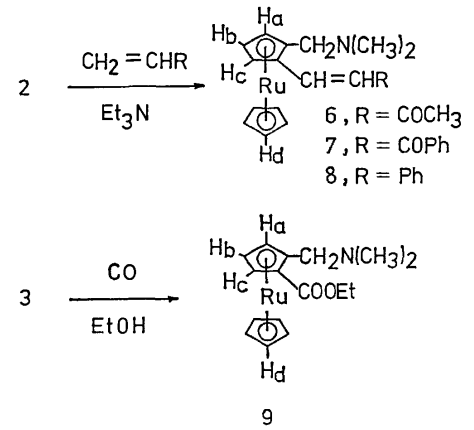

Fig. 2. Reactions of palladium(II) complexes.

1,2-Disubstituted ferrocenes exhibited one peak, while the 1,3-isomers showed two peaks in the region near 900 cm^{-1}, as the characteristic absorption band of

Table 3. Properties and analyses of 1,2-disubstituted ruthenocenes (**6**—**9**)

6	Pale yellow oil. Found: C, 57.18; H, 5.80; N, 3.74%. Calcd for $C_{17}H_{21}NORu$: C, 57.40; H, 5.92; N, 3.91%; mol wt, 356. IR(Nujol): 1655 (C=O); 1615, 965 cm^{-1} (*trans* -CH=CH-). MS: M^+ 356.
7	Pale yellow heavy oil. Found: C, 63.28; H, 5.41; N, 3.16%. Calcd for $C_{22}H_{23}NORu$: C, 63.52; H, 5.53; N, 3.34%; mol wt, 418. IR(Nujol): 1660 (C=O); 1605, 965 cm^{-1} (*trans* -CH=CH-). MS: M^+ 418.
8	Pale yellow oil. Found: C, 64.22: H, 4.80; N, 3.37%. Calcd for $C_{21}H_{23}NRu$: C, 64.59; H, 4.93; N, 3.58%; mol wt, 390. IR(Nujol): 1625, 955 cm^{-1} (*trans* -CH=CH-). MS: M^+ 390.
9	Pale yellow oil. Found: C, 53.15; H, 5.71: N, 3.66%. Calcd for $C_{16}H_{21}NO_2Ru$: C, 53.32; H, 5.87; N, 3.88%; mol wt, 360. IR(Nujol): 1715 cm^{-1} (COOEt). MS: M^+ 360.

the C–H out-of-plane bending mode on the ferrocene ring.[13] The IR spectra of compounds **6**, **7**, **8**, and **9** showed one peak at *ca.* 910 cm^{-1}. The infrared frequencies of the C–H bending modes of ruthenocene are similar to those of ferrocene.[14] Taking the evidences into account, it has been confirmed that **6**, **7**, **8**, and **9** are 1,2-disubstituted ruthenocenes. Furthermore, in the ^1H NMR spectra of **6**, **7**, and **8**, the *N*-methylene protons appear as doublets in contrast to those of **1** containing no substituent at the *ortho*-position of the dimethylaminomethyl group (Tables 1 and 2). This result, intimating the steric heterogeneity of the *N*-methylene protons in **6**, **7**, and **8**, supports the above conclusions. The coupling constnats of the doublets corresponding to olefinic protons are 16 Hz, and the absorption bands of the C=C linkage are located at *ca.* 1600 and 960 cm^{-1} in **6**, **7**, and **8** (Tables 2 and 3). This indicates that the olefinic protons occupy a *trans* position relative to each other.

Experimental

Materials. All the melting points are uncorrected. (Dimethylaminomethyl)ruthenocene (**1**) was prepared according to the method described by Hofer and Schlögl.[15]

Measurements. The ^1H NMR spectra were determined in $CDCl_3$ with a JEOL JNM-PMX-60 spectrometer (60 MHz) and a Hitachi R-22 spectrometer (90 MHz) at room temperature. All the chemical shifts are expressed in δ (ppm; downfield from the internal standard Me_4Si). The IR spectra were measured using KBr disks, Nujol mulls (4000—650 cm^{-1}) and Nujol mulls mounted on thin polythene windows (700—200 cm^{-1}) with Hitachi 215 and ÉPI-L spectrometers. The mass spectra were obtained on a JEOL JMS-07S mass spectrometer and a Hitachi RMU-6M mass spectrometer, using a direct insertion probe at an ionization energy of 70 eV. The molecular weight was determined in $CHCl_3$ with a Hitachi 115 vapor pressure osmometer.

Di-μ-chloro-bis[2-(dimethylaminomethyl)ruthenocenyl]dipalladium(II) (2). A mixture of lithium tetrachloropalladate(II) (2.28 g, 8.7 mmol) and sodium acetate trihydrate (1.18 g, 8.7 mmol) in ethanol (50 ml) was stirred for 20 min at room temperature. To the reaction mixture, a solution of (dimethylaminomethyl)ruthenocene (**1**) (2.5 g, 8.7 mmol) in ethanol (100 ml) was added, and the mixture was stirred for 5 min at room temperature. The yellow precipitate was filtered and dried, and the crude product was column-chromatographed on silica gel. The first band, eluted with chloroform, yielded di-μ-chloro-bis[2-(dimethylaminomethyl)-ruthenocenyl]dipalladium(II) (**2**) (2.9 g, 78%). The solid (**2**) was insoluble in all common solvents; mp 163—166 °C (dec). IR(Nujol): 323, 258, and 216 cm^{-1} (bridged Pd–Cl).

Chloro[2-(dimethylaminomethyl)ruthenocenyl](triphenylphosphine)-palladium(II) (3). A mixture of the complex **2** (1.9 g, 2.2 mmol) and triphenylphosphine (1.16 g, 4.4 mmol) in benzene (50 ml) was stirred for 12 h at room temperature. After removal of the solvent *in vacuo*, the column chromatography of the residue on silica gel (chloroform) gave chloro[2-(dimethylaminomethyl)ruthenocenyl](triphenylphosphine)palladium(II) (**3**) (2.7 g, 88%); mp 220—225 °C (dec) (chloroform). IR(Nujol): 357 cm^{-1} (terminal Pd–Cl). Found: C, 53.84; H, 4.39; N, 2.20%. Calcd for $C_{31}H_{31}ClRuPPd$: C, 53.85; H, 4.52; N, 2.03%; mol wt, 691.

Acetylacetonato[2-(dimethylaminomethyl)ruthenocenyl]palladium(II) (4). A suspension of the complex **2** (1.0 g, 1.16 mmol) and thallium(I) acetylacetonate (0.07 g, 2.3 mmol) in benzene (50 ml) was stirred for 3 h at room temperature, and filtered. The filtrate was evaporated *in vacuo*, and the residue was purified by column chromatography on silica gel (chloroform) to give acetylacetonato[2-(dimethylaminomethyl)ruthenocenyl]palladium(II) (**4**) (0.68 g, 60%); mp 162—165 °C(dec) (chloroform). IR(KBr): 1620 and 1550 cm^{-1} (acac group). Found: C, 43.66; H, 4.75; N, 2.91%. Calcd for $C_{18}H_{23}RuNPd$: C, 43.87; H, 4.70; N, 2.84%; mol wt, 493.

Reduction of Complex 2 with Lithium Aluminum Hydride. A mixture of the complex **2** (1.0 g, 1.16 mmol) and lithium aluminum hydride (0.044 g, 1.16 mmol) in dry ether (100 ml) was stirred for 4 h at room temperature. After the addition of moist ether and water, the reaction mixture was extracted three times with ether which had been washed with water and brine, and then dried over anhydrous sodium sulfate. The removal of the solvent gave **1** in 95% yield as brownish plates from petroleum ether; mp 38—41 °C (lit,[15] 39—42 °C). The ^1H NMR, IR, and mass spectra of **1** were consistent with those of an authentic sample.

Reduction of Complex 2 with Lithium Aluminum Deuteride. The reduction of the complex **2** (1.0 g) with lithium aluminum deuteride (0.044 g) in dry ether (100 ml) was conducted under the same conditions as in the proceeding experiment. After recrystallization from petroleum ether, the product (mp 39—42 °C) was identified as 1-(dimethylaminomethyl)ruthenocene-2-*d* (**5**) on the basis of the following evidence: ^1H NMR($CDCl_3$): δ 2.20 (s, 6H, $-N(CH_3)_2$); 3.10 (s, 2H, $-CH_2-$); 4.5—4.6 ppm (m, 8H, ruthenocene ring protons). MS: M^+ 289. Found: C, 54.08; H, 5.43; N, 4.91%. Calcd for $C_{13}H_{16}DRuN$: C, 53.96; H, 5.57; N, 4.84%; mol wt, 289.

General Procedure for the Reaction of Complex 2 with Olefins. In a closed vessel, a mixture of the complex **2** (1.0 g, 1.16 mmol) and an olefin (5 mmol) and triethylamine (0.30 g, 3 mmol) in toluene (50 ml) was stirred for 5 h at 80 °C under a nitrogen atmosphere. The reaction mixture was cooled and filtered to remove precipitated palladium, and the filtrate was evaporated *in vacuo*. The residue was dissolved in chloroform which had been washed with water and brine, and dried over anhydrous magnesium sulfate. After removal of the solvent, purification of the crude product by column chromatography (silica gel–chloroform) gave 1-alkenyl-2-(dimethylaminomethyl)ruthenocenes (**6**, **7**, **8**) in 91, 89, and 94% yields, respectively.

Carbonylation of Complex 3 in Ethanol. In an autoclave, a suspension of the complex **3** (1.3 g, 1.9 mmol) in ethanol (50 ml) was stirred for 50 h at 100 °C under a carbon monoxide pressure of 80 atm. The reaction mixture was filtered to remove precipitated palladium, and the filtrate was evaporated *in vacuo*. The residue was dissolved in chloroform and column chromatographed on silica gel (chloroform) to afford 1-(dimethylaminomethyl)-2-(ethoxycarbonyl)ruthenocene (**9**) (0.27 g, 40%). The structure of the 1,2-disubstituted ruthenocenes has been confirmed by elemental analysis and the ^1H NMR, IR, and mass spectra (Tables 2 and 3).

References

1) A. C. Cope and R. W. Siekman, *J. Am. Chem. Soc.*, **87**, 3272 (1965).

2) A. C. Cope and E. C. Friedrich, *J. Am. Chem. Soc.*, **90**, 909 (1968).

3) a) P. M. Maitlis, "The Organic Chemistry of Palladium," Academic Press, New York (1971), Vol. 1, p. 82; b) J. Tsuji, *Yuki Gosei Kagaku Kyokai Shi*, **35**, 10 (1977); *ibid.*, **35**, 94 (1977); c) S. I. Murahashi, *Kagaku No Ryoiki*, **31**, 319 (1977).

4) a) H. Alper, *J. Organomet. Chem.*, **80**, C29 (1974); b) J. C. Gaunt and B. L. Shaw, *J. Organomet. Chem.*, **102**, 511 (1975); c) A. Kasahara, T. Izumi, and M. Maemura, *Bull. Chem. Soc. Jpn.*, **50**, 1878 (1977).

5) a) J. M. Duff and B. L. Shaw, *J. Chem. Soc., Dalton Trans.*, **1972**, 219; b) J. M. Duff, B. E. Mann, B. L. Shaw, and B. Turtle, *ibid.*, **1974**, 139.

6) a) K. Nakamoto, "Characterization of Organometallic Compounds," ed by M. Tsutsui, Interscience, New York (1969), Part 1, p. 73; b) G. Davidesen, *Organomet. Chem. Rev. (A)*, **8**, 235 (1971).

7) A. C. Cope, J. M. Kliegman, and E. C. Friedrich, *J. Am. Chem. Soc.*, **89**, 287 (1967).

8) a) H. Takahashi and J. Tsuji, *J. Organomet. Chem.*, **10**, 511 (1967); b) J. M. Thompson and R. F. Heck, *J. Org. Chem.*, **40**, 2667 (1975).

9) a) D. R. Fahey, *Chem. Commun.*, **1970**, 417; b) D. R. Fahey, *J. Organomet. Chem.*, **27**, 283 (1971).

10) a) S. I. Murahashi, Y. Tanabe, M. Yamamura, and I. Moritani, *Tetrahedron Lett.*, **1974**, 3749; b) M. Yamamura, I. Moritani, and S. I. Murahashi, *Chem. Lett.*, **1974**, 1423.

11) a) J. Tsuji, *Acc. Chem. Res.*, **2**, 144 (1969); b) M. Julia, M. Duteil, and J. Y. Lallemand, *J. Organomet. Chem.*, **102**, 239 (1975); c) R. A. Holton, *Tetrahedron Lett.*, **1977**, 355.

12) T. Izumi, K. Endo, O. Saito, I. Shimizu, M. Maemura, and A. Kasahara, *Bull. Chem. Soc. Jpn.*, **51**, 663 (1978).

13) a) K. L. Rinehart, Jr., K. L. Motz, and S. Moon, *J. Am. Chem. Soc.*, **79**, 2749 (1957); b) M. Rosenblum and R. B. Woodward, *ibid.*, **80**, 5443 (1958); c) M. Rosenblum, *ibid.*, **81**, 4530 (1959); d) M. Rosenblum and W. G. Howells, *ibid.*, **84**, 1167 (1962); e) M. Rosenblum, W. G. Howells, A. K. Banerjee and C. Bennett, *ibid.*, **84**, 2726 (1962).

14) E. R. Lippincott and R. D. Nelson, *Spectrochim. Acta*, **10**, 307 (1958).

15) O. Hofer and K. Schlögl, *J. Organomet. Chem.*, **13**, 443 (1968).

Trans-esterification Reaction Catalyzed by Alkoxo(triphenylphosphine)copper(I) Complexes

Minoru KUBOTA, Takakazu YAMAMOTO, and Akio YAMAMOTO*

Research Laboratory of Resources Utilization, Tokyo Institute of Technology, Nagatsuta, Midori-ku, Yokohama 227

(Received June 2, 1978)

Alkoxocopper and phenoxocopper complexes ROCu $(PPh_3)_n$ (PPh_3=triphenylphosphine; n=1 for R=n-C_3H_7 or i-C_3H_7; n=2 for R=CH_3, C_2H_5, CH_2=$CHCH_2$, $C_6H_5CH_2$, or C_6H_5) react with esters undergoing exchange of the RO group with carboxylic esters. The alkoxocopper and phenoxocopper complexes are found to be excellent catalysts for the trans-esterification of carboxylic esters, dimethyl carbonate, and trimethyl phosphite with alcohols and phenols. A comparison of the ability of the isopropoxocopper complex as trans-esterification catalyst with that of aluminum isopropoxide and titanium isopropoxide shows the superiority of the isopropoxocopper complex. The rate of trans-esterification between p-nitrophenyl acetate and phenol follows the second-order rate law $R=k$[p-nitrophenyl acetate][phenol], the activation energy of the reaction being estimated to be 12.4 kcal/mol. A mechanism comprising a nucleophilic attack on the copper-bound carbonyl group of the ester by alcohol is proposed.

Although metal alkoxides and phenoxides are widely utilized as reagents and catalysts for organic syntheses, reports on the utilization of copper alkoxides for organic syntheses are limited.[1] This seems to be due to the availability of only a few stable and well-characterized alkoxocopper and phenoxocopper compounds. In the preceding paper a report was given on the preparation of a series of stable alkoxocopper and phenoxocopper complexes formulated as ROCu-$(PPh_3)_n$ (PPh_3=triphenylphosphine) by the reaction of $CH_3Cu(PPh_3)_2(ether)_{0.5}$ with alcohols and phenol.[2]

In this paper we describe the utilization of the alkoxocopper and phenoxocopper complexes $ROCu(PPh_3)_n$ as the trans-esterification catalyst.

Results and Discussion

Alkoxo and Phenoxo Group Exchange Reactions between $ROCu(PPh_3)_n$ and Esters. Prior to exploration of the catalytic activities of the alkoxocopper and phenoxocopper complexes for trans-esterification, stoichiometric exchange reactions betweeen $ROCu(PPh_3)_n$ and esters were examined in order to find the general trend of the exchange reactions of the RO–Cu complexes against esters. The following exchange reactions were carried out between $ROCu(PPh_3)_n$ and acetic esters:

$$ROCu(PPh_3)_n + CH_3COOR' \xrightarrow{-5\,^\circ C} R'OCu(PPh_3)_n + CH_3COOR \quad (1)$$

R: CH_3(**1a**), C_2H_5(**1b**), n-C_3H_7(**1c**), allyl(**1d**), i-C_3H_7(**1e**), benzyl(**1f**), C_6H_5(**1g**), n=1 for **1c** and **1e**, n=2 for the others, **1a**, **1c**, and **1f** have diethyl ether as the solvent of crystallization. The results are summarized in Table 1.

Yields of the exchanged esters were determined by means of gas chromatography and those of R'OCu-

Table 1. Alkoxo and phenoxo group exchange reaction between $ROCu(PPh_3)_n$ and CH_3COOR'[a]

$ROCu(PPh_3)_n + CH_3COOR' \longrightarrow R'OCu(PPh_3)_n + CH_3COOR$

$ROCu(PPh_3)_n$	%-Yields[b] of products $R'OCu(PPh_3)_n$ and CH_3COOR				
	R'=C_6H_5	R'=vinyl	R'=benzyl	R'=allyl	R'=C_2H_5
R=CH_3 (**1a**)	92 (89)	96 (75)[c]	82 (75)	76 (61)	46 d)
R=C_2H_5 (**1b**)	78 (70)	93 (22)[c]	78 (69)	74 (56)	— —
R=n-C_3H_7 (**1c**)	87 (84)	76 —	75 d)	56 d)	25 d)
R=allyl (**1d**)	96 (91)	32 (15)[c]	48 (50)	— —	20 d)
R=i-C_3H_7 (**1e**)	82 (75)	82 —	51 d)	42 d)	18 d)
R=benzyl (**1f**)	95 (92)	84 (69)	— —	33 d)	17 d)
R=C_6H_5 (**1g**)	—	NO[e]	NO[e]	NO[e]	NO[e]

a) Reaction conditions: −5 °C for 12 h for complexes **1a**—**1f**: room temperature for 12 h for complex **1g**. b) Upper figures, %-yield of CH_3COOR; figures in parentheses, % yield of the isolated $R'OCu(PPh_3)_n$. c) C-Bonded acetoxyvinylcopper complex with formation of acetaldehyde. d) A mixture of the starting complex and produced complex was obtained but separation of the mixture was difficult. e) The starting $PhOCu(PPh_3)_2$ was recovered unreacted after 1—2 days.

$(PPh_3)_n$ were calculated from the weights of the isolated complexes. The starting alkoxocopper and phenoxocopper complexes are arranged in the increasing order of stability of the complexes, **1a**<**1b**<**1c**<**1d**<**1e**<**1f**<**1g**,[2] as judged by the decomposition points of the alkoxocopper complexes. Acetic esters are arranged in the decreasing order of the stability of the produced complexes $R'OCu(PPh_3)_n$.

It is seen that, in most cases, the RO group of $ROCu(PPh_3)_n$ can be exchanged with the R'O group of CH_3COOR' even at −5 °C and the yield of the product apparently depends on the relative stability of the complex $R'OCu(PPh_3)_n$ produced. The considerably high yields of products on employment of vinyl acetate seem to be due to high stability of the six-membered C-bonded acetoxyvinylcopper complex formed in the reaction.[2,3] When the starting complex is very stable such as the phenoxocopper complex **1g**, the exchange reaction with alkyl and alkenyl acetates scarcely proceeds. The reaction of **1c** and **1e** with phenyl acetate gave a new phenoxocopper complex containing only one PPh_3 ligand $C_6H_5OCuPPh_3$, whereas $C_6H_5OCu(PPh_3)_2$ has been obtained by the reaction of $CH_3Cu(PPh_3)_2 \cdot 0.5Et_2O$ with phenol.[2] The alkoxo and phenoxo group exchange reaction between $ROCu(PPh_3)_n$ and ester is not restricted to the esters of acetic acid. Employment of other various alkyl and aryl carboxylates also leads to the exchange reaction below room temperature indicating that the RO ligands bonded to copper have high lability toward the attack of esters.

The alkoxo and phenoxo group exchange reaction on copper may proceed through one of the concerted four center mechanisms as shown by Eqs. 2 and 3 or through an oxidative addition of esters to copper (Eq. 4).

$$CH_3COOR' + ROCuL_n \longrightarrow \text{(I)} \longrightarrow CH_3COOR + R'OCuL_n \quad (2)$$

$$CH_3COOR' + ROCuL_n \longrightarrow \text{(II)} \longrightarrow CH_3COOR + R'OCuL_n \quad (3)$$

$$CH_3COOR' + ROCuL_n \longrightarrow \text{(III)} \longrightarrow CH_3COOR + R'OCuL_n \quad (4)$$

The existence of carboxylic ester-coordinated metal complexes is well known and Lappert showed that the carbonyl group in esters is bonded to metal.[4] Equations 2 and 3 show that the ester coordination to the alkoxocopper complex facilitates the nucleophilic attack on the carbonyl group by the alkoxo group. Since esters can add oxidatively to transition metal compounds such as Ni(0)[5] and Mo(0)[6] complexes with the cleavage of the bond between acyl and alkoxyl groups, the mechanism expressed by Eq. 4 is also conceivable.

Trans-esterification Catalyzed by Alkoxocopper and Phenoxocopper Complexes. Alkoxocopper and phenoxocopper complexes catalyze trans-esterification of carboxylic esters, dialkyl carbonates, and trialkylphosphines under mild conditions. The results are summarized in Table 2.

When an equimolar amount of an ester and an alcohol is used and the free energy change in the trans-esterification is small, as in the ester interchange between methyl carboxylates and ethanol (Table 2, Nos. 1 and 4,), about half of the starting ester is interchanged with alcohol. The extent of ester interchange increases with increase in the amount of alcohol (Nos. 4, 5, and 19). An ester with a bulky alkyl group such as *t*-butyl acetate did not undergo the interchange reaction smoothly (No. 3).

The trans-esterification of alkenyl carboxylates presents a special case. Vinyl acetate and isopropenyl acetate were converted into alkyl acetate in high yields by the exchange reaction with alcohols. In these cases, however, alkenols which may be produced as intermediates are considered to have been converted into their stabler tautomers, acetaldehyde and acetone.

$$CH_2{=}CH(R')(OCOCH_3) + R''OH \xrightarrow{CuOR(PPh_3)_n} CH_2{=}CH(R')(OH) + CH_3COOR'' \quad (5)$$

$$CH_2{=}CH(R')(OH) \longrightarrow CH_3{-}C(=O){-}R'$$

Since the amount of acetaldehyde was much smaller than that of methyl acetate in No. 5, the major part of acetaldehyde seems to be further converted into polyaldols by copper complex.[7] When the starting ester has more than two alkoxyl groups as in dimethyl fumarate, dimethyl carbonate, and trimethyl phosphite, a mixture of partially and fully interchanged prodcuts was obtained, the ratio between the products depending upon the relative amount of alcohol to ester.

A comparison of the catalytic activity of i-$C_3H_7OCuPPh_3$ with that of typical trans-esterification catalysts at 0 °C is given in Table 3. We see that i-$C_3H_7OCuPPh_3$ has much higher activity than the corresponding aluminum and titanium alkoxides and an activity comparable to that of i-C_3H_7ONa which is a much stronger base than i-$C_3H_7OCuPPh_3$. Thus the present system is expected to provide synthetic utility specially when applied to systems which are susceptible to attack of strong base.

TABLE 2. TRANS-ESTERIFICATION OF CARBOXYLIC ESTERS

No.	Ester (mmol)	Alcohol	Molar ratio (alcohol/ester)	Catalyst[a]	Temp (°C)	Time (h)	Products (%-yield/starting ester)
1	CH_3COOCH_3 (20)	C_2H_5OH	1.0	**1b** (0.16)	−5	12	$CH_3COOC_2H_5$ (41)
2	$C_6H_5COOCH_3$ (10)	C_2H_5OH	2.0	**1b** (0.32)	0	12	$C_6H_5COOC_2H_5$ (59)
3	CH_3COO-t-C_4H_9 (10)	C_2H_5OH	6.0	**1b** (0.32)	0	12	$CH_3COOC_2H_5$ (6)
4	CH_2=$C(CH_3)COOCH_3$ (10)	C_2H_5OH	1.0	**1b** (0.32)	0	12	CH_2=$C(CH_3)COOC_2H_5$ (48)
5	CH_2=$C(CH_3)COOCH_3$ (6.8)	C_2H_5OH	9.0	**1b** (0.32)	0	24	CH_2=$C(CH_3)COOC_2H_5$ (73)
6	CH_3COOCH=CH_2 (60)	CH_3OH	1.0	**1a** (0.32)	−5	12	CH_3COOCH_3 (91), CH_3CHO (20)
7	$CH_3COOC(CH_3)$=CH_2 (30)	C_2H_5OH	2.0	**1b** (0.32)	0	12	$CH_3COOC_2H_5$ (100), CH_3COCH_3 (100)
8	CH_3OCOCH=$CHCOOCH_3$ (10)	C_2H_5OH	2.0	**1b** (0.32)	0	12	C_2H_5OCOCH=$CHCOOC_2H_5$ (49), CH_3OCOCH=$CHCOOC_2H_5$ (42)
9	CH_3OCOCH=$CHCOOCH_3$ (10)	C_2H_5OH	10.0	**1b** (0.32)	0	12	C_2H_5OCOCH=$CHCOOC_2H_5$ (73), CH_3OCOCH=$CHCOOC_2H_5$ (10)
10	$(CH_3O)_2CO$ (20)	C_2H_5OH	2.0	**1b** (0.32)	0	12	$(C_2H_5O)_2CO$ (7), $C_2H_5O(CH_3O)CO$ (48)
11	$(CH_3O)_2CO$ (20)	C_2H_5OH	10.0	**1b** (0.32)	0	12	$(C_2H_5O)_2CO$ (63), $C_2H_5O(CH_3O)CO$ (34)
12	$P(OCH_3)_3$ (10)	C_2H_5OH	4.0	**1b** (0.32)	0	12	$P(OEt)_3$ (18), $P(OEt)_2OMe$ (37), $P(OMe)_2OEt$ (41)
13	$P(OCH_3)_3$ (20)	C_2H_5OH	10.0	**1b** (0.32)	0	12	$P(OEt)_3$ (60), $P(OEt)_2OMe$ (37), $P(OMe)_2OEt$ (2)
14	$CH_3COOCH_2C_6H_5$ (20)	i-C_3H_7OH	3.0	**1e** (0.32)	0	12	$CH_3COOCH(CH_3)_2$ (70)
15	CH_3COO-p-$C_6H_5NO_2$ (20)	C_6H_5OH	2.0	**1g** (0.30)	r.t.[b]	12	$CH_3COOC_6H_5$ (57)
16	CH_3COO-p-$C_6H_5OCH_3$ (20)	C_6H_5OH	2.0	**1g** (0.30)	r.t.[c]	12	$CH_3COOC_6H_5$ (17)
17	$CH_3COOC_2H_5$ (20)	C_6H_5OH	1.0	**1g** (0.30)	50[d]	10	no reaction proceeds
18	CH_3COOCH_3 (20)	C_2H_5OH	1.0	**1g** (0.30)	r.t.	12	$CH_3COOC_2H_5$ (55)
19	CH_2=$C(CH_3)COOCH_3$	C_2H_5OH	20.0	**1g** (0.30)	55[e]	1	CH_2=$C(CH_3)COOC_2H_5$ (94)

a) **1a**=$CH_3OCu(PPh_3)_2 \cdot 0.5Et_2O$, **1b**=$C_2H_5OCu(PPh_3)_2$, **1e**=$i$-$C_3H_7OCuPPh_3$, **1g**=$C_6H_5OCu(PPh)_2$. b) In 15 ml of toluene. c) In 10 ml of toluene. d) In 5 ml of toluene. e) In 10 ml of THF.

TABLE 3. COMPARISON OF CATALYTIC ACTIVITIES OF i-$C_3H_7OCuPPh_3$ **1e** WITH THOSE OF $Al(O$-i-$C_3H_7)_3$, $Ti(O$-i-$C_3H_7)_4$, AND i-C_3H_7ONa FOR THE TRANS-ESTERIFICATION OF $CH_3COOCH_2C_6H_5$ WITH i-C_3H_7OH[a]

Catalyst	Yield of CH_3COO-i-C_3H_7 (%)
i-$C_3H_7OCuPPh_3$	70
$Ti(O$-i-$C_3H_7)_4$	20
$Al(O$-i-$C_3H_7)_3$	negligible
i-C_3H_7ONa	76

a) The reactions were carried out at 0 °C for 12 h using 0.32 mmol of the catalyst, 20 mmol of benzyl acetate and 60 mmol of isopropyl alcohol.

Figure 1 shows the time course of the trans-esterification of p-nitrophenyl acetate with phenol catalyzed by $C_6H_5OCu(PPh_3)_2$ under the conditions where the ratio of p-nitrophenyl acetate to phenol or that of phenol to p-nitrophenyl acetate was kept at 100. The data obtained under the two different situations fit the same curve. The first-order plot (log Co/C *vs.* t) of the data in Fig. 1 gives a straight line indicating that the rate of trans-esterification is proportional to both the concentration of p-nitrophenyl acetate and that of phenol:

$$R = k[p\text{-nitrophenyl acetate}][\text{phenol}] \quad (6)$$

When the molar ratio of p-nitrophenyl acetate to phenol is unity, the time course of conversion follows the second-order rate law supporting the validity of Eq. 6. From the temperature dependence of the second-order rate constant k (Table 4) the activation energy for trans-esterification was calculated to be E_a=12.4 kcal/mol. The rate of trans-esterification increases linearly with increase in the catalyst concentration.

Mechanism of Trans-esterification. A simple extension of the observation on stoichiometric exchange reactions between esters and the alkoxocopper complexes to catalytic trans-esterification promoted by the alkoxocopper complexes leads to the following mechanism comprising two steps, (1) the exchange between the ester and the alkoxocopper, and (2) the exchange between the alcohol used and the newly formed alkoxo-

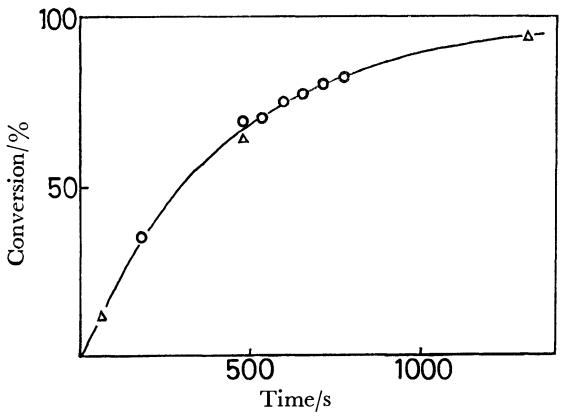

Fig. 1. Trans-esterification of *p*-nitrophenyl acetate with phenol catalyzed by $C_6H_5OCu(PPh_3)_2$. (a) ○, CH_3COO-*p*-$C_6H_4NO_2$ = 0.5 mmol (90 mg), C_6H_5OH = 50 mmol (4.70 g), catalyst = 85 mg, in this case the conversion is based on CH_3COO-*p*-$C_6H_4NO_2$. (b) △, CH_3COO-*p*-$C_6H_4NO_2$ = 50 mmol (9.00 g), C_6H_5OH = 0.5 mmol (47 mg), catalyst = 85 mg, in this case the conversion is based on C_6H_5OH. Solvent = toluene (10 ml) Temp = 50 °C.

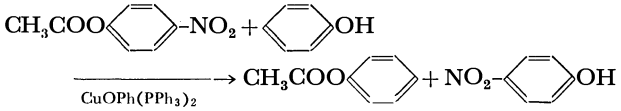

Table 4. Temperature dependence of the second-order rate constant k in the trans-esterification of CH_3COO-*p*-$C_6H_4NO_2$ with C_6H_5OH[a]

Temp (K)	$1/T$	k(l·mol^{-1}·s^{-1})
323	3.10×10^{-3}	0.8×10^{-4}
353	2.84×10^{-3}	4.0×10^{-4}
383	2.61×10^{-3}	17.0×10^{-4}
	E_a = 12.4 kcal/mol	

a) Catalyst = $C_6H_5OCu(PPh_3)_2$ (0.13 mmol). [CH_3COO-*p*-$C_6H_5NO_2$] = [C_6H_5OH] = 1.0 mol/l. Solvent = toluene.

copper complex.:

$$R^1COOR^2 + R^3OCuL_n \longrightarrow R^2OCuL_n + R^1COOR^3$$
$$R^2OCuL_n + R^3OH \longrightarrow R^3OCuL_n + R^2OH$$

$$R^1COOR^2 + R^3OH \xrightarrow[ROCuL_n]{} R^1COOR^3 + R^2OH \quad (7)$$

Such a trans-esterification reaction does not seem to constitute the main mechanistic pathway for the following reasons. (a) The phenoxocopper complex **1g**, which undergoes exchange reaction with neither aliphatic esters nor alcohols, catalyzes the trans-esterification between methyl acetate and ethanol. (b) The exchange reaction between *p*-NO_2–$C_6H_4OCu(PPh_3)_2$ and phenol is extremely slow as compared to the relatively fast trans-esterification between *p*-nitrophenyl acetate and phenol catalyzed by **1g**. (c) The kinetic results expressed by Eq. 6 are not compatible with the stepwise mechanism shown by Eq. 7.

From the available experimental evidence we propose that the trans-esterification reaction proceeds through the copper-assisted nucleophilic replacement mechanism as shown below:

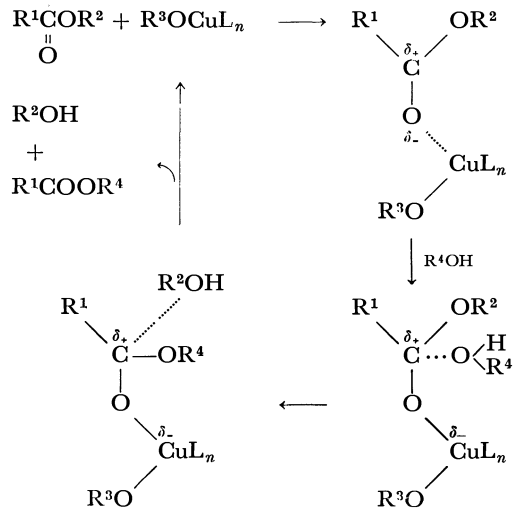

In view of the loosening of the carbonyl group in esters on their coordination to metal compounds as shown by infrared work by Lappert,[4c] the nucleophilic attack of the carbonyl carbon whose electron density decreases by coordination of the carbonyl group to metal is plausible. The mechanism is in line with the second-order rate equation, provided that the attack of alcohol on the metal-coordinated ester is the rate-determining step. According to the reaction mechanism the activation energy for the trans-esterification consists of the energy for the coordination of R^1COOR^2 to $R^3OCu(PPh_3)_n$ and that for the nucleophilic attack of R^4OH to the reaction intermediate.

Experimental

General. Preparation and the reaction of copper complexes were carried out in Schlenk type flasks under deoxygenated nitrogen or argon, or in a vacuum. Solvents were dried by the usual procedure, distilled, and stored in argon or nitrogen. IR spectra were recorded on a Hitachi Model 295 spectrophotometer. Microanalysis of carbon, hydrogen and nitrogen was carried out by Mr. T. Saito in our laboratory with a Yanagimoto CHN Autocorder Type MT-2.

Materials. Esters used in the reaction were sufficiently pure as checked by gas chromatography. Alkoxocopper and phenoxocopper complexes **1a**—**1g** were prepared as reported in the preceding paper.[2] *p*-Nitrophenoxocopper complex *p*-$O_2NC_6H_4OCu(PPh_3)_2$ was prepared similarly; yield = 90%. Found: C, 69.7; H, 4.69; N, 2.10%. Calcd for $C_{42}H_{34}CuNO_3P_2$: C, 69.5; H, 4.68; N, 1.93%. IR (KBr): 1580, 1505, 1307, 1280 cm^{-1}. NMR (C_6D_6): δ 6.48 (d, 2H), 7.0 (m, 18H), 7.4 (m, 12H), 8.04 (d, 2H).

Stoichiometric Exchange Reactions between $ROCu(PPh_3)_n$ and Carboxylic Esters. Phenyl acetate (64 mg, 0.47 mmol) was added to **1c** (200 mg, 0.47 mmol) suspended in 2 ml of diethyl ether at −5 °C. Stirring of the mixture at −5 °C for 12 h gave 0.41 mmol (87% per **1c**) of propyl acetate and a white precipitate. The white precipitate was recrystallized from toluene and dried in a vacuum to give a new phenoxocopper complex having one PPh_3 ligand, $C_6H_5OCuPPh_3$ (172 mg, 84% per **1c**). Found: C, 68.3; H, 4.50%. Calcd for $C_{24}H_{20}CuOP$: 68.8; H, 4.78%. IR(KBr): 1580, 1270 cm^{-1}. Other stoichiometric exchange reactions

of alkoxocopper and phenoxocopper complexes with carboxylic esters were carried out in a similar manner.

Catalytic Trans-esterification. Methyl acetate (1.48 g, 20 mmol) was added to an ethyl alcohol (0.92 g, 20 mmol) solution of **1c** (68 mg, 0.16 mmol) at −5 °C. Stirring of the solution at the temperature for 12 h afforded 8.2 mmol of ethyl acetate as determined by gas chromatography. Trans-esterification of carboxylic esters and trimethyl phosphite was carried out in a similar manner.

Kinetic Study. Kinetic study on the trans-esterification of CH_3COO-*p*-$C_6H_4NO_2$ by C_6H_5OH was carried out in a Schlenk type flask immersed in a thermostatted oil bath. The solvent, reactants, and catalyst were transferred in an atmosphere of nitrogen. The time-dependent conversion was measured by pipetting out each fraction of the solution at a set time and analyzing it by gas chromatography.

References

1) (a) H. Weingarten, *J. Org. Chem.* **29**, 977 (1964); (b) H. Weingarten, *ibid.*, **29**, 3624 (1964); (c) T. Tsuda, T. Hashimoto, and T. Saegusa, *J. Am. Chem. Soc.*, **94**, 658 (1972); (d) T. Tsuda, T. Nakatsuka, T. Hirayama, and T. Saegusa, *J. Chem. Soc., Chem. Commun.*, **1974**, 620; (e) T. Tsuda, T. Nakatsuka, and T. Saegusa, 22nd Symposium on Organometallic Chemistry Japan, Kyoto (1974), Abstract 211A; (f) T. Kawaki and H. Hashimoto, *Bull. Chem. Soc. Jpn.*, **45**, 1499 (1972); (g) W. T. Reichle, *Inorg. Chim. Acta*, **5**, 325 (1971).

2) M. Kubota and A. Yamamoto, *Bull. Chem. Soc. Jpn.*, **51**, 2909 (1978).

3) M. Kubota, A. Miyashita, S. Komiya, and A. Yamamoto, *J. Organomet. Chem.*, **139**, 111 (1977).

4) (a) D. C. Bradley, D. C. Hancock, and W. Wardlaw, *J. Chem. Soc.*, **1952**, 2773; (b) O. A. Osipov and Yu. B. Kletenik, *Zh. Obshch. Khim.*, **29**, 1375 (1959); (c) M. F. Lappert, *J. Chem. Soc.*, **1961**, 817 and references cited therein.

5) J. Ishizu, T. Yamamoto, and A. Yamamoto, *Chem. Lett.*, **1976**, 1091.

6) T. Tatsumi, H. Tominaga, M. Hidai, and Y. Uchida, *Chem. Lett.*, **1977**, 37.

7) T. Yamamoto, S. Konagaya, and A. Yamamoto, *J. Polym. Sci., Polym. Lett.*, **16**, 7 (1978).

Reactions of Spiro[2.6]nona-4,6,8-triene Derivatives with Acids and Bases. Rearrangement to a Heptafulvene Derivative and Formation of Ether Linkage Compounds

Takashi TODA,* Katsuhiro SAITO,† and Toshio MUKAI

Department of Chemistry, Faculty of Science, Tohoku University, Aoba, Aramaki, Sendai 980

†*Department of Chemistry, Nagoya Institute of Technology, Gokiso-cho, Showa-ku, Nagoya 466*

(Received June 2, 1978)

Reaction of dimethyl *trans*-spiro[2.6]nona-4,6,8-trien-1,2-dicarboxylate with phenyllithium afforded *trans*-1,2-bis(hydroxydiphenylmethyl)spiro[2.6]nona-4,6,8-triene (**2**) in a good yield. Spirotriene **2** is very sensitive to acids and gave 8-(2,2-diphenylvinyl)heptafulvene accompanied with a quantitative amount of benzophenone by acid treatments. Although **2** is stable to basic reagents, upon treating with sodium hydride, **2** afforded 11-hydroxydiphenylmethyl-8-oxa-9-diphenyltricyclo[5.4.0.$0^{1,10}$]undeca-2,4-diene, and its double bond isomers. Mechanisms of the above reactions are discussed.

Spiro[2.6]nona-4,6,8-triene system is of interest from the view point of spiro conjugation.[1,2] Although some spiro[2.6]nonatriene derivatives have been synthesized,[3-9] chemical properties of this class of compounds have not been well known in detail.[7-11] We designed to introduce hydroxyl groups to this system and to investigate its properties to acids and bases. We wish to report here the results obtained and discuss about mechanisms of these reactions.

Reductions of dimethyl *trans*-spiro[2.6]nona-4,6,8-trien-1,2-dicarboxylate (**1**)[7,8] by lithium aluminium hydride gave several unidentified mixtures, and reactions of **1** with Grignard reagents (benzylmagnesium chloride or methylmagnesium iodide) also gave several intractable products which did not possess a cyclopropane moiety or a cycloheptatriene ring. Presumably skeletal rearrangements took place by the actions of the Grignard reagents or lithium aluminium hydride as Lewis acids. However, *trans*-1,2-bis(hydroxydiphenylmethyl)spiro[2.6]nona-4,6,8-triene (**2**) was obtained in 80% yield by reaction of **1** with excess phenyllithium.

Spirotriene **2** is very sensitive toward acidic reagents. When **2** was treated with organic or mineral acids, or even with silica gel, the colorless solution of **2** turned to dark red, and it gave a product (**3**) which possesses a strong absorption band at 385 nm in its UV spectrum, and is a very unstable entity. When **3** was allowed to stand at room temperature in neat, the color of **3** disappeared within one hour as shown in Fig. 1, and a mixture of resinous substances and one mole of benzophenone were obtained.

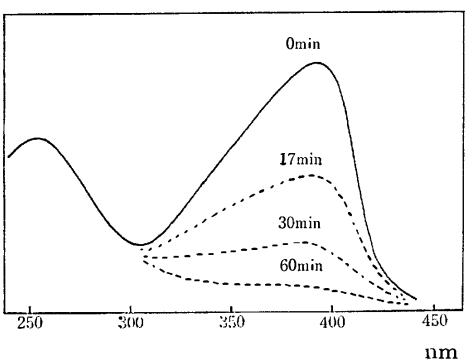

Fig. 1.

Considering that spiro[2.6]nonatriene derivatives have been known to give heptafulvene derivatives by acid treatments[3,4] and the UV spectrum of **3** is similar to those of heptafulvene derivatives,[12] structure of **3** was supposed to be 8-(2,2-diphenylvinyl)heptafulvene. Exhaustive catalytic hydrogenation of a freshly prepared reaction mixture of **2** with silica gel gave a hydrocarbon (**4**) in 75% yield and benzophenone in a good yield, after consumption of five mole of hydrogen. Hydrocarbon **4** shows the following spectral properties. Mass: *m/e*, 292 (9%, molecular ion peak, $C_{22}H_{28}$) and *m/e*, 167 (base peak, Ph_2CH^+). NMR (in CCl_4): δ ppm; 1.8—2.3 (multiplet, 17 H), 3.8 (triplet, 1 H, benzyl proton), and 7.2 (broad singlet, 10 H). These data suggest that the structure of **4** is 1-cycloheptyl-3,3-diphenylpropane, confirming the structure of **3** to be 8-(2,2-diphenylvinyl)heptafulvene. Scheme of these reactions is shown in Fig. 2.

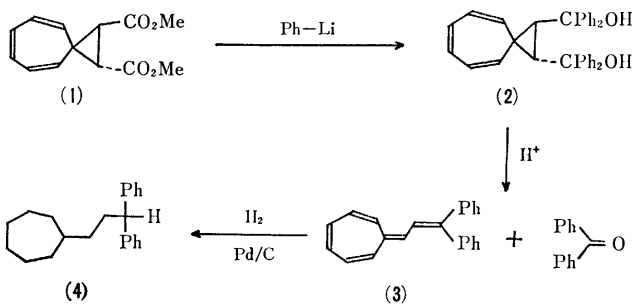

Fig. 2.

Spirotriene **2** is stable toward basic reagents. Reactions of **2** with refluxing pyridine, triethylamine, or 4 M sodium hydroxide in refluxing dioxane resulted in complete recovery of **2**. On the other hand, treatment of **2** with excess sodium hydride in dry dioxane afforded colorless crystalline substances (**5**, **6**, and **7**). Products ratios depended on the temperature and the reaction period as shown in Table 1.

Physical data of **5**, **6**, and **7** are summarized in Table 2—4. These products show the same elemental analyses ($C_{35}H_{30}O_2$) and molecular ion peaks in mass spectra (M^+, 482). Acid treatments of these products gave **3** and benzophenone, suggesting the structures of them to be analogous to that of **2**. The IR and NMR spectral studies in deuterium oxide cleared that each

Table 1.

Condition		Product yields (%) 2 (recv.)	5	6	7
Room temp	300 h	12	63	0	0
Reflux	6.5 h	0	4	44	17
Reflux	20 h	0	0	0	43

Table 2.

	UV λ_{max}^{MeOH} nm (log ε)	IR ν^{KBr} cm^{-1}	Mass *m/e* (%)
5	255 (4.18)	3550 1600	482(M^+, 3), 269(9), 197(16), 196(100), 167(8), 105(40)
6	260 (4.07)	3595 1590	482(M^+, 2), 269(9), 196(100) 118(17), 105(78)
7	277 (4.10)	3600 1600	482(M^+, 5), 286(100), 105(84)

compound possesses one hydroxyl group and the other oxygen is in an ether linkage.

Structures of **5**, **6**, and **7** were determined to be 11-hydroxydiphenylmethyl-8-oxa-9,9-diphenyltricyclo-[5.4.0.0^{1,10}]undeca-3,5-diene, 2,4-diene, and 4,6-diene, respectively, as shown in Fig. 3, from their NMR spectra with double and triple resonance techniques. Assignment of the NMR spectra were deduced from their coupling patterns which clearly showed each proton's relations in the seven membered rings of them as shown in Tables 3 and 4. Investigation of their Dreiding model indicated that the chemical shifts of H_{11} should appear more lower fields than those of H_{10} by the different anisotropy effect of the phenyl groups at C_9 and C_{12}.

These structures could reasonably be explained also by their UV spectra. The absorption maxima of them shift to longer wavelength in the order of **5**, **6**, and **7**, being well coincident with that **5** has only one isolated diene chromophore, but **6** and **7** possess diene systems conjugated with a cyclopropane and a terminal vinyl ether linkage conjugated with a cyclopropane, respectively.

Thermal reactions of these three products under the basic conditions cleared the relation of them that the isomerization took place between **5** and **6**, and **5** isomerized to **7**, but **7** did not isomerized to **5** or **6** as shown in Fig. 3, and these facts confirmed the structures of them.

Although the best model compound α,α-diphenyl-β-(7-cycloheptatrienyl)ethyl alcohol could not be prepared in pure state, as models of the ether linkage formation of **2**, reactions of 7-cycloheptatrienylmethyl

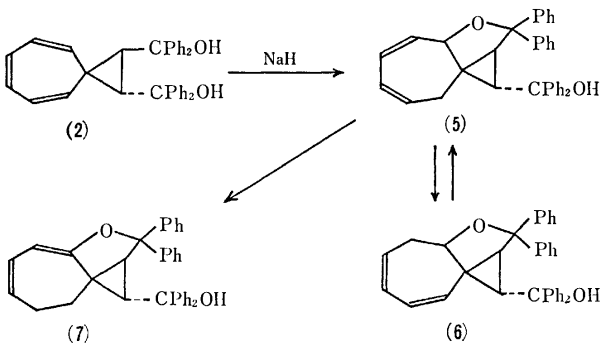

Fig. 3.

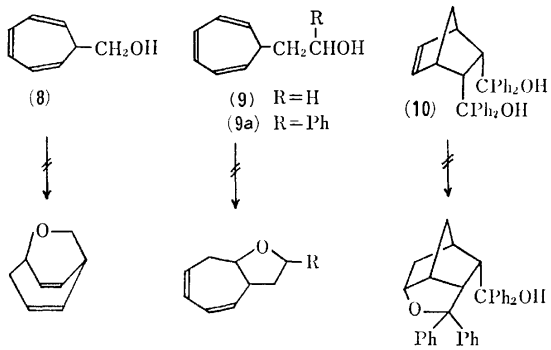

Fig. 4.

Table 3. NMR spectral data (chemical shifts, ppm, and coupling pattern)

	OH	H_2 a	H_2 b	H_3	H_4	H_5	H_6 a	H_6 b	H_7	H_{10}	H_{11}	H_{Ph}
5	1.65 (1H) s	2.52 (1H) d	2.92 (1H) d, d	5.21 (2H) m		5.46 (1H) d, d, d	5.92 (1H) d, d		4.55 (1H) d, d	1.84 (1H) d	2.78 (1H) d	6.9—7.6 (20H) m
6	1.93 (1H) s	5.92 (1H) d, d		5.5 (3H) m			2.60 (1H) d, d, d	2.85 (1H) d, d, d	4.22 (1H) d, d	1.67 (1H) d	2.95 (1H) d	6.8—7.5 (20H) m
7	1.62 (1H) s	1.9 (2H) m		2.25 (2H) m	5.41 (1H) d, d, d	5.87 (1H) d, d	5.63 (1H) d			2.02 (1H) d	2.80 (1H) d	6.9—7.5 (20H) m

s: singlet, d: doublet, d, d: double doublet, d, d, d: triple doublet, m: multiplet.

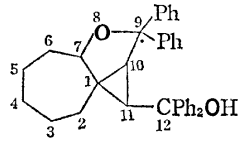

Table 4. Coupling constants (Hz)

	5	6	7
J_{2-2}	20 (2a—2b)		
J_{2-3}	3.5 (2b—3)	11	
J_{2-4}		3	4 (2a—4) 6 (2b—4)
J_{2-7}	0.5 (2b—7)		
J_{4-5}	4		12
J_{5-6}	11	3 (5—6a) 4.5 (5—6b)	
J_{5-7}	2		
J_{6-6}		18 (6a—6b)	
J_{6-7}	2	9 (6a—7) 5 (6b—7)	
J_{10-11}	4	4.5	4.5

alcohol (**8**),[13] β-(7-cycloheptatrienyl)ethyl alcohol (**9**),[14] α-phenyl-β-(7-cycloheptatrienyl)ethyl alcohol (**9a**), and *cis-endo*-1,2-bis(hydroxydiphenylmethyl)-bicyclo[2.2.1]hept-5-ene (**10**)[11] with sodium hydride under the same conditions as the case of **2** were investigated, but resulted in the complete recovery of the starting alcohols. Reactions of cycloheptatriene with benzyl alcohol or triphenylmethyl alcohol under the same conditions also resulted in the complete recovery of the starting substances.

Discussion

Mechanism of the rearrangement of **2** to **3** by acid treatments can be considered as shown in Fig. 5 by following reasons. First of all, ring creavage reactions of cyclopropane derivatives by acidic reagents are well known, and furthermore, a cycloheptatrienium ion (**11**) is a very stable ion. Secondary, dehydration reaction of **2** should proceed readily, because **2** is a benzyl alcohol. Finally, benzophenone is a stable compound: thus, elimination of benzophenone from **11** should not need high energy. From these reasons, the rearrangement of **2** to **3** seems to proceed readily.

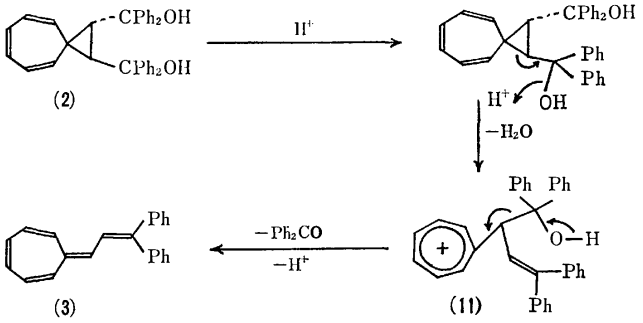

Fig. 5.

There are several plausible explanations about reaction mechanisms of the formation of **5** from **2**. The first one is direct alkoxide anion attack on double bonds. However, the reactions of **8**, **9**, and **10** did not give any ether compounds as described before. Steric requirements of **8**, **9**, and **10** are good enough for an ether linkage formation, because sterically analogous compounds such as α-(diazomethyl)-α'-(7-cycloheptatrienyl)methyl ketone gave a corresponding bond formation product by its decomposition reaction.[15] Also, it is well known that *endo*-bicyclo[2.2.1]hept-5-en-2-carboxylic acid afforded the lactone derivative by acid treatments. These results indicate that direct alkoxide anion attack on double bonds of **2** is not reasonable.

The second is an explanation by radical mechanisms. Color of the reaction mixture of **2** become deep blue during the reactions suggesting a formation of some radical species. ESR spectrum measurement of this reaction mixture did not show, however, any evidence of a radical formation. Also, if alkoxide radical or cycloheptatrienyl radical formed under the reaction conditions, the corresponding radicals would form in the reactions of **8**, **9**, and **10**, and some reactions should take place in these cases. So that radical mechanisms can not be negrected completely, but not very likely.

The third and the most probable one is a mechanism *via* norcaradiene intermediate. Valence tautomerism between cycloheptatriene and norcaradiene systems is well known phenomenon.[16,17] This tautomerism is also possible between **2** and its valence isomer (**2a**) which should be very strained one. Therefore, if once this strained tricyclic system formed in the reaction mixture, the intramolecular alkoxide anion attack takes place readily to give the ether compound **5**. The Dreiding model of **2a** indicates that the ether linkage formation is possible between alkoxide oxygen and C_1 (*ac.* 2.4 Å). Also, the most favorable conformer of **2a** is that the alkoxide oxygen comes nearby norcaradiene and the big phenyl groups stick to the outside of norcaradiene.

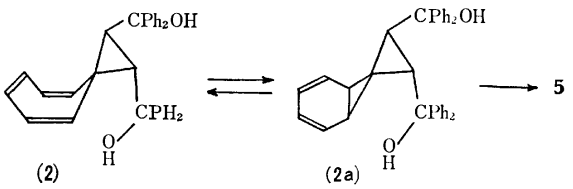

Fig. 6.

Recently, some examples of addition reactions of anionoid reagents with unsaturated or strained compounds have been reported.[18,19] Especially, addition reaction of amines to strained double bonds such as 9,9'-difluolenyridene[20] is a good example of this type of reaction.

The interconversions of **5**, **6**, and **7** are thermal 1,5-hydrogen shift reactions.[21] The diene system of **7** is conjugated with ether linkage constructing the vinyl ether skeletone, and therefore, **7** seems to be the most stable isomer of all of them.

Experimental

All melting and boiling points were uncorrected. IR spectra were measured in carbon tetrachloride solutions or potasium bromide disks, and UV spectra in methanol solutions. PMR spectra were measured with Varian T-60 or HA-100 spectrometer with deuteriochloroform or carbon tetrachloride as solvent and tetramethylsilane as internal

standard. Mass spectra were measured with Hitachi RMU 6D spectrometer at 70 eV by direct method.

*Reactions of **1** with Grignard Reagents and Lithium Aluminium Hydride.* (a) Reaction of **1** (468 mg, 2 mmol) with benzylmagnesium chloride (16 mmol) in anhydrous ether (30 ml) with ordinal method gave an yellow oil (1.436 g). Distillation of the oil afforded benzyl alcohol (50—60 °C/0.5 Torr, 300 mg), diphenylethane (65—70 °C/0.5 Torr, 85 mg), and an yellow oily residue (950 mg). Silica gel TLC (hexane, benzene, and methanol; 6 : 3 : 1) gave colorless oily mixtures (381 mg) which showed a broad absorption band at 1775 cm^{-1} in its IR spectrum. (b) Reaction of **1** (234 mg, 1 mmol) with methylmagnesium iodide (8 mmol) also gave none of clear products. (c) Reaction of **1** (300 mg, 1.3 mmol) with lithium aluminium hydride (1.2 g, 32 mmol) in boiling anhydrous tetrahydrofuran (30 ml) with ordinary method gave unidentified oily mixtures (162 mg) which still showed a broad carbonyl band at 1730 cm^{-1} in its IR spectrum.

*Reaction of **1** with Phenyllithium.* A solution of **1** (936 mg, 4 mmol) in anhydrous ether (30 ml) was added to a solution of phenyllithium (30 mmol) in anhydrous ether (20 ml) at 0 °C during 30 min with stirring. After further stirring for 13 h at room temperature, the reaction mixture was decomposed with water, and extracted with ether. Evaporation of the solvent and recrystallization of the residue from acetone gave **2** (1.58 g, 84%), mp 223—225 °C. Found: C, 87.16; H, 6.30%. Calcd for $C_{35}H_{30}O_2$: C, 87.06; H, 6.05%.

*Reactions of **2** with Acids.* A solution of **2** (1.0 g, 2.1 mmol) in 0.1 N sulfuric acid-dioxane (50 ml) was stirred for 1 h at 0 °C, and then added water (100 ml). The reaction mixture was extracted with benzene. A brown tarry material (1.0 g) obtained by evaporation of the solvent was chromatographed on alumina to give benzophenone (377 mg, 98%) by petroleum ether-benzene (9 : 1) and intractable unidentified tarry materials (600 mg). Treatments of **2** with hydrochloric acid, acetic acid, or silica gel gave the almost identical results with that of the case of sulfuric acid.

*Hydrogenation of **3**.* A mixture of **2** (1.0 g, 2.1 m mol), silica gel (10 g, 60—100 mesh), and benzene (70 ml) was stirred at room temperature for 1.5 h. Separation of the silica gel, and following hydrogenation of the filtrate with paradium carbon (10%, 400 mg) gave a pale yellow oil (1.0 g) after absorption of hydrogen (250 ml, 11 mmol). Alumina column chromatography of this oil gave a colorless oil (540 mg) by petroleum ether, benzophenone (278 mg, 74.5%) by petroleum ether-benzene (8 : 2), and diphenylmethyl alcohol (73 mg, 20%) by ether. Distillation of the colorless oil (bath temp 110 °C/0.2 Torr) gave **4** (454 mg, 74.7%). Found: C, 90.16; H, 9.63%. Calcd for $C_{22}H_{28}$: C, 90.35; H, 9.65%.

*Reactions of **2** with Sodium Hydride.* (a) A mixture of **2** (200 mg, 0.4 mmol), 55% sodium hydride (400 mg, 9 mmol), and anhydrous dioxane (10 ml) was stirred at room temperature for 330 h. The reaction mixture was filtered and the residual solid was decomposed with water and extracted with benzene. Combined organic layer was washed with water and dried over sodium sulfate. Evaporation of the solvent afforded an yellow oily material (335 mg). Purification of this oil with silica gel TLC (benzene) gave recovery of **2** (25 mg, 12%, R_f=0.5) and an yellow tarry material (156 mg, R_f=0.75). Crystallization of the tar from petroleum ether-benzene, and further recrystallization from ethyl acetate yielded pure **5** (125 mg, 63%), mp 115 °C. Found: C, 86.74; H, 6.54%. Calcd for $C_{35}H_{30}O_2$: C, 87.10; H, 6.27%. (b) A mixture of **2** (800 mg, 1.6 mmol), 55% sodium hydride (1.6 g, 37 mmol), and anhydrous dioxane (50 ml) was refluxed for 6.5 h. The same treatment as above afforded **5** (34 mg, 4.2%, R_f=0.75), colorless crystals of **6** (mp 150—155 °C, 351 mg, 44%, R_f=0.85), and **7** (mp 170—174 °C, 136 mg, 17%, R_f=0.9). Recrystallization of **6** and **7** from ethyl acetate raised their mps to 164 and 180 °C, respectively. Found: C, 87.10; H, 6.33% for **6**. Found: C, 86.76; H, 6.43% for **7**. (c) A mixture of **2** (1.0 g, 2.1 mmol), 55% sodium hydride (3.0 g, 70 mmol), and anhydrous dioxane (50 ml) was refluxed for 20 h. After the same treatment as above, the obtained yellow oil was chromatographed on alumina. An yellow oily resinous material (460 mg) which was eluted with benzene was recrystallized from ethyl acetate to give pure **7** (430 mg, 43%).

*Acid Treatments of **5**, **6**, and **7**.* A solution of **5** (10 mg, 0.02 mmol) in methanol (5 ml) containing a drop of conc sulfuric acid was allowed to stand at room temperature for 6 h. UV spectrum of this solution was identical with that of **3**, and gas chromatographic study showed existence of benzophonone. Treatments of **6** and **7** under the same conditions as above showed the identical results as the case of **5**.

*Interconversion of **5**, **6**, and **7**.* A solution of **5** (15 mg, 0.03 mmol) and 55% sodium hydride (30 mg, 7 mmol) in anhydrous dioxane (2 ml) was refluxed for 9 h. Silica gel TLC (benzene) showed three spots at the parts coincident with **5** (R_f=0.75), **6** (R_f=0.85), and **7** (R_f=0.9). By the same procedure, reaction of **6** showed the same three spots as the case of **5** on silica gel TLC, but reaction of **7** showed no other spot except one due to itself, and this spot diminished by prolonged refluxing (about one day).

*Reactions of **8**, **9**, and **10** with Sodium Hydride.* (a) A solution of **8** (1.34 g, 11 mmol) and 55% sodium hydride (2.4 g, 56 mmol) in anhydrous dioxane (10 ml) was stirred for 230 h at room temperature. The starting alcohol **8** (1.32 g, 98%) was recovered by the same treatment as the case of the reaction of **2** with sodium hydride. (b) Reaction of **9** (1.41 g) with sodium hydride under the same conditions as above resulted in recovery of the starting alcohol (1.34 g, 95%). (c) Reaction of **10** (500 mg) with sodium hydride under the same conditions as above resulted in recovery of the starting alcohol (485 mg, 97%).

Reactions of Cycloheptatriene with Benzyl Alcohol and Triphenylmethyl Alcohol. (a) A mixture of cycloheptatriene (1.8 g, 20 mmol), benzyl alcohol (16 g, 148 mmol), 55% sodium hydride (3.0 g, 70 m mol), and anhydrous dioxane (10 ml) was refluxed for 17 h. The starting alcohol was recovered quantitatively by the same treatments as above. (b) By the same procedure as above, reaction of cycloheptatriene with triphenylmethyl alcohol resulted in almost quantitative recovery of triphenylmethyl alcohol.

Preparation of α-Phenyl-β-(7-cycloheptatrienyl)ethyl Alcohol. To a solution of phenyl magnesium bromide prepared from 3.58 g of bromobenzene in 30 ml of ether, a solution of 2.0 g of (7-cycloheptatrienyl)acetaldehyde[22] in 20 ml of ether was added dropwise with stirring and under nitrogen atomsphere. After 5 h, an ordinal workup gave 1.40 g of the colorless needles of **9a**: mp 41—43 °C from hexane-ether. Found: C, 84.89; H, 7.64%. Calcd for $C_{15}H_{16}O$: C, 84.87; H, 7.60%.

We are indebted to Prof. Yusaku Ikegami for ESR spectrum measurements.

References

1) H. E. Simmons and T. Fukunaga, *J. Am. Chem. Soc.*, **89**, 5208 (1967).
2) A. Tajiri and T. Nakajima, *Tetrahedron*, **27**, 6089 (1972).
3) M. Jones, Jr. and E. W. Petrillo, Jr., *Tetrahedron Lett.*, **1969**, 3953.
4) C. J. Rostek and W. M. Jones, *Tetrahedron Lett.*, **1969**, 3957.
5) T. Toda, K. Saito, and T. Mukai, *Tetrahedron Lett.*, **1972**, 1981.
6) L. W. Christensen, E. E. Waali, and W. M. Jones, *J. Am. Chem. Soc.*, **94**, 2118 (1972).
7) W. M. Jones and C. L. Ennis, *J. Am. Chem. Soc.*, **89**, 3069 (1967).
8) T. Mukai, T. Nakazawa, and K. Isobe, *Tetrahedron Lett.*, **1968**, 505.
9) E. E. Waali and W. M. Jones, *J. Am. Chem. Soc.*, **95**, 8114 (1974).
10) K. Saito, T. Toda, and T. Mukai, *Bull. Chem. Soc. Jpn.*, **47**, 331 (1974).
11) T. Toda, K. Saito, and T. Mukai, *Chem. Lett.*, **1973**, 1123.
12) W. von E. Doering and D. W. Wiley, *Tetrahedron*, **11**, 183 (1960). T. Nozoe, T. Mukai, K. Osaka, and N. Shishido, *Bull. Chem. Soc. Jpn.*, **34**, 1384 (1961). Y. Kitahara, K. Doi, and T. Kato, *Bull. Chem. Soc. Jpn.*, **37**, 1747 (1964); D. J. Bertelli, C. Goleria, and D. L. Drength, *J. Am. Chem. Soc.*, **86**, 3329 (1964).
13) G. D. Sargent, N. Lorrey, and S. Reigh, *J. Am. Chem. Soc.*, **75**, 27 (1967).
14) K. Conrow, *J. Am. Chem. Soc.*, **81**, 5461 (1959).
15) W. von E. Doering and W. R. Roth, *Angew. Chem.*, **75**, 27 (1963); W. von E. Doering, B. M. Ferrier, E. T. Fossels, J. M. Hartenstein, M. Jones, Jr., G. Klumpp, R. M. Rubin, and M. Saunders, *Tetrahedron*, **23**, 3947 (1967).
16) E. Ciganeck, *J. Am. Chem. Soc.*, **87**, 393 (1965); **89**, 1454 (1967); **93**, 2207 (1971); H. J. Reigh, E. Ciganeck, and J. D. Roberts, *J. Am. Chem. Soc.*, **92**, 5166 (1970); T. Toda, M. Nitta, and T. Mukai, *Tetrahedron Lett.*, **1967**, 4401. M. Görlitz and H. Günther, *Tetrahedron*, **25**, 4467 (1969).
17) G. Maier, *Angew. Chem. Int. Ed. Engl.*, **6**, 402 (1967). T. Toda, *J. Soc. Org. Synth. Chem. Jpn.*, **30**, 412 (1972).
18) H. Pines, *Synthesis*, **1974**, 309.
19) N. Imai, T. Narita, and T. Tsuruta, *Tetrahedron Lett.*, **1971**, 3517; N. Imai, T. Narita, and T. Tsuruta, *Bull. Chem. Soc. Jpn.*, **46**, 1242 (1973); T. Kauffmann and E. Koppelmann, *Angew. Chem.*, **84**, 261 (1972); S. W. Stoley and A. W. Oweddal, *J. Am. Chem. Soc.*, **96**, 1918 (1974).
20) L. A. Pinck and G. H. Hilbert, *J. Am. Chem. Soc.*, **57**, 2398 (1935).
21) K. Conrow, *J. Am. Chem. Soc.*, **83**, 2343 (1961). A. P. ter Borg, H. Kloosterziel, and N. van Meurs, *Proc. Chem. Soc.*, **1962**, 359. A. P. ter Borg, H. Kloosterziel, and N. van Meurs, *Recl. Trav. Chim. Pays-Bas*, **82**, 717 (1963). W. R. Roth, *Angew. Chem.*, **75**, 921 (1963). E. Weth and A. S. Dreiding, *Proc. Chem. Soc.*, **1964**, 59. T. Nozoe and K. Takahashi, *Bull. Chem. Soc. Jpn.*, **38**, 665 (1965).
22) M. E. Vol'pin, I. S. Akhrem, and D. N. Kursanov, *Zh. Obshch. Khim.*, **30**, 159 (1960).

Direct Synthesis of 2,2-Diaryl-3-methyl-2,3-dihydrobenzothiazoles from 3-Methyl-2,3-dihydrobenzothiazole-2-thione and Some Mechanistic Aspects

Kin-ya AKIBA,* Hiroaki SHIRAISHI, and Naoki INAMOTO
Department of Chemistry, Faculty of Science, The University of Tokyo, Hongo, Tokyo 113
(Received June 9, 1978)

Reactions of 3-methyl-2,3-dihydrobenzothiazole-2-thione (**1**) and 3-methyl-2-(methylthio)benzothiazolium iodide with Grignard reagents gave 2,2-disubstituted 3-methyl-2,3-dihydrobenzothiazole (**2**) as a major product as well as 2,2′-disubstituted 3,3′-dimethyl-2,2′,3,3′-tetrahydrobi(2-benzothiazolyl) (**3**). Reactions of **1** with organolithiums gave **2** as a major product. The results demonstrate that the formation of **3** is due to the presence of transition metals as an impurity in magnesium.

As previously reported,[1] reactions of 3-substituted 2-nitrosoimino-2,3-dihydrobenzothiazoles with Grignard reagents have been shown to give 2,2,3-trisubstituted 2,3-dihydrobenzothiazoles as well as other types of products.

It is known that Grignard reagents and organolithiums can react with thiocarbonyl group at sulfur atom.[2] On the other hand, Beak *et al.*[3] have reported that phenyllithium attacks on carbon atom of the thiocarbonyl group on *N*,*N*-dimethylthiobenzamide. Thus, occurrence of C-2 attack with Grignard reagents is expected in 3-methyl-2,3-dihydrobenzothiazole-2-thione (**1**) among other possibilities. On the other hand, reactions of 3-methyl-2-(methylthio)benzothiazolium salt (**8**) with Grignard reagents can be expected to give also 2,2-disubstituted 2,3-dihydrobenzothiazoles. This paper describes synthesis of 2,2-disubstituted 3-methyl-2,3-dihydrobenzothiazoles (**2**) from **1**, **8**, and related compounds.

The reaction of 3-methyl-2,3-dihydrobenzothiazole-2-thione (**1**) with excess Grignard reagents in refluxing benzene for 1.5—4 h under nitrogen afforded 2,2-disubstituted 3-methyl-2,3-dihydrobenzothiazole (**2**) together with 2,2′-disubstituted 3,3′-dimethyl-2,2′,3,3′-tetrahydrobi(2-benzothiazolyl) (**3**) as a minor product.

The presence of unchanged magnesium did not affect considerably the product ratio of **2** to **3** (see Table 1).

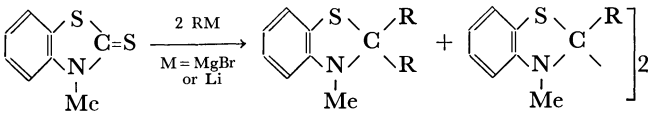

1 **2** **3**

a: R=Ph, **b**:R=*p*-ClC$_6$H$_4$, **c**: R=*p*-MeC$_6$H$_4$
d: R=*p*-MeOC$_6$H$_4$, **e**: R=Et, **f**: R=Bu

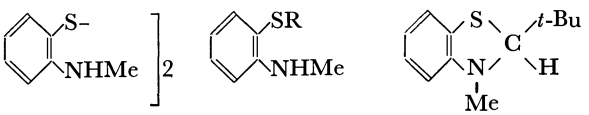

4 **5** **a**: R=Et **6**
b: R=Ph

The reaction of **1** with ethylmagnesium bromide gave also **2e** along with bis[*o*-(methylamino)phenyl] disulfide (**4**) and ethyl *o*-(methylamino)phenyl sulfide (**5a**). Refluxing of **1** with *t*-butylmagnesium bromide in benzene for 42 h gave 2-*t*-butyl-3-methyl-2,3-dihydrobenzothiazole (**6**) in 16% yield together with the recovered **1** (77%). Formation of the by-product (**3**) was encountered when phenyl and *p*-chlorophenyl Grignard reagents were employed.

Table 1. Reactions of **1** with Grignard reagents

R	**2** (%)	**3** (%)	Other (%)
Ph	**2a**, 67	**3a**, 23	
Ph[a]	**2a**, 60	**3a**, 19	
p-ClC$_6$H$_4$	**2b**, 58	**3b**, 21	
p-MeC$_6$H$_4$	**2c**, 84	—	
p-MeOC$_6$H$_4$	**2d**, 84	—	
Et[a]	**2e**, 54	—	**4**, 19: **5a**, trace
t-Bu	**6**, 16	—	recovered **1**, 77

a) In the presence of unchanged magnesium.

Table 2. Reactions of **1** with organolithiums

R	**2** (%)	Other (%)
Ph	**2a**, 42	**5b**, 19
Et	**2e**, 65	
Bu	**2f**, 58	**7**, 12

Reactions of **1** with organolithiums proceeded at room temperature and gave mainly **2**. The results are summarized in Table 2. In the cases of phenyl- and butyllithiums, **5b**[1,4] and 2-butylidene 3-methyl-2,3-dihydrobenzothiazole (**7**) were also isolated. The formation of **7** is explained by deprotonation of an intermediate (*A*) by butyllithium[5] as mentioned later.

Table 3 summarizes the results of reactions of **8** with Grignard reagents.

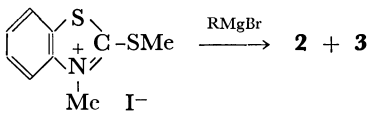

8

Table 3. Reactions of **8** with Grignard reagents

R	Condition	**2** (%)	**3** (%)	**2**/**3**
Ph	r.t., 1.5 h; then 80 °C, 0.5 h	**2a**, 54	**3a**, 25	2.1
Ph	r.t., 0.5 h; then 80 °C, 0.5 h[a]	**2a**, 48	**3a**, 37	1.3
p-MeC$_6$H$_4$	r.t., overnight	**2c**, 50	—	>10
p-MeC$_6$H$_4$	r.t., 0.5 h; then 80 °C, 0.5 h	**2c**, 43	**3c**, 28	1.5
p-ClC$_6$H$_4$	r.t., overnight	**2b**, 41	**3b**, 7	
p-MeOC$_6$H$_4$	r.t., overnight	**2d**, 85	—	

a) In the presence of unchanged magnesium.

The results reveal that the *para*-methoxyphenyl Grignard reagent bearing an electron-donating group tends to give **2** preferentially, whereas electron-withdrawing groups attached to the aromatic ring of Grignard reagents and also higher temperature would stimulate producing the compound **3**.

In the case of *t*-butylmagnesium bromide, **6** was obtained in 31% yield. The salt (**8**) can react with the Grignard reagents at room temperature, but the yield of **2** was less than those with reaction of **1** because of heterogeniety of the system.

Formation of **2** in the reactions of **1** or **8** can be rationalized by assuming the intermediacy of benzothiazolium salt (**A**) as follows.

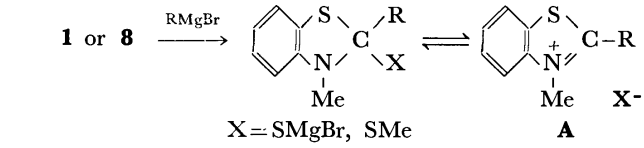

Dimerized products have also been obtained by the reaction of 3-methylbenzothiazolium,[6] 2-substituted 1,3-benzoxathiolium,[7] and 1,3-benzodithiolium salts[8] with Grignard reagents. Thereupon, reactions of 3-methyl-2-phenylbenzothiazolium iodide (**9a**) with aryl Grignard reagents were examined. The results are summarized in Table 4.

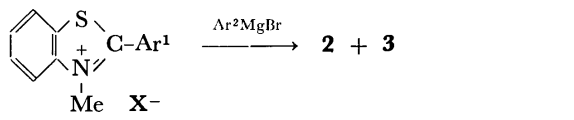

9: X=I
10: X=ClO_4
a: Ar^1=Ph
b: Ar^1=*p*-ClC_6H_4
c: Ar^1=*p*-$MeOC_6H_4$

a: Ar^1=Ar^2=Ph
g: Ar^1=Ph, Ar^2=*p*-MeC_6H_4
h: Ar^1=*p*-ClC_6H_4, Ar^2=*p*-MeC_6H_4
i: Ar^1=*p*-$MeOC_6H_4$, Ar^2=*p*-MeC_6H_4

Table 4. Reactions of **9a** with aryl Grignard reagents

Ar^1	Ar^2	Condition	**2** (%)	**3a** (%)	**2/3a**
Ph	Ph	r.t., overnight	**2a**, 31	6	5.2
Ph	Ph	r.t., 0.5 h; then 60 °C, 0.5 h	**2a**, 39	51	0.76
Ph	*p*-MeC_6H_4	r.t., 0.5 h; then 60 °C, 0.5 h	**2g**, 43	31	1.4

The yield of **3** also increased at a higher temperature.

A possible pathway for the formation of **3** would involve reduction of the intermediate **A** or **9** with an Mg–$MgBr_2$ complex in the reaction mixture. In fact, **9a** could be reduced to **3a** with the Mg–$MgBr_2$ complex in refluxing benzene in almost quantitative yield. Another possibility is that one-electron transfer from the Grignard reagent to *A* or **9** would provide the radical intermediate (**B**), which may give **2**, **3**, and the corresponding biphenyl derivative.

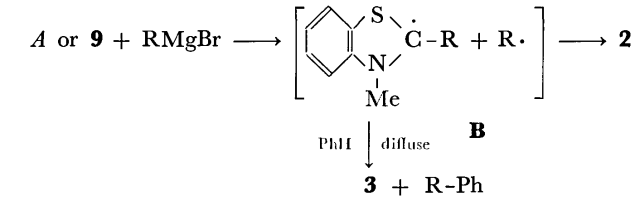

Indeed, the formation of biphenyl (21% after correction) was observed, when **9a** was treated with phenylmagnesium bromide in refluxing benzene. The interesting results from *p*-tolylmagnesium bromide solutions prepared from two kinds of magnesium metals [reagent grade: Mg-1 and 99.9% purity: Mg-2], which were treated with **9** and **10** in refluxing benzene, are summarized in Table 5.

Table 5. Effect of purity of magnesium on reactions of **9** or **10** with *p*-tolylmagnesium bromide

Mg	**9** or **10**	**2** (%)	**3** (%)	*Bis-p-tolyl* (%) [a]
Mg-1	**9a**	**2g**, 39	**3a**, 28	20
	9b	**2h**, 76	**3b**, 15	5
	9d	**2i**, 63	**3d**, 20	16
	10c	**2i**, 39	**3d**, 42	14
Mg-2	**9a**	**2g**, 82	**3a**, trace	0
	10a	**2g**, 81	**3a**, trace	0
	10b	**2h**, 82	**3b**, trace	0
	10c	**2i**, 86	**3d**, 2	0
	10c [b]	**2i**, 9	**3d**, 41	55

a) After correction of blank experiment. b) In the presence of a microspatula of anhydrous cobalt(II) chloride.

The results clearly showed that the pure magnesium (Mg-2) provided **2** preferentially and bis-*p*-tolyl was not detected. However, **3** could be obtained as a major product together with a significant amount of bis-*p*-tolyl when the reaction of **10** was carried out in the presence of a small amount of cobalt(II) chloride.

The fact that **3** is always accompanied by a significant amount of bis-*p*-tolyl using Mg-1 or Mg-2 plus cobalt(II) chloride shows that these two products are formed catalyzed by some transition metals present in magnesium as an impurity. This is supported by the fact that *p*-methylbiphenyl was not detected in the reaction mixture by careful gas chromatographic analysis which means that free *p*-toyl radical was not generated during the reaction, thus, in turn, eliminating one-electron transfer mechanism.

In the reaction of **10a** with *p*-tolymagnesium bromide prepared from Mg-2, the presence of an excess magnesium showed no effect, indicating that the reduction of *A* or **9** with the Mg–$MgBr_2$ complex to give **3** does not take place under the reaction conditions using pure magnesium.

In order to prepare 2,2-diaryl derivatives of **2**, the present reaction of **1** with aryl Grignard reagents is recommended and magnesium of higher purity should be used for selective formation of **2** and for suppression of **3** as a by-product.

Experimental

*3-Methyl-2,3-dihydrobenzothiazole-2-thione (**1**)*,[9] mp 92—94 °C (lit, 88—89 °C), 3-methyl-2-(methylthio)benzothiazolium

iodide (**8**),[10] mp 147—148 °C (lit, 148 °C (dec)), and 3-methyl-2-phenylbenzothiazolium iodide (**9a**),[11] mp 217—218 °C (lit, 218 °C (dec)), were prepared according to the reported methods.

*2-Aryl-3-methylbenzothiazolium Iodide (**9**).* *p*-Substituted benzaldehyde (80 mmol) was allowed to react with *o*-aminobenzenethiol (80 mmol) in ethanol (50 ml) for 1 h at 0 °C with stirring to afford 2-arylbenzothiazoline. The resulting thiazoline (60 mmol) was treated with dibenzoyl peroxide (60 mmol) in dichloromethane (250 ml) to give 2-arylbenzothiazole.[12] The benzothiazole (12 mmol) was heated with methyl iodide (40 mmol) at 100 °C in a sealed tube for 20 h to give 2-aryl-3-methylbenzothiazolium iodide (**9**) which was recrystallized from methanol; *p*-chloro derivative (**9b**), yield 80%, mp 253—256 °C (dec) (lit,[13] 224—225 °C) and *p*-methoxy derivative (**9d**), yield 87%, mp 197—198 °C (dec) (lit,[13] 199 °C).

*2-Aryl-3-methylbenzothiazolium Perchlorates (**10**).*[13] A solution of *o*-(methylamino)benzenethiol (69 mmol) and *p*-substituted benzoyl chloride (69 mmol) in benzene (60 ml) was stirred at room temperature for 0.1—1 h and then refluxed for 0.5 h. The resulting precipitates were collected; *p*-chloro chloride, mp 225 °C (dec) and *p*-methoxy chloride mp 191—196 °C (dec). To an aqueous solution of the chloride was added an excess amount of sodium perchlorate and the resulting precipitates were recrystallized from methanol; *p*-chloro (**10b**), yield 85%, mp 239—243 °C, and *p*-methoxy perchlorates (**10c**), yield 80%, mp 195.6—196.7 °C.

The following reactions were carried out under nitrogen.

*Reactions of 3-Methyl-2,3-dihydrobenzothiazole-2-thione (**1**) with Grignard Reagents. General Procedure.* An ethereal solution (20—30 ml) of the Grignard reagent (20—25 mmol), which was filtered through a glass filter, was added to a solution of **1** (905 mg, 5 mmol) in benzene (25—35 ml) and the mixture was refluxed for a time shown below. After addition of 10% aq ammonium chloride, the reaction mixture was extracted with dichloromethane, the extract was dried ($MgSO_4$), and the solvent was removed. The residue was submitted to dry column chromatography (DCC: SiO_2) to separate reaction products.

1) With Phenylmagnesium Bromide: The mixture was refluxed for 3 h. After addition of 10% aq sulfuric acid, evolved hydrogen sulfide was passe dthrough aq lead(II) acetate to give lead(II) sulfide (814 mg, 68%). Separation of the residue by DCC (CH_2Cl_2 : hexane=1 : 4) gave 3-methyl-2,2-diphenyl-2,3-dihydrobenzothiazole (**2a**; 1.021 g, 67%), mp 142—143 °C (from EtOH) (lit,[1a] 142—143 °C), and 3,3′-dimethyl-2,2′-diphenyl-2,2′,3,3′-tetrahydrobi(2-benzothiazolyl) (**3a**; 259 mg, 23%), mp 166—167 °C (from EtOH); NMR ($CDCl_3$): δ 2.24 (s, 6H) and 6.0—8.2 (m, 18H).

Found: C, 74.19; H, 5.26; N, 6.21%, Calcd for $C_{28}H_{24}N_2S_2$: C, 74.30; H, 5.34; N, 6.19%.

2) With p-Chlorophenylmagnesium Bromide: The mixture was refluxed for 4 h. Separation by DCC (CH_2Cl_2: hexane= 1 : 4) gave 2,2-di-*p*-chlorophenyl-3-methyl-2,3-dihydrobenzothiazole (**2b**; 1.079 g, 58%) and 2,2′-di-*p*-chlorophenyl-3,3′-dimethyl-2,2′,3,3′-tetrahydrobi(2-benzothiazolyl) (**3b**; 281 mg, 21%).

2b: did not solidify and was purified by molecular distillation; NMR ($CDCl_3$): δ 2.58 (s, 3H) and 6.3—7.5 (m, 12H).

Found: C, 64.76; H, 3.99; N, 3.63%. Calcd for $C_{20}H_{15}NCl_2S$: C, 64.52; H, 4.06; N, 3.70%.

3b: mp 203—204 °C (from PhH–EtOH); NMR ($CDCl_3$): δ 2.71 (s, 6H) and 6.0—8.1 (m, 16H).

Found: C, 64.33; H, 4.00; N, 5.37%. Calcd for $C_{28}H_{22}N_2Cl_2S_2$: C, 64.48; H, 4.25; N, 5.37%.

3) With p-Tolylmagnesium Bromide: The mixture was refluxed for 3 h. Separation by DCC (CCl_4) gave 3-methyl-2,2-di-*p*-tolyl-2,3-dihydrobenzothiazole (**2c**; 1.398 g, 84%), mp 143—144 °C (from EtOH) (lit,[1a] 141—141.5 °C).

4) With p-Methoxyphenylmagnesium Bromide: The mixture was refluxed for 1.5 h. Separation by DCC (CH_2Cl_2: hexane=1 : 1) gave 2,2-di-*p*-methoxyphenyl-3-methyl-2,3-dihydrobenzothiazole (**2d**; 1.532 g, 84%), mp 87—88 °C (from EtOH); NMR ($CDCl_3$): δ 2.61 (s, 3H), 3.85 (s, 6H), 6.3—7.2 (m, 4H), and 7.29 (ABq, $\Delta\delta$=32 Hz, J=9.5 Hz, 8H).

Found: C, 72.72; H, 5.86; N, 3.90%. Calcd for $C_{22}H_{21}NO_2S$: C, 72.70; H, 5.82; N, 3.85%.

5) With Ethylmagnesium Bromide: Filtration of the Grignard reagent was not carried out. The mixture was refluxed for 4 h. Separation by DCC (CH_2Cl_2 : hexane=1 : 4) and then preparative thin layer chromatography (PTLC) (SiO_2, CH_2Cl_2 : hexane=1 : 4) gave 2,2-diethyl-3-methyl-2,3-dihydrobenzothiazole (**2e**; 555 mg, 54%), bis[*o*-(methylamino)phenyl] disulfide (**4**; 133 mg, 19%), mp 66 °C (lit,[14] 64—68 °C), and ethyl *o*-(methylamino)phenyl sulfide (**5a**; 6 mg) (by IR and NMR[15]).

2e: oily material; NMR ($CDCl_3$): δ 0.95 (t, J=7.5 Hz, 6H), 1.3—2.2 (m, 4H), 2.70 (s, 3H), and 6.12—7.12 (m, 4H); MS: *m/e* 207 (M^+, 8%) and 178 (M^+ −Et, 100).

6) With t-Butylmagnesium Bromide: The mixture was refluxed for 42 h. Separation by DCC (CH_2Cl_2 : hexane= 1 : 4) gave recovered **1** (700 mg, 77%) and oily 2-*t*-butyl-3-methyl-2,3-dihydrobenzothiazole (**6**; 166 mg, 16%) (by NMR[1a]).

*Reaction of **1** with Organolithiums.* *1) With Phenyllithium*: Phenyllithium (40 mmol) in ether (30 ml) was added to **1** (905 mg, 5 mmol) in benzene (30 ml) and the mixture was stirred at room temperature for 15 min. After addition of 10% aq ammonium chloride and then usual work-up, the residue was submitted to DCC (SiO_2, CH_2Cl_2 : hexane= 1 : 4) and then PTLC (SiO_2, CH_2Cl_2 : hexane=1 : 4) to afford **2a** (635 mg, 42%) and oily *o*-(methylamino)phenyl sulfide (**5b**; 206 mg, 19%) (by IR and NMR[16]).

2) With Ethyllithium: To ethyllithium (20 mmol) in pentane (20 ml) was added **1** (905 mg, 5 mmol) in benzene (30 ml) and the mixture was stirred for 1 h. After usual work-up, **2e** (672 mg, 65%) was obtained by DCC (SiO_2, CH_2Cl_2 : hexane=1 : 4).

3) With Butyllithium: To butyllithium (50 mmol) in hexane (31 ml) was added **1** (1.812 g, 10 mmol) in benzene (30 ml) and the mixture was stirred for 1 h. After usual work-up, oily 2,2-dibutyl-3-methyl-2,3-dihydrobenzothiazole (**2f**; 1.536 g, 58%) (by IR and NMR[1c]) and oily 2-butylidene-3-methyl-2,3-dihydrobenzothiazole (**7**; 238 mg, 12%) were isolated by DCC (SiO_2, CH_2Cl_2 : hexane=1 : 1) and then PTLC (SiO_2, $CHCl_3$). **7** gradually changed to a solid on standing.

7: NMR ($CDCl_3$) : δ 0.6—1.9 (m, 7H), 3.01 (s, 3H), 4.65 (br s, 1H), and 6.9—7.4 (m, 4H); MS: *m/e* 205 (M^+, 100%) and 162 (M^+−Pr, 46).

*Reactions of 3-Methyl-2-(methylthio)benzothiazolium Iodide (**8**) with Grignard Reagents.* General procedure was almost the same as that for **1**.

1) With Phenylmagnesium Bromide: The mixture was stirred at room temperature for 1.5 h and then refluxed for 0.5 h. By DCC (CH_2Cl_2 : hexane=1 : 4), **2a** (818 mg, 54%) and **3a** (273 mg, 25%) were obtained.

2) With p-Chlorophenylmagnesium Bromide: The mixture was stirred overnight. By DCC (CH_2Cl_2 : hexane=1 : 4), **2b** (763 mg, 41%) and **3b** (86 mg, 7%) were obtained.

3) With p-*Tolylmagnesium Bromide*: The mixture was stirred overnight. By DCC (CCl_4), **2c** (823 mg, 50%) was obtained.

Similar reaction was carried out using **8** (808 mg, 2.5 mmol) and the Grignard reagent (10 mmol) under stirring for 0.5 h at room temperature and then refluxing for 0.5 h. **2c** (359 mg, 43%) and 3,3′-dimethyl-2,2′-di-*p*-tolyl-2,2′,3,3′-tetrahydrobi(2-benzothiazolyl) (**3c**: 166 mg, 28%), mp 163—165 °C (from EtOH); NMR (CCl_4): δ 2.29 (s, 6H), 2.94 (s, 6H), and 5.8—7.9 (m, 16H).

Found: C, 74.87; H, 5.86; N, 5.81%. Calcd for $C_{30}H_{28}N_2S_2$: C, 74.96; H, 5.87; N, 5.83%.

4) With p-*Methoxyphenylmagnesium Bromide*: The mixture was stirred overnight. By DCC (CH_2Cl_2: hexane=1 : 1), **2d** (1.515 g, 83%) was obtained.

5) With t-*Butylmagnesium Bromide*: The mixture was stirred overnight, and **6** (325 mg, 31%) was obtained by DCC (CH_2Cl_2 : hexane=1 : 4).

*Reactions of 3-Methyl-2-phenylbenzothiazolium Iodide (**9a**) with Grignard Reagents.* *1) With Phenylmagnesium Bromide*: Phenylmagnesium bromide (2 mmol) in ether (5 ml) was added to **9a** (353 mg, 1.0 mmol) in benzene (15 ml) and the mixture was stirred overnight. After usual work-up and PTLC (SiO_2, CCl_4), **2a** (93 mg, 31%), and **3a** (13 mg, 6%) were obtained.

Similar reaction was carried out using **9a** (883 mg, 2.5 mmol) and the Grignard reagent (5 mmol) under stirring at room temeperature for 0.5 h and then refluxing for 0.5 h, and **2a** (295 mg, 39%) and **3a** (289 mg, 51%) were obtained.

2) With p-*Tolylmagnesium Bromide*: *p*-Tolylmagnesium bromide (3 mmol) in ether (3 ml) was added to **9a** (353 mg, 1.0 mmol) in benzene (15 ml) and the mixture was stirred for 0.5 h and then refluxed for 0.5 h. After usual work-up and PTLC (SiO_2, CCl_4), 3-methyl-2-phenyl-2-*p*-tolyl-2,3-dihydrobenzothiazole (**2g**; 137 mg, 43%) and **3a** (70 mg, 31%) were obtained.

2g: mp 110.5—112.0 °C (from EtOH); NMR ($CDCl_3$); δ 2.30 (s, 3H), 2.52 (s, 3H), and 6.1—7.4 (m, 13H); MS; *m/e* 317 (M^+, 37%), 240 (100), and 226 (76).

Found: C, 79.46; H, 6.03; N, 4.33%. Calcd for $C_{21}H_{19}NS$: C, 79.45; H, 6.03; N, 4.41%.

*Reaction of **9a** with Mg–$MgBr_2$.* To a mixture of Mg and $MgBr_2$, prepared from magnesium (122 mg, 5 mmol) and 1,2-dibromoethane (470 mg, 2.5 mmol) in ether (10 ml), was added **9a** (883 mg, 2.5 mmol) in benzene (10 ml) and the mixture was stirred for 14 h and then refluxed for 1 h. After usual work-up, the residue was recrystallized from methanol to give **3a** (550 mg, 97%).

Determination of Biphenyl. An ethereal solution (10 ml) of phenylmagnesium bromide (8 mmol) was prepared. The Grignard solution (2.6 ml) and naphthalene as an internal standard were added to **9a** (353 mg, 1 mmol) in benzene (10 ml) and the mixture was refluxed for 49 min. Separately, the Grignard solution (2.6 ml), benzene (10 ml), and naphthalene were refluxed for 40 min. Based on gas chromatographic analysis (OV-1, 2m, 120 °C), the amount of biphenyl was 0.352 mmol and 0.142 mmol, respectively, indicating the net formation of biphenyl (0.210 mmol, 21%).

*Reactions of 2-Aryl-3-methylbenzothiazolium Salts (**9** or **10**) with* p-*Tolylmagnesium Bromide.* *General Procedure*: *p*-Tolylmagnesium bromide was prepared from magnesium (2.431 g, 0.1 mol) and *p*-bromotoluene (17.104 g, 0.1 mol) in ether (100 ml), using magnesium of reagent grade (Mg-1) and 99.9% magnesium (Mg-2), respectively, and filtered through glass wool.

To a suspension of **9** or **10** (2.5 mmol) in benzene (20 ml) was added the Grignard solution (5 mmol) at 78 °C and the mixture was heated as 76—80 °C for 1 h under stirring. A small aliquot was taken for gas chromatography. After addition of 1.5 M sulfuric acid, the reaction mixture was extracted with benzene, the extract was dired ($MgSO_4$), and evaporated. The residue was submitted to DCC (SiO_2, CH_2Cl_2: hexane=1 : 4; 1 : 1 for Mg-1 and **9c**). When the separation was incomplete, the yields were calculated based on the peak area of the NMR. The yields of bis-*p*-tolyl were determined by gas chromatography (OV-1, 120 °C) using biphenyl as an internal standard, and corrected by the amount produced after heating the Grignard solution in benzene without **9** or **10** under the same conditions. The results were listed in Table 5.

Physical data of new products are as follows.

2h: mp 145—146 °C (from MeOH–pentane); NMR ($CDCl_3$) : δ 2.27 (s, 3H), 2.51 (s, 3H), and 6.15—7.42 (m, 12H); MS : 353 (M^+ +2, 11%), 351 (M^+, 25), 262 (22), 260 (58), and 240 (100).

Found: C, 71.77; H, 5.19; N, 3.82%. Calcd for $C_{21}H_{18}NSCl$: C, 71.68; H, 5.16; N, 3.98%.

2i, mp 120.5—122.0 °C (from EtOH–pentane); NMR ($CDCl_3$): δ 2.33 (s, 3H), 2.59 (s, 3H), 3.75 (s, 3H), and 6.24—7.50 (m, 12H); MS : 347 (M^+, 46%), 256 (100), and 240 (92).

Found: C, 76.01; H, 6.19; N, 3.85%. Calcd for $C_{22}H_{21}NOS$: C, 76.05; H, 6.09; N, 4.03%.

3d: mp 182.0—183.5 °C (from MeOH–pentane); NMR ($CDCl_3$): δ 2.65 (s, 6H), 3.72 (s, 6H), and 5.90—7.95 (m, 16H); MS 512 (M^+, 0.8%), 256 (100), 241 (67), 226 (28), 198 (30), and 150 (16).

Found: C, 70.06; H, 5.54; N, 5.16%. Calcd for $C_{30}H_{28}N_2O_2S_2$: C, 70.28; H, 5.50, N, 5.46%.

References

1) a) K. Akiba, T. Kawamura, M. Hisaoka, and N. Inamoto, *Bull. Chem. Soc. Jpn.*, **48**, 3262 (1975); b) M. Hisaoka, K. Akiba, and N. Inamoto, *ibid.*, **48**, 3266 (1975); c) K. Akiba, M. Hisaoka, T. Kawamura, and N. Inamoto, *ibid.*, **48**, 3270 (1975).

2) a) P. Beak and J. W. Worley, *J. Am. Chem. Soc.*, **92**, 4142 (1970); b) M. Dagonneau and J. Vialle, *Tetrahedron*, **30**, 3119 (1974); c) A. Ohno, K. Nakamura, M. Uohama, S. Oka, T. Yamabe, and S. Nagata, *Bull. Chem. Soc. Jpn.*, **48**, 3718 (1975).

3) P. Beak, J. Yamamoto, and C. J. Upton, *J. Org. Chem.*, **40**, 3052 (1975).

4) D. Seebach, W. Lubosch, and D. Enders, *Chem. Ber.*, **109**, 1309 (1976).

5) J. R. Owen, *Tetrahedron Lett.*, **1969**, 2709.

6) K. Akiba, Y. Ohara, M. Hisaoka, and N. Inamoto, *Heterocycles*, **3**, 567 (1975).

7) I. Degani, R. Fochi, and P. Tundo, *Gazz. Chim. Ital.*, **105**, 907 (1975).

8) I. Degani and R. Fochi, *J. Chem. Soc., Perkin Trans. 1*, **1976**, 1886.

9) K. Baker and H. E. Fierz-David, *Helv. Chim. Acta*, **33**, 2011 (1950).

10) D. J. Fry and J. D. Kendall, *J. Chem. Soc.*, **1951**, 1716.

11) L. M. Clark, *J. Chem. Soc.*, **127**, 973 (1925).

12) F. J. Goetz, *J. Heterocyclic Chem.*, **4**, 80 (1967).

13) D. L. Garmaise, G. Y. Paris, J. Komlossy, and C. H. Chambers, *J. Med. Chem.*, **12**, 30 (1969).

14) C. D. Harries and E. Loewenstein, *Ber.*, **27**, 861 (1894).

15) K. Akiba, H. Shiraishi, and N. Inamoto, *Bull. Chem. Soc. Jpn.*, **52**, 263 (1979).

16) M. Hisaoka, K. Akiba, and N. Inamoto, *Bull. Chem. Soc. Jpn.*, **48**, 3274 (1975).

Reactions of 4*H*-1-Benzothiopyran-4-ones and Related Compounds with Dimethyl Sulfate†

Hiroyuki NAKAZUMI* and Teijiro KITAO
Department of Applied Chemistry, College of Engineering, University of Osaka Prefecture, Sakai, Osaka 591

(Received June 9, 1978)

4*H*-1-Benzothiopyran-4-ones (thiochromones) and isomeric 2*H*-1-benzothiopyran-2-ones (thiocoumarins) have been allowed to react with dimethyl sulfate (DMS) to study the differences in reactivity on methylation. Methylation of 2-methyl(thiochromones) with DMS afforded the blue colored dimerization products, 4-(4-methoxy-1-benzothiopyran-2-ylidenemethyl)-2-methyl-1-benzothiopyrylium perchlorates, while that of 7-methoxy-4-methyl(thiocoumarin) gave the *O*-methylated yellow salt, 2,7-dimethoxy-4-methyl-1-benzothiopyrylium perchlorate. Methylations of oxa analogues (coumarins) and aza analogues (2-quinolones) of thiocoumarins with DMS have also been examined. It has been found that the ease of formation of methylation products is affected by the hetero atom and carbonyl group.

In a previous paper,[1] the spectral characterization of 4*H*-1-benzothiopyran-4-ones (thiochromones) was proposed to distinguish them from 2*H*-1-benzothiopyran-2-ones (thiocoumarins). However, it was very difficult to distinguish only on the basis of spectral data. The methylation of these compounds with dimethyl sulfate (DMS) is an attempt to distinguish them. Tolmachev *et al.*[2] reported the methylation of 2-methyl(thiochromone), however, the systematic study of the methylation of thiochromones, thiocoumarins and the oxa analogues (coumarins) and the aza analogues (2-quinolones) with DMS have not been reported. In this paper, the differences in methylation of these heterocyclic compounds with DMS will be reported.

Experimental

All the melting points are uncorrected. Infrared spectra were recorded on a Hitachi ESI-S2 spectrophotometer using KBr pellets. ^{1}H-NMR spectra were taken on a Hitachi R-24A spectrometer with tetramethylsilane as an internal standard. Elemental analyses were recorded on a Yanaco CHN recorder MT-2. DTA-TG analysis was taken on a Rigaku DTA-TG instrument at 10 °C/min under nitrogen.

*4-(4-Methoxy-1-benzothiopyran-2-ylidenemethyl)-2-methyl-1-benzothiopyrylium Perchlorate Derivatives (**2a**—**2c**).* 2-Methyl(thiochromone)[1] **1a** (3.5 g) was added to dimethyl sulfate (2 ml). The mixture was stirred at 70 °C for 5 h and after cooling, H_2O (2 ml) was added to the reaction mixture, followed by the addition of 60% $HClO_4$ (4 ml). The resulting solid was separated, and washed with MeOH, $CHCl_3$, and EtOH, and recrystallized from glacial acetic acid to give **2a** in 32% yield. From the first filtrate, starting material **1a** was recovered in 15% yield.

The other 1-benzothiopyrylium perchlorates (**2b** and **2c**) were similarly prepared in 30—40% yield together with the starting materials (**1b** and **1c**). **2a**(X=H): mp 225 °C; λ_{max} (acetone) 590 nm (ε 6.28×10^4); NMR(CF_3COOH)δ= 3.35 (3H, s), 4.65 (3H, s), 5.78 (2H, s), and 8.20—8.90 ($\approx$9H, m); Found: C, 56.19; H, 3.70%; Calcd for $C_{21}H_{17}O_5S_2Cl$: C, 56.19; H, 3.79%. **2b**(X=OCH_3): mp >300 °C; λ_{max} (acetone) 596 nm(ε 6.92×10^4); NMR(CF_3COOH) δ= 3.20, 4.05, 4.25, 4.65, 5.55, and 7.60—8.80 (integral values could not be measured due to the poor solubility of **2b**); Found: C, 54.49; H, 4.18%; Calcd for $C_{23}H_{21}O_7S_2Cl$: C, 54.28; H, 4.13%. **2c**(X=Cl): mp>300 °C; λ_{max} (acetone) 590 nm(ε 5.22×10^4); NMR(CF_3COOH) δ=3.35 (3H, s), 4.65(3H, s), 5.75 (2H, s) and 7.80—8.90 ($\approx$7H, m); Found: C, 48.12; H, 2.73%; Calcd for $C_{21}H_{15}O_5S_2Cl_3$: C, 48.70; H, 2.90%.

*4-(1-Benzothiopyran-2-ylidenemethyl)-2-methyl-1-benzothiopyrylium Perchlorate (**3**).* A suspension of $AlCl_3$ (2.6 g) in THF (40 ml) was added to a solution of $LiAlH_4$ (0.8 g) in THF. To the resulting solution, a solution of 2-methyl(thiochromone) (3.5 g) in THF (40 ml) was added dropwise at 25—30 °C. After standing for 30 min at 30 °C, H_2O (4 ml) and then 6M-H_2SO_4 (10 ml) was added to the reaction mixture. After filtration, the filtrate was condensed and extracted with ether. To the extract 70% $HClO_4$ (5 ml) and H_2O (10 ml) were added, and the resulting solid was washed with ether and methanol to give **3**: mp 250 °C; NMR(CF_3COOH) δ=2.85 (3H, s), 5.40 (2H, s), and 7.80—8.10 ($\approx$10H, m); λ_{max} (acetone) 616 nm(ε 6.14×10^4); Found: C, 57.47; H, 3.78%; Calcd for $C_{20}H_{15}S_2O_4Cl$: C, 57.35; H, 3.58%.

*2,7-Dimethoxy-4-methyl-1-benzothiopyrylium Perchlorate (**6**).* Compound **6** was prepared from **4**[1] by a method similar to that for compound **2a** and a reaction time of 10 h in 10% yield with the starting materials. Mp 166—168 °C; λ_{max} (acetone) 386 nm(ε 1.10×10^4); NMR(CF_3COOH) δ=3.09 (3H, s), 4.14 (3H, s), 4.60 (3H, s), 7.60—7.80 (3H, m), and 8.57 (1H, m); Found: C, 44.92; H, 4.12%; Calcd for $C_{12}H_{13}O_6SCl$: C, 44.93; H, 4.06%.

*4-Methoxy-2H-1-benzothiopyran-2-one (**7**).* Compound **7** was prepared from 4-hydroxy-2*H*-1-benzothiopyran-2-one **5**[3] by a method similar to that for compound **2a**: yield 33%; mp 126—128 °C; ν_{CO} 1635 cm^{-1}; MS(80 eV), *m/e*(rel intensity), 192 (100), 164 (64), 149 (85), and 136 (10); NMR ($CDCl_3$)δ=4.00 (3H, s), 6.10 (1H, s), 7.40—7.50 (3H, m), and 8.15 (1H, m); Found: C, 62.58; H, 4.12%; Calcd for $C_{10}H_8O_2S$: C, 62.50; H, 4.17%.

*2,7-Dimethoxy-4-methylquinolinium Perchlorate (**11**).* Compound **10**[4] (1.0 g) was added to dimethyl sulfate (8.4 g) with stirring. The mixture was heated at 70 °C for 4 h and after cooling, H_2O (7 ml) was added, followed by 60% $HClO_4$ (10 ml). The resulting solid was filtered after standing at room temperature for several hours. Recrystallization from EtOH gave quinolinium perchlorate **11**: yield 41%; dec 245 °C; NMR (CF_3COOH) δ=3.00 (3H, s), 4.10 (3H, s), 4.30 (3H, s), 7.20—7.55 (3H, m), and 8.30 (1H, m); Found: C, 47.15; H, 4.57; N, 4.25%; Calcd for $C_{12}H_{14}NO_6Cl$: C, 47.45; H, 4.61; N, 4.61%.

*2,7-Dimethoxy-4-methylquinoline (**12**).* Quinolinium

† A preliminary report of this work was presented at the 10th Congress of Heterocyclic Chemistry, Tsukuba, October 1977.

salt **11** (0.1 g) was dissolved in MeOH (5 ml), and 10% aqueous NaOH was added to this solution until the pH was 10. The resulting solid was collected and recrystallized from MeOH–H_2O solution to give 2,7-dimethoxy-4-methylquinoline **12**: mp 67—68 °C; NMR($CDCl_3$) δ=2.60 (3H, s), 3.95 (3H, s), 4.05 (3H, s), 6.63 (1H, s), and 7.20—7.80 (3H, m); Found: C, 70.68; H, 6.40; N, 6.47%; Calcd for $C_{12}H_{13}NO_2$: C, 70.94; H, 6.40; N, 6.90%.

*1,4-Dimethyl-2-methoxyquinolinium Perchlorate (**15**).* Compound **15** was prepared from **13**[5] by a method similar to that for compound **11**: yield 54%; mp 161—162 °C; NMR(CF_3COOH) δ=3.00 (3H, s), 4.30 (3H, s), 4.50 (3H, s), 7.45 (1H, s), and 7.80—8.45 (4H, m); Found: C, 50.01; H, 4.84; N, 4.73%; Calcd for $C_{12}H_{14}NO_5Cl$: C, 50.09; H, 4.87; N, 4.78%.

*4-Methyl-2-methoxyquinolinium Perchlorate (**16**).* Compound **14**[6] was allowed to react with DMS by a method similar to that for compound **11**. After treating with 60% $HClO_4$, the reaction mixture was allowed to stand overnight at room temperature. The resulting solid was separated by filtration, and recrystallization from MeOH afforded quinolinium perchlorate **15** (yield 11%). Another quinolinium perchlorate **16** was isolated by the evaporation of the filtrate of compound **15** and purified by repeated recrystallization from MeOH. It was found that compound **16** contained one molecule of water of crystallization by means of TG and DTA. Yield 50%; mp 157 °C; NMR(CF_3COOH) δ=3.05 (3H, s), 4.45 (3H, s) 7.45 (1H, s), and 7.70—8.40 (4H, m); Found: C, 45.79; H, 4.84; N, 5.27%; Calcd for $C_{11}H_{12}NO_5Cl\cdot H_2O$: C, 45.28; H, 4.80; N, 4.80%.

*4-Methyl-2-(methylthio)quinolinium Perchlorate (**17**) and 7-Methoxy-4-methyl-2-(methylthio)quinolinium Perchlorate (**18**).* Compound **17** was prepared by a method similar to that for compound **11** from 4-methylquinoline-2-thione:[7] yield 26%, mp 226—228 °C; NMR(CF_3COOH) δ=2.95 (6H, s) and 7.60—8.40 (5H, m); Found: C, 45.53; H, 4.30; N, 5.11%; Calcd for $C_{11}H_{12}NO_4SCl$: C, 45.60; H, 4.15; N, 4.84%. Compound **18** was similarly prepared from 7-methoxy-4-methylquinoline-2-thione (mp 240 °C; Found: C, 64.60; H, 5.44; N, 7.08%) which was obtained by the reaction of 7-methoxy-4-methyl-2-quinolone with P_2S_5 in benzene for 6 h under reflux: yield 38%; dec 250 °C; NMR (CF_3COOH) δ=2.95 (6H, s), 4.10 (3H, s), and 7.45—8.30 (4H, m); Found: C, 44.79; H, 4.46; N, 4.69%; Calcd for $C_{12}H_{14}NO_5SCl$: C, 45.07; H, 4.38; N, 4.38%.

*7-Methoxy-4-(7-methoxy-4-methylbenzopyran-2-ylidenemethyl)-2-(methylthio)benzopyrylium Perchlorate (**19**).* 7-Methoxy-4-methyl-2*H*-benzopyran-2-thione was obtained by the reaction of 7-methoxy-4-methyl(coumarin) with P_2S_5 in benzene: yield 64%; mp 135 °C; lit,[8] 136 °C. Treatment of the thiocarbonyl derivative with DMS at 70 °C and then with 60% $HClO_4$ gave a red product. Recrystallization from glacial acetic acid gave **19**: yield 23%; NMR(CF_3COOH) δ=3.10 (6H, s), 4.20 (6H, s), 5.20 (2H, s), and 7.50—8.50 ($\approx$7H, m); λ_{max}(acetone) 556 nm (ε 5.98×10^4); Found: C, 56.85; H, 4.46%; Calcd for $C_{23}H_{21}O_8SCl$: C, 56.04; H, 4.26%.

Results and Discussion

The Methylation of Thiochromones and Thiocoumarins. Traverso[9] has reported that 4-methoxythiopyrylium perchlorate, as the *O*-methylated product, was formed when 4*H*-thiopyran-4-one reacted with DMS followed by treatment with perchloric acid. In the case of 2-methyl(thiochromone) **1a**, a blue salt was found under the same conditions. The structure of this blue salt **2a** has been determined as 4-(4-methoxy-1-benzothiopyran-2-ylidenemethyl)-2-methyl-1-benzothiopyrylium perchlorate, on the basis of the NMR spectrum and elemental analyses. The structure has been also supported by ESCA.[10] The reactions of 7-methoxy-2-methyl- and 7-chloro-2-methyl(thiochromones) with DMS also gave blue 1-benzothiopyrylium salts **2b** and **2c**, respectively, with the starting materials. The blue 1-benzothiopyrylium salts have visible absorption maxima in the region 590—596 nm similar to that of a thiacyanine dye, which was prepared by the cyclodehydration of 4-(phenylthio)-2-butanone with polyphosphoric acid.[11] Tolmachev *et al.*[2] have reported that a similar 1-benzothiopyrylium salt was obtained by the reaction of 2-methyl(thiochromone) **1a** with methyl *o*-nitrobenzenesulfonate in toluene. A possible mechanism for the formation of **2a—c** is given in Scheme 1:

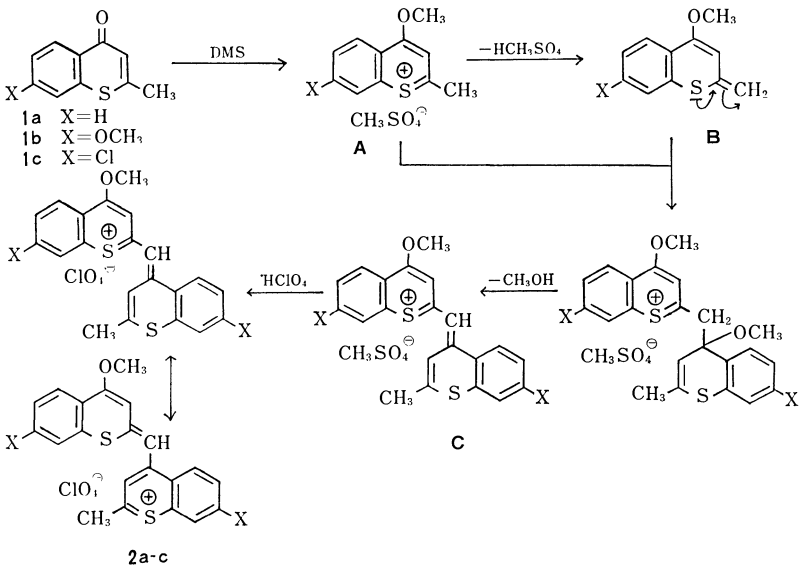

Scheme 1.

i.e. an initial attack of DMS to 2-methyl(thiochromone) derivatives leading to the *O*-methylated derivative **A**. Deprotonation could then occur to give **B**. The condensation of **B** with **A** would lead to **C**, and an anion exchange of ClO_4^- would afford the products **2a**—**c**.

Furthermore, 2-methyl(thiochromone) **1a** was reduced by aluminum hydride to 2-methyl-4*H*-1-benzothiopyran-4-ol, and the latter converted to the blue 1-benzothiopyrylium salt **3** with perchloric acid (Scheme 2). From these results, it appears that the methyl group at the 2-position of thiochromone derivatives has activated hydrogens.

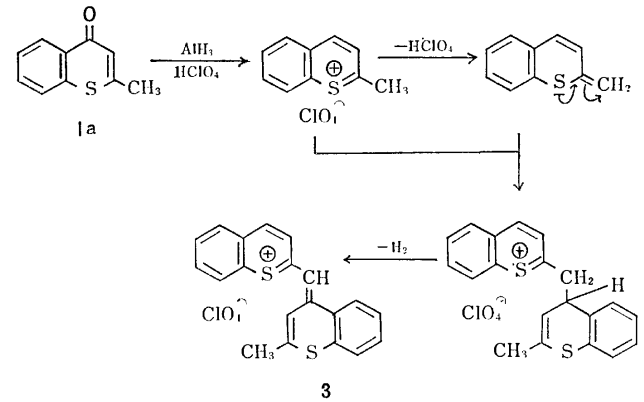

Scheme 2.

Methylation of 7-methoxy-4-methyl(thiocoumarin) **4**, the isomer of 7-methoxy-2-methyl(thiochromone) **1b**, with DMS gave a yellow salt. This yellow salt was identified with 2,7-dimethoxy-4-methyl-1-benzothiopyrylium perchlorate **6** as the *O*-methylated product of **4**. In the case of 4-hydroxy(thiocoumarin) **5**, 4-methoxy(thiocoumarin) **7** was isolated as the *O*-methylated product at the 4-position of **5** (Scheme 3). The different methylation mechanisms between 2-methyl(thiochromone) and 4-methyl(thiocoumarin) derivatives may be utilized to distinguish them.

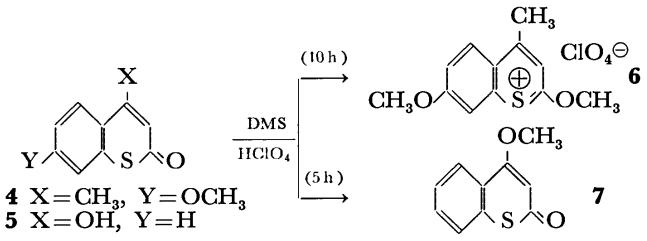

Scheme 3.

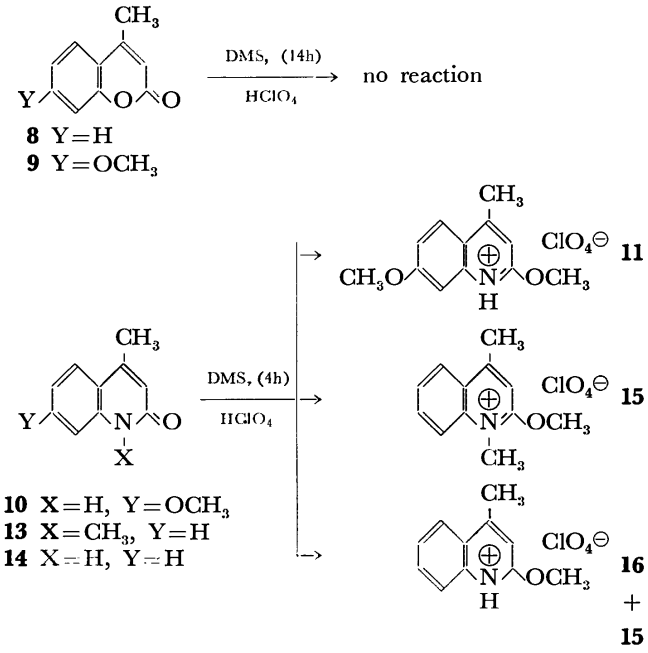

Scheme 4.

The Methylation of Oxa and Aza Analogues of Thiocoumarins with DMS. A comparison of the methylation of oxa analogues (coumarins) and aza analogues (2-quinolones) of 4-methyl(thiocoumarin) derivatives with DMS is summarized in Scheme 4. No methylation reaction occur, however, between coumarin derivatives (**8** and **9**) and DMS, even under the prolonged reaction time. In the cases of 2-quinolone derivatives (**10**, **13**, and **14**), *O*- and/or *N*-methylated products were obtained. The structures of quinolinium salts **11** and **16** could be identified by the treatment of **11** or **16** with base. For example, the 2-methoxyquinoline derivative **12** was obtained by the treatment of **11** with 10% aqueous NaOH. Similarly, 1,4-dimethyl-2-quinolone **13** gave the *O*-methylated 2-methoxy derivative **15**. In the case of 4-methyl-2-quinolone **14**, the 2-methoxy derivative **16** and the dimethylated quinolinium salt **15** were obtained. This result showed that the competitive *N*-methylation and *O*-methylation of **14** proceeded. From a comparison of the methylation of these heterocyclic compounds, it may be seen that methylation at the carbonyl group of heterocyclic compounds containing a nitrogen and/or sulfur atom readily occurs, but in the case of heterocyclic compounds containing an oxygen atom no methylation

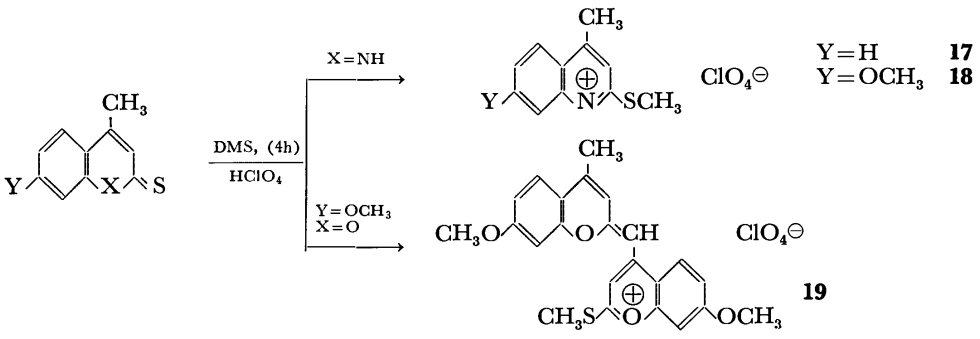

Scheme 5.

occurs.

The Methylation of Heterocyclic Compounds Containing a Thiocarbonyl Group with DMS. Reactions of 2-quinolone and coumarin derivative(s) with phosphorus pentasulfide in benzene afforded the thiocarbonyl derivatives, which were subsequently treated with DMS (Scheme 5). In the cases of the quinoline derivatives, colorless *S*-methylated products **17** and **18** were obtained, respectively. While 7-methoxy-4-methyl-2*H*-benzopyran-2-thione afforded a red compound, 7-methoxy-4-(7-methoxy-4-methylbenzopyran-2-ylidenemethyl)-2-(methylthio)benzopyrylium salt **19**, the structure of which was assigned by analogy of **2a—c**, based on the NMR spectrum and elemental analyses. This observation shows that the formation of the benzopyrylium salt proceeds easier in the case of 2*H*-benzopyran-2-thione containing a thiocarbonyl group than in the case of coumarins containing a carbonyl group.

The authors wish to acknowledge the assistance of Kohzo Higuchi and Tohru Ohtsuki.

References

1) H. Nakazumi and T. Kitao, *Bull. Chem. Soc. Jpn.*, **50**, 939 (1977).
2) A. I. Tolmachev and V. P. Sribnaya, *Zh. Obshch. Khim.*, **32**, 383, (1962).
3) A. Ruwet, C. Draguet, and M. Renson, *Bull. Soc. Chim. Belg.*, **79**, 639 (1970).
4) E. Späth and O. Brunner, *Ber.*, **57**, 1246 (1924).
5) L. Knorr, *Ann. Chem.*, **236**, 106 (1886).
6) L. Knorr, *Ann. Chem.*, **236**, 78 (1886).
7) E. Rosenhauer, H. Hoffmann, and W. Heuser, *Ber.*, **62**, 2732 (1929).
8) F. M. Dean, J. Goodchild, and A. W. Hill, *J. Chem. Soc., C*, **1969**, 2192.
9) G. Traverso, *Chem. Ber.*, **91**, 1224 (1958).
10) H. Nakazumi, T. Yoshida, S. Sawada, and T. Kitao, *Nippon Kagaku Kaishi*, **1976**, 849.
11) B. D. Tilak, H. S. Desai, C. V. Deshpande, S. K. Jain, and V. M. Vaidya, *Tetrahedron*, **22**, 7 (1966).

Dry Ozonation of Friedelane and Friedelin[1)]

Eri AKIYAMA, Masahiro TADA,† Takahiko TSUYUKI, and Takeyoshi TAKAHASHI*

Department of Chemistry, Faculty of Science, The University of Tokyo, Hongo, Bunkyo-ku, Tokyo 113

†*Laboratory of Bioorganic Chemistry, Tokyo University of Agriculture and Technology, Fuchu, Tokyo 183*

(Received June 16, 1978)

Dry ozonation of friedelane afforded 18β,19β-epoxyfriedelane, 19-oxofriedelane, 16-oxofriedelane, 21-oxofriedelane, friedelin, and a new compound, 15-oxofriedelane. Friedelin, on dry ozonation, gave 3,16-dioxofriedelane, 3,19-dioxofriedelane, and new compounds, 18β,19β-epoxyfriedelan-3-one and 3,15-dioxofriedelane. It was shown that the oxidation occurred at D and E rings regioselectively in the dry ozonation.

It has been known that ozone reacts slowly with saturated hydrocarbons in solution to give alcohols and ketones.[2)] Mazur *et al.*[3-6)] and Beckwith *et al.*[7,8)] have demonstrated that ozone adsorbed on silica gel reacts efficiently with saturated hydrocarbons,[3,4)] *t*-alcohols,[4)] bromides,[5)] acetates,[4,7,8)] bromo acetate,[6)] and ketone.[8)] This procedure, named dry ozonation, has been developed as a useful synthetic method for stereoselective hydroxylation of tertiary carbon atoms of organic compounds. Recently this dry ozonation reaction has been shown to be also applicable to oxidative conversion of primary amines to nitro compounds.[9)]

Hitherto only a few investigations on functionalization of unactivated carbon atoms in triterpene skeletons have been reported[10,11)] in contrast with investigations on the steroidal compounds.[12)] In connection with the studies on synthesis of friedelane derivatives, the dry ozonation reaction was applied to functionalization of an unactivated carbon atom of a friedelane skeleton. It is shown that friedelane (**1**) and its 3-oxo derivative, friedelin (**2**), on dry ozonation, gave 15-, 16-, and 21-oxo derivatives.

Friedelane (**1**)[13)] was adsorbed on silica gel (*ca.* 100 times weight of **1**). The silica gel was then cooled to −78 °C and saturated with ozone at this temperature. After warming to room temperature, the reaction products were eluted from the silica gel and examined by TLC. It was shown that the starting material was completely consumed and only a complex mixture of unidentified polar products with extremely low R_f value was detected. No spot corresponding to mono-oxygenated products such as tertiary alcohols or ketones was observed on the TLC. Beckwith *et al.*[7)] reported that a substrate adsorbed on silica gel was oxidized with ozone generated by desorption from the silica gel, and not directly with adsorbed ozone. And they pointed the importance of the maintenance of a high partial pressure of ozone during the warm-up period.

To obtain optimum conditions for the formation of the mono-oxygenated products, dependence of reaction temperature and ozone concentration on their yields was examined. The reaction at higher temperature increased in the conversion of friedelane and in the formation of the unidentified products, but decreased in the yields of the mono-oxygenated products. It was found that the following reaction temperature gave a fairly good result for the formation of the mono-oxygenated products, although the conversion yield of friedelane was less than 20%. The silica gel saturated with ozone at −78 °C was kept at −65 to −60 °C and ozone was desorbed gradually by sweeping with a slow stream of nitrogen at this temperature range, and then the silica gel was warmed up to room temperature. Ozone concentration was shown to be independent of the yields and silica gel (Wakogel C 200; 10 g) was saturated enough with a flow of 3% ozone in oxygen at flow rate of 50 ml/min for 1 h at −78 °C.

Under these conditions, friedelane (**1**; 100 mg) adsorbed on silica gel (10 g) was oxidized with ozone. The unchanged friedelane (**1**: 82 mg) was recovered and a mixture (*ca.* 19 mg; corresponding to 18% conversion) of mono-oxygenated products was obtained and was subjected to separation by preparative TLC, alumina column, and/or HPLC.

18β,19β-Epoxyfriedelane[14)] (**3**; yield[15)] 48%), 19-oxofriedelane[14)] (**4**; yield[15)] 2%), 16-oxofriedelane[16)] (**5**; yield[15)] 11%), and friedelin (**2**; yield[15)] 0.8%) were obtained and identified by comparison with their authentic samples, respectively. Two new carbonyl compounds (**6** and **7**) were also obtained in 11 and 1% yields,[15)] respectively.

The compound (**6**), $C_{30}H_{50}O$, mp 239—240 °C, showed a carbonyl absorption at 1700 cm^{-1} in the IR spectrum and an AB quartet signal at δ_A 2.15 and δ_B

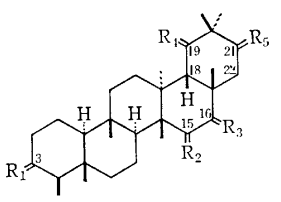

	R_1	R_2	R_3	R_4	R_5
1	H_2	H_2	H_2	H_2	H_2
2	O	H_2	H_2	H_2	H_2
4	H_2	H_2	H_2	O	H_2
5	H_2	H_2	O	H_2	H_2
6	H_2	O	H_2	H_2	H_2
6-d_2	H_2	O	D_2	H_2	H_2
7	H_2	H_2	H_2	H_2	O
8	H_2	O	O	H_2	H_2
11	O	H_2	H_2	O	H_2
12	O	H_2	O	H_2	H_2
13	O	O	H_2	H_2	H_2

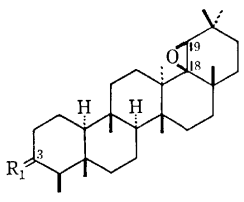

	R_1
3	H_2
10	O

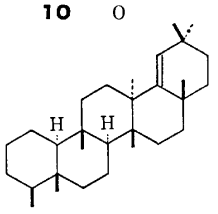

9

2.50 (J_{AB}=18 Hz) in the PMR spectrum. These observations indicate the presence of a grouping ■–CO–CH_2–■ (■ refers to a quaternary carbon atom). The carbonyl group of this compound was inferred to be located either at C-15 or C-16 from the characteristic fragment peaks in the high resolution mass spectrum[17] (Fig. 1). The spectral data of the carbonyl compound (**6**) was different from those of 16-oxofriedelane (**5**).[16] Therefore, the ketone (**6**) was deduced to be 15-oxofriedelane.

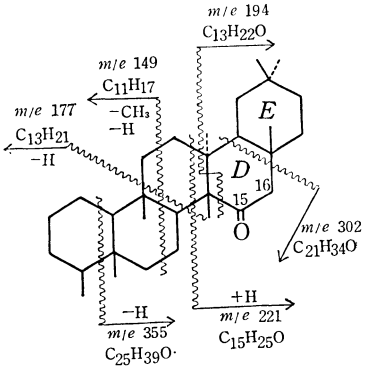

Fig. 1.

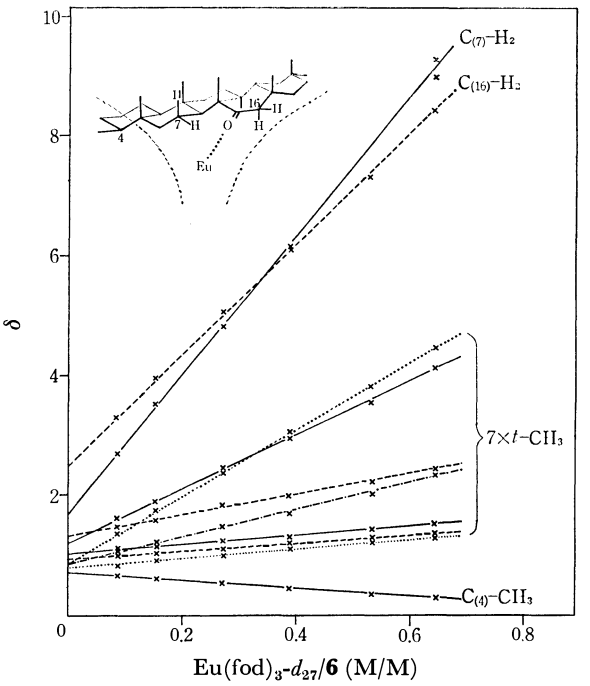

Fig. 2. Induced paramagnetic shifts for 15-oxofriedelane (**6**) in a 5% (w/v) in $CDCl_3$.

This conclusion was confirmed by spectral and chemical evidence. The intact friedelane-framework without skeletal rearrangement during the reaction was shown for **6** by its reduction under forced Wolff-Kishner conditions to afford friedelane (**1**). The carbonyl group at C-15 is so hindered that a half amount of **6** was left unchanged even though under these reduction conditions. On tretament with sodium deuterioxide, the compound (**6**) gave a deuteriated product (**6**-d_2), whose molecular ion peak was observed at *m/e* 428. In PMR measurement of **6** using Eu(fod)$_3$-d_{27} as a shift reagent, a doublet due to a secondary methyl group at C-4 suffered an upfield shift and a multiplet due to a methylene group caused condsierable downfield shift, which was much larger than that for the α-methylene protons (at C-16) adjacent to the carbonyl group (Fig. 2). Provided that the carbonyl group locates at C-15 and the shift reagent is associated with the carbonyl oxygen atom, these observations were reasonably expalined. The secondary methyl group at C-4 which would be placed outside of a cone area suffered upfield shift. The methylene group which caused downfield shift could be assigned to $C_{(7)}$–H_2 because of the nearest proximity of the shift reagent.

Oxidation with selenium dioxide, the compound (**6**) gave 15,16-dioxofriedelane (**8**), mp 280—281 °C, IR 1720 and 1700 cm^{-1}, MS *m/e* 440 (M^+). The dione (**8**) was shown to be identical with that obtained from 16-oxofriedelane (**5**) by the same treatment.

The other carbonyl compound (**7**), mp 237—240 °C, $[\alpha]_D$+117°, was shown to possess a grouping ■–CO–CH_2–■ based on the IR spectrum (1720 cm^{-1}) and on an appearance of a doublet as an H_A-part (δ 2.60, d, J=12 Hz) of an AB quartet in the PMR spectrum. In the PMR spectrum using Eu(fod)$_3$-d_{27} as a shift reagent, an H_B-part of the AB

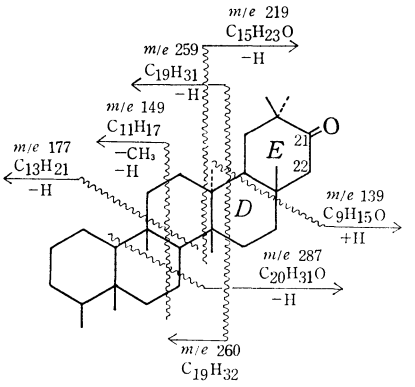

Fig. 3.

quartet was observed. The investigation on the fragmentation pattern in the high resolution mass spectrum revealed that the carbonyl group of **7** must locate on either D or E ring, that is, on either 15-, 16-, 19-, 21-, or 22 carbon atom[17] (Fig. 3). Thus the structure of **7** could be either 21- or 22-oxofriedelane, because the remaining three compounds had been already identified as the products of this reaction.

Courtney and Gascoigne isolated several friedelane derivatives from *Siphonodon australe* Benth.,[18] one of which was shown to be 3,21-dioxofriedelane.[19] In this structure determination, 21-oxofriedelane was prepared and the melting point (241—242 °C), $[\alpha]_D$ value (+152°), and the main fragment peaks (*m/e* 259, 177, and 149) were described.[18,20] On the other hand, 22-oxofriedelane has not been reported yet. Unfortunately direct comparison could not be made because no authentic 21-oxofriedelane left in Courtney's laboratory. However, the physical constants and mass fragmentation pattern were nearly

the same as those of the authentic 21-oxofriedelane. From these facts together with the spectral data, it is probable that the compound (**7**) would be 21-oxofriedelane (**7**), not 22-oxofriedelane.

Although 18β,19β-epoxyfriedelane (**3**) was obtained as the main product in the dry ozonation of friedelane (**1**), the epoxide (**3**) could be considered to be a secondary reaction product formed from friedel-18-ene (**9**) by oxidation with ozone. Initial attack of ozone to a methine hydrogen atom at C-18 would give unstable 18β-hydroxyfriedelane, which could be immediately dehydrated to form friedel-18-ene (**9**). It is known that the methine hydrogen atom at C-18 is susceptible to reaction with bromine to give friedel-18-ene (**9**)[13,21] through 18-bromofriedelane which could not be isolated, and that friedel-18-ene (**9**) in solution is easily epoxidized by ozone.[14,22]

Dry ozonation of friedel-18-ene (**9**) under the same conditions as above, gave the epoxide (**3**) in 53% yield together with the unchanged **9** (in 12% yield) and unidentified polar materials. 19-Oxofriedelane (**4**), however, could not be detected in the reaction mixture. This implies that 19-oxofriedelane (**4**) would be produced by direct insertion of ozone into $C_{(19)}$–H followed by oxidation, not through friedel-18-ene (**9**).

Friedelin (**2**) was then subjected to dry ozonation under the same conditions as above. However eaxmination of the reaction mixture by TLC showed that most of the starting material (**2**) remained unchanged. The low reactivity seems to be due to the presence of an electron-withdrawing carbonyl group at C-3.[4,5] After saturation with ozone at −78 °C, the silica gel was warmed to −15 °C and ozone was desorbed by sweeping with a stream of nitrogen at this temperature. The reaction mixture was separated as before.

Friedelin (**2**) was recovered in 32% yield. 3,16-Dioxofriedelane[16] (**12**; yield[15] 3%), a new epoxy ketone (**10**; yield[15] 12%), and a mixture of two diketones (**11** and **13**) were obtained. The epoxy ketone (**10**), $C_{30}H_{48}O_2$, mp 266—269 °C (with decomposition), showed a carbonyl absorption band at 1710 cm^{-1} and a singlet at δ 2.56 in the PMR spectrum, which could be easily assignable to a 19α-H by comparison with that (δ 2.56, s) of 18β,19β-epoxyfriedelane (**3**). The epoxy ketone (**10**) was subjected to the Birch reduction, the Jones oxidation, and then the Huang-Minlon reduction to afford 19-oxofriedelane (**4**). Thus the epoxy ketone (**10**) was shown to be formulated as 18β,19β-epoxyfriedelan-3-one.

The mixture of diketones (**11** and **13**), giving one spot on TLC, was separated by HPLC to afford **11** (yield[15] 1%), mp 264—266 °C, IR 1708 and 1680 cm^{-1} and **13** (yield[15] 3%), mp 280.5—281.5 °C, IR 1710 and 1700 cm^{-1}. On the Huang-Minlon reduction, the mixture (**11** and **13**) gave a mixture of 19-oxofriedelane (**4**) and 15-oxofriedelane (**6**). Therefore, the structutes of the diketones (**11** and **13**) were determined to be 3,19- and 3,15-dioxofriedelanes, respectively.

The dry ozonation of both friedeleane (**1**) and friedelin (**2**) resulted in the preferential introduction of a carbonyl group into hindered positions such as 15-, 16-, 19-, and 21-carbon atoms. These findings seem to be important and useful for synthesis of these carbonyl compounds hitherto unaccessible by other synthetic procedures. The reason why these sterically hindered ketones were produced is explained as follows.[7,8] If A ring moiety of friedelane (**1**) is preferentially adsorbed on the surface of silica gel due to sterical accessibility and a carbonyl group on A ring of friedelin (**2**) is apt to combine with the adsorbent, and if these molecules are ordered ideally in a close-packed array, it would be expected that the terminal moiety of these molecules, D or E ring, would be exposed for the attack by ozone.

Experimental

General Procedures. IR spectra were measured in KBr disk using a Hitachi EPI-G2 spectrometer. CD and ORD measurements were carried out on a JASCO Model J-20 spectrometer. Optical rotations were measured on a JASCO DIP-SL polarimeter. Mass spectra were taken on a Hitachi RMU-6-Tokugata mass spectrometer and high resolution mass spectra on a Hitachi RMH-2 mass spectrometer operating at 70 eV with a direct inlet system. The relative intensity observed in low resolution mass spectra was expressed in % in the parentheses. PMR spectra were measured using a JEOL 4H-100 (100 MHz) or a Hitachi R-20 (60 MHz) spectrometer. Chemical shifts were expressed in δ downfield from TMS as an internal standard, and coupling constants in Hz. HPLC analyses were carried out at room temperature using a Liquid Chromatograph Model ALC/GPC 202/401 (Waters Assoc.) with an RI detector (column: μ-Porasil 1/8(inch)×1(foot); pressure *ca.* 500 psi). GLC was carried out using a Shimadzu Gas Chromatograph 4APF equipped with a hydrogen flame ionization detector (column: OV-1 at 280 °C). Ozone was generated from an Ozonizer Model O-1-2 (Nippon Ozon) and silica gel (Wakogel C-200) was used for adsorbent. Analytical TLC was carried out on Kieselgel G (E. Merck, Darmstadt) and Alumina B-10-F (Wako) in 0.25 mm thickness, and preparative TLC on Kieselgel PF_{254} (E. Merck, Darmstadt) in 0.5 mm thickness. Wakogel C-200 (Wako) and Activated Alumina (Showa Chem.) were used for column chromatography. Melting points were measured on a Mel-temp capillary melting point apparatus (Laboratory Devices) and were uncorrected.

*Dry Ozonation of Friedelane (**1**).* Silica gel (10 g) was mixed with a solution of friedelane (**1**; 100 mg) in hexane (20 ml) and shaken well. After the solvent was removed in a rotary evaporator, the silica gel was heated at 100 °C for 1 h and then deactivated with water (0.4 ml). The silica gel was placed in a reaction vessel, cooled to −78 °C and saturated with ozone at a flow rate of 50 ml/min for 1 h. The reaction vessel was maintained at −65 to −60 °C and a slow stream of nitrogen was passed through the silica gel for 1.5 h and then the vessel was warmed gradually to room temperature. The silica gel, on which the reaction products were adsorbed, was placed on the top of a column of silica gel (1 g), and hexane (200 ml) was eluted to afford the unchanged friedelane (**1**; 82 mg). Successive elution with benzene (150 ml) gave a mixture (*ca.* 19 mg) of monooxygenated friedelanes, which showed six spots on TLC (SiO_2). The mixture was further separated by preparative TLC (3 plates (20×20 cm), developed with hexane–benzene (1:1); detection: iodine) to give six components with R_f 0.7, 0.65, 0.5, 0.4, 0.25, and 0.2. The least polar fraction [9 mg; mp 268—271 °C; IR 1000, 940, and 920 cm^{-1}; PMR

δ 2.56 (1H, s); MS *m/e* (%) 426 (M^+; 33), 411 (11), 297 (17), 257 (28), 149 (78), and 135 (100)] was identified to be 18β,19β-epoxyfriedelane (**3**) by comparison with an authentic sample.[14] The structure of the second component was left undetermined because of paucity of the material. The third product [0.4 mg; mp 230—231 °C; IR 1675 cm^{-1}; PMR δ 2.17 (1H, s); MS *m/e* (%) 426 (M^+; 10), 411 (18), 259 (36), 217 (30), 139 (100), and 149 (28)] was shown to be 19-oxofriedelane (**4**).[14]

The fourth component with R_f 0.4 (**6**; 2 mg) was shown to be 15-oxofriedelane (**6**) based on spectral data and chemical conversion (*vide infra*). The fifth component (**5**) was found to contain a small quantity of unidentified material by TLC (Al_2O_3) and the mass spectrum. This dry ozonation was repeated seven times and the component with R_f 0.25 was collected. The combined material (23 mg) was subjected to separation by column chromatography on alumina (10 g). Elution with hexane–benzene (2:1) afforded 16-oxofriedelane[16] [**5**; 14 mg, mp 270—272 °C; IR 1680 cm^{-1}; PMR δ 0.78, 0.84, 0.95, 1.05, 1.17, 1.28 (each 3H, s; *t*-Me), 2.15 and 2.37 (2H, ABq, J=19 Hz; $C_{(15)}$-H_2); MS *m/e* 426 (M^+; 21), 411 (17), 274 (8), 259 (20), 149 (100), and 109 (75)] and a mixture of unidentified alcohols (7 mg).

Although the sixth component was inferred to be a mixture from the PMR spectrum, no separation could be attained by TLC (Al_2O_3). The HPLC examination (solvent system: 1.5% ether-hexane; flow rate: 0.9 ml/min) revealed that the fraction consisted of 21-oxofriedelane (**7**; 0.2 mg, R_t 17 min) and friedelin (**2**; 0.15 mg, R_t 20 min). The material (18 mg), obtained by repeating the dry ozonation of friedelane (each 250 mg, 12 times), was subjected to separation by HPLC under the same conditions as above to afford friedelin (**2**; 4 mg) and 21-oxofriedelane [**7**; 6 mg, mp 237—240 °C; $[\alpha]_D$ +117° (*c* 0.12, $CHCl_3$); ORD $[\alpha]_{280}$ −2320° and $[\alpha]_{325}$ +3490°; IR 1720 cm^{-1}; PMR δ 2.60 (1H, d, J=12 Hz; $C_{(22)}$–H); MS *m/e* (%) 426 (M^+; 3), 411 (7), 259 (22), 217 (16), 177 (15), and 149 (100); High resolution mass spectrum: *m/e* 426.3878 ($C_{30}H_{50}O$), 411.3646 ($C_{29}H_{47}O$), 287.2383 ($C_{20}H_{31}O$), 260.2483 ($C_{19}H_{32}$), 259.2420 ($C_{19}H_{31}$), 219.1835 ($C_{15}H_{23}O$), 177.1602 ($C_{13}H_{21}$), 149.1330 ($C_{11}H_{17}$), and 139.1115 ($C_9H_{15}O$). The fragmentation patterns were shown in Fig. 3].

*15-Oxofriedelane (**6**).* Mp 239—240 °C (recrystallized from ethyl acetate); $[\alpha]_D$ +38° (*c* 1.5, $CHCl_3$); CD $[\theta]_{300}$ −215 (*c* 0.1, dioxane); IR 1700 cm^{-1}; PMR δ 0.77, 0.86, 0.89, 0.95, 1.00, 1.20, 1.32 (each 3H, s, *t*-Me), 2.15 and 2.50 (2H, ABq, J=18 Hz; $C_{(16)}$–H_2); MS *m/e* (%) 426 (M^+; 19), 411 (90), 393 (64), 355 (10), 221 (54), 194 (100), 177 (20), and 149 (41); High resolution mass spectrum: *m/e* 426.3874 ($C_{30}H_{50}O$), 411.3681 ($C_{29}H_{47}O$), 355.2912 ($C_{25}H_{39}O$), 302.2569 ($C_{21}H_{34}O$), 221.1941 ($C_{15}H_{25}O$), 194.1646 ($C_{13}H_{22}O$), 177.1665 ($C_{13}H_{21}$), and 149.1343 ($C_{11}H_{17}$). Found: C, 84.73; H, 11.89%. Calcd for $C_{30}H_{50}O$: C, 84.44; H, 11.81%. The fragmentation patterns in the high resolution mass spectrum and PMR spectral data using Eu(fod)$_3$-d_{27} as a shift reagent were given in Figs. 1 and 2.

*Wolff-Kishner Reduction of 15-Oxofriedelane (**6**).* A mixture of sodium (100 mg) in diethylene glycol (5 ml) was heated at 180 °C under a nitrogen atmosphere. To the solution, anhydrous hydrazine (1 ml) and 15-oxofriedelane (**6**; 13 mg) were added and the mixture was refluxed overnight. After excess of hydrazine was removed by distillation, the reaction mixture was heated under reflux at 210 °C overnight. After usual treatment, the reaction product was subjected to separation by preparative TLC, developed with hexane-benzene (1:1) to afford friedelane (**1**; 2 mg), mp 248.5—249 °C together with the unchanged starting material (**6**; 2 mg).

*Treatment of 15-Oxofriedelane (**6**) with Sodium Deuterioxide.* A mixture of 15-oxofriedelane (**6**; 2 mg) and sodium deuterioxide prepared from sodium (10 mg) and deuterium oxide (0.5 ml) in dioxane (1 ml) was heated under reflux for 14 h under nitrogen. The reaction mixture was poured into water, extracted with benzene–ether, washed with dilute hydrochloric acid and successively with aqueous sodium hydrogencarbonate, and then dried over magnesium sulfate. This procedure was repeated twice to give deuteriated 15-oxofriedelane, which was found to consist of 15-oxofriedelane-d_2 (**6**-d_2; 90.2%), -d_1 (7.1%), and -d_0 (2.6%) by mass spectrometry.

*Conversion of 15-Oxofriedelane (**6**) into 15,16-Dioxofriedelane (**8**).* A mixture of 15-oxofriedelane (**6**; 5 mg) and selenium dioxide (17 mg) in acetic acid (5 ml) was heated under reflux for 6 h. Since TLC examination of the reaction mixture showed that a considerable amount of the starting material was left unchanged, heating was continued for 16 h after addition of selenium dioxide (5 mg). After cooling and removal of metallic selenium, the reaction mixture was extracted with ether and worked up as usual to give a residue, which was subjected to separation by preparative TLC (developed with benzene). The unchanged 15-oxofriedelane (**6**; *ca.* 1 mg) was recovered and 15,16-dioxofriedelane [**8**; 2 mg, mp 280—281 °C; IR 1720 and 1700 cm^{-1}; PMR δ 0.78, 0.86, 0.96, 1.02, 1.20, 1.39, and 1.54 (each 3H, s, *t*-Me); MS *m/e* (%) 440 (M^+; 94), 412 (70), 288 (98), 260 (100), and 177 (53)] was obtained.

*Conversion of 16-Oxofriedelane (**5**) into 15,16-Dioxofriedelane (**8**).* i) A mixture of 16-oxofriedelane (**5**; 4 mg) and selenium dioxide (17 mg) in acetic acid (5 ml) was heated under reflux (bath temperature 135 °C) for 6 h. After additional selenium dioxide (10 mg) was added, the reaction mixture was heated under reflux (bath temperature 150 °C) overnight. The same treatment and purification as above gave unchanged 16-oxofriedelane (**5**; *ca.* 1 mg) and 15,16-dioxofriedelane [**8**; 2 mg, mp 280—280.5 °C; IR 1720 and 1700 cm^{-1}; PMR δ 0.78, 0.86, 0.96, 1.02, 1.20, 1.39, and 1.54 (each 3H, s, *t*-Me); MS *m/e* (%) 440 (M^+; 94), 425 (9), 412 (70), 288 (98), 260 (100), and 177 (53)]. ii) A mixture of 16-oxofriedelane (**5**; 5 mg), selenium dioxide (18 mg), and dioxane (2 ml) in a sealed tube was heated at 180 °C for 4 h. After usual treatment, 15,16-dioxofriedelane (**8**) was obtained nearly quantitatively.

*Dry Ozonation of Friedel-18-ene (**9**).* Friedel-18-ene (**9**) was prepared from friedelane (**1**) according to the known procedures[13] and purified by passing through a column of silica gel impregnated with 30% silver nitrate. The purity of the friedel-18-ene (**9**) was examined by GLC, which confirmed the absence of friedelane (R_t 4.3 and 3.7 min for **1** and **9**, respectively).

Friedel-18-ene (**9**; 125 mg) was adsorbed on silica gel (13 g) and oxidized with ozone by the same procedures as above. The reaction product (127 mg), obtained from the silica gel-product mixture by elution with ethyl acetate, was subjected to separation by column chromatography of silica gel (15 g) and eluted with hexane (100 ml), hexane-benzene (3:1, 40 ml), benzene (100 ml), and then with ethyl acetate (100 ml). From the hexane fraction, friedel-18-ene (**9**; 15 mg) was recovered and the fraction eluted with hexane–benzene gave 18β,19β-epoxyfriedelane (**3**; 60 mg). A mixture (*ca.* 5 mg), obtained from the benzene fraction, showed three spots on TLC, but none of the products corresponding to these spots was identical with any one of the products obtained by the dry ozonation of friedelane (**1**).

Dry Ozonation of Friedelin (2). Friedelin (**2**; 420 mg) in chloroform (150 ml) was adsorbed on silica gel (50 g) and the solvent was removed in a rotary evaporator. The silica gel was cooled to −78 °C and saturated with ozone for 2 h under the same conditions as above. A slow stream of nitrogen was passed through the silica gel kept at −15 °C, and the temperature was raised to room temperature.

The reaction product (450 mg), eluted from the silica gel with ethyl acetate, was dissolved in benzene and passed through a column of silica gel (40 g). Elution was carried out with the following solvents: benzene (500 ml), benzene–ether (10:1, 500 ml), and ethyl acetate (500 ml). From the benzene fraction, friedelin (**2**; 70 mg) was recovered. The fraction (168 mg), eluted with benzene–ether, gave three spots on TLC (SiO_2) and subjected to separation by preparative TLC (15 plates (20×20 cm), developed with benzene–chloroform–ether (20:2:1), detection: iodine) to afford three fractions with R_f 0.45, 0.38, and 0.25.

The least polar fraction gave an epoxy ketone (**10**; 50 mg), mp 266—269 °C (with decomposition); $[\alpha]_D$ −6° (*c* 1.2, $CHCl_3$); IR 1710, 1115, 1080, 920, and 835 cm^{-1}; PMR δ 2.0—2.5 (3H, m, $-C\underline{H}_2-CO-C\underline{H}-$) and 2.56 (1H, s; $C_{(13)}$–H); MS *m/e* (%) 440 (M^+; 24), 425 (7), 368 (16), 311 (17), 154 (100), and 127 (99); Found: C, 81.65; H, 10.93%. Calcd for $C_{30}H_{48}O_2$: C, 81.76; H, 10.98%.

The second fraction with R_f 0.38 was shown to be a mixture of two components by HPLC (solvent system: 15% ether–hexane, flow rate: 0.5 ml/min) and separated into 3,19-dioxofriedelane (**11**; 4 mg, R_t 21 min) and 3,15-dioxofriedelane (**13**; 12 mg, R_t 24 min). *3,19-Dioxofriedelane (11)*: Mp 264—266 °C; IR 1708 and 1680 cm^{-1}; PMR δ 2.0—2.5 (3H, m; $-C\underline{H}_2-CO-C\underline{H}-$) and 2.20 (1H, br s; $C_{(18)}$–H); MS *m/e* (%) 440 (M^+; 9), 425 (11), 422 (5), 407 (3), 273 (25), 231 (16), 191 (11), and 139 (100). *3,15-Dioxofriedelane (13)*: Mp 280.5—281.5 °C; $[\alpha]_D$ +20° (*c* 0.67, $CHCl_3$); IR 1710 and 1700 cm^{-1}; PMR δ 2.16 and 2.55 (2H, ABq, J=19 Hz; $C_{(16)}$–H_2); MS *m/e* (%) 440 (M^+; 52), 425 (59), 422 (12), 407 (29), 355 (48), 201 (58), and 194 (100).

The third fraction with R_f 0.25 was identified to be 3,16-dioxofriedelane[16] (**12**; 13 mg), mp 294—295.5 °C; IR 1720 and 1690 cm^{-1}; PMR δ 0.73, 0.97, 1.05, 1.20, 1.29 (each 3H, s, *t*-Me), 0.90 (6H, s, 2×*t*-Me), and 1.8—2.6 (5H, m; $C_{(2)}$–H_2, $C_{(4)}$–H, and $C_{(15)}$–H_2); MS *m/e* (%) 440 (M^+; 48), 425 (52), 355 (36), 273 (29), 220 (43), 219 (33), 163 (31), and 109 (100).

Conversion of 18β,19β-Epoxyfriedelan-3-one (10) into 19-Oxofriedelane (4). A solution of 18β,19β-epoxyfriedelan-3-one (**10**; 19 mg) in ethylamine (30 ml) was placed in a flask equipped with a Dry Ice-condenser, and lithium (30 mg) and *t*-butyl alcohol (1 drop) were added with stirring. Blue color of the solution faded within 1 h and aqueous solution of ammonium chloride (300 mg) and then water were added. The reaction product was extracted with chloroform and washed with dilute hydrochloric acid, sodium hydrogencarbonate solution, and brine, and dried over sodium sulfate. Evaporation gave a residue (20 mg), which was dissolved in benzene–ether (10:1) and filtered through a column of silica gel to give a diol (19 mg).

A solution of the diol (19 mg) in acetone (50 ml) was cooled with ice-bath and the Jones reagent (0.2 ml) was added to the solution with stirring at 2 °C for 2 h and the stirring was continued at 20 °C for 3 h. Excess of the oxidizing reagent was destroyed by addition of methanol and the product was extracted with chloroform. The crude material, obtained by usual treatment, was purified by preparative TLC (2 plates (20×20 cm), developed with benzene–ether (10:1), detection:iodine) followed by recrystallization from ethyl acetate to give 3,19-dioxofriedelane (**11**; 14.5 mg), mp 255—257 °C; IR 1708 and 1680 cm^{-1}; PMR δ 2.20 (1H, br. s; $C_{(18)}$–H) and 2.0—2.5 (3H, m; $C_{(2)}$–H_2 and $C_{(4)}$–H).

A mixture of 3,19-dioxofriedelane (**11**; 13 mg), above obtained, hydrazine hydrate (2 ml), and sodium hydroxide (200 mg) in diethylene glycol (30 ml) was heated under reflux for 3 h. Excess of the hydrazine was removed by slow distillation until the temperature of the vapor reached to 205 °C, and the heating was continued for 4.5 h. After usual work-up, the product was dissolved in benzene and purified by passing through a column of alumina to afford 19-oxofriedelane (**4**; 4 mg), mp 230—231 °C; IR 1675 cm^{-1}; PMR δ 2.20 (1H, s; $C_{(18)}$–H); MS *m/e* (%) 426 (M^+; 9), 411 (18), 259 (36), 217 (29), 149 (27), and 139 (100).

Reduction of a Mixture of 3,19- and 3,15-Dioxofriedelanes (11 and 13). A mixture (6 mg) of 3,19- and 3,15-dioxofriedelanes (**11** and **13**), obtained as the second fraction with R_f 0.38 in the dry ozonation of friedelin (**2**) (*vide supra*), was heated under reflux with hydrazine hydrate (2 ml), potassium hydroxide (200 mg), and diethylene glycol (20 ml) for 2 h under a nitrogen atmosphere. Excess of the hydrazine was distilled off until the vapor temperature reached to 205 °C, and the mixture was refluxed for 4.5 h. Usual treatment and separation by preparative TLC (1 plate (20×20 cm), developed with hexane–benzene (1:1), detection: iodine) gave 19-oxofriedelane (**4**; 1 mg) and 15-oxofriedelane (**6**; 2 mg). *19-Oxofriedelane (4)*: Mp 230.5—232 °C; IR 1675 cm^{-1}; MS *m/e* (%) 426 (M^+; 10), 411 (17), 259 (36), 217 (30), 149 (30), and 139 (100). *15-Oxofriedelane (6)*: Mp 238—238.5 °C; IR 1700 cm^{-1}; MS *m/e* (%) 426 (M^+; 20), 411 (90), 393 (65), 355 (10), 221 (53), 194 (100), 177 (20), and 149 (39).

The authors are grateful to Professor Tohru Kikuchi, Toyama University for a gift of spectral chart copies of 16-oxofriedelane (**5**) and 3,16-dioxofriedelane (**12**).

References

1) A part of this work was reported in a preliminary form: E. Akiyama, M. Tada, T. Tsuyuki, and T. Takahashi, *Chem. Lett.*, **1978**, 305.

2) J. R. Durland and H. Adkins, *J. Am. Chem. Soc.*, **61**, 429 (1939); M. C. Whiting, A. Z. N. Bolt, and J. H. Parish, *Adv. Chem. Ser.*, **77**, 4 (1968); G. A. Hamilton, B. S. Ribner, and T. M. Hellman, *ibid.*, **77**, 15 (1968); C. C. Schubert and R. N. Pease, *J. Am. Chem. Soc.*, **78**, 2044 (1956); D. G. Williamson and R. J. Cvetanovic, *ibid.*, **92**, 2949 (1970); T. M. Hellman and G. A. Hamilton, *ibid.*, **96**, 1530 (1974); J. E. Batterbee and P. S. Bailey, *J. Org. Chem.*, **32**, 3899 (1967).

3) H. Varkony, S. Pass, and Y. Mazur, *J. Chem. Soc., Chem. Commun.*, **1974**, 437.

4) Z. Cohen, E. Keinan, Y. Mazur, and T. H. Varkony, *J. Org. Chem.*, **40**, 2141 (1975).

5) E. Keinan and Y. Mazur, *Synthesis*, **1976**, 523.

6) Z. Cohen, E. Keinan, Y. Mazur, and A. Ulman, *J. Org. Chem.*, **41**, 2651 (1976).

7) A. L. J. Beckwith, C. L. Bodkin, and T. Duong, *Aust. J. Chem.*, **30**, 2177 (1977).

8) A. L. J. Beckwith and T. Duong, *J. Chem. Soc., Chem. Commun.*, **1978**, 413.

9) E. Keinan and Y. Mazur, *J. Org. Chem.*, **42**, 844 (1977).

10) R. Kasai, K. Shinzo, O. Tanaka, and K. Kawai, *Chem. Pharm. Bull.*, **22**, 1213 (1974).

11) *E.g.*, References for the partial conversion utilizing the Barton reaction and the relating photochemical reactions: T. Fukuda, T. Tsuyuki, Y. Tanahashi, and T. Takahashi, *Bull. Chem. Soc. Jpn.*, **38**, 1808 (1965); **40**, 370 (1967); T. Hoshino, T. Tsuyuki, and T. Takahashi, *ibid.*, **40**, 389 (1967); R. B. Boar, L. Joukhadar, M. de Luque, J. F. McGhie, D. H. R. Barton, D. Arigoni, H. G. Brunner, and R. Giger, *J. Chem. Soc., Perkin Trans. 1*, **1977**, 2104.

12) *Cf.* R. O. Kan, "Organic Photochemistry," McGraw-Hill, New York (1966), p. 233; R. Breslow, *Chem. Soc. Rev.*, **1**, 553 (1972); R. Breslow, S. Baldwin, T. Flechtner, P. Kalicky, S. Liu, and Washburn, *J. Am. Chem. Soc.*, **95**, 3251 (1973); R. Breslow, R. J. Corcoran, B. B. Snider, R. J. Doll, P. L. Khanna, and R. Kaleya, *ibid.*, **99**, 905 (1977); R. Breslow and L. M. Maresca, *Tetrahedron Lett.*, **1977**, 623. And references cited therein. J. E. Baldwin, A. K. Bhatnagar, and R. W. Harper, *Chem. Commun.*, **1970**, 659; J. E. Gurst, Y. M. Sheikh, and C. Djerassi, *J. Am. Chem. Soc.*, **95**, 628 (1973); P. S. Scholl and M. R. van de Mark, *J. Org. Chem.*, **38**, 2376 (1973).

13) V. V. Kane and R. Stevenson, *Tetrahedron*, **15**, 223 (1961).

14) T. Tsuyuki, T. Hoshino, M. Ito, and T. Takahashi, *Bull. Soc. Chim. Fr.*, **1968**, 2895.

15) Yields were calculated based on the converted starting material.

16) T. Kikuchi, M. Takayama, T. Toyoda, M. Arimoto, and M. Niwa, *Chem. Pharm. Bull.*, **21**, 2243 (1973).

17) *Cf.* H. Hirota, Y. Moriyama, T. Tsuyuki, Y. Tanahashi, T. Takahashi, Y. Kato, and H. Satoh, *Bull. Chem. Soc. Jpn.*, **48**, 1884 (1975).

18) J. L. Courtney and R. M. Gascoigne, *J. Chem. Soc.*, **1956**, 2115.

19) B. J. Clarke, J. L. Courtney, and W. Stern, *Aust. J. Chem.*, **23**, 1651 (1970).

20) J. L. Courtney and J. S. Shannon, *Tetrahedron Lett.*, **1963**, 13.

21) F. Kohen and R. Stevenson, *J. Org. Chem.*, **30**, 2479 (1965).

22) Formation of 3β-acetoxy-18β,19β-epoxyfriedelane on ozonation of 3β-acetoxyfriedel-18-ene was described: Y. Tanahashi, Y. Moriyama, T. Takahashi, F. Patil, J.-F. Biellmann, and G. Ourisson, *Bull. Soc. Chim. Fr.*, **1966**, 1670.

Synthesis of 8- and 10-Methyl-substituted 8,9,10,11-Tetrahydro-7*H*-cycloocta[*de*]naphthalenes and Their 9-Oxo Derivatives

Toshihiro KAMADA

National Chemical Laboratory for Industry, 1-1-5 Honmachi, Shibuya-ku, Tokyo 151

(Received June 23, 1978)

A novel and convenient method for the synthesis of the 8,9,10,11-tetrahydro-7*H*-cycloocta[*de*]naphthalene ring system is described. Reaction of diethyl acetonedicarboxylate and 1,8-bis(bromomethyl)naphthalene gave the eight-membered pericyclized compound, diethyl 9-oxo-8,9,10,11-tetrahydro-7*H*-cycloocta[*de*]naphthalene-8,10-dicarboxylate, which was then converted, through several steps, into various kinds of 8- and 10-methyl-substituted 8,9,10,11-tetrahydro-7*H*-cycloocta[*de*]naphthalenes and their 9-oxo derivatives, as well as the unsubstituted compounds, 8,9,10,11-tetrahydro-7*H*-cycloocta[*de*]naphthalene and 8,9,10,11-tetrahydro-7*H*-cycloocta[*de*]naphthalen-9-one. The hydrocarbon, 8,8,10,10-tetramethyl-8,9,10,11-tetrahydro-7*H*-cycloocta[*de*]-naphthalene was prepared from 8,8,10,10-tetrakis(tosyloxymethyl)-8,9,10,11-tetrahydro-7*H*-cycloocta[*de*]naphthalene.

Despite considerable current interest in the chemistry of peri-substituted naphthalenes,[1] few studies have been made on the eight-membered pericyclized naphthalene derivatives, 8,9,10,11-tetrahydro-7*H*-cycloocta[*de*]naphthalenes (**1**). The only compound of this ring system so far known is the unsubstituted hydrocarbon **1a**, which was synthesized by Nelsen and Gillespie in five steps from acenaphthylene.[2] Recently, as a part of studies on the chemistry of pericyclic naphthalene derivatives, a report was given on the syntheses of some derivatives of **1a** starting from 1,8-naphthalenedicarboxylic anhydride.[3] A novel and convenient method was worked out for the synthesis of the tetrahydrocycloocta[*de*]naphthalene ring **1**, which can be applied to the syntheses of various substituted compounds of this ring system besides **1a**. This paper deals with the syntheses of several 8- and 10-methyl-substituted 8,9,10,11-tetrahydro-7*H*-cycloocta[*de*]naphthalenes (**2a**—**7a**) as well as some 9-oxo derivatives (**1b**—**7b**) which do not seem to have been reported.

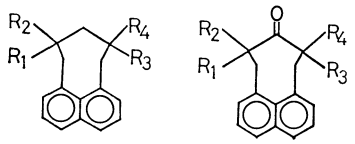

(**a**) (**b**)

1; $R_1=R_2=R_3=R_4=H$
2; $R_1=CH_3$, $R_2=R_3=R_4=H$
3; $R_1=R_3=CH_3$, $R_2=R_4=H$
4; $R_1=R_4=CH_3$, $R_2=R_3=H$
5; $R_1=R_2=CH_3$, $R_3=R_4=H$
6; $R_1=R_2=R_3=CH_3$, $R_4=H$
7; $R_1=R_2=R_3=R_4=CH_3$

For the formation of the tetrahydrocycloocta[*de*]-naphthalene skeleton **1**, diethyl acetonedicarboxylate (**8**) was allowed to react with 1,8-bis(bromomethyl)-naphthalene (**9**) prepared from 1,8-naphthalenedicarboxylic anhydride.[3] By the reaction between equimolar amounts of **8** and **9** in refluxing ethanol, using sodium ethoxide as a condensing agent, diethyl 9-oxo-8,9,10,11-tetrahydro-7*H*-cycloocta[*de*]naphthalene-8,10-dicarboxylate (**10**) with the desired peri-eight-membered ring was obtained. Compound **10**, when treated with

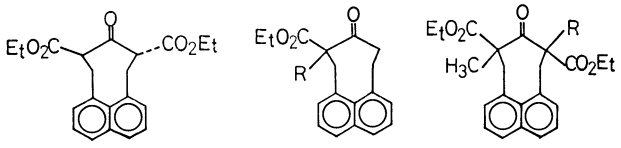

10 **11** **12**

a; R=H, **b**; R=CH_3

sodium ethoxide in ethanol, underwent deethoxycarbonylation to yield ethyl 9-oxo-8,9,10,11-tetrahydro-7*H*-cycloocta[*de*]naphthalene-8-carboxylate (**11a**). Alkaline hydrolysis of the β-keto esters **10** and **11a** was accompanied by decarboxylation to afford 8,9,10,11-tetrahydro-7*H*-cycloocta[*de*]naphthalen-9-one (**1b**). The Clemmensen reduction of ketone **1b** gave the parent hydrocarbon **1a** identical with that previously reported.[2]

Methylation of the β-keto ester **10** gave a mixture from which diethyl 8-methyl-9-oxo-8,9,10,11-tetrahydro-7*H*-cycloocta[*de*]naphthalene-8,10-dicarboxylate (**12a**) and diethyl 8,10-dimethyl-9-oxo-8,9,10,11-tetrahydro-7*H*-cycloocta[*de*]naphthalene-8,10-dicarboxylate (**12b**) were isolated by fractional crystallization in 60 and 22% yields, respectively. Repeated methylation of **10** with excess of the reagents afforded only **12b**. By alkaline hydrolysis and concurrent decarboxylation the monomethyl keto diester **12a** was converted almost in a quantitative yield into 8-methyl-8,9,10,11-tetrahydro-7*H*-cycloocta[*de*]naphthalen-9-one (**2b**), which afforded the corresponding hydrocarbon **2a** on Clemmensen reduction.

On the other hand, alkaline treatment of dimethyl keto diester **12b** in boiling dioxane yielded a mixture of geometrical isomers, which was separated by recrystallization to give *cis*-8,10-dimethyl-8,9,10,11-tetrahydro-7*H*-cycloocta[*de*]naphthalen-9-one (**3b**) and its *trans* isomer **4b** in 64 and 23% yields, respectively. **4b** was also prepared more efficiently from keto diester **10** having a *trans* structure by the following reaction. **10** was reduced by lithium aluminum hydride to give triol **13a**, which was converted by treatment with methanesulfonyl chloride in pyridine into dimesylate **13b**. Treatment of **13b** with excess lithium aluminum hydride in boiling ether afforded *c*-8,*t*-10-dimethyl-

8,9,10,11-tetrahydro-7*H*-cycloocta[*de*]naphthalen-*r*-9-ol (**13c**), which, on Jones oxidation, gave the desired *trans*-8,10-dimethyl ketone **4b** in a 40% overall yield from **10**.

Monomethyl keto diester **12a** was then converted into 8,8,10-trimethyl-8,9,10,11-tetrahydro-7*H*-cycloocta-[*de*]naphthalen-9-ol (**14c**) through the same steps as in the preparation of **13c** from the keto diester **10**. Reduction of **12a** with lithium aluminum hydride gave a triol **14a**, which, on treatment with 2 mol of methanesulfonyl chloride in pyridine, was converted into **14b**. Subsequent hydrogenolysis of **14b** with lithium aluminum hydride afforded a 59% overall yield of the trimethyl alcohol **14c**. Similarly, 8,8,-10,10-tetramethyl-8,9,10,11-tetrahydro-7*H*-cycloocta-[*de*]naphthalen-9-ol (**15c**) was derived from the dimethyl keto diester **12b** in a 78% yield by the successive reduction, mesylation and hydrogenolysis (**12b**→**15a**→**15b**→**15c**). On the other hand, methylation of the keto monoester **11a** gave ethyl 8-methyl-9-oxo-8,9,10,11-tetrahydro-7*H*-cycloocta[*de*]naphthalene-8-carboxylate (**11b**), which was then converted, on reactions similar to the above through a diol **16a** and a monomesylate **16b**, into 8,8-dimethyl-8,9,10,11-tetrahydro-7*H*-cycloocta[*de*]naphthalen-9-ol (**16c**) in only 12% overall yield from **11a**. Each of the methyl alcohols **14c**, **15c**, and **16c** was oxidized by Jones reagent to give the corresponding α-methyl ketones, **6b**, **7b**, and **5b**, respectively.

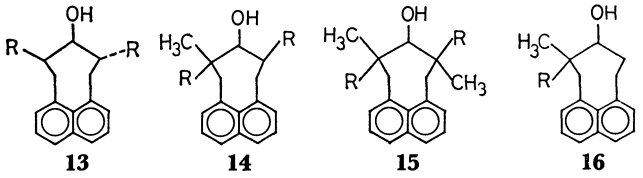

13 **14** **15** **16**

a; R=CH_2OH, **b**; R=CH_2OMs, **c**; R=CH_3

cis-8,10-Dimethyl ketone **3b** underwent Clemmensen reduction to give only the corresponding hydrocarbon **3a**, while the *trans*-dimethyl ketone **4b** gave, on Clemmensen reduction, a mixture of three compounds, which was isolated by chromatography on alumina to yield the desired *trans*-8,10-dimethyl-8,9,10,11-tetrahydro-7*H*-cycloocta[*de*]naphthalene (**4a**) (48% yield) along with the *trans*-dimethyl alcohol **13c** (8%) and its acetate **17** (26%), the acetoxyl group being derived from the solvent (acetic acid). The carbonyl groups of the *gem*-dimethyl ketone **5b** and the trimethyl ketone **6b** were smoothly reduced by Wolff-Kishner reactions to afford the corresponding hydrocarbons, 8,8-dimethyl-8,9,10,11-tetrahydro-7*H*-cycloocta[*de*]naphthalene (**5a**) and 8,8,10-trimethyl-8,9,10,11-tetrahydro-7*H*-cycloocta[*de*]naphthalene (**6a**), respectively.

An attempt to transform **6b** into **6a** by Clemmensen reduction resulted in the formation only of intractable substances with a small amount of **6b**. On the other hand, Clemmensen reduction of the tetramethyl ketone **7b** produced only the tetramethyl alcohol **15c** instead of the hydrocarbon **7a**, while by the Wolff-Kishner procedure **7b** was recovered unchanged with a small amount of alcohol **15c**. Hydrogenolysis of

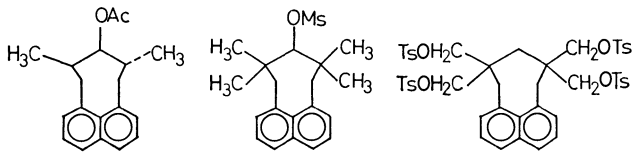

17 **18** **19**

the mesylate ester of the tetramethyl alcohol **15c** (**18**) using the same conditions as in the transformation of **13b** into **13c** caused only *O*-mesyl bond cleavage to regenerate **15c**. The great difficulty in effecting these reactions might be caused by steric hindrances,[4,5] expected to greatly increase in highly methylated compounds such as **6** and **7**, as compared to those in the lower homologs (**1**—**5**).

8,8,10,10-Tetrakis(tosyloxymethyl)-8,9,10,11-tetrahydro-7*H*-cycloocta[*de*]naphthalene (**19**), which is expected as another precursor of compound **7a**, was prepared according to the method previously reported.[3] Treatment of the tosylate **19** with lithium aluminum hydride in ether led to hydrogenolysis of the tosyloxy groups to yield, with an unidentified compound, the desired hydrocarbon, 8,8,10,10-tetramethyl-8,9,10,11-tetrahydro-7*H*-cycloocta[*de*]naphthalene (**7a**).

Experimental

All the melting points were uncorrected. The IR spectra were determined on a JASCO IR-G spectrometer calibrated with polystyrene. The proton NMR spectra were determined on a Varian HA-100D spectrometer (at 100 MHz) using chloroform-*d*, acetone-d_6 and pyridine-d_5 as solvents, and tetramethylsilane as an internal standard; the spectra of compounds **4a**, **4b**, and **10**, which changed markedly around or below room temperature, were measured under cooling, while other samples were measured at room temperature. Mass spectra were determined on a CEC 21-110B instrument.

*Diethyl 9-Oxo-8,9,10,11-tetrahydro-7*H*-cycloocta*[de]*naphthalene-8,10-dicarboxylate (**10**).* 1,8-Bis(bromomethyl)naphthalene (**9**) was prepared from 1,8-naphthalenedicarboxylic anhydride.[3]

To a stirred and cooled (at 0 °C) solution of sodium ethoxide in ethanol (prepared from 11.6 g of sodium and 1.14 l of absolute ethanol) was added quickly a solution of diethyl acetonedicarboxylate (**8**) (52 g) in dry dimethyl sulfoxide (0.14 l, distilled on calcium hydride) and absolute ethanol (0.14 l). After 8 min stirring a solution of the dibromide **9** (80 g) in dry dimethyl sulfoxide (0.86 l) was added over a period of 3 min and the mixture was stirred under reflux for 30 min. The reaction mixture was then poured into cracked ice and water (*ca.* 5 l) and the resulting cloudy solution was left at room temperature for 3 days. The precipitated solid was collected and crystallized from ethanol, giving the desired peri-eight-membered ring compound **10** as colorless fine needles (28 g, 31%); mp 146—147 °C; MS : *m/e* 354.146 (M^+ ($^{12}C_{21}{}^1H_{22}{}^{16}O_5$)=354.147); IR (Nujol): ν_{max} 1707 (ketone C=O), 1742 cm^{-1} (ester C=O); NMR ($CDCl_3$): δ 1.26 and 1.33 (each 3H, t, J=7.1 Hz, CH_3).
Found: C, 70.83; H, 6.15%. Calcd for $C_{21}H_{22}O_5$: C, 71.17 : H, 6.26%.

The crude keto diester **10** (20 g) was refluxed with a solution of sodium hydroxide (12 g) in ethanol (400 ml) and water (600 ml) for 30 h. After treatment with hydrochloric acid, the precipitated solid was collected and recrystallized from methanol to give *8,9,10,11-tetrahydro-7*H*-cycolocta*[de]*naph-*

*thalen-9-one (**1b**)* (10.8 g, 92%) as colorless needles; mp 195—196 °C; MS : *m/e* 210.103 (M^+ ($^{12}C_{15}{}^1H_{14}{}^{16}O_1$)= 210.103); IR (Nujol): ν_{max} 1695 cm^{-1} (C=O); NMR ($CDCl_3$): δ 2.80 (4H, t, J=7.1 Hz, 8,10-H), 3.77 (4H, t, J=7.1 Hz, 7,11-H).
Found: C, 85.80; H, 6.56% Calcd for $C_{15}H_{14}O$: C, 85.86; H, 6.71%.

Ethyl 9-Oxo-8,9,10,11-tetrahydro-7H-cycloocta[de]*naphthalene-8-carboxylate (**11a**).* 2.5 g of the keto diester **10** was treated with a solution of sodium ethoxide in ethanol (prepared by dissolving 7.0 g of sodium in 500 ml of absolute ethanol) and the mixture was stirred vigorously for 3 days. The reaction mixture was then acidified, diluted with water (*ca.* 2 l) and left at room temperature for 16 days. The crystals formed were removed by filtration and recrystallized from ethaonl to give the keto monoester **11a** (1.48 g, 75%) as colorless needles; mp 128—129 °C; MS : *m/e* 282.126 (M^+ ($^{12}C_{18}{}^1H_{18}{}^{16}O_3$)=282.126); IR (Nujol): ν_{max} 1705 (ketone C=O), 1744 cm^{-1} (ester C=O); NMR ($CDCl_3$): δ 1.32 (3H, t, J=7.0 Hz, CH_3), 4.28 (2H, q, J=7.0 Hz, $C\underline{H}_2CH_3$).
Found: C, 76.27; H, 6.33%. Calcd for $C_{18}H_{18}O_3$: C, 76.57; H, 6.43%.

Diethyl 8-Methyl-9-oxo-8,9,10,11-tetrahydro-7H-cycloocta[de]*naphthalene-8,10-dicarboxylate (**12a**).* A solution of the crude keto diester **10** (18.5 g) in dry dimethyl sulfoxide (50 ml) was added to a solution of sodium ethoxide prepared by dissolving 1.44 g of sodium in 300 ml of absolute ethanol. To this mixture was added a solution of methyl iodide (6 ml) in absolute ethanol (40 ml) over a period of 5 min and the mixture was stirred overnight at room temperature. The reaction mixture was poured into water and the resulting solid was collected. Recrystallization of this solid from ethanol (500 ml) gave 11.2 g (60%) of the monomethyl compound **12a** as colorless needles; mp 129—130 °C; IR (Nujol): ν_{max} 1715 (ketone C=O), 1733, and 1738 cm^{-1} (ester C=O); NMR ($CDCl_3$): δ 1.01 (3H, s, CH_3), 1.20 and 1.28 (each 3H, t, J=6.7 and 7.1 Hz, respectively, CH_3).
Found: C, 71.80; H, 6.36%. Calcd for $C_{22}H_{24}O_5$: C, 71.72; H, 6.57%.

The mother liquor from the above was concentrated to yield 4.4 g (22%) of *diethyl 8,10-dimethyl-9-oxo-8,9,10,11-tetrahydro-7H-cycloocta*[de]*naphthalene-8,10-dicaroboxylate (**12b**).* The compound was prepared more efficiently (80%) by repeating the methylation procedure described above and obtained as colorless prisms by recrystallization from ethanol; mp 162—163.5 °C; IR (Nujol): ν_{max} 1709 (ketone C=O), 1734 cm^{-1} (ester C=O); NMR ($CDCl_3$): δ 0.95 and 1.76 (each 3H, s, CH_3), 1.22 and 1.31 (each 3H, t, J=6.8 and 7.1 Hz, respectively, CH_3).
Found: C, 72.50; H, 6.80%. Calcd for $C_{23}H_{26}O_5$: C, 72.23; H, 6.85%.

Ethyl 8-Methyl-9-oxo-8,9,10,11-tetrahydro-7H-cycloocta[de]*naphthalene-8-carboxylate (**11b**).* To a stirred solution of sodium ethoxide in ethanol (prepared by dissolving 0.18 g of sodium into 25 ml of absolute ethanol) was added a solution of the keto monoester **11a** (0.26 g) in dry dimethyl sulfoxide (10 ml) and the mixture was stirred for 2 h at room temperature. A solution of methyl iodide (2 ml) in absolute ethanol (10 ml) was then added and the mixture was stirred for 20 h at room temperature. The reaction mixture was concentrated, mixed with saturated salt solution and extracted with ethyl acetate. The extracts were washed with saturated salt solution and dried over sodium sulfate, the solvnet then being evaporated. The residue was chromatographed on alumina with hexane as eluant to give the monomethyl keto ester **11b** (0.26 g, 94%). This was recrystallized from ethanol for analysis (needles); mp 106—106.5 °C: IR (Nujol): ν_{max} 1705 (ketone C=O), 1728 and 1721 cm^{-1} (ester C=O); NMR ($CDCl_3$): δ 1.26 (3H, s, CH_3), 1.30 (3H, t, J=7.0 Hz, CH_3), 4.28 (2H, q, J=7.0 Hz, $OC\underline{H}_2CH_3$).
Found: C, 76.87; H, 6.50%. Calcd for $C_{18}H_{18}O_3$: C, 76.57; H, 8.43%.

8-Methyl-8,9,10,11-tetrahydro-7H-cycloocta[de]*naphthalen-9-one (**2b**).* Methyl keto diester **12a** (1.53 g) was refluxed with a solution of potassium carbonate (1.5 g) in dioxane (35 ml) and water (25 ml) for 3 days. The reaction mixture was treated with hydrochloric acid and the precipitated solid was collected. The solid was recrystallized from ethanol to give 0.93 g (99%) of the monomethyl ketone **2b** as colorless needles; mp 158—159 °C; IR (Nujol): ν_{max} 1694 cm^{-1} (C=O); NMR ($CDCl_3$): δ 1.20 (3H, d, J=6.8 Hz, CH_3).
Found: C, 85.79; H, 7.23%. Calcd for $C_{16}H_{16}O$: C, 85.68; H, 7.19%.

cis-*8,10-Dimethyl-8,9,10,11-tetrahydro-7H-cycloocta*[de]*naphthalen-9-one (**3b**).* Dimethyl keto diester **12b** (9.83 g) was refluxed with a solution of sodium hydroxide (6 g) in dioxane (0.5 l) and water (0.5 l) for 3 days. After treatment with hydrochloric acid the precipitated solid was collected and recrystallized from ethanol, giving 4.0 g (64%) of the *cis*-dimethyl ketone **3b** as colorless needles; mp 230—231 °C; IR (Nujol): ν_{max} 1694 cm^{-1} (C=O); NMR ($CDCl_3$): δ 0.97 (6H, d, J=6.8 Hz, CH_3).
Found: C, 85.70; H, 7.91%. Calcd for $C_{17}H_{18}O$: C, 85.67; H, 7.61%. On concentration of the above mother liquor, 1.43 g (23%) of the *trans* isomer **4b** was obtained. The compound was prepared more efficiently from the keto diester **10** as follows.

trans-*8,10-Dimethyl-8,9,10,11-tetrahydro-7H-cycloocta*[de]*naphthalen-9-one (**4b**).* Keto diester **10** (11 g) was stirred under reflux with lithium aluminum hydride (6 g) in dry ether (0.5 l) and dry benzene (0.1 l) for 12 days. The reaction mixture was treated with hydrochloric acid and the precipitated solid was collected and dried *in vacuo* to give 6.32 g (75%) of *8,10-bis(hydroxymethyl)-8,9,10,11-tetrahydro-7H-cycloocta*[de]*naphthalen-9-ol (**13a**)*; mp 165—166 °C; IR (Nujol): ν_{max} 3250 and 3420 (sh) cm^{-1} (OH); NMR (pyridine-d_5): δ 5.82 and 6.20 (br, OH).

To a stirred solution of triol **13a** (2.6 g) in pyridine (15 ml) was added dropwise a solution of methanesulfonyl chloride (1.5 ml) in pyridine (6 ml) over a period of 1 min. The mixture was stirred for 40 h at room temperature. The reaction mixture was then poured into ice water and the resulting solid was collected. Recrystallization of this solid from ethanol yielded 2.75 g (68%) of c-*8*,t-*10-bis(mesyloxymethyl)-8,9,10,11-tetrahydro-7H-cycloocta*[de]*naphthalen-r-9-ol (**13b**)* as a colorless microcrystalline solid; mp 167.5—169 °C; IR (Nujol): ν_{max} 3540 (OH), 1171 and 1350 cm^{-1} (mesyl ester); NMR (pyridine-d_5–$CDCl_3$ (2 : 1)): δ 6.14 (br, OH), 3.02 and 3.14 (each 3H, s, mesyl group).

To a stirred and boiled suspension of lithium aluminum hydride (*ca.* 6 g) in dry ether (0.3 l) was added a solution of the dimesylate **13b** (6.5 g) in dry benzene (0.1 l) over a period of 5 min. The mixture, after further addition of dry ether (0.1 l), was stirred under reflux for 14 days. The reaction mixture was then poured into ice-hydrochloric acid (*ca.* 4 l) and the mixture was allowed to stand at room temperature for 30 days. The precipitated solid was collected and chromatographed on alumina with benzene as eluant, yielding 2.65 g (73%) of c-*8*,t-*10-dimethyl-8,9,10,11-tetrahydro-7H-cycloocta*[de]*naphthalen-r-9-ol (**13c**).* The compound was further pruified by recrystallization from benzene-petroleum ether; mp 135—135.5 °C; IR (Nujol): ν_{max} 3440 and 3570 cm^{-1} (OH); NMR ($CDCl_3$) : δ 0.85 (3H, d, J=7.0 Hz, CH_3), 1.18 (3H, d, J=6.9 Hz, CH_3)

and 1.26 (s, OH).
Found: C, 84.80; H, 8.50%. Calcd for $C_{17}H_{20}O$: C, 84.95; H, 8.39%.

To a stirred and cooled (at 0 °C) solution of the dimethyl alcohol **13c** (0.747 g) in acetone (75 ml) was added dropwise the Jones reagent (prepared from 13.4 g of chromic anhydride in 25 ml of water and 12 ml of concentrated sulfuric acid) over a period of 5 min. The resulting mixture was stirred at 0 °C for 30 min. After addition of 2-propanol, the insoluble substance was removed by filtration and washed with acetone. The filtrate and washings were combined, concentrated, mixed with water and left to stand overnight. The solid precipitated was collected and chromatographed on alumina (deactivated on exposure to air) with benzene as eluant to give the *trans*-dimethyl ketone **4b** (0.59 g, 80%).

Ketone **4b** was recrystallized from aqueous ethanol to give colorless needles; mp 126—127 °C; IR (Nujol) : ν_{max} 1692 cm^{-1} (C=O); NMR ($CDCl_3$) : δ 0.94 and 1.45 (each 3H, d, J=6.5 Hz, CH_3).
Found: C, 85.60; H, 7.71%. Calcd for $C_{17}H_{18}O$: C, 85.67; H, 7.61%.

Using the same sequence of reactions as in the preparation of **4b** from **10**, compounds **6b**, **7b**, and **5b** were prepared from the corresponding keto esters **12a**, **12b**, and **11b**, through the steps, (**12a**→**14a**→**14b**→**14c**→**6b**), (**12b**→**15a**→**15b**→**15c**→**7b**), and (**11b**→**16a**→**16b**→**16c**→**5b**), respectively.

*8-Methyl-8,10-bis(hydroxymethyl)-8,9,10,11-tetrahydro-7*H*-cycloocta*[de]*naphthalen-9-ol* (**14a**) (Yield, 87%); mp 168—169 °C; IR (Nujol): ν_{max} 3220 and 1030 cm^{-1} (OH); NMR (pyridine-d_5): δ 1.58 (s, CH_3), 5.6 (br, OH). *8-Methyl-8,10-bis(mesyloxymethyl)-8,9,10,11-tetrahydro-7*H*-cycloocta*[de]*naphthalen*-9-*ol* (**14b**) (Yield, 71%); mp 103—104 °C; IR (Nujol): ν_{max} 3560 (OH), 1344 and 1175 cm^{-1} (mesyl ester); NMR ($CDCl_3$): δ 1.22 and 1.21 (each s, CH_3), 2.77, 3.02, 2.98 and 3.06 (each s, mesyl group), the complex methyl signals indicate that **14b** is a mixture of isomers. *8,8,10-Trimethyl-8,9,10,11-tetrahydro-7*H*-cycloocta*[de]*naphthalen-9-ol* (**14c**) (Yield, 95%); mp 114.5—116 °C; IR (Nujol): ν_{max} 3335 cm^{-1} (OH); NMR ($CDCl_3$): δ 0.75, 1.05, 1.18, 1.21, and 1.27 (each s, CH_3), the unexpectedly complicated methyl proton signals of **14c** suggest that **14c** is a mixture of isomers; Found: C, 85.20; H, 8.69%. Calcd for $C_{18}H_{22}O$: C, 84.99; H, 8.72%. *8,8,10-Trimethyl-8,9,10,11-tetrahydro-7*H*-cycloocta*[de]*naphthalen-9-one* (**6b**) (Yield, 85%); colorless needles (from benzene–petroleum ether); mp 124.5—125 °C; IR (Nujol): ν_{max} 1696 cm^{-1} (C=O); NMR ($CDCl_3$): δ 0.99 (3H, d, J=6.8 Hz, CH_3), 0.92 and 1.43 (each 3H, s, CH_3). Found: C, 85.89; H, 8.09%. Calcd for $C_{18}H_{20}O$: C, 85.67; H, 7.99%.

*8,10-Dimethyl-8,10-bis(hydroxymethyl)-8,9,10,11-tetrahydro-7*H*-cycloocta*[de]*naphthalen-9-ol* (**15a**) (Yield, 93%); mp 171—172 °C; IR (Nujol): ν_{max} 3275 and 1030 cm^{-1} (OH); NMR (pyridine-d_5): δ 1.42 and 1.72 (each 3H, s, CH_3), 5.78 (br, OH). *8,10-Dimethyl-8,10-bis(mesyloxymethyl)-*8,9,10,11*-tetrahydro-7*H*-cycloocta*[de]*naphthalen-9-ol* (**15b**) (Yield, 92%); mp 155—156 °C; IR (Nujol): ν_{max} 3570 (OH), 1376 and 1174 cm^{-1} (mesyl ester); NMR (acetone-d_6): δ 1.12 and 1.34 (each s, CH_3), 3.01 and 3.15 (each s, mesyl group) and 4.08 (br, OH). *8,8,10,10-Tetramethyl-8,9,10,11-tetrahydro-7*H*-cycloocta*[de]*naphthalen-9-ol* (**15c**) (Yield, 90%); mp 177—178 °C; IR (Nujol): ν_{max} 3460 and 3600 cm^{-1} (OH); NMR ($CDCl_3$): δ 0.90 and 1.21 (each 6H, s, CH_3) and 1.41 (s, OH); Found: C, 85.30; H, 9.23%. Calcd for $C_{19}H_{24}O$: C, 85.02; H, 9.01%. *8,8,10,10-Tetramethyl-8,9,10,11-tetrahydro-7*H*-cycloocta*[de]*naphthalen-9-one* (**7b**) (Yield, 82%); colorless needles (from benzene–petroleum ether); mp 133—133.5 °C; IR (Nujol): ν_{max} 1683 cm^{-1}(C=O); NMR ($CDCl_3$): δ 0.92 and 1.48 (each 6H, s, CH_3); Found: C, 85.86; H, 8.27%. Calcd for $C_{19}H_{22}O$: C, 85.67; H, 8.33%.

*8-Methyl-8-hydroxymethyl-8,9,10,11-tetrahydro-7*H*-cycloocta-*[de]*naphthalen-9-ol* (**16a**) (Yield, 60%); mp 138—139 °C; IR (Nujol): ν_{max} 3330 cm^{-1}(OH); NMR ($CDCl_3$–pyridine-d_5 (2:1)): δ 1.34 (s, CH_3), 5.20 and 5.74 (each br, OH). Treatment of **16a** with 1 mol of methanesulfonyl chloride in pyridine under the same conditions as in the preparation of **13b** from **13a** afforded *8-methyl-8-mesyloxymethyl-8,9,10,11-tetrahydro-7*H*-cycloocta*[de]*naphthalen-9-ol* (**16b**); IR (neat): ν_{max} 3530 (OH), 1340 and 1170 cm^{-1} (mesyl ester). *8,8-Dimethyl-8,9,10,11-tetrahydro-7*H*-cycloocta*[de]*naphthalen-9-ol* (**16c**) (Yield, *ca.* 20% from **16a**); mp 114.5—115.5 °C; IR (Nujol): ν_{max} 3300 cm^{-1}(OH); NMR ($CDCl_3$): δ 0.92 and 1.09 (each 3H, s, CH_3), 1.24 (s, OH); Found: C, 84.70; H, 8.45%. Calcd for $C_{17}H_{20}O$: C, 84.95; H, 8.39%. *8,8-Dimethyl-8,9,10,11-tetrahydro-7*H*-cycloocta*[de]*naphthalen-9-one* (**5b**) (Yield, 66%); mp 110—111 °C; IR (Nujol): ν_{max} 1695 cm^{-1} (C=O); NMR ($CDCl_3$): δ 0.93 and 1.42 (each 3H, s, CH_3); Found: C, 85.78; H, 7.80%. Calcd for $C_{17}H_{18}O$: C, 85.67; H, 7.61%.

*8,9,10,11-Tetrahydro-7*H*-cycloocta*[de]*naphthalene* (**1a**), *8-Methyl-8,9,10,11-tetrahydro-7*H*-cycloocta*[de]*naphthalene* (**2a**), cis-*8,10-Dimethyl-8,9,10,11-tetrahydro-7*H*-cycloocta*[de]*naphthalene* (**3a**) and trans-*8,10-Dimethyl-8,9,10,11-tetrahydro-7*H*-cycloocta*[de]*naphthalene* (**4a**). The compounds were prepared by Clemmensen reductions of the corresponding 9-ketones, **1b**, **2b**, **3b**, and **4b**, respectively, by the following procedure.

The ketone (1.0 g) in benzene (30 ml) was stirred under reflux for 30 h with amalgamated zinc (34 g), concentrated hydrochloric acid (100 ml) and acetic acid (150 ml). The mixture was cooled and extracted with ether repeatedly. The ether extracts were worked up as usual to leave a brown oil, which was purified by chromatography on alumina with hexane as eluant. The products were obtained as colorless needles by recrystallization from aqueous alcohol.

Compound **1a** (Yield, 92%); mp 57.5—58 °C (lit, mp 55—56 °C[2]); MS: *m/e* 196.126 (M^+($^{12}C_{15}{}^1H_{16}$)=196.125) (Found: C, 91.71; H, 8.26%); the compound showed spectral features similar to those reported by Nelsen and Gillespie.[2]

Compound **2a** (Yield, 74%); mp 40—41 °C; NMR ($CDCl_3$): δ 1.02 (CH_3); Found: C, 91.50; H, 8.60%. Calcd for $C_{16}H_{18}$: C, 91.37; H, 8.63%.

Compound **3a** (Yield, 63%); mp 116—117 °C; NMR ($CDCl_3$): δ 0.84 (6H, d, J=6.8 Hz, CH_3); Found: C, 90.80; H, 8.90%. Calcd for $C_{17}H_{20}$: C, 91.01; H, 8.99%.

Compound **4a** (Yield, 48%); mp 65—66 °C; NMR ($CDCl_3$): δ 0.80 (3H, d, J=6.7 Hz, CH_3) and 1.22 (3H, d, J=7.0 Hz, CH_3); Found: C, 91.30; H, 9.03%. Calcd for $C_{17}H_{20}$: C, 91.01; H, 8.99%. After **4a** had been obtained, further elution with benzene afforded the acetate ester of the *trans*-dimethyl alcohol **13c** (**17**) (Yield, 26%); mp 141.5—142 °C, whose IR spectrum (Nujol) showed absorptions at 1734 and 1241 cm^{-1} characteristic of the acetate ester group, and whose NMR spectrum [($CDCl_3$): δ 0.77 and 1.18 (each 3H, d, J=7.0 Hz, CH_3) and 1.85 (3H, s, acetyl CH_3)] was in line with the structure. Further elution with ethyl acetate gave the *trans*-dimethyl alcohol **13c** (Yield, 8%), whose melting point and spectral data were identical with those of the authentic sample prepared from **13b**.

*8,8-Dimethyl-8,9,10,11-tetrahydro-7*H*-cycloocta*[de]*naphthalene* (**5a**). *gem*-Dimethyl ketone **5b** (0.22 g), potassium hydroxide (0.4 g), hydrazine hydrate (0.5 ml) and diethylene glycol (7 ml) were combined and refluxed at 130—140 °C for 1.5 h. The condenser was then removed and the reddish

solution heated until the temperature reached 200 °C. After 15 h reflux at this temperature, the cooled reaction mixture was diluted with water, acidified and extracted with ethyl acetate. The organic extracts were washed with saturated brine solution, dried over sodium sulfate and finally concentrated to give a light brown solid. Chromatography on alumina using hexane as eluant yielded 0.18 g (86%) of the 8,8-dimethyltetrahydrocycloocta[*de*]naphthalene **5a**; mp 69—70 °C; NMR ($CDCl_3$): δ 0.80 and 1.16 (each 3H, s, CH_3). Found: C, 91.25; H, 8.80%. Calcd for $C_{17}H_{20}$: C, 91.01; H, 8.99%.

*8,8,10-Trimethyl-8,9,10,11-tetrahydro-7*H*-cycloocta*[de]*naphthalene (**6a**).* Trimethyl ketone **6b** (0.3 g) was subjected to Wolff-Kishner reduction using the same procedure as in the preparation of **5a**. The crude product was chromatographed on alumina with hexane as an eluant to give 0.2 g (70%) of the hydrocarbon **6a**; mp 89—90 °C; NMR ($CDCl_3$): δ 0.80 (3H, d, J=6.8 Hz, CH_3), 0.81 and 1.16 (each 3H, s, CH_3). Found: C, 90.56; H, 9.46%. Calcd for $C_{18}H_{22}$: C, 90.70; H, 9.30%.

*8,8,10,10-Tetramethyl-8,9,10,11-tetrahydro-7*H*-cycloocta*[de]*naphthalene (**7a**).* 8,8,10,10-Tetrakis(tosyloxymethyl)-8,9,10,11-tetrahydro-7*H*-cycloocta[*de*]naphthalene (**19**) was prepared from tetraethyl 1,1,3,3-propanetetracarboxylate and 1,8-bis(bromomethyl)naphthalene (**9**).[3]

To a stirred and boiled slurry of excess lithium aluminum hydride in dry ether (0.3 l) was added a solution of the tosylate **19** (2.0 g) in dry ether (0.1 l) over a period of 5 min. The mixture, after further addition of dry ether (0.1 l), was stirred under reflux for 3 days and cooled. The reaction mixture was poured onto ice-hydrochloric acid and the mixture was extracted with ether. The ethereal extracts were combined, washed with saturated brine solution and dried over sodium sulfate. After removal of the solvent the residue was taken up in a small amount of hexane–benzene and chromatographed on alumina. Elution with hexane gave 0.24 g (44%) of the desired tetramethyltetrahydrocycloocta[*de*]naphthalene **7a**. Further elution with benzene yielded an unidentified compound (0.14 g), which, after recrystallization from hexane, melted at 160—161 °C. Hydrocarbon **7a** was recrystallized from aqueous ethanol to give colorless needles; mp 112—113 °C; NMR ($CDCl_3$): δ 0.74 and 1.29 (each 6H, s, CH_3). Found: C, 90.68; H, 9.34%. Calcd for $C_{19}H_{24}$: C, 90.41; H, 9.59%.

The author wishes to thank Dr. Yo-ichiro Mashiko, ex-director of this Laboratory, and Dr. Osamu Yamamoto for their encouragement and valuable discussions. The author also thanks Dr. Nobuhide Wasada for the measurements of high-resolution mass spectra.

References

1) V. Balasubramanian, *Chem. Rev.*, **66**, 567 (1966).
2) S. F. Nelsen and J. P. Gillespie, *J. Am. Chem. Soc.*, **95**, 2940 (1973).
3) T. Kamada, N. Wasada, and O. Yamamoto, *Bull. Chem. Soc. Jpn.*, **49**, 275 (1976).
4) O. H. Wheeler, "The Chemistry of the Carbonyl Groups," ed by S. Patai, International Publishers, New York (1966), Chap. 11, and references cited therein.
5) H. Schmid and Karrer, *Helv. Chim. Acta*, **32**, 1371 (1949).

Photochemical and Thermal Reactions of Cyclohexadienone Oximes

Renji OKAZAKI, Masako WATANABE, and Naoki INAMOTO*

Department of Chemistry, Faculty of Science, The University of Tokyo, Hongo, Tokyo 113

(Received July 1, 1978)

Photolysis of (*E*)-1-hydroxyimino-2,4,5-tri-*t*-butyl-6-methyl-2,4-cyclohexadiene (**1**) and the corresponding (*Z*)-isomer in methanol, benzene, or pentane afford 1,3,5-tri-*t*-butyl-5-cyano-1,3-cyclohexadiene (**3**), 5-*t*-butyl-7-cyano-2,2,3,8,8-pentamethyl-3,4,6-nonatriene (**4**), 5-*t*-butyl-3-cyano-2,2,7,8,8-pentamethyl-3,4,6-nonatriene (**5**), 5-*t*-butyl-7-cyano-2,3,3,8,8-pentamethyl-1,4,6-nonatriene (**6**), 5-*t*-butyl-3-cyano-7-methoxy-2,2,7,8,8-pentamethyl-3,5-nonadiene (**7**), 5-*t*-butyl-7-cyano-7-methoxy-2,2,3,8,8-pentamethyl-3,5-nonadiene, and 2,4-di-*t*-butyl-6-cyano-7,7-dimethyl-1,3,5-octatriene (**9**). The presence of an oxaziridine in the reaction mixture has been confirmed by iodometry. The photoreaction in the presence of 1,3-pentadiene or oxygen gives essentially the same results, suggesting the involvement of the singlet excited state in these photoreactions. Thermal Beckmann rearrangement of **1** has been conducted for comparison to give only **6**, **7**, and **9**. The photochemical formation of **3**—**9** has been rationalized in terms of the "free" cyclopentadienyl cation formed by ionic α-cleavage of the oxime. Photoreaction of 1-hydroxyimino-2,4,6-tri-*t*-butyl-2,4-cyclohexadiene with one alkyl group at 6-position gives 5-*t*-butyl-7-cyano-2,3,8,8-tetramethyl-1,4,6-nonatriene, 5-*t*-butyl-3-cyano-8-methoxy-2,2,7,8-tetramethyl-4,6-nonadiene, 5-*t*-butyl-7-cyano-2-methoxy-2,3,8,8-tetramethyl-3,5-nonadiene, and 1,3-di-*t*-butyl-5-cyano-3-methoxy-6,6-dimethyl-1,4-heptadiene.

Since the first report on photo-Beckmann rearrangement by de Mayo in 1963,[1] there have been numerous reports on the photoreaction of oximes.[2] There are also many investigations concerning cyclohexadienones.[3,4] On the contrary, however, there has been no report on the photoreaction of cyclohexadienone oximes, probably because of the limited availability of the material.

Since we recently discovered the facile one-step synthesis of oximes of cyclohexadienones from the reactions of 2,4,6-tri-*t*-butylnitroso(or nitro)benzene with Grignard reagents,[5,6] we undertook the study on the photoreaction of these sterically hindered cyclohexadienone oximes[7] and a full account is described in this paper.

Reaction Products. Irradiation of (*E*)-1-hydroxyimino-2,4,6-tri-*t*-butyl-6-methyl-2,4-cyclohexadiene (**1**) in solution (methanol, pentane, or benzene) (medium pressure mercury lamp, Pyrex-filter) afforded 1,3,5-tri-*t*-butyl-5-cyano-1,3-cyclohexadiene (**3**), 5-*t*-butyl-7-cyano-2,2,3,8,8-pentamethyl-3,4,6-nonatriene (**4**), 5-*t*-butyl-3-cyano-2,2,7,8,8-pentamethyl-3,4,6-nonatriene (**5**), 5-*t*-butyl-7-cyano-2,3,3,8,8-pentamethyl-1,4,6-nonatriene (**6**), 5-*t*-butyl-3-cyano-7-methoxy-2,2,7,8,8-pentamethyl-3,5-nonadiene (**7**), 5-*t*-butyl-7-cyano-7-methoxy-2,2,3,8,8-pentamethyl-3,5-nonadiene (**8**), and 2,4-di-*t*-butyl-6-cyano-7,7-dimethyl-1,3,5-octatriene (**9**) along with some recovered **1** and the isomer **2**. The yields of the products and the reaction conditions are shown in Table 1.

When (*Z*)-oxime (**2**) was irradiated under the identical conditions, isomerization into **1** was observed at first and the final products and their yields were essentially the same as those from **1**.

Formation of oxaziridine (**10**), which is considered to be an intermediate leading to an amide in photo-Beckmann rearrangement[2] and in some cases characterized in solution,[8] was also observed in the reaction of **1** in methanol; treatment of the reaction solution, after irradiation for 3.8 h, with sulfuric acid and potassium iodide, followed by titration of the liberated iodine and the subsequent titration of the consumption of the acid,[9] indicated the yield of the oxaziridine was about 6%.

The structural assignment of **3**, **7**, and **9** is straightforward from their analytical and spectral data, and it was confirmed by the chemical behavior as shown in Scheme 1.

Treatment of **7** with trifluoroacetic acid in benzene led to formation of **9** (95%), which was also obtained in irradiation of **1** in benzene for 4 h (14%). Triene (**9**) underwent cyclization to give **3** (96%) upon irradiation with Pyrex-filtered light for 6 h in methanol, suggesting that **3** is a secondary product formed *via* **9**.

Ether (**7**) is not a precursor of other products, be-

TABLE 1. YIELDS (%) OF PRODUCTS IN PHOTOREACTIONS OF **1** AND **2**

Starting material	Solvent	Reaction time (h)	Yields (%)								
			1	**2**	**3**	**4**	**5**	**6**	**7**	**8**	**9**
1	Methanol	7.5	11	6	19	11	7	5	16	2	1
2	Methanol	7.5	0	6	33	5	—	3	22	3	—
1	Pentane	9.3	—	—	5	11	7	—	—	—	—
1	Benzene	4.0	9	4	11	tr	6				14
1	Methanol[a)]	7.5	8	10	12	6	8	2	17	2	—
1	Methanol[b)]	7.5		7	19	13	8	3	16	2	1

a) In the presence of 1,3-pentadiene. b) In the presence of oxygen.

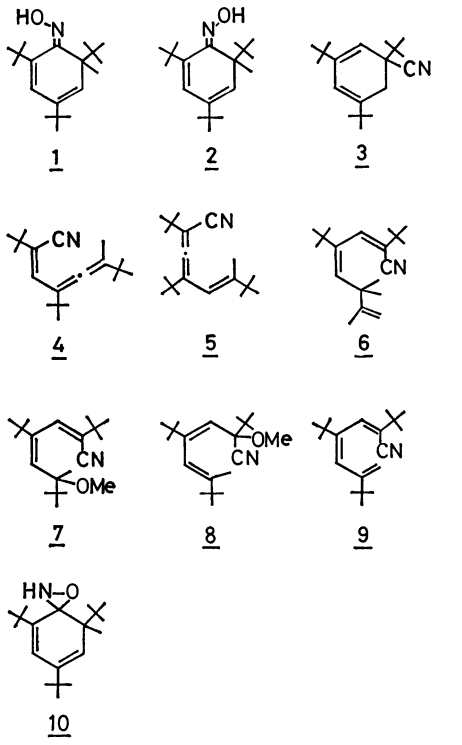

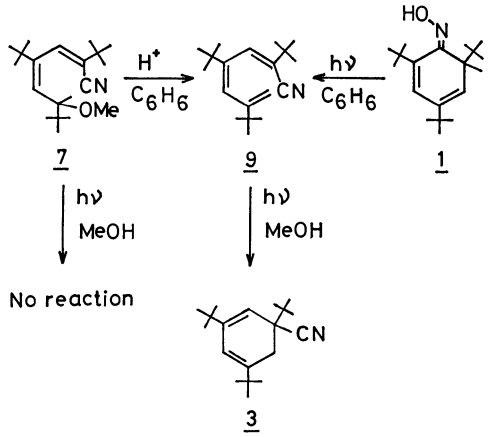

Scheme 1.

cause no change was observed in the irradiation of **7** for 7.5 h in methanol.

The NMR spectrum of **6** showed two *t*-butyl groups (δ 1.08 and 1.19), two methyl protons attached to the saturated carbon (1.19), methyl protons bound to the olefinic carbon (1.68) splitting with a small coupling constant, two equivalent olefinic protons (4.70) appeared as multiplet, and two olefinic protons (5.42 and 6.38) appeared as a doublet. The IR spectrum showed the presence of cyano (2235 cm^{-1}) and terminal methylene (889 cm^{-1}) groups. The UV spectrum of **6** had an absorption maximum at 257 nm which is consistent with the structure of a conjugated diene.

The NMR spectrum of **8** showed three *t*-butyl groups (δ 1.02 and 1.15 (1:2)), methyl protons bound to the olefinic carbon (1.83), methoxyl protons (3.35), and olefinic protons (5.04 and 5.42). The signal of the methyl protons shows a small coupling constant, suggesting that the methyl group may be attached to a fully substituted olefinic carbon. The IR spectrum showed the existence of a cyano group (2225 cm^{-1}), although absorption intensity was very week. This phenomenon suggests that the cyano group is located on the carbon to which an ether group attaches[10]. The UV spectrum of **8** had absorption maxima at 234(sh) and 262(sh) nm which indicated a conjugated diene and ruled out the structure (**11**).

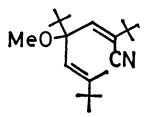

The long range coupling of two olefinic protons indicates the presence of a double bond between these protons and is consistent with this assignment.

The IR spectra of **4** and **5** indicated the existence of an allenic group (1950 cm^{-1}). Their ^{1}H-NMR spectra showed three *t*-butyl groups (δ 1.08 (18 H) and 1.21 (9 H) for **4**, δ 1.05, 1.10, and 1.28 for **5**), a methyl group on sp^2 carbon (δ 1.81 for **4**, 1.72 for **5**), and an olefinic proton (δ 6.36 for **4**, 6.56 for **5**). Since both of the methyl protons appeared as singlet and the coupling constant between the olefinic proton and the methyl protons was estimated to be very small, it is impossible from ^{1}H-NMR spectra to determine whether the methyl groups are bound to an olefinic carbon or an allenic carbon. The mass spectra of those products were similar to each other. The ^{13}C-NMR spectrum of **4** showed an allenic carbon at 198.5 ppm, a cyano group at 117.5 ppm, and a methyl group on sp^2 carbon at 14.4 ppm. Single resonance spectrum showed the signal of the cyano carbon splitted to doublet ($^3J_{CH}$=15.8 Hz). This coupling suggested the existence of β-proton, therefore, the cyano and methyl groups must be bound to olefinic and allenic carbons, respectively. These facts support the structure **4**. Therefore, **5** is considered to be an isomeric allene as shown, although satisfactory elemental analysis and ^{13}C-NMR spectrum could not be obtained because of paucity of the sample. That **4** and **5** have an allenic structure isomeric each other, was also established by catalytic hydrogenation.

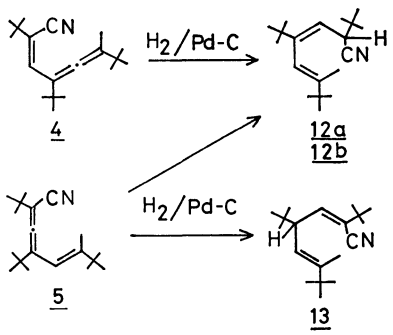

Thus, hydrogenation of **4** afforded conjugated diene **12a** as a result of the reduction of the allenic group followed by 1,5-hydrogen shift, while hydrogenation

of **5** afforded **12b** and **13**. The signal pattern of NMR spectra of **12a** and **12b** resembled each other but their chemical shifts were slightly different, suggesting they are geometric isomers having the same gross structure. They are probably (**12A**) and (**12B**), although the spectral data are insufficient to establish which is which.

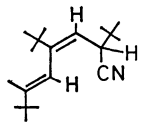

12 A

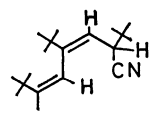

12 B

Thermal Beckmann Rearrangement. Reaction of **1** with 2-chloro-1-methylpyrimidinium fluorosulfate[11] followed by quenching with methanol, gave **6** (9%), **7** (6%), and **9** (46%).

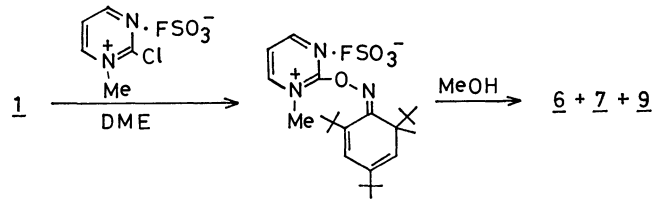

Reaction Mechanism. The products (**3**—**9**) are considered to be formed *via* heterolytically produced pentadienyl cation as depicted in Scheme 2. Since the photoreaction of **1** was not quenched by 1,3-pentadiene and oxygen, it probably proceeds *via* the singlet state.

Isomerization between oximes **1** and **2** occurs at first, as generally observed in the reaction of oximes. From this photochemical equilibrium mixture is formed oxaziridine (**10**), which probably reverts to the oxime mixture photochemically, thermally, and/or during the treatment with silica gel. Heterolytic α-cleavage and fission of the N–O bond of the oxime afford pentadienyl cation (**14**), with formal canonical structures (**14a**), (**14b**), and (**14c**). Whether these bond cleavages are simultaneous or stepwise could not be established experimentally, but involvement of nitrenium ion (**15**)

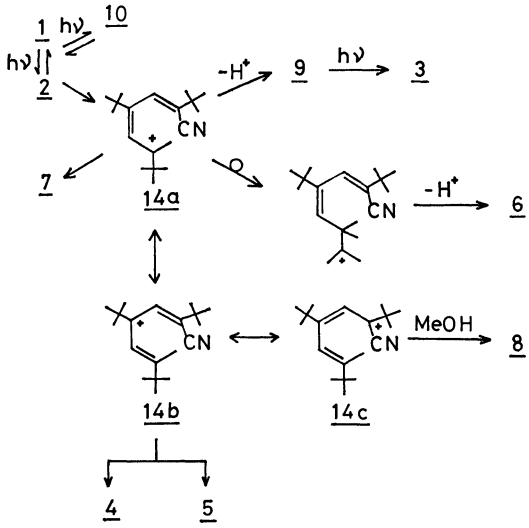

Scheme 2.

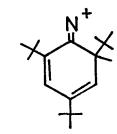

15

seemes unlikely in view of the known propensity of this kind of nitrenium ion to undergo intramolecular C–H insertion.[12] However, the possibility that oxaziridine (**10**) is a direct precursor of **14** can not be eliminated completely, although it appears quite unlikely.

The most obvious feature of this photoreaction is that all the products are formed *via* ionic processes. Contrary to frequent observations of nitrile formation in the ground state Beckmann rearrangement, photo-Beckmann fission is observed only rarely,[2] and more importantly the formation of nitriles in the excited state reaction has been explained by a homolytic process.[13,14]

The present reaction represents the first and unequivocal example of a heterolytic α-cleavage of an oxime. There seem two reasons for the facile heterolytic α-cleavage; one is that the carbonium ion formed is a stabilized pentadienyl cation with two alkyl groups on its terminal and the other is that oxaziridine, even if it is formed, would suffer strain by bulky *t*-butyl groups, thus reverting to the starting oxime.

The heterolytic pathway seems to be operative even in nonpolar solvent such as pentane, although the reaction is apparently more complex; the products identified were **3**, **4**, and **5** (Table 1).

The discrepancy in the products between the excited and ground state reactions is most likely due to the difference in nature of an intermediate in both reactions. The products of the thermal Beckmann fission are only those that are formally derived from canonical structure **14a**, suggesting the participation of the solvent (for **7**) and neighboring bonds (for **6** and **9**) in the product forming process. On the contrary, in the photoreaction, the pentadienyl cation **14** appears to be formed as a "free" carbonium ion without such assistance. The formation of the products (**4**, **5**, and **8**), characteristic of the excited state reaction, is reasonably explained in terms of canonical structures (**14b**) and (**14c**), that is, deprotonation from **14b** affords **4** and **5** and addition of methanol to **14c** gives **8**. This reactivity is most likely accounted for in the light of characteristics of a "free" (or "hot") carbonium ion[15] that reactions occur at a position(s) other than that where a carbonium ion is initially generated.

This sort of "free" carbonium ions have recently been invoked in the photoreactions of alkyl and vinyl halides in order to rationalize the difference in reactivity between the photochemical and solvolytic reactions.[16,17]

Photoreaction of 2,4-Cyclohexadienone Oxime with One Alkyl Group at 6-Position. In order to examine the relationship between structure and reactivity in the photoreaction of 2,4-cyclohexadienone oximes, the photoreaction of the oxime with only one alkyl group at the 6-position was carried out.

Irradiation of 1-hydroxyimino-2,4,6-tri-*t*-butyl-2,4-

cyclohexadiene (**16**) in methanol (medium pressure mercury arc, Pyrex-filter) for 17.5 h afforded 5-*t*-butyl-7-cyano-2,3,8,8-tetramethyl-1,4,6-nonatriene (**17**), 5-*t*-butyl-3-cyano-8-methoxy-2,2,7,8-tetramethyl-4,6-nonadiene (**18**), and recovered oxime **16**. When the reaction time was prolonged to 36.5 h products obtained were **17**, **18**, 5-*t*-butyl-7-cyano-2-methoxy-2,3,8,8-tetramethyl-3,5-nonadiene (**19**), and 1,3-di-*t*-butyl-5-cyano-3-methoxy-6,6-dimethyl-1,4-heptadiene (**20**).

The yield of the products and the reaction conditions are shown in Table 2.

Table 2. Yields (%) of products in photoreaction of **16**

Solvent	Reaction time (h)	Yields (%)				
		16	**17**	**18**	**19**	**20**
Methanol	17.5	6	20	18	—	—
Methanol	36.5	0	19	8	14	5

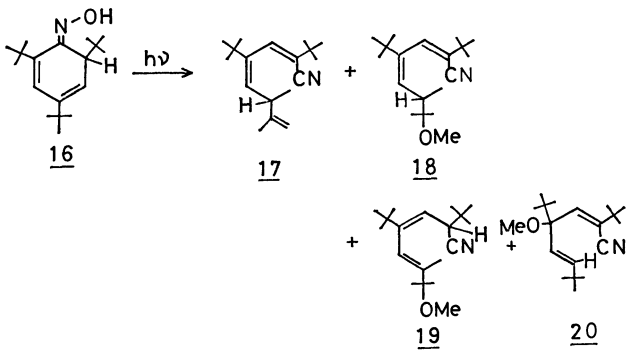

Irradiation (Pyrex-filtered light in methanol, 11.5 h) of **18** led to formation of **19** (94%). This suggests that **19** is a secondary product from **18** *via* photochemically allowed antarafacial 1,5-hydrogen shift.[18]

Elimination of methanol from **18** by trifluoroacetic acid in benzene, which converted **7** to **9**, was unsuccessful, probably because stabilization of carbonium ion formed is not sufficient in this case.

Although satisfactory elemental analysis could not be obtained, the structure of the products were confirmed by their spectral data.

The ^{1}H-NMR spectrum of **18** showed two *t*-butyl groups (δ 1.09 and 1.25), two methyl groups (1.00), methine proton with intricate splitting (1.85—2.46), methoxyl protons (3.08), and two olefinic protons (5.34 and 6.41), one methyl signal appearing as a doublet at δ 0.98.

The ^{13}C-NMR spectrum showed the presence of a cyano carbon at 117.4, three methyl carbons (δ 23.3, 21.6, and 14.2), a methoxyl carbon (48.8), and a tertiary carbon α to oxygen (77.1).

Molecular ion peak on the mass spectrum of **18** was not observed, but the fact that the base peak was *m/e* 73, assignable to $[(CH_3)_2(OCH_3)C]^+$, is consistent with the structure proposed in view of high stability of $[(CH_3)_2(OCH_3)C]^+$ and pentadienyl radical.

The easy 1,5-prototropy of **18** leading to **19** remains to be accounted for. Considering interactions between bulky *t*-butyl groups, configuration of **18** may be favorable for such a 1,5-hydrogen migration. It is interesting that similar phenomenon was observed in the hydrogenation of allene (**4**) as described before. The signal patterns of the NMR spectra of **12** and **19** resemble each other.

Formation of **20** can be explained formally by the reaction of methanol with pentadienyl cation with a canonical structure similar to **14b** shown in Scheme 2.

Therefore, the reaction of oxime (**16**) is essentially the same as that of **1** in the sense that it proceeds mainly *via* heterolytic α-cleavage, although the reaction is more complex.

Experimental

All melting points were not corrected. The IR and UV spectra were recorded with Hitachi EPI-G2 and EPS-3 spectrophotometers respectively. The ^{1}H-NMR and ^{13}C-NMR spectra were measured with Hitachi R-20B (60 MHz) and JEOL JNM-FX60 spectrometers using tetramethylsilane as an internal standard. The mass spectra were recorded with a Hitachi RMU-6L mass spectrometer. The photolyses were carried out using a 100 W medium pressure mercury lamp with a Pyrex filter, and nitrogen gas was passed through the solution before (about 15 min) and during irradiation unless otherwise noted. Gas chromatographic separation was performed using a JEOL-750 (versamide 900) unless otherwise noted.

Photolysis of (E)-1-Hydoxyimino-2,4,6-tri-t-butyl-6-methyl-2,4-cyclohexadiene (1) in Methanol. Oxime **1**[6] (450 mg, 1.55 mmol) in methanol (90 ml) was irradiated at 0—5 °C for 7.5 h. The solvent was removed under reduced pressure and the residue was subjected to preparative thin layer chromatography (TLC) (SiO_2, hexane-dichloromethane (4 : 1)) to be divided into five fractions.

The first fraction gave 28 mg (6%) of (*Z*)-isomer of (**1**).[6]

The second (white crystals) was a mixture of **4** (42 mg), **6** (16 mg), **8** (10 mg, 2%), and **9** (5 mg, 1%) according to the peak area on the gas chromatogram. Each product was isolated by means of gas chromatography (GLC) (in glass column at 135 °C). **4**: mp 54.0—55.0 °C (from methanol); IR (KBr) : 2220 (CN) and 1950 cm^{-1} (C=C=C); ^{1}H-NMR (CCl_4) : δ 1.08 (s, 18H), 1.21 (s, 9H), 1.81 (s, 3H), and 6.36 (s, 1H); ^{13}CNMR ($CDCl_3$) : 198.5 ppm, 136.4, 122.7, 117.5, 112.9, 109.9, 35.6, 34.3, 34.0, 29.5, 29.1, 28.8, and 14.4; λ_{max} (hexane) : 270.5 nm (ε 9060); MS : *m/e* 273 (M^+, 22%), 258 (17), 217 (40), 202 (100), 160 (29), and 57 (59). Found: C, 83.72; H, 11.71; N, 5.00%. Calcd for $C_{19}H_{31}N$: C, 83.45; H, 11.43; N, 5.12%. **6**: mp 48.5—49.5 °C (from methanol); IR (KBr) : 2235 (CN) and 889 cm^{-1} (C=CH$_2$); NMR (CCl_4) : δ 1.08 (s, 9H), 1.19 (s, 15H), 1.68 (d, J= 0.8 Hz, 3H), 4.07 (m, 2H), 5.42 (d, J=1.5 Hz, 1H), and 6.38(d, J=1.5 Hz, 1H); λ_{max} (hexane) : 257 nm (ε 1530); MS : *m/e* 273 (M^+, 6.7%), 258 (14), 216 (38), 202 (37), 160 (30), and 57 (100). **8** : oil; IR ($CHCl_3$) : 2225 cm^{-1} (CN); NMR (CCl_4) : δ 1.02 (s, 9H), 1.15 (s, 18H), 1.83 (d, J= 1.3 Hz, 3H), 3.35 (s, 3H), 5.04 (d, J=2.3 Hz, 1H), and 5.42 (m, 1H); λ_{max} (hexane) : 234(sh) (ε 4060) and 262(sh) nm (1500); MS : *m/e* 305 (M^+, 0.4%), 202 (13), 160 (12), and 57 (100). **9** : oil; IR (neat) : 2225 (CN), 1609, and 899 cm^{-1} (C=CH$_2$); NMR (CCl_4) : δ 1.09 (s, 9H), 1.13 (s, 9H), 1.18 (s, 9H), 4.68 (dd, J=1.5 Hz, 1H), 4.95 (d, J=1.5 Hz, 1H), 6.09 (dd, J=1.5 Hz, 1H), and 6.50 (d, J=1.5 Hz, 1H); λ_{max} (hexane): 262 nm (ε 6700); MS: *m/e* 273 (M^+, 1.5%), 217 (23), 160 (64), 57 (100), and 41 (46),

The third farction was a mixture of **3** (80 mg, 19%), **5**

(31 mg, 7%), **4** (3 mg, total yield 11%), and **6** (6 mg, total yield 5%) according to the peak area on the gas chromatogram, and they were purified by preparative GLC to give each product in a pure state. **3**: mp 137.1—137.8 °C (from methanol); IR (KBr) : 2235 cm^{-1} (CN); NMR (CCl_4) : δ 1.10 (s, 18H), 1.14 (s, 9H), 2.22 (d, J=2.4 Hz, 1H), 2.31 (s, 1H), 5.29 (d, J=1.7 Hz, 1H), and 5.95 (m, 1H); λ_{max} (hexane): 261 nm (ε 5950); MS : *m/e* 273 (M^+, <1%), 160 (13), and 57 (100). Found: C, 83.15; H, 11.67; N, 5.28%. Calcd for $C_{19}H_{31}N$: C, 83.45 : H, 11.43; N, 5.12%. **5** : oil; IR (neat) : 2225 (CN) and 1950 cm^{-1} (C=C=C); NMR (CCl_4) : δ 1.05 (s, 9H), 1.10 (s, 9H), 1.28 (s, 9H), 1.72 (s, 3H), and 6.56 (s, 1H); λ_{max} (hexane) : 258 nm (ε 14900); MS : *m/e* 273 (M^+, 6%), 217 (43), 202 (100), 160 (22), and 57 (80).

The fourth fraction (144 mg) was a mixture of **7** (78 mg, 16%) and recovered oxime **1** (48 mg, 11%) according to the signal intensity on the NMR spectrum. **7**: oil; IR (neat) : 2220 cm^{-1} (CN); NMR (CCl_4) : δ 0.88 (s, 9H), 1.12 (s, 9H), 1.18 (s, 3H), 1.22 (s, 9H), 3.16 (s, 3H), 5.55 (d, J= 1.8 Hz, 1H), and 6.50 (d, J=1.8 Hz, 1H); λ_{max} (hexane): 259(sh) (ε 3380), 306(sh) (1530), and 325(sh) nm (920); MS : *m/e* 273 (M^+-CH_3OH, <1%), 160 (16), and 57 (100).

*Photolysis of (Z)-1-Hydroxyimino-2,4,6-tri-t-butyl-6-methyl-2,4-cyclohexadiene (**2**) in Methanol.* Methanol solution (80 ml) of oxime (**2**) (394 mg, 1.35 mmol) was irradiated for 7.5 h under the same conditions as those of the photolysis of oxime **1**. After the removal of the solvent, the reaction products were analyzed by a combination of preparative TLC and GLC as described above for **1** (see Table 1).

*Photolysis of Oxime (**1**) in Pentane or Benzene.* Oxime **1** (450 mg, 1.55 mmol) in pentane or benzene (90 ml) was irradiated (9.3 h for the pentane solution and 4 h for the benzene solution) under the same conditions as those of the photolysis in methanol. The products were purified by TLC (see Table 1).

*Photolysis of Oxime (**1**) in the Presence of 1,3-Pentadiene.* Oxime (**1**) (450 mg, 1.55 mmol) and 1,3-pentadiene (608 mg, 8.9 mmol) in methanol (90 ml) was irradiated for 7.5 h. The reaction products were analyzed by TLC and GLC as above (see Table 1).

*Photolysis of Oxime (**1**) in the Presence of Oxygen in Methanol.* Oxime (**1**) (450 mg, 1.55 mmol) was dissolved in methanol (90 ml). After being flashed with oxygen, the solution was irradiated for 7.5 h at 0—5 °C, during which oxygen was passed through. The identification and determination of the yields of the reaction products were carried out by TLC and GLC (see Table 1).

*Determination of the Oxaziridine Concentration and "B.O. value" in the Photolysis of Oxime (**1**) in Methanol.* Oxime (**1**) (450 mg, 1.55 mmol) in methanol (90 ml) was irradiated under the same conditions as those of the photolysis in methanol. After irradiation for 3.8 h, a part of the solution (10 ml) was treated with sulfuric acid (0.01767 N, 50 ml) and potassium iodide (1 g), and then the liberated iodine was titrated with a standard solution of sodium thiosulfate (0.010029 N, 1.95 ml). Then the amount of the acid consumed to liberate iodine was determined by back titration with 0.009280 N potassium hydroxide. The amount of the species which liberated iodine was 0.00978 mmol (6%) and that of consumed acid was 0.036 mmol, thus the "B. O. value" being 3.68. This value suggested that the species was oxaziridine[9].

*Reaction of **7** with Trifluoroacetic Acid.* To a benzene solution (40 ml) of **7** (39 mg, 0.13 mmol), a drop of trifluoroacetic acid was added with stirring. After additional stirring for 26 h at room temperature, the solvent was removed under reduced pressure to give 33 mg (95%) of **9** as yellow tar (by NMR).

*Photoreaction of **9** in Methanol.* A mixture of trienes (**9**) and (**6**) (64.8 mg), which contained 57.6 mg (0.21 mmol) of **9** according to the GLC (DOS column, 180 °C) was dissolved in methanol (13 ml) in a Pyrex glass tube, flashed with nitrogen, and was externally irradiated for 6.3 h at 0—5 °C. TLC purification afforded 12 mg of **6** as white crystals and 55 mg (96%) of **3** (by NMR).

*Test for Photostability of **7** in Methanol.* Product **7** (99 mg, 0.32 mmol) in methanol (90 ml) was irradiated for 7.8 h under the same conditions as those of the photolysis of oxime **1** in methanol. Removal of the solvent resulted in almost complete recovery of **7** (97 mg) according to GLC. Some very small peaks other than that of **7** were observed by GLC, but they were not **3**, **4**, **5**, **6**, **8**, and **9**.

*Hydrogenation of **4**.* A solution of **4** (78 mg, 0.29 mmol) in ethanol (8 ml) and acetic acid (0.05 ml) was hydrogenated over 10% palladium on charcoal (30 mg) under atmospheric pressure for at room temperature. After the mixture was filtered and the catalyst was washed with ethanol, the solvent was evaporated from the combined filtrates under reduced pressure. The residue was chromatographed on alumina with carbon tetrachloride as eluent to give 51 mg of colorless tarry material, which was purified by preparative GLC to give 11 mg (14%) of **12a** as a colorless oil: NMR (CCl_4): δ 1.01 (s, 9H), 1.13 (s, 18H), 1.84 (d, J=1.6 Hz, 3H), 3.17 (d, J=10.8 Hz, 1H), 5.18 (dd, J=2.2 and 10.8 Hz, 1H), and 5.41 (m, 1H).

*Hydrogenation of **5**.* A solution of **5** (40 mg, 0.15 mmol) in ethanol (6 ml) containing a few drops of acetic acid was hydrogenated over a spatula of 10% palladium on charcoal under atmospheric pressure for 22 h at room temperature. After treatment similar to that mentioned above was obtained 26 mg of colorless tarry material, which was further purified by the preparative GLC to give 11 mg (27%) of **13** as colorless crystals and 8 mg (19%) of **12b** as colorless tar. **13**: NMR (CCl_4): δ 0.90 (s, 9H), 1.07 (s, 9H), 1.19 (s, 9H), 1.71 (d, J=1.5 Hz, 1H), 3.24 (dd, J=9.8 and 10.6 Hz, 1H), 5.09 (dd, J=1.5 and 9.8 Hz, 1H), and 5.86 (d, J=10.6 Hz, 1H); λ_{max} (hexane): 240(sh) nm (ε 8200); MS: *m/e* 275 (M^+, 1%). **12**: NMR (CCl_4): δ 0.99 (s, 9H), 1.08 (s, 9H), 1.15 (s, 9H), 1.62 (d, J=1.5 Hz, 3H), 2.94 (d, J=11.2 Hz, 1H), 5.25 (dd, J=1.5 and 11.2 Hz, 1H), and 5.61 (m, 1H); MS: *m/e* 275 (M^+, <1%).

*Reaction of Oxime (**1**) with 2-Chloro-1-methylpyrimidinium Fluorosulfate.* A mixture of 179 mg (0.62 mmol) of oxime (**1**) and 173 mg (0.68 mmol) of pyrimidinium salt in anhydrous 1,2-dimethoxyethane (6 ml) was stirred at room temperature under argon atmosphere. After 8.3 h, absolute methanol (20 ml) was added. After stirring for 17.4 h at room temperature, the reaction mixture was poured into water, and the mixture was extracted with dichloromethane. The extract was washed with water and dried over anhydrous magnesium sulfate. Removal of the solvent afforded 156 mg of yellow, partly crystalline material, which was subjected to preparative TLC (SiO_2, hexane–dichloromethane (5:1)) to give **9** (79 mg, 46%), **6** (15 mg, 9%), and **7** (12 mg, 6%).

*Photolysis of 1-Hydroxyimino-2,4,6-tri-t-butyl-2,4-cyclohexadiene (**16**) in Methanol.* a) Oxime (**16**)[19] (450 mg, 1.62 mmol) in methanol (90 ml) was irradiated at 0—5 °C for 17.5 h. The solvent was removed *in vacuo*, and the residue was subjected to preparative TLC (SiO_2, hexane–dichloromethane (4:1)) to give two fractions.

One fraction was 129 mg of yellow, partly crystalline material. According to the peak area on the GLC, it seemed

to be a mixture of **17** (85 mg, 20%), recovered oxime (**16**) (28 mg, 6%), and 16 mg of unidentified materials. **17** was isolated by GLC as colorless tarry material. **17**: IR (neat): 2220 (CN) and 889 cm^{-1} ($C=CH_2$); NMR (CCl_4): δ 1.10 (s, 9H), 1.19 (d, $J=7$ Hz, 3H), 1.26 (s, 9H), 1.63 (dd, $J=1.2$ Hz, 3H), 2.8 (m, 1H), 4.60 (m, 2H), 5.27 (dd, $J=9$ and 1.2 Hz, 1H), and 6.46 (d, $J=1.2$ Hz, 1H); MS: *m/e* 259 (M^+, 2.5%), 203 (21), 202 (21), 188 (36), 146 (23), and 57 (100).

Another fraction was 197 mg of brown tar, which was again purified with preparative TLC (SiO_2, hexane–dichloromethane (1:1)) to afford **18** (84 mg, 18%) as pale yellow tar; IR (neat): 2220 cm^{-1} (CN); ^{1}H-NMR (CCl_4): δ 0.98 (d, $J=7$ Hz, 3H), 1.00 (s, 6H), 1.09 (s, 9H), 1.25 (s, 9H), 1.85—2.46 (m, 1H), 3.08 (s, 3H), 5.34 (dd, $J=10.5$ and 2.2 Hz, 1H), and 6.41 (d, $J=2.2$ Hz, 1H); ^{13}C-NMR ($CDCl_3$): 143.9 ppm, 140.0, 128.5, 127.8, 117.4, 77.1, 48.8, 40.3, 36.6, 35.3, 29.3, 28.9, 23.2, 21.6, and 14.2; λ_{max} (hexane): 250 nm (ε 2580); MS: *m/e* 276 (M^+-CH_3, <1%), 73 (100), and 57 (31).

b) Oxime (**16**) (343 mg, 1.24 mmol) in methanol (80 ml) was irradiated as described in a) except that the reaction time was 36.5 h. Similar treatment gave 38 mg (19%) of **17**, 19 mg (5%) of **20**, 50 mg (14%) of **19**, and 29 mg (8%) of **18**. **19** was purified by GLC. **19**: IR (neat): 2225 cm^{-1} (CN); NMR (CCl_4): δ 0.99 (s, 9H), 1.12 (s, 9H), 1.29 (s, 6H), 1.81 (d, $J=2.4$ Hz, 3H), 3.08 (s, 3H), 3.17 (d, $J=10.2$ Hz, 1H), 5.13 (dd, $J=10.2$ and 2.4 Hz, 1H), and 5.55 (m, 1H); λ_{max} (hexane): 293(sh) nm (ε 970); MS: *m/e* 259 (M^+-CH_3OH, 6%), 244 (15), 202 (25), 188 (21), 146 (39), and 57 (100). **20**: IR (neat): 2220 cm^{-1} (CN); NMR (CCl_4): δ 0.99 (s, 9H), 1.14 (s, 9H), 1.25 (s, 9H), 3.27 (s, 3H), 5.24 (d, $J=14.4$ Hz, 1H), 5.75 (d, $J=14.4$ Hz, 1H), and 6.28 (s, 1H); MS: *m/e* 276 (M^+-CH_3, 1%), 234 (54), 202 (21), 193 (32), 188 (13), 178 (32), 146 (14), and 57 (100).

*Photoreaction of **18** in Methanol.* Diene (**18**) (56 mg, 0.19 mmol) in methanol (80 ml) was irradiated for 11.5 h under the same conditions as those of the photolysis of oxime (**16**). Removal of the solvent afforded 53 mg (94%) of **19** and a trace of recovered **18** (by GLC).

References

1) J. H. Amin and P. de Mayo, *Tetrahedron Lett.*, **1963**, 1585.

2) For reviews, see a) A. Padwa, *Chem. Rev.*, **77**, 37 (1977); b) H. Suginome, *Kagaku No Ryoiki*, **30**, 578 (1976); c) H. Ohta and K. Tokumaru, *Yuki Gosei Kagaku Kyokai Shi*, **30**, 1006 (1972).

3) K. Schaffner, *Adv. Photochem.*, **4**, 81 (1966); P. J. Kropp, *Org. Photochem.*, **1**, 1 (1967); T. Matsuura and K. Ogura, "Organic Photochemistry," ed by T. Matsuura and H. Nozaki, Nankodo, 1970, Chap. 10.

4) G. Quinkert, *Angew. Chem., Int. Ed. Engl.*, **14**, 790 (1975); *Pure Appl. Chem.*, **33**, 285 (1973) and references cited therein.

5) R. Okazaki, Y. Inagaki, and N. Inamoto, *Chem. Commun.*, **1974**, 414; Y. Inagaki, R. Okazaki, and N. Inamoto, *Bull. Chem. Soc. Jpn.*, **48**, 621 (1975).

6) R. Okazaki, Y. Inagaki, and N. Inamoto, *Chem. Lett.*, **1974**, 1503; Y. Inagaki, R. Okazaki, and N. Inamoto, *Bull. Chem. Soc. Jpn.*, **48**, 3727 (1975).

7) Preliminary report: R. Okazaki, M. Watanabe, and N. Inamoto, *Tetrahedron Lett.*, **1977**, 4515.

8) T. Oine and Y. Mukai, *Tetrahedron Lett.*, **1969**, 159.

9) E. Schmitz, R. Ohme, and D. Murauski, *Chem. Ber.*, **98**, 2516 (1965).

10) L. J. Bellamy, "The Infra-red Spectra of Complex Molecules," John Wiley & Sons, New York (1964), Chap. 15.

11) M. Shiono, Y. Echigo, and T. Mukaiyama, *Chem. Lett.*, **1976**, 1397. We thank Prof. Mukaiyama for the salt.

12) P. T. Lansbury, "Nitrenes," ed by W. Lowski, Interscience Publisher, New York (1970), Chap. 11.

13) T. Sato and H. Obase, *Tetrahedron Lett.*, **1967**, 1633.

14) A. Stojiljkvic and R. Tasovac, *Tetrahedron Lett.*, **1970**, 1405.

15) For a discussion of the concept of "free" ions, see J. T. Keating and P. S. Skell, "Carbonium Ions," Wiley Interscience, New York (1970), Vol. 2, Chap. 15.

16) a) P. J. Kropp, G. S. Poindexter, N. J. Pienta, and D. C. Hamilton, *J. Am. Chem. Soc.*, **98**, 8135 (1976); b) S. A. McNeely and P. J. Kropp, *ibid.*, **98**, 4319 (1976).

17) S. Kobayashi, T. Kitamura, H. Taniguchi, M. Mishima, M. Fujio, and Y. Tsuno, Abstracts of 26th IUPAC Congress, IV 7B202, Tokyo (1977).

18) E. F. Kiefer and J. Y. Fukunaga, *Tetrahedron Lett.*, **1969**, 993.

19) L. R. C. Barclay, I. T. McMaster, and J. K. Burgess, *Tetrahedron Lett.*, **1973**, 3947.

Studies on Biologically Active Pteridines. I. The Synthesis of 6-(1*R*)[and (1*S*)]-(1-Hydroxyethyl)- and 6-(1*S*)[and (1*R*)]-(1,2-Dihydroxyethyl)-2-amino-4-hydroxypteridines

Takashi SUGIMOTO* and Sadao MATSUURA

Department of Chemistry, College of General Education, Nagoya University, Chikusa-ku, Nagoya 464

(Received July 4, 1978)

2-Amino-4-hydroxy-6-[(1*S*)-1, 2-dihydroxyethyl]pteridine has been synthesized by the condensation of 2, 4, 5-triamino-6-hydroxypyrimidine and D-threose phenylhydrazone, followed by oxidation of the intermediate carried out by adding the condensate to a mixture of $K_3[Fe(CN)_6]$, KI, and H_2O_2 in an acidic solution. The 6-(1*R*)-1, 2-dihydroxyethyl isomer and the 6-(1*R*)[and (1*S*)]-1-hydroxyethyl analogues have also been synthesized in a similar way. By applying the present method, biopterin has been obtained in 28% yield.

The 5,6,7,8-tetrahydro derivatives of various 2-amino-4-hydroxypteridines with an alkyl or polyhydroxyalkyl substituent at the 6-position act as a cofactor for tyrosine hydroxylase.[1,2] However, the cofactor activities of the pteridines vary depending on the structure of the side chain; tetrahydrobiopterin having an L-*erythro*-1,2-dihydroxypropyl side chain has been found to be the most active cofactor.[1,3,4] Indeed, tetrahydrobiopterin is the natural cofactor of phenylalanine hydroxylase[5] and is also thought to be the natural cofactor of tyrosine hydroxylase.[6] Recently the four stereochemical isomers of biopterin, *i.e.* 6-L-*erythro*-, 6-D-*erythro*-, 6-L-*threo*-, and 6-D-*threo*-1,2-dihydroxypropyl-2-amino-4-hydroxypteridines have been synthesized[7] and the cofactor activities of their 5,6,7,8-tetrahydro derivatives for tyrosine hydroxylase examined.[4] The L-*erythro* and D-*threo* isomers, both of which have the same configuration at the 1-position(C-1) of the side chain, exhibited similar cofactor characteristics. The D-*erythro* and L-*threo* isomers, both of which have the same, though reversed C-1 configuration compared to the others, behaved in a similar fashion as cofactor. However the latter pair were less active than the former pair. These results suggest that the cofactor activities are controlled to a fair extent by the configuration at C-1 of the side chain.[4] Consequently an examination of the cofactor characteristics of several tetrahydrobiopterin analogues having a side chain at the 6-position with an asymmetric carbon only at the 1-position(C-1) is required. This paper describes the synthesis of 6-[(1*S*)-1,2-dihydroxyethyl]- and 6-[(1*R*)-1,2-dihydroxyethyl]-2-amino-4-hydroxypteridines(**4a** and **4b**) and the 6-(1*R*)[and (1*S*)]-1-hydroxyethyl analogues(**4c** and **4d**).

Previously biopterin(**4e**) was prepared in 8% yield by the condensation of 2,4,5-triamino-6-hydroxypyrimidine(**1**) with 5-deoxy-L-arabinose phenylhydrazone (**2e**) and the subsequent oxidation of the intermediate tetrahydropteridine(**3e**).[7] This method has been one of the best methods for the synthesis of biopterin and its analogues. The first attempt to synthesize the required (1,2-dihydroxyethyl)pteridine(**4a**), in analogy to the above method, was by the condensation of **1** with D-threose phenylhydrazone(**2a**) and oxidation of the intermediate(**3a**). The main product was, however, the 6-unsubstituted 2-amino-4-hydroxypteridine(**4f**), formed by the loss of the 6-side chain during the oxidation of the tetrahydropteridine intermediate(**3a**), most probably, *via* a quinonoid dihydropteridine.[7-9] The same pteridine(**4f**) was also formed as the main product from **1** and 4-deoxy-D-erythrose phenylhydrazone (**2c**). These results suggested that the 1-hydroxyethyl or 1,2-dihydroxyethyl side chain of **3** is more susceptible to cleavage than the 1,2-dihydroxypropyl or 1,2,3-trihydroxypropyl group and hence the different oxidation conditions are required. By examining the oxidation conditions, it was found that cleavage could be reduced to a great exent by adding the solution of **3a** quickly into an aqueous acidic solution (pH 2—3) of $K_3[Fe(CN)_6]$, KI, and H_2O_2; a reverse addition, that is the addition of the oxidizing agents to the solution of **3a**, gave the 6-unsubstituted pteridine(**4f**) as the main product together with a small amount of **4a**.

Heating D-threose phenylhydrazone(**2a**) with **1** gave an orange red solution of, probably, the intermediate tetrahydropteridine(**3a**). Additional heating resulted in the development of a dark red solution, from which

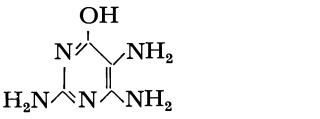

1

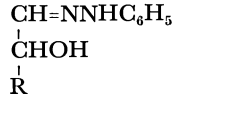

2

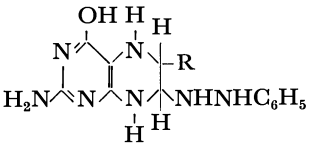

3

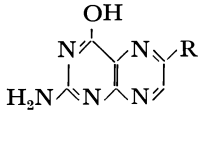

4

R=

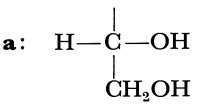

a

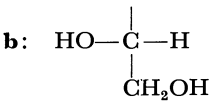

b

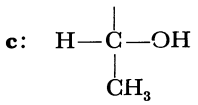

c

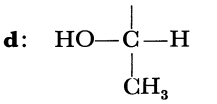

d

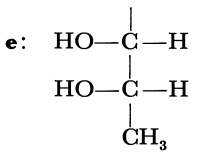

e

f: H—

TABLE 1. THE pK_a VALUES AND UV SPECTRA OF 6-(1-HYDROXYETHYL)- AND 6-(1,2-DIHYDROXYETHYL)-2-AMINO-4-HYDROXYPTERIDINES

Compound	pK_a	pH of aqueous buffer and ionic species[a]	λ_{max} (log ε)[b]
4a	2.45±0.02	0.0(+)	247(3.92), 321(3.78)
	8.05±0.02	5.5(○)	235(3.95), 274(4.02), 345(3.66)
		10.5(−)	254(4.24), 363(3.73)
4b	2.41±0.02	0.0(+)	247(3.91), 321(3.77)
	8.00±0.02	5.5(○)	235(3.92), 274(3.99), 345(3.63)
		10.5(−)	254(4.21), 363(3.70)
4c	2.57±0.02	0.0(+)	247(3.89), 321(3.75)
	8.14±0.02	5.5(○)	235(3.91), 273(3.98), 345(3.62)
		10.5(−)	253(4.19), 363(3.69)
4d	2.52±0.02	0.0(+)	246(3.89), 320(3.76)
	8.10±0.02	5.5(○)	235(3.93), 273(3.99), 345(3.64)
		10.5(−)	253(4.19), 263(3.70)

a) Ionic species are shown by +(monocation), ○(neutral molecule), and −(monoanion).
b) Wavelength in nm measured in aqueous buffer of given pH.

the pteridine(**4a**) could be obtained only in a poor yield. Oxidation of the intermediate(**3a**) to **4a** was most effective by adding the solution of **3a** quickly into an acidic solution of the above oxidizing agents, followed by stirring under oxygen; paper chromatograms showed that **4a** was formed as the main product together with a trace of **4f**. Column chromatographic isolation on Florisil gave **4a** as ivory needles (27%), which were shown to be free from the possible 7-substituted isomer by oxidation to the known 2-amino-4-hydroxypteridine-6-carboxylic acid by potassium permanganate.[10] The structure of the product was confirmed to be **4a** from the pK_a values and UV spectra (Table 1), which were very similar to those of biopterin (**4e**).[7]

The other three pteridines(**4b**, **4c**, and **4d**) were similarly prepared from the pyrimidine(**1**) and a corresponding tetrose phenylhydrazone(**2b**, **2c**, or **2d**). The present method was applied to the synthesis of biopterin(**4e**) which was obtained in the pure crystalline state in 28% yield.

Experimental

The elemental analyses were conducted at the Analytical Section, Meijo University, Nagoya, The pK_a values were determined spectroscopically and the UV spectra measured on a Shimadzu UV-300 spectrophotometer.

*2-Amino-4-hydroxy-6-[(1S)-1,2-dihydroxyethyl]pteridine (**4a**).* To a solution of D-*threo*-5,5-bis(ethylsulfonyl)-4-pentene-1,2,3-triol[11] (5.0 g) in water (50 ml), concentrated aqueous ammonia (0.5 ml) was added. After stirring at pH 9—10 and at room temperature for 10 h, the resulting suspension was adjusted to pH 3—4 with formic acid and filtered. Phenylhydrazine (1.8 g) was added to the filtrate and the solution stirred at pH 2—3 and 25 °C for 1 h. The solution of the formed phenylhydrazone (**2a**) was added to a solution of 2,4,5-triamino-6-hydroxypyrimidine (**1**) dihydrochloride[12] (2.5 g) dissolved in a mixture of water (100 ml) and methanol (150 ml). The solution was stirred under nitrogen at 25 °C for 1 h and then under reflux for 20 min. The orange red solution, after being chilled in an ice bath, was poured into an ice chilled aqueous solution (150 ml) containing potassium hexacyanoferrate(III) (15 g), potassium iodide (2.5 g), 35% hydrogen peroxide (10 ml), and formic acid (5 ml). The mixture was stirred vigorously under bubbling oxygen at 5—10 °C for 1 h and at 25—30 °C for 3 h. The mixture was evaporated to dryness under reduced pressure and the residue extracted with 2% aqueous ammonia (500 ml). The extract was concentrated to about 200 ml under reduced pressure, adjusted to pH 2—3 with hydrochloric acid, and placed on a Florisil column (4.5×35 cm). The column was first eluted with 0.25 M formic acid (4 l) until the inorganic salts, blue colored materials, and small amount of blue fluorescent compounds were removed from the column. The column was then eluted with water (4 l). Evaporation of the eluate under reduced pressure gave a solid which was extracted with 2% ammonia (150 ml). The extract was evaporated to dryness under reduced pressure and the residue extracted with 2% ammonia (150 ml). Concentration of the extract to about 70 ml under reduced pressure and acidification with formic acid (pH 3—4) gave a solid, which crystallized from water to give ivory needles (710 mg) of **4a**, mp> 300 °C (Found: C, 41.98; H, 3.98; N, 30.85%. Calcd for $C_8H_9N_5O_3 \cdot 0.3H_2O$: C, 41.98; H, 4.24; N, 30.61%).

*2-Amino-4-hydroxy-6-[(1R)-1,2-dihydroxyethyl]pteridine (**4b**).* L-Arabinose diethyl dithioacetal[13] (5.0 g) was degraded to L-erythrose according to the method of Hough and Taylor[11] by oxidation to L-*erythro*-5,5-bis(ethylsulfonyl)-4-pentene-1,2,3-triol with aqueous peroxypropionic acid and by subsequent treatment with dilute ammonia. After treatment with phenylhydrazine, condensation of the resulting L-erythrose phenylhydrazone (**2b**) with **1** in a similar manner to that for **4a** gave the (1*R*)-1,2-dihydroxyethyl compound (**4b**) as ivory needles in 22% yield, mp>300 °C (Found: C, 41.98; H, 3.95; N, 30.77%. Calcd for $C_8H_9N_5O_3 \cdot 0.3H_2O$: C, 41.98; H, 4.24; N, 30.61%).

*2-Amino-4-hydroxy-6-[(1R)-1-hydroxyethyl]pteridine (**4c**).* 5-Deoxy-D-arabinose diethyl dithioacetal (5.5 g), prepared according to the method of Green and Rembold[13] by lithium aluminium hydride reduction of 5-tosyl-D-arabinose diethyl dithioacetal, was degraded to 4-deoxy-D-erythrose as above. The erythrose was treated with equimolar phenylhydrazine (2.4 g) and the resulting phenylhydrazone (**2c**; unisolated) was condensed with **1** (dihydrochloride, 4.5 g) and subsequently oxidized in the same way as that used for **4a** to give ivory needles (650 mg, 15% yield) of **4c**, mp>300 °C (from water)(Found: C, 43.33; H, 4.61; N, 31.82%. Calcd for

$C_8H_9N_5O_2 \cdot 0.8H_2O$: C, 43.35; H 4.87; N, 31.61%).

*2-Amino-4-hydroxy-6-[(1S)-1-hydroxyethyl]pteridine (**4d**).* By replacing 5-deoxy-D-arabinose diethyl dithioacetal by 5-deoxy-L-arabinose diethyl dithioacetal[13] in the foregoing procedure, the (1*S*)-1-hydroxyethyl compound (**4d**) was obtained as ivory needles in 9% yield, mp >300 °C (from water) (Found: C, 42.54; H, 4.48; N, 30.86%. Calcd for $C_8H_9N_5O_2 \cdot H_2O$: C, 42.66; H, 4.93; N, 31.10%).

*Biopterin (**4e**).* The condensation of 2,4,5-triamino-6-hydroxypyrimidine(**1**) dihydrochloride (5.0 g) and 5-deoxy-L-arabinose phenylhydrazone (**2e**) (5.5 g), followed by oxidation and chromatographic isolation in a manner similar to that used for **4a**, gave biopterin (1.56 g, 28% yield) as colorless needles.

The authors would like to thank Mrs. N. Nishioka for the measurement of pK_a values.

References

1) A. R. Brenneman and S. Kaufman, *Biochem. Biophys. Res. Commun.*, **17**, 177 (1964).
2) T. Nagatsu, K. Mizutani, I. Nagatsu, S. Matsuura, and T. Sugimoto, *Biochem. Pharmacol.*, **19**, 1945 (1972).
3) Y. Numata, K. Ikuta, T. Kato, T. Nagatsu, T. Sugimoto, and S. Matsuura, *Biochem. Pharmacol.*, **24**, 1998 (1975).
4) Y. Numata, T. Kato, T. Nagatsu, T. Sugimoto, and S. Matsuura, *Biochem. Biophys. Acta*, **480**, 104 (1977).
5) S. Kaufman, *Proc. Natl. Acad. Sci. U.S.A.*, **50**, 1085 (1963).
6) S. Kaufman, "Frontiers in Catecholamine Research," ed by E. Usdin and S. H. Snyder, Pergamon Press, Oxford (1973), pp. 53—60.
7) T. Sugimoto and S. Matsuura, *Bull. Chem. Soc. Jpn.*, **48**, 3767 (1975).
8) M. Viscontini and E. Möhlmann, *Helv. Chim. Acta*, **42**, 836 (1959).
9) S. Matsuura, T. Sugimoto, C. Kitayama, and M. Tsusue, *J. Biochem. (Tokyo)*, **83**, 19 (1978).
10) R. Tschesche, B. Hess, I. Ziegler, and H. Machleit, *Justus Liebigs Ann. Chem.*, **658**, 193 (1962).
11) L. Hough and T. J. Taylor, *J. Chem. Soc.*, **1955**, 1212.
12) T. Sugimoto and S. Matsuura, *Research Bulletin (Dept. of General Education, Nagoya Univ.)*, **12**, 24 (1968).
13) B. Green and H. Rembold, *Chem. Ber.*, **99**, 2162 (1966).

Allylic Oxidation of Methyl 2-Alkenoates

Mitsuru NAKAYAMA,* Shuzo SHINKE, Yoichi MATSUSHITA,
Susumu OHIRA, and Shûichi HAYASHI
Department of Chemistry, Faculty of Science, Hiroshima University, Higashisenda-machi, Hiroshima 730

(Received July 3, 1978)

Allylic oxidation of methyl 2-alkenoates with chromium trioxide in a mixture of acetic anhydride and acetic acid afforded methyl 4-oxo-2-alkenoates.

The allylic oxidation of cycloalkenes to cycloalkenones with chromium trioxide in acetic acid has been reported.[1] However, the oxidation of methyl 2-alkenoates with the above reagent has not yet been reported.

We wish to report the allylic oxidation of methyl 2-alkenoates with a modified reagent prepared from chromium trioxide in a mixture of acetic anhydride and acetic acid. This reagent has the advantage that it is readily available and the reaction is rapid and efficient. The resulting product gave methyl 4-oxoalkanoates, which can be converted into cyclopentenones,[2] by reduction with zinc in acetic acid[3] or titanium trichloride.[4]

The methyl 2-alkenoates (**1a**—**f**) were prepared by a Wittig reaction using methoxycarbonylmethylenetriphenylphosphorane[5] of the corresponding aldehydes in good yields.

When methyl 2-decenoate (**1a**) was treated by the chromium trioxide–(p ridine)$_2$–dichloromethane s stem[6] or *t*-butyl chromate reagent[7] under several reaction conditions, the oxidation product was not obtained. On the other hand, **1a** was more slowly oxidized with chromium trioxide in acetic acid to give methyl 4-oxo-2-decenoate (**2a**). The addition of acetic anhydride to the above solution, however, resulted in a rapid oxidation. Consequently, the oxidation of **1a** was carried out in a mixture of acetic anhydride and glacial acetic acid (1:2) with chromium trioxide.

The oxidation of **1a** for 50 min with chromium trioxide in acetic anhydride and acetic acid (1:2) containing 1:1, 1.5:1, 3:1, 3.5:1, and 5:1 molar ratios of chromium trioxide to **1a** gave conversions to **2a** of 10, 20, 38, 57, and 80%, respectively. It is clear from the data that 5 mol equivalents of the reagent are required for complete conversion to ketone. With less than the 5:1 molar ratio extremely slow oxidation occurs.

Preparation of methyl 4-oxo-2-alkenoates (**2a**—**f**) was carried out by this method (Table 1).

The reagent was prepared by addition of chromium trioxide (50 mmol) in small portions to a mixture of acetic anhydride and glacial acetic acid under ice-cooling. Into the solution of the above reagent, methyl 2-alkenoates (**1a**—**f**) (10 mmol) were added with stirring. The optimal conditions for formation of methyl 4-oxo-2-alkenoates (**2a**—**f**) with minimum recovery of starting material were maintained by keeping a temperature at 15—25 °C for moderate times; if the temperature was allowed to rise to 30 °C, the desired product was obtained in a poor yield in the same reaction period. It was determined by gas chromatography that methyl 4-oxo-2-alkenoates (**2a**—**f**) were the sole reaction products.

Table 1. Allylic oxidation of methyl 2-alkenoates (**1**) with chromium trioxide

$$R\text{-}CH_2\text{-}CH{=}CH\text{-}COOCH_3 \xrightarrow[Ac_2O\text{-}AcOH]{CrO_3} R\text{-}\overset{\overset{O}{\|}}{C}\text{-}CH{=}CH\text{-}COOCH_3$$

(**1**) (**2**)

Substrate	R	Molar ratio of **1** : CrO_3	Time (min)	Product (% yield)[a,b]
1a	n-C_6H_{13}	1 : 1	50	**2a** 10
1a	n-C_6H_{13}	1 : 1.5	50	**2a** 20
1a	n-C_6H_{13}	1 : 3	50	**2a** 38
1a	n-C_6H_{13}	1 : 3.5	50	**2a** 57
1a	n-C_6H_{13}	1 : 5	50	**2a** 80
1b	C_2H_5	1 : 5	30	**2b** 50
1c	n-C_3H_7	1 : 5	30	**2c** 72
1d	n-C_4H_9	1 : 5	40	**2d** 77
1e	n-C_5H_{11}	1 : 5	40	**2e** 86
1f	$CH_3OOC(CH_2)_7$	1 : 5	60	**2f** 78

a) Isolated yields. b) The products were gas chromatographically pure (>99%).

In each case the product was the conjugated unsaturated ketone in which the double bond is located in its original position. Also, the fact that methyl 11-methoxycarbonyl-2-undecenoate (**1f**) gave only the corresponding 4-oxo-2-undecenoate (**2f**) [IR, 1740, 1710 cm^{-1}; NMR δ 3.63, 3.79 (each 3H, s), 2.24, 2.60 (each 2H, br t, J=7 Hz), 6.53, 7.02 (each 1H, d, J=16 Hz) ppm] shows that the methylene group next to the double bond is selectively oxidized.

On the other hand, the oxidation of 3-alkene-2-ones with chromium trioxide under the same conditions gave 3-alkene-2,5-diones in poor yields (26—34%) (n-C_7—n-C_{11}), along with aliphatic acids resulting from cleavage of the double bond in the original ketones.

The resulting **2a**—**f** were easily reduced with titanium trichloride[4] to give methyl 4-oxoalkanoates (**3a**—**f**) in good yields. They are key intermediates for the preparation of cyclopentenone derivatives.[2] From the above results, the syntheses of **3a**—**f** can be achieved in three steps from the corresponding aliphatic aldehydes in moderate yields.

Table 2. Characteristics of methyl 4-oxo-2-alkenoates (**2a—e**)

Compd	Bp, °C/Torr	Mp, °C	Mass, *m/e*	IR, cm^{-1}	^{1}H-NMR, δ ppm
2a	135.0—136.0/13	44.0—46.5	198 (M^+) 167 128 113	1735 1710 1175	3.78 (3H, s) 6.53 (1H, d, J=16 Hz) 7.01 (1H, d, J=16 Hz)
2b	80.0—81.5/16.5	33.5—35.0	142 (M^+) 128 113 111	1735 1710 1175	3.82 (3H, s) 6.57 (1H, d, J=16 Hz) 7.05 (1H, d, J=16 Hz)
2c	103.0—105.0/13	38.0—39.5	156 (M^+) 128 125 113	1735 1710 1175	3.82 (3H, s) 6.55 (1H, d, J=16 Hz) 7.03 (1H, d, J=16 Hz)
2d	115.0—116.0/10.5	35.5—37.0	170 (M^+) 139 128 113	1735 1705 1175	3.82 (3H, s) 6.53 (1H, d, J=16 Hz) 7.02 (1H, d, J=16 Hz)
2e	126.0—126.5/12	46.0—47.5	184 (M^+) 153 128 113	1735 1705 1170	3.78 (3H, s) 6.50 (1H, d, J=16 Hz) 6.98 (1H, d, J=16 Hz)

Table 3. Semicarbazones of methyl 4-oxo-2-alkenoates (**2a—f**)

Compd	Mp, °C[a]	Formula	Found (Calcd), (%)		
			C	H	N
2a	128.5—130.0	$C_{12}H_{21}O_3N_3$	56.35 (56.45)	8.32 (8.29)	16.61 (16.46)
2b	149.0—149.5	$C_9H_{13}O_3N_3$	48.40 (48.23)	6.64 (6.58)	21.21 (21.10)
2c	162.5—164.0	$C_9H_{15}O_3N_3$	50.85 (50.69)	7.14 (7.09)	19.93 (19.71)
2d	150.0—151.5	$C_{10}H_{17}O_3N_3$	53.11 (52.85)	7.61 (7.54)	18.68 (18.49)
2e	125.0—126.5	$C_{11}H_{19}O_3N_3$	54.73 (54.75)	7.89 (7.94)	17.50 (17.41)
2f	97.0— 99.0	$C_{15}H_{25}O_5N_3$	55.08 (55.03)	7.70 (7.70)	12.56 (12.84)

a) All the semicarbazones were purified by recrystallization from methanol.

Experimental

Boiling points are uncorrected and melting points were determined on a Yanagimoto micro hot-stage and are uncorrected. The mass spectra were determined on a Hitachi RMS-4 mass spectrometer at 70 eV. The IR spectra were recorded with a Hitachi EPI-G3 grating spectrometer. All ^{1}H-NMR spectra were measured in a CCl_4 solution using a Varian T-60 NMR spectrometer with TMS as an internal standard. The GLC was carried out on a Shimadzu GC-4B, with SE-30 (2%) (3 mm×2 m) and at a temperature 140 °C, unless otherwise noted.

*Preparation of Methyl 2-Alkenoates (**1a—f**).* To a solution of methoxycarbonylmethylenetriphenylphosphorane[5] (22 mmol) in anhydrous benzene (*ca.* 60 ml), was added an appropriate aldehyde (20 mmol) in anhydrous benzene (*ca.* 5 ml) under nitrogen atmosphere. The solution was refluxed for 6 h and then cooled to room temperature. After evaporating the solvent in a reduced pressure, hexane was added to give precipitates. The precipitates were collected by filtration and washed with hexane. The combined solvents were evaporated and the resulting residue was distilled under reduced pressure. Yield; **1a**, 82% (bp 126—128 °C/14 Torr); **1b**, 91% (bp 63—65 °C/16 Torr); **1c**, 90% (bp 77—79 °C/16 Torr); **1d**, 78% (bp 103—104 °C/24 Torr); **1e**, 85% (bp 108—109 °C/12 Torr). The structures of **1a—e** were confirmed by examining their mass, IR, and NMR spectra.

*Methyl 11-Methoxycarbonyl-2-undecenoate (**1f**)*: Yield, 97% [from methyl 9-formylnonanoate (bp 122 °C/3 Torr)[8]]. Bp 152—154 °C/2 Torr; MS *m/e* 256(M^+), 225, 157, 87; IR 1745, 1735, 1665, 1180, 1145 cm^{-1}; NMR δ 1.33 (12H, br s), 1.98—2.45 (4H, m), 3.60, 3.65 (each 3H, s), 5.70 (1H, dt, J=16, 1.5 Hz), 6.84 (1H, dt, J=16, 7 Hz).

General Oxidation Procedure. The reagent was prepared by addition of chromium trioxide (50 mmol) in small portions to a mixture of acetic anhydride (12.5 ml) and glacial acetic acid (25 ml), followed by dilution with benzene (25 ml) under ice-cooling. Into the solution of the above reagent, **1** (10 mmol) in benzene (5 ml) was added dropwise with stirring. The reaction temperature was kept below 20 °C. The methyl 2-alkenoates were consumed in moderate times (the times required are shown in the Table 1) as confirmed by TLC. The reaction mixture was diluted with water, neutralized with aqueous sodium hydroxide solution, and extracted with ether. After being dried over anhydrous sodium sulfate, the extract was concentrated and the resulting residue was distilled under reduced pressure or crystallized from hexane to give **2** (Tables 1, 2, 3, and below).

*Methyl 11-Methoxycarbonyl-4-oxo-2-undecenoate (**2f**)*: Mp 54—55 °C (colorless needles from hexane); MS *m/e* 239 (M−31), 157, 128, 113; IR 1740, 1710, 1175 cm^{-1}; NMR δ 1.12—1.95 (10H, br s), 2.24, 2.60 (each 2H, br t, J=7 Hz), 3.63, 3.79 (each 3H, s), 6.53, 7.02 (each 1H, d, J=16 Hz). GLC: temperature program: 5 °C/min, from 150 to 200 °C. Found: C, 62.19; H, 8.40%. Calcd for $C_{14}H_{22}O_5$: C, 62.20; H, 8.20%.

*Reduction of Methyl 4-Oxo-2-alkenoates (**2a—f**).* Into a solution of **2** (3.5 mmol) in acetone (*ca.* 20 ml) cold titanium trichloride aqueous solution (20%, 8 mmol) was added under nitrogen atmosphere. The mixture was stirred for 40 min at room temperature, then poured into 50 ml of brine, and extracted with ether. The extract was concentrated and the residue was chromatographed on a silica gel column, eluting with ethyl ether–hexane (1 : 1). Yield, **3a**, 91% (M^+ *m/e* 200); **3b**, 88% (M^+ *m/e* 144); **3c**, 93% (M^+ *m/e* 158); **3d**, 90% (M^+ *m/e* 172); **3e**, 87% (M^+ *m/e* 186); **3f**, 87% (M^+ *m/e* 272). The structures of **3a—f** were confirmed by examining their IR and NMR spectra.

The present work was partially supported by a Grant-in-Aid for Scientific Research from the Ministry of Education.

References

1) F. C. Whitmore and G. W. Pedlow, *J. Am. Chem. Soc.*, **63**, 758 (1941); H. Erdtman and L. Malmborg, *Acta Chem. Scand.*, **24**, 2252 (1970).

2) L. Novák, G. Baán, J. Marosfalvi, and C. Szántay, *Tetrahedron Lett.*, **1978**, 487.

3) L. F. Fieser and M. Fieser, "Reagents for Organic Synthesis," (1967), Vol. 1, p. 1276 and references cited therein.

4) L. C. Blaszczak and J. E. McMurry, *J. Org. Chem.*, **39**, 258 (1974).

5) O. Isler, H. Gutmann, M. Montavon, R. Rüegg, G. Ryser, and P. Zeller, *Helv. Chim. Acta*, **40**, 1242 (1957).

6) W. G. Dauben, M. Lorber, and D. S. Fullerton, *J. Org. Chem.*, **34**, 3587 (1969); J. E. Shaw and J. J. Sherry, *Tetrahedron Lett.*, **1971**, 4379.

7) C. W. Marshall, R. E. Ray, I. Laos, and B. Riegel, *J. Am. Chem. Soc.*, **79**, 6308 (1957).

8) S. B. Thakur, K. S. Jadhav, and S. C. Bhattacharyya, *Indian J. Chem.*, **12**, 893 (1974).

Conformational Effect on the Bridgehead Reaction of Bicyclo[3.3.1]nonan-2-ones. A Facile Bridgehead Deuteration of a Bicyclo[3.3.1]nonan-2-one Derivative with the Cyclohexanone Ring Locked in the Boat Conformation

Kiyoyuki YAMADA,* Shunichi MANABE, Yoshinori KYOTANI,
Masaaki SUZUKI, and Yoshimasa HIRATA
Department of Chemistry, Faculty of Science, Nagoya University, Chikusa, Nagoya 464

(Received July 3, 1978)

Five bicyclo[3.3.1]nonan-2-ones, two known (**1**, **3**) and three new ones (**2**, **4**, **5**) were prepared. The hydrogen-deuterium exchange reaction at the bridgehead position of the bicyclo[3.3.1]nonan-2-one system was examined under mild basic conditions (2 M NaOMe-MeOD, 33 °C, 22 h) using these five bicyclo[3.3.1]-nonan-2-ones. Virtually no deuteration took place at the bridgehead in each case of the bicyclic ketones (**1**, **2**, **3**, **4**), whereas one deuterium was incorporated into the bridgehead of the ketone (**5**). ^{13}C NMR spectroscopy was employed for the unambiguous determination of the site(s) of deuteration in all cases studied. The enhanced bridgehead acidity of (**5**) could be explained in terms of the locked boat conformation of the cyclohexanone ring contained in (**5**).

Schaefer and Lark[1] observed in 1965 that deuteration of the bridgehead position of bicyclo[3.3.1]nonan-2-one (**1**) occurred under basic conditions (*e.g.*, 77.2% deuteration: 0.1 M NaOD–D_2O, 95 °C, 40 days), and discussed the importance of the boat conformation of the ketone-bearing ring for stabilization of the bridgehead enolate. In 1975, Nickon and his coworkers[2] demonstrated that the bridgehead acidity of brendan-2-one (**6**) possessing the boat-locked bicyclo[3.2.1]-octan-2-one system was largely enhanced, resulting in the hydrogen-deuterium exchange at C-3 in **6** under mild conditions (92% deuteration: 4.84 M NaOD in MeOD, 25 °C, 69 h). Further they revealed that the enhanced bridgehead acidity of **6** was neither due to the "s" character of the carbon in the bridgehead C–H nor due to inductive stabilization of the carbanion by the carbonyl, but due to the facile formation of the corresponding enolate, which could be rationalized in terms of the Wiseman's postulate.[3]

We herein describe our results on the hydrogen-deuterium exchange reaction at the bridgehead position of the bicyclo[3.3.1]nonan-2-one system under the basic conditions milder than those[1] of Schaefer and Lark. The bicyclo[3.3.1]nonan-2-ones employed in the present studies are **1**, **2**, **3**, **4**, and **5**, among which the last one is a 4-homoisotwistane derivative and contains the cyclohexanone ring held rigidly in the boat conformation by the two-carbon bridge. The two known compounds, **1**[4] and **3**[6] were prepared by the modified procedures of Cope and his coworkers[5] and of Marvell and his colleagues,[6] respectively. Other three new compounds (**2**, **4**, **5**) were synthesized as follows. The acetal ketone (**2**) was synthesized from a diastereomeric mixture (*exo*-ol:*endo*-ol, 7:4) of the keto alcohol (**7**)[5] by the following sequence: (i) acetylation to give the keto acetate (**8**); (ii) acetalization affording the acetal acetate (**9**); and (iii) alkaline hydrolysis to yield the acetal alcohol(**10**) and subsequent oxidation (chromium trioxide–pyridine). Methylation of **2** with methyl iodide–sodium hydride in 1,2-dimethoxyethane gave the ketone (**4**). The tricyclic ketone (**5**) was synthesized from the keto alcohol (**11**),[7] which was converted to the corresponding thioacetal alcohol (**12**). Desulfurization of **12** with Raney nickel afforded the alcohol (**13**), oxidation of which with chromium trioxide in pyridine gave the tricyclic ketone (**5**) (The numbering system shown in **5**, although it differs from that based on the IUPAC rule, is used in the present paper for convenience of comparing ^{13}C chemical shifts with those of other bicyclo[3.3.1]nonan-2-ones).

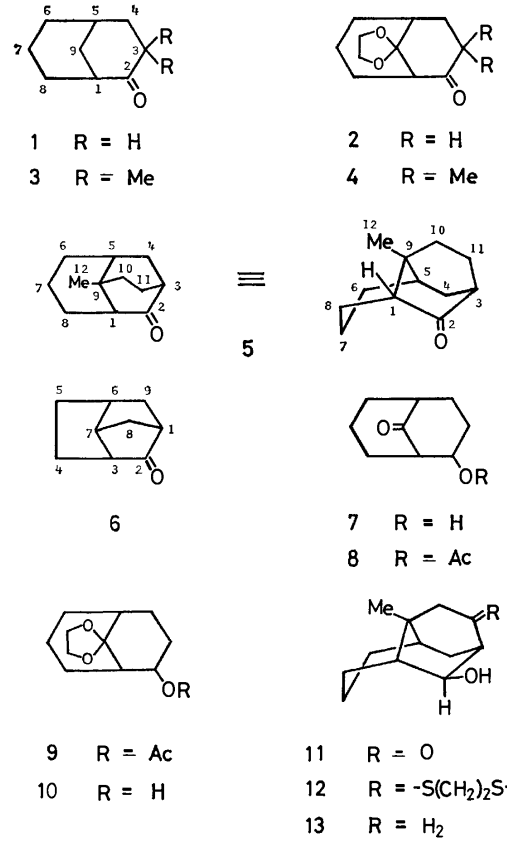

Bridgehead Hydrogen Exchange. The hydrogen-deuterium exchange reaction for each of the bicyclo-[3.3.1]nonan-2-ones (**1**, **2**, **3**, **4**, **5**) was carried out in deuteriomethanol in the presence of sodium methoxide (2.0 M NaOMe–MeOD) at 33 °C for 22 h, and the extent of deuteration was determined by mass spectrometry.[8] The results are summarized in Table 1. The location of the deuterium(s) in each product was

Table 1. Deuterium incorporation by bicyclo-[3.3.1]nonan-2-ones
(2.0 M NaOMe-MeOD at 33 °C for 22 h)

Compound	Mass spectral d assay (rel %±1)[a]			
	d_0	d_1	d_2	d_3
1	33	45	19	3
2	30	44	23	3
3	97	3		
4	100	0		
5	5	95		

a) Average of five mass spectral scans; corrected for ^{13}C.

proved by ^{13}C NMR spectroscopy (*cf.* Table 2). Most of the ^{13}C NMR chemical shift assignments for the bicyclo[3.3.1]nonan-2-ones, shown in Table 2, were made by the application of chemical shift theory[9–11] and single frequency off-resonance decoupling (sford) experiments, and further in some cases [in particular in **5**] with the aid of deuterium isotope shifts[12–15] and comparisons with structurally related compounds.[15,16] Although assignments of some signals remained uncertain for each compound (Table 2), there was no ambiguity as to the determination of the site(s) of deuteration.

Under the present exchange conditions the ketone (**2**) was shown to incorporate up to 2 equivalents of deuterium (**2**-d_1 44% and **2**-d_2 23%), the site of deuteration being shown to be C-3 as expected (*vide post*), and the incorporation of deuterium into the bridgehead position (C-1) was found to occur to an extremely small extent (3%). The site of deuteration in **2** was proved by the deuterium isotope effects in proton-noise decoupled ^{13}C NMR spectra:[12–14] on deuteration of **2** the singlet at δ 37.99 (C-3) was shifted upfield by 0.32 ppm to become a triplet due to ^{13}C–D coupling (J_{C-D}=19.6 Hz), and the singlet at δ 23.73 (C-4) was broadened and shifted upfield by *ca.* 0.06 ppm. The result on the deuteration of the ketone (**1**) was virtually the same as that of the ketone (**2**) (sce Table 1). The ketone (**3**), which possesses the gem dimethyl groups at C-3, was deduced to have the different conformation(s) regarding the cyclohexanone ring from that of the ketone (**1**). It was thus expected that the ketone (**3**) might exhibit reactivity at the bridgehead different from that of **1**. However, there was no significant incorporation of deuterium into the ketone (**3**) under the exchange conditions. No deuterium was incorporated into the bridgehead of the ketone (**4**) which has the gem dimethyl groups at C-3.

In contrast to the bicyclic compounds, **3** and **4**, the ketone (**5**) was found to be monodeuterated (95% d_1), and further it was established by ^{13}C NMR spectroscopy (*vide post*) that the deuterium was located at the bridgehead position (C-1) of **5**, excluding the possibility of deuteration by the mechanism of homoenolization.[13] It is known that homoenolization can only be effected under conditions (*e.g.*, *t*-BuOK–*t*-BuOH, 185 °C, 150 h) much more vigorous than those employed in the present studies. In the ^{13}C NMR spectrum of the monodeuterated compound (**5**-d_1) the signal at δ 52.28 assigned to the bridgehead (C-1) apparently disappeared. The ^{13}C chemical shift differences between **5**-d_1 and **5** [δ(**5**-d_1)−δ(**5**)] are shown in **5A**, and these magnitudes

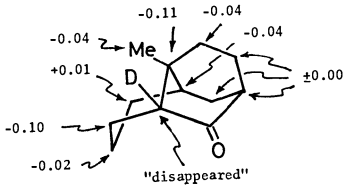

5A

Table 2. ^{13}C chemical shifts of bicyclo[3.3.1]nonan-2-ones[a,b]

Carbon	**1**	**2**	**3**	**4**	**5**	**5**-d_1
1	45.06(d)	54.65(d)	42.89(d)	53.17(d)	52.28(d)	"disappeared"
2	217.06(s)	213.73(s)	220.28(s)	221.22(s)	221.89(s)	221.89(s)
3	39.08(t)	37.99(t)	42.89(s)	41.74(s)	43.40(d)	43.40(d)
4	27.43(t)	23.70(t)	40.95(t)	39.98(t)	29.39(t)	29.39(t)
5	26.16(d)	35.41(d)	26.50(d)	36.61(d)	35.04(d)	35.00(d)
6	31.95(t)[c]	30.47(t)[c]	35.00(t)[c]	31.85(t)[c]	24.69(t)	24.70(t)
7	20.12(t)	18.76(t)	19.40(t)	18.31(t)	16.68(t)	16.66(t)
8	29.79(t)[c]	27.45(t)[c]	32.81(t)[c]	30.08(t)[c]	24.02(t)	23.92(t)
9	32.55(t)[c]	109.77(s)	29.52(t)[c]	109.48(s)	34.13(t)	34.02(s)
10					33.40(t)	33.36(t)
11					27.92(t)	27.92(t)
Ketal CH_2		64.23(t)		64.18(t)		
Ketal CH_2		64.50(t)		64.33(t)		
3-Me			26.77(q)	29.06(q)		
3-Me			31.28(q)	32.77(q)		
9-Me					23.00(q)	22.96(q)

a) Spectra taken in $CDCl_3$ at 20 MHz on a Varian CFT-20 spectrometer; chemical shifts are in parts per million relative to tetramethylsilane. b) The letter in parentheses refers to the signal multiplicity obtained from single frequency off-resonance decoupling experiments: s=singlet, d=doublet, t=triplet, q=quartet. c) Assignments may be interchanged among these signals in each vertical column.

of the upfield shifts for sp^3 carbons both geminal and vicinal to deuterium are in good agreement with those reported for deuterated 4-homoisotwistanes,[15] which has the same carbon skeleton as **5**, and for some bicyclic compounds[12c,12d,13,14] (*e.g.*, isotope shifts of carbons geminal to deuterium, 0.12 ± 0.04 ppm[12e]). Further some signals in the ^{13}C NMR spectrum of the deuterated ketone (**5**-d_1) were shown to be broadened by geminal (C-8 and C-9) and vicinal (C-5, C-7, C-10, and C-12) ^{13}C–D couplings. Thus the site of deuteration in **5** was proved to be C-1. It should be noted in this case that the ^1H NMR spectral analysis was not a reliable method of determining the deuterated site of **5**, because the signal due to H-1 could not unambiguously be identified.

Among the five bicyclo[3.3.1]nonan-2-ones (**1**, **2**, **3**, **4**, **5**) examined, the ketone (**5**) was a sole member that underwent deuteration at the bridgehead position under the exchange conditions of the present studies. As in the case of brendan-2-one (**6**),[2] the enhanced bridgehead acidity of **5** would be ascribed to the locked boat conformation of the cyclohexanone ring, in which the dihedral angle between the C(1)–H bond and the p-orbital of the carbonyl carbon is as small as *ca.* 30° from the examination of Dreiding models: this small value of the dihedral angle between the interacting orbitals would not only be favorable for removal of the proton at C-1 but result in the stabilization of the bridgehead enolate formed. On the other hand, the ketonic ring is conformationally flexible in each of the bicyclic analogs (**1**, **2**, **3**, **4**). Under the exchange conditions the flexible ketonic ring presumably can not assume the genuine boat conformation like that in **5** owing to the steric compression within the molecule, but exist as an another conformer such as a deformed boat (or as an equilibrium mixture of conformers other than boat), in which the dihedral angle discussed above is not so small as that (*ca.* 30°) in **5**, making removal of the bridgehead proton more difficult.

From the present studies it is concluded that the bicyclo[3.3.1]nonan-2-one system with the ketonic ring kept rigidly in the boat form shows the enhanced bridgehead acidity in comparison with that possessing the conformationally flexible ketonic ring.

Experimental

Melting points and boiling points are uncorrected. IR spectra were taken with a JASCO Model IRS or JASCO DS-402G spectrometer in $CHCl_3$. ^1H-NMR spectra were obtained in $CDCl_3$ using a Varian HA-100D (100 MHz) or NV-21 (90 MHz) instrument: chemical shifts (δ) are reported in ppm downfield from internal TMS. ^{13}C-NMR spectra were obtained in $CDCl_3$ (concentration, 0.3—0.4 mmol/ml) on a Varian CFT-20 spectrometer operating 20 MHz in the Fourier transform mode: chemical shifts are given in relative to internal TMS. Low resolution mass spectra were determined on a Hitachi RMU-6C mass spectrometer equipped with a heating inlet system as well as a direct inlet system and operating with an ionization energy of 70 eV. High resolution mass spectra were determined on a JEOLCO GMS-01SG mass spectrometer. Silica gel 60 F_{254} (No. 5715) and 60 PF_{254} (No. 7747) (E. Merck, A. G., Germany) were used for TLC: thickness employed was 1.50 mm for preparative TLC. Organic solutions were washed with saturated NaCl solution, dried over anhydrous Na_2SO_4, and evaporated by a vacuum rotary evaporator.

*Bicyclo[3.3.1]nonan-2-one (**1**).* A solution of a diastereomeric mixture (*exo*-ol:*endo*-ol, 4:7) of the keto alcohol (**7**)[5] (350 mg) and $BF_3\cdot OEt_2$ (0.15 ml, distilled from CaH_2) in *1,2*-ethanedithiol (5 ml) was stirred at room temperature for 40 min and diluted with ether (150 ml). The mixture was washed with 5 M NaOH (5×6 ml) and water (6 ml), and dried. On evaporation of the solvent there remained a colorless oil, which was purified by preparative TLC ($CHCl_3$–EtOAc, 3:1), giving 510 mg (98%) of a diastereomeric mixture of the thioacetal alcohol as a colorless liquid: IR 3460 cm^{-1}; ^1H-NMR (90 MHz) 3.10—3.50 (4H, complex m), 4.04 and 4.41 (total 1H, m each); MS 230 (M^+). To a solution of the diastereomeric mixture of the thioacetal alcohol (510 mg) in EtOH (12 ml) was added W-2 Raney nickel (*ca.* 8 g). The suspension was refluxed for 40 min and filtered. The filtrate was evaporated, affording a solid, which was purified by preparative TLC ($CHCl_3$–EtOAc, 3:1), affording a diastereomeric mixture of the alcohol (299 mg, 96%) as a colorless solid: IR 3650 cm^{-1}; ^1H-NMR (90 MHz) 3.60 and 3.90 (total 1H, m each); MS 140 (M^+). Found: *m/e* 140.1212. Calcd for $C_9H_{16}O$: 140.1201. A suspension of CrO_3 (420 mg) in dry pyridine (11 ml) was added to a cooled (0 °C) solution of the diastereomeric mixture of the alcohol (299 mg) in dry pyridine (3.6 ml) with stirring. The mixture was stirred at room temperature for 12 h and diluted with ether (250 ml). The precipitates were filtered through a pad of Super Cel and washed with ether thoroughly. The combined filtrates were washed with 2 M HCl and water, dried, and concentrated. Purification of the oily residue by preparative TLC ($CHCl_3$) gave **1** (160 mg, 54%) as colorless crystals: mp 127—132 °C (sealed tube) (lit, mp 135—137 °C[17] and 129—137 °C[4b]); IR 1695 cm^{-1}; ^1H-NMR (100 MHz) 2.40—2.70 (3H, complex m); MS 138 (M^+). Found: *m/e* 138.1052. Calcd for $C_9H_{14}O$: 138.1045.

*3,3-Dimethylbicyclo[3.3.1]nonan-2-one (**3**).* A solution of **1** (185 mg, 1.34 mmol) in dry 1,2-dimethoxyethane (DME, 1.1 ml) was added to a stirred suspension of NaH [250 mg of 55% mineral oil dispersion (*ca.* 4.5 mmol), three times washed with dry hexane and dried *in vacuo*] in dry DME (5.6 ml) under nitrogen. Methyl iodide (1.67 ml, 26.6 mmol) was added to the suspension, and the mixture stirred at room temperature for 26 h. After an excess amount of NH_4Cl was added, the mixture was concentrated, cooled (0 °C), diluted with water (4 ml), and extracted with $CHCl_3$ (3×10 ml). The combined $CHCl_3$ extracts were washed with water (3 ml), dried, and evaporated, giving a residue, purification of which by preparative TLC ($CHCl_3$) afforded **3** (104 mg, 47%) as a colorless liquid: IR 1686 cm^{-1}; ^1H-NMR (90 MHz) 1.12 (3H, s), 1.17 (3H, s), 2.44 (1H, m); MS 166 (M^+). Found: *m/e* 166.1361. Calcd for $C_{11}H_{18}O$: 166.1358.

*9-Oxobicyclo[3.3.1]non-2-yl Acetate (**8**).* A solution of a diastereomeric mixture (*exo*-ol:*endo*-ol, 4:7) of the keto alcohol (**7**)[5] (150 mg) in acetic anhydride (1.2 ml) and dry pyridine (2.9 ml) was stirred at room temperature for 12 h, and concentrated. The residue was purified by preparative TLC ($CHCl_3$–EtOAc, 5:1) to give the diastereomeric mixture of **8** (188 mg, 98%) as a colorless liquid: bp 178—181 °C/1 mmHg; IR 1733, 1723 cm^{-1}; ^1H-NMR (90 MHz) 2.01 and 2.06 (total 3H, s, each), 5.11 and 5.33 (total 1H, m each); MS 196 (M^+). Found: *m/e* 196.1085. Calcd for $C_{11}H_{16}O_3$: 196.1099.

9,9-Ethylenedioxybicyclo[3.3.1]non-2-yl Acetate (9). To a solution of the diastereomeric mixture of **8** (198 mg) in toluene (7 ml) were added *p*-toluenesulfonic acid monohydrate (7 mg) and ethylene glycol (0.9 ml). The stirred mixture was refluxed for 4 h using a Dean-Stark water separator to remove the water. After cooling, the mixture was washed with saturated $NaHCO_3$ solution (5 ml), dried, and concentrated. The residue was purified by preparative TLC ($CHCl_3$–EtOAc, 5:1), affording the diastereomeric mixture of **9** (234 mg, 97%) as a colorless liquid: IR 1723 cm^{-1}; ^{1}H-NMR (90 MHz) 2.04 (3H, s), 3.80—4.30 (4H, complex m), 5.01 and 5.25 (total 1H, m each); MS 240 (M^+). Found: *m/e* 240.1366. Calcd for $C_{13}H_{20}O_4$: 240.1362.

9,9-Ethylenedioxybicyclo[3.3.1]nonan-2-ol (10). To a solution of the diastereomeric mixture of **9** (234 mg) in tetrahydrofuran (THF, 5.8 ml) was added a mixture of H_2O (1.2 ml)–10% NaOH (1.6 ml)–MeOH (5.8 ml). The mixture was stirred at room temperature for 40 min and passed through a column of ion-exchange resin (H form, Amberlite CG-50 Type-I) (3.5 g). The column was further washed with MeOH (20 ml) for complete elution of the product. The combined mixtures were concentrated and the residue was dissolved in EtOH (30 ml). The solution was evaporated to give a residue, purification of which by preparative TLC ($CHCl_3$–EtOAc, 7:1) yielded the diastereomeric mixture of **10** (191 mg, 99%) as a colorless liquid: IR 3580, 3500 (broad) cm^{-1}; ^{1}H-NMR (90 MHz) 3.70—4.10 (4H, m, A_2B_2 type), 3.90 and 4.20 (total 1H, m each); MS 198 (M^+). Found: *m/e* 198.1247. Calcd for $C_{11}H_{18}O_3$: 198.1256.

9,9-Ethylenedioxybicyclo[3.3.1]nonan-2-one (2). To a stirred solution of the diastereomeric mixture of **10** (191 mg) in dry pyridine (2.9 ml) was added under cooling (0 °C) a suspension of CrO_3 (260 mg) in dry pyridine (7.1 ml) in one portion. The mixture was stirred at room temperature for 13 h, diluted with ether (150 ml), and filtered through a pad of Super Cel. The solid residue was washed with ether (40 ml). The combined filtrates were washed with water repeatedly until the washing became colorless, dried, and concentrated. The residue was purified by preparative TLC ($CHCl_3$–EtOAc, 7:1), giving **2** (160 mg, 85%) as a colorless liquid: IR 1700 cm^{-1}; ^{1}H-NMR (100 MHz) 3.95 (4H, s); MS 196 (M^+). Found: *m/e* 196.1108. Calcd for $C_{11}H_{16}O_3$: 196.1099.

9,9-Ethylenedioxy-3,3-dimethylbicyclo[3.3.1]nonan-2-one (4). To a stirred suspension of NaH [276 mg of 55% mineral oil dispersion (*ca.* 5 mmol), three times washed with dry hexane and dried *in vacuo*] in dry DME (6.1 ml) was added a solution of **2** (290 mg, 1.48 mmol) in dry DME (1.2 ml) under nitrogen. To the suspension MeI (1.84 ml, 29.3 mmol) was added, and the mixture stirred at room temperature for 29 h. An excess amount of NH_4Cl was added and, after 10 min, the mixture was concentrated. The residue was cooled, diluted carefully with water (5 ml), and extracted with $CHCl_3$ (4×10 ml). The combined $CHCl_3$ extracts were washed with water (5 ml), dried, and concentrated to afford an oily residue, purification of which by preparative TLC ($CHCl_3$) yielded **4** (164 mg, 50%) as colorless crystals: mp 54—56 °C; IR 1685 cm^{-1}; ^{1}H-NMR (90 MHz) 1.20 (3H, s), 1.24 (3H, s), 2.47 (1H, m), 3.93 (4H, s); MS 224 (M^+). Found: *m/e* 224.1408. Calcd for $C_{13}H_{20}O_3$: 224.1412.

Tricyclic Thioacetal Alcohol (12). A mixture of the crystalline keto alcohol (**11**)[7] (179 mg) and $BF_3 \cdot OEt_2$ (0.1 ml, distilled from CaH_2) in *1,2*-ethanedithiol (4 ml) was stirred at room temperature for 30 min, and diluted with saturated $NaHCO_3$ solution (5 ml) under cooling (0 °C). The mixture was extracted with $CHCl_3$ (4×10 ml). The combined $CHCl_3$ extracts were dried and concentrated. The residue was dissolved in toluene and the solution evaporated: this procedure was repeated for complete removal of *1,2*-ethanedithiol present in the residue. The resulting residue was purified by preparative TLC ($CHCl_3$–EtOAc, 8:1), giving the tricyclic thioacetal alcohol (**12**) (268 mg, 97%) as colorless crystals: mp 77—78 °C; IR 3400 (broad) cm^{-1}; ^{1}H-NMR (90 MHz) 0.90 (3H, s), 3.20—3.70 (4H, m, A_2B_2 type), 4.05 (1H, m); MS 270 (M^+). Found: *m/e* 270.1120. Calcd for $C_{14}H_{22}OS_2$: 270.1112.

Tricyclic Alcohol (13). A suspension of **12** (265 mg) and W-2 Raney nickel (*ca.* 4 g) in EtOH (25 ml) was refluxed for 45 min and filtered. The filtrate was concentrated to afford **13** (176 mg, 99%) as colorless crystals: mp 145—147 °C (sealed tube); IR 3660, 3440 (broad) cm^{-1}; ^{1}H-NMR (90 MHz) 0.87 (3H, s), 3.85 (1H, broad s); MS 180 (M^+). Found: *m/e* 180.1497. Calcd for $C_{12}H_{20}O$: 180.1514.

Tricyclic Ketone (5). Under cooling (0 °C) a suspension of CrO_3 (247 mg) in dry pyridine (6.2 ml) was added to a stirred solution of **13** (210 mg) in dry pyridine (2.8 ml) at one time. The mixture was stirred at room temperature for 13 h, diluted with ether (80 ml), and filtered through a pad of Super Cel. The solid residue was washed with ether repeatedly. The combined filtrates were washed with 1.5 M HCl (4×15 ml) and water (4×10 ml), dried, and concentrated. The resulting oily residue was purified by preparative TLC ($CHCl_3$) to yield the tricyclic ketone (**5**) (170 mg, 82%) as colorless crystals: mp 130—133 °C (sealed tube; sublimed at 40 °C/20 mmHg); IR 1714 cm^{-1}; ^{1}H-NMR (90 MHz) 1.01 (3H, s), 1.87 (1H, m), 2.34 (1H, m); MS 178 (M^+). Found: *m/e* 178.1353. Calcd for $C_{12}H_{18}O$: 178.1358.

Deuterium Exchange Reaction. In each run a ketone (0.05—0.5 mmol) was dissolved in a 2.0 M NaOMe solution in MeOD (≥99%, CEA, France) containing 9.4 molar equivalents of NaOMe and the solution was stirred at 33 °C for 22 h under nitrogen. The exchange reaction was repeated at least twice for each ketone, and it was confirmed that the extent of deuteration was reproducible. An example of the representative procedure follows. A solution of the ketone (**5**) (12.8 mg, 0.072 mmol) in 0.34 ml (0.68 mmol of NaOMe) of 2.0 M NaOMe in MeOD was stirred at 33 °C for 22 h under nitrogen, and then diluted with 1 ml of D_2O (≥99.75%, CEA, France). The mixture was extracted with hexane (4×8 ml). The combined organic extracts were washed with D_2O (5 ml), dried over anhydrous Na_2SO_4, and concentrated. The residue was purified by preparative TLC ($CHCl_3$), affording 9.4 mg (74%) of pure **5** as colorless crystals. The sample was analyzed for deuterium content by mass spectrometry.

References

1) J. P. Schaefer and J. C. Lark, *J. Org. Chem.*, **30**, 1337 (1965).

2) A. Nickon, D. F. Covey, F. Huang, and Y-N. Kuo, *J. Am. Chem. Soc.*, **97**, 904 (1975).

3) a) J. R. Wiseman, *J. Am. Chem. Soc.*, **89**, 5966 (1967); b) J. R. Wiseman and W. A. Pletcher, *J. Am. Chem. Soc.*, **92**, 956 (1970).

4) a) E. N. Marvell, D. Sturmer, and C. Rowell, *Tetrahedron*, **22**, 861 (1966); b) J. P. Schaefer, J. C. Lark, C. A. Flegal, and L. M. Honig, *J. Org. Chem.*, **32**, 1372 (1967).

5) A. C. Cope, D. L. Nealy, P. Scheiner, and G. Wood, *J. Am. Chem. Soc.*, **87**, 3130 (1965).

6) E. N. Marvell, G. J. Gleicher, D. Sturmer, and K. Salisbury, *J. Org. Chem.*, **33**, 3393 (1968).

7) K. Yamada, M. Aratani, Y. Hayakawa, H. Nakamura, H. Nagase, and Y. Hirata, *J. Org. Chem.*, **36**, 3653 (1971).
8) K. Biemann, "Mass Spectrometry, Organic Chemical Applications," McGraw-Hill, New York (1962), Chap. 5.
9) G. C. Levy and G. L. Nelson, "Carbon-13 Nuclear Magnetic Resonance for Organic Chemists," Wiley-Interscience, New York (1972).
10) J. B. Stothers, "Carbon-13 NMR Spectroscopy," Academic Press, New York (1972).
11) G. E. Maciel in "Topics in Carbon-13 NMR Spectroscopy," ed by G. C. Levy, Wiley-Interscience, New York (1974), Vol. 1, Chap. 2.
12) a) G. L. Lebel, J. D. Laposa, B. G. Sayer, and R. A. Bell, *Anal. Chem.*, **43**, 1500 (1971); b) R. A. Bell, C. L. Chan, and B. G. Sayer, *J. Chem. Soc., Chem. Commun.*, **1972**, 67; c) J. B. Stothers, C. T. Tan, A. Nickon, F. Huang, R. Sridhar, and R. Weglein, *J. Am. Chem. Soc.*, **94**, 8581 (1972); d) D. H. Hunter, A. L. Johnson, J. B. Stothers, A. Nickon, J. L. Lambert, and D. F. Covey, *J. Am. Chem. Soc.*, **94**, 8582 (1972); e) H. N. Colli, V. Gold, and J. E. Pearson, *J. Chem. Soc., Chem. Commun.*, **1973**, 408; f) A. P. Tulloch and M. Mazurek, *J. Chem. Soc., Chem. Commun.*, **1973**, 692; g) A. L. Johnson, J. B. Stothers, and C. T. Tan, *Can. J. Chem.*, **53**, 212 (1975); h) A. P. Tulloch, *Can. J. Chem.*, **55**, 1135 (1977).
13) J. B. Stothers in Ref. 11, Chap. 6.
14) N. K. Wilson and J. B. Stothers in "Topics in Stereochemistry," ed by E. L. Eliel and N. L. Allinger, Wiley-Interscience, New York (1974), Vol. 8.
15) Y. Fujikura, K. Aigami, N. Takaishi, H. Ikeda, and Y. Inamoto, *Chem. Lett.*, **1976**, 507.
16) K. M. Majerski, Z. Majerski, and E. Pretsch, *J. Org. Chem.*, **41**, 686 (1976).
17) J. P. Ferris and N. C. Miller, *J. Am. Chem. Soc.*, **85**, 1325 (1963).

Nitration of Hexamethylbenzene and Hexamethylbenzene-d_{18} in Acetic Acid. Deuterium Isotope Effect on the Product Distribution. Mechanism of Side-chain Substitution of Arenes[1)]

Hitomi SUZUKI,* Tadashi MISHINA, and Terukiyo HANAFUSA
Department of Chemistry, Faculty of Science, Hiroshima University, Higashi-sendamachi, Hiroshima 730
(Received July 4, 1978)

The reaction in acetic acid of hexamethylbenzene and hexamethylbenzene-d_{18} with nitric acid in the dark has been investigated under various conditions using a high-pressure liquid chromatographic method. Pentamethylbenzyl nitrate, pentamethylphenylnitromethane, pentamethylbenzyl acetate, and pentamethylbenzyl alcohol were formed immediately after the mixing of reactants; their relative amounts remained almost unchanged up to nearly 50% conversion. The addition of sodium nitrite gave little influence on the composition of the product mixture, while urea was found to depress somewhat the formation of nitromethane. In the presence of lithium nitrate, the reaction was modestly accelerated and the nitrate formation seems to be slightly favored over the nitromethane formation. Hexamethylbenzene-d_{18} reacted with nitric acid at the same rate as the non-labeled hydrocarbon did, but the benzyl nitrate/phenylnitromethane ratio in the product mixture was considerably higher in the former. Based on the quantitative data obtained, the mechanism for the side-chain substitution has been discussed in terms of the S_N1' pathway: nitronium ion makes an *ipso* attack on the substrate to form the arenium ion, which releases a proton from the activated methyl group *para* to the site of attack to give the 3-methylene-6-nitro-1, 4-cyclohexadiene intermediate (**7**). Heterolytic fission of the C–N bond in **7** will form a benzyl cation-nitrite anion pair, which recombines at the benzylic carbon atom *via* a C–N bond or *via* a C–O bond, giving benzyl nitrite or phenylnitromethane, respectively. Benzyl nitrite will be further converted into benzyl nitrate and benzyl alcohol, while benzyl acetate will arise from the incorporation of solvent molecules into the ion-pair.

When treated with an electrophile at low or room temperature, polyalkylated aromatic compounds often undergo substitution on a side-chain to yield benzylic compounds. The recent literature contains a variety of examples of such unusual substitution, which include chlorination,[2,3)] bromination,[4)] nitration,[5)] nitrooxylation,[5)] acetamidation,[6)] sulfonation,[7)] thiocyanation,[8)] and others.[9,10)] Although the first report on the side-chain nitration of polyalkylbenzenes under heterolytic conditions appeared nearly seventy years ago,[11)] the mechanistic aspect of this unique reaction had received little attention until very recently, probably because of the wide-spread misbelief that all the side-chain substitutions of arenes should proceed through the homolytic process. In the past decade, however, increasing attention has been focused on this aspect of non-conventional electrophilic substitutions. The accumulation of experimental evidence now provides substantial support for the view that alkylbenzenes may undergo side-chain substitution through a heterolytic mechanism involving a primary electrophilic attack at the aromatic ring: an *ipso* attack of an electrophile to form a benzenium ion is followed by a proton loss from the alkyl substituent to yield a methylenecyclohexadiene intermediate, which is then transformed into benzylic compounds. This type of reaction usually takes place in competition with the normal ring substitution and could be classified as a branched-off process of the ordinary S_E2 reaction.

Based on the product studies and kinetic evidence, several mechanistic propositions have been made for the side-chain substitution,[7,12,13)] but the actual mechanism is not yet fully understood. For *nitration*, the two propositions shown in Schemes 1 and 2, both referring to a methylenecyclohexadiene intermediate (**7**), appear to merit consideration:

Mechanism A:[14)] nucleophilic attack of nitrite or nitrate ions to the terminal methylene carbon atom in **7**, redistribution of electrons to regain the aromatic system, and departure of the nitro group as an anion.

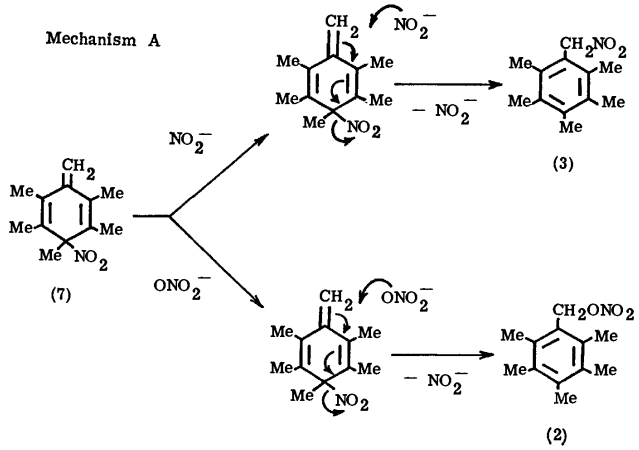

Scheme 1.

Mechanism B:[15)] heterolytic fission of the C–N bond in **7** to form a benzyl cation-nitrite anion pair (**8**) and subsequent recombination of these ions at the benzylic carbon atom either *via* a C–N bond or *via* a C–O bond.

In order to differentiate between these two possibilities, we have reinvestigated the nitration of hexamethylbenzene (**1**) and its perdeuterated derivative using the high-pressure liquid chromatographic method and now present the first quantitative data, which provide support for the mechanism B in which the side-chain substituted products are formed from the methylenecyclohexadiene intermediate through the intervention of an ion-pair.

Mechanism B

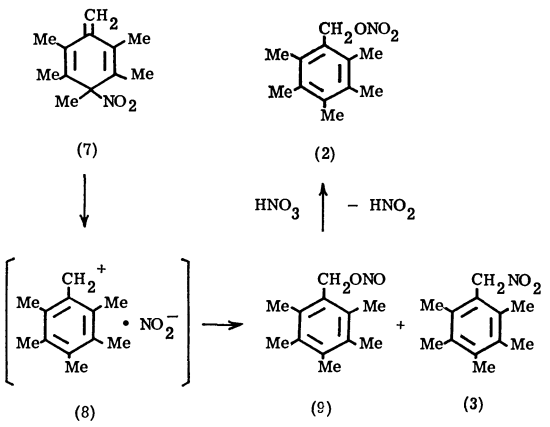

Scheme 2.

Experimental

All melting points were taken on a hot stage apparatus and are uncorrected. The IR, PMR, UV, and mass spectra were obtained using the same procedure and apparatus described in the previous paper[20] of this series, unless otherwise stated.

Acetic acid and nitric acid (d=1.5) of guaranteed grade were dried over phosphorus pentaoxide and carefully redistilled before use. Hexamethylbenzene (**1**; mp 163—164 °C),[21] pentamethylbenzyl nitrate (**2**; mp 95—97 °C),[22] pentamethylphenylnitromethane (**3**; mp 86—88 °C),[22] pentamethylbenzyl acetate (**4**; mp 84—86 °C),[23] and pentamethylbenzyl alcohol (**5**; mp 160—161 °C)[23] were prepared as described in the literature. Pentamethylbenzyl nitrite (**9**; mp 23.5—24 °C; bp 88 °C/3 mmHg)[24] was obtained by the reaction of alcohol **5** with nitrosyl chloride in pyridine.

Hexamethylbenzene-d_{18} was prepared according to the procedure of Koptyug and Shubin[25] with the indicated modification; a solution of 1,2,4,5,6,6-hexamethyl-3-methylene-1,4-cyclohexadiene (1.5 g)[26] in trifluoroacetic acid-*d* (10 ml) was allowed to stand at 70 °C for 15 min under nitrogen and then the solvent was removed under reduced pressure. A fresh 10 ml portion of trifluoroacetic acid-*d* was added to the solid residue and the solution was again worked up in a similar manner. This process was repeated until a total of seven exchanges had been performed. The progress of the isotopic exchanges was monitored by PMR spectroscopy. The solution was then diluted with deuterium oxide (6 ml) and kept under nitrogen for 72 h. The resulting oil was extracted with benzene and the organic layer was washed with saturated aqueous sodium carbonate and water, dried over sodium sulfate, and the solvent removed under reduced pressure. The crude solid obtained was placed on the top of an alumina column and eluted with light petroleum. Evaporation of the early eluate followed by recrystallization of the residue from methanol gave perdeuterated hydrocarbon as colorless plates, 0.16 g (10%). The deuterium content determined by mass spectroscopy was 99.3 atom %. Mp 165—166 °C. IR (Nujol): ν_{max} 2240, 2190, 2110, 2070, 1410, 1030, and 900 cm^{-1}.

Product analyses were performed with a high-pressure liquid chromatograph JASCO Model FLC A-700, equipped with a UV detector (Model UVIDEC-100) and a maximum 700 kg/cm^2 solvent delivery system with constant-flow capacities. The separations were made on a 500×2 mm stainless-steel column packed with JASCO-Pack SS-05 (available from Japan Spectroscopic Co., Hachioji, Tokyo). A computerized reporting integrator, Hewlett-Packard Model 3380-A, was used to estimate the concentration of each component. The eluting solvent was a water-saturated mixture of dichloromethane and hexane; the flow rate was 1.0 ml/min at a pressure of 180 kg/cm^2; the column temperature was ambient; and the injection volume was 2 μl. A 10 μl precision sampling pressure-lock syringe was used for sample injection. Determinations were made at 275 nm with UV units full scale. The difference in absorbance between the ordinary and fully deuterated compounds was negligible. Minor peaks which appeared at higher conversion were neglected.

All *kinetic measurements* were started by adding 10 ml of a solution of nitric acid (0.20 M) in acetic acid at 15 °C to 10 ml of a solution of hexamethylbenzene (0.02 M) and 3,5,6-trinitro-1,2,4-trimethylbenzene as internal standard (0.001 M) in the same solvent preequilibrated to the same temperature. The mixture was left at 15.0±0.1 °C for a suitable time which depended on the reaction rate. The products of reaction were identified by isolation and direct comparison with the authentic specimens. All products are known.

At predetermined times, each aliquot (5 ml) was drawn from the kinetic sample and transferred to a 50 ml separatory funnel containing ether (20 ml); the mixture was immediately washed with two 20 ml portions of cold distilled water, a suspension of calcium carbonate (*ca.* 0.5 g) in water (20 ml), and again distilled water (20 ml). The organic layer was separated and dried over anhydrous sodium sulfate, and the solvent was removed by flash rotary evaporation. The residual oil was dissolved in 4 ml of a 4:6 mixture of dichloromethane and hexane. An aliquot of the solution was withdrawn and injected immediately for analysis. This procedure should be carried out as quickly as possible to minimize errors arising from partial hydrolysis of the prod-

Table 1. Correction factors for the product determination

Compound	Relative molar extinction coefficient at 275 nm[a]	Relative extraction efficiency
Hexamethylbenzene	0.13	1.61
Pentamethylbenzyl nitrate	0.61	1.04
Pentamethylphenylnitromethane	0.67	1.05
Pentamethylbenzyl acetate	0.41	1.06
Pentamethylbenzyl alcohol	0.36	0.813
3,5,6,-Trinitro-1,2,4-trimethylbenzene[b]	1.00	1.00

a) In a water-saturated 4:6-mixture of dichloromethane and hexane. b) Of over fifty compounds examined, this compound was found to be best as the internal standard for liquid chromatography, since it satisfied the following requirements: to be soluble in reaction medium, extracting solvent, and eluant; to be stable throughout the reaction and work-up; to have no effect on the course of the reaction; to be well resolved from all the components of the product mixture on the chromatogram and have an elution order which promotes accuracy in the determination with two different solvent systems; and to have an appropriate intensity of UV absorption at the wavelength used for determination.

ucts. When a kinetic sample to be analyzed was first discharged into water and the products were extracted with ether from the aqueous layer, significant amounts of nitrate were hydrolyzed to alcohol. All the determinations were checked against the control experiments.

Appropriate corrections were made for the errors arising from the difference in loss of each component during the sample preparation, the correction factors being determined using the mixed standard solutions of authentic specimens. The relative molar extinction coefficient at 275 nm and the relative extraction efficiency of each component are shown in Table 1, with the internal standard as unity.

Results and Discussion

Before beginning our work, we made a systematic search for a substrate and an analytical method which could afford reliable quantitative data for side-chain nitrations of arenes. From the many alkyl aromatics examined, hexamethylbenzene (**1**) was chosen as the best, since it was found to give a clean, simple product mixture at low conversion. For the quantitative determination of the nitration product from **1**, the high-pressure liquid chromatographic method was found to be best; none of the other chromatographic procedures, such as GLC, TLC, and column, was found to give reliable and reproducible data, owing to the side reactions which inevitably took place during the separation.

Several reports have appeared on the nitration of **1**, but quantitative data are not yet available. Willstätter and Kubli treated **1** with benzoyl nitrate in carbon tetrachloride and obtained bis(pentamethylbenzyl) ether (**12**) and a bis(nitromethyl)tetramethylbenzene in an unspecified yield.[11] Smith and Harris carried out the nitration of **1** with fuming nitric acid in the presence of sulfuric acid and obtained as much as 22% yield of 5,6-dinitro-1,2,3,4-tetramethylbenzene (**14**).[27] A significant proportion of the starting material that had remained unaccounted for in their work was found by one of the present authors to be a complicated mixture of **2**, **3**, nitropentamethylbenzene (**13**), 6-nitro-2,3,4,5-tetramethylbenzyl nitrate (**14**), 5,6-bis(nitrooxymethyl)-1,2,3,4-tetramethylbenzene (**16**), pentamethylbenzaldehyde (**17**), and several other unidentified carbonyl compounds, nitrites, and aliphatic nitro compounds.[22] Illuminati and his coworkers nitrated **1** in acetic acid and obtained a mixture of **2**, **3**, and pentamethylbenzyl acetate (**4**).[28] Detsina and Koptyug reported the formation of 2,3,-4,5,6,6-hexamethyl-2,4-cyclohexadien-1-one (**18**) from the reaction of **1** with nitric acid in fluorosulfuric acid at −70 °C.[10] Fischer and his coworkers investigated the nitration of **1** in acetic anhydride at low temperature and obtained, besides various aromatic products, several extremely labile addition products, one of which was identified as 1,2,3,4,5,6-hexamethyl-3,6-dinitro-1,4-cyclohexadiene (**19**).[29]

The reaction of **1** with an excess of nitric acid was carried out in acetic acid at 15.0 °C in the dark. After aqueous work-up a mixture of nitrate **2**, nitromethane **3**, acetate **4**, and alcohol **5** was obtained as initial products. All these four products were formed immediately after the mixing of reactants and their relative amounts studied as a function of time remained almost unchanged up to nearly 50% conversion (Fig. 1). The sum of the concentration of **1** and these four products accounted for nearly all of the stoichiometric concentration, showing that even if some products other than **2** to **5** were formed, their concentrations were very small. The relative distribution of the products is given in Table 2. At higher conversions, these

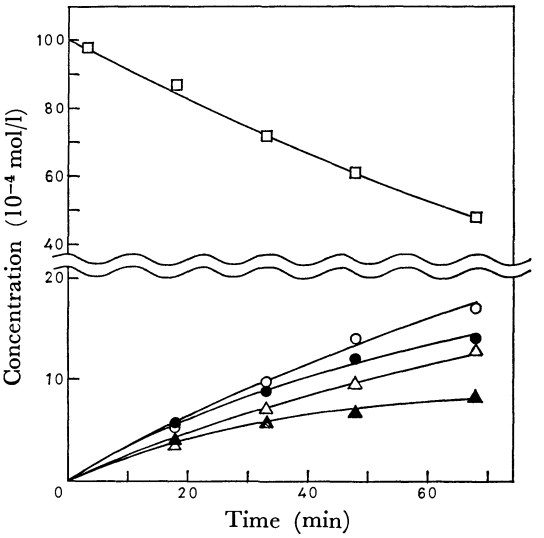

Fig. 1. Reaction of hexamethylbenzene with nitric acid in acetic acid.
□: Hexamethylbenzene,
○: pentamethylbenzyl nitrate,
●: pentamethylbenzyl acetate,
△: pentamethylphenylnitromethane,
▲: pentamethylbenzyl alcohol.

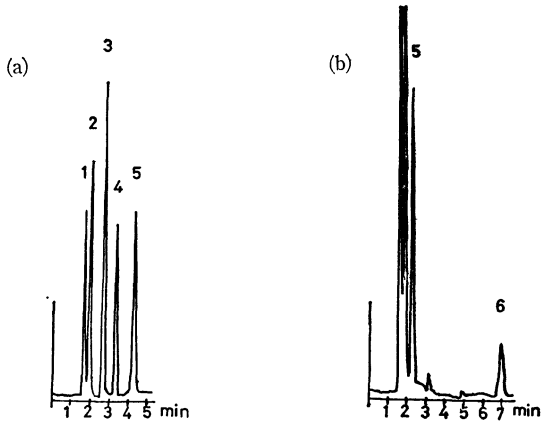

Fig. 2. Liquid chromatograms of the nitration product of hexamethylbenzene.
(a) With a water-saturated 4:6 mixture of dichloromethane and hexane as eluant.
(b) With a water-saturated 8:2 mixture of dichloromethane and hexane as eluant.
1: Hexamethylbenzene,
2: pentamethylbenzyl nitrate,
3: pentamethylphenylnitromethane,
4: internal standard,
5: pentamethylbenzyl acetate,
6: pentamethylbenzyl alcohol.

Table 2. Product distribution and product ratio in the reaction of hexamethylbenzene with nitric acid in acetic acid[a)]

Reaction	Reaction time (min)	Conversion (%)	Product distribution (%)[b)] Nitrate **2** and alcohol **5**	Nitromethane **3**	Acetate **4**	Product ratio (**2**+**5**)/**3**	(**2**+**3**+**5**)/**4**
Standard[c)]	60—73	61—68	44.3±2.0	26.0±2.2	29.8±1.3	1.74±0.25	2.35±0.17
Sodium nitrite added							
0.0039 M	70	70	44	27	30	1.6	2.4
0.0143 M	70	69	44	26	30	1.7	2.3
			(43)[d)]	(27)	(30)	(1.6)	(2.3)
Urea added							
0.0127 M	72	61	50	17	33	2.9	2.0
0.0507 M	72	52	52	15	33	3.5	2.0
			(44)	(26)	(30)	(1.7)	(2.3)
Lithium nitrate added							
0.200 M	66	81	48	23	29	2.1	2.4
			(44)	(28)	(28)	(1.6)	(2.6)
Other solvent added							
12% Acetic anhydride							
	30	93	38	29	33	1.3	2.0
20% Dichloromethane							
	73	65	49	28	23	1.8	3.3
40% Dichloromethane							
	73	50	53	29	18	1.8	4.6
			(45)	(25)	(30)	(1.8)	(2.3)
Hexamethylbenzene-d_{18}[e)]							
	60	66	55	14	31	3.9	2.2
		(65)	(42)	(28)	(30)	(1.5)	(2.3)
	90	73	57	12	32	4.8	2.1
		(72)	(42)	(27)	(31)	(1.6)	(2.2)

a) Hexamethylbenzene, 0.01 M; nitric acid, 0.10 M; reaction temperature, 15.0±0.1 °C. b) Mole percentages determined by high-pressure liquid chromatography using digital integration. c) Averaged value of eight runs. d) Numerals in parentheses refer to the values obtained by control experiments. e) Control experiments demonstrated that deuterium was not exchanged with solvent under any reaction conditions employed.

initial products gradually underwent further reaction with the reagent or solvent. Mechanism A requires that the nitro compound **3** be formed as the main product at sufficiently high nitrous acid concentration; that is, the amount of **3** would be multiplied during the progress of the reaction, as nitrous acid accumulates. According to Scheme 1, the increase in the concentration of nitrite ions in the reaction system is expected to favor the formation of nitromethane **3**. Added sodium nitrite, however, gave little influence on the composition of the product mixture. The role of urea as an added material was somewhat perplexing. Although the yellow coloration of the reaction mixture due to the liberated nitrogen dioxide was suppressed by the addition of small amounts of urea, the product composition remained little affected. However, in the presence of large amounts of urea, the nitrate formation seems to be favored, as shown in Table 2. Urea itself or its salt might be involved in the reaction process, but the situation is not clear at present.

Added lithium nitrate in low concentrations has little effect on the product composition. However, in the presence of large amounts of lithium nitrate (>0.1 M), the reaction was modestly accelerated and the nitrate formation seems to be favored over the nitromethane formation. These findings are not consistent with mechanism A, which assumes the reaction of triene intermediate **7** with external nitrate and nitrite ions for the respective formation of benzyl nitrate and phenylnitromethane. Mechanism B assumes the recombination of a benzyl cation with an ambident nitrite ion in the ion-pair. Thus, replacement of protium by deuterium in the cationic portion of the ion-pair is expected to increase the localized positive charge at the benzylic carbon atom due to the decrease in hyperconjugative electron release, as well as due to the more electronegative character of the perdeuteriomethyl group as compared to methyl group. Such an effect will favor the recombination at the oxygen atom of the ambident nitrite ions, leading to the preferential formation of benzyl nitrate or nitrite, while the secondary isotope effect would be of less significance in the product determination step in the mechanism A. In order to use the deuterium labeling as a probe into the ion-pair intermediate **8**, hexamethylbenzene-d_{18} was prepared from 1,1,2,3,4,5,6-heptamethylbenzenium chloride[26)] by the exchange of hydrogens with trifluoroacetic acid-*d* and subjected to nitration under the same conditions as applied to **1**. The perdeuterated hydrocarbon reacted with the reagent

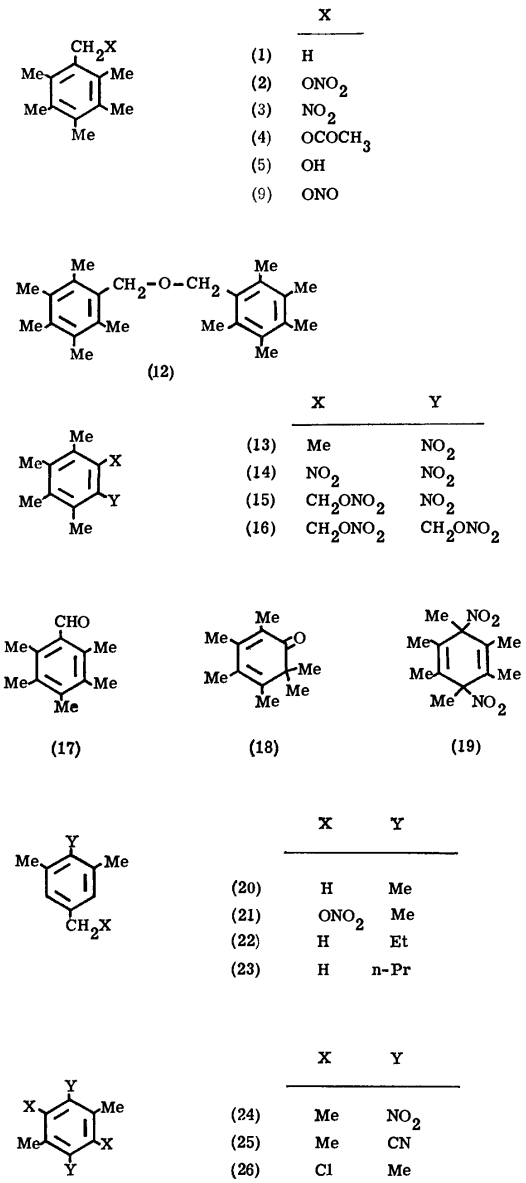

Scheme 3.

at the same rate as the non-labeled one did. In this case, however, the amount of nitrate was found to increase considerably at the expense of nitromethane, while the amount of acetate did not change very much (Table 2). These results are compatible with Scheme 2, but not with Scheme 1.

It is noteworthy that the molar ratio of acetate **4** to the sum of other three products (**2**+**3**+**5**) remains almost unaffected by the presence of sodium nitrite, urea, and lithium nitrate, as well as by the replacement of protium in **1** by deuterium. Similarly, the molar ratio of nitromethane **3** to the sum of nitrate and alcohol (**2**+**5**) is not very much affected. These trends may be taken to indicate that recombination of initially formed intermediates in **8** is a major pathway to nitrate and nitromethane, while acetate is formed through the nucleophilic capture of carbenium ion intermediate by solvent, possibly *via* a solvent-separated ion-pair (**11**). Pentamethylbenzyl nitrite (**9**) is known to be readily converted into a mixture of nitrate and alcohol in the presence of nitric acid.[24] Part of the nitrate may arise also from the reaction of ion-pair **8** with nitric acid, possibly *via* ion-pair (**10**), since the increase in the concentration of lithium nitrate was found to have a positive effect on the nitrate formation.[30] Alcohol **5** is probably formed partly from the reaction of **9** with nitric acid and partly from the hydrolysis of **2** and **9** during the aqueous work-up. Polymethylbenzyl nitrites are not highly stable and readily undergo hydrolysis to benzyl alcohols in aqueous media. However, they solvolyse quite slowly in anhydrous acetic acid.

Generally speaking, the side-chain nitration and nitrooxylation of arenes in acetic acid are not sensitive to addenda such as sodium nitrite, urea, and lithium nitrate as long as their concentrations are not very high. In contrast, acetic anhydride exhibited a strong accelerating effect on the reaction and produced a profound effect on the product distribution. Even at the first stages of the reaction, liquid chromatograms of the product revealed a complicated pattern of composition, suggesting the occurrence of various competing side reactions. The addition of dichloromethane to the reaction system, as expected, depressed the acetate formation in favor to the formation of nitrate and nitromethane, leading to the increase in the molar ratio (**2**+**3**+**5**)/**4**. However, the ratio (**2**+**5**)/**3** remained unchanged again. Thus, all the results obtained in our study may be rationalized in terms of the heterolytic mechanism involving the formation of ion-pairs and their conversion to the benzylic compounds, as shown in Scheme 4.

Recently Kochi has made the suggestion of a possible intervention of radical cationic species in the side-chain chlorination of alkyl aromatics, on the basis of his observation of ESR signal during the chlorination of **1**.[13] He extended his idea to the side-chain nitration,[31] suggesting a mechanism in which one electron is transferred from the aromatic substrate to a nitronium ion to form an arene cation radical and nitrogen dioxide (Scheme 5). However, this scheme does not explain the results of our product study: the cation radical derived from 1,2,3,5-tetramethylbenzene (**20**) has a positive charge distribution on the ring carbons in the decreasing order: $C_2 \gg C_5 \gg C_1$, $C_3 > C_4$, C_6.[32] Thus, the proton loss should occur preferentially at the 2-methyl group to form 2,4,6-trimethylbenzyl radical and yield its descendents as major products. This is consistent with the result obtained by anodic oxidation of **20** to a mixture of heptamethyldiphenylmethanes,[32] and the results obtained by the reaction of **20** either with *N*-bromosuccinimide under homolytic conditions[33] or with cerium ammonium nitrate in acetic acid.[33] However, it is not consistent with the results obtained by the nitration of **20**, where the only side-chain substituted product was 3,4,5-trimethylbenzyl nitrate (**21**) or its derivative.[34] With 2-ethyl-1,3,5-trimethylbenzene (**22**) and 2-propyl-1,3,5-trimethylbenzene (**23**), side-chain substitution occurs exclusively at the 5-methyl group.[35]

3,6-Dinitro-1,2,4,5-tetramethylbenzene (**24**),[36] 1,2,-

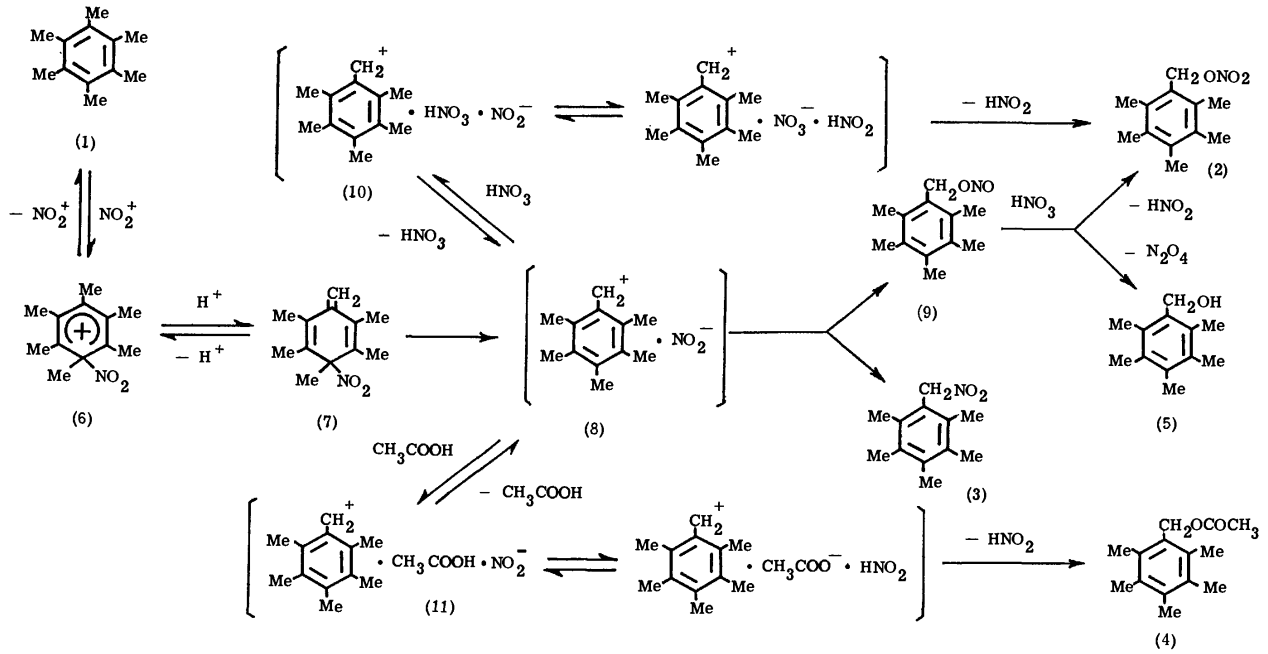

Scheme 4.

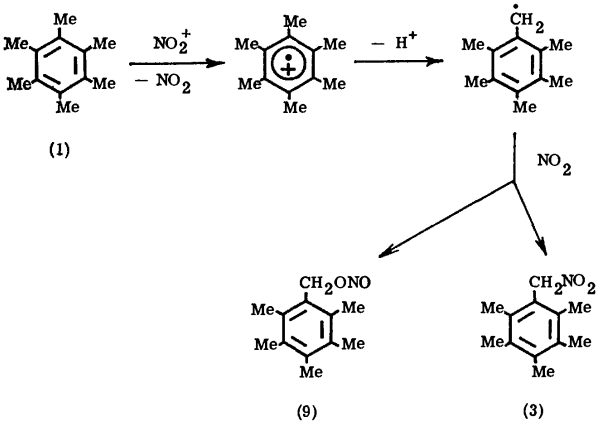

Scheme 5.

4,5-tetramethylbenzene-3,6-dicarbonitrile (**25**),[20] and tetrachloro-*p*-xylene (**26**)[37] are all quite stable towards the action of transition metallic oxidizing agents which are thought to react *via* electron-transfer mechanism, but these compounds still undergo a smooth reaction with concentrated nitric acid at room temperature, giving the corresponding benzyl nitrates in good yields. The low efficacy of nitronium tetrafluoroborate to produce side-chain substituted products from **1** provides further evidence against the suggested scheme 5. Therefore, the electron-transfer mechanism does not seem to possess a sound ground on which the formation of a variety of side-chain nitration and nitrooxylation products should be rationalized.

The present findings are highly suggestive of a pathway involving an ion-pair intermediate; nitrate **2** and nitromethane **3** are formed from an intimate ion-pair **8**, and acetate **4** arises from a solvent-separated ion-pair **11**. Full discussion of this problem awaits more detailed data, in particular, direct evidence of isolating the triene intermediate.

We are grateful to the Ministry of Education and the Saneyoshi Scientific Foundation for financial support of this work.

References

1) The reaction of polysubstituted aromatics. Part LII; Part LI: H. Suzuki, T. Mishina, and T. Hanafusa, *Bull. Chem. Soc. Jpn.*, **51**, 3099 (1978).
2) E. Baciocchi, A. Ciana, G. Illuminati, and C. Pasini, *J. Am. Chem. Soc.*, **87**, 3953 (1965).
3) H. Hart, J. L. Reilly, and J. B.-C. Jiang, *J. Org. Chem.*, **42**, 2684 (1977).
4) P. B. D. de la Mare, N. S. Isaacs, and P. D. McIntyre, *Tetrahedron Lett.*, **1976**, 4835.
5) For reviews see H. Suzuki, *Synthesis*, **1977**, 217; B. Moodie and K. Schofield, *Acc. Chem. Res.*, **9**, 287 (1976).
6) H. Suzuki and T. Hanafusa, *Bull. Chem. Soc. Jpn.*, **46**, 3607 (1973); E. Hunziker, J. R. Penton, and H. Zollinger, *Helv. Chim. Acta*, **54**, 2043 (1971).
7) H. Cerfontain, A. Koeberg-Telder, C. Ris, and C. Schenk, *J. Chem. Soc., Perkin Trans. 2*, **1975**, 966.
8) E. Baciocchi, P. Faggioni, and G. Illuminati, *Gazz. Chim. Ital.*, **103**, 1311 (1973).
9) H. Suzuki, *Bull. Chem. Soc. Jpn.*, **42**, 2618 (1969); H. Suzuki and K. Kawamura, *ibid.*, **45**, 1945 (1972); M. M. King and R. H. Brown, *Tetrahedron Lett.*, **1975**, 3995.
10) A. N. Detsina and V. A. Koptyug, *Zh. Org. Khim.*, **8**, 2215 (1972).
11) R. Willstätter and H. Kubli, *Ber.*, **42**, 4151 (1909).
12) For a general review of non-conventional electrophilic aromatic substitution, see S. R. Hartshorn, *Chem. Soc. Rev.*, **3**, 167 (1974).
13) J. K. Kochi, *Tetrahedron Lett.*, **1974**, 4305.
14) A. Fischer and J. N. Ramsay, *J. Am. Chem. Soc.*, **96**, 1614 (1974); *Can. J. Chem.*, **52**, 3960 (1974).
15) H. Suzuki, H. Yoneda, and T. Hanafusa, *Bull. Chem. Soc. Jpn.*, **48**, 2116 (1975), and other papers in the series. While studying the nitration of 4,6-dihalo-[16] and 4,6-dinitro-1,2,3,5-tetramethylbenzene,[17] we noticed the failure of the

original Baciocchi-Illuminati mechanism, which assumes a cyclic intramolecular transfer of an electrophile from ring to an *ortho* side-chain,[2,18] and proposed in 1971 an alternative possibility involving an ion-pair path for the side-chain nitrooxylation of arenes.[16] Later, a similar idea was adopted by Baciocchi and his coworkers in explaining the side-chain chlorination.[19]

16) H. Suzuki, K. Nakamura, and M. Takeshima, *Bull. Chem. Soc. Jpn.*, **44**, 2248 (1971).
17) H. Suzuki and K. Nakamura, *Bull. Chem. Soc. Jpn.*, **45**, 2534 (1972).
18) H. Suzuki, K. Nakamura, and K. Maruyama, *Bull. Chem. Soc. Jpn.*, **41**, 1487 (1968); H. Suzuki and K. Nakamura, *ibid.*, **43**, 473 (1970).
19) E. Baciocchi, L. Mandolini, and A. Patara, *Tetrahedron Lett.*, **1975**, 2268.
20) H. Suzuki, M. Koge, A. Inoue, and T. Hanafusa, *J. Chem. Soc., Chem. Commun.*, **1977**, 341; *Bull. Chem. Soc. Jpn.*, **51**, 1168 (1978).
21) L. I. Smith, *Org. Synth.*, Coll. Vol. II, 248 (1943).
22) H. Suzuki, *Bull. Chem. Soc. Jpn.*, **43**, 879 (1970).
23) O. Jacobsen, *Ber.*, **22**, 1217 (1889).
24) H. Suzuki, K. Nakano, T. Mishina, and T. Hanafusa, *Nippon Kagaku Kaishi*, **1978**, 1049.
25) V. A. Koptyug, V. G. Shubin, and D. V. Korchagina, *Tetrahedron Lett.*, **1965**, 1535.
26) W. von E. Doering, M. Saunders, H. G. Boyton, H. W. Earhart, E. F. Wadley, W. R. Edwards, and G. Laber, *Tetrahedron*, **4**, 178 (1958).
27) L. I. Smith and S. A. Harris, *J. Am. Chem. Soc.*, **57**, 1289 (1935).
28) R. Astolfi, E. Baciocchi, and G. Illuminati, *Chem. Ind. (Rome)*, **53**, 1153 (1971).
29) A. Fischer, personal communication (1977).
30) Nitrations with nitric acid alone, or with nitric acid/dichloromethane and nitric acid/nitromethane, all of these would probably follow a path involving ion-pair **10**, since they afford in most cases benzyl nitrates as the sole side-chain substituted products.
31) J. K. Kochi, personal communication (1977).
32) K. Nyberg, *Acta Chim. Scand.*, **25**, 2499 (1971).
33) E. Baciocchi, L. Mandolini, and C. Rol, *Tetrahedron Lett.*, **1973**, 3787.
34) To be published.
35) H. Suzuki, M. Sawaki, and R. Sakimoto, *Bull. Chem. Soc. Jpn.*, **45**, 1515 (1972).
36) H. Suzuki and K. Nakamura, *Synthesis*, **1972**, 606.
37) H. Suzuki, K. Ishizaki, S. Maruyama, and T. Hanafusa, *J. Chem. Soc., Chem. Commun.*, **1975**, 51; *Bull. Chem. Soc. Jpn.*, **48**, 2112 (1975).

Improved Synthesis of Antimycin A_3

Shimpei ABURAKI and Mitsuhiro KINOSHITA*
Department of Applied Chemistry, Faculty of Engineering, Keio University, Hiyoshi, Kohoku-ku, Yokohama 224
(Received July 8, 1978)

An improved synthesis of antimycin A_3 was accomplished by a suitable lactonization of 3-*O*-benzyl or 3-*O*-isovaleryl derivative (**10a** or **10b**) of (2*R*, 3*R*, 4*S*)-4-(*N*-benzyloxycarbonyl-L-threonyloxy)-2-butyl-3-hydroxypentanoic acid, which was synthesized by starting from the corresponding 3-*O*-benzyl or 3-*O*-isovaleryl derivative (**4a** or **4b**) of methyl 2-*C*-butyl-2, 5-dideoxy-β-L-arabinofuranoside, respectively. Acid hydrolysis of **4a** or **4b** followed by reduction with sodium borohydride afforded 3-*O*-benzyl or 3-*O*-isovaleryl-1, 3, 4-pentanetriol (**5a** or **5b**), respectively. Tritylation of **5a** or **5b** followed by succesive 4-*O*-acylation with *N*-benzyloxycarbonyl-*O*-*t*-butyl-L-threonine, detritylation, oxidation with chromium trioxide-acetic acid-pyridine, and de-*t*-butylation gave the hydroxy ester acid **10a** or **10b**, respectively. Lactonization of **10a** or **10b** through its 2-pyridinethiol ester **11a** or **11b** activated with silver perchlorate afforded the corresponding nine-membered dilactone derivative **12a** or **12b** in 33 or 13% yield, respectively. Removal of *N*,*O*-protecting groups of **12a** by hydrogenolysis, followed by successive *N*- and *O*-acylation gave the antimycin A_3 precursor, (3*S*, 4*R*, 7*R*, 8*R*, 9*S*)-3-(2-benzyloxy-3-nitrobenzoylamino)-4, 9-dimethyl-7-butyl-8-isovaleryloxy-1, 5-dioxonane-2, 6-dione derived from **12b**.

Antifungal antibiotic antimycin A complex has a unique nine-membered dilactone structure. In the first total synthesis[1,2] of antimycin A_3 (**1**), one of the major components of the complex, the dilactone intermediate, (3*S*,4*R*,7*R*,8*R*,9*S*)-3-benzyloxycarbonyl-amino-7-butyl-4,9-dimethyl-8-isovaleryloxy-1,5-dioxonane-2,6-dione (**12b**) was synthesized by lactonization of (2*R*, 3*R*,4*S*)-4-(*N*-benzyloxycarbonyl-L-threonyloxy)-2-butyl-3-isovaleryloxypentanoic acid (**10b**) prepared by the condensation of (±)-2,3-*threo*-3,4-*erythro*-2-butyl-4-hydroxy-3-isovaleryloxypentanoic acid *t*-butyl ester with *N*-benzyloxycarbonyl-*O*-*t*-butyl-L-threonine. The lactonization of **10b** was effected only with trifluoroacetic anhydride in hot benzene, but the yield of **12b** was extremely poor.[2]

We briefly communicated[3] the synthesis of deisovalerylblastmycin (**2**) which constitutes a new route for the stereospecific synthesis of antimycin A involving an improved lactonization step. We now describe in full the improved synthesis of antimycin A_3.[3] Since the first synthesis of antimycin A_3, studies have progressed in the field of macrolide synthesis, new lactonization methods being found to be effective for the synthesis of large lactone compounds.[4] It was expected that the yield of the medium lactone ring formation such as lactonization of the hydroxy ester acid **10b** would also be enhanced by appropriate modification in the structure of the reactant or by choice of a more suitable method for lactonization of the reactant.

The structural modification undertaken was an exchange of the 3-isovaleryloxy group of **10b** by benzyloxy group convertible into the former after lactonization. The modified hydroxy ester acid, (2*R*,3*R*,4*S*)-4-(*N*-benzyloxycarbonyl-L-threonyloxy)-3-benzyloxy-2-butylpentanoic acid (**10a**) was synthesized through the stereospecific route (Fig. 1) starting from the sugar derivative **3**.[5] The route was utilizable for the stereospecific synthesis of **10b**.

Lactonization of **10a** or **10b** through its 2-pyridinethiol ester **11a** or **11b** activated with silver perchlorate by the method of Gerlach and Thalmann[6] effectively afforded the corresponding dilactone intermediate **12a** or **12b** in 33 or 13% yield, respectively. The comparatively high yields are in contrast with the 0.8% yield[2] of **12b** obtained by the trifluoroacetic anhydride method. The dilactone derivative **12a** was converted into the 3-(2-benzyloxy-3-nitrobenzoylamino)-8-hydroxydilactone **15**, a synthetic precursor of the antibiotic deisovalerylblastmycin (**2**).[3] Isovalerylation of **15** afforded the antimycin A_3 precursor **16** which had been derived from **12b** *via* the amino dilactone derivative **13b**[2](Fig. 3). The synthesis of antimycin A_3 was thus improved through the route *via* **12a** effectively provided by suitable lactonization of the modified hydroxy ester acid **10a**. Moreover, the previous route *via* **12b** was also useful in the antimycin A_3 synthesis by the improved lactonization of **10b**.

Results and Discussion

Methyl 2-*C*-butyl-2,5-dideoxy-β-L-arabinofuranoside (**3**) was converted into the 3-*O*-benzyl derivative **4a** with benzyl bromide and sodium hydride in THF or into the 3-*O*-isovalerate **4b** with isovaleric anhydride in pyridine. Acid hydrolysis of **4a** followed by sodium borohydride reduction gave (2*S*,3*R*,4*S*)-3-*O*-benzyl-2-butyl-1,3,4-pentanetriol (**5a**) in 94% yield. Acid hydrolysis of **4b** followed by reduction with sodium borohydride in 70% ethanol at −10 °C afforded an 8:1 mixture of desired 3-*O*-isovaleryl triol (**5b**) and its positional isomer, 4-*O*-isovalerate (**5b'**)in a total yield of 97%. The formation of **5b'** was probably due to the 3→4 *O*-acylmigration proceeding under basic conditions in the borohydride reduction step.

Tritylation of **5a** with triphenylmethyl chloride in pyridine at 40 °C gave the 3-*O*-benzyl-1-*O*-trityl-1,3,4-pentanetriol (**6a**) quantitatively. Acylation of the 4-hydroxyl group of **6a** with excess *N*-(benzyloxycarbonyl)-*O*-*t*-butyl-L-threonine in the presence of dicyclohexylcarbodiimide (DCCI) and pyridine afforded the condensation product **7a** in 74% yield. Tritylation of the 8:1 mixture of **5b** and **5b'** at room temperature gave 3-*O*-isovaleryl-1-*O*-trityl-1,3,4-pentanetriol (**6b**) in

74% yield after being subjected to chromatography. However, when the reaction with **5b** was conducted at 40 °C, the major product was the isomer, 4-*O*-isovaleryl-1-*O*-trityl-1,3,4-pentanetriol (**6b'**), presumably formed from **6b** by the 3→4 *O*-acyl migration. Condensation of **6b** with the threonine derivative by the DCCI method afforded the ester **7b** in 65% yield.

Detritylation of **7a** and **7b** with 90% acetic acid gave the corresponding alcohols, **8a** and **8b** in 95 and 62.2% yields, respectively. Oxidation of **8a** and **8b** with a mixture of chromium trioxide, acetic acid and pyridine[7] afforded the corresponding ester acids, **9a** and **9b** in 76 and 96% yields, respectively.

The *t*-butyl groups of **9a** and **9b** were removed by treatment with trifluoroacetic acid to give (2*R*,3*R*,4*S*)-4-(*N*-benzyloxycarbonyl-L-threonyloxy)-3-benzyloxy-2-butylpentanoic acid (**10a**) and (2*R*,3*R*,4*S*)-4-(*N*-benzyloxycarbonyl-L-threonyloxy)-3-isovaleryloxy-2-butylpentanoic acid (**10b**), respectively.

In contrast with **10b**, the modified hydroxy ester acid **10a** afforded no cyclization product on treatment with trifluoroacetic anhydride in hot benzene by the same procedure as that for **10b**.[2] IR spectroscopy revealed that the major product of the reaction was the *O*-trifluoroacetyl derivative of **10a**.

The hydroxy acids **10a** and **10b** were converted into the corresponding 2-pyridinethiol esters, **11a** and **11b** by action of di-2-pyridyl disulfide and triphenylphosphine according to Mukaiyama *et al.*[8] in good yields after being subjected to chromatography. By the method of Gerlach and Thalmann,[6] the intramolecular cyclization of **11a** and **11b** was effected in about 0.01 M benzene solution with a 1.5 equivalent amount of silver perchlorate to yield the corresponding dilactone derivatives, **12a** and **12b** in 33 and 13.4% yields, respectively. In the cyclization of **11a** with silver perchlorate, no formation of intermolecular cyclization product was observed, the hydroxy ester acid **10a** being recoverd in good yield. Cyclization of **11a** carried out in a 0.00 M solution showed no improvement in the yield of **12a**.

According to the method of Corey and Nicolaou,[9] the crude 2-pyridinethiol ester **11a** was refluxed in a 0.005 M xylene solution to afford the sole intramolecular cyclization product in 13.7% yield. The product was distinguishable from **12a** in the ring coupling constants ($J_{7,8}$=4.0 and $J_{8,9}$=9.2 Hz), suggesting that the product might be **12a'**, the 7-epimer of **12a**.

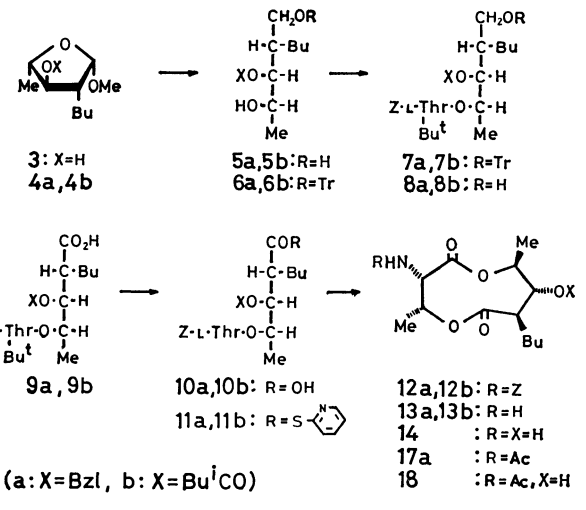

Fig. 1.

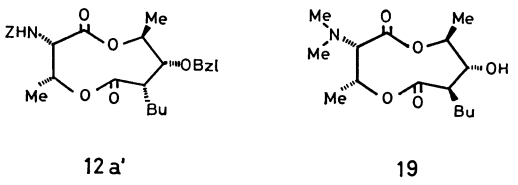

12a' 19

Fig. 2.

Hydrogenolysis of **12a** with palladium black in methanol under hydrogen atmosphere at 50 p.s.i. afforded the *N*-debenzyloxycarbonylated dilactone **13a**, *O*-debenzylation of which was effected *via* the *N*-acetyl derivative **17a** to afford **18**, the *N*-acetyl derivative of the amino hydroxy dilactone **14**. Hydrogenolysis of **12a** with palladium black in methanol containing a small amount of hydrogen chloride under hydrogen atmosphere at 50 p.s.i. gave the hydrochloride of **14**, which was selectively *N*-acylated with 2-benzyloxy-3-nitrobenzoic acid *N*-hydroxysuccinimide ester[10] to afford **15** in 72% yield. On the other hand, hydrogenolysis of **12a** with palladium black in methanol at 40 °C under hydrogen atmosphere at 50 p.s.i. yielded the dimethylamino hydroxy dilactone **19** whose structure was determined by its PMR and mass spectrum.

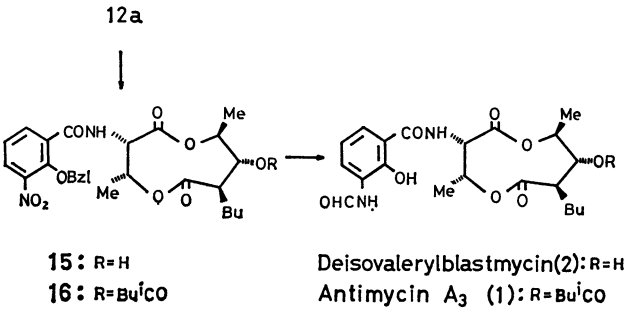

Fig. 3.

The *N*-acylamino hydroxy dilactone **15** was *O*-isovalerylated with isovaleric anhydride in pyridine to afford (3*S*,4*R*,7*R*,8*R*,9*S*)-3-(2-benzyloxy-3-nitrobenzoylamino)-4,9-dimethyl-7-butyl-8-isovaleryloxy-1,5-dioxonane-2,6-dione (**16**),[2] the antimycin A_3 precursor, in 88% yield.

Experimental

Melting points were determined on a micro hot stage and are uncorrected. IR spectra were taken on a Hitachi 225 Spectrophotometer, Mass spectra on a JMS-D-100, and PMR spectra on Varian A-60D and HA-100D Spectrometers using TMS as an internal standard. Optical rotations were measured with a Zeiss Photoelectroic Precision Polarimeter. CD spectra were taken on a JASCO J-20 Spectropolarimeter. TLC was carried out on Wakogel B-5 and silica gel column chromatography on Wakogel C-200 which was activated at 110 °C for 1 h. Concentration was carried out at reduced pressure below 40 °C.

*Methyl 3-O-Benzyl-2-C-butyl-2,5-dideoxy-β-L-arabinofuranoside (**4a**).* A suspension of 55% NaH (450 mg, 10.3 mmol) in THF(9 ml) was added to a solution of methyl 2-*C*-butyl-2,5-dideoxy-β-L-arabinofuranoside (**3**)[5] (1.29 g, 6.83 mmol) and stirred at room temperature for 2 h. Benzyl bromide (1.22 ml, 10.3 mmol) was added to the mixture and stirred at room temperature overnight. The reaction mixture was poured into cold water (50 ml) and extracted with ethyl acetate. The organic layer was washed with saturated aqueous NaCl solution, dried, and evaporated. The residue was chromatographed on silica gel(150 g) with benzene-ethyl acetate (30 : 1) to afford a colorless syrup of **4a** (1.54 g, 81%) : $[\alpha]_D^{21}$ −98°(*c* 1.1, $CHCl_3$); PMR($CDCl_3$) δ 1.32 (d, 4-CH_3, J=6.4 Hz), 3.44(s, OCH_3), 3.36 (dd, H-3, $J_{2,3}$= 4.0, $J_{3,4}$=6.1 Hz), 4.25 (dq, H-4), 4.68 (s, CH_2Ph), and 4.76 (d, H-1, $J_{1,2}$=1.8 Hz).

Found: C, 73.65; H, 9.27%. Calcd for $C_{17}H_{26}O_3$: C, 73.34; H, 9.41%.

*Methyl 3-O-Isovaleryl-2-C-butyl-2,5-dideoxy-β-L-arabinofuranoside (**4b**).* A mixture of **3** (1.08 g, 5.71 mmol), isovaleric anhydride (1.72 ml, 8.1 mmol) and pyridine (10 ml) was kept at room temperature for 2 days. The reaction mixture was poured into cold water (20 ml) and extracted with chloroform. The combined extracts were washed with saturated aqueous NaCl solution, dried, and evaporated. The residue was chromatographed on silica gel (150 g) with benzene-ethyl acetate(50 : 1) to afford an essentially pure sample of **4b** as a pale yellow syrup (1.52 g, 98%): PMR ($CDCl_3$) δ 0.97[d, 6H, $CH(CH_3)_2$, J=6.6 Hz], 1.33 (d, 3H, 4-CH_3, J=6.5 Hz), 3.40 (s, 3H, OCH_3), 4.08 (dq, H-4, $J_{3,4}$=5.9 Hz), 4.61 (dd, H-3, $J_{2,3}$=3.9 Hz), and 4.70 (d, H-1, $J_{1,2}$=1.8 Hz).

*(2S,3R,4S)-3-O-Benzyl-2-butyl-1,3,4-pentanetriol (**5a**).* A solution of **4a** (1.53 g) in a mixture of dioxane (44 ml) and 1 M HCl (11 ml) was kept at room temperature for 3 days. The reaction mixture was neutralized with solid $NaHCO_3$, the filtrate being evaporated. The residue was chromatographed on silica gel (150 g) with benzene-ethyl acetate (6 : 1) to give the free sugar (1.14 g). Unchanged **4a** recovered on chromatography was again subjected to hydrolysis and chromatography to afford an additional amount of the free sugar (260 mg). The total yield was 1.40 g (97%).

The free sugar (1.40 g, 5.30 mmol) was dissolved in 70% ethanol (28 ml), $NaBH_4$ (100 mg, 2.65 mmol) being added to the solution. The solution was stirred at room temperature for 2 h and then concentrated.The residue was taken in ethyl acetate (50 ml), and the mixture was washed with saturated aqueous NaCl solution, dried, and evaporated to afford a colorless syrup of **5a**(1.37 g, 94% overall yield based on **4a**). A portion of this product was chromatographed on silica gel with benzene-ethyl acetate (6 : 1) to give an analytical sample: $[\alpha]_D^{21}$ +1°, $[\alpha]_{365}^{21}$ −18° (*c* 0.4, $CHCl_3$); PMR ($CDCl_3$) δ 1.31 (d, 4-CH_3, J=6.4 Hz), 3.52 (dd, H-3, $J_{2,3}$= 3.4 and $J_{3,4}$=6.0 Hz), and 4.73 (s, CH_2Ph).

Found: C, 72.22; H, 9.77%. Calcd for $C_{16}H_{26}O_3$: C, 72.14; H, 9.84%.

*(2S,3R,4S)-2-Butyl-3-O-isovaleryl-1,3,4-pentanetriol (**5b**).* A solution of **4b** (1.55 g) in a mixture of dioxane (36 ml) and 2 M HCl (10.7 ml) was kept at 40 °C for 2 days. The reaction mixture was neutralized (pH 4) with solid $NaHCO_3$ and evaporated. The residue was extracted with ethyl acetate and the extract was evaporated. The residual syrup was chromatographed on silica gel (35 g) with benzene-ethyl acetate (15 : 1) to afford a colorless syrup of the free sugar (941 mg, 64%) and **4b** (395 mg, 25.5%). Free sugar: PMR ($CDCl_3$) δ 0.98[d, $CH(CH_3)_2$, J=6.8 Hz], 1.33 (d, 4-CH_3, J=6.3 Hz), 4.25 (dq, H-4, $J_{3,4}$=4.6 Hz), 4.65 (dd, H-3, $J_{2,3}$=3.2 Hz), and 5.22 (d, H-1, $J_{1,2}$=1.9 Hz). A solution of $NaBH_4$(124 mg, 2.17 mmol) in 70% ethanol (2.5 ml) was added under stirring to a solution of the free sugar (847 mg, 3.28 mmol) in 70% ethanol (17 ml) cooled at −10 °C. After being stirred at 0 °C for 1 h, the reaction mixture was neutralized with 2 M HCl and evaporated to dryness. The residue was extracted with ethyl acetate, the combined extracts being washed with saturated aqueous NaCl solution, dried, and evaporated to afford a crude syrup of **5b**(826 mg, 97%), which was used for subsequent synthesis. A portion of this sample (54.5 mg) was chromatographed on silica gel (5.5 g) with benzene-ethyl acetate (3 : 1) to give **5b**(R_f 0.12, 43.3 mg, 81%) and its positional isomer, 2-butyl-4-*O*-isovaleryl-1,3,4-pentanetriol (**5b'**) (R_f 0.26, 10 mg, 19%). **5b**: PMR($CDCl_3$) δ 0.98[d, $CH(CH_3)_2$, J=6.2 Hz], 1.21(d, 4-CH_3, J=6.3 Hz), 2.51(s, 2H, OH), *ca.* 3.6(m, 2H, H-1,1'), 4.00(dq, H-4, $J_{3,4}$=7.0 Hz), and 4.91(dd, H-3, $J_{2,3}$=3.8 Hz). Isomer of **5b**: PMR($CDCl_3$) δ 0.98[d, $CH(CH_3)_2$, J=6.5 Hz], 1.32(d, 4-CH_3, J=6.3 Hz), *ca.* 2.1 (m, 2H, OH), *ca.* 3.8(m, 3H, H-1,1',3), and 5.07(dq, H-4, $J_{3,4}$=5.9 Hz).

*(2S,3R,4S)-4-O-(N-Benzyloxycarbonyl-O-t-butyl-L-threonyl)-3-O-benzyl-2-butyl-1-O-trityl-1,3,4-pentanetriol (**7a**).* Triphenylmethyl chloride (1.68 g, 6.02 mmol) was added to a solution of **5a** (1.34 g, 5.03 mmol) in dry pyridine (6.7 ml) and the solution was allowed to stand at 40 °C overnight. Water (30 ml) was added to the reaction mixutre under cooling and the mixture was extracted with chloroform (20 ml×3). The combined extracts were washed with saturated aqueous NaCl solution, dried and evaporated to afford 1-*O*-tritylated product **6a** (2.56 g, 100%), which was used in the next reaction without purification. A solution of **6a** (2.56 g, 5.03 mmol) in dry ether (3.8 ml) and dry pyridine (0.43 ml) was added to a solution of DCCI (1.14 g, 5.54 mmol) in dry ether (3.1 ml) under ice-cooling. To this solution was added slowly a solution of *N*-benzyloxycarbonyl-*O*-*t*-butyl-L-threonine (1.71 g, 5.52 mmol) in dry ether (3.1 ml) under cooling and stirred at 5 °C for 3 days. A solution of DCCI (1.14 g) and pyridine (0.43 ml) in dry ether (3.8 ml) and a solution of the threonine derivative (1.71 g) in dry ether (3.1 ml) were then added successively and the mixture was kept at 5 °C for 3 days. After removal of *N,N'*-dicyclohexylurea (DCU) by filtration, the filtrate was washed with saturated aqueous $NaHCO_3$ solution and saturated aqueous NaCl solution, dried, and evaporated. The residue (9 g) was chromatographed on silica gel (450 g) with benzene-ethyl acetate (50 : 1) to give a pure sample of the condensation product **7a**: colorless syrup (2.96 g, 74%); $[\alpha]_D^{21}$ +3°, $[\alpha]_{365}^{21}$ +26° (*c* 0.39, $CHCl_3$); PMR($CDCl_3$) δ 1.07 (s, OBu^t), 1.20(d, 4-CH_3, J=6.3 Hz), 1.29[d, CH_3 of threonine, J=6.7 Hz], 3.16(d, H-1, $J_{1,2}$=5.2 Hz), 3.72 (dd, H-3, $J_{2,3}$=5.5, $J_{3,4}$=2.8 Hz), 4.56 (ABq, CH_2Ph), 5.06(ABq, CH_2Ph of benzyloxycarbonyl), 4.54(dq, H-4), and 5.60(d, NH, J=9.2 Hz).

Found: C, 76.76; H, 7.78; N, 2.02%. Calcd for $C_{51}H_{61}NO_7$: C, 76.56; H, 7.69; N, 1.75%.

*(2S,3R,4S)-2-Butyl-3-O-isovaleryl-1-O-trityl-1,3,4-pentanetriol (**6b**).* a) A solution of the crude **5b**(796 mg, 3.05 mmol) and triphenylmethyl chloride (1.70 g, 6.10 mmol) in dry pyridine (8 ml) was kept at room temperature for 3 days. The reaction mixture was poured into water and extracted with chloroform. The extracts were washed with saturated aqueous NaCl solution, dried, and evaporated to afford a yellow syrup (1.7 g), which was chromatographed on silica gel (150 g) with benzene-ethyl acetate (50 : 1) to afford a homogeneous sample of **6b** [R_f 0.70 (6 : 1 benzene-

ethyl acetate), 1.13 g, 74%]: PMR ($CDCl_3$) δ 0.95[d, $CH(CH_3)_2$, J=6.8 Hz], 1.21 (d, 4-CH_3, J=7.5 Hz), *ca.* 3.1 (m, 2H, H-1,1'), 5.07(dd, H-3, $J_{2,3}$=4.7, $J_{3,4}$=6.3 Hz), and *ca.* 7.3(m, 15H, CPh_3).

Found: C, 78.48; H, 8.30%. Calcd for $C_{33}H_{42}O_4$: C, 78.85; H, 8.42%.

b) A homogeneous sample of **5b** (11.6 mg, 0.0445 mmol) was treated with triphenylmethyl chloride (49.6 mg, 0.178 mmol) in dry pyridine (0.23 ml) at 40 °C for 2 days and the mixture was worked up in the same manner as described above and chromatographed with the same solvent system to afford **6b**(R_f 0.70, 9.7 mg, 43.3%) and its isomer, 4-*O*-isovalerate **6b'**(R_f 0.80, 12.3 mg, 55%): PMR($CDCl_3$) δ 0.92[d, $CH(CH_3)_2$, J=6.4 Hz], 1.24(d, 4-CH_3, J=6.1 Hz), *ca.* 2.8(m, 1H, OH), *ca.* 3.3(m, 2H, H-1,1'), *ca.* 3.8(m, 1H, H-3), 4.97(dq, H-4, $J_{3,4}$=5.2 Hz), and *ca.* 7.3(m, 15 H, CPh_3).

(2S,3R,4S)-4-O-(N-Benzyloxycarbonyl-O-t-butyl-L-threonyl)-2-butyl-3-O-isovaleryl-1-O-trityl-1,3,4-pentanetriol (7b). A solution of *N*-benzyloxycarbonyl-*O*-*t*-butyl-L-threonine (319 mg, 2.28 mmol) in dry ether (0.7 ml) was added dropwise under stirring to a cooled solution of DCCI (231 mg, 1.12 mmol), **6b** (471 mg, 0.937 mmol), and dry pyridine (0.075 ml, 2.07 mmol) in dry ether (0.62 ml). The mixture was stirred at 0 °C for 3 days, during which time the same amount of DCCI, pyridine, and the threonine derivative were added twice. The reaction mixture was worked up in the same manner as described in the preparation of **7a**. The crude product (5.11 g) was chromatographed on silica gel (80 g) with benzene-ethyl acetate (50 : 1) to afford **7b** (484 mg, 65%) as a syrup: PMR($CDCl_3$), δ 0.99 [d, $CH(CH_3)_2$, J=6.6 Hz], 1.09 (s, OBu^t), 1.19(d, CH_3 of threonine, J=6.5 Hz), 1.21 (d, 4-CH_3, J=7.6 Hz), 3.09 (m, 2H, H-1,1'), 4.1—4.2(m, 2H, H-2',3'), 5.15(ABq, CH_2Ph), 5.2—5.3(m, 3H, NH, H-3,4), and *ca.* 7.4(m, Ph).

Found: C, 74.69; H, 8.00; N, 1.78%. Calcd for $C_{30}H_{49}NO_8$: C, 74.12; H, 8.00; N, 1.76%.

(2S,3R,4S)-4-O-(N-Benzyloxycarbonyl-O-t-butyl-L-threonyl)-3-O-benzyl-2-butyl-1,3,4-pentanetriol (8a). A solution of **7a** (1.97 g, 2.47 mmol) in 90% aqueous acetic acid (40 ml) was kept at 40 °C for 15 hr and then evaporated to afford a pale yellow syrup (1.84 g). Chromatography of the syrup on silica gel (100 g) with benzene-ethyl acetate (15:1) gave a colorless syrup of **8a**(1.30 g, 95%): $[\alpha]_D^{21}$ +3°, $[\alpha]_{365}^{21}$ +18° (*c* 0.95, $CHCl_3$).

Found: C, 69.08; H, 8.43; N, 2.44%. Calcd for $C_{32}H_{47}NO_7$: C, 68.91; H, 8.49; N, 2.51%.

(2S,3R,4S)-4-O-(N-Benzyloxycarbonyl-O-t-butyl-L-threonyl)-2-butyl-3-O-isovaleryl-1,3,4-pentanetriol (8b). Treatment of **7b** (736 mg) with 90% aqueous acetic acid (16.6 ml) at room temperature for 1 day followed by evaporation afforded a yellow syrup (920 mg), which was chromatographed on silica gel (60 g) with benzene-ethyl acetate (6:1) to give a pure sample of **8b** as a colorless syrup (318 mg, 62.2%): $[\alpha]_D^{22}$ −10°(*c* 2.4, $CHCl_3$); IR_{max}($CHCl_3$, 0.1 M) 3500(OH), 3430(NH), and 1715 cm^{-1} (ester and amide); PMR($CDCl_3$) δ 1.00[d, $CH(CH_3)_2$, J=6.5 Hz], 1.16(s, OBu^t), *ca* 1.2 (m, 6H, 4-CH_3, 3'-CH_3), 3.6 (m, 3H, H-1,1', OH), *ca* 4.2 (m, 2H, H-2',3'), 5.16 (s, CH_2Ph), 5.2—5.7 (m, 3H, NH, H-3,4), and 7.39 (s, Ph).

Found: C, 65.23; H, 8.78; N, 2.41%. Calcd for $C_{30}H_{47}NO_8$: C, 65.31; H, 8.95; N, 2.54%.

(2R,3R,4S)-4-(N-Benzyloxycarbonyl-O-t-butyl-L-threonyloxy)-3-benzyloxy-2-butylpentanoic Acid (9a). A solution of **8a** (1.18 g, 2.11 mmol) in a chromium trioxide-acetic acid-pyridine reagent† (26.2 ml, 8.44 mmol) was kept at room temperature overnight. The reaction mixture was diluted with cold water (50 ml) and extracted with ether (20 ml×3). The combined extracts were washed with saturated aqueous NaCl solution, dried, and evaporated. The residual syrup (1.19 g) was chromatographed on silica gel (100 g) with hexane-benzene-acetone-acetic acid (40:20:1:2) to afford a pure sample of **9a**; colorless syrup (920 mg, 76%): $[\alpha]_D^{23}$ +3°, $[\alpha]_{365}^{23}$ +14° (*c* 2.4, $CHCl_3$), PMR($CDCl_3$) δ 1.09 (s, OBu^t), 1.19(d, 4-CH_3, J=6.5 Hz), 1.31(d, CH_3 of threonine, J=6.8 Hz), 3.78(dd, H-3, $J_{2,3}$=8.0, $J_{3,4}$=4.2 Hz), 4.66 (ABq, CH_2Ph), 5.10(dq, H-4), 5.11(ABq, CH_2Ph of benzyloxycarbonyl), and 5.62(d, NH, J=10.0 Hz).

Found: C, 67.27; H, 7.95; N, 2.32%. Calcd for $C_{32}H_{45}NO_8$: C, 67.23; H, 7.93; N, 2.45%.

(2R,3R,4S)-4-(N-Benzyloxycarbonyl-O-t-butyl-L-threonyloxy)-2-butyl-3-isovaleryloxypentanoic Acid (9b). A sample of **8b** (292 mg, 0.53 mmol) was oxidized with the chromium trioxide reagent (6.6 ml, 2.13 mmol) at room temperature for 1.5 h. Work-up of the product in the same way as in the preparation of **9a** afforded a brown syrup (299 mg), which was chromatographed on silica gel (30 g) with hexane-benzene-acetone-acetic acid (40:20:1:2) to give a pure sample of **9b**(287 mg, 96%) as a colorless syrup: $[\alpha]_D^{23}$ +5.1°(*c* 1.4, $CHCl_3$); PMR($CDCl_3$) δ 0.99[d, $CH(CH_3)_2$, J=6.5 Hz], 1.13(s, OBu^t), *ca.* 1.2(m, 6H, 4-CH_3, 3'-CH_3), *ca.* 4.2(m, 2H, H-2',3'), 5.19(s, CH_2Ph), 5.0—5.6(m, 3H, NH, H-3,4), 6.5(br, 1H, COOH), and 7.40(s, Ph).

Found: C, 63.59; H, 8.44; N, 2.61%. Calcd for $C_{30}H_{47}NO_9$: C, 63.69; H, 8.38; N, 2.48%.

Hydroxy Ester Acid (10a). A solution of **9a**(855 mg) in trifluoroacetic acid (10 ml) was allowed to stand at room temperature for 10 min and then evaporated below 10 °C to afford **10a** (770 mg, quantitative), which was used in the next reactions after being thoroughly dried at 0.01 Torr.

Hydroxy Ester Acid (10b). Treatment of **9b**(287 mg) with trifluoroacetic acid (3.5 ml) at room temperature for 10 min gave **10b** (248 mg, 96%) after evaporation: IR ($CHCl_3$) 3600—2800(COOH), and 1730 cm^{-1}(ester and amide); PMR($CDCl_3$) δ 1.03[d, $CH(CH_3)_2$, J=6.4 Hz], *ca.* 1.3(m, 6H, 4-CH_3, 3'-CH_3), 4.2—4.5(m, 2H, H-2',3'), 5.20 (s, CH_2Ph), 5.1—5.4(m, 2H, H-3,4), *ca.* 5.9(br, 1H, NH), 7.1—7.5(br, 1H, COOH), and 7.41(s, 5H, Ph).

(3S,4R,7R,8R,9S)-8-Benzyloxy-3-benzyloxycarbonylamino-7-butyl-4,9-dimethyl-1,5-dioxonane-2,6-dione (12a). A sample of **10a** (300 mg, 0.582 mmol) was dissolved in dry benzene (3 ml), triphenylphosphine (458 mg, 1.75 mmol) and di-2-pyridyl disulfide (385 mg, 1.75 mmol) then being added to the solution. After the mixture had been kept for 30 min at room temperature, the reaction mixture was evaporated and the residue (1.2 g) was chromatographed on silica gel (40 g) with benzene-acetone (10:1) to afford the 2-pyridinethiol ester **11a** (160 mg) as a yellow syrup. A solution of silver perchlorate†† (53.5 mg, 0.235 mmol) in dry benzene (0.5 ml) was added to a stirred solution of **11a** (143 mg, 0.235 mmol) in dry benzene (23.5 ml) and the mixture was stirred at room temperature for 1 h. The precipitates were filtered off and washed with benzene. The combined filtrate and washings were evaporated and the residue was chromatographed on silica gel (15 g) with benzene-ethyl acetate (50:1) to afford **12a** (38.6 mg, 33%) as colorless crystals and **10a** (94 mg, 66%). Analytical sample of **12a** was obtained by recrystallization from ethyl acetate as colorless needles: mp 118.5—119.5 °C; $[\alpha]_D^{23}$ +53°(*c* 0.73, $CHCl_3$); IR(CCl_4,

† The reagent consists of chromium trioxide (1 g), acetic acid (30 ml) and pyridine (1 ml).

†† The silver perchlorate used was thoroughly dried over P_2O_5 at 50—60 °C under reduced pressure (1 Torr) for 10 h.

0.1 M) 3432 and 1744 cm^{-1}; PMR($CDCl_3$) δ 1.28(d, 4-CH_3, J=6.8 Hz), 1.43(d, 9-CH_3, J=6.5 Hz), 2.46(m, H-7), 3.46(dd, H-8, $J_{7,8}$=9.5 Hz), 4.65(s, OCH_2Ph), 4.90(dq, H-9, $J_{8,9}$=9.5 Hz), 4.91(dd, H-3, $J_{3,NH}$=9.0 Hz), 5.12(s, $COOCH_2Ph$), and 5.54(dq, H-4, $J_{3,4}$=7.5 Hz); Found: *m/e* 497.244. Calcd for $C_{28}H_{35}NO_7$: M, 497.2413.

Found: C, 67.50; H, 7.04; N, 2.66%. Calcd for $C_{28}H_{35}NO_7$: C, 67.58; H, 7.09; N, 2.82%.

Lactonization of ***10a*** *by Corey-method. (Formation of 7-Epimer* ***12a'****).* Triphenylphosphine (130 mg, 0.494 mmol) and di-2-pyridyl disulfide (109 mg, 0.494 mmol) were added to a solution of **10a** (170 mg, 0.229 mmol) in dry xylene(0.85 ml), which was then stirred at room temperature for 5 h under argon atmosphere. The resulting solution was diluted with dry xylene (60 ml) and refluxed for 72 h under argon. The reaction mixture was evaporated and the residue (400 mg) was chromatographed on silica gel (20 g) with benzene–ethyl acetate (50:1) to afford a syrup of **12a'** (22.4 mg, 13.7%). This was chromatographed twice on silica gel with hexane–acetone (5:1) to give an analytical sample: $[\alpha]_D^{23}$ 0°(*c* 1.65, $CHCl_3$); IR(CCl_4, 0.1 M), 3435 and 1732 cm^{-1}; PMR($CDCl_3$) δ 1.29(d, 4-CH_3, J=6.8 Hz), 1.32 (d, 9-CH_3, J=6.2 Hz), 2.85(m, H-7), 3.72(dd, H-8, $J_{7,8}$= 4.0, $J_{8,9}$=9.2 Hz), 4.55(ABq, H-9), 5.11(s, $COOCH_2Ph$), and 5.15 (dq, H-4).

Found: *m/e* 497.2405. Calcd for $C_{28}H_{35}NO_7$: M, 497.2413.

Found: C, 67.68; H, 7.27; N, 2.58%. Calcd for $C_{28}H_{35}NO_7$: C, 67.58; H, 7.09; N, 2.82%.

*(3S,4R,7R,8R,9S)-3-Benzyloxycarbonylamino-7-butyl-4,9-dimethyl-8-isovaleryloxy-1,5-dioxonane-2,6-dione (****12b****).* Triphenylphosphine (224 mg, 0.930 mmol) and di-2-pyridyl disulfide (205 mg, 0.930 mmol) were added to a solution of **10b** (237 mg, 0.465 mmol) in dry benzene (2.4 ml). After being kept at room temperature for 1 h, the reaction mixture was evaporated and the residue (423 mg) was chromatographed on silica gel (15 g) with benzene–acetone (10:1) to afford a yellow syrup of **11b** (280 mg) containing a small amount of pyridone. The sample of **11b** (130 mg) was dissolved in dry benzene (21.5 ml), a solution of anhydrous silver perchlorate (67 mg) in dry toluene (0.35 ml) being added to the solution. The mixture was stirred at room temperature for 1 h and the insoluble matter was filtered off and washed with benzene. The combined filtrate and washings were evaporated and the residue (159 mg) was chromatographed on silica gel (15 g) with benzene–ethyl acetate (30:1) to afford a crystalline mass of **12b** (14.1 mg, 13.4%). Recrystallization from ether–petroleum ether gave colorless needles: mp 109—110 °C; $[\alpha]_D^{22}$ +55° (*c* 1.24, $CHCl_3$); IR (KBr) 1760, 1738, and 1693 cm^{-1}; $[\theta]_{228}^{18}$ −688 (in MeOH); PMR($CDCl_3$) δ 0.98[d, $CH(CH_3)_2$, J=6.5 Hz], 1.26(d, 9-CH_3, J=6.2 Hz), 1.28(d, 4-CH_3, J=7.0 Hz), 2.46(m, 1H, H-7), 4.94(dq, H-9, $J_{8,9}$=9.8 Hz), 4.96(dd, H-8, $J_{7,8}$=9.8 Hz), 5.05(dd, H-3, $J_{3,4}$=7.8, $J_{3,NH}$ =8.5 Hz), 5.12(s, CH_2Ph), 5.50(d, NH), 5.55(dq, H-4), and 7.34 (s, Ph).

Found: C, 63.74; H, 7.58; N, 2.76%. Calcd for $C_{26}H_{37}NO_8$: C, 63.52; H, 7.59; N, 2.85%.

*(3S,4R,7R,8R,9S)-3-Amino-7-butyl-4,9-dimethyl-8-hydroxy-1,5-dioxonane-2,6-dione (****14****) Hydrochloride.* A solution of **12a** (59.7 mg) in methanol (1 ml) was adjusted to pH 3 with a methanolic hydrogen chloride. The solution was shaken with freshly prepared palladium black in a Paar apparatus under a hydrogen atmosphere (50 p.s.i.) for 1 h. The filtered solution was evaporated to afford the crystalline hydrochloride of **14** (37.3 mg) quantitatively.

*(3S,4R,7R,8R,9S)-3-(2-Benzyloxy-3-nitrobenzoylamino)-4,9-dimethyl-7-butyl-8-hydroxy-1,5-dioxonane-2,6-dione (****15****).* A solution of **14** hydrochloride (37.3 mg, 0.120 mmol), 2-benzyloxy-3-nitrobenzoic acid *N*-hydroxysuccinimide ester (49.3 mg, 0.133 mmol) in dry THF (0.38 ml) was adjusted to pH 8 with triethylamine and kept at 40 °C for 2 days and then evaporated. The residue was chromatographed on silica gel (11 g) with benzene–acetone (6:1) to afford **15** (45.6 mg, 72%) as colorless crystals: mp 164.5—165.5 °C (ethyl acetate–petroleum ether); $[\alpha]_D^{20}$ +35° (*c* 0.71, $CHCl_3$).

Found: C, 61.42; H, 6.19; N, 5.15%. Calcd for $C_{27}H_{32}N_2O_9$: C, 61.35; H, 6.10; N, 5.30%.

*(3S,4R,7R,8R,9S)-3-(2-Benzyloxy-3-nitrobenzoylamino)-4,9-dimethyl-7-butyl-8-isovaleryloxy-1,5-dioxonane-2,6-dione (****16****).* A solution of **15** (9.0 mg, 0.017 mmol) and isovaleric anhydride (0.007 ml, 0.034 mmol) in dry pyridine (0.1 ml) was allowed to stand at room temperature for 5 h and then evaporated. The residue was chromatographed on silica gel with benzene–acetone (6:1) to give **16** (9.1 mg, 88%) as colorless crystals: mp 164.5—165.5 °C; $[\alpha]_D^{18}$ +55° (*c* 0.40, $CHCl_3$) δ 0.99 [d, $CH(CH_3)_2$, J=6.4 Hz], 1.29 (d, 9-CH_3, J=5.8 Hz), 1.11(d, 4-CH_3, J=6.8 Hz), 2.5(m, 1H, H-7), 4.86(dq, H-9, $J_{8,9}$=9.9 Hz), 5.06(dd, H-8, $J_{7,8}$=9.8 Hz), 5.19(dd, H-3, $J_{3,4}$=7.5 Hz), 5.16(s, CH_2Ph), 5.56(dq, H-4), 7.35 (dd, H-5'), 8.05 (d, 3-NH, $J_{3,NH}$=7.2 Hz), 7.96(dd, H-4' or H-6', $J_{4',5'}$ or $J_{5'6'}$=8.0 Hz), and 8.26 (dd, H-6' or H-4').

Found: C, 61.93; H, 6.74; N, 4.29%. Calcd for $C_{32}H_{40}N_2O_{10}$: C, 62.73; H, 6.58; N, 4.57%.

*(3S,4R,7R,8R,9S)-3-Acetylamino-7-butyl-4,9-dimethyl-8-hydroxy-1,5-dioxonane-2,6-dione (****18****).* A sample of **12a** (30 mg) was hydrogenolyzed with palladium black in methanol at room temperature for 15 min under a hydrogen atmosphere (50 p.s.i.) to afford a colorless syrup of **13a** (21.7 mg). Acetylation of **13a** (21.7 mg) with acetic anhydride (0.012 ml) in methanol (0.44 ml) at room temperature for 2 h gave the 3-*N*-acetyl derivative **17a** (22.1 mg, 91%) as colorless crystals: mp 156—157 °C (ethyl acetate–petroleum ether); $[\theta]_{722}^{20}$ −10660 (MeOH).

Found: C, 65.16; H, 7.68; N, 3.40%. Calcd for $C_{22}H_{31}NO_6$: C, 65.16; H, 7.71; N, 3.45%.

A sample of **17a** (9.9 mg) was hydrogenolyzed for 3 h by the same procedure as described above to afford **18** (7.7 mg) as a colorless solid. Recrystallization from ethyl acetate–petroleum ether gave colorless needles: mp 148 °C (decomp); $[\alpha]_D^{22}$ +68° (*c* 0.54, $CHCl_3$); $[\theta]_{217}^{20}$ −16000 (MeOH); IR (CCl_4, 0.1 M) 3540, 3430, 1735, and 1677 cm^{-1}; PMR ($CDCl_3$) δ 1.27(d, 4-CH_3, J=6.8 Hz), 1.43(d, 9-CH_3, J= 6.2 Hz), 2.07(s, *N*-Ac), 2.32(m, H-7), 3.56(dd, H-8, $J_{7,8}$= 9.5, $J_{8,9}$=9.5 Hz), 4.81(dq, H-9), 5.10(dd, H-3, $J_{3,4}$=7.8, $J_{3,NH}$=7.8 Hz), 5.55(dq, H-4); δ(CD_3OD) 1.26(d, 4-CH_3, J=6.5 Hz), 1.37(d, 9-CH_3, J=6.2 Hz), 2.02(s, OAc), 2.25(m, H-7), 3.35 (dd, H-8, $J_{7,8}$=9.7, $J_{8,9}$=10.0 Hz), 4.66(dq, H-9), 5.06(d, H-3, $J_{3,4}$=7.5 Hz), and 5.43(dq, H-4).

Found: C, 57.11; H, 7.91; N, 4.37%. Calcd for $C_{15}H_{25}NO_6$: C, 57.13; H, 7.99; N, 4.44%.

*(3R,4R,7R,8R,9S)-7-Butyl-4,9-dimethyl-3-dimethylamino-8-hydroxy-1,5-dioxonane-2,6-dione (****19****).* A sample of **12a** (42.5 mg) was hydrogenolyzed with palladium black in methanol at 40 °C for 1 h under a hydrogen atmosphere (50 p.s.i.). The product was purified by silica gel chromatography with hexane–acetone (5:1) to give a colorless syrup of **19** (26 mg): *m/e* 301(M^+); PMR($CDCl_3$) δ 1.41 (d, 4-CH_3, J=6.2 Hz), 1.41(d, 9-CH_3, J=6.0 Hz), 2.25[s, 6H, $N(CH_3)_2$], 3.45(dd, H-8, $J_{7,8}$=9.3, $J_{8,9}$=9.3 Hz), 3.45 (d, H-3, $J_{3,4}$=6.8 Hz), 4.66(dq, H-9), and 5.22(dq, H-4).

The authors wish to thank Dr. Hiroshi Naganawa, Institute of Microbial Chemistry, for the measurements of PMR spectra, Mr. Saburo Nakada for carrying

out the microanalyses, and Mr. Hiromitsu Matsuzaki for his technical assistance. Financial support by the Asahi Glass Foundation for Contribution to Industrial Technology is acknowledged.

References

1) M. Kinoshita, M. Wada, S. Aburaki, and S. Umezawa, *J. Antibiot. (Tokyo)*, **24**, 724 (1971).
2) M. Kinoshita, S. Aburaki, M. Wada, and S. Umezawa, *Bull. Chem. Soc. Jpn.*, **46**, 1279 (1973).
3) S. Aburaki and M. Kinoshita, *Chem. Lett.*, **1976**, 701.
4) a) K. C. Nicolaou, *Tetrahedron*, **33**, 683 (1977); b) S. Masamune, G. S. Bates, and J. W. Corcoran, *Angew. Chem. Int. Ed. Engl.*, **16**, 585 (1977).
5) S. Aburaki, N. Konishi, and M. Kinoshita, *Bull. Chem. Soc. Jpn.*, **48**, 1254 (1975).
6) H. Gerlach and A. Thalmann, *Helv. Chim. Acta*, **57**, 2661 (1974).
7) J. C. Sheehan, H. G. Zachan, and W. B. Lawson, *J. Am. Chem. Soc.*, **80**, 3349 (1958).
8) T. Mukaiyama, M. Araki, and H. Takei, *J. Am. Chem. Soc.*, **95**, 4763 (1973).
9) E. J. Corey and K. C. Nicolaou, *J. Am. Chem. Soc.*, **96**, 5614 (1974).
10) M. Kinoshita and S. Umezawa, *Bull. Chem. Soc. Jpn.*, **42**, 854 (1969); **43**, 897 (1970).

Methylation of Pyrimidine 2′-Deoxynucleosides with Trimethyl Phosphate

Toshizumi TANABE,* Kiyoshi YAMAUCHI, and Masayoshi KINOSHITA
Department of Applied Chemistry, Osaka City University, Sumiyoshi-ku, Osaka 558
(Received July 10, 1978)

The reactions of thymidine, deoxyuridine, and deoxycytidine with trimethyl phosphate (TMP) were studied in a homogeneous water solution at 37—60 °C and pH 7—10. Three pyrimidine deoxynucleosides were methylated mainly at the N-3 position to afford their 3-methyl derivatives. The methylation rate at the N-3 position was found to be dependent on the pH of reaction medium. At pH 10, thymidine and deoxyuridine were methylated much faster than deoxycytidine, the tendency being reversed at pH 7.

Most chemical carcinogens such as polycyclic aromatics, aromatic amines, and azo compounds have recently been found to be activated *in vivo* by oxidizing enzymes to alkylate nucleic acids, causing mutagenic or carcinogenic effects.[1] Since intrinsic alkylating agents such as dialkyl sulfates, alkyl alkanesulfonates, and diazo alkanes also have mutagenicity or carcinogenicity, many studies have been carried out on their actions on nucleic acids and their components.[2-7]

We reported the alkylation of five main nucleic acid-bases with trialkyl phosphates such as trimethyl,[8] triethyl,[9] and triallyl phosphates[10] (TMP, TEP, and TAP). From the results, TMP and TEP appear to be suitable for the alkylation of nucleic acids and their components because of their high solubility in water and moderate reactivity which enables the alkylating reactions to take place homogeneously in an aqueous phase. Methylation study with TMP seems to be worthy of further studies, since many methylated nucleosides are present in nucleic acids from various sources.

We have studied the methylation of pyrimidine deoxynucleosides such as thymidine (**1**), deoxyuridine (**2**), and deoxycytidine (**3**) with TMP in homogeneous aqueous phase of pH 7—12 at 37 and 60 °C.

The characterization of the products from these reactions is given in the following. The effect of pH of reaction mixtures on methylation rate is also discussed.

Results and Discussion

The reactions were carried out at 37 and 60 °C by stirring a mixture of a deoxynucleoside and TMP in water at an appropriate pH. The products were isolated by extraction and column chromatography and identified by means of UV and NMR spectra. Melting point and R_f value were also employed for the identification of products. The yields of the products were determined by means of UV spectra. The results are summarized in Tables 1 and 2.

*Thymidine (**1**) and Deoxyuridine (**2**).* Most methylation studies on thymidine (**1**) so far reported were conducted using diazomethane in water–ether[3] or methanol–ether[2,5] solution. The results indicate that diazomethane methylated **1** at the N-3 position chiefly to afford 3-methylthymidine (**4**) with co-formation of a small amount of O^4-methylthymidine. Treatment of DNA with *N*-methyl-*N*-nitrosourea, a possible source of diazomethane *in vivo*, has been reported to afford 3-

Table 1. Methylation of thymidine (**1**) and deoxyuridine (**2**)[a]

Deoxynucleosides (dNu)	Temp (°C)	pH	Mole ratio (TMP/dNu)	Product	Yield (%)[b] 6 h	12 h	24 h	48 h
Thymidine(**1**)	37	7	15	3-Methylthymidine(**4**)	0	0	0	trace
1	37	8	15	**4**	13	17	22	26
1	37	9	15	**4**	24	34	50	61
1	37	10	15	**4**	35 (30)[c]	42 (43)	76 (63)	81 (81)
1	37	10	7.5	**4**	—	37	55	78
1	37	10	30	**4**	—	71	89	97
1	37	10	60	**4**	—	84	90	100
1	37	11	15	**4**	46	65	83	93
1	37	12	15	**4**	42	63	80	87
				3,O^5′-Dimethylthymidine	trace	trace	3	5
1	60	7	15	**4**	—	14	15	22
1	60	10	15	**4**	83	96	—	—
Deoxyuridine(**2**)	37	8	15	3-Methyldeoxyuridine(**5**)	—	11	16	23
2	37	9	15	**5**	16	28	47	71
2	37	10	15	**5**	37 (34)[c]	55 (53)	73 (72)	88 (88)
2	37	11	15	**5**	67	77	86	95

a) Reaction size: a deoxynucleoside (0.25 mmol) + TMP (1.9 mmol, 3.8 mmol, 7.5 mmol, or 14.3 mmol) + H_2O (5.0 ml) at 37 or 60 °C. b) Spectroscopic yield. c) The yields in parentheses are those of the reactions of **1** and **2** with TMP in the same vessels.

Table 2. Methylation of deoxycytidine (3)[a]

Temp (°C)	pH	Mole ratio (TMP/3)	Product	Yield (%)[b] 24 h	48 h	72 h
37	7	15	3-Methyldeoxycytidine(**6**)	4	9	13
37	7	30	**6**	12	15	25
37	7	60	**6**	17	23	30
37	10	15	**6**	4	6	7
			3-Methyldeoxyuridine(**5**)	0	trace	4
37	10	30	**6**	6	9	13
			5	0	1	4
37	10	60	**6**	13	18	21
			5	3	2	4
37	12	30	**5**	0	trace	1
			$O^{x'}$-Methyldeoxycytidine	1	4	5
60	7	15	**6**	37	59	68
60	10	15	**5**	33	53	63
			3,$O^{x'}$-Dimethyldeoxyuridine	0	4	5

a) Reaction size: deoxycytidine (0.25 mmol) + TMP (3.8 mmol, 7.5 mmol, or 14.3 mmol) + H_2O (5.0 ml) at 37 or 60 °C. b) Spectroscopic yield.

methyl- and O^4-methylthymidines in addition to several methylated purine nucleosides.[11] On the other hand, little is known about the alkylation of deoxyuridine (**2**) which is present merely as the precursor of **1** in living systems.

The present reactions of **1** with TMP in an aqueous phase gave the results as shown in Table 1. Methylation occurs at the N-3 position of **1** to afford 3-methylthymidine (**4**) as the sole product at pH 7—11. However, when the pH is raised to 12, thin-layer chromatography of the reaction mixture shows two spots. One product (low R_f) was isolated and identified as **4**, the other product being assigned as 3,$O^{5'}$-dimethylthymidine by comparison of its UV spectrum and R_f value with those of an authentic sample.

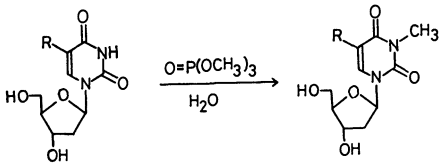

1: R = CH_3
2: R = H

4: R = CH_3
5: R = H

The methylation rate of **1**, particularly the formation of **4**, was found to be dependent on the pH of reaction medium. In the pH region 7—11 at 37 °C, the higher the pH, the faster the methylation rate. For instance, **4** was produced quantitatively in the reaction at pH 11, while the reaction hardly proceeded at pH 7. However, when the pH of reaction mixture was raised from 11 to 12, no noticeable increase in methylation rate was observed at the N-3 position of **1**. The results suggest that methylation of **1** occurs most likely in a bimolecular fashion between the anionic form of **1** and TMP, since the dissociation of the N-3 proton of **1** (pK_a:9.8)[12] gradually increases in the pH range 7—11. At pH 11, the N-3 proton dissociates nearly completely, the methylation rate at the N-3 position under present conditions becoming maximum. The pH change from 11 to 12 might not affect the methylation rate at the N-3 position of **1**.

The formation of a small amount of 3,$O^{5'}$-dimethylthymidine in the reaction at pH 12 may also be attributed to the dissociation of 5'-OH group ($pK_a > 13$) to the oxido anion and its subsequent reaction with TMP.

The rise in reaction temperature and increase in the mole ratio of TMP to **1** also accelerated the methylation rate (Table 1).

Methylation of deoxyuridine (**2**) with TMP gave almost the same result as that of methylation of **1**, **2** being methylated at the N-3 position to give 3-methyldeoxyuridine (**5**), whose yields increased gradually with the rise of pH of the reaction mixture. However, the reaction of TMP with a mixture of **1** and **2** at pH 10 showed that **2** is methylated at the N-3 position faster than **1**, probably because the pK_a value of the former is smaller, *e.g.* 9.2 and 9.8, respectively.[12]

*Deoxycytidine (**3**).* Several reports have appeared on the alkylation of cytidine and deoxycytidine (**3**).[3-7] Treatment of cytidine with diazomethane in water–ether[3] and dimethyl sulfate in DMF[4] caused methylation at the N-3 position of cytosine ring. However, **3** remains unchanged in the reaction with diazomethane in methanol–ether solution.[5] Sun and Singer studied methylation and ethylation of cytidine and **3** in detail using alkyl iodide, ethyl methanesulfonate, and diethyl sulfate, and observed the formation of 3-alkyl derivatives along with a small extent of alkylation at exocyclic 4-amino group of cytosine ring.[6]

In the present reactions, methylation took place smoothly at the N-3 position to afford 3-methyldeoxycytidine (**6**) at pH 7, while the reaction at pH 10 gave a mixture of **6** and 3-methyldeoxyuridine (**5**) (Table 2).

The production of **5** under alkaline conditions can be attributed to alkaline hydrolysis of **6**, since the analogous compound, 1,3-dimethylcytosine was trans-

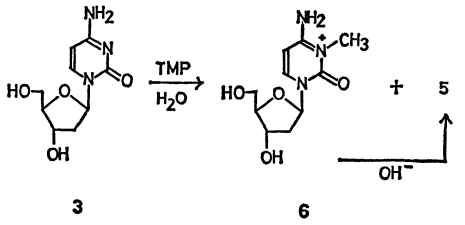

formed into 1,3-dimethyluracil and the conversion of **3** into **2** was not observed under similar conditions. Since the deprotonation of the pyrimidine ring of **3**, established to exist in the amino form,[13] does not take place under the present conditions, the formation of **6** would occur most likely by the attack of TMP on the neutral N-3 position of the amino form of **3**.

The methylation rate at the N-3 position showed a slight dependence on the pH of reaction medium, which is, however, opposite to that observed in the methylation of **1**. That is, the methylation rate decreased with the increase of pH. Especially, at pH 12, methylation hardly occurred at the N-3 position of **3**, while deoxyribose moiety was methylated in a small amount. A similar trend of **3** or cytidine to resist methylation at the N-3 position under alkaline conditions has recently been reported by Kuśmierek *et al.*[7]

The above reactions thus reveal that **1** and **2** more easily undergo methylation than **3** under alkaline conditions, whereas **3** is methylated smoothly under neutral conditions. This remarkable dependence of the reactivity of **1**, **2**, and **3** on the pH of reaction mixture is useful in view of synthesis, allowing selective methylation of these deoxynucleosides (**1**, **2**, and **3**) by tretament with TMP at a suitable pH. Smooth methylation of **3** at the N-3 position at pH 7 is noteworthy from a biological point of view, since alkylation at the N-3 position of cytosine residues in nucleic acids is believed to be one of the most harmful reactions to result in mutagenicity or carcinogenicity on mice,[14] phage T4V[15] *etc.* Apparently, a Watson-Crick type of base pairing between cytosine bases and guanine bases is no longer possible by methylation of the former at the N-3 position.

Experimental

Melting points are uncorrected. UV spectra were measured with a Hitachi 3T spectrometer. NMR spectra were recorded on a Hitachi Perkin-Elmer R-20 with a dilute solution in deuterioxide and tetramethylsilane as an outside standard or 3-(trimethylsilyl)propionic acid-d_4 sodium salt as an internal standard. Thin-layer chromatography was performed on silica gel [GF_{254} (type 60), Merck] or aluminum oxide [PF_{254} (type 150), Merck] using a mixture of chloroform and methanol. Column chromatography was carried out using silica gel (Merck, Art. 7734, 70—230 mesh) or aluminum oxide (Merck, Art. 1097).

Commercial thymidine (**1**), deoxyuridine (**2**), and deoxycytidine (**3**) as well as TMP were used without further purification.

Spectroscopic Determination of Yields. A mixture of deoxynucleoside (0.25 mmol) and TMP (1.9 mmol, 3.8 mmol, 7.5 mmol, or 14.3 mmol) in water (5.0 ml) was stirred at 37 or 60 °C at an appropriate pH maintained throughout the reaction by occasional addition of 2 M sodium hydroxide, with an error of about ±pH 0.3. At an appropriate reaction time, 4 μl of reaction mixture was spotted on a thin-layer chromatography plate, which was developed immediately with chloroform–methanol (5 : 1 for the reaction of **1** and **2**, and 5 : 2 for that of **3**).

The reaction mixture of **1** with TMP at pH 7—11 showed two spots (**1** and **4**) on TLC (R_f; **1** : 0.07, **4** : 0.23), and a new spot (R_f; 0.38) at pH 12. This was found to be 3,$O^{5'}$-dimethylthymidine by comparison of UV spectrum and R_f value of authentic sample; UV λ_{max} (H_2O) nm : pH 1, 266.0, pH 7, 267.0, pH 13, 267.0. In the reaction of **2** with TMP at pH 7—11, two spots corresponding to **2** and **5** were observed (R_f; **2** : 0.25, **5** : 0.46). Thin-layer chromatography of the reaction mixture of **3** with TMP at 37 °C showed two spots (**3** and **6**) at pH 7 and three spots (**3**, **6**, and **5**) at pH 10 (R_f; **3** : 0.22, **6** : 0.10, **5** : 0.79).

After each spot on TLC was scraped separately from the plate, the substance on the spot was extracted with 3 ml of water. From the absorbance of the solution, the yield of each product was calculated by means of a procedure similar to that described in a previous paper.[8]

Isolation of Products. *3-Methylthymidine (**4**)*: A mixture of **1** (1.20 g, 5.0 mmol) and TMP (10.5 g, 75.0 mmol) in water (15 ml) was stirred at 60 °C and pH 10. After 12 h, the spot of **1** disappeared on thin-layer chromatography of the reaction mixture. The reaction mixture was then neutralized with concentrated hydrochloric acid. After water had been removed from the reaction mixture, the residue was purified by silica gel column chromatography (2.5×35 cm). Elution with chloroform afforded unchanged TMP, **4** being obtained by subsequent elution with chloroform–methanol (7 : 1). Evaporation of the solvent afforded **4** as viscous liquid which crystallized on the addition of diethyl ether (1.13 g, 89.0%); mp 132—133.5 °C (from water) (when recrystallized compound was dried imperfectly, it melted at 84—86 °C) (lit,[16] 132.5—134.0 °C), NMR (D_2O) δ= 1.88 (3H, d, J=1.2 Hz, 5-C**H**$_3$), 2.33 (2H, complex m, 2′-C**H**$_2$), 3.28 (3H, s, N^3-C**H**$_3$), 3.81 (2H, complex m, 5′-C**H**$_2$), 4.03 (1H, complex m, 4′-C**H**), 4.45 (1H, complex m, 3′-C**H**), 6.31 (1H, t, J=7 Hz, 1′-C**H**), and 7.69 (1H, d, J=1.2 Hz, **H**^{6}); UV λ_{max} (H_2O) nm : pH 1, 265.5, pH 7, 266.0, pH 13, 266.0 (lit,[5] pH 1, 265.0, pH 7, 266.0, pH 13, 267.0).

*3-Methyldeoxyuridine (**5**)*: Compound **3** hydrochloride (0.52 g, 2.0 mmol) and TMP (4.2 g, 30.0 mmol) were stirred in water (20 ml, pH 10, NaOH) at 60 °C for 48 h. The reaction mixture was then neutralized with concentrated hydrochloric acid and extracted with chloroform to remove unchanged TMP. The water layer was concentrated to give a residue, which was then purified by silica gel column chromatography (2×33 cm). Elution with chloroform–methanol (7 : 1) provided **5** (120 mg, 25%); mp 109—110 °C (from ethyl acetate–hexane) (lit,[17] 98—100 °C), NMR (D_2O) δ=2.41 (2H, complex m, 2′-C**H**$_2$), 3.32 (3H, s, -C**H**$_3$), 3.85 (2H, complex m, 5′-C**H**$_2$), 4.10 (1H, complex m, 4′-C**H**), 4.45 (1H, complex m, 3′-C**H**), 6.03 (1H, d, J=8Hz, **H**^{5}), 6.39 (1H, t, J=7 Hz, 1′-C**H**), and 7.97 (1H, d, J=8 Hz, **H**^{6}); UV λ_{max} (H_2O) nm : pH 1, 262.5 (log ε 4.12), pH 7, 262.5 (log ε 4.12), pH 13, 263.0 (log ε 4.13).

*3-Methyldeoxycytidine (**6**)*: A mixture of deoxycytidine hydrochloride (1.30 g, 5.0 mmol) and TMP (18.8 g, 134 mmol) in water (50 ml, pH 7) was stirred for 100 h. Alumina thin-layer chromatography of the reaction mixture developed with methanol showed a faint spot of **3** (R_f : 0.12) and a distinct spot of **6** (R_f : 0.72). The reaction mixture was extracted with chloroform in order to remove unchanged

TMP. The water layer was concentrated to give a residue, which was then purified by alumina column chromatography (2.5×40 cm). Elution with methanol afforded the salt of 3-methyldeoxycytidine with dimethyl hydrogen phosphate. Since the phosphate salt was hygroscopic, it was converted into the hydrochloride salt according to the procedure of Furukawa *et al.*[18] (0.78 g, 57%); mp 250 °C (dec); NMR (D_2O) δ=2.55 (2H, complex m, 2′-C**H**$_2$), 3.67 (3H, s, -C**H**$_3$), 3.95 (2H, complex m, 5′-C**H**$_2$), 4.22 (1H, complex m, 4′-C**H**), 4.60 (1H, complex m, 3′-C**H**), 6.30 (1H, d, J=8Hz, **H**^{5}), 6.49 (1H, t, J=7 Hz, 1′-C**H**), and 8.26 (1H, d, J=8 Hz, **H**^{6}); UV λ_{max} (H_2O) nm: pH 1, 279.0, pH 7, 279.0, pH 13, 269.0. The free form of **6** was obtained by subsequent treatment of the hydrochloride salt with anionic exchange resin (Dowex 1×2, 100—200 mesh, OH form); mp 169—171 °C; Found: C, 49.94; H, 6.24; N, 17.29%. Calcd for $C_{10}H_{15}N_3O_4$: C, 49.78; H, 6.27; N, 17.42%.

References

1) L. N. Ferguson, *Chem. Soc. Rev.*, **4**, 289 (1975).
2) P. B. Farmer, A. B. Foster, M. Jarman, and M. J. Tisdale, *Biochem. J.*, **135**, 203 (1973).
3) J. A. Haines, C. B. Reese, and L. Todd, *J. Chem. Soc.*, **1964**, 1406.
4) P. Brookes and P. D. Lawley, *J. Chem. Soc.*, **1962**, 1348.
5) O. M. Friedman, G. N. Mahapatra, B. Dash, and R. Stevenson, *Biochim. Biophys. Acta*, **103**, 286 (1965).
6) L. Sun and B. Singer, *Biochemistry*, **13**, 1905 (1974).
7) J. T. Kuśmierek, J. Giziewicz, and D. Shugar, *Biochemistry*, **12**, 194 (1973).
8) K. Yamauchi, T. Tanabe, and M. Kinoshita, *J. Org. Chem.*, **41**, 3691 (1976).
9) T. Tanabe, K. Yamauchi, and M. Kinoshita, *Bull. Chem. Soc. Jpn.*, **49**, 3224 (1976).
10) T. Tanabe, K. Yamauchi, and M. Kinoshita, *Bull. Chem. Soc. Jpn.*, in press.
11) P. D. Lawley, D. J. Orr, S. A. Shah, P. B. Farmer, and M. Jarman, *Biochem. J.*, **135**, 193 (1973).
12) "Handbook of Biochemistry and Molecular Biology," ed by G. D. Fasman, CRC Press, Cleaveland (1975), Vol. 1.
13) H. T. Miles, *J. Am. Chem. Soc.*, **85**, 1007 (1963).
14) G. Kolmark, *C. R. Trav. Lab. Carlsberg, Ser. Physiol.*, **26**, 205 (1956).
15) S. D. Kononova and L. L. Gumanov, *Dokl. Akad. Nauk SSSR*, **198**, 1442 (1971).
16) H. T. Miles, *J. Am. Chem. Soc.*, **79**, 2565 (1957).
17) K. Kikugawa, M. Ichino, and T. Ukita, *Chem. Pharm. Bull.*, **17**, 785 (1969).
18) Y. Furukawa, K. Kobayashi, Y. Kanai, and M. Honjo, *Chem. Pharm. Bull.* **13**, 1273 (1965).

A New Synthetic Method for Some Pyrazolo[4,3-*d*]pyrimidines[1]

Hisashi TAKEI,* Nobuyoshi YASUDA, and Hidetsugu TAKAGAKI

Departmentt of Life Chemistry, Tokyo Institute of Technology, Nagatsutacho, Midori-ku, Yokohama 227

(Received July 20, 1978)

3,7-Dihydroxy- and 3-substituted 7-hydroxypyrazolo[4,3-*d*]pyrimidines were synthesized from diethyl oxaloacetate and ethyl acylpyruvates *via* ethyl 4-amino-5-oxo-2-pyrazoline-3-carboxylate hydrochloride and ethyl 5-substituted 4-amino-3-pyrazolecarboxylates, respectively.

Purine antagonists have been shown to be chemotherapeutic agents against various tumors.[2] Some of pyrazolo[4,3-*d*]pyrimidine derivatives, which are purine analogue, have been also found to have this antagonism.[3] It thus seemed desirable to investigate the synthesis of the pyrazolo[4,3-*d*]pyrimidine ring system.

Recently, some carbon linked nucleoside antibiotics have been found in nature. Among these, formycin and formycin B[4] were characterized as 7-amino- and 7-hydroxy-3-β-D-ribofuranosylpyrazolo[4,3-*d*]pyrimidine, respectively. The structural characterization of the antibiotics has also regenerated a great interest in the synthesis of the pyrazolo[4,3-*d*]pyrimidine ring system.

The first reported sytnthesis of the ring system was that of Behrend,[5] who utilized 5-amino-6-methyluracil for the preparation of 5,7-dihydroxypyrazolo-[4,3-*d*]pyrimidine. Rose[6] has accomplished the synthesis of the ring system by diazotization of 4-alkyl-5-amino-6-methylpyrimidine followed by an intramolecular coupling. This method is quite satisfactory but definitely restricted to the substituent at position 7 of pyrazolo[4,3-*d*]pyrimidine, since 5-amino-6-methylpyrimidine substituted at position 4 with a hydroxyl, mercapto, or amino group upon diazotization couples to give the oxadiazole, thiadiazole, or triazole ring. Robins and his coworkers[7] synthesized the ring system from 4-nitro-3-pyrazolecarboxylic acid, and Townsend and his coworkers[8] have also synthesized 5,7-disubstituted 3-methylpyrazolo[4,3-*d*]pyrimidines from ethyl 5-methyl-4-nitro-3-pyrazolecarboxylate. But these nitropyrazole methods do not seem to be applicable for the synthesis of sugar derivatives, because nitration was performed in fuming sulfuric acid. The investigation of the synthesis of oxoformycin has appeared in the literature.[9] Formycin B was totally synthesized by Acton and his coworkers[10] in 1971 from 2,3,5-tri-*O*-benzyl-β-D-ribofuranosyldiazomethane as a key intermediate. Arabinosyl analogue was also synthesized by a similar method.[11]

In this paper, we describe a convenient synthesis of 3,7-dihydroxy- and 3-substituted 7-hydroxypyrazolo-[4,3-*d*]pyrimidines starting from diethyl oxaloacetate and ethyl acylpyruvates, respectively, under mild conditions in high yields.

Treatment of diethyl oxaloacetate (**1**) with hydrazine hydrate (1 equiv) in ethanol at room temperature gave ethyl 5-oxo-2-pyrazoline-3-carboxylate (**2**) in 88% yield. Introduction of N_2O_3 gas into an ethanol solution of **2** resulted in the formation of ethyl 4-nitroso-5-oxo-2-pyrazoline-3-carboxylate (**3**) in 95% yield. Catalytic hydrogenation of this nitroso compound **3** over 20% Pd–C in ethanol in the presence of hydrochloric acid at room temperature afforded ethyl 4-amino-5-oxo-2-pyrazoline-3-carboxylate hydrochloride (**4**) in 88% yield. When **3** was hydrogenated in acetic acid in the presence of acetic anhydride at room temperature, ethyl 4-acetamido-5-oxo-2-pyrazoline-3-carboxylate (**5**) was obtained in 75% yield. Treatment of the hydrochloride **4** with formamidine acetate (3 equiv) and triethylamine (5 equiv) in boiling 2-ethoxyethanol gave 3,7-dihydroxypyrazolo[4,3-*d*]pyrimidine (**6**) in 92% yield. The structure was confirmed by spectral data and elemental analysis.

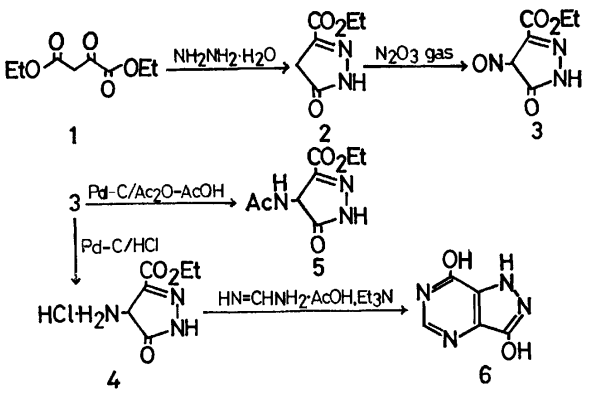

Scheme 1.

Ethyl 5-methyl-3-pyrazolecarboxylate (**8a**)[12] could not be nitrosated at position 4 of the pyrazole ring by the introduction of N_2O_3 gas. Therefore it was decided to introduce the nitroso group prior to the ring closure. Ethyl acetopyruvate (**7a**) was nitrosated to the corresponding hydroxyimino derivative (**9a**) with N_2O_3 gas in ethanol at room temperature. The reaction of this hydroxyimino derivative **9a** with hydrazine dihydrochloride (1 equiv) in water at 0 °C gave blue crystalline ethyl 5-methyl-4-nitroso-3-pyrazolecarboxylate (**10a**). By treatment with excess sodium dithionite in ethyl acetate and water at room temperature, this nitroso compound **10a** was readily reduced to ethyl 4-amino-5-methyl-3-pyrazolecarboxylate (**11a**) in 47% yield, based on ethyl acetopyruvate **7a**. Acetylation of this amino compound **11a** with acetic anhydride in pyridine gave ethyl 4-acetamido-1-acetyl-5-methyl-3-pyrazolecarboxylate (**13a**) in a quantitative yield. On the other hand, when acetylation was carried out in acetic acid, ethyl 4-acetamido-5-methyl-3-pyrazolecarboxylate (**12a**) was obtained in a quantitative yield. The reaction of the amino compound **11a** with formamidine acetate (3 equiv) in boiling 2-

ethoxyethanol afforded a quantitative yield of 7-hydroxy-3-methylpyrazolo[4,3-*d*]pyrimidine (**14a**).

Similarly, 7-hydroxy-3-phenylpyrazolo[4,3-*d*]pyrimidine (**14b**) was obtained as follows. Ethyl benzopyruvate (**7b**) was nitrosated to its hydroxyimino derivative (**9b**). This hydroxyimino derivative **9b** was converted to greenish blue crystalline ethyl 4-nitroso-5-phenyl-3-pyrazolecarboxylate (**10b**) by the reaction with hydrazine dihydrochloride (1 equiv). Reduction of the nitroso compound **10b** by excess sodium dithionite gave ethyl 4-amino-5-phenyl-3-pyrazolecarboxylate (**11b**) in 46% yield, based on ethyl benzopyruvate **7b**. Acetylation of **11b** with acetic anhydride in pyridine gave a complex result. When acetylation was carried out in acetic acid, however, ethyl 4-acetamido-5-phenyl-3-pyrazolecarboxylate (**12b**) was obtained in a quantitative yield. The reaction of the amino compound **11b** with formamidine acetate (3 equiv) in boiling 2-ethoxyethanol gave 7-hydroxy-3-phenylpyrazolo[4,3-*d*]pyrimidine (**14b**) in a quantitative yield. The structure was confirmed by spectral data and elemental analysis.

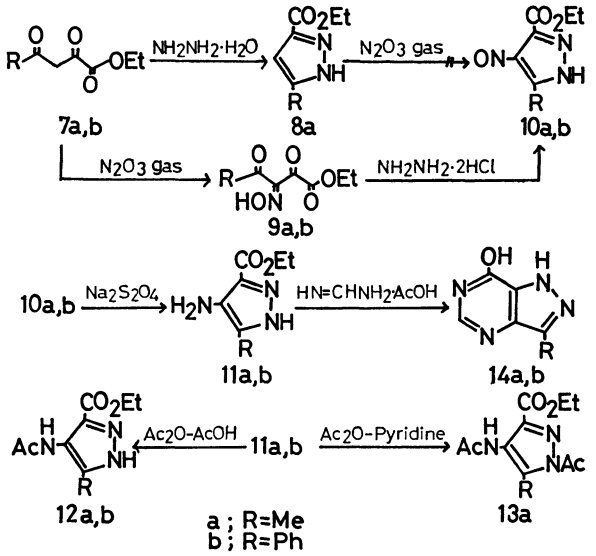

Scheme 2.

Table 1. UV absorption data for certain substituted pyrazoles and pyrazolo[4,3-*d*]pyrimidines

Compound	pH 1(HCl)		95% EtOH		pH 11(NaOH)	
	λ_{max}(nm)	ε_{max}	λ_{max}(nm)	ε_{max}	λ_{max}(nm)	ε_{max}
2	211	8910	223	10080	225	11580
	256	4020	260	2920	295	2460
3	261	9460	261	8590	300	10400
	357	3660	357	4130	369	5190
4	281	8100	281	7920	253	7600
					288[a]	5460
5	245	6450	245	6580	234	5710
	288	4480	290	4550	302	2950
6	230	10830	231[b]	10530[b]	238	10360
	271	3910	288[b]	4680[b]	285[a]	3800
	288	4600	332[b]	6200[b]	315	5120
	332	4080			332	7040
10a	273[a]	6130	212	8370	329	14740
	303	10020	275[a]	6420	333	15950
			303	10110		
10b	237	12450	237	12490	229	13860
	332	4060	332	4340	341	8010
11a	218	6540	208	5720	236	6380
			296	4900		
11b	223	18980	228	20680	255	22690
			309	9430	288[a]	10340
12a	217	8140	217	7900	230	9200
	259[a]	4620	254[a]	4240	253	13000
12b	225	21790	225	21630	247	24380
13a	221	8040	221	8740	257	8290
	265	3720	265	3830		
14a	281	6470	226	6450	226	9000
					281	8560
					288	8690
					300[a]	5600
14b	232	11590	214[a]	10760	248	13380
			231	12040		

a) Shoulder. b) These values were measured in water.

TABLE 2. ELEMENTAL ANALYSES OF CERTAIN SUBSTITUTED PYRAZOLES AND PYRAZOLO[4,3-*d*]PYRIMIDINES

	Compound	Found (%)			Calcd (%)		
		C	H	N	C	H	N
2	$C_6H_8O_3N_2$	46.36	5.18	18.08	46.15	5.16	17.94
3	$C_6H_7O_4N_2$	39.14	3.85	22.96	38.92	3.81	22.70
4	$C_6H_{10}O_3N_3Cl$[a)]	35.17	5.14	21.01	34.71	4.85	20.24
5	$C_8H_{11}O_4N_3$	44.93	5.21	19.60	45.07	5.20	19.71
6	$C_5H_4O_2N_4$	39.61	2.64	37.04	39.48	2.65	36.84
10a	$C_7H_9O_3N_3$	45.84	4.76	23.22	45.90	4.95	22.94
10b	$C_{12}H_{11}O_3N_3$[a)]	59.90	4.67	17.95	58.77	4.52	17.14
11a	$C_7H_{11}O_2N_2$	49.62	6.61	25.09	49.69	6.55	24.84
11b	$C_{12}H_{13}O_2N_3$	62.36	5.69	18.32	62.32	5.67	18.17
12a	$C_9H_{13}O_3N_3$	51.27	6.22	19.86	51.17	6.20	19.90
12b	$C_{14}H_{15}O_3N_3$	61.62	5.61	15.65	61.53	5.53	15.38
13a	$C_{11}H_{15}O_4N_3$	52.05	6.04	16.80	52.15	5.97	16.59
14a	$C_6H_6ON_4$	47.76	4.05	37.54	48.00	4.03	37.32
14b	$C_{11}H_8ON$	62.14	3.84	26.61	62.25	3.80	26.40

a) These compounds were unstable.

UV absorption data and elemental analyses of these pyrazoles and pyrazolo[4,3-*d*]pyrimidines are listed in Tables 1 and 2.

Experimental

All the melting points are uncorrected.

*Ethyl 5-Oxo-2-pyrazoline-3-carboxylate (**2**).* To a solution of diethyl oxaloacetate (**1**) (19.8 g, 0.1 mol) in 50 ml of ethanol, 80% hydrazine hydrate (6.25 g, 0.1 mol) in 50 ml of ethanol was added dropwise at room temperature. After the solution was stirred for 2 h, the solvent was removed under diminished pressure. The residual solid was recrystallized from ethyl acetate to yield 13.7 g (88%) of **2**. An analytical sample was obtained by an additional recrystallization from ethyl acetate, mp 183—184 °C.

*Ethyl 4-Nitroso-5-oxo-2-pyrazoline-3-carboxylate (**3**).* Into a solution of **2** (15.6 g, 0.1 mol) in 100 ml of ethanol, N_2O_3 gas generated by dropping concd hydrochloric acid to sodium nitrite was introduced at room temperature until the disappearance of **2** was confirmed by TLC. Then the solvent was removed under diminished pressure, and the residual yellow crystals of **3** were recrystallized from ethyl acetate, yield 17.6 g (95%). An analytical sample was obtained by two additional recrystallizations from ethyl acetate, mp 170—172 °C (dec).

*Ethyl 4-Amino-5-oxo-2-pyrazoline-3-carboxylate Hydrochloride (**4**).* The nitroso compound **3** (1.85 g, 0.01 mol) was dissolved in 50 ml of ethanol containing 2 ml of concd hydrochloric acid. A small amount of 20% Pd–C was added and stirred under hydrogen atmosphere. After 450 ml of hydrogen was absorbed, the solution was filtered and evaporated *in vacuo*. The residue was dissoved in a small amount of ethanol and 1.83 g (88%) of **4** was precipitated by the addition of ether. An analytical sample was obtained by an additional reprecipitation from ethanol and ether, mp 160 °C (dec).

*Ethyl 4-Acetamido-5-oxo-2-pyrazoline-3-carboxylate (**5**).* The nitroso compound **3** (3.70 g, 0.02 mol) was dissolved in 150 ml of acetic acid and 6 ml of acetic anhydride. A small amount of 20% Pd–C was added and stirred under hydrogen atmosphere. After 900 ml of hydrogen was absorbed, the solution was filtered and evaporated *in vacuo*. When ether was added to the residue, white crystals of **5** were precipitated, 3.20 g (75%). An analytical sample was obtained by recrystallization from water, mp 189.5—190 °C.

*3,7-Dihydroxypyrazolo[4,3-d]pyrimidine (**6**).* A mixture of **4** (519 mg, 2.5 mmol), formamidine acetate (780 mg, 7.5 mmol), and triethylamine (1.26 g, 12.5 mmol) in 10 ml of 2-ethoxyethanol was refluxed for 1 h under argon atmosphere. Crystals were precipitated when the solution was allowed to stand at room temperature. The precipitate was filtered and recrystallized from water to yield 350 mg (92%) of **6**. An analytical sample was obtained by an additional recrystallization from water, mp>300 °C.

*Ethyl α-(Hydroxyimino)acetopyruvate (**9a**) and Ethyl α-(Hydroxyimino)benzopyruvate (**9b**).* Into a solution of **7a** (15.8 g, 0.1 mol) in 100 ml of ethanol, N_2O_3 gas was introduced at room temperature until the disappearance of **7a** was confirmed by TLC. Then the solvent was removed under diminished pressure and water was added. The aqueous solution was extracted three times with ether and the combined organic layer was dried over anhydrous sodium sulfate. Evaporation of ether *in vacuo* gave a yellow oil of almost pure **9a**. The oily **9a** was used for the next step without further purification. The benzoyl derivative **9b** was obtained as an oil from ethyl benzopyruvate **7b** in a similar manner.

*Ethyl 5-Methyl-4-nitroso-3-pyrazolecarboxylate (**10a**).* To a solution of **9a** obtained from **7a** (3.16 g, 0.02 mol) in 50 ml of water, hydrazine dihydrochloride (2.08 g, 0.02 mol) in 50 ml of water was added dropwise and stirred at 0 °C until the disappearance of **9a** was confirmed by TLC. Then the solution was extracted with ether and the organic layer was dried over anhydrous sodium sulfate. When the solvent was removed under diminished pressure below 40 °C, blue crystals of **10a** were obtained. An analytical sample was obtained by using silica-gel column chromatography eluted with benzene–ethyl acetate (9 : 1), mp 95—98 °C (dec).

*Ethyl 4-Nitroso-5-phenyl-3-pyrazolecarboxylate (**10b**).* Greenish blue crystals of **10b** were obtained from **9b** in a manner similar to that described for **10a** when the removal of the solvent was carried out under an ice-cooled bath. An analytical sample was obtained by using silica-gel column chromatography eluted with benzene–ethyl acetate (5 : 1), mp 26 °C (dec).

*Ethyl 4-Amino-5-methyl-3-pyrazolecarboxylate (**11a**).* To a mixture of **10a** obtained from **7a** (3.16 g, 0.02 mol) in

50 ml of ethyl acetate and 50 ml of water, sodium dithionite was added to the mixture until the disappearance of **10a** was confirmed by TLC. Then the organic layer was separated and the aqueous layer was extracted with ethyl acetate. The combined organic layer was dried over anhydrous sodium sulfate and the solvent was removed under diminished pressure. The crude product was recrystallized from benzene to yield 1.60 g (47% from **7a**) of **11a**. An analytical sample was obtained by an additional recrystallization from benzene, mp 96—96.5 °C.

*Ethyl 4-Amino-5-phenyl-3-pyrazolecarboxylate (**11b**).* In a manner similar to that described for **11a**, **11b** was obtained from **7b** (2.20 g, 0.01 mol) and recrystallized from benzene to yield 1.06 g (46% from **7b**). An analytical sample was obtained by an additional recrystallization from benzene, mp 145—146 °C.

*Ethyl 4-Acetamido-5-methyl-3-pyrazolecarboxylate (**12a**).* A solution of **11a** (85 mg, 0.5 mmol) in acetic acid (5 ml) and acetic anhydride (26 mg, 2.5 mmol) was stirred at room temperature for 30 min. The solution was neutralized with aqueous sodium hydrogencarbonate solution and extracted with ethyl acetate. The organic layer was dried over anhydrous sodium sulfate and evaporated *in vacuo* to yield 106 mg (quantitative) of **12a**. An analytical sample was obtained by recrystallization from ethyl acetate, mp 176—177 °C.

*Ethyl 4-Acetamido-5-phenyl-3-pyrazolecarboxylate (**12b**).* In a similar manner, **12b** was obtained in a quantitative yield (137 mg) from **11b** (116 mg, 0.5 mmol). An analytical sample was obtained by recrystallization from ethyl acetate, mp 182.5—183 °C.

*Ethyl 4-Acetamido-1-acetyl-5-methyl-3-pyrazolecarboxylate (**13a**).* A solution of **11a** (169 mg, 1 mmol) in pyridine (5 ml) and acetic anhydride (510 mg, 5 mmol) was stirred at room temperature for 2 days and then the solvent was removed under diminished pressure. The crude product was recrystallized from benzene–hexane to yield 253 mg (quantitative) of **13a**, mp 152—153 °C.

*7-Hydroxy-3-methylpyrazolo[4,3-d]pyrimidine (**14a**).* A mixture of **11a** (338 mg, 2 mmol) and formamidine acetate (624 mg, 6 mmol) in 10 ml of 2-ethoxyethanol was refluxed for 1 h under argon atmosphere. Then the solvnet was removed under diminished pressure and the residue was recrystallized from water to yield 300 mg (quantitative) of **14a**. An analytical sample was obtained by an additional recrystallization from water, mp>300 °C (lit,[7] >300 °C).

*7-Hydroxy-3-phenylpyrazolo[4,3-d]pyrimidine (**14b**).* Crude **14b** was obtained from **11b** (231 mg, 1 mmol) in a similar manner. Recrystallization of crude **14b** from *N,N*-dimethylformamide gave 211 mg (quantitative) of **14b**. An analytical sample was obtained by an additional recrystallization from *N,N*-dimethylformamide, mp>300 °C.

This research was supported in part by a Kurata Research Grant.

References

1) These pyrazolo[4,3-*d*]pyrimidines and intermediate pyrazoles have many tautomeric structures. But, in this paper we provisionally describe one representative tautomeric structure.

2) R. K. Robins, *J. Am. Chem. Soc.*, **78**, 784 (1956).

3) H. E. Skipper, R. K. Robins, and J. R. Thompson, *Proc. Soc. Exp. Biol. Med.*, **89**, 594 (1955).

4) M. Mori, E. Ito, T. Takita, G. Koyama, and H. Umezawa, *J. Antibiot., Ser A*, **17**, 96 (1964); G. Koyama, K. Maeda, H. Umezawa, and Y. Iitake, *Tetrahedron Lett.*, **1966**, 597.

5) R. Behrend, *Ann.*, **231**, 213 (1888).

6) F. L. Rose, *J. Chem. Soc.*, **1952**, 3448; F. L. Rose, *ibid.*, **1954**, 4116.

7) R. K. Robins, L. B. Holum, and F. W. Furcht, *J. Org. Chem.*, **21**, 833 (1956); R. K. Robins, F. W. Furcht, A. D. Grauer. and J. W. Jones, *J. Am. Chem. Soc.*, **78**, 2418 (1956).

8) R. A. Long, J. F. Gerster, and L. B. Townsend, *J. Heterocycl. Chem.*, **7**, 867 (1970).

9) M. Bebek, J. Farkas, and F. Sorm, *Tetrahedron Lett.*, **1970**, 4611; J. Farkas and F. Sorm, *Collect. Czech. Chem. Commun.*, **37**, 2798 (1972).

10) E. M. Acton, K. J. Ryan, D. W. Henry, and L. Goodman, *Chem., Commun.*, **1971**, 986.

11) E. M. Acton, A. N. Fujisawa, L. Goodman, and D. W. Henry, *Carbohydr. Res.*, **33**, 135 (1974).

12) C. Musante, *Gazz. Chim. Ital.*, **75**, 121 (1945).

A Simple Total Synthesis of (+)-Ferruginol, (+)-Sempervirol, and (+)-Podocarpa-8(14)-en-13-one

Takashi MATSUMOTO* and Shuji USUI

Department of Chemistry, Faculty of Science, Hiroshima University, Higashisenda-machi, Hiroshima 730

(Received July 20, 1978)

The Wittig reaction of (*R*)-(−)-α-cyclocitral with (3-isopropyl-4-methoxybenzyl)-, (4-isopropyl-3-methoxybenzyl)-, and (3-methoxybenzyl)triphenylphosphonium chloride afforded the styryl derivatives which were partially hydrogenated to the corresponding dihydro derivatives (**18**, **26**, and **27**). Intramolecular cyclization of **18** and **26** with anhydrous aluminium chloride followed by demethylation with boron tribromide gave (+)-ferruginol and (+)-sempervirol. The similar cyclization of **27** gave (+)-13-methoxypodocarpa-8, 11, 13-triene. This was reduced with lithium in liquid ammonia in the presence of ethanol and then treated with dilute hydrochloric acid to give (+)-podocarpa-8(14)-en-13-one, a versatile intermediate for natural diterpene synthesis.

In previous papers,[1-3] we have reported the syntheses of highly-oxygenated tricyclic diterpenes, *i.e.* taxodione (**1**), royleanone (**2**), 7-oxoroyleanone (**3**), taxoquinone (**4**), horminone (**5**), 7α-acetoxyroyleanone (**6**), dehydroroyleanone (**7**), cryptojaponol (**8**), and inuroyleanol (**9**), using ferruginol (**10**) as an useful key intermediate. We also reported the synthesis of sempervirol (**11**), which is a rare tricyclic diterpene phenol possessing an isopropyl group at the C-12 position. All these syntheses started from natural (−)-abietic acid (**12**). To complete these previous works, we planned to devise a more efficient and general synthetic method for the optically active tricyclic diterpenes to achieve the total syntheses of the above natural products. This paper will describe the simple total syntheses of (+)-ferruginol (**10**), (+)-sempervirol (**11**), and (+)-13-methoxypodocarpa-8,11,13-triene (**13**),[4] which was easily converted into (+)-podocarpa-8(14)-en-13-one (**14**),[5-9] a versatile intermediate for naturally-occurring diterpenes.

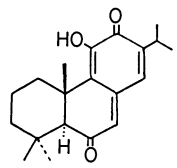

1

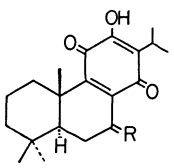

2 R = H_2
3 R = O

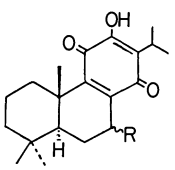

4 R = β-OH
5 R = α-OH
6 R = α-OAc

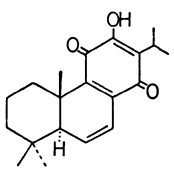

7

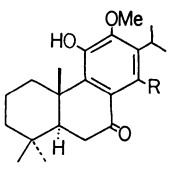

8 R = H
9 R = OH

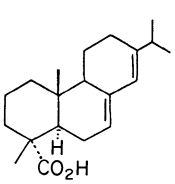

12

(*R*)-(−)-α-Cyclocitral (**15**)[10] prepared from (±)-α-cyclogeranic acid was chosen as a starting material. The Wittig reaction of **15** with (3-isopropyl-4-methoxybenzyl)triphenylphosphonium chloride (**16**) in hexane in the presence of butyllithium gave 3-(3-isopropyl-4-ethoxystyryl)-2,4,4-trimethyl-1-cyclohexene (**17**). The stereochemistry of the newly formed double bond in **17** was assigned as the *trans*-configuration because of the vicinal coupling constant (J=15 Hz) between the olefinic protons in the NMR spectrum. The compound **17** in ethanol was submitted to partial catalytic hydrogenation over Pd–C at room temperature to give the corresponding phenethyl derivative (**18**). This was treated with anhydrous aluminium chloride in benzene and gave a mixture of two intramolecular cyclization products. The chromatographic purification of the mixture afforded ferruginyl methyl ether (**19**) and its *cis*-isomer (**20**) in a ratio of 1:1. The *cis*-configuration of the A/B ring junction in **20** was supported by its NMR spectrum, which showed a signal due to the $C_{4\beta}$ methyl group in the high field, δ 0.40 ppm, because of the shielding effect of the aromatic ring. The demethylation of **19** with boron tribromide in dichloromethane gave ferruginol (**10**). However, since the optical rotation ([α]$_D$+33.2°) was somewhat lower than that of the natural product,[2] this was further purified *via* the benzoate (**21**) to give the optically pure compound (**10**), [α]$_D$+55.0°.

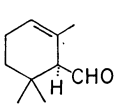

15

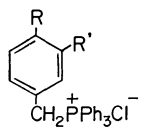

16 R=OMe, R'=i-Pr
22 R=i-Pr, R'=OMe
23 R=H, R'=OMe

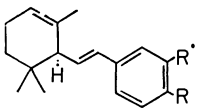

17 R=OMe, R'=i-Pr
24 R=i-Pr, R'=OMe
25 R=H, R'=OMe

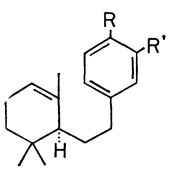

18 R=OMe, R'=i-Pr
26 R=i-Pr, R'=OMe
27 R=H, R'=OMe

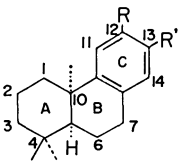

20 R=OMe, R'=i-Pr
29 R=i-Pr, R'=OMe
31 R=H, R'=OMe

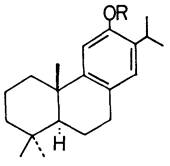

10 R=H
19 R=Me
21 R=COPh

Similarly, **15** was condensed respectively with (4-isopropyl-3-methoxybenzyl)triphenylphosphonium chlo-

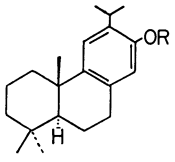

11 R = H
28 R = Me
30 R = Ac

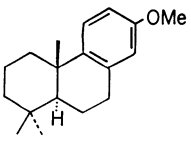

13

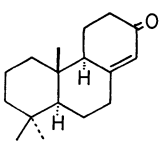

14

ride (**22**) and (3-methoxybenzyl)triphenylphosphonium chloride (**23**) in the presence of butyllithium to afford the styryl derivatives (**24** and **25**), which were then hydrogenated in the presence of Pd–C to yield the corresponding phenethyl derivatives, **26** and **27**, respectively. The intramolecular cyclization of **26** with anhydrous aluminium chloride gave semperviryl methyl ether (**28**) and its *cis*-isomer (**29**).[3] The *trans*-compound (**28**) was demethylated with boron tribromide to give sempervirol (**11**), $[\alpha]_D$+38.0°. The purification of **11** *via* the acetate (**30**) gave the optically pure sample (**11**), $[\alpha]_D$+60.2°. The compound **27** was also cyclized with anhydrous aluminium chloride to give 13-methoxypodocarpa-8,11,13-triene (**13**),[4] which was purified by crystallization along with its *cis*-isomer (**31**). The conversion of racemic **13** into racemic podocarpa-8(14)-en-13-one (**14**) has already been reported by Barltrop and Rogers[11] and Church *et al.*[12] The synthetic optically-active **13** was similarly reduced with lithium in liquid ammonia in the presence of ethanol and then treated with dilute hydrochloric acid to give the α,β-unsaturated ketone (**14**), mp 61.5—62.5 °C, $[\alpha]_D$+40.4°, a degradation product of natural diterpenes, *e.g.* isophyllocladene (**32**)[5] and manool (**33**).[5,6,9] The optically-active ketone (**14**) has already been transformed into isophyllocladene (**32**),[13] manool (**33**),[7] phyllocladene (**34**),[13] hibaone (**35**),[14] sclareol (**36**),[7] manoyl oxide (**37**),[7] anticopalic acid (**38**),[15,16] *trans*-abienol (**39**),[17] and isoabienol (**40**).[17] Therefore, the present work can be regarded as the total syntheses of the above natural diterpenes.

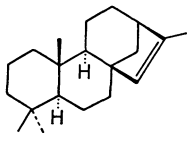

32

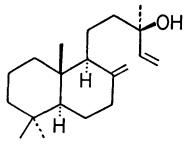

33

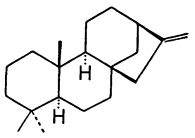

34

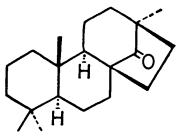

35

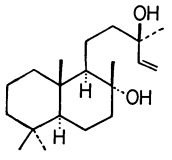

36

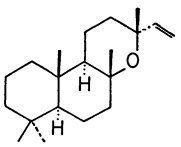

37

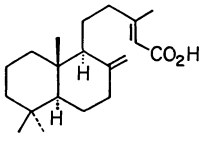

38

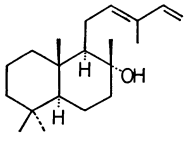

39

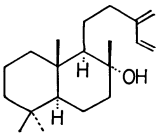

40

Experimental

All melting points are uncorrected. The IR spectra and optical rotations were measured in chloroform, and the NMR spectra in carbon tetrachloride at 60 MHz, with tetramethylsilane as the internal standard, unless otherwise stated. The chemical shifts are presented in terms of δ values; s: singlet, bs: broad singlet, d: doublet, bd: broad doublet, dd: double doublet, t: triplet, m: multiplet. Column chromatography was performed using Merck silica gel (0.063 mm).

*(R)-(−)-α-Cyclocitral (**15**).*[10] (−)-α-Cyclogeraniol[10,18] (4.11 g, $[\alpha]_D$ −117° (EtOH)) prepared from (±)-α-cyclo geranic acid, and dicyclohexylcarbodiimide[19] (16.5 g) were dissolved in dimethyl sulfoxide (15 ml) and benzene (15 ml). Anhydrous phosphoric acid[20] (7 ml, 1 M solution in dimethyl sulfoxide) was added at 5 °C, and the mixture was stirred at this temperature for 4 h. Dry ether (50 ml) was added, followed by a solution of oxalic acid (6.72 g) in methanol (7 ml). After 30 min, the *N,N'*-dicyclohexylurea was removed by filtration and washed with ether. The filtrate was washed with water, dried over sodium sulfate, and then evaporated. The crude product was purified by column chromatography on silica gel using hexane–benzene (1:4) as the eluent to yield **15** (2.90 g: 72%), $[\alpha]_D$ −711° (EtOH), NMR: 0.89 and 0.97 (each 3H and s, $-\dot{C}(CH_3)_2$), 1.60 (3H, d, J=1.5 Hz, $=\dot{C}CH_3$), 5.69 (1H, bs, $-CH=\dot{C}-$), 9.34 (1H, d, J=5 Hz, −CHO).

*(3-Isopropyl-4-methoxybenzyl)triphenylphosphonium Chloride (**16**).* A solution of 3-isopropyl-4-methoxybenzyl chloride[21] (5.71 g) and triphenylphosphine (7.54 g) in dry benzene (10 ml) was refluxed for 5 h and the precipitate (**16**) (7.80 g, mp 253—259 °C) was collected. The filtrate was further refluxed for 3 h to give some additional salt (1.20 g, mp 251—254 °C).

*3-(3-Isopropyl-4-methoxystyryl)-2,4,4-trimethyl-1-cyclohexene (**17**).* A solution of butyllithium in hexane (15%; 2.9 ml) was added at room temperature to a suspension of **16** (2.660 g) in hexane (13 ml) under a stream of nitrogen. The mixture was stirred for 1 h and a solution of **15** (549 mg) in hexane (2.0 ml) was added at 5 °C. After stirring at 5—10 °C for 4 h, the mixture was acidified with dilute hydrochloric acid, extracted with ether, and the extract was washed with brine, dried over sodium sulfate, and then evaporated. The residue was triturated with hexane, and the precipitated triphenylphosphine oxide was removed by filtration. The filtrate was evaporated and the residue (1.208 g) was purified by column chromatography on silica gel (50 g) using hexane as the eluent to give **17** (852 mg: 79%) as an oil, $[\alpha]_D$ −273°, NMR: 0.90 and 0.94 (each 3H and s, $-\dot{C}(CH_3)_2$), 1.21 (6H, d, J=7 Hz, $-CH(C\underline{H}_3)_2$), 1.63 (3H, bs, $=\dot{C}CH_3$), 3.27 (1H, m, $-C\underline{H}(CH_3)_2$), 3.79 (3H, s, $-OCH_3$), 5.40 (1H, m, $-CH=\dot{C}-$), 5.76 (1H, dd, J=8 and 15 Hz, $-\dot{C}H-C\underline{H}=CH-$), 6.25 (1H, d, J=15 Hz, $-\dot{C}H-CH=C\underline{H}-$), 6.63 (1H, d, J=9 Hz), 7.04 (1H, d, J=2 Hz), and 7.04 (1H, dd, J=2 and 9 Hz) (aromatic protons). Found: C, 84.62; H, 10.10%. Calcd for $C_{21}H_{30}O$: C, 84.51; H, 10.13%.

*3-(3-Isopropyl-4-methoxyphenethyl)-2,4,4-trimethyl-1-cyclohexene (**18**).* A suspension of **17** (852 mg) and 5% Pd–C (300 mg) in ethanol (8.0 ml) was stirred at room temperature in an atmosphere of hydrogen. After one equivalent of hydrogen had been absorbed (*ca.* 80 min), the mixture was filtered. The filtrate was evaporated and the residue (828 mg) was purified by column chromatography on silica

gel (80 g) using hexane as the eluent to afford **18** (790 mg: 92%) as an oil, $[\alpha]_D$ −89.3°, NMR: 0.88 and 0.99 (each 3H and s, $-\dot{C}(CH_3)_2$), 1.19 (6H, d, J=7 Hz, $-CH(C\underline{H}_3)_2$), 1.68 (3H, bs, $=\dot{C}CH_3$), 3.26 (1H, m, $-C\underline{H}(CH_3)_2$), 3.77 (3H, s, $-OCH_3$), 5.28 (1H, m, $-CH=\dot{C}-$), 6.59 (1H, d, J=9 Hz), 6.83 (1H, dd, J=2 and 9 Hz), and 6.88 (1H, d, J=2 Hz) (aromatic protons). Found: C, 83.66; H, 10.73%. Calcd for $C_{21}H_{32}O$: C, 83.94; H, 10.73%.

Intramolecular Cyclization of ***18***. Anhydrous aluminium chloride (370 mg) was added at 30 °C to a solution of **18** (814 mg) in dry benzene (8.0 ml). The mixture was stirred at 30—33 °C for 30 min, decomposed with dilute hydrochloric acid, and then extracted with ether. The ether extract was washed with brine, dried over sodium sulfate, and evaporated. The crude product was chromatographed on silica gel (80 g) using hexane as the eluent to give the *cis*-isomer (**20**) (363 mg: 45%) as an oil, $[\alpha]_D$ −28.0°, NMR: 0.40 (3H, s, $C_{4\beta}$–CH_3), 0.93 (3H, s, $C_{4\alpha}$–CH_3), 1.14 (3H, s, C_{10}–CH_3), 1.16 (6H, d, J=7 Hz, $-CH(C\underline{H}_3)_2$), 3.19 (1H, m, $-C\underline{H}(CH_3)_2$), 3.78 (3H, s, $-OCH_3$), 6.63 and 6.69 (each 1H and s, C_{11}–H and C_{14}–H). Found: C, 84.21; H, 10.85%. Calcd for $C_{21}H_{32}O$: C, 83.94; H, 10.73%. Further elution gave the *trans*-isomer (**19**) (352 mg: 43%) as an oil, $[\alpha]_D$ +35.9°, NMR: 0.95 (6H, s, $-\dot{C}(CH_3)_2$), 1.16 (6H, d, J=7 Hz, $-CH(C\underline{H}_3)_2$), 1.19 (3H, s, C_{10}–CH_3), 3.18 (1H, m, $-C\underline{H}(CH_3)_2$), 3.74 (3H, s, $-OCH_3$), 6.55 and 6.67 (each 1H and s, C_{11}–H and C_{14}–H). Found: C, 84.24; H, 10.96%. Calcd for $C_{21}H_{32}O$: C, 83.94; H, 10.73%.

*Ferruginyl Benzoate (****21****).* A solution of **19** (384 mg) and boron tribromide (0.30 ml) in dichloromethane (4.0 ml) was allowed to stand at 0—5 °C for 2 h. The solution was then poured into water and extracted with ether. The extract was washed with brine, dried, and then evaporated to dryness. The crude product was purified by column chromatography on silica gel (40 g) using hexane–benzene (1:1) as the eluent to give ferruginol (**10**) (349 mg: 95%), $[\alpha]_D$ +33.2°, as an oil. The IR and NMR spectra were identical with those of an authentic sample.[2]

The above ferruginol (349 mg) was benzoylated at 50—55 °C for 3 h with benzoyl chloride (0.3 ml) in pyridine (3.5 ml). After the usual work-up, the crude product was chromatographed on silica gel (40 g) using hexane–benzene (1:1) as the eluent to give ferruginyl benzoate (**21**) (409 mg) which was recrystallized from ethanol, mp 154.5—156 °C, $[\alpha]_D$ +60.1°, IR: 1728 cm^{-1}, NMR: 0.96 (6H, s, $-\dot{C}(CH_3)_2$), 1.18 (6H, d, J=7 Hz, $-CH(C\underline{H}_3)_2$), 1.21 (3H, s, C_{10}–CH_3), 6.86 and 6.89 (each 1H and s, C_{11}–H and C_{14}–H), 7.3—7.7 (3H, m) and 8.1—8.3 (2H, m) (aromatic protons). The IR and NMR spectra were identical with those of authentic benzoate which was prepared from natural ferruginol. Found: C, 83.32; H, 9.02%. Calcd for $C_{27}H_{34}O_2$: C, 83.03; H, 8.78%.

*Ferruginol (****10****).* A mixture of **21** (134 mg) and lithium aluminium hydride (15 mg) in dry ether (2.0 ml) was refluxed for 1 h. After the usual work-up, the product was purified by column chromatography on silica gel (10 g) using hexane–benzene (1:1) as the eluent to give ferruginol (**10**) (93 mg: 94%) as an oil, $[\alpha]_D$ +55.0° (lit,[2] $[\alpha]_D$ +57.5°); IR: 3605, 3350 cm^{-1}; NMR: 0.91 (6H, s, $-\dot{C}(CH_3)_2$), 1.10 (3H, s, C_{10}–CH_3), 1.19 (6H, d, J=7 Hz, $-CH(C\underline{H}_3)_2$), 3.09 (1H, m, $-C\underline{H}(CH_3)_2$), 4.73 (1H, bs, –OH), 6.41 and 6.68 (each 1H and s, C_{11}–H and C_{14}–H). Found: C, 84.13; H, 10.49%. Calcd for $C_{20}H_{30}O$: C, 83.86; H, 10.56%.

*(4-Isopropyl-3-methoxybenzyl)triphenylphosphonium Chloride (****22****).* A solution of 4-isopropyl-3-methoxybenzyl chloride[22] (3.34 g) and triphenylphosphine (4.41 g) in dry benzene (5 ml) was refluxed for 6 h. The precipitate was collected and recrystallized from chloroform–benzene to give crystals (6.40 g: 82%), mp 222—225 °C.

*3-(4-Isopropyl-3-methoxystyryl)-2,4,4-trimethyl-1-cyclohexene (****24****).* A suspension of **22** (4.460 g) in hexane (22 ml) was treated with a solution of butyllithium in hexane (15%; 4.8 ml) under a stream of nitrogen and then with a solution of **15** (921 mg) in hexane (2.0 ml), as described for the preparation of **17**. The crude product was chromatographed on silica gel (100 g) using hexane as the eluent to give **24** (956 mg: 53%), $[\alpha]_D$ −320°, NMR: 0.89 and 0.95 (each 3H and s, $-\dot{C}(CH_3)_2$), 1.17 (6H, d, J=7 Hz, $-CH(C\underline{H}_3)_2$), 1.63 (3H, bs, $=\dot{C}CH_3$), 3.25 (1H, m, $-C\underline{H}(CH_3)_2$), 5.42 (1H, m, $-CH=\dot{C}-$), 5.83 (1H, dd, J=8 and 15 Hz, $-\dot{C}H-C\underline{H}=CH-$), 6.28 (1H, d, J=15 Hz, $-\dot{C}H-CH=C\underline{H}-$), 6.69 (1H, overlap), 6.75 (1H, dd, J=2 and 8 Hz), and 7.02 (1H, d, J=8 Hz) (aromatic protons). Found: C, 84.71; H, 10.10%. Calcd for $C_{21}H_{30}O$: C, 84.51; H, 10.13%.

*3-(4-Isopropyl-3-methoxyphenethyl)-2,4,4-trimethyl-1-cyclohexene (****26****).* A mixture of **24** (956 mg), 5% Pd–C (300 mg), and ethanol (10 ml) was subjected to catalytic hydrogenation at room temperature for *ca.* 60 min as described for the preparation of **18**. After the usual work-up, the crude product was purified by column chromatography on silica gel (90 g) using hexane as the eluent, to afford **26** (765 mg: 80%) as an oil, $[\alpha]_D$ −98.7°, NMR: 0.88 and 0.99 (each 3H and s, $-\dot{C}(CH_3)_2$), 1.16 (6H, d, J=7 Hz, $-CH(C\underline{H}_3)_2$), 1.69 (3H, bs, $=\dot{C}CH_3$), 3.22 (1H, m, $-C\underline{H}(CH_3)_2$), 3.78 (3H, s, $-OCH_3$), 5.27 (1H, m, $-CH=\dot{C}-$), 6.50 (1H, overlap), 6.58 (1H, dd, J=2 and 8 Hz), and 6.97 (1H, d, J=8 Hz) (aromatic protons). Found: C, 84.22; H, 10.66%. Calcd for $C_{21}H_{32}O$: C, 83.94; H, 10.73%.

Intramolecular Cyclization of ***26***. A mixture of **26** (395 mg), anhydrous aluminium chloride (180 mg), and dry benzene (4.0 ml) was treated at 30 °C for 30 min. After the usual work-up, the crude product was chromatographed on silica gel (40 g) using hexane as the eluent, to give the *cis*-isomer (**29**) (188 mg: 48%), $[\alpha]_D$ −24.7°, NMR: 0.37 (3H, s, $C_{4\beta}$–CH_3), 0.92 (3H, s, $C_{4\alpha}$–CH_3), 1.11 (3H, s, C_{10}–CH_3), 1.17 (6H, d, J=7 Hz, $-CH(C\underline{H}_3)_2$), 3.22 (1H, m, $-C\underline{H}(CH_3)_2$), 3.74 (3H, s, $-OCH_3$), 6.32 and 6.96 (each 1H and s, C_{14}–H and C_{11}–H). Found: C, 83.67; H, 10.84%. Calcd for $C_{21}H_{32}O$: C, 83.94; H, 10.73%.

Further elution gave semperviryl methyl ether (**28**) (151 mg: 38%), $[\alpha]_D$ +35.0°, NMR: 0.95 (6H, s, $-\dot{C}(CH_3)_2$), 1.15 (3H, s, C_{10}–CH_3), 1.16 (6H, d, J=7 Hz, $-CH(C\underline{H}_3)_2$), 3.19 (1H, m, $-C\underline{H}(CH_3)_2$), 3.73 (3H, s, $-OCH_3$), 6.32 and 6.94 (each 1H and s, C_{14}–H and C_{11}–H). Found: C, 83.92; H, 10.79%. Calcd for $C_{21}H_{32}O$: C, 83.94; H, 10.73%.

*Semperviryl Acetate (****30****).* A solution of **28** (283 mg) and boron tribromide (0.20 ml) in dichloromethane (3.0 ml) was allowed to stand at 0 °C for 2 h. The crude product was purified by column chromatography on silica gel (30 g) to give sempervirol (**11**) (249 mg: 92%), $[\alpha]_D$ +38.0°, which was treated at 50 °C for 2 h with acetic anhydride (0.20 ml) and pyridine (2.5 ml). The product was chromatographed on silica gel (25 g) using hexane–benzene (1:1) as the eluent and then recrystallized from ethanol to give the acetate (**30**), mp 92—94 °C, $[\alpha]_D$ +55.4° (lit,[23] mp 92—93 °C, $[\alpha]_D$ +51°), IR: 1750 cm^{-1}, NMR: 0.93 (6H, s, $-\dot{C}(CH_3)_2$), 1.15 (6H, d, J=7 Hz, $-CH(C\underline{H}_3)_2$), 1.18 (3H, s, C_{10}–CH_3),

2.21 (3H, s, $-OCOCH_3$), 6.52 (1H, bs, C_{14}–H), 7.04 (1H, s, C_{11}–H). Found: C, 80.41; H, 9.90%. Calcd for $C_{22}H_{32}O_2$: C, 80.44; H, 9.83%.

Sempervirol (11). A mixture of **30** (105 mg) and lithium aluminium hydride (15 mg) in dry ether (2.0 ml) was refluxed for 1 h. After the usual work-up, the product was purified by column chromatography on silica gel (10 g) using hexane–benzene (1:1) as the eluent, to afford sempervirol (**11**) (90 mg: 98%), $[\alpha]_D$ +60.2°; IR: 3605, 3340 cm^{-1}; NMR: 0.92 (6H, s, $-\dot{C}(CH_3)_2$), 1.13 (3H, s, C_{10}–CH_3), 1.19 (6H, d, J=7 Hz, $-CH(CH_3)_2$), 3.10 (1H, m, $-CH(CH_3)_2$), 4.59 (1H, bs, –OH), 6.18 (1H, s, C_{14}–H), 6.92 (1H, s, C_{11}–H). Found: C, 83.78; H, 10.50%. Calcd for $C_{20}H_{30}O$: C, 83.86; H, 10.56%.

3-(3-Methoxystyryl)-2,4,4-trimethyl-1-cyclohexene (25). A solution of butyllithium in hexane (15%; 2.8 ml) was added to a suspension of (3-methoxybenzyl)triphenylphosphonium chloride (**23**)[24] (mp 159—165 °C, 2.39 g) in dry benzene (20 ml) under a stream of nitrogen and stirred at room temperature for 15 min. After the addition of a solution of **15** (434 mg) in dry benzene (2.0 ml), the mixture was stirred for 6 more hours and then treated as described for the preparation of **17**. The crude product was purified by column chromatography on silica gel (40 g) using hexane–benzene (4:1) as the eluent to give **25** (411 mg: 56%) as an oil, $[\alpha]_D$ −345°, NMR: 0.89 and 0.94 (each 3H and s, $-\dot{C}(CH_3)_2$), 1.63 (3H, bs, $=\dot{C}CH_3$), 3.76 (3H, s, $-OCH_3$), 5.42 (1H, m, $-CH=\dot{C}-$), 5.92 (1H, dd, J=8 and 15 Hz, $-\dot{C}H-CH=CH-$), 6.32 (1H, d, J=15 Hz, $-\dot{C}H-CH=CH-$). Found: C, 84.03; H, 9.29%. Calcd for $C_{18}H_{24}O$: C, 84.32; H, 9.44%.

3-(3-Methoxyphenethyl)-2,4,4-trimethyl-1-cyclohexene (27). A mixture of **25** (1090 mg), 5% Pd–C (600 mg), and ethanol (10 ml) was subjected to catalytic hydrogenation as described for the preparation of **18**. After the usual work-up, the product was purified by column chromatography on silica gel (100 g) using hexane–benzene (95:5) as the eluent to give **27** (785 mg: 71%) as an oil, $[\alpha]_D$ −113°, NMR: 0.88 and 0.99 (each 3H and s, $-\dot{C}(CH_3)_2$), 1.68 (3H, bs, $=\dot{C}CH_3$), 3.73 (3H, s, $-OCH_3$), 5.28 (1H, m, $-CH=\dot{C}-$). Found: C, 83.72; H, 10.19%. Calcd for $C_{18}H_{26}O$: C, 83.66; H, 10.14%.

Intramolecular Cyclization of 27. A mixture of **27** (780 mg), anhydrous aluminium chloride (450 mg), and dry benzene (10 ml) was stirred at 30 °C for 30 min. After the treatment by a method similar to that used for **18**, the crude product was chromatographed on silica gel (80 g) using hexane–benzene (9:1) as the eluent to give the *cis*-isomer (**31**) (285 mg: 36%) as an oil, $[\alpha]_D$ −21.9°, NMR: 0.38 (3H, s, $C_{4\beta}$–CH_3), 0.92 (3H, s, $C_{4\alpha}$–CH_3), 1.11 (3H, s, C_{10}–CH_3), 3.70 (3H, s, $-OCH_3$), 6.44 (1H, overlap, C_{14}–H), 6.53 (1H, dd, J=2.5 and 8.5 Hz, C_{12}–H), 7.06 (1H, d, J=8.5 Hz, C_{11}–H). Found: C, 83.37; H, 10.23%. Calcd for $C_{18}H_{26}O$: C, 83.66; H, 10.14%.

Further elution gave the *trans*-isomer (**13**) (291 mg: 37%), $[\alpha]_D$ +41.4°, which was recrystallized from methanol to afford an optically pure sample (138 mg), mp 84.5—86 °C, $[\alpha]_D$ +53.9° (lit,[4] mp 86—88 °C, $[\alpha]_D$ +54°), NMR: 0.93 (6H, s, $-\dot{C}(CH_3)_2$), 1.13 (3H, s, C_{10}–CH_3), 3.67 (3H, s, $-OCH_3$), 6.40 (1H, overlap, C_{14}–H), 6.51 (1H, dd, J=3 and 8 Hz, C_{12}–H), 7.01 (1H, d, J=8 Hz, C_{11}–H). Found: C, 83.42; H, 10.18%. Calcd for $C_{18}H_{26}O$: C, 83.66; H, 10.14%.

(+)-Podocarpa-8(14)-en-13-one (14). According to the method of Church *et al.*,[12] the compound **13** (138 mg) in dry ether (7.0 ml) was reduced with lithium (110 mg) in liquid ammonia (*ca.* 20 ml) in the presence of ethanol (5.0 ml) and then treated with dilute hydrochloric acid. The crude product was purified by column chromatography on silica gel (5.0 g) using ether–benzene (3:97) as the eluent, followed by recrystallization from petroleum ether to afford the enone (**14**), mp 61.5—62.5 °C, $[\alpha]_D$ +40.4° (lit,[8] mp 62—65 °C, $[\alpha]_D$ +41°); IR: 1656, 1617 cm^{-1}; NMR: 0.83, 0.90, and 0.94 (each 3H and s, $-\dot{C}(CH_3)_2$ and C_{10}–CH_3), 5.73 (1H, bs, C_{14}–H). Found: C, 83.00; H, 10.78%. Calcd for $C_{17}H_{26}O$: C, 82.87; H, 10.64%.

References

1) T. Matsumoto and S. Harada, *Chem. Lett.*, **1976**, 1311.

2) T. Matsumoto, Y. Ohsuga, S. Harada, and K. Fukui, *Bull. Chem. Soc. Jpn.*, **50**, 266 (1977); T. Matsumoto, Y. Ohsuga, and K. Fukui, *Chem. Lett.*, **1974**, 297.

3) T. Matsumoto, S. Imai, T. Matsubayashi, F. Tsunenaga, and K. Fukui, *Chem. Lett.*, **1972**, 1159.

4) R. Hodges and R. A. Raphael, *J. Chem. Soc.*, **1960**, 50.

5) P. K. Grant and R. Hodges, *Tetrahedron Lett.*, **1959**, 21; P. K. Grant and R. Hodges, *Tetrahedron*, **8**, 261 (1960); P. K. Grant and R. Hodges, *J. Chem. Soc.*, **1960**, 5274.

6) J. A. Barltrop, D. Giles, J. R. Hanson, and N. A. Rogers, *J. Chem. Soc.*, **1962**, 2534.

7) E. Wenkert, J. R. Mahajan, M. Nussim, and F. Schenker, *Can. J. Chem.*, **44**, 2575 (1966).

8) D. E. U. Ekong and J. I. Okogun, *Chem. Commun.*, **1967**, 72.

9) R. C. Cambie, K. N. Joblin, and A. F. Preston, *Aust. J. Chem.*, **24**, 2365 (1971).

10) C. H. Eugster, R. Buchecker, Ch. Tscharner, G. Uhde, and G. Ohloff, *Helv. Chim. Acta*, **52**, 1729 (1969).

11) J. A. Barltrop and N. A. J. Rogers, *J. Chem. Soc.*, **1958**, 2566.

12) R. F. Church, R. E. Ireland, and J. A. Marshall, *J. Org. Chem.*, **31**, 2526 (1966).

13) D. K. M. Duc, M. Fetizon, and S. Lazare, *J. Chem. Soc., Chem. Commun.*, **1975**, 282.

14) D. K. M. Duc, M. Fetizon, and J. P. Flament, *J. Chem. Soc., Chem. Commun.*, **1972**, 886; *Tetrahedron*, **31**, 1897 (1975).

15) D. D. K. Manh, M. Fetizon, and M. Kone, *Tetrahedron*, **31**, 1903 (1975).

16) G. Ohloff, *Justus Liebigs Ann. Chem.*, **615**, 134 (1958).

17) P. F. Vlad, A. G. Russo, and C. Kuang-fang, *Zh. Obsch. Chim.* (English Ed.), **39**, 423 (1969).

18) D. J. Bennett, G. R. Ramage, and J. L. Simonsen, *J. Chem. Soc.*, **1940**, 418.

19) K. E. Pfitzner and J. G. Moffatt, *J. Am. Chem. Soc.*, **87**, 5670 (1965).

20) L. F. Fieser and M. Fieser, "Reagents for Organic Synthesis," John Wiley and Sons, Inc., New York (1967), p. 860.

21) T. Matsumoto, S. Usui, and T. Morimoto, *Bull. Chem. Soc. Jpn.*, **50**, 1575 (1977).

22) T. Matsumoto, S. Usui, and K. Fukui, *Chem. Lett.*, **1976**, 241.

23) L. Mangoni and R. Caputo, *Tetrahedron Lett.*, **1967**, 673.

24) G. S. Grinenko, E. V. Popova, and V. I. Maksimov, *Zh. Org. Khim.*, **7**, 935 (1971); *Chem. Abstr.*, **75**, 77122x (1971).

A New Synthetic Method for Methyl Dihydrojasmonate from a Butadiene Telomer

Jiro Tsuji,* Kazuyuki Kasuga, and Takashi Takahashi
Tokyo Institute of Technology, Meguro, Tokyo 152
(Received July 19, 1978)

Ethyl 2-acetyl-4, 9-decadienoate, easily obtained by the palladium catalyzed telomerization of butadiene with ethyl acetoacetate, was selectively hydrogenated to ethyl 2-acetyl-9-decenoate using $RuCl_2(PPh_3)_3$ as a catalyst. Deacetylation, followed by hydrolysis produced 4-decenoic acid, which was converted into acid chloride. The $AlCl_3$-promoted cyclization gave 2-pentyl-2-cyclopentenone, from which methyl dihydrojasmonate was prepared.

Methyl dihydrojasmonate (**7**) is an important fragrant compound. A number of synthetic approaches for this ester have been reported.[1,2] We now wish to report a simple synthetic method for methyl dihydrojasmonate starting from an easily available butadiene telomer, which has functionality suitable for the synthesis of jasmonate. Palladium catalyzed telomerization of butadiene with various nucleophiles affords a variety of interesting telomers,[3] which can be used for syntheses of various natural products. We have already reported the syntheses of queen substance,[4] royal jelly acids,[5,6] civetone,[7] Matsutake alcohol,[8,9] pellitorine,[10] Recifeiolide,[11] and diplodialide[12] from various telomers. Butadiene and ethyl acetoacetate react readily using a palladium catalyst to give ethyl 2-acetyl-4,9-decadienoate (**1**) in a high yield.[13] This compound has the right carbon numbers and suitable functionality for a facile synthesis of 2-pentyl-2-cyclopentenone, an important precursor of dihydrojasmonate. Thus the compound **1** is a good starting compound for dihydrojasmonate.

Results and Discussion

The synthesis of methyl dihydrojasmonate using the butadiene telomer **1** was carried out by the following sequence of reactions.

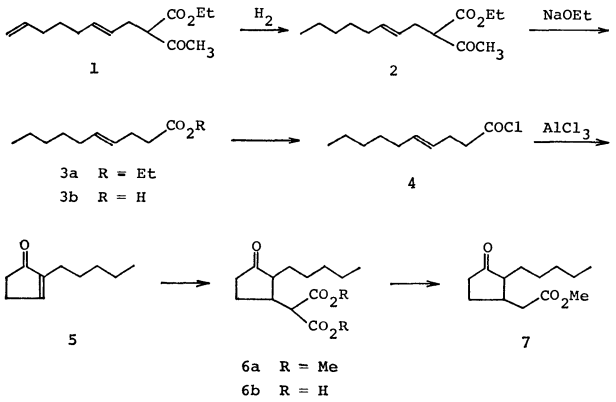

Fig. 1.

Regioselective hydrogenation of the terminal double bond of ethyl 2-acetyl-4,9-decadienoate (**1**) without attacking the internal double bond was achieved easily by homogeneous hydrogenation using $RuCl_2(PPh_3)_3$ as a catalyst under mild conditions.[14] The acetyl group of **2** was removed by the treatment with sodium ethoxide in ethanol to give ethyl 4-decenoate (**3a**) in 83% yield. Then the ester **3a** was hydrolyzed with a base to give 4-decenoic acid (**3b**) in 89% yield. The acid has a double bond at the position suitable for an acid catalyzed intramolecular cyclization to form a cyclopentenone ring. At first, the direct cyclization of the acid **3b** was attempted by using polyphosphoric acid, but the yield of the cyclopentenone was only 20%. In order to carry out the more efficient cyclization, the acid **3b** was converted to the more reactive acid chloride **4**. Then the intramolecular acylation of the double bond was carried out by using $AlCl_3$ in dichloromethane. By this method, the desired 2-pentyl-2-cyclopentenone (**5**) was obtained in 53% yield. The structure of **5** was confirmed by elemental analysis, and mass and NMR spectra. The conversion of **5** to methyl dihydrojasmonate (**7**) is the known reaction.[15] The Michael addition of dimethyl malonate (65.5% yield), followed by hydrolysis produced the diacid **6b**. Decarboxylation and methylation gave methyl dihydrojasmonate (**7**), which was identified by comparing its NMR and IR spectra with those of an authentic sample.

Experimental

NMR spectra were recorded by a Hitachi R-24A spectrometer at 60 MHz. Chemical shifts (δ) are given in ppm relative to an internal standard of TMS. IR spectra were recorded with a JASCO IRA-2 spectrometer. Ethyl 2-acetyl-4,9-decadienoate (**1**) was prepared according to the method of Hata *et al.*[13]

*Regioselective Hydrogenation of Ethyl 2-Acetyl-4,9-decadienoate (**1**).* A mixture of **1** (5.55 g, 23.3 mmol) and $RuCl_2(PPh_3)_3$ (87.6 mg, 0.09 mmol) in dry ethanol (15 ml) and dry benzene (15 ml) was pressured to 30 atm with hydrogen in a 100 ml autoclave and stirred at room temperature for 5 h. When the hydrogen pressure decreased to 19 atm, the autoclave was opened and the solvent was evaporated. Distillation of the residue afforded ethyl 2-acetyl-4-decenoate (**2**), bp 105—106 °C/1 Torr; 5.28 g (94% yield): IR (neat) 2920, 1740, 1718 cm^{-1}; NMR (CCl_4) 0.87 (t, J=4.8 Hz, 3H), 1.25 (t, J=7.2 Hz, 3H), 1.04—1.65 (m, 6H), 1.75—2.05 (m, 2H), 2.09 (s, 3H), 2.20—2.55 (m, 2H), 3.27 (t, J=7.2 Hz, 1H), 4.08 (q, J=7.2 Hz, 2H), 5.15—5.45 (m, 2H).

*Ethyl 4-Decenoate (**3a**).* Sodium metal (412 mg, 17.9 mmol) was dissolved in dry ethanol (50 ml) to which the ester **2** (8.62 g, 35.9 mmol) was added. The resulting mixture was refluxed for 6 h and neutralized with acetic acid. Ethanol was evaporated, and the residue was extracted

with ether. The extract was washed with brine and dried over sodium sulfate. After removal of ether, distillation of the residue gave **3a**, bp 114 °C/6 Torr; 5.9 g (83% yield): IR (neat) 2920, 1734 cm^{-1}; NMR (CCl_4) 0.87 (t, J=4.8 Hz, 3H) 1.05—1.50 (m, 6H), 1.22 (t, J=7.2 Hz, 3H), 1.55—2.13 (m, 4H), 2.13—2.33 (bs, 2H), 8.02 (q, J=7.2 Hz, 2H), 5.15—5.45 (m, 2H).

*4-Decenoic Acid (**3b**).* An aqueous KOH solution (2.51 g, 44.8 mmol in 20 ml) was added to a solution of **3a** (5.9 g, 29.8 mmol) in methanol (20 ml). The resulting mixture was stirred for 6 h at room temperature. The reaction mixture was washed with hexane and acidified with 6 M HCl. Methanol was evaporated and the aqueous phase was extracted with dichloromethane. The extract was dried over magnesium sulfate. The crude acid **3b** was obtained after evaporation of the solvent (4.1 g, 81% yield): IR (neat) 3000, 2930, 1705 cm^{-1}; NMR (CCl_4) 0.87 (t, J=4.8 Hz, 3H), 1.05—1.53 (m, 6H), 1.53—2.13 (m, 4H), 2.20—2.48 (bs, 2H), 5.24—5.53 (m, 2H), 10.84 (bs, 1H).

*Cyclization of **3b** with Polyphosphoric Acid.* A mixture of the acid **3b** (510 mg, 3 mmol) and polyphosphoric acid (1.6 g) was stirred at 95 °C for 4 h. Crushed ice and water were then added. The mixture was stirred until it became homogeneous and ether extraction was carried out. The extract was washed with saturated $NaHCO_3$ solution and brine, and dried over sodium sulfate. After evaporation of ether, the cyclized product was isolated by column chromatography (silica gel using hexane/ether as an eluent) (95 mg, 21% yield.

*4-Decenoyl Chloride (**4**).* A mixture of acid **3b** (1.5 g, 8.82 mmol) and thionyl chloride (1.26 g, 10.6 mmol) was heated at 60 °C under nitrogen for 5 h. The chloride **4** was obtained by distillation at 62.5 °C/1.5 Torr; (1.52 g, 91% yield): IR (neat) 2940, 1800 cm^{-1}; NMR (CCl_4) 0.88 (t, J=4.8 Hz, 3H), 1.07—1.75 (m, 6H), 1.77—2.65 (m, 4H), 2.74—3.07 (m, 2H), 5.26—5.55 (m, 2H).

*Cyclization of **4** by $AlCl_3$.* A mixture of **4** (600 mg, 3.18 mmol) and $AlCl_3$ (506 mg, 3.81 mmol) in dry dichloromethane (10 ml) was stirred at 0 °C for 2 h. Ice water (20 ml) was added and the aqueous phase was extracted with ether. The extract was washed sequentially with cold saturated $NaHCO_3$ and brine, and dried over sodium sulfate. The pure enone **5** was obtained by column chromatography (silica gel using hexane/ether as an eluent) after removal of ether (255 mg, 53% yield): IR (neat) 2920, 1700, 1630 cm^{-1}; NMR (CCl_4) 0.89 (t, J=4.8 Hz, 3H), 1.08—1.80 (m, 6H), 1.80—2.35 (m, 4H), 2.35—2.70 (m, 2H), 7.04—7.23 (m, 1H). Found: C, 78.56; H, 10.44%. Calcd for $C_{10}H_{16}O$: C, 78.90; H, 10.59%. MS *m/e* 152 (M^+).

*The Michael Addition of **5**.* Sodium metal (23.5 mg, 1.02 mmol) was dissolved in dry methanol (3 ml) and dimethyl malonate (261 mg, 1.98 mmol) was added under nitrogen at 0 °C. After 15 min, the enone **5** (171 mg, 1.13 mmol) in dry methanol (3 ml) was added dropwise during 15 min at −10 °C. After the addition, the reaction mixture was poured into a cold saturated NH_4Cl and the aqueous phase was extracted with ether. The combined organic layer was washed with brine and dried over magnesium sulfate. The addition product **6a** was isolated by column chromatography (silica gel using hexane/ether as an eluent) (209 mg, 65.5% yield): IR (neat) 2930, 1755, 1735 cm^{-1}; NMR (CCl_4) 0.90 (t, J=4.8 Hz, 3H), 1.05—1.58 (m, 8H), 1.80—2.30 (m, 6H), 3.40 (d, J=7.2 Hz, 1H), 3.71 (s, 6H).

*Methyl Dihydrojasmonate (**7**).* To aqueous NaOH (36.8 mg, 0.92 mmol) in 1 ml was added **6a** (125 mg, 0.44 mmol) in THF (2 ml). The resulting mixture was stirred for 1 h at room temperature. The solution was acidified with sulfuric acid, and refluxed for 3 h. Then, the product was extracted with ether. The extract was dried over sodium sulfate. After evaporation of ether, crude dihydrojasmonic acid was obtained. This crude acid was dissolved in dry methanol (2 ml) and the solution was heated at 40 °C for 3 h in the presence of a catalytic amount of sulfuric acid. Methanol was evaporated and the residue was extracted with ether. The ether extract was washed with cold saturated $NaHCO_3$ and brine, and dried over sodium sulfate. After evaporation of ether, pure methyl dihydrojasmonate **7** was isolated by column chromatography (silica gel using hexane/ether as an eluent) (70 mg, 70% yield): IR (neat) 2940, 1740, 1440, 1170 cm^{-1}; NMR (CCl_4) 0.88 (t, J=4.8 Hz, 3H), 1.07—1.60 (m, 8H), 1.85—2.65 (m, 8H), 3.60 (s, 3H). MS, *m/e* 226 (M^+). The IR and NMR spectra were identical with those of an authentic sample.

References

1) Reviews: a) R. A. Ellison, *Synthesis*, **1973**, 397; b) T. L. Ho, *Synth. Commun.*, **4**, 265 (1974).
2) S. Torii, H. Tanaka, and Y. Kobayashi, *J. Org. Chem.*, **42**, 3473 (1977) and references cited therein.
3) J. Tsuji, *Acc. Chem. Res.*, **6**, 8 (1973).
4) J. Tsuji, K. Masaoka, and T. Takahashi, *Tetrahedron Lett.*, **1977**, 2268.
5) J. Tsuji and H. Yasuda, *J. Organomet. Chem.*, **131**, 133 (1977).
6) J. Tsuji, K. Masaoka, T. Takahashi, A. Suzuki, and N. Miyaura, *Bull. Chem. Soc. Jpn.*, **50**, 2507 (1977).
7) J. Tsuji and T. Mandai, *Tetrahedron Lett.*, **1977**, 3285.
8) J. Tsuji, K. Tsuruoka, and K. Yamamoto, *Bull. Chem. Soc. Jpn.*, **49**, 1701 (1976).
9) J. Tsuji, T. Mandai, *Chem. Lett.*, **1977**, 975.
10) J. Tsuji, H. Nagashima, T. Takahashi, and K. Masaoka, *Tetrahedron Lett.*, **1977**, 1917.
11) J. Tsuji, T. Yamakawa, and T. Mandai, *Tetrahedron Lett.*, **1978**, 565.
12) J. Tsuji and T. Mandai, *Tetrahedron Lett.*, **1978**, 1817.
13) G. Hata, K. Takahashi, and A. Miyake, *J. Org. Chem.*, **36**, 2116 (1971).
14) J. Tsuji and H. Suzuki, *Chem. Lett.*, **1977**, 1083.
15) E. Demole, E. Lederer, and D. Mercier, *Helv. Chim. Acta*, **45**, 685 (1962).

Continuous Removal of Heavy Metals by the Lime Sulfurated Solution (Calcium Polysulfide) Process

Toshiro ARATANI,* Shigeki YASUHARA,† Hitoshi MATOBA††
and Takeo YANO

Department of Chemical Engineering, College of Engineering, University of Osaka Prefecture, Mozu-Ume, Sakai, Osaka 591

(Received July 1, 1978)

A continuous wastewater treatment system was developed for the Lime Sulfurated Solution Process which had already been tested in a batch, stirred tank and ascertained to be an effective chemical precipitation process. The removability of heavy metals was investigated with the continuous treatment system, consisting of a plant composed of H_2S desorber, reactor, thickener, sand filter, and H_2S desorber. The sulfide ion dissolved in treated water was desorbed as H_2S by a mixed gas of air and CO_2 and recycled in the reactor to precipitate heavy metals. It has been found that: (1) by the recycling use of H_2S, the continuous treatment system can remove heavy metals with less coagulant than in the batch, stirred vessel, (2) desorption of the dissolved sulfide ion by the mixed gas decreases the sulfide ion concentration in the treated water below 0.2 ppb, and (3) the conditions for the removal of heavy metals can be detected immediately by a sulfide ion electrode meter.

The development of a continuous processing system is of great practical importance to economically treat wastewater. In previous work,[1-3] an effective heavy metal removal process, *i.e.*, the CaS_x process, which utilized the lime sulfurated solution as a single coagulant, had been proposed and investigated kinetically,[1] for the removal condition for heavy metals,[2] and the simultaneous removal of heavy metal, phosphate, and COD substances.[3] These investigations had, however, been conducted in a batch, stirred vessel. On the engineering scale, *i.g.*, the wastewater treatment plant, continuous operation has been desirable, since continuous processing reduces the operating costs. It is, therefore, necessary to devise a suitable continuous processing system for the CaS_x process. The removal of heavy metals from the system also needs investigation.

According to a previous work,[1] reaction scheme for the CaS_x process is represented by Eqs. 1 to 4.

$$CaS_x + 3/2\,O_2 \longrightarrow CaS_2O_3 + (x-2)S, \quad (1)$$

$$CaS_x + CO_2 + H_2O \longrightarrow CaCO_3 + H_2S + (x-1)S, \quad (2)$$

$$M^{2+} + CaS_2O_3 + H_2O \longrightarrow MS + CaSO_4 + 2H^+, \quad (3)$$

$$M^{2+} + H_2S \longrightarrow MS + 2H^+. \quad (4)$$

In the batch operation, the H_2S liberated by Eq. 2 is partly lost to the gas (air or CO_2) blown into the water to decompose the coagulant (CaS_x),[2] and so an amount of coagulant, more than the stoichiometric amount calculated from Eqs. 1 to 4 is required. In the present study, a continuous treatment system suited to the CaS_x process was realized on the bench scale. The plant was devised to recycle the H_2S in Eq. 2. In the plant, the H_2S liberated was scrubbed by the wastewater, and the dissolved sulfide ion recovered as H_2S from the treated water and re-used to precipitate heavy metals. The efficiency of the H_2S recycling plant was investigated with regard to the removal of heavy metals and the recycling of H_2S. The desorption of the dissolved sulfide ion from the treated water was also investigated.

Experimental

Continuous Processing Plant. Figure 1 shows the total system for the continuous CaS_x process. Simulated wastewater containing heavy metal was continuously fed to the top of the reactor. The reactor was made of a multistage vibrating disc column (MVDC) consisting of 15 stages (100 mm in height pet stage and 100 mm in inner diameter). The MVDC was used as the reactor, since it had excellent gas-liquid contacting ability even in the presence of suspended solid particles.[4] The coagulant, CaS_x solution was continuously injected into the 7th stage of the MVDC reactor. At the upstream stages from the injection point (1st to 7th stage), H_2S gas generated at the downstream stages (8th to 15th stage) was scrubbed by the wastewater and caught on reacting with the heavy metals in the wastewater. The CaS_x decomposed when it came into contact with the gas introduced from the bottom of the reactor. The precipitation of heavy metals by the decomposed CaS_x proceeded mainly at the downstream stages. The suspended solid particles were sedimented in the thickener of 300 mm both in diameter and height. The supernatant liquid was further clarified by a sand filter (150 mm diameter and 200 mm depth), packed with 120 mesh silica sand of 100 mm thickness. The clarified water was stripped of dissolved sulfide ions in the desorber, where the clarified water was contacted in countercurrent with the gas blown for the CaS_x decomposition. The gas used for the desorption was a mixture of air and CO_2 at predetermined volume ratio. The effluent water (treated water) from the desorber was removed as regards heavy metals and sulfide ions. The desorber was made up of an irrigated packed bed with 1/2″ Rasching ring.[5] The bed had a diameter of 150 mm and a height of 1 m. Air, according to a previous paper,[2] requires 60 to 90 min to decompose the CaS_x solution. The long processing time in the batch operation was known to require a large volume of the reactor for continuous operation. A mixed gas of air and CO_2 at various volume ratios was tested to determine the optimum conditions for heavy metal precipitation. The exit gas from the H_2S desorber was blown into the bottom of the reactor, and with this flow of gas, the H_2S, which was recovered by blowing gas into the desorber, was re-used to precipitate the heavy metals in the reactor. The other gas exiting from the top of the reactor was removed perfectly for H_2S, at the

† Present address: Matsushita Electric Works Co., Ltd., Kitashinkai, Yokkaichi 510.

†† Present address: Ataka Kogyo Co., Ltd., Sueyoshi-bashi, Minami-ku, Osaka, 542.

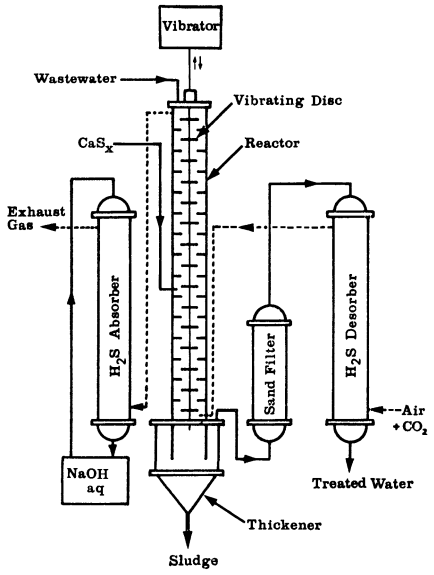

Fig. 1. Continuous heavy metal treatment system for the CaS_x process.

H_2S absorber (the same dimension of irrigated packed bed as the H_2S desorber was used). As the absorbing liquor, 5% NaOH aqueous solution was used.

Method. The simulated wastewater was prepared by dissolving the heavy metal nitrates into ordinary water, and stored in a tank (500 dm^3). The simulated wastewater was not temperature controlled, since the removal of heavy metals with the CaS_x process had already been found to be not severely affected by temperature.[2] First, the whole space of the plant, except the absorber and desorber, was filled with ordinary water. Continuous operation was started by the injection of the coagulant (CaS_x solution), followed by blowing of the gas for the CaS_x decomposition. Finally, the simulated wastewater was introduced. Samples were taken at predetermined time intervals from the outlets of the reactor, thickener, sand filter, and desorber. The samples from the reactor and thickener were filtered by membranes of various pore sizes, and the heavy metal concentrations were determined on an atomic absorption spectrophotometer. Samples from the sand filter and the desorber were directly determined for heavy metal concentrations. The sulfide ion concentration was measured by an ion meter with sulfide ion electrodes (Orion Research Inco., Model 94-16 and 90-02). Since the pH of the sample affects the detected sulfide ion concentration, the pH's of the samples were adjusted by adding a portion of 2 M-NaOH to give a pH of 10.0. The ion meter was calibrated with Na_2S of known concentration at pH=10.0. The flow rates of the wastewater and the blowing gas were set at 500 cm^3/min and 14 dm^3/min respectively. Liquid hold-up's in the reactor, thickner, sand filter, and desorber were measured to be 20, 20, 5, and 1 dm^3, respectively. With the base of these flow rates, the retention times of the reactor, thickener, sand filter, and desorber were calculated, respectively, as 40, 40, 10, and 2 min (the sum total was 92 min). The vibrating frequency of the disc in the MVDC reactor was set at 1.5 Hz with an amplitude of 19 mm, that is, at a vibrating speed of 2.85 cm/s, effective for the fine dispersion of the gas.[4]

Results and Discussion

The preliminary investigation was with simulated wastewater contaminated solely with Cd^{2+}. Figure 2 shows the change in Cd^{2+} concentration in the treated water from the start of the operation. Approximately four times the total retention time (92 min×4=368 min=6 h) was found sufficient for the steady state to be attained. In Fig. 3, the steady state concentration of Cd^{2+} has been plotted against the CO_2 vol % to air of the blowing gas. 8.5 vol % of CO_2 was found to be the optimum condition for the removal of Cd^{2+}, when R_m (the mole ratio of sulfur in the injected CaS_x per Cd^{2+} in the simulated wastewater) was 10 or 15, for C_{in} (the inlet concentration of Cd^{2+})=75 ppm. Consequently, the blowing gas containing 8.5 vol % of CO_2 was utilized in the following experiments. Figure 4 shows the steady state concentration of Cd^{2+} in the treated water plotted against R_m. The continuous plant can remove Cd^{2+}, even with R_m=5.0 for C_{in}=100 ppm, *i.e.*, closely at the stoichiometric amount of the coagulant (R_m=4.7 to 5.4).[2] This compares to the batch processing which needs more units of coagulant as shown by the dotted line in Fig. 4, for C_0=100 ppm. The economization of coagulant is mainly attributed to the recycling of H_2S.

Figure 5 shows the sulfide ion concentration detected by the ion meter against R_m. The keys in Fig. 5, *i.e.*, R_0, T_0, and *O* indicate the samples taken from the reactor, thickener, and desorber, respectively. The treated water (key: *O*) was found to be desorbed as

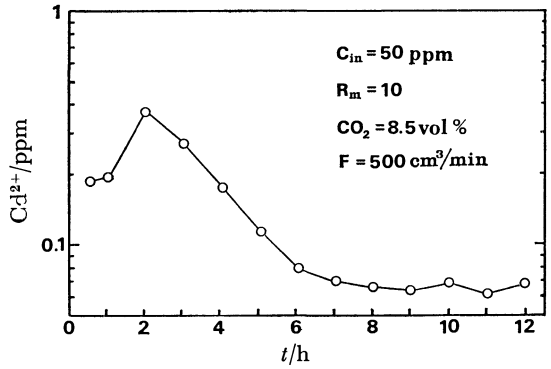

Fig. 2. Attainment to the steady state concentration with the continuous processing of Cd^{2+}.

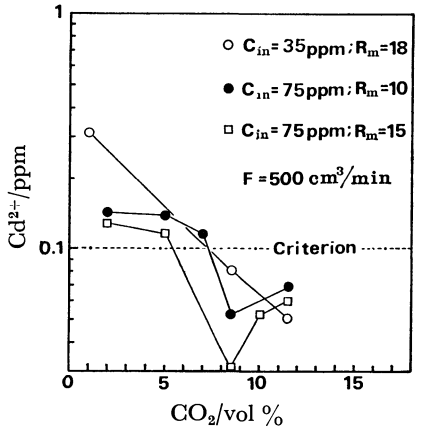

Fig. 3. Steady state concentration of Cd^{2+} *vs.* CO_2 vol % in the blowing gas.

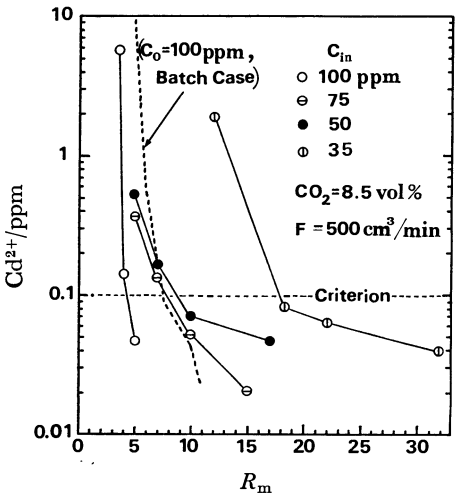

Fig. 4. Steady state concentration of Cd^{2+} *vs.* R_m.

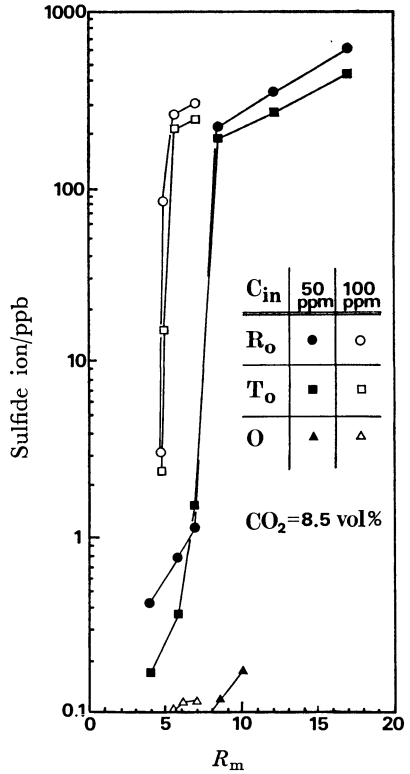

Fig. 5. Detected sulfide ion concentration by ion meter *vs.* R_m.
R_o: reactor outlet, T_o: thickener outlet, O: desorber outlet.

to have the sulfide ion concentration below 0.2 ppb. In water, H_2S is known to dissociate as shown by Eqs. 5 and 6, with dissociation constants of $K_1=[H^+][HS^-]/[H_2S]_{aq}=10^{-7.1}$ and $K_2=[H^+][S^{2-}]/[HS^-]=10^{-12.4}$ at 20 °C.[6]

$$(H_2S)_{aq} \overset{K_1}{\rightleftharpoons} HS^- + H^+, \quad (5)$$

$$HS^- \overset{K_2}{\rightleftharpoons} S^{2-} + H^+. \quad (6)$$

From Eqs. 5 and 6, the mole fractions of $(H_2S)_{aq}$, HS^-, and S^{2-} are represented as functions of pH;

$$[H_2S]_{aq}/C_{TDS} = 1/Q, \quad (7)$$

$$[HS^-]/C_{TDS} = 10^{-7.1+pH}/Q, \quad (8)$$

$$[S^{2-}]/C_{TDS} = 10^{-19.5+2pH}/Q, \quad (9)$$

where $Q=1+10^{-7.1+pH}+10^{-19.5+2pH}$ and C_{TDS} is the total molar concentration of the dissolved sulfides ($C_{TDS}=[H_2S]_{aq}+[HS^-]+[S^{2-}]$). The pH of the treated water with the blowing gas with 8.5 vol % of CO_2 was measured as 6.1. At pH=6.1, the mole fractions of $(H_2S)_{aq}$, HS^-, and S^{2-} calculated from Eqs. 7, 8, and 9 are 0.909, 0.09, and 10^{-7}, respectively. As reported by Ohkawa and Sakai,[7] H_2S in water can be desorbed better on the acidic side, since $(H_2S)_{aq}$ is more readily stripped than HS^- and S^{2-} which need to pass through the associating reaction to $(H_2S)_{aq}$ (Eqs. 5 and 6). 90.9% of C_{TDS} was found to be $(H_2S)_{aq}$ at pH=6.1; the low pH is a direct consequence of the acidity of the CO_2 gas. Thus, the use of CO_2 mixed gas for the CaS_x decomposition is desirable from the view point of H_2S desorption. The reason for the adjustment of the samples pH to 10.0 can be explained from Eqs. 7, 8, and 9 as follows. At pH=10.0, the mole fractions of $(H_2S)_{aq}$, HS^-, and S^{2-} are estimated as 0.001, 0.995, and 0.004, respectively. Therefore, the detected sulfide ion by a pair of electrodes can be said to be almost equal to C_{TDS}.

Figure 5 indicates that the R_m values crossing down the criterion for Cd^{2+} in Fig. 4 for C_{in}=50 and 100 ppm agrees closely with the R_m values of Fig. 5 when the sulfide ion concentration shows steep increase. This good agreement of R_m values suggests that the optimum conditions for Cd^{2+} removal can be detected immediately by measuring the sulfide ion concentration at the outlet of the reactor.

The agglomeration of precipitates is known to be accelerated by the solid particle concentration, or the number of particles existing in the water. To increase the solid particle concentration in the reactor, the precipitated sludge was recycled from the thickener to the top of the reactor by a peristaltic pump at 30 cm³/min. Figure 6 shows a result of Cd^{2+} removal with and without the sludge recycle. The sludge recycle was found to be effective in reducing the amount of coagulant as can be seen from Fig. 7. In Fig. 7, the abscissa is converted from R_m in Fig. 4 to $C_s=R_m\times C_{in}$, C_s being defined as the total sulfur atom concentration injected with the coagulant. Since the sulfur atoms added give rise to equivalent moles of metal sulfide and solid sulfur particles, as seen from Eqs. 1 to 4, C_s can be interpreted as the solid particle concentration generated by the CaS_x process. Since the Cd^{2+} concentration in Fig. 7 shows a single correlation with the solid particle concentration, C_s, the precipitation of heavy metals may depend solely on the solid particle concentration of the water. The recycling of the sludge will increase the solid particle concentration and may work effectively to precipitate heavy metals with less coagulant.

Figure 8 shows the result of the continuous processing of wastewater simultaneously contaminated with 25 ppm of Cd^{2+}, 100 ppm of Pb^{2+} and Zn^{2+}, 40 ppm of Cu^{2+}, and 5 ppm of Cr(VI) and Hg^{2+}. Figure 8 indicates that R_m=5.0, *i.e.*, nearly stoichiometric

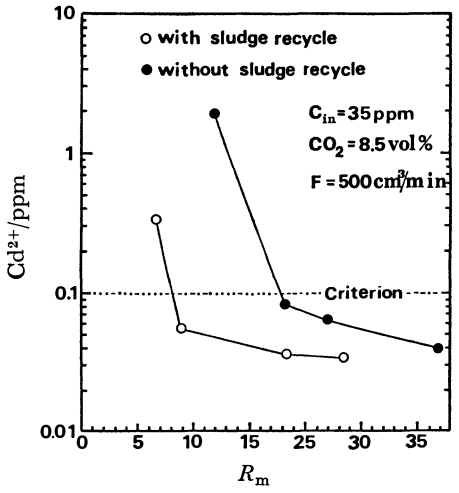

Fig. 6. Removal of Cd^{2+} with and without sludge recycle.

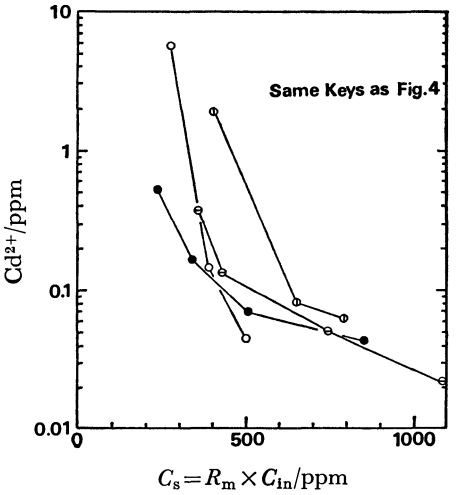

Fig. 7. Cd^{2+} *vs.* solids particle concentration or the sulfur atom concentration.

amount of coagulant is sufficient for the removal of contaminants. The removal concentrations are approximately proportional to the solubilities of the respective sulfides; 6.0×10^{-18} ppb for HgS, 1.62×10^{-10} ppb for CuS, 2.58×10^{-6} ppb for CdS, 2.0×10^{-6} ppb for PbS, 1.1×10^{-3} ppb for ZnS, and 8.3×10^{-2} ppb for $Cr(OH)_3$ at pH=7.0.[6] Cr(VI), Pb^{2+}, and Zn^{2+} show deviations from the order of solubility. The batch processing data shows a higher residual concentration for Zn^{2+}; the reason for this is not evident at present, but it is felt that the particle size of the precipitate may be concerned.

The samples taken from the outlets of the reactor and the thickener were filtered by membranes of various pore sizes, and the residual heavy metals concentrations were determined by atomic absorption, the results of which are shown in Fig. 9. Cr(VI) and Pb^{2+} are found to be finer in gain size. The growth of precipitates was shown to take place in the thickener. Figure 9 also shows that the precipitates grow to about 8 μm and this is thought sufficient for sand filtration.

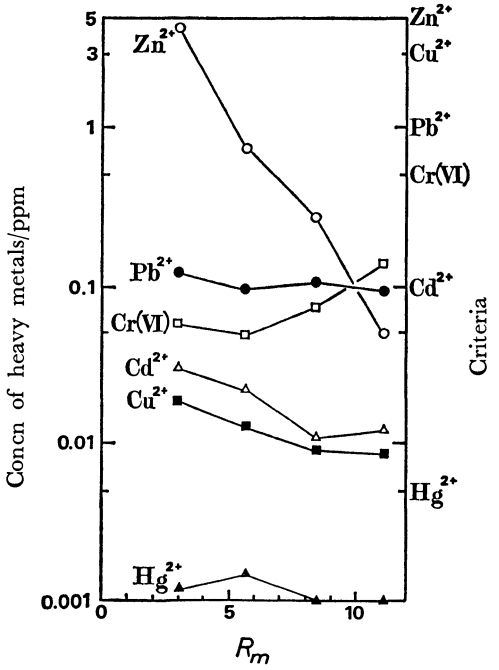

Fig. 8. Simultaneous removal of heavy metals by the continuous CaS_x process.

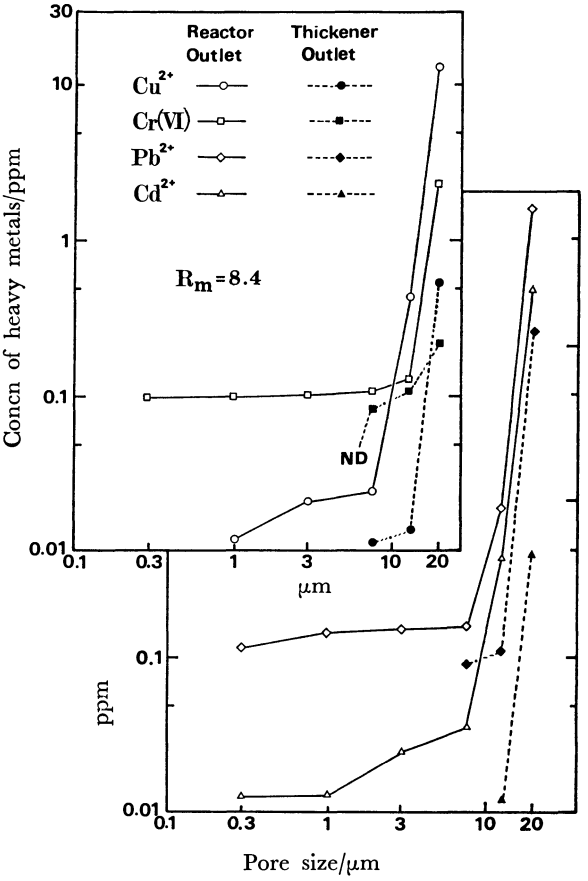

Fig. 9. Residual concentration of heavy metals *vs.* pore size of membrane filter.

Conclusion

Continuous CaS_x process study has lead to the following conclusions.

1) The amount of coagulant needed for the heavy metal removal can be lowered by recycling H_2S in the continuous operating plant.

2) The solid particle concentration in the reactor depends on the removability, which may explain the effective precipitation of Cd^{2+} by the recycling of the sludge.

3) The condition for removal of heavy metals can be detected by an electrode type ion meter. This simple method may enable the plant to be operated automatically with the least amount of coagulant.

4) The desorption of sulfide ions from the treated water can be effectively attained by the blowing gas or air containing CO_2.

The authors wish to thank Assoc. Prof. Kei Miyanami of the University of Osaka Prefecture, Prof. Ryuzo Ito of Osaka University, Profs. Takataro Suda, Yoshiki Sanoh, and Mr. Kiyochika Yahikozawa of Shinshu University for their useful discussions.

The present work was partially supported by a Grant-in-Aid for Developmental Scientific Research from the Ministry of Education, No. 185210.

References

1) K. Yahikozawa, T. Aratani, R. Ito, T. Suda, and T. Yano, *Bull. Chem. Soc. Jpn.*, **51**, 613 (1978).

2) T. Aratani, K. Yahikozawa, H. Matoba, S. Yasuhara, and T. Yano, *Bull. Chem. Soc., Jpn.*, **51**, 1755 (1978).

3) T. Aratani, Y. Nakata, H. Matoba, S. Yasuhara, and T. Yano, *Bull. Chem. Soc. Jpn.*, **51**, 2705 (1978).

4) K. Miyanami, K. Tojo, and T. Yano, *J. Chem. Eng. Jpn.*, **6**, 518 (1973).

5) "Chemical Engineers' Handbook," 4th ed, ed by J. H. Perry, McGraw-Hill, New York (1963).

6) "Stability Constants of Metal-Ion Complexes," The Chemical Society, London (1964).

7) H. Ohkawa and N. Sakai, Presentation No. A302, the 40th Annual Meeting of the Soc. of Chem. Engr. of Japan, Nagoya, April 1975.

8) V. G. Levich, "Physicochemical Hydrodynamics," Prentice-Hall, N. J. (1962).

NOTES

BULLETIN OF THE CHEMICAL SOCIETY OF JAPAN, VOL. 52 (1), 223—224 (1979)

On the Mechanism of Formation of Furotropones from (4-Halogeno-2-butenyloxy)tropones

Hitoshi TAKESHITA,* Kozo TAJIRI, and Isao KOUNO

Research Institute of Industrial Science, 86, Kyushu University, Hakozaki, Fukuoka 812

(Received July 21, 1978)

Synopsis. Pyrolysis of 2-[(*E*)-4-bromo-3-butenyloxy]-tropone and 2-[(*E*)-4-bromo-2-methyl-2-butenyloxy]tropone produced 3-methyl-3-vinyl-2,3-dihydro-8*H*-cyclohepta[*b*]-furan-8-one and 3-isopropylidene-2,3-dihydro-8*H*-cyclo-hepta[*b*]furan-8-one, which established the involvement of 3,3-sigmatropy for furotropone formation.

Previously, the one-step production of furotropones and difurotropones by application of the Claisen rearrangement to some bifunctional troponyl allyl ethers has been reported.[1,2] There are two possible mechanisms, *i.e.*, route a, 3,3-sigmatropy followed by dehydrohalogenation, and route b, a direct S_N2'-type elimination from the allyl ethers.[3]

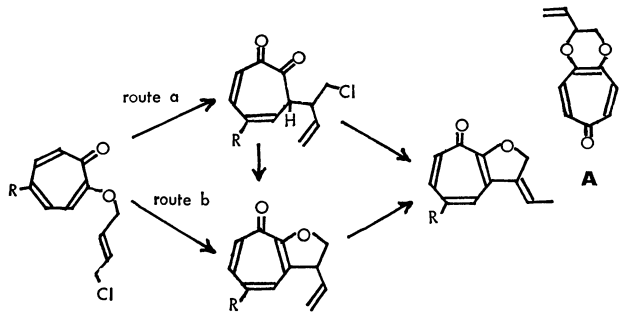

R=H, OH or O-CH_2CH=H-CH_2Cl

Chart 1.

It is important to establish the mechanism to discover the synthetic versatility for furotropones. Using an unsymmetrical halogenide, (*E*)-1,4-dibromo-2-methyl-2-butene (**1**), route a was shown to be correct by the following experiments.[4]

1 was introduced into an anhydrous solution of potassium tropolonate, prepared from tropolone (**2**), potassium hydroxide and 18-crown-6-(CE) in benzene, and refluxed for 7 h to form the isomeric ethers, **3** and **4**. The ethers were separated by high-pressure liquid chromatography. The major product (**3**), a colorless liquid, 35%, was shown to be 2-[(*E*)-4-bromo-3-methyl-2-butenyloxy]tropone [$\delta^{5)}$:1.89(3H, d, J=1 Hz), 3.97(2H, s), 4.68(2H, d, J=6 Hz), 5.89(1H, tq, J=6, 1Hz), and 6.6—7.3(5H, m)] and **4**, a colorless liquid, 18% identified as 2-[(*E*)-4-bromo-2-methyl-2-butenyloxy]tropone [δ:1.83(3H, d, J=1 Hz), 4.01(2H, s), 4.57(2H, s), 5.91(1H, tq, J=8, 1 Hz), and 6.6—7.2 (5H, m)].

The *o*-dichlorobenzene solution of **3** when heated at 180 °C for 10 min gave product **5**, a colorless liquid, 13% yield other than the deallylation product, **2**. The NMR spectrum of **5**[δ:1.47(3H, s), 4.42(1H, d, J=13 Hz), 4.49(1H, d, J=13 Hz), 5.19(1H, d, J=17 Hz), 5.27(1H, d, J=10 Hz), 6.98(1H, dd, J=17, 10 Hz), and 6.8—7.2(4H, m)] was deduced as 3-methyl-3-vinyl-2,3-dihydro-8*H*-cyclohepta[*b*]furan-8-one. Similarly, **4** afforded **6**, a colorless liquid, 24%, together with 45% of deallylated **2**. The NMR spectrum of **6** [δ: 1.80(3H, t, J=2 Hz), 2.12(3H, t, J=3 Hz), 5.20 (2H, m), and 6.6—7.2(4H, m)] was compatible with 3-isopropylidene-2,3-dihydro-7*H*-cyclohepta[*b*]furan-8-one.

The specific formation of **5** from **3** and **6** from **4** established the involvement of 3,3-sigmatropy followed by dehydrobromination. Consequently the previous results may be interpreted in terms of a 3,3-process.

The absence of primary rearrangement products is thought to be a facile cyclization into the dihydrofuran derivatives. Kitahara *et al.*[6] observed the spontaneous cyclization of 3-allyltropolone when treated with bromine.

Experimental

Reaction of Tropolone (2) with (E)-1,4-Dibromo-2-methyl-2-butene (1): Formation of Isomeric Ethers, 3 and 4. The

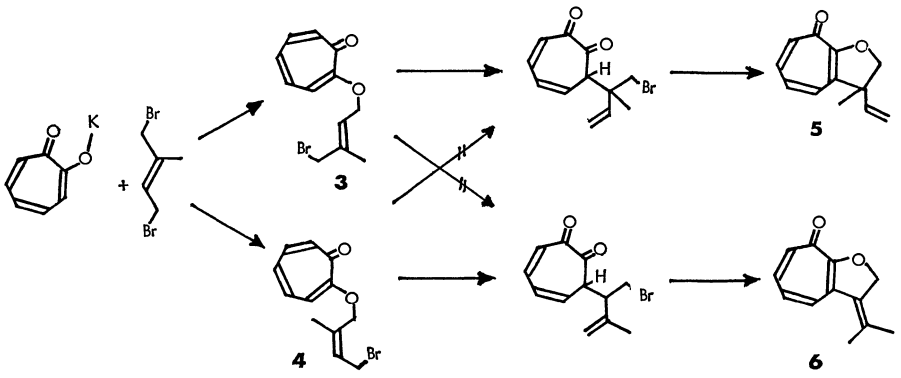

Chart 2.

potsasium salt of **2** (275 mg), the crown ether (CE, 450 mg) and **1**[7] (1.0 ml) were mixed in benzene (20 ml) and refluxed for 7 h. The mixture was, after removal of the solvent, fractionated on a silica gel column to give colorless liquids, **4**, 46 mg (10%) [Found: *m/e*, 268, 270 (M^+, double peaks for $C_{12}H_{13}O_2Br$). *ν*: 2980, 1625, 1595, 1580, 1490, 1285, 1190, 1090 cm^{-1}], from benzene–ether (80 : 20), and **3**, 170 mg (37%) [Found: 268, 270 (M^+). *ν*: 2980, 1625, 1595, 1580, 1490, 1290, 1195, 1092 cm^{-1}], from the same solvent. Analytical samples were obtained by high-pressure liquid chromatography (Micropolasil, hexane–ethyl acetate).

Thermal Reaction of ***3***: *Formation of* ***5***. An *o*-dichlorobenzene solution (5 ml) of **3** (35.8 mg) was heated on an oil bath and refluxed for 10 min. Silica gel column chromatography of the mixture produced **2**, 3.5 mg (37%), and subsequently a colorless oil, **5**, 1.9 mg (13%) [Found: C, 76.30; H, 6.59%. Calcd for $C_{12}H_{12}O_2$: C, 76.57; H, 6.43%. *ν*: 2900, 1615, 1565, 1480, 1430, 1000 cm^{-1}].

Thermal Reaction of ***4***: *Formation of* ***6***. Similarly, **4** (22 mg) was heated in *o*-dichlorobenzene (5 ml), and refluxed for 10 min. Silica gel chromatography of the mixture gave a colorless oil, **6**, 2.2 mg (24 %) [Found: *m/e*, 188.0722 (M^+). Calcd for $C_{12}H_{12}O_2$: 188.0769. *ν*: 2980, 1615, 1570, 1480, 1430 cm^{-1}], together with hydrolyzed **2**, 2.7 mg (45%).

References

1) H. Takeshita, I. Kouno, and K. Miyake, *Kyushu Daigaku Seisan Kagaku Kenkyusho Hokoku*, **66**, 1 (1977).

2) H. Takeshita, K. Tajiri, and I. Kouno, *Heterocycles*, **6**, 1101 (1977).

3) A dihydro-1,4-dioxin derivative (**A**) has been isolated in the condensation reaction of 5-hydroxytropolone and *trans*-1,4-dichloro-2-butene.

4) The condensation of **2** to *trans*-1,4-dichloro-2-pentene was unsuccessful.

5) The NMR spectra were obtained in $CDCl_3$ solutions at 100 MHz by a JEOL FX 100 Model spectrometer, and the chemical shifts expressed in δ values from the internal standard, Me_4Si.

6) H. Shimanouchi, T. Ashida, Y. Sasada, M. Kakudo, I. Murata, and Y. Kitahara, *Bull. Chem. Soc. Jpn.*, **40**, 779 (1967).

7) **1** was prepared by the bromination of isoprene in CCl_4 solution, and was used without purification. Gas-liquid chromatographic analysis revealed the presence of isomers (less than 10%).

BULLETIN OF THE CHEMICAL SOCIETY OF JAPAN, VOL. 52 (1), 225—226 (1979)

Effect of Inorganic Additives on the Reactions of Isomeric Transition-Activated ^{80}Br and ^{82}Br in the Gaseous HBr–CH_4 System

Kenjiro KONDO* and Masuo YAGI

Laboratory of Nuclear Science, Tohoku University, Tomizawa, Sendai 982

(Received March 6, 1978)

Synopsis. The effects of various inorganic additives with and without dipole moments on the product yield distributions have been examined in the CH_4–$H^{80m}Br$ and CH_4–$H^{82m}Br$ systems. Indications were that the ion-clusters formed in the reactions of IT-activated ^{80}Br and ^{82}Br play an important role in determining individual product yield distributions.

It has been reported that isomeric transition (IT)-activated ^{80}Br and ^{82}Br undergo only thermal ionic reactions in the $H^{80m}Br$–CH_4 and $H^{82m}Br$–CH_4 systems, and that the large isotope effect observed can be explained in terms of the difference in decay schemes between ^{80m}Br and ^{82m}Br.[1,2] The γ-transition of ^{82m}Br to the ground state is attained in a single transition and fully converted. The ^{80m}Br has two successive transitions through the intermediate with a half-life of 7.4 ns, and the first stage is fully converted and the second is partially converted (61%). The organic yield of ^{80m}Br therefore can be classified into the following two types;[2] Processes A (39%): internal conversion (IC)+37 keV γ-ray emission; Process B (61%): IC+IC. The chemical effect due to Process A is essentially identical to that of ^{82m}Br. The above isotope effect has been explained by assuming that complex ions CH_4Br^+ or $HBrBr^+$ produced *via* the thermal ionic process interact with the surroundings to form an ion-cluster, and that the second IC in Process B occurs in such a cluster.[2] This has been qualitatively supported from the experimental results obtained in the condensed phase.[2] The aim of this paper is to confirm the presence of ion-clusters in the reactions of IT-activated ^{80}Br and ^{82}Br in the CH_4–$H^{80m}Br$ and CH_4–$H^{82m}Br$ systems by the addition of polar and/or nonpolar molecules, since the polarizability of molecules is one of the most important controlling factors in ion-cluster formation. The ratio of HBr to CH_4 and total pressure in all samples were kept constant at 0.1±0.01 and 660±30 mmHg respectively. Details of experimental procedures may be found elsewhere.[1–3]

Results and Discussion

The effects of inorganic additives (0.3 mf) on the yield distribution in both systems are shown in Table 1. Here, X and Y in the Table are CH_2BrCl and $CH_3CHBrCl$ respectively in the HCl additive experiment. In the case of the H_2S additive, X is thought to be CH_2BrSH. The minor products in low yields (≈0.1%) in other additive experiments have not been identified. CH_3Br yields were larger with ^{80m}Br than ^{82m}Br, while CH_2Br_2 yields with ^{82m}Br were much greater than with ^{80m}Br. Table 2 shows the normalized yields Y due to Process B, which have been calculated by the following equation:[2]

$$Y(\%) = \frac{100}{61}(^{80m}\text{Br-yield} - 0.39 \text{ of } ^{82m}\text{Br-yield}).$$

As previously reported, the isotope effect in both systems can be elucidated by comparing the yields due to Process B with ^{82m}Br yields.[2] The yield ratios of CH_3Br to CH_2Br_2 were 0.2—0.7 for ^{82m}Br and more than unity for Process B. CH_3Br yields in both systems were not affected by the addition of non-polar molecules without dipole moments, while a slight decrease in CH_3Br yields was observed in the system of polar ad-

TABLE 1. EFFECT OF INORGANIC ADDITIVES ON THE YIELD DISTRIBUTION OF ORGANIC PRODUCTS FORMED BY THE IT-ACTIVATED ^{80}Br AND ^{82}Br REACTIONS WITH CH_4
($H^{80m}Br$ or $H^{82m}Br/CH_4$=0.1±0.01, total pressure: 660±30 mmHg)

Additive (0.3 mf)	Org. yield (%)		CH_3Br (%)		X (%)		CH_2Br_2 (%)		Y (%)	
	^{80m}Br	^{82m}Br	^{80m}Br	^{82m}Br	^{80m}Br	^{82m}Br	^{80m}Br	^{82m}Br	^{80m}Br	^{82m}Br
none	4.2	4.5	1.6	0.8	0	0	2.6	3.7	0	0
Kr	3.9	4.4	1.4	0.7	0	0	2.6	3.7	0	0
Xe	4.0	4.2	1.6	0.9	0	0	2.4	3.3	0	0
CO_2	4.0	4.1	1.5	0.7	0.1	0.1	2.4	3.3	0	0
O_2	4.1	4.1	1.5	0.9	0.1	0.1	2.3	3.0	0.2	0.1
N_2	4.0	4.3	1.6	0.9	0	0	2.4	3.4	0	0
CO	2.9	2.6	1.3	0.9	0.1	0	1.4	1.7	0.1	0
HBr	3.1	3.1	1.3	0.5	0	0	1.8	2.6	0	0
H_2S	2.9	4.2	1.1	0.5	1.3	2.6	0.4	1.1	0.1	0
HCl	4.2	4.0	1.2	0.7	1.0	1.5	1.5	1.8	0.5	0
SO_2	2.1	2.2	1.5	0.8	0.1	0.1	0.5	1.2	0	0.1

The experimental errors were 7—15% for ^{80m}Br and less than 10% for ^{82m}Br.

Table 2. Effect of additives on the yield distribution of organic products formed *via* process (B) in the $H^{80m}Br$-CH_4 system
($H^{80m}Br/CH_4=0.1\pm0.01$, total pressure: 660 ± 30 mmHg)

Additive (0.3 mf)	Ionization potential (eV)	Dipole moment (Debye)	Org. yield (%)	CH_3Br (%)	X (%)	CH_2Br_2 (%)	Y (%)
none	—	—	4.0	2.1	0	1.9	0
Kr	13.9	0	3.7	1.8	0	1.9	0
Xe	12.1	0	3.8	2.0	0	1.8	0
CO_2	14.1	0	3.9	2.0	0.1	1.8	0
O_2	12.5	0	4.1	1.9	0.1	1.9	0.2
N_2	15.5	0	3.8	2.0	0	1.8	0
CO	14.1	0.112	3.0	1.6	0.1	1.2	0.1
HBr	11.6	0.82	3.1	1.8	0	1.3	0
H_2S	10.4	0.97	2.1	1.5	0.5	0	0.1
HCl	13.8	1.08	4.4	1.6	0.7	1.3	0.8
SO_2	13.1	1.47	2.0	1.9	0.1	0	0
Br	11.8	0					
CH_4	12.9	0					

ditives with dipole moments. CH_2Br_2 yields in both systems showed a sharp decrease by the addition of polar molecules, contrary to the results for non-polar additives.

The $^{80}Br^+$ and $^{82}Br^+$ ions formed by IT processes react with CH_4 and/or HBr to form collision complex ions, CH_4Br^+ and/or $HBrBr^+$ at first, as has been reported previously.[1,2] Further, these thermal ions are thought to have ample opportunity to form ion-clusters. Loeb has proposed the following equation indicating that an ion-cluster is formed when the potential energy between the ion and molecule is greater than the relative kinetic energy of the ion,[4]

$$\frac{(D-1)\beta}{8\pi Nr^4}/KE \geq 1,$$

where D is the dielectric constant of additive molecules, N, the number of molecules per cm^3, r, the distance between the ion and molecule, β, the statistical weight factor and KE, the relative kinetic energy of the ion. The ratio was found to be 3.4 for CH_4 at 660 mmHg ($D=1.00094$, $r=3\times10^{-8}$ cm[1]) and 0.5 assumed for β) and therefore it is reasonable to presume the formation of ion-clusters in the ^{82}Br and ^{80}Br reactions. Since the potential energies between the ion and nonpolar additives are smaller than for CH_4, and moreover the concentration of CH_4 is larger than those of the additives, the ion-cluster thus formed in the case of nonpolar additives contains mainly CH_4 and/or HBr molecules. In addition polar additives play an important role in cluster formation since the potential energies between the ion and additives are much greater than those for nonpolar additives. Consequently, the ion-cluster thus formed contains an appreciable number of additives as constituents.

The formation of $CH_3{}^{82}Br$ in the CH_4–$H^{82m}Br$ system has been explained energetically by the H^+ transfer reaction from $CH_4{}^{82}Br^+$ to CH_4 and/or HBr as previously reported.[2]

Similarly, the fact that $CH_3{}^{82}Br$ yields were almost constant in the present experiment can be explained on the basis of the exothermicity of the H^+ transfer reaction from $CH_4{}^{82}Br^+$ to CH_4 and/or additives. On the other hand, the $CH^{82}BrBr^+$ ion formed by the ion-molecule reaction of $CH_4{}^{82}Br^+$ with HBr is considered to be a precursor for $CH_2{}^{82}BrBr$. $CH^{82}BrBr$ formed by charge neutralization of $CH^{82}BrBr^+$ undergoes H-abstraction to give $CH_2Br^{82}Br$.[1,2] In the presence of polar additives, $CH_4{}^{82}Br^+$ is effectively surrounded by these molecules in the process of ion-cluster formation, therefore the concentration of HBr in the vicinity of $CH_4{}^{82}Br^+$ decreases, and eventually the above reaction leads to the $CH_2{}^{82}BrBr$ formation being hindered by the addition of polar molecules. Thus the remarkable decrease in $CH_2{}^{82}BrBr$ yields in polar additives can be explained qualitatively.

The second IC in Process B proceeds in an ion-cluster like a condensed phase. Therefore, the molecular explosion following the second IC is responsible for the chemical effect due to Process B. Although no precise information on the IT activated ^{80}Br reactions under such condition is available, both the ion-molecule reactions and primary radical recombinations in the clusters appear to be responsible for product formation. Previously it has been pointed out that radical reactions are not concerned with the formation of CH_3Br and CH_2Br_2.[1,2] This does not always mean however that the primary recombination involving ^{80}Br-radicals does not occur. In Process B that $CH_3Br>CH_2Br_2$ may be qualitatively interpreted by the above assumption since similar results were obtained in the solid CH_4–$H^{80m}Br$ system.[2] Furthermore, it is assumed that ion-molecule reactions also contribute to product formation, judging from the similarity of reaction products in both ^{82m}Br and Process B. The effect of additives on the CH_3Br and CH_2Br_2 yields in Process B may be explained in terms of the difference in concentration of polar and nonpolar molecules contained in the clusters in the same manner as ^{82m}Br. However the details of the reaction mechanisms must await until further experiments are conducted.

References

1) K. Kondo and M. Yagi, *Bull. Chem. Soc. Jpn.*, **51** 372 (1978).
2) K. Kondo and M. Yagi, *Bull. Chem. Soc. Jpn.*, **51**, 1284 (1978).
3) M. Yagi and K. Kondo, *Radiochem. Radioanal. Lett.*, **14**, 123 (1973).
4) L. B. Loeb, "Basic Processes of Gaseous Electronics," University of California Press, Berkley and Los Angeles (1961), p. 45.

BULLETIN OF THE CHEMICAL SOCIETY OF JAPAN, VOL. 52 (1), 227—228 (1979)

Far-infrared Absorption of Non-dipolar Liquid Mixtures

Kenji FUJIWARA,† Shun-ichi IKAWA,* and Masao KIMURA*

Department of Chemistry, Faculty of Science, Hokkaido University, Sapporo 060

(Received May 11, 1978)

Synopsis. Far-infrared absorptions of some non-dipolar liquid mixtures have been observed. The changes of the intensities with mixing ratio were examined on the basis of a formula derived for the difference between absorption intensities before and after mixing, to get information about the mixing state.

The far-infrared absorption of a non-dipolar liquid arises mainly from the bimolecular collisions and thus the absorption of a mixture of the non-dipolar liquids contains valuable information about the mixing state.[1,2] In the present study, the far-infrared absorptions were measured for benzene+cyclohexane, benzene+carbon disulfide, benzene+1,4-dioxane, and carbon disulfide+cyclohexane mixtures. The results were examined by means of a refined formula derived for the difference between the absorption intensities before and after mixing, to get information about the mixing state.

Experimental

The spectral measurements were performed at room temperature with the apparatus described previously.[3] The absorption coefficients were obtained by the equation:

$$\alpha(\nu) = \ln(I_1/I_2)/(l_2 - l_1), \quad (1)$$

where I_1 and I_2 are the transmitted intensities for the two sample thicknesses, l_1 and l_2, respectively. Thus the effects of the surface- and internal-reflection were minimized. The integrated intensities, $A=\int\alpha(\nu)\mathrm{d}\nu$, were estimated in a range from 10 to 220 cm^{-1}, except for samples containing 1,4-dioxane, for which integrations were performed over a range from 10 to 170 cm^{-1}. Spectroscopic grade samples were used for carobn disulfide, benzene, cyclohexane, and 1,4-dioxane. The observed spectra for pure liquids were consistent with the results previously reported.[1,2,4]

Theoretical

If the absorption arises from the bimolecular collisional process[1,2] in addition to the intramolecular process, the absorption intensity for a neat liquid is expressed as follows:

$$A = A_a/v_a + A_{aa}/v_a^2,$$

where v_a is the molar volume and A_a and A_{aa} denote the absorptions due to the intramolecular vibrations and the bimolecular collisions respectively. Let us consider the mixture of a and b components with volume ratio of $x/(1-x)$. The excess volume of mixing is ignored, since it is less than 1 vol % for ordinary organic liquids.[5] The absorption intensity before mixing is provided by the average of those of the neat liquids concerned as follows:

$$A_0 = x(A_a/v_a + A_{aa}/v_a^2) + (1-x)(A_b/v_b + A_{bb}/v_b^2), \quad (2)$$

where subscripts a and b indicate the two components. After mixing, the collision between the different species also takes part in the absorption and the intensity is expressed as follows:

$$A_m = x(A_a/v_a + \varphi_{aa}xA_{aa}/v_a^2) + (1-x)[A_b/v_b + \varphi_{bb}(1-x)A_{bb}/v_b^2] + 2x(1-x)\varphi_{ab}A_{ab}/v_av_b, \quad (3)$$

where φ_{aa}, φ_{bb}, and φ_{ab} are the relative ease of the three types of collision. These quantities represent the mixing state of the mixture. In the case of random mixing, all the three values are equal to unity. In general, however, these values are dependent upon the mixing ratio and are different from each other. They can probably be replaced by the probabilities of the intermolecular bond formation. Then the number ratio of the three types of bond, a–a, b–b, and a–b, is given by $f^2\varphi_{aa}:(1-f)^2\varphi_{bb}: 2f(1-f)\varphi_{ab}$, where f is the mole fraction of component a. According to Schulze,[6] these values are interrelated as follows:

$$\varphi_{ab} = \varphi, \quad \varphi_{aa} = \frac{1-\varphi+\varphi f}{f}, \quad \varphi_{bb} = \frac{1-\varphi f}{1-f}. \quad (4)$$

Since φ_{aa}, φ_{bb}, and φ are all positive, $0<\varphi<\min(f^{-1}, (1-f)^{-1})$. Besides, the limit of $\varphi(f)$ is unity as f approaches 0 or 1. The relationships among f, x, and the number of moles in unit volume, N, are $f=v_bx/[v_bx+v_a(1-x)]$, and $N=[fv_a+(1-f)v_b]^{-1}$. From Eqs. 2, 3, and 4 the difference between the absorption intensities before and after mixing is given by

$$\Delta A_m = A_m - A_0 = -N^2f(1-f)[(\varphi+v_b/v_a-1)A_{aa} + (\varphi+v_a/v_b-1)A_{bb}-2\varphi A_{ab}]. \quad (5)$$

Hereafter, ΔA_m is referred to as the absorption of mixing, by analogy with the heat of mixing.

In the case of random mixing, in which the φ value is unity, Eq. 5 becomes:

$$\Delta A_m = -Cf(1-f)[fv_a+(1-f)v_b]^{-2}, \quad (6)$$

where

$$C = (v_b/v_a)A_{aa} + (v_a/v_b)A_{bb} - 2A_{ab}.$$

If the molar volumes of the components are equal, *i.e.*, $v_a=v_b$, the f-dependence of ΔA_m is simply parabolic.

Results and Discussion

The integrated intensities obtained are plotted against the mole fraction f in the upper parts of Fig. 1(a—d). The standard errors for spectral measurements are indicated by the vertical bars. The solid line shows the intensity before mixing, A_o. For a mixture of two components with different molar

† Present address: Canon Inc., Torite, Ibaragi.

volumes, the mole fraction is nonlinear to the volume fraction. The molar volumes of benzene, cyclohexane, carbon disulfide, and 1,4-dioxane are 88.9, 108.1, 60.3, and 85.2 cm^3/mol, respectively. Then the A_0 curve for the benzene+1,4-dioxane mixture is almost straight, whereas that for the carbon disulfide+cyclohexane mixture shows the largest deviation from a straight line.

The absorptions of mixing, ΔA_m, are shown in the lower parts of Fig. 1(a—d) on an expanded scale. As may be seen in Eq. 5, the absorptions due to the monomolecular processes, A_a and A_b, are cancelled out in ΔA_m. Thus the intramolecular vibrational bands, such as the bands at 150 cm^{-1} of 1,4-dioxane and at 240 cm^{-1} of cyclohexane, contribute little to the values of ΔA_m. The broken lines in Fig. 1 show the values calculated from Eq. 6 with C values adjusted. For the benzene+cyclohexane and benzene+carbon disulfide mixtures, good fits were obtained between the observed and calculated values of ΔA_m. Therefore, the condition of random mixing may hold for these mixtures. The sign of ΔA_m for the benzene+cyclohexane mixture is negative, whereas that for the benzene+carbon disulfide mixture is positive. For the a+b mixture, the sign of ΔA_m is determined by the sign of C, *i.e.*, $(v_b/v_a)A_{aa}+(v_a/v_b)A_{bb}-2A_{ab}$. For the benzene+cyclohexane system, the molar volumes of the two components, v_a and v_b, are approximately equal and the benzene–benzene absorption, A_{aa}, is much stronger than the cyclohexane–cyclohexane absorption, A_{bb}. Therefore, the positive value of C shows that A_{aa} is the dominant absorption. For the benzene+carbon disulfide system, the negative value of C means that A_{ab} is larger than the average of A_{aa} and A_{bb}, which is approximately equal to that of $(v_b/v_a)A_{aa}$ and $(v_a/v_b)A_{bb}$. Davies and Chamberlain[2] considered that the positive sign of ΔA_m was due to a complex or sticky collision interaction between different species. However, as mentioned above, the sign of ΔA_m depends upon the magnitudes of the three types of binary absorption, A_{aa}, A_{bb}, and A_{ab}, which does not necessarily represent directly the strength of the intermolecular bondings.

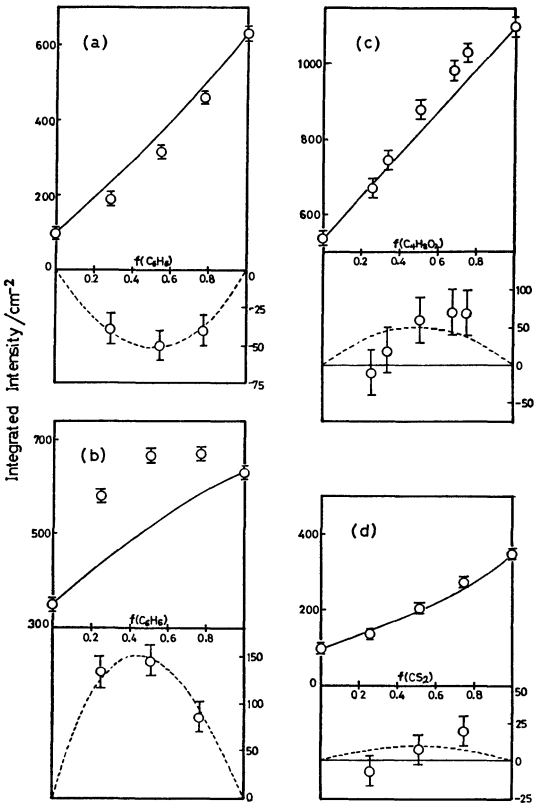

Fig. 1. The mole fraction dependency of the integrated absorption intensity (the upper part) and the absorption of mixing (the lower part) of liquid mixtures:
(a) benzene+cyclohexane,
(b) benzene+carbon disulfide,
(c) benzene+1,4-dioxane,
(d) carbon disulfide+cyclohexane.
The vertical bars indicate the standard errors. The solid lines represent the intensities before mixing. The broken lines represent the values calculated from Eq. 6 with the adjusted C values.

For the benzene+1,4-dioxane and carbon disulfide+cyclohexane mixtures, the observed values of ΔA_m seem to deviate from a symmetrical parabolic curve. Because of a moderately strong interaction between benzene and 1,4-dioxane,[7] the value of φ may change with mole fraction and cause the deviation from the random mixing model.[6] On the other hand, if the absorption due to trimolecular collisions is taken into account, the analytical form for the absorption of mixing will contain a term which has its maximum at $f=2/3$ or $1/3$. This term might also bring about the asymmetry of the ΔA_m curve. Although, at the present stage, it is not clear how much the trimolecular collision contributes to the absorption, it seems probable that the trimolecular absorption is considerably smaller than the bimolecular absorption[8] and that the main features of ΔA_m curve are governed by the latter. Then the deviation in the f-dependence of ΔA_m from Eq. 6 may be ascribed to the deviation in the mixing state from the random mixing. In order to get further insight into the mixing state, theoretical studies about the f-dependence of φ are needed.

References

1) G. W. F. Pardoe, *Trans. Faraday Soc.*, **66**, 2699 (1970).
2) G. J. Davies and J. Chamberlain, *J. Chem. Soc., Faraday Trans. 2*, **69**, 1739 (1973).
3) K. Sato, Y. Ohkubo, T. Moritsu, S. Ikawa, and M. Kimura, *Bull. Chem. Soc. Jpn.*, **51**, 2493 (1978).
4) S. K. Garg, J. E. Bertie, H. Kilp, and C. P. Smyth, *J. Chem. Phys.*, **49**, 2551 (1968).
5) J. S. Rowlinson, "Liquids and Liquid Mixtures," 2nd ed, Butterworths, London (1969).
6) V. W. Schulze, *Z. Anorg. Chem.*, **261**, 297 (1950).
7) A. W. Andrews and K. W. Morcom, *J. Chem. Thermodynamics*, **3**, 519 (1971).
8) A. Rastogi and R. P. Lowndes, *J. Phys. B*, **10**, 495 (1977).

BULLETIN OF THE CHEMICAL SOCIETY OF JAPAN, VOL. 52 (1), 229—230 (1979)

Molecular Structure of 5β,6β-Isopropylidenedioxy-15,16,17-trinorgrayan-10(20)-ene-3,14-dione as Revealed by X-Ray Methods

Akio FURUSAKI,* Shinsei GASA, and Takeshi MATSUMOTO
Department of Chemistry, Faculty of Science, Hokkaido University, Sapporo 060
(Received June 13, 1978)

Synopsis. The molecular structure of the title compound has been determined by means of the X-ray method. The A, B, and C rings take half-chair, chair, and chair conformations, respectively, while the heterocyclic ring is of envelope form.

We report herewith on an X-ray study of the molecular structure of 5β,6β-isopropylidenedioxy-15,16,17-trinorgrayan-10(20)-ene-3,14-dione (**1**), obtained from the tetracyclic diterpene grayanotoxin II (**2**). Compound **1** was used as a link in the relay total synthesis of **2**.[1] The present study was undertaken in order to know the exact stereostructure and conformation of **1**.

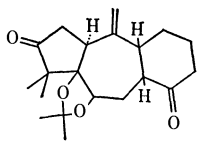

1

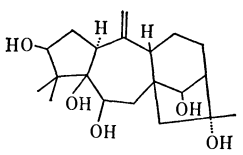

2

Experimental

Single crystals of **1** were obtained as colorless plates or columns from an ethereal solution. A crystal with dimensions of $0.2\times0.2\times0.4$ mm^3 was used for the X-ray measurement. The crystal data are as follows: $C_{20}H_{28}O_4$, mp 208—211 °C; space group $P2_12_12_1$; $a=9.500(3)$, $b=21.524(4)$, $c=8.758(3)$ Å; $Z=4$, $D_c=1.233$ g·cm^{-3}. Both the cell dimensions and diffraction intensities were measured on a Rigaku four-circle diffractometer using Cu $K\alpha$ radiation ($\lambda=1.5418$ Å) monochromatized with an LiF crystal. The intensities obtained were corrected for the Lorentz and polarization factors, but not for the absorption or the extinction effect. In the range of 2θ-values up to 140°, 1871 unique structure factor magnitudes above $\sigma(F_0)$ were selected for the structural study.

Structure Determination

The structure was determined by means of the Monte Carlo direct method.[2] The starting set was composed of the 10 strongest reflections given in Table 1. Tentative phase values for these reflections were derived from successively generated random numbers. In order to extend this tentative phase set, 10 cycles of the tangent procedure were performed using 380 E-values above 1.30. In this manner, the 40th phase set was extended to 367 phases, showing a low R_k-value of 23.5% ($R_k=\Sigma||E_o|-k|E_c||/\Sigma|E_o|$).[3] An E-map computed with these phases revealed the locations of all 24 non-hydrogen atoms.

It is of interest to compare the 40th random phase set with the correct phases calculated with the final atomic parameters. All the 10 reflections are not assigned phase values close to their correct phases (see Table 1). Great differences of 0.335π, π, and 0.434π can be seen for the (1 2 8), (3 0 7), and (2 19 3) reflections, respectively. It should be noted that, in spite of such great errors, this random phase set could lead to the correct structure. The structure thus obtained was refined by the block-diagonal-matrix least-squares method, first with isotropic temperature factors and then with anisotropic ones. The value $R=\Sigma||F_o|-k|F_c||/\Sigma|F_o|$ was reduced to 9.5%. After 28 hydrogen atoms had been found in a difference Fourier map, the least-squares refinement was repeated including these hydrogen atoms with isotropic temperature factors. For the refinement, the following weighting scheme was used:

$$W = 1/\{\sigma(F_0)^2 \exp(AX^2+BY^2+CXY+DX+EY)\},$$

where $X=|F_o|$ and $Y=\sin\theta/\lambda$. Coefficients A, B, C, D, and E were determined from $(\Delta F)^2$ values in each cycle. In this way, the R value reached 4.5%. The final parameters for the non-hydrogen atoms are given in Table 2.

Table 1. The 40th phase set and correct phases (in $10^{-3}\pi$)

	h	k	l	$\|E\|$	Correct	No. 40
1	1	22	0	3.47	500	500
2	3	18	0	3.26	1500	1500
3	2	16	4	3.03	330	500
4	4	3	7	2.98	1384	1500
5	0	18	7	2.84	1000	1000
6	1	2	8	2.84	1915	250
7	3	0	7	2.67	1500	500
8	2	19	3	2.61	66	500
9	0	9	8	2.60	500	500
10	5	13	3	2.58	632	500

The calculations for the present study were carried out on a FACOM 230-75 computer at the Computing Center of Hokkaido University, using our own programs. The atomic scattering factors were taken from International Tables for X-Ray Crystallography (1962), Vol. III. The tables of the observed and calculated structure factors are kept at the Chemical Society of Japan (Document No. 7911).

Results and Discussion

The molecular framework of **1** and the torsion angles for the tetracyclic system are shown in Figs. 1 and 2, respectively. Of the two five-membered rings, the A ring takes a somewhat distorted half-

Table 2. Final atomic parameters and estimated standard deviations

The β_{22} values are multiplied by 10^5 and the others by 10^4. The temperature factors are defined as $\exp(-\beta_{11}h^2-\beta_{22}k^2-\beta_{33}l^2-\beta_{12}hk-\beta_{13}hl-\beta_{23}kl)$.

Atom	x/a	y/b	z/c	β_{11}	β_{22}	β_{33}	β_{12}	β_{13}	β_{23}
O(1)	1638 (4)	4094 (2)	7025 (3)	209 (4)	401 (7)	151 (3)	−36 (3)	−153 (7)	−6 (3)
O(2)	−1272 (2)	4424 (1)	3950 (2)	110 (2)	175 (3)	106 (2)	16 (2)	−14 (4)	2 (2)
O(3)	−1514 (3)	4342 (1)	1389 (2)	177 (3)	192 (4)	116 (2)	29 (2)	−72 (5)	8 (2)
O(4)	−2260 (3)	2721 (1)	−1629 (2)	155 (3)	355 (6)	107 (3)	−15 (2)	−41 (5)	−4 (2)
C(1)	−454 (3)	3359 (1)	4168 (3)	92 (2)	164 (4)	87 (3)	1 (2)	−5 (5)	8 (2)
C(2)	−192 (3)	3478 (1)	5885 (3)	134 (3)	200 (5)	90 (3)	7 (2)	−23 (6)	7 (2)
C(3)	985 (3)	3947 (1)	5905 (3)	119 (3)	219 (6)	120 (3)	9 (2)	−52 (6)	−10 (3)
C(4)	1215 (3)	4210 (1)	4292 (3)	98 (3)	188 (5)	131 (3)	−5 (2)	−15 (6)	−9 (2)
C(5)	−166 (3)	4015 (1)	3477 (3)	92 (2)	150 (4)	91 (3)	−1 (2)	2 (5)	2 (2)
C(6)	−198 (3)	4055 (1)	1721 (3)	126 (3)	169 (4)	96 (3)	−17 (2)	11 (5)	16 (2)
C(7)	−112 (3)	3447 (1)	816 (3)	102 (3)	197 (5)	88 (3)	−20 (2)	23 (5)	7 (2)
C(8)	−1483 (3)	3061 (1)	825 (3)	81 (2)	195 (5)	93 (3)	0 (2)	−1 (5)	6 (2)
C(9)	−1780 (3)	2669 (1)	2284 (3)	87 (2)	175 (4)	105 (3)	−13 (2)	0 (5)	3 (2)
C(10)	−1815 (3)	3055 (1)	3734 (3)	105 (3)	158 (4)	97 (3)	−11 (2)	12 (5)	15 (2)
C(11)	−790 (3)	2107 (1)	2396 (3)	136 (3)	167 (5)	131 (3)	−7 (2)	−39 (6)	5 (2)
C(12)	−876 (4)	1700 (1)	970 (4)	151 (4)	192 (5)	183 (5)	3 (3)	−26 (8)	−22 (3)
C(13)	−539 (4)	2078 (2)	−459 (4)	123 (3)	288 (7)	147 (4)	−7 (3)	15 (6)	−48 (3)
C(14)	−1483 (3)	2630 (1)	−549 (3)	88 (3)	259 (6)	102 (3)	−27 (2)	19 (5)	−2 (2)
C(15)	2520 (3)	3872 (2)	3622 (5)	91 (3)	339 (8)	187 (5)	−9 (3)	13 (7)	−34 (4)
C(16)	1513 (4)	4906 (1)	4358 (4)	151 (4)	219 (6)	167 (4)	−38 (3)	−25 (8)	−11 (3)
C(17)	−2975 (4)	3098 (2)	4551 (4)	124 (3)	273 (7)	138 (4)	−27 (3)	72 (6)	−16 (3)
C(18)	−1958 (3)	4697 (1)	2661 (4)	144 (4)	189 (5)	132 (4)	20 (2)	−48 (7)	4 (2)
C(19)	−1539 (5)	5374 (1)	2478 (5)	224 (6)	183 (6)	208 (5)	27 (3)	−69 (11)	17 (3)
C(20)	−3538 (4)	4635 (2)	2830 (5)	142 (4)	360 (10)	225 (7)	35 (4)	−96 (10)	−2 (4)

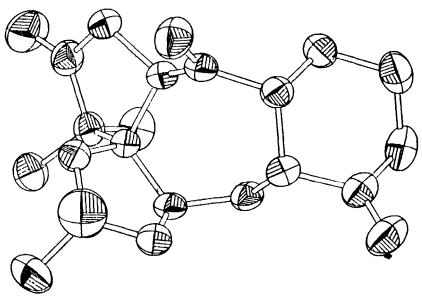

Fig. 1. The molecular framework of **1**.

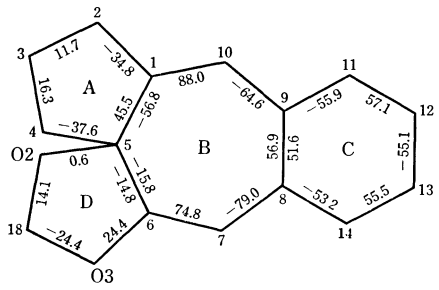

Fig. 2. The torsion angles (°) for the tetracyclic system. For the sake of clarity, only the torsion angles relevant to atoms which form the same ring are given in the ring.

chair form with an approximate two-fold rotation axis through the C(3) atom; the C(16) and O(2) atoms are equatorial and axial, respectively. On the other hand, the D ring takes an almost exact envelope form with an approximate mirror plane through the O(3) atom; the C(19) atom is axial. As a result of such ring conformations, the C(16) and C(19) atoms maintain a distance of 3.482(6) Å from each other. The seven-membered B ring takes a chair-like form and is nearly symmetrical with respect to a plane which runs through the C(9) atom, bisecting the C(5)–C(6) bond nearly perpendicularly. The six-membered C ring has a somewhat flattened chair form in which the axial positions in the C ring of the grayanane skeleton become equatorial and *vice versa*. All the observed bond distances and angles are normal; the average values for $C(sp^3)$–$C(sp^3)$, $C(sp^2)$–$C(sp^3)$, C=C, C–O, and C=O bond distances are 1.54, 1.51, 1.32, 1.43, and 1.21 Å, respectively.

References

1) S. Gasa, N. Hamanaka, S. Matsunaga, T. Okuno, N. Takeda, and T. Matsumoto, *Tetrahedron Lett.*, **1976**, 553.
2) A. Furusaki, *Acta Crystallogr.*, in press.
3) J. Karle and I. L. Karle, *Acta Crystallogr.*, **21**, 849 (1966).

BULLETIN OF THE CHEMICAL SOCIETY OF JAPAN, VOL. 52 (1), 231—232 (1979)

The Principle of Corresponding States at Elevated Pressure

Kenji KUBOTA* and Kazuyoshi OGINO

Department of Pure and Applied Sciences, College of General Education, University of Tokyo, Komaba, Meguro-ku, Tokyo 153

(Received June 14, 1978)

Synopsis. The principle of corresponding states was examined at elevated pressure, and the validity of the assumption that the external degrees of freedom of the solution are given by linearity in the weight fraction of the components was examined without any model by use of the superposition method.

The principle of corresponding states[1,2] has been investigated extensively. Especially, the theory of moderately concentrated polymer solution thermodynamics[3,4] has shown newer development and made great success by the aid of the free volume theory.[5] In this theory, themodynamic quantities of the solution are represented by the characteristic parameters and the interaction energy parameter. This theory emphasizes the importance of the volume dependence of the free energy, and it is the elementary problem how the quantities characterizing the properties of the mixture are related to those of the respective components.[6] In this point, several model theories have been presented,[2-4] but, it is scarce that the characteristic parameters of the mixture are determined directly form P-V-T relations of it and are compared with those of respective components.[6,7] Moreover, it is of great importance that the volume dependence of the free energy should be examined from the pressure effect.[7] In this note, we examined the validity both of the principle of corresponding states at elevated pressure and of the assumption that the external degrees of freedom of the solution are given by linearity in the weight fraction of the components by use of the superposition method.

The examined systems are nitrobenzene,[8] aniline,[8] their mixture,[9] bromobenzene,[8] chlorobenzene,[8] *trans*-decalin,[10] and poly(dimethylsiloxane)[11] for the investigation of the principle of corresponding states at elevated pressure, and nitrobenzene-aniline,[9] poly(dimethylsiloxane)-benzene,[7] and poly(isobutylene)-benzene[12] for the investigation of the assumption for the external degrees of freedom.

According to the principle of corresponding states, the equation of states is represented by

$$f(\tilde{P},\ \tilde{V},\ \tilde{T}) = 0,\quad \tilde{P} = P/P^*,\quad \tilde{V} = V/V^*,\quad \tilde{T} = T/T^*, \tag{1}$$

where tilde and asterisk signify respectively the reduced quantities and the characteristic parameters. These characteristic parameters are related to each other by the relation

$$P^*V^* = T^*S^*, \qquad S^* = ck, \tag{2}$$

where c is the external degrees of freedom, and V^* and c are expressed in per gram.

Using these relations, thermal expansion coefficient and isothermal compressibility can be made to be dimensionless and reduced as follows:

$$\begin{aligned} \alpha T &= (\partial \ln V/\partial \ln T)_P = (\partial \ln \tilde{V}/\partial \ln \tilde{T})_{\tilde{P}} = \tilde{\alpha}\tilde{T}, \\ \beta P &= (\partial \ln V/\partial \ln P)_T = (\partial \ln \tilde{V}/\partial \ln \tilde{P})_{\tilde{T}} = \tilde{\beta}\tilde{P}. \end{aligned} \tag{3}$$

Accordingly, αT and βP are the universal functions of reduced quantities and should be expressed by a master curve. Since $\tilde{P} \simeq 0$ at atmospheric pressure, because P^* for these substances are few thousands bars, αT at atmospheric pressure plotted against $\ln T$ or $\ln V$ can be superposed by shifting along the abscissa. As $\beta P = \tilde{\beta}\tilde{P}$ gives $\ln\beta = \ln\tilde{\beta} - \ln P^*$, the curves of $\ln\beta$ *vs.* $\ln T/a_{T^*}$ can be superposed by shifting along the ordinate, since for the same value of T/a_{T^*}, $\tilde{T}$ is same each other. From these shift factors, a_{T^*} from αT *vs.* $\ln T$, a_{V^*} from αT *vs.* $\ln V$, and a_{P^*} from $\ln\beta$ *vs.* $\ln T/a_{T^*}$, the ratios of the characteristic parameters to those of the reference substance are obtained:

$$a_{P^*} = P^*/P_1^*,\quad a_{V^*} = V^*/V_1^*,\quad a_{T^*} = T^*/T_1^*, \tag{4}$$

where 1 implies the reference substance. The ratio of the external degrees of freedom are given from these by

$$c/c_1 = a_{P^*}a_{V^*}/a_{T^*}. \tag{5}$$

Moreover, at the same value of P/a_{P^*}, αT *vs.* $\ln T/a_{T^*}$ should give the well superposed one curve. By use of a_{T^*} and a_{V^*}, the universal relation of V/a_{V^*} *vs.* T/a_{T^*} is also obtained. This correspeonds to the intersection of $f(\tilde{P},\tilde{V},\tilde{T})$ with $\tilde{T}$-$\tilde{V}$ surface of $\tilde{P}$-$\tilde{V}$-$\tilde{T}$ space. In this way, without any model theory the characteristic parameter (ratio) is determined and the principle of corresponding states at elevated pressure is examined.

The superposed curves of αT *vs.* $\ln T/a_{T^*}$ at 1, 400, and 800 bar for nitrobenzene (reference substance)—P_1 in Figs. 1 and 2—are shown in Fig. 1. They are well superposed and show that a^*'s in Eqs. 4 determined at atmospheric pressure is proper even for elevated pressure and does not change with pressure. This is shown also in Fig. 2 for the relation between T/a_{T^*} and V/a_{V^*} at various pressures. Though it is not shown in Figs. 1 and 2 (since the range of αT is beyond that of these Figs.), the superposition is well performed for poly(dimethylsiloxane)-benzene and poly(isobutylene)-benzene mixtures. Therefore, at elevated pressure the principle of corresponding states is valid and the superposition is applicable.

The relation of the external degrees of freedom for nitrobenzene-aniline, poly(dimethylsiloxane)-benzene, and poly(isobutylene)-benzene mixtures determined as the above with the weight fraction could not be expressed by linearity. For example, c/c_1 *vs.* weight fraction of aniline for nitrobenzene-aniline mixture is shown in Fig. 3. In all cases, negative discrepancy

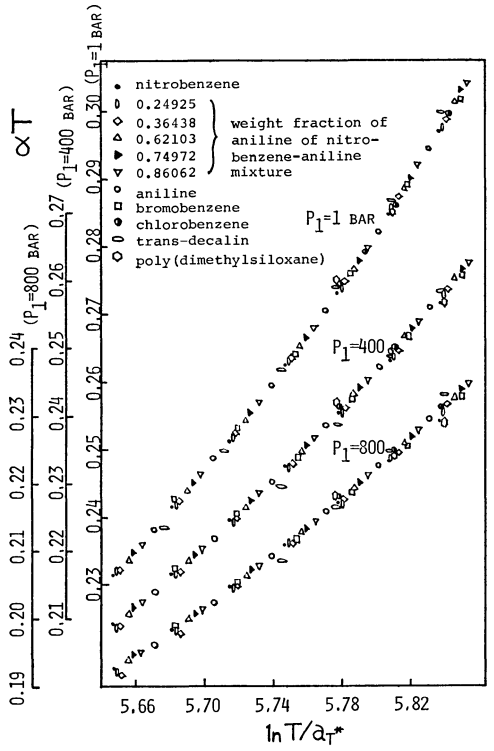

Fig. 1. The superposed curve of αT plotted against $\ln T/a_T*$. The indicated pressure, P_1, is for nitrobenzene (reference substance).

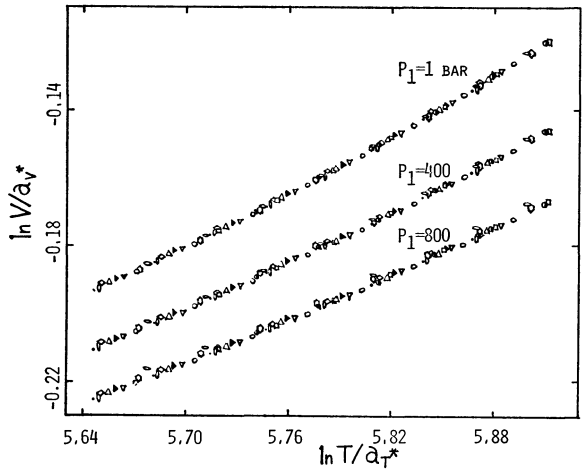

Fig. 2. The superposed curve of $\ln V/a_V*$ *vs.* $\ln T/a_T*$. The symbols for the substances are same as in Fig. 1.

was observed. In poly(dimethylsiloxane)–benzene the discrepancey is about 1.4% at 50% weight fraction and in poly(isobutylene)–benzene that is about 0.9% at 50%. This discrepancy corresponds to Q_{12}, entropy correction term of the new Flory theory.[3] This implies that the relation of the external degree of freedom with concentration much influences to the theoretical prediction for the solution thermodynamics, and the assumption of linearity is open to further consideration.

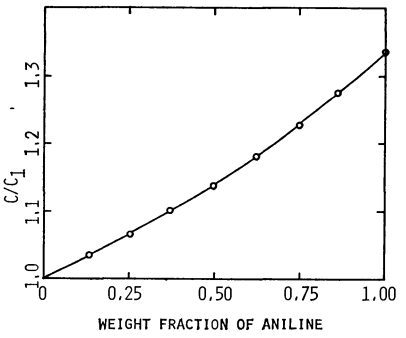

Fig. 3. The relation of the ratio of the external degrees of freedom of nitrobenzene–aniline mixture with weight fraction of aniline.

Table 1. Characteristic parameters at 30 °C and atmospheric pressure determined by use of the newer Flory theory

	$P*$ (Bar)	$V*$ (cm³/g)	$T*$ (K)
Nitrobenzene	7198	0.6898	5863
trans-Decalin	5063	0.9487	5726
Poly(dimethylsiloxane)	3390	0.8410	5563

For comparison, the characteristic parameters determined by the newer Flory theory for nitrobenzene, *trans*-decalin, and poly(dimethylsiloxane) are tabulated in Table 1. These are the values obtained at 30 °C and atmospheric pressure.

References

1) I. Prigogine, "The Molecular Theory of Solutions," North-Holland Publishers, Amsterdam (1957).
2) R. Simha and A. J. Halvik, *J. Am. Chem. Soc.*, **86**, 197 (1964).
3) P. J. Flory, *Discuss. Faraday Soc.*, **49**, 7 (1970).
4) D. Patterson and G. Delmas, *Discuss. Faraday Soc.*, **49**, 98 (1970).
5) For example, B. E. Eichinger and P. J. Flory, *Trans. Faraday Soc.*, **64**, 2035 (1968).
6) H. Noguchi and T. Nose, *Kobunshi Ronbunshu*, **33**, 293 (1976).
7) K. Kubota, Y. B. Kim, K. Kubo, and K. Ogino, *Rept. Progr. Polym. Phys. Jpn.*, **20**, 43 (1977).
8) R. E. Gibson and O. H. Loeffler, *J. Am. Chem. Soc.*, **61**, 2515 (1939).
9) R. E. Gibson and O. H. Loeffler, *J. Am. Chem. Soc.*, **61**, 2877 (1939).
10) G. V. Schulz and M. Lechner in "Light Scattering from Polymer Solutions," ed by M. B. Huglin, Academic Press, New York 1971.
11) K. Kubota and K. Ogino, *Macromolecules*, in press.
12) J. A. R. Renuncio and J. M. Prausnitz, *Macromolecules*, **9**, 324 (1976).

BULLETIN OF THE CHEMICAL SOCIETY OF JAPAN, VOL. 52 (1), 233—234 (1979)

A Refinement of the Crystal Structure of Creatine Monohydrate

Yoshihiro KATO,* Yoshitaka HAIMOTO, and Kiichi SAKURAI
Department of Physics, Osaka Kyoiku University, Tennoji-ku, Osaka 543

(Received July 10, 1978)

Synopsis. The crystal structure of creatine monohydrate has been refined from three-dimensional X-ray data. This refinement introduces minor modifications to the positional and thermal parameters and confirmed the zwitter ion structure.

Mendel and Hodgkin[1] have determined the crystal structure of creatine monohydrate from three-dimensional X-ray data and inferred that the structure of the molecule corresponds to that of a zwitter ion. They calculated the *h0l* structure factors including hydrogen atoms placed at the probable positions, but the intensity data were not accurate enough to warrant the hydrogen atom positions. The present paper describes a refinement of the structure, which has determined the positions of the hydrogen atoms and confirmed that the molecule adopts a zwitter ion form.

Experimental

The intensities of 1411 independent reflections were measured visually from Cu $K\alpha$ Weissenberg photographs taken about b ($k=0$—4) and c ($l=0$). The cross-section of the crystal used was 0.35×0.35 mm. Corrections for Lorentz and polarization factors were applied in the usual way, but no correction for absorption was made. The lattice constants were determined from photographs taken with a Buerger's back-reflection Weissenberg camera calibrating the camera radius by using a silver wire. The crystal data are as follows: $a=12.510(6)$, $b=5.048(1)$, $c=12.191(1)$ Å, $\beta=108.9(3)°$, $P2_1/c$, $Z=4$.

Refinement of the Structure

Using the positional and thermal parameters taken from the previous determination,[1] the three-dimen-

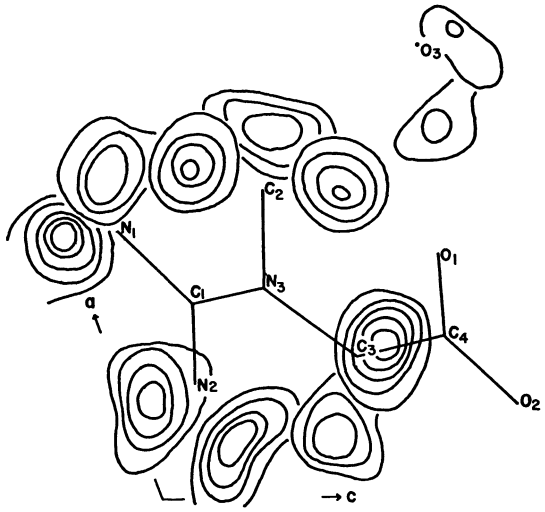

Fig. 1. A composite representation of the three-dimensional difference map on (010). Contours are at intervals of 0.1 e Å^{-3} begining with 0.1 e Å^{-3}.

Table 1. Atomic coordinates and their standard deviations

	x	M & H[a]	y	M & H[a]	z	M & H[a]
N_1	0.2894(2)	0.289	0.4702(8)	0.472	0.3083(2)	0.306
N_2	0.1184(2)	0.119	0.3678(8)	0.370	0.3277(2)	0.329
N_3	0.2255(2)	0.224	0.7147(8)	0.715	0.4351(2)	0.434
C_1	0.2113(2)	0.211	0.5217(9)	0.520	0.3582(2)	0.358
C_2	0.3308(3)	0.331	0.8674(11)	0.874	0.4719(3)	0.472
C_3	0.1507(3)	0.148	0.7429(9)	0.744	0.5049(3)	0.502
C_4	0.1705(2)	0.170	0.5408(9)	0.542	0.6012(2)	0.600
O_1	0.2568(2)	0.256	0.3950(7)	0.397	0.6250(2)	0.625
O_2	0.0981(2)	0.098	0.5289(7)	0.529	0.6520(2)	0.651
O_3	0.4848(2)	0.484	0.3577(8)	0.356	0.6891(3)	0.689
$H(N_1)$	0.362		0.550		0.322	
$H(N_1)$	0.278		0.340		0.243	
$H(N_2)$	0.111		0.226		0.270	
$H(N_2)$	0.051		0.422		0.345	
$H(C_2)$	0.354		0.935		0.404	
$H(C_2)$	0.395		0.723		0.511	
$H(C_2)$	0.325		1.010		0.526	
$H(C_3)$	0.069		0.717		0.450	
$H(C_3)$	0.156		0.920		0.535	
$H(O_3)$	0.402		0.395		0.674	
$H(O_3)$	0.496		0.555		0.729	

a) The coordinates given by Mendel and Hodgkin.

Table 2. Anisotropic temperature factors and their standard deviations ($\times 10^4$) expressed in the form $\exp\{-(B_{11}h^2+B_{22}k^2+B_{33}l^2+B_{12}hk+B_{13}hl+B_{23}kl)\}$

	B_{11}	B_{22}	B_{33}	B_{12}	B_{13}	B_{23}
N_1	35 (2)	664 (21)	57 (2)	−25 (9)	52 (3)	−34 (10)
N_2	30 (2)	671 (21)	60 (2)	−36 (9)	43 (3)	−74 (10)
N_3	40 (2)	555 (18)	44 (2)	−17 (9)	39 (3)	−7 (9)
C_1	32 (2)	525 (20)	38 (2)	12 (9)	23 (3)	7 (10)
C_2	52 (2)	688 (28)	78 (3)	−108 (13)	62 (4)	−53 (14)
C_3	42 (2)	602 (23)	47 (2)	35 (10)	43 (3)	−12 (11)
C_4	30 (2)	540 (21)	38 (2)	7 (9)	26 (3)	−30 (9)
O_1	36 (1)	719 (19)	75 (2)	125 (8)	52 (3)	144 (10)
O_2	33 (1)	802 (19)	56 (2)	33 (8)	51 (2)	65 (9)
O_3	35 (2)	783 (21)	107 (3)	−65 (9)	42 (3)	−20 (12)

Table 3. Interatomic distances (Å) and bond angles (°)

		M & H[a]			M & H[a]
N_1–C_1	1.334 (6)	1.35	$N_1C_1N_2$	117.1 (4)	118
N_2–C_1	1.346 (6)	1.32	$N_1C_1N_3$	121.1 (4)	121
N_3–C_1	1.324 (6)	1.32	$N_2C_1N_3$	121.8 (4)	121
N_3–C_2	1.466 (7)	1.49	$N_3C_3C_4$	114.3 (4)	113
N_3–C_3	1.462 (6)	1.46	$C_1N_3C_2$	120.3 (4)	121
C_3–C_4	1.514 (6)	1.51	$C_1N_3C_3$	121.3 (4)	119
C_4–O_1	1.260 (6)	1.25	$C_2N_3C_3$	116.9 (4)	117
C_4–O_2	1.253 (6)	1.25	$C_3C_4O_1$	118.9 (4)	121
O_1–O_3	2.709 (6) [b]	2.71[b]	$C_3C_4O_2$	116.9 (4)	118
			$O_1C_4O_2$	124.1 (4)	123

a) The values given by Mendel and Hodgkin. The standard deviations in all bond lengths are 0.01 Å and those in bond angles are 4°. b) Hydrogen-bond distances.

sional refinements were carried out by the block-diagonal least-squares method for non-hydrogen atoms. The weighting scheme of the type $1-\exp(-15\,s^2)$ with $s=\sin\theta/\lambda$ was used. At a later stage of the refinement, hydrogen atoms were included in the calculations with a fixed thermal parameter ($B=3.5$ Å^2) and fixed positional parameters deduced from an F_o-F_c Fourier synthesis (Fig. 1). The final R value was 0.096. The final positional parameters are given in Table 1 together with those reported by Mendel and Hodgkin.[1] The thermal parameters are given in Table 2. A list of the observed and calculated structure factors are kept in the office of the Chemical Society of Japan (Document No. 7906).

The calculations were carried out on a NEAC SYSTEM 800 computer of the Computation Center of Osaka University using the program *HBLS V* written by Y. Okaya and T. Ashida for the least-squares refinement.

Description and Discussion of the Structure

The atoms N_1, N_2, C_1, and N_3 of the guanidine group are on the plane $0.2226X-0.6380Y+0.7371Z-1.6408=0$, and C_3, C_4, O_1, and O_2 are on the plane $0.3177X+0.6774Y+0.6634Z-6.3695=0$, where X, Y, and Z are referred to the orthogonal axes a, b, and c^* (Å). These planes intersect at an angle of 82.7° with each other. The interatomic distances and bond angles are listed in Table 3, which shows that these values are in good agreement with those reported by Mendel and Hodgkin.[1]

The F_o-F_c Fourier synthesis indicated clearly all the hydrogen atoms (Fig. 1). The four hydrogen atoms attached to the guanidine group are about 1 Å away from N_1 and N_2 atoms, while there appears no hydrogen peak around the carboxyl group, which shows that the hydrogen atom of the carboxyl group is transferred to the guanidine group. The molecule of creatine, therefore, corresponds conclusively to that of a zwitter ion in the crystal.

Reference

1) H. Mendel and D. C. Hodgkin, *Acta Crystallogr.*, **7**, 443 (1954).

BULLETIN OF THE CHEMICAL SOCIETY OF JAPAN, VOL. 52 (1), 235—236 (1979)

Radical-Ion Interaction. Diphenylmethyl and Triphenylmethyl Radicals Generated by the Dissociative Electron Attachment to Halogenated Compounds in Rigid Matrices

Tatsuo IZUMIDA, Yoshio TANABE, Tsuneki ICHIKAWA, and Hiroshi YOSHIDA*

Faculty of Engineering, Hokkaido University, Kita-ku, Sapporo 060

(Received July 21, 1978)

Synopsis. Dissociative electron attachment to diphenylmethyl halides and triphenylmethyl halides in a γ-irradiated 3-methylhexane matrix at 77 K generates free radicals temporarily associated with a counterpart halide ion. The association is indicated by changes in the fluorescence and excitation spectra of the radicals as well as the charge-transfer excitation band of the radical-ion complexes.

Temporary radical-ion association has been indicated by the fluorescence spectrophotometric method for benzyl radicals[1-3] and the methyl-substituted derivatives (at the phenyl ring[2] and at the methylene position[4]) generated by the dissociative electron attachment to the corresponding halogenated compounds such as benzyl halides in organic glassy matrices γ-irradiated at 77 K. The radical-ion interaction causes the wavelength shift and the change in the vibration band structure of the benzyl spectra as well as the decrease in the fluorescence lifetime. The interaction has also been indicated by the charge-transfer band of the benzyl radical-halide ion complexes in nonpolar hydrocarbon matrices. The interaction is absent in a polar ethanol matrix probably because of the solvation of the halide ions. The temporary radical-ion association before complete dissociation appears as a general feature in solid state radiation chemistry and adds a new aspect to the molecular spectroscopy of radical intermediates. The study was extended to diphenylmethyl and triphenylmethyl radicals, because they show a similar absorption character to that of the benzyl radicals.[5-8] The triphenylmethyl radical shows an intense near-UV absorption due to the allowed $A_2''\leftarrow E''$ transition and a weak visible absorption due to the forbidden $A_1''\leftarrow E''$ transition. The assignment is based on the assumed D_{3h} symmetry of the radical. The forbidden transition is observable because of a slight deviation from the assumed planar configuration.[7] A similar assignment may be applicable to the diphenylmethyl radical.

Experimental

Diphenylmethane, dephenylmethyl chloride (Ph_2CHCl) and bromide (Ph_2CHBr), and triphenylmethyl chloride (Ph_3CCl) and bromide (Ph_3CBr), of analytical grade, were used as received. The solvents, 3-methylhexane (3MHx) and ethanol (EtOH), were purified as described elsewhere.[2] The solutions (10^{-2}—10^{-3} mol·dm^{-3}) were prepared under vacuum of *ca.* 10^{-5} Torr, sealed in quartz tubes (i.d. 4 mm), frozen by liquid nitrogen into the glassy state, and irradiated at 77 K with ^{60}Co γ-rays to a dose of *ca.* 5×10^4 rad or with unfiltered light from a high pressure mercury lamp. The fluorescence and fluorescence excitation spectra of the irradiated samples were recorded with a conventional fluorescence spectrophotometer (Hitachi, Model MPF-2A) at 77 K.

Results and Discussion

Diphenylmethyl Radical. When the diphenylmethyl (Ph_2CH) radical is generated by the dissociative electron attachment to Ph_2CHCl in the γ-irradiated EtOH matrix, the highest peak in the fluorescence spectrum is at 523 nm and the highest peak in the excitation spectrum is at 337 nm as shown in Fig. 1A. These spectra are essentially the same as those reported previously.[5-7] The excitation spectrum in the visible region is however too weak to be recorded. Although the vibration band structure is not well resolved, as is usually the case for glassy matrix samples, the peaks mentioned above indicate the wavelength of the 0-0 band for the electronic transitions in the near-UV and visible regions. The photolysis of Ph_2CH_2 gives also

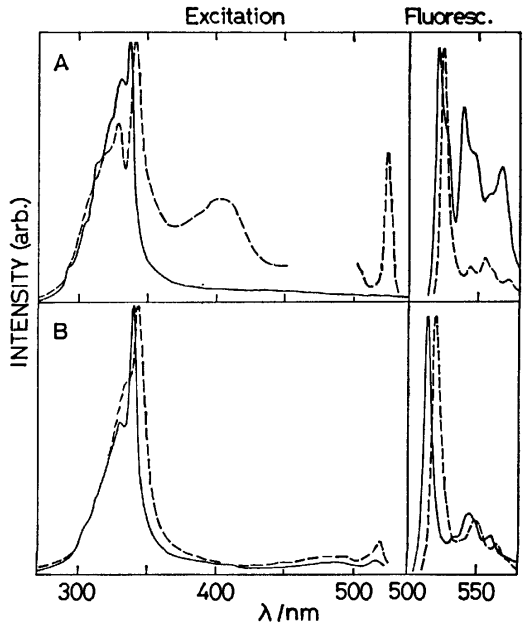

Fig. 1. Fluorescence and excitation spectra of (A) Ph_2CH radical generated from Ph_2CHCl and (B) Ph_3C radical generated from Ph_3CCl (——) in the EtOH matrix and (- - -) in the 3MHx γ-irradiated at 77 K. The spectral shape in the wavelength 460—500 nm shown by the dashed curve in A could not be determined because of the resonance lines of the Xe lamp used as a excitation source. Th excitation wavelengths and the monitoring one are generally at the highest peak of the fluorescence spectra and the excitation ones.

Table 1. Fluorescence and excitation spectra of diphenylmethyl and triphenylmethyl radicals generated by dissociative electron attachment to the corresponding halo-compounds in 3-methylhexane and ethanol matrices at 77 K

Radical	Source	Matrix	Wavelength (nm) Fluorescence[a]	Excitation[b]	CT-band[c]
$\dot{C}H(C_6H_5)_2$	$CH(C_6H_5)_2Cl$	3 MHx	526	342	405
		EtOH	523	337	—
	$CH(C_6H_5)_2Br$	3 MHx	526	341	460[e]
		EtOH	523	336	—
$\dot{C}(C_6H_5)_3$	$C(C_6H_5)_3Cl$	3 MHx	520 (515)[d]	344 (341)	—
		EtOH	514 (513)	341 (342)	—
	$C(C_6H_5)_3Br$	3 MHx	519 (515)	345 (340)	—
		EtOH	514 (513)	341 (341)	—

a) The 0-0 band of the fluorescence spectrum. b) The 0-0 band of the near-UV excitation spectrum. c) The peak of the CT excitation spectrum. d) The figures in parentheses give the wavelength after melting and refreezing of the irradiated samples. e) A satellite peak was observed at 395 nm.

the same spectra except that they overlap with the spectra of the benzyl radical attributed to the loss of a phenyl ring from the parent molecule. The Ph_2CH radical generated from Ph_2CHCl in the γ-irradiated 3MHx matrix gives a different spectra from those observed from the EtOH matrix (Fig. 1A): the spectra shift to the red, and the vibration band structure so changes that the 0-0 band comparatively increases in intensity. The visible excitation spectrum becomes intense enough to be recorded. These features are the same as those observed for the benzyl radicals and have been interpreted as the effect of the proximity of the halide ions to the radicals.[2] A similar phenomenon has been observed for the Ph_2CH radical from Ph_2CHBr, as representatively shown for the spectral red-shift in Table 1. In the EtOH matrix, the halide counter-ion is solvated with polar matrix molecules, so that the radical-ion interaction no longer affects the spectra of the Ph_2CH radical.

The radical-ion interaction has also been indicated by the presence of a broad unstructured excitation band at 405 nm observed from Ph_2CHCl in the 3MHx matrix (Fig. 1A). A similar band has been recorded for Ph_2CHBr at 460 nm with a satellite peak at 395 nm. Assignment has been made to the CT band of the Ph_2CH radical-halide ion complexes; the former having a large electron affinity acts as an electron acceptor, and the latter with a small ionization energy (the electron affinity of Cl and Br atom is 3.61 and 3.36 eV[9]) as an electron donor. The CT transition energy approximates to. $h\nu_{CT}=IP(X^-)-EA(R\cdot)+E_s(R\cdot\!-\!-X^-)-E_s(R^-\!-\!-X)$, where IP and EA represent the ionization energy and the electron affinity, and E_s is the solvation energy before and after the transition. $E_s(R\cdot\!-\!-X^-)$ can be expressed approximately by Born's formula, $E_s(X^-)=(e^2/2r)(1-1/D)$, where r is the effective radius of the halide ion and D is the dielectric constant of the matrix. The difference in the CT transition energy between 3.1 eV (405 nm) and 2.7 eV (460 nm) of 0.4 eV for Cl^- and Br^- as a counter-ion agrees well with 0.45 eV, the difference of $IP(X^-)+E_s(X^-)$ calculated from the dielectric constant, 2.0, for 3MHx[10] and the ionic radius, 0.164 and 0.180 nm for Cl^- and Br^-.[11] The energy difference between the main peak and the satellite one, 0.44 eV, observed for the Ph_2CH–Br^- complex may be interpreted as being due to the splitting of the CT excited state caused by the large separation between the $^2P_{3/2}$ and $^2P_{1/2}$ states of the bromine atom, 0.459 eV.

Triphenylmethyl Radical. Triphenylmethyl (Ph_3C) radicals generated from Ph_3CCl and Ph_3CBr in the γ-irradiated EtOH and 3MHx matrices give the spectra, as shown in Fig. 1B, of which the spectroscopic parameters are given in Table 1. The "free" Ph_3C radical in the EtOH matrix shows a visible fluorescence spectrum as well as a weak excitation spectrum in the visible region and an intense one in the near UV region. The Ph_3C radical in the 3MHx matrix shows a red-shift of the spectra (see Table 1) and an increase in spectral intensity in the visible region. The above observations indicate a radical-ion interaction for the Ph_3C radical.

Removal of the halide counter-ion produces further evidence for the interaction. The Ph_3C radical is so stable that it persists on melting the irradiated samples. The spectra of the Ph_3C radical in the 3MHx matrix changes and becomes identical with the spectra observed from the EtOH matrix, when examined after melting and refreezing. This change has been attributed to the removal of the counter-ion. The spectra observed from the EtOH matrix show no change upon melting and refreezing, since the radical is initially "effectively free" from the counter-ion in the matrix.

No CT band was recorded for the Ph_3C radical-halide ion complex in the 3MHx matrix. The intermolecular conformation adequate to the CT interaction is sterically inhibited for the bulky Ph_3C radical. However, the present investigation gives spectroscopic evidence for the temporary radical-ion association for the Ph_3C radical, as well as for the Ph_2CH radical, generated by the dissociative electron attachment in the irradiated nonpolar 3MHx matrix at 77 K.

References

1) M. Irie, M. Shimizu, and H. Yoshida, *Chem. Phys. Lett.*, **25**, 102 (1974).
2) M. Irie, M. Shimizu, and H. Yoshida, *J. Phys. Chem.*, **80**, 2008 (1976).
3) T. Izumida, T. Ichikawa, and H. Yoshida, *J. Phys. Chem.*, in press.
4) T. Saito and H. Yoshida, *Bull. Chem. Soc. Jpn.*, **47**, 3167 (1974).
5) I. Orman and G. Poter, *Proc. R. Soc. London, Ser. A*, **230**, 399 (1955).
6) G. N. Lewis, D. Lipkin, and T. T. Magel, *J. Am. Chem. Soc.*, **66**, 1579 (1944).
7) T. L. Chu and S. I. Weissman, *J. Chem. Phys.*, **22**, 21 (1954).
8) T. Okamura, K. Obi, and I. Tanaka, *Chem. Phys. Lett.*, **20**, 90 (1973).
9) R. S. Berry and C. W. Reimann, *J. Chem. Phys.*, **38**, 1540 (1963).
10) L. Kevan, "Advances in Radiation Chemistry, ed by M. Burton and J. L. Magee, John Wiley, N. Y. (1974), Vol. 4, p. 188.
11) B. S. Gourary and F. J. Adrian, *Solid State Phys.*, **1K**, 127 (1960).

BULLETIN OF THE CHEMICAL SOCIETY OF JAPAN, VOL. 52 (1), 237—238 (1979)

Kinetics on the Formation and Transformation of Alkoxy-derived $SrSiO_3$

Osamu YAMAGUCHI,* Kenzo MATSUMOTO, and Kiyoshi SHIMIZU*

Department of Applied Chemistry, Faculty of Engineering, Doshisha University, Karasuma Imadegawa, Kamigyo-ku, Kyoto 602

(Received April 17, 1978)

Synopsis. A metastable modification of $SrSiO_3$ was formed at 850—910 °C from mixed powders prepared by the alkoxy-method. Crystallization isotherms were best described by the first-order equation and the activation energy was determined as 130 kcal/mol. The kinetics on the transformation of metastable to stable $SrSiO_3$ was also studied.

Though $SrSiO_3$ is known only in the pseudo-wollastonite modification,[1] Takahashi and Roy[2] reported that a new modification is obtained by heating the $SrSiO_3$ glass prepared by the splat-cooled method. It was found that this compound, apparently metastable, is formed during the course of heating of alkoxy-derived $SrSiO_3$. The present study is concerned with the kinetics on the formation of metastable $SrSiO_3$ and the transformation of metastable into stable $SrSiO_3$.

Experimental

Silicon ethoxide used was of guaranteed purity. Strontium methoxide was prepared by the reaction of strontium metal and dehydrated methyl alcohol. The purity of strontium metal used was 99%. A mixture of these alkoxides with the mole ratio $Sr^{2+}/Si^{4+}=1:1$ was prepared, and then poured into aqueous solution of ammonia at *ca.* 30 °C. The temperature was slowly raised up to 90 °C with stirring. The mixed powders hydrolyzed in this way were washed repeatedly with hot distilled water and dried at 40 °C under reduced pressure. The average particle size of the mixed powders is approximately 400—500 Å.

Results and Discussion

The TG of the mixed powders was carried out in the air from room temperature to 1000 °C(Fig. 1). The weight loss of 11% up to 650 °C is attributed to the loss of absorbed H_2O, NH_3(aq), and organic residue from the parent alcohol. DTA of the mixed powders was also performed. Two exothermic reactions were observed at 850—910 °C and 950—1020 °C. From the results of X-ray diffraction, the reactions were found to be the crystallization of metastable $SrSiO_3$ from an amorphous phase and the transformation of metastable into stable $SrSiO_3$, respectively.

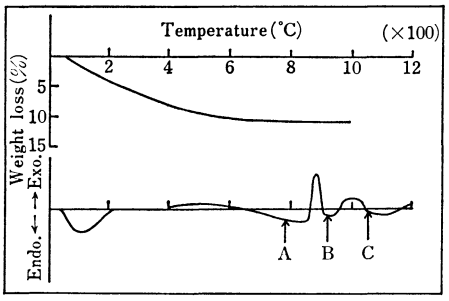

Fig. 1. TG and DTA curves of alkoxy-derived powder. Arrows show the temperatures at which the starting material was heated to obtain three specimens for X-ray diffraction.

Figure 2 shows the variation of X-ray diffraction patterns of $SrSiO_3$ with increasing temperature. The mixed powders as a raw material were amorphous, no significant changes being observed up to 820 °C. The peaks corresponding to metastable $SrSiO_3$[2] appeared after heat treatment at 850 °C for 20 min, and the intensity increased rapidly up to 900 °C. The specimen heated at 1050 °C showed an X-ray diffraction pattern of only stable $SrSiO_3$.[3]

Figure 3 shows the fraction of the metastable $SrSiO_3$

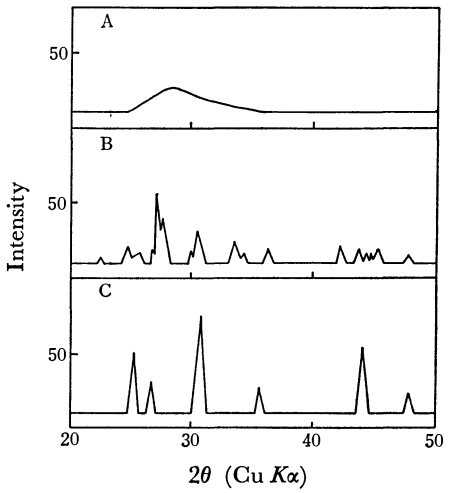

Fig. 2. X-Ray diffraction patterns for alkoxy-derived $SrSiO_3$ powder.
A: 780 °C, B: 920 °C, C: 1050 °C.
Heating rate: 600 °C/h.

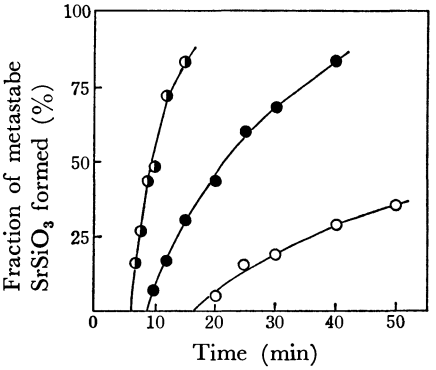

Fig. 3. Formation of metastable $SrSiO_3$ as a function of time at different temperatures.
○: 850 °C, ●: 870 °C, ◑: 890 °C.

crystallization determined for 850, 870, and 890 °C. The mixed powders were pre-heated at 400 °C for 15 min. The fraction of crystallization of each specimen was determined from the height of $d=3.28$ Å($2\theta=27.2°$) which is the strongest line of the metastable $SrSiO_3$ spectrum. A well-crystallized specimen was obtained by heating the alkoxy-derived mixed powders at 900 °C for 30 min. Calcium fluoride was used as a standard material. Induction periods were observed, attempts being made to fit the results to kinetic laws by considering the induction periods. The data can be interpreted in terms of the first-order equation. Figure 4 shows the first-order plots of $-\ln(1-\alpha)$ against t, where α is the fraction of crystallization and t time. The rate constants were determined from the slopes of straight lines. The value of activation energy calculated from the Arrhenius plot was *ca.* 130 kcal/mol. This represents the activation energy employed for establishing active nucleation centers.[4]

Figure 5 shows the fraction of the transformation of metastable into stable $SrSiO_3$ as a function of time at different temperatures. The specimens heated at 900 °C for 30 min were used as starting material. The

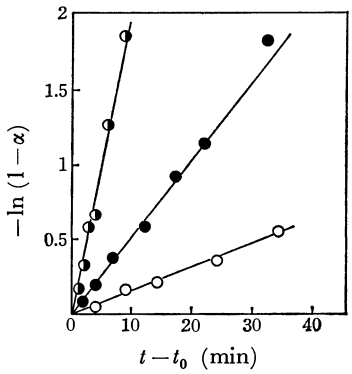

Fig. 4. First-order plots of the data of Fig. 3.
○: 850 °C, ●: 870 °C, ◑: 890 °C.

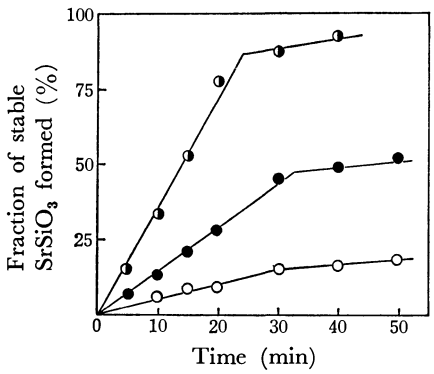

Fig. 5. Phase transformation from metastable to stable $SrSiO_3$ as a function of time at different temperatures.
○: 950 °C, ●: 970 °C, ◑: 990 °C.

fraction of transformation was established by determining the decrease of height of the strongest line($d=3.28$ Å) in the metastable diffraction pattern. Transformation isotherms were described by the zero-order equation $\alpha=kt$, where α is the fraction of transformation, t time and k the rate constant of propagation.[4] The result suggests that the transformation, which might take place in two processes(Fig. 5, broken line), is due to only a rearrangement of atoms or ions within the crystal, no penetration of a new phase from the surface being required. The values of activation energy were *ca.* 143 kcal/mol and 44 kcal/mol for initial and final stages, respectively.

References

1) E. T. Carson and L. S. Wells, *J. Res. Nat. Bur. Stand.*, **51**, 73 (1953).
2) T. Takahashi and R. Roy, *J. Am. Ceram. Soc.*, **58**, 348 (1975).
3) X-Ray powder data file (ASTM card 6-0415).
4) R. W. Grimshaw, J. Hargreaves, and A. L. Roberts, *Trans. Brit. Ceram. Soc.*, **55**, 36 (1956).

BULLETIN OF THE CHEMICAL SOCIETY OF JAPAN, VOL. 52 (1), 239—240 (1979)

Effect of Gelatin on the Reduction of Cobalt(II) in Thiocyanate Solutions at Mercury Electrodes

Eiki ITABASHI* and Kumiko TAKAYA
Miyagi University of Education, Aoba, Aramaki, Sendai 980

(Received May 19, 1978)

Synopsis. Reduction of cobalt(II) in thiocyanate solutions at mercury electrodes has been greatly accelerated in the presence of small amounts of gelatin. This accelerating effect results in an inhibition of the amalgamation of electrodeposited Co(0)SCN^-, which reacts chemically to yield CoS and CN^-. Both CoS and CN^- further stimulate the reduction of cobalt(II).

Recently, it has been shown that the reduction of cobalt(II) in thiocyanate solution at a hanging mercury drop electrode(HMDE) is accelerated by the reduction products of thiocyanate ions, cyanide and sulfide ions, produced by the chemical reduction of thiocyanate ion with the electroreduced metallic cobalt.[1] It is expected that the reduction rate of cobalt(II) in thiocyanate solution is further stimulated by the presence of surfactants, because the amalgamation of the electrodeposited cobalt is known to be inhibited by the presence of some surfactants.[2,3] It was indeed found that the reduction of cobalt(II) in thiocyanate solutions at dropping and stationary mercury electrodes was greatly accelerated in the presence of low concentrations of gelatin. This paper deals with the characteristics of the reduction wave of the above-mentioned system.

Experimental

The dropping mercury electrode(DME) had a flow rate of 0.95_6 mg s^{-1} at the controlled drop time of 4.95 s in deaerated 0.5 mol dm^{-3} $NaNO_3$ solution at −0.65 V *vs.* SCE for a mercury height of 60 cm. All the other experimental details were the same as previously described.[1] In Fig. 1, "current" means the maximum current observed just before the fall of the mercury drop.

Results and Discussion

The influence of gelatin on the dc polarograms is shown in Fig. 1. Cobalt(II) in dilute thiocyanate solution gave a pre-wave which was produced at potentials more negative than those for the usual hydrated cobalt(II) reduction wave. This pre-wave increased in height with increase in thiocyanate concentration up to *ca.* 0.1 mol dm^{-3}. The present experiments, however, were performed with dilute thiocyanate solution, because the most significant effect of gelatin has been observed at a thiocyanate concentration below 0.03 mol dm^{-3}. Upon the addition of gelatin to the solution, the pre-wave increased in height with increase in concentration of gelatin up to *ca.* 5×10^{-3} %. With further addition of gelatin above 1×10^{-2} %, the opposite effect was observed. When trace amounts of gelatin was added, the maximum wave accompanying the hydrated cobalt(II) reduction

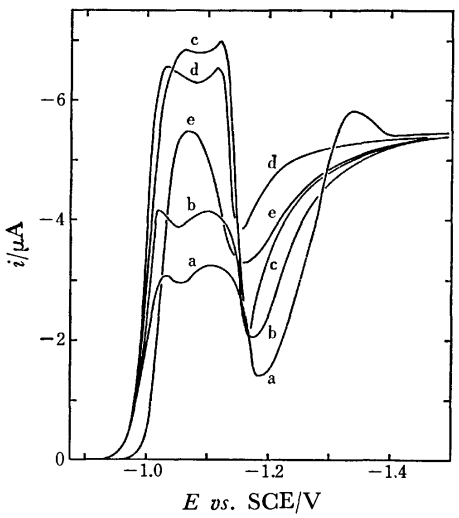

Fig. 1. Effect of concn of gelatin on the d.c. polarograms of 1 mmol dm^{-3} cobalt(II) in 0.01 mol dm^{-3} NaSCN and 0.49 mol dm^{-3} $NaClO_4$ at 25 °C. Gelatin concentration/%: (a), 0; (b), 1×10^{-3}; (c), 2×10^{-3}; (d), 5×10^{-3}; (e), 2×10^{-2}.

wave observed at potentials more negative than −1.20 V was completely suppressed, and the hydrated cobalt(II) reduction wave shifted to somewhat less negative potentials. Such a shift of the reduction potential appears to be generally characteristic of the hydrated cobalt(II) reduction wave. There have been several investigations on the positive shift of the hydrated cobalt(II) reduction wave in the presence of low con-

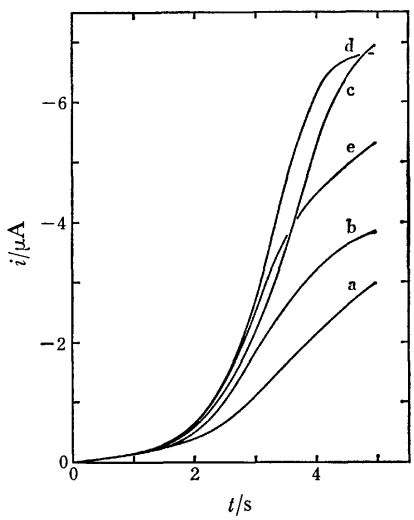

Fig. 2. Effect of concn of gelatin on the *i-t* curves with a DME at −1.05 V *vs.* SCE. Conditions are the same as Fig. 1.

centrations of some surfactants.[2,3]

The influence of gelatin on the current-time (*i-t*) curves for the pre-wave during the life of a mercury drop is shown in Fig. 2. The instantaneous current in a dilute thiocyanate solution in the absence of gelatin varies exponentially. This clearly indicates that the reaction mechanism of the pre-wave in dilute thiocyanate solution is autocatalytic in nature. The theoretical treatment of Laviron[4] predicts that the *i-t* curve varies exponentially for the catalytic polarographic wave involving a product of the electrode reaction. In the presence of gelatin, the *i-t* curves exhibit a sigmoid shape.

Figure 3 illustrates the influence of gelatin on the *i-t* curve obtained with a HMDE. In the potential region corresponding to the polarographic pre-wave, the *i-t* curves exhibited a maximum. With trace amounts of gelatin present, the diffusion-controlled current level is reached within several seconds. The falling portion after a maximum in the presence of gelatin follows an $i\text{-}t^{-1/2}$ relationship, indicating a diffusion-controlled mechanism.

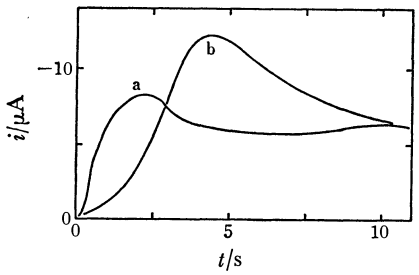

Fig. 3. *i-t* curves with a HMDE for the reduction of 1 mmol dm^{-3} cobalt(II) in 0.01 mol dm^{-3} NaSCN and 0.49 mol dm^{-3} $NaClO_4$ solutions in the absence (a) and presence (b) of 5×10^{-3}% gelatin. Electrode potential −1.05 V.

It has been recognized that the amalgamation of freshly deposited iron-group metals is inhibited by the presence of some surfactants.[2,3] The increase of the pre-wave height in the presence of small amounts of gelatin is accounted for by assuming an inhibition of the amalgamation of electrodeposited $Co(0)SCN^-$, which in part reacts chemically to yield CoS and CN^-. Cobalt sulfide as well as cyanide ion stimulates further reduction of cobalt(II). $Co(II)\text{–}CN^-$ complex is more easily reduced at the mercury electrode than the $Co(II)\text{–}SCN^-$ complex.[1] With large concentrations of gelatin present, the pre-wave becomes suppressed, gelatin then replacing the adsorbed thiocyanate ions from the surface of the electrode.

References

1) E. Itabashi, *J. Electroanal. Chem. Interfacial Electrochem.*, **88**, 205 (1978).
2) V. Ivanov and Z. A. Iofa, *Russ. J. Phys. Chem., Engl. Transl.*, **36**, 571 (1962); *ibid.*, **38**, 1026 (1964).
3) I. M. Kolthoff and P. Mader, *Anal. Chem.*, **41**, 924 (1969); *ibid.*, **42**, 1762 (1970).
4) E. Laviron, *J. Electroanal. Chem. Interfacial Electrochem.*, **52**, 355 (1974).

BULLETIN OF THE CHEMICAL SOCIETY OF JAPAN, VOL. 52 (1), 241—242 (1979)

Dynamic Calibration and Memory Effect for Fluoride Ion Selective Electrode

Yoshio UMEZAWA,* Minoru NAGATA,† Katsuhiko SAWATARI, and Shizuo FUJIWARA

Department of Chemistry, Faculty of Science, The University of Tokyo, Hongo, Tokyo 113

(Received June 9, 1978)

Synopsis. The dynamic calibration of the F^- ion selective electrode was briefly evaluated in terms of the memory effect of the electrode by analyzing the NBS urine standard.

Liberti and Pinto[1] reported the "dynamic" calibration for the iodide ion selective electrode, where the electrode response after a selected time is compared with a calibration curve obtained by contacting the electrodes with standard solutions for the same time. Thus we can continuously monitor quickly changing concentrations, although the response is not necessarily rapid. For most of the solid membrane electrodes such as the fluoride ion electrode, the response time is less than 30 s when we define the response time as the time necessary to cover 95% of the equilibrium potential. The 95% attainment of the equilibrium potential involves about 30% error in the concentration at around 10^{-5} M of F^- ions. If we define the response time as the time to reach 0.2 mV pre-equilibrium potential, for example, the resulting error is 0.2% in terms of concentration, but causes much longer response time as shown in Table 1. This result implies that in the case of ordinary analysis, we are inherently using the dynamic calibration procedure, because final potentials are read in several minutes at longest. On the other hand, one of the main factors which affects the accuracy of results for ion selective electrodes at lower concentration range seems to be the "memory effect." Usually, the calibration curve is constructed by changing the concentration from low to high. In most cases, the concentration of the sample is located at around the middle of the calibration curve. This means one has to come back from higher concentration to lower one to measure the analyte concentration in the sample right after making calibration curves. Hence, the electrode inevitably remembers the higher concentrations of the previous runs causing an error in analysis even when the electrode surface is thoroughly rinsed after each run. This would also hold true for continuous analyses where the concentration could change up and down in a short time.

TABLE 1. RESPONSE TIME FOR F^- ION SELECTIVE ELECTRODE[a)]

Concn of F^- ion(M)	Response time(min)[b)]
2×10^{-7}	200
5×10^{-7}	40
1×10^{-6}	24
5×10^{-6}	22
1×10^{-5}	18
2×10^{-5}	11
1×10^{-4}	5
1×10^{-3}	2

a) F^- ion selective electrode of DKK. b) Necessary time to reach 0.2 mV pre-equilibrium potential.

† Present adress: Denki Kagaku Keiki Co., Kichijoji-kitamachi 4-13-14, Musashino-shi, Tokyo 180.

In the present study, the dynamic calibration procedure was briefly evaluated in terms of the memory effect of the fluoride ion selective electrode by estimating the minimum time required for accurate F^- ion determination in the NBS human urine standard as illustrative example for natural samples. If the dynamic calibration works also satisfactorily for the natural systems, it would be extremely useful for clinical or environemental analysis where rapid and continuous measurements are highly desirable.

Experimental

In order to obtain precise and accurate hard copies of the potential *vs.* time profile of the ion selective electrodes, a special experimental set-up was made.[2] The analog output from the ion selective electrode is first converted into frequencies followed by counting, serialization, and finally data acquisition with a minicomputer. The precision of analog to digital conversion is 0.1 mV.

The dried urine fluoride standard sample (NBS SRM No. 2671) was dissolved in TISAB (Total ionic strength adjustment buffer) solution. The TISAB solution was prepared by dissolving 1 M NaCl, 0.25 M CH_3COOH, 0.75 M CH_3COONa, and 0.001 M sodium citrate in 1 litre of deionized and distilled water. The value recommended by NBS for the fluorine content in this solution is $(4.39\pm0.43)\times10^{-5}$ M (reliability 95%). The result of determination of fluoride ion in this NBS sample by fluoride ion selective electrode coincides with the value recommended by NBS. The total fluorine for the same solution by AlF molecular absorption spectrometry in carbon rod furnace[3] coincides with that of ion selective electrodes and of the NBS value within experimental error.[4] It seems that very little matrix effect exists and almost all fluorine containing species are of the form of free fluoride ion in the dissolved NBS standard sample. The magnitude of the error in the NBS value is rather large presumably due to the average of different lots. Thus, each bottle from the NBS probably contains a homogenous sample and the resulting analytical value should have higher precision. The response time of the fluoride ion selective electrode was examined with four electrode specimens, one from TOA and the other three from DKK. It was found that except for one from DKK which exhibited slightly slower response, three showed almost equal response time (Table 1). Therefore, the experiment concerning the memory effect was performed by using two electrode specimens from DKK, both of which gave virtually the same results (Tables 2 and 3).

Chemicals of analytical grade were used. Water was deionized and distilled. Fluoride ion selective electrodes from Denki Kagaku Keiki Co. (DKK) and TOA Dempa Co., Ltd., were used. An Ag/AgCl electrode of TOA Model HS 305 DP was used as a reference electrode. All fluoride ion selective electrodes were rinsed, excess water being wiped off before and after each run. For the dissolved NBS sample, the response time obtained is virtually equal to or slightly shorter than that of the ordinary F^- ion standard solution.

The measurement was performed in a constant temperature bath in a constant temperature room, both thermostated at 20±0.5 °C. The sample solution was stirred with a magnetic stirrer.

Results and Discussion

Table 2 shows the apparent concentration of F^- ions in the NBS standard urine sample obtained through the dynamic calibration curves at different waiting times. We deal with two cases: Analysis of the NBS sample is made after the measurements of 1) 1×10^{-4} M and 2) 1×10^{-5} M of the standard solutions for the calibration curves. The F^- ion concentrations for the NBS sample lies between these concentrations. The apparent concentration of F^- ions obtained in the NBS standard urine sample is initially higher than the NBS value for case 1) and gradually decreases to a nearly steady state value, C_1, in about 9 min. This value is consistent with the NBS value, indicating that the memory effect is completely removed. For actual analyses where the concentration of the analyte is not known, it is not clear whether the error from the memory effect is still involved in the C_1 value. Thus the following experiment corresponding to case 2) was performed. The apparent F^- concentration obtained in the NBS standard is initially lower than that of the NBS recommended value in contrast to case 1, increasing gradually to a steady state value, C_2, in about 6 min. The value is also consistent with the NBS value. From these results, it can be concluded that the most accurate method to remove the memory effect completely is to obtain the value C_0 which lies on the asymptotic line between the two concentration-time profiles, nearly equal to both C_1 and $C_2(C_1 \fallingdotseq C_2)$. This procedure may be called "double calibration." The memory free accurate result can be obtained when the waiting time exceeds 6—9 min. The lower the concentration of the analyte, the lower the accuracy (Table 3). However, even in the presence of the memory effect, we can still obtain fairly accurate results with a *ca.* 20 % error for 10^{-5} M NBS urine standard solution at a waiting time of 6 s.

Table 2. Determination of F^- ion in NBS urine sample[a] through dynamic calibration procedure for F^- ion selective electrode (see text.)

Waiting time (s)	Analysis A[b] ($\times10^{-5}$ M)	Analysis B[b] ($\times10^{-5}$ M)
6	5.40	3.40
9	5.20	3.65
12	5.15	3.75
15	5.05	3.90
18	4.95	3.85
30	4.90	4.25
60	4.65	4.35
120	4.55	4.40
300	4.50	4.45
420	4.50	4.45
540	4.45	4.45
600	4.45	4.40
1200	4.45	4.45
1800	4.45	4.45
3600	4.35	

a) The NBS value: $(4.39\pm0.43)\times10^{-5}$ M. b) Apparent concentrations A and B obtained after measurement of 1×10^{-4} M and 1×10^{-5} M, respectively, of standard solutions.

Table 3. Determination of F^- ion in diluted NBS urine sample[a] through dynamic calibration procedure for F^- ion selective electrode

Waiting time(s)	Apparent concn($\times10^{-6}$ M)[b]
30	8.05
60	5.68
300	4.70
600	4.30
1200	4.30
1500	4.25
1800	4.25
2400	4.20
3000	4.15

a) Concentration, one order of magnitude lower than that of Table 2. The same NBS sample but different lot from that of Table 2. b) Obtained after the measurement of 1×10^{-4} M standard solution.

The authors thank Prof. K. Fuwa and Mr. K. Tsunoda, The University of Tokyo, for valuable comments on the NBS standard sample. Thanks are also due to Denki Kagaku Keiki Co., for the use of several electrode specimens.

References

1) L. Liberti and A. Pinto, *Anal. Chem.*, **49**, 2377 (1977).
2) K. Sawatari, Y. Imanishi, Y. Umezawa, and S. Fujiwara, *Bunseki Kagaku*, **27**, 180 (1978).
3) K. Tsunoda, K. Fujiwara, and K. Fuwa, *Anal. Chem.*, **49**, 2035 (1977).
4) K. Chiba, B. Sc. Thesis, The University of Tokyo (1978).

BULLETIN OF THE CHEMICAL SOCIETY OF JAPAN, VOL. 52 (1), 243—244 (1979)

Absorption and Circular Dichroism Spectra of Bis(ethylenediamine)-(1,3-diamine)cobalt(III) Complexes

Kazuo KASHIWABARA, Masaaki KOJIMA, Sumio ARAKAWA,[1] and Junnosuke FUJITA*

Department of Chemistry, Faculty of Science, Nagoya University, Chikusa, Nagoya 464

(Received June 30, 1978)

Synopsis. New bis(ethylenediamine)cobalt(III) complexes containing various 1,3-diamines have been prepared and resolved (or separated) into optical isomers. The preferred conformations of six-membered 1,3-diamine chelate rings in these complexes seem to be reflected on the absorption and circular dichroism spectra.

In the previous papers,[2,3] we reported that the stable conformations of flexible six-membered chelate rings in some tris(1,3-diamine)cobalt(III) complexes can be elucidated from their absorption and circular dichroism(CD) spectra in the region of the first absorption band. In this note, we have extended such studies to cobalt(III) complexes of the type, $[Co(en)_2(1,3\text{-diamine})]^{3+}$. The diamines used here are (*R,R*)- and (*R,S*)-2,4-pentanediamine(ptn), (*S,S*)- and (*R,S*)-1,3-diphenyl-1,3-propanediamine(dppn), (*S*)-1,3-butanediamine(bn), and (*S*)-1-phenyl-1,3-propanediamine(phtn).

Experimental

Ligands. 1,3-Diamines were prepared by the methods described previously; (*R,R*)- and (*R,S*)-ptn,[4] (*S,S*)- and (*R,S*)-dppn,[5] (*S*)-bn,[6] and (*S*)-phtn.[7]

Complexes. The $[Co(en)_2(1,3\text{-diamine})]^{3+}$ complexes were prepared from 1,3-diamine and *trans*-$[CoCl_2(en)_2]Cl$ in dimethyl sulfoxide according to a method similar to that for $[Co(en)_2(tn)]^{3+}$ (tn=trimethylenediamine).[8] The separation (or resolution) of diastereomers (or enantiomers) except the *R,S*-dppn complex were achieved by SP-Sephadex column chromatography using a 0.2 mol·dm^{-3} Na_2SO_4 or a 0.2 mol·dm^{-3} sodium $(+)_{589}$-tartrate solution as the eluent. The racemic $[Co(en)_2(R,S\text{-dppn})]Br_3\cdot 3H_2O$ complex was resolved with $K_3[Co(S\text{-cysu})_3]\cdot 6H_2O$(cysu=cysteinesulfinato(2−)-SN).[9] The addition of an aqueous solution (30 cm^3) of the resolving agent (1.4 g) to an aqueous solution (30 cm^3) of the complex(1.5 g) gave immediately orange precipitate, which was recrystallized from hot water several times. The product was suspended in water and 1 mol·dm^{-3} hydrobromic acid(20 cm^3) was added to the suspension. The solution became orange and insoluble material ([Co(*S*-Hcysu)$_3$]) was filtered off. The filtrate was evaporated to dryness and the residue was recrystallized from water to give Λ-$[Co(en)_2(R,S\text{-dppn})]Br_3\cdot 3H_2O$.

The results of elemental analysis are given in Table 1.

Measurements. Absorption and CD spectra were recorded on a Hitachi 323 spectrophotometer and a JASCO J-20 Spectropolarimeter, respectively.

Table 1. Analytical data of the complexes

Complex	C/%		H/%		N/%	
	Found	Calcd	Found	Calcd	Found	Calcd
Δ-$[Co(en)_2(R,R\text{-ptn})](ClO_4)_3$	18.48	18.65	5.07	5.22	14.50	14.50
Λ-$[Co(en)_2(R,R\text{-ptn})](ClO_4)_3$	18.70	18.65	5.21	5.22	14.69	14.50
Λ-$[Co(en)_2(R,S\text{-ptn})](ClO_4)_3$	18.80	18.65	4.96	5.22	14.58	14.50
Δ-$[Co(en)_2(S,S\text{-dppn})]Br_3\cdot 3H_2O$	33.06	32.64	5.82	5.77	11.87	12.02
Λ-$[Co(en)_2(S,S\text{-dppn})]Br_3\cdot 2.5H_2O$	32.81	33.06	5.20	5.70	12.10	12.18
Λ-$[Co(en)_2(R,S\text{-dppn})]Br_3\cdot 3H_2O$	32.85	32.64	5.54	5.77	12.11	12.02
Δ-$[Co(en)_2(S\text{-bn})](ClO_4)_3\cdot H_2O$	16.60	16.46	4.89	5.18	14.42	14.40
Λ-$[Co(en)_2(S\text{-bn})](ClO_4)_3\cdot H_2O$	16.59	16.46	5.21	5.18	14.37	14.40
Δ-$[Co(en)_2(S\text{-phth})]Cl_3\cdot 0.5H_2O$	35.32	35.11	7.16	7.02	19.11	18.90
Λ-$[Co(en)_2(S\text{-phtn})]Cl_3\cdot 2.5H_2O$	32.47	32.48	7.40	7.34	17.37	17.48

Table 2. Data of the first absorption and CD bands of the complexes in water

$[Co(en)_2(L)]^{3+}$	Configuration (Conformation of L)[a]	Absorption $\bar{\nu}/10^3$ cm^{-1} (ε)	CD $\bar{\nu}/10^3$ cm^{-1} ($\Delta\varepsilon$)
L=*R,R*-ptn	$\Delta(\lambda)$	21.19 (88.2)	20.01 (−1.42)
			22.88 (+0.16)
R,R-ptn	$\Lambda(\lambda)$	21.10 (98.8)	20.49 (+1.61)
R,S-ptn	Λ(ch)	21.05 (97.5)	20.41 (+1.21)
S,S-dppn	$\Delta(\lambda)$	21.03 (98.1)	20.04 (−1.71)
S,S-dppn	$\Lambda(\lambda)$	20.94 (129)	20.70 (+1.82)
R,S-dppn	Λ(ch)	20.90 (124)	20.36 (+0.93)
R-bn[b]	Δ(ch, λ)	21.10 (92.9)	20.28 (−1.18)
R-bn[b]	Λ(ch, λ)	21.05 (94.6)	20.28 (+1.05)
S-phtn	Δ(ch, λ)	21.00 (104)	20.16 (−1.29)
S-phtn	Λ(ch, λ)	20.94 (113)	20.37 (+1.08)

a) The conformations of L(1,3-diamine) are those with equatorially disposed substituents, and the λ and ch represent the λ-skew and the chair conformations, respectively. b) The absolute configuration of *S*-bn used in the Experiment was changed to its enantiomorph, *R*-bn, since the skew conformations of the other 1,3-diamine chelate rings studied here are all stabilized in the λ-form.

Results and Discussion

Table 2 shows that the peak positions of the first absorption bands for diastereomeric complexes of a given 1,3-diamine shift to higher energies in the order of the *meso*-diamine complex, Λ- and Δ-isomers of the optically active diamine. The *meso* and active diamine chelates listed in Table 2 will be stabilized in the chair and the λ-skew conformations, respectively, since these conformers have substituents disposed equatorially. The *R*-bn and *S*-phtn chelate rings can also take the chair conformation with an equatorial substituent (*vide infra*). The λ-skew conformers in the Δ- and Λ-configurations form the *lel* and the *ob* structures, respectively.[10] Thus, the order of the shift in the absorption bands corresponds to that of chair, $\Lambda(\lambda)$-(*ob*), and $\Delta(\lambda)$(*lel*) structures. This order agrees with the results obtained for some tris(1,3-diamine)cobalt-(III) complexes.[2,3] These findings will also be utilized for determining the absolute configuration of 1,3-diamine ligands.

The energy differences in the absorption bands between each pair of diastereomers of the *R*-bn and *S*-phtn complexes are smaller than those of cases of the ptn and dppn complexes. This fact suggests that the *R*-bn and *S*-phtn chelate rings are in equilibrium between the λ-skew and the chair conformations.

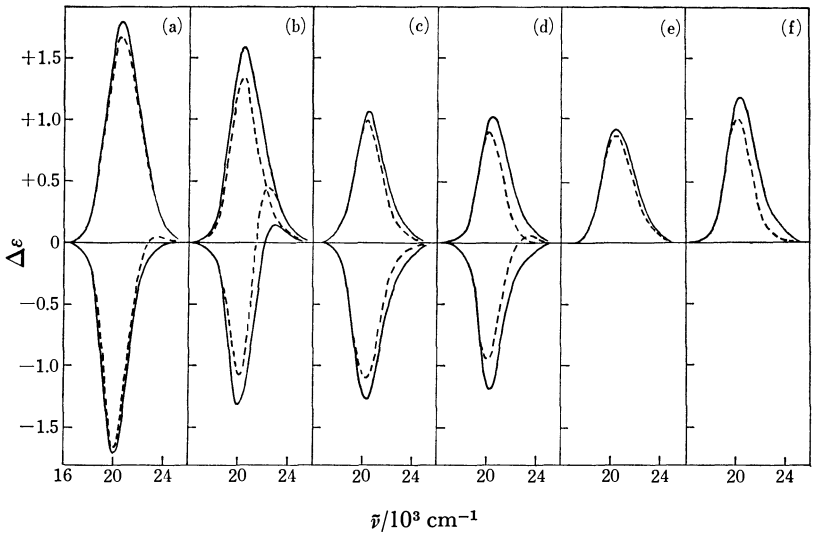

Fig. 1. CD spectra of $[Co(en)_2(L)]^{3+}$ in water (——) and in 0.2 mol·dm^{-3} Na_2SO_4 (----). L; (a) *S,S*-dppn, (b) *R,R*-ptn, (c) *S*-phtn, (d) *R*-bn, (e) *R,S*-dppn, and (f) *R,S*-ptn.

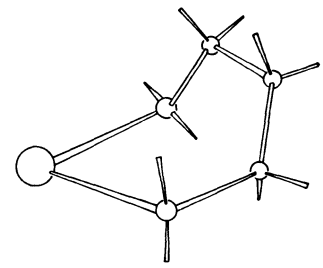

Fig. 2. The envelope conformation of a 1,3-diamine chelate ring.

As stated above, these chelate rings can also take the chair conformation. Molecular models suggest that the difference in the structure between the $\Delta(ch)$ and $\Lambda(ch)$ isomers is smaller than that between the $\Lambda(\lambda)(ob)$ and $\Delta(\lambda)(lel)$ isomers. Hence, the former two isomers give the first absorption bands with a small energy difference from each other.

In Fig. 1 are shown the CD spectra in water in the absence or the presence of sulfate ions. All the complexes show a typical CD pattern for a tris-diamine complex, and their absolute configurations can be assigned on the basis of the CD sign as shown in Table 2. In the presence of sulfate ions, all the complexes diminish the CD strength. Such a phenomenon is known to be caused by increase in the amounts of the $lel_3(\Delta(\lambda\lambda\lambda)$ or $\Lambda(\delta\delta\delta))$ conformer due to ion-association between a complex and a sulfate ion; the lel_3 conformer is the most effective structure in forming an ion-pair through hydrogen bonding between the amino protons and the sulfate ion,[11] and since the CD sign due to the vicinal effect of a λ ligand is positive opposite to that due to the configurational effect of a Δ isomer, the CD strength of the $lel_3(\Delta(\lambda\lambda\lambda))$ conformer should be smaller than those of other conformers such as lel_2ob $(\Delta(\lambda\lambda\delta))$ or $lelob_2(\Delta(\lambda\delta\delta))$.[2] For the present complexes of the optically active diamines, the Δ-isomers will be stabilized in the $\Delta(\lambda\lambda\lambda)(lel_3)$ conformer and reduced their CD strengths in the presence of sulfate ions. On the other hand, the Λ-isomers can form the $\Lambda(\delta\delta\delta)(lel_3)$ conformer with difficulty, since the δ forms of the present 1,3-diamine chelate rings involve axially disposed substituents. Similar conformers with one axial substituent are fomed for the *meso*-diamine complexes in the lel_3 form. These conformers will be unstable because of large steric interactions between the substituent and the ethylenediamine ligand. However, when these 1,3-diamine chelate rings take a conformation as shown in Fig. 2, the complex can have the same set of three N–H bonds as that in the lel_3 conformer, and can form a stable ion-pair with a sulfate ion. Such a conformer involves a *cis* form around a skeletal carbon-carbon bond (envelope type), and will be unstable compared with typical chair and skew forms. However, it seems to be much more stable than conformers with axial substituents in an octahedral complex. Although the vicinal contribution of this conformer to CD is unknown at present, the CD change of the Λ- and *meso*-diamine complexes caused by the addition of sulfate ions will also be related to such a conformational change of the 1,3-diamine chelate rings.

The authors wish to thank the Ministry of Education for Scientific Research Grant-in-Aid No. 243013.

References

1) Present address: Department of Chemistry, Wayne State University, Detroit, Michigan 48202, U. S. A.
2) M. Kojima, M. Fujita, and J. Fujita, *Bull. Chem. Soc. Jpn.*, **50**, 898 (1977).
3) M. Kojima and J. Fujita, *Bull. Chem. Soc. Jpn.*, **50**, 3237 (1977).
4) B. Bonsnich and J. MacB. Harrowfield, *J. Am. Chem. Soc.*, **94**, 3426 (1972).
5) S. Arakawa, K. Kashiwabara, J. Fujita, and K. Saito, *Bull. Chem. Soc. Jpn.*, **50**, 2108 (1977).
6) E. Balieu, P. M. Boll, and E. Larsen, *Acta Chem. Scand.*, **23**, 2191 (1969).
7) M. Kojima and J. Fujita, Presented at the 27th Symposium on Coordination Chemistry (Japan), 3B06(1977).
8) H. Ogino and J. Fujita, *Bull. Chem. Soc. Jpn.*, **48**, 1836 (1975).
9) L. S. Dollimore and R. D. Gillard, *J. Chem. Soc. Dalton Trans.*, **1973**, 933.
10) E. J. Corey and J. C. Bailar, Jr., *J. Am. Chem. Soc.*, **81**, 2620(1959).
11) R. Larsson, S. F. Mason, and B. J. Norman, *J. Chem. Soc., A*, **1966**, 301.

BULLETIN OF THE CHEMICAL SOCIETY OF JAPAN, VOL. 52 (1), 245—246 (1979)

Crystal Distortion and Cation Distribution in the System $La_{1/3}NbO_3$–WO_3

Yasuyoshi Torii

Government Industrial Research Institute, Nagoya, Hirate-machi, Kita-ku, Nagoya 462

(Received June 30, 1978)

Synopsis. It has been found that WO_3 is soluble in $La_{1/3}NbO_3$ up to *ca.* 35 mol %. The solid solutions showed an ordered perovskite structure. The orthorhombic distortion changes into a tetragonal one at 20 mol %. The temperature dependence of the tetragonality of typical samples has been examined and the nature of the tetragonal distortion discussed.

$La_{1/3}NbO_3$ is an orthorhombically distorted structure containing two perovskite subcells.[1] Iyer *et al.* reported that the perovskite-type unit cell contains a preferential distribution of La^{3+} ions on alternate c-planes, as shown in Fig. 1.[2] WO_3, on the other hand, is well-known to have a perovskite structure without A-site ions. A-site deficient perovskites with a wide range of non-stoichiometry, such as $La_{1-x}TiO_3$[3] (x=0.03—0.33) and $Sr_{1-x}NbO_3$[4] (x=0.05—0.30), have been reported to be of simple perovskite structure type. $La_{2/3}TiO_3$ is an exception and has the same ordered structure as $La_{1/3}NbO_3$.[5] It is of interest crystallographically to understand how solid solutions between $La_{1/3}NbO_3$ and WO_3 can be formed and whether such ordered arrangement is maintained. The present paper describes the structural properties of this system.

Experimental

The samples were prepared by conventional ceramic techniques, using La_2O_3, Nb_2O_5, and WO_3 as starting materials. Two-cycle firing was carried out in air at 1050—1270 °C for several hours, the samples being left to cool in the furnace. The products were analyzed by X-ray diffraction method, using Cu $K\alpha$ radiation. The lattice constants were determined from the best resolved lines of (004), (020), and (200), which appeared at 2θ=46—47°. Observed intensities were obtained from the diffractometer tracing by weighing the relative areas under the peaks. The theoretical intensities of the reflection lines were calculated according to a method previously reported.[6]

Results and Discussion

The $La_{1/3}NbO_3$–WO_3 system showed single-phase patterns similar to that for $La_{1/3}NbO_3$ up to a composition containing 35 mol % WO_3. In a 40 mol % WO_3 sample, a further phase appeared in small amounts besides the perovskite-like compound. The room temperature lattice constants are shown in Fig. 2. The crystal lattice became contracted by the partial substitution of W^{6+} ions for Nb^{5+} ions. The $c/2a$ ratio decreased with increasing amounts of WO_3. The orthorhombic distortion changed into a tetragonal one at 20 mol % WO_3 and the tetragonality decreased with further increase of WO_3, but the perovskite subcell did not become cubic. The decrease in crystal distortion is probably attributable to the size effect of B-site ions. The intensities of superstructure lines were also observed to decrease with increasing amounts of WO_3. The relative intensities of the typical lines of (001), (011), and (111) are shown by the solid lines in Fig. 3, the intensities of which depend on the La^{3+} ion concentration in this type of perovskite structure. It is impossible, however, to neglect the effect of high scattering power of the W^{6+} ion on intensity. In this respect the partial substitution of Mo^{6+} ions is more favored since the two scattering powers of the Nb^{5+} and Mo^{6+} ions are nearly equal. Unfortunately attempts to prepare solid solutions in the $La_{1/3}NbO_3$–MoO_3 system failed. In order to examine the cation distribution, the theoretical intensities of superstructure lines were calculated using Iyer's crystal data,[2] the results of which are shown by the broken lines in Fig. 3 in comparison with the observed values. Good agreement between the calculated and the observed intensities was obtained. Therefore, the ordered ar-

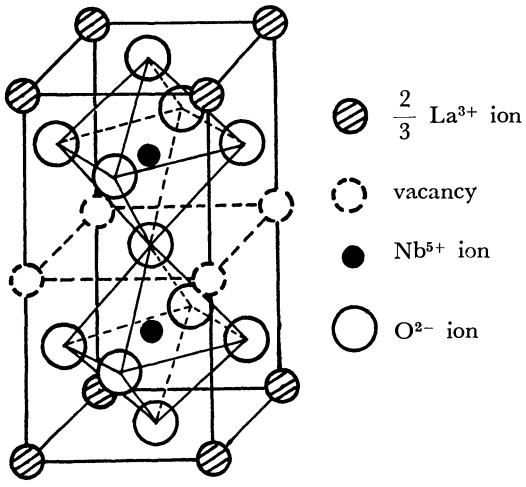

Fig. 1. Crystal structure of $La_{1/3}NbO_3$.

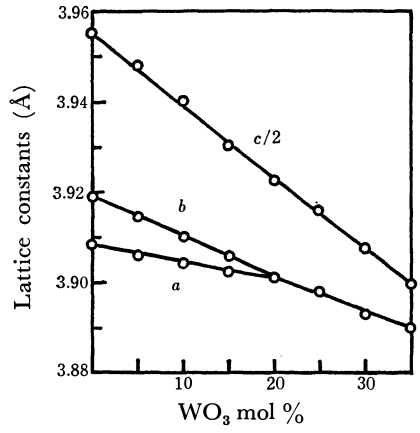

Fig. 2. Lattice constants in the $La_{1/3}NbO_3$–WO_3 system.

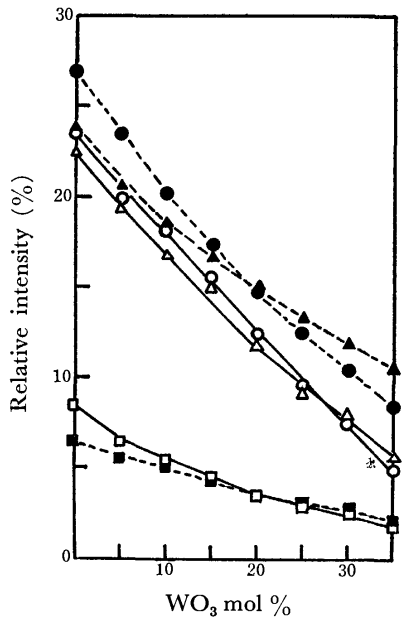

Fig. 3. Observed intensities *vs.* those caluculated for typical superstructure lines in this system.
○: $I_{obsd}(001)$, ●: $I_{calcd}(001)$,
△: $I_{obsd}(011)$, ▲: $I_{calcd}(011)$,
□: $I_{obsd}(111)$, ■: $I_{calcd}(111)$.
$I_{obsd}(001)$ represents observed intensity of (001) line, and $I_{calcd}(111)$ represents the sum of the calculated intensities of (111) and (003) lines which appeared at the nearly same value of 2θ.

rangement of La^{3+} ions as shown in Fig. 1 is completely maintained in the solid solution in the $La_{1/3}NbO_3$–WO_3 system. This is quite different from the situations showing simple perovskite phases of composition $La_{1-x}TiO_3$ (x=0.03—0.30), except $La_{2/3}TiO_3$ (x=0.33) with the ordered structure.

Figure 4 shows the variation of lattice constants of $La_{1/3}NbO_3$ with temperature. The orthorhombic subcell changes into a tetragonal one above *ca.* 190 °C. The $c/2a$ ratio is almost independent of temperature. For the 20 mol % WO_3 sample, the crystal lattice gradually expands with temperature, and the tetragonality remains almost unchanged. The superstructure lines for both samples did not disappear even at 1000 °C. Generally, the low symmetry of ordinary perovskites is expected to improve at high temperatures. It is likely that $La_{1/3}NbO_3$ and its solid solutions differ from ordinary perovskites in the nature of tetragonal distortion. In $La_{1/3}NbO_3$ two Nb^{5+} ions are located at $\pm(1/2, 1/2, z)$, z=0.262. The intensities of the superstructure lines are relatively sensitive to the atomic

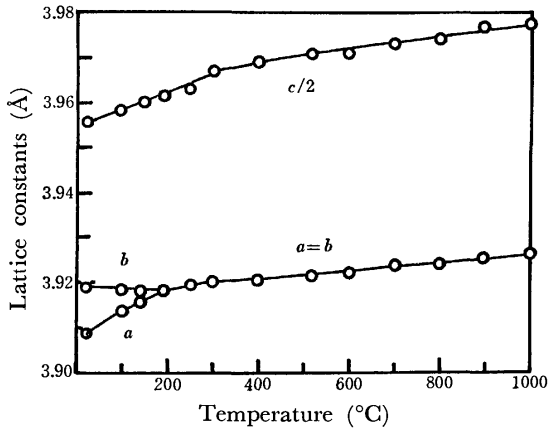

Fig. 4. Temperature dependence of lattice constants for $La_{1/3}NbO_3$.

z parameter from the structure factor. With increase in the z value, the (001) line tends to become weaker while the (011) line becomes stronger. For example, the calculated values of (001) and (011) lines for the 20 mol % WO_3 sample were 16.0 and 9.9 at z=0.25, and 14.7 and 14.9 at z=0.262, respectively. The corresponding observed values were 12.4 and 11.8, respectively. It becomes apparent that the differences between the calculated and observed intensities decrease by the deviation of Nb^{5+} and W^{6+} ions from the B positions of $\pm(1/2, 1/2, 1/4)$. In terms of charge balance, this antiparallel displacement of Nb^{5+} and W^{6+} ions with high valency is considered an important role for the formation of this type of superstructure, where the corner sites are occupied by corresponding amounts of La^{3+} ion and the vertical edge centre sites are vacant. It might be related to the origin of superstructure that the tetragonality in $La_{1/3}NbO_3$ and its solid solution remains nearly unchanged with temperature.

References

1) H. P. Rooksby, E. A. D. White, and S. A. Langston, *J. Am. Ceram. Soc.*, **48**, 447 (1965).
2) P. N. Iyer and A. J. Smith, *Acta Crystallogr.*, **23**, 740 (1967).
3) M. Kestigian and R. Ward, *J. Am. Chem. Soc.*, **77**, 6199 (1955).
4) D. Ridgley and R. Ward, *J. Am. Chem. Soc.*, **77**, 6132 (1955).
5) M. Abe and K. Uchino, *Mater. Res. Bull.*, **9**, 147 (1974).
6) Y. Torii and K. Hasegawa, *Bull. Chem. Soc. Jpn.*, **50**, 2638 (1977).

BULLETIN OF THE CHEMICAL SOCIETY OF JAPAN, VOL. 52 (1), 247—248 (1979)

Electrode Reactions of Several Transition Metal Ions in Aqueous Polyelectrolyte Solutions as Studied by DC and Fourier Transform Polarography

Noboru IMAI,* Michio HIROTA, Yoshio UMEZAWA, and Shizuo FUJIWARA

Department of Chemistry, Faculty of Science, The University of Tokyo, Hongo, Bunkyo-ku, Tokyo 113

(Received August 2, 1978)

Synopsis. The kinetic parameters, k_s for several metal ions are decreased down to 1/10—1/50 in the presence of sodium polyacrylate, although the diffusion of metal ions in the same system differs little with and without sodium polyaclylate.

The electrochemical behavior of proteins and macromolecules has been gaining popularity in recent years.[1,2] In a preceding paper,[3] the diffusion coefficient of transition metal ions in polyelectrolyte solutions has been studied polarographically. However, due to the complexity of overall reactions involved, we could not discuss the following two effects separately; i) adsorption of polyelectrolytes on the surface of the mercury electrode, ii) complex formation of metal ions with polyelectrolytes.

In the present study, the effect of polyacrylate on the reduction process of transition metal ions at the surface of the dropping mercury electrode (DME) will be studied briefly in terms of the adsorption, complex formation with metal ions, and the influence on the kinetic parameters of metal ions.

Sodium polyacrylate (M.W. 2500—7500) purchased from WAKO Chemicals Co. was purified as reported previously.[3] In all cases, 1 M $NaClO_4$ was added to 5 mM polyacrylate aqueous solution in order to make the IR drop of the solution minimum. A saturated calomel electrode (SCE) was used as the reference electrode. The flow rate of mercury was 7.52 mg/s at a mercury column height of 40 cm in 1 M $NaClO_4$ solution at an open circuit. All measurements were performed at (25.0±0.5) °C. The standard rate constant (k_s) and the transfer coefficient (α) were determined using FT polarography, where details of the analysis were also described in the previous paper.[4] Two kinds of the AC potentials with the frequencies of 55.8 and 173.6 Hz and an amplitude (ΔE) of 5 mV were used. Simulations for obtaining k_s and α were performed on a HITAC 8700/8800 system at the Computer Center, The University of Tokyo, using the FORTRAN program written and kindly given by Prof. D. E. Smith.

Adsorption of Polyelectrolyte on DME. From the electrocapillary curves for 1 M $NaClO_4$ solutions with and without sodium polyacrylate, poly(acrylic acid) adsorbs on the DME only when the concentration of proton reaches a value of *ca.* 10 mM. The differential capacity of the interface with and without poly(acrylic acid) were obtained from the fundamental AC current measured by the Fourier Transform AC polarography using the equation

$$C = \frac{I}{f\Delta E},$$

where ΔE is the amplitude of the applied AC voltage, I the resulting fundamental AC current and f the frequency in Hz. The great decrease in the value of capacitance was observed in the presence of polyacrylic acid. This is interpretable in terms of the decrease in the double layer charge due to the adsorption of neutral poly(acrylic acid). No frequency dependence was observed from 55.8 to 173.6 Hz. This result implies that the adsorption equilibrium is fast enough as compared with the time scale of 0.02—0.006 s.

Diffusion Current. As shown in Table 1, the magnitude of diffusion currents of metal ions in 5 mM sodium polyacrylate is dependent on the proton ion concentration of the sample solution. When the value of pH decreases, the magnitude of diffusion currents increases to reach the value in 1 M $NaClO_4$ solution without sodium polyacrylate.

TABLE 1. pH DEPENDENCE OF DIFFUSION CURRENTS FOR METAL IONS WITH AND WITHOUT SODIUM POLYACRYLATE
(Diffusion current μA)

HNO_3 added	No polyacrylate		5 mM polyacrylate		
	0 mM	0 mM	1 mM	3 mM	10 mM
$MnCl_2$	8.2	6.3	7.1	8.3	N[a]
$CoCl_2$	9.4	5.3	6.3	8.1	N
$ZnSO_4$	9.6	N	N	N	9.3
$Pb(NO_3)_2$	11.0	N	N	N	10.8
$Cd(NO_3)_2$	9.8	N	N	N	9.6

a) N: The diffusion currents could not be measured due to the interference of the hydrogen wave and precipitation of hydroxides for Mn(II), Co(II) and Zn(II), Pb(II), Cd(II), respectively.

Possible mechanisms for change in diffusion currents in the presence of sodium polyacrylate are: i) decrease in diffusion coefficient of metal ions due to the complex formation with polyacrylate and/or ii) blocking effect of poly(acrylic acid) adsorbed layer on the diffusion of metal ions. Of these two, the mechanism ii) should be pronounced when the pH values decrease, because the formation of the adsorbed blocking layer, if any, is enhanced in lower pH ranges. However, the observed phenomenon is opposite to expectation from the mechanism ii). From these results, it is concluded that the increase in diffusion currents of metal ions with lower pH is explained in terms of the increase in the diffusion constant through dissociation

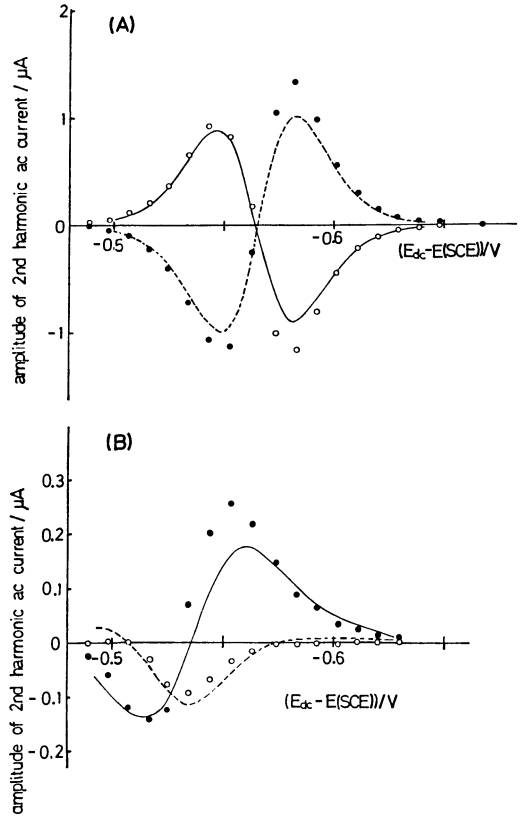

Fig. 1. The second harmonic AC polarogram of cadmium(II) ion with and without sodium polyacryate. ○: In-phase component, ●: quadrature component 2 mM Cd(II) and 1 M $NaClO_4$, (A) no sodium polyacrylate. (B) 5 mM sodium polyacrylate and 10 mM HNO_3.

of polyacrylate ligand from metal ions in acidic media.

Kinetics. Although the adsorbed layer of polyacrylic acid on the DME did not affect the diffusion current of metal ions at low pH regions (see preceding section), the kinetic parameters for the electrode reaction of these metal ions were greatly influenced by this adsorption layer. The kinetic parameters of electrode reactions with and without sodium polyacrylate was obtained through the second harmonic AC polarogram. Typical examples of the second harmonic polarogram for Cd(II) ion with and without sodium polyacrylate in acidic media are shown in Fig. 1, where the computer simulation were performed on these curves using the theoretical equation for the quasi-reversible 2nd harmonic polarogram.[7] The second harmonic polarograms with and without sodium polyacrylate differ appreciably each other.

Table 2. Kinetic parameters (k_s, α) with and without sodium polyacrylate

		α	k_s[c]/cm s^{-1}
$CdSO_4$	a)	0.15[d]	0.45[d]
	b)	0.30±0.02	0.0083±0.0005
$Pb(NO_3)_2$	a)	0.61[e]	10.2[e]
	b)	0.70±0.06	0.19±0.08
$Zn(NO_3)_2$	a)	0.30±0.04	$(3.0\pm1.0)\times10^{-3}$
	b)		$(4\pm2)\times10^{-4}$ [f]

a) No sodium polyacrylate. b) 5 mM sodium polyacrylate, $[HNO_3]=10$ mM. c) Observed rate constant. d) Values from Ref. 5. e) Values from Ref. 6. f) A well-defined second harmonic polarogram were not obtained. Therefore, k_s values roughly estimated from DC polarography.

The kinetic parameters obtained are summarized in Table 2. It is seen that in the presence of 5 mM polyacrylic acid, the value of k_s decreases down to 1/10—1/50 of those obtained without poly(acrylic acid). The shift of half-wave potential and the change in the slope for log $(i/(i_d-i))$ *vs.* E relation were obtained upon the addition of poly(acrylic acid). It is interesting to note that even if the value of kinetic parameters for Pb(II) and Cd(II) decreased upon adding poly(acrylic acid), the DC polarographic parameters such as $\Delta E_{1/2}$ and log $(i/(i_d-i))$ *vs.* E plot for those ions with and without sodium polyacrylate exhibit little change, indicating the electrode reaction for those system is still fast enough as compared with the DC polarographic time scale ($<5\times10^{-4}$ cm s^{-1}).

In conclusion, an electron transfer from the electrode to the metal ions becomes restricted appreciably in the presence of sodium polyacrylate, although the diffusion of metal ions in the same system differs little with and without sodium polyacrylate.

References

1) M. Senda and T. Ikeda, *Bunseki* **36**, 780 (1977).
2) M. Niki, T. Yagi, H. Inokuchi, and K. Kimura, *J. Electrochem. Soc.* **124**, 1889 (1977).
3) H. Kojima and S. Fujiwara, *J. Phys. Chem.*, **74**, 4126 (1970).
4) M. Hirota, Y. Umezawa, H. Kojima, and S. Fujiwara, *Bull. Chem. Soc. Jpn.*, **47**, 2486 (1974).
5) T. Biegler, E. R. Gonzales, and R. Parsons, *Collect. Czech. Chem. Commun.*, **36**, 414 (1971).
6) H. P. Agarwal, *Electrochim. Acta*, **16**, 1395 (1971).
7) M. Hirota, Ph. D. Thesis, Univ. of Tokyo, (1975).

BULLETIN OF THE CHEMICAL SOCIETY OF JAPAN, VOL. 52 (1), 249—250 (1979)

Synthesis and Characterization of (Salicylideneaminoalkyl)phosphonatocopper(II) and [(*N*-Salicylideneglycylamino)alkyl]phosphonatocopper(II)

Ichiro MURASE* and Arthur E. MARTELL†

Laboratory of Chemistry, College of General Education, Kyushu University, Ropponmatsu, Chuo-ku, Fukuoka 810

† *Department of Chemistry, Texas A & M University, College Station, Texas 77843, U. S. A.*

(Received August 28, 1978)

Synopsis. The titled compounds have been synthesized by a template reaction of aminoalkylphosphonic acids or glycylaminoalkylphosphonic acids and salicylaldehyde with copper(II) ion. The square-planar structures have been proposed by analogy with corresponding structures of *N*-salicyclideneglycine or *N*-salicylideneglycylglycine chelates. The deprotonated peptide nitrogen coordination was confirmed by IR-spectra for the phosphonopeptides chelates.

Since (2-aminoethyl)phosphonic acid has been discovered from some living organisms,[1-6] the aminoalkylphosphonic acids have attracted chemical and biological interest in the recent years. Several investigations have been reported for the syntheses of phosphonopeptides[7-9] and phosphonolipids[10] as well as aminoalkylphosphonic acids.[11-13]

It is well known that amino acids or peptides form Schiff bases with salicylaldehyde in the presence of a metal ion as a template and the stable copper(II) chelates have been isolated.[14] Because aminoalkylphosphonic acids and phosphonopeptides are phosphonic analogues of amino acids and peptides, similar metal chelate formation can be expected for these compounds. In the present investigation we have isolated salicylidene derivatives of (aminomethyl)phosphonic acid, (2-aminoethyl)phosphonic acid, (glycylaminomethyl)phosphonic acid, and [2-(glycylamino)-ethyl]phosphonic acid as a copper(II) chelate. This paper deals with synthesis of the copper(II) chelates and characterization of their structural similarity with those of amino acids and peptides by means of electronic and infrared spectroscopy.

Experimental

Reagents. (Aminomethyl)phosphonic acid,[12] (2-aminoethyl)phosphonic acid,[11] (glycylaminomethyl)phosphonic acid,[8] and [2-(glycylamino)ethyl]phosphonic acid[8] were prepared by slight modification of the previous reports.

Sodium [2-(N-Salicylideneamino)ethyl]phosphonatocuprate(II), Na[Cu(saepo)]. (2-Aminoethyl)phosphonic acid (0.63 g, 5 mmol) and salicylaldehyde (0.61 g, 15 mmol) were dissolved in 50 ml of 50% ethanol containing sodium hydroxide (0.6 g, 15 mmol) and powdered copper(II) acetate monohydrate (1.0 g, 5 mmol) was added. The mixture was heated on a water bath for a few minutes and bright green crystals were formed. They were recrystallized from hot water and air dried. Yield 0.4 g. Found: C, 31.45; H, 3.68; N, 4.16%. Calcd for $C_9H_{11}NO_5PCuNa \cdot H_2O$: C, 30.98; H, 3.76; N, 4.02%.

Sodium [(Salicylideneamino)methyl]phosphonatocuprate(II), Na[Cu(sampo)]. The procedure was the same as given for the preparation of Na[Cu(saepo)], using (aminomethyl)-phosphonic acid in place of (2-aminoethyl)phosphonic acid and bright green crystals were obtained in a yield of 0.5 g. Found: C, 30.12; H, 2.93; N, 4.34%. Calcd for $C_8H_7NO_4PCuNa \cdot H_2O$: C, 30.34; H, 2.87; N, 4.42%.

Barium [(N-Salicylideneglycylamino)ethyl]phosphonatocuprate(II), Ba[Cu(sgaepo)]. [2-(Glycylamino)ethyl]phosphonic acid (0.18 g, 1mmol) and salicylaldehyde (0.12 g, 1 mmol) were suspended in 20 ml of water and aqueous sodium hydroxide was added to give a clear solution. To this was added copper-(II) acetate monohydrate (0.2 g, 1 mmol) and the mixture was heated on a water bath, while aqueous sodium hydroxide was added to adjust a pH of 9. After ten minutes, the insoluble precipitate was filtered off and saturated barium chloride solution was added to the filtrate. The resulting blue-violet crystals were filtered and recrystallized from hot water and air dried. Yield 0.4 g. Found: C, 26.57; H, 2.67; N, 5.50%. Calcd for $C_{11}H_{11}N_2O_5PCuBa \cdot H_2O$: C, 26.36; H, 2.62; N, 5.59%.

Barium [(N-Salicylideneglycylamino)methyl]phosphonatocuprate-(II), Ba[Cu(sgampo)]. The procedure was the same as employed for the preparation of Ba[Cu(sgaepo)], but with (glycylaminomethyl)phosphonic acid in place of [2-(glycylamino)ethyl]phosphonic acid. Violet needles were obtained in a yield of 0.4 g. Found: C, 24.39; H, 2.51; N, 5.65%. Calcd for $C_{10}H_9N_2O_5PCuBa \cdot H_2O$: C, 24.66; H, 2.28; N, 5.75%.

Measurements. The infrared spectra were determined in potassium bromide disks by means of a Hitachi EPI-S2 spectrophotometer, while the electronic spectra were measured with a Hitachi EPS-3T spectrophotometer.

Results and Discussion

As described in the experimental section, copper(II) chelate formation is a typical template reaction and proceeded smoothly with equimolar aminoalkylphosphonic acid or glycylaminoalkylphosphonic acid, sali-

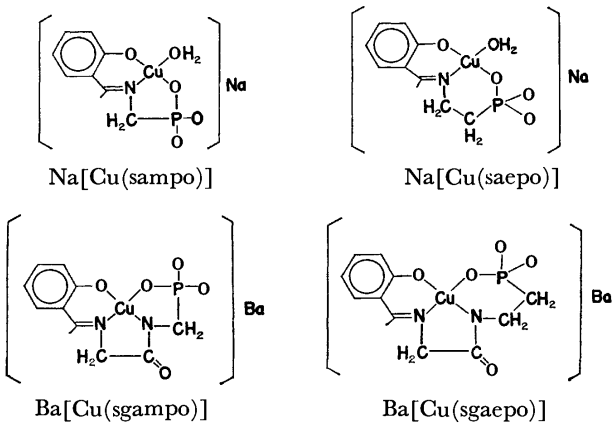

Na[Cu(sampo)] Na[Cu(saepo)]

Ba[Cu(sgampo)] Ba[Cu(sgaepo)]

Fig. 1. Structures of sodium [(salicylideneamino)alkyl]-phosphonatocuprate(II) and barium [(*N*-salycylidene-glycylamino)alkyl]phosphonatocuprate(II).

Table 1. Absorption spectra of the copper(II) chelates in water

Chelate	λ_{max} (nm)	log ε	Chelate	λ_{max} (nm)	log ε
Na[Cu(sampo)]	680	1.99	Ba[Cu(sgampo)]	566	2.10
Na[Cu(saepo)]	700[a]	—	Ba[Cu(sgaepo)]	596	2.08
Cu(sg)[b]	662	1.98	Na[Cu(sgg)]	575	2.20

a) Refrecting spectrum. b) Ref. 14.

Table 2. Infrared spectra of phosphonopeptides and their copper(II) chelates (cm^{-1})

Compound	Amide I	Amide II	$\left(P\langle^{O}_{O}\right)^{-}$	$\left(P\langle^{O}_{O}\right)^{2-}$
H_3(gampo)[a]	1665	1552	1116 1046	—
Ba[Cu(sgampo)]	1590	—	—	1104 1047
H_3(gaepo)[b]	1693	1584	1160 1145	—
Ba[Cu(sgaepo)]	1580	—	—	1096 1045

a) (Glycylaminomethyl)phosphonic acid. b) [2-(Glycylamino)ethyl]phosphonic acid.

cylaldehyde, and copper(II) acetate in an alkaline medium. The probable structures of these chelates are formulated in Fig. 1 by analogy with the corresponding structures of the amino acid and peptide chelates. The elemental analyses also agreed with these formulations.

The electronic spectra of the copper(II) chelates exhibit one broad band due to d-d transition in the visible region. They are shown in Table 1 and compared with those of *N*-salicylideneglycinatocopper(II), Cu(sg) and sodium *N*-salicylideneglycylglycinatocuprate(II), Na[Cu(sgg)]. The close similarity in the absorption maximum and the intensity between the phosphonatocopper and the glycinatocopper clearly indicates the same geometry around the metal ion, *i.e.* square-planar as previously discussed.[14] It is interesting to note that the ligand field strength of the amine-phosphonate coordination is nearly equal to that of amine-carboxylate coordination. In the case of the phosphonopeptide chelates, Ba[Cu(sgampo)] and Ba[Cu(sgaepo)], the amide nitrogen coordinates to the metal ion by deprotonation. This conclusion is supported by the similarity of the ligand field strength to that of Na[Cu(sgg)] in which the coordination of the deprotonated amide nitrogen has been recognized.[14]

Kim and Martell[15] have studied infrared spectra of coordinated peptide in D_2O by varying pD, and assigned the carbonyl band at different solution conditions. The peptide carbonyl band of glycylglycine which exists as a zwitter ion appears at 1665 cm^{-1} and it shifts to 1625 cm^{-1} on coordination through the carbonyl oxygen to the copper(II) ion in acidic solution. The 1625 cm^{-1} band further shifts to 1610 cm^{-1} in alkaline solution and this was interpreted as direct evidence for the ionization of the peptide NH hydrogen. Similar spectral changes were observed in the solid state for the phosphonopeptide chelates as shown in Table 2, and peptide nitrogen coordination in these complexes is indicated. The amide I band (C=O stretching vibration) in the free ligands shifts to lower wave number and the amide II band (NH deformation vibration) disappears on metal chelate formation. This indicates the deprotonation of the amide nitrogen and the resulting delocalization of charge in the $N=C\diagup^{O}$ linkage. The P–O stretching bands of the monoanion in the free ligands also shift to lower wave number on metal chelate formation because of proton ionization to form the dianion.

It is concluded from the present investigation that aminoalkylphosphonic acids and their peptides with amino acids have properties that are similar to those of amino acids and peptides in metal chelate formation so far as copper(II) ion is concerned. Although aminophosphonate peptide derivatives have been described in this paper, there is another fundamentally different type of phosphonopeptide that may be formed; such as $H_2N(CH_2)_nP(O)(OH)NHCH_2COOH$ having a P–N linkage. Synthesis of such phosphonopeptides and investigation of their metal-chelating property are in progress at our laboratories.

References

1) M. Horiguchi and M. Kandatsu, *Nature(London)*, **184**, 901 (1959).
2) J. S. Kittredge, E. Roberts, and D. G. Simonsen, *Biochemistry*, **1**, 624 (1962).
3) L. D. Quin, *Biochemistry*, **4**, 324 (1966).
4) A. J. Koning, *Nature (London)*, **210**, 113 (1966)
5) T. Hori, O. Itasaka, H. Inoue, and K. Yamada, *J. Biochem. (Tokyo)*, **56**, 447 (1964).
6) J. A. Alhadeff and G. D. Davies, Jr., *Biochemistry*, **9**, 4866 (1970); *Biochim. Biophys. Acta*, **244**, 2111 (1971).
7) M. Hariharan, S. Chaberek, and A. E. Martell, *Synth. Commun.*, **3**, 375 (1973).
8) M. Hariharan, R. J. Motekaitis, and A. E. Martell, *J. Org. Chem.*, **40**, 470 (1975).
9) K. Yamauchi, M. Kinoshita, and H, Imoto, *Bull. Chem. Soc. Jpn.*, **45**, 2528; 2531 (1972).
10) E. Baer and N. Z. Stancev, *J. Biol. Chem.*, **239**, 3209 (1964).
11) G. M. Kosolapoff, *J. Am. Chem. Soc.*, **69**, 2112 (1947).
12) J. R. Chambers and A. F. Isbell, *J. Org. Chem.*, **29**, 832 (1964).
13) A. F. Isbell, J. P. Berry, and L. W. Tansey, *J. Org. Chem.*, **37**, 4399 (1972).
14) A. Nakahara, *Bull. Chem. Soc. Jpn.*, **32**, 1195 (1959).
15) M. K. Kim and A. E. Martell, *Biochemistry*, **3**, 1169 (1964).

BULLETIN OF THE CHEMICAL SOCIETY OF JAPAN, VOL. 52 (1), 251—252 (1979)

Friedel-Crafts Reaction of Benzene with 2-Phenylpentanedioic Anhydride

Iwao HASHIMOTO

Department of Industrial Chemistry, Wakayama Technical College, Noshima, Nada-cho, Gobo 649-15

(Received December 21, 1977)

Synopsis. The reaction of benzene with 2-phenylpentanedioic anhydride in the presence of $AlCl_3$ afforded a mixture of 1,2,3,4-tetrahydro-4-oxo-1-naphthalenecarboxylic acid, 4-benzoyl-2-phenylbutanoic acid and the isomeric 4-benzoyl-4-phenylbutanoic acid. The relative yields among the products were markedly affected by a change in the polarity of the solvent.

In a previous paper[1] the $AlCl_3$-catalyzed acylation of benzene with 2-phenylbutanedioic anhydride (**1**) was reported. Competitive inter- and intramolecular acylations were reported in the above reaction system. It was also reported that either the oxonium compound or the acylium ion, which were derived from the interaction between **1** and $AlCl_3$, were the actual acylating agents. Therefore, in order to obtain more information on the actual acylating agent in the Friedel-Crafts reaction with the dibasic acid anhydride, it was necessary to investigate the Friedel-Crafts reaction with a higher dibasic acid anhydride.

Only a few works between benzene and 2-phenylpentanedioic anhydride (**2**) have so far been described[2,3] that **2** acylated intermolecularly benzene to give only 2-phenyl substituted keto acid under Friedel-Crafts conditions, although intramolecular reaction took place with sulfuric acid as catalyst.

In the present study the Friedel-Crafts reaction of benzene with **2** was conducted in various solvents having different polarities, and the solvent effect examined in connection with the reaction mechanism.

The reaction of **2** with $AlCl_3$ in a large excess of benzene gave a mixture of 1,2,3,4-tetrahydro-4-oxo-1-naphthalenecarboxylic acid (**3**), 4-benzoyl-2-phenylbutanoic acid (**4**) and the isomeric 4-benzoyl-4-phenylbutanoic acid (**5**), as is shown in Table 1. However, the total yield of these keto acids was lower than that obtained from the acylation of benzene with **1** under similar reaction conditions, and the yield of **3** was always over the sum of those of **4** and **5**. This suggested that the intramolecular acylation of **2** with $AlCl_3$, even in a large excess of benzene, predominates over the intermolecular reaction of **2** on benzene in the presence of $AlCl_3$. A decrease in the amount of $AlCl_3$ from 20 to 10 mmol did not largely affect the distribution of products.

In more polar solvents such as 1,2-dichloroethane, the reaction of **2** with a limited amount of benzene predominantly gave **3** using 20 mmol of $AlCl_3$, accompanied by a small amount of **5** and a trace of **4**. Furthermore, in the case of 10 mmol of $AlCl_3$ on the reaction in 1,2-dichloroethane, **3** was exclusively obtained with a trace amount of **5**.

In nitrobenzene, the most polar solvent used, the reaction of **2** with benzene, in the presence of 30 mmol of $AlCl_3$, gave **3** almost exclusively. The intramolecular acylation of **2** with $AlCl_3$ in nitrobenzene overwhelmingly predominated over the intermolecular acylation of **2** on benzene in the presence of $AlCl_3$. The use of 30 mmol of $AlCl_3$ without benzene increased the yield of **3** to 79%.

These results imply that the solvent variations in the reaction of **2** with benzene in the presence of $AlCl_3$ markedly affect the relative yield among, **3**, **4**, and **5**; thus, an increase of polarity of solvent led to an increasing yield of **3** and the decreasing yields of **4** and **5**. From this, the following reaction paths may be formulated in consideration of the results obtained in the acylation of benzene with **1**.[1]

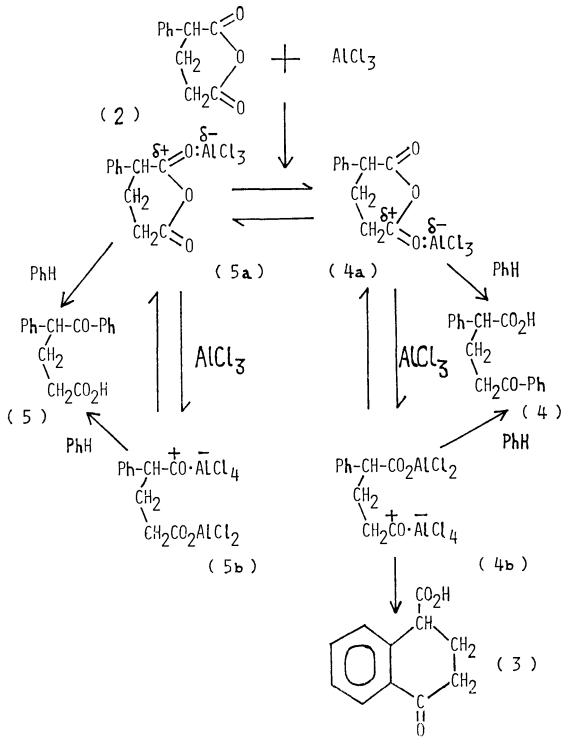

Scheme 1.

As delineated in Scheme 1, the oxonium compounds (**4a** and **5a**) possibly intermolecularly acylate benzene to give **4** and **5**, and also the acylium ions (**4b** and **5b**) afford **3**, **4**, and **5** by the intra- and intermolecular acylations. Since the above reaction gives **3** as the main product, which is obtained by way of **4b** and since the yield of **3** increases with increasing polarity of solvent, it may be assumed that the actual acylating agent in the reaction using **2** is a type of acylium ion. This is because the acylium ion bearing a more centered positive charge than the oxonium compound appears to be markedly influenced by a change of the polarity of solvent; hence, **4b** and **5b** reacted intermolecularly

Table 1. Acylation of benzene with 2-phenylpentanedioic anhydride at 30 °C

Solvent	Reaction time (h)	$AlCl_3$ (mmol)	C_6H_6 (mmol)	Product yields (%)[a]		
				3	**4**	**5**
None[b]	2	20	550	38	11	26
	2	10	550	23	5	13
$(ClCH_2)_2$ 25 ml	5	5	10	11	0	trace
	5	10	10	44	0	trace
	5	20	10	50	trace	8
	24	20	10	51	trace	7
	5	20	20	51	trace	14
	5	20	—	66	—	—
$C_6H_5NO_2$ 25 ml	24	20	10	66	0	trace
	24	30	10	70	0	trace
	24	30	20	65	trace	1
	24	30	—	79	—	—
None[b]	2	concd H_2SO_4 100	550	6	0	0
None[b]	2	CF_3SO_3H 5	550	23	0	0

a) Calculated on the basis of the amount of 2-phenylpentanedioic anhydride used (10 mmol). b) The reaction was carried out at 60 °C, excess benzene being used as solvent.

with benzene to give **4** and **5**, respectively, although **4b** afforded **3** intramolecularly.

In nonpolar solvents such as benzene, the intermolecular acylations with **4b** and **5b** on the benzene molecule are possibly due to the low solvation of benzene, although the intramolecular acylation of **4b** predominates over the intermolecular acylations of **4b** and **5b** on benzene even in a large excess of benzene. In the intermolecular acylations, **5b** having an electron-attracting phenyl group closer to the acylium cation is preferred to **4b**. Hence the formation of **5** is more favored than **4**.

The highly charged acylium ions (**4b** and **5b**) may be strongly solvated by nitrobenzene to form a bulky acylating agent, and consequently the attack by such bulky agents upon benzene becomes intermolecularly difficult. Indeed, only the intramolecular acylation of **4b** occurred in nitrobenzene to give **3**, since the effect of solvent on the closely-located internal acylium ion and benzene ring is small.

If the phenyl group occupies a quasi axial position in **4a**, the formation of **3** should proceed with a direct intramolecular cyclization as follows:

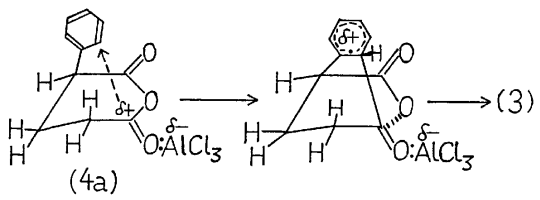

Scheme 2.

However, the observed solvent effect can not be explained, because the effect of solvent upon the oxonium compound (**4a**) should be much less marked than for the acylium ion (**4b**). Moreover, the strained transition state, being caused by the intramolecular approach of $\overset{\delta+}{>}C{=}O{:}\overset{\delta-}{AlCl_3}$ to the benzene ring in **4a**, would have so high an energy that it would be improbable.

Since it is known[4] that trifluoromethanesulfonic acid is a very effective catalyst for the acylation of arenes, the reaction of **2** with a large excess of benzene in the presence of trifluoromethanesulfonic acid or concd sulfuric acid was attempted. However, only the intramolecular acylation of **2** occurred and the yield of **3** was considerably lower compared with the case using $AlCl_3$.

Experimental

Material. Compound **2** was prepared according to the method of Horning *et al.*

Acylation of Benzene with 2 in the Presence of $AlCl_3$. The procedure paralleled the acylation with **1** described in an earlier paper.[1]

Analyses of the Products. All keto acids were esterified with an ethereal solution of diazomethane and then analyzed by GLPC employing a Yanagimoto G-800T model on a 1.5 m × 3 mm column packed with Apieson Grease M (5 wt %) on Celite 545 of 80—100 mesh with a He flow of 40 ml/min at 228 °C. All methyl esters were identified by comparison of their retention times with those of authentic samples. The retention times of the methyl esters of **2**,[2] **3**,[2] **4**,[2,5] and **5**[5,6] were 1.0, 1.4, 4.2, and 5.6 min, respectively. 4-Chlorobenzophenone was used as the internal standard for the GLPC determination.

The author wishes to thank Professor Yoshiro Ogata, Nagoya University, for his valuable discussions.

References

1) I. Hashimoto and R. Takatsuka, *Bull. Chem. Soc. Jpn.*, **50**, 2495 (1977).
2) E. C. Horning and A. F. Finelli, *J. Am. Chem. Soc.*, **71**, 3204 (1949).
3) E. Berliner, "Organic Reactions," John Wiley & Sons, New York (1949), Vol. 5, p. 247.
4) F. Effenberger and G. Epple, *Angew. Chem. Int. Ed. Engl.*, **11**, 299 (1972).
5) I. Heilbron, "Dictionary of Organic Compounds," 4th ed, Eyre and Spottiswoode Publishers, London (1965), Vol. 1, p. 364.
6) E. Knoevenagel, *Ber.*, **21**, 1351 (1888).

BULLETIN OF THE CHEMICAL SOCIETY OF JAPAN, VOL. 52 (1), 253—254 (1979)

Preparation and Spectra of 9-(*p*-Vinylphenyl)anthracene

Akio MUKOH,* Sukekatsu NOZAKI,† Akira HAGITANI,† and Hirosada MORISHITA

Hitachi Research Laboratory, Hitachi Ltd., Hitachi, Ibaraki 319

†*Department of Chemistry, College of Science, St. Paul's University, Toshima-ku, Tokyo 171*

(Received March 7, 1978)

Synopsis. A novel vinyl monomer containing the polyaromatic ring, 9-(*p*-vinylphenyl)anthracene, was prepared by the Grignard reaction of anthrone and *p*-vinylphenylmagnesium halides which could be obtained either from *p*-bromostyrene or *p*-chlorostyrene. The results and the spectra of products are discussed.

Recently, many investigations of organic polymers[1] with polyaromatic rings in the side-chains have been carried out from the optical and electrical interests. 9-(*p*-Vinylphenyl)anthracene (IV) is a promising new vinyl monomer which can be used to prepare one such organic polymer. The authors wish to report on the preparation of IV by the Grignard reaction as follows.

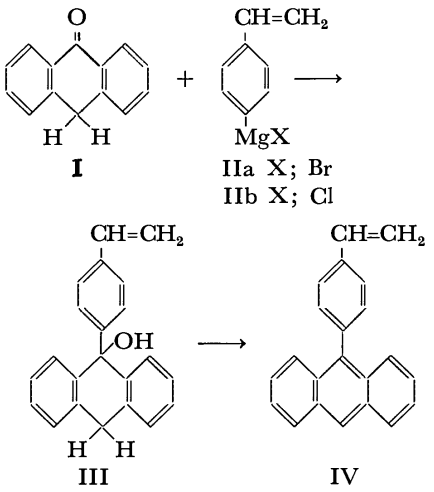

p-Vinylphenylmagnesium halide (IIa) was synthesized by the Grignard reaction of *p*-bromostyrene and magnesium in accordance with Cazes' report.[2] A method using inexpensive *p*-chlorostyrene in place of *p*-bromostyrene was also investigated.

The results are given in Table 1. It was observed that *p*-vinylphenylmagnesium halides can be produced in yields of more than 80% either from *p*-bromostyrene or *p*-chlorostyrene. In the case of *p*-chlorostyrene the yield increased remarkably with the rises in the reaction temperature.

The reaction mixture of *p*-vinylphenylmagnesium halides with I was analyzed by thin layer chromatography(TLC) on alumina, and six spots were detected at R_f 0.94, 0.58, 0.49(main spot), 0.36, 0.25 and at the starting point. These spots were observed in the cases both chlorostyrene or bromostyrene was used. They were assigned to IV, anthraquinone (V), unreacted I, major product III, bianthrone-9-yl (VI) and the polymer of IV, respectively. TLC was presumed to produce V and IV by oxidation or hydration.[3] The spot at R_f 0.25 was identical with that which appeared when purified I was allowed to stand in a benzene solution for several days. It has been reported that I produces bianthrone-9-yl in benzene by photoreaction.[4] Bianthrone-9-yl (VI) was prepared by a known method,[5] and was found to be identical with the product (R_f 0.25) which formed in the reaction mixture. The spots at R_f 0.94 and at the starting point showed a strong blue fluorescence under UV irradiation (366 mm), and therefore, were characterized as polyaromatic compounds.

The overall yield of IV based on I was about 20% when III was separated, purified and then treated with phosphorus pentaoxide (Method A). On the other hand, when the reaction mixture from the reaction of I and *p*-vinylphenylmagnesium halide was directly treated with phosphorus pentaoxide without separating or purifying III, the yield of IV increased to about 40% (Method B). IV was also recrystallized from isopropyl alcohol after treatment with phosphorus pentaoxide without using column chromatography, and a high yield of IV was obtained as shown in Table 2 (the maximum overall yield 44%) (Method C). Table 2 shows the relation of the molar ratio of I to *p*-vinylphenylmagnesium halide and the yield of IV. The yield is maximum at a molar ratio of about 1.3.

In the NMR signals of IV quartet 1H at τ=3.24, doublet 1H at τ=4.29 and doublet 1H at τ=4.82 coincide well with the signals of the α,β-proton of the vinyl group of styrene. Further, the spin-spin coupling constants $J_{\alpha\beta}$=1.72, $J_{\alpha\beta'}$=10.8 and $J_{\beta\beta'}$=1.7 for the

TABLE 1. YIELDS OF GRIGNARD REAGENTS FROM STYRYL HALIDES

Styryl halide 0.1 mol	Mg mol	THF ml	Reaction temp °C	Reaction time h	Grignard reagent (IIa, IIb) yield, %[a]
p-Bromo	0.1	80	60—65	1.5	90.5 (IIa)
p-Bromo	0.1	80	70—75	1.5	95.5 (IIa)
p-Chloro	0.1	70	60—65	1.5	80.5 (IIb)
p-Chloro	0.2	140	70—75	1.5	94.9 (IIb)

a) Determined by acid titration method.

TABLE 2. YIELDS OF 9-(*p*-VINYLPHENYL)ANTHRACENE (IV) BY DIRECT SYNTHESIS (METHOD C)

Starting material	Anthrone (I)/(IIa or IIb)[a] Molar ratio	Reaction time h	Reaction temp °C	Yield of IV % Crude	Pure
IIa	1	3	20—25	19	—
IIa	1	3	Reflux	36	—
IIa	1.3	4	Reflux	52	—
IIa	1.5	4	Reflux	52	36
IIa	2.0	4	Reflux	45	—
IIa	2.5	4	Reflux	13	—
IIb	1.5	4	Reflux	51	44

a) Assuming that Grignard reaction of styryl halide with magnesium gives IIa (or IIb) in quantity.

Table 3. Ultraviolet spectra of 9-phenylanthracene and its derivatives

Compound	Solvent	λ_{max} nm (log ε)					
9-Phenylanthracene[a)]	CH_2Cl_2	259 (5.13)	318 (3.09)	332 (3.46)	350 (3.78)	368 (3.97)	387 (3.93)
9-Phenylanthracene[b)]	C_2H_5OH	256 (5.09)	—	331 (3.44)	347 (3.77)	365 (3.94)	385 (3.94)
9-(*p*-Vinylphenyl)-anthracene (IV)	CH_2Cl_2	258 (5.12)	—	332 (3.45)	349 (3.81)	367 (4.01)	387 (3.97)
9-(*p*-Vinylphenyl)-anthracene (IV)	C_2H_5OH	256 (5.09)	—	331 (3.44)	348 (3.79)	365 (3.96)	384 (3.98)
9-(*p*-Toryl)anthracene[b)]	C_2H_5OH	255 (5.12)	—	331 (3.54)	346 (3.84)	364 (4.00)	383 (3.97)

a) S. C. Dikerman, D. de Souza, and P. Wolf, *J. Org. Chem.*, **30**, 1981 (1965). b) D. Mosnaim, *Tetrahedron*, **25**, 3485 (1969).

vinyl group of IV also coincide well with the coupling constants of styrene.[6,7]

It is known that, when phenyl groups are introduced into anthracene rings, the overall ultraviolet absorption shifts to the longer wavelength region[8,9] and is scarcely affected by the position of the phenyl group or the kind of substitutes bonded to that group. As shown in Table 3, IV shows the same absorption as other 9-monophenylanthracene derivatives in the UV spectra.

Experimental

All compounds were shown to be pure by TLC with alumina B-5 or silica gel C-100 (Wako Pure Chemicals Co., Ltd., Tokyo) as absorbent on glass plates using benzene as the eluent, and with UV and iodine vapor for visualization. IR spectra were recorded using a Hitachi Model EPI-2 IR spectrometer. NMR spectra were recorded on Hitachi Model H-60 NMR spectrometer in deuteriobenzene.

p-Chlorostyrene and p-Bromostyrene[10]: *p*-Chlorostyrene and *p*-bromostyrene were synthesized by dehydration of *p*-hals-(α-hydroxyethyl)benzene with $KHSO_4$. *p*-Chlorostyrene was obtained in yield 67.9%: bp 50.5—51 °C/2 mmHg (lit, 65 °C/4 mmHg). *p*-Bromostyrene was obtained in yield 72.7%: bp 85—85.5 °C/11 mmHg (lit, 87—88 °C/12 mmHg).

9-(p-Vinylphenyl)-9-hydroxy-9,10-dihydroanthracene (III): A solution of 2.75 g of *p*-bromostyrene in 6 ml of THF was added dropwise during 1 h to a mixture of metal magnesium ribbon (0.37 g) and 10 ml of dry THF under mild refluxing. After the magnesium had disappeared, a solution of 2.91 g of I dissolved in 60 ml of dry THF was dropped into the above Grignard reagent (IIa) solution with stirring. The mixture was refluxed for 5 h, cooled and then hydrolyzed with 24 ml of 1.5 M HCl containing ice. An organic layer was extracted with ethyl ether and evaporated to dryness. Recrystallizations with methanol, and petroleum ether-benzene (9:1) in that order, gave 1.12 g (25.1%) of III: mp 132—135 °C; IR bands at 3300 and 1150 cm^{-1} (–OH), 907 and 990 cm^{-1} (–CH=CH_2). Calcd for $C_{22}H_{18}O$: C, 88.56; H, 6.08%. Found: C, 88.16; H, 6.74%.

9-(p-Vinylphenyl)anthracene (IV) Method A): Ten grams of phosphorus pentaoxide was added to a solution of 1.12 g of III dissolved in 22 ml of carbon tetrachloride with stirring at room temperature. Stirring was continued overnight. A solution was then extracted with ethyl ether was evaporated to dryness, taken up in toluene and chromatographed over a 2.5×30 cm column containing 42 g of silica gel. Elution of the column with isopropyl alcohol gave a crude product of IV, which was recrystallized twice with isopropyl alcohol, giving 0.77 g (73.2%) of IV: mp 166—168 °C; IR bands at 910 and 995 cm^{-1} (CH=CH_2), NMR signals (C_6D_6, internal TMS) τ: 1.67 (s, 1 anthracene ring C-10H), 1.99—2.20 (m, 4 anthracene ring C-1, C-4, C-5, and C-8H), 2.59—2.85 (m, 8 aromatic H), 3.24 (q, 1 vinyl α-H), 4.29 (d, 1 vinyl β-H), 4.82 (d, 1 vinyl β′-H). Calcd for $C_{22}H_{16}$: C, 94.25; H, 5.75%. Found: C, 94.26; H, 5.56%.

Method B): In the method described for III, a crude solid of III which was obtained by reaction IIa with I was dissolved in anhydrous benzene containing phosphorus pentaoxide (2% by weight of the benzene) and stirred overnight at room temperature. A solution was then extracted with ethyl ether and evaporated to dryness. The residue was chromatographed as in Method A, giving a crystalline of IV in yield of 40.5% which was recrystallized with isopropyl alcohol.

Method C): In the method described for III, 15.8 g of I in anhydrous benzene (125 ml) was added dropwise to Grignard reagent (IIb) prepared from 14.7 g of *p*-chlorostyrene in THF (50 ml). To the reaction mixture was added 7.6 g of phosphrous pentaoxide in 150 ml of anhydrous benzene with stirring overnight at room temperature. Subsequently, the addition of 332 ml of hexane and filtration left 13.5 g of a solid, which was insoluble in hexane. The filtrate was evaporated to dryness, giving a crude solid of IV which gave 10.0 g (43.7%) of pure product after recrystallization with isopropyl alcohol.

References

1) See, for example, H. Mikawa and S. Kusabayashi, "Semiconductive Polymers," Kohdansha Co., Ltd., Tokyo (1977).
2) J. Cazes, *C. R. Acad. Sci.*, **247**, 1874 (1958).
3) T. Nagai and E. Funakubo, *Kogyo Kagaku Zasshi*, **64**, 1053 (1961).
4) A. Schönberg and A. Mustafa, *J. Chem. Soc.*, **1945**, 657.
5) D. Cohen, L. T. Millar, and K. E. Richards, *J. Chem. Soc.*, **1968**, 793.
6) T. Shimizu, S. Matsuoka, S. Hattori, and K. Senda, *J. Phys. Soc. Jpn.*, **14**, 683 (1959).
7) R. W. Fessenden and J. S. Waugh, *J. Chem. Phys.*, **31**, 996 (1959).
8) S. C. Dickerman, D. D. Souza, and P. Wolf, *J. Org. Chem.*, **30**, 1981 (1965).
9) S. C. Dickerman, M. Klein, and G. B. Vermont, *J. Org. Chem.*, **29**, 3695 (1964).
10) C. S. Marvel and G. L. Schertz, *J. Am. Chem. Soc.*, **65**, 2054 (1943).

BULLETIN OF THE CHEMICAL SOCIETY OF JAPAN, VOL. 52 (1), 255—256 (1979)

α-Chlorination of Long-chain Aliphatic Acids[1)]

Yoshiro OGATA,* Toshiyuki SUGIMOTO, and Morio INAISHI

Department of Applied Chemistry, Faculty of Engineering, Nagoya University, Chikusa-ku, Nagoya 464

(Received March 24, 1978)

Synopsis. Chlorination of long-chain aliphatic acids with a Cl_2–O_2 mixture in the presence of chlorosulfuric acid at 85 °C gave the corresponding α-chloro acids in good yields (*ca.* 90%) along with a little amount of aliphatic α-sulfo acids, but no α,α-dichloro acids.

Halogenation of aliphatic acids can occur *via* either a free-radical[2)] or a acid-catalyzed mechanism.[3,4)] The radical halogenation occurs at random positions, while the acid-catalyzed halogenation tends to give α-halo acid. Hell-Volhard-Zelinsky (H-V-Z) procedure using phosphorus tribromide gives exclusively α-bromo acid. However, the application of H-V-Z reaction to chlorination of long-chain aliphatic acids often gives α,α-dichloro acids along with α-chloro acids; the extent of α,α-dichlorination increases with the progress of reaction.[5,6)]

We have reported that aliphatic acids can be α-chlorinated by molecular chlorine in the presence of strong protic acids such as chlorosulfuric[7-9)] or fuming sulfuric acid[7)] and a radical trapper such as molecular oxygen. Here we wish to report the application of this chlorination method to higher fatty acids, *e.g.*, dodecanoic acid.

Results and Discussion

Dodecanoic acid was chlorinated in the presence of chlorosulfuric acid with a gaseous mixture of molecular chlorine and oxygen which acts as a radical trapper.[10)] The effect of reaction time on the yield is shown in Fig. 1. Within initial one hour, the yield of α-chlorododecanoic acid increased with progress of the reaction, but after one hour the yield was no more increased, but kept constant (*ca.* 90%). The substrate acid disappeared gradually until only a trace remained after 1 h.

The resulting mixture was extracted with ether and washed with water containing sodium chloride. The washing, after standing for a few days, afforded colorless crystals (0.1—0.6 g) of sodium 1-carboxy-1-undecanesulfonate, $[CH_3(CH_2)_9CH(SO_3Na)CO_2H]$, which is an expected product in view of the known formation of α-sulfo acid in the reaction of aliphatic acid with sulfur trioxide,[11-13)] fuming sulfuric acid,[11)] or chlorosulfuric acid.[11)]

Even the chlorination of dodecanoic acid for more than one hour gave α-monochlorododecanoic acid with no α,α-dichloro acid; further, no α,α-dichloro acid was detected in the attempted chlorination of α-chlorododecanoic acid as a substrate. Whereas, α,α-dichlorination occurs as easy as α-chlorination by H-V-Z procedure.[5,6)] Thus our procedure has the advantage that there is no contamination by dichloro acid, which is due to the low reactivity of α-chloro acid as well as gradual consumption of $ClSO_3H$ with the progress of reaction.

The mechanism may involve the addition of molecular chlorine to a ketene intermediate.[14)]

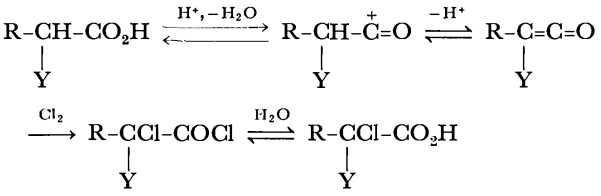

When Y=H and R=$C_{10}H_{21}$, alkyl substituted ketene is formed, while α-chloro acid (Y=Cl) gives chloro substituted ketene, which is less reactive to electrophilic chlorine addition; hence the reaction gives only α-monochlorination.

Figure 2 shows that the α-chlorination increases with increasing amount of catalyst acid, while the total yield of α-chlorinated product decreases, since there is a considerable amount of loss as α-sulfonated compound. In short, the optimum conditions for the highest yield and the lowest loss of the substrate are obtained with *ca.* 10 mmol of chlorosulfuric acid (1/5 equivalent of substrate).

The effect of reaction temperature on the yield is

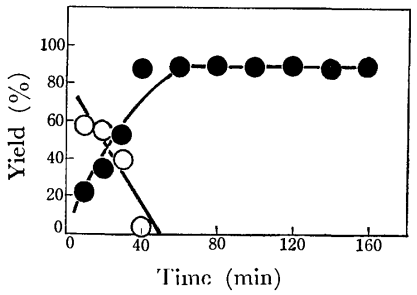

Fig. 1. Effect of reaction time on α-chlorination of dodecanoic acid (50 mmol) in the presence of chlorosulfuric acid (12.5 mmol) at 85 °C. ●: α-Chlorododecanoic acid, ○: dodecanoic acid.

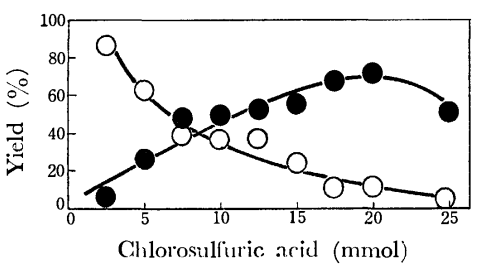

Fig. 2. Effect of amount of chlorosulfuric acid on α-chlorination of dodecanoic acid (50 mmol) at 85 °C for 30 min. ●: α-Chlorododecanoic acid, ○: dodecanoic acid.

Table 1. Yields and physical properties for α-chloro acids

α-Chloro acid	Yield %	Mp (°C)	IR $\nu_{C=O}$ (cm^{-1})	NMR[c] α-H (δ ppm)
$CH_3(CH_2)_5CHCO_2H$ (Cl)	90	liquid	1720[a]	4.17
$CH_3(CH_2)_7CHCO_2H$ (Cl)	89	liquid	1720[a]	4.15
$CH_3(CH_2)_9CHCO_2H$ (Cl)	90	36—37	1720[b]	4.17
$CH_3(CH_2)_{11}CHCO_2H$ (Cl)	91	41—42	1715[b]	4.15
$CH_3(CH_2)_{13}CHCO_2H$ (Cl)	92	52—53	1720[b]	4.15

a) Neat. b) KBr. c) CCl_4.

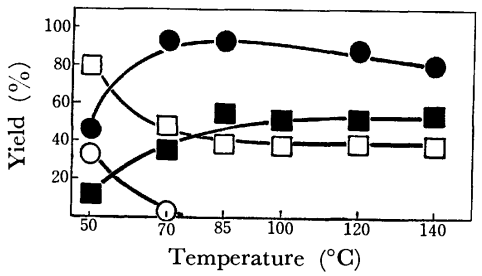

Fig. 3. Effect of temperature on α-chlorination of dodecanoic acid (50 mmol) in the presence of chlorosulfuric acid (12.5 mmol) for 30 or 120 min. ■: α-Chlorododecanoic acid (30), □: dodecanoic acid (30), ●: α-chlorododecanoic acid (120), and ○: dodecanoic acid (120 min).

less important (Fig. 3), probably because the favorable effect of increasing rate is compensated with the reverse effects of a decrease of chlorine solubility and an acceleration of α-sulfonation with increasing temperature.

This method can generally be applied to α-chlorination of other long-chain aliphatic acids with satisfactory yields. The optimum conditions for α-chlorination are as follows: A mixture of 50 mmol of substrate acid and 12.5 mmol of chlorosulfuric acid is heated at 85 °C for 60 min. The yields and physical properties for identification of α-chloro acids are listed in Table 1. Little effect of structure, *i.e.*, length of the chain, on the yield was observed.

The mechanism may involve the addition of molecular chlorine to a ketene intermediate.[14]

Experimental

Chlorosulfuric acid (1.45 g 12.5 mmol) was added gradually with stirring to substrate acid (50 mmol) and the mixture was heated slowly to 85 °C. The mixture of chlorine and oxygen in a molar ratio of 2:1 was bubbled into it for 60 min. After completion of the reaction chlorine was removed by introducing nitrogen, the mixture was cooled to room temperature, and extracted with ether (60 ml). The extract was washed with aqueous sodium chloride (20 ml) for three times. Ether was removed at 60 °C under reduced pressure. The residual material was cooled to freeze and dried *in vacuo*. The product was esterified with diazomethane[15] in ether and analyzed on a Yanagimoto G 180 gas chromatograph using a copper column packed with PEG 20 M 10% on Chromosorb WAW or Apiezon Grease L 15% on Celite 545.

The isolated α-chloro fatty acids (C_8—C_{16}) were identified by comparing the ^1H NMR and IR spectra with those of authentic samples. NMR and IR spectra were measured by means of a Hitachi R-24B NMR spectrometer and Perkin-Elmer Model 337 IR spectrophotometer, respectively.

References

1) Contribution No 246.
2) M. S. Kharasch and H. C. Brown, *J. Am. Chem. Soc.*, **62**, 925 (1940).
3) H. J. Harwood, *Chem. Rev.*, **62**, 99 (1962).
4) O. V. Sonntag, *Chem. Rev.*, **52**, 237 (1953).
5) H. H. Guest and C. M. Goddard, Jr., *J. Am. Chem. Soc.*, **66**, 2074 (1944).
6) R. L. Rodin and H. Gershon, *J. Org. Chem.*, **38**, 3919 (1973).
7) Y. Ogata, T. Harada, K. Matsuyama, and T. Ikejiri, *J. Org. Chem.*, **40**, 2960 (1975).
8) Y. Ogata and T. Ikejiri, *Nippon Kagaku Kaishi*, **1975**, 1517.
9) Y. Ogata and T. Sugimoto, *Chem. Ind. (London)*, **1977**, 538.
10) M. L. Poutsma, *J. Am. Chem. Soc.*, **87**, 2161 (1965).
11) F. Gunther and J. Hetger, U. S. Pat. 1 926 442; *Chem. Abstr.*, **27**, 6001 (1933).
12) J. K. Weil, L. P. Witnauer, and A. J. Stirton, *J. Am. Chem. Soc.*, **75**, 2526 (1953).
13) E. E. Gilbert, *Chem. Rev.*, **62**, 549 (1962).
14) Y. Ogata, T. Harada, and T. Sugimoto, *Can. J. Chem.*, **55**, 1268 (1977).
15) J. K. Weil, R. G. Bistline, Jr., and A. J. Sterton, *Org. Synth.*, Coll. Vol. IV, 250 (1963).

BULLETIN OF THE CHEMICAL SOCIETY OF JAPAN, VOL. 52 (1), 257—258 (1979)

Synthesis of 4,8-Dimethyl-5,7-nonamethyleneazulene

Shinji KUROKAWA* and Arthur G. ANDERSON, Jr.†

Department of Chemistry, Faculty of Education, Saga University, Honjo-machi, Saga 840

† *Department of Chemistry, University of Washington, Seattle, Washington, 98195, U. S. A.*

(Received April 10, 1978)

Synopsis. The title compound has been prepared from 2,6-dimethyl-3,5-nonamethylenepyrylium perchlorate and from 1,2,6-trimethyl-3,5-nonamethylenepyridinium iodide in low yield by reaction with sodium cyclopentadienide. The UV, visible and PMR spectra of the title compound are correlated with the structure.

Electrophilic substitution was used to prepare the intermediate for cyclization to a 1,3-meta-bridged azulene, 1,3-(5-cyano-6-oxoundecamethylene)azulene.[1] This route was not possible for the formation of a 5,7-bridge. The later synthesis of 3,5-bridged pyrylium perchlorate (**1**) and pyrydinium iodide (**2**)[2] made available compounds needed for a 5,7-bridged azulene by the Hafner route.

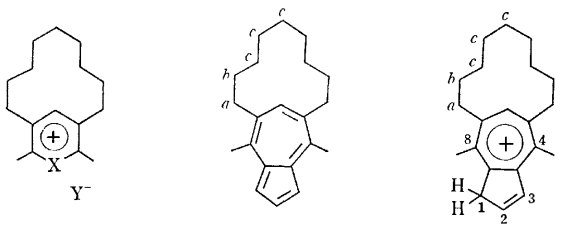

1: X=O, Y=ClO_4 **3** **4**
2: X=NMe, Y=I

Reaction of sodium cyclopentadienide with **1** or **2** gave a low (≤0.3%) yield of the title compound (**3**) as violet crystals. The PMR spectrum of **3** in trifluoroacetic acid corresponded well to the structure of the conjugate acid (**4**).

A molecular model of **3** did not show steric strain such that appreciable distortion of the azulene ring would occur. Distortion of the ring should cause a larger bathochromic shift of the ultraviolet absorption than is caused by the tetraalkyl substitution, and ring distortion would also probably cause lower intensity of absorption and loss of fine structure.[3] Comparison of the ultraviolet spectrum with those of the best model compounds in the literature (4,8-,[4] 4,5-,[5] and 4,7-dimethylazulenes[6]) showed a shift to longer wavelengths for **3**, but the principal maximum at 581 nm agreed well with 578 nm calculated by Plattner's rule.[6] The absence of ring distortion was also indicated by the high intensities (log ε 3.87 to 4.87) and the retention of fine structure.

The model of **3** showed the *c* methylenes over the pi-electron cloud of the aromatic ring in the sterically favoured conformations. The model also showed significant steric restrictions to rotational conversions from the many unsymmetric to the two symmetric conformations of the bridge. In agreement with the model, the PMR signal for the *c* methylenes (δ 1.25) is at higher field[7] than that for the *b* methylenes (δ 1.78) which are nearer to the plane of the azulene ring. Comparison with the spectrum of 5,7-dimethylazulene[8] showed a shift inversion for the 2- and 6-hydrogens: δ 7.48 and 7.61, respectively, for **3**, *vs.* δ 7.81 and 7.42. This may be explained by two factors: the very small concentration of **3** in the PMR solution would cause the 6-H signal to shift downfield, but would have little effect on the 2-H signal,[9] and the effective shielding of the 6-H would be decreased by the asymmetrical interaction with the bridge hydrogens.[10] The observed nonequivalence of 1-H and 3-H (δ 7.19 and 7.28) seems due to the asymmetrical magnetic anisotropy effect of the bridge. The small amount of material obtained did not permit experiments concerned with this point.

Experimental

PMR spectra (δ) were taken on a Hitachi R-22 spectrometer with TMS as internal standard, for **3**, with a Hitachi A-1600 signal averaging analyzer. MS were obtained at 70 eV on a Hitachi RMS-4 instrument. UV and visible spectra were recorded on a Hitachi 624 digital spectrometer with a Hitachi 056 recorder. IR spectra were taken on a JASCO A-3 spectrometer. Mps are uncorrected.

*2,6-Dimethyl-3,5-nonamethylenepyrylium Perchlorate (**1**).* This compound was prepared from cyclododecene [166 g (1 mol) purified by distillation; bp 111—116 °C/12 Torr] and acetic anhydride (511 g, 5 mol) in the presence of 70% perchloric acid[2] except that stirring was continued for 2 h at room temperature after addition of the acid. Recrystallization of the product from 1% perchloric acid gave 41.3 g (12.4%) of **1** as pale yellow crystals, mp 181—182 °C (lit,[2] 170 °C). IR (KBr) 3020, 2890—2940, 2855, and 1606 cm^{-1}. PMR (CF_3COOH) δ=2.94 (6H, s, CH_3), 3.02 (4H, t, *J*= 6.0 Hz, *a*), 2.00 (4H, symmetrical m, *b*), 1.28 (10H, unsymmetrical m, *c*), and 8.80 (1H, s, pyrylium H).

*1,2,6-Trimethyl-3,5-nonamethylenepyridinium Iodide (**2**).* Dry ammonia gas was bubbled into a suspension of 50.8 g (0.153 mol) of vacuum-dried **1** in 300 cm^3 of dry *t*-butyl alcohol for 2 h[2] to give 24.26 g (68.6%) of 2,6-dimethyl-3,5-nonamethylenepyridine, bp 140—142 °C/3 Torr; UV_{max} (cyclohexane) 197 (log ε 4.3), 217 (3.9), 273 (3.5) and 280^{sh} nm (3.5); IR (liquid film) 2930, 2855, and 1445 cm^{-1}; PMR ($CDCl_3$) δ=1.04 (10H, m, *c*), 1.64 (4H, m, *b*), 2.64 (4H, t, *J*=6.5 Hz, *a*), 2.41 (6H, s, CH_3) and 7.20 (1H, s, 4-H).

The pyridine [5.13 g (0.222 mol)] was mixed with 5 cm^3 (0.08 mol) of methyl iodide. After 12 h, an additional 5 cm^3 of methyl iodide was added. After 12 h, removal of excess methyl iodide (reduced pressure) left **2** as a yellowish hygroscopic crystalline mass.

*4,8-Dimethyl-5,7-nonamethyleneazulene (**3**). A. From **1**.* To sodium cyclopentadienide prepared from 4.6 g (0.07 mol) of cyclopentadiene and 2.9 g (0.06 mol) of sodium hydride in 30 cm^3 of THF under dry nitrogen, was added 6.7 g (0.02 mol) of **1** in 15 cm^3 of THF (30 min) and the mixture stirred

for 2 h. Two-thirds of the solvent was removed, 300 cm^3 of water was added, and the whole was extracted several times with petroleum ether. The solvent was evaporated and the residue chromatographed on 20 g of silica gel (petroleum ether eluant). Extraction of the blue-green fraction with 85% phosphoric acid, dilution of the extracts with ice water, extraction of the aqueous solution with petroleum ether, evaporation of the solvent, and chromatography with petroleum ether of the residue on 25 g of silica gel gave 16.7 mg (0.3%), mp *ca.* 89 °C.

The crude product (66.8 mg, 0.239 mmol) in petroleum ether was retreated with 85% phosphoric acid as described above. Chromatography on 25 g of silica gel (petroleum ether) and rechromatography on 7 g of silica gel (hexane–benzene, 9:1) gave 23.4 mg of **3** as blue-violet crystals. Passage over Amberlite IRC-50 (CG-50 type) (80% ethanol) gave 9.82 mg (0.04%) of violet plates from 80% ethanol, mp 109—110 °C; pure by GLC, UV_{max} (cyclohexane) 253 (log ε 4.71), 292 (4.87), 298 (4.85), 340 (3.97), 350 (4.06), and 365 nm (3.87); 565^{sh} (ε 829), 581 (875), 600 (816), 627^{sh} (666), 660^{sh} (361), and 690 nm (196). IR (CCl_4) 2920, 2850, and 1460 cm^{-1}. PMR (CCl_4, 90 MHz), δ= 1.25 (10H, broad s, *c*), 1.78 (4H, m, *b*), 2.88 (6H, s, CH_3), 3.05 (4H, m, J=6.0 Hz, *a*), 7.19 (1H, dd, J=4.0 and 1.5 Hz, 1- or 3-H), 7.28 (1H, m, overlapping 7.19 signal, 1- or 3-H), 7.48 (1H, q, J=4.0 Hz, 2-H) and 7.61 (1H, s, 6-H). MS *m/e* 280 (M^+ for $C_{21}H_{28}$, base peak) [M^+=280.218 ($C_{21}H_{28}$= 280.219)].

B. From **2**.[11] Sodium cyclopentadienide (from 3.8 g (0.078 mol) of sodium hydride and 7.4 cm^3 (0.09 mol) of cyclopentadiene) in 10 cm^3 of THF was added to the vacuum dried ($CaCl_2$) pyridinium iodide (**2**) from 0.222 mol of pyridine. The mixture was stirred for 2.5 h and the solvent was removed. A petroleum ether solution of the violet solid was washed (H_2O), dried (Na_2SO_4), separated from the solvent, and chromatographed on 80 g of silica gel (petroleum ether–benzene, 9:1). The green zone (86.23 mg) was purified as described for the crude product in *A* to give 2.12 mg (0.034%) of **3**.

A solution of **3** in trifluoroacetic acid showed PMR signals corresponding to **4**, δ=1.33 (10H, *c*), 2.10 (4H, *b*), 3.05 (6H, 4-CH_3 and 8-CH_3), 3.46 (4H, *a*), 4.20 (2H, 1-CH_2), 7.68 (2H, 2-H and 3-H), and 8.78 (1H, 6-H).

The authors wish to express their thanks to Professor Yuho Tsuno and Professor Hitoshi Takeshita of Kyushu University for kind measurements of FT-NMR spectra. Thanks are also due to Dr. Mitsuru Nakayama of Hiroshima University for kind measurements of mass spectra. The present work was partially carried out in the Department of Chemistry, University of Washington, and partially supported by a Grant-in-Aid for Scientific Research from the Ministry of Education.

References

1) A. G. Anderson, Jr. and R. D. Breazeale, *J. Org. Chem.*, **34**, 2375 (1969).

2) A. T. Balaban, *Tetrahedron Lett.*, **1968**, 4643.

3) D. J. Cram and G. R. Knox, *J. Am. Chem. Soc.*, **83**, 2204 (1961).

4) Pl. A. Plattner and E. Heilbronner, *Helv. Chim. Acta*, **31**, 804 (1948).

5) W. Herz and J. L. Rogers, *J. Am. Chem. Soc.*, **75**, 4499 (1953).

6) Pl. A. Plattner, *Helv. Chim. Acta*, **24**, 283E (1941); Pl. A. Plattner and E. Heilbronner, *ibid.*, **30**, 910 (1947); Pl. A. Plattner, A. Fürst, and K. Jirasek, *ibid.*, **30**, 1320 (1947).

7) J. S. Waugh and R. W. Fessenden, *J. Am. Chem. Soc.*, **79**, 846 (1957); N. L. Allinger, M. A. DaRooge, and R. B. Hermann, *ibid.*, **83**, 1974 (1961); W. S. Lindsay, P. Stokes, L. G. Humber, and V. Boekelheide, *ibid.*, **83**, 943 (1961); D. J. Wilson, V. Boekelheide, and R. W. Griffin, Jr., *ibid.*, **82**, 6302 (1960).

8) The data on 5,7-dimethylazulene were kindly provided by Dr. R. W. Alder of the University of Bristol.

9) W. S. Schneider, H. J. Bernstein, and J. A. Pople, *J. Am. Chem. Soc.*, **80**, 3497 (1958); D. Meuche, B. B. Molloy, D. M. Reid, and E. Heilbronner, *Helv. Chim. Acta*, **46**, 2483 (1963).

10) N. S. Bhacca and D. H. Williams, "Application of NMR Spectroscopy in Organic Chemistry," Holden-Day, San Francisco (1964), p. 4.

11) Following the procedure of B. R. Pai, P. S. Santhanum, and M. Srinivasan, *Tetrahedron*, **22**, 3417 (1966). Application of the conditions of K. Ziegler and K. Hafner, U. S. Patent 2805266, Sept. 3, 1957 gave no azulenic product.

BULLETIN OF THE CHEMICAL SOCIETY OF JAPAN, VOL. 52 (1), 259—260 (1979)

Allylation of Nucleic Acid-Bases with Triallyl Phosphate

Toshizumi TANABE,* Kiyoshi YAMAUCHI, and Masayoshi KINOSHITA
Department of Applied Chemistry, Osaka City University, Sumiyoshi-ku, Osaka 558

(Received May 12, 1978)

Synopsis. Triallyl phosphate alkylated uracil (N-1), thymine (N-1), cytosine (N-1), adenine (N-3 and N-9), and guanine (presumably N-1 or N-7) in a water solution at 60 °C (pH values were 10—10.5 for uracil, thymine, cytosine, and adenine, and 12 for guanine), giving the corresponding allyl derivatives in considerable yields.

Many modified nucleosides are present in various tRNAs and have been considered to play important roles in their biogenesis.[1] Since most of the modified nucleosides are methylated at nitrogen atoms of base moieties, methylation studies of nucleic acid-bases or nucleosides have been carried out using various alkylating agents, such as dimethyl sulfate,[2-4] diazomethane,[5] and methyl iodide.[6,7] Previously, we reported methylation[8] and ethylation[9] of nucleic acid-bases in an aqueous phase by means of trimethyl and triethyl phosphate (TMP and TEP).

In this paper, we wish to describe the reactions of nucleic acid-bases such as uracil (**1**), thymine (**2**), cytosine (**3**), adenine (**7**), and guanine (**10**) with triallyl phosphate (TAP) in an aqueous phase. These reactions may be interest since there is a class of nucleic acid components which are substituted by allyl or isopentenyl groups like triacanthine.[10] Moreover, the present reactions are considered to resemble the biosynthesis of cytokinin which involves a transfer of an allylic group from Δ^2-isopentenyl pyrophosphate to the 6-amino group of adenine ring.[11]

The reactions were carried out at 60 °C by stirring a mixture of a base and 2 molar excess of TAP in water. (The pH values were maintained at 10—10.5 for **1**, **2**, **3**, and **7**, and 12 for **10** throughout the reactions by the occasional addition of 4 M sodium hydroxide.)

Generally, **1** and **2** have been known to be alkylated with alkyl halides to give mainly 1-alkyl derivatives.[12,13] In the present reactions of **1** and **2** with TAP, 1-allyluracil (**4**) and 1-allylthymine (**5**) were obtained in 12 and 13% yields, respectively. The preference for the alkylation at the N-1 position was also observed in the ethylation of **1** and **2** with TEP,[9] while TMP methylated these two pyrimidine bases at both the N-1 and the N-3 positions in almost equal amounts.[8]

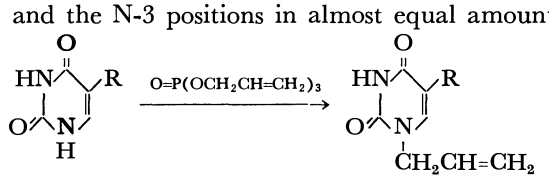

1: R=H
2: R=Me
4: R=H 12%
5: R=Me 13%

In cytosine (**3**), alkylation has been reported to take place mainly at the N-3 position in the reaction with dimethyl sulfate in DMF,[2] while TMP and TEP alkylated **3** at the N-1 position predominantly.[8,9] The present reaction of **3** with TAP occurred at the N-1 position to provide 1-allyl derivative (**6**) in 15% yield.

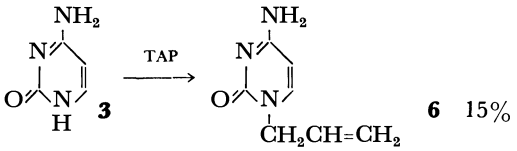

3 **6** 15%

Thus, triallyl phosphate was found to alkylate the above pyrimidines (**1**, **2**, and **3**) mainly at the N-1 position to give 1-allyl derivatives. The difficulty in alkylation at the N-3 position is attributed to the steric hindrance around the N-3 position of **1**, **2**, and **3** by two adjacent carbonyl or amino groups.

Meanwhile, adenine (**7**) was alkylated by TAP at the N-3 and the N-9 positions to afford 3-allyladenine (**8**) and 9-allyladenine (**9**) in 35 and 31% yields. Although **7** is generally known to be alkylated at the N-3 position under neutral conditions[3,4,14,15] and at the N-9 position under alkaline conditions,[7] alkylations with trialkyl phosphates such as TMP,[8] TEP,[9] and TAP in alkaline aqueous phase tend to take place at the N-3 and the N-9 positions in almost equal ratios.

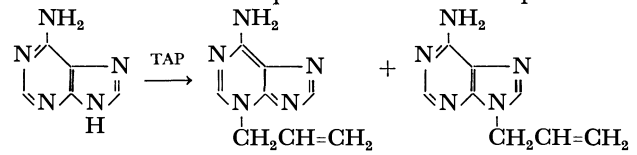

7 **8** 35% **9** 31%

Most of guanine (**10**), on the other hand, remained unchanged in the reaction with TAP, because of the sparing solubility of **10** and TAP in water. (More than 70% of **10** was recovered.) But the reaction mixture, which was obtained after removing the unchanged **10**, showed eight product-spots on its thin-layer chromatography. Identification of these products, however, remained unsolved; the spectra of the isolated compounds did not resemble those of any known alkylated guanines.

Based on the above experiments, TAP was found to alkylate all five main nucleic acid-bases at various positions. This rather strong alkylating property of TAP may originate from its conjugated structure. The reactivity order of nitrogen atoms in each nucleic acid-base except **10**[16] toward TAP in weakly alkaline aqueous phase was found as follows; uracil, thymine, and cytosine: N-1>N-3; adenine:N-9, N-3>N-7, N-1.

Experimental

Melting points are uncorrected. The UV spectra were measured with a Hitachi EPS-3T spectrometer. The NMR spectra were recorded on a Hitachi 3T spectrometer, with a dilute solution in deuterium oxide, deuteriochloroform, or dimethyl-d_6 sulfoxide. Tetramethylsilane was used as the internal and outside standard. Mass spectra were obtained using a JEOL 01SG-2 spectrometer. Column chromatography was carried out using silica gel (Merck, Art. 7734, 70—230 mesh).

Commercially available uracil, thymine, cytosine, adenine,

and guanine were used without further purification. Triallyl phosphate was prepared by the procedure of Toy and Costello.[17]

*1-Allyluracil (**4**).* A mixture of **1** (1.23 g, 1.1 mmol) and TAP (5.10 g, 30.0 mmol) in water (15 ml) was stirred at 60 °C. The suspension was maintained at pH 9—10 throughout the reaction by the occasional addition of 4 M sodium hydroxide. After stirring for 48 h, the reaction mixture was neutralized with concentrated hydrochloric acid and extracted with chloroform. Unchanged **1** was recovered from the water layer (0.76 g, 63%). The organic layer was concentrated to give a residue which afforded crystalline 1-allyluracil (**4**, 0.20 g, 12%) by the addition of hexane; mp 106—108 °C; NMR ($CDCl_3$) δ=4.40 (2H, complex m, $-CH_2-CH=CH_2$), 5.08—5.57 (2H, complex m, $-CH_2-CH=CH_2$), 5.60—6.40 (1H, complex m, $-CH_2-CH=CH_2$), 5.78 (1H, d, J=7 Hz, **H**^{5}), 7.28 (1H, d, J=7 Hz, **H**^{6}), and 10.48 (1H, bs, N^3–**H**); UV, λ_{max} (H_2O) nm: pH 1, 266.0 (log ε 4.05), pH 7, 266.0 (log ε 4.00), pH 13, 265.0 (log ε 3.84); Found: C, 55.35; H, 5.04; N, 18.62%. Calcd for $C_7H_8N_2O_2$: C, 55.25; H, 5.30; N, 18.41%.

*1-Allylthymine (**5**).* A reaction of **2** (1.20 g, 10.0 mmol) with TAP (5.10 g, 30.0 mmol) in water (15 ml) at 60 °C for 48 h afforded **5** (0.20 g, 13%) after a procedure similar to that described above; mp 96—97 °C (from methanol); NMR ($CDCl_3$) δ=1.94 (3H, d, J=1.2 Hz, $-CH_3$), 4.35 (2H, complex m, $-CH_2-CH=CH_2$), 5.02—5.50 (2H, complex m, $-CH_2-CH=CH_2$), 5.50—6.30 (1H, complex m, $-CH_2-CH=CH_2$), 7.02 (1H, d, J=1.2 Hz, **H**^{6}), and 9.80 (1H, bs, N^3–**H**); UV, λ_{max} (H_2O) nm: pH 1, 272.0 (log ε 3.96), pH 7, 272.0 (log ε 3.95), pH 13, 272.0 (log ε 3.82); Found: C, 57.76; H, 5.98; N, 16.75%. Calcd for $C_8H_{10}N_2O_2$: C, 57.82; H, 6.07; N, 16.86%. Unchanged **2** was recovered in 67% yield (0.80 g).

*1-Allylcytosine (**6**).* A mixture of **3** (1.00 g, 0.9 mmol) and TAP (5.10 g, 30.0 mmol) was stirred in water (10 ml, pH 9—10, NaOH) at 60 °C for 48 h. The reaction mixture was then neutralized by concentrated hydrochloric acid and extracted with chloroform to remove the unchanged TAP. The water layer was concentrated to give a residue, which was then separated by silica gel chromatography (2×50 cm). Elution with chloroform–methanol (5:2) provided the salt of **6** with diallyl hydrogen phosphate (0.46 g) and unchanged **3** diallyl hydrogen phosphate (1.52 g, 59%). The salt of **6** was subsequently treated with an anionic exchange resin (Dowex 1×8, 200—400 mesh, OH form). Elution with water gave the free form of **6** (0.20 g, 15%); mp 245—247 °C (sublime); NMR (D_2O) δ=4.37 (2H, complex m, $-CH_2-CH=CH_2$), 4.85—5.48 (2H, complex m, $-CH_2-CH=CH_2$), 5.52—6.30 (1H, complex m, $-CH_2-CH=CH_2$), 5.99 (1H, d, J=7 Hz, **H**^{5}), and 7.48 (1H, d, J=7 Hz, **H**^{6}); UV, λ_{max} (H_2O) nm: pH 1, 282.0 (log ε 4.19), pH 7, 274.0 (log ε 4.01), pH 13, 274.0 (log ε 4.00); Found: C, 54.38; H, 5.76; N, 27.21%. Calcd for $C_7H_9N_3O\cdot 0.2H_2O$: C, 54.33; H, 6.08; N, 27.13%.

*3- and 9-Allyladenines (**8** and **9**).* Compound **7** (1.35 g, 10.0 mmol) and TAP (5.20 g, 31.0 mmol) was stirred in water (10 ml, pH 10, NaOH) at 60 °C for 48 h. After the reaction mixture was neutralized by hydrochloric acid, the resulting solution was concentrated to give a residue which was subsequently mixed with ethanol and separated from undissolved substances. The residue which was obtained after concentrating the ethanolic solution was then purified with a silica gel column (3×50 cm). Elution with chloroform–methanol (10:1) provided **9** (0.57 g, 31%); mp 162 °C (from benzene) (lit,[18] 163 °C); NMR ($CDCl_3$) δ=4.75—5.00 (2H, complex m, $-CH_2-CH=CH_2$), 5.05—5.53 (2H, complex m, $-CH_2-CH=CH_2$), 5.75—6.55 (1H, complex m, $-CH_2-CH=CH_2$), 6.32 (2H, bs, $-NH_2$), 7.88 (1H, s, **H**^{2}), and 8.46 (1H, s, **H**^{8}); UV, λ_{max} (H_2O) nm: pH 1, 259.5 (log ε 4.11), pH 7, 261.0 (log ε 4.11), pH 13, 261.0 (log ε 4.11). The subsequent elution with the same solvent afforded crude **8** contaminated with some phosphate, which was then treated with an anionic exchange resin (Dowex 1×8, 200—400 mesh, OH form). Elution with water gave **8** (0.64 g, 35%); mp 207—210 °C (from methanol) (lit,[15] 199—201 °C); NMR (D_2O) δ=4.40—5.06 (2H, complex m, $-CH_2-CH=CH_2$), 5.06—5.50 (2H, complex m, $-CH_2-CH=CH_2$), 5.58—6.50 (1H, complex m, $-CH_2-CH=CH_2$), 7.80 (1H, s, **H**^{2}), and 8.06 (1H, s, **H**^{8}); UV, λ_{max} (H_2O) nm: pH 1, 274.0 (log ε 4.22), pH 7, 274.0 (log ε 4.10), pH 13, 274.0 (log ε 4.06).

*Allylation of Guanine (**10**).* Compounds **10** (2.50 g, 16.6 mmol) was suspended in a mixture of TAP (10.2 g, 60.0 mmol) and water (100 ml, pH 12, NaOH) at 60 °C. After stirring for 48 h, undissolved **10** (1.83 g, 73%) was recovered by filtration and the resulting solution was extracted with toluene to remove unchanged TAP. The water layer was developed on silica gel [GF_{254} (type 60), Merck] thin-layer chromatography using chloroform–methanol (5:1), and showed eight unidentified spots. After concentrating the water solution, the residue was mixed with ethanol and separated from the undissolved substances. The residue which was obtained after concentrating the alcoholic solution was purified by silica gel chromoatography (3×55 cm). Two kinds of effluents were obtained, using chloroform–methanol (8:1) as the developing solvent. One of them showed a single spot on silica gel TLC, which turned out to be monoallylguanine from its mass spectrum (0.03 g, 1%); *m/e*: 191; UV λ_{max} (H_2O) nm: pH 1, 251, 275(s), pH 13, 280.0. The other effluent (0.01 g) seemed to be a mixture of monoallyl- and diallylguanines, since there were two spots on its silica gel TLC and its mass spectrum showed *m/e* 231 and 191.

References

1) J. A. McClosky and S. Nishimura, *Acc. Chem. Res.*, **10**, 403 (1977).
2) P. Brookes and P. D. Lawley, *J. Chem. Soc.*, **1962**, 1348.
3) J. W. Jones and R. K. Robins, *J. Am. Chem. Soc.*, **84**, 1914 (1962).
4) C. B. Pal, *Biochemistry*, **1**, 558 (1962).
5) J. A. Haines, C. B. Reese, and L. Todd, *J. Chem. Soc.*, **1962**, 5281.
6) J. W. Jones and R. K. Robins, *J. Am. Chem. Soc.*, **85**, 193 (1963).
7) M. Rasmussen and H. -S. Chan, *Aust. J. Chem.*, **28**, 1031 (1975).
8) K. Yamauchi, T. Tanabe, and M. Kinoshita, *J. Org. Chem.*, **41**, 3691 (1976).
9) T. Tanabe, K. Yamauchi, and M. Kinoshita, *Bull. Chem. Soc. Jpn.*, **50**, 3021 (1977).
10) N. J. Leonard and J. A. Deyrup, *J. Am. Chem. Soc.*, **84**, 2148 (1962).
11) Y. Taya, Y. Tanaka, and S. Nishimura, *Nature*, **271**, 545 (1978).
12) G. E. Hilbert and J. B. Johnson, *J. Am. Chem. Soc.*, **52**, 2001 (1930).
13) E. Wittenburg, *Chem. Ber.*, **99**, 2380 (1966).
14) N. J. Leonard and R. A. Lauren, *J. Am. Chem. Soc.*, **85**, 2026 (1963).
15) N. J. Leonard and T. Fujii, *J. Am. Chem. Soc.*, **85**, 3719 (1963).
16) The reactivity of nitrogen atoms in guanine was uncertain due to the low extent of allylation reaction, but methylation by TMP and ethylation by TEP have suggested the following order: N-1>N-7>N-3>N-9.
17) A. D. Toy and J. R. Costello, U. S. Patent 2754315 (1950).
18) K. Kondo, K. Kuwata, and K. Takemoto, *Makromol. Chem.*, **160**, 341 (1972).

BULLETIN OF THE CHEMICAL SOCIETY OF JAPAN, VOL. 52 (1), 261—262 (1979)

Autoxidation of Thujopsene in Carboxylic Acid Media. Co-preparation of Mayurone and 3-Thujopsanone

Kazuo ABE* and Masaaki ITO

Chemistry Laboratory, Department of General Education, Higashi Nippon Gakuen University, Onbetsu, Hokkaido 088-01

(Received May 22, 1978)

Synopsis. *cis*-(−)-Thujopsene has been autoxidized by perculation molecular oxygen through carboxylic acid solution, giving mayurone and 3-thujopsanone in fair yields. An investigation on the reaction conditions is described.

In a previous paper,[1] the autoxidation of thujopsene (**1**) to mayurone and other carbonyl compounds was reported utilizing metal chelate catalysts in dioxane. The reaction of thujopsene however, with a bismuth-(III) sulfate catalyst in carboxylic acid media gave a neopentyl type ester (**2**),[2] which differed from the general reactions of olefins.[3] This paper reports the autoxidation of **1** in carboxylic acid media to give mayurone and 3-thujopsanone in fair yields.

Experimental

Melting points were determined with a Shimadzu micro melting point apparatus and are uncorrected. The NMR spectra were recored on a JEOL JNM-PMX spectrometer using TMS as the internal standard. The IR spectra were determined on a Shimadzu IR-400 spectrometer and optical rotations on a Shimadzu polarisacchari meter. GLC analyses were performed on a Shimadzu GC-4B apparatus with a 1.5 m glass column packed with 10% OV-17, at 200 °C. The thujopsene used was purified by distillation of Cedar H oil (Takasago Perfumery Co., Ltd.) through a concentric column; bp 120 °C/10 Torr. The organic acids used were commercial, extra-pure reagents.

*General Procedure for Autoxidation of Thujopsene (**1**) in Carboxylic Acid.* Into a stirred solution of **1** (4.09 g, 20 mmol) in an organic acid or dioxane (0.4 mol), was passed a stream of dry oxygen at a rate of 66 ml/min at 75 °C for 20 h, using a catalyst in some cases. After removal of the organic acid under reduced pressure, the solution of the resulting residue was washed with water, the ether layer dried over anhydrous sodium sulfate, and the solvent removed. The reaction mixture was analyzed by GLC. In the case of preparation of main products, the reaction mixture was distillated. The corresponding fractions were collected and subsequently recrystallized.

*Isolation of (−)-3-Thujopsanone (**4**).* Into a stirred solution of thujopsene **1** (30.7 g, 0.15 mol) in propionic acid (333 g, 4.5 mol), a dry stream of oxygen was passed at the rate of 200 ml/min at 75 °C for 30 h. After removal of propionic acid under reduced pressure, the reaction mixture was distilled through a concentric column to collect the distillate with a bp of 138—139 °C/8 Torr on chilling a crystalline matter deposited. Recrystallization of the crystals from pentane gave 2.6 g of **4** as colorless crystals, further purified by sublimation; mp 71.3—71.8 °C; $[\alpha]_D^{20}$ −85.5° (*c* 16.4, CCl_4); IR (CCl_4) 1712 cm^{-1} (C=O); NMR ($CDCl_3$) δ 0.61 (3H, s, CH_3), 1.10 (3H, s, CH_3), 1.23 (6H, d, $2CH_3$, J=6 Hz), 1.66 (1H, d, 4-$CH_2(\alpha)$, J=14 Hz), 2.22 (1H, d, 4-$CH_2(\beta)$, J=14 Hz), 2.45 (1H, q, 2-H, J=7 Hz). Found: C, 81.61; H, 10.88%. Calcd for $C_{15}H_{24}O$: C, 81.76; H, 10.98%.

Results and Discussion

The oxidation of *cis*-(−)-thujopsene (**1**) with molecular oxygen in a series of organic acids from acetic to isovaleric gave mayurone (**3**) and (−)-thujopsanone (**4**) in yields as shown in Fig. 1. The reactions always gave **3**, **4**, and **5**, regardless of the carboxylic acid used. The highest yields were obtained in propionic acid which has the highest pK_a value in the series of organic acid used. Addition of $CoCl_2 \cdot 6H_2O$ in the above reaction system (in $C_2H_5CO_2H$) did not influence the

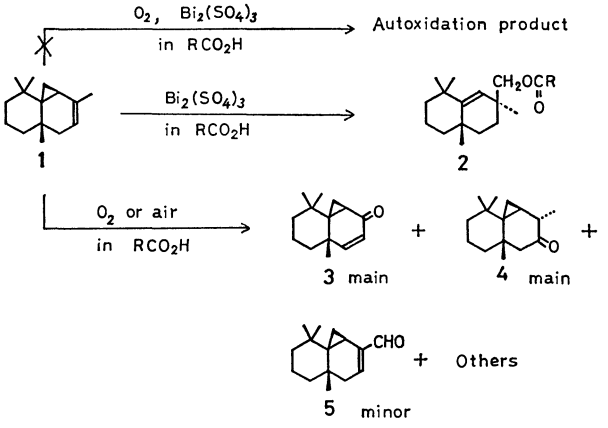

Scheme 1.

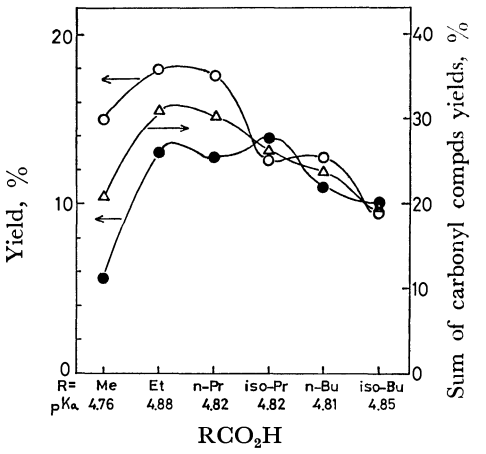

Fig. 1. Yield of carbonyl compounds—carboxylic acid profiles for the autoxidation in carboxylic acid media. Thujopsene 20 mmol, RCO_2H 0.4 mol, O_2 66 ml/min, at 75 °C for 20 h.
○: Mayurone, ●: 3-thujopsanone, △: sum of carbonyl compds.

yields of **3** and **5** but decreased the yield of **4**. Benzoyl peroxide did not give catalytic effect.

The autoxidation without catalyst in dioxane was significantly different from the same reaction in organic acid media. The addition of Co(II) complex catalyst in the system gave a higher yield of **3** and only a little of **4**,[1] the results of which are summarized in Table 1.

Table 1. Autocatalytic oxidation of thujopsene (20 mmol) at 75 °C for 20 h under perculating oxygen (66 ml/min)

Reaction	Distribution of products, %		
	Mayurone **3**	(−)-3-Thujopsanone **4**	Thujopsenal **5**
In $C_2H_5CO_2H$	20.2	13.2	0.6
In $C_2H_5CO_2H$,			
$CoCl_2 \cdot 6H_2O$ 2 mmol	16.7	1.1	0.3
4 mmol	20.9	1.1	0.6
6 mmol	22.1	1.2	0.6
10 mmol	20.8	1.0	0.5
In $C_2H_5CO_2H$,			
BPO 0.2 mmol	17.4	12.3	0.4
1 mmol	17.0	11.0	0.6
In dioxane[a]	1.7	2.1	0.6
In dioxane			
Co(II) complex[a]	27.4	5.6	4.9

a) This work, *cf.* Ref. 1.

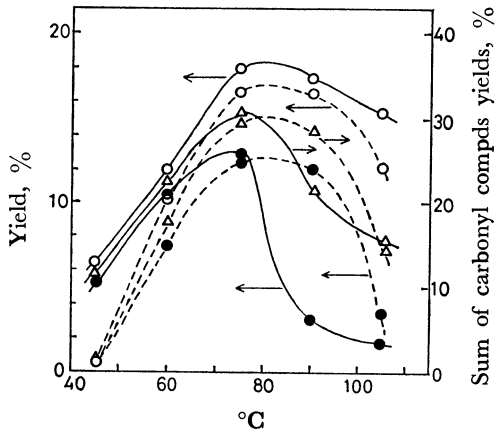

Fig. 2. Yield of carbonyl compounds—reaction temperature profiles for the autoxidation in carboxylic acid media.
Thujopsene 20 mmol, propionic acid 0.4 mol, O_2 or air 66 ml/min for 20 h.
○: Mayurone, ●: 3-thujopsanone, △: sum of carbonyl compds, ——: O_2, ----: air.

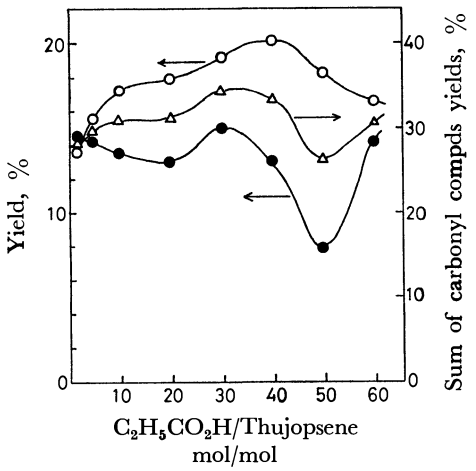

Fig. 3. Yield of carbonyl compounds—amount of carboxylic acid used profiles for the autoxidation in propionic acid media.
O_2 66 ml/min, at 75 °C for 20 h.
○: Mayurone, ●: 3-thujopsanone, △: sum of carbonyl compds.

The optimum conditions for autoxidation were found in propionic acid. To obtain higher yields of carbonyl compounds, the reaction must be conducted at 70 °C using 40—30 mole parts of thujopsene as shown in Figs. 2 and 3.

The GLC of the reaction product (propionic acid/thujopsene=40/1, oxygen 66 ml/min, 75 °C for 20 h) indicated that the main products were **3** and **4**. The IR and NMR spectra of products **3** and **5** were coincident with those of authentic samples. The structure of **4** was confirmed by analytical and spectral analysis and also by the LAH reduction of **4** which afforded (+)-3-neothujopsanol which have been prepared by the hydroboration of thujopsene.[4] It was found that an unidentified product of the autocatalytic oxidation[1] of thujopsene with metal chelate catalyst was identical with (−)-3-thujopsanone (**4**).

The authors wish to express their gratitude to Takasago Perfumery Co., Ltd., for the donation of crude thujopsene.

References

1) M. Ito, T. Nishimura, and K. Abe, *Bull. Chem. Soc. Jpn.*, **45**, 1914 (1972).
2) K. Abe and M. Ito, *Bull. Chem. Soc. Jpn.*, **51**, 319 (1978).
3) S. Suzuki, Y. Moro-oka, and T. Ikawa, *Chem. Lett.*, **1976**, 29.
4) S. P. Acharya and H. C. Brown, *J. Org. Chem.*, **35**, 3874 (1970).

BULLETIN OF THE CHEMICAL SOCIETY OF JAPAN, VOL. 52 (1), 263—264 (1979)

Reactions of 2-Hydroxyimino-3-methyl-2,3-dihydrobenzothiazole Derivatives with Grignard Reagents and Organolithiums

Kin-ya AKIBA,* Hiroaki SHIRAISHI, and Naoki INAMOTO

Department of Chemistry, Faculty of Science, The University of Tokyo, Hongo, Tokyo 113

(Received June 9, 1978)

Synopsis. Reactions of 2-hydroxyimino-3-methyl-2,3-dihydrobenzothiazole derivatives (**1**) with Grignard reagents gave 2-hydroxyimino (**1e**) and 2-(substituted imino)-3-methyl-2,3-dihydrobenzothiazoles as major products, where **1e** was reduced by excess Grignard reagents to 2-imino derivative. On the other hand, reactions of **1** with organolithiums afforded *o*-(methylamino)phenyl sulfides as a major product.

As reported previously, reactions of 3-substituted 2-nitrosoimino-2,3-dihydrobenzothiazoles with Grignard reagents[1] and organolithiums[2] give products through attacks on the C-2 and the sulfur atom in the ring and the nitrogen atom of the nitroso group, depending on the type of nucleophiles.[3] Therefore, it is interesting to examine reactions of 2-hydroxyimino-3-methyl-2,3-hydrobenzothiazole derivatives (**1**) with the same kind of nucleophiles, expecting to see whether these can be controlled to effect ring-expansion[4,5] by changing the nature of leaving groups.

Reactions of 2-hydroxyimino-3-methyl-2,3-dihydrobenzothiazole derivatives (**1**) with Grignard reagents gave 2-hydroxyimino- (**1e**), 2-imino- (**2**), and 2-(substituted imino)-3-methyl-2,3-dihydrobenzothiazoles (**3**), bis[*o*-(*N*-cyanomethylamino)phenyl] disulfide (**4**), bis[*o*-(methylamino)phenyl] disulfide (**5**), and *o*-(methylamino)phenyl sulfide (**6**), depending on the substituent of **1** and reaction conditions. The results are summarized in Table 1.

The tosyloxyimino (**1a**) and benzoyloxyimino derivatives (**1b**) reacted easily in ether–benzene at room temperature, whereas the trimethylsilyloxyimino (**1c**), methoxyimino (**1d**), and hydroxyimino derivatives (**1e**) reacted only in refluxing benzene.

The possible reaction centers in **1** are a) the nitrogen atom in the imino group, b) the α-atom in the X group, c) the sulfur atom, d) the C-2 atom on the ring.

The formation of **2** is due to *in situ* reduction of **1e** by excess Grignard reagent, which is formed through an attack on the X group (path b). The formation of **4** and **5** is attributable to the presence of ring-opening equilibrium of Grignard type reagent of **2**, which was established in a previous paper.[4] The sulfide **6** is formed through an attack on the sulfur atom in the ring (path c).

Thus, **1a** reacts mainly by path a showing high ability of *p*-toluenesulfonate as a leaving group,[6] **1b**, **1c**, and **1d** do almost exclusively by path b producing Grignard type reagent of **1e** *in situ*.

The interesting point in the reaction of **1** with organolithiums is that path c is observed in a comparable extent with paths a and b, respectively, in the cases of **1a** and **1c**, which was not the case with Grignard reagents.[2] Moreover, **1d** reacts exclusively by path c in dramatic contrast to the result with ethylmagnesium bromide which followed path b almost exclusively. The results are summarized in Table 2.

The high thiophilicity of organolithiums compared with Grignared reagents has been observed in the reaction of the nitrosoimino derivatives with these organometalloids[2] and also in that of thioketones.[7] Conversion of an intermediate, *o*-(*N*-cyanomethylamino)phenyl sulfide (**A**), in to **6** was confirmed by the formation of benzophenone of the corresponding amount in the reaction with phenyllithium.

Table 1. Reactions of **1** with Grignard reagents

1	R	Condition	1e(%)	2(%)	3(%)	4(%)	5(%)	6(%)
1a	*p*-MeC_6H_4	Et_2O-PhH, r. t.	—	—	69	—	—	—
1a	Et	Et_2O-PhH, r. t.	—	—	72	12	—	—
1b	*p*-MeC_6H_4	Et_2O-PhH, r. t.	78	—	—	—	—	—
1c	Et	PhH, reflux	—	78	4	—	3	—
1d	Et	PhH, reflux	—	72	—	—	—	—
1e	Et	PhH, reflux	—	85	—	—	6	6

Table 2. Reactions of **1** with organolithiums

1	R	1e(%)	3(%)	5(%)	6(%)	Ph_2CO(%)
1a	Bu	12	16	12	34	—
1c	Ph	42	—	—	36	32
1d	Bu	—	—	—	90	—
1d	Ph	—	—	—	91	89

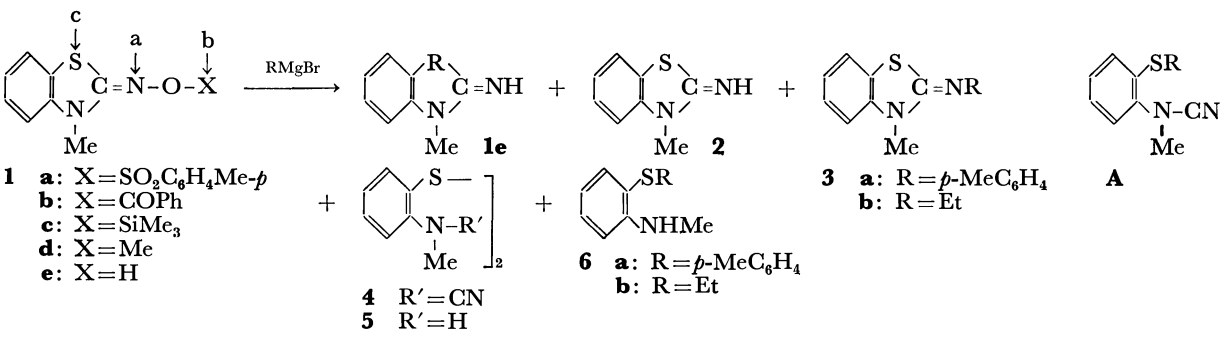

Experimental

2-Hydroxyimino-3-methyl-2,3-dihydrobenzothiazole (**1e**) was prepared by the reported method,[9] mp 203—204 °C (lit, 202—203 °C).

3-Methyl-2-tosyloxyimino- (**1a**), 2-benzoyloxyimino-3-methyl- (**1b**), 3-methyl-2-trimethylsilyloxyimino- (**1c**), and 3-methyl-2-methoxyimino-2,3-dihydrobenzothiazole (**1d**) were prepared from **1e** and the corresponding halides with base (triethylamine or sodium methoxide) in yields of 80, 69, 87, and 59%, respectively, with correct elemental analyses.

1a: mp 167—169 °C (from benzene–hexane). NMR ($CDCl_3$): δ 2.44 (s, 3H), 3.34 (s, 3H), 6.65—7.95 (m, 8H).

1b: mp 140—142 °C (from methanol). NMR ($CDCl_3$): δ 3.55 (s, 3H), 6.90—7.55 (m, 7H), 8.10—8.25 (m, 2H).

1c: bp 152 °C/3.5 mmHg, mp 49—50 °C. NMR ($CDCl_3$): δ 0.15 (s, 9H), 3.39 (s, 3H), 7.4—7.6 (m, 4H).

1d: bp 125—127 °C/115 mmHg, mp 47—48 °C (from hexane). NMR (CCl_4): δ 3.30 (s, 3H), 3.82 (s, 3H), 6.62—7.30 (m, 4H).

The following reactions were carried out under nitrogen.

*Reaction of Tosyloxyimino Derivative (**1a**).* *1) With p-Tolylmagnesium Bromide*: *p*-Tolylmagnesium bromide (4.5 mmol) in ether (15 ml) was added dropwise to a solution of **1a** (1.00 g, 3.0 mmol) in benzene (15 ml) at room temperature, and the mixture was stirred for 0.5 h. The reaction mixture was treated with 10% aq ammonium chloride (25 ml), extracted with dichloromethane and the dried extract was evaporated. The residue was submitted to dry column chromatography (DCC) (SiO_2, hexane: CH_2Cl_2=1:1) to afford 3-methyl-2-*p*-tolylimino-2,3-dihydrobenzothiazole (**3a**), yield 523 mg, (69%), mp 92—93 °C (from MeOH). NMR ($CDCl_3$): δ 2.34 (s, 3H), 3.55 (s, 3H), and 6.80—7.42 (m, 8H); MS: *m/e* 254 (M^+, 100%).

The compound (**3a**) was identical in every data with the authentic sample prepared from p-toludine and 3-methyl-2-methylthiobenzothiazolium iodide.[10]

2) With Ethylmagnesium Bromide: Ethylmagnesium bromide (3.9 mmol) in ether (15 ml) was added dropwise to **1a** (1.00 g, 3 mmol) in benzene (30 ml) and the mixture was stirred for 1 h. After usual work-up and DCC (SiO_2, CH_2Cl_2:AcOEt-4:1), 274 mg of **1a** was recovered, and oily 2-ethylimino-3-methyl-2,3-dihydrobenzothiazole (**3b**) (302 mg, 72%) and bis[*o*-(*N*-cyanomethylamino)phenyl] disulfide (**4**) (42 mg, 12%), mp 141 °C (lit,[11] 140—141 °C), were isolated.

3b: NMR ($CDCl_3$): δ 1.30 (t, J=7 Hz, 3H), 3.25 (q, J=7 Hz, 2H), 3.40 (s, 3H), and 6.79—7.40 (m, 4H).

*Reaction of Benzoyloxyimino Derivative (**1b**) with p-Tolylmagnesium Bromide* in benzene at room temperature afforded, after usual work-up, **1e** in 78% yield.

*Reaction of Hydroxyimino Derivative (**1e**) with Ethylmagnesium Bromide.* Ethylmagnesium bromide (17 mmol) in ether (15 ml) was added to **1e** (500 mg, 2.8 mmol) in warm benzene (30 ml) and the mixture was refluxed for 3 h. After usual work-up and DCC (SiO_2, CH_2Cl_2:AcOEt=4:1) followed by preparative thin-layer chromatography (PTLC) (SiO_2, CH_2Cl_2:hexane=1:1), 40 mg of **1e** was recovered, and 2-imino-3-methyl-2,3-dihydrobenzothiazole (**2**) (357 mg, 85%) mp 122—123 °C (lit,[12] 123 °C), bis[*o*-(methylamino)phenyl] disulfide (**5**) (22 mg, 6%), mp 66—67 °C (lit,[13] 67—68 °C), and ethyl *o*-(methylamino)phenyl sulfide (**6b**) (24 mg, 6%) were obtained.

6b: IR (neat): 3350 cm^{-1}; NMR ($CDCl_3$): δ 1.18 (t, J=7 Hz, 3H), 2.72 (q, J=7 Hz, 2H), 2.85 (s, 3H), and 6.5—7.5 (m, 4H); MS: *m/e* 167 (M^+, 100%).

*Reaction of Trimethylsilyloxyimino Derivative (**1c**) with Ethylmagnesium Bromide* in refluxing benzene (1.5 h) gave, after the same procedure as the preceding one, **2** (78%), **3b** (4%), and **5** (3%).

*Reaction of Methoxyimino Derivative (**1d**) with Ethylmagnesium Bromide* in refluxing benzene (3 h) gave, after usual work-up, **2** (72%).

*Reaction of **1a** with Butyllithium.* Butyllithium (10 mmol) in hexane (6 ml) was added to **1a** (836 mg, 2.5 mmol) in benzene (35 ml) and the mixture was stirred for 2 h. After usual work-up, the residue was submitted to DCC (SiO_2, CH_2Cl_2) and then PTLC (SiO_2, CH_2Cl_2: AcOEt=10:1 and then CH_2Cl_2:hexane=1:1) to give **1e** (53 mg, 12%), butyl *o*-(methylamino)phenyl sulfide (**6d**) (165 mg, 34%), 2-butylimino-3-methyl-2,3-dihydrobenzothiazole (**3d**) (86 mg, 16%), and bis[*o*-(methylamino)phenyl] disulfide (**5**) (42 mg, 12%).

3d: oily material; NMR ($CDCl_3$): δ 0.8—1.8 (m, 7H), 3.20 (t, J=7 Hz, 2H), 3.39 (s, 3H), and 6.7—7.4 (m, 4H).

6d: oily material; IR (neat): 3360 cm^{-1}; NMR ($CDCl_3$): δ 0.7—1.0 (m, 3H), 1.2—1.7 (m, 4H), 2.71 (t, J=7 Hz, 2H), 2.89 (s, 3H), 4.80 (bs, 1H), and 6.5—7.5 (m, 4H).

*Reaction of **1c** with Phenyllithium.* Phenyllithium (36 mmol) in ether (20 ml) was added to **1c** (756 mg, 3.0 mmol) in benzene (30 ml) and the mixture was stirred for 1 h. After usual work-up, **1e** (225 mg, 42% after recrystallization from methanol) precipitated from the residue. DCC of the filtrate gave benzophenone (173 mg, 32%), mp 47 °C, and *o*-(methylamino)phenyl phenyl sulfide (**6c**)[2] (233 mg, 36%) (by IR and NMR[2]).

*Reaction of **1d** with Butyllithium* in benzene afforded, after usual work-up and DCC (SiO_2, CH_2Cl_2:hexane=1:4), butyl *o*-(methylamino)phenyl sulfide (**6d**) (90%).

*Reaction of **1d** with Phenyllithium* in benzene afforded, after usual work-up, benzophenone (89%) and **6c** (91%).

References

1) a) K. Akiba, T. Kawamura, M. Hisaoka, and N. Inamoto, *Bull. Chem. Soc. Jpn.*, **48**, 3262 (1975); b) M. Hisaoka, K. Akiba, and N. Inamoto, *ibid.*, **48**, 3266 (1975); c) K. Akiba, M. Hisaoka, T. Kawamura, and N. Inamoto, *ibid.*, **48**, 3270 (1975).

2) M. Hisaoka, K. Akiba, and N. Inamoto, *Bull. Chem. Soc. Jpn.*, **48**, 3274 (1975).

3) For review of these and related reactions see: K. Akiba and N. Inamoto, *Heterocycles*, **7**, 1131 (1977).

4) K. Akiba, K. Ishikawa, and N. Inamoto, *Chem. Lett.*, **1976**, 1111.

5) E. Fanghaenel, *J. Prakt. Chem.*, **318**, 127 (1976).

6) S. S. Pelosi and R. E. Lyle, *Chem. Eng. News*, **1964**, 45.

7) P. Beak and J. W. Worley, *J. Am. Chem. Soc*, **92**, 4144 (1970).

8) K. Akiba, M. Hisaoka, N. Inamoto, T. Ohta, and H. Kuroda, *Chem. Lett.*, **1975**, 347.

9) K. Fuchs and E. Grauaug, *Ber.*, **61**, 2194 (1928).

10) D. J. Fry and J. D. Kendall, *J. Chem. Soc.*, **1951**, 1716.

11) K. Akiba, I. Fukawa, N. Nomura, and N. Inamoto, *Bull. Chem. Soc. Jpn.*, **45**, 1867 (1972).

12) E. Besthorn, *Ber.*, **43**, 1519 (1910).

13) C. D. Harries and E. Loewenstein, *Ber.*, **27**, 861 (1894).

BULLETIN OF THE CHEMICAL SOCIETY OF JAPAN, VOL. 52 (1), 265—266 (1979)

Carbon-13 Chemical Shifts of Retinal Isomers and Their Schiff Bases as Models of Visual Chromophores

Yoshio INOUE,* Yasuo TOKITÔ, Shigeki TOMONOH, and Riichiro CHÛJÔ

Department of Polymer Chemistry, Tokyo Institute of Technology, O-okayama, Meguro-ku, Tokyo 152

(Received June 23, 1978)

Synopsis. Carbon-13 NMR spectra have been observed for 11- and 13-*cis*-retinals and their Schiff base linkage compounds with butylamine as a model compound of visual chromophore. The chemical shift changes on going from retinal to Schiff base. The changes in chemical shifts of polyene carbons were discussed in correlation with the changes of π-electron densities.

The visual mechanism in the vertebrate is mainly controlled by rhodopsin composed of the vitamin A_1 aldehyde isomer, 11-*cis*-retinal, and the lipoprotein, opsin. Absorption of the photon by a visual pigment induces immediate isomerization of the retinal from the 11-*cis*- to *all-trans*-isomer. This isomerization act as a trigger for stimulating the nerve.

When the 11-*cis*-retinal, which has an absorption maximum at 380 nm, forms the visual pigment by combination with opsin, a large bathochromic shift is observed.[1] In order to understand the origin of this spectral shift, it is necessary to know the electronic structure of polyene chain of retinal. Since experimental results suggest that the retinal is bonded through a Schiff base linkage to the ε-amino group of a lysine residue in a opsin,[2–5] the Schiff base compound of retinal with butylamine, *N*-retinylidenebutylamine (NRB), have been used as a model for the rhodopsin. The change in carbon-13 chemical shifts of the conjugated polyene carbon atoms on going from *all-trans*-retinal to *all-trans*-NRB can be correlated quite well with that in π-electron density.[6,7]

We have investigated the changes in the π-electron densities of polyene carbon atoms on going from 11-*cis* and 13-*cis*-retinals to their Schiff base linkage compounds with butylamine by observing the carbon-13 NMR chemical shifts. The polyene aldehyde 13-*cis*-retinal is considered the chromophores of the membrane protein, bacteriorhodopsin.[8]

Experimental

11- and 13-*cis*-retinals were prepared by the photoisomerization of *all-trans*-retinals in ethanol in the sunlight. The resulting mixture of retinal isomers was fractionated on a column of sodium aluminosilicate by eluting with petroleum ether. Each crude isomer was purified by repeated crystallization from petroleum ether at −15 °C. Details of the methods of preparation for the *all-trans*-retinal and the Schiff base compound of retinal isomer have been reported.[7]

Carbon-13 NMR spectra were observed on a JEOL JNM PS-100 spectrometer linked with a PFT-100 Fourier transform system at 25.14 MHz. All measurements were carried out immediately after dissolution of sample in CCl_4 in 8 mm o.d. glass tubes in the dark. Chemical shifts were measured as downfield shifts from internal tetramethylsilane. The carbon-13 NMR spectra of 11- and 13-*cis*-retinals were assigned according to the results published.[9,10] All peaks in the carbon-13 NMR spectra of NRB have been assigned by use of various techniques.[7]

Results and Discussion

The chemical shifts of the conjugated polyene chain carbons in *cis*-retinal isomers and their Schiff base linkage compounds are given in Table 1 together with the data of *all-trans*-retinal and *all-trans*-NRB for the sake of comparison. The chemical shifts of the NRB are expressed as the chemical shift differences $\Delta\delta$, the differences between chemical shifts of retinal and those of corresponding NRB, in which the positive and negative signs indicate the downfield and upfield shifts, respectively. The numbering of the carbons, for example in *all-trans*-NRB, is given as shown in the following.

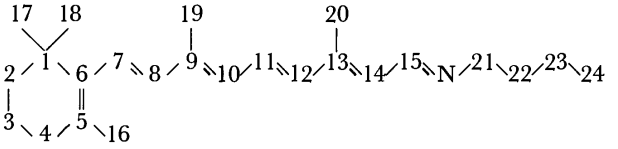

For all isomers the peaks assigned to the odd-numbered carbons show large upfield shifts and the peaks assigned to the even-numbered carbons show small downfield shifts by formation of the Schiff base com-

TABLE 1. THE CARBON-13 CHMICAL SHIEFTS OF CONJUGATED CHAIN CARBONS ON RETINAL ISOMERS AND THEIR SCHIFF BASE COMPOUNDS (NRB)

Carbon No.	11-*cis*		13-*cis*		*all-trans*[c]	
	Retinal[a]	NRB[b]	Retinal[a]	NRB[b]	Retinal[a]	NRB[b]
5	131.5	−0.7	131.7	−0.6	131.7	−1.0
6	139.8	0.1	139.4	0.5	139.8	−0.1
7	130.9	−1.9	130.9	−1.6	130.9	−2.2
8	139.8	0.5	139.8	0.2	139.4	0.3
9	142.6	−2.6	142.3	−2.9	142.1	−3.6
10	128.0	1.3	131.8	0.8	131.7	0.6
11	132.6	−3.8	134.5	−4.0	133.5	−4.9
12	132.6	1.8	129.0	1.0	137.1	1.4
13	155.5	−10.5	154.2	−10.4	154.7	−10.6
14	131.9	0.9	129.8	1.0	131.2	1.1
15	191.5	−30.8	190.2	−30.7	191.5	−31.3

a) Chemical shifts were measured as downfield shifts from internal tetramethylsilane and are expressed in terms of ppm. The estimated error in chemical shifts is less than 0.1 ppm. b) Chemical shifts of NRB are expressed as downfield (plus) and upfield (minus) shifts from the corresponding carbon of retinal. c) The chemical shifts of *all-trans*-retinal and *all-trans*-NRB were taken from Refs. 6 and 7.

pounds. Table 1 also indicates the presence of the gradients in the chemical shifts differences $\Delta\delta$ along the polyene chain from $C(15)$ to $C(5)$.

The carbon-13 chemical shifts of conjugated π-electron systems are generally dominated by the contribution from the paramagnetic term, being related to the π-electron density and π-bond order.[11] According to the data of X-ray analysis[12] and resonance-enhanced Raman spectra,[13] and the results of CNDO/2 MO calculation,[7] there are neither collapse of the bond alternation nor remarkable difference of the π-bond order between *all-trans*-retinal and *all-trans*-NRB. The constancy of the π-bond order may be also valid in the *cis*-isomers. Thus the changes of the chemical shifts can be explained by those of π-electron densities on the polyene chain.[7,11]

When the terminal atom of the polyene chain changes from oxygen to nitrogen, the total π-electron density of the conjugated polyene carbons of NRB increases due to the decrease in electronegativity at the polyene terminal. The carbon-13 chemical shifts differences show that an increase in total π-electron density leads to the increase in π-electron density at the odd-numbered carbons of NRB. It is noticeable that the chemical shifts in the conjugated polyene carbons of NRB are distributed in a relatively narrow range of approximately 30 ppm, whereas those of corresponding retinal isomers are in a range of 60 ppm. The decrease in the chemical shift range indicates that the delocalization of π-electron on the polyene chain is induced by the formation of Schiff base linkage.

The chemical shift differences $\Delta\delta$ of the odd-numbered polyene carbons of *all-trans*-NRB are slightly larger than those of the corresponding carbons in 11- and 13-*cis*-NRB's. This result may reflect the fact that the changes in π-electron density induced by the formation of the Schiff base are slightly larger on the *all-trans* polyene chain than on the *cis*-chain.

The authors are grateful to Dr. Yasuhiro Miyoshi of the Department of Botany, The University of Tokyo, for his valuable discussion.

References

1) G. Wald and P. K. Brown, *J. Gen. Physiol.*, **37**, 189 (1953).
2) D. Bownds, *Nature (London)*, **216**, 1178 (1967).
3) M. Akhtar, P. T. Blosse, and P. B. Dewhurst, *Chem. Commun.*, **1967**, 631.
4) M. O. Hall and A. D. E. Bacharach, *Nature (London)*, **225**, 637 (1970).
5) W. J. DeGrip, S. L. Bonting, and F. J. M. Daemen, *Biochim. Biophys. Acta*, **303**, 189 (1973).
6) Y. Tokitô, Y. Inoue, R. Chûjô, and Y. Miyoshi, *Org. Magn. Reson.*, **7**, 485 (1975).
7) Y. Inoue, Y. Tokitô, R. Chûjô, and Y. Miyoshi, *J. Am. Chem. Soc.*, **99**, 5592 (1977).
8) D. Oesterhelt, M. Meentzen, and L. Schuhmann, *Eur. J. Biochem.*, **40**, 453 (1973).
9) R. Rowan, III, and B. D. Sykes, *J. Am. Chem. Soc.*, **96**, 7000 (1974).
10) R. S. Becker, S. Berger, D. K. Dalling, D. M. Grant, and R. J. Pugmire, *J. Am. Chem. Soc.*, **96**, 7008 (1974).
11) M. Karplus and J. A. Pople, *J. Chem. Phys.*, **38**, 2803 (1963).
12) T. Hamanaka and T. Mitsui, paper read at the 12th Meeting of the Biophysical Society of Japan, Tokyo, Preprints, 1973, p. 81.
13) M. E. Heyde, D. Gill, R. G. Kilponen, and L. Rimai, *J. Am. Chem. Soc.*, **93**, 6776 (1971).

BULLETIN OF THE CHEMICAL SOCIETY OF JAPAN, VOL. 52 (1), 267—268 (1979)

A Convenient Synthesis of α-(2-Benzothiazolylthio)alkanoates by Cleavage of β-Keto Esters with 2-Benzothiazolesulfenamides

Sigeru TORII,* Hideo TANAKA, and Hiroshi OKUMOTO

Department of Industrial Chemistry, School of Engineering, Okayama University, Okayama 700

(Received June 26, 1978)

Synopsis. α-(2-Benzothiazolylthio)alkanoates were prepared by the reaction of β-keto esters with 2-(morpholinothio)benzothiazole in refluxing alcohols. Sulfenylating cleavage of α-methoxycarbonylcycloalkanones afforded the corresponding ω-alkoxycarbonyl- and/or ω-carbamoyl-α-(2-benzothiazolylthio)alkanoates.

In a previous paper, it has been shown that the direct cross-coupling reaction of disulfides with amines by an electrochemical procedure provides a variety of sulfenamides **2** in high yields.[1] Several investigations demonstrate that the sulfenamides **2** and their related compounds can be used for sulfenylation of active hydrogen compounds.[2,3] It was previously reported that sulfenylation of ethyl acetoacetate (**1**, R^1=Me, R^2=H, R^3=Et) with sulfenamides **2** (Y=Ph, R^4, R^5=alkyl) in CH_2Cl_2 gives ethyl α-(phenylthio)acetoacetate (**4**, R^1=Me, R^2=H, R^3=Et, Y=Ph) *via* the intermediate **5**.[3] However, sulfenylating cleavage of β-keto esters **1** with **2** into the corresponding α-sulfenyl esters **3** has not yet been realized. In this paper, we wish to report an efficient synthesis of α-sulfenylalkanoates **3** from β-keto esters **1** by the action of 2-benzothiazolesulfenamides **2**.

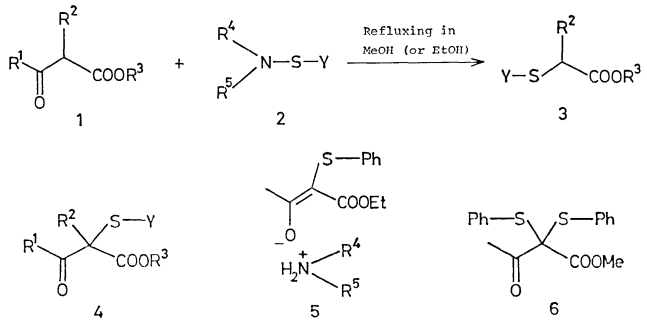

The reaction of equimolar amounts of methyl acetoacetate (**1a**, R^1=R^3=Me, R^2=H) with sulfenamide **2a** (Y=Ph, R^4, R^5=$(CH_2CH_2)_2O$) in refluxing methanol for 7 h afforded methyl (phenylthio)acetate (**3a**) along with disulfenylated product **6** (8%) (Table 1, entry 1). On the other hand, the reaction of **1a**

TABLE 1. REACTION OF METHYL ACETOACETATE WITH SULFENAMIDES **2**

Entry		Sulfenamide **2** Y[b]	R^4	R^5		Product **3** Y[b] (R^3=Me)	Yield[a] %
1	**2a**	Ph	$-CH_2CH_2OCH_2CH_2-$		**3a**	Ph	61[c]
2	**2b**	BT	$-CH_2CH_2OCH_2CH_2-$		**3b**	BT	92
3	**2c**	BT	$-(CH_2)_5-$		**3b**	BT	81
4	**2d**	BT	H	Cyclohexyl	**3b**	BT	73
5	**2e**	T	$-(CH_2)_5-$		**3c**	T	21
6	**2f**	(*N*-(Phenylthio)phthalimide)					—

a) Isolated yield. b) BT= 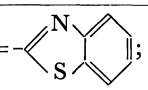 ; T=. c) Disulfenylated compound **6** was also produced in 8% yield.

TABLE 2. REACTION OF β-KETO ESTERS WITH (2-BENZOTHIAZOLE)SULFENAMIDE **2b**

Entry		β-Keto ester **1** R^1	R^2	R^3	Solvent		Product **3** (Y=BT) R^2	R^3	Yield[a] %
7	**1b**	Me,	n-C_6H_{13},	Me	MeOH	**3d**	n-C_6H_{13}	Me	98
8	**1c**	$-(CH_2)_3-$		Me	MeOH	**3e**	$(CH_2)_3COOMe$	Me	99
9	**1c**	$-(CH_2)_3-$		Me	EtOH	**3f**	$(CH_2)_3COOEt$	Me	73
10	**1c**	$-(CH_2)_3-$		Me	Benzene	**3g**	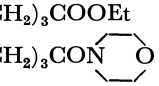	Me	97
11	**1c**	$-(CH_2)_3-$		Me	CH_2Cl_2	**3g**	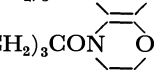	Me	87
12	**1d**	$-(CH_2)_3-$		Et	MeOH	**3h**	$(CH_2)_3COOMe$	Et	92
13	**1d**	$-(CH_2)_3-$		Et	EtOH	**3i**	$(CH_2)_3COOEt$	Et	58
14	**1e**	$-(CH_2)_4-$		Me	MeOH	**3j**	$(CH_2)_4COOMe$	Me	99

a) Isolated yield.

with various 2-benzothiazolesulfenamides **2b—d** (Y= 2-benzothiazolyl (BT)) furnished **3b** (Y=BT, R^2=H) as a sole product in high yields (entries 2—4). In contrast, thiocarbamoylsulfenamide **2e** (entry 5) afforded only 21% of the desired α-sulfenyl ester **3c** as well as complex materials. In entry 6, most of *N*-(phenylthio)phthalimide (**2f**) was recovered.

Above all, it was found that 2-benzothiazolesulfenamide **2b** is the most effective reagent for the conversion of **1a** into the corresponding α-sulfenylacetates **3**. The results of sulfenylation of α-substituted β-keto esters **1** (R^1, R^2=alkyl) with **2b** in refluxing alcohols are shown in Table 2. Thus, α-alkoxycarbonylcycloalkanones **1** afforded the corresponding ω-alkoxycarbonyl-α-sulfenylalkanoates **3** (R^2=$(CH_2)_n$COOMe (or COOEt)) (entries 8, 9, 12, 13, and 14), indicating that regioselective nucleophilic attack with alcohols, providing the ω-ester groups, was encountered.

When the reaction of 2-methoxycarbonylcyclopentanone (**1c**) with **2b** was carried out in benzene or CH_2Cl_2, the corresponding methyl 5-morpholinocarbonyl-2-sulfenylpentanoate **3g** was isolated in good yields (entries 10 and 11). This result demonstrates that nucleophilic attack of morpholine provided by the sulfenylation to the ketonic carbonyl of **4** [Y=BT, R^1, R^2=$(CH_2)_3$, R^3=Me] would occur preferentially in aprotic solvent.

Experimental

All the melting and boiling points are uncorrected. IR spectra were determined with a JASCO IRA-I infrared spectrometer. NMR spectra were obtained at 100 MHz with a JEOL MH-100 spectrometer.

*Methyl (Phenylthio)acetate (**3a**).* A MeOH solution (3 ml) of $AcCH_2COOMe$ (70 mg, 0.6 mmol) and **2a** (110 mg, 0.6 mmol) was heated to reflux for 7 h. The solution was concentrated *in vacuo* and the residue was chromatographed (SiO_2, benzene–hexane–AcOEt, 10/10/1). The first coming elute gave **6** (16 mg, 8%): bp 119—123 °C/0.003 Torr; IR (neat) 3060, 3030 (HC=C), 1723, 1712 cm^{-1} (C=O); NMR ($CDCl_3$) δ 2.30 (s, 3, CH_3), 3.59 (s, 3, CH_3O), 7.10—7.82 (m, 10, HC=C). Found: C, 61.50; H, 4.99%. Calcd for $C_{17}H_{16}O_3S_2$: C, 61.42; H, 4.85%.

The second fraction afforded **3a** (67 mg, 61%): bp 38—40 °C/0.007 Torr (lit,[4a] bp 87—90 °C/0.3 Torr); IR (neat) 3046 (HC=C), 1734 cm^{-1}; NMR ($CDCl_3$) δ 3.70 (s, 2, CH_2), 3.76 (s, 3, CH_3O), 7.30—7.72 (m, 5, HC=C).

*Methyl (2-Benzothiazolylthio)acetate (**3b**).* A MeOH solution (3 ml) of $AcCH_2COOMe$ (116 mg, 1.0 mmol) and **2b** (252 mg, 1.0 mmol) was heated to reflux for 7 h. Evaporation of the solvent followed by column chromatography (SiO_2, benzene–hexane–AcOEt, 10/10/1) gave **3b** (219 mg, 92%): mp 74—75 °C (Et_2O–hexane, 1/2); IR (Nujol) 3050 (HC=C), 1743 cm^{-1} (C=O); NMR ($CDCl_3$) δ 3.70 (s, 3, CH_3O), 4.12 (s, 2, CH_2), 7.06—7.86 (m, 4, HC=C). Found: C, 50.20; H, 3.81%. Calcd for $C_{10}H_9NO_2S_2$: C, 50.19; H, 3.79%.

The reaction of β-keto esters **1** with **2b—c** was carried out in a similar manner to that above (Tables 1 and 2). Physical properties and spectral data of the products **3c—j** are as follows.

*Compound **3c**:* Bp 64—68 °C/0.006 Torr; IR (neat) 1734 cm^{-1} (C=O); NMR ($CDCl_3$) δ 1.72 (br, 6, CH_2), 3.75 (s, 3, CH_3O). 3.92—4.40 (m, 4, CH_2N), 4.18 (s, 2, CH_2S). Found: C, 46.14; H, 6.23%. Calcd for $C_9H_{15}NO_2S_2$: C, 46.32; H, 6.48%.

*Compound **3d**:* Bp 123—126 °C/0.005 Torr; IR (neat) 3053 (HC=C), 1739 cm^{-1}; NMR ($CDCl_3$) δ 0.87 (t, 3, J=6 Hz, CH_3), 1.05—2.19 (m, 10, CH_2), 3.72 (s, 3, CH_3), 4.61 (t, 1, J=7 Hz, CH), 7.11—7.91 (m, 4, HC=C). Found: C, 59.38; H, 6.42%. Calcd for $C_{16}H_{21}NO_2S_2$: C, 59.41; H, 6.54%.

*Compound **3e**:* Bp 124—126 °C/0.008 Torr; IR (neat) 3050 (HC=C), 1732 cm^{-1} (C=O); NMR ($CDCl_3$) δ 1.58—2.27 (m, 4, CH_2), 2.35 (t, 2, J=7 Hz, CH_2CO), 3.61 (s, 3, CH_3O), 3.72 (s, 3, CH_3O), 4.66 (t, 1, J=7 Hz, CH), 7.14—7.90 (m, 4, HC=C). Found: C, 53.03; H, 4.87%. Calcd for $C_{15}H_{17}NO_4S_2$: C, 53.08; H, 5.05%.

*Compound **3f**:* Bp 121—123 °C/0.009 Torr; IR (neat) 3050 (HC=C), 1732 cm^{-1} (C=O); NMR ($CDCl_3$) δ 1.22 (t, 3, CH_3), 1.62—2.26 (m, 4, CH_2), 2.35 (t, 2, J=7 Hz, CH_2CO), 3.73 (s, 3, CH_3O), 4.07 (q, 2, CH_2O), 4.66 (t, 1, J=7 Hz, CH), 7.09—7.94 (m, 4, HC=C). Found: C, 54.32; H, 5.41%. Calcd for $C_{16}H_{19}NO_4S_2$: C, 54.37; H, 5.42%.

*Compound **3g**:* Bp 147—150 °C/0.006 Torr; IR (neat) 3060 (HC=C), 1733, 1640 cm^{-1} (C=O); NMR ($CDCl_3$) δ 1.65—2.31 (m, 4, CH_2), 2.40 (t, 2, J=7 Hz, CH_2CO), 3.28—3.78 (m, 8, NCH_2CH_2O), 3.79 (s, 3, CH_3O), 4.76 (t, 1, J=7 Hz, CH), 7.24—8.06 (m, 4, HC=C). Found: C, 54.64; H, 5.52%. Calcd for $C_{18}H_{22}N_2O_4S_2$: C, 54.80; H, 5.62%.

*Compound **3h**:* Bp 124—126 °C/0.009 Torr; IR (neat) 3065 (HC=C), 1735 cm^{-1} (C=O); NMR ($CDCl_3$) δ 1.25 (t, 3, CH_3), 1.63—2.25 (m, 4, CH_2), 2.37 (t, 2, J=7 Hz, CH_2CO), 3.62 (s, 3, CH_3O), 4.19 (q, 2, CH_2O), 4.63 (t, 1, J=7 Hz, CH), 7.11—7.95 (m, 4, HC=C). Found: C, 54.24; H, 5.59%. Calcd for $C_{16}H_{19}NO_4S_2$: C, 54.37; H, 5.42%.

*Compound **3i**:* Bp 124—126 °C/0.006 Torr; IR (neat) 3050 (HC=C), 1730 cm^{-1} (C=O); NMR ($CDCl_3$) δ 1.24 (t, 3, CH_3), 1.26 (t, 3, CH_3), 1.67—2.28 (m, 4, CH_2), 2.38 (t, 2, J=7 Hz, CH_2CO), 4.14 (q, 2, CH_2O), 4.26 (q, 2, CH_2O), 4.70 (t, 1, J=7 Hz, CH), 7.24—8.03 (m, 4, HC=C). Found: C, 55.65; H, 5.86%. Calcd for $C_{17}H_{21}NO_4S_2$: C, 55.56; H, 5.76%.

*Compound **3j**:* Bp 125—128 °C/0.006 Torr; IR (neat) 3058 (HC=C), 1739 cm^{-1} (C=O); NMR ($CDCl_3$) δ 1.32—2.22 (m, 6, CH_2), 2.31 (t, 2, J=7 Hz, CH_2CO), 3.63 (s, 3, CH_3O), 3.73 (s, 3, CH_3O), 4.64 (t, 1, J=7 Hz, CH), 7.08—8.04 (m, 4, HC=C). Found: C, 54.20; H, 5.43%. Calcd for $C_{16}H_{19}NO_4S_2$: C, 54.37; H, 5.42%.

References

1) S. Torii, H. Tanaka, and M. Ukida, *J. Org. Chem.*, **43**, 3223 (1978).

2) For a review of the chemistry of sulfenamide derivatives: (a) C. Brown and B. T. Grayson, *Int. J. Sulfur Chem.*, **5**, 93 (1970); (b) F. A. Davis, *ibid.*, **8**, 71 (1973).

3) (a) T. Mukaiyama, S. Kobayashi, and T. Kumamoto, *Tetrahedron Lett.*, **1970**, 5115; (b) In the aprotic solvent the stable ammonium salt **5** would serve to prevent further sulfenylation reaction: T. Kumamoto, S. Kobayashi, and T. Mukaiyama, *Bull. Chem. Soc. Jpn.*, **45**, 866 (1972).

4) Syntheses of α-sulfenyl esters : (a) R. G. Hiskey and F. I. Carroll, *J. Am. Chem. Soc.*, **83** 4649 (1961); (b) B. M. Trost, T. N. Salzmann, and K. Hiroi, *ibid.*, **98**, 4887 (1976).

BULLETIN OF THE CHEMICAL SOCIETY OF JAPAN, VOL. 52 (1), 269—270 (1979)

The Photo-Beckmann Rearrangement of A-Nor-5α-cholestan-3-one Oxime[1)]

Hiroshi SUGINOME,* Hiroshi TAKEDA, and Tadashi MASAMUNE
Department of Chemistry, Faculty of Science, Hokkaido University, Sapporo 060

(Received July 3, 1978)

Synopsis. The photo-Beckmann Rearrangement of A-nor-5α-cholestan-3-one oxime affords 4-aza-5α-cholestan-3-one and 3-aza-5α-cholestan-4-one as the only lactams.

In previous papers,[2)] we reported the photo-Beckmann rearrangement of some cholestanone oximes and A-nor-5β-cholestan-3-one oxime.

In this paper, we report on an investigation of the photo-Beckmann rearrangement of A-nor-5α-cholestan-3-one oxime (**3**) which is complementary to the previous communications.[2)]

The parent ketone, A-nor-5α-cholestan-3-one (**2**),[2b,6)] has been prepared either by oxidative decarboxylation of 3-hydroxy-A-nor-5α-cholestane-3-carboxylic acid,[4)] prepared *via* three steps from cholest-4-en-3-one, with sodium bismuthate[5)] or by ozonization of 3-isopropylidene-A-nor-5α-cholestane (**1**) prepared *via* 4 steps from cholest-4-en-3-one.[6)] In the present experiment, the 3-one (**2**) was prepared by the latter method which afforded a significantly better overall yield from cholest-4-en-3-one. We have found that the reported yield for the ozonization step (12%) could be significantly improved by a modified procedure (64%, see Experimental).

The new oxime (**3**), prepared by the standard method, exhibited no deshielded proton signal due to the 2-H or the 5-αH at *ca.* τ 6.6 in the ^{1}H NMR spectrum as for the 5β-isomer.[2b)] This is expected since no proton eclipsed by the C=N bond of the hydroxyimino group is present in the oxime (**3**). The Beckmann rearrangement with thionyl chloride afforded 4-aza-5α-cholestan-3-one (**4**) as the sole product, indicating the configuration of the hydroxyimino group as depicted.

The photo-Beckmann rearrangement of the oxime (**3**) in methanol was carried out under the same procedure as for the photo-Beckmann rearrangement of cholestanone oxime previously reported.[2b)] As in the case of A-nor-5β-cholestan-3-one-oxime, irradiation of the oxime led to a mixture of products from which 4-aza-5α-cholestan-3-one (**4**) (6%) and 3-aza-5α-cholestan-4-one (**5**) (4%) were isolated as the only lactams together with A-nor-5α-cholestan-3-one (**2**) (4%) and unchanged oxime (**3**) (9%) by careful preparative TLC. Examination by TLC proved that no 5β isomers of the lactams (**4**) or (**5**) [*e.g.*,(**6**)] were formed.

Thus, it was again proved that the chirality of the migrating group in the oxime is retained during the photo-rearrangement.[2,7)]

The lactam (**5**) has been prepared by a method[3)] which involved 5 steps from 3,4-secocholest-5-ene-3,4-dioic acid. The present result may provide another route for this rather inaccessible lactam.

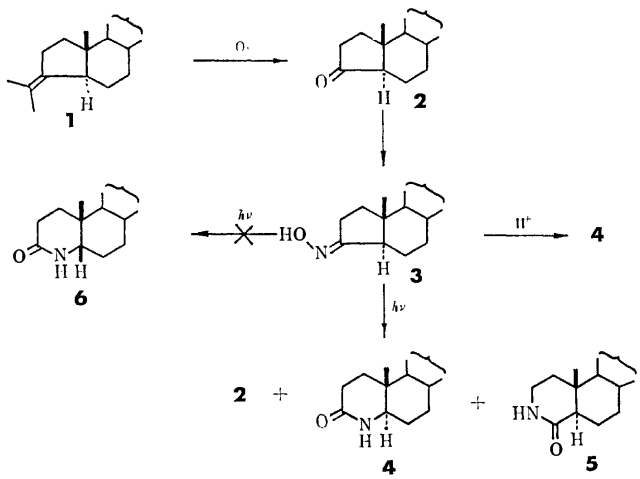

Scheme.

Experimental

For instruments used and general procedure see Ref. 2b. The mass spectra were taken with a Hitachi JMS-D 300 spectrometer using a direct inlet system (source temperature *ca.* 180 °C) in the Faculty of Pharmaceutical Sciences. Only fragment peaks of the relative intensities of over 20% are described. The infrared spectrum was taken with a model 260-10 Hitachi infrared spectrophotometer.

A-Nor-5α-cholestan-3-one (2).[2b,6)] This ketone was prepared either by the procedure of Camerino *et al.*[5)] or by the procedure of Biellmann and Ourisson.[6)] A modified procedure for ozonization of 3-isopropylidene-A-nor-5α-cholestane by Biellmann afforded a better yield of the ketone. Namely,

TABLE 1. NMR PARAMETERS (100 MHz) FOR THE KETONE, THE OXIME AND THE LACTAMS IN $CDCl_3$ SOLUTION
[Chemical shifts (τ) and splittings (Hz; in parentheses)]

Compound	18-H	19-H	2-CH_2	5-αH	Others
2	9.32	9.24	a)	a)	
3	9.32	9.29	a)	a)	OH 1.79 br (s)
4	9.32	9.10	7.59 (dd) (4 and 9)	6.95 (dd) (6 and 10)	NH 3.80 (s) ($W_{1/2}$ 4.8)
5	9.33	9.10	6.68 br (d) (9)	a)	

a) Unassignable.

3-isopropylidene-A-nor-5α-cholestane (2 g) in a mixed solvent of dichloromethane and methanol was ozonized at −72 °C. The temperature of the solution was raised to room temperature without adding sodium borohydride. After removal of the solvent, the residue (2.2 g) was subjected to column chromatography (silica gel, Wako C-200, 150 g). Elution with hexane afforded the starting material (41 mg). Further elutions with a 3 : 1 mixture of benzene and hexane afforded the ketone (1.21 g, 64%). This was recrystallized from methanol (1.12 g). Mp 103—106 °C (lit,[6] mp 106 °C). Biellmann[6] reports a yield of 12% for this ozonization step.

A-Nor-5α-cholestan-3-one Oxime (3). The 3-ketone (**2**) (270 mg), hydroxylamine hydrochloride (193 mg) and sodium acetate trihydrate (386 mg) in methanol (35 ml) and water (5 ml) were stirred for 3h. The solution was neutralized with 10% sodium hydrogencarbonate and was extracted with ether. The ethereal solution was worked up in usual way. The residue was recrystallized from methanol to yield the oxime (265 mg). Mp 167—168 °C; $[\alpha]_D^{22}$ +18.4 (*c* 1.0 $CHCl_3$); Found: C, 80.17; H, 11.87; N, 3.31%. Calcd for $C_{26}H_{45}NO$: C, 80.56; H, 11.70; N, 3.61%; IR 3288 (OH), 970, 934, and 905 cm^{-1}; MS (70 eV), *m/e* (rel. intensity), 41 (24.2), 43 (32.0), 55 (33.1), 109 (21.4), 112 (42.0), 217 (24.8), 233 (35.8), 356 (21.7), 370 (100), 371 (32.9), 372 (28.0), 387 (32.4, M^+).

The Beckmann Rearrangement of the Oxime (3). A stirred solution of the oxime (200 mg) in dioxane (6 ml) and ether (2 ml) was cooled to 5 °C. To this solution was added thionyl chloride (1 ml) and the solution was stirred for 1 min. The crystals which appeared in the solution were collected by filtration to afford the crude lactam (112 mg). The filtrate was extracted with ether-water. The ethereal solution was washed with aq sodium hydrogencarbonate solution and with water and dried (Na_2SO_4). The crude product was subjected to preparative TLC with a 4 : 1 mixture of dichloromethane and diethyl ether to afford the crude lactam (53 mg) as a least mobile fraction. The combined crude lactam (**4**) (165 mg, 83%) was recrystallized from methanol. Mp 252—255 °C (lit,[3] 253—255 °C); $[\alpha]_D^{22}$ +43.1 (*c*, 1.0 $CHCl_3$). MS (70 eV), *m/e* (rel. intensity), 41 (20.2), 43 (32.1), 55(28.3), 56 (40.5), 57 (24.0), 98 (37.4), 112 (26.0), 232 (82.4), 233 (50.9), 234 (23.3), 248 (21.3), 372 (24.3), 387 (100, M^+), 388 (30.2).

The Photo-Beckmann Rearrangement of the Oxime (3). The oxime (570 mg) in methanol (500 ml) was irradiated with a 15-W low pressure mercury arc in an atmosphere of nitrogen for 68 h. After removal of the solvent, the residue was extracted with ethyl acetate and the solution was worked up as usual. The TLC has shown the products to be a complex mixture. The crude photolyzate was subjected to preparative TLC (Wakogel B-5F) with a 4 : 1 mixture of dichloromethane and diethyl ether. Seven fractions A, B,C,D,E,F and G were obtained in order of decreasing mobility. The fraction A (37 mg) was the crude parent ketone and this was purified by preparative TLC (a 4 : 1 mixture of benzene and diethyl ether)followed by two recrystallizations to yield pure ketone (20 mg, 4%). The fractions B (20 mg), D (28 mg), E (23 mg), and G (164 mg) were an intractable mixture and they were not identified. The crystalline fraction C (90 mg) was recrystallized to yield the recovered oxime (50 mg, 9%). The fraction F (209 mg) was a mixture of two lactams and this was again subjected to preparative TLC with a 1 : 1 mixture of ethyl acetate and diethyl ether. Developments were made twice. The more mobile crystalline lactam (30 mg, 5%) was recrystallized from methanol to yield the lactam (**5**), (20 mg) in two crops. Mp 225 °C. (lit,[3] 225—227 °C). The less mobile crystalline lactam (34 mg, 6%) was recrystallized from methanol to yield the lactam (**4**) (25 mg). Mp 252—255 °C (lit,[3] mp 253—255 °C); $[\alpha]_D^{22}$ +43.1 (*c* 1.0 $CHCl_3$); MS (70 eV), *m/e* (rel. intensity). 41 (19.7), 43(27.0), 55 (28.1), 57 (20.1), 99 (25.5), 112 (42.3), 125 (42.2), 232 (78.5), 233 (34.0), 234 (23.1), 372 (21.9), 287 (100, M^+), and 388 (30.3).

We thank Mrs. T. Okayama and Miss H. Maki for H^1 NMR measurements.

References

1) Photoinduced Transformations. Part 40. Part 39. H. Suginome, H. Umeda, S. Sugiura, and T. Masamune, *J. Chem. Res.*, (*S*), 380 (1978); (*M*) 4520.

2) a) H. Suginome and H. Takahashi, *Tetrahedron Lett.*, **1970**, 5119; *Bull. Chem. Soc. Jpn.*, **47**, 687 (1974); b) H. Suginome and F. Yagihashi, *J. Chem. Soc., Perkin Trans. 1*, **1977**, 2488.

3) C. W. Shoppee, R. W. Killick, and G. Krüger, *J. Chem. Soc.*, **1962**, 2275.

4) G. H. Whitham and J. A. F. Wickramasinghe, *J. Chem. Soc.*, **1965**, 5416.

5) B. Camerino and V. Valcavi, *Gazz. Chim. Ital.*, **93**, 723, 735 (1963); B, Camerino, B. Pateli, and R. Sciaky, *Gazz. Chim. Ital.*, **93**, 1165 (1963).

6) J. F. Biellmann and G. Ourisson, *Bull. Soc. Chim. Fr.*, **1962**, 331.

7) H. Suginome, *Kagaku No Ryoiki*, **30**, 578 (1976).

BULLETIN OF THE CHEMICAL SOCIETY OF JAPAN, VOL. 52 (1), 271—272 (1979)

The Selective Elimination of Secondary Alkyl Group from Trialkylborane by the Successive Treatments with Anisole and Dimethyl Sulfoxide. A Supply of the Synthetic Intermediate for Primary Alkyl Derivatives

Yuzuru MASUDA, Masayuki HOSHI and Akira ARASE*

Department of Applied Chemistry, Kitami Institute of Technology, Kitami, Hokkaido 090

(Received July 7, 1978)

Synopsis. Secondary alkyl group of trialkylborane, derived from terminal olefin and borane, was selectively eliminated by the successive treatments with anisole and dimethyl sulfoxide. By the use of the resulting trialkylborane as the synthetic intermediate for primary alkyl derivatives, the contaminations of secondary alkyl derivatives were greatly reduced.

In the hydroboration of simple straight-chain terminal olefins, boron atom is placed on the terminal carbon atom, 95%, and on the internal carbon atom, 5%,[1] giving a mixture of trialkylboranes. For example, 1-pentene gives a mixture of tripentylborane (91%), dipentyl(1-methylbutyl)borane (6%), and pentylbis(1-methylbutyl)borane and tris(1-methylbutyl)borane (3%).[2] Accordingly, when these trialkylboranes are used as the synthetic intermediates, in some cases, contamination of the secondary alkyl derivative to the primary alkyl derivative is unavoidable.[3]

The authors previously reported that the mixed trialkylborane, which contained the primary and the secondary alkyl groups on the same boron atom, eliminated the secondary alkyl group preferentially to the primary alkyl group on heating in dimethyl sulfoxide (Eq. 1).[4]

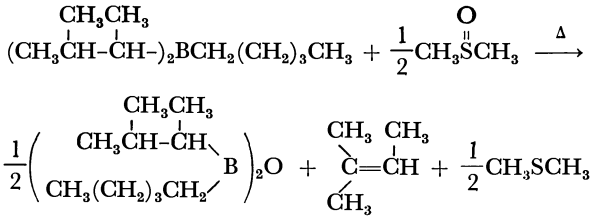

(1)

The present work was undertaken with a view to obtain trialkylboranes in which the amount of the secondary alkyl group was considerably small by the selective elimination of the secondary alkyl group of the trialkylboranes, prepared from terminal olefins by the hydroboration with borane.

To achieve the selective and effective elimination of the secondary alkyl group from the mixed trialkylborane, several reaction procedures were examined by using the reaction of trihexylborane, prepared from 1-hexene, with dimethyl sulfoxide. After the reaction, the amounts of hexyl and 1-methylpentyl group were estimated from the amounts of hexanols obtained by the alkaline hydrogen peroxide oxidation of the reaction mixture.

By the direct reaction only with dimethyl sulfoxide, it was not able to obtain a satisfactory result (Table 1). This insufficient result seemed to be caused by the progress of the isomerization of the primary alkyl group to the secondary alkyl group in nearly neat trihexylborane during the elimination reaction with dimethyl sulfoxide.[5] Accordingly, anisole, which had a significant effect on the migration of the boron atom from the terminal carbon atom to the internal carbon atom,[5] was used as shown in Scheme 1. Thus, trihexylborane was heated in anisole followed by the reaction with dimethyl sulfoxide.

Table 1. Residual hexyl groups after the reaction with dimethyl sulfoxide[a]

Anisole[b] (ml)	DMSO / R_3B (mmol) / (mmol)	Temperature, °C (treatment with DMSO)	Residual hexyl group (%)	Hexyl/1-Methylpentyl
None	0.5 / 4	160	87.1	95 / 5
None	1 / 4	160	85.1	95 / 5
None	4 / 4	160	81.8	96 / 4
None	12 / 4	160	67.0	97 / 3
2	0.2 / 4	160	97.5	98 / 2
2	0.2 / 4	170	97.5	99 / 1
2	0.5 / 4	170	84.3	99 / 1

a) Carried out for 2 h. b) Pretreatment with anisole was carried out at 170 °C for 2 h.

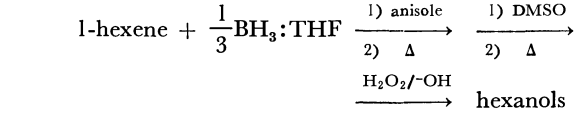

Scheme 1.

By this procedure, the ratio of hexyl group and 1-methylpentyl group was greatly improved to 99:1, and 97.5% of hexyl group remained on the boron atom (Table 1).

By the same procedure, high proportions of the primary alkyl group were also realized in the reactions of trialkylboranes derived from other terminal olefins. The results are listed in Table 2.

Actually, the 1-alkanols thus formed by the oxidation with alkaline hydrogen peroxide, could be separated from the reaction mixtures effectively by column chromatography. For example, 1-octanol was obtained in 89% yield accompanied by only 0.5% of 2-octanol.

On the other hand, neat trialkylboranes could be distilled from the reaction mixtures. For example, essentially pure tripentylborane was distilled from the reaction mixture in 85% yield (75—76 °C/12 mmHg).

Then we undertook another reactions to confirm the usefulness of this procedure. Thus, after the treatments with anisole and dimethyl sulfoxide, trihexylborane was allowed to react with aqueous iron(III) chloride, aqueous copper(II) bromide and aqueous

Table 2. Residual alkyl group of some trialkylboranes after the successive treatments with anisole[a] and dimethyl sulfoxide[b]

R_3B (4 mmol) from olefin	Residual alkyl group (%)	*prim*-Alkyl/*sec*-Alkyl
1-Butene	86.3	99 / 1
1-Pentene	95.2	99 / 1
1-Octene	92.7	99 / 1
1-Dodecene	93.3	99 / 1

a) Carried out by using 2 ml of anisole at 170 °C for 2 h. b) Carried by using 0.2 mmol of DMSO at 170 °C for 2 h.

Table 3. Reactions of trihexylborane[a] with aqueous iron(III) chloride,[b] aqueous copper(II) bromide[c] and aqueous methyl vinyl ketone[d] after the treatments[e] with anisole and dimethyl sulfoxide

Reagent (mmol)	Product, mmol		Hexyl/1-Methylpentyl
Iron(III) chloride (24)	1-Chlorohexane	5.80	98 / 2
	2-Chlorohexane	0.09	
Copper(II) bromide (24)	1-Bromohexane	6.31	99 / 1
	2-Bromohexane	0.09	
Methyl vinyl ketone (6)	2-Decanone	2.41	98 / 2
	5-Methyl-2-nonanone	0.05	

a) 4 mmol of trihexylborane was used. b) The reaction was carried out at 55 °C for 48 h. c) The reaction was carried out at 55 °C for 48 h. d) The reaction was carried out at 20 °C for 2 h. e) The treatments were carried out by using 2 ml of anisole at 170 °C for 2 h, and then by using 0.2 mmol of DMSO at 170 °C for 2 h.

methyl vinyl ketone. The results are presented in Table 3.

As previously reported, the reactions of trialkylboranes with these reagents provide simple and convenient synthetic methods for chloroalkane,[3b] bromoalkane[3b] and 2-alkanone[3a] from various types of olefins. These reactions have a characteristic that the secondary alkyl group reacts with these reagents preferentially to primary alkyl group when both alkyl groups are on the same boron atom. Accordingly, in the direct reactions of these reagents with trialkylborane, prepared from terminal olefin and borane, appreciable amounts of secondary alkyl derivatives were involved in the reaction mixtures, that is, 8% of 2-chlorohexane, 5% of 2-bromohexane and 15% of 5-methyl-2-nonanone in the respective reactions. However, after the treatments with anisole and dimethyl sulfoxide, the proportions of the secondary alkyl derivatives were greatly reduced in the reactions with the same reagents.

We have not fully examined how trialkylboranes changed by the treatment with anisole. However, this procedure seems to have a practical value when trialkylboranes, derived from terminal olefins, are used as the synthetic intermediates for primary alkyl derivatives.

Experimental

Materials. Commercial 1-butene, 1-pentene, 1-hexene, 1-octene, 1-dodecene, anisole and dimethyl sulfoxide were dried over molecular sieve-5A and distilled before use. Commercial iron(III) chloride and copper(II) bromide were used without any purification.

Successive Treatments of Trialkylborane with Anisole and Dimethyl Sulfoxide. The following procedure is representative. A dry 50-ml flask, equipped with a magnetic stirring bar, a septum inlet and a reflux condenser, was flushed with argon. In the flask, 12 mmol of 1-hexene was hydroborated with 4 mmol of borane in tetrahydrofuran in the usual procedure.[6] After the addition of a 2 ml portion of anisole, tetrahydrofuran was removed under reduced pressure. Then the solution was heated at 170 °C for 2 h, followed by the reaction with 0.2 mmol of dimethyl sulfoxide at 170 °C fro 2 h. Then 4 ml of tetrahydrofuran was added to the solution and the solution was oxidized with alkaline hydrogen peroxide. The lower aqueous layer was separated and extracted with ethyl ether. The combined extracts and upper layer were analyzed by GLC, demonstrating that 11.6 mmol of 1-hexanol (96.7%) was obtained accompanied by 0.10 mmol of 2-hexanol (0.8%).

Isolation of 1-Octanol. From the organic layer, derived from 24 mmol of 1-octene in a similar manner as above, tetrahydrofuran and ethyl ether were removed. Then the reaction mixture was put on a dry silica gel column (Wako Q-50). Anisole was first eluted by benzene and then octanols were eluted by ethyl ether. Thus, 21.4 mmol of 1-octanol and 0.12 mmol of 2-octanol were obtained.

Reactions of Trihexylborane with Iron(III) Chloride, Copper(II) Bromide and Methyl Vinyl Ketone. After the treatments of trihexylborane with anisole and dimethyl sulfoxide as above, the aqueous solutions of these reagents were added to the solution respectively, and the reactions were carried out in similar manners as described in the previous reports.[3] The amounts of the reaction products were estimated by GLC.

References

1) H. C. Brown and B. C. Subba Rao, *J. Am. Chem. Soc.*, **78**, 5964 (1962); *ibid.*, **81**, 6423 (1959).

2) A. Arase, Y. Masuda, M. Itoh, M. Itoh, and A. Suzuki, *Nippon Kagaku Kaishi*, **1972**, 395.

3) See, for example; (a) A. Suzuki, A. Arase, H. Matsumoto, M. Itoh, H. C. Brown, M. M. Rogic, and M. W. Rathke, *J. Am. Chem. Soc.*, **89**, 5708 (1967); (b) A. Arase, Y. Masuda, and A. Suzuki, *Bull. Chem. Soc. Jpn.*, **47**, 2511 (1974). (c) A. Arase and Y. Masuda, *Chem. Lett.*, **1975**, 419. (d) A. Arase and Y. Masuda, *Chem. Lett.*, **1976**, 785.

4) A. Arase, Y. Masuda, M. Itoh, M. Itoh, and A. Suzuki, *Kogyo Kagaku Zasshi*, **74**, 1416 (1971).

5) A. Arase, K. Kihara, Y. Masuda, M. Itoh, and A. Suzuki, *Kogyo Kagaku Zasshi*, **73**, 1155 (1970).

6) G. Zweifel and H. C. Brown, "Organic Reactions," John Wiley and Sons, Inc., London (1963), Vol. 13, p. 1.

BULLETIN OF THE CHEMICAL SOCIETY OF JAPAN, VOL. 52 (1), 273—274 (1979)

Simple and Practical Routes to 4,5-Benzocycloheptenone. Ring Enlargement of 3,4-Dihydro-2-ethoxynaphthalene and 2-Alkoxynaphthalenes with Dichlorocarbene

Tadao, UYEHARA,* Akio ICHIDA, Makoto FUNAMIZU,† Hirofumi NANBU, and Yoshio KITAHARA††

Department of Chemistry, Faculty of Science, Tohoku University, Aoba, Aramaki, Sendai 980

(Received August 15, 1978)

Synopsis. An addition of dichlorocarbene generated by a phase-transfer reaction, to 3,4-dihydro-2-ethoxynaphthalene gave 7,7-dichloro-6-ethoxy-2,3-benzobicyclo[4.1.0]-hept-2-ene, from which 4,5-benzocycloheptenone was derived in preparative yield. 2-Methoxy- and 2-ethoxynaphthalene were converted into 2-chloro-4,5-benzotropone in 33 and 66% yield, respectively, by treatment with large excess of ethyl trichloroacetate and sodium methoxide.

4,5-Benzo-4-cyclohepten-1-one (**1**) is an important compound to obtain 4,9-methano[11]annulenone (**2**),[1] a ten-pi-electron analog of tropone. During investigation of polycondensed novel aromatics containing a methano-eleven-membered ring, we were in need of large amount of **1**.

Standard synthetic methods of **1** are intramolecular acylations of diethylbenzene derivatives (**3**, Z= CO_2R,[2] CN,[3] and $CO_2^-M^{+4}$), derived from *o*-xylene *via* once or twice of elongation of the side chains, under the basic conditions followed by decarboxylation. The other procedure is ring enlargement of β-tetralone enamine (**4**) using dichlorocarbene, generated from sodium trichloroacetate, to give 2-chloro-4,5-benzo-2,4-cycloheptadien-1-one (**5**), from which the ketone **1** is derived by catalytic hydrogenation.[5] The latter is relatively simple to handle, but the yield of the crucial compound **5** is not high enough. Parham *et al.* have reported that 2-chloro-4,5-benzo-2,4,6-cycloheptatrien-1-one (**6**) is obtained from 2-methoxynaphthalene by the treatment with ethyl trichloroacetate and sodium methoxide.[6] The benzotropone **6** should be converted into the desired ketone **1**, easily. However, the optimum conditions to obtaine **6** were not established. We wish to describe a simple route to the ketone **5** in a practical yield and a reaction to give **6** more than 65% yield.

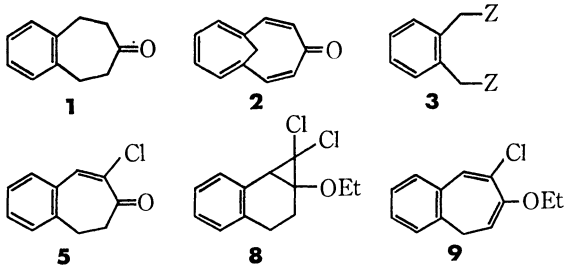

1 **2** **3** **5** **8** **9**

In order to use dichlorocarbene generated from inexpensive reagents: chloroform, 50% aqueous sodium hydroxide and a phase-transfer catalyst: and to avoid multiple additions of the carbene to a 1:1 adduct, we chose 2-ethoxy-3,4-dihydronaphthalene (**7**) as the substrate. The addition of dichlorocarbene to the enol ether **7**, which was derived easily from β-tetralone, proceeded smoothly to give the adduct (**8**), as colorless oil, which decomposed slowly on silica gel TLC. An attempt of purification of the adduct by distillation *in vacuo* was not successful: elimination of hydrogen chloride proceeded under the conditions to form 1,2-benzo-4-chloro-5-ethoxy-1,3,5-cycloheptatriene (**9**). Compound **9** was obtained cleanly in 86% yield (from **7**), when a solution of the adduct **8** in pyridine was heated under reflux for 90 min under a nitrogen atmosphere. Conversion of the enol ether **9** into the ketone **5** was performed with heating under reflux for 90 min in a mixture of methanol and hydrochloric acid. Catalytic hydrogenation of **5** in the presence of potassium acetate gave 4,5-benzo-4-cyclohepten-1-one **1** in an excellent yield.[5]

It has been reported that a treatment of 2-methoxynaphthalene with 0.75 equiv of the carbene source (ethyl trichloroacetate) and sodium methoxide gives the benzotropone **6** in 13% yield with recover of 73% of the naphthalene.[6] In order to know synthetic utility of the ring enlargement, we changed the ratios of the carbene source and the base to the substrate. When 7 equiv of the carbene source and sodium methoxide were used, **6** was obtained in 33% yield with unexpected by-products (**10**, **11** and **12**; in 6.0, 23.0 and 0.2%, respectively).[7] Replacement of the substrate to 2-ethoxynaphthalene (**13**) gave better results. The yield of **6** was increased to 66%, when **13** was treated with 7 equiv of ethyl trichloroacetate and 8 equiv of sodium methoxide. Catalytic hydrogenation of the tropone **6** gave the ketone **1** in 97% yield.

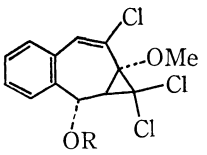

10 R=Me
11 R=CH_2CHCl_2
12 R=$CH(CHCl_2)_2$

Experimental

Instruments. Melting points were determined on Thomas Hoover MP Apparatus using an uncorrected thermometer. NMR spectra were recorded with a JEOL JNM-PMX-60 spectrometer or a Varian Model A-60 spectrometer using tetramethylsilane as an internal standard. IR spectra were measured with a Hitachi Model 215 grating infrared spectrophotometer.

† Present address: Department of Chemistry, College of General Education, Yamagata University, Koshirakawa, Yamagata 990.

†† Deceased February 4, 1976.

*2-Ethoxy-3,4-dihydronaphthalene (**7**).*[8] A solution of β-tetralone (15.2 g, 0.104 mol), ethyl orthoformate (41.6 g, 0.312 mol) and *p*-toluenesulfonic acid (50 mg) in ethanol (60 ml) was heated under reflux for 40 min. Removal of the solvent followed by distillation gave **7** (16.95 g, 93.7%) : bp 84—86 °C/0.2 Torr; NMR (CCl_4) δ=1.34 (3H, t, J=7.0 Hz), 2.21—3.0 (4H, m), 3.89 (2H, q, J=7.0 Hz), 5.63 (1H, s) and 6.72—7.02 (4H, m).

*1,2-Benzo-4-chloro-5-ethoxy-1,3,5-cycloheptatrine (**9**).* To a solution of **7** (16.54 g, 95 mmol) and benzyltrimethylammonium chloride (262 mg) in chloroform (38.7 ml) was added dropwise 50% aqueous sodium hydroxide (38.4 g) at 0 °C under an inert atmosphere (N_2). The mixture was allowed to warm to room temperature and stirred for 14 h. The mixture was diluted with dichloromethane and water, and the organic layer was separated. After dried over magnesium sulfate, evaporation of the solvent to dryness *in vacuo* (0.06 Torr, 4 h) gave **8** (24.03 g) as brown oil: NMR (CCl_4) δ=1.24 (3H, t, J=7.0 Hz), 2.15—2.94 (4H, m), 2.64 (1H, s), 3.74 (1H, q, J=7.0 Hz), 3.77 (1H, q, J=7.0 Hz) and 6.95—7.26 (4H, m). A mixture of **8** (24 g, 93.5 mmol) and dry pyridine (36.5 ml) was heated under reflux for 90 min. Pyridinium hydrochloride was removed by filtration and the filtrate was diluted with water and extracted with three portions of ether (60 ml each). The extract was washed successively with 10% hydrochloric acid, water and brine, and dried over magnesium sulfate. Evaporation of the solvent followed by distillation gave **9** (17.8 g, 86.4%) as pale yellow oil: bp 113 °C/0.05 Torr; IR (neat) 1684 (m), 1630 cm^{-1} (s); NMR (CCl_4) δ=1.20 (3H, t, J=7.0 Hz), 2.85 (2H, d, J=7.4 Hz), 3.60 (2H, q, J=7.0 Hz), 4.88 (1H, t, J=7.4 Hz), 7.08—7.19 (4H, m), 7.23 (1H, s).

*2-Chloro-4,5-benzo-2,4-cycloheptadien-1-one (**5**).* A suspension of **9** (17.6 g, 80.1 mmol) in a mixture of concd hydrochloric acid (0.143 ml), methanol (20 ml) and water (5.7 ml) was heated under reflux for 90 min. White precipitate was formed, after addition of ice (30 g) followed by vigorous stirring. The product was filtered, washed with water, dried over calcium chloride *in vacuo* and recrystallized from hexane (13.66 g, 88.6%). **5**: mp 66.5—67.5 °C (lit,[5] 63—65 °C)

*2-Chloro-4,5-benzo-2,4,6-cycloheptatrien-one (**6**).* To a mixture of dry sodium methoxide (21.6 g, 0.4 mol), 2-ethoxynaphthalene (8.6 g, 0.05 mol) and dry ether (50 ml) was added dropwise with vigorous stirring a solution of ethyl trichloroacetate (62.76 g, 0.35 mol) in ether (50 ml) under a nitrogen atmosphere below 0 °C. The reaction mixture was kept at 0 °C for an additional hour, and then allowed to stand over night at room temperature, whereupon water was added and extracted with ether. The extract was dried over sodium sulfate, concentrated and chromatographed on a dry column of silica gel (240 g, Wako C-200). Elution with hexane gave a mixture of 2-ethoxynaphthalene, ethyl trichloroacetate and less polar products (*ca.* 10 g). 2-Chlorobenzotropone **6** was eluted with hexane–benzene (2 : 1) and benzene, and recrystallized from hexane (6.3 g, 66%). **6**: mp 103—104 °C (lit,[6] 105—106 °C).

*4,5-Benzo-4-cyclohepten-1-one (**1**). Hydrogenation of **5**:* The chloro ketone **5** (25 g, 0.130 mol) and potassium acetate (14 g, 0.143 mol) were suspended in ethanol (150 ml) and hydrogenated at atmospheric pressure over 5% Pd on charcoal (0.9 g). After 20 h the catalyst was filtered, the solvent was removed *in vacuo* and the residue was dissolved in ether. The etherial solution was washed with water, aqueous sodium hydrogencarbonate and brine, and dried over sodium sulfate. Evaporation of the ether to dryness gave white solid (20.2 g, 97%). **1** : mp 41—42 °C (lit,[4] 41—42 °C).

*Hydrogenation of **6**:* A mixture of **6** (3.2 g, 16.6 mmol), potassium acetate (2.1 g, 21.4 mmol) and methanol (50 ml) was hydrogenated over 5% Pd–C (0.1 g) for 96 h. The product **1** was obtained as colorless needles (2.6 g, 98%) from hexane.

References

1) W. Grimme, J. Reisdarff, W. Jünemann, and E. Vogel, *J. Am. Chem. Soc.*, **92**, 6335 (1970).

2) a) A. F. Tifley, *J. Chem. Soc.*, **1928**, 2571; b) G. D. Ewing and L. A. Paquette, *J. Org. Chem.*, **40**, 2965 (1975).

3) C. W. Muth, D. O. Steiniger, and Z. B. Papanastassiou, *J. Am. Chem. Soc.*, **77**, 1006 (1955).

4) B. Kubota and T. Isemura, *Bull. Chem. Soc. Jpn.*, **6**, 103 (1931).

5) U. K. Pandit, S. A. G. DeGraaf, C. T. Braams, and J. S. T. Raaphorst, *Recl. Trav. Chim. Pays-Bas*, **91**, 799 (1972).

6) W. E. Parham, D. A. Bolon, and E. E. Schweizer, *J. Am. Chem. Soc.*, **83**, 603 (1961).

7) Elucidation of the structures and formation mechansims of the by-products will be published soon.

8) Reduction of 2-ethoxynaphthalene with sodium and ethanol (*Org. Synth.*, Coll. Vol. IV, 903) gave **7** less than 75% of purity.

BULLETIN OF THE CHEMICAL SOCIETY OF JAPAN, VOL. 52 (1), 275—276 (1979)

The Reaction of Copper(I) Methyltrialkylborates with 1-(1-Pyrrolidinyl)-6-chloro-1-cyclohexene

Kinji YAMADA, Takashi YANO, Norio MIYAURA, and Akira SUZUKI*
Faculty of Engineering, Hokkaido University, Sapporo 060

(Received August 3, 1978)

Synopsis. The reaction between copper(I) methyltrialkylborates readily obtainable from organoboranes and 1-(-1-pyrrolidinyl)-6-chloro-1-cyclohexene was found to give corresponding alkylation products which are readily hydrolyzed to alkylated cyclohexanones.

Recently, we have reported that lithium methyltrialkylborates readily undergo cation exchange reaction by copper(I) halides to give copper(I) methyltrialkylborates, which in turn successfully add to acrylonitrile, ethyl acrylate, 1-acyl-2-vinylcyclopropane[1] and ethyl propiolate.[2] These borate complexes also react with benzylic bromides,[3] aroyl chlorides,[4] allylic chlorides, propargylic bromides,[5] and ethyl β-bromoacrylates.[6] In an attempt to develop the reaction of such borate complexes, we examined the possibility of a coupling reaction with 1-(1-pyrrolidinyl)-6-chloro-1-cyclohexene.

To a solution of copper(I) methyltripropylborate obtained from lithium methyltripropylborate and copper(I) iodide (Eq. 1), 1-(1-pyrrolidinyl)-6-chloro-1-cyclohexene was addde at 0 °C and stirred at room temperature. After the reaction was complete, the residual organoborane was oxidized with alkaline hydrogen peroxide under the usual conditions. VPC analysis revealed the formation of 2-propylcyclohexanone (**3**) and 2-methylcyclohexanone (**4**) in 31 and 11% yields, respectivley (Eq. 2). Although the

$$R_3B + MeLi \rightarrow (R_3BMe)Li \xrightarrow{CuX} \underset{\mathbf{1}}{(R_3BMe)Cu} \qquad (1)$$

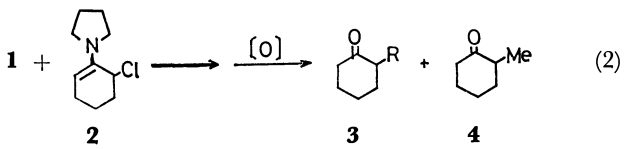

2 **3** **4** (2)

formation of an undesirable by-product, 2-methylcyclohexanone (**4**) formed by attack of methyl group in the borate was observed, it was found that such yields are markedly dependent upon copper(I) halides and solvents employed, as shown in Table 1. The reaction using copper(I) cyanide and 1,2-dimethoxyethane (DME) as a solvent was effective for the circumvention of formation of the by-product. This reaction is applicable to other representative organoboranes. In each case, the desired alkylated cyclohexanones were obtained in good yields (Table 1).

It is well known that enamines formed from cyclanones react with reactive alkyl halides at the β-carbon atom to afford an immonium salt, which is readily hydrolyzed to the monoalkylated ketone. Allylic, propargylic and benzylic halides as well as α-halo ketones, α-halo esters, and α-halo nitriles give good results, but yields are only fair with saturated alkyl halides[7]. On the other hand, the present reaction overcomes such a difficulty, which makes possible to introduce saturated alkyl groups at the α-carbon atom of cyclohexanones.

Table 1. Reaction of copper(I) methyltrialkylborates with 1-(1-pyrolidinyl)-6-chloro-1-cyclohexene

R_3B	CuX	Solvent	R'X	Yield (%)[a] of **3** or **6**
Propyl	CuI	THF		31 (11)
	CuBr	THF		32 (10)
	CuCl	THF		29 (7)
	CuCN	THF		53 (6)
	CuCN	DME		60 (13)
Butyl	CuCN	DME		81 (n. a.)[b]
Isobutyl	CuCN	DME		83 (n. a.)[b]
Hexyl	CuCN	DME		70 (n. a.)[b]
Propyl	CuCN	DME	Allyl bromide	59 (n. a.)[b]
	CuCN	DME	Benzyl bromide	59 (n. a.)[b]
	CuCN	DME	Dimethyl sulfate	37 (n. a.)[b]

a) Based on the chloroenamine (**2**) employed and the yields of methylcyclohexanone are shown in parentheses.
b) Not analyzed.

Recently, Cantacuzene *et al.*,[8] reported the alkylation of 1-(1-pyrrolidinyl)-6-chloro-1-cyclohexene (**2**) with Grignard reagents, For example, 2-butylcyclohexanone and 6-butyl-6-(1-pyrrolidinyl)bicylo[3.1.0]hexane were obtained in the ratio of 30:70: the ratio varied with different Grignard reagents (Eq. 3). However, any formation of such a cyclopropane derivative was not observed in the present reaction of copper(I) borates.

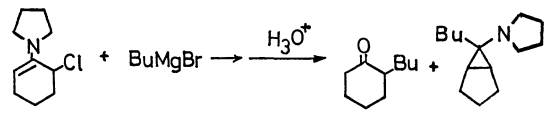

2 (3)

The present reaction, although the mechanism is still unknown, appears to proceed through the enamine (**5**) as an intermediate, because treatment of the reaction mixture, without alkaline hydrogen peroxide oxidation, with relatively active alkyl halides such as allylic and benzylic bromides or dimethyl sulfate pro-

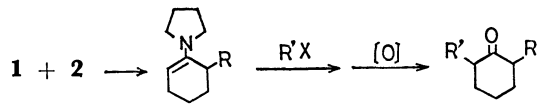

5 **6** (4)

duced the corresponding disubstituted cyclohexanone (**6**) (Eq. 4).

Combination of these two reactions, namely, the reaction of borate complexes with chloroenamine (**2**) and subsequent alkylation by alkyl halides, provides a convenient synthetic procedure for disubstituted cyclohexanones from organoboranes.

Experimental

Materials. Commercial copper(I) halides and alkyl halides were used. The solvents were purified by distillation before use. 1-(1-Pyrrolidinyl)-6-chloro-1-cyclohexene was prepared from 2-chlorocyclohexanone and pyrrolidine by the Blazejenski's method.[8] Trialkylbroanes were prepared from diborane and olefins *via* hydrobroation.[9]

The IR and NMR spectra were taken on a Hitachi-Perkin Elmer Model 125 spectrophotometer and a Hitachi R-22 spectrometer at 90 MHz using tetramethylsilane as an internal standard.

General Procedure. The following procedures for the preparation of 2-propylcyclohexanone and 2-allyl-6-propylcyclohexanone are representative.

A dry 100 ml-flask equipped with a septum inlet and a magnetic stirring bar was flushed with dry nitrogen. The flask was charged under dry nitrogen atmosphere with 0.89 g (9 mmol) of copper(I) cyanide and 12 ml of dry 1,2-dimethoxyethane. To this mixture was added lithium methyltripropylborate[1] (9 mmol in THF) at 0 °C and stirred for 5 min. Then 0.84 ml (6 mmol) of 1-(1-pyrrolidinyl)-6-chloro-1-cyclohexene was gradually added and the mixture was stirrred for 2 h at room temperature. After the reaction was complete, the residual organoborane was oxidized with 3 ml of 3 M aqueous NaOH and 3 ml of 30%-H_2O_2 at room temperature for 2 h. The products were extracted with ether. The combined extracts were washed with saturated NaCl solution and dried over anhydrous sodium sulfate. The ether solution thus obtained was analyzed by VPC, revealing the formation of 2-propylcyclohexanone (5.4 mmol, 60%).

The procedure for the preparation of 2-allyl-6-propylcyclohexanonone is as follows: To the reaction mixture obtained by the same procedure described above was added allyl bromide (3.06 g, 18 mmol), followed by refluxing for 3 h and allowed to stand over night at room temperature. Analysis by VPC after alkaline hydrogen peroxide oxidation indicated the presence of 3.54 mmol (59% yield) of 2-allyl-6-propylcyclohexanone. Although 2-allyl-6-methylcyclohexanone formed as a by-product was not analyzed, the quantity was little.

Identification of the Products. In all cases analytically pure samples were obtained by preparative VPC with Varian autoprep Model-2800 and characterized by NMR, IR, and mass spectra, refractive indices, and elemental analyses.

2-Propylcyclohexanone: n_D^{20}=1.4558 (lit,[10] 1.4538). Found: C, 76.96; H, 11.50%. Calcd for $C_9H_{16}O$: C, 77.09; H, 11.50%. Mass; *m/e*=140 (M^+). IR (CCl_4); 1710 cm^{-1}. NMR (CCl_4); δ, 0.91 (3H, t, J=6 Hz), 1.09—1.45 (4H, m), 1.46—2.50 (9H, m).

2-Butylcyclohexanone: n_D^{20}=1.4576 (lit,[10] 1.4545). Found: C, 77.30; H, 11.61%. Calcd for $C_{10}H_{18}O$: C, 77.56; H, 11.76%. Mass; *m/e*=154 (M^+). IR (CCl_4); 1710 cm^{-1}. NMR (CCl_4); δ, 0.90 (3H, t, J=6 Hz), 1.05—1.55 (6H, m), 1.60—2.50 (9H, m).

2-Isobutylcyclohexanone: n_D^{20}=1.4477. Found: C, 77.52; H, 11.62%. Calcd for $C_{10}H_{18}O$: C, 77.86; H, 11.76%. Mass; *m/e*=154 (M^+). IR (CCl_4); 1710 cm^{-1}. NMR (CCl_4); δ, 0.87 (6H, d, J=5.5 Hz), 1.1—2.4 (12H, m).

2-Hexylcyclohexanone: n_D^{20}=1.4580. Found: C, 78.74; H, 11.90%. Calcd for $C_{12}H_{22}O$: C, 79.06; H, 12.16%. Mass; *m/e*=182 (M^+). IR (CCl_4); 1700 cm^{-1}. NMR (CCl_4); δ, 0.90 (3H, t, J=6 Hz), 1.15—1.45 (8H, m), 1.50—2.40 (9H, m).

2-Allyl-6-propylcyclohexanone: Found: C, 79.43; H, 10.94%. Calcd for $C_{12}H_{20}O$: C, 79.74; H, 11.18%. Mass; *m/e*=180 (M^+). IR (CCl_4); 1700 cm^{-1}. NMR (CCl_4); δ, 0.90 (3H, t, J=6 Hz), 1.15—1.55 (4H, m), 1.55—2.60 (10H, m), 4.8—5.15 (2H, m), 5.5—6.0 (1H, m).

2-Benzyl-6-propylcyclohexanone: n_D^{20}=1.5210. Found: C, 83.47; H, 9.52%. Calcd for $C_{16}H_{22}O$: C, 83.43; H, 9.63%. Mass; *m/e*=230 (M^+). IR (CCl_4); 1700 cm^{-1}. NMR (CCl_4); δ, 0.90 (3H, t, J=6 Hz), 1.10—1.40 (4H, m), 1.55—2.60 (8H, m), 7.20 (5H, m).

2-Methyl-6-propylcyclohexanone: n_D^{20}=1.4561. Found: C, 78.04; H, 11.77%. Calcd for $C_{10}H_{18}O$: C, 77.86; H, 11.76%. Mass; *m/e*=154 (M^+). IR (CCl_4); 1710 cm^{-1}. NMR (CCl_4); δ, 0.96 (3H, t, J=6 Hz), 0.94 (3H, d, J=5.5 Hz), 1.1—1.5 (4H, m), 1.5—2.4 (8H, m).

References

1) N. Miyaura, M. Itoh, and A. Suzuki, *Tetrahedron Lett.*, **1976**, 255.

2) K. Yamada, N. Miyaura, M. Itoh, and A. Suzuki, *Bull. Chem. Soc. Jpn.*, **50**, 3431 (1977).

3) N. Miyaura, M. Itoh, and A. Suzuki, *Synthesis*, **1976**, 655.

4) N. Miyaura, M. Sasaki, M. Itoh, and A. Suzuki, *Tetrahedron Lett.*, **1977**, 173.

5) N. Miyaura, M. Itoh, and A. Suzuki, *Bull. Chem. Soc. Jpn.*, **50**, 2199 (1977).

6) N. Miyaura, M. Sasaki, M. Itoh, and A. Suzuki, *Tetrahedron Lett.*, **1977**, 3369.

7) For reviews, see (a) C. A. Buehler and D. E. Pearson, "Survey of Organic Synthesis," John Wiley & Sons, New York (1970), Vol. 1, p. 703; (b) C. A. Buehler and D. E. Pearson, "Survey of Organic Synthesis," John Wiley & Sons, New York (1977), Vol. 2, p. 599; (c) J. Mathieu and J. Weill-Raynal, "Formation of C-C Bonds," Georg Thieme Pub., Stuttgart (1975), Vol. 2, p. 264.

8) J. C. Blazejenski, D. Cantacuzene, and C. Wakselman, *Tetrahedron*, **29**, 4233 (1973).

9) H. C. Brown, "Organic Syntheses *via* Boranes," John-Wiley, New York (1975).

10) "Atlas of Spectral Data and Physical Constants for Organic Compounds," 2nd ed, CRC Press, Ohio (1975).

Correlation between Electron Capture Response and Chemical Structure for Benzyl Chlorides

Tsugio KOJIMA,* Masaru SATOUCHI,† and Yasukazu TANAKA

Department of Industrial Chemistry, Faculty of Engineering, Kyoto University, Yoshida, Kyoto 606

†*Department of Industrial Chemistry, Shiga Prefectural Junior College, Hikone, Shiga 522*

(Received March 6, 1978)

In the dissociative electron capture reaction of benzyl chlorides, all the substituents in the para position except for *t*-butyl group tend to decrease the activation energy, those in the meta position having no influence on the activation energy. This can be explained in terms of the contribution of a para substituent to the stabilization of the incipient radical in the transition state resulting from the delocalization of the odd electron. The resonance effect of the para substituent was compared with that obtained in the phenylation of substituted benzenes with phenyl radical, where phenylcyclohexadienyl radical is formed as an intermediate. The resonance effects in these two reactions agree, supporting the reaction mechanism proposed.

The principle of electron capture detection is based on the electron attachment to a molecule. Since an electron capture detector (ECD) gives data concerning only the probability of electron attachment to a molecule, the information obtained is not useful. However, if the temperature dependence of the electron capture coefficient is measured and analyzed, we can obtain useful information on the chemical structure of the molecule.[1-3]

Wentworth and coworkers studied the electron attachment phenomenon on kinetics using the steady-state approximation, giving the electron capture response to the concentration of a capturing species in terms of electron capture coefficient K.[4-6] According to Wentworth's theory, the molecular electron affinity or activation energy for an electron attachment accompanying a bond dissociation is obtained from K.

We proposed that the dissociative electron capture reaction of alkyl and aryl halides proceeds by a mechanism similar to that of S_N2 reaction.[1-2] In the case of alkyl halides the magnitude of the activation energy is determined by the stability of the transition state, which depends upon the extent to which the odd electron on the α-carbon atom is delocalized by resonance. Although reports have appeared on the relative electron attachment coefficients for different organic compounds, little is known about the electron capture reaction in view of nucleophilic reaction. It is interesting to test this reaction model with various classes of compounds.

In the present paper, the results of measurements of activation energy in the electron capture reaction of benzyl chlorides are given, the substituent effect on the activation energy being discussed in terms of the reaction mechanism proposed for alkyl halides.[1]

Experimental

A modified Shimadzu GC-2C model gas chromatograph was used. The ECD employed was of a concentric type with 15 mCi nickel-63 as radioactive source. Applied voltage was supplied as a pulse through a pulse generator with an amplitude of 28 V, a pulse period of 3200 μs, and a pulse width of 3.2 μs; the electron capture reaction proceeded under field free conditions.

Glass columns (0.4 cm × 100 cm and 0.4 cm × 40 cm) were packed with Durapak (Carbowax 400/Porasil C), temperature being maintained at 70 or 100 °C. Nitrogen was used as a carrier gas. The oxygen in the carrier gas was removed by passing the gas through a tube packed with copper(I) chromate pellets. Another tube packed with Molecular Sieve 5A was used for the removal of moisture. The tubes were inserted between the cylinder of the carrier gas and the GC inlet.

Reagents except for commercial ones were synthesized. *m*-Methoxybenzyl chloride and *p*-*t*-butylbenzyl chloride: *m*-Methoxy- and *p*-*t*-butylbenzoic acids were reduced to the corresponding benzyl alcohols with lithium aluminum hydride in ether solution. They were converted into benzyl chlorides by chlorination with concd hydrochloric acid at 80 °C for 2 h. Alkylbenzyl chlorides were synthesized by the chlorination of alkyltoluenes with chlorine gas or sulfinyl chloride.

The compounds synthesized were identified by GC-MS technique. The sample solution was prepared by dilution with benzene to a concentration such that the detector current decreases to about a half of the back ground current.

The electron capture coefficient K was calculated by the following equation derived by Wentworth and Chen:[5]

$$\frac{F}{S}\int\frac{(I_b-I_e)}{I_e}dx = Kn, \qquad (1)$$

where F is the flow rate of the carrier gas in l/min, S the chart speed in cm/min, n the amount of sample injected in moles. I_b and I_e are the detector current without and with a capturing species in the detector, respectively. Since the detector signal proportional to (I_b-I_e) was converted into the signal proportional to $(I_b-I_e)/I_e$ through an analog convertor,[3] the integral term of the above equation corresponds to the peak area on the chromatogram.

Results and Discussion

The mode of the electron capture reaction for a halogen compound depends upon the organic group bonding to the halogen atom. An aklyl halide captures a free electron dissociatively (Eq. 2), while an aryl halide dose so before the bond dissociation of the carbon-halogen bond (Eq. 3).[2,4]

$$RX + e^- \longrightarrow R\cdot + X^- \qquad (2)$$

$$ArX + e^- \longrightarrow ArX^{\cdot-} \longrightarrow Ar\cdot + X^- \qquad (3)$$

The type of reaction can be judged by means of the Arrhenius plot of ln K. According to Wentworth's theory,[5] the temperature dependence of K is expressed by the following equations:

$$\ln K = \ln Z - E^*/RT \quad \text{(dissociative)}, \qquad (4)$$

$$\ln KT^{3/2} = \ln Z + EA/RT \quad \text{(nondissociative)}, \qquad (5)$$

where E^* and EA are activation energy and molecular electron affinity, respectively; R is the gas constant, T the absolute temperature of the detector and Z the pre-exponential factor. The Arrhenius plot of ln K might be linear with a negative slope of E^*/R for the dissociative case and with a positive slope of EA/R for the nondissociative case.

In a previous paper,[1] it was proposed that the dissociative electron capture reaction of an alkyl halide can be assumed to be similar to the S_N2 reaction in solution and the sp^3 orbital on the α-carbon atom changes to an sp^2 orbital with the approach of a free electron to an alkyl halide. The linear relationship observed between the activation energy and the change in internal energy was explained.

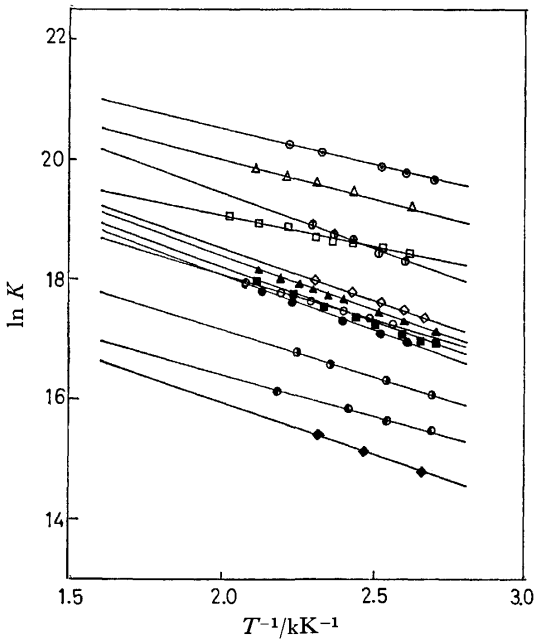

Fig. 1. Arrhenius plots of electron capture coefficients for benzyl chlorides.
● Benzyl chloride, ◆ *m*-methylbenzyl chloride, ○ *p*-methylbenzyl chloride, ▲ *p*-*t*-butylbenzyl chloride, △ *m*-chlorobenzyl chloride, ◑ *p*-chlorobenzyl chloride, ■ *m*-methoxybenzyl chloride, ◐ *p*-methoxybenzyl chloride, ⊙ *p*-phenylbenzyl chloride, △ *p*-cyanobenzyl chloride, ⓘ *m*-nitrobenzyl chloride, □ *p*-nitrobenzyl chloride.

It is of interest to see if this reaction model is adequate in the electron capture reaction of benzyl chlorides. It will be useful if the variation of activation energies for benzyl chlorides with various substituents is explained.

The Arrhenius plots of ln K for benzyl chlorides with various substituents in the aromatic ring are shown in Fig. 1. Since all the plots are linear with negative slopes, benzyl chlorides capture free electron dissociatively as in the case of alkyl halides. The activation energies E^* calculated by the least-squares method are given in Table 1.

A question may be raised whether the α-carbon atom is the reaction center, or the α-carbon atom is attacked

Table 1. Activation energies for benzyl chlorides

Compound	E^*[a] / kcal mol^{-1}
Benzyl chloride	3.6±0.1[b]
m-Methylbenzyl chloride	3.4±0.2
p-Methylbenzyl chloride	3.2±0.2
p-Ethylbenzyl chloride	3.1±0.2
p-Isopropylbenzyl chloride	3.2±0.2
p-*t*-Butylbenzyl chloride	3.6±0.1
m-Chlorobenzyl chloride	3.5±0.2
p-Chlorobenzyl chloride	3.0±0.1
m-Methoxybenzyl chloride	3.6±0.1
p-Methoxybenzyl chloride	3.0±0.1
p-Phenylbenzyl chloride	2.5±0.2
p-Cyanobenzyl chloride	2.6±0.1
m-Nitrobenzyl chloride	3.5±0.2
p-Nitrobenzyl chloride	2.0±0.1

a) Activation energy. b) Standard deviation.

by a free electron. The activation energy of 8.6 kcal/mol[2] or 9.25 kcal/mol[7] observed for chlorobenzene corresponds to the energy of the barrier for electron attachment to the benzene nucleus of the compound. When the benzene nucleus is substituted by a more electron-withdrawing group, the electron attachment to the benzene nucleus occurs more easily.[2] Therefore, when a free electron attacks the benzene nucleus of benzyl chloride, the activation energy should be greater than 8.6 kcal/mol. However, the activation energy of benzyl chloride is only 3.6 kcal/mol (Table 1). It can be concluded that in analogy with alkyl halides, the α-carbon atom is attacked by a free electron in the electron capture reaction of benzyl chloride.

All the activation energies of benzyl chlorides in Table 1 are smaller than those of alkyl chlorides by 6—8 kcal/mol. A comparison of K shows that benzyl chloride reacts with a free electron faster than alkyl chlorides by a factor of 1000—3000. The enhanced reactivity of benzyl chloride over the corresponding alkyl chloride has also been observed in S_N2 reaction in solution.[8]

It seems that the transition state of the dissociative electron capture reaction for benzyl chloride has a

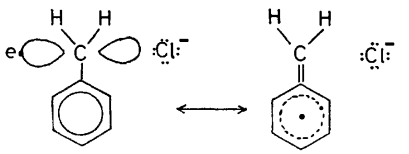

Scheme A.

structure as shown in Scheme A. It is expected from the structure that the accepted odd electron on the α-carbon atom is delocalized by the overlapping of the π orbital on the benzene ring with the p orbital on the α-carbon atom and the stabilization of the transition state due to such resonance affords the enhanced reactivity for benzyl chloride.

In the substituted benzyl chlorides, it is necessary to take into account the contribution of substituents to the resonance through the benzene ring. The substituent effect in the electron capture reaction can be illustrated

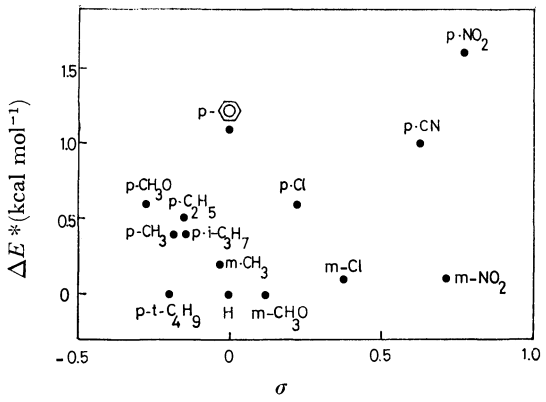

Fig. 2. Relationship between activation energy and Hammett substituent constant.

by a plot, ΔE^* $(=E_H^*-E_X^*)$ *vs.* the Hammett σ constant, where the subscripts H and X are used to represent benzyl chloride and the benzyl chloride substituted by a group X, respectively (Fig. 2). The relationship between the electron capture coefficient K and the rate constant k in the dissociative electron capture reaction is given by

$$\ln K = \ln k_{12} - \ln k_D, \tag{6}$$

where k_D is the rate constant of the reaction between a positive ion produced from a molecule of the carrier gas and a free electron, k_{12} is the rate constant of the dissociative process of benzyl chlorides as given by Eq. 2.[5-7] Using the Arrhenius equation, we have

$$\ln k_{12} = \ln Z' - \frac{E^*}{RT}. \tag{7}$$

k_D is almost temperature independent as pointed out by Wentworth and Chen.[5] Hence, $\ln(K_X/K_H)$ is nearly equal to $\ln(k_{12,X}/k_{12,H})$. Since it is reasonable to presume that the pre-exponential factor Z' is nearly equal for all the benzyl chlorides investigated, ΔE^* (ordinate, Fig. 2) is approximately equal to the difference in $\ln k_{12}$ between the benzyl chloride substituted by a group X and benzyl chloride. Thus, Fig. 2 can be considered to be Hammett plot which enables us to evaluate the substituent effect in the electron capture reaction.

We see that the plots for meta-substituted benzyl chlorides are linear with a slope near to zero. This can be explained as follows. In the transition state for benzyl chlorides, the negative charge is localized on the chlorine atom as shown in Scheme A. Consequently, a group in meta position does not contribute to the stabilization of the transition state by the inductive effect. The odd electron can conjugate only with the π electrons in the aromatic ring and the conjugative system can not be extended to meta substituents. The resonance effect, therefore, for all meta-substituted benzyl chlorides should be equal to that for benzyl chloride itself.

On the other hand, no simple relation exists between ΔE^* and the Hammett σ constant for para-substituted benzyl chlorides. The plot is concave downward. Both electron releasing groups except for *t*-butyl group and electron withdrawing groups tend to decrease the activation energy. This indicate that, in the transition state of para-substituted benzyl chlorides, the odd electron accepted on the α-carbon atom can conjugate not only with the π electrons in the aromatic ring, but with the electrons in the para substituent through the π electron system of the aromatic ring. Consequently, para substituents contribute to the stabilization of the transition state through hydrogen atom hyperconjugation and electron donating or electron accepting resonance as shown in Scheme B. The resonance effect of the para

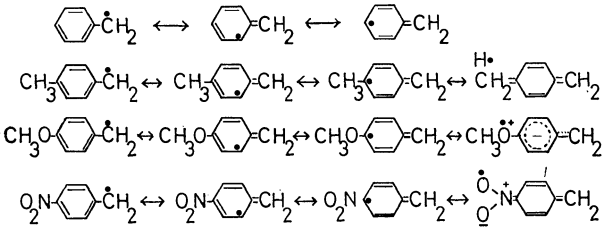

Scheme B.

substituents decreases in the order: NO_2>CN, C_6H_5 >CH_3O, Cl>*iso*-C_3H_7, C_2H_5, CH_3>H. As *t*-butyl group has no hydrogen atom capable of participating in the hyperconjugation, the resonance effect for *t*-butylbenzyl chloride is equal to that for benzyl chloride itself. The order is in line with that of the substituent effect found in polarographic reduction of benzyl halides.[9,10]

A similar substituent effect has been reported in the phenylation of substituted benzenes with phenyl radical. Ito and coworkers observed that for all benzene compounds the ortho and para positions are more reactive than the meta position. The relative reactivity of the para position does not satisfy the Hammett relation, being usually larger than that expected from the Hammett equation by an increment of τ_p as expressed by

$$\log (k_{X(p)}/k_H) = \rho\sigma_p + \tau_p, \tag{8}$$

where $k_{X(p)}/k_H$ is the partial rate constant of the para position of the benzene substituted by a group X in phenylation, ρ is the Hammett reaction constant for the phenylation estimated from the Hammett plot for the meta substituent and σ_p is the Hammett substituent constant for para position.[11] τ_p is regarded as a measure of the conjugative effect.

The value of τ_p for a substituent is approximately constant for each substituted benzene irrespective of the nature of attacking radical. It is accepted that the homolytic phenylation proceeds through the rate determining step of the addition of a phenyl radical to the aromatic ring, a phenylcyclohexadienyl radical being formed as an intermediate. When the substitution occurs in the para position to a substituent, the odd electron in the transition state can conjugate with the electrons in the substituent. Consequently, the value of τ_p indicates the extent to which the incipient radical in the transition state of the addition of a phenyl radical to a substituted benzene is stabilized by resonance.

Thus, ΔE^* and τ_p can be considered to show identical character, and the validity of our proposal on the mechanism of the dissociative electron capture reaction for benzyl chlorides should be judged by a comparison of ΔE^* and τ_p. As shown in Table 2, the conjugative effect expressed in energy term $2.3RT\tau_p$ is almost equal

TABLE 2. COMPARISON OF THE CONJUGATIVE EFFECT OF PARA-SUBSTITUENTS OBSERVED IN ELECTRON CAPTURE REACTION OF BENZYL CHLORIDES WITH THAT OBSERVED IN PHENYLATION OF SUBSTITUTED BENZENES BY PHENYL RADICAL

Substituent	ΔE^{*} [a] / kcal mol^{-1}	τ_p [b]	$2.3RT\tau_p$ [c] / kcal mol^{-1}
CH_3	0.4	0.09	0.2
Cl	0.5	0.16	0.3
CH_3O	0.6	0.14	0.3
NO_2	1.6	0.9	1.8

a) The conjugative effect of para substituents observed in electron capture reaction of benzyl chlorides. b) Values taken from Ref. 11. c) $T=423$ K.

to ΔE^{*} at 423 K, the average temperature of ECD. The agreement between ΔE^{*} and τ_p shows that our proposal is valid. Thus, the substituent effect is explained by assuming the reaction mechanism of the electron capture reaction for benzyl chlorides analogous to that of alkyl halides.

Conclusion

An extensive study has been made on the substituent effect on the electron capture reaction of benzyl chlorides. We concluded that the electron capture reaction of benzyl chlorides is a kind of S_N2 reaction in analogy with alkyl halides. The enhanced reactivity of a para-substituted benzyl chloride over the corresponding meta isomer and benzyl chloride itself can be explained on the basis of a mechanism similar to the S_N2 reaction. Our proposal on the mechanism of the electron capture reaction will be useful for understanding the relationship between the activation energy measured and the chemical structure of the sample molecule and for identifying peaks on the chromatogram for separation of halogen compounds by GC-ECD system.

References

1) T. Kojima, Y. Tanaka, and M. Satouchi, *Anal. Chem.*, **48**, 1760 (1976).
2) M. Satouchi and T. Kojima, *Bunseki Kagaku*, **25**, 764 (1976).
3) T. Kojima and M. Satouchi, *Bunseki Kagaku*, **22**, 1428 (1972).
4) W. E. Wentworth, E. Chen, and J. E. Lovelock, *J. Phys. Chem.*, **70**, 445 (1966).
5) W. E. Wentworth and E. Chen, *J. Gas. Chromatogr.*, **5**, 170 (1967).
6) W. E. Wentworth, R. S. Becker, and R. Tung, *J. Phys. Chem.*, **71**, 1652 (1967).
7) J. C. Steelhammer and W. E. Wentworth, *J. Chem. Phys.*, **51**, 1802 (1969).
8) R. G. Pearson, S. H. Langer, F. V. Williams, and W. J. McGuire, *J. Am. Chem. Soc.*, **74**, 5130 (1952).
9) G. Klopman, *Helv. Chim. Acta*, **44**, 1908 (1961).
10) A. Streitwieser, Jr. and C. Perrin, *J. Am. Chem. Soc.*, **86**, 4938 (1964).
11) R. Ito, T. Migita, N. Morioka, and O. Shimamura, *Tetrahedron*, **21**, 955 (1965).

Effect of Pressure on Iodine Complexes. I. Absorption Spectra of the Visible Iodine Bands with Diethyl Ether, Diethyl Sulfide, and Diethyl Selenide in Heptane

Seiji SAWAMURA, Yoshihiro TANIGUCHI, and Keizo SUZUKI*

Department of Chemistry, Faculty of Science and Engineering, Ritsumeikan University, Kita-ku, Kyoto 603

(Received April 13, 1978)

Absorption spectra of the visible I_2 band of I_2 complexes with Et_2O, Et_2S, and Et_2Se in heptane have been measured up to 3300 bar at 25 °C. The equilibrium constants and volume changes accompanying complex formation, the molar extinction coefficients and the absorption maxima have been estimated. The volume changes were found comparable with those estimated from the X-ray data of the I_2 complexes in the crystalline state. The enhancement of the molar extinction coefficient and the blue shift of the visible I_2 band with increasing pressure have been established. The results suggest a decrease in the bond distance between an n-donor and I_2, compared with the spectroscopic properties of the I_2 complex at 1 bar. The decrease has been estimated as 0.008 nm with increasing pressure up to 3300 bar.

There have been several investigations of iodine (I_2) complexes as examples of charge transfer (CT) complexes from both the experimental and theoretical point of view.[1] Pressure effects on the I_2 complexes with π-donors such as benzene, toluene, and mesitylene have been studied by Ham,[2] and Kwun and Lentz,[3] where it was concluded that the equilibrium constants accompanying complex formation increased with increasing pressure. There has yet been no investigation of I_2 complexes with n-donor such as ether or amines under high pressure.

In the study of the I_2 complex at 1 bar, not only a CT band but also a I_2 band in the visible region (visible I_2 band) has been reported.[1] The I_2 band shifts to blue (to shorter wavelength) very largely with complex formation, and the shift is larger with stronger n-donors. Thus the blue shift in the visible I_2 band has been a useful indication of CT interaction. Furthermore, the molar extinction coefficients of the visible I_2 bands increase with stronger n-donors. Consequently the investigation of the visible I_2 bands of the I_2 complexes with n-donors under high pressure has been interesting. Recently by measuring the visible absorption spectra pressure effect on I_2 complex with diethyl ether (Et_2O) in heptane has been studied.[4] The present report is an extention of the work using diethyl sulfide (Et_2S) and diethyl selenide (Et_2Se) as n-donors in heptane.

Experimental

The purification of I_2 and heptane has been described in a preceding paper.[4] Et_2S (Wako Pure Chemical Co., Ltd.) was dried with calcium chloride and fractionally distilled, bp 91—92 °C (lit,[5] bp 92 °C). Et_2Se was synthesized by the method of Bird and Challenger,[6] n_D^{20} 1.4790, bp 107—108 °C (lit,[7,8] n_D^{20} 1.4768, bp 108 °C). The method of measuring the absorption spectra under high pressure has been described in a preceding paper.[4]

Results and Discussion

The absorption spectra of the Et_2S–I_2 complex in Fig. 1 show an isosbestic point at 490 nm. The absorption band at 522 nm decreases and at 438 nm increases with increasing pressure. The former band has been ascribed as free I_2 (I_2 in heptane) and the latter the complexed I_2 with Et_2S.[6] In the Et_2Se–I_2 complex absorption spectra similar to Fig. 1 were observed with an isosbestic point at 470 nm. The absorption spectra of the Et_2O–I_2 complex have been described previously.[4]

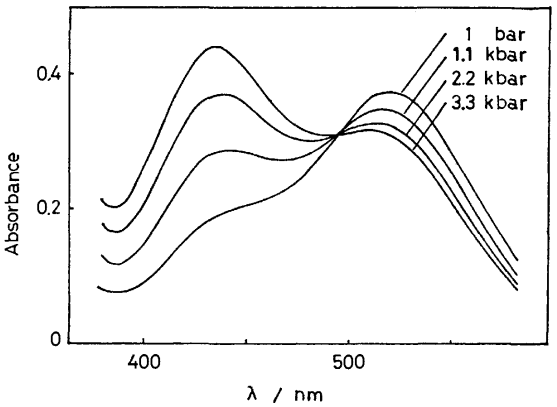

Fig. 1. Visible I_2 absorption spectra of mixed solution of Et_2S and I_2 in heptane at 25 °C and various pressures. Et_2S: 1.4×10^{-3} mol dm^{-3}, I_2: 5.0×10^{-4} mol dm^{-3}. The absorptions are not corrected for compression.

Equilibrium Constants. The equilibrium constants accompanying complex formation and the molar extinction coefficients have been estimated by the Benesi-Hildebrand equation[10]

$$\frac{X_A}{A} = \frac{V}{K\varepsilon l}\frac{1}{X_D} + \frac{V}{\varepsilon l}, \quad (1)$$

where K is the equilibrium constant in mole fractions accompanying complex formation, A the absorbance of the mixed solution of I_2 and donor, ε the molar extinction coefficient of the complex, l the path length, X_A and X_D the initial mole fractions of I_2 and donor, respectively, and V the molar volume of the solution which has been assumed to be equal to that of the solvent under each pressure.[11] The value of the initial concentration of I_2 in units of mol dm^{-3} ($[I_2]$) used by Benesi and Hildebrand[10] depends on the pressure. The value in mole fraction units (X_A) has been utilized in Eq. 1 with the following relation:

$$X_A = [I_2]V. \quad (2)$$

TABLE 1. EQUILIBRIUM CONSTANTS (K), MOLAR EXTINCTION COEFFICIENTS (ε_{max}) AND ABSORPTION MAXIMA (λ_{max}) OF VARIOUS I_2 COMPLEXES IN HEPTANE AT 25 °C

P / bar	K[a]	ε_{max} / mol^{-1} dm^3 cm^{-1}	λ_{max} / nm
Free I_2[b]			
1		900±30	522.0±0.5
1100		900±30	520.5±0.5
2200		900±30	519.5±0.5
3300		900±30	518.0±0.5
Et_2O–I_2			
1	6.1±1.0[c]	980±60	462.5±1.5
	5.9[d]	950[d]	462[d]
1100	8.4±1.2[c]	980±60	460.0±1.5
2200	11.0±1.2[c]	980±60	458.0±1.5
3300	12.1±1.6[c]	980±60	456.0±1.5
Et_2S–I_2			
1	1320±210	1820±70	438.0±0.5
	1430[c]	1960[c]	435[d]
1100	2010±670	1830±70	435.5±0.5
2200	2480±600	1970±70	433.5±0.5
3300	3360±1200	2120±70	432.0±0.5
Et_2Se–I_2			
1	6600±900	2730±60	435.5±0.5
			436[f]
1100	13500±6000	2780±60	433.0±0.5
2200	20900±10000	2930±60	431.5±0.5
3300	26300±11000	3020±60	430.0±0.5

a) In mole fraction units. b) I_2 in heptane. c) Ref. 4. d) Ref. 9. f) Ref. 13, in CCl_4.

The values of K and ε have been evaluated from the intercept and the slope of the plot of X_A/A *vs.* $1/X_D$, the results of which are shown in Table 1 together with the spectroscopic data.

The volume changes, ΔV, accompanying formation of the I_2 complexes have been calculated from the following equation and the slopes of the ln K *vs.* P plot as shown in Table 2:

$$\left(\frac{\partial \ln K}{\partial P}\right)_T = -\frac{\Delta V}{RT}. \quad (3)$$

TABLE 2. VOLUME CHANGES (ΔV) ACCOMPANYING THE FORMATION OF I_2 COMPLEXES AT 25 °C (cm^3 mol^{-1})

	Et_2O–I_2	Et_2S–I_2	Et_2Se–I_2
ΔV_{vis}[b]	−6.7±1.0[c]	−8.1±1.2	−14.6±4.0
ΔV_{theor}[b]	−6.4[c]	−8.9	−9.8

a) From visible I_2 band and Eq. 3. b) From Eq. 4. c) Ref. 4.

In the preceding paper[4] the volume change accompanying the formation of the Et_2O–I_2 complex was estimated from Eq. 4, assuming that the I_2 complex is formed along the axis of cylinder having a radius equal to the van der Waals radius for the iodine atom:

$$\Delta V = (\pi r^2 \Delta d) N_A, \quad (4)$$

where N_A is Avogadro's number, r the radius of the cylinder, and Δd the contraction of the cylinder accompanying complex formation estimated by the following equation:

$$\Delta d = d_X - (d_D + d_A), \quad (5)$$

where d_X is the bond distance of the complex estimated from the X-ray data of the crystal, and d_D and d_A are van der Waals radii for the donor atom (O) and the acceptor atom (I), respectively. In the same manner the volume changes for the Et_2S–I_2 and Et_2Se–I_2 complexes have been estimated with the bond distance for 1,4-dithiane–I_2[14] and 1,4-diselenane–I_2[15] complexes in the crystal for d_X, van der Waals radii[16] of the sulfur and selenium atoms for d_D, and van der Waals radius of the iodine atom for d_A and r, the results of which are shown in Table 2. These values are comparable with those estimated from the pressure dependence of the equilibrium constants.

Spectroscopic Properties. Absorption maxima (λ_{max}) of the visible I_2 band are shown in Table 1. The values of λ_{max} for free I_2 were determined directly from the observed absorption. In the Et_2S–I_2 and Et_2Se–I_2 complexes, these were determined from the observed absorptions under the condition that $X_D \gg X_A$, where the absorption of free I_2 could be neglected. The λ_{max} values of the Et_2O–I_2 complex have been estimated from the observed absorption by subtracting the absorption of the free I_2 calculated from the equilibrium constant of the Et_2O–I_2 complex and the molar extinction coefficient of free I_2. All of the λ_{max} values shifted to blue with increasing pressure; Ham failed to observe any blue shift in the visible absorption spectra of I_2 in heptane up to 2000 bar.[2] The molar extinction coefficients (ε_{max}) of the visible I_2 band at λ_{max} increased with increasing pressure in Et_2S–I_2 and Et_2Se–I_2 complexes (Table 1). In the Et_2O–I_2 complex and free I_2, however, ε_{max} was not enhanced.

The pressure effect of the increase in ε_{max} accompanying the blue shift of λ_{max} is similar to the property of I_2 complexes with n-donors at 1 bar as shown in Fig. 2, where the value of ε_{max} is larger in the I_2 complex whose λ_{max} is at shorter wavelength. Mulliken and Person explained this as follows.[1] The visible I_2 band corresponds to the excitation of an electron from the π_g MO to the σ_u MO of I_2 molecule. Since the latter MO is strongly antibonding, the size of the σ_u MO must be larger than that of the π_g MO. When the I_2 molecule, coupled with a donor in a I_2 complex, is excited by absorption of visible light, its suddenly swollen size ($\sigma_u \leftarrow \pi_g$) increases the repulsion energy between I_2 and the donor, which causes the blue shift of the visible I_2 band. The shift should be greater, the more compact the I_2 complex. The enhanced intensity of the visible I_2 band is presumably explained in terms of the increased mixing of the excited state of the visible I_2 band with the higher excited states of the I_2 complex, as a result of the shift of the excited state of the visible I_2 band to higher energy. Such a explanation may be suited for the pressure effects on the I_2 complex, that is, the blue shift of λ_{max} and the enhancement of ε_{max} of the visible I_2 band, implying a decrease in the bond distance between I_2 and the n-donor.

The values of the slope in Fig. 2 have been estimated to be 0.01, 0.12, 0.81, and 0.95 mol^{-1} dm^3 cm^{-1}/cm^{-1} at band maxima of free I_2, Et_2O–I_2, Et_2S–I_2, and Et_2Se–

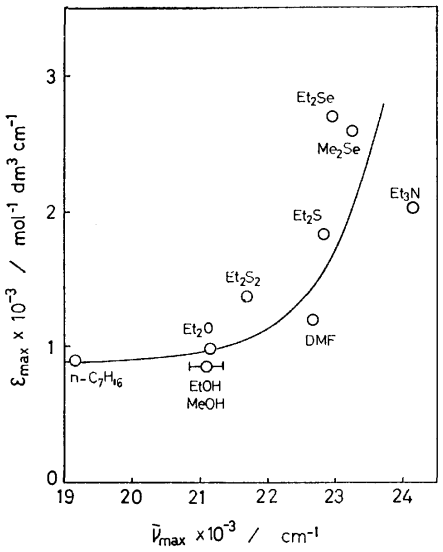

Fig. 2. Relation between ε_{max} and $\tilde{\nu}_{max}$ at visible I_2 band of I_2 complexes with n-donors at 1 bar. References 1 and 17 were utilized. $\tilde{\nu}_{max}=1/\lambda_{max}$.

TABLE 3. THE INCREASES IN THE MOLAR EXTINCTION COEFFICIENTS AT λ_{max} OF VISIBLE I_2 BANDS WITH INCREASING PRESSURE UP TO 3300 bar (mol^{-1} dm^3 cm^{-1})

	Free I_2	Et_2O–I_2	Et_2S–I_2	Et_2Se–I_2
$\Delta\varepsilon_{obsd}$	0	0	300	290
$\Delta\varepsilon_{est}$	1.4	36	267	285

$\Delta\varepsilon=\varepsilon_{max}$ (at 3300 bar) $-\varepsilon_{max}$ (at 1 bar). The subscripts "obsd" and "est" represent the observed value in Table 1 and the estimated one from Fig. 2, respectively.

I_2 complexes, respectively. The blue shifts of the visible I_2 bands with increasing pressure up to 3300 bar have been estimated as 140 cm^{-1} for free I_2, 300 cm^{-1} for Et_2O–I_2 and Et_2Se–I_2 complexes, and 330 cm^{-1} for Et_2S–I_2 complex from Table 1. The amount of increase in ε_{max} corresponding to the blue shift of the visible I_2 band with increasing pressure up to 3300 bar may be estimated from the slope of the curve in Fig. 2. These values shown in Table 3 are comparable with the observed ones. This result may support that Mulliken's explanation is suited for the pressure effect on I_2 complexes.

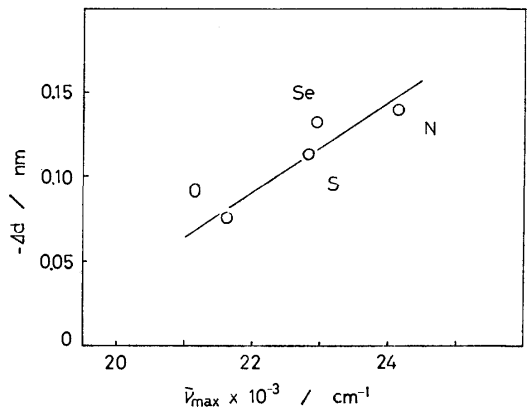

Fig. 3. Relation between $-\Delta d$ and $\tilde{\nu}_{max}$ of visible I_2 bands with several n-donors at 1 bar. O: Et_2O–I_2, S: Et_2S–I_2, Se: Et_2Se–I_2, N: Me_3N–I_2, Δd: see Eq. 5. For the estimation of Δd, van der Waals radii[16] of O, S, Se, N, and I atoms and X-ray data of 1,4-dioxane–I_2 (O),[18] 1,4-dithiane–I_2 (S),[14] 1,4-diselenane–I_2 (Se),[15] and Me_3N–I_2 (N)[19] complexes in their crystals were utilized.

In I_2 complexes with n-donors at 1 bar, it has been found that the decreases in distance between the n-donors and I_2 accompanying complex formation are larger with stronger n-donors.[14,15,18,19] These values are also related to the absorption maxima of the visible I_2 bands in Fig. 3, suggesting the blue shift of the visible I_2 band by the increase in the repulsion force between a n-donor and I_2. The value of $-\Delta d$ in Fig. 3 represents a decrease in the interatomic distance between an n-donor atom and an iodine atom accompanying formation of the I_2 complex (refer to Eq. 5). A linear relation between $-\Delta d$ and the absorption maxima ($\tilde{\nu}_{max}$) of the visible I_2 band has been obtained, and the slope has been estimated to be 2.7×10^{-5} nm/cm^{-1}. The blue shift of 300 cm^{-1} in the visible I_2 band of Et_2Se–I_2 complex with increasing pressure up to 3300 bar has been observed. The value of $-\Delta d$ corresponding to this blue shift may be estimated as 0.008 nm from the slope in Fig. 3.

We wish to thank Professor H. Tsubomura of Osaka University for his useful discussion and advice.

References

1) R. S. Mulliken and W. B. Person, "Molecular Complexes," Wiley-Interscience, New York (1969), pp. 137—162.
2) J. Ham, *J. Am. Chem. Soc.*, **76**, 3881 (1954).
3) O. C. Kwun and H. Lentz, *Z. Phys. Chem. (Frankfurt)*, **96**, 177 (1975).
4) S. Sawamura, Y. Taniguchi, and K. Suzuki, *Chem. Lett.*, **1977**, 823.
5) D. T. McAllan, T. V. Currum, R. A. Dean, and F. A. Fidler, *J. Am. Chem. Soc.*, **73**, 3627 (1951).
6) M. L. Bird and F. Challenger, *J. Chem. Soc.*, **1942**, 570.
7) M. P. Pascal, *C. R. Acad. Sic.*, **156**, 1904 (1913).
8) L. Pieverling, *Ann*, **185**, 331 (1877).
9) H. Tsubomura and R. P. Lang, *J. Am. Chem. Soc.*, **83**, 2085 (1961).
10) H. A. Benesi and J. H. Hildebrand, *J. Am. Chem. Soc.*, **71**, 2703 (1949).
11) H. E. Eduljee, D. M. Newitt, and K. E. Weal, *J. Chem. Soc.*, **1951**, 3086.
12) S. M. Brandon, M. Tamres, and S. Searles, Jr., *J. Am. Chem. Soc.*, **82**, 2129 (1960).
13) A. V. Smolentsev, I. P. Gol'dshtein, E. N. Gur'yanova, L. M. Kataeva, E. G. Kataev, and K. A. Kocheshkov, *Dokl. Akad. Nauk SSSR*, **219**, 1416 (1974).
14) G. Y. Chao and J. D. McCullough, *Acta Crystallogr.*, **13**, 727 (1960).
15) G. Y. Chao and J. D. McCullough, *Acta Crystallogr.*, **14**, 940 (1961).
16) L. Pauling, "The Chemical Bond," Cornell Univ. Press, New York (1967), p. 152.
17) H. C. Tse and M. Tamres, *J. Phys. Chem.*, **81**, 1367 (1977).
18) O. Hassel, *Acta Chem. Scand.*, **19**, 2259 (1965).
19) K. O. Stroemme, *Acta Chem. Scand.*, **13**, 268 (1959).

Effect of Pressure on Iodine Complexes. II. Absorption Spectra of the Charge Transfer Bands with Diethyl Ether, Diethyl Sulfide, and Diethyl Selenide in Heptane

Seiji SAWAMURA, Yoshihiro TANIGUCHI, and Keizo SUZUKI*

Department of Chemistry, Faculty of Science and Engineering, Ritsumeikan University, Kita-ku, Kyoto 603

(Received April 13, 1978)

Absorption spectra of the CT bands of I_2 complexes with Et_2O, Et_2S, and Et_2Se in heptane have been measured up to 4400 bar at 25 °C. The equilibrium constants and the volume changes accompanying complex formation, and the molar extinction coefficients and absorption maxima have been estimated. The volume changes were comparable with those estimated by the visible I_2 bands and by the X-ray data of the I_2 complexes in the crystalline state. In the CT bands of Et_2S–I_2 and Et_2Se–I_2 complexes inversion of shift from red to blue has been observed with increasing pressure though the CT band of Et_2O–I_2 complex shifted only through red. This inversion appears to be characteristic of the strong CT complex. Enhancement of the molar extinction coefficient of the CT band has been found with increasing pressure suggesting enhancement of the CT interaction between I_2 and the n-donor.

In previous papers[1,2] I_2 complexes with diethyl ether (Et_2O), diethyl sulfide (Et_2S), and diethyl selenide (Et_2Se) have been studied as an example of a n-σ complex under high pressure measuring the visible I_2 band. Enhancement of the molar extinction coefficient and the blue shift of the visible I_2 band have been observed with increasing pressure, and the decrease in bond distance between the n-donor and I_2 with increasing pressure up to 3300 bar was estimated as 0.008 nm. The I_2 complex has not only a visible I_2 band but also a charge transfer (CT) band. Then information about the pressure effect on the I_2 complex can be also found by measuring the latter band. The pressure effect on the CT band of the I_2 complexes with Et_2O, Et_2S, and Et_2Se in heptane has consequently been studied.

Experimental

The purification of reagents and the method of measuring the absorption spectra under high pressure are the same as described previously.[1,2]

Results and Discussion

Equilibrium Constants. The CT absorption spectra of the Et_2S–I_2 complex are shown in Fig. 1, and as can be seen the absorption spectra are free from component bands. Similar distinct CT absorption spectra have been observed in the Et_2Se–I_2 complex. The equilibrium constants (K) accompanying complex formation and the molar extinction coefficients (ε_{max}) of these CT bands have been estimated from the Benesi-Hildebrand equation.[2] The CT band of the Et_2O–I_2 complex overlaps the I_2 band in the ultraviolet region (Fig. 2). For the estimation of K and ε_{max} of the Et_2O–I_2 complex, a modified Benesi-Hildebrand equation has been used as previously described.[1] These results are shown in Table 1 together with the spectroscopic data.

The volume changes, ΔV, accompanying complex formation have been calculated from the pressure dependence of $\ln K$.[1,2] These are shown in Table 2. The volume changes estimated from the CT band of the I_2 complex in the present work is comparable with that previously estimated from the visible I_2 band in each complex[2] and furthermore comparable with that estimated from the X-ray data of the I_2 complex.[2]

Spectroscopic Properties. The absorption maxima (λ_{max}) of the CT bands of several I_2 complexes are

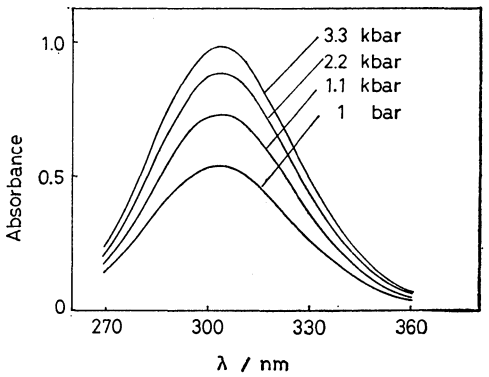

Fig. 1. CT absorption spectra of mixed solution of Et_2S and I_2 in heptane at 25 °C and various pressures. Et_2S: 2.4×10^{-3} mol dm^{-3}, I_2: 5.5×10^{-5} mol dm^{-3}. The absorptions are not corrected for compression.

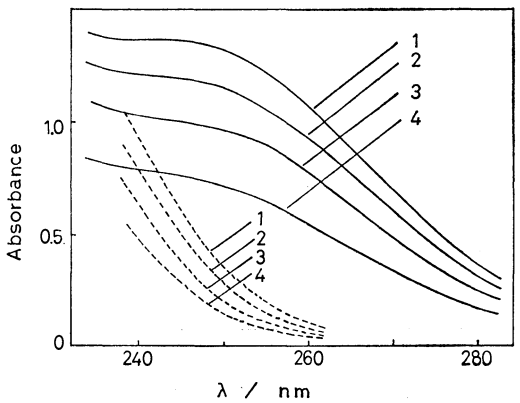

Fig. 2. CT absorption spectra of mixed solution of Et_2O and I_2 in heptane at 25 °C and various pressures. Et_2O: 0.57 mol dm^{-3}, I_2: 3.0×10^{-4} mol dm^{-3}. Dotted lines indicate absorption spectra of I_2 (3.0×10^{-4} mol dm^{-3}) in heptane. 1: 3300 bar, 2: 2200 bar, 3: 1100 bar, 4: 1 bar. The absorptions are not corrected for compression.

Table 1. Equilibrium constants (K), molar extinction coefficients (ε_{max}) and absorption maxima (λ_{max}) of various I_2 complexes in heptane at 25 °C

P / bar	K[a]	ε_{max} / mol^{-1} dm^3 cm^{-1}	λ_{max} / nm
Et_2O–I_2			
1	4.1±1.0[b]	7100±1200	250.8±0.5
	5.9[c]	5650[c]	252[c]
1100	6.9±1.0[b]	7200±1200	252.2±0.5
2200	8.6±1.3[b]	7200±1200	252.6±0.5
3300	10.3±1.3[b]	7200±1200	252.8±0.5
Et_2S–I_2			
1	1460±170	21600±1200	302.7±0.3
	1430[d]	29800[d]	302[d]
1100	2170±340	21900±1200	303.2±0.3
2200	3420±530	22200±1200	303.3±0.3
3300	4570±860	22600±1200	303.2±0.3
4400			302.4±0.2
Et_2Se–I_2			
1	10400±1600	31400±1000	314.2±0.3
			315[e]
1100	19000±4500	32000±1000	314.6±0.3
2200	25000±6700	33900±1000	315.0±0.3
3300	38100±8900	34400±1000	314.8±0.3
4400			314.1±0.2

a) In mole fractions. b) Mean value of K at 250 and 254 nm. c) Ref. 3. d) Ref. 4. e) Ref. 5 in CCl_4.

Table 2. Volume changes (ΔV) accompanying the formation of I_2 complexes at 25 °C (cm^3 mol^{-1})

	Et_2O–I_2	Et_2S–I_2	Et_2Se–I_2
ΔV_{CT}[a]	−7.5±1.0	−10.0±1.2	−13.5±3.0
ΔV_{vis}[b]	−6.7±1.0	−8.1±1.2	−14.6±4.0
ΔV_{theor}[c]	−6.4	−8.9	−9.8

a) From CT band (this work). b) From visible I_2 band (Ref. 2). c) From a theoretical estimation (Ref. 2).

shown in Table 1. In Et_2O–I_2 complex the λ_{max} values of the CT band have been estimated from the observed absorption by subtracting that of the free I_2, which has been calculated from the equilibrium constant of this complex and the molar extinction coefficient of free I_2. In Et_2O–I_2 complex λ_{max} showed a red shiftt with increasing pressure. The red shift has been generally observed in π-π complexes.[6-11] Two explanations have been proposed for the red shift of the CT band with increasing pressure. One is the enhancement of the dielectric constant of the solvent by compression.[6,11,12] This effect stabilizes the excited state of the CT complex rather than the ground state as the dipole moment of the former state is much larger than that of the latter. The other reason is the decrease in the bond distance between a donor and an acceptor,[8,9] supposing that the distance between a donor and an acceptor at the potential minimum of the ground state is larger than that of the excited state.

In Et_2S–I_2 and Et_2Se–I_2 complexes the λ_{max} of the CT band shifted to red with increasing pressure, and then to blue (Table 1). Such an unusual pressure shift from red to blue has been observed only in CT complex between hexamethylbenzene (HMB) and tetracyanoethylene (TCNE).[7,8,11] Gott and Maisch attributed the blue shift in the HMB–TCNE complex under high pressure to the onset of steric hindrance between the nitrogen atoms of TCNE and the methyl groups of HMB.[7] This explanation does not appear to be valid for Et_2S–I_2 and Et_2Se–I_2 complexes because of the absence of steric hindrance. The bond energies of these complexes in nonpolar solvents are 33, 41, and 32 kJ mol^{-1} for Et_2S–I_2,[4] Et_2Se–I_2,[5] and HMB–TCNE complexes,[13] respectively. These values are larger than those of other CT complexes (≈20 kJ mol^{-1}) which indicate normal red shifts of the CT bands with increasing pressure.[6-11] Therefore the unusual pressure shift, namely the inversion of shift with increasing pressure up to several thousand bars may be a character of the complex with strong CT interaction.

The increases in ε_{max} of the CT bands up to 3300 bar are shown in Table 3 as $\Delta\varepsilon_{obsd}$. The same magnitude of $\Delta\varepsilon_{obsd}$ value has been generally observed in π-π complexes.[7-11] The enhancement of ε_{max} of the CT band may be ascribed to the decrease in the bond distance between a donor and an acceptor with increasing pressure as the overlap integral increases due to the decrease in bond distance as expected by Mulliken,[14] implying enhancement of the CT interraction. This explanation supports the preceding conclusion, that is, a decrease in the bond distance of 0.008 nm between I_2 and an n-donor with increasing pressure up to 3300 bar.[2] Furthermore the amount of increase in the overlap integral accompanying decrease in the bond distance is expected to be larger in the stronger CT complex since the overlap integral

Table 3. The increases in the molar extinction coefficients at the CT absorption maxima with increasing pressure up to 3300 bar (mol^{-1} dm^3 cm^{-1})

	Et_2O–I_2	Et_2S–I_2	Et_2Se–I_2
$\Delta\varepsilon_{obsd}$	100±1200	1000±1200	3000±1000
$\Delta\varepsilon_{est}$	2200	2400	2200

$\Delta\varepsilon=\varepsilon$ (at 3300 bar) $-\varepsilon$ (at 1 bar), where ε is the molar extinction coefficient at the CT absorption maximum. The subscripts "obsd" and "est" represent the observed value in Table 1 and the estimated value from Fig. 3, respectively.

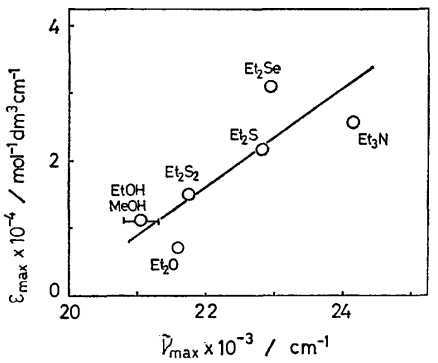

Fig. 3. Relation between ε_{max} of CT band and $\tilde{\nu}_{max}$ of visible I_2 band of I_2 complexes with n-donors at 1 bar. References 15 and 16 were utilized. $\tilde{\nu}_{max}=1/\lambda_{max}$.

increases exponentially with decrease in bond distance. This may explain the $\Delta\varepsilon_{obsd}$ values in Table 3 being larger with stronger n-donors (O<S<Se).

A relation between ε_{max} of the CT bands and λ_{max} (or $\bar{\nu}_{max}$) of the visible I_2 bands of the I_2 complexes with n-donors is expected at 1 bar since it is established that the former values are larger and the latters are at shorter wavelengths with stronger n-donors.[15] This relation is shown in Fig. 3 with a straight line of slope 7.3 mol^{-1} dm^3 cm^{-1}/cm^{-1}. From this slope we can estimate the increases in ε_{max} of the CT bands corresponding to the previously observed blue shifts of the visible I_2 bands, that is, 300 cm^{-1} for Et_2O–I_2 and Et_2-Se–I_2 complexes and 330 cm^{-1} for Et_2S–I_2 complex with increasing pressure up to 3300 bar.[2] These blue shifts suggest enhancement of the CT interaction with increasing pressure. The results are shown in Table 3 as $\Delta\varepsilon_{est}$ and compared with the observed values. The values of $\Delta\varepsilon_{est}$ appear to be the same order of magnitude as the $\Delta\varepsilon_{obsd}$ values and this supports the hypothesis that the increase in ε_{max} of the CT band with increasing pressure is due to the enhancement of the CT interaction between I_2 and the n-donor.

We wish to thank Professor H. Tsubomura of Osaka University for his useful discussion and advice.

References

1) S. Sawamura, Y. Taniguchi, and K. Suzuki, *Chem. Lett.*, **1977**, 823.
2) S. Sawamura, Y. Taniguchi, and K. Suzuki, *Bull. Chem. Soc. Jpn.*, **52**, 281 (1979).
3) S. M. Brandon, O. P., M. Tamres, and S. Searles, Jr., *J. Am. Chem. Soc.*, **82**, 2129 (1960).
4) H. Tsubomura and R. P. Lang, *J. Am. Chem. Soc.*, **83**, 2085 (1961).
5) A. V. Smolentsev, I. P. Gol'dshtein, E. N. Gur'yanova, L. M. Kataeva, E. G. Kataev, and K. A. Kocheshkov, *Dokl. Akad. Nauk SSSR*, **219**, 1416 (1974).
6) J. Ham, *J. Am. Chem. Soc.*, **76**, 3881 (1954).
7) J. R. Gott and W. G. Maisch, *J. Chem. Phys.*, **39**, 2229 (1963).
8) A. H. Ewald, *Trans. Faraday Soc.*, **64**, 733 (1968).
9) Y. Torihashi, Y. Furutani, K. Yagii, N. Mataga, and A. Sawaoka, *Bull. Chem. Soc. Jpn.*, **44**, 2985 (1971).
10) O. C. Kwun and H. Lentz, *Z. Phys. Chem. (Frankfurt)*, **96**, 177 (1975).
11) T. Nakayama and J. Oasugi, *Rev. Phys. Chem. Jpn.*, **45**, 79 (1975); T. Nakayama, M. Sasaki, and J. Osugi, *ibid.*, **46**, 57 (1976).
12) A. H. Ewald and J. A. Scudder, *J. Phys. Chem.*, **76**, 249 (1972).
13) G. Briegleb, J. Czekalla, and G. Reuss, *Z. Phys. Chem. (Frankfurt)*, **30**, 333 (1961).
14) R. S. Mulliken, *J. Am. Chem. Soc.*, **74**, 811 (1952).
15) R. S. Mulliken and W. B. Person, "Molecular Complexes," Wiley-Interscience, New York (1969), pp. 137—162.
16) H. C. Tse and M. Tamres, *J. Phys. Chem.*, **81**, 1367 (1977).

A Molecular Orbital Approach to the Electrophilicity of H and OH Radicals

Akira IMAMURA* and Kimihiko HIRAO

Department of Chemistry, Shiga University of Medical Science, Setatsukinowa-cho, Otsu, Shiga 520-21

(Received April 28, 1978)

We tried to explain the electrophilicity of radical reagents such as H and OH radicals in the aromatic substitution reaction by using the molecular orbital theory. The delocalization energy of π electrons was decomposed into two parts: one is the energy due to the delocalization from a substrate to a reagent and another is that from a reagent to a substrate. The former was considered to be a measure of the electrophilicity and the latter of the nucleophilicity. The decomposition of the delocalization energy into two parts was carried out by modifying the relevant core resonance integrals as appropriate. The result indicated that the delocalization energy for the electrophilicity was much larger than that for the nucleophilicity for both radicals. Thus, H and OH radicals should be electrophilic in nature, in good agreement with the experimental facts. Finally, the origin of the electrophilicity was discussed in connection with the height of the relevant energy levels by following a perturbational approach.

Chemical reactivities of OH and H radicals have been extensively studied in connection with the radiobiological reaction mechanism.[1-6] In many studies of the reaction mechanisms of OH and H radicals, it has been shown that OH and H radicals are electrophilic in nature.[1,2] A beautiful proof for the electrophilicity of the OH radical was published by Anbar *et al.*:[2] they measured the relative rates of reaction of OH radicals with many benzene derivatives and substituted benzoate ion, and found that a plot of the reaction rate against Hammett's σ value is nearly linear, with $\rho = -0.41$, indicating the electrophilicity of the OH radical.

Molecular orbital studies of the reaction mechanism of the OH radical have also been carried out by many researchers.[10-12] In these studies, the electrophilicity of the OH radical was indicated by the electron transfer quantity from the substrate to the OH radical. This quantity, however, can only be used as a qualitative measure of the electrophilicity, since this quantity should be the difference of two electron transfer quantities, from substrate to OH radical and *vice versa*.

In the present paper, we used the unrestricted SCF method in the INDO approximation and calculated, separately, the stabilization energies due to the delocalization of electrons from radical reagent to substrate and those due to the delocalization of electrons from substrate to radical reagent. Obviously, the former can be considered to be a measure of the nucleophilicity of the radical reagent and the latter a measure of the electrophilicity. From the results obtained, OH and H radicals were found to have much more electrophilicity than nucleophilicity, in good agreement with the experimental data.[1,2]

Method of Calculations

First of all, we assumed that the transition state of the reaction between benzene and the radical reagent is the tetrahedral intermediate, as shown in Fig. 1. This model for the transition state has been used in many theories for the chemical reactivity, especially in the frontier electron theory of Fukui *et al.*[7,8] The geometry of the tetrahedral intermediate was tentatively assumed at follows: C–C bond = 1.397 Å, C–H bond = 1.084 Å, C–O bond = 1.360 Å, O–H bond = 0.967 Å, all bond angles except for those including the tetrahedral carbon = 120°, bond angles including tetrahedral carbon = 109°28′, ∠COH = 107°18′, and the H atom of the OH group and the H atom of the CH bond are assumed to be in the trans form. Although the C–O and C–H bond lengths of the tetrahedral carbon atom in the transition state may be different from those used in the present article, it is difficult to determine the bond lengths in the transition state. However, the relative magnitude of the stabilization energies for delocalization of electrons from the substrate to the reagent and *vice versa* can probably be estimated by using the above-mentioned geometry.

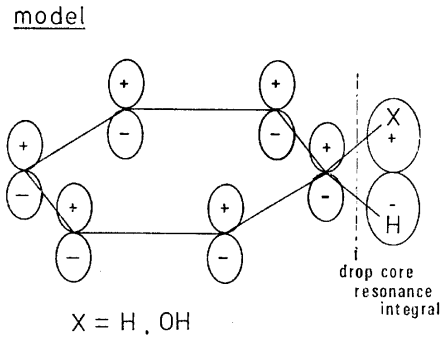

Fig. 1. The model for the tetrahedral intermediate. The orbital at the most right is the pseudo π orbital.

It has been well known that the chemical reactivity of aromatic substitution is mainly governed by the magnitude of the stabilization energy due to the delocalization of π electrons between benzene π orbitals and the pseudo π orbital which is formed from the attacking radical reagent and the remaining hydrogen atom.[7,8] In order to estimate the delocalization energy of π electrons, first, the total energy of the molecule was calculated by using the unrestricted SCF method with INDO approximation[9] after dropping all core resonance integrals between π atomic orbitals on the benzene moiety and the pseudo π orbital. This gives the total energy without the delocalization of π electrons. Next, the total energy of the molecule was calculated after partially including the core resonance integrals between π atomic orbitals and the pseudo π^* orbital, so as to include only the effect of the delocalization of π electrons from the substrate to the radical reagent, and not from

the radical reagent to the substrate. The difference between these two total energies can be considered to be a measure of the electrophilicity of the radical reagent in question:

$$E_{\text{electrophilicity}} = E(\text{including the delocalization from the substrate to the radical reagent}) - E(\text{without the delocalization of } \pi \text{ electrons}), \quad (1)$$

where E is the total energy calculated under the restriction described in the parentheses. In a similar manner, we can obtain a measure of the nucleophilicity of the radical reagent by the following equation:

$$E_{\text{nucleophilicity}} = E(\text{including the delocalization from the radical reagent to the substrate}) - E(\text{without the delocalization of } \pi \text{ electrons}). \quad (2)$$

In calculating a measure of the electrophilicity as well as the nucleophilicity, the core resonance integrals between π atomic orbitals on the benzene moiety and the pseudo π orbital should be modified in order to include the delocalization of π electrons from the substrate to the radical reagent or *vice versa*. That is, for a measure of the electrophilicity, the core resonance integrals between atomic orbitals in question should be modified so that the core resonance integrals between the occupied π molecular orbitals on the benzene moiety and the vacant pseudo π^* molecular orbitals have the same value as those obtained by using the usual core resonance integrals between atomic orbitals, and the resonance integral between other molecular orbitals is always zero. Of course, the molecular orbitals which are used for calculating the core resonance integral have to be those obtained without the effect of the delocalization of π electrons, namely, by dropping the core resonance integrals between π and pseudo π atomic orbitals. The values of the core resonance integrals required can be calculated by the procedure described below.

Molecular orbitals obtained by dropping all the core resonance integrals between π atomic orbitals on benzene and pseudo π orbitals can be classified into two groups: one is those containing only π atomic orbitals on a benzene moiety and the other, the pseudo π orbitals as well as σ atomic orbitals of benzene. Thus, the molecular orbitals can be represented as follows:

$$\phi_{\pi i} = \sum_r C_{\pi i,r}\chi_r, \quad (3)$$

$$\phi_{\sigma j} = \sum_s C_{\sigma j,s}\chi_s, \quad (4)$$

where $\phi_{\pi i}$ denotes a molecular orbital containing only π atomic orbitals on the benzene ring, and $\phi_{\sigma j}$ denotes that containing pseudo π orbitals as well as σ atomic orbitals of benzene. From Eq. 3, an atomic orbital, χ_r, can be represented by a linear combination of molecular orbitals $\phi_{\pi i}$, as shown in the following. Equation 3 is multiplied by the coefficient $C_{\pi i,r_1}$ and the resulting equations are added for all i:

$$\sum_i C_{\pi i,r_1}\phi_{\pi i} = \sum_r\sum_i C_{\pi i,r_1}C_{\pi i,r}\chi_r = \sum_r \chi_r \sum_i C_{\pi i,r_1}C_{\pi i,r} = \sum_r \chi_r \delta_{rr_1} = \chi_{r_1}, \quad (5)$$

where r_1 designates one of the π atomic orbitals $\{\chi_r\}$. Thus, we have

$$\chi_r = \sum_i C_{\pi i,r}\phi_{\pi i}. \quad (6)$$

Similarly,

$$\chi_s = \sum_j C_{\sigma j,s}\phi_{\sigma j}. \quad (7)$$

By using Eqs. 6 and 7, we can represent a core resonance integral between atomic orbitals χ_r and χ_s as the sum of core resonance integrals between molecular orbitals $\phi_{\pi i}$ and $\phi_{\sigma j}$:

$$I_{rs} = \int \chi_r h^\circ \chi_s d\tau = \sum_i\sum_j C_{\pi i,r}C_{\sigma j,s}\int \phi_{\pi i} h^\circ \phi_{\sigma j} d\tau = \sum_i\sum_j C_{\pi i,r}C_{\sigma j,s}I_{ij}, \quad (8)$$

where I_{rs} and I_{ij} are the core resonance integral between the atomic orbitals χ_r and χ_s, and that between the molecular orbitals $\phi_{\pi i}$ and $\phi_{\sigma j}$, respectively, and h° means the one electron Hamiltonian. By modifying Eq. 8, we can obtain the value of the core resonance integral between atomic orbitals which gives the core resonance integrals between any specified molecular orbitals $\phi_{\pi i_1}$ and $\phi_{\sigma j_1}$ correctly and gives zero for the core resonance integrals between other molecular orbitals. That is,

$$I_{rs} = \sum_{(i_1-j_1)} C_{\pi i_1,r}C_{\sigma j_1,s}I_{i_1 j_1}, \quad (9)$$

where (i_1-j_1) means that the summation should cover only some specified molecular orbitals $\phi_{\pi i_1}$ and $\phi_{\sigma j_1}$. It is proved below that the core resonance integrals, I_{rs}, in Eq. 9 give the core resonance integrals between molecular orbitals $\phi_{\pi i_1}$ and $\phi_{\sigma j_1}$ correctly and give zero values for others. Consequently, when the vacant molecular orbitals localized in the radical moiety and the occupied molecular orbitals are chosen for i_1 and j_1, respectively, we can calculate the delocalization energy for the electrophilicity given by Eq. 1. The proof is as follows:

$$\begin{aligned} I_{ij} &= \sum_r\sum_s C_{\pi i,r}C_{\sigma j,s}\int \chi_r h^\circ \chi_s d\tau = \sum_r\sum_s C_{\pi i,r}C_{\sigma j,s}I_{rs} \\ &= \sum_r\sum_s C_{\pi i,r}C_{\sigma j,s}\sum_{(i_1-j_1)} C_{\pi i_1,r}C_{\sigma j_1,s}I_{i_1 j_1} \\ &= \sum_{(i_1-j_1)} I_{i_1 j_1}\left(\sum_r C_{\pi i,r}C_{\pi i_1,r}\right)\left(\sum_s C_{\sigma j,s}C_{\sigma j_1,s}\right) \\ &= \sum_{(i_1-j_1)} I_{i_1 j_1}\delta_{ii_1}\delta_{jj_1}. \end{aligned} \quad (10)$$

Equation 10 indicates that I_{ij} is equal to the correct value only when $i=i_1$ and $j=j_1$ and is zero otherwise. Consequently, when molecular orbitals $\phi_{\pi i_1}$ cover all occupied orbitals, and $\phi_{\sigma j_1}$ cover all vacant pseudo π^* orbitals, the SCF calculations with the core resonance integrals of Eq. 9 should give a measure of the electrophilicity. On the other hand, when molecular orbitals $\phi_{\pi i_1}$ cover all vacant orbitals, and $\phi_{\sigma j_1}$ cover all occupied pseudo π orbitals, a measure of the nucleophilicity must be given.

The procedure of the calculations can be summarized as follows. (i) The total energy of the molecule in the transition state is calculated with the unrestricted SCF method in the INDO approximation after dropping all the core resonance integrals between the π atomic orbitals on the benzene moiety and the pseudo π orbital. (ii) By using the molecular orbitals obtained in step (i), the core resonance integrals between π atomic orbitals and pseudo π atomic orbitals are modified according to

Eq. 9 in order to take the electrophilic or the nucleophilic nature into account. (iii) The modified core resonance integrals are employed to calculate the total energy of the molecule in the transition state with the delocalization of π electrons, which corresponds to the electrophilic or the nucleophilic nature. (iv) A measure of the electrophilicity or the nucleophilicity of the radical reagent can be obtained by calculating the difference between energies obtained in steps (i) and (iii).

Results and Discussion

The electrophilicity of H and OH radicals was studied according to the procedure described. However, the procedures for H and OH radicals are slightly different owing to the symmetrical character of the pseudo π orbital; that is, in the case of the H radical, the pseudo π orbital is antisymmetric with respect to the reflection in the plane containing the benzene ring, but is lacking in the symmetry for the OH radical. Consequently, the results for H and OH radicals will be shown separately in the following.

H Radical. The unrestricted SCF method is applied to the tetrahedral intermediate of the benzene attacked by the H radical (see Fig. 1) in the INDO approximation. The obtained energy levels are as indicated in Fig. 2 when the delocalization of π electrons is prohibited. As is clearly shown in Fig. 2, the energy level of the pseudo π orbital for α-spin is much lower than that for β-spin owing to the effect of the spin polarization. The delocalization energy for the measure of the nucleophilicity of the H radical is obtained when the core resonance integrals are retained only between the pseudo π orbital and the vacant π^* molecular orbitals on the benzene moiety for α-spin, as shown by arrows in Fig. 2. On the other hand, the measure of the electrophilicity can be calculated by retaining the core resonance integrals between the pseudo π^* orbital and the occupied π molecular orbitals on the benzene moiety for β-spin.

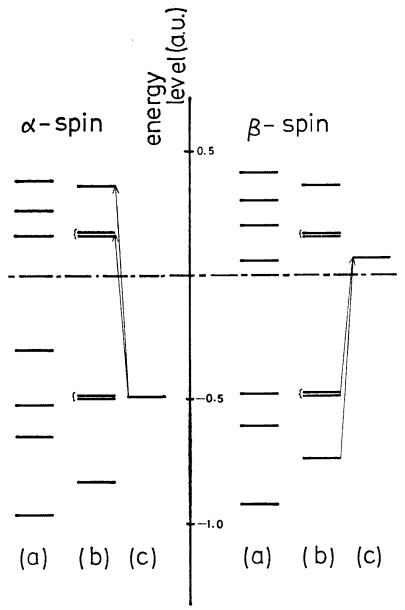

Fig. 2. Energy level diagrams of π molecular orbitals for the tetrahedral intermediate attacked by H radical. (a) The energy levels obtained by the usual UHF calculation. (b) The energy levels of benzene π molecular orbitals obtained by the UHF calculation after dropping core resonance integrals shown in Fig. 1. (c) The energy levels of pseudo π orbital obtained by the procedure in (b). The arrows in the figure indicate the direction of electron delocalization.

Table 1. Total energies of tetrahedral intermediate attacked by H radical with various types of delocalization effects

Interacting MO[a] (α-spin)	Interacting MO[a] (β-spin)	Total energy[b]	Delocalization energy[b]
all	all	−46.312	0.315
none	none	−45.998	0.0
pseudo π-all π^*	none	−46.060	0.063
none	all π-pseudo π^*	−46.161	0.164
pseudo π-all π^*	all π-pseudo π^*	−46.236	0.238
pseudo π-$\begin{matrix}\text{all } \pi^* \\ \text{all } \pi\end{matrix}$	none	−46.096	0.098
none	$\begin{matrix}\text{all } \pi \\ \text{all } \pi^*\end{matrix}$-pseudo π	−46.180	0.182

a) Interacting MO means molecular orbitals which retain the core resonance integrals between themselves.
b) In a.u.

The obtained results are listed in Table 1. The third line indicates the nucleophilicity and the fourth line the electrophilicity of the H radical. Obviously, the delocalization energy for the electrophilicity is much larger than that for the nucleophilicity. Consequently, it should be concluded that the H radical is electrophilic in nature for the radical reaction with benzene, in accordance with the experimental fact that the H radical behaves like an electrophilic reagent in the abstraction reaction[1] (although this reaction is somewhat different from the model used in the present article). The fifth line of Table 1 includes the delocalization energy obtained by retaining core resonance integrals for the electrophilicity as well as the nucleophilicity. The delocalization energy in the fifth line is nearly equal to the sum of the delocalization energies in the third and the fourth lines, that is, the delocalizations of α-spin and β-spin electrons affect each other only slightly. The delocalization energy in the sixth line was obtained by including the core resonance integrals between the pseudo π orbital and all the π molecular orbitals on benzene moiety for α-spin, that is, the effect of the nucleophilicity as well as the redistribution of α-spin electrons were included in the value of the delocalization energy. Similarly, the delocalization energy in the seventh line includes the effect of the electrophilicity as well as the redistribution of the β-spin electrons. By comparing the values in the sixth and the seventh lines with those in the fourth and fifth lines, the redistribution effect is found not to be negligibly small, although the delocalization energy corresponding to the nucleophilicity and the electrophilicity are somewhat larger than those for the redistribution effect. In conclusion, for the H radical the delocalization energy for the electrophilicity was found to be the most important contribution to the total delocalization energy.

TABLE 2. CHARGE DISTRIBUTIONS OF TETRAHEDRAL INTERMEDIATE ATTACKED BY H RADICAL WITH VARIOUS TYPES OF DELOCALIZATION EFFECTS[a)]

Interacting MO[b)] (α-spin)	Interacting MO[b)] (β-spin)	H_1	H_2	H_3	C_1	C_2	C_3	C_4	H
all	all	−0.021	−0.027	−0.024	0.118	−0.007	0.032	0.008	−0.029
none	none	−0.024	−0.026	−0.024	0.039	0.018	0.024	0.024	−0.011
pseudo π-all π^*	none	−0.031	−0.030	−0.027	−0.035	0.007	0.029	0.012	0.049
none	all π-pseudo π^*	−0.012	−0.020	−0.019	0.193	0.040	0.015	0.046	−0.133
pseudo π-all π^*	all π-pseudo π^*	−0.012	−0.024	−0.022	0.112	0.027	0.021	0.032	−0.066
pseudo π-$\begin{matrix}\text{all } \pi \\ \text{all } \pi^*\end{matrix}$	none	−0.033	−0.035	−0.029	−0.002	−0.050	0.052	−0.036	0.099
none	$\begin{matrix}\text{all } \pi \\ \text{all } \pi^*\end{matrix}$-pseudo π^*	−0.012	−0.018	−0.018	0.158	0.069	0.001	0.076	−0.148

a) The numbering of the atom is as below: b) The meaning of "Interacting MO" is given in Table 1.

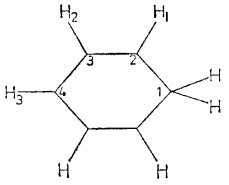

In Table 2, charge distributions of the tetrahedral intermediate were given for the various cases corresponding to the calculations in Table 1. It is obvious that the charges on the hydrogen atoms bonded to the tetrahedral carbon atom can help in determining the direction of the electron delocalization. The charge on the hydrogen atom in the third line is positive, in accordance with the fact that the calculations of the third line give a measure for the nucleophilicity. Similarly, the negative charge on the hydrogen in the fourth line corresponds with the calculations for the electrophilicity. The charges listed in the sixth and the seventh lines indicate that the inclusion of the redistribution effect makes the positive hydrogen more positive and the negative hydrogen more negative. As a result, the sum of the charges of the hydrogen atom in the sixth and seventh lines leads to a slightly negative charge, which corresponds to the value of the charge in the first line.

OH Radical. For the calculation of the electrophilicity of the OH radical, the tetrahedral intermediate of the benzene attacked by an OH radical (see Fig. 1) was subjected to the unrestricted SCF calculations in the INDO approximation. However, this intermediate has no symmetry for the reflection in the plane containing the benzene ring. In other words, the pseudo π and π^* orbitals don't localize in the parts of the H atom and OH group attached to the tetrahedral carbon atom, but these orbitals spread over the σ skeleton of the whole molecule. Because of the delocalizing character of the pseudo π and π^* orbitals, it becomes rather difficult to discriminate the pseudo π and π^* orbitals from other orbitals. In addition to this, the core resonance integrals between the $2p\pi$ atomic orbitals and the other 2s or 2p atomic orbitals of the same atom are apparently non-zero, using Eq. 9, since the values of $C_{\sigma j,s}$ for a pseudo π or π^* orbital are non-zero because of the spreading character of the pseudo π or π^* orbital.

In order to overcome these undesirable developments, the molecular orbitals $\psi_{\sigma j}$ given by Eq. 4 were transformed into the localized molecular orbitals according to the procedure of Edmiston and Ruedenberg.[13] After this procedure, it becomes quite easy to pick up the pseudo π or π^* orbital. Furthermore, if the transformed orbital is localized completely, the core resonance integral between $2p\pi$ and 2s or $2p\sigma$ atomic orbitals, which is apparently non-zero if one uses canonical molecular orbitals, becomes completely zero if one uses localized molecular orbitals, since the value of $C_{\sigma j,s}$ in Eq. 9 vanishes. Usually, transformed orbitals don't localize completely, and hence the undesirable development cannot be completely excluded, but its contribution is expected to be significantly diminished. Therefore, the degree of localization given by Eq. 11 was calculated to check the validity of the calculations.

$$\text{Degree of localization} = \sum_{\substack{r \\ (\text{OH.H})}} C_{ir}^2, \qquad (11)$$

where r in the summation covers all atomic orbitals on the OH group and H atom attached to the tetrahedral carbon atom.

TABLE 3. THE DEGREE OF LOCALIZATION OF CANONICAL AND LOCALIZED MOLECULAR ORBITALS[a)]

Molecular orbital[b)]	1	2	3	4	5
Canonical MO (α-spin)	0.782	0.533	0.506	0.464	0.411
Localized MO (α-spin)	0.980	0.962	0.908	0.786	0.767
Canonical MO (β-spin)	0.988	0.474	0.414		
Localized MO (β-spin)	0.956	0.766	0.519		

a) The degree of localization was calculated by using Eq. 11. b)The numbering of molecular orbitals is in the decreasing order of the degree of localization.

Table 4. Total energies of tetrahedral intermediate attacked by OH radical with various types of delocalization fefects using localized molecular orbitals

Interacting MO[a] (α-spin)	Interacting MO[a] (β-spin)	Total energy[b]	Delocalization energy[b]
all	all	−63.879	0.428
none	none	−63.451	0.0
pseudo π-all π	none	−63.538	0.087
none	all π-pseudo π^*	−63.623	0.171

a) The meaning of "interacting MO" is the same as that in Table 1. b) In a.u.

Table 5. Total energies of tetrahedral intermediate attacked by OH radical with various types of delocalization effects using canonical molecular orbitals

Interacting MO[a] (α-spin)	Interacting MO[a] (β-spin)	Total energy[b]	Delocalization energy[b]
all	all	−63.879	0.428
none	none	−63.451	0.0
pseudo π-all π	none	−63.517	0.066
none	pseudo π-all π^*	−63.626	0.175

a) The meaning of "interacting MO" is the same as that in Table 1. b) In a.u.

The degree of the localization for some transformed molecular orbitals is listed in Table 3, and compared with that for the corresponding canonical molecular orbitals. Obviously, the degree of localization increases remarkably by the transformation of the molecular orbital. The measure of the electrophilicity of the OH radical was calculated in a similar manner to that of the H radical by using the transformed molecular orbitals. The results thus obtained are collected in Table 4. It is clearly indicated that the OH radical is quite electrophilic in nature, in agreement with the experimental data.[1,2] In order to investigate the effect of the localization of molecular orbitals, the same calculations were carried out by using canonical molecular orbitals. Table 5 contains the results which indicate the essential features of the electrophilicity of the OH radical. That is, by comparing Tables 4 and 5, the delocalization energy for the measure of the electrophilicity is much larger than that for the nucleophilicity, regardless of the degree of the localization. In other words, the conclusion that the OH radical is electrophilic in nature is valid independently of the degree of the localization for the molecular orbitals in question. In Table 6, charge distributions corresponding to the calculations of Table 4 are listed. This indicates that the electrophilicity of the OH radical is reflected in the negative charges of the H atom and OH group attached to the tetrahedral carbon atom. That is, when the conjugation of π electrons is completely prohibited between pseudo π or π^* orbital and benzene π molecular orbitals, the charge on the tetrahedral group is somewhat negative (−0.110). When the effect of the nucleophilicity is taken into account, it becomes slightly positive (+0.003), and when the effect of the electrophilicity is taken into account, it becomes quite negative (−0.352). As a sum of these two effects, the considerable negative charge on the group results. This feature for OH radicals is quite similar to that for H radicals.

Concluding Remarks. In the present article, the electrophilicity of H and OH radicals was quantitatively evaluated by separating the delocalization energy in the nucleophilic and the electrophilic ones. The obtained result is in good agreement with the experimental fact that H and OH radicals are electrophilic in nature. In the present paragraph, we will discuss briefly the origin of the electrophilicity of H and OH radicals. Since the measure of the electrophilicity is a kind of delocalization energy, it should be very effective for the analysis of the electrophilicity of H and OH radicals to use the concept of the perturbation method.

In Figs. 2 and 3, the energy levels for zero-th order wave functions are given for H and OH radicals. As is well known, the delocalization energy is approximately proportional to the core resonance integral between pseudo π or π^* orbital and benzene π molecular orbitals, and is inversely proportional to the energy difference between pseudo π and benzene unoccupied π^* molecular orbitals or pseudo π^* and benzene occupied π orbitals. The above-metioned reasoning is applicable only when the uncoupled approximation[14,15] in the SCF perturbation method is valid. The present approach has its

Table 6. Charge distributions of tetrahedral intermediate attacked by OH radical with various types of delocalization effects using localized molecular orbitals

Interacting MO[b] (α-spin)	Interacting MO[b] (β-spin)	C_1	C_2	C_3	C_4	H	O	H(O)[c]	(H, OH)[d]
all	all	0.292	−0.042	0.034	0.011	−0.053	−0.317	0.164	−0.206
none	none	0.166	−0.016	0.028	0.020	−0.008	−0.289	0.187	−0.110
pseudo π-all π	none	0.103	−0.028	0.032	0.008	0.069	−0.264	0.198	0.003
none	all π-pseudo π^*	0.309	0.007	0.019	0.045	−0.150	−0.361	0.159	−0.352

a) The numbering of the atom is as below:

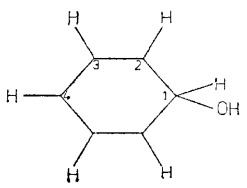

b) The meaning of "Interacting MO" is the same as that in Table 4. c) The hydrogen atom in the group. d) The sum of the charges on the group of H and OH atoms.

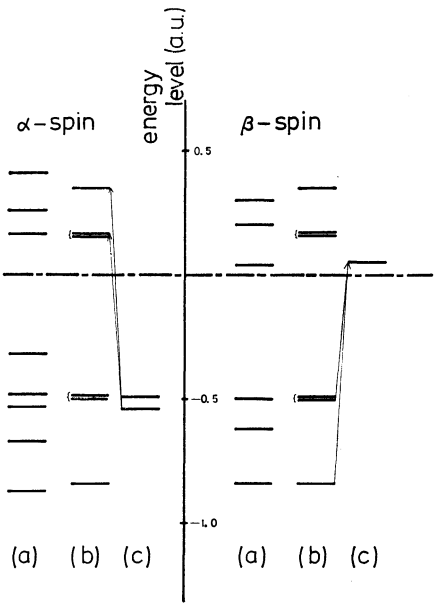

Fig. 3. Energy level diagrams of π molecular orbitals for the tetrahedral intermediate attacked by OH radical. The meaning of (a), (b), and (c) is the same as that in Fig. 2.

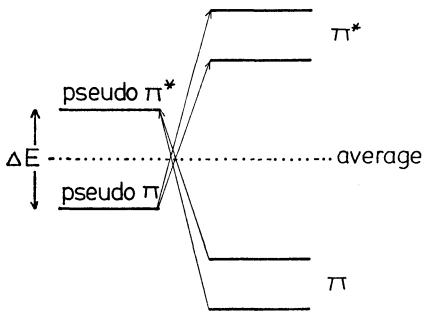

Fig. 4. Schematical energy levels for the perturbational approach to the present method.

special characteristics in the feature of the distribution of energy levels: that is, by using the unrestricted SCF method the energy level for an odd electron splits into two different values, for occupied α-spin and unoccupied β-spin levels. Thus, the dependence of the delocalization energy upon the height of the energy levels should be classified into two factors; one is the average height of the two split levels for an odd electron and the other is the magnitude of splitting of these two levels. This situation is schematically shown in Fig. 4. As is evident from this figure, the lower the average height of the two energy levels is, the more electrophilic the radical reagent is. On the other hand, a large magnitude of splitting of the two energy levels results in large values for the measures of both the electrophilicity and the nucleophilicity.[16] From the heights of the energy levels in Figs. 2 and 3, H and OH radicals can be inferred to be electrophilic in nature, although the quantitative evaluation of the delocalization energy is not accessible, owing to the contribution of the core resonance integral between pseudo π or π^* orbital and benzene π molecular orbitals. In conclusion, the electrophilicity of the radical reagent may qualitatively be predicted by the average of the two energy levels of pseudo π and π^* orbitals and the magnitude of their splitting. As to other radical reagents, analysis will soon be carried out in order to investigate whether the above-mentioned conclusion holds or not. Furthermore, the abstraction reaction of a hydrogen atom, as well as a halogen atom, by the reagent was subjected to an analysis similar to that in the present article and was published.[17]

The authors are very grateful to Prof. T. Masuda of Tokyo Metropolitan University for suggesting this problem and for stimulating discussion. We are also grateful to Dr. T. Minato for his considerable assistance with the computer program of localized molecular orbitals. The numerical calculations were carried out on the FACOM 230-75 at the Computer Center of Kyoto University. This research was supported in part by a Scientific Grant from the Ministry of Education.

References

1) G. A. Russell, "Free Radicals," ed by J. K. Kochi, John Wiley & Sons, New York, N. Y. (1973), Vol. 1, p. 275.
2) M. Anbar, D. Meyerstein, and P. Neta, *J. Phys. Chem.*, **70**, 2660 (1966).
3) H. Taniguchi, K. Fukui, S. Ohnishi, H. Hatano, H. Hasegawa, and T. Maruyama, *J. Phys. Chem.*, **72**, 1926 (1968).
4) H. Taniguchi, H. Takagi, and H. Hatano, *J. Phys. Chem.*, **76**, 135 (1972).
5) T. Masuda, H. Shinohara, and M. Kondo, *J. Radiat. Res.*, **16**, 153 (1975).
6) H. Shinohara, T. Masuda, and M. Kondo, *J. Radiat. Res.*, **17**, 230 (1976).
7) K. Fukui, "Theory of Orientation and Stereoselection," Springer-Verlag, Berlin (1974), p. 34.
8) K. Fukui, T. Yonezawa, and C. Nagata, *Bull. Chem. Soc. Jpn.*, **27**, 423 (1954).
9) J. A. Pople and D. L. Beveridge, "Approximate Molecular Orbital Theory," McGraw-Hill, New York, N. Y. (1970).
10) H. Fujimoto, S. Yamabe, T. Minato, and K. Fukui, *J. Am. Chem. Soc.*, **94**, 9205 (1972).
11) S. Nagase, K. Takatsuka, and T. Fueno, *J. Am. Chem. Soc.*, **98**, 3838 (1976).
12) S. Nagase and T. Fueno, *Bull. Chem. Soc. Jpn.*, **49**, 2920 (1976).
13) C. Edmiston and K. Ruedenberg, *Rev. Mod. Phys.*, **35**, 457 (1963).
14) R. M. Stevens, R. M. Pitzer, and W. N. Lipscomb, *J. Chem. Phys.*, **38**, 550 (1963).
15) P. W. Langhoff, M. Karplus, and R. P. Hurst, *J. Chem. Phys.*, **44**, 505 (1966).
16) The magnitude of the splitting of the energy levels can be approximately represented as Eq. 12 by using the first order perturbation theory.
$$\Delta E = \sum_r \sum_s (P^{\alpha}_{rs} - P^{\beta}_{rs})(rr|ss) C^{\alpha}_{ir} C^{\alpha}_{is} \qquad (12)$$
where superscripts α and β denote α and β spins, respectively, and the number of α spin electrons is greater by one than that of β spin electrons.
17) H. Shinohara, A. Imamura, T. Masuda, and M. Kondo, *Bull. Chem. Soc. Jpn.*, **51**, 1917 (1978).

Liquid Structure of Carbon Tetrachloride and Long-range Correlation

Keiko NISHIKAWA* and Yoshitada MURATA†

Department of Chemistry, Faculty of Science, Gakushuin University, Mejiro, Toshima-ku, Tokyo 171

(Received May 20, 1978)

The diffraction of liquid CCl_4 was measured by using the energy-dispersive X-ray diffractometer. The fine structure was observed for the first time in the present study. The existence of the fine structure in the diffraction pattern shows the long-range correlation "directly." The bcc cluster model for liquid CCl_4 is presented on the basis of the long-range correlation. The calculated intensity of the model is in good agreement with the observed one.

We constructed an energy-dispersive X-ray diffractometer using a solid state detector for the determination of liquid structure. The details were reported in a previous paper.[1)]

The energy-dispersive method has various merits in comparison with the traditional angle-dispersive method. First, a higher resolution of the s-value ($s=4\pi \sin\theta/\lambda$, λ: wavelength, 2θ: scattering angle) can be obtained. The resolution of the s-value is determined by the following equation:

$$\Delta s/s = \Delta E/E + \cot\theta \cdot \Delta\theta. \quad (1)$$

In the energy-dispersive diffractometer, the first term on the right side of Eq. 1 is nearly 0.01 and much larger than in a conventional angle-dispersive one. The second term in the angle-dispersive one, on the other hand, is several times as large as that in the energy-dispersive one. Since $\cot\theta \cdot \Delta\theta$ is less than 0.01 in our apparatus, the resolution $\Delta s/s$ is consequently a half of that in the conventional angle-dispersive diffractometer. Second, in the energy-dispersive method the scattering intensity is hardly affected by fluctuation in the primary beam intensity. Thirdly, it is possible to expand the observable region of the s-value, and hence the intensity data over the range of $s=0.15$—30 Å^{-1} can be obtained by our energy-dispersive X-ray diffractometer. Fourth, such accessories as a sample holder operated at high or low temperature can be mounted easily, since the design of the diffractometer is simple.

The scattering intensity from liquid CCl_4 was measured by taking advantage of the energy-dispersive method. Carbon tetrachloride has been studied well by the angle-dispersive method,[2–7)] and several models for liquid CCl_4 have been proposed by Narten *et al.*,[5)] Egelstaff *et al.*,[9)] Reichelt *et al.*[6)] and Narten.[7)] We reported the scattering intensity of liquid CCl_4 and its electron radial distribution function in a previous paper,[1)] but the analysis of the data obtained by energy-dispersive method was described mainly. In the present study it is shown that liquid CCl_4 has a long-range correlation at room temperature. A new model which explains the observed scattering intensity and the long-range correlation is presented.

Scattering Intensity and Radial Distribution Function

Details of the measurement and data analysis were described elsewhere.[1)] The absorption and Compton correction are more difficult in the energy-dispersive method than in the angle-dispersive one and these may be thought to be a demerit in energy-dispersive diffractometry, but these difficulties were resolved.[1)] The reduced intensity $i(s)$ was obtained in electron units after these corrections. The weighted structure function $si(s)$ is shown in Fig. 1 and agrees fairly well with the recent data for CCl_4 obtained by Narten[7)] except for the fine structure.

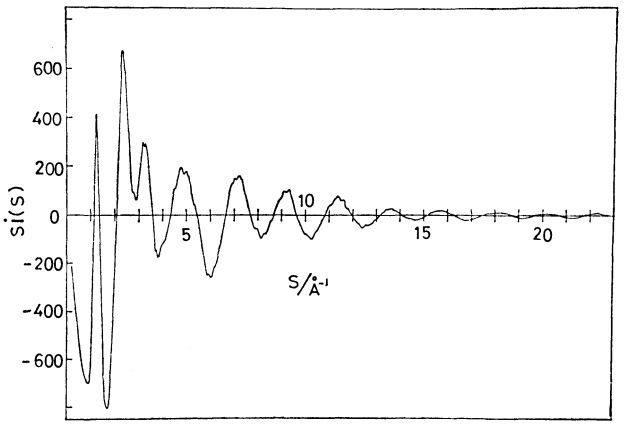

Fig. 1. Weighted structure function $si(s)$ for liquid CCl_4 at room temperature.

The electron radial distribution function from which the bulk density is subtracted, $4\pi r^2(\rho-\rho_0)$, is obtained by the Fourier transformation of $si(s)$,

$$4\pi r^2(\rho-\rho_0) = \frac{2r}{\pi \sum_j Z_j^2} \sum_s si(s) \cdot \sin(sr) \cdot \Delta s, \quad (2)$$

where ρ is the radial distribution function, ρ_0 the bulk density and Z_j the atomic number of a component atom j. The radial distribution function derived from Eq. 2 includes the distribution of the electron cloud. The

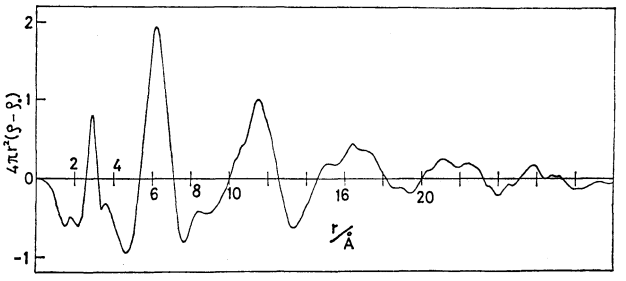

Fig. 2. Electron radial distribution function from which the bulk density was subtracted, $4\pi r^2(\rho-\rho_0)$.

† Present address: The Institute for Solid State Physics, The University of Tokyo, Roppongi, Minato-ku Tokyo 106.

Table 1. Intramolecular distances and associated root mean-square amplitudes
The values in parentheses indicate the standard deviations.

i	j	r_{ij}(Å)	l_{ij}(Å)	Reference	
C	Cl	1.768(6)	0.069(9)	Present work	(liquid)
		1.773(3)	0.079(9)	Ref. 5	
		1.767(3)	0.055(8)	Ref. 6	
		1.766(3)	0.043(4)	Ref. 7	
		1.765(2)	0.051(2)	Ref. 8	(gas)
Cl	Cl	2.889(2)	0.086(6)	Present work	(liquid)
		2.896(5)	0.092(3)	Ref. 5	
		2.886	0.070(9)	Ref. 6	
		2.884	0.078(3)	Ref. 7	
		2.886(2)	0.070(1)	Ref. 8	(gas)

electron radial distribution function of CCl_4 at room temperature is shown in Fig. 2.

The intramolecular parameters of CCl_4 were obtained by the least-squares fit of the calculated intensity of the free molecule to the observed intensity of the liquid at s-values larger than 8 Å^{-1}. These parameters are listed in Table 1 with those obtained by other experiments.[5-8] The interatomic distances are in good agreement with each other within experimental errors.

The Fine Structure in the Scattering Intensity and the Long-Range Correlation

Figure 2 shows that liquid CCl_4 at room temperature has long-range correlation. The information on the long-range correlation in liquid is confined in the region of $s<2$ Å^{-1}, but it is also recognized elsewhere. Figure 1 shows that the intensity curve has fine structure of short periodicity at small s-values.†† The fine structure near the top and the bottom of the halos at $s=3.2$ and 4.7 Å^{-1} was reproducible not only in repeated measurements but also in measurements at different scattering angles. The separation between the peaks in this fine structure were 0.2—0.3 Å^{-1}, which was larger than the estimated resolution in the s-value ($\Delta s=0.14$ Å^{-1} at those s-values) in our experiment. The difference between the collected counts at the top and the bottom of these small waves was about 500 counts, which were larger than the statistical random error ($\sqrt{n}=170$, where total counts $n=3\times10^4$). In the energy-dispersive method, the scattering intensity is hardly affected by fluctuations of the incident beam intensity. Therefore, the statistical random error given by the square root of the total counts at each position is the main origin of the noise.

To examine the relation between the fine stricture and the long-range correlation in liquid CCl_4, the inverse Fourier transformation of the experimental data was conducted. Each peak in the observed radial distribution function was expressed approximately by

$$G(r) = A\exp[-4(\ln 2)(r-r_0)^2/w^2] - B, \quad (3)$$

where A is the peak height measured from the average values at the minimum points, w the full width at half maximum, and B the difference between the zero line and the average minimum values. Figure 3 shows the curve for the inverse Fourier transformation for each Gaussian function $G(r)$. The curve (1), (2), (3), (4), (5), and (6) in Fig. 3(a) correspond to the peaks at the maximum positions $r_0=3.8$, 6.3, 8.3, 11.4, 16.3, and 21.5 Å, respectively. The summation of these curves is

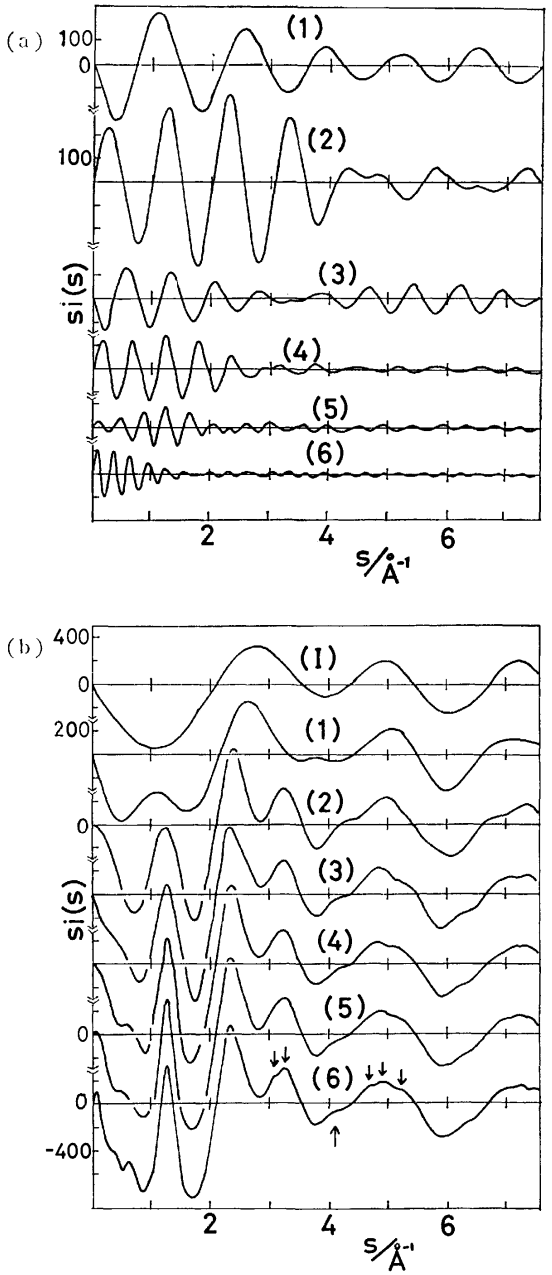

Fig. 3. (a) The inverse Fourier transformation function of the Gaussian function given by Eq. 3. Curves (1), (2), (3), (4), (5), and (6) correspond to the functions with $r_0=3.8$, 6.3, 8.3, 11.4, 16.3, and 21.5 Å, respectively. (b) The uppermost curve (I) is the inverse Fourier transformation function of the intramolecular part. Curve (n) is the sum of curves (1), (2)—(n) of Fig. 3(a) and curve (I).

†† The fine structure at large s-values is random noise, since the ratio of the reduced intensity $i(s)$ to the total scattering intensity is small.

shown in Fig. 3(b). The uppermost curve (I) is the inverse Fourtier transformation of the intramolecular contribution. Curve (n) in Fig. 3(b) represents the sum of curves (1), (2),$\cdots$(n) of Fig. 3(a) and curve (I). The fine structure indicated by the small arrows is in good agreement with the experimental intensity (Fig. 1), *e.g.*, the shoulder peak on the left side of the fourth halo, at $s \simeq 4$ Å^{-1}, appears due to the peaks at $r_0 = 6.3$ and 8.3 Å. The two small waves on the top of the third halo at $s \simeq 3.2$ Å^{-1} may be due to the scattering intensities corresponding to peaks at $r_0 = 16.3$ and 21.5 Å.

It has been concluded that the long-range correlation is not caused by experimental error nor by errors in the data analysis and this is supported by the following consideration. The electron radial distribution function, $4\pi r^2(\rho - \rho_0)$, computed using the intensity data obtained by Narten[7] shows a long-range correlation similar to Fig. 2. However, fine structure was not been observed in the intensity data. The fine structure represents "directly" that the molecules in the liquid phase have a long-range order in the arrangement. The presence of this fine structure had never been detected until the energy-dispersive method was applied to liquids in the present experiment.

Structure of Liquid CCl_4

The molecular arrangement in liquid CCl_4 was drawn on the basis of the following experimental results; (1) the small peak around 3.8 Å in the electron radial distribution function shows the nearest neighbor distance between chlorine atoms belonging to different molecules, and (2) the peaks with respect to the long-range correlation of molecular arrangement appear at integral multiples of about 5.7 Å, *i.e.* $r_0 = 11.4$, 16.3, and 21.5 Å. The peak at 3.8 Å is assigned to the Cl–Cl pair in the partial distribution function derived from X-ray and neutron diffractions by Narten.[7] That the peaks appear in equal intervals may show that CCl_4 molecules are arranged linearly. Consequently it is assumed that the three-fold axes of the CCl_4 molecules are linear. A chlorine atom of one molecule lies in the hollow formed by the three off-axis chlorine atoms of the other molecules. The distance between chlorine atoms belonging to different molecules is 3.8 Å, as shown in Fig. 4(a). Moreover, it is assumed that the average orientation is set in the eclipsed form for the chlorine atoms. In this arrangement, molecules form a body-centered cubic lattice, hereafter called a bcc cluster model. Since the nearest neighbor distance between chlorine atoms is 3.8 Å, the nearest neighbor distance referred to the molecular centers, *i.e.* the carbon atoms, is given by 5.77 Å and the second nearest neighbor distance is 6.77 Å, which corresponds to the lattice constant of the bcc lattice. Figure 4(b) shows the bcc cluster containing 15 CCl_4 molecules. The packing shown in Fig. 4(a) is similar to the "Apollo model" presented by Egelstaff *et al.*[9] They assumed that both molecules were freely oriented about the three-fold axes. However, neither the scattering intensity nor the distribution function was calculated for this model.

Of course, the liquid can never be the crystal. The

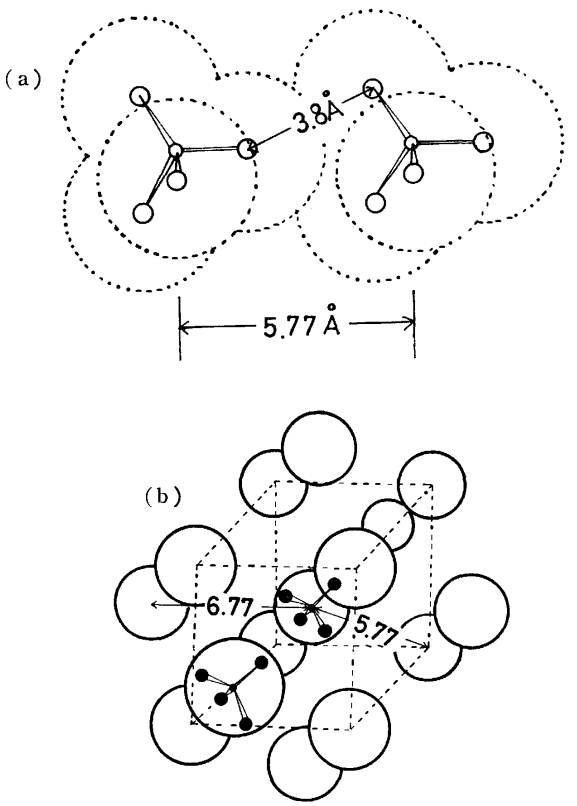

Fig. 4. (a) Packing model for liquid CCl_4. Small circles denote carbon atoms and large circles chlorine atoms. Van der Waals spheres of chlorine atoms are shown by dotted circles. (b) The bcc cluster model for liquid CCl_4 with 15 molecules. CCl_4 molecules are shown by circles. The orientation of all molecules is same as that described in the circles. The cube shown by broken lines forms the bcc unit cell.

molecule in the liquid phase lies around the equilibrium position, which forms the cluster. The cluster must have the same density as the actual liquid. We never mean that clusters with a density different from uniform medium exist actually—here "cluster" means a representation of the region where one molecule "feels" the "structure." The cluster is not rigid, but the structure becomes gradually loose as the molecules separate from the center of the cluster, *i.e.* the distance between molecules in the cluster is smeared as they are separated from each other. The smearing effect is treated with the increase of the root mean-square amplitude l_{ij} of the interatomic distance r_{ij}. The structure outside the cluster is a uniform medium.

The reduced intensity function may be computed from the equation,

$$i(s) = \frac{1}{N}\sum\sum_{i \neq j} f_i f_j \frac{\sin(sr_{ij})}{sr_{ij}} \exp(-l_{ij}^2 s^2/2) + i_c, \quad (4)$$

where N is the number of CCl_4 molecules contained in the cluster. In the cluster model, the first term series in Eq. 4 must be terminated at the end of the cluster. The second term in Eq. 4 complements a fault due to this termination. This correction corresponds to placing a uniform and structureless medium outside the cluster. This is depicted in Fig. 5. The sphere surrounded by

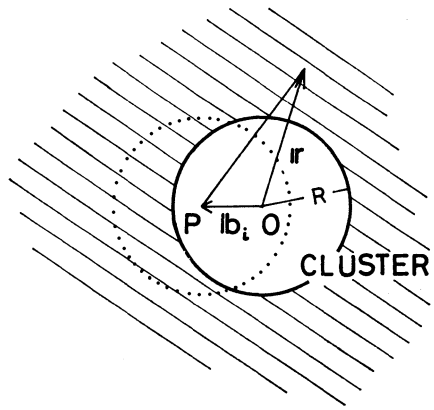

Fig. 5. A schematic illustration of the model used for the calculation of the correction term i_c in the reduced intensity $i(s)$.

the solid line is the cluster, in which the structure exists and the stripped region is the uniform medium. The continuous medium of the unit volume has a scattering factor $\langle F\rangle\rho_0$, where ρ_0 is the number density of CCl_4 in the liquid and $\langle F\rangle$ is the average scattering factor of CCl_4 in the continuous medium. The scattering intensity due to interference between the cluster and the continuous medium becomes,

$$i_c = \frac{1}{N}\sum_i\{f_i\langle F\rangle\rho_0 \exp(-l_i^2s^2/2)\int\exp(i(\boldsymbol{s}\cdot\boldsymbol{r}-\boldsymbol{b}_i))\mathrm{d}v_r\}, \quad (5)$$

where the origin is taken at the center of the cluster, $\boldsymbol{b}_i$ is the position vector of the i-th atom with a scattering factor f_i and l_i is the root mean-square amplitude of b_i. The integration in Eq. 5 is performed beyond the sphere of the cluster to infinity, that is over the stripped region of Fig. 5. The average scattering factor $\langle F\rangle$ is given by

$$\langle F\rangle = f_C + 4f_{Cl}\frac{\sin(sr_{C-Cl})}{sr_{C-Cl}}. \quad (6)$$

In Eq. 5 the atom around the periphery of the cluster effectively "feels" a much smaller cluster size than the atom at the center. On the other hand, the cluster means the representation of the region where one molecule "feels" the "structure." All molecules in the liquid must sit at the center of the cluster, when the second term of Eq. 4 is estimated. The surrounding of a molecule in a liquid is spherically symmetric except for near positions, and then the cluster radius R should be the same for all molecules. When the i-th atom is located at P (Fig. 5), the second term of Eq. 4 is integrated over the continuous medium beyond the dotted sphere. Therefore, it is reasonable to modify Eq. 5:

$$\begin{aligned} i_c &= \frac{1}{N}\sum_i f_i\langle F\rangle\rho_0\langle\exp(-is\cdot b_i)\rangle\exp(-l_i^2s^2/2) \\ &\quad\times\int_R^\infty\exp(is\cdot r)\mathrm{d}v_r \\ &= -\frac{1}{N}\sum_i f_i\langle F\rangle\rho_0\frac{\sin(sb_i)}{sb_i}\exp(-l_i^2s^2/2) \\ &\quad\times\frac{4\pi}{s^3}[\sin(sR)-sR\cos(sR)]. \end{aligned} \quad (7)$$

This equation is an extension of the formula derived by Warren.[10]

With a cluster radius R equal to 8.4 Å, the best agreement between the calculated and experimental intensities was obtained. This value, 8.4 Å, is reasonable, since the effective radius of the cluster containing 15 CCl_4 molecules, namely, the distance between the center of the cluster and the farthest chlorine atom is 8.54 Å. The weighted structure function, $si(s)$, with respect to the bcc cluster model with 15 CCl_4 molecules was calculated and is shown over the range from s=0—6

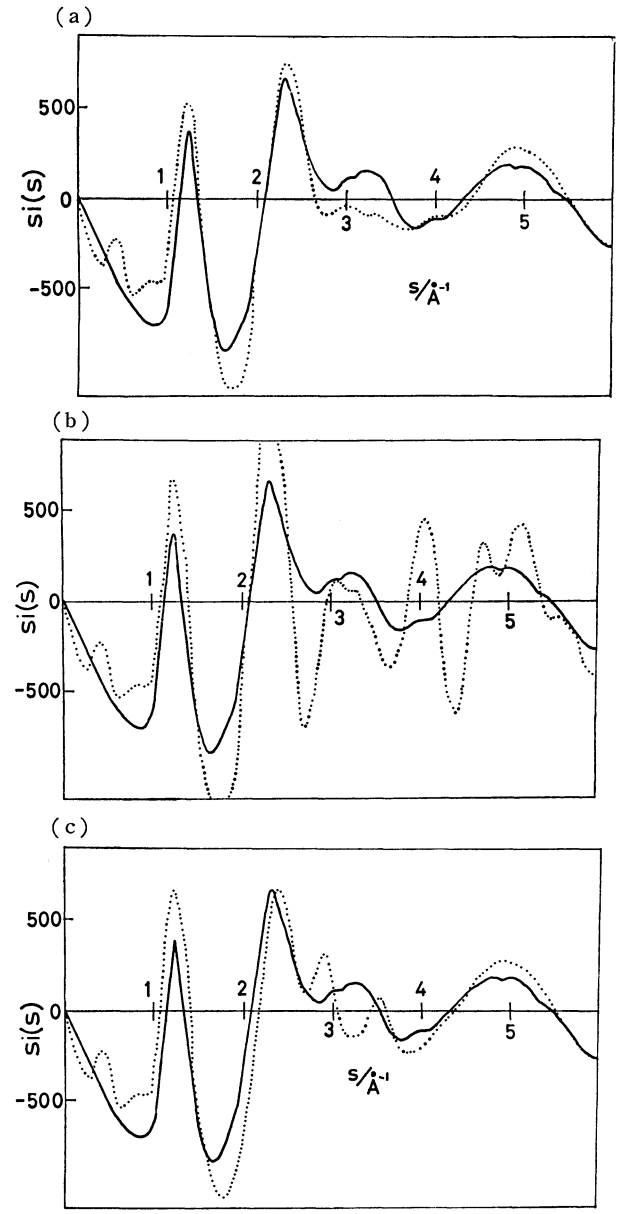

Fig. 6. Weighted structure function $si(s)$ for liquid CCl_4. (a) Solid line: experimental intensity. Dotted line: calculated intensity for the bcc cluster model with 15 CCl_4 molecules. (b) Solid line: experimental intensity. Dotted line: calculated intensity for the bcc cluster model neglecting the root mean square amplitude. (c) Solid line: experimental intensity. Dotted line: calculated intensity for the bcc model modified by the freely rotating molecules.

Table 2. Root mean-square amplitudes assumed for the calculated intensity of Figs. 6(a) and (c)

r_{ij}(Å)	l_{ij}(Å)
1.77 (C-Cl, intramolecule)	0.069
2.89 (Cl-Cl, intramolecule)	0.086
3—4	0.25
4—6	0.30
6—8	0.35
over 8	0.40

Å^{-1} in Fig. 6(a). The intensity curve in s-values larger than 6 Å^{-1} is almost the same as that of the free molecule of CCl_4. The full line is the observed intensity, and the dotted line shows the calculated intensity, where the root mean-square amplitude l_{ij} used is listed in Table 2. The fine structure on the fourth halo does not appear in the dotted line in Fig. 6(a). However, if the smearing effect is neglected, that is, l_{ij} is assumed to be zero in Eq. 4, the fine structure appears as shown in Fig. 6(b). The periodicity in the calculated intensity agrees well with the fine structure of the experimental intensity indicated by the full line. Therefore, the molecular arrangement of the bcc cluster explains the fine structure in the scattering intensity.

The dotted line in Fig. 6(c) corresponds to the bcc cluster model modified by the freely rotating molecules. In the model of the free rotation, the halo at 3.3 Å^{-1} splits into two peaks at 2.9 and 3.6 Å^{-1}, which differs from the experimental intensity. The possibility of a free rotation model is excluded by the distance between the nearest neighbor molecules, 5.77 Å, which is smaller than the van der Waals diameter of CCl_4, 7 Å. Consequently the barrier is too high for the molecule to rotate independently.

In the calculated intensity two small peaks appear at s=0.4 and 0.9 Å^{-1} as shown by the dotted line in Fig. 6(a) and this represents a discrepancy between the calculated and observed intensities. These peaks are, however, not significant. The intensity calculated by use of only the first term of Eq. 4 agrees well with the dotted line of Fig. 6(a) in the region of $s>1$ Å^{-1}. On the other hand, the second term of Eq. 4 dominates the region of s=0—1 Å^{-1}. In this region the weighted intensity curve without i_c has a strong peak, as shown by the solid line in Fig. 7. The dotted line in Fig. 7 shows the correction term, $-si_c$. These large values were subtracted in the calculation of the reduced intensity in the region of s=0—1 Å^{-1}.

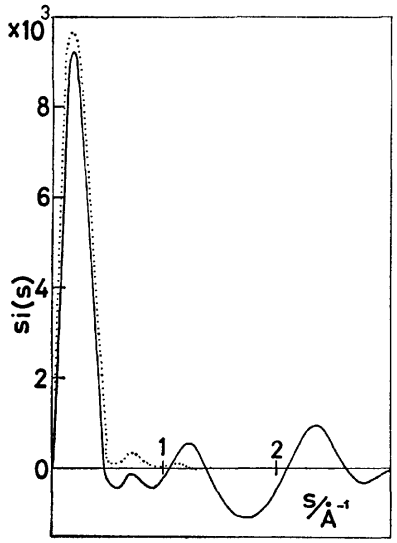

Fig. 7. The effect of the correction of Eq. 7. The full line is the weighted intensity neglecting the correction term i_c. The dotted line shows the correction term, $-si_c$.

The calculated intensity of the bcc cluster model is in good agreement with the observed intensity, not only in the main peaks at $s\simeq 1.2$ and 2.3 Å^{-1} but also in the fine structure around s=3—4 Å^{-1} (Fig. 6(a)). However disagreement in the intensity around s=3 Å^{-1} was observed. This discrepancy may be caused by the analysis, since it is difficult to derive the reduced intensity $i(s)$ from the total scattering intensity in this region.[1] Further possible source of the discrepancy may be the small cluster size and the large root mean-square amplitude assumed in this model.

In the present model, the peak in the radial distribution at 6.3 Å consists of two kinds of radial distances refering to the molecular centers, 5.77 and 6.77 Å, in which 8 and 6 molecules are contained, respectively. The equal interval in the peak in the radial distribution, *i.e.* 5.77, 11.4, 16.3, and 21.5 Å, is explained from the bcc cluster model.

The first and second nearest neighbor distances of the molecular center, 5.77 and 6.77 Å, happen to coincide with the model presented by Narten *et al.*,[5] as shown in Table 3 in spite of a different model. Narten *et al.* assumed at first the "crystal" of the space group Pa3,

Table 3. The distance between molecular centers r and the number of the pair n in the two models of liquid CCl_4

bcc cluster model		Pa3 model	
r(Å)	n	r(Å)	n
5.77	8	5.77	6
6.77	6	6.13	1
		6.77	6

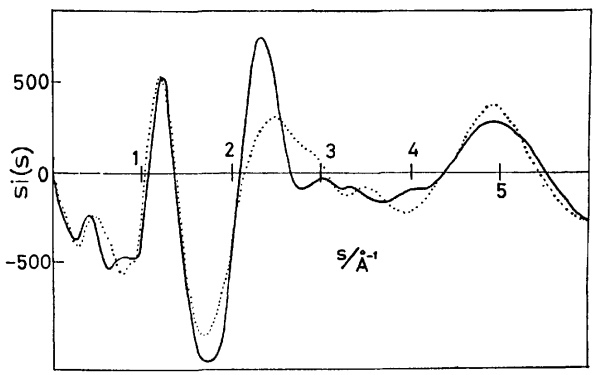

Fig. 8. Weighted structure function for liquid CCl_4. Solid line: bcc cluster model with 15 CCl_4 molecules. Dotted line: Pa3 model with 14 CCl_4 molecules.

which is the space group in the close-packing structure of Group IV halides *e.g.* SnI_4.[11] Next, the "ideal structure" was distorted by the least-squares fit to the observed diffraction data of the liquid. In order to compare the bcc cluster model with the distorted close-packing model, $si(s)$ of the close-packing model (Pa3 model) was calculated using Eq. 4 and the parameters given by Narten *et al.* The result is shown in Fig. 8 together with the intensity calculated from the bcc model. The agreement between both intensities fairly well in the positions of the main peaks, but differences exist in the region $s \simeq 2.5$—3.5 Å^{-1} and in the fine structure. Therefore, the long-range correlation demonstrated by the present study is important for estimating the liquid structure, and the measurements including the fine structure are necessary. For this purpose the energy-dispersive method is superior to the angle-dispersive one.

We are indebted to Prof. T. Iijima of Gakushuin University for helpful disscussions and reading of the manuscript. The present work was partially supported by Grant-in-Aid for Scientific Research from the Ministry of Education.

References

1) Y. Murata and K. Nishikawa, *Bull. Chem. Soc. Jpn.*, **51**, 411 (1978).
2) A. Eisenstein, *Phys. Rev.*, **63**, 304 (1943).
3) E. E. Bray and N. S. Gingrich, *J. Chem. Phys.*, **11**, 351 (1943).
4) R. W. Gruebel and G. T. Clayton, *J. Chem. Phys.*, **46**, 639 (1967).
5) A. H. Narten, M. D. Danford, and H. A. Levy, *J. Chem. Phys.*, **46**, 4875 (1967).
6) G. Reichelt, J. U. Weidner, and W. Zimmermann, *Ber. Bunsenges. Phys. Chem.*, **78**, 1050 (1974).
7) A. H. Narten, *J. Chem. Phys.*, **65**, 573 (1976).
8) Y. Morino, Y. Nakamura, and T. Iijima, *J. Chem. Phys.*, **32**, 643 (1960).
9) P. A. Egelstaff, D. I. Page, and J. G. Powles, *Mol. Phys.*, **20**, 881 (1971).
10) B. E. Warren, *Phy. Rev.*, **45**, 657 (1934).
11) F. Meller and I. Fankuchen, *Acta Crystallogr.*, **8**, 343 (1955).

The γ-Ray Induced Oxidation of Cyclohexene in the Liquid Dinitrogen Oxide at −18 °C

Shun-ichi HIROKAMI,† Laszlo WOJNAROVITS,†† and Shin SATO*

Department of Applied Physics, Tokyo Institute of Technology, Ookayama, Meguro-ku, Tokyo 152

(Received June 6, 1978)

The γ-radiolysis of a cyclohexene–dinitrogen oxide mixture in the liquid phase at −18 °C has been studied and the results compared with that of the radiolysis of a cyclohexene–carbon dioxide mixture in the liquid phase.[5] The oxidation reaction initiated by oxygen atoms produced in the direct radiolysis of dinitrogen oxide or carbon dioxide is common for both solutions, the products being cyclohexene oxide, cylohexanone, and cyclopentanecarbaldehyde. In the dinitrogen oxide solution, however, two other oxidation processes have to be considered in order to interpret the material balance of products and the formation of other oxygenated compounds: cyclohexanol, 2-cyclohexenol, and 2-cyclohexenone. A possible reaction mechanism is discussed.

Recently the liquid phase γ-radiolysis of the carbon dioxide solution of hydrocarbons has been extensively investigated.[1–6] It is now believed that the liquid phase γ-radiolysis of carbon dioxide provides a conventional source of oxygen atoms. However, in this system, the formation of a small amount of cyclohexanol with a G-value of 0.2 has been observed under optimum conditions. This compound has not been observed in the gas phase reaction of oxygen atoms with cyclohexene. There has been much speculation on the precursor of cyclohexanol, one of which is the O^- ion.

Dinitrogen oxide is a well-known electron scavenger, widely used in radiation chemistry and O^- or N_2O^- ions are believed to be formed by electron scavenging.[7] Since dinitrogen oxide, like carbon dioxide, is a good solvent for hydrocarbon, the γ-radiolysis of a cyclohexene–dinitrogen oxide mixture at −18 °C has been studied and compared with the results obtained with a carbon dioxide solution.[5]

Experimental

The experimental procedure is the same as that described in a previous paper.[5] Impurities in cyclohexene (Tokyo Kasei Co.) were less than 0.5%, estimated by gas chromatography with a 2-m PEG-600 column of 20% w/w on celite. Dinitrogen oxide (Takachiho Shoji Co.) contained no detectable impurities, confirmed by gas chromatography with a 5 m dimethyl sulfolane column of 20% w/w on celite. In order to calculate the G-value, the absorbed dose was estimated by Fricke dosimetry assuming a proportionality between the absorbed dose and the electron density of the solution.

Results

The G-values of the noncondensable products, nitrogen and hydrogen, are shown in Fig. 1 as a function of the electron fraction ε of N_2O. The result is similar to that of the radiolysis of mixtures of various hydrocarbons and dinitrogen oxide.[1,8]

Figure 2 shows the G-values of cyclohexene oxide, cyclohexanone, and cyclopentanecarbaldehyde. In the γ-radiolysis of a cyclohexene–CO_2 mixture, the three products were explained in terms of the addition reaction of oxygen atoms to cyclohexene. The electron fraction dependence of G(cyclohexene oxide) in Fig. 2 is very similar to that obtained with a cyclohexene–CO_2 mixture;[5] however, G(cyclohexanone) deviates from the

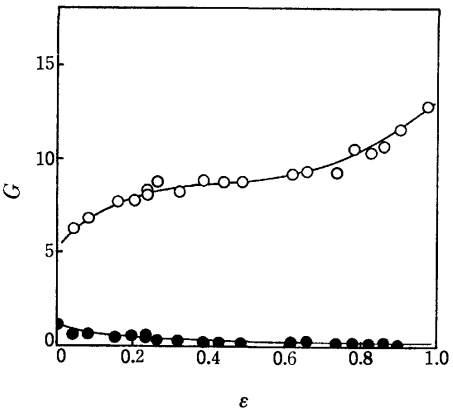

Fig. 1. The G-values of nitrogen (○) and hydrogen (●) from a cyclohexene–dinitrogen oxide mixture as a function of the electron fraction ε of dinitrogen oxide.

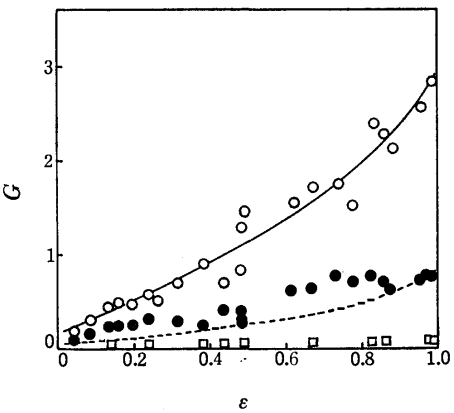

Fig. 2. The G-values of cyclohexene oxide (○), cyclohexanone (●), and cyclopentanecarbaldehyde (□) as a function of the electron fraction of dinitrogen oxide. The dashed curve was drawn by assuming G(cyclohexanone)/G(cyclohexene oxide+cyclohexanone)=0.2, the ratio which was obtained in the radiolysis of a cyclohexene–carbon dioxide mixture.

† Present address: Faculty of Pharmaceutical Sciences, Toyama Medical and Pharmaceutical University, Sugitani, Toyama 930-01.

†† Present address: Institute of Isotopes of the Hungarian Academy of Sciences, H-1525, Budapest, P. O. B. 77.

curve drawn on the assumption that G(cyclohexanone)/G(cyclohexene oxide+cyclohexanone)=0.2, the ratio obtained in the γ-radiolysis of a cyclohexene–CO_2 mixture. The deviation suggests that there is another process for the formation of cyclohexanone.

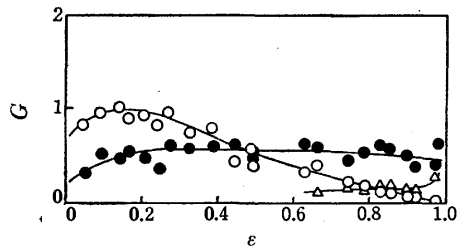

Fig. 3. The G-values of cyclohexanol (○), 2-cyclohexenol (●), and 2-cyclohexenone (△) as a function of the electron fraction of dinitrogen oxide.

Figure 3 shows the G-values of other oxygen containing compounds: cyclohexanol, 2-cyclohexenol, and 2-cyclohexenone, the yields of which were very small in the radiolysis of the carbon dioxide solution.

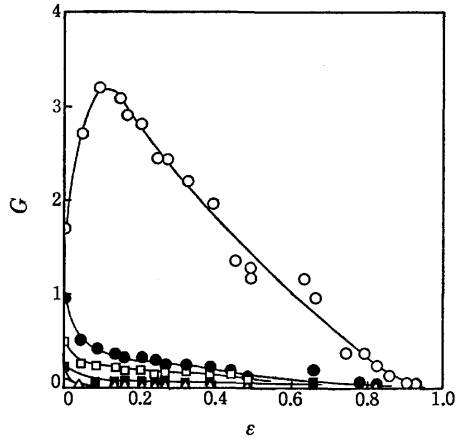

Fig. 4. The G-values of bi(2-cyclohexenyl) (○), cyclohexane (●), 2-cyclohexenylcyclohexane (□), bicyclohexyl (■), and 2-cyclohexenyl-1-cyclohexene (△) as a function of the electron fraction of dinitrogen oxide.

Figure 4 shows the G-values of hydrocarbon products. Bi(2-cyclohexenyl) shows a peculiar dependence on the electron fraction of N_2O; at low concentration of N_2O, the G-value increases with increase in the electron fraction of N_2O until it reaches a maximum at ε=0.1 after which it decreases.

Discussion

Oxygen Atom Reactions. The dependence of G(cyclohexene oxide) on the electron fraction of N_2O (Fig. 2) is similar to that for the G-value of this compound on the electron fraction of CO_2 obtained in the γ-radiolysis of a cyclohexene–CO_2 mixture. On the other hand, cyclohexene oxide is known to be one of the main products in the gas phase reaction of oxygen atoms with cyclohexene.[5] The formation of cyclohexene oxide in the present experiment, therefore, may be ascribed to the reaction of oxygen atoms produced in the direct radiolysis of N_2O with cyclohexene.

$$N_2O \rightsquigarrow N_2 + O \quad (1)$$

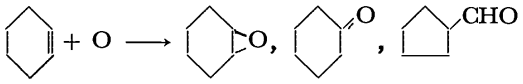

(2)

Cyclopentanecarbaldehyde is a minor product among the three compounds.

At high electron fractions, above 0.6, of N_2O, a slight deviation is observed from the linearity between G-(cyclohexene oxide) and ε. This deviation may be due to another process for the formation of oxygen atoms which is interrupted by the presence of cyclohexene:

$$N_2O^+ + N_2O^- \longrightarrow N_2 + O + N_2O, \quad (3)$$

$$N_2O^+ + \text{cyclo-}C_6H_{10} \longrightarrow N_2O + \text{cyclo-}C_6H_{10}^+. \quad (4)$$

A similar process has been discussed in the case of the cyclohexene–CO_2 mixture.[5]

Reactions of N_2O^- (or O^-) Ions. Dinitrogen oxide is a well-known scavenger. Nitrogen molecules are produced as the consequence of electron scavenging. However, the detailed mechanism for the formation of nitrogen has not been established.[9–11]

According to the discussion of Wakeford and Freeman,[12] the main reactions initiated by ionization in the γ-radiolysis of cyclohexene may be described as follows:

$$\text{cyclo-}C_6H_{10} \longrightarrow \text{cyclo-}C_6H_{10}^+ + e^- \quad (5)$$

$$\text{cyclo-}C_6H_{10}^+ + e^- \longrightarrow \cdot + H \quad (6)$$

$$H + \text{cyclo-}C_6H_{10} \longrightarrow \cdot \quad (7)$$

$$2 \cdot \longrightarrow \quad (8)$$

$$\longrightarrow + \quad (9)$$

$$\cdot + \cdot \longrightarrow \quad (10)$$

$$\longrightarrow + \quad (11)$$

$$2 \cdot \longrightarrow \quad (12)$$

$$\longrightarrow + \quad (13)$$

When a small amount of N_2O is present in this system, N_2O interrupts the neutralization reaction. According to the mechanism proposed by Sambrook and Freeman for the radiolysis of hydrocarbons containing N_2O,[8] the succeeding reactions may be written as follows:

$$e^- + N_2O \longrightarrow N_2O^- \text{ (or } N_2 + O^-) \quad (14)$$

$$N_2O^- + \text{cyclo-}C_6H_{10} \longrightarrow N_2 + OH^- + \cdot \quad (15)$$

$$OH^- + \text{cyclo-}C_6H_{10}^+ \longrightarrow H_2O + \text{C}_6\text{H}_9\cdot \quad (16)$$

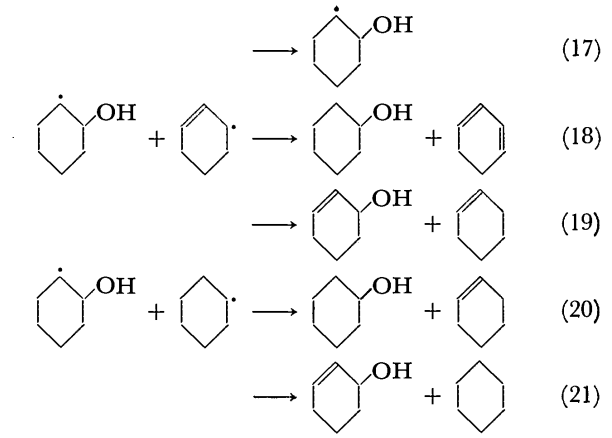

(17)–(21)

The increase of G(bi(2-cyclohexenyl)) and the decrease in G-values of other hydrocarbon products upon addition of N_2O can be explained by this reaction mechanism. However, the increase of $G(N_2)$ with the increase in ε is too great to be explained by the above mechanism.[10] The neutralization reaction which does not lead to the formation of any products,

$$\text{cyclo-}C_6H_{10}^+ + e^- \longrightarrow \text{cyclo-}C_6H_{10}, \quad (22)$$

may play an important role in the present reaction system. The fraction of the neutralization reaction not leading to the formation of any products has not been determined even in the radiolysis of cyclohexane for which numerous studies have been published. There is some evidence to show that this fraction is negligibly small.[13]

When ε is larger than 0.1, N_2O suppresses the formation of bi(2-cyclohexenyl) (Fig. 4). This suggests that the N_2O^- or O^- ions are reactive to N_2O molecules. For this reaction, two processes are energetically possible;[9]

$$N_2O^- + N_2O \longrightarrow N_2 + NO + NO^-, \quad (23)$$

$$\longrightarrow 2N_2 + O_2^-. \quad (24)$$

In mass spectrometry,[14] Reaction 23 is the main process and if the same is true here, then the G-value of the electrons from cyclohexene should be of the order of $G(N_2)$; *i.e.*, about 5—7, since one nitrogen molecule corresponds to one electron captured by N_2O. On the other hand, if Reaction 24 is the main process, the G-value of the electrons should be in the range 2.5—3.5. The latter value is consistent with the W-value obtained in the gas phase,[15] Reaction 22 not being necessarily involved in the reaction mechanism. From the present experiment it is impossible to determine which Reaction, 23 or 24, is more dominant. However, in order to explain the deviation of G(cyclohexanone) from the dashed curve (Fig. 2), Reaction 24 has been tentatively used as follows:

$$\text{cyclo-}C_6H_{10}^+ + O_2^- \longrightarrow \text{C}_6\text{H}_9\cdot + HO_2\cdot \quad (25)$$

$$\text{C}_6\text{H}_9\cdot + HO_2\cdot + C_6H_{10} \longrightarrow \text{C}_6\text{H}_9\text{OH} + \text{C}_6\text{H}_8\text{O} \quad (26)$$

At present, no completely self-consistent reaction scheme for the formation of all oxygen containing products can be proposed.

Material Balance. Since the origin of oxygen atoms in the present system is dinitrogen oxide, the G-value of nitrogen should be equal to the sum of the G-values of oxygen containing products. However, the observed G-value of oxygen containing products does not reach 20% of the G-value of nitrogen. Sambrook and Freeman suggested that most of the oxygen containing product is water.[8] The G-value of water in the present experiment could not be measured because of experimental difficulties. However, if the rest of the oxygen containing products is water, hydrocarbon products such as bi(2-cyclohexenyl) should not decrease with an increase in ε, since two hydrogen atoms in water molecule should be supplied from cyclohexene. No material balance was given by Sambrook and Freeman for hydrocarbon products in their experiments.

In conclusion, the γ-ray induced oxidation of cyclohexene in liquid dinitrogen oxide occurs through three processes. The precursor in the first process is the oxygen atom produced by the direct radiolysis of dinitrogen oxide. The second process proceeds by the reaction of N_2O^- or O^- ions, produced by the electron scavenging of the N_2O molecule. The third process is not clear; the precursor may be produced in the reaction of N_2O^- or O^- ions with N_2O. It might be O_2^- ions.

References

1) S. Sato, K. Hosoya, S. Shishido, and S. Hirokami, *Bull. Chem. Soc. Jpn.*, **45**, 2308 (1972).
2) K. Ishizaki and S. Sato, *Chem. Lett.*, **1975**, 123.
3) H. Sakurai, K. Akimoto, S. Toki, and S. Takamuku, *Chem. Lett.*, **1975**, 469.
4) A. Hori, S. Takamuku, and H. Sakurai, *J. Chem. Soc., Chem. Commun.*, **1976**, 686.
5) L. Wojnarovits, S. Hirokami, and S. Sato, *Bull. Chem. Soc. Jpn.*, **49**, 2956 (1976).
6) A. Hori, S. Takamuku, and H. Sakurai, *J. Org. Chem.*, **42**, 2318 (1977).
7) S. Sato, R. Yugeta, K. Shinsaka, and T. Terao, *Bull. Chem. Soc. Jpn.*, **39**, 156 (1966).
8) T. E. M. Sambrook and G. R. Freeman, *J. Phys. Chem.*, **78**, 32 (1974).
9) J. M. Warman, K.-D. Asmus, and R. H. Schuler, *Adv. Chem. Ser.*, **82**, 25 (1968).
10) Y. Hatano, K. Takeuchi, and S. Takao, *J. Phys. Chem.*, **77**, 586 (1973).
11) G. R. Freeman and T. E. M. Sambrook, *J. Phys. Chem.*, **78**, 102 (1974).
12) B. R. Wakeford and G. R. Freeman, *J. Phys. Chem.*, **68**, 2635 (1964).
13) H. Karasawa, E.-R. Kim, and S. Sato, *Bull. Chem. Soc. Jpn.*, **50**, 1670 (1977).
14) P. J. Chantry, *J. Chem. Phys.*, **51**, 3380 (1969).
15) L. M. Hunter and R. H. Johnsen, *J. Phys. Chem.*, **71**, 3228 (1967).

A Kinetic Study of the Simultaneous Dealkylation and Disproportionation of Cumene over Silica-Alumina[1]

Jun-ichiro TAKE,* Yoichi TOZAWA, and Yukio YONEDA

Department of Synthetic Chemistry, Faculty of Engineering, The University of Tokyo, Hongo, Bunkyo-ku, Tokyo 113

(Received June 8, 1978)

Cumene has been passed over a silica–alumina bed at low temperature (210 to 254 °C) and at cumene pressures of 0.003 to 0.023 atm. Both dealkylation and disproportionation occurred simultaneously and independently of each other. The disproportionation/dealkylation ratio increased with decrease in temperature and/or an increase in cumene pressure. The dealkylation and disproportionation reactions followed a Langmuir-Hinshelwood model with inhibition by the reactant. The dealkylation has been interpreted in terms of a unimolecular surface reaction, while the disproportionation reaction in terms of a bimolecular surface reaction. The heat of adsorption of cumene and the entropy loss of cumene on adsorption were much larger for the dealkylation sites than for the disproportionation sites. These results indicated that dealkylation was catalyzed by strong acid sites, while disproportionation by weak acid sites. The dealkylation had a much higher activation energy than the disproportionation reaction. The activation energy for dealkylation (33.5 kcal mol^{-1}) was in good agreement with that predicted on the assumption that the previously reported LFER (linear free-energy relationship) in the alcohol dehydration holds for alkylbenzene dealkylation.

The catalytic dealkylation of cumene has been employed as a standard test for characterizing acidic cracking catalysts. The kinetics have been investigated in detail at high temperatures (above 300 °C) by Prater and Lago,[2] Horton and Maatman,[3] and Wojciechowski and coworkers.[4,5] Under the conditions where the reverse reaction is negligible, the accepted kinetic scheme of this reaction is

$$C + S \rightleftharpoons CS \longrightarrow \text{products}, \quad (1)$$

where C represents cumene, S, an active site, and CS, cumene adsorbed on an active site. It has been shown that the bond-breaking step, CS→products, is the rate-determining step.[2,6,7]

Cumen is known to undergo disproportionation to benzene and diisopropylbenzenes in the presence of a Friedel-Crafts catalyst.[8,9] Therefore, under favorable conditions, cumene disproportionation may take place on acidic cracking catalysts. However, little attention has been paid hitherto to this reaction over acidic cracking catalysts. The present study intends to obtain kinetic data on the nature of the active sites for cumene dealkylation and disproportionation, as well as about the nature of the two reactions, under the conditions where both reactions take place simultaneously.

Recently, it has been reported that the activation energy for the bond-breaking step in the catalytic dehydration of alkanols (ROH) on silica–alumina has a linear relationship with the heterolytic bond dissociation energy for the C–O bond in alcohols, $D(R^+OH^-)$.[10] Mochida and Yoneda[7] reported that the apparent activation energy for the dealkylation of monoalkylbenzenes (RPh, where R=alkyl and Ph=phenyl) over silica–alumina had a linear relationship with the enthalpy change of the hydride abstraction from the corresponding paraffin, $\Delta H_c^+(R)$. This enthalpy change, in its turn, linearly correlates with $D(R^+Ph^-)$ for RPh. Therefore, the present study also intends to establish whether the LFER (linear free-energy relationship) obtained in the alcohol dehydration holds in the catalytic dealkylation of monoalkylbenzenes.

Experimental

Materials. The silica–alumina (SA-1, 13% Al_2O_3) was obtained from the same source.[6,7,10] Cumene of GR grade from Tokyo Kasei was percolated through two columns packed with silica gel and active alumina, and stored over a mixture of active alumina and Molecular Sieve 4A under nitrogen. Gas-chromatographic analysis of the cumene indicated a purity of 99.2 mol%; the impurities were *m*- and *p*-xylenes which did not affect the reactions to any detectable extent. Hydrogen, used as a diluent gas, was purified by passing it through a Deoxo column and then a Dry Ice–ethanol temperature trap.

Apparatus and Procedures. Experiments were conducted in a continuous flow-type reactor, the details of which have been given in a previous paper.[10] Catalyst charges of 0.19—0.26 g were used depending mainly on the reaction temperature. The catalyst was activated in a hydrogen stream with a flow rate of 40 STP ml min^{-1} for 2 h at 450 °C. The temperature was then lowered to the reaction temperature (210—254 °C) and additional hydrogen was admitted from another inlet. After the total flow rate of hydrogen had been adjusted to about 300 STP ml min^{-1}, cumene was introduced from a microfeeder. The desired partial pressure was attained about 30 min later.

Subsequently, a portion of the effluent gas was led through a 6-way sampling-valve to a gas-liquid chromatograph with a flame ionizing detector for analysis at intervals of 5—10 min. An analysing column of Silicone DC-11 (2-m long) was used at 140 °C. In some experiments, a column of VZ-7 (6-m long) was also used at 0 °C for analysis of lighter hydrocarbon products.

A total of five kinetic runs were made at 210—254 °C. In each run lasting for 7—8 h at constant temperature, the run was divided into several periods in which the partial pressure of cumene was altered over the range of 0.003—0.023 atm (by changing the feed rate). Each period lasted for 60—80 min, including an initial 30 min period for the attainment of steady-state conditions (no samples taken). In the subsequent period of 30—50 min, the effluent gas was analysed at least four times.

Treatment of Data. A plot of the cumene conversion to each product against the reciprocal space velocity was linear through the origin in the region of total conversion below 8%, indicating that the differential-reactor conditions were met.

Since the total conversion of cumene was kept below this level in all runs, the rate of formation of the i product, v_i, was calculated by

$$v_i = x_i F/W, \quad (2)$$

where x_i is the fractional conversion to the i product, F, the feed rate of cumene (mol min^{-1}) and W, the catalyst weight(g).

Slow catalyst aging occurred during the run, necessitating correction of the data on a common basis. The bracketing sequence of Sinfelt[11] was adopted for this purpose: periods at a chosen standard condition were repeated between periods at other conditions. The rates of formation of the dealkylation and disproportionation products were plotted separately as a function of run time. Smooth curves were drawn through the data of the standard periods to obtain the aging curves. Intermediate run periods were then corrected to a common reference time using the following relationships, since the aging curves were linear as will be stated below:

$$\alpha = (v_r^s - v_t^s)/v_r^s,$$
$$v_r = v_t/(1-\alpha),$$

where α is the degree of catalyst aging, v_r^s and v_t^s, the reaction rates for standard conditions at reference time r and another time t, respectively, and v_r and v_t, the reaction rates for other conditions at times r and t, respectively.

Sample analyses in each period consistently gave the same product composition, implying that the catalyst aging was negligible in that period. Therefore, each period was represented by the reaction rates and run time averaged over that period. Typical plots of the rates of formation as a function of run time are presented in Fig. 1. Other temperature conditions gave a similar catalyst aging pattern, indicating that the catalyst activity declined slowly and linearly with increasing run time. The standard periods were operated at a cumene pressure of 0.003—0.004 atm. The reference time was t/min= 50 in Fig. 1.

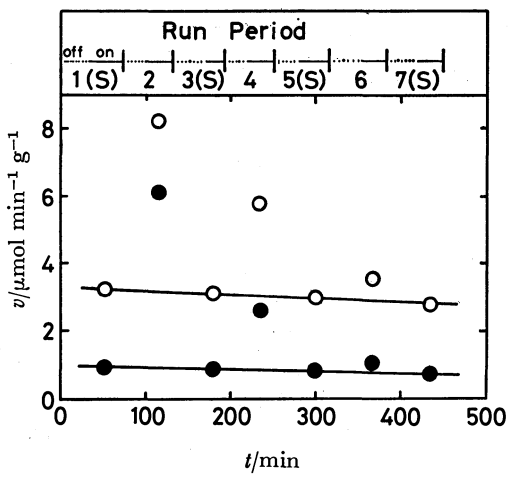

Fig. 1. Catalyst aging for run at 220 °C.
○ and ● denote the rates of dealkylation and disproportionation, respectively, (s), the standard period.

Results

Diffusion Effects. The mass transfer effects were assessed by running at constant partial pressure (0.023 atm) and temperature (250 °C) and by varying the total flow rate of the diluent gas over the range of 100 to 400 STP ml min^{-1}. The reaction rates for dealkylation and disproportionation did not change when the total flow rate was higher than 180 STP ml min^{-1}, indicating that the external diffusion effects were negligible under such conditions. The diluent gas has therefore been passed at a flow rate of about 300 STP ml min^{-1} in all kinetic runs.

The internal diffusion effects have been examined using the Weisz formula,[12]

$$\Phi = \frac{dN}{dt}\frac{1}{C_0}\frac{R^2}{D_{eff}},$$

where dN/dt is the reaction rate in mol s^{-1} cm^{-3}, C_0, the reactant concentration in mol cm^{-3}, R, the catalyst particle radius in cm, and D_{eff}, the effective diffusion constant in cm^2 s^{-1}. In the present study, the limits for these coefficients are as follows: $dN/dt = 5\times10^{-7}$ mol s^{-1} cm^{-3} as the total reaction rate of cumene, $C_0 = 1\times10^{-7}$ mol cm^{-3}, $R = 5\times10^{-3}$ cm, and $D_{eff} = 10^{-3}$ cm^2 s^{-1} for the system of silica–alumina and cumene.[12] These values give a Φ of 1.3×10^{-1}, from which the effectiveness factor is evaluated to be very close to 1 for zero- to second-order reactions.[12] Consequently, the internal diffusion effects on the reaction rates have been concluded to be negligible.

Table 1. Product composition from cumene on silica–alumina

t °C	p[a] atm	Molar ratios of products[b,c] P	DPB	P+DPB	B	DPB/P
210	0.02	0.59	0.39	0.98	1.00	0.66
230	0.02	0.70	0.33	1.03	1.00	0.47
254	0.02	0.80	0.19	0.99	1.00	0.24
254	0.01	0.85	0.12	0.97	1.00	0.14

a) Cumene partial pressure. b) P=propene, DPB=*m*- and *p*-diisopropylbenzenes, B=benzene. c) Normalized to benzene=1.00.

Reaction Products. The reaction products were propene (P), benzene (B), and *m*- and *p*-diisopropylbenzenes (DPB); *o*-diisopropylbenzene was not formed to any detectable extent. Table 1 presents typical data on the product composition. Other temperature and partial pressure conditions gave a similar product composition. On the basis of these data, the following points emerge: (a) propene is consistently smaller in the amount of formation than benzene, indicating reactions other than dealkylation, (b) the amount of propene plus diisopropylbenzenes is equal to that of benzene, (c) the DPB/P ratio changes depending upon the temperature and cumene pressure, *i.e.*, the lower-temperature and/or higher-cumene pressure conditions favor the formation of diisopropylbenzenes.

The formation of propene undoubtedly results from the dealkylation of cumene. The possible reactions which form diisopropylbenzenes are the disproportionation of cumene, the alkylation of cumene with propene, and the alkylation of benzene with propene. The existence of one of the three reactions, in addition to that of dealkylation, accounts for observation (b), P+DPB=B. As mentioned in Experimental, a plot of the cumene conversion to each product against the residence time

was linear through the origin, indicating that the two isomers of diisopropylbenzene are primary products. Therefore, the last two of the three reactions are unimportant for the formation of diisopropylbenzenes under these experimental conditions. The rates of formation of diisopropylbenzenes and propene thus give the rates of disproportionation, v_D, and dealkylation, v_C, respectively. In some experiments, the difference in the amounts of benzene and propene was taken as the amount of diisopropylbenzenes formed. The ratio of the meta to the para isomers was 1.3—1.6 for all runs.

Kinetics. The rate data were first subjected to a simple power low rate equation. The plots of log v_C and log v_D *versus* log p(cumene pressure) indicated that the kinetic expressions were more complex than a simple first- or second-order reaction.

Subsequently, the data was analysed using the Langmuir-Hinshelwood theory. Best fits were found when dealkylation was assumed to be controlled by a single-site surface reaction, namely,

$$v_C = \frac{k_C K_C p}{1+K_C p}, \quad (3)$$

and disproportionation by a dual-site surface reaction,

$$v_D = k_D\left(\frac{K_D p}{1+K_D p}\right)^2, \quad (4)$$

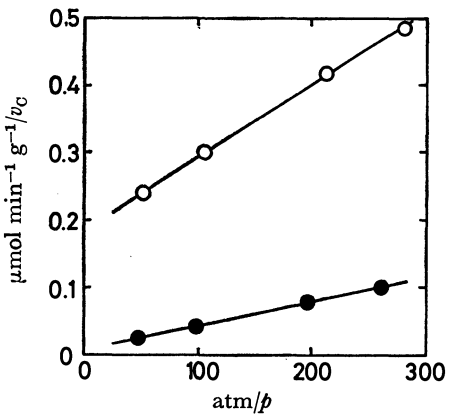

Fig. 2. Correlation of dealkylation rates with Eq. 3.
○: 210 °C, ●: 254 °C.

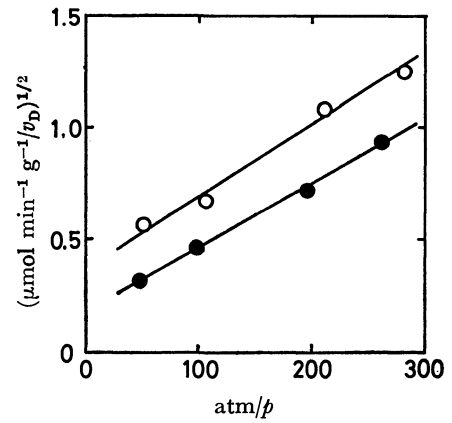

Fig. 3. Correlation of disproportionation rates with Eq. 4.
○: 210 °C, ●: 254 °C.

TABLE 2. RATE AND ADSORPTION-EQUILIBRIUM CONSTANTS FOR CUMENE DEALKYLATION AND DISPROPORTIONATION

t / °C	Dealkylation k_C / μmol min⁻¹ g⁻¹	Dealkylation K_C / atm⁻¹	Disproportionation k_D / μmol min⁻¹ g⁻¹	Disproportionation K_D / atm⁻¹
210	5.33	175	7.31	114
220	12.7	93.5	12.7	88.9
230	20.4	84.0	16.6	79.0
240	40.6	54.0	25.0	71.4
254	105	27.4	39.1	53.3

where k_C and k_D are the rate constants for dealkylation and disproportionation, respectively, K_C and K_D, the adsorption equilibrium constants of cumene for the dealkylation and disproportionation sites, respectively. Figures 2 and 3 show typical plots for these equations. The proposed fit to the equations is good and the values for the rate and adsorption-equilibrium constants obtained from each plot are given in Table 2. The plots of log k and log K *versus* $1/T$ were ideally linear. The activation energies (E_A), the pre-exponential factors (A), the heats of adsorption (Q_a), and the entropies of adsorption (ΔS_a) were calculated from the plots, the results of which are included in Table 3.

TABLE 3. ARRHENIUS PARAMETERS, HEATS OF ADSORPTION, AND ENTROPIES OF ADSORPTION FOR CUMENE DEALKYLATION AND DISPROPORTIONATION[a)]

	Dealkylation	Disproportionation
E_A/kcal mol⁻¹	33.5	19.4
log (A/μmol min⁻¹ g⁻¹)	15.9	9.67
Q_a/kcal mol⁻¹	20.1	8.1
ΔS_a/cal K⁻¹ mol⁻¹	−31.4	−7.4

a) E_A is the activation energy, A, the pre-exponential factor, Q_a and ΔS_a, the heat and entropy of adsorption, respectively.

Discussion

The Nature of the Dealkylation, Disproportionation, and Active Sites. The kinetic model which best correlates the rate data on the dealkylation at low temperatures is identical with that which has generally been accepted for the same reaction at higher temperatures (Eq. 1). This implies that the low-temperature dealkylation of cumene is rate-determined by a unimolecular surface reaction of cumene adsorbed on an active site. The disproportionation of cumene has kinetically been shown to be rate-determined by a bimolecular surface reaction of the adjacent, absorbed molecules of cumene. The cumene disproportionation is therefore the same in the kinetic model as the disproportionation of toluene[13)] and mesitylene[14)] over acidic solid catalysts. The reactions are clearly different from each other in the number of cumene molecules which participate in the respective rate-determining steps. This difference gives rise to an increase of the disproportionation/dealkylation ratio with an increase in the partial pressure of cumene. In addition, the dealkylation has a higher activation energy

than the disproportionation, as shown in Table 3 and the disproportionation/dealkylation ratio, therefore, decreases steeply with increase in temperature (Table 1).

For the dealkylation, the adsorbed cumene has generally been supposed to be a σ-complex with the proton attached at the substituted position. Accordingly, the rate-determining step in the kinetic model corresponds to a break of the C(phenyl)–C(isopropyl) bond in the σ-complex. Previous LFER studies on the dealkylation of monoalkylbenzenes[6,7] has shown that bond-breaking in the rate-determining step is heterolytic. The alkylbenzene disproportionation in the presence of Friedel-Crafts catalysts has been accepted as rate-determined by the nucleophilic attack of an arene on an arene cation.[8,9,15] The nature of the arene cation does not seem to have been established: a σ-complex[8] of the same type as proposed for the alkylbenzene dealkylation and a π-complex[9] have been suggested; a benzyl cation has also been proposed for the disproportionation of primary alkylbenzenes.[15]

Since the adsorption equilibrium constant measures the strength of the interactions of an adsorbing molecule with an active site, the nature of active sites should be reflected in the constant. If the dealkylation and disproportionation occurred, respectively, *via* a unimolecular and a bimolecular reaction of the surface species present on the same active sites, the same adsorption equilibrium constant would kinetically be observed for the two reactions. The data in Table 2 clearly shows that the adsorption equilibrium constants for the two reactions are different in magnitude. This difference in the adsorption equilibrium constant is emphasized by the data in Table 3, where the Q_a and ΔS_a values are clearly different for the two reactions. The heat of adsorption of cumene is notably smaller for the disproportionation sites than for the dealkylation sites. These results, therefore, indicate that the active sites differ in nature, probably in acidic nature. Dealkylation is catalyzed by strong acid sites, while disproportionation by weak acid sites.

The difference in the heat of adsorption also suggests that the surface species on the disproportionation sites are more mobile than those on the dealkylation sites and this is confirmed by a comparison of the entropy data in Table 3. As shown, cumene in the gas phase has an entropy loss of about 31 cal K^{-1} mol^{-1} when it is adsorbed on the dealkylation sites, while the entropy loss markedly decreases when cumene is adsorbed on the disproportionation sites. An entropy loss of 31 cal K^{-1} mol^{-1} is comparable to that for immobile adsorption, which has been estimated to be 39 cal K^{-1} mol^{-1} under the present experimental conditions.[16] It has therefore been deduced that cumene molecules adsorbed on the disproportionation sites are, probably, relatively free on the surface. This viewpoint is in line with the nature of the disproportionation reaction, since a bimolecular surface reaction necessitates mobile adsorbed molecules.

Finally, it must be said that the correct kinetics for disproportionation were not obtained assuming the following two possible mechanism: a Rediel-type mechanism with the rate-determining step involving reaction between an adsorbed cumene molecule and another cumene molecule in the gas phase, a Langmuir-Hinshelwood mechanism with the rate-determining step in which a cumene molecule chemisorbed on the dealkylation site reacts with another cumene molecule chemisorbed on the adjacent site which differs in nature from the dealkylation sites.

Activation Energy for Dealkylation. Recently, it has been found that, in the catalytic dehydration of alkanols over silica–alumina, the activation energy for the bond-breaking step has a linear relationship with the heterolytic bond dissociation energy for the C–O bond in the alcohols, $D(R^+OH^-)$.[10] The activation energy for the bond-breaking step in the cumene dealkylation has consequently been determined. The silica–alumina catalyst used for both dehydration and dealkylation was from the same batch and was activated in the same way. The alcohol dehydration and the alkylbenzene dealkylation belong to an olefin-forming elimination reaction catalyzed by acids. Therefore, it is necessary to establish whether the LFER obtained in the alcohol dehydration holds in the alkylbenzene dealkylation. The $D(R^+Ph^-)$ value for cumene has been calculated to be 220 kcal mol^{-1} using the reported values for the standard heats of formation of cumene, the isopropyl cation, and the phenyl anion, as shown in Table 4. This $D(R^+Ph^-)$ value is equal in magnitude to the $D(R^+OH^-)$ value for *s*-butyl alcohol. The assumption that the LFER in the alcohol dehydration holds in the alkylbenzene dealkylation predicts an activation energy of 32 kcal mol^{-1} for the bond-breaking step in the cumene dealkylation. The predicted value is very close to the observed one (33.5 kcal mol^{-1}, Table 3).

Table 4. Heterolytic bond dissociation energy and related thermodynamic quantities[a]

R	$\Delta H^\circ_f(R^+)$[b] / kcal mol^{-1}	$\Delta H^\circ_f(RPh)$[c] / kcal mol^{-1}	$D(R^+Ph^-)$[d] / kcal mol^{-1}
Et	219.0	7.12	241
n-Pr	207.8	1.87	235
i-Pr	191.7	0.94	220
n-Bu	200.7	−3.30	233
i-Bu	198.7	−5.15	233
s-Bu	183.3	−4.17	216
t-Bu	166.6	−5.42	201
$\Delta H^\circ_f(Ph^-)$[e]/kcal mol^{-1} = 29.0			

a) ΔH°_f is the standard heat of formation, D, the heterolytic bond dissociation energy, EA, the electron affinity, Et=ethyl; Pr=propyl; Bu=butyl; Ph=phenyl. b) See Ref. 10 and references cited therein. c) D. S. Stull, E. F. Westrum, Jr., and G. C. Sinke, "Chemical Thermodynamics of Organic Compounds," John Wiley & Sons, New York (1969). d) Calculated according to $D(R^+Ph^-) = \Delta H^\circ_f(R^+) + \Delta H^\circ_f(Ph^-) - \Delta H^\circ_f(RPh)$. e) Calculated according to $\Delta H^\circ_f(Ph^-) = \Delta H^\circ_f(Ph) - EA(Ph)$ using $\Delta H^\circ_f(Ph)$/kcal mol^{-1} = 80.0[f] and $EA(Ph)$/kcal mol^{-1} = 51.0.[g] f) D. M. Golden and S. W. Benson, *Chem. Rev.*, **69**, 125 (1969). g) A. F. Gaines and F. M. Page, *Trans. Faraday Soc.*, **59**, 1266 (1963).

The apparent activation energies for the monoalkylbenzene dealkylation have been reported by Mochida

and Yoneda,[7] under the conditions where the reaction was nearly first-order in the reactant using silica–alumina taken from the same batch as used in the present work. The numerical values of the apparent activation energies reported in Ref. 7 are as follow (in kcal mol^{-1}): 17 ± 4 (ethylbenzene); 14.5 ± 2 (propylbenzene); 14.5 ± 1.5 (butylbenzene); 11 ± 3.5 (cumene); 11 ± 2 (*s*-butylbenzene); 10 ± 1 (*t*-butylbenzene). The assumption[6] that the heat of adsorption is approximately the same for all the alkylbenzenes used has been used here. Using the observed value for the heat of adsorption of cumene on the dealkylation sites (Table 3), the activation energies for the zero-order dealkylation, namely, for the bond-breaking step in the dealkylation may be calculated as the sum of the apparent activation energies and the heat of adsorption of cumene. The calculated values and the values predicted from the LFER in the alcohol dehydration and the $D(R^+Ph^-)$ values shown in Table 4 are (given in kcal mol^{-1} as the calculated, the predicted): 37 ± 4, 37 (ethylbenzene); 35 ± 2, 35 (propylbenzene); 35 ± 1.5, 35 (butylbenzene); 31 ± 3.5, 32 (cumene); 31 ± 2, 31 (*s*-butylbenzene); 30 ± 1, 28 (*t*-butylbenzene). The activation energy calculated for the cumene dealkylation is in good agreement with that observed in the present study. Also, the agreement between the calculated and the predicted values is excellent for all the alkylbenzenes used, though the equality in the heat of adsorption has been assumed as above. Therefore, it is likely that the LFER observed in the alcohol dehydration holds, at least approximately, in the alkylbenzene dealkylation, as shown in Fig. 4.

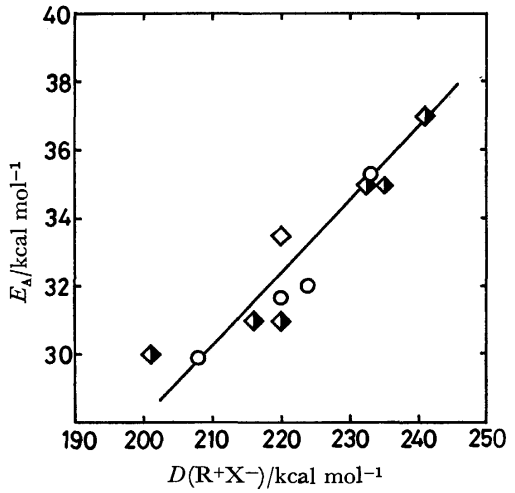

Fig. 4. Correlation of activation energies for alcohol-dehydration and alkylbenzene-dealkylation over silica–alumina with heterolytic bond dissociation energies for the C–X bond. ○: Alcohol-dehydration;[10] ◇ and ◆: observed and calculated activation energies, respectively, for alkylbenzene-dealkylation (see text).

References

1) A preliminary report of this work was presented at the 30th National Meeting of the Chemical Society of Japan, Osaka, April 1974.
2) C. D. Prater and R. M. Lago, *Adv. Catal.*, **8**, 293 (1956).
3) W. B. Horton and R. W. Maatman, *J. Catal.*, **3**, 113 (1964).
4) D. R. Campbell and B. W. Wojciechowski, *J. Catal.*, **20**, 217 (1971).
5) D. A. Best and B. W. Wojciechowski, *J. Catal.*, **31**, 74 (1973).
6) I. Mochida and Y. Yoneda, *J. Catal.*, **7**, 386 (1967).
7) I. Mochida and Y. Yoneda, *J. Catal.*, **8**, 223 (1967).
8) D. A. McCaulay and A. P. Lien, *J. Am. Chem. Soc.*, **75**, 2411 (1953).
9) H. C. Brown and C. R. Smoot, *J. Am. Chem. Soc.*, **78**, 2176 (1956).
10) J. Take, T. Matsumoto, and Y. Yoneda, *Bull. Chem. Soc. Jpn.*, **51**, 1612 (1978).
11) J. H. Sinfelt, *Chem. Eng. Sci.*, **23**, 1181 (1968).
12) P. B. Weisz, *Z. Phys. Chem. (NF)*, **11**, 1 (1957).
13) Y. Izumi and T. Shiba, *Bull. Chem. Soc. Jpn.*, **37**, 1797 (1964).
14) C. W. Pukanic and F. E. Massoth, *J. Catal.*, **28**, 304 (1973).
15) A. Streitwieser, Jr., and L. Reif, *J. Am. Chem. Soc.*, **82**, 5003 (1960).
16) C. Kemball, *Adv. Catal.*, **2**, 233 (1950).

NQR and NMR Studies of Boron Trihalide-Trimethylamine Complexes

Tsutomu OKUDA,* Hideta ISHIHARA, Koji YAMADA, and Hisao NEGITA
Department of Chemistry, Faculty of Science, Hiroshima University, Hiroshima 730
(Received June 9, 1978)

The character of the B–X bond (X=Cl, Br, and I) in BX_3–TMA complexes (TMA=trimethylamine) has been studied on the basis of the results of the nuclear quadrupole resonance (NQR). The ionic character of the B–X bond decreased in the order as expected from the electronegativity of the halogen atoms. The temperature dependence of the halogens on the NQR frequencies has been examined for BBr_3– and BI_3–TMA. For BBr_3–TMA, all the observed resonance lines faded out far below the melting point and this has been attributed to the hindered rotation of the BBr_3 group about the B–N bond, as with BCl_3–TMA.

The crystal structure of BX_3–TMA complexes has been recently determined by X-ray analysis[1] and the atomic arrangement about the boron atom is shown to be approximately tetrahedral and that the B–N bond distance decreases with increasing atomic weight of the halogen atom. It is of interest to examine the character of the B–X and B–N bonds in these complexes. Furthermore, for BCl_3–TMA, the reorientation of the methyl and trimethylammonio groups is known to affect the temperature dependence of the ^{35}Cl NQR frequencies[2] and consequently a study of the temperature dependence of the NQR frequencies for BBr_3– and BI_3–TMA will elucidate dynamic properties of the crystals.

Experimental

BCl_3 and BBr_3 were prepared by heating a mixture of potassium tetrafluoroborate with aluminum(III) chloride or bromide, respectively, up to 140—170 °C.[3] BI_3 was prepared from sodium hydroborate and iodine according to the method of Schumb *et al.*[4] The complexes BCl_3– and BBr_3–TMA were prepared by the dropwise addition of a dichloromethane solution of BX_3 to a dichloromethane solution of TMA under dry nitrogen. For the complex BI_3–TMA, a similar procedure was conducted using benzene as a solvent. BCl_3– and BBr_3–TMA were recrystallized from ethanol and BI_3–TMA from benzene. The compound obtained was dried in a vaccum desiccator. The elemental analyses of these complexes agreed well with theoretical values. Found: C, 20.47; H, 5.26; N, 7.75%. Calcd for $C_3H_9NBCl_3$: C, 20.44; H, 5.14; N, 7.94%. Found: C, 11.86; H, 3.01; N, 4.56%. Calcd for $C_3H_9NBBr_3$: C, 11.64; H, 2.93; N, 4.52%. Found: C, 7.96; H, 2.05; N, 3.09%. Calcd for $C_3H_9NBI_3$: C, 8.00; H, 2.01; N, 3.10%.

NQR spectra were observed on an oscilloscope using a super-regenerative oscillator with frequency modulation. NMR were observed using a broad line NMR spectrometer, JES-ME 1 from JEOL Co., Ltd.

Results and Discussion

NQR of BX_3–TMA. The NQR frequencies of boron trihalides and their complexes are listed in Table 1. Each NQR line for BBr_3, BI_3, and their complexes was split into a doublet by the boron isotope, ^{10}B and ^{11}B.[6] However, the frequencies are listed only for the halogen atoms linked to the ^{11}B atom. Each complex has two resonance lines with an intensity ratio of 1 to 2 and this is consistent with the X-ray analysis.[1] The weaker resonance line in each complex is due to the halogen atom on the symmetry plane and the stronger to the two halogen atoms symmetrically located with respect to this plane.

It has been established that the B–X bond in BX_3 has a considerably large double bond character.[5,6] When BX_3 forms a complex with TMA, the BX_3 molecule is deformed from a planar to a pyramidal configuration. As a direct consequence most of the double bond character of the B–X bond is lost *i.e.*, the asymmetry parameter of the halogen atoms becomes very small as shown in BI_3–TMA. For ^{35}Cl and ^{81}Br atoms, the quadrupole coupling constant, e^2Qq/h, is obtained from the equation,

$$\nu = (1/2)(e^2Qq/h)(1+\eta^2/3)^{1/2}, \quad (1)$$

where ν is the resonance frequency and η the asymmetry parameter. For BCl_3– and BBr_3–TMA, the asymmetry parameter has been assumed to be zero. For ^{127}I atom,

Table 1. NQR parameters at 77 K

Compound	Nucleus	Frequency(MHz)	Intensity ratio	η	e^2Qq/h (MHz)
BCl_3[a]	^{35}Cl	21.582		0.54	41.208
BCl_3–TMA[b]	^{35}Cl	21.532	1		43.064
		21.779	2		43.558
BBr_3[c]	^{81}Br	146.43		0.45	283.45
BBr_3–TMA	^{81}Br	144.28	1		288.56
		147.20	2		294.40
BI_3	^{127}I	ν_1 214.00		0.453	1186.3
		ν_2 342.95			
BI_3–TMA	^{127}I	ν_1 186.65	2	0.066	1238.4
		ν_2 371.19			
		ν_1 190.48	1	0.066	1263.9
		ν_2 378.84			

a) Ref. 5. b) Ref. 2. c) Ref. 6.

the quadrupole coupling constant and asymmetry parameter can be derived from the frequency ratio, ν_1/ν_2 (ν_1 and ν_2 are the frequencies corresponding to the $\pm1/2\leftrightarrow\pm3/2$ and $\pm3/2\leftrightarrow\pm5/2$ transitions, respectively). The quadrupole coupling constants thus obtained are listed in Table 1.

The Character of the B–X Bond. The amount of the unbalanced p-electron, U_p, is given by[7]

$$U_p = |e^2Qq/e^2Qq_0|, \quad (2)$$

where e^2Qq_0/h is the quadrupole coupling constant for the free halogen atom (−109.746, 643.032, and −2292.712 MHz for ^{35}Cl, ^{81}Br, and ^{127}I, respectively). Assuming that the B–X bond is represented by the resonance between B–X, $B^-{=}X^+$, and B^+X^-, U_p is then related to the ionic character, i, and the double bond character, f, expressed by[6,8]

$$U_p = (1-i)(1-s)-(f/2)\{1-(1-2s)\varepsilon\}, \quad (3)$$

where s is the fractional s character of the B–X bond and ε the correction for the increase in field gradient attributed to the positive fractional charge at the halogen atom.[8] In addition, the double bond character is related to the asymmetry parameter expressed by

$$\eta = (3/2)f(1+\varepsilon)/U_p. \quad (4)$$

Thus, U_p, i, and f can be deduced from Eqs. 2—4, by selecting s=0.15 and ε to be 0.14, 0.13, and 0.12 for Cl, Br, and I, respectively,[9] the results of which are listed in Table 2.

TABLE 2. THE NATURE OF THE B–X BOND

Compound	U_p	i(%)	f(%)
BCl_3	0.376	50	12
BCl_3–TMA[a)]	0.395	54	0
BBr_3	0.441	42	12
BBr_3–TMA[a)]	0.455	47	0
BI_3	0.517	32	14
BI_3–TMA[a)]	0.544	35	2

a) For each complex, the weighted-mean value of the two resonance lines is listed.

In each complex, U_p is greater than that of the halogens in BX_3 caused largely by the loss of double bond character upon complex formation. In addition, the ionic character of the complexes decreases in the order, chloride>bromide>iodide which is consistent considering the electronegativity of the halogen atoms.

Attempts to obtain the quadrupole coupling constant of the ^{11}B atom at 13 MHz in each complex gave neither first-order nor second-order splitting. The quadrupole coupling constant of the ^{11}B atom in each complex was however estimated to be less than 500 kHz from the line-width of the polycrystalline sample. This value was far less than *ca.* 2.5 MHz for BX_3.[10] Consequently, in the complex, the B–N bond and the three B–X bonds are arranged almost tetrahedrally and thus each bond may be regarded as equivalent.

The Temperature Dependence of the NQR Frequencies. For BCl_3–TMA, it has been established that the reorientation of the methyl and trimethylammonio groups affects the ^{35}Cl NQR line, *i.e.*, the temperature coefficient of the NQR frequency varied at 100 and 204 K, respectively.[2] A similar phenomenon was however not observed for both BBr_3– and BI_3–TMA.

For BBr_3–TMA, the resonance lines faded out in the noise level at about 285 K, which far below the melting point, 511 K, as seen for BCl_3–TMA. The resonance lines became increasingly broad from 260 K, although the accurate evaluation of line-widths could not be made, since each NQR line was a doublet. The disappearance of the NQR line may be caused by the hindered rotation of the BBr_3 group. It is known that the activation energies of the reorientation of trimethylammonio group in BCl_3– and BBr_3–TMA are greater than those of BH_3– and BF_3–TMA.[11] This suggests that in BCl_3– and BBr_3–TMA, the molecule rotates as a whole, that is, the triemethylammonio and BX_3 groups do not rotate independently. For BBr_3–TMA, the frequency of this motion or the rotation of the BBr_3 group reaches 10^4—10^5 Hz in the vicinity of 285 K and approaches the NQR frequency.[12] Therefore, rotation of the BBr_3 group or the whole molecule is thought to induce broadening of NQR lines. Moreover, at a particular rate of rotation, averaging of the field gradient will occur along the axis of rotation reducing the NQR frequency to[13]

$$\nu_T = \nu_Q(3\cos^2\theta-1)/2, \quad (5)$$

where ν_T is the averaged NQR frequency, ν_Q the NQR frequency of the stationary molecule, and θ the angle between the B–Br bond and the axis of rotation. An attempt to observe the resonance lines above room temperature however was unsuccessful.

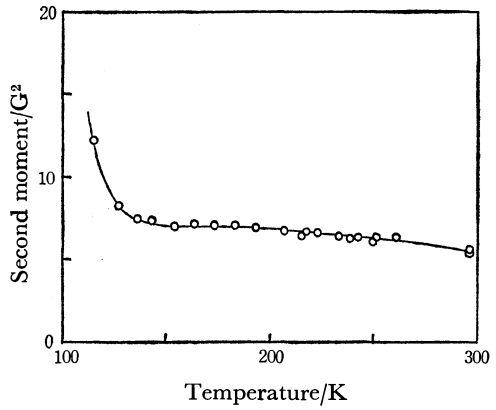

Fig. 1. Temperature dependence of the second moment of ^1H NMR spectrum for BI_3–TMA.

TABLE 3. CALCULATED SECOND MOMENTS FOR BI_3–TMA

Group		Second moment (G^2)
CH_3	$N(CH_3)_3$	
Static	Static	28.6
Rotating	Static	9.7
Rotating	Rotating	1.6

For BI_3–TMA, the resonance lines could be observed up to 353 K at which time the sample began to turn brown. For this complex, the second moment of ^1H NMR spectrum was approx. 7.5 G^2 from 113 to 300 K

as shown in Fig. 1. The theoretical second moment was calculated on the basis of the crystal structure[1] based on the same assumptions for the hydrogen position as for Ref. 11, the results of which are listed in Table 3. The reorientation of the trimethylammonio group is not expected in this temperature range, from a comparison of the observed with the calculated values.

References

1) P. H. Clippard, J. C. Hanson, and R. C. Taylor, *J. Cryst. Mol. Struct.*, **1**, 363 (1971).
2) D. F. R. Gilson and R. M. Hart, *Can. J. Chem.*, **48**, 1976 (1970).
3) E. L. Gamble, *Inorg. Synth.*, **3**, 27 (1950).
4) W. C. Schumb, E. L. Gamble, and M. D. Banus, *J. Am. Chem. Soc.*, **71**, 3225 (1949).
5) J. A. S. Smith and D. A. Tong, *J. Chem. Soc., A*, **1971**, 173.
6) T. Chiba, *J. Phys. Soc. Jpn.*, **13**, 860 (1958).
7) C. H. Townes and A. L. Schawlow, "Microwave Spectroscopy," McGraw-Hill, New York (1955), Chap. 9.
8) E. A. C. Lucken, "Nuclear Quadrupole Coupling Constants," Academic Press, London and New York (1969), Chap. 7.
9) B. P. Dailey and C. H. Townes, *J. Chem. Phys.*, **23**, 118 (1956).
10) P. A. Casabella and T. Oja, *J. Chem. Phys.*, **50**, 4814 (1969).
11) C. T. Yim and D. F. R. Gilson, *Can. J. Chem.*, **48**, 515 (1970).
12) T. T. Ang and B. A. Dunell, *Can. J. Chem.*, **52**, 1840 (1974).
13) R. Sh. Lotfullin and G. K. Semin, "Advances in Nuclear Quadrupole Resonance," ed by J. A. S. Smith, Heyden, London (1977), Vol. 2, p. 1.

Magnetic Studies on Basic Salts of Copper, Dicopper Arsenate Hydroxide, Dicopper Hydroxide Phosphate, and Dicopper Oxide Sulfate

Takeshi Asai,* Hiroshi Saheki,† and Ryôiti Kiriyama††

The Institute of Scientific and Industrial Research, Osaka University, Yamadakami, Suita 565

(Received June 10, 1978)

Magnetic susceptibilities, χ, of $Cu_2AsO_4(OH)$, $Cu_2(OH)PO_4$, and Cu_2OSO_4 have been measured from 4.2 to 360 K to establish the role of the OH^- and O^{2-} ions in the magnetic superexchange interaction. The former two compounds showed a broad maximum for χ at 118 and 110 K, respectively. Although the crystal structure is three-dimensional, only a tetramer model with two parameters can explain the temperature dependence of χ, since the hydroxide anion causes a strong magnetic interaction which is limited to four copper atoms between which the anion is intermediary. The magnetic susceptibility of Cu_2OSO_4 obeyed the Curie-Weiss law above 140 K with a Weiss constant of -56 K. At 16 K the compound transformed into a ferrimagnetic phase, the effective megneton number of which is 0.11 at 4.2 K. A canted ferrimagnetic structure has been proposed and the canting angle estimated. In the superexchange interaction, only hydroxide and oxide anions are significant and both anions behave similarly.

Copper oxide compounds are a group of substances whose magnetic behavior has been widely studied. The magnetic properties of many oxoacid copper salts have also drawn much interest and have been examined theoretically and magnetochemically. However, little work has been published on hydroxide compounds. Escoffier and Gauthier published the Curie and the Weiss constants for 15 basic copper salts.[1] Diot *et al.* studied copper hydroxide and found its transition to an antiferromagnetic phase at about 20 K from measurements of magnetic susceptibility and specific heat.[2] Abrahams *et al.* reported that $CuIO_3(OH)$ showed signs of a phase transition into an antiferromagnetic state at 162 K.[3] Hatfield and coworkers found a linear relationship between the exchange energy $2J$ and the bridging angle of the OH^- anion for a series of di-μ-hydroxo-copper(II) complexes.[4] The observed correlation was explained quantitatively[5] as well as qualitatively[6] by means of MO's. All experiments indicated that the hydroxide anion has the potential to bring about a stronger magnetic interaction between copper(II) spins.

In order to elucidate the superexchange interaction *via* the hydroxide anion, the magnetic susceptibilities of three basic salts of copper, $Cu_2AsO_4(OH)$, $Cu_2(OH)PO_4$, and Cu_2OSO_4, have been measured from 4.2 to 360 K. The compounds have similar chemical compositions, and contain, as a common structural feature,[7,8] a trigonal bipyramid and an octahedron of oxygen atoms around a central copper atom. They were chosen as a suitable series of compounds to establish the magnetic behavior of the hydroxide and the oxide anions.

Experimental

Preparation. Samples of $Cu_2AsO_4(OH)$ and $Cu_2(OH)PO_4$ were prepared hydrothermally at 130—140 °C[9] and identified by X-ray diffraction.[7] Dicopper oxide sulfate, Cu_2OSO_4, was obtained by the thermal decomposition of $CuSO_4 \cdot 5H_2O$ at 650 °C over 10 h.[10] During this process the reacting material was removed from the furnace, ground and re-heated several times. This technique was found necessary because, otherwise, the decomposition reaction proceeded only at the reagent surface owing to sintering of the product, Cu_2OSO_4, resulting in a mixture of $CuSO_4$, Cu_2OSO_4, and CuO. The product was identified by powder X-ray diffraction.[8] The reagent used are of superpure grade (Wako Pure Chemical Industries, Ltd.). Found: Cu, 44.89; As, 26.03%. Calcd for $Cu_2AsO_4(OH)$: Cu, 44.90; As, 26.47%. Found: Cu, 53.00; P, 12.88%. Calcd for $Cu_2(OH)PO_4$: Cu, 53.16; P, 12.96%.

Magnetic Measurements. The magnetic susceptibility was measured from 4.2 to 360K using powder samples. A Faraday balance was employed and calibrated for $CoHg(SCN)_4$.[11] Susceptibility values were corrected for diamagnetism; the values were -1.18, -1.02, and -0.93 mm^3 mol^{-1} for the arsenate, phosphate, and sulfate, respectively.[12] The temperature of the sample was measured by a calibrated 0.03% Co: Au or constantan *vs.* Cu thermocouple.

Results and Discussion

Crystal Structures.[7,8] The crystal structures of $Cu_2(OH)PO_4$ and Cu_2OSO_4 are projected in Fig. 1. As a common structural feature, they contain two kinds of oxygen polyhedra coordinating to the copper atoms; a trigonal bipyramid and an octahedron. In this paper the center of the trigonal bipyramid will be designated

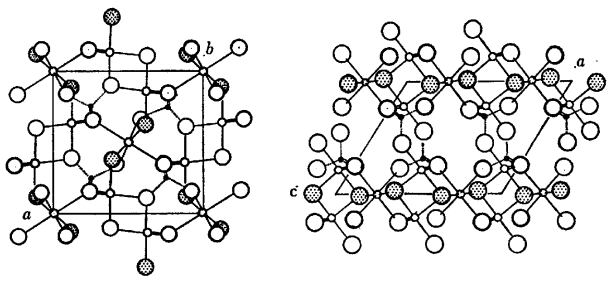

Fig. 1. Projection of the crystal structures of (a) $Cu_2(OH)PO_4$ and (b) Cu_2OSO_4. Symbols are Cu: middle circle, O: large circle and P or S: small solid circle. Oxygen atoms belonging to the hydroxide or the oxide anions are shaded. The octahedron in $Cu_2(OH)PO_4$ has the diad axis along the c axis, while that in Cu_2OSO_4 has a center of symmetry. They form a linear chain perpendicular to the projection plane.

† Present address: Mitsui Aluminum Co., Ltd., 80 Yotsuyama-cho, Omuta 836.

†† Emeritus professor of Osaka University.

as site A and that of the octahedron as site B. The octahedron shares two opposite edges with two neighboring octahedra to form a linear chain. The two trigonal bipyramids constitute a dimer by sharing an edge. The dimeric unit, the linear chain of the octahedra, and the anion tetrahedra share corners thereby forming a three-dimensional network.

An oxide anion has the tendency to form tetrahedral bonds with four metallic cations.[13] Consequently, the oxide anion in Cu_2OSO_4 can occupy the position which lies on the shared edge of the linear chain and simultaneously on that of the dimer. The dimeric unit connects two linear chains by the oxide anions. Since other oxygen corners of the dimer are shared with the same linear chains, the two kinds of coordination polyhedra construct a two-dimensional network. This network is joined with neighboring ones only by the tetrahedra of an SO_4^{2-} anion, and as a result, each copper atom has 5 or 6 copper neighbors through the intermediate oxide anions.

In contrast, the hydroxide anion can make bonds with, at most, three metal atoms.[14] This limitation brings about a remarkable difference in the manner of linkage of the polyhedra between $Cu_2(OH)PO_4$ and Cu_2OSO_4. The hydroxide anion in $Cu_2(OH)PO_4$ lies on a shared edge of the linear chain, but in the dimer it is located on a corner not belonging to the shared edge. The dimer joins two linear chains by the hydroxide anions and two more chains by other oxygen atoms. In this case, therefore, a three-dimensional network is built of the coordination polyhedra, independent of the phosphate tetrahedra. Also in the phosphate the copper atom has 5 or 6 copper neighbors, two or three of which are connected with the copper atoms by the hydroxide anions.

The crystal structure of $Cu_2AsO_4(OH)$ is isomorphous with that of $Cu_2(OH)PO_4$.[15] The phosphate, however, belongs to the space group Pnnm and the arsenate to $P2_1nm$,[16] a subgroup of Pnnm, and so it appears necessary to take into account some deformation of the coordination polyhedra in $Cu_2AsO_4(OH)$.

Magnetic Properties of $Cu_2AsO_4(OH)$ and $Cu_2(OH)PO_4$. The magnetic susceptibilities, χV_m, of $Cu_2AsO_4(OH)$ and $Cu_2(OH)PO_4$ have been plotted as a function of temperature in Figs. 2 and 3. The two compounds exhibit a similar temperature dependence on χV_m; a broad maximum around 110 K accompanied by a large decrease below that temperature. The sharp increase of χV_m with decreasing temperature below 10 K has been attributed to paramagnetic impurities. There was, however, a distinct difference between the maximum susceptibilities, $\chi_{max} V_m$, for the arsenate and the phosphate, which were 39.8 and 49.7 $mm^3\,mol^{-1}$, respectively. The temperature, T_{max}, at which the susceptibility is a maximum, was 118 K for $Cu_2AsO_4(OH)$ and 110 K for $Cu_2(OH)PO_4$. Such large values of T_{max} indicate that the magnetic interaction between copper(II) spins is very strong in these compounds. Since the two values of T_{max} are similar, the large difference in $\chi_{max} V_m$ has been attributed to differences in the magnetic interaction and the g-factor.

The susceptibility obeyed the Curie-Weiss law, $\chi V_m = C/(T-\theta)$, above 200 K. However, in the course of the analysis given below, the temperature of measurement was found so low that only formal values of the Curie and the Weiss constants were obtained.

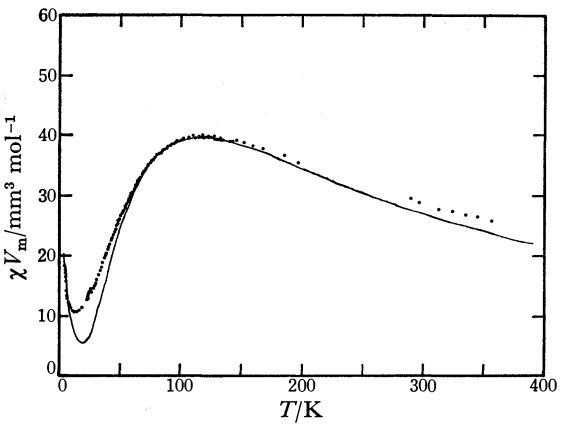

Fig. 2. Temperature dependence of the magnetic susceptibility of $Cu_2AsO_4(OH)$. The solid line shows the calculated susceptibility for the tetramer model with parameters of $g=2.02$, $J=-68$ K and $J'/J=-3.0$ plus a contribution from paramagnetic impurities.

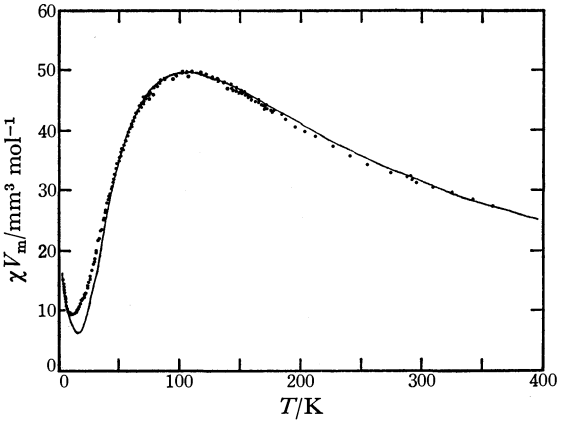

Fig. 3. Temperature dependence of the magnetic susceptibility of $Cu_2(OH)PO_4$. The solid line shows the calculated susceptibility for the tetramer model with parameters of $g=2.16$, $J=-62$ K and $J'/J=-2.4$ plus a contribution from paramagnetic impurities.

Several magnetic models have been tested in order to investigate the magnetic interaction in these hydroxide compounds. However, since the susceptibility below T_{max} decreases significantly, only cluster models containing an even number of copper(II) spins are admissible. Furthermore, the possible models has been confined to the following two cases taking into account the symmetry relationship between the copper atoms.

(1) The tetramer model in which two copper atoms at site A and two at site B are connected by two hydroxide anions as depicted in Fig. 4. The interaction energy for this spin system may be written as follows:

$$H = -2J(\boldsymbol{S}_1\boldsymbol{S}_2+\boldsymbol{S}_2\boldsymbol{S}_3+\boldsymbol{S}_3\boldsymbol{S}_4+\boldsymbol{S}_4\boldsymbol{S}_1)-2J'(\boldsymbol{S}_1\boldsymbol{S}_3). \quad (1)$$

Solving the equation for the case of $S=1/2$ for all spins, the magnetic susceptibility is given by Eq. 2:[17]

$$\chi V_m = \frac{Lg^2\mu_B^2}{kT} \times \frac{\exp(x)+\exp(2x-x')+\exp(2x)+5\exp(3x)}{1+3\exp(x)+4\exp(2x-x')+3\exp(2x)+5\exp(3x)}, \quad (2)$$

where $x=2J/kT$ and $x'=2J'/kT$.[18]

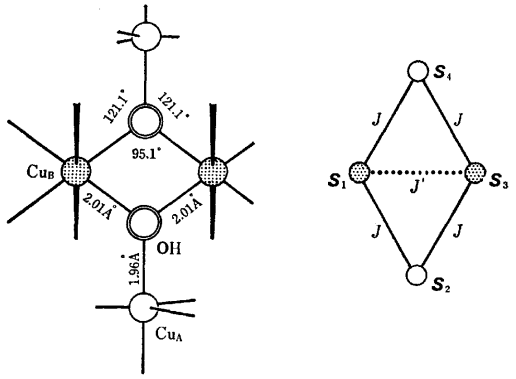

Fig. 4. Schematic drawing of the tetramer unit (left), and interaction scheme in it (right). The unit has a point symmetry of C_{2h} with the diad axis passing through the Cu_B atoms.

(2) Two kinds of dimers. One of the dimers is composed of two copper atoms on site A and the other on site B. The susceptibility for this system is obtained by adding the two Bleaney-Bowers equations with the respective values for the g-factor and J.[17,18]

$$\chi V_m = (L\mu_B^2/3kT)\sum_{i=A,B} g_i^2\left[1+\frac{1}{3}\exp(-2J_i/kT)\right]^{-1} \quad (3)$$

The former model gave good agreement between the calculated and observed values, whereas in the latter $Cu_2(OH)PO_4$ gave an unreasonable value for the g-factor and $Cu_2AsO_4(OH)$ poorer agreement than in the tetramer model. Consequently the tetramer model has been thought suitable for these compounds. The values of g, J, and J'/J, which gave the best fit to the observed susceptibility, are 2.02 ± 0.04, -68 ± 1 K and <-1.5 for the arsenate, and 2.16 ± 0.04, -62 ± 2 K and -2.4 ± 1.5 for the phosphate. The susceptibilities calculated from these parameters are shown in Figs. 2 and 3. The large standard deviation of J'/J arises from Eq. 2 in that χV_m shows low sensitivity to J'/J when this parameter is less than -1. In the case of Cu_2AsO_4-(OH) the small g value further diminished the sensitivity to J'/J, which prevented the absolute value of this parameter being found.

As the large values of T_{max} suggest, the deduced values of J are very large. Such strong magnetic interaction must be brought about by a superexchange interaction *via* intermediate anions, since the separation between copper atoms exceeds 2.96 Å. It is also noteworthy that J and J' have opposite signs; the interaction between a copper spin on site A and that on site B is antiferromagnetic, whereas the interaction between two copper spins on site B is ferromagnetic (Fig. 4). It is widely recognized that there is a correlation between the parameter J and interatomic angle relevant to the superexchange interaction. The angle of Cu_B–OH–Cu_B' is 95.1° and that of Cu_A–OH–Cu_B is 121.1° in $Cu_2(OH)PO_4$ (Fig. 4), and consequently the signs expected from this correlation are consistent with those obtained from the present study.

As described earlier, the coordination polyhedra form a three-dimensional network and no isolated clusters are found in the crystal structure. Nevertheless, only the tetramer model could explain the temperature dependence of the magnetic susceptibility. This indicates that the hydroxide anion, which joins three copper atoms in the tetramer unit, makes the main contribution to the magnetic interaction between copper(II) spins, whereas the phosphate oxygen atoms have a negligible effect on the interaction. It is surprising that the difference between the roles is very large, because the interatomic distances and angles relevant to the superexchange interaction are similar for both types of oxygen atoms.

The susceptibility of $Cu_2AsO_4(OH)$ can be explained on the basis of the tetramer model. The magnitude of the obtained J value is similar to that of the phosphate and the signs of both J and J' are the same as those of the phosphate. This supports the assertion that the two compounds are isomorphous. Agreement between the observed and calculated susceptibility values was poorer for $Cu_2AsO_4(OH)$ than for $Cu_2(OH)PO_4$. Introduction of the anisotropic parameters, $J_\parallel$, $J_\perp$, $J_\parallel'$, and $J_\perp'$, into Eq. 1 proved no appreciable improvement. It appears, therefore, that the superexchange interaction through an arsenate oxygen atom makes some contribution to the magnetic behavior of $Cu_2AsO_4(OH)$.

In contrast with the values of J and J', the values of the g-factor differ from each other and this difference largely accounts for the difference in $\chi_{max}V_m$ between the two compounds. This indicates that the local environment at the copper site, and thus at the sites of the intermediary oxygen atoms in $Cu_2AsO_4(OH)$ vary considerably from those in $Cu_2(OH)PO_4$. This may explain the different effects of the arsenate and the phosphate oxygen atoms on the magnetic interaction. Further structural study is both necessary and desirable.

Magnetic Properties of Cu_2OSO_4. The magnetic susceptibility of Cu_2OSO_4 is shown in Figs. 5 and 6. It may be seen that as the temperature decreases, the

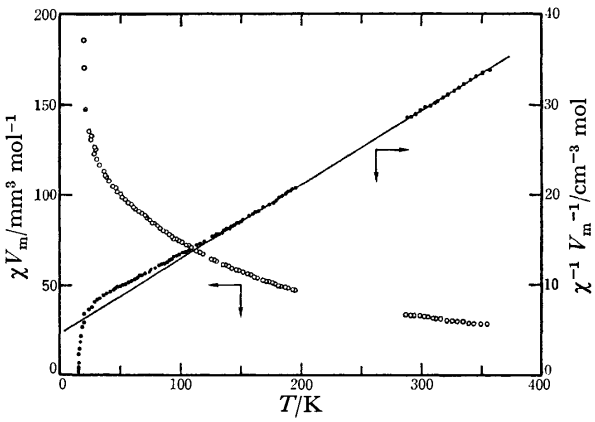

Fig. 5. Temperature dependence of the magnetic susceptibility (○) and its inverse (●) of Cu_2OSO_4 in the paramagnetic region. The solid line shows the Curie-Weiss relation obtained by the least-squares fit.

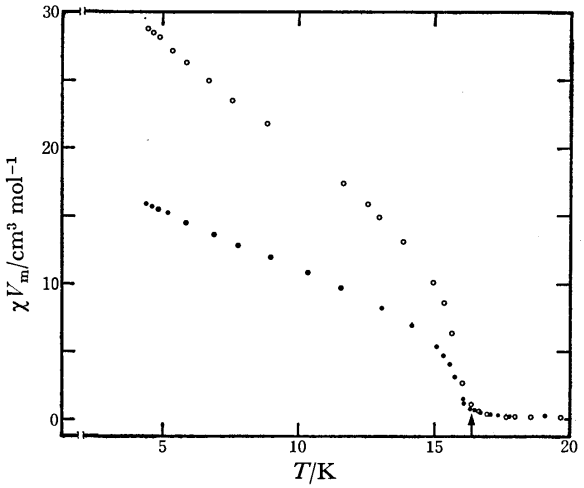

Fig. 6. Temperature dependence of the apparent magnetic susceptibility of Cu_2OSO_4 in the ordered phase. The arrow shows the transition temperature. ○: 22 kA m^{-1}, ●: 55 kA m^{-1}.

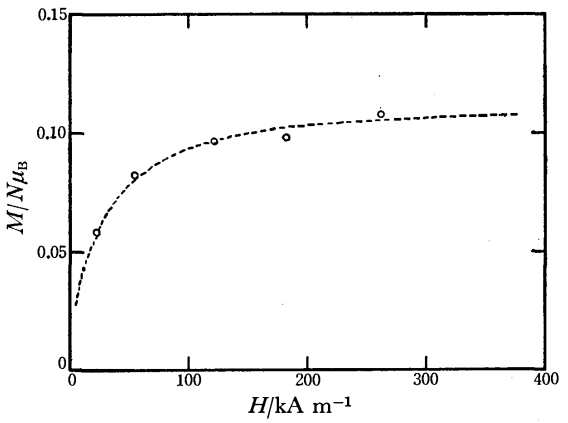

Fig. 7. Magnetization as a function of the magnetic field strength. Quantity N is a number of copper atoms per unit volume.

susceptibility increases monotonically and the Curie-Weiss law is obeyed above 140 K. The effective number of Bohr magnetons, p, and the Weiss constant, θ, have been deduced to be 1.96 ± 0.01 and -56 ± 2 K. Below 30 K the susceptibility increases rapidly and finally becomes dependent on the magnetic field strength, indicating a transition to an ordered phase with spontaneous magnetization. The transition temperature was found to be 16 ± 1 K. In Fig. 7 the magnetization, M, at 4.2 K is plotted as a function of the magnetic field strength, H, and from this plot the effective magneton number, n_B, has been evaluated as 0.11 ± 0.01.

The small value of n_B and the negative value of θ indicate that the spin-ordered state is ferrimagnetic. In order to determine the ferrimagnetic structure, it has been assumed that the magnetic space group of Cu_2OSO_4 can be obtained by changing each element of the crystallographic space group, C2/m, for a primed or unprimed magnetic symmetry element. Thus the spontaneous magnetization can only arise in the magnetic space groups of C2/m and C2′/m′.[19] In Fig. 8 the

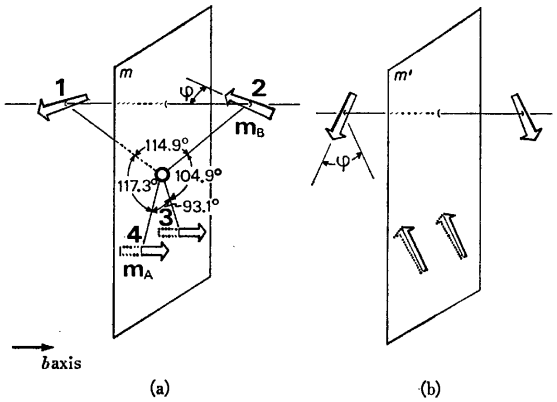

Fig. 8. Arrangement of the magenetic moments in the two possible magnetic space groups of (a) C2/m and (b) C2′/m′. Angles are the interatomic ones about the intermediary oxide anion.

arrangement of the magnetic moments is shown for the two space groups. In the case of C2/m, the moments of the copper cations on sites A, $\boldsymbol{m}_A$, are all parallel to the b axis. Those on sites B, $\boldsymbol{m}_B$, are divided into two sublattices. The components perpendicular to the b axis compensate for each other, whereas the components along the b axis remain unchanged. The net moment from $\boldsymbol{m}_B$ must be antiparallel to $\boldsymbol{m}_A$ so that the compound is ferrimagnetic. From the observed n_B the canting angle, φ, has been estimated as 38.7°, assuming that both m_A and m_B are equal to one μ_B. The discussion also holds in the case of C2′/m′, except for the direction of the spontaneous magnetization and the value of φ (Fig. 8b).[20] Therefore this compound probably has a canted ferrimagnetic structure.[21]

As cited earlier, the coordination polyhedra in Cu_2OSO_4 form a two-dimensional network. In this network layer the copper atoms form a kagomé-like lattice and the oxide anion is intermediate in every pair of adjacent copper atoms. The magnetic interaction can extend through the layer, as expected from the presence of the ordered state, assuming the oxide anion plays an important role. Since the interatomic distance between copper atoms exceeds 2.9 Å, the superexchange interaction governs the magnetic behavior of Cu_2OSO_4. The sulfate oxygen atoms afford interaction paths with long Cu–O separations of 2.14 and 2.52 Å. On the other hand, the interatomic distances of Cu–O (oxide anion) are short; 1.87(×2), 1.91, and 2.01 Å. In addition, judging from the Cu–O distances in the coordination polyhedra, three copper atoms with a half-filled 3d orbital direct their lobes towards the oxide anion. For the magnetic interaction in Cu_2OSO_4, therefore, the oxide anion assumes important role, whereas the sulfate oxygen atoms contribute a negligible effect.

Since the four Cu–O (oxide anion) distances are similar, the sign and magnitude of the superexchange interaction appears to mainly depend on the interatomic angles Cu–O–Cu′. Then the following relations hold among the parameters, J_{ij}:

$$|J_{12}| > |J_{13}| = |J_{23}|,\quad J_{12} \approx J_{14} = J_{24},$$
and J_{12}, J_{13}, $J_{23} < 0$, and $J_{34} > 0$

where the suffixes, i and j, refer to the numbering given in Fig. 8a. The statement that the interaction between copper(II) spins on sites B, J_{12}, is strong and antiferromagnetic appears, at first sight, to be conflicting with the ferrimagnetic structure discussed above, in which the main components of the $\boldsymbol{m}_B$'s are arranged ferromagnetically. However, this ferrimagnetic structure is a direct result of competing antiferromagnetic interactions. If the magnetic moments $\boldsymbol{m}_B$ are ordered antiferromagnetically, the interaction of $\boldsymbol{m}_A$ with two $\boldsymbol{m}_B$'s cancels out. Canting of $\boldsymbol{m}_B$'s brings the moment $\boldsymbol{m}_A$ some energy gain, which accompanies some energy loss for a pair of $\boldsymbol{m}_B$'s. The canting angle is thus determined by delicate balancing between energy loss and gain. The following simple formalism explains the canting angle quantitatively and supports the arguments made above. On the basis of the ferrimagnetic structure in Fig. 8 and including the interaction between the four copper moments, the interaction energy of the system, E, is given as a function of the angle, φ_{ij}, between the moments $\boldsymbol{m}_i$ and $\boldsymbol{m}_j$.

$$E = 2(N_{13}+N_{14})m^2 \cos(180°-\varphi) + N_{12}m^2 \cos(2\varphi) + N_{34}m^2 \quad (4)$$

The parameter, N_{ij}, is proportional to J_{ij}. The relationship of $N_{13}=N_{23}$ and $N_{14}=N_{24}$ holds on the basis of the symmetry, and $m_1=m_2=m_3=m_4=m$ is assumed. Setting $\partial E/\partial\varphi=0$, the canting angle is obtained.

$$\varphi = \cos^{-1}\{(N_{13}+N_{14})/2N_{12}\} \quad (5)$$

Substituting $\varphi=38.7°$, deduced from the magnetic space group of C2/m, and $N_{14}\approx N_{12}$, ratio of N_{13}/N_{12} is calculated to be 0.5. In the case of C2′/m′ it is in the range from 0.95 to 0.5 depending on the value of φ.[20] These values are comparable with the value of 0.5, obtained by application of the relationship between $2J$ and the bridging angle for the di-μ-hydroxo-copper(II) complexes.[4,6] The calculated values mean that both J_{12} and J_{13} have the same sign and that the interaction J_{12} is stronger than J_{13}.

Comparison of the Hydroxides and the Oxide. The magnetic behavior of the hydroxides, $Cu_2AsO_4(OH)$ and $Cu_2(OH)PO_4$, and the oxide, Cu_2OSO_4, are remarkably different; the former behaves like a cluster, whereas the latter like an ordered phase. This difference does not stem from the different roles in the magnetic behavior between the hydroxide and the oxide anions. On the contrary, the magnetic interaction induced by both anions has been explained qualitatively on the same principle. Rather the different magnetic behavior has its origin in the following: (1) mainly hydroxide or oxide anions contribute to the magnetic interaction, and (2) they are arranged in a different manner in the coordination polyhedra. The oxide anions occupy the trans positions in the octahedron and participate in every shared edge. Thus the interaction path extends infinately in the layer parallel to the (001) plane. The hydroxide anions occupy the cis positions in the octahedron and participate in every two shared edges. Moreover, it makes three bonds with copper atoms. Since other oxygen atoms give no appreciable effect, the magnetic interaction is localized within the four copper atoms bridged by two hydroxide anions. This explains the success of the tetramer model in spite of the three-dimensional network structure.

References

1) P. Escoffier and J. Gauthier, *C. R. Acad. Sci.*, **252**, 271 (1961).
2) M. Diot, P. Turlier, and J.-C. Volta, *C. R. Acad. Sci., Ser. B*, **274**, 225 (1972).
3) S. C. Abrahams, R. C. Sherwood, J. L. Bernstein, and K. Nassau, *J. Solid State Chem.*, **8**, 274 (1973).
4) D. L. Lewis, W. E. Hatfield, and D. J. Hodgson, *Inorg. Chem.*, **11**, 2216 (1972); K. T. McGregor, N. T. Watkins, D. L. Lewis, R. F. Drake, D. J. Hodgson, and W. E. Hatfield, *Inorg. Nucl. Chem. Lett.*, **9**, 423 (1973).
5) P. J. Hay, J. C. Thibeault, and R. Hoffmann, *J. Am. Chem. Soc.*, **97**, 4884 (1975).
6) D. J. Hodgson, *Prog. Inorg. Chem.*, **19**, 173 (1975).
7) E. M. Walitzi, *Tschermaks Mineral. Petrogr. Mitt.*, **8**, 614 (1963).
8) E. Flügel-Kahler, *Acta Crystallogr.*, **16**, 1009 (1963).
9) Gmelins Handbuch der Anorganischen Chemie, [8], Nr. 60, Kupfer, Teil B, Lief. 2, Verlag Chemie, Weinheim (1961), pp. 924, 953.
10) Gmelins Handbuch der Anorganischen Chemie, [8], Nr. 60, Kupfer, Teil B, Lief. 2, Verlag Chemie, Weinheim (1961), pp. 496, 588.
11) B. N. Figgis and R. S. Nyholm, *J. Chem. Soc.*, **1958**, 4190.
12) Landolt-Börnstein Zahlenwerte und Funktionen, Neue Serie, Gruppe II, Band II, Springer, Berlin (1966), pp. 1—16.
13) G. Bergerhoff and J. Paeslack, *Z. Kristallogr., Kristallgeom., Kristallphys., Kristallchem.*, **126**, 112 (1968).
14) V. Baran, *Coord. Chem. Rev.*, **6**, 65 (1971).
15) H. Heritsch, *Z. Kristallogr., Kristallgeom., Kristallphys., Kristallchem.*, **99**, 466 (1938); H. Strunz, "Mineralogische Tabellen," 5. Auflage, Akademische Verlagsgesellschaft, Leipzig (1970), p. 70.
16) E. M. Walitzi, *Tschermaks Mineral. Petrogr. Mitt.*, **8**, 275 (1962).
17) E. A. Boudreaux and L. N. Mulay, "Theory and Applications of Molecular Paramagnetism," Wiley-Interscience, New York (1976), Chap. 7.
18) Note that V_m in Eqs. 2 and 3 is defined by the formulas of $Cu_2AsO_4(OH)$ and $Cu_2(OH)PO_4$.
19) W. Opechowski and R. Guccione, "Magnetism," ed by G. T. Rado and H. Suhl, Academic Press, New York (1965), Vol. 2A, p. 105.
20) In the case of C2′/m′, the canting angle cannot be determined from n_B alone, but takes a value from 12.6° to 38.7°.
21) D. H. Martin, "Magnetism in Solids," The M. I. T. Press (1967), Chap. 1.

Adsorption of Water on FeOOH as Studied by Electrical Conductivity Measurements

Katsumi KANEKO* and Katsuya INOUYE

Department of Chemistry, Faculty of Science, Chiba University, Yayoi-cho, Chiba 280

(Received June 12, 1978)

Changes in the electrical conductivity of synthetic α-, β-, and γ-FeOOH crystals with the amount of adsorbed water were measured at 30 °C and various frequencies (dc, 100—10 MHz). The conductivity variations of water-adsorbed FeOOH with temperature were also examined over the range from −140 to 140 °C. For the adsorption coverages between 0 and 0.5, the electronic conduction increased with the coverage due to the transfer of electrons from chemisorbed water molecules to the FeOOH crystal. The decrease in activation energy for conduction with chemisorption was observed. The conductivity increase due to the chemisorption is related to the characteristic surface structure of each FeOOH polymorph. In the coverage range 0.7—2, protons in the adsorbed water layer transport electrical charges. The linear relationships between the logarithm of conductivity and the logarithm of the relative pressure of water vapor suggest the presence of clusters of physisorbed water molecules on FeOOH surfaces. A steep change in protonic conductivity by a factor of 10^2—10^4 was observed at a temperature close to −5 °C. The change seems to be caused by an order-disorder transition of protons in the adsorbed water layer.

Both O and OH on the surfaces of semiconductors and metal oxides play an important role in chemisorption.[1,2] Iron hydroxide oxide (FeOOH) crystal containing O and OH offers an ideal system for investigating the mechanism of chemisorption, since the geometrical positions of the surfaces O and OH can be derived by X-ray diffraction[3-5] and neutron diffraction[6-8] in crystallographic studies. α-, β-, and γ-FeOOH are found as minerals and as the main components in atmospheric corrosion products of iron. Electronmicroscopic observation reveals the presence of the predominant plane for each FeOOH, the index of which has been determined by selected-area electron diffraction.[9] With reference to these results, the surface characteristics of each FeOOH can be discussed by examining the structure of the predominant plane. It is anticipated that the adsorption sites for gaseous molecules are the characteristic O and OH on the predominant planes.

FeOOH is produced through an electrochemical process on the iron surface in the atmospheric environments, when water film of necessary thickness exists. The rust formed further promotes the adsorption of water on the iron surface. There is no doubt that water exhibits a particular activity to the FeOOH surface.

Kaneko *et al.* examined the adsorption process of water molecules on synthetic α-, β-, and γ-FeOOH by dielectric measurements.[10] They postulated that water molecules are adsorbed on two kinds of OH in (100) planes for α-FeOOH, OH and tunnels for β-FeOOH, and OH in (010) planes for γ-FeOOH; the adsorbed water layer forms a regular structure. The adsorption process was supported by thermodynamic study.[11] However, they were unable to discuss the electronic factors in the water adsorption. In the present work, the changes in electrical conductivity of synthetic FeOOH crystals with the amount of adsorbed water have been measured in order to elucidate the mechanism of chemisorption and the structure of adsorbed water.

Experimental

α-, β-, and γ-FeOOH were synthesized by procedures similar to those described in an earlier paper.[12] The X-ray diffraction of the samples gave patterns of pure, well-crystallized crystals. The BET surface areas obtained by use of N_2 adsorption at liquid nitrogen temperature were 69, 34, and 66 m^2/g for α-, β-, and γ-FeOOH, respectively.

Adsorption of Water and Electrical Conductivity. Sample disks made by applying a pressure of 150 kg/cm^2 were set between silver-plated brass electrodes in a glass cell of 215 cm^3. The sample disk was evacuated under a pressure of 10^{-5} Torr at 100 °C for 14 h prior to the adsorption measurement. The amount of adsorbed water was measured at 30 °C with use of a conventional volumetric apparatus with a silicone-oil manometer in the range of relative pressure 0—0.7. The water vapor was evolved from $BaCl_2 \cdot 2H_2O$. It took an hour to reach the adsorption equilibrium. Variations of electrical conductivity with the amount of adsorption at 30 °C and various frequencies (dc, 100—10 MHz) were measured by the same method as reported previously.[13] The conductivity of water-adsorbed FeOOH was also examined at different temperature in the range −140—140 °C. For the dc conductivity measurements, voltage in the range 0.1—100 V was applied. The current-voltage relationship for samples with submonolayer-adsorbed water obeyed Ohm's law, while that for samples with adsorbed water exceeding the monolayer deviated from the law.

Results and Discussion

FeOOH crystals exhibit an n-type electronic conduction *in vacuo*,[14,15] *i.e.*, the negative sign in Seebeck voltage and a conductivity decrease caused by introducing oxygen. The conductivity of samples with adsorbed H_2O of the coverage below 0.5 decreased by more than 25% of the initial value within a minute after the introduction of oxygen. The decrease is an evidence of electronic conduction. On the other hand, the exposure of samples with H_2O coverage above 0.7 to the oxygen gas brought about an instantaneous increase in conductivity. A fact of particular interest is that the water-adsorbed β-FeOOH (coverage 1.0) evolved hydrogen gas by applying dc 100 V at 30 °C for 265 h, which was detected by a mass spectrometer (Hitachi RMU-7M). No hydrogen gas was evolved from the water-adsorbed γ-FeOOH under the same conditions as those for the above-mentioned β-FeOOH specimen. No evolution of H_2 seems to be due to the progress of the reductive

reaction of γ-FeOOH to Fe_3O_4 consuming the protons at the specimen-electrode interface.[16] Thus, the protonic conduction is assumed for water-adsorbed FeOOH of coverage above 0.7. In view of the facts mentioned above as well as the dependence of conductivity on frequency, temperature, and adsorption of water described later, it is suggested that the electrical transport in the water-adsorbed FeOOH consists of electronic and protonic conductions. The total electrical conductivity of the specimen is assumed to be the sum of the electronic conducitivity σ_{el} and the protonic one σ_p.

$$\sigma = \sigma_{el} + \sigma_p. \quad (1)$$

σ is nearly equal to σ_{el} for the samples of adsorption coverage less than 0.5. In the coverage range 0.7—2, σ is close to σ_p. In the range 0.5—0.7, σ_{el} is comparable to σ_p.

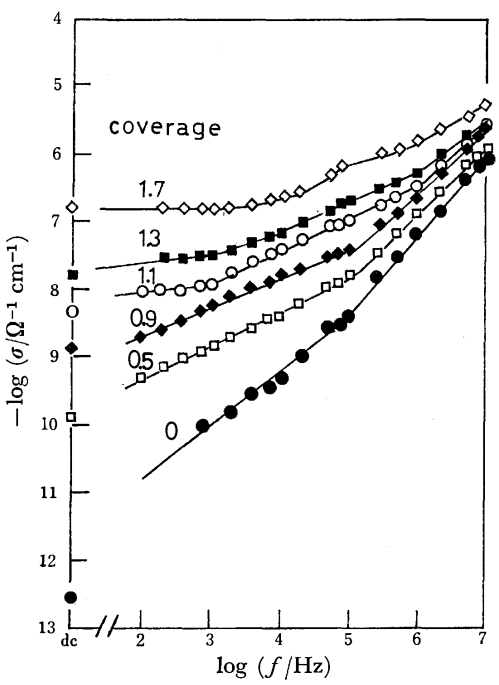

Fig. 1. Frequency dependence of electrical conductivity of γ-FeOOH at 30 °C at various coverages of adsorbed water (●: θ=0, □: θ=0.5, ◆: θ=0.9, ○: θ=1.1, ■: θ=1.3, and ◇: θ=1.7).

The frequency dependence of conductivity of γ-FeOOH measured at 30 °C for different values of coverage θ of adsorbed water is shown in Fig. 1. The logarithm of conductivity of pure γ-FeOOH (θ=0) shows linear dispersion with the logarithm of frequency, suggesting the hopping of d-electrons in the t_{2g}-orbital of Fe^{2+} to that of adjacent Fe^{3+}.[17,18] In the coverage range 0.5—1, it appears that the more water is adsorbed, the more vague is the dispersion in the lower frequency range, probably because of the contribution of the protonic conduction to the dc conduction. The dispersion of conductivity in the lower frequency range disappeared for samples with adsorbed water exceeding the monolayer; dc protonic conduction through adsorbed water layer overwhelms the dc electronic conduction. Water molecules seem to be partly chemisorbed in the coverage range 0—0.5, and physisorbed in the coverage range 0.7—2. Discussion is given in two parts, chemisorption and physisorption.

Chemisorption

Change of Physisorption to Chemisorption. The excess d-electrons of Fe^{2+} in pure FeOOH crystals move in a hopping process with mobility proportional to $\exp(-W_H/kT)$, where W_H is the hopping energy. The activation energy E for conduction of pure FeOOH crystals is nearly equal to the hopping energy W_H, if the Fe^{2+} concentration n does not change with temperature. Taking into account the interaction between Fe^{2+} ions, E can be given by

$$E \approx W_H = W_H^\circ - c\frac{e^2}{d}, \quad (2)$$

where W_H° is the hopping energy in the case where there is no interaction between carriers, e the electronic charge, c a constant, and d the average Fe^{2+}–Fe^{2+} distance. The value d is approximately given by[14]

$$d = 2\left(\frac{3}{4\pi n}\right)^{1/3}. \quad (3)$$

It is accepted that the water molecule with negative electron affinity is apt to give an electron to the oxide surface.[19,20] A portion of water molecules physisorbed on the FeOOH crystals by hydrogen bonding can be chemisorbed through a charge-transfer interaction.[21] The chemisorbed water molecule donates an electron to the t_{2g} orbital of Fe^{3+} according to the thermal excitation process:

$$H_2O \text{ (chemisorbed)} \longrightarrow H_2O^+ \text{ (chemisorbed)} + e(t_{2g}), \quad (4)$$

where $e(t_{2g})$ denotes the electron in the t_{2g} orbital. The ionization energy of the chemisorbed water molecule is denoted by E_i hereafter. The electron-transfer from water to the FeOOH surface results in an increase of the carrier concentration n; the activation energy for conduction decreases with increase in the amount of chemisorption owing to shallowing of the polarization-well of the carrier. The Fe^{2+}–Fe^{2+} distance d (Eq. 2) changes with the chemisorption of water. When the initial number of carriers, n_0, is much larger than the number of electrons donated from chemisorbed water, the hopping energy for the water-chemisorbed FeOOH is given by

$$W_H = W_H^\circ - \frac{ce^2}{2}\left(\frac{4\pi n_0}{3}\right)^{1/3} - \frac{ce^2}{6}\left(\frac{4\pi}{3n_0^2}\right)^{1/3} N_m\theta \exp(-E_i/kT), \quad (5)$$

where N_m is the number of adsorbed water molecules in monolayer at 30 °C. Equation 5 can be simplified to

$$W_H = W_H(\text{none}) - g\theta, \quad (6)$$

where W_H(none) is the hopping energy for FeOOH without water-chemisorption,

$$W_H(\text{none}) = W_H^\circ - \frac{ce^2}{2}\left(\frac{4\pi n_0}{3}\right)^{1/3}, \quad (7)$$

and g is given by

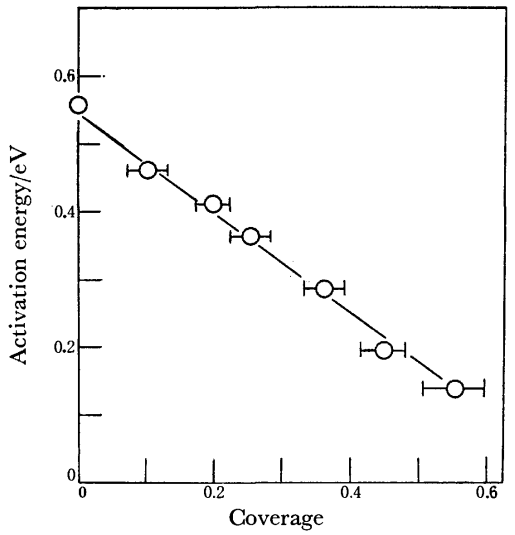

Fig. 2. Relationship between the activation energy and the coverage of adsorbed water for γ-FeOOH.

$$g = \frac{ce^2}{6}\left(\frac{4\pi}{3n_0^2}\right)^{1/3} N_m \exp(-E_i/kT). \quad (8)$$

Equation 6 shows that the hopping energy decreases in proportion to the coverage θ at a certain temperature.

Equation 6 holds for γ-FeOOH (Fig. 2); the activation energy for dc conduction at 30 °C decreases linearly with coverage; the slope of the straight line gives a g value of 0.71 eV. Taking the values $c=0.6$, $n_0=2\times10^{20}$ cm^{-3}, and $N_m=7\times10^{14}$ cm^{-2} in Eq. 8 we obtain $E_i=0.03$ eV. Thus, it is concluded that water molecules less than 15% of monolayer give electrons to γ-FeOOH at 30 °C, since the factor of $\exp(-E_i/kT)$ is about 0.3 and the upper limit of coverage for the chemisorption is 0.5.

Effect of the Surface Structure. Equation 6 requires a linear relationship between the logarithm of conductivity, log σ, and coverage θ, since log σ is proportional to the activation energy E ($\log\sigma \propto (W_H - g\theta)/kT$). Figures 3—5 show the linear relationships between log σ at dc and θ for γ-, α-, and β-FeOOH. The linear relationships

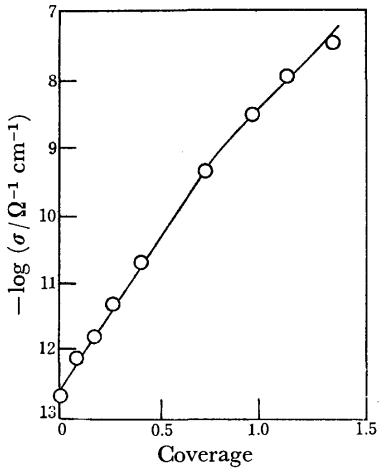

Fig. 3. Relationship between dc electrical conductivity and the coverage of adsorbed water at 30 °C for γ-FeOOH.

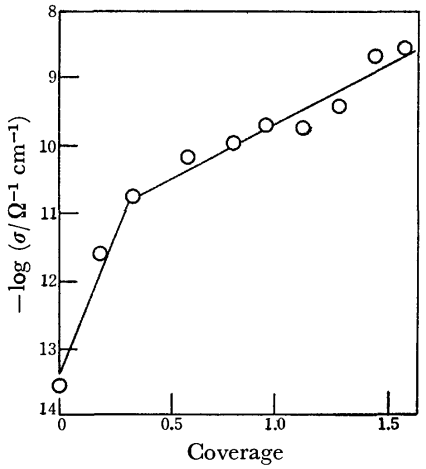

Fig. 4. Relationship between dc electrical conductivity and the coverage of adsorbed water at 30 °C for α-FeOOH.

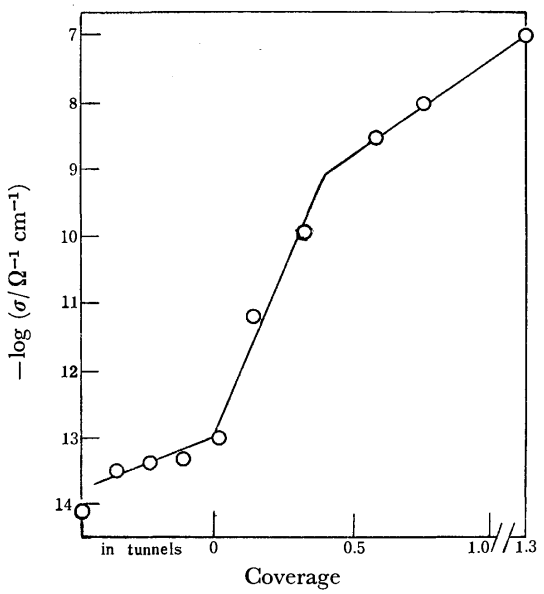

Fig. 5. Relationship between dc electrical conductivity and the coverage of adsorbed water at 30 °C for β-FeOOH.

break at an inherent coverage for each FeOOH, which can be ascribed to the change in E_i. The coverage at which the line breaks relates to the number of the particular adsorption sites on the crystal surface.

Ewing[3] postulated that the crystal structure of γ-FeOOH is built up of layers parallel to the (010) plane, each layer being made up of octahedra embracing iron atoms at centers of octahedra and linked together by sharing corners (Fig. 6(A)); the layers are joined to each other by hydrogen bonds. The linear relationship for γ-FeOOH (Fig. 3) in a wide range of coverage up to 0.8 is in line with the fact that the predominant (010) plane of γ-FeOOH has only one kind of OH as the water-adsorption site. However, the linearity breaks at the coverage of 0.8, since the protonic conduction through the bilayer of adsorbed water prevails over the electronic conduction.

The surface structure of α-FeOOH is shown in Fig. 6 (B).[4] Water molecules up to a coverage of 0.3 are

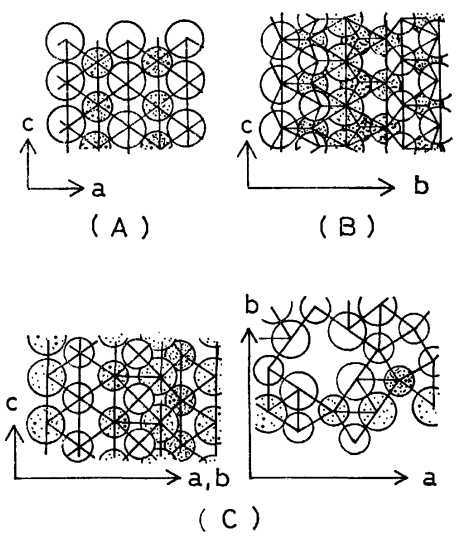

Fig. 6. Structure of the predominant surface of γ-FeOOH (A), α-FeOOH (B), and β-FeOOH (C). Large circle denotes OH^- and small circle O^{2-}.

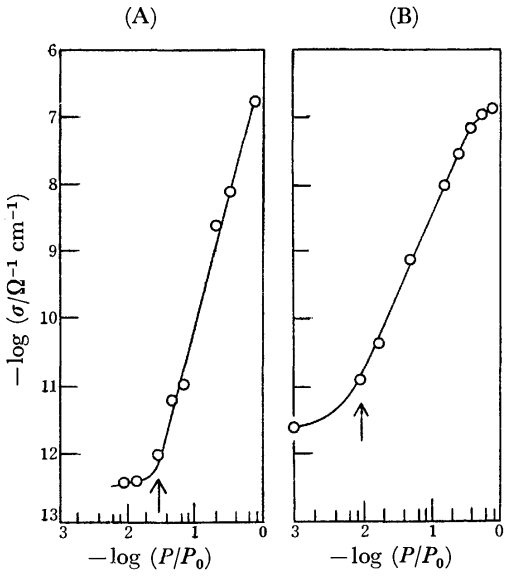

Fig. 7. Proportionality between log σ at dc and log (P/P_0) for β-FeOOH (A) and γ-FeOOH (B).

adsorbed on the hydroxyls in the groove of the (100) plane of α-FeOOH; the line in Fig. 4 breaks at 0.3.

Mackay[5] showed that β-FeOOH has a hollandite structure having tunnels parallel to the c-axis, in which Cl^- and H_2O can be occluded (Fig. 6(C)). The vacant part in the tunnel, produced by the removal of Cl^-, is the most active site for water adsorption, and the number of the adsorption site can be determined by the Cl^- content in the tunnel. The adsorption begins when water molecules enter the tunnels. The abscissa in Fig. 5 represents the coverage of the sites in tunnels and that of the outer surface (coverage: 0—1.3). We see that the conductivity-increase of β-FeOOH due to the adsorption in the tunnel is less conspicuous than that due to the adsorption on the outer surface. The linear relationship between log σ and θ in the coverage range from 0 to *ca.* 0.5 is ascribed to the transformation of physisorbed water molecules with bifurcated hydrogen bonding to chemisorption.

When water is desorbed from each FeOOH sample at 30 °C under a pressure of 10^{-5} Torr for several hours, the conductivity is reduced to the order of the original value for the sample without adsorbed water; the chemisorption of water appears to be reversible. It seems that the chemisorbed water molecules are connected to the FeOOH surface by both hydrogen bonds and weak charge-transfer bonds.

Physisorption

Clusters of the Physisorbed Water Molecules. The protonic conduction through the physisorbed water layer seems to predominate over the d-electron conduction in a restricted coverage range. In the coverage range 0.7—2, log σ is proportional to the logarithm of relative pressure, $\log(P/P_0)$, at 30 °C, where P and P_0 are the vapor pressure and the saturated one, respectively. Figure 7 shows the relationship between log σ at dc and $\log(P/P_0)$ for β- and γ-FeOOH. The lines on the right side of the bending point (indicated by an arrow, Fig. 7) correspond to the region of protonic conduction. When the linear relationship is expressed by

$$\sigma \propto (P/P_0)^s, \tag{9}$$

s values obtained from the slope of each line are: α-FeOOH, 1.1; β-FeOOH, 4.1; and γ-FeOOH, 2.2.

The adsorbed water layer is supposed to consist of solid-like two-dimensional clusters of water molecules. The relation given by Eq. 9 is interpreted by the presence of the clusters of adsorbed water molecules. The protonic conduction in the adsorbed water layer requires the production of protons by the ionic dissociation of water molecules. The dissociation of H_2O is determined by two bonding states, *i.e.*, the bonding between an adsorbed molecule and the surface, and that between adsorbed molecules. The proton formation from associated water molecules should differ from that of a single molecule. The association of m molecules on the FeOOH surface can be expressed by

$$m\mathrm{H_2O(g)} = m\mathrm{H_2O(ads)};\quad K_{\mathrm{ads}}, \tag{10}$$

$$m\mathrm{H_2O(g)} = (\mathrm{H_2O(ads)})_m;\quad K_{\mathrm{ass}}. \tag{11}$$

The number of association, m, is determined by the field strength of the surface. The dissociation equilibrium of a proton can be written as

$$(\mathrm{H_2O(ads)})_m = \mathrm{H^+} + (\mathrm{H_2O(ads)})_{m-1}\mathrm{OH^-};\quad K_{\mathrm{dis}}, \tag{12}$$

where (g) and (ads) denote gaseous water molecule and adsorbed one, respectively. The equilibrium constants for Eqs. 10, 11, and 12 are denoted by K_{ads}, K_{ass}, and K_{dis}, respectively. From Eqs. 10—12 the concentration of protons, p, is given by

$$p = \sqrt{K_{\mathrm{ads}}K_{\mathrm{ass}}K_{\mathrm{dis}}}P^{m/2}. \tag{13}$$

We see that σ_p is proportional to $P^{m/2}$, the mobility changing slightly with the adsorption of water. m is found to be $2s$ from a comparison of Eqs. 13 and 9.

The number of association m suggests a model of the cluster on the surface of each FeOOH, as shown in Fig. 8. For α-FeOOH (Fig. 8(A)), two molecules in the b-axis direction (dark circles) tend to form a dimer (m=2). When all grooves exposed on the β-FeOOH

surface are filled with H_2O at a coverage of 0.3, H_2O molecules can come into contact with the six nearest neighbors; in this case m equals 7 (Fig. 8(C)). The adsorbed water molecules on γ-FeOOH surfaces (Fig. 8(B)) are connected to each other by tetrahedral hydrogen bonding (Fig. 11), the m value approaching 5.

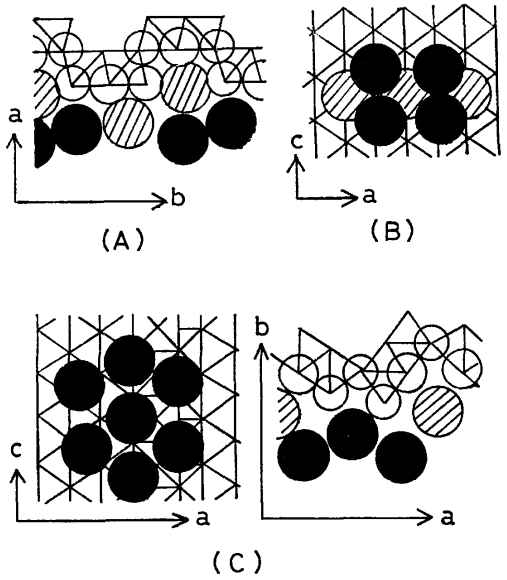

Fig. 8. Associated structures of water molecules physisorbed on α-FeOOH (A), γ-FeOOH (B), and β-FeOOH (C). Large and small circles denote OH^- and O^{2-}, respectively. Hatched circle and dark one denote the adsorbed water molecule contributing to the electronic conduction and to the protonic conduction, respectively.

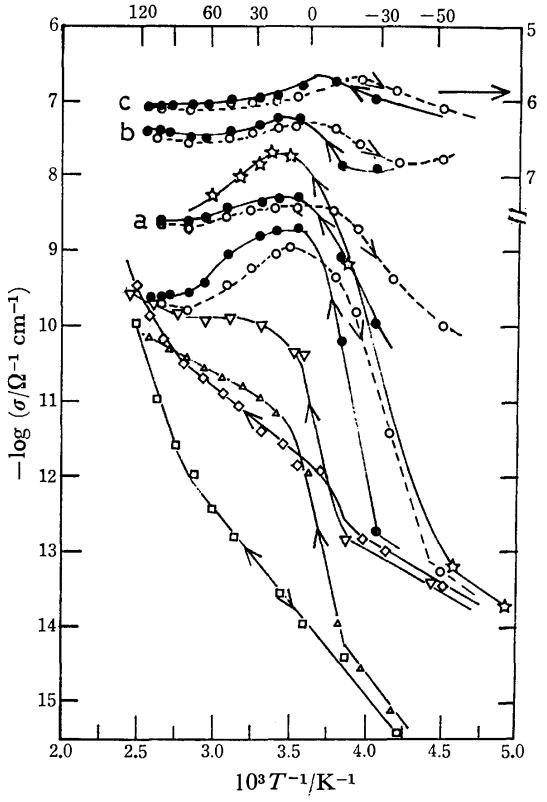

Fig. 9. Temperature dependence of electrical conductivity of γ-FeOOH with adsorbed water of various coverages.
dc: $\theta=0$ (□), $\theta=0.3$ (◇), $\theta=0.5$ (△), $\theta=0.7$ (▽), $\theta=1$ (●,○), and $\theta=1.5$ (☆). $\theta=1$ (●,○): 1 kHz (a), 100 kHz (b), and 7 MHz (c).

Phase Transition of Adsorbed Water Layer. The proton conduction through the adsorbed layer shows characteristic temperature dependence. Figure 9 shows the temperature dependence of the dc electrical conductivity of γ-FeOOH with adsorbed water of different coverages ($\theta=0$—1.5 at 30 °C). The coverage determined at 30 °C increases with a lowering in temperature due to the condensation of vapor on the samples below 30 °C. It decreases with rise in temperature due to the desorption above 30 °C. The linear $\log\sigma$ *vs.* $1/T$ relationships for the coverage above 0.5 become nearly vertical in the range from −40 to −5 °C. The higher the coverage, the lower the temperature at which conductivity jumps. The $\log\sigma$ *vs.* $1/T$ relationships of water-adsorbed samples ($\theta=1$ and 1.5) have maxima at 10 °C. The $\log\sigma$ *vs.* $1/T$ relationships of γ-FeOOH ($\theta=1$ at 30 °C) at different frequencies are also shown in Fig. 9. The higher the frequency, the smaller the change in conductivity with temperature. The conductivities at 1 and 10 kHz reach maxima at 10 °C with rise in temperature. On the other hand, the conductivity at 7 MHz has no maximum at 10 °C, but at -7 ± 3 °C, where dc and lower frequency conductivities increase vertically with rise in temperature. The hysteresis of conductivity-temperature change was observed at all frequencies.

The steep change in conductivity in the temperature range from −40 to −5 °C may be due to a phase transition of the adsorbed water layer. All the phenomena observed appear to be similar to a solid-liquid transition of water in porous solids, which shows freezing-point depression.[23–25] However, the phase transition does not seem to be the solid-liquid transition for two reasons: (1) The adsorbed water layer of

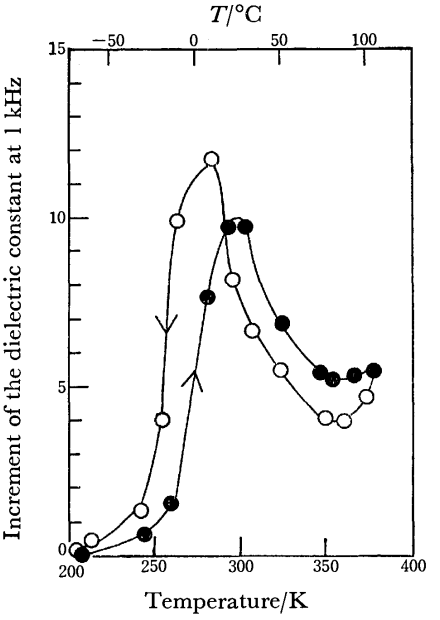

Fig. 10. Temperature dependence of the increment of the dielectric constant at 1 kHz of γ-FeOOH covered with adsorbed water ($\theta=1$ at 30 °C).

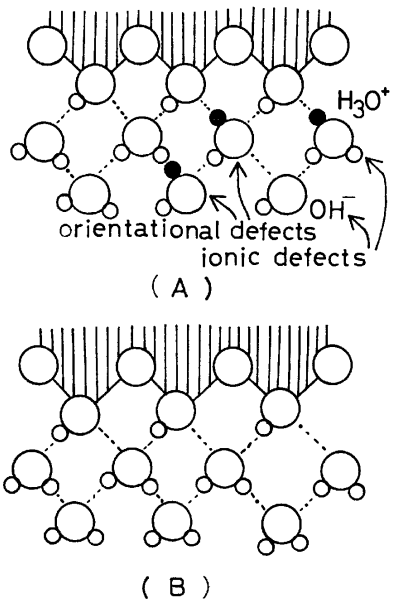

Fig. 11. Hydrogen-disordered (A) and hydrogen-ordered (B) structures of bilayer of water adsorbed on γ-FeOOH. Small, open circle denotes a hydrogen atom. Small, black circle denotes the misplaced hydrogen atom (or ion). Large circle denotes an oxygen atom (or ion).

thickness less than three molecular layers can not be regarded as a liquid phase. (2) The phase transition between ice I and liquid water causes no significant conductivity changes, since the electrical conductivity of ice I at -20 °C is 10^{-8}—10^{-10} Ω^{-1} cm^{-1} [26] and that of liquid water 10^{-9} Ω^{-1} cm^{-1}.[27] The variations of dielectric constant with temperature should also be taken into consideration. Figure 10 shows the temperature dependence of the dielectric constant for γ-FeOOH at 1 kHz ($\theta=1$ at 30 °C). The results are referred to the dielectric studies on polymorphs of ice by Whalley *et al.*,[28,29] who argued that an order-disorder transition of the position of hydrogen atoms affects the dielectric constant. It seems that the phase transition of the adsorbed water layer on the FeOOH surface is not a solid-liquid transition but an order-disorder transition of hydrogen atoms. A model of the order-disorder transition of hydrogen atoms in the adsorbed water layer on γ-FeOOH is shown in Fig. 11. The disordered adsorbed-water layer containing many orientational and ionic defects would result in high dielectric constant and high conductivity. The electrical conduction at dc and that at frequencies higher than 100 kHz arise from the migration of ionic (protonic) defects and the formation of orientational defects, respectively.[30] Most orientational defects appear at the temperature of order-disorder transition; the conductivity at 7 MHz reaches maximum at the transition temperature. The fact that H_2O-adsorbed FeOOH ($\theta=1$ or 1.5) has the highest protonic conductivity at 10 °C might be related to the maximum of the adsorbed water in the disordered state at the temperature. The hysteresis observed can be attributed to a strong interaction between the adsorbed water and the FeOOH surface. The strong interaction also promotes the dissociation of water. Gallagher and Phillips[31,32] observed the hydrogen-exchange between hydroxyls of FeOOH and water.

The authors wish to acknowledge the Special Research Grant for Environmental Science (R-32-303020) from the Ministry of Education.

References

1) E. McCafferty, V. Pravdic, and A. C. Zettlemoyer, *Trans. Faraday Soc.*, **66**, 1720 (1970).
2) H. P. Boehm, *Discuss. Faraday Soc.*, **52**, 264 (1971).
3) F. J. Ewing, *J. Chem. Phys.*, **3**, 420 (1935).
4) F. J. Ewing, *J. Chem. Phys.*, **3**, 203 (1935).
5) A. L. Mackay, *Mineral. Mag.*, **32**, 545 (1960).
6) J. B. Forsyth, I. G. Hedley, and C. E. Johnson, *J. Phys. C*, **1**, 179 (1968).
7) A. Szytula, M. Balanda, and Z. Dimitrijevic, *Phys. Status Solidi A*, **3**, 1033 (1970).
8) A. Oles, A. Szytula, and A. Wanic, *Phys. Status Solidi*, **41**, 173 (1970).
9) G. W. van Oosterhout, *Acta Crystallogr.*, **13**, 932 (1960).
10) K. Kaneko, M. Serizawa, T. Ishikawa, and K. Inouye, *Bull. Chem. Soc. Jpn.*, **48**, 1764 (1975).
11) T. Ishikawa, K. Kaneko, and K. Inouye, *Nippon Kagaku Kaishi*, **1975**, 1635.
12) K. Kaneko and K. Inouye, *Bull. Chem. Soc. Jpn.*, **47**, 1139 (1974).
13) K. Kaneko and K. Inouye, *Nippon Kagaku Kaishi*, **1973**, 1075.
14) K. Kaneko and K. Inouye, *J. Chem. Soc., Faraday Trans. 1*, **72**, 1258 (1976).
15) K. Kaneko and K. Inouye, *Bull. Chem. Soc. Jpn.*, **49**, 3689 (1976).
16) A ferromagnetic black compound was formed at the interface between electrode (either Au- or Ag-plated) and H_2O-adsorbed γ-FeOOH after applying a dc potential of 10 V at 30 °C for 30 h. The compound appears to be Fe_3O_4 from electron-diffraction studies. No such compound was found on the surface of H_2O-adsorbed α- or β-FeOOH specimens by the application of dc 100 V at 30 °C for 70 h.
17) M. Pollak and T. H. Geballe, *Phys. Rev.*, **122**, 1742 (1961).
18) A. K. Jonscher, *Nature*, **250**, 191 (1974).
19) H. O. Pritchard, *Chem. Rev.*, **52**, 529 (1953).
20) K. Hauffe, *Adv. Catal.*, **7**, 213 (1955).
21) R. S. Mulliken, *J. Am. Chem. Soc.*, **74**, 811 (1952).
22) W. Meyer and H. Neldel, *Phys. Z.*, **38**, 1014 (1937).
23) Y. Morioka, J. Kobayashi, and I. Higuchi, *J. Colloid Interface Sci.*, **42**, 156 (1973).
24) C. Hodgson and R. McIntosh, *Can. J. Chem.*, **38**, 958 (1960).
25) R. Defay, I. Prigogine, and A. Bellemans, "Surface Tension and Adsorption," translated by D. H. Everett, Longmans, Green & Co., Ltd. London (1966), Chap. 15.
26) A. von Hippel, *J. Chem. Phys.*, **54**, 145 (1971).
27) S. Barret and G. Briere, *J. Chim. Phys.*, **62**, 970 (1965).
28) R. K. Chan, D. W. Davidson, and E. Whalley, *J. Chem. Phys.*, **43**, 2376 (1965).
29) G. J. Wilson, R. K. Chan, D. W. Davidson, and E. Whalley, *J. Chem. Phys.*, **43**, 2384 (1965).
30) P. V. Hobbs, "Ice Physics," Clarendon Press, Oxford (1974), Chap. 2.
31) K. J. Gallagher and D. N. Phillips, *Trans. Faraday Soc.*, **64**, 785 (1968).
32) K. J. Gallagher and D. N. Phillips, *Chimia*, **23**, 465 (1969).

ESR Study of SeO_2^- Radical in an Irradiated Single Crystal of Triglycine Selenate in the Vicinity of Phase Transition Temperature

Yashige KOTAKE* and Keiji KUWATA

Department of Chemistry, Faculty of Science, Osaka University, Toyonaka, Osaka 560

(Received June 12, 1978)

Detailed observations of the angular dependence of ESR spectra of SeO_2^- radicals formed by X-ray irradiation of a single crystal of ferroelectric triglycine selenate were carried out. Two kinds of SeO_2^- radicals were produced due to the difference in manner of selenium-oxygen bond scission. In spite of the difference in stability of radicals in TGSe and those in TGS, the behavior of SeO_2^- radicals in the phase transition region is in line with that expected from the result of X-ray diffraction study of TGS.

Various aspects of ferroelectric phase transition have been clarified by ESR technique with use of paramagnetic probes such as radiation damage and doped metal ions. As regards triglycine sulfate (TGS), X- or γ-ray irradiation has been effective for producing paramagnetic probes which are stable up to the transition temperature.[1-7] However, the stability of the resulting radicals in TGS and isomorphous triglycine selenate differs a great deal. In TGS, radicals from glycines II and III are stable while in TGSe those from acid ions are stable, indicating that the environments of radicals differ from each other. It is interesting to see whether the difference influences the behavior of radicals upon phase transition, resulting in a behavior differing from that expected from the result of X-ray diffraction study on TGS.

In view of the fact that the radicals are good probes for watching microscopic behavior of phase transition, the difference in the behavior of yielded radicals in isomorphous crystals might supply useful information.

In the mechanism of the phase transition in TGS, Hoshino *et al.*[8] postulated that acid ions change their structure and orientation at the phase transition point, and that they are located on the mirror planes at $b=1/4$ and 3/4 in the paraelectric phase. In isomorphous triglycine fluoberyllate (TGBe) the behavior of fluoberyllate ion has been studied by making use of ^{9}Be quadrupole perturbed NMR in deuterated crystals.[9] The results were in line with those of the X-ray diffraction study, the fluoberyllate ions being on the mirror planes at $b=1/4$ and 3/4 in the paraelectric phase.

No ESR study using paramagnetic probes has been reported for such behavior of acid ions mainly because of the lack of suitable probes.

The objective of this work is to clarify whether the stable radical produced from acid ions in TGSe reflects the general behavior of acid ions in TGS and its isomorphous crystals.

Experimental

Single crystals of TGSe were grown from aqueous solutions by slow cooling. After being irradiated by X-ray at room temperature for 1 h, the crystal was aged at room temperature for several weeks in order to reduce the unstable radicals produced from glycines.

The ESR spectrometer employed was operated at X-band, the second derivative signal being recorded. The position of the absorption line was determined by using DPPH as a standard. The temperature of the sample was controlled by a nitrogen gas stream and measured by a copper-constantan thermocouple attached to the crystal.

Results and Discussion

Stability of Radicals. In TGS two radical species are observed immediately after irradiation at room temperature.[3] They are assigned to $\dot{C}H_2COO^-$ produced from glycine I and $NH_3^+\dot{C}HCOO^-$ from glycines II and III. $\dot{C}H_2COO^-$ radicals have a half life of about one week at room temperature, while $NH_3^+\dot{C}HCOO^-$ is stable for a long period of time. In the case of TGSe, SeO_2^- radicals are formed from selenate ions in addition to radicals from glycines. The yield of the radicals from glycines is low, and they have a half life of several weeks. SeO_2^- radicals are quite stable, no decrease in signal intensity being observed. The difference in the stability of radicals formed from acid ions might be ascribed to the reactivity of the radical. However, the difference in the stability of the $NH_3^+\dot{C}HCOO^-$ radical indicates that the hydrogen-bonded network which stabilizes the radical is different. The radicals located in the network might give microscopic information on the difference in the surrounding which cannot be obtained from macroscopic properties such as Curie temperature and transition entropy.

Angular Dependence of SeO_2^- Radicals. The stable radical species produced in irradiated TGSe has been assigned to SeO_2^- radicals by Suzuki and Abe[10] by comparison of the principal values of hf-tensors of ^{77}Se with those of various oxy radicals of selenium. However, the structure and alignment of the radical has not been clarified in connection with the crystal structure.

The present results of angular dependence show that there are two major radicals which give eminent peaks in all of the three perpendicular planes. Figure 1 shows the observed angular dependence of the two species denoted by S1 and S2 in both the para- and ferroelectric phases. Weaker signals appear in certain directions.

The results of the tensor analysis with repect to a'bc orthogonal coordinate are given in Table 1, where $a' \perp c$ lies in the ac plane. Both species S1 and S2 change the alignment upon phase transition. However, the principal values remain unchanged. Though there is a considerable discrepancy in the direction cosines, the principal values coincide with those of Suzuki and Abe.[10] In view of the difference in the angular dependence in

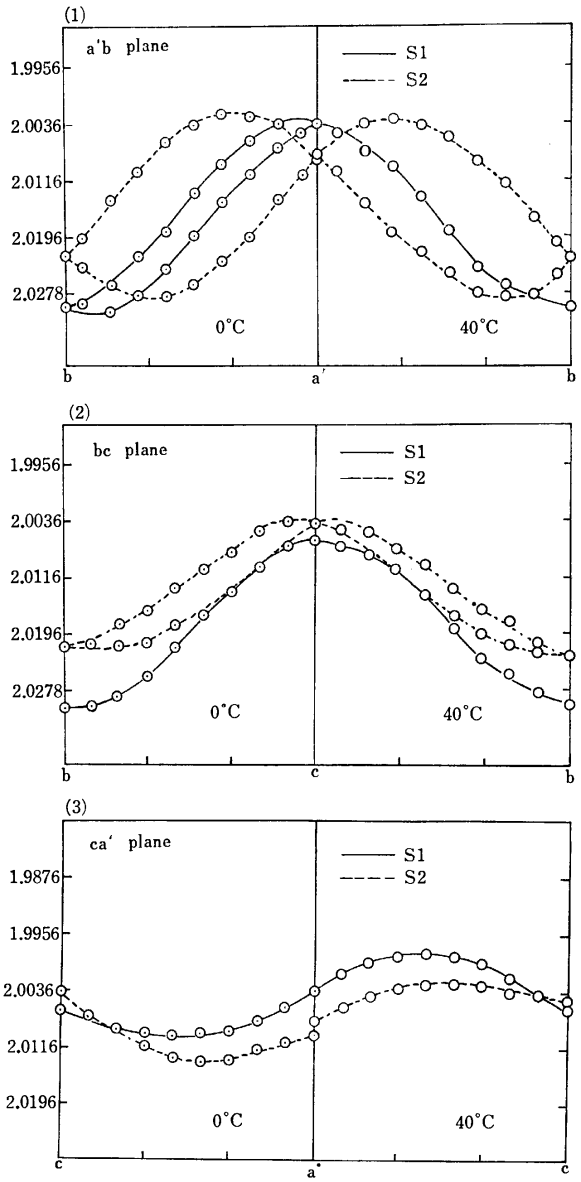

Fig. 1. Angular dependence of the ESR spectra of SeO_2^- radicals in the para- (40 °C) and ferroelectric (0 °C) phases. The magnetic field is applied parall to the crystallographic planes: (1) a'b plane, (2) bc plane, and (3) ca' plane.

TABLE 1. *g*-TENSORS OF SeO_2^- RADICALS IN IRRADIATED TGSe CRYSTALS IN THE FERRO- (0 °C) AND THE PARAELECTRIC (40 °C) PHASES

	g	*a'*	*b*	*c*
S1 0 °C	2.028	0.067	±0.995	0.076
	2.009	−0.591	±0.022	0.803
	1.999	0.804	±0.096	0.586
S1 40 °C	2.027	0.0	1.0	0.0
	2.013	−0.585	0.0	0.811
	1.994	0.811	0.0	0.585
S2 0 °C	2.024	0.365	±0.898	0.246
	2.007	−0.573	±0.012	0.819
	2.000	0.733	±0.439	0.518
S2 40 °C	2.026	0.290	±0.829	0.470
	2.006	−0.600	±0.217	0.769
	2.001	0.739	±0.516	0.432

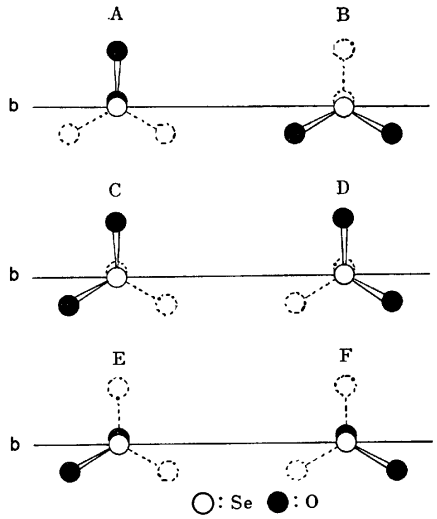

Fig. 2. Possible spatial configurations of SeO_2^- radicals produced from SeO_4^{2-} ion in TGSe crystals. The horizontal line shows the b-axis. S1 was assigned to B and S2 to E or F.

both the para- and ferroelectric phases, the most striking feature is that the site splitting of S1 in the ferroelectric phase disappears in the paraelectric phase.

There are six possible spatial configurations for SeO_2^- radicals in the paraelectric phase of TGSe crystals as shown in Fig. 2. Two of them (A, B) have mirror planes perpendicular to the b-axis. From the fact that the direction of the maximum principal value of the *g*-tensors in SeO_2^- corresponds to the direction combining two oxygen atoms[11,12] S1 is assigned to SeO_2^- of configuration B. The direction cosines of S2 have no such characteristics of S1 (Table 1) and are ascribed to configurations E and F in Fig. 2. The two configurations are crystallographically equivalent in the paraelectric phase. In the ferroelectric phase ESR spectra of configurations E and F should give a slightly different angular dependence caused by the different bond lengths of the two selenium-oxygen bonds, but this was not shown by experimental results.

The direction cosines of S1 and S2 show that S1 almost exactly keeps the configurations of the mother selenate ions even after the loss of two oxygen atoms. The direction cosines of SeO_2^- radicals calculated on the X-ray diffraction data for configurations B and F are given in Table 2. There is a considerable displacement of S2 from the site of the mother selenate ions as compar-

TABLE 2. CALCULATED DIRECTION COSINES FOR CONFIGURATIONS B AND F

Configuration	*a'*	*b*	*c*	Difference[a] (degree)
B g_{max}	0	1	0	0
B g_{int}	−0.44	0	0.89	11
B g_{min}	0.89	0	0.44	11
F g_{max}	0.39	±0.53	0.76	24
F g_{int}	−0.89	±0.44	0.15	41
F g_{min}	0.24	±0.72	0.63	34

[a] The angular deviation of the observed direction of S1 from B and that of S2 from F.

ed with the case of S1. This is reasonably explained by the fact that S1 has mirror symmetry but not S2. The selenate ions are stabilized by a network having a mirror symmetry because of the symmetry of the crystal. After the loss of two oxygen atoms S2 is forced to have asymmetric hydrogen bond system possibly causing displacement to seek a stable position.

Scission of Selenium–Oxygen Bonds. According to the crystal structure determined by X-ray diffraction[8] and neutron diffraction,[13] glycine I and one of the oxygen atoms in a sulfate ion are bonded by a short hydrogen bond (0.254 nm) in the TGS crystal. This is the shortest hydrogen bond connecting sulfate ion and neighboring glycines, the involved sulfur–oxygen bond having the longest bond length (0.148 nm) in a sulfate ion. In TGSe one of the lost oxygen in SeO_2^- corresponds to the oxygen atom with the longest sulfur–oxygen bond. The scission behavior of the selenate ion is in line with the fact that in a single crystal the breakage of the bond by irradiation tends to occur along the shortest hydrogen bond.[14]

Behavior of SeO_2^- Radical upon Phase Transition. As shown by the angular dependence of the *g*-value of the SeO_2^- radical, the orientations of radicals in the para- and ferroelectric phases differ. Particularly in the case of S1 disappearance of the site splitting was clearly observed in the a'b plane. In the bc plane the site splitting was too small as compared with linewidth even in the ferroelectric phase.

In the ferroelectric phase, the direction combining two oxygen atoms in SeO_2^- of configuration B has a finite angle with the b-axis, due to the lack of mirror symmetry. X-Ray diffraction study has shown that in TGS the sulfate ions do not have tetrahedral symmetry in the ferroelectric phase. In isomorphous TGSe, two selenium-oxygen bonds in SeO_2^- are thought to have a different bond length, causing the slightly different configurations of B in the ferroelectric phase. On the other hand, in the paraelectric phase the change of the structure makes the angle zero, resulting in mirror planes perpendicular to the b-axis. The result of tensor analysis shows the behavior to be consistent with that predicted by the result of X-ray diffraction study.[8] It should be noted that the behavior of radicals shows no influence expected from the difference in the stability of radicals. The magnitude of the site splitting gradually tends to zero without line broadening. It is hard to explain the absence of the line broadening in terms of the dynamic order-disorder mechanism.[15] It this system, the dynamic order-disorder mechanism assumes the interchange of two sites of S1 by thermal motion. When the interchange rate becomes greater, the site splitting should become smaller with exchange broadening.

The magnitude of the site splitting of S1 is not large enough as compared with the linewidth in the phase transition region. It was found that the alignment of S1 and S2 has a suitable relation for the observation of the change of the spectral feature in the critical region. In a certain direction, *i.e.* when the external field is slightly off from the b- and c-axis, each component of the signals from S1 and S2 completely collapses in the paraelectric phase because of the different temperature dependence of the alignment. The doublet splitting in this direction is sufficiently large in the ferroelectric phase to observe the temperature dependence. Figure 3 shows the difference between the resonance fields of the signals of S1 and S2 as a function of temperature. The plot shows that the change has a second order nature, the behavior of the radicals being in line with that of TGS.[16]

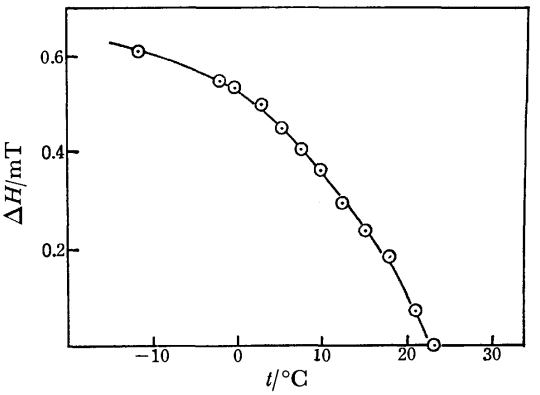

Fig. 3. Temperature dependence of the separation of ESR signals of S1 and S2. The magnetic field is applied slightly off from the b- and c-axis.

References

1) D. W. Ovenall and K. A. Muller, *Helv. Phys. Acta*, **34**, 786 (1961).
2) R. Blinc, S. Detoni, I. Levstek, M. Pintar, S. Proberaj, and M. Schara, *J. Phys. Chem. Solids*, **20**, 187 (1962).
3) T. Kato and R. Abe, *J. Phys. Soc. Jpn.*, **26**, 948 (1969).
4) T. Kato, R. Abe, and I. Suzuki, *J. Phys. Soc. Jpn. Suppl.*, **28**, 123 (1970).
5) W. Windsh, M. Welter, and W. Driesel, *Ferroelectrics*, **8**, 551 (1974).
6) Y. Kotake and I. Miyagawa, *J. Chem. Phys.*, **64**, 3169 (1976).
7) J. L. Yeh and I. Miyagawa, *J. Phys. Chem. Solids*, **38**, 1371 (1977).
8) S. Hoshino, Y. Okaya, and R. Pepinsky, *Phys. Rev.*, **115**, 323 (1959).
9) R. Blinc, J. Slak, and J. Stepisnik, *J. Chem. Phys.*, **55**, 4848 (1971).
10) I. Suzuki and R. Abe, *J. Phys. Soc. Jpn.*, **31**, 179 (1971).
11) P. W. Atkins, M. C. R. Symons, and H. W. Wardale, *J. Chem. Soc.*, **1964**, 5215.
12) L. Jardine, D. E. O'Reilly, and T. Tsang, *J. Chem. Phys.*, **48**, 1417 (1968).
13) M. I. Kay and R. Kleinberg, *Ferroelectrics*, **5**, 45 (1973).
14) See for example, M. Iwasaki, K. Minakata, K. Nunome, and K. Tagami, *J. Chem. Phys.*, **57**, 3187 (1972) and M. Iwasaki and K. Toriyama, *Chem. Phys. Lett.*, **41**, 59 (1976).
15) R. Blinc, M. Mali, R. Osredkar, A. Prelesnik, I. Zupancic, and L. Ehrenberg, *J. Chem. Phys.*, **55**, 4843 (1971).
16) F. Jona and G. Sirane, "Ferroelectric Crystals," Pergamon, Oxford, (1962).

The Crystal Structures of Methylammonium Hexachlorostannate(IV) in the High- and Low-temperature Phases Studied by X-Rays

Katsuki KITAHAMA,* Hideko KIRIYAMA, and Yoshihisa BABA

The Institute of Scientific and Industrial Research, Osaka University, Yamadakami, Suita, Osaka 565

(Received June 28, 1978)

The title compound crystallizes in the trigonal space group $R\bar{3}m$ with $a=7.171$, $c=21.952$ Å, and $Z=3$ at 298 K. The crystal structures at 298 and 120 K, as well as the lattice parameters in the temperature range 113—298 K, have been determined by X-rays, in order to elucidate the mechanism of the phase transition occurring at $T_t=156$ K. The structure of the high-temperature phase is essentially the same as that determined by Wyckoff, except for the discrimination between C and N atoms. No change in the space group nor in the basic structure was detected over the temperature range studied, in spite of a strong suggestion from previous ^{35}Cl-NQR measurements. A small but significant anomaly associated with the transition is recognized in the c axis, which retains almost the same length near and below T_t. As a result, the lattice shrinkage below T_t becomes increasingly anisotropic as the temperature is lowered, whereas the thermal expansion above it is relatively isotropic.

In a series of hexahalo complexes of quadrivalent metal ions, A_2MX_6, the compounds of methylammonium cations, $A=CH_3NH_3^+$, are of much interest, because dumbell-like cations and octahedral anions co-exist in their structures. According to Wyckoff, a crystal of methylammonium hexachlorostannate(IV) has an anti-fluorite type structure which is deformed by elongation of the cubic unit-cell parallel to [111].[1] A phase transition in this compound was found at 156 K from an anomaly in the frequency of chlorine-35 NQR (nuclear quadrupole resonance) measured by Kume *et al.*[2] In our laboratory, molecular motions of both cation and anion have been studied by means of magnetic resonance of ^{1}H and ^{35}Cl nuclei. The results of PMR (proton magnetic resonance) revealed that the total cations are rapidly reorienting about their three-fold axes even at very low temperatures.[3] It was also suggested that the motion of cations makes a minor contribution to the occurrence of the phase transition. On the other hand, the ^{35}Cl-NQR spin-lattice relaxation time, T_1, showed a distinct reduction in the vicinity of the phase transition temperature, T_t.[4] This anomalous behavior of ^{35}Cl-T_1 has been explained in terms of the softening of some rotary lattice mode of anion octahedra, $[SnCl_6]^{2-}$, in analogy with K_2PtBr_6.[5]

The present X-ray study was undertaken to make clear the change in crystal structure and/or in lattice constants on passing through the phase transition and to check the transition mechanism suggested from the NQR results. Discrimination between C and N atoms of the cation will be accomplished as well.

Experimental

Polycrystalline $(CH_3NH_3)_2SnCl_6$ was prepared by the same method as in the previous paper.[3] Single crystals were obtained as hexagonal plates by the slow cooling of a 6 mol/dm^3 HCl solution.

All single crystals used were sealed in glass capillary tubes to protect them from moisture. Cooling was achieved by blowing a stream of cold nitrogen gas over a crystal. The temperature of a sample was stabilized within ±0.5 K during measurements of the lattice constants and within ±1.0 K during exposure of X-ray photographs and also throughout the intensity data collection at 120 K.

A single crystal with dimensions $0.3\times0.3\times0.15$ mm was used throughout the measurements described below. The crystal was mounted on a Rigaku four-circle diffractometer with the a-axis along the ϕ-axis of the goniostat. Intensity data at 120 and 298 K and the lattice parameters from 113 to 298 K were measured with graphite monochromatized Mo $K\alpha$ radiation. Diffraction peaks were centered automatically in the measurement of the cell constants. The lattice parameters at a given temperature were refined by a least-squares method based on the setting angles (2θ, ω, χ, and ϕ) of nine reflections. The results are summarized in Table 1.

Table 1. Lattice parameters for $(CH_3NH_3)_2SnCl_6$ at various temperatures

T/K	a/Å	c/Å	V/Å^3
298	7.171	21.952	977.6
293	7.169	21.944	976.7
233	7.137	21.859	964.3
213	7.130	21.828	961.0
193	7.119	21.810	957.2
173	7.108	21.790	953.4
153	7.098	21.790	950.7
133	7.090	21.791	948.6
120	7.082	21.790	946.5
113	7.077	21.789	945.1

e.s.d.'s for a and c are less than 0.004 and 0.009 Å, respectively. Space group : $R\bar{3}m$ (throughout the temperature range). $Z=3$, $F.W.=395.54$ g mol^{-1}, $F(000)=570$ e cell^{-1}, $\rho_{obsd}=1.989$ g cm^{-3} (at 293 K), $\rho_{calcd}=2.018$ g cm^{-3} (at 293 K).

The intensity data at the two temperatures were collected in a 2θ range of 0—60° by using the 2θ-ω scan technique. Of 402 independent reflections at 298 K and of 392 ones at 120 K, 383 reflections at 298 K and 364 ones at 120 K were observable ($F_o>3\sigma_{CS}$); these were used in the present analysis and refinement. No correction was made for absorption (μ for Mo $K\alpha=31.3$ cm^{-1}).

Structure Determination and Refinement

Weissenberg and precession photographs of zero- and upper-layers showed that the space group is either R32, R3m, or $R\bar{3}m$ at both 120 and 298 K, and that no change in crystal symmetry occurs on passing through the phase transition. By judging from the solutions of the structure, the space group was determined to be $R\bar{3}m$

for both phases.

The positional parameters of the Cl atom reported by Wyckoff,[1] together with the isotropic thermal parameters of the Sn and Cl atoms, were refined by least-squares methods with the intensity data collected at 298 K. Using the intensity data phased with these coordinates, three-dimensional electron density maps were calculated. The position of the C atom was clearly distinguished from that of the N atom; the peaks assigned to C and N atoms were as high as 8.0 and 11.0 e/Å^3, respectively. Successive difference Fourier syntheses did not yield any hydrogen position. The block-diagonal least-squares refinement with anisotropic thermal parameters was continued until the maximum shift of any parameter was less than one-fifth of its associated e.s.d. The structure in the low-temperature phase was determined at 120 K by almost the same procedure as described above.

The atomic scattering factors for Sn^{4+}, Cl^-, C, and N and the anomalous dispersion corrections f' and f'' for Sn and Cl were taken from the International Tables for X-Ray Crystallography, Vol. IV.[6] The quantity minimized in the refinement was $\sum w(|F_o|-k|F_c|)^2$ with unit weight for all reflections. The final residual values, $R[=\sum||F_o|-|F_c||/\sum|F_o|]$, of 0.052 and 0.062 were obtained at 298 and 120 K, respectively. The final positional and thermal parameters of non-hydrogen atoms at the two temperatures are presented in Table 2. The coordinates for all H atoms were calculated by assuming their existence on the crystallographic mirror planes, the staggered conformation of the $CH_3NH_3^+$ ions, and the bond lengths and angles: N–H=1.03 Å, C–H=1.09 Å, C–N–H=109.47°, and N–C–H=109.47°. Thus the assumed positions are also included in Table 2. The main interatomic distances and angles are given in Table 3. A list of the observed and calculated structure factors at 120 and 298 K has been deposited with the Chemical Society of Japan (Document No. 7904).

All computations were made on a NEAC 2200/700 at the computer center, Osaka University, using local modifications of RSSFR-5, HBLS-IV, and RSDA-4 in the UNICS program system,[7] and the stereoscopic drawing program ORTEP.[8]

Table 2. Positional (x_j) and thermal parameters (B_{ij}/Å^2) for $(CH_3NH_3)_2SnCl_6$ in hexagonal coordinate system

Estimated standard deviations are given in parentheses. The anisotropic thermal factors are of the form: $T=\exp[-1/4(h^2a^{*2}B_{11}+\ldots+2klb^*c^*B_{23})]$.

Atom	Wyckoff notation		120 K	298 K
Sn	3 a	$x=y=z=0$		
		$B_{11}(=B_{22}=2B_{12})$	0.32(4)	1.98(5)
		B_{33}	1.20(5)	4.17(7)
		$B_{13}=B_{23}=0$		
Cl	18 h	$x(=-y)$	0.1617(4)	0.1599(4)
		z	0.0632(1)	0.0628(1)
		$B_{11}(=B_{22})$	2.29(16)	3.52(17)
		B_{33}	1.40(7)	4.59(11)
		B_{12}	1.90(9)	2.37(10)
		$B_{13}(=-B_{23})$	−0.07(6)	−0.32(9)
N	6 c	$x=y=0$		
		z	0.2738(8)	0.2729(9)
		$B_{11}(=B_{22}=2B_{12})$	5.14(71)	7.74(84)
		B_{33}	5.21(69)	8.56(92)
		$B_{13}=B_{23}=0$		
C	6 c	$x=y=0$		
		z	0.2039(9)	0.2051(11)
		$B_{11}(=B_{22}=2B_{12})$	4.51(121)	5.69(126)
		B_{33}	0.95(61)	4.10(102)
		$B_{13}=B_{23}=0$		
H(N)[a]	18 h	$x(=-y)$	−0.0792	−0.0782
		z	0.2895	0.2885
H(C)[a]	18 h	$x(=-y)$	0.0838	0.0827
		z	0.1872	0.1886

a) This position is assumed. See text.

Table 3. Interatomic distances (l/Å) and angles (θ/°)

		120 K	298 K
(a) $[SnCl_6]^{2-}$ octahedron			
Sn–Cl	*6 times*	2.415(2)	2.417(3)
Cl–Sn–Cl^{i}	*6 times*	90.71(6)	90.72(7)
Cl–Sn–Cl^{ii}	*6 times*	89.29(6)	89.28(7)
Cl–Cl^{i}	*6 times*	3.436(2)	3.439(3)
Cl–Cl^{iii}	*6 times*	3.394(3)	3.396(2)
(b) CH_3–NH_3^+ ion			
C–N		1.522(25)	1.487(30)
(c) Between ions			
Cl···Cl^{iv}	*twice*	3.646(16)	3.732(19)
C···Cl	*3 times*	3.652(16)	3.703(20)
C···Cl^{vi}	*6 times*	3.824(7)	3.863(9)
N···Cl^{v}	*3 times*	3.404(13)	3.458(14)
N···Cl^{vi}	*6 times*	3.542(2)	3.587(2)
N–C···Cl	*3 times*	147.09(17)	147.57(20)
C–H(C)···Cl	*3 times*	129.0	128.6
N–C···Cl^{vi}	*6 times*	67.82(27)	68.17(33)
C–H(C)···Cl^{vi}	*6 times*	113.3	113.6
C–N···Cl^{v}	*3 times*	141.80(17)	141.46(19)
N–H(N)^{vii}···Cl^{v}	*3 times*	135.4	136.1
C–N···Cl^{vi}	*6 times*	88.73(27)	89.19(29)
N–H(N)^{vii}···Cl^{vi}	*6 times*	132.4	133.3
Symmetry code			
none	x,	$-x$,	z,
i	x,	$2x$,	z,
ii	$-x$,	$-2x$,	$-z$,
iii	$2x$,	x,	$-z$,
iv	x,	$-1+2x$,	z,
v	$2/3-2x$,	$1/3-x$,	$1/3+z$,
vi	$2/3-x$,	$1/3+x$,	$1/3-z$,
vii	$-2x$,	$-x$,	z,

Results and Discussion

Crystal Structure. The structure described by Wyckoff[1] was confirmed to be essentially correct. The present study showed that there is no change in the basic structure in moving between the high- and low-temperature phases. This finding is an important piece of structural information about the phase transition which will be discussed later.

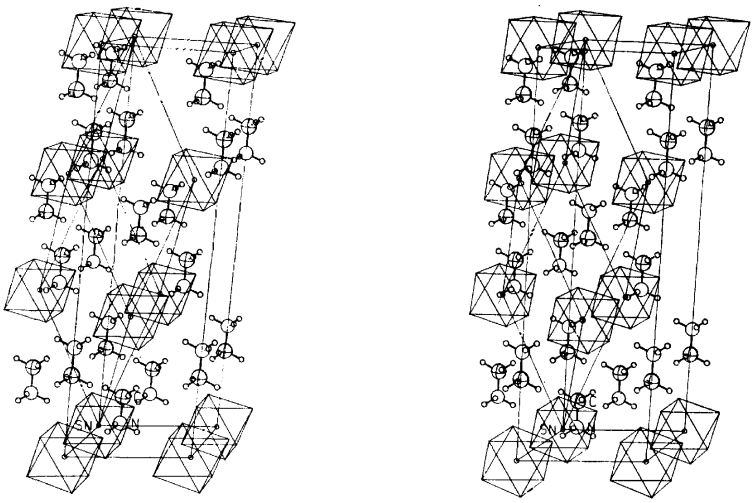

Fig. 1. Stereoscopic drawings of the crystal structure of $(CH_3NH_3)_2SnCl_6$.

The crystal consists of dumbell-like $CH_3NH_3^+$ ions and octahedral $[SnCl_6]^{2-}$ ions. These ions are arranged, in principle, in an antifluorite-type structure like K_2PtCl_6, but the real unit cell is deformed rhombohedrally by elongation along one body-diagonal of the cube. The C–N axes of cations are parallel to the hexagonal c-axis thus obtained. The packing of both ions and the relation between the unit cell in the hexagonal coordinate system ($Z=3$) and that in the rhombohedral coordinate system ($Z=1$) are illustrated in Fig. 1. It is clear that each ion species forms separate layers parallel to the hexagonal basal plane. The octahedron layer seems to be stabilized by electrostatic interaction between the negatively charged octahedra and the positively charged NH_3^+ groups of cations. Then the layers of octahedra are held together by van der Waals interactions between CH_3 residues and Cl atoms. Because the locations of the Cl atoms do not deviate largely from a close-packing of Cl atoms, the stacking sequence of chlorine sheets can be regarded as ABCABC along the hexagonal c-axis.

In the crystal lattice, each cation is tetrahedrally surrounded by four complex anions, while each anion has eight cation neighbors. The CH_3 group of a cation faces the triangle of Cl atoms coming from the same octahedron. The equivalent three C···Cl distances (3.70 Å) are shorter than the van der Waals distance (2.0+1.8=3.8 Å), and much shorter than the corresponding value (3.90 Å) found in CH_3NH_3Cl.[9] However, a reasonable assumption of tetrahedral angles around a methyl carbon atom leads us to speculate that the C–H bond should deviate greatly from the C···Cl direction; the C–H···Cl angle is estimated to be 129° from the coordinates given in Table 2. Therefore, the methyl group of a cation only has contact with three Cl atoms, and can scarcely form C–H···Cl type hydrogen bonds.

The other end of the cation, *i.e.* the NH_3 group, has nine Cl neighbors, three from each of the three $[SnCl_6]^{2-}$ ions. The nine N···Cl distances (three 3.46 and six 3.59 Å) are rather long compared with those in such chloride compounds as: CH_3NH_3Cl (N···Cl=3.18 Å),[9] NH_4Cl (3.35 Å),[10] $NH_4HgCl_3\cdot H_2O$ (3.31—3.41 Å),[11] $C_4N_2O_3H_9Cl\cdot H_2O$ (3.18—3.30 Å),[12] and $C_5H_{10}O_4N\cdot C$ (3.16—3.21 Å).[13] On the other hand, the N···Cl distances in the present $(CH_3NH_3)_2SnCl_6$ are comparable to the 3.55 Å reported for $(NH_4)_2SnCl_6$.[14] As evidenced by the Sn–Cl distance of 2.417 Å at 298 K, as well as the ^{35}Cl-NQR frequency of 15.815 MHz at 300 K,[2] the Sn–Cl bond nature is far less ionic and, consequently the effective charge on the Cl^- ion may be appreciably reduced. Furthermore, each hydrogen atom of an NH_3 group is probably pointed toward nearly the center of a triangle of Cl atoms, forming a trifurcated hydrogen-bond. However the average H···Cl distance (2.75 Å) is too large, and also the average N–H···Cl angle (134°) is too small, for a significant hydrogen-bond interaction. Such an arrangement of the H atoms or a very weak hydrogen-bonding scheme is supported by the PMR results described previously.[3] Thus, the $CH_3NH_3^+$ ion can exhibit the reorientation about its three-fold axis as a whole, instead of the individual or uncorrelated motions of CH_3 and NH_3 groups with different activation energies which are recognized in typical CH_3NH_3Cl and other related compounds.[15,16]

The C–N distances were determined to be 1.49 and 1.52 Å at 298 and 120 K, respectively. Each value, especially the room temperature one, is quite usual for normal single-bond lengths between carbon and quaternary nitrogen atoms, in comparison with those in $(CH_3NH_3)_2MnCl_4$,[17] $(CH_3NH_3)_2ZnCl_4$,[18] and CH_3NH_3Cl.[9] It may be noted that the C–N distance in the high-temperature phase is a little shorter than in the low-temperature one. Such a tendency has been established in chloride perovskite-layer-compounds and interpreted in terms of a change in motion of methylammonium ions.[17,19] But a tilting motion of the C–N bond relative to the c-axis expected above T_t cannot be confirmed by the present study, because the difference in C–N distance is only twice the associated e.s.d. (Table 3).

Thermal Expansion. The lattice constants and the unit-cell volumes are plotted against temperature in Fig. 2, where the ordinate scales are normalized to the

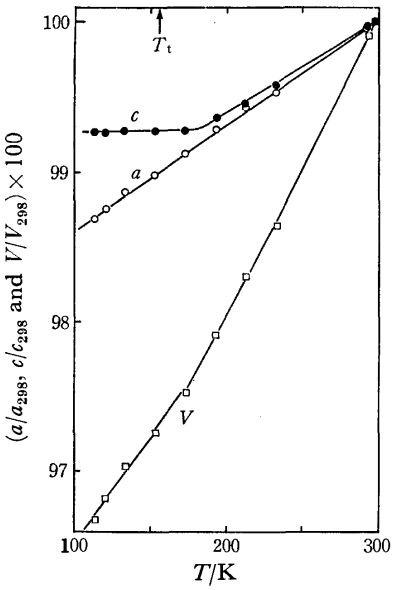

Fig. 2. Variation of a/a_{298}, c/c_{298} and V/V_{298} with temperature, where a_{298} *etc.* stand for the lattice constants at 298 K.

respective values at 298 K. The a-axis length increases steadily with a thermal expansion coefficent $(1/a)da/dT$ of 0.7×10^{-5} over the whole temperature range. On the other hand, the c-axis remains at almost the same length between 120 and 180 K (across T_t), above which it starts to increase with a linear coefficient $(1/c)dc/dT$ of 0.6×10^{-5}. Although this anomaly should be reflected in the volume change, its effect may be largely masked by the more effective expansion of the a-axis. Consequently the unit-cell volume appears to change continuously near T_t, indicating that the phase transition is approximately of a higher order. It is therefore concluded that the detectable change in structure on the phase transition is only the anomaly of the c-axis length. This finding may help us to understand the mechanism of the phase transition.

Very recently, we have found a similar structural phase transition in the trigonal phase of the tellurium(IV) complex, $(CH_3NH_3)_2TeCl_6$, which is isomorphous with the tin(IV) complex.[20]

Phase Transition. The present X-ray work showed that the basic structures are identical above and below T_t. Among the three space groups allowed for a diffraction symmetry of $\bar{3}$m, only R$\bar{3}$m was preferred for both phases. The ^{35}Cl-NQR results, however, suggested the softening of some rotary phonon of the anion octahedra as a mechanism of the phase transition.[2,4] If this is the case, the appearance of a superstructure and/or a small deviation from the space group R$\bar{3}$m would be expected in the low-temperature phase. The first possibility was easily excluded because no extra spot nor superstructure spot was detected on the X-ray photographs in spite of long exposure. On the other hand, the second possibility is likely to happen if the rotary mode of $[SnCl_6]^{2-}$ octahedra about the c-axis, *i.e.* their three-fold axes, softens at the Γ point of the Brillouin zone.

Hence, this possibility was checked by permitting the lowering of the diffraction symmetry. It is evident that all the Cl atoms are equivalent even below T_t, because a single ^{35}Cl-NQR line is observable in the low-temperature phase.[2] Accordingly, the diffraction symmetry should be $\bar{3}$ and then the space group is limited to R$\bar{3}$. Actually the refinement of the low-temperature structure in R$\bar{3}$ yielded a rather poor *R*-value of 0.066. In this trial, however, the Cl atom is displaced only by 0.004 Å, which corresponds to a 0.13° rotation of the $[SnCl_6]^{2-}$ octahedra about the c-axis. Such a very small displacement is of no significance, since it is less than twice of its associated e.s.d. Additionally, taking into account the thermal ellipsoid of the Cl atom, which was rather spherical in the low-temperature phase, we cannot pick out the rotation of $[SnCl_6]^{2-}$ octahedra, at least positively.

In this connection, there arose a new question of whether or not the single crystal might be twinned when it was cooled down below T_t. The shift of the Cl position to either side of the mirror plane in R$\bar{3}$m will produce the identical structure, regardless of its orientation. If such twinning occurs, both individual crystals must be related to each other by a 180° rotation about the [210] direction, followed by a 180° rotation about the c-axis. The diffraction intensity in this case can be expressed by $xF^2(hkl)+yF^2(\bar{k}\bar{h}l)$ instead of the usual $F^2(hkl)$, where x and y stand for the volume fractions of both individuals. Therefore, when the twin effect is neglected, the refinement of the low-temperature structure may lead us to unreasonable positional parameters or incredible thermal parameters, especially for the Cl atom. However, as described previously, the results refined in R$\bar{3}$m (Table 2) as well as the electron density maps are good enough to exclude the occurrence of any twinning.

In conclusion, the X-ray study cannot provide any evidence to support the transition mechanism which has been ascribed to a softening of some rotary lattice mode of the anion octahedra. It is therefore conceivable that the rotation angle of the $[SnCl_6]^{2-}$ ion expected for the low-temperature phase is too small to be detected by the present X-ray experiments. On the other hand, an alternative mechanism was proposed from the structural anomaly in the c-spacing. That is, the phase transition in this compound may be primarily triggered by softening of some acoustic mode at the zone center, because it is accompanied by the bulk deformation but not by any change in the structure.

The authors wish to express their thanks to Professor Emeritus Ryôiti Kiriyama for his continuous encouragement and fruitful discussion. This work was partially supported by a Grant-in-Aid for Scientific Research from the Ministry of Education (No. 154141).

References

1) R. W. G. Wyckoff, *Am. J. Sci.*, **16**, 349 (1928).
2) Y. Kume, R. Ikeda, and D. Nakamura, *J. Magn. Reson.*, **20**, 276 (1975).
3) R. Ikeda, Y. Kume, D. Nakamura, Y. Furukawa, and H. Kiriyama, *J. Magn. Reson.*, **24**, 9 (1976).
4) Y. Furukawa, H. Kiriyama, and R. Ikeda, *Bull. Chem.*

Soc. Jpn., **50**, 1927 (1977).
5) R. L. Armstrong, *J. Magn. Reson.*, **20**, 214 (1975).
6) "International Tables for X-Ray Crystallography," Kynoch Press, Birmingham (1974), Vol. IV, pp. 71—98 and 148—150.
7) "UNICS Program System," ed by T. Sakurai, Crystallographic Society of Japan (1967).
8) C. K. Johnson, ORTEP. Oak Ridge National Laboratory Report ORNL-3794 (1965).
9) E. W. Hughes and W. L. Lipscomb, *J. Am. Chem. Soc.*, **68**, 1970 (1946).
10) R. W. G. Wyckoff, "Crystal Structures," 2nd ed, Interscience Publishers, New York (1963), Vol. 1, p. 104.
11) K. Sagisawa, K. Kitahama, H. Kiriyama, and R. Kiriyama, *Acta Crystallogr., Sect. B*, **30**, 1603 (1974).
12) T. F. Koetzie, W. C. Hamilton, and R. Parthasarathy, *Acta Crystallogr., Sect. B*, **28**, 2083 (1972).
13) A. Sequeira, H. Rajagopal, and R. Chidambaram, *Acta Crystallogr., Sect. B*, **28**, 2514 (1972).
14) J. A. Lerbscher and J. Trotter, *Acta Crystallogr., Sect. B*, **32**, 2671 (1976).
15) S. Albert and J. A. Ripmeester, *J. Chem. Phys.*, **58**, 541 (1973).
16) J. Tsau and D. F. R. Gilson, *Can. J. Chem.*, **48**, 717 (1976).
17) I. Mikhail, *Acta Crystallogr., Sect. B*, **33**, 1317 (1977); **33**, 1321 (1977).
18) B. Morosin and K. Emerson, *Acta Crystallogr., Sect. B*, **32**, 294 (1976).
19) G. Chapuis, H. Arend, and R. Kind, *Phys. Status Solidi A*, **31**, 449 (1975).
20) K. Kitahama and H. Kiriyama, Abstr. No. 2J18, 37th National Meeting of the Chemical Society of Japan, Yokohama, April 1978; *Acta Crystallogr., Sect. A*, S302 (1978).

The Low-Energy π,π^* S-S Absorption Spectra of 1,4-Dimethyl- and 1,4-Dichloroanthraquinones

Akira KUBOYAMA

National Chemical Laboratory for Industry, Shibuya-ku, Tokyo 151

(Received July 6, 1978)

The very broad absorption band of 1,4-dichloroanthraquinone, which corresponds to the allowed $^1B_{2u}\pi,\pi^*$ band of anthraquinone (AQ), is shown to consist of two π,π^* bands with comparable intensities. The band which corresponds to the ^1A_g forbidden band of AQ is at longer wavelengths than the band corresponding to the $^1B_{2u}$ band of AQ. MO calculations were made, and MCD spectra and 77 K absorption spectra were measured. The very broad absorption band of 1,4-dimethyl-AQ can probably be similarly interpreted. The strong visible π,π^* bands of 1,4- and 1,5-disubstituted AQ's are shown to arise from the ^1A_g and $^1B_{2u}$ bands of AQ respectively.

In the π,π^* S-S absorption spectrum of anthraquinone (AQ) the $^1B_{2u}$ band near 330 nm is the only one so far found in the wavelength region longer than 300 nm.[1-3] According to the P-P-P method[4] calculations,[2,3] a forbidden ^1A_g level is predicted to be located close to this allowed $^1B_{2u}$ level. However, few experimental facts about this ^1A_g forbidden state have been reported.[5] Recently, we noticed that 1,4-dimethyl-AQ seems to show a rather intense band corresponding to the ^1A_g band on the longer wavelength side of the band corresponding to the $^1B_{2u}$ band, and that the P-P-P method calculations support this interpretation. We have therefore studied the π,π^* S-S absorption spectra of various symmetrically substituted dimethyl-AQ's and dichloro-AQ's in this wavelength region.

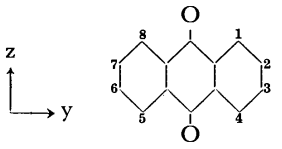

(AQ)

Experimental

Measurements. The absorption spectra were measured with a Cary 14 M recording spectrophotometer, using cyclohexane as solvent. A Dewar vessel and 1 mm-path cells[6] were used to obtain the absorption spectra at 77 K, using heptane as solvent. The magnetic circular dichroism (MCD) spectra were obtained by a J-40 circular dichroism spectrometer of the Japan Spectroscopic Co., Ltd.,[7] with a magnetic field of 3500 Gauss, using cyclohexane as solvent.

Materials. Commercially-available AQ was zone-refined (mp 286.6—287.2 °C). Commercially-available 1,4-dimethyl-AQ and 1-chloro-AQ were purified by vacuum sublimation (mp 141.0—142.0 °C and 159.0—160.5 °C). Commercially-available 2,3-dimethyl-AQ and 1,5-dichloro-AQ were twice recrystallized, from a toluene and cyclohexane (1:2) mixture and from acetic acid respectively (mp 207.5—208.8 °C and 243.3—244.0 °C). According to the method described in the literature,[8] 1,4-dichloro-AQ was synthesized, purified by liquid chromatography on alumina using toluene as developer, and obtained as yellow crystals[9] (mp 190.5—191.0 °C). Commercially-available heptane and cyclohexane of spectrograde quality were used.

Results. The absorption and MCD spectra obtained are shown in Figs. 1—4. The wavelengths and molar absorption coefficients of the absorption maxima in these absorption spectra are shown in Table 1. The MCD spectra were obtain-

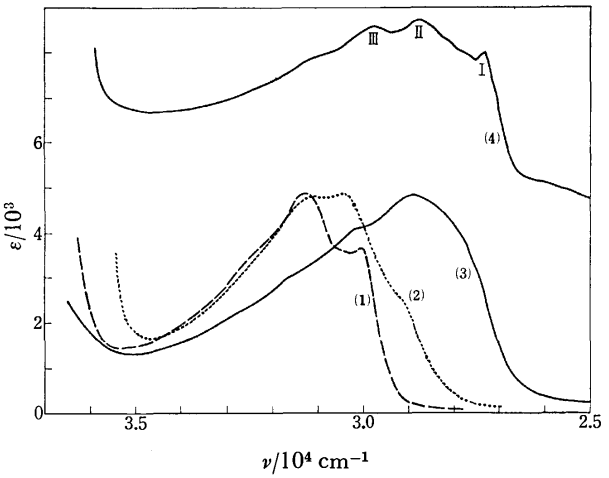

Fig. 1. Absorption spectra of AQ, 2,3-dimethyl-AQ, and 1,4-dimethyl-AQ in solutions.
1) AQ, 2) 2,3-dimethyl-AQ, 3) 1,4-dimethyl-AQ, 4) 1,4-dimethyl-AQ. Solvent: 1)—3) cyclohexane, 4) heptane. Temperature: 1)—3) room temperature, 4) 77K. The ordinates for 2) and 4) are arbitrary.

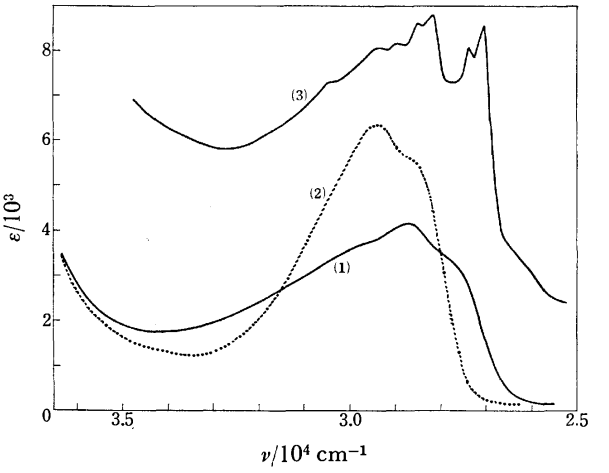

Fig. 2. Absorption spectra of 1,4-dichloro-AQ and 1,5-dichloro-AQ in solutions.
1) 1,4-Dichloro-AQ, 2) 1,5-dichloro-AQ, 3) 1,4-dichloro-AQ. Solvent; 1), 2) cyclohexane, 3) heptane. Temperature: 1), 2) room temperature, 3) 77 K. The ordinate for 3) is arbitrary.

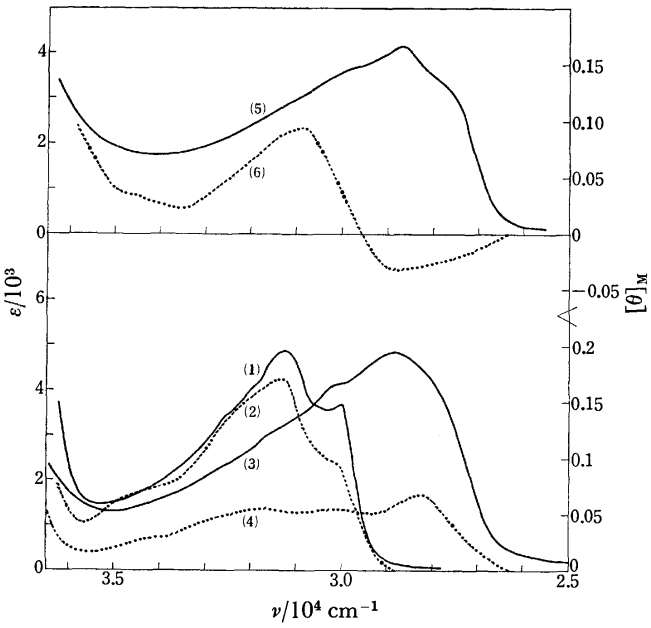

Fig. 3. Absorption and MCD spectra of AQ, 1,4-dimethyl-AQ, and 1,4-dichloro-AQ in the cyclohexane solutions.
1), 2) AQ, 3), 4) 1,4-Dimethyl-AQ, 5), 6) 1,4-Dichloro-AQ. The solid and dotted curves are the absorption and MCD spectra respectively, where the left and right side ordinates are used respectively.

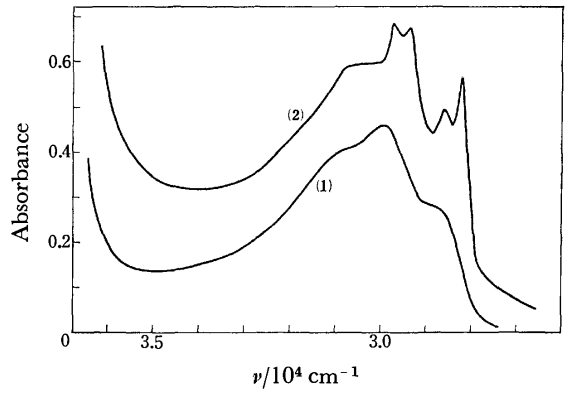

Fig. 4. Absorption spectra of 1-chloro-AQ in the heptane solutions.
1) Room temperature, 2) 77 K. The ordinate is arbitrary.

ed with a relatively high noise-level, because of using the low magnetic field. However, their accuracy is thought to be not so low as to affect the discussion in this work.

Calculations

Method. The electronic integral values for AQ in the P-P-P method[4] were the same as those[3] previously used. To account for the effect of methyl-group substitution, the core Coulomb integral of the substituted

TABLE 1. WAVELENGTHS AND MOLAR ABSORPTION COEFFICIENTS OF THE ABSORPTION MAXIMA

	λ (nm)	ε	Solvent	Temperature
AQ	333	3680	Cyclohexane	Room temp
	320	4870		
	≈308			
1,4-Dimethyl-AQ	346	4850	Cyclohexane	Room temp
	≈331.5(sh)			
	366.5		Heptane	77 K
	347.5			
	336.5			
	320			
2,3-Dimethyl-AQ	≈344(sh)		Cyclohexane	Room temp
	328.5			
	321.5			
1,4-Dichloro-AQ	≈361.5(sh)		Cyclohexane	Room temp
	348	4120		
	≈337(sh)			
	369.5		Heptane	77 K
	354.5			
	350.5			
	346			
	340			
1,5-Dichloro-AQ	≈351(sh)		Cyclohexane	Room temp
	339.5	6330		
1-Chloro-AQ	≈349(sh)		Heptane	Room temp
	335			
	≈323(sh)			
	355		Heptane	77 K
	350			
	340.5			
	337			
	≈326(sh)			

TABLE 2. CALCULATED RESULTS FOR THE DIMETHYL AQ'S

	No.	Symmetry	E(eV)	f_y	f_z
AQ	1	^1A_g	4.17	0	0
	2	$^1B_{2u}$	4.25	0.081	0
	3	$^1B_{3g}$	4.42	0	0
1,4-Dimethyl-AQ	1	$^1A_1$	4.09	0.076	0
	2	$^1A_1$	4.22	0.075	0
	3	$^1B_2$	4.42	0	0.001
1,5-Dimethyl-AQ	1	^1A_g	4.13	0	0
	2	^1B_u	4.19	0.149	0.002
	3	^1A_g	4.43	0	0
1,8-Dimethyl-AQ	1	$^1A_1$	4.13	0	0.001
	2	$^1B_2$	4.19	0.148	0
	3	$^1B_2$	4.43	0.002	0
2,3-Dimethyl-AQ	1	$^1A_1$	4.17	0.000	0
	2	$^1A_1$	4.25	0.065	0
	3	$^1B_2$	4.35	0	0.044
2,6-Dimethyl-AQ	1	^1A_g	4.16	0	0
	2	^1B_u	4.25	0.065	0.011
	3	^1A_g	4.38	0	0
2,7-Dimethyl-AQ	1	$^1A_1$	4.17	0	0.000
	2	$^1B_2$	4.22	0.054	0
	3	$^1B_2$	4.39	0.003	0

carbon atoms was taken as −9.00 eV, considering only the inductive effect of the methyl group, as in the previous work.[3] The core Coulomb integral and two-center electron repulsion integral of chlorine atoms and the core resonance integral of the C–Cl bonds were taken as −25.00, 14.30, and −0.75 eV respectively.[10] In the calculations, the lowest thirty singly-excited configurations were included. The dimension of the AQ skeleton in the AQ derivatives was that of AQ.[3] The bond length of the C–Cl bonds was assumed to be 1.75 Å.

Results. The calculated results for the three lowest-energy singlet excited states of AQ and the symmetrically substituted dimethyl-AQ's are shown in Table 2: the first column indicates the numbering of the states in order of increasing excitation energies (calculated). In Fig. 5, the calculated results for 1,4-dichloro-AQ, taking −0.75 and −1.50 eV for the core Coulomb integral values of the C–Cl bonds, are shown together with that for AQ.

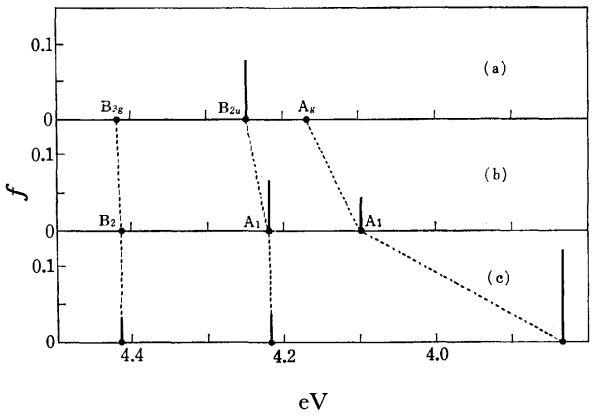

Fig. 5. Comparisons of the calculated excitation energies and oscillator strengths of the low-energy π,π^* states of AQ and 1,4-dichloro-AQ.
a) AQ, b) 1,4-dichloro-AQ (β(C–Cl) = −0.75 eV), c) 1,4-dichloro-AQ (β(C–Cl) = −1.50 eV).

Discussion

The absorption band of AQ in Fig. 1 has been theoretically and experimentally assigned to the $^1B_{2u}$ band by many authors.[1-3] In the absorption band of 1,4-dimethyl-AQ in Fig. 1, the absorption maximum is at far longer wavelengths than those for AQ and 2,3-dimethyl-AQ, and the half-width (5170 cm^{-1}) is far larger than those for the latter (3850 and 4210 cm^{-1} respectively). In Fig. 2, the absorption spectrum of 1,4-dichloro-AQ, which is far broader than that of 1,5-dichloro-AQ, is similar to that of 1,4-dimethyl-AQ in position and shape. The absorption spectra of 1,8-dichloro-AQ[11] and 2,6-dichloro-AQ[12] reported by other authors in this wavelength region are similar to those of 1,5-dichloro-AQ and AQ respectively in position and shape. From these facts, it may be considered that in 1,4-dimethyl-AQ and 1,4-dichloro-AQ, a band corresponding to that ^1A_g band appears with a considerable intensity on the longer wavelength side of the band corresponding to the $^1B_{2u}$ band.

In Table 2, the three lowest-energy π,π^* states, the Nos. 1—3 states, of all the dimethyl-AQ's correspond to the Nos. 1—3 states of AQ: the ^1A_g, $^1B_{2u}$, and $^1B_{3g}$ states respectively. As may be seen in Table 2, only in 1,4-dimethyl-AQ does the No. 1 state have a relatively large oscillator strength; there its energy is considerably lower than that of the ^1A_g state of AQ. Similar calculated results were obtained for 1,4-dichloro-AQ. These calculated results support the above assignment of the π,π^* spectra of 1,4-dimethyl-AQ and 1,4-dichloro-AQ. In these two AQ's, on the basis of the calculated results, it has been proved that the excitations to the Nos. 1 and

2 states have the character of a charge-transfer from the carbon atoms of the 1- and 4-positions and the 5- and 8-positions, respectively, to the carbonyl groups.

In the absorption spectra of 1,4-dimethyl-AQ and 1,5-dichloro-AQ, the two $^1A_1$ bands corresponding to the excitations to the Nos. 1 and 2 states can not be discriminated by the usual dichroism measurements. In this work, therefore, their MCD spectra and that of AQ[13] in this wavelength region have been measured. Since these compounds have no electronic degenerate states, all the MCD spectra obtained are B-type.[13,14] In Fig. 3, the MCD spectrum of 1,4-dichloro-AQ consists of a negative and a positive band in the longer and shorter wavelength regions, respectively, while those of AQ and 1,4-dimethyl-AQ show only a positive spectrum. On the basis of these results, the absorption spectrum of 1,4-dichloro-AQ may be concluded to consist of two absorption bands, one of which is at longer wavelengths than the other. This result proves the previous assignment of the spectrum of 1,4-dichloro-AQ to be correct. On the other hand, the sign of the MCD in the longer wavelength region of the absorption spectrum of 1,4-dimethyl-AQ is opposite to that for 1,4-dichloro-AQ. In general, the MCD for originally forbidden bands may be expected to depend strongly on the substituents, as in the case of the L_b bands of benzene derivatives.[15] In 1,4-dimethyl-AQ, the calculated results show that the electron-donative inductive effect of the two methyl groups plays an important role in the intensity enhancement of the longer wavelength $^1A_1$ band. On the other hand, in 1,4-dichloro-AQ, the calculated results show that the electron-attractive resonance effect of the two chlorine atoms does so. Therefore, this difference of the electronic property between these two substituents may be expected to bring about the above mentioned difference of the MCD sign.

In the absorption spectra of 1,4-dichloro-AQ (Fig. 2) and 1-chloro-AQ (Fig. 4) in the heptane solutions at 77 K, four sharp peaks[16] are observed in the longer wavelength region; they may be assigned to the $^1A_1$ band corresponding to the ^1A_g band of AQ. In the absorption spectrum of 1-chloro-AQ in the heptane solution at room temperature (Fig. 4), therefore, the shoulder on the longer wavelength side may also be assigned in the same way. In the absorption spectrum of 1,4-dimethyl-AQ at room temperature (Fig. 1), a small but relatively sharp shoulder is observed near 330 nm on the broad absorption curve; this may be considered to belong to the $^1A_1$ band corresponding to the $^1B_{2u}$ band of AQ. This peak may correspond to Peak III in the 77 K spectrum (Fig. 1), and the sharp Peak I in the latter spectrum may be considered to belong to the $^1A_1$ band corresponding to the ^1A_g band of AQ, as in the case of 1,4-dichloro-AQ. On the basis of the theoretically and experimentally obtained results for the absorption spectrum of 1,4-dimethyl-AQ, it may be considered that the assignment of that spectrum is also likely to be correct.

In Fig. 5, an increase of the absolute value of the core Coulomb integral of the C–Cl bonds means an increase of the electron-donative power of the chlorine atoms. In 1,4-dichloro-AQ (Fig. 5), the lower $^1A_1$ level (the No. 1 level) drops significantly and its oscillator strength becomes strikingly larger, with an increase in the absolute value of that integral, while the higher $^1A_1$ level (the No. 2 level) shows almost no change and its oscillator strength becomes considerably smaller. On the other hand, in 1,5-dichloro-AQ, the ^1A_g levels are the forbidden levels, and the ^1B_u level drops considerably and its oscillator strength becomes markedly larger with an increase in the absolute value of that integral. On the basis of these calculated results, the strong π,π^* bands of 1,4-dihydroxy-AQ[17] and 1,4-diamino-AQ[18,19] and 1,5-dihydroxy-AQ[17] and 1,5-diamino-AQ[18] in the visible range may be concluded to arise from the $^1A_g \leftarrow {}^1A_g$ and $^1B_{2u} \leftarrow {}^1A_g$ transitions of AQ respectively, and the relatively weak π,π^* bands of 1,4-dihydroxy-AQ and 1,4-diamino-AQ near 330 nm to arise from the $^1B_{2u} \leftarrow {}^1A_g$ transition of AQ. This conclusion about the spectra of these 1,4-disubstituted AQ's is consistent with the polarized absorption spectra of 1,4-diamino-AQ reported by Inoue *et al.*[19] and Labhart.[20]

The author is grateful to Mr. A. Takakuwa of the Japan Spectroscopic Co., Ltd., and to Prof. M. Miwa and Dr. T. Komiyama of Seikei University for their helpful cooperation in obtaining the MCD spectra.

References

1) H. R. Drott and H. H. Dearman, *J. Chem. Phys.*, **47**, 1876 (1967); A. Kuboyama and S. Yabe, *Bull. Chem. Soc. Jpn.*, **40**, 2475 (1967); H. Inoue, T. Hoshi, and Y. Tanizaki, *Nippon Kagaku Zasshi*, **92**, 25 (1971).

2) K. Nishimoto and L. S. Foster, *Theor. Chim. Acta*, **4**, 155 (1966); L. Leibovici and J. Deschamps, *ibid.*, **4**, 321 (1966); T. L. Kunii and H. Kuroda, *Rep. Compt. Cent. Univ. Tokyo*, **1**, No. 1, 163 (1968).

3) A. Kuboyama, S. Matsuzaki, M. Takagi, and H. Arano, *Bull. Chem. Soc. Jpn.*, **47**, 1604 (1974); *Tokyo Kogyo Shikensho Hokoku*, **69**, 492 (1974).

4) R. Pariser and R. G. Parr, *J. Chem. Phys.*, **21**, 466, 767 (1953); J. A. Pople, *Trans. Faraday Soc.*, **49**, 1375 (1953).

5) N. S. Strokach and D. N. Shigorin, *Opt. Spectrosc.*, **43**, 34 (1977).

6) A. Kuboyama, R. Yamazaki, S. Yabe, and Y. Uehara, *Bull. Chem. Soc. Jpn.*, **42**, 10 (1969); *Tokyo Kogyo Shikensho Hokoku*, **64**, 465 (1969).

7) By courtesy of the Japan Spectroscopic Co., Ltd., an instrument in its laboratory was used.

8) M. Phillips, *J. Am. Chem. Soc.*, **48**, 3198 (1926).

9) In Ref. 8, orange crystals were obtained.

10) A. Kuboyama, F. Kobayashi, and S. Morokuma, *Bull. Chem. Soc. Jpn.*, **48**, 2145 (1975); *Tokyo Kogyo Shikensho Hokoku*, **71**, 180 (1976).

11) H. Hartmann and E. Lorenz, *Z. Naturforsch., Teil A*, **7**, 360 (1952).

12) M. Nepras, M. Vecera, J. Borecky, and M. Jureck, *Collect. Czech. Chem. Commun.*, **28**, 2706 (1963).

13) H. H. Dearman, *J. Chem. Phys.*, **58**, 2135 (1973).

14) A. D. Buckingham and P. J. Stephens, *Ann. Rev. Phys. Chem.*, **17**, 399 (1966).

15) J. G. Foss and M. E. McCarville, *J. Am. Chem. Soc.*, **89**, 30 (1967).

16) In Figs. 1, 2, and 4, sharp peaks in the 77 K spectra may appear due to the Shpol'skii effect (E. V. Shpol'skii, *Sov. Phys. Usp.*, **3**, 372 (1960); **5**, 522 (1962); **6**, 411 (1963)).
17) A. Morton and W. T. Earlam, *J. Chem. Soc.*, **1941**, 159, N. A. Shcheglova, D. N. Shigorin, and N. S. Dokunikhin, *Russ. J. Phys. Chem.*, **38**, 1067 (1964).
18) R. H. Peters and H. H. Sumner, *J. Chem. Soc.*, **1953**, 210; DMS, "UV Atlas of Organic Compounds," Butterworths (1968), B8/13, B8/14.
19) H. Inoue, T. Hoshi, J. Yoshino, and Y. Tanizaki, *Bull. Chem. Soc. Jpn.*, **45**, 1018 (1972).
20) H. Labhart, *Chimia*, **15**, 20 (1961).

Ab initio LCAO MO SCF CI Calculations on the Electronic Structure of the Cyclopropenyl Cation

Toshikazu TAKADA* and Kimio OHNO

Department of Chemistry, Faculty of Science, Hokkaido University, Kita-ku, Sapporo 060

(Received July 14, 1978)

Ab initio LCAO MO SCF and limited CI calculations are carried out on the electronic structure of the $C_3H_3^+$ ion. Two kinds of basis sets are used, namely the minimal STO's and the minimal STO's plus 3d orbitals on each carbon atom. With the latter basis, the equilibrium C–C distance is calculated to be 1.389 Å. It is predicted that the C–C bond distance of $C_3H_3^+$ is shorter than that of C_6H_6. The calculated C–C stretching force constant is 7.92 mdyn/Å and is close to the experimental value 6.59 mdyn/Å. Contour diagrams of the charge distribution of valence electrons are drawn and it is revealed that the calculated C–C bonds are bent and have two maxima in charge density. In terms of population analysis of localized MO's, it is shown that the C–H bond in this molecule has a higher s-character than the C–H bonds in C_2H_4 and C_6H_6 and is close to an sp hybrid. This is in accord with a very large NMR coupling constant $J_{^{13}C-H}$. From CI calculations of low lying excited states, singlet σ-π^* states ($^1A_1''$, $^1E''$, $^1A_2''$) are calculated to be lower than the singlet π-π^* state ($^1E'$).

The cyclopropenyl cations are the smallest ring systems which have two π-electrons and satisfy the Hückel $4n+2$ rule. Their electronic structures are of great interest since the molecules are highly strained. The simplest one, $C_3H_3^+$, has been synthesized by Breslow and Groves.[1] The D_{3h} configuration of the ion is indicated on the basis of the IR and NMR spectra.[1] One might think that the C–C bonds in this system would be weaker than the usual C–C bonds such as those in C_6H_6 and thus the equilibrium C–C bond distance would be longer and the C–C stretching force constant smaller. Apparently, this is not the case. X-Ray diffraction shows that trisdimethylaminocyclopropenyl cation has a regular triangle cyclopropenyl ring with a C–C bond length of 1.363 Å[2] and that the C–C bond length of triphenylcyclopropenyl cation is 1.373 Å.[3] These values are significantly smaller than the C–C bond distance of 1.397 Å[4] in C_6H_6. From IR spectra, the Urey-Bradley force constant of the ring C–C stretching of $C_3H_3^+$ has been estimated to be 6.590 mdyn/Å,**,[5] which is larger than the C_6H_6 value of 5.78 mdyn/Å.[6]

In spite of these immense theoretical interest, there have been only three *ab initio* all-electron calculations on $C_3H_3^+$ as far as the authors are aware. Clark carried out *ab initio* LCAO SCF MO calculations on both $C_3H_3^+$ and $C_3H_3^-$ and discussed the aromaticity and antiaromaticity.[7] Ha, Graf and Günthard reported an extensive *ab initio* LCAO SCF MO investigation on $C_3H_3^+$, C_3H_3, and $C_3H_3^-$ and discussed the geometry and stability of these species.[8] Their basis set consists of Gaussian lobe functions and is approximately of the double zeta quality. Radom, Hariharan, Pople, and Schleyer also carried out *ab initio* LCAO SCF MO calculation on $C_3H_3^+$ using STO-3G and 6-31G and obtained the equilibrium structure of the ion.[9]

In this paper, the results of *ab initio* LCAO MO SCF CI calculations on $C_3H_3^+$ are reported. The C–C bond distance is varied and the equilibrium C–C distance and the C–C stretching force constant are calculated and are compared with experiment. The occupied MO's are transformed into localized MO's and the nature of the C–C and C–H bonds is discussed in terms of the contour diagrams of the charge distribution and the population analysis of these localized MO's. CI calculations of the low lying excited states are carried out for the first time and the character of these states is discussed.

Method of Calculations

The wave functions of $C_3H_3^+$ are obtained by *ab initio* LCAO MO SCF and CI calculations. Two kinds of basis sets are used. One is the minimal STO's. The other is the minimal STO's plus 3d orbitals on each carbon atom. One reason for adding the 3d orbitals is to hope for a better description of the bent C–C bonds. The former basis is called Min. and the latter Min.+C3d, hereafter. The orbital exponents adopted are shown in Table 1. The values of H1s and C1s, 2s and 2p orbitals are optimized for C_6H_6 by Hehre, *et al.*[10] The exponents of C3d orbitals are optimized for CO by Nesbet.[11] In the evaluation of molecular integrals, these STO's are expanded in terms of GTO's; the H1s and C1s, 2s and 2p orbitals are expanded by five GTO's and the C3d orbitals by three GTO's, respectively. The expansion coefficients are those given by Stewart.[12]

Table 1. Orbital exponents

H1s	1.21
C1s	5.67
2s, $2p_v$,[a] $2p_h$,[b] $2p_z$	1.71
$3d_{z^2}$, $3d_{h^2-v^2}$, $3d_{hv}$	1.895
$3d_{hz}$, $3d_{vz}$	1.429

a) The v axis is pointing towards the partner H atom.
b) The h axis is in the molecular plane and perpendicular to the v axis.

In the CI calculations, configuration state functions are constructed as follows. All single and double excitations are considered from $2a_1'$, $2e'$, $3a_1'$, $3e'$, and $1a_2''$ to $1e''$, $1a_2'$, $4e'$, $4a_1'$, $2e''$, $2a_2''$, $5e'$, $5a_1'$, and $3e''$ orbitals (These orbitals are indicated by * in Table 2 in Section 3.). Other molecular orbitals are excluded, that

** This value is obtained by assuming that the C–C bond distance of $C_3H_3^+$ is equal to that of triphenylcyclopropenyl cation.

is, $1a_1'$ and $1e'$ as core and the orbitals whose energies are greater than 1.0 a.u. This is called occupation Scheme I. In another choice, occupation Scheme II, only single and double excitations from the four highest occupied MO's $3a_1'$, $3e'$, and $1a_2''$ to the six lowest unoccupied MO's $1e''$, $1a_2'$, $4e'$, and $4a_1'$ are taken into account. The method of the first order interacting space proposed by McLean and Liu[13] is employed in order to reduce the number of configuration state functions without sacrificing the accuracy too much.

The D_{3h} configuration is assumed in the present calculations. This configuration is indicated on the basis of the IR and NMR spectra[1] and is supported theoretically by Ha and others.[8] The C–H internuclear distance is fixed at 1.09 Å which is the observed C–H distance in C_6H_6.[14] The calculation is repeated for the following six C–C distances, 1.300, 1.350, 1.375, 1.400, 1.425, and 1.500 Å. The calculated energy curve is expressed as a fifth degree polynominal of the C–C distance and the minimum energy, the equilibrium C–C distance and the C–C stretching force constant are determined.

In order to investigate the nature of C–C and C–H bonds of the system, the resulting MO's are transformed into localized MO's by a unitary transformation. The measure of localization proposed by Hall[15] and applied extensively by Edmiston and Ruedenberg[16] is adopted. This is to maximize the total self-energy of the orbitals. The unitary transformation is applied only to the valence MO's. Namely the three lowest MO's, $1a_1'$ and $1e'$, are omitted since, in our opinion, the distinction between valence electrons and inner-shell electrons is more fundamental than the requirement of "localization."

Results and Discussion

The calculated potential curves are illustrated in Fig. 1. In the ground state CI calculations, the occupation Scheme I is used. The orbital energies are given in Table 2. The values in the parentheses are those

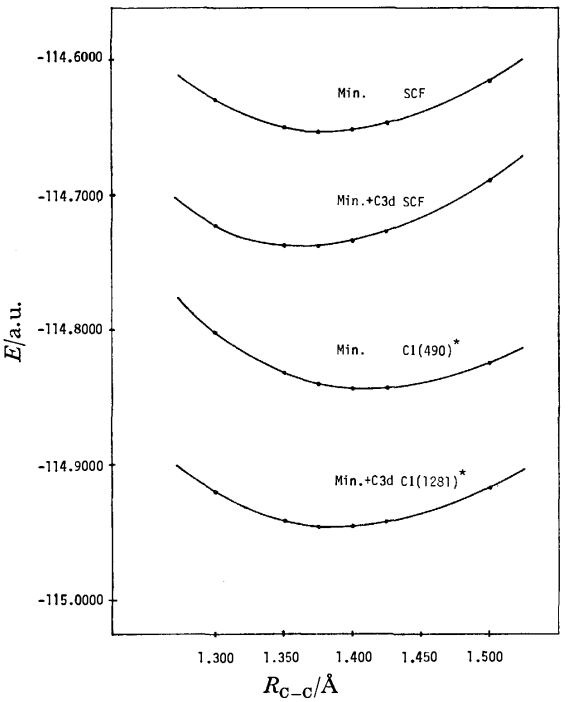

Fig. 1. Potential curves of $C_3H_3^+$.
* Dimension of CI solved in C_{2v} symmetry.

Table 2. Molecular orbital energies of $C_3H_3^+$ (a.u.)

		Occupation		Present study R_{C-C}=1.375Å(R_{C-C}=1.400 Å)		Ha R_{C-C}=1.400Å
		I	II	Min.	Min.+C3d	
occ.	$1a_1'$	2	2	−11.6167(−11.6113)	−11.5898(−11.5878)	−11.8156
	$1e_1'$	2	2	−11.6154(−11.6102)	−11.5886(−11.5869)	−11.8137
	$2a_1'$	*	2	−1.5260 (−1.5017)	−1.4983 (−1.4755)	−1.6192
	$2e'$	*	2	−1.0651 (−1.0614)	−1.0602 (−1.0573)	−1.1359
	$3a_1'$	*	*	−0.9813 (−0.9754)	−0.9711 (−0.9659)	−1.0588
	$3e'$	*	*	−0.7956 (−0.7874)	−0.7799 (−0.7728)	−0.8770
	$1a_2''$	*	*	−0.7735 (−0.7571)	−0.7574 (−0.7430)	−0.8385
unocc.	$1e''$	*	*	−0.0612	−0.0905	
	$1a_2'$	*	*	0.2160	0.1912	
	$4e'$	*	*	0.2411	0.2245	
	$4a_1'$	*	*	0.2951	0.2269	
	$2e''$	*	0	—	0.5249	
	$2a_2''$	*	0	—	0.5755	
	$5e'$	*	0	0.6826	0.6306	
	$5a_1'$	*	0	—	0.6639	
	$3e''$	*	0	—	0.6921	
	$6a_1'$	0	0	—	1.0808	
	$1a_1''$	0	0	—	1.1593	
	$6e'$	0	0	—	1.2783	
	$7e'$	0	0	—	1.5378	
	$2a_2'$	0	0	—	1.7914	
	$8e'$	0	0	—	2.0630	

TABLE 3. C–C EQUILIBRIUM BOND DISTANCE AND C–C STRETCHING FORCE CONSTANT OF $C_3H_3^+$

	SCF				CI		
	This work				This work		Obsd
	Min.	Min.+C3d	Ha[a]	Radom[b]	Min.	Min.+C3d	
Total energy(a.u.)	−114.6549	−114.7388	−114.7442	−115.00369	−114.8444	−114.9466	—
C–C eq. bond dis. (Å) R^e_{C-C}	1.383	1.365	1.40	1.377	1.413	1.389	1.373[c],1.363[d]
Force constant (mdyn/Å) k_{C-C}	9.56	9.19	—	—	8.07	7.92	6.59[e]

a) See Ref. 8. b) See Ref. 9. c) See Ref. 3. d) See Ref. 2. e) See Ref. 5.

for the C–C bond distance of 1.400 Å, which is used by Ha and others.[8] Although their absolute values are larger than our values by 0.08—0.23 a.u., the order is the same and the relative positions are very similar between the two calculations.

Equilibrium C–C Bond Distance and the C–C Stretching Force Constant. By using the results shown in Fig. 1, the equilibrium C–C bond distance R^e_{C-C} and the stretching force constant k_{C-C} are determined. First, R^e_{C-C} and $k_{A_1'}$ (stretching force constant of totally symmetric vibrational mode) are calculated by expanding the potential curves in terms of a polynominal of fifth degree. Next, if we neglect the cross terms such as $\Delta r_1 \Delta r_2$ in the expansion, k_{C-C} is one third of $k_{A_1'}$. By using this relation, k_{C-C} is estimated. The R^e_{C-C} and k_{C-C} are given in Table 3 with the results of the previous calculations. It is noted that the C–C bond distance becomes larger and the C–C stretching force constant smaller by the CI calculation in comparison with the SCF results. The calculated C–C distance by CI with the Min.+C3d basis is close to the observed values at the substituted cyclopropenyl cations.[2,3] The equilibrium C–C distance of C_6H_6 is calculated to be 1.39 Å in the SCF calculation by Newton and others.[17] Since the calculated value of R^e_{C-C} of $C_3H_3^+$ at the SCF level is smaller than this value, the equilibrium C–C distance of $C_3H_3^+$ is expected to be smaller than that of C_6H_6. The C–C bond distance of $C_3H_3^+$ has not been determined experimentally so far.

The calculated C–C stretching force constants are improved by CI and the CI results are in fair agreement with experiment. However, it is difficult to say whether the C–C stretching force constant of $C_3H_3^+$ would be greater than that of C_6H_6, or not. One will have to calculate the stretching force constant of C_6H_6 in the same manner and to compare the result with that of $C_3H_3^+$.

Charge Distribution and Localized Molecular Orbitals. The σ-bonds of three membered ring molecules would have the maxima of charge distribution outside the ring, that is, the bonds are bent. X-Ray diffraction showed that cyclopropane has such bent bonds.[18] In order to examine whether the calculated C–C bonds of $C_3H_3^+$ are bent or not, the contour diagrams of the charge distribution of the valence electrons are drawn, using the ground state wave functions obtained by the Min. and Min.+C3d SCF calculations and are shown in Figs. 2 and 3, respectively. The contributions of the three lowest molecular orbitals, $1a_1'$ and $1e'$, are excluded since they consist of mainly carbon core orbitals. According to these figures, the C–C bonds of

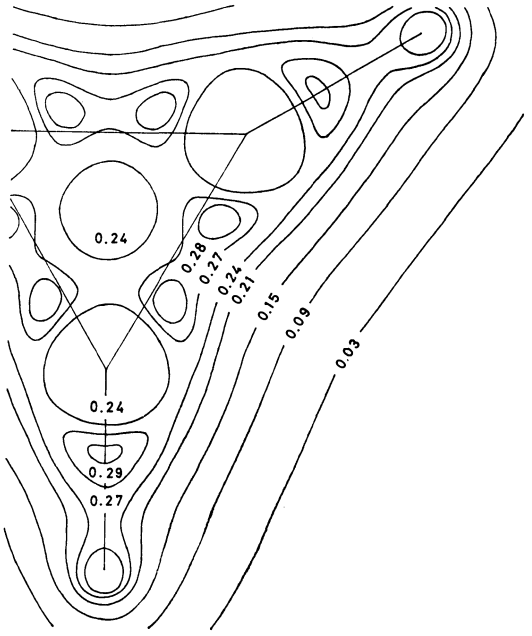

Fig. 2. Valence electron density (e/a.u.^{3}) in $C_3H_3^+$ obtained from Min. SCF.

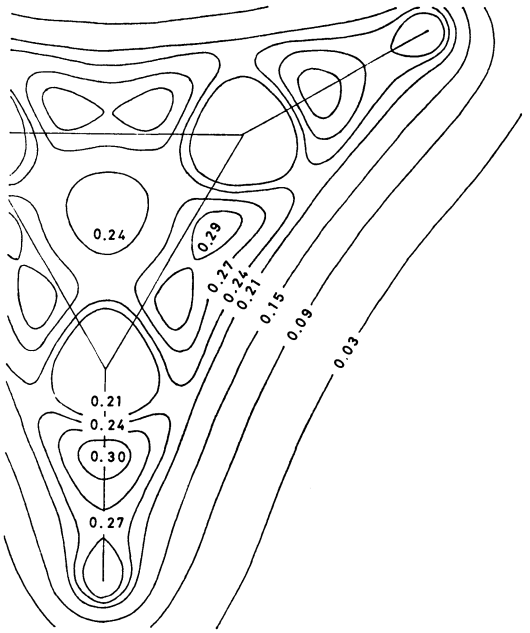

Fig. 3. Valence electron density (e/a.u.^{3}) in $C_3H_3^+$ obtained from Min.+C3d SCF.

$C_3H_3^+$ are bent having the two maxima of charge density. Ha and others also reported a similar diagram of $C_3H_3^+$.[8] However, because of the existence of the inner-shell electrons, the positions of the maxima of C–C and C–H bonds and the degree of the bending were not so clear. It is interesting to note that the charge density in the C–C and C–H bond regions increases by the addition of 3d orbitals, as is clear from Figs. 2 and 3.

The localized MO's have certain advantages over cannonical MO's in describing a bond. The occupied MO's are thus transformed into the localized MO's by the Edmiston and Ruedenberg procedure.[16] This is carried through with the Min. basis. The contour diagrams of charge distribution of the localized MO's

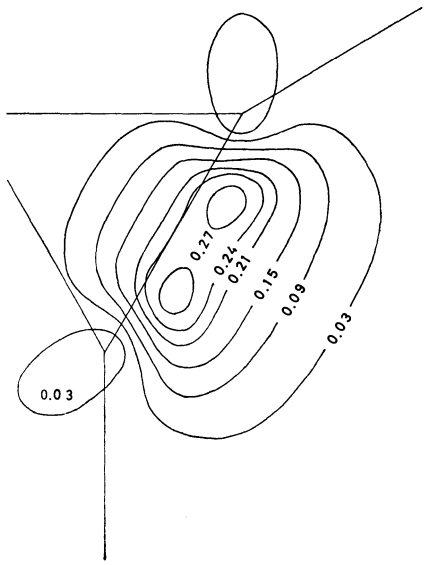

Fig. 4. Electron density (e/a.u.^{3}) of two electrons in a localized C–C orbital in $C_3H_3^+$.

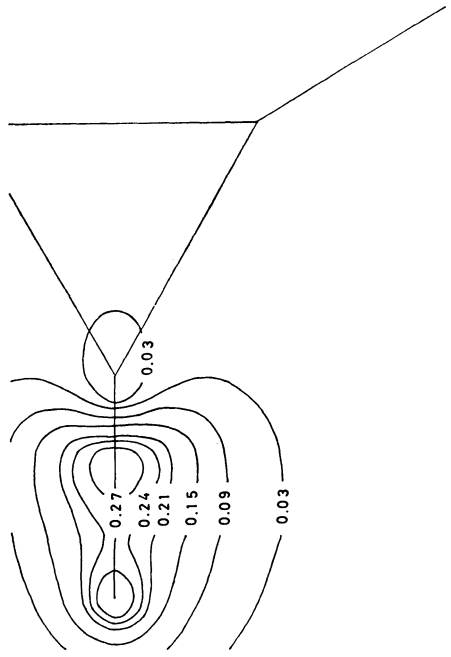

Fig. 5. Electron density (e/a.u.^{3}) of two electrons in a localized C–H orbital in $C_3H_3^+$.

Table 4. Ratios of the hybrid orbitals and $J_{^{13}C-H}$

	sp^x		$J_{^{13}C-H}$(Hz)
	C–C	C–H	
C_2H_4	1.74	1.85[a]	157[b]
C_6H_6	1.73	1.87[a]	159[b]
$C_3H_3^+$	2.28	0.99	265[c]

a) See Ref. 20. b) See Ref. 21. c) See Ref. 1.

corresponding to the C–C and C–H bonds are illustrated in Figs. 4 and 5, respectively.

The ratio of 2s and 2p orbitals in a hybrid sp^x is estimated by the coefficients of these localized MO's. The values of x are given by $(C_{2ph}^2+C_{2pv}^2)/C_{2s}^2$, where C_{2s}, C_{2ph}, and C_{2pv} are the coefficients of STO's in the localized MO's. Newton and others reported the ratio for several molecules determined by the same procedure.[19,20] The ratio for $C_3H_3^+$ is compared with their results of C_2H_4 and C_6H_6 in Table 4. It is seen that the localized MO's of C_2H_4 and C_6H_6 are rather similar to the sp^2 hybrid orbitals in the region around the carbon nuclei. In the same region, the C–H bond orbital of $C_3H_3^+$ has a higher s-character than C_2H_4 and C_6H_6 and is closer to an sp hybrid. Breslow pointed out that the ^{13}C–H coupling constant $J_{^{13}C-H}$ of NMR spectra of $C_3H_3^+$ is quite large.[1] The values of coupling constant of C_2H_4, C_6H_6,[21] and $C_3H_3^+$ are also included in Table 4. As was shown by Ramsey,[22] the Fermi contact term which gives a dominant contribution to the constant, is proportional to the density of s-electrons at the two nuclei. In Table 4, this relation is seen to hold approximately, namely, $1/3: 1/2 \simeq 159: 265$.

Low Lying Excited States. The electronic structure

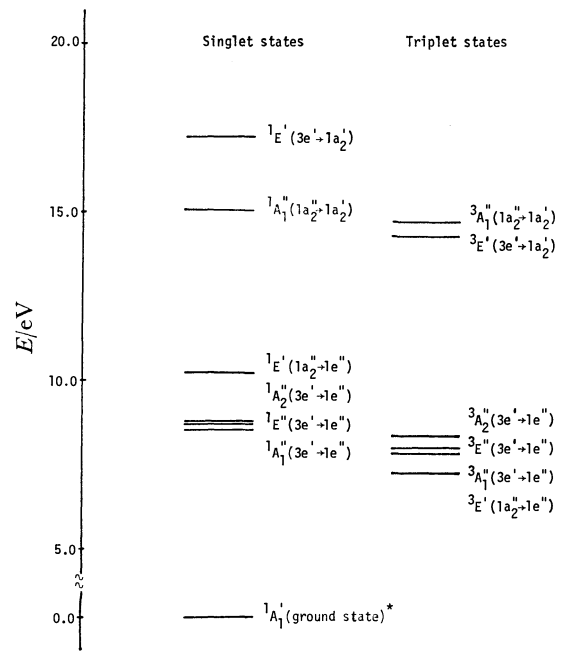

Fig. 6. Excitation energies of $C_3H_3^+$.
* -114.8003 a.u. obtained by CI calculation with occupation II basis. Dimension of CI is 140 in C_{2v} symmetry.

of excited states in highly strained molecules is of considerable experimental and theoretical interest. The excitation energies of $C_3H_3^+$ has never been measured, probably because of its instability. CI calculations of the low lying excited states of $C_3H_3^+$ are carried out for the geometry with the C–C bond distance of 1.400 Å and the results are given in Fig. 6. In these calculations, the occupation Scheme II is used. The values in Fig. 6. are the excitation energies of the π-$\pi^*(1a_2'' \rightarrow 1e'')$, π-$\sigma^*(1a_2'' \rightarrow 1a_2')$, σ-$\pi^*(3e' \rightarrow 1e'')$, and σ-$\sigma^*(3e' \rightarrow 1a_2')$ states. It should be noted that the singlet σ-π^* states ($^1A_1''$, $^1E''$, $^1A_2''$) are lower than the singlet π-π^* state ($^1E'$). All excited states are represented well by a single configuration except for the singlet σ-σ^* state ($^1E'$) and in these states the weights of the leading configurations are as big as 82—96%. In the singlet σ-σ^* state ($^1E'$), the weight of leading configuration is 47% and that of $(3a_1')^2(3e')^3(1a_2'')^2(4e')^1$ is 36%.

Conclusions

The LCAO MO SCF and CI calculations are carried out on the electronic structure of $C_3H_3^+$ and the following conclusions are obtained.

1. The calculated C–C bond distance of $C_3H_3^+$ is 1.389 Å. This is close to the experimental values of the substituted cyclopropenyl cations. The C–C distance of $C_3H_3^+$ is expected to be shorter than that of C_6H_6. The C–C stretching force constant is calculated to be 7.92 mdyn/Å, and is close to the experimental value of 6.59 mdyn/Å.

2. The contour diagram of the charge distribution of valence electrons indicates that the σ-bonds of $C_3H_3^+$ are bent outwardly.

3. The ratio, x of a hybrid orbital sp^x to be found in $C_3H_3^+$ is estimated by the coefficients in the localized MO's. The value x of the C–H bond is 0.99 reflecting that the bond has a larger s-character, compared with the C–H bonds in C_2H_4 and C_6H_6. This is in accord with the very large NMR coupling constant J^{13}_{C-H} of the ion.

4. The low lying excited states of $C_3H_3^+$ are calculated by the CI calculations. The singlet σ-π^* state ($^1A_1''$, $^1E''$, $^1A_2''$) are lower than the singlet π-π^* state ($^1E'$).

We wish to thank Professor Fukashi Sasaki, Professor Hiroshi Kashiwagi, Dr. Kiyoshi Tanaka, and Dr. Hiroshi Tatewaki for helpful suggestions and discussions. Thanks are also due to Dr. Kiyoshi Tanaka, Dr. Hiroshi Tatewaki, Mr. Tsutomu Nomura, and Dr. Takeshi Noro for making their CI program package COMICAL available. The calculations reported in this paper were carried out on the FACOM 230-75 computer at the Hokkaido University Computing Center.

References

1) R. Breslow and J. T. Groves, *J. Am. Chem. Soc.*, **92**, 984 (1970).
2) A. T. Ku and M. Sundaralingam, *J. Am. Chem. Soc.*, **94**, 1688 (1972).
3) M. Sundaralingam and L. H. Jensen, *J. Am. Chem. Soc.*, **88**, 198 (1966).
4) A. Langseth and B. P. Stoicheff, *Can. J. Phys.*, **34**, 350 (1956).
5) Z. Yoshida, S. Hirota, and H. Ogoshi, *Spectrochim. Acta*, **30A**, 1105 (1974).
6) T. Shimanouchi, The Molecular Force Field in "Physical Chemistry," ed by H. Eyring, D. Henderson, and W. Jost, Academic Press, New York (1970), Vol. 4, Chap. 6.
7) D. T. Clark, *Chem. Commun.*, **1969**, 637.
8) T.-K. Ha, F. Graf, and Hs. H. Günthard, *J. Mol. Struct.*, **15**, 335 (1973).
9) L. Radom, P. C. Hariharan, J. A. Pople, and P. V. R. Schleyer, *J. Am. Chem. Soc.*, **98**, 10 (1976).
10) W. J. Hehre, R. F. Stewart, and J. A. Pople, *J. Chem. Phys.*, **51**, 2657 (1969).
11) R. K. Nesbet, *J. Chem. Phys.*, **40**, 3619 (1964).
12) R. F. Stewart, *J. Chem. Phys.*, **52**, 431 (1970).
13) A. D. McLean and B. Liu, *J. Chem. Phys.*, **58**, 1066 (1973).
14) "Tables of Interatomic Distances and Configuration in Molecules and Ions," ed by L. E. Sutton, The Chem. Soc., London (1958).
15) G. G. Hall, *Rept. Prog. Phys.*, **23**, 1 (1959).
16) C. Edmiston and K. Ruedenberg, *Rev. Mod. Phys.*, **35**, 457 (1963).
17) M. D. Newton, W. A. Lathan, W. J. Hehre, and J. A. Pople, *J. Chem. Phys.*, **52**, 4064 (1970).
18) A. Hartman and F. L. Hirshfeld, *Acta Crystallogr.*, **20**, 80 (1966).
19) M. D. Newton, E. Switkes, and W. N. Lipscomb, *J. Chem. Phys.*, **53**, 2645 (1970).
20) M. D. Newton and E. Switkes, *J. Chem. Phys.*, **54**, 3179 (1971).
21) L. M. Jackman and S. Sternhell, "Application of Nuclear Magnetic Resonance Spectroscopy in Organic Chemistry," Pergamon, New York (1969).
22) N. F. Ramsey, *Phys. Rev.*, **91**, 303 (1953).

Molecular Motion in Ammonium Hydrogendifluoride Studied by Pulsed NMR

Yoshihiro FURUKAWA* and Hideko KIRIYAMA

The Institute of Scientific and Industrial Research, Osaka University, Yamadakami, Suita, Osaka 565

(Received July 17, 1978)

The proton and fluorine-19 spin-lattice relaxation times, T_1 and $T_{1\rho}$, in polycrystalline ammonium hydrogendifluoride were measured in the temperature range 142—345 K to elucidate the molecular motion of cation and anion. Below 200 K, the relaxation rates of both nuclei can be accounted for by dipolar interactions modulated *via* the isotropic reorientation of NH_4^+ ions. The log $T_{1\rho}$ *versus* $1/T$ curves above 200 K exhibit two distinct minima, suggesting that two crystallographically nonequivalent HF_2^- ions undergo 180°-flips about their two-fold axes with different correlation times. The activation energy of the NH_4^+ reorientation was determined to be 25.5 ± 1.0 kJ/mol from the T_1 data, while those of the 180°-flips were estimated from the $T_{1\rho}$ data to be about 40 and 60 kJ/mol for the two types of anions. These relaxation mechanisms have been confirmed by further experiments on a partially deuterated sample.

A series of alkali-metal hydrogendifluorides have occasioned much interest in the very short, nearly symmetric hydrogen-bond of the $[F\text{–}H\text{–}F]^-$ ion and in the motional state of such a dumbbell-like anion. The hydrogendifluorides of heavy alkali-metals, such as K, Rb, and Cs, transform to cubic phases at high temperatures because rapid, random reorientations of linear HF_2^- ions give rise to an effectively cubic symmetry.[1] It was also recognized from the previous NMR measurements that the HF_2^- ions are 180°-flipping in the low-temperature phase.[2,3] On the other hand, the compounds of light alkali-metals such as Li and Na, and of NH_4^+, have no phase transitions, suggesting that even if the 180°-flip motion takes place, it persists up to their melting points. The NH_4^+ ion has some freedom of reorientation and a possibility of forming another type of hydrogen bond between $N(NH_4^+)$ and $F(HF_2^-)$ in addition to the hydrogen bond in an $[F\text{–}H\text{–}F]^-$ ion just described. It is therefore worthwhile to investigate the ionic motions of nearly spherical NH_4^+ and dumbbell-like HF_2^- ions in NH_4HF_2 crystals and to compare the results obtained with those in potassium hydrogendifluoride.[3]

The crystal structure of NH_4HF_2 contains four chemical formula units in its orthorhombic cell; the HF_2^- ions are distinguished between two crystallographically nonequivalent $HF_2^-(1)$ and $HF_2^-(2)$, whereas the ammonium ions are all equivalent.[4] The crystal structure can be described as a superstructure of the caesium chloride type, although it is distorted by the presence of rod-shaped HF_2^- ions and by interionic hydrogen bonds.

In this paper, the results of pulsed NMR of both ^1H and ^{19}F nuclei in NH_4HF_2 are reported, and models of the isotropic reorientation of the NH_4^+ ion and the two types of 180°-flipping of the HF_2^- ions are proposed.

Experimental

Powdered NH_4HF_2 was prepared from an aqueous solution of NH_4F and a slight excess of HF acid; it was then recrystallized twice from the aqueous solution. The sample used was identified from its X-ray powder diffraction pattern.[4]

A Bruker B-KR 322s frequency-variable, pulsed NMR spectrometer was employed to determine the magnetic relaxation times, T_1 and $T_{1\rho}$, of ^1H and ^{19}F nuclei. The spin-lattice relaxation time, T_1, was measured by use of the 180°-t-90° pulse sequence at 60 and 20 MHz for ^1H and at 56.442 and 18.814 MHz for ^{19}F nuclei. The relaxation time in the rotating frame, $T_{1\rho}$, was determined by the spin-locking method. The temperature of the sample was controlled to within ±0.5 K by using an Ohkura EC 61 temperature controller and was measured with a copper-constantan thermocouple calibrated before measurements.

Results

Figure 1 shows the temperature dependences, as a semilogarithmic plot *versus* inverse temperature, of proton $T_1(H)$ and fluorine-19 $T_1(F)$ obtained at 60 and 56.442 MHz respectively, together with the $T_{1\rho}(H)$ at the r.f. field strength 10 G. The $T_{1\rho}(F)$ could not be measured because of its poor signal, resulting from a very short free-induction-decay (FID). Below about 200 K, the magnetization-recovery curve for the T_1 process of either nucleus became markedly non-exponential, owing to heteronuclear H–F dipole interaction.[5] The recovery curve was, therefore, resolved into two exponential terms, according to the equation $<I_0-I_z>/2I_0=A\exp(-t/T_1')+B\exp(-t/T_1'')$; here I_z and I_0 are the z-components of the I-spin (^1H or ^{19}F) magnetization at time t and at thermal equilibrium, respectively, A and B are constants, and T_1' and T_1'' denote the short and long relaxation times, respectively.[3] Above 200 K, although the recovery curve was slightly non-exponential, the T_1 value as well as the $T_{1\rho}$ one was approximated by a single relaxation time, which was defined as the time necessary for the $<I_0-I_z>/2I_0$ to fall to $1/e$ of its initial value. The frequency dependence of the T_1 value was examined by additional measurements at 20 MHz for ^1H and 18.814 MHz for ^{19}F nuclei; these plots were omitted from Fig. 1 for simplicity.

The log $T_1(H)$ *vs.* $1/T$ curve at 60 MHz exhibits a deep T_1 minimum at $kK/T\approx4.4$; the corresponding $T_{1\rho}$ minimum occurs at $kK/T\approx6.6$. Two additional $T_{1\rho}$ minima are recognized at $kK/T\approx3.0$ and 4.0, indicating that the molecular motions of NH_4^+ and/or HF_2^- ions are rather complex within the crystal lattice.

In order to uncover further details of the ionic motion in the high-temperature region, the measurements of the $T_1(F)$ and $T_{1\rho}(F)$ were extended to a sample of partially deuterated NH_4HF_2. The results are shown as

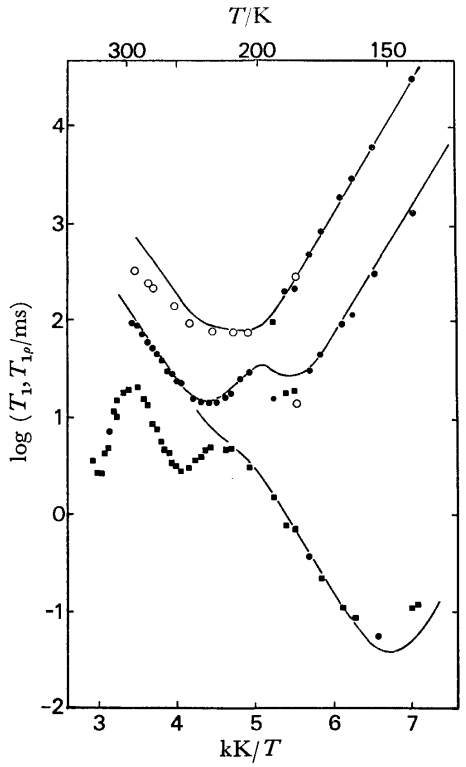

Fig. 1. Temperature dependences of spin-lattice relaxation times in NH_4HF_2: (●) T_1(H) at 60 MHz, (○) T_1(F) at 56.442 MHz, and (■) $T_{1\rho}$(H) at 10 G. The solid lines indicate the calculated temperature dependences of T_1 and $T_{1\rho}$(H) for randomly reorienting NH_4^+ ions.

experimental points in Fig. 2. The deuterium content was estimated to be about 65% from the ratio of the T_1(F) minimum value for the nondeuterated sample to that for the partially deuterated one; these minima will be assigned to the NH_4^+ isotropic reorientation later.

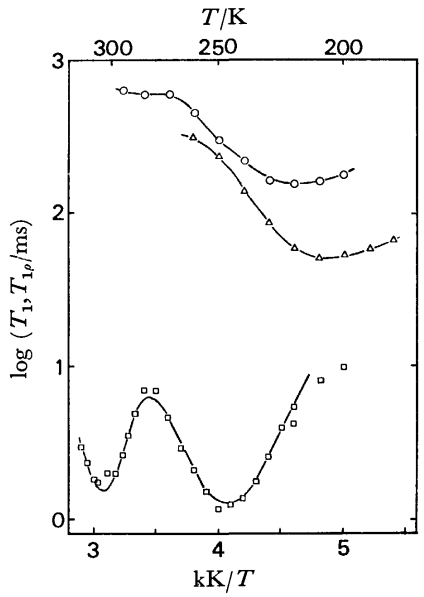

Fig. 2. Temperature dependences of spin-lattice relaxation times in 65% *d*-NH_4HF_2: (○) T_1(F) at 56.442 MHz, (△) T_1(F) at 18.814 MHz, and (□) $T_{1\rho}$(F) at 6.5 G. The lines are drawn to guide the eye.

Isotropic Reorientation of NH_4^+ Ions. The relaxation process for T_1 below room temperature is ascribable to NH_4^+ isotropic reorientation, because such a short T_1(H) minimum as 14 ms is characteristic of NH_4^+ reorientation. In this case, the ^1H relaxation rate is governed mainly by the intraionic H–H dipolar interaction and partially by the interionic dipolar interactions, $H(NH_4^+)$–$H(NH_4^+)$ and $H(NH_4^+)$–$H(HF_2^-)$, and the heteronuclear $H(NH_4^+)$–$F(HF_2^-)$ one. Among these, the contribution of the homonuclear H–H interaction to the ^1H relaxation rate is expressed as follows:

$$T_1(\mathrm{HH})^{-1} = (2/3)\gamma_H^2 \Delta M_{HH} f(\omega_H, \tau_H), \quad (1a)$$

$$f(\omega, \tau) = \tau/(1+\omega^2\tau^2) + 4\tau/(1+4\omega^2\tau^2). \quad (1b)$$

The quantity ΔM_{HH} is the reduction in the second moment of the ^1H absorption spectrum due to the H–H dipolar interaction associated with the NH_4^+ reorientation; τ_H stands for the correlation time for the NH_4^+ motion; the other symbols have their usual meaning.

On the other hand, the relaxation due to heteronuclear dipole interaction between ^1H and ^{19}F nuclei can be expressed by the following pair of coupled equations:[5]

$$\mathrm{d}\langle I_z\rangle/\mathrm{d}t = -\langle I_z - I_0\rangle/T_1(\mathrm{IS}) - \langle S_z - S_0\rangle/T_1'(\mathrm{IS}), \quad (2a)$$

$$\mathrm{d}\langle S_z\rangle/\mathrm{d}t = -\langle I_z - I_0\rangle/T_1'(\mathrm{SI}) - \langle S_z - S_0\rangle/T_1(\mathrm{SI}), \quad (2b)$$

where I and S stand for H and F, respectively. Each relaxation time in Eq. 2 can be calculated in the same manner as with $(NH_4)_2BeF_4$.[5] Thus,

$$T_1(\mathrm{FH})^{-1} = (3/16)\gamma_F^2 \Delta M_{FH} g(\omega_F, \omega_H, \tau_H), \quad (3a)$$

$$T_1'(\mathrm{FH})^{-1} = (3/16)\gamma_F^2 \Delta M_{FH} g'(\omega_F, \omega_H, \tau_H), \quad (3b)$$

$$g(\omega_I, \omega_S, \tau) = \tau/[1+(\omega_I-\omega_S)^2\tau^2] + 3\tau/(1+\omega_I^2\tau^2) + 6\tau/[1+(\omega_I+\omega_S)^2\tau^2], \quad (3c)$$

$$g'(\omega_I, \omega_S, \tau) = -\tau/[1+(\omega_I-\omega_S)^2\tau^2] + 6\tau/[1+(\omega_I+\omega_S)^2\tau^2]. \quad (3d)$$

The ΔM_{FH} is again the reduction in the ^{19}F second moment due to the F–H dipolar interaction *via* the NH_4^+ reorientation. By taking into account the abundances of ^1H and ^{19}F nuclei in the crystal,[5] the ^1H relaxation rates due to the heteronuclear H–F interaction, $T_1(\mathrm{HF})^{-1}$ and $T_1'(\mathrm{HF})^{-1}$, can be easily related to Eq. 3. The $T_1(\mathrm{FF})^{-1}$ of course, need not be considered because the F–F dipole interaction is not modulated *via* the NH_4^+ reorientation. The observed relaxation rates are given by the eigenvalues of the relaxation matrix:

$$\begin{pmatrix} T_1(\mathrm{HH})^{-1} + T_1(\mathrm{HF})^{-1} & T_1'(\mathrm{HF})^{-1} \\ T_1'(\mathrm{FH})^{-1} & T_1(\mathrm{FH})^{-1} \end{pmatrix}.$$

The ΔM_{HH} value was first evaluated from the atomic positions as determined by X-rays.[4] It was too large to explain the observed T_1(H) minimum, because of the rather short N–H distance (0.88 Å) used. So the values of ΔM_{HH} and ΔM_{FH} were recalculated by taking the r(N–H) distance as 1.059 Å (corresponding to 1.73 Å for the r(H···H) distance in a tetrahedral NH_4^+ ion)[6] and the two nonequivalent r(F–F) distances as 2.297 and 2.291 Å in both hydrogen-centered $[F\text{–}H\text{–}F]^-$ ions.[7] For the rigid lattice model, the theoretical second moments thus obtained are M_{HH}=41.80, M_{HF}=30.01 G^2 for ^1H and M_{FF}=4.18, M_{FH}=84.97 G^2 for ^{19}F nuclei. On the other hand, a model of the NH_4^+

isotropic reorientation yields $M_{HH}=5.55$, $M_{HF}=26.56$, $M_{FF}=4.18$, and $M_{FH}=75.20$ G^2. By substituting the calculated second moments into Eqs. 1 and 3 and by diagonalizing the relaxation matrix, one can calculate the following T_1 minimum values for the two nuclei: $T_1(H)_{min}=14.3$ and $T_1(F)_{min}=79.5$ ms. The experimental values to be compared with these T_1 minima were 13.5 and 73 ms, respectively. The good agreement between the calculated and experimental values indicates that the NH_4^+ isotropic reorientation is responsible for the relaxation process in this temperature region. The activation energy, E_a, of the NH_4^+ reorientation was determined to be 25.5 ± 1.0 kJ/mol from the slope of the log T_1' (or T_1'') *vs.* $1/T$ line on its low-temperature side, by assuming that $\tau=\tau_0\exp(E_a/RT)$. The solid lines for T_1(H) and T_1(F) in Fig. 1 were calculated from Eqs. 1 and 3 with the relaxational parameters, τ_0 and E_a, listed in Table 1.

Table 1. Relaxational parameters in NH_4HF_2

	E_a/kJ mol^{-1}	τ_0/s	Motion
NH_4^+	25.5 ± 1.0	2.5×10^{-15}	isotropic
HF_2^-(1)	≈60	$\approx10^{-15}$	180°-flip
HF_2^-(2)	≈40	$\approx10^{-14}$	180°-flip
HF_2^- in KHF_2[a]	50.5	6.4×10^{-15}	180°-flip

a) Ref. 3.

In the weak collision limit, $T_{1\rho}$(H) is given by the equation corresponding to Eqs. 1 and 3 for T_1(HH), *etc*:[5]

$$T_{1\rho}(H)^{-1} = (1/3)\gamma_H^2\Delta M_{HH}f_\rho(\omega_H, \tau_H) + (3/32)\gamma_H^2\Delta M_{HF}g_\rho(\omega_H, \omega_F, \tau_H), \quad (4a)$$

$$f_\rho(\omega_I, \tau) = 3\tau/(1+4\omega_{1I}^2\tau^2) + 5\tau/(1+\omega_I^2\tau^2) + 2\tau/(1+4\omega_I^2\tau^2), \quad (4b)$$

$$g_\rho(\omega_I, \omega_S, \tau) = 4\tau/(1+\omega_{1I}^2\tau^2) + \tau/[1+(\omega_I-\omega_S)^2\tau^2] + 9\tau/(1+\omega_I^2\tau^2) + 6\tau/[1+(\omega_I+\omega_S)^2\tau^2]. \quad (4c)$$

Although our experimental condition ($H_1=\omega_{1H}/\gamma_H=10$ G) wasn't sufficient for the weak collision limit, we tried to approximate the problem by this limit. Thus, the theoretical log $T_{1\rho}$(H) *vs.* $1/T$ curve was calculated from Eq. 4 with the same relaxational parameters as those in the T_1 calculation. As compared in Fig. 1, the overall agreement between the calculation and the observation is good, except for the temperature range above 200 K.

180°-Flipping of HF_2^- Ions. The relaxational behavior above 200 K is rather complicated. The $T_{1\rho}$ data in Figs. 1 and 2 clearly suggest the presence of other relaxational processes. The FID signals of both nuclei show no lengthening due to self-diffusion of the NH_4^+ or HF_2^- ions, even at the highest temperature of measurement (345 K). Hence, the 180°-flip motion of the HF_2^- ion becomes of much interest, because it can contribute to the relaxation rates of both nuclei in the high temperature region, as evidenced in the low-temperature phase of potassium hydrogendifluoride.[2,3]

If that is the case, at temperatures higher than 200 K the $T_{1\rho}$(H) in NH_4HF_2 may be governed by the H–F dipolar interaction modulated *via* the 180°-flips of the HF_2^- ions. The two crystallographically nonequivalent HF_2^- ions may have different correlation times, τ_1, and τ_2, for their individual 180°-flips. If these correlation times are greatly different from each other, then the two corresponding $T_{1\rho}$ minima would be well separated, as can be seen in Fig. 1. The ^{1}H relaxation rate due to the H–F dipolar interaction *via* the 180°-flip is given in a spatial average form as follows:[3]

$$T_{1\rho}(HF)^{-1} = \gamma_H^2\gamma_F^2\hbar^2/80\sum_F[r_{HF}(\beta)^{-6}+r_{HF}(\delta)^{-6} - r_{HF}(\beta)^{-3}r_{HF}(\delta)^{-3}(3\cos^2\Delta_{\beta\delta}-1)]g_\rho(\omega_H, \omega_F, \tau_i), \quad (5)$$

where τ_i stands for τ_1 and τ_2, β and δ denote two positions of a given F atom, $r_{HF}(\beta)$ is the distance between the hydrogen and the fluorine atom at a β-site, and $\Delta_{\beta\delta}$ is the angle between two H–F internuclear vectors. In the actual calculation based on Eq. 5, four hydrogen atoms of a rapidly rotating NH_4^+ ion were located at the center of the ion, in the usual manner.

On the other hand, the $T_{1\rho}$(F) in the 65% *d*-NH_4HF_2 may be governed by the homonuclear F–F dipolar interaction. The relaxation rate due to 180°-flipping of water molecules has been derived by Look and Lowe.[8] In order to apply the Look and Lowe equation to the present case, the equation was modified to hold for two independent correlation times. The results are presented only in the $T_{1\rho}^{-1}$ form for a single crystal:

$$T_{1\rho}(FF)^{-1} = 3\gamma_F^4\hbar^2I_F(I_F+1)/64N\sum_{i\neq j}[\zeta^{(0)}J(2\omega_{1F}, \tau_i) + 10\zeta^{(1)}J(\omega_F, \tau_i)+\zeta^{(2)}J(2\omega_F, \tau_i) + \xi^{(0)}J(2\omega_{1F}, \tau_j)+10\xi^{(1)}J(\omega_F, \tau_j) + \xi^{(2)}J(2\omega_F, \tau_j)+\eta^{(0)}J(2\omega_{1F}, \tau_{ij}) + 10\eta^{(1)}J(\omega_F, \tau_{ij})+\eta^{(2)}J(2\omega_F, \tau_{ij})], \quad (6a)$$

$$\zeta^{(q)} = |\chi_{ij}^{(q)}(\beta_i, \beta_j)+\chi_{ij}^{(q)}(\beta_i, \delta_j)-\chi_{ij}^{(q)}(\delta_i, \beta_j) -\chi_{ij}^{(q)}(\delta_i, \delta_j)|^2, \quad (6b)$$

$$\xi^{(q)} = |\chi_{ij}^{(q)}(\beta_i, \beta_j)-\chi_{ij}^{(q)}(\beta_i, \delta_j)+\chi_{ij}^{(q)}(\delta_i, \beta_j) -\chi_{ij}^{(q)}(\delta_i, \delta_j)|^2, \quad (6c)$$

$$\eta^{(q)} = |\chi_{ij}^{(q)}(\beta_i, \beta_j)-\chi_{ij}^{(q)}(\beta_i, \delta_j)-\chi_{ij}^{(q)}(\delta_i, \beta_j) +\chi_{ij}^{(q)}(\delta_i, \delta_j)|^2, \quad (6d)$$

$$\tau_{ij}^{-1} = \tau_i^{-1} + \tau_j^{-1}, \quad (6e)$$

$$J(\omega, \tau) = \tau/(1+\omega^2\tau^2), \quad (6f)$$

where $\chi_{ij}^{(q)}$ ($q=0$, 1, and 2) is the usual orientation function.[8] When $\tau_i=\tau_j$, of course, Eq. 6 is identical with the Look and Lowe equation. As a powdered sample was used in this study, Eq. 6 was spatially averaged before use.[9]

In addition, the interionic F–H dipolar interaction also contributes to $T_{1\rho}$(F). This contribution can be estimated from Eq. 5, taking into account the extent of the deuteration. The contribution from ^{2}H nuclei was neglected because γ_F is very large compared with γ_D.

The summations in Eqs. 5 and 6 were carried out up to six or eight neighboring ions around a central HF_2^-(1) or HF_2^-(2) ion, respectively. By using the parameters thus obtained, and Eqs. 5 and 6 for $T_{1\rho}$'s, the minimum values of $T_{1\rho}$ were evaluated. In this calculation, the correlation time for the 180°-flip of the HF_2^-(2) ions was assumed to be shorter than that of the HF_2^-(1) ions, for a reason to be described later. These values

Table 2. Calculated and experimental values of $T_{1\rho}$ minima due to the 180°-flips of the HF_2^- ions

$T_{1\rho}$(H) was measured at 10 G in NH_4HF_2 and $T_{1\rho}$(F) was at 6.5 G in the 65% *d*-NH_4HF_2.

	$T_{1\rho}(H)_{min}$/ms		$T_{1\rho}(F)_{min}$/ms	
	Calcd	Exptl	Calcd	Exptl
$HF_2^-(1)$	2.4	2.2	1.2	1.7
$HF_2^-(2)$	2.5	1.9	1.1	1.2

are compared with the experimental ones in Table 2. The agreement is fairly good, supporting the idea that the 180°-flip motions of the nonequivalent, linear HF_2^- ions are separately excited at high temperatures. The values of E_a and the pre-exponential factor τ_0 were roughly estimated in a conventional way; these results are included in Table 1 together with those for the NH_4^+ ions.

Discussion

The T_1 observed at all temperatures and the $T_{1\rho}$ in the low-temperature region were well explained by the random reorientation of the NH_4^+ ion, rather than by its C_2 reorientation predicted from the site symmetry (2) of the ammonium nitrogen. An activation energy E_a of 25.5 kJ/mol in the present NH_4HF_2 suggests that the hydrogen-bonds between N(NH_4^+) and F(HF_2^-) atoms are rather strong, as was anticipated from the short N–F distances (2.797 Å twice and 2.822 Å twice)[4] and also from the highly ionic charge on the F atom ($-0.83e$).[10] The values of E_a and the N(H)···F distance in NH_4HF_2 are intermediate between those found in NH_4F (42 kJ/mol, 2.71 Å)[11] and NH_4BF_4 (6.3 kJ/mol, 2.92 Å);[12] an E_a value of 3—5 kJ/mol in NH_4PF_6 is the lowest one,[13] but the N···F distance (2.4 Å) seems to be too small to compare with the above three, possibly owing to the highly disordered structure.[14] These comparisons indicate that the activation energy for the NH_4^+ reorientation strongly depends on the NH···F hydrogen-bond distance as well as on the dimensions of a combined anion.

On the other hand, the $T_{1\rho}$ data above 200 K could be interpreted in terms of the stepwise 180°-flip motions of the two nonequivalent HF_2^- ions. According to the X-ray results, the intraion F–(H)–F bond distances in both HF_2^- ions are nearly the same within the experimental errors, whereas the interionic hydrogen-bond distances F···(H)N significantly differ from each other (2.797 for $HF_2^-(1)$ and 2.822 Å for $HF_2^-(2)$ ions).[4] It was therefore expected that the latter $HF_2^-(2)$ ion would be more mobile and be characterized by a lower activation energy, *i.e.* a shorter correlation time. The preceding analysis of the $T_{1\rho}$ data based on this assumption yielded approximate E_a values of 60 for $HF_2^-(1)$ and 40 kJ/mol for $HF_2^-(2)$, both of which are roughly comparable to the 50 kJ/mol obtained in KHF_2 (Table 1).[3] However, the difference of E_a in the ammonium salt seems to be too large to arise from the difference in the hydrogen-bond strength alone. This finding leads us to point out that the different HF_2^- ions take different pathways of flipping. For an isolated molecular ion, the two-fold (C_2) axis of flip cannot be defined uniquely on the molecular mirror plane, because the symmetry of the ion is ∞/m ($D_{\infty h}$). Furthermore, the X-ray results, especially the strongly anisotropic temperature factors, provided valuable information on the ionic motion. That is, the maximum amplitude of either fluorine atom due to ionic libration is observed perpendicular to the mean plane of the three hydrogen-bonds, one of which is intraionic and the other two interionic.[4] As can be seen in Fig. 3, both types of HF_2^- ions locate at the sites of the same symmetry 2/m, but the ionic axis of $HF_2^-(1)$ is perpendicular to the mirror plane (100), while the axis of $HF_2^-(2)$ ion lies on this mirror plane. Under these circumstances, the $HF_2^-(2)$ ion may rotate about the ionic and crystallographic C_2 axis, *i.e.* on the plane (100), without destroying any initial site symmetry. In contrast to this, the flipping pathway of the $HF_2^-(1)$ ion about the C_2-axis, which lies on the hydrogen-bonded plane, does break down the site symmetry and then the motion is highly hindered by the repulsion from the neighboring fluorine atoms, when the linear anion goes across the crystal mirror plane. Although this explanation is only a simple and tentative one, it seems likely that such a steric hindrance contributes to the difference in the activation energies.

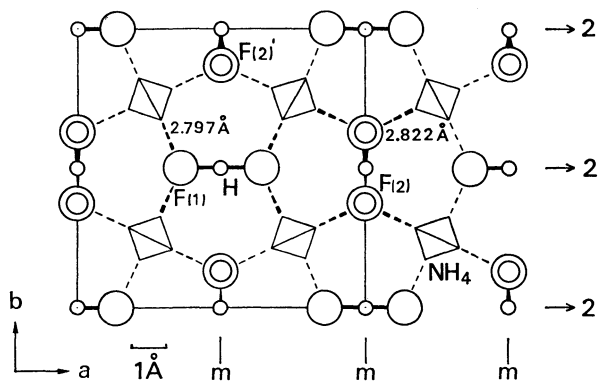

Fig. 3. The crystal structure of NH_4HF_2 projected along the c axis after McDonald.[4]

The authors are grateful to Professor Emeritus Ryôiti Kiriyama for his continued interest and encouragement. This work was partly supported by a Grant-in-Aid for Scientific Research from the Ministry of Education (No. 047076).

References

1) R. Kruh, K. Fuwa, and T. E. McEver, *J. Am. Chem. Soc.*, **78**, 4256 (1956).
2) Yu. G. Kriger, S. P. Gabuda, and N. K. Moroz, *Fiz. Tverd. Tela (Leningrad)*, **17**, 3420 (1975) [*Sov. Phys. Solid State*, **17**, 2239 (1976)]; Yu. G. Kriger, N. K. Moroz, and S. P. Gabuda, *ibid.*, **18**, 891 (1975) [*ibid.*, **18**, 514 (1976)].
3) Y. Furukawa and H. Kiriyama, *Bull. Chem. Soc. Jpn.*, **51**, 3438 (1978).
4) T. R. R. McDonald, *Acta Crystallogr.*, **13**, 113 (1960).
5) D. E. O'Reilly, E. M. Peterson, and T. Tsang, *Phys.*

Rev., **160**, 333 (1967).
6) D. E. O'Reilly and T. Tsang, *J. Chem. Phys.*, **46**, 1291 (1967).
7) H. L. Carrell and J. Donohue, *Israel J. Chem.*, **10**, 195 (1972).
8) D. C. Look and I. J. Lowe, *J. Chem. Phys.*, **44**, 2995 (1966).
9) K. Sagisawa, H. Kiriyama, and R. Kiriyama, *Bull. Chem. Soc. Jpn.*, **51**, 1942 (1978).
10) P. Van Hecke, H. W. Spiess, and U. Haeberlen, *J. Magn. Reson.*, **22**, 103 (1976).
11) L. E. Drain, *Discuss. Faraday Soc.*, **19**, 200 (1955).
12) J. J. Van Rensburg and J. C. A. Boeyens, *J. Solid State Chem.*, **5**, 79 (1972).
13) L. Niemela and J. Tuohi, *Ann. Univ. Turku., Ser. A*, **1**, 12 (1970).
14) R. W. G. Wyckoff, "Crystal Structures," 2nd ed, Interscience Publishers, New York (1965), Vol. 3, p. 326.

Vibrational Spectra and Rotational Isomerism of 2-Chloro- and 2-Bromoethyl Methyl Sulfides

Hiroatsu MATSUURA,* Nobuyuki MIYAUCHI, Hiromu MURATA, and Masaaki SAKAKIBARA†

Department of Chemistry, Faculty of Science, Hiroshima University, Higashisenda-machi, Hiroshima 730

†*Faculty of General Education, Tottori University, Koyama-cho, Tottori 680*

(Received July 17, 1978)

The Raman and infrared spectra of 2-chloro- and 2-bromoethyl methyl sulfides $CH_3SCH_2CH_2X$ (X=Cl and Br) were measured for the liquid and crystalline solid states. The vibrational frequencies of these molecules were calculated by the use of the force constants transferred from unbranched alkyl sulfides and alkyl halides. The rotational isomerism was studied on the basis of the spectral observations and the calculations, and the following conclusions were obtained. (1) In the crystalline solid state, both the chloride and the bromide take the molecular form with the *gauche* conformation about the (C)S–C(C) axis and the *trans* conformation about the (S)C–C(X) axis. (2) In addition to this form (GT), three other forms (TG, GG, and TT) coexist in the liquid state, the GT form being the most stable. (3) The sulfur atom is suggested to lower the energy of the *trans* conformation of the (S)C–C(X) axis.

The vibrational spectra of unbranched alkyl halides have been studied extensively by many investigators. The rotational isomerism of these molecules was thoroughly examined in recent studies[1,2] by analyzing the spectra in conjunction with the systematic calculations of normal coordinates. These studies provided us with essential knowledge on the conformational stability of the halide molecules. In the present study, we deal with 2-halogenoethyl methyl sulfides $CH_3SCH_2CH_2X$ (X=Cl and Br), in which halogen and sulfur atoms are simultaneously involved, in order to examine the effect of the sulfur atom on the conformation of the halide part. Another interest is the reversed effect, namely the effect of the halogen atom on the conformation of the sulfide part. The rotational isomerism of alkyl sulfides has also been investigated systematically in a series of recent studies.[3–5]

Experimental

2-Chloroethyl methyl sulfide was purchased from Tokyo Kasei Kogyo Co., Ltd. and was distilled prior to the Raman and infrared measurements. 2-Bromoethyl methyl sulfide was prepared from 2-methylthioethanol (Tokyo Kasei Kogyo Co., Ltd.) and phosphorus tribromide and was distilled under reduced pressure (bp 64 °C at 25 mmHg).

The measurements of Raman spectra were made on a JEOL JRS-400D spectrophotometer with a Coherent Radiation CR-2 or CR-3 argon ion laser. The Raman spectra were obtained for the liquid state at various temperatures and the crystalline solid state at liquid nitrogen temperature. The infrared spectra were recorded on a Perkin-Elmer 621 spectrophotometer and Hitachi EPI-G2 and EPI-L spectrophotometers. The crystalline solid sample for the infrared measurements was obtained by depositing vapor of the substance onto a cooled window and annealing it repeatedly.

Normal Coordinate Treatment

The calculations of the normal coordinates for 2-chloro- and 2-bromoethyl methyl sulfides were carried out by an MVIB system,[6] which is a program system consisting of various program units combined functionally with one another to calculate vibrational frequencies, modes and other information on the normal vibrations from minimal input data of only a name of the molecule and its conformation. This program system is adapted for a HITAC 8800/8700 Computing System at the University of Tokyo.

The force constants associated with the sulfur and halogen parts were transferred from the unbranched alkyl sulfides[6] and alkyl halides.[7] The force constants for the (S)C–C(X) stretching and the methylene-methylene interactions were transferred from the corresponding alkyl halides. No further adjustment of the force constants was made. The transferred values were found to be accurate enough for determining the existing rotational isomers from their vibrational frequencies. Structural parameters used in the calculations were the same as those of the corresponding parts of the sulfides and halides.[6,7]

Results

The Raman spectra of 2-chloro- and 2-bromoethyl methyl sulfides are shown in Figs. 1—4, and the observed and calculated frequencies and the vibrational assignments based on the potential-energy distributions are listed in Tables 1 and 2. Considering possible molecular forms to be in the staggered conformations, we have for a 2-halogenoethyl methyl sulfide molecule five rotational isomers, TT, TG, GT, GG, and GG′, where the first and second conformation symbols in each isomer designation are those for the (C)S–C(C) and (S)C–C(X) axes, respectively. The symbols T and G imply *trans* and *gauche*, respectively, in accordance with the convention generally accepted.[8]

The following general spectral features are observed for the two halogeno sufildes. (1) As expected, the spectra have combined features of alkyl halides and sulfides. (2) The number of the bands observed in the crystalline solid state is less than that in the liquid state. The former corresponds to what is expected for one molecular form. (3) The relative intensities in the liquid-state Raman spectra vary with the change of temperature.

The rotational isomers existing in each state of aggregation and their relative stabilities will be considered below. The results are summarized in Table 3.

2-Chloroethyl Methyl Sulfide. The key bands for studying molecular conformations of this molecule are the bands due to the S–CH_2 stretching, C–Cl stretching and skeletal deformation vibrations.[1,4,5] The C–S stretching (CH_3–S and S–CH_2) and C–Cl stretching frequencies are expected to be in the range between 800 and 600 cm^{-1}, where the CH_2 rocking frequencies are also likely to be.

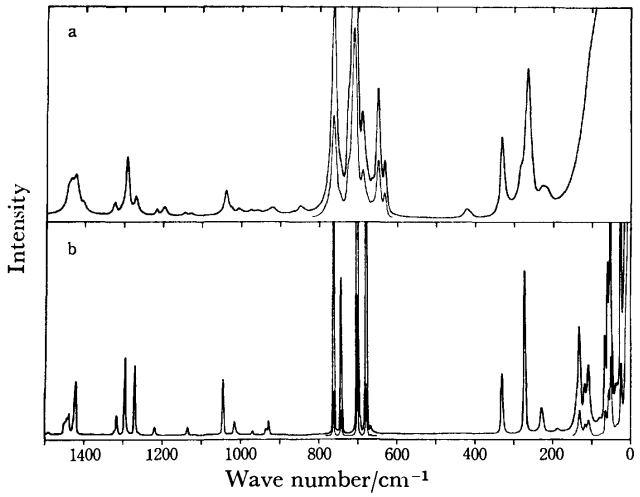

Fig. 1. Raman spectra of 2-chloroethyl methyl sulfide.
a: Liquid, b: crystalline solid.

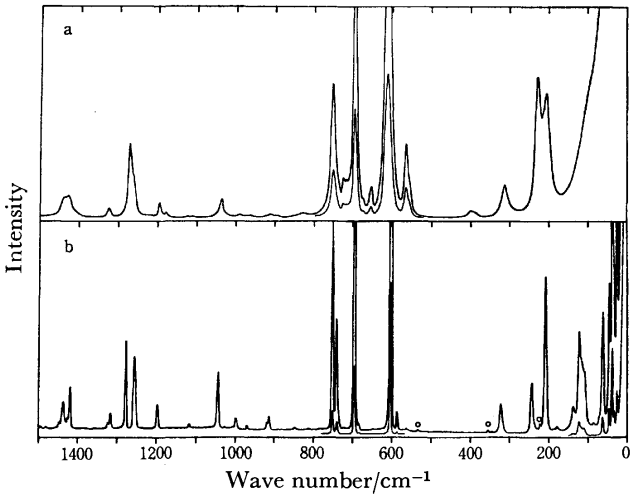

Fig. 3. Raman spectra of 2-bromoethyl methyl sulfide.
a: Liquid, b: crystalline solid.
○: Spurious emission line from the Ar^+ laser.

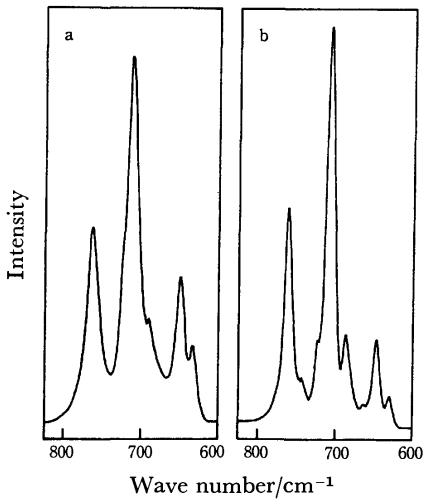

Fig. 2. Raman spectra of 2-chloroethyl methyl sulfide in the liquid state.
a: 110 °C, b: −55 °C.

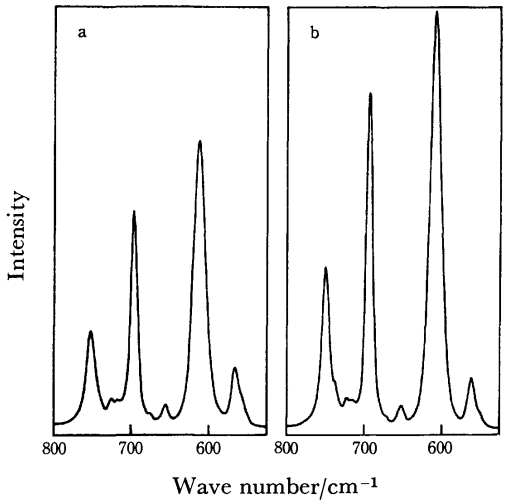

Fig. 4. Raman spectra of 2-bromoethyl methyl sulfide in the liquid state.
a: 25 °C, b: −30 °C.

Table 1. Observed and calculated frequencies and assignments of 2-chloroethyl methyl sulfide

Observed frequency (cm^{-1})[a]				Assignment[b]
Liquid		Crystalline solid		
Raman	Infrared[c]	Raman	Infrared[c]	
		1512 VW		Overtones
		1491 VW		
		1450 W	1451 W,sh	CH_2(Cl) scis (TG 1450, GG 1442, GT 1433, TT 1433), CH_3 ip-d-deform (TT 1444, GT 1442, GG 1441, TG 1440), CH_3 op-d-deform (GT 1432, TG 1432, GG 1432, TT 1432), (S) CH_2 scis (TG 1420, TT 1420, GG 1415, GT 1410)
		1447 W	1445 W,sh	
1442 W,sh	1443 S	1443 W		
1436 W	1438 S	1439 W	1439 M	
1425 W	1428 S	1427 W,sh		
		1423 M	1421 M	
1407 VW, sh	1406 W			

TABLE 1. Continued

Observed frequency (cm^{-1})[a]				Assignment[b]
Liquid		Crystalline solid		
Raman	Infrared[c]	Raman	Infrared[c]	
1322 VW	1327 W	1322 VW 1316 W	1324 W 1318 W	CH_3 s-deform (TG 1325, GG 1324, TT 1323, GT 1322)
	1306 M,sh			$CH_2(Cl)$ wag (TG 1318, GG 1316)
1293 M	1296 M	1295 M	1301 M	$CH_2(Cl)$ wag (GT 1307, TT 1306)
1271 VW	1280 M	1270 M 1260 VW	1272 W	(S)CH_2 twist (TT 1280, GT 1277), (S) CH_2 wag (TG 1277, GG 1277)
1218 VW	1219 S	1218 W	1221 M	(S)CH_2 wag (GT 1219, TT 1217)
1198 VW				(S)CH_2 twist (GG 1199, TG 1198)
1144 VW	1144 VW,sh			$CH_2(Cl)$ twist (GG 1149)
1132 VW	1130 W	1135 VW	1135 M	$CH_2(Cl)$ twist (GT 1147, TG 1147, TT 1147)
1038 W	1040 W	1046 M	1046 W	CC stretch (TT 1030, TG 1023, GT 1019)
1027 VW,sh	1028 W			CC stretch (GG 1008)
1006 VW	1008 W	1016 W	1016 M	$CH_2(Cl)$ rock (TT 986, GT 975)
975 VW	977 W			CH_3 ip-rock (GG 972, TG 968, TT 965)
960 VW	961 W	969 VW	970 M	CH_3 ip-rock (GT 960), CH_3 op-rock (TG 958, GG 957, TT 956)
922 VW	927 W	933 VW 927 W	929 W	CH_3 op-rock (GT 957), $CH_2(Cl)$ rock (TG 948, GG 941)
863 VW	866 VW			(S)CH_2 rock (TG 881)
845 VW	848 W			(S)CH_2 rock (GG 863)
763 S	764 W	763 S	764 W	$SC(H_2)$ stretch (GT 773, TT 770)
745 W, sh	746 W	745 M	745 W	(S)CH_2 rock (TT 754, GT 742), $C(H_3)S$ stretch (TT 736)
724 S, sh				$C(H_3)S$ stretch (TG 726, GG 723)
710 VS	712 S	703 VS 695 VW	705 S	CCl stretch (GT 719)
688 M	688 S	680 S	686 S 679 S	$C(H_3)S$ stretch (GT 697), CCl stretch (TT 697)
		667 VW	668 W	^{13}CCl stretch ? (GT)
663 W	667 W, sh			$SC(H_2)$ stretch (TG 669)
648 S	651 W			$SC(H_2)$ stretch (GG 659), CCl stretch (TG 651)
632 W	634 VW			CCl stretch (GG 643)
422 VW	415 W			SCC deform (TG 423)
412 VW, sh				CCCl deform (GG 387)
332 M	328 VW	333 M	329 W	CSC bend (GT 337, TT 335, GG 327)
282 W, sh				CCCl deform (TT 288)
265 S	258 VW	274 M	267 W	CCCl deform (TG 266, GT 257)
226 W				CSC bend (TG 216)
218 W, sh		228 W		SCC deform (GT 204, GG 200)
		188 VW		
		140 W,sh		
		132 M		
		120 W		
≈100 sh		107 W		
		78 VW		Torsions and lattice vibrations
		65 M		
		60 M		
		53 S		
		40 W		
		28 S		

a) VS: very strong, S: strong, M: medium, W: weak, VW: very weak, sh: shoulder. b) All the calculated frequencies for the individual rotational isomers are given in parentheses except for those of the CH stretching and torsional vibrations and the lowest skeletal deformation frequency for the TT form (133 cm^{-1}, SCC deform) which are not included in the table. c) The infrared spectra in the region below 250 cm^{-1} were not measured.

The Raman and infrared spectra of the crystalline solid state exhibit four distinct bands at 763, 745, 703, and 680 cm^{-1}, the fourth being a doublet in the infrared spectrum. Since a single molecular form exists in this state as is evident from the number of the bands observed in the whole region, the four bands are assigned to the CH_3–S, S–CH_2, and C–Cl stretching, and one of the two CH_2 rocking vibrations. The least strong Raman band at 745 cm^{-1} is assignable to the CH_2 rocking vibration by considering that Raman intensities for the C–S or C–Cl stretching vibration are generally stronger than those for the rocking vibration. Previous studies indicated that the C–S stretching frequencies for the P_C conformation (the sulfur atom is *trans* to a carbon atom) and the P_H conformation (the sulfur atom is *trans* to a hydrogen atom) are 745—760 and 645—670 cm^{-1}, respectively,[9] and that the C–Cl stretching frequencies for the P_C conformation (the chlorine atom is *trans* to a carbon atom) and the P_H conformation (the chlorine atom is *trans* to a hydrogen atom) are 720—730

Table 2. Observed and calculated frequencies and assignments of 2-bromoethyl methyl sulfide

Observed frequency (cm^{-1})[a]				Assignment[b]
Liquid		Crystalline solid		
Raman	Infrared[c]	Raman	Infrared[c]	
		1503 VW		
≈1490 VW		1493 VW	1492 VW	Overtones
		1479 VW		
		1446 VW	1449 W	
1437 W	1433 S	1434 W	1435 M	CH_2(Br) scis (TG 1451, GG 1443, GT 1435, TT 1435), CH_3 ip-d-deform (TT 1444, GT 1442, GG 1442, TG 1441), CH_3 op-d-deform (GT 1432, GG 1432, TG 1432, TT 1432), (S) CH_2 scis (TG 1418, TT 1418, GG 1413, GT 1408)
1427 W		1424 W	1432 M,sh	
		1417 M	1419 M	
1408 VW,sh	1409 W,sh			
1323 W	1322 W	1323 VW 1316 W	1323 VW 1316VW,sh	CH_3 s-deform (TG 1323, TT 1323, GT 1322, GG 1322)
	1282 W,sh			(S)CH_2 wag (GG 1288, TG 1288)
1270 M	1268 M	1276 M	1277 M	(S)CH_2 wag (GT 1272, TT 1269)
1259 M, sh	1255 M	1256 M 1252 M,sh	1255 W	(S)CH_2 twist (GG 1267, TG 1267, TT 1265, GT 1262)
1193 W	1192 S	1197 W	1198 S	CH_2(Br) wag (GT 1200, TT 1199)
1177 VW				CH_2(Br) wag (GG 1179, TG 1179)
1121 VW				CH_2(Br) twist (TT 1127)
1112 VW	1107 M	1116 VW	1114 M	CH_2(Br) twist (GT 1126, GG 1118, TG 1117)
1036 W	1035 W	1045 M	1043 W	CC stretch (TT 1020, TG 1014, GT 1009, GG 1000)
989 VW	989 W	998 W	999 M	CH_3 ip-rock (GG 970, GT 969, TG 967, TT 965)
975 VW	972 W,sh	970 VW	969 M	CH_3 op-rock (TT 960, GT 958, GG 958, TG 958)
960 VW	959 M			(S)CH_2 rock (TT 947)
911 VW	908 W	920 VW 913 W	914 W	CH_2(Br) rock (GT 931, GG 917), (S)CH_2 rock (TG 928)
896 VW	891 VW,sh			CH_2(Br) rock (TG 866)
828 VW	827 W			(S)CH_2 rock (GG 850)
752 S	751 W,sh	750 S	751 W	SC(H_2) stretch (GT 759, TT 751)
739 M,sh	738 W	741 M	738 W	CH_2(Br) rock (TT 748), (S)CH_2 rock (GT 737)
725 W	723 VW,sh			C(H_3)S stretch (TT 727, TG 726)
718 W				C(H_3)S stretch (GG 723)
697 VS	691 W	695 VS 683 VW	695 W	C(H_3)S stretch (GT 698)
675 VW,sh				SC(H_2) stretch (TG 665)
655 W	651 VW			SC(H_2) stretch (GG 653)
613 VS	607 S	601 VS	600 S 595 S	CBr stretch (GT 630, TT 625)
		585 W	579 VW	^{13}CBr stretch ? (GT)
565 M				CBr stretch (TG 556)
555 W,sh	557 W			CBr stretch (GG 553)
401 VW				SCC deform (TG 405)
392 VW	389 VW			SCC deform (GG 363)
313 W	313 VW	320 W	320 VW	CSC bend (TT 329, GG 321, GT 318)
228 S		242 M		CCBr deform (TG 246, GT 216), SCC deform (TT 235)
215 M,sh				CSC bend (TG 214)
207 S		207 S		SCC deform (GT 200)

TABLE 2. Continued

Observed frequency (cm^{-1})[a]				Assignment[b]
Liquid		Crystalline solid		
Raman	Infrared[c]	Raman	Infrared[c]	
		177 VW		Torsions and lattice vibrations
		136 W		
		122 M		
		117 M,sh		
≈100 sh		109 M		
		84 VW		
		61 M		
		45 S		
		37 VS		
		32 S		
		25 S		

a) See a) of Table 1. b) All the calculated frequencies for the individual rotational isomers are given in parentheses except for those of the CH stretching and torsional vibrations and the lowest skeletal deformation frequencies for the TT form (125 cm^{-1}, CCBr deform) and for the GG form (89 cm^{-1}, CCBr deform) which are not included in the table. c) See c) of Table 1.

and 650—660 cm^{-1}, respectively.[10,11] These frequency-conformation correlations show that the 763 cm^{-1} band of 2-chloroethyl methyl sulfide corresponds definitely to the C–S stretching of $P_{C'}$, and therefore is assigned to the C–S stretching of P_{Cl}. Thus, the (S)C–C(Cl) axis in this molecule is determined to be in the *trans* conformation and the molecular conformation is either TT or GT. No observation of the C–Cl stretching band of P_H also suports this conformation. The band at 703 cm^{-1} (710 cm^{-1} in the liquid state) is assigned to the C–Cl stretching of the P_S conformation with reference to the P_C frequency of 720—730 cm^{-1}. The remaining band at 680 cm^{-1} is then assigned to the CH_3–S stretching vibration. All of these vibrational assignments are confirmed by the normal coordinate calculations as shown in Table 1.

The conformation about the (C)S–C(C) axis is found to be in *gauche* in the solid state by examining the skeletal deformation vibrations as mentioned below. The Raman bands are observed in this state at 333, 274, and 228 cm^{-1} between 500 and 180 cm^{-1} (the corresponding frequencies in the liquid state are 332, 265, and 223 cm^{-1}). On the other hand, the normal coordinate calculations give the frequencies of 335 and 288 cm^{-1} in the same range for the TT form and 337, 257, and 204 cm^{-1} for the GT form. The number of the observed bands and their frequencies are explained only by the GT form. The Raman band at 282 cm^{-1}, which is observed in the liquid state but disappears on solidification, is in fact assigned to the TT form.

Close examinations of the observed Raman and infrared spectra, incorporated with the results of the normal coordinate calculations (Table 1), indicate that the TG, GG, and TT forms coexist in the liquid state in addition to the GT form. The frequencies of the observed bands which are assigned only to a single molecular form are 863, 663, and 422 cm^{-1} (TG form), 845, 632, and 412 cm^{-1} (GG form), and 282 cm^{-1} (TT form). The existence of the GG′ form is not certain but this conformation is quite unlikely to exist as suggested from the expected large steric repulsions.

The liquid-state Raman spectra were measured at higher and lower temperatures in order to study the relative conformational stabilities among the existing rotational isomers (Fig. 2). Although most of the individual Raman bands are more or less overlapped by other bands, it is evidently shown that the bands due to the GT form increase at lower temperature as compared with the bands due to the other forms. The GT form is thus found to be the most stable in the liquid state. The relative conformational stability for the other forms is not definitive from the present spectral measurements.

2-Bromoethyl Methyl Sulfide. The S–CH_2 and C–Br stretching frequencies are useful in determining the conformation about the (S)C–C(Br) axis, similarly to the case of 2-chloroethyl methyl sulfide for which the S–CH_2 and C–Cl stretching frequencies have been used.

In the crystalline solid state, the distinct bands are observed at 750, 741, 695, and 601 cm^{-1} in the range between 800 and 500 cm^{-1}. The 601 cm^{-1} band (613 cm^{-1} in the liquid state) is assigned to the C–Br stretching vibration of the P_S conformation, since the C–Br stretching frequencies for the P_C and P_H conformations of alkyl bromides are 635—645 and 555—565 cm^{-1}, respectively,[12] and the corresponding frequency for the P_S conformation is expected to be lower than the P_C frequency on account of a heavier atom of sulfur. The P_H frequencies of the C–Br stretching vibration is observed, in fact, at 565 and 557 cm^{-1} in the liquid state. Thus, the (S)C–C(Br) axis is determined to be in the *trans* conformation and the molecular conformation in the solid state is either TT or GT. The 741 cm^{-1} band, which is the least strong of the four Raman bands and corresponds to the 745 cm^{-1} band of the chloride, is assigned to the CH_2 rocking vibration. The band at 750 cm^{-1} is associated with the S–CH_2 vibration of the P_{Br} conformation in accord with the P_C frequency of 745—760 cm^{-1}, and the band at 695 cm^{-1} is assigned to the CH_3–S stretching vibration. It is noted that the

Table 3. Rotational isomers of 2-halogenoethyl methyl sulfides

	$CH_3SCH_2CH_2Cl$	$CH_3SCH_2CH_2Br$
Liquid[a]	GT, TG, GG, TT	GT, TG, GG, TT
Crystalline solid	GT	GT

a) For both 2-chloro- and 2-bromoethyl methyl sulfides, the GT form is the most stable in the liquid state.

C–Br stretching Raman band is stronger than the C–S stretching Raman band. For the chloride, a similar observation is also made that the C–Cl stretching vibration gives rise to a stronger Raman intensity than the C–S stretching vibration.

In the solid-state spectra, the bands are observed at 320, 242, and 207 cm^{-1} in the region between 500 and 180 cm^{-1}.[13] The TT form gives two calculated frequencies of 329 and 235 cm^{-1} in this region and the GT form three calculated frequencies of 318, 216, and 200 cm^{-1}. The comparison of the observed and calculated frequencies readily leads to the conclusion that the molecular conformation in the solid state is the GT form. Thus, the normal coordinate calculation is shown to be important in determining the conformation about the (C)S–C(C) axis in both cases of the chloride and the bromide.

In the liquid-state spectrum, there appear several bands which are not found in the solid-state spectrum. These are reasonably assigned to the rotational isomers other than the GT form on the basis of the spectral analyses and the results of the normal coordinate calculations. Of the bands observed only in the liquid state, the following bands are associated exclusively with a single rotational isomer: 960 cm^{-1} (TT form), 896, 675, 565, 401, and 218 cm^{-1} (TG form), and 828, 718, 655, 555, and 392 cm^{-1} (GG form). The GT, TG, GG, and TT forms are thus found to coexist in the liquid state, but the GG′ form is again unlikely to exist. If the GG′ form existed, the Raman spectrum would exhibit a band around 270 cm^{-1}, since the normal coordinate calculation on this form gives this frequency for a quasi-totally symmetrical deformation of the molecular skeleton.

The Raman spectra in the liquid state at higher and lower temperatures (Fig. 4) show the relative intensities of the bands assigned to the GT form are stronger at lower temperature than those assigned to the other forms. Accordingly the GT form is the most stable in the liquid state similarly to the case of the chloride.

Discussion

The rotational isomerism of 2-chloroethyl methyl sulfide has been studied by Hayashi[14] and the molecular form in the solid state has been reported to be either GT or TT.

In the present study, the following results on the rotational isomerism have been obtained for 2-chloro- and 2-bromoethyl methyl sulfides in common. (1) The molecular form in the crystalline solid state is the GT form. (2) The GT, TG, GG, and TT forms coexist in the liquid state, the GT form being the most stable.

For both 2-chloro- and 2-bromoethyl methyl sulfides, the GT form is the most stable in the liquid state, the (C)S–C(C) and (S)C–C(X) axes being in the *gauche* and *trans* conformations, respectively. The previous studies on unbranched alkyl sulfides indicated that the *gauche* conformation about the (C)S–C(C) axis is slightly more stable than the *trans* conformation[3–5,15,16] and for ethyl methyl sulfide the enthalpy difference between the *trans* and *gauche* conformation was shown to be $\Delta H_{T-G}=140\pm50$ cal mol^{-1} in the liquid state.[15] Accordingly, the conformational stability of the (C)S–C(C) part in the halogeno sulfides is in line with that for other sulfides.

The most stable isomer of the halogeno sulfide molecules takes the *trans* conformation about the (S)C–C(X) axis. For unbranched alkyl halides, the *gauche* (C)C–C(X) axis was found to be slightly more stable than the *trans* axis.[1] The conformational stability of the (O)C–C(X) axis in halogeno ethers was also studied and the *gauche* conformation was found to be more stable than the *trans* conformation.[17] Accordingly, the stability of the (S)C–C(X) axis is different from that of the (C)C–C(X) or (O)C–C(X) axis.

The Raman spectrum of 2-bromoethyl methyl sulfide in the liquid state (Fig. 3) shows that the C–Br stretching band at 613 cm^{-1} due to the *trans* (S)C–C(Br) conformation is much stronger than the corresponding bands at 565 and 555 cm^{-1} due to the *gauche* conformation.[18] For 2-bromoethyl methyl ether, however, the C–Br stretching Raman band of the *trans* (O)C–C(Br) conformation at 668 cm^{-1} is weaker than that of the *gauche* conformation at 571 cm^{-1} (Fig. 4 of Ref. 17) in contrast with the case of 2-bromoethyl methyl sulfide. This spectral difference for the two molecules suggests the difference of the conformational stability of the (S)C–C(Br) and (O)C–C(Br) axes as mentioned above, on the assumption that the ratio of the Raman intensity, per molecule, of the *trans* conformation to that of the *gauche* conformation does not change for these molecules. The validity of this assumption may be diagnosed in part by examining the coupling of these C–Br stretching vibrations with other vibrations. The calculated potential-energy distributions indicate that the bands assigned to the C–Br stretching have contributions from other vibrations less than 20% in any case of 2-bromoethyl methyl sulfide and 2-bromoethyl methyl ether. Accordingly, the assumption can be approximately valid for discussing the relative conformational stability.

For 1-bromobutane, the C–Br stretching Raman band of the *trans* (C)C–C(Br) conformation is weaker than the corresponding band of the *gauche* conformation (Fig. 11 of Ref. 1), similarly to the case of 2-bromoethyl methyl ether, but the intensity ratio of the *trans* to *gauche* band is larger than that of 2-bromoethyl methyl ether. Hence, the *gauche* conformation of the (O)C–C(Br) axis is shown to be more stabilized than the *gauche* conformation of the (C)C–C(Br) axis on the assumption of the constant Raman intensity ratio. The spectral observations on the above-mentioned molecules give a suggestion that a sulfur atom lowers, as compared with a carbon atom, the energy of the *trans* conformation but an oxygen atom lowers the energy of the *gauche* confor-

mation of the (A)C–C(X) axis, where A is S or O and X is a halogen atom.

Part of the Raman and infrared measurements for 2-chloroethyl methyl sulfide was made on the spectrometers in the laboratory of Professor Mitsuo Tasumi, the University of Tokyo, to whom the authors wish to express their gratitude.

References

1) Y. Ogawa, S. Imazeki, H. Yamaguchi, H. Matsuura, I. Harada, and T. Shimanouchi, *Bull. Chem. Soc. Jpn.*, **51**, 748 (1978).

2) H. Matsuura, S. Imazeki, Y. Ogawa, M. Sakakibara, I. Harada, and T. Shimanouchi, to be published.

3) M. Sakakibara, H. Matsuura, I. Harada, and T. Shimanouchi, *Bull. Chem. Soc. Jpn.*, **50**, 111 (1977).

4) M. Ohta, Y. Ogawa, H. Matsuura, I. Harada, and T. Shimanouchi, *Bull. Chem. Soc. Jpn.*, **50**, 380 (1977).

5) Y. Ogawa, M. Ohta, M. Sakakibara, H. Matsuura, I. Harada, and T. Shimanouchi, *Bull. Chem. Soc. Jpn.*, **50**, 650 (1977).

6) T. Shimanouchi, H. Matsuura, Y. Ogawa, and I. Harada, *J. Phys. Chem. Ref. Data*, **7**, No. 4 (1978).

7) T. Shimanouchi, H. Matsuura, Y. Ogawa, and I. Harada, to be published.

8) T. Shimanouchi, Y. Ogawa, M. Ohta, H. Matsuura, and I. Harada, *Bull. Chem. Soc. Jpn.*, **49**, 2999 (1976).

9) N. Nogami, H. Sugeta, and T. Miyazawa, *Bull. Chem. Soc. Jpn.*, **48**, 2417 (1975).

10) S. Mizushima, T. Shimanouchi, K. Nakamura, M. Hayashi, and S. Tsuchiya, *J. Chem. Phys.*, **26**, 970 (1957).

11) J. J. Shipman, V. L. Folt, and S. Krimm, *Spectrochim. Acta*, **18**, 1603 (1962).

12) F. F. Bentley, N. T. McDevitt, and A. L. Rozek, *Spectrochim. Acta*, **20**, 105 (1964).

13) The frequency of the second band was found to decrease with increasing temperature in the solid state (240 cm^{-1} at -70 °C and 235 cm^{-1} at -30 °C) and the 228 cm^{-1} band in the liquid state is thus identified as the corresponding band.

14) M. Hayashi, *Nippon Kagaku Zasshi*, **80**, 1084 (1959).

15) N. Nogami, H. Sugeta, and T. Miyazawa, *Bull. Chem. Soc. Jpn.*, **48**, 3573 (1975).

16) N. Nogami, unpublished work.

17) H. Matsuura, M. Kono, H. Iizuka, Y. Ogawa, I. Harada, and T. Shimanouchi, *Bull. Chem. Soc. Jpn.*, **50**, 2272 (1977).

18) A similar observation is not made for 2-chloroethyl methyl sulfide because of overlapping of the C–Cl and C–S stretching bands and of unnegligible coupling of these vibrational modes.

The Photochemical Reaction of Benzo[*c*]cinnoline. II. Photo-reduction in Acidic 2-Propanol

Hiroyasu INOUE,* Yukimi HIROSHIMA, and Norio MAKITA

Department of Applied Chemistry, Faculty of Technology, Kanagawa University, Kanagawa-ku, Yokohama 221

(Received July 22, 1978)

The photochemical reduction of benzo[*c*]cinnoline in strongly acidic 2-propanol (4 M HCl) has been studied using light of wavelength longer than 400 nm. The photoproduct has been identified as 5,6-dihydrobenzo[*c*]-cinnoline. The quantum yields for product formation, which are the same as that for the disappearance of the reactant, have been measured under various conditions. In contrast to the poor phosphorescent property of benzo[*c*]cinnoline, the protonated species has been found to phosphoresce with significant efficiency. The lowest triplet state energy has been estimated to be 51 kcal/mol. The results of the quenching showed that the photo-reduction was attributed to the lowest excited triplet state of protonated benzo[*c*]cinnoline. The pK_a value in the reactive state is lower than that in the ground state.

Several nitrogen heterocyclic compounds in electronically excited states have been shown to undergo hydrogen atom abstraction from solvent molecules. The photo-reductions of acridine and phenazine, for example, have been extensively studied, and the reactive states in the photo-reduction shown to be the lowest excited $n\pi^*$ singlet states.[1,2] The photo-reduction of phenazine has also been studied in acidic media, and the $n\pi^*$ singlet state mechanism proposed.[3] For quinoline and pyrimidine derivatives in acidic alcohol solutions, however, photoalkylation has been observed.[4,5]

In a previous paper[6] it was reported that the photo-irradiation of benzo[*c*]cinnoline in strongly acidic (4M HCl) alcoholic solution led to the formation of 2,2′-diaminobiphenyl or carbazole as the final product depending on the excitation wavelength and the alcohol used as the solvent. In both reactions the final products are formed by the subsequent reactions of the initially formed intermediate which is characterized by absorption bands at 240, 270, and 316 nm. In the case of benzo[*c*]cinnoline in acidic 2-propanol, irradiation with light of a wavelength longer than 400 nm gives the intermediate compound, but no subsequent reaction occurs.[7]

In this paper, the initial photoreaction of benzo[*c*]-cinnoline under certain conditions will be reported. Although some results indicate that the photoproduct is 5,6-dihydrobenzo[*c*]cinnoline, further evidence will be given for the identification of the product. This will be followed by a discussion of the reactive state of the reactant on the basis of the quantum yields for the reaction under various conditions.

Experimental

Materials. Benzo[*c*]cinnoline was obtained from Aldrich Chemical Co. and recrystallized from ethanol; mp 155 °C (lit,[8] 156 °C). 2-Propanol, a Kokusan Works reagent, was purified by refluxing in sodium hydroxide solution and subsequent distillation. Purified 2-propanol was shown to be free from aldehydes by GLC analysis.[9] Anthracene, pyrene, fluoranthene, *trans*-1,3-pentadiene, and naphthalene, which were used in quenching experiments, were purified by recrystallization or distillation.

Light Source and Irradiation. A 500 W high pressure mercury arc lamp (Ushio USH-500) was used as the visible light source with a Corning glass filter (CS3-73) which cut off light shorter than 400 nm. All irradiations were carried out at room temperature. The solution of the reactant was flushed with nitrogen passed through a pyrogallol solution for 30 min prior to and during the irradiation. Acidities of the solution were adjusted with HCl.

Actinometry and Analysis. The intensities of light transmitted by the sample solution and solvent respectively were measured to determine the quantum yields of the photoreaction using a potassium ferrioxalate solution as actinometer.[10] Two cylindrical cells (diameter: 4.5 cm, length: 3 cm) were used in the actinometry. The disappearance of benzo[*c*]-cinnoline and the appearance of the product were determined spectrophotometrically. The molar extinction coefficients of the ultraviolet absorption bands of the photoproduct have been determined previously.[6]

Measurements. Ultraviolet absorption spectra were taken with a Shimadzu UV-200 spectrophotometer using 1 cm quartz cells. Emission spectra were recorded on a Shimadzu RF-500 spectrofluorimeter.

Chemical Reduction of Benzo[c]*cinnoline with Lithium Aluminium Hydride.* Benzo[*c*]cinnoline was chemically reduced by a large excess of lithium aluminium hydride in tetrahydrofuran under nitrogen at room temperature. After 30 min the solution was acidified by the addition of HCl and the absorption spectrum of the reduced compound was measured.

Results and Discussion

Photoproduct in Acidic Aqueous 2-Propanol. Figure 1 shows the spectral change caused by irradiation of the reactant (6.7×10^{-5} M) in acidic (4 M HCl) aqueous 2-propanol. The photo-reaction was completed in 140 min giving rise to a photoproduct having bands at 240, 270, and 316 nm. The existence of three isosbestic points at 235, 270, and 324 nm and the quantitative recovery of benzo[*c*]cinnoline by aeration of the irradiated solution indicate the absence of a side reaction.

In order to identify the product as 5,6-dihydrobenzo-[*c*]cinnoline (monoprotonated form in strongly acidic solution), the chemical hydrogenation of the reactant was attempted. The hydrogenation was performed by treating the tetrahydrofuran solution of benzo[*c*]-cinnoline with lithium aluminium hydride. The solution of the resulting reduced compound was acidified and the absorption spectrum determined. The observed spectrum is presented in Fig. 2. The chemically reduced compound has been considered to be 5,6-dihydrobenzo-

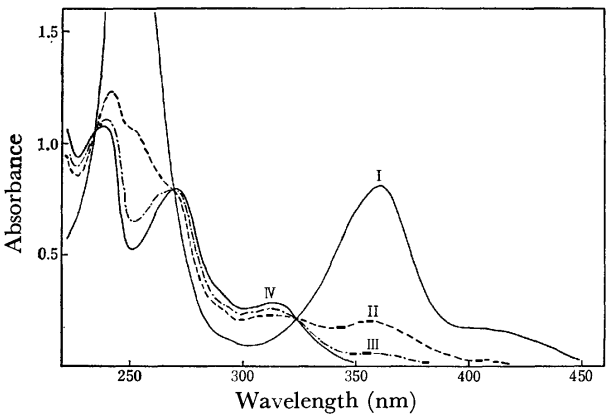

Fig. 1. Spectral change of the 4 M HCl 2-propanol solution of benzo[*c*]cinnoline (6.7×10^{-5} M) caused by irradiation with light longer than 400 nm. Irradiation time (min); I: 0, II: 30, III: 60, IV: 140.

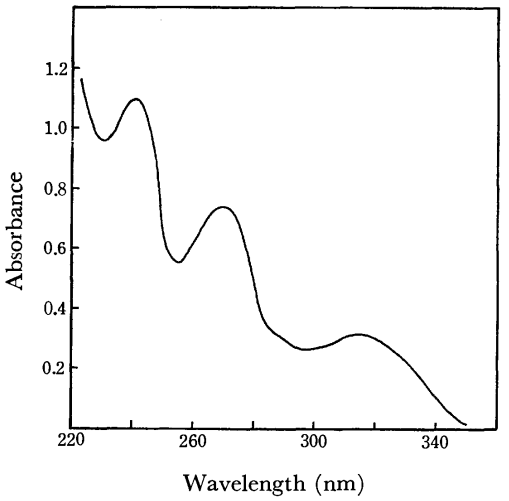

Fig. 2. Absorption spectrum of the acidified tetrahydrofuran solution of the compound prepared by reduction of benzo[*c*]cinnoline with $LiAlH_4$.

[*c*]cinnoline. As seen from Figs. 1 and 2, the absorption spectra of the products formed by the two methods show good agreement. Consequently, the photoproduct has been identified as 5,6-dihydrobenzo[*c*]cinnoline.

Quantum Yields for the Photo-reduction under Various Conditions. The quantum yield for the disappearance of the reactant coincides with that for product formation, thus indicating that 5,6-dihydrobenzo[*c*]-cinnoline is the only photoproduct from the reactant in the present experimental conditions. As seen from Fig. 3, the quantum yield remained constant with variation in the irradiation time (15—120 min) and in the initial concentration of the reactant (4.0×10^{-5}—5.2×10^{-4} M). The average quantum yield has been determined to be 5.5×10^{-3}. For the photo-reduction of phenazine in alcoholic solution, the concentration dependence of the quantum yield has been established and interpreted in terms of self quenching.[11] However, the result shown in Fig. 3b indicates that such self-quenching is absent in the present photo-reduction in the concentration range studied here.

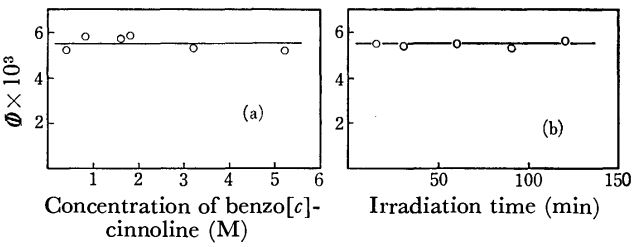

Fig. 3. Dependence of quantum yields for the photoreduction: (a) on the initial concentration of the reactant; (b) on irradiation time.

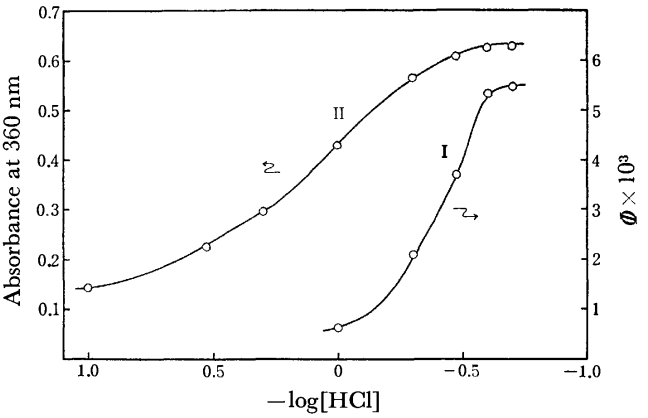

Fig. 4. Quantum yields for the photoreduction (I) and absorption intensity of the 360 nm band (II) at various concentrations of HCl.

It has been found that the quantum yield changes with variation in the acidity of the solution. Curve I in Fig. 4 shows the quantum yield at various concentrations of hydrochloric acid. In Fig. 4 the absorbances of protonated benzo[*c*]cinnoline at 360 nm have also been plotted against the acid concentration (curve II). From this curve the apparent pK_a of the conjugate acid of benzo[*c*]cinnoline in the ground state has been determined to be 0.1 in a mixed solvent of 2-propanol and water (1 : 1) at 20 °C. Since only the protonated species of the reactant can be excited with visible light, curve I may be regarded as reflecting the equilibrium situation of the protonation at the reactive state in the photo-reduction. From curve I the pK_a at the reactive state, which can be assigned as the lowest triplet state as described below, has been estimated to be −0.4. Therefore, the basicity of the reactant in the lowest triplet state is considered to be lower than that in the ground state and this behavior is in contrast to that for other nitrogen heterocyclic compounds which have higher pK_a values in the lowest triplet states than in the ground states.[12–14]

Since hydrochloric acid was used to acidify the solution the quenching effect of chloride ion needs to be examined in view of the fact that in some cases halide ions act as fluorescence quenchers[15] and exibit a quenching effect as in the photo-reduction of acridine.[16] In the present case, the quantum yield has been found to be unaffected on addition of sodium chloride in the concentration range up to 0.05 M.

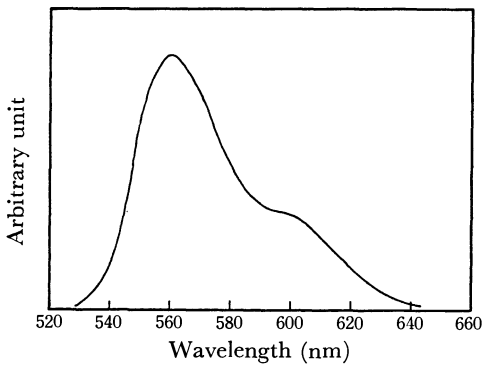

Fig. 5. Phosphorescence spectrum of protonated benzo[c]cinnoline in 4 M HCl aqueous 2-propanol at 77 K. Excitation wavelength 420 nm.

Therefore, it is not necessary to correct the results concerning the effect of acid concentration on the quantum yield presented in Fig. 4 for changes in chloride ion concentration.

Emission Spectra of Protonated Benzo[c]*cinnoline.* It has been established that benzo[*c*]cinnloine exibits fluorescence, but does not phosphorescence with a significant quantum yield.[17] The lowest triplet state has been assigned as of the $\pi\pi^*$ type and the energy determined to be 52.0 kcal/mol from the $S_0 \rightarrow T_1$ absorption spectrum.[18] On the other hand, little is known concerning the excited states of the protonated species. In order to study the behavior of protonated benzo[*c*]cinnoline in electronically excited states, the emission spectra have been measured. In contrast to the non-phosphorescent property of the unprotonated species, the phosphorescence emission could be observed for the protonated species by means of a conventional spectrofluorimeter at 77 K, the observed phosphorescence band is shown in Fig. 5. On the other hand, the intensity of the fluorescence band at 490 nm decreased with increasing acid concentration. Since the phosphorescence band has no fine structure, the position of the 0-0 transition can not be determined precisely. Nevertheless, the wavelength of the peak (560 nm) may indicate the approximate energy of the lowest triplet state (E_T), that is, E_T has been estimated to be 51 kcal/mol. Recently, Lin *et al.*[19] have observed the enhanced phosphorescence band in isopentane solution containing fluorinated alcohols which can form hydrogen bonds with benzo[*c*]cinnoline. The spectra have fine structure and the shortest wavelength peaks are at approximately 550 nm.

Quenching in the Photo-reduction. In order to investigate the reactive state of the reactant in the photoreduction, quenching experiments were conducted. Quenching during the photo-reduction has been studied quantitatively through measurements of the quantum yields. In consideration of the estimated value of the lowest triplet state of the reactant (E_T=51 kcal/mol), the following compounds have been employed in the quenching experiments, naphthalene (E_T=60.9 kcal/mol), *trans*-1,3-pentadiene (E_T=59.2 kcal/mol), fluoranthene (E_T=52.9 kcal/mol), pyrene (E_T=48.2 kcal/mol), and anthracene (E_T=42.7 kcal/mol).[20] Under the present experimental conditions, none of these compounds can absorb the irradiated light.

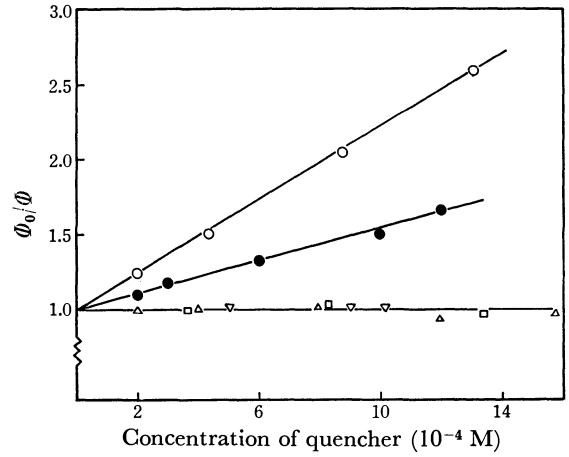

Fig. 6. Stern-Volmer plots for the photoreduction.
○: Anthracence, ●: pyrene, ▽: fluoranthene, △: *trans*-1,3-pentadiene, □: naphthalene.

The quenching experiments were performed using a fixed concentration of the reactant and variations in the quencher concentration. The quenching data are presented in Fig. 6, where Φ_0/Φ have been plotted against the quencher concentrations. The quantities Φ and Φ_0 are the quantum yields with and without quencher, respectively. As can be seen from Fig. 6, pyrene and anthracene act effectively as quenchers for the photo-reduction and the Stern-Volmer plots give straight lines, thus indicating that a single excited state participates in the photo-reduction. Fluoranthene, *trans*-1,3-pentadiene, and naphthalene exibited no influence on the quantum yield. Taking into account the lowest triplet state energies of the reactant and the quenchers, the triplet-triplet energy transfers from the protonated benzo[*c*]cinnoline donor to the pyrene and anthracene acceptors are considered possible, whereas such energy transfer are impossible in other cases. These situations reflect the results obtained here. Therefore, the observed quenching effects have been interpreted in terms of the triplet-triplet energy transfer. This is also indicated by the phosphorescence quenching data as shown in Fig. 7, where I_0/I has been plotted against the concentration of pyrene acceptor. The quantities I and I_0 are phosphorescence intensities at 560 nm with and

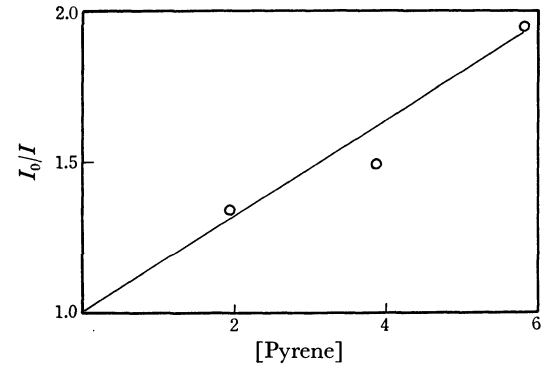

Fig. 7. Phosphorescence quenching plots of protonated benzo[*c*]cinnoline by the pyrene acceptor.
Excitation wavelength: 362 nm. Concentration of benzo[*c*]cinnoline: 1.04×10^{-4} M.

without pyrene. It is evident that pyrene acts as a triplet quencher.

The lowest excited singlet state energy of the protonated benzo[*c*]cinnoline has been estimated to be 68 kcal/mol from the longest wavelength absorption band at 420 nm. This value is lower than that of any compound used in the quenching experiments,[20] and therefore, the singlet-singlet energy transfer may be dismissed as responsible for the observed quenching. From the absorption and emission spectra, no evidence was obtained for the ground state complexing and the exciplex formation between the reactant and the quenchers.

Consequently, the results suggest that the reactive state in the photo-reduction in strongly acidic aqueous 2-propanol is the lowest excited triplet state of protonated benzo[*c*]cinnoline.

References

1) D. G. Whitten and Y. J. Lee, *J. Am. Chem. Soc.*, **93**, 961 (1971).

2) G. A. Davis, J. D. Gresser, and P. A. Carapellucci, *J. Am. Chem. Soc.*, **93**, 2179 (1971).

3) D. N. Bailey, D. K. Roe, and D. M. Hercules, *J. Am. Chem. Soc.*, **90**, 6291 (1968).

4) F. R. Stermitz, C. C. Wei, and C. M. O'Donnell, *J. Am. Chem. Soc.*, **92**, 2745 (1970).

5) M. Ochiai, E. Mizuta, Y. Asahi, and K. Morota, *Tetrahedron*, **24**, 5861 (1968).

6) Part I of this series: H. Inoue, T. Sakurai, and F. Tanaka, *Bull. Chem. Soc. Jpn.*, **48**, 924 (1975).

7) The photoproduct has no absorption at wavelength longer than 400 nm.

8) G. M. Badger, J. H. Seidler, and B. Thomson, *J. Chem. Soc.*, **1951**, 3207.

9) If 2-propanol is contaminated with aldehydes, the initial photo-reduction is followed by the subsequent reaction to give 2,2′-diaminobiphenyl to be published.

10) C. G. Hatchard and C. A. Parker, *Proc. R. Soc. London, Ser. A*, **235**, 518 (1956).

11) T. Iwaoka, S. Niizuma, and M. Koizumi, *Bull. Chem. Soc. Jpn.*, **43**, 2786 (1970).

12) G. Jackson and G. Porter, *Proc. R. Soc. London, Ser. A*, **260**, 13 (1961).

13) J. S. Brinen, D. D. Rosebrook, and R. C. Hirst, *J. Phys. Chem.*, **67**, 2651 (1963).

14) Z. R. Grabowski and A. Grabowska, *Z. Phys. Chem. (Neue Folge)*, **101**, 197 (1976).

15) Th. Förster, "Fluoreszenz Organischer Verbindugen," Vandenhoeck and Ruprecht (1951), p. 183.

16) F. Wilkinson and J. T. Dubois, *J. Chem. Phys.*, **48**, 2651 (1968).

17) E. Lippert, W. Lüder, F. Moll, W. Nägele, H. Boss, H. Prigge, and I. Seibold-Blankenstein, *Angew. Chem.*, **73**, 695 (1961).

18) R. M. Hochstrasser and C. Marzzacco, *J. Chem. Phys.*, **45**, 4681 (1966); **49**, 971 (1968).

19) C. T. Lin and J. A. Stikeleather, *Chem. Phys. Lett.*, **38**, 561 (1976).

20) S. L. Murov, "Handbook of Photochemistry," Marcel Dekker (1973), p. 3.

CNDO/2 Parametrizations and the Applications to Some Organo-sulfur Molecules: $(CH_2SH)_2$, $(CH_2SCH_3)_2$, CH_3SCH_2SH, and $CH_3SCH_2SCH_3$[1]

Masaru OHSAKU,* Norihisa BINGO, Wataru SUGIKAWA, and Hiromu MURATA

Department of Chemistry, Faculty of Science, Hiroshima University, Higashisenda-machi, Hiroshima 730

(Received July 31, 1978)

The CNDO/2 spd′ parametrizations of K_d, β_C, ζ_S, and β_S have been performed. Some of the valence and torsional angles of 1,2-ethanedithiol $(CH_2SH)_2$, 1,2-bis(methylthio)ethane $(CH_2SCH_3)_3$, methanethiol, ethanethiol, (methylthio)methanethiol CH_3SCH_2SH, and bis(methylthio)methane $CH_3SCH_2SCH_3$ have been optimized. In order to obtain further information on the rotational isomerism, CNDO/2 spd′ and sp calculations have been conducted for the molecules with variations in torsional angle.

Recently semi-empirical MO calculations have been widely applied and subsequently modified, *e.g.*, to the molecules including 2nd- and 3rd-row elements.[2,3] The authors have previously investigated the vibrational spectra of 1,2-ethanedithiol $(CH_2SH)_2$,[4] 1,2-bis(alkylthio)ethane $RSCH_2CH_2SR$ (R=Me, Et, *n*-Pr, and *n*-Bu),[5,6] bis(alkylthio)methane $RSCH_2SR$ (R=Me, Et, *n*-Pr, and *n*-Bu),[7-9] and (methylthio)methanethiol CH_3SCH_2SH.[10] With $(CH_2SH)_2$, electron diffraction[11] and EHMO[12] studies have been reported. The molecular structure of ethanethiol EtSH has appeared recently,[13-16] while for methanethiol MeSH and EtSH, the MINDO/3 calculations were performed;[17] however the MINDO/3 calculations do not always faithfully reproduce the experimental geometries. With oxygen analogs such as dimethoxymethane $CH_3OCH_2OCH_3$, the experimental structural analysis[18] and the theoretical conformational analyses by the semi-empirical and non-empirical methods have been attempted.[19]

In the present paper, to avoid the complexity of *ab initio* calculations, several of the CNDO/2 parameters have been reasonably optimized and the CNDO/2 method applied to examine the stable geometries of the molecules concerned. The CNDO/2 calculations have also been conducted on the oxygen analogs, 1,2-ethanediol $(CH_2OH)_2$, 1,2-dimethoxyethane $(CH_2OCH_3)_2$, and 1-methoxy-2-methylthioethane $CH_3OCH_2CH_2SCH_3$. The results of the CNDO/2 calculations will be compared with the observed values.

Optimization of Parameters

The Fock matrix[20] in the CNDO/2 method[21,22] can be expressed by

$$F_{\mu\mu} = -(1/2)(I_\mu + A_\mu) + [(P_{AA} - Z_A) - (1/2)(P_{\mu\mu} - 1)]\gamma_{AA} + \sum_{B \neq A} (P_{BB} - Z_B)\gamma_{AB} \quad (\mu \text{ on A}),$$

$$F_{\mu\nu} = (1/2)KS_{\mu\nu}(\beta_A + \beta_B) - (1/2)P_{\mu\nu}\gamma_{AB} \quad (\mu \text{ on A}, \nu \text{ on B}),$$

where the notations are the same as those used by Pople *et al.*[21] The constant K of the off-diagonal core matrix element has been given by Pople *et al.*[21] as unity in relation to the first-row elements, and 0.75 in the 2nd-row elements. In this paper, hereafter K_d will replace K in relation to the 2nd-row elements. The constant β is the bonding parameter, and this will be estimated reasonably. The orbital exponent ζ is included in the radial distance r multiplied by a decaying exponential $\exp(-\zeta r)$.

SCF calculations using the parameters of Pople *et al.*[21] (POPLE) sometimes diverge for certain molecules having more than two 2nd-row elements. Moreover the POPLE method gives the organo-sulfur molecules rather larger dipole moments and higher energy barriers for internal rotation than observed. In order to overcome the first difficulty, the density matrix method,[23-25] and others have been used, but suffer from the disadvantage of requiring a lot of computation time. Consequently the value of the constant K_d has been varied. With reference to previous works,[26-28] K_d has been assumed to be 0.492 on the basis of the smoothness of the SCF using the molecular geometry of $(SiH_3)_2O$.[29] The ζ and β values have been optimized in relation to carbon and sulfur atoms. In the course of the parametrizations, the molecular geometry of T-EtSH,[13] and initial parameters reported[21] have been adopted. The optimizations have been made in the order:

i) β_C has been estimated using ζ_C as the Slater value to reproduce the observed r(C–C) of ethane.[30]

ii) ζ_S was then deduced using the revised β_C to fit the observed r(C–S) of T-EtSH.[13]

iii) β_S was optimized using the revised ζ_S to reproduce the observed ϕ(CSH) of T-EtSH.[13]

iv) Steps ii) and iii) were repeated until the two parameters, ζ_S and β_S, did not vary very much. In the present case, nine cycles were repeated. The parameters finally obtained are summarized in Table 1 together with those reported,[3,21] and the relation between ζ_S and β_S is shown in Fig. 1. The orbital exponents previously estimated by Clementi *et al.*[31] and Burns[32] are included. The ζ_S obtained here is larger than that

TABLE 1. CNDO/2 PARAMETERS, β IN eV

	Present work	Pople[a]	Höjer[b]
K_d	0.492	0.75	1.0
β_H	−9.	−9.	−7.00
β_C	−16.97	−21.	−15.00
β_S	−31.79	−18.15	−11.39
ζ_H	1.2	1.2	1.2
ζ_C	1.625	1.625	1.6083[c]
ζ_S	1.867	1.8167	2.1223[c]

a) From Ref. 21. b) From Ref. 3. c) Transferred from Ref. 31.

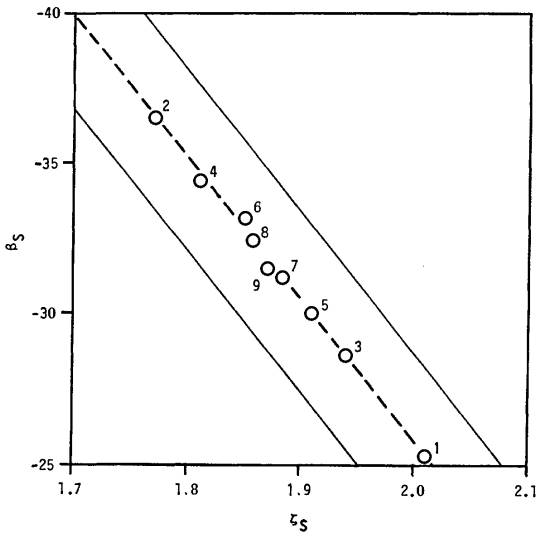

Fig. 1. Correlation plot of β_S *vs.* ζ_S.
Figures show the number of the repeated cycles.

used by Pople *et al.*[21] and smaller than that used by Clementi *et al.*[31] For β_S, a fairly small value was obtained. Hereafter, the method with the revised parameters will be employed as the MCNDO method. The method with K_d set at 0.492 and the others as the original ones[21] is named the KCNDO method. These methods have been applied to some of organo-sulfur molecules, and an attempt has been made to obtain information on the molecular conformations of these molecules.

Results and Discussion

Molecular geometries used were as follows: for $(CH_2SH)_2$— the geometry reported[11] except ϕ(CSH), for $(CH_2SCH_3)_2$, CH_3SCH_2SH, and $CH_3SCH_2SCH_3$, r(C–H)=1.09 Å, r(C–S)=1.82 Å, r(C–C)=1.54 Å, r(S–H)=1.335 Å. The angles around the carbon atom have been assumed as tetrahedral, and for MeSH[33] and EtSH[13,15] those observed. The dihedral angles were 180° and 60° for the T and G forms, respectively. The angles calculated and observed, and the stability of the molecules are summarized in Tables 2 and 3.

$(CH_2SH)_2$ and $(CH_2SCH_3)_2$. Using the molecular geometry reported above, optimizations were made on ϕ(CSH) of $(CH_2SH)_2$ and ϕ(CSC) of $(CH_2SCH_3)_2$. The calculated ϕ(CSH) are 95.5 and 96.5° for the MCNDO and POPLE methods respectively. The observed ϕ(CSH) has been reported as 90.5°[11] which is much smaller than those of the other thiols; MeSH: ϕ(CSH)=96.5°,[33] and T-EtSH: 96°13′.[13] With the ϕ(CSC) of

Table 2. Calculated and observed angles

Molecule		MCNDO	KCNDO	POPLE	sp	MINDO/3[d]	Obsd	Ref.
$(CH_2SH)_2$	ϕ(CSH)	95.5°		96.5°	101.9°		90.5°	11
$(CH_2SCH_3)_2$	ϕ(CSC)	115.5°						
MeSH	ϕ(CSH)	94.4°		94.5°	101.1°	111.9°	96.5°	33
T-EtSH	ϕ(CSH)	96.2°		97°	102.7°	105.1°	96°13′ 95.23°	13 14
G-EtSH	ϕ(CSH)	97.7°		98.5°	101.9°		96° 95.23°	15,16 14
	τ(C–S)	67°	64°	65°	<60°		61°45′ 58.75°	15,16 14
H_2S	ϕ(HSH)	92.7°		99° [a] 92.8°	99.5°	97°	92.06°	e)
H_2S_2	ϕ(SSH)	96.2°		95.7°	102.2°	102.9°	95° 91°21′	f) g)
n-PrSH	ϕ(CSH)	96.6°		97.2°	106.5°	96.4°		
CH_3SCH_2SH	ϕ(CSC)	113° [b]	107° [b]	113° [b]	103°			
	ϕ(CSH)	99°	<93.5°	99.5°	101.5°			
	τ(C–S)	75°	c)	76°	<40°			
$CH_3SCH_2SCH_3$	ϕ(CSC)	113°	107°	113°	103°			
	τ(C–S)	75°	77°	75°	63.5°			
MeOMe	ϕ(COC)						111°43′	43
$CH_3OCH_2OCH_3$	ϕ(COC)						114.2°	18
	τ(C–O)						66.3°	18
POM	ϕ(COC)						110°53′	45
	τ(C–O)						77°23′	45
MeSMe	ϕ(CSC)					115.4°	98°52′	44
PES	ϕ(CSC)						109.5°	34
PTM	ϕ(CSC)						106°52′	35
	τ(C–S)						65°59′	35

a) From Ref. 26. b) Assumed. c) Not performed. d) From Ref. 17. e) R. L. Cook, F. C. De Lucia, and P. Helminger, *J. Mol. Struct.*, **28**, 237 (1975). f) D. P. Stevenson and J. Y. Beach, *J. Am. Chem. Soc.*, **60**, 2872 (1938). g) G. Winnewisser, M. Winnewisser, and W. Gordy, *J. Chem. Phys.*, **49**, 3465 (1968). Geometries; $(CH_2SH)_2$: TGT, $(CH_2SCH_3)_2$: TGT, MeSH: from Ref. 33, EtSH: from Refs. 13 and 15, H_2S: e), H_2S_2: g) in G, *n*-PrSH: r(C–H)=1.09 Å, r(C–C)=1.54 Å, r(C–S)=1.82 Å, r(S–H)=1.335 Å, ϕ(CSH)=96.5°, angles around carbon atom=tetrahedral in TT, CH_3SCH_2SH: GT, $CH_3SCH_2SCH_3$: GG.

Table 3. Stability as a function of internal rotation angle

Molecule	Stability
$HOCH_2CH_2OH$	
Calcd	TTT $\underset{0.03}{>}$ TGT $\underset{1.88}{>}$ TGG $\underset{1.81}{>}$ GGG $\underset{0.25}{>}$ GTG′ $\underset{0.01}{>}$ GTG
Obsd[a]	–G–, –T–
$HSCH_2CH_2SH$	
Calcd MCNDO	TGT $\underset{0.18}{>}$ TGG $\underset{3.03}{>}$ GGG $\underset{14.9}{>}$ TTT $\underset{0.31}{>}$ GTG $\underset{0.20}{>}$ GTG′
sp	TGT $\underset{0.32}{>}$ TTT $\underset{1.17}{>}$ TGG $\underset{1.30}{>}$ GTG $\underset{0.01}{>}$ GTG′ $\underset{0.17}{>}$ GGG
Obsd	–T–, –G–[b]
	TGT, TGG, GTG′, TTT, GGG, GTG, one or more other rotamers[c]
$CH_3OCH_2CH_2OCH_3$	
Calcd	TGT $\underset{0.05}{>}$ TTT $\underset{2.83}{>}$ TGG $\underset{2.78}{>}$ GGG $\underset{0.06}{>}$ GTG′ $\underset{0.21}{>}$ GTG
Obsd[d]	TGT, TTT, one or more other rotamers
$CH_3OCH_2CH_2SCH_3$	
Calcd MCNDO	GGT $\underset{2.01}{>}$ TGG $\underset{6.24}{>}$ TTG $\underset{0.91}{>}$ GTT $\underset{0.87}{>}$ GTG $\underset{0.27}{>}$ TGT $\underset{6.26}{>}$ GGG $\underset{1.23}{>}$ TTT $\underset{3.68}{>}$ GTG′
sp	TGT $\underset{0.25}{>}$ TTT $\underset{1.55}{>}$ TGG $\underset{0.25}{>}$ TTG $\underset{1.00}{>}$ GGT $\underset{0.35}{>}$ GTT $\underset{1.40}{>}$ GGG $\underset{0.44}{>}$ GTG′ $\underset{0.03}{>}$ GTG
Obsd[e]	TTG, TGG, TGT, TTT, GTG or GTG′, GGT
$CH_3SCH_2CH_2SCH_3$	
Calcd MCNDO	TGG $\underset{9.73}{>}$ GGG $\underset{1.51}{>}$ TGT $\underset{0.58}{>}$ GTG $\underset{9.28}{>}$ TTT $\underset{2.37}{>}$ GTG′
sp	TGT=TTT $\underset{2.20}{>}$ TGG $\underset{1.71}{>}$ GTG′ $\underset{0.01}{>}$ GTG $\underset{0.45}{>}$ GGG
Obsd	GTG′, GGG, one or more other rotamers[f]
	TGT, TTT, GTG′, GGG, one or more other rotamers[g]
CH_3SCH_2SH	
Calcd MCNDO	GT $\underset{0\ 18}{>}$ GG $\underset{0.97}{>}$ GG′ $\underset{18.8}{>}$ TG $\underset{0.96}{>}$ TT
sp	TT $\underset{0.99}{>}$ GT $\underset{0.45}{>}$ TG $\underset{1.61}{>}$ GG $\underset{1.31}{>}$ GG′
Obsd[h]	GG, GT, GG′, TG, TT
$CH_3SCH_2SCH_3$	
Calcd MCNDO	GG $\underset{18.7}{>}$ TG $\underset{16.5}{>}$ TT $\underset{229.}{>}$ GG′
sp	TT $\underset{1.06}{>}$ TG $\underset{1.73}{>}$ GG $\underset{265.}{>}$ GG′
Obsd[i,j]	GG, TG, TT

Small figures indicate the energy difference, in kcal/mol. —, stable form in the crystalline solid state. a) From Ref. 36. b) From Ref. 4a. c) From Ref. 4b. d) From Ref. 37. e) From Ref. 38. f) From Ref(s). 5 (and 38). g) From Ref. 6. h) From Ref. 10. i) From Ref. 7. j) From Ref. 8. Geometries; $(CH_2OH)_2$: from Ref. 12, $(CH_2OCH_3)_2$ and $CH_3OCH_2CH_2SCH_3$: r(C–O)=1.41 Å, ϕ(COC)=111°49′, referred from M. Hayashi and K. Kuwada, Preprint of the 32nd National Meeting of the Chemical Society of Japan, Vol. 1, (1975) p. 121, and assumed r(C–H)=1.09 Å, r(C–C)=1.54 Å, r(C–S)=1.82 Å, ϕ(CSC)=99°, angles around carbon atom=tetrahedral.

$(CH_2SCH_3)_2$, 115.5° was obtained which corresponds well to the 115.4° of MeSMe and 115.6° of MeSEt estimated by the MINDO/3 method.[17] However, the calculated value 115.5° is somewhat larger than that observed for poly(ethylene sulfide) (PES) 109.5°[34] and poly(thiomethylene) (PTM) 106°52′.[35]

The calculations were conducted for each of six typical forms with ϕ(CSH)=95.5° in $(CH_2SH)_2$ and ϕ(CSC)=115.5° in $(CH_2SCH_3)_2$. The stability from the calculated energy is in the order, TGG>GGG>TGT>GTG>TTT>GTG′ for $(CH_2SCH_3)_2$. It had been previously concluded[6] that the conformation about the C–C bond in the crystalline state is the G conformation. From the CNDO/2 calculations (KCNDO) assuming the four typical forms, TGT, GGG, TTT, and GTG′, the conclusion drawn is that the TGT form is the best form to explain the stable crystalline solid state.[6] The main reason for the difference in stability between the present and previous calculations is due to the difference in geometry used. For $(CH_2SH)_2$ nearly the same order to that of $(CH_2SCH_3)_2$ was obtained. The sp calculations[22] have also been conducted for these molecules. With $(CH_2SH)_2$, the CNDO/2 spd′ or sp calculation suggests that the most stable form is the TGT form. From this, it appears that the previous conclusion,[4a] in which mainly the TTT and TGT molecular forms exist in the gaseous and liquid states and the TTT form alone persists in the solid state, is of doubtful validity. As a result, it may be concluded that the stable form in the crystalline solid state is the TGT form.

With $(CH_2SCH_3)_2$, if the observed spectra demon-

strate[5,38] the mutual exclusion rule between the IR and Raman spectra, the actual molecular form in the crystalline solid state should be either the TTT or the GTG′ form. However, the CNDO/2 spd′ calculation does not support this conclusion, although the TTT form has been shown to be the fairly stable form from the sp calculation.

$(CH_2OH)_2$, $(CH_2OCH_3)_2$, and $CH_3OCH_2CH_2SCH_3$. The vibrational spectra, normal coordinate treatments, and conformational analyses of $(CH_2OH)_2$[36] and $(CH_2OCH_3)_2$[37] have been studied extensively. Recently, the vibrational spectra and rotational isomerism of $CH_3XCH_2CH_2YCH_3$ (X, Y=O or S) have been published.[38] The CNDO/2 calculations for these molecules have been conducted assuming the typical forms, the results of which are summarized in Table 3. The stability, determined with the aid of the CNDO/2 calculations for $(CH_2OCH_3)_2$ agree excellently with the observed, TGT>TTT>TGG>TTG,[38] although the present calculation was not performed on the TTG form. With $CH_3OCH_2CH_2SCH_3$, the observed frequencies[38] in the crystalline solid state can be well explained by the GGT form—the most stable form calculated from the MCNDO method—as well as by the TTG form, which was concluded as the stable form in the crystalline solid state.[38]

MeSH and EtSH. The relations between the bond order, bond lengths, and force constants have been reported by Coulson.[39,40] It has been previously shown that a linear relationship exists between the bond length r(X–H) and the X–H stretching frequency and the bond order matrix elements, $P_{1sH,nSX}$ calculated by the POPLE method, where n is 2 or 3, and X is C, N, or Si.[41] The same is true in this case as shown in Fig. 2. These results, therefore, imply that most of the X–H stretching force constant K(X–H) can be explained in terms of the relation between the 1s AO of hydrogen and the ns AO of the X atom.

The angles ϕ(CSH), ϕ(HSH), and ϕ(SSH) of the molecules having the S–H bond are excellently reproduced, both by the POPLE and MCNDO methods (Table 2). The torsional angle is also fairly well reproduced. However, the sp calculations, in general, do not agree with the observed ones very well. With EtSH, the energy difference has been found and is summarized in Table 4. The experimental value obtained from the calorimetric data gives the stability G>T and the difference 0.3 kcal/mol,[42] and recent microwave data[14] the value 0.406 kcal/mol. The observed values are well explained by the calculations. The MCNDO method is refined a little in the energy difference.

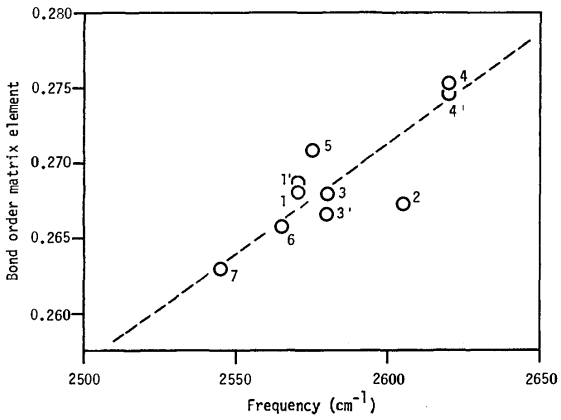

Fig. 2. Correlation plot of $P_{1sH.3sS}$ *vs.* ν_{SH}—POPLE.
1: $(CH_2SH)_2$, 2: MeSH, 3: EtSH, 4: H_2S, 5: H_2S_2, 6: *n*-PrSH, 7: CH_3SCH_2SH.
IR data (observed in the gaseous state except 7); 1: from Ref. 4a, 2: I. W. May and E. L. Pace, *Spectrochim. Acta, Part A*, **24**, 1605 (1968), 3: N. Sheppard, *J. Chem. Phys.*, **17**, 79 (1949), 4: J. W. Nibler and G. C. Pimentel, *J. Mol. Spectrosc.*, **26**, 294 (1968), 5: M. K. Wilson and R. M. Badger, *J. Chem. Phys.*, **17**, 1232 (1949), 6: M. Hayashi, Y. Shiro and H. Murata, *Bull. Chem. Soc. Jpn.*, **39**, 112 (1966), 7: from Ref. 10.
Geometries; 1: TGT, 1′: TTT, 2: from Ref. 33, 3: from Ref. 13 in T, 3′: from Ref. 15 in G, 4: e of Table 2 with r(S–H)=1.3362 Å, 5: g of Table 2 in T, 6: see geometry listed in Table 2, 7: TT. $(CH_2SH)_2$: we have at first carried out the calculations using r(S–H)=1.4 Å then we have obtained an extraordinarily low value of $P_{1sH.3sS}$: 0.2554. On the other hand the infrared frequency does not lie off the ordinary value. Therefore, we have assumed r(S–H)=1.335 Å only in these calculations (bond order calculations).

Table 4. Energy difference (ΔE, kcal/mol), energy barrier height (V, kcal/mol), and dipole moment (D.M., Debye) of MeSH and EtSH

	MCNDO	KCNDO	POPLE	Obsd
ΔE, T-EtSH–G-EtSH	1.06	2.20	1.87	0.406[a] 0.3[b]
V-SH, MeSH	1.38	0.91	1.75	1.27[c]
V-Me, EtSH	9.42	6.84	14.25	3.260[d] 3.305[a] 3.75[b]
V-SH, EtSH	4.41	2.65	6.17	1.305[d] 1.258[a] 1.42[b]
D.M., MeSH	2.345	1.893	2.443	1.48[c]
T-EtSH	2.139	2.238	2.454	1.560[e] 1.58[a]
G-EtSH	2.223	2.248	2.512	1.61[a]

a) From Ref. 14. b) From Ref. 42. c) From Ref. 33. d) From Ref. 16. e) From Ref. 13. Geometries; MeSH: from Ref. 33, T-EtSH: from Ref. 13, G-EtSH: from Ref. 15, EtSH: from Ref. 13.

CH_3SCH_2SH and $CH_3SCH_2SCH_3$. The optimized angles are shown in Table 2 along with the observed values for dimethyl ether (MeOMe),[43] dimethyl sulfide (MeSMe),[44] $CH_3OCH_2OCH_3$,[18] poly(oxymethylene) (POM),[45] PES,[34] and PTM.[35] For the ϕ(CSC) of the molecules now of interest, it can be expected that the value is larger than that of MeSMe[44] and smaller than that of PTM.[35] The sp calculations reproduce the values as expected except for the τ(C–S) of CH_3SCH_2SH, but the spd′ calculations are somewhat too large. The CNDO/2 calculations were then performed with variations in the torsional angle. From the analyses of the vibrational spectra it has been concluded that for CH_3SCH_2SH only one form exists, the GG form in the crystalline solid state as compared with five

forms, GG, GT, TG, GG′, and TT, which coexist in the liquid and gaseous states.[10] With $CH_3SCH_2SCH_3$, the order of the stability has been reported as: GG>TG>TT≫GG′.[7,8] By the MCNDO method using the assumed geometry $\phi(CSC)=99°$ and $\phi(CSH)=96.5°$, the order for CH_3SCH_2SH has been established as: GT>GG>GG′>TG>TT, and for $CH_3SCH_2SCH_3$ as: GG>TG>TT≫GG′. With $CH_3SCH_2SCH_3$, the most stable form GG is well explained by the MCNDO method, the stable structure corresponding with that of the oxygen analog, $CH_3OCH_2OCH_3$.[18,19] With CH_3SCH_2SH, however, the most stable form has been calculated as GT by the MCNDO method, but this does not agree perfectly with the observed one.[10] In the course of the analyses of the IR spectra of this molecule, the most stable form expected was the GG or GT form. From the frequency shift of the S–H stretching vibration by D substitution it has been concluded that the most stable form is the GG. In the molecule CH_3SCH_2SH, the conformation about the bond CH_3SCH_2–SH is indeed very difficult to explain, since hydrogen is a very light and small atom. It may be concluded that the conformation about the bond CH_3S–CH_2SH is reproduced by the spd′ calculations. In the case of $CH_3SCH_2SCH_3$, it has been previously stated that the GG′ form is not the stable form even in the liquid state.[7,8] On the other hand the GG′ form has been taken into consideration for CH_3SCH_2SH.[10] These situations are well reproduced by the CNDO/2 method.

The sp calculations explain fairly well the geometries of CH_3SCH_2SH and $CH_3SCH_2SCH_3$ as reported above, but do not explain the stability. In the case of two sulfur atoms in a molecule, the interactions between the d-orbitals may play an important role in the conformational stability. Therefore, it is better to use the spd′ calculation for the molecules having more than two sulfur atoms in a molecule than the sp calculation.

The conclusions drawn are that the use of the POPLE and MCNDO parameters give fairly good ϕ(CSH) and internal rotation angles for simple aliphatic thiols. The present calculations also show that the molecular geometry reported for $(CH_2SH)_2$[11] appears ambiguous, in particular in ϕ(CSH) and r(S–H). The energy barrier is better reproduced by the MCNDO method than by the POPLE one (Table 4). The dipole moment in general decreases in the order: POPLE>MCNDO>KCNDO and in these respects, the MCNDO method is better than the original CNDO/2 method. The angle ϕ(CSH) for RSH is better reproduced by the CNDO/2 spd′ method than by the MINDO/3 method.[17]

The CNDO/2 method now used, however, may not reproduce the energy difference itself between the rotational isomers which is very important in the analysis of rotational isomerism. Therefore in the CNDO/2 parameters there may be still some ambiguities, in particular relating to the 2nd-row elements. Generally, from the vibrational data and normal coordinate treatment, it is very difficult to determine which rotational isomer is more stable when the calculated frequencies of the rotational isomers are almost identical. In order to overcome this difficulty, the CNDO/2 method is helpful.

The authors wish to thank Prof. Akira Imamura of Shiga University of Medical Science for his kind advice. All calculations were performed at the Computing Center of Hiroshima University.

References

1) Presented in part at the 35th National Meeting of the Chemical Society of Japan, Sapporo, August 1976.
2) For example, the references cited in A. Veillard. *Chem. Phys. Lett.*, **33**, 15 (1975); Th. Weller, D. Klöpper, and H.-J. Köhler, *Chem. Phys. Lett.*, **36**, 475 (1975).
3) G. Höjer and S. Meza, *Acta Chem. Scand.*, **26**, 3723 (1972).
4) a) M. Hayashi, Y. Shiro, T. Oshima, and H. Murata, *Bull. Chem. Soc. Jpn.*, **38**, 1734 (1965); b) M. Ohsaku and H. Murata, *J. Mol. Struct.*, in press.
5) M. Hayashi, Y. Shiro, T. Oshima, and H. Murata, *Bull. Chem. Soc. Jpn.*, **39**, 118 (1966).
6) M. Ohsaku and H. Murata, *Spectrochim. Acta, Part A*, **34**, 869 (1978).
7) M. Ohsaku, Y. Shiro, and H. Murata, *Bull. Chem. Soc. Jpn.*, **45**, 113 (1972).
8) M. Ohsaku, *Bull. Chem. Soc. Jpn.*, **47**, 965 (1974).
9) M. Ohsaku, *Spectrochim. Acta, Part A*, **31**, 1271 (1975).
10) M. Ohsaku, Y. Shiro, and H. Murata, *Bull. Chem. Soc. Jpn.*, **45**, 3035 (1972).
11) I. Hargittai and Gy. Schultz, *J. Chem. Soc., Chem. Commun.*, **1972**, 323; Gy. Schultz and I. Hargittai, *Acta Chim. Acad. Sci. Hung.*, **75**, 381 (1973).
12) N. Hadjiliadis and T. Theophanides, *Chim. Chronika*, **2**, 37 (1973).
13) M. Hayashi, H. Imaishi, and K. Kuwada, *Bull. Chem. Soc. Jpn.*, **47**, 2382 (1974).
14) R. E. Schmidt and C. R. Quade, *J. Chem. Phys.*, **62**, 3864 (1975).
15) M. Hayashi, J. Nakagawa, and K. Kuwada, *Chem. Lett.*, **1975**, 1267.
16) J. Nakagawa, K. Kuwada, and M. Hayashi, *Bull. Chem. Soc. Jpn.*, **49**, 3420 (1976).
17) M. J. S. Dewar, D. H. Lo, and C. A. Ramsden, *J. Am. Chem. Soc.*, **97**, 1311 (1975).
18) E. E. Astrup, *Acta Chem. Scand.*, **25**, 1494 (1971).
19) a) I. Tvaroška and T. Bleha, *J. Mol. Struct.*, **24**, 249 (1975). b) D. G. Gorenstein and D. Kar, *J. Am. Chem. Soc.*, **99**, 672 (1977).
20) C. C. J. Roothaan, *Rev. Mod. Phys.*, **23**, 69 (1951).
21) J. A. Pople, D. P. Santry, and G. A. Segal, *J. Chem. Phys.*, **43**, S129 (1965); J. A. Pople and G. A. Segal, *J. Chem. Phys.*, **43**, S136 (1965); J. A. Pople and G. A. Segal, *J. Chem. Phys.*, **44**, 3289 (1966); J. A. Pople and D. L. Beveridge, "Approximate Moleculer Orbital Theory," McGraw-Hill, New York, N. Y. (1970).
22) D. P. Santry and G. A. Segal, *J. Chem. Phys.*, **47**, 158 (1967).
23) R. McWeeny, *Proc. R. Soc. London, Ser. A*, **235**, 496 (1956).
24) A. T. Amos, *Mol. Phys.*, **5**, 91 (1962).
25) A. Imamura and H. Fujita, *J. Chem. Phys.*, **61**, 115 (1974).
26) D. P. Santry, *J. Am. Chem. Soc.*, **90**, 3309 (1967).
27) J. D. Bene and H. H. Jaffé, *J. Chem. Phys.*, **48**, 1807 (1968).
28) T. Morita, *Kagaku No Ryoiki*, **29**, 455 (1975).
29) A. Almenningen, O. Bastiansen, V. Ewing, K. Hedberg, and M. Trætteberg, *Acta Chem. Scand.*, **17**, 2455 (1963).

30) D. E. Shaw, D. W. Lepard, and H. L. Welsh, *J. Chem. Phys.*, **42**, 3736 (1965).
31) E. Clementi and D. L. Raimondi, *J. Chem. Phys.*, **38**, 2686 (1963).
32) G. Burns, *J. Chem. Phys.*, **41**, 1521 (1964).
33) T. Kojima and T. Nishikawa, *J. Phys. Soc. Jpn.*, **12**, 680 (1957); T. Kojima, *J. Phys. Soc. Jpn.*, **15**, 1284 (1960).
34) Y. Takahashi, H. Tadokoro, and Y. Chatani, *J. Macromol. Sci., Part B*, **2**, 361 (1968); K. Tai and H. Tadokoro, *Macromolecules*, **7**, 507 (1974).
35) G. Carazzolo and G. Valle, *Makromol. Chem.*, **90**, 66 (1966).
36) H. Matsuura and T. Miyazawa, *Bull. Chem. Soc. Jpn.*, **40**, 85 (1967).
37) R. G. Snyder and G. Zerbi, *Spectrochim. Acta, Part A*, **23**, 391 (1967).
38) Y. Ogawa, M. Ohta, M. Sakakibara, H. Matsuura, I. Harada, and T. Shimanouchi, *Bull. Chem. Soc. Jpn.*, **50**, 650 (1977).
39) C. A. Coulson, *Proc. Soc. London, Ser. A*, **169**, 413 (1935).
40) For electronic population analysis: R. A. Mulliken, *J. Chem. Phys.*, **23**, 1833, 1841, 2338, and 2343 (1955).
41) N. Bingo, M. Ohsaku, and H. Murata, *J. Sci. Hiroshima Univ.*, **A40**, 317 (1976).
42) D. Smith, J. P. Devlin, and D. W. Scott, *J. Mol. Spectrosc.*, **25**, 174 (1968).
43) U. Blukis, P. H. Kasai, and R. J. Myers, *J. Chem. Phys.*, **38**, 2753 (1963).
44) L. Pierce and M. Hayashi, *J. Chem. Phys.*, **35**, 479 (1961).
45) H. Tadokoro, T. Yasumoto, S. Murahashi, and I. Nitta, *J. Polym. Sci.*, **44**, 266 (1960).

Conformational Transition of Poly(L-glutamic acid) in Aqueous Decylammonium Chloride Solution

Iwao SATAKE,* Takeshi GONDO,† and Hideo KIMIZUKA†

Department of Chemistry, Faculty of Science, Kagoshima University, Korimoto, Kagoshima 890

†*Department of Chemistry, Faculty of Science, Kyushu University, Hakozaki, Higashiku, Fukuoka 812*

(Received August 5, 1978)

The cooperative binding of decylammonium chloride to poly(L-glutamic acid) (PLG) was studied by the potentiometric measurement of the binding isotherm at pH 7.9. Circular dichroism spectra were also measured as a function of the degree of binding of surfactant ion (x). It was shown that the coil to α-helix transition of PLG-surfactant complex takes place with a change in x. PLG did not undergo an appreciable conformational change in the range of x below 0.55. But the helical content increased suddenly with further increase in x. An abrupt increase in the helical content of PLG-surfactant complex can be well interpreted in terms of the hydrophobic interaction among bound surfactant ions. On the basis of the theoretical analysis of the cooperative binding isotherm, it was concluded that the formation of a micelle-like cluster consisting of at least eight surfactant ions is required for the stabilization of a surfactant induced helical structure.

The conformational transition of polypeptide in surfactant solution is of special interest in connection with the effect of surfactant on protein structure. Although most studies so far reported have been confined to the conformational changes of poly(L-ornithine) (PLO) homologs with side chain R=$-(CH_2)_nNH_2$, some interesting features of such transition have been clarified.

PLO (n=3)[1,2] and its homologs (n=5—7)[3] adopt helical conformation in neutral solution of sodium dodecyl sulfate (SDS). The coil to helix transition of PLO is also noted in solution of sodium n-alkyl sulfate with 8 to 16 carbon atoms.[2] In contrast, however, poly(L-lysine)(PLL, n=4) assumes β-structure in neutral solutions of sodium decyl sulfate (SDeS) and its longer chain homologs,[2,4-8] while it assumes helical structure in sodium octyl sulfate solution.[2] Upon raising the pH of SDS solution, PLL undergoes a reversible β to helix transition.[7-9] These conformational changes occur even in the concentration of SDS much lower than the critical micelle concentration (CMC), suggesting a highly cooperative binding of surfactant ions to polypeptide.[2,7,8,10] An acidic solution of SDS causes poly(L-arginine) to undergo a coil to helix transition and poly(L-histidine) to change from a coil to β-structure.[11] In view of these observations, it is likely that the hydrophobic interaction between electrostatically bound surfactant ions plays a predominant role in the conformational change of charged polypeptide in surfactant solution. However, little is known about the factors which influence the type of a resulting conformation.

One might expect a similar conformational change of anionic polypeptide in cationic surfactant solution. The purpose of the present paper is to determine the binding isotherm of decylammonium ion to poly(L-glutamic acid)(PLG) and to find a correlation between the degree of binding and a resulting conformational change as inferred from circular dichroism (CD) spectra.

Experimental

Materials. PLG (Miles-Yeda Ltd., molecular weight 50000) was converted to sodium salt by dissolving it into dilute sodium hydroxide solution and then dializing against distilled water. The polypeptide concentration was determined by micro-Kjeldahl nitrogen analysis. Decylammonium chloride (DeAC) was prepared from 99% decylamine (Nakarai Chemicals Ltd.) according to a method described by Kolthoff and Strickes.[12] The pK_a of DeAC in 10^{-2} mol/dm³ KCl solution was determined from pH titration to be 10.4 at 25 °C.

Binding Isotherm Measurement. Since PLG is a typical polyelectrolyte, the apparent dissociation constant (K) depends not only on the degree of dissociation (α), but on added salt concentration. For instance, in 5×10^{-3} mol/dm³ NaCl, the pK value varies from 4.45 at α=0 to 6.0 at α≈0.9.[13] This means that about 10% of carboxylic acid groups remain still undissociated even at pH 7. In order to secure the complete dissociation of PLG, therefore, all experiments were performed with buffered solution at pH 7.9, which contains 4.32×10^{-3} mol/dm³ sodium borate and 7.36×10^{-3} mol/dm³ hydrochloric acid. The binding isotherm of DeAC to PLG was determined potentiometrically at 25 °C, using a poly(vinyl chloride)(PVC) plastic electrode which had been shown to respond to tetraalkylammonium ions.[14] The cell constructed was as in the following.

Reference electrode (Ag-AgCl)|1 mol/dm³ NH_4NO_3 Agar bridge|Reference solution (DeAC, 5.238×10^{-4} mol/dm³)|PVC membrane|Sample solution ($C_p=3.18\times10^{-4}$ residue mol/dm³; DeAC, C_t; Borate buffer)|1 mol/dm³ NH_4NO_3 Agar bridge| Reference electrode (Ag-AgCl),

where, C_p denotes the concentration of PLG in residue mol/dm³ and C_t, the total concentration of DeAC, respectively. The PVC membrane was prepared by dissolving 0.6 g of PVC into mixed solution of 2.4 cm³ of bis(2-ethylhexyl) phthalate and 2.4 cm³ of 10^{-4} mol/dm³ DeAC in tetrahydrofuran. The solution was then poured onto a covered glass dish and allowed tetrahydrofuran to evapolate slowly. A resulting film 0.30 mm thick was fixed to a PVC tube of 9 mm diameter by the use of a tetrahydrofuran solution of PVC. The electromotive force (EMF)(E) of the cell was measured with a Corning Digital 112 Research pH Meter with an accuracy of ±0.1 mV. Prior to the measurements on PLG solutions, the PVC membrane was calibrated with solutions of DeAC. Figure 1 shows the semilogarithmic plots of EMF *vs.* DeAC concentration. A linear relation with a slope of 57.9 mV suggests that the PVC membrane responds to surfactant ion exclusively in the concentration range studied. The concentration of PLG was

kept constant throughout a series of experiments.

Circular Dichroism. The CD spectra were obtained at 25 °C with a JASCO Automatic Recording Spectropolarimeter J-40A, using 1 cm path length cell equipped with water-circulating jacket. The spectra were recorded 3.5—4 h after mixing, because an appreciable time dependence was found during first 2—3 h.

Results and Discussion

In order to estimate the degree of binding (x) of decylammonium ion to PLG, it is necessary to assume that the polypeptide ions in an excess salt solution do not affect appreciably the activity coefficient of free surfactant ion.[10] On this assumption, which is compatible with a theoretical prediction,[15] x may be given as

$$x = C_b/C_p = (C_t - C_f)/C_p, \quad (1)$$

where, C_b represents the bound surfactant ion concentration and C_f, the free surfactant ion concentration which can be determined from Fig. 1.

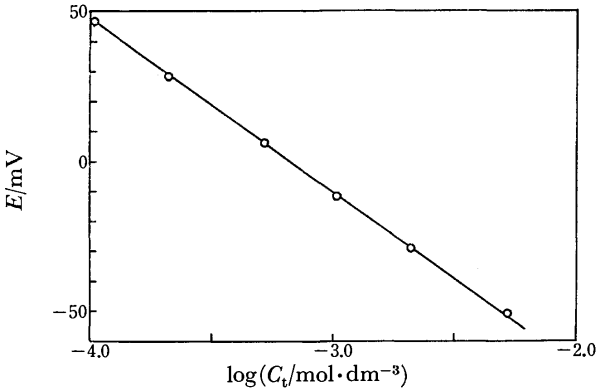

Fig. 1. Plots of EMF (E) of the cell *vs.* the logarithm of decylammonium chloride concentration in the absence of PLG at 25 °C.

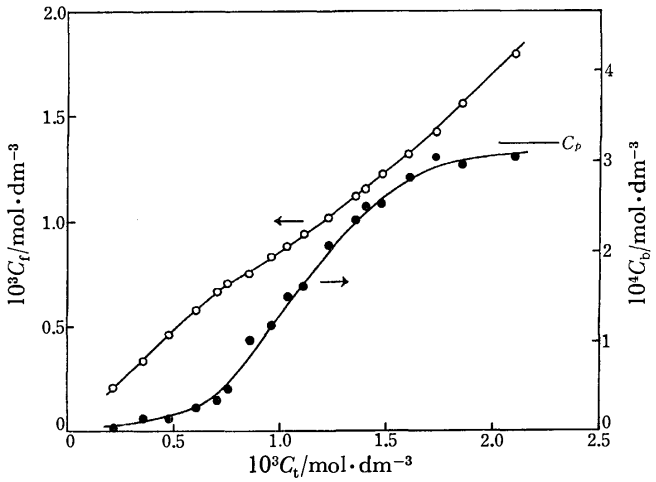

Fig. 2. Plots of C_f and C_b *vs.* C_t at 25 °C. C_p=3.18 $\times 10^{-4}$ residue mol/dm³. Arrows indicate the ordinate to be applied.

In Fig. 2, C_f and C_b observed with constant PLG concentration of 3.18×10^{-4} residue mol/dm³ are plotted against the total concentration of DeAC, C_t. Through a broad kink at about 7×10^{-4} mol/dm³, C_t first increases

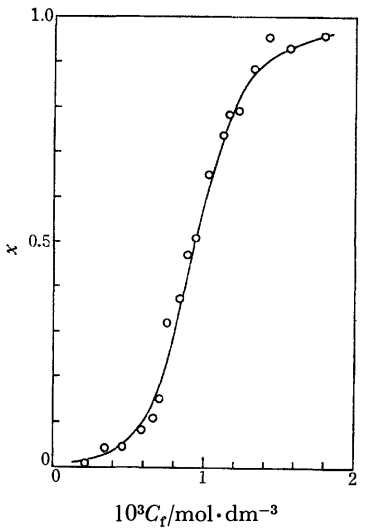

Fig. 3. The binding isotherm of decylammonium chloride to PLG at 25 °C.

almost linearly with increasing C_t and then increases gradually with further increase in C_t. In accordance with the change in C_f, C_b shows a sigmoidal increase with C_t and approaches eventually to PLG concentration, C_p. Figure 3 shows the binding isotherm of DeAC to PLG calculated from Fig. 2. Since the carboxylic acid groups of PLG are completely ionized at pH 7.9, decylammonium ion can interact electrostatically with carboxylate group, giving rise to an ion pair. As was pointed out by Satake and Yang,[10] however, the binding process of surfactant ion to polypeptide ion becomes cooperative because of an additional hydrophobic interaction among bound surfactant ions. In these circumstances, the bound surfactant ions will cluster side by side onto polypeptide chain even in small degree of binding and cause the binding isotherm to rise steeply in narrow range of C_f. This is indeed the case for the present result shown in Fig. 3, where x increases more rapidly than predicted by simple statistical binding model. In this connection, it is interesting to compare the present binding isotherm with those of sodium decyl sulfate to PLL and PLO.[10] In the case of PLL, the binding isotherm was found to rise almost vertically at a certain value of C_f, indicating a highly cooperative binding of decyl sulfate ion. This in turn results in a micellar clustering on the polypeptide chain similar to the micelle formation process of the surfactant alone above its CMC. On the other hand, the binding isotherm for PLO is not so sharp as for PLL,[10] but is still sharp as compared with the present result. These facts imply that the cooperativity in surfactant ion binding to polypeptide depends virtually on the total alkyl chain length of the complex species, *i.e.*, the sum of alkyl chain length of bound surfactant ion and polypeptide side group. The type of ionic group seems to play, if any, a minor role.

On the basis of Zimm-Bragg theory[16] for helix-coil transition, Satake and Yang[10] derived the following expression for the cooperative binding of small ions to polymer;

$$2x - 1 = (y-1)/[(1-y)^2 + 4yu^{-1}]^{1/2}, \quad (2)$$

where

$$y = C_f/(C_f)_{x=0.5}. \quad (3)$$

In Eqs. 2, and 3, u denotes a parameter, which is a measure of cooperativity, defined by

$$u = \exp[(2E_{01}-E_{11}-E_{00})/kT], \quad (4)$$

where, E_{ij} represents the interaction energy between neighboring i-j pairs, and suffix 0 and 1 refer to an unbound and a surfactant-bound polypeptide side chain respectively. The estimation of u can easily be attained by using a relation,

$$(dx/d\ln C_f)_{x=0.5} = u^{1/2}/4. \quad (5)$$

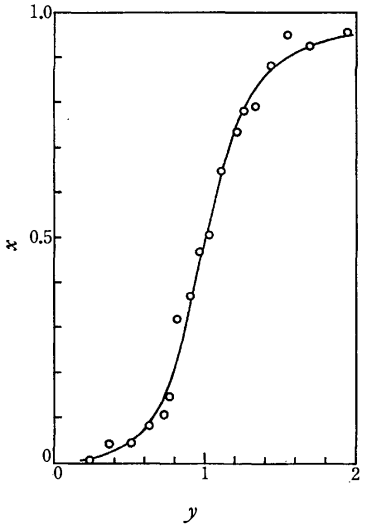

Fig. 4. Comparison of calculated and observed binding isotherm for PLG at 25 °C. ○, observed; solid line, calculated isotherm from Eq. (2) with $u=40$.

The most reliable value of u for the present system was found to be 40, reflecting well the cooperative nature of the binding process. The value of $u=40$ corresponds to an interchange energy $(2E_{01}-E_{11}-E_{00})$ of 9.12 kJ at 25 °C. Figure 4 shows the comparison of the calculated binding isotherm from Eq. 2 with $u=40$ with the observed one. The agreement is quite satisfactory over nearly whole range of x. As would be anticipated, the value of u obtained above is considerably small as compared with that of 77 for SDeS–PLO system.[10] This may reasonably be ascribed to a change in hydrophobic interaction between neighboring groups, arising from a difference in the alkyl chain length of polypeptide side group. According to a foregoing treatment,[10] the average cluster size ($\bar{m}$) of bound surfactant ions, *i.e.*, the average number of bound surfactant ions which constitute a one-dimensional micellar cluster on the polypeptide chain, is given as

$$\bar{m} = 2x(u-1)/[\{4x(1-x)(u-1)+1\}^{1/2}-1]. \quad (6)$$

In Table 1, the calculated values of $\bar{m}$ from Eq. 6 with $u=40$ are given as a function of x. It should be noted

Table 1. The calculated value of $\bar{m}$ as a function of x

x	0.1	0.2	0.3	0.4	0.5	0.55	0.6	0.7	0.8	0.9
$\bar{m}$	2.7	3.8	4.9	6.0	7.3	8.1	9.0	11.4	15.2	24.4

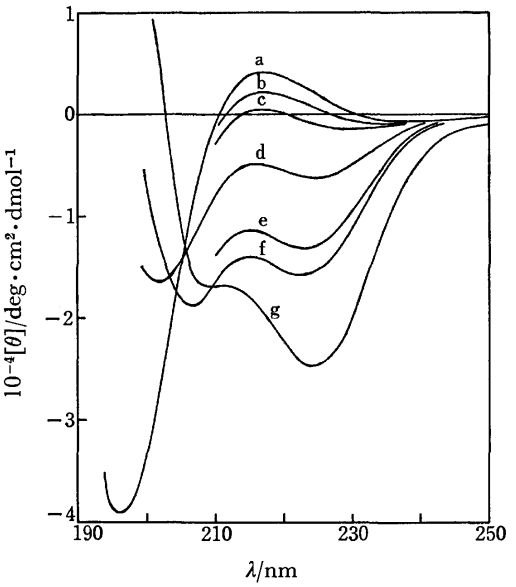

Fig. 5. The change in CD spectrum of PLG with respect to x at 25 °C.
a, 0; b, 0.35; c, 0.56; d, 0.64; e, 0.72; f, 0.80; g, 1 (C_t=0.1515 mol/dm³).

that the cluster size of bound surfactant ions increases rapidly with increasing x.

It is of great interest to find an interrelation between the degree of binding (x) or the average cluster size ($\bar{m}$) and the conformational change induced by surfactant ion binding. To this end, CD spectra were measured under the same experimental conditions as for binding isotherm measurement. Figure 5 shows the change in CD spectrum with respect to x. In the absence of surfactant, the CD spectrum of PLG is characterized by two extrema, a maximum centered at 217 nm with mean residue ellipticity, $[\theta]_{217}$, of 4300 and a deep minimum at 196 nm with $[\theta]_{196}$ of −39000. An additional shallow minimum is also observed at around 235 nm. These features agree well with the CD spectra observed for PLG[17] and PLL[18,19] in their random conformations. With increasing degree of binding, the CD spectrum of PLG tends to approach progressively to a typical spectrum which has a double minimum characteristic of α-helical conformation. A similar change in CD spectrum with surfactant concentration has been found for PLL in SDS solution[2,7] as well as for PLO in solutions of SDS[2] and SDeS.[10] At a concentration above CMC, where x may virtually be regarded as unity, the CD spectrum shows a deep minimum centered at 224 nm with $[\theta]_{224}$ of −25000 and a well defined shoulder located at 209—210 nm with $[\theta]_{209}$ of −17000. Hence, the ordered conformation of PLG in DeAC solution can reasonably be identified as an α-helical structure. It must be kept in mind, however, that the CD spectrum of surfactant induced helical conformation is somewhat different in shape and magnitude from those of helical PLG and PLL in water.[1,2,11] In the absence of surfactant, a double minimum of helical PLG or PLL has been found to locate at 221—222 nm with $[\theta]_{222}$ of −(32000—40000) and at 207—209 nm with $[\theta]_{207-209}$ of −(33000—39000).[17-20] Unfortunate-

ly, there is no conclusive evidence that accounts for the observed decrease in CD minima of helical polypeptide in surfactant solution. Grourke and Gibbs[1] have assumed that the environment produced by the bound surfactant ions affects the rotatory strengths of n-π^* and π-π^* transitions. Nevertheless, it seems equally probable that the surfactant induced helical structure contains small amounts of random conformation. It is true that the above situation makes it difficult to estimate the precise percentage of helix in PLG–DeAC complex, but $[\theta]_{222}$ is still available for a measure of helix content.

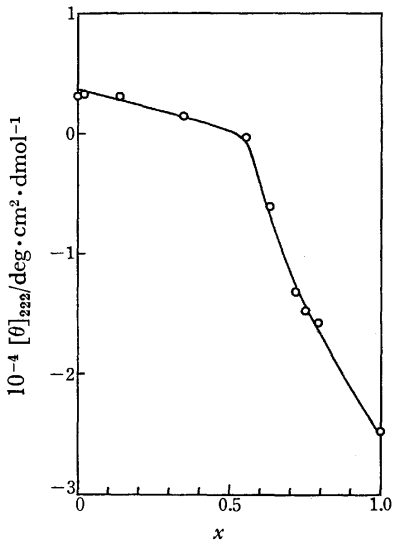

Fig. 6. Plots of $[\theta]_{222}$ *vs.* x at 25 °C. Value at $x=1$ is that in 0.1515 mol/dm³ decylammonium chloride solution.

In Fig. 6, $[\theta]_{222}$ is plotted as a function of x. A clear kink occurs at $x\approx0.55$, through which the magnitude of $[\theta]_{222}$ increases sharply with further increase in x. This implies that PLG does not undergo an appreciable coil to helix transition unless more than 50% of carboxyl groups are bound to decylammonium ions and that a helical structure of the complex become stable only when x exceeds this critical value. An abrupt increase in $[\theta]_{222}$ with x was also observed by Satake and Yang[10] for PLO in SDeS solution. In this case, however, the kink point locates at $x=0.3$—0.4, which corresponds to the average cluster size ($\bar{m}$) of bound decyl sulfate ions of 7—8.[10] This, in turn, corresponds to the number of residues included in two helical turns of α-helical structure. On the basis of these observations, they assumed that the hydrophobic interaction of each bound surfactant ion with another one locating one turn above or below is essential for the formation of a stable helical structure. If this is also valid for PLG–DeAC system, the kink point in $[\theta]_{222}$ *vs.* x plot should appear at x which corresponds to $\bar{m}=7$—8. In addition, the critical x value for the present system will be slightly large as compared with that for PLO–SDeS system, since the binding process is less cooperative in the former than in the latter. The estimation of $\bar{m}$ given in Table 1 supports well the above predictions. As would be expected, the critical value of $x=0.55$ corresponds to $\bar{m}\approx8$.

The authors wish to thank Prof. M. Tanaka and Prof. G. Sugihara, both of Fukuoka University and also to Prof. T. Inaba of Saga University for their helping in CD measurements.

References

1) M. J. Grourke and J. H. Gibbs, *Biopolymers*, **5**, 586 (1967).
2) I. Satake and J. T. Yang, *Biochem. Biophys. Res. Commun.*, **54**, 930 (1973).
3) Y. W. Tseng and J. T. Yang, *Biopolymers*, **16**, 921 (1977).
4) P. K. Sarkar and P. Doty, *Proc. Natl. Acad. Sci. U.S.A.*, **55**, 981 (1966).
5) L. K. Li and A. Spector, *J. Am. Chem. Soc.*, **91**, 220 (1969).
6) W. Mattice and W. H. Harrison III, *Biopolymers*, **15**, 559 (1976).
7) M. M. Feldshtein, A. B. Zezin and J. J. Gragerova, *Biokhimiya*, **37**, 305 (1972).
8) A. B. Zezin, M. M. Feldshtein, V. P. Merzlov and J. J. Maletina, *Molekulyarnaya Biologia*, **7**, 174 (1973).
9) I. Satake and J. T. Yang, *Biopolymers*, **14**, 1841 (1975).
10) I. Satake and J. T. Yang, *Biopolymers*, **15**, 2263 (1976).
11) R. W. McCord, E. W. Blakeney, Jr., and W. L. Mattice, *Biopolymers*, **16**, 1319 (1977).
12) I. M. Kolthoff and W. Stricks, *J. Phys. Colloid Chem.*, **52**, 915 (1948).
13) M. Nagasawa and A. Holtzer, *J. Am. Chem. Soc.*, **86**, 538 (1964).
14) T. Higuchi, C. R. Illian and J. L. Tossounian, *Anal. Chem.*, **42**, 1674 (1970).
15) G. S. Manning, *J. Chem. Phys.*, **51**, 924 (1969).
16) B. H. Zimm and J. K. Bragg, *J. Chem. Phys.*, **31**, 526 (1959).
17) "Conformation of Biopolymers," ed by G. N. Ramachandran, Academic Press, New York (1967), Vol. 1, p. 157.
18) R. Townend, T. F. Kumosinski, S. N. Timasheff, G. D. Fasman and B. Davidson, *Biochem. Biophys. Res. Commun.*, **23**, 163 (1966).
19) N. Greenfield and G. D. Fasman, *Biochemistry*, **8**, 4108 (1969).
20) G. Holzwarth and P. Doty, *J. Am. Chem. Soc.*, **87**, 218 (1965).

The Crystal and Molecular Structure of Benzanilide

Setsuo KASHINO,* Kuniaki ITO,† and Masao HAISA

Department of Chemistry, Faculty of Science, Okayama University, Tsushima, Okayama 700

(Received August 7, 1978)

The crystal structure of benzanilide has been determined from Weissenberg photographs using Cu $K\alpha$ radiations and refined to an R value of 0.075 for 766 independent reflections. The crystals are monoclinic, space group C2/c, $Z=4$, with $a=24.34(4)$, $b=5.325(3)$, $c=8.012(8)$ Å, $\beta=107.2(3)°$, $D_m=1.32$ and $D_x=1.321$ g cm^{-3}. Dihedral angle between the benzene rings is 62.6°, and each benzene ring makes dihedral angle of 31.3 and 31.6° with the plane of amido group as found in Kevlar and Nomex polymers. The molecules related by a ***b***-translation are linked together by N-H···O hydrogen bond [N···O 3.112(6), H···O 2.03 Å, N-H···O 157°] to form a chain along ***b***. The chains are held together primarily by dipole forces of carbonyl groups of the molecules related by inversion centers to form a sheet parallel to the *bc* plane. The sheets are stacked along ***a*** with disorder by van der Waals interactions.

The present work forms a part of studies on the relationship between molecular conformation and crystal structure of aromatic compounds containing amido group.[1] One particular interest is in a comparison of the compounds in which two benzene rings are separated by two bonding atoms. Another aspect is of a model compound of the polymer chains in poly(*p*-phenyleneterephthalamide) (Kevlar) and poly(*m*-phenyleneisophthalamide) (Nomex). Their conformations have been explained to be governed primarily by torsion about the exocyclic bonds.[2-4]

Experimental

Crystals were grown from an ethanol solution by slow evaporation as hexagonal plates with developed (100) and bounded by {001} and {011}. Systematic absences were *hkl* with $h+k$ odd, and *h0l* with l odd, hence the space group was Cc or C2/c. During the analysis Cc was ruled out. The density was measured by flotation in aqueous KI solution.

Crystal Data: Benzanilide, $C_{13}H_{11}NO$, $Mr=197.2$, mp 161—162 °C, monoclinic, space group C2/c, $a=24.34(4)$, $b=5.325(3)$, $c=8.012(8)$ Å, $\beta=107.2(3)°$, $V=992(3)$ Å^3, $D_m=1.32$, $D_x=1.321$ g cm^{-3}, $Z=4$, μ(Cu $K\alpha$)$=6.89$ cm^{-1}, $F(000)=416$.

Intensity data were collected on Weissenberg photographs for the layers *h0l* to *h4l* by using a specimen of dimensions 0.3 × 2.0 × 0.4 mm. The intense reflections, particularly 002, were accompanied by diffuse streaks elongated along a^*. Intensities of 766 independent reflections were visually estimated and corrected for Lorentz and polarization factors and for spot shape. Inter-layer scaling was made according to the exposure time (about 40 h for each layer). Wilson's plot gave $B=6.99$ Å^2. Distribution of E-values preferred to centrosymmetrical space group.

Structure Determination and Refinement

The structure was solved from a Patterson map and refined by block-diagonal least-squares calculations. Analysis based on the space group Cc gave extraordinary values of bond lengths and angles even at the stage of R value of 0.087. Therefore the space group C2/c was adopted by assuming the disorder with occupancy factor 0.5 about the twofold rotation axis. A difference Fourier map (Fig. 1) at the stage of $R=0.10$ revealed the H atoms. For further refinements the H atoms were included with their thermal parameters ($B=6.99$ Å^2) and fixed positional parameters deduced from the geometry of the molecule. The weighting scheme used was: $w=1.0$ for $0<|F_o|\leq 5.0$, $w=(5.0/|F_o|)^2$ for $|F_o|>5.0$. The final R value was 0.075 for 766 non-zero reflections.

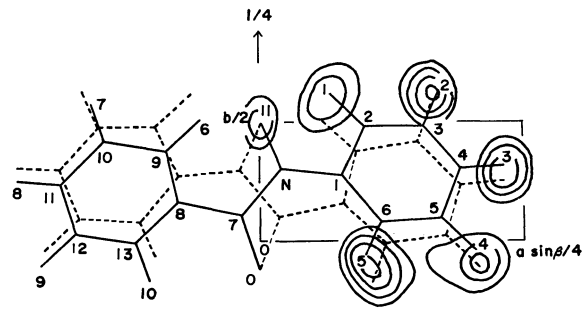

Fig. 1. Difference Fourier map at the stage of $R=0.10$. Contours are depicted for positive x region, at intervals of 0.1 e Å^{-3} starting at 0.1 e Å^{-3}. The molecular frames are based on the final positional parameters.

TABLE 1. THE FINAL POSITIONAL PARAMETERS (×10^4) OF THE NON-HYDROGEN ATOMS WITH STANDARD DEVIATION IN PARENTHESES

For all the atoms the occupancy factor is 0.5.

	x	y	z
C(1)	771(2)	2764(10)	2581(6)
C(2)	985(3)	4802(11)	1826(7)
C(3)	1540(3)	4834(14)	1881(9)
C(4)	1901(2)	3029(12)	2742(7)
C(5)	1718(2)	1036(10)	3547(6)
C(6)	1140(2)	843(10)	3461(6)
C(7)	−175(2)	1083(11)	2435(7)
C(8)	−778(2)	1640(10)	2377(7)
C(9)	−904(2)	3817(9)	3197(6)
C(10)	−1497(2)	4215(11)	3132(7)
C(11)	−1906(2)	2396(12)	2224(8)
C(12)	−1757(3)	283(12)	1433(9)
C(13)	−1196(2)	−58(11)	1494(8)
N	188(2)	3020(9)	2533(6)
O	0	−1197(6)	2500

† Present address: Marugo Kogyo Co., Chayamachi, Kurashiki 710.

TABLE 2. THE POSITIONAL PARAMETERS ($\times 10^3$) OF THE HYDROGEN ATOMS

	x	y	z
H(1)	66	617	109
H(2)	169	633	128
H(3)	231	317	281
H(4)	204	−38	428
H(5)	99	−58	409
H(6)	−57	504	388
H(7)	−163	575	378
H(8)	−232	258	219
H(9)	−208	−104	75
H(10)	−106	−167	84
H(11)	0	500	250

Atomic scattering factors were taken from International Tables for X-Ray Crystallography.[5] The computations were carried out on an NEAC 2200-500 computer at the Okayama University Computer Center. The programs used were HBLS-5 and DAPH.[6] The final atomic parameters are listed in Tables 1 and 2.[7]

Results and Discussion

Molecular Structure. Bond lengths and angles are given in Fig. 2. The least-squares planes of the benzene rings and the amido group and the displacement of the atoms from the planes are listed in Table 3. The dihedral angles of two benzene ring-planes with respect to the amido group plane are 31.3 and 31.6°. These values are close to those in Kevlar and Nomex and consistent with the value calculated from the π-bond energy and the steric interaction.[4]

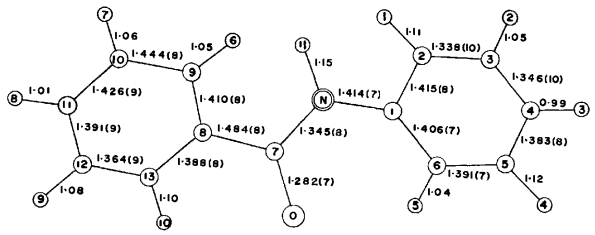

Fig. 2. The molecular structure: (a) bond lengths (Å) and numbering of atoms, (b) bond angles (°).

It is interesting to compare the competitive interactions between the resonance effect of the benzene ring and the steric hindrance of attached atoms to the ring. Table 4 lists the torsion angles about the exocyclic

TABLE 3. THE LEAST-SQUARES PLANES AND DISPLACEMENTS (Å) OF THE ATOMS FROM THE PLANES $X=ax+cz\cos\beta$, $Y=by$, $Z=cz\sin\beta$.

(I) Amido group			
$0.0447X-0.0016Y-0.9992Z+1.9276=0$			
C(1)[a]	0.0083	H(11)	−0.0145
N[a]	−0.0182	C(2)	0.6152
C(7)[b]	0.0205	C(6)	−0.6317
O[a]	−0.0094	C(9)	−0.6525
C(8)[a]	−0.0008	C(13)	0.6319
(II) Benzene ring (1)			
$0.0626X-0.5203Y-0.8517Z+2.3766=0$			
C(1)[a]	0.0075	C(5)[a]	−0.0133
C(2)[a]	−0.0209	C(6)[a]	0.0098
C(3)[a]	0.0180	N	−0.1203
C(4)[a]	−0.0007	C(7)	0.4270
(III) Benzene ring (2)			
$0.1099X+0.5173Y-0.8488Z+1.3545=0$			
C(8)[a]	−0.0076	C(13)[a]	0.0091
C(9)[a]	0.0036	C(7)	−0.0390
C(10)[a]	−0.0008	N	0.5250
C(11)[a]	0.0018	O	−0.6643
C(12)[a]	−0.0059		
Dihedral angles (°) between the planes			
(I) and (II)	(I) and (III)	(II) and (III)	
31.3	31.6	62.6	

a) Atoms used for the calculation of the planes.

bonds in the series of compounds, *p*-R–Ph–XY–Ph–R′-*p*, where the central part XY is such as CH=N, N=N, CH=CH (these are isoelectronic), and so on, and the substituents R and R′ are confined to relatively small groups for the sake of brevity A survey of the crystal structures of this series shows that the molecules in the crystals are classified into either centrosymmetrical or non-centrosymmetrical group, the present one belonging to the latter The former is visualized only when X and Y are identical or isoelectronic and R and R′ are also identical. The torsion angles are in general very small, suggesting the electronic delocalization extended over the central part between benzene rings. Large torsion angles occur only when X and Y are attached by bulky substituents (*e.g.* CN) or of sp^3 hybrid type missing conjugation. Even in this case parallelism of two benzene rings is maintained.

On the other hand, when X and Y or R and R′ are different the two benzene rings lose the parallelism and make in general large dihedral angle near 60°. In the non-centrosymmetrical group the torsion angles about each exocyclic bond differ greatly from each other in general. The disordered structure is, however, observed only when these torsion angles are similar to each other as in the present compound.

It is of interest to note that *N*-(*p*-chlorobenzylidene)-*p*-chloroaniline shows dimorphism where the Pccn form[8] belongs to the non-centrosymmetrical group while $P\bar{1}$ form[9] belongs to the centrosymmetrical one. They are conformational dimorphs, showing disorder about twofold rotation axis and inversion center respectively.

Crystal Structure. The crystal structure viewed along **c** is illustrated in Fig. 3. The four possible cells

Table 4. Molecular conformations of the series of compounds, *p*-R–Ph–XY–Ph–R′-*p*

The torsion angles (°) about X–C (aromatic) and Y–C (aromatic) bonds are denoted by $\widehat{\text{XPh}}$ and $\widehat{\text{YPh}}$ respectively, and the dihedral angles (°) between the benzene rings are by $\widehat{\text{PhPh}}$. The values were calculated based on the atomic coordinates in the literatures

Compound	R	XY	R′	Space group	Z	Disordered about	$\widehat{\text{XPh}}$	$\widehat{\text{YPh}}$	$\widehat{\text{PhPh}}$
Centrosymmetrical group									
(I)	Cl	CH=N	Cl	$P\bar{1}$	1	$\bar{1}$	0.1	−0.1	0
(II)	Cl	N=N	Cl	$P2_1/c$	2		1.0	−1.0	0
(III)	Br	CH=N	Br	$P2_1/a$	2	$\bar{1}$	2.2	−2.2	0
(IV)	Br	N=N	Br	$P2_1/c$	2		1.5	−1.5	0
(V)		CH=CH		$P2_1/a$	4[a]	$\bar{1}$	2.8	−2.8	0
							6.6	−6.6	0
(VI)	Me	CH=N	Me	$P2_1/c$	2	static positional	3.5	−3.5	0
						disorder	6.6	−6.6	0
(VII)		N=N		$P2_1/a$	4[a]	$\bar{1}$	5.8	−5.8	0
(VIII)	Br	CF=CF	Br	Pccn	4		9.0	−9.0	0
(IX)	Me	N=N	Me	$P2_1/a$	2	1	11.2	−11.2	0
(X)		C(CN)=C(CN)		C2/c	4		25.2	−25.2	0
(XI)	Me	CH_2–CH_2	Me	I2/a	4		71.8	−71.8	0
(XII)		CH_2–CH_2		$P2_1/a$	2		72.7	−72.7	0
(XIII)		CF_2–CF_2		$P2_1/a$	2		85.1	−85.1	0
Non-centrosymmetrical group									
(XIV)	EtOOC	NO=N	COOEt	$P\bar{1}$	2		−1.5	1.5	0.4
(XV)	EtO	N=N	OEt	$P2_1/c$	4		6.7[b]	8.8[b]	2[b]
(XVI)	O_2N	CH=N	NMe_2	$P2_1/c$	4		−4.2	8.9	5.1
(XVII)	MeO	NO=N	OMe	$P2_1/a$	4		3.6	20.1	22.6
(XVIII)	Me_2N	NO=N		$P2_1/c$	4		2.1	31.3	32.6
(XIX)	Cl	CH=N	Cl	Pccn	4	2	26.5	26.5	49.6
(XX)	Me_2N	CH=N	NO_2	$P\bar{1}$	4[a]		10.3	41.4	52.9
							5.2	50.7	56.3
(XXI)		CO–O		$P2_1/c$	4		65.1	−9.8	55.7
(XXII)	MeO	CH_2–CO	OMe	$P2_1/c$	4		63.6	−0.8	62.2
(XXIII)		CO–NH		C2/c	4	2	29.4	37.3	62.6
(XXIV)		CH=N		$P2_1/c$	4		9.9	56.8	65.5
(XXV)	Me	CH=N	NO_2	$P2_1/c$	4		6.3	53.4	59.0
(XXVI)	HOOC	CH=N		$P2_1/c$	4		13.8	41.4	54.6

(I) *N*-(*p*-Chlorobenzylidene)-*p*-chloroaniline (metastable form).[9] (II) *trans*-*p*,*p*′-Dichloroazobenzene.[10] (III) *N*-(*p*-Bromobenzylidene)-*p*-bromoaniline.[11] (IV) *trans*-*p*,*p*′-Dibromoazobenzene.[12] (V) *trans*-Stilbene.[13] (VI) *N*-(*p*-Methylbenzylidene)-*p*-methylaniline (form III).[14] (VII) *trans*-Azobenzene.[15] (VIII) *p*,*p*′-Dibromo-α,α′-difluorostilbene[16] (IX) *p*-Azotoluene.[17] (X) *trans*-α,β-Dicyanostilbene.[18] (XI) 4,4′-Dimethyldibenzyl.[19] (XII) Dibenzyl.[20] (XIII) 1,2-Diphenyltetrafluoroethane.[21] (XIV) Ethyl *p*-azoxybenzoate.[22] (XV) 4,4′-Azodiphenetole.[23] (XVI) *p*-Nitrobenzylidene-*p*-dimethylaminoaniline.[24] (XVII) *p*-Azoxyanisole.[25] (XVIII) β-*p*-Dimethylaminoazoxybenzene.[26] (XIX) *N*-(*p*-Chlorobenzylidene)-*p*-chloroaniline (stable form).[8] (XX) *p*-Dimethylaminobenzylidene-*p*-nitroaniline.[24] (XXI) Phenyl benzoate.[27] (XXII) Deoxyanisoin.[28] (XXIII) Benzanilide (this work). (XXIV) Benzylidenaniline.[29] (XXV) *p*-Methylbenzylidene-*p*-nitroaniline.[29] (XXVI) Benzylideneaniline-*p*-carboxylic acid.[29]

a) The unit cell contains two kinds of molecules. b) Dihedral angles reported in the literature.

Table 5. Four possible cells

Space group	Mode of sheet formation	Resulting sheet	Short contacts (Å) in the sheet C···H	Energy of dipole interactions (kcal/mol)	Mode of sheet stacking	Short contacts(Å) between the sheets H···H	Short contacts(Å) between the sheets C···H	Interaction energy[a] (kcal/mol)
$P2_1/n$	$\bar{1}$	*A*	2.73, 2.76	−2.9	2_1	2.52	3.13	−32.1
$C\bar{1}$	$\bar{1}$	*A*			$\bar{1}$	2.39	3.02	−32.0
$P2_1/c$	*c*-glide	*B*	2.51, 2.54	−2.0	2_1	2.52	3.13	−31.5
Cc	*c*-glide	*B*			*n*-glide	2.39	3.02	−31.5

a) Intermolecular interaction energy for twelve nearest neighbors calculated by assuming the universal potential of Kitaigorodsky[30] for the intermolecular contacts smaller than 10 Å.

TABLE 6. CHARACTERISTIC FEATURES OF THE CHAINS OF AMIDO GROUPS RELATED BY A TRANSLATION

Compound	Space group	Dimension (Å) of axis along which the chain extends	N···O hydrogen bond length (Å)	Dihedral angle (°) between the amido group and benzene ring
(I)	C2/c	b=5.325	3.112	31.3
(II)	P1	c=5.27	—	30
(III)	$P2_1/n$	b=5.19[a)]	—	30
(IV)	$P2_12_12_1$	c=4.972	2.868	39.8
(V)	Cc	b=4.83	2.954	42.4
(VI)	$P2_1$	c=4.66	3.050	46.4

(I) Benzanilide (this work). (II) Nomex.[4)] (III) Kevlar.[4)] (IV) 4-Chloro-dipropylacetanilide. (V) 2-Acetyl aminofluorenone (Haisa *et al.*, unpublished data). (VI) Phenylurea.[32)]

a) The first setting is chosen.

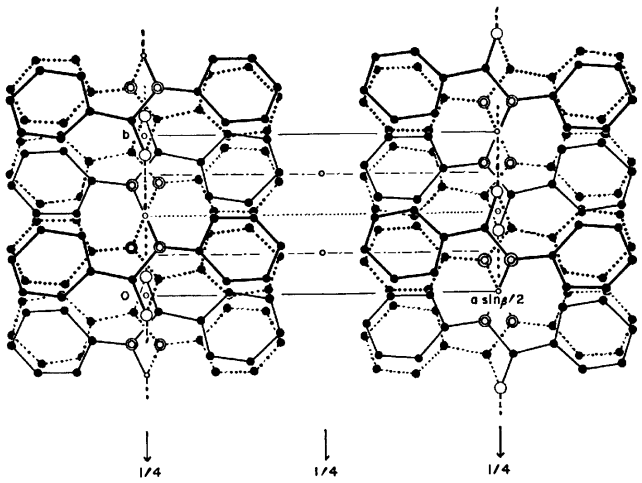

Fig. 3. The crystal structure viewed along ***c***. Arrangement of the molecules shown by solid lines corresponds to that in the $P2_1/n$ cell. The disordered molecules about twofold rotation axis are shown by dotted lines.

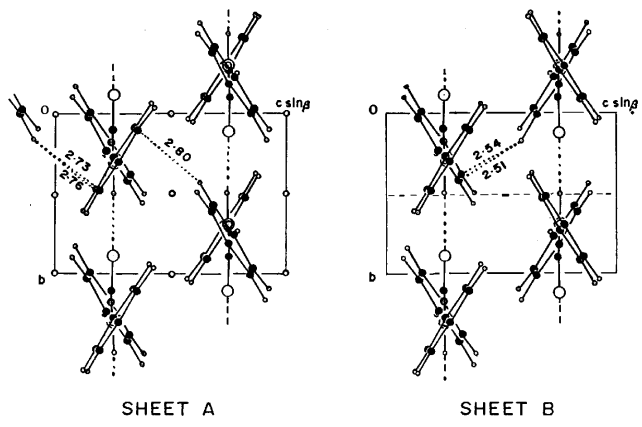

Fig. 4. Two possible arrangements of the chains in the sheets. Short intermolecular contacts are shown by dotted lines, and hydrogen bonds by broken lines.

which generate the apparent space group C2/c by adding the symmetry operation 2 for disordering are listed in Table 5. In the cells, the molecules related by a ***b***-translation are linked together by N–H···O hydrogen bond [N···O 3.112(6), H···O 2.03 Å, N–H···O 157, H···O=C 161°] to form a chain along ***b***. The chains are held together primarily by dipole interactions of the carbonyl groups of the molecules related by inversion centers or c-glide plane to form a sheet A or B parallel to the bc plane. Packing arrangement of the chains in the sheets is illustrated in Fig. 4. The sheets are stacked along ***a*** by van der Waals forces.

As seen from Table 5 and Fig. 4, the sheet A seems to prefer to the sheet B from the viewpoint of the molecular interactions. Concerning to the inter-sheet interactions, there are no significant differences among the stacking modes.

Disordered Structure. Disordering in the chain is not plausible, because it would result in an unexpectedly short intermolecular C···C contact of 3.03 Å. The disorder can be explained by a random stacking of the sheets A by two kinds of operations, 2_1 and $\bar{1}$, with an equal probability. In fact, the continuous streaks are elongated along a^* and no doubling of cell dimension a is observed.

The disordering of the present compound and the Pccn form of *N*-(*p*-chlorobenzylidene)-*p*-chloroaniline is similar in the axis about which disorder occurs, and the torsion angles around the central bond, but in the latter the disordering occurs by random arrangement of the molecular units.

Comparison of the Crystal Structure with the Related Compounds. The chains of amido groups related by a translation have been observed also in the related compounds as shown in Table 6. The dimension of the axis along which the chain extends becomes smaller with increasing the dihedral angle between the amido group and benzene ring. It is noted that the arrangement of the chains in the sheet (Fig. 4) is similar to that of Kevlar,[4)] irrespective of the difference in the symmetry operation relating the chains.

References

1) M. Haisa, S. Kashino, Y. Matsuzaki, R. Kawai, and K. Kunitomi, *Acta Crystallogr., Sect. B*, **33**, 2449 (1977).

2) M. G. Northolt and J. J. Van Aarsten, *J. Polym. Sci., Polym. Lett., Ed.*, **11**, 333 (1973).

3) H. Kakida, Y. Chatani, and H. Tadokoro, *J. Polym. Sci., Polym. Phys. Ed.*, **14**, 427 (1976).

4) K. Tashiro, M. Kobayashi, and H. Tadokoro, *Macromolecules*, **10**, 413 (1977).

5) "International Tables for X-Ray Crystallography," Kynoch Press, Birmingham (1962), Vol. III, p. 202.

6) "The Universal Crystallographic Computing System-

Osaka," The Computation Center, Osaka University (1973).
7) Lists of structure factors and anisotropic thermal parameters have been deposited at the Chemical Society of Japan (Document No. 7908).
8) J. Bernstein and I. Izak, *J. Chem. Soc., Perkin Trans. 2*, **1976**, 429.
9) J. Bernstein and D. M. J. Schmidt, *J. Chem. Soc., Perkin Trans. 2*, **1972**, 951.
10) H. Hope and D. Victor, *Acta Crystallogr., Sect. B*, **25**, 1849 (1969).
11) J. Bernstein and I. Izak, *J. Cryst. Mol. Struct.*, **5**, 257 (1975).
12) A. G. Amit and H. Hope, *Acta Chem. Scand.*, **20**, 835 (1966).
13) A. Hoekstra, P. Meertens, and A. Vos, *Acta Crystallogr., Sect. B*, **31**, 2813 (1975).
14) J. Bernstein and I. Bar, *Acta Crystallogr., Sect. B*, **32**, 1609 (1976).
15) C. J. Brown, *Acta Crystallogr.*, **21**, 146 (1966).
16) L. A. Cetkina and G. A. Gol'der, *Zh. Strukt. Khim.*, **8**, 106 (1967).
17) C. J. Brown, *Acta Crystallogr.*, **21**, 153 (1966).
18) S. C. Wallwork, *Acta Crystallogr.*, **14**, 375 (1961).
19) C. J. Brown, *Acta Crystallogr.*, **7**, 97 (1954).
20) D. W. J. Cruickshank, *Acta Crystallogr.*, **2**, 65 (1949).
21) D. W. J. Cruickshank, G. A. Jeffrey, and S. C. Nyburg, *Z. Kristallogr.*, **112**, 385 (1959).
22) W. R. Krigbaum and P. G. Barber, *Acta Crystallogr., Sect. B*, **27**, 1884 (1971).
23) J. L. Galigné, *Acta Crystallogr., Sect. B*, **26**, 1977 (1970).
24) H. Nakai, M. Shiro, K. Ezumi, S. Sakata, and T. Kubota, *Acta Crystallogr., Sect. B*, **32**, 1827 (1976).
25) W. R. Krigbaum, Y. Chatani, and P. G. Barber, *Acta Crystallogr., Sect. B*, **26**, 97 (1970).
26) J. Browning, D. A. R. Happer, and B. R. Penfold, *J. Cryst. Mol. Struct.*, **4**, 187 (1974).
27) J. M. Adams and S. E. Morsi, *Acta Crystallogr., Sect. B*, **32**, 1345 (1976).
28) H. G. Norment and I. L. Karle, *Acta Crystallogr.*, **15**, 873 (1962).
29) H. B. Bürgi and J. D. Dunitz, *Helv. Chim. Acta*, **53**, 1747 (1970).
30) A. I. Kitaigorodsky, "Molecular Crystals and Molecules," Academic Press, New York (1973), pp. 386—394.
31) C. Cohen-Addad, *Acta Crystallogr., Sect. B*, **29**, 157 (1973).
32) S. Kashino and M. Haisa, *Acta Crystallogr., Sect. B*, **33**, 855 (1977).

Chemical Reactivity of Würster's Salts at Very High Pressure

Akifumi ONODERA,* Tadayoshi SAKATA,† Hiroshi TSUBOMURA, and Naoto KAWAI

Faculty of Engineering Science, Osaka University, Toyonaka, Osaka 560

(Received August 9, 1978)

The electrical and chemical properties of some Würster's salts have been studied under the static pressure of up to 250 kbar. In most cases the resistances of the salts decreased to the respective minima and then rose irreversively with increasing pressure. Spectral observations on the recovered specimens revealed that such behavior is associated with chemical reaction induced by the pressure. This reaction takes place more readily in the salts of *p*-phenylenediamine cation radical than in those of Würster's red or Würster's blue radicals.

Recent high-pressure studies on organic solid materials have shown that a number of charge transfer complexes[1-5] and ion radical salts[6-9] cause chemical changes above one hundred kilobars†† or so. The occurrence of chemical reaction is unequivocally indicated by the peculiar behavior in electrical resistance of the specimen showing a minimum on the way of increasing pressure and monotonic rise on the way of decreasing pressure. The samples recovered after the application of pressure were chemically analysed and the reaction mechanisms were elucidated.[2-4]

In a previous paper[4] we reported the pressure-induced chemical reactions in three charge transfer (CT) complexes of *p*-chloranil with aromatic diamines. In the crystalline state of CT complexes the donor and acceptor molecules are generally stacked alternately in columns. The crystals of ion radical salts, on the other hand, are made up of columns of ion radicals. The interactions between adjacent molecules within a column are strong while the interaction between columns are much weaker. Therefore, the chemical reactivities of ion radical salts would be different from those in CT complexes.

The present investigation was undertaken to see chemical reactivity at very high pressure in a series of ion radical salts derived from *p*-phenylenediamine (PD), *N*,*N*-dimethyl-*p*-phenylenediamine and *N*,*N*,*N*′,*N*′-tetramethyl-*p*-phenylenediamine The counter ions were iodide, bromide and perchlorate. The electrical resistance measurements of the radical salts were carried out under various pressures and the reaction products recovered after the application of high pressure were analysed spectroscopically.

Experimental

Materials. *p*-Phenylenediamine bromide (PDB) and *p*-phenylenediamine iodide (PDI) were prepared by the reaction of *p*-phenylenediamine with the respective halogens in methanol. Würster's red bromide (WRB) and Würster's red iodide (WRI) were obtained by the reaction of *N*,*N*-dimethyl-*p*-phenylenediamine with the respective halogens in methanol. *p*-Phenylenediamine perchlorate (PDP), Würster's red perchlorate (WRP) and Würster's blue perchlorate (WBP) were prepared by the oxidation of dissolved amine perchlorate and sodium perchlorate with bromine in ethanol.[10] The radical salts were submitted for elementary analyses on formation and were compressed within a week.

† Present address: Institute for Molecular Science, Olazaki, Aichi 444.

†† 1 bar=10^5 Pa.

High-pressure System. The materials described above were compressed in a split sphere-type apparatus.[11] The apparatus is composed of cube, sphere and cylinder, all split up and assembled in a layered structure as shown in Fig. 1. A sphere made of hardened steel is equally divided into six segments, each with a square face at the front. Three out of the six segments are placed in a hemispherical space on the upper part of a cylinder. Similarly, the second assemblage is constructed using the remaining three segments. The two assemblages are set opposed and joined so that a cubic cavity whose ⟨111⟩ direction is parallel to the axis of cylinders is formed in the center of the join.

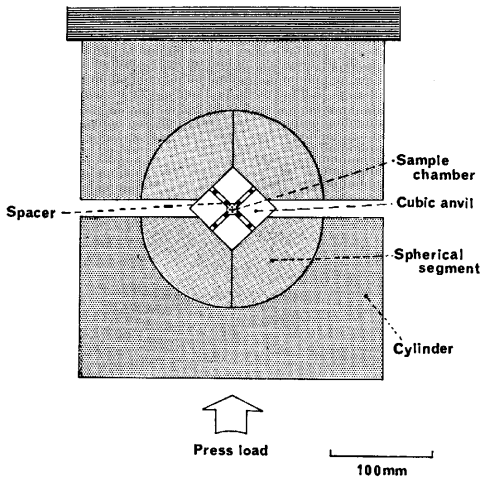

Fig. 1. A schematic drawing of the high-pressure apparatus.

An assemblage of eight cubic anvils made of cemented tungsten carbide is placed in the cubic cavity. A corner of each cubic anvil is truncated to form a triangular face. When the eight cubic anvils are put together an octahedral hollow space is formed in the center of the assemblage. Into this space is placed an octahedral pressure-transmitting medium made of pyrophyllite ($Al_2O_3 \cdot 4SiO_2 \cdot H_2O$). Crushable spacers made of cardboard are sandwiched in the gaps among the eight cubic anvils. When the two cylinders containing a split sphere and cubes are compressed in a uniaxial press, the thickness of the spacers decreases and quasi-hydrostatic high pressure is generated in the octahedral chamber. The pressures are calibrated by measuring the sharp resistance changes at the phase transitions of Bi (Bi_{I-II} at 25 kbar, Bi_{V-VI} at 74 kbar), ZnTe (127 kbar), Pb (132 kbar), ZnS (153 kbar), GaAs (177 kbar) and GaP (222 kbar).[12-16]

As shown in Fig. 2 the sample is enclosed within a Teflon capsule which is inserted into a hole drilled from a face to face of the ocatahedral chamber. Two platinum electrodes

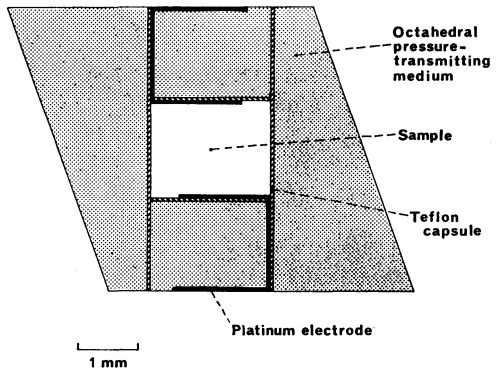

Fig. 2. A cross section of the octahedral pressure chamber.

for resistance measurements are taken out of the octahedron and are in contact with the top faces of the two of the eight cubic anvils. Electrical insulation between the anvils is provided by cardboard spacers and also by thin sheets of mica.

Measurements. The electrical resistance of the samples under pressure is measured *via* two cubic anvils with a Keithley 160B digital multimeter. The resistance of the cubic anvils is low enough to be neglected. On the other hand, the resistance of the pressure-transmitting medium is higher than that of any of the present samples by more than one order of magnitude. Thus the observed resistance reflects substantially the behavior of the sample. For the recovered samples after the application of pressure, the electronic spectra are obtained on the KBr disks with a Shimadzu Model MPS-50L multipurpose spectrometer. The vibrational spectra are obtained on a JASCO JRA-1 type diffraction grating infrared spectrometer using a similar KBr method.

Results

PD Cation Radical Salts. In Fig. 3 the electrical resistance of PDP is plotted on a logarithmic scale as a function of pressure. The resistance drops rapidly with pressure up to about 130 kbar. At higher pressure the resistance begins to rise. A noticeable upward drift of the resistance continues while the pressure is kept fixed. Beyond 200 kbar the resistance begins to decrease slowly. The resistance changes on the unloading process as shown by a dotted line in the diagram.

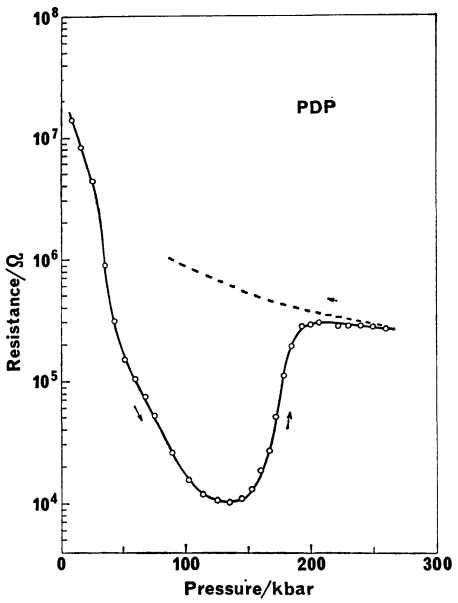

Fig. 3. Electrical resistance *versus* pressure for PDP.

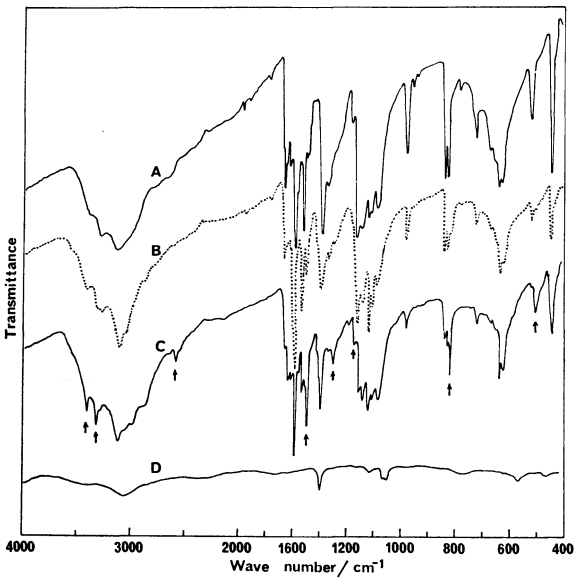

Fig. 4. Infrared spectra.
A: PDP at 1 bar, B: the sample recovered after the application of 140 kbar, C: the sample recovered after the application of 180 kbar, D: the sample recovered after the application of 220 kbar.

Figure 4 shows the infrared (IR) spectra of PDP before and after the compression. It should be noted that there was no appreciable change in the spectrum for the specimen compressed to pressures lower than 130 kbar, where a minimum appears in the electrical resistance. At 140 kbar new bands become to appear on the IR spectrum B, and at 180 kbar they become stronger as shown by the spectrum C. The bands indicated by arrows in Fig. 4, at 3420, 3330, 2590, 1505, 1300, 1195, 820, and 505 cm^{-1}, are assigned to 4-aminophenylammonium perchlorate, [PDH$^+$][ClO_4^-]. This was confirmed by the comparison of the bands with those in the IR spectrum of the synthesized authentic sample. The spectrum D is quite simple, suggesting that the product at higher pressure is polymeric. In the spectra of the high-pressure products in Fig. 4, there remain the bands responsible for the starting material, showing that the reaction in this system is rather slow.

Figure 5 shows the electronic absorption spectra of PDP and its reaction products recovered after the application of pressure, all specimens containing equal amounts of PDP in each of the KBr pellets. In the spectrum of PDP at 1 bar, the band at 13000 cm^{-1} is assigned to the charge transfer between cation radicals, whereas the peaks at 28800 and 35500 cm^{-1} are due to the local excitation between cation radicals.[17] As seen in Fig. 5 the band at 13000 cm^{-1} becomes weaker and shifts to blue with increasing pressure. The intensities of the peaks at 28800 and 35500 cm^{-1} decrease and the peaks shift to red with increasing pressure. The spectrum

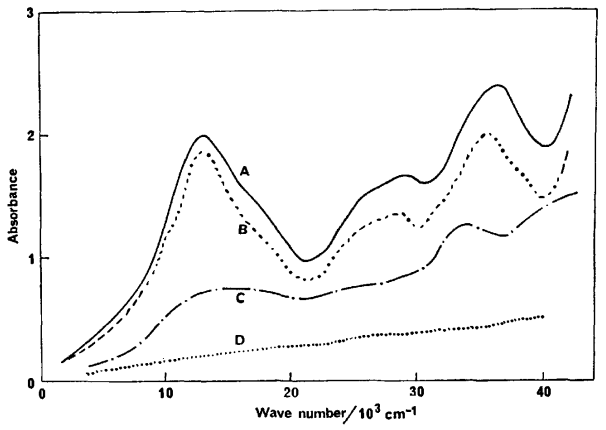

Fig. 5. Electronic absorption spectra.
A: PDP at 1 bar, B: the samle recovered after the application of 140 kbar, C: the sample recovered after the application of 180 kbar, D: the sample recovered after the application of 220 kbar.
The weight concentration of the above samples are epual to each other.

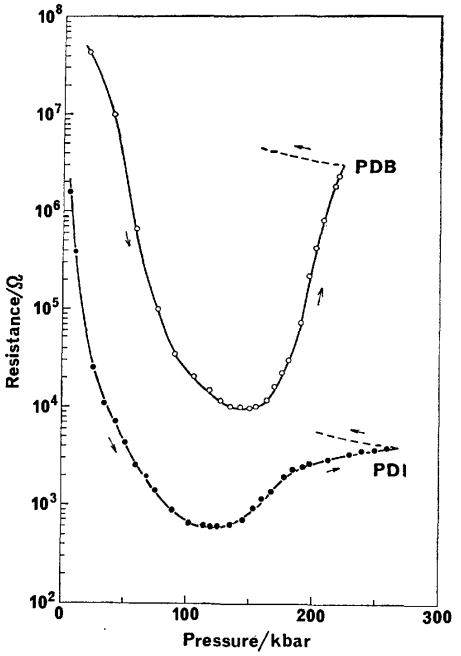

Fig. 6. Electrical resistance *versus* pressure for PDB and PDI.

C in Fig. 5 is well accounted for by a formation of $[PDH^+][ClO_4^-]$. In coincidence with the IR spectrum D in Fig. 4, the spectrum D in Fig. 5 is quite simple.

Figure 6 shows the electrical resistance *versus* pressure curves for PDB and PDI. The resistance of PDI is lower than that of PDB by about one order of magnitude throughout the pressure range covered. The resistance of PDB decreases by approximately four orders of magnitude when pressurized to 150 kbar, where a minimum appears. Above this pressure the electrical resistance of PDB begins to increase. As the pressure is released the resistance increases monotonously, suggesting that chemical reaction takes place in PDB above 150 kbar. The electrical resistance of PDI decreases by compression to about 120 kbar, above which it begins to rise. The behavior is irreversible on unloading process. This again suggests that chemical reaction takes place. The recovered PDI specimens were inspected after the application of pressures up to 200 kbar. Both the IR and electronic absorption spectra of compressed PDI were quite similar to those of compressed PDP. This shows that the high-pressure product of PDI is $[PDH^+][I^-]$.

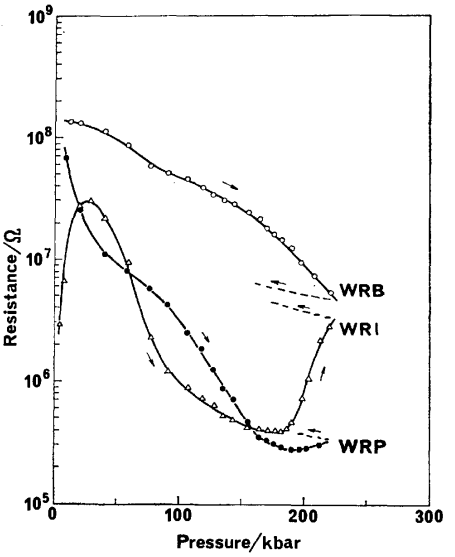

Fig. 7. Electrical resistance *versus* pressure for WRP, WRB, and WRI.

WR Cation Radical Salts. Figure 7 shows the electrical resistance of WRP, WRB, and WRI as a function of pressure. The resistance of these WR radical salts at high pressure are higher than those of PD radical salts. For WRP there appears a broad minimum around 190 kbar. The electrical resistance of WRP changes on unloading process in a different way from that shown on compression, indicating chemical reaction. The resistance of WRB decreases monotonously up to the highest pressure applied in this work. There might be a minimum in resistance at higher pressure. The resistance of WRI first increases to about 40 kbar, then decreases and after a broad minimum it increases again. The first increase of resistance is not well understood at present. From the resistance-pressure curve, the solid-state reaction in WRI seems to take place at a pressure of 180 kbar. No attempt was made to recover the specimen after the application of pressure and to carry out its spectral inspection.

WB Cation Radical Salt. Figure 8 shows the change of electrical resistance of WBP as a function of pressure. There appear two minima, the first at about 25 kbar, and the second around 220 kbar. WBP transforms at ambient pressure from the orthorhombic to monoclinic structure near 190 K. The pressure dependence of this transition temperature is reported to be 10 deg/kbar.[18] The linear extrapolation to room temperature locates the transition pressure at about 11 kbar, which is much less than the first minimum pressure. It is not certain whether or not the first

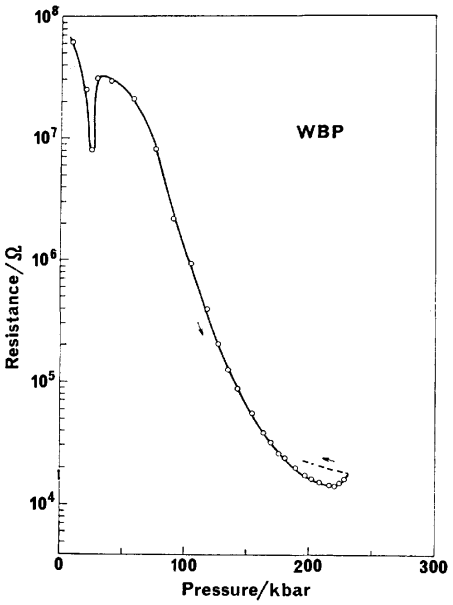

Fig. 8. Electrical resistance *versus* pressure for WBP.

minimum reflects the phase transition. Since the resistance drifts upward after the second minimum and increases irreversibly on decreasing pressure, the second minimum is attributable to chemical reaction, as in the case of PD radical salts, WRP and WRI.

Discussion

The product of the high-pressure reaction in PDP is, as described earlier, $[PDH^+][ClO_4^-]$. A possible scheme for the reaction to $[PDH^+][ClO_4^-]$ from PDP is as follows.

i) Proton transfer between ClO_4^- and PD cation radicals, yielding semi-quinone type radical and $HClO_4$.

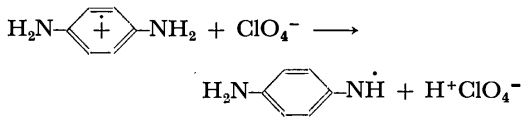

ii) Disproportionation between two radicals to form neutral PD and *p*-benzoquinone diimine.

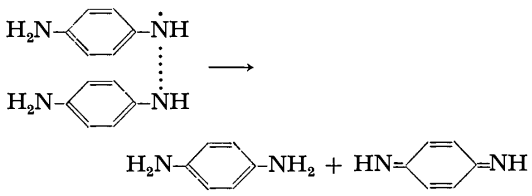

iii) Addition of $HClO_4$ to PD.

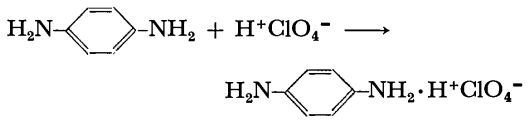

When PDP crystal is heated at 120 °C under vacuum, a solid-state reaction takes place within several hours. The products are PD, 4,4′-diaminoazobenzene (AZ), N^1, N^4-bis(*p*-aminophenyl)-2,5-diamino-1,4-benzoquinone diimine (Bandrowski's base, BB) and its polymer, among which BB-polymer and PD are predominant.[19] These materials are not recognized in the spectra of the high-pressure product of PDP. In order that BB[20] be produced by the linkage of three adjacent PD molecules in the crystalline state, the PD molecule to be centered should rotate to a certain amount because they are stacked in parallel face to face positions. This rotation will be facilitated in solids at higher temperature in vacuo, while it will be rather retarded under high pressure. BB is also synthesized by the reaction of PD cation radical with the parent molecule in ethanol solution.[21] The requisite linkage of three molecules for the formation of BB would be much easier in the solution than in the solid state.

Table 1. Pressure at which a minimum appears in the electrical resistance of respective Würster's salts

Cation radical	Counter ion		
	ClO_4^-	Br^-	I^-
	P_{min}/kbar		
PD^+	130	150	120
WR^+	190	>230	180
WB^+	25 220	a)	a)

a) Not measured.

Table 1 lists P_{min}, the pressure at which the electrical resistance shows minimum. As described earlier, P_{min} reflects the commencement of solid-state reaction. In PD radical salts P_{min} increases with the order; iodide, perchlorate and bromide. The reactivity[19] of the PD radical salt in the thermal reaction at ambient pressure becomes lower in the same sequence, indicating that the chemical reactivity in PD radical salts at high pressure is similar to the thermal reaction at 1 bar, although the products and hence the mechanisms are different. In the WR radical salts, the chemical reactivity at high pressure decreases with the order; WRI, WRP and WRB, in coincidence with the salts of PD radical. The counter ions are, therefore, very effective in the chemical reactivity in PD and WR radical salts at high pressure.

For PDP, WRP, and WBP, on the other hand, the chemical reactivity decreases at high pressure as the cation radical changes in the order PD, WR, and WB. The order holds also for salts of bromide and iodide. This sequence of chemical reactivity may be attributed to the difference in the number of active protons in PD, WR, and WB molecules, respectively.

In some of the present radical salts the interplanar spacing of cation radicals is quite short with respect to that calculated from the van der Waals distances. The separation is 3.105 Å in WRB[22] and 3.550 Å in WBP,[23] respectively, which is to be compared with that of tetrathiafulvalenium (TTF) cation radical in TTF salts. The spacing of TTF molecules is 3.57 Å in $TTFBr_{0.8}$,[24] 3.56 Å in TTF_7I_5[25] and 3.48 Å in TTF-TCNQ (tetracyanoquinodimethane),[26] respectively. These TTF cation radical salts undergo chemical reactions at pressures below 50 kbar,[8,9] whilst much higher

pressures are required for the reactions in Würster's salts. Therefore, the short spacing of the cation radicals does not necessarily facilitate the chemical reactivity of the compressed radical salts. Partial charge transfer, prevailing in the TTF cation radical salts,[24,27] seems to be more effective in causing the chemical changes at high pressure. This is evidenced by the pressure-induced chemical reaction of TCNQ anion radical salts[7-9] in which is also observed partial charge transfer.

This work was supported in part by the Ministry of Education under the Grant-in-Aid for Scientific Research, No. 054164.

References

1) W. H. Bently and H. G. Drickamer, *J. Chem. Phys.*, **42**, 1573 (1965).
2) V. C. Bastron and H. G. Drickamer, *J. Solid State Chem.*, **3**, 550 (1971).
3) M. I. Kuhlman and H. G. Drickamer, *J. Am. Chem. Soc.*, **94**, 8325 (1972).
4) T. Sakata, A. Onodera, H. Tsubomura, and N. Kawai, *J. Am. Chem. Soc.*, **96**, 3365 (1974).
5) A. Onodera, T. Sakata, H. Tsubomura, and N. Kawai, Proc. 4th Int'l Conf. High Pressure, Kyoto (1974) p. 713.
6) R. B. Aust, G. A. Samara, and H. G. Drickamer, *J. Chem. Phys.*, **41**, 2003 (1964).
7) I. Shirotani, A. Onodera, and N. Sakai, *Bull. Chem. Soc. Jpn.*, **48**, 167 (1975).
8) A. Onodera, I. Shirotani, Y. Hara, and H. Anzai, High Pressure Science and Technology: 6th AIRAPT Conf., Boulder (1977) p. 498.
9) A. Onodera, I. Shirotani, and H. Anzai, in preparation.
10) L. Michaelis and S. Granik, *J. Am. Chem. Soc.*, **65**, 1747 (1943).
11) N. Kawai, M. Togaya, and A. Onodera, *Proc. Jpn. Acad.*, **49**, 623 (1973).
12) A. Ohtani, S. Mizukami, M. Katayama, A. Onodera, and N. Kawai, *Jpn. J. Appl. Phys.*, **16**, 1843 (1977).
13) A. Ohtani, A. Onodera, and N. Kawai, *Rev. Sic. Instrum.*, in press.
14) G. J. Piermarini and S. Block, *Rev. Sci. Instrum.*, **46**, 973 (1975).
15) F. P. Bundy, *Rev. Sci. Instrum.*, **46**, 1318 (1975).
16) K. J. Dunn and F. P. Bundy, *Rev. Sci. Instrum.*, **49**, 365 (1978).
17) Y. Oohashi and T. Sakata, *Bull. Chem. Soc. Jpn.*, **46**, 765 (1973).
18) R. C. Hughes, A. W. Merkl, and H. M. McConnell, *J. Chem. Phys.*, **44**, 1720 (1966).
19) T. Sakata, T. Fujita, and H. Tsubomura, 32th National Meeting of the Chemical Society of Japan, Tokyo, April 1975.
20) E. Bandrowski, *Ber.*, **27**, 480 (1894).
21) T. Sakata, M. Hiromoto, T. Yamagoshi, and H. Tsubomura, *Bull. Chem. Soc. Jpn.*, **50**, 43 (1977).
22) J. Tanaka and N. Sakabe, *Acta Crystallogr., Sect. B*, **24**, 1345 (1968).
23) J. L. de Boer and A. Vos, *Acta Crystallogr., Sect. B*, **28**, 835 (1972).
24) S. J. LaPlaca, P. W. R. Corfield, R. Thomas, and B. A. Scott, *Solid State Commun.*, **17**, 635 (1975).
25) J. J. Daly and F. Sanz, *Acta Crystallogr., Sect. B*, **31**, 620 (1975).
26) T. J. Kistenmacher, T. E. Phillips, and D. O. Cowan, *Acta Crystallogr., Sect. B*, **30**, 763 (1974).
27) W. D. Grobman, R. A. Pollak, D. E. Eastman, E. T. Mass, Jr., and B. A. Scott, *Phys. Rev. Lett.*, **32**, 534 (1974).

Magnetic Susceptibility and Low-field ESR of an Organic Ion-radical Salt, Tri-*p*-tolylaminiumyl Chloroantimonate

Toshio YOSHIOKA†

Department of Chemistry, Faculty of Science, Kyoto University, Sakyo-ku, Kyoto 606

(Received August, 9, 1978)

The static magnetic susceptibility and the low-field ESR spectra (33.6 and 135 MHz) of powder samples of tri-*p*-tolylaminiumyl chloroantimonate were measured above 1.7 K. A broad maximum in the susceptibility, which indicates an antiferromagnetic interaction, was observed at 6.0 K; this is consistent with the results of the proton NMR measurements. In the low-field ESR spectra, broadening of the $g=2$ absorption line and distinct appearance of the $g=4$ absorption line were observed in the temperature region below T_m, the temperature at which the susceptibility is maximum. The results are interpreted by assuming that the magnetic behavior is due to antiferromagnetic Heisenberg linear chains. An abrupt decrease in the $g=2$ absorption intensity and a rapid increase in the $g=2$ absorption linewidth were also found in the temperature range from 3.5 to 2.5 K, while a slight rise in the susceptibility was observed below 2.5 K. These anomalies may imply a magnetic-phase transition in the vicinity of 2.5 K.

There have been many investigations regarding the magnetic properties of the stable organic free radicals. A deviation from the Curie-Weiss law and a broad maximum in the susceptibilities of some ion-radical salts with plate-like structures have been observed above the temperature of liquid nitrogen.[1] The anomalous behavior arises from the strong interaction between adjacent radicals and has been interpreted in terms of the exchange-coupled pair model or the linear Ising model. The mechanism of such a strong interaction is considered to be the charge-transfer stabilization. However, the magnetic behavior of ion-radical salts which have small Weiss constants had never been studied in the low-temperature region.

In triarylaminiumyl radical salts, the cations are considered to have propeller-like structures similar to those of triarylmethylium salts,[2] so that the exchange interaction between adjacent radicals is expected to be small compared with that of plate-like ion-radical salts. The static magnetic susceptibilities from 77 to 300 K and the proton NMR spectra from 1.5 to 77 K have been measured on powder samples of some triarylaminiumyl radical salts by the present author and his co-workers.[3] The static magnetic susceptibilities of tri-*p*-tolylaminiumyl chloroantimonate (TTA·$SbCl_5$) obeyed the Curie-Weiss law, with a Weiss constant of $\theta=-10$ K, and a broad maximum in the paramagnetic shift of its proton NMR spectra was found in the vicinity of 6.0 K. The broadening of the shifted lines was also observed below 4.2 K. This behavior cannot be explained by the anisotropic broadening.[3,4] In order to clarify the magnetic behavior of TTA·$SbCl_5$ at low temperatures, the static magnetic susceptibility and low-field ESR (33.6 and 135 MHz) measurements were carried out for temperatures above 1.7 K. Precise and absolute values of susceptibility can be obtained from the static magnetic measurements. Information concerning the dynamical behavior of the spin system near the zero field can be obtained from the low-field ESR (LF-ESR) measurements. In this paper the author will report the results of these measurements and discuss the exchange interaction, spin correlation, and abnormal ESR behavior in the TTA·$SbCl_5$ salt. The tri-*p*-tolylaminiumyl cation, TTA, has the molecular structure shown in Fig. 1.

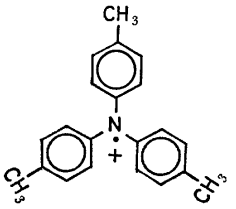

Fig. 1. Molecular structure of the tri-*p*-tolylaminiumyl cation, TTA.

Experimental

The tri-*p*-tolylamine was prepared by the method of Walter and was purified by repeated recrystallization.[5] The TTA·$SbCl_5$ was prepared according to the method of Wieland.[6] To a solution of the tri-*p*-tolylamine in benzene was added a chloroform solution of $SbCl_5$ under cooling. By addition of benzene a deep blue crystalline product with a metallic luster was obtained from the solution. After filtration, the product was quickly washed with benzene and dried *in vacuo*, mp 114—116 °C. The results of the elementary analysis were described in the previous paper.[3]

The static magnetic susceptibilities were measured for powder samples of 70—90 mg in a field of 8.8 kG from 1.7 to 100 K by means of the torsion balance described elsewhere.[7] No ferromagnetic impurities were found in samples by checking the field dependence of magnetization up to 12 kG at 4.2 K. The temperatures were measured with an AuCo–Cu thermocouple and a carbon resistor calibrated by measuring not only the magnetic susceptibility of Mn-Tutton salt, but also the vapor pressures of liquid helium, liquid hydrogen, and liquid nitrogen. The LF-ESR spectra (33.6 and 135 MHz) were observed using a Robinson type spectrometer[8] and a Benedek-Kusida type spectrometer,[9] respectively. Details of the apparatus for the LF-ESR measurements have been described elsewhere.[10] The sensitivity of the Robinson type spectrometer with respect to temperature variations was checked by measuring the absorption intensity of the proton NMR, which is inversely proportional to the temperature. A conventional cryostat was used, and tem-

† Present address: Fibers Research Laboratories, Toray Industries, Inc., Sonoyama, Otsu 520.

Table 1. Results from susceptibility measurements

	χ_d / 10^{-4} emu·mol^{-1}	θ / K	T_m / K	χ_m / 10^{-4} emu·mol^{-1}	p	J/k / K
TTA·$SbCl_5$[a]	−3.4	−10	6.0	188	0.94	−4.7
TANOL[b]	−1.1	−6	6.5	226	1.00	−5.0
p-Cl-BDPA[b]	−2.8	−6	5.6	196	1.00	−4.4

a) This work. b) Ref. 12.

peratures were determined using an Allen-Bradley carbon resistor calibrated against the vapor pressures of liquid helium, hydrogen, and nitrogen.

Results and Discussion

Susceptibility. The diamagnetic correction was made using Pascal's constant. The diamagnetic susceptibility, χ_d, is listed in Table 1. In the temperature range above 15 K, the paramagnetic susceptibility, χ_p, of TTA·$SbCl_5$ follows the Curie-Weiss law, with a Weiss constant of $\theta=-10$ K and a spin concentration of $p=0.94$. As the temperature is lowered below 15 K, it deviates from the Curie-Weiss law and reaches a broad maximum at 6.0 K, as is shown in Fig. 2. After passing through the maximum, it decreases comparatively slowly down to 2.5 K. However, below 2.5 K it increases slightly as the temperature is lowered. In the region from 3.0 to 77 K, the behavior of the susceptibility is consistent with that of the relative susceptibility obtained from the proton paramagnetic shift.[3]

The *g*-value of TTA·$SbCl_5$ is nearly isotropic, so that it is not appropriate to discuss its magnetic properties on the basis of the linear Ising model. Therefore, the susceptibility data have been analyzed using the pair model and the one-dimensional Heisenberg model based on Bonner and Fisher's calculation.[11] The kT_m/J ratio is 1.28 for the one-dimensional Heisenberg model and 1.25 for the pair model, where T_m is the temperature at which the susceptibility reaches its maximum value and J is the exchange coupling constant. The J value for each model can be estimated from the T_m value

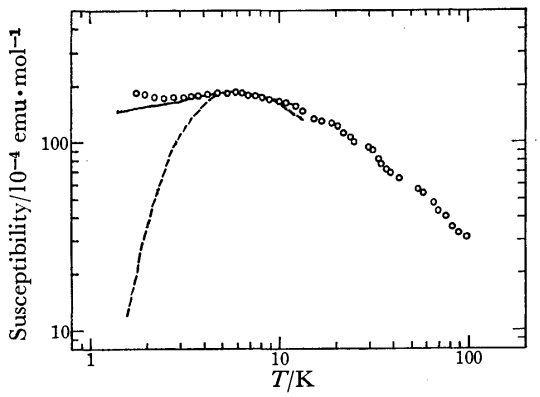

Fig. 2. Magnetic molar susceptibility of TTA·$SbCl_5$. The open circles represent the experimental values. The solid line and the dashed line are the theoretical curves for the one-dimensional Heisenberg model of $J=-4.7$ K and for the pair model of $J=-4.9$ K, respectively, which are fitted at $T_m=6.0$ K.

obtained experimentally. In Fig. 2, the paramagnetic susceptibility is compared with the theoretical curves for the one-dimensional Heisenberg model of $J=-4.7$ K and for the pair model of $J=-4.9$ K, which are fitted at the temperature T_m. It can be seen from Fig. 2 that the observed value above 2.5 K fits the one-dimensional Heisenberg model better than the pair model. However, the maximum value of the observed susceptibility, $\chi_m=188\times10^{-4}$ emu/mol, is 20% lower than the former theoretical $\chi_m=225\times10^{-4}$ emu/mol; it is 40% lower than the latter theoretical $\chi_m=296\times10^{-4}$ emu/mol. The difference between the experiment and the theory is not due to a poor spin concentration, but to the some other effect, for the spin concentration is equal to 0.94 in the temperature range above 15 K. The one-dimensional Heisenberg interaction has not been observed in ion-radical salts. It is interesting that the ion-radical salt, TTA·$SbCl_5$, studied here exhibits a one-dimensional Heisenberg interaction. In the crystalline state, the cation radicals with a propeller-like configuration may form chain-like arrays of molecules. The propeller-like structure of the cation radical, TTA, may restrict pairing of electron spins and dimerization of molecules in the crystalline state compared with a plate-like structure. The resulting parameters are summarized in Table 1, together with those of one-dimensional Heisenberg antiferromagnets typical of organic neutral radicals, 2,2,6,6-tetramethyl-4-hydroxy-1-piperidinyloxyl (TANOL) and 9-(α-fluorenylidene-*p*-chlorobenzyl)-9-fluorenyl (*p*-Cl-BDPA).[12] The exchange parameter J for TTA·$SbCl_5$ is as large as that for the organic neutral radicals. The mechanism of such a weak interaction may be attributable to the overlap of π-orbitals occupied by the unpaired electron rather than to the charge-transfer stabilization. The slight rise in the susceptibility below 2.5 K may be attributable to a magnetic-phase transition rather than to paramagnetic impurities. Such a slight rise in the susceptibility has also been found near a magnetic-phase transition into an antiferromagnetic state in the case of some organic neutral radicals.[12,13] This will be discussed below on the basis of the LF-ESR results.

LF-ESR. The LF-ESR absorption spectra of TTA·$SbCl_5$ exhibit a single line which has an exchange-narrowed Lorentzian shape at room temperature. The temperature dependences of the 33.6 MHz ESR and 135 MHz ESR spectra are shown in Figs. 3 and 4, respectively. The linewidth, which was taken to be the peak-to-peak linewidth of the first derivative of the $g=2$ absorption spectrum, started to increase as the temperature was decreased below T_m, where the susceptibility went through a broad maximum. The

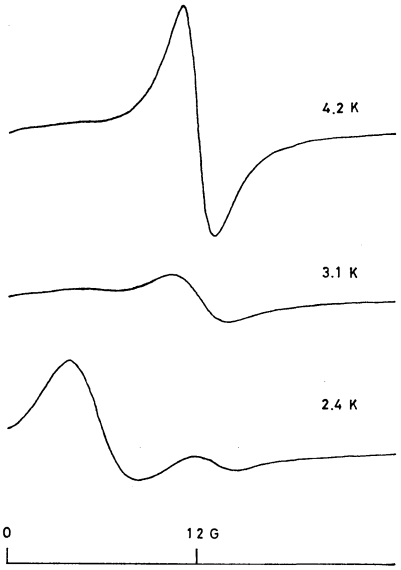

Fig. 3. The LF-ESR spectra of TTA·$SbCl_5$ measured at 33.6 MHz. The 2.4 K signal is amplified thirty three times compared with the 4.2 and 3.1 K signals.

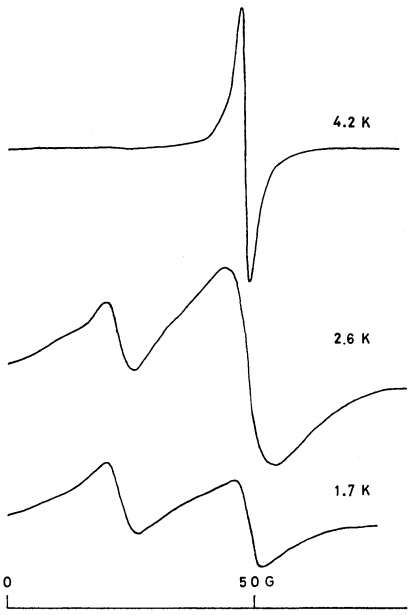

Fig. 4. The LF-ESR spectra of TTA·$SbCl_5$ measured at 135 MHz.

signal intensity, which was defined as the product of the square of the linewidth and the amplitude of the first derivative of the $g=2$ absorption line, measured at 33.6 MHz, was almost constant in the region from 4.2 to 3.5 K. In the temperature range from 3.5 to 2.5 K, an abrupt decrease in the signal intensity and a rapid increase in the linewidth were found. The temperature dependence of the linewidth and signal intensity measured at 33.6 MHz is shown in Fig. 5. Below 2.5 K the linewidth measured at 135 MHz decreased rapidly, as is shown in Fig. 6. The $g=4$ absorption could not be observed at room temperature or at liquid nitrogen temperature. Below the temperature at which the susceptibility deviated from the Curie-Weiss law, the

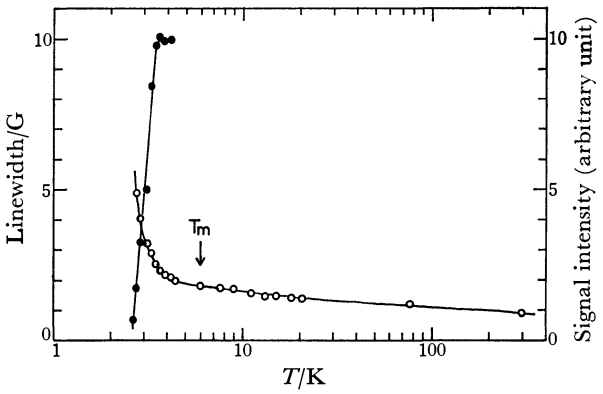

Fig. 5. Temperature dependence of the LF-ESR linewidth (-○-) and signal intensity (-●-) measured at 33.6 MHz.

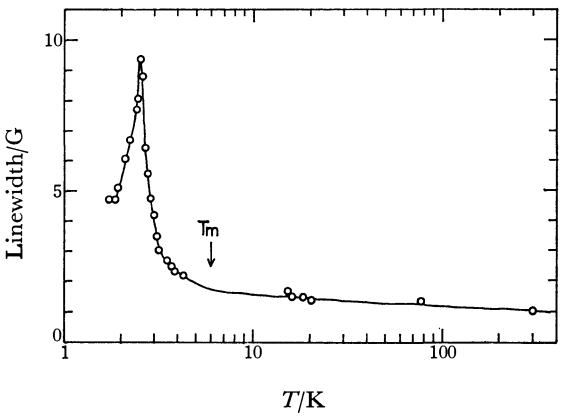

Fig. 6. Temperature dependence of the LF-ESR linewidth measured at 135 MHz.

$g=4$ absorption was detected as the temperature was lowered. At fixed temperature, the ratio of the intensity of the $g=4$ resonance absorption to that of the $g=2$ absorption was larger in the 33.6 MHz ESR spectrum than in the 135 MHz ESR spectrum.

It is well-known that the signal intensity of the ESR absorption line is proportional to the magnetic susceptibility in the paramagnetic state. The relative susceptibility, obtained from the signal intensity, agrees qualitatively with the static magnetic susceptibility for temperatures above 3.5 K. In Fig. 7, the relative susceptibility, obtained from the signal intensity, is compared with the static magnetic susceptibility and the theoretical curves for the one-dimensional Heisenberg model of $J=-4.7$ K and the pair model of $J=-4.9$ K, which are normalized at 4.2 K. In a one-dimensional Heisenberg system, a rapid decrease in the signal intensity is not observed below the temperature of maximum susceptibility.[14] In a pair-like system, the signal intensity decreases in direct proportion to the static magnetic susceptibility below the temperature of maximum susceptibility. The observed deviation from the static magnetic susceptibility below 3.5 K, consisting in an abrupt decrease in the signal intensity of the ESR line, indicates the occurrence of a reorganization of the energy spectrum involving a decrease in the number of

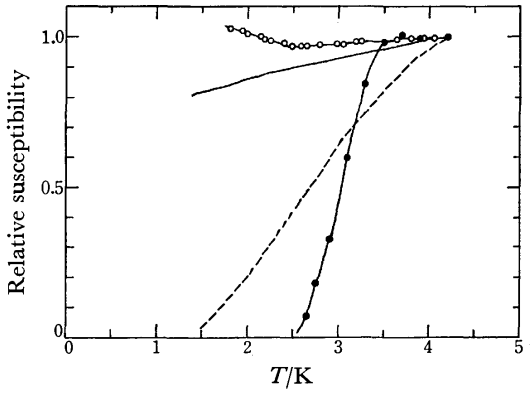

Fig. 7. Comparison between the static magnetic susceptibility (-○-) and the relative susceptibility obtained from the LF-ESR signal intensity (-●-). The solid line and the dashed line represent the theoretical curves for the one-dimensional Heisenberg model of $J=-4.7$ K and the pair model of $J=-4.9$ K, respectively. The experimental plots and the theoretical curves are normalized at 4.2 K.

spins possessing a paramagnetic property. Recent magnetic resonance measurements revealed that some organic neutral radicals go into a long-range ordered antiferromagnetic state in a sufficiently low temperature region.[15] The abrupt decrease in the signal intensity of the ESR line of TTA·$SbCl_5$ may imply a magnetic-phase transition from the short-range ordered state to the long-range ordered state in the vicinity of 2.5 K. In the temperature range from 3.8 to 3.2 K, such an abrupt decrease in the signal intensity of 33.6 MHz ESR line has also been observed for *p*-Cl-BDPA,[16] which undergoes a magnetic-phase transition to an antiferromagnetic state at 3.25 K.[17] Delocalization of the unpaired electron on the three *p*-tolyl rings or the chloroantimonate anion with a diamagnetic formula[3] may play some role in an exchange interaction leading to a long-range ordered state, such as the interchain exchange interaction.

In the case of LF-ESR, precise linewidth data can be obtained even in powder samples, because any contribution to the linewidth from the anisotropy of the *g*-values is excluded. The LF-ESR line is narrowed by the strong exchange interaction in the high-temperature region. It has been reported that, in several organic neutral radicals, the LF-ESR linewidth *versus* temperature below T_m of maximum susceptibility can be fitted to the following empirical relation:[14]

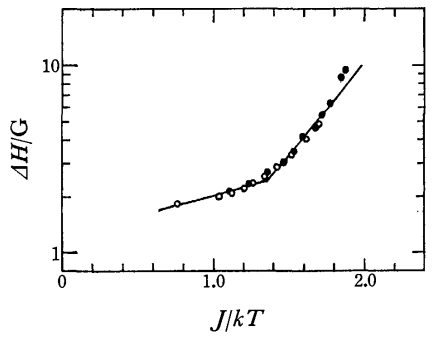

Fig. 8. LF-ESR linewidth (ΔH) *versus* J/kT. ○: 33.6 MHz, ●: 135 MHz.

$$\Delta H = \alpha \exp(\beta J/kT), \quad (1)$$

where α and β are constant and where J means the absolute value of the exchange coupling constant. The parameters of temperature dependent LF-ESR linewidth for TTA·$SbCl_5$ are summarized in Table 2, together with those for some organic neutral radicals.[14,16] The β values for TTA·$SbCl_5$ were determined to be 0.50 in the region from 6.0 to 3.5 K and to be 2.30 in the region from 3.5 to 2.5 K, by plotting the linewidth against the reciprocal of the temperature, as is shown in Fig. 8. The β value is considered to be associated with the correlation mechanism of exchange motion, which may be related to the magnetic interaction of the system. It is interesting that the first β value for TTA·$SbCl_5$ is nearly equal to the β value for TANOL, which has a one-dimensional Heisenberg interaction.[12] The broadening of the resonance with the first β value is attributable to an increase in the correlation for exchange motion because of short-range magnetic ordering below the temperature of maximum susceptibility. Such a broadening was not found above 1.7 K in tri-*p*-tolylaminiumly perchlorate (TTA·ClO_4); its susceptibility obeyed the Curie-Weiss law with a Weiss constant of $\theta=-0.5$ K.[3] The second β value for TTA·$SbCl_5$ is much larger than the β values for the radicals with one-dimensional Heisenberg or pair-like interaction. The rapid increase in linewidth with the second β value may be the result of the critical fluctuation of electron spins in the vicinity of the transition temperature, which may simultaneously cause the abrupt decrease in the signal intensity in the range from 3.5 to 2.5 K. It may be appropriate to use one parameter in place of $\beta J/k$ in Eq. 1, because the J parameter is considered to be insignificant in this temperature

Table 2. Parameters for temperature dependent LF-ESR linewidth and magnetic interaction

	α / G	β	J/k / K	Magnetic interaction
TTA·$SbCl_5$[a] 2.5—3.5 K	0.1	2.30	4.7	——
TTA·$SbCl_5$[a] 3.5—6.0 K	1.2	0.50	4.7	one-dimensional
TANOL[b]	3.6	0.48	5.0	Heisenberg interaction
Porphyrexide[b]	3.0	0.95	5.9	
Cl-porphyrexide[b,c]	1.1	0.93	18.2	pair-like interaction
Solvent-free DPPH[d]	0.7	0.70	8.8	

a) This work. b) Ref. 14. c) Monochloroporhyrexide. d) α,α-Diphenyl-β-picryl hydrazyl recrystallized from ether. Refs. 16 and 18.

range. The behavior of the $g=2$ resonance can be related to the broadening of the shifted lines in the proton NMR spectra below 4.2 K. The residual resonance measured at 135 MHz below 2.5 K is probably due to paramagnetic impurities.

In the high-temperature region, the $g=4$ resonance, which is probably caused by a forbidden transition due to dipolar interaction, cannot be detected,[14,19] for the strong exchange interaction averages the dipolar coupling.[20] The appearance of the $g=4$ resonance at low temperatures can be explained by an increase in the correlation time for exchange motion, as is expected from the linewidth of the $g=2$ resonance and the susceptibility data. Below 3.5 K the behavior of the $g=4$ resonance was independent of the temperature in spite of the anomalies of the $g=2$ resonance. This cannot be explained now.

Conclusions

1. The static magnetic susceptibility of TTA·$SbCl_5$, as well as the relative susceptibility obtained from the paramagnetic shift, can be described by the one-dimensional Heisenberg model of $J/k=-4.7$ K in the temperature range above 2.5 K, although the maximum value of the observed susceptibility is 20% lower than the theoretical value.

2. The broadening of the $g=2$ absorption line and the distinct appearance of the $g=4$ absorption line in the LF-ESR spectra are attributable to the effects of short-range magnetic ordering below the temperature of the susceptibility maximum.

3. The following anomalies may imply a magnetic-phase transition in the vicinity of 2.5 K: 1) the rise of the susceptibility below 2.5 K, 2) the abrupt decrease in the $g=2$ absorption intensity and the rapid increase in the $g=2$ absorption linewidth in the temperature range from 3.5 to 2.5 K, 3) the broadening of the shifted lines in the proton NMR spectra below 4.2 K.

The author would like to express his appreciation to Professor Yasuo Deguchi for his continuous encouragement throughout this work. He also wishes to thank Drs. Hiroaki Ohya-Nishiguchi and Jun Yamauchi for their illuminating discussions and Dr. Kohji Watanabe for his advice on the preparation of the samples.

References

1) D. B. Chesnut and W. D. Phillips, *J. Chem. Phys.*, **35**, 1002 (1961); R. G. Kepler, *ibid.*, **39**, 3528 (1963); H. Nishiguchi, *Bull. Chem. Soc. Jpn.*, **40**, 1587 (1967); Y. Sato, M. Kinoshita, M. Sano, and H. Akamatu, *ibid.*, **40**, 2539 (1967); **42**, 3051 (1969); J. Tanaka, M. Inoue, M. Mizuno, and K. Horai, *ibid.*, **43**, 1998 (1970).

2) W. Otting and H. Kainer, *Chem. Ber.*, **87**, 1205 (1954); D. W. A. Sharp, *J. Chem. Soc.*, **1957**, 4804.

3) T. Yoshioka, K. Watanabe, and H. Ohya-Nishiguchi, *Bull. Chem. Soc. Jpn.*, **48**, 2533 (1975).

4) T. Yoshioka, H. Ohya-Nishiguchi, and Y. Deguchi, *Bull. Chem. Soc. Jpn.*, **47**, 430 (1974).

5) R. I. Walter, *J. Am. Chem. Soc.*, **77**, 5999 (1955).

6) H. Wieland, *Ber.*, **40**, 4260 (1907).

7) M. Mekata, *J. Phys. Soc. Jpn.*, **17**, 796 (1962).

8) F. N. H. Robinson, *J. Sci. Instrum.*, **36**, 481 (1959).

9) G. B. Benedek and T. Kusida, *Phys. Rev.*, **118**, 46 (1960).

10) M. A. Garstens, L. S. Singer, and A. H. Ryan, *Phys. Rev.*, **96**, 53 (1954).

11) J. C. Bonner and M. E. Fisher, *Phys. Rev. A*, **135**, 640 (1964).

12) J. Yamauchi, *Bull. Chem. Soc. Jpn.*, **44**, 2301 (1971).

13) N. Azuma, J. Yamauchi, K. Mukai, H. Ohya-Nishiguchi, and Y. Deguchi, *Bull. Chem. Soc. Jpn.*, **46**, 2728 (1973).

14) T. Yoshioka, *Bull. Chem. Soc. Jpn.*, **50**, 1372 (1977).

15) S. Saito and T. Sato, *Phys. Lett. A*, **44**, 2301 (1971); K. Uchino, J. Yamauchi, H. Ohya-Nishiguchi, and Y. Deguchi, *Bull. Chem. Soc. Jpn.*, **47**, 285 (1974); T. Yoshioka, J. Yamauchi, H. Ohya-Nishiguchi, and Y. Deguchi, *ibid.*, **48**, 335 (1975); O. Takizawa, T. Yoshioka, H. Ohya-Nishiguchi, and Y. Deguchi, *Chem. Lett.*, **1976**, 223.

16) T. Yoshioka, H. Ohya-Nishiguchi, and J. Yamauchi, unpublished work.

17) J. Yamauchi, K. Adachi, and Y. Deguchi, *Chem. Lett.* **1972**, 733; *J. Phys. Soc. Jpn.*, **35**, 443 (1973).

18) T. Fujito, T. Enoki, H. Ohya-Nishiguchi, and Y. Deguchi, *Chem. Lett.*, **1972**, 557.

19) R. S. Rhodes, J. H. Burgess, and A. S. Edelstein, *Phys. Rev. Lett.*, **6**, 462 (1961).

20) V. I. Konovalov and S. M. Ryabchenko, *Soviet Physics-Solid State*, **8**, 2833 (1967).

Gas and Solid Phase Photoelectron Spectra of 5,6,11,12-Tetraphenylnaphthacene (Rubrene)

Takashi TAKAHASHI, Yoshiya HARADA,* Naoki SATO,** Kazuhiko SEKI,**
Hiroo INOKUCHI,** and Shoji FUJISAWA***

Department of Chemistry, College of General Education, The University of Tokyo, Komaba, Meguro, Tokyo 153
***Institute for Molecular Science, Myodaiji, Okazaki 444*
****Department of Chemistry, Faculty of Science, Toho University, Miyama, Funabashi 274*

(Received August 24, 1978)

The gas and solid phase UV photoelectron spectra of rubrene were measured. In the molecule there is little conjugation of π-electrons between four substituent phenyl groups and the naphthacene skeleton owing to the effect of the steric hindrance of the phenyl groups. Therefore, the lower IP bands in the gas phase spectrum could be correlated to the π-bands in the photoelectron spectra of benzene and naphthacene. The features of the solid phase spectrum are similar to those of the gas phase one except for a large peak due to inelastically scattered electrons. The polarization energy due to the molecular ion in the solid, the peak to peak difference between the gas and solid phase spectra, was observed to be 0.6 eV, which is about half the polarization energy for naphthacene. This means that rubrene molecules are loosely packed in the solid as a result of the steric hindrance of four phenyl groups.

The compound 5,6,11,12-tetraphenylnaphthacene (rubrene) has aroused considerable chemical interest, since Moureu *et al.*[1] observed that its solution became colourless when irradiated in the presence of air. Subsequently, it was established that the change in colour is due to the formation of a transannular compound:[2]

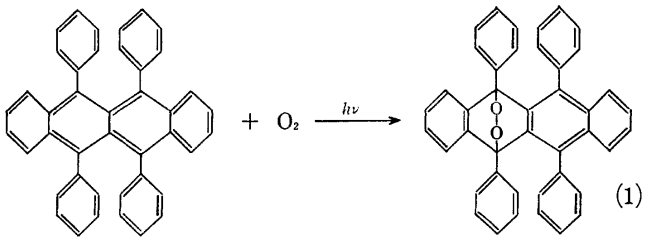

rubrene (1) rubrene peroxide

Recently we have studied the photooxidation process (1) in solid phase by ultraviolet photoelectron spectroscopy.[3] In the course of the study, it was necessary to assign the bands in the photoelectron (PE) spectrum of rubrene.

We therefore present the PE spectra of rubrene for gas and solid phases, and a subsequent analysis of the electronic structure in comparison with that of the unsubstituted compound, naphthacene.

Experimental

Rubrene was purified by vacuum sublimation. The gas phase He I spectrum was recorded on a Perkin-Elmer PS-18 photoelectron spectrometer. The temperature of the sample was kept at 280 °C during the experiment.

The He I spectrum of solid rubrene was measured using an ultra high vacuum spectrometer constructed at our laboratory (the University of Tokyo), the details of which will be described elsewhere.[3] A 180° hemispherical analyzer of 5 cm mean radius was used for electron energy analysis. The solid phase photoelectron spectrum was also obtained with 7.75 eV† monochromatic light which was provided by a 0.5 m Seya-Namioka type monochromator fitted with a hydrogen discharge lamp. In this case a spherical retarding type analyzer was used with an ac-modulation method. Rubrene films were prepared by vacuum sublimation *in situ* onto copper substrates. The thickness of the films was controlled by means of a quartz osicillator monitor and was about 15 nm.

Results and Discussion

Gas Phase Spectrum. Figure 1 shows the gas phase spectrum of rubrene. The observed lower ionization potentials (*IP*'s) are listed in the first column of Table 1. Since four substituent phenyl groups in the rubrene molecule are considered to be rotated out of the molecular plane owing to the effect of steric hindrance,†† little conjugation of π-electrons between the phenyl groups and the naphthacene skeleton is expected. Therefore, bands in the lower *IP* region of the rubrene spectrum can be correlated to the π-bands in the photoelectron spectra of benzene[4,6] and naphthacene.[5]

The correlation is listed in Table 1 for the bands 1 to

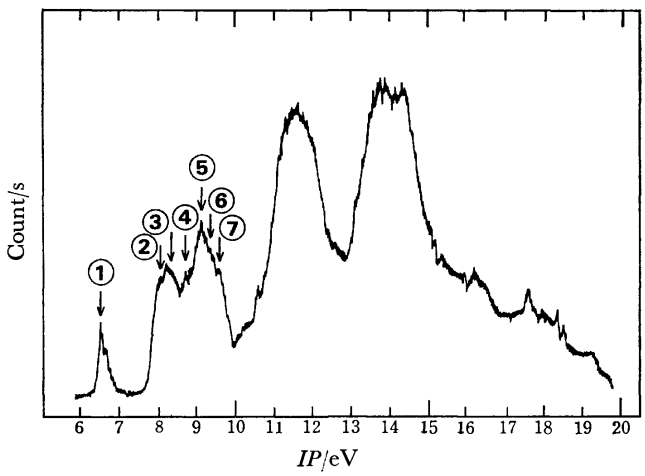

Fig. 1. Gas phase He I photoelectron spectrum of rubrene.

† Throughtout this paper 1 eV = 1.62×10^{-19} J.

†† The conformation of rubrene has not been determined experimentally.

Table 1. Vertical ionization potentials of rubrene and related compounds with assignment

Rubrene	Vertical *IP*/eV: Benzene[c]	Vertical *IP*/eV: Naphthacene[d]	ΔIP/eV[a]	Partial electron density[b]
① 6.52		6.97($2a_u\pi$)	0.45	0.148
② 8.0_5		8.41($3b_{1u}\pi$)	0.3_8	0.048
③ 8.3_0		8.41($2b_{2g}\pi$)	0.1_1	0.000
④ 8.7_5	9.24 ($1e_{1g}\pi_3$)			
⑤ 9.15	9.24 ($1e_{1g}\pi_2$)	9.56($1a_u\pi$)	0.41	0.044
⑥ 9.4		9.70($2b_{3g}\pi$)	0.3	0.034
⑦ 9.6		10.25($1b_{2g}\pi$)	0.6_5	0.112

a) The difference between the IP value of naphthacene and that of rubrene b) partial π-electron density due to the orbital of naphthacene at one of the substituted positions (5-, 6-, 11-, and 12-positions). c) Refs. 4 and 6. d) Ref. 5.

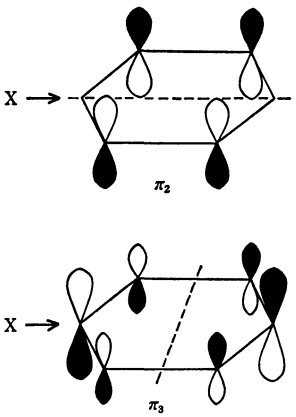

Fig. 2. The $1e_{1g}$ π-orbitals of benzene. X represents a substituent.

7 in Fig. 1. The 9.24 eV band of benzene has been assigned to the degenerate π_2 and π_3 orbitals.[6] At the point of substitution, the π_2 orbital has a node, while the π_3 has its maximum electron density (Fig. 2). Accordingly, on substitution, the π_2 orbital may be relatively unaffected, whereas the π_3 may have its energy lowered relative to the π_2. Thus, in Table 1 we assign the bands at 8.7_5 and 9.15 eV of rubrene to the π_3 and π_2 orbitals, respectively. This assignment is supported by the fact that the bands ascribable to the π_2 and π_3 orbitals are also found in the *IP* region 8.8—9.3 eV of the photoelectron spectrum of 5,10-diphenylanthracene.[7] Moreover, it has been observed that the bands corresponding to the 8.7_5 and 9.15 eV bands of rubrene remain in the photoelectron spectrum of a rubrene peroxide film (*cf.* Eq. 1).[3] Although the intensities of the bands ④ and ⑤ involving the ionization of four benzene rings are much stronger than those of the bands ⑥ and ⑦, they are not strong enough in comparison with the intensities of the bands ① to ③. The transmission coefficient ($\propto \Delta E/E$; E, the energy of photoelectrons) of the energy analyzer used may partly account for this effect.

When the naphthacene molecule is substituted by phenyl groups, similar effect as above can be expected; the shift of the π-orbital energy may become greater, the larger the partial π-electron density due to the orbital at the position of substitution.††† In Table 1 the differences between the *IP* values of naphthacene and those of rubrene (π-orbital energy shifts) are shown in comparison with the π-electron densities of naphthacene at one of the substituted positions (5-, 6-, 11-, and 12-positions). The electron densities were calculated on the basis of the Pariser-Parr-Pople method. It can be seen from Table 1 that the correlation of the *IP* shift with the π-electron density is satisfactory. This supports the present assignment of the bands in the lower *IP* region of the rubrene spectrum.

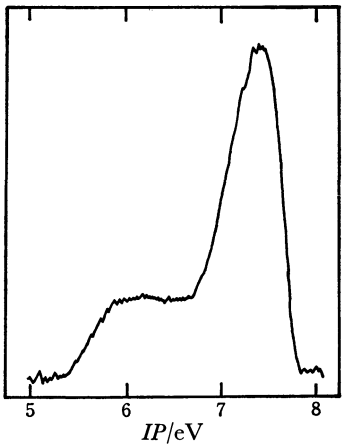

Fig. 3. Solid phase photoelectron spectrum of rubrene for $h\nu$=7.75 eV.

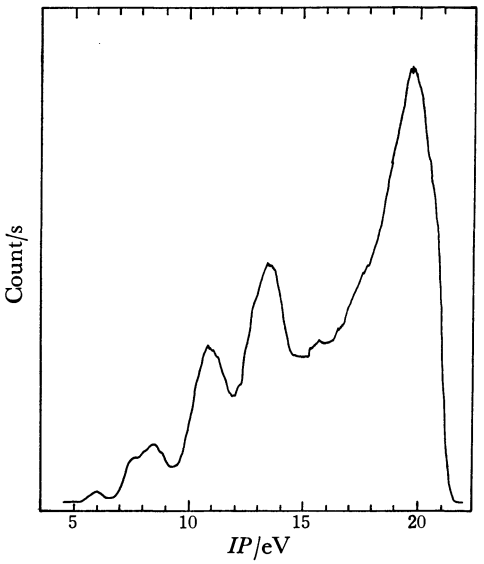

Fig. 4. Solid phase photoelectron spectrum of rubrene for $h\nu$=21.22 eV.

††† When a π LCAO MO, $\phi_i=\sum_k C_{ik}\chi_k$, is perturbed by a substituent X, the first-order perturbation energy of the MO is expressed by $\Delta E_i=\int \phi_i^* \hat{H}' \phi_i dv=\sum_{k,l} C_{ik}^* C_{il} H'_{kl}$, where $\hat{H}'$ is the perturbation operator and $H'_{kl}=\int \chi_k^* \hat{H}' \chi_l dv$. Let s be the number of the carbon atom substituted by X, H'_{ss} is considered to be much larger than the other H'_{kl}'s. Neglecting them, we have $\Delta E_i \fallingdotseq |C_{is}|^2 H'_{ss}$; the MO energy shift is proportional to the partial π-electron density $|C_{is}|^2$ due to ϕ_i at the position of substitution.

Solid Phase Spectrum. Figures 3 and 4 show the photoelectron spectra of solid rubrene for photon energies of 7.75 and 21.22 eV, respectively. The numbers on the abscissas indicate the ionization potential, which could be obtained by a spherical retarding type analyzer for $h\nu=7.75$ eV. In Fig. 3 only the first band located at 6.0 eV appears in the spectrum because of the small photon energy. The value of its adiabatic *IP* (threshold energy) is 5.3 eV. As can be seen from Figs. 1 and 4, the appearance of the solid phase spectrum for 21.22 eV is similar to that of the gas phase one except for a large peak due to inelastically scattered electrons. This behaviour means that the features of the solid phase spectrum are mostly associated with the valence bands. Further, it is found from Figs. 1 and 4 that the peak positions of the solid phase spectrum are lowered by *ca.* 0.6 eV relative to those of the gas. The shift corresponds to the polarization energy due to the molecular ion left in solid after a photoelectron is removed. In the case of naphthacene the polarization energy is observed to be around 1.1 eV,[8] which is about twice as large as that for rubrene. Being non-planar as a result of the steric hindrance of four phenyl groups, rubrene molecules are considered to be loosely packed in solid. This seems to be the reason for the small polarization energy for rubrene.‡

The authors are grateful to Dr. Koichi Ohno, the University of Tokyo, for his helpful discussion. The π-electron densities of the naphthacene molecule were calculated by him.

References

1) C. Moureu, C. Dufraisse, and P. M. Dean, *C. R. Acad. Sci.*, **182**, 1440 (1926).
2) "1,4-Cycloaddition Reactions," ed by J. Hamer, Academic, New York (1967), Chap. 10.
3) Y. Harada *et al.*, *Chem. Phys. Lett.*, to be published.
4) E. Lindholm, *Faraday Discuss. Chem. Soc.*, **54**, 200 (1973).
5) W. Schmidt, *J. Chem. Phys.*, **66**, 828 (1977).
6) D. W. Turner, C. Baker, A. D. Baker, and C. R. Brundle, "Molecular Photoelectron Spectroscopy," Wiley, London (1970).
7) R. Boschi, E. Clar, and W. Schmidt, *J. Chem. Phys.*, **60**, 4406 (1974).
8) K. Seki, H. Inokuchi, and Y. Harada, *Chem. Phys. Lett.*, **20**, 197 (1973).

‡ The values of the polarization energy for benzene, naphthalene and anthracene are 1.15, 1.1, and 1.2 eV, respectively (W. D. Grobman and E. E. Koch, "Photoemission in Solids I," ed by M. Cardona and L. Ley, Springer, Berlin (1978)). Thus the polarization energy is fairly constant for the aromatic molecules, benzene to naphthacene, which suggests that its value depends on the molecular packing in the crystal, irrespective of the size of the molecule.

High Resolution Infrared Spectrum of Chlorine Dioxide: The v_2 Fundamental Band

Yoshiaki HAMADA and Masamichi TSUBOI*

Faculty of Pharmaceutical Sciences, University of Tokyo, Hongo, Bunkyo-ku, Tokyo 113

(Received August 26, 1978)

Fourier transformed infrared absorption spectrum of gaseous ClO_2 has been obtained with the resolution of 0.06 cm^{-1}. The rotational structure of the bending fundamental band ($v_2=1\leftarrow0$) was analyzed. Rotational constants determined were in good agreement with previous microwave results. The band center was now fixed at 447.675 ± 0.030 cm^{-1}, and five centrifugal distortion constants for the $v_2=1$ state were also newly determined.

Extensive spectroscopic and kinetical studies have been started on photochemically produced molecules originating from chlorofluorocarbons, since it was disclosed that they are partially on charge of destruction of ozone in the upper atmosphere.[1] ClO_2 is one of the reaction products which appears in the final step in the Cl and O chain, and is considered to exist in the lower layer of the stratosphere, but has never been detected yet.[2]

It is thought to be important to study ClO_2 spectroscopically in the various regions of radiation in the laboratory system to give more detailed understanding of stratospheric reactions. Curl *et al.* have intensively studied the microwave spectrum, and determined a number of molecular parameters involving spin-rotation interaction constants.[3–8] Since infrared spectrum had first been observed by Bailey and Cassie,[9] some infrared works[10–12] were reported without any high resolution. The higher vibrational levels of the electronic ground state were mainly obtained by means of the electronic absorption spectrum[13] or fluorescence spectrum.[14]

We have recently observed the infrared spectrum by a Fourier transform spectrometer and partially by a diode laser spectrometer. This is a report of an analysis of the bending fundamental band ($v_2=1\leftarrow0$) in the 415—510 cm^{-1} region. 8 rotational transitions of $v_2=1$ state were observed in the microwave spectrum by Mariella and Curl.[8] The results of our infrared analysis will be compared with the microwave results.

Experimental

ClO_2 was prepared by the reaction of oxalic acid and potassium chlorate in dilute sulfuric acid at 60 °C.[15] The product was condensed in a dry ice bath, and then distilled in vacuum. The sample with the vapour pressure (about 1 mmHg) at dry ice temperature was introduced into a multiple reflection cell, whose optical path length was 10 m.

The spectrum was obtained by a Nicolet 7199 Fourier transform spectrometer. 128 scans of interferometer were accumulated (38 sec per scan) to construct an interferogram, and this was Fourier-transformed (it took about 30 min.) into an ordinary spectrum of 4000—400 cm^{-1} region. The maximum distance of the moving mirror is 8 cm, and by the use of Happ-Genzel apodization function to remove the ripple of the spectral curve the actual width (full width at half miximum) was found to reach 0.07 cm^{-1}. The peak separation of 0.05 cm^{-1} was found to be recognizable. To confirm the accuracy of the wavenumber scale, some of the atmospheric CO_2 and H_2O lines overlapped on the ClO_2 spectrum were compared with the standard spectral data.[16] The wavenumber precision was found to be better than ±0.02 cm^{-1}.

Analysis

Neglect of the Spin-Rotation Interaction. The spin-rotation constants for the $v_2=1$ state are known to be almost the same as those for the ground state.[8] In Fig. 1, the spin splitting patterns in the ground state are shown, on the basis of the following equations:

$$F_1 = \left\{\left[a-a_0\pm\frac{1}{2}b\delta_{1,K}\right]N(N+1)-3aK^2 + 9a^2K^2\left[1-\frac{K^2}{(N+1)^2}\right]\Big/4\bar{B}\right\}\Big/2(N+1), \quad (1)$$

$$F_2 = -\left\{\left[a-a_0\pm\frac{1}{2}b\delta_{1,K}\right]N(N+1)-3aK^2 + 9a^2K^2\left[1-\frac{K^2}{N^2}\right]\Big/4\bar{B}\right\}\Big/2N, \quad (2)$$

where

$$a_0 = -\frac{1}{3}(\varepsilon_{aa}+\varepsilon_{bb}+\varepsilon_{cc}),$$

$$a = -\frac{1}{6}(2\varepsilon_{aa}-\varepsilon_{bb}-\varepsilon_{cc}),$$

$$b = -\frac{1}{2}(\varepsilon_{bb}-\varepsilon_{cc}),$$

and

$$\bar{B} = \frac{1}{2}(B+C).$$

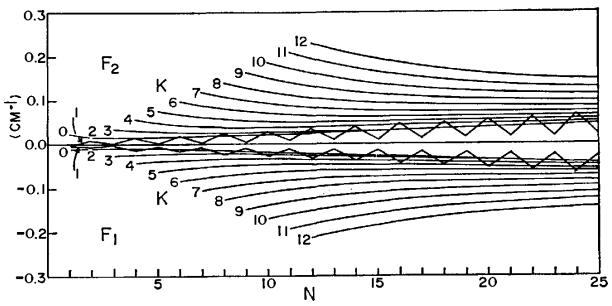

Fig. 1. Spin splitting pattern of $^{35}ClO_2$ in the ground state. Deviations, F_1 and F_2, caused by the spin rotation interaction, from pure rotational levels are shown. F_1 is for $N=J-S$, and F_2 for $N=J+S$, where N is the quantum number of rotational angular momentum, S is the quantum number of electron spin angular momentum, and J is the quantum number of total angular momentum. The calculations were made on Eqs. 1 and 2, where it was assumed that $a_0=0.017798$, $a=0.014262$, and $b=0.003679$ cm^{-1}.

ε's are spin-rotation interaction constants defined by

$$\mathcal{H}_{s.r.} = \varepsilon_{aa}N_aS_a + \varepsilon_{bb}N_bS_b + \varepsilon_{cc}N_cS_c, \quad (3)$$

where $\mathcal{H}_{s.r.}$ is the Hamiltonian for the spin-rotation interaction. As may easily be seen in Fig. 1, the spin-splitting should reach as much as 0.1 cm^{-1}, for lines of ^{P}R- and ^{R}P-branches if K is as high as 10 or so. These lines, however, have practically no intensity to be detected. The next largest spin-splitting is expected to occur in the lines of ^{R}Q- and ^{P}Q-branches, but these are so badly overlapped on one another. Absorption lines in the ^{R}R- and ^{P}P-branches are well separated from one another and intense enough. The spin-splittings for these lines are, however, always less than 0.05 cm^{-1} (our resolution). We, therefore, neglect the spin-rotation interaction in our present analysis.

Assignments of the Observed Peaks. The assignments were made on the basis of a comparison of the observed and calculated spectra. In the calculation, rotational matrices were trancated so as to include the elements with the K value which is higher by three than the maximum K we need. This makes the eigenvalues significant at least for 7 decimal digits. The ground state energy levels were calculated with the constants given by the microwave spectroscopy.[18] In an early stage of the analysis, the rotational constants A, B, and C of the $v_2=1$ state given by Mariella and Curl[8] were used to predict the J structures of low K sub-branches. Here essentially no single lines were detected, but most of the strong transitions were reasonably assigned to the observed peaks. In Fig. 2, part of the calculated spectrum is shown along with the observed spectrum.

At first sight, we can see ^{R}Q- and ^{P}Q-branches that make clusters: especially, $^{P}Q_K$ with $K\geqq 7$ give narrow and intense absorption peaks. These confirm the K-numbering. We can next recognize the strong absorptions formed by the turning head of the progressions in the $^{P}Q_2$, $^{P}Q_3$, $^{R}Q_1$, and $^{R}Q_2$ branches. The J-numbering for these progressions is of great merit for the following assignments in the low K region, because this allows us to fix the size of asymmetry, $B-C$. The absorption lines with $J=10$—30 in the $^{R}R_0$ and $^{P}R_1$ branches in the higher frequency region than the band center, and those in the $^{P}P_1$ and $^{R}P_0$ branches in the lower frequency region than the band center are the most intense ones in the whole band. They form progressions with nearly equal spacings.

Towards the high frequency end of the band, some of the ^{R}R branch lines are piled up to construct a progression with fairly regular spacing of about 0.6 cm^{-1}. From this we can determine the $\bar{B}'=1/2(B'+C')$ value. The J-numbering of this progression is rather straightforward, because we can use the ground state combination differences with the ^{P}P branch lines located in the other end of the band. The assignments are proceeded to reach reasonable intensity pattern.

We used the sample of ClO_2 with isotopes of natural abundance. This means that $^{35}ClO_2$ is mixed with $^{37}ClO_2$ with the ratio 3: 1. Hence difficulty was that not all absorption lines should necessarily be assigned to any transition of $^{35}ClO_2$. Also it happened that some fairly strong absorption was buried behind the $^{37}ClO_2$ absorption and made no apparent peak. No attempt was made to analyze $^{37}ClO_2$ spectrum in our present work.

Determination of the Molecular Constants. Upper state term values were calculated by adding the ground state rotational levels to the observed frequencies. The ground state rotational and centrifugal constants were fixed, as given in Table 1, in this work. Then, the term values were used for the least squares fitting to obtain the parameters of the following Hamiltonian:[17]

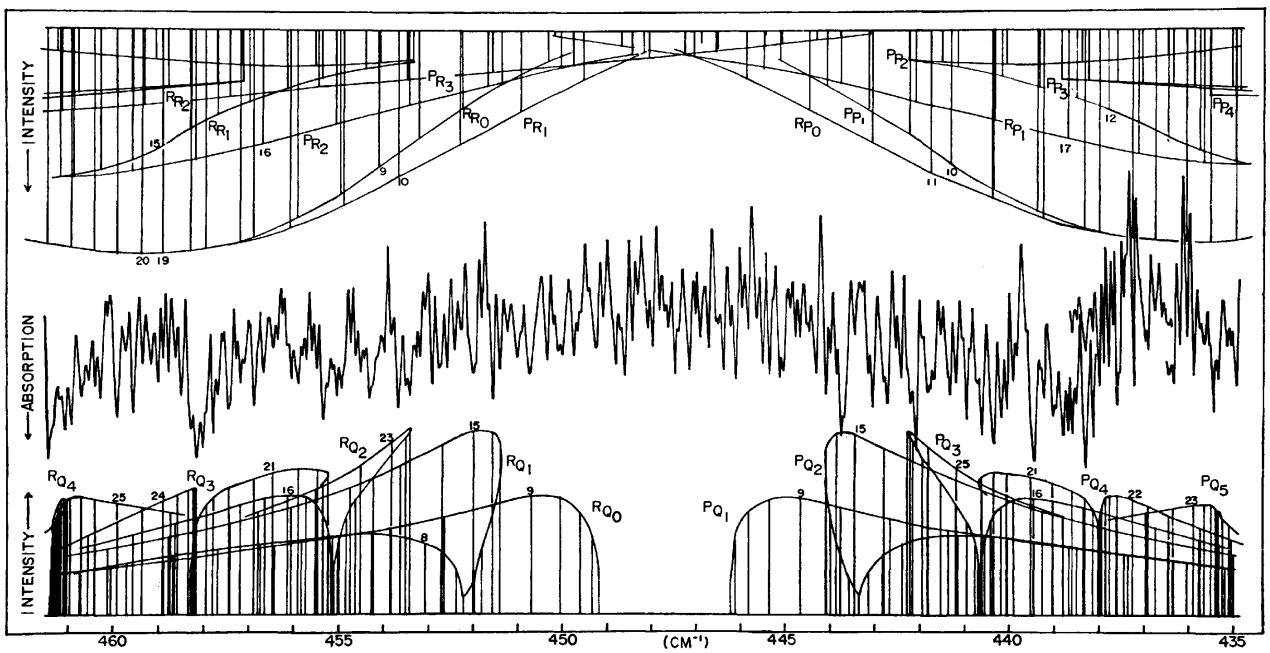

Fig. 2. The infrared absorption spectrum of ClO_2 in the 461—435 cm^{-1} region. Upper is the calculated pattern of R- and P- branches. Lower is the calculated pattern of Q-branches. The observed spectrum is shown in the middle.

Table 1. Molecular constants of $^{35}ClO_2$[a]

	(000)[b]	This work(010)	Previous data
ν_0		447.675(11)	447.3[c]/447.9[d]
A	1.737225(50)	1.77052(24)	1.77052(20)[e]
B	0.331982(7)	0.332021(59)	0.331682(60)
C	0.277993(6)	0.277215(46)	0.277202(60)
Δ_J	$2.335(334)\times10^{-7}$	$1.127(224)\times10^{-7}$	
Δ_{JK}	$-4.003(1000)\times10^{-6}$	$-2.714(222)\times10^{-6}$	
Δ_K	$6.905(300)\times10^{-5}$	$7.580(107)\times10^{-5}$	
δ_J	$7.67(100)\times10^{-8}$	$-2.714(222)\times10^{-9}$	
δ_K	$5.67(300)\times10^{-7}$	$-4.72(1365)\times10^{-6}$	

a) Units are in cm^{-1}. Uncertainties (3σ) in parentheses are in units of the last significant figure. b) The higher order centrifugal distortion constants $H_J=7\times10^{-7}$, $H_{JK}=2\times10^{-5}$, $H_{KJ}=-1\times10^{-4}$, $H_K=1\times10^{-3}$, $h_J=3\times10^{-7}$, $h_{JK}=-3\times10^{-4}$, in units of MHz, were used to calculate the ground state rotational energies, and the same values were assumed for $v_2=1$ state. c) Ref. 11 from IR spectrum. d) Ref. 11 from UV spectrum. e) Ref. 8.

$$\begin{aligned}\mathscr{H} = {} & \nu_0 + AP_a^2 + BP_b^2 + CP_c^2 - \Delta_J P^4 - \Delta_{JK}P^2P_a^2 \\ & - \Delta_K P_a^2 - 2\delta_J P^2(P_b^2-P_c^2) - \delta_K[P_a^2(P_b^2-P_c^2) \\ & + (P_b^2-P_c^2)P_a^2] + H_J P^6 + H_{JK}P^4P_a^2 + H_{KJ}P^2P_a^4 \\ & + H_K P_a^6 + 2h_J P^4(P_b^2-P_c^2) + h_{JK}P^2[P_a^2(P_b^2-P_c^2) \\ & + (P_b^2-P_c^2)P_a^2] + h_K[P_a^4(P_b^2-P_c^2) \\ & + (P_b^2-P_c^2)P_a^4]. \qquad (4)\end{aligned}$$

From totally 452 term values, ranging J up to 47, and K up to 15, first 9 parameters were determined. The parameters of P^6-term were fixed to the ground state values. There could not seen any systematic deviation in the residuals (observed-calculated) in the final least squares fit. Therefore, it has been concluded that the higher centrifugal distortion constants are not necessary to be included as variables.

Discussion

In Table 1, the final set of parameters are compared with the previous results. As described in the preceding chapter, the precision of the observed line position is better than ±0.02 cm^{-1}. Therefore, (in combination with the calculated error ±0.01 cm^{-1}), the standard error is estimated to be ±0.03 cm^{-1} for the band center.

The rotational constant B has a meaningful discrepancy between the microwave and our infrared analysis. This may be attributed to the fact that, in microwave analysis, Curl *et al.* assumed the same centrifugal distortion constants in $v_2=1$ state as in the ground state, and used only 4 rotational transitions of low J's of $K=0$ and 1 in their least squares fit.

As was pointed by Pliva and Telfair,[19] the term values of the upper state are strongly correlated with the ground state parameters. We should realize, therefore, that from an infrared term value analysis, such as what we have done in the present work, the differences ΔA, ΔB, ΔC, *etc.* of the parameters in the upper and ground states are determined rather than their absolute values of the parameters themselves. Even if the ground state parameters are revised in future, ΔA, ΔB, ΔC,···values fixed here will remain significant.

The authors wish to express their deep appreciation to Dr. S. Saëki and Dr. S. Kondo for their kindness in affording us their Fourier transform infrared facilities in the National Chemical Laboratory for Industry. Their thanks are also due to Dr. T. Nakagawa for his computer program in calculating the absorption intensities.

References

1) M. J. Molina and F. S. Rowland, *Nature*, **249**, 810 (1974).
2) T. Ogawa, *J. Met. Soc. Jpn.*, **54**, 294 (1976).
3) R. F. Curl, Jr., J. L. Kinsey, J. G. Baker, J. C. Baird, G. R. Bird, R. F. Heidelberg, T. M. Sugden, D. R. Jenkins, and C. N. Kenney, *Phys. Rev.*, **121**, 1119 (1961).
4) R. F. Curl, Jr., R. F. Heidelberg, and J. L. Kinsey, *Phys. Rev.*, **125**, 1993 (1962).
5) R. F. Curl, Jr., *J. Chem. Phys.*, **37**, 779 (1962).
6) M. G. Krishna Pillai and R. F. Curl, Jr., *J. Chem. Phys.*, **37**, 2921 (1962).
7) W. M. Tolles, J. L. Kinsey, R. F. Curl, and R. F. Heidelberg, *J. Chem. Phys.*, **37**, 927 (1962).
8) R. P. Mariella, Jr. and R. F. Curl, Jr., *J. Chem. Phys.*, **52**, 757 (1970).
9) C. P. Bailey and A. B. D. Cassie, *Proc. Roy. Soc. (London), Ser. A*, **137**, 622 (1932).
10) A. H. Nielsen and P. J. H. Wolts, *J. Chem. Phys.*, **20**, 1878 (1952).
11) A. W. Richardson, R. W. Redding, and J. C. D. Brand, *J. Mol. Spectrosc.*, **20**, 93 (1969).
12) A. W. Richardson, *J. Mol. Spectrosc.*, **35**, 43 (1970).
13) J. B. Coon and E. Ortiz, *J. Mol. Spectrosc.*, **1**, 81 (1957).
14) R. F. Curl, Jr., K. Abe, J. Bissinger, C. Bennett, and F. K. Tittel, *J. Mol. Spectrosc.*, **48**, 72 (1973).
15) G. Brauer, "Handbuch der Praeparativen Anorganischen Chemie," Ferdinand Enke, Publisher, Stuttgart (1960).
16) "IUPAC Table of Wavenumbers for the Calibration of Infrared Spectrometers," 2nd ed, ed by A. R. H. Cole, Pergamon Press, (1977).
17) J. K. G. Watson, *J. Chem. Phys.*, **46**, 1935 (1967).
18) The tentatively determined constants involving the P^6-term were kindly supplied by Drs. T. Tanaka and K. Tanaka; they newly added 21 rotational lines to Curl's 18 rotational lines.
19) J. Pliva and W. B. Telfair, *J. Mol. Spectrosc.*, **53**, 221 (1974).

Interdiffusion of Zinc Ions in Aluminium Cobalt(II) Oxide and Aluminium Nickel(II) Oxide

Kunihito KOUMOTO,* Takao MATSUBARA, Masasuke TAKATA, and Hiroaki YANAGIDA

Department of Industrial Chemistry, Faculty of Engineering, The University of Tokyo, Hongo, Bunkyo-ku, Tokyo 113

(Received October 5, 1978)

The interdiffusion coefficients $\tilde{D}$ of Zn^{2+} ions in aluminium cobalt(II) oxide (cobalt aluminate) and aluminium nickel(II) oxide (nickel aluminate) were measured. In the former $\tilde{D}$ is independent of the concentration of the composition-dependent cation vacancies, while in the latter it decreases with increase in the concentration of cation vacancies. The difference in the distribution of cations and cation vacancies in the spinel lattice has a great effect on the interdiffusion coefficients of Zn^{2+} ions. The results were interpreted by means of the vacancy mechanism for Co^{2+} and Ni^{2+} ions and the interstitial or interstitialcy mechanism for Zn^{2+} ions. The activation energy is independent of the concentration of Zn^{2+} ions or cation vacancies; 355 kJ mol^{-1} for cobalt aluminate and 364 kJ mol^{-1} for nickel aluminate.

The vaporization rate of ZnO from the spinel solid solution of the ZnO–CoO–Al_2O_3 system was more pronounced than from that of the ZnO–NiO–Al_2O_3 system above 1300 °C in air.[1] It was suggested that the diffusion of Zn^{2+} ions in the spinel phase might be a rate determining process during the course of vaporization of ZnO. Thus the measurements of the diffusivity of Zn^{2+} ions and its dependence on the concentration of the composition-dependent cation vacancies in aluminium cobalt(II) oxide (cobalt aluminate) and aluminium nickel(II) oxide (nickel aluminate) were undertaken in the present work.

When $(A_x^{2+}B_{1-x}^{2+})O\cdot M_2^{3+}O_3$ forms a solid solution of $(A_xB_{1-x})O\cdot nM_2O_3$ with M_2O_3, the concentration of the composition-dependent cation vacancies is $(n-1)/(9n+3)\times 100$ cation site percent, increasing with the increase of n up to the solubility limit.

Studies have been carried out on the ionic diffusion in spinels. However, most of them are concerned with perfect spinels having no composition-dependent cation vacancies. Only a few studies on the defective spinels have appeared. Ando and Oishi[2] reported that the self-diffusion coefficients of oxygen ions in $MgO\cdot 1.2Al_2O_3$ and $MgO\cdot 2.2Al_2O_3$ single crystal spinels are close to those in $MgO\cdot Al_2O_3$ spinel. Morkel and Schmalzried[3] found for various kinds of spinels that the self-diffusion coefficients of cations in perfect spinels differ from those in defective spinels. Dieckmann and Schmalzried[4] measured the dependence of self-diffusion coefficient of iron ions in magnetite on oxygen partial pressure and found that the diffusion mechanism changes with the change in P_{O_2}. Yamaguchi *et al.*[5] proposed a vacancy mechanism of Ni^{2+} ion diffusion in magnesium aluminate on the basis that the interdiffusion coefficient of Ni^{2+} ions increases in proportion to the increase in the concentration of the composition-dependent cation vacancies.

The dependence of interdiffusion coefficients of Zn^{2+} ions on the concentration of the composition-dependent cation vacancies was found to differ in the two systems investigated in the present study. The mechanism of cation diffusion is also discussed.

Experimental

Material. The spinel powders of compositions $(Zn_xCo_{1-x})O\cdot nAl_2O_3$ and $(Zn_xNi_{1-x})O\cdot nAl_2O_3$ ($x=0$, 0.2; $n=1.0$—1.2) were synthesized from basic zinc carbonate, basic cobalt carbonate, basic nickel carbonate, and gibbsite of reagent grade. The pellets, diam. 10 mm and thickness 2—4 mm, were obtained by hot-pressing the spinel powders in a carbon mold under the pressure 260 kg/cm^2 at 1000 °C for 2 h. The pellets were further sintered densely for 1—2 h at 1700 °C to give the relative density colse to that of a single crystal. They were polished with SiC abrasives and diamond paste, and the diameters and thicknesses were measured with a micrometer. The sintering degrees, apparent density/theoretical density, calculated for a cation vacancy model, were 80—85%.

Diffusion Measurements. Interdiffusion between pure polycrystalline cobalt aluminate (or nickel aluminate) ($x=0$) and the spinel solid solution containing Zn^{2+} ions ($x=0.2$) was studied, the concentration of the composition-dependent cation vacancies being the same in both compositions (n is equal). The diffusion couple, made by giving the polished surfaces an intimate contact, was interposed between alumina plates. Annealing was carried out in the air in a vertical tube furnace with a SiC heating element. Temperature was measured with a calibrated Pt–Pt 13% Rh thermocouple. Although ZnO vaporized from the diffusion couples during the course of annealing, its amount was almost negligible in the diffusional zone near the interface. Annealing was carried out at 1320—1540 °C over a period of 24—96 h. After annealing, the diffusion couple was embedded in epoxy resin and cut perpendicular to the diffusion interface with a diamond cutter. The cut surface was polished carefully with SiC grains and diamond paste and then coated with gold by vacuum sputtering. The specimens were mounted on the sample holder and analyzed by an electron probe microanalyzer. They were moved perpendicular to the diffusion interface at 50 μm/min while the electron beam was kept fixed; the intensity profile of Zn $K\alpha$ radiation was then obtained. The microprobe was calibrated using standard samples having compositions $(Zn_xCo_{1-x})O\cdot Al_2O_3$ and $(Zn_xNi_{1-x})O\cdot Al_2O_3$, where $x=0.05$, 0.1, and 0.2. The standards were mounted and polished following the procedure for the diffusion couples. The relative intensity of Zn $K\alpha$ radiation to that of Al $K\alpha$ radiation showed good linearity as regards the concentration of Zn^{2+} ions in both cases.

Results and Discussion

The intensity profile of Zn $K\alpha$ radiation obtained by electron microprobe analysis was smoothed so as to average the statistical fluctuations. The curve thus obtained was considered to represent the concentration distribution of Zn^{2+} ions in the diffusion couple as the intensity of Al $K\alpha$ radiation was constant throughout the diffusional zone. A typical profile is shown in Fig. 1. The concentration curves were not apparently

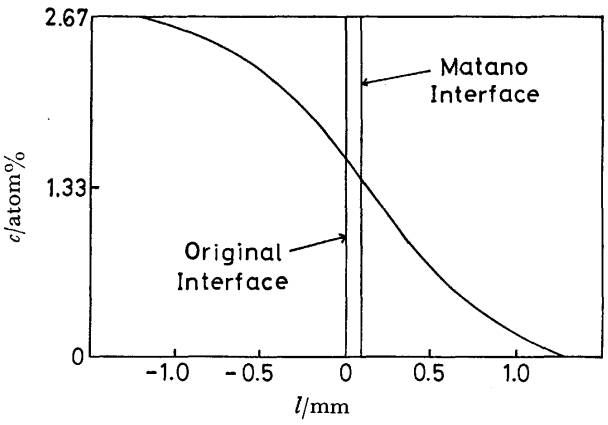

Fig. 1. Concentration profile of Zn^{2+} ions in $CoO \cdot 1.1\text{-}Al_2O_3$ annealed at 1540 °C for 48 h.

symmetrical as regards the original interface, and the Matano interface in all cases was determined graphically. The concentration-dependent diffusion coefficients were calculated by the Boltzmann-Matano solution:

$$D(c') = (-1/2t)(dx/dc)_{c=c'} \int_0^{c'} x dc,$$

where t is the annealing time, x the distance, and c, c' the concentration of Zn^{2+} ions. When Matano's method is used, the molar volume change caused by diffusion should be taken into acount as pointed out by Prager[6] and Balluffi.[7] In the present diffusion couples, however, the maximum molar volume changes due to the diffusion of Zn^{2+} ions were 0.14 and 0.48% for cobalt aluminate and nickel aluminate, respectively, as calculated from the lattice constants reported by Romeijn.[8] The changes were not significant and the effect of the molar volume change on diffusion coefficients was negligible.

Cobalt Aluminate. Interdiffusion coefficients $\tilde{D}$ of Zn^{2+} ions in cobalt aluminate are plotted against the concentration of Zn^{2+} ions in Fig. 2. The coefficient decreased with the increase in the concentration of Zn^{2+} ions in the perfect spinel which has no composition-dependent cation vacancies, while that of Zn^{2+} ions in the defective spinels turned out to be approximately independent of the concentration of Zn^{2+} ions. The value remained almost unchanged with the change in the concentration of cation vacancies.

Morkel and Schmalzried[3] found that the self-diffusion coefficient of Co^{2+} ions in $Co_{0.85}Al_{2.10}O_4$ ($\fallingdotseq CoO \cdot 1.235\text{-}Al_2O_3$) is larger than that in $CoAl_2O_4$ ($=CoO \cdot Al_2O_3$). This suggests the vacancy mechanism for the diffusion of Co^{2+} ions in cobalt aluminate. If the diffusion of Zn^{2+} ions were also to occur by the vacancy mechanism in

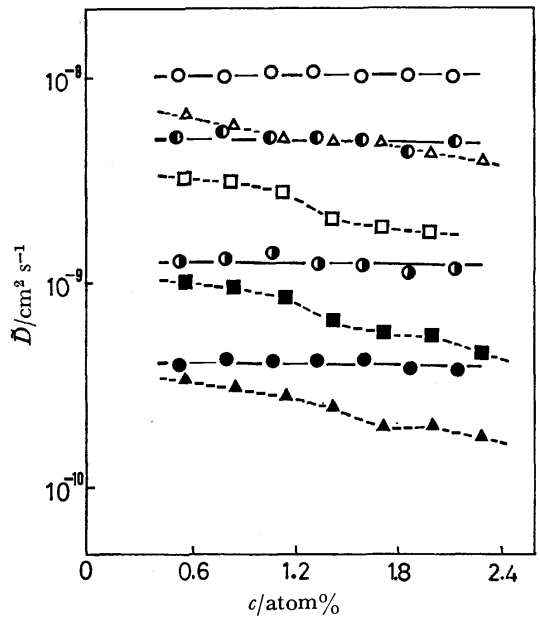

Fig. 2. Interdiffusion coefficients of Zn^{2+} ions in $CoO \cdot nAl_2O_3$ as a function of the concentration of Zn^{2+} ions. $n=1.0$: △ (1540 °C), □ (1470 °C), ■ (1400 °C), ▲ (1320 °C); $n=1.1$: ○ (1540 °C), ◐ (1470 °C), ◑ (1400 °C), ● (1320 °C).

cobalt aluminate, the interdiffusion coefficients would increase with the increase in the concentration of the composition-dependent cation vacancies, but this was not the case.

According to Darken's binary diffusion equation, when two kinds of ions interdiffuse, the effect of diffusion of the first ions on the interdiffusion coefficient increases with the increase in the concentration of the second ions. Thus, the diffusion of Zn^{2+} ions comes to play an important role as the concentration of Zn^{2+} ions decreases

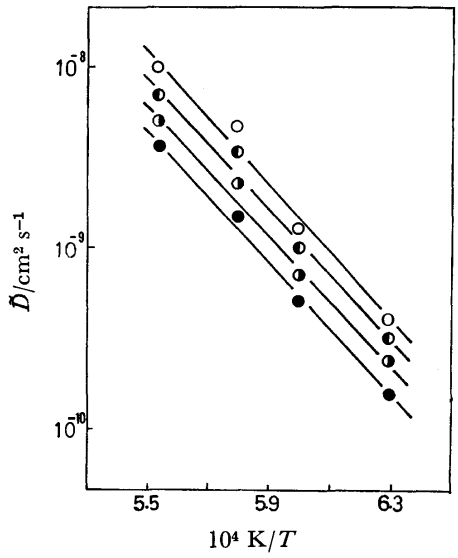

Fig. 3. Arrhenius plots of interdiffusion coefficients of Zn^{2+} ions for $CoO \cdot nAl_2O_3$.
○: $\varepsilon_{Zn} < 2.5$ ($n=1.1$, 1.2), ◐: $c_{Zn}=0.0$ ($n=1.0$), ◑: $c_{Zn}=1.0$ ($n=1.0$), ●: $c_{Zn}=2.0$ ($n=1,0$), where c_{Zn} is the concentration of Zn^{2+} ions in atomic percent.

(the concentration of Co^{2+} ions increases). The so-called impurity diffusion coefficients of Zn^{2+} ions for both perfect and defective spinels obtained by extrapolating interdiffusion coefficients to zero concentration of Zn^{2+} ions were the same within experimental errors. The Arrhenius plot shown in Fig. 3 is expressed as follows:

$$D_i = 2.1 \times 10^2 \exp(-355000/RT) \quad (cm^2/s),$$

where D_i is the impurity diffusion coefficient, R the molar gas constant, and T the absolute temperature. These results give no evidence for the vacancy mechanism of Zn^{2+} ion diffusion.

In general, the spinel structure consists of cubic close-packed oxygen ions with 1/8 of tetrahedral and 1/2 of octahedral interstices occupied by cations. The rest of the interstices are vacant as no-cation sites or interstitial sites. The structural formula for $(Zn_{0.5}Co_{0.5})O \cdot 2Al_2O_3$ spinel can be written as[1]

$$[Zn_{0.28}Co_{0.28}Al_{0.44}](Al_{1.86}\square_{0.14})O_4,$$

where $\square$ denotes cation vacancies, and [ ] and ( ) tetrahedral and octahedral sites, respectively. Thus, even though the concentration of the composition-dependent cation vacancies increases as $n>1.0$, the cation vacancies tend to occupy octahedral sites having little influence on the diffusion of Zn^{2+} ions on tetrahedral sites. The above formula represents only approximate distribution of cations and cation vacancies in the spinel lattice. There still remains the possibility of the existence of interstitial cations (especially Zn^{2+} ions) and octahedral Co^{2+} ions which could not be detected by the X-ray diffraction method. Consequently, the present result in which the interdiffusion coefficient is essentially independent of the concentration of the composition-dependent cation vacancies in cobalt aluminate could be explained on the assumption that Zn^{2+} ions diffuse through the spinel lattice *via* interstitial sites and not *via* octahedral sites.

Nickel Aluminate. Interdiffusion coefficients $\tilde{D}$ of Zn^{2+} ions in nickel aluminate obtained at 1470 °C are plotted as a function of the concentration of Zn^{2+} ions in Fig. 4. The interdiffusion coefficient is strongly dependent on the concentration of Zn^{2+} ions in each spinel with different concentration of cation vacancies. This is also the case for other annealing temperatures.

As is clear from Fig. 4, the interdiffusion coefficient decreases with increase in the concentration of the composition-dependent cation vacancies within the range of at least 1.45 cation site percent (corresponding to $n=1.2$) at low concentration of Zn^{2+} ions. It should be considered, as Yamaguchi *et al.*[5] reported, that the diffusion of Ni^{2+} ions in nickel aluminate occurs by the vacancy mechanism. The fact that $\tilde{D}$ increases with the increase in the concentration of Zn^{2+} ions in the cases of $n=1.15$ and 1.2 may support this suggestion. However, the present results deny the vacancy mechanism for the diffusion of Zn^{2+} ions in nickel aluminate.

The approximate structural formula of $(Zn_{0.5}Ni_{0.5})O \cdot 2Al_2O_3$ spinel is given by[1]

$$[Zn_{0.28}Ni_{0.14}Al_{0.44}\square_{0.14}](Ni_{0.14}Al_{1.86})O_4.$$

This indicates that both Zn^{2+} ions and cation vacancies prefer tetrahedral sites in nickel aluminate. Thus, when the concentration of the composition-dependent cation vacancies increases in nickel aluminate, they predominantly occupy tetrahedral sites causing the decrease in the interdiffusion coefficient of Zn^{2+} ions on tetrahedral sites. The decrease in the interdiffusion coefficient of Zn^{2+} ions should correspond to the decrease in the concentration of interstitial Zn^{2+} ions which are considered to be mobile as compared to those at normal cation sites, if the interstitial or interstitialcy mechanism for the diffusion of Zn^{2+} ions is assumed.

The activation energy obtained from the Arrhenius plots in Fig. 5 is nearly independent of the concentration of Zn^{2+} ions and the composition-dependent cation

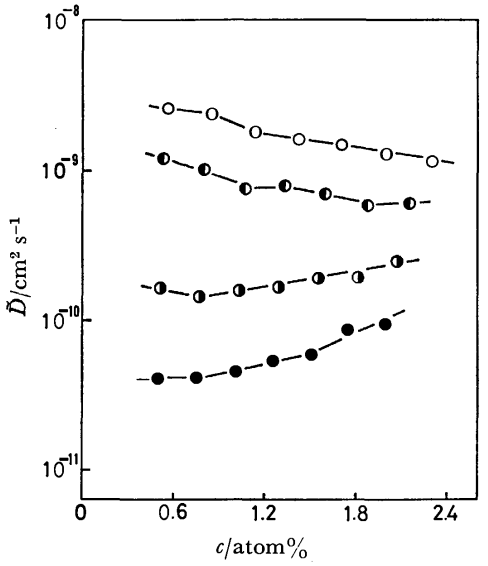

Fig. 4. Interdiffusion coefficients of Zn^{2+} ions in $NiO \cdot nAl_2O_3$ at 1470 °C as a function of the concentration of Zn^{2+} ions.
○: $n=1.0$, ◐: $n=1.1$, ◑: $n=1.15$, ●: $n=1.2$.

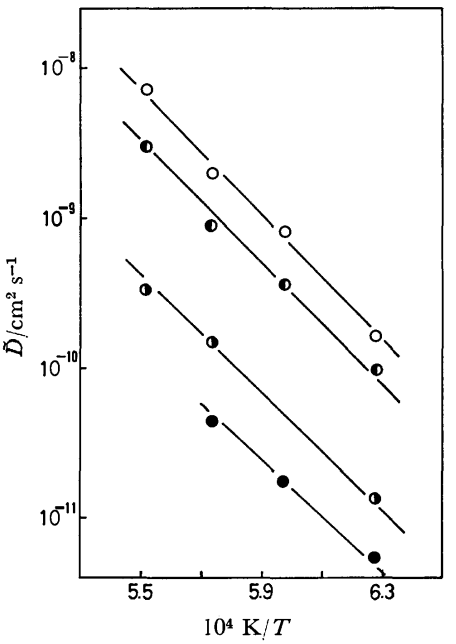

Fig. 5. Arrhenius plots of interdiffusion coefficients of Zn^{2+} ions for $NiO \cdot nAl_2O_3$.
○: $n=1.0$, ◐: $n=1.1$, ◑: $n=1.15$, ●: $n=1.2$.

vacancies, the average value calculated being 364 kJ mol^{-1}.

Contribution of Grain Boundary Diffusion. The contribution of grain boundary diffusion to the diffusion coefficients should be considered when polycrystalline specimens are used for diffusion measurements. The contribution can be detected by measuring the difference in diffusion coefficients between a single crystal and a polycrystal in an experiment on the coupling of two crystals. By this method, Yamaguchi *et al.*[5] found no contribution for the diffusion of Ni^{2+} ions in magnesium aluminate. In the present work, it was difficult to obtain single crystals of aluminates containing Zn^{2+} ions because of the high vapor pressure of ZnO at high temperatures, so that the contribution of grain boundary diffusion could not be made clear.

Enhancement of anion diffusion at grain boundaries has been reported for Al_2O_3,[9] MgO,[10] and alkali halides.[11] However, no evidence has been found for grain boundary enhancement of cation diffusion in spinels. The contribution of grain boundary diffusion was not taken into consideration in interpreting the present results.

The authors wish to thank Messrs. T. Ohta and T. Akiba of Chichibu Cement Co., Ltd. for their assistance in the electron microprobe analysis.

1) K. Koumoto and H. Yanagida, *Yogyo Kyokai Shi*, **85**, 193 (1977).
2) K. Ando and Y. Oishi, *J. Chem. Phys.*, **61**, 625 (1974).
3) A. Morkel and H. Schmalzried, *Z. Phys. Chem. (Frankfurt am Main)*, **Bd. 32**, S. 76 (1962).
4) R. Dieckmann and H. Schmalzried, *Ber. Bunsenges. Phys. Chem.*, **81**, 344 (1977).
5) G. Yamaguchi, M. Nakano, and M. Tosaki, *Bull. Chem. Soc. Jpn.*, **42**, 2801 (1969).
6) S. Prager, *J. Chem. Phys.*, **21**, 1344 (1953).
7) R. W. Balluffi, *Acta Metall.*, **8**, 871 (1960).
8) F. C. Romeijn, *Philips Res. Rep.*, **8**, 321 (1953).
9) Y. Oishi and W. D. Kingery, *J. Chem. Phys.*, **33**, 480 (1960).
10) H. Hashimoto, M. Hama, and S. Shirasaki, *J. Appl. Phys.*, **43**, 4828 (1972).
11) J. F. Laurent and Jacques Benard, *C. R. Acad. Sci. (Paris)*, **241**, 1204 (1955).

The Crystal and Molecular Structure of Dichloro[1,3-bis(di-*t*-butylphosphino)propane]platinum(II) Chlorobenzene Solvate

Masahiro HARADA, Yasushi KAI, Noritake YASUOKA, and Nobutami KASAI*

Department of Applied Chemistry, Faculty of Engineering, Osaka University, Yamadakami, Suita, Osaka 565

(Received September 9, 1978)

X-Ray crystal structure analysis of $[PtCl_2\{(t\text{-}Bu)_2P(CH_2)_3P(t\text{-}Bu)_2\}]\cdot 0.5C_6H_5Cl$ has been carried out. Crystals belong to monoclinic system: $a=11.532(2)$, $b=14.984(5)$, $c=16.455(4)$ Å, $\beta=106.96(2)°$, space group $P2_1/c$ with $Z=4$. The structure, solved by the heavy-atom method, has been refined anisotropically by least-squares procedure to $R=0.056$ for 5019 non-zero reflections. The coordination around the platinum atom is approximately square-planar, however, it showed a slight deviation toward the tetrahedral geometry; Pt–P=2.281(3) and 2.282(3), Pt–Cl=2.359(3) and 2.362(3) Å, P–Pt–P=99.05(9) and Cl–Pt–Cl=83.18(11)°.

In co-operation with the studies on a series of bis(di-substituted phosphino)alkaneplatinum complexes by Sei Otsuka and his coworkers,[1] we have carried out the determination of X-ray molecular structures of these complexes. Recently, we have reported the crystal and molecular structures of dichloro[1,2-bis(di-*t*-butylphosphino)ethane]platinum(II) (**1**) and its chlorobenzene solvate.[2] We report here the crystal structure analysis of dichloro[1,3-bis(di-*t*-butylphosphino)propane]platinum(II) (**2**) chlorobenzene solvate.

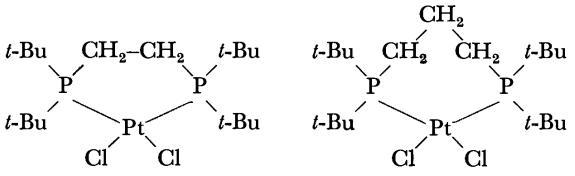

Experimental

Crystals of $[PtCl_2\{(t\text{-}Bu)_2P(CH_2)_3P(t\text{-}Bu)_2\}]\cdot 0.5C_6H_5Cl$ were kindly provided by Professor Sei Otsuka and co-workers. The space group was uniquely determined as $P2_1/c$ from the preliminary Weissenberg photographs. Accurate unit-cell dimensions were determined at 20 °C by a least-squares fit of 2θ values of high order reflections measured on a Rigaku automated, four-circle diffractometer. The crystal data are given in Table 1.

TABLE 1. CRYSTAL DATA OF $[PtCl_2(\{(t\text{-}Bu)_2PC(H_2)P(t\text{-}Bu)_2\})]\cdot 0.5C_6H_5Cl$

$C_{14}H_{26.5}P_2Cl_{2.5}Pd$	*F.W.* 654.77
Monoclinic	Space group $P2_1/c$
$a=11.532(2)$ Å	$D=1.61$ g cm^{-3}
$b=14.984(5)$	$Z=4$
$c=16.455(4)$	$D=1.599$ g cm^{-3}
$\beta=106.96(2)°$	μ(Mo $K\alpha$)=57.94 cm^{-1}
$U=2719.8(12)$ Å^3	

A crystal with dimensions of *ca.* $0.2\times 0.2\times 0.3$ mm, sealed in a thin-walled glass capillary tube, was mounted on the diffractometer for the intensity data collection. Graphite-monochromatized Mo $K\alpha$ radiation was used. The θ—2θ scan technique was employed. The integrated intensity was determined by scanning over the peak at a rate of 4° min^{-1}, and substracting the background obtained by averaging the two values measured for 6 s at both ends of a scan. The scan width was calculated by the equation: $\Delta(2\theta)=(2.4+0.69\tan\theta_c)°$, where θ_c is the calculated value of the Bragg angle using λ (Mo $K\alpha_1$)=0.70926 Å. The starting angle of the scan was $(2\theta_c-1.2)°$. Usual Lorentz and polarization corrections were applied, but absorption correction was ignored. Throughout the data collection four standard reflections were measured after every 60 reflections, which remained constant within the error limits. A total of 5936 independent reflections was measured out to a 2θ value of 54°, and of these 917 reflections were less than $3\sigma(F)$ and they were recorded as $F_o=0$.

Solution and Refinement of the Structure

The structure was solved by the heavy atom method and was refined by the block-diagonal least-squares procedure. HBLS V program was used,[3] the function minimized being $\sum w(|F_o|-k|F_c|)^2$. Starting from isotropic temperature factors, anisotropic thermal parameters were introduced in the refinement. When the R value decreased to 0.086 the Fourier map calculated revealed an existence of the chlorobenzene molecule disordered near a crystallographic center of symmetry, and they were then included in the refinement. How-

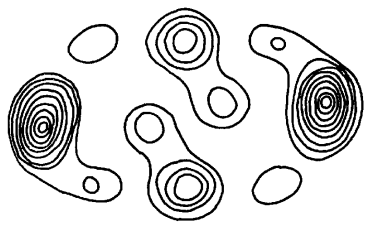

(a)

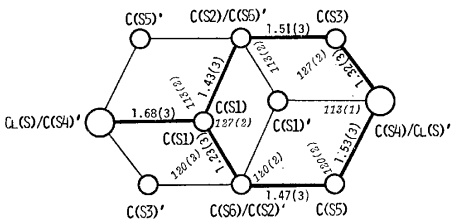

(b)

Fig. 1. Disordered structure of chlorobenzene (a) Electron density map. (b) A pair of disoldered half molecules.

TABLE 2. ATOMIC FRACTIONAL COORDINATES AND THERMAL PARAMETERS ALONG WITH THEIR ESTIMATED STANDARD DEVIATIONS IN PARENTHESES

Anisotropic temperature factors are expressed in the form: $\exp[-(\beta_{11}h^2+\beta_{22}k^2+\beta_{33}l^2+\beta_{12}hk+\beta_{13}hl+\beta_{23}kl)]$.

Atom	x	y	z	β_{11}	β_{22}	β_{33}	β_{12}	β_{13}	β_{23}
Pt	0.45637(3)	0.18692(2)	0.24936(2)	0.00567(2)	0.00346(1)	0.002841(13)	0.00059(3)	0.00189(3)	0.00180(2)
Cl(1)	0.3692(2)	0.1125(2)	0.3435(2)	0.0095(2)	0.00612(15)	0.00496(12)	0.0010(3)	0.0059(3)	0.0049(2)
Cl(2)	0.6166(2)	0.0851(2)	0.3039(2)	0.0079(2)	0.00516(13)	0.0067(1)	0.0038(3)	0.0040(3)	0.0049(2)
P(1)	0.2785(2)	0.2609(2)	0.19134(15)	0.0058(2)	0.00452(12)	0.00314(9)	0.0009(2)	0.0021(2)	0.0025(2)
P(2)	0.5758(2)	0.2610(2)	0.18284(15)	0.0059(2)	0.00387(11)	0.00336(9)	0.0006(2)	0.0032(2)	0.0016(2)
C(1)	0.2843(9)	0.3507 8)	0.1152(7)	0.0078(9)	0.0062(6)	0.0043(5)	0.0040(12)	0.0042(10)	0.0056(9)
C(2)	0.3725(10)	0.3387(9)	0.0646(7)	0.0097(10)	0.0073(7)	0.0040(5)	0.0019(14)	0.0040(11)	0.0040(9)
C(3)	0.5034(9)	0.3562(7)	0.1153(7)	0.0075(8)	0.0054(5)	0.0052(5)	0.0011(11)	0.0058(11)	0.0062(9)
C(10)	0.1574(9)	0.1817(8)	0.1241(7)	0.0065(8)	0.0070(7)	0.0044(5)	0.0015(12)	−0.0001(10)	0.0021(9)
C(11)	0.0359(11)	0.2296(11)	0.0794(11)	0.0077(11)	0.0081(9)	0.0099(10)	−0.003(2)	−0.004(2)	0.005(2)
C(12)	0.213(2)	0.1365(14)	0.0567(10)	0.020(2)	0.0145(15)	0.0062(8)	−0.017(3)	0.010(2)	−0.011(2)
C(13)	0.1278(13)	0.1019(9)	0.1745(9)	0.016(2)	0.0063(7)	0.0059(7)	−0.005(2)	0.001(2)	0.0033(11)
C(20)	0.2175(9)	0.3260(7)	0.2689(7)	0.0080(9)	0.0058(6)	0.0043(5)	0.0034(11)	0.0066(11)	0.0021(8)
C(21)	0.1365(10)	0.4050(8)	0.2284(8)	0.0091(10)	0.0053(6)	0.0068(7)	0.0046(12)	0.0048(13)	0.0022(10)
C(22)	0.3302(10)	0.3671(9)	0.3366(8)	0.0098(11)	0.0065(7)	0.0054(6)	0.0010(14)	0.0025(13)	−0.0004(10)
C(23)	0.1444(12)	0.2682(9)	0.3149(9)	0.0130(13)	0.0068(7)	0.0079(8)	0.001(2)	0.014(2)	0.0045(12)
C(30)	0.7022(9)	0.3233(7)	0.2627(7)	0.0067(8)	0.0047(5)	0.0052(5)	−0.0008(10)	0.0038(10)	0.0015(8)
C(31)	0.7799(11)	0.3773(8)	0.2171(8)	0.0108(11)	0.0063(7)	0.0065(7)	−0.0063(14)	0.0072(14)	0.0007(11)
C(32)	0.6435(10)	0.3876(8)	0.3120(8)	0.0087(10)	0.0054(6)	0.0068(6)	0.0001(12)	0.0056(13)	−0.0019(10)
C(33)	0.7877(10)	0.2644(8)	0.3308(7)	0.0092(10)	0.0054(6)	0.0049(5)	0.0004(12)	0.0000(12)	0.0002(9)
C(40)	0.6356(10)	0.1878(7)	0.1086(8)	0.0095(10)	0.0053(6)	0.0053(5)	0.0020(12)	0.0061(12)	0.0008(9)
C(41)	0.6556(14)	0.2409(10)	0.0334(8)	0.018(2)	0.0088(9)	0.0047(6)	0.003(2)	0.012(2)	0.0012(12)
C(42)	0.5402(11)	0.1136(8)	0.0726(8)	0.0115(12)	0.0061(7)	0.0060(6)	−0.0034(15)	0.0068(14)	−0.0038(11)
C(43)	0.7574(11)	0.1423(8)	0.1549(9)	0.0107(11)	0.0058(7)	0.0075(7)	0.0042(14)	0.009(2)	−0.0011(11)
C(S1)	0.976(2)	−0.0136(15)	0.5247(11)	0.009(2)	0.0059(11)	0.0026(7)	−0.005(2)	0.001(2)	−0.0009(14)
C(S3)	1.007(2)	0.073(2)	0.4075(14)	0.012(2)	0.0051(11)	0.0037(9)	0.002(3)	0.000(2)	−0.001(2)
C(S5)	1.157(2)	−0.0281(14)	0.4872(15)	0.007(2)	0.0050(11)	0.0061(12)	0.002(2)	0.002(2)	−0.005(2)
C(S2)	0.9251(11)	0.0517(8)	0.4618(7)	0.0129(13)	0.0048(6)	0.0048(5)	0.0006(14)	0.0018(13)	−0.0013(9)
Cl(S)/C(S4′)	1.1146(6)	0.0376(5)	0.4136(4)	0.0176(7)	0.110(4)	0.0062(3)	−0.0127(9)	0.0114(8)	−0.0058(6)

ever, peaks assigned for Cl(S), C(S2), C(S4), and C(S6) (or C(S4)′, C(S6)′, Cl(S)′, and C(S2)′) could not be resolved (Fig. 1), and the unresolved Cl(S)/C(S4)′ (or C(S4)/Cl(S)′) and C(S2)/C(S6)′ (or C(S6)/C(S2)′) atoms were treated as peaks of a hypothetic (Cl+C)/2 and a single carbon atoms, respectively.

The final R value is 0.080 (0.056 for non-zero reflections). The weighting scheme employed was: $w=(\sigma(F)^2+0.03289|F_o|+0.00159|F_o|^2)^{-1}$ for $|F_o|>0$ and $w=0.06036$ for $|F_o|=0$. The atomic scattering factors used were those of neutral atoms given in International Tables for X-Ray Crystallography, Vol. IV,[4] and those for the hypothetic (Cl+C)/2 atom were assumed as the mean value of those for Cl and C. The effect of the anomalous dispersion of Pt, Cl, and P atoms was included in the calculation: the values of $\Delta f'$ and $\Delta f''$ being also taken from the International Tables for X-Ray Crystallography.[5]

The final positional and thermal parameters are listed in Table 2.†

Results and Discussion

Molecular Structure. A stereoscopic drawing of the molecule is given in Fig. 2. Bond lengths and bond angles are listed in Table 3. Selected bond lengths and

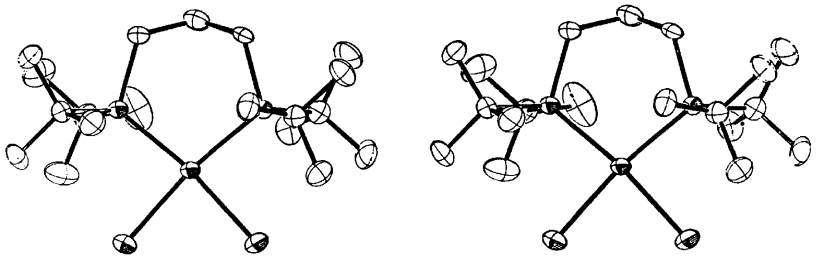

Fig. 2. Stereoscopic drawing of $[PtCl_2\{(t\text{-}Bu)_2P(CH_2)_3P(t\text{-}Bu)_2\}]$.

† The table of observed and calculated structure factors is kept as Document No. 7910 at the Chemical Society of Japan.

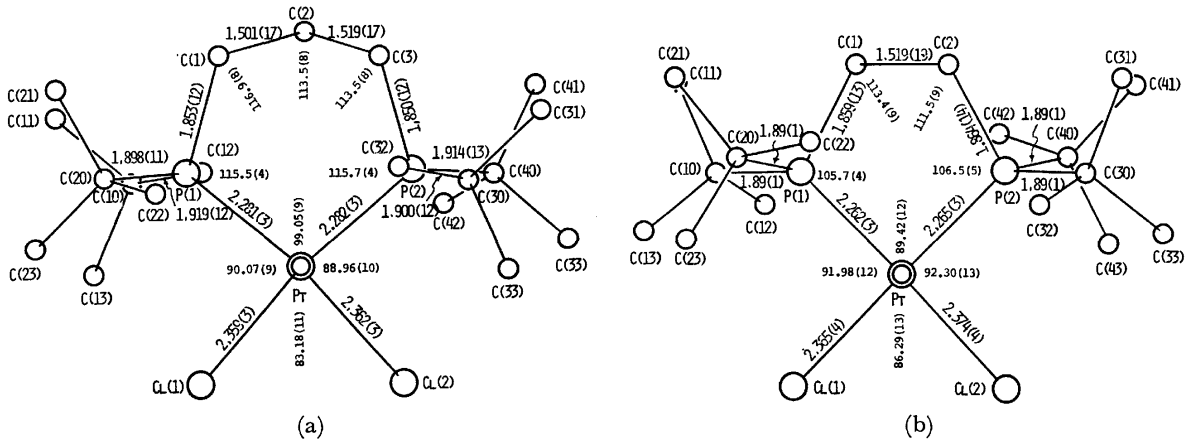

Fig. 3. Selected bond lengths and bond angles in (a) $[PtCl_2\{(t\text{-}Bu)_2P(CH_2)_3P(t\text{-}Bu)_2\}]$ compared with those in (b) $[PtCl_2\{(t\text{-}Bu)_2P(CH_2)_2P(t\text{-}Bu)_2\}]$.

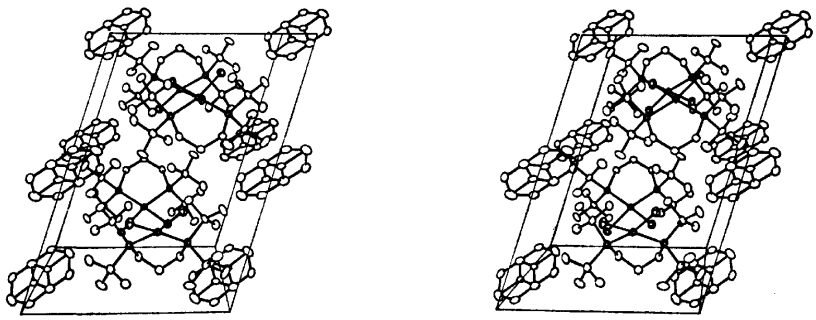

Fig. 4. Stereoscopic drawing of molecular packing in the unit cell. Disordered chlorobenzene molecules are shown.

bond angles are compared with those of **1**[2] in Fig. 3.

The co-ordination around the platinum atom can be described as approximately square-planar, however, the remarkable feature is that, different from **1**, there observed a slight distortion towards the tetrahedral geometry (Table 4). The dihedral angle between two planes defined by P(1), Pt, and P(2) and Cl(1), Pt, and Cl(2) is 12.0°.

The Pt–P bond lengths [2.281(3) and 2.282(2) Å] are significantly longer, whereas the Pt–Cl bond lengths [2.359(3) and 2.362(3) Å] are slightly shorter than those observed in **1** (Fig. 3). The shortening of the Pt–Cl lengths in the present complex indicates that the *trans*-influence of the phosphorus atoms is somewhat less than that in **1** because of the distortion of the $5d6s6p^2$ hybrid orbitals of the platinum atom.[6]

The P(1)–Pt–P(2) angle [99.05(9)°] is considerably greater than the corresponding angle in **1** [89.42(2)°], and other three angles around the platinum atom are smaller than the corresponding angles in **1**. This widening of the P–Pt–P angle in the present complex is probably due to an increased number of methylene groups in bis(di-*t*-butylphosphino)alkane ligand, which results in a distortion of dsp^2 hybrid orbitals of the platinum atom. Similar coordination geometry is observed in $[cis\text{-}PtCl_2(PMe_3)_2]$,[7] in which there seems to exist a steric repulsion between *cis*-PMe_3 groups.

As is found in **1** two P–C(CH_2) bond lengths [1.853(12) and 1.850(11) Å] are shorter than four P–C(*t*-Bu) bonds [1.919(12), 1.898(11), 1.900(12) and 1.914(13) Å].

The Pt–P–C(CH_2) angles [115.5(4) and 115.7(4)°] are about 10° larger than the corresponding angles in **1**. This is also probably affected by the increased number of methylene groups.

In the central propane moiety, the C(1)–C(2) and C(2)–C(3) bonds [1.50(2) and 1.52(2) Å] have normal single bond length, and bond angles around the C(1), C(2), and C(3) show slight deviations from the tetrahedral angle, however these are not significant except the P(1)–C(1)–C(2) [116.9(8)°]. The conformations about the C(1)–C(2) and C(2)–C(3) bonds are both nearly gauche. The torsion angles P(1)–C(1)–C(2)–C(3) and P(2)–C(3)–C(2)–C(1) are −75.7 and 80.3° respectively. The displacements of three methylene carbon atoms, C(1), C(2), and C(3) from the plane defined by Pt, P(1), and P(2) are 0.01, −0.67, and 0.13 Å, respectively.

Bond lengths and bond angles in *t*-butyl groups are normal values [1.55 Å and 109.4°]. Two *t*-butyl groups attached to the same phosphorus atom are mutually in a staggered position.

Solvated Chlorobenzene Molecule. In the crystal 0.5 chlorobenzene molecule per one platinum complex is contained. There observed a disorder of chlorobenzene molecules: a pair of molecules with 0.5 occupancy being related by a crystallographic center of

Table 3. Bond lengths and bond angles

Bond lengths [l/Å]			
Pt–P(1)	2.281(3)	C(10)–C(11)	1.56(2)
Pt–P(2)	2.282(2)	C(10)–C(12)	1.59(2)
Pt–Cl(1)	2.359(3)	C(10)–C(13)	1.549(19)
Pt–Cl(2)	2.362(3)	C(20)–C(21)	1.534(17)
P(1)–C(1)	1.853(12)	C(20)–C(22)	1.570(17)
P(2)–C(3)	1.850(11)	C(20)–C(23)	1.551(19)
P(1)–C(10)	1.919(12)	C(30)–C(31)	1.554(18)
P(1)–C(20)	1.898(11)	C(30)–C(32)	1.538(18)
P(2)–C(30)	1.900(12)	C(30)–C(33)	1.537(17)
P(2)–C(40)	1.914(13)	C(40)–C(41)	1.54(2)
C(1)–C(2)	1.501(17)	C(40)–C(42)	1.556(18)
C(2)–C(3)	1.519(17)	C(40)–C(43)	1.547(19)
Bond angles [ϕ/°]			
P(1)–P–Pt(2)	99.05(9)	Cl(1)–Pt–Cl(2)	83.18(11)
P(1)–Pt–Cl(1)	90.07(9)	P(2)–Pt–Cl(1)	167.87(9)
P(1)–Pt–Cl(2)	168.79(10)	P(2)–Pt–Cl(2)	88.96(10)
Pt–P(1)–C(1)	115.5(4)	Pt–P(2)–C(3)	115.7(4)
Pt–P(1)–C(10)	110.8(4)	Pt–P(2)–C(3)	110.9(4)
Pt–P(1)–C(20)	115.7(4)	Pt–P(2)–C(40)	114.1(4)
C(1)–P(1)–C(10)	102.9(5)	C(3)–P(2)–C(30)	99.1(5)
C(1)–P(1)–C(20)	100.1(5)	C(3)–P(2)–C(40)	104.0(5)
C(10)–P(1)–C(20)	110.8(5)	C(30)–P(2)–C(40)	112.1(5)
P(1)–C(1)–C(2)	116.9(8)	P(2)–C(3)–C(2)	113.5(8)
C(1)–C(2)–C(3)	113.5(8)		
P(1)–C(10)–C(11)	113.0(9)	P(2)–C(30)–C(31)	110.9(8)
P(1)–C(10)-C(12)	107.0(10)	P(2)–C(30)–C(32)	107.8(8)
P(1)–C(10)–C(13)	114.0(9)	P(2)–C(30)–C(33)	115.0(8)
P(1)–C(20)–C(21)	113.8(8)	P(2)–C(40)–C(41)	112.5(9)
P(1)–C(20)–C(22)	106.6(8)	P(2)–C(40)–C(42)	107.8(9)
P(1)–C(20)–C(23)	113.7(8)	P(2)–C(40)–C(43)	112.5(9)
C(11)–C(10)–C(12)	111.1(12)	C(31)–C(30)–C(32)	109.5(10)
C(11)–C(10)–C(13)	107.5(11)	C(31)–C(30)–C(33)	108.3(10)
C(12)–C(10)–C(13)	104.0(12)	C(32)–C(30)–C(33)	105.2(10)
C(21)–C(20)–C(22)	106.2(10)	C(41)–C(40)–C(42)	108.6(11)
C(21)–C(20)–C(23)	107.1(10)	C(41)–C(40)–C(43)	107.2(11)
C(22)–C(20)–C(23)	109.2(10)	C(42)–C(40)–C(43)	108.2(11)

Table 4. Least-squares planes through various groups of atoms, the deviations (l/Å) of the atoms from the plane and the dihedral angles between the selected planes

Equation of the plane is of the form $AX+BY+CZ+D=0$, where X, Y, Z, and D are measured in Å unit: $X=ax+cz\cos\beta$, $Y=by$, $Z=cz\sin\beta$.

a. Coordination plane Pt, Cl(1), Cl(2), P(1) and P(2)

$-0.1284X-0.6595Y-0.7407Z+5.2821=0$

Pt	Cl(1)	Cl(2)	P(1)	P(2)
0.006	−0.169	0.173	0.179	−0.169

b. Plane defined by C(1), C(2), and C(3)

$0.0312X-0.9634Y+0.2663Z+4.4943=0$

c. Plane defined by Pt, P(1), and P(2)

$-0.0284X-0.6624Y-0.7486Z+4.9089=0$

d. Plane defined by Pt, Cl(1), and Cl(2)

$-0.2356X-0.6508Y-0.7218Z+5.6135=0$

Dihedral angles [ϕ/°]

between planes *a* and *b* 64.3

c and *d* 12.0

symmetry. Figure 1(b) shows a drawing of a disordered molecular pair. Owing to the difficulty resolving each of the overlapped peaks in two (Fig. 1(a)), the Cl(S)/C(S4)′ (or C(S4)/Cl(S)′) and C(S2)/C(S6)′ (or C(S(6)/C(S2)′) atoms are drawn as a single hybrid (Cl+C)/2 and single carbon atoms. Consequently, bond lengths and bond angles shown in Fig. 1(b) are less satisfactory.

Crystal Structure. The crystal structure is shown in Fig. 4 as a stereoscopic drawing. Pairs of disordered chlorobenzene half molecules are also shown on the center of symmetry. All the intermolecular atomic contacts are the usual van der Waals distances.

Computations throughout the present study were carried out on a NEAC 2200-700 computer at Osaka University. Figures 2, 4, and 5 were drawn on a NUMERICON 7000 systems at Osaka University with a local version of ORTEP.[8]

The authors wish to express their deep thanks to Professor Sei Otsuka and his coworkers for providing crystals and helpful discussions.

References

1) S. Otsuka, unpublished work.
2) M. Harada, Y. Kai, N. Yasuoka, and N. Kasai, *Bull. Chem. Soc. Jpn.*, **49**, 3472 (1976).
3) T. Ashida, The Universal Crystallographic Computing System-Osaka, The Computation Center, Osaka University (1973), p. 55.
4) "International Tables for X-Ray Crystallography," The Kynoch Press, Birmingham (1974), Vol. IV, p. 71.
5) "International Tables for X-Ray Crystallography," The Kynoch Press, Birmingham (1974), Vol. IV, p. 148.
6) J. Chatt and L. A. Duncanson, *J. Chem. Soc.*, **1953**, 2939.
7) G. G. Messmer, E. L. Amma, and J. A. Ibers, *Inorg. Chem.*, **6**, 725 (1967).
8) C. K. Johnson, "ORTEP, Report ORNL-3794," Oak Ridge National Laboratory, Oak Ridge, Tennessee (1965).

Thermodynamic Studies on Phase Transitions of Potassium Thiocyanate and Ammonium Thiocyanate Crystals

Yoshio KINSHO,† Natsuo ONODERA,†† Minoru SAKIYAMA, and Syûzô SEKI*

Department of Chemistry, Faculty of Science, Osaka University, Toyonaka, Osaka 560

(Received September 16, 1978)

Heat capacities of KSCN and NH_4SCN crystals were measured by adiabatic calorimetry in the temperature range between 13 K and the melting points. Molar volume of NH_4SCN was also determined above room temperature. Entropy change for the II-I transition of KSCN (414.54 K, essentially higher order but accompanied with the first order component) is 6.26 J K^{-1} mol^{-1} (=1.09 R ln 2), which is of similar magnitude with our previous value (*Bull. Chem. Soc. Jpn.*, **36**, 1025 (1963)). Entropy change for the III-II transition of NH_4SCN (360.1 K, first order) is 10.01 J K^{-1} mol^{-1} and apparent entropy change for the II-I transition of NH_4SCN (392.8 K, higher order) is 2.85 J K^{-1} mol^{-1} (=0.49 R ln 2) in spite of possibly similar nature of the transition with the II-I transition of KSCN. A possibility has been suggested that the entropy change might be approximately R ln 2 if the transition was not interfered with the III-II trasition and the premelting.

In the previous paper,[1] thermodynamic studies were reported which had been carried out on potassium thiocyanate (KSCN) crystal by use of a conduction calorimeter above room temperature in combination with the infrared studies and its apparently higher order transition at 414.5 K was interpreted in terms of orientational disorder of thiocyanate ions in the higher temperature phase††† of the crystal. In parallel with these studies X-ray diffraction study was also reported by Yamada and Watanabé.[2]

In the present paper we have studied the thermodynamic behavior of NH_4SCN crystal and reinvestigated that of KSCN crystal. Ammonium thiocyanate crystal, which consists of two kinds of polyatomic ions, undergoes two phase transitions below the melting point.††† A significant volume decrease on heating was observed for the III-II transition by Bridgman in his high pressure experiments.[3] X-Ray diffraction study on phase III showed that the crystal is monoclinic with four pairs of ions per unit cell (β=97.4°, a=0.43 nm, b=0.72 nm, c=1.30 nm) arrayed in a layered structure.[4] A thermoanalytical study on the system KSCN–NH_4SCN showed that both compounds formed solid solution in phases I and II over the entire composition range.[5] Hence, both crystals are possibly isomorphous with each other in these phases and the II-I transitions in these crystals are possibly of similar nature. Pressure dependence of the II-I transition temperature for these crystals were studied and its thermodynamic implication was discussed.[6,7]

Heat capacity measurements for ammonium thiocyanate crystal above room temperatures by conduction calorimetry and for ammonium thiocyanate and potassium thiocyanate crystals below 300 K by adiabatic calorimetry had been completed before 1969.[8] Heat capacities obtained by conduction and adiabatic methods for the both compounds showed discrepancies at 300 K. Subsequently, Vanderzee and Westrum reported the results of heat capacity measurements below 340 K for both salts.[9] Their results also showed discrepancies with our results obtained by conduction calorimetry. Further measurements of heat capacities above ordinary temperature were carried out by adiabatic calorimetry for these crystals, in order to examine the validity of our previous conclusion on the phase transition of potassium thiocyanate and to elucidate the mechanism of phase transitions of ammonium thiocyanate. In this paper, heat capacities of these crystals at temperatures above 13 K and below the melting points and molar volumes of ammonium thiocyanate above room temperatures are reported.

Experimental

Materials. Commercial potassium thiocyanate (Wakō, special grade) was purified by repeated recrystallization from methanol solutions followed by drying under vacuum (≈0.1 Pa) at 373 K and loaded into the calorimeters under dry nitrogen atmosphere. The nitrogen was exchanged with helium, when helium was used as heat exchange gas.

Commercial ammonium thiocyanate (Wakō, special grade) used for calorimetry and dilatometry was purified by repeated crystallization from 50% aqueous methanol solution and methanol solutions. The crystal was dried under vacuum (≈0.1 Pa) through heating and cooling cycles around the III-II transition temperature. In spite of the precaution, examination of the heat capacity behavior indicated the presence of a small amount of methanol occluded in the crystals by showing an excess heat capacity at 176 K with magnitude similar to that observed by Vanderzee *et al.*[9] The anomaly was attributed to the melting of CH_3OH–NH_4SCN eutectic mixture by them. Loading into the calorimeters and substitution of nitrogen with helium were carried out as for the potassium salt.

Calorimetric Procedures. Measurements between 13 and 300 K for both compounds were carried out by adiabatic calorimetry using a cryostat, a gold calorimeter cell, and a control system described elsewhere.[10] The calorimetric sample of potassium thiocyanate had a mass corrected to buoyancy of 30.141 g and its heat capacity ranged from 35% of the total at 13K to 59% at 300 K. The contribution from nitrogen (heat exchange gas except in series IV of Table 1) including the effects of its melting and vaporization or that from helium (heat exchange gas in series IV) was subtracted properly. The mass of the calorimetric sample of ammonium thiocyanate corrected to buoyancy was 22.227 g and contri-

† Present address: Kurosaki Plant, Mitsubishi Chemical Industries Ltd., Yahata-nishi-ku, Kitakyushu, Fukuoka 806.

†† Present address: Japan Information Center of Science and Technology, Chiyoda-ku, Tokyo 100.

††† Crystalline phases are denoted as I, II, (and III) from higher temperature side for both crystals.

bution of its heat capacity to the total ranged from 44% at 13 K to 66% at 298 K. Contribution of helium packed in the calorimeter was corrected properly. The original heat capacities for both compounds, determined in 1968 in terms of NBS-55 temperature scale below 90 K and in terms of International Temperature Scale of 1948 (IPTS-48) between 90 and 300 K, were converted to the values in terms of IPTS-68 in this paper.[11,12]

Measurements above 300 K for both compounds were performed by adiabatic calorimetry using a calorimetric system described elsewhere,[13] and a gold calorimeter-cell equipped with eight internal radial vanes and two silver shields. Temperature was measured by a Tinsley type 5187-L platinum resistance thermometer calibrated in terms of IPTS-68 against a Leeds-Northrup type 8163 platinum resistance thermometer. Lead wires in the calorimetric system were replaced with copper wires (0.2 mm in diameter) covered with glass-fiber. The mass of calorimetric sample (corrected for buoyancy) was 32.799 g for the potassium salt and 23.485 g for the ammonium salt. Contribution of the heat capacity to the total was 46—50% for the former and 52—55% for the latter in the temperature range where no heat capacity anomaly was observed. Contribution from helium enclosed in the calorimeter was corrected properly.

Dilatometry. A glass dilatomer with internal volume of *ca.* 10 cm^3 was used. Confining liquid was mercury. The mass of ammonium thiocyanate crystal packed in the dilatometer was 6.262 g. Temperature of the dilatometer was detected by a copper-constantan thermocouple. Molar volume for phase III was calculated on the basis of the molar volume at 295 K obtained from X-ray diffraction data.[15] For other phases X-ray diffraction data[15] at 362 K was employed for the calculation.

Results and Discussion

Potassium Thiocyanate. Enthalpy increase per 1 K is presented in Tables 1 and 2 for temperatures below and above 300 K, respectively. Molar heat capacity was obtained by applying curvature correction and shown in Fig. 1 over the entire temperature range. The curves for both temperature ranges are smoothly connected with each other at 300 K. The molar heat capacity below 330 K is in agreement with the values reported by Vanderzee *et al.*[9] within 1%.

Relative enthalpy $[H°(T)-H°(400\ K)]$ plotted against temperature is shown in Fig. 2. Enthalpies from the three series of measurements are in good agreement with each other except for those above 414.5 K for Series VI, in which temperature increments around 414.5 K were small. A small but distinct discontinuity is observed at 414.54 K, which was assigned to the transition temperature as given in Table 3. A small discontinuity (0.20 $cm^3\ mol^{-1}$) is found at the same temperature also in the molar volume *vs.* temperature curve as shown in Fig. 7. These findings indicate unambiguously that the transition is a higher order transition accompanied with the first order component as suggested by Klement.[7] The transition was interpreted as a higher order transition previously by the present authors[1] and by Yamada and Watanabé[2] and as a first order one with a small volume change by Bridgman.[3] Both conclusions are partly correct in view of the present findings.

As shown in Fig. 1, a straight line connecting the points at 300 and 438 K on the heat capacity curve was drawn for the estimation of a "normal" heat capacity in the transition region.[1] Vanderzee and Westrum showed that the difference between experimental and calculated heat capacities of potassium thiocyanate crystal deviates from ±1% limits above 310 K.[9] This fact is in harmony with the present selection of 300 K as the lower temperature limit of the transition region. Transition enthalpy and entropy thus determined are given in Table 3 together with contributions from the

TABLE 1. ENTHALPY INCREMENTS PER 1 K OF POTASSIUM THIOCYANATE CRYSTAL BELOW 300 K

T/K	$\Delta H/\Delta T$ / J K^{-1} mol^{-1}	ΔT/K
	Series I	
12.81	1.109	3.473
15.94	2.312	2.775
19.23	4.075	1.627
20.84	5.186	1.619
	Series II	
17.38	2.998	1.873
19.37	4.197	2.111
21.48	5.689	2.097
23.77	7.522	2.482
26.33	9.743	2.647
29.12	12.330	2.943
32.40	15.699	3.600
35.72	18.625	3.061
38.60	21.60	2.694
41.56	24.32	3.224
44.63	27.07	2.924
47.63	29.48	2.692
50.23	31.84	2.523
	Series III	
71.11	45.22	3.432
74.43	46.81	3.196
77.58	48.14	3.111
80.65	49.49	3.033
83.65	50.60	2.971
86.59	51.72	2.913
89.32	52.74	2.854
92.15	53.57	2.810
94.94	54.50	2.768
99.03	55.76	5.433
104.41	57.33	5.303
109.65	58.75	5.189
114.79	60.00	5.093
119.84	61.20	5.006
125.55	62.42	5.336
130.84	63.53	5.256
135.42	64.44	3.895
139.93	65.33	5.136
145.04	66.28	5.077
149.14	67.06	3.145
153.20	67.80	4.987
159.69	68.93	5.912
165.57	69.85	5.850
171.39	70.74	5.793
177.15	71.68	5.736
182.85	72.50	5.684
188.51	73.32	5.633
194.12	74.16	5.579
199.68	74.96	5.535
205.18	75.90	5.486
216.04	77.48	5.401
221.41	78.20	5.353
226.75	78.94	5.321
232.04	79.78	5.281
237.30	80.41	5.248
242.53	81.10	5.215
247.79	81.77	5.311
253.01	82.51	5.148
258.14	83.10	5.119
266.54	84.50	6.098
272.61	85.31	6.054
278.63	86.22	6.005
284.61	87.10	5.959
290.54	88.00	5.914
296.42	89.00	5.866
301.17	89.83	3.641
	Series IV	
24.87	8.527	2.801
27.92	11.230	3.311
31.31	14.467	3.542
34.18	17.389	2.214
36.75	19.752	2.948
39.94	22.86	3.460
43.21	25.85	3.095
46.17	28.45	2.831
48.90	30.74	2.639
52.01	33.14	3.588
55.47	35.65	3.350
58.72	37.88	3.167
61.82	39.87	3.027
64.78	41.83	2.905
67.63	43.39	2.805
70.40	44.78	2.721
73.08	46.12	2.649
75.70	47.22	2.592

Table 2. Enthalpy increments per 1 K of potassium thiocyanate crystal above 300 K

T/K	$\Delta H/\Delta T$ / J K^{-1} mol^{-1}	ΔT/K	T/K	$\Delta H/\Delta T$ / J K^{-1} mol^{-1}	ΔT/K
	Series I			Series IV	
317.40	92.26	3.007	413.03	254.9	1.716
320.37	92.89	2.993	414.21	775.6	0.709
323.33	93.70	2.978	415.31	291.3	1.562
326.26	94.95	2.957	417.40	118.85	2.726
329.25	95.09	3.340	420.08	114.42	2.776
332.55	95.45	3.326			
335.83	97.07	3.294		Series V	
339.09	96.43	3.302			
342.34	98.05	3.272	301.27	88.99	6.713
345.76	99.32	3.706	305.85	89.72	3.023
349.42	100.06	3.687	308.85	90.25	3.015
353.07	101.21	3.663	311.82	91.20	2.995
356.68	102.55	3.636	314.79	91.59	2.987
	Series II			Series VI	
363.83	104.43	3.606	406.60	158.74	1.562
367.37	106.53	3.553	408.10	167.29	1.514
370.86	108.25	3.516	409.54	178.49	1.455
374.32	110.09	3.481	410.91	193.79	1.381
377.75	112.20	3.446	412.19	220.0	1.272
381.13	114.56	3.409	413.34	266.3	1.117
384.42	117.82	3.353	414.05	356.3	0.429
387.72	119.32	3.330	414.39	568.0	0.296
390.96	124.68	4.249	414.53	4404	0.045
394.17	127.41	3.211	414.55	4176	0.047
397.30	132.39	3.142	414.63	939.6	0.191
400.36	138.25	3.066	415.78	125.47	2.340
403.37	146.30	3.178	418.10	116.88	2.425
406.43	158.43	3.030	420.46	113.87	2.456
			422.71	112.73	2.461
	Series III		425.12	110.25	2.487
			427.53	109.53	2.493
408.11	168.35	2.920	429.93	109.25	2.494
410.85	194.18	2.668	432.23	108.86	2.497
413.21	271.4	2.130	434.62	107.82	2.506
414.62	942.2	0.774	437.03	108.44	2.498
416.66	119.03	3.531	439.42	108.92	2.490
420.15	114.51	3.601			
423.70	110.40	3.661			

first order component of the transition. The total entropy change of 6.26 J K^{-1} mol^{-1} is equal to 1.09 R ln 2. The previous conclusion of the present authors[1] that the transition entropy may be interpreted principally in terms of two-fold orientational disorder of thiocyanate ions in phase II need not be altered at all.

Volume thermal expansion coefficient was calculated from the dilatometric data given in Appendix. Plots of the heat capacity below the transition temperature against the thermal expansion coefficient is shown in Fig. 3. The plots below 412.2 K was approximated with a straight line as shown in the figure. Pressure dependence of transition temperature $(dT/dp)_{tr}$ was

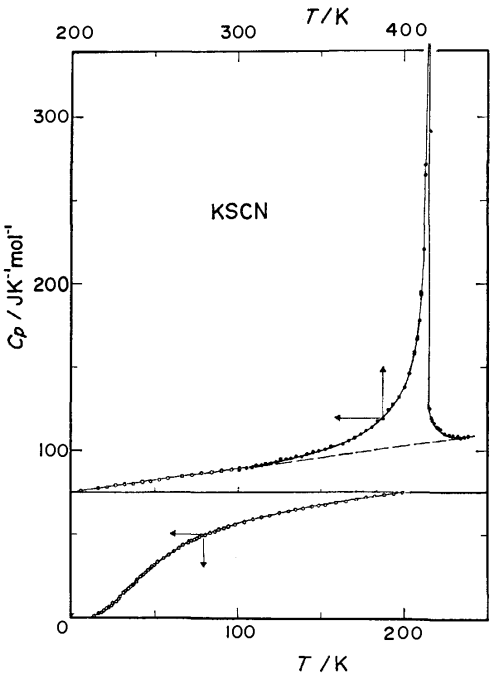

Fig. 1. Molar heat capacity of potassium thiocyanate crystal in the regions 12—300 K(○) and 300—410 K(●). Estimated normal heat capacity is drawn with a broken line.

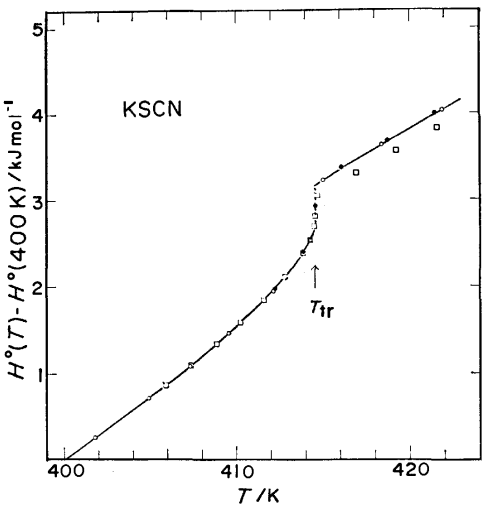

Fig. 2. Relative enthalpy $[H^\circ(T)-H^\circ(400\ \mathrm{K})]$ of potassium thiocyanate crystal around the II-I transition temperature.
○: Series II and III, ●: Series IV, □: Series VI.

Table 3. Transition temperatures, enthalpies, and entropies of potassium thiocyanate and ammonium thiocyanate crystals

Crystal	Transition	T/K	ΔH_{tr} / kJ mol^{-1}	ΔS_{tr} / J K^{-1} mol^{-1}
KSCN	II-I	414.54±0.02	2.53 (0.50)[a]	6.26 (1.21)[a]
NH_4SCN	III-II	360.1 ±0.1	3.61±0.03	10.01±0.08
	II-I	392.8 ±0.1	1.14	2.85

a) Contribution from the first order component.

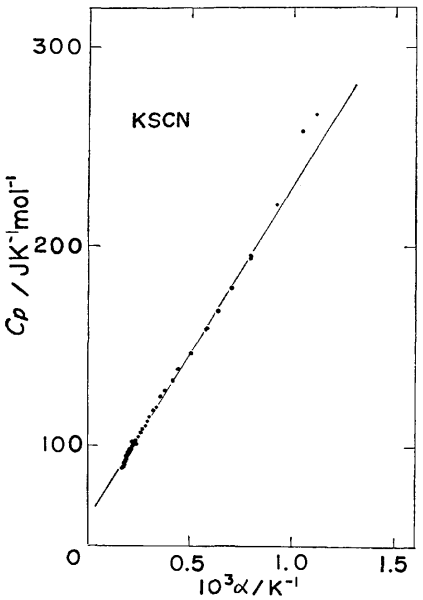

Fig. 3. Molar heat capacity *vs.* thermal expansion coefficient plot of potassium thiocyanate crystal below 414.5 K.

calculated from the slope of the straight line on the basis of the Pippard's relation,[14]

$$C_p = \left(\frac{dp}{dT}\right)_{tr} V_m T_{tr} \alpha + \text{const},$$

where C_p, the molar heat capacity, V_m, the molar volume, α, the thermal expansion coefficient and T_{tr}, the transition temperature. The calculated value for $(dT/dp)_{tr}$ is 0.134 K MPa^{-1}, while the observed value[6] is 0.172 K MPa^{-1}.

For the first order component of the transition, the Clausius-Clapeyron equation was applied with the volume change of 0.20 cm^3 mol^{-1} and the entropy change of 1.21 J K^{-1} mol^{-1}. The calculated value for $(dT/dp)_{tr}$ is 0.165 K MPa^{-1}, which is rather in good agreement with the observed value.[6]

Ammonium Thiocyanate. Plot of the molar volume against temperature is shown in Fig. 4. Molar volumes calculated from the X-ray diffraction data by Pistorius[15] is also shown in the figure. As stated above, the dilatometric values were calculated with reference to the X-ray diffraction data at 295.2 and 361.7 K. Agreement is especially good for the temperature dependence of molar volume in phase II. Part of the molar volume *vs.* temperature curve around the II-I transition temperature is enlarged and presented in the enclosed portion. It is not clear whether a discontinuity in molar volume is present at the transition temperature or not. In the III-II transition, a discontinuous volume decrease (*ca.* 6% of the molar volume) took place on heating. Significant superheating and supercooling were also observed as will be explained below.

Changing topics to the discussion of heat capacity data, the effect of thermal decomposition upon the heat capacity values will be given. One of the principal reactions which ammonium thiocyanate crystal undergoes at higher temperatures may be the dissociation reaction into gaseous ammonia and gaseous isothiocyanic acid:

$$NH_4SCN(c) \longrightarrow NH_3(g) + HNCS(g). \quad (1)$$

The dissociation pressure comes up to 101.325 kPa at 443 K.[16] Now, for the dissociation effect molar heat capacities were corrected approximately by using the following equation:

$$\Delta C_p = \Delta H_r^\circ(T) \cdot \frac{MV_g}{2mRT}\left(\frac{dp}{dT} - \frac{p}{T}\right), \quad (2)$$

where ΔC_p is the correction to molar heat capacity, m, the mass of the sample in the calorimeter, M, the molar mass, V_g, the volume available for the gaseous species in the calorimeter, and $\Delta H_r^\circ(T)$, the standard enthalpy of reaction. In the derivation of the equation, the gases were assumed to be ideal and only the direct effect of the dissociation was taken into account. Here, V_g was found to be 18.0 cm^3. $\Delta H_r^\circ(T)$ for each of the phases

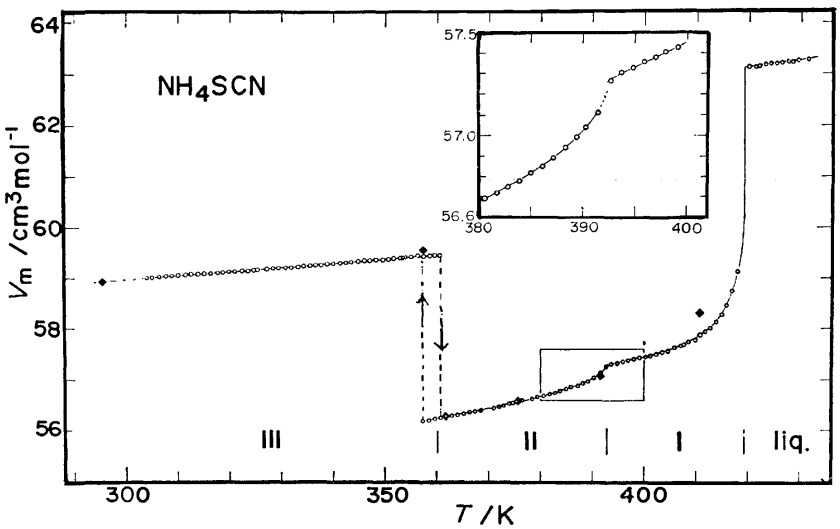

Fig. 4. Molar volume of ammonium thiocyanate in the crystalline and liquid phases.
○: Dilatometric data, ◆: X-ray diffraction data.[15]

was assumed to be independent of temperature for simplicity, *i.e.* 140 kJ mol^{-1} for the liquid phase, 149, 152, and 160 kJ mol^{-1} for the phases I, II, and III, respectively. These values were evaluated from standard enthalpies of formation at 298.15 K of the relevant species,[17] relative enthalpy $[H°(T)-H°(298.15\ K)]$ of ammonium thiocyanate, and molar heat capactites of the gaseous species.[17] The relative enthalpy of ammonium thiocyanate was calculated from the observed (uncorrected) molar heat capacities for the crystal below 400 K, while the molar heat capacities of the crystal above 400 K and of the liquid phase were assumed to be 130 J K^{-1} mol^{-1}. The observed enthalpies of transition as will be given below, and the enthalpy of melting (9.2 kJ mol^{-1}) determined by conduction calorimetry[8] were also utilized to estimate ΔH_r°. Dissociation pressure and its temperature dependence given in Eq. 2 were derived with reference to the dissociation pressure of 101.325 kPa at 443 K on the basis of the Van't Hoff's equation,

$$\ln p = -\frac{\Delta H_r^\circ(T)}{2RT} + \text{const.} \qquad (3)$$

The correction term to molar heat capacity, ΔC_p, amounted to 0.10, 0.29, 0.61, and 1.21 J K^{-1} mol^{-1} at 360, 378, 393, and 407 K, respectively. Enthalpy increase per 1 K of the crystal corrected as above for the dissociation effect are tabulated for temperatures below 300 K and above 278 K in Tables 4 and 5, respectively. No correction was made upon the data of Table 4 for the effect of eutectic melting of NH_4SCN–CH_3OH mentioned above. Molar heat capacities were calculated by applying curvature correction for the

Table 4. Enthalpy increments per 1 K of ammonium thiocyanate crystals below 300 K

T/K	$\Delta H/\Delta T$ / J K^{-1} mol^{-1}	ΔT/K	T/K	$\Delta H/\Delta T$ / J K^{-1} mol^{-1}	ΔT/K
Series I			Series IV		
101.84	57.71	3.243	13.11	1.812	3.328
105.06	59.20	3.181	16.16	3.208	2.822
108.22	60.63	3.129	18.66	4.755	2.162
112.23	62.38	4.902	20.96	6.305	2.458
117.07	64.50	4.785	23.41	8.106	2.451
121.81	66.45	4.683	26.10	10.255	2.957
			29.19	12.641	3.217
Series II			31.95	14.896	3.315
			34.63	17.141	3.057
79.58	46.55	3.359	37.94	19.655	3.562
82.89	48.30	3.261	41.30	22.14	3.171
86.11	50.02	3.173	44.33	24.41	2.893
89.25	51.61	3.097	47.12	26.37	2.683
92.31	53.10	3.029	49.72	28.31	2.517
95.31	54.56	2.967	52.73	30.37	3.527
98.25	55.98	2.910	56.15	32.57	3.307
101.13	57.46	2.855	59.37	34.63	3.133
			62.42	36.69	2.990
Series III			65.32	38.53	2.869
			68.17	40.10	2.770
124.55	67.69	5.776	70.91	41.81	2.717
130.26	70.01	5.638	73.57	43.33	2.599
135.83	72.21	5.515	76.14	44.73	2.531
141.29	74.35	5.403	78.64	46.04	2.469
146.64	76.43	5.300	81.08	47.37	2.413
151.89	78.48	5.204			
157.05	80.38	5.117	Series V		
162.12	82.09	5.040			
167.12	84.33	4.959	215.16	100.04	5.726
172.04	85.56	4.895	220.84	101.87	5.652
176.90	87.25	4.827	226.43	103.63	5.582
181.69	88.86	4.764	231.97	105.59	5.508
186.79	90.62	5.613	237.44	107.28	5.445
192.36	92.51	5.533	242.84	109.08	5.381
197.85	94.30	5.456	248.18	110.78	5.321
203.26	96.14	5.381	253.46	112.49	5.262
208.60	97.88	5.313	258.69	114.08	5.207
213.87	99.39	5.246	263.86	115.70	5.154
			269.33	117.48	5.851
			275.14	119.13	5.790
			280.89	120.93	5.726
			286.58	122.82	5.653
			292.22	124.15	5.612
			297.79	125.70	5.560

Table 5. Enthalpy increments per 1 K of ammonium thiocyanate crystal above 300 K

T/K	$\Delta H/\Delta T$ / J K^{-1} mol^{-1}	ΔT/K	T/K	$\Delta H/\Delta T$ / J K^{-1} mol^{-1}	ΔT/K
Series I			339.62	138.7	3.718
			343.30	139.1	3.712
298.84	124.9	3.635	346.94	140.2	3.695
302.44	126.1	3.622	350.56	141.3	3.679
306.05	126.8	3.607	352.71	140.0	1.910
311.40	129.0	7.130	354.54	141.9	1.888
316.73	130.6	3.542	356.37	143.0	1.879
320.25	131.1	3.529	358.19	143.2	1.877
321.96	131.7	3.489	360.74	142.7	0.607
324.31	132.0	1.216			
325.52	132.5	1.216	Series V		
326.73	133.1	1.214			
			368.06	145.8	3.390
Series II			371.51	149.7	3.540
			375.03	157.8	3.560
320.55	132.3	2.011	378.41	168.7	3.314
322.58	132.4	2.117	381.67	171.2	3.285
326.53	135.1	1.977	384.92	179.9	3.174
328.46	135.2	1.978	387.96	201.4	2.969
			390.71	257.2	2.525
Series III			392.47	374.0	0.994
			393.86	152.1	1.797
326.80	133.6	2.093	396.53	146.0	3.566
328.76	134.5	1.939	399.17	144.4	1.744
330.65	135.5	1.968			
332.56	134.6	1.964	Series VI		
334.46	137.8	1.946			
336.37	137.7	1.945	396.94	146.5	3.537
338.24	139.0	1.943	400.46	146.3	3.556
			403.90	148.5	3.525
Series IV			407.20	154.6	3.444
			409.39	167.5	1.695
335.96	137.3	3.737			

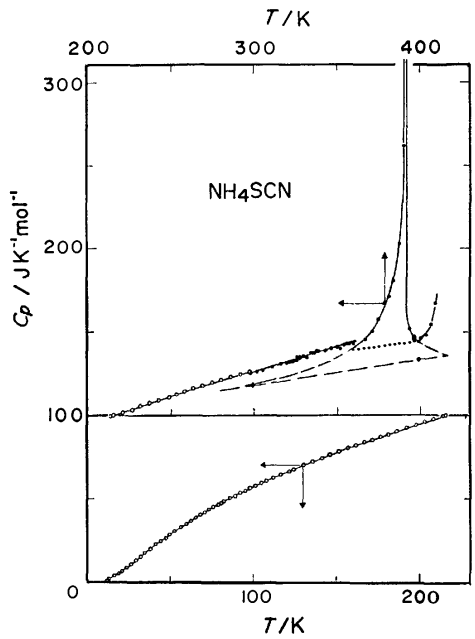

Fig. 5. Molar heat capacity of ammonium thiocyanate crystal. Experimental values are shown by empty and filled circles for the regions 13—300 K and 300—410 K, respectively. Estimated normal molar heat capacities at 300 and 400 K for phase II are shown by filled squares. For dotted and broken lines, see the text.

enthalpy increments and shown in Fig. 5 for the entire temperature range.

Another reaction to be taken into consideration will be the decomposition of ammonium thiocyanate in the solid state. The decomposition reaction in the liquid state was studied above 423 K by Kodama *et al.* in some detail.[24] The equilibrium composition of the reaction product at 423 K was 67% in ammonium thiocyanate, 30% in thiourea and 3% in other products. In the following discussion, only the isomerization

$$NH_4SCN \longrightarrow (NH_2)_2CS$$

will be considered. This reaction is exothermic at 298.15 K with the standard enthalpy of reaction of $-9.6\,kJ\,mol^{-1}$, which has been calculated from enthalpies of formation of the both compounds in the solid states.[17] In the present study, the significant increase of temperature drift of the calorimeter in the cooling direction was observed above 402 K, which brought about difficulty in the precise measurement of molar heat capacity. Two molar heat capacity data above 402 K tabulated in Table 3 were obtained under the abnormal condition and would be influenced significantly with the isomerization reaction.

Increase in molar heat capacity above 402 K may be interpreted in the following way. Molar heat capacity of thiourea crystal at 298.15 K ($108.91\,J\,K^{-1}\,mol^{-1}$)[19] is considerably lower than that of ammonium thiocyanate crystal (*ca.* $125\,J\,K^{-1}\,mol^{-1}$) at the same temperature and the former crystal shows no phase transition between 298 and 400 K, while the latter undergoes two phase transitions in the same temperature range. Accordingly, the above-mentioned isomerization reaction as a solid state reaction would certainly continue to be exothermic up to 400 K. However, the system NH_4SCN-$(NH_2)_2CS$ shows a eutectic point at 373 K with the mole fraction of thiourea of 0.3.[5] Thus a small amount of crystalline thiourea formed by the solid-state isomerization would melt immediately together with ammonium thiocyanate to give a melt rich in ammonium thiocyanate. From the analysis of equilibria between ammonium thiocyanate and thiourea in the liquid phase, enthalpy of reaction for the isomerization in the liquid state was determined to be $-9.1\,kJ\,mol^{-1}$.[24] A thermochemical cycle involving both the species in the liquid and solid states shows that net change in enthalpy from ammonium thiocyanate crystal to thiourea liquid *via* thiourea crystal is almost neutral. On the other hand, ammonium thiocyanate in the liquid state would be converted to thiourea more rapidly than in the solid state, but the conversion is only of the order of 1% after 1 h even at 413 K.[18] Although the enthalpies of melting of ammonium thiocyanate and of isomerization in the liquid state into thiourea are of similar magnitude with opposite sign, realized net result would be the predominance of endothermic effect due to the melting of ammonium thiocyanate. Summerizing, the increase in molar heat capacity above 402 K may be interpreted in terms of premelting of ammonium thiocyanate crystal, triggered and accelerated by the isomerization into thiourea.

Transition temperature for III-II transition was determined to be $360.1_5 \pm 0.1$ K by monitoring the temperature of the calorimeter under the adiabatic condition when the crystal transformed partially. Superheating and supercooling of the crystal were observed, when the crystal was heated up or cooled down through the transition range by a small temperature head between the calorimeter and the adiabatic jacket. Transition enthalpy and entropy are given in Table 3. The above-mentioned findings together with the discontinuous volume change in this transition reveal that the transition is of the first-order type. In phases I and II, the crystal forms mixed crystal with potassium thiocyanate crystal over the entire composition range[5] and they are possibly isomorphous. The crystal of ammonium thiocyanate in phase III is characterized with open structure with hydrogen bonding between essentially stationary ammonium ions and thiocyanate ions. In phase II, the orientation of the ammonium ions would be statistically disordered so that the crystal may be isomorphous with the potassium salt.

Application of the Clausius-Clapeyron equation for the III-II transition with the volume change of $3.42\,cm^3\,mol^{-1}$ (from X-ray diffraction[15]) and the entropy change of $10.0\,J\,K^{-1}\,mol^{-1}$ (the present study) gave $-0.342\,K\,MPa^{-1}$ for $(dT/dp)_{III\text{-}II}$, which agreed with the observed value of Bridgman,[3] $-0.334\,K\,MPa^{-1}$.

Transition temperature of the II-I transition of the ammonium salt was determined to be 392.8 ± 0.1 K from the plot of relative enthalpy $[H^\circ(T) - H^\circ(361\,K)]$ against temperature. It is not certain from the relative enthalpy plot whether the transition is accompanied with a first-order component as observed for the potassium salt. Thermal expansion coefficient α of ammonium

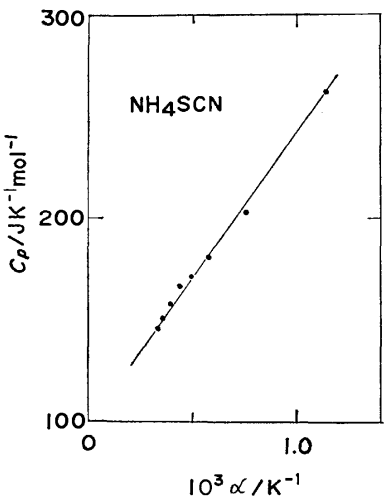

Fig. 6. Molar heat capacity *vs.* thermal expansion coefficient plot of ammonium thiocyanate crystal below 392.8 K in phase II.

thiocyanate crystal in phase II was calculated from the dilatometric data in Fig. 7 and the heat capacities were plotted against the thermal expansion coefficient as shown in Fig. 6. The plots below 385 K was approximated with a straight line. The value of $(dT/dp)_{II-I}$ calculated from the slope of the straight line with the value of V_m of 57.0 $cm^3\,mol^{-1}$ on the basis of the Pippard's relation[14] is 0.155 K MPa^{-1}, while the observed value[7] is 0.126 K MPa^{-1}.

It is difficult to draw a reasonable "normal" molar heat capacity curve for phase II in Fig. 5. An obvious but tentative solution is to draw a straight line between the points at 360 and 398 K on the smoothed curve as shown by a dotted line in the figure. Transition enthalpy and entropy thus obtained are tabulated in Table 3. As stated above, the II-I transition in potassium thiocyanate and ammonium thiocyanate crystals should be similar in nature. Although the II-I transition of the ammonium salt is of essentially higher-order type as indicated in the heat capacity curve, the transition entropy 0.49 R ln 2 calculated as above is considerably lower than the expected value, R ln 2.

One possible interpretation of the apparent smallness of this transition entropy is that the crystal transforms from phase III into phase II which has been disordered to some extent with respect to the orientation of thiocyanate ions. A support to this is that thermal expansion coefficient of the ammonium salt at the lowest temperature in phase II is considerably higher than the corresponding value for the potassium salt at 300 K (see Figs. 3 and 6). The entropy change for the III-II transition is 10.0 J $K^{-1}\,mol^{-1}$, which is of sufficient magnitude to include a part of the contribution from the disordering process of thiocyanate ions in addition to the entropy change related with the orientational disorder of ammonium ions. In this respect, the adoption of the normal heat capacity as given above is in conflict with the supposition that orientation of thiocyanate ions has been disordered to some extent even at the lowest temperature in phase II.

This supposition leads to the suggestion that hypothetical heat capacity for phase II below the III-II transition temperature is lower than the one observed for phase III. Furthermore it is to be recalled that normal heat capacities have not been determined adequately for phase I by the interference with the premelting described above. Thus, the normal heat capacities for phase I should be lower than the observed values above 402 K.

Application of the Kopp's law using ("normal") heat capacities of ammonium chloride,[20] potassium thiocyanate, and potassium chloride[20] gave 125 and 153 J $K^{-1}\,mol^{-1}$ for heat capacities at 300 and 400 K, respectively, which agree rather well with heat capacities of phase III observed at 300 K and extrapolated to 400 K and are therefore higher than expected for phase II.

Chihara and Nakamura[21] showed that heat capacity of ammonium chloride at 300 K was anomalously higher than the value calculated as a sum of Debye heat capacity and contributions from internal vibrations and harmonic (or anharmonic) vibration of ammonium ions. The anomaly had been pointed out earlier by Sakamoto.[22] Linear extrapolation of heat capacities of ammonium chloride at 500 and 600 K,[20] where the crystal is in the higher temperature phase, to 300 and 400 K gives 80 and 82 J $K^{-1}\,mol^{-1}$ for heat capacities of ammonium chloride, respectively. Adoption of these values leads to 118 and 133 J $K^{-1}\,mol^{-1}$ at 300 and 400 K, respectively, for ammonium thiocyanate.

Potassium and ammonium thiocyanate crystals are of cesium chloride type structure, while potassium and ammonium chloride crystals are of sodium chloride structure, in the relevant phases. This fact seems to lend support to the latter estimation of "normal" heat capacities.

A possible hypothetical "normal" heat capacity curve is thus drawn in Fig. 5 by a broken line, which is obtained by assuming that "normal" heat capacities are 118 and 133 J $K^{-1}\,mol^{-1}$ at 300 and 400 K as shown by filled squares, respectively, and that it changes linearly between these temperatures. Anomalous heat capacities are also extrapolated smoothly to lower and higher temperatures as shown in the figure with broken lines. Hypothetical total entropy of transition for II-I transition thus obtained is 5.22 J $K^{-1}\,mol^{-1}$, which is equal to 0.91 R ln 2. Klement discussed the apparent entropy decrease with increasing polarizability of the cation observed for corresponding transitions of KSCN, RbSCN, NH_4SCN, and TlSCN.[7] However, the present analysis suggests a possibility that transition entropy for the ammonium salt would be compatible with the value of the isomorphous potassium salt, if the transition was not interfered with the III-II phase transition and the premelting.

Appendix

The molar volume of potassium thiocyanate crystal from 300 to 460 K has been reported only briefly in a previous paper.[23] Temperature dependence of the molar volume around 415.5 K (II-I transition temperature) is shown in detail in Fig. 7. Obviously, a small discontinuity of the molar volume can be observed in the small interval of 415.5—415.7

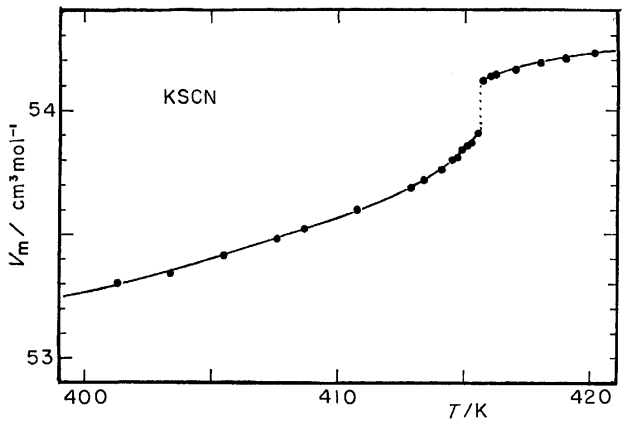

Fig. 7. Molar volume of potassium thiocyanate crystal around the II-I transition temperature.

K. Magnitude of the discontinuity amounts to 0.20 cm^3 mol^{-1}, which corresponds to 0.39% of the molar volume. The presence of the discontinuity had been shown implicitly as ΔV_t in Table 1 of the previous paper[23] before Klement pointed out from an analysis of molar volume data supplied by the authors.[7] However, the values of $\Delta V_t/V_t$, ΔV_t and t.p. given in the Table[23] are not correct and should read 0.39%, 0.20 cm^3 mol^{-1}, and 141.4 °C, respectively.

References

1) M. Sakiyama, H. Suga, and S. Seki, *Bull. Chem. Soc. Jpn.*, **36**, 1025 (1963).
2) Y. Yamada and T. Watanabé, *Bull. Chem. Soc. Jpn.*, **36**, 1032 (1963).
3) P. W. Bridgman, *Proc. Am. Acad. Arts Sci.*, **51**, 55 (1915); **72**, 235 (1938).
4) Z. V. Zvonkova and G. S. Zhdanov, *Zh. Fiz. Khim.*, **23**, 1495 (1949).
5) J. B. Wrzesnewsky, *Z. Anorg. Chem.*, **74**, 95 (1912).
6) C. W. F. T. Pistorius, J. B. Clark, and E. Rapoport, *J. Chem. Phys.*, **48**, 5123 (1968).
7) W. Klement, Jr., *Bull. Chem. Soc. Jpn.*, **49**, 2148 (1976).
8) Unpublished results of the present authors, part of which has been cited in Ref. 9.
9) C. E. Vanderzee and E. F. Westrum, Jr., *J. Chem. Thermodyn.*, **2**, 417 (1970).
10) H. Suga and S. Seki, *Bull. Chem. Soc. Jpn.*, **38**, 1000 (1965).
11) R. E. Bedford, M. Durieux, R. Muijlwijk, and C. R. Barber, *Metrologia*, **5**, 47 (1969).
12) T. B. Douglas, *J. Res. Natl. Bur. Stand., Sect. A*, **73**, 451 (1969).
13) N. Onodera, A. Kimoto, M. Sakiyama, and S. Seki, *Bull. Chem. Soc. Jpn.*, **44**, 1463 (1971).
14) a) A. B. Pippard, *Phil. Mag.*, **1**, 473 (1956); b) A. B. Pippard, "The Elements of Classical Thermodynamics," Cambridge University Press (1964), p. 140.
15) Appendix II of Ref. 7.
16) N. W. Luft, *Ind. Chem.*, **31**, 502 (1955).
17) D. D. Wagman, W. H. Evans, V. B. Parker, I. Halow, S. M. Bailey, and R. H. Schumm, "Selected Values of Chemical Thermodynamic Properties," NBS Technical Note 270-3, U.S. Government Printing Office, Washington, D.C. (1968).
18) S. T. Talreja, P. M. Oza, and P. S. Rao, *Bull. Chem. Soc. Jpn.*, **40**, 2427 (1967).
19) E. F. Westrum, Jr., and E. Chang, *Colloq. Int. C. N. R. S.*, **156**, 163 (1967).
20) "JANAF Thermochemical Tables," 2nd ed, NSRDS-NBS-37, U.S. Government Printing Office, Washington, D.C. (1971).
21) H. Chihara and M. Nakamura, *Bull. Chem. Soc. Jpn.*, **45**, 133 (1972).
22) Y. Sakamoto, *J. Sci. Hiroshima Univ.*, **A18**, 95 (1954).
23) T. Shinoda, H. Suga, and S. Seki, *Bull. Chem. Soc. Jpn.*, **33**, 1314 (1960).
24) S. Kodama, T. Fukushima, S. Nose, and J. Nakajima, *Kogyo Kagaku Zasshi*, **56**, 49 (1953).

The Crystal Structure of *fac*(*N*)-*Δ*-Tris(L-asparaginato)-cobalt(III) Trihydrate

Masao SEKIZAKI

College of Liberal Arts, Kanazawa University, Marunouchi, Kanazawa 920

(Received May 9, 1978)

The crystal structure of tris(L-asparaginato)cobalt(III) trihydrate, $[Co(L\text{-}H_2NCOCH_2CHNH_2COO)_3]\cdot 3H_2O$, has been determined by the X-ray diffraction method, and refined by a block-diagonal least-squares method to give $R=0.055$ for 1302 non-zero reflections. The crystals are orthorhombic with a space group $P2_12_12_1$, $a=39.082(4)$, $b=7.523(2)$, $c=6.643(2)$ Å, and $Z=4$. The complex molecule has a slightly distorted octahedral coordination with *fac*(*N*)-*Δ* geometry. The three bidentate ligand ions form five-membered planar chelate rings with coordination through amino nitrogen and carboxyl oxygen atoms. The amide groups of the two side-chains approach the central atom, and the oxygen atoms are connected through intramolecular hydrogen bonds. Another amide group is, however, far from the central atom. The complex molecules are hydrogen-bonded to one another to form layers parallel to the (100) plane. These layers are piled up through hydrogen bonds to complete a three-dimensional network.

Transition metal complexes of L-asparaginate ion (L-2-aminosuccinamate ion, $L\text{-}H_2NCOCH_2CHNH_2COO^-$) have been widely investigated,[1–5] and it has been concluded that the ligand ion is terdentate or bidentate. The terdentate ligand occupies the *facial* positions of the octahedron and the amide group is of *N*-[3] or *O*-coordination.[4] The coordination modes of the bidentate ligand are various.[2,5] According to the spectroscopic investigation by Takenaka and Shibata[2] on the stereochemistry of trivalent cobalt complexes, the bidentate ligand may coordinate through amino nitrogen and carboxyl oxygen atoms forming a five-membered chelate ring, and the amide group may remain free. If this assumption is correct, the bulky side-chain including the amide group is expected to have considerable effects on the neighboring molecules in the crystal. To ascertain these effects and to confirm the assumed structure, a single-crystal structure analysis of tris(L-asparaginato)cobalt(III) trihydrate has been carried out.

Experimental

The crystals which were prepared by Professor Muraji Shibata of Kanazawa University were dark pink needles. A crystal was shaped into a ball with the diameter of *ca.* 0.05 mm, and the intensities were measured on a Philips PW1100 four-circle diffractometer with Cu $K\alpha$ radiation ($\lambda=1.5418$ Å) monochromated by a graphite plate. The θ-2θ scan technique was used at a scan rate of 0.0666°/s in θ with a scan width of $(1.20+0.20\tan\theta)°$. The intensities of the three reference reflections were monitored every 2 h and remained constant within experimental error during data collection. Of 1392 independent reflections measured up to $\theta=65°$, 1302 with $|F|>3\sigma$ were used for the structure analysis. No corrections were made for absorption and extinction effects ($\mu r=0.2$). Cell dimensions were obtained by a least-squares method based on 17 2θ values measured by diffractometry.

Crystal data:
$Co(H_2NCOCH_2CHNH_2COO)_3\cdot 3H_2O$. *F.W.*=506.31. $a=39.082$ (4), $b=7.523$ (2), and $c=6.643$ (2) Å. $U=1953$ (2) Å^3. $Z=4$. $D_x=1.722$ g cm^{-3}. Orthorhombic. Space group $P2_12_12_1$. $\mu=78$ cm^{-1} (Cu $K\alpha$ radiation, $\lambda=1.5418$ Å).

Determination and Refinement of the Structure

The coordinates of the cobalt atom were determined from a Patterson map; successive Fourier syntheses gave the approximate skeletal structure. The block-diagonal least-squares refinement was carried out based on 1302 reflections with a unit weight. The atomic scattering factors were taken from the International Tables for X-Ray Crystallography.[6]

After several cycles of refinement with isotropic temperature factors the *R*-value became 0.077. At this stage the oxygen and nitrogen atoms of each amide group could be distinguished by interatomic distances. Anisotropic temperature factors were, then, introduced for all the non-hydrogen atoms with the anomalous scattering factor of the cobalt atom for Cu $K\alpha$ radiation ($f'=-2.464$, $f''=3.608$).[6] The *R*-value was reduced to 0.064. Of all 27 hydrogen atoms, 23 appeared in a difference Fourier map. Their positional parameters were refined with isotropic temperature factors of 4.0 Å^2. Four hydrogen atoms attached to C(3) and O(1w) could not be found. The final *R*-value was 0.055. The final atomic parameters are listed in Table 1, and a list of the observed and calculated structure amplitudes has been deposited with the Chemical Society of Japan (Document No. 7903).

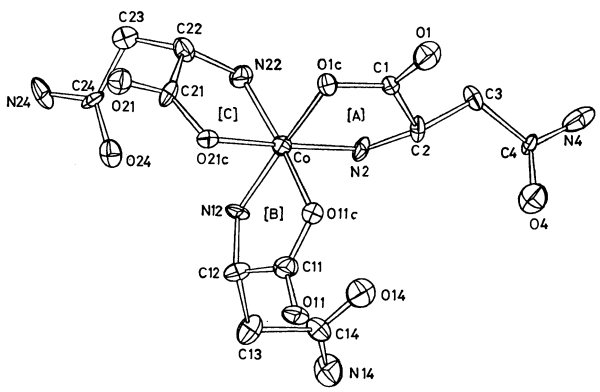

Fig. 1. The molecular structure and the absolute configuration with the anisotropic thermal ellipsoids of the atoms at 50% probability level.

The absolute configuration of the complex was determined by a comparison of the absolute configuration of the coordinated ligand ion with that of the free ligand molecule, and by a comparison of the *R*-values between the correct structure (0.055) and the mirror image (0.116). To confirm the result, another set of reflections ($\bar{h}\bar{k}l$) was measured by diffractometry with Cu $K\alpha$ radiation. All 363 Friedel pairs satisfying $|F(hkl)|/|F(\bar{h}\bar{k}l)| < 0.9$ or > 1.1 gave coincident intensity relations with those calculated, except for 14 weak pairs.

The refinement of the structure and the drawing of thermal ellipsoids were carried out with HBLS-IV[7] and ORTEP[8] programs, respectively. Other calculations were carried out with programs written by the author. A FACOM 230-35 computer at the Data Processing Center of Kanazawa University and a

Table 1a. Final atomic parameters and their estimated standard deviations in parentheses
Thermal parameters are in the form: $\exp[-(h^2\beta_{11}+k^2\beta_{22}+l^2\beta_{33}+hk\beta_{12}+hl\beta_{13}+kl\beta_{23})]$.
Values are multiplied by 10^4.

Atom	x	y	z	β_{11}	β_{22}	β_{33}	β_{12}	β_{13}	β_{23}
Co	1143(1)	7107(3)	9043(3)	2(1)	56(3)	87(4)	0(2)	−0(2)	0(8)
O(1c)	1206(2)	6236(11)	6376(11)	3(1)	88(15)	92(20)	−2(5)	−10(5)	34(31)
O(1)	1610(2)	5560(13)	4173(13)	4(1)	179(20)	95(20)	−16(6)	−7(7)	23(41)
C(1)	1522(3)	5883(15)	5896(19)	2(1)	83(20)	129(28)	0(7)	−2(8)	101(53)
C(2)	1786(3)	5990(16)	7615(18)	1(1)	90(22)	126(29)	6(7)	−8(8)	−34(49)
N(2)	1595(3)	6105(14)	9571(14)	2(1)	117(20)	65(23)	−11(6)	−8(6)	−16(37)
C(3)	2049(3)	4504(16)	7542(21)	3(1)	88(23)	196(36)	8(7)	−15(9)	88(54)
C(4)	2411(3)	5188(18)	7863(19)	1(1)	128(25)	135(32)	−12(7)	−8(8)	115(51)
O(4)	2491(3)	6769(12)	7983(15)	4(1)	94(17)	246(27)	6(6)	7(7)	−80(40)
N(4)	2649(3)	3845(16)	7966(18)	5(1)	136(23)	168(30)	−30(8)	4(9)	−18(50)
O(11c)	1349(2)	9295(11)	8326(12)	3(1)	78(15)	128(21)	−2(5)	−4(6)	40(33)
O(11)	1408(2)	12103(11)	9303(14)	4(1)	54(13)	198(24)	−0(6)	1(7)	72(38)
C(11)	1325(3)	10520(16)	9666(18)	4(1)	86(23)	117(32)	−9(8)	−9(9)	18(46)
C(12)	1156(3)	10060(15)	11624(17)	3(1)	75(20)	91(25)	−8(8)	9(9)	3(40)
N(12)	1097(3)	8132(11)	11720(14)	4(1)	26(15)	93(21)	−0(6)	−3(7)	27(33)
C(13)	1365(3)	10695(18)	13462(19)	3(1)	130(26)	117(32)	−11(8)	−5(8)	−97(50)
C(14)	1731(3)	9973(16)	13476(17)	4(1)	80(21)	66(26)	7(8)	−1(8)	−9(41)
O(14)	1852(3)	9264(12)	11946(13)	5(1)	138(20)	126(22)	−6(6)	−2(7)	−13(39)
N(14)	1901(3)	10198(16)	15170(17)	4(1)	165(25)	164(30)	19(8)	16(8)	−11(50)
O(21c)	710(2)	8081(11)	8297(12)	3(1)	63(14)	151(22)	−3(5)	−2(6)	61(33)
O(21)	161(2)	7429(11)	7882(13)	3(1)	84(17)	152(22)	0(5)	−2(6)	−32(34)
C(21)	460(3)	7012(16)	8397(16)	2(1)	96(21)	58(24)	−9(7)	−2(7)	−85(46)
C(22)	528(3)	5119(15)	9092(20)	3(1)	65(20)	133(29)	5(7)	−13(9)	−10(52)
N(22)	890(3)	4979(14)	9782(15)	3(1)	99(19)	90(24)	−14(7)	−12(7)	28(39)
C(23)	271(3)	4475(15)	10665(18)	3(1)	67(21)	88(28)	−1(7)	8(8)	−45(44)
C(24)	241(3)	5707(15)	12455(18)	2(1)	56(20)	132(29)	−10(6)	10(8)	5(43)
O(24)	396(2)	7161(11)	12512(12)	3(1)	77(14)	126(19)	11(5)	−4(6)	−71(36)
N(24)	31(3)	5202(14)	13931(17)	5(1)	122(21)	109(24)	15(7)	−25(8)	21(47)
O(1w)[a]	2356(3)	224(12)	9105(16)	6(1)	111(18)	213(26)	3(6)	−12(9)	39(46)
O(2w)[a]	833(3)	3849(12)	13945(15)	5(1)	136(18)	157(23)	−5(6)	6(8)	−89(43)
O(3w)[a]	536(3)	1360(13)	6448(21)	7(1)	104(19)	518(50)	6(7)	−29(11)	75(55)

a) Oxygen atoms of the water molecules.

Table 1b. Positional parameters of hydrogen atoms ($\times 10^3$)
The e.s.d.'s are 15—17 ($\times 10^3$).

	x	y	z		x	y	z
H(C2)	194	702	740	H(C22)	49	445	775
H(N2-a)	178	716	1061	H(N22-a)	85	464	1133
H(N2-b)	158	484	996	H(N22-b)	99	393	899
H(N4-a)	267	428	884	H(C23-a)	34	317	1117
H(N4-b)	258	173	812	H(C23-b)	0	421	991
H(C12)	88	1080	1181	H(N24-a)	17	413	1359
H(N12-a)	125	753	1232	H(N24-b)	3	588	1528
H(N12-b)	79	785	1200	H(2w-a)	89	485	1493
H(C13-a)	120	1038	1463	H(2w-b)	108	436	1402
H(C13-b)	139	1215	1346	H(3w-a)	57	−10	679
H(N14-a)	219	1024	1512	H(3w-b)	75	288	583
H(N14-b)	176	981	1664				

FACOM 230-75 computer at the Computation Center of Nagoya University were used.

Description of the Structure and Discussion

The molecular structure is shown in Fig. 1, together with the thermal ellipsoids of the non-hydrogen atoms. The bond distances and angles are listed in Table 2. The projections of the crystal structure on the (010) and (100) planes are shown in Figs. 2 and 3, respectively. The hydrogen bonds are shown in these figures and in Table 3.

The three ligand ions act bidentately through amino nitrogen and carboxyl oxygen atoms forming three five-membered chelate rings in the *Δ* configuration. The cobalt atom is, thus, surrounded by three nitrogen atoms and three oxygen atoms in *fac*(*N*) geometry. This structural feature agrees with the assumption based on the spectroscopic investigation by Takenaka and

Table 2. Interatomic distances and angles within the complex molecule

Co–O(1c)	1.90(1)Å	Co–O(11c)	1.89(1)Å	Co–O(21c)	1.91(1)Å
Co–N(2)	1.95(1)	Co–N(12)	1.95(1)	Co–N(22)	1.94(1)
C(1)–O(1c)	1.30(2)	C(11)–O(11c)	1.28(2)	C(21)–O(21c)	1.27(2)
C(1)–O(1)	1.22(2)	C(11)–O(11)	1.26(2)	C(21)–O(21)	1.26(2)
C(1)–C(2)	1.54(2)	C(11)–C(12)	1.50(2)	C(21)–C(22)	1.52(2)
C(2)–N(2)	1.50(2)	C(12)–N(12)	1.47(2)	C(22)–N(22)	1.49(2)
C(2)–C(3)	1.52(2)	C(12)–C(13)	1.54(2)	C(22)–C(23)	1.53(2)
C(3)–C(4)	1.52(2)	C(13)–C(14)	1.53(2)	C(23)–C(24)	1.51(2)
C(4)–O(4)	1.23(2)	C(14)–O(14)	1.24(2)	C(24)–O(24)	1.25(2)
C(4)–N(4)	1.38(2)	C(14)–N(14)	1.32(2)	C(24)–N(24)	1.33(2)
O(1c)–C(1)–O(1)	122(2)°	O(11c)–C(11)–O(11)	122(2)°	O(21c)–C(21)–O(21)	123(2)°
O(1c)–C(1)–C(2)	116(2)	O(11c)–C(11)–C(12)	118(2)	O(21c)–C(21)–C(22)	118(2)
O(1)–C(1)–C(2)	121(2)	O(11)–C(11)–C(12)	120(2)	O(21)–C(21)–C(22)	119(2)
C(1)–C(2)–C(3)	113(2)	C(11)–C(12)–C(13)	112(1)	C(21)–C(22)–C(23)	113(2)
C(1)–C(2)–N(2)	108(1)	C(11)–C(12)–N(12)	110(1)	C(21)–C(22)–N(22)	109(1)
C(3)–C(2)–N(2)	114(1)	C(13)–C(12)–N(12)	111(1)	C(23)–C(22)–N(22)	113(2)
C(2)–C(3)–C(4)	112(2)	C(12)–C(13)–C(14)	113(1)	C(22)–C(23)–C(24)	113(1)
C(3)–C(4)–O(4)	125(2)	C(13)–C(14)–O(14)	120(2)	C(23)–C(24)–O(24)	121(2)
C(3)–C(4)–N(4)	113(2)	C(13)–C(14)–N(14)	116(2)	C(23)–C(24)–N(24)	117(2)
O(4)–C(4)–N(4)	122(2)	O(14)–C(14)–N(14)	124(2)	O(24)–C(24)–N(24)	122(2)
Co–O(1c)–C(1)	115(1)	Co–O(11c)–C(11)	115(1)	Co–O(21c)–C(21)	115(1)
Co–N(2)–C(2)	109(1)	Co–N(12)–C(12)	110(1)	Co–N(22)–C(22)	110(1)
O(1c)–Co–N(2)	85(1)	O(11c)–Co–N(12)	86(1)	O(21c)–Co–N(22)	86(1)
O(1c)–Co–O(11c)	91(1)	O(11c)–Co–O(21c)	89(1)	O(21c)–Co–O(1c)	90(1)
N(2)–Co–N(12)	94(1)	N(12)–Co–N(22)	93(1)	N(22)–Co–N(2)	96(1)

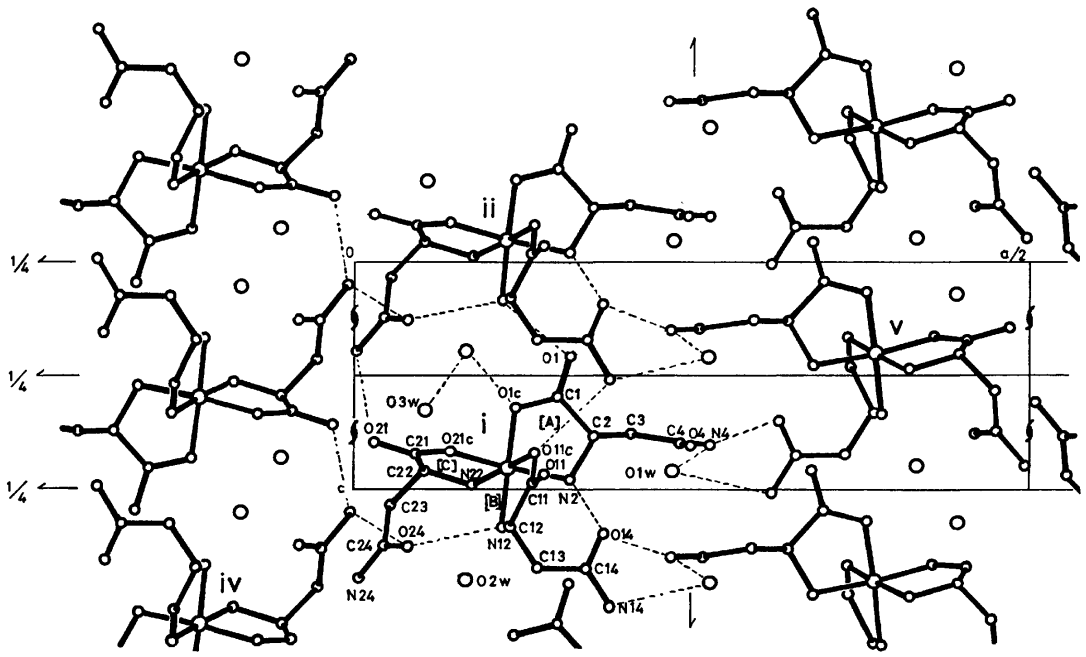

Fig. 2. Projection of the structure on the (010) plane. Dashed lines exhibit hydrogen bonds.

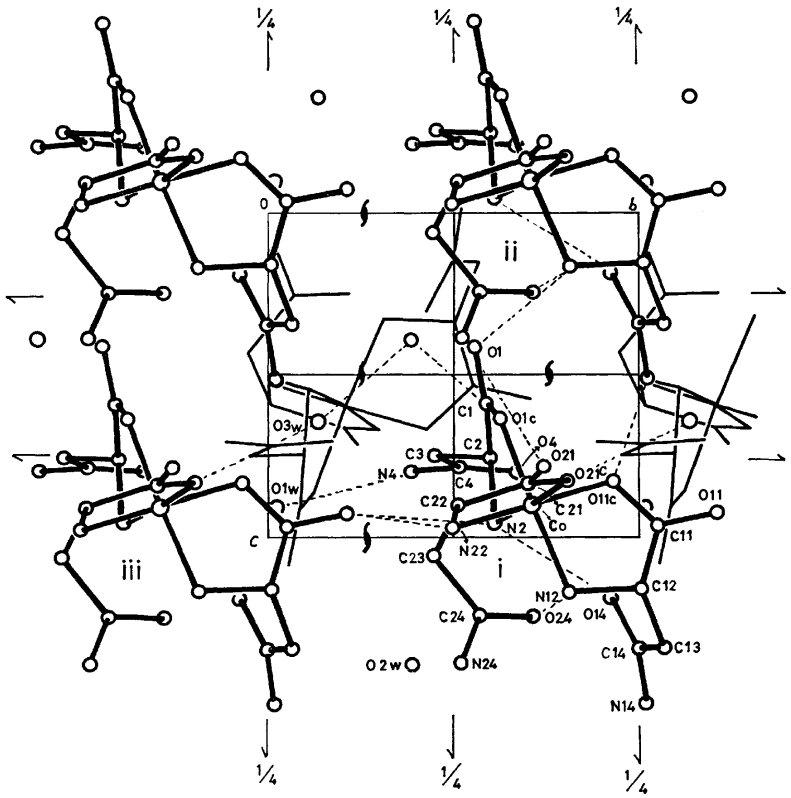

Fig. 3. Projection of the structure on the (100) plane.

TABLE 3. SHORT CONTACTS DUE TO HYDROGEN BONDS

Key to symmetry operations			
i	x	y	z
ii	x	y	$-1+z$
iii	x	$-1+y$	z
iv	$-x$	$1/2+y$	$5/2-z$
v	$1/2-x$	$1-y$	$-1/2+z$

D———H.....A[a]			D–A	D–H	A–H
$N^{I}(2)$	Ha	$O^{I}(14)$	3.02Å	1.28Å	1.83Å
$N^{I}(12)$	Hb	$O^{I}(24)$	2.88	1.23	1.66
$N^{II}(12)$	Ha	$O^{I}(1)$	3.23	0.86	2.37
$O^{I}(3w)$	Hb	$O^{II}(2w)$	2.76	1.47	1.49
$O^{II}(2w)$	Ha	$O^{I}(1c)$	2.82	1.02	1.87
$N^{II}(14)$	Hb	$O^{I}(11c)$	3.09	1.17	1.98
$N^{II}(24)$	Hb	$O^{I}(21)$	3.15	1.03	2.14
$N^{I}(2)$	Hb	$O^{III}(11)$	3.10	0.98	2.22
$N^{I}(22)$	Hb	$O^{III}(11)$	2.98	1.02	2.16
$O^{I}(3w)$	Ha	$O^{III}(21c)$	2.84	1.13	1.78
$N^{IV}(24)$	Ha	$O^{I}(24)$	2.99	0.99	2.75
$N^{I}(4)$	Hb	$O^{V}(14)$	3.12	1.62	2.46
$N^{V}(14)$	Ha	$O^{I}(1w)$	3.00	1.13	1.93

a) D, hydrogen donor; A, hydrogen acceptor.

Shibata.[2]

The Co–N bond lengths are 1.94—1.95 Å, which are longer than the Co–O bond lengths (1.89—1.91 Å). The coordination bond angles of the chelate rings are 85—86°. Thus the octahedron is slightly distorted. Each of the three five-membered chelate rings is nearly planar within 0.15 Å. Two side-chains of chelate rings **[B]** and **[C]** turn their amide groups toward the central atom, so that O(14) and O(24) are connected with N(2) and N(12), respectively, through intramolecular hydrogen bonds (Fig. 2 and Table 3). The side-chain of ring **[A]** is far from the central atom, and N(4) is hydrogen-bonded with O(14) of the neighboring molecule v.

The molecules i and ii are connected with one another through several hydrogen bonds to form columns parallel to the c axis. These columns are combined with each other by hydrogen bonds between molecules i and iii (Fig. 3), thus forming layers along the (100) plane. A three-dimensional network is completed by piling up of an infinite number of these layers through hydrogen bonds.

The author is grateful to Professor Muraji Shibata of Kanazawa University for the supply of crystals, and also to Professor Seiji Sugiura, Department of Mineralogy, Kanazawa University, for the use of the diffractometer.

References

1) H. Takenaka and M. Shibata, *Chem. Lett.*, **1976**, 535.
2) H. Takenaka and M. Shibata, *Bull. Chem. Soc. Jpn.*, **49**, 2133 (1976).
3) M. Sekizaki, *Bull. Chem. Soc. Jpn.*, **51**, 1991 (1978).
4) F. S. Stephens, R. S. Vagg, and P. A. Williams, *Acta Crystallogr., Sect. B*, **31**, 841 (1975).
5) D. R. Williams, *Chem. Revs.*, **72**, 203 (1972).
6) "International Tables for X-Ray Crystallography," Kynoch Press, Birmingham (1974), Vol. IV.
7) T. Ashida, "Universal Crystallographic Computation Program System (UNICS)," ed by T. Sakurai, The Crystallographic Society of Japan, Tokyo (1967).
8) C. K. Johnson, Oak Ridge National Laboratory Report ORNL-3794 (1965).

Stereochemistry of Cobalt(III) Complexes with Sulfur-containing Amino-carboxylate. Mixed Cobalt(III) Complexes with L-Methioninate or *S*-Methyl-L-cysteinate and L- or D-Aspartate

Takashi ISAGO, Kozo IGI,† and Jinsai HIDAKA*

Department of Chemistry, University of Tsukuba, Ibaraki 300-31

(Received May 29, 1978)

Four kinds of $[Co(N)_2(O)_3(S)]$ type mixed complexes, (L- or D-aspartato)(L-methioninato), and (L- or D-aspartato) (*S*-methyl-L-cysteinato)cobalt(III) complexes have been prepared and chromatographically separated into their three geometrical isomers, *trans(N)*, *trans(SO)* and *trans(SN)*, respectively. The isomers were identified from their electronic absorption and PMR spectra. The absolute configurations of sulfur atoms in the ligands after coordination were suggested on the basis of their PMR spectra. The circular dichroism spectra of the isomers were considered in relation to their geometrical configurations.

Bis(terdentate) type Co(III) complexes containing α-amino-carboxylates have been extensively investigated during the past several years.[1-9] However, the relationship between their geometrical configurations and CD spectra remains unsolved because of the peculiarity of configurational chirality. For example, $[Co(L\text{-asp})_2]^-$ (L-asp=L-aspartate) was prepared and separated into their three geometrical isomers,[1] but their configurational assignments on the basis of their CD spectra were unsuccessful.[1,10,11] As for the isomers of $[Co(L\text{-met})_2]^+$ and $[Co(L\text{-smc})_2]^+$ (L-met=L-methioninate and L-smc=*S*-methyl-L-cysteinate),[3,12,13] which have biochemically important functions and quite similar frameworks to those of $[Co(L\text{-asp})_2]^-$, their three isomers have been assigned on the basis of their absorption spectral behavior due to the coordinated sulfur atom of the ligand, though the sulfur atom takes *R* or *S* configuration after coordination. Recently, Yamanari *et al.*[14] reported the preparation and separation of the isomers of two kinds of mixed type cobalt(III) complexes, [(2-aminoethylthio)acetato](L-methioninato) and [3-(2-aminoethylthio)propionato](L-methioninato)cobalt-(III), and suggested the vicinal CD contribution due to the chiral sulfur atom of L-methioninate by applying an additivity rule for the CD curves of their diastereomeric pairs. In these circumstances, it is significant to investigate the properties of the mixed Co(III) complexes with L- or D-aspartate and L-methioninate or *S*-methyl-L-cysteinate. In the present work, the mixed Co(III) complexes, [Co(L-asp)(L-met)], [Co(D-asp)(L-met)], [Co(L-asp)(L-smc)], and [Co(D-asp)(L-smc)], have been prepared and chromatographically separated into their three geometrical isomers, respectively. The isomers have been characterized from their electronic absorption and PMR spectra. The absolute configurations of sulfur atoms after coordination were also suggested on the basis of their PMR spectra. Their CD spectra were discussed mainly in relation to the geometrical configurations of the isomers.

Experimental

Preparation and Separation of Isomers. *(L-Aspartato)(L-methioninato)cobalt(III)*, *[Co(L-asp)(L-met)]*: A solution containing 0.9 g of L-aspartic acid and 1.1 g of L-methionine in 20 cm³ of water was adjusted to pH 8 by the addition of sodium hydroxide aqueous solution. This was added to a a hot solution (*ca.* 65 °C) containing 1.6 g of cobalt(II) chloride hexahydrate in 30 cm³ of water. 3.0 g of lead dioxide and 0.5 g of activated charcoal were gradually added to the solution, which was then stirred at 65 °C for 30 min, the color of the solution turning violet. The mixture was filtered in order to remove the excess of lead dioxide and charcoal after cooling to room temperature. The filtrate was passed through an anion-exchange column of Dowex 1-X8 (Cl^- form, 200—400 mesh, 4.5×20 cm) and successively through a cation-exchange column of Dowex 50W-X8 (Na^+ form, 100—200 mesh, 4.5×20 cm) in order to obtain a solution containing the neutral species which are the isomers of [Co(L-asp)(L-met)]. The eluate was concentrated to 5—10 cm³. Chromatographic seapration was then carried out through a cation-exchange column of Dowex 50W-X8 (Na^+ form, 200—400 mesh, 3.0×120 cm). The adsorbed band was eluted with water at a rate of 0.4 cm³/min. Three colored bands, dark violet (F-1), purple (F-2) and reddish violet (F-3) were eluted in succession. Here the F-2 isomer followed closely after the F-1 isomer. The three eluates were separately concentrated to dryness in a rotary evaporator below 30 °C. The F-2 isomer was recrystallized from hot water, and the F-1 and F-3 isomers were recrystallized from as little water as possible by adding ethanol. The F-2, isomer was less soluble in water. The F-1 isomer formed needle crystals, the F-2 isomer flaky crystals and the F-3 isomer hexagonal crystals. Found for F-1: C, 28.21; H, 5.25; N, 7.31%. Calcd for $[Co(L\text{-asp})(L\text{-met})]\cdot 2.5H_2O = CoC_9H_{15}N_2O_6S\cdot 2.5H_2O$: C, 28.20; H, 5.26; N, 7.31%. Found for F-2: C, 31.57; H, 4.52; N, 8.24%. Calcd for $[Co(L\text{-asp})(L\text{-met})] = CoC_9H_{15}N_2O_6S$: C, 31.96; H, 4.42; N, 8.24%. Found for F-3: C, 30.24; H, 4.85; N, 7.85%. Calcd for $[Co(L\text{-asp})(L\text{-met})]\cdot H_2O = CoC_9H_{15}N_2O_6S\cdot H_2O$: C, 30.34, H, 4.81; N, 7.86%.

(D-Aspartato)(L-methioninato)cobalt(III), *[Co(D-asp)(L-met)]*: Preparation was carried out according to a method similar to that for [Co(L-asp)(L-met)] by using an anion-exchange column (Dowex 1-X8, Cl^- form) and a cation-exchange column (Dowex 50W-X8, Na^+ form). Chromatographic separation was carried out through a column of QAE-Sephadex A-25 (Cl^- form, 3.3×250 cm) instead of Dowex 50W-X8 (Na^+ form, 200—400 mesh, 3.0×120 cm). The adsorbed band was eluted with water at a rate of 0.3 cm³/min. Three colored bands, gray-violet (G-1), reddish violet (G-2), and pink-violet (G-3) were eluted in succession. The G-2

† Present address: Department of Chemistry, Washington State University, Pullman, Washington 99164.

isomer followed colsely after the G-1 isomer. The three eluates were separately concentrated to dryness in a rotary evaporator below 30 °C. The G-1 and G-3 isomers were recrystallized from hot water and the G-2 isomer was recrystallized from as little water as possible by adding ethanol. The G-1 and G-3 isomers were sparingly soluble in water and the G-2 isomer was very soluble in water. The G-1 isomer formed needle crystals and the G-3 isomer rod crystals whereas the G-2 isomer was powdery. Found for G-1: C, 30.51; H, 4.95; N, 7.80%. Calcd for [Co(D-asp)(L-met)]·H_2O=$CoC_9H_{15}N_2O_6S\cdot H_2O$: C, 30.34; H, 4.81; N, 7.86%. Found for G-2: C, 26.78; H, 4.85; N, 6.92%. Calcd for [Co(D-asp)(L-met)]·$2H_2O$·0.5NaCl = $CoC_9H_{15}N_2O_6S\cdot 2H_2O\cdot 0.5NaCl$: C, 26.79; H, 4.75; N, 6.94%. Found for G-3: C, 28.82; H, 4.68; N, 7.49%. Calcd for [Co(D-asp)(L-met)]·$2H_2O$=$CoC_9H_{15}N_2O_6S\cdot 2H_2O$: C, 28.88; H, 5.12; N, 7.49%.

(L-Aspartato)(S-methyl-L-cysteinato)cobalt(III), *[Co(L-asp)(L-smc)]*: A solution containing 1.2 g of L-aspartic acid and 1.2 g of *S*-methyl-L-cysteine in 20 cm^3 of water was adjusted to pH 6 by the addition of sodium hydroxide aqueous solution. This was added to a hot solution (*ca.* 65 °C) containing 2.0 g of cobalt(II) chloride hexahydrate in 30 cm^3 of water. 3.0 g of lead dioxide and 0.5 g of activated charcoal were gradually added to the solution which was then stirred at 65 °C for 30 min, the color of the solution turning violet. After the mixture had been filtered, the filtrate was passed through an anion-exchange column and then a cation-exchange column in order to obtain a solution containing the neutral species which are the isomers of [Co(L-asp)(L-smc)]. Chromatographic separation was carried out by a method similar to that for [Co(D-asp)(L-met)], using a column of QAE-Sephadex A-25 (Cl^- form, 3.3×250 cm). Three colored bands, purple (H-1), dark violet (H-2), and light purple (H-3) were eluted in succession. The H-2 isomer followed closely after the H-1 isomer. The three eluates were separately concentrated to dryness in a rotary evaporator below 30 °C. Each crude product was recrystallized from as little water as possible by addition of ethanol. The H-3 isomer formed needle crystals whereas the H-1 and H-2 isomers were powdery. Found for H-1: C, 25.42; H, 4.69; N, 7.30%. Calcd for Co(L-asp)(L-smc)]·$3H_2O$=$CoC_8H_{13}N_2O_6S\cdot 3H_2O$: C, 25.40; H, 5.06; N, 7.41%. Found for H-2: C, 24.76; H, 4.68; N, 7.27%. Calcd for [Co(L-asp)(L-smc)]·$3.5H_2O$=$CoC_8H_{13}N_2O_6S\cdot 3.5H_2O$: C, 24.81; H, 5.20; N, 7.23%. Found for H-3: C, 26.27; H, 4.76; N, 7.64%. Calcd for [Co(L-asp)(L-smc)]·$2H_2O$=$CoC_8H_{13}N_2O_6S\cdot 2H_2O$: C, 26.67; H, 4.76; N, 7.78%.

(D-Aspartato)(S-methyl-L-cysteinato)cobalt(III), *[Co(D-asp)(L-smc)]*: The preparation was carried out according to a method similar to that for [Co(L-asp)(L-smc)]. Chromatographic separation was accomplished according to a method similar to that for [Co(L-asp)(L-met)], using a column of Dowex 50W-X8 (Na^+ form, 200—400 mesh, 3.0×120 cm). Three colored bands, purple (I-1), gray-violet (I-2), and light purple (I-3) were eluted in succession. The I-2 isomer followed closely after the I-1 isomer. The three eluates were separately concentrated to dryness in a rotary evaporator below 30 °C. The I-2 and I-3 isomers were recrystallized from hot water and the I-1 isomer was recrystallized from as litlte water as possible by adding ethanol. The I-2 isomer was sparingly soluble in water. The I-2 isomer formed needle crystals and the I-3 isomer cubic crystals whereas the I-1 isomer was powdery. The yields of the I-1 and I-2 isomers were rather small. Found for I-1: C, 26.50; H, 4.90; N, 7.72%. Calcd for [Co(D-asp)(L-smc)]·$2H_2O$=$CoC_8H_{13}N_2O_6S\cdot 2H_2O$: C, 26.67; H, 4.76; N, 7.78%. Found for I-2: C, 29.31; H, 4.08; N, 8.57%. Calcd for [Co(D-asp)(L-smc)]=$CoC_8H_{13}N_2O_6S$: C, 29.64; H, 4.04; N, 8.64%. Found for I-3: C, 27.78; H, 4.58; N, 8.22%. Calcd for [Co(D-asp)(L-smc)]·H_2O=$CoC_8H_{13}N_2O_6S\cdot H_2O$: C, 28.08; H, 4.42; N, 8.19%.

Measurements. Electronic absorption spectra were measured with a JASCO UVIDEC-1 spectrophotometer in aqueous solution. CD spectra were recorded with a JASCO J-20 spectropolarimeter. Proton magnetic resonance spectra were recorded in deuterium oxide or trifluoroacetic acid (CF_3COOH) on a JEOL JUM-MH-100 NMR spectrometer with DSS as an internal reference. All measurements were carried out at room temperature.

Results and Discussion

Absorption Spectra and Configurational Assignment. Three geometrical isomers are possible for the present $[Co(N)_2(O)_3(S)]$ type complex because of the stereospecific regulation by the coordinated terdentate ligands. The three isomers for each of [Co(L-asp)(L-met)], [Co(D-asp)(L-met)], [Co(L-asp)(L-smc)], and [Co(D-asp)(L-smc)] are shown in Fig. 1. The isomers are designated as *trans(N)*, *trans(SO)*, and *trans(SN)* with respect to the coordinated atoms, N, O, and S. The absorption spectra of the isomers of [Co(L- or D-asp)(L-met)] are shown in Fig. 2 and their data are summarized in Table 1. For all the isomers the first absorption bands are located at around 19000 cm^{-1} and the charge transfer bands due to the coordinated sulfur atoms at around 33000 cm^{-1}. The second absorption bands appear as shoulders on the lower energy side of the thioether charge transfer bands. The shape of the first absorption band for each of the isomers can be expected from the semi-empirical calculation[15] on the basis of the ligand field order N>S>O.[16–18] The first absorption band of the *trans(N)* isomer is expected to show a well separated minor component on the lower energy side of the major one, that of the *trans(SN)* isomer a broad band, and the *trans(SO)* isomer a sharp band. As seen in Fig. 2 and Table 1, the F-1 isomer of [Co(L-asp)(L-met)] shows an explicit shoulder on the lower energy side of the major peak (19600 cm^{-1}), and the G-1 isomer of [Co(D-asp)(L-met)] a peak on the lower energy side of the major one (19600 cm^{-1}). Thus F-1 and G-1 isomers are assigned to *trans(N)* form. The similar splitting pattern was also observed for the *trans(N)* isomers of $[Co(L\text{-met})_2]^+$,[3] $[Co(L\text{-smc})_2]^+$,[12] and $[Co(L\text{-asp})_2]^-$.[1] The F-2 isomer of [Co(L-asp)(L-met)] shows a broad band and the G-2 isomer of [Co(D-asp)(L-met)] a broad band with a vague shoulder on the higher energy side, while the F-3 isomer of [Co(L-asp)(L-met)] and the G-3 isomer of [Co(D-asp)(L-met)] show apparently a sharp band. These absorption patterns indicate that the F-2 and G-2 isomers are *trans(SN)* form and the F-3 and G-3 ones *trans(SO)* form in accordance with the expected splittings which were estimated semiempirically.[15] A similar treatment was successfully applied to the isomers of bis[(2-aminoethylthio)acetato]cobalt(III) complex.[18] The present assignment is in line with that based on the PMR spectra (*vide post*). The absorption spectra of the isomers of [Co(L- or D-asp)(L-smc)] are shown in Fig. 3 and their

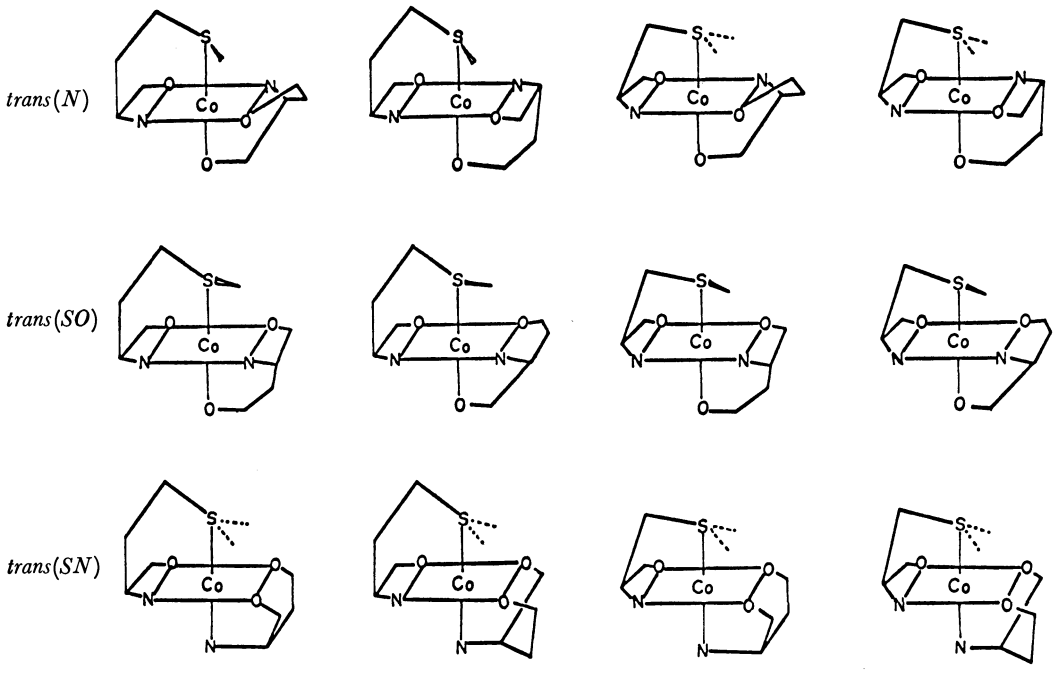

Fig. 1. Three geometrical isomers of [Co(L-asp)(L-met)] (a), [Co(D-asp)(L-met)] (b), [Co(L-asp)(L-smc)] (c) and [Co(D-asp)(L-smc)] (d).

TABLE 1. ABSORPTION DATA OF ISOMERS OF [Co(L- OR D-asp)(L-met)] AND [Co(L- OR D-asp)(L-smc)]
Wave numbers and log ε values (in parentheses) are given in 10^3 cm^{-1} and mol^{-1} dm^3 cm^{-1}, respectively.

Isomer	First absorption band	Second absorption band	Charge transfer band
trans(*N*)-[Co(L-asp)(L-met)]	16.8 (1.60)[a]	26.3 (2.13)[a]	33.0 (3.94)
	19.6 (1.93)		41.7 (4.03)[a]
			46.9 (4.11)
trans(*N*)-[Co(D-asp)(L-met)]	16.7 (1.76)	26.3 (2.23)[a]	32.5 (3.98)
	19.6 (1.97)		42.6 (4.13)[a]
			46.5 (4.18)
trans(*N*)-[Co(L-asp)(L-smc)]	16.7 (1.73)[a]	26.3 (2.09)[a]	33.9 (3.93)
	19.6 (1.99)		41.7 (4.04)[a]
			47.6 (4.11)
trans(*N*)-[Co(D-asp)(L-smc)]	16.4 (1.67)	26.3 (1.99)[a]	33.3 (3.93)
	19.6 (1.93)		43.5 (4.05)[a]
			47.2 (4.08)
trans(*SN*)-[Co(L-asp)(L-met)]	18.9 (2.15)	26.7 (2.34)[a]	33.6 (3.95)
			43.5 (4.08)[a]
			45.5 (4.09)
trans(*SN*)-[Co(D-asp)(L-met)]	18.2 (2.00)	26.3 (2.27)[a]	33.3 (3.95)
			43.5 (4.10)[a]
			45.2 (4.11)
trans(*SN*)-[Co(L-asp)(L-smc)]	19.2 (2.22)	26.7 (2.33)[a]	34.5 (3.93)
			43.5 (4.10)[a]
			46.7 (4.17)
trans(*SN*)-[Co(D-asp)(L-smc)]	18.5 (2.14)	26.3 (2.26)[a]	33.9 (3.94)
			42.6 (4.13)[a]
			47.8 (4.16)
trans(*SO*)-[Co(L-asp)(L-met)]	18.5 (2.15)	26.3 (2.07)[a]	32.9 (4.02)
			45.5 (4.18)
trans(*SO*)-[Co(D-asp)(L-met)]	18.9 (2.28)	26.3 (2.14)[a]	33.2 (4.02)
			45.2 (4.13)
trans(*SO*)-[Co(L-asp)(L-smc)]	18.2 (2.22)	26.3 (2.06)[a]	33.1 (3.95)
			45.7 (3.95)
trans(*SO*)-[Co(D-asp)(L-smc)]	18.7 (2.29)	26.7 (2.05)[a]	33.6 (3.93)
			45.0 (4.10)

a) A shoulder.

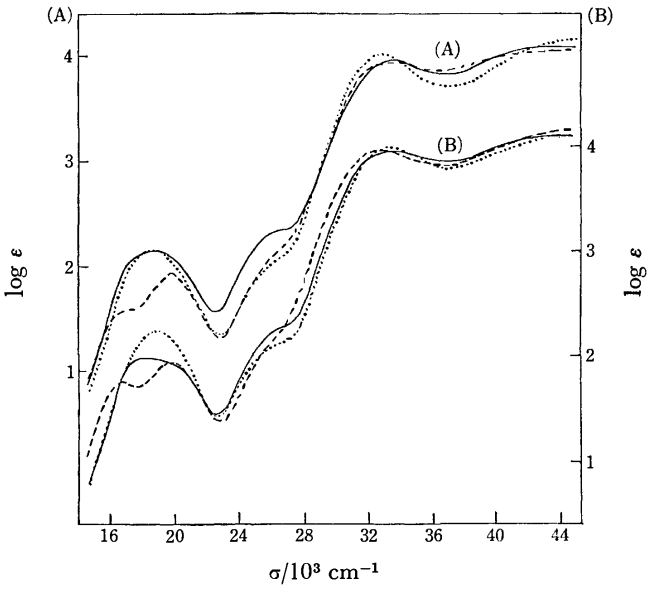

Fig. 2. Absorption spectra for the isomers of [Co(L-asp)-(L-met)] (A); F-1 (——), F-2 (——), and F-3 (·····) and [Co(D-asp)(L-met)] (B); G-1 (——), G-2 (——), and G-3 (·····).

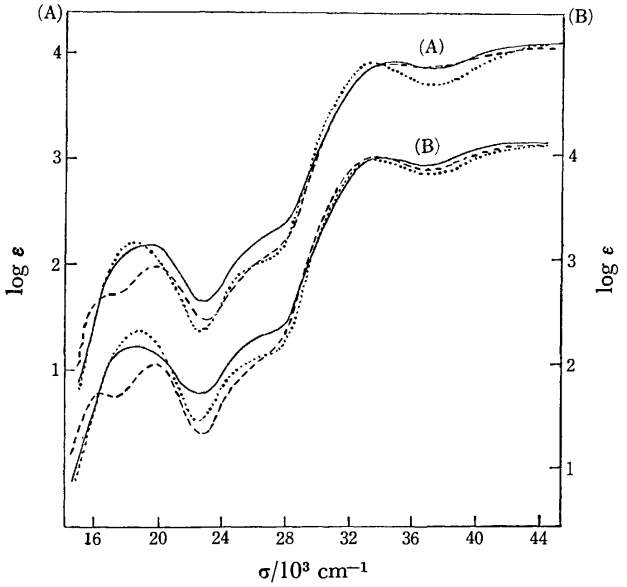

Fig. 3. Absorption spectra for the isomers of [Co(L-asp)-(L-smc)] (A); H-1 (——), H-2 (——) and H-3 (·····) and [Co(D-asp)(L-smc)] (B); I-1 (——), I-2 (——), and I-3 (·····).

data are summarized in Table 1. The splitting behavior of their first absorption bands is very similar to that of the corresponding isomers of L-methioninato complex. Thus the H-1, H-2, and H-3 isomers of [Co(L-asp)(L-smc)] are assigned to *trans(SN)*, *trans(N)*, and *trans(SO)* forms, respectively. As for the [Co(D-asp)(L-smc)], the I-1, I-2, and I-3 isomers are assigned to *trans(SN)*, *trans(N)*, and *trans(SO)* forms, respectively.

Proton Magnetic Resonance Spectra. Proton magnetic resonance spectra of the isomers isolated were measured in D_2O or trifluoroacetic acid. Representative spectra are shown in Fig. 4. The sulfur atom of a thioether

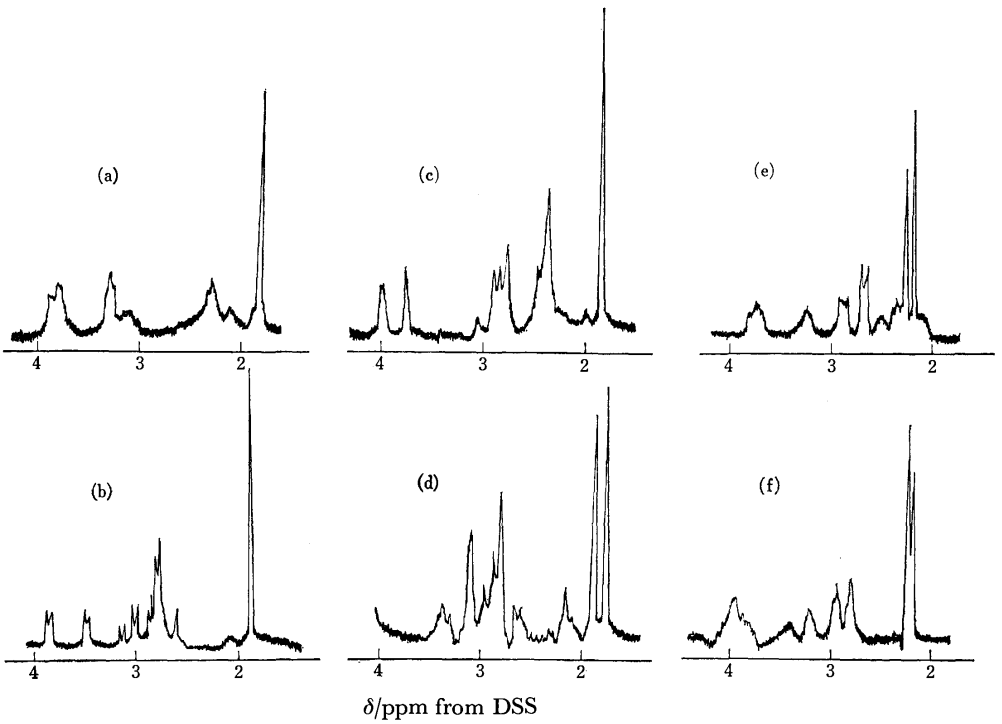

Fig. 4. The representative PMR spectra for the isomers of [Co(L- or D-asp)(L-met)] and [Co(L- or D-asp)(L-smc)]: (a) *trans(SO)*-[Co(L-asp)(L-met)] in CF_3COOH, (b) *trans(SO)*-[Co(L-asp)(L-smc)] in D_2O, (c) *trans(N)*-[Co(L-asp)(L-met)] in D_2O, (d) *trans(N)*-[Co(L-asp)(L-smc)] in D_2O, (e) *trans(SN)*-[Co(D-asp)(L-met)] in D_2O and (f) *trans(SN)*-[Co(D-asp)(L-smc)] in D_2O.

ligand becomes chiral by coordination, leaving on itself a single lone-pair which can give a fixed configuration for the donor center at ordinary temperature.[14] The sulfur atom of L-methioninate or *S*-methyl-L-cysteinate should take *R* or *S* configuration after coordination. Taking the chiral sulfur atom into consideration, two isomers of another type are expected for each of the three geometrical isomers. Each reacted solution was separated chromatographically into three bands (*trans*-(*N*), *trans*(*SN*), and *trans*(*SO*) isomers), the detailed fractions of each separated band showing similar CD spectra. This suggests that the isomers due to the configuration *R* or *S* of the chiral sulfur atom are not separable from each other by the present procedure or the sulfur atom is coordinated stereoselectively. As seen in Figs. 4 and 5, the F-3, G-3, H-3, and I-3 isomers assigned to *trans*(*SO*) from their absorption spectra show a single peak (1.87[1.88] ppm for F-3, [2.00] ppm for G-3, 1.90 ppm for H-3 and 1.98 ppm for I-3. Chemical shifts in trifluoroacetic acid are shown in the brackets) in the *S*-methyl proton region, respectively. It seems that sulfur atoms of these isomers selectively take either *R* or *S* configuration. Molecular model constructions indicate that the *S*-methyl group of *trans*(*SO*) isomer has a significant steric interaction with the amino group of L- or D-aspartate chelate when the sulfur atom takes *R* configuration, while no interaction arises for *S* configuration. A similar result was obtained for the sulfur atoms of *trans*(*S*)-[Co(L-smc)$_2$]$^+$ [12,13] which has a similar framework to the present *trans*(*SO*) isomers. On the other hand, the F-2, G-2, H-1, and I-1 isomers assigned to *trans*(*SN*) show two peaks (2.27, 2.16 ppm for F-2; 2.13, 2.25 ppm for G-2; 2.19, 2.33 ppm for H-1, and 2.21, 2.26 ppm for I-1) in the *S*-methyl proton region, respectively (Figs. 4 and 5). The results indicate that each of the isomers contains the sulfur atoms of both *R* and *S* configurations. Molecular models reveal that the sulfur atoms of *trans*(*SN*) isomers can easily coordinate in both configurations *R* and *S* (Fig. 1). The F-1 and G-1 isomers assigned to *trans*(*N*) show a single peak (1.82 ppm for F-1 and 1.79 ppm for G-1) due to the *S*-methyl protons of L-methioninate, respectively. These *trans*(*N*) isomers seem to take *R* configuration, since the *S*-methyl group is *S* configuration interacts with the amino group of L- or D-aspartate (Fig. 1). However, the H-2 and I-2 isomers assigned similarly to *trans*(*N*) show two peaks (1.91, 1.80 ppm for H-2 and 1.90, 1.78 ppm for I-2) due to the *S*-methyl protons of *S*-methyl-L-cysteinate, respectively (Figs. 4 and 5). This indicates that both of the isomers contain the sulfur atoms of both *R* and *S* configurations. The difference between the *trans*(*N*)-L-methioninato and *S*-methyl-L-cysteinato isomers is attributed to the situation in which the steric interaction between the *S*-methyl group in *S*-configuration and the adjacent amino group of aspartate is more serious in orientation of *S*-methyl group for the six-membered chelate ring of L-methioninato isomers than for the five-membered ring of *S*-methyl-L-cysteinato isomers (Fig. 1). The consideration on the basis of their PMR spectra and molecular model constructions is in line with the structural arguments from their first absorption band patterns.

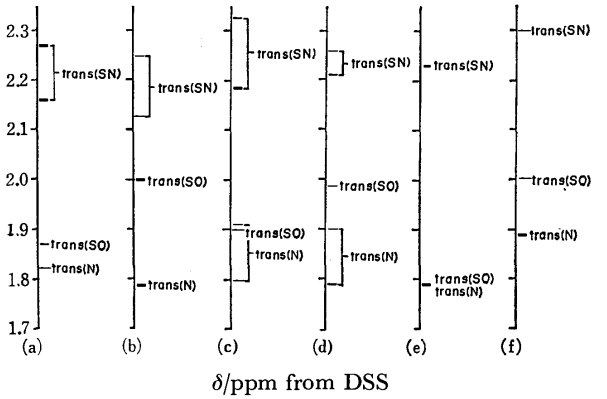

Fig. 5. The distribution of the *S*-methyl protons' chemical shifts: (a) [Co(L-asp)(L-met)], (b) [Co(D-asp)(L-met)], (c) [Co(L-asp)(L-smc)], (d) [Co(D-asp)(L-smc)], (e) [Co(ida)(L-met)], and (f) [Co(ida)(L-smc)].

The chemical shifts of *S*-methyl protons of the twelve isomers isolated are summarized in Fig. 5 with those of six isomers of (iminodiacetato)(L-methioninato) and (iminodiacetato)(*S*-methyl-L-cysteinato)cobalt(III).[20] The PMR spectra were measured in D_2O except for *trans*(*SO*)-[Co(D-asp)(L-met)] which was measured in trifluoroacetic acid because of its low solubility in D_2O. The values can be arranged in order in accordance with their geometries (Figs. 1 and 5). The chemical shifts of the *trans*(*N*) isomers (F-1, G-1, H-2, and I-2) and *trans*(*SO*) isomers (F-3, G-3, H-3, and I-3) appear in a higher magnetic field (1.7—2.0 ppm) than those of the *trans*(*SN*) isomers (F-2, G-2, H-1, and I-1) (2.1—2.4 ppm). The chemical shifts of *trans*(*SO*) isomers are similar to those of *trans*(*N*) ones, though the former has a tendency to a slightly lower field (Fig. 5). This is understandable from the fact that the oxygen atom occupies the trans position to the sulfur atom for the *trans*(*N*) and *trans*(*SO*) isomers, whereas the nitrogen

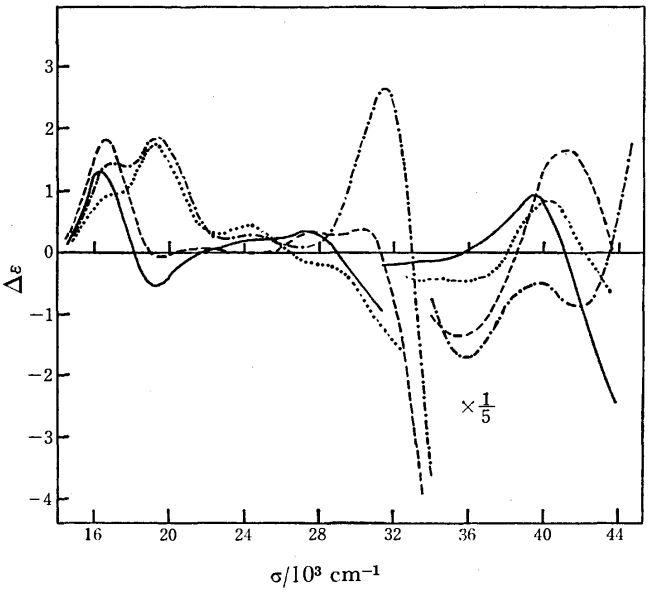

Fig. 6. CD spectra of *trans*(*N*) complexes: [Co(L-asp)(L-met)](-·-·-), [Co(D-asp)(L-met)](——), [Co(L-asp)(L-smc)](·····), and [Co(D-asp)(L-smc)] (——).

Table 2. CD data of isomers of [Co(L- or D-asp)(L-met)] and [Co(L- or D-asp)(L-smc)]
Wave numbers and $\Delta\varepsilon$ values (in parenthese) are given in 10^3 cm^{-1} and mol^{-1} dm^3 cm^{-1}, respectively.

Isomer	First absorption band	Second absorption band	Charge transfer band
trans(*N*)-[Co(L-asp)(L-met)]	16.9(+1.47) 19.4(+1.90)	24.4(+0.29)	31.3(+2.65) 35.7(−8.54) 42.0(−0.46) 45.9(+12.7)
trans(*N*)-[Co(D-asp)(L-met)]	16.6(+1.86) 19.5(−0.07) 21.3(+0.07)	27.8(+0.33)	29.9(+0.38) 35.7(−6.67) 41.2(+8.26)
trans(*N*)-[Co(L-asp)(L-smc)]	16.9(+0.93)[a] 19.2(+1.75)	24.1(+0.44)	35.5(−2.33) 40.0(+4.15)
trans(*N*)-[Co(D-asp)(L-smc)]	16.4(+1.25) 19.2(−0.52)	25.0(+0.18) 27.2(+0.31)	31.5(−0.98) 39.2(+4.35) 47.2(−2.97)
trans(*SN*)-[Co(L-asp)(L-met)]	16.5(+0.66) 18.3(−1.55) 20.5(+0.78)	26.2(+0.66)	31.1(+1.44) 35.7(−5.74) 44.4(+19.5)
trans(*SN*)-[Co(D-asp)(L-met)]	17.8(−1.29) 20.5(+0.90)	25.0(+0.34)	30.3(+0.53) 34.5(−6.20) 39.2(+5.72)
trans(*SN*)-[Co(L-asp)(L-smc)]	16.5(+0.15) 18.0(−0.20) 20.0(+1.04)	26.7(+0.44)	34.5(−5.83) 43.9(+14.2)
trans(*SN*)-[Co(D-asp)(L-smc)]	17.2(−1.44) 20.5(+0.98)	25.5(+0.24)	34.4(−6.75) 40.0(+8.41) 47.6(−8.41)
trans(*SO*)-[Co(L-asp)(L-met)]	17.6(+1.48) 20.6(−0.46)	26.3(−0.73)	38.5(+1.22) 45.0(+12.5)
trans(*SO*)-[Co(D-asp)(L-met)]	17.3(+0.43) 20.2(−0.83)	26.8(−0.59)	34.5(−1.90) 44.1(+13.1)
trans(*SO*)-[Co(L-asp)(L-smc)]	17.5(+2.52) 20.4(−0.70)	25.1(−1.05)	32.8(−13.0) 42.9(+17.1)
trans(*SO*)-[Co(D-asp)(L-smc)]	17.3(+1.36) 20.2(−0.83)	24.5(−0.89)	33.3(−13.5) 42.9(+18.6)

a) A shoulder.

atom occupies the trans position for the *trans*(*SN*) isomers. The results are in line with the PMR spectra for the isomers of (L- or D-aspartato)(L-2,4-diaminobutyrato)cobalt(III) complexes.[19] In these complexes, the carbon proton adjacent to the coordinated nitrogen atom resonates at a higher magnetic field when oxygen atom occupies trans position to the nitrogen atom than when nitrogen atom occupies the same position.

Circular Dichroism Spectra. The CD curves of *trans*(*N*)-[Co(L- or D-asp)(L-met)] and [Co(L- or D-asp)-(L-smc)] are shown in Fig. 6 and their data are summarized in Table 2. In the first absorption band region, the two L-aspartato complexes, [Co(L-asp)(L-met)] and [Co(L-asp)(L-smc)], show two positive CD bands which correspond to their absorption components (Table 1). This CD pattern is similar to that of *trans*(*N*)-[Co(L-asp)$_2$]$^-$ [1] and of *trans*(*N*)-[Co(L-met)$_2$]$^+$ [3] The replacement of the ligand L-aspartate by D-aspartate reveals a negative CD component at the higher energy side, though the positive CD band at the lower energy side remains unchanged. A similar CD behavior was observed for the curves of *trans*(*SN*) isomers (Fig. 7 and Table 2). In this isomer, however, the replacement of the D-aspartate to L-aspartate reveals a positive CD component at the lower energy side in contrast with the case of *trans*(*N*) isomers, the CD band at the higher energy side remaining unchanged. The CD curves of *trans*(*SO*) isomers show a similar CD pattern (+ and − from the lower energy) to each other in the corresponding region,

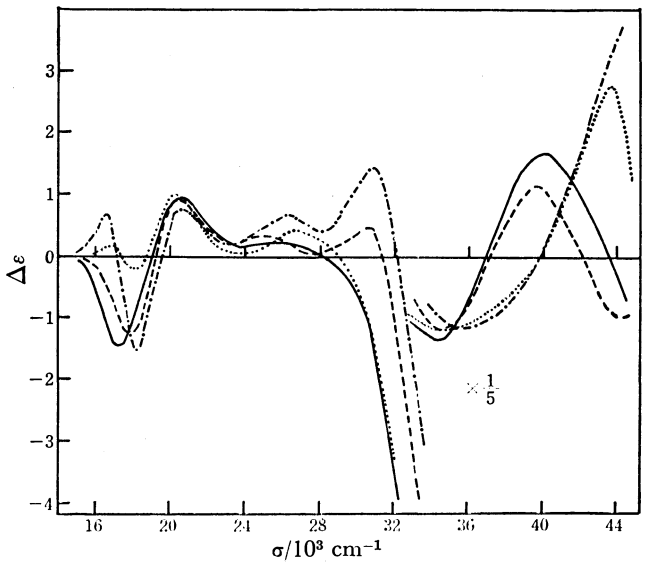

Fig. 7. CD spectra of *trans*(*SN*) complexes: [Co(L-asp)-(L-met)](-•-•-), [Co(D-asp)(L-met)](——), [Co(L-asp)-(L-smc)](·····), and [Co(D-asp)(L-smc)] (——).

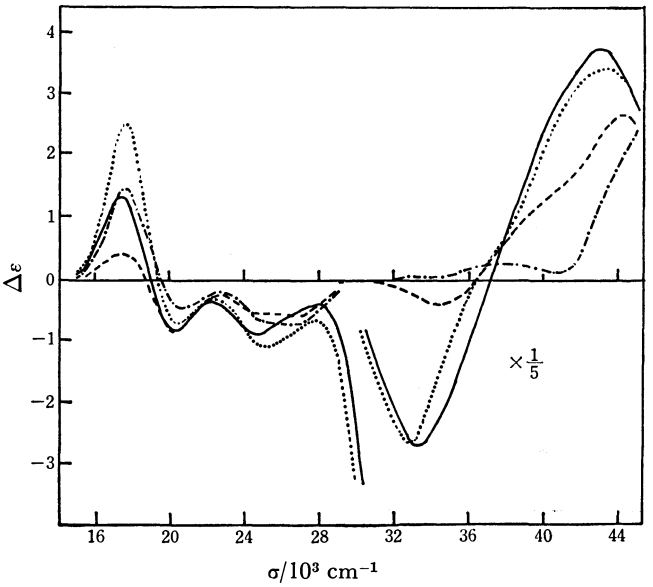

Fig. 8. CD spectra of *trans(SO)* complexes: [Co(L-asp)-(L-met)](-·--·-), [Co(D-asp)(L-met)](——), [Co(L-asp)-(L-smc)](·····), and [Co(D-asp)(L-smc)](——).

though the positive CD band intensities significantly differ from each other (Fig. 8 and Table 2). This pattern might be related to the situation where the first absorption components of *trans(SO)* isomer are close to each other. These observations approximately suggest that the LL mixed or DL mixed type complexes of each of three isomers show a similar CD pattern regardless of L-methioninate coordination or *S*-methyl-L-cysteinate one, the CD pattern depending mainly on the L- or D-aspartate coordination in the first absorption band region.

The three isomers of [Co(L-asp)(L-met)] are very similar in framework to the corresponding isomers of $[Co(L\text{-}asp)_2]^-$ or $[Co(L\text{-}met)_2]^+$. As an example, the *trans(N)* isomer of the mixed complex corresponds to *trans(N)*-$[Co(L\text{-}asp)_2]^-$, the *trans(SN)* isomer to *trans*-(O_5)-$[Co(L\text{-}asp)_2]^-$ and the *trans(SO)* isomer to *trans*(O_6)-$[Co(L\text{-}asp)_2]^-$, respectively. The *trans(SN)* and *trans(SO)* isomers of [Co(L-asp)(L-met)] are quasiantipodal in framework as in the case of the *trans*(O_5) and *trans*(O_6) isomers of $[Co(L\text{-}asp)_2]^-$. In fact, the CD curves of the *trans(SN)* and *trans(SO)* isomers reflect their antipodal relationship in the first and second absorption band region, though the *trans(SN)* isomer shows a positive CD band (16500 cm^{-1}), which suggests a lowering of molecular symmetry or the vicinal CD contributions (Fig. 9). A similar consideration is also applicable to each pair of the *trans(SO)* and *trans(SN)* isomers of [Co(D-asp)(L-met)] or [Co(L- or D-asp)(L-smc)] (Figs. 7 and 8). The quasiantipodal relationship in framework and CD curve is better for the DL mixed complexes than for the LL mixed ones, being especially good for the *trans(SO)* and *trans(SN)* isomers of [Co(D-asp)(L-met)]. From these observations in the first and second absorption band regions, it seems that the CD patterns of the complexes are understandable in relation to their frameworks so far as the present terdentate ligands are concerned. It was suggested that the sulfur chirality of

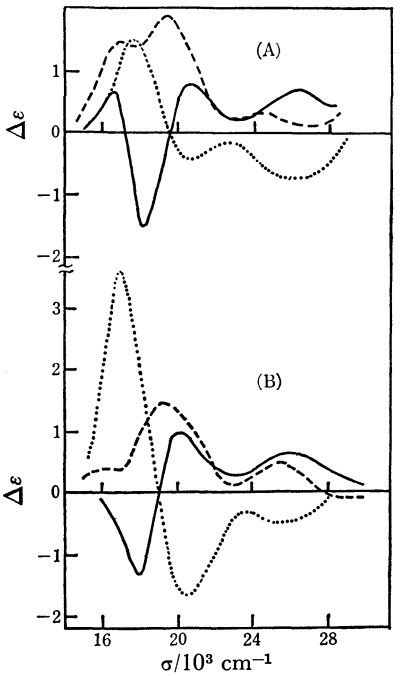

Fig. 9. The CD spectra for isomers of [Co(L-asp)(L-met)] (A), [*trans(N)*(——), *trans(SN)*(——), and *trans(SO)* (·····)] and $[Co(L\text{-}asp)_2]^-$ (B), [*trans(N)*(——), *cis(N)*-*trans*(O_5)(——), and *cis(N)trans*(O_6)(·····)].

the coordinated L-methioninate has large vicinal CD contribution in the first absorption band region.[14] In the present case, however, the CD curves of *trans(N)*-[Co(L-asp)(L-met)], in which the coordinated sulfur atom is assigned to *R* configuration, are similar to those of *trans(N)*-[Co(L-asp)(L-smc)] which contains two kinds of chiral sulfur atoms, *R* and *S* configurations (Fig. 4 and Table 2). It seems that in the present mixed complexes the framework of isomer determines dominantly the CD pattern in the first absorption band region. In the thioether charge transfer band region (30000—35000 cm^{-1}), the CD curves of the twelve isomers are classified apparently into two groups. L-Methioninato complexes show a positive CD band regardless of L- or D-aspartate coordination, though it is only a trend for the *trans(SO)* isomers. In contrast, no CD band appears for the *S*-methyl-L-cysteinato complexes (Figs. 6—8). The sulfur atoms of *trans(N)*-L-methioninato complexes take *R* configuration and *trans(N)*-*S*-methyl-L-cysteinato one contain two kinds of chiral sulfur atoms, *R* and *S* configurations. The *trans(SN)* isomers contain the sulfur atom of both *R* and *S* configurations for both the L-methioninato and *S*-methyl-L-cysteinato complexes. The *trans(SO)* isomers take only *S* configuration. From the information on their PMR spectra, it is assumed that the CD spectra in this region apparently depend mainly on L-methioninate coordination or *S*-methyl-L-cysteinate one, though the influence of the CD bands in the highest energy region (35000—44000 cm^{-1}) should be taken into consideration.

References

1) S. Yamada, J. Hidaka, and B. E. Douglas, *Inorg. Chem.*,

10, 2187 (1971).
2) K. Hosaka, H. Nishikawa, and M. Shibata, *Bull. Chem. Soc. Jpn.*, **42**, 277 (1969).
3) J. Hidaka, S. Yamada, and Y. Shimura, *Chem. Lett.*, **1974**, 1487.
4) L. J. Zompa, *Chem. Commun.*, **1969**, 783.
5) S. Bagger, K. Gibson, and C. S. Sorensen, *Acta Chem. Scand.*, **26**, 2503 (1972).
6) W. A. Freeman and C. F. Liu, *Inorg. Chem.*, **7**, 764 (1968).
7) C. F. Liu and J. A. Ibers, *Inorg. Chem.*, **8**, 1911 (1969).
8) W. A. Freeman and C. F. Liu, *Inorg. Chem.*, **9**, 1191 (1970).
9) Y. Nakayama, S. Ooi, and H. Kuroya, *Bull. Chem. Soc. Jpn.*, **49**, 151 (1976).
10) I. Oonishi, S. Sato, and Y. Saito, *Acta Crystallogr., Sect. B*, **31**, 1318 (1975).
11) J. I. Legg and J. A. Neal, *Inorg. Chem.*, **12**, 1805 (1973).
12) J. Hidaka and Y. Shimura, presented at the XVI I.C.C.C., Dublin, Ireland (1974), Paper 1.7a.
13) P. de Meester and D. J. Hodgson, *J. Chem. Soc. Dalton. Trans.*, **1976**, 618.
14) K. Yamanari, J. Hidaka, and Y. Shimura, *Bull. Chem. Soc. Jpn.*, **50**, 2451 (1977).
16) G. H. Searle and E. Larsen, *Acta Chem. Scand.*, **A30**, 143 (1976).
17) K. Yamanari, J. Hidaka, and Y. Shimura, *Bull. Chem. Soc. Jpn.*, **50**, 2299 (1977).
18) K. Yamanari, J. Hidaka, and Y. Shimura, *Bull. Chem. Soc. Jpn.*, **50**, 2643 (1977).
19) M. Watabe, K. Onuki, and S. Yoshikawa, *Bull. Chem. Soc. Jpn.*, **48**, 687 (1975).
20) To be submitted.

X-Ray Diffraction Studies on the Structures of Tetra- and Higher-ammine Complexes of Copper(II) Ion in Aqueous Solution

Toshio YAMAGUCHI and Hitoshi OHTAKI*

Department of Electronic Chemistry, Tokyo Institute of Technology at Nagatsuta, Nagatsuta-cho, Midori-ku, Yokohama 227

(Received June 11, 1978)

From X-ray scattering measurements on ammoniacal aqueous solutions of copper(II) chloride at the NH_3/Cu mole ratios of 4.8 and 5.0, four ammonia molecules at the equatorial position and other two water molecules at the axial one were found to be coordinated to a copper(II) ion at the distance of 2.03 and 2.33 Å, respectively. The radial distribution curve obtained for an aqueous solution of copper(II) chloride saturated with ammonia ($NH_3/Cu=11.2$) showed that a higher ammine copper(II) complex than the tetraamminecopper(II) ion is formed in the solution. The complex has a distorted octahedral form in which the equatorial Cu–N bond distance is 1.93 Å. The axial apices of the octahedron at the distance of 2.30 Å are occupied by either an ammonia molecule and a water molecule or two ammonia molecules. The present study shows that the structures of the tetra- and higher-ammine copper(II) complexes in solution are different from those in crystal.

A number of methods have been applied for investigating the formation of ammine complexes of copper(II) ion. For a long time the tetraamminecopper(II) ion has been believed to have a square planar structure. In 1968 Tomlinson and Hathaway[1] studied the structures of pentaammine- and hexaamminecopper(II) salts in the solid state by means of electronic, ESR, and infrared spectra, together with magnetic moment measurements, and they suggested that the configuration of the pentaammine complex of copper(II) ion is a tetragonal pyramid and that the hexaammine complex has also the pentaammine moiety so that the complex should be described as $Cu(NH_3)_5X_2\cdot NH_3$ having a free ammonia molecule in the lattice. Romano and Bjerrum[2] also proposed the tetragonal pyramid form for the pentaammine complex in aqueous solution.

While numerous crystal structures have been reported for the tetraammine complexes of copper(II) ion,[3–6] no structural data have been reported for the complex in solution. For penta- and hexaamminecopper(II) complexes, many powder X-ray data have been reported,[7,8] but few crystallographic data are available because of low stability of the crystals.

The present X-ray diffraction study for ammoniacal aqueous solutions of copper(II) chloride with the NH_3/Cu mole ratios of 4.8 and 5.0 has been undertaken in order to clarify the structure of the tetraamminecopper(II) complex in solution. An aqueous solution of copper(II) chloride saturated with ammonia has also been examined to determine the structure of a higher-ammine complex of copper(II).

Experimental

Preparation and Analysis of Sample Solutions. The tetraammine copper(II) chloride solutions were prepared by dissolving recrystallized copper(II) chloride (Wako Pure Chemicals. Co., reagent grade) into concentrated ammoniacal aqueous solutions (Wako Pure Chemicals. Co., reagent grade) and by adding gaseous ammonia (99.99%) to the solutions (A and B) in order to obtain prescribed stoichiometric ratios of NH_3/Cu, in which the tetraaminecopper(II) ion is expected to be predominant in the solutions according to the formation constants of ammine copper(II) complexes.[9] The distribution of the ammine complexes of copper(II) ion is shown in Fig. 1. An ammoniacal copper(II) chloride solution (C) of a high ammonia concentration was also prepared by introducing gaseous ammonia into a tetraammine copper(II) chloride solution to saturation (the NH_3/Cu mole ratio was about 11).

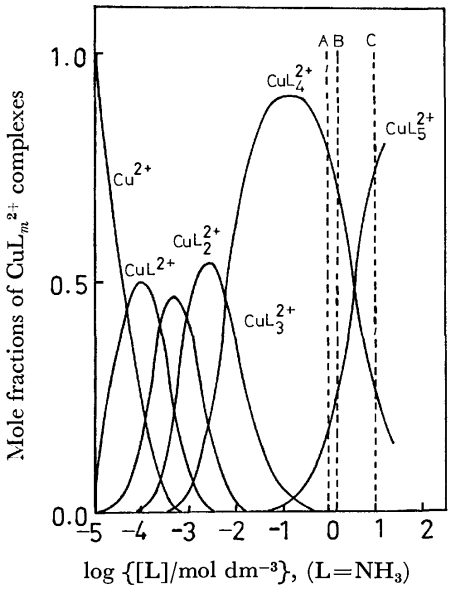

Fig. 1. The distribution of copper(II) ammine complexes as a function of the free ammonia concentration by assuming the formation constants in the literature[16] to be valid.

The concentration of the copper(II) ion was determined both by EDTA titration using a BT indicator and by electrogravimetry as metallic copper on a platinum gauze. The results of the two different methods agreed each other within 0.2%. The concentration of total ammonia was determined by the Kjeldahl method. The concentration of the chloride ion was determined from the stoichiometry of copper(II) chloride.

The density of the solutions was determined pycnometrically.

The compositions of the solutions are given in Table 1.

X-Ray Scatterings. The X-ray diffractometer used, methods of measurements and data treatment have been previously described.[10–12] Mo $K\alpha$ radiation ($\lambda=0.7107$ Å) was used for the measurements. The measurements were

TABLE 1. THE COMPOSITION (g-atoms/dm^3) AND THE STOICHIOMETRIC VOLUME V PER COPPER ATOM IN THE SOLUTIONS

Solution	Cu	Cl	N	O	H	$\frac{NH_3}{Cu}$	$\frac{V}{Å^3}$	Density / g cm^{-3}
A	2.108	4.217	10.21	39.60	109.9	4.8	787.6	1.171
B	2.180	4.360	10.87	39.91	112.4	5.0	761.6	1.171
C	1.541	3.083	17.30	30.70	113.3	11.2	1077.0	1.055

carried out over the range of $1°<\theta<70°$ (2θ is the scattering angle), corresponding to the range 0.31 Å$^{-1}<s<16.6$ Å^{-1} ($s=4\pi \sin\theta/\lambda$). Times required to accumulate 40000 counts at each angle were recorded. The whole angle range was scanned twice. The scattered intensities were corrected for background, polarization, absorption and Compton modified radiation, and then scaled to absolute units by conventional ways.[10-12] The values of coherent, incoherent and anomalous scatterings were the same as those used in previous papers.[11,12] The reduced intensities $i(s)$ obtained by subtraction of independent atomic scatterings from the scattered intensities thus deduced, were Fourier transformed into radial distriction functions, $D(r)$, after smoothing correction.[12] Residual systematic errors appearing in the small r region of the $D(r)$ curves were also corrected. The theoretical peak for a given atom pair i-j was calculated in the previous manner.[12]

Results and Discussion

The scaled coherent intensity curves, the observed $s\cdot i(s)$ values, the $D(r)$, and $(D(r)-4\pi r^2\rho_0)$ curves where ρ_0 is the bulk electron density obtained for solutions A, B, and C are shown in Figs. 2—5, respectively.

Solutions A and B. As can be seen in Fig. 1, the tetraamminecopper(II) ion is the predominant species in solutions A and B. The $D(r)$ and $(D(r)-4\pi r^2\rho_0)$ curves obtained for the both solutions are very similar except for $r>5$ Å and show four peaks around 1.0, 2.1, 3.3, and 4.3 Å. The smallest broad peak around 1 Å is attributed to both O–H and N–H bonds within water and ammonia molecules, respectively. The peak centered at 3.3 Å is mainly attributed to the interaction between chloride ions and water molecules.[13]

The location of the second major peak at about 2.1 Å is consistent with interatomic distances between Cu(II) and nitrogen atoms within the square-planar tetraamminecopper(II) ion in the crystalline state.[3-6] However, the area under the peak was found to be larger than the area calculated from only four Cu–N bonds. Therefore, it is expected that the copper complex may have an octahedral structure and the axial copper–ligand bond within the octahedral coordination may also contribute to the area under the peak. By assuming that the equatorial Cu(II)–N bonds are the same as those in the crystalline state, the interactions due to the four Cu–N bonds were subtracted from the $D(r)$ and $(D(r)-4\pi r^2\rho_0)$ curves. The values of 2.03 Å for the Cu–N distance and 0.0020 Å^2 for the temperature factor calculated from spectroscopic data[14] were adopted for the calculation. The result is shown in Fig. 6 (fine solid line). A hump still remaining around 2.3 Å may be due to the axial copper(II)–ligand bonds. The location of this hump ruled out the possibility of axial Cu(II)–Cl bonding, since the Cu–Cl distance was reported to be about 2.6 Å.[15] It is therefore assumed that water molecules occupy the axial sites of Cu(II). The Cu–OH_2(axial) distance, as well as the Cu–NH_3(equatorial) one, within the tetraamminecopper(II) complex were determined by the trial-and-error method so that subtraction of the calculated peaks of the assumed structure of the tetraamminecopper(II) complex from the $D(r)$ and $(D(r)-4\pi r^2\rho_0)$ curves led to a smooth background curve with no indication of any other intramolecular interactions in the first coordination sphere of copper(II) ion. From the analysis, we found that two water molecules should coordinate to the tetraamminecopper(II) ion in solutions A and B.

Table 2 gives the final values estimated from the

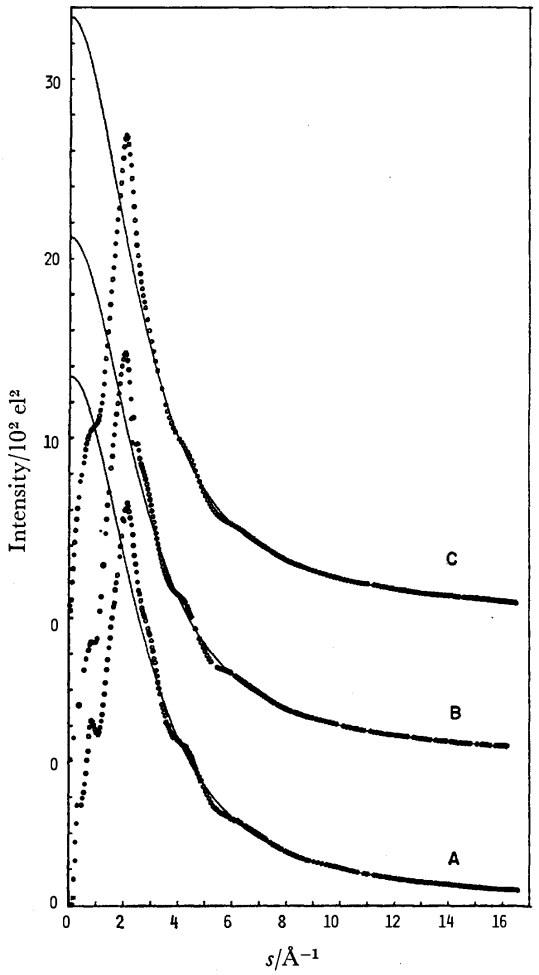

Fig. 2. Scaled coherent intensity functions (circle) and calculated independent scatterings (solid line) for ammoniacal aqueous solutions of copper(II) chloride. A. $NH_3/Cu=4.8$; B. $NH_3/Cu=5.0$; C. $NH_3/Cu=11.2$.

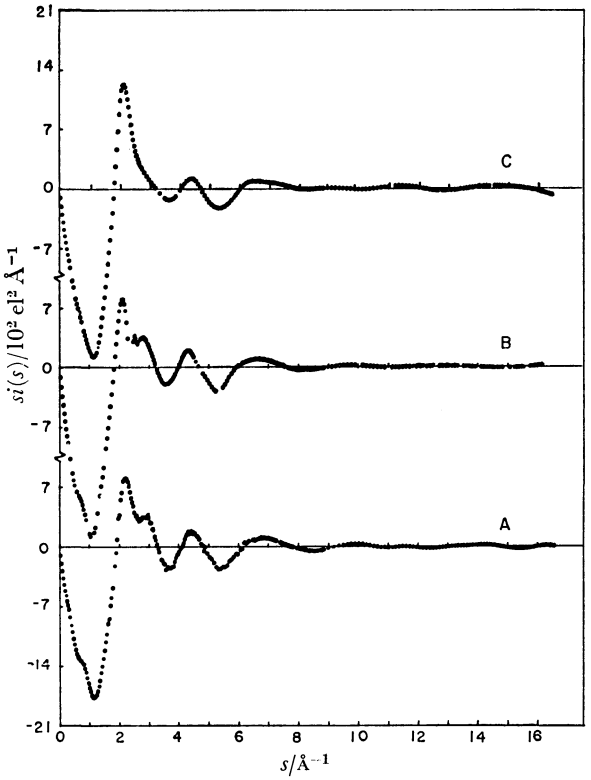

Fig. 3. Observed $s \cdot i(s)$ values of solutions A, B, and C.

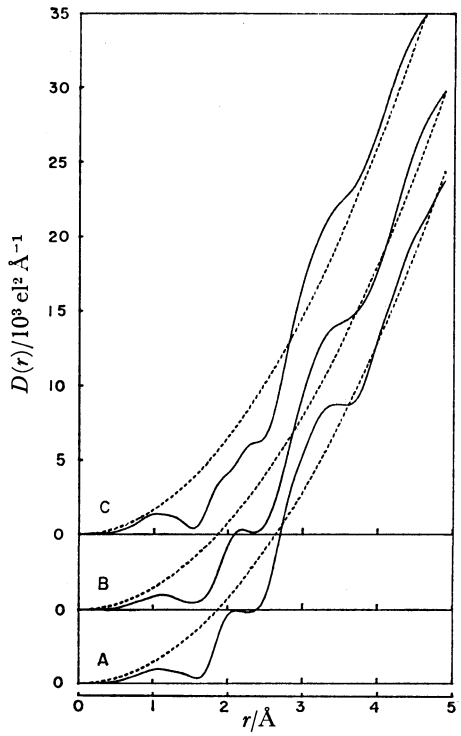

Fig. 4. Radial distribution functions $D(r)$ (solid line) and $4\pi r^2\rho_0$ (dashed line) for solutions A, B and C.

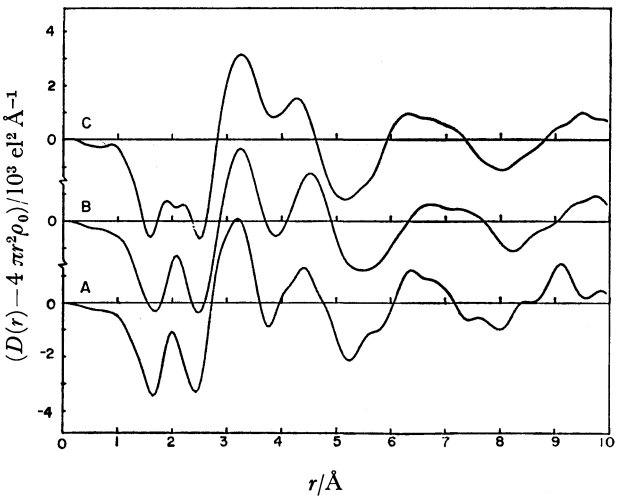

Fig. 5. The $(D(r)-4\pi r^2\rho_0)$ curves for solutions A, B, and C.

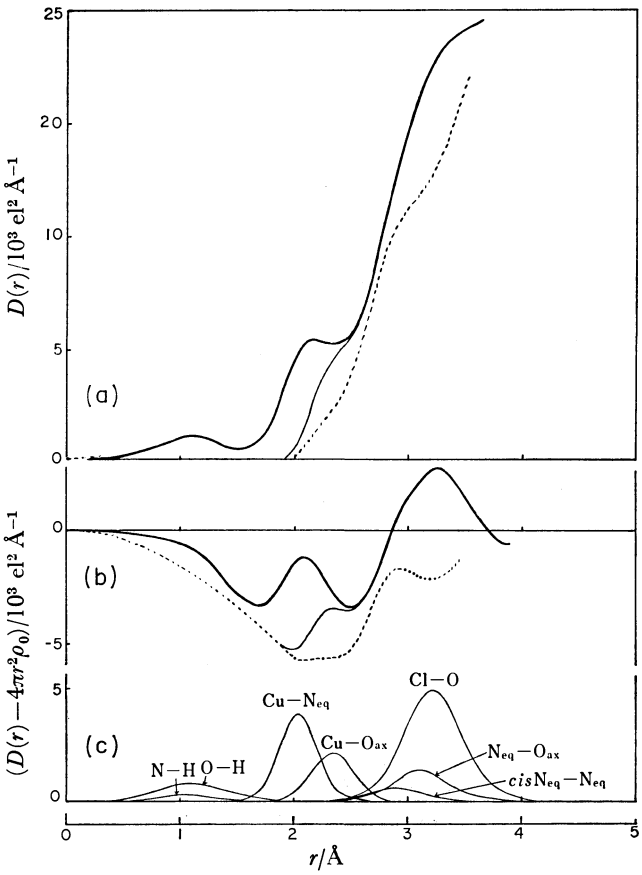

Fig. 6. (a). The $D(r)$ curve for solution A (NH_3/Cu= 4.8). The fine solid line shows the residual curve obtained subtraction of theoretical peak shape for four Cu-N_{eq} bonds from the $D(r)$ curve and the broken curve the difference between the $D(r)$ curve and theoretical peak shapes shown in (c). (b). The corre sponding $(D(r)-4\pi r^2\rho_0)$ curve. (c). The theoretical peak shapes with the parameters given in Table 2.

shape of the $D(r)$ curve in Fig. 6. The broad peak at around 2.9 Å still left in the residual radial distribution curve (broken line) may be ascribed to the O–O bonds of bulk water. The maximum at 4.3 Å in the $D(r)$ and $(D(r)-4\pi r^2\rho_0)$ curves (Figs. 4 and 5) may include the interaction between Cu(II) and water molecules within the secondary hydration shell,[16] as well as the interaction of *trans*-N···N.

TABLE 2. THE FINAL PARAMETER VALUES FOR THE DISTORTED OCTAHEDRAL STRUCTURE OF THE TETRAAMMINE COPPER(II) COMPLEX. THE VALUES IN PARENTHESES ARE THEIR ESTIMATED ERRORS

	r_{ij}/Å	b_{ij}/Å^2	n_{ij}
$Cu(NH_3)_4(OH_2)_2^{2+}$			
Cu–N_{eq}	2.03(±0.02)	0.003	4
Cu–O_{ax}	2.33(±0.03)	0.005	2
cis-$N_{eq}\cdots N_{eq}$	2.87(±0.05)	0.01	4
$N_{eq}\cdots O_{ax}$	3.09(±0.05)	0.01	8
$Cl(H_2O)_6^-$			
Cl–O	3.20(±0.05)	0.01	6

Solution C. Figure 1 shows that the predominant species is a pentaamminecopper(II) ion in solution C. As can be seen in Figs. 4 and 5, the $D(r)$ and $(D(r)-4\pi r^2\rho_0)$ curves for solution C show double peaks in the range of r=2.0—2.5 Å. The double peaks may be easily resolved into a peak with the maximum at about 1.95 Å and another one at about 2.3 Å. Other peaks at 3.3 Å and 4.2 Å also appeared in the curve C.

The first small peak located at 1.0 Å is due to the O–H bonds within water molecules and partly due to the N–H bonds within ammonia molecules. The peak at about 1.95 Å may be ascribed to the Cu(II)–N bond in the square-plane and the peak at about 2.3 Å may be ascribed to the interaction between Cu(II) and the ligands at the axial sites. The peaks located at 3.3 Å and 4.2 Å are mainly related to the Cl–O and to the Cu–OH_2 (in the second coordination layer) interactions, respectively, as previously described.

After subtracting the appropriate intramolecular interactions within the tetraamminecopper(II) ion present, as well as O–H and N–H interactions in solution C, the second and third peaks of the residual curves (fine solid line in Fig. 7) were analyzed for determining the structure of a higher-ammine complex of copper ion as illustrated in Fig. 7. The clearly defined peak at 1.93 Å was assigned to the equatorial Cu–N distance and the area under this peak gave four Cu–N bonds per Cu(II). The distance and the number of the axial copper(II)–ligand bonds were estimated after subtraction of the four equatorial Cu–N interactions from the $D(r)$ curve. The resulting curve is drawn by the chain line (—·—) in Fig. 7. The area under the peak at 2.3 Å corresponded to the Cu–NH_3 and Cu–OH_2 bonds with an equal distance (see Fig. 7c), if it is assumed that the pentaamminecopper complex is formed. However, it must be noted that another assumption of the formation of the hexaamminecopper complex can equally well explain the data. The final parameter values thus determined are summarized in Table 3. The residual radial distribution curve after subtraction of all the intramolecular interactions of the

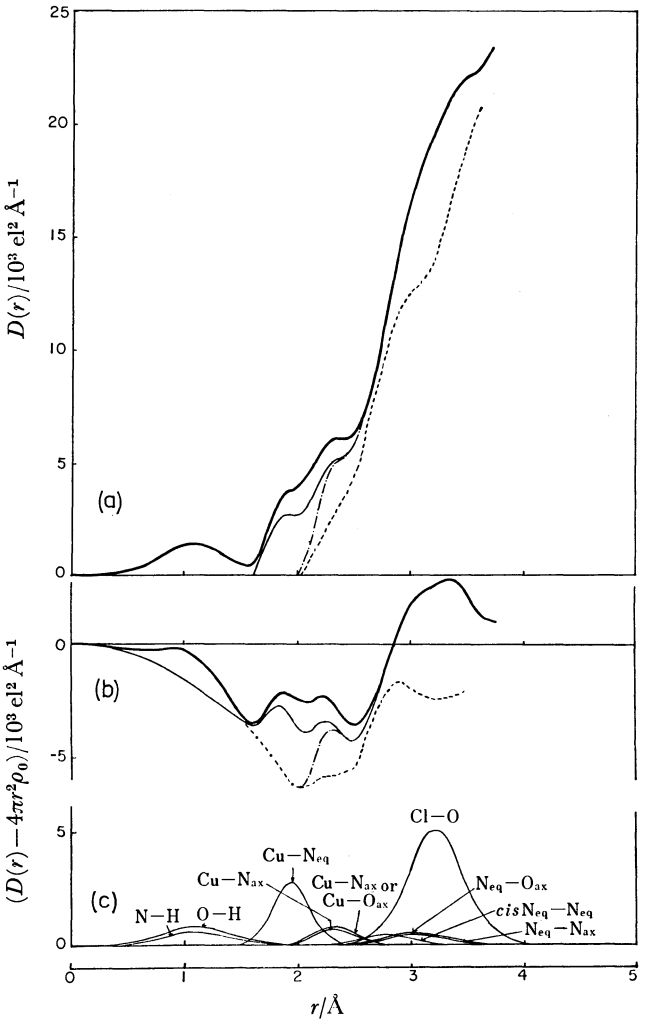

Fig. 7. (a). The $D(r)$ curve for solution C (NH_3/Cu= 11.2). The fine solid line (——) shows the residual curve obtained by subtracting the contribution of the tetraamminecopper(II) ion from the $D(r)$ curve, the chain line (-·-·-) gives the difference between the residual curve and the calculated peak shape for four Cu–N_{eq} bonds and the broken line (----) the residual curve obtained by subtraction of the theoretical peak shapes shown in (c) from the residual curve.
(b). The corresponding $(D(r)-4\pi r^2\rho_0)$ curve. (c). The theoretical peak shapes with the parameters given in Table 3.

TABLE 3. THE FINAL PARAMETER VALUES FOR THE DISTORTED OCTAHEDRAL STRUCTURE OF THE $Cu(NH_3)_5X^{2+}$ (X=NH_3 or H_2O) THE VALUES IN PARENTHESES ARE THEIR ESTIMATED ERRORS

	r_{ij}/Å	b_{ij}/Å^2	n_{ij}
$Cu(NH_3)_5X^{2+}$			
Cu–N_{eq}	1.93(±0.02)	0.003	4
Cu–N_{ax}	2.30(±0.03)	0.005	1
Cu–X_{ax}	2.30(±0.03)	0.005	1
cis-$N_{eq}\cdots N_{eq}$	2.73(+0.05)	0.01	4
$N_{eq}\cdots N_{ax}$	3.00(±0.05)	0.01	4
$N_{eq}\cdots X_{ax}$	3.00(±0.05)	0.01	4
$Cl(H_2O)_6^-$			
Cl–O	3.20(±0.05)	0.01	6

species is shown in Fig. 7 with dashed lines. The broad peak remaining at about 2.9 Å in the residual radial distribution curve may be due to the O–O interactions within bulk water. The maximum at 4.3 Å in the $D(r)$ curve (Fig. 4, curve C) may be attributable to the interaction between Cu(II) and water molecules within the secondary hydration shell.

Although it is not conclusive whether the copper(II) ion combines with five ammonia molecules and a water molecule or with six ammonia molecules in solution C, it is obvious that the complex present in the solution has not a tetragonal-pyramidal form, but a distorted octahedral structure.

In the hexaaquacopper(II) ion the Cu–OH_2-(equatorial) distance is 1.94 Å[17] and the Cu–NH_3-(equatorial) one within the tetraamminecopper(II) complex is 2.03 Å. However, we observed that the Cu–NH_3(equatorial) distance is shortened to 1.93 Å by further combination of ammonia molecules with the tetraamminecopper(II) complex. Although the reason of the change in the bond distance is not clear yet, it may be due to the lowering of the symmetry of the complex ion. The electron density of the bonds between the central copper(II) ion and the ammonia molecules at the equatorial position may also be changed with varying ligand molecules at the axial position. This may reflect to the change in the bond distances between the copper(II) ion and ligand molecules.

References

1) A. A. G. Tomlinson and B. J. Hathaway, *J. Chem. Soc., Part A*, 1905 (1968).
2) V. Romano and J. Bjerrum, *Acta Chem. Scand.*, **24**, 1551 (1970).
3) B. Morosin, *Acta Crystallogr., Sect. B*, **31**, 2220 (1975).
4) J.-C. Tedenac, É. Philippot, and M. Maurin, *Bull. Soc. Fr. Mineral Cristallogr.*, **98**, 36 (1975).
5) B. Morosin, *Acta Crystallogr., Sect. B*, **25**, 19 (1969); **32**, 1237 (1976).
6) E. Dubler and L. Linowsky, *Helv. Chim. Acta*, **58**, 2604 (1975).
7) H. Elliot and B. J. Hathaway, *Inorg. Chem.*, **5**, 885 (1966).
8) T. Distler and P. A. Vaughan, *Inorg. Chem.*, **6**, 126 (1967).
9) L. G. Sillén and A. E. Martel, "Stability Constants," Special Publication No. 17, The Chemical Society, London (1964).
10) H. Ohtaki, M. Maeda, and S. Ito, *Bull. Chem. Soc. Jpn.*, **47**, 2217 (1974).
11) H. Ohtaki, T. Yamaguchi, and M. Maeda, *Bull. Chem. Soc. Jpn.*, **49**, 701 (1976).
12) T. Yamaguchi and H. Ohtaki, *Bull. Chem. Soc. Jpn.*, **51**, 3227 (1978).
13) A. H. Narten, F. Vaslow, and H. A. Levy, *J. Chem. Phys.*, **58**, 5017 (1973).
14) B. N. Cyvin, S. J. Cyvin, K. H. Schmidt, W. Wiegeler, A. Müller, and J. Brunvoll, *J. Mol. Struct.*, **30**, 315 (1976).
15) D. L. Wertz and J. L. Tyvoll, *J. Inorg. Nucl. Chem.*, **36**, 3713 (1974).
16) W. Bol and T. Welzen, *Chem. Phys. Lett.*, **49**, 189 (1977).
17) H. Ohtaki and M. Maeda, *Bull. Chem. Soc. Jpn.*, **47**, 2197 (1974).

Single Crystal Growth of Zirconium Nitride by Modified Filament-Method

Kohzo SUGIYAMA, Kunio WATANABE, Seiji MOTOJIMA,* and Yasutaka TAKAHASHI

Department of Synthetic Chemistry, Faculty of Engineering, Gifu University, Kakamigahara, Gifu 504

(Received June 2, 1978)

Single crystals of zirconium nitride (ZrN) have been grown by the modified filament-method from a gas mixture of $ZrCl_4$, N_2, H_2, and Ar. The cubic crystals grew at 2000—2200 °C with a gas flow ratio $2N_2/ZrCl_4$ of 2—6, and evaporation of ZrN took place above 2400 °C. Linear growth rates along the <100> direction have been measured in terms of sequential micrographs, and attained a maximum of 60—75 μm/min at 2100—2200 °C. The atomic ratio N/Zr of grown crystals increased with an increase of the flow ratio $2N_2/ZrCl_4$, and reached a constant of 0.93 above the flow ratio of 3.

Zirconium nitride, a representative interstitial compound of NaCl-type structure, has desirable properties such as high melting point (2982 °C,[1] 3700 ±70 °C at P_{N_2} 60 atm[2]), high hardness (≈2500 kg/mm²),[3] metallic conductivity and high resistivity at high temperature.

The preparation of single crystals of refractory compounds is difficult because of the high melting point. Crystal growth using a floating zone technique[4] is the only way by which single crystals have been successfully grown. Single crystals of the nitride,[5] diboride,[6] and carbide[7] of titanium have been grown by the authors using a modified filament-method, which has the advantages of simple procedure and apparatus. In this paper, the single crystal growth of zirconium nitride by the modified filament-method will be described.

Experimental

Apparatus and Growth Procedure. The apparatus is analogous to that used in previous experiments on titanium nitride crystal growth.[5] A tungsten filament (99.0% pure) 30 mm long and 0.3 mm thick was tightly bound to iron electrodes 5.8 mm thick. Another short tungsten wire of 0.3 mm diameter was twisted around the tungsten filament (one and a half turns) and the tips cut slantwise with a separation of 0.3—1.0 mm from the filament and pointing towards the gas inlet. The filament was located in a horizontal reaction tube (24 mm in i.d.) which was heated to 400 °C by a nichrome heater thereby keeping zirconium tetrachloride in the vapor phase. Zirconium tetrachloride was prepared by the chlorination of zirconium sponge (99.9% pure) at 550 °C, and carried into the reaction zone by argon gas. The flow rate of zirconium tetrachloride was calculated assuming quantitative chlorination to the tetrachloride. Hydrogen and nitrogen were mixed with the zirconium tetrachloride stream near the filament. The surface temperature of the growing crystals was measured by an optical pyrometer through an observation window.

Measurement of Linear Growth Rate. The growing crystals were photographed using a stereoscopic microscope every 10—20 s. A series of sequential micrographs is shown in Fig. 1. The linear growth rate along the <100> direction was obtained as the gradient from the plot of edge length versus growth time.

Atomic Ratio (N/Zr) in Crystals and the Lattice Constant. A collection of zirconium nitride crystallites was pulverized, and oxidized to zirconium dioxide at 1000 °C for 5 h in an oxygen flow. The atomic ratio N/Zr was calculated from the weight of zirconium nitride crystallites W_{ZrN} and zirconium dioxide W_{ZrO_2} using the following equation;

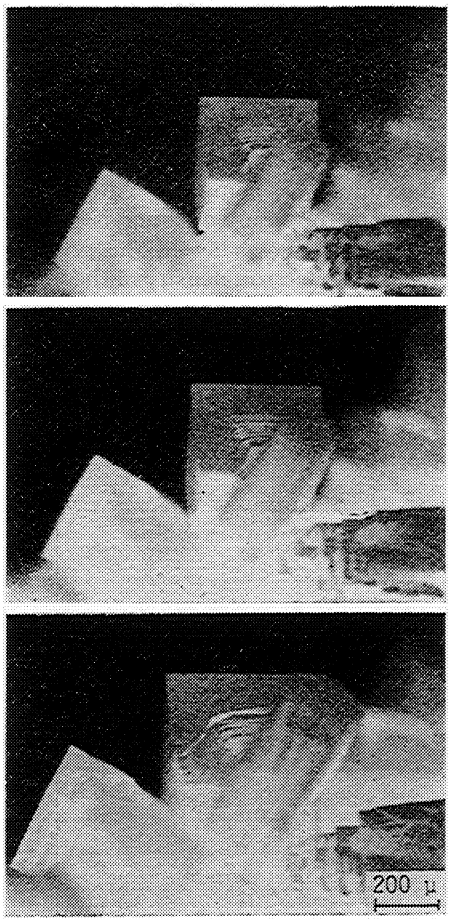

Fig. 1. Sequential micrographs of the growing crystals. Temperature: 2000 °C, $2N_2/ZrCl_4$: 5.4, $2H_2/ZrCl_4$: 10, total flow rate: 3.0 cm³/s, growth time: (A) 0 min (starting of measurement), (B) 4 min, (C) 15 min.

$$N/Zr = 8.7972(W_{ZrN}/W_{ZrO_2}) - 0.7403. \quad (2)$$

The lattice constant was determined by X-ray diffraction using annealed silicon powder as internal standard.

Micro-hardness. Micro-hardness was measured by a Vickers micro-hardness tester (Akashi, MVK-C) on the (100) and (111) facets of cubic and tetragonal pyramid crystals, respectively.

Results and Discussion

Crystal Morphology. The effect of growth temperature and source gas flow ratio $2N_2/ZrCl_4$ ("N/Zr ratio" hereafter) on crystal morphology is shown in Fig. 2, in which the sum of the flow rates of zirconium tetra-

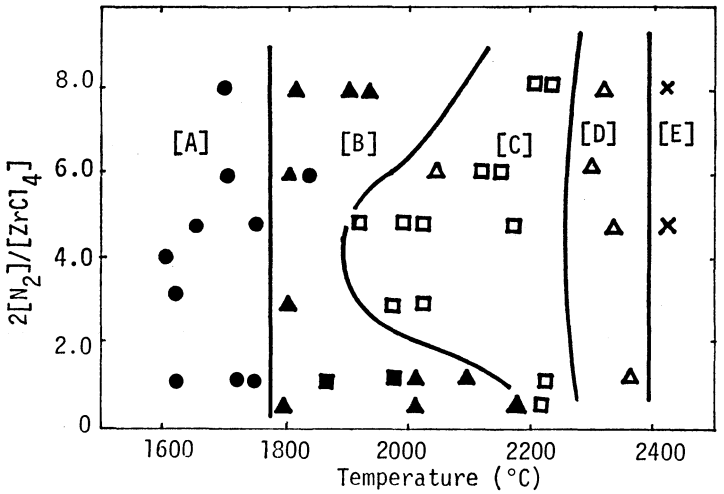

Fig. 2. Effect of the temperature and the flow ratio ($2N_2/ZrCl_4$) on crystal morphology. Total flow rate: 3.0 cm^3/s, $ZrCl_4+N_2$: 0.1 cm^3/s, $2H_2/ZrCl_4$: 3.
(●) Coatings or fine crystals, (▲) tetragonal pyramid crystals, (■) polyhedral crystals, (□) cubic crystals, (△) arrow-like or dendritic crystals, (×) no-deposition.
[A] Coating or fine crystal growth region, [B] tetragonal pyramid crystal growth region, [C] cubic crystal growth region, [D] arrow-like or dendritic crystal growth region, [E] no deposition region.

chloride and nitrogen was kept at 0.1 cm^3/s and the gas flow ratio $2H_2/ZrCl_4$ ("H/Zr ratio" hereafter) kept at 3. The crystal morphology varied with increase in growth temperature in the following order; polycrystallite or fine crystal, tetragonal pyramid, cubic, and arrow-like or dendritic. Cubic crystals grew in the temperature range of 2000—2200 °C and at a N/Zr ratio of 2—6. Above 2400 °C, the crystals did not grow and crystallites which had been deposited at a lower temperature gradually disappeared. Concerning the evaporation of zirconium nitride, Hoch *et al.*[8] have investigated the evaporation in the temperature range of 2236—2466 K. Extrapolating the data of Hoch *et al.* to 2400 °C, the evaporation rate is given by the curve B in Fig. 8, and is as fast as 85 μm/min at 2400 °C. This evaporation temperature is 200 °C higher than that of titanium nitride.[5]

The effect of growth temperature and H/Zr ratio on crystal morphology is shown in Fig. 3, in which the N/Zr ratio was kept constant at 4. The growth regions of the pyramidal and arrow-like or dendritic crystals spread to the hydrogen-rich region (Fig. 3, regions B and D). Cubic crystals grew in the temperature range of 2100—2300 °C under a H/Zr ratio below 40.

In Figs. 4 and 5, the representative morphologies of zirconium nitride crystals are shown. Large cubic or

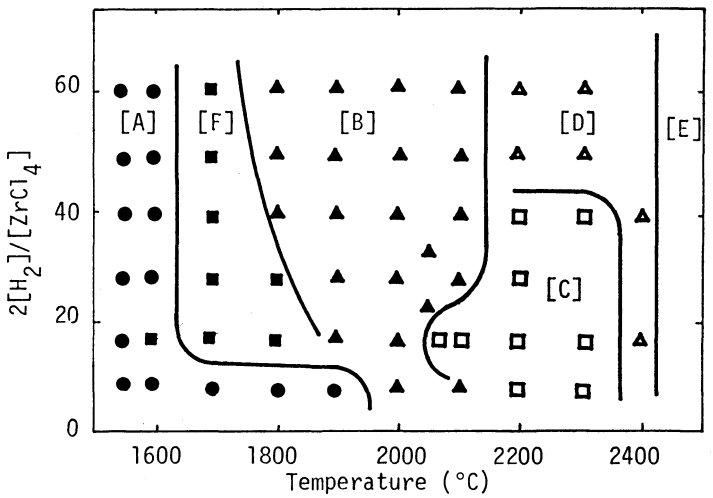

Fig. 3. Effect of the temperature and the flow ratio ($2H_2/ZrCl_4$) on crystal morphology. Total flow rate: 3.0 cm^3/s, $2N_2/ZrCl_4$: 4. [F] polyhedral crystal growth region. Signes and other notations are the same as those of Fig. 2.

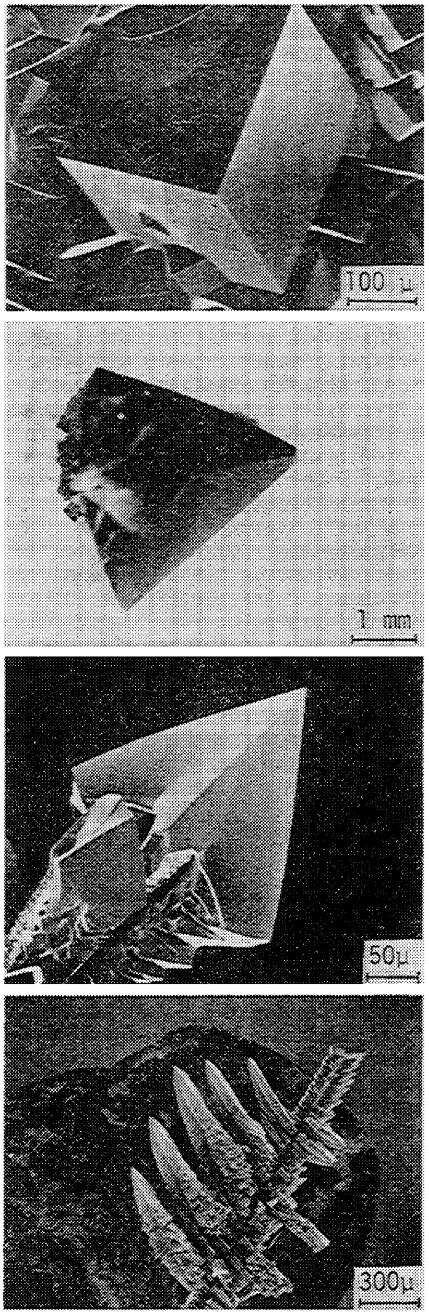

Fig. 4. Representative morphologies of zirconium nitride crystals. (A) cubic crystal, temperature: 2000 °C; $2N_2/ZrCl_4$: 4, (B) tetragonal pyramid crystals, (C) tetragonal pyramid crystal, temperature: 1800 °C; $2H_2/ZrCl_4$: 4, (D) arrow-like and dendritic crystals, temperature: 2300 °C; $2N_2/ZrCl_4$: 4.

tetragonal pyramidal crystals grew from the tips of the tungsten wire, after initial deposition of a few nuclei (Fig. 5). The largest single crystals obtained in this work were 3 mm in edge length for cubic crystals and 3.5 mm for tetragonal pyramids for 90 min growth under a condition of C- and B-regions in Fig. 2, respectively. Square pillar crystals of 10 μm thickness and 1 mm length, on which short pillar crystals branched perpendicularly, were obtained by chance on the filament close to the bound point of the electrodes (Fig. 6). X-Ray diffraction profiles of the pillar crystals are

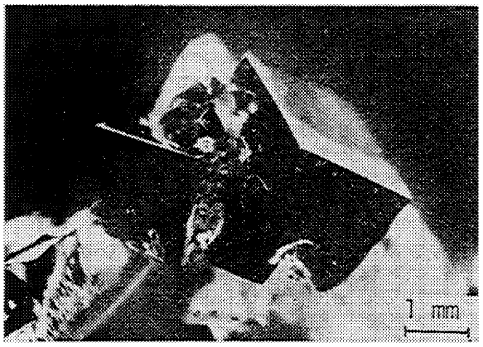

Fig. 5. Cubic crystal grown on the tip of tungsten wire.

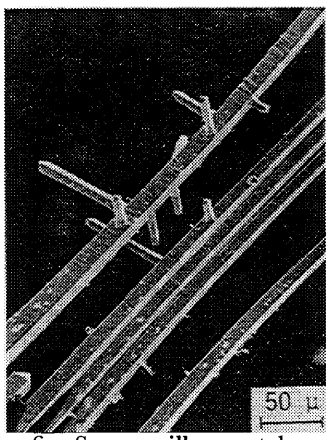

Fig. 6. Square pillar crystals.

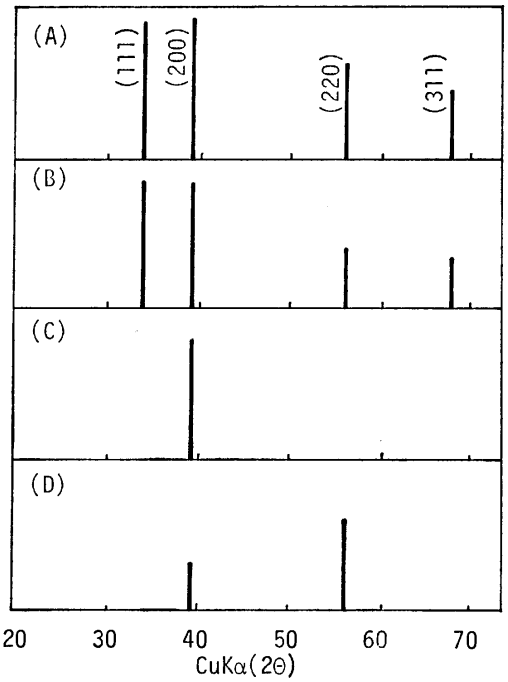

Fig. 7. X-Ray diffraction profiles (A) ZrN-ASTM (No. 2-956), (B) pulverized from crystallites, (C) a square facet of cubic crystal, (D) square pillar crystals set aside along the growth axis.

shown in Fig. 7D, together with those of pulverized crystallites (Fig. 7B) and the square facet of a cubic crystal (Fig. 7C). The pillar crystal was suspended in a

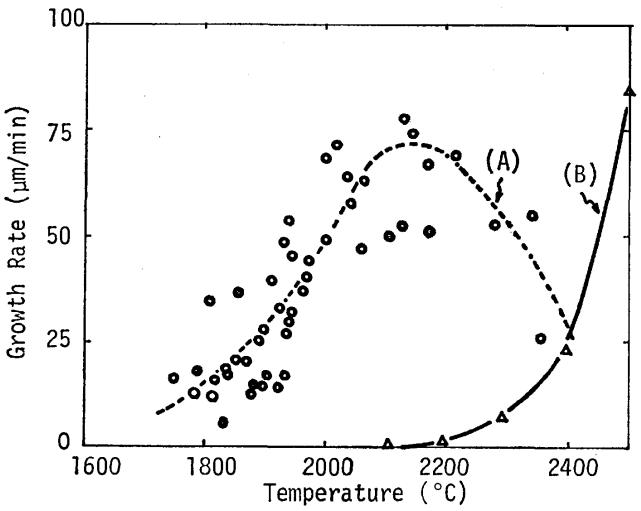

Fig. 8. (A) Effect of the temperature on the linear growth rate in <100> direction. Total flow rate: 3.0 cm^3/s, $2N_2/ZrCl_4$: 4, $2H_2/ZrCl_4$: 15. (B) Evaporation rate.[8]

drop of water, poured on to a holder plate and dried. Thus, the growth axis of the pillar crystals may be regarded as parallel to the holder plate. The two strong peaks in Fig. 7D have been assigned as (200) and (220) of the cubic lattice and thus, the growth direction is considered to be <100>.

Linear Growth Rate. Dependence on Temperature: The linear growth rate along the <100> direction of a cubic crystal was measured in the temperature range of 1700—2400 °C as shown in Fig. 8, in which the N/Zr and H/Zr ratios were kept constant at 4 and 15, respectively. The growth region for tetragonal pyramid crystals is below 1900 °C and for arrow-like crystals above 2250 °C, as seen in Fig. 2. The linear growth rate along the <100> direction in the temperature range was measured as follows; a few small cubic crystals were deposited on the tip in the temperature range C in Fig. 2, followed by decreasing or increasing the temperature to that of measurement. The growth rate increased with the increase of temperature and reached a maximum (about 75 μm/min) in the temperature range 2100—2200 °C, and decreased above 2200 °C. Dispersion of the data may be attributed to fluctuation of the nucleation site, the size and the orientation of the crystals, and the temperature of the growing crystals.

Dependence on N/Zr Ratio: The effect of the N/Zr ratio on the linear growth rate along the <100> direction was examined, where the sum of the flow rates of zirconium tetrachloride and nitrogen, and the H/Zr ratio were kept constant at 0.1 cm^3/s and 10, respectively. The maximum growth rates of 60 and 35 μm/min were measured under a N/Zr ratio of 2—3 at 2100 °C and 1.5—2.5 at 1900 °C, respectively. These values are in agreement with that of the polycrystalline growth of zirconium nitride from the same gas mixture at 1150 °C.[9]

Dependence on H/Zr Ratio: The effect of the H/Zr ratio on the linear growth rate was examined, where the N/Zr ratio was kept constant at 4. The linear growth rate increased with increase of the H/Zr ratio and the maximum was at a ratio as high as 15—18 at 2100 °C, the rate decreasing abruptly above these ratios. At a H/Zr ratio above 40, that is, a low flow ratio of zirconium tetrachloride, the growth rate along the <111> direction predominated resulting in arrow-like or dendritic growth.

Dependence on the Total Flow Rate: The effect of the total flow rate on the growth rate along the <100> directions was examined, where N/Zr and H/Zr ratios were kept constant at 4 and 10, respectively, and the temperature at 2000 °C. The growth rate increased with increase of the total flow rate approaching a constant value of 45 μm/min above a flow rate of 3 cm^3/s which corresponds to a linear velocity at the growth temperature of about 5 cm/s.

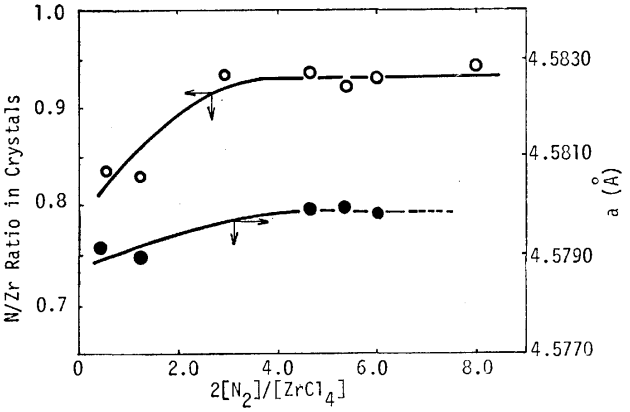

Fig. 9. Effect of flow ratio ($2N_2/ZrCl_4$) on the atomic ratio (N/Zr) and the lattice constant in ZrN crystals. Temperature: 2000—2100 °C, total flow rate: 3.0 cm^3/s, $2H_2/ZrCl_4$: 15.

The Atomic Ratio N/Zr in Crystals and Lattice Constant. The influence of the N/Zr ratio in input gas on the atomic ratio N/Zr in crystals and the lattice constant are shown in Fig. 9, in which the crystals were grown in the temperature range of 2000—2100 °C and with a H/Zr ratio of 15. The atomic ratio N/Zr in crystals increased with the increase of N/Zr ratio in input gas attaining a constant value of 0.93 at a flow ratio above 3. Zirconium nitride exists over a broad composition range corresponding to $ZrN_{0.55-1.0}$[10] and $ZrN_{1.54-1.0}$ at 1500 °C.[11] The stoichiometric composition of ZrN could not be obtained in the present work and the lowest atomic ratio N/Zr was about 0.83.

The lattice constants of zirconium nitride crystals were 4.579 Å for a sample of N/Zr=0.83 and 4.580 Å for that of 0.93. These values are slightly larger than those reported in the literature; *i.e.* 4.5755 Å (N/Zr=0.89),[12] 4.564 Å (N/Zr=1.0),[13] and 4.5755 Å (N/Zr=0.93).[14] The deviations of the constants from the literature may arise from the presence of oxygen in the crystal lattice,[15] although the presence of oxygen in the crystal was below the detectable limit of electron probe microanalysis.

Micro-hardness. Micro-hardness was measured on the (100) and (111) facets of cubic and tetragonal pyramid crystals, respectively. The hardness varied from 1500 to 1600 kg/mm^2, irrespective of the crystal

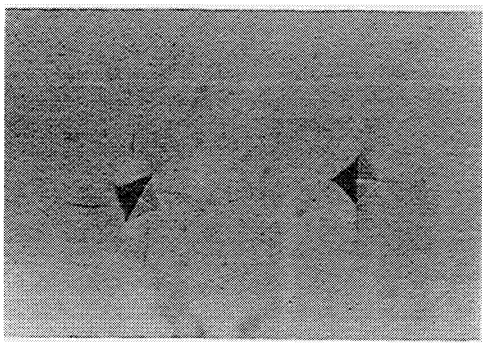

Fig. 10. Typical marks impressed on the (100) facet of a cubic crystal by a pyramidal diamond indenter in Vickers microhardness tester.

facets. These values are somewhat smaller than that reported by Hill *et al.*[3] Typical marks impressed on the (100) facet of cubic crystals by a pyramidal diamond indenter are shown in Fig. 10. Slip lines can be seen in the <110> direction irrespective of the orientation of the indenter, which is in agreement with the slip direction of titanium nitride.[16]

References

1) L. E. Toth, "Transition Metal Carbides and Nitrides," in "Refractory Materials," ed by J. L. Margrave, Academic Press, New York and London (1971), Vol. 7.
2) M. A. Eron'yan, R. G. Avarbe, and T. A. Nikol'skaya, *Zh. Prikl. Khim. (Leningrad)*, **46**, 428 (1973); *Chem. Abstr.* **78**, 140540 m (1973).
3) R. J. Hill, S. Scheuermann, and R. Lucariello, *Thin Solid Films*, **40**, 217 (1977).
4) A. N. Christensen, *J. Cryst. Growth.*, **33**, 99 (1976).
5) S. Motojima, K. Baba, K. Kitatani, Y. Takahashi, and K. Sugiyama, *J. Cryst. Growth*, **32**, 141 (1976).
6) K. Sugiyama, S. Iwakoshi, S. Motojima, and Y. Takahashi, *J. Cryst. Growth*, **43**, 533 (1978).
7) K. Sugiyama, H. Mizuno, S. Motojima, and Y. Takahashi, unpublished data.
8) M. Hoch, D. P. Dingledy, and H. L. Johnston, *J. Am. Chem. Soc.*, **77**, 304 (1955).
9) T. Takahashi, H. Itoh, and S. Noguchi, *Nippon Kagaku Kaishi*, **1975**, 627.
10) E. K. Stromes, *M. T. P. Int. Rev. Sci., Inorg. Chem. Ser.* **I**, 37 (1972).
11) E. D. Rudy and F. Benesovsky, *Monatsh. Chem.*, **92**, 415 (1961).
12) C. R. Houska, *J. Phys. Chem. Solids*, **25**, 359 (1964).
13) G. V. Samsonov and T. S. Verkhoglyanova, *Dopov. Akad. Nauk Ukr. RSR*, **1962**, 48.
14) J. G. Desmaison and W. W. Smeltzer, *J. Electrochem. Soc.*, **122**, 354 (1975).
15) N. Schönberg, *Acta Chem. Scand.*, **8**, 627 (1954).
16) F. W. Vahldiek and S. A. Mersol, *J. Less-Common Met.*, **55**, 265 (1977).

Polysoap as a New Titrant for the Determination of Sodium Dodecylbenzenesulfonate by Colloid Titration

Toshiro Ono, Haruo Miyata, and Kyoji Tôei*

Department of Chemistry, Faculty of Science, Okayama University, Tsushima-naka 3-1-1, Okayama 700

(Received June 12, 1978)

A colloid titration method for the determination of sodium dodecylbenzenesulfonate (LAS) with poly(4-vinyl-1-pentylpyridinium bromide) (polysoap) is described. The end-point detection is based on the measurement of turbidity, the transmittance at 420 nm or 680 nm being used for the determination. The most successful results were obtained by titrating LAS ($1—7.5\times10^{-4}$ N) with 2.5×10^{-3} N polysoap solution. The purity of commercial LAS was found to be 81—84%.

Colloid titration is widely used for the determination of polyelectrolytes. Usually, Cat-Floc (poly(diallyldimethylammonium chloride)) and PVSK (potassium poly(vinyl sulfate)) are used as polycationic and polyanionic titrants, respectively.[1] Anionic surfactants, however, can not be titrated with Cat-Floc, since Cat-Floc can not form polyion complexes with anionic surfactants stoichiometrically.

When a long aliphatic chain is introduced into the polycation to enhance the bonding strength of polycationic titrants with sodium dodecylbenzenesulfonate, the chain is combined firmly with the dodecyl group of the surfactant by hydrophobic bonding. An attempt was made to synthesize a cationic titrant by introducing methyl, ethyl, propyl, butyl, pentyl, hexyl, or octyl group into poly(4-vinylpyridine) in order to form poly(4-vinyl-1-alkylpyridinium halide). The longer the chain, the stronger the bonding strength, the solubility in water decreasing. No standard solution of hexyl and octyl derivatives (2.5×10^{-3} N) can be prepared since they are hardly soluble in water. Thus, poly(4-vinyl-1-pentylpyridinium bromide)(polysoap), synthesized by Menschutkin's reaction,[2] was used as a new cationic titrant. It can combine with sodium dodecylbenzenesulfonate (LAS) stoichiometrically. For the titration of LAS, turbidimetry[3] was used to observe the end-point at wavelengths 420 or 680 nm. Titration was carried out slowly near the end-point.

Experimental

Synthesis of Polysoap. Poly(4-vinyl-1-pentylpyridinium bromide) was synthesized as follows: An equimolecular mixture of pentyl bromide(3 M) and 4-vinylpyridine(3 M) in nitrobenzene was refluxed at 100 °C for several hours. After steam distillation to remove the nitrobenzene and the unreacted reagents, polysoap was obtained as a solid.

Apparatus. Turbidity was measured with a Metrohm Spectrocolorimeter E 1009 equipped with a titration cylinder cell(diameter 35 mm), titration curve being recorded with a Metrohm Potentiograph E 336. pH was measured with a Hitachi-Horiba M 5 pH meter.

Reagents. PVSK solution. Potassium poly(vinyl sulfate) (Wako Pure Chemical Industries Ltd., degree of esterification 92.6%) was dissolved in distilled water to prepare a 2.5×10^{-3} N solution. The factor of the PVSK solution was determined by titrating a standard solution of 2.5×10^{-3} N hexadecylpyridinium chloride monohydrate,[4] stored for several days over a silica gel desiccator, using Toluidine Blue as an indicator.

Polysoap solution. Poly(4-vinyl-1-pentylpyridinium bromide) was dissolved in distilled water to prepare a 2.5×10^{-3} N solution. The solution (10 ml) was diluted to 50 ml with distilled water in a 100 ml cylinder cell and titrated automatically with the standardized PVSK solution using Toluidine Blue as an indicator. The titration speed was 0.37 ml min^{-1}. The end-point was indicated by the inflection point of the transmittance at 630 nm.

Sample Solutions. Standard LAS solution. Standard LAS (Wako Pure Chemical Industries Ltd., purity>99%) was dried *in vacuo* at about 50 °C, and weighed. The standard LAS solution was prepared by dissolving the LAS in distilled water to a constant volume.

Other LAS sample solutions were prepared in the same way as described above.

Titration Procedure of LAS. LAS solution was titrated directly with 2.5×10^{-3} N polysoap solution. A sample solution (2.5×10^{-3} N, 10 ml) in a 100 ml cylinder cell was diluted to 50 ml with distilled water, and titrated with the polysoap solution under mechanical stirring. In order to follow the course of titration, the transmittance at 420 or 680 nm was measured and recorded automatically. It is important to maintain a titration speed of 0.37 ml min^{-1} near the end-point.

Results and Discussion

Standardization of Polysoap. Figure 1 shows the influence of pH on the titration of polysoap with a standard solution of PVSK. The values of meq g^{-1} are constant (3.77 meq g^{-1}) in the pH range 5.0—9.5, decreasing gradually above 9.5. Since the polysoap is quaternary ammonium salt, the values of meq g^{-1} should be constant over the whole pH range 0—14. Actually, however, the pH range is restricted. This

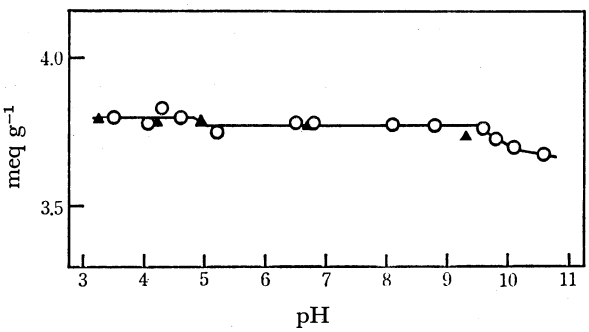

Fig. 1. Colloid titration results of polysoap. Titrant: 1×10^{-3} N PVSK. Titrating solution: 2×10^{-4} N polysoap. ○ Colorimetric, ▲ conductometric.

Table 1. Titration values of standard LAS solution

LAS total concn	Polysoap normality ($N \times 10^3$)					
	2.5	1.25	1	0.5	0.25	0.125
75×10^{-5} N	2.84 meq g^{-1} ($99._1$%)					
50	2.85($99._1$)					
25	2.85($99._5$)	2.78($97._1$)				
20			2.76($96._4$)			
15	2.85($99._2$)					
12.5		2.78($97._1$)		2.74($95._5$)		
10	2.85($99._1$)			2.73($95._2$)		
7.5		2.77($96._5$)		2.74($95._5$)		
5		2.79($97._2$)		2.72($94._8$)	2.68($93._5$)	
2.5						2.69($93._5$)

Standard LAS (Wako Pure Chemical Industries, Ltd.; purity: more than 99%).

suggests that the quaternarized reaction is incomplete, the titration results of 3.77 meq g^{-1} corresponding to 96.7% of the expected value, 3.90 meq g^{-1}. The results obtained by the conductometric method[4] with platinum electrodes coincide with those of the photometric method as shown in Fig. 1.

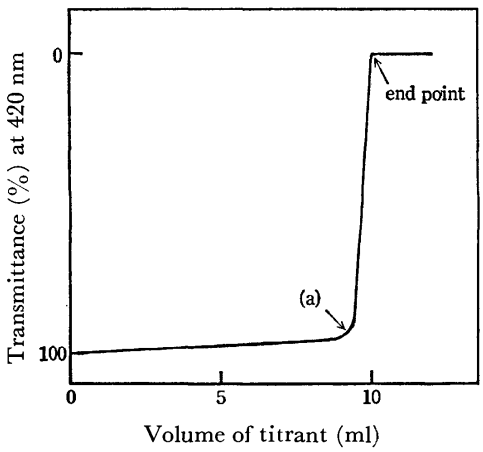

Fig. 2. Turbidimetric titration curve. Titrant: 1×10^{-3} N polysoap. Titrating solution: 2×10^{-4} N LAS(purity: more than 99%).

Turbidimetric Titration of LAS. Figure 2 shows a titration curve for LAS (50 ml of 2×10^{-4} N) titrated with polysoap solution (1×10^{-3} N). The turbidity measured at 420 nm increases gradually with the progress of titration. Near the end-point the transmittance decreases abruptly. The end-point was determined by the point where the reaction between polysoap and LAS finishes completely and the transmittance becomes zero. The titration curve is reproducible. The titration speed is 0.55 ml min^{-1} until point (a) in Fig. 2, and subsequently, 0.37 ml min^{-1}. When the titration speed is faster than 0.37 ml min^{-1} near the end-point, the results are not reproducible since the rate of reaction between polysoap and LAS is slow. When the concentration of LAS is above 2.5×10^{-3} N LAS, the wavelength 680 nm is preferable.

The titration results at various pH values are shown in Fig. 3. A constant value was obtained in the pH range 4.5—10.5. For determination of the purity of LAS,

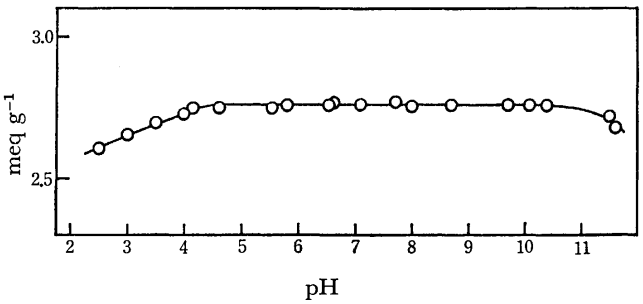

Fig. 3. Coloid titration results of LAS. Titrant: 1×10^{-3} N polysoap. Titrating solution: 2×10^{-4} N LAS.

the LAS solution can be used as it is because of its neutrality. Titration values of the standard LAS solution are given in Table 1. The concentration of LAS and polysoap is shown to have an effect on the titration value, when lower than 7.5×10^{-5} and 1.25×10^{-3} N respectively, the results becoming lower than the calculated value. Titration is impossible when the concentration of polysoap and LAS becomes higher than 10^{-2} and 10^{-3} N, respectively, since the solution becomes strongly turbid from the beginning of titration. The concentration of polysoap and LAS should be 2.5×10^{-3} and $1—7.5 \times 10^{-4}$ N, respectively.

Purity of LAS. The purity of samples was determined under the conditions described above with a 2.5×10^{-3} N polysoap solution. The results of the analysis of commercial LAS are given in Table 2. The

Table 2. Determination of the purity of LAS samples

Sample	LAS		Polysoap		LAS purity %
	concentration mg/ml	amount ml	normality $N \times 10^3$	amount ml[a]	
A	88.2/100	10.00	2.402	3.74±0.01	35.3
B_1	432.2/500	10.00	2.434	9.99±0.01	98.0
B_2	89.5/100	10.00	2.402	8.85±0.01	82.8
C	218.8/250	10.00	2.434	8.45±0.02	81.9
D	85.6/100	10.00	2.434	8.23±0.01	81.6
E	91.3/100	10.00	2.434	8.96±0.02	83.2
F	90.6/100	10.00	2.402	9.03±0.01	83.4

a) Average value of three determinations.

purity of Sample A, over twenty years old, was an abnormally low 35.3%. B_1 was an ultra pure reagent (Tokyo Kasei Kogyo Co., Ltd.). The others were of chemical pure grade, the purity being 81—84%.

Other Anionic Surfactants. As described in JIS K 0102-1974, sodium bis(2-ethylhexyl) sulfosuccinate (SSS) is used as a standard substance for the determination of anionic surfactants in water. SSS can also be titrated by the present method. The purity of SSS was found to be 95.7%. This is in line with the value 96.3% confirmed by the Japan Oil Chemists' Society.

On the other hand, the titration values of sodium dodecyl sulfate (LS) varied with the concentration of LS. The titration curve of sodium myristate show no clear end-point. These anionic surfactants can not form stable polyion complexes with polysoap.

This work was supported in part by a Grant-in-Aid for Scientific Research from the Ministry of Education.

References

1) K. Tôei and K. Kawada, *Bunseki Kagaku*, **21**, 1510 (1972).
2) V. A. Kabanov, *et al.*, *J. Polym. Sci., Part C*, **16**, 1079 (1967).
3) K. Tôei and M. Sawada, *Anal. Chim. Acta*, **80**, 383 (1977).
4) K. Tôei and T. Kohara, *Anal. Chim. Acta*, **83**, 59 (1976).

A Synthetic Study of the Solid Solutions in the Systems $La_2(CO_3)_3 \cdot 8H_2O$-$Ce_2(CO_3)_3 \cdot 8H_2O$ and $La(OH)CO_3$-$Ce(OH)CO_3$

Hisanobu WAKITA* and Setsuko KINOSHITA

Department of Chemistry, Faculty of Science, Fukuoka University, Nanakuma, Nishi-ku, Fukuoka 814

(Received, June 15, 1978)

The solid solutions in the systems $La_2(CO_3)_3 \cdot 8H_2O$-$Ce_2(CO_3)_3 \cdot 8H_2O$ and $La(OH)CO_3$-$Ce(OH)CO_3$ have been synthesized by the hydrolysis of the lanthanum–cerium trichloroacetates. The X-ray diffraction data of the solid solutions of $La_2(CO_3)_3 \cdot 8H_2O$-$Ce_2(CO_3)_3 \cdot 8H_2O$ indicated a lanthanite-type structure while the data of $La(OH)CO_3$-$Ce(OH)CO_3$ indicated a bastnaesite-type structure. The correlations between lanthanite, bastnaesite, and calkinsite, and the lanthanite-bastnaesite transformation are discussed.

Rare-earth carbonate minerals being mainly composed of lanthanum and cerium which have been reported are lanthanite, $(La,Ce)_2(CO_3)_3 \cdot 8H_2O$, calkinsite, $(La,Ce)_2(CO_3)_3 \cdot 4H_2O$, and bastnaesite, $(La,Ce)(F,OH)CO_3$.[1] Several double carbonate minerals, *e.g.*, ancylite, $(La,Ce)_x(Sr,Ca)_{2-x}(CO_3)_2(OH)_x \cdot (2-x)H_2O$, have also been described. However, because of the rare occurence and preparatory diffculties the existence and relationships between the minerals have not always been clear. The crystal structures of lanthanum carbonate octahydrate, $La_2(CO_3)_3 \cdot 8H_2O$,[2] and lanthanite, $(La,Ce)_2(CO_3)_3 \cdot 8H_2O$,[3] have been determined from X-ray diffraction studies. Despite differences in the representations of the unit cell parameters and space group, they were found to be isostructural. The principal structural features are infinite layers of RE–O(RE=La,Ce) coordination polyhedra and CO_3^{2-} groups. However the disordering of lanthanum and cerium has not been confirmed in the lanthanite-type carbonates. Furthermore, in spite of the existence with lanthanite, calkinsite which is considered to be the solid solution of lanthanum and cerium has not yet been the subject of chemical and mineralogical studies. It is not always apparent whether the structure of hydroxy-bastnaesite is isostructural with fluoro-bastnaesite or with ancylite ($x=2$).[4,5,13] Moreover, the existence of hydroxy-bastnaesite has not always been proposed.

In order to investigate the above mentioned points, solid solutions of the carbonates, changing the molar ratio of lanthanum to cerium have been synthesized at various temperatures and pressures, and the products examined by X-ray diffractometry, thermal analysis, and infrared spectroscopy.

Experimental

Synthesis of Rare-earth Carbonates. There are several precipitants for preparing rare-earth carbonates: alkali carbonates and bicarbonates, trichloroacetic acid, urea, *etc.*[6,14] Trichloroacetic acid was used as a precipitant in the present work, since it gives good crystalline products. An appropriate amount of 0.1 mol dm^{-3} lanthanum chloride solution and of 0.1 mol dm^{-3} cerium chloride solution were mixed together, maintaining a total volume of 10 cm^3. After the addition of a 5 cm^3 portion of 2.0 mol dm^{-3} trichloroacetic acid solution, the solution was adjusted with ammonia to pH 5—6 and the volume made up to 50 cm^3 with water. The solutions were placed in a thermostatted bath for a week at temperatures ranging from 50 to 80 °C and in glass autoclaves for four days at 100, 115, and 150 °C. The precipitates were filtered off, washed with water and air-dried.

X-Ray Powder Diffractometry. The X-ray powder diffractions were recorded on a Rigaku Denki Geigerflex Diffractometer, using Ni-filtered Cu $K\alpha$ radiation.

Chemical Analysis. The carbonates were analyzed by igniting weighed samples in a muffle furnace at a temperature of *ca.* 1000 °C. Loss on ignition corresponds to the CO_2+H_2O content of the sample. Both CO_2 and H_2O were determined by the routine procedure for elemental analysis for organic compounds. The ignited oxides were dissolved in perchloric acid. The determination of lanthanum and cerium in the dissolved solution was conducted according to the conventional method.

Infrared Spectra. The infrared absorption spectra of the carbonates were obtained by means of a JASCO IRA-1 spectrophotometer, using KBr pellets and the nujol mull techniques.

Thermal Analysis. The thermal decomposition processes of the carbonates were investigated with a Rigaku Denki Thermoflex thermalanalyzer. About twenty milligramme samples in shallow platinum crucibles were heated in air or in a stream of nitrogen at a heating rate of 5 °C/min.

Electron Probe Microanalysis. The compositional analyses of the carbonates were conducted by means of a JEOL JXA-5 scanning electron microscopic analyzer, using the characteristic X-rays of La $L\alpha$ and Ce $L\alpha$.

Results and Discussion

X-Ray Powder Diffractometry. The carbonates synthesized at 50 and 65 °C gave patterns similar to that of lanthanite, while the carbonates synthesized at 100 °C (5.5 atm) and 115 °C (8 atm) gave patterns similar to that of bastnaesite. The carbonates synthesized from lanthanum-rich solutions at 80 °C gave patterns consisting of those of lanthanite and bastnaesite. The molar ratio of lanthanum to cerium in the lanthanum-rich solutions was 6 or more. No precipitates appeared when the mixed solutions were kept at 150 °C. The X-ray data of the carbonates synthesized at 100 °C (5.5 atm) are shown in Table 1. An observed increase in d values with increasing molar ratio of lanthanum indicates that the carbonates formed solid solutions. Furthermore, when samples of the synthesized carbonates were physically mixed with the two end-members (*i.e.* bastnaesite lanthnum and cerium carbonate) the position and intensity of the diffraction peaks from the synthesized material could be described as just the average and sum, respectively, of the two end-members. The electron probe microanalysis also

Table 1. X-Ray powder data for bastnaesite-type carbonates

hkl	*d*(Å)							I/I_0
	La10	La8Ce2	La6Ce4	La5Ce5	La4Ce6	La2Ce8	Ce10	
002	5.031	5.022	5.002	5.000	4.994	4.991	4.988	70
300	3.661	3.655	3.642	3.639	3.635	3.627	3.622	90
302	2.955	2.952	2.942	2.939	2.936	2.932	2.927	100
004	2.504	2.505	2.497	2.497	2.494	2.491	2.489	15
330	2.112	2.107	2.100	2.098	2.096	2.092	2.090	30
304	2.066	2.064	2.058	2.057	2.055	2.052	2.051	45
332	1.944	1.942	1.936	1.934	1.933	1.929	1.926	25
600	1.827	1.825	1.818	1.817	1.815	1.812	1.810	10
602	1.716	1.714	1.709	1.707	1.706	1.702	1.700	15
334	1.612	1.611	1.607	1.605	1.604	1.602	1.601	10
a(Å)	12.68	12.66	12.62	12.61	12.59	12.56	12.55	
c(Å)	10.06	10.04	10.01	10.00	9.988	9.982	9.976	

The abbreviations used in this table are the figures of molar ratios of lanthanum and cerium in the starting solutions (1 Å=0.1 nm).

Table 2. Chemical analysis of synthesized carbonates

Lanthanite-type			Bastnaesite-type		
La : Ce Mixed	La : Ce Found	M_2O_3 : CO_2 : H_2O	La : Ce Mixed	La : Ce Found	M_2O_3 : CO_2 : H_2O
10 : 0	10 : 0	1.00 : 3.09 : 7.40	10 : 0	10 : 0	1.00 : 2.19 : 1.84
8 : 2	7.88 : 2.12	1.00 : 3.14 : 7.74	8 : 2	8.02 : 1.98	1.00 : 2.12 : 2.13
6 : 4	6.00 : 4.00	1.00 : 3.18 : 7.64	6 : 4	5.92 : 4.08	1.00 : 2.03 : 2.39
5 : 5	5.00 : 5.00	1.00 : 3.09 : 7.91	5 : 5	5.02 : 4.98	1.00 : 2.08 : 1.87
4 : 6	3.95 : 6.05	1.00 : 3.10 : 7.78	4 : 6	3.98 : 6.02	1.00 : 2.05 : 2.15
2 : 8	1.96 : 8.04	1.00 : 3.06 : 7.79	2 : 8	2.00 : 8.00	1.00 : 2.15 : 2.20
0 : 10	0 : 10	1.00 : 2.98 : 7.68	0 : 10	0 : 10	1.00 : 2.11 : 2.27

M_2O_3 is the sum of lanthanum and cerium oxides.

indicated that the bastnaesite-type carbonates formed solid solutions over the whole series. Assuming a hexagonal symmetry,[12] the unit cell parameters, *a* and *c*, were calculated from 300 and 002 diffractions respectively (Table 1). These cell parameters indicated, semiquantitatively, the molar ratios of lanthanum and cerium in bastnaesite-type carbonates. The shift of the diffraction peaks of the lanthanite-type carbonates were too small to analyze, however, the results of the electron probe microanalysis indicated that lanthanite-type carbonates formed solid solutions.

Chemical Analysis. From the results shown in Table 2, the molar ratios of lanthanum to cerium contained in the synthesized carbonates were almost equal to those in the starting solutions. In addition, it was found that the molar ratio M_2O_3: CO_2: H_2O was almost 1:3:8 for the carbonates synthesized at 50 °C under atmospheric pressure and 1:2:2 for those synthesized at 100 °C, 5.5 atm. The chemical composition of the carbonates synthesized at 50 °C agreed with the composition of lanthanite, while the composition of those synthesized at 100 °C, 5.5 atm agreed with the composition of hydroxy-bastnaesite, assuming one water molecule of adhesive moisture. From the results of X-ray diffractometry and chemical analysis, it became apparent that $La_2(CO_3)_3 \cdot 8H_2O$ and $Ce_2(CO_3)_3 \cdot 8H_2O$ form a complete series of lanthanite-type solid solutions by the isomorphous replacement of lanthanum by cerium, and that $La(OH)CO_3$ and $Ce(OH)CO_3$ form a complete series of bastnaesite-type solid solutions by the isomorphous replacement of lanthanum by cerium.

Infrared Spectroscopy. The infrared spectra of the lanthanite-type and bastnaesite-type carbonates are shown in Fig. 1. The frequencies for the four modes of the free carbonate ion are: ν_1, 1063 cm^{-1}; ν_2, 879 cm^{-1}; ν_3, 1415 cm^{-1}; and ν_4, 680 cm^{-1}. The vibrations ν_3 and ν_4 are degenerate while ν_1 is infrared-inactive for

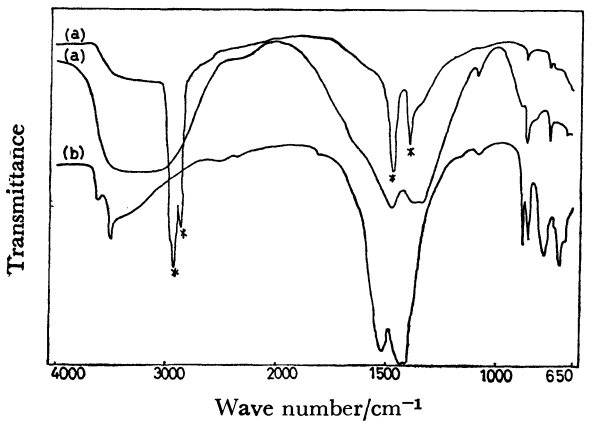

Fig. 1. Infrared absorption spectra of synthesized carbonates.
(a) Lanthanite-type (in KBr disk and in Nujol mull),
(b) bastnaesite-type (in KBr disk).

the free ion.[8] For the lanthanite-type carbonate, the ν_1 mode was just detectable while the ν_3 mode split, indicating that the D_{3h} symmetry of the free carbonate ion was lowered either to C_{2v} or to C_s. The bands in the region 2900—3500 cm^{-1}, appeared even in nujol mull, and were assigned to the absorption of water. Bands marked by a star (*) in Fig. 1 are the absorptions attributable to Nujol. For the bastnaesite-type carbonate, the ν_1 mode appeared faintly and the degenerate mode, ν_3, split. The splitting of the non-degenerate mode, ν_2, indicated that non-equivalent carbonate groups existed.[9] The sharp absorption bands at 3630 and 3480 cm^{-1} were attributed to absorptions by the OH group.[5] The shifts and changes of the absorption spectra caused by the formation of solid solutions were not observed over all the absorptions.

Thermal Analysis. The thermal analysis of the carbonates having various molar ratios of lanthanum and cerium are shown in Fig. 2-a. On the thermogravimetric curve (TG) for the lanthanite-type La10 carbonate, the following abbreviations are used: La10, $La_2(CO_3)_3 \cdot 8H_2O$; Ce10, $Ce_2(CO_3)_3 \cdot 8H_2O$; La5Ce5, $(La_{1.00}Ce_{1.00})_2(CO_3)_3 \cdot 8H_2O$. Initially there was loss of water, which corresponded to the formation of the anhydrous carbonate. Continuous raising of the temperature led to the formation of the dioxide carbonate. The final product of the decomposition was La_2O_3. From the differential scanning calorimetric curve (DSC) for the La10 carbonate, it has been established that the dehydration and decarbonatation in this decomposition process were endothermic. As for the lanthanite-type Ce10 carbonate, the loss of the CO_2 molecules after dehydration was accompanied by the oxidation of Ce^{3+}. That no peaks appeared in the DSC at *ca.* 250 °C appear to be the net result of an endothermic decomposition due to decarbonation coupled with an exothermic reaction due to the oxidation of Ce^{3+} to Ce^{4+}. Although the continuous raising of the temperature in air did not lead to the formation of the dioxide carbonate, it did lead to the formation of the dioxide carbonate, $Ce_2O_2CO_3$ at *ca.* 400 °C in a stream of nitrogen (Fig. 2-c). However, the dioxide carbonate decomposed immediately to CeO_2. The lanthanite-type La5Ce5 carbonate lost eight water molecules at one time under the heating rate used here (5 °C/min), while the formation of the dioxide carbonate did not appear in air. It did, however, appear in a stream of nitrogen. No clear peak attributable to decarbonatation appeared in the DSC at *ca.* 450 °C. As in the course of the decomposition of the Ce10 carbonate, this is the net result of endothermic and the exothermic reactions. The results of the thermal analysis of the lanthanite-type carbonates of other molar ratios were similar to that of the La5Ce5 carbonate. The end product of the La5Ce5 carbonate was a mixed La(III)-Ce(IV)-oxide. The intermediate $Ln_2O_3 \cdot xCO_2 (x<1)$ reported by other workers was not observed.[9]

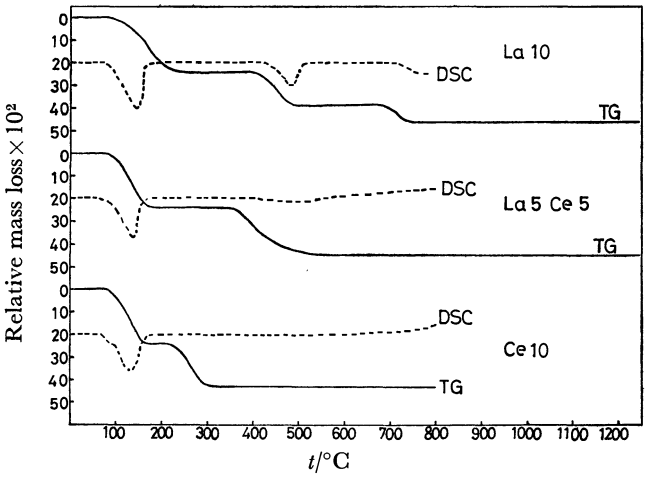

Fig. 2a. TG and DSC curves of lanthanite-type carbonates (in air).

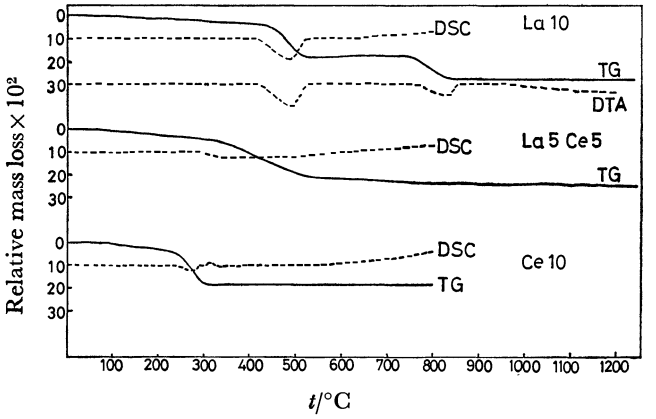

Fig. 2b. TG and DSC curves of bastnaesite-type carbonates (in air).

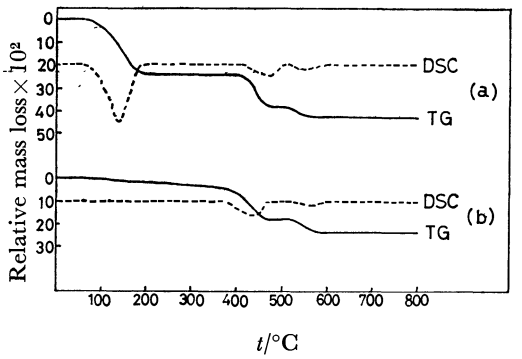

Fig. 2c. TG and DSC curves of lanthanite-type and bastnaesite-type carbonates (in nitrogen stream).
(a) $Ce_2(CO_3)_3 \cdot 8H_2O$, (b) $Ce(OH)CO_3 \cdot H_2O$.

In air:

$$La_2(CO_3)_3 \cdot 8H_2O \xrightarrow{ca.\ 80\ °C} La_2(CO_3)_3 \xrightarrow{ca.\ 400\ °C} La_2O_2CO_3\text{(IA type)} \xrightarrow{ca.\ 680\ °C} La_2O_3$$

$$(La_{1.00}Ce_{1.00})_2(CO_3)_3 \cdot 8H_2O \xrightarrow{ca.\ 80\ °C} (La_{1.00}Ce_{1.00})_2(CO_3)_3 \xrightarrow{ca.\ 330\ °C} La_2O_3 + CeO_2$$

$$Ce_2(CO_3)_3 \cdot 8H_2O \xrightarrow{ca.\ 70\ °C} Ce_2(CO_3)_3 \xrightarrow{ca.\ 210\ °C} CeO$$

In a stream of nitrogen:

$$Ce_2(CO_3)_3\cdot 8H_2O \xrightarrow{ca.\ 60\ ^\circ C} Ce_2(CO_3)_3 \xrightarrow{ca.\ 400^\circ C} Ce_2O_2CO_3 \xrightarrow{ca.\ 500\ ^\circ C} CeO_2$$

$$(La_{1.00}Ce_{1.00})_2(CO_3)_3\cdot 8H_2O \xrightarrow{ca.\ 70\ ^\circ C} (La_{1.00}Ce_{1.00})_2(CO_3)_3 \xrightarrow{ca.\ 430\ ^\circ C} (La_{1.00}Ce_{1.00})_2O_2(CO_3) \xrightarrow{ca.\ 540\ ^\circ C} La_2O_3 + CeO_2$$

Figure 2-b shows the decomposition of bastnaesite-type carbonates. For the bastnaesite-type La10 carbonate, the following abbreviations are used here: La10, $La(OH)CO_3\cdot H_2O$; Ce10, $Ce(OH)CO_3\cdot H_2O$; La5Ce5, $(La_{0.50}Ce_{0.50})(OH)CO_3\cdot H_2O$. The bastnaesite-type La10 carbonate started losing adhesive moisture *ca.* 100 °C and the main decomposition occurred at *ca.* 430 °C accompanying the formation of the dioxide carbonate. The evolution of the remaining one mole of CO_2 began at *ca.* 740 °C. The decomposition of the Ce10 carbonate was accompanied by the oxidation of Ce^{3+}. The small peak that appeared in the DSC at *ca.* 300 °C appeared to be the net result of an endothermic decomposition reaction due to the dehydration and decarbonatation and an exothermic reaction due to the oxidation of Ce^{3+} to Ce^{4+}. The La5Ce5 carbonate continuously lost weight from *ca.* 70 °C. The dioxide carbonate decomposed from the lanthanite-type and bastnaesite-type samples showed different infrared and X-ray powder diffraction spectra. According to the literature, the former was found to be IA type (monoclinic) and the latter, to be II type (hexagonal).[9]

In air:

$$La(OH)CO_3\cdot H_2O \xrightarrow{ca.\ 100\ ^\circ C} La(OH)CO_3 \xrightarrow{ca.\ 430\ ^\circ C} La_2O_2CO_3(\text{II type}) \xrightarrow{ca.\ 740\ ^\circ C} La_2O_3$$

$$(La_{1.00}Ce_{1.00})(OH)CO_3\cdot H_2O \xrightarrow{ca.\ 70\ ^\circ C} (La_{1.00}Ce_{1.00})(OH)CO_3 \xrightarrow{ca.\ 290\ ^\circ C} La_2O_3 + CeO_2$$

$$Ce(OH)CO_3\cdot H_2O \xrightarrow{ca.\ 70\ ^\circ C} Ce(OH)CO_3 \xrightarrow{ca.\ 230\ ^\circ C} CeO_2$$

In a stream of nitrogen:

$$Ce(OH)CO_3\cdot H_2O \xrightarrow{ca.\ 70\ ^\circ C} Ce(OH)CO_3 \xrightarrow{ca.\ 370\ ^\circ C} Ce_2O_2CO_3 \xrightarrow{ca.\ 510\ ^\circ C} CeO_2$$

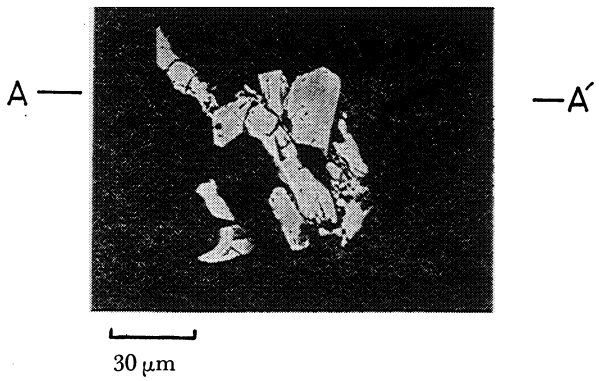

Fig. 3a. The compositional figure of the bastnaesite-type La4Ce6 carbonate.

$$(La_{1.00}Ce_{1.00})(OH)CO_3\cdot H_2O \xrightarrow{ca.\ 100\ ^\circ C} (La_{1.00}Ce_{1.00})(OH)CO_3 \xrightarrow{ca.\ 390\ ^\circ C} (La_{1.00}Ce_{1.00})_2O_2CO_3 \xrightarrow{ca.\ 550\ ^\circ C} La_2O_3 + CeO_2$$

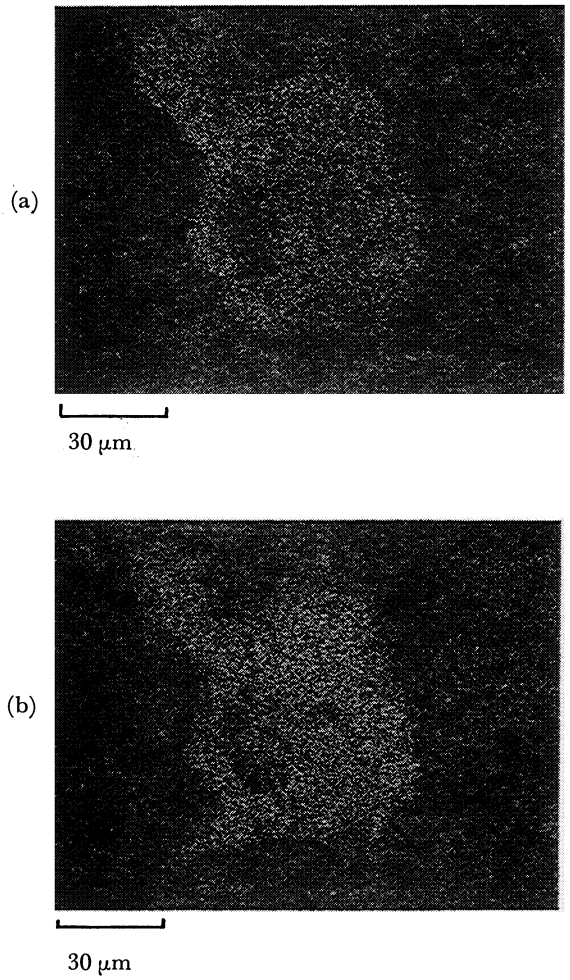

Fig. 3b. The characteristic X-ray figures of the bastnaesitetype La4Ce6 carbonate.
(a) La Lα, (b) Ce Lα.

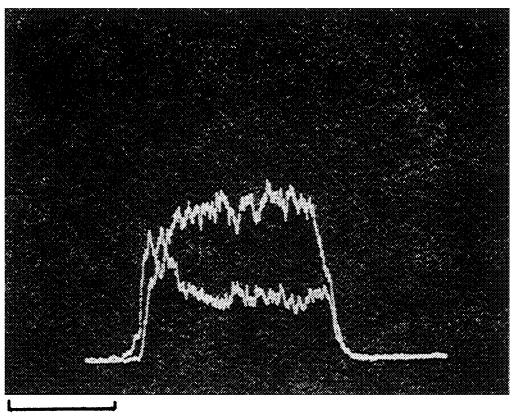

Fig. 3c. The line profiles of the bastnaesite-type La4Ce6 carbonate in A-A′ section.
Upper line: Ce *Lα*, lower line: La *Lα*.

Calkinite[10] was discovered as a late mineral associated with lanthanite in the veins in Bearpaw Mountains of Montana. Although its occurrence is very similar to that of lanthanite and the other hydrated rare earth orthocarbonate minerals synthesized, calkinsite has not been obtained as a product of the La5Ce5 carbonate or as an intermediate of the thermal decomposition of any of the synthesized rare-earth carbonates.

Lanthanite is usually rarely found associating with bastnaesite. The reason for its rare occurrence becomes clear from the above discussions and experiments. Lanthanite changed its structure and chemical composition from lanthanite- to bastnaesite-type when heated with water at 100 °C.[11,12] Thus, it is presumed that lanthanite is lacking in nature due to this thermal metamorphism.

Electron Probe Microanalysis. The compositional figure of the bastnaesite-type La4Ce6 carbonate and its characteristic X-ray figures of La $L\alpha$ and Ce $L\alpha$ are shown in Fig. 3. From the characteristic X-ray figures of La $L\alpha$ and Ce $L\alpha$ and the line profiles in a grain of the La5Ce5 carbonates, the same grain was found to contain equal molar ratios of lanthanum and cerium, indicating that the carbonate formed a solid solution. Semiquantitative analysis suggested that there was a slight difference in the composition of each grain, which might be a reflection of some "fluctuation" in this solution. The molar ratio of lanthanum to cerium contained in the crystal was also microscopically equal to that of the starting solution.

We wish to express our deep gratitude to Professor Isao Masuda, Fukuoka University and Professor Kozo Nagashima, The University of Tsukuba, for their encouragement through the course of this work.

References

1) C. Palache, H. Berman, and C. Frondel, "Dana's System of Mineralogy," 7th ed, J. Wiley, New York, N.Y. (1962), Vol. II.
2) D. B. Shinn and H. A. Eick, *Inorg. Chem.*, **7**, 1340 (1968).
3) A. D. Negro, G. Rossi, and V. Tazzoli, *Am. Mineral.*, **62**, 142 (1977).
4) A. D. Negro, G. Rossi, and V. Tazzoli, *Am. Mineral.*, **60**, 280 (1975).
5) K. Sakurai, H. Wakita, A. Kato, and K. Nagashima, *Bull. Chem. Soc. Jpn.*, **42**, 2725 (1969).
6) K. Nagashima, H. Wakita, and A. Mochizuki, *Bull. Chem. Soc. Jpn.*, **46**, 152 (1973).
7) JIS M 8401 (1956).
8) G. Herberg, "Molecular Spectra and Molecular Structure, II. Infrared and Raman Spectra of Polyatomic Molecules," D. Van Nostranc Co. Inc., New York, N.Y. (1945), p. 179.
9) R. P. Turcotte, J. O. Sawyer, and L. Eyring, *Inorg. Chem.*, **8**, 238 (1969).
10) W. T. Pecora and J. H. Kerr, *Am. Mineral.*, **38**, 1169 (1953).
11) R. Aumont, F. Genet, M. Passaret, and Y. Toudic, *C. R. Acad. Sci., Ser. C*, **272**, 314 (1971)
12) A. N. Christensen, *Acta Chem. Scand.*, **27**, 2973 (1973).
13) J. Sawyer, P. Caro, and L. Eyring, *Revue Chim. Miner.*, **10**, 93 (1973).
14) H. Wakita, *Bull. Chem. Soc. Jpn.*, **51**, 2879 (1978).

Preparation and Optical Resolution of $[Co(en)_x(dmbpy)_{3-x}]^{3+}$ ($x=0, 1$) and Related Complexes

Toshishige M. Suzuki

Government Industrial Research Institute, Tohoku, Nigatake, Haranomachi, Sendai 983

(Received June 28, 1978)

The optical resolution of $[Co(dmpy)_3]^{3+}$, $[Co(en)(dmbpy)_2]^{3+}$, $[Co(en)(bpy)_2]^{3+}$, and $[Rh(dmbpy)_3]^{3+}$(dmbpy =3,3′-dimethyl-2,2′-bipyridine) has been achieved using $(-)_D$ tris(L-cysteinsulfinato)cobaltate(III). The dmbpy complexes consist of a pair of stereo-selective enantiomers. The absorption and CD spectra of two series of complexes, $[Co(en)_x(dmbpy)_{3-x}]^{3+}$ and $[Co(en)_x(bpy)_{3-x}]^{3+}$ ($x=0$, 1, 2, 3) and also $[Rh(dmbpy)_3]^{3+}$ have been investigated. The complexes containing more than two aromatic ligands showed an exciton CD in the ligand π-π^* transition region and the band has been related to the absolute configuration of the complexes. The spectral features of dmbpy complexes are different from those of the bpy complexes and such differences have been discussed with reference to the twisting nature of dmbpy chelates.

The metal chelates of 3,3′-dimethyl-2,2′-bipyridine (dmbpy) are expected to take a non-coplanar conformation owing to the steric interactions of the substituted methyl groups. Some bis(diamine) and tetramine cobalt(III) complexes with dmbpy have been prepared and resolved.[1] It has been found that dmbpy coordinates to the cobalt(III) ion with a stereospecific conformation depending on the given configuration.[1] The absolute configurations of $(+)_D[Co(en)_2(dmbpy)]Cl(ClO_4)_2\cdot H_2O$[2] and $(-)_D[Co(R,R\text{-chxn})_2(dmbpy)]Br(ClO_4)_2\cdot H_2O$[3] (en=enthylenediamine, chxn=1,2-cyclohexanediamine) have been determined by an X-ray method to be $\Lambda(\delta\text{-dmbpy})$ and $\Delta(\lambda\text{-dmbpy})$,[4] respectively. The empirical assignments of the absolute configurations on the basis of the Cotton effects in the first d-d absorption band region[5] are consistent with the X-ray results.

Recently, $[Co(dmbpy)_3]^{3+}$, $[Co(en)(dmbpy)_2]^{3+}$, $[Co(en)(bpy)_2]^{3+}$, and $[Rh(dmbpy)_3]^{3+}$ (bpy=2,2′-bipyridine) have been prepared and resolved. The resolution of the series of complexes, $[Co(en)_x(dmbpy)_{3-x}]^{3+}$ and $[Co(en)_x(bpy)_{3-x}]^{3+}$ where $x=0$, 1, 2, 3 has now been completed. The absolute configuration of the bis and tris(diimine) cobalt(III) complexes can be estimated from the sign of the CD bands in the d-d absorption region[5] as well as in the ligand π-π^* transition region.[6] Data for the complete series of mixed complexes is necessary to elucidate the electronic state, optical activity and absolute configuration of the complexes.

In order to understand the twisted effects of dmbpy chelates, the absorption and CD spectra of dmbpy complexes have been compared with the corresponding bpy complexes, in which chelate conformation is believed to be planar.

Experimental

Materials. 3,3′-Dimethyl-2,2′-bipyridine was prepared as stated previously.[1]

$[Co(dmbpy)_3](ClO_4)_3$. This was prepared by air oxidation as described in a previous paper.[1] Oxidation with PbO_2 in place of bubbling air improved the yield. Approximately 50 mg of the complex was adsorbed on a SP-Sephadex column ($\phi 2.5\times 50$ cm) and eluted with 0.15 mol·dm^{-3} potassium $(+)_D$-tartratoantimonate(III). The eluate was fractionated and the visible absorption spectra measured. All the fractions showed very similar spectra, indicating the absence of geometrical isomers.

$(-)_D[Co(dmbpy)_3](ClO_4)_3\cdot H_2O$. The complex perchlorate (3.6 g) was converted into the bromide by treatment with an anion exchanger, Dowex 1-X8 in the bromide form. A mixture of the solution of the bromide (50 cm^3) and $K_3[Co(L\text{-cysu})_3]$(cysu=cysteinsulfinato)[7] (1.0 g) was stored in a refrigerator overnight. Needlelike crystals of the $(-)_D$-diastereoisomer were filtered, washed with water and acetone (1.4 g). The second crop of crystals (0.3 g) was obtained by concentrating the filtrate to half volume. The first and the second crystal crops were combined, recrystallized twice from hot water to give a reproducible CD spectrum. The $(-)_D$-diastereoisomer in water (20 cm^3) was treated with concentrated hydrochloric acid (1 cm^3). Yellow precipitate of $H_3[Co(L\text{-cysu})_3]$ was filtered off. The filtrate was treated with 70% perchloric acid (2 cm^3) and the yellow crystals of the perchlorate salt were collected and recrystallized from hot water. Found: C, 46.38; H, 4.25; N, 8.84%. Calcd for $C_{36}H_{36}N_6Cl_3O_{12}Co\cdot H_2O$: C, 46.59; H, 4.13; N, 9.06%.

Preparation of $[Co(en)(dmbpy)_2](ClO_4)_3$. To a solution of $[Co(dmbpy)_3](ClO_4)_3$ (1.83 g in 400 cm^3 of water) was added a 10% solution of ethylenediamine (1.2 g) and activated charcoal (0.5 g). The solution was stirred at room temperature for 15 min and then filtered. The filtrate was acidified with a few drops of concentrated hydrochloric acid and poured onto a column of SP-Sephadex ($\phi 3.0\times 40$ cm). The adsorbed band was washed with water and eluted with 0.15 mol·dm^{-3} sodium sulfate solution. The column gave four separate bands in the order of elution, I, II, III, and IV, which were $[Co(en)_3]^{3+}$, $[Co(en)_2(dmbpy)]^{3+}$, $[Co(dmbpy)_3]^{3+}$, and $[Co(en)(dmbpy)_2]^{3+}$, respectively. The eluatant of band IV was fractionated and the absorption spectra recorded. No indication for the presence of the geometrical isomer was found. The fractions were collected, evaporated to dryness and the yellow residue extracted with methanol (50 cm^3) and the extract was evaporated to dryness. The residual solid was dissolved in water (20 cm^3) and 70% perchloric acid was added (1 cm^3). The orange-yellow precipitate was filtered off and recrystallized from hot water (300 mg) Found: C, 39.52; H, 4.41; N, 10.34%. Calcd for $C_{26}H_{32}N_6Cl_3O_{12}Co$: C, 39.74; H, 4.10; N, 10.69%.

$(+)_D[Co(en)(dmbpy)_2](ClO_4)_3$. 1.2 g of perchlorate was converted into the bromide using the anion exchanger Dowex 1-X8 in the bromide form. To the solution of the bromide (50 cm^3) was added $K_3[Co(L\text{-cysu})_3]$ (0.64 g in 10 cm^3 of water) and the solution stored in a refrigerator for 3 h. The yellow crystals of the $(-)_D$-diastereoisomer were

filtered off, washed with a small amount of ethanol and finally ether, (400 mg). The filtrate was evaporated to half volume and stored in a refrigerator overnight and a second crop of crystals (60 mg) were obtained. The crystals were combined and recrystallized from hot water (300 mg). The $(+)_D$-diastereoisomer was suspended in water (5 cm^3) and stirred for 1 h with 3 $mol \cdot dm^{-3}$ hydrochloric acid (1 cm^3). The yellow precipitate was filtered off and the filtrate was treated with 70% perchloric acid (0.5 cm^3). The orange crystals of $(+)_D[Co(en)(dmbpy)_2](ClO_4)_3$ were collected and recrystallized from hot water. Found: C, 39.74; H, 4.34; N, 10.71%. Calcd for $C_{26}H_{32}N_6Cl_3O_{12}Co$: C, 39.74; H, 4.10; N, 10.69%.

[Co(en)(bpy)$_2$](ClO$_4$)$_3$·4H$_2$O. To a solution of [Co-$Cl_2(bpy)_2]Cl$ (3.8 g in 100 cm^3 of water) was added 10% ethylenediamine solution (4.8 g) and the mixture warmed at 60 °C for 3 h. Concentrated hydrochloric acid (0.5 cm^3) was added to the solution and resulting solution diluted to 1000 cm^3 and poured onto a column of SP-Sephadex (ϕ 3.5×80 cm). The adsorbed band was washed with water and eluted with 0.2 $mol \cdot dm^{-3}$ hydrochloric acid. The column gave three separate bands, I, II, III, in the order of elution, which were $[Co(bpy)_3]^{3+}$, $[Co(en)(bpy)_2]^{3+}$, and $[Co(en)_2(bpy)]^{3+}$, respectively. The effluent of band II was evaporated to dryness, the residue dissolved in water (10 cm^3) and filtered. After the addition of 70% perchloric acid (2 cm^3), the solution was placed in a refrigerator overnight and the yellow crystals were collected and recrystallized from hot water (1.3 g). Found: C, 33.16; H, 3.74; N, 10.59%. Calcd for $C_{22}H_{24}N_6$-$Cl_3O_{12}Co \cdot 4H_2O$: C, 32.96; H, 3.99; N, 10.47%.

(+)$_D$[Co(en)(bpy)$_2$](ClO$_4$)$_3$. This complex was resolved by a similar method as that for $[Co(en)(dmbpy)_2]^{3+}$ using $K_3[Co(L\text{-}cysu)_3]$. Found: C, 35.20, H, 3.28; N, 11.36%. Calcd for $C_{22}H_{24}N_6Cl_3O_{12} \cdot H_2O$: C, 35.34; H, 3.47; N, 11.23%.

(−)$_D$[Rh(dmbpy)$_3$](ClO$_4$)$_3$. This complex was prepared by a similar method to that for $[Rh(bpy)_3](ClO_4)_3$ using dmbpy instead of bpy.[8] Optical resolution was achieved using $K_3[Co(L\text{-}cysu)_3]$. Found: C, 45.29; H, 3.75; N, 8.92%. Calcd for $C_{36}H_{36}N_6Cl_3O_{12}Rh$: C, 45.33; H, 3.68; N, 8.81%.

Measurements. Absorption and CD spectra were recorded at room temperature on a Shimadzu Double 40-R spectrometer and a JASCO J-20 spectropolarimeter, respectively. PMR spectra were measured with a JNM-PMX60 and a JEOL Model 4H-100 spectrometer using DSS as the internal standard.

Results and Discussion

A 3,3′-dimethyl-2,2′-bipyridine chelate can assume dissymmetric conformations (δ and λ) and consequently eight optical isomers arise from the conformational and configurational dissymmetry are possible for a tris complex. The PMR spectra of $[Co(dmbpy)_3]^{3+}$ and $[Rh(dmbpy)_3]^{3+}$ in D_2O gave a single methyl signals at 2.55 and 2.67 ppm, respectively, indicating all the methyl groups in the complex are equivalent. Chromatographic separation of the isomers of $[Co(dmbpy)_3]^{3+}$ suggests that the complex consists of only one geometrical isomer; *i.e.*, a pair of enantiomers. Four of the eight possible isomers, $\Delta(\lambda\lambda\lambda)$, $\Lambda(\delta\delta\delta)$, $\Delta(\delta\delta\delta)$, and $\Lambda(\lambda\lambda\lambda)$, two pairs of enantiomers have D_3 symmetry in which all the methyl groups are equivalent. Figure 1 shows a schematic drawing of the two isomers, (a) $\Lambda(\delta\delta\delta)$ (*lel*) and (b) $\Lambda(\lambda\lambda\lambda)$ (*ob*). The 2C–2C′ bond of each dmbpy chelate in (a) is pseudo-parallel (*lel*) to the three-fold axis whereas in (b) it is oblique. A molecular model examination suggests that the (b) configuration has appreciable non-bonded atomic interactions between dmbpy chelates in contrast to the (a) configuration. Clearly the same relationship holds for $\Delta(\delta\delta\delta)$ and $\Lambda(\delta\delta\delta)$. Thus the tris complexes are most likely to consist of a pair of enantiomeric forms, $\Delta(\lambda\lambda\lambda)$ and $\Lambda(\delta\delta\delta)$.

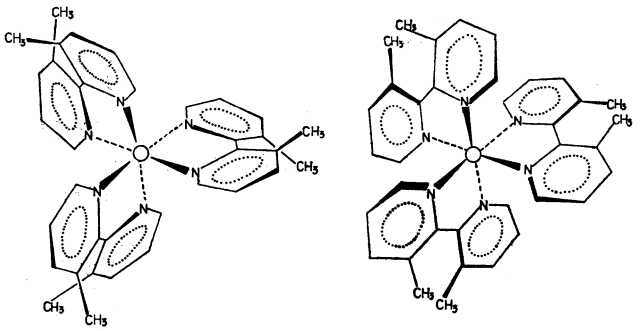

(a) (b)

Fig. 1. Schematic drawings of the two isomers of $[Co(dmbpy)_3]^{3+}$; (a) $\Lambda(\delta\delta\delta)(lel)$, (b) $\Lambda(\lambda\lambda\lambda)(ob)$.

The bis(dmbpy) complex, $[Co(en)(dmbpy)_2]^{3+}$ was obtained by treating the tris complex in aqueous solution with ethylenediamine in the presence of activated charcoal. Other species, such as $[Co(en)_2(dmbpy)]^{3+}$, $[Co(en)_3]^{3+}$ formed by disproportionation were separated on a Sephadex column. No indication for the presence of more than a pair of enantiomers was found for the bis(dmbpy) complex. Two dmbpy chelates in $[Co(en)(dmbpy)_2]^{3+}$ are expected to take the (*lel*, *lel*) form exclusively owing to similar steric requirements as described for the tris complexes.

In addition to the series of dmbpy complexes, the optical resolution of the bpy complex series, $[Co(en)_x(bpy)_{3-x}]^{3+}$ was completed by the resolution of $[Co(en)(bpy)_2]^{3+}$. Figures 2 and 3 show the absorption and CD spectra of the series where $[Co(en)_3]^{3+}$ has been excluded to avoid complications. The numerical data is listed in Table 1. The first absorption maximum for the dmbpy complex appears always at longer wavelengths than that of the corresponding bpy complex. Since the first d-d peak positions for the dmbpy complex series do not significantly vary with x (see Table), except for the $[Co(dmbpy)_3]^{3+}$ ion, dmbpy appears to lie close to ethylenediamine in the spectrochemical series. The torsional strain of the dmbpy chelate induced by twisting about the 2C–2C′ bond should more or less affect the strength of the coordination bond.

For the dmbpy complexes, strong bands have been observed in the region, 27000—31000 cm^{-1}, In the case of $[Co(dmbpy)_3]^{3+}$, the first absorption band is obscured by overlapping. The nature of the band should be a charge transfer transition, since the free ligand does not have a band in this region.[9] The peak maxima shifts to lower energy and the intensities decrease in the order, $[Co(en)_2(dmbpy)]^{3+}$, $[Co(en)(dmbpy)_2]^{3+}$, and $[Co(dmbpy)_3]^{3+}$. This is also the

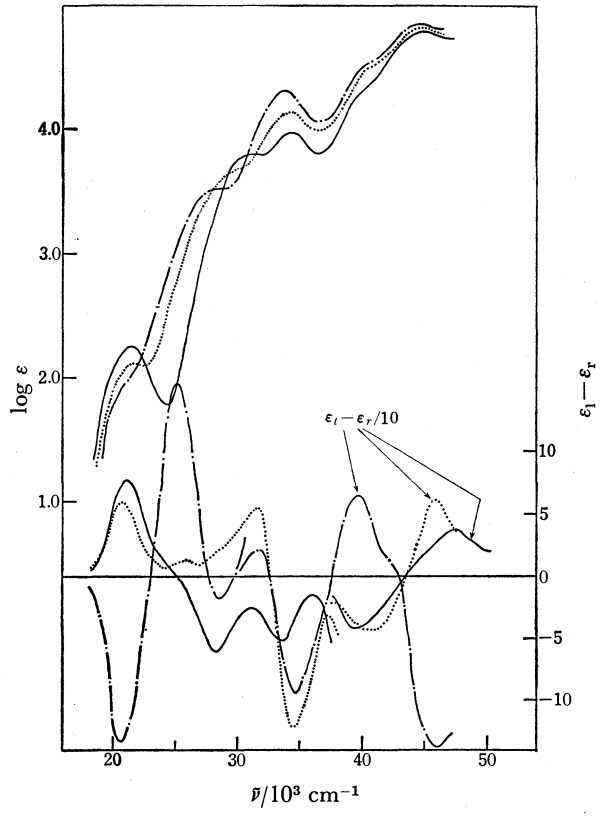

Fig. 2. Absorption and CD spectra of (——)Λ[Co(en)$_2$(dmbpy)]$^{3+}$, (·····) (+)$_D$[Co(en)(dmbpy)$_2$]$^{3+}$, and (-·-·-)(−)$_D$[Co(dmbpy)$_3$]$^{3+}$ in water.

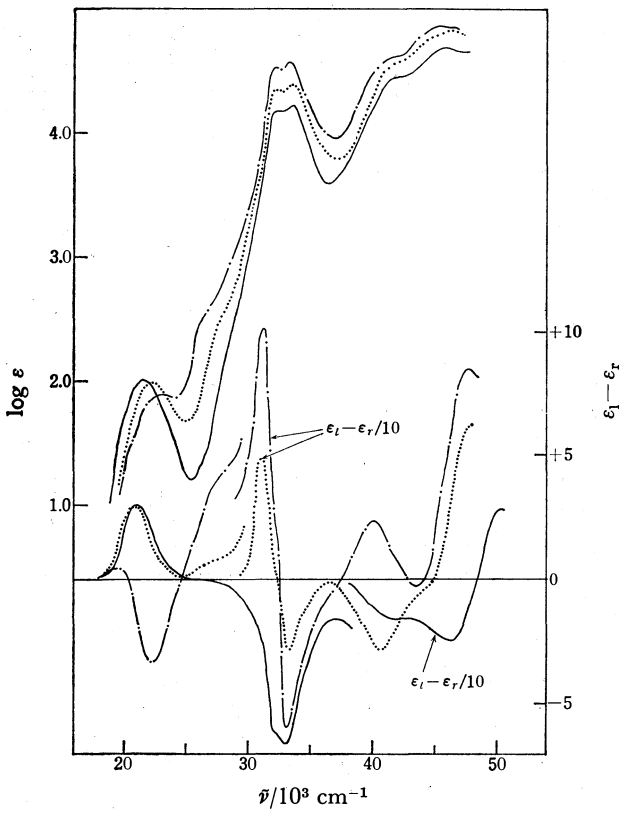

Fig. 3. Absorption and CD spectra of (——) (+)$_D$[Co(en)$_2$(bpy)]$^{3+}$, (·····) (+)$_D$[Co(en)(bpy)$_2$]$^{3+}$, and (-·-·-) (+)$_D$[Co(bpy)$_3$]$^{3+}$ in water.

Table 1. Absorption (AB) and circular dichroism (CD) spectral data in 10 cm^{-1}, (log ε) and ($\varepsilon_l-\varepsilon_r$)

Complex	AB	CD
(+)$_D$[Co(en)$_3$]$^{3+}$ a)	21.40(1.97)	20.40(+1.89)
		23.30(−0.12)
	29.50(1.93)	28.60(+0.25)
	47.10(4.36)	47.40(−31.0)
(+)$_D$[Co(en)$_2$(dmbpy)]$^{3+}$ b)	21.28(2.21)	21.05(+7.45)
	30.30(3.77)	28.17(−5.84)
	33.67(3.91)	33.78(−4.72)
		39.37(−21.1)
	44.24(4.73)	47.17(+35.7)
(+)$_D$[Co(en)(dmbpy)$_2$]$^{3+}$	21.28(2.12)	20.41(+5.81)
	sh 28.57(3.63)	25.97(+1.10)
	33.33(4.15)	31.75(+5.40)
		34.48(−12.4)
	sh 40.32(4.49)	40.98(−23.1)
	43.48(4.77)	45.87(+36.2)
(−)$_D$[Co(dmbpy)$_3$]$^{3+}$	sh 20.62(1.95)	20.83(−12.9)
	27.78(3.55)	25.12(+15.6)
	32.89(4.33)	32.05(+27.2)
		34.84(−90.2)
		39.37(+71.0)
	42.74(4.89)	sh 42.02(+16.9)
		46.30(−137.0)
(+)$_D$[Co(en)$_2$(bpy)]$^{+}$ b)	21.74(1.99)	20.70(+3.02)
	sh 31.25(4.03)	32.47(−6.64)
	32.46(4.12)	sh 45.87(−24.8)
	45.87(4.68)	49.50(+28.9)
(+)$_D$[Co(en)(bpy)$_2$]$^{3+}$	21.83(1.96)	20.62(+3.04)
	31.44(4.34)	30.96(+48.7)
	32.57(4.41)	33.00(−27.2)
	sh 40.82(4.60)	40.48(−28.1)
	45.45(4.88)	47.62(+64.4)
(+)$_D$[Co(bpy)$_3$]$^{3+}$ c)		19.80(+0.35)
	22.22(1.89)	22.22(−3.33)
	31.45(4.49)	31.15(+104)
	32.68(4.53)	33.44(−59.2)
		39.68(+23.6)
	45.05(4.84)	43.10(−4.22)
		46.51(+84.3)
(−)$_D$[Rh(dmbpy)$_3$]$^{3+}$	sh 30.49(4.41)	29.85(+19.7)
	31.45(4.46)	32.68(−35.6)
		36.50(−14.3)
	sh 42.37(4.73)	40.98(+59.8)
	sh 47.62(4.99)	46.51(−62.1)
(+)$_D$[Rh(bpy)$_3$]$^{3+}$ c)	31.45(4.56)	31.15(+145)
	32.79(4.54)	32.36(+52.1)
		sh 33.33(−37.7)
		34.38(−57.9)
	41.67(4.60)	41.67(+15.0)
		45.45(−72.5)

a) Ref. 17. b) Ref. 1. c) Ref. 7.

order of increasing steric interaction. In the case of the bpy complexes, such bands are less marked than for dmbpy complexes.

The intense absorption at about 32000—33000 cm^{-1} for all complexes is ascribed to the ligand π-π^* transition.[9,10] The band maxima for the dmbpy complexes always have lower intensities and appear at shorter

wavelengths compared with those of the bpy complexes. Single bond twisting in a conjugated system away from coplanarity is known to affect the position and/or the intensities of the π-π^* absorption bands.[11] Therefore, the spectral differences between the bpy and dmbpy series are mainly attributable to the differences in conformation of the chelate rings.

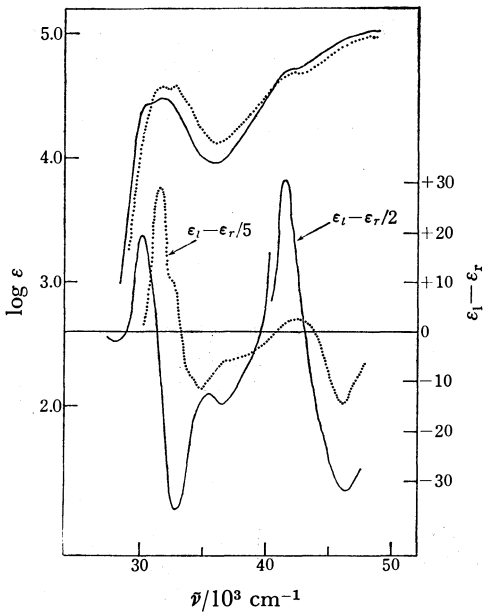

Fig. 4. Absorption and CD spectra of (——) $(-)_D$-$[Rh(dmbpy)_3]^{3+}$, and (·····) $(+)_D[Rh(bpy)_3]^{3+}$ in water.

All the CD spectral data given in Table 1 and Figs. 2—4 are for isomers derived from the less soluble diastereoisomeric salt with $[Co(L\text{-cysu})_3]^{3-}$ ion. Of these, the absolute configuration of $(+)_D[Co(en)_3]^{3+}$ [12] and $(+)_D[Co(en)_2(dmbpy)]^{3+}$ [2] have been assigned Λ by X-ray method. The empirical assignment of the absolute configuration on the basis of the dominant CD peaks in the first d-d region are consistent with Λ. The complexes containing two or three bpy or dmbpy units always give a positive-negative CD couplet from the longer wavelength side in the ligand π-π^* region. The exciton couplet CD of the π-π^* transition has been related nonempirically to the absolute configurations of the complexes; when the configuration is Λ, the negative component of the π-π^* couplet lies at a higher energy, while it lies at lower energy when the chirality is Δ.[6] From this rule, the present complexes have been assigned the Λ-configuration.

The bis complexes, $(+)_D[Co(en)(bpy)_2]^{3+}$ and $(+)_D$-$[Co(en)(dmbpy)_2]^{3+}$ exibit one positive CD band in the first d-d absorption band region, giving an assignment of Λ-configuration which is consistent with that predicted from the π-π^* exciton CD bands. On the contrary, $(+)_D[Co(bpy)_3]^{3+}$ [13] and $(-)_D[Co(dmbpy)_3]^{3+}$ gave the negative CD in the first absorption band region, which contradicts the configuration predicted from the exciton CD. The charge-transfer bands have however been located close to or overlapping the first absorption band region for the present tris complexes leading that the CD bands in this region would be complicated by the CD components associated with the charge-transfer bands. The d-d absorption bands of the bis and mono (bpy or dmbpy) complexes are relatively clear compared with those of the tris complexes and the CD bands beneath the d-d absorption appear less affected by adjacent transitions. Many bis(bpy or 1,10-phenanthroline) complexes of cobalt(III),[13–16] whose d-d absorption bands are rather isolated from adjacent bands give CD consistent with the ligang exciton CD for assigning the absolute configuration. The CD in the first absorption band region is at times greately affected by the steric and electronic circumstances of surrounding ligands,[17,18] whereas the exciton CD of tris complexes is usually very intense and not significantly affected by other transitions.[6c] Comparing the exciton CD of the present tris and bis pairs, the absolute configurations of $(+)_D[Co(bpy)_3]^{3+}$, $(+)_D[Co(en)(bpy)_2]^{3+}$, $(-)_D$-$[Co(dmbpy)_3]^{3+}$, and $(+)_D[Co(en)(dmbpy)_2]^{3+}$ have been assigned as Λ

The absorption and CD spectra of $(-)_D[Rh$-$dmbpy)_3]^{3+}$ are shown in Fig. 4 along together those of $(+)_D[Rh(bpy)_3]^{3+}$. [7] The CD patterns of the two complexes are quite similar over all the wavelength region. The intense exciton couplet CD is centered at about 33000 cm^{-1} for the bpy complex and 32000 cm^{-1} for the dmbpy complex. The patterns indicate that the absolute configuration of the complexes are assignable to Λ.

References

1) a) T. M. Suzuki, *Chem. Lett.*, **1975**, 93; b) T. M. Suzuki and T. Kimura, *Bull. Chem. Soc. Jpn.*, **50**, 391 (1977).
2) S. Sato and Y. Saito, *Acta Crystallogr., Sect. B*, in press.
3) S. Ōba, S. Sato, and Y. Saito, private communication.
4) (δ, λ) and (Δ, Λ) refer to the chelate ring conformations and the absolute configurations about the metal ion respectively, as defined in *Inorg. Chem.*, **9**, 1 (1970).
5) A. J. MacCaffery, S. F. Mason, and B. J. Norman, *J. Chem. Soc.*, **1965**, 5094.
6) a) S. F. Mason, *Inorg. Chim. Acta Rev.*, **2**, 89 (1968); b) Bosnich, *Inorg. Chem.*, **1**, 178, 2379 (1968); c) B. Bosnich, *Acc. Chem. Res.*, **2**, 266 (1969).
7) L. S. Dollimore and R. D. Gillard, *J. Chem. Soc., Dalton Trans.*, **1973**, 933.
8) P. M. Gindney, R. D. Gillard, and B. T. Heaton, *J. Chem. Soc., Dalton Trans.*, **1972**, 2621.
9) G. Favini, *Gazz. Chim. Ital.*, **94**, 1287 (1964).
10) W. R. McWhinnie and J. D. Miller, *Adv. Inorg. Chem. Radiochem.*, **12**, 135 (1969).
11) "Steric Effects in Organic Chemistry," ed by M. S. Newman, John Wiley & Sons, New York (1956), p. 481.
12) Y. Saito, K. Nakatsu, M. Shiro, and H. Kuroya, *Acta Crystallogr.*, **8**, 729 (1955); *Bull. Chem. Soc. Jpn.*, **30**, 795 (1957).
13) J. Ferguson, C. J. Hawkins, N. A. P. Kane-Maguire, and H. Lip, *Inorg. Chem.*, **8**, 771 (1969).
14) L. S. Dollimore and R. D. Gillard, *J. Chem. Soc., Dalton Trans.*, **1975**, 369.
15) A. Tatehata, *Inorg. Chem.*, **15**, 2086 (1976).
16) K. Kashiwabara, K. Igi, and B. E. Douglas, *Bull. Chem. Soc. Jpn.*, **49**, 1573 (1976).
17) M. Kojima, H. Yamada, H. Ogino, and J. Fujita, *Bull. Chem. Soc. Jpn.*, **50**, 2325 (1977).
18) R. D. Gillard, R. E. E. Hill, and R. Maskill, *J. Chem. Soc., A*, **1970**, 1447.

Kinetics of the Oxidative Addition Reaction of Iodine to (Dimethyldithiocarbamato)bis(2,4,6-trimethylphenyl isocyanide)rhodium(I)

Ryosho KUWAE, Toshio TANAKA,* and Katsuhiko KAWAKAMI

Department of Applied Chemistry, Faculty of Engineering, Osaka University, Suita, Osaka 565

(Received June 23, 1978)

The reaction of $Rh(dtc)L_2$ (dtc=$S_2CN(CH_3)_2$, L=2,4,6-$(CH_3)_3C_6H_2NC$) with an equimolar amount of iodine yields a *trans* adduct, $RhI_2(dtc)L_2$. The rate of this reaction was measured in benzene, employing a stopped-flow technique under pseudo-first-order conditions with excess iodine. The result indicates that the reaction proceeds *via* a charge transfer complex $Rh(dtc)L_2 \cdot I_2$, which is rearranged in two consecutive zero-order reactions with respect to the I_2 concentration; the rearrangement of $Rh(dtc)L_2 \cdot I_2$ to a *cis* adduct followed by isomerization to the *trans* adduct. This mechanism is supported from kinetic data for the reaction of $Rh(acac)L_2$ (acac=$CH_3COCHCOCH_3$) with I_2. It is also described that $RhI(I_3)(dtc)L_2$ and $RhI(I_3)(acac)L_2$ were obtained by reactions of $Rh(dtc)L_2$ and $Rh(acac)L_2$ with excess iodine, respectively.

Coordinatively unsaturated rhodium(I) complexes undergo oxidative addition reactions with various organic and inorganic molecules.[1,2] The interest in these reactions stems partly from their catalytic implications.[3] Recently, kinetic studies have been reported for the reactions of Rh(I) substrates with hydrogen,[4,5] oxygen,[5] organic halides,[5-7] and olefins.[5,8,9] However, little is known concerning the mechanism of the addition reactions of halogen, although various halogen adducts of Rh(I) have been isolated.[2,10-14]

This paper reports the kinetic study on the reactions of (dimethyldithiocarbamato)bis(2,4,6-trimethylphenyl isocyanide)rhodium(I), $Rh(dtc)L_2$, and (acetylacetonato)bis(2,4,6-trimethylphenyl isocyanide)rhodium(I), $Rh(acac)L_2$, with iodine giving *trans*-$RhI_2(dtc)L_2$ and -$RhI_2(acac)L_2$, respectively. The isolation of $RhI(I_3)(dtc)L_2$ and $RhI(I_3)(acac)L_2$ is also described.

Experimental

Materials. $Rh(dtc)L_2$[15] and $Rh(acac)L_2$[16] (L=2,4,6-$(CH_3)_3C_6H_2NC$, dtc=$S_2CN(CH_3)_2$, acac=$CH_3COCHCOCH_3$) were prepared as described previously. Iodine was sublimed three times. Benzene was purified by the usual method.[17]

Equimolar Reactions of $Rh(dtc)L_2$ and $Rh(acac)L_2$ with Iodine. Iodine (0.74 mmol) was added to a suspension of $Rh(dtc)L_2$ (0.74 mmol) in diethyl ether (70 ml), and the mixture was stirred for 10 h. The resulting precipitate was recrystallized from a mixture of benzene and cyclohexane to give reddish brown crystals of $RhI_2(dtc)L_2$ in a 69% yield. Found: C, 36.38; H, 3.63; N, 5.41%; mol wt, 798 in $CHCl_3$ at 37 °C. Calcd for $C_{23}H_{28}I_2N_3S_2Rh$: C, 36.00; H, 3.68; N, 5.48%; mol wt, 767.

The analogous acac complex, $RhI_2(acac)L_2$, was similarly obtained by the reaction of $Rh(acac)L_2$ with an equimolar amount of I_2 in a 68% yield. Found: C, 40.48; H, 3.97; N, 3.83%; mol wt, 754 in $CHCl_3$ at 37 °C. Calcd for $C_{25}H_{29}I_2N_2O_2Rh$: C, 40.24; H, 3.92; N, 3.75%; mol wt, 746.

Reaction of $Rh(dtc)L_2$ or $Rh(acac)L_2$ with Excess Iodine. To a suspension of $Rh(dtc)L_2$ (0.74 mmol) in diethyl ether (40 ml) was added large excess iodine (7.4 mmol), and the mixture was stirred for 15 h. The resulting precipitate was washed with diethyl ether to remove unreacted iodine and recrystallized from tetrahydrofuran (THF)–petroleum ether to give dark brown crystals of $RhI_4(dtc)L_2 \cdot 3/4THF$ in a 64% yield. Found: C, 28.85; H, 3.13; N, 3.79%. Calcd for $C_{26}H_{34}I_4N_3O_{3/4}S_2Rh$: C, 29.04; H, 3.19; N, 3.91%. This compound was prepared also by the reaction of $RhI_2(dtc)L_2$ with excess iodine in diethyl ether, and recrystallized from THF–petroleum ether.

The corresponding acac complex, $RhI_4(acac)L_2$, was similarly obtained by the reaction of $Rh(acac)L_2$ with excess iodine in a 41% yield. Found: C, 29.84; H, 2.91; N, 2.87%. Calcd for $C_{25}H_{29}I_4N_2O_2Rh$: C, 30.03; H, 2.92; N, 2.80%.

Kinetic and Other Measurements. Kinetic runs were performed by using a Union RA-413 stopped-flow spectrophotometer equipped with a 0.2 cm quartz cell in a cell holder thermostated to ±0.2 °C, under pseudo-first-order conditions by mixing a benzene solution of the Rh(I) substrate (1.0×10^{-4} M) with excess iodine in benzene ($1.0-4.0\times10^{-3}$ M). The rate of reaction was measured by following the decay of absorbance at 370 nm with time. At least five reaction curves were accumulated by a Union System-71 kinetic data processor and an average curve was recorded on a National VP-6421A X-Y recorder.

Molecular weights, infrared, and ^1H NMR spectra were measured as described elsewhere.[18] Electronic spectra in benzene or toluene were recorded on a Hitachi 124 spectrophotometer.

Results and Discussion

Characterization of Reaction Products. Table 1 shows relevant infrared frequencies (in $CHCl_3$) and ^1H NMR chemical shifts (in $CDCl_3$) of the four adducts obtained here. The 1:1 adducts exhibit two $\nu(N\equiv C)$ bands, whose frequencies are higher than those of the Rh(I) substrates, confirming the occurrence of oxidative addition reactions[10,12,13] with the retention of mutual *cis* positions of the two isocyanide ligands. The ^1H

Table 1. $\nu(N\equiv C)$ frequencies (in $CHCl_3$, cm^{-1}) and ^1H NMR chemical shifts (in $CDCl_3$, ppm) of the adducts

Adduct	$\nu(N\equiv C)$[a]	δ(dtc- or acac-Me)	δ(2,6-Me)	δ(4-Me)	δ(3,5-H)
$RhI_2(dtc)L_2$	2187, 2203	3.32	2.51	2.30	6.88
$RhI_2(acac)L_2$	2199, 2215	2.11	2.52	2.32	6.92
$RhI_4(dtc)L_2 \cdot 3/4THF$	2181, 2197	3.36	2.50	2.33	6.97
$RhI_4(acac)L_2$	2200, 2215	2.12	2.51	2.32	6.95

a) $Rh(dtc)L_2$: 2057 and 2120 cm^{-1}, $Rh(acac)L_2$: 2082 and 2147 cm^{-1}.

NMR spectrum of $RhI_2(dtc)L_2$ shows only a signal for the dtc-methyl and the isocyanide protons, respectively (Table 1), suggesting that both of the two dtc-methyl groups and the two isocyanide ligands are magnetically equivalent, respectively. These results imply that $RhI_2(dtc)L_2$ assumes an octahedral geometry, in which dtc and two isocyanides are located in an equatorial plane with the two iodide ligands in axial positions. The same geometry is suggested for $RhI_2(acac)L_2$ on the basis of infrared and ^1H NMR spectra. The ^1H NMR spectrum of a benzene-d_6 solution containing equimolar amounts (5.0×10^{-2} M) of $Rh(dtc)L_2$ or $Rh(acac)L_2$ and I_2 showed no signal other than those assignable to $RhI_2(dtc)L_2$ or $RhI_2(acac)L_2$. Thus, the stoichiometry for the addition reaction of equimolar iodine to the rhodium substrate is expressed by

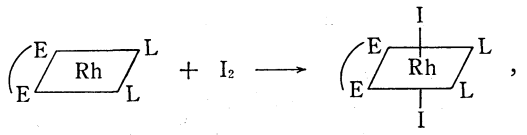

where E–E stands for dtc (E=S) or acac (E=O).

The $RhI_4(dtc)L_2$ and $RhI_4(acac)L_2$ complexes may be formulated as $RhI(I_3)(dtc)L_2$ and $RhI(I_3)(acac)L_2$ respectively, both of which involve a triiodide anion, since trivalent rhodium is known to assume a hexacoordinated geometry. Coordination of I_3^- to metal ions has been proposed for some Pt(II)[19,20] and Fe(III)[21] complexes.

Kinetics and Mechanism. As shown in Fig. 1, benzene solutions of $Rh(dtc)L_2$ and I_2 exhibit absorption maxima at 352 (ε 14000) and 500 nm (ε 1200) in the electronic spectra, respectively. Immediately after mixing of these solutions, however, appeared an absorption maximum at 370 nm, which decreased with a half-life of about 3 ms, as shown in Fig. 2. This Figure was obtained by plotting A_t-A_∞ at nine different wavelengths in the 340—400 nm range against time,

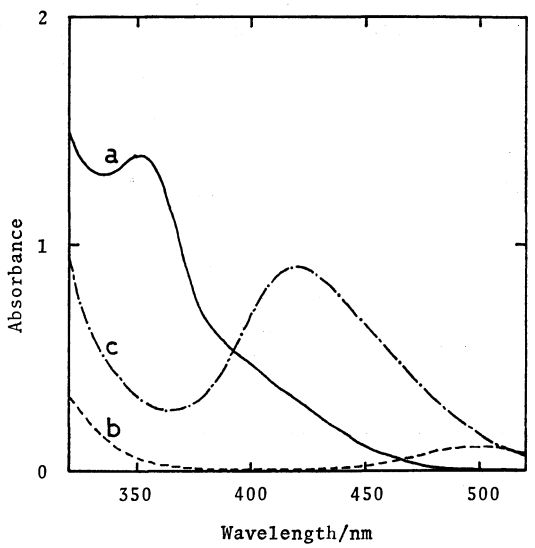

Fig. 1. Electronic spectra of $Rh(dtc)L_2$ (**a**), I_2 (**b**), and *trans*-$RhI_2(dtc)L_2$ (**c**) in benzene (1.0×10^{-4} M) at 25.1 °C; cell length 1.0 cm.

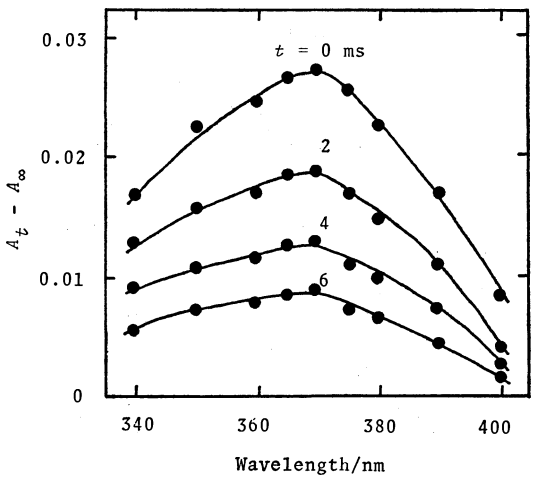

Fig. 2. Decay of the absorption band with time after mixing $Rh(dtc)L_2$ (1.0×10^{-4} M) with I_2 (1.0×10^{-3} M) in benzene at 10.0 °C.

where A_t and A_∞ are absorbances at a given wavelength at the time "t" and at the end of reaction. This result indicates the formation of a transient intermediate during the dead time of the instrument, followed by its rapid degradation. The mixing of $Rh(acac)L_2$ with excess I_2 in benzene also gave a similar short-lived absorption maximum at 360 nm (half-life; about 4 ms at 25.1 °C). In view of the fact that the absorption maxima observed in the two reaction systems do not coincide in wavelength with each other, those bands may not be associated with a common chemical species, such as the I_3^- anion, although this anion formed by mixing $(n\text{-}C_4H_9)_4NI$ with I_2 in benzene[22] exhibited an absorption maximum at 367 nm. Alternatively, the 370 nm band which occurred in the $Rh(dtc)L_2$–I_2 system may be assigned to the charge transfer (CT) transition from the dtc-sulfur atom to the I_2 molecule, by analogy with the fact that both $(CH_3)_2Sn\{S_2CN(C_2H_5)_2\}_2$[23] and $Zn\{S_2CN(n\text{-}C_4H_9)_2\}_2$[24] react with I_2 to yield short-lived absorptions at 385 and 360 nm, respectively, assignable to CT transitions of the same

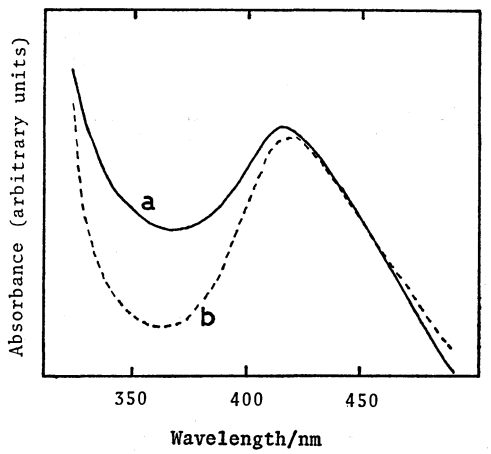

Fig. 3. Electronic spectra of toluene solutions containing equimolar quantities of $Rh(dtc)L_2$ and I_2 at −60 °C; **a** and **b** are those of the solutions prepared at −60 °C and at room temperature, respectively.

type. Similarly, the 360 nm band observed in the $Rh(acac)L_2$–I_2 system may be due to the CT transition from the acac-oxygen to I_2. This is supported from the fact that ethanol, *N*,*N*-dimethylformamide, and related oxygen-containing compounds have been reported to form CT complexes with iodine; the CT bands were observed around 250 nm.[25]

Figure 3 shows the electronic spectra of two toluene solutions both containing equimolar quantities of $Rh(dtc)L_2$ and I_2 at −60 °C; one was prepared at −60 °C (solution **a**) and the other at room temperature followed by cooling (solution **b**). No absorption maximum is observed around 370 nm for these solutions, indicating that the CT complex had already decomposed even at −60 °C. It is to be noted, however, that the absorbance in the 370 nm region is different between the spectra of solution **a** and **b**, despite the similarity in those spectra. In addition, the same spectrum as solution **b** was observed in solution **a** which was allowed to stand at room temperature for several minutes, followed by cooling down to −60 °C. The spectrum of solution **b** can be ascribed to *trans*-$RhI_2(dtc)L_2$, because it showed no change at all even in prolonged standing at room temperature. Thus, the spectrum of solution **a** may arise from another intermediate frozen at −60 °C. No direct evidence has been obtained for the configuration of the intermediate, because in nonpolar solvents such as toluene $Rh(dtc)L_2$ is not soluble at low temperatures enough to measure the ^1H NMR and infrared spectra. The intermediate is presumably assigned to *cis*-$RhI_2(dtc)L_2$. A similar *cis* addition was reported to occur in the reaction of hydrogen with some Vaska-type complexes, $IrX(CO)\{P(C_6H_5)_3\}_2$ (X=halide).[26]

The two intermediates in the present reaction were confirmed to exist also from kinetic measurements. A typical decay curve of the absorbance at 370 nm after mixing $Rh(dtc)L_2$ and excess I_2 in benzene at 10.0 °C is depicted in Fig. 4, which indicates the reaction proceeds *via* two consecutive processes with the half-lives of about 3 ms and 3 s, respectively. These two processes were followed by a much slower one in which the

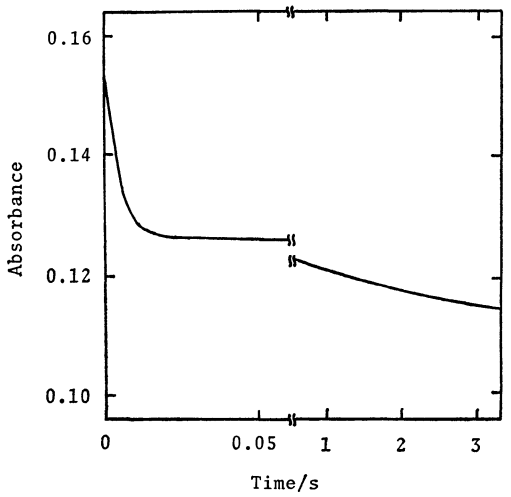

Fig. 4. Decay of the absorbance at 370 nm with time for the reaction of $Rh(dtc)L_2$ (1.0×10^{-4} M) with I_2 (1.0×10^{-3} M) in benzene at 10.0 °C.

Table 2. Observed rate constants[a] for the two consecutive processes in the reactions of $Rh(dtc)L_2$ (1.0×10^{-4} M) with excess I_2 at various temperatures

Temp °C	$[I_2]/[Rh(dtc)L_2]$	$k^{(1)}_{obsd}$ / s^{-1}	$10^3\,k^{(2)}_{obsd}$ / s^{-1}
10.0	10	206±1	216±1
	20	212±1	183±1
	30	213±1	223±1
	40	216±1	183±0
		(212±3)	(201±14)
14.5	10	331±2	318±2
	20	317±2	303±2
	30	318±2	278±1
	40	304±2	280±1
		(318±7)	(295±13)
20.1	10	543±4	579±4
	20	568±4	524±4
	30	544±4	551±3
	40	528±3	531±3
		(546±11)	(546±17)
25.1	10	785±8	1095±9
	20	779±14	1103±5
	30	722±7	1020±9
	40	746±4	1083±11
		(758±20)	(1075±25)

a) Average values in parentheses. $k^{(1)}_{obsd}$ and $10^3\,k^{(2)}_{obsd}$ are 197±1 and 83.2±0.6, respectively, for the reaction of $Rh(acac)L_2$ (1.0×10^{-4} M) with I_2 (1.0×10^{-3} M) at 25.1 °C.

trans-$RhI_2(dtc)L_2$ further reacted with excess I_2 to give $RhI(I_3)(dtc)L_2$. The last process, however, has not been kinetically analyzed, because there was little change in absorbance. The reaction rate in the two initial processes is different from each other sufficiently enough to allow the graphical determination of rate constants.[27] Plots of $\ln(A_t-A_\infty)$ *vs.* time for each process were found to be linear. Pseudo-first-order rate constants, $k^{(1)}_{obsd}$ and $k^{(2)}_{obsd}$ were obtained by the least-squares method. The results are shown in Table 2; the $k^{(1)}_{obsd}$ and $k^{(2)}_{obsd}$ are both essentially independent of the concentration of I_2 at a given temperature. Thus, the equimolar reaction of $Rh(dtc)L_2$ with I_2 is suggested to proceed *via* the CT complex, $Rh(dtc)L_2\cdot I_2$, which undergoes a rapid rearrangement probably to give *cis*-$RhI_2(dtc)L_2$, followed by isomerization to the *trans* adduct, as shown in the following scheme. The isomeri-

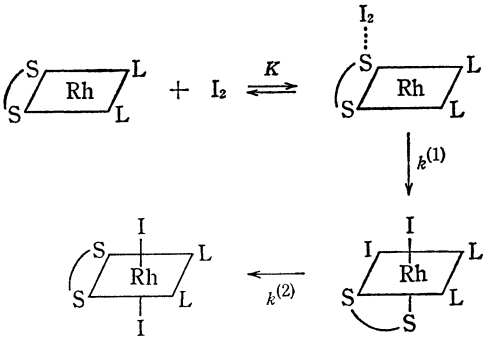

zation of the *cis* adduct to the *trans* one may be a site exchange between the equatorial iodide ligand and the axial dtc-sulfur atom *via* a rhombic twist or by a metal-sulfur bond rupture mechanism. According to this reaction scheme, $k_{obsd}^{(1)}$ can be expressed by Eq. 1.

$$k_{obsd}^{(1)} = \frac{Kk^{(1)}[I_2]}{1+K[I_2]} \quad (1)$$

When $K[I_2]$ is much greater than unity, $k_{obsd}^{(1)}$ can be reduced to $k^{(1)}$. This is consistent with the present result that $k_{obsd}^{(1)}$ is little dependent on the I_2 concentration. Since the *cis-trans* isomerization proceeds intramolecularly, the scheme also predicts $k_{obsd}^{(2)}$ being independent of $[I_2]$, which is in agreement with the results obtained. Activation parameters obtained by the Arrhenius plots for the two processes are: $\Delta H_{298}^{\ddagger(1)} = 57.7 \pm 2.0$ kJ mol^{-1}, $\Delta S_{298}^{\ddagger(1)} = 4.0 \pm 6.9$ J mol^{-1} K^{-1} for the decomposition of CT complex, and $\Delta H_{298}^{\ddagger(2)} = 75.5 \pm 3.9$ kJ mol^{-1}, $\Delta S_{298}^{\ddagger(1)} = 8.0 \pm 9.9$ J mol^{-1} K^{-1} for the *cis–trans* isomerization. The small positive values of $\Delta S_{298}^{\ddagger(1)}$ and $\Delta S_{298}^{\ddagger(2)}$ are consistent with the two proposed intramolecular processes. In addition, the $\Delta H_{298}^{\ddagger(2)}$ value is comparable to the activation enthalpies (75 to 104 kJ mol^{-1}) of *cis-trans* isomerizations of $Cr(CO)_4\{C(OCH_3)CH_3\}(PR_3)$ ($R = C_2H_5$, C_6H_{11}),[28] $Ru(CO)_4(SiCl_3)_2$,[29] and $Os(CO)_4\{Si(CH_3)_3\}_2$,[29] which have been proposed to proceed *via* intramolecular manners, supporting the formation of the *cis* isomer as a short-lived species as suggested above.

The authors are grateful to the Ministry of Education for support of this work through Grant-in-Aid for Scientific Research.

References

1) S. Carra and R. Ugo, *Inorg. Chim. Acta, Rev.*, **1**, 49 (1967).
2) J. P. Collman and W. R. Roper, *Adv. Organomet. Chem.*, **7**, 53 (1968), and the references cited therein.
3) J. P. Collman, *Acc. Chem. Res.*, **1**, 136 (1968).
4) J. Halpern and C. S. Wong, *J. Chem. Soc., Chem. Commun.*, **1973**, 629.
5) Y. Ohtani, M. Fujimoto, and A. Yamagishi, *Bull. Chem. Soc. Jpn.*, **50**, 1453 (1977).
6) A. J. Hart-Davis and W. A. G. Graham, *Inorg. Chem.*, **9**, 2658 (1970).
7) S. Otsuka and K. Ataka, *Bull. Chem. Soc. Jpn.*, **50**, 1118 (1977).
8) M. Haga, K. Kawakami, and T. Tanaka, *Inorg. Chim. Acta*, **12**, 93 (1975).
9) M. Haga, K. Kawakami, and T. Tanaka, *Inorg. Chem.*, **15**, 1946 (1976).
10) A. L. Balch and J. Miller, *J. Organomet. Chem.*, **32**, 263 (1971).
11) F. Faraone, *J. Chem. Soc., Dalton Trans.*, **1975**, 541.
12) N. S. Lewis, K. R. Mann, J. G. Gordon II, and H. B. Gray, *J. Am. Chem. Soc.*, **98**, 7461 (1976).
13) A. L. Balch, *J. Am. Chem. Soc.*, **98**, 8049 (1976).
14) J. T. Mague and M. O. Nutt, *Inorg. Chem.*, **16**, 1259 (1977).
15) T. Kaneshima, Y. Yumoto, K. Kawakami, and T. Tanaka, *Inorg. Chim. Acta*, **18**, 29 (1976).
16) T. Kaneshima, K. Kawakami, and T. Tanaka, *Inorg. Chim. Acta*, **15**, 161 (1975).
17) J. A. Riddick and E. E. Toops, Jr., "Technique of Organic Chemistry," Interscience Publishers, New York (1955), Vol. 7, p. 317.
18) T. Kaneshima, K. Kawakami, and T. Tanaka, *Inorg. Chem.*, **13**, 2198 (1974).
19) C. R. Kistner, D. A. Drew, J. R. Doyle, and G. W. Rausch, *Inorg. Chem.*, **6**, 2036 (1967).
20) K. D. Hodges and J. V. Rund, *Inorg. Chem.*, **14**, 525 (1975).
21) E. A. Pasek and D. K. Straub, *Inorg. Chim. Acta*, **21**, 23 (1977).
22) A. D. Awtrey and R. E. Connick, *J. Am. Chem. Soc.*, **73**, 1842 (1951).
23) H. Kita, K. Tanaka, and T. Tanaka, *Bull. Chem. Soc. Jpn.*, **48**, 2816 (1975).
24) H. Kita, K. Tanaka, and T. Tanaka, *Inorg. Chim. Acta*, **21**, 229 (1977).
25) R. Foster, "Molecular Complexes," Elek Science, London (1973), Vol. 1, p. 1.
26) L. Vaska and R. E. Rhodes, *J. Am. Chem. Soc.*, **87**, 4970 (1965).
27) A. A. Frost and R. G. Pearson, "Kinetics and Mechanism," 2nd ed, Wiley, New York (1961), p. 160.
28) H. Fischer, E. O. Fischer, and H. Werner, *J. Organomet. Chem.*, **73**, 331 (1974).
29) R. K. Pomeroy and W. A. G. Graham, *J. Am. Chem. Soc.*, **94**, 274 (1972).

Proton Magnetic Resonance Studies of 4-(2-Pyridylazo)resorcinol (PAR) and Its Cobalt(III) Complexes†

Katsura Mochizuki, Tasuku Ito,†† and Masatoshi Fujimoto*

Department of Chemistry, Faculty of Science, Hokkaido University, Sapporo 060

(Received July 6, 1978)

The ^1H NMR spectra of PAR, $[Co^{III}(par)_2]^-$, and $[Co^{III}(par)(dien)]^+$ were measured in D_2O solutions. The signals were assigned. The deuteration of H_7 was observed in D_2O solutions of free ligand PAR around pD 9—10, where PAR exists in the form of LH^- having an intramolecular hydrogen-bond. The significant up-field shift for the resonance of H_1 was observed in $[Co^{III}(par)_2]^-$ but not in $[Co^{III}(par)(dien)]^+$. The shift was interpreted in terms of the magnetic anisotropy due to the π-electron system of the neighboring PAR molecule in the complex. The down-field shift for the resonance of the H_5 signal of the cobalt(III) complexes reflects the structural change of PAR upon chelate-ring formation. PAR coordinates to cobalt(III) ion in planar terdentate fashion, *viz.*, in a *mer* configuration.

4-(2-Pyridylazo)resorcinol (PAR, Fig. 1(a)) has widely been used as a metallochromic indicator.[1] A number of data on the compositions and the stability constants of the PAR-chelates have been reported.[1-5] In a previous paper,[6] we confirmed in the course of the reactions between Co^{2+} and PAR and its analogs the fast formation of a transient intermediate cobalt(II) complex and the subsequent slower oxidation to cobalt(III) complex. The measurements of magnetic susceptibility have also confirmed the formation of cobalt(III) complex in the solution prepared from Co^{2+} and PAR.[7]

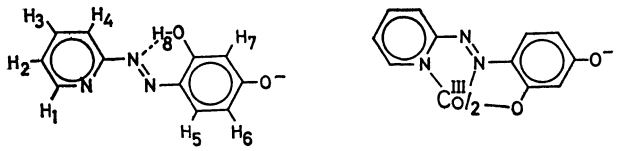

(a) (b)

Fig. 1. Structural formulae of (a) PAR with numbering of the protons and (b) its cobalt(III) complex.

As a part of serial studies on the metal chelates of PAR and its analogs,[6-8] the ^1H NMR spectra of PAR and its cobalt(III) complexes were studied in the present paper. Figure 1 shows the suggested structures of a free ligand PAR and the metal complexes of PAR. A form with an intramolecular hydrogen-bond (Fig. 1(a)) has been suggested for a free ligand PAR in solutions.[1,9] On the other hand, no direct evidence on the structures of the PAR chelates has been reported so far. The crystal structures of $[Cu(pan)(OH_2)]ClO_4$,[10] $[Ni(tan)_2]$,[11] $[Fe(tan)_2]$,[12] $[PdCl(tan)]$,[13] $[Co(tan)_2]ClO_4$,[14] and $[Cu(tan)(OH_2)_2]ClO_4$[15] have been reported, where pan and tan denote 1-(2-pyridylazo)-2-naphthol and 1-(2-thiazolylazo)-2-naphthol, respectively. The results of the X-ray analyses of these complexes suggest that the cobalt–PAR complex has the structure shown in Fig. 1(b), since PAN and TAN, as well as PAR, are *o*-hydroxy azo compounds and the PAR complexes can have the same chelate structure as the PAN and TAN complexes. Therefore, a structural change of the ligand PAR occurs upon coordination; breaking of the intramolecular hydrogen-bond and subsequent internal rotation of the resorcinol ring around the C–N bond by 180°. The main interest of the present work is to elucidate the structures of PAR and its cobalt(III) complexes in solutions by ^1H NMR measurements.

Experimental

Materials. PAR and $[Co^{III}(par)_2]$ were prepared as reported in the previous paper.[6] Deuterium oxide (99.7%), DMSO-d_6 (99.5%), and *ca.* 40% NaOD in D_2O were purchased from E. Merck, Ltd. Reagent grade materials were used unless otherwise specified.

A new complex $[Co^{III}(par)(dien)]Cl\cdot NaCl$ was prepared from $[Co^{III}Cl_3(dien)]$ after the synthetic route described for the preparation of $[Co^{III}(ida)(dien)]$ from $[Co^{III}Cl_3\cdot(dien)]$[16] (ida=iminodiacetate ion). Two grams of the monosodium salt of PAR in 75 ml H_2O were added to 50 ml of suspended aqueous solution containing 2.1 g of $[Co^{III}Cl_3(dien)]$ and 0.6 g of charcoal at 50 °C with stirring. The addition of 20 ml of 20% aqueous solution of $AgNO_3$ produced a deep red solution. The reaction mixture was stirred for 2 h at 50 °C and cooled. After the further addition of 0.3 g of NaCl, the solution was filtered. The pH of the filtrate was adjusted to 7—8 with NaOH and the solution was diluted to 400 ml with water. One hundred milliliters of this solution were passed through a column of a cation-exchange resin SP-Sephadex C-25 in the Na-form (400 mm × 30 mm i.d.) and eluted with a 0.1 mol dm^{-3} aqueous solution of NaCl at pH 7—8 (NaOH). The eluates from the main band were collected and evaporated to a small volume at 40—50 °C. The precipitated sodium chloride was filtered off and the filtrate was evaporated to dryness. A small amount of ethanol was added to the residue. The extract was filtered to remove sodium chloride. Successive filtration and extraction yield *ca.* 30 mg of deep red black crystals with golden luster. The yield was very low because of the high solubilities of the product in H_2O and ethanol. Found: C, 38.44; H, 4.74; N, 17.96%. Calcd for $C_{15}H_{21}N_6O_2Cl_2CoNa$: C, 38.40; H, 4.30; N, 17.91%. The elemental analysis shows that the isolated complex contains one mole of sodium chloride.

† Presented in part at the 1976 Summer Meeting in Hokkaido of the Chemical Society of Japan and the Japan Society for Analytical Chemistry, Kitami, July 19, 1976, Abstracts p. 12.

†† Present Address: Institute for Molecular Science, Okazaki 444.

[$Pd^{II}Cl$(par)] was synthesized by the reaction between monosodium salt of PAR and palladium(II) chloride in an aqueous solution at pH 1—2 (HCl). The precipitate which formed upon mixing of the stoichiometric amounts of the reagents was filtered off, washed with water, and dried in a desiccator over silica gel. Found: C, 36.09; H, 2.65; N, 11.43%. Calcd for $C_{11}H_8N_3O_2ClPd \cdot 0.5H_2O$: C, 36.19; H, 2.49; N, 11.51%.

Measurements. 100 MHz ^1H NMR spectra were measured with a JEOL PS-100 spectrometer. Tetramethylsilane (TMS) and sodium trimethylsilylpropanesulfonate (DSS) were used as internal standards in DMSO-d_6 and D_2O solutions, respectively. The pD (pH-meter reading $+0.40$)[17] of the D_2O solutions was adjusted with NaOD and measured in nitrogen atmosphere with a Horiba pH-meter model M-7 equipped with a small glass electrode type 1826 05T and a reference electrode type 2410.

The ^1H NMR spectra of [Co^{III}(par)$_2$] and [Co^{III}(par)-(dien)] in D_2O solutions were measured at pD *ca.* 10, where the coordinated PAR in [Co^{III}(par)$_2$] and [Co^{III}(par)-(dien)] exists in the same chemical form (*vide infra*) and the solubilities of the complexes were enough for the ^1H NMR measurements.

The ^1H NMR spectra of the 1:1 PAR-complexes, [La^{III}-(par)] and [Zn^{II}(par)], were measured with the alkaline-DMSO-d_6–D_2O solutions. The mixture of the monosodium salt of PAR and about fifty-fold excess of anhydrous La-$(NO_3)_3$ or anhydrous $ZnCl_2$ was dissolved as much as possible in 50%(v/v) DMSO-d_6–D_2O. One drop of 10% D_2O solution of NaOD was added. The solution was filtered. The red filtrate was subjected to the measurements.[18]

The ^1H NMR spectrum of [$Pd^{II}Cl$(par)] was measured with a red DMSO-d_6–D_2O solution, which was prepared by adding a small amount of 10% D_2O solution of NaOD to a green solution of the complex in 50%(v/v) DMSO-d_6–D_2O.[21]

Absorption spectra were measured at 25 °C and $I=0.1$ ($NaClO_4$) with a Hitachi recording spectrophotometer Model EPS-3T. The pH of the aqueous solution of [Co^{III}(par)-(dien)]Cl was measured with a Radiometer pH-meter 4d (Copenhagen) equipped with a glass electrode type G 202B and a reference electrode type 410.

Results and Discussion

^1H NMR Spectra of the Free Ligand. The 100 MHz spectrum of the monosodium salt of PAR in DMSO-d_6 at 90 °C is given in Fig. 2. Under these conditions the spectrum was highly resolved. Since the observed signals were well-separated from each other as compared with the coupling constants, the first-order analysis of the spin-spin coupling constants and the values of the chemical shifts allowed the assignments of the signals. The assignments were further confirmed by applying the method of double irradiation at the resonance frequencies for the protons, H_1, H_2, H_3, H_4, and H_6. In Table 1 are listed the values of the chemical shifts measured for band centers or maxima and the coupling constants evaluated from the spacings of the split signals (for numbering of the protons, see Fig. 1(a)). The significant difference in the values of J_{12} and J_{23} permitted the unambiguous assignments of H_2 and H_3. Though no direct evidence has been reported so far, the following facts suggest the presence of intramolecular hydrogen-bond for the free ligand PAR (Fig. 1(a)) in solutions: The pK_a value of the *o*-hydroxyl group (12.31) is much higher than that of the *p*-hydroxyl group (5.6)[1] and also higher than the value of pK_{a2} for resorcinol (11.06);[22] the proton-transfer reaction of the *o*-hydroxyl group of PAR proceeds slowly;[9] the IR spectrum of 4-(phenylazo)resorcinol in CCl_4 shows a broad band due to an intramolecular hydrogen-bond –OH···N= around 2860 cm^{-1}.[23] Furthermore, we observed the following facts: The resonance for the H_8, the proton of the *o*-hydroxyl group, appeared at very low field at 25 °C (see Table 1); The chemical shift of this resonance was not affected on dilution; The resonance disappeared by addition of one portion of

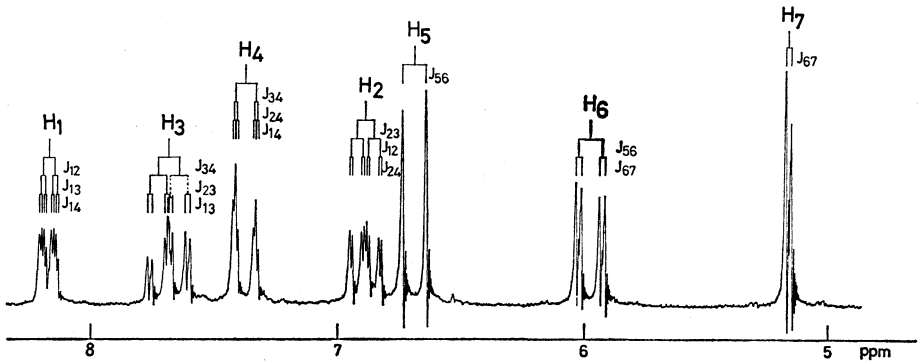

Fig. 2. 100 MHz ^1H NMR spectrum of the monosodium salt of PAR in DMSO-d_6 at 90 °C.

Table 1. ^1H NMR spectral data of the free ligand PAR[a]

	H_1	H_2	H_3	H_4	H_5	H_6	H_7	H_8
Chemical shift[b]	8.17	6.90	7.68	7.38	6.69	5.99	5.18	16.59[d]
	J_{12}	J_{23}	J_{34}	J_{56}	J_{13}	J_{24}	J_{67}	J_{14}	J_{57}
Coupling constant[c]	4.9	7.0	8.4	9.7	2.0	1.4	2.3	1.1	≃0

a) Data for the monosodium salt in DMSO-d_6 at 90 °C. b) In ppm referred to TMS. c) In Hz. d) At 25 °C. The resonance for H_8 diminished at 90 °C.

D_2O. These results directly show the presence of an intramolecular hydrogen-bond in the free PAR.[24]

^{1}H NMR spectra of PAR in D_2O solutions were measured in the range of pD 9—14, where PAR exists in the form of LD^- and L^{2-} as revealed in the electronic absorption spectra.[1)†††] In the pD range, where two species of PAR are in equilibrium, only the averaged ^{1}H NMR spectrum of LD^- and L^{2-} was observed instead of the simple sum of each spectrum. The chemical shifts of the protons H_1, H_5, and H_7 moved to lower field with increasing concentration of NaOD, while that of H_6 was almost invariable with varying pD. Figure 3 shows the plots of the chemical shifts of H_5 and H_7 *vs.* pD. From these plots, the pK_a value for the acid-dissociation of the *o*-hydroxyl group in D_2O

$$LD^- \overset{K_a}{\rightleftharpoons} L^{2-} + D^+$$

was determined to be 12.8 ± 0.3, which is reasonable compared with the literature value 12.31 determined spectrophotometrically in H_2O.[1)] Figure 4(a) shows the ^{1}H NMR spectrum of the free ligand PAR in D_2O solution at pD 9.3, which corresponds to the spectrum of LD^- as is clear from Fig. 3.

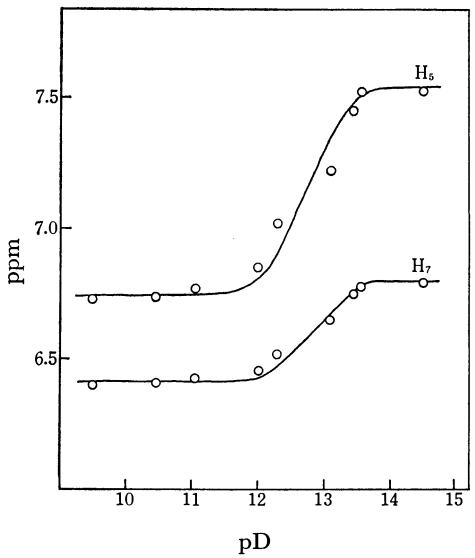

Fig. 3. Plots of the chemical shifts corresponding to H_5 and H_7 *vs.* pD.

In the course of the experiments on the pD-dependency of the ^{1}H NMR spectra, it was found that the proton H_7 was deuterated in D_2O solutions. The intensity of the signal for H_7 decreased with the lapse of time. At the same time, the signal shape of the H_6 resonance changed gradually. The rate of the deuteration depended strongly on the pD of the solution. The deuteration of H_7 can be distinctly observed in Fig. 4(a). The integrated intensity for the signal of H_7 in the spectrum (a) is considerably less than that for one proton. In addition the H_6–H_7 coupling observed in the resonance for H_6 has almost disappeared (see the signal shape of the H_6 resonance in Fig. 2). The plot of the integrated intensity of the H_7 signal *vs.* time allowed the kinetic measurements of the deuteration. The half-times of the deuteration at room temperature at pD 9.3 and *ca.* 14 were found to be 80 min and 2.5 day, respectively. The deuteration proceeds much faster in LD^- than in L^{2-}. The LD^- species of PAR has an intramolecular hydrogen-bond, which may affect the electronic state of the carbon atom bonded to H_7 so as to facilitate the H–D exchange in D_2O. In fact, no corresponding deuteration was observed in L^{2-}, $[Co^{III}(par)_2]$, and $[Co^{III}(par)(dien)]$ containing no intramolecular hydrogen-bond.

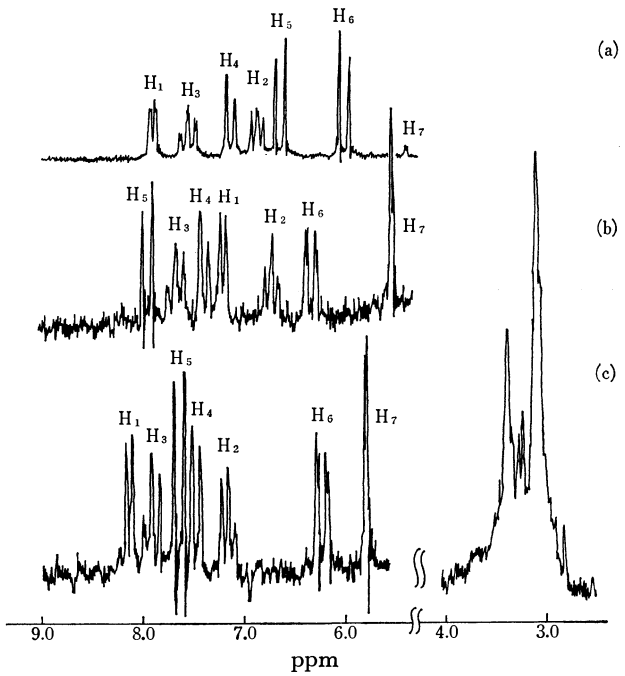

Fig. 4. ^{1}H NMR spectra in D_2O solution of (a) PAR at pD 9.3, (b) $[Co^{III}(par)_2]$, and (c) $[Co^{III}(par)(dien)]$ at pD *ca.* 10.

^{1}H NMR Spectra of the Cobalt(III) Complexes. Figure 4(b) shows the ^{1}H NMR spectrum of $[Co^{III}(par)_2]$ in D_2O solution at pD *ca.* 10. Under this condition $[Co^{III}(par)_2]$ exists in the form of $[Co^{III}L_2]^-$.[6)] The spectrum indicates that two ligand molecules in $[Co^{III}L_2]^-$ are magnetically and chemically equivalent. The ^{1}H NMR spectrum of $[Co^{III}(par)(dien)]$ at pD *ca.* 10 is shown in Fig. 4(c). The integrated intensities of the signals showed the presence of seven aromatic protons and six methylene protons (complex multiplet centered at *ca.* 3.2 ppm) corresponding to the coordinated ligands PAR and dien, respectively. As will be described later, $[Co^{III}(par)(dien)]$ exists in the form of $[Co^{III}L(dien)]^+$ at pD *ca.* 10.

Small couplings were not clearly observed in the spectra of $[Co^{III}L_2]^-$ and $[Co^{III}L(dien)]^+$ because of the low solubilities of the complexes in D_2O. However, comparison of the spectrum of the free ligand with those of the cobalt(III) complexes revealed that the spin-spin couplings in PAR remained essentially unchanged upon coordination, though the chemical shifts of some protons changed considerably. All the

††† Hereafter, "PAR" stands for L^{2-}, LH^-, LH^{*-}, LHH^*, and/or LD^-, where H* denotes the proton of the *p*-hydroxyl group.

signals of $[Co^{III}L_2]^-$ and $[Co^{III}L(dien)]^+$ were unambiguously assigned by the analysis of the coupling constants. The coupling constant J_{12} is smaller than J_{23} in the cobalt(III) complexes as well. The assignments are given in Table 2.

Table 2. ^1H NMR chemical shifts of LH^-, $[Co^{III}L_2]^-$, and $[Co^{III}L(dien)]^+$ a)

	H_1	H_2	H_3	H_4	H_5	H_6	H_7
LH^- b)	7.90	6.86	7.56	7.13	6.63	6.00	5.40
$[Co^{III}L_2]^-$ c)	7.23	6.75	7.70	7.41	7.98	6.37	5.56
$[Co^{III}L(dien)]^+$ d)	8.14	7.16	7.92	7.48	7.64	6.23	5.78

a) In D_2O. Chemical shifts in ppm referred to DSS.
b) Monosodium salt. At pD 9.3. c) At pD *ca.* 10.
d) Chloride. At pD *ca.* 10.

The resonance of H_1 in $[Co^{III}L_2]^-$ shows a definite up-field shift compared with that in free PAR. On the other hand, such an up-field shift was not observed for the H_1 resonance of $[Co^{III}L(dien)]^+$ (see Table 2). In order to clarify whether the difference in chemical shift of H_1 is caused by the number of PAR molecules in the complex, we measured ^1H NMR spectra of the PAR chelates of other metal ions containing only one PAR ligand, $[Pd^{II}ClL]^-$, $[La^{III}L]^+$, and $[Zn^{II}L]^0$, in 50%(v/v) DMSO-d_6–D_2O mixed solvents containing one drop of *ca.* 10% NaOD.[18,21] No up-field shift of the H_1 signal was observed for these complexes. Spectral pattern of these complexes was very similar to that of $[Co^{III}L(dien)]^+$ but not to that of $[Co^{III}L_2]^-$. A careful inspection of molecular models reveals a plausible explanation for the up-field shift of the H_1 signal of $[Co^{III}(par)_2]$. The proton H_1 of one PAR molecule in $[Co^{III}(par)_2]$ is disposed close to and above the azo group of the other PAR molecule, only when two PAR molecules coordinate to cobalt(III) ion in planar fashion as terdentate ligands. In view of this fact and the above-mentioned observations, the large up-field shift can reasonably be explained as being caused by the magnetic anisotropy due to the π-electron system of the azo group in the neighboring ligand PAR. The up-field shift of the H_1 signal would not be expected for free PAR, $[Co^{III}L(dien)]^+$, $[Pd^{II}ClL]^-$, $[La^{III}L]^+$, and $[Zn^{II}L]$, since the proton H_1 in these compounds cannot experience the chemical environment as described above.

Similar up-field shifts have been observed for the *ortho*-protons of pyridyl nitrogen in $[M(phen)_3]^{n+}$ [25] (M=Fe(II), Ru(II), Zn(II), and Co(III)), in $[Co^{III}(phen)_2(en)]^{3+}$,[26] and in $[Fe^{II}(bipy)_3]^{2+}$.[27] One of the β-methylene protons in tris-(*N*,*N'*-dibutyl-2,3-butanediimine)iron(II) complex has been also reported to show similar large up-field shifts.[28] The up-field shifts observed in these complexes have been interpreted in terms of the ring current of the neighboring aromatic ligands[26,27] or in terms of the magnetic anisotropy due to the imine bonds of the neighboring ligands.[28]

Another remarkable feature found in the ^1H NMR spectra of cobalt(III)–PAR complexes in comparison with that of the free PAR is a large difference in the chemical shift of the proton H_5. The H_5 signal appears at 6.63 ppm in the free ligand at pD 9.3, while the corresponding signal appears at 7.98 ppm in $[Co^{III}L_2]^-$ and 7.64 ppm in $[Co^{III}L(dien)]^+$ at pD *ca.* 10. As was discussed before, around pD 10 the free ligand PAR and the cobalt(III) complexes have the structures shown in Figs. 1(a) and 1(b), respectively. The terdentate and planar coordination of PAR molecule is accompanied by an internal rotation of resorcinol ring moiety around C–N axis by 180°. The molecular model suggests that the coordination of PAR causes a fairly strong strain in the complexes especially for the bond angle around cobalt(III) ion. The bond angles, N(pyridine)–Co–N(azo) and N(azo)–Co–O, are expected to be significantly smaller than 90°. As a result, a fairly close contact appears between the proton H_5 and the azo group. The proton H_5 in such a chemical environment would be susceptible to the effect of the magnetic anisotropy due to the π-electron system of the azo group in addition to the effect of the ring current of the resorcinol ring. The location of the proton H_5 in such an environment causes a down-field shift when the complexes are in the magnetic field.

Very similar situation has been found in the crystal structure of $[Co^{III}(tan)_2]$.[14] The X-ray analysis of $[Co^{III}(tan)_2]$ shows that the bond angles around the cobalt atom within the chelate ring are compressed to 84.9 and 81.6° and that the coordinated TAN is deformed due to the in-plane close contact around the azo group. The significant down-field shift of the H_5 signal observed for the cobalt(III) complexes of PAR can be ascribed to the structural change of PAR upon chelate-ring formation.

On the basis of the ^1H NMR studies, it is concluded that PAR coordinates to cobalt(III) ion in planar fashion as a terdentate ligand, namely, in the *mer* configuration.

Acid-Base Behavior of $[Co^{III}(par)(dien)]$. In order to confirm the chemical species of $[Co^{III}(par)(dien)]$ present under the conditions of the ^1H NMR measurements, the absorption spectra were measured in aqueous solutions at various pH. Figure 5 shows the pH-

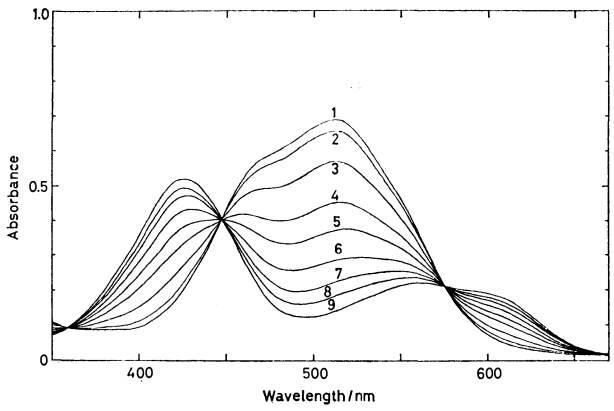

Fig. 5. Absorption spectra of the aqueous solution of $[Co^{III}(par)(dien)]$ as a function of pH at 25 °C and I=0.1 ($NaClO_4$). pH=8.88 (1), 5.79 (2), 5.06 (3), 4.60 (4), 4.33 (5), 4.01 (6), 3.67 (7), 3.34 (8), and 2.36 (9).

dependence of the absorption spectrum of [Co^{III}(par)-(dien)]. Well-defined isosbestic points were observed at 359, 447, and 576 nm, which demonstrate the presence of a simple equilibrium. The spectral change with varying pH was fully reversible. In view of the inertness of the cobalt(III) complexes against the ligand dissociation, the pH-dependence of the spectrum can be attributed to the protonation-deprotonation equilibrium of a *p*-hydroxyl group of the coordinated PAR in [Co^{III}(par)(dien)]. From the plot of absorbance at 500 nm *vs.* pH, the value of pK_a for the acid-dissociation

$$[Co^{III}LH^*(dien)]^{2+} \overset{K_a}{\rightleftharpoons} [Co^{III}L(dien)]^+ + H^+$$

was determined to be 4.52±0.03. The average value of the acid-dissociation constants for pK_{a1}([Co^{III}-(LH^*)$_2$]$^+$) and pK_{a2}([$Co^{III}L(LH^*)$]) has been reported to be 4.1.[6] Around pH 10, where the ^{1}H NMR measurements were carried out, [Co^{III}(par)(dien)] exists only in the form of [$Co^{III}L$(dien)]$^+$.

References

1) S. Shibata, "2-Pyridylazo Compounds in Analytical Chemistry," in "Chelates in Analytical Chemistry," ed by H. A. Flaschka and A. J. Barnard, Jr., Marcel Dekker, Inc., New York (1972), Vol. 4, p. 1.

2) T. Iwamoto, *Bull. Chem. Soc. Jpn.*, **34**, 605 (1961).

3) M. Hniličková and L. Sommer, *Collect. Czech. Chem. Commun.*, **26**, 2189 (1961).

4) "Stability Constants," Special Publication No. 17, The Chemical Society (London) (1964), p. 657; "Stability Constants, Supplement No. 1," Special Publication No. 25, The Chemical Society (London) (1971), p. 661.

5) R. G. Anderson and G. Nickless, *Analyst*, **92**, 207 (1967); **93**, 13, 20 (1968).

6) K. Mochizuki, T. Imamura, T. Ito, and M. Fujimoto, *Bull. Chem. Soc. Jpn.*, **51**, 1743 (1978).

7) T. Iwamoto and M. Fujimoto, *Anal. Chim. Acta*, **29**, 282 (1963).

8) T. Onodera and M. Fujimoto, *Bull. Chem. Soc. Jpn.*, **44**, 2003 (1971); K. Mochizuki, T. Imamura, T. Ito, and M. Fujimoto, *Chem. Lett.*, **1976**, 1207; **1977**, 1239.

9) N. Yoshida and M. Fujimoto, *Bull. Chem. Soc. Jpn.*, **49**, 1557 (1976).

10) S. Ooi, D. Carter, and Q. Fernando, *Chem. Commun.*, **1967**, 1301.

11) M. Kurahashi, *Bull. Chem. Soc. Jpn.*, **47**, 2067 (1974).

12) M. Kurahashi, A. Kawase, K. Hirotsu, M. Fukuyo, and A. Shimada, *Bull. Chem. Soc. Jpn.*, **45**, 1940 (1972).

13) M. Kurahashi, *Bull. Chem. Soc. Jpn.*, **47**, 2045 (1974).

14) M. Kurahashi, *Chem. Lett.*, **1974**, 1271; *Bull. Chem. Soc. Jpn.*, **49**, 3053 (1976).

15) M. Kurahashi, *Chem. Lett.*, **1974**, 63.

16) J. I. Legg and D. W. Cooke, *Inorg. Chem.*, **5**, 594 (1966).

17) R. G. Bates, "Determination of pH," 2nd ed, John Wiley and Sons, Inc., New York (1973), p. 375.

18) The stability constants and the acid-dissocation constants for the present systems in aqueous media have been reported to be $K_{La(par)}=10^{9.2}$,[19] $K_{Zn(par)}=10^{11.9\pm0.1}$,[20] $K_{Zn(par)_2}=10^{10.3\pm0.2}$,[20] and $K(ZnL^{2-} + H^+ \rightleftharpoons ZnLH^*) = 10^{5.90\pm0.05}$.[20] Though the value of $K(LaL^- + H^+ \rightleftharpoons LaLH^*)$ has not been reported so far, it is expected to be in the order of magnitude *ca.* 10^6 from the corresponding values of *K* for other lanthanide(III)–PAR systems.[19] These values suggest that in the sample solutions used for the ^{1}H NMR measurements the complexes are predominantly present as 1:1 complexes with the dissociated *p*-hydroxyl group of the coordinated PAR.

19) L. Sommer and H. Novotná, *Talanta*, **14**, 457 (1967).

20) M. Tanaka, S. Funahashi, and K. Shirai, *Inorg. Chem.*, **7**, 573 (1968).

21) In the red solution, the PAR coordinated in the palladium(II) complex was considered to be present as L^{2-}. See T. Yotsuyanagi, H. Hoshino, and K. Aomura, *Anal. Chim. Acta*, **71**, 349 (1974).

22) M. Bartusek and L. Sommer, *J. Inorg. Nucl. Chem.*, **27**, 2397 (1965).

23) Y. Matsunaga, Private communication.

24) J. A. Pople, W. G. Schneider, and H. J. Bernstein, "High-Resolution Nuclear Magnetic Resonance," McGraw-Hill, New York (1959), Chap. 15.

25) J. D. Miller and R. H. Prince, *J. Chem. Soc.*, **1965**, 3185, 4076.

26) H. Ito, J. Fujita, and T. Ito, *Bull. Chem. Soc. Jpn.*, **44**, 723 (1971).

27) S. Castellano, H. Gunther, and S. Ebersole, *J. Phys. Chem.*, **69**, 4166 (1965).

28) T. Ito and N. Tanaka, *J. Inorg. Nucl. Chem.*, **32**, 155 (1970).

A Study of the Ligand Exchange Reaction of Tetrakis(μ-trifluoroacetato)-dimolybdenum(II) in Acetonitrile by ^{19}F NMR Spectroscopy

Kazunori TERAMOTO, Yoichi SASAKI,* Kouto MIGITA,† Masamoto IWAIZUMI,† and Kazuo SAITO*

Department of Chemistry, Faculty of Science, Tohoku University, Aoba, Aramaki, Sendai 980

†*Chemical Research Institute of Non-aqueous Solutions, Tohoku University, Katahira, Sendai 980*

(Received July 5, 1978)

The dimeric molybdenum(II) complex, $Mo_2(CF_3COO)_4$, forms $Mo_2(CF_3COO)_4\cdot(CH_3CN)_2$ in acetonitrile, where solvent molecules are attached to positions trans to the metal–metal bond (apical positions). The rate of ligand exchange between $Mo_2(CF_3COO)_4$ ($(1.31—8.28)\times10^{-2}$ M; M=mol dm^{-3}) and CF_3COONa ($(1.31—4.56)\times10^{-1}$ M) was measured in acetonitrile by the use of ^{19}F NMR spectroscopy. The rate is independent of the total concentration of CF_3COONa and is linearly dependent on that of $Mo_2(CF_3COO)_4$. The first-order rate constant (k_{ex}) is $(1.1\pm0.2)\times10^4$ s^{-1} (25 °C), and the activation parameters are $\Delta H^{\ddagger}=(8.2\pm0.8)$ kcal mol^{-1} and $\Delta S^{\ddagger}=(-15\pm3)$ cal K^{-1} mol^{-1}. Under the given conditions the complex seems to exist as $Mo_2(CF_3COO)_4\cdot CF_3COO^-$, where the underlined ligand occupies one of the apical positions, and the following mechanism is proposed (solvent molecules are omitted; asterisks indicate the molecule substituting for the coordinated ligand).

$$Mo_2(CF_3COO)_4\cdot\underline{CF_3COO^-} + {}^*CF_3COO^- \overset{\text{fast}}{\rightleftharpoons} Mo_2(CF_3COO)_4\cdot{}^*\underline{CF_3COO^-} + CF_3COO^-$$

$$Mo_2(CF_3COO)_4\cdot{}^*\underline{CF_3COO^-} \xrightarrow{k_s} Mo_2(CF_3COO)_3({}^*CF_3COO)\cdot\underline{CF_3COO^-}$$

The k_{ex} corresponds to k_s.

Bivalent molybdenum forms diamagnetic compounds having strong metal–metal bonds such as $Mo_2(RCOO)_4$ (R=CH_3, CF_3, *etc.*), $Mo_2X_8^{4-}$ (X$^-$=Cl$^-$ and Br$^-$), and $Mo_2(SO_4)_4^{4-}$, with bond distances of about 2.1 Å.[1-5] Their structures in the crystalline state[1,2,4] and their spectroscopic properties[2,5] have been widely studied, but little attention has been drawn to their reactivities in solution.[6,7] The first and only report on the kinetics of the substitution reaction describes the substitution of acetate ions for the chloride ligands of $Mo_2Cl_8^{4-}$ to give $Mo_2(CH_3COO)_4$, and a dissociative mechanism was suggested.[7]

We have examined the solubility and stability of several dimeric molybdenum(II) complexes in various solvents in search of a simple system suitable for elucidating the substitution properties still further. Tetrakis(μ-trifluoroacetato)dimolybdenum(II), $Mo_2(CF_3COO)_4$ [I] (Fig. 1), in acetonitrile seemed suitable for our purpose. The Mo–Mo bond length of this compound is 2.090 Å, and the four trifluoroacetate ligands are equivalent in the crystalline state.[8] This paper reports on the results of a kinetic study of its ligand exchange reaction with sodium trifluoroacetate in acetonitrile by the use of ^{19}F NMR spectroscopy.

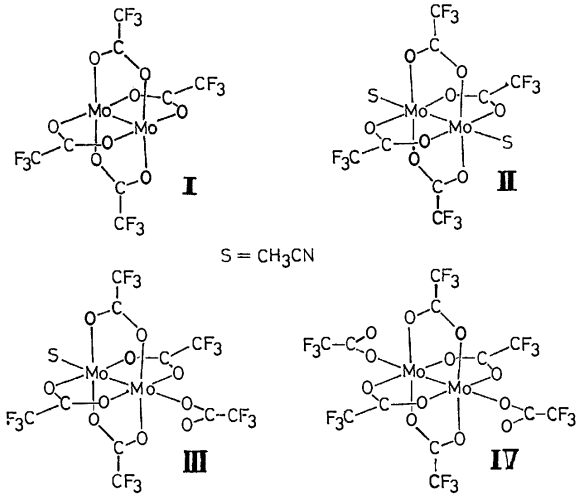

Fig. 1. Various forms of $Mo_2(CF_3COO)_4$ in solution. $Mo_2(CF_3COO)_4$ [I], $Mo_2(CF_3COO)_4\cdot(CH_3CN)_2$ [II], $Mo_2(CF_3COO)_4\cdot(CF_3COO)(CH_3CN)^-$ [III], and $Mo_2(CF_3COO)_4\cdot(CF_3COO)_2^{2-}$ [IV].

Experimental

Materials. Tetrakis(μ-trifluoroacetato)dimolybdenum(II) was prepared by the known method,[8] and sublimed before measurement of the ^{19}F NMR and electronic absorption spectra. Sodium trifluoroacetate (special grade reagent) was used without further purification. Acetonitrile was distilled twice over diphosphorus pentaoxide. Dichloromethane was distilled twice. Methanol (special grade reagent) was used without distillation. Each solvent was stored *in vacuo* over Linde 4a molecular sieves. The water content in each solvent was estimated to be as low as 5×10^{-3} M (M=mol dm^{-3}) using a Karl-Fischer titration.

Measurements. Electronic absorption spectra were measured using a Hitachi 323 Recording Spectrophotometer. The ^{19}F NMR spectra were recorded with a JEOL JNM-PM-100 high resolution NMR spectrometer operating at 94 MHz, with a variable temperature probe. Chemical shifts are recorded with respect to the internal standard CF_2Cl_2 (Freon 12).

Sample Preparation. Weighed samples of the complex and sodium trifluoroacetate were placed in an NMR tube, into which the solvent was introduced through a vacuum line. The molar concentration of each component was calculated from the volume of the prepared sample solution at room temperature, and expressed as $[Mo_2(CF_3COO)_4]_T$ and $[CF_3COO^-]_T$. Sample solutions were stored in liquid nitrogen for as long as a month without deterioration.

Evaluation of the Mean Life Time of the Coordinated and Free Ligands. A general method for studying a system involving two exchange sites[9] was applied to the present system. In the slow exchange region where two separate peaks are observed, the following equations were used:

$$\tau_c^{-1} = (W_c - W_c^{\circ}), \quad (1)$$

$$\tau_f^{-1} = (W_f - W_f), \quad (2)$$

where τ_c and τ_f are the mean life times of the coordinated and free ligands, and W_c and $W_c°$ (or W_f and $W_f°$) are the half line widths in Hz at half-height of the signal of the coordinated (or free) ligand of the sample solution and of the solution without free (or coordinated) ligand, respectively. In the fast exchange region where the two peaks coalesce completely, the following equation was used:

$$\tau_c^{-1} = \frac{4\pi p_c p_f^2 (\Delta\nu)^2}{W_{cf} - p_c W_c° - p_f W_f°}, \quad (3)$$

where p_c and p_f are the mole fractions of two exchanging species, W_{cf} is the half line width in Hz at half-height of the signal of the coalesced peak, and $\Delta\nu$ is the chemical shift difference in Hz between the signals of the coordinated and the free ligand (ν_c and ν_f) both measured in the absence of each other. The following equation should hold.

$$p_c/\tau_c = p_f/\tau_f \quad (4)$$

In the region of intermediate exchange, τ_c^{-1} was obtained by comparison of the observed spectra with the calculated spectra.[10] A Nihon-minicon NOVA-01 was used for the calculation.

The $W_c°$ and $W_f°$ values showed small temperature dependence. The values at any temperature between −40 and 70 °C were estimated from the calibration curves for the temperature dependence. The ν_c and ν_f gave no appreciable temperature dependence over the temperature range from −40 to 70 °C. The $\Delta\nu$ value was 306 Hz at all temperatures.

Results and Discussion

Structure of the Complex in Acetonitrile. Various compounds are known which have the general formula: $Mo_2(CF_3COO)_4 \cdot L_n^{m-}$ ($n=1$, $m=0$, L=$(C_6H_5)_3P$;[11] $n=2$, $m=0$, L=pyridine (py)[12] and CH_3OH;[11] $n=1$, $m=1$, $L^-=Cl^-$, CF_3COO^- *etc.*; $n=2$, $m=2$, $L^-=Br^-$ and Cl^-[13]). X-Ray crystallography disclosed that $Mo_2(CF_3COO)_4 \cdot (py)_2$ has two weakly coordinated pyridine molecules at both positions trans to the metal–metal bond (hereafter called apical positions).[12] The other L's are believed to coordinate similarly to the molybdenum ion.[11,13]

The ν(Mo–Mo) stretching frequency observed by Raman spectroscopy is sensitive to the apical ligand. The ν(Mo–Mo) value of solid $Mo_2(CF_3COO)_4$ is 397 cm^{-1},[8] while those of the compounds containing apical ligands are between 386 ($n=2$, L=CH_3OH) and 368 cm^{-1} ($n=2$, L=py) in the solid state.[11-13] The value for the solid $Mo_2(CF_3COO)_4 \cdot (CH_3OH)_2$ is 386 cm^{-1}.[13] On the other hand $Mo_2(CF_3COO)_4$ has ν(Mo–Mo) values of 397 and 383 cm^{-1} in dichloromethane and methanol respectively.[12] The two apical positions must be occupied by solvent molecules in methanol and remain vacant in dichloromethane. The ν(Mo–Mo) values in acetone and diethylether are 385 and 383 cm^{-1} respectively,[12] and these solvent molecules are also likely to occupy the apical positions. Acetonitrile solution could not be used in similar studies because the solvent itself gives strong Raman bands in the region of interest. On the other hand, Cotton and Norman found that the energy of the electronic transition of $Mo_2(CF_3COO)_4$ at *ca.* 430 nm in various solvents decreases as the ν(Mo–Mo) decreases.[12] Thus the coordination of solvent molecules at the apical positions lowers the energy of electronic transition. The electronic absorption spectra of $Mo_2(CF_3COO)_4$ in dichloromethane, methanol and acetonitrile are shown in Fig. 2. The peak positions are at 428 (ε, 95 cm^{-1} M^{-1}), 434 (118), and 434 nm (112), respectively. From these spectra it is concluded that $Mo_2(CF_3COO)_4$ is present as $Mo_2(CF_3COO)_4 \cdot (CH_3CN)_2$ (II) (Fig. 1) in acetonitrile.

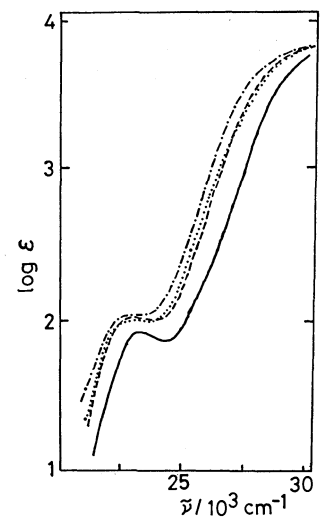

Fig. 2. The electronic absorption spectra of $Mo_2(CF_3COO)_4$ in CH_2Cl_2 (——), methanol (– – –), acetonitrile (·····) and in acetonitrile containing 4.6×10^{-2} M of CF_3COONa (-·-·-).

The Species in the Presence of the Free Ligand. A complex, $[(C_2H_5)_4N][Mo_2(CF_3COO)_4 \cdot (CF_3COO)]$, has been isolated from an equimolar mixture of $Mo_2(CF_3COO)_4$ and $[(C_2H_5)_4N][CF_3COO]$ in dichloromethane.[12] On addition of sodium trifluoroacetate to an acetonitrile solution of $Mo_2(CF_3COO)_4$, the peak position at 434 nm shifts to slightly longer wavelengths with an increase in strength (Fig. 2). This change may be caused by the substitution of trifluoroacetate ion(s) for acetonitrile in apical position(s). The following reactions are believed to be involved,

$$[Mo_2(CF_3COO)_4 \cdot \underline{(CH_3CN)_2}] + CF_3COO^- \overset{K_1}{\rightleftharpoons} \underset{(II)}{} \quad [Mo_2(CF_3COO)_4 \cdot \underline{(CF_3COO)}\,\underline{(CH_3CN)}]^- + CH_3CN, \quad (5)$$
$$\underset{(III)}{}$$

$$[Mo_2(CF_3COO)_4 \cdot \underline{(CF_3COO)}\,\underline{(CH_3CN)}]^- + CF_3COO^- \overset{K_2}{\rightleftharpoons} [Mo_2(CF_3COO)_4 \cdot \underline{(CF_3COO)_2}]^{2-} + CH_3CN. \quad (6)$$
$$\underset{(III)}{} \qquad \underset{(IV)}{}$$

The underlined ligands denote the ligand at the apical positions. The change in electronic absorption spectra is too small to enable the evaluation of K_1 and K_2. However, as Fig. 3 shows, appreciable amounts of III and/or IV (Fig. 1), must be present when the free ligand concentration is ≧0.01 M in the *ca.* 5×10^{-3} M complex solution.

^{19}F NMR Spectra in Acetonitrile. The ^{19}F NMR spectrum of the complex in acetonitrile (*ca.* 4×10^{-2} M)

Table 1. ^{19}F NMR chemical shifts(with respect to CF_2Cl_2 as an internal standard) of acetonitrile solutions of $Mo_2(CF_3COO)_4$ and CF_3COONa, and reciprocals of mean life time of the complexed ligand and activation energies for the ligand exchange reaction

Run	$[Mo_2(CF_3COO)_4]_T$ / 10^{-2} M	$[CF_3COO^-]_T$ / 10^{-1} M	Chemical shift/ppm[b] at −40 °C	Chemical shift/ppm[b] at 70 °C	τ_c^{-1}(25 °C)[c] / 10^3 s^{-1}	E_a[d] / kcal mol^{-1}
1	4.85	1.31	67.2, 70.5	68.9	3.2	9.6
2	5.26	1.46	67.4, 70.8	69.1	2.8	8.2
3	5.81	4.56	67.2, 70.8	70.7	2.5	9.1
4	1.51	2.10	67.4, 70.9	70.5	2.6	8.0
5	2.82	2.68	67.4, 70.9	69.8	2.5	8.4
6	8.28	1.71	67.5, 70.9	68.8	2.4	9.1
7[a]	5.46	2.67	67.2, 70.0	69.2	3.7	9.0
8	4.90	8.68	67.5, 70.8	70.8	—	—
9	3.41	10.40	67.6[e], 67.7, 71.1	70.6	—	—

a) $(C_2H_5)_4NClO_4$=0.7 M. b) Error, ±0.3. c) Error, ±0.3. d) Error, ±0.5. e) Doublet.

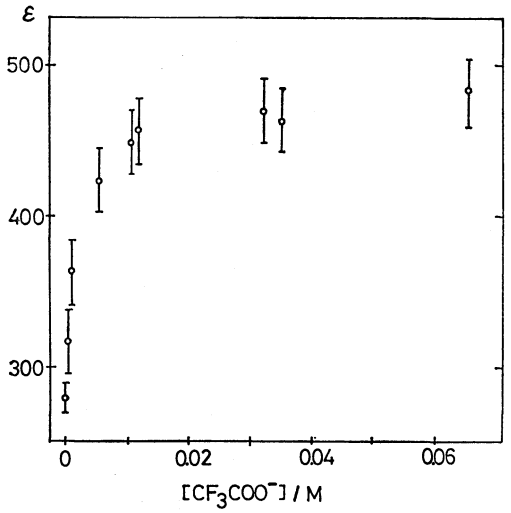

Fig. 3. The change in apparent molar absorption coefficient (ε) at 390 nm of $Mo_2(CF_3COO)_4$ in acetonitrile with a change in concentration of added CF_3COONa.

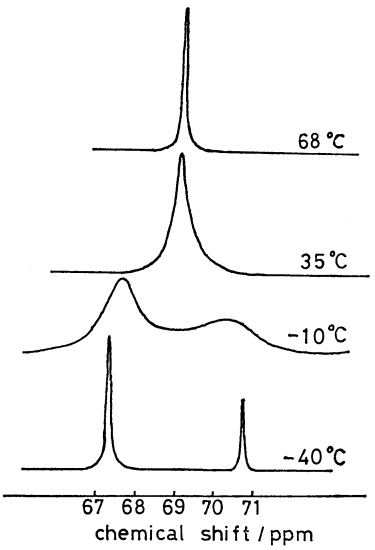

Fig. 4. An example of the temperature dependence of the ^{19}F NMR spectra of an acetonitrile solution of $Mo_2(CF_3COO)_4$ and CF_3COONa ($[Mo_2(CF_3COO)_4]=5.26\times10^{-2}$ M and $[CF_3COONa]=0.146$ M). Chemical shifts are shown with respect to CF_2Cl_2 as an internal reference.

shows one sharp peak upfield from the reference peak at 67.6 ppm over a temperature range of −40 to 70 °C, suggesting that the four trifluoroacetate ligands are magnetically equivalent. Hence, no significant change in the basic structure of I occurs, except for coordination of the solvent molecules at the apical positions. Sodium trifluoroacetate (*ca.* 0.58 M) has one sharp band at 71.0 ppm in acetonitrile.

The temperature dependence over the temperature range from −40 to 70 °C of the ^{19}F NMR spectra of the solutions (Table 1) containing both the complex and the free ligand is exemplified in Fig. 4 (run 2 in Table 1). A similar dependence was observed for runs 1 and 3—7. The following observations were made for these solutions: (a) the positions of the two peaks (67.2—67.5 and 70.8—70.9 ppm) at a low temperature (−40 °C in Fig. 4) coincide with those of the complex and of the free ligand; (b) the p_c and p_f values obtained from the ratio of the integral strengths of the two peaks can be expressed by

$$p_c/p_f = 4[Mo_4(CF_3COO)_4]_T/[CF_3COO^-]_T; \quad (7)$$

(c) the chemical shift of the coalesced peak at a high temperature (68 °C in Fig. 4) is close to the value determined from the expression, $67.6\times p_c+71.0\times p_f$; (d) the τ_c^{-1} values estimated from each of the two separate peaks (Eqs. 1 and 2) are in reasonable agreement with each other; (e) plots of log (τ_c^{-1}) against T^{-1} give straight lines (Fig. 5). All of these observations support the conclusion that the temperature dependence of the ^{19}F NMR spectra can be interpreted by chemical exchange of the bridging trifluoroacetate with "free" CF_3COO^- ("free" includes both the apical and the free ligands).

The values of τ_c^{-1} at 25 °C and the activation energy (E_a) were calculated from the best fit lines of Arrhenius plots, and are summarized in Table 1. In order to see the kinetic salt effect, $(C_2H_5)_4NClO_4$ was added to the reaction mixture (run 7). Addition of 0.7 M $(C_2H_5)_4NClO_4$ did not change the pattern of the temperature

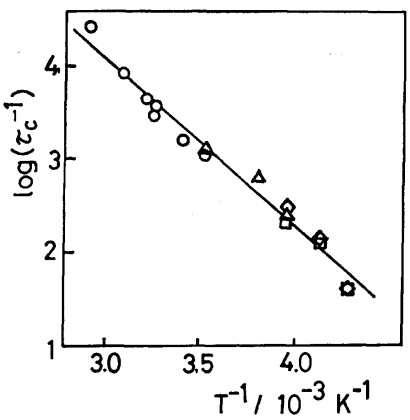

Fig. 5. An example of a plot of log (τ_c^{-1}) *vs.* T^{-1}. τ_c^{-1} values were obtained from Eq. 5 from the coalesced peak (○), by spectral simulation (△), from Eq. 1 from the peak in the coordinated ligand region (□), or from Eqs. 2 and 3 from the peak in the free ligand region (◇) ($[Mo_2(CF_3COO)_4]=5.81\times10^{-2}$ M and $[CF_3COONa]=0.456$ M). The solvent is acetonitrile.

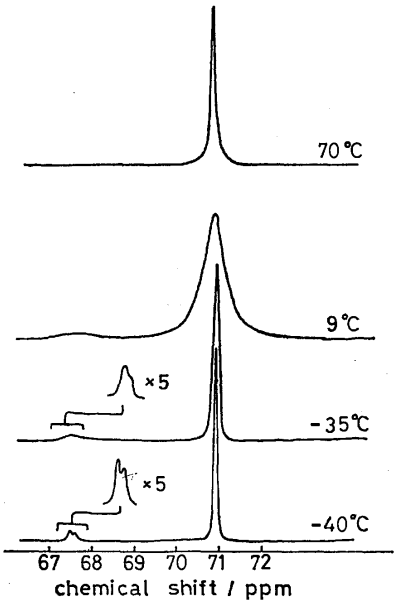

Fig. 6. Temperature dependence of the ^{19}F NMR spectra of an acetonitrile solution of $Mo_2(CF_3COO)_4$ (3.41 $\times10^{-2}$ M) and CF_3COONa (1.04 M) (run 9 in Table 1).

dependence of the signals, but gave a slight increase in τ_c^{-1}.

The Arrhenius plot for run 8 gave a concave curve. In run 9, the signal peak in the coordinated ligand region splits at a low temperature (Fig. 6). Thus, the ^{19}F NMR spectra of the solutions containing more than 0.8 M sodium trifluoroacetate cannot be interpreted by simple chemical exchange.

Rate Law for the Exchange Reaction. The result of run 7 indicates that the kinetic salt effect is not significant over the range of concentrations of reactants in runs 1—6. Sodium trifluoroacetate is almost completely dissociated into sodium and trifluoroacetate ions in acetonitrile (dielectric constant: 35.95 at 25 °C).[13]

The τ_c^{-1} values in Table 1 are almost equal to one another, and seem to be independent of both $[CF_3COO^-]_T$ and $[Mo_2(CF_3COO)_4]_T$. The τ_f^{-1} value depends linearly on the ratio p_c/p_f, as is expected from Eq. 4. This was confirmed from the τ_f^{-1} values obtained from the peak in the free ligand region by Eq. 2. Thus the rate (R) of the exchange reaction is independent of $[CF_3COO^-]_T$ and is linearly dependent on $[Mo_2(CF_3COO)_4]_T$,

$$R = 4\tau_c^{-1}[Mo(CF_3COO)_4]_T = k_{ex}[Mo_2(CF_3COO)_4]_T, \quad (8)$$

where R and k_{ex} are the rate and the first order rate constant of the exchange, respectively, of one of the four coordinated ligands. The rate constant and activation parameters were determined to be $k_{ex}=(1.1\pm0.2)\times10^4$ s^{-1} (25 °C), $\Delta H^*=(8.2\pm0.8)$ kcal mol^{-1} and $\Delta S^*=(-15\pm3)$ cal K^{-1} mol^{-1}.

Mechanism of Ligand Exchange. The electronic absorption spectra showed that an appreciable amount of III and/or IV is present in the solutions of runs 1—7. Therefore, more than three non-equivalent circumstances are involved for the trifluoroacetate. Only two ^{19}F NMR signals were observed at −40 °C, however, for runs 1—7. The ratios of the integral strengths of the two signals (Eq. 7) suggest that the signal due to the apical ligand must be included in the peak in the free ligand region.

The solution of run 9 which contained a larger amount of the "free" ligand, gives two peaks in the complex region. The two peaks are most likely due to the bridging ligands of III and IV, and the single peak of runs 1—7 in this region to the bridging ligand of III.[14]

Equation 9 can be applied to the runs 1—7.

$$[CF_3COO^-]_T = [CF_3COO^-]_F + [CF_3COO^-]_A = [CF_3COO^-]_F + [Mo_2(CF_3COO)_4]_T, \quad (9)$$

where the suffices A and F denote the apical ligand of III and uncoordinated free ligand, respectively. An appreciable amount of added trifluoroacetate exists as the apical ligand (48.4% for run 6). The peak position of the apical ligand is very close to that of the free ligand, since, at −40 °C, no shift of the "free" ligand peak (coalesced peak of the free and the apical ligand) is observed upon addition of the complex (Table 1). This suggests very weak coordination at the apical positions.

The following mechanism is proposed for runs 1—7.

$$[Mo_2(CF_3COO)_4\cdot\underline{CF_3COO}]^- + {}^*CF_3COO^- \overset{\text{fast}}{\rightleftharpoons} [Mo_2(CF_3COO)_4\cdot{}^*\underline{CF_3COO}]^- + CF_3COO^-, \quad (10)$$

$$[Mo_2(CF_3COO)_4\cdot{}^*\underline{CF_3COO}]^- \xrightarrow{k_s} [Mo_2(CF_3COO)_3({}^*CF_3COO)\cdot\underline{CF_3COO}]^-, \quad (11)$$

where the asterisks indicate the molecule substituting for the coordinated ligand. The first process is proposed to be fast, and the exchange rate is expressed by

$$R = k_s[Mo_2(CF_3COO)_4\cdot CF_3COO^-] = k_s[Mo_2(CF_3COO)_4]_T. \quad (12)$$

This equation is of the same form as the experimentally

obtained equation (Eq. 8). The observed rate constant, k_{ex}, is equal to k_s.

An alternative assignment for the ^{19}F NMR spectra of runs 1—7 could be proposed by considering that both II and III are present in the solutions and that their interconversion (Eq. 5) was fast with respect to the ^{19}F NMR time scale (so that the signals of coordinated CF_3COO^- of II and III coalesced completely). However, such a consideration does not account for the rate law (Eq. 8), unless II and III give identical exchange rates.

Comparison with Other Reactions. Few kinetic studies are reported on the substitution reactions of the compounds containing strong metal–metal bond such as Mo^{II}–Mo^{II} or Re^{III}–Re^{III}. Mureinik studied the reaction of acetate ions with $[Mo_2Cl_{8-n}(H_2O)_n]^{(4-n)-}$ (partially aquated form of $Mo_2Cl_8^{4-}$) to give $Mo_2(CH_3COO)_4$ in aqueous acid solutions ($[H^+]=0.05$—1.95 M with HCl or *p*-toluenesulfonic acid) at 25 °C by the stopped-flow method.[7] The entry of the first and the third acetate ions was kinetically analyzed. At a constant $[H^+]$, the following rate law (Eq. 13) was obtained for the first step.

$$k_{obsd} = \frac{b[CH_3COOH][Mo_2Cl_{8-n}(H_2O)_n^{(4-n)-}]}{1+a[CH_3COOH]} \quad (13)$$

The rate law was explained by the following dissociative mechanism.

$$[Mo_2Cl_{8-n}(H_2O)_n]^{(4-n)-} \rightleftarrows [Mo_2Cl_{8-n}(H_2O)_{n-1}]^{(4-n)-} + H_2O$$

$$[Mo_2Cl_{8-n}(H_2O)_{n-1}]^{(4-n)-} + CH_3COOH \longrightarrow [Mo_2Cl_{8-n}(H_2O)_{n-2}(CH_3COO)]^{(5-n)-} + H_3O^+ \quad (14)$$

A similar proposal was also put forth for the third step. We suggest that the rate law (Eq. 13) may also be explained by the following mechanism, which is similar to that proposed for our reaction.

$$[Mo_2Cl_{8-n}(H_2O)_n]^{(4-n)-} + CH_3COOH \overset{fast}{\rightleftarrows} [Mo_2Cl_{8-n}(H_2O)_n\cdot\underline{CH_3COO}]^{(5-n)-} + H^+$$

$$[Mo_2Cl_{8-n}(H_2O)_n\cdot\underline{CH_3COO}]^{(5-n)-} \longrightarrow [Mo_2Cl_{8-n}(H_2O)_{n-2}(CH_3COO)]^{(5-n)-} + 2H_2O \quad (15)$$

Further information, such as activation parameters, would be necessary to make a more definitive conclusion about the mechanism of this reaction.

The kinetics of the substitution of tributylphosphine or thiourea for the halide ligands of $Re_2X_8^{2-}$ ($X^-=Cl^-$ or Br^-), and of chloride ions for the bromide ligands of $Re_2Br_8^{2-}$ in methanol at 25 °C, have been studied by the stopped-flow method.[16] The following general rate law was given:

$$k_{obsd} = \frac{k_s+k_LK[L]}{1+K[L]}, \quad (16)$$

where L is the incoming ligand. The following mechanism was proposed (the charges are omitted, and S denotes methanol).

$$\begin{array}{ccc} Re_2X_8(S) & \xrightarrow{k_s} & Re_2X_7(S) + X^- \\ K\uparrow\downarrow +L & & +L\downarrow \text{fast} \\ Re_2X_8L & \xrightarrow{k_L} & \text{product} \end{array}$$

Although the detailed structure of the species Re_2X_8L was not given, L coordinates most likely at the apical position. Thus, we suggest that the rate-determining-step is the intramolecular rearrangement between X and either S or L, for the k_S or k_L path, respectively. Such a mechanism is similar to that proposed for our reaction.

Mono-oxo metal ions, such as $Mo^{V}O^{3+}$ and $V^{IV}O^{2+}$ have strong metal–oxygen bonds comparable to the metal–metal bond Mo–Mo, and their trans (apical) sites are vacant or weakly coordinated. The substitution of Cl^- for $OP(C_6H_5)_3$ in $Mo^{V}OCl_3\{OP(C_6H_5)_3\}_2$ and for $OP\{N(CH_3)_2\}_3$ in $Mo^{V}OCl_3[OP\{N(CH_3)_2\}_3]_2$ was claimed to occur first at the apical position followed by an intramolecular rearrangement to the basal position.[17] This process is similar to that of our ligand exchange. A similar mechanism is also proposed for the substitution reactions of oxovanadium(IV) complexes at the basal site.[18] The activation parameters for these reactions are close to those of our reaction. A substitution mechanism involving initial attack at the apical position, followed by rearrangement to the basal position would be a common feature of complexes containing strong metal–metal and metal–oxo bonds.

The rate of halide substitution at the apical positions of $Re_2(C_2H_5COO)_4\cdot X_2$ ($X^-=Cl^-$ or Br^-) in acetonitrile was reported to be *ca.* 10^{-3} s^{-1} at 25 °C.[19] On the other hand, the rate of process (10) for our Mo(II) complex is fast ($>10^4$ s^{-1}). It is difficult to explain such a big difference at the present stage. The difference in the oxidation state of metal ions, the electronic charge of the $M_2(RCOO)_4$ unit, and/or the d-orbitals involved (3d or 4d) may be important.

We are grateful to the Ministry of Education for a Grant-in-aid. We thank Mrs. R. Tanaka of the Institute of Non-aqueous Solution, for operating the NMR spectrometer, and Professor N. Tanaka and Dr. Y. Kato of the Department of Chemistry for simulation of the NMR spectra.

References

1) F. A. Cotton, *Chem. Soc. Rev.*, **4**, 27 (1975); *J. Less-Common Met.* **54**. 3 (1977).

2) J. San Filippo, Jr., H. J. Sniadoch, and R. L. Grayton, *J. Less-Common Met.*, **54**, 13 (1977); S. Onaka, *Kagaku No Ryoiki*, **31**, 1034 (1977).

3) Recent reports on the preparations of new compounds, D. A. Edwards and J. J. Maguire, *Inorg. Chim. Acta*, **25**, L47 (1978); E. Hochberg and E. H. Abbott, *Inorg. Chem.*, **17**, 506 (1978); T. Nimry and R. A. Walton, *Inorg. Chem.*, **17**, 510 (1978); P. Vella and J. Zubieta, *J. Inorg. Nucl. Chem.*, **40**, 477 (1978).

4) J. V. Brencic, I. Leban, and P. Segedin, *Z. Anorg. Allg. Chem.*, **427**, 85 (1976); F. A. Cotton, M. Extine, and L. D. Gage, *Inorg. Chem.*, **17**, 172 (1978).

5) P. E. Haycock, D. S. Urch, C. D. Garner, J. H. Hillier, and G. R. Mitcheson, *J. Chem. Soc., Chem. Commun.*, **1978**, 262; P. E. Fanwick, D. S. Martin, F. A. Cotton, and T. R. Webb, *Inorg. Chem.*, **16**, 2103 (1977);W. C. Trogler, E. I. Solomon, and H. B. Gray, *Inorg. Chem.*, **16**, 3031 (1977); I. H. Hillier, C. D. Garner, G. R. Mitcheson, and M. F. Guest, *J. Chem. Soc., Chem. Commun.*, **1978**, 204.

6) F. A. Cotton, B. A. Frenz, E. Pederson, and T. R.

Webb, *Inorg. Chem.*, **14**, 391, 399 (1975); H. J. Baxendale, C. D. Garner, R. G. Senior, and P. Sharpe, *J. Am. Chem. Soc.*, **98**, 638 (1976).

7) R. J. Mureinik, *Inorg. Chim. Acta*, **23**, 103 (1977).

8) F. A. Cotton and J. G. Norman, Jr., *J. Coord. Chem.*, **1**, 161 (1971).

9) J. A. Pople, W. G. Schneider, and H. J. Bernstein, "High-Resolution Nuclear Magnetic Resonance," McGraw Hill, New York (1959).

10) Y. Arata, "Zoku Jikkenkagaku Koza," ed by M. Kotake, Maruzen, Tokyo (1967). Vol. 12, p. 135.

11) A. P. Ketteringham and C. Oldham, *J. Chem. Soc., Dalton Trans.*, **1973**, 1067.

12) F. A. Cotton and J. G. Norman, Jr., *J. Am. Chem. Soc.*, **94**, 5697 (1972).

13) C. D. Garner and R. G. Senior, *J. Chem. Soc., Dalton Trans.*, **1975**, 1171.

14) G. J. Janz and R. P. T. Tomkins, "Nonaqueous Electrolytes Handbook," Academic Press, New York (1972), Vol I.

15) The assignment means that $W_f°$, $W_c°$, ν_f and ν_c are not appropriate to evaluate τ_f^{-1} and τ_c^{-1} (Eqs. 1—3), and the corresponding values of the coalesced peak of the free and apical ligands and of the bridging ligand of III should be used instead. However since the latter values are not estimated (even at −40 °C the chemical exchange is not frozen), the former values were used without any correction. The τ_f^{-1} and τ_c^{-1} values obtained do not appear to be unreasonable.

16) M. J. Hynes, *J. Inorg. Nucl. Chem.*, **34**, 366 (1972).

17) C. D. Garner, M. R. Hyde, F. E. Mabbs, and V. I. Routledge, *J. Chem. Soc., Dalton Trans.*, **1975**, 1175, 1180; **1977**, 1198.

18) M. Nishizawa and K. Saito, *Bull. Chem. Soc. Jpn.*, **51**, 483 (1978); M. Nishizawa and K. Saito, *Inorg. Chem.*, **17**, 3676 (1978), and references cited therein.

19) T. R. Webb and J. H. Espenson, *J. Am. Chem. Soc.*, **96**, 6289 (1974).

Synthesis and Structure of a Hexa-coordinated Vanadium(IV) Complex Aquaoxo[*N*-(2-pyridylmethyl)iminodiacetato]vanadium(IV) Dihydrate

Shun'ichiro Ooi, Masato Nishizawa,*,† Keiji Matsumoto, Hisao Kuroya, and Kazuo Saito†

Chemistry Department, Faculty of Science, Osaka City University, Sugimoto-cho, Sumiyoshi-ku, Osaka 558

†*Chemistry Department, Faculty of Science, Tohoku University, Aoba, Aramaki, Sendai 980*

(Received July 22, 1978)

A new complex, aquaoxo[*N*-(2-pyridylmethyl)iminodiacetato]vanadium(IV) dihydrate [VO(pmida)(H_2O)]·$2H_2O$ has been synthesized and its crystal structure determined by the X-ray method. The triclinic crystals obtained from water or aqueous ethanol solution are twinned and contain 2 mol of lattice water. The unit cell contains four formula units and the structure was analyzed on the assumption that the space group is $P\bar{1}$. The positional and thermal parameters were refined to $R=0.115$. The vanadium atom has a distorted octahedral coordination and deviates by 0.39 Å from the equatorial plane, which is composed of two cis carboxylate oxygens, a water molecule and the pyridine nitrogen. Vanadyl oxygen and tertiary nitrogen occupy the axial sites. Absorption spectra indicated that the structure is maintained in an aqueous solution of pH 3.0 to 4.9. This geometrical isomer seems to be formed selectively in an aqueous medium.

Many vanadium(IV) complexes have strong V=O bonds[1] and exhibit characteristic distorted molecular structure. X-Ray crystallography has disclosed that the V=O bond length (1.56 to 1.63 Å)[2–11] is shorter than that of the trans ligand to vanadium (2.18 to 2.51 Å). Sometimes the trans site remains vacant. The vanadium(IV) ion is above the equatorial plane by 0.26 to 0.41 and 0.48 to 0.58 Å in the complexes with coordination numbers 6[2–11] and 5,[12] respectively.

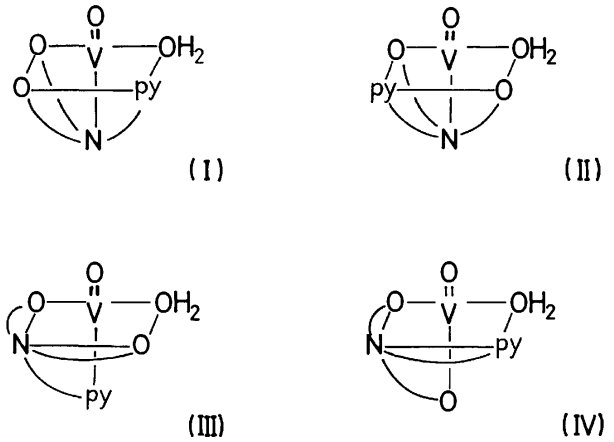

Fig. 1. The possible geometrical isomers of [VO(pmida)(H_2O)].

With a view toward studying the kinetics of direct ligand substitution at the equatorial site,[13] we have synthesized a new complex aquaoxo[*N*-(2-pyridylmethyl)iminodiacetato]vanadium(IV) dihydrate [VO(pmida)(H_2O)]·$2H_2O$. There can be four geometrical isomers depending on the coordination mode of the quadridentate $pmida^{2-}$ ion (Fig. 1). The structure has been determined by the X-ray method, and the properties in aqueous solution have been studied spectroscopically.

Experimental

Materials. The ligand, 2-pyridylmethyliminodiacetic acid H_2pmida,[14] and bis(acetylacetonato)oxovanadium(IV) [$VO(acac)_2$][15] were synthesized by known methods. Equimolar amounts of [$VO(acac)_2$] and H_2pmida (0.01 mol) were heated in acetonitrile (200 cm^3) at 83 °C for 30 min with vigorous stirring. The blue violet precipitate was filtered off, washed with aqueous ethanol and recrystallized by the following two methods. When a large amount of ethanol was added to the aqueous solution of the raw product, a pale violet powder was obtained within a few hours, which was washed with aqueous ethanol (1+1, v/v) and ethanol, and dried *in vacuo* at room temperature. (Yield 60%) Found C, 38.86; H, 4.11; N, 8.98%. Calcd for $C_{10}H_{12}N_2O_6V$: C, 39.10; H, 3.91; N, 9.12%.

When a small amount of ethanol was added to the aqueous solution, blue violet crystals precipitated very slowly (*e.g.* 10 days) with 2 mol of lattice water. Found C, 34.70; H, 4.64; N, 8.12%. Calcd for $C_{10}H_{16}N_2O_8V$: C, 35.00; H, 4.67; N, 8.17%.

The magnetic moment of the dihydrate was 1.7 Bohr magnetons at room temperature. This value is normal to those of VO^{2+} complexes with a $3d^1$ configuration.

Structure Determination. *Crystal Data*: $C_{10}H_{16}N_2O_8V$, $M=343.19$, Triclinic, $a=19.54(2)$, $b=10.846(4)$, $c=6.829(3)$ Å, $\alpha=102.56°(4)$, $\beta=87.64°(8)$, $\gamma=92.84°(9)$, $D_m=1.62$, $D_c=1.62$ g/cm^3, $Z=4$, μ(Cu $K\alpha$)$=149.9$ cm^{-1}, space group $P\bar{1}$ or P1. The structure analysis was carried out on the basis of the $P\bar{1}$ space group.

The Laue symmetry was determined from the Weissenberg and precession photographs. The unit cell dimensions were obtained by a least-squares analysis of fifteen 2θ values measured on a Philips PW 1100 four circle diffractometer by the use of Cu $K\alpha$ radiation.

The blue violet plate-like crystals of the dihydrate were usually twinned. Recrystallization was repeated in an attempt to obtain single crystals by taking precession photographs, but all the efforts were unsuccessful.

The precession photographs showed clearly the presence of two individuals in twin orientation. Both have a common a* axis and the reciprocal lattice of one crystal of the twin is related to that of the other by a rotation of 180° about the a* axis. This was confirmed by the intensity measurements ($2\theta \leq 40°$) for each constituent in a twinned crystal. The intensities of the corresponding reflections were different from each other in every twin crystal; in the crystal used for X-ray data measurements, the intensity ratio was found to be 6.88: 1.

Data Collection: Intensity data for the major individual of the twin were collected on the diffractometer by use of nickel-filtered Cu $K\alpha$ radiation. A crystal with dimensions $0.07\times 0.10\times 0.13$ mm^3 was mounted so that the a axis is roughly parallel to ϕ axis. The crystal-to-detector distance and the

detector aperture were 195 mm and 3×3 mm, respectively. The scan rate and the scan width are 0.030° s^{-1} and (0.7+0.2 tan θ)°, respectively. Background counts were measured for (scan time/2)$\sqrt{I_b/I_{int}}$ at each side of the scan range (I_b, mean background intensity obtained from the preliminary background measurements for 5 s at each side of the peak; I_{int} is the total number of counts divided by total scan time). A total of 3080 reflections having $I_t-2\sqrt{I_t}>I_b$ were collected in the $2\theta\leq120°$ range (I_t, intensity at the top of the peak), but 2584 reflections for which $I>2\sigma(I)$ were used in the structure analysis. Intensity data were corrected for the *Lp* factor[16] but not for absorption.

For each reflection no estimation was made of the error derived from the diffraction due to the minor crystal. However, a tentative calculation suggested that under these experimental conditions the intensity from a reciprocal lattice point is liable to suffer from disturbance due to the diffraction from the minor individual; the disturbance is possibly significant unless a reciprocal lattice point of the major is separated from the neighboring point due to the minor by more than 0.013 $Å^{-1}$. Of the 2584 reflections 1027 were under such circumstances but the error induced in the structure amplitude is about 8% on an average.[17] Therefore, all 2584 reflections were used for the structure analysis in the initial stage.

Table 1. Positional and thermal parameters

	x	y	z	B/Å^2
V(1)	0.1605(1)	0.4260(2)	0.3791(3)	2.00(4)
O(1)	0.3681(5)	0.4497(10)	0.3641(14)	3.7(2)
O(2)	0.2575(4)	0.4672(8)	0.4494(12)	2.3(2)
O(3)	0.1589(4)	0.5910(7)	0.2898(11)	1.9(1)
O(4)	0.2502(5)	0.7082(10)	0.0858(15)	4.1(2)
O(5)	0.1785(5)	0.2468(8)	0.3967(13)	2.7(2)
O(6)	0.1148(5)	0.4710(9)	0.5793(13)	2.9(2)
N(1)	0.0832(5)	0.3517(10)	0.1752(15)	2.4(2)
N(2)	0.2176(5)	0.3796(9)	0.0721(14)	2.0(2)
C(1)	0.0171(7)	0.3698(13)	0.2201(20)	2.9(3)
C(2)	−0.0341(8)	0.3318(15)	0.0760(22)	3.8(3)
C(3)	−0.0136(8)	0.2732(15)	−0.1179(22)	3.8(3)
C(4)	0.0549(8)	0.2515(14)	−0.1643(22)	3.4(3)
C(5)	0.1038(7)	0.2912(12)	−0.0161(19)	2.5(2)
C(6)	0.1780(7)	0.2647(13)	−0.0490(20)	2.9(3)
C(7)	0.2900(7)	0.3413(14)	0.1188(21)	3.1(3)
C(8)	0.3068(7)	0.4265(13)	0.3249(19)	2.5(2)
C(9)	0.2197(7)	0.4915(12)	−0.0151(19)	2.4(2)
C(10)	0.1924(6)	0.6041(12)	0.1255(18)	2.1(2)
V′(1)	0.3376(1)	0.9451(2)	0.8745(3)	2.03(4)
O′(1)	0.1292(5)	0.9378(9)	0.9001(14)	3.2(2)
O′(2)	0.2408(4)	0.9751(8)	0.9626(12)	2.1(2)
O′(3)	0.3373(4)	1.1036(8)	0.7673(12)	2.0(2)
O′(4)	0.2914(5)	1.2068(10)	0.5559(15)	4.0(2)
O′(5)	0.3191(5)	0.7663(8)	0.9144(13)	2.7(2)
O′(6)	0.3844(5)	1.0044(9)	1.0622(14)	3.2(2)
N′(1)	0.4139(5)	0.8669(10)	0.6624(15)	2.2(2)
N′(2)	0.2797(5)	0.8759(10)	0.5779(14)	2.0(2)
C′(1)	0.4807(8)	0.8836(14)	0.6961(22)	3.3(3)
C′(2)	0.5310(9)	0.8337(17)	0.5561(26)	5.0(4)
C′(3)	0.5110(9)	0.7595(15)	0.3773(24)	4.3(3)
C′(4)	0.4418(8)	0.7458(14)	0.3344(23)	3.9(3)
C′(5)	0.3937(7)	0.7964(12)	0.4832(19)	2.6(3)
C′(6)	0.3187(7)	0.7646(12)	0.4571(19)	2.5(2)
C′(7)	0.2083(7)	0.8345(12)	0.6466(19)	2.4(2)
C′(8)	0.1902(7)	0.9247(12)	0.8495(19)	2.5(3)
C′(9)	0.2776(7)	0.9848(13)	0.4793(20)	3.0(3)
C′(10)	0.3022(7)	1.1039(12)	0.6083(19)	2.5(2)
O(WA)	0.3886(6)	0.5687(10)	0.7734(17)	4.9(2)
O(WB)	0.0356(6)	0.9014(11)	0.6045(17)	5.1(3)
O(WC)	0.0994(5)	0.0435(9)	0.3022(14)	3.6(2)
O(WD)	0.4787(9)	0.4074(14)	0.1131(22)	8.1(4)

Structure Determination and Refinement: The positions of V atoms were obtained from the Patterson map and those of the remaining nonhydrogen atoms were found from successive Fourier syntheses. The positional and isotropic thermal parameters were refined by the least-squares method. The minimized function was $\sum W(|F_o|-|F_c|)^2$. The weighting scheme was as follows: $W=0.3$ for $F_o<9.8$ and $W=1.0$ for $F_o>9.8$. Several cycles of the least-squares calculations reduced R to 0.109. In the subsequent refinement, zero weight was assigned to the 1027 reflections. The structure converged with $R=0.115$. In the final cycle no parameters were varied by more than 0.3 σ.

Atomic scattering factors of V^0, O, N, and C were taken from Ref. 18. Observed and calculated structure factors are available (Document No. 7902; in the F_o-F_c table those reflections for which zero weight was given in the leasts quares calculation, are marked with asterisks). Table 1 lists final atomic parameters. All computations were carried out on the FACOM 230-60 computer of Osaka City University, by the use of the RSSFR-5, HBLS-IV, and DAPH programs in the UNICS.[19]

Other Measurements. The electronic spectra were recorded with a Hitachi 323 Spectrometer in aqueous solution and by the reflectance method. Infrared spectra were recorded with a JASCO IR-Al Spectrometer in KBr disks. The pH titration was performed with a Metrohm E300B titrator under nitrogen atmosphere. The Magnetic susceptibility was measured by the Gouy method.

Results and Discussion

Crystal Structure. The crystal structure viewed down from the c axis is shown in Fig. 2. Although no H atoms were found in the structure analysis, possible hydrogen bonds are indicated by dotted lines. The unit cell comprises two crystallographically independent complexes which are discerned by atom numberings primed and unprimed. They are very similar in geometry and have virtually equal dimensions, except that they are enantiomeric to each other. Table 2 indicates that chemically equivalent bond lengths and angles are in reasonable agreement with each other. The elevation and projection of the complex are shown in Fig. 3 in which one antipode is depicted. The vanadium ion has a distorted octahedral coordination; the vanadyl oxygen and tertiary amino nitrogen occupy axial positions, while the equatorial plane consists of the pyridine nitrogen, water oxygen and two cis carboxylate oxygen atoms. The bond lengths and angles are listed in Table 2, and the deviation of the atoms from the least-squares plane in Table 3.

The V atom deviates from the equatorial plane by 0.39 Å toward the oxo ligand. This value is comparable with that (0.39 Å) in $Na_2[(VO)_2(ttha)]\cdot10H_2O$[2] ($H_6$ttha, triethylenetetraaminehexaacetic acid), in which the complex has a centrosymmetric dimer structure but is similar to the present complex in the context that each V atom is surrounded octahedrally by 4O and 2N (cis

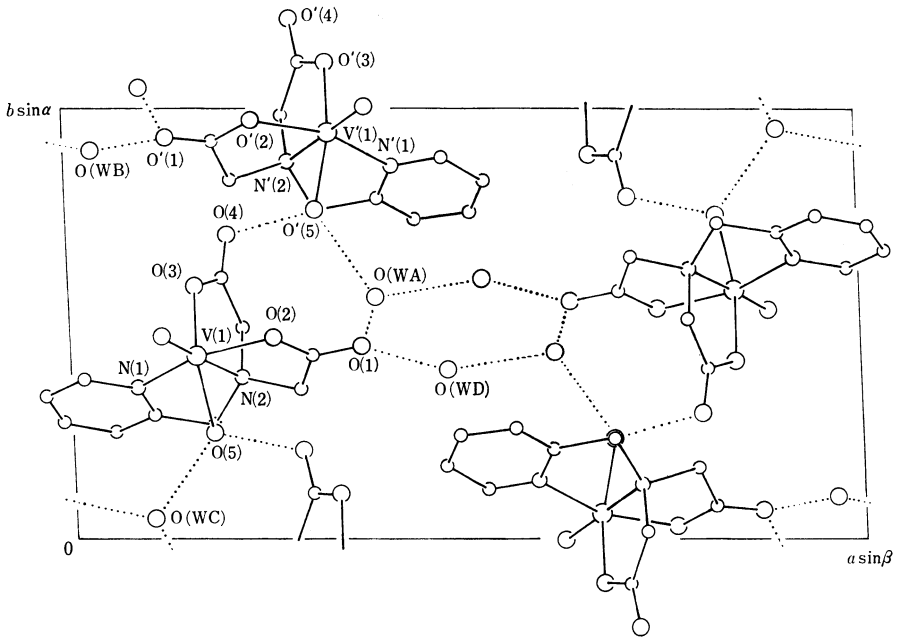

Fig. 2. The crystal structure viewed down the c axis. The dotted lines indicate possible O–H···O hydrogen bonds.

Table 2. Interatomic distances and bond angles

Bond lengths (l/Å)				Bond angles (ϕ/°)			
V–O(2)	1.98(1)	V'–O'(2)	1.98(1)	C(6)–N(2)–C(7)	110(1)	C'(6)–N'(2)–C'(7)	112(1)
V–O(3)	2.02(1)	V'–O'(3)	2.01(1)	C(7)–N(2)–C(9)	113(1)	C'(7)–N'(2)–C'(9)	112(1)
V–O(5)	2.02(1)	V'–O'(5)	2.03(1)	C(6)–N(2)–C(9)	115(1)	C'(6)–N'(2)–C'(9)	114(1)
V–O(6)	1.60(1)	V'–O'(6)	1.60(1)	N(2)–C(6)–C(5)	107(1)	N'(2)–C'(6)–C'(5)	108(1)
V–N(1)	2.11(1)	V'–N'(1)	2.11(1)	C(6)–C(5)–N(1)	117(1)	C'(6)–C'(5)–N'(1)	118(1)
V–N(2)	2.30(1)	V'–N'(2)	2.32(1)	C(5)–N(1)–V	117.5(9)	C'(5)–N'(1)–V'	118.3(9)
N(2)–C(6)	1.53(2)	N'(2)–C'(6)	1.53(2)	N(2)–C(7)–C(8)	105(1)	N'(2)–C'(7)–C'(8)	107(1)
C(6)–C(5)	1.49(2)	C'(6)–C'(5)	1.50(2)	C(7)–C(8)–O(2)	119(1)	C'(7)–C'(8)–O'(2)	118(1)
C(5)–N(1)	1.38(2)	C'(5)–N'(1)	1.36(2)	C(8)–O(2)–V	121.2(8)	C'(8)–O'(2)–V'	121.6(8)
N(2)–C(7)	1.56(2)	N'(2)–C'(7)	1.53(2)	C(7)–C(8)–O(1)	118(1)	C'(7)–C'(8)–O'(1)	118(1)
C(7)–C(8)	1.55(2)	C'(7)–C'(8)	1.55(2)	O(1)–C(8)–O(2)	123(1)	O'(1)–C'(8)–O'(2)	124(1)
C(8)–O(2)	1.29(2)	C'(8)–O'(2)	1.30(2)	N(2)–C(9)–C(10)	113(1)	N'(2)–C'(9)–C'(10)	113(1)
C(8)–O(1)	1.24(2)	C'(8)–O'(1)	1.23(2)	C(9)–C(10)–O(3)	120(1)	C'(9)–C'(10)–O'(3)	121(1)
N(2)–C(9)	1.46(2)	N'(2)–C'(9)	1.49(2)	C(10)–O(3)–V	119.7(8)	C'(10)–O'(3)–V'	119.4(8)
C(9)–C(10)	1.49(2)	C'(9)–C'(10)	1.47(2)	C(9)–C(10)–O(4)	118(1)	C'(9)–C'(10)–O'(4)	118(1)
C(10)–O(3)	1.30(2)	C'(10)–O'(3)	1.31(2)	O(4)–C(10)–O(3)	122(1)	O'(4)–C'(10)–O'(3)	121(1)
C(10)–O(4)	1.23(2)	C'(10)–O'(4)	1.27(2)	N(1)–C(1)–C(2)	122(1)	N'(1)–C'(1)–C'(2)	123(1)
N(1)–C(1)	1.33(2)	N'(1)–C'(1)	1.33(2)	C(1)–C(2)–C(3)	118(1)	C'(1)–C'(2)–C'(3)	118(2)
C(1)–C(2)	1.42(2)	C'(1)–C'(2)	1.39(2)	C(2)–C(3)–C(4)	120(1)	C'(2)–C'(3)–C'(4)	119(2)
C(2)–C(3)	1.39(2)	C'(2)–C'(3)	1.37(3)	C(3)–C(4)–C(5)	120(1)	C'(3)–C'(4)–C'(5)	119(2)
C(3)–C(4)	1.38(2)	C'(3)–C'(4)	1.39(3)	C(4)–C(5)–N(1)	120(1)	C'(4)–C'(5)–N'(1)	121(1)
C(4)–C(5)	1.40(2)	C'(4)–C'(5)	1.40(2)	C(5)–N(1)–C(1)	120(1)	C'(5)–N'(1)–C'(1)	119(1)

Bond angles (ϕ/°)			
O(2)–V–N(1)	152.6(4)	O'(2)–V'–N'(1)	152.4(4)
O(3)–V–O(5)	163.7(4)	O'(3)–V'–O'(5)	163.0(4)
O(6)–V–O(2)	107.2(4)	O'(6)–V'–O'(2)	107.4(4)
O(6)–V–O(3)	95.4(4)	O'(6)–V'–O'(3)	95.7(4)
O(6)–V–O(5)	100.9(4)	O'(6)–V'–O'(5)	101.3(5)
O(6)–V–N(1)	100.2(5)	O'(6)–V'–N'(1)	100.1(5)
O(6)–V–N(2)	172.1(4)	O'(6)–V'–N'(2)	172.0(5)
O(2)–V–O(3)	88.5(4)	O'(2)–V'–O'(3)	87.5(4)
O(3)–V–N(1)	89.2(4)	O'(3)–V'–N'(1)	92.3(4)
N(1)–V–O(5)	88.1(4)	N'(1)–V'–O'(5)	85.8(4)
O(5)–V–O(2)	86.6(4)	O'(5)–V'–O'(2)	86.5(4)
V–N(2)–C(6)	105.1(7)	V'–N'(2)–C'(6)	106.2(7)
V–N(2)–C(7)	104.7(8)	V'–N'(2)–C'(7)	104.0(7)
V–N(2)–C(9)	108.6(8)	V'–N'(2)–C'(9)	107.4(8)

Possible hydrogen bonds (l/Å)

Symmetry code

I $1-x, 1-y, 1-z$: II $-x, 1-y, 1-z$;
III $x, 1+y, 1+z$; IV $x, -1+y, z$;
V $x, y, 1+z$

O(1)···O(WA)	2.85(2)
O(1)···O(WD)	2.70(2)
O(5)···O(WC)	2.61(1)
O(5)···O'(4^{IV})	2.59(1)
O'(1)···O(WB)	2.73(2)
O'(1)···O(WC^{III})	2.79(1)
O'(5)···O(WA)	2.58(1)
O'(5)···O(4^{V})	2.59(1)
O(WA)···O(WD^{I})	2.72(2)
O(WB)···O(WC^{II})	2.75(2)

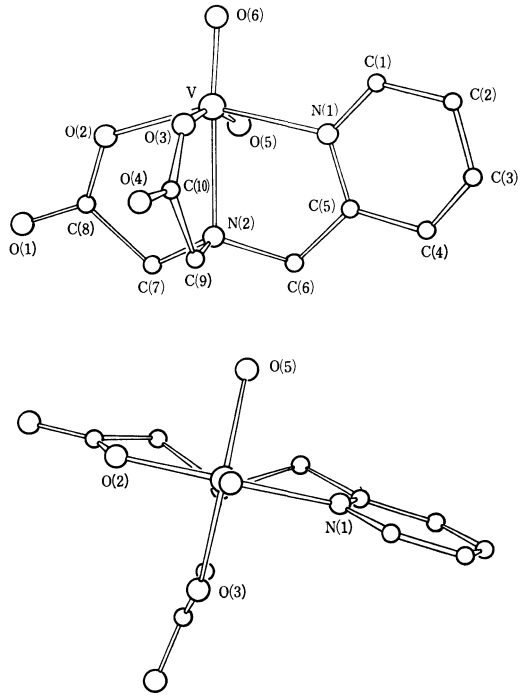

Fig. 3. The elevation and projection of the complex.

Table 3. Deviations (Δd/Å) of atoms from several mean planes

(1)	[N(1), O(2), O(3), O(5)] plane N(1) 0.15, O(2) 0.07, O(3) −0.12, O(5) −0.06, V −0.38
(1′)	[N′(1), O′(2), O′(3), O′(5)] plane N′(1) 0.09, O′(2) 0.10, O′(3) −0.10, O′(5) −0.09, V′ −0.39
(2)	[V, N(1), N(2)] plane C(5) 0.28, C(6) 0.78
(2′)	[V′, N′(1), N′(2)] plane C′(5) −0.26, C′(6) −0.70
(3)	[V, N(2), O(2)] plane C(7) 0.73, C(8) 0.31, O(1) 0.33
(3′)	[V′, N′(2), O′(2)] plane C′(7) −0.69, C′(8) −0.28, O′(1) −0.31
(4)	[V,N(2), O(3)] plane C(9) −0.02, C(10) 0.12, O(4) 0.40
(4′)	[V′, N′(2), O′(3)] plane C′(9) 0.04, C′(10) −0.14, O′(4) −0.37

positions) atoms. In square pyramidal oxovanadium(IV) complexes the deviation of V atom from the equatorial plane ranges from 0.48 to 0.58 Å,[12] whereas in the octahedral complexes this deviation is in the range 0.26—0.41 Å.

The axial ligation thus decreases the deviation, with the O donor giving more marked effect than the N donor. This is in accord with the larger mean L_{eq}–V–L_{eq} angles for *trans*(*O*) than for *trans*(*N*). The V=O bond length (1.60 Å) agrees well with that in the ttha complex.[2] The lengths in the 6-coordinate complexes range from 1.56 to 1.63 Å, differing little from those in the 5-coordinate complexes.[12] The salpn complex [VO(salpn)] (salpn, *N*,*N*′-disalicylidene-1,2-propanediamine) has V=O··· V=O chain in the crystals, and a rather strong intermolecular interaction is expected. Even in this compound the V=O length (1.633(9) Å) is not significantly different from those in the 5-coordinate complexes.

Selbin *et al.* summarized IR frequencies of various oxovanadium(IV) complexes and indicated that the ν(V=O) depends on the variety of ligands.[20] However, there seems to be an overall trend as follows: (1) VO^{2+} complexes with coordination number 5 give ν(V=O) higher than 995 cm^{-1};[21] (2) on the other hand, VO^{2+} complexes with coordination number 6 give lower ν(V=O)'s; *e.g.*, 976, 955,[22] and 854 cm^{-1} for $(NH_4)_2$-$[VO(oxalato)_2(H_2O)]\cdot H_2O$, $[VO(acac)_2$(4-phenylpyridine)] and [VO(salpn)], respectively. The present complex with coordination number 6 gives ν(V=O) at 985 cm^{-1}. It appears as if VO^{2+} complexes with coordination number 5 and 6 have ν(V=O) values higher than and lower than 990 cm^{-1}, respectively, and this figure can serve as a criterion for discriminating the coordination number of VO^{2+} complexes.[23] Correlation could be also expected between the V=O bond length and ν(V=O). However, the variation of the bond length should be very small and a more accurate measurement is desirable.

The axial V–N(2) bond with the tertiary amino nitrogen agrees in length with the corresponding value in $[(VO)_2(ttha)]^{2-}$ but is longer by 0.15 Å than the equatorial V–N(sp^3) bond in the ttha complex. Such a difference is attributed to the trans influence of the oxo ligand.

The 5-membered chelate rings are of the envelope conformation, the ring composed of O(3), C(10), C(9), N(2), and V has relatively planar structure. However, the other two rings are considerably puckered up. Figure 4 shows, as an example, the projection and elevation of the chelate ring which includes the pyridine moiety. The firm disposition of the equatorial bonds may be responsible for such a puckering. Bond lengths and angles in the pmida ligand are normal. The length of the hydrogen bonding (Table 2) range from 2.59 to 2.85 Å, which are normal for lattice waters in coordination compounds.

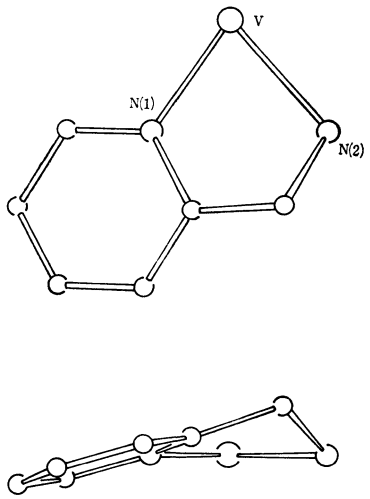

Fig. 4. The projection and elevation of the chelate ring in which pyridine moiety participates.

Table 4. Some structural parameters of 6-coordinate oxovanadium(IV) complexes

	Deviation[b] (d/Å)	L_{eq}–V–L_{eq}[c] (ϕ/°)	V=O (l/Å)	V–O_{eq}[d] (l/Å)	V–N_{eq} (l/Å)	V–L_{ax} (l/Å)
[VO(pmida)(H_2O)]·2H_2O[a]	0.39	157.9	1.60(1)	O(COO⁻) 2.00 O(H_2O) 2.02(1)	2.11(1)(sp^2)	N(sp^3) 2.31(1)
Na_2[($VO)_2$(ttha)]·10H_2O[2]	0.39	156.6	1.605(8)	O(COO⁻) 1.933	2.163(5)(sp^3)	N(sp^3) 2.294(7)
[VO(2,6-pyridinedicarboxylato)($H_2O)_2$]·2H_2O[3]	0.408	156.6	1.59(1)	O(COO⁻) 2.02(2) O(H_2O) 2.03(1)		N(sp^2) 2.18(1)
$(NH_4)_2$VO$(NCS)_4$·5H_2O[4]	0.26	163	1.62(6)		2.04(3)(sp)	O(H_2O) 2.22(5)
$VOSO_4$·5H_2O[5]	0.281		1.591(5)	O(H_2O) 2.040 O(SO_4) 1.983(5)		O(H_2O) 2.223(5)
$(NH_4)_2$[VO$(ox)_2(H_2O)$]·H_2O[6]	0.302	161.9	1.594(3)	O(COO⁻) 2.004 O(H_2O) 2.033(3)		O(COO⁻) 2.184(3)
$VOSO_4$·3H_2O[7]	0.36	159.4	1.559(8)	O(SO_4) 2.017 O(H_2O) 2.065		O(H_2O) 2.284(8)
$VOSO_4$[8]	0.31	162.2	1.59(2)	O(SO_4) 2.03		O(SO_4) 2.28(2)
VO$(acac)_2$(4-Ph-py)[9]	0.22		1.58(1)			
[VO$(acac)_2]_2$(dioxane)[10]			1.62	O(acac) 1.99		O(dioxane) 2.51
VO(salpn)[11]	0.31		1.633(9)	O(C–O⁻) 1.945(9)	2.11(1)(sp^2)	O(V=O) 2.213(9)

a) Present work. b) The deviation of the V atom from the equatorial plane; in every complex four atoms defining the equatorial plane are disposed in a more or less tetrahedral configuration with respect to the plane. The four atoms in the 2,6-pyridinedicarboxylato complex have significant deviations (±0.196 Å), and hence it might be inadequate here to define an "equatorial" plane. However, as is seen in the Table, the "devia tion" of the V atom as well as the L_{eq}–V–L_{eq} value in the 2,6-pyridinedicarboxylato complex have features similar to those of the other complexes with an axial N ligand. c) Mean value of two L_{eq}–V–L_{eq} angles; the two L_{eq}'s denote the ligand atoms which are trans to each other in the equatorial plane. d) In case there are more than two chemically equivalent bonds, the average value of their lengths is listed.

Of the four possible isomers of this complex, the present product seems to involve the least strain, because coordination of the two acetate oxygens in trans positions (II and III in Fig. 1) brings about a larger strain in the chelates. The pyridine ring is parallel to the z-axis. The d^1 electron of VO(2+) is believed to occupy d_{xy} orbital and the delocalization of this electron to the π-orbital of the pyridine moiety should be favorable.

Structure in the Aqueous Solution. The complex gave a pK_a value 6.4 at 25 °C and an ionic strength of 1.0 ($NaClO_4$). Hence, the complex is mostly (>98%) present in the aqua from below pH 4.7. The electronic absorption peaks are at 258, 350, 572, and 765 nm with molar extinction coefficients of 4940, 304, 16, and 27 cm^{-1} M^{-1}, respectively at pH 3.0 to 4.9. The reflectance spectrum of the solid dihydrate in the range from 340 to 700 nm gave peaks at 354 and 570 nm, suggesting that the complex maintains the same skeletal structure in aqueous solution of pH below 4.7 as in the crystalline state.

Complex formation between the aqueous solution of oxovanadium(IV) sulfate (0.008 M) and $pmida^{2-}$ (0.01 M) is indicated by the visible absorption peaks at 572 and 765 nm with molar extinction coefficients 15 and 26 cm^{-1} M^{-1}, respectively (*vide supra*) at pH 3.0. The visible peaks are so sensitive to the environment of oxovanadium(IV) ions as to be useful for identifying the complexes.[1] Therefore, it appears as if the present product was formed selectively from among the four possible structures.

The authors wish to thank Dr. Hiroshi Yokoi, Chemical Research Institute of Non-aqueous Solutions, Tohoku University for the measurement of the magnetic moment.

References

1) J. Selbin, *Chem. Rev.*, **65**, 153 (1965).
2) G. D. Fallen and B. M. Gatehause, *Acta Crystallogr., Sect. B*, **32**, 71 (1976).
3) B. H. Bersted, R. L. Belford, and I. C. Paul, *Inorg. Chem.*, **7**, 1557 (1968).
4) A. C. Hazell, *J. Chem. Soc.*, **1963**, 5745.
5) C. J. Ballhausen, B. F. Djurinskij, and K. J. Watson, *J. Am. Chem. Soc.*, **90**, 3305 (1968).
6) R. E. Oughtred, E. S. Raper, and H. M. M. Shearer, *Acta Crystallogr., Sect. B*, **32**, 82 (1976).
7) F. Theobald and J. Galy, *Acta Crystallogr., Sect. B*, **29**, 2732 (1973).
8) P. Kierkegaard and J. M. Longo, *Acta Chem. Scand.*, **19**, 1906 (1965).
9) M. R. Caira, J. M. Haigh, and L. R. Nassimbeni, *Inorg. Nucl. Chem. Lett.*, **8**, 109 (1972).
10) K. Dichmann, G. Hamer, S. C. Nyburg, and W. F. Reynolds, *Chem. Commun.*, **1970**, 1295.
11) M. Mathew, A. J. Carty, and Gus J. Palenik, *J. Am. Chem. Soc.*, **92**, 3197 (1970).
12) F. S. Molinaro and J. A. Ibers, *Inorg. Chem.*, **15**, 2278 (1976).
13) M. Nishizawa and K. Saito, *Inorg. Chem.*, **17**, 3676 (1978).
14) T. M. Suzuki, in preparation.
15) R. A. Rowe and M. M. Jones, *Inorg. Synth.*, **5**, 115 (1957).
16) J. Hornstra and B. Stubbe, PW 1100 Data Processing program, Philips Research Laboratories, Eindhoven, Holland.
17) The expected error in a troublesome reflection was calculated on the assumption that the diffracted X-ray beams

from the major and minor crystals are coincidentally lined. Of the 2584 structure factors, only 27 ones were found to have errors greater than 20%.

18) "International Tables for X-Ray Crystallography," Vol. IV, Kynoch Press, Birmingham, (1974), p. 71.

19) "The Universal Crystallographic Computation Program System," Crystallographic Society of Japan (1968).

20) J. Selbin, L. H. Holmes, Jr., and S. P. McGlynn, *J. Inorg. Nucl. Chem.*, **25**, 1359 (1963).

21) The *N*,*N'*-bis(1-methyl-3-oxobutylidene)ethylenediamine complex gives ν(V=O) of 982 cm^{-1} in acetonitrile, the solvent molecule with a large donating power being possibly coordinated to V(IV) at the apical site.

22) M. R. Caira, J. M. Haigh, and L. R. Nassimbeni, *J. Inorg. Nucl. Chem.*, **34**, 3171 (1972).

23) The very low value for [VO(salpn)], 854 cm^{-1}, should be due to the strong V=O···V interaction.

Phase Equilibria in the Er_2O_3–V_2O_3–V_2O_5 System at 1200 °C

Kenzo KITAYAMA,* Tadashi SUGIHARA, and Takashi KATSURA

Department of Chemistry, Faculty of Science, Tokyo Institute of Technology, Ookayama, Meguro-ku, Tokyo 152

(Received August 8, 1978)

The phase equilibria in the Er_2O_3–V_2O_3–V_2O_5 system have been established at 1200 °C. In this system, Er_2O_3, $Er_8V_2O_{17}$($4Er_2O_3 \cdot V_2O_5$), $ErVO_3$, $ErVO_4$, V_nO_{2n-1}(n: 2 to 7), and VO_2 found to be stable, $Er_8V_2O_{17}$, $ErVO_4$, V_2O_3, and VO_2 of which had non-stoichiometric compositions. On the basis of the phase equilibria, the standard Gibbs energies for the reactions,

$$ErVO_3 + 1/2O_2 = ErVO_4, \quad (1)$$

$$3Er_2O_3 + 2ErVO_3 + O_2 = Er_8V_2O_{17}, \quad (2)$$

have been determined to be -121 ± 1 and -256 ± 1 kJ, respectively. It has been shown that the standard Gibbs energy for Sm, Er, and Lu in Eq. 1 decreases linearly with increasing ionic radius of lanthanoid.

In previous papers,[1,2] the phase equilibria in the Sm_2O_3–V_2O_3–V_2O_5 and the Lu_2O_3–V_2O_3–V_2O_5 systems were reported at 1200 °C. In both systems, the existence of the V_nO_{2n-1} (n: 2 to 7) phases were confirmed. In the former system, $Sm_{10}V_2O_{20}$($5Sm_2O_3 \cdot V_2O_5$), $SmVO_3$, and $SmVO_4$, and in the latter, $LuVO_3$, $LuVO_4$, $Lu_7V_3O_{16}$, $Lu_2V_2O_7$, and LuV_4O_8 were stable as ternary compounds. On the basis of these phase equilibria, the standard Gibbs energies for the reactions related to the ternary compounds have been determined.

It has been reported that $ErVO_3$ is only the stable ternary compound in the Er_2O_3–V_2O_3 system, and that it belongs to the orthorhombic crystal system.[3,4] Recently, Brusset *et al.*[5,6] have studied the phase equilibria in the Er_2O_3–V_2O_5 system in the temperature range from 600 to 1500 °C, and found the existence of $4Er_2O_3 \cdot V_2O_5$ and $5Er_2O_3 \cdot V_2O_5$ in addition to the established tetragonal $ErVO_4$ phase, and concluded that $4Er_2O_3 \cdot V_2O_5$ is stable at temperatures from 1350 to 1500 °C, and $5Er_2O_3 \cdot V_2O_5$ from 1250 to 1500 °C.[5] Brusset *et al.*[7] reported that the $4Er_2O_3 \cdot V_2O_5$ phase belongs to the monoclinic system, and determined the relative intensities, spacings and assignments of the index of this phase. The precise phase equilibria in the Er_2O_3–V_2O_3–V_2O_5 system have, however, not been investigated.

The objectives of the present study have been (1) to establish the detailed phase equilibria in the Er_2O_3–V_2O_3–V_2O_5 system at 1200 °C in order to clarify the stable ternary compounds, (2) to calculate the Gibbs energies of the reactions for ternary compounds, and (3) to ascertain, prior to pursuing the complete studies of the Ln–V–O system (Ln: La, Ce, Pr, Nd, Sm, Eu, Gd, Tb, Dy, Ho, Er, Tm, Yb, Lu, and Y), wether or not there exists a linear relationship between the standard Gibbs energy of reaction and the ionic radius of the lanthanoid, as found in the Ln–Fe–O system.[8] Er_2O_3 has been selected as one of the lanthanoid sesquioxides in this paper.

Experimental

Analytical grades of Er_2O_3 (99.9% purity) and V_2O_5, made by heating guaranteed reagent grade NH_4VO_3 in air for 24 h at 500 °C, have been employed as starting materials. The desired ratios of Er_2O_3/V_2O_5 were obtained by mixing the appropriate quantities thoroughly in an agate mortar under ethyl alcohol. The mixtures thus obtained were treated by procedures previously described.[1]

Apparatus and procedures for controlling the partial pressure of oxygen, for keeping the temperature constant, the method of thermogravimetry, the criterion for establishing equilibrium, the method of identification of solid phases after quenching, of lattice constant determination, the method of measurement of the actual oxygen partial pressure, and the method of wet chemical analysis are the same described in previous papers.[1,9–11] On the basis of the previous results,[1] the weight of sample measured at an oxygen partial pressure of 10^{-12} atm has been chosen as the standard reference weight for thermogravimetry.

Results and Discussion

Phase Equilibria. Seven starting samples with different Er_2O_3/V_2O_5 ratios of 5.67, 4.00, 2.33, 1.50, 1.00, 0.667, and 0.250 were prepared. Figure 1 illustrates, as an example, the relationship between the oxygen partial pressure and the composition change, W_{O_2}/W_T, for samples with Er_2O_3/V_2O_5 ratios of 5.67, 1.50, and 0.250. W_{O_2} represents the weight gain of the samples assuming the reaction, $V_2O_3+O_2=V_2O_5$, were completed. Table 1 gives the results of the phase identification after quenching, and Fig. 2 illustrates the phase diagram. The following phases were found to be stable under the present experimental conditions; Er_2O_3(R), $ErVO_4$(B), $ErVO_3$(C), V_2O_3(D), V_3O_5(E), V_4O_7(F), V_5O_9(G), V_6O_{11}(H), V_7O_{13}(I), VO_2(J), and $Er_8V_2O_{17}$(N) ($4Er_2O_3 \cdot V_2O_5$). The letters in parentheses are the abbreviations of compounds. The existence of the $4Er_2O_3 \cdot V_2O_5$ phase contradicts the results of Brusset *et al.*[5] The stoichiometric existence of Er_2O_3 has been certified by Kitayama and Katsura.[12] As seen in Fig. 2, the phases $ErVO_4$, V_2O_3, VO_2, and $Er_8V_2O_{17}$ are of non-stoichiometric composition. The relationship between N_O/N_d and log P_{O_2} values for the solid solutions has been obtained using the results of thermogravimetric analysis and the method of least squares. Here, N_O/N_d indicates the deviation of the oxygen atoms from the stoichiometric composition d.[1,10] The empirical equations for $Er_8V_2O_{17}$ and $ErVO_4$ have been obtained as

$$N_O/N_{Er_8V_2O_{17}} = 0.0443 \log P_{O_2} + 0.108$$

and

$$N_O/N_{ErVO_4} = 0.0236 \log P_{O_2} + 0.180,$$

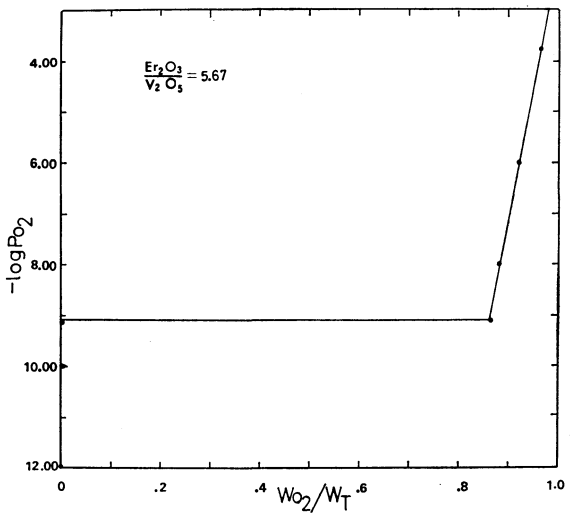

Fig. 1-1. The relationship between $-\log P_{O_2}$ and weight gains of the sample, $Er_2O_3/V_2O_5=5.67$.

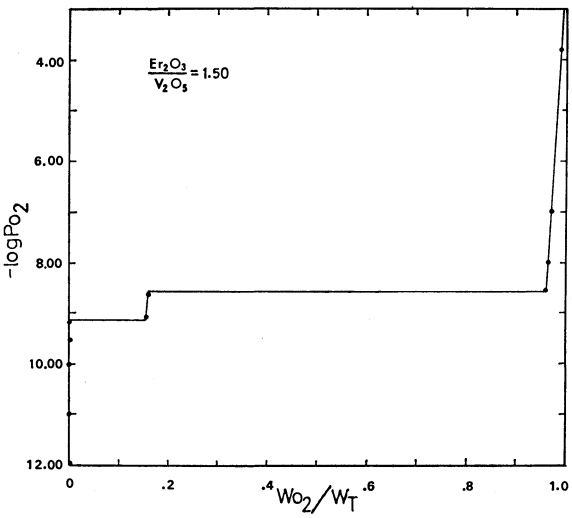

Fig. 1-2. The relationship between $-\log P_{O_2}$ and weight gains of the sample, $Er_2O_3/V_2O_5=1.50$.

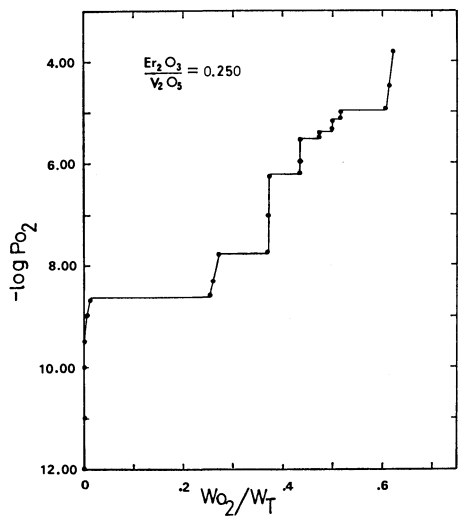

Fig. 1-3. The relationship between $-\log P_{O_2}$ and weight gains of the sample, $Er_2O_3/V_2O_5=0.250$.

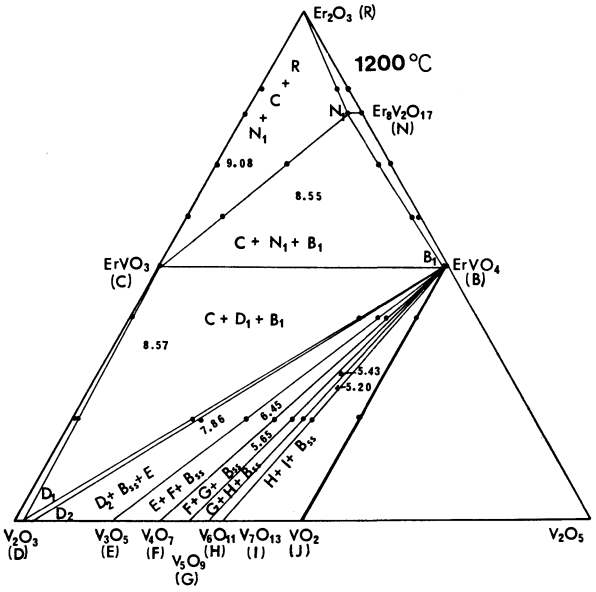

Fig. 2. Phase equilibria in the Er_2O_3–V_2O_3–V_2O_5 system at 1200 °C. Numerical values in three solid phases regions are the oxygen partial pressures in terms of $-\log P_{O_2}$. Abbreviations are the same as those in Table 2.

Table 1. Identification of phases

Starting material (mol %)		$-\log P_{O_2}$ (atm)	Time (h)	Phase
Er_2O_3	V_2O_5			
0.85	0.15	12.00	5	$Er_2O_3+ErVO_3$
		9.50	18	$Er_2O_3+ErVO_3$
		9.00	24	$Er_2O_3+Er_8V_2O_{17}$
		8.50	25	$Er_2O_3+Er_8V_2O_{17}$
		0.68	19	$Er_2O_3+Er_8V_2O_{17}$
0.70	0.30	12.00	5	$Er_2O_3+ErVO_3$
		9.50	18	$Er_2O_3+ErVO_3$
		8.50	25	$ErVO_4+Er_8V_2O_{17}$
		0.68	19	$ErVO_4+Er_8V_2O_{17}$
0.40	0.60	12.00	5	$ErVO_3+V_2O_3$
		9.50	18	$ErVO_3+V_2O_3$
		9.00	24	$ErVO_3+V_2O_3$
		8.50	25	$ErVO_4+V_2O_3$
		8.00	27	$ErVO_4+V_2O_3$
		7.00	25	$ErVO_4+V_3O_5$
		5.75	34	$ErVO_4+V_4O_7$
		5.50	34	$ErVO_4+V_5O_9$
		5.30	40	$ErVO_4+V_6O_{11}$
		5.10	44	$ErVO_4+V_7O_{13}$
		4.50	48	$ErVO_4+VO_2$
0.20	0.80	12.00	5	$ErVO_3+V_2O_3$
		9.50	18	$ErVO_3+V_2O_3$
		9.00	24	$ErVO_3+V_2O_3$
		8.50	25	$ErVO_4+V_2O_3$
		8.00	27	$ErVO_4+V_2O_3$
		7.00	25	$ErVO_4+V_3O_5$
		5.75	34	$ErVO_4+V_4O_7$
		5.50	34	$ErVO_4+V_5V_9$
		5.30	40	$ErVO_4+V_6O_{11}$
		5.10	44	$ErVO_4+V_7O_{13}$
		4.50	48	$ErVO_4+VO_2$

Table 2. Compositions, stability ranges in oxygen partial pressures, and activities in solid solutions

Component	Composition	Symbol	$-\log P_{O_2}$	$\log a_i$
$Er_8V_2O_{17}$	$Er_8V_2O_{17.0}$	N	0.68[a]—2.44[b]	0.489
	$Er_8V_2O_{16.8}$	N_1	9.08	0
$ErVO_3$	$ErVO_{3.00}$	C	8.55 —12.00[c]	0
$ErVO_4$	$ErVO_{4.00}$	B	0.68[a]—7.63[b]	5×10^{-3}
	$ErVO_{3.98}$	B_1	8.55	0

a) Stability range in log P_{O_2} may be higher than -0.68. b) These values were obtained by extrapolation using the thermogravimetric values. c) Stability range in log P_{O_2} may be lower than -12.00.

respectively.

In Table 2, the compositions, the stability ranges in oxygen partial pressures, and the abbreviations of the compounds are tabulated. As given in Table 2, $Er_8V_2O_{17}$ has a composition ranging from $Er_8V_2O_{16.8}$ at $\log P_{O_2}=-9.08$ to $Er_8V_2O_{17.0}$ at $\log P_{O_2}=-2.44$. $ErVO_3$ exhibites no deviation from the stoichiometric composition within the limits of experimental error. The deviation from the stoichiometric composition of $ErVO_4$ extends up to $ErVO_{3.98}$ at $\log P_{O_2}=-8.55$.

The lattice constants for $ErVO_4$, $ErVO_3$, and $Er_8V_2O_{17}$ are given in Table 3 together with the previous data.[3-5,7,13] The values obtained in this study are in reasonable agreement with previous results. As seen from Table 3, the non-stoichiometric dependence of the lattice constants for $Er_8V_2O_{17}$ has not been observed, and this may be due to compensation of the V^{4+} ion for the V^{5+} ion and the corresponding oxygen deficiency on the cell volume. The results for the V–O binary system have been reported in a previous paper.[1]

Calculation of Standard Gibbs Energy of Reaction. On the basis of the phase equilibria, the standard Gibbs energy of reaction to form the $ErVO_4$ and $Er_8V_2O_{17}$ compounds can be calculated by referring to the following reactions:

$$ErVO_3 + 1/2O_2 = ErVO_4, \quad (1)$$

$$3Er_2O_3 + 2ErVO_3 + O_2 = Er_8V_2O_{17}. \quad (2)$$

The standard Gibbs energies of these reactions can be directly calculated by adopting the equilibrium oxygen partial pressures corresponding to Eqs. 1 and 2. Here, the activity of each component, $ErVO_4$ and $Er_8V_2O_{17}$ at the composition of B_1 and N_1 in Fig. 2, respectively, was set equal to unity. The standard Gibbs energy of each reaction was calculated from the equation, $\Delta G^\circ=-RT\ln K$, where R is the gas constant, T the absolute temperature, and K the equilibrium constant. The detailed method of obtaining the equilibrium constant K, has been described by Kimizuka and Katsura.[14] In this study, the standard Gibbs energy for Reactions 1 and 2 found to be -121 ± 1 and -256 ± 1 kJ, respectively.

In similar studies,[1,2] Kitayama and Katsura determined the standard Gibbs energies of reaction for $SmVO_4$ and $LuVO_4$ to be -127 ± 1 and -116 ± 1 kJ, respectively. Thus by utilizing this data, the relationship between the standard Gibbs energy of reaction (expressed as $LnVO_3+1/2O_2=LnVO_4$ (Ln; Sm, Er, and Lu)) and the ionic radius of Ln^{3+} ion may be found. The value of each ionic radius has been determined by Shannon and Prewitt[15] to be Sm^{3+} 1.09, Er^{3+} 1.00, and Lu^{3+} 0.97Å with a coordination number of 8. Although the data was limited, the standard Gibbs energy of the reaction was found to decrease linearly with increasing ionic radius. A similar trend in the Fe-lanthanoid-perovskite system has been established.[8,16] It is conceivable that the thermodynamic properties of Ln–V–O compounds are closely related to the structural stability. In order to demonstrate this the study of the phase equilibria in the Ln–V–O system needs further research.

The authors wish to thank Dr. Tadao Kanzaki, Tokyo Institute of Technology, for the reading of this manuscript.

References

1) K. Kitayama and T. Katsura, *Bull. Chem. Soc. Jpn.*, **50**, 889 (1977).
2) K. Kitayama and T. Katsura, *Bull. Chem. Soc. Jpn.*, **51**, 1358 (1978).
3) G. J. McCarthy, C. A. Sipe, and K. E. McIlvried, *Mater. Res. Bull.*, **9**, 1279 (1974).
4) B. Reuter, *Colloq. Int. C. N. R. S.*, **1965**, 1053.
5) H. Brusset, F. Madaule-Aubry, B. Blanck, and A. Deboichet, *Bull. Soc. Chim. Fr.*, **1969**, 15.
6) H. Brusset, F. Madaule-Aubry, B. Blanck, J. P. Glaziou, and J. P. Laude, *Can. J. Chem.*, **49**, 3700 (1971).
7) H. Brusset, R. Mahe, and J. P. Laude, *Bull. Soc. Chim. Fr.*, **1973**, 495.
8) T. Katsura, K. Kitayama, T. Sugihara, and N. Kimizuka, *Bull. Chem. Soc. Jpn.*, **48**, 1809 (1975).
9) T. Katsura and H. Hasegawa, *Bull. Chem. Soc. Jpn.*, **40**, 561 (1967).

Table 3. Unit cell dimensions of compounds

Compound	$-\log P_{O_2}$	a(Å)	b(Å)	c(Å)	β	V(Å^3)	Reference
$ErVO_4$	0.68	7.094±0.001		6.271±0.001		315.6±0.1	present
		7.101±0.002		6.274±0.003			5
		7.0975		6.2723			4
$ErVO_3$	12.00	5.260±0.001	5.590±0.001	7.566±0.001		222.5±0.1	present
		5.256	5.581	7.559		221.8	3
		5.262	5.604	7.578			4
$Er_8V_2O_{17}$	0.68	10.45±0.02	8.42±0.02	16.05±0.10	98.08±0.23	1397±9	present
	8.50	10.47±0.02	8.39±0.02	16.01±0.07	98.56±0.18	1391±7	present
		10.498±0.003	8.399±0.003	16.104±0.011	98.13±0.04		7

10) N. Kimizuka and T. Katsura, *J. Solid State Chem.*, **13**, 176 (1975).
11) T. Katsura and A. Muan, *Trans. Soc. Min. Eng. AIME*, **230**, 77 (1964).
12) K. Kitayama and T. Katsura, *Bull. Chem. Soc. Jpn.*, **49**, 998 (1976).
13) X-Ray powder data, Card 17-260, A.S.T.M.
14) N. Kimizuka and T. Katsura, *J. Solid State Chem.*, **15**, 151 (1975).
15) R. D. Shannon and C. T. Prewitt, *Acta Crystallogr., Sect. B*, **25**, 925 (1969); **26**, 1046 (1970).
16) T. Katsura, T. Sekine, K. Kitayama, T. Sugihara, and N. Kimizuka, *J. Solid State Chem.*, **23**, 43 (1978).

Reaction of Bis[2-hydroxy-1-(2,6-dimethyl-4-methoxyphenyl)ethyl] Ethers with Tosyl Chloride

Munehiro NAKATANI and Tsunao HASE*

Department of Chemistry, Faculty of Science, Kagoshima University, Kagoshima 890

(Received March 8, 1978)

In the reaction with tosyl chloride in pyridine, the meso isomer (**2a**) of bis[2-hydroxy-1-(2,6-dimethyl-4-methoxyphenyl)ethyl] ether rearranged to give arylacetaldehyde (**3**) and 2-arylmethyl-4-aryl-1,3-dioxolane (**4**), and the racemic isomer (**2b**) afforded **3**, **4**, and 2,6-diaryl-1,4-dioxane. The aryl migration in this reaction has been confirmed by the use of the deuterated compounds, **2a-D** and **2b-D**, respectively, substituted with deuteriums at the 2,2-positions.

The meso (**1a**) and racemic (**1b**) isomers of bis(2-hydroxy-1-mesitylethyl) ether gave the corresponding tosylates with tosyl chloride in pyridine at 80 °C in high yields, respectively.[1] The reaction of the *p*-methoxy compounds, **2a** and **2b**, with the same reagent, on the contrary, gave no tosylate. At 80 °C or higher, these compounds afforded the rearranged products, in which migration of a *p*-anisyl group was observed. Under reflux, **1a** and **1b** were also observed to give results similar to those of **2a** and **2b**, except for the formation of the tosylates. The reaction of **2a** and **2b** with tosyl chloride by a mechanism similar to that reported by earlier investigators for the solvolysis of *p*-methoxyneophyl tosylate will be reported.[3i]

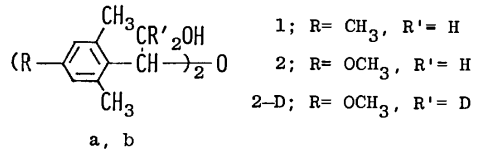

Fig. 1.

Results and Discussion

Synthesis of Bis[2-hydroxy-1-(2,6-dimethyl-4-methoxyphenyl)ethyl] Ethers (2). The meso **2a** and racemic compound **2b** have been synthesized from 2,6-dimethyl-4-methoxybenzaldehyde[2] by a method similar to the synthesis of bis(2-hydroxy-1-mesitylethyl) ethers (**1a** and **1b**).[1] Deuterated compounds **2a-D** and **2b-D** were prepared by the reduction of *meso*- and *dl*-bis(α-methoxycarbonyl-2,6-dimethyl-4-methoxybenzyl) ethers with lithium aluminium deuteride. With a large excess of the deuteride, 3,3,5,5-tetradeuterio-2,6-bis(2,6-dimethyl-4-methoxyphenyl)-1,4-dioxanes (**5a-D** and **5b-D**) were obtained as by-products, respectively. From a comparison of the PMR spectra of **2a** and **2b** with those of the *p*-methyl compounds, **1a** and **1b**, it became clear that the low-melting isomer, **2a**, is meso and the high-melting one, **2b**, is racemic.

Reaction of Bis[2-hydroxy-1-(2,6-dimethyl-4-methoxyphenyl)ethyl] Ethers (2) with Tosyl Chloride in Pyridine. The mild refluxing of **2a** with five equivalents of tosyl chloride in pyridine afforded 2,6-dimethyl-4-methoxyphenylacetaldehyde (**3**) in a 57% yield, and 2-(2,6-dimethyl-4-methoxyphenylmethyl)-4-(2,6-dimethyl-4-methoxyphenyl)-1,3-dioxolane (**4**) in a 42% yield. A similar treatment of the racemic isomer **2b** gave **3**(5%), **4**(24%) and 2,6-bis(2,6-dimethyl-4-methoxyphenyl)-1,4-dioxane (**5**) in a 42% yield. The IR spectrum of **3** shows the presence of a formyl group (1716, 2720, and 2830 cm^{-1}) and the PMR spectrum the presence of two benzyl protons (δ 3.55 ppm) coupling (2 Hz) to a formyl proton (δ 9.60 ppm).

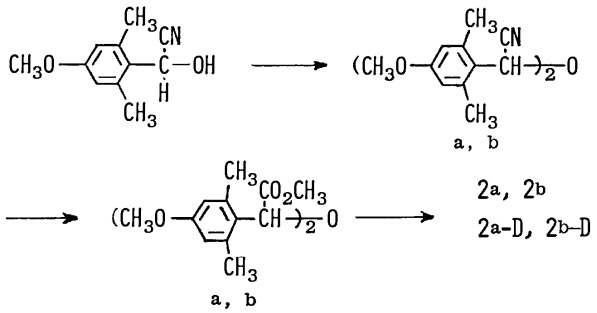

Fig. 2.

Since the IR spectra of **4** and **5** show no absorption band attributable to hydroxyl and carbonyl groups, the oxygen atoms are probably present as ether linkages. The PMR spectrum of **4** revealed the acetal moiety. The signal (δ 5.00 ppm) for the proton at C-2 is coupled (4 Hz) to the benzyl protons (δ 3.10 ppm), whereas the C-4 proton (δ 5.28 ppm) is coupled (each 8 Hz) to C-5 protons (δ 3.75 and 3.99 ppm) which are coupled (8 Hz) to each other. These nuclear spin-spin interactions have been confirmed by spin-decoupling techniques. Treatment of **4** with hydrochloric acid gave **3**. The PMR spectrum of **5** shows a overlapped ABX system for the protons on C-3 and C-5 (AB part), and C-2 and C-6 (X part) (see Experimental) which led to the tentative assignment of the 2,6-diarylsubstituted-1,4-dioxane structure, **5**. This structure was confirmed by the reaction of **2b** with concd hydrochloric acid to give **5**

The route to **3** and **4** must involve a *p*-anisyl migration to the adjacent carbon atom, and this assumption has been proved by the use of deuterated compounds, **2a-D** (meso) and **2b-D** (racemic). The reaction of **2a-D** with tosyl chloride gave a mixture of two aldehydes (the ratio of **3-D-1** and **3-D-2** was 1 : 1); **3-D-1** [PMR: δ 9.97 ppm (br s, Ar–CD_2C<u>H</u>O)] and **3-D-2** [PMR: δ 3.55 (br s, Ar–C<u>H</u>D–CDO)], a 1,3-dioxolane **4-D** and a small amount of tosylate (7%) with a composition of $C_{36}H_{38}D_4O_9S_2$, mp 118 °C. The reaction of **2b-D** also afforded **3-D-1**, **3-D-2**, **4-D**, and a tosylate (14%), mp 115 °C, but did not give **5-D**. Compared with the reaction of

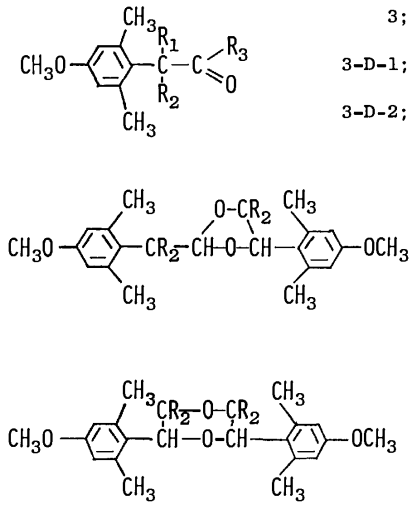

Fig. 3.

2a and **2b**, there may be present the isotope effect of deuterium in these reactions, but no conclusion may be drawn from these experimental results. The hydrolysis of dioxane **4-D** with concd hydrochloric acid in methanol afforded a mixture of the aldehydes(the ratio of **3-D-1** and **3-D-2** was 1: 1), 2,2-dideuterio-2-(2,6-dimethyl-4-methoxyphenyl)ethanal dimethyl acetal (**6**), and 1,1-dideuterio-2-methoxy-2-(2,6-dimethyl-4-methoxyphenyl)ethanol (**7**). The mass spectrum of the mixture of **3-D-1** and **3-D-2** showed a molecular ion peak at *m/e* 180 and these ratios of the **3-D-1** and **3-D-2** aldehydes were established by estimating the peak areas of the signals due to benzyl and formyl protons in the PMR spectra. Structure **6** and **7** have been assigned on the basis of the spectral data. The mass spectrum of **6** displayed fragment peaks which have been assigned to

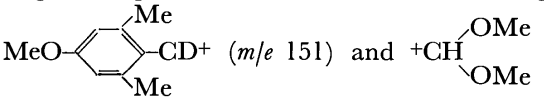

(*m/e* 151) and (*m/e* 75).

The PMR spectrum showed the proton (δ 4.50 ppm) at C-1 and two equivalent methoxyl groups (δ 3.39 ppm) in the dimethyl acetal moiety, but did not show a benzyl proton. The mass spectrum of **7** however showed a fragment peak which has been assigned to

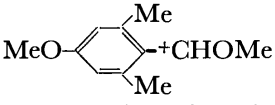

(*m/e* 179) and the PMR spectrum showed one benzyl proton (δ 4.86 ppm). This structure has been confirmed by direct comparison with a specimen synthesized by an established route. The tosylate of **2b-D** afforded a mixture of the aldehydes (the ratio of **3-D-1** and **3-D-2** was *ca.* 1: 1) in pyridine under reflux.

Many studies have been reported on the aryl migration in the solvolysis of tosylates.[3] Winstein *et al.*[3i] investigated the solvolysis rates of *p*-methoxyneophyl tosylate on various solvents and established that it underwent ionization in pyridine to give a rearranged product. In these experiments, it may be assumed that the tosylate formed from **2** undergoes ionization followed by the migration of the *p*-anisyl group to the adjacent carbon atom to give the rearranged products, **3** and **4**. Although there may be several mechanisms by which the formation of **3**, **4**, and **5** can be explained, Scheme 1 is the simplest.

Experimental

All the melting points are uncorrected. IR and UV spectra were recorded with Shimadzu IR-27C and Shimadzu UV-210A spectrophotometers. PMR spectra were measured with JEOL JNM 60 and JNM 100 apparatus (with TMS as an internal standard).

Cyanohydrin of 2,6-Dimethyl-4-methoxybenzaldehyde. A mixture of 2,6-dimethyl-4-methoxybenzaldehyde[2] (2 g) and anhydrous HCN (2 ml) was kept with CaO (400 mg) in a sealed tube at 50 °C for 2 h. The reaction mixture was acidified with dil H_2SO_4 followed by extraction with ether to give the cyanohydrin (1.8 g, 79%) as needles, mp 122—123 °C (acetone–petroleum ether). Found: C, 69.23; H, 6.91; N, 7.30%. Calcd for $C_{11}H_{13}NO_2$: C, 69.09; H, 6.85; N, 7.33% IR (Nujol); 3380 and 2250 cm^{-1}. PMR ($CDCl_3$); δ 2.53 (6H, s, Ar–C$\underline{H}_3$), 3.02 (1H, s, –O$\underline{H}$), 3.82 (3H, s, –OC$\underline{H}_3$), 5.83 (1H, s, –C$\underline{H}$OH), and 6.60 ppm (2H, s, Ar–$\underline{H}$). From the mother liquor, yellow crystals were obtained in a 2% yield, mp 215 °C. Found: C, 66.11; H, 5.66; N, 22.23%. Calcd for $C_{14}H_{14}N_4O$: C, 66.12; H, 5.55; N, 22.04%. IR (Nujol): 3580, 3400, 2360, and 2306 cm^{-1}. UV $(EtOH)_{max}$: 251.5 (ε 13500), 260 (15900), and 277 nm (18900). PMR (DMSO): δ 2.50 (6H, s), 3.43 (2H, br), 3.82 (4H, s), 6.72 (2H, s), and 7.35 ppm (2H, br).

Bis(α-cyano-2,6-dimethyl-4-methoxybenzyl) Ethers. The cyanohydrin (2 g) was refluxed with a catalytic amount of TsOH in dry benzene (500 ml) for 6 h. The crude product gave a mixture of ethers in a 65% yield (the ratio of meso and racemic forms was 5: 7), which was recrystallized from EtOH to give the racemic isomer as plates, mp 132—133 °C. Found: C, 72.74; H, 6.58; N, 7.97%. Calcd for $C_{22}H_{24}N_2O_3$: C, 72.50; H, 6.64; N, 7.69%. IR (Nujol): 1378, 1140, and 1050 cm^{-1}. PMR ($CDCl_3$): δ 2.38 (12H, s, Ar–C$\underline{H}_3$), 3.80 (6H, s, –OC$\underline{H}_3$), 5.75 (2H, s, –C$\underline{H}$–O–), and 6.59 ppm (4H, s, Ar–$\underline{H}$).

meso- *and* dl-*Bis(α-methoxycarbonyl-2,6-dimethyl-4-methoxybenzyl) Ethers.* Into a mixture of the above ethers (2 g) in abs EtOH (100 ml), dry HCl gas was passed for 5 h at 45—50 °C. The solvent was removed *in vacuo*, and the residue hydrolyzed with 30% aq KOH in ethylene glycol for 3 h. After acidification with dil HCl, the reaction mixture was extracted with ether and the ether extract methylated with

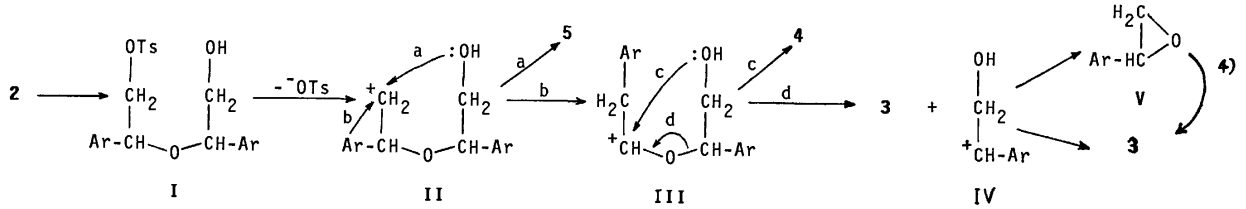

Scheme 1.

diazomethane. The crude product was chromatographed over silica gel. Elution with $CHCl_3$ containing acetone (0.5% v/v) gave a meso ester (1.3 g, 52%) as prisms from EtOH, mp 123—124 °C. Found: C, 66.79; H, 7.08%. Calcd for $C_{24}H_{30}D_7$: C, 66.96; H, 7.02%. IR (Nujol): 1765, 1745, 1380, 1200, 1140, and 1070 cm^{-1}. PMR ($CDCl_3$): δ 2.16 (12H, s, Ar–C$\underline{H}_3$), 3.71 (6H, s, –$CO_2C\underline{H}_3$), 3.77 (6H, s, Ar–O$C\underline{H}_3$), 5.45 (2H, s, Ar–C$\underline{H}$–O–), and 6.54 ppm (4H, s, Ar–$\underline{H}$). Further elution with $CHCl_3$ containing acetone (3% v/v) gave the racemic isomer (0.9 g, 39%) as prisms from EtOH, mp 173—174 °C. Found: C, 67.04; H, 7.13%. IR (Nujol): 1750, 1380, 1220, 1190, 1140, and 1065 cm^{-1}. PMR ($CDCl_3$): δ 2.19 (12H, s, Ar–C$\underline{H}_3$), 3.68 (6H, s, –$CO_2C\underline{H}_3$), 3.79 (6H, s, Ar–O$C\underline{H}_3$), 5.24 (2H, s, Ar–C$\underline{H}$–O–), and 6.56 ppm (4H, s, Ar–$\underline{H}$).

*Bis[2-hydroxy-1-(2,6-dimethyl-4-methoxyphenyl)ethyl] Ethers (**2a** and **2b**).* The meso and racemic ethers (1 g) were reduced with $LiAlH_4$ (0.5 g) in ether to give **2a** (760 mg, 87%) and **2b** (810 mg, 93%) respectively as needles from acetone–hexane. **2a**; mp 114—115 °C. Found: C, 70.31; H, 8.20%. Calcd for $C_{22}H_{30}O_5$: C, 70.56; H, 8.08%.

IR (Nujol): 3300, 1195, 1145, 1100, and 1067 cm^{-1}. PMR ($CDCl_3$): δ 2.20 (12H, br s, Ar–C$\underline{H}_3$), 2.92 (2H, br s, –O$\underline{H}$), 3.63 (2H, dd, J=4.5 and 12 Hz, –CH–C(H)–OH), 3.72 (6H, s, –O$C\underline{H}_3$), 4.15 (2H, dd, J=9 and 12 Hz, –CH–C($\underline{H}$)–OH), 5.07 (2H, dd, J=4.5 and 9 Hz, Ar–C$\underline{H}$(–CH_2–)O–), and 6.43 ppm (4H, s, Ar–$\underline{H}$). **2b**; mp 167—168 °C. Found: C, 70.51; H, 8.12%. IR (Nujol): 3250, 1310, 1196, 1140, 1090, 1068, and 1045 cm^{-1}. PMR ($CDCl_3$): δ 1.50 (6H, br s, Ar–C$\underline{H}_3$), 2.51 (6H, br s, Ar–C$\underline{H}_3$), 2.17 (2H, br s, –O$\underline{H}$), 3.66 (2H, dd, J=5 and 11.5 Hz, –CH–C(H)–OH), 3.72 (6H, s, –O$C\underline{H}_3$), 4.05 (2H, dd, J=9 and 11.5 Hz, –CH–C($\underline{H}$)–OH), 4.70 (2H, dd, J=5 and 9 Hz, Ar–C$\underline{H}$(–CH_2–)O–), and 6.53 ppm (4H, br s, Ar–$\underline{H}$).

Reduction of meso- *and* dl-*Bis(α-methoxycarbonyl-2,6-dimethyl-4-methoxybenzyl) Ethers with Lithium Aluminium Deuteride.* i) The meso and racemic ethers (430 mg, 1 mmol) were reduced with $LiAlD_4$ (76 mg, 2 mmol) in ether under reflux to give **2a-D** (352 mg, 93%) and **2b-D** (349 mg, 92%), respectively. **2a-D**; mp 114—115 °C. PMR ($CDCl_3$): δ 2.20 (12H, br s, Ar–C$\underline{H}_3$), 2.75 (2H, br s, –O$\underline{H}$), 3.73 (6H, s, –O$C\underline{H}_3$), 5.09 (2H, s, Ar–C$\underline{H}$(–CD_2–)O–), and 6.52 ppm (4H, s, Ar–$\underline{H}$). **2b-D**; mp 166—167 °C. PMR ($CDCl_3$): δ 1.57 (6H, br s, Ar–C$\underline{H}_3$), 2.27 (1H, s, –O$\underline{H}$), 2.57 (1H, s, –O$\underline{H}$), 2.58 (6H, br s, Ar–C$\underline{H}_3$), 3.75 (6H, s, –O$C\underline{H}_3$), 4.74 (2H, s, Ar–C$\underline{H}$(–CD_2–)O–), and 6.58 ppm (4H, br s, Ar–$\underline{H}$).

ii) The meso ether (200 mg, 0.47 mmol) was allowed to react with $LiAlD_4$ (180 mg, 4.7 mmol) in ether under reflux and the complex decomposed with dil HCl to give **2a-D** (163 mg, 91%) and **5a-D** (8 mg, 5%). **5a-D**; mp 243—244 °C. Found: C, 73.52; H, 7.77%. Calcd for $C_{22}H_{24}D_4O_4$: C, 73.31; H, 8.03%. IR (Nujol): 1306, 1280, 1142, 1100, and 1060 cm^{-1}. MS: *m/e* (rel intensity) 360 (M^+, 1),164 (100), 148 (18), 135 (23), 121 (29), 105 (25), and 91 (35). The racemic isomer (200 mg, 0.47 mmol) was treated with $LiAlD_4$ (180 mg, 4.7 mmol) in a manner similar to that described above to give **2b-D** (142 mg, 72%) and **5b-D** (37 mg, 22%). **5b-D**; mp 252—253 °C. Found: C, 73.35; H, 7.71%. IR (Nujol): 1306, 1280, 1150, 1135, 1090, 1062, and 1000 cm^{-1}. MS: *m/e* (rel intensity) 360 (M^+, 4), 180 (1), 164 (100), 148 (13), 135 (17), 121 (23), 105 (14), and 91 (25).

*Reaction of Bis[2-hydroxy-1-(2,6-dimethyl-4-methoxyphenyl)ethyl] Ethers (**2a** and **2b**) with Tosyl Chloride.* i) The ether **2a** (110 mg, 0.29 mmol) was mildly refluxed with tosyl chloride (550 mg, 2.3 mmol) in pyridine (10 ml) for 1 h. The reaction mixture was poured into ice water and extracted with ether. The ether layer was washed with dil HCl and water, and dried. The crude product afforded an oily **3** (29 mg, 56%) and **4** (43 mg, 42%), mp 113—114 °C. **3**; IR ($CHCl_3$): 2830, 2720, 1716, 1200, 1140, and 1060 cm^{-1}. PMR ($CDCl_3$): δ 2.17 (6H, s), 3.55 (2H, d, J=2 Hz), 3.64 (3H, s), 6.49 (2H, s), and 9.6 ppm (1H, t, J=2 Hz). 2,4-Dinitrophenylhydrazone of **3**; mp 168—169 °C. Found; C, 56.91; H, 5.04; N, 15.61%. Calcd for $C_{17}H_{18}N_4O_5$: C, 56.98; H, 5.06; N, 15.64%. Oxidation of **3** with chromium(VI) oxide in acetic acid gave 2,6-dimethyl-4-methoxy-phenylacetic acid, mp 144—145 °C. Found: C, 68.13; H, 6.55%. Calcd for $C_{11}H_{14}O_3$: C, 68.02; H, 6.74%. **4**; Found: C, 74.23; H, 8.09%. Calcd for $C_{22}H_{28}O_4$: C, 74.13; H, 7.92%. IR ($CHCl_3$): 1180, 1140, 1118, and 1040 cm^{-1}. MS: *m/e* (rel intensity) 356 (M^+, 2), 207 (25), 179 (28), 162 (10), 149 (100), 138 (11), 119 (18), 105 (8), and 91 (18). PMR ($CDCl_3$): δ 2.39 (12H, s), 3.10 (2H, d, J=4 Hz), 3.75 (1H, t, J=8 Hz), 3.78 (6H, s), 3.99 (1H, t, J=8 Hz), 5.00 (1H, t, J=4 Hz), 5.28 (1H, t, J=8 Hz), and 6.68 ppm (4H, br s). Both evaporation to dryness of the water layer and acetylation of the residue did not give any isolable product.

ii) The racemic isomer **2b** (110 mg, 0.29 mmol) was treated with tosyl chloride (550 mg, 2.3 mmol) in a manner similar to that described above to give **3** (5 mg, 10%), **4** (24 mg, 23%) and **5** (43 mg, 42%). **5**; mp 244 °C. Found: C, 73.96; H, 7.86%. Calcd for $C_{22}H_{28}O_4$: C, 74.13; H, 7.92%. IR ($CDCl_3$): 1190, 1177, 1148, 1100, and 1065 cm^{-1}. MS: *m/e* (rel intensity) 356 (M^+, 15), 178 (14), 163 (34), 162 (100), 149 (88), 105 (6), and 91 (13). PMR ($CDCl_3$): δ 2.46 (12H, s), 3.66 (6H, s), 3.79 and 3.88 (4H, AB in ABX, J_{AX}=10, J_{BX}=6 Hz, $J_{AB}\simeq 0$), 4.99 (2H, X in ABX, J_{AX}=10 and J_{BX}=6 Hz), and 6.46 ppm (4H, s).

*Reaction of Bis[2,2-dideuterio-2-hydroxy-1-(2,6-dimethyl-4-methoxyphenyl)ethyl] Ethers (**2a-D** and **2a-D**) with Tosyl Chloride.* i) The meso compound, **2a-D** (210 mg, 0.56 mmol), was allowed to react with tosyl chloride (1.1 g, 4.6 mmol) in pyridine (20 ml) for 1 h. After the usual work-up, when the crude product was dissolved in a solution of benzene–hexane (1: 1), a tosylate (28 mg, 8%) precipitated, mp 128 °C from EtOH. Found: C, 63.31; H, 6.39%. Calcd for $C_{36}H_{38}D_4O_9S_2$: C, 62.94; H, 6.29%. PMR ($CDCl_3$): δ 1.94 (6H, br s, Ar–C$\underline{H}_3$), 2.04 (6H, br s, Ar–C$\underline{H}_3$), 2.48 (6H, s, Ar–C$\underline{H}_3$), 3.78 (6H, s, –O$C\underline{H}_3$), 5.20 (2H, s, Ar–C$\underline{H}$–O–), 6.57 (4H, br s, Ar–$\underline{H}$), 7.58 (4H, d, J=9 Hz, Ar–$\underline{H}$), and 8.05 ppm (4H, d, J=9 Hz, Ar–$\underline{H}$). The mother liquor afforded a mixture (79 mg) of **3-D-1** and **3-D-2**, and **4-D** (42 mg, 21%). The mixture of **3-D-1** and **3-D-2**; PMR ($CDCl_3$): δ 2.27 (6H, s), 3.55 (0.5H, br s), 3.79 (3H, s), 6.71 (2H, s), and 9.97 ppm (0.5H, s). **4-D**; PMR ($CDCl_3$): δ 2.41 (12H, s), 3.80 (6H, s), 5.13 (1H, s), 5.42 (1H, s), and 6.73 ppm (2H, s).

ii) The racemic isomer **2b-D** (214 mg, 0.57 mmol) afforded a mixture (50 mg) of **3-D-1** and **3-D-2** (1: 1), **4-D** (52 mg, 26%), and a tosylate (55 mg, 15%), mp 115 °C. Found:

C, 62.77; H, 6.03%. PMR ($CDCl_3$): δ 1.47 (6H, br s, Ar-C$\underline{H}_3$), 2.38 (6H, br s, Ar-C$\underline{H}_3$), 2.43 (6H, br s, Ar-C$\underline{H}_3$), 3.77 (6H, s, -OC$\underline{H}_3$), 4.70 (2H, s, Ar-C$\underline{H}$-O-), 6.50 (2H, br d, J=2 Hz, Ar-$\underline{H}$), 6.59 (2H, br d, J=2 Hz, Ar-$\underline{H}$), 7.40 (4H, d, J=8.5 Hz, Ar-$\underline{H}$), and 7.80 ppm (4H, d, J=8.5 Hz, Ar-$\underline{H}$).

*Hydrolysis of Acetal (**4-D**) with Hydrochloric Acid in Methanol.* Acetal **4-D** (30 mg) was refluxed with 4 M HCl (6 ml) in MeOH (10 ml) for 1 h. The crude product afforded a mixture (7 mg) of **3-D-1** and **3-D-2**, and an oil **6** (8 mg) and **7** (15 mg). **6**; Found: C, 68.72; H, 8.80%. Calcd for $C_{13}H_{18}D_2O_2$: C, 69.00; H, 9.06%. MS: *m/e* (rel intensity) 226 (M^+, 2), 151 (9), and 75 (100). IR ($CHCl_3$): 1315, 1180, 1145, 1130, 1065, and 1000 (sh) cm^{-1}. PMR ($CDCl_3$): δ 2.38 (6H, s), 3.39 (6H, s), 3.83 (3H, s), 4.50 (1H, br s), and 6.74 ppm (2H, s). **7**; Found: C, 67.52; H, 8.53%. Calcd for $C_{12}H_{16}D_2O_3$: C, 67.90; H, 8.70%. MS: *m/e* (rel intensity) 213 ($M+1^+$, 2), and 179 (100). IR ($CHCl_3$): 3580, 3460, 1305, 1140, 1095, 1085, 1000, and 963 cm^{-1}. PMR ($CDCl_3$): δ 2.33 (1H, br s), 2.42 (6H, s), 3.30 (3H, s), 3.83 (3H, s), 4.86 (1H, s), and 6.72 ppm (2H, s).

*Preparation of 1,1-Dideuterio-2-methoxy-2-(2,6-dimethyl-4-methoxyphenyl)ethanol (**7**).* α-Cyano-2,6-dimethyl-4-methoxybenzylalcohol (1.3 g) was refluxed with a catalytic amount of TsOH in abs MeOH for 12 h. The crude product gave 0.72 g (52%) of α-cyano-2,6-dimethyl-4-methoxybenzyl methyl ether, bp 204—206 °C/27 mmHg. Found: C, 70.19; H, 7.39; N, 7.17%. Calcd for $C_{12}H_{15}NO_2$: C, 70.22; H, 7.37; N, 6.82%. PMR ($CDCl_3$): δ 2.45 (6H, s), 3.48 (3H, s), 3.76 (3H, s), 5.41 (1H, s), and 6.69 ppm (2H, s). The methyl ether (500 mg) was hydrolyzed in abs EtOH (50 ml) with dry HCl at 50 °C for 3 h. The crude product gave 420 mg (75%) of α-methoxy-(2,6-dimethyl-4-methoxyphenyl)-acetamide, mp 156—157 °C from benzene. Found: C, 64.59; H, 7.70; N, 6.16%. Calcd for $C_{12}H_{17}NO_3$: C, 64.55; H, 7.68; N, 6.27%. IR (Nujol): 3350, 3130, and 1675 cm^{-1}. PMR ($CDCl_3$): δ 2.38 (6H, s), 3.30 (3H, s), 3.83 (3H, s), 5.20 (1H, s), 6.74 (2H, s), and 6.5—7.1 ppm (2H, br s, -N$\underline{H}_2$). The amide (240 mg) was hydrolyzed in ethylene glycol (10 ml) with aq 30% KOH to give α-methoxy-(2,6-dimethyl-4-methoxyphenyl)acetic acid, mp 101—102 °C from benzene–hexane. Found: C, 64.12; H, 7.21%. Calcd for $C_{12}H_{16}O_4$: C, 64.27; H, 7.19%. IR (Nujol): 3300—2200 and 1718 cm^{-1}. PMR ($CDCl_3$): δ 2.00—2.40 (1H, -O$\underline{H}$), 2.40 (6H, s), 3.37 (3H, s), 3.82 (3H, s), 5.30 (1H, s), and 6.73 ppm (2H, s). The carboxylic acid (85 mg) was reduced with $LiAlD_4$ (40 mg) in ether to give 68 mg (81%) of **7**.

Treatment of the tosylate of **2b-D** in pyridine. The tosylate (70 mg) of **2b-D** was boiled in pyridine (10 ml) for 4 h and gave a mixture (17 mg) of **3-D-1** and **3-D-2** (54:46).

The authors would like to express their deep gratitude to Dr. M. Nakayama, Hiroshima University, for the mass spectra and Dr. K. Shibata, Osaka City University, for the elemental analyses.

References

1) M. Nakatani, T. Kamikawa, T. Hase, and T. Kubota, *Bull. Chem. Soc. Jpn.*, **50**, 945 (1977).

2) C. T. Davis and T. A. Geissmann, *J. Am. Chem. Soc.*, **76**, 3507 (1954).

3) a) D. J. Cram, *J. Am. Chem. Soc.*, **71**, 3863, 3875, 3883 (1949); **74**, 2159 (1952); b) S. Winstein, B. K. Morse, E. Grunwald, K. S. Screiber, and J. Corse, *ibid.*, **74**, 1113 (1952); c) S. Winstein, M. Brown, K. C. Schreiber, and A. H. Schlesinger, *ibid.*, **74**, 1140 (1952); d) S. Winstein and H. Marshall, *ibid.*, **74**, 1120 (1952); e) S. Winstein, C. R. Lindegren, H. Marshall, and L.L. Ingraham, *ibid.*, **75**, 147 (1953); f) A. H. Fainberg, G. C. Robinson, and S. Winstein, *ibid.*, **78**, 2777 (1956); g) C. C. Lee, G. P. Slater, and J. W. T. Spinks, *Can. J. Chem.*, **35**, 1417 (1957); h) C. C. Lee, R. Tkachuk, and G. P. Slater, *Tetrahedron*, **7**, 206 (1959); i) S. G. Smith, A. H. Fainberg, and S. Winstein, *J. Am. Chem. Soc.*, **83**, 618 (1961); j) H. C. Brown, K. J. Morgan, and F. J. Chloupek, *ibid.*, **87**, 2137 (1965).

4) R. Lagrave, *Ann. Chim.*, **8**, 363 (1927).

Reaction of Dimethyl Phosphonate with Ketene Dimethyl Dithioacetal Derivatives. An Alternative Method to Prepare *s*-Alkylphosphonates

Mitsuji YAMASHITA,* Tadaaki MIYANO, Takashi WATABE, Hiromi INOKAWA,†
Hiroshi YOSHIDA, Tsuyoshi OGATA, and Saburo INOKAWA*,††

Department of Synthetic Chemistry, Faculty of Engineering, Shizuoka University, Johoku, Hamamatsu 432
†*Department of General Education, Shizuoka Women's Junior College, Nunohashi, Hamamatsu 432*

(Received May 6, 1978)

Reaction of dimethyl phosphonate with phenylketene dimethyl dithioacetal derivatives have been investigated to prepare *s*-alkylphosphonates. The addition reactions of phosphonate were accelerated in dithioacetal derivatives in the following order: –SMe<–SOMe≪–SO_2Me. The reaction of β,β-bis(methylsulfonyl)styrene (**7**) with dimethyl phosphonate followed by the catalytic reduction afforded dimethyl α-methylbenzylphosphonate in 74% yield from compound **7**. The reaction of 1-methylsulfinyl-1-methylthio-4-phenyl-1-butene with dimethyl phosphonate gave dimethyl (2-methylthio-1-phenethylvinyl)phosphonate in 21% yield.

Dialkyl phosphonates rapidly add to strongly activated C=C double bonds in the presence of basic catalysts, and the initial adducts are generally protonated to give phosphonates.[1] In previous papers, the reaction of phosphorus compounds with the 5,6-unsaturated 6-nitro-*xylo*-hexofuranose derivatives to give the 5-phosphino and 5-phosphinyl derivatives of D-glucose, that were *s*-alkylphosphorus derivatives, were reported.[2] The present paper deals with an alternative preparative method for *s*-alkylphosphonate.

Results and Discussion

The reaction of (*E*)-β-methylsulfinyl-β-methylthiostyrene (**1**)[3] with dimethyl phosphonate in the presence of sodium methoxide under a nitrogen atmosphere at room temperature for a month afforded dimethyl (*Z*)-(2-methylthio-1-phenylvinyl)phosphonate (**3**) in 10% yield, but no corresponding initial adduct **2** was isolated. The photochemical reaction of compound **1** with dimethyl phosphonate or *O,O*-dimethyl thiophosphonate[4] afforded no such addition products as compound **2**, but gave the (*Z*)-isomer **4**,[3a] where the SMe signal in the NMR spectrum shifted from δ 2.25 to 2.45.

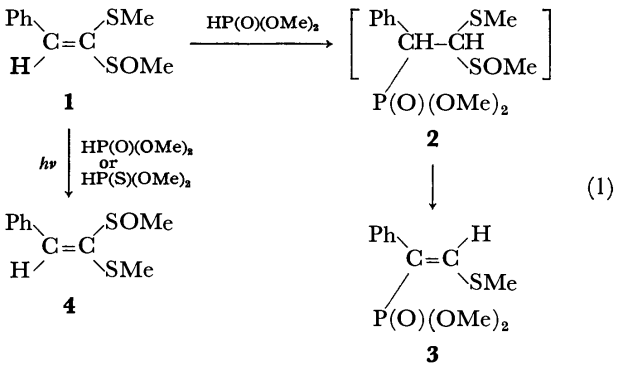

(1)

β,β-Bis(methylsulfinyl)styrene (**5**) has been prepared from compound **1** by the action of hydrogen peroxide in acetic acid.[5] The reaction of **5** with dimethyl phosphonate in the presence of sodium methoxide at room temperature for 2 weeks gave dimethyl (2-methylsulfinyl-1-phenylvinyl)phosphonate (**6**, 10% yield), which contained *E* and *Z* stereoisomers in the ratio of 1 : 1. The acid catalyzed reactions (*e.g.*, *p*-toluenesulfonic acid) of compounds **1** and **5** with dimethyl phosphonate were unsuccessful.

Oxidation of **1** with hydrogen peroxide in refluxing acetic acid afforded β,β-bis(methylsulfonyl)styrene (**7**) in 30% yield.[6] Compound **7** reacted with ethanol to give 1-ethoxy-2,2-bis(methylsulfonyl)-1-phenylethane (**8**) in excellent yield. The reaction of **7** with dimethyl phosphonate under a nitrogen atmosphere at 60 °C for 16 h gave the corresponding adduct **9** in 95% yield. It appears that the addition of phosphonate to ketene dimethyl dithioacetal derivatives is accelerated in the order –SMe<–SOMe≪–SO_2Me bearing in mind the reaction conditions.

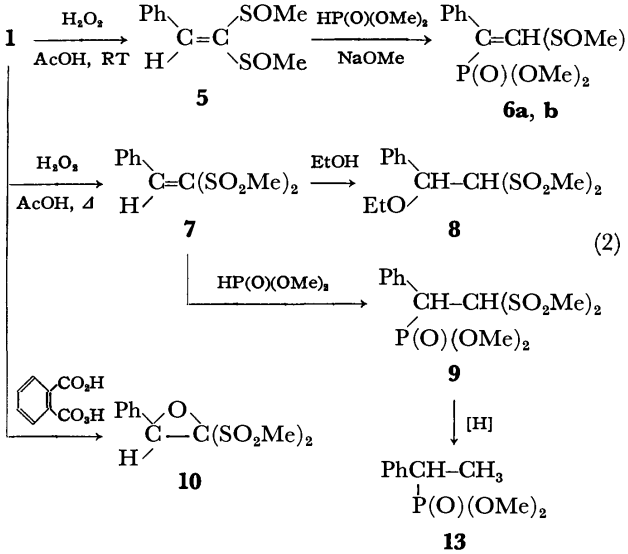

(2)

The oxidation of **1** with hydrogen peroxide in acetic anhydride–acetic acid (1 : 1 v/v), or monoperoxyphthalic acid in ether gave the epoxide **10** in moderate yields. The reaction of 1-methylsulfinyl-1-methylthio-4-phenyl-1-butene (**11**)[7] with dimethyl phosphonate at 120 °C for 30 h afforded dimethyl (2-methylthio-1-phenethylvinyl)phosphonate (**12**) in 21% yield. The catalytic reduction of **3**, **6**, and **9** with Raney nickel gave dimethyl

†† Present address: Department of Chemistry, Faculty of Science, Okayama University, Tsushima, Okayama 700.

α-methylbenzylphosphonate (**13**) in 70—90% yields.

The Michaelis-Arbuzov and Michaelis-Becker reactions are important processes to prepare compounds having phosphorus-carbon bonds.[8] However, in some instances the reactions have been unsuccessful *e.g.*, the reaction of 3-*O*-benzyl-5-bromo-5,6-dideoxy-1,2-*O*-isopropylidene-β-L-idofuranose with sodium methylphosphide gave only olefinic products.[9] The addition reactions of phosphonates to ketones or hydrazones followed by 1 or 2 steps afforded *s*-alkylphosphonates in moderate yields.[10] The reaction described in this paper is an alternative method for the preparation of *s*-alkylphosphonates from esters as well as aldehydes.

The reaction of **1** and **5** with dimethyl phosphonate to give compounds **3** and **6** may be written as Eq. 1, *i.e.*, the initially formed adduct spontaneously loses methanesulfenic acid.[11] Compound **7** gave the corresponding adduct **9** attributed to the slow departure of methanesulfinic acid in this reaction condition.

Experimental

Material. Methyl methylthiomethyl sulfoxide was supplied by Nippon Soda Company, Ltd.

Measurements. Melting and boiling points were uncorrected. The ^{1}H-NMR spectra were run on Hitachi-Perkin-Elmer R-20 (60 MHz) and Hitachi R-24 (60 MHz) spectrometers with tetramethylsilane as an internal standard. The IR spectra were measured by Hitachi-Perkin-Elmer 337 and Japan Optics Laboratory A-3 infrared spectrophotometers.

*Reaction of (E)-β-Methylsulfinyl-β-methylthiostyrene (**1**) with Dimethyl Phosphonate.* Compound **1**[3] (1.5 g) was added to the mixture of dimethyl phosphonate (2 g) and sodium methoxide (1 g). After the introduction of nitrogen gas, the mixture was allowed to stand for 1 month at room temperature. Neutralization of the reaction mixture followed by extraction of the chloroform solution with saturated sodium chloride solution and evaporation of the volatile materials *in vacuo* afforded a syrup (R_f value 0.2, silica gel, eluent; benzene: ethyl acetate=1: 1 v/v). Purification of the syrup by column chromatography afforded 0.2 g of dimethyl (*Z*)-(2-methylthio-1-phenylvinyl)phosphonate (**3**, 10% yield). IR (neat) 1250 cm^{-1} (P=O); NMR ($CDCl_3$) δ 2.43 (s, 3H, SMe), 3.73 (d, J_{POCH}=12.0 Hz, 6H, POMe), 7.24 (d, J_{PCCH}=44.3 Hz, 1H, CH), and 7.34 (5H, Ph).

*Synthesis of β,β-Bis(methylsulfinyl)styrene (**5**).*[5] Treatment of **1** (5 g) with 35% aqueous hydrogen peroxide (4 ml) in acetic acid (15 ml) at room temperature for 30 h afforded the oxidation product, which was extracted with chloroform. Evaporation of the solvent followed by recrystallization from ethanol afforded 2.7 g of compound **5** (*meso* form, 51% yield), mp 113—115 °C (lit,[5] mp 112—113 °C).

*Synthesis of β,β-Bis(methylsulfonyl)styrene (**7**).*[6] Treatment of **1** (1.3 g) with 35% aqueous hydrogen peroxide (2.5 ml) in refluxing acetic acid (5 ml) for 6 h followed by neutralization of the reaction mixture, extraction of the chloroform solution with water, and evaporation of the solvent *in vacuo* afforded 1.3 g of a crude product (87% yield). Recrystallization from benzene–hexane gave 0.47 g of the pure compound **7** (30% yield), mp 136—137 °C. IR (KBr) 1330 and 1160 cm^{-1} (SO_2); NMR ($CDCl_3$) δ 3.20 and 3.30 (s, 6H, SO_2Me), 7.6 (5H, Ph), and 8.48 (s, 1H, CH).

Found: C, 45.83; H, 4.66%. Calcd for $C_{10}H_{12}O_4S_2$: C, 46.15; H, 4.65%.

*Synthesis of 1,1-Bis(methylsulfonyl)-2-phenyloxirane (**10**).* Treatment of **1** (6 g) with 35% aqueous hydrogen peroxide (10 ml) in acetic anhydride (25 ml)–acetic acid (25 ml) for 5 days at room temperature followed by the same work-up as cited above afforded 3.5 g of **10** (42% yield), mp 158—160 °C. IR (KBr) 1330 and 1160 cm^{-1} (SO_2); NMR ($CDCl_3$) δ 2.55 and 3.08 (s, 6H, SO_2Me), 4.98 (s, 1H, CH), and 7.38 (5H, Ph).

Found: C, 43.33; H, 4.54%. Calcd for $C_{10}H_{12}O_5S_2$: C, 43.48; H, 4.35%.

Oxidation of **1** (3 g) with monoperoxyphthalic acid (5.6 g) in ether at room temperature for 4 days afforded **10** (2.6 g) in 70% yield.

*Reaction of **5** with Dimethyl Phosphonate.* The mixture of dimethyl phosphonate (4.7 g), sodium methoxide (0.6 g), and **5** (1.5 g) in tetrahydrofuran (8 ml) under a nitrogen atmosphere was allowed to react for 2 weeks at room temperature. After the work-up as described for **1** with dimethyl phosphonate, the *E* and *Z* isomers of dimethyl (2-methylsulfinyl-1-phenylvinyl)phosphonate (**6a** and **6b**, 0.14g) were obtained in 10% yield. NMR ($CDCl_3$) δ 2.30 and 2.58 (s, 3H, SOMe), 3.63 and 3.65 (d, J_{POCH}=12.0 Hz, 6H, POMe), and 6.70—7.68 (m, 6H, Ph and CH).

*Reaction of **7** with Dimethyl Phosphonate.* A mixture of **7** (0.5 g) with an excess of dimethyl phosphonate (2 g) was heated for 16 h at 60 °C under a nitrogen atmosphere in a sealed tube. The removal of excess phosphonate *in vacuo* afforded dimethyl 2,2-bis(methylsulfonyl)-1-phenylethylphosphonate (**9**, *dl*-form, 0.67 g) in 95% yield, mp 154—157 °C. NMR ($CDCl_3$) δ 3.13 and 3.48 (s, 6H, SO_2Me), 4.15 and 4.35 (d, J_{POCH}=12.0 Hz, 6H, POMe), 4.50—6.00 (m, 2H, CH–CH), and 7.75—8.75 (m, 5H, Ph).

Found: C, 38.86; H, 5.17%. Calcd for $C_{12}H_{19}O_7PS_2$: C, 38.92; H, 5.14%.

*Reaction of **7** with Ethanol.* Reaction of **7** (1.3 g) with a large excess of hot ethanol (10 ml) afforded 1.36 g of adduct **8** (87% yield) in 72% yield from compound **1**, mp 145—149 °C. NMR ($CDCl_3$) δ 1.34 (t, J_{HH}=7.5 Hz, 3H, C–Me), 3.40 (s, 6H, SO_2Me), 3.83 (q, J_{HH}=7.5 Hz, 2H, O–CH_2), 4.45 and 5.84 (m, 2H, CH–CH), and 7.65 (m, 5H, Ph).

Found: C, 46.92; H, 5.96%. Calcd for $C_{12}H_{18}O_5S_2$: C, 47.04; H, 5.92%.

*Reaction of **11** with Dimethyl Phosphonate.* The reaction of **11**[7] (0.4 g) with dimethyl phosphonate (2.0 g) proceeded at 120 °C for 30 h. Evaporation of excess dimethyl phosphonate *in vacuo* afforded a syrup, which on separation by preparative TLC (silica gel, eluent: ethyl acetate) afforded phosphonate **12** in 21% yield. The reaction in the presence of *p*-toluenesulfonic acid gave a similar result. NMR (CCl_4) δ 2.12 (s, 3H, SMe), 2.00—2.90 (m, 4H, CH_2CH_2), 3.73 (d, J_{POCH}=12.0 Hz, 6H, POMe), and 7.05—7.50 (m, 6H, Ph and CH).

*Catalytic Hydrogenolysis of **9**.* Treatment of **9** (0.50 g) with hydrogen in the presence of Raney nickel (W-2) for 6 h in refluxing ethanol (20 ml) followed by filtration and evaporation afforded an oily material. The product in chloroform was washed with aqueous sodium hydrogencarbonate, and then dried over sodium sulfate. Evaporation of the solvent *in vacuo* gave dimethyl α-methylbenzylphosphonate (**13**) in 78% yield, bp 119—120 °C/1.5 mmHg (lit,[10b] bp 150—152 °C/2 mmHg). NMR (CCl_4) δ 1.40 (dd, J_{PCCH}=18.6 Hz and J_{HH}=7.5 Hz, 3H, C–Me), 3.00 (dq, J_{PCH}=23.0 Hz and J_{HH}=7.5 Hz, 1H, CH), 3.30 and 3.48 (d, J_{POCH}=10.3 Hz, 6H, POMe), and 7.16 (m, 5H, Ph).

Similar treatment of **3** and **6** afforded the same phosphonate in 70 and 90% yields, respectively.

References

1) A. J. Kirby and S. G. Warren, "The Organic Chemistry of Phosphorus," Elsevier, Amsterdam (1967), p. 53.

2) H. Takayanagi, M. Yamashita, K. Seo, H. Yoshida, T. Ogata, and S. Inokawa, *Carbohydr. Res.*, **38**, C19 (1974); H. Takayanagi, K. Seo, M. Yamashita, H. Yoshida, T. Ogata, and S. Inokawa, *ibid.*, **63**, 105 (1978).

3) a) K. Ogura and G. Tsuchihashi, *Tetrahedron Lett.*, **1972**, 1383; b) K. Ogura and G. Tsuchihashi, *ibid.*, **1972**, 2681.

4) H. Tomioka and Y. Izawa, *Yuki Gosei Kagaku Kyokai Shi*, **34**, 901 (1976).

5) G. Tsuchihashi, K. Ogura, and C. Mochizuki, Japan Patent, Kokai 74108043; *Chem. Abstr.*, **83**, 9497p (1975).

6) S. R. Sandler and W. Karo, "Organic Functional Group Preparations," Academic Press, New York, N. Y. (1968), Vol. 1, p. 501.

7) K. Ogura, S. Furukawa, and G. Tsuchihashi, *Chem. Lett.*, **1974**, 659.

8) G. M. Kosolapoff and C. Maier, "Organo Phosphorus Compounds," John Wiley, London (1976), Vol. 7, p. 22.

9) S. Inokawa, K. Yoshida, H. Yoshida, and T. Ogata, *Carbohydr. Res.*, **26**, 230 (1973).

10) a) T. Gomyo, H. Yoshida, T. Ogata, H. Inokawa, and S. Inokawa, *Nippon Kagaku Kaishi*, **1974**, 1093; b) S. Inokawa, Y. Nakatsukasa, M. Horisaki, M. Yamashita, H. Yoshida, and T. Ogata, *Synthesis*, **1977**, 179.

11) a) C. Walling and L. Bollyky, *J. Org. Chem.*, **29**, 2699 (1964); b) T. J. Wallace. J. E. Hofmann, and A. Schriesheim, *J. Am. Chem. Soc.*, **85**, 2739 (1963).

Electron-transfer Reduction of α-Substituted Ketones and 1,2-Diketones with Benzenethiol Mediated by Iron Polyphthalocyanine

Hiroo INOUE,* Tadashi NAGATA, Hiroyuki HATA, and Eiji IMOTO

Department of Applied Chemistry, College of Engineering, University of Osaka Prefecture, Sakai, Osaka 591

(Received May 10, 1978)

Iron polyphthalocyanine (Fe-poly PC) has been found to act as an electron-transfer reagent in the reductions of α-substituted ketones, α-bromodeoxybenzoin (**1a**), 2-bromopropiophenone (**1b**), α,α-bis(phenylthio)deoxybenzoin (**4**), and 1,2-diketones, benzil (**5**) and 4,5-octanedione (**8**), with benzenethiol. The α-bromo ketones (**1a** and **1b**) have been debrominated to their parent ketones. **4** has been reduced to α-(phenylthio)deoxybenzoin and deoxybenzoin *via* the cleavage of the carbon-sulfur bond, and **5** and **8** to the corresponding α-hydroxy ketones. The ability of Fe-poly PC to perform these reactions is superior to that of iron phthalocyanine (Fe-PC), particularly those reactions in dry benzene. The catalytic action of Fe-poly PC and Fe-PC becomes evident when methanol or 80 vol % aqueous methanol is used as solvent. Furthermore, the reductions of related compounds by the Fe-poly PC-benzenethiol system are described.

Iron polyphthalocyanine (Fe-poly PC) is an electroconductive polymer which has iron(II) ions in a conjugated system.[1] It has been shown that Fe-poly PC is catalytically active for the oxidation of hydrocarbons with oxygen[2] and the reductive dehalogenation of α-halo ketones with 1-benzyl-1,4-dihydronicotinamide.[3] In these reactions, Fe-poly PC assists the transfer of the electron from an electron donor to an electron acceptor to promote the reduction of the electron acceptor coupled to the oxidation of the electron donor. Furthermore, the catalytic effects increase with an increase in the degree of the conjugation of the phthalocyanine polymer. The function of Fe-poly PC may be due to the nature of iron ions bridged with an electron-transferring ligand.[4] Similar phenomena have been observed in the catalytic action of copper polyphthalocyanine on the decomposition of hydrogen peroxide[5] and the exchange reaction between hydrogen and deuterium.[6]

To further explore the catalytic behavior of Fe-poly PC, the reactions of α-substituted ketones and 1,2-diketones (electron acceptors) with benzenethiol (electron donor) have been conducted in the presence of Fe-poly PC. In this paper, the characteristic of Fe-poly PC as an electron-transfer reagent is reported. Some of the results described here have been communicated in a preliminary report.[7]

Results and Discussion

The Properties of Fe-PC and Fe-poly PC. The visible absorption spectrum of Fe-PC and Fe-poly PC using a KBr disk showed absorption maxima at 677 and 725 nm respectively which agrees with previous data.[2] The absorption of Fe-poly PC is shifted towards the longer wavelength by 48 nm at 725 nm compared with Fe-PC. Thus, Fe-poly PC is a stronger electron donor than Fe-PC.

The value of ρ_{20} of the electrical conductivity of Fe-poly PC was 2×10^6 ohm-cm and it is apparent that Fe-poly PC has a better electron-conducting property than Fe-PC ($>10^9$ ohm-cm[8]). Furthermore, the catalytic activity of Fe-poly PC in the oxidation of acetaldehyde ethylene acetal with oxygen at room temperature was similar to that of the previously prepared Fe-poly PC.[2] On the other hand, Fe-PC did not show any activity. In this paper, Fe-PC and Fe-poly PC which have these properties have been used.

Reductive Dehalogenation of α-Halo Ketones. Function of Fe-poly PC: In the absence of Fe-poly PC, α-bromodeoxybenzoin (**1a**) and 2-bromopropiophenone (**1b**) did not react under nitrogen with benzenethiol in dry benzene at 80 °C. In 80 vol % aqueous methanol, α-phenylthio ketones (**2a** and **2b**) were obtained in high yields, as Table 1 shows. The reaction of 2-bromoacetophenone (**1c**) with benzenethiol gave 2-(phenylthio)-acetophenone (**3c**) even in dry benzene. In these reactions, the reductive debromination of **1a**, **1b**, and **1c** did not occur. Furthermore, Fe-poly PC did not react under similar conditions with **1a**, **1b**, and **1c**. When Fe-poly PC (iron ion: α-bromo ketone molar ratio=1 : 1) was suspended in a solution containing α-bromo ketones (**1**) and benzenethiol in dry benzene or 80 vol% aqueous methanol and the solution heated at 80 °C (under conditions similar to those used in the absence of Fe-poly PC), the debromination products (**2**) were produced (Table 1).

$$\underset{\mathbf{1}}{\mathrm{PhCOCHR}}(\mathrm{Br}) + \mathrm{PhSH} \xrightarrow{\text{Fe-poly PC}} \mathrm{PhCOCH_2R} + \underset{\mathbf{3}}{\mathrm{PhCOCHR}}(\mathrm{SPh}) + \mathrm{PhSSPh}$$
$$\mathbf{2}$$

(**a**, R=Ph; **b**, R=CH_3; **c**, R=H)

The product yields decreased in the following order; **2a**>**2b**>**2c**, while those of the α-phenylthio ketones increased inversely. Benzenethiol was oxidized to diphenyl disulfide when the α-bromo ketones were reduced to the parent ketones, respectively. However, the amount of diphenyl disulfide was ambiguous, since benzenethiol was readily oxidized to diphenyl disulfide in air in the presence of Fe-poly PC.

The reaction of **1a** with benzenethiol in the presence of Fe-poly PC conducted at a molar ratio of iron ion to **1a** of 1: 10 selectively produced **2a**, as shown in Table 1. From this it is apparent that Fe-poly PC acts

Table 1. The effects of Fe-poly PC on the reactions of α-bromo ketones with benzenethiol[a)]

α-Bromo ketone	Solvent[b)]	Molar ratio, Fe ion/**1**	Time, h	Yield, %[c)]		Unreacted **1**, %[c)]
				2	**3**	
1a	B	0	24	0	0	89
1a	B	0.1	120	34	0	49
1a	B	1	12	67	0	—
1a	WM	0	1/12	0	96	<1
1a	WM	0.1	2	67	0	23
1a	WM	1	1/12	87[d)]	0	—
1b	B	0	24	0	0	100
1b	B	1	96	56	7	22
1b	WM	0	1/12	0	80	20
1b	WM	1	1/2	58	24	0
1c	B	0	24	0	34	66
1c	WM	1	24	16	62	22

a) α-Bromo ketone; 2.8×10^{-2} mol/l. PhSH: α-bromo ketone molar ratio; 4: 1. Solvent; 6 cm³, 80 °C. b) B; benzene. WM; 80 vol % aqueous methanol. c) The amounts were determined by means of GLC. Based on 1. d) Isolated yield; 70%.

as a catalyst for the reductive debromination. It has been reported that the organic halogen compounds are reduced by iron porphyrins[9)] and thiols are oxidized by $Fe(CN)_6^{3-}$ and iron(III) octanoate to disulfides.[10)] Furthermore, the carbon-halogen bond reductions with metals and metal complexes and electrolysis have been explained in terms of an initial conversion of RBr to R· by one-electron reduction.[11)] The formation of the ketone (**2**) along with diphenyl disulfide indicates that Fe-poly PC undergoes cleavage of the C–Br bond of the α-bromo ketones (**1**), followed by hydrogen abstraction from benzenethiol to give the parent ketone (**2**). This reaction is coupled to the reduction of the oxidized Fe-poly PC with benzenethiol giving the original Fe-poly PC and diphenyl disulfide. For **1a** and **1b**, the rate of reduction of the C–Br bond

$$\mathbf{1} + \text{Fe-poly PC} \longrightarrow [\text{PhCOĊHR}][\text{Fe-poly PC}]^{\text{oxd}}\text{Br}^- \xrightarrow{\text{PhSH}} \mathbf{2} + \text{Fe-poly PC} + \text{HBr}$$

promoted by Fe-poly PC is considerably faster than that for the formation of the α-phenylthio ketones (**3a** and **3b**).

The function of Fe-poly PC accelerating the reductive debromination of **1a** was compared with that of Fe-PC.

Table 2. A comparison of the catalytic action between Fe-poly PC and Fe-PC in the reduction of **1a** with benzenethiol[a)]

Fe-complex	Solvent	Temp, °C	Time, h	Yield, %[b)]	
				2a	**3a**
Fe-poly PC	B	80	12	67	0
Fe-poly PC	WM	80	1/12	87	0
Fe-poly PC	WM	25	1/2	47	0
Fe-PC	B	80	24	37	17
Fe-PC	WM	80	1/12	59	40
Fe-PC	WM	25	1/2	31	13

a) **1a**; 2.8×10^{-2} mol/l. PhSH: **1a** molar ratio; 4: 1. Fe ion: **1a** molar ratio; 1: 1. Solvent; 6 cm³. b) The amounts were determined by means of GLC. Based on **1a**.

As Table 2 shows, Fe-PC underwent the reduction of **1a** with benzenethiol to **2a**, but the reduction rate was slower than that in the case of Fe-poly PC. In addition, the reaction was accompanied by the formation of **3a**. Thus, it has been concluded that Fe-poly PC is more effective than Fe-PC as an electron-transfer reagent in the reductive debromination of **1a**.

Acceleration Using Ethyl Iodide: In order to make possible the reduction of **1c** with benzenethiol in dry benzene in the presence of Fe-poly PC, ethyl iodide was added to the reaction system, since the exchange of the bromo substituent with iodine was expected to facilitate the reduction by Fe-poly PC. As is to be expected, after a reaction of 72 h, **2c** was obtained in 88% yield, along with **3c** in 16% yield (**1c**; 2.8×10^{-2} mol/l, PhSH; 1.1×10^{-1} mol/l, the ethyl iodide: **1c** molar ratio; 10: 1, the iron ion: **1c** molar ratio; 1: 1, and 80 °C). The reaction of **1c** with ethyl iodide in the presence of Fe-poly PC without benzenethiol in dry benzene gave 2-iodoacetophenone in a quantitative yield after a reaction time of 6 h (**1c**; 2.8×10^{-2} mol/l, the ethyl iodide: **1c** molar ratio; 10: 1, the iron ion: **1c** molar ratio; 1: 1, and 80 °C). When Fe-PC, Cu-PC, K_2-PC, and H_2-PC were used instead of Fe-poly PC, 2-iodoacetophenone was not obtained under similar conditions. 2-Iodoacetophenone was reduced instantaneously with benzenethiol in the absence of Fe-poly PC at room temperature to give **2c**

$$\mathbf{1c} + \text{EtI} \xrightarrow[C_6H_6]{\text{Fe-poly PC}} \text{PhCOCH}_2\text{I} + \text{EtBr}$$

quantitatively. Thus, Fe-poly PC performs the reduction of **1c** to **2c** by promoting the exchange reaction of the bromo substituent with iodine of ethyl iodide.

$$\text{PhCOCH}_2\text{I} + \text{PhSH} \longrightarrow \text{PhCOCH}_3 + \text{PhSSPh} + \text{HI}$$

Reductive Cleavage of Carbon-Sulfur Bond of α,α-Bis(phenylthio)deoxybenzoin (4). Fe-poly PC and Fe-PC made possible the reduction of **4** with benzenethiol in dry benzene to give mainly **3a**, as illustrated in Table 3. Furthermore, in the case of Fe-poly PC, **2a** was produced in addition to **3a**, although the yield of **2a** was lower. The ability of Fe-poly PC to form **2a** and/or **3a** was

Table 3. The reduction of **4** with benzenethiol in the presence of Fe-poly PC or Fe-PC in dry benzene (24 h)[a]

Fe-complex	Temp, °C	**2a** %[c]	**3a** %[c]	Unreacted **4** %[c]
None	14—16	0	0	98
Fe-poly PC	14—16	0	19	75
Fe-poly PC	80	15	84	0
Fe-PC	14—16	0	16	83
Fe-PC[b]	80	0	46	53

a) The concentation of **4**; 5×10^{-2} mol/l, Fe ion: **4** molar ratio; 1:1; and the PhSH: **4** moar ratio; 10:1. b) Time of 72 h; **3a** and **2a**: 93 and 0. c) Isolated yields. Based on **4**.

superior to that of Fe-PC. When the reaction was conducted using methanol as a solvent, however, **2a** was not produced even in the presence of Fe-poly PC (**3a** was obtained in 48% yield after a reaction of 24 h at

$$\underset{\text{SPh}}{\overset{|}{\text{PhCOCPh}}}\underset{\text{SPh}}{\overset{|}{}} + \text{PhSH} \xrightarrow{\text{Fe-poly PC}} \mathbf{2a} + \mathbf{3a} + \text{PhSSPh}$$

4

14—16 °C). In these reactions, benzenethiol was oxidized to diphenyl disulfide. Fe-poly PC and Fe-PC acted as a catalyst in reactions conducted in an iron ion: **4** molar ratio of 1: 10 in methanol.

In an analogy with α-halo ketones, the reaction proceeds *via* the reductive cleavage of the carbon-sulfur bond of **4** by Fe-poly PC or Fe-PC, followed by the reaction with benzenethiol to give **3a**.

$$\mathbf{4} + \text{Fe-poly PC} \longrightarrow [\text{PhCOC}^{\cdot}(\text{SPh})\text{Ph}][\text{Fe-poly PC}]^{\text{oxd}}\text{PhS}^{-} \xrightarrow{\text{PhSH}} \mathbf{3a} + \text{PhSSPh} + \text{Fe-poly PC}$$

Reduction of 1,2-Diketones and Their Related Compounds. Benzil (**5**) was reduced with benzenethiol in the presence of Fe-poly PC (the iron ion: **5** molar ratio; 1: 1) in dry benzene at 80 °C to afford benzoin (**6**) as the reduction product. The amount of **6** produced increased slowly with time until an almost constant value. The maximum yield of **6** was 70% with Fe-poly PC and 16% with Fe-PC. This phenomenon was not observed when methanol was substituted for benzene where the reaction proceeded much more rapidly than in benzene.

As Table 4 illustrates, results at the iron ion: **5** molar

$$\underset{\mathbf{5}}{\text{PhCOCOPh}} + \text{PhSH} \xrightarrow{\text{Fe-poly PC}} \underset{\mathbf{6}}{\overset{\text{OH}}{\overset{|}{\text{PhCOCHPh}}}} + \text{PhSSPh}$$

ratio of 1: 10 indicate that Fe-poly PC and Fe-PC act as catalysts for the reduction of **5** with benzenethiol in methanol. The rate of the formation of **6** catalyzed by Fe-poly PC was faster by a factor of about 25. Furthermore, the reduction of **5** by the Fe-poly PC- or Fe-PC–benzenethiol system in dry benzene was promoted by triethylamine, as shown in Table 5.

Table 5. The effect of triethylamine on the reduction of **5** by the Fe-poly PC or Fe-PC–benzenethiol system[a]

Fe-complex	Molar ratio Et_3N/Fe ion	Temp, °C	Yield,[b] **6**, %	Unreacted[b] **5**, %
Fe-poly PC	0	r.t.	10	87
Fe-poly PC	5	r.t.	38	60
Fe-poly PC	1	80	85	10
Fe-poly PC	5	80	90	8
Fe-PC	0	r.t.	<3	>97
Fe-PC	5	r.t.	11	89
Fe-PC	1	80	72	27
Fe-PC	5	80	88	12

a) **5**; 0.5 mmol. PhSH/**5** molar ratio; 10. $n=1$. Solvent; C_6H_6 (10 cm^3). Time; 24 h. b) Isolated yields. Based on **5**.

The catalytic reaction is best rationalized by assuming either a partial or complete electron transfer to form either a charge-transfer complex or the ion radical (**7**), followed by the reaction of **7** with benzenethiol giving **6** and the original Fe-poly PC. The benzenethiolate anion produced by triethylamine facilitates the regeneration of the original Fe-poly PC from **7**.

$$\mathbf{5} + \text{Fe-poly PC} \longrightarrow [\text{PhCOC}^{\cdot}\text{Ph}][\text{Fe-poly PC}]^{\text{oxd}} \quad \underset{\mathbf{7}}{\overset{|}{\text{O}^-}} \xrightarrow{\text{PhSH}} \mathbf{6} + \text{Fe-poly PC}$$

4,5-Octanedione (**8**) and ethyl benzoylformate (**9**) were reduced to the corresponding α-hydroxy carbonyl compounds by the Fe-poly PC–benzenethiol system in methanol at 80 °C (Table 6). The reduction of **9**

Table 4. The reduction of **5** with benzenethiol in the presence of Fe-poly PC or Fe-PC[a]

Fe-complex	Molar ratio Fe ion/**5**	Solvent[b]	Temp, °C	Time, h	Yield,[c] **6**, %	Unreacted[c] **5**, %
Fe-poly PC	1	B	80	72	60	38
Fe-poly PC	1	M	50	3	74	23
Fe-poly PC	1	M	80	24	97	0
Fe-poly PC	0.1	M	80	3	64	30
Fe-PC	1	B	80	168	16	83
Fe-PC	1	M	50	3	20	75
Fe-PC	1	M	80	24	95	0
Fe-PC	0.1	M	80	72	58	36

a) **5**; 0.5 mmol. Solvent; 10 cm^3. PhSH/**5** molar ratio; 10. b) B; C_6H_6. M; MeOH. c) Isolated yields. Based on **5**.

Table 6. The reduction of **8**, **9**, **10**, and **11** by the Fe-poly PC–benzenethiol system[a)]

Compd	Time, h	Product (Yield, %)[b)]
$C_3H_7COCOC_3H_7$ (**8**)	24	$C_3H_7CH(OH)COC_3H_7$ (69)
$PhCOCOOC_2H_5$ (**9**)	120	$PhCH(OH)COOC_2H_5$(37)
PhCOCH=CHCOPh (**10**)	24	$PhCOCH_2CH_2COPh$(21), $PhCOCH_2CH(SPh)COPh$(73)
PhCO(Ph)C=NPh (**11**)	24	PhCO(Ph)CHNHPh(78)

a) **8**, **9**, **10**, and **11**; 0.5 mmol. Solvent; MeOH (10 cm³). PhSH/Substrate molar ratio; 10. Fe ion: Substrate molar ratio; 1: 1. 80 °C. b) Isolated yields. Based on substrate.

proceeded very slowly. 1,4-Diphenyl-2-butene-1,4-dione (**10**) was reduced under similar conditions to 1,4-diphenyl-1,4-butanedione in low yield, because of the addition of benzenethiol to the double bond of **10** giving 1,4-diphenyl-1-phenylthio-1,4-butanedione. Furthermore, the Fe-poly PC–benzenethiol system was favorable for reducing the >C=N– bond of the Schiff's base (**11**) of **5**, as illustrated in Table 6.

A Characteristic of Fe-poly PC. As described above, Fe-poly PC and Fe-PC assisted the transfer of an electron from benzenethiol to the electron-accepting group at the α-position in the carbonyl group. However, Fe-poly PC differed from Fe-PC in the following respects:

(1) The electron-transfer reduction by Fe-poly PC proceeded more smoothly than by Fe-PC and in particular, a remarkable difference in reactivity was observed in the reduction of the 1,2-diketone **5** in aprotic solvents such as benzene.

(2) Fe-poly PC showed higher selectivity than Fe-PC for the reductive debromination of the α-bromo ketone **1a** giving the parent ketone **2a**.

(3) The reduction of **4** with the benzenethiol–Fe-poly PC system gave **2a** in addition to the α-phenylthio ketone **3a**, while, in the case of Fe-PC, **2a** was not obtained.

The last observation, (3) cannot be explained by the difference in oxidation-reduction potential between Fe-poly PC and Fe-PC. In the case of Fe-poly PC, there is the possibility that the reduction of **4** and the oxidation of benzenethiol may occur on a separate iron site with the assistance of the electron-transfer between iron ions bridged by the conjugated ligand. This probable function of Fe-poly PC may permit the reduction of **4** to **2a**.

Experimental

Materials. α-Bromo ketones (**1**), α-phenylthio ketones (**3**), **4**, **8**, **10**, **11**, and Fe-PC were prepared as described in the literature.[12] **5** and **9** were purchased. Fe-poly PC was prepared by the method described in a previous paper[2]: C, 53.16; H, 2.72; N, 17.71; Fe, 6.6%: λ_{max} (KBr method); 725 nm: ρ_{20}; 2×10^6 ohm-cm. Powdered Fe-poly PC and Fe-PC, reprecipitated from sulfuric acid solution with water, were used for the above reactions.

General Procedure for Reaction and Isolation of Product. All reactions were performed similarly in reaction tubes (90-cm³ total capacity). A typical reaction is described: a solution of a mixture of **5** (0.105 g; 0.5 mmol) and benzenethiol (0.551 g; 5 mmol) in dry benzene (10 cm³) was placed in the reaction tube and cooled with liquid nitrogen; the air was removed under a reduced pressure of 1 mmHg and, after melting the tube, was filled with nitrogen gas. The replacement by nitrogen gas procedure was repeated 4—5 times. The resulting solution was cooled with liquid nitrogen and to the frozen solution. Fe-poly PC (432 mg) corresponding to 0.5 mmol of Fe was added under nitrogen and degassed under a reduced pressure of 1 mmHg. After the reaction tube was sealed, the solution was melted and vigorously stirred at 80 °C. After a reaction time of 72 h, the Fe-poly PC was filtered and washed with dry benzene. The filtrate was extracted with a 10% sodium carbonate solution, dried over magnesium sulfate, and the benzene removed. The residue was submitted to chromatography on silica gel. Elution with benzene and chloroform gave 0.143 g of diphenyl disulfide (mp 58—59 °C), 0.040 g (38% recovery) of **5** (mp 94—95 °C), and 0.017 g (60%) of **6** (mp 131—132 °C). When methanol was used instead of benzene as a reaction solvent, and excess of benzene was added to the filtrate and the resulting solution worked up in a similar manner to that described for benzene.

The reactions of **1** with benzenethiol in the absence or presence of Fe-poly PC and Fe-PC in 80 vol % aqueous methanol were conducted as follows. Benzenethiol was added under nitrogen to degassed 80 vol % aqueous methanol dispersed by Fe-poly PC or Fe-PC. The resulting solution was frozen, the α-bromo ketones (**1**) added the reaction tube sealed. After the reaction, the products were isolated in a manner similar to that described above.

Analyses. The determination of the products and the unreacted materials in most experiments were conducted by means of GLC, using a silicone HV grease, 80—100 mesh column. After the Fe-poly PC or Fe-PC was removed by filtration, the filtrate was treated with a 10% sodium carbonate solution and submitted to GLC analysis, with biphenyl or 1,2-diphenylethane as an internal standard. The amounts of the products derived from **4**, **5**, **8**, **9**, **10**, and **11**, respectively, were determined satisfactorily by means of chromatography on silica gel. The products were eluted with carbon tetrachloride, benzene, and chloroform, and identified by comparing the IR and NMR spectra with that authentic specimens.

References

1) J. E. Katon, "Organic Semiconducting Polymers," Marcel Dekker Inc., New York (1970), Chap. 3.

2) H. Inoue, Y. Kida, and E. Imoto, *Bull. Chem. Soc. Jpn.*, **38**, 2214 (1965); *idid.*, **40**, 184 (1967); *ibid.*, **41**, 684, 692 (1968).

3) H. Inoue, R. Aoki, and E. Imoto, *Chem. Lett.*, **1974**, 1157.

4) The redox reactions between metal ions through the bridging ligand have been studied extensively: A. Haim, *Acc. Chem. Res.*, **8**, 264 (1975); D. Dolphin and R. H. Felton, *ibid.*, **7**, 26 (1974).

5) S. Z. Roginskii, A. A. Berlin, O. A. Golovina, E. S. Dokukina, M. M. Sakharov, and L. G. Cherkashina, *Kinet. Katal.*, **4**, 431 (1963).

6) G. J. K. Acres and D. D. Eley, *Trans. Faraday Soc.*, **60**, 1157 (1964).

7) H. Inoue, H. Hata, and E. Imoto, *Chem. Lett.*, **1975**, 1241.
8) P. Day, G. Scregg, and R. J. P. Williams, *Nature*, **197**, 589 (1963).
9) C. E. Castro, *J. Am. Chem. Soc.*, **86**, 2310 (1964).
10) G. Capozzi and G. Modena, "The Chemistry of the Thiol Group," ed by S. Patai, Part 2, Wiley, New York (1975), Chap. 17 and references therein.
11) H. O. House, "Modern Synthetic Reactions," ed by W. A. Benjamin, California (1972), p. 221; J. Casanova and L. Eberson, "Electrochemistry of the Carbon-Halogen Bond," ed by S. Patai, Wiley, New York (1973), p. 979.
12) I. J. Borowitz, P. E. Rusek, and Virkhaus, *J. Org. Chem.*, **34**, 1595 (1969); P. Z. Bedoukian, *J. Am. Chem. Soc.*, **67**, 1430 (1945); L. M. Long, *ibid.*, **68**, 2159 (1946); R. M. Cowper and L. H. Davidson, *Org. Synth.*, Coll. Vol. II, 480 (1943); R. E. Lutz, *ibid.*, Coll. Vol. III, 248 (1955); J. M. Snell and S. M. McElvain, *ibid.*, Coll. Vol. II, 114 (1943); P. A. Barrett, C. E. Dent, and R. P. Linstead, *J. Chem. Soc.*, **1936**, 1719.

Ligand Effects of Amine Chelates in the Decomposition of 1,2,3,4-Tetrahydro-1-naphthyl Hydroperoxide Catalyzed by Cobalt(II) and Copper(II) Salts

Teruaki YAMADA and Yoshio KAMIYA*

Department of Reaction Chemistry, Faculty of Engineering, The University of Tokyo, Bunkyo-ku, Tokyo 113

(Received May 15, 1978)

The ligand effects of 2,2′-bipyridine, ethylenediamine, and diethylenetriamine on the rate of decomposition of 1,2,3,4-tetrahydro-1-naphthyl hydroperoxide catalyzed by cobalt(II) decanoate and copper(II) decanoate in chlorobenzene were kinetically studied. The results were compared with the redox potentials measured in nonaqueous media and the spectral data of cobalt(II) and copper(II) complexes. It was found that the catalytic activity of Me(II) decanoate–ethylenediamine, or –diethylenetriamine complex (Me=Co, Cu) becomes maximum at 1/2 the molar ratio of ethylenediamine to Me(II), or at 1/3 that of diethylenetriamine to Me(II), and that further addition of these amines deactivates the catalysts. The activity of copper(II) decanoate increased from $k=0$ to $k=1.4\times10^{-3}$ s^{-1} on addition of 2,2′-bipyridine when the molar ratio of 2,2′-bipyridine to copper(II) decanoate was 0—4. No maximum activity was observed in copper(II) decanoate–2,2′-bipyridine system. A large excess of 2,2′-bipyridine, 150 times the quantity of copper(II) salt, did not decrease the decomposition rate in contrast to the case of the cobalt(II) decanoate–2,2′-bipyridine system. The difference in ligand effect of ethylenediamine, diethylenetriamine and 2,2′-bipyridine on cobalt(II) ion and copper(II) ion was discussed on the basis of the properties of these complexes.

The decomposition reaction of hydroperoxide catalyzed by transition metal complex, regarded as an important initiation reaction in autoxidation, has been extensively studied[1] during the last decade. Most of the studies afforded kinetic data presenting many kinds of reaction schemes and disclosing the outline of the reaction. However, no detailed account was given, and the relation between the structure and property of metal complex and its catalytic activity in the decomposition of hydroperoxide not being made clear. Clarification of this problem would be profitable not only for industrial chemistry but also for a new field of autoxidation in life science.

In a previous paper,[2] we reported the new finding of maximum activity in the decomposition reaction of 1,2,3,4-tetrahydro-1-naphthyl hydroperoxide catalyzed by cobalt(II) decanoate–2,2′-bipyridine in chlorobenzene, giving explanation on the basis of the change of redox potentials, spectral data and structural variations of catalysts. In this paper we report the ligand effect of 2,2′-bipyridine and aliphatic amines such as ethylenediamine, diethylenetriamine on cobalt(II) decanoate and copper(II) decanoate.

Experimental

Materials. Cobalt (II) decanoate ($CoDe_2$) and copper (II) decanoate ($CuDe_2$) were prepared by the conventional method[3] and used after being dried in a vacuum at 70 °C for 5 h. Elemental analyses were carried out on $CoDe_2$ and $CuDe_2$. Found: C, 58.2; H, 10.0%. Calcd for $CoDe_2[Co(C_{10}H_{19}O_2)_2]$: C, 59.8; H, 9.0%. Found: C, 58.0; H, 9.6%. Calcd for $CuDe_2[Cu(C_{10}H_{19}O_2)_2]$: C, 59.1; H, 9.4%. 1,2,3,4-Tetrahydro-1-naphthyl hydroperoxide (THP) was prepared by the autoxidation of 1,2,3,4-tetrahydronaphthalene (tetralin) and recrystallized from heptane.[4] Ethylenediamine (en), diethylenetriamine (dien), 1,6-hexanediamine, 1,4-butanediamine, 2,2′-bipyridine (bpy) and 2,2′: 6′,2″-terpyridine (tpy) were purified before use. A mixed solution of the metal decanoate and the amine chelate were allowed to stand at room temperature for 15 h to equilibrate and then subjected to reactions and measurements.

Measurements. The decomposition of THP proceeded in chlorobenzene at 45 °C, the rate of decomposition being determined by iodometry. The redox potentials of catalysts were measured by cyclic voltammetry in dichloromethane at room temperature with use of tetrabutylammonium perchlorate as a supporting electrolyte. A saturated calomel electrode was used as a reference electrode. The concentration of complex was less than 10 mM. Infrared spectra were recorded as Nujol mulls on a JASCO-IRA 2 spectrophotometer. Details of experimental procedures were reported.[2]

Results and Discussion

Effect of Ethylenediamine and Diethylenetriamine on Cobalt(II) Salt. The effect of ethylenediamine and that of diethylenetriamine on the rate of the $CoDe_2$-catalyzed decomposition of THP in chlorobenzene are shown in Figs. 1 and 2, respectively. The rate of decomposition increases with the addition of the amines, maximum activities being found at the molar ratio [en]/[$CoDe_2$]=

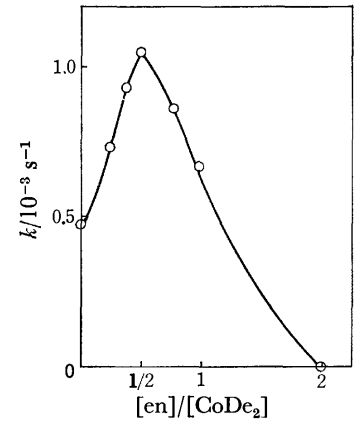

Fig. 1. Effect of ethylenediamine on the rate of decomposition of THP catalyzed by $CoDe_2$ in chlorobenzene at 45 °C.
[$CoDe_2$]$=2\times10^{-4}$ M, [THP]$=5\times10^{-2}$ M.

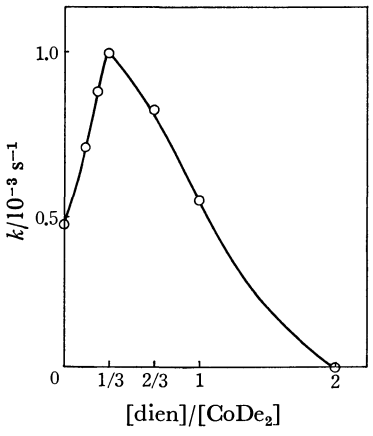

Fig. 2. Effect of diethylenetriamine on the rate of decomposition of THP catalyzed by $CoDe_2$ in chlorobenzene at 45 °C.
[$CoDe_2$]$=2\times10^{-4}$ M, [THP]$=5\times10^{-2}$ M.

1/2, [dien]/[$CoDe_2$]$=1/3$. The maximum value, almost the same in both systems, is one third of that of $CoDe_2$–bpy system. Unlike the case of the $CoDe_2$–bpy system, the $CoDe_2$ catalyst was deactivated by the amines at the raios [en]/[$CoDe_2$], [dien]/[$CoDe_2$] higher than 2.

The difference in activation of catalyst between the $CoDe_2$–bpy system and the $CoDe_2$–en, –dien systems can be attributed to the difference in electron donative force between 2,2′-bipyridine and two aliphatic amines; coordination of 2,2′-bipyridine having strong electron donative force causes an increase in the reductive force of cobalt(II) ion and weakening in the Co–O(decanoate) bond strength, resulting in facile coordination of hydroperoxide to the central cobalt(II) ion as well as the acceleration of cleavage of hydroperoxide molecule. Since ethylenediamine and diethylenetriamine do not have such a strong electron donative force as 2,2′-bipyridine, they can only change the reductive force of cobalt(II) ion moderately and not weaken the Co–O (decanoate) bond strength, resulting in smaller catalytic activities of the $CoDe_2$–en, –dien than that of the $CoDe_2$–bpy system. The IR data of the $CoDe_2$–en and $CoDe_2$–dien complexes given in Table 1 support our view. The shift of C–O stretching band to a higher wave number with an increase in the amount of 2,2′-bipyridine added as in the case of $CoDe_2$–bpy system shows the weakening in the Co–O(decanoate) bond strength. No shift of C–O stretching band upon the addition of ethylenediamine or diethylenetriamine suggests a very small effect due to the amines on the Co–O(decanoate) bond strength. The redox potentials of the $CoDe_2$–en complexes and the $CoDe_2$–dien complexes in dichloromethane or in *N,N*-dimethylformamide could not be obtained. No new C-T band or remarkable change in visible and ultraviolet spectra could be found.

The difference in the deactivation of catalyst between the $CoDe_2$–bpy complex and the $CoDe_2$–en, –dien complexes can be attributed to the difference in their steric factors. In the $CoDe_2$–bpy system, the steric hindrance makes it difficult for the second 2,2′-bipyridine to coordinate to a cobalt(II) ion. But in the $CoDe_2$–en, –dien systems, the steric hindrance of the amines smaller than that of 2,2′-bipyridine makes easier the coordination of the second ethylenediamine, diethylenetriamine to a cobalt(II) ion. Occupation of the coordination site by the amines may inevitably result in the deactivation of the $CoDe_2$ catalyst.

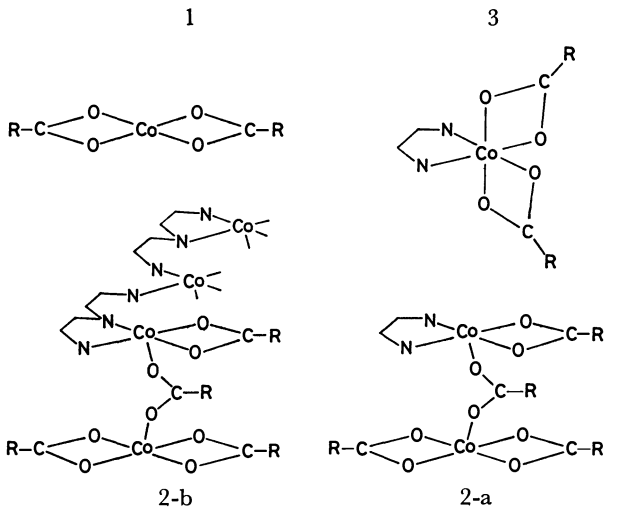

Fig. 3. Proposed structure of $CoDe_2$–en, –dien complexes.
1) $CoDe_2$, 2-a) $CoDe_2$–en (1: 1/2), 2–b) $CoDe_2$–dien (1: 1/3), 3) $CoDe_2$–en (1: 1).

Table 1. Infrared absorption bands and decomposition rates of THP for $CoDe_2$–en, $CoDe_2$–dien and $CoDe_2$–bpy complexes

Complex	C–$O_{st.}$, cm^{-1}	$k/10^{-3}$ s^{-1}
$CoDe_2$	1550	0.5
$CoDe_2$–en(1: 1/2)	1550	1.1
(1: 1)	1550	0.7
(1: 2)	1550	0.0
$CoDe_2$–dien(1: 1/3)	1550	1.1
(1: 2/3)	1550	0.9
(1: 1)	1550	0.5
(1: 2)	1550	0.0
$CoDe_2$–bpy(1: 1/2)	1570	3.7
(1: 1)	1590	1.3
(1: 2)	1595	1.3

The appearance of maximum suggests that the same structural variation[2] as that of the $CoDe_2$–bpy system occurs. Figure 3 shows the proposed structures of $CoDe_2$–en, –dien complexes. $CoDe_2$ (Structure 1) has a lower activity, which can be attributed to its poor reductive force. $CoDe_2$–en (1: 1/2) or $CoDe_2$–dien (1: 1/3) (Structure 2-a, 2-b) has the highest activity. This structure has a vacant coordination site and an adequate reductive force. $CoDe_2$–en (1: 1) (Structure 3) shows relatively low activity, the structure having a strong reductive force but no vacant coordination site.

From the value of the ratio [Chelate]/[Metal] of maximum activity in $CoDe_2$–bpy, $CoDe_2$–en, and $CoDe_2$–dien systems, one metal to one N atom complex seems to have the highest activity. An exceptional case is the $CoDe_2$–2,2′: 6′,2″-terpyridine system. A maximum

value was found at the ratio [tpy]/[$CoDe_2$]=1/2 instead of 1/3. Steric difficulty would not allow all the pyridine rings to coordinate to a cobalt(II) ion.

Figure 4 shows the effect of the length of carbon chain in aliphatic amine on the rate of the $CoDe_2$–catalyzed decomposition of THP in chlorobenzene. The ability of activation or deactivation of the added amines decreases with an increase in the carbon number of the carbon chain. This can be explained by the fact that their chelate effect decrease with increase in the carbon number of the carbon chain; the decrease of the chelate effect would decrease the ability of activation and deactivation.

Effect of 2,2′-Bipyridine on Copper(II) Salt. The effect of 2,2′-bipyridine on the rate of the $CuDe_2$–catalyzed decomposition of THP in chlorobenzene is shown in Fig. 5. The catalytic activity of $CuDe_2$ increases monotonously with the addition of 2,2′-bipyridine, the activity curve becoming a gradual slope in the ratio [bpy]/[$CuDe_2$] higher than 1. The k value at [bpy]/[$CuDe_2$]=1—2 is close to that of the $CoDe_2$–bpy complexes at [bpy]/[$CoDe_2$]=1—2 (Table 2).

The redox potentials of $CuDe_2$–bpy complexes measured in dichloromethane by cyclic voltammetry are given in Table 2 with the values of $CoDe_2$–bpy complexes. The shift of redox potentials to the negative direction with the addition of 2,2′-bipyridine, a tendency similar to the case of $CoDe_2$–bpy system, will help to elucidate the increase in activity. The decomposition of hydroperoxide by copper(II) complex has been studied extensively.[5] Some workers reported that the coordination of 2,2′-bipyridine to copper(II) ion increases the catalytic activity of copper(II) complex.[6] The decomposition reaction of hydroperoxide by copper(II) ion proceeds with Cu(II)/Cu(I) redox reaction, the difficulty of reproduction of copper(I) ion giving new schemes differing from those of cobalt(II) and manganese(II) systems. The rate-determining step seems to be the decomposition process of the copper–

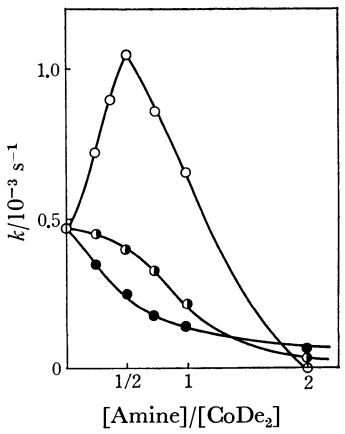

Fig. 4. Effect of aliphatic amines on the rate of decomposition of THP catalyzed by $CoDe_2$ in chlorobenzene at 45 °C.
(-●-) 1,6-Hexanediamine, (-◑-) 1,4-butanediamine, (-○-) ethylenediamine.
[$CoDe_2$]=2×10^{-4} M, [THP]=5×10^{-2} M.

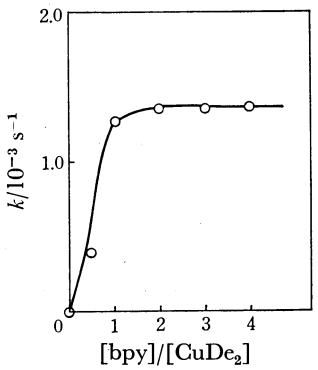

Fig. 5. Effect of 2,2′-bipyridine on the rate of decomposition of THP catalyzed by $CuDe_2$ in chlorobenzene at 45 °C.
[$CuDe_2$]=2×10^{-4} M, [THP]=5×10^{-2} M.

Table 2. Comparison of voltammetric data with the decomposition rates of THP for $CuDe_2$–bpy and $CoDe_2$–bpy complexes

Complex	Electrode reaction	$E_{1/2}$, V[a]	$k/10^{-3}$ s^{-1}
$CuDe_2$	Cu(II)+e⟶Cu(I)	−0.43[b]	0.0
	Cu(I)−e⟶Cu(II)	−0.36[b]	
$CuDe_2$–bpy (1 : 1/2)	Cu(II)+e⟶Cu(I)	−0.56	0.4
	Cu(I)−e⟶Cu(II)	−0.40	
(1 : 1)	Cu(II)+e⟶Cu(I)	−0.64	1.3
	Cu(I)−e⟶Cu(II)	−0.43	
(1 : 2)	Cu(II)+e⟶Cu(I)	−0.67	1.4
	Cu(I)−e⟶Cu(II)	−0.43	
$CoDe_2$	Co(II)−e⟶Co(III)	0.80	0.5
	Co(III)+e⟶Co(II)	0.84	
$CoDe_2$–bpy (1 : 1/2)	Co(II)−e⟶Co(III)	0.67	3.7
	Co(III)+e⟶Co(II)	0.70	
(1 : 1)	Co(II)−e⟶Co(III)	0.60	1.3
	Co(III)+e⟶Co(II)	0.63	
(1 : 2)	Co(II)−e⟶Co(III)	0.59	1.3
	Co(III)+e⟶Co(II)	0.59	

a) Potential sweep rate: 0.05 V/s. (V *vs.* SCE). b) Decanoic acid (10^{-3} M) added to raise the solubility of $CuDe_2$ to dichloromethane.

hydroperoxide complex. The redox force of copper ion might be the main factor of catalytic activity. The shift of redox potential to the negative direction shows an increase of reductive force of copper(I) ion which accelerates the cleavage of the hydroperoxide molecule, and also an increase of electron density of the copper ion which stabilizes[7] the copper–hydroperoxide complex. The increase in activity can be attributed to the change of the redox potential of catalyst.

The fact that the redox potential of copper(II) complexes is smaller than that of cobalt(II) complex is reasonable from their ionization potentials. The increase of catalytic activity upon the addition of 2,2′-bipyridine in the $CuDe_2$–bpy system or in the $CoDe_2$–bpy system can be explained by the change of their redox potentials. From a comparison of the activity of copper(II) complexes with that of cobalt(II) complexes, the small defference between the two activities can not be explained by the large difference between their redox potentials; the $CuDe_2$–bpy (1 : 2) complex has almost the same activity as that of the $CoDe_2$–bpy (1 : 2) complex, in spite of the large difference in the redox potential between the $CuDe_2$–bpy (1 : 2) complex and the $CoDe_2$–bpy (1 : 2) complex. This suggests that the $CuDe_2$–bpy system has a reaction mechanism differing from the $CoDe_2$–bpy system.

A maximum activity observed in the $CoDe_2$–bpy system[2] was absent in the $CuDe_2$–bpy system This is explained as follows: With an increase of added 2,2′-bipyridine the concentration of the inactive $CuDe_2$ may change to the active $CuDe_2$–bpy complex having a different structure from the five coordination $CoDe_2$–bpy (1 : 1/2) type complex. Formation of the five coordination complex with 2,2′-bipyridine will be difficult for $CuDe_2$. In acetic acid, no catalytic activity was found on both $Cu(OAc)_2$ and $Cu(OAc)_2$–bpy (1 : 1) complex.

The effect of a large amount of 2,2′-bipyridine on $CoDe_2$ and $CuDe_2$ is given in Table 3. The activity of $CoDe_2$ decreases to half the value of $CoDe_2$ with the addition of one hundred times of 2,2′-bipyridine. However, $CuDe_2$ could not be deactivated by the addition of one hundred fifty times of 2,2′-bipyridine. This can be explained by the difficult addition of three 2,2′-bipyridine to copper(II) ion. The $CuDe_2$–bpy (1 : 1) complex has no absorption band in the 350 —400 nm region. However, C-T band (λ_{max}=380 nm) was found on the $CuDe_2$–bpy (1 : 100) complex.

Table 3. Decomposition rates of THP for $CoDe_2$–bpy and $CuDe_2$–bpy complexes in chlorobenzene at 45 °C

Complex	$k/10^{-3}$ s^{-1}
$CoDe_2$	0.49
$CoDe_2$–bpy(1 : 1)	1.32
(1 : 50)	0.56
(1 : 100)	0.28
(1 : 150)	0.27
$CuDe_2$	0.00
$CuDe_2$–bpy(1 : 1)	1.40
(1 : 50)	0.91
(1 : 100)	1.76
(1 : 150)	1.78

[Metal]=2×10^{-4}M, [THP]=5×10^{-2} M.

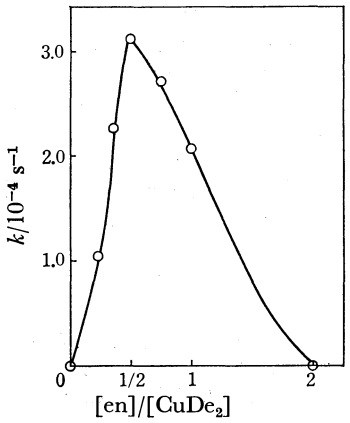

Fig. 6. Effect of ethylenediamine on the rate of decomposition of THP catalyzed by $CuDe_2$ in chlorobenzene at 45 °C.
[$CuDe_2$]=2×10^{-4} M, [THP]=5×10^{-2} M.

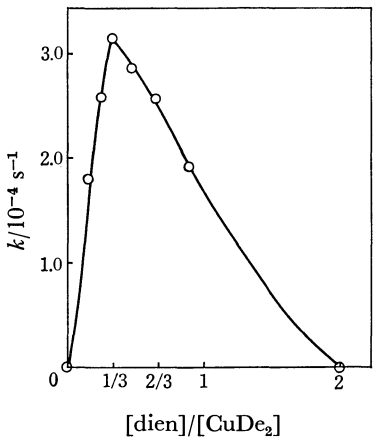

Fig. 7. Effect of diethylenetriamine on the rate of decomposition of THP catalyzed by $CuDe_2$ in chlorobenzene at 45 °C.
[$CuDe_2$]=2×10^{-4} M, [THP]=5×10^{-2} M.

Effect of Ethylenediamine and Diethylenetriamine on Copper(II) Salt. The effect of ethylenediamine and that of diethylenetriamine on the rate of the $CuDe_2$-catalyzed decomposition of THP in chlorobenzene are shown in Figs. 6 and 7, respectively. They show the same pattern as that of the $CoDe_2$–en and $CoDe_2$–dien systems. The rate increases with the addition of ethylenediamine or diethylenetriamine, the maximum activities being found at the ratio of [en]/[$CuDe_2$]=1/2 and [dien]/[$CuDe_2$]=1/3. $CuDe_2$ was deactivated by the amines at the ratio [en]/[$CuDe_2$], [dien]/[$CuDe_2$] higher than 2. The maximum values were one third of those of the $CoDe_2$–en, –dien systems. Appearance of a maximum in these systems suggests that the same structural variation occurs as in the $CoDe_2$–bpy system in $CuDe_2$–en, –dien systems. The order of maximum values is $CoDe_2$–bpy>$CoDe_2$–en, –dien>$CuDe_2$–en, –dien.

The following conclusions on the ligand effect were obtained from our results. 1) The catalytic activities of cobalt(II) ion and copper(II) ion in the deocmposition

of THP change with the concentration of amine chelate added. 2) Aliphatic amine chelate acts as a deactivator and aromatic amine chelate as an activator. 3) In most cases a maximum activity was found at the molar ratio of [Chelate]/[Metal] = 1/(Number of N atom of chelate). 4) All the effects of chelate ligands can be explained in terms of the variation of structure or electrochemical and spectral property of catalyst.

References

1) R. Hiatt, K. C. Irwin, and C. W. Gould, *J. Org. Chem.*, **33**, 1430 (1968); N. M. Emanuel, Z. K. Maizus, and I. P. Skibida, *Angew. Chem. Int. Ed. Engl.*, **8**, 97 (1969); R. A. Sheldon and J. K. Kochi, *Adv. Catal.*, **25**, 272 (1976).

2) T. Yamada and Y. Kamiya, *Bull. Chem. Soc. Jpn.*, **51**, 830 (1978).

3) F. W. Heaton and N. Uri, *J. Lipid Res.*, **2**, 152 (1961).

4) N. Rabjohn, *Org. Synth.*, Coll. Vol. IV, 895 (1963).

5) J. K. Kochi, *J. Am. Chem. Soc.*, **84**, 774, 3271 (1962); J. K. Kochi and H. E. Maines, *J. Org. Chem.*, **30**, 1862 (1965); J. K. Kochi, *Science*, **155**, 145 (1967); J. K. Kochi, *J. Am. Chem. Soc.*, **90**, 4038, 4616 (1968); J. K. Kochi, *J. Org. Chem.*, **36**, 3095, 3103 (1971).

6) A. J. Chalk and J. F. Smith, *Trans. Faraday Soc.*, **53**, 1325 (1967); H. Sigel, C. Flierl, and R. Griesser, *J. Am. Chem. Soc.*, **91**, 1061 (1969); H. Sigel, *Angew. Chem. Int. Ed. Engl.*, **8**, 167 (1969).

7) H. Sigel, *Angew. Chem. Int. Ed. Engl.*, **11**, 851 (1972).

Further Study of Methanol Carbonylation Catalyzed by Cobalt, Rhodium, and Iridium Catalysts

Tsutomu MIZOROKI,* Toshio MATSUMOTO, and Atsumu OZAKI

Research Laboratory of Resources Utilization, Tokyo Institute of Technology, Nagatsuta-cho, Midori-ku, Yokohama 227

(Received May 31, 1978)

The effect of iodide ion was examined in methanol carbonylation with use of Co-, Rh-, and Ir-catalysts. Sodium iodide gives no noticeable effect on carbonylation catalyzed by Rh-catalyst to give acetic acid, and retards that catalyzed by Ir-catalyst. Methyl iodide is effective for methanol carbonylation with Co-catalyst in the presence of hydrogen to give mainly acetaldehyde, which is readily hydrogenated to ethanol during the course of carbonylation on addition of a catalytic amount of $Ru_3(CO)_{12}$. Sodium iodide is also effective for acetaldehyde formation, although it strongly retards the hydrogenation of acetaldehyde with Ru-catalyst. The different effect of iodide ion on methanol carbonylation catalyzed by Co-, Rh-, or Ir-catalyst is discussed in terms of neucleophilicity of the active catalyst species.

Methyl iodide is known as an efficient promoter for methanol carbonylation with Co-, Rh-, or Ir-catalyst. A reaction scheme involving an oxidative addition of methyl iodide has been accepted in Rh- or Ir-catalyzed carbonylation.[1] It has been pointed out that the presence of iodide ion promotes the oxidative addition of methyl iodide to rhodium(I) complexes.[2] The rate of methanol carbonylation with Co-catalyst increases with addition of iodide ion,[3] although no detailed discussion has been made on the role of iodide ion. It has not been clarified why Co- catalyst gives preferentially acetaldehyde when methanol carbonylation is performed in the presence of hydrogen,[4] while all attempts for acetaldehyde formation were unsuccessful with the use of Rh- or Ir-catalyst.

The present work was undertaken to elucidate the effect of iodide ion on methanol carbonylation as well as the significance of Co-catalyst in the acetaldehyde formation.

Experimental

Carbonylation was carried out according to the procedure described in a previous paper.[5] $Co_2(CO)_8$, $RhCl_3 \cdot 3H_2O$, and $IrCl_4 \cdot H_2O$ were used as catalyst precursors. $Co_2(CO)_8$ was prepared by reduction of cobalt carbonate suspended in toluene with a synthesis gas ($CO/H_2=1$, 150 kg/cm^2) at 170 °C. Methyl iodide (extra pure grade, Tokyo Kasei), $Ru_3(CO)_{12}$ (Strem Chemicals) and all the other materials were commerical products and used without purification. Acetophenone has been found to be useful solvent for preventing the formation of dimethyl ether during the course of Rh- of Ir-catalyzed methanol carbonylation.[5] However, it was readily hydrogenated to give 1-phenylethanol and ethylbenzene during the course of carbonylation when a mixture of carbon monoxide and hydrogen was used. Thus, methyl benzoate was used as the solvent in the present work. It was also partially transformed into benzoic acid during the carbonylation. The amount of benzoic acid formed was taken into account to evaluate the methyl-balance of product solutions.

The product solutions were analyzed by means of gas chromatography (carrier gas of He). A glass column of Diethylene Glycol Succinate Polyester (3 mmϕ, 3 m) was used at 100—200 °C for carboxylic acids, and two copper columns of 3,3′-oxydipropionitrile (3 mmϕ, 5 m) and PEG-400 (3 mmϕ, 3 m) were separately used at 70 °C for acetaldehyde, methyl iodide, acetaldehyde dimethyl acetal, methyl acetate, ethyl acetate, methanol, and ethanol. Methane in gaseous products was also analyzed by gas chromatography using a copper column of VZ-7 (3 mmϕ, 3m) at room temperature.

Results and Discussion

Carbonylation with $Co_2(CO)_8$. The carbonylation of methanol (125 mmol) with $Co_2(CO)_8$ (1 mmol) in the presence of methyl iodide (10 mmol) was carried out in methyl benzoate (20 ml) at 173 °C under 30—75 kg/cm^2 of carbon monoxide (CO 98%) for 3 h, giving practically no acetic acid. Under the same reaction conditions, both Rh- and Ir-catalysts almost quantitatively converted methanol into acetic acid (115 mmol, 90% yield) within a shorter reaction period (0.5 h). When a mixture of carbon monoxide and hydrogen (100 kg/cm^2, $CO/H_2=1$) was used for the $Co_2(CO)_8$-catalyzed carbonylation of methanol under similar conditions, appreciable amounts of C_2-oxygenated compounds such as methyl acetate, acetaldehyde and ethanol were obtained. The results are shown in Fig. 1. Analytical results of product solutions are represented by S_1, S_2, and M with the following definitions.

$$\text{total AcOH (mmol)} = [\text{AcOH}] + [\text{AcOMe}] + [\text{AcOEt}]$$

$$\text{total AcH (mmol)} = [\text{AcH}] + [\text{DMA}]$$

(DMA = acetaldehyde dimethyl acetal)

$$\text{total EtOH (mmol)} = [\text{EtOH}] + [\text{AcOEt}]$$

$$\text{total } C_2 \text{ (mmol)} = [\text{total AcOH}] + [\text{total AcH}] + [\text{total EtOH}]$$

$$S_1\ (\%) = 100 \times \{([\text{total AcH}] + [\text{total EtOH}])/[\text{total } C_2]\}$$

$$M\ (\%) = 100 \times \{([\text{AcOH}] + [\text{EtOH}] + 2[\text{AcOEt}] + 2[\text{AcOMe}] + 3[\text{DMA}] + [\text{CH}_3\text{I}] + [\text{CH}_3\text{OH}])/([\text{CH}_3\text{OH}]_0 + [\text{CH}_3\text{I}]_0 + [\text{PhCO}_2\text{H}])\}$$

$$S_2\ (\%) = 100 \times [\text{total EtOH}]/[\text{total } C_2]$$

S_1 and S_2 are the selectivities to total C_2-oxygenated products and ethanol respectively, and M is the percent methylbalance, where $[CH_3OH]_0$ and $[CH_3I]_0$ are molar amounts of methanol and methyl iodide initially charged. The amount of methyl group introduced from methyl benzoate during the course of carbonylation is evaluated from the amount of benzoic acid, $[PhCO_2H]$,

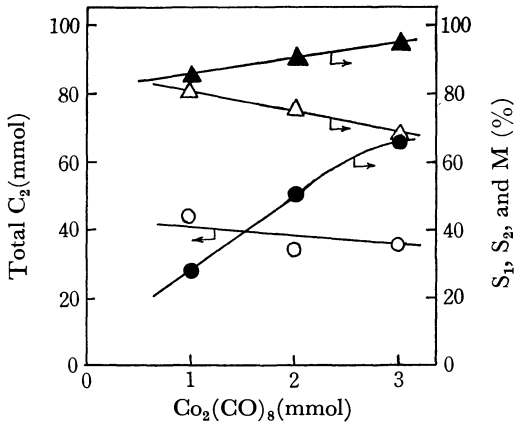

Fig. 1. Effect of the amount of $Co_2(CO)_8$ on methanol homologation in methyl benzoate solvent.
Total C_2(mmol)-○, S_2(%)-● M(%)-△, and S_1(%)-▲.

Table 1. Effect of $Ru_3(CO)_{12}$ on the hydrogenation of acetaldehyde formed CH_3OH 125 mmol, CH_3I 5 mmol, $Co_2(CO)_8$ 1 mmol. $PhCO_2CH_3$ 20 ml, press. 100 kg/cm² ($CO/H_2=1$) at room temp, temp 173 °C, and react. time 2 h.

	Run 1	Run 2	Run 3	Run 4[a]
$Ru_3(CO)_{12}$ (mmol)	0	0.038	0.075	0.075
Total AcH (mmol)	30.4	17.0	4.5	0.5
(DMA mmol)	(8.8)	(2.5)	(0.9)	(tr.)
Total EtOH (mmol)	8.2	25.4	29.8	5.5
(Acetate mmol)	(tr.)	(1.0)	(0.9)	(tr.)
Total AcOH (mmol)	3.9	4.0	4.6	1.8
(Acetate mmol)	(tr.)	(tr.)	(tr.)	(tr.)
CH_3I (mmol)	2.5	3.2	3.6	4.4
Total C_2 mmol	42.5	46.4	38.9	7.8
S_1 (%)	19	55	75	71

a) Without $Co_2(CO)_8$.

remaining in the product solutions. A low methyl-balance indicates an increase in dimethyl ether and methane formed, since neither C_3 nor C_4-compounds were detected in product solutions. Figure 1 shows that the selectivity to ethyl alcohol (S_2) increases with increase in the amount of $Co_2(CO)_8$, despite no increase in total C_2-compounds, suggesting that the Co-catalyst mostly works as a hydrogenation catalyst for the acetaldehyde formed. In fact, $Co_2(CO)_8$ and its tertiaryphosphine derivatives are known to be active for the hydrogenation of aldehydes under oxo reaction conditions,[6] where the active species is the hydridocarbonyl.

A rapid hydrogenation of the acetaldehyde formed is desirable in order to examine the effects of methyl iodide and iodide ion on the methanol carbonylation to give acetaldehyde, otherwise the acetaldehyde is readily transformed into dimethyl acetal, resulting in consumption of 3 mol of methanol for a dimethylacetal formation ($2CH_3OH+CH_3CHO \rightarrow CH_3CH(OCH_3)_2+H_2O$). Since the hydrogenation catalyst should work in the presence of carbon monoxide, some carbonyl compounds were examined. It was found that $Ru_3(CO)_{12}$ is much more efficient for the hydrogenation of acetaldehyde than $Co_2(CO)_8$ under the methanol carbonylation conditions[7] as shown in Table 1. It is apparent that the selectivity to ethanol is remarkably increased by the addition of a catalytic amount of $Ru_3(CO)_{12}$. Although $Ru_3(CO)_{12}$ shows a small activity for methanol carbonylation (run 4), its contribution can be neglected in runs 2 and 3. The effects of methyl iodide and sodium iodide on the Co-catalyzed carbonylation were then examined in the presence of $Ru_3(CO)_{12}$. The results are summarized in Table 2. The favorable effect of methyl iodide on methanol carbonylation levels off at higher concentration as shown by the change in total C_2-compounds (runs 1—3). The increase in methyl iodide lowers the methyl-balance, presumably due to an increase in dimethyl ether formation. Sodium iodide is also effective for carbonylation without lowering the methyl-balance (runs 4—6), where small amounts of methyl iodide were detected in the product solutions. The amount of total C_2-compounds is the largest when both methyl iodide and sodium iodide are added (runs 7 and 8). It should be noted, however, that the $Ru_3(CO)_{12}$-catalyzed hydrogenation of acetaldehyde is almost completely inhibited by the addition of sodium iodide. Since the $Ru_3(CO)_{12}$-catalyzed hydrogenation of acetaldehyde takes palce in the absence of sodium iodide (runs 1—3), it can be concluded that methyl iodide supplies no appreciable amount of iodide ion during the course of Co-catalyzed methanol carbonylation, the rate of which is enhanced by both methyl iodide and iodide ion (runs 7 and 8).

In this respect, the chemical reaction of $Co_2(CO)_8$, the catalyst precursor, with iodides should be referred

Table 2. Effect of iodide ion on the $Co_2(CO)_8$–$Ru_3(CO)_{12}$ catalyzed methanol homologation CH_3OH 125 mmol, press. 100 kg/cm² ($CO/H_2=1$) at room temp, $Co_2(CO)_8$ 1 mmol, $Ru_3(CO)_{12}$ 0.075 mmol, $PhCOOCH_3$ 20 ml, temp 173 °C, and time 2 h.

Run	CH_3I (mmol)	NaI (mmol)	Residual CH_3I (mmol)	Total AcH (mmol)	Total EtOH (mmol)	Total AcOH (mmol)	Total C_2 (mmol)	Methyl-balance (%)	CH_4 (mmol)
1	5	0	2.7	1.8	29.8	4.6	36	88	14.0
2	10	0	7.0	5.8	33.3	6.0	45	63	—
3	15	0	10.5	9.6	29.5	3.9	43	58	3.3
4	0	5	0.5	19.0	7.8	1.5	28	95	2.5
5	0	10	0.6	26.5	2.9	1.6	31	104	2.0
6	0	15	0.5	42.1	6.9	3.9	53	105	3.3
7	5	5	2.8	50.8	2.5	3.7	57	101	—
8	5	10	3.0	74.1	1.9	7.3	83	104	5.3

to. It is known that $Co_2(CO)_8$ undergoes disproportion in polar solvents to give $Co(CO)_4^-$ ($3Co_2(CO)_8+2nL\rightarrow 2[CoL_n][Co(CO)_4]_2+8CO$, L=solvent).[8] In fact, $Co_2(CO)_8$ dissolves in methyl benzoate with evolution of carbon monoxide. When sodium iodide is present in the solution, the carbon monoxide ligands of $Co(CO)_4^-$ may be partly replaced by iodide ion giving rise to an increase in nucleophilicity of the complex. It is also known that methyl iodide undergoes an oxidative addition to $Co(CO)_4^-$ to give $CH_3Co(CO)_4$,[9] the oxidation state of which is lower than that of methyl rhodium(III) and iridium(III) complexes. The difference of oxidation state seems to constitute the main reason why cobalt catalyst behaves differently.

$$CH_3I + Co(CO)_4^- \longrightarrow CH_3Co(CO)_4 + I^-$$
$$\Updownarrow$$
$$CH_3COCo(CO)_3$$

If the methanol carbonylation with Co-catalyst proceeds through a nucleophilic attack of the anion complex on the carbon of methyl iodide, the observed enhancement with iodide ion is reasonable. In view of the low oxidation state of the cobalt intermediate, an electrophilic oxidative addition of hydrogen would take place readily giving rise to the predominant formation of acetaldehyde.

Carbonylation with Rh- or Ir-catalysts. In the acetic acid synthesis catalyzed by Rh-complex, kinetic[5,10] and spectroscopic studies[2] have made it clear that the rate-determining step is the oxidative addition of methyl iodide to Rh(I) complex. The oxidative addition seems to take place through a nucleophilic attack of rhodium(I) species on the carbon of methyl iodide to give methyl rhodium(III) complex, which is readily transformed into the acetyl complex. Coordination of iodide ion evidently produces a highly nucleophilic rhodium(I) anion, resulting in an increase in the rate of oxidative addition of methyl iodide. The enhancement by iodide ion has been found by Forster upon addition of Bu_4NI in the oxidative addition of methyl iodide to $[Rh(AsPh_3)_2(CO)I]$ or $[Rh(SbPh_3)_2(CO)I]$ in dichloromethane solvent.[11]

The effect of iodide ion on the rate of Rh-catalyzed methanol carbonylation was examined by adding sodium iodide under the conditions given in Table 3 except that $RhCl_3\cdot 3H_2O$ was used instead of $IrCl_4\cdot H_2O$ as the catalyst precursor. No appreciable effect of iodide ion was found on the rate of carbonylation. The inconsistency, however, can be understood by taking into account the fact that the predominant species during the course of the Rh-catalyzed carbonylation in the presence of an excess methyl iodide is anionic rhodium(I) complex, $[Rh(CO)_2I_2]^-$, spectroscopically verified by Forster.[11] Thus, no appreciable enhancement was observed by the addition of sodium iodide.

On the other hand, in the acetic acid synthesis with Ir-catalyst in acetophenone solvent, the predominant species is an Ir(III) complex, acetyl iridium(III) being a plausible form with its methanolysis being rate-determining.[12] If the methanolysis proceeds *via* an electrophilic attack of the acetyl iridium(III) complex on the oxygen of methanol, replacement of the neutral ligands such as carbon monoxide and solvent molecule by iodide ion should lower the rate of methanolysis because of the decrease in the electrophilicity of iridium(III) species. Thus the effect of iodide ion on the Ir-catalyzed acetic acid synthesis was examined (Table 3). It is apparent that the addition of sodium iodide decreases the yield of acetic acid. The observed retardation of acetic acid synthesis by iodide ion is reasonably explained by the electrophilic attack of acetyl iridium(III) species on methanol being the rate-datermining step as discussed in a previous paper.[12]

As regards the lack of hydrogen activation by Rh- and Ir-catalysts in methanol carbonylation in spite of their high catalytic activities for olefin hydroformylation, the carbonylation of ethylene with Rh- or Ir-catalyst was carried out under methanol carbonylation conditions. The results are summarized in Table 4. Methanol carbonylation as well as ethylene hydroesterification which forms methyl propionate (propionic acid was not detected) take place (runs 1 and 2). Hydrogen, however, gives no appreciable effect on either carbonylation (runs 3 and 4), since the amounts of total acetic acid and methyl propionate are almost the same regardless of introduction of hydrogen. Hydroformylation of ethylene proceeds under the same conditions (runs 5 and 6), while it is completely suppressed by addition of methyl iodide (runs 7 and 8). The results are explained by the following simplified scheme on the assumption that the oxidative addition of methyl iodide takes place on rodium(I) and iridium(I) complexes and that acetyl complexes of high oxidation state(III) thus formed are more rapidly attacked by methanol than hydrogen molecule. Preferential formation of methyl propionate can also be realized by an electrophilic attack of propionyl rhodium(III) and iridium(III) complexes,

Table 3. Effect of iodide ion on the Ir-catalyzed acetic acid synthesis

CH_3OH 125 mmol, $IrCl_4\cdot H_2O$ 0.25 mmol, P_{CO} 30 kg/cm² at room temp, temp 173 °C, and time 2 h.

Run	CH_3I (mmol)	NaI (mmol)	Residual CH_3I (mmol)	Total AcOH (mmol)	Yield (%)
1	0.75	0	0.22	51	41
2	1.25	0	0.51	54	43
3	0	1.25	0.35	44	35
4	0	2.50	0.59	25	20
5	0.75	1.25	0.89	37	30
6	1.25	1.25	1.24	44	35

Table 4. Carbonylation of ethylene under methanol carbonylation conditions
P_{c_2}' 40 kg/cm,[2a] P_{CO} 20 kg/cm^2,[a] $PhCOCH_3$ 20 ml,[b] temp 156 °C, and time 1 h.

Run	Catalyst (mmol)	CH_3I (mmol)	CH_3OH (mmol)	P_{H_2}[a] (kg/cm)	Total AcOH(mmol)	$EtCO_2CH_3$[c] (mmol)	EtCHO (mmol)
1	$RhCl_3 \cdot 3H_2O$ (0.5)	10	125	20	23	63	12
2	$IrCl_4 \cdot H_2O$ (0.25)	10	125	20	27	29	5.1
3	$RhCl_3 \cdot 3H_2O$ (0.5)	10	125	0	21	59	tr.
4	$IrCl_4 \cdot H_2O$ (0.25)	10	125	0	29	24	tr.
5	$RhCl_3 \cdot 3H_2O$ (0.5)	0	0	20	0	0	14
6	$IrCl_4 \cdot H_2O$ (0.25)	0	0	20	0	0	7.4
7	$RhCl_3 \cdot 3H_2O$ (0.5)	10	0	20	0	0	tr.
8	$IrCl_4 \cdot H_2O$ (0.25)	10	0	20	0	0	tr.

a) Partial pressure at room temperature. b) No hydrogenation of benzophenone observed at this temperature.
c) No propionic acid observed.

formed from ethylene and the corresponding hydride complexes, on methanol, as shown in the scheme.

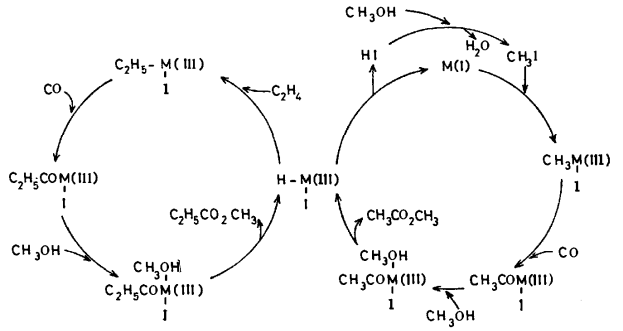

Scheme 1. Reaction scheme on the Rh- or Ir-catalyzed carbonylation in the presence of methyl iodide (M=Rh or Ir).

References

1) J. F. Roth, J. H. Craddock, A. Hershman, and F. E. Paulik, *Chemtech*, **1971**, 600.
2) D. Forster, *J. Am. Chem. Soc.*, **19**, 951 (1975).
3) T. Mizoroki and M. Nakayama, *Bull. Chem. Soc. Jpn.*, **41**, 1628 (1968).
4) J. Berty and L. Marko, *Chem. Tech. (Berlin)*, **8**, 260 (1965); T. Mizoroki and M. Nakayama, *Bull. Chem. Soc. Jpn.*, **37**, 236 (1964); **39**, 1477 (1966).
5) T. Matsumoto, K. Mori, T. Mizoroki, and A. Ozaki, *Bull. Chem. Soc. Jpn.*, **50**, 2337 (1977).
6) E. R. Tucci, *Ind. Eng. Chem. Prod. Res. Dev.*, **7**, 125 (1968); F. E. Paulik, *Catal. Rev.*, **6**, 49, (1972).
7) Patent (USA 3285948) claims that the addition of ruthenium chloride increases the selectivity to ethanol in the methanol homologation with Co-catalyst.
8) I. Wender, H. W. Sternberg, and M. Orchin, *J. Am. Chem. Soc.*, **74**, 1216 (1952); F. Calderazzo, R. Ercoli, and G. Natta, "Organic Syntheses *via* Metal Carbonyls Vol. 1," Interscience Publishers, New York, London, Sydney (1968), p. 83.
9) R. F. Heek and D. S. Breslow, *J. Am. Chem. Soc.*, **84** 2499 (1962); **85**, 2779 (1963).
10) J. Hjortkjaer and V. W. Jensen, *Ind. Eng. Chem. Prod. Res. Dev.*, **15**, 46 (1976).
11) D. Forster, *J. Am. Chem. Soc.*, **98**, 846 (1976).
12) T. Matsumoto, T. Mizoroki, and A. Ozaki, *J. Catal.*, **51**, 96 (1978).

Thermal and Acid-catalyzed Decomposition of 3,6-Diphenyl-1,4-bis-(phenylsulfonyl)-1,4-dihydro-1,2,4,5-tetrazine[1]

Suketaka Ito,* Akikazu Kakehi, Yumo Tanaka, Kazuyoshi Yoshida, and Toshiyuki Matsuno

Department of Industrial Chemistry, Faculty of Engineering, Shinshu University, Wakasato, Nagano 380

(Received June 5, 1978)

Thermolysis of the title dihydrotetrazine in boiling toluene gives benzenesulfonic anhydride, *S*-phenyl benzenethiosulfonate, and small amounts of diphenyl disulfide and a rearrangement product, 3,6-diphenyl-1,2-bis(phenylsulfonyl)-1,2-dihydro-1,2,4,5-tetrazine, together with 3,6-diphenyl-1,2,4,5-tetrazine. On the other hand, the treatment with concentrated sulfuric acid affords 3,6-diphenyl-1,4-dihydro-1,2,4,5-tetrazine in good yield. On the basis of the kinetic parameters obtained for the thermolysis, the mechanism was discussed.

3,6-Diphenyl-1,4-bis(*p*-tolylsulfonyl)-1,4-dihydro-1,2,4,5-tetrazine (**1**), obtained by the reaction of 5-phenyltetrazole with *p*-toluenesulfonyl chloride, yields 3,6-diphenyl-1,2,4,5-tetrazine (**2**) when heated at its melting point or treated with ethanolic potassium hydroxide at room temperature, and *p*-toluenesulfonic acid alone was isolated as a by product.[2]

The thermal decomposition of 2-*p*-tolylsulfonyl-5-phenyltetrazole[3] was also reported:[4] this reaction gave traces of **2** together with other products and should not proceed *via* **1** as an intermediate, and further details are unavailable for the decomposition reaction of **1** and its homologs.

The present paper deals with the thermolysis and the acid-catalyzed dephenylsulfonylation of 3,6-diphenyl-1,4-bis(phenylsulfonyl)-1,4-dihydro-1,2,4,5-tetrazine (**3**).

Results and Discussion

Preparation and Thermolysis of Dihydrotetrazine. Dihydrotetrazine (**3**) was obtained in good yields by treating *N*-(phenylsulfonyl)benzohydrazonoyl chloride with triethylamine in THF[4,5] (Scheme 1).

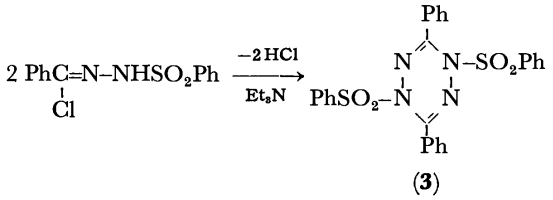

Scheme 1.

In the IR spectra, dihydrotetrazine **3** exhibits a characteristic peak at 1320 cm^{-1} (strong) which should be assigned to the 1,4-dihydrotetrazine ring vibration. Compound **3** is thermolabile and melt with decomposition to give tetrazine **2**; a partial decomposition is also observed below the melting point. Furthermore, **3** altered gradually to **2** at room temperature when dissolved in a polar solvent such as DMF or DMSO.

The thermolysis of **3** was carried out in the following two procedures: (A) Keeping at 150—155 °C for 30 min in a sealed tube without solvent; (B) refluxing a toluene solution for 20 h. The IR spectrum of the resulting dark red solid from Procedure A showed the formation of benzenesulfonic anhydride (**4**), a portion of which could be isolated as a sparingly soluble part in benzene.

The precipitation of anilinium benzenesulfonate (**5**) was observed when aniline was added to the chloroform solution of the product from Procedure A or the reaction mixture in toluene from Procedure B. Work-up gave 3,6-diphenyl-1,2-bis(phenylsulfonyl)-1,2-dihydro-1,2,4,5-tetrazine (**6**), *S*-phenyl benzenethiosulfonate (**7**), diphenyl disulfide (**8**), and benzenesulfonanilide (**9**) along with 3,6-diphenyl-1,2,4,5-tetrazine (**2**) and anilinium benzenesulfonate (**5**). The results are summarized in Table 1.[6]

Table 1. Thermolysis of dihydrotetrazine **3**

Reaction condition[a]	Yield (%) of product[b]					
	2	**6**	**7**	**8**	**9**	**5**
A	98	0	24	6	62	70
B	88	3	26	3	58	52

a) A: Kept at 150—155 °C for 30 min in a sealed tube without solvent with subsequent treatment with aniline. B: Refluxed in toluene for 20 h with subsequent treatment with aniline. b) Yield as mole per cent based on **3**.

When ethanol was added to the primary reaction mixture from Procedure A or B, ethyl benzenesulfonate was obtained. Compounds **5** and **9** or ethyl benzenesulfonate should be derived from **4** formed in the reaction. Thus, the thermal decomposition reaction may be formulated as follows (Scheme 2).

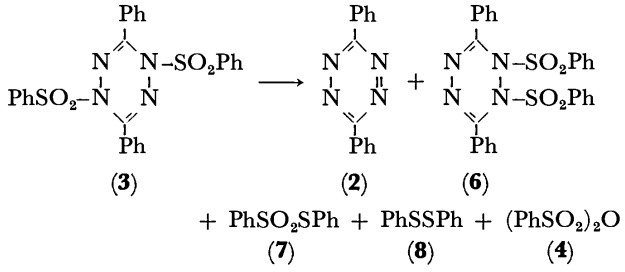

Scheme 2.

Compound **6** decomposed when heated at its melting point, giving the same products as those obtained from **3**. No promotion of reaction was observed when benzoyl peroxide was added in the thermolysis of **3** in toluene

Kinetics and Mechanism. In order to obtain some kinetic data, the thermolysis of **3** in toluene was conducted in Pyrex tubes under nitrogen atmosphere at 110,

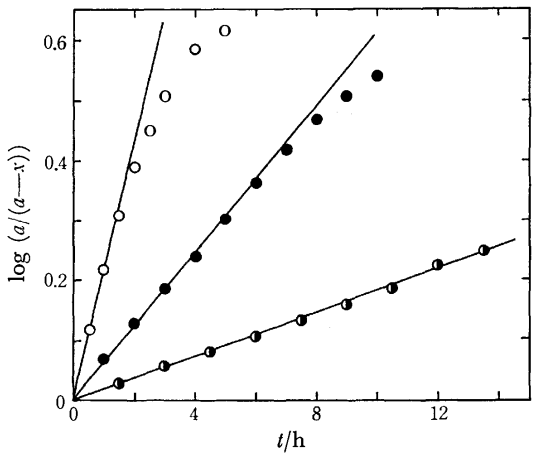

Fig. 1. First order plots for the thermolysis of dihydrotetrazine **3** in toluene.
○: 130 °C, ●: 120 °C, ◑: 110 °C; $[3]_0=1.95$ mmol·l^{-1}.

120, and 130 °C. The course of decomposition was followed by measuring the tetrazine absorption at 550 nm.

Since the reaction is not simple as has been shown above, the integral method cannot be employed for the kinetic determination: thus any good linear relationship may be hardly found in the first order plots (Fig. 1) and also in the second order ones for the reaction.

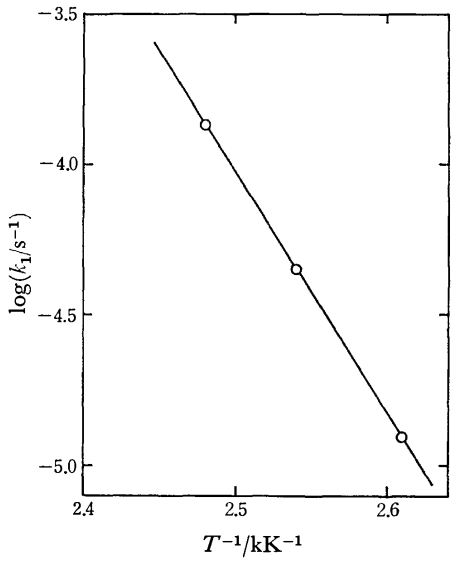

Fig. 2. Arrhenius plots for the thermolysis of dihydrotetrazine **3** in toluene.

The decomposition reaction of **3** to **2** was analyzed by the initial rate method, which showed the reaction to obey good first order kinetics and gave $k_1(h^{-1})=0.493$(130 °C); 0.162(120 °C); 0.0447(110 °C). The plots of log k_1 *vs.* $1/T$ are given in Fig. 2, from which the Arrhenius parameters, $E_a(=154$ kJ/mol) and $\Delta S^*(=61$ J/(K mol)), were obtained.

When the solvent toluene was replaced by DMSO, plots of yield of tetrazine *vs.* time gave a curve with an inflection point (Fig. 3, Curve II), but almost no

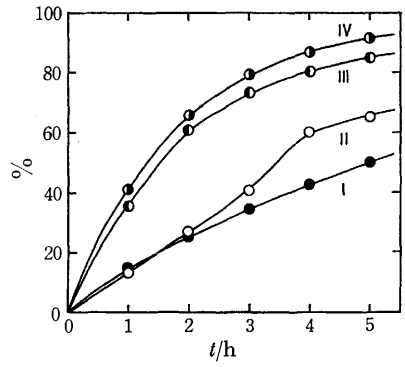

Fig. 3. Plots of yield of tetrazine **2** *vs.* time for the thermolysis of dihydrotetrazine **3**.
●: In toluene/N_2, ○: in DMSO/N_2, ◐: in DMSO with TosOH/N_2, ◑: in DMSO with TosOH/O_2; $[3]_0=1.95$ mmol l^{-1}, [TosOH]=2.0 mmol l^{-1}; temp: 120 °C.

difference in the reaction rate at the initial period between DMSO and toluene could be detected.

In view of the fact that the reaction is not promoted by a radical initiator and that the ΔS^* value is positive, the following route can be given as a possible mechanism for the thermolysis of **3**, in which benzenesulfonic benzenesulfinic anhydride (**10**) is postulated as an intermediate for **4** and **7**.

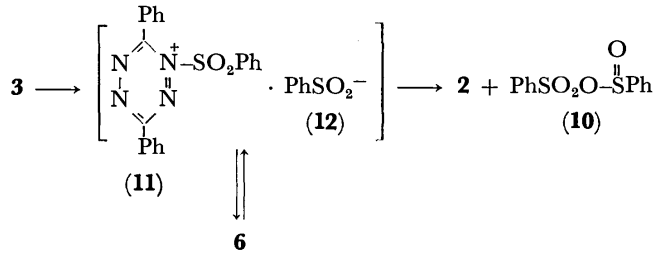

Scheme 3.

Since, as has been described, little difference in the rate at the initial reaction period is found between DMSO (polar) and toluene (less polar), the intermediate, [**11**·**12**], should exist as an intimate ion pair.[8] The formation of **6** can be explained by the recombination of **11** and **12** (internal return).

The thermolability of **3** is possibly due to the nonaromaticity of eight-electron dihydrotetrazine system,

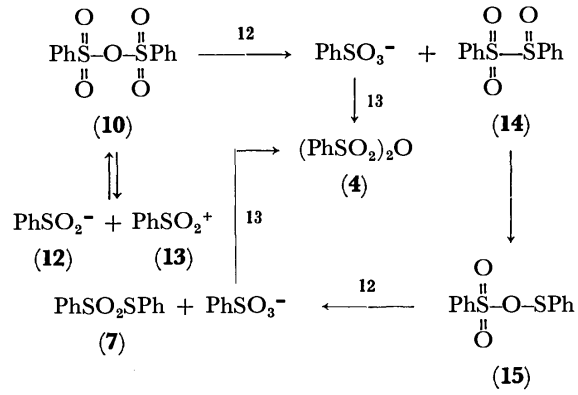

Scheme 4.

which alters to a stable aromatic six-electron one by releasing **12**.[9] Mass spectroscopic data (*vide post*) may be consistent with the collapse of **3** to **11** and **12**.

The formation of *S*-phenyl benzenethiosulfonate (**7**) and benzenesulfonic anhydride (**4**) can be well interpreted by the intermediacy of benzenesulfonic benzenesulfinic anhydride (**10**) (Scheme 4).

p-Toluenesulfonic *p*-toluenesulfinic anhydride has been postulated as the primary intermediate in the reaction of *p*-toluenesulfonyl chloride with sodium *p*-toluenesulfinate, from which *S*-*p*-tolyl *p*-toluenethiosulfonate and sodium *p*-toluenesulfonate are formed.[10] Anhydride **10** corresponds to carboxylic *p*-toluenesulfinic anhydride which has been proposed as an intermediate for the formation of carboxylic anhydride and *S*-*p*-tolyl *p*-toluenethiosulfonate in the reaction of sodium *p*-toluenesulfinate with acyl chloride.[11]

The intermediacy of sulfinyl sulfone **14** and sulfenic sulfonic anhydride **15** and the rearrangement **14** to **15** have been also proposed for the formation of *S*-*p*-tolyl *p*-toluenethiosulfonate in the disproportionation of *p*-toluenesulfinic acid under acidic conditions.[12]

From Scheme 4, the following stoichiometric formula can be obtained:

$$3[PhSO_2^+ + PhSO_2^-] \longrightarrow \underset{(4)}{2(PhSO_2)_2O} + \underset{(7)}{PhSO_2SPh}$$

This formula is consistent with that of the disproportionation of *p*-toluenesulfinic acid,[12] and in agreement with the experimental results obtained (Table 1). The formation of diphenyl disulfide (**8**) can be explained in terms of the air oxidation of benzenethiolate ion[13] generated by the hydrolysis of thiosulfonate **7**.[12]

The characteristic feature of Curve II shown in Fig. 3 suggests that the reaction in DMSO may involves an autocatalyzed process as a parallel one,[14] which may be due to benzenesulfonic acid formed from traces of moisture and **4**. In the initial presence of *p*-toluenesulfonic acid a pronounced catalysis took place (Fig. 3, Curve III), and a further promotion of reaction was observed under oxygen atmosphere (Curve IV).

In general, DMSO accelerates ionic processes and can also function as an oxidizing agent itself, thus the primary product of the acid-catalyzed reaction in DMSO may be dephenylsulfonylated dihydrotetrazine, which would be oxidized to **2** by DMSO.[15] The acid-catalyzed dephenylsulfonylation will be discussed later.

An acceleration of reaction was observed also when a small amount of *p*-toluenesulfonic acid was added in the thermolysis of **3** in toluene, but this effect of acid was less remarkable than when DMSO was used as the solvent.

Structure Assignment of **6**. Compound **6** also decomposes somewhat higher temperature, giving the same products as those of **3**. The IR spectrum of **6** is simpler than that of **3**, and shows a medium peak at 1284 cm^{-1} (νSO_2: 1370, 1171 cm^{-1}) and none at near 1320 cm^{-1}. The peak at 1284 cm^{-1} might be attributed to the 1,2-dihydrotetrazine ring vibration.

The mass spectrum of **6** also differs from that of **3** in some respects: it is particularly characteristic that the peaks of *m/e* 105, 222, and 244 of **6** are far weaker than those of **3** in intensity (Table 2). The fragment ions

Table 2. Mass spectral data of dihydrotetrazines **3** and **6** (Major peaks)

m/e	Assignment	Relative abundance[a]	
		3	**6**
516	M^+	0.8	0.3
375	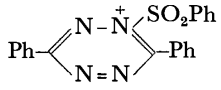	47	83
250	$[PhSO_2\text{–}S\text{–}Ph]^+$	2.1	4.5
244	$Ph\text{–}C^+N\text{–}SO_2Ph$	15	0.2
234	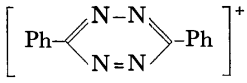	8.0	19
222	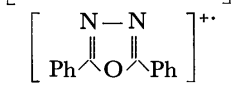	3.8	0.3
141	$PhSO_2^+$	69	71
125	$PhSO^+$	9.3	9.4
109	PhS^+	3.4	5.7
105	$PhC{\equiv}O^+$	23	2.0
103	$PhC{\equiv}N^+$	56	93
77	Ph^+	100	100
65	$C_5H_5^+$	3.0	4.3
51	$C_4H_3^+$	19	26

a) Ionizing energy: 75 eV.

of *m/e* 105, 222, and 244 as assigned in Table 2 may be produced from the 1,4-dihydrotetrazine structure as shown in Scheme 5. In conclusion, compound **6** must be a structural isomer of **3**, thus **6** can be assigned to be 3,6-diphenyl-1,2-bis(phenylsulfonyl)-1,2-dihydro-1,2,4,5-tetrazine. The peak of *m/e* 250 is possibly the parent peak of *S*-phenyl benzenethiosulfonate (**7**) formed by the partial thermolysis of **3** and **6** in the ionization chamber, which may be supported by the appearance of its fragment ions, *m/e* 125, 109, and 65.[16,17]

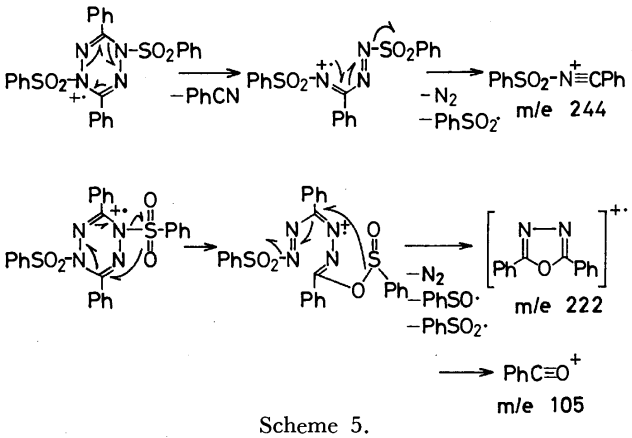

Scheme 5.

Acid-catalyzed Decomposition of **3**. When **3** was treated with concentrated sulfuric acid at room temperature, 3,6-diphenyl-1,4-dihydro-1,2,4,5-tetrazine (**16**: 86%) and benzoic acid (12%) were obtained. Treatment of **3** with refluxing 1-butanol gave 4-amino-3,5-diphenyl-1,2,4-triazole (as benzenesulfonate, **17**: 54%), butyl benzoate (42%), and **2** (24%) together with small amounts of butyl benzenesulfonate, benzenesulfonic acid,

and **7**. The formation of dibutyl ether was also confirmed (Scheme 6).

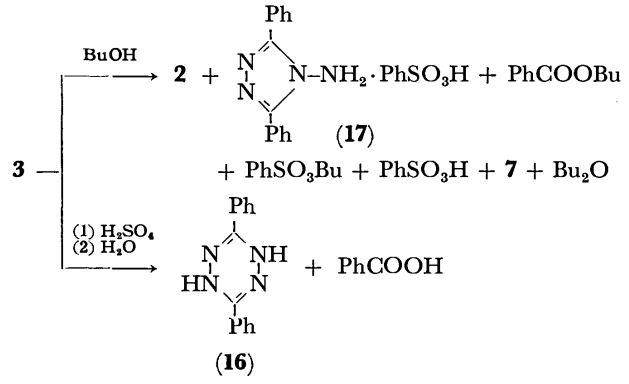

Scheme 6.

The formation of **16** can be interpreted in terms of the *N*-protonation of **3** followed by the removal of benzenesulfonyl ion. The reaction in refluxing 1-butanol is explained as follows: the thermal decomposition of **3** takes place in part to give **2** and benzenesulfonic anhydride (**4**), and acid catalysis by benzenesulfonic acid generated from **4** leads to the formation of **16** as an intermediate The acid-catalyzed rearrangement[18] and hydrolysis[19] of the intermediate **16** should afford **17** and benzoic acid, respectively. A part of **2** obtained here may be derived from **16** by air-oxidation.

Experimental

Melting points were determined with a Yanagimoto micro-melting point apparatus Model MP-S3 and are uncorrected. The microanalysis was performed on a Perkin-Elmer elemental analyzer Model 240. The IR, VIS, and MS spectra were recorded with a JASCO DS-301, a Hitachi EPU-2A, and a JEOL JMS-013G-2 spectrometer, respectively. *N*-(Phenylsulfonyl)benzohydrazonoyl chloride was prepared by the method reported.[20]

Preparation of **3**. A solution of triethylamine (5.5 g, 54 mmol) in THF (20 ml) was added dropwise to a solution of *N*-(phenylsulfonyl)benzohydrazonoyl chloride (14.8 g, 50 mmol) in THF (60 ml) under cooling (ice water) and stirring. The reaction mixture was stirred additionally for 1 h at room temperature. After removal of the separated triethylamine hydrochloride by filtration, the THF solution was concentrated and washed with aqueous ethanol to give fairly pure dihydrotetrazine **3** as yellow solids. The product was purrified by crystallization from benzene–hexane (Yield: 11.6 g, 22 mmol, 45 mol %).

Mp 151—156 °C (dec), IR (KBr, cm^{-1}): 1320 (Ring); 1367, 1183 (νSO_2). Found: C, 60.21; H, 3.93; N, 10.81%; M^+, 516. Calcd for $C_{26}H_{20}N_4O_4S_2$: C, 60.44; H, 3.90; N, 10.84%; M, 516.

Thermolysis of **3**. *Procedure A*: Dihydrotetrazine **3** (2.58 g, 5 mmol) was heated in a sealed tube at 150—155 °C for 30 min. The resulting dark red mass was dissolved in chloroform (50 ml). To the chloroform solution, aniline (2 g) was added and the mixture was allowed to stand for a few hours. The separated precipitates (anilinium benzenesulfonate, **5**: 0.89 g, 3.5 mmol) were filtered, and the filtrate was washed with 10% sodium hydroxide solution followed by dilute hydrochloric acid and dried. After removal of the solvent, the residue was dissolved in hot ethanol. Diphenyltetrazine **2** (1.11 g, 4.7 mmol) separated upon cooling was filtered, and the filtrate was concentrated and then chromatographed on a silica gel (15 g) column, using hexane and benzene as the eluents, to give diphenyl disulfide (**8**: 0.06 g, 0.3 mmol), **2** (0.05 g, 0.2 mmol), and *S*-phenyl benzenethiosulfonate (**7**: 0.30 g, 1.2 mmol). Benzenesulfonanilide (**9**: 0.72 g, 3.1 mmol) was isolated by acidification from the aqueous sodium hydroxide washings above obtained. Treatment of the primary product (dark red mass) with benzene gave a small amount of benzenesulfonic anhydride (**4**) as a sparingly soluble matter.

All the products obtained were identified by comparison with authentic specimens.

Procedure B: A solution of **3** (2.58 g) in 15 ml of toluene dried over sodium wire was refluxed for 20 h. Addition of a solution of aniline (2 g) in toluene (5 ml) to the red reaction mixture led to the precipitation of **5** (0.64 g, 2.6 mmol), which was filtered from the hot toluene solution. Removal of the solvent from the toluene filtrate followed by treatment with chloroform gave pale cream-colored precipitates (**6**: 0.07 g, 0.14 mmol) which after recrystallization from DMF–ethanol melted at 168—171 °C with decomposition.

IR (KBr, cm^{-1}): 1284 (Ring); 1370, 1171 (νSO_2). Found: C, 60.45; H, 3.92; N, 11.00%; M^+, 516. Calcd for $C_{26}H_{20}N_4O_4S_2$: C, 60.44; H, 3.90; N, 10.84%; M, 516.

The chloroform filtrate was worked up in the same manner that used in Procedure A. **2**: 1.04 g (4.4 mmol); **7**: 0.32 g (1.3 mmol); **8**: 0.03 g (0.14 mmol); **9**: 0.68 g (2.9 mmol).

The results of thermolysis are summarized in Table 1.

Thermolysis of **6**. Compound **6** (0.52 g, 1 mmol) was heated in a sealed tube at 170—173 °C for 20 min. The resulting dark red mass was treated in the same manner that used in the thermolysis of **3** (Procedure A). **2**: 0.21 g (0.90 mmol); **5**: 0.18 g (0.72 mmol); **7**: 0.04 g (0.16 mmol); **8**: trace; **9**: 0.14 g (0.60 mmol).

Kinetic Measurement. Rates for the formation of **2** in toluene (and in DMSO[21]) were determined spectrophotometrically by the usual sealed-ampoule technique. In a typical experiment, 10 ampoules each containing *ca.* 6.5 ml of solution of **3** in dry toluene were prepared. They were sealed after being flashed with dry nitrogen. The reaction mixture was taken out from each ampoule after quenching by cooling, and the absorbance of the mixture was determined at 550 nm. The rate constants were obtained by means of the initial rate method.

Reaction of **3** *with Sulfuric Acid*. A solution of **3** (2.58 g, 5 mmol) in chloroform (15 ml) was stirred vigorously with concentrated sulfuric acid (10 ml) for 1 h at room temperature. The sulfuric acid layer was poured into water to give light fine needles, which were filtered and identified to be 3,6-diphenyl-1,4-dihydro-1,2,4,5-tetrazine (**16**). Yield: 1.01 g (4.3 mmol); mp 194—195 °C (lit,[22] mp 191—193 °C).

From the aqueous filtrate, salting-out with sodium sulfate followed by extraction with ether gave benzoic acid (0.07 g, 0.6 mmol).

Reaction of **3** *with Boiling Butanol*. A solution of **3** (2.58 g) and 1-butanol (15 ml) was refluxed for 15 h. Dibutyl ether was detected from the reaction mixture by means of GLC. Addition of ethanol (15 ml) followed by cooling the solution led to the precipitation of **2** (0.28 g, 1.2mmol). Removal of the solvent from the alcohol filtrate gave a residue, which was treated with ether and filtered. The solids (**17**: 1.07 g; 2.7 mmol) obtained were confirmed to be fairly pure by IR spectroscopy, and melted at 193—195 °C after recrystallization from ethanol.

IR (KBr, cm^{-1}): 3240 (brd)(νNH_3^+); 1240, 1158, 1120 (νSO_2). Found: C, 60.68; H, 4.56; N, 14.41%. Calcd for

$C_{20}H_{18}N_4O_3S$: C, 60.90; H, 4.60; N, 14.20%. Dissolution of this product in pyridine followed by dilution with water gave 4-amino-3,5-diphenyl-1,2,4-triazole, mp 260—262 °C. (lit,[18] mp 263 °C).

Benzenesulfonic acid was removed by washing with water from the ether filtrate above obtained; butyl benzoate (0.37 g, 2.1 mmol), butyl benzenesulfonate (0.02 g, 0.09 mmol), **7** (0.04 g, 0.16 mmol), and **2** (trace) were determined by means of gas or liquid (column) chromatography.

References

1) Presented in part at the 37th National Meeting of the Chemical Society of Japan, Yokohama, April 1978.

2) R. Huisgen, H. J. Strum, and M. Seidel, *Chem. Ber.*, **94**, 1555 (1961).

3) This compound is regarded as the primary intermediate in the reaction of 5-phenyltetrazole with *p*-toluenesulfonyl chloride.[2]

4) S. Wawzonek and J. N. Kellen, *J. Org. Chem.*, **38**, 3627 (1973).

5) S. Ito, Y. Tanaka, and K. Yoshida, Abstracts of the Meeting of the Tokai Branch of the Chemical Society of Japan, Matsumoto, November 1972, p. 1; Abstracts of the 28th National Meeting of the Chemical Society of Japan, Tokyo, April 1973, Vol. III, p. 1371.

6) The original presence of aniline in the reaction in boiling toluene gave a similar result: phenyl *p*-aminophenyl sulfide and/or sulfoxide, which would form by the reaction of benzenesulfinic acid with aniline,[7] could not be found.

7) O. Hinsberg, *Ber.*, **36**, 113 (1903).

8) E. S. Gould, "Mechanism and Structure in Organic Chemistry," Henry Holt and Co., New York (1960), p. 580.

9) The release of **12** from **3** in the first step of reaction may be supported by the fact that 3,6-di(*p*-nitrophenyl)- and 3,6-di(*p*-cyanophenyl)-1,4-bis(phenylsulfonyl)-1,4-dihydro-1,2,4,5-tetrazine prepared from the corresponding hydrazonoyl chlorides are stable thermally as compared with **3**.[5]

10) F. P. Corson and R. G. Pews, *J. Org. Chem.*, **36**, 1654 (1971).

11) M. Kobayashi, *Bull. Chem. Soc. Jpn.*, **39**, 967 (1966).

12) J. L. Kice and K. W. Bowers, *J. Am. Chem. Soc.*, **84**, 605 (1962).

13) D. S. Tarbell, in "Organic Sulfur Compounds," ed by N. Kharasch, Pergamon Press, London (1961), Vol. 1, Chap. 10, p. 97.

14) T. Kagiya, "Kagaku-hanno no Sokudoron-teki Kenkyu-ho," Kagaku-dojin, Kyoto (1970), p. 218.

15) Dihydrotetrazine **16** is known to be oxidized to tetrazine **2** by air. When **16** was warmed in DMSO under nitrogen atmosphere, the fast formation of **2** was observed.

16) The mass spectrum of *S*-phenyl benzenethiosulfonate has appeared: S. Kozuka, H. Takahashi, and S. Oae, *Bull. Chem. Soc. Jpn.*, **43**, 129 (1970).

17) The fragment ion of *m/e* 65 should be assigned to be $C_5H_5^+$ generated from PhS^+ by the loss of C=S.

18) A. Pinner, *Ber.*, **27**, 1004 (1894); "Beilsteins Handbuch der Organischen Chmie," Bd 26, Hauptwerke (1937), p. 83.

19) Water should be furnished by the acid-catalyzed dehydration of butanol.

20) S. Ito, Y. Tanaka, and A. Kakehi, *Bull. Chem. Soc. Jpn.*, **49**, 762 (1976).

21) Commercial reagent-grade DMSO was used without purification.

22) B. Holmberg, *Arkiv Kemi*, **9**, 47 (1955); *Chem. Abstr.*, **50**, 11325c (1956).

Radiation-induced Reactions of Pyridinecarboxylic Esters in Acidic Alcoholic Solutions. Substitution by Alkyl and Hydroxyalkyl Groups and Reduction of Carboxylic Esters to Alcohol[1)]

Kazuhito NAKAMURA, Yukari MORITA, Toru SUZUKI, Toru SUGIYAMA, and Akira SUGIMORI*

Department of Chemistry, Faculty of Science and Technology, Sophia University, Kioi-cho 7, Chiyoda-ku, Tokyo 102

(Received October 4, 1978)

The main reactions of pyridinecarboxylic esters induced by Co-60 γ-rays in acidic alcoholic solutions are: 1) substitution on the pyridine ring by alkyl or hydroxyalkyl groups derived from solvent alcohols, and 2) reduction of carboxylic esters to alcohol (hydroxymethyl group). Substitution is dominant in methanol solutions and reduction is dominant in 2-propanol solutions. Carboxylic esters at the 2- and 4-positions are selectively reduced to alcohols. Alkylation results from the attack by hydrogen atoms and hydroxylalkyl radicals. Reduction of carboxylic esters to alcohol is effected by the hydroxyalkyl radicals derived from the radiolysis of alcohols.

Radiation-induced reactions of pyridinecarboxylic acid derivatives including biologically important nicotinamide and nicotinic acid have not yet been thoroughly investigated at least on the basis of product analysis. Schachinger and Heindle reported the radiation-induced hydroxylation for the model compounds of NAD (nicotinamide adenine dinucleotide) in aqueous solutions.[2)] Swallow suggested the formation of a "dimer" during the X-ray irradiation of certain model compounds for NAD.[3)] By means of pulse radiolysis technique, intermediates formed by the reaction of pyridinecarboxylic acid derivatives with reactive species from the radiolysis of water and with the hydroxyalkyl radicals formed during the irradiation of aqueous alcohol have been investigated.[4,5)]

The radiation-induced reactions of esters of 2-, 3-, and 4-pyridinecarboxylic acids and of 2,5-pyridinedicarboxylic acid have been studied and compared with the work of Minisci *et al.* on the free radical substitution,[6)] and our work on the photochemical reactions.[7)]

Experimental

Materials. 2-Pyridinecarboxylic esters were synthesized by the reaction of acid chloride prepared from 2-pyridinecarboxylic acid (GR grade reagent of Tokyo Kasei Co.) with alcohols. The esters were purified by means of vacuum distillation and finally by preparative TLC before use. Commercial methyl and ethyl esters of 3- and 4-pyridinecarboxylic acid (GR grade reagent of Tokyo Kasei Co.) were purified by vacuum distillation. Dimethyl 2,5-pyridinedicarboxylate prepared by the esterification of 2,5-pyridinedicarboxylic acid (GR grade reagent of Tokyo Kasei Co.) in the presence of hydrogen chloride was used after recrystallization from methanol (mp 158 °C).

Gamma-irradiation. Solutions containing 0.03 mol dm^{-3} of pyridinecarboxylic esters and 0.05 mol dm^{-3} of sulfuric acid were deaerated by bubbling nitrogen gas for 20 min before irradiation. The solutions were irradiated with the Co-60 γ-irradiation facility of Japan Atomic Energy Research Institute in Takasaki. The normal dose rate and dose were 5×10^5 rad h^{-1} and 1.0×10^7 rad, respectively.

Isolation of Products. The irradiated solutions (each *ca.* 100 cm^3) were concentrated under reduced pressure to about 3 cm^3. After the neutralization with aqueous sodium hydrogencarbonate or sodium carbonate solutions, the products were extracted 7 times each with 5 cm^3 of dichloromethane. The extract was dried over anhydrous sodium sulfate. After concentrating the solution, the products were separated by means of TLC. Except for the methylated products of methyl 3-pyridinecarboxylate, products were obtained in pure form.

Identification of Products. Reduction Products: The identification of 2- and 4-hydroxymethylpyridine was carried out by the comparison of their NMR and IR spectra with those of authentic ones.

Methyl 6-hydroxymethyl-3-pyridinecarboxylate from dimethyl 2,5-pyridinedicarboxylate was identified from the following basis. IR (KBr disc) 3350 (OH), 1725 cm^{-1} (ester C=O); NMR ($CDCl_3$) δ=9.26 (1H, d, J=2.1 Hz, H at 2-position), 8.38 (1H, dd, J=8.0 and 2.1 Hz, H at 4-position), 7.46 (1H, d, J=8.0 Hz, H at 5-position), 4.90 (2H, s, $C\underline{H}_2$-OH), 4.02 (3H, s, $C\underline{H}_3OCO$-); MS (70 V) *m/e* (relative intensity) 167 (77), 166 (100), 138 (57), 137 (23), 136 (36), 108 (15), 106 (11), 79 (35), 78 (45), 59 (11), 53 (12), 52 (15), 51 (30), and 50 (16).

The position of the reduction was confirmed by MS. The difference of the mass-spectrometric behavior between methyl esters at the 2- and 3-positions on the pyridine ring is seen in the following fragmentation patterns.

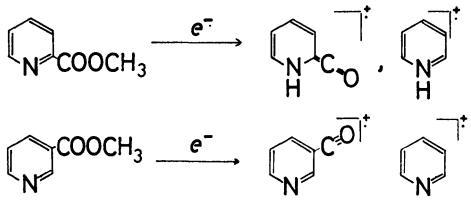

For the methyl ester of 2-pyridinecarboxylic acid, McLafferty-type fragmentation (intramolecular hydrogen abstraction by the N atom of pyridine) occurs and the peak of $(M-30)^+$ and $(M-58)^+$ are observed, whereas for the methyl ester of 3-pyridinecarboxylic acid the intramolecular hydrogen abstraction cannot occur and the peaks of $(M-31)^+$ and $(M-59)^+$ are observed. This assignment was supported by using methyl-d_3-2-pyridinecarboxylate.

In the mass spectra of the reduction product from dimethyl 2,5-pyridinedicarboxylate, the $(M-59)^+$ peak was observed but the peak of $(M-58)^+$ was very low and the peak of $(M-31)^+$ was higher than that of $(M-30)^+$. Peaks of $(M-29)^+$, $(M-30)^+$, and $(M-31)^+$ can be partly ascribed to the decomposition of the hydroxymethyl moiety of the product. This fact indicates that the reduction occurred at the 2-position.

Alkylation Products: Methyl 6-methyl-3-pyridinecarboxylate was identified by comparison with the authentic sample synthesized by the method of Graf.[8]

Methyl esters of 4-methyl-2-pyridinecarboxylic, 6-methyl-3-pyridinecarboxylic and 2-methyl-4-pyridinecarboxylic acids were identified by the accordance of their NMR spectra with those obtained by Deady *et al.*[9] The alkylated products in the reaction in alcohols other than in methanol were identified by the comparison of NMR spectra with the corresponding methylated products from the reaction of methyl esters in methanol solutions.

The structures of methyl 4,6-dimethyl-2-pyridinecarboxylate which was obtained only in a small amount and methyl 4,6-dimethyl-3-pyridinecarboxylate which was obtained only in a mixture was presumed on the basis of NMR spectra.

Methyl 4,6-dimethyl-2-pyridinecarboxylate, NMR ($CDCl_3$) δ=7.75 (1H, s, H at 3-position), 7.12 (1H, s, H at 5-position), 3.98 (3H, s, $C\underline{H}_3OCO$–), 2.60 (3H, s, $C\underline{H}_3$), and 2.38 (3H, s, $C\underline{H}_3$)

Methyl 4,6-dimethyl-3-pyridinecarboxylate, NMR ($CDCl_3$) δ=8.88 (1H, s, H at 2-position), 6.95 (1H, s, H at 5-position), 3.90 (3H, s, $C\underline{H}_3OCO$–), 2.59 (3H, s, $C\underline{H}_3$), and 2.54 (3H, s, $C\underline{H}_3$).

Methyl 2-hydroxymethyl-4-pyridinecarboxylate was identified by the comparison of its spectral data with those obtained by Ninomiya *et al.*[10]

Methyl 6-hydroxymethyl-4-methyl-2-pyridinecarboxylate: mp 27.0—28.5 °C; IR (KBr disc) 3350 (OH) and 1725 cm^{-1} (ester C=O); NMR ($CDCl_3$) δ=7.81 (1H, d, J=1 Hz, H at 3-position), 7.30 (1H, d, J=1 Hz, H at 5-position), 4.79 (2H, s, $HOC\underline{H}_2$–), 3.98 (3H, s, $C\underline{H}_3OCO$–), 2.45 (3H, s, $C\underline{H}_3$–); MS (70 V), *m/e* (relative intensity), 181 (38), 180 (57), 166 (13), 152 (8), 151 (9), 148 (11), 124 (8), 123 (100), 122 (11), 121 (10), 120 (14), 119 (7), 105 (35), 93 (8), 92 (8); Found: C, 60.80; H, 4.87; N, 7.68%; M^+, 181 Calcd for $C_9H_{10}NO_3$: C, 59.94; H, 5.59; N, 7.77%; M, 181.

Determination of the Yields of Products. For the determination of the yields of the alkylated and hydroxyalkylated products the gravimetric method after the separation by TLC was applied. The composition of the methylation products from methyl 3-pyridinecarboxylate, which could not be separated by means of TLC was estimated by NMR. For the study of the effect of the acid concentration on the reaction of ethyl 2-pyridinecarboxylate in ethanol, the yields of the products were determined by means of gas-chromatography (column, Carbowax 20M or Triton QS 15; temperature, 160—180 °C). For the determination of the yields of hydroxymethylpyridines, gas-chromatography was employed.

Calculation of the Electronic States. The electronic states of pyridinecarboxylic esters were calculated using the CNDO/2 program (Q.C.P.E. 141) prepared by Pople, Beveridge and Dobosh and arranged by Kihara, Fujikawa, and Aoyama. The structural parameters obtained for 3-pyridinecarboxylic acid[11] was used as a basis. For the other structural parameters, the generally accepted values are substituted, and the structure of the ester group in 3-pyridinecarboxylic ester is assumed for 2- and 4-pyridinecarboxylic esters.

Results and Discussion

The main reactions of pyridinecarboxylic esters in acidic alcoholic solutions under Co-60 γ-irradiation are: 1) the substitution on the pyridine ring by alkyl and/or hydroxyalkyl groups which originate from the solvent alcohols, and 2) the reduction of alkoxycarbonyl group to hydroxymethyl group. Whether reduction or alkylation (or hydroxyalkylation) is predominant depends on the structure of the substrates and on the alcohols used as the solvents.

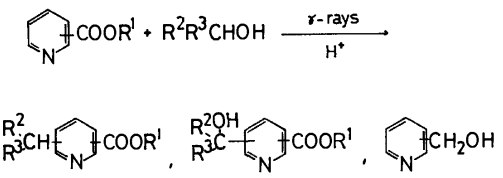

Alkylation and Hydroxyalkylation. Results on the radiation-induced alkylation and hydroxyalkylation in 2-, 3-, and 4-pyridinecarboxylic esters are summarized in Table 1. Except for 4-pyridinecarboxylic ester, alkyla-

Table 1. Radiation-induced alkylation and hydroxyalkylation of pyridinecarboxylic esters

[Substrate]=0.03 mol dm^{-3}; [H_2SO_4] =0.05 mol dm^{-3}; dose rate, 5×10^5 rad h^{-1}; dose, 10^7 rad.

Substrate	Alcohol	Additive (Concn of additive)	Position and group introduced	*G*-value
Methyl 2-pyridinecarboxylate	MeOH		4-Methyl-	1.29
			4,6-Dimethyl-	0.10
			4-Methyl-6-hydroxymethyl-	0.16
	MeOH	I_2(0.015 mol dm^{-3})	No methylated product	
Ethyl 2-pyridinecarboxylate	EtOH		4-Ethyl-	0.12
			6-Ethyl-	0.01
	EtOH	$FeCl_3$ (0.03 mol dm^{-3})	4-Ethyl-	0.02
Butyl 2-pyridinecarboxylate	*n*-BuOH		4-Butyl-	0.10
			6-Butyl	0.08
Isopropyl 2-pyridinecarboxylate	*i*-PrOH		6-Isopropyl	0.02
Methyl 3-pyridinecarboxylate	MeOH		4-Methyl-	0.21
			6-Methyl-	0.58
			4,6-Dimethyl-	0.31
	MeOH	I_2 (0.015 mol dm^{-3})	No methylated product	
Ethyl 3-pyridinecarboxylate	EtOH		6-Ethyl-	1.42
Methyl 4-pyridinecarboxylate	MeOH		2-Methyl	0.16
			2-Hydroxymethyl	0.23
	MeOH	I_2 (0.015 mol dm^{-3})	No methylated product	

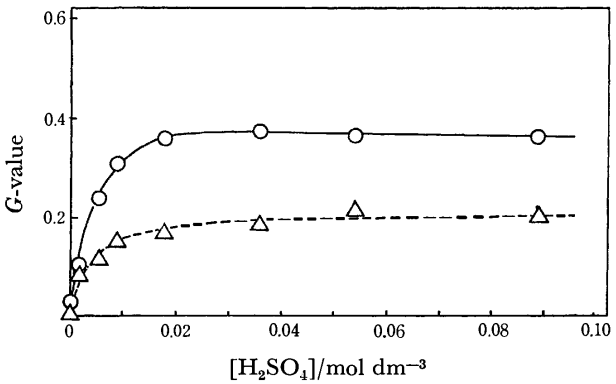

Fig. 1. Effect of the concentration of sulfuric acid on the radiation-induced ethylation and reduction of ethyl 2-pyridinecarboxylate.
-△- Ethyl 4-ethyl-2-pyridinecarboxylate, -○- 2-hydroxymethylpyridine. [Ethyl 2-pyridinecarboxylate]= 0.03 mol dm^{-3}; dose rate, 4×10^5 rad h^{-1}; dose, 8×10^6 rad.

tion is dominant over hydroxyalkylation. Figure 1 shows that the alkylation occurs in an acidic environment where pyridinecarboxylic ester is in the cationic pyridinium form.

The fact that the alkylation is completely inhibited by iodine and iron(III) chloride shows that the reaction proceeds *via* free radical intermediates. However, there is a difference between the radiation-induced reaction and the free radical reaction of pyridine derivatives in alcohol, where hydroxyalkylation is dominant over alkylation.[6] In both cases hydroxyalkyl radicals are expected to play an important role.

Free radical substitution of pyridinium compounds has been investigated by Minisci and his coworkers.[6] According to them, alkyl radicals bring about alkylation and hydroxyalkyl radicals hydroxyalkylation.

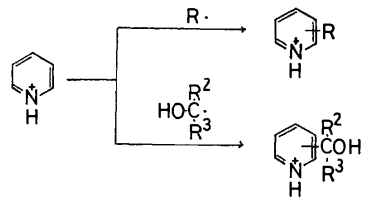

Reported *G*-values (radiation-chemical yield) for primary reactive species from the radiolysis of methanol are 2.0 for electron, 1.1 for H·, 0.2 for ·OH, 0.2 for $\cdot CH_3$, and 2.7 for $\cdot CH_2OH$, respectively.[12] The fact that alkylation is favored over hydroxyalkylation in radiation-induced reactions is not consistent with the higher *G*-value of $\cdot CH_2OH$ and lower *G*-value of $\cdot CH_3$.

The difference between the radiation-induced reaction and the free radical-initiated reaction in alcohol is the participation of hydrogen atoms in the former. (Under the acidic conditions which we employed, electrons should be very effectively converted to hydrogen atoms and the formation of 3.1H· per 100 eV of absorbed radiation energy is expected.) Radiation-induced alkylation can be explained by the initial attack of H

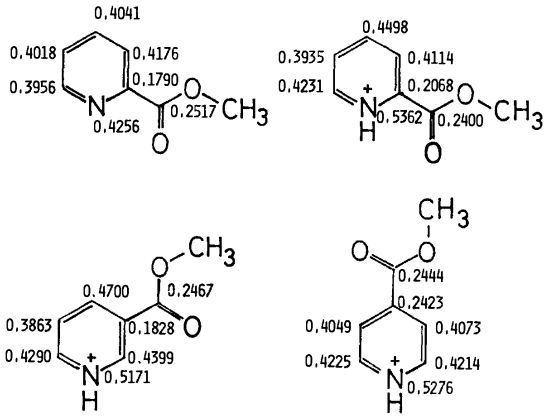

Fig. 2. Free valence in π-electronic systems of pyridine carboxylic esters calculated by CNDO/2.

atoms to the nitrogen atom, which has the greatest free valence among the atoms constituing the pyridine ring (Fig. 2), followed by the attack of hydroxyalkyl radicals and the elimination of water.

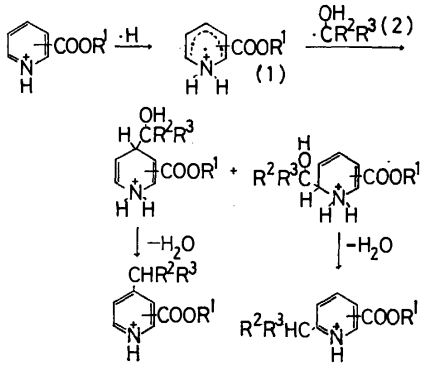

As to the alkylation and hydroxyalkylation, the radiation induced reaction is similar to the photoreaction;[13] alkylation is predominant over hydroxyalkylation and the alkylation occurs at α- and γ-position of pyridine nucleus. Photochemically excited pyridinium abstracts a hydrogen atom from alcohol to give the intermediate (**1**) and hydroxyalkyl radical (**2**). This should be the reason of the similarity between the radiation-induced reaction and the photochemical reaction.

Reduction of Carboxylic Ester to Alcohol. The remarkable reaction induced by ionizing radiation is the reduction of the carboxylic ester group to the hydroxymethyl group. In Table 2, *G*-values for the reduction of methyl esters of pyridinecarboxylic acids in several alcohols are summarized.

Among the esters of monocarboxylic acids, 2- and 4-pyridinecarboxylic esters are reduced to alcohols, whereas 3-pyridinecarboxylic ester is not reduced. In dimethyl 2,5-pyridinedicarboxylate, the carboxylic ester at the α-position is selectively reduced. The efficiency of the reduction is higher in the secondary alcohol than in the primary alcohols.

As to the intermediacy of the aldehyde, no conclusion has been made: among the products from methyl 2-pyridinecarboxylate we could not identify 2-pyridinecarbaldehyde and the irradiation of 2-pyridinecarbalde-

Table 2. Dependence of G-values for reduction of alkyl pyridinecarboxylates to hydroxymethylpyridines on alcohol

[Substrate]$=0.03$ mol dm^{-3}; [H_2SO_4]$=0.05$ mol dm^{-3}; dose rate, 5×10^5 rad h^{-1}; dose, 10^7 rad.

Substrate	Alcohol	G(Hydroxymethylpyridine)
Methyl 2-pyridinecarboxylate	MeOH	0.012
	EtOH	0.54
	n-PrOH	0.46
	n-BuOH	0.40
	i-PrOH	0.93
Ethyl 3-pyridinecarboxylate	MeOH	0.0
	EtOH	0.0
Ethyl 4-pyridinecarboxylate	EtOH	0.13
Dimethyl 2,5-pyridinedicarboxylate[a)]	MeOH	0.03
	i-PrOH	0.26

a) Reduction product is methyl 6-hydroxymethyl-3-pyridinecarboxylate (the product reduced at 2-position of the substrate).

hyde in 2-propanol gave only small amount of 2-hydroxymethylpyridine.

The reduction is brought about by free radicals produced by ionizing radiation, because the reduction is inhibited by iodine and iron(III) chloride. As is seen in Fig. 1, the reduction occurs in acidic conditions.

As the reducing species, hydroxyalkyl radicals and hydrogen atoms should be taken into consideration. Solvated electrons cannot participate in the reduction, because they should react with H^+ rather than with the substrate.

A small amount of 2-hydroxymethylpyridine was obtained in the sun-light irradiation of methyl 2-pyridinecarboxylate in ethanol in the presence of acetone. In this system, the formation of hydroxymethyl radicals is expected.

Table 3. Pai-electron density and π-bond order of the carbonyl moiety in pyridinecarboxylic esters calculated by CNDO/2

Compound	π-Electron density		π-Bond order
	C	O	
Methyl 2-pyridinecarboxylate (neutral form)	0.8243	1.3043	0.8818
Methyl 2-pyridinecarboxylate (pyridinium form)	0.8576	1.2553	0.8885
Methyl 3-pyridinecarboxylate (pyridinium form)	0.8468	1.2769	0.8885
Methyl 4-pyridinecarboxylate (pyridinium form)	0.8546	1.2419	0.8913

The above fact suggests that the reducing species are hydroxyalkyl radicals. The series of $E_{1/2}$ *vs.* SCE -1.30 V ($(CH_3)_2\dot{C}OH$), -1.18 V (CH_3–$\dot{C}HOH$), and -0.98 V ($\cdot CH_2OH$)[14] correlates well with the G-values for the reduction.

The correlation between the reactivity for the reduction and the electronic state of pyridinecarboxylic esters (Table 3) is not so significant. Among the calculated π-electron densities and π-bond orders, the π-electron densities at O atoms of the carbonyl moiety of the substrates show the correlation to the reactivities.

The authors wish to express their hearty thanks to Professor L. W. Deady of La Trobe University in Australia and Professor Ichiya Ninomiya of Kobe Women's College of Pharmacy for sending us the spectral data of pyridinecarboxylic acid derivatives. We also would like to thank Mr. Susumu Kumon and Miss Kuniko Yamada of Shin-Nihon Jitsugyo Co. for obtaining the mass spectra.

The present work was partially supported by a Grant-in-Aid for Scientific Research from the Ministry of Education Science and Culture (No. 147026).

References and Note

1) Preliminary report, K. Nakamura, T. Sugiyama, T. Suzuki, and A. Sugimori, *Chem. Lett.*, **1977**, 1203.

2) L. Schachinger and B. Heindle, *Atomkernenergie*, **24**, 121 (1974).

3) A. J. Swallow, *Biochem. J.* **61**, 197 (1955); G. Stein and A. J. Swallow, *J. Chem. Soc.*, **1958**, 306.

4) U. Brühlmann and E. Hayon, *J. Am. Chem. Soc.*, **96**, 6169 (1974).

5) M. Simić and M. Ebert, *Int. J. Radiat. Phys. Chem.*, **3**, 259 (1971).

6) F. Minisci, *Synthesis*, **1973**, 1; F. Minisci and O. Porta, *Adv. Heterocycl. Chem.*, **16**, 123 (1974).

7) F. Takeuchi, T. Sugiyama, T. Fujimori, K. Seki, Y. Harada, and A. Sugimori, *Bull. Chem. Soc. Jpn.*, **47**, 1245 (1974); T. Sugiyama, T. Furihata, Y. Edamoto, R. Hasegawa, G. P. Satô, and A. Sugimori, *Tetrahedron Lett.*, **1974**, 4339.

8) R. Graf, *J. Prakt. Chem.*, **133**, 19 (1933).

9) L. W. Deady, P. M. Harrison, and R. D. Topson, *Org. Magn. Reson.*, **7**, 41 (1975); L. W. Deady, private communication.

10) I. Ninomiya, private communication.

11) W. B. Wright and G. S. D. King, *Acta Crystallogr.*, **6**, 317 (1953).

12) J. W. T. Spinks and R. J. Woods, "An Introduction to Radiation Chemistry," 2nd ed, John Wiley, New York (1976), p. 415.

13) The photoreactions of pyridinecarboxylic esters consist of alkylation (hydroxyalkylation) and alkoxylation. Whether alkylation or alkoxylation is dominant depends on the structure of the pyridinecarboxylic esters and the reaction conditions. Concerning the alkylation (and hydroxyalkylation), the photoreaction of pyridinecarboxylic esters are similar to radiation-induced reactions. Ref. 7.

14) J. Lilie, G. Beck, and A. Henglein, *Ber. Bunsenges. Phys. Chem.*, **75**, 458 (1971).

Thermal Decomposition of Coal-related Aromatic Compounds in Hydrogen-donating Solvent

Tadashi YAO and Yoshio KAMIYA*

Department of Reaction Chemistry, Faculty of Engineering, The University of Tokyo, Bunkyo-ku, Tokyo 113

(Received June 23, 1978)

In order to elucidate the reaction mechanism of coal dissolution in the hydrogen-donating solvent, twenty aromatic compounds related to coal were treated at 450 °C in the presence of tetralin. Diphenylmethane and bibenzyl slowly decomposed giving alkylbenzenes almost quantitatively. Diphenylmethanol and benzophenone were hydrogenated to diphenylmethane, and benzyl phenyl ketone to a mixture of diphenylmethane and bibenzyl. Diphenyl ether and dibenzofuran are very stable, di-2-naphthyl ether decomposing slowly and benzyl phenyl ether or dibenzyl ether very rapidly. The conversion of aromatic compounds by thermolysis can be correlated as a function of bond dissociation energy. The bond rupture of coal-related polynuclear aromatic compounds at 450 °C was concluded to occur mainly at methylene or ether structures. Addition of phenolic compounds or quinoline is very effective for the decomposition of di-2-naphthyl ether. The effect of phenolic compounds and quinoline on the thermal decomposition of aromatic ether was discussed on the basis of stabilization of transition state due to solvation.

Thermal treatment of coal at 400—450 °C in hydrogen-donating solvent results in successful dissolution of coal and high yield of solvent refined coal[1] (SRC) containing small amounts of sulfur compounds and mineral matters. This is a most promising coal liquefaction process because of very simple and non-catalyzed reaction.

However, the fundamental chemistry of coal liquefaction has received little attention, a very limited number of compounds[2,3] being subjected to thermal treatment. Recently, the thermolysis[4–6] of a number of diarylalkanes and phenolic compounds was studied to elucidate the reaction mechanism.

The most important and interesting reaction in coal liquefaction[7,8] should be the deoxyganation and subsequent dissolution reaction of coal, which starts at 400 °C and almost finishes at 450 °C, resulting in the formation of the solvent refined coal with carbon contents of 86—88% on maf basis independent of coalification grade of the feed coal. Oxygen containing structures should play an important part in the coal liquefaction reaction. It is essential to know what kinds of oxygen containing structure are decomposed and what kind of structure is formed at coal liquefaction temperatures.

We wish to report in this work on the thermal decomposition of diaryl ethers along with other types of coal model structure, and also on the additive effect of phenols and quinoline for the scission of ether linkage. We found that a diaryl ether with polynuclear aromatic is decomposed at coal liquefaction temperature, and that phenols[9] accelerate the liquefaction of coal strongly depending on the character of coal. The effect of additives would be most important for finding out good solvent character for coal liquefaction.

Experimental

Tetralin and 1-methylnaphthalene of reagent grade were used after washing with sulfuric acid, alkali, and water and the subsequent distillation at 70 °C under reduced pressure. Various additives and model compounds were of grade. Some of them were used after recrystallization.

Samples were put into a 300 ml magnetic stirring (500 rpm) autoclave. After being pressurized with 15 kg/cm² of hydrogen, the autoclave was heated to the reaction temperature within 45 min and maintained at the temperature for the desired reaction time.

At the completion of a run, the autoclave was cooled by an electric fan to room temperature and the autoclave gases were vented through a gas meter and analyzed by gas chromatography. Liquid portions of the samples were subjected to gas chromatographic analysis in order to determine the composition of solvent.

Results and Discussion

Thermal Treatment of Tetralin and 1-Methylnaphthalene. In order to investigate the stability of solvent, thermal treatment of tetralin and 1-methylnaphthalene was carried out at 450 °C for 30 min. Their conversion was 3.0 and 1.5%, respectively, indicating that they are very stable under the reaction conditions.

The consumed tetralin was explained to be converted into naphthalene (23%), decalin (40%) and alkylbenzenes (30%), although thermal decomposition of tetralin has been reported by many workers[6,10,11] to yield dihydronaphthalene, decalin, methylindane and ethylbenzene. Only 44% of consumed 1-methylnaphthalene was recovered as naphthalene, indicating considerable formation of polymerized products according to GLC analysis.

Thermal Treatment of Various Aromatic Compounds. In order to study the reaction of coal structure, twenty aromatic compounds were chosen as the coal model and treated at 450 °C. Conversion of the reaction and the detected products are given in Table 1.

Polynuclear aromatic was found to be partially hydrogenated by tetralin. Heredy and coworkers[12] demonstrated that –CHR–, $-CH_2-$, and $-CH_2-CH_2-$ bridges connect aryl groups in coal. However, diphenylmethane and bibenzyl were thermally decomposed slowly giving benzene and toluene almost quantitatively.

Recently, the thermal decomposition of diarylalkanes such as bibenzyl and 1,3-diphenylpropane has been studied by Sato and coworkers[6] and Collins and coworkers.[4,5] These compounds were confirmed to decompose into alkylbenzenes very slowly as a function of carbon chain length at 400 °C.

TABLE 1. REACTION PRODUCTS FROM THE THERMAL TREATMENT OF AROMATIC COMPOUNDS RELATED TO COAL IN THE PRESENCE OF TETRALIN

Charge (mmol)			Reaction conditions		Conversion (%)		Product (mol % to reacte model compound)
Model compound	Tetralin	1-Methyl-naphthalene	Temp (°C)	Time (min)	Model compound	Tetralin	
Naphthalene	78.1 226	—	450	60	2.8	7.2	—
1-Methylnaphthalene	141.0 217	—	450	30	3.3	8.3	—
Phenanthrene	16.9 301	—	450	60	0.8	9.1	9,10-Dihydrophenanthrene 70
Diphenylmethane	6.1 220	141	450	30	1.7	8.0	Benzene 100, Toluene 95
Bibenzyl	16.6 217	140	450	30	31.1	11.2	Toluene 207
Bibenzyl	27.5 300	—	450	60	54.1	21.4	Toluene 194
Diphenyl ether	5.9 220	141	450	30	0	8.0	—
Benzyl phenyl ether	5.4 287	80	400	30	100	12.7	Toluene 71, Phenol 66, Benzyl phenol 17
Dibenzyl ether	5.1 220	141	400	30	65	9	Toluene 100, PhCHO, PhH, $PhCH_2OH$
Di-2-naphthyl ether	11.2 228	141	450	60	12.6	11.9	2-Naphthol 84
Dibenzofuran	6.1 218	141	450	30	3.3	12	—
Benzyl benzoate	4.7 219	141	450	30	100	13.1	Benzene 53, Toluene 98
Benzophenone	5.7 224	141	450	30	29.4	11.2	Diphenylmethane 100
Benzyl phenyl ketone	16.2 435	—	450	30	25.3	9.1	Bibenzyl 37, Diphenylmethane 37, Benzene 5, Toluene 7
1-Naphthol	7.1 223	141	450	30	1.4	10.7	—
2-Naphthol	6.9 214	141	450	30	1.4	11.2	—
Diphenylmethanol	5.7 218	141	450	30	79	10.2	Diphenylmethane 96
1,4-Naphthoquinone	6.4 218	141	450	30	100	16.2	1-Naphthol 74, Naphthalene
2-Naphthoic acid	5.5 218	141	450	30	100	9.3	Naphthalene
Diphenylamine	6.1 218	141	450	30	8.2	12.4	Benzene 60, Aniline(trace)
Diphenyl sulfide	5.6 222	141	450	30	10.7	10.8	Benzene 183

When the molar ratio of tetralin to a mixture of 1-methylnaphthalene and tetralin were increased from zero to 1.0, the conversion of bibenzyl increased from 14 to 30%. This can be attributed to the capability of hydrogen donation of solvent, since the conversion reaches almost a constant value at the equimolar mixture of tetralin and 1-methylnaphthalene.

Although diphenyl ether and dibenzofuran were very stable at 450 °C, di-2-naphthyl ether decomposed slowly and benzyl ethers completely.

The apparent activation energy for the thermal decomposition of benzyl phenyl ether was calculated to be about 50 kcal/mol from the data obtained at 320—350 °C, since the first order rate constants were 1.39×10^{-4} at 320 °C, 5.19×10^{-4} at 340 °C and 9.52×10^{-4} s^{-1} at 350 °C, respectively.

These results indicate that highly aromatic ether linkages will be broken to a great extent at coal liquefaction temperatures resulting in a main source of phenolic groups of the dissolved coal.

Naphthols were confirmed to be very stable against thermal treatment. Diphenylmethanol and benzophenone were stable against decomposition but hydrogenated to form diphenylmethane quantitatively. Benzyl phenyl ketone was found to be paritally hydrogenated or decarbonylated to form diphenylalkanes. 1,4-Naphthoquinone was completely eliminated and hydrogenated to naphthol and dihydroxynaphthalene as reported by Brower.[13]

Carboxylic acid and carboxylate were completely decarboxylated to the parent hydrocarbons. Carboxylic acid is quite stable in a glass apparatus, but decomposes completely in a stainless steel autoclave.[13]

Generally, the conversion of aromatic compounds by thermal treatment can be correlated as a function of bond dissociation energy of the weakest structure of the substrate as shown in Table 2 and Fig. 1. A few exceptions observed in the cases of benzophenone, benzyl benzoate and naphthoic acid can be ascribed to hydrogenation or the wall effect.

Effect of Phenolic Compounds on the Thermal Decomposition of Aromatic Ethers. According to the results given in Table 1, the bond scission of oxygen containing polynuclear aromatic structure of coal at coal liquefaction

TABLE 2. BOND DISSOCIATION ENERGIES OF TEN AROMATIC COMPOUNDS

Structure of bond	Bond dissociation energy (kcal/mol)	Remark
$PhCH_2$–Ch_2Ph	64.5	Ref. 14, 15
$PhCH_2$–Ph	78.4	Ref. 15
PhO–Ph	86.0	Ref. 14, 15
PhO–CH_2Ph	50	Ref. 16
PhCOO–CH_2Ph	66.4	Ref. 14
PhCO–Ph	87.5	Ref. 16
Naph–CH_3	100	Ref. 14
Ph_2CH–OH	78	Ref. 14
Ph–Ph	118.1	Ref. 16
$PhCH_2CO$–CH_2Ph	65.4	Ref. 14

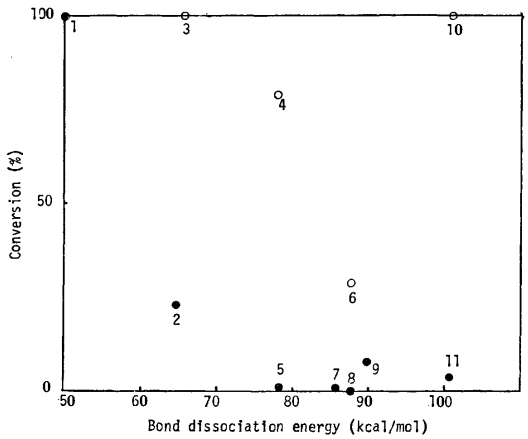

Fig. 1. Relation between the bond dissociation energy and the conversion of aromatic compounds.
1: Benzyl phenyl ether, 2: bibenyl, 3: benyl benzoate, 4: diphenylmethanol, 5: diphenylmethane, 6: benzophenone 7: diphenyl ether, 8: naphthol, 9: diphenylamine, 10: 2-naphthoic acid, 11: 1-methylnaphthalene.

temperature 400—450 °C seems to occur mainly at methylene or ether structures. Thus, a study of the characteristics of these structures in the thermolysis is important.

It has been proposed that the units of coal structure are linked by ether linkages.[17,18] Recently, Ruberto and his coworkers[19] concluded that a significant portion of the oxygen in solid subbituminous coal occurs in saturated ether functional groups α- or β- to the aromatic moieties or as furan systems. Ignasiak and Gawlak[20] concluded from the increase in hydroxyl functions in the protonated coal concentrate that for each 4.6 ruptured covalent bond two were ether linkages.

As shown in Table 1 the decomposition of di-2-naphthyl ether proceeds slowly. We have chosen this ether and studied in detail the effect of various phenols on the decomposition of the aromatic ether since phenols remarkably enhance coal dissolution among the several types of oxygenated compounds.[9]

The thermal decomposition of bibenzyl is not affected by the addition of phenol or *p*-cresol (Table 3). In contrast, the decomposition of di-2-naphthyl ether increases remarkably in the presence of phenolic compounds (Table 4). The effect seems to increase with increase in the electron donating property of substituent on the benzene nucleus.

The effect of hydroquinone and *p*-methoxyphenol is remarkable. However, no decisive argument can be made since they can not be recovered sufficiently, indicating that very complicated side reactions take place.

Although 1-naphthol is quite stable against thermal decomposition (Table 1), its recovery after the thermolysis of dinaphthyl ether is not successful. This is in line with our previous findings[9] that about half the amount of naphthol can be recovered after the dissolution of coal in contrast to the very high recovery of phenol and *p*-cresol. This indicates that a naphthyloxyl radical is decomposed into alkylbenzene or alkylnaphthalene after reacting with some other free radicals.

Phenolic compounds might enhance the rate of decomposition of aromatic ether by solvating transition state of the scission of ether linkage and by hydrogen transfer to the formed alkoxyl radicals.

Effect of Quinoline. Quinoline shows no effect on the decomposition of bibenzyl, but considerably increases the conversion of dinaphthyl ether as in the cases of phenols (Tables 3 and 4).

The yield of 2-naphthol from dinaphthyl ether was

Table 3. Effect of phenol and quinoline on the thermal decomposition of bibenzyl at 450 °C for 60 min

Charge (mmol)				Conversion (%)		
Phenol		Bibenzyl	Tetralin	Bibenzyl	Tetralin	Phenol
1-Methylnaphthalene	70.2	16.7	225.7	35.5	12.3	5.7
Phenol	107.1	16.5	226.2	33.1	12.2	1.5
Quinoline	76.8	16.6	226.1	35.6	10.9	18.6

Table 4. Effect of phenols and quinoline on the thermal decomposition of di-2-naphthyl ether at 450 °C for 60 min

Charge (mmol)				Conversion (%)		Yield (mol % to reacted ether)
Phenols or quinoline		Di-2-naphthyl ether	Tetralin	Dinaphthyl ether	Phenol or quinoline	2-Naphthol
1-Methylnaphthalene	141	11.2	228.4	11.5	5.0	67.4
Phenol	210	11.1	230.0	17.1	1.5	57.2
p-Cresol				21.0		
p-Methoxyphenyl[a]	135.3	14.5	225.5	49.5	100	61.3
p-Phenylphenol	117.6	11.1	225.7	34.1	0	54.2
2,4,6-Trimethylphenol	147.0	11.3	226.1	26.0	3.5	30.0
1-Naphthol	138.7	11.2	225.7	33.7	22.1	—
Hydroquinone[b]	182	11.2	225.8	63.4	57.7	24.0
Quinoline	154	11.2	226.5	23.6	22.1	7.0

a) *p*-Methoxyphenol was converted into phenol, hydroquinoline, and benzene. b) Hydroquinone was mostly converted into phenol and benzene.

lowered in the presence of quinoline, suggesting that a considerable amount of naphthyloxyl radical was reacted with quinoline as a result of close interaction between the ether and quinoline during the course of thermal decomposition reaction.

Accelerating Effect Due to Additives on the Rupture of Ether Linkage. Phenols are weak acids and polar solvent, and often enhance the thermal decomposition of covalent bond. However, we could observe no accelerating effect due to phenol on the decomposition of bibenzyl. Pyridine bases accelerate the depolymerization of coal.[10,21] Thus, phenols and quinoline should participate directly in the scission of ether linkage.

Huyser and Van Scoy[22] observed that the thermal decomposition of di-*t*-butyl peroxide is remarkably accelerated in acetic acid or *t*-butyl alcohol. They ascribed this effect to the solvation of *t*-butoxyl radical by the solvents.

Mahoney and Da Rooge[23] found that the hydrogen abstraction from phenols by phenoxyl radicals proceeds very rapidly in spite of very low enthalpy change. Howard and Furimsky[24] suggested that the hydrogen atom transfer between peroxyl radical and phenol involves the formation of a hydrogen bonded free radical reactant complex.

A phenoxyl radical from the thermal decomposition of aromatic ether can be stabilized by solvation or hydrogen bonding with phenolic compounds, giving rise to the subsequent hydrogen transfer reaction from phenols or hydrogen donor solvents.

Stabilization of the transition state of bond dissociation or the formed alkoxyl radical might be the best explanation for the rate enhancement, since quinoline also remarkably accelerates the decomposition of dinaphthyl ether. Alkoxyl radical would be electron donor and phenols or quinoline electron acceptors.

In view of bond dissociation energy, phenolic compounds having electron supplying substituent such as naphthol and *p*-methoxyphenol can be easily converted into phenoxyl radicals by reacting with the phenoxyl radicals resulting from the thermal decomposition of ether structure, and will result in further decomposition reaction including deoxygenation reaction.

Easiness of bond rupture of an ether depends strongly on its chemical structure. Diphenyl ether and dibenzofuran are quite stable against thermal treatment at 450 °C, while dibenzyl ether and benzyl phenyl ether can be completely decomposed at 400 °C.

Almost all $-CH_2-O-$ linkages in coal structure would be ruptured at temperatures below 400 °C and diaryl ether with polynuclear aromatic moderately at coal liquefaction temperatre. Some coals containing aliphatic ether structure would be decomposed remarkable at lower temperatures and their decomposition would not be affected by the addition of phenols or pyridine bases. Some coals containing polynuclear aromatic diaryl ethers would be decomposed effectively by the addition of phenolic compounds or pyridine bases.

Financial support from the Sunshine Project Promotion Headquarters, Agency of Industrial Science and Technology, is acknowledged.

References

1) Coal Liquefaction Symposium, *Preprints Div. Fuel Chem. Am. Chem. Soc.*, **20** (1) (1975), **21** (5) (1976).
2) R. Brucker and G. Koelling, *Brennstoff Chem.*, **46**, 41 (1965).
3) D. Hausigk, G. Koelling, and F. Ziegler, *Brennstoff Chem.*, **50**, 8 (1969).
4) C. J. Collins, V. F. Raaen, B. M. Benjamin, and G. W. Kabalka, *Fuel*, **56**, 107 (1977).
5) C. J. Collins, B. M. Benjamin, V. F. Raaen, P. H. Maupin, and W. H. Roark, *Preprints Div. Fuel Chem. Am. Chem. Soc.*, **22** (2) 206 (1977).
6) Y. Sato, T. Yamakawa, R. Onishi, H. Kameyama, and A. Amano, *J. Jpn. Petrol. Inst.*, **21**, 110 (1978).
7) Y. Kamiya, *J. Fuel Soc. Jpn.*, **56**, 319 (1977).
8) Y. Kamiya, *J. Fuel Soc. Jpn.*, **57**, 12 (1978).
9) Y. Kamiya, H. Sato, and T. Yao, **57**, 681 (1978).
10) R. C. Neavel, *Fuel*, **55**, 237 (1976).
11) D. Kang, L. L. Anderson, and W. H. Wiser, *Preprint Div. Fuel Chem. Am. Chem. Soc.*, **22** (2), 160 (1977).
12) L. A. Heredy, A. E. Kostyo, and M. B. Neuworth, *Fuel*, **41**, 221 (1962), **43**, 414 (1964), **44**, 125 (1965).
13) K. R. Brower, *Fuel*, **56**, 245 (1977).
14) "Handbook of Chemistry and Physics," 57th ed, CRC (1976), pp. F231, 328.
15) "Handbook of Chemistry," 2nd ed, Maruzen (1975), p. 976.
16) S. W. Benson, *J. Chem. Educ.*, **52**, 502 (1965).
17) C. H. Fisher and A. Eisner, *Ind. Eng. Chem.*, **29**, 1371 (1937).
18) Y. Takegami, S. Kajiyama, and C. Yokokawa, *Fuel*, **42**, 291 (1963).
19) R. G. Ruberto, D. C. Cronauer, D. M. Jewell, and K. S. Seshadri, *Fuel*, **56**, 17, 25 (1977).
20) B. S. Ignasiak and M. Gawlak, *Fuel*, **56**, 216 (1977).
21) D. W. Van Krevelen, "Coal Science," Elsevier (1961), p. 177.
22) E. S. Huyser and R. M. Van Scoy, *J. Org. Chem.*, **33**, 3524 (1968).
23) L. R. Mahoney and M. A. Da Rooge, *J. Am. Chem. Soc.*, **89**, 5619 (1967).
24) J. A. Howard and E. Furimsky, *Can. J. Chem.*, **51**, 3788 (1973).

Synthesis and Reactions of *o*-Benzothioquinonemethides

Renji OKAZAKI, Kazuhiko SUNAGAWA, Kyung-Tae KANG, and Naoki INAMOTO*
Department of Chemistry, Faculty of Science, The University of Tokyo, Hongo, Tokyo 113
(Received June 26, 1978)

Photoreactions of 1,2-benzodithiole-3-thione with olefins (cyclopentene, cyclohexene, cyclooctene, and 2,3-dimethyl-2-butene) afforded deep blue *o*-thioquinonemethides (**4**) in high yields. The thione **4** is equilibrated with a colorless head-to-head dimer having an eight-membered ring. The mode of the dimerization has been discussed in comparison with other *o*-quinonoid compounds. Cycloaddition reactions of **4** with electron-deficient acetylenes and olefins gave rise to [4+2] adducts. It was confirmed that these cycloadditions proceeded stereoselectively as well as regioselectively. Reactions of **4** with diphenylketene, phenyl isocyanate, and phenyl isothiocyanate led to six-membered 1:1 adducts. Reduction by hydride reagents has been also described.

Chemistry of *o*-quinonoid compounds has extensively been investigated in recent years because of the interesting chemical and physical properties and the synthetic application.[1,2] However, there had been no report concerning *o*-thioquinonemethides, when we started this study, except those which described their existence as a transient species.[3]

Our previous study on the photochemical reactions of 1,2,4-dithiazole-3-thiones or 1,2-dithiole-3-thiones (**1**) with olefins leading to the corresponding 1:1 adducts (**2**)[4] suggested that a similar ring-opening-cycload-

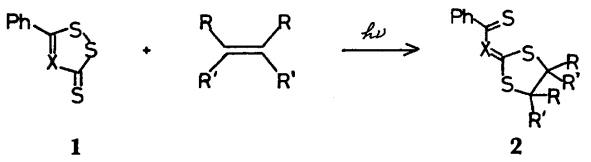

1 **2**

X=N, CH, CPh

dition reaction with 1,2-benzodithiole-3-thione (**3**) would give 6-methylene-2,4-cyclohexadiene-1-thione (referred to *o*-thioquinonemethide hereafter) (**4**) (see below), and indeed this expectation was fulfilled.[5,6] The purpose of this paper is to describe a detailed account of the preparation and some reactions of *o*-thioquinonemethides (**4**) thus formed.

Results and Discussion

Synthesis of o-*Benzothioquinonemethides and Equilibrium with Dimers.* Irradiation of benzo-1,2-dithiole-3-thione (**3**) in the presence of an olefin (cyclopentene, cyclohexene, cyclooctene or 2,3-dimethyl-2-butene) afforded deep blue *o*-thioquinonemethide (**4**). The structure of **4** was established by its cycloaddition leading to [4+2] adduct (see below) and analogy with the photoproducts from **1** and olefins.[4] The color of the

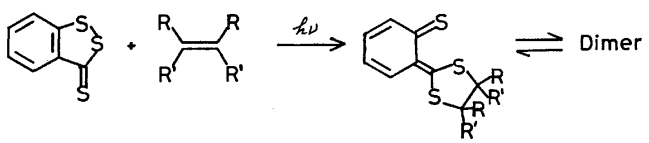

3 **4** **5**

a: RR=$(CH_2)_3$ R'=H 68%
b: RR=$(CH_2)_4$ R'=H 89%
c: RR=$(CH_2)_6$ R'=H 84%
d: R=R'=CH_3 87%

Table 1. Electronic spectra of **4b** in various solvents [a]

Solvent	λ_{max}(nm) (ε)[b]		
cyclohexane	262(5010)	355(700)	580(≈0)
benzene		354(1460)	585(915)
ethanol	264(6100)	350(1940)	580(1180)
dichloromethane	269(10900)	351(4050)	584(2610)

a) Concentration: 1.23×10^{-4} mol/l (as a monomer).
b) Apparent molar extinction coefficient.

Table 2. Electronic spectra of **4** in dichloromethane[a]

4	λ_{max} (nm)(ε)		
4a	267(7480)	350(2200)	585(1390)
4b	269(10900)	351(4050)	584(2610)
4c	269(10000)	350(3720)	584(2380)
4d	—[b]	351(10500)	585(6660)

a) Concentration: $1.23—1.27\times10^{-4}$ mol/l (as a monomer).
b) Could not be determined at this concentration. In 0.492×10^{-4} mol/l, λ_{max} 269 nm (ε 23500).

solution of **4** depends on solvent, temperature, and irradiation with light (Tables 1 and 2). For example, the color of **4b** is deep blue in dichloromethane or tetrahydrofuran (THF) at room temperature, but in cyclohexane it is almost colorless. Recrystallization of **4b** from carbon tetrachloride at −23 °C affords white crystals, the dissolution of which in an appropriate solvent, however, leads to a deep blue solution. The colorless cyclohexane solution of **4b** turns blue on heating or irradiation, but the blue color is discharged when the solution is left at room temperature. These facts and the dependence of the UV spectrum of **4b** on the concentration suggest that **4** is equilibrated with a colorless aggregate. It was found that the aggregate was a dimer on the basis of cryoscopic measurement of the molecular weight for the adduct with cyclohexene (**5b**) in cyclohexane (Found 542, Calcd 532). Other *o*-thioquinonemethides **4a**, **4c**, and **4d** behave similarly, although the blue color of the solution of **4d** is the strongest in any solvent as expected by the highest apparent molar extinction coefficient among **4a**—**4d** (Table 2). It is obvious that the 580 nm band responsible for the blue color is due to the monomer. Although the value of 580 nm is in the range of n-π^* band of conjugate thiones,[4,7] the absorption of **4** is considered to be of π-π^* nature, because the extinction coefficient is too high

for n-π^* bands. In this connection, it is interesting that the visible absorption of **4** bears a close resemblance to that of 6-allylidene-2,4-cyclohexadiene-1-thione (**6**) generated from a photoreaction of 2*H*-thiochromene at 77 K in a rigid matrix (a broad band with its center around 570 nm), though no molar extinction coefficient was given for the latter.[3b]

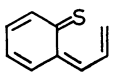

6

Since the intensity change of the 270 and 350 nm bands parallels that of the 580 nm band, the former two are also due to the monomer.

When **4b** was heated in refluxing xylene for 45 min under argon, **3** was formed in a quantitative yield.

Structure of the Dimer. Since the NMR spectrum of the cyclohexene adduct (**5b**) in carbon tetrachloride at −20 °C, where it is almost colorless and hence essentially dimeric, shows eight proton signals between δ 7.3—9.0 ascribed to aromatic or olefinic protons, the dimerization should occur using the thiocarbonyl and/or ketene thioacetal units. The absence of the 580 nm band in the spectrum of **5b** in cyclohexane suggests that it represents that of the dimer, which shows no strong absorption above 300 nm. These facts imply that [4+2] and [2+2] type adducts can be eliminated among many possible structures of the dimer, because they must have a conjugated ketene thioacetal(s) which should have a strong band above 350 nm [*e.g.*, for **7**, λ_{max} 345 nm (ε 6760)][8] or a conjugated thione(s) which should have an absorption in the visible region.[4,7] The dimer, therefore, must be **8** or **9** of [4+4] type.

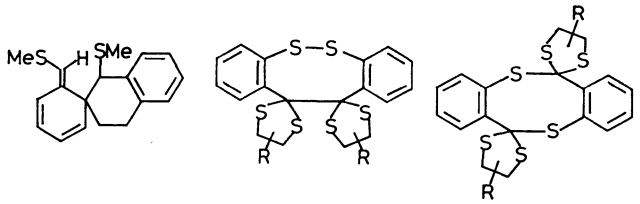

7 **8** **9**

Since it is reasonably assumed that **4a**—**4d** have almost identical molar extinction coefficients each other, irrespective of the substituents of the 1,3-dithiolane ring, the data in Table 2 show that the proportion of the monomer increases with increasing bulkiness of the added olefins, that is, the dissociation into the monomer increases with bulkiness of the thioacetal moiety of the dimer **5**. This fact is more compatible with a head-to-head dimer (**8**) than a head-to-tail dimer (**9**) in view of the higher steric repulsion between the two dithiolane rings in the former.

Desulfurization of **4b** with Raney nickel leading to bibenzyl (5%) along with toluene (41%) is another piece of evidence for the head-to-head structure, although the possibility can not be excluded that the former may be formed from the monomer.[9]

More confirmative evidence comes from isolation of another [4+4]dimer of **4d**.[5b] When **4d** was allowed to react with enamine (**10**) at 60 °C in THF–acetonitrile, a colorless crystalline compound (**11**) with a molecular formula of $(C_{13}H_{16}S_3)_2$ (from elemental analysis and molecular weight determination) was obtained in 38% yield.

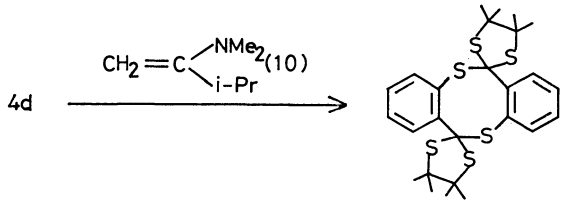

11

The NMR spectrum of the dimer (**5d**) obtained from the photochemical reaction showed four singlets due to the methyl groups (δ 1.22, 1.33, 1.57, and 1.76), while the new dimer (**11**) from above reaction had a singlet (δ 1.52) in the methyl region along with aromatic multiplet (δ 7.0—8.3). The difference can be readily accounted for if we consider that the 11*H*,12*H*-dibenzodithiocin ring of **5d** is less symmetric than that of **11** because of the steric interaction between the two dithiolane rings. Thus, we conclude that the photodimer (**5d**) and the new dimer (**11**) are a head-to-head and a head-to-tail [4+4] type dimers, respectively, although X-ray analysis will be necessary for the final answer.

Dimer (**11**) is thermally stable and does not show thermal equilibrium with the monomer, although it dissociates into an equilibrium mixture of **4d** and **5d** as evidenced by UV and NMR spectra.

It should be noted here that the mode of dimerization of **4** under normal conditions (*i.e*, the formation of a head-to-head dimer) parallels that of *o*-quinodimethanes (**12a-c**)[8,10,11] rather than that of benzothietes (**13a, b**) leading to **14a,b**,[12,13] which might proceed *via* *o*-thioquinonemethide.

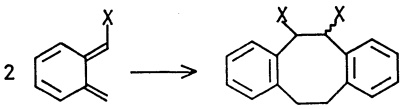

12

a: X=CONHR[10]
b: X=SMe[8]
c: X=P(O)(OMe)$_2$[11]

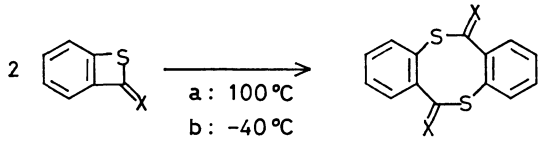

13 **14**

a: X=H_2
b: X=O

It has been reported that quinodimethane (**15**) is stable at −40 °C in *N*,*N*-dimethylformamide but undergoes dimerization, followed by elimination of methanethiol, to give **16**.[14]

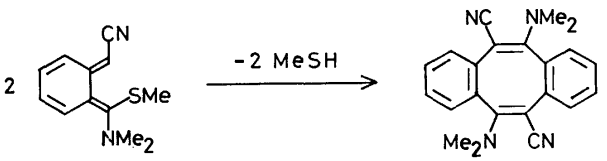

15 16

The reason for these different chemical behaviors is not clear, but one possible explanation is involvement of homolytic processes in the dimerization of **4** and **12**.

Reactions of o-*Thioquinonemethides. a) Reactions with Acetylenes or Olefins*: The *o*-thioquinonemethide (**4**) is a strong enophile and rapidly reacts with acetylenes and olefins having electron-withdrawing groups at room temperature to afford 1,4-cycloaddition adducts. The reaction of **4b** with dibenzoylacetylene and *N*-phenylmaleimide gave **17** (83%) and **18** (93%) respectively. The regioselectivity and stereoselectivity of the cycloaddition were examined with mono- and di-substituted olefins, respectively. Reaction of **4b** with methyl vinyl ketone in refluxing benzene for 5 min afforded only one kind of 1: 1 adduct (**19**) in a quantitative yield. Raney nickel desulfurization of the product gave 3-methyl-4-phenyl-2-butanone (**20**, 64%) and 3-methyl-4-phenyl-2-butanol (**21**, 12%), thus establishing the regioselectivity of the reaction. Acrylamide reacted with **4b** to give 1: 1 adduct (**22**, 64%), the similarity of whose NMR spectrum to that of **19** suggested the same regioselectivity also in this case.

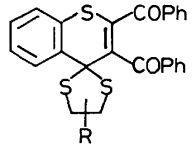

17

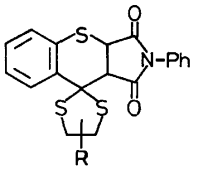

18

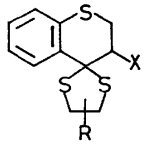

19: X=$COCH_3$
22: X=$CONH_2$

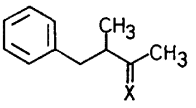

20: X=O
21: X=H, OH

When maleonitrile and fumaronitrile were allowed to react with **4b** in dichloromethane at room temperature for 1 or 2 days, *cis*- (**23a**) and *trans*-adducts (**23b**) were obtained in 66 and 88% yields, respectively. The NMR spectra of the crude reaction products from both dicyanoolefins showed the presence of two methine protons α to a cyano group which appeared as two sets of double doublets of AX type. The intensity ratio of the two double doublets was about 4: 1 (J_{AX}=3.4 Hz for the both doublets) for **23a** and about 5: 1 (J_{AX}= 9.1 Hz for the both doublets) for **23b**. In light of the reported values[10] of 4.5 ($J_{HR'}$) and 10 Hz ($J_{H,R'}$) for similar compounds **24** and **25** respectively, the coupling constants observed for **23a** and **23b** indicate they are *cis*- and *trans*-adducts respectively, the stereoselectivity of the cycloaddition thus being established.

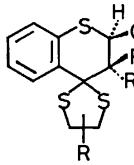

23

a: R^1=CN, R^2=H
b: R^1=H, R^2=CN

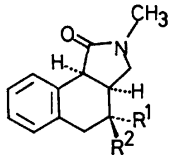

24: R^1=H, R^2=Cl
25: R^1=Cl, R^2=H

The stereoselectivity for cycloaddition of **4** with olefins is noteworthy, because it means the cycloaddition of **4** proceeds probably in a concerted manner, although possible contribution of ionic canonical structure (**26**) might lead to a stepwise ionic reaction resulting in non-stereoselective addition.

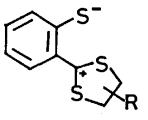

26

The two sets of the spectra for **23a** and **23b** are considered to correspond to two isomers with respect to the direction of the cyclohexane ring. We previously isolated such a sort of isomers in cycloadditions of similar conjugated systems.[15] Recrystallization of **23a** and **23b** gave pure specimens of the corresponding major isomers.

We previously reported that **4** also reacted with electron-rich olefins (*i.e.*, enamines) to give [4+2]adducts.[16]

b) Reactions with Heterocumulenes: Reaction with diphenylketene proceeds very rapidly at room temperature to afford a mixture of **27** and **28** in 73% yield. The primary product (**27**) is unstable and easily isomerizes to **28** or decomposes to **4b** when heated or left on silica gel for a long time. The thioester (**28**) is stable and purified by usual work-up.

4b reacts with phenyl isocyanate at room temperature for 6 days to afford **29** in 88% yield.

Major reaction product with phenyl isothiocyanate in benzene at 80 °C for 21 h was **31** (73%). Although **31** is stable in the presence of the excess isothiocyanate,

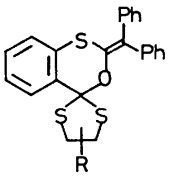

27

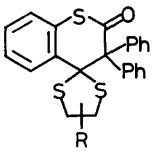

28

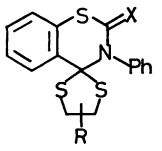

29: X=O
30: X=S

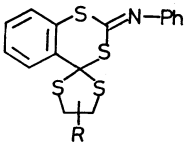

31

it decomposes mainly to **4b** and phenyl isothiocyanate when the isothiocyanate is removed. A compound tentatively assigned as **30** was also isolated in the decomposition product.

c) Reduction and Other Reactions: Reduction with hydride reducing reagents (lithium aluminum hydride and sodium bis(2-methoxyethoxy)dihydridaluminate) followed by methylation were carried out in order to get **32** which would be formed from the dimer (**5b**). The product, however, was not an expected one but **33** (64%) when quenched with aqueous alkali and methyl iodide or **34** (24%) when quenched with dilute sulfuric acid. The formation of these products can be explained in terms of the preferential attack of the hydride on **4b** because of much higher reactivity of **4b** than that of **5b** and/or of facile decomposition of intermediate **35**, even if it is formed from the dimer **5b**.

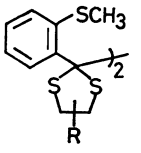

32

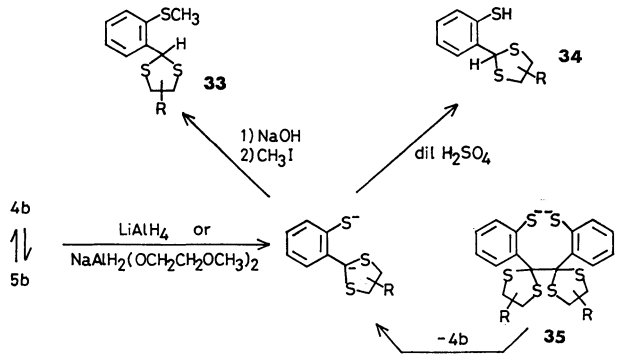

Thiophenol (**34**) was unstable and was gradually oxidized by atmospheric oxygen to afford **4b**.

4b did not react with diphenyldiazomethane or phenyldiazomethane, which readily reacts with thiones to afford episulfides.[17] This is in marked contrast with the reactivity of similar conjugate thiones **2** (X=CH, CPh) which react with diphenyldiazomethane to give **36**.[15]

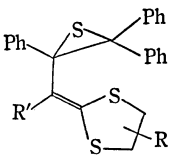

36: R′=H, Ph

Inertness of **4b** toward these diazomethanes is indicative of a greater contribution of the ionic resonance structure of type **26** for **4** as expected from its aromatic stabilization.

Experimental

NMR spectra were recorded with a Hitachi R-20B or R-24 spectrometer using tetramethylsilane as an internal standard. UV and visible absorption spectra were recorded on a Hitachi ESP-3 spectrophotometer. IR spectra were taken with a Hitachi EPI-G2 spectrometer (beam energy 70 eV). Molecular weights were measured with a Hitachi 117 Molecular Weight Apparatus (vapor pressure osmometry in benzene at 40 °C). All the melting points were not corrected.

Synthesis of o-Thioquinonemethides (4). A solution of 1,2-benzodithiole-3-thione (**3**)[18] (460 mg, 2.5 mmol) and cyclohexene (7 ml) in ether (70 ml) was irradiated under nitrogen for 45 min with 100 W medium pressure mercury lamp through Pyrex filter. After 35 or 40 min the color of the solution turned deep blue. The reaction mixture was subjected to dry column chromatography (DCC) (SiO_2, 2: 1 benzene–hexane) to give **4b** (614 mg, 89%). Essentially the same result was obtained when benzene was used as solvent. Recrystallization from carbon tetrachloride at −23 °C afforded white crystals, whose color gradually changed pale blue upon standing under diffused light. Mp 166—167 °C (dec); NMR (CCl_4): δ 1.0—2.5 (br s, 8H), 3.3—4.4 (m, 2H), and 6.8—7.8 (m, 4H); UV (cyclohexane at 7 °C): λ_{max} 260 nm (ε 1.04×10^4). For the spectra in other solvents, see Table 2. Found: C, 58.99; H, 5.20; S, 35.59%. Calcd for $C_{13}H_{14}S_3$: C, 58.60; H, 5.30; S, 36.10%. There formed slightly green crystals when the reaction solution in ether was stood overnight at −5—0 °C. The crystals thus formed, after filtration and washing with ether, were pure enough for further use without purification. The yield of the crystals was about 60%.

Photoreactions of **3** with cyclopentene, cyclooctene, and tetramethylethylene were carried out in a similar way, the yield, after DCC, being 68, 84, and 87%, respectively. In the case of the last olefin, the color of the reaction solution turned deep blue after 10 minutes' irradiation. These *o*-thioquinonemethides were purified by recrystallization from dichloromethane and methanol. **4a**: mp 159—161 °C (dec); NMR ($CDCl_3$): δ 1.7—2.3 (br s, 6H), 3.8—4.4 (m, 2H), and 6.8—7.9 (m, 4H). Found: C, 57.65; H, 4.90; S, 37.35%. Calcd for $C_{12}H_{12}S_3$: C, 57.10; H, 4.79; S, 38.10%. **4c**: mp 153—154 °C (dec); NMR ($CDCl_3$): δ 1.1—2.4 (m, 12H), 3.3—3.9 (m, 1H) 4.0—4.4 (m, 1H), 6.9—7.1 (m, 2H), and 7.25—7.90 (m, 2H). Found: C, 61.46; H, 6.30; S, 32.22%. Calcd for $C_{15}H_{18}S_3$: C, 61.18; H, 6.16; S, 32.66%. **4d**: mp 137—140 °C (dec); NMR ($CDCl_3$): δ 1.22, 1.33, 1.57, and 1.76 (s, 3H each), 6.8—7.4 (m, 3H), and 7.8—8.0 (m, 1H). Found: C, 58.38; H, 6.33; S, 35.06%. Calcd for $C_{13}H_{16}S_3$: C, 58.16; H, 6.01; S, 35.83%.

Desulfurization of 4b. Tetrahydrofuran (THF) solution (8 ml) of **4b** (576 mg, 2.16 mmol) and 5 g of Raney nickel (W-4) were stirred for 6 h at room temperature and then refluxed for 4 h. The reaction solution was analyzed by high speed liquid chromatography (Hitachi 634; column: Hitachi 3010; solvent: 10: 1 methanol–28%NH_4OH (v/v)) for toluene (41%) and bibenzyl (4.6%).

Reaction of 4d with 2-Dimethylamino-3-methyl-1-butene. To **4d** (523 mg, 1.95 mmol) in a mixture (13 ml) of THF and acetonitrile (1: 3) was added 2-dimethylamino-3-methyl-1-butene (**10**; 410 mg, 3.6 mmol) and the solution was heated at reflux temperature for 6.5 h. DCC (SiO_2, 1: 1 hexane–

dichloromethane) afforded **11** (200 mg, 0.745 mmol, 38%) as white crystals. Mp 190—191 °C (from hexane); NMR ($CDCl_3$): δ 1.52 (s, 24H), 7.1—7.6 (m, 6H), and 7.9—8.1 (m, 2H). UV (EtOH): λ_{max} (log ε) 250 (sh) nm (4.22); mol wt: Found 568. Calcd for $(C_{13}H_{16}S_3)_2$ 537. Found: C, 58.02; H, 6.26; S, 35.75%. Calcd for $C_{26}H_{32}S_6$: C, 58.16; H, 6.01; S, 35.83%.

*Reaction of **4b** with N-Phenylmaleimide.* A benzene solution (4 ml) of **4b** (55 mg, 0.21 mmol) and *N*-phenylmaleimide (38 mg, 0.22 mmol) was stood overnight at room temperature. After evaporation of the solvent, the residue was purified by preparative layer chromatography (PLC) (SiO_2, benzene) to give white crystals **18** (82 mg, 93%). Mp 217—218 °C (ethanol); NMR ($CDCl_3$) δ 1.0—2.2 (m, 8H), 3.6—4.0 (m, 1H), 4.0—4.3 (m, 1H), 4.45 (s, 2H), 6.8—7.4 (m, 8H), and 8.1—8.4 (m, 1H). IR (KBr): 1710 cm^{-1} (C=O); MS: *m/e* 439 (M^+, 5%), 326 (45), and 184 (100). Found: C, 62.98; H, 4.80; N, 3.08; S, 21.67%. Calcd for $C_{23}H_{21}NO_2S_3$: C, 62.84; H, 4.82; N, 3.19; S, 21.88%.

*Reaction of **4b** with Dibenzoylacetylene.* A solution of dibenzoylacetylene (51 mg, 0.22 mmol) and **4b** (53 mg, 0.20 mmol) in benzene (4 ml) was stood overnight at room temperature. Purification by PLC (SiO_2, benzene) and recrystallization from benzene-ethanol gave **17** (83 mg, 83%) as pale yellow crystals: mp 181—183 °C; NMR ($CDCl_3$): δ 0.9—2.3 (m, 8H), 3.7—4.1 (m, 2H), and 7.0—8.2 (m, 14H); IR (KBr): 1650 and 1665 cm^{-1} (C=O); MS: *m/e* 500 (M^+, 4%), 370 (100), and 105 (80). Found: C, 69.59; H, 4.95; S, 19.13%. Calcd for $C_{29}H_{24}O_2S_3$: C, 69.57; H, 4.83; S, 19.21%.

*Reaction of **4b** with Methyl Vinyl Ketone.* A benzene solution (100 ml) of the ketone (0.82 ml, 10 mmol) and **4b** (1.01 g, 3.8 mmol) was refluxed for 5 min. The solvent was evaporated and the residue was recrystallized from benzene to afford **19** (835 mg). The filtrate was subjected to PLC (SiO_2, 1:1 dichloromethane-hexane) to afford **19** (438 mg). The total yield was 1.273 g (100%). Mp 155—156 °C (from benzene); NMR ($CDCl_3$): δ 1.0—2.5 (m, 8H), 2.25 (s, 3H), 2.8—4.4 (m, 5H), 6.8—7.4 (m, 3H), 8.1—8.4 (m, 1H); IR (KBr): 1715 cm^{-1} (C=O); MS: *m/e* 336 (M^+, 2%), 184 (81), and 43 (100). Found: C, 60.79; H, 6.07; S, 28.49%. Calcd for $C_{17}H_{20}OS_3$: C, 60.67; H, 6.00; S, 28.58%.

*Raney Nickel Desulfurization of **19**.* To a solution of **19** (803 mg, 2.4 mmol) in benzene (50 ml) was added Raney nickel (W-4) prepared from Raney alloy (7 g) and the mixture was refluxed for 2.5 h with stirring. Raney nickel was removed by filtration and the filtrate was evaporated under reduced pressure. The residue was subjected to DCC (SiO_2, 1:1 dichloromethane-hexane) to afford oily compounds **20** (246 mg, 63.5%) and **21** (45 mg, 11.5%). **20**: NMR (CCl_4): δ 1.04 (d, J=6 Hz, 3H), 1.95 (s, 3H), 2.1—3.0 (m, 3H), and 7.0—7.3 (m, 5H); MS: *m/e* 162 (M^+, 5.9%) and 43 (100); IR (neat): 1710 cm^{-1} (C=O). **21**: NMR (CCl_4): δ 0.79, 0.83 (a pair of doublet due to diastereomers, J=7 Hz, 3H), 1.15 (d, J=5 Hz, 3H), 1.64 (br s, 1H, disappeared by D_2O), 2.0—3.1 (m, 3H), 3.4—3.9 (m, 1H), and 7.1 (br s, 5H); MS: *m/e* 164 (M^+, 2.3%) and 91 (100); IR (neat): 3100—3600 cm^{-1} (OH).

*Reaction of **4b** with Acrylamide.* A dichloromethane solution (50 ml) of acrylamide (1.163 g, 16.4 mmol), **4b** (248 mg, 0.94 mmol), and a small amount of hydroquinone was allowed to stand at room temperature for a week. The solution was washed with water, dried (Na_2SO_4), and the solvent was evaporated. The residue was washed with a small amount of dichloromethane to give white crystals **22** (198 mg, 63.8%). Mp 242.5—243.0 °C (dec) (from ethanol); NMR (DMSO-d_6): δ 1.0—2.3 (m, 8H), 2.9—4.2 (m, 7H), 6.7—7.6 (m, 3H), and 8.0—8.4 (m, 1H); MS: *m/e* 337 (M^+, 11%), 184 (84), and 179 (100); IR (KBr): 3480, 3370 (NH), 1695 cm^{-1} (C=O). Found: C, 56.95; H, 6.09; N, 4.10; S, 28.11%. Calcd for $C_{16}H_{19}NOS_3$: C, 56.94; H, 5.67; N, 4.15; S, 28.50%.

*Reactions of **4b** with Fumaronitrile and Maleonitrile.* Fumaronitrile (238 mg, 3.05 mmol) and **4b** (396 mg, 1.48 mmol) dissolved in dichloromethane (30 ml) were stood for 2 days at room temperature. After removal of the solvent, the NMR (in $CDCl_3$) of the residue was taken for methine protons of the dihydrobenzothiopyran ring. The two methine protons appeared as two sets of AX type double doublet whose intensity ratio was 5:1; the major one: δ 3.69, 3.84, 4.67, and 4.82; the minor one: δ 3.80, 3.54, 4.52, and 4.67. No signal due to *cis*-isomer **23a** was observed. In order to remove excess fumaronitrile the crude reaction mixture was twice washed with ethanol giving **23b** (453 mg, 88%). Since some isomerization was observed during purification by TLC (SiO_2), **23b** thus obtained was purified by repeated recrystallization from ethyl acetate to give a pure specimen of the major isomer; mp 154—157 °C; NMR ($CDCl_3$): δ 1.78 (m, 8H), 4.27 (m, 2H), 3.76 (d, J=9.1 Hz, 1H), 4.74 (d, J=9.1 Hz, 1H), 7.25 (m, 3H), and 8.25 (m, 1H); IR (KBr): 2240 cm^{-1} (CN); MS: *m/e* 344 (M^+, 17%) and 184 (100). Found: C, 59.43; H, 4.57; N, 8.26; S, 27.87%. Calcd for $C_{17}H_{16}N_2S_3$: C, 59.27; H, 4.68; N, 8.13; S, 27.92%.

Dichloromethane solution (20 ml) of maleonitrile (154 mg, 1.97 mmol) and **4b** (263 mg, 0.99 mmol) was stood for 1 day at room temperature. The crude reaction mixture was checked for the methine protons by NMR as above. There were found two sets of double doublets, the chemical shifts being δ 4.06, 4.12, 5.07, and 5.13 for the major one, and 4.12, 4.19, 4.92, and 4.99 for the minor one with no signal of **23b**. The reaction mixture was washed with ethanol to afford **23a** (276 mg, 66%), which was recrystallized from ethyl acetate to give the major isomer contaminated with a small amount of the minor isomer (by NMR); mp 168—170 °C; NMR ($CDCl_3$): δ 1.84 (m, 8H), 3.98 (m, 2H), 4.04 (d, J=3.4 Hz, 1H), 5.08 (d, J=3.4 Hz, 1H), 7.15 (m, 3H), and 8.17 (m, 1H); IR (KBr): 2240 cm^{-1} (CN); MS: *m/e* 344 (M^+, 17%) and 184 (100). Found: C, 59.54; H, 4.76; N, 8.20; S, 27.68%. Calcd for $C_{17}H_{16}N_2S_3$: C, 59.27; H, 4.68; N, 8.13; S, 27.92%.

*Reaction of **4b** with Diphenylketene.* Diphenylketene (260 mg, 1.34 mmol) in benzene (10 ml) was added slowly to a solution of **4b** (261 mg, 0.98 mmol) in benzene (20 ml).

The color of the solution turned very rapidly from deep blue to yellow, but slowly reverted to blue. After all the solution was added the color did not revert to blue. The solution was kept at 40 °C for 30 min. After removal of the solvent, the residue was subjected to DCC (SiO_2, 1:3 chloroform-carbon tetrachloride) at about 0 °C to give two fractions, one (201.8 mg) containing **27** and **28** and the other (126.8 mg) containing **28**. PLC (SiO_2, 1:1 hexane–ether) was twice carried out at about 0 °C to obtain **27**, but it was unstable because of isomerization to **28** or decomposition to **4b** when heated in solution or left on silica gel for a long time. The total yield of **27** and **28** was 73%. **28** was stable and purified by recrystallization from ethanol. **28**: mp 222.0—223.5 °C (from ethanol); NMR ($CDCl_3$): δ 1.0—2.5 (m, 8H), 2.5—3.0 (m, 1H), 3.2—4.6 (m, 1H), 6.7—7.6 (m, 13H), and 8.3—8.7 (m, 1H); MS: *m/e* 460 (M^+, 3%) and 184 (100); IR (KBr): 1670 cm^{-1} (C=O). Found: C, 69.92; H, 5.20; S, 20.56%. Calcd for $C_{27}H_{24}OS_3$: C, 70.40; H, 5.25; S, 20.88%. **27**: NMR ($CDCl_3$): δ 1.0—2.3 (m, 8H), 3.3—3.7 (m, 2H), 6.7—7.5 (m, 13H), and 7.6—8.1 (m, 1H); IR (KBr): 1587 1580 cm^{-1} (C=C).

*Reaction of **4b** with Phenyl Isocyanate.* A benzene solution (50 ml) of **4b** (536 mg, 2.0 mmol) and phenyl isocyanate

(242 mg, 2.0 mmol) was allowed to stand for 6 days at room temperature. The solvent was evaporated under reduced pressure and the residue was subjected to DCC (SiO_2, chloroform) to give **29** (677 mg, 88%). Mp 164.5—166.0 °C (from benzene); NMR ($CDCl_3$): δ 1.0—2.3 (m, 8H), 3.5—3.9 (m, 2H), 7.1—7.6 (m, 8H), and 8.1—8.4 (m, 1H); IR (KBr): 1650 cm^{-1} (C=O); MS: *m/e* 385 (M^+, 0.4%) and 119 (100). Found: C, 62.20; H, 4.86; N, 3.53; S, 24.70%. Calcd for $C_{20}H_{19}NOS_3$: C, 62.30; H, 4.97; N, 3.63; S, 24.95%.

*Reaction of **4b** with Phenyl Isothiocyanate.* A solution of **4b** (246 mg, 0.92 mmol) and phenyl isothiocyanate (249 mg, 1.84 mmol) in benzene (25 ml) was refluxed for 21 h under argon atmosphere. The solvent was evaporated and the residue was subjected to PLC (SiO_2, benzene) to give crude **31** (269 mg, 73%). Although **31** was stable in solution in the presence of excess phenyl isothiocyanate, it was unstable, if the isothiocyanate was removed, and slowly decomposed to **4b** and phenyl isothiocyanate, thus precluding the isolation of an analytically pure specimen. Among the decomposition product there was formed a small amount of product (15 mg, 4%) tentatively assigned as **30**. **31**: mp 46—52 °C (white crystals from hexane); NMR (CCl_4): δ 1.0—2.4 (m, 8H), 3.6—4.1 (m, 2H), 6.7—7.5 (m, 8H), and 7.9—8.3 (m, 1H); UV (cyclohexane): λ_{max} (ε) 318 (7330), 275 (11400), and 244 (sh) nm (17200); IR (KBr): 1565 cm^{-1} (CN). **30**: NMR (CCl_4): δ 1.0—2.0 (m, 8H), 3.6—3.9 (m, 2H), 7.1—7.5 (m, 8H), and 7.9—8.3 (m, 1H); IR (KBr): no band due to C=N.

*Reduction of **4b** with Lithium Aluminum Hydride.* Lithium aluminum hydride (120 mg, 3.2 mmol) was added to a THF solution (50 ml) of **4b** (269 mg, 1.0 mmol) with stirring under nitrogen atmosphere, and the mixture was refluxed for 5 h. Though a small amount of **4b** still remained, 10% aq sodium hydroxide and methyl iodide (0.5 ml) were added successively with stirring. The solvent was evaporated under reduced pressure, and ether was added. The ethereal solution was washed with water, dried and the ether was evaporated. The residue was subjected to DCC (SiO_2, 1: 1 hexane–ether) to give **33** (184 mg, 64.4%) and a trace amount of 2-methylthiobenzyl alcohol (by NMR). When the reaction mixture was treated with dil sulfuric acid instead of aq sodium hydroxide and methyl iodide, the product was **34** (24%), which was unstable and was rapidly oxidized by air to afford **4b**. **33**: mp 107.0—109.0 °C (from ethanol); NMR ($CDCl_3$): δ 1.0—2.5 (m, 8H), 2.49 (s, 3H), 3.7—4.1 (m, 2H), 6.38 (s, 1H), 7.1—7.4 (m, 3H), and 7.8—8.2 (m, 1H); MS: *m/e* 282 (M^+, 19%) and 153 (100). Found: C, 59.60; H, 6.17; S, 33.89%. Calcd for $C_{14}H_{18}S_3$: C, 59.53; H, 6.42; S, 34.05%. **34**: NMR ($CDCl_3$): δ 1.0—2.5 (m, 8H), 3.55 (s, 1H), 3.6—4.0 (m, 2H), 6.14 (s, 1H), 7.0—7.5 (m, 3H), and 7.7—8.2 (m, 1H).

References

1) For reviews, see R. Gompper, *Angew. Chem. Int. Ed. Engl.*, **8**, 312 (1969); H. U. Wagner and R. Gompper, "The Chemistry of the Quinonoid Compounds," ed by S. Patai, John Wiley & Sons, (1974), Chap. 18; R. Okazaki, *Yuki Gosei Kagaku Kyokai Shi*, **34**, 439 (1976).

2) T. Kametani, H. Nemoto, H. Ishikawa, K. Shiroyama, and K. Fukumoto, *J. Am. Chem. Soc.*, **98**, 3378 (1976); T. Kametani, C. V. Loc, T. Higa, M. Koizumi, M. Ihara, and K. Fukumoto, *ibid.*, **90**, 2306 (1977); K. P. C. Vollhardt, *Acc. Chem. Res.*, **10**, 1 (1977); W. Oppolzer, *Angew. Chem. Int. Ed. Engl.*, **16**, 10 (1977) and references cited therein.

3) a) G. Jacquim, J. Nasielski, G. Billy, and M. Remy, *Tetrahedron Lett.*, **1973**, 3655; b) R. S. Becker and J. Kolc, *J. Phys. Chem.*, **72**, 997 (1968).

4) R. Okazaki, K. Okawa, and N. Inamoto, *Chem. Commun.*, **1971**, 843; R. Okazaki, F. Ishii, K. Ozawa, and N. Inamoto, *Chem. Lett.*, **1972**, 9; R. Okazaki, F. Ishii, K. Okawa, K. Ozawa, and N. Inamoto, *J. Chem. Soc., Perkin Trans. 1*, **1975**, 270. See also, P. de Mayo and H. Y Ng, *Teteahedron Lett.*, **1973**, 1561.

5) Preliminary reports: a) R. Okazaki and N. Inamoto, *Chem. Lett.*, **1974**, 1439; b) R. Okazaki, F. Ishii, K. Sunagawa, and N. Inamoto, *ibid.*, **1978**, 51; c) R. Okazaki, K.-T. Kang, and N. Inamoto, *ibid.* **1978**, 55.

6) Similar results have been reported independently by Prof. de Mayo. P. de Mayo and H. Y. Ng, *J. Chem. Soc., Chem. Commun.*, **1974**, 877; *Can. J. Chem.*, **55**, 3763 (1977).

7) D. H. R. Barton, L. L. Choi, R. H. Hess, M. M. Pechet, and C. Wilshir, *J. Chem. Soc., Chem. Commun.*, **1975**, 557.

8) J. Bornstein, J. E. Shields, and J. H. Supple, *J. Org. Chem.*, **32**, 1499 (1967).

9) For reductive dimerization in Raney nickel desulfurization, see, for example, A. Lüttringhaus and R. Deckert, *Angew. Chem.*, **67**, 275 (1955).

10) W. Oppolzer, *J. Am. Chem. Soc.*, **93**, 3833 (1971).

11) T. H. Chau and K. T. Nwe, *Tetrahedron Lett.*, **1973**, 3601.

12) W. J. M. van Tilborg and R. Plomp, *J. Chem. Soc., Chem. Commun.*, **1977**, 130; *Recl. Trav. Chim. Pays-Bas*, **96**, 282 (1977).

13) O. L. Chapman and C. L. McIntosh, *J. Am. Chem. Soc.*, **92**, 7001 (1970).

14) R. Gompper, E. Kutter, and H. Kast, *Angew. Chem.*, **70**, 147 (1967).

15) R. Okazaki, M. O-oka, and N. Inamoto, *J. Chem. Soc., Chem. Commun.*, **1976**, 562; M. O-oka, A. Kitamura, R. Okazaki, and N. Inamoto, *Bull. Chem. Soc. Jpn.*, **51**, 301 (1978).

16) F. Ishii, R. Okazaki, and N. Inamoto, *Tetrahedron Lett.*, **1976**, 4283; R. Okazaki, F. Ishii, and N. Inamoto, *Bull. Chem. Soc. Jpn.*, **51**, 309 (1978).

17) A. Schönberg, B. König, and E. Singer, *Chem. Ber.*, **100**, 767 (1967) and references cited therein.

18) F. S. Fowkes and E. W. McClelland, *J. Chem. Soc.*, **1941**, 187.

Syntheses and Spectral Observation on the Structure of Several 2(1*H*)-Pyridinethionato Zinc Complexes

Mitsuo MASAKI,* Satoshi MATSUNAMI, Takayuki KIMURA,† and Tokio OSHIMA†

Polymer Research Laboratory, Ube Industries, Ltd., Minami-Kaigan, Goi, Ichihara, Chiba 290

†*Central Research Laboratory, Ube Industries Ltd., Nishihon-Machi, Ube, Yamaguchi 755*

(Received June 28, 1978)

Although bis[2(1*H*)-pyridinethionato]zinc (**1**) is prepared by the reaction of 2(1*H*)-pyridinethione with zinc chloride in the presence of stoichiometric amount of sodium hydroxide, a similar reaction in the presence of a large excess amount of the base gave μ_4-oxo-hexakis-μ-[2(1*H*)-pyridinethionato-(*N*,*S*)]-tetrazinc (**2**) which is the first example of L_6Zn_4O (L=ligand) type complexes having heterocyclic thiolato groups as ligands. The complex **2** was also prepared by several routes, which involve hydrolysis of **1** and the reaction of **1** with zinc oxide. In these complexes 2(1*H*)-pyridinethionato ligand acts as a bidentate or bridging ligand. Attempts to convert bis-(4,6-dimethyl-2-pyridylthio)zinc or bis(1-oxido-2-pyridylthio)zinc into a complex of L_6Zn_4O type were failed. Complexes of L_6Zn_4O type were also prepared when L were 2-thiazolidinethionato, 5-methyl-2-thiazolidinethionato, and 1-methyl-4-imidazoline-2-thionato.

In the previous papers,[1,2] the synthesis and the molecular structure of dichlorobis[2(1*H*)-pyridinethionato]-tin(IV) were reported. The 2(1*H*)-pyridinethionato ligands act as bidentate ligands in the complex, which has an octahedral structure resulted from the intra-molecular four-membered (Sn, S, C, and N) chelate rings formation.

Several metal (Ru,[3,4] Ir,[5] Fe,[6] Rh,[7] Hg[8]) derivatives of 2(1*H*)-pyridinethione have been reported. The 2-pyridylthio group acts as a bidentate,[3,5] unidentate,[6-8] or bridging ligand.[4]

We have studied zinc derivatives of 2(1*H*)-pyridinethione. This paper deals with the transformation of bis[2(1*H*)-pyridinethionato]zinc (**1**) into a new zinc complex, μ_4-oxo-hexakis-μ-[2(1*H*)-pyridinethionato-(*N*,*S*)]-tetrazinc (**2**) and an observation on the coordination of 2(1*H*)-pyridinethionato ligand in **1** and **2**. This paper also describes syntheses of several new zinc derivatives of heterocyclic thiols.

Results and Discussion

Syntheses. Bis[2(1*H*)-pyridinethionato]zinc (**1**) is briefly reported in a patent,[9] but no characterization of **1** is described. The zinc derivative **1** was obtained as a sole product when the molar ratio of the three reactants was stoichiometric (2: 1: 2), as shown in Eq. 1.

$$2PySH + ZnCl_2 + 2NaOH \longrightarrow (PyS)_2Zn + 2NaCl + 2H_2O \quad (1)$$

$$8PySH + 4ZnCl_2 + 10NaOH \longrightarrow (PyS)_6Zn_4O + 8NaCl + 2PySNa + 9H_2O \quad (2)$$

When the reaction was performed in the presence of a large excess amount of sodium hydroxide, a new complex μ_4-oxo-hexakis-μ-[2(1*H*)-pyridinethionato-(*N*,*S*)]-tetrazinc (**2**) was found to be formed according to Eq. 2.

The complex **2** was best prepared by the reaction in a molar ratio of 3: 2: 4 as shown in Scheme 1. The composition of **2** was determined by elemental analyses, alternative synthetic reactions, and the reaction with 2(1*H*)-pyridinethione giving again **1**. The complex **2** was alternatively prepared by several routes as shown in Scheme 1.

$$6PySH + 4ZnCl_2 + 8NaOH \xrightarrow{-8NaCl,\ -7H_2O} \mathbf{2}$$

$$4\,\mathbf{1} + H_2O \underset{}{\overset{-2PySH}{\rightleftharpoons}} \mathbf{2}$$

$$3\,\mathbf{1} + ZnO \longrightarrow \mathbf{2}$$

$$6PySH + 4ZnO \xrightarrow{-3H_2O} \mathbf{2}$$

Scheme 1. Syntheses of μ_4-oxo-hexakis-μ-[2(1*H*)-pyridinethionato-(*N*,*S*)]-tetrazinc (**2**).

When a suspension of **1** in water was refluxed for 1 h, **2** was obtained as an insoluble product and 2(1*H*)-pyridinethione was recovered from the aqueous solution in a quantitative yield based on the equation shown in Scheme 1. A treatment of **1** with zinc oxide in a molar ratio of 3: 1 in refluxing acetonitrile also gave **2**. A reaction of 2(1*H*)-pyridinethione and zinc oxide in a molar ratio of 3: 2 in 1,2-dichloroethane yielded **2**. In contrast, complex **1** was obtained by the reaction of the same reagents in a molar ratio of 2: 1 in boiling benzene with azeotropical removal of water formed.[10]

When **2** was treated with twice molar amount of 2(1*H*)-pyridinethione in boiling benzene under azeotropical removal of water produced, **1** was again obtained in a quantitative yield.

Bis(4,6-dimethyl-2-pyridylthio)zinc (**3**) was prepared from 4,6-dimethyl-2(1*H*)-pyridinethione by a reaction similar to Eq. 1 and by a reaction of bis(4,6-dimethyl-2-pyridyl) disulfide with zinc dust.[11] Transformations of **3** and bis(1-oxido-2-pyridylthio)zinc into the complexes of L_6Zn_4O (L=ligand) type were attempted by heating L_2Zn compounds in water, but the major amount of starting materials was recovered, and the expected complexes could not be obtained.

Although a large number of bis(organo ligand)zinc are known, there have been reported only four types of L_6Zn_4O complex formed with alkanecarboxylato,[12] *O*,*O*-dialkyl(or diaryl)phosphorodithioato,[13] dialkylphosphinothioato,[14] and 1,3-diphenyltriazenato.[15] The complex **2** is the first example of oxotetrazinc complex, where the ligand is a heterocyclic thiolato group. Syntheses of several other complexes of L_6Zn_4O type where L is a heterocyclic thiolato group were examined. Complexes of L_6Zn_4O type were synthesized by the re-

TABLE 1. HEXAKIS-μ-(HETEROCYCLIC THIOLATO)-μ_4-OXO-TETRAZINC

Product	Mp	IR (cm^{-1})	Found / Calcd (%) C	H	N	S
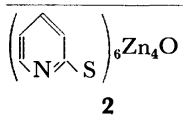 **2**	above 340 °C (dec)[25]	1590s, 1545m, 1455s, 1410s, 1270m, 1155m, 1135s(sh), 1130s, 1085m, 1050m, 1010m, 775m, 765m, 755m, 725m, 645w, 540m, 530m, 515m, 495w, 445w, 415w, 360w, 265m(br)	38.61 38.40	2.47 2.58	8.74 8.96	20.33 20.50
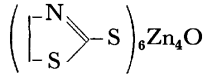	above 170 °C (dec)	1500s, 1450w, 1310m, 1200w, 1040s, 980s, 940m, 510m (br), 435w, 325w	22.01 21.91	2.41 2.45	8.43 8.52	38.85 38.99
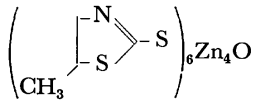	175—220 °C(dec) [EtOH]	1505s, 1440m, 1375m, 1305m, 1195m, 1025s, 1005s (sh), 920m, 510m (br), 460w (sh), 385w, 350w, 305w	27.09 26.91	3.29 3.39	7.64 7.85	36.15 35.92
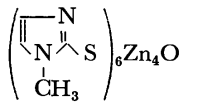 **8**	above 255 °C (dec)	1535w, 1455s, 1415m, 1370s, 1315m, 1285m, 1145s, 735m (br), 690s, 515m (br), 315w, 220m (br)	29.92 30.14	2.89 3.16	17.65 17.57	20.33 20.11

action of 2-thiazolidinethione (**4**), 5-methyl-2-thiazolidinethione (**5**), 1-methyl-4-imidazoline-2-thione (**6**) with zinc chloride in the presence of sodium hydroxide (molar ratio of 3: 2: 4) in an aqueous solution. The results are shown in Table 1. However, L_2Zn derivatives of these five membered heterocyclic thiols could not be prepared by the reaction of the thiols with zinc chloride in the molar ratio of 2: 1. Bis(1-methyl-4-imidazoline-2-thionato)zinc (**7**) could be prepared only by the reaction of hexakis-μ-(1-methyl-4-imidazoline-2-thionato)-μ_4-oxo-tetrazinc (**8**) with the thione **6**. Attempts to prepare L_2Zn derivatives of **4** and **5** were unsuccessful by analogous reactions from the corresponding L_6Zn_4O type complexes.

Observation on Structure. The MS spectrum (double focus) of **1** exhibits a very weak dizinc-containing polyisotopic molecular ion (*m/e* 568) as the highest mass feature, which corresponds to the parent peak of the dimer. Three dizinc-containing molecular ions observed at *m/e* 490 (M—Py), 458 (major peak, M—PyS), 426 (M—PyS—S) seem to be fragments derived from the dimer, and a monozinc-containing molecular ion at *m/e* 316 [$(PyS)_2ZnS$] is also indicative for dimeric structure of **1**. Molecular weight measurement (osmometry) showed that **1** was dimeric in 4-methyl-2-pentanone.[16]

The IR spectrum of **1** exhibits bands due to ring vibration at 1595 (s), 1545 (s), 1455 (s, doublet), 1420 (s, doublet), 1020 (m), 645 cm^{-1} (w), and the bands due to C–H bending vibration at 765(sh) and 755 cm^{-1} (s).[1,17] The bands at 1020 and 645 cm^{-1} have shoulders. The absorption pattern is close to that of dichlorobis[2(1*H*)-pyridinethionato]tin(IV).[18] This fact suggests that 2(1*H*)-pyridinethionato ligands act as bidentate ligands. These bands all shifted in higher frequency region in comparison with the corresponding bands of di-2-pyridyl disulfide.[1] The shift can be interpreted by the coordination of pyridine nucleus through nitrogen to tin atom. A strong intensity absorption band appears at 1135 cm^{-1} in the spectrum of **1**, which can be assigned to C=S stretching since 2(1*H*)-pyridinethione shows the strong absorption of C=S stretching at the same position.[19] This band indicates the presence of 2(1*H*)-pyridinethionato ligand of thione form, whose coordination to zinc through sulfur atom is weak as in the iridium complex.[5] Based on these spectral data 2(1*H*)-pyridinethionato ligands act as bidentate or bridging one and **1** seems not monomeric.

Molecular weight of **2** could not be determined owing to the low solubility to the ordinary solvent for osmometric measurement. The MS spectrum (chemical ionization with isobutane) of **2** exhibits the zinc-containing, polyisotopic molecular ion (*m/e* 839) as the highest mass feature which corresponds to species resulting from loss of one pyridyl group and one oxygen atom from [M+H]. The remaining major peaks (*m/e* 743, 568, 459) in the spectrum can be assigned to species resulting from loss of one or more 2(1*H*)-pyridinethionato groups, zinc atoms, and oxygen atom from [M+H] or [M].

The IR absorption pattern of **2** in the region higher than 600 cm^{-1} is very close to that of **1**, except that the bands at 1455, 1410, 1010, and 645 cm^{-1} in **2** are all single peaks. This fact seems to suggest that six 2(1*H*)-pyridinethionato ligands in **2** are in chemically similar states. The characteristic absorption band of **2** is a broad triplet with medium intensity, whose peaks are at 540, 530, and 515 cm^{-1}. The broad and strong intensity absorption bands of zinc oxide in the 540—400 cm^{-1} spectral region were replaced with the triplet bands, when zinc oxide was allowed to react with **1** to give **2**. The triplet bands can be ascribed to Zn–O bond, since the absorptions of zinc–sulfur vibrations have been described to appear in the region lower than 401 cm^{-1} in several compounds containing Zn–S bond,[20] and the absorptions due to Zn–N bond are found between 250 and 200 cm^{-1} in complexes of pyridine compound with zinc halides.[21] The band at 526 cm^{-1} in hexa-μ-acetato-(O,O')-μ_4-oxo-tetrazinc has been assigned to $\nu(Zn_4O)$.[22]

The structures of L_6Zn_4O complexes where L is AcO, $(BuO)_2PS_2$, or Ph_2N_3 have been determined by X-ray analyses.[12a,13a,15] The replacement of –O–C–O–, –S–P–S–, or –N–N–N– moiety in the structures of those complexes with –S–C–N– moiety gives a possible structure for **2** as shown in Fig. 1. The IR spectral observation mentioned above supports the structure for **2**.

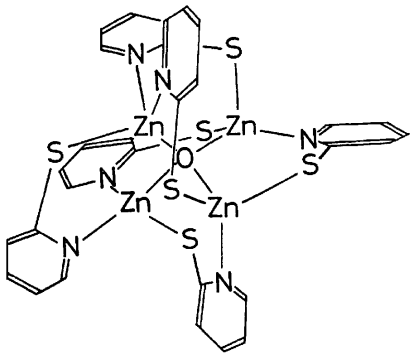

Fig. 1. A possible structure for **2**.

The transformation of **1** into **2** can be explained by the substitution of one 2(1*H*)-pyridinethionato ligand in the dimer of **1** with oxygen of water or zinc oxide and the simultaneous or subsequent coupling of two $(PyS)_3Zn_2$ group through the oxygen, as shown in Eq. 3 or 4.

$$2(PyS)_3Zn_2(SPy) + H_2O \longrightarrow [(PyS)_3Zn_2]_2O + 2HSPy \quad (3)$$

$$2(PyS)_3Zn_2(SPy) + ZnO \longrightarrow [(PyS)_3Zn_2]_2O + Zn(SPy)_2 \quad (4)$$

$$[2Zn(SPy)_2 \longrightarrow (PyS)_3Zn_2(SPy)]$$

Bis(4,6-dimethyl-2-pyridylthio)zinc (**3**) is monomeric based on the molecular weight (osmometry) and MS spectrum. No remarkable difference is observed in the IR spectrum of C=C/C=N stretching region and C=S stretching region between **3** and bis(4,6-dimethyl-2-pyridyl) disulfide. Furthermore, there was not recognized such a shift of bands due to ring vibration and C–H bending vibration as observed between **1** and the corresponding disulfide. These data show that **3** is a simple zinc salt of a thiol and no such strong coordination of pyridine ring through nitrogen on metal is observed as in the case of **1**. This may be a reason why **3** could not be converted to a complex of L_6Zn_4O type.

Experimental

All the melting points were determined in a liquid bath placing a cut edge of capillary outside of the bath, and were uncorrected. The IR spectra were measured with a Hitachi Perkin-Elmer 225 and a Hitachi EPI-G2 Grating Infrared Spectrometer. The molecular weight was determined in 4-methyl-2-pentanone with a Hitachi 115 Vapor Pressure Osmometer. The MS spectra were measured with a Hitachi M60 Mass Spectrometer equipped with computer system 002B, a Hitachi M52 Mass Spectrometer, or a JMS-01SG-2 Double Focus Mass Spectrometer.

Materials. Commercial anhydrous zinc chloride was used after drying over phosphorus pentaoxide. Commercial 2(1*H*)-pyridinethione, 2-thiazolidinethione (**4**), and 1-methyl-4-imidazoline-2-thione (**6**) were used after recrystallization. 5-Methyl-2-thiazolidinethione (**5**) was prepared by the procedure previously reported.[23]

Bis[2(1H)-pyridinethionato]zinc (1). a) Reaction of 2(1H)-Pyridinethione with Zinc Chloride in the Presence of Base: To an aqueous solution of sodium hydroxide (1/2 M, 20 ml) was added 2(1*H*)-pyridinethione (1.11 g, 10 mmol). To the resulting solution was added drop by drop a solution of zinc chloride (95%, 0.72 g, 5 mmol) in water (15 ml) with stirring at 20 °C and the mixture was stirred at 20 °C for 2 h. The resulting slightly yellowish precipitate was filtered and washed with water (50 ml) to give 1.41 g (99%) of **1**; mp 248—251 °C.[24] Mol wt, Found: 603; Calcd (dimer): 571. Found: C, 42.07; H, 2.75; N, 9.68; S, 22.46%. Calcd for $C_{10}H_8N_2S_2Zn$: C, 42.04; H, 2.82; N, 9.81; S, 22.45%.

b) Reaction of 2(1H)-Pyridinethione with Zinc Oxide: To a suspension of zinc oxide (0.81 g, 10 mmol) in benzene (150 ml) was added 2(1*H*)-pyridinethione (2.44 g, 22 mol). A mixture was stirred at room temperature for 1 h and then refluxed for 5 h, during which boiling benzene was gradually distilled out to remove water azeotropically, while dried benzene was supplied to the mixture at intervals. The precipitate was collected by filtration and washed with benzene (60 ml) to give 2.73 g (96%) of slightly yellowish powder. The IR spectrum of the powder was identical with that of **1**.

μ_4-Oxo-hexakis-μ-[2(1H)-pyridinethionato-(N,S)]tetrazinc (2). a) Reaction of 2(1H)-Pyridinethione with Zinc Salt in the Presence of Base in Water: A solution of zinc chloride (95%, 0.72 g, 5 mmol) in water (30 ml) was added drop by drop to a solution of 2(1*H*)-pyridinethione (0.83 g, 7.5 mmol) in 1/2 M aqueous sodium hydroxide (20 ml) with stirring at room temperature. After stirring the mixture at room temperature for 22 h, the precipitate was collected by filtration and washed with water (50 ml) to give 1.12 g (96%) of colorless crystalline powder: mp above 340 °C (gradually dec).[25] MS (CI): *m/e* 839 $[(PyS)_5Zn_4SH]$, 820 $[(PyS)_5(Py)Zn_3]$, 743 $[(PyS)_5Zn_3H]$, 727 $[(PyS)_4(Py)Zn_3OH]$, 664 $[(PyS)_4Zn_3S]$, 632 $[(PyS)_4Zn_3]$, 608, 568 $[(PyS)_4Zn_2]$, 554 $[(PyS)_3Zn_3S]$, 536 $[(PyS)_3(Py)Zn_2]$, 491 $[(PyS)_3Zn_2SH]$, and 459 $[(PyS)_3Zn_2H]$.

b) Hydrolysis of 1: A suspension of **1** (10.0 g, 35 mmol) in water (200 ml) was refluxed for 1 h. The precipitate was collected by filtration and washed with water (50 ml) to give 8.13 g (99%) of colorless crystalline powder. The IR spectrum of the solid was identical with that of **2**. The filtrate separated from **2** and washings were combined and concentrated under reduced pressure. The residue was extracted with acetone (100 ml). The acetone extract was concentrated under reduced pressure to give 1.95 g (100%) of 2(1*H*)-pyridinethione as yellow crystals; mp 124—126 °C (lit, mp 125 °C[26]). When **1** was treated in boiling water for 28 h, the same product was obtained without further decomposition. Found: C, 38.48; H, 2.66; N, 8.96; S, 20.25; Zn, 27.43%. Calcd: Zn, 27.87%.

c) Reaction of 1 with Zinc Oxide: A mixture of **1** (4.29 g, 15 mmol) and zinc oxide (0.41 g, 5 mmol) in acetonitrile (100 ml) was refluxed for 4 h. The precipitate was collected by filtration and washed with acetonitrile (40 ml) to give 4.54 g (97%) of colorless crystalline powder. The IR spectrum of the solid was identical with that of **2**.

d) Reaction of 2(1H)-Pyridinethione with Zinc Oxide: Zinc oxide (1.63 g, 20 mmol) was added to a solution of 2(1*H*)-pyridinethione (3.34 g, 30 mmol) in 1,2-dichloroethane (100 ml) and the mixture was stirred at room temperature for 5 h. The precipitate was collected by filtration and washed with 1,2-dichloroethane (40 ml) to give 4.41 g (94%) of crystalline powder. The IR spectrum of the solid was iden-

tical with that of **2**.

*Reaction of **2** with 2(1H)-Pyridinethione.* To a solution of 2(1*H*)-Pyridinethione (0.53 g, 4.8 mmol) in benzene (100 ml) was added **2** (1.88 g, 2 mmol) and the mixture was refluxed for 5 h, during which boiling benzene was gradually distilled out in order to remove water azeotropically, while dried benzene was supplied to the mixture at intervals. The precipitate was collected by filtration and washed with benzene (50 ml) to give 2.22 g (97%) of slightly yellowish solid. The IR spectrum of the solid was essentially identical with that of **1**.

Bis(4,6-dimethyl-2-pyridylthio)zinc (3). *a) Reaction of 4,6-Dimethyl-2(1H)-pyridinethione with Zinc Chloride in the Presence of Base*: To an aqueous solution of sodium hydroxide (1/2 M, 4.6 ml) was added 4,6-dimethyl-2(1*H*)-pyridinethione 0.28 g, 2 mmol). To the resulting solution was added drop by drop a solution of zinc chloride (95%, 0.14 g, 1 mmol) in water (20 ml) with stirring at 20 °C and the mixture was stirred for 2.5 h. The precipitate was collected by filtration and washed with water to give 0.29 g of colorless solid. The solid was recrystallized from 90 ml of ethanol to give 0.10 g (29%) of prisms; mp 250—252 °C (dec). IR (KBr): 1595s, 1545 s, 1450 m, 1395 m, 1370 m, 1275 m, 1205 m, 1135 m, 875 m, 840 m, 825 m, 535 w, 530 m, 430 w, 270 w(br), and 235 m(br) cm^{-1}. Mol wt, Found: 364; Calcd (monomer): 342. MS(EI): *m/e* 340 (M), 325, 307, and 202. Found: C, 49.15; H, 4.65; N, 8.24; S, 18.81%. Calcd for $C_{14}H_{16}N_2S_2Zn$: C, 49.20; H, 4.72; N, 8.20; S, 18.76%.

b) Reaction of Bis(4,6-dimethyl-2-pyridyl) Disulfide with Zinc Dust: A mixture of bis(4,6-dimethyl-2-pyridyl)disulfide (5.00 g, 18 mmol) and zinc dust (1.18 g, 18 mg atom) in benzene (100 ml) was refluxed for 26 h. The reaction mixture was filtered to give 4.53 g of a mixture of white powdery solid and zinc dust, which was extracted by Soxhlet's extractor with benzene for 10 h. Colorless crystals were obtained from the extract. Yield 3.08 g (50%); mp 251—252 °C (dec). The IR spectrum of the crystals was identical with that of **3** obtained in a).

Bis(1-methyl-4-imidazoline-2-thionato)zinc (7). A mixture of hexakis-μ-(1-methyl-4-imidazoline-2-thionato)-μ_4-oxotetrazinc (**8**) (0.96 g, 1 mmol) and 1-methyl-4-imidazoline-2-thione (**6**) (0.46 g, 4 mmol) in benzene (100 ml) was refluxed for 15 h, during which benzene was gradually distilled out in order to remove water azeotropically, while dried benzene was supplied to the mixture at intervals. The precipitate was collected by filtration and washed with benzene (50 ml) to give 1.11 g of colorless solid. The solid (0.48 g) was added again to a solution of **6** (0.46 g, 4 mmol) in benzene (200 ml). The mixture was refluxed for 2.5 h, during which benzene was distilled out and supplied in the same manner mentioned above. The precipitate was collected by filtration and washed with benzene (50 ml) to give 0.44 g of colorless solid; mp above 300 °C (gradually dec). IR (KBr): 1575w, 1535m, 1455s, 1410m, 1370s, 1315m, 1285s, 1145s, 1085w, 955m, 725m (br), 690s, 510m, 435w, 315w, and 250w cm^{-1}. MS(CI): *m/e* 853 [$(LS)_5Zn_4S$] (LSH=**6**), 837 [$(LS)_5LZn_3$-H], 547 [$(LS)_3LZn_2$-H], 467 [$(LS)_3Zn_2$], 403 [$(LS)L_2Zn_2$], 331, 291 [$(LS)_2ZnH$], and 115 [LSH_2]. Found: C, 33.16; H, 3.25; N, 19.26; S, 21.84%. Calcd for $C_8H_{10}N_4S_2Zn$: C, 32.94; H, 3.46; N, 19.26; S, 21.98%.

References

1) M. Masaki and S. Matsunami, *Bull. Chem. Soc. Jpn.*, **49**, 3274 (1976).

2) M. Masaki, S. Matsunami, and H. Ueda, to *Bull. Chem. Soc. Jpn.*, **51**, 3298 (1978).

3) S. R. Fletcher and A. C. Skapski, *J. Chem. Soc., Dalton Trans.*, **1972**, 635; P. Powell, *J. Organomet. Chem.*, **65**, 89 (1974).

4) J. D. Gilbert and G. Wilkinson, *J. Chem. Soc., A*, **1969**, 1749.

5) C. K. Brown, D. Georgiou, and G. Wilkinson, *J. Chem. Soc., Dalton Trans.*, **1973**, 929.

6) G. Le Borgne and D. Grandjean, *J. Organomet. Chem.*, **92**, 381 (1975).

7) R. W. Mitchell, J. D. Ruddick, and G. Wilkinson, *J. Chem. Soc., A*, **1971**, 3224.

8) L. F. Sytsma and R. J. Kline regarded the ligand in the methylmercury derivative of 2(1*H*)-pyridinethione as an unidentate ligand: *J. Organomet. Chem.*, **54**, 15 (1973). However, A. J. Canty and A. Marker described recently that a weak intramolecular coordination of nitrogen on mercury is not excluded in the complex: *Aust. J. Chem.*, **29**, 1383 (1976).

9) E. C. Ladd, Can. Patent 501851 (1954); *Chem Abstr.*, **50**, 6740c (1956).

10) The reaction of 2(1*H*)-pyridinethione and zinc oxide in a molar ratio of 2: 1 in water gave a product, the elemental analyses of which exhibit a composition of $(PyS)_2$-Zn_2O.

11) The reaction of bis[1-naphthyl(thiocarbonyl)] disulfide with zinc dust is known to give bis[1-naphthyl(thiocarbonyl)-thio]zinc: A. Schönberg, *Ber.*, **66**, 1932 (1933). Bis(allylthio)zinc is estimated to be an intermediate in the reaction of diallyl disulfide with zinc dust giving diallyl sulfide: F. Challenger and D. Greenwood, *J. Chem. Soc.*, **1950**, 26.

12) a) H. Koyama and Y. Saito, *Bull. Chem. Soc. Jpn.*, **27**, 112 (1954); b) W. L. Mead, W. K. Reid, and H. B. Silver, *Chem. Commun.*, **1968**, 573; J. Charalambous, R. G. Copperthwaite, S. W. Jeffs, and D. E. Shaw, *Inorg. Chim. Acta*, **14**, 53 (1975); *Chem. Abstr.*, **83**, 70093v (1975).

13) a) A. J. Burn and B. W. Smith, *Chem. Commun.*, **1965**, 394; b) D. R. Dakternieks and D. P. Graddon, *Aust. J. Chem.*, **23**, 1989 (1970).

14) S. Meriani, G. Nardin, and A. Ripamonti, *Inorg. Chem.*, **6**, 1931 (1967).

15) M. Corbett and B. F. Hoskins, *Inorg. Nucl. Chem. Lett.*, **6**, 261 (1970).

16) A referee pointed out a possibility that **1** may be polymeric and dissociates into dimeric form in 4-methyl-2-pentanone. Although a higher association of the dimer is possible in crystalline state, the dimeric form seems to be a basic unit for bis[2(1*H*)-pyridinethionato]zinc based on not only MS data of crystals and osmometric molecular weight determination, but also the reaction of **2** with benzoyl chloride giving chlorotris[2(1*H*)-pyridinethionato]dizinc and benzoylthiopyridine: S. Matsunami, S. Fujimura, K. Okimoto, and M. Masaki, submitted for publication to *Bull. Chem. Soc. Jpn.*

17) In a previous report,[1] we assigned the band at 710 or 720 cm^{-1} in di-2-pyridyl disulfide or 2(1*H*)pyridinethionatotin(IV) complex to a C-H bending vibration based on literatures: S. P. Sinha, *Spectrochim. Acta*, **20**, 879 (1964); H. Shindo and N. Ikekawa, *Chem. Pharm. Bull.*, **4**, 192 (1965). However, it seems to be more probable to assign these bands to C–C ring deformations: N. S. Gill and H. J. Kingdon, *Aust. J. Chem.*, **19**, 2197 (1966). Complexes **1** and **2** also exhibit medium intensity bands at 725 cm^{-1} assignable to the C-C ring deformation. The shift of the bands to higher frequency region compared with that of di-2-pyridyl disulfide seems also to indicate the coordination of pyridine nucleus to zinc.

18) The bands corresponding to those bands at 1455, 1420, 1020, and 645 cm^{-1} in **1** are singlets in the spectrum of dichlorobis[2(1*H*)-pyridinethionato]tin(IV).

19) A. R. Katrizky and R. A. Jones, *J. Chem. Soc.*, **1960**,

2947.

20) I. M. Cheremisina and S. V. Larionov, *Izv. Akad. Nauk SSSR, Ser, Khim.*, **10**, 2150 (1971); G. E. Coats and D. Ridley, *J. Chem. Soc.*, **1965**, 1870; M. R. Hunt, A. G. Krueger, L. Smith, and G. Winter, *Aust. J. Chem.*, **24**, 53 (1971); J. E. Förster, M. Vargas, and H. Müller, *J. Organomet. Chem.*, **59**, 97 (1973); D. M. Adams and J. B. Cornell, *J. Chem. Soc., A*, **1968**, 1299.

21) M. Keeton and A. B. P. Lever, *Inorg. Chem.*, **10**, 47 (1971); R. J. H. Clark and C. W. Williams, *Inorg. Chem.*, **4**, 350 (1965); C. Postmus, J. R. Ferraro, and W. Wozniak, *Inorg. Chem.*, **6**, 2030 (1967).

22) W. P. Griffith, *J. Chem. Soc., A*, **1969**, 2270.

23) C. S. Dewey and R. A. Bafford, *J. Org. Chem.*, **30**, 491 (1965).

24) In our previous description, we recorded for **1** the value of 240 °C, at which this compound began to decompose: M. Masaki, S. Matsunami, K. Okimoto, and S. Fujimura, Japan Kokai 88970 (1976); *Chem. Abstr.*, **85**, 178503j (1976). The value was obtained by a measurement which was done by setting a capillary in a sulfuric acid bath. The sample might be exposed to the vapor of sulfuric acid, which could be introduced from a cut edge of the capillary placed inside of the bath.

25) In the measurement of mp, it was observed that the product began coloring gradually at about 340 °C and decomposed and melted at 380—385 °C.

26) W. Markwald, W. Klemm, and H. Trabert, *Chem. Ber.*, **33**, 1556 (1900).

Substituent Effects in Heterogeneous Catalysis. III. Competitive Hydrogenation of Cyclohexanone and 2-Alkylcyclohexanones over Platinum Group Metals

Teiji CHIHARA and Kazunori TANAKA*

The Institute of Physical and Chemical Research, Wako-shi, Saitama 351

(Received July 3, 1978)

Cyclohexanone (**1**) and one of its 2-alkyl (methyl, ethyl, or propyl) derivatives (**2**) were hydrogenated competitively at 30 °C in cyclohexane over platinum group metals. The alkyl derivatives **2** were all less reactive than **1** on all the catalysts used. The relative reactivity R_2/R_1 was given by $\log_{10}(R_2/R_1)=\sigma^{**}+\kappa$, with σ^{**} depending only upon the substituent and κ upon the catalyst. The greater the substituent size, the more negative was the substituent constant σ^{**}. The catalyst-dependent constant κ was in general more negative for a catalyst metal having a smaller atomic radius. The above empirical rate expression has been interpreted based on the absolute reaction rate theory. The σ^{**} values calculated on this theoretical ground were in excellent agreement with the observed values.

Substituent effects in homogeneous reactions have been extensively studied, but relatively little work on heterogeneous catalysis has been reported. Especially, the influence of catalyst properties on the substituent effects is still to be explored. Although the application of Hammett-type equations to heterogeneous catalysis was attempted by Kraus,[1] it was successful for only half of the data tested. Besides, it is not always clear why the relative hydrogenation rate should correlate with σ or σ^*. Thus it seems desirable to seek a new approach to the substituent effects in heterogeneous catalysis. The present series of studies has this primary aim. In the first paper[2] of this series, methyl substituent effects in cyclohexanone (**1**) hydrogenation were investigated by means of competitive reactions of cyclohexanone and one of its methyl derivatives over platinum group metals. The relative rates observed were discussed in relation to the reaction mechanism and the atomic radius of the catalyst metal.

The present work extends this comparative study to include 2-ethyl- and 2-propylcyclohexanone (**2e** and **2p**). The main purpose of this extension is to see how the substituent size affects the hydrogenation rate. The experiments with 2-methylcyclohexanone (**2m**) were repeated to make a comparison with **2e** and **2p** under strictly identical conditions including catalyst preparation and preservation.

Experimental

Materials. Cyclohexane (Wako Pure Chemical Ind., "special grade") was used without further purification after determining its purity to be 99.96% by GLPC on an Apiezon Grease L column. **1** and **2m** were also commercial products and distilled before use. **2e** was prepared by hydrogenation of 2-acetylphenol over Raney-Ni[3] followed by chromic acid oxidation.[4] Distillation under reduced pressure gave **2e** as a liquid: bp 71.0 °C/17 mmHg. **2p** was prepared in a similar manner using 2-allylphenol as the starting material. Distillation under reduced pressure gave **2p** as a liquid: 86.7 °C/17.5 mmHg. The purity of these ketones was greater than 99% by gas chromatography.

All the catalysts used were unsupported metal powders, and prepared by reduction of the corresponding metal oxides or hydroxides. The procedure for the preparation was described previously[2] except for Pt. The Pt catalyst was prepared using $PtCl_2$ (Mitsuwa Yakuhin Kagaku KK) as a starting material. To a hot suspension of $PtCl_2$ (1 g) in dilute HCl (2000 ml) was added 5—10% aqueous NaOH in small portions until the pH reached 8. The resulting black hydroxide suspension was simmered for 30 min and then filtered off. The hydroxide was washed repeatedly with water until the washings were neutral, transferred into a 100 ml autoclave, and about 20 ml of water was added. The hydroxide was reduced with stirring for 20 min at temperatures up to 30 °C and an initial hydrogen pressure of 80 atm. The resulting metal black was filtered off, washed with water until the washings were neutral, dried under reduced pressure, and stored over silica gel.

Kinetic Procedures. Competitive hydrogenations were conducted at 30 °C and in hydrogen of atmospheric pressure using an equimolar mixture of **1** and **2** in cyclohexane (0.5 mol/l of each ketone). Reaction mixtures were analyzed by gas chromatography on a column of 10 wt % bis(2,3-dihydroxypropyl) ether on 60—80 mesh C-22 SK. Of the two peaks due to the isomer mixture of any *cis*- and *trans*-2-alkylcyclohexanols, the one having the shorter retention time was assigned to the cis isomer and the other to the trans.[5] Details on the experimental procedure and the design of the glass reaction vessel have been given before.[2]

Data Treatments. In dealing with competitive reactions on solid catalysts it is usual to assume (i) that the reaction rate is proportional to the surface concentration of the adsorbed substrate, and (ii) that the substrate adsorption during reaction obeys the Langmuir isotherm. Applying these assumptions to our reaction systems leads to the following two rate expressions:

$$-\mathrm{d}C_1/\mathrm{d}t = k_1K_1C_1/(1+K_1C_1+K_2C_2), \quad (1)$$

$$-\mathrm{d}C_2/\mathrm{d}t = k_2K_2C_2/(1+K_1C_1+K_2C_2), \quad (2)$$

where C is the concentration, t is the time, k is the rate constant, and K is the adsorption equilibrium constant. Combining Eqs. 1 and 2 and defining R by

$$R_1 \equiv -\mathrm{d}C_1/C_1\mathrm{d}t, \quad (3)$$

$$R_2 \equiv -\mathrm{d}C_2/C_2\mathrm{d}t, \quad (4)$$

we obtain a relative rate expression such as

$$\frac{R_2}{R_1} = \frac{k_2K_2}{k_1K_1} = \log\left(\frac{C_{2(\mathrm{i})}}{C_2}\right)\Big/\log\left(\frac{C_{1(\mathrm{i})}}{C_1}\right), \quad (5)$$

where subscript (i) refers to the initial state at $t=0$. Equation 5 serves to calculate relative rates from competitive hydrogenation data.

For more rigor, the role of hydrogen should be taken into account in Eqs. 1 and 2. However, we can ignore this because whatever the involved hydrogen kinetics, we are always led to Eq. 5 by cancellation.

Results

Reaction Products. With respect to the cis/trans ratio for the product alcohol, Pd was rather cis selective (cis%; 85 for **2m**, 73 for **2e**, and 77 for **2p**). The other metals were less selective, and the observed cis% fell in the rather narrow range 58—73 for all the substrates **2m**, **2e**, and **2p**.

In the hydrogenation of **1** and **2** over Pt, more hydrogen was consumed than expected from stoichiometry for complete hydrogenation to the corresponding alcohols. This is probably due to accompanying hydrogenolysis. However, the extent of hydrogenolysis did not exceed 5% of the total conversion of the ketone. In the case of Pd, two unidentified gas chromatographic peaks (one from **1** and one from **2**) developed as the hydrogenation proceeded, but each of the by-products was always less than 2% of the corresponding alcohol. For the rest of the catalysts, there were no indications of any side reactions. Thus it is reasonable to evaluate R_2/R_1 based on Eq. 5 which ignores side reactions.

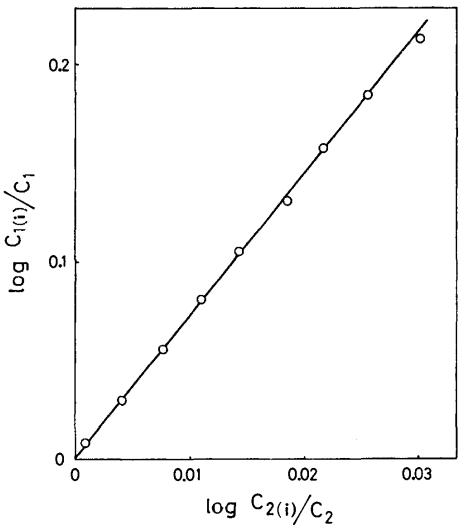

Fig. 1. A typical linear plot according to Eq. 5, observed for **1** and **2e** in competitive hydrogenation on Ir.

Substituent Effects. The log-log plots drawn according to Eq. 5 were linear, with the exception of that for Pt catalyst, which exhibited a slight curvature. Figure 1 shows a typical linear log-log plot observed on Ir. The values for relative reactivity R_2/R_1 were determined from the slope of the straight lines or from the tangent to the curved line at zero conversion. In repeated runs using the same reaction mixture and catalyst, the R_2/R_1 values observed were usually reproducible to within 5%. All the R_2/R_1 values for the same catalyst were averaged, and $\log(R_2/R_1)$ was plotted in Fig. 2a against the atomic radius of the catalyst metal. Here the atomic radius is one-half the internuclear distance between nearest neighbors in the metal crystal

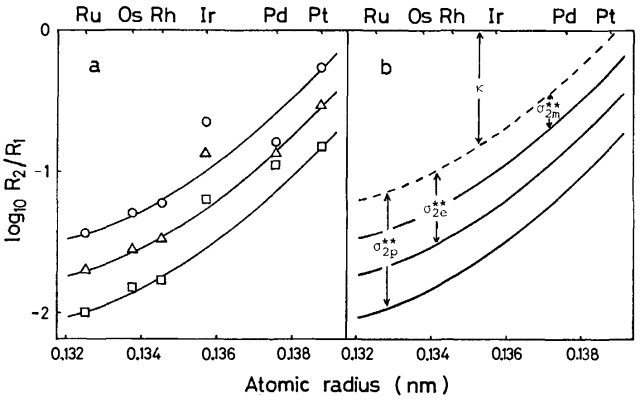

Fig. 2. Alkyl substituent effects in cyclohexanone hydrogenation.
○: **2m**, △: **2e**, □: **2p**.
κ: catalyst-dependent constant, σ^{**}: substituent constant.

which is stable under room conditions. In regard to the **2m/1** system, the general trend observed earlier (Fig. 2, Ref. 2) was reproduced here: the greater the atomic radius the greater the relative reactivity. In general the agreement on the R_{2m}/R_1 value itself is fairly good between the present and earlier experiments.

Of particular interest in Fig. 2a is the parallelism of the three correlation lines for the **2m/1**, **2e/1**, and **2p/1** systems with almost identical spacings. The distances between the adjacent data points for Ir also resemble these spacings. In what follows we are mainly concerned with explaining these apparent identities.

Discussion

Empirical Formulations. Figure 2b is a reproduction of Fig. 2a with omission of the data points. In order to derive an empirical expression for the observed relative rates, let us draw a reference line, shown as a dotted line in Fig. 2b: although the location and physical meaning of this reference line is defined later by our reaction model, at this point suffices it to say that the reference line lies between the horizontal line at $\log_{10}(R_2/R_1)=0$ and the correlation line for the **2m/1** system. We refer to the distance between the horizontal and reference lines as κ (catalyst-dependent constant) and the distances between the reference and correlation lines as σ^{**} (substituent constant): the subscript to σ^{**} indicates the substituted ketone. Obviously, the relative reactivity can be written as

$$\log_{10}(R_2/R_1) = \sigma^{**} + \kappa. \quad (6)$$

One may speculate that σ^{**} is related to the substrate size and κ to the catalyst property. It will be demonstrated below that such speculation may indeed be justified on the basis of the absolute reaction rate theory.

Theoretical Treatment. Now we aim at deriving Eq. 6. The argument developed herein is not intended to be very rigorous. Since we are dealing with heterogeneous catalysis in the liquid phase, we will be forced to be rather speculative and to employ a few ad hoc approximations. One of the basic assumptions we

make is that when converted to the activated complex, ketones **1** and **2** are adsorbed on the catalyst and are "immobile" with complete loss of translational and rotational freedom.

In deriving Eq. 5 we have assumed that both **1** and **2** are in adsorption equilibrium during reaction. Then, the overall hydrogenation rate must be controlled by one of the following steps: (i) the reaction of adsorbed ketone with adsorbed hydrogen to form a half-hydrogenated intermediate, (ii) the reaction of this intermediate with adsorbed hydrogen to form adsorbed alcohol, or (iii) the desorption of the adsorbed alcohol. If step (i) is rate-determining, the overall rate will be given by[6]

$$-\frac{dC_1}{dt} = C_{H_s}^{1/2} C_1 C_s \frac{kT}{h} \frac{f_1^{\neq}}{F_{H_s}^{1/2} F_{1(l)} f_s} \exp\left(\frac{-\varepsilon_1}{kT}\right), \quad (7)$$

$$-\frac{dC_2}{dt} = C_{H_s}^{1/2} C_2 C_s \frac{kT}{h} \frac{f_2^{\neq}}{F_{H_s}^{1/2} F_{2(l)} f_s} \exp\left(\frac{-\varepsilon_2}{kT}\right), \quad (8)$$

where factor kT/h has its usual meaning, f is the complete partition function, F is the partition function per unit volume, ε is the apparent activation energy, *i.e.*, the true activation energy subtracted by the heat of adsorption, subscript s indicates a vacant dual site that can accommodate both an adsorbed ketone molecule and a hydrogen atom, subscript l refers to the liquid state, and superscript $\neq$ indicates the activated complex. It is to be noted that we are dealing with competitive reactions and that **1** and **2** are not very much different in molecular size. This permits us to make an approximation that the adsorption site s is common to reactions of both **1** and **2**. Hence we can regard quantities C_s and f_s as identical for Eqs. 7 and 8. Combining Eqs. 7 and 8 and referring to Eqs. 3 and 4 we have

$$R_2/R_1 = (F_{1(l)} f_2^{\neq} / F_{2(l)} f_1^{\neq}) \exp\{-(\varepsilon_2 - \varepsilon_1)/kT\}. \quad (9)$$

Even if we consider step (ii) or (iii) as the rate-determining, we will still be led to Eq. 9 by cancellation. Thus, Eq. 9 can be regarded as a general expression which is applicable to different kinetics or different rate-determining steps.

Since the activated complex has been assumed to possess no translational and rotational freedom, we need to consider merely its vibration. Thus

$$f^{\neq} = f_{vib}^{\neq}. \quad (10)$$

We are not aware of any theories of liquids which permit us to formulate F_l exactly. However, what is needed herein is merely the ratio $F_{1(l)}/F_{2(l)}$, not the F_l formulation itself. The ratio can be estimated by an extension of Keii's idea.[7] As a rough approximation, let us suppose that Henry's law holds for the dissolution of **1** and **2** in cyclohexane and also that the Henry's-law constant is the same for these two ketones. Then

$$F_{1(l)}/F_{2(l)} = F_{1(g)}/F_{2(g)}, \quad (11)$$

where subscript g refers to the gas phase. The substitution of F_g for F_l underlies the conventional theoretical treatments of isotope effect problems in liquid phase reactions. A fair success in such treatments[8,9] gives indirect further support to Eq. 11. The F_g is usually expressed by

$$F_g = \frac{(2\pi mkT)^{3/2}}{h^3} \frac{8\pi^2 (8\pi^3 I)^{1/2} (kT)^{3/2}}{\sigma h^3} f_{vib}, \quad (12)$$

where m is the mass, I is the product of the three principal moments of inertia, and σ is the symmetry number. Applying Eq. 12 to both ketones **1** and **2**, taking Eqs. 9, 10, and 11 into account, and omitting the symmetry number[10] we obtain

$$\frac{R_2}{R_1} = \left(\frac{m_1}{m_2}\right)^{3/2} \left(\frac{I_1}{I_2}\right)^{1/2} \left[\frac{f_{2.vib}^{\neq} f_{1.vib}}{f_{1.vib}^{\neq} f_{2.vib}}\right] \exp\left\{\frac{-(\varepsilon_2 - \varepsilon_1)}{kT}\right\}. \quad (13)$$

Let us consider the magnitude of the quantity in the square brackets. Most stretching and bending molecular vibrations related to the C–C, C–H, and C=O bonds absorb at frequencies higher than 1000 cm^{-1}, and hence their contributions to the partition function are negligible. Some skeletal and adsorption-bond vibrations probably absorb at lower frequencies, thus contributing somewhat to the partition function. However, these contributions are expected to cancel out almost completely in the square brackets. Therefore, it might not be a serious error to set the quantity in the square brackets equal to unity. Based on this approximation Eq. 13 can be reduced to

$$\log_{10}(R_2/R_1) = \frac{3}{2}\log_{10}(m_1/m_2) + \frac{1}{2}\log_{10}(I_1/I_2) - \frac{\varepsilon_2 - \varepsilon_1}{2.303kT}. \quad (14)$$

The first and second terms of the right side of Eq. 14 depend only upon the substrates, while the third term probably reflects the catalyst property. Our empirical expression 6 becomes identical to the theoretical Eq. 14, if we put

$$\sigma^{**} = \frac{3}{2}\log_{10}(m_1/m_2) + \frac{1}{2}\log_{10}(I_1/I_2), \quad (15)$$

and

$$\kappa = -(\varepsilon_2 - \varepsilon_1)/2.303kT. \quad (16)$$

Substituent Constants. As evident from Eq. 15, σ^{**} depends only upon the m and I values of the substrates under comparison. In order to calculate I exactly, all the probable conformations of the cyclohexanone ring and the substituted alkyl group should be considered with the appropriate statistical weight. However, owing to a lack of necessary data for such a rigorous treatment, we had to be content with an approximation in which only the most likely conformation is considered. The actually assumed conformation was the chair form with the alkyl substituent in the equatorial position. For the sake of convenience, all the carbon atoms of the substituent were set so as to lie in the C(2)–C(1)=0 plane. The bond lengths and bond angles used were: r(C=C)=0.124 nm, r(C–C)=0.154 nm, r(C–H)=0.109 nm; ϕ{C(2)–C(1)–C(6)}=117°, ϕ{C(1)–C(2)–C(7)}=113.25°, any other ϕ (C–C–C)=109.5°, ϕ(H–C–H)=

Table 1. Theoretical values for σ^{**}

Paired substrates	$\frac{3}{2}\log_{10}\frac{m_1}{m_2}$	$\frac{1}{2}\log_{10}\frac{I_1}{I_2}$	σ^{**}	
2m/1	−0.087	−0.20	−0.29	(σ_{2m}^{**})
2e/1	−0.16	−0.41	−0.57	(σ_{2e}^{**})
2p/1	−0.23	−0.61	−0.84	(σ_{2p}^{**})

109.5°. The details of I calculations based on these data will be published elsewhere, and the σ^{**} values and related data are summarized in Table 1.

Turning back to Fig. 2b, it is seen that one can calculate $\Delta\sigma^{**}$ values ($\sigma^{**}_{2e}-\sigma^{**}_{2m}$ and $\sigma^{**}_{2p}-\sigma^{**}_{2m}$) from the experimental data. In Table 2 the experimental and theoretical $\Delta\sigma^{**}$ values are compared. The agreement between theory and experiment is remarkable except for Pd. The exceptional result with Pd is not unexpected since the reaction mechanism is complex for this metal.[11-13]

TABLE 2. COMPARISON OF EXPERIMENTAL AND THEORETICAL $\Delta\sigma^{**}$

	Catalyst	$\Delta\sigma^{**}$	
		$\sigma^{**}_{2e}-\sigma^{**}_{2m}$	$\sigma^{**}_{2p}-\sigma^{**}_{2m}$
Observed	Ru	−0.27	−0.54
	Rh	−0.25	−0.54
	Pd	(−0.074)	(−0.153)
	Os	−0.27	−0.53
	Ir	−0.28	−0.55
	Pt	−0.27	−0.56
	Average[a)]	−0.27	−0.54
Calcd from Eq. 15		−0.28	−0.55

a) Averaged over all the metals except Pd.

Catalyst-Dependent Constant. We are now brought to the question why κ is invariant among the three reaction systems: **2m/1**, **2e/1**, and **2p/1**. This constancy means that ε is the same for the three **2**'s. The constancy of ε is explained by assuming a particular model for the activated complex of **2** that is adsorbed on the catalyst. Figure 3 illustrates the assumed model.

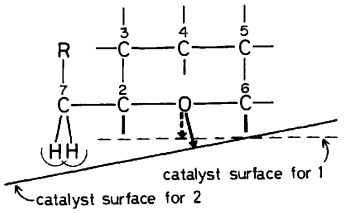

Fig. 3. Adsorption model for substituted (**2**) and unsubstituted cyclohexanone (**1**). R=H, methyl, or ethyl.

Important in this assumption is that in the case of **2m** one hydrogen at the C(7) position points away from the catalyst surface while the other two hydrogens point toward it. It must be this "pointing away" hydrogen that is replaced by a methyl or ethyl group upon going from **2m** to **2e** or **2p**. In this situation, no significant difference is expected among these **2**'s either in the heat of adsorption or in activation energy. As for **1**, however, it lacks the excess repulsive interaction between the substituent and the catalyst surface. Consequently, as shown in Fig. 3, the adsorption bond for **1** is probably shorter and hence stronger compared with that for **2**.

For both **1** and **2**, there must be two different forms of adsorption depending upon which face of the six-membered ring is directed toward the catalyst surface. By cis-addition of two hydrogen atoms from the catalyst side, one form is converted to the cis alcohol, and the other to the trans alcohol. In general both forms must be quite different from each other in adsorption strength. Thus, in principle, one should treat the rates of cis- and trans-alcohol formation separately in a theoretical consideration such as the one we made above. Nevertheless, we have been quantitatively successful in $\Delta\sigma^{**}$ correlation without such a separation. This is presumably aided by the observed fortuitous practical constancy of cis/trans ratio for different substrate ketones.

Concluding Remarks. Looking back at Eq. 14, let us remember that relative reactivity R_2/R_1 in a competitive reaction depends only upon the masses and the moments of inertia provided that $\varepsilon_1=\varepsilon_2$. Such conditions would be brought about if the substituent neither affects the functional group nor interacts with the catalyst surface. In other words, these conditions will be realized when the polar, steric, and "anchor" effects of the substituent are absent or negligible. The requirement for such substituent inertness may be fulfilled by an inactive substituent like alkyls unless they interact with the catalyst surface upon adsorption. Thus, the theoretical treatment presented in this paper would be expected to find a wider use even beyond ketone hydrogenation.

Measuring R_2/R_1 at various temperatures would provide a means to test the validity of our reaction model and its theoretical treatment: in Eq. 14 $\log(R_2/R_1)$ should vary linearly with the reciprocal of absolute temperature if $\varepsilon_1\neq\varepsilon_2$, and be temperature independent if $\varepsilon_1=\varepsilon_2$.

We are indebted to Mr. Okio Nomura of this laboratory for his help in deriving Eq. 14 and in making numerical calculations of the moment of inertia. It is a pleasure to acknowledge the helpful discussions with Dr. Takayoshi Kobayashi and Mr. Yasuaki Kawamura, both of this Institute, Professor Samuel Siegel of University of Arkansas, and Professor Robert W. Taft, Jr., of University of California at Irvine. Thanks are also extended to Dr. John M. Morris of University of Melbourne and Dr. F. Scott Howell of Sophia University for their linguistic comments on the original manuscript of this paper.

References

1) M. Kraus, "Advances in Catalysis," ed by D. D. Eley, H. Pines, and P. B. Weisz, Academic Press, New York (1967), Vol. 17, p. 75.

2) K. Tanaka, Y. Takagi, O. Nomura, and I. Kobayashi, *J. Catal.*, **35**, 24 (1974).

3) H. E. Ungnade and A. D. McLaren, *J. Am. Chem. Soc.*, **66**, 118 (1944).

4) L. T. Sandborn, *Org. Synth*, Coll. Vol. I, 340 (1932).

5) R. Komers, and K. Kochloefl, *Collect, Czech. Chem. Commun.*, **28**, 46 (1963).

6) S. Glasstone, K. J. Laidler, and H. Eyring, "The Theory of Rate Processes," McGraw-Hill (1941), pp. 377—378. Notice that the concentration of dual sites $(1/2)SC_S^2/L$ in this reference is represented by C_s in this paper.

7) T. Keii, *Nature*, **202**, 1331 (1964).

8) H. C. Urey, *J. Chem. Soc.*, **1947**, 562.
9) R. Nakane and T. Watanabe, "Shin Jikken Kagaku Koza," ed by Nippon Kagaku Kai, Maruzen, Tokyo (1975), Vol. 11, p. 193.
10) K. J. Laidler, "Chemical Kinetics," McGraw-Hill, New York (1965), pp. 84—85.
11) Y. Takagi, S. Teratani, and K. Tanaka, *J. Catal.*, **27**, 79 (1972).
12) Y. Takagi, S. Teratani, and K. Tanaka, "Proceedings of the Fifth International Congress on Catalysis," ed by J. W. Hightower, North-Holland, Amsterdam (1973), p. 757.
13) T. Chihara and K. Tanaka, *Chem. Lett.*, **1977**, 843.

Substituent Effects in Heterogeneous Catalysis. IV. Adsorption Estimations during Competitive Hydrogenation of Cyclohexanone and Its 2-Alkyl Derivatives

Teiji CHIHARA and Kazunori TANAKA*

The Institute of Physical and Chemical Research, Wako-shi, Saitama 351

(Received July 3, 1978)

Cyclohexanone (**1**) and its 2-alkyl derivatives (2-methyl-, 2-ethyl-, and 2-propylcyclohexanone (**2m**, **2e**, and **2p**)) were hydrogenated both individually and competitively in pairs (**1**+**2**) in cyclohexane using Ru/Al_2O_3, Rh/Al_2O_3, and Pt/Al_2O_3 as catalysts. For all the catalysts, the reaction rates in competitive reaction decreased in the sequence, **1**≫**2m**>**2e**>**2p**, while those in individual reaction were in the relation, **1**>**2m**≈**2e**≈**2p**. By the analysis of these kinetic data, the relative values of adsorption equilibrium constants have been estimated for **2m**, **2e**, and **2p**. These experimental values are in good agreement with the theoretical ones which have been derived on the basis of statistical mechanics using an adsorption model characterized by immobile adsorption of the substrate ketones.

The first[1] and third papers[2] of this series dealt with alkyl substituent effects in cyclohexanone (**1**) hydrogenation catalyzed by platinum group metals. The substituent effects were studied by means of competitive hydrogenation of **1** and its alkyl derivatives (2-methyl-, 2-ethyl-, and 2-propylcyclohexanone abbreviated subsequently to **2m**, **2e**, and **2p**). The logarithm of the observed relative rates was expressed as the sum of substituent constant σ^{**} and catalyst-dependent constant κ;

$$\log_{10}(R_2/R_1) = \sigma^{**} + \kappa. \quad (1)$$

A theoretical relative-rate expression corresponding to this empirical one (1) was derived on the basis of Eyring's rate equation using a simple reaction model in which the substrate ketones lose the translational and rotational freedom at the transition state. Comparing the empirical and theoretical relative-rate expressions, σ^{**} was quantitatively correlated as a function of the mass and the moment of inertia of the two substrate ketones under comparison. On the other hand, it is generally accepted in heterogeneous catalysis that the relative rate R_2/R_1 in competitive reaction can be expressed as

$$R_2/R_1 = (k_2/k_1)(K_2/K_1), \quad (2)$$

where k is the rate constant referred to the unit fraction of the surface covered and K is the adsorption equilibrium constant.

Thus we can now question whether k_2/k_1 or K_2/K_1 makes the chief contribution to σ^{**}. The main purpose of the present work is to resolve this question by estimating these relative values. The results are considered in the light of a statistical-mechanical treatment of adsorption equilibrium.

It is more or less conventional to compare the adsorption of the two reaction substrates by subjecting them to both individual and competitive reactions and by analyzing the obtained comparative data. This conventional technique was used in the present work. The catalysts chosen were Ru/Al_2O_3, Rh/Al_2O_3, and Pt/Al_2O_3, all in the form of pellets. At the beginning, adsorption estimations on the same powder metal catalysts that were used in the previous work were attempted but failed owing to the difficulty in obtaining a good reproducibility in catalytic activity.

Experimental

Materials and Apparatus. Commercial cyclohexane (Wako Pure Chemical Ind., "Special grade") was used as received. Compounds **1** and **2m** were also commercial products and distilled before use. The preparation of **2e** and **2p** has been described previously.[2] The catalysts chosen were Ru/Al_2O_3, Rh/Al_2O_3, and Pt/Al_2O_3, each containing 0.5 wt % of the metal. They were all purchased from Engelhard Industries in the form of pellets (1/8 inch diameter). The glass reaction vessel has already been illustrated in detail.[1]

Kinetic Procedure. In order to obtain reliable kinetic data from a series of individual reaction runs using the same kind but different batches of catalyst, the catalytic activity must be very similar for all the runs. Such a requisite was realized by pretreating the catalyst in the following fashion. One to ten catalyst pellets were weighed into a small glass test tube, and about 10 ml of cyclohexane was added. The test tube was placed in a 100-ml autoclave. The autoclave was charged with hydrogen to about 80 atm, heated to 80 °C, and allowed to stand at that temperature for 20 min with occasional gentle swirling by hand. No significant hydrogen consumption was observed during this pretreatment.

Then, the catalyst pellets were transferred to the glass reaction vessel pre-charged with cyclohexane that had already been made air-free by hydrogen flushing, care being taken to minimize the time of exposure of the catalyst to air. The reaction vessel was connected to a hydrogen reservoir and flushed repeatedly with hydrogen. Freshly distilled **1** and/or **2** were introduced into the reaction vessel by a syringe. The volume of the reaction solution thus prepared was made to be exactly 5 ml by adjusting the volume of the cyclohexane precharge and by standardizing the flushing procedure. The reaction was allowed to start by shaking the reaction vessel at 30 °C and in hydrogen of atmospheric pressure, and the reaction mixture was sampled at appropriate time intervals for the following 2 h (up to a conversion of *ca.* 5%). The activity of all the catalysts remained constant during this initial period of reaction. The reaction mixtures sampled were analyzed using a gas chromatograph.

Results

Relative Rates. Under our reaction conditions the rate of individual hydrogenations of **1** or **2** was proportional to the catalyst weight but unaffected by the fre-

Table 1. The observed rates

Catalyst	Competitive reaction		Individual reaction					
	Ketone pair	R_2/R_1	Ketone	$10^8R_1'$ mol/s g-cat		$10^8R_2'$ mol/s g-cat		R_2'/R_1'
				0.5[a]	1[a]	0.5[a]	1[a]	
Ru/Al_2O_3			**1**	3.63	3.27			
	1+2m	0.086	**2m**			1.40	1.40	0.41
	1+2e	0.051	**2e**			1.57	1.55	0.45
	1+2p	0.029	**2p**			1.38	1.38	0.40
Rh/Al_2O_3			**1**	21.7	18.2			
	1+2m	0.134	**2m**			9.2	8.0	0.43
	1+2e	0.072	**2e**			9.7	10.0	0.49
	1+2p	0.040	**2p**			7.8	9.2	0.43
Pt/Al_2O_3			**1**	60	58			
	1+2m	0.45	**2m**			30	30	0.51
	1+2e	0.23	**2e**			33	32	0.55
	1+2p	0.13	**2p**			30	27	0.48

a) Initial concentration of substrate ketone in mol/l.

quency at which the reaction vessel was shaken. It has also been observed that the hydrogenation rate is practically independent of ketone concentrations down to 0.5 mol/l or less for all the catalysts. The data on individual hydrogenations in Table 1 were all obtained in this concentration-independent region. Let us assume that R_1', the rate of individual hydrogenation of **1**, may be expressed by

$$R_1' = k_1K_1C_1/(1+K_1C_1), \quad (3)$$

where k is the rate constant. From the above-mentioned zero order kinetics in C_1, it follows that $K_1C_1 \gg 1$ in Eq. 3. Thus we have

$$R_1' = k_1. \quad (4)$$

Since the same argument holds for ketone **2**, we are led to

$$R_2'/R_1' = k_2/k_1. \quad (5)$$

Numerical values for R' were all estimated from the linear plot of product alcohol concentrations against reaction time. It is to be noted that R_2' represents the sum of the rates of cis- and trans-alcohol formation. The observed cis/trans ratio of product alcohols did not significantly differ for the three substrate ketones on a certain catalyst.

The observed values for R_1' and R_2' are given in Table 1. Interestingly enough, on each catalyst the R_2' values for **2m**, **2e**, and **2p** agree to within experimental error. In contrast R_1' is twice as great as R_2'.

Also included in Table 1 are the R_2/R_1 values, the relative rates in competitive reaction. The two characteristic features observed previously for unsupported metal catalysts were reproduced here with the Al_2O_3-supported catalysts. One of them is that, for all the catalysts, R_2/R_1 decreases in the sequence **2m**>**2e**>**2p**, *i.e.*, as the substituent size becomes larger. The other is that the R_2/R_1 value for a particular **2** decreases in the sequence Pt/Al_2O_3, Rh/Al_2O_3, Ru/Al_2O_3, *i.e.*, in the order of decreasing atomic radius of the catalyst metals. This indicates that the alkyl substituent effect in cyclohexanone hydrogenation is more pronounced for a metal having a shorter atomic radius.

Relative Adsorption. Let us derive equations which will serve to obtain some relative adsorption data. Applying Eqs. 2 and 5 to the **1-2m** pair system and combining the resulting equations yields

$$\log (K_{2m}/K_1) = \log (R_{2m}/R_1) - \log (R_{2m}'/R_1'). \quad (6)$$

Similarly for the **1-2e** pair system we have

$$\log (K_{2e}/K_1) = \log (R_{2e}/R_1) - \log (R_{2e}'/R_1'). \quad (7)$$

In these two equations we can equate the last terms to each other, as the fair agreement was obtained between R_{2m}' and R_{2e}'. Then, from Eqs. 6 and 7,

$$\log (K_{2e}/K_{2m}) = \log (R_{2e}/R_1) - \log (R_{2m}/R_1). \quad (8)$$

Analogous considerations with respect to the **1-2m** and **1-2p** pairs lead to

$$\log (K_{2p}/K_{2m}) = \log (R_{2p}/R_1) - \log (R_{2m}/R_1). \quad (9)$$

Equations 8 and 9 indicate that the relative adsorption equilibrium constants can be estimated experimentally using the relative rate data listed in Table 1. The results of actual calculations are given in Table 2 under the heading "Observed."

Table 2. Observed and calculated relative adsorption equilibrium constants

Catalyst		Obsd	Calcd
Ru/Al_2O_3	$\log_{10}(K_{2e}/K_{2m})$	−0.24	−0.28
	$\log_{10}(K_{2p}/K_{2m})$	−0.46	−0.55
Rh/Al_2O_3	$\log_{10}(K_{2e}/K_{2m})$	−0.27	−0.28
	$\log_{10}(K_{2p}/K_{2m})$	−0.53	−0.55
Pt/Al_2O_3	$\log_{10}(K_{2e}/K_{2m})$	−0.28	−0.28
	$\log_{10}(K_{2p}/K_{2m})$	−0.54	−0.55

Discussion

We intend herein to derive theoretical expressions corresponding to Eqs. 8 and 9, based on statistical mechanics employing a simple model for competitive ketone adsorption during hydrogenation. Let us recall that our reaction systems consist of a solid catalyst and a

cyclohexane solution of **1** and **2** under hydrogen of atmospheric pressure. We assume that during reaction both **1** and **2** are in adsorption equilibrium competing for the same adsorption sites. We also assume that the adsorption of the solvent and the product alcohols is negligible. The latter assumption seems reasonable in view of the use of nonpolar cyclohexane as the solvent and of our concern about only the initial stage of reactions up to a conversion of 5%.

Employing the Langmuir adsorption model, the partition function Q_a for the adsorbed phase is given by

$$Q_a = \{L!/M_1!M_2!(L-M_1-M_2)!\}q_{1(a)}^{M_1}q_{2(a)}^{M_2}, \quad (10)$$

where L is the number of adsorption sites, M is the number of adsorbed molecules, q is the molecular partition function, and subscript a refers to the adsorbed state. The chemical potential of adsorbed molecules **1** is expressed as

$$\mu_{1(a)} = (-\partial kT \ln Q_a/\partial M_1)_{L,M_2,T,V} = -kT\{-\ln M_1+\ln (L-M_1-M_2)+\ln q_{1(a)}\}. \quad (11)$$

Similarly for adsorbed molecules **2**,

$$\mu_{2(a)} = -kT\{-\ln M_2+\ln (L-M_1-M_2)+\ln q_{2(a)}\}. \quad (12)$$

On the other hand, the partition function Q_l for a ternary solution containing N_1, N_2, and $N_{s(olvent)}$ molecules of the indicated constituents is approximately described by[3,4]

$$Q_l = \frac{(N_1+N_2+N_s)!}{N_1!N_2!N_s!}q_{1(l)}^{N_1}q_{2(l)}^{N_2}q_{s(l)}^{N_s}, \quad (13)$$

where the subscript l refers to the liquid state. Based on Eq. 13 the chemical potentials of **1** and **2** in the solution are given by

$$\mu_{1(l)} = -kT\{\ln (N_1+N_2+N_s)-\ln N_1+\ln q_{1(l)}\} \quad (14)$$

and

$$\mu_{2(l)} = -kT\{\ln (N_1+N_2+N_s)-\ln N_2+\ln q_{2(l)}\}. \quad (15)$$

Since at adsorption equilibrium the relations

$$\mu_{1(l)} = \mu_{1(a)}, \quad \mu_{2(l)} = \mu_{2(a)} \quad (16)$$

hold, Eqs. 11, 12, 14, and 15 yield

$$\frac{M_2/N_2}{M_1/N_1} \equiv \frac{K_2}{K_1} = \frac{q_{1(l)}q_{2(a)}}{q_{2(l)}q_{1(a)}}. \quad (17)$$

We now come to the problem of how to express the molecular partition functions in Eq. 17. If the adsorbed **1** and **2** are immobile with loss of translational and rotational freedom, only $q_{vib(ration)}$ should be considered. Thus

$$q_{2(a)}/q_{1(a)} = (q_{2,vib(a)}/q_{1,vib(a)}) \exp\{-(w_2-w_1)/kT\}, \quad (18)$$

where w is the heat of adsorption. On the other hand, until now no theories of liquids have been developed which allow one to express exactly the molecular partition function q for a molecule in the liquid phase. As an approximation, however, it is often assumed that the internal molecular motions of a molecule in the liquid phase are identical with those of the same molecule in the gas phase.[5,6] Employing this assumption for our reaction solutions would not be seriously in error, because nonpolar cyclohexane is used as the solvent and we eventually deal with only relative values of like olecules. The problem of seeking a q_l expression now reduces to that of evaluating merely the translational partition function $q_{tr(l)}$. According to Eyring and Hirschfelder[5] $q_{tr(l)}$ can be expressed as $q_{tr(gas)}$ times v_f, where v_f represents the free volume. Then we have

$$q_l = \frac{(2\pi mkT)^{3/2}}{h^3}v_f\frac{8\pi^2(8\pi^3I)^{1/2}(kT)^{3/2}}{\sigma h^3}q_{vib}, \quad (19)$$

where m is the mass, I is the product of the three principal moments of inertia, and σ is the symmetry number. Applying Eq. 19 to both ketones **1** and **2** we obtain

$$\frac{q_{2(l)}}{q_{1(l)}} = \left(\frac{m_2}{m_1}\right)^{3/2}\left(\frac{I_2}{I_1}\right)^{1/2}\left(\frac{v_{f,2}}{v_{f,1}}\right)\left(\frac{q_{2,vib}}{q_{1,vib}}\right), \quad (20)$$

where the symmetry numbers are omitted since we are eventually concerned with rate processes.[7,8] An approximation

$$v_{f,1} = v_{f,2} \quad (21)$$

reduces Eq. 20 to

$$\frac{q_{2(l)}}{q_{1(l)}} = \left(\frac{m_2}{m_1}\right)^{3/2}\left(\frac{I_2}{I_1}\right)^{1/2}\left(\frac{q_{2,vib}}{q_{1,vib}}\right). \quad (22)$$

Alternatively, one can derive Eq. 22, as was done in the preceding paper,[2] by assuming Henry's law and the identical Henry's-law constants for the dissolution of **1** and **2** in cyclohexane. Inserting Eqs. 18 and 22 into Eq. 17 yields

$$\frac{K_2}{K_1} = \left(\frac{m_1}{m_2}\right)^{3/2}\left(\frac{I_1}{I_2}\right)^{1/2}\left(\frac{q_{1,vib}q_{2,vib(a)}}{q_{2,vib}q_{1,vib(a)}}\right) \times \exp\left\{\frac{-(w_2-w_1)}{kT}\right\}. \quad (23)$$

Applying Eq. 23 to substrates **2m** and **2e** and combining the resulting equations gives

$$\frac{K_{2e}}{K_{2m}} = \left(\frac{m_{2m}}{m_{2e}}\right)^{3/2}\left(\frac{I_{2m}}{I_{2e}}\right)^{1/2}\left(\frac{q_{2m,vib}q_{2e,vib(a)}}{q_{2e,vib}q_{2m,vib(a)}}\right) \times \exp\left\{\frac{-(w_{2e}-w_{2m})}{kT}\right\}. \quad (24)$$

In Eq. 24 we assume as an approximation that

$$w_{2m} = w_{2e}, \quad (25)$$

$$q_{2m,vib}q_{2e,vib(a)}/q_{2e,vib}q_{2m,vib(a)} = 1. \quad (26)$$

Approximation 25 is consistent with the observed identity $R'_{2m}=R'_{2e}$ because this identity can be interpreted as indicating that **2m** and **2e** are similar not only in the transition state but also in the adsorbed state. Approximation 26 also seems to be justified based on this resemblance in the adsorbed state although we can hardly develop rigorous arguments based on the concept of normal vibrations. Let us divide each substrate molecule into two parts: the carbonyl group and the rest. The rest part would undergo little or no change when the substrate molecule goes from the dissolved to the adsorbed state. Thus, merely considering the carbonyl group will suffice for estimating the value for the left-hand side of Eq. 26. With this in mind we could equate $q_{2m,vib}$ to $q_{2e,vib}$ since there seems to be no significant difference between **2m** and **2e** in the nature of the carbonyl group. Nor can we expect any significant difference between $q_{2m,vib(a)}$ and $q_{2e,vib(a)}$ in view of the above-discussed resemblance between the adsorbed **2m** and **2e**. Thus we are led to approximation 26. Approximations 25 and 26 reduce Eq. 24 to

$$\log (K_{2e}/K_{2m}) = \frac{3}{2}\log (m_{2m}/m_{2e}) + \frac{1}{2}\log (I_{2m}/I_{2e}). \quad (27)$$

By applying a similar argument to the **2m-2p** pair system we are led to

$$\log (K_{2p}/K_{2m}) = \frac{3}{2}\log (m_{2m}/m_{2p}) + \frac{1}{2}\log (I_{2m}/I_{2p}). \quad (28)$$

Equations 27 and 28 correspond to Eqs. 8 and 9, respectively. In Table 2, the theoretical values for relative adsorption equilibrium constants predicted by Eqs. 27 and 28 are compared with the observed values based on Eqs. 8 and 9. The agreement between theory and experiment is excellent.

Concluding Remarks. The most important experimental results are summarized in two reactivity sequences: **1**$\gg$**2m**$>$**2e**$>$**2p** in competitive hydrogenation and **1**$>$**2m**$\approx$**2e**$\approx$**2p** in individual hydrogenation. The identity of the three **2**'s in the latter sequence suggests that the reactivity of the carbonyl group itself and the interaction of the substituent with the catalyst surface remain unchanged when the methyl is replaced by the ethyl or propyl group. In other words, these three substituents are very similar in their chemical nature, and can be considered as "pseudo-isotopes." The observed reactivity sequence in competitive reaction is regarded as reflecting the effect of these pseudo-isotopes upon substrate adsorption. Indeed, the results in competitive reaction have been quantitatively accounted for based on this concept by means of a statistical mechanical treatment. As for the immobile adsorption model employed in this theoretical treatment, it was referred to by Glasstone *et al.*[9] as early as 1941 as the "entropy of activation in adsorption."

We thank Dr. F. Scott Howell of Sophia University for his linguistic comments on the original manuscript of this paper.

References

1) K. Tanaka, Y. Takagi, O. Nomura, and I. Kobayashi, *J. Catal.*, **35**, 24 (1974).
2) T. Chihara and K. Tanaka, *Bull. Chem. Soc. Jpn.*, **52**, 507 (1979).
3) E. A. Moelwyn-Hughes, "Physical Chemistry," 2nd revised ed, Pergamon Press, London (1961), pp. 820—821.
4) G. S. Rushbrooke, "Introduction to Statistical Mechanics," The Clarendon Press, Oxford (1951), Chap. 18.
5) H. Eyring and J. Hirschfelder, *J. Phys. Chem.*, **41**, 249 (1937).
6) E. A. Moelwyn-Hughes, "Physical Chemistry," 2nd revised ed, Pergamon Press, London (1961), p. 730.
7) K. J. Laidler, "Chemical Kinetics," McGraw-Hill, New York (1965), pp. 84—85.
8) D. M. Bishop and K. J. Laidler, *J. Chem. Phys.*, **42**, 1688 (1965).
9) S. Glasstone, K. J. Laidler, and H. Eyring, "The Theory of Rate Processes," McGraw-Hill, New York (1941), pp. 396—399.

ortho-Disubstituted *F*-Benzenes. I. Preparation of (*F*-Benzo)heterocyclic Compounds from *F*-Aniline and the Reactions of Some Intermediate (*F*-Phenyl)amino Compounds†

Yoshinari INUKAI,†† Yoshitsugu OONO, Takaaki SONODA, and Hiroshi KOBAYASHI*

Research Institute of Industrial Science, Kyushu University 86, Hakozaki, Fukuoka 812

††*Department of Organic Synthesis, Faculty of Engineering, Kyushu University 36, Hakozaki, Fukuoka 812*

(Received July 3, 1978)

With the intention of achieving the selective *ortho*-disubstitution of *F*-aniline *via* intramolecular nucleophilic cyclization, syntheses of some requisite intermediate (*F*-phenyl)amino compounds and (*F*-benzo)heterocyclic compounds were investigated. 2-Phenyl-*F*-benzoxazole, 2-phenyl-*F*-benzimidazole, and 2,3-dihydro-1,4-(*F*-denz)-oxazin-3-one were obtained from the respective precursors: benz-*F*-anilide, *N*-(*F*-phenyl)benzamidine, and hydroxyacet-*F*-anilide. 2-Phenyl-*F*-benzothiazole was obtained by treating benz-*F*-anilide with phosphorus pentasulfide. Hydrolytic dehalogenation of haloacet-*F*-anilide failed to give hydroxyacet-*F*-anilide, but it was obtained successfully by catalytic debenzylation of benzyloxyacet-*F*-anilide. The reactions of iodoacet-*F*-anilide with silver nitrate and acetate yielded 2-nitrate and 2-acetate, respectively. The reaction with diamminesilver(I) nitrate resulted in a reductive deiodination which gave acet-*F*-anilide. This exceptional reactivity was ascribed to the strong electron-withdrawing effect of the *F*-phenyl group.

There have been reports of several procedures for attaining *ortho*-disubstituted *F*-benzenes;[1] rather inaccessible starting substances were used, however.[2] The reactions of monosubstituted *F*-benzenes with nucleophiles yielded predominantly *para*-disubstituted derivatives.[3] The *ortho*-disubstitution by nucleophilic reactions occurred only in a few cases where the attacking nucleophile was chemically bonded to the preceding substituent group so as to be oriented to the *ortho*-position.[4] This might constitute another useful procedure for obtaining *ortho*-disubstituted benzenes from readily available monosubstituted ones, if a wide variety of actual or potential nucleophiles could be bonded to the preceding substituent. The nucleophiles include not only actual nucleophilic agents but also their protected derivatives and the functional groups which are readily convertible to effective nucleophilic agents. As shown in Scheme 1, the nucleophile to be introduced into the *ortho*-position is linked to the substituent with one to three atoms in between, so that a five- to seven-membered heterocyclic ring is formed as an intermediate by nucleophilic cyclization. The resulting heterocyclic ring is cleaved to the final *ortho*-disubstituted *F*-benzene.[5,6]

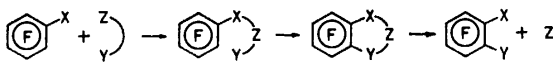

Scheme 1.

This paper will report on the *F*-benzo-heterocyclic compounds and precursory (*F*-phenyl)amino compounds which were obtained in the course of the investigation of the *ortho*-substitution on *F*-aniline (**1**) *via* intramolecular nucleophilic cyclization.

Results and Discussion

Preparation of Precursory (F-Phenyl)amino Compounds. Nucleophiles such as amine nitrogen, oxylate oxygen, and thiolate sulfur are regarded as the most effective cyclizing agents for replacing the fluorine atom on an *F*-phenyl nucleus. On the other hand, *F*-aniline nitrogen is also an actual nucleophile, and the linkage formation of *F*-aniline onto a ligand to prepare the precursory(*F*-phenyl)amino compounds can be achieved by nuclephilic attack of *F*-aniline nitrogen onto the carbocationic site of a ligand carrying a nucleophile. In a reaction of this type, the oxygen nucleophile has to be protected in the form of a carbonyl, ester, ether, or some other group containing oxygen, lest it should interfere with the *F*-aniline nitrogen nucleophile. The terminal halides can also be taken as equivalents, because they are hydrolyzable into a hydroxyl group.

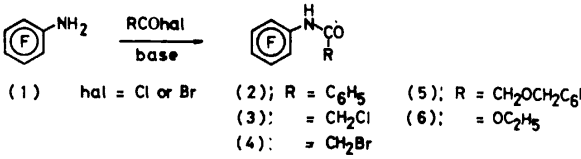

(1) hal = Cl or Br (2); R = C_6H_5 (3); = CH_2Cl (4); = CH_2Br (5); R = $CH_2OCH_2C_6H_5$ (6); = OC_2H_5

Scheme 2.

Acylation was one of the most convenient methods to afford the requisite precursors. *F*-Aniline (**1**), whose amine nitrogen is much less basic than the ordinary one,[7] reacted with various acyl halides to give the corresponding amides (**2**—**5**) and carbamate (**6**) in a similar manner to that for ordinary aromatic primary amines. The reactions proceeded in the presence of bases such as pyridine or aqueous alkali generally in good yield.

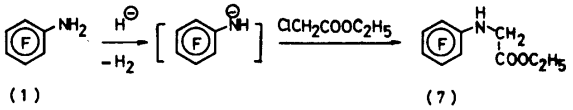

(1) (7)

Scheme 3.

Upon ethoxycarbonylmethylation on the amine nitrogen, *F*-aniline had to be activated by deprotonation; in practice, chloroacetate gave *N*-(*F*-phenyl)glycinate (**7**) by being refluxed with sodium hydride in DMF.

† Presented in part before the 8th International Symposium on Fluorine Chemistry at Kyoto, Japan, 1976.

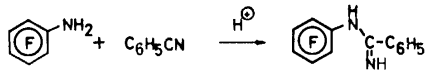

(1) (8)

Scheme 4.

The reaction with the nitrile carbon proceeded by the protonation of the nitrile; thus benzonitrile afforded *N*-(*F*-phenyl)benzamidine (**8**) in the presence of anhydrous *p*-toluenesulfonic acid.[8]

Intramolecular Nucleophilic Cyclization. The carbonyl oxygen in benz-*F*-anilide (**2**) and the imino nitrogen in benzamidine (**8**) could work as nucleophilic agents at the cyclization step. Upon being refluxed in the presence of sodium hydride in DMF, these two compounds gave strongly fluorescent 2-phenyl-*F*-benzoxazole (**9**) and 2-phenyl-*F*-benzimidazole (**10**), respectively, presumably by the nucleophilic attack of anionic intermediates to the *ortho*-fluorine on the *F*-phenyl nucleus. Since acet-*F*-anilide (**11**) yielded 2-methyl-*F*-benzoxazole (**12**) in much lower yield,[9] the phenyl group on the side chain favored the intramolecular cyclization reaction, probably due to the steric effect of its bulkiness and the resonance stabilization of the conjugated structure of the benzylideneamine type. The same effects have been invoked, in part, to explain the similar trend in the relative ease of formation of polyfluorinated benzofuran and indole derivatives from the base-catalyzed cyclization of the precursory β-(*F*-phenyl)ketones.[10]

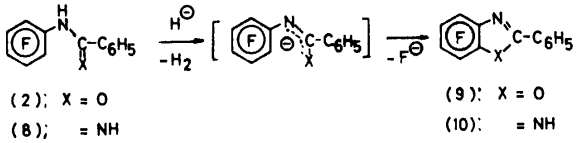

(2): X = O (9): X = O
(8): = NH (10): = NH

Scheme 5.

Introduction of sulfur atom as a nucleophilic agent was effected by replacing the carbonyl oxygen of benz-*F*-anilide (**2**) by refluxing with phosphorus pentasulfide in pyridine. The reaction proceeded to give directly the cyclized 2-phenyl-*F*-benzothiazole (**13**), without isolation of an expected intermediate, thiobenz-*F*-anilide (**14**).

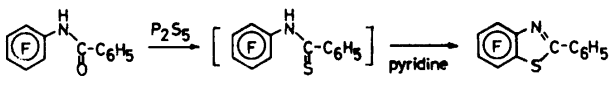

(2) (14) (13)

Scheme 6.

The present heteroaromatic compounds were isolated in fairly good yields, but against our purpose they were so stable that the cleavage of these five-membered rings was unsuccessful.

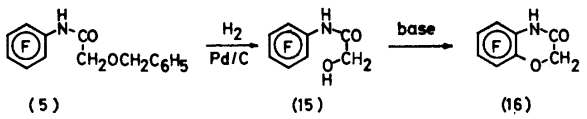

(5) (15) (16)

Scheme 7.

Formation of six-membered heterocyclic rings was attained by the cyclization of hydroxyacet-*F*-anilide (**15**), which was derived from benzyloxyacet-*F*-anilide (**5**) by reductive debenzylation. Nucleophilic cyclization of the 2-hydroxy compound (**15**) gave 2,3-dihydro-1,4-(*F*-benz)oxazin-3-one (**16**) by way of alcoholate anionic intermediate. The ring fission of this compound seems more facile than the simple 2,3-dihydro-1,4-(*F*-benz)-oxazine (**17**), whose heterocyclic ring could not be cleaved.[5]

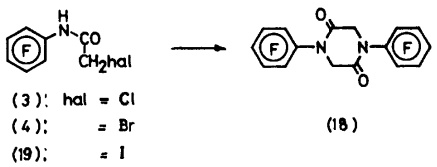

(3): hal = Cl
(4): = Br (18)
(19): = I

Scheme 8.

*Reactions of Haloacet-*F*-anilides with Nucleophiles.* Searching for a shorter route from *F*-aniline to the 2-hydroxy compound (**15**), we attempted to hydrolyze haloacet-*F*-anilides under various conditions. In the reactions of chloroacet-*F*-anilide (**3**) with potassium carbonate in anhydrous DMF, as well as that of bromoacet-*F*-anilide (**4**) with tetrabutylammonium hydroxide in a benzene–water mixture, the only isolated solid product was 1,4-di(*F*-phenyl)-2,5-piperazinedione (**18**). The attempted hydrolysis of haloacet-*F*-anilides (**3**) and (**4**) to the 2-hydroxy compound (**15**) in aqueous alkaline media afforded no definite products. Iodoacet-*F*-anilide (**19**), which was derived from chloroacet-*F*-anilide (**3**) by treatment with sodium iodide in acetone, gave the same result as above when treated with alkali in an aqueous solvent. In the reactions with silver nitrate and acetate, the haloacet-*F*-anilides (**19**) and (**4**) gave the respective esters (**20**) and (**21**). Hydrolytic fission at the O–N or O–C bond of the esters, however, did not proceed either in acidic or in basic media; instead the amide N–C bond was cleaved to give the parent *F*-aniline (**1**).

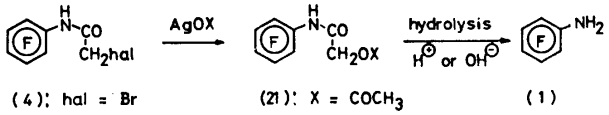

(4): hal = Br (21): X = $COCH_3$ (1)
(19): = I (20): = NO_2

Scheme 9.

On the other hand, when treated with diamminesilver(I) in aqueous THF at room temperature in the dark, the 2-iodo compound (**19**) afforded unexpectedly acet-*F*-anilide (**11**), accompanied by immediate precipitation of yellow silver iodide, the yield being almost quantitative. This reductive dehalogenation seemed to proceed specifically in aqueous THF; otherwise, for example in aqueous dioxane, the 2-iodo compound (**19**)

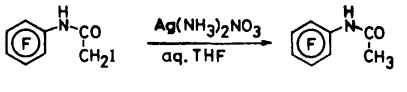

(19) (11)

Scheme 10.

gave only the piperazinedione derivative (**18**) in poor yield.

This unusual reactivity of the iodoacet-*F*-anilide (**19**), in comparison with unfluorinated iodoacetanilide,[11] suggested that the *F*-phenyl group exerted its electron-withdrawing effect up to the γ-position. Evidence might be adduced for this in the reaction of di(*F*-phenyl)-methyl bromide[12] and bromomethyl *F*-phenyl ketone[13] with nucleophiles. Further studies of the cleavage of the heterocyclic rings and the effects of the *F*-phenyl group are under way in this laboratory.

Experimental

Melting points were uncorrected. IR spectra were obtained with a JASCO DS-403G spectrometer. ^{1}H-chemical shifts were recorded on a Varian A-60 against the internal TMS reference. ^{19}F-NMR shifts were recorded on a JEOL PS-100 as the positive values downfield from the internal *F*-benzene reference. MS were obtained with JEOL JMS-07 and 01SG spectrometers. Electronic absorption and fluorescence spectra were recorded on HITACHI 200-20 and MDF-4 spectrometers, respectively. *F*-Aniline (**1**) was prepared according to the methods by Forbes[14] and Birchall.[15]

Benz-F-*anilide* (**2**). A mixture of *F*-aniline (2.00 g, 11 mmol), benzoyl chloride (5.00 g, 40 mmol), and 20% aqueous potassium carbonate (50 ml) was heated under reflux for 2 h. The cooled mixture was poured into ice-water and a solid product was collected by filtration. Recrystallization from benzene gave white plates of benz-*F*-anilide (**2**) melting at 188—189 °C (2.45 g, 78%). IR (KBr): 1670 cm^{-1} (C=O). Found: C, 54.28; H, 2.29; N, 4.89%. Calcd for $C_{13}H_6NF_5O$: C, 54.37; H, 2.11; N, 4.88%.

Chloroacet-F-*anilide* (**3**). Into a mixture of *F*-aniline (4.00 g, 22 mmol), anhydrous pyridine (4.05 g, 51 mmol), and absolute ether (70 ml), chloroacetyl chloride (7.00 g, 62 mmol) was added dropwise over 30 min with stirring. The mixture was refluxed for an additional 1 h, cooled, and filtered. The filtrate was washed with water, 10% aqueous sodium hydroxide, and water, successively, and evaporated to dryness after being dried over magnesium sulfate. Recrystallization of the residual solid from cyclohexane gave white needles, mp 108—109 °C, of chloroacet-*F*-anilide (**3**) (4.67 g, 88%). IR (CCl_4): 2950 and 2920 (CH), 1720 cm^{-1} (C=O). Found: C, 37.02; H, 1.17; N, 5.40%. Calcd for $C_8H_3NClF_5O$: C, 37.07; H, 1.27; N, 5.26%.

Bromoaceto-F-*anilide* (**4**). *F*-Aniline (5.00 g, 27 mmol) was worked up with bromoacetyl bromide (14.56 g, 72 mmol) in a manner similar to the above. Recrystallization from cyclohexane gave white needles, mp 113—114 °C, of bromoacet-*F*-anilide (**4**) (7.55 g, 91%). IR (CCl_4): 2950 and 2920 (CH), 1715 cm^{-1} (C=O). Found: C, 31.67; H, 1.02; N, 4.49%. Calcd for $C_8H_3NBrF_5O$: C, 31.61; H, 1.00; N, 4.61%.

Benzyloxyacet-F-*anilide* (**5**). Into a mixture of *F*-aniline (5.00 g, 27 mmol), anhydrous pyridine (13.7 g, 173 mmol), and absolute ether (50 ml), benzyloxyacetyl chloride[16] (10.8 g, 58 mmol) was added dropwise over 30 min with stirring. The reaction mixture was refluxed for an additional 1 h, then cooled to room temperature and filtered. The filtrate was washed with water, 10% aqueous sodium hydroxide, diluted hydrochloric acid, and water, successively, and then dried over magnesium sulfate. The residue obtained after evaporation was recrystallized from cyclohexane to give benzyloxyacet-*F*-anilide (**5**) (8.30 g, 92%) of white plates, mp 129—130 °C. IR (KBr): 3000 (CH), 1670 cm^{-1} (C=O). ^{1}H-NMR ($CDCl_3$): 4.2 (s, 2H, $COCH_2O$), 4.7 (s, 2H, OCH_2), 7.4 (s, 5H, arom.), 7.8—8.1 ppm (br s, 1H, NH). Found: C, 54.62; H, 3.19; N, 4.03%. Calcd for $C_{15}H_{10}NF_5O_2$: C, 54.39; H, 3.04; N, 4.23%.

Ethyl (F-*Phenyl*)*carbamate* (**6**). Into an ice-chilled solution of *F*-aniline (2.00 g, 10.9 mmol) in ethanol (20 ml) was added with stirring the separate solutions of ethyl chloroformate (2.00 g, 18.4 mmol) in ethanol (5 ml) and aqueous sodium carbonate (1.20 g in 2 ml) simultaneously over 10 min. The resulting solution was kept stirring for an additional 30 min at 0 °C. It was then diluted with ethanol and the resulting precipitates were filtered out. The filtrate was poured into a large amount of water to give crude precipitates, which were recrystallized from petroleum ether (bp 40—60 °C) to afford white fibrous ethyl (*F*-phenyl)carbamate (**6**), mp 81 °C (sublimable). The yield was up to 40%. Found: C, 42.37; H, 2.37; N, 5.49%. Calcd for $C_9H_6NF_5O_2$: C, 42.36; H, 2.51; N, 5.45%.

Ethyl N-(F-*Phenyl*)*glycinate* (**7**). A DMF solution of *F*-aniline (5.00 g, 27.3 mmol in 30 ml) was added dropwise into a suspension of sodium hydride (27.1 mmol) in DMF (20 ml) with stirring. Into the resulting green mixture, after the evolution of hydrogen ceased, was added ethyl chloroacetate (5.00 g, 40.8 mmol). The mixture was refluxed for 1 h with stirring, then cooled and extracted with ether. The ethereal extract was washed with diluted hydrochloric acid and water, successively, and dried over magnesium sulfate. The dried extract was distilled under reduced pressure, and the fraction boiling at 100—135 °C/5 Torr was crystallized from cyclohexane–ethanol to give ethyl *N*-(*F*-phenyl)glycinate (**7**) (1.56 g, 21%) of white needles, mp 64—65 °C. IR(KBr): 2990 (CH), 1728 (C=O), 1265 and 1230 cm^{-1} (C–N). Found: C, 44.90; H, 3.11; N, 4.98%. Calcd for $C_{10}H_8NF_5O_2$: C, 44.62; H, 3.00; N, 5.20%.

N-(F-*Phenyl*)*benzamidine* (**8**). A mixture of *F*-aniline (3.00 g, 16.4 mmol), benzonitrile (2.70 g, 26.2 mmol), and anhydrous *p*-toluenesulfonic acid (26.5 mmol) was kept stirring at 180—200 °C for 5 h. The resulting solid was washed with ether, 20% aqueous sodium hydroxide, and water, successively, and was recrystallized from cyclohexane–ethanol to give *N*-(*F*-phenyl)benzamidine (**8**) (2.55 g, 55%) in white needles melting at 127—128 °C. IR (CCl_4): 3500 and 3400 (NH), and 1640 cm^{-1} (C=N). ^{1}H-NMR ($CDCl_3$): 4.8—5.2 (br s, 2H, NH), 7.0—8.0 ppm (m, 5H, arom.). Found: C, 54.47; H, 2.63; N, 9.76%. Calcd for $C_{13}H_7N_2F_5$: C, 54.56; H, 2.47; N, 9.79%.

2-Phenyl-F-*benzoxazole* (**9**). Benz-*F*-anilide (**2**) (0.50 g, 1.75 mmol) dissolved in anhydrous DMF (15 ml) was added dropwise into a mixture of sodium hydride (2.5 mmol) and anhydrous DMF (15 ml) over 30 min under a dry nitrogen atmosphere. The mixture was refluxed for an additional 2 h, then extracted with ether. The ethereal extract was washed with diluted hydrochloric acid and water, successively, dried over magnesium sulfate, and evaporated to dryness. The residual solid was chromatographed on a neutral alumina column. From the fraction eluted with benzene, 0.43 g (92%) of 2-phenyl-*F*-benzoxazole (**9**) was obtained. Recrystallization from methanol gave white needles melting at 125.2—125.7 °C.[17] IR (KBr): 1540 cm^{-1} (C=N). UV: λ_{max} (EtOH); 293 (log ε 4.40), 287.5 (4.40), 283 (4.40), 236 nm (3.99). Fluorescence spectra (EtOH): emission λ_{max}; 349 nm and exitation λ_{max}; 295 nm. ^{19}F-NMR ($CDCl_3$): 0.4 (1F), 2.5 (1F), 3.1 (1F), 11.2 ppm (1F). Found: C, 58.68; H, 2.09; N, 5.28; F, 29.3%; M$^+$, 267.

2-Phenyl-F-*benzimidazole* (**10**). The benzamidine (**8**) (0.50 g, 1.75 mmol) dissolved in anhydrous DMF (15 ml) was added dropwise into sodium hydride (2.5 mmol) in anhydrous

DMF (15 ml) over 30 min under a dry nitrogen atmosphere. The mixture was refluxed for an additional 2 h, and subsequently worked up in a manner similar to that described in the oxazole (**9**). A chromatographic fraction eluted with THF gave white needles of 2-phenyl-*F*-benzimidazole (**10**) (0.25 g, 54%), mp 221—222 °C after recrystallization from ethanol. UV: λ_{max} (EtOH); 293 (log ε 4.25), 288 (4.24), 242 nm (4.14). Fluorescence spectra (EtOH): emission λ_{max}; 332 nm and exitation λ_{max}; 312 nm. ^{19}F-NMR (ethyl acetate): 5.1 (2F), 8.0 ppm (2F). Found: C, 58.60; H, 2.39; N, 10.41; F, 28.4%; M$^+$, 266.055. Calcd for $C_{13}H_6N_2F_4$: C, 58.66; H, 2.27; N, 10.52; F, 28.6%; M, 266.058.

*2-Phenyl-*F*-benzothiazole (**13**).* A mixture of benz-*F*-anilide (**2**) (1.45 g, 5.0 mmol), phosphorus pentasulfide (2.20 g, 10.0 mmol), and anhydrous pyridine (20 ml) was refluxed for 12 h. The cooled mixture was poured into water. The resulting solid was filtered off, washed with water, and then chromatographed on a silica gel column. Evaporation of the solvent from a hexane–benzene fraction, and recrystallization from cyclohexane resulted in 2-phenyl-*F*-benzothiazole (**13**) (1.10 g, 77%) in a white powder, mp 133.0—133.5 °C. IR (KBr): 1640 cm^{-1} (C=N), UV: λ_{max} (EtOH); 295 (log ε 4.30), 253 nm (4.08). ^{19}F-NMR ($CDCl_3$): 3.2 (1F), 4.1 (1F), 15.4 (1F), 25.1 ppm (1F). Found: C, 55.19; H, 1.97; N, 4.77; F, 26.3%; M$^+$, 283. Calcd for $C_{13}H_5NF_4S$: C, 55.13; H, 4.95; F, 26.8%; M, 283. The sulfur test using sodium nitroprusside was positive.

*2,3-Dihydro-1,4-(*F*-benz)oxazine-3-one (**16**).* The 2-benzyloxy compound (**5**) (5.40 g, 16 mmol) dissolved in ethyl acetate (50 ml) was hydrogenated in the presence of 5% palladium on charcoal (1.00 g) under atmospheric pressure at room temperature. The catalyst was filtered out and the filtrate was evaporated to dryness. Recrystallization from benzene gave hydroxyacet-*F*-anilide (**15**) (3.50 g, 89%) in a white powder, mp 99—100 °C. IR (KBr): 3240 cm^{-1} (OH). ^{1}H-NMR ($CDCl_3$): 3.0—3.4 (br s, 1H, OH), 4.3 (s, 2H, CH_2), 7.9—8.3 ppm (br s, 1H, NH). Found: C, 39.86; H, 1.81; N, 5.64%. Calcd for $C_8H_4NF_5O_2$: C, 39.85; H, 1.67; N, 5.81%.

A mixture of hydroxyacet-*F*-anilide (**15**) (2.00 g, 8.3 mmol), anhydrous potassium carbonate (2.00 g, 14 mmol), and anhydrous DMSO (50 ml) was kept stirring at 110 °C for 22 h. Then the cooled mixture was poured into ether. The ethereal solution was washed with diluted hydrochloric acid and water, dried over magnesium sulfate, and evaporated to dryness. The resulting solid was purified by chromatography on a silica gel column. A fraction eluted by benzene was recrystallized from benzene to give 2,3-dihydro-1,4-(*F*-benz)-oxazin-3-one (**16**) (0.66 g, 36%) in white needles, mp 194.0—195.5 °C measured in a sealed tube. ^{1}H-NMR (acetone-d_6): 4.7 (s, 2H, CH_2), 9.5—10.3 ppm (br s, 1H, NH). UV: λ_{max} (EtOH); 240 (log ε 4.83), 209 nm (4.18). Found: C, 43.50; H, 1.53; N, 6.15; F, 35.5%; M$^+$, 221. Calcd for $C_8H_3NF_4O_2$: C, 43.46; H, 1.37; N, 6.33; F, 34.4%; M, 221.

*Iodoacet-*F*-anilide (**19**).* Chloroacet-*F*-anilide (**3**) (2.00 g, 8.2 mmol) dissolved in anhydrous acetone (10 ml) was treated with sodium iodide (2.00 g, 13 mmol) in anhydrous acetone (10 ml) for 3 h in the dark. The mixture was poured into ether and filtered. The filtrate was evaporated to give a solid, which was sublimed at 150—160 °C. The sublimate was recrystallized from benzene to give white needles, mp 152.5—153.0 °C, of iodoacet-*F*-anilide (**19**) (2.10 g, 80%). IR (CCl_4): 2910 and 2840 (CH), 1720 cm^{-1} (C=O). Found: C, 27.67; H, 0.89; N, 3.91%. Calcd for $C_8H_3NF_5IO$: C, 27.37; H, 0.86; N, 3.99%.

*(Nitrooxy)acet-*F*-anilide (**20**).* Into the iodoacet-*F*-anilide (**19**) (1.00 g, 3.0 mmol) in THF (10 ml) was added silver nitrate (1.00 g, 5.9 mmol) dissolved in water (10 ml). The solution was left standing in the dark for 9 h at room temperature. The mixture was then filtered and the filtrate was extracted with ether. Evaporation of the dried extract and recrystallization of the residue from aqueous methanol resulted in (nitrooxy)acet-*F*-anilide (**20**) (0.35 g, 41%) in white needles, mp 156.8—158.8 °C. IR (KBr): 3080, 3040, and 3000 (CH), 1690 (C=O), 1640 and 1630 cm^{-1} (ONO_2) ^{1}H-NMR ($CDCl_3$): 5.2 (s, 2H, CH_2), 7.2—7.5 ppm (br s, 1H, NH). Found: C, 33.67; H, 1.18; N, 9.87%. Calcd for $C_8H_3N_2F_5O_4$: C, 33.58; H, 1.06; N, 9.79%.

A mixture of bromoacet-*F*-anilide (**4**) (0.50 g, 1.6 mmol) dissolved in THF (10 ml) and silver nitrate (0.80 g, 4.7 mmol) dissolved in water (10 ml) was refluxed for 5 h in the dark with stirring. The subsequent working up gave the nitrate (**20**) (0.07 g, 15%), while 0.18 g (36%) of the starting material was recovered.

When chloroacet-*F*-anilide (**3**) was treated in the same manner as above, it remained unreacted and was recovered almost quantitatively.

*Acetoxyacet-*F*-anilide (**21**).* A mixture of bromoacet-*F*-anilide (**4**) (2.00 g, 6.6 mmol), silver acetate (2.00 g, 12 mmol), and acetic acid (32 ml) was refluxed with stirring for 5 h in the dark, and then left standing at room temperature overnight. The resulting precipitates were filtered out and the filtrate was evaporated to give an oily residue, which was solidified immediately. The residue was chromatographed on a neutral alumina column. An eluate with benzene–acetone (10: 1) was evaporated and the residue was recrystallized from benzene to give acetoxyacet-*F*-anilide (**21**) (1.40 g, 75%) in white needles, mp 85.5—87.0 °C. IR (KBr): 3000 (CH), 1760 (ester C=O), 1690 cm^{-1} (amide C=O). ^{1}H-NMR (acetone-d_6): 2.1 (s, 3H, CH_3), 4.8 (s, 2H, CH_2), 9.0—9.4 ppm (br s, 1H, NH). Found: C, 42.23; H, 2.29; N, 4.80%. $C_{10}H_6NF_5O_3$: C, 42.41; H, 2.14; N, 4.96%.

*Reactions of Haloacet-*F*-anilides with Bases.* *1*: A mixture of chloroacet-*F*-anilide (**3**) (1.00 g, 4.1 mmol), anhydrous potassium carbonate (0.25 g, 1.8 mmol), and anhydrous DMF (20 ml) was refluxed for 1 h with stirring. The cooled mixture was poured into ether. The ethereal solution was washed with diluted hydrochloric acid and water, successively, and evaporated to dryness. The residue was chromatographed on a neutral alumina column. The benzene eluate was evaporated and the residue was recrystallized from aqueous methanol to afford 1,4-di(*F*-phenyl)2,5-piperazinedione (**18**) (0.35 g, 41%) in white plates, mp 178—179 °C. Further purification was effected by recrystallization from cyclohexane–benzene to afford a specimen of white needles melting at 180.0—180.5 °C.[10b] IR (KBr): 2900 (CH), 1690 (C=O), 1330 and 1130 cm^{-1} (C–N). ^{1}H-NMR ($CDCl_3$): 4.5 ppm (s, CH_2). Found: C, 43.28; H, 1.09; N, 6.10%; M$^+$, 446.009.

When treated with potassium hydroxide in aqueous dioxane, chloroacet-*F*-anilide (**3**) was recovered unchanged almost quantitatively.

2: A mixture of bromoacet-*F*-anilide (**4**) (0.50 g, 1.6 mmol), benzene (15 ml), and aqueous tetrabutyl ammonium hydroxide (1.6 mmol, 10 ml) was heated for 4 h with stirring. The benzene layer was separated and the aqueous layer was extracted with ether. The organic layer were combined and evaporated to give 0.23 g (63%) of the piperazinedione (**18**) after recrystallization from cyclohexane–benzene.

3: Into the iodoacet-*F*-anilide (**19**) (0.50 g, 1.5 mmol) in 50% aqueous THF (10 ml) was added diamminesilver(I) nitrate (5.0 mmol) in 50% aqueous THF (50 ml); the solution was left standing for 20 h in the dark. The mixture was filtered and the filtrate was extracted with ether. Evapo-

ration of the dried extract (crude yield 0.35 g) and recrystallization of the residue from aqueous methanol afforded acet-*F*-anilide (**11**) (0.17 g, 51%) in white needles, mp 135—136 °C. IR(KBr): 3240 (NH), 3060, 3020, and 2980 (CH), 1685 cm^{-1} (C=O). ^{1}H-NMR ($CDCl_3$): 2.2 (s, 3H, CH_3), 7.2—7.5 ppm (br s, 1H, NH). Found: C, 42.82; H, 1.81; N, 6.36%. The product was identified by comparison with an authentic specimen.[18]

4: Bromoacet-*F*-anilide (**4**) (0.50 g, 1.6 mmol) in 50% aqueous THF (10 ml) was added into diamminesilver nitrate (4.2 mmol) in 50% aqueous THF (10 ml); the mixture was refluxed for 5 h in the dark with stirring. After being worked up in the same manner as above, 0.06 g (16%) of the piperazinedione (**18**) was obtained.

5: When treated in the above manner, chloroacet-*F*-anilide (**3**) remained unreacted to be recovered almost quantitatively.

We wish to express our sincere thanks to Professor Keihei Ueno of Kyushu University for his continuous encouragement throughout this study. We are also grateful to Professor Nobuhiko Ishibashi of Kyushu University for use of the fluorescence spectrophotometer and to Messrs. Akira Kito and Atsushi Iyoda of the Government Industrial Research Institute at Osaka for the measurements of the ^{19}F-NMR spectra.

References

1) According to the revised nomenclature of highly fluorinated organic compounds by J. A. Young, *J. Chem. Document.*, **14**, 98 (1974); *J. Fluorine Chem.*, **6**, 571 (1975).

2) For examples: a) N. Ishikawa and T. Tanabe, *Kogyo Kagaku Zasshi*, **73**, 447 (1970); b) C. Tamborski and E. J. Soloski, *J. Organomet. Chem.*, **20**, 245 (1969); c) G. M. Brooke and B. S. Furniss, *J. Chem. Soc.*, **1967**, 869; d) L. P. Anderson, W. J. Feast, and W. K. R. Musgrave, *J. Chem. Soc., C*, **1969**, 211.

3) L. S. Kobrina, "Fluorine Chemistry Reviews," ed by P. Tarrant, Marcel Dekker, New York (1974), Vol. 7, Chap. 1.

4) For examples: a) G. G. Yakobson, G. G. Furin, L. S. Kobrina, and N. N. Voroshtsov, *J. Gen. Chem., USSR*, **37**, 1221 (1967); b) L. S. Kobrina, G. G. Furin, and G. G. Yakobson, *ibid.*, **38**, 505 (1968); c) L. S. Kobrina, G. G. Furin, and G. G. Yakobson, *J. Org. Chem., USSR*, **6**, 512 (1970).

5) J. Burdon, V. A. Damodaran, and J. C. Tatlow, *J. Chem. Soc.*, **1964**, 763.

6) a) N. N. Vorozhtsov, V. A. Barkhash, A. T. Prudchenko, and T. I. Khomenko, *Dokl. Akad. Nauk SSSR* **164**, 1046 (1965): *Chem. Abstr.*, **64**, 2045f (1966); b) A. T. Prudchenko, L. P. Vovdenko, V. A. Barkhash, and N. N. Vorozhtsov, *Khim. Geterotsikl. Soedin.*, **1968**, 967: *Chem. Abstr.*, **70**, 106308s (1969); c) G. S. Schegoleva, A. K. Petrov, V. A. Barkhash, and N. N. Vorozhtsov, *ibid.*, **1970**, 278: *Chem. Abstr.*, **26**, 140675t (1972); d) S. A. Osadchii and V. A. Barkhash, *J. Org. Chem., USSR*, **6**, 1639 (1970); e) G. S. Shchegoleva, I. S. Isaev, T. F. Ardyukova, and V. A. Barkhash, *Izv. Sib. Otd. Akad. Nauk SSSR*, **1**, 90 (1971): *Chem. Abstr.* **76**, 13587r (1972).

7) V. M. Vlasov and G. G. Yakobson, *Russ. Chem. Rev.*, **43**, 781 (1974).

8) a) P. Oxyley and W. F. Shorter, *J. Chem. Soc.*, **1946**, 147; b) J. -A. Gautier, M. Miocque, and C. C. Jarnoux, "The Chemistry of the Amidines and Imidates," ed by S. Patai, John Wiley & Sons, New York (1975), Chap. 7, p. 290.

9) When treated in the manner described for the benzoxazol (**9**), acet-*F*-anilide (**11**) gave 2-methyl-*F*-benzoxazole (**12**) mp 45—46 °C,[19] with 10% yield.

10) a) G. M. Brooke, W. K. R. Musgrave, and T. R. Thomas, *J. Chem. Soc., C*, **1971**, 3596; b) G. M. Brooke, W. K. R. Musgrave, R. J. D. Rutherford, and T. W. Smith, *Tetrahedron*, **27**, 5653 (1971).

11) Under identical reaction conditions iodoacetanilide remained unreacted and could be recovered upon being treated with diamminesilver(I) nitrate.

12) R. Filler and F. P. Avonda, *J. Chem. Soc., Chem. Commun.*, **1972**, 943.

13) V. A. Barkhash, O. J. Andreevskaya, and N. N. Vorozhtsov, *Dokl. Akad. Nauk SSSR*, **166**, 1343 (1966); *Chem. Abstr.*, **64**, 17517f (1966).

14) E. J. Forbes, R. D. Richardson, and J. C. Tatlow, *Chem. Ind. (London)*, **1958**, 630.

15) J. M. Birchall, R. N. Haszeldine, and A. R. Parkinson, *J. Chem. Soc.*, **1962**, 4966.

16) S. G. Fridman, *Zh. Obshch. Khim.*, **24**, 642 (1954); *Chem. Abstr.*, **49**, 6231b (1955).

17) The present compound was presumably identical with that reported by J. M. Birchall, R. N. Haszeldine, J. Nikokavouras, and E. S. Wilks, *J. Chem. Soc., C*, **1971**, 562, though it was somewhat different from the latter in mp and UV spectrum.

18) G. M. Brooke, E. J. Forbes, R. D. Richardson, M. Stacey, and J. C. Tatlow, *J. Chem. Soc.*, **1965**, 2088.

19) Literature in Ref. 17.

Spectroscopic Studies of Solvent Effects on Intramolecular Hydrogen Bonding in *N*-Substituted Salicylamides

Michio KONDO

Central Research Laboratories, Sankyo Co., Ltd., Hiromachi 1-2-58, Shinagawa-ku, Tokyo 140

(Received July 6, 1978)

It has been found from absorption and emission spectra that the intramolecular hydrogen bonds between the phenolic hydroxyl and carbonyl group of *N*-methylsalicylamide and *N*-methyl-5-chlorosalicylamide survive in DMSO as well as in 1,2-dichloroethane, whereas those of *N,N*-dimethylsalicylamide and *N,N*-dimethyl-5-chlorosalicylamide are disrupted in DMSO. The solvent dependence of the ^{1}H and ^{13}C chemical shifts of these compounds are also well related to the intramolecular hydrogen bonding.

The first absorption bands of benzoic acid, benzamide, phenol, and salicylic acid are located at 280 (heptane),[1] 279 (solvent not identified),[2] 278 (hexane),[3] and 303 nm (0.1 M $HClO_4$),[4] respectively. The red shift of the first band of salicylic acid, compared with those of the other three compounds, have been ascribed to the intramolecular hydrogen bonding between the phenolic hydroxyl and carbonyl groups.

In salicylamide and *N*-methylsalicylamide, the first absorption bands are located very close to that of salicylic acid, suggesting a planar structure involving intramolecular hydrogen bonds as in salicylic acid molecules. In the case of *N,N*-dimethylsalicylamide, on the other hand, steric interaction between the ring proton-6 and the N–CH_3 group distorts the planar structure.

DMSO is known as a powerful solvent capable of forming intermolecular hydrogen bonds with various polar groups of solute molecules. An almost exclusive intermolecular hydrogen bond between the phenolic hydroxyl and DMSO molecules has been assumed for a number of *o*-substituted phenols.[5]

It is well established that a molecule having intramolecular hydrogen bonds, such as methyl salicylate[6] or *N*-methylsalicylamide,[7] undergo the so-called proton transfer in the excited singlet state, resulting in a significantly red-shifted emission band.

These observations suggest that the absorption and emission spectra of salicylamides are dependent upon the solvent wherein the intramolecular hydrogen bond is replaced by intermolecular hydrogen bonds with solvent molecules or not. In this paper, the spectroscopic behavior of *N*-methylsalicylamide (**1**), *N,N*-dimethylsalicylamide (**2**) and the corresponding amides of 5-chlorosalicylic acid (**3** and **4**) will be reported in the binary solvent system of 1,2-dichloroethane (DCE) and DMSO. The ^{1}H and ^{13}C NMR spectral changes of these compounds, upon changing the solvent from $CDCl_3$ to DMSO, will also be described.

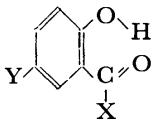

	X=NHCH$_3$	N(CH$_3$)$_2$
Y=H	**1**	**2**
Cl	**3**	**4**

Experimental

N-methyl- and *N,N*-dimethylsalicylamide were prepared by the condensation of methyl salicylate with the appropriate amine in methanol. 5-Chlorosalicylamides were also prepared in a similar way. The absorption and emission spectra were recorded on a Hitachi spectrophotometer, Model 356, and a Hitachi fluorescence spectrophotometer, Model MPF-2, respectively. The ^{1}H and ^{13}C NMR spectra were recorded on a Varian XL-100A-15 spectrometer at room temperature. The sample concentrations were 2% for ^{1}H NMR and 5—10% w/v for ^{13}C NMR measurements, unless otherwise noted. The ^{13}C NMR spectra were recorded at FT mode operation.

Results and Discussion

Absorption Spectra. In Fig. 1 are shown the absorption spectra of **1** and **2** in the binary solvent system of DCE and DMSO. The first absorption band of **2** in DCE has a peak at 297 nm and comparison of this value with that for phenol and salicylic acid, suggests the existence of intramolecular hydrogen bonds. With increase in DMSO content, this band shows a progressive decrease in intensity accompanied by the appearance of a new band at 280 nm, an isosbestic point being clearly seen at 285 nm. This observation suggests the existence of an equilibrium between two molecular species in solution. Therefore, the new absorp-

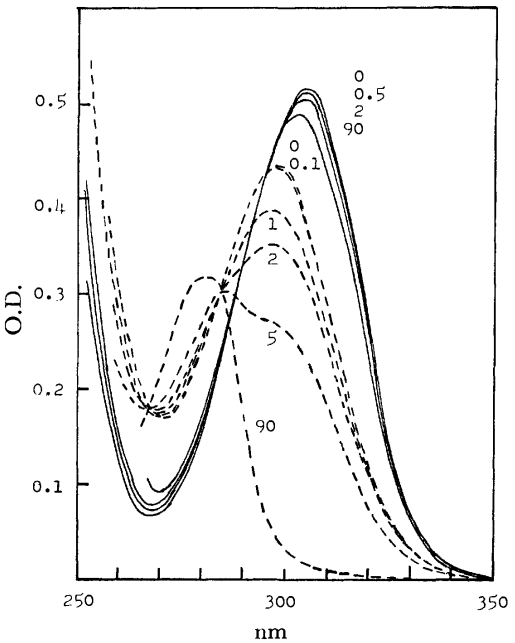

Fig. 1. The absorption spectra of **1** (——; 1.1×10^{-4} M) and **2** (-——; 1.1×10^{-4} M) in binary solvent system of DCE and DMSO. The numbers given on the curves indicate the contant of DMSO (% v/v).

ion band may reasonably be ascribed to molecules of which the intramolecular hydrogen bond is replaced by intermolecular hydrogen bonds with DMSO molecules. As anticipated the absorption spectrum of the methyl ether of **2** did not show any variation with the change in solvent composition.

A DCE solution of **1** shows the first absorption band at 304.5 nm, suggesting intramolecular hydrogen bonding. Addition of DMSO to this solution caused no appreciable change in both the position and intensity of this band. Even in a solution composed of 90% DMSO, the absorption maximum of **1** was located at 302 nm, with a trivial decrease in absorbance. The absorption spectrum of the methyl ether of **1** was almost independent of solvent composition and the first absorption band was located at 287 nm, much lower than that of **1** in 90% DMSO and higher by about 10 nm than that of benzamide. It may be concluded from these observations that the intramolecular hydrogen bond in **2** is almost disrupted in DMSO but not in **1**.

Similar behavior was observed for **3** and **4** in the same binary solvent system.

Emission Spectra. In DCE solution, the emission bands of **1**, **2**, **3**, and **4** are located at about 440, 460, 450, and 465 nm respectively. The large Stokes' shifts may be ascribed to the intramolecular proton transfer in the lowest excited state— often observed for many compounds having intramolecular hydrogen bonds.[6-8]

In 90% DMSO solution, **1** and **3** exhibited emission spectra similar to those in DCE solution, both in peak positions (429, 436 nm) and intensities. This similarity suggests that strong intramolecular interactions between the two substituents of **1** and **3** survive in the lowest excited singlet state in DMSO as well as in DCE and that intramolecular proton transfer takes place. The emission spectra of **2** and **4** in 90% DMSO solution were located at 348 and 400 nm, respectively and these large blue shifts suggest species without intramolecular hydrogen bonding between the phenolic OH and the carbonyl oxygen.

^1H NMR Spectra. The ^1H NMR spectral measurements were conducted on **3** and **4** because of easier analysis of the ring proton signals. The results are summarized in Table 1.

The phenolic hydroxyl proton of **3** appeared as a sharp signal at about the same field in $CDCl_3$ and DMSO (δ 12.11 and 12.68, respectively), much lower than the fields where **4** resonates, implying that the intramolecular hydrogen bond of **3** survives even in DMSO. The phenolic OH proton of **4** dissolved in $CDCl_3$ was observed as a very broad signal at about δ 9.6, indicating that the intramolecular hydrogen bond in **4** is much weaker than that in **3**. The broadness of this signal may be ascribed to the average of two molecular conformations, one with intramolecular hydrogen bonds and the other without, on the NMR time scale. Conversely in DMSO, the phenolic OH proton resonates at δ 8.8 as a broad signal. It can be said therefore that intermolecular hydrogen bonds between the phenolic OH of **4** and DMSO molecules exist exclusively.

Table 1. ^1H CHEMICAL SHIFTS IN ppm DOWNFIELD FROM TMS

Compd	Solvent	OH	NH	NCH_3	H-3	H-4	H-6
3	$CDCl_3$	12.11[s]	6.24[b]	3.02	*ca* 6.9	7.33	7.26
	DMSO	12.68[s]	8.95[b]	2.83	6.92	7.40	7.89
4	$CDCl_3$	9.6[b]	—	2.74	6.86	7.28	7.79
	DMSO	8.8[b]	—	2.59	6.67	7.17	7.63

s: Sharp. b: Broad.

The $N-CH_3$ signal for **4** was observed as a singlet in both solvents, $CDCl_3$ and DMSO. Hirota *et al.*[9] observed a singlet signal for the $N-CH_3$ groups of **2** in CD_2Cl_2 at room temperature but at low temperature discovered two discrete signals. The signal coalescence at room temperature was ascribed to the rapid rotation, on the NMR time scale, of the $N(CH_3)_2$ group around the amide bond, CO–N. From the MO calculation the bond, CO–N, is expected to have a reduced double bond character owing to the intramolecular hydrogen bonding of the carbonyl group with the phenolic OH group.[9] In DMSO the intramolecular hydrogen bond of **2** and **4** are considered to be disrupted from the UV spectroscopic point of view. Therefore, in terms of ^1H NMR spectroscopy it is expected that **2** and **4** dissolved in DMSO are very similar to *N,N*-dimethylbenzamide (**5**). It has been reported for **5** that $N-CH_3$ is a broad singlet at room temperature, when dissolved in $CDCl_3$.[10] However, two discrete signals were observed for an aqueous solution of **5**.[11] The methyl ether of **2**, the UV spectrum of which is very similar to that of **2** in DMSO, showed two discrete signals for the two $N-CH_3$ groups in both solvents, $CDCl_3$ and DMSO, at room temperature. This indicates that the intramolecular interaction of the phenolic OH with the $CON(CH_3)_2$ group in **2**

Table 2. ^{13}C CHEMICAL SHIFTS IN ppm DOWNFIELD FROM TMS

Carbon	**1**		**2**		**3**		**4**	
	$CDCl_3$	DMSO	$CDCl_3$[a]	DMSO	$CDCl_3$[a]	DMSO	$CDCl_3$[a]	DMSO
C-1	114.6	115.2	117.3	124.4	115.3	116.6	118.5	126.3
C-2	161.8	160.4	159.2	153.2	160.1	158.6	157.7	152.1
C-3	118.8	117.5	118.0	115.6	120.2	119.3	119.4	117.3
C-4	134.5	133.6	132.5	129.9	134.0	133.1	132.4	129.5
C-5	119.0	118.5	118.3	118.9	123.3	122.2	123.2	122.5
C-6	125.7	127.5	128.6	127.8	124.9	127.0	128.0	127.3
C=O	171.1	169.8	171.9	168.6	169.5	168.1	170.6	166.9
$N-CH_3$	26.5	26.0	38.2	b)	26.5	26.0	38.4	b)

a) Saturated solution. b) A very broad signal.

and **4** can not be neglected even in DMSO.

When the solvent was changed from $CDCl_3$ to DMSO the ring proton-6 of **3** shifted downfield, whereas that of **4** shifted a little upfield. With the same solvent change the amide proton signal of **3** shifted downfield as much as 2.71 ppm, while the phenolic OH signal shifted downfield much less. This indicates that strong intermolecular interactions of this compound with DMSO molecules occur through the amide proton. This intermolecular hydrogen bonding makes the ring proton-6 subject to the electric field due to the polar S–O group of the intermolecularly hydrogen bonded DMSO molecule, resulting in the lower field resonance of this proton. For the ring proton-6 in **4**, this type of deshielding may be negligible in DMSO. Possible internal rotation around the C_{ring}–CO bond, induced by the disruption of the intramolecular hydrogen bond, may be responsible for the slight upfield shift of proton-6.

^{13}C NMR Spectra. The ^{13}C chemical shifts of the four compounds are given in Table 2. Signal assignments for **3** and **4** could be readily made on the basis of the chemical shifts given for methyl salicylate in $CDCl_3$,[12] the chlorine-substituent constant, and the relative intensities. However, identification of the C-3 and C-5 signals of **1** and **2** is not so simple because of the close proximity. Fortunately, the C-3 signal showed additional fine splitting due to long range spin coupling with the OH proton when it was fixed by the intramolecular hydrogen bond with the carbonyl oxygen. This identified the C-3 signal in $CDCl_3$. Recording several ^{13}C spectra of **2** in mixed solvent systems of $CDCl_3$ and DMSO with varied compositions was applied to correlate the two sets of signals of C-3 and C-5 in $CDCl_3$ and DMSO solutions.

The pronounced DMSO-induced shifts (Table 3) were observed for C-1, C-2, and C–O in **2** and **4**; the carbonyl carbon and C-2 shifted upfield while the C-1 shifted downfield. These shifts can not be attributed to the usual solvent effects and since these carbons are closely related to the intramolecular hydrogen bond, it is reasonable to attribute the observed shifts to the replacement of intramolecular hydrogen bonds by the formation of intermolecular hydrogen bonds with DMSO molecules. It is reasonable to explain the observed upfield shifts of the carbonyl carbons in terms of the disruption of the intramolecular hydrogen bonds, since the carbonyl carbon of salicylaldehyde was shown to resonate at lower fields by 3.6 and 3.0 ppm than those of the *m*- and *p*-isomers, respectively.[13] Similarly, the upfield shifts of the carbonyl carbon, upon changing from acid to ester, has been ascribed to impossibility of hydrogen bond formation in the latter.[14]

Table 3. DMSO-induced shifts ($\delta_{DMSO} - \delta_{CDCl_3}$)

Carbon	**1**	**2**	**3**	**4**
C-1	0.6	7.1	1.3	7.8
C-2	−1.4	−6.0	−1.5	−5.6
C-3	−1.3	−2.4	−0.9	−2.1
C-4	−0.9	−2.6	−0.9	−2.9
C-5	−0.5	0.6	−1.1	−0.7
C-6	1.8	−0.8	2.1	−0.7
C=O	−1.3	−3.3	−1.4	−3.7
N–CH_3	−0.5	—	−0.5	—

Secondary effects, such as changes in the degree of conjugation between the ring and the substituents induced by the disruption of the intramolecular hydrogen bond, may be responsible for the observed shifts for the other carbons.

References

1) J. Tanaka, *Bull. Chem. Soc. Jpn.*, **36**, 833 (1963).
2) C. J. Seliskar, O. S. Khalil, and S. P. McGlynn, "Excited States," ed by E. C. Lim, Academic Press, New York and London (1974), Vol. 1, p. 278.
3) M. Ito, *J. Mol. Spectrosc.*, **4A**, 125 (1960).
4) S. G. Schulman and H. Gershon, *J. Phys. Chem.*, **72**, 3297 (1968).
5) M. T. Tribble and J. G. Traynham, *J. Am. Chem. Soc.*, **91**, 379 (1969).
6) A. Weller, *Z. Elektrochem.*, **60**, 1144 (1956).
7) M. Kondo, *Bull. Chem. Soc. Jpn.*, **49**, 2679 (1976).
8) H. Shizuka, K. Matsui, T. Okamura, and I. Tanaka, *J. Phys. Chem.*, **79**, 2731 (1975).
9) M. Hirota and K. Todokoro, *Chem. Lett.*, **1974**, 777.
10) P. K. Korver, K. Spaargaren, P. J. van der Haak, and Th. J. de Boer, *Org. Magn. Reson.*, **2**, 295 (1970).
11) M. Nakano and T. Higuchi, *J. Pharm. Sci.*, **57**, 183 (1968).
12) Y. Takeuchi and H. Ishizuka, "C-13 NMR, Kiso to Ōyō," ed by S. Fujiwara, Kodansha, Tokyo (1976), p. 278.
13) A. Mathias, *Tetrahedron* **22**, 217 (1966).
14) D. H. Marr and J. B. Stothers, *Can. J. Chem.*, **45**, 225 (1967).

Reduction of 6,6-Disubstituted Fulvenes and 1,2-Benzoheptafulvene by Naphthalene Radical Anion

Akira Oku,* Mitsuhiro Yoshida, and Kenkichi Matsumoto

Department of Chemistry, Kyoto Institute of Technology, Matsugasaki, Sakyo-ku, Kyoto 606

(Received July 12, 1978)

Structural effects of fulvenes in the electron transfer reaction were examined by using naphthalene radical anion (**1**) as a homogeneous electron source in aprotic media. The reduction of 6,6-diphenylfulvene (**2**) with **1** in THF at −78 °C gave 3-benzhydrylcyclopentadiene (34%) and its 2-isomer (13%). The structures were determined by hydrogenation and by the reaction with *N*-phenylmaleimide. The reaction of 6,6-dimethylfulvene (**3**) with **1** gave bi(2-isopropylidene-3-cyclopentenyl) as the major product (39%) besides bi(2-isopropyl-1,3-cyclopentadienyl) (5%). The reaction of 3,3′,4′,5,5′,6,6′-heptamethyl-1,2-benzoheptafulvene (**4**) with **1** gave 3,3′,4,4′,5,5′,-6′,7-octamethyl-1,2-benzo-1,3,6-cycloheptatriene (32%) and 3,3′,4′,5,5′,6,6′,7-octamethyl-1,2-benzo-1,3,5-cycloheptatriene (18%). These product structures as well as the CH_3I- and D_2O-quenching of the reduction intermediates indicate that **2** is reduced by the EEC-mechanism and **3** by the ECC-mechanism, whereas the results are rather complicated in the case of **4** to distinguish between EEC and ECC mechanism.

In the study of chemical reactions *via* electron transfer mechanism, it often turns out necessary to clarify the specificity of the reaction and correlate it with electrochemical processes. In the reduction of olefins by means of Birch-type reductions[1] and stable aromatic hydrocarbon radical anions[2] which proceeds quite rapidly under homogeneous and aprotic conditions,[3] the following mechanisms have hitherto been accepted: (i) two succeeding electron transfer steps followed by a chemical reaction (EEC mechanism), and (ii) an electron transfer step followed by two chemical reactions (ECC mechanism).[4] The ECE mechanism (two electron transfer steps intercepted by protonation) generally involved in electrolytic reductions is negligible in the case of reductions by aromatic radical anions. Nevertheless, radical anion $R^{\cdot-}$ is the initially formed common chemical species in all these routes, but its behavior thereafter varies depending upon the reaction conditions[5] and the structure of substrates.

$$R \xrightarrow{e} R^{\cdot-} \begin{cases} \xrightarrow{e} [R]^{2-} \xrightarrow{2H^+} RH_2 & \cdots\cdots\text{EEC} \\ \xrightarrow{H\cdot} [RH]^- \xrightarrow{H^+} RH_2 & \cdots\cdots\text{ECC} \\ \xrightarrow{H^+} [RH]\cdot \xrightarrow{e} [RH]^- \xrightarrow{H^+} RH_2 & \cdots\text{ECE} \\ \xrightarrow{e} [R]^{2-} \xrightarrow{R} [R\text{–}R]^{2-} \xrightarrow{2H^+} RH\text{–}RH & \cdots\cdots\text{EECC} \\ \xrightarrow{\text{coupling}} [R\text{–}R]^{2-} \xrightarrow{2H^+} RH\text{–}RH & \cdots\cdots\text{ECC} \end{cases}$$

In order to ascertain the structural effects that control the reaction paths and product structures, the authors chose some fulvenes as one type of olefin models, *i.e.*, 6,6-diphenylfulvene (**2**), 6,6-dimethylfulvene (**3**), and 1,2-benzoheptafulvene (**4**), and examined their behavior in chemical electron transfer reactions in aprotic media. Sodium naphthalene (**1**) in tetrahydrofuran (THF) was employed as a homogeneous electron source and was used with the reactant ratio of [reductant]/[fulvene]=2 in all reactions.

Results and Discussion

Reduction of 6,6-Diphenylfulvene (2) by Sodium Naphthalene. The reaction of diphenylfulvene (**2**)[6] with sodium naphthalene (**1**)[7] in THF at −78 °C gave a viscous oil as the major product (47%). Its mass spectrum showed the parent ion peak at m/e=232 which is equivalent to a hydrogenated structure, **2**+2H. The NMR spectrum indicated that the product molecule involves two allylic methylene hydrogen and has an unsymmetrical geometry. Therefore, among five possible [**2**+2H]-structures **5**—**9**, only **5** and **6** satisfy the NMR observations. In addition, VPC as well as NMR

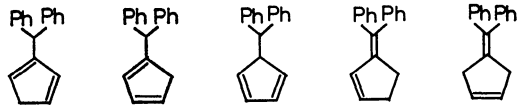

5 6 7 8 9

analysis indicated that the product consisted of two components with the ratio of *ca.* 3/1. Their separation was unsuccessful and the product was treated as a mixture in elucidating their structures in the following chemical transformations.

In catalytic hydrogenation (Pd/C), the mixture absorbed exactly 1 mol hydrogen per the molecular weight 232, giving the hydrogenated product **10** as the sole product. This supports that the structures of products are **5** and **6**, though the question of choosing the major isomer still remains unsolved. To know this answer, the mixture was treated with *N*-phenylmaleimide (**11**). The structure of the obtained adduct (isolated yield 40%) was ascribed to **12** with the support of mass spectrum (M^+=405) and NMR (the number of olefinic hydrogen per molecule was one), and consequently the major isomer was proved to be **5**, but not **6**. This structure agrees with the one previously proposed for the single reduction product isolated in the reaction of **2** with sodium metal in diethyl ether.[8]

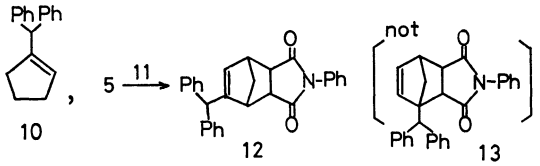

10 12 13

The D_2O-quenching technique in this reaction system seems inadequate to elucidate the carbanion intermediates, because cyclopentadiene hydrogens are so susceptible to the H/D exchange that excessive amount of deuterium incorporated in **5** and **6** (d_3 28%, d_4 18%).[9] Instead, the reaction was quenched by methyl iodide (which was added until the reaction mixture was decolorized) to give methylated products, which consisted of dimethylated (**2**+2Me), and monomethylated (**2**+Me +H) products with the ratio of 88: 12 (isolated total yield was 42% after repeated column chromatography). In contrast, no methyl group was introduced into the H_2O-quenched products in the treatment with methyl iodide under basic conditions. These results support that the trapped intermediate is a dianion. Additionally, the product structures **5** and **6** are indicative of the formation of dianion **14** as their precursor in which negative charges are separated so that the repulsive force can be minimized and both benzhydryl and cyclopentadienyl systems are contributing to stabilizing the separated charge (Scheme 1). The intermediacy of **14** is also compatible with the polarographic data of **2** ($^1E_{1/2}$= −1.30, $^2E_{1/2}$= −1.78 V *vs.* SCE; *cf.* naphthalene −2.6 V),[10] although the structures of the electrolytic reduction products have not been reported yet.

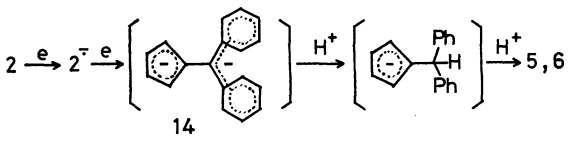

Scheme 1.

Reduction of 6,6-Dimethylfulvene (3) by Sodium Naphthalene. When 6,6-dimethylfulvene (**3**)[11] was treated under the same conditions as in the case of **2** (−78 °C in THF), only one product was detectable by VPC analysis (isolated yield 39%, air-sensitive) in addition to the formation of resinous solids. The mass spectrum showed M^+ peak at m/e=214, which is equivalent to the formula, 2×**3**+2H. In the NMR spectrum, the proton spin coupling pairs are: i) allylic methyl protons at 1.80 with olefinic proton at 5.90, ii) methylene protons at 2.20 with both olefinic protons at 5.90 and 6.26.[12] However, no coupling was observed between methine proton at 3.1 and olefinic proton at 6.26. Therefore, among several possible structures, **16** seems to be most explainable of the above-mentioned NMR observation.

Before isolating products, the crude reaction mixture was mixed with maleimide **11** at −50 °C and the mixture was warmed up to ambient tempeature. A solid product was isolated (5%), M^+ was 560. In its NMR spectrum, the absorption at 0.97 is ascribable to isopropyl methyl protons which couple with the methine proton (J=7.5 Hz) concealed in other protons around 2.0; this methine proton also couples with the olefinic proton at 5.90; a pair of doublet (AB-Type) appears at 1.45—2.10 which is ascribable to the apical methylene protons; the integrated intensity of the olefinic proton relative to the methyl is 1/6. These spectral data support the adduct structure **18**, thus proving the presence of another product **17** as a minor component.

When **3** was treated with **1** at 0 °C, a new product **19** (65%) was obtained in addition to **16** (15%). This product (mp 156 °C) showed the M^+ peak at 342 which is equivalent to [2×**3**+2H+naphthalene], but the structure is not elucidated yet. The same product was also formed when **3** was added into **1** at −78 °C (inverse dropping method).

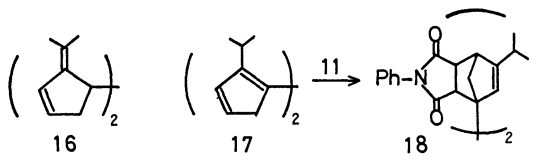

In contrast to the reaction of **2**, **3** is anticipated to show an entirely different behavior and give different product due to the methyl substituents at C-6 position. In fact, no possible monomeric product was formed, but dimeric products **16** and **17** were obtained. These structures are entirely different from the reported one in the reduction of **3** by sodium metal.[8] The formation of dimers can be most reasonably explained in terms of ECC mechanism (route *a*) or ECEC mechanism (route *b*)[4] (Scheme 2), although the averaged polarographic two-electron reduction potential of **3** was reported to be −1.90 V *vs.* SCE,[13] so far not low enough to rule out an EECC mechanism. In this Scheme, the C–C bond

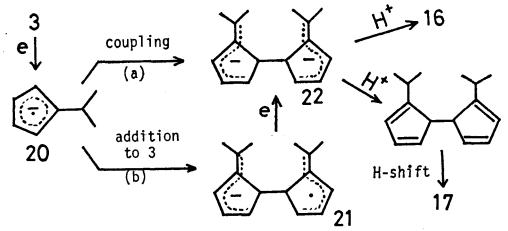

Scheme 2.

formation by either radical coupling (route *a*) or addition (route *b*) takes place more favorably between C-1 positions rather than between C-6 positions, because the latter position is sterically more crowded and the bonding at C-1 positions results in the formation of stable dienyl conjugation in **22** (or **21**). Another evidence against EEC mechanism was obtained in the reaction using an inverse dropping method (in which **3** was added into **1** at −78 °C); no monomeric product was obtained but **16**, **17**, and **19**. If any EEC mechanism had been involved, then a significant change in the products would have been observed. Scheme 2 postulates the derivation of **16** and **17** from an identical intermediate **22**; probably the protonation on the C-2 position of **22** takes place more favorably than on C-6 due to the difference in the stability between secondary and tertiary carbanions.

Reduction of 1,2-Benzoheptafulvene (4) by Sodium Naphthalene. Unsubstituted heptafulvene and its simple homologues are usually unstable and difficult to prepare.[14] In the present study, 3,3′,4′,5,5′,6,6′-heptamethyl-1,2-benzoheptafulvene (**4**)[15] was chosen as a model of seven-membered fulvene system, though not the most suitable, but because it is stable and has the unsymmetrically substituted structure easy to elucidate

the reduction products.

The reduction of **4** with **1** was carried out at −40 °C and two isomeric products, 3,3′,4,4′,5,5′,6′,7-octamethyl-1,2-benzo-1,3,6-cycloheptatriene (**23**) and 3,3′,4′,5,5′,6,6′,7-octamethyl-1,2-benzo-1,3,5-cycloheptatriene (**24**), were isolated (total yield 50%, **23**/**24**=64/36). Both of them showed the identical M^+ peaks in their mass spectra (254, equivalent to **4**+2H) and their NMR spectra did not show the presence of exo methylene protons. Thus the exo double bond was preferably reduced. These isomers were able to be separated by VPC and their structures were determined independently by the NMR analysis (see the Experimental section). Consequently,

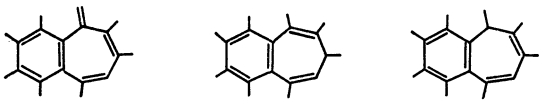

4 23 24

the major product was ascribed to the structure **23** and the minor to **24**. The fact that the isomer ratio **23**/**24** stayed almost unchanged (63—66/37—34) throughout the reaction period (3 h at −40—0 °C) and that deuterium was not incorporated when a mixture of **23** and **24** was treated by NaOD in D_2O, rules out the possibility of base-induced isomerization between products.

Table 1. *d*-Distribution in the D_2O-quenched products **23** and **24**

Run	Compound	Treatment	*d*-Distribution, %		
			d_0	d_1	d_2
1	**23**	—[a]	19	43.5	37.5
2	**24**	—[a]	26	40	34
3	**23**	D/H[b]	20.1	45.4	34.2
4	**23**	H/D[c]	20.2	45.2	34.6

a) After D_2O quenching. b) The D_2O-quenched product was treated with 15% $NaOD/D_2O$ at 25 °C for 10 h. c) The D_2O-quenched product was treated with 15% $NaOH/H_2O$ at 25°C for 10 h.

The geometrical and electronic structure of benzoheptafulvene **4** is essentially different from pentafulvenes and its immediate comparison with **2** and **3** in the reduction behavior seems complicated. The D_2O quenching technique of the reaction of **4** incorporated 34—37% d_2 and 40—44% d_1 in both products **23** and **24** (see Table 1), whereas the standard experiment in which the mixture of **23** and **24** was treated with 15% $NaOD/D_2O$ or $NaOH/H_2O$ did not show any appreciable H/D exchange. In so far as the formation of these dideuterio compounds is concerned, a rational species to be protonated seems to be dianion intermediate **27** which can be formed by the EEC mechanism (route *a* in Scheme 3). However, the extent of the d_2-incorporation was not high enough to exclude the ECC (route *b* or *b′* in Scheme 3) or ECEC mechanism.

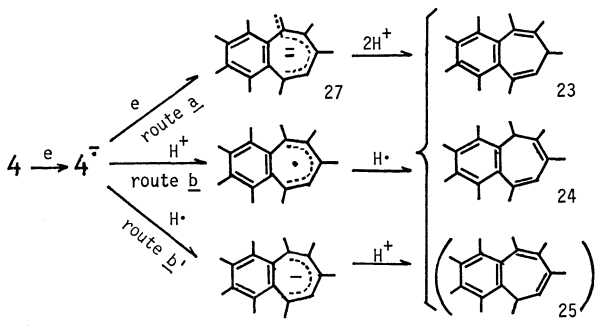

Scheme 3.

Experimental

General. The NMR spectra were measured by Varian T-60A and HA-100 spectrometers and chemical shifts were expressed in δ units. The mass spectra were measured by Hitachi RU-6L GC-MS spectrometer with the chamber voltage of 80 eV. Generally, the reductions were carried out by the method of dropping the reductant into fulvenes (normal dropping method) unless otherwise stated.

Sodium Naphthalene (1). Under the atmosphere of purified nitrogen, a THF solution of **1** was prepared from sodium metal and naphthalene, the latter recrystallized repeatedly from methanol before use. The amount of reagents which were charged initially for the preparation of **1** was kept constant at 0.5 g atom Na/0.5 mol naphthalene/liter THF throughout all experiments.[16]

Pentafulvenes. 6,6-Diphenylfulvene (**2**) and 6,6-dimethylfulvene (**3**) were prepared from cyclopentadiene according to the reported methods.[6,11]

3,3′,4′,5,5′,6,6′-Heptamethyl-1,2-benzoheptafulvene (4). Heptafulvene **4** was prepared by the reduction of the corresponding 4-Cl derivative (**4a**) which was obtained by the reaction of octamethylnaphthalene (OMN) with dichlorocarbene. The alternative 4-Br derivative (**4b**)[17] can also be used though the reaction of OMN with CBr_2 yielded 6-Br isomer as a by-product.[15]

Under a gentle stream of purified N_2, a THF solution of **1** (10 ml) was added dropwise to a cooled (−78 °C) solution of **4a** (1.28 g, 4.5 mmol) in THF (50 ml) over 10 min. After additional stirring for 20 min, the solution was decolorized by a mixture of H_2O and THF (2+10 ml). Solvent was removed and the residue, dissolved in Et_2O, was washed with aq NaCl and dried. Naphthalene was removed by sublimation and the residue was chromatographed through a silica gel column (pet. ether) to yield 0.55 g of **4** (49%); mp 104—105 °C, M^+ 252. ^{1}H-NMR (CCl_4) 1.66 and 1.92 (3H each, q, J=0.5 Hz, 5- and 6-Me), 2.06 (3H, d, J=1.4 Hz, 3-Me), 2.18 (3H, s), 2.20 (3H, s), 2.21 (3H, s), 2.29 (3H, s), 4.75 and 5.03 (1H each, dd, J=2.2 Hz, exo CH_2), 5.99 (1H, bs, J=1.4 Hz, 4-H).

Reduction of 6,6-Diphenylfulvene (2) by 1. **2** (4.7 g, 20.4 mmol) was dissolved in 50 ml of dry THF and the solution was bubbled through by N_2 for 10 min at ambient temperature. The solution was cooled to −72——78 °C and a THF solution of **1** (40 mmol) was added dropwise over 30 min. After additional stirring (1 h at −78 °C) of the colored solution (dark crimson purple), a mixture of H_2O and THF (3+10 ml) was added and the solution was warmed up to ambient temperature. The solution was diluted by Et_2O (100 ml), washed with water repeatedly till the aq layer showed pH=7.0, and dried over anhyd $MgSO_4$. After removing solvents, the residue was chromatographed through a silica gel column (pet. ether). The first fraction consisted mainly of naphthalene and the second one contained reduction products 3-benzhydrylcyclopentadiene (**5**) and its 2-isomer (**6**) as a mixture. A resinous substance trapped in the column was incapable of being identified. The products **5** and **6** could not be

separated satisfactorily by such attempted means as TLC and VPC. Yield of the mixture, 2.2 g (47%). Isomer ratio **5**/**6**=34/13 (by NMR). M^+, 232. NMR (CCl_4) 2.80—3.00 (2H, m+m′, coupling with H at 5.15 and 5.7—6.0), 5.15 (1H, m, coupling with H at 2.80—3.0 and 6.45), 5.70—6.00 (1H, m+m′, coupling with H at 2.80—3.0 and 6.2—6.45), 6.20—6.45 (2H, d+m′, coupling with H at 5.70—6.0 and 5.15), 7.20 (10H, bs).

Reduction of **2** *by* **1**, *D_2O-Quenching*: The procedure was essentially the same with that described above except that 99.9% D_2O was used as the quencher instead of H_2O. The product mixture showed an analogous VPC chromatogram to that of the H_2O-quenched products. The deuterium content of the products was determined by mass spectrometry: d_0 5.0, d_1 14.6, d_2 26.1, d_3 28.8, d_4 18.2%.

Reduction of **2** *by* **1**, *CH_3I-Quenching*: The solution of the reaction mixture of **2** (4.7 g, 20 mmol) and **1** (50 mmol) was quenched by methyl iodide (5.7 g, 40 mmol in 30 ml of THF) at −78 °C. After stirring for 40 min, the temperature was gradually raised to 0 °C and the mixture was worked-up with water and Et_2O. The organic residue was chromatographed three times through silica gel columns (pet. ether) to isolate methylated products, 2.9 g (42%). The VPC-mass spectral analysis showed that this consisted of dimethylated (88%) and monomethylated product (12%). The NMR showed methyl protons (6H at 1.8—2.0) relative to other aliphatic protons (2H at 2.6—2.8 and 2H at 5.5—6.5) and aromatic protons (10H at 7.15). The mass spectral analysis of the isolated dimethyl-product showed the M^+ peak at 260 (**2**+2Me) consistent with the dimethylated structure and that of the monomethylated product at 246 (**2**+Me+H), although the methylated positions were not elucidated.

Catalytic Hydrogenation of the Mixture **5**+**6**: A mixture of **5** and **6** (0.64 g, 2.8 mmol) was hydrogenated over Pd/C (0.13 g) in EtOH (13 ml) at 25 °C. The solution absorbed 61.3 ml H_2 (calcd 61.6 ml for one double bond) over 6.5 h to afford 1-benzhydryl cyclopentene (**10**). IR (C=C) 1600 cm^{-1} (CCl_4). NMR (CCl_4) 1.5—2.3 (6H, m), 4.7 (1H, bs), 5.2 (1H, dd, J_1=4, J_2=2 Hz), 7.1 (10H, s). Only one eluting spot was shown by TLC.

*Reaction of the Mixture (***5**+**6***) with N-Phenylmaleimide (***11***)*: Under N_2 atmosphere, a solution of **11** (0.53 g, 3 mmol, in 5 ml of benzene) was mixed with a benzene solution of **5** and **6** (0.70 g, 3 mmol in 5 ml), (slightly exothermic). The mixture was heated in a sealed tube at 60 °C for 2 h to give colorless solids of adduct **12**. 0.49 g (40%), mp 247.0—248.5 °C. NMR (acetone-d_6) 1.60 and 2.00 (1H each, dd, J=9 Hz, apical CH_2), 3.23 (1H, m), 3.45—3.55 (3H, m, coupling with H at 1.60, 2.00, and 5.52, bridgehead), 4.60 (1H, d, J=2 Hz, coupling with H at 5.52, benzhydryl), 5.52 (1H, m, olefinic), 6.70—7.60 (15H, m, ArH). Found: C, 82.85; H, 5.64; N, 3.34%; M^+, 405. Calcd for $C_{28}H_{23}NO_2$: C, 82.94; H, 5.72; N, 3.45%; M, 405.

*Reduction of 6,6-Dimethylfulvene (***3***) by* **1**. Under N_2 stream, **1** (51 mmol in 92 ml of THF) was added over 30 min to a freshly distilled **3** (2.70 g, 25.5 mmol, in 50 ml of THF) at −76 °C. The rate of decoloration of the radical anion was slow compared with that in the case of **2**. After additional stirring for 30 min, H_2O (0.9 ml in 25 ml of THF) was added and the solution was warmed up to ambient temperature. After working-up, the obtained mixture showed three TLC spots. The ethereal solution of the products, 210 ml, was divided into two parts, 160 and 50 ml, and the former was chromatographed first through a silica gel column (pet. ether) to remove polymeric products, and then by VPC (PEG 20M) to separate three fractions corresponding to the TLC spots. The first two fractions were di- and tetrahydronaphthalene, and the third fraction, liquid, was determined to be a dimeric product **16**, bi(2-isopropylidene-3-cyclopentenyl), 1.05 g (39%), by the following spectral data. NMR (CCl_4) 1.80 (6H, bs, allylic Me, slightly coupling with H at 5.90), 2.20 (2H, m, coupling with H at 3.10, 5.90, and 6.26), 3.10 (1H, m, coupling with H at 2.20), 5.90 (1H, m, coupling with H at 2.20, 6.26 by J=6 Hz, and slightly with 1.80), 6.26 (1H, a pair of t, coupling with H at 5.90 by J=6, with H at 2.20 by J=2 Hz). M^+ 214.

Reaction of the Product Mixture Obtained from **3** *with* **11**: The latter of the divided solution (50 ml) prepared in the preceding experiment was mixed with **11** (0.65 g, 3.8 mmol) under N_2 at 0 °C and the mixture was stirred for 15 h. White solids of adduct **18** separated, 0.12 g (5.3%), mp 300 °C. NMR ($CDCl_3$) 0.97 (12H, splitted d, J=7.5 Hz, isopropyl Me), 1.62 and 1.93 (2H each, dd, J=8 Hz, apical), 1.45—2.10 (2H, concealed, coupling with Me), 3.46 (6H, m, coupling with H at 5.90, bridgehead), 5.90 (2H, m, olefinic, coupling with H at 1.45—2.10 and 3.46), 7.30 (10H, m, ArH). Found: C, 77.31; H, 6.59; N, 4.81%; M^+, 560. Calcd for $C_{18}H_{18}NO_2$: C, 77.12; H, 6.47; N, 5.00%; M, 560.

Reduction of **4** *by* **1**. A solution of **4** (200 mg, 0.83 mmol) in dry THF (30 ml) was treated by a THF solution of **1** (1.8 mmol) at −40 °C for 1 h under N_2. The initially dark-green colored solution turned brown-red, which was then decolorized by a mixture of H_2O and THF (1+3 ml) at −30 °C. The mixture was extracted with Et_2O, washed with water and dried ($MgSO_4$). After removing naphthalene by sublimation, the residue was analyzed by VPC (PEG 20M, 2 m) to show two products. They could not be separated by TLC but by preparative VPC, where the first eluting fraction was **23** and the second was **24** (total yield 50%, **23**/**24**=64/36). **23**, liquid, M^+ 254. NMR (CCl_4) 1.10 (3H, d, J=12 Hz), 1.80 (6H, bs), 1.85 (3H, d, J=1.2 Hz), 2.1—2.25 (12H, m, plus concealed 1H coupling with Me at 1.10 as well as with H at 5.54), 5.54 (1H, dq, J=7.0 and 1.2 Hz). **24**, liquid, M^+ 254. NMR (CCl_4) 1.10 (3H, d, J=12 Hz), 1.63 (3H, bs), 1.79 (3H, bs), 2.04 (3H, d, J=1.5 Hz), 2.11 (3H, s), 2.17 (6H, s), 2.24 (3H, s), 3.75 (1H, q, J=12 Hz), 6.05 (1H, bs, coupling with Me at 2.04). The product ratio **23**/**24** stayed almost constant (63−66/37−34) during the reaction period.

The financial support of this work from the *Asahi Glass Foundation for the Contribution to Industrial Technology* is acknowledged with gratitude. We are also grateful for the Grant-in-Aid for Scientific Research from the Ministry of Education (No. 355372).

References

1) For examples: a) A. J. Birch and H. F. Smith, *Quart. Rev. (London)*, **12**, 17 (1958); b) W. H. Smith and A. J. Bard, *J. Am. Chem. Soc.*, **97**, 6491 (1975), and references cited therein.

2) K. Suga and S. Watanabe, *Bull. Chem. Soc. Jpn.*, **40**, 1257 (1967); D. Y. Myers, R. R. Grabbe, and D. D. Gardner, *Tetrahedron Lett.*, **1973**, 533.

3) Review: N. L. Holy, *Chem. Rev.*, **74**, 243 (1974).

4) M. M. Baizer, "Organic Electrochemistry," ed by M. M. Baizer, Marcel Dekker, Inc., New York, (1973), pp. 269, 682.

5) For the effects of ion pairs, see M. Szwarc, *Acc. Chem. Res.*, **2**, 87 (1969); **5**, 169 (1972); S. Bank and B. Bockrath, *J. Am. Chem. Soc.*, **93**, 430 (1971); **94**, 6076 (1972); **97**, 567 (1975).

6) J. Baldwin, "Experimental Organic Chemistry," 2nd ed, McGraw-Hill, New York (1970), p. 56.

7) D. E. Paul, D. Lipkin, and S. J. Weissman, *J. Am. Chem. Soc.*, **78**, 116 (1965); see also Ref. 3.
8) W. Schlenk and E. D. Bergmann, *Justus Liebigs Ann. Chem.*, **479**, 42, 60 (1930).
9) V. A. Mironov, E. V. Sobolov, and A. N. Elizarova, *Tetrahedron*, **19**, 1939 (1963); S. McLean and P. Haynes, *ibid.*, **21**, 2313, 2329, and 2343 (1965).
10) A. J. Fry, "Synthetic Organic Electrochemistry," Harper and Raw, New York (1972), p. 93.
11) H. Pines and V. N. Ipatieff, *J. Am. Chem. Soc.*, **61**, 1076 (1939).
12) J. Hine an D. B. Knight, *J. Org. Chem.*, **35**, 3946 (1970).
13) S. Wawzonek and J. W. Fan, *J. Am. Chem. Soc.*, **68**, 2541 (1946).
14) Review: E. D. Bergmann, *Chem. Rev.*, **68**, 41 (1968).
15) A. Oku, T. Hino, and K. Matsumoto, *J. Org. Chem.*, **40**, 695 (1975).
16) The actual concentration of the naphthalene radical anion in THF was determined by a carefully devised colorimetric titration method using standardized acetic acid; usually *ca.* 80% of the initially charged amounts of chemicals produced the soluble active reductant.
17) H. Hart and A. Oku, *J. Org. Chem.*, **37**, 4269 (1972).

Reactions of 2′-Hydroxyisoflavone and 2′-Hydroxy-2-methylisoflavones with Metal Salts

Kazu KUROSAWA* and Fukuo ARAKI

Department of Chemistry, Faculty of Science, Kumamoto University, Kumamoto 860

(Received July 17, 1978)

Reactions of four 2′-hydroxy-2-methylisoflavones with lead(IV) acetate gave the corresponding 10b-acetoxy-5a-methyl-5a,10b-dihydrobenzofuro[2,3-*b*][1]benzopyran-11-ones in 21—25% yields and 2-(2-methyl-4-oxo-4*H*-chromen-3-yl)-*p*-benzoquinones in 27—46% yields. Reactions of the isoflavones with manganese(III) acetate gave the ketones in 1—25% yields. Reaction of 2′-hydroxy-4′,7-dimethoxyisoflavone with lead(IV) acetate gave 10b-acetoxy-3,8-dimethoxy-5a,10b-dihydrobenzofuro[2,3-*b*][1]benzopyran-11-one, and 3,8-dimethoxybenzofuro-[2,3-*b*][1]benzopyran-11-one.

In the lead(IV) acetate oxidation of organic compounds in which a hydroxyl group and a double bond or a hydrogen are located in a spatially suitable position, an oxidative cyclization has been found.[1,3-7] Manganese(III) acetate oxidations of the compounds have also been reported to give cyclic products.[2-5,7] It could be expected that the reaction of 2′-hydroxy-2-methylisoflavone with metal salts might give a dehydrorotenoid by the removal of hydrogens from the hydroxyl and methyl groups. The dehydrorotenoid can be transformed into a rotenoid, which is known as a fish poison. It is also expected that the reaction of 2′-hydroxyisoflavone with metal salts would give benzofuro-[2,3-*b*][1]benzopyran-11-one, which has been found in natural sources as Lisetin.[8] Lisetin was synthesized from Piscerythrone, which was also a natural product, by the oxidation with potassium hexacyanoferrate.[8] However, this method is not applicable to water insoluble 2′-hydroxyisoflavones (described later).

2′-Hydroxy- and 2′-hydroxy-2-methylisoflavones (Ia—e) were prepared by partial demethylation of the corresponding 2′-methoxyisoflavones with aluminium chloride. The structures of new isoflavones were determined by examining their NMR and IR spectra, and by elemental analyses.

The reaction of 2′-hydroxy-4′,7-dimethoxy-2-methylisoflavone (Ib) with lead(IV) acetate in hot acetic acid gave two products, IIb and IIIb (Table 1, entry 3). The NMR spectrum of IIb ($C_{20}H_{18}O_7$, mp 186—188 °C) indicated that it is an acetate (δ 2.20) with a methyl group (δ 1.79), two methoxyl groups (δ 3.71 and 3.81), and six aromatic protons {δ 6.3—6.8 (4H, m), 7.35 (1H, d, J=8.5 Hz) and 7.75 (1H, m)}. The IR spectrum showed carbonyl absorptions at 1710 and 1760 cm^{-1}. These spectroscopic properties are consistent with the structure of 10b-acetoxy-3,8-dimethoxy-5a-methyl-5a,10b-dihydrobenzofuro[2,3-*b*][1]benzopyran-11-one (IIb) (Fig. 1). The NMR spectrum of IIIb ($C_{18}H_{14}O_6$, mp 237 °C) indicated the presence of a methyl group (δ 2.29), two methoxyl groups (δ 3.90 and 3.95), two singlet protons (δ 6.11 and 6.72), and three aromatic protons {δ 6.85—7.05 (2H, m) and 8.13 (1H, d, J=8.5 Hz)}. The IR spectrum exhibited multiple absorptions at 1630—1660 cm^{-1} and a carbonyl absorption at 1700 cm^{-1}. The spectroscopic evidence suggested that the structure of IIIb is to be 2-(7-methoxy-2-methyl-4-oxo-4*H*-chromen-3-yl)-5-methoxy-*p*-benzoquinone (IIIb). The reactions of Ib with lead(IV) acetate in acetic acid at room temperature and in benzene at reflux temperature gave less satisfactory results (entries 4 and 5). When Ib was treated with aqueous potassium hexacyanoferrate, the starting material was recovered unchanged.

Three other 2′-hydroxy-2-methylisoflavones (Ia, Ic, and Id) also gave the corresponding 10b-acetoxy-5a-methyl-5a,10b-dihydrobenzofuro[2,3-*b*][1]benzopyran-11-ones (IIa, IIc, and IId) and 2-(4-oxo-4*H*-chromen-3-yl)-*p*-benzoquinones (IIIa, IIIc, and IIId), respectively, in the oxidation with lead(IV) acetate. The reaction of Ib with manganese(III) acetate gave a dimeric compound, IV ($C_{40}H_{34}O_{14}$, mp 300 °C), together with IIb (entries 6, 7, and 10). IIIb was not obtained in these cases. The NMR spectrum of IV was similar to that of IIb, except for the presence of *para*-related protons {δ 7.24 (s) and 6.35 (s)} instead of the one set of three aromatic protons in IIb. The reactions of Ia, Ic, and Id with manganese(III) acetate gave IIa, IIc, and IId, respectively, in less satisfactory yields (entries 2, 12, and 14).

The reaction of 2′-hydroxy-4′,7-dimethoxyisoflavone (Ie) with lead(IV) acetate yielded two products, IIe and V. When the reaction was conducted at room temperature, IIe was the major product (entry 15). At reflux temperature, however, V was the major product (entry 17). The structures of these products were again elucidated by examining their NMR and IR spectra, and are shown in Fig. 1. It appears that the removal of acetic acid from IIe would give V and, in fact, the heating of IIe up to 250 °C yielded V in quantitative yield. The thermal elimination of acetic acid from IIe IIe suggests that the stereochemistry of the 5a-hydrogen and the 10b-acetoxyl group would be *cis*. This also leads to the prediction that the stereochemistry of 5a-methyl and 10b-acetoxyl groups in IIa—d would be *cis*, which is the more stable conformation predicted from molecular models.

In conclusion, the reactions of 2′-hydroxy-2-methylisoflavones (Ia—d) with lead(IV) acetate and manganese(III) acetate did not yield the expected dehydrorotenoids, but gave new dihydrobenzofuro-[2,3-*b*][1]benzopyran-11-ones (IIa—d), while the reaction of 2′-hydroxyisoflavone gave benzofuro[2,3-*b*][1]-benzopyran-11-one (V). The latter reaction can be utilized as a synthetic method for benzofuro[2,3-*b*][1]-benzopyran-11-one.

Table 1. The reactions of 2′-hydroxyisoflavones with metal salts

Entry	Compd	Reaction conditions: Oxidant	Molar ratio of I: oxidant	Solvent	Temp (°C)	Time (h)	Product (% yield)[a]			
1	Ia[9]	$Pb(OAc)_4$	1:1.5	AcOH	100	0.5	IIa (25)	IIIa (45)		
2	Ia	$Mn(OAc)_3 2H_2O$	1:3	AcOH	100	1.0	IIa (1)			
3	Ib	$Pb(OAc)_4$	1:1.5	AcOH	100	0.5	IIb (25)	IIIb (46)		
4	Ib	$Pb(OAc)_4$	1:1.5	AcOH	R.T.	2.0	IIb (21)	IIIb (28)		
5	Ib	$Pb(OAc)_4$	1:1.5	benzene	80	1.0	IIb (5)	IIIb (17)		
6	Ib	$Mn(OAc)_3 2H_2O$	1:1	AcOH	100	0.5	IIb (16)		IV (3)	
7	Ib	$Mn(OAc)_3 2H_2O$	1:3	AcOH	100	0.5	IIb (25)		IV (29)	
8	Ib	$Mn(OAc)_3 2H_2O$	1:3	AcOH	R.T.	72	IIb (7)			
9	Ib	$Mn(OAc)_3 2H_2O$	1:3	benzene	80	720	IIb (9)			
10	Ib	$Mn(OAc)_3 2H_2O$	1:6	AcOH[b]	100	4.5	IIb (14)		IV (9)	
11	Ic	$Pb(OAc)_4$	1:1.5	AcOH	100	0.5	IIc (22)	IIIc (27)		
12	Ic	$Mn(OAc)_3 2H_2O$	1:3	AcOH	100	0.5	IIc (9)			
13	Id	$Pb(OAc)_4$	1:1.5	AcOH	100	0.5	IId (24)	IIId (43)		
14	Id	$Mn(OAc)_3 2H_2O$	1:3	AcOH	100	0.5	IId (10)			
15	Ie[10]	$Pb(OAc)_4$	1:1.5	AcOH	R.T.	2.0	IIe (22)			V (8)
16	Ie	$Pb(OAc)_4$	1:1.5	AcOH	100	0.5	IIe (19)			V (17)
17	Ie	$Pb(OAc)_4$	1:1.5	AcOH	reflux	0.5				V (35)
18	Ie	$Mn(OAc)_3 2H_2O$	1:3	AcOH	100	0.3	IIe (10)			V (7)

a) Yield is based on the amount of isoflavone consumed. b) Two equivalents of Ac_2O were added.

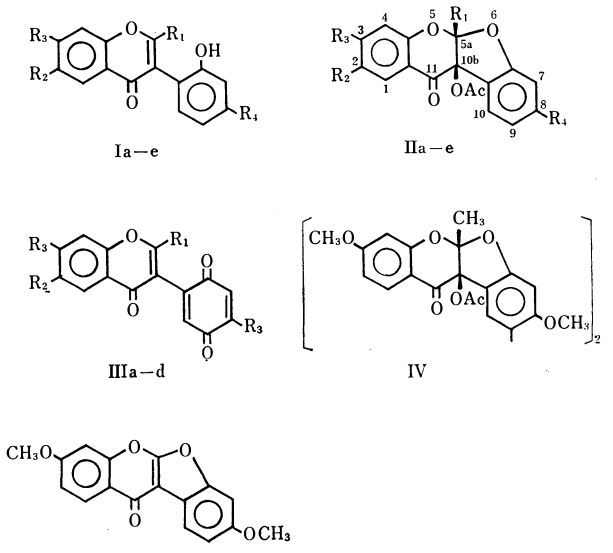

a $R_1=CH_3$, $R_2=R_4=H$, $R_3=OCH_3$
b $R_1=CH_3$, $R_2=H$, $R_3=R_4=OCH_3$
c $R_1=CH_3$, $R_2=R_3=OCH_3$, $R_4=H$
d $R_1=CH_3$, $R_2=R_3=R_4=OCH_3$
e $R_1=H$, $R_2=H$, $R_3=R_4=OCH_3$

Fig. 1.

Experimental

All ^1H NMR spectra were recorded with a Hitachi NMR spectrometer with TMS as an internal standard. The IR spectra were recorded with a JSACO grating spectrometer. The UV spectra were recorded with a Hitachi EPS-3T spectrophotometer, while the mass spectrum was recorded with a JEOL JMS-01 SG-2 mass spectrometer. Melting points were determined on a Yanagimoto hot-stage and are uncorrected.

Preparation of 2-Methylisoflavones. A typical procedure for the preparation of 2-methylisoflavone was as follows. A mixture of a phenyl benzyl ketone (0.5 g), sodium acetate (0.5 g) acetic anhydride (2 ml), and acetic acid (2 ml) was heated under reflux for 12 h. The reaction mixture was poured into ice water and the precipitates were collected.

2-Hydroxy-4,5-dimethoxyphenyl 2-methoxybenzyl ketone[11] gave 2-methyl-2′,6,7-trimethoxyisoflavone, mp 172—173 °C (EtOH) in a 31% yield. IR ($CHCl_3$) 1640 cm^{-1} (C=O); UV (MeOH) λ_{max} (ε) 288 (11900) and 324 nm (10200); NMR ($CDCl_3$) δ=2.18 (3H, s, CH_3), 3.72 (3H, s, OCH_3), 3.92 (6H, s, $2\times OCH_3$), 6.83 (1H, s, $H_{(8)}$), 6.95—7.43 (4H, m, $H_{(3'-6')}$), and 7.51 (1H, s, $H_{(5)}$). Found: C, 69.94; H, 5.60%. Calcd for $C_{19}H_{18}O_5$: C, 69.92; H, 5.56%.

2-Hydroxy-4,5-dimethoxyphenyl 2,4-dimethoxybenzyl ketone[12] yielded 2-methyl-2′,4′,6,7-tetramethoxyisoflavone, mp 175—177 °C (EtOH) in a 31% yield. IR ($CHCl_3$) 1635 cm^{-1} (C=O); UV (MeOH) λ_{max} (ε) 291 (12200) and 325 nm (9700); NMR ($CDCl_3$) δ=2.20 (3H, s, CH_3), 3.78 (3H, s, OCH_3), 3.82 (3H, s, OCH_3), 3.95 (6H, s, $2\times OCH_3$), 6.4—7.4 (2H, m, $H_{(3')}$ and $H_{(5')}$), 6.89 (1H, s, $H_{(8)}$), 7.18 (1H, m, $H_{(6')}$), 7.57 (1H, s, $H_{(5)}$). Found: C, 67.10; H, 5.82%. Calcd for $C_{20}H_{20}O_6$: C, 67.40; H, 5.66%.

Preparation of 2′-Hydroxy-2-methylisoflavones (Ib—d). A typical procedure for the preparation of 2′-hydroxy-2-methylisoflavone was as follows. A mixture of a 2′-methoxy-2-methyl isoflavone (10 mmol), aluminium chloride (20 mmol), and nitrobenzene (50 ml) was heated at 100 °C for 1 h. After the removal of the nitrobenzene under reduced pressure, the resulting mixture was triturated with 2 M hydrochloric acid. The precipitates were collected and recrystallized.

2′-Hydroxy-4′,7-dimethoxy-2-methylisoflavone (Ib): Mp 224—225 °C ($CHCl_3$); 44% yield; IR (KBr) 3300 (OH) and 1620 cm^{-1} (C=O); UV (MeOH) λ_{max} (ε) 247 (25000), 251 (25300), and 290 nm (15700); NMR (CF_3COOH) δ=2.70 (3H, s, CH_3), 4.02 (3H, s, OCH_3), 4.17 (3H, s, OCH_3), 6.75—7.59 (5H, m), and 8.59 (1H, m, $H_{(5)}$). Found: C, 69.42; H, 5.05%. Calcd for $C_{18}H_{16}O_5$: C, 69.22; H; 5.16%.

2′-Hydroxy-6,7-dimethoxy-2-methylisoflavone (Ic): Mp 251—253 °C ($CHCl_3$); 27% yield; IR (KBr) 3240 (OH) and

1630 cm^{-1} (C=O), UV (MeOH) λ_{max} (ε) 298 (13600) and 324 nm (11700); NMR (CF_3COOH) δ=2.79 (3H, s, CH_3), 4.20 (3H, s, OCH_3), 4.28 (3H, s, OCH_3), 7.21—7.53 (4H, m, $H_{(3'-6')}$), 7.58 (1H, s, $H_{(8)}$), and 7.86 (1H, s, $H_{(5)}$). Found: C, 69.50; H, 5.20%. Calcd for $C_{18}H_{16}O_5$: C, 69.22; H, 5.16%.

2′-Hydroxy-2-methyl-4′,6,7-trimethoxyisoflavone (Id): Mp 241 °C ($CHCl_3$–C_6H_6); 23% yield; IR (KBr) 3200 (OH) and 1620 cm^{-1} (C=O); UV (MeOH) λ_{max}(ε) 291 (16100) and 324 nm (12900); NMR (CF_3COOH) δ=2.71 (3H, s, CH_3). 4.03 (3H, s, OCH_3), 4.19 (3H, s, OCH_3), 4.25 (3H, s, OCH_3), 6.72—6.98 (3H, m, $H_{(3')}$, $H_{(5')}$ and $H_{(6')}$), 7.51 (1H, s, $H_{(8)}$), and 7.80 (1H, s, $H_{(5)}$). Found: C, 66.36; H, 5.35%. Calcd for $C_{19}H_{18}O_6$: C, 66.66; H, 5.30%.

Oxidations of 2′-Hydroxy-2-methylisoflavanoes (Ia—d) and 2′-Hydroxyisoflavone with Lead(IV) Acetate. A typical oxidation of 2′-hydroxyisoflavone was as follows. A mixture of a 2′-hydroxyisoflavone (1 mmol), lead(IV) acetate[13] (1.5 mmol), and a solvent (20 ml) was heated at an appropriate temperature for the time shown in the Table 1. After the removal of the solvent, the resulting reaction mixture was triturated with water and extracted with chloroform. The chloroform solution was evaporated and separated on TLC using chloroform as developing solvent.

Ia yielded 10b-acetoxy-3-methoxy-5a-methyl-5a,10b-dihydrobenzofuro[2,3-*b*][1]benzopyran-11-one (IIa): mp 136—137 °C (EtOH); 25% yield; IR ($CHCl_3$) 1700 (C=O) and 1760 cm^{-1} (OAc); UV (MeOH) λ_{max} (ε) 287 nm (16900); NMR ($CDCl_3$) δ=1.79 (3H, s, CH_3), 2.20 (3H, s, OAc), 3.79 (3H, s, OCH_3), 6.51—7.50 (6H, m), and 7.68 (1H, d, J=8.5 Hz, $H_{(1)}$) (Found: C, 66.92; H, 4.73%. Calcd for $C_{19}H_{16}O_6$: C, 67.05; H, 4.75%); and 2-(7-methoxy-2-methyl-4-oxo-4*H*-chromen-3-yl)-*p*-benzoquinone (IIIa): mp 180 °C (C_6H_6–light petroleum); 45% yield; IR ($CHCl_3$) 1650 and 1680 cm^{-1} (C=O); UV (MeOH) λ_{max}(ε) 226 (30500), 246 (30400), 252 (30000), and 297 nm (14700); NMR ($CDCl_3$) δ=2.30 (3H, s, CH_3), 3.91 (3H, s, OCH_3), 6.75—7.06 (5H, m, $H_{(3)}$, $H_{(5)}$, $H_{(6)}$, $H_{(6')}$, and $H_{(8')}$), and 8.05 (1H, d, J=8.5 Hz, $H_{(5')}$) (Found: C, 68.80; H, 4.10%. Calcd for $C_{17}H_{12}O_5$: C, 68.91; H, 4.08%).

Ib gave 10b-acetoxy-3,8-dimethoxy-5a-methyl-5a,10b-dihydrobenzofuro[2,3-*b*][1]benzopyran-11-one (IIb): mp 186—188 °C (EtOH); 5—25% yields; IR ($CHCl_3$) 1710 (C=O) and 1760 cm^{-1} (OAc); UV (MeOH) λ_{max} (ε) 233 (13700) and 284 nm (15800); NMR ($CDCl_3$) δ=1.79 (3H, s, CH_3), 2.20 (3H, s, OAc), 3.71 (3H, s, OCH_3), 3.81 (3H, OCH_3), 6.31—6.71 (4H, m, $H_{(2)}$, $H_{(4)}$, $H_{(7)}$, and $H_{(9)}$), 7.37, (1H, m, $H_{(10)}$), and 7.73 (1H, d, J=8.5 Hz, $H_{(1)}$) (Found: C 64.65; H, 4.90%. Calcd for $C_{20}H_{18}O_7$: C, 64.56; H, 4.90%); and 2-(7-methoxy-2-methyl-4-oxo-4*H*-chromen-3-yl)-5-methoxy-*p*-benzoquinone (IIIb): mp 237 °C (EtOH); 17—46% yields; IR ($CHCl_3$) 1630—1660 and 1700 cm^{-1} (C=O); UV (MeOH) λ_{max} (ε) 223 (23700), 247 (25400), 252 (27200), and 298 nm (15900); NMR ($CDCl_3$) δ=2.29, (3H, s, CH_3), 3.90 (3H, s, OCH_3), 3.95 (3H, s, OCH_3) 6.11 (1H, s, $H_{(6)}$), 6.72 (1H, s, $H_{(3)}$), 6.85—7.05 (2H, m, $H_{(6')}$ and $H_{(8')}$), 8.13 (1H, d, J=8.5 Hz, $H_{(5')}$)(Found: C, 65.96; H, 4.32%. Calcd for $C_{18}H_{14}O_6$: C, 66.25; H, 4.32%).

Ic yielded 10b-acetoxy-2,3-dimethoxy-5a-methyl-5a,10b-dihydrobenzofuro[2,3-*b*][1]benzopyran-11-one (IIc): mp 207—209 °C (EtOH); 22% yield; IR ($CHCl_3$) 1700 (C=O) and 1760 cm^{-1} (OAc); UV (MeOH) λ_{max} (ε) 286 (14200) and 347 nm (8800); NMR ($CDCl_3$) δ=1.79 (3H, s, CH_3), 2.21 (3H, s, OAc), 3.82 (3H, s, OCH_3), 3.91 (3H, s, OCH_3), 6.61 (1H, s, $H_{(4)}$), 7.22 (1H, s, $H_{(1)}$), 6.70—7.50 (3H, m, $H_{(7)}$, $H_{(8)}$, and $H_{(9)}$), and 7.56 (1H, m, $H_{(10)}$) (Found: C, 64.63; H, 4.92%. Calcd for $C_{20}H_{18}O_7$: C, 64.86; H, 4.90%); and 2-(6,7-dimethoxy-2-methyl-4-oxo-4*H*-chromen-3-yl)-*p*-benzoquinone (IIIc): mp 192—193 °C (EtOH); 27% yield; IR ($CHCl_3$) 1650 and 1680 cm^{-1} (C=O); UV (MeOH) λ_{max} (ε) 289 (12000) and 323 nm (13400); NMR ($CDCl_3$) δ=2.30 (3H, s, CH_3), 3.95 (3H, s, OCH_3), 3.98 (3H, s, OCH_3) 6.79—6.83 (4H, m, $H_{(3)}$, $H_{(5)}$, $H_{(6)}$, and $H_{(8')}$, and 7.45 (1H, s, $H_{(5')}$) (Found: C, 66.10; H, 4.31%. Calcd for $C_{18}H_{14}O_6$: C, 66.25; H, 4.32%).

Id gave 10b-acetoxy-5a-methyl-2,3,8-trimethoxy-5a,10b-dihydrobenzofuro[2,3-*b*][1]benzopyran-11-one (IId): mp 180—183 °C (EtOH); 24% yield; IR (KBr) 1700 (C=O) and 1760 cm^{-1} (OAc); UV (MeOH) λ_{xam} (ε) 286 (14900) and 347 nm (9300); NMR ($CDCl_3$) δ=1.79 (3H, s, CH_3), 2.20 (3H, s, OAc), 3.75 (3H, s, OCH_3), 3.82 (3H, s, OCH_3), 3.91 (3H, s, OCH_3), 6.57 (1H, s, $H_{(1)}$), 7.18 (1H, s, $H_{(1)}$), 6.29—6.59 (2H, m, $H_{(7)}$ and $H_{(9)}$), and 7.38 (1H, m, $H_{(10)}$) (Found: C, 62.80; H, 5.08%. Calcd for $C_{21}H_{20}O_8$: C, 62.99; H, 5.04%); and 2-(6,7-dimethoxy-2-methyl-4-oxo-4*H*-chromen-3-yl)-5-methoxy-*p*-benzoquinone (IIId): mp 222—227 °C (EtOH); 43% yield; IR (KBr) 1630 and 1700 cm^{-1} (C=O); UV (MeOH) λ_{max} (ε) 322 nm (14900); NMR ($CDCl_3$) δ=2.29 (3H, s, CH_3), 3.85 (3H, s, OCH_3), 3.92 (3H, s, OCH_3), 3.98 (3H, s, OCH_3), 6.02 (1H, s, $H_{(6)}$), 6.73 (1H, s, $H_{(8')}$), 6.84 (1H, s, $H_{(3)}$), and 7.45 (1H, s, $H_{(5')}$) (Found: C, 63.74; H, 4.55%. Calcd for $C_{19}H_{16}O_7$: C, 64.04; H, 4.53%).

Ie yielded 10b-acetoxy-3,8-dimethoxy-5a,10b-dihydrobenzofuro[2,3-*b*][1]benzopyran-11-one(IIe): mp 150 °C (EtOH); IR ($CHCl_3$) 1710 (C=O) and 1760 cm^{-1} (OAc); UV (MeOH) λ_{max} (ε) 233 (13900), 283 (15500), and 311 nm (inf.) (8760); NMR ($CDCl_3$) δ=2.18 (3H, s, OAc), 3.77 (3H, s, OCH_3), 3.81 (3H, s, OCH_3), 6.45—6.70 (5H, m, $H_{(2)}$, $H_{(4)}$, $H_{(5a)}$, $H_{(7)}$, and $H_{(9)}$), 7.29 (1H, m, $H_{(10)}$), and 7.71 (1H, d, J=8.5 Hz, $H_{(1)}$) (Found: C, 63.95; H, 4.54%. Calcd for $C_{19}H_{16}O_7$: C, 64.04; H, 4.53%); and 3,8-dimethoxybenzofuro[2,3-*b*][1]benzopyran-11-one (V): mp 235 °C ($CHCl_3$); IR (KBr) 1658 cm^{-1} (C=O); UV (MeOH) λ_{max} (ε) 261 (30500), 287 (16600), and 311 nm (inf.) (9330); NMR (CF_3COOH) δ=4.08 (3H, s, OCH_3), 4.15 (3H, s, OCH_3), 7.10—7.60 (4H, m, $H_{(2)}$, $H_{(4)}$, $H_{(7)}$, and $H_{(9)}$), 8.10 (1H, d, J=8.5 Hz, $H_{(1)}$), and 8.52 (1H, d, J=8.5 Hz, $H_{(10)}$) (Found: C, 68.80; H, 4.10%. Calcd for $C_{17}H_{12}O_5$: C, 68.91; H, 4.08%).

Oxidations of Ia—e with Manganese(III) Acetate. A typical oxidation of 2′-hydroxyisoflavone with manganese(III) acetate was as follows. A mixture of 2′-hydroxyisoflavone (1 mmol), manganese(III) acetate dihydrate[14] (3 mmol), and a solvent (20 ml) was heated at an appropriate temperature for the time shown in Table 1. After the removal of the solvent, the resulting mixture was triturated with water and extracted with chloroform. The chloroform solution was evaporated and the resulting mixture was separated on TLC using chloroform as developing solvent and by recrystallization.

Ia gave IIa: mp 136—137 °C, 1% yield. Ib yielded IIb: mp 186—188 °C, 7—25% yields; and IV: mp 300 °C (EtOH–$CHCl_3$), 3—29% yields; IR ($CHCl_3$) 1710 (C=O) and 1760 cm^{-1} (OAc); UV (MeOH) λ_{max} (ε) 289 nm (33400); NMR ($CDCl_3$) δ=1.81 (3H, s, OCH_3), 2.20 (3H, s, OAc), 3.60 (3H, s, OCH_3), 3.82 (3H, s, OCH_3), 6.35 (1H, s, $H_{(7)}$), 6.53—6.70 (2H, m, $H_{(2)}$ and $H_{(4)}$), 7.24 (1H, s, $H_{(10)}$), and 7.75 (1H, m, $H_{(1)}$) (Found: C, 64.79; H, 4.64%. Calcd for $C_{40}H_{34}O_{14}$: C, 65.03; H, 4.64%), *m/e* 738 (M^+). Ic gave IIc: mp 207—209 °C, 9% yield. Id yielded IId: mp 180—183 °C, 10% yield. Ie gave IIe: mp 150 °C, 10% yield; and V: mp 235 °C, 7% yield.

The Thermal Decomposition of IIe. 10b-Acetoxy-3,8-di-

methoxy-5a,10b-dihydrobenzofuro[2,3-*b*][1]benzopyran-11-one (IIe) (0.1 mmol) was heated at 250 °C for 10 min. The NMR spectrum of the residue was identical with that of V in every respect.

The authors wish to thank Mr. Shuichi Ueda at Taiho Pharmaceutical Co., Ltd., Tokushima, for measuring the mass spectrum.

References

1) F. F. Stephens and J. D. Bower, *J. Chem. Soc.*, **1949**, 2971.
2) K. Kurosawa, *Bull. Chem. Soc. Jpn.*, **42**, 1456 (1969).
3) K. Kurosawa and J. Higuchi, *Bull. Chem. Soc. Jpn.*, **45**, 1132 (1972).
4) K. Kurosawa, Y. Sasaki, and M. Ikeda, *Bull. Chem. Soc. Jpn.*, **46**, 1498 (1973).
5) K. Nogami and K. Kurosawa, *Bull. Chem. Soc. Jpn.*, **47**, 505 (1974).
6) K. Kurosawa and K. Nogami, *Bull. Chem. Soc. Jpn.*, **49**, 1955 (1976).
7) S. Ueda and K. Kurosawa, *Bull. Chem. Soc. Jpn.*, **50**, 193 (1977).
8) C. P. Falshaw, W. D. Ollis, J. A. Moore, and K. Magnus, *Tetrahedron*, Supplement No. 7, 333 (1966).
9) J. M. Sehgal and T. R. Seshadri, *Proc. Indian Acad. Sci.*, **42A**, 36 (1955); *Chem. Abstr.*, **50**, 8631e (1956).
10) K. Aghoramarthy, A. S., Kukla, and T. R. Seshadri, *Curr. Sci. (India)*, **30**, 218 (1961); *Chem. Abstr.*, **56** 3443b (1962).
11) R. V. M. Campbell, S. H. Harper, and A. P. Kemp, *J. Chem. Soc., C*, **1969**, 1787.
12) V. K. Kakra, A. S. Kukla, and T. R. Seshadri, *Indian J. Chem.*, **5**, 607 (1967). *Chem. Abstr.*, **69**, 59134z (1968).
13) L. F. Audrieth, *Inorg. Synth.*, **3**, 47 (1950).
14) P. J. Andruilis, Jr., M. J. S. Dewar, R. Dietz, and R. L. Hunt, *J. Am. Chem. Soc.*, **88**, 5473 (1966).

Syntheses of Polymerizable Carbodiimides Bearing a Terminal Vinyl Group

Hiroyoshi KAMOGAWA,* Masato NANASAWA, Shigeki UEHARA, and Keisuke OSAWA

Department of Applied Chemistry, Yamanashi University, Takeda 4, Kofu, Yamanashi 400

(Received July 22, 1978)

N-(*p*- or *m*-Vinylphenyl)-*N'*-isopropyl- and cyclohexylcarbodiimides (**3**) have been synthesized in reasonable yields by first synthesizing the substituted ureas by the reactions of *p*- or *m*-vinylaniline with isopropyl or cyclohexyl isocyanate in THF and the subsequent dehydration with *p*-toluenesulfonyl chloride in pyridine. The monomers **3** were found to polymerize smoothly with AIBN to afford vinyl polymers bearing the corresponding carbodiimide units as pendants in more or less cross-linked forms. The cross-linked insoluble polymers thus obtained can act as a dehydrative coupling agent in reactions such as the formation of peptide linkages.

Carbodiimides are one of the most versatile dehydrative coupling agents, especially for use in peptide syntheses.[1] An attempt to use carbodiimide units as pendants of vinyl polymers prepared by polymer reactions has been reported,[2] thereby assuring ready separation of carbodiimide reagents after reaction.

The authors have been interested in the syntheses of vinyl carbodiimide monomers and the preparation of vinyl polymers bearing carbodiimide units as pendants by the radical polymerization of the monomers thus synthesized. The carbodiimide polymers thus synthesized can act as polymer reagents in dehydration and other reactions characteristic of low molecular weight carbodiimides such as dicyclohexylcarbodiimide.

Results and Discussion

Carbodiimide monomers have been synthesized as follows.

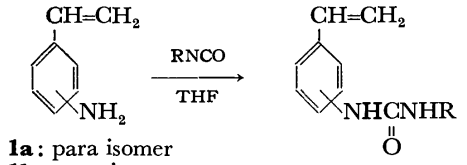

1a: para isomer
1b: meta isomer

2a1: *p*-isomer; R=isopropyl
2a2: *p*-isomer; R=cyclohexyl
2a3: *p*-isomer; R=phenyl
2b1: *m*-isomer; R=isopropyl
2b2: *m*-isomer; R=cyclohexyl
2b3: *m*-isomer: R=phenyl

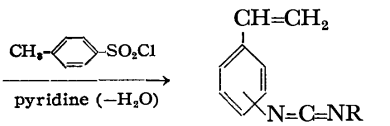

3a1: *p*-isomer; R=isopropyl
3a2: *p*-isomer; R=cyclohexyl
3b1: *m*-isomer; R=isopropyl
3b2: *m*-isomer; R=cyclohexyl

Substituted ureas (**2**) have been readily synthesized from vinylanilines (**1**) and isocyanates in tetrahydrofuran (THF) in satisfactory yields, as indicated in Table 1. The conversions of ureas to the corresponding carbodiimides (**3**) were however not successful in all cases. Thus, ureas **2a3** and **2b3** did not provide the corresponding carbodiimides in pure forms, presumably due to the poor stability of the products; the yields of other carbodiimides, as indicated in Table 1, were not high. The synthetic route described here however appears to be useful, since it can be easily conducted and, starting from the readily available **1**, the desired products (**3**) are obtained in two steps.

Table 1. Substituted ureas and carbodiimide monomers synthesized

Compound	Yield, %	Mp, °C	Bp, °C/mmHg
2a1	88.2	148—150	—
2a2	73.8	178—180	—
2a3	80.3	203—204	—
2b1	81.2	118—120	—
2b2	87.3	149—150	—
2b3	90.9	162—163	—
3a1	62.8	—	97/0.7
3a2	29.0	—	105/3.0
3b1	48.1	—	98/1.0
3b2	40.7	—	128/1.0

As indicated in Table 2, the solution polymerization of the monomer **3**, alone and in the presence of styrene, proceeded smoothly to give homogeneous polymer solutions. Monomers **3a1** and **3a2** were exceptional in that the solutions gave gels. The homopolymers of **3b** became insoluble in THF once precipitated into methanol, indicating that the N=C bonds of the carbodiimide portions in the monomers and polymers participated, more or less, in the polymerizations. The IR spectra of the **3a** polymers indicated a decrease in the intensities of the –N=C=N– absorptions at 2100 cm^{-1} compared with those of the corresponding monomers, together with characteristic absorptions for vinyl polymers containing carbodiimide units as pendant. Copolymerizations with styrene overcame the poor solubility characteristic: copolymers Nos. 4 and 7 in Table 2 are completely soluble in organic solvents, although the contents of the carbodiimide units are considerably lower than those calculated for the monomers employed. It appears, however, that the practical merits of the carbodiimide polymers are displayed when they are employed in the cross-linked insoluble forms and compensate for this fault.

The dehydrative coupling functions of the carbodiimide polymers have been investigated especially for the following amino acid combination:

TABLE 2. SOLUTION POLYMERIZATION OF **3** MONOMERS[a]

No.	Monomer	Conversion %	3-Content[c] in polymer, %	$[\eta]$[d] dl/g	Remark on polymer
1	**3a2**	52.2	100	—	Homogeneous polymerization but converted to an insoluble gel
2	**3b1**	52.0	100	0.22	Soluble in hot pyridine
3	**3b1**-St (50)[b]	64.8	44	0.18	Soluble in pyridine
4	**3b1**-St (33)[b]	44.2	15	0.23	Soluble in organic solvents
5	**3b2**	30.2	100	0.22	Soluble in hot pyridine
6	**3b2**-St (50)[b]	55.2	48	0.22	Soluble in hot pyridine
7	**3b2**-St (33)[b]	49.9	19	0.20	Soluble in organic solvents

a) 30% Total monomers and 1% AIBN/monomers in THF; 70 °C×24 h. b) 3 mol % in monomers (St= styrene). c) By CHN analyses (mol %). d) In THF at 25 °C.

TABLE 3. FORMATION OF PEPTIDE LINKAGE WITH **3** POLYMER

No.	Polymer	**6** obtained, mol / g-polymer
1	**3b1**-St (1: 1) copolymer[a]	0.33
2	**3a1** Homopolymer[b]	0.25
3	**3a1**-St (1: 1) copolymer[b]	0.22

a) Obtained by solution polymerization. b) Obtained by precipitation polymerization.

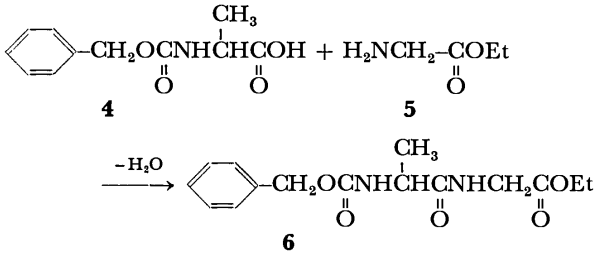

Table 3 indicates the results obtained which indicate that the cross-linked insoluble polymers of **3** play the role of polymer reagent inducing the desired reaction in a heterogeneous system. As expected, the capacity as a polymer reagent is dependent upon the origin of the **3** polymer. Thus, No. 1 polymer in Table 3 with a gel structure is superior to No. 3 with a somewhat macroreticular structure. A more detailed investigation is however required for a complete evaluation of the effects of both chemical and physical structures.

Experimental

The IR, ^{1}H-NMR, and mass spectra were recorded on a Hitachi 215 spectrophotometer, a JNM-PMX 60 spectrophotmeter, and a Hitachi RMU-6 MG spectrometer, respectively, under standard measurement conditions. Elemental analyses were conducted using a Perkin-Elmer 250 instrument.

N-*(p-Vinylphenyl)*-N′-*isopropylurea* (**2a1**). To a solution of *p*-vinylaniline (2.0 g, 17 mmol), prepared by the alkaline dehydration of 2-(*p*-aminophenyl)ethanol,[3] in anhydrous THF (20 ml), isopropyl isocyanate (1.5 g, 17 mmol) was added gradually at room temperature with stirring, the resulting solution being allowed to stand overnight at room temperature. The solvent was then removed by evaporation *in vacuo* at 50 °C, followed by recrystallizations from THF–petroleum ether which gave white needles.

Found: C 70.54; H, 7.78; N, 13.24%. Calcd for $C_{12}H_{16}N_2O$: C, 70.56; H, 7.90; N, 13.71%. IR(KBr) 3300 (NH), 2860—3000 (alkyl), 1620 (C=O), 1580 (phenyl), 990, 900 (vinyl) cm^{-1}; NMR ($CDCl_3$) δ 1.1 (d, 6 H, Me), 3.8 (m, 1 H, CH), 5.1 (d, 1 H, C<u>H</u>$_2$=CH–), 5.5 (d, 1 H, C<u>H</u>$_2$=CH–), 5.7 (s, 1 H, N<u>H</u>CHMe$_2$), 6.6 (q, 1 H, CH$_2$=C<u>H</u>–), 7.2 (s, 4 H, ArH), 7.8 (s, 1 H, NHAr) ppm; Mass (*m/e*) 207 (M$^+$, 67), 118, 119 (100).

N-(*p*-Vinyl-phenyl)-*N*′-cyclohexylurea (**2a2**) and *N*-(*p*-vinylphenyl)-*N*′-phenylurea (**2a3**) were synthesized in the same manner to afford fine colorless needles and a colorless powder, respectively, their analytical data being also satisfactory.

N-*(m-Vinylphenyl)*-N′-*cyclohexylurea* (**2b2**). By applying the same reaction procedure as that for the synthesis of **2a1**, cyclohexyl isocyanate (5.2 g, 42 mmol) and *m*-vinylaniline (**1b**: 5.0 g, 42 mmol), prepared by the Al_2O_3 dehydration of 1-(*m*-aminophenyl)ethanol,[4] produced a white powder (**2b2**) which was recrystallized from THF–petroleum ether.

Found: C, 73.25; H, 8.39; N, 11.50%. Calcd for $C_{15}H_{20}N_2O$: C, 73.37; H, 8.52; N, 11.48%. IR(KBr) 3350 (NH), 2860, 2940 (cyclohexyl), 1620 (C=O), 1560 (phenyl), 995, 910 (vinyl) cm^{-1}; NMR (DMSO-d_6+$CDCl_3$) δ 1.1—1.9 (m, 10 H, 5 CH$_2$), 2.8 (s, 1 H, –CH ), 5.2 (d, 1 H, C<u>H</u>$_2$=CH–), 5.7 (d, 1 H, C<u>H</u>$_2$=CH–), 5.7 (s, 1 H, –NH– ), 6.6 (q, 1 H, CH$_2$=C<u>H</u>–), 6.8—7.6 (m, 4 H, ArH), 8.0 (s, 1 H, ArNH) ppm; Mass (*m/e*) 244 (M$^+$, 18), 119 (100). *N*-(*m*-Vinylphenyl)-*N*′-isopropylurea (**2b1**) and *N*-(*m*-vinylphenyl)-*N*′-phenylurea (**2b3**) were synthesized in the same manner to afford fine colorless crystals with satisfactory analytical data in both instances.

N-*(p-Vinylphenyl)*-N′-*isopropylcarbodiimide* (**3a1**). To a solution of **2a1** (1.5 g, 7.4 mmol) and 4-*t*-butylcatechol (0.1 g) in anhydrous pyridine (20 ml) *p*-toluenesulfonyl chloride (2.8 g, 15 mmol) was added dropwise and the resulting solution heated at 70 °C for 2 h. The reaction mixture was then poured into iced water and extracted with ether (200 ml), the organic layer being washed with water and dried over anhydrous sodium sulfate, followed by distillation *in vacuo* to afford a pale brown liquid. Found: C, 77.91; H, 7.50; N, 14.58%. Calcd for $C_{12}H_{14}N_2$: C, 77.38; H, 7.58; N, 15.04%. IR ($CHCl_3$) 2870—2920 (alkyl), 2120 (–N=C=N–), 1600 (phenyl), 990, 900 (vinyl) cm^{-1}; NMR ($CDCl_3$) δ 1.3 (d, 6 H, 2 Me), 3.7 (m, 1 H, CH), 5.2 (d, 1 H, C<u>H</u>$_2$=CH–), 5.6 (d, 1 H, C<u>H</u>$_2$=CH–), 6.6 (q, 1 H, CH$_2$=C<u>H</u>–), 6.8—7.5 (m, 4 H, ArH) ppm; Mass (*m/e*) 186 (M$^+$, 100). *N*-(*p*-Vinylphenyl)-*N*′-cyclohexylcarbodiimide (**3a2**) was synthesized in the same manner to afford a colorless liquid.

N-*(m-Vinylphenyl)*-N′-*cyclohexylcarbodiimide* (**3b2**). The same reaction procedure as that for **3a1** was applied to afford a colorless liquid.

Found: C, 79.60; H, 8.18; N, 12.23%. Calcd for $C_{15}H_{18}N_2$:

C, 79.61, H, 8.02, N, 12.38%. IR ($CHCl_3$) 2860—2930 (alkyl), 2120 (–N=C=N–), 1580 (phenyl), 990, 900 (vinyl) cm^{-1}; NMR ($CDCl_3$) δ 1.1—1.9 (m, 10 H, 5 CH_2), 3.5 (m, 1 H, –CH<), 5.3 (d, $C\underline{H}_2$=CH–), 5.8 (d, 1 H, $C\underline{H}_2$=CH–), 6.7 (q, 1 H, CH_2=C<u>H</u>–), 6.9—7.6 (m, 4 H, ArH) ppm. Mass (*m/e*) 226 (M^+, 13), 144 (100).

N-(*m*-Vinylphenyl)-*N'*-isopropylcarbodiimide (**3b1**, a colorless liquid) was synthesized in the same manner.

The analytical data for the synthesized carbodiimide monomers not shown above were satisfactory.

Solution Polymerization of 3 Monomers. A solution of the total monomers (1.0 g) and 2,2'-azobisisobutyronitrile (AIBN: 0.01 g) in THF (2.3 ml) was placed in a Pyrex glass ampoule, which was evacuated, flushed with nitrogen, sealed, and allowed to stand for 24 h at 70 °C. Precipitation of the contents into methanol provided the polymer. All polymers of **3** thus synthesized indicated IR absorptions at 2860 and 2930 cm^{-1} attributable to vinyl polymer backbones together with sharp peaks at 2100 cm^{-1} characteristic of –N=C=N– bonds. For the determination of intrinsic viscosities [η], 20% of the contents were set aside without precipitation and diluted with THF for use in viscosimetry (Ostwald).

Precipitation Polymerization of 3 Monomers. A solution of total monomers (5 g) containing 10% divinylbenzene and AIBN (0.05 g) in heptane (8—15 ml) was stirred at 70 °C for 6—8 h under a nitrogen atmosphere. After 3—4.5 h, heptane (8—10 ml) was further added and stirring continued. The precipitated polymer was washed with petroleum ether and extracted overnight with ether using a Soxhlet extractor. Yields of 60—75% were obtained.

Formation of Peptide Linkage with 3 Polymer. Typically, *N*-benzyloxycarbonyl-L-alanine (**4**: 0.8 g, 4 mmol) and glycine ethyl ester (**5**: 0.4 g, 4 mmol) were dissolved in THF (50 ml). The No. 1 copolymer in Table 3, extracted with anhydrous THF, was then added and the mixture stirred at room temperature overnight. The reaction mixture was centrifuged, the supernatant solution evaporated *in vacuo* at 50 °C, the residue dissolved in chloroform, and the resulting solution washed first with aqueous hydrochloric acid, then with aqueous sodium carbonate, followed by evaporation *in vacuo* to give colorless crystals.

References

1) A. C. Cope, *Org. React.*, **12**, 205 (1962).
2) N. M. Weinshenker and C. M. Shen, *Tetrahedron Lett.*, **1972**, 3281, 3283.
3) H. Kamogawa, *J. Polym. Sci., A-1*, **7**, 725 (1969).
4) G. Manecke and G. Kossmehl, *Makromol. Chem.*, **70**, 112 (1964).

Syntheses of Chlorozinc Complexes of 2(1*H*)-Pyridinethione and Their Mutual Transformations

Satoshi MATSUNAMI, Susumu FUJIMURA, Kiyomi OKIMOTO, and Mitsuo MASAKI*

Polymer Research Laboratory, Ube Industries, Ltd., Minami-Kaigan, Goi, Ichihara, Chiba 290

(Received July 22, 1978)

Three types of zinc complexes, chlorotris[2(1*H*)-pyridinethionato]dizinc (**3**), dichlorotetrakis[2(1*H*)-pyridinethionato]trizinc (**4**), and chloro[2(1*H*)-pyridinethionato]zinc (**5**) were produced by the reactions of bis[2(1*H*)-pyridinethionato]zinc (**2**) and zinc chloride. The product in the reactions varies depending on the solvent. The mutual transformation reactions among **3**, **4**, **5**, **2**, and oxohexakis[2(1*H*)-pyridinethionato]tetrazinc were described. The formations of **5**, **4**, and **3** were explained by stepwise additions of **2** to zinc chloride based upon a view that these complexes are the adducts of **2** with zinc chloride in molar ratios of 1: 1, 2: 1, and 3: 1. Analogously, the correlation of the known polynuclear zinc complexes was systematically rationalized by stepwise additions of L_2Zn (L=ligand) to ZnX_2 (X=Cl or OH) or ZnO.

In a previous paper,[1] we reported on the formation of oxohexakis[2(1*H*)-pyridinethionato]tetrazinc (**1**) from bis[2(1*H*)-pyridinethionato]zinc (**2**)[2] and on the mutual transformations between **1** and **2**. Various types of polynuclear zinc complexes have been reported. They include L_8Zn_5O (L=ligand group),[2] L_6Zn_4O,[3] L_2Zn_2O,[4] L_5Zn_3X (X=chlorine atom or hydroxyl group),[5] $L_4Zn_4X_4$,[6] $L_4Zn_3X_2$,[7] and L_3Zn_2X[8] type complexes. The types of complexes are different depending on the kind of the ligand. Correlations between these types of complexes have not been elucidated, probably owing to the lack of report on the formation of different type of polynuclear zinc complexes formed with the same ligand.[9]

This paper describes the syntheses of chlorozinc complexes, L_3Zn_2Cl, $L_4Zn_3Cl_2$, and LZnCl where L is 2(1*H*)-pyridinethionato group, and mutual transformations among the three complexes and the complexes **1** and **2**, which contribute a systematization of polynuclear zinc complexes.

Results and Discussion

The transformation of **2** into oxocomplex **1** has been explained by the fission of one of four 2(1*H*)-pyridinethionato ligands in the complex **2**.[1,2] When **2** was treated with a half-molar equivalent of benzoyl chloride in 1,2-dichloroethane (EDC), one of four 2(1*H*)-pyridinethionato groups was removed as the *S*-benzoyl derivative, and chlorotris[2(1*H*)-pyridinethionato]dizinc (**3**) was obtained quantitatively. The complex **3** is a new complex and the characterization will be described later. The complex **3** was also obtained by a reaction of **2** with zinc chloride in a molar ratio of 3: 1 in diethyl ether. A treatment of **2** with a large excess molar amount of zinc chloride (in a molar ratio of 1: 1) in ethanol gave **3**, but the same reaction in acetone afforded another product, dichlorotetrakis[2(1*H*)-pyridinethionato]trizinc (**4**). The complex **4** could be obtained by the reaction of **3** with an excess molar amount of zinc chloride (in a molar ratio of 2: 3) in acetone. When **2** was treated with an excess molar amount of zinc chloride (in a molar ratio of 1: 2) in ethyl acetate, the third complex, chloro[2(1*H*)-pyridinethionato]zinc (**5**) was isolated. The complex **5** could be obtained also by the treatment of **4** with zinc chloride in ethyl acetate. The complexes **4** and **5** are also new compounds and the characterization will be described later. When **5** was treated in acetone, **4** was recovered. The treatment of **4** in ethanol gave **3**. The complexes **3**, **4**, and **5** all could be converted to oxocomplex **1** when they were treated in boiling water.

The experimental results for the formation of the complexes can be rationalized as shown in Scheme 1.

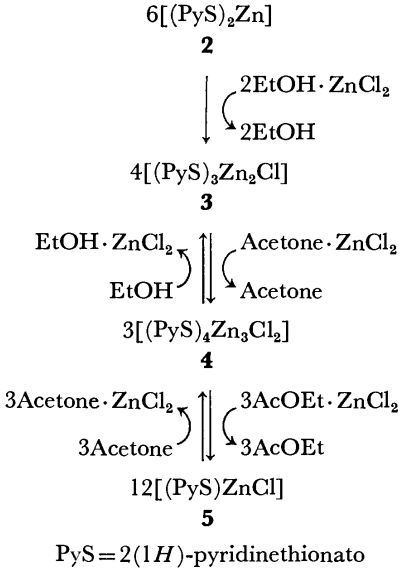

PyS=2(1*H*)-pyridinethionato

Scheme 1.

The formation of a product in a specific solvent can be rationalized by a ligand exchange reaction of zinc chloride between the reactant and the solvent.

The complexes **3**, **4**, and **5** can be viewed as adducts of bis[2(1*H*)-pyridinethionato]zinc with zinc chloride in molar ratios of 3: 1, 2: 1, and 1: 1, respectively. The complex **1** is on a same level with the complex **3**, since **1** is an adduct of bis[2(1*H*)-pyridinethionato]zinc with zinc oxide in a molar ratio of 3: 1.

In a similar idea various types of polynuclear zinc complexes reported hitherto can be made systematic as shown in Scheme 2, in which a thick arrow signifies an addition of a unit of L_2Zn. A stepwise addition of L_2Zn to ZnX_2 or ZnO leads to a formation of each level of zinc complexes. The several types of complexes put in brackets are not yet reported. The stability of

complex could be depend on the kind of the ligand and the conditions under which the formation was performed. The solvent is a very important factor as illustrated in Scheme 1 for 2(1*H*)-pyridinethionato zinc complexes. From Scheme 2, one can predict the presence of complexes containing four and five units of $(PyS)_2Zn$, $(PyS)_8Zn_5Cl_2$ or $(PyS)_8Zn_5O$ and $(PyS)_{10}Zn_6Cl_2$ or $(PyS)_5Zn_3Cl$, but they are not yet isolated. One may be able to isolate them when appropriate solvents are found.

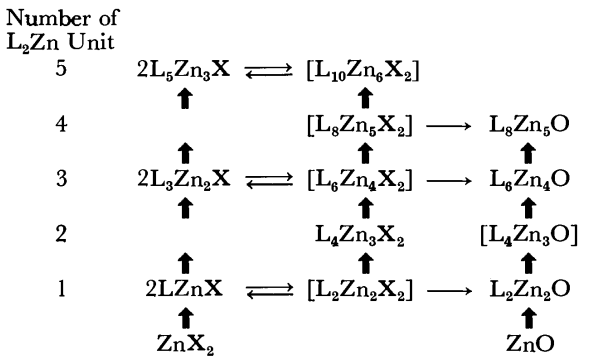

Scheme 2. Complex types (complexes in brackets are unknown).

In a previous report,[1] we have described a probable formation of oxobis[2(1*H*)-pyridinethionato]dizinc in the reaction of 2(1*H*)-pyridinethione and zinc oxide in a molar ratio of 2: 1 in water. Oxotetrakis[2(1*H*)-pyridinethionato]trizinc can be estimated to be produced in an appropriate solvent, since the same level chlorocompound **4** is moderately stable.

Characterization of the Complexes. The compositions of the three complexes **3**, **4**, and **5** were determined by elemental analyses (C, H, Cl, N, and S). The complexes **3**, **4**, and **5** were obtained as powdery crystals, respectively. The powder X-ray analyses showed the independent spectrum for the three complexes and the contamination of free zinc chloride in the complexes was not observed.

Thermal analysis curves of **3**, **4**, and **5** show single and sharp endothermic peaks at 297, 303, and 295 °C, respectively. The mixture prepared by mixing any two of the complexes **2**, **3**, **4**, and **5** give thermal analysis curves showing broad endothermic peaks at temperatures different from those of the endothermic peaks for **2**, **3**, **4**, and **5**, except the mixture of **4** and **5** whose curve shows a sharp endothermic peak but at 287 °C. These facts indicate for the three complexes **3**, **4**, and **5** to be independent compounds, respectively.

The IR spectrum of the complex **3** exhibits bands due to C=C/C=N stretching vibration at 1595 (s), 1555 (s), 1445 (s), and 1420 cm^{-1} (s), a band due to C=S stretching vibration at 1135 cm^{-1} (s), bands due to ring vibration at 1020 (m) and 650 cm^{-1} (w), and bands due to C–H bending vibration at 770 (s), 765 (sh), and 760 cm^{-1} (sh). The absorption patterns of the corresponding bands in **1**, **2**, **4**, and **5** are similar to that of bands in **3**, except that the spectrum of **2** shows doublet peaks or peaks with a shoulder at 1455, 1420, 1020, and 645 cm^{-1} and that the spectrum of **4** and **5** show a doublet peak or a peak with a shoulder at 650 cm^{-1}. The fact thet the absorption patterns of these bands of **3**, **4**, and **5** are similar to that of the bands of **1** indicates that the 2(1*H*)-pyridinethionato ligands act as bidentates and bridging ligands in the complexes **3**, **4**, and **5**.[1]

The mass spectra of **3**, **4**, and **5** exhibit several fragmentation ions containing zinc, 2(1*H*)-pyridinethionato ligand, and/or chlorine. The peak pattern of the MS spectra of **3**, **4**, and **5** differ depending on the temperature of the inlet part to which the samples were introduced. The peak pattern of the MS feature higher than *m/e* 209[(PyS)ZnCl] are shown in Table 1. The changes of peak patterns of the three compounds depending on

Table 1. Mass spectral data for thionatozinc complexes (*m/e*)

Compound	Temperature[a] 120 °C	150 °C	180 °C
$(PyS)_3Zn_2Cl$ **3**	458[$(PyS)_3Zn_2$] 284[$(PyS)_2Zn$] 209[(PyS)ZnCl)]	458[$(PyS)_3Zn_2$] 284[$(PyS)_2Zn$] 209[(PyS)ZnCl]	490[$(PyS)_3Zn_2S$] 458[$(PyS)_3Zn_2$] 284[$(PyS)_2Zn$] 220[$(PyS)_2$] 209[(PyS)ZnCl]
$(PyS)_4Zn_3Cl_2$ **4**		458[$(PyS)_3Zn_2$] 284[$(PyS)_2Zn$] 209[(PyS)ZnCl]	490[$(PyS)_3Zn_2S$] 458[$(PyS)_3Zn_2$] 394[$(PyS)_3Zn$] 383[$(PyS)_2Zn_2Cl$] 362[$(PyS)_2(py)Zn$] 284[$(PyS)_2Zn$] 220[$(PyS)_2$] 209[(PyS)ZnCl]
$[(PyS)ZnCl]_n$ **5**	284[$(PyS)_2Zn$] 209[(PyS)ZnCl]	284[$(PyS)_2Zn$] 209[(PyS)ZnCl]	458[$(PyS)_3Zn_2$] 383[$(PyS)_2Zn_2Cl$] 362[$(PyS)_2(py)Zn$] 284[$(PyS)_2Zn$] 209[(PyS)ZnCl]

a) The temperature at which the spectra were measured.

the temperature are clearly different, respectively. This phenomena can not be rationalized at present, but the results indicate that the complexes **3**, **4**, and **5** are independent compounds. Although there is no certain evidence, **5** seems to be not monomeric. This is suggested by the high melting point of **5** and by MS peak of **5** at *m/e* 284[$(PyS)_2Zn$] which was observed in the spectra measured even at 120 °C.

Experimental

All melting points were determined in a liquid bath unless otherwise mentioned and were uncorrected. The powder X-ray diffraction was measured on a Rigaku D_2 X-ray diffractometer. The thermal analyses were performed on a Rigaku 8085 differencial scanning calolimeter. The IR spectra were measured in KBr disks with a Hitachi Perkin-Elmer 225 and a Hitachi EPI-G2 grating infrared spectrometer. The mass spectra were measured with a Hitachi M52 mass spectrometer.

Materials. Commercial anhydrous zinc chloride was used after drying over diphosphorus pentaoxide. Bis[2(1*H*)-pyridinethionato]zinc (**2**) was prepared by the method previously reported.[1] Commercial benzoyl chloride was distilled before its use.

Chlorotris[2(1H)-pyridinethionato]dizinc (3). a) Reaction of 2 with Zinc Chloride in Ethanol: A solution of zinc chloride (95 %, 0.43 g, 3.0 mmol) in ethanol (30 ml) was added to a suspension of **2** (0.86 g, 3.0 mmol) in ethanol (40 ml) with stirring at room temperature and the mixture was stirred at room temperature for 12 h. The precipitate was collected by filtration, washed with ethanol (80 ml), and dried at 70 °C for 24 h under reduced pressure to give 0.98 g (98%) of colorless crystalline powder; mp 294—298 °C. Found: C, 36.35; H, 2.57; Cl, 7.09; N, 8.16; S, 19.14%. Calcd for $C_{15}H_{12}ClN_3S_3Zn_2$: C, 36.27; H, 2.44; Cl, 7.14; N, 8.46; S, 19.37%. Molecular weight of the product could not be determined owing to the poor solubility in most organic solvent except *N,N*-dimethylformamide, in which the product was partly hydrolyzed with a slight amount of water contained in the solvent.

b) Reaction of 2 with Zinc Chloride in Diethyl Ether: Zinc chloride (95%, 0.72 g, 5.0 mmol) was treated with **2** (4.29 g, 15.0 mmol) in diethyl ether (100 ml) at room temperature for 17 h. The precipitate was collected by filtration and washed with diethyl ether (20 ml) to give 4.93 g (99%) of **3** as colorless crystalline powder; mp 294—298 °C. The IR spectrum of the powder was identical with that of the product obtained in a). Thermal analysis curve of the solid exhibits an endothermic peak at 297 °C.[11]

c) Reaction of 2 and Benzoyl Chloride: A solution of benzoyl chloride (2.81 g, 20 mmol) in 1,2-dichloroethane (EDC) (40 ml) was added drop by drop to a suspension of **2** (11.43 g. 40 mmol) in EDC (110 ml) with stirring at room temperature and the mixture was stirred for 18.5 h. The precipitate was collected by filtration and washed with EDC (20 ml) to give 9.90 g (100%) of **3** as colorless crystalline powder. The IR spectrum of the powder was identical with that of the product obtained in a). The filtrate separated from **3** and washings were combined and concentrated under reduced pressure. Diethyl ether (70 ml) was added to the residue and filtered leaving insoluble materials. A solution of zinc chloride (95%, 1.38 g, 9.6 mmol) in diethyl ether (50 ml) was added to the filtrate and the mixture was stirred at room temperature for 21.5 h. The precipitate was collected by filtration and washed with diethyl ether (20 ml) to give 4.74 g (84%) of bis(2-benzoylthiopyridine)dichlorozinc (**6**) as colorless solid. The IR spectrum of the solid was identical with that of authentic sample.

Bis(2-benzoylthiopyridine)dichlorozinc (6). A solution of zinc chloride (95%, 0.72 g, 5 mmol) in diethyl ether (30 ml) was added drop by drop to a solution of 2-benzoylthiopyridine[12] (2.15 g, 10 mmol) in diethyl ether (20 ml) with stirring at room temperature. The precipitate was collected by filtration and washed with diethyl ether (20 ml) to give 2.73 g (96 %) of colorless powder; mp 182—185 °C. Found: C, 50.76; H, 3.05; Cl, 12.67; N, 4.70; S, 11.19%. Calcd for $C_{24}H_{18}Cl_2N_2O_2S_2Zn$: C, 50.85; H, 3.20; Cl, 12.51; N, 4.94; S, 11.31%.

Dichlorotetrakis[2(1H)-pyridinethionato]trizinc (4). a) Reaction of 2 with Zinc Chloride: A solution of zinc chloride (95%, 4.30 g, 30 mmol) in acetone (45 ml) was added to a suspension of **2** (8.57 g, 30 mmol) in acetone (150 ml) with stirring at room temperature and then the mixture was stirred at room temperature for 4 h. The precipitate was collected by filtration and washed with acetone (90 ml) to give 10.48 g (99%) of colorless crystalline powder; mp 305—308 °C. Thermal analysis curve of the powder exhibits an endothermic peak at 303 °C. Found: C, 33.72; H, 2.28; Cl, 10.13; N, 7.75; S, 17.89%. Calcd for $C_{20}H_{16}Cl_2N_4S_4Zn_3$: C, 33.94; H, 2.28; Cl, 10.02; N, 7.94; S, 18.12%. Molecular weight of the product could not be determined owing to the poor solubility in most organic solvent except *N,N*-dimethylformamide, in which the product was partly hydrolyzed with a slight amount of water contained in the solvent.

b) Reaction of 3 with Zinc Chloride: Zinc chloride (95%, 0.27 g, 1.8 mmol) was treated with **3** (0.60 g, 1.2 mmol as monomer) in acetone (110 ml) at room temperature. The mixture was refluxed for 3 h and stirred at room temperature for 7 h. The precipitate was collected by filtration and washed with acetone (50 ml) to give 0.63 g (99%) of **4** as colorless solid; mp 304—307 °C. The IR spectrum of the solid was identical with the product obtained in *a)*.

Chloro[2(1H)-pyridinethionato]zinc (5). a) Reaction of 2 with Zinc Chloride: A solution of zinc chloride (95%, 0.44 g, 3.0 mmol) in ethyl acetate (50 ml) was added to a suspension of **2** (0.43 g, 1.5 mmol) in ethyl acetate (40 ml) with stirring at room temperature and then the mixture was refluxed for 5 h. The precipitate was collected by filtration and washed with ethyl acetate (100 ml) under dried nitrogen atmosphere to give 0.62 g (98%) of colorless crystalline powder; mp 296—298 °C. Thermal analysis curve of the powder exhibits an endothermic peak at 295 °C. Found: C, 28.65; H, 1.66; Cl, 16.95; N, 6.50; S, 15.31%. Calcd for $C_5H_4ClNSZn$: C, 28.46; H, 1.91; Cl, 16.80; N, 6.64; S, 15.20%.[13]

b) Reaction of 4 with Zinc Chloride: Zinc chloride (95%, 0.43 g, 3.0 mmol) was treated with **4** (1.06 g, 1.5 mmol as monomer) in ethyl acetate (80 ml) at room temperature. The mixture was refluxed for 4 h and stirred at room temperature for 9 h. The reaction mixture was treated in the similar manner as in a) to give 1.19 g (94%) of **5** as colorless crystalline powder; mp 296—298 °C. The IR spectrum of the powder was identical with the product obtained in *a)*.

Transformation of 5 into 4 in Acetone. A suspension of **5** (4.22 g, 20 mmol as monomer) in acetone (100 ml) was refluxed for 35 h. The precipitate was collected by filtration and washed with acetone to give 3.43 g (5 mmol, 97%) of **4** as colorless crystalline powder; mp 304—307 °C. The IR spectrum of the powder was identical with that of **4** obtained above. A solution of triphenylphosphine oxide (1.26 g, 4.5 mmol) in acetone (50 ml) was added to a portion (30.0 g) of the combined solution (85.9 g) of the filtrate separated from **4** and washings. The mixture was concentrated under reduced pressure and the residue was treated with ethyl acetate (50 ml). The insoluble materials were collected by filtration and washed with ethyl

acetate (30 ml) to give 1.08 g of colorless solid; mp 236—241 °C (on a hot plate). The IR spectrum of the solid was identical with that of authentic dichlorobis(triphenylphosphine oxide)-zinc.[14] This result shows that at least 4.5 mmol (89%) of zinc chloride is generated by the above treatment of **5** in acetone.

*Transformation of **4** into **3** in Ethanol.* A suspension of **4** (4.25 g, 6 mmol as monomer) in ethanol (100 ml) was refluxed for 9 h. The precipitate was collected by filtration and washed with ethanol (50 ml) to give 3.83 g (7.7 mmol, 96%) of **3** as colorless crystalline powder; mp 298—300 °C. The IR spectrum of the powder was identical with that of **3** obtained above. A solution of triphenylphosphine oxide (1.45 g, 5.2 mmol) in ethanol (20 ml) was added to the combined solution of the above filtrate and washings. The mixture was concentrated under reduced pressure and the residue was treated with ethyl acetate (50 ml). The insoluble materials were collected by filtration and washed with ethyl acetate to give 1.36 g of colorless solid; mp 236—240 °C (on a hot plate). The IR spectrum of the solid was identical with that of authentic dichlorobis-(triphenylphosphine oxide)zinc.[14] This result shows that 2.0 mmol (100%) of zinc chloride is generated by the above treatment of **4** in ethanol.

*Hydrolysis of **3** in Water.* A suspension of **3** (1.49 g, 3 mmol as monomer) in water (100 ml) was refluxed for 1 h. The precipitate was collected by filtration and washed with water (40 ml) to give 1.06 g (1.1 mmol) of **1** as colorless crystalline powder; mp above 340 °C (gradually dec).[15] The IR spectrum of the powder was identical with that of authentic sample **1**. The filtrate separated from **1** and washings were combined and the mixture was concentrated under reduced pressure. Ethyl acetate (50 ml) was added to the residue and the mixture was stirred. The insoluble materials were collected by filtration and washed with ethyl acetate (15 ml) to give 0.38 g (1.1 mmol, of dichlorobis[2(1*H*)-pyridinethione]zinc (**7**) as slightly yellowish crystalline powder; mp 248—256 °C (on a hot plate). The IR spectrum of the powder was identical with that of authentic sample **7**.[16] The filtrate separated from **7** and washings were combined and mixed with a solution of triphenylphosphine oxide (0.31 g, 1.1 mmol) in ethyl acetate (30 ml). The precipitate was collected by filtration and washed with ethyl acetate to give 0.27 g (0.4 mmol) of dichlorobis(triphenylphosphine oxide)zinc as slightly yellowish solid; mp 235—239 °C (on a hot plate). The IR spectrum of the solid was identical with that of authentic sample.[14]

*Hydrolysis of **4** in Water.* A suspension of **4** (4.25 g, 6 mmol as monomer) in water (100 ml) was refluxed for 2 h. The reaction mixture was treated in a similar manner as in the hydrolysis of **3**. The products were 2.76 g (2.9 mmol) of **1**; mp above 340 °C (gradually dec),[15] 1.00 g (2.8 mmol) of **7**; mp 246—254 °C (on a hot plate), and 2.11 g (3.0 mmol) of dichlorobis(triphenylphosphine oxide)zinc; mp 236—239 °C (on a hot plate). The IR spectra of the products were identical with those of authentic samples.

*Hydrolysis of **5** in Water.* A suspension of **5** (1.69 g, 8 mmol as monomer) in water (70 ml) was refluxed for 1 h. The reaction mixture was treated in a similar manner as in the hydrolysis of **3**. The products were 0.93 g (1.0 mmol) of **1**; mp above 340 °C (gradually dec),[15] 0.32 g (0.9 mmol) of **7**; mp 245—255 °C (on a hot plate), and 2.04 g (2.9 mmol) of dichlorobis(triphenylphosphine oxide)zinc; mp 238—242 °C (on a hot plate). The IR spectra of the products were identical with those of authentic samples.

References

1) M. Masaki, S, Matsunami, T. Kimura, and T. Oshima, *Bull. Chem. Soc. Jpn.*, **52**, 502 (1979).

2) Bis[2(1*H*)-pyridinethionato]zinc has been estimated to be dimeric based on the data of mass spectrum and osmometric molecular weight determination.[1] However, since the result is not conclusive, molar ratios of **2** and other reagents in the reactions were calculated based on $(C_5H_4NS)_2Zn$ unit in this report.

3) M. Braid and R. H. Schmitt, Fr. Patent 1525721 (1968); *Chem. Abstr.*, **71**, 14839h (1969).

4) H. Koyama and Y. Saito, *Bull. Chem. Soc. Jpn.*, **27**, 112 (1954); J. Charalambous, R. G. Copperthwaite, S. W. Jeffs, and D. E. Shaw, *Inorg. Chim. Acta*, **14**, 53 (1975); A. J. Burn and G. W. Smith, *Chem. Commun.*, **1965**, 394; S. Meriani, G. Nardin, and A. Ripamonti, *Inorg. Chem.*, **6**, 1931 (1967); M. Corbett and B. F. Hoskins, *Inorg. Nucl. Chem. Lett.*, **6**, 261 (1970); D. Johnstone, J. E. Fergusson, and W. T. Robinson, *Bull. Chem. Soc. Jpn.*, **45**, 3721 (1972).

5) T. Mito, S. Nara, M. Nagata, and M. Yukitomi, Japan Patent, 21419 (1974); *Chem. Abstr.*, **82**, 99229j (1976).

6) J. P. Farve, *Bull. Soc. Chim. Fr.*, **1968**. 237.

7) L. J. Porter, D. D. Perrin, and R. W. Hay, *J. Chem. Soc., A*, **1969**, 118.

8) J. D. Citron and R. E. Tarney, Ger. Offen. Patent 2513778 (1975); *Chem. Abstr.*, **84**, 32375b (1976).

9) a) S. Komura, R. Harima, T. Misawa, T. Goto, T. Masatomi, T. Nishi, Y. Shimizu, and Y. Nakacho, Japan Kokai Patent 70343 (1975); *Chem. Abstr.*, **83**, 178576u (1975); M. Z. Gurevich, T. M. Sas, V. V. Zelentsov, B. D. Stepin, and N. E. Mazzpova, *Zh. Neorg. Khim.*, **20**, 452 (1975); *Chem. Abstr.*, **82**, 179843v (1975); V. V. Sher, E. I. Markova, L. G. Khanakova, G. N. Kuz'mina, and P. I. Sanin, *Neftekhimiya*, **13**, 876 (1973); *Chem. Abstr.*, **89**, 95168z (1974); b) S. Kacani and L. Stefanka, Czech. Patent 124384 (1967).

10) Two types of complexes formed with 2(3*H*)-benzothiazolethionato ligand have been reported independently.[6,9b] But it is not clear whether the products described in the papers are identical or not, since no characterization of the products have been demonstrated, unfortunately.

11) For the preparation of **3**, diethyl ether is recommended for the reaction solvent, since the perfect removal of the solvent from the product is easy.

12) Y. Ueno, S. Asakawa, and E. Imoto, *Nippon Kagaku Zasshi*, **89**, 101 (1968).

13) When the same reaction was carried out by stirring the mixture of **2** and zinc chloride in ethyl acetate at room temperature for 2 h and the precipitate was collected by filtration under undried atmosphere, the product obtained was different from **5**. Mp 293—298 °C. The IR spectrum of the product exhibits medium intensity bands at 1590, 1510, and 1370 cm^{-1} in addition to bands of **5** and shows a medium intensity multiplet around 3100 cm^{-1}, while the intensity of the corresponding band in **5** is weak.

14) R. H. Pickard and J. Kenyon, *J. Chem. Soc.*, **80**, 262 (1906).

15) In the measurement of mp, it was observed that the product began to be colored gradually at about 340 °C and melted at 380—385 °C with decomposition.

16) For the preparation of **7**, an aqueous solution of zinc chloride was used instead of its ethanolic solution in the previous paper: B. P. Kennedy and A. B. P. Lever, *Can. J. Chem.*, **50**, 3488 (1972).

Synthesis of Viscumamide and Its Analogs

Atsushi SAKURAI* and Yasuaki OKUMURA

Department of Chemistry, Faculty of Science, Shizuoka University, Ohya, Shizuoka 422

(Received July 26, 1978)

Viscumamide, cyclo(-L-Leu-L-Ile-L-Leu-L-Ile-L-Leu-) (**1a**) and its three analogs, cyclo(-L-Leu-L-Leu-L-Leu-L-Leu-L-Leu-), cyclo(-L-Leu-L-Ile-L-Leu-L-Leu-L-Leu-), and cyclo(-L-Ile-L-Ile-L-Leu-L-Leu-L-Leu-) were synthesized by the *N*-hydroxysuccinimide ester method. The yields in the cyclization step were low due to a strong intermolecular association even at high dilution, which causes cyclodimerization and other polymerization. Chromatographic and spectroscopic comparison of synthetic **1a** with natural viscumamide showed their identity. The structure of viscumamide was confirmed to be **1a**.

In a paper on the constituents of the mistletoe, *Viscum album* Linn. *var. coloratum* Ohwi, we reported on the isolation and structure of viscumamide, a new cyclic pentapeptide, which was assigned to be cyclo(-L-leucyl-L-isoleucyl-L-leucyl-L-isoleucyl-L-leucyl) (**1a**).[1]

In order to confirm the structure of viscumamide, we attempted to synthesize the cyclic peptide **1a** and three analogous cyclic peptides which consist of L-leucine and L-isoleucine.

This paper deals with the synthesis of these cyclic pentapeptides, and the chromatographic and spectroscopic comparison of synthetic **1a** with natural viscumamide.

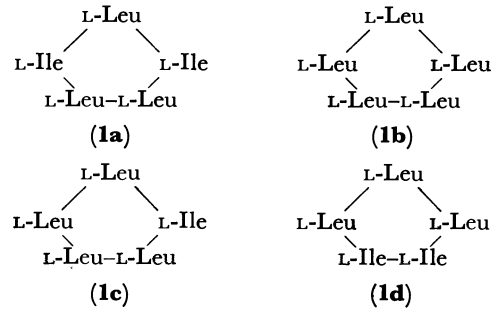

The synthesis of **1a** is outlined in Scheme 1. The *N*-hydroxysuccinimide ester method[2] was employed throughout the coupling reactions, the removal of benzyloxycarbonyl (Z) groups of the intermediates being performed by the action of hydrogen bromide in acetic acid.[3] Z-L-Leucine *N*-hydroxysuccinimide ester (-ONSu) (**2a**)[2] was coupled with L-isoleucine in the presence of sodium hydrogencarbonate to yield needles of Z-L-leucyl-L-isoleucine (**3a**) in 92% yield. Z-Dipeptide **3a** was then transformed into Z-L-leucyl-L-isoleucine *N*-hydroxysuccinimide ester (**4a**) as an oil by treatment with *N*-hydroxysuccinimide (HONSu) and dicyclohexylcarbodiimide (DCC) in dioxane. Purification of the substance by crystallization was unsuccessful. Z-Dipeptide ester **4a** was coupled with L-leucine in the same way as described above to yield Z-L-leucyl-L-isoleucyl-L-leucine (**5a**) as fine crystals in 67% yield based on **3a**. After removal of the Z group of the Z-tripeptide **5a** by the action of hydrogen bromide in acetic acid, the resulting tripeptide hydrobromide (**6a**) was coupled with Z-dipeptide ester **4a** to yield Z-L-leucyl-L-isoleucyl-L-leucyl-L-isoleucyl-L-leucine (**7a**) as fine crystals in 56% yield. Z-Pentapeptide **7a** was transformed into the corresponding *N*-hydroxysuccinimide ester (**8a**) as fine

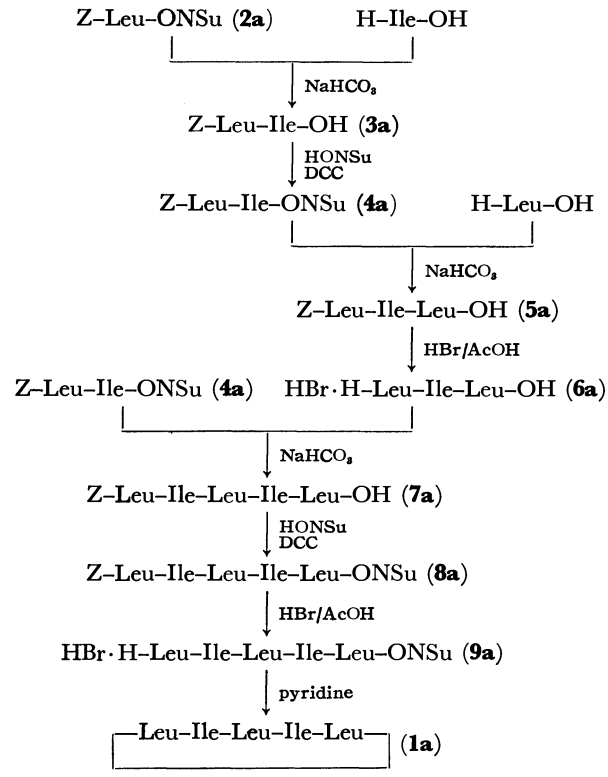

Scheme 1.

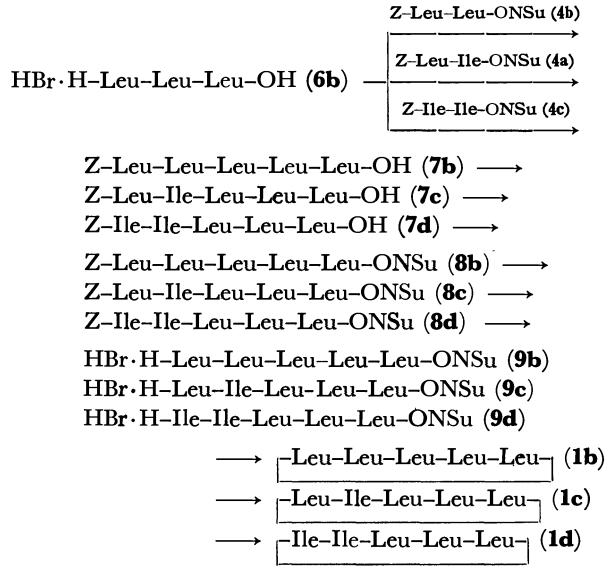

Scheme 2.

crystals in 71% yield by the reaction with *N*-hydroxysuccinimide and dicyclohexylcarbodiimide in *N*,*N*-dimethylformamide (DMF) followed by separation from *N*,*N'*-dicyclohexylurea (DCU) by extraction with ethyl acetate. After removal of the Z group of the Z-pentapeptide ester **8a** in the same way as described above, the pentapeptide hydrobromide (**9a**) thus obtained was cyclized in pyridine at 40 °C by the high dilution method.[4] Purification through silica gel column, followed by chromatography on alumina, gave cyclo(-L-leucyl-L-isoleucyl-L-leucyl-L-isoleucyl-L-leucyl) (**1a**) as colorless needles in 6.5% yield.

Cyclic pentapeptides (**1b**, **1c**, and **1d**) were synthesized in the same way as described for the preparation of **1a** (Scheme 2). **2a** was chosen as the starting material and the peptide chains were extended stepwise to yield Z-L-leucyl-L-leucyl-L-leucine (**5b**). After removal of the Z group, the resulting tripeptide hydrobromide (**6b**) was coupled with the Z-dipeptide esters **4b**, **4a**, and **4c** to yield Z-pentapeptides **7b**, **7c**, and **7d**, respectively. The Z-pentapeptides were transformed into the corresponding *N*-hydroxysuccinimide esters **8b**, **8c**, and **8d**. After removal of the Z-groups, the resulting pentapeptide ester hydrobromides (**9b**, **9c**, and **9d**) were respectively cyclized and purified in the same way as described for the preparation of **1a** affording cyclic pentapeptides **1b**, **1c**, and **1d** as colorless needles in 6.5%, 4.5%, and 4.4% yields, respectively.

Cyclodimerization has been shown to occur predominantly with tripeptides and with pentapeptides.[5-7] Significant differences in the yield of cyclization have been observed to depend on the configuration of the amino acids in the open peptide chain.[8-10]

The yields in the cyclization step were low due to dimerization and other polymerization, since the pentapeptide esters (**9a**, **9b**, **9c**, and **9d**) consist of five L-amino acids, undergoing strong intermolecular association even at high dilution.

Racemization during this synthesis seems negligible, since the specific rotation value of synthetic **1a** is −56° which is identical with that of natural viscumamide.[11] Synthetic **1a** was identical with natural viscumamide in the infrared absorption spectrum (Fig. 1), the proton magnetic resonance spectrum (Fig. 2), and thin layer

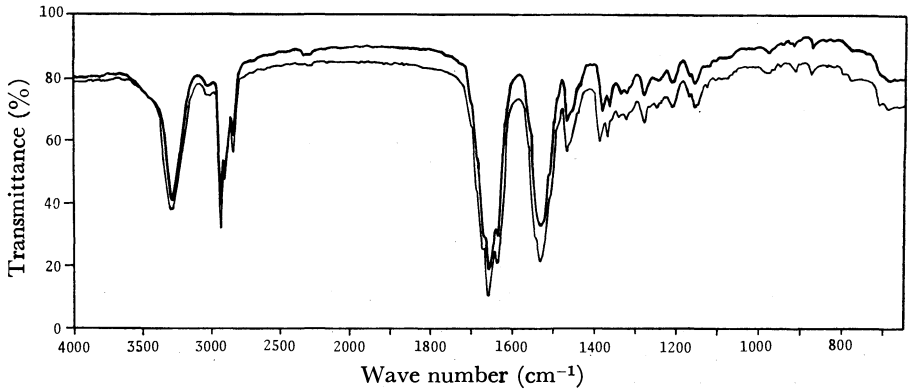

Fig. 1. Infrared absorption spectra of synthetic **1a** (heavy line) and natural viscumamide (light line) in KBr disk.

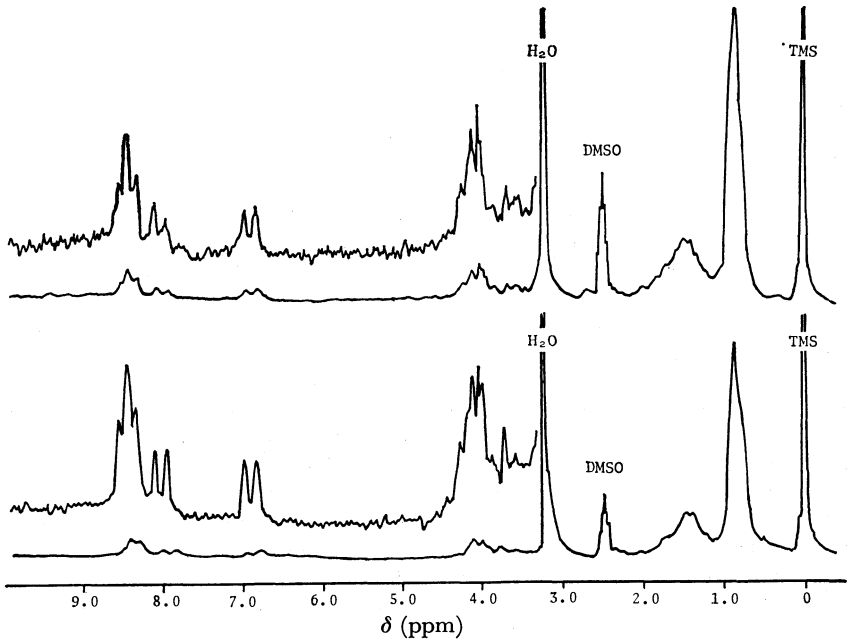

Fig. 2. Proton magnetic resonance spectra of synthetic **1a** (lower) and natural viscumamide (uper) in DMSO-d_6 at 30 °C.

chromatography with various solvent systems (Table 1). The results indicate that the structure of viscumamide is confirmed to be cyclo(-L-leucyl-L-isoleucyl-L-leucyl-L-isoleucyl-L-leucyl) (**1a**).

Experimental

All melting points are uncorrected. The proton magnetic resonance spectra were measured with a JEOL JNM PFT-60 NMR spectrometer at 60 MHz with tetramethylsilane as an internal standard. The infrared absorption spectra were measured with a Hitachi EPI-G3 recording spectrophotometer. The optical rotations were measured with a Union PM-101 polarimeter. Thin layer chromatography (TLC) was carried out on silica gel (Wakogel B-10).

Z-L-Leu-L-Lle-OH (3a). A solution of Z-L-Leu-ONSu[2] (**2a**) (72.5 g, 0.2 mol) in ethanol (1 l) was added to a solution of L-isoleucine (26.4 g, 0.2 mol) and sodium hydrogencarbonate (33.6 g, 0.4 mol) in water (1 l). After being stirred at room temperature overnight, the solution was acidified with 2M hydrochloric acid, and then ethanol was removed under reduced pressure below 40 °C. The precipitate separated from aqueous solution was dissolved in ethyl acetate (300 ml), and the solution was washed with water and dried over sodium sulfate. Hexane (300 ml) was added and the solution was chilled in a refrigerator. **3a** was obtained as colorless needles: mp 125—126 °C (lit,[9] 101—101.5 °C); yield, 62.8 g (83%); $[\alpha]_D^{25}$ $-5.0\pm0.2°$ (*c* 1.0, EtOH). (Found: C, 63.53; H, 8.19; N, 7.37%).

Z-L-Leu-L-Leu-OH (3b). **3b** was obtained in the same way as described above from **2a** (72.5 g, 0.2 mol) and L-leucine (26.4 g, 0.2 mol); colorless needles: mp 117—118 °C (lit,[9] 97.5—98.5 °C); yield, 63.5 g (88%); $[\alpha]_D^{25}$ $-25.0\pm0.2°$ (*c* 1.0, EtOH). (Found: C, 63.51; H, 8.22; N, 7.34%).

Z-L-Ile-L-Ile-OH (3c). **3c** was obtained in the same way as described above from Z-L-Ile-ONSu[2] (**2b**) (18.9 g, 50 mmol) and L-isoleucine (6.6 g, 50 mmol); colorless needles: mp 128—129 °C; yield, 16.7 g (88%); $[\alpha]_D^{25}$ $-8.9\pm0.2°$ (*c* 1.0, EtOH). (Found: C, 63.54; H, 8.20; N, 7.37%).

Z-L-Leu-L-Ile-ONSu (4a). DCC (30.9 g, 0.15 mol) was added at 0 °C to a solution of **3a** (56.8 g, 0.15 mol) and HONSu (17.3 g, 0.15 mol) in dry dioxane (300 ml). After being stirred at 0 °C for 4 h and then at room temperature overnight, DCU separated was filtered off and washed with dioxane. The combined filtrate and washings were evaporated to dryness under reduced pressure. **4a** was obtained as a colorless oil: yield, 67.8 g (95%); IR 1815 and 1785 (succinimide), and 1740 cm^{-1} (ester C=O).

Z-L-Leu-L-Leu-ONSu (4b). **4b** was obtained in the same way as described above from **3b** (62.5 g, 0.17 mol), HONSu (19.0 g, 0.17 mol), and DCC (34.0 g, 0.17 mol); colorless oil: yield, 76.9 g (98%); IR 1817 and 1787 (succinimide), and 1743 cm^{-1} (ester C=O).

Z-L-Ile-L-Ile-ONSu (4c). **4c** was obtained in the same way as described above from **3c** (15.1 g, 40 mmol), HONSu (4.6 g, 40 mmol), and DCC (8.3 g, 40 mmol); colorless oil: yield, 18.1 g (95%); IR 1817 and 1787 (succinimide), and 1742 cm^{-1} (ester C=O).

Z-L-Leu-L-Ile-L-Leu-OH (5a). L-Leucine (5.2 g, 40 mmol) and **4a** (15.0 g, 40 mmol) were treated in the same way as described for the preparation of **3a**. Concentration of the mixture under reduced pressure followed by chilling in a refrigerator gave the precipitate, which was collected and washed with water. Recrystallization from ethanol gave 13.2 g (67%) of **5a** as colorless fine crystals: mp 182—183 °C; $[\alpha]_D^{25}$ $-53.4\pm0.4°$ (*c* 0.5, EtOH). Found: C, 63.25; H, 8.52; N, 8.36%. Calcd for $C_{26}H_{41}N_3O_6$: C, 63.52; H, 8.41; N, 8.55%.

Z-L-Leu-L-Leu-L-Leu-OH (5b). **5b** was obtained in the same way as described above from **4b** (59.4 g, 0.13 mol) and L-leucine (16.4 g, 0.13 mol); colorless fine crystals: mp 102—104 °C; yield, 39.9 g (65%); $[\alpha]_D^{25}$ $-51.0\pm0.4°$ (*c* 0.5, EtOH). Found: C, 63.53; H, 8.63; N, 8.24%. Calcd for $C_{26}H_{41}N_3O_6$: C, 63.52; H, 8.41; N, 8.55%.

Z-L-Leu-L-Ile-L-Leu-L-Ile-L-Leu-OH (7a). **5a** (12.3 g, 25 mmol) was treated with 30% hydrogen bromide in acetic acid (25 g) at room temperature for 1 h, dry ether (100 ml) and dry hexane (200 ml) being added to the solution. Chilling of the solution gave the precipitate which was collected by filtration, washed with dry hexane, and dried in a desiccator over sodium hydroxide overnight; yellowish powder **6a**: yield, 11.9 g.

To a solution of **4a** (11.9 g, 25 mmol) in ethanol was added a solution of the tripeptide hydrobromide (**6a**) (11.9 g) and sodium hydrogencarbonate (6.3 g, 75 mmol) in a mixture of water (250 ml) and ethanol (200 ml). The mixture was treated in the same way as described for the preparation of **5a**. Recrystallization from 2-propanol gave **7a** as colorless fine crystals: mp 262—265 °C (dec); yield, 10.1 g (56%, based on **5a**); $[\alpha]_D^{25}$ $-57\pm2°$ (*c* 0.1, EtOH). Found: C, 63.39; H, 9.04; N, 9.63%. Calcd for $C_{38}H_{63}N_5O_8$: C, 63.57; H, 8.85; N, 9.76%.

Z-L-Leu-L-Leu-L-Leu-L-Leu-L-Leu-OH (7b). **7b** was obtained as colorless fine crystals in the same way as described above from the tripeptide hydrobromide (**6b**) prepared from **5b** (12.3 g, 25 mmol) and **4b** (11.9 g, 25 mmol): mp 263—266 °C (dec); yield, 12.4 g (69%, based on **5b**); $[\alpha]_D^{25}$ $-67\pm2°$ (*c* 0.1, EtOH). Found: C, 63.29; H, 9.08; N, 9.58%. Calcd for $C_{38}H_{63}N_5O_8$: C, 63.57; H, 8.55; N, 9.76%.

Z-L-Leu-L-Ile-L-Leu-L-Leu-L-Leu-OH (7c). **7c** was obtained as colorless fine crystals in the same way as described above from the tripeptide hydrobromide (**6b**) prepared from **5b** (12.3 g, 25 mmol) and **4a** (11.9 g, 25 mmol): mp 243—246 °C (dec); yield, 9.7 g (54%, based on **5b**); $[\alpha]_D^{25}$ $-31\pm2°$ (*c* 0.1, EtOH). Found: C, 63.33; H, 9.07; N, 9.61%. Calcd for $C_{38}H_{63}N_5O_8$: C, 63.57; H, 8.55; N, 9.76%.

Z-L-Ile-L-Ile-L-Leu-L-Leu-L-Leu-OH (7d). **7d** was obtained as colorless fine crystals in the same way as described above from the tripeptide hydrobromide (**6b**) prepared from **5b** (12.3 g, 25 mmol) and **4c** (11.9 g, 25 mmol): mp 256—258 °C (dec); yield, 9.5 g (53%, based on **5b**); $[\alpha]_D^{25}$ $-42\pm2°$ (*c* 0.1, EtOH). Found: C, 63.13; H, 9.13; N, 9.62%. Calcd for $C_{38}H_{63}N_5O_8$: C, 63.57; H, 8.55; N, 9.76%.

Z-L-Leu-L-Ile-L-Leu-L-Ile-L-Leu-ONSu (8a). DCC (2.7 g, 13 mmol) was added at 0 °C to a solution of **7a** (8.6 g, 12 mmol) and HONSu (1.7 g, 15 mmol) in DMF (500 ml). After being stirred at 0 °C for 8 h and then at room temperature for 16 h, deposited DCU was filtered off and washed with DMF. The combined filtrate and washings were evaporated to dryness under reduced pressure. The residue was extracted twice with hot ethyl acetate (150 ml) to remove DCU and then recrystallized from 2-propanol. **8a** was obtained as colorless fine crystals: mp 249—250 °C (dec); yield, 6.9 g (71%); $[\alpha]_D^{25}$ $-55\pm2°$ (*c* 0.1, EtOH); IR (Nujol) 1819 and 1789 (succinimide), and 1746 cm^{-1} (ester C=O). Found: C, 67.67; H, 8.41; N, 10.04%.

Calcd for $C_{42}H_{66}N_6O_{10}$: C, 61.89; H, 8.16; N, 10.31%.

Z-L-Leu-L-Leu-L-Leu-L-Leu-L-Leu-ONSu (8b). **8b** was obtained as colorless fine crystals in the same way as described above from **7b** (8.6 g, 12 mmol), HONSu (1.7 g, 15 mmol), and DCC (2.7 g, 13 mmol): mp 237—238 °C (dec); yield, 6.4 g (65%); $[\alpha]_D^{25}$ $-67\pm2°$ (*c* 0.1, EtOH); IR (Nujol) 1817 and 1790 (succinimide), and 1746 cm^{-1} (ester C=O).

Found: C, 61.75; H, 8.55; N, 10.13%.

Calcd for $C_{42}H_{66}N_6O_{10}$: C, 61.89; H, 8.16; N, 10.31%,

Z-L-Leu-L-Ile-L-Leu-L-Leu-L-Leu-ONSu (8c). **8c** was obtained as colorless fine crystals in the same way as described above from **7c** (8.6 g, 12 mmol), HONSu (1.7 g, 15 mmol), and DCC (2.7 g. 13 mmol): mp 248—250 °C (dec); yield, 6.7 g (69%); $[\alpha]_D^{25}$ −69±2° (*c* 0.1, EtOH); IR (Nujol) 1819 and 1790 (succinimide), and 1742 cm^{-1} (ester C=O). Found: C, 61.82; H, 8.49; N, 10.14%. Calcd for $C_{42}H_{66}N_6O_{10}$: C, 61.89; H, 8.16; N, 10.31%.

Z-L-Ile-L-Ile-L-Leu-L-Leu-L-Leu-ONSu (8d). **8d** was obtained as colorless fine crystals in the same way as described above from **7d** (8.6 g, 12 mmol), HONSu (1.7 g, 15 mmol), and DCC (2.7 g, 13 mmol): mp 243—245 °C (dec); yield, 6.8 g (70%); $[\alpha]_D^{25}$ −51±2° (*c* 0.1, EtOH); IR (Nujol) 1817 and 1788 (succinimide), and 1745 cm^{-1} (ester C=O). Found: C, 61.80; H, 8.41; N, 10.20%. Calcd for $C_{42}H_{66}N_6O_{10}$: C, 61.89; H, 8.16; N, 10.31%.

Cyclo(-L-Leu-L-Ile-L-Leu-L-Ile-L-Leu-) (1a). **8a** (5.7 g, 7 mmol) was treated with 20% hydrogen bromide in acetic acid (15 g) in the same way as described for the preparation of **6a**. The pentapeptide ester hydrobromide (**9a**) (yellowish powder; yield, 5.1 g (96%)) thus obtained was dissolved in DMF (1 l), and the solution was added dropwise into pyridine (2 l) with stirring at 40 °C over a period of 12 h; stirring at room temperature was then continued for 12 h. The solvent was removed under reduced pressure, and the residue was dissolved in hot chloroform (250 ml). The solution was subject ed to chromatography on a column of silica gel (100 g). After the column had been eluted with chloroform (400 ml), elution with a mixture of ethyl acetate and ethanol (19: 1) (400 ml) gave the desired product, as determined by TLC. The effluent was evaporated to dryness under reduced pressure, giving a brownish powder which was dissolved in chloroform (100 ml) and then further purified by column chromatography on alumina (100 g). The column was washed with chloroform (200 ml) and successively with ethyl acetate (200 ml). Elution with a mixture of ethyl acetate and ethanol (19: 1) (200 ml) followed by recrystallization from ethanol gave 257 mg (6.5 %) of cyclic pentapeptide (**1a**) as colorless needles: mp >300 °C; $[\alpha]_D^{20}$ −56±2° (*c* 0.1, EtOH); MS (70 eV), M^+ *m/e* 565; PMR (DMSO-d_6, amide protons, at 30 °C) δ=8.68 (1H, d, J=6.6 Hz), 8.58 (2H, d, J=7.2 Hz), 8.15 (1H, d, J=9.0 Hz), and 6.97 ppm (1H, d, J=9.0 Hz); IR (KBr) 3300, 3050, and 1535 (amide NH), 1680, 1661, and 1638 cm^{-1} (amide C=O). Found: C, 63.39; H, 9.89; N, 12.22%. Calcd for $C_{30}H_{55}N_5O_5$: C, 63.68; H, 9.80; N, 12.38%.

Cyclo(-L-Leu-L-Leu-L-Leu-L-Leu-L-Leu-L-Leu-) (1b). **1b** (238 mg, 6.0% based on **8b**) was obtained and purified in the same way as described above *via* HBr·H-L-Leu-L-Leu-L-Leu-L-Leu-L-Leu-ONSu (**9b**) (yellowish powder; 5.2 g (98%)) from **8b** (5.7 g, 7 mmol); colorless needles: mp >300 °C; $[\alpha]_D^{20}$ −67 ±2° (*c* 0.1, EtOH); MS (70 eV), M^+ *m/e* 565; PMR (DMSO-d_6, amide protons, at 30 °C) δ=8.71 (1H, d, J=7.2 Hz), 8.53 (1H, d, J=6.6 Hz), 8.18 (1H, d, J=6.6 Hz), 7.63 (1H, d, J=9.0 Hz), and 7.23 ppm (1H, d, J=9.0 Hz); IR (KBr) 3290, 3060, and 1540 (amide NH), and 1659, 1651, and 1640 cm^{-1} (amide C=O). Found: C, 63.85; H, 9.68; N, 12.40%. Calcd for $C_{30}H_{55}N_5O_5$: C, 63.68; H, 9.80; N, 12.38%.

Cyclo(-L-Leu-L-Ile-L-Leu-L-Leu-L-Leu-) (1c). **1c** (178 mg, 4.5% based on **8c**) was obtained and purified in the same way as described above *via* HBr·H-L-Leu-L-Ile-L-Leu-L-Leu-L-Leu-ONSu (**9c**) (yellowish powder; yield, 5.1 g (95%)) from **8c** (5.7 g, 7 mmol); colorless needles: mp >300 °C; $[\alpha]_D^{15}$ −71 ±2° (*c* 0.1, EtOH); MS (70 eV), M^+ *m/e* 565; PMR (DMSO-d_6, amide protons, at 30 °C) δ=8.59 (1H, d, J=7.8 Hz), 8.40 (1H, d, J=8.4 Hz), 8.33 (1H, d, J=7.8 Hz), 8.04 (1H, d, J=8.4 Hz), and 7.19 ppm (1H, d, J=8.4 Hz); IR (KBr) 3350, 3310, 3050, and 1520 (amide NH), and 1658 and 1652 cm^{-1} (amide C=O). Found: C, 63.59; H, 10.03; N, 11.98%. Calcd for $C_{30}H_{55}N_5O_5$: C, 63.68; H, 9.80; N, 12.38%.

Cyclo(-L-Ile-L-Ile-L-Leu-L-Leu-L-Leu-) (1d). **1d** (175 mg, 4.4% based on **8d**) was obtained and purified in the same way as described above *via* HBr·H-L-Ile-L-Ile-L-Leu-L-Leu-L-Leu-ONSu (**9d**) (yellowish powder; yield, 5.3 g (99%)) from **8d** (5.7 g, 7 mmol); colorless needles: mp >300 °C; $[\alpha]_D^{15}$ −52 ±2° (*c* 0.1, EtOH); MS (70 eV), M^+ *m/e* 565; PMR (DMSO-d_6, amide protons, at 30 °C) δ=8.53 (1H, d, J=7.8 Hz), 8.33 (1H, d, J=7.8 Hz), 8.11 (1H, d, J=9.0 Hz), 8.06 (1H, d, J=7.8 Hz), and 7.67 ppm (1H, d, J=9.0 Hz); IR (KBr) 3300, 3050, and 1530 (amide NH), and 1658 and 1650 cm^{-1} (amide C=O). Found: C, 63.66; H, 10.01; N, 12.26%. Calcd for $C_{30}H_{55}N_5O_5$: C, 63.66; H, 9.80; N, 12.38%.

Comparison of Viscumamide with Synthetic Cyclopentapeptides. The specific rotation value, mass spectrum, proton magnetic resonance spectrum, and infrared absorption spectrum of synthetic viscumamide **1a** were identical with those of the authentic sample. A thin layer chromatographic comparison of viscumamide with the synthetic cyclopentapeptides is given in Table 1.

Table 1. Thin layer chromatography of cyclopentapeptides

Solvents[a]	Substances				
	Viscumamide	**1a**	**1b**	**1c**	**1d**
I	0.36	0.36	0.36	0.38	0.44
II	0.50	0.50	0.55	0.57	0.58

a) Solvents: I=chloroform–methanol (95: 5), II=ethyl acetate.

The authors wish to express their thanks to Dr. Takayuki Naito, Bristol-Banyu Research Institute, and to Dr. Shosuke Yamamura, Meijo University, for the microanalyses.

References

1) Y. Okumura and A. Sakurai, *Bull. Chem. Soc. Jpn.*, **46**, 2190 (1973).
2) G. W. Anderson, J. E. Zimmerman, and F. M. Callahan, *J. Am. Chem. Soc.*, **86**, 1839 (1964).
3) D. Ben-Ishai and A. Berger, *J. Org. Chem.*, **17**, 1564 (1952).
4) H. Sugano, H. Abe, M. Miyoshi, T. Kato, and N. Izumiya, *Bull. Chem. Soc. Jpn.*, **47**, 698 (1974).
5) J. C. Seehan, M. Goodman, and W. L. Richardson, *J. Am. Chem. Soc.*, **77**, 6391 (1955).
6) R. Schwyzer and P. Sieber, *Helv. Chim. Acta*, **41**, 2186 and 2190 (1958); R. Schwyzer and B. Group, *ibid.*, **41**, 2199 (1958); R. Schwyzer, J. P. Carrion, B. Group, H. Nolting, and T. K. Aung, *ibid.*, **47**, 441 (1964).
7) M. Rothe, K. D. Steffen, and I. Rothe, *Angew. Chem.*, **75**, 1206 (1963).
8) R. Schwyzer and T. K. Aung, *Helv. Chim. Acta*, **45**, 859 (1962).
9) C.-S. Yang, K. Blaha, and J. Rudinger, *Collect. Czech. Chem. Commun.*, **29**, 2633 (1964).
10) P. M. Hardy, G. W. Kenner, and R. C. Scheppard, *Tetrahedron*, **19**, 95 (1963).
11) The specific rotation value of this substance has been recorded as $[\alpha]_D^{25}$ −49.1° (*c* 0.2, EtOH) by the use of an ORD spectrophotometer.[1] This value was recorded as $[\alpha]_D^{20}$ −54 ±2° (*c* 0.1, EtOH) by the use of a polarimeter under the same conditions as those of synthetic **1a**.

High Pressure Organic Chemistry. III.[1] Diels-Alder Reaction of Thiophene with Maleic Anhydride

Hiyoshizo KOTSUKI,* Hitoshi NISHIZAWA,* Sachio KITAGAWA, Masamitsu OCHI, Nakamichi YAMASAKI, Kiyoshi MATSUOKA, and Takashi TOKOROYAMA†

Faculty of Science, Kochi University, Asakura, Kochi 780

†*Faculty of Science, Osaka City University, Sumiyoshi-ku, Osaka 558*

(Received August 11, 1978)

The Diels-Alder reaction of thiophene with maleic anhydride has been investigated under conditions of very high pressure. The Diels-Alder adduct was obtained in dichloromethane at 100 °C and 15 kbar; above a pressure of 15 kbar the reaction was highly accelerated. From the spectral data and chemical evidence it has been suggested that the adduct has the *exo*-configuration. The reactions in various solvents and with other dienophiles have also been examined.

Recently much attention has been focused on the application of high pressure techniques in the field of synthetic organic chemistry.[2] In general, the pressure dependence of the rate constant on the reaction may be written as follows:

$$\frac{\delta \ln k}{\delta P} = -\frac{\Delta V^*}{RT}$$

where ΔV^*, the activation volume, represents the difference in volume between the reactants and the transition state. If ΔV^* is negative, *i.e.*, the volume of the transition state is smaller than the volume of the reactants, the rate k will increase with increasing pressure. The activation volume for a number of organic reactions has been determined and [4+2] cycloaddition reactions, typically the Diels-Alder reaction, are known to have a relatively large activation volume (−25——50 cm³/mol)[2,3] being the most favorable case at high pressure.

In line with this theory the [4+2] cycloaddition reactions at high pressures have been investigated and it has been shown that the use of high pressure (10—40 kbar) is a very valuable tool for synthetic organic chemistry.[4-6]

In a preliminary paper it was reported that the Diels-Alder reaction of thiophene with maleic anhydride, which had never undergone reaction under the usual conditions, had effectively proceeded at very high pressures.[1b] This paper will report a more detailed investigation.

Results and Discussion

Cycloaddition between Thiophene and Maleic Anhydride. It is well documented that thiophene itself does not undergo the Diels-Alder reaction.[7] Recently, however, there have been reports that some thiophene derivatives do combine with extremely reactive dienophiles such as dicyanoacetylene and dimethyl acetylenedicarboxylate.[8] The only recorded thiophene derivatives which are able to react with maleic anhydride in a Diels-Alder manner are thiophenc 1,1-dioxide[9] and 2,5-dimethoxythiophene.[10]

The authors anticipated that thiophene would react with maleic anhydride if the reaction were performed under high pressure conditions overcoming the high aromatic character.

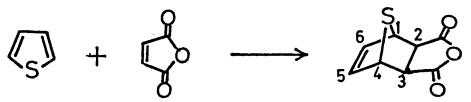

1 2 3

Initially, the reaction of thiophene with maleic anhydride in dichloromethane at 15 kbar and room temperature was attempted considering the thermal lability of the cycloadduct or the enhancement of the reverse reaction. After 3 days, however, reaction had not occurred and reaction without solvent or with a Lewis acid catalyst (*e.g.* $MgCl_2$) was also fruitless. This demonstrates a striking absence of diene character in thiophene and contrasts remarkably with furan.[4b] The reaction was examined at higher temperatures at 15 kbar for 3 h in dichloromethane when the reaction did occur (Table 1). Inspection of Table 1 reveals that the most favorable

Table 1. Temperature dependence of the yield[a] in the adduct **3** between thiophene and maleic anhydride

Room temp	40 °C	80 °C	100 °C	120 °C	150 °C
No reaction	No reaction	8%	37—47%	18%	Decomposition

a) The yield based on the isolated materials.

results are obtained at 100 °C. Thus, from the reaction mixture a highly crystalline compound **3**,[11] mp 159.5—161.5 °C, of molecular formula $C_8H_6O_3S$ (MS, M^+ 182) was obtained in yields of 37—47% after recrystallization from ether or chloroform. It is suggested that **3** has an *exo*-configuration from the spectral data and chemical evidence as follows. In the ^1H NMR spectra (Table 2), the C_2 and C_3 protons appear at δ 3.63 as a doublet (J=1 Hz) and when the dihedral angle between the protons at C_1 and C_2 (C_3 and C_4) is considered the indication is that **3** has an *exo*-configuration. This assignment is in good agreement with the data of the adducts between furan and maleic anhydride, showing that the *exo*-adduct **6** resembles **3** rather than the *endo*-adduct.[12]

Further supporting evidence has been obtained as follows. Adduct **3** was subjected to methanolysis to give the monomethyl ester **4**. As expected **4** did not undergo

TABLE 2. ^{1}H NMR SPECTRAL DATA (δ ppm)

Compd	C_1,C_4–H	C_2,C_3–H	C_5,C_6–H	
3[a]	4.59 (2H, m)	3.63 (2H, d, J=1 Hz)	6.61 (2H, dd, J=2, 3 Hz)	
4[b]	4.29 (2H, m)	3.15 (1H, d, J=9 Hz) 3.24 (1H, d, J=9 Hz)	6.51 (2H, dd, J=2, 2.5 Hz)	-COOMe 3.63 -COOH 8.81
5[c]	4.29 (2H, dd, J=2, 2.5 Hz)	3.16 (2H, s)	6.48 (2H, dd, J=2, 2.5 Hz)	-COOMe 3.68
6[a]	5.34 (2H, m) 5.34[d]	3.26 (2H, s) 3.25[d]	6.56 (2H, m) 6.53[d]	
8[c]	5.12 (2H, m) 5.10[e]	3.43 (2H, dd, J=2, 3 Hz) 3.41[e]	6.54 (2H, d, J=1 Hz) 6.52[e]	-COOMe 3.63 3.62[e]

a) $CDCl_3$–DMSO-d_6 (1 : 1), b) $CDCl_3$–Acetone-d_6 (2 : 1). c) $CDCl_3$. d) Ref. 12. e) Ref. 13.

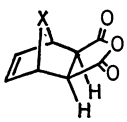

X=S **3**
X=O **6**

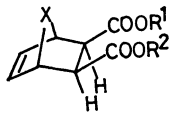

X=S, R^1=Me, R^2=H **4**
X=S, R^1=R^2=Me **5**
X=O, R^1=R^2=H **7**

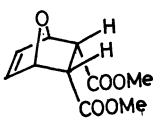

8

iodolactonization (I_2–KI).[13] The corresponding dimethyl ester **5**, which is formally regarded as the Diels-Alder product of thiophene with dimethyl maleate, was prepared from **4** by careful methylation with diazomethane.[14] In the ^{1}H NMR spectra of **5** (Table 2) the C_2 and C_3 protons appeared at δ 3.16 as a singlet. In the ^{1}H NMR spectra of the *exo*-adduct **7** between furan and maleic acid the C_2 and C_3 protons were reported to appear at δ 2.61 as a singlet.[13,15] Moreover, in the case of the *endo*-adduct **8** between furan and dimethyl maleate, which was prepared under similar conditions as reported by Dauben and Krabbenhoft,[4b] the C_2 and C_3 protons appear at δ 3.43 as a doublet of doublets (J=2, 3 Hz)[16] and contrasts remarkably with these results.

The exclusive formation of the *exo*-adduct **3** in the Diels-Alder reaction of thiophene with maleic anhydride is predictable on the basis of the preferential production of the thermodynamically stable adduct at higher temperature.[17] However, it would be premature to say whether **3** represents the kinetic product.

Since the reaction of thiophene with maleic anhydride has been proven efficient in giving an adduct, an investigation of the reactions between thiophene and other dienophiles has been undertaken. However all attempted reactions of thiophene with dimethyl maleate, dimethyl fumarate, methyl acrylate, acrylonitrile, or acrylaldehyde under the same conditions (100 °C, 15 kbar, 3 h, the concentrations of the reactants were 3 M in CH_2Cl_2) were unsuccessful and no adduct formation was observed. At higher temperatures the reaction was too vigorous to give the adduct, thus dimethyl maleate isomerized completely to dimethyl fumarate. Acrylonitrile and acrylaldehyde readily polymerized even in the presence of an inhibitor such as hydroquinone.

Thus sole criterion of high pressure is insufficient to bring about the reaction of thiophene with dienophiles less reactive than maleic anhydride.

Effect of Solvent. It is usually recognized that the conventional Diels-Alder reaction is little affected by the solvent.[17] However, under high pressure conditions the choice of solvent becomes important and there have been various studies on the kinetic solvent effects in Diels-Alder reactions.[3,18] Unfortunately these studies have been limited to relatively low pressures (*ca.* 2 kbar max.), and little information is available in the pressure range from 10 to 20 kbar. Consequently an investigation of the solvent effect in the Diels-Alder reaction of thiophene with maleic anhydride has been undertaken and the results are summarized in Table 3. In a previous paper the low yield in benzene (Run 11) was assumed to be due to the freezing of the reaction medium at 15 kbar.[1b] According to the Simon equation the freezing temperature of substances is dependent on pressure.[19] The estimated freezing point of benzene at 4 kbar is *ca.* 100 °C, so that freezing of the reaction medium appears to be probable. The interpretation based on freezing temperature of solvent is plausible in the cases of dichloromethane, chloroform, and carbon tetrachloride (Runs

TABLE 3. SOLVENT DEPENDENCE OF THE YIELD IN THE ADDUCT **3** (100 °C, 3 h)

Run	Solvent	Pressure(kbar)	Yield(%)[a]	
1		10	6	
2	CH_2Cl_2	15	43	22 kbar[b]
3		20	47	
4		10	3	
5	$CHCl_3$	15	42	12 kbar[b]
6		20	42	
7		10	No reaction	
8	CCl_4	15	12	4 kbar[b]
9		20	21	
10	$CHCl_2CHCl_2$	15	47	
11	C_6H_6	15	7	
12	$C_6H_5CH_3$	15	Trace[c]	
13	C_6H_5Cl	15	20	
14	C_6H_5Br	15	5	
15	C_6H_5CN	15	29	
16	$C_6H_5COCH_3$	15	Trace[c,d]	
17	CH_3CN	15	39	
18	AcOEt	15	17	
19	Et_2O	15	Trace[c]	
20	CH_3COCH_3	15	No reaction[d]	

a) The values are the average of two or more runs. b) The estimated freezing point is 100 °C at this pressure. See Ref. 19. c) Only trace amounts of adduct were detected by TLC. d) A considerable amount of polymeric substances was obtained.

1—9). In this connection it can be seen that *at pressures above 15 kbar the reaction is highly accelerated!* The fact that at 20 kbar, a respectable increase of product yield was observed in carbon tetrachloride (Run 9) leads to the assumption that the reaction proceeds to some extent in the frozen state,[20] although further experiments were necessary. In addition the results in Table 3 suggest that the adduct formation should increase in aromatic solvents having an electron withdrawing substituent (Runs 13 and 15) rather than ones having an electron donating substituent (Runs 11 and 12). This may be explained in terms of the specific solute-solvent interactions such as the charge transfer complex formation between maleic anhydride and benzene or toluene which would become significant at high pressure.[21,22]

The very low yield of product in ether, acetone, and acetophenone can not be explained.

Experimental

Apparatus. Figure 1 shows a schematic version of the high pressure apparatus used which consists essentially of a press frame, the upper and bottom drive cylinders, an induction heater and a sample cylinder. The sample cylinder, shown in Fig. 2, has been fabricated from a SUS-27 multiplex cylinder subject to autofrettage and a hardened S-3 tool steel cylinder or sintered tungsten carbide cylinder (80 mm long and 50 mm diameter). The piston made from hardened S-3 tool steel or sintered tungsten carbide has a diameter of 12 mm. The reaction vessel has been made from Teflon which is a good container for most organic substrates and pressure transmitter at elevated temperatures (below 300 °C). Talc and stainless steel disks have been used to prevent leakage from the Teflon vessel. The pressure generated in the reaction vessel can not be directly read on the pressure gauge and so has been calibrated using the change in volume of $AgNO_3$ (9.8 kbar) and KBr (17.9 kbar) and the resistivity of Bi I–II (25.3 kbar) at room temperature. The leakage from the Teflon vessel containing the reactants and solvent has been checked and appears to be negligible.

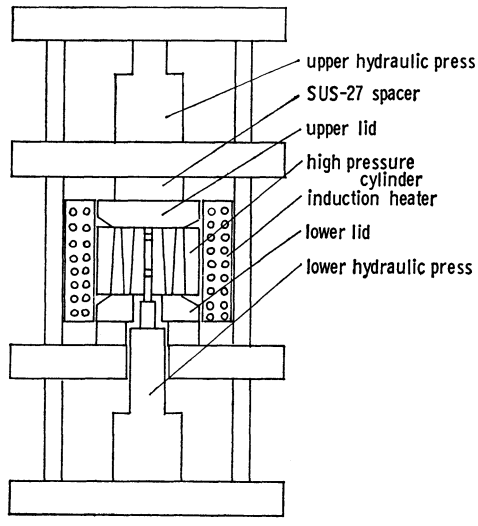

Fig. 1. Schematic version of high pressure apparatus.

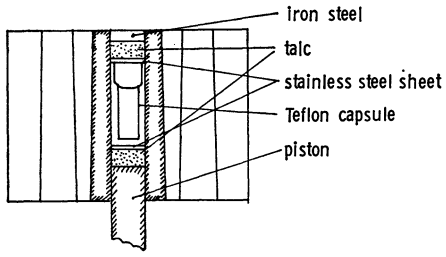

Fig. 2. Detailed schematic version of the sample cylinder.

The procedure for a high pressure reaction is as follows. The reaction vessel (*ca.* 0.85 ml capacity) is filled completely with the reactants dissolved in an appropriate solvent and covered with Teflon lid. The reaction vessel and the piston are forced into the bore of a sample cylinder by synchronously raising the upper and bottom drive cylinders hydraulically until the desired pressure is attained. To conduct a reaction at elevated temperatures, the sample cylinder system is inserted into the induction heater and heated to the desired temperature measured by an alumel-chromel thermocouple. After the experiment the sample cylinder is cooled to room temperature by a fan and the pressure released. A representative temperature-pressure diagram is shown in Fig. 3 in the experiment at 150 °C and 15 kbar for 3.5 h.

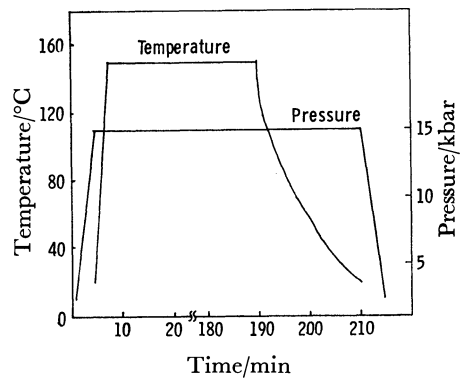

Fig. 3. Representative temperature-pressure diagram at 150 °C and 15 kbar for 3.5 h.

All high pressure reactions were performed at a concentration of 3 M of the reactants in the dried solvents.

General. All melting points are uncorrected. ^1H NMR spectra were obtained on a JEOL-MH-100 spectrometer using TMS as the internal standard. ^{13}C NMR spectra were obtained at 25.05 MHz on a JEOL-FX-100 spectrometer. The IR spectra were measured with a JASCO infrared spectrophotometer Model IRA-1 and the mass spectra on a Hitachi Model M-52 spectrometer.

TLC was conducted using Merck's precoated Kieselgel 60 (5721) and for column chromatography, Wakogel C-200 (74—149 μ) was employed.

Diels-Alder Reaction of Thiophene with Maleic Anhydride. The general procedure is as follows. A CH_2Cl_2 solution (1 ml) of thiophene (3 mmol) and maleic anhydride (3 mmol) was injected into the Teflon reaction vessel. The reaction vessel was heated to 100 °C at 15 kbar for 3 h. After cooling of the reaction mixture and the release of pressure, the solvent was evaporated and the product recrystallized from ether or chloroform to give pure **3** in 37—47% yield: mp 159.5—161.5 °C (from $CHCl_3$), 159—160 °C (from Et_2O); IR (Nujol) 1850, 1795, 1085, 943, and 920 cm^{-1}; ^1H NMR spectrum (Table 2); ^{13}C NMR spectrum (Table 4); MS (20 eV), *m/e* (rel intensity),

Table 4. ^{13}C NMR spectral data of **3** and **5** (in $CDCl_3$)[a]

	3	5
C-1, C-4	54.2(d)	54.0(d)
C-2, C-3	52.0(d)	50.2(d)
C-5, C-6	139.8(d)	139.8(d)
C=O	169.2(s)	171.8(s)
CH_3		52.2(q)

a) Chemical shifts are expressed in ppm downfield from the ^{13}C NMR of TMS.

182 (36, M^+), 110 (27), 84 (44), 78 (100), 66 (25), 45 (12).

Found: C, 52.80; H, 3.32%. Calcd for $C_8H_6O_3S$: C, 52.74; H, 3.32%.

Methanolysis of Adduct **3**. Two ml of an absolute MeOH solution of adduct **3** (200 mg) was stirred at 40 °C for 5 days under a N_2 atmosphere.[23] After removal of excess MeOH the crude product, which still contained a small amount of starting anhydride (R_f 0.61, 4: 1 C_6H_6–AcOEt) on TLC, was obtained as a viscous oil. A pure sample of the monomethyl ester **4** was obtained in crystalline form after column chromatography on silica gel: mp 123—124 °C (from Et_2O); IR (Nujol) 3200—2600, 1740, 1710, 1245, 1210, and 1185 cm^{-1}; ^1H NMR spectrum (Table 2); MS (30 eV), *m/e*, 214 (M^+).

Found: C, 50.42; H, 4.66%. Calcd for $C_9H_{10}O_4S$: C, 50.46; H, 4.70%.

Methylation of the Monomethyl Ester **4**. The monomethyl ester **4** (123 mg) was treated conventionally with a small excess of diazomethane. After the renewed addition of diazomethane succeeded in producing a pale yellow coloration (*ca.* 1 min on standing at 0 °C), the excess of reagent was instantly decomposed with the minimum amount of AcOH and the solution evaporated *in vacuo* (below 45 °C).[14] The crude product with an unpleasant odor was purified by column chromatography on silica gel (eluted with $CHCl_3$) and 100 mg of dimethyl ester **5** was obtained as a colorless and odorless oil which crystallized on standing in the refrigerator: mp 73—73.5 °C (from Et_2O–petroleum ether); IR (Nujol) 1745, 1585, 1335, 1225, 1215, 1160, and 1035 cm^{-1}; ^1H NMR spectrum (Table 2); ^{13}C NMR spectrum (Table 4); MS (70 eV), *m/e*, 228 (M^+).

Found: C, 52.67; H, 5.28%. Calcd for $C_{10}H_{12}O_4S$: C, 52.62; H, 5.30%.

Hiyoshizo Kotsuki acknowledges a Grant-in-Aid for Scientific Research from the Ministry of Education. The authors wish to thank Mr. Kazumi Hojo for his preliminary experiments in this study.

References

1) a) A part of this work was presented at the 18th Symposium on High Pressure, Kyoto, November, 1977; b) This work was reported in a preliminary form: H. Kotsuki, S. Kitagawa, H. Nishizawa, and T. Tokoroyama, *J. Org. Chem.*, **43**, 1471 (1978).

2) For some reviews in this area, see a) D. vor der Brück, R. Bühler, C. C. Heuck, H. Plieninger, K. E. Weale, J. Westphal, and B. Wild, *Chem.-Ztg.*, **94**, 183 (1970); b) R. C. Neuman, Jr., *Acc. Chem. Res.*, **5**, 381 (1972) and earlier reviews cited therein; c) D. Bieniek and F. Korte, *Naturwissenschaften*, **59**, 529 (1972); d) G. Jenner, *Angew. Chem.*, **87**, 186 (1975); e) T. Asano and A. Sera, *Yuki Gosei Kagaku Kyokai Shi* , **35**, 535 (1977); f) A. Sera, *Kagaku*, **32**, 510 (1977); g) H. Thies, *Chimia*, **32**, 79 (1978).

3) J. R. McCabe and C. A. Eckert, *Acc. Chem. Res.*, **7**, 251 (1974), and references cited therein.

4) a) W. G. Dauben and A. P. Kozikowski, *J. Am. Chem. Soc.*, **96**, 3664 (1974); b) W. G. Dauben and H. O. Krabbenhoft, *ibid.*, **98**, 1992 (1976); c) W. G. Dauben and H. O. Krabbenhoft, *J. Org. Chem.*, **42**, 282 (1977).

5) J. A. Gladysz, S. J. Lee, J. A. V. Tomasello, and Y. S. Yu, *J. Org. Chem.*, **42**, 4170 (1977).

6) K. Matsumoto, Y. Ikemi-Kono, and T. Uchida, *J. Chem. Soc., Chem. Commun.*, **1978**, 543.

7) For most recent review, see R. M. Acheson, "An Introduction to the Chemistry of Heterocyclic Compounds," 3rd ed, Wiley, New York, N. Y. (1976), p. 157.

8) a) R. Helder and H. Wynberg, *Tetrahedron Lett.*, **1972**, 605; b) H. J. Kuhn and K. Gollnick, *ibid.*, **1972**, 1909; c) H. J. Kuhn and K. Gollnick, *Chem. Ber.*, **106**, 674 (1973); d) D. N. Reinhoudt, W. P. Trompenaars, and J. Geevers, *Tetrahedron Lett.*, **1976**, 4777; e) K. Kobayashi and K. Mutai, *Chem. Lett.*, **1977**, 1149.

9) H. Wollweber, "Diels-Alder-Reaktion," Georg Thieme Verlag, Stuttgart (1972), p. 72.

10) J. M. Baker, P. R. Huddleston, and S. W. Shutler, *J. Chem. Soc., Perkin Trans. 1*, **1975**, 2483.

11) For another approach to this model, see R. K. Murray, Jr., J. S. Polley, S. S. Abdel-Meguid, and V. W. Day, *J. Org. Chem.*, **42**, 2127 (1977).

12) a) F. A. L. Anet, *Tetrahedron Lett.*, **1962**, 1219: b) M. W. Lee and W. C. Herndon, *J. Org. Chem.*, **43**, 518 (1978).

13) T. A. Eggelte, H. de Koning, and H. O. Huisman, *Tetrahedron*, **29**, 2491 (1973).

14) With an excess of reagent and/or a long time the 1,3-dipolar cycloaddition to the C_5–C_6 double bond easily occurred.

15) The hydrolysis of adduct **3** failed to give the dicarboxylic acid derivative. Adduct **3** was slightly hydrolyzed in refluxing water and with this treatment the reaction product became contaminated with a considerable amount of unidentified impurities. See also Ref. 23.

16) H. Kotsuki and H. Nishizawa, unpublished results. The reaction was performed in CH_2Cl_2 at 15 kbar and room temperature for 18 h and only the almost pure *endo*-isomer was obtained as a colorless oil.

17) J. Sauer, *Angew. Chem.*, **79**, 76 (1967).

18) a) J. R. McCabe and C. A. Eckert, *Ind. Eng. Chem., Fundam.*, **13**, 168 (1974); b) K. Seguchi, A. Sera, and K. Maruyama, *Bull. Chem. Soc. Jpn.*, **47**, 2242 (1974); c) See also K. Tamura and T. Imoto, *ibid.*, **48**, 369 (1975).

19) The Simon equation may be expressed in the following form: $(P-P_0)/a=(T/T_0)^c-1$. For a number of substances each parameter is listed in the literature: S. E. Babb, Jr., *Rev. Mod. Phys.*, **35**, 400 (1963).

20) *Cf.* I. C. Paul and D. Y. Curtin, *Acc. Chem. Res.*, **6**, 217 (1973).

21) a) W. G. Barb, *Trans. Faraday Soc.*, **49**, 143 (1953); b) H. W. Offen, "Electron-donor-acceptor Complexes at High Pressures," in "Molecular Complexes," ed by R. Foster, Elek Science, London (1973), Vol. 1, Chap. 3; c) For a study of charge transfer complexes at ultra-high pressure, see T. Sakata, A. Onodera, H. Tsubomura, and N. Kawai, *J. Am. Chem. Soc.*, **96**, 3365 (1974), and the references cited therein; d) For a general discussion, see R. Foster, "Organic Charge-Transfer Complexes," Academic (1969).

22) A referee has pointed out the participation of the solvent in the activated complex rather than the charge transfer complex formation between maleic anhydride and

solvent. The importance of such a feature cannot be excluded. However, the authors have concluded that the charge transfer complex formation is significant in this reaction since the stability of the complex is enhanced at high pressure: A. H. Ewald, *Trans. Faraday Soc.*, **64**, 733 (1968). See also Ref. 21b.

23) A significant amount of the starting material (*ca.* 20%) remained unchanged on ^{1}H NMR even after refluxing for 2 days under a N_2 atmosphere. In this case the reaction mixture was colored yellow and difficult to purify.

Light-induced Conformational Changes of Polypeptides. Photoisomerization of Azoaromatic Polypeptides

Akihiko UENO,* Jun-ichi ANZAI, Tetsuo OSA, and Yoshinori KADOMA†

Pharmaceutical Institute, Tohoku University, Aobayama, Sendai 980

†*Institute for Medical and Dental Engineering, Tokyo Medical and Dental University, 2-Chome, Surugadai, Kanda, Chiyoda-ku, Tokyo 101*

(Received August 15, 1978)

Copolymers of β-benzyl L-aspartate with β-*m*- or *p*-(phenylazo)benzyl L-aspartate were prepared in order to investigate the effect of side-chain photoisomerization on their conformations. These polymers in 1,2-dichloroethane show a CD band at 222 nm characteristic of left-handed α-helices. After irradiation, remarkable changes of the 222 nm band were observed for both *meta* and *para* copolymers with more than 50% azo residues. The decrease in ellipticity observed for the *meta* copolymers indicates that photoisomerization induces a significant instability in the left-handed α-helical conformation. On the other hand, the *para* copolymers change their sign from positive to negative by irradiation, confirming the reversal in the helix sense. In the course of subsequent relaxation of the irradiated *para* copolymer with 59% azo residues, an abrupt change in the CD spectra was found above 50% *cis* followed by a gradual change on decreasing the content of *cis* isomers. Concerning the polymers with azoaromatic side chains including copolymers with γ-benzyl L-glutamate, the helical sense seems to affect appreciably the sign of the side-chain CD bands.

The conformation of substituted benzyl esters of poly(aspartic acid) is determined by the nature and position of the substituent. Revesal in the helix sense from left- to right-handed α-helix is induced by the *para* substitution of the benzene ring of poly(β-benzyl L-aspartate) (PBLA) with a methyl, cyano, or nitro group.[1] Furthermore, the chlorine substituted PBLAs assume different handed helices depending on the position of the chlorine atom attached to the benzene ring.[2] From these observations a geometrical change such as *cis-trans* isomerization of the appropriate side chains might be expected to reverse the helix sense. Such a system, if realized, can be compared with visual purple, rhodopsin, since its polypeptide part (opsin) undergoes a conformational change induced by *cis-trans* photoisomerization of its chromophoric part (retinal). In nature, this light-induced conformational change is a trigger which excites the nerve cells of the retinal rods. From this view point, we prepared some copolymer series containing azobenzene moieties in their side chains. Photoisomerization of a polypeptide side chain itself was reported for the copolymers of L-*p*-(phenylazo)phenylalanine[3] and also for poly(γ-cinnamyl L-glutamate).[4] However, no conformational change could be induced by irradiation probably because of their conformational stability. In a previous paper,[5] we reported the results of the copolymer series of γ-benzyl L-glutamate with β-*m*- or *p*-(phenylazo)benzyl L-aspartate, and showed evidence supporting the following processes which occur independently.

$$\text{random coil} \underset{\Delta}{\overset{h\nu}{\rightleftharpoons}} \text{right-handed helix} \qquad (1)$$

$$\text{left-handed helix} \underset{\Delta}{\overset{h\nu}{\rightleftharpoons}} \text{random coil} \qquad (2)$$

Reversal in helix sense could be attained for these copolymer series. In this paper, the results of copolymer series of β-benzyl L-aspartate with β-*m*- or *p*-(phenylazo)benzyl L-aspartate (*meta* or *para* copolymer series) are described. The following process which involves reversal in the helix sense has been confirmed to occur for some of these polymers.

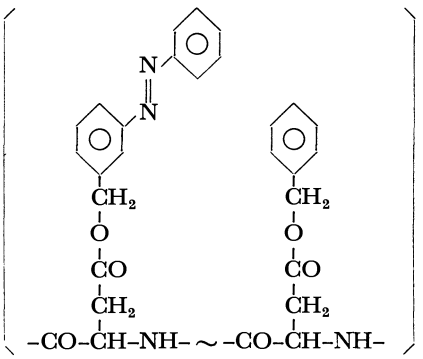

meta copolymer series

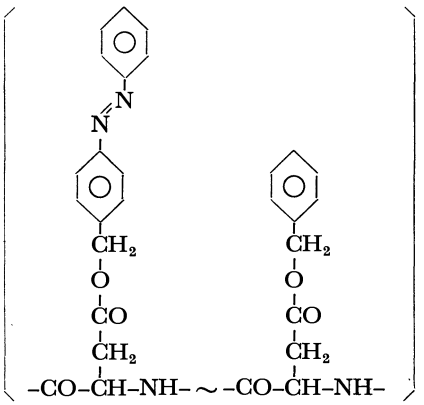

para copolymer series

$$\text{left-handed helix} \underset{\Delta}{\overset{h\nu}{\rightleftharpoons}} \text{right-handed helix} \qquad (3)$$

The side-chain *cis* isomer, formed by irradiation, undergoes subsequent relaxation in the dark back to the original *trans* form. The light-induced conformational changes are, therefore, reversible, and provide a unique system which responds to light signals in an on-off fashion.

Results and Discussion

The ultraviolet and visible spectrum of poly[β-*m*-

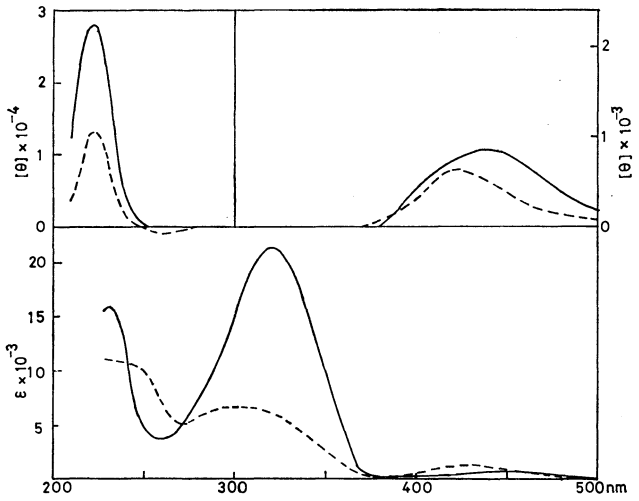

Fig. 1. CD and ultraviolet-visible spectra of mPALA in 1,2-dichloroethane before (——) and after (----) irradiation.

(phenylazo)benzyl L-aspartate] (mPALA) is essentially that of azobenzene itself (Fig. 1).[7] The band at 320 nm is attributed to π-π^* transition (ε=22000) and that at 450 nm to n-π^* transition (ε=700).[8] The irradiated polymer shows a spectrum resembling that of *cis*-azobenzene reported by Gerson *et al.*[7] The important aspect of the spectrum after irradiation is the decrease in absorption intensity in the π-π^* transition region. All of the *meta* and *para* copolymer series show similar spectra with various intensities corresponding to their content of azo residues.

The circular dichroism (CD) spectra of *meta* copolymer series before and after irradiation show dichroic bands associated with the n-π^* transitions of the main-chain amide and side-chain azo chromophores at 222 nm and 420—450 nm, respectively. No dichroic band was observed in the region of the π-π^* transition of the chromophore. The values of $[\theta]$ at the extrema are plotted against the content of azo residues (mol % of (phenylao)benzyl L-aspartate in copolymers) (Fig. 2).

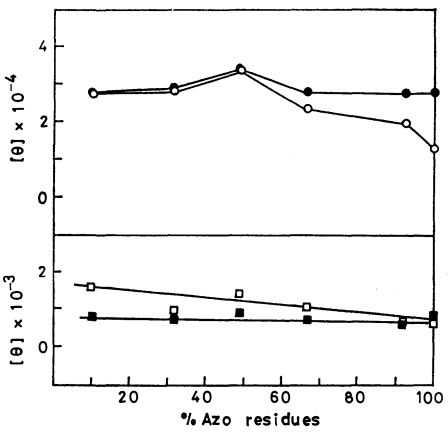

Fig. 2. Variation of maximum ellipticities associated with the side-chain n-π^* (■,□) and the amide n-π^* (●,○) transitions before (■,●) and after (□,○) iradiation for *meta* copolymer series as a function of the azo content.

Molar ellipticities of the side-chain band were calculated with use of the molar concentration of azo residues. The spectra around 222 nm before irradiation are almost independent of the copolymer composition, and are very similar to those of poly(β-methyl L-aspartate) which assumes a left-handed α-helical conformation.[9] These observations suggest that overlapping of allowed transitions of side-chain chromophores with those from the peptide backbone is either small or absent in the polymers.[10] The values of $[\theta]$ at 222 nm do not seem to be affected by irradiation for the copolymers with azo residues of smaller than 50%. However, the values decrease for the copolymers of 67 and 92% azo contents and mPALA (Figs. 2 and 7). The value of $[\theta]$ at 222 nm is generally used to characterize the helicity, the decreased values indicating the increase in instability for the left-handed α-helices of the polymers. The value of $[\theta]_{222}$=28000 for mPALA is reduced to 13000 by irradiation (Figs. 1 and 2), confirming the formation of an appreciable amount of random-coil form. Its reduced specific viscosity, η_{sp}/c (c=0.1 in 1,2-dichloroethane), measured at 25 °C changes from 0.23 to 0.49 by photoirradiation. This suggests the increased volume induced by collapse of the helical form.

Proton NMR spectra at 100 MHz were measured for mPALA (Fig. 3) in order to obtain further evidence for the partial helix-coil transition. The spectrum of the fully helical mPALA in 0.3% v/v trifluoroacetic acid/deuteriochloroform (TFA/$CDCl_3$) solution shows a peak at 4.37 ppm from α-CH proton and a broad doublet at 3.28 and 2.76 ppm from the β-CH_2 protons. The spectrum of the random-coil form of mPALA in 3% v/v TFA/$CDCl_3$ solution shows a peak at 4.86 ppm from the α-CH proton (shoulder of the peak from the benzyl CH_2

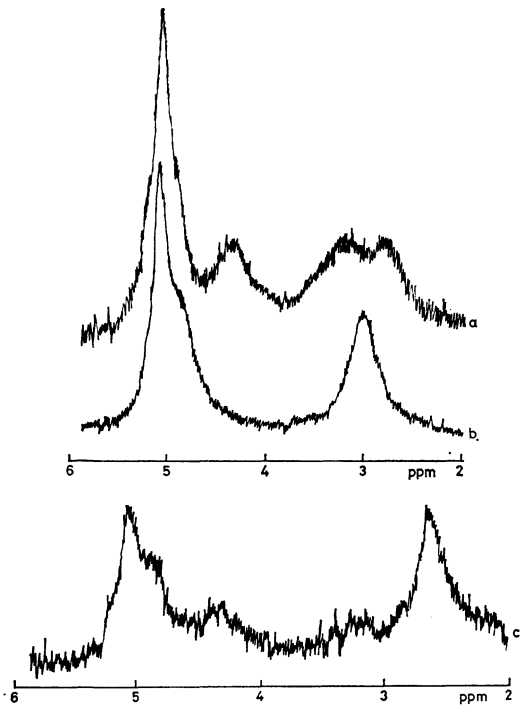

Fig. 3. 100-MHz NMR Spectra of mPALA. a; α-Helix (0.3% v/v TFA/$CDCl_3$), b; random coil (3% v/v TFA/$CDCl_3$), c; mPALA after irradiation ($CDCl_3$).

protons) and a single peak at 3.01 ppm from the β-CH_2 protons. The chemical shifts are close to those reported for the L-aspartate polymers.[11] The spectrum of mPALA after irradiation in $CDCl_3$ shows a complex pattern. The two α-CH chemical shifts observed at 4.40 and 4.90 ppm correspond to the α-helix and the random-coil peaks, respectively. Another change to be noted is that for the β-CH_2 resonance, which shows a sharp peak at 2.66 ppm probably from the random-coil form overlapped by the high field component of the β-CH_2 doublet of the helix. Compared with the chemical shift of the random coil caused by TFA addition, it is shifted upfield. The cause of the shift is unknown, but it might be due to the absense of TFA or a ring current effect of formed *cis* isomers. The results of NMR spectra might be in line with those of CD spectra.

The signs of the n-π^* CD band of the side-chain azo chromophores are always positive, not changing on photoirradiation (Fig. 2). The values of $[\theta]$ before and after irradiation are independent of the content of azo residues, which confirms side chain-main chain interactions as the origin of the dichroism band.

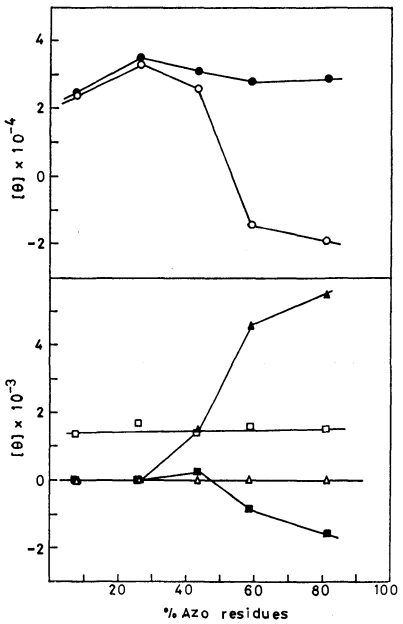

Fig. 4. Variation of maximum or minimum ellipticities associated with the side-chain n-π^* (■,□) π-π^* (▲,△) and the amide n-π^* (●,○) transitions before (■,▲,●) and after (□,△,○) irradiation for *para* copolymer series as a function of the azo content.

The CD spectra of *para* copolymer series show dichroic bands associated with the side-chain π-π^* transition as well as the n-π^* transitions of the main chain amide and side-chain azo chromophores. The values of $[\theta]$ at the extrema before and after irradiation are plotted against the content of azo residues (Fig. 4). All the spectra around 222 nm before irradiation are essentially those for the left-handed α-helices. The spectra after irradiation differ remarkably from those before irradiation for the copolymers of 59 and 81% azo contents (Fig. 7). These copolymers before irradiation display maxima with the values of $[\theta]_{222}=28000$ for 59% azo copolymer and $[\theta]_{215}=29000$ for 81% azo copolymer,[12] after irradiation minima with the values of $[\theta]_{224}=-14000$ for the former and $[\theta]_{222}=-19000$ for the latter. These observations demonstrate the reversal in the helix sense of these copolymers. Some indication of double trough is also consistent with helix reversal. Since the absolute values of $[\theta]$ are appreciably smaller than the value of $\approx$40000 reported for right-handed α-helices,[13] the copolymers after irradiation cannot be entirely right-handed helices. In contrast to the above polymers, the effect of irradiation on conformation is negligible for the polymers with smaller amount of azo residues. Certain amount of azo residues is necessary to cause the pronounced conformational changes. A critical azo content seems to exist at about 50%.

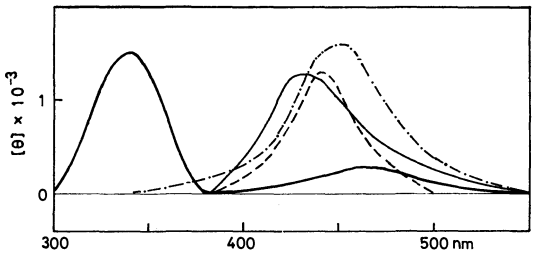

Fig. 5. CD spectra associated with the side-chain transitions of *para* copolymer series in 1,2-dichloroethane. Before irradiation: azo content 43% (——). After irradiation: azo content 7.4% (– – –), 26% (-·-·-), 43% (——).

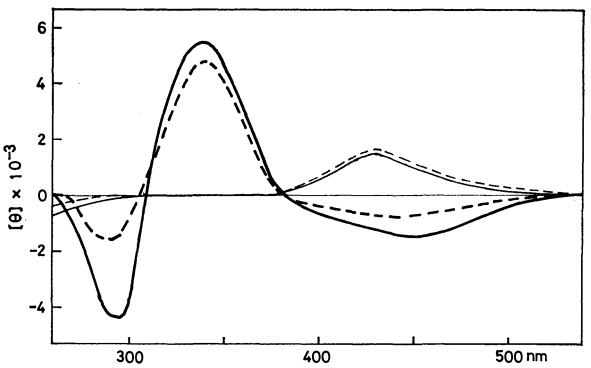

Fig. 6. CD spectra associated with the side-chain transitions of *para* copolymer series in 1,2-dichloroethane. Before irradiation: azo content 59% (– – –), 81% (——). After irradiation: azo content 59% (– – –), 81% (——).

The CD spectra associated with the side-chain n-π^* and π-π^* transitions of *para* copolymer series before and after irradiation are shown in Figs. 5 and 6.[14] Before irradiation, the CD spectra of the two copolymers with azo residues of 7.4 and 26% exhibit no dichroism in the region of the side-chain π-π^* transition, whereas the spectra of the copolymers with more azo residues exhibit distinct dichroism bands in the region. A distinct difference in the observed π-π^* CD bands exists between the copolymer with 43% azo residues and the copolymers

with more azo residues. A simple positive band is observed for the former while the spectra of the latter are rather complicated, showing a peak in the 340-nm region and a trough in the 295-nm region with a crossover near 310 nm. The separation of these bands is small, confirming the assignment of the band to exciton resonance coupling[15] of spatially adjacent azoaromatic chromophores.[16] The side chains of these polymers are allowed to arrange themselves in close packing in favor of the delocalization of the electronic excitation. Such exciton resonance coupling was also observed in the π-π^* transition region of azo chromophores by Goodman *et al.*[10] for some azoaromatic polypeptides composed of (phenylazo)phenylalanine or its analogues. In the case of (phenylazo)benzyl L-aspartate polymers, the exciton resonance coupling seems to be very difficult because of the allowed movement of the side chains and the relatively large distances between the side chains. In fact, it does not appear for other copolymer series of (phenylazo)benzyl L-aspartate involving the copolymer series with γ-benzyl L-glutamate. Thus it might be possible only when some steric requirements are satisfied concerning the side-chain conformation.

In the region of the side-chain n-π^* transition, circular dichroism is absent or small before irradiation for the copolymers with azo residues smaller than 40%. On further increase in azo residues, there appears a positive band and subsequently a negative band. It is difficult to explain the complicated spectral behavior. Nevertheless, we believe that the origin of the band is side chain-main chain interaction since there must be a profound difficulty for the electronic interactions between the adjacent side chains due to a small value for the transition moment of the n-π^* transition and the large distance between the side chains.

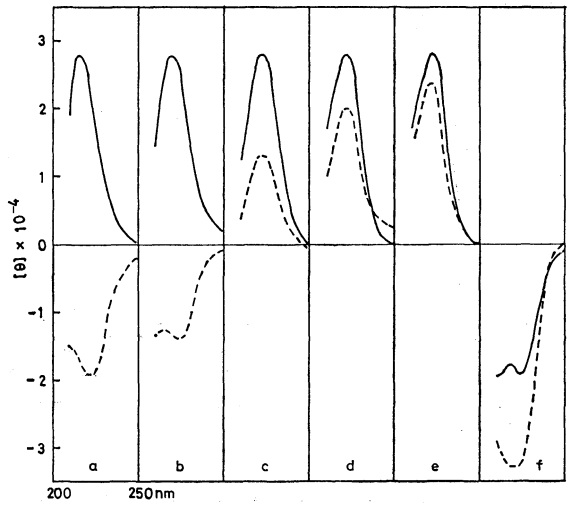

Fig. 7. CD spectra associated with the amide n-π^* transition before (——), and after (– – –) irradiation in 1,2-dichloroethane for the polymers which undergo light-induced conformational changes. a, b; *para* Copolymers with azo residues of 81 and 59% respectively. c, d, e; *meta* Copolymers with azo residues of 100, 92, and 67% respectively. f; Copolymer of *β-m*-(phenylazo)benzyl L-aspartate and γ-benzyl L-glutamate (89: 11).

Photoirradiation causes significant changes in the side-chain CD bands of the *para* copolymers. The dichroic band associated with the π-π^* transition vanishes. On the other hand, a positive band appears in the region of the n-π^* transition. The complete disappearance of the π-π^* CD band, in spite of the presence of about 20% *trans* isomers in the photostationary state, indicates the importance of *trans-trans* side-chain interactions for this CD band. The intensity of the azo n-π^* transition after irradiation does not depend on the content of azo residues in the copolymers (Fig. 4), which assumes side chain-main chain interactions as the origin of this band.

The CD spectra associated with the peptide n-π^* transition of the polymers which undergo light-induced conformational changes are summarized in Fig. 7. The spectral changes induced by irradiation can be classified into three types; left-handed to right-handed helix (*para* copolymers with azo residues of 59 and 81%), left-handed helix to random coil (*meta* copolymers with azo residues of 100, 92, and 67%) and random coil to right-handed helix (copolymer of *β-m*-(phenylazo)benzyl L-aspartate and γ-benzyl L-glutamate; 89: 11). We cannot obtain the spectra of pure *cis* azoaromatic polypeptides since 100% conversion could not be attained in our experimental conditions (about 80% *cis* in the photostationary state). Thus the conformational changes cannot be regarded as those occurring between pure *trans* and pure *cis* polypeptides.

TABLE 1. CD SIGNS OF THE SIDE-CHAIN n-π^* AND π-π^* BANDS[a]

Copolymer series[b]	Helix sense	Before irradiation		After irradiation
		n-π^*	π-π^*	n-π^*
meta	right	−		−
meta	left	+		+
para	right	−	−	+
para	left	+	+	+

a) Signs for the copolymers showing exciton resonance coupling are not included. b) Copolymer series of γ-benzyl L-glutamate with *β-m-* and *p*-(phenylazo)-benzyl L-aspartate are also designated as *meta* and *para* copolymer series.

The signs of the side-chain CD bands are summarized in relation to the helical senses in Table 1. Konishi and Hatano showed that the CD signs of the α-band on aromatic side-chain chromophores in many ester derivatives of poly(glutamic acid) and poly(aspartic acid) are determined by the helical sense of polymers, positive for left-handed helices and negative for right-handed helices.[17] Concerning the (phenylazo)benzyl L-aspartate copolymers including copolymers with γ-benzyl L-glutamate, we also find that the CD signs of the side-chain n-π^* and π-π^* bands are determined by the backbone conformation of the polymers, positive for left-handed helices and negative for right-handed helices though some exceptions are present. Exceptional behavior is encountered for the *para* copolymers which show exciton resonance coupling and the right-handed *para* copoly-

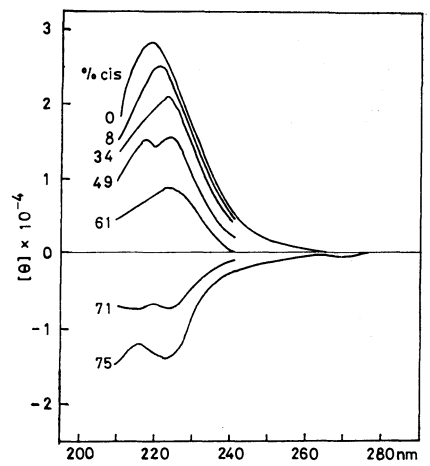

Fig. 8. CD Spectra of *para* copolymer with 59% azo residues at different *cis* contents in the course of relaxation.

mers after irradiation. So far there is no explanation for these exceptions.

The relaxation process back to the original state was studied for the *para* copolymer with 59% azo residues by CD spectra.[18] The CD spectra associated with the amide n-π^* transition change in a complicated manner in the course of relaxation (Fig. 8).[19] The behavior of the CD change can be attributed to the mixing of different conformations. After complete decay of the side-chain chromophores into the *trans* isomers the original CD spectrum was again obtained. The values of $[\theta]$ at 222 nm in the course of relaxation are plotted against the *cis* content (Fig. 9). It shows an abrupt change of $[\theta]_{222}$ at more than 50% *cis*. It should be noted that the transition is caused by variation in the ratio of different configurations of the side chains. The usual conformational transitions involving reversal in helix sense have been shown on copolymers composed of different amino acids such as β-benzyl L-aspartate and substituted benzyl L-aspartate by variation in the monomer ratios.[1] The present result demonstrates that the energy required for the conformational change comes

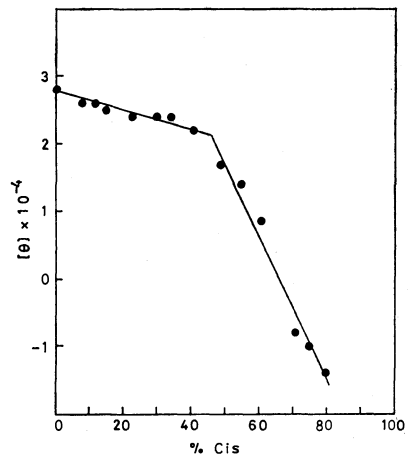

Fig. 9. Variation of $[\theta]$ values around 222 nm for *para* copolymer with 59% azo residues as a function of *cis* content.

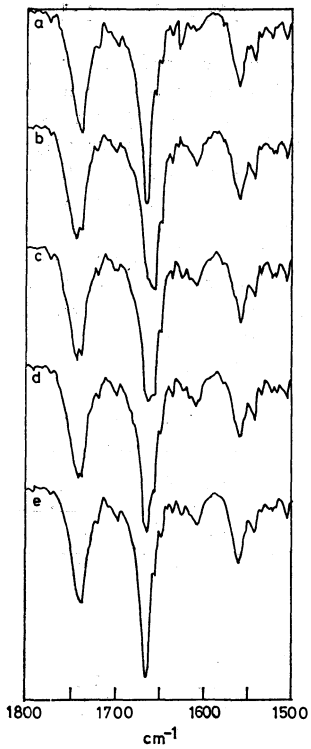

Fig. 10. Infrared spectra of the *para* copolymer with 59% azo residues before (a) and after (b; 0 min, c; 20 min, d; 50 min, e; 20 h) irradiation.

from *cis* forms in the side chain, or light energy.

The infrared spectra of the *para* copolymer with 59% azo residues in the course of relaxation are shown in Fig. 10. Before irradiation, the spectrum of the copolymer shows the amide I at 1665 cm^{-1}, the amide II at 1560 cm^{-1} and the ester carbonyl at 1738 cm^{-1} characteristic of left-handed α-helices.[1c] On the other hand, the spectrum after irradiation shows shifted bands, the amide I at 1655 cm^{-1}, the amide II at 1558 cm^{-1} and the ester carbonyl at 1744 cm^{-1}, characteristic of right-handed α-helices. In the spectrum, absorptions attributable to the left-handed helix remain as shoulders. Thus the polymer after irradiation is not purely right-handed helical but contains left-handed conformation. The spectrum after 20 min shows comparable absorption intensities of both helices. The spectrum is finally restored to the original one.

Conclusion

The light-induced reversal in polypeptide helix sense was observed for the *para* copolymers which contain more than 50% azo residues. The conformational change occurs abruptly at more than 50% *cis*. Thus, the light-induced conformational change enables the polypeptides to act as elements which response to light in an on-off fashion. The system as well as systems such as left-handed helix to random coil and random coil to right-handed helix can be compared with visual purple, rhodopsin. Return to the original state is promoted by an isomerase for rhodopsin, but occurs spontaneously in these systems.

Experimental

All polymers were prepared according to the procedure described previously[5] with various ratios of β-benzyl L-aspartate *N*-carboxy anhydride (NCA) and β-*m*- or *p*-(phenylazo)-benzyl L-aspartate NCA. Mole percentage of azo residues in the copolymers was estimated from their nitrogen contents obtained by elemental analyses. The reduced specific viscosity, η_{sp}/c, of each polymer was measured for a 0.1% 1,2-dichloroethane solution at 25 °C. Viscosity measurement could not be carried out for poly[β-*p*-(phenylazo)benzyl L-aspartate] and the *para* copolymer with 81% azo residues due to their poor solubility in 1,2-dichloroethane. The data on these polymers are summarized in Table 2.

Table 2. Yields and viscosities of azoaromatic polypeptides

Copolymer series	mol % azo NCA[a]	mol % azo residues[b]	Yield		η_{sp}/c[c]
			mg	%	
meta	10	9.7	235	54	1.13
meta	30	32	125	77	0.66
meta	50	49	65	63	0.44
meta	70	67	41	52	0.79
meta	90	92	28	42	0.23
meta	100	100	218	75	0.23
para	10	7.4	216	69	0.55
para	30	26	79	65	0.71
para	50	43	103	62	0.59
para	70	59	80	29	0.66
para	90	81	66	47	d)
para	100	100	63	61	e)

a) mol % of β-*m*- or *p*-(phenylazo) benzyl L-aspartate NCA reacted with β-benzyl L-aspartate NCA. b) Determined from the nitrogen content of elemental analysis. c) Measured for 0.1% 1,2-dichloroethane solutions at 25 °C. d) Almost insoluble. e) Insoluble.

Photoirradiation was carried out with a 500-W xenon lamp. A Corning 7-37 filter was used to pass the light of 320—380 nm. The *cis* content was calculated from the absorbance at 320 nm assuming that the absorbance is essentially proportional to the concentration of the *trans* isomer in view of the low extinction of the *cis* isomer for the wavelength.[20] Ultraviolet and visible spectra were measured with a JASCO UVIDEC-1 spectrophotometer using 3×10^{-5} M (azo residues) solutions. NMR spectra were recorded on a JEOL PS-100 spectrometer. Solutions of *ca.* 10 mg/ml were prepared in $CDCl_3$ containing tetramethylsilane as an internal reference. CD spectra were recorded on a JASCO J-20 circular dichrograph apparatus at 25 °C with cell thickness 0.1 and 0.01 cm using 0.3—1 mg/ml solutions. Due to the absorption of solvent, no spectra could be obtained below 210 nm. Molar ellipticities were calculated for the band around 222 nm by use of molar concentration of the amide group, while the molar concentration of the azo residues was used for the calculation of the ellipticities associated with the extrinsic bands. No CD spectrum of poly[β-*p*-(phenylazo)benzyl L-aspartate] could be measured due to its insolubility in 1,2-dichloroethane. As for the *para* copolymer with 81% azo residues, soluble part was used. On the irradiated solutions, special care was taken in order to accomplish the spectral measurements quickly.

References

1) (a) M. Hashimoto and J. Aritomi, *Bull. Chem. Soc. Jpn.*, **39**, 2707 (1966); (b) M. Hashimoto, *ibid.*, **39**, 2713 (1966); (c) M. Hashimoto and S. Arakawa, *ibid.*, **40**, 1698 (1967); (d) C. Toniolo, M. L. Falxa, and M. Goodman, *Biopolymers*, **6**, 1579 (1968); (e) M. Goodman, C. M. Deber, and A. M. Felix, *J. Am. Chem. Soc.*, **84**, 3773 (1962); (f) J. B. Aragao and M. H. Loucheux, *J. Chim. Phys.*, **1974**, 1578; (g) D. F. Bradley, M. Goodman, A. Felix, and R. Records, *Biopolymers*, **4**, 607 (1966); (h) M. Goodman, A. M. Felix, C. M. Deber, A. R. Brause, and G. Schwartz, *Biopolymers*, **1**, 371 (1963); (i) M. H. Loucheux and C. Duflot, *Biopolymers*, **14**, 469 (1975).

2) E. H. Erenrich, R. H. Andreatta, and H. A. Sheraga, *J. Am. Chem. Soc.*, **92**, 1116 (1970).

3) M. Goodman and M. L. Falxa, *J. Am. Chem. Soc.*, **89**, 3863 (1967).

4) Y. Kadoma, A. Ueno, K. Takeda, K. Uno, and Y. Iwakura, *J. Polym. Sci., Polym. Chem. Ed.*, **13**, 1545 (1975).

5) A. Ueno, J. Anzai, T. Osa, and Y. Kadoma, *Bull. Chem. Soc. Jpn.*, **50**, 2995 (1977).

6) A. Ueno, J. Anzai, T. Osa, and Y. Kadoma, *J. Polym. Sci., Polym. Lett. Ed.*, **15**, 407 (1977).

7) F. Gerson, E. Heibronner, A. van Ween, and B. M. Wepster, *Helv. Chim. Acta*, **43**, 1889 (1960).

8) H. H. Jaffe, Y. Si-Jung, and R. W. Gerdner, *J. Mol. Spectrosc.*, **2**, 120 (1958).

9) D. W. Urry, *Ann. Rev. Phys. Chem.*, **19**, 477 (1968).

10) Goodman *et al.* prepared some azoaromatic polypeptides composed of (phenylazo)phenylalanine or its analogues, and observed the spectra around 222 nm significantly perturbed from those typical for α-helices due to the overlapping of transitions of the side-chain chromophores with those from the peptide backbone. (a) M. Goodman and A. Kossoy, *J. Am. Chem. Soc.*, **88**, 5010 (1966); (b) M. Goodman and E. Benedetti, *Biochemistry*, **7**, 4226 (1968); (c) E. Benedetti, A. Kossoy, M. L. Falxa, and M. Goodman, *ibid.*, **7**, 4234 (1968); (d) E. Benedetti and M. Goodman, *ibid.*, **7**, 4242 (1968).

11) E. M. Bradbury, B. G. Carpenter, C. Crane-Robinson, and H. Goldman, *Macromolecules*, **5**, 557 (1971); (b) L. Paolillo, P. A. Temussi, and E. Trivellone, *Biopolymers*, **10**, 2555 (1971); (c) L. Paolillo, P. A. Temussi, E. M. Bradbury, and C. Crane-Robinson, *ibid.*, **11**, 2043 (1972).

12) The appreciable shift from 222 nm to the shorter wavelength for the para copolymer with 81% azo residues suggests that it takes a perturbed conformation of the left-handed α-helix.

13) G. Holzwarth and P. Doty, *J. Am. Chem. Soc.*, **87**, 218 (1965).

14) The [θ] values of the side-chain CD bands of the *para* copolymer with 59% azo residues reported[7] differ from those given here since the values in this paper are calculated based on the molar concentrations of the azo residues.

15) (a) W. Moffitt, *Proc. Natl. Acad. Sci. U. S. A.*, **42**, 736 (1956); (b) M. Kasha, *Radiat. Res.* **20**, 55 (1963); (c) W. Rhodes, *J. Am. Chem. Soc.*, **83**, 3609 (1961).

16) The precipitous appearance of the exciton resonance coupling on increasing azo residues might indicate that the azo residues are not distributed at random in the copolymers with high azo residues.

17) Y. Konishi and M. Hatano, *J. Polym. Sci., Polym. Lett. Ed.*, **14**, 351 (1976).

18) The half-life of this copolymer is 730 min at 40 °C starting from the photostationary state.

19) No time parameter is given in Fig. 8 since the solution is occasionally warmed for the convenience of measurements covering wide *cis* percentages.

20) C. S. Paik and H. Morawetz, *Macromolecules*, **5**, 171 (1972).

The Partial Reduction of Carboxylic Acids to Aldehydes *via* 3-Acylthiazolidine-2-thiones with Diisobutylaluminum Hydride and with Lithium Tri-*t*-butoxyaluminum Hydride

Toshio IZAWA and Teruaki MUKAIYAMA*

Department of Chemistry, Faculty of Science, The University of Tokyo, Hongo, Bunkyo-ku, Tokyo 113

(Received August 31, 1978)

3-Acylthiazolidine-2-thiones, easily prepared from carboxylic acids and readily available thiazolidine-2-thione, were reduced to the corresponding aldehydes either with diisobutylaluminum hydride in toluene at −78—−40 °C in 70—90% yields or with lithium tri-*t*-butoxyaluminum hydride in tetrahydrofuran at −20—0 °C in 80—90% yields. The present method appears to be applicable to the synthesis of aldehydes from both aromatic and aliphatic derivatives having chloro, bromo, nitro, and noncojugated double bond, except for the reduction of α,β-unsaturated derivatives with lithium tri-*t*-butoxyaluminum hydride and of cyano derivative with diisobutylaluminum hydride. Completion of the reduction is indicated by disappearance of the original yellow color of the reaction mixture.

One of the most convenient synthetic routes to aldehydes is the utilization of readily available carboxylic acids. Many methods have been reported for the partial reduction of such acid derivatives to the corresponding aldehydes by catalytic hydrogenation (the Rosenmund reduction) or by use of various hydride reducing agents. For example, carboxylic esters were converted into the corresponding aldehydes with aluminum hydride reagents, such as diisobutylaluminum hydride (DIBAH),[1a] sodium aluminum hydride,[1b] sodium bis(methoxyethoxy)aluminum hydride,[1c] and bis(dialkylamino)aluminum hydride.[1d] The partial reduction of various carboxamides was also carried out with lithium aluminum hydride,[1e] lithium di- and triethoxyaluminum hydride,[1f] or bis(dialkylamino)aluminum hydride.[1g] Moreover, the lithium tri-*t*-butoxyaluminum hydride (LTBA) reductions of acyl halides[1h] and of phenyl esters[1i] provided mild synthesis of aldehydes. The reduction is widely applied to the syntheses of natural products.[2] However, in most cases the desired aldehydes are often contaminated by further reduced products, *i.e.*, alcohol and/or amine.

In the preceding communications,[3,4] we reported preliminary results of the partial reduction of 3-acylthiazolidine-2-thiones **1** to aldehydes **2** with DIBAH or with LTBA. We now wish to describe the reaction in detail.

In order to determine the optimum conditions for the synthesis of 3-phenylpropanal (**2a**) from 3-(3-phenylpropionyl)thiazolidine-2-thione (**1a**), the effect of molar ratio of the reducing agents to **1a** was studied first. The reduction with the hydrides, DIBAH and LTBA, was carried out in toluene at −78—−40 °C, and in tetrahydrofuran (THF) at −20—0 °C, respectively. The results are summarized in Table 1.

Table 1. Effects of molar ratio[a] of reducing agent to **1**

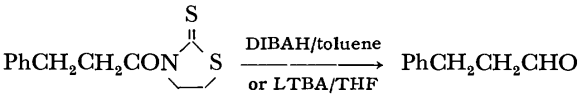

1a **2a**

DIBAH[b]			LTBA[c]		
Molar ratio	Mode of addn.[d]	Yield (%)[e]	Molar ratio	Mode of addn.[d]	Yield (%)[e]
1.2	N	91	1.1	N	87
1.2	R	85	1.15	N	89
1.5	N	93	1.2	R	85
2.1	N	90	2.4	N	57
4.0	N	69			

a) Hydride/**1a**. b) Reduction carried out at −78 °C for 0.25—4.5 h and then at −50—−40 °C for 1—1.5 h. c) Reduction carried out at −20 °C for 1—1.5 h and then at 0 °C for 1—4 h. d) N: normal addition (addition of **1a** in a solid state to hydride in solution); R: reverse addition (addition of DIBAH in solution or of LTBA in a solid state to **1a** in solution). e) Isolated yield by TLC (silica gel) or by distillation.

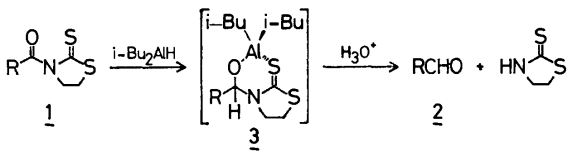

The table shows that no decrease in the yield of **2a** can be found with change in the molar ratio of DIBAH to **1a** from 1.2 to 2.1 equivalents. **2a** was isolated in 67% yield even when 4.0 equivalents of DIBAH were employed. The results are reasonably ratioalized by considering an aluminum-contained six-membered chelate intermediate **3** produced by the reaction of **1** with DIBAH. The chelate complex of the resulting aluminum alkoxide **3** is inert toward the further reduction under the reaction conditions. Thus, aldehyde **2** is liberated after quenching the reaction mixture with dilute acid. On the other hand, in the case of LTBA, employment of a slight excess amount of reducing agent gave the best results. The yield of **2a** decreased to 57% when 2.4 equivalents of LTBA were introduced. This is explained by assuming that the reduction of **1a** is much faster than that of **2a** generated in the reaction mixture before hydrolysis, in contrast with the case of DIBAH; the employment of excess LTBA causes the overreduction of **2a**. Moreover, longer reaction time and the mode of addition of the reactants did not significantly affect the yields of aldehydes. When a

stoichiometric amount of reducing agents was employed, the desired aldehyde was always contaminated with a small amount of starting material.

Thus, 3-acylthiazolidine-2-thiones **1** derived from representative carboxylic acids were converted into the corresponding aldehydes **2** with DIBAH by employing the optimum reduction conditions. In the case of DIBAH, when **1** is a solid mass, normal addition generally gave slightly better results than the reverse one (normal addition: **1** in a solid state added to DIBAH in toluene; reverse addition: DIBAH in toluene added to **1** in toluene). And when an oily substance, reverse addition gave better results than the normal one. On the other hand, in the case of LTBA, the mode of addition did not significantly affect the yields of aldehydes **2** (normal addition: **1** in a solid state added to LTBA in THF; reverse addition: LTBA in a solid state added to **1** in THF). The results are summarized in Table 2.

TABLE 2. PREPARATION OF ALDEHYDEES **2** IN THE REDUCTION OF 3-ACYLTHIAZOLIDINE-2-THIONES **1** WITH DIBAH AND WITH LTBA

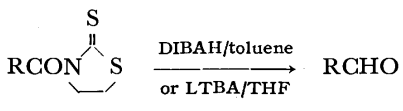

1 **2**

	R	DIBAH Mode of addn.	DIBAH Yield[a] (%)	LTBA Mode of addn.	LTBA Yield[a] (%)
a	$PhCH_2CH_2$	N[b]	93	N	89
		R[c]	85	R	(85)
b	$PhCH_2$	N	64	R	(69)[d]
c	CH_3CH_2PhCH	R	75	R	(86)
d	$PhCH_2CH_2CH_2$	N	90	N	86
e	$CH_3(CH_2)_{15}CH_2$	N	82	N	85[e]
f	$CH_2{=}CH(CH_2)_7CH_2$	R	74	R	(78)
g	$CH_3(CH_2)_3$-$(PhCH_2O)CH$	R	80	R	(91)[f]
h	$Br(CH_2)_9CH_2$	N	88	R	80
i	$NC(CH_2)_9CH_2$	N	—[g]	R	71
j	Ph	N	(49)	R	(83)
k	*p*-ClC_6H_4	N	84	N	86
l	*p*-$O_2NC_6H_4$	N	89	R	88
m	PhCH=CH	R	74	R	—[g]
n	*p*-$ClC_6H_4CH{=}CH$	N	70	R	—[g]

a) Isolated yield by TLC (silica gel). Numbers in parentheses indicate the yield by distillation. Bp (bath temp) °C/mmHg; **2a**: 120—140/20, **2b**: 105—135/24, **2c**: 110—130/21, **2f**: 130—140/30, and **2j**: 120—140/95. Bp of **2g**: 101—105 °C/0.9 mmHg. b) N: normal addition. c) R: reverse addition. d) Reaction carried out at −20 °C for 5 h. e) Reaction carried out at 0 °C for 4 h and then at room temp for 4 h. f) Reaction carried out at −40 °C for 2 h. g) Isolation of aldehydes not tried.

The yields of the reduction of 3-acylthiazolidine-2-thiones **1** to aldehydes **2** with DIBAH and with LTBA are generally good to high, *i.e.*, 70—90 and 80—90%, respectively, both in the cases of aliphatic and aromatic derivatives with a few exceptions. When the reduction of 3-(phenylacetyl)thiazolidine-2-thione (**1b**) with LTBA was carried out under similar conditions, only a polymerized product was obtained. Phenylacetaldehyde (**2b**) was isolated in 69% yield by keeping the reaction temperature −20 °C throughout the reduction. The α-benzyloxy derivative **1g** was very susceptible to the reduction with LTBA even at −40 °C to give 2-benzyloxyhexanal (**2g**) in 91% yield. The reduction of 3-(11-cyanoundecanoyl)thiazodine-2-thione (**1i**) with LTBA proceeded smoothly to afford 11-cyanoundecanal (**2i**) in 71% yield, but the same reaction was not observed with use of 1.2 equivalents of DIBAH and, when 2.2 equivalents of DIBAH were employed, 51% yield of dodecanedial was isolated. In the case of α,β-unsaturated derivatives, **1m** and **1n**, the reduction with LTBA gave no satisfactory results.

Various aldehydes possessing other substituents in the same molecules, such as bromo, chloro, nitro, and nonconjugated double bond, were easily obtained in good yields.

It is concluded that the present method is widely applicable to the partial reduction of various carboxylic acids *via* 3-acylthiazolidine-2-thiones, and the yields of the corresponding aldehydes are comparable or preferable to those of the conventional methods.[1] Further advantages of the present procedure is simplicity of the reaction, 3-acylthiazolidine-2-thione **1** being simply added to the reducing agent or *vice versa*, and that the completion of the reaction is clearly indicated by disappearance of the original yellow color of the reaction mixture.

Experimental

General. Melting and boiling points are uncorrected. ^1H NMR spectra were recorded on a Hitachi R-24 spectrometer with Me_4Si as an internal standard. IR spectra were taken on a Hitachi EPI-G2 spectrophotometer. MS data were obtained on a Hitachi RMU-6L at 70 eV. CH_2Cl_2 was dried over P_2O_5, distilled over CaH_2, and stored over molecular sieves 4A. Toluene was distilled over Na and then stored over molecular sieves 4A. THF was distilled over Na, followed by redistillation over $LiAlH_4$ before use.

DIBAH was synthesized by the pyrolysis of *i*-Bu_3Al according to the procedure of Ziegler *et al.*[5] LTBA was prepared from $LiAlH_4$ and *t*-BuOH according to a similar method of Brown and McFarlin.[6]

Reduction was carried out under argon atmosphere, all the apparatus being dried before use.

Materials. Acyl chlorides were either obtained commercially or synthesized from carboxylic acids and $SOCl_2$ according to standard methods.

*Preparation of 3-Acylthiazolidine-2-thiones **1a**—**1n**.* **A**: A CH_2Cl_2 (5 ml) solution of acyl chloride (20 mmol) was added dropwise to an ice-cooled, stirred CH_2Cl_2 (20 ml) suspension of thiazolidine-2-thione (2.38 g, 20 mmol) and Et_3N (2.12 g, 21 mmol) over the period of 1 h. The resulting mixture was stirred at room temperature for 1 h, and then washed with H_2O and brine, the organic layer being dried (Na_2SO_4) and concentrated. Purification of the products **1a**—**n** was accomplished by recrystallization or by column chromatography on silica gel using PhH as an eluent: yields 80—95%. The physical data for **1a**—**n** are given in Table 3.

Table 3. Physical data of 3-acylthiazolidine-2-thiones **1**

1	Mp °C	Found (Calcd), % C	H	N	S	X	IR ν_{CO} cm^{-1}	NMR δ($CDCl_3$)
1a	66.0—67.5 (CH_2Cl_2–Et_2O)[a]	57.59 (57.34	5.21 5.21	5.51 5.57	25.22 25.48)		1685	3.0 (t, J=7 Hz, 2H), 3.2 (t, J=7 Hz, 2H), 3.6 (t, J=7 Hz, 2H), 4.5 (t, J=7 Hz, 2H), 7.25 (s, 5H)
1b	84.5—85.5 (CH_2Cl_2–Et_2O)	55.38 (55.67	4.60 4.67	5.71 5.90	26.93 26.98)		1700	3.1 (t, J=7.5 Hz, 2H), 4.45 (t, J=7.5 Hz, 2H), 4.6 (s, 2H), 7.25 (s, 5H)
1c	oil	59.00 (58.88	5.77 5.70	5.39 5.28	23.94 24.13)		1700	0.85 (t, J=8 Hz, 3H), 1.5—2.5 (m, 2H), 3.05 (t, J=7.5 Hz, 2H), 4.4 (t, J=7.5 Hz, 2H), 5.75 (t, J=7.5 Hz, 1H), 7.3 (s, 5H)
1d	85.5 (CH_2Cl_2–Et_2O)	59.05 (58.88	5.76 5.70	5.09 5.28	23.97 24.13)		1690	1.95 (m, 2H), 2.65 (m, 2H), 2.9—3.4 (m, 4H), 4.45 (t, J=7.5 Hz, 2H), 7.15 (s, 5H)
1e	54—63 (hexane)	65.94 (65.40	10.34 10.19	3.76 3.63	16.26 16.60)		1705	0.8 (t, 3H), 1.25 (m, 30H), 3.2 (m, 2H), 3.25 (t, J=7 Hz, 2H), 4.55 (t, J=7 Hz, 2H)
1f	oil	59.08 (58.91	8.35 8.12	4.90 4.91	22.03 22.43)		1705	1.2—2.5 (m, 14H), 3.25 (t, J=7 Hz, 2H), 3.3 (t, J=8 Hz, 2H), 4.6 (t, J=8 Hz, 2H), 4.8 (m, 1H), 5.05 (m, 1H), 5.5—6.2 (m, 1H)
1g	oil	59.22 (59.41	6.71 6.54	4.54 4.33	20.09 19.80)		1705	0.9 (t, 3H), 0.9—2.1 (m, 6H), 3.15 (t, J=8 Hz, 2H), 4.4 (t, J=8 Hz, 2H), 4.5 (s, 2H), 5.75 (m, 1H), 7.3 (s, 5H)
1h[b]	66.0—66.5 (Et_2O–hexane)	45.03 (45.89	6.92 6.60	3.71 3.82	17.15 17.48	20.77 21.81)	1695	1.2—2.1 (m, 16 H), 3.1—3.6 (m, 6 H), 4.6 (t, J=7 Hz, 2H)
1i	75.5—76.5 (CH_2Cl_2–Et_2O)	57.88 (57.67	8.04 7.74	8.90 8.96	20.84 20.49)		1690	1.1—2.05 (m, 16 H), 2.35 (t, J=7 Hz, 2H), 3.25 (t, J=7 Hz, 2H), 3.3 (t, J=7 Hz, 2H) 4.6 (t, J=7 Hz, 2H)
1j	112.5—113.5 (CH_2Cl_2–Et_2O)	53.63 (53.79	4.09 4.06	6.26 6.27	28.30 28.68)		1675	3.4 (t, J=7 Hz, 2H), 4.5 (t, J=7 Hz, 2H), 7.2—8.0 (m, 5H)
1k	118.0—119.0 (CH_2Cl_2–Et_2O)	46.47 (46.60	2.97 3.13	5.40 5.43	24.56 24.88	13.86 13.75)	1680	3.4 (t, J=7 Hz, 2H), 4.5 (t, J=7 Hz, 2H), 7.3 (d, J=8 Hz, 2H), 7.7 (d, J=8 Hz, 2H)
1l	168.5—170.0 (THF–Et_2O)	45.00 (44.78	2.86 3.01	10.67 10.44	23.79 23.87)		1670	3.5 (t, J=7 Hz 2H), 4.55 (t, J=7 Hz, 2H), 7.75 (d, J=18 Hz, 2H), 8.25 (d, J=18 Hz, 2H)
1m	84.5—85.5 (CH_2Cl_2–Et_2O)	57.56 (57.81	4.30 4.45	5.60 5.62	25.56 25.68)		1670	3.3 (t, J=7 Hz, 2H), 4.55 (t, J=7 Hz, 2H), 7.4 (m, 5H), 7.65 (d, J=15.5 Hz, 1H), 7.95 (d, J=15.5 Hz, 1H)
1n	132.0—132.5 (CH_2Cl_2–Et_2O)	50.73 (50.79	3.41 3.55	5.13 4.94	22.57 22.57	12.98 12.49)	1670	3.4 (t, J=7 Hz, 2H), 4.6 (t, J=7 Hz, 2H), 7.45 (m, 5H), 7.55 (d, J=15 Hz, 2H), 7.9 (d, J=15 Hz, 1H)

a) Recrystallization solvents. b) MS, *m/e*, 367 and 365 (M^+), 249 and 247, 120, and 119.

Table 4. Spectrum data of aldehydes **2**

Aldehyde	IR ν_{CO} cm^{-1}	NMR δ(CCl_4)
2a	1730	2.5—3.0 (m, 4H), 7.15 (s, 5H), 9.7 (t, J=1.5 Hz, 1H)
2b	1730	3.5 (d, J=2.5 Hz, 2H), 7.2 (m, 5H), 9.6 (t, J=2.5 Hz, 1H)
2c	1730	0.85 (t, J=8 Hz, 3H), 1.85 (m, 2H), 3.3 (dt, J=2, 8 Hz 1H), 7.2 (m, 5H), 9.55 (d, J=2 Hz, 1H)
2d	1730	1.9 (m, 2H), 2.1—2.8 (m, 4H), 7.2 (s, 5H), 9.55 (t, J=1.5 Hz, 1H)
2e	1730	0.9 (t, J=6 Hz, 3H), 1.3 (m, 30H), 2.4 (m, 2H), 9.8 (t, J=1.5 Hz, 1H)
2f	1730	1.2—2.6 (m, 16H), 4.75 (br s, 1H), 5.0 (br d, 1H), 5.7 (m, 1H), 9.7 (br s, 1H)
2g	1730	0.9 (t, 3H), 0.9—1.9 (m, 6H), 3.6 (m, 1H), 4.4 (d, J=12 Hz, 1H), 4.65 (d, J=12 Hz, 1H), 7.25 (s, 5H), 9.55 (br s, 1H)
2h	1710	1.1—2.1 (m, 14 H), 2.35 (m, 2 H), 3.35 (d, J=6.5 Hz, 2H), 9.7 (t, J=1.5 Hz, 1H)
2i	1720	1.1—2.1 (m, 14H), 2.1—2.6 (m, 4H), 9.75 (t, J=1.5 Hz, 1H)
2j	1700	7.2—7.6 (m, 3H), 7.6—8.0 (m, 2H), 9.5 (s, 1H)
2k	1690	7.5 (d, J=8.5 Hz, 2H), 7.75 (d, J=8.5 Hz, 2H), 9.5 (s, 1H)
2l	1705	8.15 (d, J=8.5 Hz, 2H), 8.45 (d, J=8.5 Hz, 2H), 10.2 (s, 1H)[a]
2m	1680	6.45 (dd, J=16, 7.5 Hz, 1H), 7.4 (d, J=16 Hz, 1H), 7.4 (m, 4H), 9.7 (d, J=7.5 Hz, 1H)
2n	1690	6.6 (dd, J=16, 7.5 Hz, 1H), 7.4 (d, J=16 Hz, 1H), 7.4 (m, 4H), 9.7 (d, J=7.5 Hz, 1H)

a) $CDCl_3$ used as a sovent.

B: A CH_2Cl_2 (1 ml) solution of Et_3N (2.23 g, 22 mmol) was added at −20 °C to a stirred CH_2Cl_2 (20 ml) suspension of carboxylic acid (10 mmol), thiazolidine-2-thione (1.19 g, 10 mmol), and 2-chloro-1-methylpyridinium iodide (2.81 g, 11 mmol), and the mixture was stirred at room temperature for 1.5 h—overnight. The resulting mixture was washed with

H_2O, 1M HCl and brine, dried (Na_2SO_4), and evaporated. Purification of the products was performed by the method described above.

General Procedure for the Reduction with DIBAH. Normal Addition: 3-Acylthiazolidine-2-thione **1** (1.0 mmol) in a solid state was added in one portion to a stirred toluene (2 ml) solution of DIBAH (171 mg, 1.2 mmol) at −78 °C. The mixture was stirred for 0.25—2 h at this temperature, and then at −50—−40 °C till the yellow color of the reaction mixture disappeared (0.5—3 h). To the mixture were successively added 1M H_2SO_4 (*ca.* 0.5 ml), petroleum ether (*ca.* 20 ml) (or CH_2Cl_2 (*ca.* 20 ml) in the cases of **1i**, **1k**, **1l**, and **1n**), and Na_2SO_4 (*ca.* 1 g), and the resulting white precipitate was filtered off. The organic filtrate was dried (Na_2SO_4) and concentrated *in vacuo*, and the desired aldehyde **2** was purified by thin layer chromatography on silica gel using PhH and/or CH_2Cl_2 as a developing solvent.

Reverse Addition: A toluene solution (0.5 ml) of DIBAH (171 mg, 1.2 mmol) was injected to a stirred toluene (2 ml) suspension or solution of **3** at −78 °C, and the mixture was stirred at this temperature until completion of the reaction (1—2 h), followed by repetition of *Normal Addition* to give product **2**. The results and physical data for **2a**—**n** are given in Tables 2 and 3, respectively.

General Procedure for the Reduction with LTBA. Normal Addition: Crystalline **3** (1.0 mmol) was added at once to a stirred THF (2 ml) solution of LTBA (305 mg, 1.2 mmol) at −20 °C. The mixture was stirred for 0.5—5 h at this temperature and then at 0 °C until the orginal yellow color of the reaction mixture disappeared (0.5—7 h). After successive addition of 1M H_2SO_4 (*ca.* 0.5 ml), petroleum ether (*ca.* 20 ml) (or CH_2Cl_2 (*ca.* 20 ml) in the case of **1i**, **1k**, **1l**, and **1n**), and saturated Na_2SO_4 solution (*ca.* 0.5 ml), the organic layer was separated from the white pasty mass by decantation, dried (Na_2SO_4), and evaporated *in vacuo*. Thin layer chromatography of the residue on silica gel developed with PhH and/or CH_2Cl_2 gave aldehyde **2**.

Reverse Addition-A: Powdered LTBA (305 mg, 1.2 mmol) was added in one portion to a stirred THF (2 ml) solution or suspension of **3** (1.0 mmol) at −20 °C, followed by repetition of the procedure described above to afford compound **2**.

Reverse Addition-B: The preceding reaction was repeated with use of LTBA (1.53 g, 6.0 mmol), **3** (5.0 mmol), and THF (10 ml). After completion of the reaction, 1 M H_2SO_4 (*ca.* 2 ml), petroleum ether (*ca.* 80 ml), and saturated Na_2SO_4 solution (*ca.* 4 ml) were successively added to the resulting mixture, and the organic layer was decanted, washed with H_2O and brine, and dried (Na_2SO_4). Removal of the solvent *in vacuo*, followed by short-path distillation of the residual oil afforded aldehyde **2**. The results are given in Table 2, the physical data being identical with those of **2** prepared by the reduction with DIBAH.

References

1) a) L. I. Zakharkin and I. M. Khorlina, *Tetrahedron Lett.*, **1962**, 619; b) L. I. Zakharkin, V. V. Gavrilenko, D. N. Maslin, and I. M. Khorlina, *Tetrahedron Lett.*, **1963**, 2087; c) J. Vit, *Org. Chem. Bull.*, **42**, 1 (1970) [*Chem. Abstr.*, **74**, 99073 (1971).]; d) M. Muraki and T. Mukaiyama, *Chem. Lett.*, **1975**, 215, and references therein; e) H. A. Staab and H. Baunling, *Justus Liebigs Ann. Chem.*, **654**, 119 (1962); f) H. C. Brown and A. Tsukamoto, *J. Am. Chem. Soc.*, **86**, 1089 (1964), and references therein; g) M. Muraki and T. Mukaiyama, *Chem. Lett.*, **1975**, 875, and references therein; h) H. C. Brown and B. C. S. Rao, *J. Am. Chem. Soc.*, **80**, 5377 (1958), and references therein; i) P. M. Weismann and H. C. Brown, *J. Org. Chem.*, **31**, 283 (1966), and references therein.

2) For example, C. Szantay, L. Toke, and P. Kolopits, *J. Org. Chem.*, **31**, 1337 (1966); R. Baudouy, P. Crabbe, A. E. Greene, C. Le Drian, and A. F. Orr, *Tetrahedron Lett.*, **1977**, 2973.

3) T. Izawa and T. Mukaiyama, *Chem. Lett.*, **1977**, 1443.

4) T. Izawa and T. Mukaiyama, *Chem. Lett.*, **1978**, 409.

5) K. Ziegler, H. G. Gellert, H. Lehmkuhl, W. Pfahl, and K. Zogel, *Justus Liebigs Ann. Chem.*, **629**, 11 (1960).

6) H. C. Brown and R. F. McFarlin, *J. Am. Chem. Soc.*, **80**, 5372 (1958).

Reduction of Some Sulfides and Ethers with Aromatic Rings by Electrochemically Generated Solvated Electrons

Mikio MIYAKE,* Yoshihiro NAKAYAMA, Masakatsu NOMURA, and Shōichi KIKKAWA

Department of Applied Chemistry, Faculty of Engineering, Osaka University, Yamadakami, Suita, Osaka 565

(Received June 23, 1978)

The reduction of some sulfides and ethers has been investigated in 0.5 M LiCl–HMPA solutions with and without alcohol (methanol, ethanol, and 2-propanol). Diphenyl sulfide underwent cleavage to produce benzene as the main product. The hydrogenated products of benzene have been obtained in 35 and 50 mol % alcohol solutions, and the increased dependence on ethanol (*i.e.*, H^+) concentrations in the solutions has been established. The cleavage reaction was affected by the ease of α-hydrogen abstraction from the alcohol. The cleavage reaction has been elucidated as proceeding *via* a one-electron transfer mechanism, while the hydrogenation proceeded *via* a two-electron transfer mechanism. The estimation of current efficiencies supports this mechanism. Hexyl phenyl sulfide cleaved in the manner similar to that for diphenyl sulfide with a current efficiency of about 80% whereas only the hydrogenated products were obtained from benzo[*b*]thiophene and dibenzothiophene. Fission of the C–S bond of tetrahydrothiophene has been achieved by this method. Some ethers examined exhibited *approx.* the same behavior as the corresponding sulfides.

Aromatic clusters have been effectively reduced in hexamethylphosphoric triamide (HMPA)–ethanol solutions by electrochemically generated solvated electrons;[1–4] cyclohexane,[2] dihydronaphthalene,[3] and cyclooctane[4] were obtained mainly from benzene, naphthalene, and cyclooctadiene, respectively. The solvent system with HMPA and proton donor appears to provide the most strongly reducing conditions which cannot be achieved by ammonia and amine solvents.[5] Itoh *et al.* have reported the cleavage reactions of aryl decyl ethers in alkali metal–HMPA–THF systems.[6] From these reports, it appears that the solubilization of pitch and coal is efficiently conducted in HMPA solutions by solvated electrons in a manner similar to Benkeser reductions[7] and reductive alkylations.[8]

Prior to the investigation of the reactions of pitch and coal, it is necessary to obtain fundamental information about the reactions using model substances, *i.e.*, the factors which influence the two competitive reactions (the hydrogenation of aromatic clusters and the cleavage of C–X bonds where X denotes oxygen and sulfur atoms) and the reaction mechanisms. To this end, the reduction of some sulfides and ethers which contain aromatic rings has been performed using electrochemically generated solvated electrons in 0.5 M lithium chloride–HMPA solutions with and without alcohol. The reduction of diphenyl sulfide has been investigated thoroughly, since diphenyl sulfide is considered to be the simplest compound containing both aromatic rings and C–X (X: O, S) bonds.

In the investigation, the solvated electrons have been generated electrochemically, since this method achieves the desired rate and amount of solvated electrons easily by controlling the electrolytic current and the quantity of electricity passed, respectively. This feature is a great advantage for mechanistic investigations.

Experimental

Reagents. HMPA was dried on calcium oxide under vacuum and subsequently distilled from calcium hydride at 267 Pa. The middle fraction collected was then stored over molecular sieves 3A in a desiccator containing diphosphorus pentoxide. Methanol, ethanol, and 2-propanol were distilled from magnesium powder activated with iodine, and stored in the same manner as HMPA. The second distillation of the solvents was conducted prior to use. Lithium chloride was dried at 200 °C for 6 h prior to use.

Reactants such as diphenyl sulfide, benzo[*b*]thiophene, dibenzothiophene, tetrahydrothiophene, diphenyl ether, dibenzofuran, and tetrahydrofuran were obtained commercially. Isobenzofuran[9] and hexyl phenyl sulfide[10] were synthesized according to the general procedures. Dibenzothiophene and dibenzofuran were purified by recrystallization from methanol, and the others by distillation. The purity was checked by GLC.

Apparatus. The electrolytic vessel was a special H-type cell of 30 cm^3 total capacity. On the side wall, there were gas outlets with taps and a connecting glass tube to maintain the pressure of gas between the two rooms.

Pt electrodes (1×1 and 3×3 cm) served as cathode and anode, respectively. Before use, they were dipped in saturated sodium hydroxide solution, aqua resia, washed with deionized water, and dried in a desiccator under vacuum.

To generate the solvated electrons, a constant current of 5 mA/cm^2 was supplied by a galvanostat (Hokuto Denko Co., HA-104). When high currents (25 and 50 mA/cm^2) were needed, a DC power supply (Yamabishi Electric Co., Ltd, YVR-550) was used in place of the galvanostat. A linear scanning unit (Hokuto Denko Co., LS-2D) and a HA-104 potentiostat were employed for cyclic voltammometry experiments. The voltammograms were recorded by an X-Y recorder (Yokogawa Electric Works Ltd., 3077). In this case, the potential was measured against Ag/0.1 M $AgClO_4$ in HMPA with a sweep rate of 3.3 mV/s.

Procedure. The preparation of the solution and the electrolysis were performed in a drybox containing diphosphorus pentoxide. The reactant (6 mmol) and HMPA or HMPA–alcohol solution (6 cm^3) containing 0.5 M lithium chloride was poured into each compartment of the cell and immediately the rubber stoppers with the electrodes and gas inlets were set. The cell was placed in a paraffin liquid bath containing Dry Ice and the temperature of the electrolyte maintained at 15 °C. Before electrolysis, dried nitrogen gas was bubbled through the cell for about 30 min, and then the cell was sealed and the catholyte agitated with a magnetic stirrer. The electrolysis was performed with a constant current of 10 mA for 18 h, except when specified otherwise. The amount of electricity passed was checked by a copper coulomb meter. During electrolysis, the cathode potential was not measured, since it was reported as reasonably constant

in a similar system.[2]

Analyses of Products. The products were analyzed mainly by GLC without any treatment. The GLC analyses were performed on a Shimadzu GC-4BPTF with a 4.5 m × 3 mm column packed with 20% Silicone SE-30 on Uniport B. On occasion, GC-MS (GC: Hitachi M5201, column: Silicone OV-1 on Uniport KS, MS: Hitachi RMU-6MG) spectra were taken to identify the products. To obtain further information about the products, most of the catholytes were hydrolyzed by hydrochloric acid, and the aqueous solutions extracted with ether. The presence of lithium sulfide was examined by colorimetry using sodium pentacyanonitrosylferrate (III). Hydrogen sulfide and hydrogen gas were analyzed by GLC (Shimadzu GC-3AH with a 3 m × 3 mm column packed with Silica gel 60—80 mesh).

Results and Discussion

Cyclic Voltammometry. The electrolytic decomposition of ethanol in HMPA solution is thought to be suppressed by the preferential adsorption of HMPA on the electrode surface.[2] However, when the ethanol concentration becomes high, the ethanol decomposes, and the current efficiency for the generation of solvated electrons decreases. Therefore, in order to study the maximum alcohol concentration where the alcohol is not decomposed electrolytically, cyclic voltammograms were measured on the Pt electrode in 0.5 M lithium chloride–HMPA–ethanol solution with various ethanol concentrations, and the results are given in Fig. 1. The reduction waves at *approx.* −3.4 V *vs.* Ag/0.1 M Ag^+ are attributed to the generation of solvated electrons from the electrode, since the standard electrode potential of solvated electrons has been reported to be −3.4 V *vs.* Ag/0.1 M Ag^+ in HMPA,[12] and the solutions turned dark blue where the ethanol concentrations were less than 50 mol %.[1,13,14] When the ethanol concentration was increased up to 50 mol %, a further peak was observed at about −2.0 V. This peak became high in 67 mol % solution, and hydrogen gas evolved from the electrode surface in the potential region more negative than −1.5 V. This peak is apparently connected to the electrolytic decomposition of the ethanol.

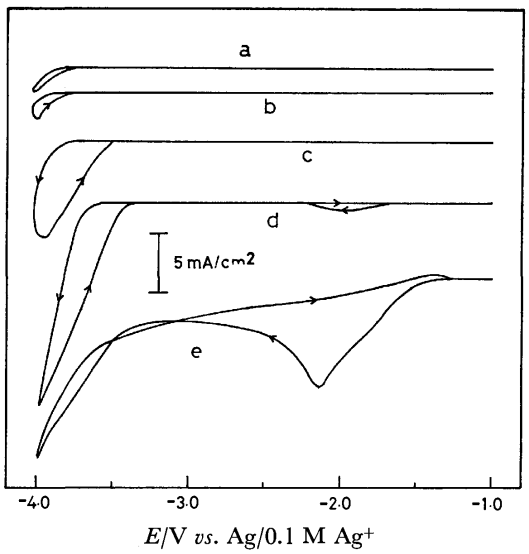

Fig. 1. Cyclic voltammograms on the Pt electrode in 0.5 M LiCl–HMPA–ethanol solutions. Ethanol concentration; a: 0, b: 14, c: 35, d: 50, and e: 67 mol %. Sweep rate: 3.3 mV/s.

On the basis of the above results, solutions with an alcohol concentration less than 50 mol % have been adopted for the following study. The detailed analysis of the cyclic voltammograms will appear in another report.

The cyclic voltammograms of solutions containing diphenyl sulfide gave the same pattern as in Fig. 1. Consequently, it was confirmed that no diphenyl sulfide was reduced electrolytically under the present experimental conditions.

Cleavage Reaction of Diphenyl Sulfide. Diphenyl sulfide was reduced by electrochemically generated solvated electrons. Tables 1 and 2 show the results in HMPA solutions with various ethanol concentrations and three types of 50 mol % alcohols, respectively. It should be remembered that in Table 2 the acidity of the alcohol, *i.e.*, the proton concentration in the solution decreased in the order, methanol > ethanol > 2-propanol, while the ease of α-hydrogen abstraction from the alcohol decreased in the reverse order.[15] It was found from Tables 1 and 2 that benzene was formed as the main product indicating that the cleavage reaction proceeded in preference to the hydrogenation of the aromatic ring of diphenyl sulfide.

Several reports have appeared on the cleavage reaction of diphenyl sulfide by solvated electrons.[16,17] Based on these reports, the following three reactions are possible for the present system:

$$\mathrm{Ph\text{–}S\text{–}Ph} + e^-_{solv} \longrightarrow [\mathrm{Ph\text{–}S\text{–}Ph}]^{\cdot-} \xrightarrow{e^-_{solv}} \mathrm{Ph}^- + {}^-\mathrm{S\text{–}Ph}, \quad (1)$$

Table 1. Reduction products of diphenyl sulfide in HMPA–ethanol solutions

Ethanol concn, mol%	Yield of product, %						Conv.,[g] %	Total current efficiency,[g] %
	PhH[a]	1,4-CHD[b]	1,3-CHD[c]	CHE[d]	PhPh[e]	Others[f]		
50	32.7	10.3	1.6	1.3	tr	0.8	46.4	67.2
35	42.1	8.2	1.1	1.1	tr	3.2	54.3	69.6
14	65.1	0.0	0.0	0.0	1.8	0.0	66.9	61.4
0	84.8	0.0	0.0	0.0	1.8	2.4	88.9	79.4

a) Benzene. b) 1,4-Cyclohexadiene. c) 1,3-Cyclohexadiene. d) Cyclohexene. e) Biphenyl. f) Alkylbenzenes (toluene and ethylbenzene), alkyl phenyl sulfides (methyl phenyl sulfide and ethyl phenyl sulfide), and dibenzothiophene. g) 6 mmol of diphenyl sulfide was used. Quantity of electricity passed was 648 Q.

Table 2. Reduction products of diphenyl sulfide in HMPA–alcohol solutions

Alcohol[a]	Yield of product,[b] %						Conv.,[c] %	Total current efficiency,[c] %
	PhH	1,4-CHD	1,3-CHD	CHE	PhPh	Others		
MeOH	24.8	9.8	tr	1.6	tr	1.9	36.8	56.4
EtOH	32.7	10.3	1.6	1.3	tr	0.8	46.4	67.2
i-PrOH	59.6	3.9	tr	tr	0.4	0.7	64.4	64.8

a) Concentration was 50 mol %. b) Notations of products are the same as in Table 1. c) Obtained by the same conditions as in Table 1.

$$\mathrm{Ph\text{–}S\text{–}Ph} + e^-_{solv} \longrightarrow [\mathrm{Ph\text{–}S\text{–}Ph}]^{\cdot} \longrightarrow \mathrm{Ph}\cdot + {}^-\mathrm{S\text{–}Ph} \quad (2)$$

$$\mathrm{Ph\text{–}S\text{–}Ph} + e^-_{solv} \longrightarrow [\mathrm{Ph\text{–}S\text{–}Ph}]^{\cdot} \longrightarrow \mathrm{Ph}^- + \cdot\mathrm{S\text{–}Ph} \quad (3)$$

where e^-_{solv} denotes the solvated electron.

The results in Tables 1 and 2 indicate that the higher the ethanol concentration and acidity of the alcohol, the lower the conversion and benzene yield. These results imply that the protons in the solutions have no effect on the rate of benzene formation. Moreover, Table 2 shows that both the benzene yield and conversion depend on the ease of α-hydrogen emission of the alcohol. It can therefore be presumed that benzene is formed mainly according to Eq. 2, followed by hydrogen abstraction by the phenyl radical from the solvent,

$$\mathrm{Ph}\cdot + \mathrm{RH} \longrightarrow \mathrm{PhH} + \mathrm{R}\cdot \quad (4)$$

where RH denotes the solvent (HMPA or alcohol). The detailed discussion of the further reaction of R· is beyond the scope of this paper.

Benzenethiol is expected *via* Eq. 2 as the pair product of benzene but remained undetected. It was detected quantitatively, however, after hydrolysis of the catholyte by hydrochloric acid. Since neither lithium sulfide nor hydrogen sulfide was detected in the products, the benzenethiolate formed by Eq. 2 is assumed to react with the lithium cation which is present in high concentration to produce lithium benzenethiolate.

The formation of biphenyl, as minor products (Tables 1 and 2), is attributed to the coupling of the phenyl radicals and supports the validity of the reaction mechanism *via* Eq. 2. Cleavage of diphenyl sulfide was reported to proceed also by Eq. 2 when it was cleaved by potassium metal in liquid ammonia.[17]

Estimation of current efficiencies demonstrates almost conclusively that the cleavage reaction proceeds *via* the one-electron mechanism (Eq. 2), since the current efficiency for the formation of benzene estimated by the two-electron mechanism (Eq. 1) sometimes exceeds 100 % despite an ionic reaction without the existence of a radical chain reaction.

Hydrogenation Reaction of the Aromatic Ring. As shown in Table 1, 1,4- and 1,3-cyclohexadiene and cyclohexene were produced in 35 and 50 mol% ethanol–HMPA solutions. These products are believed to be formed by hydrogenation of the benzene, since no hydrogenated product of diphenyl sulfide without cleavage was detected. The ratio of hydrogenated products to benzene was high in 50 mol % ethanol solution compared with that in 35 mol %. Moreover, as may be seen from Table 2, the ratio increased depending on the acidity of the alcohol used. Therefore, the hydrogenation of the benzene is considered to be proton associated.

Krapcho and Bothner-By proposed a hydrogenation mechanism for benzene as shown in Scheme 1, which was obtained from alkali metal–liquid ammonia–alcohol systems.[18] The results in Tables 1 and 2 may be interpreted by this mechanism. The mechanism has also been supported by the hydrogenation of some unsaturated hydrocarbons in HMPA–alcohol solutions by electrochemically generated solvated electrons.[1–3] The rate determining step in this reaction is considered to be Eq. 6, since the availability of the hydroxyl proton of the alcohol will be rather low due to formation of a hydrogenated complex between alcohol and HMPA, in a manner similar to that for ethylenediamine solution,[19] and the hydrogenation was affected by the concentration and the acidity of the alcohol adopted. The same rate determining step was proposed by Krapcho and Bothner-By.[18]

According to the present mechanism, the production of one cyclohexadiene molecule from diphenyl sulfide requires three solvated electrons, *i.e.*, one for cleavage of diphenyl sulfide (Eq. 2) and two for hydrogenation of the benzene produced (Eqs. 5 and 7). Similarly, one cyclohexene molecule consumes five electrons. The total current efficiencies thus estimated are listed in Tables 1 and 2.

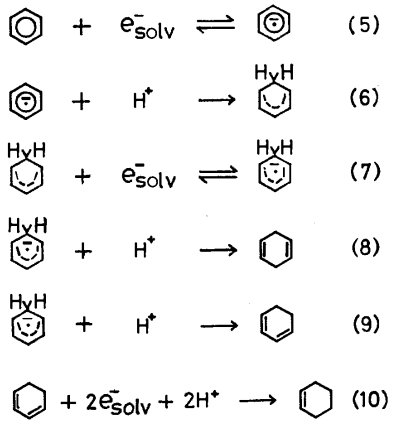

Scheme 1.

Effects of Current Density and Sulfide Concentration. Sternberg *et al.* proposed that the reduction rate of benzene by solvated electrons was proportional to benzene, solvated electron, and proton concentrations.[2] If a similar argument is applicable to the reduction of diphenyl sulfide, then the rate of cleavage of diphenyl sulfide is expected to increase when the concentration

Table 3. Effects of current density and diphenyl sulfide concentration on reduction of diphenyl sulfide[a)]

Current density, mA/cm²	Diphenyl sulfide, mmol	Yield of product,[b)] % PhH	1,4-CHD	1,3-CHD	CHE	Others	Conv.,[c)] %	Total current efficiency,[c)] %
5[d)]	6[d)]	32.7 (29.4)	10.3 (27.6)	1.6 (4.3)	1.3 (5.8)	0.8	46.4	67.2
25	6	44.6	6.6	2.2	1.6	0.6	55.3	67.2
50	6	35.5	6.9	0.9	1.1	0.1	44.4	58.4
5	12	30.2 (54.2)	0.5 (2.7)	0.0 0.0	tr (tr)	0.9	31.0	57.2

a) Solution: 0.5 M LiCl–HMPA–50 mol % EtOH. b) Notations of products are the same as in Table 1. Current efficiency is shown in the parenthesis. c) Quantity of electricity passed was 648 Q. d) Usual conditions.

of diphenyl sulfide and the generation rate of solvated electrons (*i.e.*, current density) are raised. Therefore, to establish the most suitable reaction conditions for the reduction of diphenyl sulfide, the reactions were carried out at various current densities and diphenyl sulfide concentrations, the results of which are summarized in Table 3. The conversion and benzene yield increased as expected when the current density was raised from 5 to 25 mA/cm². On the contrary, when the current density was raised to 50 mA/cm², the total current efficiency, the conversion, and the yield of benzene derivatives decreased, and a large amount of hydrogen gas was evolved—the generation mechanism has been discussed by Sternberg *et al.*[2)] It was found that a large increase in the current density such as 50 mA/cm² was not suitable for the reduction of diphenyl sulfide.

Doubling of the concentration of diphenyl sulfide produced a doubling of the current efficiency of benzene production (denoted in the parentheses in Table 3).

Reduction of Some Other Sulfides. In the case of diphenyl sulfide, the cleavage reaction proceeded preferentially compared to the hydrogenation under the present experimental conditions. This result, however, is not applicable to all sulfides having a phenyl group. Therefore, the reduction of some sulfides has been investigated in a similar manner, the results of which are given in Table 4 where the main products and current efficiencies are summarized. Products obtained after hydrolysis are designated in parentheses.

Table 4. Reduction products of some sulfides in HMPA solutions

Reactant	Hexyl phenyl sulfide	Benzo[*b*]-thiophene	Dibenzo-thiophene	Tetra-hydro-thiophene
Ethanol concn, mol %	0 50	0 50	0 50	0 50
Current efficiency of main product, %	*n*-C_6H_{14} 55.5 39.0 *n*-$C_{12}H_{26}$ 21.2 3.2 *n*-C_6H_{12} 2.8 0.0 PhH 0.7 0.4 (PhSH)[c)]	3,4-Di-hydro-benzo[*b*]-thiophene 0.0 53.8	2H-[a)] 0.0 3.6 4H-[b)] 0.0 7.6	*n*-BuSH 45.5 3.7 (*n*-Bu)$_2$S 10.2 4.8 *n*-BuSEt 0.0 4.2
Total current efficiency, %	80.2 42.6	0.0 53.8	0.0 11.2	55.7 12.7

a) Dihydro product. b) Tetrahydro product. c) Detected after hydrolysis.

Hexyl phenyl sulfide underwent cleavage in a similar manner to diphenyl sulfide, that is, the reduction was not accelerated in the presence of ethanol and benzenethiol was detected quantitatively after hydrolysis of the catholyte. The formation of hexane and the coupling of hexyl radicals as the main products suggests that β-cleavage took place predominantly (Eq. 11). The course

$$C_6H_{13}\overset{\beta}{-}S\overset{\alpha}{-}Ph \xrightarrow{e^-_{sol'v}} C_6H_{13}\cdot + {}^-S\text{–}Ph \qquad (11)$$

of cleavage of aryl decyl ethers by alkali metals was investigated in HMPA–THF solvents by Itoh *et al.* where it was suggested that highly polar solvents and small alkali metals favor β-cleavage.[6)] This suggestion is supported here.

In the case of benzo[*b*]thiophene and dibenzothiophene, only the hydrogenated products were obtained in 50 mol % ethanol–HMPA solution and in HMPA solution without ethanol, no reaction occurred. The C–S bonds of these sulfides are considered to be more stable than those of the alkyl phenyl and diphenyl sulfides. It has been reported that the hydrogenation of dibenzothiophene proceeds in preference to the cleavage of C–S bonds when reduced in ethylenediamine by

Table 5. Reduction products of some ethers in HMPA solutions

Reactant	Diphenyl ether	Isobenzo-furan	Dibenzo-furan	Tetrahydro-furan
Ethanol concn, mol %	0 50	0 50	0 50	0 50
Current efficiency of main product,[a)] %	PhH 41.5 43.7 1,4-CHD 0.0 1.7 CHE 0.0 1.1 (PhOH)	3,4-di-hydro-benzo-furan 0.0 61.4	2H- 0.0 1.6 4H- 0.0 2.2	*n*-BuOH 0.0 11.5 *n*-BuOEt 0.0 8.8 *n*-C_4H_{10} tr 0.0
Total current efficiency, %	41.5 46.5	0.0 61.4	0.0 3.8	tr 20.3

a) Notations of products are the same as in Tables 1 and 4.

electrochemically generated solvated electrons, and that no sulfur was eliminated until partial hydrogenation of the aromatic ring had taken place.[20]

The reduction of tetrahydrothiophene was attempted to establish whether the cyclic sulfide can be cleaved by the present method. This compound was selected because it was considered the simplest representative of the completely hydrogenated thiophenes. As shown in Table 4, tetrahydrothiophene cleaved, although the current efficiencies were relatively low compared with those of the diphenyl and hexyl phenyl sulfides.

Reduction of Some Ethers. The reduction of some ethers was conducted to compare the behavior with that of the sulfides. The results in Table 5 show that the ethers were reduced in the same way as the corresponding sulfides. In the case of tetrahydrofuran in HMPA solution without ethanol, the high resistivity of the solution caused no appreciable reaction.

The authors would like to express their sincere thanks to Professor Hideo Tamura and Associate Professor Hiroshi Yoneyama at Osaka University for their helpful suggestions and assistance with the DC power supply and linear scanning unit. The present work was partially supported by a Grant-in-Aid for Scientific Research from the Ministry of Education.

References

1) H. W. Sternberg, R. E. Markby, I. Wender, and D. M. Mohilner, *J. Am. Chem. Soc.*, **89**, 186 (1967).
2) H. W. Sternberg, R. E. Markby, I. Wender, and D. M. Mohilner, *J. Am. Chem. Soc.*, **91**, 4191 (1969).
3) T. Asahara, M. Seno, and H. Kaneko, *Bull. Chem. Soc. Jpn.*, **41**, 2985 (1968).
4) T. Asahara, M. Seno, T. Ibuki, and H. Asagahara, *Yukagaku*, **22**, 27 (1973).
5) L. A. Avaca and A. Bewick, *J. Chem. Soc., Perkin Trans. 2*, **1972**, 1709.
6) M. Itoh, S. Yoshida, T. Ando, and N. Miyaura, *Chem., Lett.*, **1976**, 271.
7) L. Reggel, R. Raymond, S. Friedman, R. A. Friedel, and I. Wender, *Fuel*, **37**, 126 (1968).
8) H. W. Sternberg and C. L. D. Donne, *Fuel*, **53**, 172 (1974).
9) M. Nakazaki, "Yūkikagōbutsu Gōseihō," Gihōdō, Tokyo (1966), Vol. 8.
10) D. J. Cram and G. S. Hammond, "Organic Chemistry," 2nd ed, McGraw-Hill, New York (1964), p. 253.
11) "Bunseki-kagaku Jikken," ed by Y. Uzumasa, Kagaku-dōzin, Kyoto (1965), p. 183.
12) Y. Kanzaki and S. Aoyagui, *J. Electroanal. Chem.*, **36**, 297 (1972).
13) J. M. Brooks and R. R. Dewald, *J. Phys. Chem.*, **72**, 2655 (1968).
14) R. Catterall, L. P. Stodulski, and M. C. Symons, *J. Chem. Soc., Inorg.*, **1968**, 437.
15) W. E. Truce and J. J. Breiter, *J. Am. Chem. Soc.*, **84**, 1621 (1962).
16) R. Gerdil and E. A. C. Lucken, *J. Chem. Soc.*, **1963**, 5444.
17) R. A. Rossi and J. F. Bunnett, *J. Am. Chem. Soc.*, **96**, 112, (1974).
18) A. P. Krapcho and A. A. Bothner-By, *J. Am. Chem. Soc.*, **81**, 3658 (1959).
19) J. R. Brandon and L. M. Dorfman, *J. Chem. Phys.*, **53**, 3849 (1970).
20) H. W. Sternberg, C. L. D. Donne, and I. Wender, *Fuel*, **47**, 219 (1968).

Thermodynamics of Steady States: "Resistance Change" Transitions in Steady-state Systems

R. J. TYKODI

Department of Chemistry, Southeastern Massachusetts University, North Dartmouth, Massachusetts 02747, U.S.A.

(Received August 1, 1977)

Some one-current steady-state systems showing a discontinuous change in flow resistance at a point of instability—forced vaporization of carbon tetrachloride, Bénard instability in a horizontal layer of fluid heated from below, Taylor instability in the Couette flow of a liquid between coaxial rotating cylinders—are analyzed from a thermodynamic point of view: the behavior of the rate of entropy production and of the local potential (thermokinetic potential) for the system at the point of instability is explored. A multi-current situation involving a flip-flop current *vs.* voltage relation for the flow of electric current across a porous charged membrane is also commented on briefly.

Continuing my studies[1-6] of the thermodynamics of steady-state systems, I examine here the thermodynamic properties of several one-current steady-state systems, each of which develops an instability in its flow behavior and undergoes a discontinuous change in flow resistance. The "resistance change" transition at a point of instability for a steady-state system is in some respects analogous[7-9] to a phase transition in a thermo-static system. I shall first briefly discuss the "resistance change" transition in general terms; and I shall then discuss specifically the forced vaporization of carbon tetrachloride, Bénard instability in a horizontal layer of fluid heated from below, and Taylor instability in the Couette flow of a liquid between coaxial rotating cylinders. Finally I shall comment briefly on a multi-current example showing a flip-flop current-voltage relation for the flow of electric current across a porous charged membrane.

1. General Considerations (One-current Situations). Consider a fluid in a state of thermo-static equilibrium characterized by the variables T_σ, P_σ, $\mu_\sigma^{(1)}, \cdots$—a fluid system in the equilibrium state σ, for short. Relabel the set of equilibrium state variables in the following fashion: $\{T_\sigma, P_\sigma, \mu_\sigma^{(1)} \cdots\} \equiv \{\sigma_1, \sigma_2, \sigma_3, \cdots\} \equiv \{\sigma_i\}$. By changing some of the boundary conditions, induce the steady flow of a current Y in the fluid system. Use the equilibrium state σ as a reference state; the current Y will then depend on the departure of variables of the type σ_i from their reference state values. For each state of steady current flow, the rate of entropy production $\theta \equiv \dot{S}$(system) $+\dot{S}$(surroundings) takes the form

$$\theta = Y\Omega \geq 0, \tag{1}$$

where Ω is the affinity[1] conjugate to the current Y; both Y and Ω measure, in a certain sense, the "distance" of the steady-flow state from the reference equilibrium state σ. In addition to the rate of entropy production, another thermodynamic concept, the local potential (also called the generalized entropy production or the thermokinetic potential[5,10,11])— first introduced by Glansdorff and Prigogine[7,12,13]— is of use in discussing "resistance change" transitions. When the Pfaffian differential form (for a one-current situation)

$$\mathrm{d}F_\sigma = Y\mathrm{d}\Omega \tag{2}$$

is integrable under the given experimental conditions, the resulting quantity F_σ is the local potential:[5,7,10-13]

$$F_\sigma = \int Y\mathrm{d}\Omega = \int_0^Y Y(\partial\Omega/\partial Y)_\sigma \mathrm{d}Y. \tag{3}$$

The local potential F_σ (when it exists) is never negative, has a minimum at the point where $Y=0$, and satisfies the condition

$$0 < (\partial^2 F_\sigma/\partial\Omega^2)_\sigma|_{Y=0} = (\partial Y/\partial\Omega)_\sigma|_{Y=0}. \tag{4}$$

Glansdorff and Prigogine[7,12,13] found the local potential concept to be very useful for discussing the temporal evolution of a system with fixed boundary conditions as it passed through a sequence of transient states toward some stable steady state. I discussed in an earlier paper[5] the role played by the local potential (thermokinetic potential) in thermodynamic analyses of *all steady state* situations. In this paper I am somewhat more interested in the behavior of the rate of entropy production at "resistance change" transitions than in the behavior of the local potential; I shall, however, keep both quantities in view.

Consider again a fluid system in the equilibrium state σ. By successive manipulations of the boundary conditions establish a series of steady-flow states in the system with monotonically increasing values of the current Y. Observe θ as Y increases. If the plot of θ *vs.* Y shows a jump or a kink — a point of discontinuity in θ or in $\partial\theta/\partial Y$ — we have a point of instability, a point at which the fluid system undergoes a "resistance change" transition. It is the thermodynamic properties of the fluid system at the point of instability that I intend to discuss — in macroscopic phenomenological terms.

Let $\partial\Omega/\partial Y$ be the (differential) flow resistance, let the subscript c refer to the point of instability, and let ΔZ be the jump in an arbitrary property Z at the point of instability, *i.e.* let $\Delta Z \equiv Z(Y_c+0) - Z(Y_c-0)$. We have then

$$\Delta\theta = Y_c\Delta\Omega, \tag{5}$$

$$\Delta\partial\theta/\partial Y = \Delta\Omega + Y_c\Delta\partial\Omega/\partial Y, \tag{6}$$

$$\Delta\partial^2\theta/\partial Y^2 = 2\Delta\partial\Omega/\partial Y + Y_c\Delta\partial^2\Omega/\partial Y^2, \tag{7}$$

$$\Delta\partial^m\theta/\partial Y^m = m\Delta\partial^{m-1}\Omega/\partial Y^{m-1} + Y_c\Delta\partial^m\Omega/\partial Y^m \quad (m = 2, 3, 4, \cdots). \tag{8}$$

In the canonical procedure, some parts of the boundary are maintained at the reference state values σ_i, and other parts are varied in condition so as to control the current Y. The partial derivatives in Eqs. 6—8

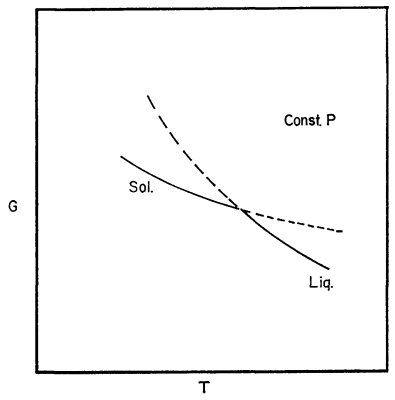

Fig. 1. Relative stability of the solid and liquid phases, at constant pressure, in a one-component system.

are thus at constant σ_i where appropriate.

"Resistance change" transitions in steady state systems are in some respects analogous[7-9] to thermostatic phase transitions where the phase with the lower Gibbs function value is the more stable one (see Fig. 1). Prigogine[7,8,12,13] considers the local potential F_σ to be the analog of the Gibbs function for "resistance change" transitions; for one-current steady-state situations there is no advantage in considering F_σ rather than θ, and I shall devote primary consideration to θ.

For stable steady states it is always true that[6,14]

$$\partial^2\theta/\partial Y^2 > 0, \quad \partial\Omega/\partial Y > 0; \tag{9}$$

and for "resistance change" transitions where both the upper ($Y > Y_c$) and lower ($Y < Y_c$) branches have metastable extensions beyond Y_c we anticipate that

$$\Delta\theta = 0, \quad \Delta\Omega = 0, \quad \Delta\partial\theta/\partial Y < 0, \tag{10}$$

i.e. we expect a kink in the θ *vs.* Y plot reflecting [Eq. 6] a discontinuous change in the flow resistance with $\Delta\partial\Omega/\partial Y < 0$: pipes spring leaks, vigorously rubbed paper tears, screwdrivers often shear the slotted heads of screws — in short, *processes usually take the path of least resistance.* If, however, the transition point is a point of intrinsic instability for one or both of the upper and lower branches, *i.e.* if one or both of the branches do not have metastable extensions beyond Y_c, then Eq. 10 must be modified — more about this later.

Rather than continuing in general terms, it will be better if we look at the special cases that we are interested in.

2. Forced Vaporization of Carbon Tetrachloride. Consider a pure liquid in equilibrium with its vapor in a glass cell in a thermostat of temperature T. Let P_0 be the equilibrium vapor pressure of the liquid at temperature T. Reduce the pressure of the vapor to a pressure $P < P_0$, and establish a steady rate of vaporization of the liquid:

$$\text{liquid}(T, P_0) \rightarrow \text{vapor } (T, P). \tag{11}$$

The rate of entropy production for the forced vaporization process[15] is

$$\theta = -\dot{G}/T = \dot{\xi}[(\mu_{liq} - \mu_{vap})T^{-1}] = Y\Omega, \tag{12}$$

where $\dot{\xi}$ is the reaction velocity (amount vaporized per unit time) for Reaction 11 and I have neglected

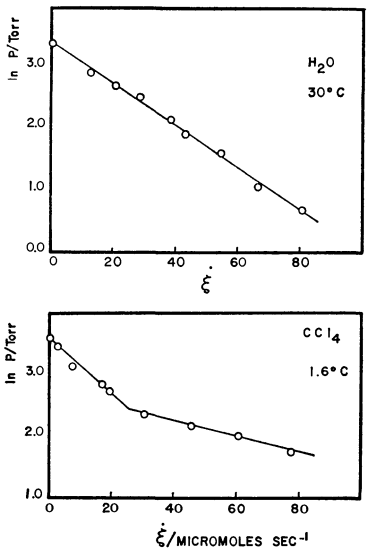

Fig. 2. Plots of $\ln P$ *versus* $\dot{\xi}$ for the steady forced vaporization of water at 30 °C and of carbon tetrachloride at 1.6 °C; P in Torr and $\dot{\xi}$ in μmol s^{-1}. Data of Alty and Nicoll.[17]

kinetic energy terms. Treating the vapor as an ideal gas $\{\mu_{liq} - \mu_{vap} = RT \ln (P_0/P)\}$ we have

$$\theta/R = \dot{\xi} \ln(P_0/P), \tag{13}$$

where R is the gas constant. Steady vaporization has been studied by Alty[15-17] and by Erikson;[15,18,19] nonsteady vaporization has been studied by Spangenberg and Rowland.[20]

Figure 2 shows the data of Alty and Nicoll[17] for the steady forced vaporization of water and of carbon tetrachloride; the current is given in micromoles per second and the pressure is measured in Torr. There is clear evidence in the carbon tetrachloride data for a discontinuous change in flow resistance at $\dot{\xi}_c = 25$ μmol/s; the two flow regimes show the following behavior:

$$\ln P = \ln P_0 - A\dot{\xi}, \qquad (0 \le \dot{\xi} \le \dot{\xi}_c), \tag{14}$$

$$\ln P = \ln P_* - B\dot{\xi}, \qquad (\dot{\xi}_c \le \dot{\xi}), \tag{15}$$

$$\theta/R = A\dot{\xi}^2, \quad F_\sigma/R = \frac{1}{2}A\dot{\xi}^2, \quad (0 \le \dot{\xi} \le \dot{\xi}_c), \tag{16}$$

$$\theta/R = B\dot{\xi}^2 + (A-B)\dot{\xi}_c\dot{\xi},$$

$$F_\sigma/R = \frac{1}{2}B\dot{\xi}^2 + \frac{1}{2}(A-B)\dot{\xi}_c^2, \quad (\dot{\xi}_c \le \dot{\xi}), \tag{17}$$

where $-A$ and $-B$ are the slopes of the two line segments and P_* is the intercept on the line $\dot{\xi} = 0$ of the (extrapolated) line segment with slope $-B$. Values for A and B, in seconds per micromole, are $A = 0.045$, $B = 0.013$. Figure 3 is a graph of $10^6\theta/R$ *vs.* $\dot{\xi}$ for the carbon tetrachloride data, calculated from Eqs. 16 and 17 after insertion of the appropriate numerical values of A, B, and $\dot{\xi}_c$. The dashed and dotted curves are potential hysteresis curves extending the observed behavior into unstable regions. We see that at the

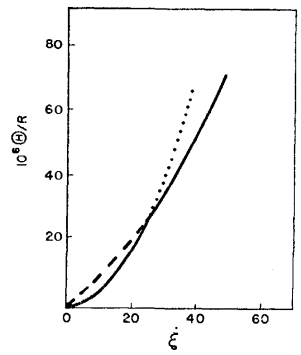

Fig. 3. Plot of $10^6\theta/R$ *versus* $\dot{\xi}$ for the steady forced vaporization of carbon tetrachloride at 1.6 °C. Data af Alty and Nicoll.[17]

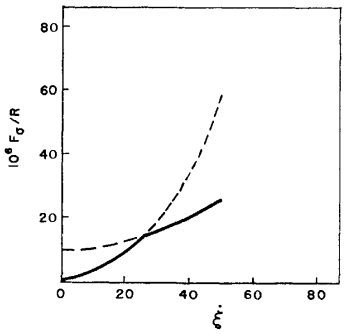

Fig. 4. Plot of $10^6F_\sigma/R$ *versus* $\dot{\xi}$ for the steady forced vaporiization of carbon tetrachloride at 1.6 °C. Data of Alty and Nicoll.[17]

transition point

$$\Delta\{\partial(\theta/R)/\partial\dot{\xi}\}_T = (B-A)\dot{\xi}_c < 0, \tag{18}$$

i.e. the discontinuous change is to a configuration of lower rate of entropy production.

Figure 4 shows that the behavior of the local potential F_σ at the transition point is somewhat similar to the behavior of θ: the branch with the lower value of F_σ is the more stable. In the case of F_σ, however, the metastable extension of the upper branch does not go through the origin of coordinates.[7]

In the carbon tetrachloride case, for fixed T, we have the transition point values θ_c, $\dot{\xi}_c$, P_c; if we repeat the experiment at another value of T we produce a new set of transition point values. In general then the thermodynamic data are the values of T, θ_c, $\dot{\xi}_c$, and P_c at the transition point (for a given apparatus configuration); and, from a thermodynamic point of view, we are interested in derivatives of the type $d\theta_c/d\dot{\xi}_c$, $d\dot{\xi}_c/dT$, $dP_c/d\dot{\xi}_c$, *etc.* Whereas in the somewhat analogous case of a phase transition in a thermo-static system we have the Clapeyron equation ($dP/dT = \Delta S/\Delta V$) to help us out in determining the slope of the phase coexistence line, in the present case we have no such useful general result.

2.1 Expectations and Queries: For the steady forced vaporization of carbon tetrachloride we have

$$\Delta\partial^2(\theta/R)/\partial\dot{\xi}^2 = 2(B-A) < 0, \tag{19}$$

$$\Delta\partial^n(\theta/R)/\partial\dot{\xi}^n = 0 \quad (n = 3, 4, 5, \cdots). \tag{20}$$

Equations 20 are consequences of the linear form of the given current-affinity relation; they, therefore, cannot be expected to have any *general* validity. Relation 19 will merit further investigation; is it generally true that

$$\Delta\partial^2\theta/\partial Y^2 < 0\ ? \tag{21}$$

The physics of the steady forced vaporization process supplies us with some reasonable expectations concerning the behavior of the transition point variables. If the dominant feature of the transition point is the temperature gradient in the liquid in the vicinity of the liquid-vapor interface, then, since the heat of vaporization is a decreasing function of the temperature, we expect to find that

$$d\dot{\xi}_c/dT > 0, \tag{22}$$

to establish the same sort of temperature gradient at a higher temperature we have to pump off the vapor faster because the heat of vaporization now has a lower value. Note that

$$\frac{d(\theta_c/R)}{dT} = \frac{d\dot{\xi}_c}{dT}(\ln P_0 - \ln P_c) + \dot{\xi}_c\left(\frac{d\ln P_0}{dT} - \frac{d\ln P_c}{dT}\right). \tag{23}$$

Now we expect the coefficient A in Eq. 14 to be a decreasing function of temperature,[15,18,19,21] so, given Eq. 22, $d\ln P_c/dT$ should be positive. It is conceivable, then, that $d\ln P_c/dT$ might be large enough to make the right hand side of Eq. 23 vanish, leading to the result that, for a given liquid and a given apparatus configuration,

$$\theta_c = \text{const.} \tag{24}$$

Relation 24 would imply, for this type of experiment, an intrinsic limit to the rate of entropy production that the initial liquid configuration could support; in order to pass beyond the critical rate of entropy production, the liquid would have to change its configuration. An observation analogous to this is that small droplets of liquid have an intrinsic limit (at low to moderate pressures) to the degree of superheat that they can sustain.[22]

If Relation 24 were found to hold, then it would follow that for forced vaporization

$$d\theta_c/dY_c = 0 \tag{25}$$

and, consequently, that

$$d\Omega_c/dY_c = -\Omega_c/Y_c < 0. \tag{26}$$

It is hard to see how Relation 26 could possibly be true, and in section 3 I show that it is very unlikely the Relation 24 can hold true.

The carbon tetrachloride data in Fig. 2 clearly show a "resistance change" transition; the studies of Spangenberg and Rowland[20] indicate that such behavior should regularly occur in forced vaporization experiments; yet the data for water in Fig. 2 and other published results of forced vaporization experiments[15,16,18,19] do not clearly show evidence of "resistance change" transitions. What controls the presence or absence of such transitions? I shall discuss this matter at the

end of the section on Bénard instability, but, to anticipate that discussion, what we need in forced vaporization experiments are a closer spacing of points in the ln P *vs.* $\dot{\xi}$ plots and more attention given to the depth of the liquid layer as an experimental parameter.

3. Bénard Instability. Sandwich a thin layer of fluid between two heat reservoirs (a, b) of temperatures T_a and T_b, with reservoir a above and b below the layer of fluid. By making $T_b \neq T_a$ we can generate a steady flow of heat through the fluid layer from one reservoir to the other. Characterize a reference thermo-static equilibrium state of the fluid by the variables T_a, P_a. Make T_b progressively larger than T_a. A sequence of states of steady heat flow results which ultimately shows an instability: thermal expansion causes the fluid to be less dense at the bottom of the layer than at the top— the layer becomes "top heavy;" eventually conductive heat flow gives way to convective heat flow. The sudden onset of a pattern of convective heat flow is referred to as the Bénard instability;[23,24] it is another example of a "resistance change" transition.

Let $T_b > T_a$ and let $\dot{Q}$ be the rate of influx of heat to the upper reservoir (reservoir a); take state a (T_a, P_a) as the reference state, then

$$\theta = Y\Omega = \dot{Q}\left(\frac{1}{T_a} - \frac{1}{T_b}\right) = \dot{Q}(T_b - T_a)/T_a T_b, \tag{27}$$

$$(\partial\Omega/\partial Y)_{T_a} = (1/T_b)^2[\partial(T_b - T_a)/\partial\dot{Q}]_{T_a}. \tag{28}$$

Schmidt and Milverton[25] immersed two circular brass plates, a fixed distance apart, into a tank of water. They passed a steady electric current I through a resistor of resistance ω affixed to the underside of the lower plate. If f is the fraction of the electrical energy dissipated per unit time by the resistor that passes directly from the lower plate to the upper one through the intervening layer of water, then

$$\dot{Q} = f\omega I^2, \tag{29}$$

$$\theta = \dot{Q}\left(\frac{1}{T_a} - \frac{1}{T_b}\right) = \frac{f\omega I^2(T_b - T_a)}{T_a T_b}, \tag{30}$$

$$T_0^2\theta/f\omega = I^2(T_b - T_a)(T_0^2/T_a T_b), \tag{31}$$

where T_0 is an additional reference temperature introduced for computational convenience. Figure 5 is a plot of $(T_b - T_a)(T_0^2/T_a T_b)$ *vs.* I^2, with $T_0 = 291$ K, of the data listed for Experiment 4 in the paper of Schmidt and Milverton;[25] the distance of separation between the plates was 5.5 mm. There is again clear evidence for a "resistance change" transition, and a plot of $T_0^2\theta/f\omega$ *vs.* I^2 would be qualitatively of the same shape as that of Fig. 3: at the point of transition the configuration of lower rate of entropy production is the more stable, and Relations 9, 10, and 21 are valid. Similarly a plot of $T_0^2 F_a/f\omega$ *vs.* I^2 would be qualitatively of the same shape as that of Fig. 4.

In the case of Bénard instability the thermodynamic variables characterizing the transition point are θ_c, $\dot{Q}_c$, $(T_a^{-1} - T_b^{-1})_c$ or $(T_b - T_a)_c$, T_a, and P_a (depending on the experimental setup, P_a may or may not be an independent variable). We are again interested in quantitites such as $\partial\theta_c/\partial\dot{Q}_c$, $\partial\Omega_c/\partial Y_c$, $\partial\dot{Q}_c/\partial T_a$, *etc.* We

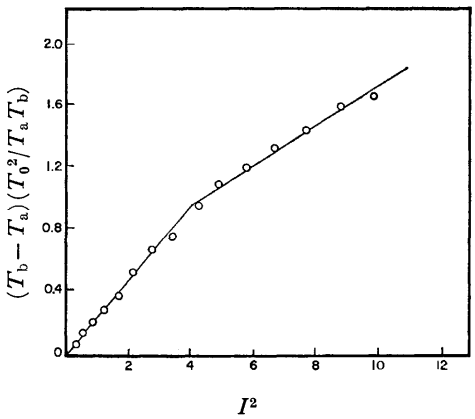

Fig. 5. Plot of $(T_b - T_a)(T_0^2/T_a T_b)$ *versus* I^2, with $T_0 = 291$ K. Data of Schmidt and Milverton.[25]

get some help from hydrodynamic stability theory[23] in this case. The (dimensionless) Rayleigh number $R_\#$ is defined to be

$$R_\# = g\alpha(T_b - T_a)\lambda^3/\kappa\nu, \tag{32}$$

where g is the gravitational acceleration, λ is the thickness of the fluid layer, and α, κ, and ν are the coefficients of volume expansion, thermometric conductivity, and kinematic viscosity, respectively. Stability theory[23] shows that at the point of Bénard instability

$$R_{\#c} = 1708. \tag{33}$$

In the conductive heat flow regime $\dot{Q} = D(T_b - T_a) \times \kappa\rho C_V/\lambda$, where D is the area through which the heat current flows, ρ is the density of the fluid, and C_V is the specific heat of the fluid; consequently

$$\theta_c \approx D(1708\nu/g\alpha T_a)^2(\kappa^3\rho C_V/\lambda^7), \tag{34}$$

where I have set $T_a T_b \approx T_a^2$. Since ν, α, κ, ρ, and C_V are all functions of the reference temperature T_a, the rate of entropy production θ_c for a given fluid with fixed values of D and λ, is apt to be a complicated function of T_a; and a relation such as Eq. 24 is not apt to be satisfied.

3.1 Forced Vaporization Reconsidered: With respect to the hydrodynamic stability of a layer of liquid, heating from below and cooling from above are much the same thing. The instability in the forced vaporization of carbon tetrachloride should thus be of the same nature as the Bénard instability, and the sensitivity of the Bénard instability to the thickness of the fluid layer [Eq. 32] indicates the advisability of treating the depth of the vaporizing liquid as an experimental variable in the forced vaporization case. (The forced vaporization problem is a more complicated one than the Bénard problem in that the temperature gradient in the vaporizing liquid has a complicated 3-dimensional structure[20] whereas the temperature gradient in the Bénard case is a simple 1-dimensional one.)

The data of Alty and Nicoll[17] displayed in Fig. 2 were all gathered in the same apparatus at the same fixed depth for the liquid layer. At the point of instability for the carbon tetrachloride the difference between the thermostat temperature T and the temperature T_s at the surface of the vaporizing liquid was $T - T_s = 7.5$ K. If we assume the geometric factors of

the two experiments displayed in Fig. 2 to be the same (same apparatus, same depth of liquid, same 3-dimensional structure for the thermal gradients) and if we scale the water data according to Eq. 33, relative to the carbon tetrachloride data, *i.e.* if we say that

$$[\alpha(T-T_s)/\kappa v]_{c,\ H_2O} = [\alpha(T-T_s)/\kappa v]_{c,\ CCl_4}, \qquad (35)$$

we find a predicted value of $T-T_s \approx 59$ K at the point of instability for water under the given experimental conditions at 30 °C — such a value is far outside the range of experimental conditions displayed in Fig. 2.

In Alty's other experiments[16] and in Erikson's experiments[18,19] the depth of the liquid layer was an uncontrolled variable, so the resulting data were not gathered in such a way as to highlight the onset of Bénard-type instability. Note that Erikson did see evidence of convection currents in some of his experiments.[18] As I mentioned previously, what is needed in forced vaporization experiments is strict control of the depth-of-liquid variable — and a closer spacing of experimental points in plots of $\ln P$ *vs.* $\dot{\xi}$ (for a fixed depth of liquid). Also, as I mentioned in my discussion of Eq. 34, Relation 24 is unlikely to have any validity whatsoever.

4. Taylor Instability. Place a sample of liquid between two coaxial cylinders; put the device in thermal communication with a thermostat of temperature T, and rotate one of the cylinders at a constant angular velocity γ by exerting on it a torque N. (The case of simultaneous rotation of both cylinders is also of interest, but I do not consider it in this paper.) The simple Couette flow between the cylinders ultimately becomes unstable at $\gamma=\gamma_c$, and toroidal Taylor vortices form at the point of instability[24,26-28] — another example of a "resistance change" transition. As in the previous case, the instability is correlated with the critical value of a dimensionless combination of fluid properties — the Taylor number.[26]

The rate of entropy production for a given angular velocity γ is

$$\theta = \gamma(N/T) = Y\Omega. \qquad (36)$$

To analyze the Taylor instability we need experimental data in the form of N *vs.* γ plots (plots of driving torque *versus* angular velocity) so as to be able to see discontinuities in N and/or $\partial N/\partial\gamma$ at $\gamma=\gamma_c$. The usual experimental procedure,[26-28] however, is to measure the torque on the *stationary cylinder* as a function of the angular velocity γ. The measurements of Donnelly[28] show a discontinuity in the torque on the stationary cylinder at γ_c, *i.e.* the fluid shows a discontinuous increase in apparent viscosity at the point of instability. What do these results imply concerning the variation of N with γ? Until we have some direct measurements or dependable calculations of the N, γ relationship, we cannot be sure of the implication; we can, however, explore some of the possibilities.

Suppose that the N, γ relation turns out to be similar in nature to the torque-on-the-stationary-cylinder, γ relation: suppose that $\Delta N\neq 0$, $\Delta\partial N/\partial\gamma>0$, and the configuration of *higher* rate of entropy production (and of higher local potential) is the more stable one beyond γ_c. What would be the thermodynamic implications of such a result? The idea here is to pursue the analogy to thermo-static phase transitions. If both phases have metastable regimes extending out beyond the transition point (Fig. 1, *e.g.*), then we are dealing with a problem of *relative stability* and the phase with the smaller Gibbs function value is the more stable. But it is also possible to have a phase transition point such that one of the phases reaches an *absolute limit of stability* at the transition point and has no metastable existence out beyond the transition point — the order-disorder transition in β-brass, for example.[29] For "resistance change" transitions, then, where each configuration has a metastable extension beyond the point of instability (in one direction or the other) the question of relative stability is decided by having the configuration of lower rate of entropy production (or lower local potential) more stable (Fig. 3, *e.g.*). But if a given configuration approaches an inflection point in the θ, Y plot, *i.e.* $\partial^2\theta/\partial Y^2$ approaches zero, it approaches an intrinsic limit of stability [see Eq. 9]: at the point where $\partial^2\theta/\partial Y^2=0$ the configuration must change to some other stable configuration; it is no longer a question of relative stability but an absolute requirement for a change of configuration. Under such circumstances $\Delta\partial\Omega/\partial Y$ could just as well be positive as negative, and we could even have a discontinuity in Ω (and F_σ): $\Delta\Omega\neq 0$ ($\Delta F_\sigma\neq 0$). The requirement for such a point of intrinsic instability would be

$$0 = \partial^2\theta/\partial Y^2 = 2(\partial\Omega/\partial Y) + Y_c(\partial^2\Omega/\partial Y^2), \qquad (37)$$

and we should have

$$Y_c = -2(\partial\Omega/\partial Y)/(\partial^2\Omega/\partial Y^2) \qquad (38)$$

as $Y\rightarrow Y_c-0$.

If the transition point is a point of intrinsic instability for both the upper ($Y>Y_c$) and lower ($Y<Y_c$) branches, we cannot say anything *a priori* about $\Delta\theta$ or $\Delta\partial\Omega/\partial Y$. If the transition point is a point of intrinsic instability for the lower branch and if the upper branch has a metastable extension below Y_c, then we can make the following observations relative to the transition point: i) it is not possible, under these circumstances, to have $\Delta\theta<0$ since the extension of the upper branch into the region $0\leq Y<Y_c$ would be more stable (would have a lower θ value) than the experimental lower branch; ii) it is not possible to have $\Delta\theta=0$ and $\Delta\partial\theta/\partial Y>0$ for the same reason as in i) — the extension of the upper branch into the region $0\leq Y<Y_c$ would be more stable than the experimental lower branch; iii) it is possible, but not likely, to have $\Delta\theta=0$ and $\Delta\partial\Omega/\partial Y<0$ — it is improbable to expect the lower branch to just "happen" to intersect the upper branch at the point of intrinsic instability; iv) it is possible, and likely, to have $\Delta\theta>0$ and either $\Delta\partial\Omega/\partial Y>0$ or $\Delta\partial\Omega/\partial Y<0$ — at the point of intrinsic instability it is highly probable that the lower branch will be some distance away from the upper branch, hence a jump discontinuity in θ (and in Ω) — and in F_σ — will occur, with no necessary restrinction on the sign of the change in slope $\Delta\partial\Omega/\partial Y$. Note that if $\Delta\partial\Omega/\partial Y>0$ then there *must* be a discontinuity in θ (and in Ω) — see Fig. 6.

If the N, γ relation for the Taylor instability proves to have $\Delta N\neq 0$ at $\gamma=\gamma_c$ the most likely explanation

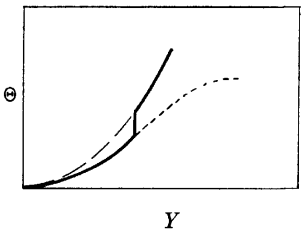

Fig. 6. Example: point of intrinsic instability with $\Delta\theta>0$ and $\Delta\partial\Omega/\Omega Y>0$.

will be that the transition point is a point of intrinsic instability for the lower branch. Points of intrinsic instability are special cases of the "bifurcations" and "catastrophes" discussed by Nicolis and Prigogine.[30]

5. A Multi-current Situation — Flip-Flop Current vs. Voltage Relation. Interpose a sintered glass membrane between aqueous sodium chloride solutions of concentrations 0.01 and 0.1 M; place inert electrodes on opposite sides of the membrane and impose a voltage $\Delta\phi$ between the electrodes; exert an excess pressure ΔP on the more concentrated solution. Keep the concentration difference and the pressure difference across the membrane fixed and measure the electric current I induced by the impressed voltage $\Delta\phi$. (Maintain the entire system at a constant temperature T.)

Let subscript 1 indicate water and subscript 2 indicate sodium chloride, and let a single prime designate the more concentrated solution and a double prime designate the less concentrated solution. Then, if the experiment is conducted in a steady-state fashion, we have[31]

$$T\theta = -(\dot{n}_1'\mu_1'+\dot{n}_2'\mu_2'+\dot{n}_1''\mu_1''+\dot{n}_2''\mu_2'') + I\Delta\phi, \tag{39}$$

and

$$\begin{aligned} T\theta &= \dot{n}_1'(\mu_1''-\mu_1') + \dot{n}_2'(\mu_2''-\mu_1') + I\Delta\phi \\ &= Y_1\Omega_1 T + Y_2\Omega_2 T + Y_3\Omega_3 T, \end{aligned} \tag{40}$$

since $\dot{n}_1'+\dot{n}_1''=0$ and $\dot{n}_2'+\dot{n}_2''=0$. If we treat the sodium chloride solutions as "ideal" we can say that

$$\begin{aligned} \mu_1' - \mu_1'' &= \int_{P''}^{P'} \overline{V}_1\,dP + RT\ln(X_1'/X_1'') \\ &= \langle\overline{V}_1\rangle\Delta P + RT\ln(X_1'/X_1''), \end{aligned} \tag{41}$$

$$\begin{aligned} \mu_2' - \mu_2'' &= \int_{P''}^{P'} \overline{V}_2\,dP + RT\ln(C_2'/C_2'') \\ &= \langle\overline{V}_2\rangle\Delta P + RT\ln(C_2'/C_2''), \end{aligned} \tag{42}$$

where X_i is the mole fraction, $\overline{V}_i$ the partial molar volume, $\langle\overline{V}_i\rangle$ the average partial molar volume over the pressure interval ΔP, and C_i the concentration (moles per liter) of component i. Let $\dot{n}_1'\langle\overline{V}_1\rangle+\dot{n}_2'\langle\overline{V}_2\rangle\approx\dot{V}'$ and evaluate X_1'/X_1'' by setting molarities approximately equal to molalities. Impose the restriction on $\dot{n}_1'$ and $\dot{n}_2'$ that they keep the ratio n_1'/n_2' constant (*i.e.* constant C_2'). Upon substitution of the appropriate numerical values, we get

$$T\theta \approx -\dot{V}'\Delta P - 1.4\,\dot{n}_2'RT + I\Delta\phi. \tag{43}$$

Experiments measuring the current-voltage relationship for this type of experiment were carried out by H. Jahnke and reported on by Franck.[32] Figure 7 shows the I *vs.* $\Delta\phi$ relation for various fixed pressure differences for one series of experiments carried out by Jahnke. The rather spectacular form of the I, $\Delta\phi$ relation is explained by Kobatake[8] in the following way: " ... under the external conditions studied here, the Poiseuille pressure flow transports fluid from the more concentrated to the less concentrated solution, while the electro-osmotic flow caused by the potential gradient tends to carry fluid in the opposite direction. With increasing $\Delta\phi$, the electro-osmotic flow becomes appreciable, outweighs the pressure flow, and eventually changes the direction of mass flow from negative to positive. Calculations show that this change of the direction of mass flow occurs discontinuously when $\Delta\phi$ reaches a certain value, when the pressure difference ΔP is larger than a critical value ΔP_c. Correspondingly, the average salt concentration in the membrane is lowered, *i.e.* the membrane is occupied with the less concentrated solution... The effect of this change in concentration in the membrane is reflected in the I *vs.* $\Delta\phi$ relationships depicted in [Fig. 7]."

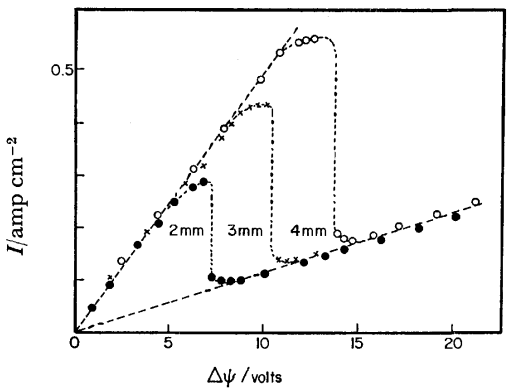

Fig. 7. Plots of I *versus* $\Delta\phi$ for the system of a sintered glass membrane and NaCl solutions of 0.01 and 0.1 M with various fixed pressure differences. Data of Jahnke as reported by Franck.[32]

The results reported by Franck[32] do not include data for $\dot{V}'$ and $\dot{n}_2'$ so we cannot actually calculate $T\theta$ for the experiment. It seems reasonable to expect, however, that at the critical value $\Delta\phi_c$ of the voltage $T\theta$ will actually show a discontinuous *decrease*. If such is indeed the case, it must be because the point $\Delta\phi=\Delta\phi_c$ is a point of intrinsic instability ($\partial^2\theta/\partial Y^2\to 0$) for *both* the upper ($\Delta\phi=\Delta\phi_c+0$) and lower ($\Delta\phi=\Delta\phi_c-0$) branches of the I *vs.* $\Delta\phi$ relation, *i.e. neither* branch has a metastable extension beyond the point $\Delta\phi=\Delta\phi_c$.

Kobatake[8] has analyzed Jahnke's experiments in terms of the local potential:

$$TF_\sigma = T\int\Sigma_i Y_i d\Omega_i = \int_0^{\Delta\phi} I d\Delta\phi + f(\Delta P, \Delta\mu_2). \tag{44}$$

By an elementary theorem of the calculus[33] the integral in Eq. 44 is continuous at the point $\Delta\phi_c$, so TF_σ does not have a discontinuity at the flip-flop point.

6. Summary. I have considered the behavior

of the rate of entropy production θ and the local potential F_σ for several one-current steady-state situations showing "resistance change" transitions — forced vaporization of carbon tetrachloride, Bénard instability, and Taylor instability. For these cases the behavior of the local potential is qualitatively similar to the behavior of the rate of entropy production. The complexity of the thermodynamic relations pertaining to the transition point depends upon whether the branches intersecting at the transition point have metastable extensions beyond that point. I also considered (briefly) a multi-current situation showing a flip-flop current-voltage relation at the transition point; here θ and F_σ seemingly show different kinds of behavior—F_σ is continuous at the transition point whereas θ appears to undergo a discontinuous change (it seems that *neither* of the branches intersecting at the transition point has a metastable extension beyond that point).

References

1) R. J. Tykodi, "Thermodynamics of Steady States," Macmillan, New York (1967).
2) R. J. Tykodi, *J. Chem. Phys.*, **47**, 1879 (1967).
3) R. J. Tykodi, *Am. J. Phys.*, **38**, 586 (1967).
4) R. J. Tykodi, *Bull. Chem. Soc. Jpn.*, **44**, 1001 (1971).
5) R. J. Tykodi, *J. Chem. Phys.*, **57**, 37 (1972).
6) R. J. Tykodi, *Physica*, **72**, 341 (1974).
7) "Non-Equilibrium Thermodynamics, Variational Techniques and Stability," ed by R. J. Donnelly, R. Herman, and I. Prigogine, University of Chicago Press, Chicago (1966), pp. 3—16.
8) Y. Kobatake, *Physica*, **48**, 301 (1970).
9) "Fluctuations, Instabilities, and Phase Transitions," ed by T. Riste, Plenum, New York (1975).
10) J. C. M. Li, *J. Appl. Phys.*, **33**, 616 (1962).
11) J. C. M. Li, *J. Phys. Chem.*, **66**, 1414 (1962).
12) P. Glansdorff and I. Prigogine, *Physica*, **30**, 351 (1964).
13) P. Glansdorff and I. Prigogine, "Thermodynamic Theory of Structure, Stability and Fluctuations," Wiley-Interscience, London (1971).
14) Ref. 1, Chap. 3.
15) Ref. 1, Chap. 2.
16) T. Alty, *Proc. R. Soc. London, Ser. A*, **131**, 554 (1931).
17) T. Alty and F. Nicoll, *Can. J. Res.*, **4**, 547 (1931).
18) T. A. Erikson and R. J. Tykodi, *J. Chem. Phys.*, **33**, 46 (1960).
19) T. A. Erikson and R. J. Tykodi, J. of Heat Transfer, Trans. ASME, Vol. 91, Series C. Number 2 (May 1969), p. 221.
20) W. G. Spangenberg and W. R. Rowland, *Phys. Fluids*, **4**, 743 (1961).
21) R. J. Tykodi and T. A. Erikson, *J. Chem. Phys.*, **31**, 1521 (1959).
22) R. C. Reid, *Am. Scientist*, **64**, 146 (1976).
23) S. Chandrasekhar, "Hydrodynamic and Hydromagnetic Stability," Oxford U. P., Oxford (1961), Chap. II.
24) Ref. 7, pp. 165—197.
25) R. J. Schmidt and S. W. Milverton, *Proc. R. Soc. London, Ser. A*, **152**, 586 (1935).
26) Ref. 23, Chap. VII.
27) G. I. Taylor, *Proc. R. Soc. London, Ser. A*, **157**, 546 (1936).
28) R. J. Donnelly, *Proc. R. Soc. London, Ser. A*, **246**, 312 (1958).
29) E. A. Guggenheim, "Thermodynamics," 2nd ed, North-Holland Pub. Co., Amsterdam (1950), pp. 276—285.
30) G. Nicolis and I. Prigogine, "Self-Organization in Nonequilibrium Systems," Wiley, New York (1977).
31) Ref. 1, Chaps. 4, 13.
32) U. F. Franck, Z. Elektrochem., *Ber. Bunsenges. Phys. Chem.*, **67**, 657 (1963).
33) D. V. Widder, "Advanced Calculus," 2nd ed, Prentic-Hall, Englewood Cliffs (1961), p. 178.

Synthesis and Sintering of Active Manganese(II) Zinc Ferrite Powders†

M. N. Sankarshana MURTHY,* C. E. DESHPANDE, P. P. BAKARE, and (Mrs.) J. J. SHROTRI

National Chemical Laboratory, Poona 411008, India

(Received January 10, 1978)

Manganese(II) monoxide which is spontaneously oxidized in air is stabilized by solid solution with zinc oxide and then employed as a raw material in the synthesis of manganese(II) zinc ferrites in an inert atmosphere, giving thereby no chance for Mn^{2+} to get oxidized. Sintering is done in a static controlled atmosphere created by the thermal dissociation of pellets of active iron(III) oxide kept in oxygen-free nitrogen along with the ferrite toroids. The ferrite formation and the sintering are performed at 950 and 1150 °C respectively by employing active oxide raw materials.

The synthesis of manganese(II) zinc ferrites is complicated by the need to have all the manganese as Mn^{2+}, while a small amount of Fe^{2+} is also needed in order to reduce the magnetocrystalline anisotropy or magnetostriction.[1,2] It is not possible to employ manganese(II) monoxide directly as the raw material since this oxide is not stable in air. Conventional methods employ a higher stable oxide of manganese as the raw material[3] or allow the manganese(II) monoxide to get oxidized during the initial calcination.[4] The reduction of Mn^{2+} is subsequently performed by a current of an inert gas such as nitrogen that sweeps off the oxygen produced by the thermal dissociation of the ferrite at the sintering temperature which is usually between 1200 and 1300 °C. Calculated small concentrations of oxygen are mixed with the nitrogen current in order to effect the optimum thermal reduction of Fe^{3+} to Fe^{2+}. This oxygen concentration has to vary with temperature during the sintering cycle so as to cope with the temperature variation of the partial pressure of oxygen in thermal equilibrium with the ferrite.

Quite apart from the complexity and expense of maintaining the flowing current of the controlled atmosphere with varying oxygen concentrations at different temperatures, it is difficult to know in such a process the stage at which the reduction of Mn^{3+} to Mn^{2+} is complete. Even if this reduction is complete, the Mn^{2+} may or may not be situated completely at the correct lattice sites in the spinel. The Mn^{2+} can enter the spinel lattice only after it is formed by the thermal reduction of Mn^{3+}; but the possibility of harmful non-spinel forming solid state reactions before such a reduction cannot be ruled out. The site-preference for Mn^{3+} is obviously different from that for Mn^{2+} during the solid state reaction among the component oxides. The manganese has to move to the correct lattice site in the ferrite spinel after the subsequent reduction of Mn^{3+} to Mn^{2+}; but this migration in the solid matrix may or may not be complete during the sintering run. One can then expect a considerable degree of non-reproducibility in the final properties of the ferrite even when all the synthetic parameters have been apparently kept constant; and in fact this non-reproducibility of properties is a bugbear in the synthesis of these ferrites.

This difficulty has been overcome in the present investigation by stabilizing the MnO by solid solution with ZnO. It is then possible to prepare the ferrite without oxidation of Mn^{2+}. There is subsequently no need to maintain a running current of the controlled atmosphere in order to reduce the Mn^{3+}. The controlled atmosphere is now necessary only to prevent the oxidation of Mn^{2+} as well as an undue thermal reduction of Fe^{3+}. A static controlled atmosphere suffices for this purpose; and this can be easily obtained by an inert gas in the presence of suitable metallic oxides placed in the high temperature zone. These oxides can supply the required oxygen to the ambient atmosphere by thermal dissociation.

Experimental

(1) Preparation of Raw Materials. Manganese(II) oxalate precipitated from filtered solutions of manganese(II) chloride (AnalaR) and ammonium oxalate (Laboratory Reagent) was washed free from chloride and dried in vacuum. Zinc oxalate prepared similarly could be dried in air at 70°C due to its greater thermal stability. Iron(III) oxide was prepared by adding a concentrated purified iron(III) nitrate solution into an excess of aqueous ammonia. After decanting the supernatent liquid, the precipitate was heated to 250 °C to give pure and active iron(III) oxide. These pure raw materials could be easily estimated gravimetrically; manganese as $MnSO_4$, zinc and iron as the respective oxides by direct ignition.

(2) Preparation of MnO-ZnO Solid Solution. The oxalates of manganese and zinc were mixed in the required proportion and decomposed in a flowing current of oxygen-free nitrogen obtained by passing the cylinder gas through a column of heated reduced copper.[5] The carbon monoxide was disposed off by direct burning. After the evolution of gases ceased, the powder was degassed at 750 °C in order to remove carbon monoxide in particular that is tenaciously chemisorbed by MnO.[6] The system was cooled before taking out the charge which had a fine orange colour and could be safely exposed to air. Chemical analysis revealed the presence of manganess fully as Mn^{2+}.

(3) Preparation of the Ferrite Powder. The above powder containing ZnO and MnO was thoroughly mixed with the requisite amount of iron(III) oxide, pressed as such into pellets and then heated to 950 °C for 8 h in a static atmosphere of pure nitrogen. After cooling, the pellets were found to have become strongly magnetic. They were ground and ball-milled.

(4) Sintering. The sintering of toroids pressed with this ferrite powder could also be done without allowing the Mn^{2+} to get oxidized. The powder was pressed into toroids —3.6 cm o.d., 1.6 cm i.d., 1 cm thickness, employing a

† Communication No: 2223.

Table 1. Measurements on sintered manganese(II) zinc ferrite toroids made by the technique described in the paper

Sr. No.	Composition (mol %)			μ_i(initial permeability)		Loss factor $\frac{\tan\delta}{\mu_i}\times 10^6$ at 4 kHz	Curie point °C	Density g cm^{-3}	D.F.[a] × 10^6	T.F.[b] × 10^6
	Fe_2O_3	ZnO	MnO	at 4 kHz	at 100 kHz					
1	51.75	20.25	28	2640	2621	1.15	135	4.72	0.87	1.06
2	51.71	23.13	25.26	2800	2762	1.72	125	4.72	0.45	1.74
3	52.00	19.25	28.75	2720	2701	1.53	150	4.77	1.09	1.42
4	53.06	17.8	29.14	2729	2571	2.7	160	4.82	1.08	0.13

a) D.F.: Disaccommodation factor defined as $(\mu_1-\mu_2)/\mu_1^2 \log (t_2/t_1)$ where μ_1 and μ_2 are the initial permeabilities at 10 min (t_1) and 100 min (t_2) respectively after demagnetization at 23 °C. b) T.F.: Temperature factor defined as $1/\mu^2\, d\mu/dT$ where T is the temperature.

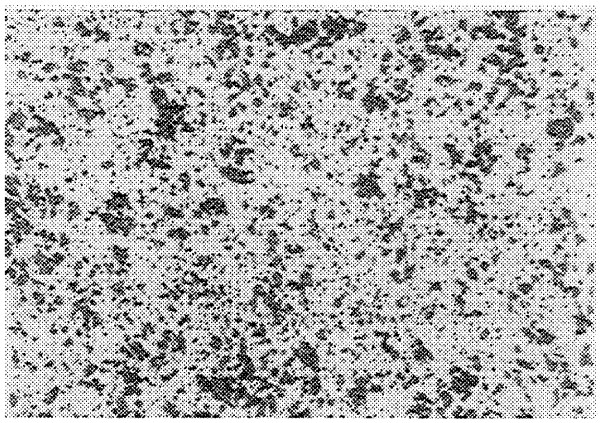

Fig. 1. Photomicrographs of ferrites (present technique) sintered at 1150 °C. Magnification × 100.

volatilizable binder such as camphor. The binder was distilled off in a current of purified nitrogen. The sintering was then done as per the technique given below.

It was however also possible to employ a binder such as polyvinyl alcohol that needs to be burnt out. The Mn^{2+} did of course get oxidized in the process, but subsequent satisfactory reduction could be effected in a run at 1050 °C for eight hours in a static atmosphere of oxygen-free nitrogen and in the presence of a calculated amount of iron powder (pressed as such into pellets) in the closed system. The iron in the hot zone got oxidized by the oxygen given out by the thermal dissociation of the oxidized ferrite; and the reduction of Mn^{3+} back to Mn^{2+} could be effected quantitatively as checked by subsequent chemical analysis. The amount of iron needed in the above reduction was not very critical and a little excess was found to do no harm. After cooling, the toroids contained all the manganese as Mn^{2+}.

These toroids were then sintered in static nitrogen at 1150 °C for 12 h in the presence of iron(III) oxide pellets meant to generate the required partial pressure of oxygen in the closed system. Here again it was found that the quantity of iron(III) oxide to be kept was not very critical so long as it exceeded a certain minimum amount depending on the quantity of ferrite to be sintered. This could be easily determined by slight trial. The temperature of 1150 °C proved to be the correct sintering temperature to give satisfactory grains (Fig. 1). The furnace was cooled after sintering, at a rate of about 25 °C per hour till about 500 °C when the power was switched off. The toroids were taken out after cooling to room temperature and examined for their properties (Table 1). Each of the compositions given in the table was repeated four times and the variation in any of their properties was never more than ±15% of the mean values given in the table. No additives were tried in order to reduce the losses still further.

Discussion

The above technique virtually enables us to use MnO itself as the raw material in the preparation of manganese(II) zinc ferrites. In fact, it was found that even 1 mol % of ZnO in MnO stabilizes the lattice in air[7] so that such an analysed solid solution can be prepared once and for all, and used regularly as a raw material for the synthesis of this ferrite, adding the required balance of ZnO along with the Fe_2O_3 afterwards. It is therefore possible to effect the spinel formation at a relatively low temperature and then sinter the ferrite at a higher temperature just as in the case of nickel zinc or any other ferrite. In a conventional technique on the other hand these two processes are combined into one since the thermal reduction of Mn^{3+} to Mn^{2+} at the sintering temperature is a prerequisite for the spinel formation. Since manganese is present as Mn^{2+} right from the start, the spinel formation occurs at the lowest temperature at which the component oxides can at all react with one another; and it is possible to lower this temperature considerably by employing very active oxides produced by the effervescent decomposition of precipitated compounds at low temperatures —MnO and ZnO by the decomposition of their respective precipitated oxalates, and Fe_2O_3 during the effervescent decomposition of ammonium nitrate produced at the time of precipitation from iron(III) nitrate with ammonia. The preparation of the ferrite powder could be accomplished even at a temperature lower than 950 °C used here. This temperature was employed in order to get the bigger particles necessary for a higher pressed density. The burning of the binder at 800 °C—while it oxidizes the Mn^{2+} and renders the burnt toroids totally non-magnetic—can be expected not to disturb the various ions from their lattice sites. Subsequent reduction at 1050 °C in a closed system filled with pure nitrogen and in the presence of iron powder in the hot zone effects an *in situ* reduction of Mn^{3+} to Mn^{2+}. The iron gets oxidized by the oxygen given out by the thermal dissociation of the oxidized ferrite and thereby reduces all the manganese to Mn^{2+}. It is obvious from the above that the Mn^{2+} should be expected to

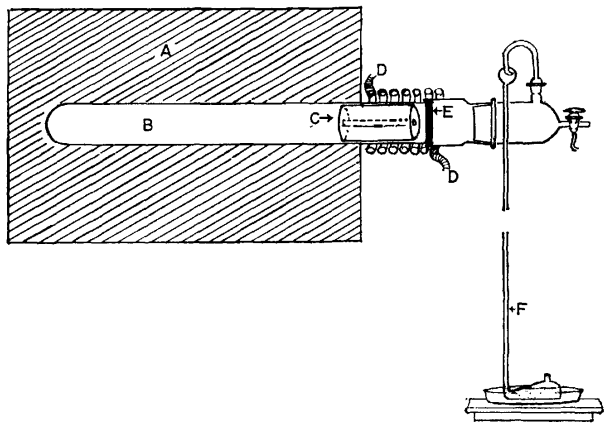

Fig. 2. Experimental arrangement for sintering manganese(II) zinc ferrites.
(A) Furnace; (B) sintering chamber in a recrystallized alumina tube; (C) cylindrical firebrick piece (with an axial bore) to act as a radiation shield on the glass joints; (D) coil for circulation of water to cool the outer end of the furnace tube; (E) attachment of the alumina tube to a ground glass joint with an epoxy resin; (F) manometer-cum-mercury seal.

be fully present at the appropriate lattice sites in the spinel, thereby eliminating an important cause of uncertainty of the results. A little excess iron can obviously do little harm since reduction, if any, of Fe^{3+} to Fe^{2+} at this stage can be easily corrected during the final sintering at 1150 °C in the presence of an excess of active iron(III) oxide pellets. This iron(III) oxide dissociates at the sintering temperature into Fe_3O_4 and oxygen, thereby providing the correct partial pressure of oxygen required to leave an optimum small concentration of Fe^{2+} in the sintered ferrite. The relatively lower temperatures of processing minimise the loss of zinc oxide from the ferrite. Since the dissociation pressure of iron(III) oxide is independent of the quantity of the oxide and depends only on the temperature, the quantity of iron(III) oxide to be placed in the hot zone of the sintering furnace is not very critical provided however, it is sufficient to maintain the correct dissociation pressure of oxygen in the sintering chamber. The mercury seal (Fig. 2) employed during the sintering run and the previous reduction serves to release the pressure during the heating. Since the dissociation pressure of oxygen in equilibrium with the ferrite varies with temperature in the same way as for the iron(III) oxide, the composition of the ambient atmosphere during the entire sintering run adjusts itself automatically at each temperature. The concentration of Fe^{2+} in the sintered ferrite is therefore fixed only by its composition and sintering temperature but not the vagaries of an externally controlled atmosphere; thereby eliminating one uncertain and sensitive parameter determining the ferrite properties. These properties can be varied in other ways such as variation of composition. This simplifies the technique considerably in every way. As mentioned in the introduction, sintering in a static controlled atmosphere whose composition adjusts itself automatically at each temperature is a great advantage over a flowing current of gas whose composition has to be externally adjusted from time to time.

The authors are grateful to Dr. A. P. B. Sinha who has kindly encouraged this work with his keen interest and valuable suggestions. The P. P. U. of Armament Research and Development Establishment, Poona, have kindly prepared the dies and helped in pressing; and this valuable help is most gratefully acknowledged. Grateful thanks are also due to Mr. S. S. Ali, Merado, Poona, for taking the photomicrographs.

References

1) G. Winkler, "Magnetic Properties of Materials," ed by J. Smit, McGraw Hill, New York (1971), p. 52.
2) Keizo Ohta, *J. Phys. Soc. Jpn.*, **18**, 685 (1963).
3) M. A. Strivens and G. Chol, "Ferrites," ed by Y. Hoshino, S. Iida, and M. Sugimoto, Univ. of Tokyo Press, Tokyo (1971), p. 239.
4) Y. Schichijō, G. Asano, and E. Takama, *J. Appl. Phys.*, **35**, 1646 (1964).
5) P. W. Schenk, "Handbook of Preparative Inorganic Chemistry," 2nd ed, ed by George Brauer, Translation ed by R. F. Riley, Academic Press, New York (1963), Vol. I, p. 458.
6) D. O. Hayward and B. M. W. Trapnell, "Chemisorption," Butterworths, London (1964), p. 85, Table 8.
7) C. E. Deshpande, L. M. Pant, and M. N. Sankarshana Murthy, *Indian J. Chem.*, **16A**, 251 (1978).

Medium Effect on the Ionisation Constants of Some Hydroxy Derivatives of 1-Ethyl-2-styrylpyridinium and -quinolinium Iodides

M. R. Mahmoud,* R. Abd-El-Hamide, and K. A. Idriss
Chemistry Department, Faculty of Science, Assiut University, Assiut, Egypt

(Received February 13, 1978)

The pK_a values of 1-ethyl-2-(4 or 2-hydroxystyryl)pyridinium and -quinolinium iodides in different organic solvent–water mixtures were determined. The organic solvents used are methanol, ethanol, acetone, DMF and DMSO. The ionisation of the compounds under investigation depends largely on both the proportion and the nature of the organic co-solvent used. The ionisation constant decreases with increase in the proportion of the organic co-solvent in the medium. The major important effect responsible for this is the difference in the stabilization of base by donor hydrogen bond from solvent molecules. The free energy of solvation of both acid and proton by electrostatic interaction and that of the base by donor hydrogen bond from solvent molecules were calculated. The effect of the molecular structure of the compound on pK_a is also discussed.

So far only a few studies seem to have appeared on the ionisation of hydroxystyryl derivatives.[1] The pK_a values of some hydroxy derivatives of 1-ethyl-2-styrylpyridinium and -quinolinium iodides in pure aqueous medium were determined by Mahmoud *et al.*[2] However, it is known that the hydroxystyryl derivatives are quite interesting compounds because of their application as photosensitizers[3,4] and use as antiseptics, trypanocidal and anticarcinogenic agents.[5-8]

We have investigated the ionisation of some hydroxystyryls in aqueous solutions containing varying proportions of organic solvents (methanol, ethanol, acetone, *N*,*N*-dimethylformamide, dimethyl sulfoxide). The pK_a values have been determined and discussed in terms of solvent properties.

Experimental

Materials and Solutions. The hydroxystyryl dyes used are 1-ethyl-2-(4-hydroxystyryl)pyridinium iodide I, 1-ethyl-2-(2-hydroxystyryl)pyridinium iodide II, 1-ethyl-2-(4-hydroxystyryl)quinolinium iodide III and 1-ethyl-2-(2-hydroxystyryl)quinolinium iodide IV. These derivatives were synthesized by the reaction of the corresponding aldehyde with 1-ethyl-2-methylpyridinium iodide or 1-ethyl-2-methylquinolinium iodide using piperidine as a condensation reagent.[9,10] The products obtained were crystallized several times from ethanol. The compounds used for the preparation of the derivatives and the organic solvents were of high purity (A. R. or spectrograde). Stock solutions 10^{-3} M of the compounds were prepared by dissolving the solid in the solvent. pH control was achieved by using a modified universal buffer solution.[11]

To account for the difference in acidity, basicity, dielectric constant and ion activities in partially aqueous solutions relative to pure aqueous ones, the pH values of the former solutions were corrected making use of the attempts described by Douheret[12]

$$pH^* = pH(R) - \delta,$$

where pH* is the corrected reading and pH(R) is the meter reading obtained in a partially aqueous medium, where the pH-meter is standardized using aqueous buffer.

The values of δ of the aqueous buffer solutions containing varying proportions of each of the organic solvents under investigation were determined by Douheret.[12,13]

Apparatus. The absorption spectra were measured on a UNICAM S.P 8000 Spectrophotometer within the wavelength range 300—700 nm using 1 cm matched silica cells. The pH-measurements were carried out at 25 °C with a UNICAM MK_2 pH-meter, equipped with the usual glass and calomel electrodes, accurate to ±0.005 unit. The temperature was controlled by placing the solutions as well as the pH-meter in an air thermostat accurate to ±0.5 °C.

Results and Discussion

The visible absorption spectra of the compounds measured either in buffer solutions or in those containing different proportions of an organic solvent (methanol, ethanol, acetone, DMF, and DMSO) show mainly two bands (Fig. 1). The spectra of solutions with low pH are characterized by only one visible band mainly due to the absorption by species with non-ionised OH-group. This band was assigned to an intramolecular charge transfer transition.[2] Its intensity decreases with increase in pH in media of pH≥7. At the same time another band appears at longer wavelength, its intensity increasing with increase in pH. The behaviour can be explained as follows. With increase in the pH of the medium, the ionisation of the proton starts which in turn increases the proportion of the ionised form in solution, making the energy barrier of the intramolecular CT smaller.

The results (Tables 1 and 2) indicate that the λ_{max} of the band responsible for the absorption by the free base exhibits a clear red shift on increasing the proportion of the organic solvent in the medium, λ_{max} for the band of the acid shifting slightly.

The spectra of the compounds (I—IV) in all media investigated display clear isosbestic points, showing the existence of equilibrium of the form

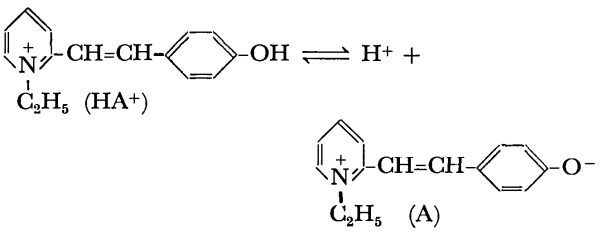

The absorbance —pH curves obtained at selected wavelengthes (Fig. 2) are typical of dissociation and association types, revealing the existence of one acid-base equilibrium in each case.

Table 1. Mean values of pK_a for compounds I(1.50×10^{-5} M) and II(4×10^{-5} M) and the λ_{max} values of the non-ionised and ionised forms in different water-organic solvent mixtures at 25 °C

Organic co-solvent	% (w/w) of organic solvent	Mole fraction of organic solvent	Dielectric constant of the medium 25 °C	Compound I			Compound II		
				pK_a	λ_{max}, nm		pK_a	λ_{max}, nm	
					non-ionic form	ionic form		non-ionic from	ionic form
—	Zero	Zero	78.40	8.32	359	427	8.17	355	436
Methanol	7.92	0.046	76.24	8.46	359	430	8.20	358	438
	15.84	0.0957	73.81	8.58	360	435	8.26	359	444
	23.76	0.149	71.06	8.66	362	440	8.35	360	448
	31.68	0.2067	67.92	8.82	365	446	8.45	361	452
Ethanol	7.91	0.0325	76.60	8.58	360	430	8.20	348	425
	15.82	0.0685	74.50	8.68	362	436	8.30	350	435
	23.73	0.1085	72.07	8.82	365	446	8.40	356	440
	31.64	0.1533	69.15	9.06	367	453	8.58	357	452
Acetone	7.92	0.026	76.85	8.65	363	436	8.30	356	440
	15.84	0.0552	75.06	8.80	366	447	8.46	358	448
	23.78	0.0883	72.90	9.16	369	452	8.62	360	456
	31.68	0.1258	70.28	9.32	372	462	8.75	362	460
DMF	15.82	0.0443	76.52	8.60	366	448	8.25	360	444
	23.76	0.0714	75.35	8.71	367	451	8.36	362	452
	31.60	0.1022	74.47	8.84	368	456	8.50	363	458
	38.00	0.131	72.77	8.92	370	459	8.62	364	466
DMSO	15.82	0.04156	77.08	8.57	363	439	8.20	358	445
	23.76	0.0671	76.50	8.64	364	442	8.30	360	450
	31.60	0.0963	75.42	8.73	367	450	8.45	364	460
	44.04	0.1537	73.80	8.85	369	458	8.58	365	467

Table 2. Mean values of pK_a for III(1.07×10^{-5} M) and IV(4×10^{-5} M) and the λ_{max} values of the non-ionised and ionised forms in different water-organic solvent mixtures at 25 °C

Organic co-solvent	% (w/w) of organic solvent	Mole fraction of organic solvent	Dielectric constant of the medium 25 °C	Compound III			Compound IV		
				pK_a	λ_{max}, nm		pK_a	λ_{max}, nm	
					non-ionic from	ionic form		non-ionic form	ionic form
—	Zero	Zero	78.40	8.04	400	487	7.96	392	488
Methanol	7.92	0.046	76.24	8.12	402	492	7.98	393	492
	15.84	0.0957	73.81	8.20	408	499	8.10	397	498
	23.76	0.149	71.06	8.30	410	506	8.25	399	504
	31.68	0.2067	67.92	8.40	413	513	8.35	401	511
Ethanol	7.91	0.0325	76.60	8.12	408	496	8.08	392	494
	15.82	0.0685	74.50	8.25	409	505	8.19	398	502
	23.73	0.1085	72.07	8.35	412	515	8.30	400	511
	31.64	0.1533	69.15	8.55	417	527	8.40	402	520
Acetone	7.92	0.026	76.85	8.27	406	503	8.20	395	500
	15.84	0.0552	75.06	8.40	408	510	8.35	398	510
	23.78	0.0883	72.90	8.52	410	518	8.52	400	518
	31.68	0.1258	70.28	8.70	414	528	8.60	403	526
DMF	15.82	0.0443	76.25	8.15	409	512	8.10	394	504
	23.73	0.0714	75.35	8.23	412	520	8.22	396	516
	31.60	0.1022	74.47	8.30	413	526	8.35	398	522
	38.00	0.1310	72.77	8.40	413	532	8.48	401	530
DMSO	15.82	0.04156	77.08	8.20	406	500	8.10	395	500
	23.76	0.0671	76.50	8.26	407	507	8.25	397	508
	31.60	0.0963	75.42	8.35	411	517	8.36	400	516
	44.08	0.1537	73.80	8.45	413	528	8.45	402	526

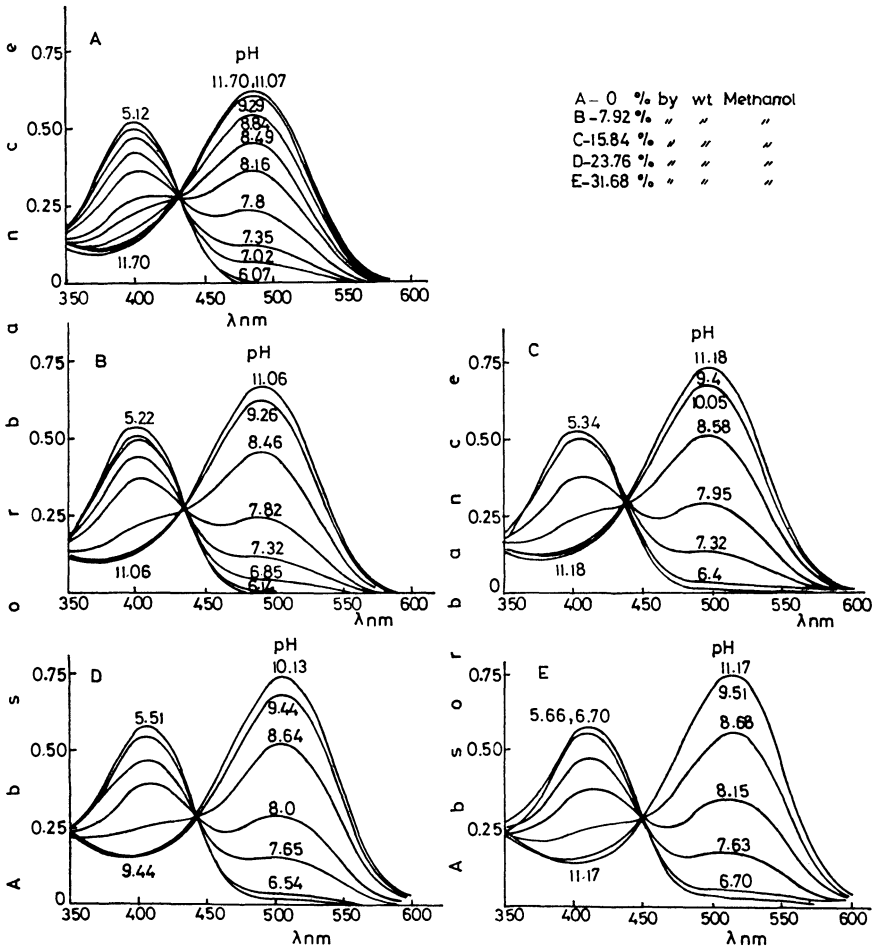

Fig. 1. Absorption spectra of 1.07×10^{-5} M 1-ethyl-2-(4-hydroxystyryl)quinolinium iodide III solution containing different percentages of methanol.

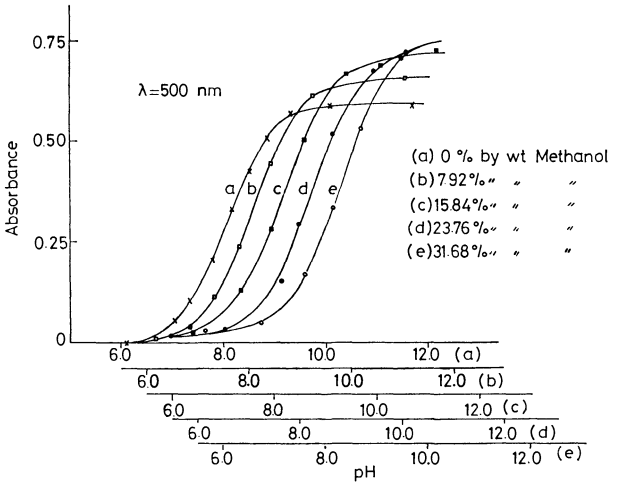

Fig. 2. Absorbance-pH curves for 1-ethyl-2-(4-hydroxystyryl)quinolinium iodide III in universal buffer solutions containing different percentages of methanol.

The acid dissociation constant, pK_a, of the compounds in different media was determined from the variation of absorbance with pH with use of three different spectrophotometric methods viz half-height, limiting absorbance and Colleter methods.[14,15] The results are given in Tables 1 and 2.

It is evident that the pK_a values depend largely on both the proportion and the nature of the organic solvent. The ionisation constant decreases with increase in the amount of solvent in the medium. This behaviour is the opposite of that observed with *p*-dimethylaminostyryl derivatives.[16]

According to Coetzee and Ritchie,[17] the acidity constant in aqueous medium $K_{a(1)}$ is related to that in partially aqueous medium $K_{a(2)}$ by means of

$$K_{a(1)} = K_{a(2)}\frac{\gamma_{H^+}\gamma_A}{\gamma_{HA^+}}, \quad (1)$$

where the γ is the activity coefficient of the subscripted species in a partially aqueous medium relative to that in a pure one. It is known that the electrostatic effect resulting from the change in dielectric constant of the medium will operate on the activity coefficient of the charged species only, its magnitude being inversely proportional to the radius of the ionic species considered.[18] Consequently the magnitude of this effect on the proton exceeds that on the acid (HA^+). Thus, the ionisation constant of the compounds is expected to decrease with increase in the proportion of the organic solvent in the medium, which is in line with the results given in Tables 1 and 2.

However, in the light of the relation given by Charlot and Tremillon,[19] giving the variation of pK_a with

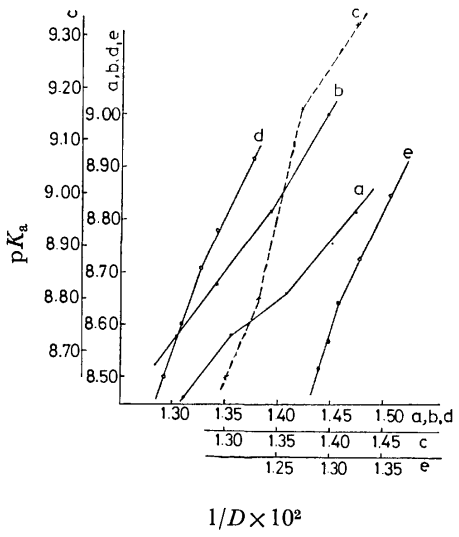

Fig. 3. Variation of pK_a of compound I in aqueous organic solvent mixture with $1/D$ of the medium at 25 °C.
a: Methanol, b: ethanol, c: acetone, d: DMF, e: DMSO.

dielectric constant (D), the plots of pK_a against $1/D$ are not strictly linear (Fig. 3). This indicates that the decrease in the ionisation constant of these compounds, though mainly governed by the dielectric constant effect, is strongly influenced also by other solvent effects. The behaviour can be interpreted by calculating the change in the ionisation constant produced by electrostatic effect (ΔpK_{el}) for compounds I and III in the presence of each organic solvent (31.60 % by wt). The calculation was made by means of the Bron equation,[18] valid for large radii,[20] and following the principles described by Tremillion.[21] The following equation is obtained for the calculation of ΔpK_{el} value:

$$\Delta pK_{el} = \frac{Ne^2}{4.6RT}\left[\frac{1}{r_{HA^+}} - \frac{1}{r_{H_3O^+}}\right]\left[\frac{1}{D_{mix}} - \frac{1}{D_{H_2O}}\right],$$

where N=Avogadro's number, e=electron charge, r=radius of ion expressed in Å, D=dielectric constant, $r_{H_3O^+}=r_{H_2O}=1.93$ Å. The radius of the monovalent cation (HA^+) was determined by assuming that its density is approximately equal to the one belonging to the corresponding non-quaternized derivative. The densities of the non-quaternized derivatives of compounds I and III were determined by means of the technique developed by Clark and White.[22]

$$d = \frac{m \times d_{Hg}}{m+w},$$

where d_{Hg}=density of mercury m=weight of the non-quaternized compound in the air, w=the weight to be added to the pan in order to level the fixed mark on the stem back to the surface of Hg. The density values obtained for the non-quaternized derivatives of compounds I and III are 1.1055 and 1.2685 gm/cm^3, respectively; thus the calculated radii are 4.30 and 4.42 Å respectively. Hydrogen bonding, solvent basicity, despersion forces and proton-solvent interaction effects are commonly recognized as influencing factors in the ionisation constants of acids in the presence of organic solvent.

We can attribute the decrease in the ionisation constant of each compound due to increase in the proportion of organic solvent in the medium to the following effects besides the electrostatic effect.

(a) Decrease in the ionisation of the OH group of the compound (*i.e.* high pK_a) caused by the relatively low basicity of alcohols or acetone with respect to water.

(b) The high stabilization of the base (A) by donor hydrogen bond in pure aqueous medium relative to that in presence of organic solvent. This is presumably due to the greater tendency of water molecules to donate hydrogen bond as compared with other solvent molecules.[17] Increase in solvent proportion in the aqueous medium will result in an increase in the activity coefficient of the base, thereby causing decrease in the ionisation constant of the compound (*i.e.* high pK_a).

Since the organic co-solvent is characterized by high polarizability relative to water, the base would be more highly stabilized by dispersion forces in solvent–water mixtures than in water. On the other hand, the proton is expected to be highly stabilized in partially aqueous media relative to pure ones through proton-solvent interactions. Thus, the ionisation constant of the compound should increase with increase in the amount of the organic co-solvent in the medium. However, this is not the case (Tables 1 and 2). We see that the dispersion forces and proton-solvent interactions do not appear to be of much importance in the ionisation of the hydroxystyryl derivatives.

The results (Tables 1 and 2) indicate that the variation of pK_a values in solutions containing either the same percentage or more or less the same mole fraction (≈ 0.1) of alcohol or acetone appears to be in the order:

methanol < ethanol < acetone.

This is presumably due to the decrease in the tendency of the solvent molecules to donate hydrogen bond to the base on going from methanol to acetone. This was deduced from the fact that the tendency of alcohol to associate with solutes through H- bond decreases with increase in the molecular weight of alcohol.[23] Acetone is characterized by a very weak tendency to donate hydrogen bond.[17]

The decrease in ionisation with decrease in the donor hydrogen-bond character of the organic co-solvent is in line with the fact that the difference in the stabilization of the base by donor-hydrogen bond from solvent molecules is a major factor responsible for the increase in pK_a resulting from the increase in the amount of the solvent in the medium.

It is evident that the pK_a value in presence of the poorer donor-hydrogen bond DMF or DMSO is less than either the one obtained in the presence of the same amount or nearly the same mole faction (≈ 0.10) of acetone or ethanol (Tables 1 and 2). This can be attributed to the high basic character of the former solvents, reflecting itself in the construction of a strong acceptor hydrogen bond from the OH group of the non-ionised form and thus facilitating the ionisation process of the OH group (*i.e.* low pK_a).

TABLE 3. VALUES OF ΔpK_{el}, ΔpK_{nonel}, ΔG_{el}, and ΔG_{nonel} OBTAINED FOR COMPOUNDS I and III

Solvent	$+\Delta pK_t$		$+\Delta pK_{el}$		$+\Delta pK_{nonel}$		$+\Delta G_{el}$ cal/mol 25 °C		ΔG_{nonel} kcal/mol 25 °C	
	I	III	I	III	I	III	I	III	I	III
31.68 wt % Methanol	0.50	0.36	0.065	0.067	0.435	0.293	89.1	91.8	0.60	0.40
31.64 wt % Ethanol	0.74	0.51	0.058	0.060	0.682	0.450	79.5	82.3	0.94	0.62
31.68 wt % Acetone	1.00	0.66	0.051	0.052	0.949	0.608	69.9	71.3	1.30	0.83
31.60 wt % DMF	0.52	0.26	0.023	0.024	0.497	0.236	31.5	32.9	0.68	0.32
31.60 wt % DMSO	0.41	0.31	0.017	0.018	0.393	0.292	23.3	24.7	0.54	0.40

The free energy of solvation of both the acid and proton by electrostatic interactions and that of the base, by donor hydrogen bond, which are equal to the free energy of transfer due to electrostatic (ΔG_{el}) and non-electrostatic (ΔG_{nonel}) interactions respectively were calculated for compounds I and III in the presence of each organic solvent (31.60% by wt) (Table 3). It is evident that the ΔG_{nonel} value of the same base becomes less positive on going from acetone→ethanol→methanol. This is in line with the increase in hydrogen bond donor character of the solvent in the same direction. On the other hand, the less positive value of ΔG_{nonel} obtained in the presence of DMF or DMSO with respect to the same percentage of the other solvents can be attributed to the high basicity of these solvents.

The observed red shift in λ_{max} belonging to the base and observed as the proportion of the organic solvent in the medium increases, can be interpreted as follows. Increase of the latter would cause an increase of the free negative charge on the oxygen atom of the base. This is due to the weak tendency of the molecules of the solvent in forming donor hydrogen bond with the oxygen atom relative to water moleucles. This in turn will reflect itself in the increase of the intramolecular charge transfer from oxygen atom to the delocalized molecular orbital of the pyridinium (I, II) and quinolinium (III, IV) cations (*i.e.* increase of the induced dipole moment of the molecule), and thus a lower excitation energy is required. This behaviour can be considered as further evidence for the fact that the donor hydrogen bond from solvent molecules to the base is important in the ionisation process of the hydroxystyryl derivatives.

Effect of Molecular Structure on pK_a. The results (Tables 1 and 2) show that the pK_a values of the 1-ethyl-2-(hydroxystyryl)quinolinium iodides (III, IV) are smaller than the corresponding ones belonging to the 1-ethyl-2-(hydroxystyryl)pyridinium iodides (I, II). This is presumably due to the high co-planarity of compounds III and IV resulting from the greater bulk of the heterocyclic moiety attached to the -CH=CH- centre. This leads to an increase in the intramolecular CT from the phenyl moiety, affording a lower negative charge density on the aromatic system resulting in weaker bonding of the proton (low pK_a value).

The pK_a values of the 4-hydroxy derivatives (I,III) are greater than the ones belonging to the 2-hydroxy derivatives (II, IV). This is probably due to the high inductive effect of the OH group on 2-position of styryl group which facilitates liberation of the proton from the compound (low pK_a value).

References

1) L. H. Feldman, A. M. Herz, and I. M. Regan, *J. Phys. Chem.* **72**, 2008 (1968).
2) M. R. Mahmoud, Z. H. Khalil, and R. M. Issa, *Acta Chim. Acad. Sci. Hung.*, **87**, 121 (1975).
3) J. M. Eder and L. Luppocramer "Ausfurliches Handbuch der Photographie," (1932), Band III, Teil 3.
4) T. Takahashi and K. Sato, *Yakugaku Zasshi*, 467 (1958).
5) M. Banno, *Kanko Shikiso*, **34**, 1 (1955).
6) L. K. Mushkalo, *Zh. Obshch. Khim.*, **29**, 1030, 1034 (1959).
7) C. Bahner, C. Cook, J. Dale, J. Fain, E. Franklin, J. Goan, W. Stump, J. Wilson, *J. Org. Chem.* **22**, 682 (1957).
8) C. Bahner, J. Dale, J. Fain, E. Franklin, J. Goan, W. Stump, M. West, and J. Wilson, *J. Org. Chem.*, **22**, 1110 (1957).
9) A. P. Phillips, *J. Org. Chem.*, **12**, 333 (1947).
10) G. T. Pilyugin, I. N. Chernyuk, *Zh. Obshch. Khim.*, **31**, 1585 (1961).
11) H. T. S. Britton, "Hydrogen Ions," Chapman & Hall, London (1952), p. 364.
12) G. Douheret, *Bull. Soc. Chim. Fr.*, **1967**, 1412.
13) G. Douheret, *Bull. Soc. Chim. Fr.*, **1968**, 3122.
14) R. M. Issa, H. Sadek, and I. I. Izzat, *Z. Phys. Chem. N. F.*, **74**, 17 (1971).
15) J. C. Colleter, *Ann. Chem. (Paris)*, **1960**, 415.
16) M. R. Mahmoud and R. Abd-El-Hamide, *Indian J. Chem.*, in press.
17) J. F. Coetzee and C. D. Ritchie, "Solute-Solvent Interactions," Marcel Dekker Ltd., New York, London (1969), p. 221.
18) M. Born, *Z. Phys.*, **1920**, 45.
19) G. Charlot and B. Tremillon, "Chemical Reactions In Solvents and Melts," Pergamon Press (1969), p. 55.
20) L. G. Hepler, *Aust. J. Chem.*, **17**, 587 (1964).
21) B. Tremillon, "Chemistry in Non-Aqueous Solvents," Publishing company, Dordrecht, Holland (1974), p. 232.
22) P. W. Clark and J. White, *Trans. Brit. Ceram. Soc.*, **49**, 305 (1950).
23) F. Frank and D. J. G. Ives, *Quart. Rev.*, **20**, 1 (1966).

Temperature and Composition Dependences of Transport Processes in Glass-forming Molten Mixtures of $Zn(NO_3)_2 \cdot 6.27H_2O$ and $CoCl_2$

Nurul ISLAM,* Kunwar Pal SINGH, and Satendra KUMAR
Department of Chemistry, Aligarh Muslim University, Aligarh 202001, India

(Received May 31, 1978)

Density, viscosity, and electrical conductivity of glass-forming mixtures of zinc nitrate hexahydrate and anhydrous cobalt chloride were measured as functions of temperature and concentration. Non-Arrhenius temperature dependence of equivalent conductance, Λ and fluidity, ϕ has been discussed in terms of a three parameter equation derived from Adam-Gibbs model. A linear correlation has been obtained between the preexponential parameter, A_Y and the ideal glass transition temperature, T_0. The composition dependence of Λ and ϕ has been described by the expression derived from the Adam-Gibbs equation on the criteria of constant T/T_0, where T is the absolute temperature, and a modification to this expression has been made. An attempt has been made to describe the concentration dependence of $\Lambda\eta$ product in terms of modified Adam-Gibbs equation.

Much attention has been paid to describe the variation in mass transport properties of glass-forming melts with temperature. In doing so, several empirical and theoretical expressions[1-5] have been developed. On the other hand, expressions for describing the concentration dependence of transport properties are still in the process of development. In recent communications,[3,6,7] such expressions by modifying the basic equations for explaining the temperature dependence of transport behaviors of mixtures of molten salts have been proposed. The purpose of the present investigation on $Zn(NO_3)_2 \cdot 6.27H_2O$–$CoCl_2$ glass-forming melts is to test the applicability of these concentration-dependent equations and to improve them accordingly. Importance of selecting such systems has been discussed elsewhere.[3]

Experimental

Zinc nitrate hexahydrate (BDH; mp 36.4 °C) was used as solvent in molten state and the solute, anhydrous cobalt chloride was added to it at about 50 °C, to prepare mixtures of molten salts of several concentrations. Anhydrous cobalt chloride was prepared[8] from the recrystallized hexahydrate salt using purified thionyl chloride (Riedel). Water of crystallization of hydrated zinc nitrate was estimated volumetrically[9] before using in sample preparation. The ratio H_2O/Zn^{2+} was found to be 6.27. Accuracy of such an analysis was checked by taking hydrated calcium nitrate of known H_2O/Ca^{2+} ratio and was found to be within ± 0.01.

Densities were measured using pycknometer of 0.01 ml divisions. Viscosities and electrical conductivities were measured with calibrated Cannon-Ubbelohde viscometer[10] (β=6.26 cSt/s) and a Philips Model PR 9500 conductance bridge along with capillary-type cell[11] (cell constant= 758.5 cm^{-1} at 25 °C), respectively. Overall accuracy of these measurements were estimated to be better than $\pm 2.5\%$. Measurements were made in a descending as well as in an ascending order of temperature ranging between 298 to 358 ± 0.02 K.

Results and Discussion

It may be interesting to compare the extent of dissolution of $CoCl_2$ in molten $Zn(NO_3)_2 \cdot 6.27H_2O$ and $Cd(NO_3)_2 \cdot 4.1H_2O$.[7] Anhydrous $CoCl_2$ dissolves up to approximately 30 mol % in the former and approximately 12 mol % in the latter case. The difference in the solubilities of $CoCl_2$ in these molten solvents may be due to the presence of associated species like MNO_3^+, where M=Cd^{2+} and Zn^{2+}. Addition of anhydrous solute to the above hydrated melts appear to facilitate the formation of MNO_3^+ species through the dehydration of an equivalent amount of hydrated cations, $M(H_2O)_n^{2+}$. The maximum solubility of $CoCl_2$ may refer to the optimum concentration of MNO_3^+ obtained. Accordingly, higher solubility of $CoCl_2$ in $Zn(NO_3)_2 \cdot 6.27H_2O$ than in $Cd(NO_3)_2 \cdot 4.1H_2O$ is inferred to a higher association constant for $ZnNO_3^+$ than for $CdNO_3^+$ species. Furthermore, difference in the number of water molecules coordinated to the metallic cations may also be responsible for the difference in solubilities of $CoCl_2$ in these solvents.

The temperature dependence of measured densities of $Zn(NO_3)_2 \cdot 6.27H_2O$–$CoCl_2$ systems was found to be linear (*cf.* Table 1). The fluidity, ϕ and equivalent conductance, Λ show non-Arrhenius temperature behaviors in the range 298 to 358 K (*cf.* Table 2). These data can be expressed by the following expression,[5] when the exponential parameter, k_Y is almost constant:

$$Y = A_Y \exp\left[-k_Y/T \ln (T/T_0)\right], \quad (1)$$

where, $Y=\phi$ or Λ and A_Y, k_Y, and T_0 are empirical parameters. The values of the best fit parameters obtained in the condition described above are displayed in Table 3 along with standard deviation in Y. Plots of log Y *vs.* $1/T \ln (T/T_0)$ (Fig. 1) show linear relationship indicating the applicability of the above equation to the present system.

The values of A_ϕ and A_Λ decrease linearly with increasing composition of $CoCl_2$, whereas T_0 increases (Fig. 2). Such variations in A_ϕ, A_Λ, and T_0 are in accordance with the explanations given earlier.[3,6,12]

Based on the nature of composition dependences of A_Y and T_0, they may be correlated[13] as

$$A_Y = \alpha - \beta T_0, \quad (2)$$

where $\alpha = A_{0Y} + T_{0(0)} Q_{1Y}/Q_{2Y}$, and $\beta = Q_{1Y}/Q_{2Y}$. A_{0Y} and $T_{0(0)}$ are the values of A_Y and T_0 for the pure solvent, respectively. Q_{1Y} and Q_{2Y} are the slopes of the linear plots (Fig. 2) of A_Y and T_0 *versus* composition, respectively. Such an observation may be visualized through the inverse relationship[6] between preexponential factor, A_Y and the rigidity of the system and also the direct dependence[3,14] of ideal glass transition

Table 1. Computed parameters for density equation, $\rho(\mathrm{g\,cm^{-3}}) = a - bT(\mathrm{K})$ of $Zn(NO_3)_2 \cdot 6.27H_2O$-$CoCl_2$ melts

Co^{2+} mol %	a g cm^{-3}	$b\times10^3$	Std dev in ρ	V_m cm^3 mol^{-1}
0.00	2.1848	1.1553	0.94×10^{-3}	166.92
5.11	2.2117	1.1903	0.56×10^{-3}	160.67
10.14	2.2158	1.1757	0.47×10^{-3}	155.17
15.30	2.2241	1.1557	0.38×10^{-3}	149.12
20.52	2.2235	1.1236	0.23×10^{-3}	143.50
25.32	2.2616	1.1861	0.37×10^{-3}	137.71
30.20	2.2528	1.1290	0.33×10^{-3}	132.56

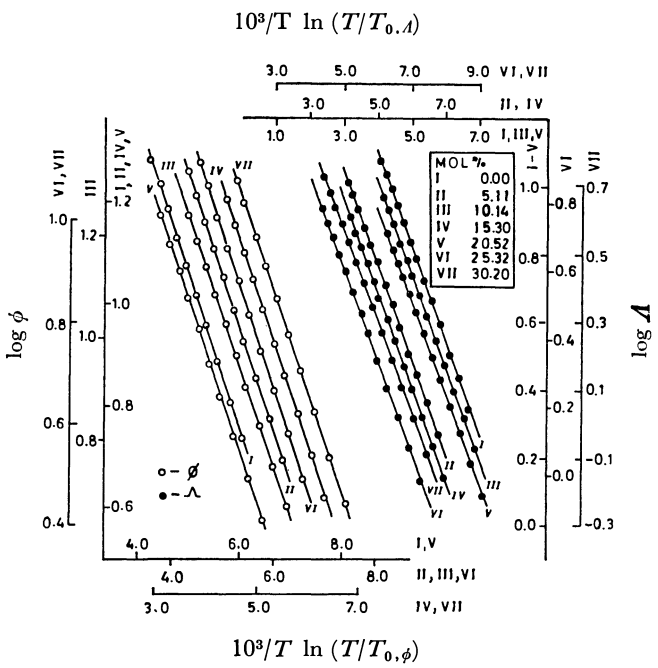

Fig. 1. Plots of log Y *vs.* $1/T \ln(T/T_0)$ for $Zn(NO_3)_2 \cdot 6.27H_2O$-$CoCl_2$ melts.

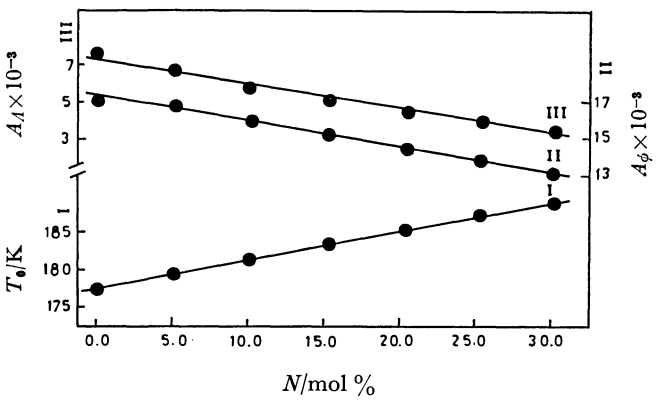

Fig. 2. Variation of T_{0Y} (average of $T_{0,\phi}$ and $T_{0,\Lambda}$, and A_Y (A_ϕ for II and A_Λ for III) with composition for $Zn(NO_3)_2 \cdot 6.27H_2O$-$CoCl_2$ melts.

temperature, T_0 upon the rigidity of the system, *i.e.* upon the coulombic interactions or cohesive energy[14] of the system. The rigidity of the system under investigation may increase with increase in concentration of $CoCl_2$ which is responsible for the variation of

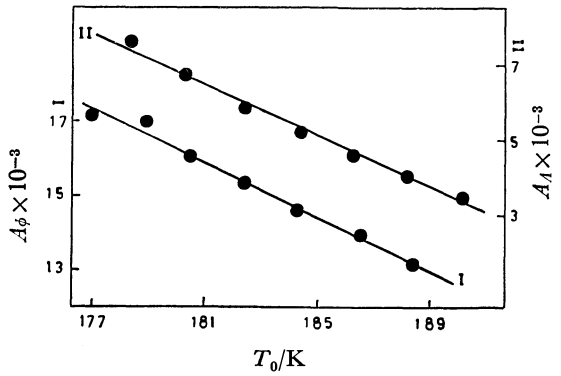

Fig. 3. Plots of A_ϕ and A_Λ *vs.* T_{0Y} (average of $T_{0,\phi}$ and $T_{0,\Lambda}$) for $Zn(NO_3)_2 \cdot 6.27H_2O$-$CoCl_2$ melts.

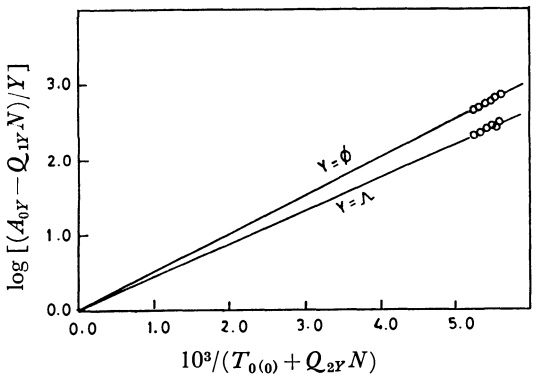

Fig. 4. Plots of $\log[(A_{0Y}-Q_{1Y}N)/Y]$ *vs.* $1/(T_{0(0)}+Q_{2Y}N)$ for $Zn(NO_3)_2 \cdot 6.27H_2O$-$CoCl_2$ melts.

A_Y terms with T_0 linearly but inversely. Linear plots of $A_{Y(=\phi \text{ or } \Lambda)}$ *versus* T_0 (an average of $T_{0,\phi}$ and $T_{0,\Lambda}$ has been taken) (Fig. 3) further emphasize the validity of Eq. 2.

To describe the composition dependence of transport processes, an isoenergetic equation was suggested in earlier publication[6] based upon the Vogel-Tammann-Fulcher equation. However, Eq. 1 which is based upon Adam-Gibbs model is more satisfactory in describing the physical changes in the properties of fused salts and supercooled liquids. In view of this notion Eq. 1 was modified recently[7] by considering T_0 as the basis for the corresponding temperature, T and at T/T_0=constant=c, to

$$Y = A_Y \exp[-k_Y/T_0 c \ln c], \quad (3)$$

and by substituting the linear variations[6] of A_Y and T_0 we obtain

$$Y = (A_{0Y}-Q_{1Y}N) \exp[-k_Y/(T_{0(0)}+Q_{2Y}N)c \ln c], \quad (4)$$

where the symbols have their usual significances. To test the applicability of Eq. 4, the values of $Y(=\phi$ or $\Lambda)$ at constant, c=1.5 were calculated from Eq. 3 and were in turn least-squares fitted to Eq. 4. Computer fitted values of empirical constants, A_{0Y}, $T_{0(0)}$, Q_{1Y}, and Q_{2Y} are given in Table 4. The linearity of the plots of $\log[(A_{0Y}-Q_{1Y}N)/Y]$ *versus* $1/(T_{0(0)}+Q_{2Y}N)$ which pass through origin (Fig. 4) supports the feasibility of Eq. 4. However, it may be noted that Eq. 4 is not capable of correlating directly the measured transport data with the composition. A prior calculation of the transport property at constant c value is

Table 2. Equivalent conductance (cm^2 equiv^{-1} Ω^{-1}) and fluidity[a] (P^{-1}) data as a function of temperature for $Zn(NO_3)_2 \cdot 6.27H_2O$-$CoCl_2$ melts

T/K	Co^{2+}/mol %						
	0.00	5.11	10.14	15.30	20.52	25.32	30.20
298.0	2.2018	1.8449	1.6788	1.3715	1.2240	0.9611	0.8067
303.0	2.7154	2.3135	2.0531	1.7029	1.5276	1.2051	1.0328
308.0	3.2798	2.7556	2.4909	2.0827	1.8662	1.4782	1.2743
	(5.4731)	(4.9810)	(4.6869)	(4.1956)	(3.7626)	(3.0931)	(2.7808)
313.0	3.9155	3.2549	2.9833	2.5202	2.2446	1.7959	1.5472
	(6.4785)	(5.9617)	(5.6028)	(5.0615)	(4.5593)	(3.7968)	(3.4258)
318.0	4.5834	3.7962	3.5126	2.9672	2.6862	2.1515	1.8564
	(7.7262)	(7.1376)	(6.7591)	(6.1107)	(5.5353)	(4.6526)	(4.2229)
323.0	5.3085	4.4806	4.1153	3.4909	3.1459	2.5729	2.2050
	(9.1206)	(8.4339)	(8.0108)	(7.2884)	(6.6203)	(5.5541)	(5.0849)
328.0	6.1060	5.0947	4.7611	4.0522	3.6636	2.9771	2.5991
	(10.445)	(9.7106)	(9.2242)	(8.4380)	(7.6614)	(6.4863)	(5.9803)
333.0	6.9042	6.0133	5.4336	4.6645	4.2118	3.4580	2.9925
	(11.963)	(11.209)	(10.702)	(9.7868)	(8.8910)	(7.5625)	(7.0034)
338.0	7.8650	6.7256	6.0507	5.2374	4.7756	3.9350	3.4046
	(13.611)	(12.809)	(12.183)	(11.217)	(10.207)	(8.8178)	(8.1453)
343.0	8.8010	7.5293	6.8128	5.8140	5.4010	4.4454	3.8546
	(15.340)	(14.464)	(13.779)	(12.709)	(11.687)	(10.055)	(9.3439)
348.0	9.8035	8.4858	7.6675	6.5285	5.8786	4.9597	4.3251
	(17.166)	(16.280)	(15.477)	(14.331)	(13.176)	(11.554)	(10.654)
353.0	10.788	9.4167	8.4510	7.2951	6.5210	5.4885	4.7842
	(19.186)	(18.194)	(17.313)	(15.981)	(14.819)	(12.985)	(11.917)
358.0	11.802	10.189	9.3328	8.0861	7.2206	6.0014	5.2936

a) Fluidity data are within parentheses.

Table 3. Computed parameters for Eq. 1 for the fluidity and equivalent conductance data of $Zn(NO_3)_2 \cdot 6.27H_2O$-$CoCl_2$ melts

Co^{2+} / mol %	A_ϕ	k_ϕ	$T_{0,\phi}$	Std dev in ϕ	A_Λ	k_Λ	$T_{0,\Lambda}$	Std dev in Λ
0.00	340.54	685.01	180.00	0.055	161.52	639.51	180.80	0.024
5.11	337.04	684.00	181.99	0.049	144.99	642.52	182.00	0.068
10.14	324.54	680.00	183.06	0.036	128.97	631.03	183.20	0.031
15.30	312.99	681.26	184.50	0.024	116.59	635.60	184.48	0.035
20.52	299.51	680.96	186.00	0.044	103.81	622.00	186.24	0.044
25.32	287.35	690.21	188.00	0.061	92.14	625.01	188.30	0.031
30.20	268.96	681.00	189.97	0.026	80.89	616.07	190.20	0.015

Table 4. Computed parameters for Eq. 4 (c=1.5) for the fluidity[a] and equivalent conductance of $Zn(NO_3)_2 \cdot 6.27H_2O$-$CoCl_2$ melts

A_{0Y}	Q_{1Y}	k_Y/K	$T_{0(0)}$/K	Q_{2Y}	Std dev in Y
161.24	2.624	631.68	178.69	0.322	0.064
(350.30)	(2.483)	(689.30)	(180.30)	(0.320)	(0.035)

a) Parameters for fluidity are within parentheses.

necessary and in order to remove this difficulty an alternative expression may be written as

$$Y = (A_{0Y} - Q_{1Y}N) \exp\{-k'_Y/T \ln [T/(T_{0(0)} + Q_{2Y}N)]\}. \quad (5)$$

The measured fluidity and equivalent conductance data at all concentrations were least-squares fitted to Eq. 5 and reasonably good fits were obtained. The values of empirical parameters, A_{0Y}, k'_Y, $T_{0(0)}$, Q_{1Y}, and Q_{2Y} are given in Table 5 and were found to be very close to those obtained from the corresponding plots. Furthermore, linear plots (Fig. 5) of $\log [(A_{0Y} - Q_{1Y}N)/Y]$ *versus* $1/T \ln [T/(T_{0(0)} + Q_{2Y}N)]$ provide graphical support to the validity of Eq. 5. Thus, we are able to describe satisfactorily the composition dependence of transport processes without depending upon the measurements as a function of temperature in the entire range of composition.

Having examined the individual behaviors of viscosity and electrical conductivity, their simultaneous representation may similarly be analysed. Walden's rule, $\Lambda\eta$=constant, fails to hold good in the cases of molten salt systems and is found to change both with temperature and concentration. The temperature dependence of $\Lambda\eta$ product for the system under investigation may quantitatively be described by the relations,[3,6]

$$\Lambda\eta = A_1 \exp [B_1/(T - T_0)] \quad (6)$$

Table 5. Computed parameters for Eq. 5 for the fluidity[a] and equivalent conductance of $Zn(NO_3)_2 \cdot 6.27H_2O$-$CoCl_2$ melts

A_{0Y}	Q_{1Y}	k_Y/K	$T_{0(0)}$/K	Q_{2Y}	Std dev in ln Y
162.9±1.1	2.66±0.004	631.4±0.50	178.5±0.04	0.324±0.001	0.055±0.007
(345.2±1.0)	(2.37±0.002)	(686.3±0.41)	(177.3±0.09)	(0.328±0.001)	(0.0396±0.004)

a) Parameters for fluidity are within parentheses.

Table 6. Best-fit parameters for Eqs. 6 and 7 for $\Lambda\eta$ product of $Zn(NO_3)_2 \cdot 6.27H_2O$-$CoCl_2$ melts

$\frac{Co^{2+}}{mol\ \%}$	A_1	B_1	$T_{0,\Lambda\eta}$	Std dev in $\Lambda\eta$	A_2	B_2	$V_{0,\Lambda\eta}$	Std dev in $\Lambda\eta$
0.00	0.4714	32.00	177.84	0.0037	0.4850	2.7148	152.75	0.0038
5.11	0.4341	30.00	179.80	0.0050	0.4487	2.4000	147.01	0.0050
10.14	0.3756	45.00	181.40	0.0035	0.3901	3.5928	142.30	0.0035
15.30	0.3464	46.00	183.33	0.0038	0.3588	3.5000	137.20	0.0037
20.52	0.3329	50.00	185.30	0.0056	0.3409	3.7348	132.50	0.0056
25.32	0.3071	55.00	187.50	0.0055	0.3278	3.6343	127.00	0.0053
30.20	0.2867	56.00	189.20	0.0028	0.2947	3·8543	122.70	0.0028

Table 7. Computed parameters for Frenkel equation for the product of equivalent conductance and viscosity of $Zn(NO_3)_2 \cdot 6.27H_2O$-$CoCl_2$ melts

$\frac{Co^{2+}}{mol\ \%}$	n	ln K	Std dev in η
0.00	1.0541	0.4411	0.006
5.11	1.0471	0.5546	0.009
10.14	1.0736	0.5581	0.007
15.30	1.0772	0.6347	0.008
20.52	1.0884	0.6354	0.012
25.32	1.0869	0.6947	0.011
30.20	1.0977	0.7536	0.006

and,

$$\Lambda\eta = A_2 \exp\left[B_2/(V-V_0)\right], \qquad (7)$$

essentially based upon the "Vogel-Tammann-Fulcher" (VTF) and the "Doolittle" equations, respectively. The empirical parameters A_1, B_1, A_2, and B_2 are the resultant of those for the individual Λ and η values in the VTF and the Doolittle equations. V is the molar volume and V_0 is the intrinsic volume at the ideal glass transition temperature, T_0. The values of the best-fit parameters for Eqs. 6 and 7 are given in Table 6. The computed values of the parameters $T_{0,\Lambda\eta}$ and $V_{0,\Lambda\eta}$ were in good agreement with those obtained independently from fluidity and conductance data, *i.e.*, $T_{0,\phi,\Lambda}$ and $V_{0,\phi,\Lambda}$ values, respectively, emphasizing further the thermodynamic nature of these parameters.

Moreover, the nature of $\Lambda\eta$ product may also be explained by Frenkel equation, $\Lambda^n\eta$=constant, K, where n is the ratio of activation energies for the viscous and the conductance flows, E_η/E_Λ. The least-squares fitted values of the parameters for this equation are given in Table 7.

An attempt has been made here to understand the composition dependence of the Walden product. It is worthy to note a monotonous decrease in $\Lambda\eta$ with increasing composition (Fig. 6) and is different from

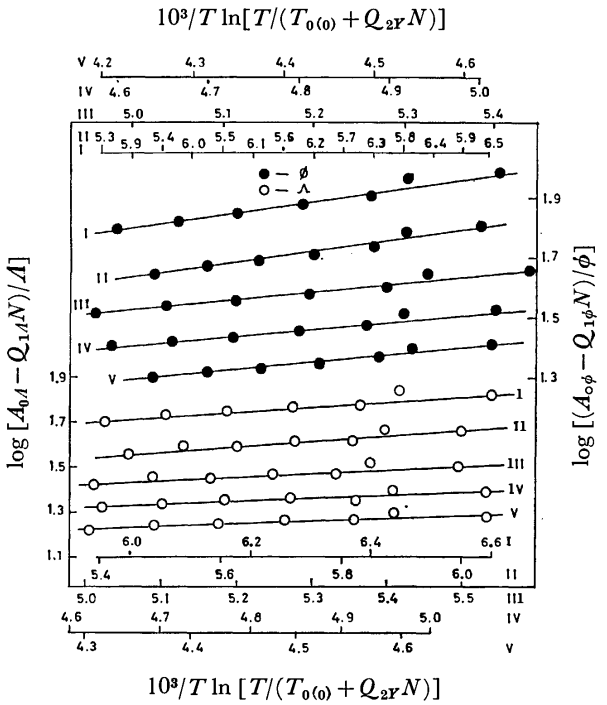

Fig. 5. Plots of $\log\left[(A_{0Y}-Q_{1Y}N)/Y\right]$ *vs.* $1/T$ $\ln\left[T/(T_{0(0)}+Q_{2Y}N)\right]$ for $Zn(NO_3)_2 \cdot 6.27H_2O$-$CoCl_2$ melts (I: 308 K, II: 318 K, III: 328 K, IV: 338 K, V: 348 K).

the behavior reported in $Ca(NO_3)_2 \cdot 3.91H_2O+CoCl_2$ and in $(C_4H_9)_4NI+CoCl_2$ melts.[3,15] As equivalent conductance decreases with increasing the composition of $CoCl_2$, the variation of $\Lambda\eta$ product of the present system seems to be mainly determined by the value of Λ. However, as the concentration increases the amount of decrease in $\Lambda\eta$ lessens thereby reflecting the contribution of viscosity as well.

Equation 5 may be written as

$$\Lambda\eta = \left(\frac{A_{0\Lambda}-Q_{1\Lambda}N}{A_{0\phi}-Q_{1\phi}N}\right)\exp\left[\frac{k'_\phi-k'_\Lambda}{T\ln[T/(T_{0(0)}+Q_{2Y}N)]}\right] \qquad (8)$$

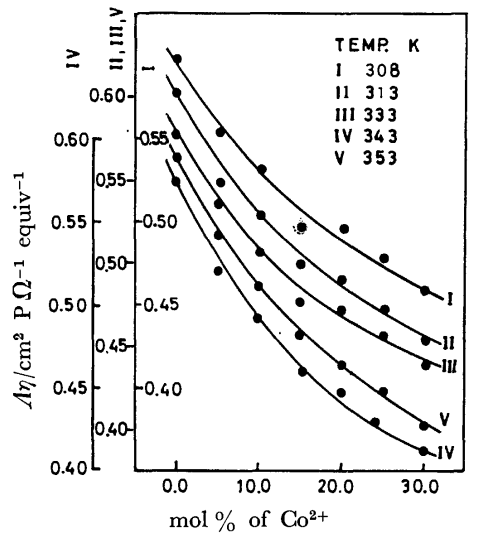

Fig. 6. Variation of $\Lambda\eta$ product with composition for $Zn(NO_3)_2 \cdot 6.27H_2O$-$CoCl_2$ melts.

for describing the composition dependence of $\Lambda\eta$ product. The ratios of the variation of A_Λ and A_ϕ with N seems to be almost independent of composition as the slopes of A_Λ and A_ϕ *vs.* N are nearly equal (Fig. 2). This indicates that the similar species are taking part in the processes of conductance and viscous flows as suggested earlier.[16] Adam and Gibbs[5] also suggested that identical species are responsible for the two kinds of flow. Therefore, the contribution of preexponential factor towards the variation of $\Lambda\eta$ with concentration seems to be negligible and Eq. 8 may be approximated to

$$\Lambda\eta = \left(\frac{A_{0\Lambda}}{A_{0\phi}}\right)\exp\left[\frac{k'_\phi - k'_\Lambda}{T\ln[T/(T_{0(0)}+Q_{2Y}N)]}\right]. \quad (9)$$

From above equation it is apparent that the difference in k_Y terms is almost constant while the denominator of the exponential term decreases with increase in concentration at a given temperature thereby resulting in a monotonous increase in the $\Lambda\eta$ product which is contrary to the observed trend. Instead, the ratio of activation energies for flow processes, $E_\phi/E_\Lambda = n$ is greater than unity, also the value of n increases with the increase in concentration of $CoCl_2$ may be responsible for the overall decrease of the $\Lambda\eta$ product with composition.

Authors are thankful to Professor W. Rahman, Head of the Department of Chemistry, for providing necessary research facilities. Financial assistance of CSIR (India) to two of them (K.P.S. and S.K.) is gratefully acknowledged. Authors are also thankful to Dr. Ismail K for his valuable suggestions during the progress of this work.

References

1) C. A. Angell, *J. Phys. Chem.*, **70**, 3988 (1966); *J. Electrochem. Soc.*, **112**, 1225 (1965).
2) C. T. Moynihan, *J. Phys. Chem.*, **70**, 3399 (1966).
3) N. Islam and Ismail K, *J. Phys. Chem.*, **79**, 2180 (1975); *ibid.*, **80**, 1929 (1976).
4) M. H. Cohen and D. Turnbull, *J. Chem. Phys.*, **31**, 1164 (1959).
5) G. Adam and J. H. Gibbs, *J. Chem. Phys.*, **43**, 139 (1965).
6) N. Islam, S. Kumar, and K. P. Singh, *Bull. Chem. Soc., Jpn.*, **51**, 2712 (1978).
7) N. Islam, S. Kumar, and K. P. Singh, *Can. J. Chem.*, **56**, 1231 (1978).
8) T. Moeller, "Inorg. Synthesis," McGraw-Hill, New York, N. Y. (1957), Vol. V, p. 153.
9) C. N. Reilly, R. W. Schmid, and F. S. Sadek, *J. Chem. Educ.*, **36**, 555 (1959); *ibid.*, **36**, 619 (1959).
10) C. Tanford, "Physical Chemistry of Macromolecules," John-Wiley and Sons, New York, N. Y. (1961), p. 329.
11) H. C. Cowen and H. J. Axon, *Trans. Faraday Soc.*, **52**, 242 (1956).
12) C. T. Moynihan, C. R. Smalley, C. A. Angell, and E. J. Sare, *J. Phys. Chem.*, **73**, 2287 (1969).
13) The Linear variation of A_Y and T_0 *vs.* N may be represented as[3,6]

$$A_Y = A_{0Y} - Q_{1Y}N,$$

and

$$T_0 = T_{0(0)} + Q_{2Y}N.$$

On rearranging the equation for T_0 and substituting into the A_Y equation, we have

$$A_Y = A_{0Y} - \frac{(T_0 - T_{0(0)})}{Q_{2Y}}Q_{1Y}$$

$$= A_{0Y} + \frac{T_{0(0)}Q_{1Y}}{Q_{2Y}} - \frac{Q_{1Y}}{Q_{2Y}}T_0,$$

$$A_Y = \alpha - \beta T_0.$$

14) C. A. Angell, *J. Phys. Chem.*, **68**, 218 (1964); *ibid.*, **68**, 1917 (1964).
15) N. Islam, M. R. Islam, B. Waris, and Ismail K, *J. Phys. Chem.*, **80**, 291 (1976).
16) M. V. Susic and S. V. Mentus, *J. Chem. Phys.*, **62**, 744 (1975).

Solvent Extraction and Spectrophotometric Determination of Palladium with 3-(2-Hydroxy-5-methylphenyl)-5-(*p*-methoxyphenyl)isoxazoline

B. K. Deshmukh* and R. B. Kharat

Department of Chemistry, Nagpur University, Nagpur 440010, India

(Received December 23, 1977)

3-(2-Hydroxy-5-methylphenyl)-5-(*p*-methoxyphenyl)isoxazoline (HMPAO) is used for the simultaneous extraction and direct photometric determination of palladium. About 46 μg of palladium was quantitatively extracted at pH 1.0—2.0 with 10 ml of 1.0×10^{-3} M HMPAO in isobutyl alcohol as a yellowish complex. It was measured spectrophotometrically at 332 nm. The system conformed to Beer's law over the concentration range 1.0—20.0 μg of palladium per ml. The colour of the complex was stable for more than 48 h. Palladium was extracted quantitatively and was determined in the presence of large excess of ions which are associated with it. The extractable species was 1:2 (Pd: HMPAO) in nature. The equilibrium constants were determined according to the methods of Yatsimirskii and Leden with suitable modification.

3-(2-Hydroxy-5-methylphenyl)-5-(*p*-methoxyphenyl)-isoxazoline (HMPAO) is the isomer of 2'-hydroxy-4-methoxy-5'-methylchalcone oxime (HMMCO). The latter has been widely used and studied for the extraction of palladium[1-3] and copper.[3,4] HMPAO has the structural formula

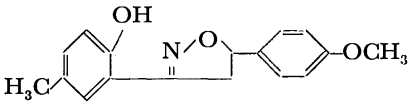

The above reagent forms a light yellow complex with palladium around pH 2.0 which can be measured spectrophotometrically at 332 nm.

The present paper deals with extraction studies of palladium with HMPAO in isobutyl alcohol. The proposed method for determination of palladium is simple, selective and sensitive.

Experimental

Apparatus and Reagent. A model DU 2 Beckman spectrophotometer with 10.0 mm quartz cells, and a model LI-10, ELICO pH meter with glass electrode and saturated calomel electrode and a Ganson Shaker were used.

HMPAO was synthesised from 2'-hydroxy-4-methoxy-5'-methylchalcone as per the method of Borkhade[5] and was crystallised from ethanol. About 0.002 M reagent in isobutyl alcohol was used. Fresh solutions were used.

A stock solution of palladium was prepared by dissolving chloride-free palladium hydroxide obtained from 1 g palladium chloride (Johnson-Matthey) in perchloric acid and was standardized gravimetrically with dimethylglyoxime.[6] The dilute solutions were prepared by appropriate dilution.

General Procedure. An aliquot of solution containing about 46 μg of palladium was taken. After addition of water, the pH of the solution was adjusted to 2.0 with 0.1 M perchloric acid or sodium hydroxide and was made to 10 ml volume. It was then transferred into a 250 ml separatory funnel. The solution was equilibrated with 10 ml of 1.3×10^{-3} M HMPAO in isobutyl alcohol for about 10 min. The light yellow organic phase was measured spectrophotometrically at 332 nm against a reagent blank similarly processed. The amount of palladium was then calculated from the calibration curve.

For interference studies a solution containing the desired ion was added before the pH adjustment.

Table 1. Spectral properties of HMPAO in isobutyl alcohol

λ_{max} / nm	Molar extinction coefficient $\times10^{-4}$	Beer's law range $\times10^{5}$ M
230	2.85	0.4—5.5
258	0.96	0.2—17.0
312	0.50	1.0—23.0

Results and Discussion

Absorption Spectra of HMPAO. The reagent HMPAO exhibits peaks of absorption at 230, 258, and 312 nm in isobutyl alcohol. Spectral data are given in Table 1.

Distribution of Reagent. A 10 ml solution of HMPAO of known concentration, $[HMPAO]_{tot}$, in the isobutyl alcohol was equilibrated with equal volume of aqueous solutions at pH 1.0—12.5 and ionic strength 0.2 M ($NaClO_4$). The concentration of HMPAO in the organic phase, $[HMPAO]_{org}$ was determined by noting the absorbance of the solution at 258 nm against the similarly processed solvent as a blank and reading from the calibration curve. The distribution ratio of HMPAO is thus:

$$D_R = [HMPAO]_{org}/[HMPAO]_{tot} - [HMPAO]_{org}.$$

The results of HMPAO for isobutyl alcohol and water system are shown in Fig. 1. The distribution decreases above pH 11.0 which may be due to dissociation of the phenolic –OH.

Proton-Ligand Stability Constant of HMPAO. If K_1^H is the proton-ligand association constant and P_R the partition constant of HMPAO, then the distribution ratio D_R can be given by[7]

$$1/D_R = 1/P_R + 1/P_R \cdot K_1^H[H^+]. \quad (1)$$

At low pH, $D_R=P_R$, Thus Fig. 1 gives the value of $\log P_R$. The $\log P_R$ for HMPAO between isobutyl alcohol and water becomes 1.82.

The negative slope region of Fig. 1 satisfies the relation

$$\log\frac{(P_R-D_R)}{D_R} = pH - \log K_1^H. \quad (2)$$

This gives the value of $\log K_1^H$ (12.08) for HMPAO (Fig. 2).

Absorption Spectrum of Pd–HMPAO Complex. The

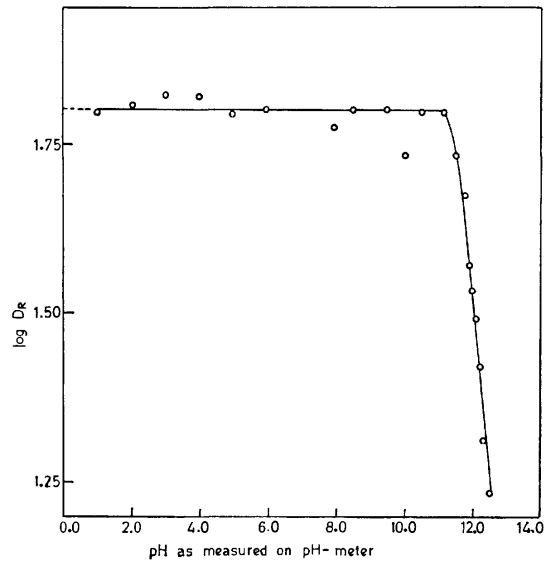

Fig. 1. Distribution of HMPAO between isobutyl alcohol and water as a function of pH-meter reading.

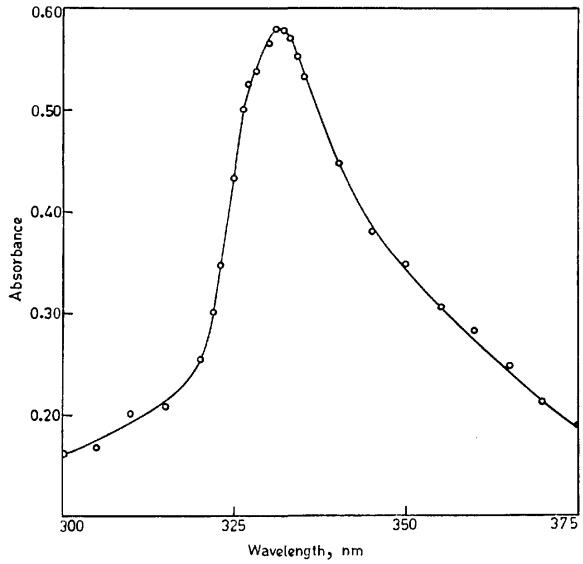

Fig. 3. Absorption spectrum of Pd(II)-HMPAO complex in isobutyl alcohol.

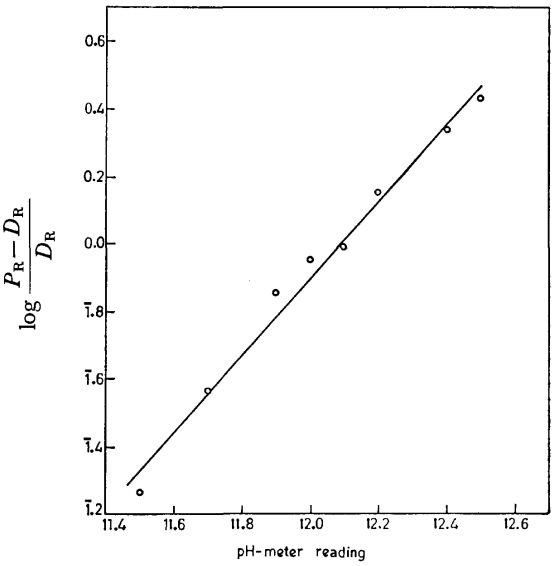

Fig. 2. Plot of $\log \frac{P_R - D_R}{D_R}$ *vs.* pH.

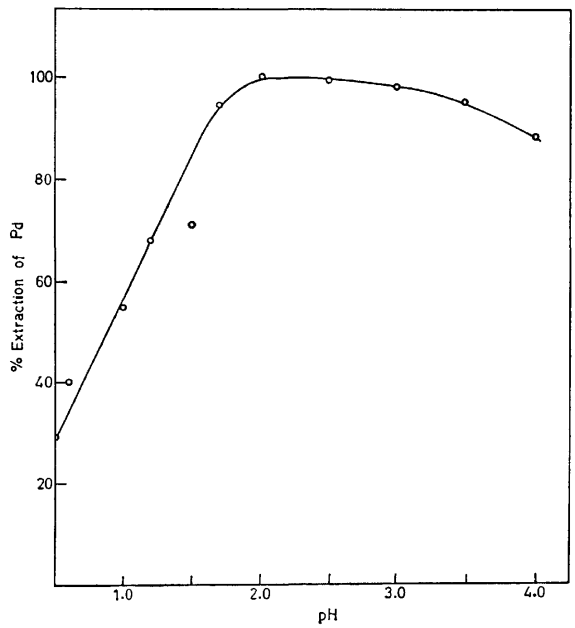

Fig. 4. Effect of pH on extraction of Pd(II).

absorption spectrum of Pd-HMPAO complex (Pd= 46 μg) extracted at pH 2.0 against the reagent similarly processed as a blank is shown in Fig. 3. The light yellow Pd-HMPAO chelate solution shows maximum absorption at 332 nm. The molar absorptivity is 1.3×10^4 at 332 nm and the sensitivity (as per Sandell's definition) is 0.0055 μg/cm^2.

Extraction as a Function of pH. The solvent extraction behaviour of Pd-HMPAO system was studied in the pH range 0.5—6.0 (Fig. 4). It was observed that the extraction is quantitative at pH 2.0. Beyond pH value 2.5 the percentage extraction decreases. Varying amounts of palladium ranging from 1.0 to 20.0 μg per ml were taken. They were extracted at pH 2.0 with 1.3×10^3 M HMPAO in isobutyl alcohol. The light yellow palladium HMPAO system followed Beer's law at 332 nm in the concentration range 1.0—20.0 μg/ml of palladium (Fig. 5). The effective working range from Ringbom curve is 1.0—6.0 μg/ml.

Stability of Colour of the Complex. The absorbance of the coloured complex was measured at interval of 0.5, 8, 16, 24, 48, 96, and 120 h. The value of the absorbance was found to be constant *viz.*, 0.575 until 48 h. The absorbance after 72 h was about 0.500.

Period of Equilibration. With all other factors constant the period of shaking was varied from 2—120 min. The extraction was quantitative when the period of equilibration exceed 10 min.

Effect of Reagent Concentration. The concentration of the reagent was varied from 2.5×10^{-4} to 2.0×10^{-3}M. Extraction was quantitative for the reagent concentration of greater than 1.3×10^{-3} M. It was incomplete

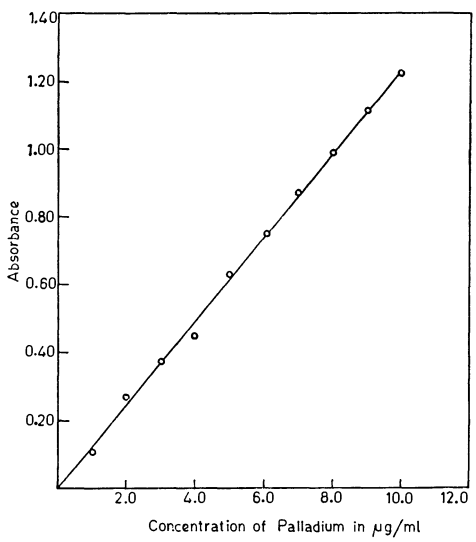

Fig. 5. Beer's law for Pd(II)-HMPAO in isobutyl alcohol.

for lower concentrations of the reagent.

Effect of Palladium Ion Concentration. The effect of Pd concentration on the extraction was examined at different pH values. It was found that the possibility of polymerization can be ruled out in the working range of metal ion concentration 1.0—20.0 μg/ml.

Effect of Ionic Strength. The distribution of palladium was studied at various concentrations of sodium perchlorate (0.2—2.0 M) at pH 2.0. The extent of extraction remains the same up to 0.8 M $NaClO_4$. Above 1.0 M, however, the extent decreases.

Effect of Solvents. Various solvents such as isobutyl methyl ketone, 1-butanol, ethyl acetate, isoamyl alcohol and cyclohexanol were also tried. However, isobutyl alcohol is preferred as it gives a clear separation of the two phases and a less reagent blank absorbance.

Effect of Diverse Ions. The interference of several ions on the extraction behaviour of palladium was studied. The tolerance limit was calculated as the amount necessary to cause ±2% error in the recovery of palladium. The results (Table 2) indicate that moderate amounts of many ions are tolerable. The ions showing strong interference include Cr(III), Sn(II), Ga(III), In(III), Tl(I), and Pt(IV).

Precision and Accuracy. The absorbance obtained for fifteen determinations of 46 μg Pd was 0.575 ±0.005 at 332 nm. Average relative and standard deviations were found to be 1.0 and 1.1%, respectively.

The method is rapid, simple and selective and permits separation and determination of palladium at tracer levels. The entire operation takes only 30 min.

Composition of the Extractable Species. The 1:2 (Pd: HMPAO) composition of the extractable species was determined by Job's[8] method as applied by Irving and Pierce[9] and slope ratio[10] method as modified by Bhatki *et al.*,[11] which was further supported by the distribution data analysis.

Table 2. Effect of diverse ions

[Pd] = 46 μg, pH = 2.0 [HMPAO] = 0.0013 M

Foreign ion	Added as[a]	Tolerance limit μg
Ag^+	$AgNO_3$	500
Al^{3+}	$Al_2(SO_4)_3$	2500
Au^{3+}	$HAuCl_4$	6000
Cd^{2+}	$CdSO_4$	5500
Co^{2+}	$CoSO_4$	12000
Cr^{3+}	$Cr(NO_3)_3$	500
Cu^{2+}	$CuSO_4$	12000
Fe^{2+}	$FeSO_4$	17000
Fe^{3+}	$Fe(NO_3)_3$	3500
Ga^{3+}	$Ga(NO_3)_3$	2600
Hg^{2+}	$HgCl_2$	20000
In^{3+}	$In(NO_3)_3$	600
Mn^{2+}	$MnCl_2$	1000
Ni^{2+}	$NiSO_4$	10000
Os^{8+}	OsO_4	500
Pt^{4+}	H_2PtCl_6	1000
Rh^{3+}	$RhCl_3$	600
Ru^{3+}	$RuCl_3$	300
Sn^{2+}	$SnCl_2$	25000
Th^{4+}	$Th(NO_3)_4$	12000
Ti^{4+}	$TiCl_4$	1000
Tl^+	$TlClO_4$	1500
VO^{2+}	$VOSO_4$	6000
Zn^{2+}	$ZnSO_4$	13000
ZrO^{2+}	$ZrOCl_2$	None
F^-	KF	22000
Cl^-	KCl	36000
Br^-	KBr	40000
SCN^-	KSCN	6000
$S_2O_3^{2-}$	$Na_2S_2O_3$	23000
SO_4^{2-}	Na_2SO_4	19000
NO_2^-	$NaNO_2$	30000
NO_3^-	$NaNO_3$	25000
$Mo_7O_{24}^{6-}$	$(NH_4)_6Mo_7O_{24}$	3000
WO_4^{2-}	Na_2WO_4	2500
PO_4^{3-}	Na_3PO_4	6000
$C_2O_4^{2-}$	$H_2C_2O_2$	6200
CH_3COO^-	CH_3COOH	1300
$Malonate^{2-}$	$(COOH)_2CH_2$	1800
$Tart^{2-}$	Tartaric acid	2200
$Citr^{3-}$	Citric acid	2400
$Ascorb^-$	Ascorbic acid	10000
$EDTA^{4-}$	EDTA (disodium salt)	800

a) Water of crystallisation omitted for the sake of brevity.

Metal-Ligand Formation Constants. The equilibrium constants of Pd–HMPAO chelate were determined from the spectrophotometric data by Yatsimirskii's[12,13] and Leden's[14] methods and are incorporated in Table 3.

It can be seen that the values of $\log k_1$, $\log k_2$, $\log \beta_{ext}$, and $\log \beta_{abs}$ obtained by different methods are in good agreement.

TABLE 3. PRIMARY PARAMETERS AND EQUILIBRIUM CONSTANTS FOR Pd(II)–HMPAO–ISOBUTYL ALCOHOL SYSTEM $\mu=0.2$ M (H^+, Na^+, ClO_4^-): Temperature $=30\pm1$ °C.

Yatsimirskii's method		Lenden's method	
Primary parameter	Stability constant	Primary parameter	Stability constant
$a_1\times10^{-8}=6.9$	$\log k_1=4.85\pm0.02$	$\phi_1\times10^{-5}=0.78$	$\log k_1=4.89\pm0.03$
$a_2\times10^{-11}=-1.58$	$\log k_2=4.71\pm0.05$	[HR]$\rightarrow$0	
$b_1\times10^{-4}=1.35$	$\log \beta_2=9.56\pm0.08$	$\phi_2\times10^{-9}=1.20$	$\log k_2=4.20\pm0.05$
$b_2\times10^{2}=-7.5$	$\log \beta_{ext}=33.36\pm0.1$	[HR]$\rightarrow$0	$\log \beta_2=9.09\pm0.08$
	$\log \beta_{abs}=31.84\pm0.1$		$\log \beta_{ext}=32.89\pm0.1$
			$\log \beta_{abs}=31.37\pm0.1$

Thanks are due to the Council of Scientific and Industrial Research (India) for sponsoring this project and awaring a research fellowship to one of the authors (B.K.D.). They are grateful to Prof. K. N. Munshi for laboratory facilities.

References

1) B. K. Deshmukh, C. N. Vyas, and R. B. Kharat, *J. Indian Chem. Soc.*, **52**, 385 (1975).
2) B. K. Deshmukh and R. B. Kharat, *J. Indian Chem. Soc.*, **53**, 1065 (1976).
3) B. K. Deshmukh and R. B. Kharat, *Z. Anal. Chem.*, **276**, 299 (1975).
4) B. K. Deshmukh and R. B. Kharat, *J. Inorg. Nucl. Chem.*, **37**, 165 (1977).
5) K. T. Borkhade, Ph. D. thesis, Nagpur University (1972).
6) A. I. Vogel, "A Text Book of Quantitative Inorganic Analysis," E.L.B.S., London (1973).
7) C. N. Reilley and F. W. McLafferty, "Advances in Analytical Chemistry and Instrumentation," John Wiley & Sons, New York (1966), Vol. 3, p. 187.
8) P. Job, *Ann. Chim.*, **9**, 113 (1928).
9) H. Irving and T. B. Pierce, *J. Chem. Soc.*, **1939**, 2565.
10) A. E. Harvey and D. L. Manning, *J. Am. Chem. Soc.*, **72**, 4488 (1950).
11) K. S. Bhatki, A. T. Rane, and M. B. Kabadi, *Proc. Symp. Chem. Coord. Compods. Agra* (1959), 89.
12) K. B. Yatsimirskii and V. P. Vasilev, "Instability Constants of Complex Compounds," Pergamon Press, New York (1960).
13) K. B. Yatsimirskii and T. I. Fedorova, *Zh. Neorg. Khim.* **1**, 2301 (1956).
14) I. Leden, *Z. Phys. Chem.*, **188A**, 160 (1941).

Rare Earth Complexes of 1-(2-Pyridylazo)-2-naphthol

I. M. Rao, D. Satyanarayana,* and Umesh Agarwala†

Department of Chemistry, Andhra University, Waltair 530003, India

† *Department of Chemistry, Indian Institute of Technology, Kanpur 208016, India*

(Received January 23, 1978)

The rare earth complexes of 1-(2-pyridylazo)-2-naphthol (PAN=Hpan) are prepared in the solid state. The analytical, molecular weight and differential thermal analysis data of the complexes indicated the metal-ligand ratio as 1:3 with the general formulae $Ln(pan)_3 \cdot H_2O$ (Ln=Pr^{3+}, Nd^{3+}, and Sm^{3+}) and $Ln(pan)_3$ (Ln=La^{3+}, Eu^{3+}, Gd^{3+}, Tb^{3+}, Dy^{3+}, Ho^{3+}, Er^{3+}, and Yb^{3+}). Based on IR, UV, and visible absorption spectra, electrical conductance and magnetic susceptibility data, an octahedral structure having the metal ion bonded through nitrogen of azo and oxygen of carbonyl groups of the ligand has been postulated to these complexes.

The solvent extraction and the potentiometric studies of the complexes of lanthanoids with 1-(2-pyridylazo)-2-naphthol(I), (hereafter referred as PAN=Hpan) have been reported in the literature.[1-4] Besides, PAN has also been used for the detection and the spectrophotometric determination of a large number of metal ions.[5-11] But the synthesis and the characterization of its rare earth metal complexes in the solid state have not so far been reported. In this communication we report

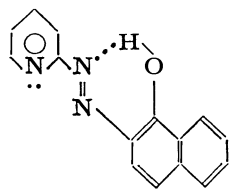

I

the preparation of the lanthanoid complexes of PAN in the solid state. Their probable structures have been established using analytical, IR, UV, and visible spectra, magnetic moment, conductivity, differential thermal analysis, and molecular weights data.

Experimental

All the chemicals used are of Analar or chemically pure grade. PAN (Riedel) was recrystallised from ethanol.[12]

Preparation of the Complexes. On slowly mixing a solution of 1 mmol of rare earth chloride in ethanol (10 ml) with a solution of 1 mmol of PAN in ethanol (40 ml) and adjusting its pH between 8 and 10 by dropwise addition of NaOH solution(0.1 M),** a dark red coloured thick precipitate was obtained. The slurry was then cooled to about 3—4 °C and kept at this temperature for 24 h. The precipitate was separated by centrifugation and it was then extracted several times with ether until the ether layer acquired no colour. The combined ethereal extract was evaporated to dryness whereby the red coloured complex of the lanthanoid was obtained. It was then kept in vacuum desiccator for about 24 h and analysed. Yield 20—25%.

In the above preparation the amount of PAN added to the metal ion solution was always less than the stoichiometric amount (1:1, in place of 3:1). If excess PAN was used, it gets extracted along with the complex into the ether layer which was difficult to remove. By using excess lanthanoid salt, its hydroxide which precipitates along with the metal complex remained unextracted in the ethereal layer.

Analysis. The analyses of the metal ions were carried out gravimetrically by the standard oxalate method.[13,14]

Carbon, hydrogen and nitrogen analyses were performed by the Micro Analytical Section of the Indian Institute of Technology, Kanpur. The analytical results are given in Table 1.

Measurements. The molecular weights of the complexes were determined cryoscopically. The measurements were carried out in purified benzene. The results are given in Table 1.

Magnetic susceptibility measurements were made using a Gouy balance at room temperature (28 °C). Mercury tetrathiocyanatocobaltate(II) was used as a calibrant. The results are given in Table 1.

The conductivity of the complexes were measured in *N,N'*-dimethyl formamide using Philips PR 9500/90 type Conductivity Measuring Bridge. The results are given in Table 2.

The electronic spectra of the ligand and the complexes were obtained in chloroform solutions using a Cary Model 14 Recording spectrophotometer. Their IR spectra were recorded with a Perkin-Elmer 521 Infrared Diffraction Grating spectrophotometer in 4000—250 cm^{-1} range. The samples were prepared as KBr pellets. Positions and assignments of the IR spectral bands of the ligand and the complexes are given in Table 3.

The differential thermal analytical curves were taken on DTA-02 UNIVERSAL (VEB Laborelektronik, Halle, DDR).

Results and Discussion

The analytical data of the complexes indicate the metal ligand ratio as 1:3 with the general formulae $Ln(C_{15}H_{10}N_3O)_3 \cdot H_2O$ (Ln=Pr^{3+}, Nd^{3+}, and Sm^{3+}) and $Ln(C_{15}H_{10}N_3O)_3$ (Ln=La^{3+}, Eu^{3+}, Tb^{3+}, Dy^{3+}, Ho^{3+}, Er^{3+}, Yb^{3+}, and Gd^{3+}). Their monomeric nature in solution is confirmed by the experimental values of the molecular weights (Table 1).

The equivalent conductance values of the complexes in DMF at 28 °C when compared with those already reported[15] indicate that they are non-electrolytes. This is further supported by their insolubility in water, and high solubility in most of the non-aqueous solvents like $CHCl_3$, CCl_4, ether, C_6H_6, *etc.* These complexes when dissolved in organic solvents are not very stable and the deep red coloured solution gradually changes to orange yellow.

PAN has been reported to be a tridentate ligand where the bonding sites to the metal ion are oxygen of the hydroxyl group after deprotonation, azo and the pyridine nitrogen atoms.[8,16-18] In order to investigate the bonding sites in the complexes the spectral and the magnetic studies have been carried out.

** 1 M=1 mol/dm^3.

Table 1. Analytical data, molecular weight and magnetic moments of the complexes

S. No.	Formula of the complex	Calcd %					Found %					Color	Mp °C	μ_{eff} (B.M.)
		mol wt	C	H	N	Metal	mol wt	C	H	N	Metal			
1	$La(C_{15}H_{10}N_3O)_3$	884	61.16	3.41	14.27	15.72	900.0	61.00	3.80	13.90	16.48	Dark red	133	Dia
2	$Pr(C_{15}H_{10}N_3O)_3 \cdot H_2O$	903	59.81	3.57	13.95	15.59	923.4	59.94	3.80	13.84	15.41	Dark red	220	3.85
3	$Nd(C_{15}H_{10}N_3O)_3 \cdot H_2O$	907	59.60	3.56	13.90	15.90	920.0	59.69	3.77	14.17	15.67	Dark red	296	3.87
4	$Sm(C_{15}H_{10}N_3O)_3 \cdot H_2O$	913	59.17	3.53	13.80	16.46	917.0	58.60	3.78	13.75	16.96	Dark red	297	1.60
5	$Eu(C_{15}H_{10}N_3O)_3$	897	60.29	3.38	14.06	16.95	912.6	60.22	3.31	14.21	16.39	Dark red	302	3.30
6	$Gd(C_{15}H_{10}N_3O)_3$	902	59.92	3.35	13.98	17.42	880.0	59.30	3.36	13.85	17.13	Dark red	305	7.30
7	$Tb(C_{15}H_{10}N_3O)_3$	904	59.81	3.35	13.95	17.59	931.3	60.00	3.50	14.10	17.74	Dark red	299	9.06
8	$Dy(C_{15}H_{10}N_3O)_3$	907	59.58	3.33	13.90	17.91	890.2	60.10	3.60	13.80	17.35	Dark red	302	10.48
9	$Ho(C_{15}H_{10}N_3O)_3$	909	59.41	3.32	13.87	18.12	926.4	59.26	3.77	14.32	18.30	Dark red	294	10.54
10	$Er(C_{15}H_{10}N_3O)_3$	912	59.27	3.32	13.82	18.34	928.1	59.64	3.88	13.35	18.34	Dark red	249	9.69
11	$Yb(C_{15}H_{10}N_3O)_3$	918	58.88	3.29	13.73	18.85	940.4	59.24	3.30	14.00	19.02	Dark red	231	4.70
12	Ligand $C_{15}H_{11}N_3O$	—	72.00	4.40	16.80	—	—	72.20	3.80	16.50	—	Orange	—	—

Table 2. Molar conductance of complexes in DMF solution temperature 28 °C

S. No.	Metal complex	Concentration mol $l^{-1} \times 10^3$	λ ohm s^{-1} cm^2
1	$La(C_{15}H_{10}N_3O)_3$	1.621	41.21
2	$Pr(C_{15}H_{10}N_3O)_3 \cdot H_2O$	0.850	6.58
3	$Nd(C_{15}H_{10}N_3O)_3 \cdot H_2O$	0.904	3.95
4	$Sm(C_{15}H_{10}N_3O)_3 \cdot H_2O$	1.109	1.99
5	$Eu(C_{15}H_{10}N_3O)_3$	1.307	1.81
6	$Gd(C_{15}H_{10}N_3O)_3$	0.878	1.01
7	$Tb(C_{15}H_{10}N_3O)_3$	1.093	0.58
8	$Dy(C_{15}H_{10}N_3O)_3$	1.009	0.51
9	$Ho(C_{15}H_{10}N_3O)_3$	0.959	0.24
10	$Er(C_{15}H_{10}N_3O)_3$	1.338	1.18
11	$Yb(C_{15}H_{10}N_3O)_3$	0.527	0.44

Table 3. Positions and assignments of the IR spectral bands of the ligand and complexes

Ligand (PAN) cm^{-1}	Complexes cm^{-1}	Assignment
3080	3080	ν(C-H)
3020	3020	ν(C-H)
1620	1550—1555	ν(C=O)
1570	1510—1515	ν(N=N)
1450	1390—1375	ν(N=N)
1230	—	δ(C-O-H)
1615, 1600, 1525, 1415, 1325, 1310, 1270, 1150, 1040, 995, 880, 850, 800, 780, 765	Same position as in the spectrum of PAN (± 5 cm^{-1})	Bands due to pyridyl and naphthyl rings
—	450—555	Two bands due to ν(M-N) + ν(M-O)

Infrared Spectra. Although the spectra of PAN and its chelates are complicated owing to the extensive overlap of a number of bands arising due to ν(N=N), ν(C=N), ν(C=C), ν(C-H) and other bending modes in the region below 1700 cm^{-1}, the systematic shifts in the positions of a few ligand bands in the spectra of the complexes suggest the probable modes of bonding in the complexes. Some of these major shifts along with the conclusions drawn from them are given below.

a) The absorption bands observed at 3020 and 3080 cm^{-1} in the spectrum of PAN are due to ν(C-H). These bands are stable in position as well as in intensity when one goes from the ligand to the metal chelates indicating that these are purely due to ν(C-H). It is interesting to note that instead of a well defined band, only a very broad and weak band appeared in the spectrum of the ligand around 3300 cm^{-1} due to ν(O-H). This suggests a strong intramolecular hydrogen bonding in the ligand which was confirmed earlier by NMR studies.[5] In the spectra of all the metal chelates except those of Pr^{3+}, Nd^{3+}, and Sm^{3+}, the intensity of the very broad band further decreased; but in the spectra of Pr^{3+}, Nd^{3+}, and Sm^{3+} chelates, the weak and broad band was evident indicating the presence of water molecule in these chelates.

b) The ligand molecule can exist in equilibrium both in azo and hydrazone forms as shown in II and III. An intense band observed at 1620 cm^{-1} in the

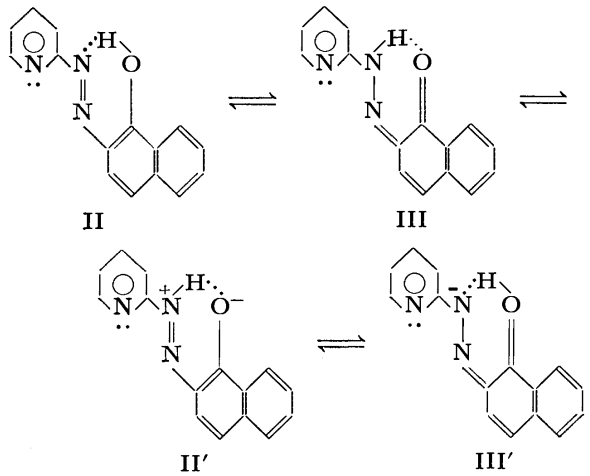

II III

II′ III′

spectrum of the ligand may be due to ν(C=O) of the hydrogen bonded ring systems of the hydrazone form. Although the carbonyl band normally should appear around 1700 cm^{-1}, such a bathochromic shift

is observed in hydrogen bonded ring systems.[19-20] The band at 1620 cm^{-1} in the ligand is shifted to lower frequencies (1550—1555 cm^{-1}) in the metal chelate spectra as a result of the involvement of the C=O··· linkage in metal chelate ring as shown in IV.

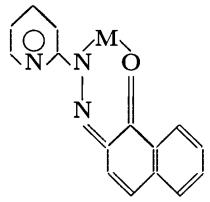

IV

c) The absorption bands due to azo linkage are generally observed at 1410 and 1570 cm^{-1}.[21] The main difficulty in the assignment of a frequency to azo linkage is that the band due to ν(N=N) would overlap with other absorption bands such as those of pyridine and/or naphthol rings. However, the positions of the two bands at 1570 and 1450 cm^{-1} present in the ligand spectrum are shifted to 1510 and 1375 cm^{-1}, respectively. These shifts suggest the linkage of the metal ion with the azo group of the ligand. Since the positions of the other pyridine bands are not changed in the spectra of the chelates, it further suggests that the pyridine moiety of the ligand is possibly not involved in bonding.

d) A band at 1230 cm^{-1} present in the spectrum of the ligand was missing from the spectra of all the chelates. Hadzi[22] has assigned a band at 1272 cm^{-1} in the spectra of similar azo compounds to the in-plane bending mode of C–O–H group. It is possible that the band at 1230 cm^{-1} may arise due to the in-plane bending mode of C–O–H and the fact that the corresponding band is missing in the spectra of metal chelates suggests the deprotonation of the C–O–H group for the bond formation. This is essential in order to keep a charge balance between the metal ion and the ligand molecules.

e) Two new bands appeared in the spectra of all the chelates between 450 and 550 cm^{-1}. They may be coupled bands having contributions from both ν(M–O) and ν(M–N).

The IR spectral study, thus, suggests the bonding of the metal ions with the oxygen atom of the carbonyl and the nitrogen of the azo groups of the ligand.

Electronic Spectra. The positions of absorption bands in the spectrum of PAN in the aqueous and non-aqueous media corresponded with those given in the literature.[7] It presented three well defined broad maxima in the visible region (555, 480, and 415 nm) besides other bands due to pyridine and 2-naphthol moiety in the UV region. The 480 nm band has two shoulders one at 465 nm and the other at 510 nm. The peaks at 555 and 510 nm may be attributed to the hydrazone form (III and III′) whereas the short wave maxima (480, 465, and 415 nm) due to azo (II and II′) chromophore.[22-25] In the spectra of all the chelates the bands at 555 nm and the shoulder band at 510 nm are intensified to a very large extent. Further, the shoulder band at 465 nm and the one at 415 nm showed a bathochromic shift ($\approx$10 nm). There was also a lowering in the intensity of the band at 460 nm. The positions of all the bands in the UV region remained practically constant. It, therefore, appears that in the chelate formation, the nitrogen atom of the azo group and the oxygen atom of the C–O–H group after deprotonation are taking part. It is interesting to note that the relative increase in the intensity of 555 and 510 nm bands and also the relative decrease in the intensity of 465 nm band compared to that of 485 nm band decreases with the increase in the atomic number of the metal ion. Similar effect is observed in the bathochromic shift of the 465 and 415 nm bands (the higher the atomic number, the lower the shift). This correlation may be due to the fact that the interaction of the metal ion decreases with the increase in atomic number.

The bands due to f-f transitions corresponding to the metal ions could not be located in the spectra of the chelates. This is what one should expect because the bands due to metal ions will be very weak ($\varepsilon\approx$ 1—10) and they will be masked by the intense bands of the ligand molecule.

Magnetic Moments. The values of the magnetic moments of the complexes are summarized in Table 1. These values compare very well with those measured for other simple compounds[26] and those calculated for the uncomplexed ions.[27,28] The relatively small differences from the calculated values of Van Vleck suggest either minor or no involvement of the 4f orbitals in the bonding.

The differential thermal analysis curves indicated in general the decomposition of the complexes around 250—300 °C. In case of Pr^{3+}, Nd^{3+}, and Sm^{3+} complexes a dehydration step beginning at about 80 °C is observed indicating the presence of water molecule in these complexes as water of hydration.

Thus, on the basis of the above studies, the octahedral structure of the complexes having metal ion bonded through nitrogen of azo and oxygen of carbonyl group of the ligand has been proposed.

The authors wish to thank Apache Chemicals, Inc. Illinois (USA) for providing rare earth oxides as gift. One of us (I. M. Rao) thank the Council of Scientific and Industrial Research, New Delhi, India, for the award of Junior Research Fellowship.

References

1) S. Shibata, *Anal. Chim. Acta*, **23**, 367 (1960).
2) S. Shibata and I. Ishiguro, *Nagoya Kogyo Gijutsu Shikensho Hokoku*, **11**, 318 (1962).
3) S. Shibata, *Anal. Chim. Acta*, **28**, 388 (1963).
4) Chang Tiao-Hsu, Lin Ai-Ling, and Y. Su-Ing, *Hua Hsuch.*, **4**, 111 (1971).
5) D. Betteridge and D. John, *Analyst*, **98**, 377 (1973).
6) K. L. Cheng and R. H. Bray, *Anal. Chem.*, **27**, 782 (1955).
7) B. F. Pease and M. B. Williams, *Anal. Chem.*, **31**, 1044 (1959).
8) S. Shibata, *Anal. Chim. Acta*, **25**, 348 (1961).
9) R. Püschel, *Z. Anal. Chem.*, **221**, 132 (1966).
10) N. Desai and H. Gandhi, *Chim. Anal. (Paris)*, **50**,

297 (1968).
11) M. Langova-Hniličkova and L. Sommer, *Folia. Fac. Sci. Nat. Univ., Purkyniahae Brno.*, **9**, 2 (1968).
12) S. Shibata in "Chelates in Analytical Chemistry," ed by H. A. Flaschka and A. J. Barnard, Jr., Marcel Dekker, New York (1972), Vol. IV, p. 17.
13) I. M. Kolthoff and P. J. Ewing, "Treatise on Analytical Chemistry," Interscience, New York (1963), Part II, Vol. 8, pp. 29, 51.
14) C. L. Wilson and D. W. Wilson, "Comprehensive Analytical Chemistry," Elsevier Pub. Co., Amsterdam (1962), Vol. 1C, pp. 449, 452.
15) W. J. Geary, *Coord. Chem. Rev.*, **7**, 81 (1971).
16) S. Ooi, D. Carter, and Q. Fernando, *Chem. Commun.*, **24**, 1301 (1967).
17) J. A. Szabō and V. Nikolasev, *Acta Phys. Chem.*, **15**, 59 (1969).
18) W. J. Geary, G. Nickless, and F. H. Pollard, *Anal. Chim. Acta*, **27**, 71 (1962).
19) R. S. Rasmussen, D. D. Tunnicliff, and R. R. Brattain, *J. Am. Chem. Soc.*, **71**, 1068 (1949).
20) L. J. Bellamy and L. Beecher, *J. Chem. Soc.*, **1954**, 4487.
21) R. J. W. Le Fevré, M. F. O'Dwyer, and R. L. Werner, *Aust. J. Chem.*, **6**, 341 (1953).
22) D. Hädzi, *J. Chem. Soc.*, **1956**, 2143.
23) A. Burawoy and I. Markowitsch, *Ann.*, **503**, 180 (1933); **504**, 71 (1933).
24) R. Kuhn and F. Bär, *Ann.*, **516** 143 (1935).
25) P. Ramart-Lucas, *Bull. Soc. Chim. Fr.*, **11**, 75 (1944).
26) T. Moeller, "Comprehensive Inorganic Chemistry," 1st ed Pergamon Press, New York (1973), Vol. 4, Chap. I, p. 11.
27) J. H. Van Vleck and A. Frank, *Phys. Rev.*, **34**, 1494, 1625 (1929).
28) F. Hund, *Z. Phys.*, **33**, 855 (1925).

Extraction-Spectrophotometric Determination of Vanadium(V) Employing N^1-Hydroxy-N^1,N^2-diarylbenzamidines and Various Adduct-forming Substances

K. S. PATEL* and R. K. MISHRA

Department of Chemistry, Ravishankar University, Raipur, M.P., India

(Received March 13, 1978)

The reactions of 16 newly synthesized N^1-hydroxy-N^1,N^2-diarylbenzamidines with vanadium(V) in presence of various adduct-forming substances have been investigated photometrically in chloroform. The present study indicated the formation of 1:2:1 metal:reagent:acetic acid or phenol and 1:2:2 metal:reagent:thiocyanate complexes. On the basis of strong synergism, which is attributed to mixed-complex formation, simple, rapid, sensitive and selective methods for the spectrophotometric determination of microgram quantities of vanadium(V) have been developed. The influence of experimental variables on the procedures have been discussed.

A number of monobasic and bidentate chelating agents[1-15] react with vanadium(V) to form 1:2 (metal: ligand) complex having a basic V=O group and an acidic V–OH group in the same molecule. The basic V=O group reacts with acidic substances like carboxylic acids, hydrogen chloride, phenols *etc.* to produce hyper- and bathochromic effects. N^1-Hydroxy-N^1,N^2-diarylbenzamidines, a new type of monobasic and bidentate chelating agents possessing the function, I, react with

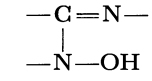

Formula I.

vanadium(V) to form coloured 1 : 2 (metal : ligand) complexes. It is very likely that the basic V=O group of the complexes reacts with acidic substances such as acetic acid, phenol, *p*-chlorophenol and 2-naphthol to produce hyper- and bathochromic effects in chloroform solution, accompanied by synergism. The formation of both 1:2:1 (metal:ligand:acetic acid or phenol) and 1:2:2 (metal:ligand:thiocyanate) complexes is adaptable to the development of sensitive and selective methods for the spectrophotometric determination of traces of the metal.

The selectivity of the method for vanadium(V) employing N^1-hydroxy-N^1,N^2-diarylbenzamidines enables the direct determination of vanadium in steels and other materials.[16] This and other excellent qualities of *N*-hydroxyamidines as reagents for vanadium(V) gave us an encouragement to search for better reagents amongst the family of *N*-hydroxyamidines. A number of compounds of the general formula, II, have, therefore, been synthesized and examined as possible reagents for vanadium(V).

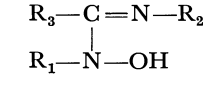

Formula II.

R_2 is phenyl, *p*-tolyl, *m*-tolyl, 2,5-dimethylphenyl, or 2-methyl-4-chlorophenyl; R_1 is phenyl, *p*-tolyl, *m*-tolyl, or *p*-chlorophenyl; R_3 is *p*-tolyl.

Of the 16 reagents examined in the present investigation N^1-hydroxy-N^1-(*p*-chlorophenyl)-N^2-(2-methyl-4-chlorophenyl)-*p*-toluamidine hydrochloride (HCPMCPTH), which has the largest molar absorptivity for its vanadium(V) complexes has been studied in detail.

Experimental

Apparatus and Solutions. A Carl Zeiss Specord recording ultraviolet-visible spectrophotometer and an ECIL UV-VIS spectrophotometer model GS-865 equipped with 1-cm quartz and silica cells were employed for recording spectra and absorbance measurements respectively. Systronic pH meter Type-322 was employed for the determination of pH values of the solutions. Twice distilled water and ethanol-free chloroform were used for solution preparations.

A stock solution of vanadium(V) was prepared by dissolving ammonium metavanadate in water and the solution standardized volumetrically with potassium permanganate.[20]

Solutions of cations were prepared from analytical reagent grade chlorides, sulfates or nitrates and those of anions were obtained by dissolving their sodium or potassium salts.

Reagents. N^1-Hydroxy-N^1,N^2-diarylbenzamidines were prepared by the condensation of equimolar quantities of *N*-aryl-*p*-toluimidoyl chloride and *N*-arylhydroxylamine in ether medium.[16,21] The resulting hydrochloride was filtered and crystallized from absolute alcohol. The free bases were obtained by treatment of hydrochlorides with dilute ammonia solution and crystallized from benzene:petroleum ether (2:1). All these compounds gave satisfactory C, H, and N analyses. 0.005 M (1 M=1 mol/dm^3) solutions of these reagents were used for extraction studies.

Procedure. Transfer an aliquot of vanadium(V) solution to a separatory funnel. Add suitable quantity of adduct-forming substance. Dilute to 25 ml with distilled water and add 10 ml of chloroform solution of the reagent. Shake the contents of the funnel vigorously for 2 min and allow the phases to separate. Dry the chloroform extract over anhydrous sodium sulfate and transfer to 25-ml volumetric flask. Dilute the extracts to 25 ml with chloroform and scan the absorption spectrum of the coloured extract against chloroform or reagent blank.

Results and Discussion

Absorption Spectra. The absorption spectra of vanadium–HCPMCPTH complex in the absence and presence of adduct-forming substances are shown in Fig. 1. When adduct-forming substances are added to chloroform solution of vanadium–HCPMCPTH complex, a hyper- and bathochromic effect is noticed which is attributed to mixed complex formation. The λ_{max} and ε depend on the nature of *N*-hydroxyamidine and the adduct-forming substance. The spectral characteristics of vanadium complexes of HCPMCPTH

Table 1. Spectral characteristics of vanadium-HCPMCPTH complex in the presence of acetic acid, thiocyanate, and phenols

Adduct-forming substance	Optimum acidity ranges of acetic acid / M	Color	λ_{max} / nm	ε / $l\,mol^{-1}\,cm^{-1}$	Optimum concn ranges from Beer's law (Optimum concn ranges from Ringbom plot) ppm of V	Sensitivity $\mu g\,cm^{-2}$ of V	Relative standard deviation[a] / %
Acetic acid	1.0—10.0	BV	580	2900	1.0—16.0 (2.0—13.0)	0.017	±0.80
Thiocyanate	0—2.0	DG	610	6500	1.0—7.0 (1.5—6.0)	0.0080	±0.60
Phenol	0—3.0	B	590	6300	1.4—7.0 (1.6—6.5)	0.0085	±0.52
p-Chlorophenol	0—2.5	B	600	6800	1.0—7.0 (1.2—6.0)	0.0075	±0.74
2-Naphthol	0—3.0	GB	620	6500	1.2—7.0 (1.5—6.4)	0.0080	±0.50

BV, blue-violet; DG, deep-green; B, blue; GB, greenish-blue; O, pH 3.0.
a) 10 measurement are made, each containing 4 ppm of V.

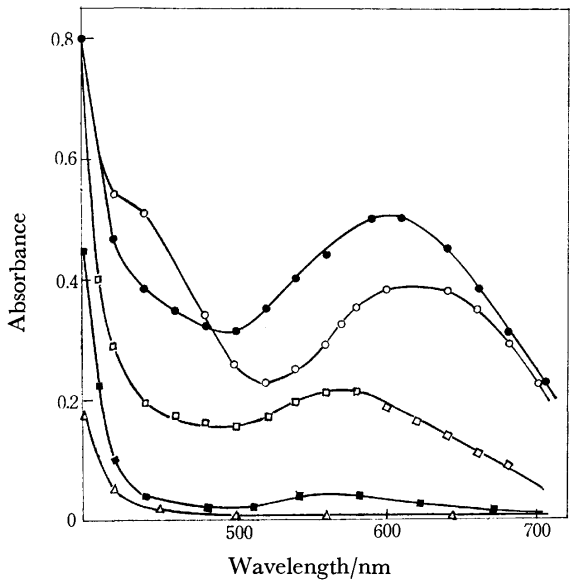

Fig. 1. Absorption spectra.
●: 7.35×10^{-5} M C_V + 0.003 M $C_{HCPMCPTH}$ + 0.03 M *p*-chlorophenol, ○: 5.84×10^{-5} M C_V + 0.003 M $C_{HCPMCPTH}$ + 0.01 M thiocyanate, □: 7.40×10^{-5} M C_V + 0.003 M $C_{HCPMCPTH}$ + 1 M acetic acid, ■: 6.40×10^{-5} M C_V + 0.003 M $C_{HCPMCPTH}$, △: 0.003 M $C_{HCPMCPTH}$.

are recorded in Table 1.

Effect of Reagents Temperature and Time. For complete extraction of vanadium(V), acetic acid system requires a 12 fold molar excess of *N*-hydroxyamidine, whereas the optimal amount of *N*-hydroxyamidine required for quantitative transfer of the metal to organic phase following thiocyanate and phenol systems are 6 and 3 fold molar excess of the reagent respectively. The thiocyanate and phenol systems necessitate 8 and 250 fold molar excess of thiocyanate and phenols respectively for complete extraction of vanadium(V). Order of addition of reagents is not critical. Variation in temperature from 20 to 35 °C does not affect the λ_{max} and absorbance of coloured systems.

The extracts of acetic acid and thiocyanate systems are stable at least 50 and 35 h respectively. The HCPMCPTH–phenol–vanadium complexes are stable in chloroform for at least 30 h at 27±2 °C.

Nature of Adducts. The composition of the adducts were determined by various methods. The ratio of vanadium to *N*-hydroxyamidine was determined by mole ratio[22] and continuous variation methods,[23] and vanadium to adductant by curve fitting method.[24] In the thiocyanate system the ratio of vanadium to thiocyanate was determined by mole ratio method and slope ratio method.[25] The results indicate that V:HOAm:L (acetic acid or phenol) ratio in adduct is 1:2:1 and in thiocyanate system V:HOAm:SCN ratio is 1:2:2 as indicated in the V(V)–8-quinolinol–thiocyanate complex.[26]

N¹-Hydroxy-N¹,N²-diarylbenzamidines as Reagents for Vanadium(V). All the 16 newly synthesized reagents were tested for their potentialities towards the spectrophotometric determination of vanadium(V). Beer's law was tested and confirmed for each system. All these compounds reacted with vanadium in presence of adduct-forming substances in a similar manner with only slight variation in the value of λ_{max} and ε. The vanadium–*N*-hydroxyamidine–acetic acid complexes possess λ_{max} in the range 570—585 nm with molar absorptivities in the range 2900—4300 $l\,mol^{-1}\,cm^{-1}$. The thiocyanato–vanadium complexes of these reagents show maximum absorption at 605—610 nm (ε=5100—6500). The vanadium complexes of the present reagents in the presence of phenol, *p*-chlorophenol and 2-naphthol have absorption maxima at 590—595 (ε=4600—6650), 595—600 (ε=4950—6800), and 590—620 nm (ε=4600—6650) respectively. The substitution of N^1-phenyl group(R_1) or N^2-phenyl group(R_2) with aryl groups has only slight bathochromic effect. Of the various group tested, *p*-chlorophenyl causes highest hyperchromic shift, when attached to hydroxylamine nitrogen atom. Substitution of R_2 with 2-methyl-4-chlorophenyl group results into the highest hyperchromic shift in the thiocyanate, *p*-chlorophenol

and 2-naphthol complexes.

Effect of Diverse Ions. To evaluate the tolerance limits for different ions, solutions containing 4 ppm of vanadium(V) and varying amounts of other ions were analyzed as described above. Absorbance errors above 2% were considered to indicate interference.

In acetic acid system, tungsten(VI) seriously interfered. The system, however, tolerates the presence of the following ions, the tolerance limits of which are given in parentheses(ppm): citrate(500); tartrate(600); fluoride(500); chloride, bromide, nitrate, or sulfate (1500); phosphate(1000); arsenate(400); phthalate (800); triethanolamine or selenate(1000); alkali elements (1500); alkaline-earth elements(1000); lanthanoid elements(1000); Ni^{2+}, Zn^{2+}, Cd^{2+}, or Hg^{2+}(800); Cu^{2+}(600); Co^{2+}(700); Sb^{3+}(750); Bi^{3+}(600), Cr^{3+} (500); Th^{4+}(800); Tl^{3+}(1000); Pb^{2+}(800); Mn^{2+}(700); Fe^{3+}(800); Be^{2+}(1000); Ti^{4+}(20); Zr^{4+}(60), and Mo^{6+} (400).

In *p*-chlorophenol system iron(III) and tungsten-(VI) interfered. However, the interference due to Fe^{3+} was eliminated by masking with trisodium phosphate. The tolerance limits for various ions are shown in parentheses(ppm): Ni^{2+}, Co^{2+}, Zn^{2+}, Cd^{2+} Hg^{2+} (600); Pb^{2+}, UO_2^{2+}(500); Mo^{6+}(200); Zr^{4+}(100); Ti^{4+} (40); Cu^{2+}(200); Bi^{3+}, Fe^{3+}(800); Sb^{3+}(600); Al^{3+}, Cr^{3+}(500), and Th^{4+}(600). Alkali and alkaline-earth elements and lanthanoid elements, chloride, bromide, iodide, fluoride, nitrate, sulfate, citrate, tartrate, arsenate, phosphate, phthalate and borate have no interfering effect.

In thiocyanate system the interference due to Fe^{3+} was removed by masking with trisodium phosphate. The tolerance limits for other ions are indicated in parentheses(ppm): Cr^{3+}, Al^{3+}(500); UO_2^{2+}(400); Zr^{4+}(100); Mo^{6+}(300); Cu^{2+}(200); Co^{2+}, Ni^{2+}, Cd^{2+}, Zn^{2+}, Hg^{2+}(500); Ti^{4+}(60); W^{6+}(20); Fe^{3+}(800); Th^{4+} (800). Alkali metals, alkaline-earths, lanthanoid elements, chloride, bromide, fluoride, nitrate, sulfate, arsenate, phosphate, phthalate, borate, citrate and tartrate have no interfering effect on the determination.

References

1) D. E. Ryan, *Analyst*, **85**, 569 (1960).
2) A. J. Blair and D. A. Pantony, *Anal. Chim. Acta*, **13**, 1 (1955).
3) H. E. Jungnickel and W. Klinger, *Z. Anal. Chem.*, **203**, 257 (1964).
4) H. Kohara, N. Ishibashi, and Y. Ito, *Bunseki Kagaku*, **16**, 315 (1967).
5) O. Menis and C. S. P. Iyer, *Anal. Chim. Acta*, **55**, 89 (1971).
6) H. Kohara, N. Ishibashi, T. Hanamura, and K. Ueno, *Bunseki Kagaku*, **15**, 938 (1966).
7) I. Kojima and M. Tanaka, *J. Inorg. Nucl. Chem.*, **29**, 1769 (1967).
8) E. M. Donaldson, *Talanta*, **17**, 583 (1970).
9) H. Kawamoto and H. Akaiwa, *Nippon Kagaku Kaishi*, **1973**, 90.
10) A. J. Blair, D. A. Pantony, and G. I. Minkoff, *J. Inorg. Nucl. Chem.*, **5**, 316 (1958).
11) F. Buscarons, J. L. Marin, and J. Claver, *Anal. Chim. Acta*, **3**, 310, 417 (1949).
12) M. Tanaka and I. Kojima, *Anal. Chim. Acta*, **41**, 75 (1968).
13) I. Kojima and M. Tanaka, *Anal. Chim. Acta*, **75**, 367 (1975).
14) I. Kojima and Y. Miwa, *Anal. Chim. Acta*, **83**, 329 (1976).
15) V. Pandu Range Rao and Y. Anjaneyulu, *Mikrochim. Acta*, **4**, 481 (1973).
16) K. Satyanarayana and R. K. Mishra, *Anal. Chem.*, **46**, 1609 (1974).
17) K. K. Deb and R. K. Mishra, *Curr. Sci.*, **45**, 134 (1976); **47**, 341 (1978).
18) K. Satyanarayana and R. K. Mishra, *Indian J. Chem.*, **13**, 295 (1975).
19) K. Satyanarayana and R. K. Mishra, *J. Indian Chem. Soc.*, **53**, 63, 469, 928 (1976).
20) G. Gharlot and D. Bezier, "Quantitative Inorganic Analysis," John Wiley, New York (1957).
21) K. K. Deb and R. K. Mishra, *J. Indian Chem. Soc.*, **53**, 178 (1976).
22) J. H. Yoe and A. L. Jones, *Ind. Eng. Chem., Anal. Ed.*, **16**, 111 (1944).
23) P. Job, *Ann. Chim. (Paris)*, **9**, 113 (1928).
24) L. G. Sillen, *Acta Chem. Scand.*, **10**, 185 (1956).
25) A. E. Harvey, Jr. and D. L. Manning, *J. Am. Chem. Soc.*, **72**, 4488 (1950).
26) V. Pandu Ranga Rao, and Y. Anjaneyulu, *J. Inorg. Nucl. Chem.*, **33**, 3567 (1971).

Studies on N^1-Hydroxy-N^1,N^2-diarylbenzamidines as Metal Complexing Agents: Extraction-Photometric Determination of Iron(III) as Thiocyanato and Azido Mixed Ligand Complexes with N^1-Hydroxy-N^1,N^2-diphenyl-*p*-toluamidine(HDPTA)

K. S. PATEL,* Kanak Kanti DEB, and Rajendra K. MISHRA
Department of Chemistry, Ravishankar University, Raipur, M.P., India
(Received June 3, 1978)

N^1-Hydroxy-N^1,N^2-diarylbenzamidines react with iron(III) in presence of thiocyanate and azide forming coloured complexes which are quantitatively extractable in benzene. The extraction of iron(III) as red Fe(III)–L–$(SCN^-)_2$ complex is quantitative at 0.1—0.6 M hydrochloric acid concentration, whereas the Fe(III)–L–$(N_3^-)_2$ complex gets quantitatively extracted into benzene at pH 1.0—2.5. The ternary iron(III)-thiocyanato complex of N^1-hydroxy-N^1,N^2-diphenyl-*p*-toluamidine(HDPTA) has a fairly large molar absorptivity (1.01×10^4 l mol^{-1} cm^{-1}) and the spectrophotometric method based on this colour reaction is highly selective as almost all common ions including Fe(II) do not interfere. The method employing the formation of ternary iron(III): HDPTA: azide complex is also highly selective.

Thiocyanate is frequently used for the spectrophotometric determination of traces of iron(III).[1] This method, which is simple, rapid, fairly sensitive and free from interference of Fe(II), and can be applied in strongly acidic medium, suffers from interference due to a large number of experimental factors. These include time of standing, thiocyanate concentration, non-linearity of Beer's law *etc.* Even the modified method[2] lacks selectivity as various elements such as manganese, zinc, cadmium, copper, nickel, coblat, titanium, uranium, and molybdenum interfere.[3,4] A recent investigation bases the formation of ternary iron(III)–thiocyanate–*N*-hydroxyethylenediamine-*N*,N^1,N^1-triacetate to develop a fairly selective spectrophotometric method,[5] but only at the expense of sensitivity.

N^1-Hydroxy-N^1,N^2-diarylbenzamidines,[6–8] a new type of reagents react with iron(III) forming blue[9] and red-purple[10] pH dependent complexes in ethanol. However, in the presence of thiocyanate these reagents produce an intensely red ternary complex which is quantitatively extractable into benzene from hydrochloric acid solutions. The present paper reports the use of N^1-hydroxy-N^1,N^2-diphenyl-*p*-toluamidine (HDPTA) and 18 analogous compounds possessing the general formula-I, for the extractive-spectrophotometric determination of microgram quantitities of iron(III). The present method is sensitive and highly

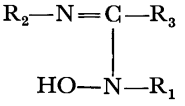

Formula I.

R_3 is *p*-tolyl; R_2 is phenyl, *p*-tolyl, *m*-tolyl, 2,5-dimethylphenyl, 2-methyl-4-chlorophenyl, or 2-methyl-5-chlorophenyl; R_1 is phenyl, *p*-tolyl, *m*-tolyl, or *p*-chlorophenyl.

selective as Fe(II) and almost all common ions including those which usually interfere with the parent thiocyanate method and other literature methods[11] do not interfere. The present paper also describes a new spectrophotometric method based on the benzene extraction of iron(III) as its ternary HDPTA and azide complex. This method, though relatively less sensitive is also very selective.

Experimental

Apparatus. A Carl-Zeiss 'Specord' UV-VIS spectrophotometer and an ECIL UV-VIS spectrophotometer model GS-865 with 1-cm matched quartz and silica cells were employed for recording the spectra and absorbance measurements respectively. A Systronic pH meter type-322 was used for determination of pH values.

Standard Iron(III) Solution. Stock solution of iron(III) was prepared by dissolving about 0.62 g of pure iron wire(E. Merck) in 50 ml of 1:3 nitric acid. It was boiled to expel oxides of nitrogen and diluted to 1 litre. This solution was standardised gravimetrically employing 8-quinolinol.[12]

One percent aqueous solutions of potassium thiocyanate and sodium azide were also prepared. All the chemicals used were of analytical reagent grade.

Preparation of N-*Hydroxyamidines.* N^1-Hydroxy-N^1,N^2-diarylbenzamidines were prepared by condensation of equimolar quantities of *N*-aryl-*p*-toluimidoyl chloride with *N*-arylhydroxylamine in ether.[13,14] The resulting hydrochloride was filtered and treated with dilute ammonia to liberate the free base. The free bases were recrystallised from petroleum ether (60—80 °C): benzene (1:2) and the hydrochlorides were crystallised from absolute ethanol. All these compounds showed infrared spectral bands characteristic of N^1-hydroxy-N^1,N^2-diarylbenzamidines.[13,14]

Solutions of *N*-hydroxyamidines (0.1%) in benzene were used for extraction purposes.

Procedure. Place an aliquot (10 ml) of iron(III) solution containing 50—120 μg of the metal in a separatory funnel. To this, add 5 ml of 1% potassium thiocyanate/sodium azide solution. Adjust the acidity to the required value and dilute to 25 ml. Introduce 25 ml of benzene solution of N^1-hydroxy-N^1,N^2-diphenyl-*p*-toluamidine (0.1%; 0.003 M) and equilibriate for 2 min. Dry the benzene extract over anhydrous sodium sulfate and measure the absorbance at the wavelength of maximum absorption against reagent blank.

Results and Discussion

Absorption Spectra. The absorption spectra of ternary thiocyanate and azide complexes of iron(III) with HDPTA are shown in Fig. 1. HDPTA reacts

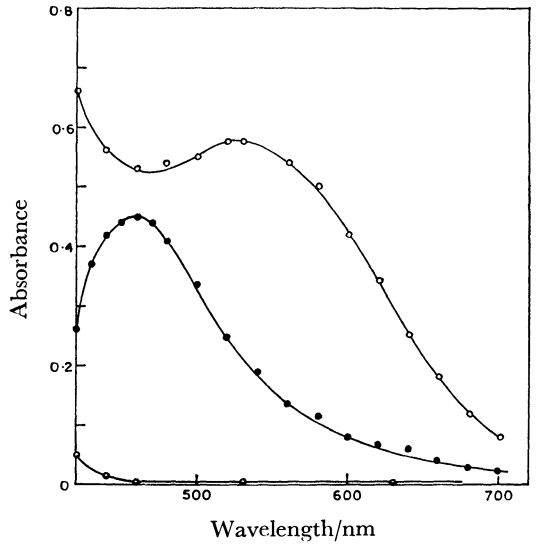

Fig. 1. Absorption spectra of ion(III) ternary complexes and reagent.
-○-: 8.47 ppm Fe(III)+0.1% HDPTA+azide,
-●-: 2.54 ppm Fe(III)+0.1% HDPTA+thiocyanate,
-◒-: 0.1% HDPTA(w/v) in benzene.

with iron(III) forming blue (λ_{max}, 580 nm) and red-purple (λ_{max}, 540 nm) pH-dependent ethanol-soluble complexes. However, in the presence of thiocyanate an intense red complex (λ_{max}, 460 nm) is developed. The wavelength of maximum absorption of the ternary iron(III)–azide–HDPTA complex is 520 nm. Both these complexes are quantitatively extractable in benzene. As the reagent (HDPTA) shows negligible absorption at 450 nm and onwards, the reagent blank can be replaced by benzene.

Effect of Variables. Various solvents such as chloroform, carbon tetrachloride, toluene, benzene *etc.* were found to extract the ternary complexes quantitatively. However, benzene was found to be the best extracting solvent as in this the sensitivity of the complexes is enhanced and complete extraction is relatively rapidly accomplished.

The acidity of the solutions were maintained with hydrochloric acid and ammonia. If the hydrochloric acid concentration of the aqueous phase in case of thiocyanate system lies in the range 0.01—1.0 M, the position of the absorption band of the benzene extract remains intact. However, the optimum acidity range was found to be 0.10—0.65 M HCl in which iron(III) was quantitatively extracted. The optimum pH range for complete extraction of iron employing HDPTA and azide was 1.0—2.5.

Generally a 30 fold molar excess of HDPTA was adequate for full colour development. In thiocyanate ternary system, a 30 and 130 fold molar excess of the ligand and thiocyanate respectively is necessary for complete extraction of iron(III). The azide ternary system requires a 25 and 100 fold molar excess of hydroxyamidine and azide respectively. The presence of HDPTA, thiocyanate, and azide in large causes no adverse effect. Order of addition of reagents was not critical in these systems.

An equilibriation period of 2 min was sufficient for complete extraction of iron(III) mixed ligand complexes. Prolonged extraction has no harmful effect on the determination. Variation of temperature of the aqueous phase from 20 to 35 °C did not affect the absorbance and λ_{max} of ternary complexes. Both the systems were stable for at least for 30 h at 27±2 °C.

Nature of Complexes. The composition of thiocyanate and azide mixed ligand complexes was determined by curve fitting method.[15] To determine the ratio of Fe(III) to HDPTA, the concentration of iron(III) was kept constant and X^- (SCN^- or N_3^-) was taken in excess and then, the concentration of HDPTA was varried. Log absorbance was plotted against log M of HDPTA. Similarly the number of X^- attached to Fe(III) were also found out. The results indicated the formation of 1:1:2 (metal: HDPTA: thiocyanate or azide) ternary complexes.

The molar absorptivities of the Fe(III): thiocyanate: HDPTA and Fe(III) : azide : HDPTA complexes are 1.01×10^4 and 4×10^3 l mol^{-1} cm^{-1} respectively. The Sandell sensitivities of the colour reactions are 0.0054 and 0.0140 μg cm^{-2} of Fe(III) for thiocyanate and azide systems respectively. The iron concentration ranges which follow Beer's law are 0.4—4.8 ppm for thiocyanate system and 0.6—12.0 ppm of Fe(III) for azide system. Ringbom plot[16] suggested optimum and effective metal concentration range of 0.8—4.0 and 2.0—11.0 ppm for thiocyanate and azide systems respectively. The relative standard deviation for the determinations based on thiocyanate and azide colour reactions are ±0.82 and ±0.60% respectively.

N^1-Hydroxy-N^1,N^2-diarylbenzamidines as Reagents for Iron(III). To study the influence of substituents on the complexing properties of the functional grouping, 18 analogues of HDPTA were synthesised and tested for their potentialities towards the extractive separation and spectrophotometric determination of iron. The absorption spectra of the ternary complexes of these reagents were scanned. The average molar absorptivities of the coloured complexes were evaluated at the wavelength of maximun absorption and on the basis of iron content. The experimental details are the same as described for HDPTA. Adherence to Beer's law was tested and confirmed for each system. It is observed that the ternary iron(III) thiocyanate complexes of N^1-hydroxy-N^1,N^2-diarylbenzamidines show maximum absorption at 460—465 nm having molar absorptivities in the range 10100—13400 l mol^{-1} cm^{-1}. Thus, substitution at azomethine or hydroxyl nitrogen atom has no effect on the position of λ_{max}. However, the substitution of the N^1-phenyl group of HDPTA with aryl substituents displayed hyperchromic effect in the order *p*-chlorophenyl>*p*-tolyl>*m*-tolyl. The replacement of the N^2-phenyl group with aryl groups also resulted into hyperchromic shifts, the order being 2-methyl-4-chlorophenyl>2,5-dimethylphenyl>2-methyl-5-chlorophenyl>*p*-tolyl>*m*-tolyl. Thus, N^1-hydroxy-N^1-(*p*-chlorophenyl)-N^2-(2-methyl-4-chlorophenyl)-*p*-toluamidine has the largest value for molar absorptivity. In azide ternary systems only slight variation in the value of λ_{max} and ε_{max} were noticed.

Effect of Diverse Ions. To study the influence

of various foreign ions, a fixed amount of iron(III) was mixed with varying amounts of diverse ions and the extraction of iron was carried out according to the recommended procedure. The tolerance limits of diverse ions(ppm) which cause an error less than ±2% are shown in parentheses.

Thiocyanate System. (0.4 M HCl; 2 ppm iron). Alkaline earth and lanthanoide elements (2000); Fluoride (800); phosphate or arsenate(1400); Cu^{2+}(100); Ni^{2+} or Co^{2+} (400); Zn^{2+}(1500); Cd^{2+}(1300); Al^{3+}(600); Cr^{3+}(500); Fe^{2+}(800); Mn^{2+}(600); Se^{4+}(300); Th^{4+} (200); Ti^{4+}(100); Zr^{4+}(700); V^{5+}(50); Mo^{6+}(15); W^{6+}(50); U^{6+}(600).

Manganese(II) inhibits colour development. However, its interference could be overcome by the addition of ammonium peroxomonosulfate.

Azide System. (pH 1.5±0.2; 6 ppm iron). Alkaline earth and lanthanoid elements (1600); Chloride (3000); sulfate(2500); Zn^{2+} or Cd^{2+}(800); phosphate (400); Ni^{2+} or Co^{2+}(400); Cu^{2+}(100); Al^{3+}(500); Cr^{3+} (450); Fe^{2+}(500); Mn^{2+}(200); Th^{4+}(500); Ti^{4+}(100); Zr^{4+}(500); Mo^{6+}(50); W^{6+}(200); U^{6+}(400).

The laboratory facilities provided by the authorities of Ravishankar University, Raipur are gratefully acknowledged.

References

1) E. B. Sandell, "Colorimetric Determination of Traces of Metals," Interscience Publishers Inc., New York (1959).
2) J. T. Woods and M. G. Mellon, *Ind. Eng. Chem., Anal. Ed.*, **13**, 551 (1941).
3) A. I. Vogel, "A Text Book of Quantitative Inorganic Analysis," Longmans, Green and Co., Ltd., London (1964), p. 786.
4) I. M. Kolthoff and E. B. Sandell, "Textbook of Quantitative Inorganic Analysis," The Macmillan Co., New York (1952), p. 636.
5) K. Yamamoto and K. Ohashi, *Anal. Chim. Acta*, **88**, 141 (1977).
6) K. Satyanarayana and R. K. Mishra, *Anal. Chem.*, **46**, 1609 (1974).
7) K. Satyanarayana and R. K. Mishra, *Indian J. Chem.*, **13**, 295 (1975).
8) K. Satyanarayana and R. K. Mishra, *J. Indian Chem. Soc.*, **53**, 928 (1976).
9) K. K. Deb and R. K. Mishra, *Curr. Sci.*, **45**, 134 (1976).
10) K. Satyanarayana and R. K. Mishra, *J. Indian Chem. Soc.*, **53**, 63 (1976).
11) F. D. Snell, C. T. Snell, and C. A. Snell, "Colorimetric Methods of Analysis," D. Van Nostrand Co., Inc., New York (1967), Vol. II.
12) A. I. Vogel, "A Textbook of Quantitative Inorganic Analysis," Longmans, Green London (1964), p. 524.
13) K. K. Deb and R. K. Mishra, *J. Indian Chem. Soc.*, **53**, 178 (1976).
14) K. Satyanarayana and R. K. Mishra, *J. Indian Chem. Soc.*, **53**, 469 (1976).
15) L. G. Sillen, *Acta Chem. Scand.*, **10**, 185 (1956).
16) A. Ringbom, *Z. Anal. Chem.*, **115**, 332 (1938).

Mutual Catalysis in the Chromium(III)–EDTA–Hydrogen Peroxide System

Mihály T. Beck* and Zoltán Tóth
Institute of Physical Chemistry, Kossuth Lajos University, H-4010 Debrecen, Hungary
(Received March 22, 1978)

Hydrogen peroxide catalyzes the reaction between hexaaquachromium(III) and ethylenediaminetetraacetic acid, while chromium(III)–EDTA complex accelerates the decomposition of hydrogen peroxide. A mechanism is suggested for the reaction on the basis of gasvolumetric and spectrophotometric experiments.

Yamamoto and Ohashi[1] reported that hydrogen peroxide accelerates the reaction between hexaaquachromium(III) and ethylenediaminetetraacetate in acidic medium. The effect was found proportional to the concentration of hydrogen peroxide. According to the mechanism suggested by the authors hydrogen peroxide oxidizes chromium(III) to chromium(IV) and/or chromium(V) which then reacts rapidly with EDTA. The chromium complex in higher oxidation state can react either with chromium(III) or with hydrogen peroxide:

$$\text{Cr(IV)-EDTA} \xrightarrow[\text{Cr(III)}]{} \text{Cr(III)-EDTA} + \text{Cr(IV)} \qquad (1)$$
$$\text{Cr(IV)-EDTA} \xrightarrow[H_2O_2]{} \text{Cr(III)-EDTA} + 1/4\,O_2$$

Analogous reactions are also assumed for the Cr(V)–EDTA complex.

However, the reactions with hydrogen peroxide were eliminated from the mechanism since no evolution of oxygen was observed for one half time. Since these reactions seem to be essential we have carried out measurements on the evolution of oxygen.

Experimental

The experimental conditions were the same as those reported by Yamamoto and Ohashi.[1]

Chromium(III) perchlorate was prepared in solution by the reduction of CrO_3 with hydrogen peroxide in perchloric acid medium.

For the experiments 0.1 M EDTA solution and 30% hydrogen peroxide solution were used. The pH was adjusted by use of 0.5 M acetate buffer. The volume of the reaction mixture was 10 ml in each case. Formation of the complex was followed by measring the absorbance of the thermostated reaction mixture (25 °C) at 545 nm using a Beckman Acta III spectrophotometer. From the measured absorbance the concentration was calculated by means of 210 $mol^{-1}\,dm^3\,cm^{-1}$ molar absorbance of the chromium(III)–EDTA complex.

The evolution of oxygen was followed gas-volumetrically. The hydrogen peroxide solution was first stirred for about 30 min to eliminate the over-saturation of solution by oxygen. Before each experiment the rate of self-decomposition of hydrogen peroxide was checked. The reaction was started when the rate became constant and—within the experimental error—equal to 0.19 ml min^{-1}. The rate of self-decomposition was considered in calculating the rate of the catalyzed reaction of hydrogen peroxide.

Results and Discussion

The decomposition of hydrogen peroxide is enhanced by hexaaquachromium(III) ions as shown in Fig. 1. The shape of the curve suggests that Cr(IV) and/or Cr(V) formed from Cr(III) are the catalysts of the decomposition of hydrogen peroxide in acidic medium. So far no information seemes to have been given on the effect of Cr(III).[2] Spitalsky[3] found that in the reaction between hydrogen peroxide and chromium(VI) the final ratio of Cr(VI): Cr(III) is determined by the initial concentration of hydrogen peroxide. He found that a considerable portion of chromium(VI) can be substituted by Cr(III) without substantial change in the catalytic effect. However, the effect of chromium(III) was not studied exclusively.

The rate of the evolution of oxygen decreases a great deal in the presence of EDTA, indicating that the EDTA complexes are less active catalysts of the decomposition than the corresponding aqua complexes. The difference in the shape of the curves in Fig. 2 shows that catalytically active EDTA complexes of the chromium are of higher oxidation state. The formation of the complex $CrEDTA(H_2O)^-$ is described by a saturation curve, the evolution of oxygen after an acceleration period becoming constant. In contrast to the result of Yamamoto and Ohashi the evolution of oxygen is considerable from the beginning of the reaction.[1]

We have also studied the effect of EDTA in the system chromium(VI)–hydrogen peroxide. Only semi-quantitative data could be obtained because of the lively evolution of oxygen. It is certain that in the presence of an excess of EDTA the total amount of chromium is present as chromium(III)–EDTA complex.

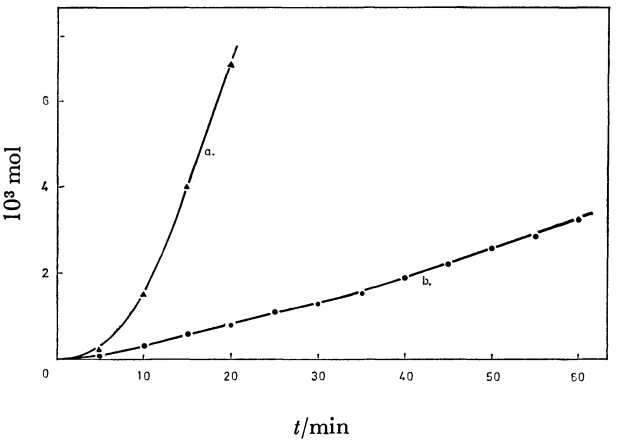

Fig. 1. Kinetic curves of evolution of oxygen in the Cr(III)–H_2O_2 system in the absence (a) and in the presence (b) of EDTA.
$[H_2O_2]=5.0$ M, $[Cr(III)]=7.35\times10^{-3}$ M, $[CH_3COO^-]=0.1$ M, $[EDTA]=2\times10^{-2}$ M, pH=3.8, $T=25.0\pm0.1$ °C, 10 ml.

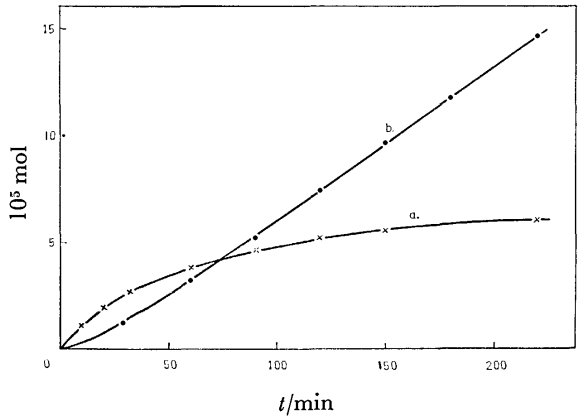

Fig. 2. Comparison of the kinetic curves of complex formation of Cr(III)-EDTA (a) and of evolution of oxygen (b) in the Cr(III)-EDTA-H_2O_2 system. Conditions are given in the legend of the Fig. 1.

When no EDTA is present, there is an equilibrium between Cr(VI) and Cr(III). The fast initial evolution of oxygen diminishes and the value observed in the system chromium(III)-EDTA-hydrogen peroxide is attained. The formation of Cr(III)-EDTA complex takes place faster when chromium is initially present as chromate.

The reaction mechanism is extremely complicated. The following types of reactions should be taken into account:

1. Redox reactions between hydrogen peroxide and aquo ions of chromium in different oxidation states.
2. Disproportionation reaction of Cr(IV) and Cr(V).
3. Redox reactions between chromium ions in different oxidation states.
4. Substitution reactions with EDTA.
5. Redox reactions betweeen hydrogen peroxide and EDTA complexes of chromium in different oxidation states.
6. Other redox and disproportionation reactions involving EDTA complexes of chromium in different oxidation states.

Starting with Cr(III) in the presence of EDTA we can disregard reactions leading to Cr(VI). In the following scheme only those redox reactions which involve hydrogen peroxide are taken into consideration, visg., reactions of type 2, 3, and 6 are also disregarded. Thus the following scheme can be written:

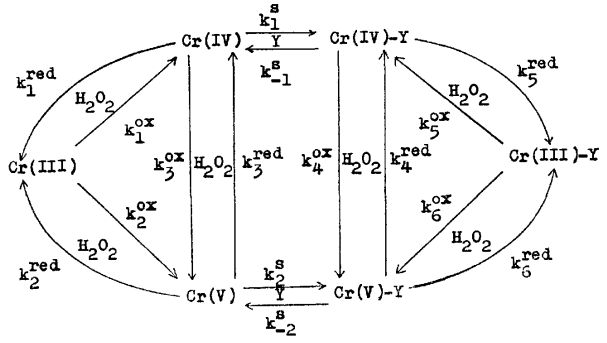

Y: EDTA. (2)

The network of reactions can be greatly simplified if we bear in mind the data referring to the rate of the formation of the Cr(III)-EDTA complex and that of the evolution of oxygen:

1. According to the rate equation given by Yamamoto and Ohashi[1] the rate determining step is the reaction between $Cr(H_2O)_6^{3+}$ and H_2O_2, k_1^{ox} and k_2^{ox} being the smallest among the rate constants.
2. In order to explain the diminishing effect of EDTA on the rate of the oxygen evolution, we should assume that the equilibrium between Cr(IV) and Cr(V) and EDTA is shifted to the formation of the complex, viz., $k_1^s \gg k_{-1}^s$ and $k_2^s \gg k_{-2}^s$.
3. According to the spectrophotometric measurements (Fig. 2. curve a) the amount of Cr(III)-EDTA complex increases steadily: $k_5^{ox} < k_5^{red}$ and $k_6^{ox} < k_6^{red}$.
4. Since the experimental data do not permit separation of paths involving Cr(IV) and Cr(V), only reactions of Cr(IV) should be considered. This makes the handling of rate equations easier.

The following simple scheme can be written:

$$\text{Cr(III)} \xrightarrow[H_2O_2]{k_1^{ox}} \text{Cr(IV)} \xrightarrow[\text{EDTA}]{k_1^s}$$

$$\text{Cr(IV)-EDTA} \underset{H_2O_2}{\overset{k_5^{ox}}{\rightleftharpoons}} \text{Cr(III)-EDTA} \quad (H_2O_2,\ -1/4\,O_2;\ k_5^{red})$$

$$k_1^s > k_5^{red} > k_1^{ox} \approx k_5^{ox}. \tag{3}$$

The condition of the steady evolution of oxygen is as follows:

$$\frac{d[O_2]}{dt} = \text{constant} = k_5^{red}[\text{Cr(IV)-EDTA}]. \tag{4}$$

This requires that

$$\frac{d[\text{Cr(IV)-EDTA}]}{dt} = 0 = k_1^{ox}[\text{Cr(III)}] - k_5^{red}[\text{Cr(IV)-EDTA}] + k_5^{ox}[\text{Cr(III)-EDTA}]. \tag{5}$$

Since the concentration of the intermediates is so small that they cannot be detected spectrophotometrically and their existence is indicated only by the shape of the rate curves of oxygen evolution, we have

$$[\text{Cr(III)}] + [\text{Cr(III)-EDTA}] \approx [\text{Cr(III)}]_0. \tag{6}$$

Thus Eq. 5 can be written as follows.

$$k_5^{red}[\text{Cr(IV)-EDTA}] = k_5^{ox}[\text{Cr(III)}]_0 - [\text{Cr(III)}](k_5^{ox} - k_1^{ox}). \tag{7}$$

Considering Eqs 4 and 7, we get

$$k_5^{ox}[\text{Cr(III)}]_0 - [\text{Cr(III)}](k_5^{ox} - k_1^{ox}) = \text{constant}. \tag{8}$$

It follows that the steady evolution of oxygen follows from the simplified scheme, if

1. $k_5^{ox} \approx k_1^{ox}$ and/or
2. $[\text{Cr(III)}] \ll [\text{Cr(III)}]_0$.

In the first stage of the reaction, before the formation of the Cr(III)-EDTA complex is completed, only the first condition is fulfilled, while in the later stage of the reactions both conditions can be satisfied. The fact that the rate of the oxygen evolution becomes

constant before the complete transformation of Cr(III) to Cr(III)–EDTA indicates that the first condition is actually satisfied:

$$k_5^{ox}[\mathrm{Cr(III)}]_0 \gg [\mathrm{Cr(III)}](k_5^{ox} - k_1^{ox}), \quad (9)$$

causing Eq. 8 to be fulfilled.

The results show that mutual catalysis takes place in the Cr(III)–EDTA–H_2O_2 system. Hydrogen peroxide accelerates the formation of Cr(III)–EDTA, which in turn catalyzes the decomposition of H_2O_2.

References

1) K. Yamamoto and K. Ohashi, *Bull. Chem. Soc. Jpn.*, **49**, 2433 (1976).
2) J. Baxendale, *Adv. Catal.*, **4**, 75 (1952).
3) E. Spitalsky, *Z. Anorg. Chem.*, **69**, 179 (1911).

Indirect Polarographic Estimation of Palladium

P. B. KALAPURNA

Department of Analytical Chemistry, Madras University, A.C. College Campus, Madras 600025, India

(Received April 10, 1978)

Chemical displacement of palladium by mercury at the DME, has been found to be quantitative (that is, instantaneous and proportional to the i_d of mercury). Therefore the mercury(I) wave has been exploited for the indirect estimation of palladium using the DME. The conditions of estimation are standardized and the method applied to a mixture (dental alloy) containing palladium. The results are within experimental accuracy. The indirect method has certain advantages over the direct methods.

Palladium has been directly estimated in the past by several workers mostly by the spectrophotometric technique using a variety of organic reagents, as for example, oximes,[1-3] azoles,[4] substituted ketones,[5-7] substituted phenols,[8-10] and sulfur compounds.[11-14] There has also been an indirect spectral method,[15] based on the catalytic action of palladium on the reduction of molybdophosphate to molybdenum blue. With but a few exceptions[16,17] the spectral estimations were restricted to ranges below 30 ppm. Another short-coming of the spectral method was that an extraction step was often necessary prior to the spectral reading, and this has been the cause to lengthen the procedure and introduce errors.

Less frequently adopted methods for the direct estimation of palladium are amperometry,[18] potentiometry,[19] stripping voltammetry,[20] and polarography.[21]

Polarographic estimations of palladium complexes at the DME (dropping mercury electrode), in the past have not been smooth-sailing. In some cases[22] the half-wave potential had been very close to the decomposition potential of the electrolyte, the wave itself being irregular at the top. In other cases,[23,24] the half-wave potential was reported to vary with concentrations of palladium, indicating the formation of more than one species. The present indirect polarographic method is free from these short-comings.

The direct polarographic estimation of palladium (without complexation) using a DME is difficult, for the reason that palladium salts are spontaneously reduced[22] to the metal by contact with mercury, the latter being more electronegative than palladium in the electromotive series of elements. An accurate method of estimation is outlined here for the indirect estimation of palladium, making use of the mercury(I) wave, which occurs due to the chemical displacement of palladium from solution. The practical range of estimation has been found to be between 10—210 ppm, (wider than many of the spectral methods, and also without encumbrance of the extraction step). This makes it a more rapid method than the conventional spectrophotometric methods.

When a solution of palladium chloride was subjected to polarography at a DME, a single wave was obtained with an half-wave potential of +0.06 V. This curve has been reported by previous workers[25] as due to mercury(I) ion liberated by the reaction.[26]

$$Pd^{2+} + 2\,Hg^0 \rightarrow Pd^0 + Hg_2^{2+}$$

This reaction is instantaneous up to 210 ppm, and the lower limit has been found to be 10 ppm, though theoretically the reaction may be stoichiometric even at much lower concentration ranges.

That the wave with a half-wave potential of +0.06 V is due to the mercury(I) ion, was confirmed by us as follows: Polarograms of palladium using a stationary platinum electrode, under the same conditions as before always showed a wave with an $E_{1/2}$ of +0.16 V. There was no wave at +0.06 V, unlike with the DME.

Polarograms of mercury(I) chloride (10^{-5} M) in the absence of palladium gave the same wave with a half-wave potential of +0.06 V, regardless, whether the electrode used was a DME or a platinum electrode.

Estimation of Palladium. A stock solution of 1×10^{-2} M palladium chloride was prepared from anhydrous palladium chloride (A.R.), by warming the aqueous solution with a drop of concentrated HCl, to ensure complete dissolution before making up to the required volume. This solution was diluted appropriately to get concentrations ranging from 10 to 225 ppm during polarography. Potassium chloride was used as a supporting electrolyte and also to keep the ionic concentration constant at 0.1 M. A 0.01% gelatin solution was used as a maximum suppressor. pH was maintained at 3.5 by the use of an appropriate Britton-Robinson buffer.[27] Polarograms were recorded after deaeration with oxygen-free nitrogen.

Instrument. A polariter PO3 Radiometer of the pen recording type with a built-in saturated calomel anode was used to record the polarograms.

The capillary characteristics were established as follows: $m=9$ mg/s, $t=1.4$ s, $h=25$ cm. A fast dropping capillary was found to be more suitable for the experiment, to minimize the chemical vitiation of the mercury surface.

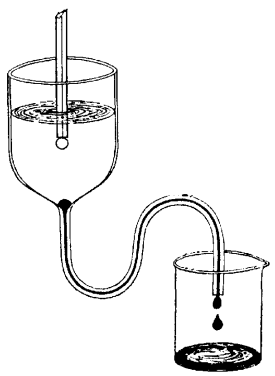

Fig. 1. Vessel used for the indirect polarographic estimation of palladium.

TABLE 1. COMPARISON OF RESULTS OBTAINED BY POLAROGRAPHY AND SPECTROPHOTOMETRY

No.	Quantity of Pd in the dental alloy (ppm)	Polarographically (ppm)	Spectrophotometrically (ppm)	Deviation between the two techniques (ppm)
1	10.65	10.55	10.60	+0.05
2	21.30	21.40	21.35	−0.05
3	31.95	32.00	32.00	0.00
4	53.05	53.00	53.05	+0.05
5	63.70	63.20	63.50	+0.30
6	74.35	74.20	74.30	+0.10
7	95.65	95.50	95.55	+0.05
8	106.30	106.40	106.20	−0.20
9	116.95	117.00	116.90	−0.10
10	137.65	137.50	137.60	+0.10
11	148.30	148.00	148.20	+0.20
12	158.95	159.80	160.00	+0.20
13	180.25	180.30	180.20	−0.10
14	190.90	191.00	190.90	−0.10
15	201.55	201.00	201.50	+0.50

Precaution was taken to avoid undue contact of solution with mercury other than the DME, so that the chemical reaction between palladium ions and non-electrodic mercury is made negligible. The polarographic vessel was drawn out into a capillary, so that the building up of the mercury pool by the drops of mercury was prevented by continuous tapping out of mercury, leaving only a droplet of negligible area of contact inside the capillary (Fig. 1). The scanning of the polarogram was done within 2 min.

The relationship between the diffusion current i_d and the concentration was found to be linear up to 210 ppm. Above this range the linearity is gradually lost by the vitiation of the surface of the mercury drop. A number of estimations were carried out with known concentrations of palladium, and the quantities were estimated by referring the i_d to the working graph.

The results obtained by the above method were checked by parallel determinations conducted by the well known spectrophotometric method[28,29] (λ_{max}= 525 nm), using *p*-nitrosodimethylaniline as the color developer and a Beckman Model B spectrophotometer as the instrument. The results of the two techniques were found totally within experimental error *vide* Table 1. In a series of fifteen experiments with 106.3 ppm of palladium, the standard deviation[30] was found to be 0.0876.

Analytical Applications. Indirect polarographic estimation of palladium through the mercury(I) wave is applicable to micro and semimicro quantities of palladium (below 50 mg). This quantity is below the macro-gravimetric limit. Micro-gravimetry is more tedious and hence the advantage of the polarographic estimation. This technique is suitable for the estimation of palladium present in hydrogenation catalysts and in dental and ornamental alloys. In alloys, palladium is generally found in association with gold, silver, and sometimes base metals like copper and zinc.

TABLE 2. R_f VALUES OF THE DIFFERENT IONS

Ion	R_f value	Remark
Gold	0.96	Moves with the solvent front
Palladium	0.84	Fine, thin band
Copper	0.74	Thin, well defined band
Zinc	0.30	Thick, diffused band, but far separated from the other ions

Before subjecting to polarography, it has to be isolated from its associates by any suitable method, a number of which are available in literature.[31-34] The method adopted in this laboratory was to separate the palladium by means of circular paper chromatography.

Isolation of Palladium from Gold, Copper, and Zinc in a Dental Alloy. The first investigation was to discover the R_f values of individual constituents, which alone will decide whether they can be separated at all. Solutions of pure metal constituents of the dental alloy (10^{-4} M) were prepared in aqua-regia. The solutions were evaporated to dryness to expel the oxides of nitrogen and made up to a required volume with 0.1 M HCl. Chromatograms were run on circular paper of diameter of 12 cm, with a central wick, and the eluent used was ethyl methyl ketone, concd HCl (A.R.) and isoamyl alcohol in the ratio of 6:3:1. After the paper was dried the bands were developed by spraying with the following reagents. (a) Hydrazinium chloride in dilute HCl for gold (Black band), (b) DMG in acid medium for palladium (Yellow band), (c) 0.1% Rubeanic acid in alcohol for copper (Green band), and (d) Dilute dithizone in chloroform for zinc (Pink band).

Table 2 shows the average R_f values of the different ions.

An appropriate quantity of the dental alloy was weighed, dissolved in 10 cm^3 of aqua regia, evaporated to expel the oxides of nitrogen and finally made up to 200 ml with 0.1 M HCl. The chromatogram was run as before. The brown band of palladium was clearly visible second from the outermost. It was cut out from the paper, and the metal extracted with 0.1 M HCl and utilized for quantitative estimation.

References

1) P. K. Paria and S. K. Majumdar, *Z. Anal. Chem.*, **275**, 265 (1975).
2) G. Popa, A. Danet, and I. Baciu, *Revta. Chim.*, **25**, 573 (1974).
3) G. Popa, A. F. Danet, and O. Maior, *Mikrochim. Acta*, **1**, 147 (1973).
4) S. R. Joshi, P. K. Srivastava, and S. N. Tandon, *Indian J. Chem.*, **11**, 590 (1973).
5) L. I. Mas'ko, V. P. Kerentseva, and M. D. Lipanova, *Zh. Anal. Khim.*, **30**, 315 (1975).
6) G. V. Taneeva, *Zh. Anal. Khim.*, **30**, 381 (1975).
7) G. H. Rizvi, Singh Rajendra Pal, *Indian J. Chem.*, **10**, 873 (1972).
8) Sh. T. Talipov, V. N. Artemov, and A. E. Martirosov, *Nauch. Trudy. tashkent. gos. Univ.*, **435**, 49 (1973); *Referat. Zh. khim.*, **19** GD, (6) 1974. Abstract No: 6G 106.
9) T. Yatsuyanagi, H. Hoshino, and K. Aomura, *Anal. Chim. Acta*, **71**, 349 (1974).

10) V. M. Ivanov, V. N. Figurovskaya, and A. I. Busev, *Zavod. Lab.*, **38**, 1311 (1972).
11) I. A. Sheka, K. F. Karlysheva, N. I. Salo, T. E. Bezmenova, and T. N. Varshavets, *Ukr. Khim. Zh.*, **40**, 1123 (1974).
12) Pitombo, R. M. Luiz, Cartaxo, Q. Elisabeth, *Talanta*, **21**, 965 (1974).
13) A. Diamantatos, *Anal. Chim. Acta*, **61**, 233 (1972).
14) L. K. Kabanova, P. M. Solozhenkin, and S. V. Usova, *Dokl. Akad. Nauk. Tadzhik. SSR*, **15**, 27 (1972).
15) R. E. Stanton, *Lab. Pract.*, **24**, 525 (1975).
16) B. I. Nabivanets and L. V. Kalabina, *Zh. Anal. Khim.*, **27**, 1134 (1972).
17) R. J. Walker and W. J. Holland, *Mickrochim. Acta*, **4**, 591 (1973).
18) A. M. Arishkevich, O. I. Pitsyk, T. V. Zamorskaya, Yu. I. Usatenko, *Zavod. Lab.*, **36**, 265 (1970).
19) A. T. Pilipenko, O. P. Ryabushko, L. A. Krivokhizhina, and N. L. Emchenko, *Ukr. Khim. Zh.*, **40**, 73 (1974).
20) G. N. Popov, V. V. Pnev, and M. S. Zakharov, *Zh. Anal. Khim.*, **27**, 1335 (1972).
21) G. W. C. Milner, "The Principles and Applications of Polarography and other Electroanalytical Processes," Longman Green and Co., London (1958).
22) J. B. Willis, *J. Am. Chem. Soc.*, **67** 547 (1945).
23) P. M. Rao and S. B. Rao, *Z. Anal. Chem.*, **272**, 128 (1974).
24) O. K. Kudra, O. V. Izbekova, V. V. Chelikidi, *Ukr. Khim. Zh.*, **42**, 1031 (1976).
25) D. Cozzi, E. F. Pantani, *Inorg. Nucl. Chem.*, **8**, 385 (1946).
26) F. Feigl, and V. Angler, "Spot Tests in Inorganic Analysis," 6th ed, Elsevier, New York (1972), p. 305.
27) J. Heyrovsky and P. Zuman, "Practical Polarography," Acad. Press., Lond. (1968), p. 179.
28) F. D. Snell and C. T. Snell, "Colorimetric Methods of Analysis," 3rd ed, Van Nostrand, London, (1967), Vol. II, p. 530.
29) F. Feigl and V. Angler, "Spot Tests in Inorganic Analysis," 6th ed, Elsevier, New York (1972), p. 383.
30) W. J. Youden, "Statistical Methods for Chemists," John Wiley and Sons, New York (1951), p. 12.
31) F. E. Beamish, *Talanta*, **14**, 991, 1133 (1967).
32) P. Senise, and L. R. M. Pitombo, *Anal. Chim. Acta*, **26**, 89 (1962).
33) S. S. Dehmlov and I. L. Preiss, *Z. Anal. Chem.*, **194**, 183 (1963).
34) S. N. Poddar, *Anal. Chim. Acta*, **28**, 586 (1964).

Quaternisation at an Sp^2 Nitrogen. II.[1] An Analysis on the Substituent Effect and on the Nature of the Transition State

G. B. BEHERA* and A. SHARMA†

Post-Graduate Department of Chemistry, Sambalpur University, Jyoti Vihar, Burla 768017, India

(Received August 1, 1977)

The kinetics of *N*-phenacylation of a number of substituted thiazoles and substituted phenacyl bromides have been investigated in nitrobenzene and in a number of other dipolar aprotic solvents. The rate constants of 2-amino-4-phenylthiazoles and 2-aminobenzothiazoles have been calculated with suitably developed equations. The deviation of the observed values from the calculated results has been ascribed to the steric effect. A seven membered hydrogen bonded transition state has been proposed on the basis of the results obtained from the substituent and medium effect.

In the field of quaternisation reactions pioneering and extensive work have been done by Menschutkin.[2] The reaction has been used successfully in the development and understanding of mechanistic principles. The quaternisation kinetics of pyridines with methyl iodide has been studied by Fischer and Vaughan[3] and Murai *et al.*[4] They observed the operation of normal substituent effect for the substituents at position 4 and a good correlation between the rate constant and pK_a with the exception of $-NH_2$, $-CO-C_6H_5$, $-COOR$, and $-CN$ groups. In an earlier study[5] on the quaternisation of thiazoles, the sulfur atom was observed to act as a resonance transmitter. The lower reactivity of 2-amino group over 2-methyl group was explained as due to the existence of an equilibrium between loose contact pairs and charge transfer complexes.

Deady *et al.*[6] also studied the rate of *N*-methylation of a number of heterocyclic compounds such as *N*-methylpyrazole, isothiazole, isoxazole and their 2 : 1 and 1 : 2 analogues; 2-methyl-benzothiazoles; 2,1,3-benzoxadiazoles; 2,1,3-benzothia (or selena) diazoles; 1,2,5-oxadiazole; and 1,2,5-thiadiazoles. They concluded a reactant-like transition state for the Menschutkin reaction. The present work was undertaken to investigate the nature of the transition state during the course of *N*-phenacylation reaction.

Results and Discussion

The reaction of 2-aminothiazole and phenacyl bromide takes place according to

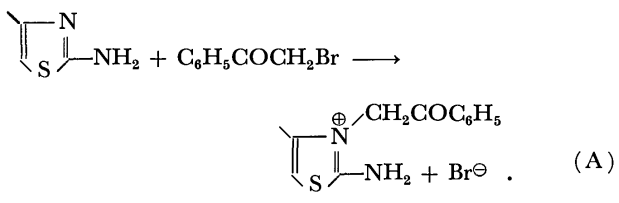

(A)

The rate data, Arrhenius parameters and the entropy of activation values for this reaction are given in Table 1. The greater rate of reactivity of **5** over **1** is ascribed to the presence of a *p*-OMe group, which stabilizes the transition state by interacting through the sulfur atom. Substantial transmission of electronic effects through the sulfur atom has been clearly shown by Davis *et al.*[7] from the ultraviolet spectral data of some sulfur amides. A mechanism of through conjugation involving p-π, d-π, p-π conjugation has been suggested for phenyl vinyl sulfides[8] and supported by CNDO/2 calculations.[9] Discussions have been made by various workers.[10]

*2-Aminobenzothiazole(**1**), 2-Amino-4-phenylthiazole(**2**), 2-Amino-4,5-diphenylthiazole(**6**), and 2-Aminopyridine(**8**).* Since the sulfur atom acts as a resonance transmitter, it can be considered equivalent to a vinyl group. Therefore, the compounds **1**, **2**, and **6** can be considered equivalent to 2-amino-6-phenylpyridine, 2-aminoquinoline, and 2-amino-5,6-diphenylpyridine, respectively. Considering compound **8** as a standard, the rate constants of **1** and **2** can be calculated by means of

$$k_1(\text{calcd}) = \frac{\beta_s}{\beta_{\text{vinyl}}} \times \frac{K_B(\text{2Ph-pyridine})}{K_B(\text{Pyridine})} \times k_8, \qquad \text{(B)}$$

and

$$k_2(\text{calcd}) = \frac{\beta_s}{\beta_{\text{vinyl}}} \times \frac{K_B(\text{Quinoline})}{K_B(\text{Pyridine})} \times k_8, \qquad \text{(C)}$$

where β_s is the resonance integral of the S atom and the vinyl group, K_B is the basicity constant of base and k_8 is the observed rate constant for compound **8**. The values of k_1 and k_2 at various temperatures and the calculated and observed rate constants are given in Table 3. The ratio falls from 10.0 at 60 °C to 3.0 at 100 °C for compound **1** whereas it changes from 1.5 to 1.3 for compound **2**. The values of energy of activation obtained with the calculated rate constants are 6.45 and 8.64 kcal mol^{-1} as against 13.40 and 9.52 kcal mol^{-1} derived from observed rate constants for compounds **1** and **2**, respectively. The agreement between the observed and calculated rate constants appears reasonable in view of the assumptions: (1) steric effect during the course of protonation and phenacylation is the same and (2) an amino group at 2-position produces the same effect in both the processes. However, for compound **2** a greater divergence is noted than for compound **1**. The discrepancy might be due to the librational freedom of the phenyl group at position 4 in compound **2**. The free libration of the phenyl group becomes restricted during the course of phenacylation due to the steric interaction of ortho hydrogen atom and the phenacyl moiety. Therefore, the plane of the phenyl group will rotate to the thermodynamically favoured conformation, *i.e.*, the planes of the π MO of the phenyl and the thiazole ring will tend to be orthogonal, causing destabilisation of the transition state. Thus the energy of activation

† Junior Research Fellow, C.S.I.R., Government of India.

obtained with observed rate constant is much higher with **2** than with **1** as compared to the same obtained from calculated rate constants.

4-(1- and 2)-Naphthylthiazoles. The greater rate of reactivity of 1-naphthyl over 2-naphthyl group at position 4 of the thiazole ring can be ascribed to both steric and electronic factors. The ratio of F_r and Z_r values for position 1 and 2 of the naphthalene are 1.12 and 1.04, respectively.[11] Brown[12] showed a good correlation between F_r and Z_r values with the reactivity parameter, $\sigma_r(\log k/k_0=\sigma_r\rho^*)$ with a deviation $\simeq$6%. The ratio of logarithm of rate constants of 4-(1- and 2)-naphthylthiazole is 0.81. Examination of the model shows that H atom at C-8 in I is nearer by 1.3 times to the H atom at C-1 (II). Thus, the ratio of rate constants of 4-(1- and 2)-naphthylthiazole in the absence of the steric effect due to the nearness of C_α–H atom would have been $0.81\times1.3=1.053$, which is in good agreement with the ratio of F_r and Z_r values. Charton[13] also concluded that E_s parameters are a function of the Van der Waals radii only.

The increased rate of reaction of **6** over **2** can be ascribed to a buttressing effect on the phenyl group at position 4 due to the same group at position 5.

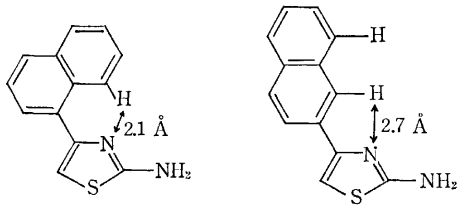

I II

The phenyl ring at position 4 interacts with the electron pair of the sulfur atom (III) and the electron density around nitrogen is relatively decreased.[14] The phenyl ring at position 5 decreases this electronic effect by sterically interfering with the group at position 4.

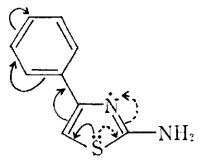

III

Reactivity of Phenacyl Bromide: The order of reactivity of the substituted phenacyl bromide is, *m*-$NO_2\simeq$ *p*-NO_2>*p*-Cl>*p*-OMe>-H (Table 3). The order of reactivity determined earlier by Rout *et al.* in the reaction of phenacyl bromides and aniline is, *p*-NO_2> *m*-NO_2>*p*-Cl>-H>-OMe.[15] The greater rate of reactivity of nitrophenacyl bromide over the unsubstituted one is in line with the transition state (IV) proposed by them and other workers[16] for similar reactions.

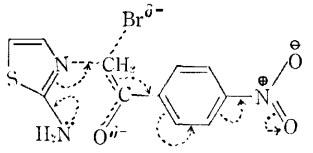

IV

The transition state is stabilised by an interaction with the $-NH_2$ group (arrows). However, it cannot explain the order of reactivity. If a hydrogen bonded structure (V) is proposed for the transition state then the effect of *p*-NO_2 and *p*-OMe groups can be understood: (i) in X=NO_2, electron withdrawing effect of

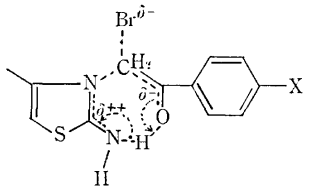

V

NO_2 is lowered by the electron movement shown in the cyclic transition state, (ii) in X=MeO, the electron movement in V is enhanced by electron donating effect of MeÖ. The possibility of such a hydrogen bonded structure is also further confirmed from IR data of 2-amino-3-phenacyl-4-phenyl-3-thiazolium bromide. The >C=O group stretching frequency occurs at 6.1—6.15 μ, whereas in acetophenone it is 5.95 μ. The shift in *o*-hydroxyacetophenone and salicylaldehyde, where chelation has been established is by 0.15 μ. Therefore, these is a case to believe that a hydrogen bonded structure also exists in the quaternary salt.

Medium Effect: With a view to understanding further the nature of the transition state, the *N*-phenacylation kinetics has been studied with 2-aminobenzothiazoles. The order of reactivity in different solvents was observed to be DMA>DMF>NB>BN>AN>BA>CB (Table 4). This is the order of decreasing dielectric constant of the solvents (AN being an exception). A plot of log *k vs.* $(D-1)/(2D+1)$, gives a straight line, AN and NB not lying on the line. This order of reactivity in different solvents also does not conform to the order of *Z* values[17] and E_T values[17] of these solvents, suggesting a nonquaternary salt-like structure for the transition state. However, there seems to be some correlation with the dipole moment of these solvents. The order of increasing dipole moment of these solvents is BN>NB>DMF>DMA>AN. There is a reversal in the order with respect to the first four solvents. Plots of ΔS^*, ΔH^* *vs.* dipole moment give straight lines whereas similar plots with $(D-1)/(2D+1)$ show a scatter.

On the basis of these evidences, a transition state (VI) is suggested for the phenacylation process of 2-aminothiazoles.

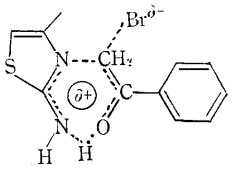

VI

Experimental

4-Substituted 2-aminothiazoles were prepared by condensation of appropriately substituted phenacyl bromide and

Table 1. Values of rate constants at different temperatures, energy of activation and entropy of activation of the quaternisation reaction of some heterocyclic bases and phenacyl bromide in nitrobenzene

Compound No.	Compound	$k \times 10^5$, s^{-1}						E kcal mol^{-1}	$-\Delta S^*$ in e.u.
		60 °C	70 °C	75 °C	80 °C	90 °C	100 °C		
1	2-Aminobenzothiazole	3.70	5.69	6.60	7.96	—	—	9.52	42.0
2	2-Amino-4-phenylthiazole	0.20	0.39	—	0.79	1.24	2.09	13.40	35.5
3	2-Amino-4-(1-naphthyl)thiazole	3.36	5.56	6.53	7.87	—	—	12.28	34.2
4[a]	2-Amino-4-(2-naphthyl)thiazole	—	0.86	1.03	1.27	—	—	9.51	45.6
5[b]	2-Amino-4-(*p*-methoxyphenyl)thiazole	—	0.80	0.90	1.12	—	—	9.43	45.1
6	2-Amino-4,5-diphenylthiazole	2.63	3.78	4.54	5.78	—	—	9.79	41.8
7[c]	2-Methylbenzimidazole	12.36	20.04	—	26.92	38.4	—	9.89	38.7
8[d]	2-Aminopyridine	24.43	30.3	—	34.08	45.6	—	8.91	40.4
9	2-Methylbenzothiazole	1.39	—	3.30	5.50	—	—	11.97	35.7
10[e]	2-Methylmercaptobenzothiazole	4.97	7.87	—	13.0	—	—	9.86	41.2

a) $k \times 10^5$ at 85 °C = 1.42. b) $k \times 10^5$ at 85 °C = 1.27. c) $k \times 10^5$ at 65 °C = 15.90. d) The data are at 40, 45, 50, and 60 °C, respectively. e) $k \times 10^5$ at 50 °C = 3.43 s^{-1}.

Table 2. Values of rate constants at different temperatures, energy of activation and entropy of activation of the reaction of 2-amino-4-phenylthiazole and phenacyl bromides in nitrobenzene

Compound	$k \times 10^5$ in s^{-1}					E kcal mol^{-1}	$-\Delta S^*$ in e.u.	ΔF^* in kcal mol^{-1}
	60 °C	70 °C	75 °C	80 °C	90 °C			
Phenacyl bromide[a]	—	0.39	—	0.79	1.24	13.40	35.5	25.5
4-Nitrophenacyl bromide[b]	1.49	1.9	—	3.80	6.60	11.75	37.1	25.8
4-Chlorophenacyl bromide[c]	—	0.51	—	1.22	1.91	13.38	34.4	25.5
4-Methoxyphenacyl bromide	0.27	0.33	0.66	0.84	—	13.21	36.0	25.9
3-Nitrophenacyl bromide	1.68	2.01	3.40	3.80	—	9.89	42.6	24.9

a) $k \times 10^5$ at 100 °C = 1.58 in s^{-1}. b) $k \times 10^5$ at 50 °C = 0.77 and at 100 °C = 13.44 in s^{-1}. c) $k \times 10^5$ at 85 °C = 1.67 in s^{-1}.

Table 3. Calculated rate constants (k_1 for 2-amino-4-phenylthiazole, k_2 for 2-aminobenzothiazole)

Temp in °C	Calcd $k_1 \times 10^5$ in s^{-1}	$\frac{k_1 \text{ calcd}}{k_1 \text{ exptl}}$	E in kcal mol^{-1}	Calcd $k_2 \times 10^5$ in s^{-1}	$\frac{k_2 \text{ calcd}}{k_2 \text{ exptl}}$	E in kcal mol^{-1}
60	2.027	10.0		3.7	1.5	
70	2.837	7.0	6.45	5.69	1.4	8.64
80	3.613	4.5		7.96	1.3	
90	4.654	4.0		—	—	
100	5.928	3.0		—	—	

thiourea in ethanol. The thiazoles obtained were crystallised twice from alcohol. The 2-aminothiazoles prepared by this method are 4-phenylthiazole, mp 150 °C (lit,[18] mp 151 °C); 4-(1-naphthyl)thiazole, mp 144 °C (lit,[19] mp 144 °C); 4-(2-naphthyl)thiazole, mp 134 °C (lit,[19] mp 135 °C); 4-(*p*-methoxyphenyl)thiazole, mp 204 °C (lit,[20] mp 204 °C) and 4,5-diphenylthiazole, mp 180 °C. 2-Methylbenzimidazole and 2-aminopyridine were of Couchlight Renal grade. They were crystallised before use. 2-Methylbenzothiazole (Schudart and Co.) was distilled before use.

Phenacyl bromide was synthesised by the bromination of acetophenone.[21] The substituted phenacyl bromides prepared by this method are 4-nitro-, mp 90 °C (lit,[22] mp 91 °C); 4-chloro-, mp 110 °C (lit,[22] mp 110 °C); 4-methoxy-, mp 72 °C(lit,[22] mp 72 °C) and 3-nitro-, mp 95 °C(lit,[22] mp 96 °C).

Purity of all the synthesised compounds has been confirmed by silica gel G TLC plate.

All the solvents used were of BDH grade. Nitrobenzene was purified by the method of Leffek and Matheson,[23] acetonitrile by that of Coetzee,[24] *N*,*N*-dimethylformamide by that of Hurt and Simpson,[25] 1-butanol by that of Goldschmidt and Mathieson[26] and chlorobenzene by that of Vogel.[27] Benzonitrile was purified by shaking with silica gel and then stirring with calcium hydroxide for two hours. After decantation, it was distilled under reduced pressure. The middle portion was cut and used. *N*,*N*-Dimethylacetamide was also used after distillation under reduced pressure.

Kinetic Procedure: The method of rate measurement by conductance method is the same as reported.[5] The pseudo first order rate constants ([Base] = 0.0025 M and [α-halo-

Table 4. Values of rate constants at different temperatures, energy of activation, entropy of activation of the quaternisation reaction of 2-aminobenzothiazoles with phenacyl bromide in different solvents

No.	Solvent	$k\times10^4$ in $M^{-1}s^{-1}$					E in kcal mol^{-1}	$-\Delta S^*$ in e.u.	ΔF^* in kcal mol^{-1}
		60 °C	70 °C	80 °C	90 °C	100 °C			
1	Nitrobenzene (NB)[a]	7.84 (3.7)	11.6 (5.67)	15.16 (7.96)	—	—	9.52	42.2	24.5
2	Acetonitrile (AN)	2.84	3.5	8.1	23.34	—	14.5	29.9	24.39
3	*N,N*-Dimethylformamide (DMF)	6.92 (2.74)	10.0 (4.37)	19.0 (9.17)	20.4 (10.7)	—	10.81	41.03	24.58
4	*N,N*-Dimethylacetamide (DMA)	4.76 (2.75)	14.64 (6.9)	22.02 (11.12)	— (16.46)	—	16.22	30.36	25.34
5	Benzonitrile (BN)	—	5.62	8.48	11.66	12.5	13.92	32.4	24.61
6	Chlorobenzene (CB)	—	1.54	3.58	5.12	3.5	10.82	44.50	25.81
7	Butyl alcohol (BA)	—	1.76	3.76	8.34	6.96	15.67	30.83	25.84

a) $k\times10^4$ at 75 °C=13.2 in $M^{-1}s^{-1}$. The rate data in parentheses in DMF, DMA, and NB refer to the first order rate constants ($k\times10^5$ in s^{-1}) by conductometric methods.

ketone]=0.05 M) were calculated from the slopes of the linear plots of log $R_t/(R_t-R_\infty)$ *versus* time, where R_t and R_∞ are the electrical resistances at time 't' and infinite time, respectively. The rate constants were reproducible within ±0.2 units.

Since the measurements of rate constants in less polar solvents by the conductance method were less satisfactory, the argentometric method was also adopted. The rate constants by both titrimetric and conductometric methods were compared in a few cases and found to agree well in conformity to the observation made by Jones *et al.*[28] A thermostated solution of phenacyl bromide (0.05 M)and 2-aminobenzothiazole (0.05 M) were mixed and the course of the reaction was studied by pipetting aliquots from the reaction mixture at different intervals of time and estimating [Br^-] argentometrically. The rate constants were calculated by employing the bimolecular rate equation.

The activation parameters were calculated by using bimolecular rate constants.

Funds for this project were kindly provided by the Council of Scientific and Industrial Research, Government of India.

References

1) Ref. 5 for Part I.
2) N. Menschutkin, *Z. Phys. Chem.*, **5**, 589 (1890).
3) A. Fischer and J. Vaughan, *J. Chem. Soc.*, **1964**, 3596.
4) K. Murai, S. Takeuchi, and C. Kimura, *Nippon Kagaku Kaishi*, **1973**, 95.
5) G. B. Behera, J. N. Kar, R. C. Acharya, and M. K. Rout, *J. Org. Chem.*, **38**, 2164 (1973).
6) L. W. Deady, M. Davis, and E. Homfeld, *Aust. J. Chem.*, **27**, 1221 (1974); **27**, 1917 (1974).
7) F. A. Davis, J. M. Kaminski, E. W. Kluger, and H. S. Freilich, *J. Am. Chem. Soc.*, **97**, 7085 (1975).
8) (a) O. Kajimoto, M. Kobayashi, and T. Fueno, *Bull. Chem. Soc. Jpn.*, **46**, 1425 (1973); (b) *ibid.*, **46**, 1422 (1973).
9) O. Kajimoto, M. Kobayashi, and T. Fueno, *Bull. Chem. Soc. Jpn.*, **46**, 2316 (1973).
10) (a) G. Cilento, *Chem. Rev.*, **60**, 147 (1960); (b) K. A. R. Mitchell, *ibid.*, **69**, 157 (1969), (c) S. Wolfe, *Acc. Chem. Res.*, **5**, 102 (1972).
11) J. A. Joule and G. F. Smith, "Heterocyclic Chemistry," Van Nostrand Rheinhold, (1972), p. 110.
12) R. D. Brown, *J. Chem. Soc.*, **1959**, 2232.
13) M. Charton, *Prog. Phys. Org. Chem.*, **8**, 247 (1971).
14) R. M. Acheson, "An Introduction to Chemistry of Heterocyclic Compounds," 2nd ed, Wiley International, (1967), p. 320.
15) M. K. Rout, G. B. Behera, and R. Rath, *Indian J. Chem.*, **6**, 202 (1965).
16) R. A. Firestone, *J. Org. Chem.*, **36**, 702 (1971); M. Litvinenko, L. A. Perelman, and A. F. Popov, *J. Org. Chem. (Russian)*, **8**, 578 (1972) (Engl. Ed.); R. P. Lutz, *J. Am. Chem. Soc.*, **90**, 3888 (1968).
17) E. M. Kosower, "An Introduction to Physical Organic Chemistry," John Wiley & Sons, N. Y. (1967).
18) D. Hurd and H. L. Herhrmeister, *J. Am. Chem. Soc.*, **71**, 4007 (1949).
19) A. Nayak, Ph. D. Thesis, Utkal University, Orissa, India, 1971.
20) B. Das and M. K. Rout, *J. Indian Chem. Soc.*, **32**, 662 (1955).
21) I. Ervin and H. Prones, *J. Org. Chem.*, **32**, 3566 (1967).
22) R. Rath, G. B. Behera, and M. K. Rout, *Indian J. Chem.*, **6**, 202 (1968).
23) K. T. Leffek and A. F. Matheson, *Can. J. Chem.*, **50**, 986 (1972).
24) J. F. Coetzee, *Pure Appl. Chem.*, **73**, 429 (1966).
25) H. D. Hurt and W. T. Simpson, *J. Am. Chem. Soc.*, **75**, 4540 (1959).
26) H. Goldschmidt and E. Mathiesen, *Z. Phys. Chem. (Leipzig)*, **121**, 153 (1926).
27) A. I. Vogel, *J. Chem. Soc.*, **1948**, 654.
28) W. M. Jones, T. G. Squires, and M. Lynn, *J. Am. Chem. Soc.*, **89**, 318 (1967).

Synthetic Studies on Terpenoids. I. Stereocontrolled Synthesis of (±)-1,2,3,4,4a,9,10,10a-Octahydro-7-methoxy-1,4a-dimethyl-10-oxophenanthrene-1β-carboxylic Acid: A Potential Intermediate for Diterpenoid Synthesis[1,2]

Ajoy K. Banerjee,* Carmen D. Ceballo, Maria N. Vallejo, and Edith H. Bolivar

Centro de Química, Instituto Venezolano de Investigaciones Científicas, I.V.I.C., Apartado 1827, Caracas, Venezuela

(Received March 6, 1978)

A stereocontrolled synthetic route to (±)-1,2,3,4,4a,9,10,10a-octahydro-7-methoxy-1,4a-dimethyl-10-oxophenanthrene-1β-carboxylic acid and its conversion to 1,2,3,4,4a,4b,5,6,7,9,10,10a-dodecahydro-10β-hydroxy-1,4a-dimethyl-7-oxophenanthrene-1β-carboxylic acid is described.

Functionalization of methyl group of abietic acid and podocarpic acid have been realized[3] with a view to synthesise potential intermediates of naturally occurring diterpenoids such as gibberellin and the diterpenoid alkaloids. Investigations towards the functionalization of C-1 methyl groups in the compounds possessing a rosane skeleton was undertaken for the construction of lactone ring of rosenonolactone[4] and the fundamental skeleton of erythroxydiol X.[5] In connection with our synthetic studies on diterpenes[6] attention was directed towards the functionalization of C-1β-methyl group of a hexahydrophenanthrene system (III) to C-1β carboxylic acid (XVI) derivative, a potential synthon for the entry into various tricyclic and tetracyclic diterpenes recently isolated.[7,8]

For the synthesis of the hexahydrophenanthrene system (III), the elimination of the carbonyl group of the ketone (I)[9] was attempted. The difficulties of the elimination of C-2 carbonyl group of I, without affecting $\Delta^{10,10a}$, by Huang-Minlon procedure or by thioacetal desulfurization sequence have already been noted by Ireland and coworkers[10] and thus requires no comment. The elimination of carbonyl groups by reduction of tosylhydrazone derivative (II) was thus attempted. The tosylhydrazone derivative II prepared following the procedure of Caglioti[11] was obtained in 85% yield. Reduction of the derivative II could not be effected either with $NaBH_4$ or $LiAlH_4$. Finally the desired hexahydrophenanthrene (III) was obtained in 60% yield by Clemmensen reduction[12] of the carbonyl group of I. In the IR spectrum the olefin (III) showed band at 1678 cm^{-1} (C=C) in and the NMR spectrum exhibited a triplet centered at δ 5.68 ppm, characteristic of C-10 hydrogen. Hydroboration of the olefin (III) under controlled conditions[13] afforded crystalline alcohol (IV) in 50% yield. When the hydroboration of the olefin (III) was carried for a prolonged period, a complex mixture was obtained from which a very little amount of the desired alcohol (IV) was obtained. The stereochemistry of this hydroxylation is important as only 10β-hydroxyl function is useful for transannular oxidation of 1β-methyl group. Inspection of molecular models of the olefin (III) shows that an approach of the hydroborating agent from α-side of the olefin is shielded by 4aα-CH_3 and 1α-CH_3. Thus the approach to β-side of 10a,10-double bond of the olefin (III) is more favoured to produce 10β-alcohol (IV). In the NMR spectrum the alcohol (IV) exhibited multiplet at δ 4.23 (m, H at C-10) with half-band width ($W_{1/2}$) of 8 Hz, characteristic of equatorial proton[14] of C-10. Further that the alcohol (IV) was indeed 10β-isomer was indicated by careful (−12 °C) Jones oxidation to the corresponding ketone (V). The ketone (V) on being equilibrated with acid or base was recovered unchanged. Many examples can be cited from the chemical literature[15] to illustrate that the low temperature Jones oxidation does not bring enolization of similar ketones and the configuration position adjacent to the carbonyl group remains undisturbed. The stability of the ketone (V) under enolizing conditions indicated that A/B ring fusion is in the more stable trans-configuration. The ketone (V) exhibited three methyl signals δ 0.96, 0.99, and 1.15 ppm which are consistent with trans A/B fusion[16] of the ketone (V). If the ketone (V) be with cis A/B ring fusion and steroidal conformation (VI) then one of the C-1 methyl groups would be present at a very high field (δ 0.52—0.56 ppm)[13] in the NMR spectrum owing to the shielding effect of aromatic ring. On the other hand the ketone (V) with cis A/B ring fusion and non-steroidal conformation (VII) would exhibit the signal of one of the C-1 methyl group in a very low field (δ 1.56 ppm) in the NMR spectrum[16] owing to the deshielding effect of C-10 carbonyl group. The benzyl protons at C-9 appeared as two doublets centered at δ 2.48 and 2.51 ppm indicating that C-10 carbonyl group is not equidistant from C-9 benzyl protons. This data is only consistent with half-boat conformation (VIII) for ring B because with half-chair conformation (IX) of ring B, these benzyl protons would appear magnetically equivalent and would appear as a singlet. The appearance of C-9 benzyl protons at δ 2.48 and 2.51 also indicated that the trans fusion of A/B ring of the ketone (V) because if A/B ring were cis-fused then the benzyl protons would have appeared at low field in the NMR spectrum. Thus the C-10a hydrogen of the ketone (V) must be β-oriented (axial) and hence also β-oriented (axial) in the alcohol (IV). The hydroboration reaction involves cis addition of B-H moiety to the double bond and this would also imply that C-10 hydroxyl group of the alcohol (IV) was also β-oriented. The reduction of the ketone (V) with $NaBH_4$ in alcohol afforded an

alcohol in 90% yield which was identical in all respects (IR and mp) with the alcohol (IV). These chemical and spectroscopic properties conclusively indicate that the alcohol (IV) bears axial 10 β hydroxy function. A byproduct of this hydroboration process that resulted in 12% yield appeared to be the olefin (X) exhibited a singlet at δ 6.01 ppm corresponding to two olefinic protons at C-10 and C-9 and a singlet at δ 2.42 ppm corresponding protons at C-10a. The olefin (X) showed absorption at λ_{max} 266 nm (log ε 3.96) characteristic of styrene band. This kind of addition-elimination sequence under mild hydroboration conditions has also been observed.[17] It is worthwhile to mention that though the addition-elimination-readdition sequences under mild hydroboration conditions have been reported previously[18] in the present case no such observation was made.

Reasonably confident that we had the alcohol (IV) with desired stereochemistry, attempt was made to oxygenate 1β-methyl group by intramolecular, transannular oxidation.[19] The alcohol (IV) was oxidized

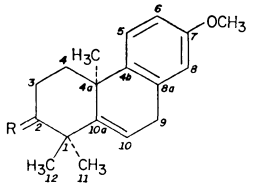

I ; R = O

II ; R = H_3C- 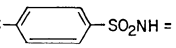 -SO_2NH =

III ; R = H,H

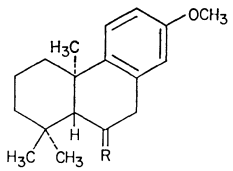

IV ; R = 

V ; R = O

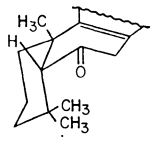

VI

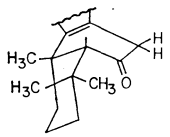

VII

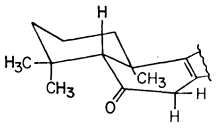

VIII

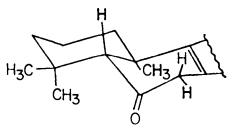

IX

in cyclohexane with lead tetraacetate in presence of iodine. The resulting product after chromatographic purification afforded cyclic ether (XI) in 10% yield whose structure was confirmed by the appearance of two doublets at δ 4.08 (1H, J=7 Hz) and δ 4.18 (1 H, J=8 Hz) (2 H at C-12) and by the disappearance of one of the methyl groups at C-1 CH_3 in the NMR spectrum. Further elution of the oxidised product afforded the ketone (V) in 42.7% yield and the lactone (XII) in 36% yield. When the alcohol (IV) was oxidized with lead tetraacetate in benzene in the absence of iodine the yield of the ether (XI) and the ketone (V) was increased to a certain extent along with the diminution in the yield of the lactone (XII).

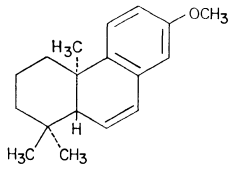

X

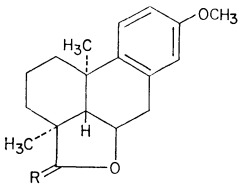

XI ; R = H,H

XII ; R = O

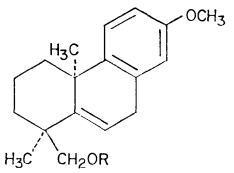

XIII ; R = AC

XIV ; R = H

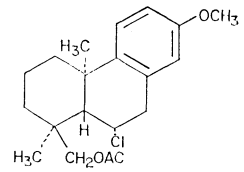

XV

Having obtained the ether (XI), the lactone (XII) and the ketone (V) from the photolytic oxidation of the alcohol (IV), attention was directed towards the transformation of these products to the desired keto acid (XVI). Treatment of the ether (XI) with pyridine hydrochloride and acetic anhydride at reflux yielded a gummy mass which on chromatographic purification afforded a product in poor yield which was identified as olefin acetate (XIII) since it exhibited IR band at 1735 (acetate C=O) and 1245 (C–O) cm^{-1} and the NMR signals at δ 2.06 (3 H, s, OAc), 4.18 (2 H, AB q, J=12 Hz, $C\underline{H}_2OAc$) and 5.55 (1 H, m, olefinic proton at C-10) ppm. Hydrolysis of this compound with 3% methanolic potassium hydroxide afforded an olefinic alcohol (XIV), the NMR spectrum of which showed peaks at δ 3.63 (2 H, AB q, J=11 Hz, CH_2OH) and 5.63 (1 H, m, olefinic proton at C-10). Beside the olefin acetate (XIII), a chlorine compound was obtained in 70% yield which was assigned to the structure (XV). The compound gave positive halogen test and in the NMR spectrum the compound (XV) showed an AB quartet of the acetate centered at δ 3.53 ppm. Refluxing of this chloro compound with 5% methanolic potassium carbonate solution gave back the ether (XI). The poor yield of the olefin acetate (XIII) can be accounted by the rapid addition of hydrogen chloride across the 10,10a-double bond of the olefin acetate (XIII). The ready transformation of the chloroacetate (XV) to the ether (XI) under weakly basic conditions strongly suggests that the halogen at position C-10 is α-oriented.

As the yield of the olefinic alcohol (XIV), which is a useful intermediate for the synthesis of keto acid (XVI), was poor, we investigated chromic acid oxidation of the ether (XI). On oxidation of the ether (XI) with chromic acid in acetic acid was obtained a nicely crystalline keto acid (XVI) in excellent yield. That the cleavage of 10β→12 ether linkage had occurred was evidenced by the disappearance of C-12

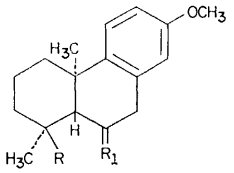

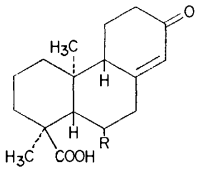

XVI ; R = COOH, R_1 = O

XVII ; R = CH_2OH, R_1 = O

XVIII ; R = CH_2OH, R_1 = 

XIX ; R = CHO, R_1 = O

XX ; R = COOH, R_1 = 

XXI ; R = COOH, R_1 = H,H

XXII, R = COOH, R_1 = 

XXIII ; R = 

XXIV ; R = H,H

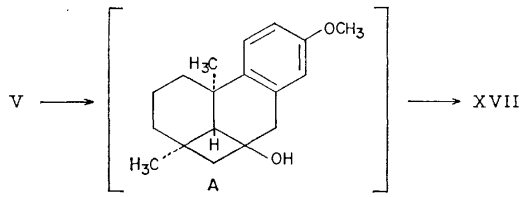

oxymethylene protons in the NMR spectrum. In the IR spectrum it showed an unresolved carbonyl band of high intensity of 1710 cm^{-1}. Its molecular weight as determined by mass spectrometry was found to be 302 which corresponded to the keto acid (XVI).

With a view to convert the ketone (V) to the keto acid (XVI) it was planned to subject the ketone (V) to photochemical reaction[20] with the hope of obtaining a cyclobutane derivative (A) which on ring cleavage would produce the keto alcohol (XVII) and this alcohol (XVII) on oxidation would afford the keto acid (XVI). Photolysis of the ketone (V) with a 200 W Hanovia high pressure mercury lamp with a Pyrex filter under oxygen free N_2 gave an oily material. Hydrolysis of the product with acetic acid yielded a gummy material which on chromatographic purification afforded an alcohol (as identified by mass spectrum and IR study) in 78% yield which was identical in all respects (IR and mp) with the alcohol (IV). Another product of this reaction showed OH band at 3320 cm^{-1} and no carbonyl band in the IR spectrum. Due to the low yield of the oily material it was not possible to investigate its chemical and spectroscopic properties. Thus the ketone (V) could not be utilised for the synthesis of keto acid (XVI).

Finally effort was made to cnovert the lactone (XII) to the desired keto acid (XVI). The lactone ring on being reduced with $LiAlH_4$ in tetrahydrofuran afforded the diol (XVIII) in excellent yield. In the NMR spectrum the diol (XVIII) exhibited an AB quartet centered at δ 3.53 ppm (2 H, J=8 Hz, CH_2OH) and the molecular weight determined by mass spectrum study was found to be 290 which corresponded to the alcohol (XVIII). The alcohol on oxidation with Jones reagent afforded the keto acid (XVI) in 50% yield and the keto aldehyde (XIX) in 35% yield. Oxidation of the keto aldehyde (XIX) with Jones reagent for a prolonged period afforded a negligible amount of the keto acid (XVI).

In order to confirm the structure of the keto acid (XVI), it was converted to its thioacetal (XX) which on desulfurization with Raney nickel afforded the acid (XXI) in 65% yield. The acid (XXI), identical in all respects (mp and IR) with authentic specimen prepared by Pelletier and Ogiso,[21] was utilized for the synthesis of resin acid degradation products. Thus keto acid (XVI) is not only a potential intermediate for the synthesis of pimarane and tetracyclic diterpenes but constitutes an alternative and elegant approach for the synthesis of resin acid degradation products.

The keto acid (XVI) on reduction with sodium borohydride[22] afforded only the alcohol (XXII) in 92% yield. In the NMR spectrum the alcohol, mp 245 °C, exhibited a multiplet at δ 4.30 (m, H at C-6) with half-band width ($W_{1/2}$) of 6 Hz, characteristic of equatorial proton. Reduction of the alcohol (XXII) by Birch procedure using lithium in liquid ammonia and ethanol afforded an oily material which without purification was treated with mineral acid to obtain α,β-unsaturated ketone (XXIII). In the IR spectrum the ketone (XXIII) showed a strong band at 1645 cm^{-1} characteristic of α,β-unsaturated ketone and in the NMR spectrum it exhibited olefinic proton at δ 5.93 (s, 1 H). The molecular weight of the ketone determined by mass spectrometry was found to be 292 which corresponded to the keto acid (XXIII). It was reported[21] that the Birch reduction of the acid (XXI) afforded α,β-unsaturated ketones (XXIV) in which hydrogen at C-4b and the methyl group at C-4a are trans to each other. By this analogy the trans relationship of C-4b hydrogen and C-4a methyl group of the keto acid (XXIII) was established. Besides the keto acid (XXIII), some oily material consisting a mixture of products (as observed from TLC) was obtained from the Birch reduction of the alcohol (XXII). The oily material exhibited a weak carbonyl band and complete absence of hydroxyl group in the IR spectrum. The formation of the oily material devoid of hydroxyl group can be explained by intramolecular participation of the hydroxyl group and examples in which a hydroxyl group influences reduction with lithium in liquid ammonia have been reported.[23]

The keto acid (XXIII) thus obtained with desired stereochemistry is a potential intermediate for the synthesis of pimarane diterpene[7] and other tetracyclic diterpene.[8] The utility of the keto acid (XXIII) in the synthesis of natural products will be reported.

Experimental

Mps were taken on a Kofler hot stage apparatus. Unless otherwise stated IR spectra measured in cm^{-1}, were recorded on a Perkin-Elmer 337 spectrometer for KBr discs of liquid films and UV spectra were measured with a Cary Model 15 spectrometer for EtOH solution, NMR spectra for solutions in deuteriochloroform on either Varian A-60 or XL-100 instrument. Chemical shifts are reported as δ units using

TMS as an internal standard. The form of signals is expressed as s=singlet, d=doublet, q=quartet and m=multiplet. Mass spectra were recorded on a Hitachi Perkin Elmer RMU-6H at 70 eV using a direct inlet system. Merck standardized alumina, activity II-III was used for column chromatography. For TLC, Merck Silica Gel G used and the spots were identified by exposure to iodine vapour. All organic extracts were washed with saturated NaCl solutions, dried over anhydrous $MgSO_4$ and evaporated under reduced pressure below 40 °C. Microanalyses were carried out by Dr. A. Bernhardt, Microanalytical Laboratory, 5251 Elbach über Engelskirchen, West Germany. The compounds described are all racemic forms.

1,2,3,4,4a,9-Hexahydro-7-methoxy-1,1,4a-trimethylphenanthrene (III). The ketone (I; 5.15 g) suspended in 20% HCl (125 ml) was heated under reflux for 24 h in the presence of amalgated mossy Zn [125 g, shaken for 15 min with $HgCl_2$ solution (120 ml containing 25 g $HgCl_2$ and 10 ml concd HCl)]. During the heating, five portions of concd HCl (6 ml) were added in 5 h intervals. After cooling, the mixture was extracted with chloroform. The chloroform extract was washed, dried and concentrated to give the olefin (III; 3.07 g, 60%), bp 110—112 °C at 0.2 mmHg (bath), *m/e* 256 (M^+) and 226 (M^+-2CH_3), δ 1.13 (3H, s), 1.22 (3H, s) 1.26 (3H, s) (1,1-CH_3), and 4a-CH_3 and 3.66 (3H, s; OCH_3). Found: C, 84.30; H, 9.42%. Calcd for $C_{18}H_{24}O$: C, 84.32; H, 9.44%.

Attempted Method for the Reduction of the Ketone (I). In a 50 ml round bottomed flask equipped with a condenser were placed ketone (I; 0.27 g), tosylhydrazine (0.25 g) and methanol (20 ml). The mixture was heated under reflux for 3 h, then cooled to room temperature. The tosylhydrazone (II; 0.39 g, 75%) obtained had mp (from methanol) 180 °C. Found: C, 86.32; H, 7.2%. Calcd for $C_{25}H_{32}O_3N_2S$: C, 86.15; H, 7.32%.

The tosylhydrazone derivative (II; 0.35 g) was dissolved in tetrahydrofuran (30 ml) and to it was added $LiAlH_4$ (0.42 g) slowly. The resulting mixture was refluxed for 8 h. The complex was decomposed by adding water followed by addition of a solution of 10% potassium hydroxide solution. The organic layer was separated and dried. On removal of the solvent a solid material was obtained which was identified as II by comparison (mp and IR).

1,2,3,4,4a,9,10,10a-Octahydro-7-methoxy-1,1,4a-trimethylphenanthren-10β-ol (IV). To a solution of the olefin (III; 2.01 g) in anhydrous ether (50 ml) at 0 °C was added $LiAlH_4$ (1.21 g). To the cold suspension was added dropwise freshly distilled boron trifluoride etherate (8 ml) in anhydrous ether (60 ml). The reaction mixture was stirred at 0 °C for 1 h and at room temperature for 4 h. The excess diborane was decomposed by addition of ice water and 10% aqueous sodium hydroxide solution (75 ml). The reaction mixture was cooled to 0 °C and then added dropwise 30% hydrogen peroxide (75 ml). The reaction mixture was allowed to warm to room temperature and stirred for 16 h. The aqueous layer was drawn off and extracted twice with ether and then combined with original ethereal solution, dried and then solvent removed. The oily material obtained was chromatographed over alumina. Elution with hexane: benzene (1:1) afforded oily olefin (X; 0.24 g, 12%), bp 115—120 °C at 0.2 mmHg (bath), *m/e* 256 (M^+), λ_{max} 266 nm (log ε 3.96), δ 1.12 (3H, s), 1.20 (3H, s), 1.24 (3H, s) (1,1-CH_3 and 4a-CH_3), 2.42 (1H, s, H-10a), 3.65 (3H, s, OCH_3) and 6.01 (2H, s) (H-10 and H-9). Found: C, 84.28; H, 9.43%. Calcd for $C_{18}H_{24}O$: C, 84.32; H, 9.44%. Further elution with benzene afforded the alcohol (IV; 1.09 g, 50%), mp (from ether) 128—130 °C, *m/e* 274 (M^+) and 256 (M^+-H_2O), ν_{max} 3480 (OH), δ 1.12 (3H, s) 1.20 (3H, s), 1.26 (3H, s) (1,1-CH_3 and 4a-CH_3), 3.68 (3H, s, OCH_3) and 4.23 (1H, m, $W_{1/2}$=8 Hz, H-10). Found: C, 78.76; H, 9.54%. Calcd for $C_{18}H_{26}O_2$: C, 78.79; H, 9.55%.

1,2,3,4,4a,9,10,10a-Octahydro-7-methoxy-1,1,4a-trimethylphenanthren-10-one (V). Jones chromic acid reagent (1 ml) was added to a solution (−12 °C) of the alcohol (IV; 0.22 g) in acetone (4 ml). The solution was stirred during 5 min maintaining the temperature −12 °C. 2-Propanol was added to destroy the excess oxidant and after the usual work-up afforded oily material which on chromatographic purification over alumina afforded the ketone (V; 0.18 g), mp 19—20 °C (from ether-hexane), *m/e* 272 (M^+), ν_{max} 1720 (C=O), δ 0.96 (3H, s), 0.99 (3H, s) and 1.15 (3H, s) (1,1-CH_3 and 4a-CH_3), 2.48 (1H), 2.51 (1H) (H-9) and 3.65 (3H, s, OCH_3). Found: C, 79.35; H, 8.86%. Calcd for $C_{18}H_{24}O_2$: C, 79.37; H, 8.88%.

Reduction of the Ketone (V). $NaBH_4$ (0.1 g) was added slowly to an ice-cooled solution of the ketone (V; 0.15 g) dissolved in methanol (20 ml). The solution was stirred at room temperature for 6 h. After acidification with dil HCl, the product was extracted with chloroform. Washing of the organic extract and evaporation yielded a solid material which on crystallization (from ether) afforded an alcohol (0.13 g, 90%) which was identical in all respects (mp and IR) with alcohol (IV).

Lead Tetraacetate Oxidation of 1,2,3,4,4a,9,10,10a-Octahydro-7-methoxy-1,1,4a-trimethylphenanthren-10β-ol (IV). A mixture of lead tetraacetate (3.70 g) and calcium carbonate (3.70 g) was dried under reduced pressure and then heated in cyclohexane (184 ml) under reflux for 30 min with stirring. Then a solution of the alcohol (IV; 2 g) in cyclohexane (40 ml) was added to the above suspension followed immediately by iodine (0.94 g). The mixture was heated under reflux 1 h with two philips 500-W photolamps. The cooled mixture was filtered and the filtered cake was washed thoroughly with ether. The combined organic solvents were washed with 1% sodium hydroxide solution and the colour of iodine was removed by washing with sodium thiosulfate solution. Subsequent washing and evaporation afforded an oily material which was chromatographed on alumina. Elution with hexane afforded the ether (XI; 0.21 g, 10%), mp (ether–hexane) 22—23 °C *m/e* 272 (M^+), δ 1.10 (3H, s), 1.23 (3H, s) (1-CH_3 and 4a-CH_3), 3.65 (3H, s, OCH_3), 4.08 (1H, d, J=7 Hz) and 4.18 (1H, d, J=8 Hz) (2H, H-12). Found: C, 79.34; H, 8.87%. Calcd for $C_{18}H_{24}O_2$: C, 79.37; H, 8.88%. Further elution with hexane: benzene (1:1) afforded the ketone (V; 0.88 g, 42.7%) Elution with benzene afforded the lactone (XII; 0.78 g, 36%), *m/e* 286 (M^+), ν_{max} 1765, δ 1.20 (3H, s) and 1.28 (3H, s) (1-CH_3 and 4a-CH_3) and 3.65 (3H, s, OCH_3). Found: C, 75.48; H, 7.72%. Calcd for $C_{18}H_{22}O_3$: C, 75.49; H, 7.74%.

1,2,3,4,4a,9-Hexahydro-1β-acetoxymethyl-7-methoxy-1,4a-dimethylphenanthrene (XIII). The ether (XI; 0.91 g) was heated under reflux with acetic anhydride (20 ml) and pyridine –HCl (0.11 g) for 6 h. The mixture was treated with cold water and extracted with ether. The ether extract was washed till neutral and then evaporated to yield a liquid which gave a positive halogen test with a copper wire. The liquid was chromatographed on alumina. Elution with hexane gave the oily olefin acetate (XIII; 90 mg, 9%), bp 118—125 °C at 0.12 mmHg (bath), *m/e* 314 (M^+) and 254 (M^+-CH_3COOH). Found: C, 76.37; H, 8.32%. Calcd for $C_{20}H_{26}O_3$: C, 76.40; H, 8.34%. Hydrolysis of the acetate (XIII; 80 mg) with 3% methanolic potassium hydroxide afforded the alcohol (XIV; 50 mg) as a yellow oil, homogeneous in TLC, *m/e* 272 (M^+). Found: C, 79.35; H, 8.86%.

Calcd for $C_{18}H_{24}O_2$: C, 79.37; H, 8.88%. Further elution with hexane:benzene (1:1) afforded a chloro compound (XV; 0.81 g, 70%) which was obtained as semi-solid material. It gave positive halogen test, δ 1.13 (3H, s), 1.61 (3H, s) (1-CH_3 and 4a-CH_3), 3.53 (2H, AB q, J=12 Hz, CH_2OAc) and 3.65 (3H, s, OCH_3). Refluxing the chloro compound (XV; 0.70 g) with 5% methanolic potassium carbonate solution afforded ether (XI, 0.48, 90%).

1,2,3,4,4a,9,10,10a- Octahydro-7-methoxy-10-oxo - 1,4a - dimethylphenanthrene-1β-carboxylic Acid (XVI). To the ether (**XI**; 0.31 g) dissolved in acetic acid (6 ml, 98%) was added a solution of CrO_3 (0.25 g) in acetic acid (5 ml, 80%) and the mixture was kept at room temperature for 40 h. The usual work-up gave the acid (**XVI**; 0.27 g, 80%), mp 256—257 °C (from ether), *m/e* 302 (M^+) and 257 (M^+-COOH), ν_{max} 1710 (unresolved acid and ketonic C=O), δ 1.23 (3H, s), 1.26 (3H, s) (1-CH_3 and 4a-CH_3) and 3.65 (3H, s, OCH_3). Found: C, 71.48; H, 7.32%. Calcd for $C_{18}H_{22}O_4$: C, 71.50; H, 7.35%.

Photolysis of the Ketone (V). The ketone (V; 0.92 g) in 95% ethanol (790 ml) saturated with potassium carbonate was irradiated for 25 h with a 200 W Hanovia high pressure lamp with a Pyrex filter under oxygen free nitrogen. On removal of the ethanol a liquid (0.89 g) was obtained which was hydrolysed with a mixture of acetic acid (20 ml), methanol (80 ml) and water (15 ml) heating under reflux for 2 h. The crude product on chromatographic purification over alumina and elution with hexane: ether (1:1) afforded the alcohol (IV, 0.72 g, 78%) identical with the foregoing sample. Further elution with hexane: ether (2:8) afforded an oily material, ν_{max} 3320 (OH). Found: C, 74.42; H, 9.01%. Calcd for $C_{18}H_{26}O_3$: C, 74.44; H, 9.03%.

Oxidation of the Diol (XVIII). The diol (XVIII; 0.14 g) in acetone (15 ml) was added Jones reagent (2 ml) and stirred at room temperature for 4 h. 2-Propanol was added to destroy the excess oxidant and then the mixture was extracted with ether. The ether extract was washed with sodium hydrogencarbonate (5%). The alkaline extract after acidification afforded the keto acid (XVI; 70 mg, 50%) identical with the foregoing sample.

The ether extract was washed, dried and evaporated to obtain the aldehyde (XIX; 40 mg, 30%), as a semi-solid mass, homogeneous in the TLC, *m/e* 286 (M^+) and 257 (M^+-CHO), ν_{max} 1685 (C=O) and 1720 (CHO). Found: C, 75.46; H, 7.72%. Calcd for: C, 75.49; H, 7.47%.

1,2,3,4,4a,9,10,10a-Octahydro-7 - methoxy - 1,4a - dimethylphenanthrene-1β-carboxylic Acid (XXI). The keto acid (XVI; 0.11 g) dissolved in chloroform (5 ml) was treated with boron trifluoride etherate (1 ml) and 1,2-ethanedithiol (4 ml). The reaction mixture was stirred for 36 h and then treated with water. The organic extract was washed, dried and on removal of the solvent was obtained the thioacetal (**XX**; 0.16 g). The crude thioacetal, mp 98—105 °C, without purification, was dissolved in absolute ethanol (50 ml) and was added to a suspension of W2 Raney nickel (20 g) in absolute ethanol (100 ml). The mixture was stirred and refluxed for 18 h. The usual work-up afforded the acid (**XXI**; 60 mg, 65%), mp (from ether) 151—152 °C. Found: C, 74.95; H, 8.38%. Calcd for $C_{18}H_{24}O_3$: C, 74.97; H, 8.39%. The mp of the acid (XXI) was not depressed on admixture with the authentic[21] sample (identical in IR and TLC properties).

1,2,3,4,4a,9,10,10a-Octahydro-10β-hydroxy-7-methoxy-1,4a-dimethylphenanthrene-1β-carboxylic Acid (XXII). To the keto acid (XVI; 0.1 g) dissolved in methanol (20 ml) and cooled to 0 °C was added sodium borohydride (15 mg) and the reaction mixture was stirred for 2 h at room temperature. After acidification with dil HCl, the product was extracted with chloroform. Washing of the organic extract and evaporating yielded the alcohol (**XXII**, 90 mg, 92%), mp (from ether) 245 °C *m/e* 304 (M^+) and 286 (M^+-H_2O), δ 1.18 (3H, s), 1.23 (3H, s) (1-CH_3 and 4a-CH_3), 3.65 (3H, s, OCH_3) and 4.30 (1H, m, $W_{1/2}$=6 Hz). Found: C, 71.01; H, 7.93%. Calcd for $C_{18}H_{24}O_4$: C, 71.02; H, 7.95%.

1,2,3,4,4a,4b,5,6,7,9,10,10a-Dodecahydro-10β-hydroxy-1,4a-dimethyl-7-oxophenanthrene-1β-carboxylic Acid (XXIII). The hydroxy acid (XXII; 0.2 g) dissolved in ether (30 ml) was added slowly to anhydrous liquid NH_3 containing lithium metal (30 mg). The mixture was stirred for 30 min and then added slowly absolute ethanol (95 ml). Stirring was continued until disappearance of the blue color; after the mixture had stood overnight at room temperature to allow the ammonia to evaporate, water was added and the reduced product was extracted with ether. The extracts were washed till neutral, dried and evaporated to obtain a semi-solid material (0.94 g) which without purification was hydrolysed on steam bath for 2 h in a mixture of methanol (20 ml), water (5 ml) and concd hydrochloric acid (10 ml). The mixture was poured into cold water and extracted with ether. The organic extract was washed till neutral, dried and evaporated. An oily material was obtained which was chromatographed over silica gel. Elution with benzene: ether (9:1) afforded α,β-unsaturated ketone (**XXIII**; 58 mg, 30%), mp (from ether) 292 °C, *m/e* 292 (M^+) and 274 (M^+-H_2O), λ_{max} EtOH 248 nm (log ε 15,500), ν_{max} 3540 (OH), 1725 (C=O) and 1665 (α,β-unsaturated C=O), δ 1.18 (3H, s), 1.23 (3H, s) (1-CH_3 and 4a-CH_3), 3.78 (1H, m, $W_{1/2}$= 8 Hz) and 5.93 (1H, s) (8-H). Found: C, 69.81; H, 8.25%. Calcd for $C_{17}H_{24}O_4$: C, 69.83; H, 8.27%.

We wish to thank Prof. R. E. Ireland, California Institute of Technology for helpful discussions during the preparation of manuscript and Consejo Nacional de Investigaciones Cientificas y Tecnologicas (CONICIT) for partial financial assistance.

References

1) Preliminary communication, A. K. Banerjee, C. D. Ceballo, M. N. Vallejo, and E. H. Bolivar, *Gazz. Chim. Ital.* **107**, 437 (1977).

2) (a) Part of this investigation was presented (A.K.B.) at 26th International Congress of Pure and Applied Chemistry, Tokyo (Japan), September, 1977 (Symposium Papers, p. 1117). (b) Dedicated to Sir Derek Barton on the occasion of his 60th birthday.

3) A. Tahara, K. Hirao and Y. Hamazaki, *Tetrahedron*, **21**, 2133 (1965).

4) R. E. Ireland and L. N. Mander, *J. Org. Chem.*, **34**, 142 (1969).

5) a) T. Nakano and A. K. Banerjee, *Tetrahedron*, **28**, 471 (1972); b) T. Nakano and A. K. Banerjee, *J. Chem. Soc.*, **1977**, 2181.

6) a) A. K. Banerjee, *Acta Cient. Venezolana*, **23**, 211 (1972); b) A. S. Sarma, A. K. Banerjee, and P. C. Dutta, *J. Chem. Soc.*, **1976**, 722; c) A. K. Banerjee, *Bull. Soc. Chim. Belg.*, **85**, 499 (1976); d) A. K. Banerjee, M. Narváez, and E. H. Bolivar, *Bull. Soc. Chim. Belg.*, **85**, 904 (1976).

7) O. Tanaka, S. Mihashi, I. Yanagisawa, T. Nikaido, and S. Shibata, *Tetrahedron*, **28**, 4523 (1972).

8) L. Canonica, B. Rindone, C. Scolastic, K. D. Han, and J. H. Kim, *Tetrahedron Lett.*, **1969**, 4801.

9) G. Stork, A. Meisels, and J. E. Davies, *J. Am. Chem. Soc.*, **85**, 3419 (1963).

10) R. F. Church, R. E. Ireland and J. A. Marshall, *J. Org. Chem.*, **31**, 2526 (1966).
11) L. Caglioti, *Org. Synth.*, **52**, 122 (1972).
12) E. L. Martin, *Org. React.*, **1**, 155 (1942).
13) J. W. Huffman and J. J. Gibs, *J. Org. Chem.*, **39**, 2501 (1974).
14) N. S. Bhaca and D. H. Williams, "Applications of NMR Spectroscopy in Organic Chemistry," Holden-Day, Inc., San Francisco (1964), p. 69.
15) H. O. House, "Modern Synthetic Reactions," 2nd ed W. Benjamin, Menlo Park, California (1972), p. 263.
16) E. Wenkert, A. Alonso, P. Beak, R. W. J. Carney, P. W. Jeffs, and J. D. McChesney, *J. Org. Chem.*, **30**, 713 (1965).
17) R. E. Ireland, private communication.
18) a) W. Herz and J. Schmid, *J. Org. Chem.*, **34**, 3464 (1969); b) B. E. Cross and P. L. Myers, *J. Chem. Soc.*, **1968**, 471; c) P. Pernelle and G. Ourisson, *J. Org. Chem.*, **30**, 1744 (1965); also see Ref. 16.
19) K. Hueslar, J. Kalvoda, G. Anner, and A. Wettstein, *Helv. Chim. Acta*, **48**, 704 (1965).
20) E. Atenburger, H. Wehrls, and K. Schaffner, *Helv. Chim. Acta*, **48**, 704 (1965).
21) A. Ogiso and S. W. Pelletier, *J. Chem. Soc., Chem. Commun.*, **1967**, 94.
22) Reduction with disiamylborane (H. C. Brown and R. S. Varma, *J. Org. Chem.*, **39**, 1631, (1974)) was not successful.
23) E. Fujita, M. Shibuya, S. Nakamura, Y. Okada, and T. Fujita, *J. Chem. Soc., Perkin Trans. 1*, **1974**, 165.

NOTES

BULLETIN OF THE CHEMICAL SOCIETY OF JAPAN, VOL. 52 (2), 614 (1979)

Photochemical Thiocyanation of Halobenzenes with Thiocyanate Anion

Kiyoko FUJIKI,* Takehiko NISHIO,† and Yoshimori OMOTE†

Department of Agricultural Chemistry, Faculty of Agriculture, Meiji University, Ikuta, Kawasaki 214
†*Department of Chemistry, University of Tsukuba, Sakura-mura, Niihari-gun, Ibaraki 300-31*

(Received July 21, 1978)

Synopsis. Halobenzenes having such an electron-donating group as amino, hydroxyl or methoxyl group at their para position were thiocyanated with sodium thiocyanate under irradiation. Also, the ring isomer of *o*-thiocyanatoaniline, 2-aminobenzothiazole, was obtained by the photoreaction of *o*-chloroaniline with sodium thiocyanate.

In spite that photochemically induced nucleophilic aromatic substitution including the photocyanation has been extensively studied[1] very few examples of photothiocyanation of aromatic compounds are known other than the reaction of phenylthallium(III) compounds with potassium thiocyanate[2] and the formation of *p*-thiocyanatoaniline from *p*-chloroaniline.[3] We now report the photothiocyanation of monosubstituted halobenzene with thiocyanate anion.

By the irradiation of *p*-substituted halobenzenes and sodium thiocyanate in water or *t*-butyl alcohol-water through quartz by a high pressure mercury lamp the corresponding *p*-substituted thiocyanatobenzenes were obtained. The results are summarized in Table 1. Under the similar conditions, *m*-chloroaniline, *m*-chlorophenol, *m*-chloronitrobenzene, or *m*-nitroanisole did not give a detectable amount of *m*-thiocyanatobenzene derivatives.

TABLE 1. PHOTOTHIOCYANATION OF *p*-SUBSTITUTED HALOBENZENES

$$R\text{-}C_6H_4\text{-}X + NaSCN \xrightarrow{h\nu} R\text{-}C_6H_4\text{-}SCN + NaX$$

R	X	Solvent	Time (h)	Yield (%)
NH_2	Cl	20% *t*-butyl alcohol	6	10.5
NH_2	Br	20% *t*-butyl alcohol	6	5.0
OH	Cl	water	18	25.0
OH	Br	water	6	13.6
OCH_3	Cl	20% *t*-butyl alcohol	11	15.3
OCH_3	Br	60% *t*-butyl alcohol	3	7.0

Irradiation of a solution of *o*-chloroaniline and sodium thiocyanate in 20% aqueous *t*-butyl alcohol afforded 2-aminobenzothiazole. There was no remarkable acceleration in the photoreaction of *p*- or *m*-chloroaniline in the presence of 18-crown-6 ether potassium thiocyanate complex in anhydrous acetonitrile. As shown in Table 1, halobenzenes having an electron-donating group at their para position can be substituted by photothiocyanation.

Experimental

UV spectra were recorded on a Hitachi EPS-3T recording spectrophotometer and IR spectra on a Hitachi EPI-G3 spectrophotometer. A Taika 100W high pressure mercury lamp was used as the irradiation source.

General Procedure for Analysis of Photothiocyanation Products from Halobenzenes. A solution of a halobenzene (0.2 mmol) and sodium thiocyanate (2 mmol) in a solvent (20 ml) was irradiated. The reaction was cheked with TLC and UV spectrum. An aliquot of the reaction mixture was analyzed by liquid partition chromatography and UV spectrum to determine the yields of products. The reaction mixture was always proved to contain unreacted halobenzene.

Photothiocyanation of p-*Chloroaniline.* A typical example for isolation and identification of photothiocyanation products from monosubstituted halobenzenes is as follows. A solution of *p*-chloroaniline (5 mmol) and sodium thiocyanate (50 mmol) in 20% aqueous *t*-butyl alcohol (500 ml) was irradiated through quartz with stirring for 4.5 h. A small amount of dark brown precipitates which appeared during the irradiation was filtered off. The filtrate was concentrated to dryness. The residue was mixed with water and extracted with ether. The ethereal layer was dried over anhydrous sodium sulfate and ether was removed under reduced pressure. The residue was crystallized from ethanol water to give colorless crystals, mp 55.5 °C,[4] which was identified with an authentic sample by mixed-melting point, UV and IR spectrum: λ_{max}^{EtOH} 262 nm, ν(KBr) 2141 cm^{-1} (SCN).

Photothiocyanation of o-*Chloroaniline. Formation of 2-Aminobenzothiazole.* The preceding procedure was used except that the *t*-butyl alcohol solution was irradiated for 50.5 h to give colorless crystals, mp 128—129.5 °C,[5] which was identified with an authentic sample by mixed-melting point and UV spectrum: λ_{max}^{EtOH} 264 nm.

Photothiocyanation of p- *or* m-*Chloroanilne in the Presence of 18-Crown-6 Ether Potassium Thiocyanate Complex.* Potassium thiocyanate (1 mmol) and 18-crown-6 ether (1 mmol) were dissolved in methanol (10 ml) and then methanol was removed under reduced pressure to give a colorless complex. A solution of the complex and *p*- or *m*-chloroaniline (0.1 mmol) in acetonitrile (10 ml) was irradiated for 5 h. The yield of the product did not increase compared with that of the reaction product in the absence of the complex.

References

1) a) J. Cornelisse and E. Havinga, *Chem. Rev.*, **75**, 353 (1975); b) J. Cornelisse, *Pure Appl. Chem.*, **41**, 433 (1975).
2) E. C. Taylor, F. Kienzle, and A. McKillop, *Synthesis*, **1972**, 38.
3) A. V. Eltsov, O. V. Kulbitskaya, and A. N. Frolov, *Zh. Org. Khim.*, **8**, 76 (1972).
4) The reported value is 56—57 °C; A. Kaji, *Nippon Kagaku Zasshi*, **81**, 1776 (1960).
5) The reported value is 132 °C; Z. H. Skraup, *Ann.*, **419**, 65 (1919).

BULLETIN OF THE CHEMICAL SOCIETY OF JAPAN, VOL. 52 (2), 615—616 (1979)

A Broad-line NMR Study on Some Pyrene Complexes: Molecular Motion and Isomorphism in the High-temperature Forms

Tamotsu INABE, Yoshio MATSUNAGA,* and Yuji YOSHIDA

Department of Chemistry, Faculty of Science, Hokkaido University, Sapporo 060

(Received July 14, 1978)

Synopsis. The pyrene complexes with six polynitro aromatic compounds are isomorphous to each other above the transition temperatures. The onset of a large degree of molecular motion has been shown from broad-line NMR measurements to occur at the transition temperature of all the six complexes.

As noted earlier,[1] crystalline pyrene complexes with 2,4-dinitrofluorobenzene (DNF), 2,4-dinitrochlorobenzene (DNC), 2,4-dinitrotoluene (DNT), 2,4-dinitrophenol (DNP), and 2,4,6-trinitrochlorobenzene (TNC) exhibit polymorphic transitions. These transitions are of considerable interest because of the isomorphism observed with the high-temperature forms. The disappearance of the specific interaction between the hydrocarbon molecule and the substituent on the acceptor molecule was speculated to be due to dynamical averaging of the interaction by the onset of a large degree of thermal motion at the transition temperature. The presence of such a molecular motion in the high-temperature forms was considered to be consistent with the relatively small enthalpy and entropy changes at the melting of these complexes. Solid state NMR has proven to be powerful tool for the detection and investigation of molecular motion in complexes;[2] therefore, this technique was employed to study the behavior in our cases.

^{1}H NMR spectra were recorded as the first derivatives at 40 MHz, using a JEOL model JES-ME-3X spectrometer with a broad-line NMR attachment, model JES-BE-1, which employs a crossed-coil system. For the measurements, the complexes were pressed in the form of rods with a diameter of 8 mm. Care was taken in recording the spectra to avoid saturation (where possible), and the modulation amplitude was kept small to avoid distortion of line shape. Second moments were calculated for both halves of the derivative curve and corrected for modulation broadening.

Differential scanning calorimetry (DSC) and X-ray diffraction measurements were made as described in a previous paper.[1] In addition to the five complexes mentioned above, the 2,4,6-trinitrotoluene (TNT) complex was found to exhibit a new phase transition at 59 °C, with an enthalpy change of 2.9 kcal mol^{-1}. The complex melts at 162 °C. The enthalpy of melting is 5.3 kcal mol^{-1}. The X-ray diffraction patterns measured using Cu $K\alpha$ radiation are schematically presented in Fig. 1 along with those of the TNC complex for comparison. Although the two acceptor molecules are almost the same in size, the patterns at room temperature are distinctly different, reflecting the nature of the particular substituent. On the other hand, the simple patterns above the transition temperatures are essentially identical and indicate that these high-temperature forms are isomorphous to each other.

The second moment of the measured spectrum is shown in Fig. 2 as a function of the temperature for each of the pyrene complexes. In all the cases, an abrupt reduction in the second moment was observed almost at the transition temperature determined by DSC. Only when the molecules in the high-tempera-

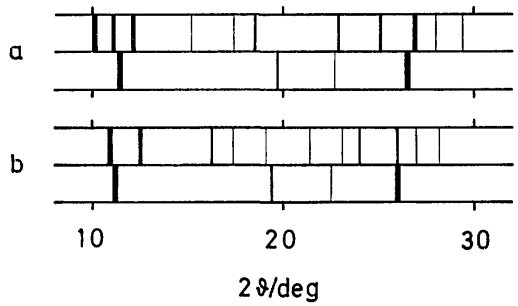

Fig. 1. X-Ray diffraction patterns of the pyrene complexes with a) TNC and b) TNT. The upper pattern for each complex was recorded at room temperature and the lower one, above the transition temperature.

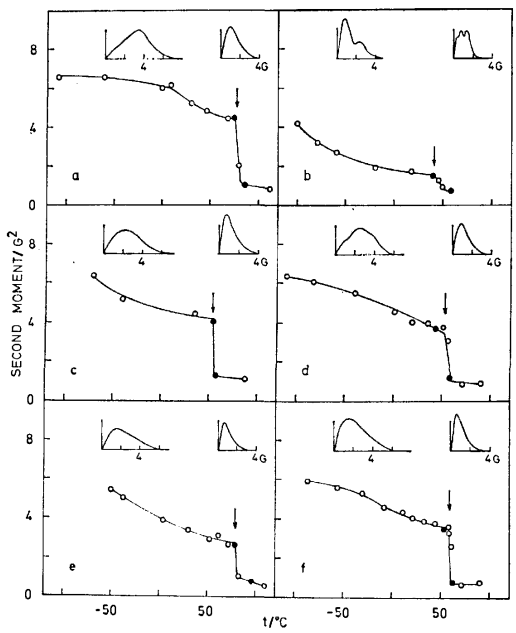

Fig. 2. Second moment values of the proton resonance for the pyrene complexes with a) DNF, b) DNC, c) DNT, d) DNP, e) TNC, and f) TNT with (inset) right halves of representative spectra recorded below (left) and above (right) the transition temperatures. The vertical arrows indicate the thermodynamic transition temperatures.

ture forms are moving fast on an NMR time-scale can one expect such coincidence of the temperatures. It must be noted that the moments observed with the high-temperature forms are in a narrow range around 1 G^2. The resonance line shape changes at the transition. Representative spectra below and above the transition temperature are inset in Fig. 2. The second moments given by these spectra are indicated by shaded circles. Thus, the presence of a large degree of molecular motion in the isomorphous high-temperature forms is now firmly established.

The largest reduction of second moment associated with the transition was found with the DNF complex, and the smallest with the DNC complex. The molecular motion in the low-temperature form of the former complex is clearly more restricted than that of the latter. This conclusion is consistent with the thermodynamic data. Although the enthalpies of melting are rather similar, namely, 5.0 kcal mol^{-1} at 119 °C and 4.2 kcal mol^{-1} at 87 °C respectively, there is a remarkable difference in the enthalpy of transition. The value for the DNF complex is as much as 4.3 kcal mol^{-1}, whereas that for the DNC complex is merely 0.57 kcal mol^{-1}. The enthalpies of transition observed for the other four complexes are in the range from 2.9 to 3.2 kcal mol^{-1}.

The second moment can be calculated from a knowledge of the positions of the nuclei in the lattice, using the formulation of Van Vleck. For such a calculation, the crystal structure is needed, but this is unknown for the present complexes. Nevertheless, the observed variation is so large that the motional characteristics may be discussed to some extent. The second moment in a polycrystalline molecular complex can be divided into an intramolecular part, from the atoms within a single donor molecule and a single acceptor molecule, and an intermolecular part between the atoms of different molecules. For the present complexes, only the former part can be approximately calculated from the molecular structure. The contribution in a pyrene molecule in a rigid lattice has been calculated to be 3.43 G^2 by Fyfe *et al.*[3] As for the acceptor molecule, we calculated the intramolecular contribution in DNF, by way of example, to be 1.5 G^2, taking bond distances of C–C=1.39, C–H =1.08, C–F=1.31, and C–N=1.46 Å, and all bond angles 120°. Then, the contribution in the basis unit of the pyrene–DNF complex becomes about 3.2 G^2 for the rigid lattice model. In order to explain the observed second moment in the high-temperature form, a reduction of the moment by some molecular motion has to be taken into consideration.

The rotation of the pyrene molecule in solids has been suggested to occur in pyrene itself and in some of the molecular complexes.[3,4] It has been pointed out that the rotational barriers found for complexes are lower than those for the parent compounds, possibly due to a general decrease in intermolecular steric effects;[2,5] thus the flat hydrocarbon molecule in the present complexes is probably rotating around the axis perpendicular to the ring plane at high temperatures. Such a motion would reduce the intramolecular contribution by a factor of one fourth.[6] Moreover, the intermolecular contribution is also significantly reduced by it. In the case of the DNF complex, the latter contribution appears to be almost nil. As has been suggested for the azulene-trinitrobenzene complex by Fyfe and Kupferschmidt,[7] it is likely that the acceptor molecule is also mobile in the high-temperature form. In addition to the pyrene complexes reported here, we have recently found a isomorphous high-temperature forms with the complexes of some other hydrocarbons. The work on these complexes is now in progress and will be the subject of forthcoming papers.

The authors wish to express their thanks to Miss Mikiko Nanba and Mr. Eiji Ochi for their collaboration.

References

1) N. Inoue and Y. Matsunaga, *Bull. Chem. Soc. Jpn.*, **51**, 90 (1978).
2) C. A. Fyfe, "Molecular Complexes," ed by R. Foster, Elek Science, London (1973), Vol. 1, pp. 209—299.
3) C. A. Fyfe, D. F. R. Gilson, and K. H. Thompson, *Chem. Phys. Lett.*, **5**, 215 (1970).
4) C. A. Fyfe, *J. Chem. Soc., Faraday Trans. 2*, **70**, 1633 (1974).
5) J. Gallier, *J. Chim. Phys.*, **73**, 893 (1976).
6) H. S. Gutowsky and G. E. Pake, *J. Chem. Phys.*, **18**, 162 (1950).
7) C. A. Fyfe and G. J. Kupferschmidt, *Can. J. Chem.*, **51**, 3774 (1973).

BULLETIN OF THE CHEMICAL SOCIETY OF JAPAN, VOL. 52 (2), 617—618 (1979)

Oxidation of Ammonia with Lattice Oxygen of Metal Oxides by Pulse Reaction Technique

Yukio KOSAKI,* Akira MIYAMOTO, and Yuichi MURAKAMI

Department of Synthetic Chemistry, Faculty of Engineering, Nagoya University, Furo-cho, Chikusa-ku, Nagoya 464

(Received July 6, 1978)

Synopsis. On V_2O_5, MoO_3, and WO_3, lattice oxygen has been found to be the active oxygen species for the *catalytic* oxidation of NH_3, whereas on MnO_2, Co_3O_4, Fe_2O_3, and NiO, adsorbed oxygen also played a significant role in the reaction. NO has been found to be an intermediate in the reaction of NH_3 with lattice oxygen.

Many studies have been reported on the reaction of hydrocarbons with the lattice oxygen of metal oxides in connection with the *catalytic* oxidation of hydrocarbons. On a number of catalysts, lattice oxygen (O^{2-}) has been found to play an important role in the *catalytic* oxidation of hydrocarbons. In a previous paper,[1] the authors investigated the *catalytic* oxidation of NH_3 on various metal oxides by a flow technique, and found that NO is an important gas phase intermediate in the oxidation of NH_3. The *catalytic* oxidation of NH_3 was shown to have a specific character, in that NH_3 is first oxidized to NO (deep oxidation product) which then reacts with NH_3 (the NO–NH_3 reaction) to form N_2 and N_2O (partial oxidation products). This is in contrast with the oxidation of hydrocarbons. In the present work, the reaction of NH_3 with the lattice oxygen of metal oxides has been studied to determine the role of lattice oxygen in the oxidation of NH_3 and the importance of NO as an intermediate in the reaction of NH_3 with metal oxides.

Experimental

Materials. The method of preparation of metal oxides has been described previously.[1] Commercial ammonia (99.9 % purity) and oxygen (99.8% purity) were used as reactants without further purification.

Apparatus. Experiments were conducted with a pulse apparatus. The reactant and product components (NH_3, N_2, N_2O, and NO) were analyzed using gas chromatography. Helium as a carrier gas (116 ml/min) was purified with titanium metal sponge heated at 750 °C. Pulses of NH_3 with various concentrations were supplied to the reactor by a 6-way valve. 0.1 g of metal oxides were used. Before injection of each sample, the metal oxides were treated with oxygen in a gas stream for 30 min at the reaction temperature in order to regulate the oxidation state of the samples.

Results and Discussion

Activities of Metal Oxides for the Reaction with Ammonia. The conversion of NH_3 (X_{NH_3}) and the selectivities to N_2, N_2O, and NO (S_{N_2}, S_{N_2O}, and S_{NO}) have been obtained for various metal oxides as functions of the reaction temperature. In order to compare the activities of the metal oxides, the authors have defined T_L^{-1}, where T_L^{-1} represents the reciprocal of the absolute temperature at which X_{NH_3} attains 20% and is a measure of the reactivity of the lattice oxygen of the metal oxide with NH_3. In Fig. 1, the value of T_L^{-1} for a metal oxide is shown against the enthalpy change (ΔH_0) for the following reaction;

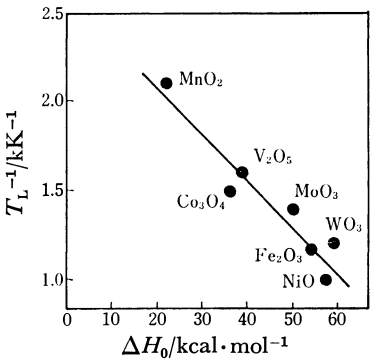

Fig. 1. Relationship between the reactivity of lattice oxygen of a metal oxide (T_L^{-1}) and the enthalpy change (ΔH_0) of the Reaction 1.

$$M_nO_m \longrightarrow M_nO_{m-1} + \frac{1}{2}O_2, \quad (1)$$

where M_nO_m represents a metal oxide before reaction. As shown in Fig. 1, a correlation was obtained between T_L^{-1} and ΔH_0 indicating that the reactivity of the metal oxide with NH_3 is determined by the enthalpy change of the Reaction 1.

In Fig. 2, the relation between T_L^{-1} and T_C^{-1} is shown, where T_C^{-1} is defined as the reciprocal of the absolute temperature at which the conversion of NH_3 in the *catalytic* oxidation of NH_3 by flow technique attains 20%.[1] As shown in Fig. 2, the metal oxides can be divided into two groups. In the first group (V_2O_5, MoO_3, and WO_3), a correlation is obtained between T_L^{-1} and T_C^{-1}, that is, T_L^{-1} is approximately equal to T_C^{-1} within the possible deviations due to the

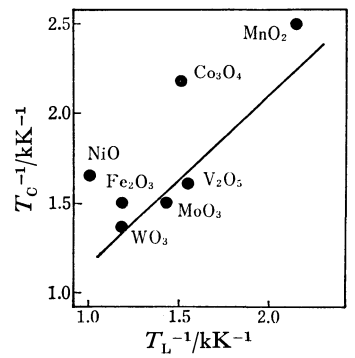

Fig. 2. Relationship between the reactivity of lattice oxygen of a metal oxide (T_L^{-1}) and the activity of the metal oxide for the *catalytic* oxidation of NH_3 (T_C^{-1}).

differences in the reaction technique (pulse or flow technique). The correlation indicates that, on a metal oxide in the first group, the oxygen species responsible for the *catalytic* oxidation of NH_3 is mainly the lattice oxygen of the metal oxide. In the second group (MnO_2, NiO, Fe_2O_3, and Co_3O_4), T_C^{-1} is greater than T_L^{-1} suggesting that on a metal oxide of the second group, in addition to the lattice oxygen, the adsorbed oxygen species such as O_2^- or O^- play a significant role in the *catalytic* oxidation of NH_3. This is in accordance with the results of thermal desorption, that is, the oxygen species, which desorbs at a lower temperature and is assigned to O_2^- or O^- species, was detected for the metal oxide of the second group.[2,3] This classification has been supported by pulse experiments on the effects of gaseous oxygen addition on pulses. The conversion of NH_3 with metal oxides of the second group was enhanced by the addition of O_2 in pulses, whereas X_{NH3} with the metal oxide of the first group was not changed. Concerning the reaction of NH_3 with metal oxides, the influence of adsorbed oxygen, formed by the treatment with gaseous oxygen before the pulse was negligibly small—the conversion of NH_3 in the first pulse was the same as that in the second pulse measured without the treatment with gaseous oxygen. Furthermore, it is considered that the lowering of the surface lattice oxygen concentration hardly occurred in the reaction of NH_3 with metal oxides at the temperature at which X_{NH3} attained 20%, since the yield of N_2, the only product at the temperature, was not changed by the increasing concentration of NH_3 in the pulse.

Nitrogen Oxide as an Intermediate in the Oxidation of Ammonia with the Lattice Oxygen of Metal Oxides. As reported in a previous paper,[1] NO plays an important role as a gas phase intermediate in the *catalytic* oxidation of NH_3 on metal oxides. This view agrees with that of Shelef *et al.*[4] and Schmidt *et al.*[5] In the oxidation of NH_3 with lattice oxygen of Co_3O_4 and V_2O_5 at 520 °C and 528 °C respectively, the conversion of NH_3 was 100

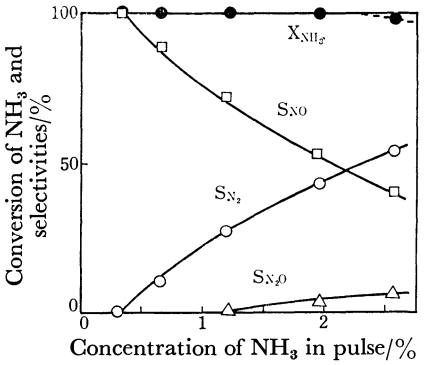

Fig. 3. Oxidation of NH_3 pulse with various NH_3 concentrations by lattice oxygen of Co_3O_4.
Reaction temperature=520 °C. Pulse size=7.42 cm³.

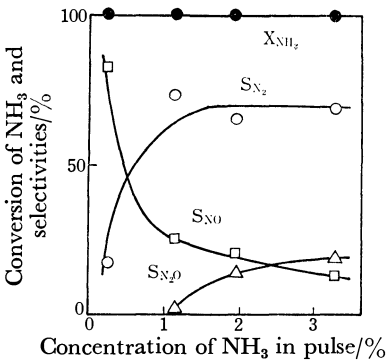

Fig. 4. Oxidation of NH_3 pulse with various NH_3 concentrations by lattice oxygen of V_2O_5.
Reaction temperature=528 °C. Pulse size=7.42 cm³.

% and all of NO, N_2, and N_2O were formed irrespective of the inlet concentration of NH_3. As the concentration of NH_3 in the pulse decreased (Figs. 3 and 4), S_{NO} increased to 100%, and S_{N2O} and S_{N2} decreased to 0%. The results can be explained by the following scheme;

$$NH_3 \xrightarrow[\text{I}]{\text{Lattice oxygen}} NO \xrightarrow[\text{II}]{NH_3} N_2,\ N_2O, \qquad (2)$$

where NH_3 is at first oxidized by lattice oxygen to NO which then reacts with NH_3 (the NO–NH_3 reaction) to form N_2 and N_2O (Step II). The NO–NH_3 reaction (Step II) takes place catalytically under the experimental conditions of the present work.[6] According to the scheme, the activity of a metal oxide is determined by Step I, whereas the selectivities to N_2 and N_2O are limited by the relative rate of Step II to that of Step I. Since Step I and Step II are a monomolecular and a bimolecular reactions respectively, the relative rate of Step II to that of Step I, should increase with an increase in the concentration of NH_3, which is in accord with the experimental results shown in Figs. 3 and 4. Furthermore, in Figs. 3 and 4, the S_{NO} on V_2O_5 decreases more markedly than that on Co_3O_4 with increasing concentration of NH_3, in accordance with the scheme, since the activity of V_2O_5 for the NO–NH_3 reaction is higher than that of Co_3O_4.[6] Thus, it is concluded that NO plays an important role as a gas phase intermediate in the reaction of NH_3 with metal oxides as well as in the *catalytic* oxidation of NH_3.

References

1) Y. Murakami, Y. Kosaki, M. Motokawa, Y. Ooyabu, and A. Miyamoto, *Nippon Kagaku Kaishi*, **1977**, 612.
2) B. Halpern and J. E. Germain, *J. Catal.*, **37**, 44 (1975).
3) N. Yamazoe, *Shokubai*, **19**, 133 (1977).
4) H. S. Gandhi and M. Shelef, *J. Catal.*, **40**, 312 (1975).
5) T. Pignet and L. D. Schmidt, *J. Catal.*, **40**, 212 (1975).
6) Y. Murakami, K. Hayashi, K. Yasuda, T. Ito, T. Minami, and A. Miyamoto, *Nippon Kagaku Kaishi*, **1977**, 173.

BULLETIN OF THE CHEMICAL SOCIETY OF JAPAN, VOL. 52 (2), 619—620 (1979)

Preparation of Potassium Glycinatotrihydroxonitrosylruthenate(II)

Toshio ISHIYAMA* and Takashi MATSUMURA

Radiation Center of Osaka Prefecture, Shinke-cho, Sakai, Osaka 593

(Received March 3, 1978)

Synopsis. A new mono-glycinato complex of hydroxonitrosylruthenium(II), K[Ru(gly)$(OH)_3$NO] was isolated by use of ion exchange resin from the product formed by the reaction of $[RuCl_3(H_2O)_2NO]$ with glycine. The complex was characterized by means of infrared, visible, and ultraviolet absorption spectra, capillary type isotachophoresis, magnetic moment and molar conductivity.

The hydroxonitrosylruthenium(II) complex with amino acid is not known. Belot and Pignon[1] studied the behavior of nitrosylruthenium in the presence of potentially complexing organic compounds. They reported that the mercapto carboxylic acids were the best complexing agents and that the complex formation of nitrosylruthenium(II) hydroxide with mercaptoacetic acid could evidenced by measuring the relative amount of dissolved species with ultra-filtration or gel chromatography. In the present paper we report on potassium glycinatotrihydroxonitrosylruthenate(II).

Experimental

Materials. Commercial ruthenium(III) chloride monohydrate (Mitsuwa Chemicals and Co.) and glycine (extra pure grade, Kishida Chemicals and Co., Ltd.) were used. Commercial Dowex 1×4 sieved to a fraction of 100—200 mesh was used as anion exchange resin. The resin was converted into the Cl-form by treatment with 2 M NaOH and 2 M NaCl in a beaker. The resin was washed with distilled water until the chloride ion was no longer detected in the washing. The Cl-form resin was dried at 60 °C for 48 h and then stored in a desiccator.

Preparation. Diaquatrichloronitrosylruthenium(II), [$RuCl_3(H_2O)_2NO$]: The complex was prepared by a modification of the method of Fletcher *et al.*[2] After the solution of nitrosyl derivative formed by the reaction of ruthenium(III) chloride with sodium nitrite has been adjusted to pH 6.4 with 2 M sodium hydroxide, the solution was evaporated to dryness and extracted with ethanol. The crystals formed by the removal of ethanol by distillation were dried *in vacuo*. (Found: Ru, 36.05; H, 1.74; N, 5.26; Cl, 39.36%. Calcd for $[RuCl_3(H_2O)_2NO]$: Ru, 36.95; H, 1.46; N, 5.12; Cl, 38.92%).

Potassium Glycinatotrihydroxonitrosylruthenate(II), K[Ru(gly)$(OH)_3$NO]: Diaquatrichloronitrosylruthenium(II) (3 g) was dissolved in 20 ml of distilled water. To this was added a solution obtained by dissolving 1.2 g of glycine in a small amount of distilled water. The resulting solution was refluxed on a hot-water bath for 3 h. This was concentrated and then cooled in a refrigerator for several days. The crystals formed were filtered and dissolved in 5 ml of distilled water. The solution was passed through a column (diam. 11 mm, height 245 mm) filled with Cl-form anion exchange resin. The adsorbed complex was eluted with 2 M KCl. After the eluent had been concentrated, potassium chloride deposited was filtered off. The crystals formed were filtered, recrystallized from water and dried *in vacuo*. The complex is insoluble in organic solvents. Found: K, 13.76; Ru, 33.80; C, 8.19; H, 2.60; N, 9.89; yield 36.84%. Calcd for K[Ru(H_2N–CH_2–COO)$(OH)_3$NO]: K, 13.24; Ru, 34.23; C, 8.13; H, 2.39; N, 9.49%.

Measurements. Potassium in the complex was determined as follows. Potassium was precipitated with 2% sodium tetraphenylborate solution. After being filtered and washed, the precipitate was dissolved in acetone. To this solution was added excess mercury(II)–EDTA, and the EDTA liberated was back-titrated with a standard zinc solution using a PAN indicator.[3] Ruthenium in the complex was determined spectrophotometerically by measuring the absorbance at 465 nm after thermal decomposition of the complex at 320 °C followed by alkali fusion.[4] Infrared absorption spectra were measured in KBr disks on a JASCO Model IR-S infrared spectrophotometer. Magnetic susceptibility was measured by the Faraday method[5] at 20 °C with a Cahn R. G. electrobalance. Molar conductivity was measured at 20 °C with Yanagimoto Model MY-7 conductivity outfit. Isotachophoresis was measured with a Shimadzu Model IP-1B capillary tube isotachophoretic analyzer as described below. 1.8 mg of potassium glycinatotrihydroxonitrosylruthenate(II) was dissolved in 500 μl of distilled water. A 10 μl portion of the aqueous solution of the sample was poured into a capillary tube, length 20 cm, inner diam. 0.57 mm. An aqueous mixture solution of 0.01 M ammediol–HCl adjusted to pH 8.8 was used as the leading electrolyte, and an aqueous mixture solution of 0.01 M β-alanine–$Ba(OH)_2$ adjusted to pH 10.9 as the terminal electrolyte. The electrophoreogram was recorded with migration current and migration time 100 μA and 20 min, respectively.

Results and Discussion

It was found from the electrophoreogram shown in Fig. 1 that the complex behaves like an anionic species in electrophoretic migration. A potential gradient inversely proportional to the mobility was obtained, the potential unit value (*PU* value) of the sample being calculated from the relative ratio of the potential gradient of leading electrolyte and the sample zone by means of the following equation:[6]

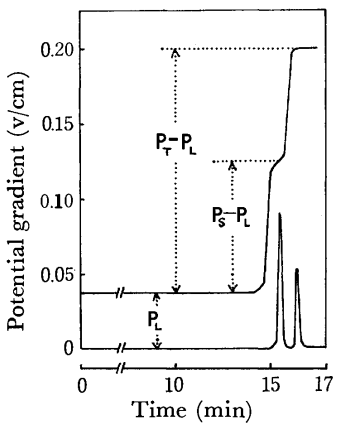

Fig. 1. Isotachophoresis of $[Ru(gly)(OH)_3NO]^-$.

$$PU \text{ value} = \frac{P_S - P_L}{P_T - P_L} = 0.531,$$

where P_S: potential gradient of the sample,
P_L: potential gradient of leading electrolyte,
P_T: potential gradient of terminating electrolyte.

The leading electrolyte has a mobility larger than that of the sample and the terminating electrolyte a smaller mobility. The *PU* value 0.531 indicates that the mobility of the complex anion is nearly intermediate between that of 0.01 M ammediol–HCl at pH 8.8 and 0.01 M β-alanine–$Ba(OH)_2$ at pH 10.9, assuming the formation of mono-glycinato complex anion of hydroxonitrosylruthenium(II) in weak alkali solution.

From the results of elemental analysis, the ratio of potassium, ruthenium, carbon, hydrogen and nitrogen of the complex was found to be 1 : 1 : 2 : 7 : 2. The molar conductivity of aqueous solution of the complex was 143.6 Ω^{-1} cm^2 mol^{-1}, showing that the complex is a 1 : 1 type electrolyte.

Table 1. The characteristic infrared absorption bands of the present Ru(II) complex (cm^{-1})

Assignment	Glycine	K[Ru(gly)$(OH)_3$NO]
ν(N–H)	3480	3400
ν(O–H)		3060
ν(O–D)		2140
ν(N–O)		1865s—1825br
Antisymmetric		
ν(COO)	1595	1603
Symmetric		
ν(COO)	1399	1395
ν(C–N)	1034	1030sh

s=strong, br=broad, sh=shoulder.

The main infrared absorption bands of the present complex are given in Table 1, together with those of the pure ligand. The absorption band at 1850 cm^{-1} was assigned to the NO^+ stretching vibration of nitrosyl group. The band shifted to the lower frequency side than that of the original complex, [$RuCl_3(H_2O)_2NO$] by the chelation of glycine. A similar observation has been reported for [$RuCl_3$(phen)NO] by Lewis *et al.*[7] The absorption band at 3400 cm^{-1} was assigned to N–H stretching vibration of the NH_2 group by comparison with the peak at 3480 cm^{-1} of glycine. The absorption band at 1030 cm^{-1} was assigned to C–N stretching vibration arising from skeleton stretching of glycine. The band at 3060 cm^{-1}, assigned to the OH stretching frequency, shifted after deuteration to 2140 cm^{-1}. The new glycinatohydroxonitrosylruthenate(II) complex was identified from the IR-data.

The electronic absorption spectrum of the complex, K[Ru(gly)$(OH)_3$NO] was measured in aqueous solution (pH=6.15), and compared with that of the starting complex, [$RuCl_3(H_2O)_2NO$] reported by Mercer *et al.*[8]

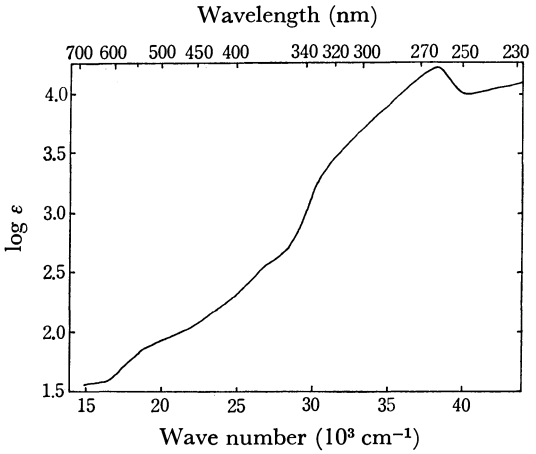

Fig. 2. Electronic spectrum of K[Ru(gly)$(OH)_3$NO] in H_2O (pH=6.15).

The spectrum is shown in Fig 2.. Potassium glycinatotrihydroxonitrosylruthenate(II), K[Ru(gly)$(OH)_3$NO] has three shoulders and a peak at 540, 390, 335, and 265 nm, respectively. The 540 nm shoulder may be assigned to the d-d transition. In spite of no appearance of an absorption band of [$RuCl_3(H_2O)_2NO$] in the ultraviolet region, the appearance of the characteristic peak of K[Ru(gly)$(OH)_3$NO] at 265 nm may be attributed to the ligation of glycine.

The observed diamagnetism of K[Ru(gly)$(OH)_3$NO] indicates that the ruthenium atom has spin-paired d^6 configuration, suggesting that the complex can be formulated by the donation from NO^+ ion. The stereochemical configuration of K[Ru(gly)$(OH)_3$NO] is not clear, but a facial or meridional formula can be proposed.

The authors wish to express their thanks to Prof. Masayasu Mori and Dr. Shigeichi Kubo, Osaka City University, for their guidance in the measurement of magnetic susceptibility. Thanks are also due to Dr. Yasuyo Shiogai, Shimadzu Seisakusho Ltd. for carrying out the isotachophoretic analysis.

References

1) Y. Belot and N. Pignon, *Health Phys.*, **15**, 443 (1968).
2) J. M. Fletcher, I. L. Jenkins, F. M. Lever, A. R. Martin, A. R. Powell, and R. Todd, *J. Inorg. Nucl. Chem.*, **1**, 378 (1955).
3) H. Flaschka and F. S. Sadek, *Chem. Anal. (Warsaw)*, **47**, 30 (1958).
4) E. D. Marshall and R. R. Rickard, *Anal. Chem.*, **22**, 795 (1950).
5) L. N. Mulay, "Magnetic Susceptibility," Wiley, New York, Sydney (1963), p. 1836.
6) J. Akiyama, T. Mizuno, and Y. Shiogai, *Shimadzu Review*, **34**, 111 (1977).
7) J. Lewis, R. J. Irving, and G. Wilkinson, *J. Inorg. Nucl. Chem.*, **7**, 32 (1958).
8) E. E. Mercer, W. M. Campbell, and R. M. Wallace, *Inorg. Chem.*, **3**, 1018 (1964).

BULLETIN OF THE CHEMICAL SOCIETY OF JAPAN, VOL. 52 (2), 621—622 (1979)

Flux Growth of Double Oxide Crystals of Tantalum and Rare-earth Elements

Yuichi YAMASAKI* and Yoshinori SUGITANI

Department of Chemistry, The University of Tsukuba, Sakura-mura, Niihari-gun, Ibaraki 300-31

(Received July 5, 1978)

Synopsis. Crystals of $GdTaO_4$, $DyTaO_4$, and $ErTaO_4$, and those of Gd_3TaO_7, Y_3TaO_7, and Er_3TaO_7 have been grown by PbF_2–PbO flux. Solid solution crystals of $YTaO_4$ and $YNbO_4$ have been obtained for the starting composition of $YTa_xNb_{1-x}O_4$($x<0.5$).

Niobium and tantalum occur in nature as fergusonite $Y(Nb,Ta)O_4$, columbite $(Fe,Mn)(Nb,Ta)_2O_6$, and samarskite $Y_4[(Nb,Ta)_2O_7]_3$, *etc.*[1] It is common for these minerals to contain radioactive elements such as U and Th as minor elements, so that they are in most cases in the 'metamict' form, giving an X-ray pattern like that of an amorphous phase. It is generally known that in inorganic compounds solid solutions are formed at any atomic ratio for Nb and Ta, and that with an increase in Ta content, the melting point of the compound increases, abruptly over 2000 °C.

The flux growth of fergusonite type crystals[2,3] $LnNbO_4$, where Ln is a rare-earth element has been reported, as have the new compounds of Ln_3NbO_7, the columbite type crystals of MNb_2O_6 and MTa_2O_6, where M is divalent transition metal. Although these compounds have high melting points, growth at temperatures below about 1300 °C has been achieved. In this paper the flux growth of the double oxides of rare-earth elements and tantalum at temperatures below 1500 °C are reported. Above 1500 °C the Pt crucible is seriously damaged.

As a typical case, the growing method of $GdTaO_4$ is given here. Other compounds can be grown, in general, in a manner similar to that for $GdTaO_4$, with some minor changes in the conditions such as the composition of the starting materials, solute-flux ratio, *etc.* Reagents of Ln_2O_3 (purity 4N) and Ta_2O_5 (purity 4N) were used for the growth experiment. As flux materials, PbF_2–PbO, Bi_2O_3–V_2O_5, and B_2O_3–$Na_2B_4O_7$ were used at various flux ratios. The purity of PbF_2 and PbO was 3N, and the others were of chemical reagent grade.

A mixture of the starting material (Gd_2O_3 5 mM+Ta_2O_5 5 mM) was put into a 20 ml platinum crucible together with the flux material (PbF_2 40 mM+PbO 10 mM), and tightly covered with a platinum lid. The crucible was placed in an electric muffle furnace kept at 1350 °C for 10 h. Cooling to 900 °C was achieved at the rate of 1—3 °C/h, program controlled. At the final temperature the crucible was taken from the furnace and air quenched to room temperature. The products obtained were washed with hot dilute HNO_3 for several hours. The crystals thus obtained were identified as the desired materials by X-ray powder diffraction.

Figure 1 shows the crystals of $GdTaO_4$ obtained by using PbF_2–PbO flux. The regular crystals are octahedral in shape, ranging in size from 0.5—2.5 mm in the longest directions.

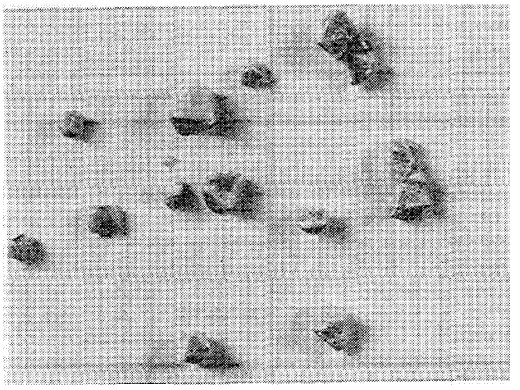

Fig. 1. Crystals of $GdTaO_4$ (1 division=1 mm).

Of the flux materials tried, only the PbF_2–PbO system was suitable for the growth of Ln–Ta–O system compounds. A list of crystals obtained from the PbF_2–PbO flux is given in Table 1, where the compounds presented in each row were obtained from the same melt. Crystals having $LnTaO_4$ composition are those with Ln=Gd, Dy, and Er. They were found to be monoclinic and isostructural with $LnNbO_4$ with a fergusonite structure, the cell parameters of which are given in Table 2. Attempts at growing other $LnTaO_4$ type compounds at higher temperatures (*i.e.* up to about 1500 °C) were not successful. Compounds of Gd_3TaO_7, Y_3TaO_7, and Er_3TaO_7 belong to the cubic system, and have been related to the Ln_3NbO_7 type crystals.[4] No analogue compounds of Ln_3TaO_7 are known in nature. Crystals which were obtained as by-products during the growth are $Pb_3Ta_2O_8$, $Pb_2Ta_2O_7$ and other unidentified crystals.

The growth of the solid solution phases of the $YTaO_4$–

Table 1. List of products obtained by flux method (PbF_2: PbO=80: 20)

Ln[a]	Products (color, shape)
La	$Pb_3Ta_2O_8$(brown, massive), $Pb_2Ta_2O_7$(yellow plates)
Ce	CeO_2(black, octahedral)
Nd	$Pb_3Ta_2O_8$[b]
Sm	$Pb_3Ta_2O_8$[b]
Eu	$Pb_3Ta_2O_8$[b]
Gd	Gd_3TaO_7(yellow plates), $GdTaO_4$(yellow, octahedral)
Dy	$DyTaO_4$(pale yellow, massive)
Y	Y_3TaO_7(pale brown, massive), $Pb_3Ta_2O_8$, $Pb_2Ta_2O_7$
Ho	$Pb_3Ta_2O_8$[b]
Er	Er_3TaO_7(pink plates), $ErTaO_4$(pale yellow, massive)

a) Ln means rare-earth element, the oxide form of which was added as one component of the starting materials. b) Compounds of rare-earth element and tantalum were not obtained.

Table 2. Lattice parameters of products having $LnTaO_4$ and Ln_3TaO_7 composition (1 Å=0.1 nm)

Product	Lattice parameter			
	a(Å)	b(Å)	c(Å)	β(°)
$GdTaO_4$	5.401(2)[a]	11.060(2)	5.071(2)	95.6(2)
$DyTaO_4$	5.352(2)	10.981(2)	5.060(2)	95.7(2)
$ErTaO_4$	5.313(2)	10.891(2)	5.040(2)	95.7(2)
Gd_3TaO_7	5.321(2)			
Y_3TaO_7	5.240(2)			
Er_3TaO_7	5.321(2)			

a) Numbers in parentheses here are estimated standard deviations in units of the last significant digit.

$YNbO_4$ series has been attempted in the temperature region below 1500 °C. Single phase crystals have been obtained for the compositions $YTa_xNb_{1-x}O_4$ with $x<0.5$. Here, the value x means the composition of the starting materials. For $x\geq 0.5$, products showing X-ray patterns corresponding to fergusonite type structure were not obtained. Significant changes in cell dimensions for the grown solid solutions were not observed within experimental error, but for a parallel increase in specific gravity with an increase in Ta content.

The authors wish to express their thanks to Professor Kozo Nagashima of the University of Tsukuba for his kind support of this work.

References

1) J. D. and E. S. Dana, "The System of Mineralogy," 7th ed, John Wiley & Sons, London (1952); H. Strunz, "Mineralogische Tabellen," 5th ed, Akad. Verlag, Leipzig (1970).
2) Y. Sugitani and K. Nagashima, *Miner. J.*, **8**, 66 (1975).
3) Y. Sugitani, *Bull. Chem. Soc. Jpn.*, **50**, 755 (1977).
4) K. Kawajiri, Y. Yamasaki, and Y. Sugitani, *Nippon Kagaku Kaishi*, **1978**, 1244.
5) Y. Yamasaki and Y. Sugitani, *Bull. Chem. Soc. Jpn.*, **51**, 3077 (1978).

BULLETIN OF THE CHEMICAL SOCIETY OF JAPAN, VOL. 52 (2), 623—624 (1979)

2,2′-Bipyridine Derivatives of Hexarhodium Carbonyl Cluster

Kenji NOMIYA* and Hisashi SUZUKI

Sagami Chemical Research Center, Nishi-Ohnuma 4-4-1, Sagamihara, Kanagawa 229

(Received July 6, 1978)

Synopsis. The properties of $[Rh_6(CO)_{12}(bpy)_2]$(bpy: 2,2′-bipyridine), prepared recently from substitution of carbonyl ligands in $[Rh_6(CO)_{16}]$ by 2,2′-bipyridine have been investigated.

Though hexadecacarbonylhexarhodium is generally considered to be a stable, rather unreactive compound, its derivatives substituted by dienes, halogens, phosphines and phosphites have been reported.[1–5] Recently we have found that the treatment of $[Rh_6(CO)_{16}]$ with 2,2′-bipyridine in dichloromethane at room temperature under nitrogen atmosphere gives rise to a successive replacement of two carbonyl groups by 2,2′-bipyridine and results in the formation of $[Rh_6(CO)_{12}(bpy)_2]$. Further replacement of carbonyl groups did not occur. Darkbrick-colored crystals were isolated from the deep brown solution. This compound is more soluble in dichloromethane and chloroform than $[Rh_6(CO)_{16}]$, and stable to air oxidation on the solid state. In the synthetic reaction unis(bipyridine)-substituted cluster was not obtained.

The IR spectrum of $[Rh_6(CO)_{12}(bpy)_2]$ in the carbonyl stretching region shows ν(CO) at 2050, 2015 cm^{-1} (terminal) and 1785 cm^{-1} (face-bridging) in dichloromethane. In comparison with $[Rh_6(CO)_{16}]$ which has sharp bands at 2075 and 2025 cm^{-1} due to terminal carbonyls and at 1801 cm^{-1} due to face-bridging carbonyl group in chloroform, all bands were shifted to the lower frequency. The symmetry (A_1+B_1) of terminal carbonyls implies that two bipyridine ligands coordinate, in place of four carbonyl groups, to the terminal sites in the trans-position of the hexarhodium unit. The coordination mode of the bipyridine ligand is similar to that of the dienes such as norbornadiene, 1,4-cyclohexadiene and 1,5-cyclooctadiene in $[Rh_6(CO)_{14}(diene)]$.[1]

Under carbon monoxide atmosphere, the bipyridine ligand of $[Rh_6(CO)_{12}(bpy)_2]$ can be readily replaced with carbon monoxide at room temperature. By monitoring IR spectra it was found that the cluster had been returned to parent carbonyl $[Rh_6(CO)_{16}]$ *via* $[Rh_6(CO)_{14}(bpy)]$ as an intermediate, the existence of which was confirmed by ^{13}C-NMR data described later. The resulting $[Rh_6(CO)_{16}]$ is almost excluded from the solution because of its low solubility.

$$\begin{array}{ccc} [Rh_6(CO)_{16}] & \xrightarrow[-CO]{bpy} & [Rh_6(CO)_{12}(bpy)_2] \\ \uparrow CO,\ -bpy & & CO \downarrow,\ -bpy \\ & & [Rh_6(CO)_{14}(bpy)] \end{array}$$

Under carbon monoxide atmosphere the direct carbonyl exchange also proceeds on the cluster during the coordinated bipyridine-CO exchange. For 100 h reaction of $[Rh_6(CO_{12})(bpy)_2]$ (27 mg) in dichloromethane (4 ml) with excess ^{13}C-enriched carbon monoxide (*ca.* 91 atom%) at room temperature, the labelled unis(bipyridine)substituted cluster was predominantly existent in the solution. The proton-decoupled ^{13}C-NMR spectrum of the cluster showed the presence of two nonequivalent carbonyl resonances at a lower field (δ 231.8, 243.2 ppm: quartet J(Rh–C) *ca.* 26 Hz) and three nonequivalent carbonyl resonances at a higher field (δ 180.2, 181.6, 184.0 ppm: doublet J(Rh–C) 71.6±0.3 Hz). As observed for $[Rh_6(CO)_{16}]$ (terminal carbonyl; δ 180.1 ppm, doublet J(Rh–C) 70.2 ±0.6 Hz, face-bridging carbonyl; δ 231.5 ppm, quartet J(Rh–C) 24.4±0.6 Hz),[6] the lower field signals are due to the face-bridging carbonyl groups and the higher field signals due to the terminal carbonyl groups. The intensity ratio of the terminal carbonyls exhibits 4: 4: 2. Since these intensities should reflect the relative abundances in this region, the spectrum is compatible with Structure (1).

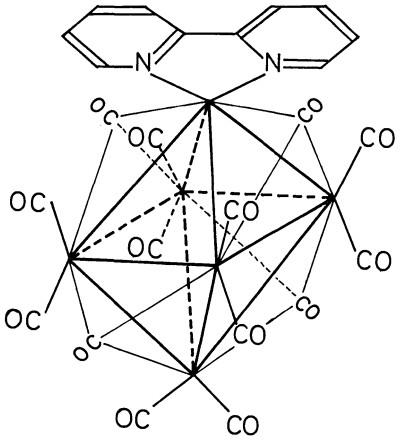

Structure (1).

The result that two resonances of the terminal carbonyls attached to the square plane in the Rh_6 unit are nonequivalent is similar to the result that two resonances of terminal carbonyls attached to the basal plane are nonequivalent relative to the apical rhodium in $[Rh_4(CO)_{12}]$.[7]

The reaction product between $[Rh_4(CO)_{12}]$ and dienes is reported to give the same product, $[Rh_6(CO)_{14}(diene)]$ obtained by the reaction of $[Rh_6(CO)_{16}]$ with dienes.[1] However, the reaction of $[Rh_4(CO)_{12}]$ with bipyridine under the aforementioned synthetic conditions produces exclusively an unidentified black solid, which is insoluble in almost organic solvents.

Experimental

^{13}C-NMR spectra were recorded in the Fourier transform

mode on a Varian Associates XL-100-15 spectrometer in dichloromethane-d_2 solution, using 0.05M $Cr(acac)_3$ as a relaxation reagent and using tetramethylsilane as an internal standard. IR spectra were recorded on a Model EPI–G3 of Hitachi Grating Infrared Spectrophotometer.

2,2′-Bipyridine was recrystallized from a mixture of ethanol and water. Hexadecacarbonylhexarhodium, $[Rh_6(CO)_{16}]$, was purchased from the commercial source (Strem Chemical Incorporated). The ^{13}CO (91 atom%) enclosed in a glass tube with a breakable seal, purchased from B.O.C. Ltd. (Prochem), was connected with vacuum line and used without further purification. Solvents, CH_2Cl_2 and CD_2Cl_2, were dried over P_2O_5, and were vacuum-distilled before use.

Preparation of $[Rh_6(CO)_{12}(bpy)_2]$. The 2,2′-bipyridine (bpy: 176 mg, 1.13 mmol) was added to $[Rh_6(CO)_{16}]$ (200 mg, 0.19 mmol) suspended in dichloromethane (10 ml) on stirring at room temperature. During the stirring the evolved carbon monoxide was evacuated from time to time and replaced with dry nitrogen. After the 100 h reaction at about 30 °C, the reaction mixture was filtered out under dry nitrogen. (The residue was dark-green and air-stable.) Excess hexane was added to the deep brown filtrate, the solution of which was kept overnight at −78 °C. The solid obtained was washed several times with hexane, recrystallized from a mixture of dichloromethane and hexane, and then dried *in vacuo*. The yield was about 30%. It was stored under nitrogen in an ice box. Found: C, 30.19; H, 1.99; N, 4.75%. Clacd for $C_{32}H_{16}O_{12}N_4Rh_6$: C, 30.33; H, 1.26; N, 4.42%.

References

1) T. Kitamura and T. Joh, *J. Organomet. Chem.*, **65,** 235 (1974).

2) B. L. Booth, M. J. Else, R. Fields, and R. N. Haszeldine, *J. Organomet. Chem.*, **27**, 119 (1971).

3) B. F. G. Johnson, J. Lewis, and P. W. Robinson, *J. Chem. Soc., A*, **1970**, 1100.

4) P. Chini, S. Martinengo, and G. Giovanni, *Gazz. Chim. Ital.*, **102,** 330 (1972).

5) G. Chiani, L. Garlaschelli, M. Manassero, U. Sartorelli, and V. G. Albano, *J. Organomet. Chem.*, **129**, C25 (1977).

6) B. T. Heaton, A. D. C. Towl, P. Chini, A. Fumagalli, D. J. A. McCaffrey, and S. Martinengo, *J. Chem. Soc., Chem. Commun.*, **1975,** 523.

7) J. Evans, B. F. G. Johnson, J. Lewis, J. R. Norton, and F. A. Cotton, *J. Chem. Soc., Chem. Commun.*, **1973**, 807.

BULLETIN OF THE CHEMICAL SOCIETY OF JAPAN, VOL. 52 (2), 625—626 (1979)

Preparations and Paramagnetic Contact Shifts of Some Tris(β-diketonato)vanadium(III) Complexes

Katsuma HIRAKI,* Masayoshi ONISHI,* Yutaka NAKASHIMA, and Yayoi OBAYASHI

Department of Industrial Chemistry, Faculty of Engineering, Nagasaki University, Bunkyo-machi, Nagasaki 852

(Received August 26, 1978)

Synopsis. New tris(dehydroacetato)-, tris(methyl acetoacetato)-, and tris(ethyl acetopyruvato)vanadium(III) complexes were prepared and characterized by IR and NMR spectroscopies. Paramagnetic contact shifts of these complexes were discussed.

Remarkable paramagnetic contact shifts have been observed for mononuclear trivalent vanadium complexes containing univalent chelate ligands such as β-diketonato,[1-3] salicylaldehydato,[4] and their related ligands,[4,5] and been applied to the investigations of the *fac-mer* stereochemistry and of electron distributions over the ligands of these complexes.[2,3,6,7] However, no work has been yet reported about a vanadium(III) complex coordinated with dehydroacetic acid (Hdac), alkyl acetoacetate, or alkyl acetopyruvate, each of which belongs to a β-diketone, possessing a characteristic substituent. This note will deal with the preparation and ^{1}H-NMR study of the new vanadium(III) complexes containing dac, methyl acetoacetato (maa), or ethyl acetopyruvato (eap) ligand.

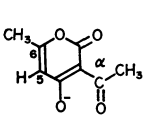

dac

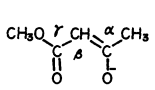

maa

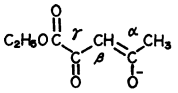

eap

Experimental

Materials. Commercial grade vanadium(III) chloride, dehydroacetic acid, and methyl acetoacetate were used without further purification. Ethyl acetopyruvate was prepared accoding to the method of Marvel *et al.*[8]

General Procedures. IR and ^{1}H-NMR spectra were measured on a Hitachi Model 285 and a JEOL Model PS-100 (100 MHz) spectrometers, respectively. Since solutions of vanadium(III) complexes appeared to be sensitive to aerial oxidation, preparations and recrystallization were carried out under a dinitrogen atmosphere.

Preparation of $[V(dac)_3]$. An aqueous solution of dehydroacetic acid (57 mmol) and sodium carbonate (30 mmol) was added to an aqueous solution of vanadium(III) chloride (19 mmol). After the mixture was refluxed for 2 h, a resulting precipitate was separated, washed with water, and dried *in vacuo*. Recrystallization from dichloromethane–petroleum ether yielded an ochre-colored solid, $[V(dac)_3]$.

Preparation of $[V(maa)_3]$. An ethanol solution of methyl acetoacetate (19.2 mmol) and an aqueous solution of sodium carbonate were added to vanadium(III) chloride (6.4 mmol) in 32 cm^3 of an ethanol–water (3: 1) solution. The mixture was stirred for 2 h at room temperature. After the solvent was evaporated, a residue was recrystallized from benzene–petroleum ether to give a greenish yellow crystal, $[V(maa)_3]$.

Preparation of $[V(eap)_3]$. Sodium ethyl acetopyruvate (30 mmol) was added to an aqueous solution of vanadium(III) chloride (9 mmol). After the reaction mixture was refluxed for 1 h, a resultant precipitate was separated, washed with water, and dried *in vacuo*. Recrystallization from diethyl ether–petroleum ether afforded a reddish brown solid, $[V(eap)_3]$. This complex is considerably sensitive to air.

Results and Discussion

Table 1 shows the yields, elemental analyses, and some properties of the complexes prepared in the present study. IR spectrum of $[V(maa)_3]$ lacked ν(C=O) near 1700 cm^{-1}, revealing that the vanadium(III) ion was coordinated with a carbonyl oxygen of the ester group to form a β-diketonato chelate ring, but not with a methoxy oxygen of the same group. Moreover, IR spectra of the three complexes exhibited complicated bands near 1510 and 1590 cm^{-1}, which were assignable to the unsymmetrical β-diketonato chelate rings. The reasons for the complicacy of these bands were probably due to the coexistence of two kinds of bonding sites in the unsymmetrical β-diketonato ligand itself, the *fac-mer* isomerism, and the coordination of the three chelate rings in different circumstances in the *mer* isomer, as elucidated by ^{1}H-NMR spectra.

Table 2 shows ^{1}H-magnetic resonances of $[V(dac)_3]$, $[V(maa)_3]$, and $[V(eap)_3]$. Four signals were detected for a given substituent on the unsymmetrical chelate ring of each of these complexes. This fact indicates that these complexes consist of *fac* and *mer* isomers, similarly to the other vanadium(III) complexes with unsymmetrical β-diketonato ligands.[2,3] Three signals of an equal intensity were ascribed to the substituents on the three

Table 1. Yields and properties of the vanadium complexes

Complex	Yield (%)	Mp[a] (°C)	Characteristic IR bands (cm^{-1})[b]		C(%)		H(%)	
			β-Diketonato ring[c]	Other ν(C=O)	Calcd	Found	Calcd	Found
$[V(dac)_3]$	78	147—150	1552, 1565	1720[d]	52.19	51.96	3.83	4.31
$[V(maa)_3]$	41	152—154	1510, 1590	—	45.47	45.62	5.34	5.36
$[V(eap)_3]$	10	63	1508, 1582	1727, 1740[e]	48.29	48.03	5.21	4.98

a) In dinitrogen atmosphere. b) In KBr disc. c) A few shoulders were observed near each band.
d) Pyrone carbonyl. e) Ester carbonyl.

Table 2. ^{1}H-NMR data of the vanadium complexes[a)]

Complex	Isomer ratio[b)] (%)		α-CH_3 δ, ppm	β-H δ, ppm	γ-Substituents δ, ppm	γ-Substituents δ, ppm
$[V(dac)_3]$	*fac*	18	50.4	—	0.8[c)]	22.1[d)]
	mer	82	54.9, 61.5, 63.5	—	1.2, 11.1, 11.6[c)]	17.2, 19.6, 22.4[d)]
$[V(maa)_3]$	*fac*	12	25.8	31.8	9.5[e)]	—
	mer	88	17.3, 21.5, 27.5	41.0, 41.5, 55.2	9.0, 10.7, 12.4[e)]	—
$[V(eap)_3]$	*fac*	17	60.2	39.9	6.0, 6.3[f,h)]	1.1[g,h)]
	mer	83	57.6, 64.0, 69.2	26.5, 45.8, 56.0		

a) Measured at 20 °C in deoxygenated $CDCl_3$ using tetramethylsilane as the internal standard. b) Calculated from α-CH_3 signals. c) 5-H. d) 6-CH_3. e) OCH_3. f) $COOCH_2$–. g) –CH_3(Et). h) Not distinguished owing to overlapping each other.

unsymmetrical chelate rings in the disparate circumstances in the *mer* isomer. The fourth signal was ascribed to that on the three unsymmetrical chelate rings in the same circumstance, *i.e.* in C_3 symmetry in the *fac* isomer. Since the fourth signal is smaller than each of the former three ones, the *fac* isomer populates in a smaller ratio than that expected for a statistical formation, which would result in a *fac*: *mer* ratio of 1 : 3 and in four signals of an equal intensity for the ring substituents.

Holm *et al.*[2)] reported that in the NMR paramagnetic shifts of tris(β-diketonato)vanadium(III) complexes, π-contact part was dominant and pseudo-contact one was negligible, and that unpaired spin of the metal was delocalized to the β-diketonato ligand. In connection with the Holm *et al.*'s explanations, the paramagnetic shifts of α-CH_3 protons of $[V(maa)_3]$, $[V(eap)_3]$, and the related (β-diketonato)vanadium(III) complexes[1–3)] were correlated to the electronic effect of the corresponding γ-substituent of the β-diketonato ligand. A value σ_R^m[9)] was used as a parameter for the electronic effect of the γ-substituent, since the β-diketonato conjugated system was reported to have a quasi-aromatic character[10)] and σ_R^m represents the term of the resonance effect of each *meta* substituent, composing Hammett value σ^m.[9)]

Figure 1 presents the paramagnetic shifts of the α-CH_3 protons[11)] against the σ_R^m values of the γ-substituents. As for $[V(maa)_3]$, α-CH_3 protons show a small shift, indicating that the methoxy group at the γ-position of the chelate ring suppresses the electron delocalization from the metal to the ligand. This is consistent with a negative σ_R^m value of the methoxy group, representing the donation of the resonance electron from this group. However, as for $[V(eap)_3]$ in which the ethoxycarbonyl group has a positive σ_R^m, meaning the small donating ability of the resonance electron, the contact shift of α-CH_3 protons is large. The linearity shown in Fig. 1 is consistent with the quasi-aromatic character of the β-diketonato systems, and supports the Holm *et al.*'s explanations[2)] about the paramagnetic shifts of the tris-(β-diketonato)vanadium(III) complexes.

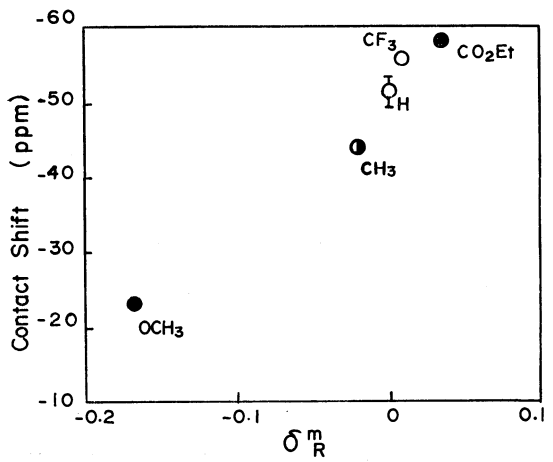

Fig. 1. Relationship between the paramagnetic shift of the α-protons and the σ_R^m value of the γ-substituent.
◑: From Ref. 1, ○: from Ref. 2, ●: from the present study. See note 11 concerning the paramagnetic shifts.

We are grateful to Mr. Katsuhiro Inada, Nagasaki University, for his help with the NMR measurements.

References

1) D. R. Eaton, *J. Am. Chem. Soc.*, **87**, 3097 (1965).
2) F. Röhrscheid, R. E. Ernst, and R. H. Holm, *Inorg. Chem.*, **6**, 1315 (1967).
3) J. G. Gordon, II, M. J. O'Connor, and R. H. Holm, *Inorg. Chim. Acta*, **5**, 381 (1971).
4) F. Röhrscheid, R. E. Ernst, and R. H. Holm, *J. Am. Chem. Soc.*, **89**, 6472 (1967).
5) F. Röhrscheid, R. E. Ernst, and R. H. Holm, *Inorg. Chem.*, **6**, 1607 (1967).
6) R. H. Holm, *Acc. Chem. Res.*, **2**, 307 (1967).
7) D. R. Eaton and K. L. Chua, *Can. J. Chem.*, **51**, 2260 (1973).
8) C. S. Marvel and E. E. Dreger, *Org. Synth.*, Coll. Vol. I, 238 (1967).
9) L. N. Ferguson, "The Modern Structural Theory of Organic Chemistry," Prentice-Hall, Inc., Englewood Cliffs, N. J. (1963), Chap. 4.
10) J. P. Collman, "Reactions of Coordinated Ligands and Homogeneous Catalysis," ed by D. H. Busch, American Chemical Society, Washington, D. C. (1963), pp. 78—98.
11) The paramagnetic shifts of the α-CH_3 protons were determined from a difference between δ-value of the complex and that of the corresponding free ligand. The δ-values for the *fac*-type complexes were used as for the γ-substituents of OCH_3, CF_3, and CO_2Et. As regards the γ-substituents of CH_3 and H, δ-value of the acetylacetonato complex and the range of four δ-values for the *fac* and *mer* isomers were adopted, respectively.

BULLETIN OF THE CHEMICAL SOCIETY OF JAPAN, VOL. 52 (2), 627—628 (1979)

O-Methylation of Aromatic (*E*)-Oximes by Dimethylsulfonium Methylide

Shigeo TANIMOTO,* Takashi YAMADERA, Toyonari SUGIMOTO, and Masaya OKANO

Institute for Chemical Research, Kyoto University, Uji, Kyoto 611

(Received May 18, 1978)

Synopsis. The reactions of dimethylsulfonium methylide with (*E*)-aldoximes and (*E*)-ketoximes proceeded smoothly at room temperature and gave moderately good yields of *O*-methyl (*E*)-aldoximes and *O*-methyl (*E*)-ketoximes, respectively. A possible scheme for the formation of *O*-methyl (*E*)-oximes has been discussed.

Metzger and coworkers[1] published a brief report on a facile methylation of nitrobenzene by dimethyloxosulfonium methylide. Additional methylation reactions with several substituted nitrobenzenes have been described by Traynelis and McSweeney.[2] Analogous *O*-methylation reactions with *o*-hydroxybenzaldehyde have been found by Holt and Lowe,[3] *i.e.*, when *o*-hydroxybenzaldehyde and dimethylsulfonium methylide (**1**) were allowed to react, *o*-methoxybenzaldehyde was isolated. The methylation reactions of anthracene and benzaldehyde phenylhydrazone with dimethyloxosulfonium methylide are also known.[1]

In this paper the facile *O*-methylation of (*E*)-aldoximes (**2a**—**2e**) and (*E*)-ketoximes (**2f**—**2k**) are reported employing **1** prepared *in situ* by the action of *t*-BuOK on trimethylsulfonium iodide in dimethyl sulfoxide (DMSO).

Hitherto, various *O*-methyl (*E*)-oximes (**3**) have been synthesized either by the reaction of a sodium (*E*)-oximate with methyl iodide[4,5] or by the action of methyl sulfate on an (*E*)-oxime under alkaline conditions.[6]

However, the above reactions proceeded with the accompanying formation of *N*-methylated oxime derivatives.[6] The present method provides an exclusive *O*-methylated (*E*)-oxime derivative (**3**). This reaction not only presents an alternative method[7] for the selective *O*-methylation of **2**, but is also of interest as an example of the utility of sulfur ylides.

When an (*E*)-oxime and **1** (generated *in situ* from trimethylsulfonium iodide and *t*-BuOK in DMSO) were allowed to react at room temperature, the corresponding *O*-methyl (*E*)-oxime (**3**) was formed in a moderately good yield. The results are listed in Table 1.

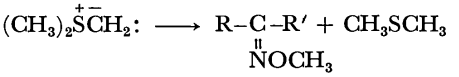

2 **1** **3**

a: R=C_6H_5, R′=H
b: R=*p*-$CH_3C_6H_4$, R′=H
c: R=*p*-ClC_6H_4, R′=H
d: R=*p*-$CH_3OC_6H_4$, R′=H
e: R=*o*-ClC_6H_4, R′=H
f: R=C_6H_5, R′=CH_3
g: R=*p*-$CH_3C_6H_4$, R′=CH_3
h: R=*p*-ClC_6H_4, R′=CH_3
i: R=*p*-BrC_6H_4, R′=CH_3
j: R=C_6H_5, R′=C_6H_5
k: R–C(=)–R′=cyclo-C_6H_{10}=

TABLE 1. *O*-METHYLATION OF (*E*)-OXIMES (**2**) BY DIMETHYLSULFONIUM METHYLIDE (**1**)

Run	(*E*)-Oxime	Product	Yield[a] (%)
1	**2a**	**3a**[b]	60
2	**2b**	**3b**[c]	51
3	**2c**	**3c**[d]	65
4	**2d**	**3d**[e]	54
5	**2e**	**3e**[f]	63
6	**2f**	**3f**[g]	91
7	**2g**	**3g**[h]	79
8	**2h**	**3h**[i]	84
9	**2i**	**3i**[j]	69
10[k]	**2j**[l]	**3j**[m]	77
11	**2k**[l]	**3k**[n]	32

a) Yield was based upon **2**, and was of the isolated product. b) Bp 86—88 °C/21 mmHg (lit,[8] 95 °C/20 mmHg). NMR ($CDCl_3$): δ 3.97 (s, 3H), 7.25—7.70 (m, aromatic 5H), 8.06 (s, 1H). c) Bp 80—83 °C/5 mmHg. Found: C, 72.32; H, 7.58; N, 9.42%. Calcd for $C_9H_{11}NO$: C, 72.45; H, 7.43; N, 9.39%. NMR ($CDCl_3$): δ 2.33 (s, 3H), 3.95 (s, 3H), 7.05—7.56 (m, aromatic 4H), 8.15 (s, 1H). d) Bp 92—94 °C/4 mmHg (lit,[6] mp 28 °C). NMR ($CDCl_3$): δ 3.95 (s, 3H), 7.20—7.58 (m, aromatic 4H), 8.00 (s, 1H). e) Bp 137—139 °C/22 mmHg (lit,[9] 129 °C/15 mmHg). NMR ($CDCl_3$): δ 3.77 (s, 3H), 3.92 (s, 3H), 6.75—7.62 (m, aromatic 4H), 8.00 (s, 1H). f) Bp 89—92 °C/6 mmHg. Found: C, 56.44; H, 4.62; N, 8.15%. Calcd for C_8H_8ClNO: C, 56.65; H, 4.75; N, 8.26%. NMR ($CDCl_3$): δ 3.97 (s, 3H), 7.12—7.98 (m, aromatic 4H), 8.49 (s, 1H). g) Bp 106—108 °C/21.5 mmHg (lit,[10] 132—135 °C/46 mmHg). NMR ($CDCl_3$): δ 2.19 (s, 3H), 3.98 (s, 3H), 6.86—7.96 (m, aromatic 5H). h) Bp 124—127.5 °C/23.5 mmHg. Found: C, 73.77; H, 8.19; N, 8.30%. Calcd for $C_{10}H_{13}NO$: C, 73.59; H, 8.03; N, 8.58%. NMR ($CDCl_3$): δ 2.16 (s, 3H), 2.29 (s, 3H), 3.95 (s, 3H), 6.96—7.68 (m, aromatic 4H). i) Bp 84—88 °C/2 mmHg. Found: C, 59.08; H, 5.42; N, 7.86%. Calcd for $C_9H_{10}ClNO$: C, 58.86; H, 5.49; N, 7.63%. NMR ($CDCl_3$): δ 2.16 (s, 3H), 4.00 (s, 3H) 7.20—7.79 (m, aromatic 4H). j) Bp 92—96 °C/2 mmHg. Found: C, 47.62; H, 4.34; N, 6.39%. Calcd for $C_9H_{10}BrNO$: C, 47.39; H, 4.42; N, 6.14%. NMR ($CDCl_3$): δ 2.16 (s, 3H), 3.98 (s, 3H), 7.33—7.68 (m, aromatic 4H). k) A considerable amount of DMSO was used as the solvent due to the small solubility of benzophenone oxime (**2j**). l) There is no geometrical isomerism. m) Purified by column chromatography on silica gel (eluent 25% ether–75% hexane). Mp 58—60 °C (lit,[11] 61—62 °C). NMR ($CDCl_3$): δ 3.97 (s, 3H), 7.17—7.65 (m, aromatic 10H). n) Bp 68—70 °C/21 mmHg (lit,[7] 50 °C/12 mmHg). NMR ($CDCl_3$): δ 1.38—2.64 (m, 10H), 3.78 (s, 3H).

On the other hand, when a potassium (*E*)-oximate (prepared *in situ* by mixing 1 equivalent of an (*E*)-oxime

and 1.5 equivalents of *t*-BuOK in DMSO) and 1.5 equivalents of trimethylsulfonium iodide were allowed to react at room temperature, the corresponding *O*-methyl (*E*)-oxime (**3**) was obtained, but the yield was very poor compared with the result in Table 1. For example, the yield of *O*-methyl (*E*)-benzaldoxime (**3a**) in this procedure was 25%. Consequently, it has to be assumed that the formation of an (*E*)-oximate anion and its subsequent attack on a trimethylsulfonium cation with the loss of neutral dimethyl sulfide occurs simultaneously in the reaction involving **1** and an (*E*)-oxime. Thus, the transition state might be represented as follows:

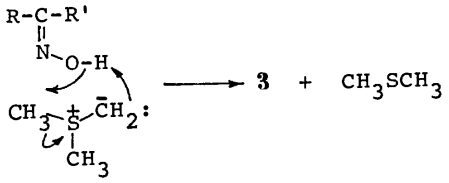

It has been reported that the methylation of sodium (*E*)-oximate by methyl iodide in ethanol always accompanies some degree of *N*-methylation, which is attributable to the ambifunctional nucleophilic character of the (*E*)-oximate anion.[8,12] However, **2** has been exclusively methylated on oxygen by the method described in this paper. The *N*-methylated oxime derivative could not be detected by NMR spectra. The selective *O*-methylation in the present reaction can be understood taking into consideration the formation of the cyclic transition state.

Experimental

Preparation of O-*Methyl* (E)-*Oximes* (*3*). *General Procedure*: A solution of trimethylsulfonium iodide (8.10 g, 39.6 mmol) in DMSO (20 ml) was placed in a 100 ml four-necked flask equipped with a reflux condenser, thermometer, gas-inlet tube, dropping funnel, and magnetic stirrer. Finely powdered *t*-BuOK (4.44 g, 39.6 mmol) was slowly added with efficient stirring at 5—10 °C, under a nitrogen atmosphere, to the solution. A DMSO solution (5 ml) of an (*E*)-oxime (26.4 mmol) was subsequently introduced dropwise at that temperature. The reaction mixture was then stirred for 5—6 h at room temperature, quenched with saturated aqueous Na_2SO_4 solution and extracted with ether. The organic extract was washed and dried over $MgSO_4$, the solvent evaporated and the residue distilled under reduced pressure.

References

1) H. Metzger, H. König, and K. Seelert, *Tetrahedron Lett.*, **1964**, 867.
2) V. J. Traynelis and Sr. J. V. McSweeney, O. P., *J. Org. Chem.*, **31**, 243 (1966).
3) B. Holt and P. A. Lowe, *Tetrahedron Lett.*, **1966**, 683.
4) S. G. Smith and D. V. Milligan, *J. Am. Chem. Soc.*, **90**, 2393 (1968).
5) W. R. Dunstan and E. Goulding, *J. Chem. Soc.*, **79**, 628 (1901).
6) O. L. Brady, F. P. Dunn, and R. F. Goldstein, *J. Chem. Soc.*, **1926**, 2386.
7) For the preparation of pure *O*-methyl (*E*)-oximes, the reaction of methoxyamine with either an aldehyde or a ketone has already been published: L. G. Donaruma, *J. Org. Chem.*, **22**, 1024 (1957).
8) E. Buehler, *J. Org. Chem.*, **32**, 261 (1967).
9) H. Lindemann and K. T. Tschang, *Chem. Ber.*, **60**, 1727 (1927).
10) G. W. Perold, A. P. Steyn, and F. V. K. Reiche, *J. Am. Chem. Soc.*, **79**, 462 (1957).
11) P. A. S. Smith and J. E. Robertson, *J. Am. Chem. Soc.*, **84**, 1197 (1962).
12) O. L. Brady and N. M. Chokshi, *J. Chem. Soc.*, **1929**, 2271.

BULLETIN OF THE CHEMICAL SOCIETY OF JAPAN, VOL. 52 (2), 629—630 (1979)

The Structure of Yahazunol, a New Sesquiterpene-substituted Hydroquinone from the Brown Seaweed *Dictyopteris undulata* Okamura

Masamitsu Ochi,* Hiyoshizo Kotsuki, Kiyoshi Muraoka, and Takashi Tokoroyama†

Faculty of Science, Kochi University, Asakura, Kochi 780

†*Faculty of Science, Osaka City University, Sugimoto-cho, Sumiyoshi-ku, Osaka 558*

(Received May 29, 1978)

Synopsis. The structure of yahazunol, an antimicrobial substance isolated from the brown seaweed *D. undulata* Okamura, was established on the basis of spectral and chemical evidence.

Fenical and coworkers have recently reported the isolation of five sesquiterpene-substituted phenols from *D. undulata* Okamura ("Shiwayahazu" in Japanese), and noted that the occurrence of these constituents was dependent upon the growth localities of the alga.[1-3] Our investigation of the phenolic components of the seaweed collected in the Bay of Tosa led to the isolation of a new sesquiterpene-substituted hydroquinone, designated as yahazunol, together with zonarol (**1**),[1] isozonarol (**2**),[1] and zonaroic acid (**3**).[3] These were all obtained in the crystalline state, contrary to previous descriptions. In this note, we will deal with the structure of this new compound. This compound was found to have a strong antimicrobial activity against some yeasts.[4]

Yahazunol (**4**), $C_{21}H_{32}O_3$, mp 127—129 °C, $[\alpha]_D^{27}$ −12° (*c* 0.10, $CHCl_3$), was isolated in 0.008% yield from a methanol extract of the fresh alga by careful silica-gel column chromatography and fractional crystallization. **4** shows hydroxylic absorptions in the IR spectrum at 3400 and 3280 cm^{-1} and forms a diacetate (**5**), $C_{25}H_{36}O_5$, mp 95—96 °C, the IR spectrum of which still shows the presence of a hydroxyl group at 3560 cm^{-1}. The ^1H NMR spectrum of **5** shows signals due to three methyl groups attached to quaternary carbon atoms at δ 0.80, 0.87, and 0.89 (3H each, s), one methyl group on an oxygenated carbon atom at δ 1.25 (3H, s), two acetoxyl groups at δ 2.28 and 2.34 (3H each, s), one benzyl methylene group at δ 2.61 and 2.68 (1H each, dd, J=15 and 5 Hz), and one 1,2,4-trisubstituted benzene ring at δ 6.90 (1H, dd, J=9 and 2 Hz), 6.96 (1H, d, J=9 Hz), and 7.12 (1H, d, J=2 Hz). In addition, the ^{13}C NMR data of **4**, as summarized in Fig. 1, indicate the presence of five methylene groups, two methine groups, one oxygen-bearing tertiary carbon atom, and two quaternary carbon atoms.

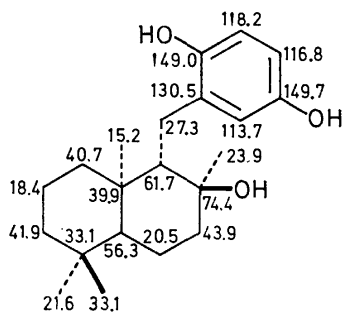

Fig. 1. Yahazunol; ^{13}C NMR data (δ/ppm) for CD_3COCD_3 solution.[5]

These facts suggest that **4** has a structure analogous to that of zonarol (**1**), in which the exocyclic methylene of **1** is displaced by a grouping $\overset{OH}{\underset{CH_3}{C}}$. This was confirmed by the following chemical correlation of **4** with **1**. The methylation of **1** with CH_3I–K_2CO_3 gave a dimethyl ether (**6**), $C_{23}H_{34}O_2$, mp 74—74.5 °C. The epoxidation of **6** with *m*-$ClC_6H_4CO_3H$ and the reduction of the resulting epoxide (**7**) with $LiAlH_4$ afforded a tertiary alcohol (**8**), which was found to be identical with the compound derived from **4** by the treatment with CH_3I–K_2CO_3.

These correlation reactions also define the configuration at C-8 of **4**. The epoxidation of **6** should occur predominantly on the sterically less crowded β-side and, hence, the C-8 hydroxyl group of **4** is β-oriented. Therefore, yahazunol must be represented by the structure **4**.

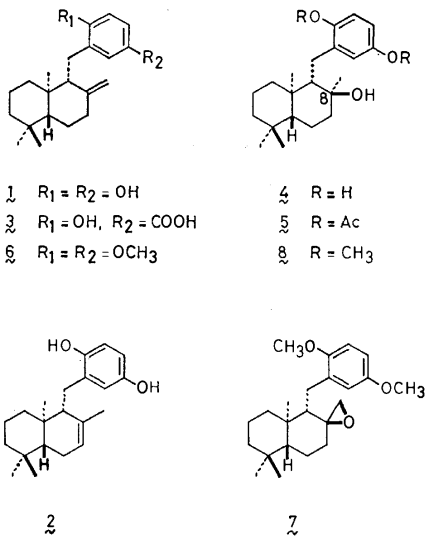

Experimental

All mp's are uncorrected. The IR spectra were recorded on a JASCO model IRA-1 spectrophotometer. The ^1H NMR spectra were determined using a JEOL PS-100 spectrometer in $CDCl_3$ solutions, with TMS as an internal standard. A Union Giken apparatus, model PM-101 was used for the measurement of the rotations.

Isolation. Fresh alga (4.3 kg), collected in the Bay of Tosa in May 1977, was chopped up and extracted with 13 liter

of methanol for 10 days. The aqueous methanol solution was washed with petroleum ether, concentrated up to about 1.5 liter and extracted with dichloromethane. The dichloromethane layer was washed with water, dried over Na_2SO_4, and evaporated to dryness. The residue (27.9 g) was subjected to repeated chromatography over silicic acid. The fractions eluted with benzene–ether (19: 1) gave zonarol (**1**)[6] (1.49 g), needles (from ether–petroleum ether), mp 173.5—174.5 °C, $[\alpha]_D^{27}$ +18° (*c* 0.10, $CHCl_3$), isozonarol (**2**)[6] (322 mg), spherulites (from benzene), mp 116—117 °C, $[\alpha]_D^{27}$ +30° (*c* 0.10, $CHCl_3$), and zonaroic acid (**3**)[6] (1.28 g), needles (from aqueous methanol), mp 108—109 °C, $[\alpha]_D^{27}$ +32° (*c* 0.10, $CHCl_3$). The fractions eluted with benzene–ether (9: 1) yielded yahazunol (**4**) (343 mg), needles (from acetone–ether), mp 127—129 °C, $[\alpha]_D^{27}$ −12° (*c* 0.10, $CHCl_3$); IR (KBr) 3400, 3280, 1625, 1507, and 1240 cm^{-1}. Found: C, 76.07; H, 9.82%. Calcd for $C_{21}H_{32}O_3$: C, 75.86; H, 9.70%.

Acetylation of ***4***. A solution of **4** (50 mg) in acetic anhydride (0.5 ml) and pyridine (0.5 ml) was allowed to stand at room temperature overnight and then worked up in the usual way to give a diacetate (**5**) (39 mg), needles (from ether–petroleum ether), mp 95—96 °C; IR (Nujol) 3560, 1760, 1745, and 1250 cm^{-1}. Found: C, 72.27; H, 8.94%. Calcd for $C_{25}H_{36}O_5$: C, 72.08; H, 8.71%.

Methylation of ***1***. To a solution of **1** (1 g) in dry acetone (10 ml) were added methyl iodide (5 ml) and anhydrous K_2CO_3 (5 g). The mixture was refluxed for 8 h, diluted with water, and extracted with ether. The ether layer was washed with water, dried over Na_2SO_4, and evaporated to dryness. The resulting gum was subjected to chromatography over silicic acid with benzene as solvent to give a dimethyl ether (**6**) (415 mg), needles (from methanol), mp 74—74.5 °C; IR (Nujol) 3080, 1645, and 890 cm^{-1}; ^1H NMR δ 3.74 and 3.80 (3H each, s). Found: C, 80.64; H, 10.01%. Calcd for $C_{23}H_{34}O_2$: C, 80.65; H, 10.01%.

Conversion of ***6*** *into* ***8***. A mixture of **6** (200 mg) and *m*-$ClC_6H_4CO_3H$ (138 mg) in dichloromethane (5 ml) was stirred at room temperature for 4 h under nitrogen atmosphere. The reaction mixture was worked up in the usual way and the resulting product was chromatographed over silicic acid with petroleum ether as solvent to give an epoxide (**7**) (110 mg). The ^1H NMR spectrum of this compound no longer showed the presence of the exocyclic methylene but the presence of a grouping $\rangle C(O)CH_2$ at δ 2.51 and 2.62 (1H each, d, J=6 Hz).

To a solution of **7** (90 mg) in dry ether (4 ml) was added $LiAlH_4$ (180 mg) dissolved in dry ether (9 ml). The mixture was stirred for 2 h at room temperature, refluxed for 1 h, and then poured into ether floated on water. The organic layer was separated, washed with water, dried over Na_2SO_4, and evaporated to dryness. The residue was subjected to chromatography over silicic acid and subsequent elution with benzene–ether (49: 1) gave a tertiary alcohol (**8**) (42 mg), oil, $[\alpha]_D^{14}$+4° (*c* 0.42, $CHCl_3$); IR (neat) 3480 cm^{-1}; ^1H NMR δ 1.28 (3H, s, $\rangle C(CH_3)OH$, which was also obtained by the tratment of **4** with CH_3I–K_2CO_3 in a similar manner to that described.

We are grateful to Professor W. Fenical, University of California, for the extract of *D. undulata* and for the IR and ^1H NMR spectra of zonarol, isozonarol, and related compounds, and to Dr. S. de Stefano, Consiglio Nazionale Delle Ricerche, Italy, for a sample of zonaroic acid. We also thank Dr. M. Taniguchi, Osaka City University, for carrying out the antimicrobial activity test.

References

1) W. Fenical, J. J. Sims, D. Squatrito, R. M. Wing, and P. Radlick, *J. Org. Chem.*, **38**, 2383 (1973).

2) W. Fenical and O. McConnell, *Experientia*, **31**, 1004 (1975).

3) G. Cimino, S. de Stefano, W. Fenical, L. Minale, and J. J. Sims, *Experientia*, **31**, 1250 (1975).

4) The results of antimicrobial activity test will be givn in detail elsewhere.

5) The ^{13}C NMR spectrum was recorded at the UCSD NMR Facility, supported by the National Institutes of Health (RR-0708). Assignments are attributed to Dr. D. J. Faulkner, University of California, to whom we are grateful.

6) These compounds are described as noncrystalline gums in the literature. See Refs. 1 and 3.

BULLETIN OF THE CHEMICAL SOCIETY OF JAPAN, VOL. 52 (2), 631—632 (1979)

Oxidation of 2,6-Dialkyl-*p*-cresols by Metal Acetates

Toshio ITAHARA* and Tsutomu SAKAKIBARA

Institute of Chemistry, College of Liberal Arts, Kagoshima University, Kagoshima 890

(Received May 30, 1978)

Synopsis. The oxidation of 2,6-dialkyl-*p*-cresols by silver(I) and palladium(II) acetate afforded the corresponding *p*-hydroxybenzyl acetates and *p*-hydroxybenzaldehydes.

Recently much attention has been focused on the selective oxidation of the methyl group of *p*-cresols. However, the selective side-chain oxidation of alkylphenols is generally attained with difficulty, *e.g.*, coupling reactions predominantly occur when 2,6-di-*t*-butyl-*p*-cresol (**1a**) is oxidized by metal salts,[1] although the oxidation of **1a** to 3,5-di-*t*-butyl-4-hydroxybenzaldehyde (**3a**) using bromine,[2] 2,3-dichloro-5,6-dicyano-*p*-benzoquinone (DDQ),[3] or oxygen in alkaline medium[4] has been reported. The oxidation of toluenes to benzyl acetates or benzaldehydes by palladium(II) acetate is however well known.[5] These observations and an interest in metal salt-catalyzed oxidations of aromatic compounds[6] led to this examination of the oxidation of *p*-cresols with palladium(II) acetate and other metal acetates. The side-chain oxidations of *p*-cresol itself and 2,4-dimethylphenol led to failure,[7] however, it was found that the *p*-methyl group of **1a** and 2,4,6-trimethylphenol (**1b**) were oxidized by silver(I) acetate and palladium(II) acetate in acetic acid. There appears to be no other reports that the products from the side-chain oxidation of *p*-cresols change depending on the amount of the oxidant used, although the oxidation of **1b** with $S_2O_8^{2-}$–Ag^+ gives 3,5-dimethyl-4-hydroxybenzylalcohol[8] and with DDQ[3] or with oxygen[4] gives 3,5-dimethyl-4-hydroxybenzaldehyde (**3b**).

Treatment of **1a** and **1b** with silver(I) acetate in acetic acid under nitrogen at 118 °C afforded 3,5-di-*t*-butyl-4-hydroxybenzyl acetate (**2a**) and 3,5-dimethyl-4-hydroxybenzyl acetate (**2b**), respectively, in good yields. When the oxidation was conducted with an excess of the metal acetate, **3** was obtained in good yield. Furthermore, the oxidation of **2** gave the corresponding **3**. The oxidation of **1** by palladium(II) acetate also resulted in the formation of **2** and **3**, but the yield of **2b** from **1b** was reduced. These results are summarized in Table 1. The attempted oxidations with other metal acetates, listed in Table 1, were unsuccessful.

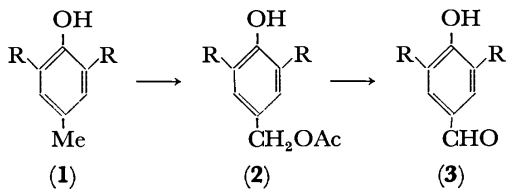

(**1**) (**2**) (**3**)

a: R = *t*-Bu
b: R = Me

Experimental

*Oxidation of **1a** by Metal Acetates.* A solution of **1a** (1 mmol) and the metal acetate (0.5—4.0 mmol) in acetic acid (30 ml) was heated at 118 °C under a nitrogen atmosphere for 5—15 h. The reaction mixture was evaporated to dryness under reduced pressure and chromatographed on a silica-gel plate (chloroform/petroleum ether) to give **1a** (recovered), **2a**, identical with a sample which was prepared according to the method described by Coppinger and Campbell,[9] and **3a**, identical with an authentic sample.[4]

*Oxidations of **1b**, **2a**, and **2b** by Metal Acetates.* The

TABLE 1. THE OXIDATION OF **1a**, **1b**, **2a**, AND **2b** BY METAL ACETATES

Substrate (1 mmol)	Metal acetate (mmol)	Reaction time (h)	Conversion (%)	Product yield (%)
1a		14	0	—
	AgOAc (1)	7	88	**2a**(78)[a]
	AgOAc (4)	14	100	**3a**(71)[a]
	$Pd(OAc)_2$ (1/2)	7	85	**2a**(69), **3a**(6)[a]
	$Pd(OAc)_2$ (1)	10	100	**2a**(40), **3a**(50)[b]
	$Pd(OAc)_2$ (2)	5	85	**2a**(35), **3a**(55)[b]
	$Cu(OAc)_2$ (1/2)	14	3	**3a**(80)[a]
	$Co(OAc)_2 4H_2O$ (1/2)	14	0	—
	$Ni(OAc)_2 4H_2O$ (1/2)	14	0	—
	$Mn(OAc)_2 4H_2O$ (1/2)	14	0	—
1b	AgOAc (1)	7	92	**2b**(77), **3b**(6)[a]
	AgOAc (4)	14	100	**2b**(20), **3b**(70)[b]
	$Pd(OAc)_2$ (1/2)	7	80	**2b**(20), **3b**(60)[b]
2a	AgOAc (1)	7	85	**3a**(70)[b]
	$Pd(OAc)_2$ (1/2)	4	100	**3a**(60)[b]
2b	AgOAc (1)	7	60	**3b**(80)[b]
	$Pd(OAc)_2$ (2)	2	87	**3b**(70)[b]

a) Isolated yield. b) Yield determined by NMR spectroscopy.

phenol **1b** was oxidized by the metal acetate and worked up as described above to yield **1b** (recovered), **2b**, mp 73—75 °C (lit,[10] 76 °C), and **3b**, identical with an authentic sample.[4]

Similar procedures were applied to the oxidations of **2a** and **2b**, the results of which are summarized in Table 1.

We wish to express our sincere thanks to Professors Teruo Matsuura and Akira Nishinaga of Kyoto University for their valuable suggestions.

References

1) C. D. Cook, *J. Org. Chem.*, **18**, 261 (1953); C. D. Cook, N. G. Nash, and H. R. Franagan, *J. Am. Chem. Soc.*, **77**, 1783 (1955).

2) T. W. Campbell and G. M. Coppinger, *J. Am. Chem. Soc.*, **74**, 1469 (1952).

3) H. D. Becker, *J. Org. Chem.*, **30**, 982 (1965).

4) A. Nishinaga, T. Itahara, and T. Matsuura, *Angew. Chem.*, **87**, 386 (1975).

5) K. Ichikawa, S. Uemura, and T. Okada, *Nippon Kagaku Zasshi*, **90**, 212 (1969); D. R. Bryant, J. E. McKeon, and B. C. Ream, *J. Org. Chem.*, **33**, 4123 (1968), *ibid.*, **34**, 1107 (1969), *Tetrahedron Lett.*, **1968**, 3371; J. M. Davidson and C. Triggs, *J. Chem. Soc., A*, **1968**, 1331.

6) T. Itahara and T. Sakakibara, *Synthesis*, 607 (1978).

7) Oxidations of *p*-cresol and 2,4-dimethylphenol by metal acetates gave coupling products.

8) R. G. R. Bacon and D. J. Munro, *J. Chem. Soc.*, **1960**, 1339.

9) G. M. Coppinger and T. W. Campbell, *J. Am. Chem. Soc.*, **75**, 734 (1953).

10) F. Wessely and E. Schinzel, *Monatsh. Chem.*, **84**, 425 (1953).

BULLETIN OF THE CHEMICAL SOCIETY OF JAPAN, VOL. 52 (2), 633—634 (1979)

Substituent Effects in Heterogeneous Catalysis. V. Steric Hindrance of Bulky Alkyl Substituents in Cyclohexanone Hydrogenation

Teiji CHIHARA and Kazunori TANAKA*

The Institute of Physical and Chemical Research, Wako-shi, Saitama 351

(Received July 3, 1978)

Synopsis. The reactivities of 2-isopropyl- and 2-*t*-butylcyclohexanone were measured relative to cyclohexanone in both individual and competitive hydrogenation over Ru/Al_2O_3, Rh/Al_2O_3, and Pt/Al_2O_3. The results obtained suggest that alkyl substitution sterically hinders much more significantly the ketone adsorption than the following surface reaction. A molecular model is presented for adsorption of each ketone.

In the preceding two reports[1,2] of this series, we studied the effect of alkyl substitution in cyclohexanone hydrogenation using 2-methyl-, 2-ethyl-, and 2-propylcyclohexanone (**2m**, **2e**, and **2p**), along with cyclohexanone (**1**) itself. Since ethyl and propyl substituents are rather flexible, little or no additional steric hindrance to adsorption is expected when going from **2m** to **2e** or **2p**. In support of this speculation, our previous work indicated that **2m**, **2e**, and **2p** exhibit almost the same reactivity in their individual hydrogenations. However, increasing the branching degree of the alkyl substituent might cause a marked increase in steric hindrance to adsorption and reactions. The main purpose of the present work is to test this anticipation by conducting individual and competitive hydrogenations of 2-isopropyl- and 2-*t*-butylcyclohexanone (**2ip** and **2tb**).

Interest in enzymatic and related reactions is growing. Although it is acknowledged that steric factors play an important role in these reactions, little is known concerning the correlation of steric factors with complexation and catalysis.[3] In heterogeneous catalysis as well, there seem to be many cases where steric factors play a part. Especially, a rigid bulky group in close proximity to the functional group in general ought to exert steric hindrance to adsorption and reactions. However, few studies have been reported about the extent of such steric hindrance. This paper describes our first attempt to study this problem.

Experimental

Compound **2ip** was prepared by hydrogenation of *o*-isopropylphenol over Raney-Ni,[4] followed by chromic acid oxidation.[5] Distillation under reduced pressure gave **2ip** as a liquid: bp 82.0 °C/20 mmHg. **2tb** was similarly prepared from *o*-*t*-butylphenol: bp 89.0 °C/19 mmHg. The catalysts used were the same commercial products that were employed in the previous work:[2] they were pelletized Ru/Al_2O_3, Rh/Al_2O_3, and Pt/Al_2O_3, each containing 0.5 wt % of the metal. Hydrogenation runs, either individual using a single ketone substrate or competitive using two ketone substrates, were conducted in cyclohexane at 30 °C and in hydrogen of atmospheric pressure. The procedure has been detailed previously.[2]

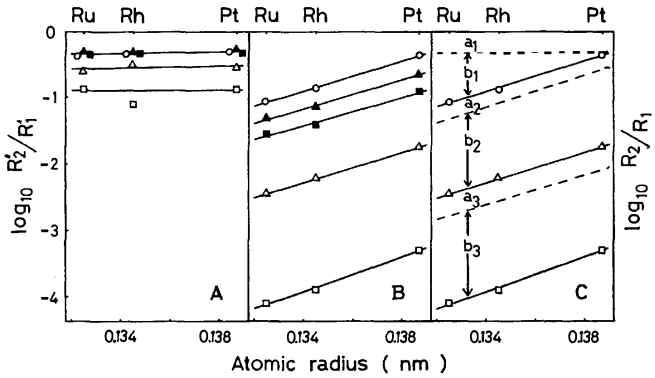

Fig. 1. Comparative data in hydrogenation of **1** and **2**.
(A) Rates of **2** relative to **1** in individual reactions;
(B) Rates of **2** relative to **1** in competitive reactions;
(C) Substituent effects in adsorption and in surface reaction.
○: **2m**, ▲: **2e**, ■: **2p**, △: **2ip**, □: **2tb**.
$a_1 \equiv \log_{10}(k_{2m}/k_1)$, $b_1 \equiv \log_{10}(K_{2m}/K_1)$
$a_2 \equiv \log_{10}(k_{2ip}/k_{2m})$, $b_2 \equiv \log_{10}(K_{2ip}/K_{2m})$
$a_3 \equiv \log_{10}(k_{2tb}/k_{2ip})$, $b_3 \equiv \log_{10}(K_{2tb}/K_{2ip})$

Results and Discussion

Individual Reactions. Preliminary experiments confirmed that in individual hydrogenation the reaction rate is zero order in ketone over a wide concentration range down to or even lower than 0.5 mol/l. The rate measurements were all made in this zero-order region, and the rates of **2** relative to **1** are plotted in Fig. 1A against the atomic radius of the catalyst metal. For comparison, the data on **2e** and **2p** obtained previously[2] are also given in Fig. 1A. It is seen that in general the relative rate R_2'/R_1' in individual reaction is not very different from metal to metal, and depends only upon the substituent itself. Another characteristic feature is that R_2'/R_1' decreases in the order **2m**=**2e**=**2p**>**2ip**>**2tb**.

In considering this activity sequence it should be noted that R_2'/R_1' is related to the reactivity of the adsorbed species by

$$R_2'/R_1' = k_2/k_1, \quad (1)$$

where k is the rate constant referred to the unit fraction of the surface covered. The observed identity **2m**=**2e**=**2p** has already[1,2] been explained by assuming for these ketones a particular adsorption model in which no additional steric hindrance is brought about when going from **2m** to **2e** and to **2p**.

Now let us consider why R_2'/R_1' decreases in the order **2m**>**2ip**>**2tb**. For these ketones we assume those adsorption models that are illustrated in Fig. 2 which represents the projection of the alkyl substituents on a

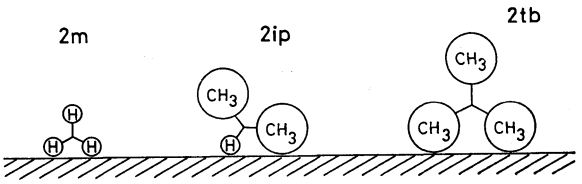

Fig. 2. The orientation of a C(7)–H or C(7)–CH_3 bond in the alkyl substituent relative to the catalyst surface for adsorbed **2m**, **2ip**, and **2tb**.

plane perpendicular to the catalyst surface. It seems very likely that the steric hindrance to adsorption due to the alkyl substituents is minimized in the assumed model. A comparison of the three ketones indicates that the bulkier the substituent, the greater the steric hindrance to adsorption that would be exerted; by bringing a C(7)–H bond more perpendicular to the catalyst surface plane when going from **2m** to **2ip**, and by directing two methyl groups toward the catalyst when going from **2ip** to **2tb**. In antiparallel with this increasing steric hindrance the adsorption strength of ketones is expected to decrease in the order **2m**>**2ip**>**2tb**. The observed order of decreasing R_2'/R_1' probably reflects this order of decreasing adsorption strength and, in turn, decreasing reactivity.

Table 1. Direct and indirect measurements of relative rate $\log_{10}(R_{2tb}/R_{2m})$

Catalyst	$\log_{10}(R_{2ip}/R_{2m})$	$\log_{10}(R_{2tb}/R_{2ip})$	$\log_{10}(R_{2tb}/R_{2m})$	
			Indirect	Direct
Pt/Al_2O_3	−1.36	−1.59	−2.95	−2.89
Rh/Al_2O_3	−1.35	−1.64	−2.99	−3.04
Ru/Al_2O_3	−1.38	−1.64	−3.02	−2.88

Competitive Reactions. The observed relative rate R_2/R_1 in competitive reaction is plotted in Fig. 1B against the atomic radius of the catalyst metal. The data for **2m**, **2e**, and **2p** were obtained directly by competitive hydrogenation with **1**, but the data for **2ip** and **2tb** were determined indirectly by hydrogenating each competitively with **2m** and then by allowing for the relative rate R_{2m}/R_1 measured by a separate experiment. The validity of this indirect procedure for determining R_2/R_1 is confirmed by the data of Table 1 which compare the directly and indirectly determined R_{2tb}/R_{2m} values. It is seen that for all the catalysts the agreement is satisfactory. Fig. 1B shows that the magnitude of the substituent effect based on **1**, *i.e.*, $\log(R_2/R_1)$, depends upon the catalyst metal whereas those for any **2** based on another, such as $\log(R_{2ip}/R_{2m})$ and $\log(R_{2tb}/R_{2ip})$, are independent of the catalyst.

As previously shown,[6] the relative rate in competitive reaction may be given by

$$R_2/R_1 = (K_2/K_1)(R_2'/R_1'), \quad (2)$$

where K is the adsorption coefficient in Langmuir's adsorption isotherm. Combining Eqs. 1 and 2 we obtain

$$\log(R_2/R_1) = \log(K_2/K_1) + \log(k_2/k_1). \quad (3)$$

Equation 3 means that the substituent effect in competitive reaction is divided into two terms; the substituent effect in adsorption and that in surface reaction. Such a division is also feasible in a comparison between different **2**'s. The extents of the two terms worked out for a few ketone pairs are given in Fig. 1C. It is seen that only b_1 varies with the catalyst. This indicates that an increase in adsorption hindrance due to methyl substitution leading **1** to **2m** varies with the catalyst, whereas that caused by further methyl substitution leading **2m** to **2ip** or leading **2ip** to **2tb** is independent of the catalyst. The reason for this unique behavior of the methyl substituent on **2m** is obscure at present although it must be related to the close proximity of that substituent to the carbonyl group. Figure 1C also shows that bulky alkyl groups hinder the adsorption markedly but the following surface reaction to a much smaller extent. Interestingly, the same trend has been observed in olefin hydrogenation by Hussey *et al.* (Table 3 or 4 in Ref. 7).

We thank Dr. F. Scott Howell of Sophia University for his linguistic comments on the original manuscript of this paper.

References

1) T. Chihara and K. Tanaka, *Bull. Chem. Soc. Jpn.*, **52**, 507 (1979).
2) T. Chihara and K. Tanaka, *Bull. Chem. Soc. Jpn.*, **52**, 512 (1979).
3) M. L. Bender, "Mechanisms of Homogeneous Catalysis from Protons to Proteins," Wiley-Interscience, New York (1971), Part 3.
4) H. E. Ungnade and A. D. McLaren, *J. Am. Chem. Soc.*, **66**, 118 (1944).
5) L. T. Sandborn, *Org. Synth.*, Coll. Vol. I, 340 (1932).
6) T. Chihara and K. Tanaka, *Chem. Lett.*, **1977**, 843.
7) A. S. Hussey, R. H. Baker, and G. W. Keulks, *J. Catal.*, **10**, 258 (1968).

BULLETIN OF THE CHEMICAL SOCIETY OF JAPAN, VOL. 52 (2), 635—636 (1979)

Oxidation of Organic Compounds with Perborates or H_2O_2–Boric Acids[1)]

Yoshiro OGATA* and Hideo SHIMIZU

Department of Applied Chemistry, Faculty of Engineering, Nagoya University, Chikusa-ku, Nagoya 464

(Received July 24, 1978)

Synopsis. Perborate oxidation of *p*-chloroaniline to 4,4′-dichloroazobenzene and H_2O_2–boric acid hydroxylation of aromatics have been studied. The kinetic behavior suggests that the so-called sodium perborate is not peroxoborate but borate peroxyhydrate, H_2O_2 acquiring stronger electrophilicity by the coordination with boric acid which acts as Lewis acid rather than protic acid.

Perborates have received little attention as reagents for organic oxidations. Metha and Vakilwala reported that sodium perborate is a satisfactory reagent for the oxidation of anilines to azo compounds.[2)] However, no report seems to have appeared on the mechanism of perborate oxidation and the systems of H_2O_2–boric acids (boric acids: H_3BO_3, HBO_2, and B_2O_3). The present note deals with our attempt to elucidate the mechanism for the oxidation of *p*-chloroaniline with perborates and hydroxylation of aromatics with H_2O_2–boric acids reagents.

Results and Discussion

Oxidation of p-*Chloroaniline.* *p*-Chloroaniline was oxidized by sodium or ammonium perborates in acetic acid to give 4,4′-dichloroazobenzene. Azobenzene is obtained as a condensation product of unreacted aniline with nitrosobenzene formed *via* phenylhydroxyamine[3,4)] (Eqs. 1 and 2).

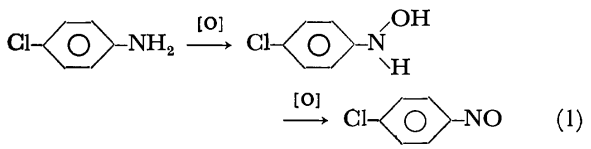

(1)

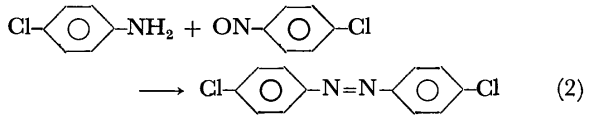

(2)

Oxidation can also be achieved by H_2O_2–AcOH. The rates of disappearance of perborates or H_2O_2 (0.02—0.04 M) were measured iodometrically in 100 or 75% aq AcOH at 50 °C, where *p*-chloroaniline is in large excess (0.5 M) (Table 1). The rates are pseudo-first order in perborates or H_2O_2: $v=k_{obsd}$[perborates or H_2O_2]. There is no possibility that the actual oxidizing agent is peracetic acid,[5)] since the rate for peracetic acid formation (Table 2) is smaller than that of aniline oxidation. Azobenzene should be produced mainly by direct oxidation of aniline with another oxidizing species.

In 100% AcOH, apparent first-order rate constants (k_{obsd}) for sodium and ammonium perborates are respectively 6.7 and 4.7 times greater than those for H_2O_2, but in 75% aq AcOH the rate constants become comparable to those with H_2O_2. This can be explained as follows: the so-called perborate is not peroxoborate but borate peroxyhydrate.[6)] Thus, in excess water, H_2O_2 is readily separated from borate, the oxidation being performed by liberated H_2O_2, where the rate is analogous to that by H_2O_2 alone. In 100% AcOH, H_2O_2 remains coordinated with boric acid which is formed from metal borate in AcOH, the electrophilicity of H_2O_2 thus increasing. When an equivalent amount of boric acid is added to H_2O_2–75% aq AcOH system, the rate increases slightly (Table 1). The protonation of H_2O_2 by boric acid is negligible in AcOH, since acetic acid is a much stronger acid than boric acid.[7)] In conclusion, boric acid should coordinate with H_2O_2 as Lewis acid but not protic acid to increase the electrophilicity of H_2O_2.

TABLE 1. RATES FOR OXIDATION OF *p*-CHLOROANILINE BY PERBORATES, H_2O_2, H_2O_2–H_3BO_3, OR AcOOH IN ACETIC ACID AT 50 °C[a)]

Oxidizing agent	$k_{obsd}\times10^5$ (s^{-1})[b)]	
	In 100% AcOH	In 75% aq AcOH
$NaBO_3$	66.0	5.33
NH_4BO_3	45.8	4.88
H_2O_2	9.8	4.06
H_2O_2–H_3BO_3[c)]	—	4.41
AcOOH	too fast to measure	too fast to measure

a) [*p*-chloroaniline]=0.5 M, [oxidizing agent]=0.02—0.04 M. The yields of 4,4′-dichloroazobenzene were *ca.* 30% in each case under these conditions. b) The pseudo-first order rate constant with respect to oxidizing agent. c) H_2O_2: H_3BO_3=1:1. H_3BO_3 is insoluble in 100% AcOH.

TABLE 2. RATES FOR THE FORMATION OF PERACETIC ACID BY SEVERAL PEROXIDE SYSTEMS IN ACETIC ACID AT 50 °C

Oxidizing agent	$k_{obsd}\times10^5$ (s^{-1})[a)]	
	In 100% AcOH	In 75% aq AcOH
$NaBO_3$	9.66	1.39
NH_4BO_3	3.30	1.17
H_2O_2	1.75	1.05
H_2O_2–H_3BO_3[b)]	—	1.25

a) The pseudo-first order rate constant with respect to the oxidizing agent. b) H_2O_2: H_3BO_3=1:1. H_3BO_3 is insoluble in 100% AcOH.

Hydroxylation of Aromatics. It has been reported that aromatic hydroxylation occurs by H_2O_2 in the presence of Lewis acid such as BF_3[8a)] or $AlCl_3$,[8b)] where the hydroxylation might take place by HO^+ formed from H_2O_2 by the coordination of Lewis acid. Aromatic compounds were hydroxylated also with H_2O_2 in ether in the presence of H_3BO_3, HBO_2, or B_2O_3 (heterogene-

Table 3. Hydroxylation of anisole and toluene by H_2O_2–boric acids in ether at 100 °C for 1 h

Substrate[a]	Yield of monohydroxylated products (%)		
	H_3BO_3	HBO_2	B_2O_3
	54.6 (56:44)[b]	35.7 (51:49)[b]	84.5 (55:45)[b]
	6.7 (73:27)[c]	4.8 (67:33)[c]	45.1 (66:34)[c]

a) Substrate is in large excess. b) Ortho *vs.* para ratio. *m*-Isomer was not detected. c) Ortho *vs.* para-meta ratio. *m*- and *p*-isomers could not be separated. *m*-Isomer would not be produced because of the electrophilic nature of the reagent.

ous) at 100 °C (Table 3),[9] no reaction taking place by H_2O_2 alone under similar conditions.

Boric acids act as Lewis acid, but not protic acid in H_2O_2–boric acids, since the yield is the highest in the case of B_2O_3, which has no proton but is considered to the strongest Lewis acid among the three. For example with H_3BO_3:

$$ArH + H_2O_2 + B(OH)_3 \xrightarrow{\text{Ether}} \begin{matrix} H \\ Ar \end{matrix}\!\!>\!O\cdots O\!<\!\begin{matrix} B(OH)_3 \\ H \end{matrix} \longrightarrow ArOH + H_2O + B(OH)_3 \quad (3)$$

On the other hand, sodium and ammonium perborates are basic and unable to form HO^+ from H_2O_2, although they can give free boric acid in acetic acid.

Experimental

Materials. The chemicals except ammonium perborate are commercial products of first grade. Ammonium perborate was prepared from ammonium borate and H_2O_2 by Tsal's method.[10] Guaranteed boric anhydride free of water was used.

Oxidation of p-*Chloroaniline.* The reactions of large excess *p*-chloroaniline (0.5 M) with sodium and ammonium perborates or H_2O_2 (0.02—0.04 M) were carried out in 100% and 75% aq AcOH at 50 °C. The reaction with H_2O_2 by addition of an equivalent amount of H_3BO_3 was carried out in 75% aq AcOH. The products were identified by GLC analysis in comparison with the corresponding authentic specimen. The rates were followed by determining the disappearance of the oxidizing agent by iodometry.

Rate for Formation of Peracetic Acid. The rates for peracetic acid formation from oxidizing agents (0.02—0.04 M) and AcOH were followed by determining the disappearance of the oxidizing agents by titration with $KMnO_4$.[11] The oxidizing agents were oxidized by $KMnO_4$, but peracetic acid formed was not oxidized.

Hydroxylation of Aromatics. A large excess of anisole (370 mmol) or toluene (435 mmol) was mixed with H_2O_2 (6 mmol) in Et_2O (10 ml). The solvent ether was removed in a vacuum until a pressure of 40 mmHg was attained. The reaction mixture was stirred vigorously with H_3BO_3, HBO_2, or B_2O_3 (15 mmol) at 100 °C for 1 h. The products were identified by GLC analysis with the authentic specimen.

References

1) Contribution No. 255.
2) S. M. Mehta and M. V. Vakilwala, *J. Am. Chem. Soc.*, **74**, 563 (1952).
3) K. M. Ibne-Rasa and J. O. Edwards, *J. Am. Chem. Soc.*, **84**, 763 (1962).
4) Y. Ogata and Y. Takagi, *J. Am. Chem. Soc.*, **80**, 3591 (1958).
5) Y. Ogata and Y. Sawaki, *Tetrahedron*, **21**, 3381 (1965).
6) G. Carpéni, *Chem. Abstr.*, **44**, 3391 g (1949).
7) pK_a's of AcOH and H_3BO_3 are 4.74 and 9.24, respectively, in water at 25 °C.
8) a) J. D. McClure and P. H. Williams, *J. Org. Chem.*, **27**, 24 (1962); b) M. E. Kurz and G. J. Johnson, *J. Org. Chem.*, **36**, 3184 (1971).
9) R. Achard and N. Crenne, *Chem. Abstr.*, **67**, 21637 m (1967).
10) M. I. Tsal, *Chem. Abstr.*, **54**, 17132 e (1959).
11) D. Swern, *Org. React.* **7**, 261 (1953).

BULLETIN OF THE CHEMICAL SOCIETY OF JAPAN, VOL. 52 (2), 637—638 (1979)

The Reaction of Methyl *cis*-Decahydro-5,8-dioxonaphthalene-1-carboxylates

Hajime IRIKAWA,* Tsuyoshi KOYAMA, and Yasuaki OKUMURA

Department of Chemistry, Faculty of Science, Shizuoka University, Oya 836, Shizuoka 422

(Received July 31, 1978)

Synopsis. Methyl *cis*-decahydro-5,8-dioxonaphthalene-1-carboxylates (**1b** and **1c**) were derived from the Diels-Alder adducts of *p*-toluquinone or *p*-xyloquinone and methyl sorbate, respectively. The ^{13}C NMR spectra of **1b** and **1c** suggest the existence of **1b** and **1c** in the form (A), which is in line with the formation of the keto γ-lactone from **1b** and of the keto alcohol from **1c**.

In our previous paper, the compound **1a**, derived from the Diels-Alder adduct of *p*-benzoquinone and methyl sorbate, was indicated to exist in the form (A) shown below.[1a] This paper deals with the conformation and reaction of methyl *cis*-decahydro-5,8-dioxonaphthalene-1-carboxylates (**1b** and **1c**).

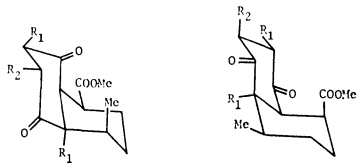

(A) (B)

1a $R_1,R_2=H$
1b $R_1=H$, $R_2=Me$
1c $R_1=Me$, $R_2=H$

The adduct (**2a**) of *p*-toluquinone and methyl sorbate was reduced with zinc to **3a**, which was converted into **1b** by catalytic hydrogenation with palladium-carbon. The Diels-Alder reaction of *p*-xyloquinone and methyl sorbate was catalyzed by aluminium chloride to afford **2b**, which was similarly reduced to **3b** and **1c**. The cis ring junction of **2b** is supported by the comparison of the physical data with those of the C-8a epimer of **2b**.[2]

The treatment of **1b** with sodium borohydride at room temperature for 2 h gave the keto γ-lactone (**4**), and that for 3 days afforded the δ-lactone (**5a**), which was also obtained from **4** by further treatment with sodium borohydride. The formation of **4** suggests that the methyl group originally in *p*-toluquinone is situated at C-6 in the adduct **2a**, since the C-8 carbonyl group was reduced more easily than the C-5 carbonyl group in **1b**. The ^{13}C NMR chemical shifts of **5a** are similar to those of **5b**[1a] within 1 ppm except for C-5, -6, and -7, which are shifted downfield by the α- and β-effects of the methyl group at C-6 in **5a**. Absence of the γ-effect on C-4a and -8 by the methyl group at C-6 in **5a** indicates the equatorial orientation of the methyl group.[3] The

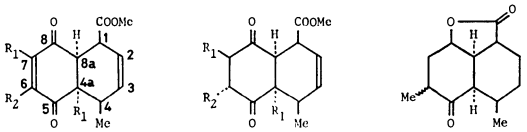

2a $R_1=H$, $R_2=Me$ **3a** $R_1=H$, $R_2=Me$ **4**
2b $R_1=Me$, $R_2=H$ **3b** $R_1=Me$, $R_2=H$

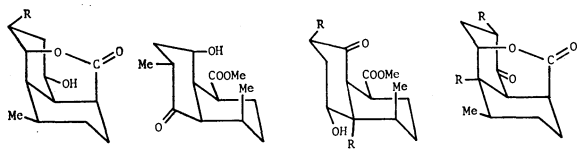

5a R=Me **6** **7a** R=Me **8a** R=Me
5b R=H **7b** R=H **8b** R=H

^{13}C chemical shift differences within 1 ppm for C-1, -3, -4, -4a, and -8a between **1a**[1a] and **1b** indicate that **1b** also exists in the form (A) with the stable equatorial methyl group at C-6. Accordingly, **4** is formed from the reduction intermediate (**6**) which is unstable because of the steric interaction between the hydroxyl group at C-8 and the methyl group at C-4. Formation of **5a** proceeds through the ring inversion, epimerization at C-6, and reduction of the C-5 carbonyl group in **6**.

On the other hand, sodium borohydride reduction of **1c** afforded the keto alcohol (**7a**), which was converted into the δ-lactone (**8a**) by methanolic hydrogen chloride. The formation of **8a** from **1c** *via* **7a** is similar to that of **8b** from **1a** *via* **7b**.[1b] It is supported by the ^{13}C NMR spectra of **7a** and **1c** that two methyl groups originally in *p*-xyloquinone are situated at C-4a and -7 in the adduct **2b**, since the signals for C-4a and -6 in **7a** are shifted upfield compared with those in **1c**. Comparison of the ^{13}C chemical shifts of **1c** with **1b** suggests that **1c** also exists in the form (A), since the signal for C-3 in **1c** is shifted upfield by the γ-gauche effect of the methyl group at C-4a. The axial proton signal at 4.02 ppm (–CH–OH, q, $J=11$ and 6 Hz) in the ^1H NMR spectrum of **7a** is in line with the ^{13}C signal for C-4 in **7a**

TABLE 1. ^{13}C CHEMICAL SHIFTS OF **1b**, **1c**, AND **7a**

Compound	**1b**	**1c**	**7a**
C-1	40.82*	38.39*	38.59*
2	17.89	18.38	19.19
3	31.45	27.43	30.72
4	30.76	34.65	32.54
4a	50.97	51.90	46.46
5	211.91**	213.12**	77.06
6	41.06*	44.43	41.31
7	42.24	39.76*	41.31*
8	208.83**	211.18**	211.59
8a	47.44	52.55	52.91
COO	173.69	174.25	175.31
OMe	51.78	51.78	51.70
C_4–Me	15.05	16.80	18.50
C_{4a}–Me		26.01	28.81
C_6–Me	13.31		
C_7–Me		16.80	14.36

*, ** Assignments are not unambiguous within indicated pair(s).

which is shifted upfield (−2.11 ppm) compared with that in **1c** by the γ-gauche effect of the hydroxyl group. Accordingly, lactonization of **7a**, which is stable in contrast to **6**, proceeds by the aid of acid through the ring inversion and epimerization at C-7.

Therefore, the formation of **4** and **7a** is in line with the structures of **1b** and **1c** in the form (A).

Experimental

Melting points are uncorrected. The IR spectra were recorded on a Hitachi infrared spectrometer EPI-G_3 in Nujol, unless otherwise stated. The ^1H and ^{13}C NMR spectra were obtained on a JEOL JNM-PFT-60 in $CDCl_3$. All the chemical shifts are expressed in term of δ (ppm downfield from internal TMS).

Preparation of ***2a***. A solution of 12.2 g of *p*-toluquinone and 12.6 g of methyl sorbate in 150 ml of benzene was refluxed for 30 h, and concentrated *in vacuo* to afford 7.80 g of **2a**: mp 108—110 °C (from EtOH); IR 1730 and 1678 cm^{-1}; ^1H NMR 0.78 (3H, d, J=7 Hz), 2.01 (3H, d, J=1.5 Hz), 3.74 (3H, s), 5.70 (1H, m), 6.20 (1H, br d, J=11 Hz), and 6.67 ppm (1H, d, J=1.5 Hz). Found: C, 67.59; H, 6.48%. Calcd for $C_{14}H_{16}O_4$: C, 67.73; H, 6.50%.

Preparation of ***3a***. Treatment of 2.00 g of **2a** with 10 g of zinc in 50 ml of AcOH at room temperature for 3 h afforded 1.86 g of **3a**: mp 148—150 °C (EtOH); IR 1734 and 1708 cm^{-1}; ^1H NMR 0.74 (3H, d, J=7 Hz), 1.16 (3H, d, J=6 Hz), 3.73 (3H, s), 5.70 (1H, m), and 6.10 ppm (1H, br d, J=10 Hz). Found: C, 67.09; H, 7.35%. Calcd for $C_{14}H_{18}O_4$: C, 67.18; H, 7.25%.

Preparation of ***1b***. Hydrogenation of 1.22 g of **3a** with 150 mg of 5% Pd–C in 70 ml of MeOH afforded 1.04 g of **1b**: mp 169—170 °C (in a sealed tube) (EtOH); IR 1732 and 1707 cm^{-1}; ^1H NMR 0.67 (3H, d, J=7 Hz), 1.13 (3H, d, J=6 Hz), and 3.70 ppm (3H, s). Found: C, 66.71; H, 8.07 %. Calcd for $C_{14}H_{20}O_4$: C, 66.64; H, 7.99%.

Preparation of ***2b***. To an ice-cold suspension of 1.3 g of powdered anhydrous $AlCl_3$ in 50 ml of dry benzene was added 4.04 g of *p*-xyloquinone and then 3.61 g of methyl sorbate. The mixture was stirred at room temperature for 3 days. Work-up in the usual manner[4] afforded 1.48 g of **2b**: mp 134—136 °C (EtOH); IR 1738 and 1673 cm^{-1}; ^1H NMR 0.75 (3H, d, J=7 Hz), 1.41 (3H, s), 1.99 (3H, d, J=1.5 Hz), 3.75 (3H, s), 5.60 (1H, m), 6.20 (1H, dd, J=10 and 1 Hz), and 6.57 ppm (1H, d, J=1.5 Hz). Found: C, 68.68; H, 6.95 %. Calcd for $C_{15}H_{18}O_4$: C, 68.68; H, 6.92%.

Preparation of ***3b***. Treatment of 1.11 g of **2b** with 5 g of zinc in 50 ml of AcOH at room temperature for 2 h afforded 0.88 g of **3b**: mp 102—103 °C (EtOH); IR 1733 and 1075 cm^{-1}; ^1H NMR 0.77 (3H, d, J=7 Hz), 1.15 (3H, d, J=6 Hz), 1.36 (3H, s), 3.73 (3H, s), 5.60 (1H, m), and 6.16 ppm (1H, br d, J=10 Hz). Found: C, 67.89; H, 7.64%. Calcd for $C_{15}H_{20}O_4$: C, 68.16; H, 7.63%.

Preparation of ***1c***. Hydrogenation of 783 mg of **3b** with 81 mg of 5% Pd–C in 40 ml of MeOH afforded 681 mg of **1c**: mp 78—79 °C diisopropyl ether); IR 1730 and 1708 cm^{-1}; ^1H NMR 0.73 (3H, d, J=7 Hz), 1.16 (3H, d, J=7 Hz), 1.40 (3H, s), and 3.68 ppm (3H, s). Found: C, 67.41; H, 8.40%. Calcd for $C_{15}H_{22}O_4$: C, 67.64; H, 8.33%.

$NaBH_4$ Reduction of ***1b*** *to* ***4***. Treatment of 620 mg of **1b** with 170 mg of $NaBH_4$ in 50 ml of MeOH at room temperature for 2 h afforded 457 mg of **4**: mp 187—188 °C (benzene); IR 1764 and 1701 cm^{-1}; ^1H NMR 1.19 (6H, d, J=6 Hz) and 4.70 ppm (1H, m, W_H=10 Hz). Found: C, 70.05; H, 8.31 %. Calcd for $C_{13}H_{18}O_3$: C, 70.24; H, 8.16%.

$NaBH_4$ Reduction of ***1b*** *to* ***5a***. Treatment of 507 mg of **1b** with 520 mg of $NaBH_4$ in 50 mg NeOH at room temperature for 3 days afforded 211 mg of **5a**: mp 169—170 °C (benzene); IR($CHCl_3$) 3430 and 1723 cm^{-1}; ^1H NMR 1.07 (6H, d, J=5 Hz), 2.97 (1H, br s, W_H=8 Hz), 3.21 (1H, br s, OH), 3.80 (1H, m, W_H=18 Hz), and 4.42 ppm (1H, br s, W_H=4 Hz); ^{13}C NMR 17.81 (C_6–Me), 19.23 (C_4–Me), 29.09 (C-3), 31.57 (C-2), 34.25 (C-7), 34.81 (C-4), 36.19 (C-6*), 36.56 (C-1*), 40.21 (C-4a), 44.35 (C-8a), 70.24 (C-8), 79.09 (C-5), and 175.63 ppm (COO). Found: C, 69.60; H, 9.22%. Calcd for $C_{13}H_{20}O_3$: C, 69.61; H, 8.99%. In a similar way, **5a** was obtained from **4** (95 mg from 173 mg of **4**).

$NaBH_4$ Reduction of ***1c*** *to* ***7a***. Treatment of 504 mg of **1c** with 160 mg of $NaBH_4$ in 20 ml of MeOH at room temperature for 4 h afforded 380 mg of **7a**: mp 124—125 °C (diisopropyl ether); IR 3510, 1728, and 1711 cm^{-1}; ^1H NMR 0.95 (3H, d, J=7 Hz), 1.00 (3H, d, J=6 Hz), 1.37 (3H, s), 3.65 (3H, s), and 4.02 ppm (1H, q, J=11 and 6 Hz). Found: C, 66.93; H, 9.22%. Calcd for $C_{15}H_{24}O_4$: C, 67.13; H, 9.02%.

Lactonization of ***7a*** *to* ***8a***. Treatment of 339 mg of **7a** with 3 ml of 5% methanolic hydrogen chloride at room temperature overnight afforded 195 mg of **8a**: mp 74—75 °C (diisopropyl ether); IR 1717 and 1709 cm^{-1}; ^1H NMR 0.90 (3H, s), 1.10 (6H, d, J=6 Hz), and 4.68 ppm (1H, d, J=2 Hz, W_H=6 Hz); ^{13}C NMR 13.59 (C_7–Me), 15.42 (C_4–Me), 24.06 (C_{4a}–Me), 29.62 (C-3), 31.08 (C-2), 36.60 (C-7*), 37.17 (C-6), 38.63 (C-4a), 41.55 (C-1 and -4*), 59.53 (C-8a), 78.84 (C-5), 172.87 (COO), and 211.26 ppm (C-8). Found: C, 71.12; H, 8.77%. Calcd for $C_{14}H_{20}O_3$; C, 71.16; H, 8.53%.

References

1) a) H. Irikawa and Y. Okumura, *Bull. Chem. Soc. Jpn.*, **51**, 2086 (1978); b) H. Irikawa and Y. Okumura, *ibid.*, **51**, 657 (1978).

2) F. Bohlmann, W. Mathar, and H. Schwarz, *Chem. Ber.*, **110**, 2028 (1977).

3) D. K. Dalling, D. M. Grant, and E. G. Paul, *J. Am. Chem. Soc.*, **95**, 3718 (1973).

4) I. Nagakura, H. Ogata, M. Ueno, and Y. Kitahara, *Bull. Chem. Soc. Jpn.*, **48**, 2995 (1975).

BULLETIN OF THE CHEMICAL SOCIETY OF JAPAN, VOL. 52 (2), 639—640 (1979)

Stereoselectivity in Hydride Reduction of [*n*.3.2]Propellanones

Yoshito TOBE,* Akifumi DOI, Koji KIMURA, and Yoshinobu ODAIRA

Department of Petroleum Chemistry, Faculty of Engineering, Osaka University, Suita-shi, Osaka 565

(Received July 31, 1978)

Synopsis. Stereoselectivity in hydride reduction of [*n*.3.2]propellanones is described. The observed stereoselectivity is attributed to conformational flexibility of the third ring, that is, from five- to eight-membered alicyclic rings.

Propellanes are compounds having three rings conjoined along a common σ bond and serve as good models for examination of steric and electronic effects among three dimensionally arranged rings.[1] From this point of view, much works have been done on the reactivity of unsaturated propellanes such as heterocyclic[2a] and [4.4.2]propellane derivatives.[2b] As part of studies on relationship between structure and reactivity of propellanes,[3] we wish to report here stereoselectivity in hydride reduction of [*n*.3.2]propellanones (**1**)—(**4**) involving a cyclobutane ring, a cyclopentanone moiety, and one of alicyclic rings from five to eight-membered rings as the third ring, and wish to emphasize that conformational flexibility of the third ring plays a key role in determining the stereochemistry of products.

[*n*.3.2]Propellanones **1**—**4** were prepared in good yields by photocycloaddition of the corresponding bicyclic enones to ethylene. Reduction of **1**—**4** with $LiAlH_4$ in ether or $NaBH_4$ in methanol gave two epimeric alcohols (exo; (**5X**)—(**8X**), endo; (**5N**)—(**8N**)), in quantitative yields, and the exo and endo stereochemistry of them were assigned on the basis of the α-hydroxy proton coupling constants according to the data reported for derivatives of bicyclo[3.2.0]heptan-2-ol.[4] The ratios of exo and endo propellanols are summarized in Table.

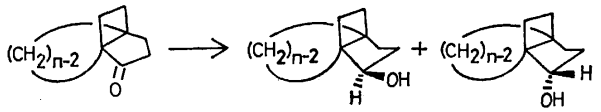

	exo	endo
1 n=5	**5X**	**5N**
2 n=6	**6X**	**6N**
3 n=7	**7X**	**7N**
4 n=8	**8X**	**8N**

TABLE 1. STEREOSELECTIVITY IN HYDRIDE REDUCTION OF [*n*.3.2]PROPELLANONES **1**—**4**

Propellanone	Exo: endo ratio	
	$LiAlH_4$	$NaBH_4$
1	91.4:8.6	87.5:12.5
2	96.4:3.6	93.5: 6.5
3	98.6:1.4	97.2: 2.8
4	99.3:0.7	98.3: 1.7

As shown in Table 1, exo alcohols are always formed almost stereoselectively and, more interestingly, the ratio of exo alcohols increases in order as the size of the third ring increases. Taking the above facts and the mechanism for metal hydride reduction of carbonyl groups into account,[6] it is reasonable to consider that endo side of propellanones **1**—**4** is sterically less hindered than exo side and the difference in the steric hindrance at exo and endo sides of each propellanones becomes greater as the third ring changes from five- to eight-membered ring. In the present system, the difference in the steric hindrance at each side of cyclopentanone moiety may be attributed to the difference in nonbonded interaction

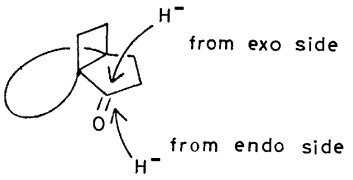

in the transition state between hydrogens of individual alicyclic ring and a hydride, which can be associated with conformational flexibility of ring systems. Namely, on account of the greater degree of conformational flexibility of the third ring in comparison with that of cyclobutane ring, such nonbonded interaction in the transition state at the endo side may be remarkably reduced compared with the exo side. In addition, the nonbonded interaction at the endo side may become smaller in order of increase in conformational flexibility of the third ring, in other words, in the increasing order in size of the third ring. Consequently, it must be concluded that conformational flexibility of the third ring plays a key role in determining the stereochemistry of the resulting alcohols in hydride reduction of [*n*.3.2]-propellanones.

Experimental

Materials. Ketones **1**,[7] **2**,[8] **3**, **4**, and 1,5-dimethylbicyclo[3.2.0]heptan-2-one were prepared in 51—73% yields by photocycloaddition of the corresponding bicyclic enones to ethylene in ether at −70 °C. **3**, IR 1710 cm^{-1}; NMR δ (CCl_4) 1.00—2.80 (m); MS *m/e* 178 (M^+). Semicarbazone, mp 203—204 °C; Found: C, 66.24; H, 8.87; N, 17.95%. Calcd for $C_{13}H_{21}ON_3$: C, 66.35; H, 9.00; N, 17.86%. **4**, IR 1710 cm^{-1}; NMR δ (CCl_4) 1.00—2.90 (m); MS *m/e* 192 (M^+). Semicarbazone, mp 216—218 °C; Found: C, 67.31; H, 9.43; N, 16.96%. Calcd for $C_{14}H_{23}ON_3$: C, 67.43; H, 9.30; N, 16.85%. 1,5-Dimethylbicyclo[3.2.0]heptan-2-one, IR 1710 cm^{-1}; NMR δ (CCl_4) 0.95 (s, 3H), 1.15 (s, 3H), 1.40—2.80 (m, 8H); MS *m/e* 138 (M^+). Semicarbazone, mp 202—204 °C; Found: C, 61.51; H, 8.78; N, 21.52%. Calcd for $C_{10}H_{17}ON_3$: C, 61.39; H, 8.88; N, 21.33%.

*$LiAlH_4$ Reduction of **1**—**4**.* A solution of a ketone in ether was added dropwise to the suspension of 5 molar excess of $LiAlH_4$ in ether and the mixture was stirred at room temperature for 12 h. Water and dilute hydrochloric acid was added carefully and the aqueous solution was extracted with

ether. The combined ethereal solution was washed with aqueous sodium hydrogencarbonate and brine, and then dried (Na_2SO_4). After evaporation of the solvent, the residue was distilled under reduced pressure to give a mixture of alcohols in 90—97% yields. Exo alcohols were separated by preparative GLC (10% FFAP or 10% DEGS) and endo ones were identified with the authentic materials prepared by Meerwein-Ponndorf reduction of ketones. The ratios of them are listed in Table.

5X, mp 95—96 °C; IR 3250, 1040 cm^{-1}; NMR δ (CCl_4) 1.00—2.40 (m, 15H), 3.72 (t, J=8.0 Hz, 1H); MS *m/e* 152 (M^+); Found: C, 77.63; H, 10.60%. Calcd for $C_{10}H_{16}O$: C, 77.89; H, 10.59%. **6X**, mp 55—57 °C; IR 3300, 1050 cm^{-1}; NMR δ (CCl_4) 1.10—2.20 (m, 16H), 3.40 (s, 1H), 3.70 (q, J=7.2 Hz, 1H); MS *m/e* 166 (M^+); Found: C, 79.15; H, 10.88. Calcd for $C_{11}H_{18}O$: C, 79.46; H, 10.92%. **7X**, mp 58—60 °C; IR 3350, 1165 cm^{-1}; NMR δ (CCl_4) 1.00—2.10 (m, 18H), 2.82 (s, 1H), 3.75 (q, J=7.6 Hz, 1H); MS *m/e* 180 (M^+); Found: C, 79.79; H, 11.33%. Calcd for $C_{12}H_{20}O$: C, 79.94; H, 11.18%. **8X**, mp 95—96 °C; IR 3300, 1040 cm^{-1}; NMR δ (CCl_4) 0.90—2.00 (m, 20H), 2.75 (s, 1H), 4.10 (q, J=7.6 Hz, 1H); MS *m/e* 194 (M^+); Found: C, 80.27; H, 11.41%. Calcd for $C_{13}H_{22}O$: C, 80.35; H, 11.41%.

*$NaBH_4$ Reduction of **1**—**4**.* A solution of a ketone in methanol was added dropwise to a solution of 2 molar excess of $NaBH_4$ in methanol and the mixture was stirred at room temperature for 12 h. The solution was poured into dilute hydrochloric acid and extracted with ether. The organic layer was washed with aqueous sodium hydrogencarbonate and brine and then dried (Na_2SO_4). Similar work-up as above gave a mixture of alcohols in 87—90% yields. The ratios of them are listed in Table.

*Preparation of **5N**—**9N** and **9X** by Meerwein-Ponndorf Reduction.* A mixture of a ketone and 2.2 molar excess of aluminum isopropoxide in isopropyl alcohol was heated until isopropyl alcohol began to distill slowly, while more alcohol was added. Heating was continued until no ketone remained (monitored by GLC). The solution was poured into ice-cooled aqueous sodium hydroxide and extracted with ether. The ether extract was washed with water and brine, and then dried (Na_2SO_4). Evaporation of the solvent afforded a mixture of alcohol in 84—89% yields. Products were separated by column chromatography on silica gel and purified by preparative GLC. The ratios of alcohols are as follows; **5X**: **5N**=32: 68, **6X**:**6N**=32: 68, **7X**: **7N**=58: 42, **8X**: **8N**=58: 42, **9X**: **9N**=35: 65.

5N, mp 93—94 °C; IR 3250, 1040 cm^{-1}; NMR δ (CCl_4) 1.00—2.60 (m, 15 H), 3.72 (d, J=3.7 Hz, 1H); MS *m/e* 152 (M^+); Found: C, 77.63; H, 10.58%. Calcd for $C_{10}H_{16}O$: C, 77.89; H, 10.59%. **6N**, mp 53—55 °C; IR 3300, 1050 cm^{-1}; NMR δ (CCl_4) 1.10—2.40 (m, 17H), 3.75 (d, J=4.0 Hz, 1H); MS *m/e* 166 (M^+); Found: C, 79.45; H, 11.16%. Calcd for $C_{11}H_{18}O$: C, 79.46; H, 10.92%. **7N**, mp 55—56 °C; IR 3400, 1040 cm^{-1}; NMR δ (CCl_4) 1.00—2.60 (m, 19H), 3.55 (d, J=3.8 Hz, 1H); MS *m/e* 180 (M^+); Found: C, 80.11; H, 11.22%. Caled for $C_{12}H_{20}O$: C, 79.94; H, 11.18%. **8N**, mp 48—50 °C; IR 3300, 1050 cm^{-1}; NMR δ (CCl_4) 1.00—2.20 (m, 21H), 3.70 (d, J=3.7 Hz, 1H); MS *m/e* 194 (M^+); Found: C, 80.63; H, 11.64. Calcd for $C_{13}H_{22}O$: C, 80.35; H, 11.41%. **9X**, mp 77—78 °C; IR 3250, 1050 cm^{-1}; NMR δ (CCl_4) 1.05 (s, 6H), 1.30—2.20 (m, 9H), 3.62 (d, J=3.8 Hz, 1H); MS *m/e* 140 (M^+). *p*-Nitrobenzoate, mp 110—111 °C; Found: C, 66.14; H, 6.63; N, 4.83%. Calcd for $C_{16}H_{19}O_4N$: C, 66.42; H, 6.62; N, 4.84%. **9N**, mp 78—79 °C; IR 3250, 1050 cm^{-1}; NMR δ (CCl_4) 0.96 (s, 3H), 1.02 (s, 3H), 1.10—2.10 (m, 9H), 3.53 (q, J=7.2 Hz, 1H); MS *m/e* 140 (M^+). *p*-Nitrobenzoate, mp 114—115 °C; Found: C, 66.14; H, 6.64; N, 4.89%. Calcd for $C_{16}H_{19}O_4N$: C, 66.42; H, 6.62; N, 4.84%.

References

1) For a review; D. Ginsburg, "Propellanes, Structure and Reactions," Verlag Chemie, Weinheim, Germany, 1975.

2) (a) D. Ginsburg, *Acc. Chem. Res.*, **7**, 286 (1974); (b) L. A. Paquette, J. M. Photis, and R. P. Micheli, *J. Am. Chem. Soc.*, **99**, 7899 (1977), and references cited therein.

3) Previous report of this series; Y. Tobe, K. Kimura, and Y. Odaira, *J. Org. Chem.*, in press.

4) Since bicyclo[3.2.0]heptan-2-ol moiety has rigid boat conformation, endo α-hydroxy proton in exo propellanol appeared as triplet or quartet with coupling constants of 7—8 Hz and exo proton in endo propellanol appeared as doublet with coupling constants of about 4 Hz. (a) S. C. Lewis and G. H. Whitham, *J. Chem. Soc., C*, 274 (1967); (b) R. G. Weiss and E. I. Snyder, *J. Org. Chem.*, **35**, 1627 (1970); (c) P. G. Gassman and J. M. Pascone, *J. Am. Chem. Soc.*, **95**, 7801 (1973); (d) E. A. Hill, R. J. Theissen, C. E. Cannon, R. Miller, R. B. Guthrie, and A. T. Chen, *J. Org. Chem.*, **41**, 1191 (1976).

Validity of this assignment is further confirmed by LIS NMR of *endo*- and *exo*-1,5-dimethylbicyclo[3.2.0]heptan-2-ol, (**9N**) and (**9X**), using $Eu(dpm)_3$. Namely, S values[5] for the methyl protons of endo isomer **9N** (exo proton, q, J=7.2 Hz) are 0.11 and 0.26 and those for exo isomer **9X** (endo proton, d, J=3.8 Hz) are 0.094 and 0.17, which are well in accord with the assigned structure.

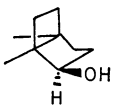

9N

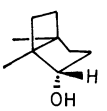

9X

5) A. F. Cockerill and D. M. Rackham, *Tetrahedron Lett.*, **1970**, 5149.

6) It has been demonstrated that the transition state geometry for reduction of carbonyl groups with metal hydrides resembles the geometry of the starting ketones and, therefore, reduction stereochemistry is determined by the relative steric hindrance to nucleophilic attack of hydrides at each side of a carbonyl group. H. O. House, "Modern Synthetic Reactions," 2nd ed, Benjamin, Menlo Park, California, 1972, p. 61.

7) R. L. Cargill, J. R. Damewood, and M. M. Cooper, *J. Am. Chem. Soc.*, **88**, 1330 (1966).

8) A. Kunai, K. Yorihiro, T. Hirata, and Y. Odaira, *Tetrahedron*, **29**, 1679 (1973).

BULLETIN OF THE CHEMICAL SOCIETY OF JAPAN, VOL. 52 (2), 641—642 (1979)

The Reaction of 1-(1-Pyrrolidinyl)acenaphthylene with Electrophilic Acetylenes[1)]

Otohiko TSUGE* and Haruyuki WATANABE

Research Institute of Industrial Science, Kyushu University 86, Hakozaki, Higashi-ku, Fukuoka 812

(Received August 25, 1978)

Synopsis. 1-(1-Pyrrolidinyl)acenaphthylene (**1**), which was prepared from acenaphthenone and pyrrolidine, reacted with dimethyl acetylenedicarboxylate to give the dihydrocyclohepta[*de*]naphthalene and dihydrofluoranthene. The reaction of **1** with methyl propiolate in benzene afforded the dihydrocyclohepta[*de*]naphthalene (**8**) and its isomeric cyclohepta[*de*]naphthalenol (**9**), whereas the Michael type adduct was formed in methanol. An interconversion between **8** and **9** was also described.

It is known that enamines derived from cyclic ketones react with activated acetylenes to yield intermediate cyclobutene adducts which undergo rearrangement with expansion of the carbocyclic ring by two carbon atoms.[2)] Application of this process to 1-aminoacenaphthylene derivatives, which might exhibit enamine-like properties, seems to provide a one-pot synthesis of cyclohepta[*de*]naphthalene compounds which are nonalternant hydrocarbons. However, no 1-aminoacenaphthylenes appeared in the literature. We now report the preparation of 1-(1-pyrrolidinyl)acenaphthylene (**1**) and its reaction with electrophilic acetylenes.

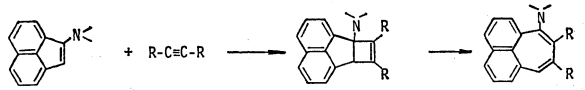

When a benzene solution of acenaphthenone was refluxed with a slight excess of pyrrolidine in the presence of *p*-toluenesulfonic acid for 1 h, the expected enamine **1** as reddish violet viscous oil was obtained quantitatively. Benzoylation of **1** with benzoyl chloride afforded 1-benzoyl-2-(1-pyrrolidinyl)acenaphtylene (**2**), mp 178—180 °C, in 87% yield.

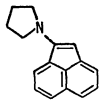

1

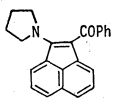

2

The reaction of **1** with dimethyl acetylenedicarboxylate (**3**) in benzene at room temperature for 3 h gave dimethyl 7-oxo-7,8-dihydrocyclohepta[*de*]naphthalene-8,9-dicarboxylate (**4**), mp 131—132 °C, and the dihydrofluoranthene (**5**), mp 191—192 °C, together with tarry materials. The compound **4** was evidently formed by hydrolysis of an initial cyclohepta[*de*]naphthalene. As shown in Scheme 1, the yields of **4** and **5** depended on the amounts of **3** used. Structural elucidation of **4** and **5** was accomplished on the basis of their spectral data.

Treatment of **4** with 3% aqueous sodium hydroxide solution under reflux for 30 min gave 7-oxo-7,8-dihydrocyclohepta[*de*]naphthalene-9-carboxylic acid (**6**), mp

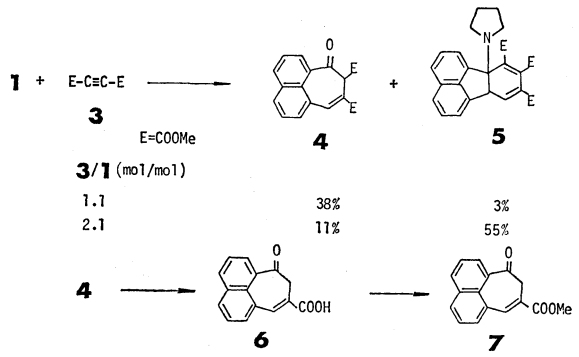

Scheme 1.

229—230 °C, in a 78% yield, evidently by hydrolysis and followed by decarboxylation. The carboxylic acid **6** was converted into the methyl ester **7**, mp 102—103 °C.

In the reaction of **1** with an equimolar amount of methyl propiolate in benzene at room temperature for 1 h, two isomers were isolated. The minor product (2.3 %), mp 115—125 °C (turned to red), as colorless prisms was proven to be methyl 7-oxo-7,8-dihydrocyclohepta[*de*]naphthalene-8-carboxylate (**8**), which is an isomer of **7**, and the major product (21%), mp 87—88 °C, as red needles was assigned to be a tautomer of **8**, methyl 7-hydroxycyclohepta[*de*]naphthalene-8-carboxylate (**9**). On the other hand, the same reaction in methanol at room temperature for 3 h gave the Michael type adduct **10**, mp 157—158 °C, in a 49% yield. (Scheme 2).

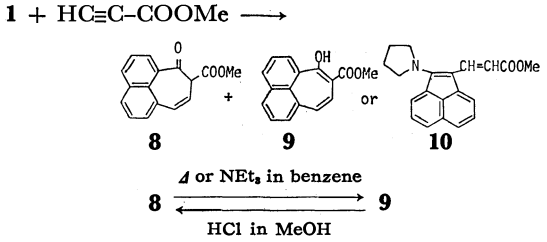

Scheme 2.

As mentioned above, dihydrocyclohepta[*de*]naphthalene **8** melted at 115—125 °C with color change to red, which suggests the transformation into red colored cyclohepta[*de*]naphthalenol **9**. In fact, heating of **8** at 130 °C for 3 h afforded **9** in a 73% yield. When treated with silica gel or triethylamine in benzene at room temperature, **8** was also converted into **9**. On the treatment with catalytic amounts of hydrochloric acid in methanol, however, **9** was partially converted into **8**.

In contrast to **8**, attempts to isomerize **7** to a cyclohepta[*de*]naphthalenol under various conditions were unsuccessful.

Experimental

1-(1-Pyrrolidinyl)acenaphthylene (1). A solution of acenaphthenone (9.1 g, 0.054 mol), pyrrolidine (4.6 g, 0.065 mol), and *p*-toluenesulfonic acid (0.9 g) in benzene (100 ml) was boiled with azeotropic removal of water. After being boiled for 1 h, the reaction mixture was concentrated *in vacuo*, and the residue was extracted with petr. ether. The extract was concentrated to give 11.8 g (*ca.* 100%) of the enamine **1** as reddish violet viscous oil. Bp 185 °C/4 mmHg; NMR (CCl_4) δ 1.85—2.25, 3.40—3.75 (each 4H, m), 5.26 (1H, s, =CH), 6.85—7.86 (6H, m); MS *m/e* 221 (M^+). Picrate of **1**: mp 164—166 °C. Found: C, 58.60; H, 4.05; N, 12.19%. Calcd for $C_{22}H_{18}N_4O_7$: C, 58.66; H, 4.03; N, 12.44%.

Benzoylation of the Enamine 1. A solution of **1** (1.3 g, 0.006 mol) and benzoyl chloride (1.3 g, 0.009 mol) in benzene (20 ml) was stirred with NEt_3 (0.9 g, 0.009 mol) at room temperature for 3 h. The reaction mixture was filtered to remove triethylamine hydrochloride, and the filtrate was evaporated *in vacuo*, followed by addition of petr. ether to give crystals. Recrystallization from EtOH afforded 1.7 g (87%) of 1-benzoyl-2-(1-pyrrolidinyl)acenaphthylene (**2**), mp 178—180 °C, as red prisms. IR (KBr) 1600 cm^{-1} ($\nu_{C=O}$); MS *m/e* 325 (M^+). Found: C, 84.89; H, 5.88; N, 4.30%. Calcd for $C_{23}H_{19}NO$: C, 84.89; H, 5.89; N, 4.30%.

Reaction of the Enamine 1 with Dimethyl Acetylenedicarboxylate (3). A solution of **1** (13.0 g, 0.059 mol) and the acetylene **3** (9.2 g, 0.065 mol) in benzene (100 ml) was stirred at room temperature for 3 h. The reaction mixture was concentrated *in vacuo*, and MeOH (20 ml) was added to the residue, giving 7.0 g (38%) of colorless crystals, mp 128—130 °C. Recrystallization from cyclohexane afforded dimethyl 7-oxo-7,8-dihydrocyclohepta[*de*]naphthalene-8,9-dicarboxylate (**4**), mp 131—132 °C, as colorless prisms. IR (KBr) 1680, 1720, 1780 cm^{-1} ($\nu_{C=O}$); NMR ($CDCl_3$) δ 3.25, 3.99 (each 3H, s), 5.46 (1H, s, >CH), 7.22 (1H, s, =CH), 7.30—8.20 (6H, m); UV λ_{max}^{EtOH} nm (log ε) 208 (4.5), 237 (4.5), 325 (4.0); MS *m/e* 310 (M^+). Found: C, 69.64; H, 4.58%. Calcd for $C_{18}H_{14}O_5$: C, 69.67; H, 4.55%.

The MeOH filtrate was concentrated *in vacuo*, and the residue was chromatographed on alumina using benzene as an eluent, giving 0.9 g (3%) of crystals. Recrystallization from MeOH afforded the dihydrofluoranthene **5**, mp 191—192 °C, as colorless prisms. IR (KBr) 1740, 1750 cm^{-1} ($\nu_{C=O}$); NMR ($CDCl_3$) δ 1.60—1.96, 3.20—3.60 (each 4H, m), 3.65, 3.72 (each 6H, s), 5.35 (1H, s, >CH), 7.25—8.20 (6H, m); UV λ_{max}^{EtOH} nm (log ε) 215 (4.8), 330 (3.8); MS *m/e* 505 (M^+). Found: C, 66.78; H, 5.45%. Calcd for $C_{28}H_{27}NO_8$: C, 66.52; H, 5.38%.

A similar reaction of **1** (11.7 g, 0.053 mol) with **3** (16.5 g, 0.116 mol) in benzene (100 ml) afforded 1.8 g (11%) of **4** and 14.8 g (55%) of **5**.

7-Oxo-7,8-dihydrocyclohepta[de]*naphthalene-9-carboxylic Acid (6) and Its Methyl Ester (7).* A suspension of dihydrocyclohepta[*de*]naphthalene **4** (5.0 g) in 3% NaOH aq solution (200 ml) was refluxed for 30 min; during which time it turned to a red solution. The solution was acidified with hydrochloric acid to give brown precipitates, which extracted with hot EtOH (150 ml). The extract was concentrated *in vacuo* to leave the residue, which on recrystallization from EtOH using charcoal afforded 1.5 g (39%) of **6**, mp 229—230 °C, as yellow prisms. IR (KBr) 2700—3100 (ν_{OH}), 1690 cm^{-1} ($\nu_{C=O}$); NMR (DMSO-d_6) δ 3.80 (2H, s, CH_2), 7.60—8.45 (7H, m, ArH+=CH); UV λ_{max}^{EtOH} nm (log ε) 225 (4.5), 243 (4.4), 320 (3.9); MS *m/e* 238 (M^+). Found: C, 75.90; H, 4.35%. Calcd for $C_{15}H_{10}O_3$: C, 75.62; H, 4.23%.

Esterification of **6** in MeOH containing H_2SO_4 afforded the methyl ester (**7**) in a 92% yield. Mp 102—103 °C; yellow prisms; IR (KBr) 1670, 1704 cm^{-1} ($\nu_{C=O}$), NMR ($CDCl_3$) δ 3.82 (2H, s, CH_2), 3.89 (3H, s), 7.30—8.20 (7H, m, ArH+=CH); MS *m/e* 252 (M^+). Found: C, 76.07; H, 4.78%. Calcd for $C_{16}H_{12}O_3$: C, 76.18; H, 4.80%.

Reaction of the Enamine 1 with Methyl Propiolate. i) A solution of **1** (2.65 g, 0.012 mol) and methyl propiolate (1.0 g, 0.012 mol) in benzene (20 ml) was stirred at room temperature for 3 h. The reaction mixture was concentrated *in vacuo*, and the residue was chromatographed on silica gel using benzene as an eluent to give crystals. The crystals were washed with hexane (50 ml) to leave red crystals. Recrystallization from petr. ether afforded 0.65 g (21%) of methyl 7-hydroxycyclohepta[*de*]naphthalene-8-carboxylate (**9**), mp 87—88 °C, as red needles. IR (KBr) 1660 cm^{-1} ($\nu_{C=O}$); NMR ($CDCl_3$) δ 3.80 (3H, s), 6.02, 6.28 (each 1H, d, =CH, J=12 Hz), 6.85—8.20 (6H, m), 14.50 (1H, s, OH); UV λ_{max}^{EtOH} nm (log ε) 217 (4.5), 250 (4.2), 370 (3.7), 450 (3.3); MS *m/e* 252 (M^+). Found: C, 76.47; H, 4.79%. Calcd for $C_{16}H_{12}O_3$: C, 76.18; H, 4.80%.

The hexane washings were evaporated *in vacuo* to leave colorless crystals, which on recrystallization from hexane afforded 0.07 g (2.3%) of methyl 7-oxo-7,8-dihydrocyclohepta[*de*]naphthalene-8-carboxylate (**8**), mp 115—125 °C (turned to red), as colorless prisms. IR (KBr) 1690, 1755 cm^{-1} ($\nu_{C=O}$); NMR ($CDCl_3$) δ 3.78 (3H, s), 4.48 (1H, dd, >CH, J=2, 5 Hz), 6.41 (1H, dd, =CH, J=5, 11 Hz), 6.98 (1H, dd, =CH, J=2, 11 Hz), 7.28—8.25 (6H, m); UV λ_{max}^{EtOH} nm (log ε) 220 (4.6), 317 (3.8), 340 (3.8), 355 (3.8); MS *m/e* 252 (M^+). Found: C, 76.29; H, 4.84%. Calcd for $C_{16}H_{12}O_3$: C, 76.18; H, 4.80%.

ii) A solution of **1** (2.65 g) and methyl propiolate (1.0 g) in MeOH (20 ml) was stirred at room temperature for 3 h; during which time crystals precipitated. Recrystallization of the crystals from EtOH afforded 1.8 g (49%) of the Michael type adduct **10**, mp 157—159 °C, as violet prisms. IR (KBr) 1690 cm^{-1} ($\nu_{C=O}$); NMR ($CDCl_3$) δ 1.69—2.05, 3.55—3.90 (each 4H, m), 3.79 (3H, s), 6.08, 8.17 (each 1H, d, =CH, J=15 Hz), 7.19—7.90 (6H, m); UV λ_{max}^{EtOH} nm (log ε) 227 (4.7), 254 (4.4), 320 (4.3), 357 (4.5), 390 (4.2), 520 (3.8); MS *m/e* 305 (M^+). Found: C, 78.04; H, 6.22; N, 4.69%. Calcd for $C_{20}H_{19}NO_2$: C, 78.66; H, 6.27; N, 4.59%.

Isomerization of Dihydrocyclohepta[de]*naphthalene (8) to Cyclohepta*[de]*naphthalenol (9). i)* Dihydrocyclohepta[*de*]naphthalene (**8**) (0.15 g) in a test tube was heated at 130 °C (bath temperature) under nitrogen for 3 h. The mixture was washed with hexane (20 ml) to leave 20 mg of unchanged **8**. From the hexane washing 0.11 g (73%) of **9** was obtained.

ii) A solution of **8** (80 mg) in benzene (20 ml) was stirred with NEt_3 (3 drops) at room temperature for 6 h. After the reaction mixture was evaporated *in vacuo* below 40 °C, a similar treatment of the residue with hexane gave 50 mg (62.5%) of **9**.

Isomerization of Cyclohepta[de]*naphthalenol (9) to Dihydrocyclohepta*[de]*naphthalene (8).* A solution of **9** (0.5 g) in MeOH (50 ml) was stirred with hydrochloric acid (1 drop) at room temperature for 7 days. The reaction mixture was poured into water, and extracted with $CHCl_3$. The extract was washed with water, dried over Na_2SO_4, and evaporated *in vacuo*. A similar treatment of the residue with hexane gave 0.15 g (30%) of **8**, together with recovery of **9** (0.3 g).

References

1) Studies of Acenaphthene Derivatives. Part 31. Part 30: O. Tsuge and M. Koga, *Heterocycles*, **6**, 411 (1977).

2) G. A. Berchtold and G. F. Uhlig, *J. Org. Chem.*, **28**, 1459 (1963); K. C. Brannock, R. D. Burpitt, V. W. Goodlett, and J. G. Thweatt, *ibid.*, **28**, 1464 (1963); K. C. Brannock, R. D. Burpitt, V. W. Goodlett, and J. G. Thweatt, *ibid.*, **29**, 818 (1964).

BULLETIN OF THE CHEMICAL SOCIETY OF JAPAN, VOL. 52 (2), 643—644 (1979)

A Novel Synthesis of δ-Amino Acid Derivatives

Takeshi IMAGAWA* and Mituyosi KAWANISI

Department of Industrial Chemistry, Faculty of Engineering, Kyoto University, Sakyo-ku, Kyoto 606

(Received October 19, 1978)

Synopsis. The Diels-Alder adducts of "anhydrochloral-urethane" with some 1,3-dienes were successfully utilized for the synthesis of some δ-amino acid derivatives by the sequence of the reactions, *viz.*, hydrogenation, dehydrochlorination, and ozonolysis.

Polar cycloaddition reactions are ingeniously utilized for the introduction of a substituent at the specific position.[1] We describe here a method of synthesis of δ-amino acid derivatives making use of the Diels-Alder adducts between "anhydrochloral-urethane" *N*-(2,2,2-trichloroethylidene)carbamates (**1**) and 1,3-dienes reported by us previously.[2]

The *exo*- and *endo*-adducts (**2** and **3**) of **1** with cyclopentadiene[2] were hydrogenated over Pd–C to afford in about 90% yields ethyl *exo*- and *endo*-3-trichloromethyl-2-azabicyclo[2.2.1]heptane-2-carboxylates (**4** and **5**), respectively. Upon treatment of **4** and **5** with sodium methoxide in refluxing benzene, ethyl 3-dichloromethylene-2-azabicyclo[2.2.1]heptane-2-carboxylate (**6**) in 60—75% yields. When **6** was oxidized with ozone in methanol, followed by treatment with dimethyl sulfide, methyl *cis*-3-ethoxycarbonylamino-1-cyclopentanecarboxylate (**7**) was obtained in 76% yield. The *cis*-configuration of **7** is evident from the consideration of the reaction course. This product (**7**) is a potential intermediate for the synthesis of an antibiotics "amidinomycin."[3]

In a similar manner, 1-ethoxycarbonyl-2-trichloromethyl-1,2,3,6-tetrahydropyridine (**8**) obtained from **1** and butadiene was converted into methyl 5-(ethoxycarbonylamino)pentanoate (**11**) by the sequence of the reactions, *viz.*, hydrogenation, dehydrochlorination, and ozonolysis.

Consequently, the present procedure has merged into a powerful synthetic route to δ-amino acid derivatives.

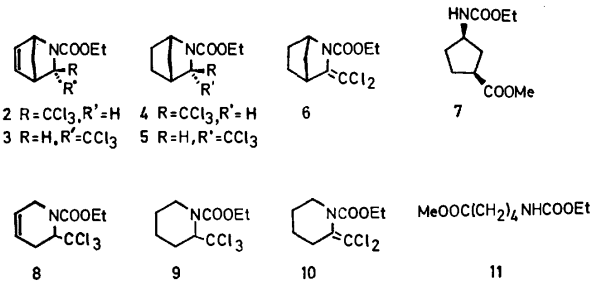

Experimental

Ethyl exo-*3-Trichloromethyl-2-azabicyclo[2.2.1]heptane-2-carboxylate (4).* A solution of 1.956 g of **2**[2] in 50 ml of ethanol was hydrogenated over 500 mg of Pd–C until 154 ml (1.0 equiv.) of hydrogen-uptake (5 min). Removal of the catalyst and the solvent, followed by distillation, gave 1.793 g (91%) of **6**: bp 132.5—135 °C/3 Torr; IR (neat): 1725 cm^{-1}; MS: *m/e* 242 (small), 240 (small), 168 (100), 140 (38), 68 (31%); NMR (CCl_4): δ 4.31 (m, H_1), 4.16 (s, H_3), 2.98 (m, H_4), 1.62 (4H, m, $2\times H_5$ and $2\times H_6$), 2.68 (bd, 10 Hz, syn-H_7), 1.23 (bd, 10 Hz, anti-H_7), 4.18 (q, 7 Hz, $COO\underline{H}_2CH_3$), 1.31 (t, 7 Hz, $COOC\underline{H}_2CH_3$). Found: C, 42.14; H, 4.93; N, 4.71%. Calcd for $C_{10}H_{14}NO_2Cl_3$: C, 41.91; H, 4.92; N, 4.89%.

Ethyl endo-*3-Trichloromethyl-2-azabicyclo[2.2.1]heptane-2-carboxylate (5).* A solution of 1.0 g of **3**[2] in 30 ml of ethanol was hydrogenated over 500 mg of 5% Pd–C until 1.14 equiv. of hydrogen-uptake. Removal of the catalyst and the solvent, followed by recrystallization from ether–petroleum ether 894 mg (89%) of **5**, mp 63.5—65.0 °C; IR (CCl_4): 1722 cm^{-1}; MS: *m/e* 242 (small), 240 (small), 168 (100), 140 (34), 96 (21), 68 (36), 67 (28%); NMR (CCl_4): δ 4.61 (m, H_1), 4.67 (d, 4.0 Hz, H_3), 3.09 (m, H_4), 1.2—2.3 (6H, m, $2\times H_5$, $2\times H_6$, and $2\times H_7$), 4.12 (q, 7.3 Hz, $COOH_2$–), 1.27 (t, 7.3 Hz, $COOCH_2$-$C\underline{H}_3$). Found: C, 42.08; H, 4.92; N, 4.66%. Calcd for $C_{10}H_{14}NO_2Cl_3$: C, 41.91; H, 4.92; N, 4.89%.

Ethyl 3-Dichloromethylene-2-azabicyclo[2.2.1]heptane-2-carboxylate (6). *From 4*: To a solution of 1.356 g of **4** in 50 ml of benzene, was added 505 mg (2 equiv.) of methanol-free sodium methoxide, and heated under reflux for 40 h. The reaction mixture was washed twice with water, dried (Na_2SO_4), and distilled to give 888 mg (75%) of **6**, bp 128—130 °C/3 Torr; IR (neat): 1740 (broad), 1646 cm^{-1}; MS: *m/e* 249 (M^+, 43), 251 (M+2, 27), 254 (M+4, 5), 214 (87), 177 (24), 151 (33), 150 (68), 149 (51), 148 (100), 144 (27), 142 (53), 114 (37), 67 (34%); NMR (CCl_4): δ 4.52 (m, H_1), 3.47 (m, H_4), 1.74 (6H, m, $2\times H_5$, $2\times H_6$, and $2\times H_7$), 4.18 (q, 7 Hz, $COOC\underline{H}_2CH_3$), 1.34 (t, $COOCH_2C\underline{H}_3$). Found: C, 47.86; H, 5.12; N, 5.32%. Calcd for $C_{10}H_{13}NO_2Cl_3$: C, 48.02; H, 5.24; N, 5.60%. *From 5*: To a solution of 582 mg of **5** in 20 ml of benzene, was added 220 mg (2 equiv.) of sodium methoxide, and heated under reflux for 9 h. The reaction mixture was worked up as described above, giving 324 mg (64%) of **6**.

Methyl cis-*3-Ethoxycarbonylamino-1-cyclopentanecarboxylate (7).* A slow stream of ozonized oxygen was bubbled into a solution of 888 mg of **6** in 40 ml of dichloromethane and 10 ml of methanol cooled to −50 °C until the blue color persisted. The solution was flushed with oxygen for 10 min, removed from the cooling bath, and added with 2 ml of dimethyl sulfide. The mixture was allowed to warm to room temp for 4 h. After evaporation of the solvent, distillation gave 715 mg (76%) of **7**, bp 137—141 °C/3 Torr; MS: *m/e* 215 (M^+, 16), 156 (20), 142 (100), 138 (25), 129 (55), 128 (30), 84 (20), 83 (21), 67 (52), 57 (23), 56 (55), 55 (23%); NMR ($CDCl_3$): δ 1.5—2.5 (8H, m), 1.26 (3H, t), 3.73 (3H, s), 4.15 (2H, q); IR (neat): 3325, 1730 (broad) cm^{-1}. Found: C, 55.58; H, 7.86; N, 6.41%. Calcd for $C_{10}H_{17}NO_4$: C, 55.80; H, 7.96; N, 6.51%.

2-Trichloromethyl-1-(ethoxycarbonyl)piperidine (9). A solution of 6.156 g of **8** in 50 ml of ethanol was hydrogenated over 3.0 g of 5% Pd–C until 538 ml (1.07 equiv.) of hydrogen-uptake. After removal of the catalyst and the solvent, distillation gave 5.578 g (90.4%) of **10**, bp 121—122 °C/4 Torr; $n_D^{25.6}$ 1.5020; IR (neat): 1720, 1735 (shoulder) cm^{-1}; MS: *m/e* 163 (100), 154 (33), 128 (30), 84 (50%). Found: C, 39.37; H, 5.15; N, 4.95%. Calcd for $C_9H_{14}NO_2Cl_3$: C, 39.37; H, 5.14; N, 5.10%.

*2-Dichloromethylene-1-(ethoxycarbonyl)piperidine (**10**).* To 1.026 g of **9** in 30 ml of benzene, was added 400 mg (2 equiv.) of sodium methoxide, and refluxed for 23 h. The reaction mixture was poured into water, and extracted with dichloromethane. The organic layer was washed with water, dried (Na_2SO_4), and distilled to give 672 mg (75%) of **10**, which solidified on standing; mp 54.0—54.7 °C; IR (Nujol): 1740 (broad), 1635 cm^{-1}; NMR (CCl_4): δ 2.82 (2H, m, $-N-CH_2-$), 1.2—2.5 (6H, complex m, $3\times CH_2$), 4.12 (bq, $COOC\underline{H}_2CH_3$), 1.28 (t, $COOCH_2CH_3$); MS: *m/e* 237 (M^+, small), 239 (M+2, small), 204 (23), 202 (75), 176 (31), 174 (100%). Found: C, 45.53; H, 5.54; N, 5.61%. Calcd for $C_9H_{13}NO_2Cl_2$: C, 45.39; H, 5.52; N, 5.88%.

*Methyl 5-(Ethoxycarbonylamino)pentanoate (**11**).* A slow stream of ozonized oxygen was bubbled into a solution of 1.427 g of **10** in 30 ml of methanol at room temp for 2 h. After the solution was flushed with oxygen for 20 min, 3 ml of dimethyl sulfide was added to the reaction mixture, and allowed to stand overnight. After evaporation of the solvent, fractional distillation gave 889 mg of crude **11**, bp 125—128 °C/3 Torr. Pure sample of **11** was obtained by preparative GLC; MS: *m/e* 203 (M^+, 14), 172 (20), 171 (22), 130 (22), 126 (27), 115 (47), 102 (100), 100 (67), 98 (54), 82 (22), 74 (37), 70 (22), 59 (37), 58 (26), 56 (61), 55 (60), 44 (23), 43 (45), 42 (30), 41 (36). Found: C, 53.35; H, 8.56; N, 6.60%. Calcd for $C_9H_{17}NO_4$: C, 53.19; H, 8.43; N, 6.89%.

References

1) R. R. Schmid, *Synthesis*, **1972**, 333.
2) T. Imagawa, K. Sisido, and M. Kawanisi, *Bull. Chem. Soc. Jpn.*, **46**, 2922 (1973).
3) H. Berger, H. Paul, and G. Hilgetag, *Chem. Ber.*, **101**, 1525 (1968).
4) Mass spectra were obtained with an ionization potential of 70 eV.

BULLETIN OF THE CHEMICAL SOCIETY OF JAPAN, VOL. 52 (2), 645—646 (1979)

Synthesis and Magnetic Behavior of Three Novel Di-μ-halobis[halo(1,2-benzoquinonedioxime)copper(II)] Complexes. Ferromagnetic Exchange Coupling

Michel MÉGNAMISI-BÉLOMBÉ
Department of Physics, Stanford University, Stanford, California 94305, U.S.A.

(Received April 8, 1978)

Synopsis. Variable-temperature magnetic susceptibilities measured from 4.2 to 300 K on the new dimeric clusters indicate ferromagnetic exchange coupling with $J=+4.63$ cm^{-1} and $J=+0.14$ cm^{-1} for di-μ-bromobis-[bromo-(4-chloro-1,2-benzoquinonedioxime)copper(II)] and di-μ-chlorobis[chloro-1,2-benzoquinonedioxime) copper(II)], respectively, and antiferromagnetic exchange coupling with $J=-0.11$ cm^{-1} for di-μ-bromobis[bromo(1,2-benzoquinonedioxime)copper(II)].

The investigation of exchange effects in paramagnetic cluster compounds has recently developed into a topic of focal and increasing interest to inorganic chemists, as well in theoretical[1] as in experimental[2,3] respect. Lately we reported[4] antiferromagnetic exchange coupling in di-μ-bromobis[bromo(dimethylglyoxime)copper(II), $[CuBr_2(dmgH)]_2$. This dimeric cluster, the first adduct of $CuBr_2$ with a 1,2-dionedioxime ligand, is isostructural[4] with the di-μ-chloro analogue.[5] We now have employed 1,2-benzoquinonedioxime(bqdH) ligands[6] to prepare the three new dimers listed above. We show in the following that, as a specific result of scientific innovation, it is possible to bring about desirable changes in magnetic properties of cluster compounds (in particular ferromagnetic orderings) by controlled chemical modifications of appropriate ligand systems.

Experimental

The brown solids were obtained in good yield by reacting equimolar solutions of the analytical grade reactants according to the equation $RR'bqdH+CuX_2 \xrightarrow[20°C]{(acetone)} CuX_2(RR'bqdH)$ (dimeric structure sketched in the Fig. 1). After washing with cold acetone and drying at ≈ 50 °C, the materials analyze as in the Table 1. The compounds are remarkably air stable, though the bromo derivatives show signs of decomposition after several weeks of exposure to air and light.

Near infrared spectra (KBr pellets) were recorded with a Perkin-Elmer 621 Grating Spectrophotometer, and X-band electron spin resonance spectra with a Varian Assoc. E-12 instrument at room temperature. Variable-temperature susceptibility data were collected at 36 different points from 4.2 to 300 K with a Superconducting Technology, Inc. SQUID-type susceptometer operating at ≈ 2 kG.[4]

Results and Discussion

The spectroscopic data are taken as conclusive evidence to infer the dimeric structure sketched in the Fig. 1. This is done by comparing the spectra with those recorded on the analogous, well-characterized

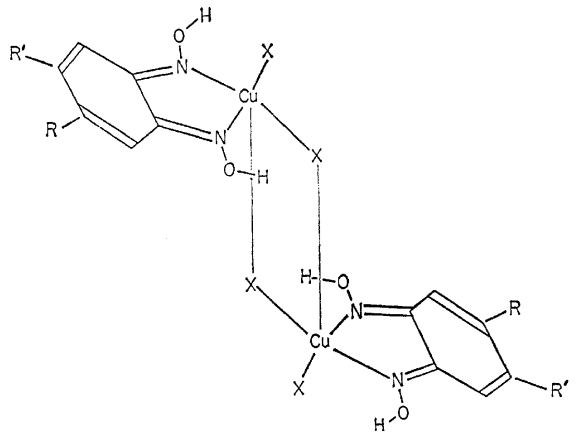

Fig. 1. Infrerred schematic structure of the $[CuX_2(RR'bqdH)]_2$ dimers (bqdH=1,2-benzoquinonedioxime):
a) R=Cl, R'=H, X=Br$^-$: $[CuBr_2(ClbqdH)]_2$,
b) R=R'=H, X=Cl$^-$: $[CuCl_2(bqdH)]_2$,
c) R=R'=H, X=Br$^-$: $[CuBr_2(bqdH)]_2$.

dimethylglyoxime Cu(II) dimers.[4,5] The striking resemblance of the two sets of spectra is interpreted as an intimate reflection of the similar ligand field geometry surrounding the Cu sites in both dimer types. This is rationalized by considering the two analogues $[CuCl_2(bqdH)]_2$ and $[CuCl_2(dmgH)]_2$,[5] which exhibit the same ESR line shape with the identical parallel g factor of 2.207, but have, as to be expected, the different perpendicular g factors of 2.056 and 2.039, respectively.

The corrected molar susceptibility data, χ_m, were fitted with a standard non-linear least-squares computer program[4,7] to the singlet-triplet equation

$$\chi_m = \frac{Ng^2\beta^2}{3k(T-\theta)}\left[1+\frac{1}{3}\exp\left(-\frac{2J}{kT}\right)\right]^{-1} + N\alpha,$$

where the exchange parameter J is defined by the Heisenberg Hamiltonian $H_{ex}=-2JS_1\cdot S_2$. The van Vleck constant, $N\alpha$, was fixed at 60×10^{-6} emu/mol for all three dimers, and the best fits gave a) $J=+4.63$ cm^{-1}, $g=1.99$, $\theta=-5.53$ K for $[CuBr_2(ClbqdH)]_2$; b) $J=+0.14$ cm^{-1}, $g=1.95$, $\theta=-0.29$ K for $[CuCl_2(bdqH)]_2$; c) $J=-0.11$ cm^{-1}, $g=1.95$, $\theta=+0.22$ K for $[CuBr_2(bqdH)]_2$. The fitting g factors differ slightly from the correspeonding isotropic values of 2.050, 2.106, and 2.050 observed with ESR, but the deviations of less than ±0.2 lie within the range expected for the observed J values to be regarded as reliable and "meaningful measurements of the exchange interaction."[3] The experimental magnetic data agreed to within 3% or less with the corresponding theoretical values

Table 1. Microanalytical data

Element	$[CuBr_2(ClbqdH)]_2$		$[CuCl_2(bqdH)]_2$		$[CuBr_2(bqdH)]_2$	
	Found(%)	Calcd(%)	Found(%)	Calcd(%)	Found(%)	Calcd(%)
C	18.20	18.20	26.35	26.44	20.09	19.94
H	1.33	1.27	2.19	2.22	1.64	1.67
N	6.95	7.08	10.16	10.28	7.68	7.75
Cl	8.90	8.95	25.82	26.01		
Br	40.12	40.37			43.63	44.21
Cu	15.70	16.05	23.11	23.31	17.50	17.58

calculated using the above equation. The intradimer exchange coupling, measured by J, is presumably mediated by a *super exchange* mechanism involving the valence orbitals of the bridging halide ligands. Substitution of the bqdH rings (Fig. 1) with electron withdrawing Cl stoms is accompanied by a remarkable increase in J value which passes from -0.11 cm^{-1} in $[CuBr_2(bqdH)]_2$ to $+4.63$ cm^{-1} in $[CuBr_2(ClbqdH)]_2$ Obviously this result demonstrates that the reported ligand-induced nephelauxetic effect[8] may provide a mechanism for modulating electron spin orderings in paramagnetic cluster compounds.

Provided this trend could prove to be generally valid, the present effect might be anticipated to have a far-reaching significance with respect to the better understanding of solid state magnetic phenomena as well as in connection with sounder studies of bonding mechanisms in coordination chemistry for the years ahead. Synthetic details of these and other new Cu(II) dimeric clusters will appear in a subsequent, more comprehensive report.

This work was supported by the National Science Foundation Grant No. DMR 76-82087-A02. The author thanks E. J. Laskowski and M. A. Novotny for experimental assistance, and Prof. W. A. Little for his encouragement.

References

1) P. J. Hay, J. C. Thibeault, and R. Hoffmann, *J. Am. Chem. Soc.*, **97**, 4884 (1975).
2) D. J. Hodgson, *Progr. Inorg. Chem.*, **19**, 173 (1975).
3) A. P. Ginsberg, *Inorg. Chim. Acta Rev.*, **5**, 45 (1971).
4) M. M. Bélombé and M. A. Novotny, *Inorg. Chem.*, submitted (and references therein).**
5) D. H. Svedung, *Acta Chem. Scand.*, **23**, 2865 (1969).
6) M. M. Bélombé, in "Synthesis and Properties of Low-Dimensional Materials," ed by J. S. Miller, Annal of the New York Academy of Sciences, New York, to be published (1978).
7) P. Gill, W. Murray, and Picken, Report DNAC 24, National Physical Laboratory, Teddington (England), August 1972.
8) M. M. Bélombé, *J. Solid State Chem.*, **22**, 151 (1977); J. W. Brill, M. M. Bélombé, and M. Novotny, *J. Chem. Phys.*, **68**, 585 (1978).
** The three-dimensional single crystal X-ray structure of $[CuBr_2(dmgH)]_2$ has now been fully solved (H. Endres, submitted to *Acta Crystallogr., Sect. B.* The results are in excellent agreement with our preliminary findings.

BULLETIN OF THE CHEMICAL SOCIETY OF JAPAN, VOL. 52 (2), 647—648 (1979)

Synthesis and Reduction of 3-Bromoflavanones

N. J. REDDY and T. C. SHARMA*
School of Studies in Chemistry, Vikram University, Ujjain, M.P., India

(Received April 14, 1978)

Synopsis. Bromination of flavanone, 6-methylflavanone, 6-methyl-4′-methoxyflavanone, and 6-methyl-3′,4′-dimethoxyflavanone with pyridinium tribromide in glacial acetic acid gives the corresponding 3-bromoflavanones, which when refluxed with thiourea in ethanol undergo reduction to flavanones.

Several reagents such as pyridinium tribromide,[1] phenyltrimethylammonium tribromide,[2,3] 2-pyrrolidone hydrotribromide,[4] (2-carboxyethyl)triphenylphosphonium tribromide,[5] and 2-bromo-2-cyano-*N*,*N*-dimethylacetamide[6] have been employed for the selective bromination of C–H α to a carbonyl group. All these reagents, however, are not equally effective and their reactivity varies with the presence of other functional groups prone to bromine reactivity.

Because of the asymmetric centres, 3-bromoflavanones exist in two racemic forms having different configurations for C_3-bromine. These compounds have been synthesized by the bromination of flavanones with bromine dissolved in a suitable solvent[7–11] or with a brominating agent like dioxane dibromide,† [12] trimethylphenyl ammonium tribromide,[13] and *N*-bromosuccinimide.[10,14–16] 3-Bromoflavanones have also been obtained by the cyclization of 2′-acetoxychalcone dibromides[17–19,22] as well as of 2-bromo-3-ethoxy-1,3-diphenyl-1-propanone.[20] A 3-bromoflavanone was synthesized by the action of copper(II) bromide on 2′-hydroxychalcone.[21] All the methods gave a mixture of cis and trans isomers.

In the present work, we have brominated four variedly substituted flavanones (I) with pyridinium tribromide in acetic acid medium. Three cases gave only the trans isomer, whereas, in the case of 6-methyl-3′,4′-dimethoxyflavanone a mixture of *trans*- and *cis*-bromoflavanones has been obtained.

Keeping in view the biological importance of thio compounds, we examined the reaction of thiourea with 3-bromoflavanones (II). Thiourea reacts with α-halo ketones[24–27] and chalcone dibromides to afford the corresponding thiazoles and chalcones[28] respectively. However, under the reaction conditions employed, the 3-bromo-flavanones undergo conversion to the corresponding flavanones (I).

In addition to flavanone only sulfur could be isolated from the reaction mixture and a positive test was obtained for the presence of HBr. In the light of these facts, a likely reaction path can be as follows.

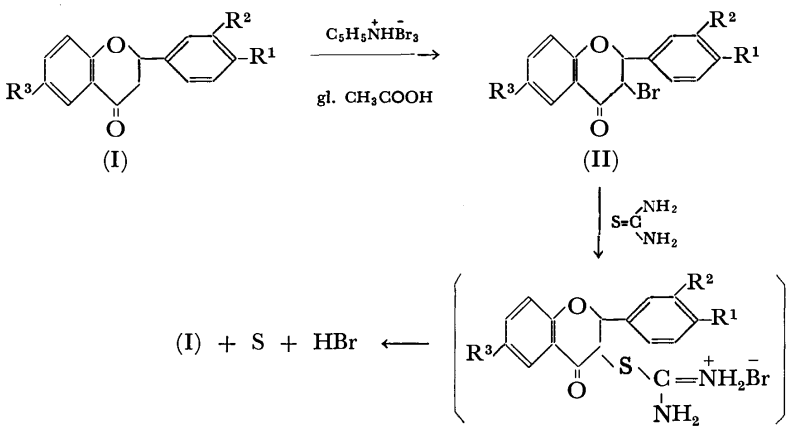

where
(a) $R^1=R^2=R^3=H$, (b) $R^1=H$; $R^2=H$, $R^3=CH_3$, (c) $R^1=OCH_3$; $R^2=H$; $R^3=CH_3$,
(d) $R^1=R^2=OCH_3$; $R^3=CH_3$

It may be mentioned that all the attempts to detect the presence of urea in the reaction mixture met with failure.

Experimental

All melting points are uncorrected. Pyridinium tribromide was prepared by following the reported procedure.[1]

trans-3-Bromoflavanone (IIa). Flavanone (Ia; 1.1 g) was dissolved in glacial acetic acid (5 ml) by warming on water-bath. To the hot solution was added pyridinium tribromide (1.6 g) in equimolar ratio in small amounts shaking the contents to expel the HBr formed. After the complete addition of the reagent, the reaction mixture was kept at room temperature for 30 min with occasional shaking. It was then diluted with cold water and 3-bromoflavanone thus obtained was crystallized from ethanol to give white crystals (0.9 g) mp 111—112 °C (lit,[12] mp 111 °C).

trans-3-Bromo-6-methylflavaone (IIb). Flavanone (Ib; 1 g) was dissolved in glacial acetic acid (5 ml) by warming on water-bath. To the hot solution was added pyridinium tribromide (1.5 g) under the conditions described above.

† *p*-Dioxane and bromine in equimolar ratio.

After 1/2 h crystals of 3-bromoflavanone separated, which were filtered, washed with water and recrystallized from ethanol to give white glistering leaflets (0.85 g) mp 127—128 °C (lit,[23] mp 127—128 °C). The dilution of the mother liquor gave (0.1 g) more of the product (IIb).
Found: C, 60.4; H, 4.3; Br, 25.1%. Calcd for $C_{16}H_{13}O_2Br$: C, 60.5; H, 4.1; Br, 25.23%.

trans-3-Bromo-4'-methoxy-6-methylflavanone (IIc). Flavanone (Ic; 1.3 g) was dissolved in glacial acetic acid (5 ml) by warming on water-bath. To the hot solution was added pyridinium tribromide (1.3 g) in small amounts. The reaction mixture was worked up as described for IIb. The solid thus obtained was crystallized from ethanol to afford white hexagonal plates (0.8 g) mp 141—142 °C (lit,[22] mp 138 °C).
Found: C, 58.6; H, 4.2; Br, 22.8%. Calcd for $C_{17}H_{15}O_3Br$: C, 58.7; H, 4.3; Br, 23.05%.

3-Bromo-3',4'-dimethoxy-6-methylflavanone (IId). Flavanone (Id, 1 g) was dissolved in glacial acetic acid (5 ml) by warming on water-bath. To the hot solution was added pyridinium tribromide (1 g) in small amounts. The reaction mixture was worked up as described for IIb. The solid thus obtained gave *cis*-3-bromo-3',4'-dimethoxy-6-methylflavanone as colourless plates (0.97 g), mp 158—159 °C (lit,[22] mp 155—156 °C) and *trans*-3-bromo-3',4'-dimethoxy-6-methylflavanone (0.21 g), mp 144—145 °C (lit,[22] mp 142—143 °C) from ethanol.
Found: C, 56.8; H, 4.4; Br, 21.6%. Calcd for $C_{18}H_{17}BrO_4$: C, 57.3; H, 4.5; Br, 21.2%.

Action of Thiourea on 3-Bromo-4'-methoxy-6-methylflavanone. A mixture of the bromoflavanone (1.7 g), thiourea (0.4 g) and ethanol (20 ml) was refluxed on water-bath for three hours. The reaction mixture was then allowed to cool to room temperature and poured into cold water. The solid thus separated was filtered and washed with water. Crystallization from ethanol afforded two products. The sparingly soluble compound on recrystallization from benzene gave yellow needles of free sulfur (0.1 g, mp 120 °C). The soluble product was found to be 4'-methoxy-6-methylflavanone (1.12 g), mp 109 °C (lit,[11] mp 108—109 °C). A mixed melting point determination with an authentic sample of flavanone showed no depression.

Action of Thiourea on 3-Bromoflavanone. A mixture of 3-bromoflavanone (1 g), thiourea (0.3 g), and ethanol (20 ml) was refluxed on water-bath for three hours. The reaction mixture was allowed to cool to room temperature and poured into cold water. The usual work up of the reaction mixture gave sulfur (0.04 g, mp 119—120 °C) and flavanone (0.62 g, mp 76 °C) (lit,[29] mp 76 °C). A mixture melting point determination with an authentic sample of flavanone showed no depression.

Action of Thiourea on 3-Bromo-6-methylflavanone. A mixture of the bromoflavanone (1.6 g), thiourea (0.5 g), and ethanol (20 ml) was refluxed on water-bath for three hours. The reaction products were worked up as usual to afford yellow needles of sulfur (0.12 g, mp 120 °C) and 6-methylflavanone (0.95 g), mp 104—105 °C (lit,[30] mp 105 °C). No depression was observed when a mixture melting point determination with an authentic sample was carried out.

Action of thiourea on 3-Bromo-3',4'-dimethoxy-6-methylflavanone. A mixture of the bromoflavanone (0.6 g), thiourea (0.3 g) and ethanol (20 ml) was refluxed on water-bath for three hours. The reaction product when worked up as described above gave sulfur (0.05 g, mp 120 °C) and 3',4'-dimethoxy-6-methylflavanone (0.34 g), mp 108 °C (lit,[11] mp 108—109 °C). The identity of flavanone was further confirmed by mixture melting point determination with an authentic sample.

Authors are thankful to Prof. M. M. Bokadia for providing laboratory facilities and to U. G. C. (New Delhi) for the award of Junior Research Fellowship to (N. J. Reddy).

References

1) C. Djerassi and C. R. Scholz, *J. Am. Chem. Soc.*, **70**, 417 (1948).
2) A. Marquet and J. Jacques, *Bull. Soc. Chim. Fr.*, **1962**, 90.
3) W. S. Johnson, J. D. Bass, and K. L. Williamson, *Tetrahedron*, **19**, 861 (1963).
4) D. V. Awang and S. Wolfe, *Can. J. Chem.*, **47**, 706 (1969).
5) V. W. Armstrong, N. H. Chishti, and R. Ramage, *Tetrahedron Lett.*, **6**, 373 (1974).
6) M. Sekiya, K. Ito, and K. Suzuki, *Tetrahedron*, **31**, 231 (1975).
7) St. V. Kostanecki, R. Levi, and J. Tambor, *Ber.*, **32**, 326 (1899).
8) G. Zemplen and R. Bognar, *Ber.*, **76**, 452 (1943).
9) C. G. Joshi and A. B. Kulkarni, *Chem. Ind. (London)*, **1956**, 124.
10) R. Bognar, M. Rakosi, G. Litker, and K. Lajos, *Magy. Kem. Foly*, **68**, 305 (1962).
11) J. W. Clark-Lewis, L. M. Jackman, and L. R. Williams, *J. Chem. Soc.*, **1962**, 3858.
12) L. Reichel and F. G. Weber, *Z. Chem.*, **6**, 233 (1966).
13) D. Brule and C. Mentzer, *C. R. Acad. Sci.*, **250**, 365 (1960).
14) K. R. Chandorkar, D. W. Pathak, and A. B. Kulkarni, *J. Scient. Ind. Res. (India)*, **21B**, 24 (1962).
15) M. Suzuki, *Nippon Kagaku Zasshi*, **82**, 885 (1962).
16) Chin-Techang, *Formosan Sci.*, **16**, 127 (1962).
17) H. K. Pendse and S. D. Limaye, *Rasayanam*, **2**, 90 (1953).
18) H. K. Pendse, *Rasayanam*, **2**, 731 (1956).
19) T. R. Seshadri and N. R. Banerjee, *Proc. Indian Acad. Sci., Sect. A*, **36**, 134 (1952).
20) K. R. Kutumbe and M. G. Marathey, *Chem. Ber.*, **96**, 913 (1963).
21) K. B. Doifode, *J. Org. Chem.*, **27**, 2665 (1962).
22) J. W. Clark-Lewis, T. McL. Spotswood, and L. R. Williams, *Aust. J. Chem.*, **16**, 107 (1963).
23) L. Reichel and F. G. Weber, *Z. Chem.*, **7**, 62 (1967).
24) L. Traumann, *Justus Liebigs Ann. Chem.*, **249**, 35 (1888).
25) M. Kopp, *Bull. Soc. Chim. Fr.*, **1950**, 582.
26) H. Erlenmeyer and W. Schoenauer, *Helv. Chim. Acta*, **24**, 172 (1941).
27) H. Patel, T. C. Sharma, and M. M. Bokadia, *Indian J. Chem.*, **8**, 376 (1970).
28) T. C. Sharma and M. M. Bokadia, *Indian J. Chem.*, **14B**, 66 (1976).
29) K. Freudenberg and L. Orthner, *Chem. Ber.*, **55**, 1748 (1922).
30) O. Dann and G. Mylius, *Ann.*, **587**, 1 (1964).

NMR Studies on Molecular Interactions Involved in Alkali Metal Halide–Amide–Glycol Ternary Systems

Naoru HAMAGUCHI, Terumichi NAKAGAWA,* and Toyozo UNO
Faculty of Pharmaceutical Sciences, Kyoto University, Sakyo-ku, Kyoto 606

(Received March 16, 1978)

Interactions in a ternary solution of alkali metal halide–amide–glycol have been investigated on the basis of NMR measurement of chemical shifts of OH proton of glycol and amidic protons of acetamide. Measurements were carried out with various alkali metal halides (MX, M=Li, Na, K, X=Cl, Br, I) and glycols (mono-, di-, tri-, and tetraethylene glycol). The dependency of the chemical shifts on solute concentration was examined with a ternary solution of potassium iodide–acetamide–ethylene glycol. The addition of alkali metal halide to respective glycols or glycolic solutions of acetamide gave rise to a change in chemical shift values. The observed changes were related to the ionic sizes of cations and anions of alkali metal halides and to the number of oxyethylene units in a glycol molecule. It was found that a large ion induces a higher magnetic field shift of resonance positions of glycolic OH proton and amidic proton at trans position than a small ion, the magnitude of the shift change being almost proportional to the concentration of ion, and halogen anion formed in glycolic solution tending to interact with hydrogen at trans position rather than at cis position. From a comparison with the values for chemical shifts of water proton in aqueous alkali metal halide solution, it is suggested that the contribution of alkali metal halide to the chemical shift changes in glycolic solution is similar to those in aqueous solution.

Some aliphatic amides interact with various inorganic salts to form stable complexes. Investigations have been made on their isolation,[1] X-ray analysis,[2,3] electric conductivity,[4–7] heat of solution,[8–14] and infrared spectra.[15] In the preceeding paper,[16] we reported that a similar interaction takes place also in gas-chromatographic stationary phase and is applicable to the specific separation of amides. The interaction between acetamide and lithium iodide in polyethylene glycol (PEG) is as strong as −2.5 kcal/mol of partial molar free energy of transfer from PEG to LiI-containing PEG, which is large enough to attain specific retardation of acetamide elution. It is difficult, however, to consider the structural aspects of the interaction from gas-chromatographic findings.

NMR spectroscopy has been extensively used for the study of aqueous electrolyte and non-electrolyte solutions. Shoolery and Alder[17] discussed the chemical shift of water proton in aqueous diamagnetic salt solution. Fabricand and Goldberg[18] investigated the relationship between proton resonance position and the ionic charge, radius, and concentration of alkali metal halide in aqueous solution, and Hinton and Ladner[19] the structure of a series of amides in aqueous solution. Sunners *et al.*[20] found the non-equivalence of two amide protons of formamide owing to the energy barrier hindering C–N bond rotation. The non-equivalence of two amide protons was also observed when the bromide ion was added to acetonitrile solution of formamide.[21] Hindman[22] studied the effect of the change in concentrations of salts of diamagnetic ions on the chemical shift of water proton. It is known from NMR measurements of ethylene proton of polyethylene glycol (PEG) that PEG associates with potassium iodide in methanol solution to behave as a polyelectrolyte. This phenomenon has been ascribed to ion-dipole interaction between potassium cation[23,24] (or, iodide anion[25]) and etherate oxygen of PEG. No paper seems to have described NMR studies on glycol solution of acetamide and/or alkali metal halide.

In connection with our gas-chromatographic studies on alkali metal halide–amide interaction in PEG stationary phase, we have attempted to consider the interaction from the NMR data of the ternary solution and to compare the results with those obtained in aqueous solution.

Experimental

A Varian A-60 NMR spectrometer operating at 60 MHz and 33.7±1.0 °C was used. Since the chemical shift of glycolic methylene proton determined by use of TMS as an internal standard is independent of addition of alkali metal halide and acetamide, it was used as a standard signal for the chemical shifts of glycolic OH proton and amidic protons.

Ethylene glycol(EG) and triethylene glycol(triEG)(Wako Pure Chemical Industry, Osaka, Japan), diethylene glycol (diEG)(Nakarai Chemicals, Kyoto, Japan), and tetraethylene glycol(tetraEG) (Tokyo Kasei Kogyo, Tokyo, Japan) were dried with sodium metal or anhydrous sodium sulfate and purified by double distillation under a reduced pressure with dry nitrogen gas bubbling. The gas-chromatographic analysis of the distilled glycols on Tenax GC column indicated no impurity peaks within the full scale recorder response of the main peak. The purity of acetamide(AA) (Wako Pure Chemical Industry) was also checked by GC using PEG 20 M column, showing a single clear peak. Alkali metal halides of reagent grade were completely dried over phosphorus pentoxide before use.

Results

The chemical shift change, $\Delta\sigma(-\Delta\delta)$, was calculated by

$$\Delta\sigma = -(\delta-\delta_0), \quad (1)$$

where δ and δ_0 are the chemical shifts(ppm) of protons in sample solution and in reference solution, respectively. Pure glycol and a solution of AA/glycol=1/9 by mole ratio were used as a reference for the measurements of the chemical shift changes of glycolic OH proton($\Delta\sigma_{OH}$) and of trans and cis (geometrical position to amide oxygen) amide protons ($\Delta\sigma_{NH,t}$, $\Delta\sigma_{NH,c}$),

TABLE 1. CHEMICAL SHIFTS AND SHIFT CHANGES OF GLYCOLIC OH PROTON AND *trans* AND *cis* AMIDE PROTONS WITH VARYING CONCENTRATIONS OF KI AND AA IN ETHYLENE GLYCOL

m_{KI}	m_{AA}	X_{KI}	X_{AA}	δ_{OH}	$\delta_{NH,c}$	$\delta_{NH,t}$	$\Delta\sigma_{OH}$	$\Delta\sigma_{NH,c}$	$\Delta\sigma_{NH,t}$
0.00	0.00	0.000	0.000	5.20	—	—	0.00	—	—
0.41	0.00	0.025	0.000	5.07	—	—	0.13	—	—
0.00	0.41	0.000	0.025	5.20	6.92	7.59	0.00	0.02	0.00
0.85	0.00	0.050	0.000	4.94	—	—	0.26	—	—
0.42	0.42	0.025	0.025	5.07	6.89	7.55	0.13	0.05	0.04
0.00	0.85	0.000	0.050	5.19	6.94	7.58	0.01	0.00	0.01
1.79	0.00	0.100	0.000	4.68	—	—	0.52	—	—
1.34	0.45	0.075	0.025	4.82	6.82	7.48	0.38	0.12	0.11
0.90	0.90	0.050	0.050	4.94	6.88	7.51	0.26	0.06	0.08
0.45	1.34	0.025	0.075	5.07	6.91	7.57	0.13	0.03	0.02
0.00	1.79	0.000	0.100	5.20	6.94	7.59	0.00	0.00	0.00
2.84	0.00	0.150	0.000	4.45	—	—	0.75	—	—
2.13	0.71	0.113	0.038	4.63	6.77	7.37	0.57	0.17	0.22
1.42	1.42	0.075	0.075	4.82	6.81	7.44	0.38	0.13	0.15
0.71	2.13	0.038	0.113	5.01	6.87	7.51	0.19	0.07	0.08
0.00	2.84	0.000	0.150	5.19	6.94	7.58	0.01	0.00	0.01
4.03	0.00	0.200	0.000			insoluble			
3.02	1.01	0.150	0.050	4.44	6.72	7.29	0.76	0.22	0.30
2.01	2.01	0.100	0.100	4.69	6.79	7.40	0.51	0.15	0.19
1.01	3.02	0.050	0.150	4.94	6.88	7.49	0.26	0.06	0.10
0.00	4.03	0.000	0.200	5.18	6.94	7.57	0.02	0.00	0.02

m; molality(mol/kg EG), X; mole fraction, δ; chemical shift(ppm), $\Delta\sigma$; chemical shift change(ppm, defined by Eq. 1).

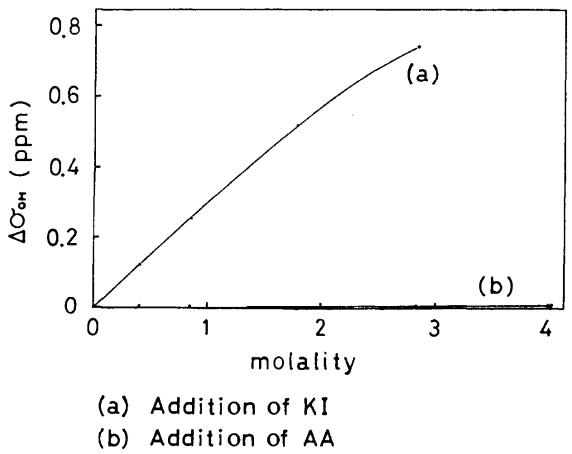

Fig. 1. Relationship between chemical shift change of glycolic OH proton and molality of KI or acetamide in ethylene glycol solution.

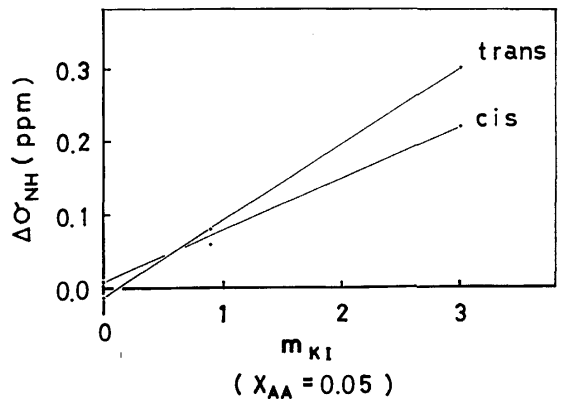

Fig. 2. Relationship between chemical shift changes of trans and cis amide protons and molality of KI at a fixed mole fraction of acetamide (X_{AA}=0.05) in ethylene glycol solution.

respectively. The results obtained in KI–EG and AA–EG binary solutions and in KI–AA–EG ternary solution, where mole fractions of KI(X_{KI}) and AA(X_{AA}) are varied from 0 to 0.2 and from 0 to 0.15, respectively, are given in Table 1. The addition of KI to EG (Fig. 1) gave rise to a high field shift of glycolic OH proton resonance position ($\Delta\sigma_{OH}>0$) proportional to the increase in its molality, whereas the addition of AA had little effect on $\Delta\sigma_{OH}$. In an aqueous solution, a linear relationship between salt concentration and $\Delta\sigma_{OH}$ of water proton was found by Fabricand and Goldberg,[18] the relationship deviating from the linearity in relatively high salt concentration range. The deviation was attributed to the shielding effect of more than one ions on a water proton. Such an effect was not clearly observed in the present case. The interstitial effect,[19] which leads to low field shift of water proton resonance position in dilute aqueous amide solution indicating the stabilization of water structure, was not observed in EG solution. The results for chemical shifts and shift changes of trans and cis amide protons with change in the concentration of KI, are also given in Table 1. It was found that two amide protons of AA give distinct resonance positions ($\delta_{NH,t}>\delta_{NH,c}$), suggesting their non-equivalence. The relationship between $\Delta\sigma_{NH,t}$ or $\Delta\sigma_{NH,c}$ and molality of KI (m_{KI}) is shown in Fig. 2 where X_{AA} is fixed at 0.05. The increasing molality of KI produces almost linear increase in both $\Delta\sigma_{NH,t}$ and

TABLE 2. THE OPTIMUM COEFFICIENTS FOR THE EQUATION, $\Delta\sigma = A \cdot m_{KI} + B \cdot m_{AA} + C$

$\Delta\sigma$		A	B	C	r_{KI}[a]	r_{AA}[a]	n[b]
$\Delta\sigma_{OH}$	EG	0.26	−0.01	0.02	0.998	−0.381	20
	diEG	0.29	−0.03	0.00	0.999	−0.893	19
	triEG	0.17	−0.08	−0.01	0.989	−0.953	19
	tetraEG	0.14	−0.10	−0.01	0.961	−0.928	21
$\Delta\sigma_{NH,t}$	EG	0.10	0.01	−0.01	0.994	0.534	15
	diEG	0.06	0.00	−0.01	0.954	−0.263	14
	triEG	0.01	−0.01	0.01	0.339	−0.317	14
	tetraEG	−0.05	−0.05	0.02	−0.755	−0.755	16
$\Delta\sigma_{NH,c}$	EG	0.07	−0.01	0.02	0.987	−0.483	15
	diEG	0.05	−0.03	0.02	0.961	−0.882	14
	triEG	0.04	−0.03	0.03	0.851	−0.807	14
	tetraEG	0.05	−0.07	0.04	0.729	−0.877	16

a) Partial correlation coefficient. b) Number of trials.

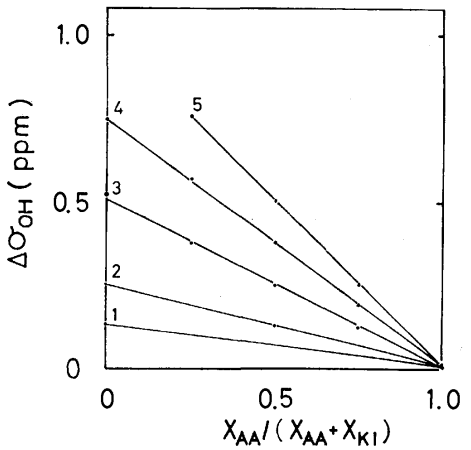

Fig. 3. Relationship between chemical shift change of glycolic OH proton and mole fraction of acetamide with varying total mole fraction of KI and acetamide in ethylene glycol solution (1; $X_{KI}+X_{AA}=0.025$, 2; 0.05, 3; 0.1, 4; 0.15, and 5; 0.2).

$\Delta\sigma_{NH,c}$, the magnitude of increase in $\Delta\sigma_{NH,t}$ being larger than that in $\Delta\sigma_{NH,c}$.

Linear relationship also holds between $\Delta\sigma_{OH}$ and mole fraction of KI (or AA) with change in total mole fraction of KI and AA in KI–AA–EG ternary solution (Fig. 3). This suggests that the contribution of KI and AA to $\Delta\sigma_{OH}$ can be expressed by a linear combination of respective molalities in the form

$$\Delta\sigma_{OH} = A\,m_{KI} + B\,m_{AA} + C, \qquad (2)$$

where the coefficients A and B represent the degree of contribution and C is the intercept. The optimum values for the coefficients were estimated by means of the least squares method using the data given in Table 1. The resulting equation is given in Table 2 along with those for $\Delta\sigma_{NH}$ in the same solution. The value for A coefficient (0.26) is almost equal to the slope of the line(a) in Fig. 1 and is far larger than coefficient B. This means that KI exerts a predominant effect on $\Delta\sigma_{OH}$ and the contribution of AA is as small as that of the intercept which should essentially be zero. With $\Delta\sigma_{NH}$, the trans amide proton seems to be more affected by the addition of KI than the cis proton.

$\Delta\sigma_{OH}$ values for four glycols added with various alkali metal halides at a mole ratio of MX/glycol=1/9 are given in Table 3. The addition of alkali metal halide except lithium chloride to EG produces high field shift of glycolic OH proton. A certain relationship seems to hold between the magnitude of the shift change and the ionic size. Thus, on the assumption that the surface charge of ion is involved in the electrostatic interaction, the squared reciprocals of ionic radii (r_c^{-2}) of anions and cations of alkali metal halides added are plotted against $\Delta\sigma_{OH}$ in EG solution (Fig. 4). It was found that the increasing r_c^{-2} of halogen anion having a cation in common is proportional to the decrease in $\Delta\sigma_{OH}$. The relationship between $\Delta\sigma_{OH}$ and cationic size indicates that the larger cation causes the more positive shift change in resonance position of glycolic OH proton (Fig. 4). However, the effect, as a whole, is smaller than that of anions; the size effect of anion on $\Delta\sigma_{OH}$ is greater than that of cation. It is of interest to compare such behavior of ions in glycolic solution with that in aqueous solution. The contribution of individual ion to $\Delta\sigma_{OH}$ of water proton in aqueous alkali metal halide solution is shown in Fig. 5. A strong resemblance is found between Figs.

TABLE 3. CHEMICAL SHIFT CHANGE OF GLYCOLIC OH PROTON OF MONO-, DI-, TRI-, AND TETRAETHYLENE GLYCOL IN THE PRESENCE OF VARIOUS ALKALI METAL HALIDES AT MOLE RATIO OF MX/GLYCOL=1/9

Salt	$\Delta\sigma_{OH}$(ppm)			
	EG	diEG	triEG	tetraEG
LiCl	−0.02	−0.15[a]	−0.24	−0.26
LiBr	0.10	−0.02	−0.14	−0.16
LiI	0.26	0.08	−0.08	−0.08
NaCl	0.19[a]	0.04[a]	−0.16[a]	−0.17[a]
NaBr	0.34	0.13	−0.04[a]	−0.04[a]
NaI	0.47	0.26	0.09	0.05
KCl	0.20[b]	0.13[b]	−0.09[a]	−0.14[a]
KBr	0.37[a]	0.17[a]	0.01[a]	−0.02
KI	0.52	0.30	0.13	0.07

a) Calculated from twice the $\Delta\sigma_{OH}$ value obtained from a solution of MX/glycol=1/19 by mole ratio. b) Calculated from four times the $\Delta\sigma_{OH}$ value obtained from a solution of MX/glycol=1/39 by mole ratio.

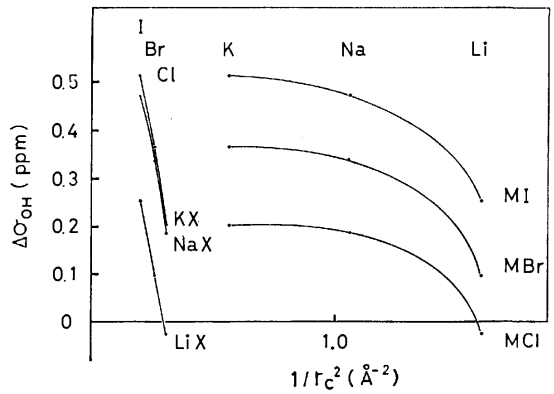

Fig. 4. Ionic size effect on the chemical shift change of glycolic OH proton in a solution of MX/EG=1/9 by mole ratio.

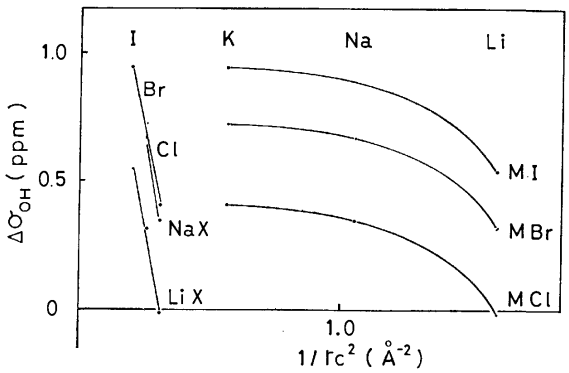

Fig. 5. Ionic size effect on the chemical shift change of water proton in a solution of MX/H_2O=1/9 by mole ratio. The data were obtained from Ref. 18 and corrected with respect to salt susceptibilities[26] according to Wiedeman law.

4 and 5.

Figure 6 shows the relationship between $\Delta\sigma_{OH}$ measured in a solution of MX/AA/EG=1/1/18 by mole ratio and the ionic sizes of alkali metal halides. As compared with Fig. 4 where mole ratio is MX/EG=1/9, Fig. 6 indicates that the general profile of $\Delta\sigma_{OH}$ remains unchanged against the variation of molality of each component, whereas the magnitude of the shift change is about half of those in Fig. 4. This suggests the additive property of $\Delta\sigma_{OH}$ with respect to the concentration of alkali metal halide in relatively low concentration region, since AA has little contribution to $\Delta\sigma_{OH}$. Figure 7 shows the cases of $\Delta_{NH,t}$ and $\Delta\sigma_{NH,c}$; $\Delta\sigma_{NH,t}$ is obviously more dependent on the ionic sizes of alkali metal halides especially on anionic size than $\Delta\sigma_{NH,c}$, although both magnitudes are smaller than that of $\Delta\sigma_{OH}$.

The contribution of individual ions to the change in $\Delta\sigma$ values was evaluated by means of analysis of variance using the data given in Figs. 6 and 7. The presumed values for $\Delta\sigma_{OH}$ and $\Delta\sigma_{NH,t}$ given as a sum of respective ions are in agreement with the observed values. The variance ratios for $\Delta\sigma_{OH}$ and $\Delta\sigma_{NH,t}$ among cations and anions are larger than the value for a level of significance at 5% ($F_4^2(0.05)=6.94$), but the variance ratio of $\Delta\sigma_{NH,c}$ is too small to recognize

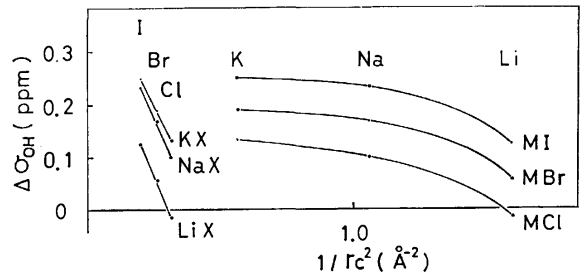

Fig. 6. Ionic size effect on the chemical shift change of glycolic OH proton in a solution of MX/AA/EG=1/1/18 by mole ratio.

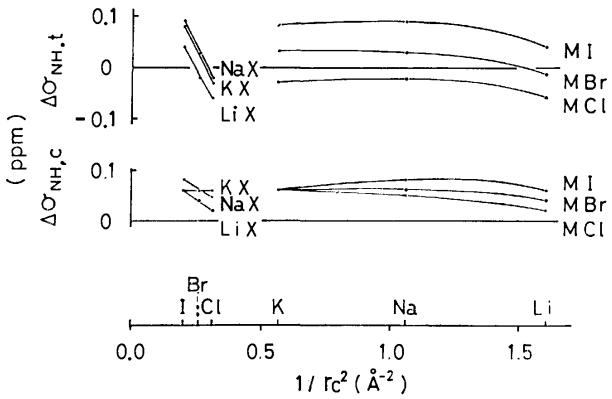

Fig. 7. Ionic size effect on the chemical shift change of amide protons in a solution of MX/AA/EG=1/1/18 by mole ratio.

significant difference. The results seem to support the idea of ionic dissociation of alkali metal halide in glycolic solution.

Experiments were also carried out for higher glycolic solutions (di-, tri-, and tetraEG). It was observed that the increase in the number of oxyethylene units in a glycol molecule is accompanied by a high field shift of OH proton resonance position of pure glycol (EG; δ=5.20, diEG; δ=4.95, triEG; δ=4.50, and tetraEG; δ=4.31). Figure 8 gives the plots of chemical shifts (δ) of glycolic OH and amide protons *vs.* mole fraction of AA (or KI) ($X_{AA}+X_{KI}=0.1$) in di, tri, and tetraEG solutions, showing the linear relationships between δ and X_{AA} (or X_{KI}) in each glycolic solution. It was found that the increase in the oxyethylene unit number is accompanied by high field shifts (decrease in δ value) of all the proton resonance positions, with which the slope, δ/X_{AA}, becomes small. As for the amide protons, the resonance positions are less dependent on the variation in X_{AA} (or X_{KI}) than that of glycolic OH proton.

The chemical shift changes ($\Delta\sigma_{OH}$, $\Delta\sigma_{NH,t}$, and $\Delta\sigma_{NH,c}$) in di-, tri-, and tetraEG solutions are expressed as functions of m_{KI} and m_{AA} as in Eq. 2 according to the method of least squares. The resulting equations, given in Table 2, indicate that $\Delta\sigma_{OH}$ receives a positive contribution($A>0$) from m_{KI} in all the glycolic solutions and a negative contribution($B<0$) from m_{AA} in di-, tri-, and tetraEG solutions. With amide protons, the A coefficient for $\Delta\sigma_{NH,t}$ decreases with increase in the number of oxyethylene units, becoming

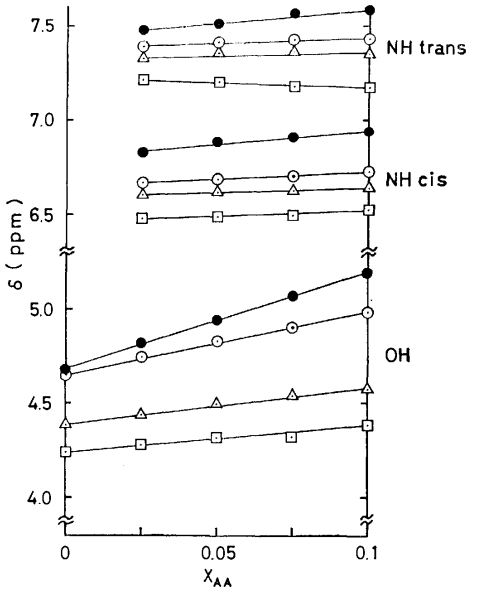

Fig. 8. Relationship between chemical shifts of glycolic OH and amide protons and mole fraction of KI (or AA) with varying oxyethylene unit number in glycol molecule. ($X_{AA}+X_{KI}=0.1$) ●; EG, ⊙; diEG, ◬; triEG, and ⊡; tetraEG.

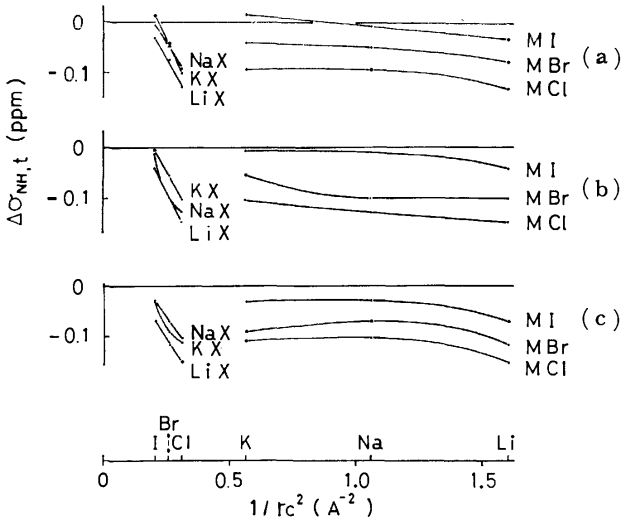

Fig. 9. Ionic size effect on the chemical shift change of trans amide proton in a solution of MX/AA/glycol= 1/1/18 by mole ratio (a; diEG, b; triEG, c; tetraEG).

negative in tetraEG solution. No such explicit change is observed in $\Delta\sigma_{NH,c}$.

The change in OH proton resonance positions of mono to tetraEG (*i.e.*, $\Delta\sigma_{OH}$) decreases with the increase in the number of oxyethylene unit in a glycol molecule with different rate among alkali metal halides added (Table 3). The tendency is almost unchanged irrespective of the addition of AA to alkali metal halide–glycol binary system. In a ternary solution consisting of MX/AA/glycol=1/1/18 by mole ratio, the variation in alkali metal halide causes a more significant difference in $\Delta\sigma_{OH}$ and $\Delta\sigma_{NH,t}$ values than in $\Delta\sigma_{NH,c}$ values in each glycol solution. This suggests that the contribution of alkali metal halide to $\Delta\sigma_{OH}$ and $\Delta\sigma_{NH,t}$ may be delivered to the individual ions. The results thus obtained by means of analysis of variance prove that the larger the anionic size, the larger the $\Delta\sigma$ values. The general profile of ionic size effect on $\Delta\sigma_{OH}$ in di-, tri-, and tetraEG solutions are similar to those in EG solution (Fig. 6). However, the magnitude of $\Delta\sigma_{OH}$ decreases with the increase in the oxyethylene unit number. A similar trend was observed in the relationship between ionic size and $\Delta\sigma_{NH,t}$ in di-, tri-, and tetraEG solutions. The difference in molecular weight of glycol produces almost no change in the ionic size effect on $\Delta\sigma_{NH,t}$ (Fig. 9). In all the glycolic solutions, the increase in anionic size gives rise to more increase in $\Delta\sigma_{NH,t}$ than in $\Delta\sigma_{NH,c}$. The $\Delta\sigma_{NH,t}$ value, however, is negative in higher glycolic solutions.

Discussion

Let us first consider the effects which might cause the change in the resonance position of glycolic OH proton. If acetamide is added to glycol, it may affect the hydrogen bondings of glycol. Since acetamide is a non-electrolyte, glycolic OH proton resonance position may be dominated by the change in the hydrogen bondings. Thus, it is assumed that a high field shift of OH proton resonance position ($\Delta\sigma_{OH}>0$) indicates a decrease in hydrogen bondings in the system. The results (Table 1 and Fig. 1) in which little increase in $\Delta\sigma_{OH}$ accompanies the addition of acetamide to ethylene glycol over the concentration range examined, suggest that the AA–EG hydrogen bond may be as strong as the EG–EG hydrogen bond. The addition of alakli metal halide to glycol, on the other hand, produces a different situation, since dissolution of alkali metal halide in glycol is accompanied by ionic dissociation. Approaching glycol molecule, the ions can interact with dipole of glycol molecule, inducing polarization of OH group, decreasing electronic shielding of OH proton to result in an apparent low field shift of OH resonance position. Thus, the observed value for the chemical shift (δ_{OH}) can be expressed as a function of the electrostatic interaction in addition to the effect on hydrogen bondings. A similar but more detailed consideration has been made with respect to water proton resonance position in aqueous electrolyte solution, the salt-effect on water structure being discussed.[22] Some physico-chemical properties of glycol (*i.e.* heat of vaporization, boiling point, and viscosity)[27] suggest that glycol as well as water may have a certain structure due to hydrogen bondings, although there is no explicit evidence. In this connection, it is interesting to note that the strong resemblance found between Figs. 4 and 5 may give a clue for understanding the behavior of ion in glycol solution.

A linear increase in $\Delta\sigma_{OH}$ with increasing KI concentration (Fig. 1) suggests that EG–EG hydrogen bondings may be decreased by the addition of KI. The results given in Table 3 and Fig. 4 indicate that, as compared with a large anion, a small anion (with large surface charge) induces more decrease in the electronic shielding of glycolic OH proton to give a smaller $\Delta\sigma_{OH}$ value.

Amidic protons at the trans and cis positions of acetamide are also involved in hydrogen bonding with glycol molecule. The addition of alkali metal halide, therefore, may have an influence on amide protons as well. The results shown in Figs. 2 and 7 may be interpreted as follows: When alkali metal halide is dissolved in an EG solution of acetamide, the ions formed give rise to apparent decrease in hydrogen bondings of amidic protons to result in high field shifts ($\Delta\sigma_{NH}>0$), halogen anion tending to interact with amide at trans position rather than at cis position.

From the results in Tables 2 and 3 and Fig. 8, it seems that the increase in the number of oxyethylene units in a glycol molecule is accompanied by enhancement of electrostatic interaction of alkali metal halide with acetamide. Such effect may be responsible for the specific retention of amide on an alkali metal halide-containing PEG as a gas-chromatographic stationary phase.

References

1) A. W. Titherley, *J. Chem. Soc.*, **79**, 413 (1901).
2) P. Piret, L. Rodrique, Y. Gobillon, and M. Van Meerssche, *Acta Crystallogr.*, **20**, 482 (1966).
3) J. P. Roux and J. C. A. Boeyens, *Acta Crystallogr., Sect. B*, **25**, 1700 (1969).
4) L. R. Dawson, T. M. Newell, and W. J. MacCreary, *J. Am. Chem. Soc.*, **76**, 6024 (1954).
5) L. R. Dawson, P. G. Sears, and R. H. Graves, *J. Am. Chem. Soc.*, **77**, 1986 (1955).
6) C. M. French and K. H. Glover, *Trans. Faraday Soc.*, **51**, 1427 (1955).
7) L. R. Dawson, E. D. Wilhoit, R. R. Holms, and P. G. Sears, *J. Am. Chem. Soc.*, **79**, 3004 (1957).
8) R. P. Held and C. M. Criss, *J. Phys. Chem.*, **69**, 2166 (1965).
9) L. Weeda and G. Somsen, *Recl. Trav. Chim. Pays-Bas*, **85**, 159 (1966).
10) G. Somsen, *Recl. Trav. Chim. Pays-Bas*, **85**, 517 (1966).
11) G. Somsen, *Recl. Trav. Chim. Pays-Bas*, **85**, 526 (1966).
12) L. Weeda and G. Somsen, *Recl. Trav. Chim. Pays-Bas*, **86**, 263 (1967).
13) L. Weeda and G. Somsen, *Recl. Trav. Chim. Pays-Bas*, **86**, 893 (1967).
14) R. P. Held and C. M. Criss, *J. Phys. Chem.*, **71**, 2487 (1967).
15) T. Uno, K. Machida, and I. Hamanaka, *Bull. Chem. Soc. Jpn.*, **34**, 1448(1961).
16) N. Hamaguchi, T. Nakagawa, and T. Uno, *J. Chromatogr.*, **147**, 151 (1978).
17) J. N. Shoolery and B. J. Alder, *J. Chem. Phys.*, **23**, 805 (1955).
18) B. P. Fabricand and S. Goldberg, *J. Chem. Phys.*, **34**, 1624 (1961).
19) J. F. Hinton and K. H. Ladner, *J. Magn. Reson.*, **6**, 586 (1972).
20) B. Sunners, L. H. Piette, and W. G. Schneider, *Can. J. Chem.*, **38**, 681 (1960).
21) R. D. Green, *Can. J. Chem.*, **47**, 2407 (1969).
22) J. C. Hindman, *J. Chem. Phys.*, **36**, 1000 (1962).
23) R. D. Lundberg, F. E. Bailey, and R. W. Callard, *J. Polym. Sci., Part A-1*, **4**, 1563 (1966).
24) Kang-Jen Liu, *Macromolecules*, **1**, 308 (1968).
25) Kang-Jen Liu and J. E. Anderson, *Macromolecules*, **2**. 235 (1969).
26) W. R. Meyers, *Rev. Modern Phys.*, **24**, 15 (1952).
27) J. A. Riddick and W. B. Bunger, "Organic Solvents," 3rd ed, Wiley-Interscience, New York (1970).

Ultrasonic Properties of Aqueous Solutions of Butylamines

Sadakatsu NISHIKAWA* and Mitsuo MASHIMA

Department of Chemistry, Faculty of Science and Engineering, Saga University, Saga 840

(Received April 27, 1978)

Ultrasonic absorption and velocity measurements were performed in aqueous solutions of *t*-butylamine and isobutylamine at 20 °C. Two relaxational absorptions were found in both solutions. One is associated with the proton transfer reaction, the rate constants being determined together with the standard volume change of the reaction. No effect was observed on K_f with change in molecular structure. The other, associated with the peak sound absorption concentration, is ascribed to the association-dissociation reaction mechanism of unionized amine molecules. The results are discussed in comparison with those of butylamine.

Ultrasonic investigations for liquid properties provide useful information on kinetic behavior. Two kinds of relaxational processes exist in aqueous solutions of amines, depending upon the concentration and molecular structure.[1,2] One is due to the proton transfer reaction observed in relatively dilute solutions. The other is associated with the peak sound absorption concentration (PSAC). These processes have been treated independently because of the complexity of the interaction between fast and slow processes. A report was given on the ultrasonic absorption of aqueous solutions of some amines. This investigation was undertaken in order to clarify the ultrasonic properties of three butylamines with different molecular structures.

Experimental

Commercial *t*-butylamine and isobutylamine (G. R. grade, Wako Chemicals Industries, Ltd.) were distilled, the purity being confirmed to be higher than 99.9% by gas chromatography. The solutions were prepared with twice distilled water.

The ultrasonic absorption measurement was carried out at the odd harmonics of 0.5, 5, and 20 MHz x-cut quartz transducers by means of pulse technique in the frequency range 6.5—220 MHz, absorption coefficient being reproducible to within ±3%. The sound velocity was measured by a sing-around method operated at 1.92 MHz. The major mechanical features of the apparatus have been reported.[3] The cells for absorption and velocity measurement were immersed in a water bath maintained at a constant temperature within ±0.001 °C. All the measurements were carried out in a dry nitrogen gas atmosphere in order to prevent the contamination of air, since the aqueous solutions of amines are highly basic.

Results and Discussion

In general, the sound absorption caused by several relaxation processes can be expressed by

$$\alpha/f^2 = \sum_i A_i/[1+(f/f_{ri})^2] + B, \quad (1)$$

where α is the absorption coefficient, f frequency, A_i relaxation amplitude for the i-th process, f_{ri} relaxation frequency and B residual absorption amplitude. Figures 1 and 2 show the representative ultrasonic absorption spectra in aqueous solutions of *t*-butylamine and isobutylamine at 20 °C. In both solutions, only a single relaxtional absorption was observed in relatively dilute solutions (less than 0.9 mol dm^{-3}). However, with increasing concentration, the experimental

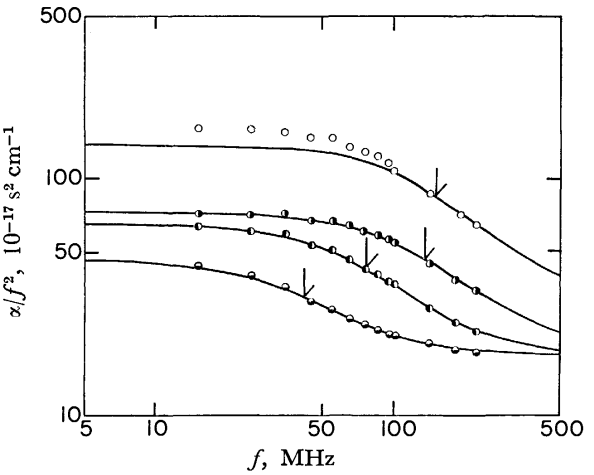

Fig. 1. Ultrasonic absorption spectra in aqueous solution of *t*-butylamine. The solid lines are the best-fit single relaxation curves and the arrows are the relaxation frequencies. ◒: 0.0154 mol dm^{-3}, ◐: 0.154 mol dm^{-3}, ◑: 0.787 mol dm^{-3}, ○: 1.69 mol dm^{-3}.

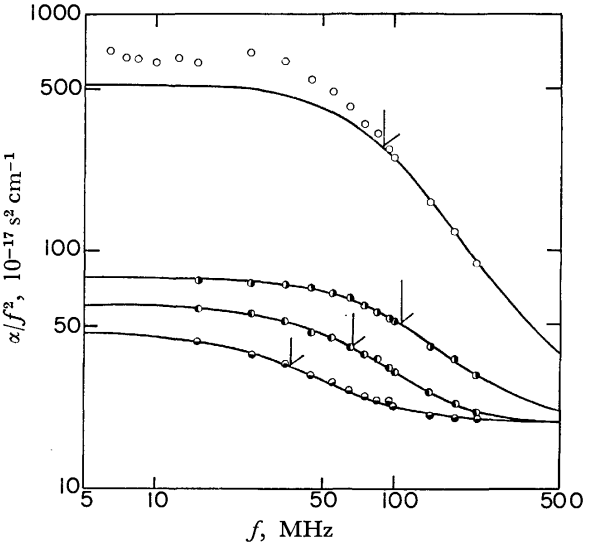

Fig. 2. Ultrasonic absorption spectra in aqueous solution of isobutylamine. ◒: 0.0447 mol dm^{-3}, ◐: 0.158 mol dm^{-3}, ◑: 0.801 mol dm^{-3}, ○: 1.81 mol dm^{-3}.

values of the absorption coefficients deviate from the single relaxational equation, *viz.*, another excess absorption appears in the same frequency range. In the case of the single relaxation process, the ultrasonic parameters, A, f, and B, were determined from the

Table 1. Ultrasonic parameters, density and pH in aqueous solutions of *t*-butylamine and isobutylamine

C_o (mol dm^{-3})	pH	ρ (g cm^{-3})	v (10^5 cm s^{-1})	A (10^{-17} s^2 cm^{-1})	B	f_r (MHz)
			[*t*-butylamine]			
0.0154	11.60	0.9982	1.4847	37	24	42
0.0386	11.76	0.9981	1.4860	55	24	45
0.0772	11.90	0.9970	1.4889	67	25	53
0.154	12.08	0.9962	1.4953	63	24	77
0.184	12.12	0.9962	1.4970	66	24	83
0.202	12.17	0.9955	1.4981	59	24	87
0.268	12.21	0.9946	1.5039	69	24	95
0.508	12.46	0.9917	1.5224	77	22	115
0.681	12.51	0.9883	1.5369	68	27	130
0.787	12.54	0.9868	1.5455	72	26	135
			[isobutylamine]			
0.0203	10.74	0.9982	1.4852	15	23	55
0.0447	11.23	0.9980	1.4870	37	25	37
0.0787	11.48	0.9976	1.4893	41	24	55
0.131	11.75	0.9968	1.4929	51	26	63
0.158	11.74	0.9966	1.4946	57	23	68
0.203	11.84	0.9959	1.4980	56	24	75
0.435	12.22	0.9931	1.5136	72	27	85
0.500	12.25	0.9916	1.5204	79	25	88
0.598	12.29	0.9911	1.5251	77	24	92
0.801	12.47	0.9879	1.5398	81	25	108
0.852	12.45	0.9875	1.5442	77	26	110

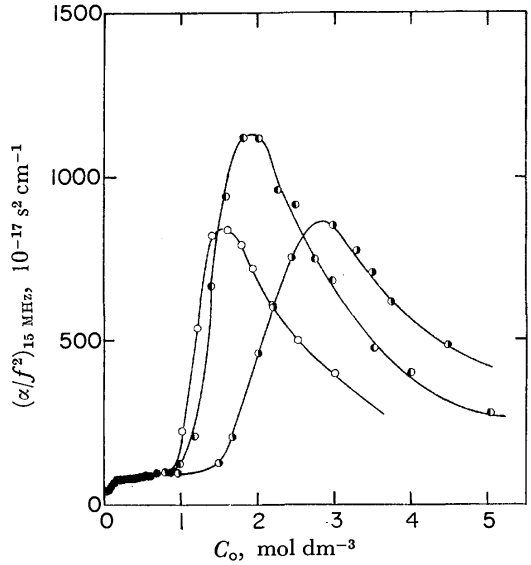

Fig. 3. Plots of α/f^2 *vs.* C_o of aqueous solutions of butylamines. ○: Butylamine, ◑: *t*-butylamine, ◐: isobutylamine.

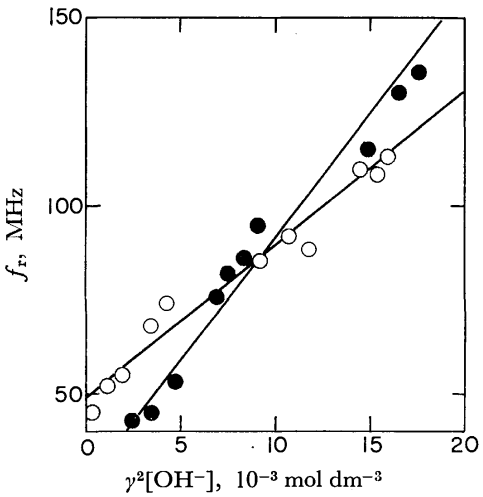

Fig. 4. Plots of f_r *vs.* γ^2[OH$^-$]. ●: *t*-Butylamine, ○: isobutylamine.

plots of α/f^2 *vs.* $[1+(f/f_r)^2]^{-1}$ so as to obtain a straight line. On the other hand, the ultrasonic parameters associates with more than one process are not easily determined because the two processes are close together. In Fig. 3 only the concentration dependence of α/f^2 at 15 MHz in the aqueous solutions is shown along with that of butylamine.[5] The most plausible mechanism of the excess absorption in the lower concentration range is the perturbation of the equilibrium associated with proton transfer[1,2,6,7] expressed by the formula

$$R\text{-}NH_3^+ + OH^- \underset{k_b}{\overset{k_f}{\rightleftharpoons}} R\text{-}NH_2 + H_2O. \quad (2)$$

The relaxation frequency for the above process can be related to the forward and backward rate constants, k_f and k_b, as repredented by

$$2\pi f_r = k_f\gamma^2([R\text{-}NH_3^+]+[OH^-]) + k_b, \quad (3)$$

$$= 2k_f\gamma^2[OH^-] + k_b, \quad (3')$$

where γ is the mean activity coefficient, which is assumed to be identical for $R\text{-}NH_3^+$ and OH^- ions,[8] and is calculated from the equation, $-\log\gamma=0.5[\sqrt{I}/(1+\sqrt{I})-0.3I]$ where I is the ionic strength. Equation 3 can be rewritten as follows, using the analytical

TABLE 2. RATE CONSTANTS AND STANDARD VOLUME CHANGE OF PROTON TRANSFER REACTION OF BUTYLAMINES

	k_f (mol dm^{-3} s^{-1})		k_b (s^{-1})			K_b (mol^{-1})	ΔV (cm^3 mol^{-1})	Ref.
	(a)	(b)	(a)	(b)	(c)			
Butylamine	4.1×10^{10}	2.5×10^{10}	1.4×10^{8}	1.1×10^{8}	1.1×10^{7}	4.44×10^{-4}	32	4
Isobutylamine	1.2×10^{10}	3.4×10^{10}	3.2×10^{8}	3.0×10^{8}	1.1×10^{7}	3.22×10^{-4}	29	This work
t-Butylamine	1.9×10^{10}	2.0×10^{10}	2.1×10^{8}	2.9×10^{8}	1.0×10^{7}	5.17×10^{-4}	24	This work

The values in column (a) were determined from the slope and intercept using Eq. 3, those in column (b) from Eq. 4, and the backward rate constants in column (c) were calculated using the dissociation constant.

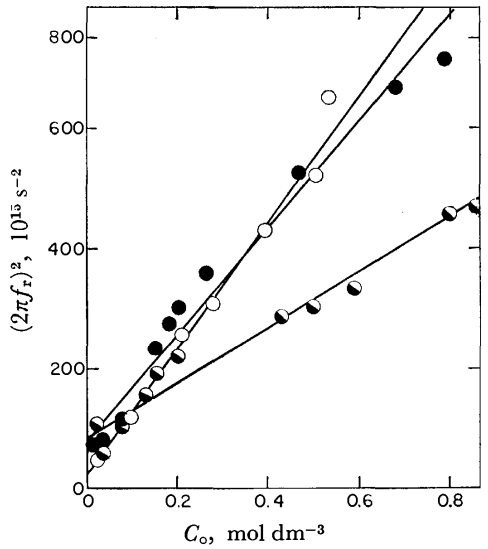

Fig. 5. Plots of $(2\pi f_r)^2$ *vs.* C_o. ○: Butylamine, ●: *t*-butylamine, ◒: isobutylamine.

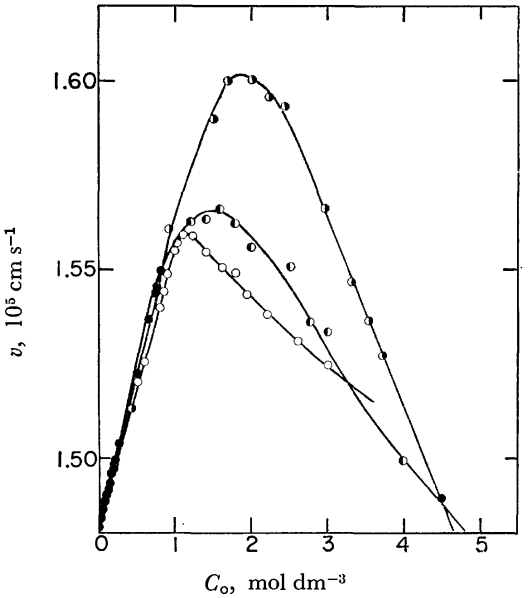

Fig. 6. Concentration dependence of the sound velocity. ○: Butylamine, ◑: *t*-butylamine, ◐: isobutylamine.

concentration, C_o, on the assumption that the activity coefficient is unity and only one equilibrium exists in the aqueous solution.

$$(2\pi f_r)^2 = 4k_f k_b C_o + k_b^2 \quad (4)$$

Figure 4 shows the plots of f_r *vs.* $\gamma^2[OH^-]$, the slope and intercept of which provide the rate constants. Figure 5 shows those of $(2\pi f_r)^2$ *vs.* C_o, from which the rate constants were also determined. In proton transfer investigations so far, the latter procedure of rate determination was carried out by means of the dissociation constants in the literature because of the uncertainty of the intercept. The forward rate constants are approximately the same in both determinations and reasonable values are obtained for the diffusion-controlled reaction. However, there are some questions in the latter determination of the backward rate constants for the following reasons. First, Eq. 4 is derived with numerous approximations. Second, the backward rate constant is determined from Eq. 4 without use of dissociation constant. However, ratio k_b/k_f is not in line with the dissociation constant even when the experimental error is taken into account. The cause of disagreement has been interpreted by the introduction of intermediate of Eq. 5.[2]

$$R\text{-}NH_3^+ + OH^- \rightleftharpoons R\text{-}NH_3^+\cdots OH^- \rightleftharpoons R\text{-}NH_2\cdots H_2O \rightleftharpoons R\text{-}NH_2 + H_2O \quad (5)$$

Actually, the rate constants, k_f and k_b, can be related by those of each steps of Eq. 5, assuming that the second and third steps equilibrate so rapidly or the stationary states are established. However, detailed discussions for each step of Eq. 5 from the rate constants obtained may not be appropriate at this stage since the rationalized mechanisms are too complicated.

The determination of the rate constants from Eq. 3, on the other hand, is a direct procedure even if the intermediate exists. The dissociation constants were calculated from the concentration dependence on pH and are very close those in the literature.[9] This means that the determination of the concentration of OH^- ion in the solutions is correct. The rate constants calculated from the above two methods (from Eqs. 3 and 4) are given in Table 2 along with the dissociation constants and the standard volume changes of the reaction which are determined from the maximum excess absorption per wavelength.[2] It can be concluded that the diffusion-controlled rate constants of butylamines may be independent of the molecular structures, *viz.*, the mobilities of butylamine molecules in aqueous solvent are approximately the same.

We consider next the absorptions which appear in the concentrated solutions of the amines. Figure 6 shows the concentration dependence of the sound velocity at 20 °C. The values of α/f^2 increase rapidly near the maximum of the sound velocity, reaching a maximum in all the solutions. The peak sound veloc-

ity concentration increases in the order, butylamine, isobutylamine and *t*-butylamine. The peak sound absorption concentration stands in the same order. We have proposed an association-dissociation reaction of unionized amine molecules as the cause of the excess absorption mechanism, since no peak sound absorption concentration is observed in aqueous solutions of amines with low hydrophobicity,[2] nor excess absorption in aqueous solution of the amine hydrochloride and in organic solvent.[1] In the cases of aqueous solutions of butylamine and pentylamine, the two relaxation processes could be treated independently since the two relaxation frequencies are far apart. However, in the aqueous solutions of *t*-butylamine and isobutylamine, the relaxation times are close to each other and can not be determined precisely. It is likely that the structure of liquid solution is altered by addition of solute molecules near the peak sound velocity concentration and the solute molecules with hydrophobicity aggregate in aqueous media. The hydrophobicity seems to be in the order of peak sound velocity concentration or peak sound absorption concentration. Williams *et al.*[10] reported the ultrasonic absorption data of various amines in the liquid phases and interpreted them in terms of conformational changes of molecules. However, no excess absorption has been observed in the pure liquids of amines. Thus, the absorption mechanism with conformational change has been ruled out from the cause of the excess absorption.

The authors wish to thank Professor Paul Hemmes, Rutgers University, for reading the manuscript and helpfull discussions.

References

1) S. Nishikawa, T. Yasunaga, and K. Takahashi, *Bull. Chem. Soc. Jpn.*, **46**, 2992 (1973).
2) S. Nishikawa, U. Otani, and M. Mashima, *Bull. Chem. Soc. Jpn.*, **50**, 1716 (1977).
3) N. Tatsumoto, *J. Chem. Phys.*, **47**, 4561 (1967).
4) S. Nishikawa, T. Nakamoto, and T. Yasunaga, *Bull. Chem. Soc. Jpn.*, **46**, 324 (1973).
5) S. Nishikawa and T. Yasunaga, *Bull. Chem. Soc. Jpn.*, **46**, 1098 (1973).
6) M. Eigen, G. Maas, and G. Schwarz, *Z. Phys. Chem. (Frankfurt am Main)*, **74**, 319 (1971).
7) G. Grimshaw and E. Wyn-Jones, *J. Chem. Soc., Faraday Trans. 2*, **69**, 168 (1973).
8) J. Kielland, *J. Am. Chem. Soc.*, **59**, 1675 (1937).
9) J. J. Christensen, R. M. Itatt, D. P. Wrathall, and L. D. Hansen, *J. Chem. Soc., B*, **1969**, 1212.
10) E. J. Williams, T. H. Thomas, E. Wyn-Jones, and W. J. Orville-Thomas, *J. Mol. Struct.*, **2**, 307 (1968).

Determination of Magnetic Susceptibilities of Paramagnetic Gases by an Improved Viscometer Method

Kazuo SUEOKA* and Toshio IKEDA†

Department of Chemistry, Johsai University, Sakado, Saitama 350-02

† *Department of Chemistry, Shizuoka University, Shizuoka 422*

(Received July 7, 1978)

An improved viscometer method has been applied to the determination of the magnetic susceptibility of a paramagnetic gas and found to be of use in the analysis of a paramagnetic gas mixed in a diamagnetic gas. The magnetic susceptibilities of oxygen and nitrogen monoxide have been determined to within ±0.5% using a saturated aqueous solution of sodium chloride as the working liquid.

The present authors reported an improved viscometer method[1] for the determination of the magnetic susceptibilities of diamagnetic liquids by measuring the time of flow of liquid under nitrogen through the capillary of a modified Ubbelohde type viscometer under an external magnetic field.

In the present study, some applications of the viscometer method will be described concerning the magnetic susceptibilities of paramagnetic gases and the analysis of paramagnetic species in a gaseous mixture, *e.g.*, oxygen in air.

Theoretical

A capillary viscometer cell of modified Ubbelohde type as shown in Fig. 1 was placed in a magnetic field so that the lower end of the capillary was in the center of the pole gap of an electromagnet, while the capillary extended vertically, through the inhomogeneous region, outside the field. The liquid in the capillary of the cell was forced to flow down by the dual action of the gravitational and magnetic forces acting on it and its enviromental gas which was in contact with the liquid and circulating in the dead space below the capillary.

Assuming a liquid of certain volume requires time t_H to flow through the capillary of the viscometer under action of an external magnetic field of strength, H, then it follows that

$$\frac{1}{t_H} = C\left[\rho_L g\tilde{h} + \frac{1}{2}(\kappa_L - \kappa_G)H^2\right], \tag{1}$$

where C is a constant determined by the geometry of the cell and the viscosity of the flowing liquid, g is the acceleration due to gravity, $\tilde{h}$ is the mean effective head of liquid, ρ_L is the density of the liquid, κ_L represents the volume magnetic susceptibility of the liquid phase (L) in equilibrium with the gas phase (G) whose susceptibility is κ_G, where the gas is supposed to dissolve in the liquid without chemical reaction (solbility β). In the absence of a field, $1/t_0 = C\rho_L g\tilde{h}$ which gives from Eq. 1:

$$\tau_G \equiv \left(\frac{t_0 - t_H}{t_H}\right)_G = \frac{H^2}{2g\tilde{h}\rho_L}(\kappa_L - \kappa_G), \tag{2}$$

where

$$\kappa_L = \kappa_L^\circ + \beta\kappa_G', \tag{3}$$

κ_L° is the volume magnetic susceptibility of the pure liquid and κ_G' that for the dissolved gas. Generally speaking, the gas considered may be mixture, the most simple case being the two component system consisting of, from the magnetic point of view, a diamagnetic (D) and a paramagnetic (P) species with respective volume fractions x_D and x_P. It is apparent that

$$x_D + x_P + x_V = 1, \tag{4}$$

where x_V is the volume fraction of the working liquid vapor with which the gases are in contact. Denoting by κ_D° and κ_P° the volume magnetic susceptibilities of the dia- and paramagnetic species respectively both in the gaseous pure states at a given temperature T and pressure P, the apparent susceptibility, κ_G, of a gas mixture may thus be written as follows:

$$\kappa_G = \kappa_D^\circ x_D + \kappa_P^\circ x_P + \kappa_V^\circ x_V, \tag{5}$$

where κ_V° denotes the susceptibility of the saturated vapor of the working liquid in the pure state at a given condition of T. Assuming the gas is in equilibrium in contact with the working liquid in the viscometer at constant temperature and pressure and denoting by β_D° and β_P° the solubilities of the two gaseous species D and P, in the pure states respectively, (under the same conditions of T and P) the solubility of a gaseous mixture composed of D and P in a certain liquid may be written as follows:

$$\beta = \beta_D^\circ x_D + \beta_P^\circ x_P. \tag{6}$$

Then, the volume fractions x_D' and x_P' of the two species (D and P) dissolved in the liquid may be expressed as follows:

$$x_D' \equiv \frac{\beta_D^\circ}{\beta}x_D, \qquad x_P' \equiv \frac{\beta_P^\circ}{\beta}x_P, \tag{7}$$

and

$$x_D' + x_P' = 1. \tag{8}$$

For the magnetic contribution, κ_G', from the gas dissolved in the liquid (L) assuming that the intermolecular interaction between the liquid and dissolved gas is not strong, in analogy to Eq. 5, it may be written as

$$\kappa_G' = \kappa_D^\circ x_D' + \kappa_P^\circ x_P'. \tag{9}$$

Converting the magnetic susceptibility of the i-th species, κ_i, per unit volume into that, χ_i, per unit mass by definition $\kappa_i \equiv \rho_i\chi_i$, and putting $\rho_L \fallingdotseq \rho_L^\circ$ (ρ_L° is the density of the pure liquid), Eq. 2 may be rewritten with the abbreviation $H^2/2g\tilde{h} \equiv K$:

$$\tau_G = K\left[\chi_L^\circ - \frac{\rho_D^\circ x_D}{\rho_L^\circ}(1-\beta_D^\circ)\chi_D^\circ - \frac{\rho_P^\circ x_P}{\rho_L^\circ}(1-\beta_P^\circ)\chi_P^\circ - \frac{\rho_V^\circ x_V}{\rho_L^\circ}\chi_V^\circ\right], \tag{10}$$

where ρ°_L, ρ°_P, and ρ°_V are the densities of the dia- and paramagnetic gases, D and P, and the vapor of the liquid in the pure states, respectively, at a given T and P. For the paramagnetic gas system ($x_P = 1-x_V$, $x_D=0$);

$$\tau_P = K\left[\chi^\circ_L - \frac{\rho^\circ_P(1-x_V)}{\rho^\circ_L}(1-\beta^\circ_P)\chi^\circ_P - \frac{\rho^\circ_V x_V}{\rho^\circ_L}\chi^\circ_V\right], \quad (11)$$

and for the diamagnetic gas system ($x_P=0$, $x_D=1-x_V$);

$$\tau_D = K\left[\chi^\circ_L - \frac{\rho^\circ_D(1-x_V)}{\rho^\circ_L}(1-\beta^\circ_D)\chi^\circ_D - \frac{\rho^\circ_V x_V}{\rho^\circ_L}\chi^\circ_V\right], \quad (12)$$

assuming t_H is measured under the same field strength, *i.e.*, with a common K. Then invariably, irrespective of the working liquid used;

$$\frac{\tau_G-\tau_D}{\tau_P-\tau_D} = \frac{x_P}{x_P+x_D} = \phi_P, \quad (13)$$

where Eq. 4 is considered and ϕ_P is the volume fraction of the paramagnetic component in the gaseous sample. From Eq. 13, it is now possible to make a magnetic a nalysis of a gaseous mixture which is known to involveonly one paramagnetic species. (See below).

In addition to this, the susceptibility of the paramagnetic species in the gaseous state may be obtained in four ways:

(i) from Eq. 10,

$$\chi^\circ_P = -\frac{\rho^\circ_L(\tau_G - K\chi^\circ_L)}{K\rho^\circ_P\phi_P(1-x_V)(1-\beta^\circ_P)}, \quad (14)$$

(ii) from Eq. 11,

$$\chi^\circ_P = -\frac{\rho^\circ_L(\tau_P - K\chi^\circ_L)}{K\rho^\circ_P(1-x_V)(1-\beta^\circ_P)}, \quad (15)$$

(iii) from Eqs. 10 and 12,

$$\chi^\circ_P = -\frac{\rho^\circ_L(\tau_G - \tau_D)}{K\rho^\circ_P\phi_P(1-x_V)(1-\beta^\circ_P)}, \quad (16)$$

(iv) from Eqs. 11 and 12,

$$\chi^\circ_P = -\frac{\rho^\circ_L(\tau_P - \tau_D)}{K\rho^\circ_P(1-x_V)(1-\beta^\circ_P)}, \quad (17)$$

where the second terms of Eqs. 10 and 12 and the last terms of Eqs. 10, 11, and 12 have been considered negligible. Allowing for a deviation of 0.5—1% (approximately -0.5×10^{-6} e.m.u.), one may use Eq. 16 or 17.

Experimental

Materials. Nitrogen and oxygen were obtained from commercial sources with purities exceeding 99.9%. The mixed gases were prepared from these. The gases and air were dried by passage through silica gel and phosphorus pentoxide; commercial 99.0% nitrogen monoxide was used without further drying. Benzene, carbon tetrachloride, 2,2,4-trimethylpentane, and cyclohexane were Dotite Primasol solvents, while toluene, ethyl acetate, hexane, heptane, and acetone were Dotite Spectrosol solvents (Dojindo Co.) and used without purification. Sodium chloride (G. R. grade) was recrystallized twice from water. The water was purified by sub-boiling distillation from a quartz still after deionization.

Capillary Cells. A detailed figure of the cell has been given in a previous paper.[1] The two types of cell used in the present work were found to have slightly different cell-

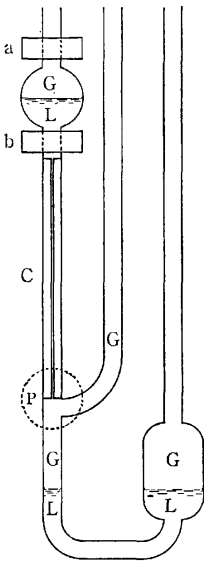

Fig. 1. Schematic representation for the G-L contact in a viscometer cell. P, the position of the pole pieces of electromagnet; a and b, detectors of viscometer; C, capillary; G, sample gas; L, working liquid.

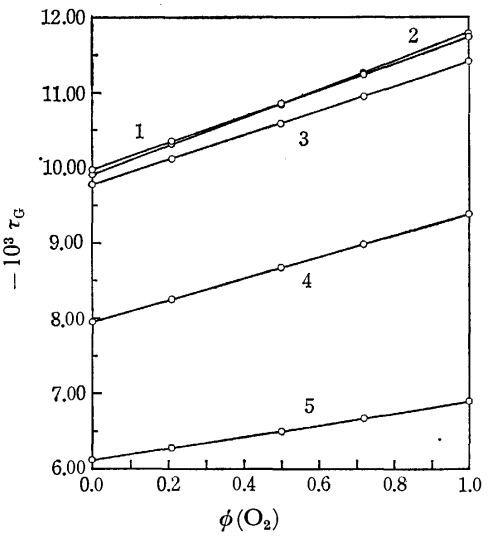

Fig. 2. Relationship between the τ-values found at a fixed magnetic-field strength of 18.8 kOe and the volume fraction of oxygen mixed with nitrogen at 20 °C. 1, Toluene; 2, water; 3, benzene; 4, acetone; 5, carbon tetrachloride.

constants, K, *i.e.*, 38.9_3 and 38.7_2 $Oe^2\,dyn^{-1}\,cm^{-1}$, respectively, at 1 kOe and $13.7_6\times10^3$ and $14.7_2\times10^3$ $Oe^2\,dyn^{-1}\,cm^{-1}$, respectively, at the respective maximum magnetic field strengths. The cell constants were determined from Eq. 12 for water under nitrogen, ignoring the second and last terms in Eq. 12 and using -0.720×10^{-6} e.m.u. for the magnetic susceptibility of pure water.[2] Figure 1 and Tables 1 and 2 are derived from using the first type cell and Fig. 2 and Table 3 from the second type.

Magnet. The electromagnet is the same type as used in the previous work.[1] The pole pieces of the magnet were set at a separation of approximately 8 mm for the first type cell and approximately 7 mm for the second type. The highest magnetic field strengths available at a maximum current of 4 A were 18.8 and 19.5 kOe, calibrated with

TABLE 1. τ-VALUES MEASURED IN VARIOUS GASES AND OXYGEN CONTENT IN DRIED AIR AT 20 °C

Liquid	$10^3\tau(N_2)$[a]	$10^3\tau(Air)$[a]	$10^3\tau(O_2)$[a]	$\phi(O_2)$[c]
Water	-9.90_7	-10.30_5	-11.79_8	0.21_0
Carbon tetrachloride	-6.11_0	-6.27_1	-6.89_2	0.20_6
Acetone	-7.95_3	-8.25_3	-9.38_6	0.20_9
Ethyl acetate	-8.57_9	-8.88_8	-10.06_5	0.20_7
Hexane	-11.95_6	-12.26_5	-13.47_0	0.20_4
Heptane	-11.95_2	-12.32_1	-13.75_2	0.20_5
2,2,4-Trimethylpentane	-12.16_7	-12.52_8	-13.86_7	0.21_2
Cyclohexane	-11.05_7	-11.40_1	-12.71_9	0.20_7
Benzene	-9.78_6	-10.13_4	-11.43_3	0.21_1
Toluene	-9.98_5	-10.35_0	-11.74_5	0.20_7
	Gas-chromatographic analysis			0.210 ± 0.005
	Literature value[b]			0.2099

a) Mean values obtained from more than 20 measurements at 18.8 kOe. b) International critical Tables, Vol. 1. c) Calculated using Eq. 12.

TABLE 2. MAGNETIC SUSCEPTIBILITY OF OXYGEN MEASURED WITH VARIOUS FLOWING LIQUIDS, IN 10^{-6} e.m.u. AT 20 °C

Liquid	ρ_L g cm^{-3}	p[a] mmHg	ρ_G[b] g cm^{-3}	β[c] cm^3 cm^{-3}	χ from air[d]	χ from oxygen
Water	0.998	17.5	0.001345	0.0333	$105._8$	$105._6$
Carbon tetrachloride	1.598	91	0.001216	0.2996	$104._6$	$106._6$
Acetone	0.792	184.8	0.001052	0.2736	$107._7$	$107._9$
Benzene	0.880	74.8	0.001244	0.2186	$109._1$	$108._4$
Toluene	0.867	22.2	0.001336	0.179	$99._9$	$101._1$
		Literature values[c,e]			104.1—108.2	

a) The vapor pressure of liquids at 20 °C: International Critical Tables, Vol. 3. b) Converted from the partial pressure of oxygen under a total pressure of 785 mmHg at 20 °C in the measuring cell, where the standard density, 0.001435 g cm^{-3} at 0 °C, 1 atm is assumed for pure oxygen (International Critical Tables, Vol. 3). c) Gmelin's Handbuch der Anorganischen Chemie, 8 Auflage. d) Assuming $\phi(O_2)=0.2099$. e) International Critical Tables, Vol. 6.

a Yokogawa gauss meter, type 3251. The magnetizing current was automatically kept at a constant value ($\pm0.01\%$) throughout the measurements.

Measurements. Prior to the measurements the liquid in the cell was saturated with the gas under study by passing the gas through the liquid for about 10 min and the dead space of the cell fully replaced by the gas by means of an operation tube connected to the cell. The τ-value was measured for nitrogen before and after every measurement of τ to check for changes in the liquid under study. Exchange of the two gases was achieved by means of 3-way stop valve that allowed either of the two gases to flow continuously through the operation tube so that the gases and the liquid in the cell was never exposed to the air. The temperature and pressure were kept constant at 20 ± 0.01 °C, and 785 ± 1 mmHg and 798 ± 1 mmHg for the first and second type cells respectively. Details of the automatic measurements have been fully described in a previous paper.[1] The density of the liquid was measured using a Shibayama Scientific Co. densimeter, type SS-D-200; more than 20 measurements were conducted to yield a mean flow time from which the magnetic susceptibility could be calculated.

Results and Discussion

The experimental results obtained at different mixing ratios of oxygen and nitrogen are shown in Fig. 2. In all cases a straight line relation may be seen, which can be expressed by the following empirical formula;

$$\tau_G = [\tau(O_2)-\tau(N_2)]\phi(O_2) + \tau(N_2), \quad (18)$$

where $\tau(O_2)$ and $\tau(N_2)$ represent the τ-values measured with a working liquid under flowing of pure oxygen and pure nitrogen, respectively, and $\phi(O_2)$ represents the volume fraction of oxygen in the gas. This equation is identical with that of Eq. 13. The volume fraction of oxygen in air was calculated with the aid of Eq. 13 from the τ-values measured on various working liquid, and the results are shown in Table 1. The observed values of $\phi(O_2)$ for air are found to be reproducible within $\pm1\%$ and are in good agreement with the literature as well as those given by gas-chromatographic analysis.

The magnetic susceptibility of pure oxygen was estimated with the aid of Eq. 15, from the experimental τ-values as listed in Table 1, where the volume fraction ϕ_P is assumed equal to 0.999, the purity of the oxygen in the gas cylinder used here, the results of which are shown in Table 2 together with the necessary physical data. In most cases, the τ-values obtained were always reproducible to within $\pm0.05\%$ and the estimated values of χ for oxygen were found to be reproducible to within $\pm0.5\%$, in good agreement with the literature except for the case of toluene. Thus, it has been demonstrated that the magnetic susceptibility

Table 3. Magnetic susceptibilities of oxygen and nitrogen monoxide, in 10^{-6} e.m.u. at 20 °C
Saturated aqueous sodium chloride used as the working liquid

H kOe	$10^3\tau(N_2)$	$10^3\tau(NO)$	$10^3\tau(O_2)$	$\kappa^{a,b)}$ NO	$\kappa^{a,b)}$ O_2	$\chi^{b,c)}$ NO	$\chi^{b,c)}$ O_2
12.2	-3.84_1	-4.14_4	-4.54_4	0.064_9	0.149_2	$49._5$	$106._7$
15.0	-5.78_3	-6.22_7	-6.84_0	0.063_2	0.149_0	$48._2$	$106._5$
17.2	-7.63_5	-8.22_7	-9.04_4	0.063_8	0.150_5	$48._7$	$107._6$
18.6	-8.98_1	-9.67_5	-10.63_5	0.063_6	0.150_2	$48._5$	$107._3$
19.5	-9.83_1	-10.58_9	-11.64_0	0.063_4	0.150_0	$48._4$	$107._3$
			Literature values[d,e]			48.7	104.1
						±0.25	—108.2

a) The volume susceptibilities at 798 mmHg. b) Calculated by taking the purities, 0.990 (NO) and 0.999 (O_2), for the ϕ_P values, and assuming 13.6 mmHg for the vapor pressure of water saturated with sodium chloride under the total pressure 798 mmHg. (International Critical Tables, Vol. 3.) c) Calculated using densities, 0.001310 g/cm³ (NO) and 0.001399 g/cm³ (O_2), at 798 mmHg. d) Gmelin's Handbuch der Anorganischen Chemie, 8 Auflage. e) International Critical Tables, Vol. 6.

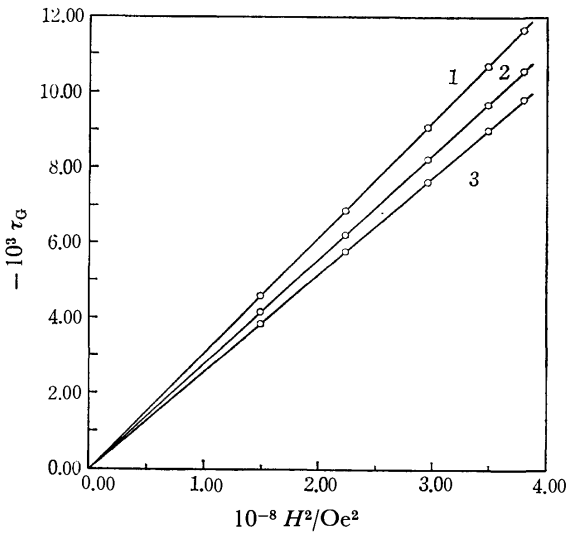

Fig. 3. Relationship between the τ-values found in different gases and the external magnetic-field strength at 20 °C when water saturated with sodium chloride was used as a working liquid. 1, Oxygen; 2, nitrogen monoxide; 3, nitrogen.

of a paramagnetic species mixed singly in diamagnetic gases may be determined by the viscometer method when the working liquid is selected and the gas non-reactive and the vapor pressure and solubility data of the gas in the liquid available. At least, all liquids used here appeared not to be denaturalized throughout the measurements, since no changes in the $\tau(N_2)$-value could be found before and after the measurement of the $\tau(O_2)$-value, were concluded.

In the case of toluene as the working liquid, a considerably low magnetic susceptibility was obtained for oxygen, the deviation being up to 6%. Such a large deviation can not be accounted for by intermolecular interactions such as the charge transfer between the dissolved oxygen and the liquid. A possible explanation may be that the solubility value of oxygen in toluene used here is somewhat erroneous since the value is too small compared with other liquids. On the other hand, the solubility data for the less-familiar gases, *e.g.*, nitrogen monoxide, are rarely found in the literature. Consequently it is advisable to use a liquid in which the solubility of gases is negligibly small, the limit of $\beta<0.001$ being sufficient. Concentrated aqueous solutions of inorganic salts having strong salting out effects may be of use. Water saturated with sodium chloride may be a liquid that can be used conveniently; *i.e.*, one volume of saturated aqueous solution dissolves only 0.00107 volumes of oxygen at 20 °C and 1 atm.[3]

The experimental results obtained by the viscometer method using saturated aqueous solutions of sodium chloride and various gases are shown in Fig. 3. In every case a straight line relation can be seen between τ and H^2, passing through the origin in agreement with Eq. 2. The saturated solution used here was found by analysis to dissolve sodium chloride at 26.17_6 wt% with a density 1.1990 g cm^{-3}, only slightly lower than that reported in the literature,[4] 26.43 wt% and 1.1999 g cm^{-3}, respectively. The magnetic susceptibility, χ_L, of this solution, measured by the present method was found to be $-0.667_8\times10^{-6}$ e.m.u., very closely in agreement with $-0.667_6\times10^{-6}$ e.m.u. estimated by Wiedemann's additivity law using the magnetic susceptibilities of -0.720 and -0.520×10^{-6} e.m.u.,[2] respectively for water and solid sodium chloride. Furthermore, the use of a saturated sodium chloride solution as the working liquid in the viscometer method at the same field strength using the same cell and measuring τ_G and τ_D separately, allowing for a maximum error of approximately ±0.5% at most, the following conventional equation, may be used instead of the more rigorous Eq. 16,

$$\kappa_P^\circ = \rho_P^\circ\chi_P^\circ = \frac{0.800_7}{(1-x_V)\phi_P}\left(\frac{\tau_G}{\tau_D}-1\right)\times10^{-6}\text{ e.m.u.}, \quad (19)$$

where two approximations, $\beta_P^\circ=0$ and $\tau_D=K\chi_L^\circ$ are assumed. From the experimental values of τ measured at different magnetic field strengths, the magnetic susceptibilities of oxygen and nitrogen monoxide have been computed using Eq. 19 and are listed in Table 3. In the range of magnetic fields investigated the results obtained were found to be in good agreement with

each other in either species of gases and those reported in the literature. However, according to the experience of the authors, the stronger the field in which the measurements are conducted, the more reliable are the results obtained. Consequently, for the magnetic susceptibilities of oxygen and nitrogen monoxide the values 107.3 and 48.4×10^{-6} e.m.u., respectively are prefered, found at 19.5 kOe, the highest level of the magnetic field strength available in the present study.

The advantages of the present method are: (1) no structural delicacy of the apparatus for its simple mechanism; (2) the measuring system since it is fully automatic, the successive analysis of a gas with respect to paramagnetic species may be possible; (3) it is easy to obtain results with considerable accuracy without taking a lot of precision; (4) the use of saturated aqueous solution of sodium chloride is very convenient for determining the susceptibility of paramagnetic gas species to a sufficient accuracy avoiding considerations of the solubility effect of gases. In addition pure sodium chloride is readily available and ample physicochemical data of its aqueous solutions exists.

References

1) K. Sueoka and T. Ikeda, *Bull. Chem. Soc. Jpn.*, **50**, 2124 (1977).

2) Landolt-Börnstein, "Zahlenwerte und Funktionen aus Physik, Chemie, Astronomie, Geophysik und Technik," Springer Verlag, Berlin (1967), II Band, 10 Teil.

3) Gmelin's Handbuch der Anorganischen Chemie, 8 Auflage, Verlag Chemie, GMBH, Weinheim/Bergstrasse (1958).

4) International Critical Tables of Numerical Data, Physics, Chemistry and Technology, McGraw-Hill (1928), Vol. 3.

The Photochemical Reaction of Benzo[c]cinnoline. III. Mechanism of Carbazole Formation

Hiroyasu INOUE,* Yukimi HIROSHIMA, and Kiyoto MIYAZAKI

Department of Applied Chemistry, Faculty of Technology, Kanagawa University, Kanagawa-ku, Yokohama 221

(Received July 22, 1978)

5,6-Dihydrobenzo[*c*]cinnoline is an intermediate in the photochemical formation of carbazole from benzo[*c*]cinnoline. The mechanism of the photo-induced carbazole formation from 5,6-dihydrobenzo[*c*]cinnoline has been studied in acidic aqueous 2-propanol of the reactant previously produced by the photo-reduction of benzo[*c*]cinnoline. It has been established that only the protonated species of the reactant undergoes photoreaction. The results of quenching experiments on quantum yields for the reaction and on the fluorescence of the reactant have shown that the reactive state is the first excited singlet state of protonated 5,6-dihydrobenzo[*c*]cinnoline. The initial step in the reaction is the hydrogen atom abstraction followed by elimination of the amino radical.

It has been reported that benzo[*c*]cinnoline in acidic alcohol solutions gives rise to carbazole under ultraviolet light irradiation.[1] 5,6-Dihydrobenzo[*c*]cinnoline has been found to be an intermediate in the carbazole formation. This intermediate is obtained in acidic 2-propanol with visible light irradiation. No subsequent reaction occurs,[2] hence the photo-induced carbazole formation from 5,6-dihydrobenzo[*c*]cinnoline can be studied using the solution thus obtained. In strongly acidic solution such as 4 M HCl aqueous 2-propanol, 5,6-dihydrobenzo[*c*]cinnoline exists in the monoprotonated form and has absorption bands at 240, 270, and 315 nm.

The purpose of this paper is to clarify the mechanism regarding the photochemical reaction of 5,6-dihydrobenzo[*c*]cinnoline to carbazole. The reactive excited state of the reactant and the mode of elimination of fragments from the reactant are of particular interest.

Experimental

Materials. Benzo[*c*]cinnoline, naphthalene, anthracene, pyrene, and 2-propanol were the same as those used previously.[2] Phenanthrene and fluorene were recrystallized from ethanol. Acetophenone was purified by distillation. *trans*-1,3-Pentadiene was used without further purification.

Irradiation. To convert benzo[*c*]cinnoline into 5,6-dihydrobenzo[*c*]cinnoline, an acidic aqueous 2-propanol solution of the former was irradiated with light of a wavelength in excess of 400 nm, obtained from a 500 W high pressure mercury arc lamp and a Corning glass filter (CS 3-73). The solution of the reactant thus prepared was irradiated with 315 nm light from a Shimadzu excitation apparatus GF-16E, equipped with a 500 W Xe lamp and a grating monochromator. All irradiations were conducted at room temperature under nitrogen to prevent oxidation of the reactant.

Measurements and Analysis. Ultraviolet spectra were measured with a Shimadzu UV-200 spectrophotometer using 1 cm cells. Fluorescence and phosphorescence spectra were recorded on a Shimadzu RF-500 spectrofluorimeter at room temperature and 77 K, respectively. The quantum yield for the carbazole formation was determined as follows. Acidic aqueous 2-propanol solution (4 M HCl) of benzo[*c*]cinnoline (1.0×10^{-4} M) was irradiated, first with light of a wavelength in excess of 400 nm for 3 h to give 5,6-dihydrobenzo[*c*]cinnoline quantitatively, and then the resulting solution was irradiated with light of wavelength 315 nm for 15 min. The actionmetry was performed together with the spectrophotometric determination of the amount of carbazole produced, a potassium ferrioxalate solution being employed as the actinometer.[3]

Results and Discussion

The quantum yield for the carbazole formation was determined to be 0.15 and this did not change with variation in the initial concentration of reactant in the range 7.5×10^{-5}—2.0×10^{-4} M. In order to estimate the energies of the lowest excited singlet and triplet states of the reactant, the fluorescence and phosphorescence spectra were measured. From the observed emission spectra presented in Fig. 1 the energies of the lowest excited singlet and triplet states were evaluated to be 82.7 and 63.4 kcal/mol, respectively. These values were determined from the wavelengths of the emission band shoulders indicated by the arrows in Fig. 1, since the emission bands have no distinct fine structures.

To identify the reactive state of the photoreaction, quenching experiments were conducted using several compounds, *e.g.* fluorene, naphthalene, acetophenone

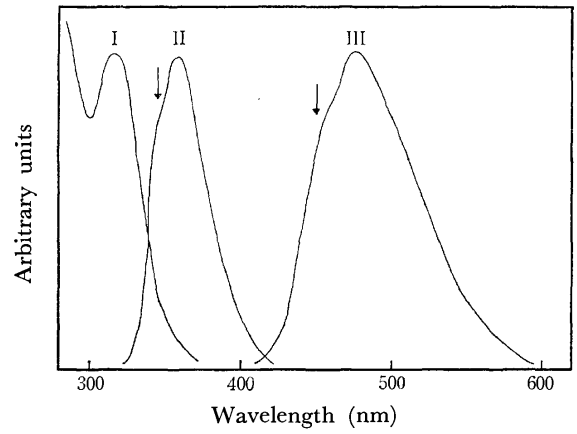

Fig. 1. Absorption and emission spectra of 5,6-dihydrobenzo[*c*]cinnoline in 4 M HCl aqueous 2-propanol. Excitation wavelength: 315 nm. I: Absorption, II: fluorescence, III: phosphorescence.

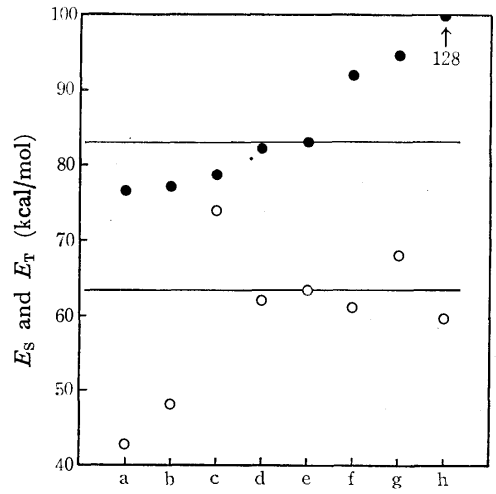

Fig. 2. Energies of the lowest excited singlet (●) and triplet (○) states for 5,6-dihydrobenzo[*c*]cinnoline and the quenchers. a: Anthracene, b: pyrene, c: acetophenone, d : phenanthrene, e : 5,6-dihydrobenzo-[*c*]cinnoline, f : naphthalene, g : fluorene, h : *trans*-1,3-pentadiene (The singlet energy was estimated from the absorption band at 223 nm).

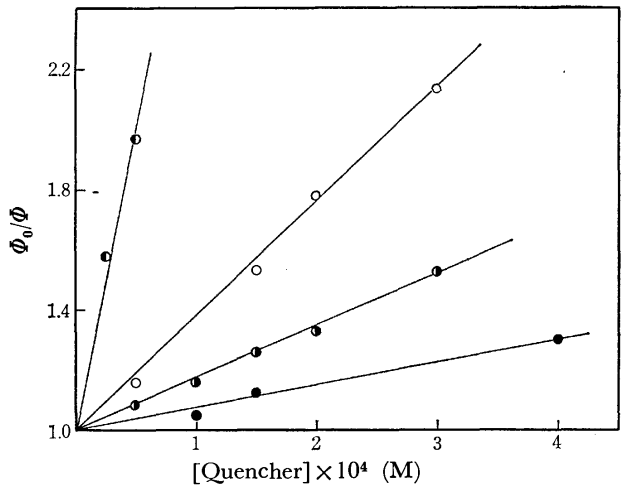

Fig. 3. Stern-Volmer plots for the carbazole formation. [5,6-dihydrobenzo[*c*]cinnoline] = 1.0×10^{-4} M.
◐: Pyrene, ○: anthracene, ◑: phenanthrene, ●: acetophenone.

pyrene, phenanthrene, anthracene, and *trans*-1,3-pentadiene. The energies of the lowest excited singlet and triplet states for these compounds in polar solvents[4] and the estimated values for 5,6-dihydrobenzo[*c*]-cinnoline are presented in Fig. 2. Fluorene, naphthalene and *trans*-1,3-pentadiene have no quenching effect, whereas phenanthrene, acetophenone, pyrene, and anthracene were found to reduce the quantum yield of the reaction. The quenching data is presented in Fig. 3 for each quencher, and the Stern-Volmer plots give straight lines.

The results can be interpreted in terms of the energy levels illustrated in Fig. 2. All effective quenchers studied have singlet energies lower than that of the reactant, whereas fluorene, naphthalene, and *trans*-1,3-pentadiene have higher singlet energies. Naphthalene and *trans*-1,3-pentadiene have triplet energies

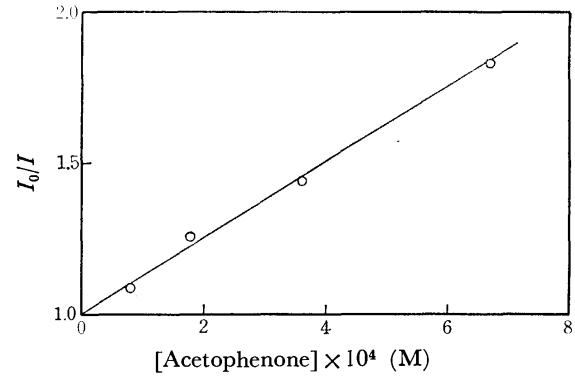

Fig. 4. Fluorescence quenching plot of 5,6-dihydrobenzo[*c*]cinnoline by acetophenone. [5,6-Dihydrobenzo[*c*]cinnoline] = 1.0×10^{-4} M.

lower than that of the reactant and do not quench the reaction, indicating the unsuitability of the triplet-triplet energy transfer as a mechanism for the quenching effect. This is also indicated in the case of acetophenone as a quencher, since this molecule has a triplet energy higher than the reactant. Consequently, the observed quenching may be ascribed to an energy transfer from the lowest excited singlet 5,6-dihydrobenzo[*c*]cinnoline to the quenchers. Further evidence for this mechanism can be given from the fluorescence quenching study using acetophenone as a quencher, the results of which are shown in Fig. 4, where the quantities I and I_0 are fluorescence intensities at 356 nm with and without acetophenone, respectively. From this figure it is evident that the fluorescent state of the reactant is deactivated with acetophenone through singlet-singlet energy transfer.

The indication is that the photoreaction proceeds through the lowest excited singlet state of the reactant and that the triplet state does not participate in the reaction.

Although benzo[*c*]cinnoline is reduced photochemically to 5,6-dihydrobenzo[*c*]cinnoline in neutral ethylene glycol[5] and poly(vinyl alcohol) film,[6] the subsequent reaction to lead carbazole does not occur in these media with the light of wavelength 315 nm. Consequently only the protonated species of the reactant undergoes the photochemical formation of carbazole.

Ammonia (NH_4Cl in acidic solution) has been found to be generated in carbazole formation. Trace amounts of ammonia in the irradiated solution have been detected using a thymol indicator,[7] but hydrazine was not detected. Subsequently the mode of the photo-elimination was examined through the determination of the fragment which participated in the ammonia formation. The amino radical ($\cdot NH_2$) is known to react with alcohol or hydrochloric acid to yield ammonia.[8] Therefore, the fragment produce in the photo-elimination is presumed to be the amino radical. If this is the case, the initial step in the reaction may be abstraction of the hydrogen atom from the solvent molecule by the reactant as illustrated below. The necessity of hydrogen atom donors in the initial step of the carbazole formation has been examined as follows. Benzo[*c*]cinnoline has been photo-reduced in poly(vinyl alcohol) film as earlier

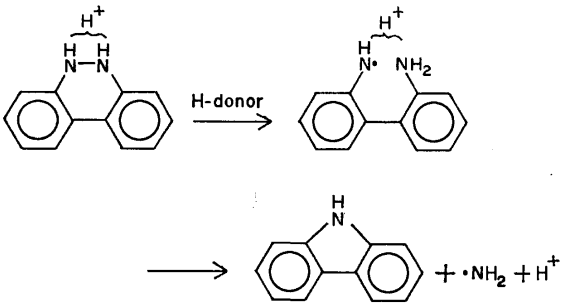

reported,[6] and the 5,6-dihydrobenzo[*c*]cinnoline thus produced has been extracted with acidic aqueous acetonitrile (4 M HCl) under nitrogen.[9] The resulting solution of 5,6-dihydrobenzo[*c*]cinnoline was irradiated with light of wavelength 315 nm, the carbazole formation was not observed at all. This supports the above assertion and consequently the direct elimination of the imino radical (NH) from the reactant can be ruled out as the mechanism of the photo-elimination to yield carbazole.

References

1) Part I of this series : H. Inoue, T. Sakurai, and F. Tanaka, *Bull. Chem. Soc. Jpn.*, **48**, 924 (1975).
2) Part II of this series : H. Inoue, Y. Hiroshima, and N. Makita, *Bull. Chem. Soc. Jpn.*, **52**, 351 (1979).
3) C. G. Hatchard and C. A. Parker, *Proc. R. Soc. London, Ser. A*, **235**, 518 (1956).
4) S. L. Murov, "Handbook of Photochemistry," Marcel Dekker, New York (1973), p. 3.
5) H. Inoue and Y. Hiroshima, unpublished results.
6) H. Inoue and M. Matsumoto, *Nippon Kagaku Kaishi*, **1974**, 203.
7) H. Fujinuma, Y. Shimada, and S. Hirano, *Bunseki Kagaku*, **20**, 131 (1971).
8) C. J. Albisetti, D. D. Coffman, F. W. Hoover, E. J. Jenner, and W. E. Mochel, *J. Am. Chem. Soc.*, **81**, 1489 (1959).
9) The absorption spectrum of the acetonitrile solution showed that 5,6-dihydrobenzo[*c*]cinnoline was present in 10^{-4} M concentration.

Miexd Monolayers of Long Normal Chain Fatty Acids with Long Normal Chain Esters. I. Fatty Acids–Ethyl Hexadecanoate System

Hirosi MATUO,* Noriaki YOSIDA, Kinsi MOTOMURA, and Ryohei MATUURA

Department of Chemistry, Faculty of Science, Kyushu University 33, Higashi-ku, Fukuoka 812

(Received July 28, 1978)

Surface pressure-area(π-A) curves of the two-component surface films of long normal chain fatty acids with ethyl hexadecanoate were measured at various compositions and temperatures. It was found that the π-A curves of the mixed monolayers vary characteristically with the number of carbon atoms of the film-forming acid. The two-dimensional phase diagrams of these systems and their partial molar enthalpy changes were obtained by taking advantage of the thermodynamic treatment of multicomponent surface films.[1,2] It was concluded that the chain length of the acid plays an important role in the thermodynamic state of the mixed monolayer.

There have been many studies of mixed monolayers at the air–water interface, aimed at elucidating the effect of the molecular structure on their state and properties.[3–5] But few studies using long normal chain esters have been reported. So we investigated mixed monolayers of long normal chain fatty acids with a long normal chain ester in order to clarify the effect of the chain length of the acid on the thermodynamic state of the two-component monolayers.

In the present study, tridecanoic(C_{13}), tetradecanoic(C_{14}), pentadecanoic(C_{15}), hexadecanoic(C_{16}), heptadecanoic(C_{17}), and octadecanoic(C_{18}) acids were employed as the fatty acids, and ethyl hexadecanoate (EH) was used as the ester. From these experiments, we constructed two-dimensional phase diagrams and calculated the partial molar enthalpy change for the respective systems. Consequently, systematic information concerning the effect of the number of carbon atoms of acid on fatty acid–ester mixed monolayers could be obtained.

Experimental

Long normal chain fatty acids employed in this experiment were obtained from Tokyo Kasei Co., Ltd. and purified by recrystallization from petroleum ether three times. Ethyl hexadecanoate(EH) was synthesized from recrystallized hexadecanoic acid and distilled ethanol by the usual method and purified by distillation. Benzene was used as the spreading solvent. To prevent the ester from hydrolysis, a 0.1 M NaCl solution was used as the substrate; this was prepared from twice distilled water and sodium chloride (Wako super special grade).

The π-A curves were measured by a Wilhelmy type surface balance. The temperature was maintained constant within ± 0.2 K during the experiment. The monolayer was compressed continuously with a constant velocity of 2.79×10^{-2} nm^2 molecule^{-1} min^{-1} and the π-A curves were reproducible within ± 0.2 mN m^{-1} at the same mean molecular area.

Results and Discussion

Surface pressure-area(π-A) curves were obtained for the C_{13}–EH, C_{14}–EH, C_{15}–EH, C_{16}–EH, C_{17}–EH, and C_{18}–EH systems at various compositions and temperatures. Typical π-A curves are shown in Fig. 1 for the C_{14}–EH system and in Fig. 2 for the C_{18}–EH system, both at 298.15 K.

For the C_{13}– EH system, the monolayers of pure

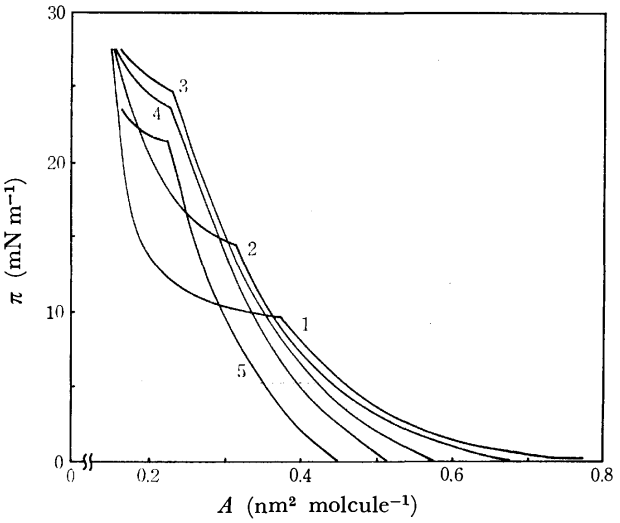

Fig. 1. Surface pressure *vs.* mean area curves of the tetradecanoic acid-ethyl hexadecanoate mixed monolayer at 298.15 K: 1, $x_2^{\pi}=1$ (ethyl hexadecanoate); 2, 0.8; 3, 0.3; 4, 0.15; 5, 0 (tetradecanoic acid).

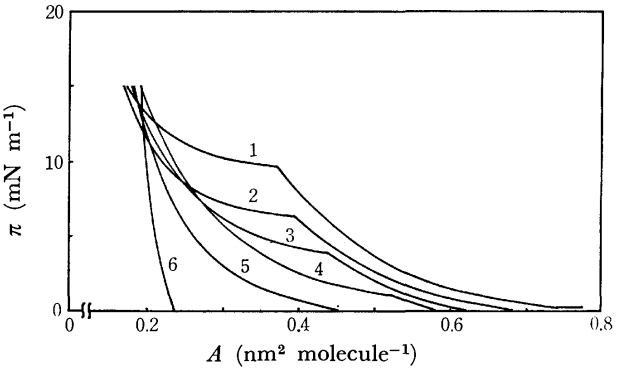

Fig. 2. Surface pressure *vs.* mean area curves of the octadecanoic acid-ethyl hexadecanoate mixed monolayer at 298.15 K: 1, $x_2^{\pi}=1$(ethyl hexadecanoate); 2, 0.9; 3, 0.8; 4, 0.7; 5, 0.5; 6, 0(octadecanoic acid).

C_{13} and EH are of the expanded type and a phase transition from liquid expanded to liquid condensed state is found over the whole range of composition at 298.15 and 288.15 K. The π^{eq}-$x_2^{\pi,e}$ curve for this system at 298.15 K is shown in Fig. 3, where π^{eq} is the phase equilibrium surface pressure which corresponds to that of the break point of π-A curve and $x_2^{\pi,e}$ indicates the mole fraction of the EH in the expanded mixed monolayer. It is seen that the curve

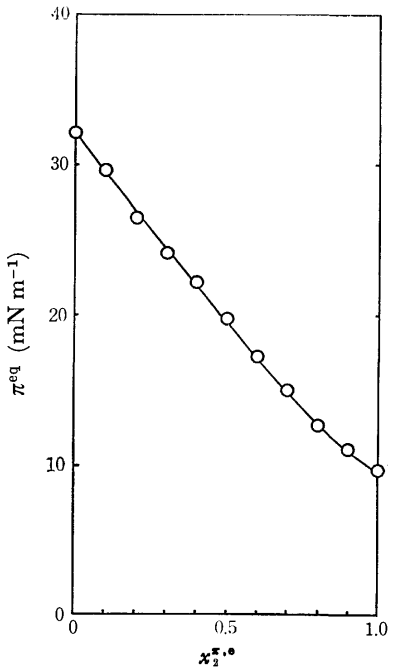

Fig. 3. π^{eq}-$x_2^{\pi,e}$ curves of the tridecanoic acid-ethyl hexadecanoate mixed monolayer at 298.15 K.

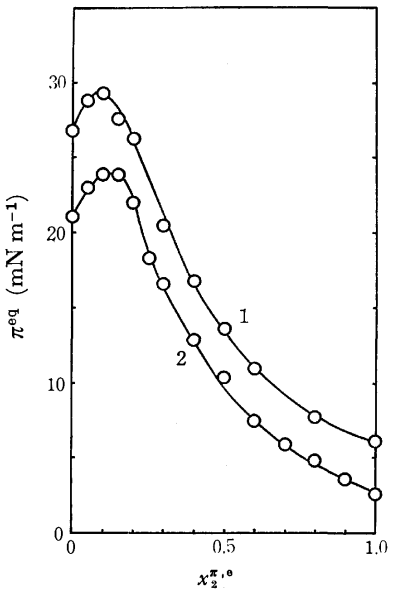

Fig. 4. π^{eq}-$x_2^{\pi,e}$ curves of the tridecanoic acid-ethyl hexadecanoate mixed monolayer at 293.15 and 288.15 K: 1, 293.15 K; 2, 288.15 K.

is of the simple, monotonous type. When the temperature is lowered, the shape of the π^{eq}-$x_2^{\pi,e}$ curve changes; it is noteworthy that at 293.15 and 288.15 K a maximum appears on the curve, as is shown in Fig. 4.

For the C_{14}–EH system, as can be seen from Fig. 1, the π^{eq}-$x_2^{\pi,e}$ curve has a maximum even at 298.15 K. The shape of the curve is similar at 293.15 and 288.15 K to that at 298.15 K, although the equilibrium surface pressure decreases gradually as the temperature is lowered, as shown in Fig. 5. We see that the composition of the maximum point is almost independent of temperature.

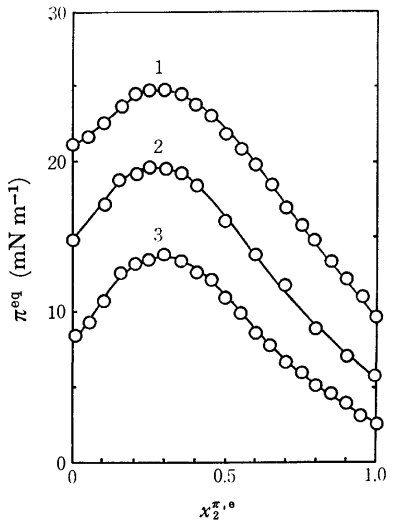

Fig. 5. π^{eq}-$x_2^{\pi,e}$ curves of the tetradecanoic acid-ethyl hexadecanoate mixed monolayer at several temperatures: 1, 298.15 K; 2, 293.15 K; 3, 288.15 K.

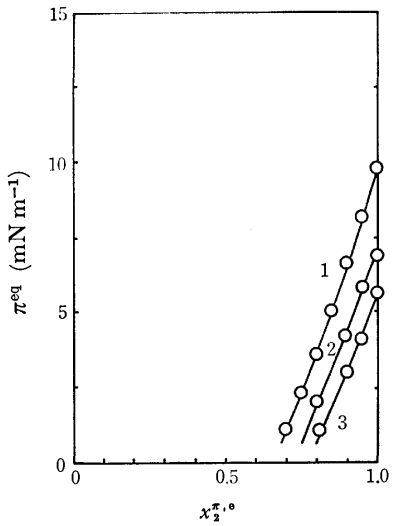

Fig. 6. π^{eq}-$x_2^{\pi,e}$ curves of the octadecanoic acid-ethyl hexadecanoate mixed monolayer at several temperatures: 1, 298.15 K; 2, 293.15 K; 3, 288.15 K.

For the C_{15}–EH and C_{16}–EH systems, the π^{eq}-$x_2^{\pi,e}$ curve is similar to that for the C_{14}–EH system, except that the maximum point shifts to the right along the $x_2^{\pi,e}$ axis; that is, the composition of the maximum becomes richer in EH as the carbon number of the fatty acid increases.

Figure 2 represents π-A isotherms of the C_{18}–EH system at 298.15 K. The π-A curve of this system is very different from the curves of the above-mentioned lower fatty acids–EH systems, in that the phase transition takes place only in a limited range of compositions. This difference may be caused by the fact that pure shorter-chain fatty acids give rise to the expanded film, while long-chain fatty acids form the condensed film at 298.15 K. The π^{eq}-$x_2^{\pi,e}$ curves for the C_{18}–EH system at various temperatures are shown in Fig. 6. It is found that the π^{eq} decreases monotonously with the decrease of $x_2^{\pi,e}$, and the lowering

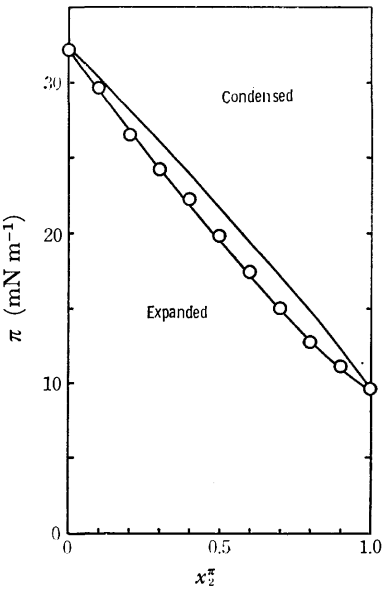

Fig. 7. Phase diagram of the tridecanoic acid-ethyl hexadecanoate mixed monolayer at 298.15 K.

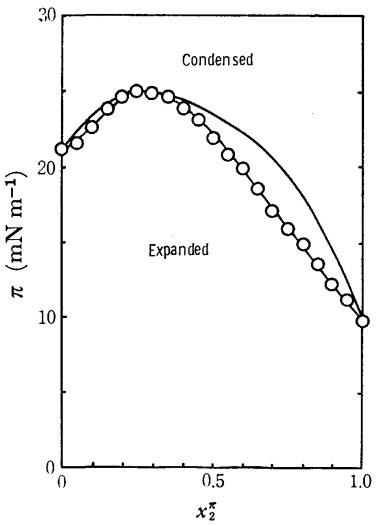

Fig. 8. Phase diagram of the tetradecanoic acid-ethyl hexadecanoate mixed monolayer at 298.15 K.

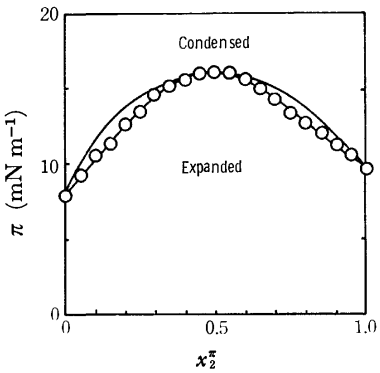

Fig. 9. Phase diagram of the pentadecanoic acid-ethyl hexadecanoate mixed monolayer at 298.15 K.

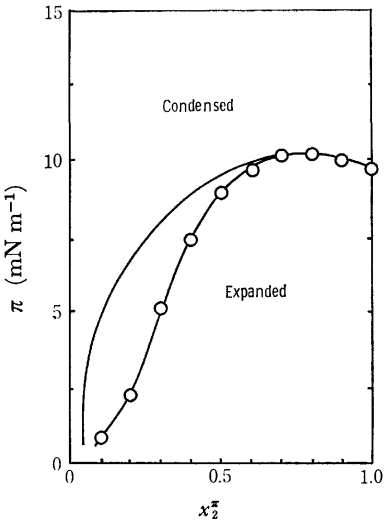

Fig. 10. Phase diagram of the hexadecanoic acid-ethyl hexadecanoate mixed monolayer at 298.15 K.

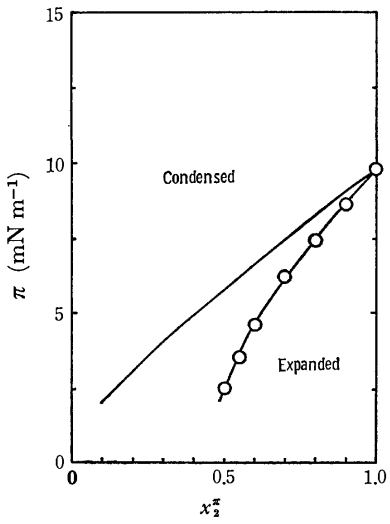

Fig. 11. Phase diagram of the heptadecanoic acid-ethyl hexadecanoate mixed monolayer at 298.15 K.

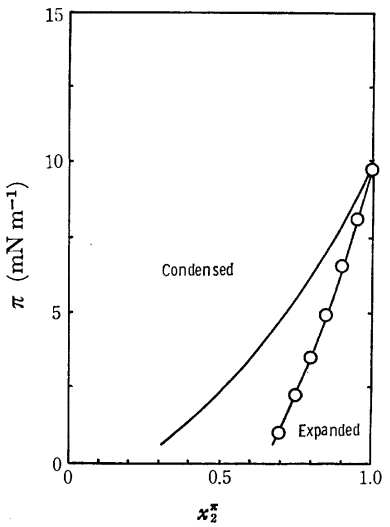

Fig. 12. Phase diagram of the octadecanoic acid-ethyl hexadecanoate mixed monolayer at 298.15 K.

TABLE 1. SURFACE PRESSURE AND COMPOSITION AT MAXIMUM POINT

System	298.15 K		293.15 K		288.15 K	
	$(\pi^{eq})_{max}$	$(x_2^{\pi})_{max}$	$(\pi^{eq})_{max}$	$(x_2^{\pi})_{max}$	$(\pi^{eq})_{max}$	$(x_2^{\pi})_{max}$
C_{13}–EH	—	—	29.3	0.1	23.9	0.12
C_{14}–EH	24.8	0.3	19.7	0.3	13.7	0.3
C_{15}–EH	16.1	0.5	11.1	0.5	6.7	0.5
C_{16}–EH	10.2	0.8	—	—	—	—

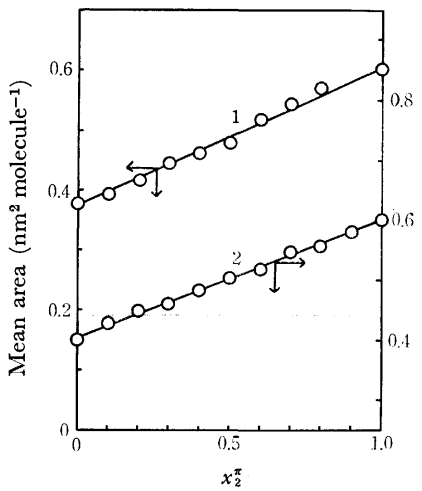

Fig. 13. Additivity of area at 2 mN m^{-1} for C_{14}–EH and C_{15}–EH systems at 298.15 K : 1, C_{14}–EH; 2, C_{15}–EH.

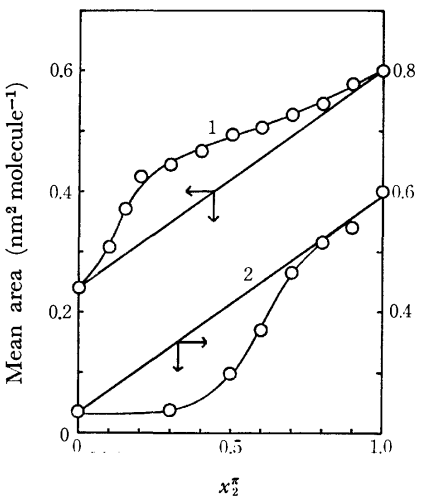

Fig. 14. Additivity of area at 2 mN m^{-1} for C_{16}–EH and C_{18}–EH systems at 298.15 K : 1, C_{16}–EH; 2, C_{18}–EH.

of temperature causes the parallel decrease in π^{eq} of this mixed monolayer. The π^{eq} disappears finally at a certain $x_2^{\pi,e}$, below which the phase transition from the expanded to the condensed film is not observed any more.

For the C_{17}–EH system we have a π^{eq}-$x_2^{\pi,e}$ curve similar to that for the C_{18}– EH system, although the phase transition region is a little wider for the former than for the latter.

Now the entire phase diagram can be constructed for each system by using thermodynamic equations previously described.[1,2] In Figs. 7 to 12 are shown the two-dimensional phase diagrams for C_{13}–EH to C_{18}–EH systems, respectively, at 298.15 K. The experimental points are indicated by open circles which give the π^{eq}-$x_2^{\pi,e}$ curve and the corresponding π^{eq}-$x_2^{\pi,c}$ curve calculated is shown by the solid line, where $x_2^{\pi,c}$ indicates the mole fraction of the EH in the condensed mixed monolayer.

The phase diagram for the C_{13}–EH system (Fig. 7) at 298.15 K is of an ideally mixing type; tow components form a continuous series of mixtures in the condensed as well as in the expanded phase. For C_{14}–EH, C_{15}–EH, and C_{16}–EH systems, a maximum appears on the phase diagram (Figs. 8, 9, and 10), where the composition of the expanded phase is equal to that of the condensed one. Therefore, this maximum may be called a two-dimensional positive azeotropic point. At this point the phase transition pressure $(\pi^{eq})_{max}$ decreases, while the mole fraction of ester $(x_2^{\pi})_{max}$ increases, with increase in the number of carbon atoms of fatty acid, as shown in Table 1. The positive azeotropy suggests that there are mutual interactions between two components in the mixed monolayer which are weaker than the interactions between the pure component molecules themselves.

In contrast to this positive azeotropy, we have observed negative azeotropy in C_{14}–D,L-α-dipalmitoyl lecithin(DPL), EH–DPL, hexadecyl acetate(HA)–DPL, 1-monopalmitin–DPL, and EH–HA systems; these results will be reported in a separate paper.

For C_{17}–EH and C_{18}–EH systems at 298.15 K the phase transition from expanded to condensed states appears only in a limited range of composition, and so the phase diagram is incomplete, as shown in Figs. 11 and 12. Because of the strong condensing effect of longer chain fatty acids, C_{17} or C_{18}, the phase transition pressure decreases remarkably with increase in the amount of the fatty acid, resulting finally in the disappearance of the expanded phase at a certain composition of the mixed monolayer.

The situation of the interaction and miscibility of two components in the mixed monolayer may also be obtained from mean molecular area A_m at constant surface pressure *vs.* mole fraction x_2^{π} relations. The A_m-x_2^{π} curves were obtained for the C_{13}–EH, C_{14}–EH, C_{15}–EH, C_{16}–EH, C_{17}–EH, and C_{18}–EH systems at 2 mN m^{-1}. Several examples are shown in Figs. 13 and 14. From these results, it is found that at 2 mN m^{-1} the simple additivity is nearly established for the C_{13}–EH, C_{14}–EH, and C_{15}–EH systems, but the curves of the C_{16}–EH, C_{17}–EH, and C_{18}–EH systems

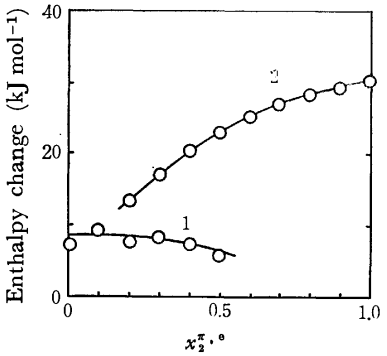

Fig. 15. Partial molar enthalpy change of the phase transition, $-(\bar{h}_i^c - \bar{h}_i^e)$ *vs.* mole fraction in the expanded monolayer, $x_2^{\pi,s}$, curves of the tetradecanoic acid–ethyl hexadecanoate at 293.15 K: 1, tetradecanoic acid; 2, ethyl hexadecanoate.

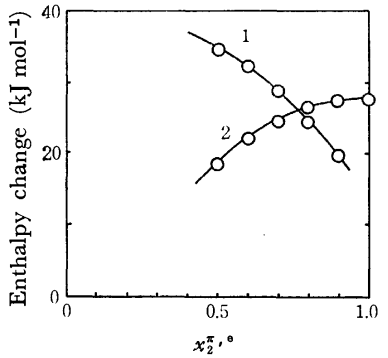

Fig. 17. Partial molar enthalpy change of the phase transition, $-(\bar{h}_i^c - \bar{h}_i^e)$ *vs.* mole fraction in the expanded monolayer, $x_2^{\pi,s}$, curves of the hexadecanoic acid–ethyl hexadecanoate at 293.15 K: 1, hexadecanoic acid; 2, ethyl hexadecanoate.

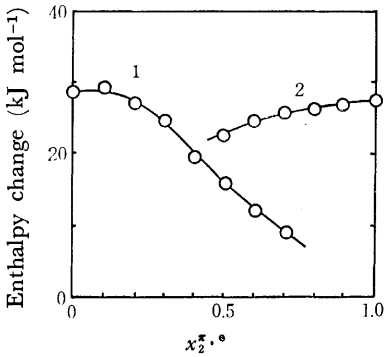

Fig. 16. Partial molar enthalpy change of the phase transition, $-(\bar{h}_i^c - \bar{h}_i^e)$ *vs.* mole fraction in the expanded monolayer, $x_2^{\pi,s}$, curves of the pentadecanoic acid–ethyl hexadecanoate at 293.15 K: 1, pentadecanoic acid; 2, ethyl hexadecanoate.

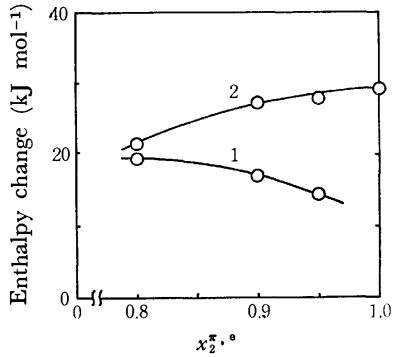

Fig. 18. Partial molar enthalpy change of the phase transition, $-(\bar{h}_i^c - \bar{h}_i^e)$ *vs.* mole fraction in the expanded monolayer, $x_2^{\pi,s}$, curves of the octadecanoic acid–ethyl hexadecanoate at 295.65 K: 1, octadecanoic acid; 2, ethyl hexadecanoate.

evidently deviate from this rule. Judging from this fact and the appearance of phase transition, it is concluded that in the former group the miscibility of two components is quite good, but in the latter group it gradually decreases with an increase in the difference of carbon number between the two components.

By the use of a thermodynamic treatment (Eqs. 38, 42, and 43 in Ref. 2), the partial molar enthalpy change accompanying the phase transition form the expanded to the condensed state was calculated for the C_{14}–EH, C_{15}–EH, C_{16}–EH, and C_{18}–EH systems; the results are shown in Figs. 15 to 18. It is difficult to make such a calculation over the whole range of composition with sufficient accuracy, and so in these figures data are shown for some limited ranges.

In the C_{14}–EH system (Fig. 15), the partial molar enthalpy change of C_{14} is small and decreases slightly, while that of EH is large and increases considerably, with increase of the composition of EH. The value of EH in the pure monolayer is larger than that of EH in the mixed monolayer. This shows that EH is more condensed in the mixed monolayer than in the pure monolayer.

In the C_{15}–EH system (Fig. 16), the partial molar enthalpy change of C_{15} decreases but the value of EH increases with the increase of $x_2^{\pi,s}$ to almost the same extent. This indicates that both C_{15} and EH are more condensed in the mixed monolayer than in the pure monolayer, respectively. In other words, the mixed monolayer of C_{15} and EH at relatively high pressure is less stable in the condensed state than in the expanded state and needs less heat for the transition from the condensed to expanded state than does the monolayer of pure components. On the contrary, in the system of negative azeotropy, such as EH–HA, EH–DPL, and so on, the monolayer is more stable in the condensed state than in the expanded state at relatively high pressure and needs much heat for the transition from the condensed to expanded state than does the monolayer of pure components.

In the C_{16}–EH system(Fig. 17), the partial molar enthalpy change of C_{16} decreases more than that of C_{15} in the C_{15}–EH system and the value of EH increases more than that of EH in the C_{15}–EH system, with increase of $x_2^{\pi,s}$. The tendency is much more pronounced in the C_{18}–EH system (Fig. 18). From these results it is seen that the partial molar enthalpy changes of acids and EH vary more rapidly with increase of the chain length of the acid. From Figs. 15 to 17, it was found that the values of partial molar

enthalpy change of acids and EH are quite close to each other at the composition of the maximum point.

In conclusion, the chain length of the acid plays an important role in the thermodynamic state of the mixed monolayer. Taking advantage of the thermodynamic treatment it is seen that the C_{13}–EH system has a cigar type phase diagram at 298.15 K, while it comes to have a maximum point when the temperature is lowered. C_{14}–EH, C_{15}–EH, and C_{16}–EH systems have maximum points in their phase diagrams at 298.15 K. They correspond to the positive azeotrope in the three-dimensional phase diagram. This result suggests that there are mutual interactions between two components in the mixed monolayer which are weaker than the interactions between the pure component molecules themselves. The composition of the maximum point gradually shifts towards the ester side, with increase of the number of carbon atoms of acids. Finally it disappears in the C_{17}–EH and C_{18}–EH systems. It was found that the miscibility, phase diagram, and the partial molar enthalpy change of these systems change successively with the difference of the chain length.

References

1) K. Motomura, *J. Colloid Interface Sci.*, **48**, 307 (1974).
2) K. Motomura, K. Sekita, and R. Matuura, *J. Colloid Interface Sci.*, **48**, 319 (1974).
3) N. Kuramoto, K. Sekita, K. Motomura, and R. Matuura, *Mem. Fac. Sci. Kyushu Univ.*, **C**, **8**, 67 (1972).
4) K. Sekita, M. Nakamura, K. Motomura, and R. Matuura, *Mem. Fac. Sci. Kyushu Univ.*, **C**, **10**, 51 (1976).
5) H. Matuo, K. Hiromoto, K. Motomura, and R. Matuura, *Bull. Chem. Soc. Jpn.*, **51**, 690 (1978).

Mixed Monolayers of Long Normal Chain Fatty Acids with Long Normal Chain Esters. II. Fatty Acids–Hexadecyl Acetate System

Hirosi MATUO,* Kinsi MOTOMURA, and Ryohei MATUURA

Department of Chemistry, Faculty of Science, Kyushu University 33, Higashi-ku, Fukuoka 812

(Received July 28, 1978)

In order to clarify the effect of molecular structure on states and properties of mixed monolayers, surface pressure-area(π-A) curves of the two-component surface films of long normal chain fatty acids with hexadecyl acetate were measured at various compositions and temperatures. By use of thermodynamic analysis, the phase diagrams and partial molar enthalpy changes were calculated. For four systems studied in the present paper it was found that the diagram and enthalpy change vary characteristically with the number of carbon atoms of acids, but the dependence on the chain length of acid in fatty acid–hexadecyl acetate systems was very different from that in fatty acid–ethyl hexadecanoate systems.

In our previous studies of fatty acid–fatty acid,[1,2] fatty acid–fatty alcohol,[3] and fatty acid–fatty ester[4] systems, it was found that the interaction, the miscibility, the state, and the thermodynamic quantities in mixed monolayers change successively with increase in the chain length of the film-forming acid. The present work has been undertaken to investigate the difference between fatty acid–hexadecyl acetate and fatty acid–ethyl hexadecanoate[4] systems, in order to elucidate the effect of molecular structure on mixing.

Experimental

The long normal chain fatty acids employed in this experiment were tetradecanoic(C_{14}), pentadecanoic(C_{15}), hexadecanoic(C_{16}), and octadecanoic(C_{18}) acids. They were purified by repeated recrystallization. Hexadecyl acetate (HA) was synthesized from distilled acetic acid and 1-hexadecanol of Tokyo Kasei Co., Ltd., and purified by distillation.

Experimental conditions were the same as described in the previous paper.[4]

Results and Discussion

Surface pressure-area(π-A) curves obtained for C_{14}–HA, C_{15}–HA, C_{16}–HA, and C_{18}–HA systems at 298.15 K are shown in Figs. 1 to 4. It was observed that in the C_{14}–HA system (Fig. 1) there is a maximum equilibrium surface pressure, similar to the C_{14}–EH system[4] at $x_2^{\pi,e}=0.05$, where $x_2^{\pi,e}$ is the mole fraction of the second component(HA) in the expanded monolayer and EH indicates ethyl hexadecanoate, as described in the previous paper.[4] In the C_{15}–HA system (Fig. 2) there is a unique result: *i.e.*, the curve has a maximum and a minimum point at $x_2^{\pi,e}=0.3$ and 0.87, respectively. This phenomenon is peculiar to the C_{15}–HA system and we have not observed it in any other systems until now. In the C_{16}–HA(Fig. 3) and C_{18}–HA(Fig. 4) systems the equilibrium surface pressure, π^{eq}, decreases monotonously with the decrease of $x_2^{\pi,e}$, but the extent of decreasing is larger in the C_{18}–HA system than in the C_{16}–HA system.

In the preceding papers[5,6] the thermodynamic equations of multicomponent monolayers were derived. Taking advantage of them (Eqs. 38, 42, and 43 in Ref. 6), we obtained the two-dimensional phase diagram and partial molar enthalpy change associated with the phase transition from an expanded to a condensed state. The diagrams of the C_{14}–HA, C_{15}–HA, C_{16}–HA, and C_{18}–HA systems are shown in Figs. 5 to 8, respectively.

The C_{14}–HA system (Fig. 5) has a maximum point in the phase diagram which is analogous to the C_{14}–EH system,[4] but the composition of the maximum

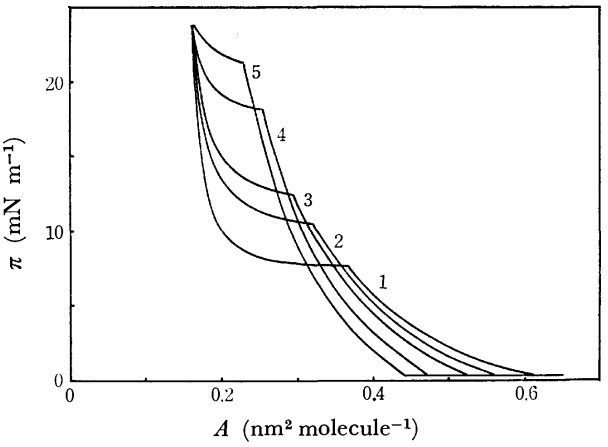

Fig. 1. Surface pressure *vs.* mean area curves of the tetradecanoic acid–hexadecyl acetate mixed monolayer at 298.15 K: 1, $x_2^{\pi}=1$(hexadecyl acetate); 2, 0.7; 3, 0.6; 4, 0.3; 5, 0(tetradecanoic acid).

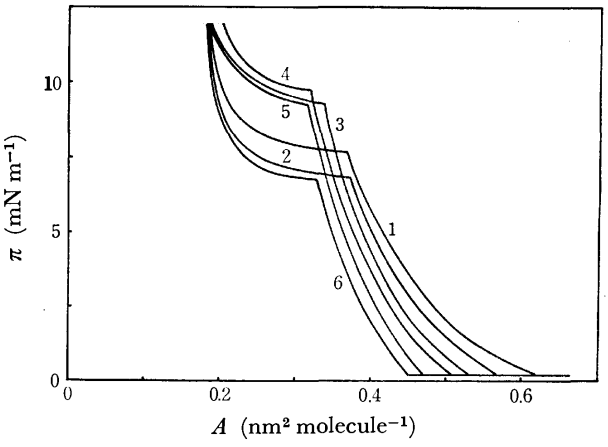

Fig. 2. Surface pressure *vs.* mean area curves of the pentadecanoic acid–hexadecyl acetate mixed monolayer at 298.15 K: 1, $x_2^{\pi}=1$(hexadecyl acetate); 2, 0.8; 3, 0.4; 4, 0.3; 5, 0.2; 6, 0(pentadecanoic acid).

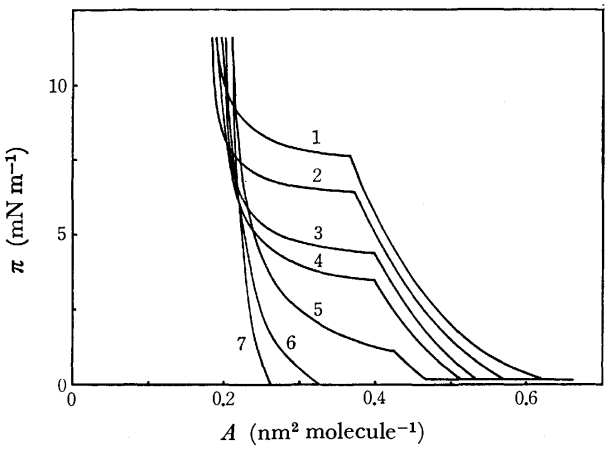

Fig. 3. Surface pressure *vs.* mean area curves of the hexadecanoic acid–hexadecyl acetate mixed monolayer at 298.15 K: 1, $x_2^{\pi}=1$(hexadecyl acetate); 2, 0.9; 3, 0.7; 4, 0.5; 5, 0.2; 6, 0.1; 7, 0(hexadecanoic acid).

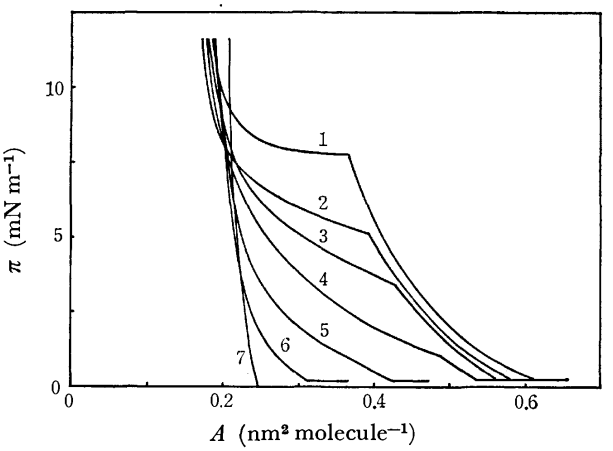

Fig. 4. Surface pressure *vs.* mean area curves of the octadecanoic acid–hexadecyl acetate mixed monolayer at 298.15 K: 1, $x_2^{\pi}=1$(hexadecyl acetate); 2, 0.95; 3, 0.9; 4, 0.8; 5, 0.7; 6, 0.6; 7, 0(octadecanoic acid).

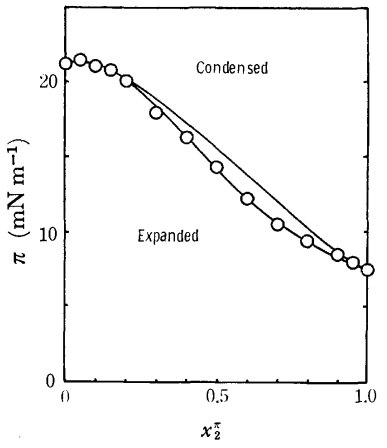

Fig. 5. Phase diagram of the tetradecanoic acid–hexadecyl acetate mixed monolayer at 298.15 K.

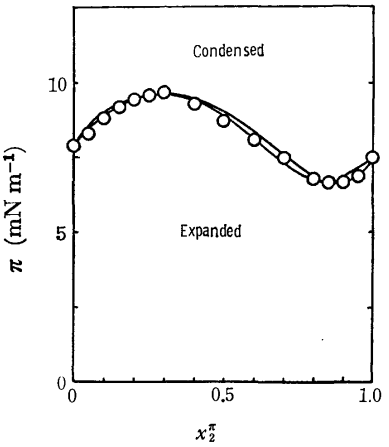

Fig. 6. Phase diagram of the pentadecanoic acid–hexadecyl acetate mixed monolayer at 298.15 K.

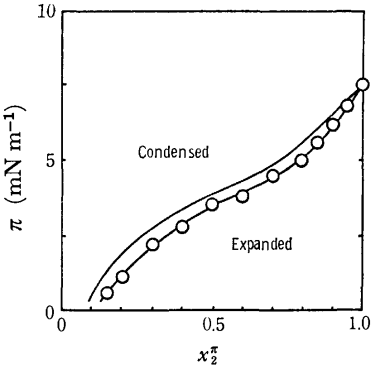

Fig. 7. Phase diagram of the hexadecanoic acid–hexadecyl acetate mixed monolayer at 298.15 K.

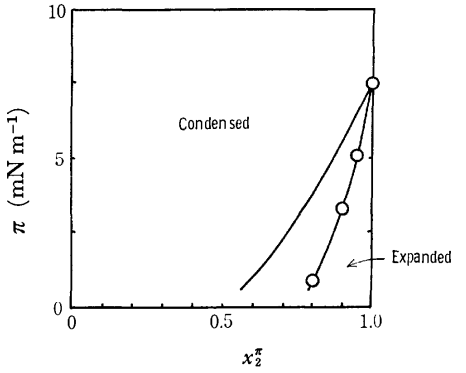

Fig. 8. Phase diagram of the octadecanoic acid–hexadecyl acetate mixed monolayer at 298.15 K.

point in the former system is $x_2^{\pi,e}=0.05$ while that in the latter system $x_2^{\pi,e}=0.3$. From the molecular structural point of view, the hydrocarbon chain of HA is longer than that of EH. It seems that C_{14} and HA are less miscible with each other than C_{14} and EH in mixed monolayer, and so in the C_{14}–HA system the composition of maximum point shifts towards the acid side more than that in the C_{14}–EH system. By using ethyl heptadecanoate, which has the same hydrocarbon chain length as HA, we investigated the mixed monolayer with C_{14}; it was found that in the C_{14}–ethyl heptadecanoate system there existed a maximum at $x_2^{\pi,e}=0.2$.[7]

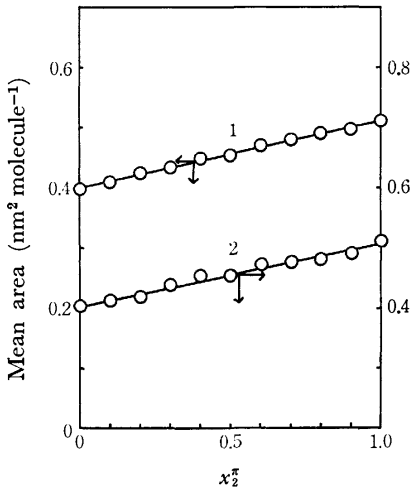

Fig. 9. Additivity of area at 2 mN m^{-1} for C_{14}–HA and C_{15}–HA systems at 298.15 K: 1, C_{14}–HA; 2, C_{15}–HA.

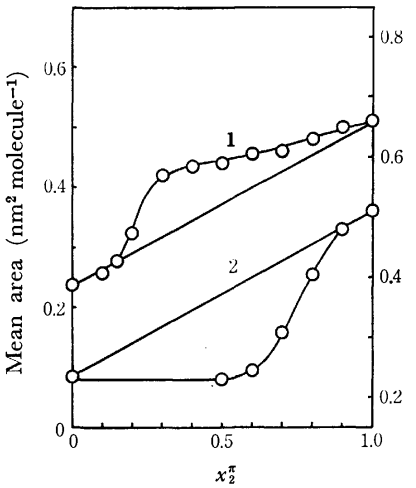

Fig. 10. Additivity of area at 2 mN m^{-1} for C_{16}–HA and C_{18}–HA systems at 298.15 K: 1, C_{16}–HA; 2, C_{18}–HA.

The diagram of the C_{15}–HA system at 298.15 K is shown in Fig. 6. There exist maximum and minimum points in this diagram at $x_2^{\pi,e}=0.3$ and 0.87, respectively. This is particularly surprising from the thermodynamic point of view and we have not observed such a result in any other system. This phase diagram shows that in the C_{15} rich region the excess free energy of the monolayer in the expanded state ($G^{E,e}$) is smaller than that in the condensed state ($G^{E,c}$), and in the HA rich region the $G^{E,e}$ is larger than $G^{E,c}$ at relatively high pressures.[8] According to thermodynamic analysis,[7] it is easily understandable that in a positive azeotrope system, which has a maximum point in the phase diagram, the mutual interaction between film-forming substances in the mixed monolayer is weaker than the interaction between the pure component molecules themselves. In other words, in the C_{15} rich region C_{15} and HA are likely to be located apart from each other, since the hydrophilic group of HA is so different from that of C_{15} that C_{15} and HA are difficult to pack together. It is thus more stable as the expanded

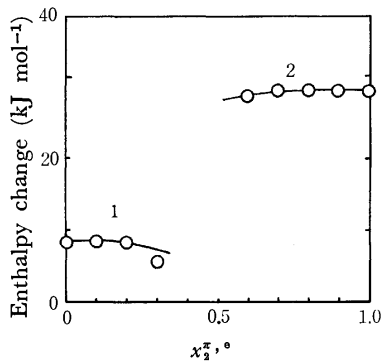

Fig. 11. Partial molar enthalpy change of the phase transition, $-(\bar{h}_i^e-\bar{h}_i^c)$ *vs.* mole fraction in the expanded monolayer, $x_2^{\pi,e}$, curves of the tetradecanoic acid–hexadecyl acetate at 293.15 K: 1, tetradecanoic acid; 2, hexadecyl acetate.

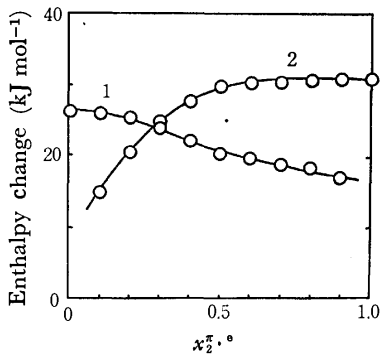

Fig. 12. Partial molar enthalpy change of the phase transition, $-(\bar{h}_i^e-\bar{h}_i^c)$ *vs.* mole fraction in the expanded monolayer, $x_2^{\pi,e}$, curves of the pentadecanoic acid–hexadecyl acetate at 295.65 K: 1, pentadecanoic acid; 2, hexadecyl acetate.

state in this region than as the condensed state. But in the HA rich region, it seems that C_{15} and HA are likely to pack together owing to the ease of packing of C_{15} and HA. In this way it is seen that the thermodynamic state of the monolayer is very much influenced by the molecular structure of the components. This is also revealed by the difference in phase diagrams between the C_{15}–HA(Fig. 6) and C_{15}–EH[4] systems.

Figure 7 represents the phase diagram of the C_{16}–HA system. This is also very different from that of the C_{16}–EH system.[4] π^{eq} decreases gradually with the decrease of $x_2^{\pi,e}$. It seems that the interaction between C_{16} and HA is complicated. In the C_{18}–HA system (Fig. 8), the diagram is analogous to that of the C_{18}–EH system.[4] But the π^{eq} decreases more rapidly with the decrease of $x_2^{\pi,e}$ than that of the C_{18}–EH system. This indicates that in the mixed monolayer HA is more condensed than EH. This can also be seen from the result of mean area *vs.* mole fraction curves (Fig. 10) and the partial molar enthalpy changes (Fig. 14).

The mean area *vs.* mole fraction curves of the mixed monolayers at 2 mN m^{-1} are shown in Figs. 9 and 10. In C_{14}–HA and C_{15}–HA systems (Fig. 9) the additivity rule is approximately established under these conditions. Owing to this result and the phase dia-

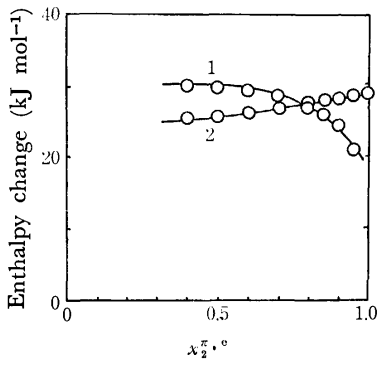

Fig. 13. Partial molar enthalpy change of the phase transition, $-(\bar{h}_i^c - \bar{h}_i^e)$ *vs.* mole fraction in the expanded monolayer, $x_2^{\pi,e}$, curves of the hexadecanoic acid–hexadecyl acetate at 298.15 K: 1, hexadecanoic acid; 2, hexadecyl acetate.

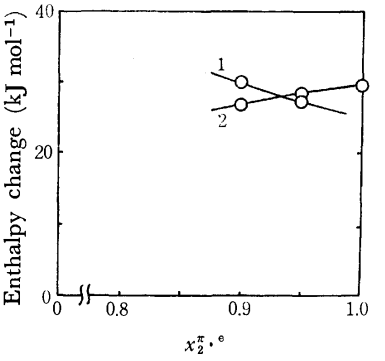

Fig. 14. Partial molar enthalpy change of the phase transition, $-(\bar{h}_i^c - \bar{h}_i^e)$ *vs.* mole fraction in the expanded monolayer, $x_2^{\pi,e}$, curves of the octadecanoic acid–hexadecyl acetate at 298.15 K: 1, octadecanoic acid; 2, hexadecyl acetate.

grams (Figs. 5 and 6), it may be said that these systems are nearly ideal at low surface pressures, but deviate appreciably from ideal behaviors as the pressure increases. In the C_{16}–HA system (Fig. 10) there is a considerable positive deviation from the additivity rule, similar to that of the C_{16}–EH system.[4] The C_{18}–HA system shows a considerable negative deviation in the expanded state, as shown by the solid line (Fig. 10), and the deviation is larger in the C_{18}–HA system than in the C_{18}–EH system.[4]

The partial molar enthalpy change was obtained from the thermodynamic analysis(Eqs. 38, 42, and 43 in Ref. 6), and they are shown in Figs. 11 to 14. In the C_{14}–HA system (Fig. 11), the enthalpy change of C_{14} gradually decreases, and that of HA slightly increases, with increase of $x_2^{\pi,e}$. Although the C_{15}–HA system has maximum and minimum points in the phase diagram, the nature of the enthalpy change, as shown in Fig. 12, is very similar to that of the C_{15}–EH system[4] which has only one maximum point in the phase diagram. The partial molar enthalpy change of C_{15} decreases, and that of HA increases considerably, with increase of $x_2^{\pi,e}$. In the C_{16}–HA system (Fig. 13), the enthalpy change of C_{16} also decreases, and the value of HA increases, with increases of $x_2^{\pi,e}$. This system shows the same tendency as the C_{16}–EH system[4] but the degree of variation of the partial molar enthalpy change is larger in the C_{16}–EH system than in the C_{16}–HA system. The characteristics of the enthalpy change of the C_{18}–HA system(Fig. 14) are similar to those of the C_{15}–HA and C_{16}–HA systems.

In conclusion, it was found that the phase diagram and partial molar enthalpy change vary with the chain length of the film-forming acid. There exists a maximum point in the C_{14}–HA system and this result is analogous to that of the C_{14}–EH system. However, in the C_{15}–HA system there is not only a maximum point but also a minimum point. This phenomenon was not observed in the C_{15}–EH or other systems, but is peculiar to the C_{15}–HA system. The C_{16}–HA system is also very different from the C_{16}–EH system. But the C_{18}–HA system is similar to the C_{18}–EH system. In this way, it is seen that the state of mixed monolayers is very much influenced by the molecular structure of film-forming components, especially by the chain length of the acid and the structure of the hydrophilic group of the ester. It seems that the structure effect is larger in mixed monolayers as the difference of the chain length between acid and ester becomes smaller.

References

1) N. Kuramoto, K. Sekita, K. Motomura, and R. Matuura, *Mem. Fac. Sci. Kyushu Univ.*, **C**, **8**, 67 (1972).
2) K. Sekita, M. Nakamura, K. Motomura, and R. Matuura, *Mem. Fac. Sci. Kyushu Univ.*, **C**, **10**, 51 (1976).
3) H. Matuo, K. Hiromoto, K. Motomura, and R. Matuura, *Bull. Chem. Soc. Jpn.*, **51**, 690 (1978).
4) H. Matuo, N. Yoshida, K. Motomura, and R. Matuura, *Bull. Chem. Soc. Jpn.*, **52**, 667 (1979).
5) K. Motomura, *J. Colloid Interface Sci.*, **48**, 307 (1974).
6) K. Motomura, K. Sekita, and R. Matuura, *J. Colloid Interface Sci.*, **48**, 319 (1974).
7) K. Motomura, T. Yano, M. Ikematsu, H. Matuo, and R. Matuura, *J. Colloid Interface Sci.*, to be published.
8) P. Gordon, "Principles of Phase Diagrams in Material Systems," McGraw-Hill, New York (1968), Chap. 4.

The Crystal and Molecular Structures of 6-Deoxyversicolorin A and Versicolorin A, Metabolites from *Aspergillus versicolor*

Keiichi FUKUYAMA,* Tamaichi ASHIDA,† Yukiteru KATSUBE, and Masao KAKUDO††

Faculty of Engineering, Tottori University, Koyama, Tottori 680

† *Faculty of Engineering, Nagoya University, Chikusa-ku, Nagoya 464*

†† *Institute for Protein Research, Osaka University, Yamadakami, Suita, Osaka 565*

(Received August 7, 1978)

The structures of 6-deoxyversicolorin A, $C_{18}H_{10}O_6$, and versicolorin A, $C_{18}H_{10}O_7$, both isolated from *Aspergillus versicolor*, have been determined by the X-ray diffraction method. Both compounds crystallized in the space group $P2_12_12_1$, with four molecules per unit cell. The cell dimensions of 6-deoxyversicolorin A are $a=9.588$, $b=18.083$, $c=7.769$ Å, and those of versicolorin A are $a=9.524$, $b=18.629$, $c=7.629$ Å. The structure was refined to $R=0.055$ for 6-deoxyversicolorin A and to $R=0.043$ for versicolorin A. Both structures are in agreement with those assigned by chemical and spectroscopic methods. There are two intramolecular hydrogen bonds in each molecule. Although an intermolecular hydrogen bond is present in versicolorin A, both structures are isotypic. The dimensions of the anthraquinone skeleton and the dihydrofuro[2,3-*b*]furan moiety are compared with those in related compounds whose structures have been determined.

The dihydrofuro[2,3-*b*]furan moiety is the common structural unit in an important class of fungel metabolites which includes aflatoxins, B_1[1] and G_1,[2] and sterigmatocystin.[3,4] The structures of these metabolites have been extensively investigated by chemical, spectroscopic, and X-ray methods. The present compounds, 6-deoxyversicolorin A (I) and versicolorin A (II), were isolated from *Aspergillus versicolor* (Vuillemin) Tiraboschi, and the structures were proposed by Elsworthy *et al.*[5] and Hamasaki *et al.*[6] respectively by means of chemical and spectroscopic methods. Both the compounds have a dihydrofuro-[2,3-*b*]furan moiety with an anthraquinone skeleton, and were shown to be biogenetic precursors of sterigmatocystin and aflatoxins.[7] The present X-ray structure analysis was carried out to compare the structures of the title compounds with those of the related metabolites of this mold which have been studied in our laboratory.

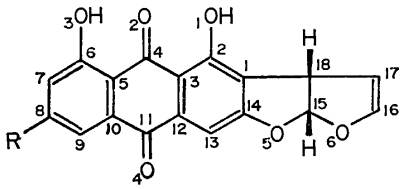

I: R=H

II: R=7OH

Experimental

Crystallographic Measurements. 6-Deoxyversicolorin A and versicolorin A were crystallized from acetone solution in the forms of orange red prisms and orange red plates respectively. Although the crystals of versicolorin A appeared to be well-developed plates, the diffraction profiles were broad and not symmetrical about the peaks. The cell constants were obtained from the least-squares treatment of the angular settings of 13 reflections. The crystal data and details of experimental conditions for each compound are summarized in Table 1. The intensities of each compound were measured on a Rigaku-Denki computer-controlled four-circle diffractometer with Ni-filtered Cu $K\alpha$ radiation. Attenuators were automatically inserted to keep the counting rate below 8000 cps. Backgrounds were counted for 10 s at the both sides of the scan range. The intensities were corrected for the Lorentz and polarization factors, but were not corrected for absorption.

TABLE 1. CRYSTAL DATA AND DETAILS OF EXPERIMENTAL CONDITIONS

	6-Deoxyversicolorin A	Versicolorin A
Molecular formula	$C_{18}H_{10}O_6$	$C_{18}H_{10}O_7$
Molecular weight	322.3	338.3
Crystal system	orthorhombic	orthorhombic
Space group	$P2_12_12_1$	$P2_12_12_1$
a	9.588(4) Å	9.524(5) Å
b	18.083(6) Å	18.629(7) Å
c	7.769(4) Å	7.629(5) Å
Z	4	4
D_x	1.589 g/cm³	1.659 g/cm³
μ(for Cu $K\alpha$)	10.4 cm⁻¹	11.2 cm⁻¹
Crystal size	0.07×0.07×0.28 mm	0.08×0.20×0.30 mm
Scan technique	ω-2θ scan	ω scan
Scan range (ω)	1.0°+0.2° tan θ	1.6°+0.15° tan θ
Scan speed (ω)	2° min⁻¹	2° min⁻¹
Maximum 2θ	120°	127°
No. of reflections measured	1180	1296
No. of non-zero reflections	1046	1160

Structure Determination of 6-Deoxyversicolorin A. The structure was solved by application of the vector-search method;[8] the rigid group used in the calculations was an anthraquinone skeleton with two oxygen atoms. A three-dimensional Fourier synthesis based on the phases due to the rigid group revealed the positions of the remaining non-hydrogen atoms. The structure was refined by the block-diagonal least-squares calculations,[9] first with isotropic and subsequently with anisotropic temperature factors for non-hydrogen atoms. All hydrogen atoms were found in a difference electron density map, and included in the subsequent refinement with isotropic temperature factors. The final refinement was made using the following weighting scheme: $w=0.0$ for $F_o=0$, $w=1.0$ for $0<F_o\leqq 22$, and $w=[1.0+0.33(F_o-22)]^{-1}$ for $22<F_o$. However, the two strongest reflections, 022 and 032, were omitted from the calculations. The final R value was 0.055 for 1044 non-zero reflections. The final atomic parameters are listed in Tables

TABLE 2. FINAL ATOMIC PARAMETERS AND e.s.d.'s ($\times 10^4$) FOR NON-HYDROGEN ATOMS

The anisotropic temperature factors are of the form: $\exp(-\beta_{11}h^2-\beta_{22}k^2-\beta_{33}l^2-\beta_{12}hk-\beta_{13}hl-\beta_{23}kl)$.

	x	y	z	β_{11}	β_{22}	β_{33}	β_{12}	β_{13}	β_{23}
(a)	6-Deoxyversicolorin A								
C(1)	8889 (5)	1043 (3)	9456 (7)	82 (6)	22 (1)	182 (11)	0 (5)	−20 (14)	−4 (7)
C(2)	8564 (5)	1687 (2)	8621 (7)	76 (5)	19 (1)	159 (9)	−12 (5)	1 (13)	−6 (7)
C(3)	7109 (5)	1879 (3)	8375 (6)	76 (5)	22 (1)	133 (9)	0 (5)	32 (13)	−16 (6)
C(4)	6749 (6)	2551 (3)	7477 (6)	100 (6)	20 (1)	141 (10)	6 (5)	23 (14)	−5 (6)
C(5)	5293 (5)	2719 (2)	7140 (7)	94 (6)	21 (1)	151 (10)	18 (5)	−52 (14)	−11 (7)
C(6)	4884 (6)	3356 (3)	6241 (7)	139 (8)	22 (2)	160 (10)	9 (6)	−30 (16)	−13 (7)
C(7)	3488 (6)	3517 (3)	5951 (8)	121 (8)	33 (2)	193 (12)	23 (6)	−31 (18)	−17 (8)
C(8)	2469 (6)	3052 (3)	6609 (8)	107 (7)	37 (2)	196 (12)	31 (6)	−41 (17)	−8 (9)
C(9)	2841 (6)	2416 (3)	7491 (8)	106 (7)	37 (2)	188 (12)	16 (7)	−16 (17)	−37 (9)
C(10)	4214 (5)	2261 (3)	7785 (7)	80 (6)	28 (2)	162 (10)	−2 (5)	−39 (14)	−27 (7)
C(11)	4605 (5)	1586 (3)	8801 (7)	78 (6)	27 (2)	167 (10)	−11 (5)	24 (14)	−11 (7)
C(12)	6089 (5)	1397 (3)	9051 (7)	92 (6)	21 (1)	151 (10)	−4 (5)	1 (14)	4 (7)
C(13)	6442 (6)	757 (3)	9922 (7)	97 (7)	27 (2)	159 (10)	−15 (6)	38 (15)	2 (7)
C(14)	7830 (6)	603 (2)	10101 (7)	120 (7)	19 (1)	148 (10)	−13 (5)	−20 (15)	12 (7)
C(15)	9829 (6)	7 (3)	10929 (8)	120 (7)	24 (1)	211 (12)	13 (6)	−83 (17)	−6 (8)
C(16)	10841 (7)	−422 (3)	8522 (9)	133 (8)	31 (2)	240 (14)	38 (7)	−55 (19)	−44 (9)
C(17)	10881 (6)	297 (3)	8261 (8)	108 (7)	34 (2)	208 (12)	25 (6)	−6 (17)	−20 (9)
C(18)	10276 (6)	677 (3)	9831 (7)	95 (6)	24 (1)	168 (10)	5 (5)	−20 (15)	−9 (7)
O(1)	9589 (4)	2129 (2)	8043 (5)	85 (4)	24 (1)	230 (8)	−8 (4)	38 (11)	10 (5)
O(2)	7690 (4)	2981 (2)	6931 (5)	106 (4)	24 (1)	202 (8)	−16 (4)	−1 (11)	37 (5)
O(3)	5838 (4)	3844 (2)	5623 (6)	136 (5)	28 (1)	243 (9)	6 (5)	−41 (13)	52 (6)
O(4)	3681 (4)	1203 (2)	9461 (6)	97 (5)	42 (2)	270 (10)	−18 (5)	40 (13)	37 (7)
O(5)	8319 (4)	−8 (2)	10936 (5)	116 (5)	25 (1)	236 (8)	−7 (4)	−24 (12)	34 (6)
O(6)	10302 (5)	−639 (2)	10072 (6)	170 (6)	24 (1)	274 (10)	30 (5)	−34 (15)	4 (6)
(b)	Versicolorin A								
C(1)	8946 (4)	1037 (2)	9391 (6)	72 (4)	21 (1)	137 (8)	1 (4)	−28 (11)	3 (5)
C(2)	8636 (4)	1683 (2)	8575 (5)	78 (5)	17 (1)	132 (8)	−6 (4)	12 (11)	−1 (5)
C(3)	7228 (4)	1877 (2)	8317 (5)	71 (4)	19 (1)	112 (7)	−1 (4)	−12 (11)	−2 (5)
C(4)	6872 (4)	2545 (2)	7473 (5)	74 (5)	18 (1)	139 (8)	6 (4)	−4 (11)	−9 (5)
C(5)	5416 (4)	2742 (2)	7187 (6)	75 (5)	19 (1)	132 (8)	−5 (4)	−10 (11)	−5 (5)
C(6)	5023 (5)	3373 (2)	6295 (6)	89 (5)	19 (1)	161 (8)	4 (4)	−1 (12)	3 (6)
C(7)	3646 (5)	3543 (2)	6001 (6)	97 (5)	17 (1)	179 (9)	3 (4)	−15 (13)	4 (6)
C(8)	2614 (5)	3088 (2)	6577 (6)	103 (6)	22 (1)	163 (9)	27 (4)	−52 (13)	−26 (6)
C(9)	2931 (5)	2449 (2)	7477 (6)	78 (5)	23 (1)	164 (9)	8 (4)	23 (12)	−4 (6)
C(10)	4319 (4)	2287 (2)	7763 (6)	75 (5)	20 (1)	128 (8)	7 (4)	−10 (11)	−12 (5)
C(11)	4651 (4)	1615 (2)	8729 (6)	73 (5)	21 (1)	140 (8)	−12 (4)	−1 (11)	1 (5)
C(12)	6161 (4)	1409 (2)	8950 (5)	75 (5)	20 (1)	117 (7)	−2 (4)	24 (10)	−9 (5)
C(13)	6458 (4)	774 (2)	9792 (6)	67 (4)	20 (1)	157 (8)	0 (4)	24 (11)	−9 (5)
C(14)	7880 (4)	603 (2)	9997 (5)	88 (5)	17 (1)	148 (8)	−5 (4)	−15 (12)	−23 (5)
C(15)	9865 (4)	12 (2)	10813 (6)	90 (5)	20 (1)	203 (9)	15 (5)	−58 (12)	3 (7)
C(16)	10913 (5)	−364 (2)	8344 (7)	100 (6)	29 (1)	200 (10)	16 (5)	−34 (14)	−29 (7)
C(17)	10981 (5)	332 (2)	8135 (7)	79 (5)	28 (1)	180 (9)	16 (4)	2 (12)	9 (7)
C(18)	10335 (4)	676 (2)	9768 (6)	66 (4)	19 (1)	165 (9)	8 (4)	−29 (11)	−3 (5)
O(1)	9725 (3)	2084 (1)	8049 (4)	70 (3)	24 (1)	208 (7)	−7 (3)	22 (9)	24 (4)
O(2)	7822 (3)	2962 (1)	6940 (4)	77 (3)	20 (1)	209 (6)	−7 (3)	0 (9)	30 (4)
O(3)	6006 (3)	3843 (2)	5723 (5)	109 (4)	22 (1)	223 (7)	−10 (3)	−29 (10)	48 (5)
O(4)	3734 (3)	1235 (2)	9343 (5)	73 (3)	38 (1)	254 (8)	−20 (3)	20 (10)	60 (6)
O(5)	8339 (3)	−2 (2)	10802 (4)	91 (3)	23 (1)	196 (6)	8 (3)	−5 (8)	56 (5)
O(6)	10335 (4)	−605 (1)	9896 (5)	128 (4)	19 (1)	241 (8)	18 (3)	2 (10)	−5 (4)
O(7)	1209 (3)	3218 (2)	6318 (5)	75 (4)	32 (1)	258 (8)	22 (3)	−54 (10)	15 (5)

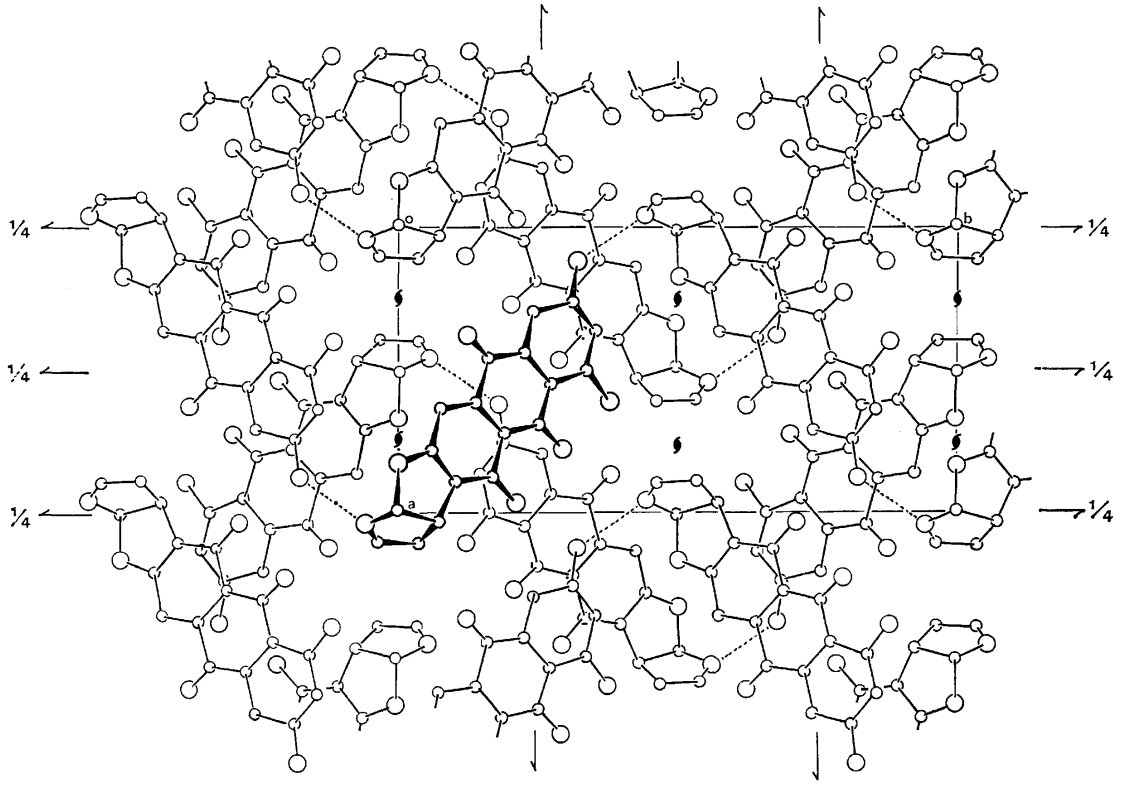

Fig. 1. The crystal structure of versicolorin A viewed along the c axis. Broken lines indicate intermolecular hydrogen bonds.

Table 3. Final positional parameters ($\times 10^3$) and isotropic temperature factors (Å^2) for hydrogen atoms

	x	y	z	B	d[a)]
(a) 6-Deoxyversicolorin A					
H(O1)	917(7)	265(3)	776(9)	4.6(17)	1.04
H(O3)	658(7)	371(3)	581(8)	4.5(16)	0.77
H(C7)	349(6)	400(3)	523(7)	2.6(13)	1.03
H(C8)	156(7)	318(3)	635(8)	4.6(16)	0.92
H(C9)	213(7)	207(3)	811(8)	4.6(17)	1.04
H(C13)	556(7)	48(3)	1066(8)	3.7(15)	1.13
H(C15)	1021(6)	−2(3)	1212(7)	2.1(11)	1.00
H(C16)	1134(6)	−81(3)	772(7)	2.9(14)	1.05
H(C17)	1122(7)	60(3)	734(8)	3.4(15)	0.96
H(C18)	1095(5)	99(3)	1054(7)	1.6(11)	1.02
(b) Versicolorin A					
H(O1)	959(6)	251(3)	757(8)	4.7(15)	0.89
H(O3)	686(7)	366(3)	600(8)	5.8(16)	0.91
H(C7)	333(6)	407(3)	544(7)	3.8(13)	1.12
H(O7)	108(6)	371(3)	581(8)	5.2(16)	1.01
H(C9)	216(6)	213(3)	785(7)	3.8(13)	0.98
H(C13)	580(7)	47(3)	1005(8)	4.3(14)	0.87
H(C15)	1014(5)	−4(3)	1218(7)	3.1(11)	1.08
H(C16)	1132(6)	−67(3)	741(8)	4.1(14)	0.99
H(C17)	1130(6)	66(3)	706(7)	3.9(13)	1.07
H(C18)	1098(5)	100(2)	1050(7)	2.5(11)	1.02

a) Length of covalent bond involving hydrogen atom in Å.

2(a) and 3(a).†††

Structure Determination of Versicolorin A. The structure was solved by the direct method with program MULTAN.[10] The refinement of versicolorin A was made in the same way as that of 6-deoxyversicolorin A. All hydrogen atoms were found in a difference electron density map after the anisotropic refinement for non-hydrogen atoms. The weighting scheme adopted in the final cycle of the refinement was: $w=0.0$ for $F_o=0$, $w=1.0$ for $0<F_o\leqq 17$, and $w=[1.0+0.11\times(F_o-17)]^{-1}$ for $17<F_o$. However, zero weight was given to the two strongest reflections, 022 and 032. The final R value was 0.043 for 1158 non-zero reflections. The final atomic parameters are listed in Tables 2(b) and 3(b).† The atomic scattering factors were taken from the International Tables for X-Ray Crystallography.[11]

Results and Discussion

The present crystallographic analysis has verified the structures of 6-deoxyversicolorin A and versicolorin A proposed by the chemical and spectroscopic methods.[5,6] The absolute configuration adopted is based on the assumption that the configuration of the dihydrofuro[2,3-*b*]furan moiety of the present molecules is the same as that of related molecules which has been established by X-ray method.[1,4,12] The crystal structure of versicolorin A is shown in

††† Lists of the observed and calculated structure factors are available from the authors on request and also kept as Document No. 7905 at the Chemical Society of Japan.

TABLE 4. BOND LENGTHS AND ANGLES FOR NON-HYDROGEN ATOMS

(a) Bond lengths (l/Å)

	6DVA	VA		6DVA	VA
C(1)-C(2)	1.370 (8)	1.387 (6)	C(1)-C(14)	1.384 (8)	1.377 (6)
C(1)-C(18)	1.514 (8)	1.512 (6)	C(2)-C(3)	1.450 (7)	1.402 (6)
C(2)-O(1)	1.344 (7)	1.340 (5)	C(3)-C(4)	1.442 (7)	1.442 (6)
C(3)-C(12)	1.412 (7)	1.422 (6)	C(4)-C(5)	1.453 (8)	1.452 (6)
C(4)-O(2)	1.265 (7)	1.259 (5)	C(5)-C(6)	1.404 (8)	1.408 (6)
C(5)-C(10)	1.417 (8)	1.416 (6)	C(6)-C(7)	1.389 (9)	1.368 (7)
C(6)-O(3)	1.358 (7)	1.354 (6)	C(7)-C(8)	1.387 (9)	1.370 (7)
C(8)-C(9)	1.386 (9)	1.408 (6)	C(8)-O(7)	—	1.374 (6)
C(9)-C(10)	1.366 (8)	1.373 (6)	C(10)-C(11)	1.501 (8)	1.487 (6)
C(11)-C(12)	1.477 (8)	1.498 (6)	C(11)-O(4)	1.236 (7)	1.217 (6)
C(12)-C(13)	1.383 (8)	1.376 (6)	C(13)-C(14)	1.367 (8)	1.400 (6)
C(14)-O(5)	1.363 (7)	1.356 (5)	C(15)-C(18)	1.543 (8)	1.538 (7)
C(15)-O(5)	1.447 (7)	1.454 (6)	C(15)-O(6)	1.418 (8)	1.417 (6)
C(16)-C(17)	1.316 (10)	1.309 (7)	C(16)-O(6)	1.368 (8)	1.381 (6)
C(17)-C(18)	1.516 (9)	1.530 (7)			

(b) Bond angles (φ/°)

	6DVA	VA		6DVA	VA
C(2)-C(1)-C(14)	119.6 (5)	120.2 (4)	C(2)-C(1)-C(18)	131.5 (5)	131.1 (4)
C(14)-C(1)-C(18)	108.9 (5)	108.7 (4)	C(1)-C(2)-C(3)	119.0 (5)	119.3 (4)
C(1)-C(2)-O(1)	119.9 (5)	116.9 (4)	C(3)-C(2)-O(1)	121.2 (5)	123.7 (4)
C(2)-C(3)-C(4)	119.7 (5)	120.6 (4)	C(2)-C(3)-C(12)	118.0 (5)	118.6 (4)
C(4)-C(3)-C(12)	122.3 (5)	120.8 (4)	C(3)-C(4)-C(5)	119.5 (5)	120.7 (4)
C(3)-C(4)-O(2)	120.7 (5)	120.5 (4)	C(5)-C(4)-O(2)	119.7 (5)	118.8 (4)
C(4)-C(5)-C(6)	122.0 (5)	122.5 (4)	C(4)-C(5)-C(10)	121.0 (5)	120.4 (4)
C(6)-C(5)-C(10)	116.9 (5)	117.0 (4)	C(5)-C(6)-C(7)	121.4 (5)	121.8 (4)
C(5)-C(6)-O(3)	121.5 (5)	120.8 (4)	C(7)-C(6)-O(3)	117.1 (5)	117.4 (4)
C(6)-C(7)-C(8)	119.5 (6)	119.5 (4)	C(7)-C(8)-C(9)	120.3 (6)	121.7 (4)
C(7)-C(8)-O(7)	—	122.9 (4)	C(9)-C(8)-O(7)	—	115.4 (4)
C(8)-C(9)-C(10)	120.1 (6)	118.0 (4)	C(5)-C(10)-C(9)	121.7 (5)	122.0 (4)
C(5)-C(10)-C(11)	118.6 (5)	120.1 (4)	C(9)-C(10)-C(11)	119.7 (5)	117.9 (4)
C(10)-C(11)-C(12)	119.9 (5)	118.4 (4)	C(10)-C(11)-O(4)	119.7 (5)	121.8 (4)
C(12)-C(11)-O(4)	120.4 (5)	119.8 (4)	C(3)-C(12)-C(11)	118.4 (5)	119.4 (4)
C(3)-C(12)-C(13)	122.0 (5)	122.6 (4)	C(11)-C(12)-C(13)	119.6 (5)	118.0 (4)
C(12)-C(13)-C(14)	117.3 (5)	116.5 (4)	C(1)-C(14)-C(13)	124.1 (5)	122.9 (4)
C(1)-C(14)-O(5)	112.6 (5)	113.7 (4)	C(13)-C(14)-O(5)	123.3 (5)	123.4 (4)
C(18)-C(15)-O(5)	107.1 (5)	107.6 (4)	C(18)-C(15)-O(6)	107.4 (5)	107.8 (4)
O(5)-C(15)-O(6)	107.9 (5)	107.3 (4)	C(17)-C(16)-O(6)	115.4 (6)	116.5 (5)
C(16)-C(17)-C(18)	108.3 (6)	107.2 (4)	C(1)-C(18)-C(15)	101.8 (5)	101.6 (4)
C(1)-C(18)-C(17)	112.3 (5)	112.5 (4)	C(15)-C(18)-C(17)	101.2 (5)	101.7 (4)
C(14)-O(5)-C(15)	109.2 (4)	108.1 (3)	C(15)-O(6)-C(16)	107.4 (5)	106.6 (4)

Fig. 1. The bond lengths and angles for non-hydrogen atoms are given in Table 4, the equations of the least-squares planes and perpendicular displacements of atoms from each plane in Table 5, and intermolecular distances in Table 6.

Hydrogen Bonds. There are two intramolecular hydrogen bonds in each molecule. The lengths of O(2)···H(O1) and O(2)···H(O3) are 1.67 and 1.87 Å respectively in 6-deoxyversicolorin A, and 1.97 and 1.75 Å respectively in versicolorin A. The angles of O(1)-H(O1)···O(2), O(3)-H(O3)···O(2), H(O1)···O(2)-C(4), and H(O3)···O(2)-C(4) are 137, 145, 105, and 101° respectively in 6-deoxyversicolorin A, and 126, 148, 107, and 102° respectively in versicolorin A. In the crystal of versicolorin A there is an intermolecular hydrogen bond, O(7)-H(O7)···O(6), which connects the molecules related by the screw axis along the b axis. The distance of H(O7)···O(6) is 1.93 Å, and the angles of O(7)-H(O7)···O(6), H(O7)···O(6)-C(15), and H(O7)···O(6)-C(16) are 143, 117, and 105° respectively. A short contact (2.865 Å) is observed in the crystal of versicolorin A between the atoms O(7) and O(1) of the molecule at $(-1+x, y, z)$; however, the final difference electron density map showed no peak in the region between these atoms. The molecular arrangements in both crystals are similar in spite of the existence of the intermolecular hydrogen bond in the crystal of versicolorin A.

Structure of Dihydrofuro[2,3-b]furan Moiety. The

TABLE 5. EQUATIONS OF LEAST-SQUARES PLANES AND DEVIATIONS OF ATOMS FROM EACH PLANE

X, Y, and Z are Cartesian coordinates in Å referred to the axes a, b, and c.

(a) Anthraquinone skeleton

6DVA: $0.004X-0.520Y-0.854Z+7.283=0$

VA: $0.001X-0.486Y-0.874Z+7.244=0$

	6DVA	VA		6DVA	VA
C(1)	0.066	0.050	C(12)	−0.011	0.006
C(2)	0.012	0.008	C(13)	0.015	0.020
C(3)	−0.011	0.005	C(14)	0.047	0.039
C(4)	−0.048	−0.039	O(2)	−0.087	−0.060
C(5)	0.011	−0.028	O(4)	−0.110	−0.100
C(6)	0.006	−0.006	C(15)[a]	0.067	0.032
C(7)	0.042	0.036	C(18)[a]	0.166	0.127
C(8)	0.039	0.063	O(1)[a]	−0.015	−0.004
C(9)	0.053	0.043	O(3)[a]	−0.038	−0.049
C(10)	0.009	0.000	O(5)[a]	0.069	0.051
C(11)	−0.029	−0.034	O(7)[a]	—	0.118

(b) C(1), C(14), C(15), C(18), and O(5) atoms

6DVA: $0.033X+0.528Y+0.848Z-7.488=0$

VA: $0.024X+0.498Y+0.867Z-7.353=0$

	6DVA	VA		6DVA	VA
C(1)	−0.024	−0.022	C(18)	0.033	0.031
C(14)	0.005	0.003	O(5)	0.022	0.021
C(15)	−0.035	−0.033			

(c) C(15), C(16), C(17), C(18), and O(6) atoms

6DVA: $0.899X+0.042Y+0.436Z-12.212=0$

VA: $0.890X+0.016Y+0.456Z-12.153=0$

	6DVA	VA		6DVA	VA
C(15)	0.036	0.032	C(18)	−0.028	−0.023
C(16)	0.013	0.013	O(6)	−0.032	−0.029
C(17)	0.012	0.008			

a) Not included in the least-squares calculation.

dihydrofuro[2,3-*b*]furan moiety has been widely found in fungal metabolites. The interatomic distances of this moiety for 10 molecules, whose structures were determined by means of X-ray crystallography, have been compared by a half-normal probability plot.[13] The slopes of the plots range from *ca.* 1.2 to 3.0 with intercept 0.0, and some of them are not straight. The plots for 6-deoxyversicolorin A-sterigmatocystin and for 6-deoxyversicolorin A-sterigmatin are shown in Fig. 2 as typical examples.†† Most of the extreme values are found between non-bonded atoms, especially between the atoms C(1), C(14), or O(5) and the atoms C(17), C(16), or O(6). This fact suggests that the environments affect the conformation of such a simple moiety.

The conformation of this moiety may be defined by the torsion angles about the C(18)–C(15) bond, and the values for these angles are listed in Table 7. The torsion angles of C(1)–C(18)–C(15)–O(5) and C(17)–C(18)–C(15)–O(6) are apt to be right-handed in helicity. However, it is difficult to generalize the conformation of this moiety, since there is no rule for the distribution of the torsion angles about the C(18)–C(15) bond except the right-handed helicity.

Structure of Anthraquinone Skeleton. The structure of the anthraquinone skeleton was also examined by the half-normal probability method. The slope of the plot (1.8) between the anthraquinone skeletons of the present compounds is not much greater than 1.0, which is in accordance with the result that the skew-senses of the skeletons of each of these compounds are similar to each other, as shown in Table 5. The slopes of the plots between the skeletons of the other molecules, averufin,[18] and versicolorin C,[19] are larger than that of the present compounds (1.8—2.5). The plot for versicolorins A and C is shown in Fig. 2 as an example. When interatomic distances greater than

†† The figures of 55 plots among these molecules are available from the authors on request.

TABLE 6. SHORT INTERMOLECULAR CONTACTS BETWEEN NON-HYDROGEN ATOMS

		6DVA	VA			6DVA	VA
O(7)	C(16)^{I}	—	3.336	O(7)	O(6)^{I}	—	2.798[a]
O(2)	C(16)^{II}	3.231	3.351	O(2)	O(6)^{II}	3.515	3.490
O(3)	C(16)^{II}	3.513	3.362	C(6)	O(1)^{III}	3.454	3.434
C(7)	O(1)^{III}	3.480	3.460	C(8)	C(4)^{III}	3.426	3.381
C(8)	O(2)^{III}	3.331	3.326	C(9)	O(2)^{III}	3.512	3.456
O(3)	C(17)^{III}	3.394	3.320	O(7)	C(4)^{III}	—	3.283
O(7)	C(5)^{III}	—	3.304	C(6)	C(18)^{IV}	3.536	3.499
C(9)	C(2)^{IV}	3.498	3.484	C(10)	C(2)^{IV}	3.435	3.451
C(10)	O(1)^{IV}	3.443	3.425	C(11)	O(1)^{IV}	3.378	3.453
O(4)	O(2)^{IV}	3.308	3.322	C(8)	O(1)^{V}	3.413	3.511
C(9)	O(1)^{V}	3.189	3.158	O(4)	C(17)^{V}	3.280	3.249
O(4)	C(18)^{V}	3.412	3.416	O(7)	O(1)^{V}	—	2.865
O(7)	O(2)^{V}	—	3.296	O(4)	C(16)^{VI}	3.487	3.474
O(5)	C(13)^{VI}	3.388	3.372	O(6)	C(11)^{VI}	3.367	3.477

Roman numeral superscripts refer to the following transformations of the coordinates:

(I) $1-x,\ 1/2+y,\ 3/2-z$ (II) $2-x,\ 1/2+y,\ 3/2-z$ (III) $-1/2+x,\ 1/2-y,\ 1-z$

(IV) $-1/2+x,\ 1/2-y,\ 2-z$ (V) $-1+x,\ y,\ z$ (VI) $3/2-x,\ -y,\ 1/2+z$

a) Hydrogen bond.

TABLE 7. TORSION ANGLES ABOUT THE C(18)-C(15) BOND

	A	B	C	D
6DVA	5.9	5.7	121.6	−110.0
VA	5.6	4.9	121.1	−110.6
ST(A)	2.1	1.8	118.6	−114.7
ST(B)	0.5	−1.5	117.0	−118.0
STERIG	4.6	3.6	121.2	−112.9
OMST	4.8	1.6	121.0	−114.6
DMST	13.6	11.2	127.8	−103.0
MTST	1.3	0.9	119.4	−117.1
AF(C)	3.2	2.8	121.1	−115.1
AF(O)	2.0	−0.1	117.7	−115.7
AF(M)	3.0	0.7	117.9	−114.1

A: C(1)-C(18)-C(15)-O(5), B: C(17)-C(18)-C(15)-O(6), C: C(1)-C(18)-C(15)-O(6), D: C(17)-C(18)-C(15)-O(5).

Abbreviation: 6DVA, 6-deoxyversicolorin A; VA, versicolorin A; ST(A) and ST(B), two crystallographically independent molecules (A and B) of sterigmatin;[15] STERIG, sterigmatocystin;[4] OMST, *O*-methylsterigmatocystin;[4] DMST, demethylsterigmatocystin;[17] MTST, 5-methoxysterigmatocystin;[16] AF(C), aflatoxin B_1 (chloroform-solvated);[1] AF(O), aflatoxin B_1 (orthorhombic form);[1] AF(M), aflatoxin B_1 (monoclinic form).[1] The sign convention of the torsion angle is such that the sign is positive if a clockwise rotation is requested of the atom (1) to eclipse atom (4) whilst looking down the (2)-(3) bond. The configurations of the moiety in these molecules are assumed to be similar to each other.

3.0 Å were excluded from the drawing, most of the extreme values were eliminated and the slopes decreased slightly to 1.6—2.2. This fact shows that the structure of the skeleton is affected by the environment, as in the case of the dihydrofuro[2,3-*b*]furan moiety. However, the difference of substituents attached to the atoms C(1), C(8), and C(14) of this skeleton does not seem to affect the short interatomic distances.

Although the interatomic distances are dependent on the cell constants, the underestimation (about 1/1.6) of e.s.d.'s can scarcely be ascribed to their error. The underestimation may be due to other sources, such as the effect of thermal motion and/or the inherent tendency of underestimation in a block-diagonal least-squares technique. The same underestimation has been reported by several authors.[14]

Average Dimensions of Dihydrofuro[2,3-b]furan Moiety and Anthraquinone Skeleton. The average dimensions of the dihydrofuro[2,3-*b*]furan moiety and the anthraquinone skeleton were calculated by using the e.s.d.'s of each length as a weight (Fig. 3). Although the e.s.d. is underestimated, this may be reasonable weighting, because the underestimation of e.s.d. for each bond length is not so different. The dimensions of the anthraquinone skeleton seem to be affected by two hydroxyl groups, O(1)H and O(3)H; the lengths of the C(3)–C(4) and C(4)–C(5) bonds are shorter than those of the C(10)–C(11) and C(11)–C(12) bonds, while the lengths of the C(4)–O(2), C(2)–C(3), and C(5)–C(6) bonds are longer than those of the C(11)–O(4), C(12)–C(13), and C(9)–C(10) bonds. Such an

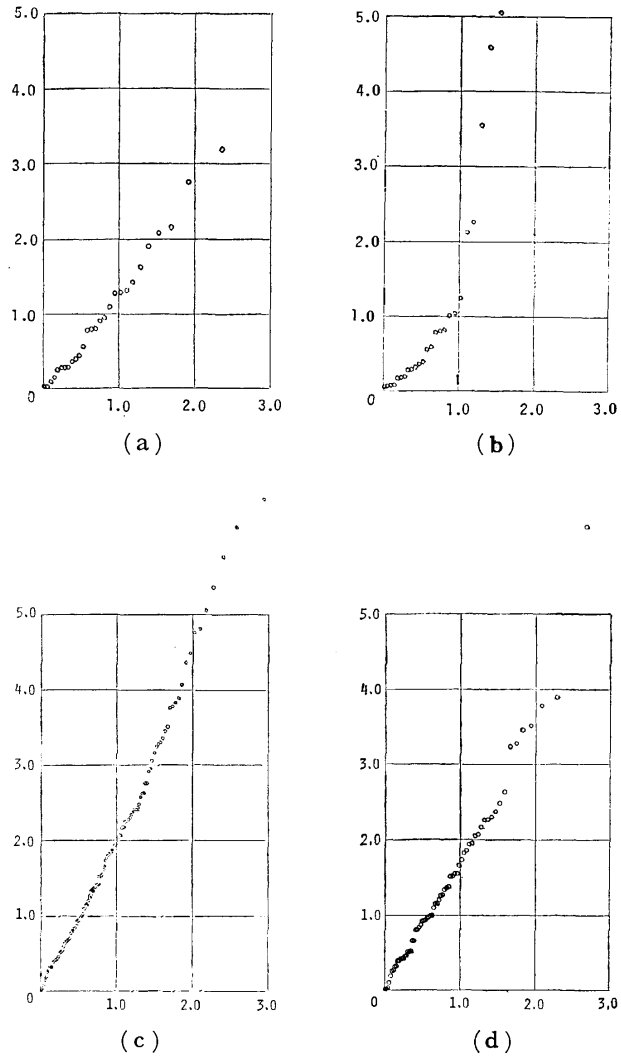

Fig. 2. Half-normal probability plot : the vertical axis is observed δp_i; the horizontal axis is the expected δp_i. $\delta p_i = |d(1)-d(2)|/\{\sigma^2(1)+\sigma^2(2)\}^{1/2}$, where d and σ are the interatomic distance and its e.s.d. respectively. (a) 6-Deoxyversicolorin A-sterigmatocystin as an example that the conformation of the dihydrofuro[2,3-*b*]furan moiety is similar to each other, (b) 6-deoxyversicolorin A-sterigmatin (B molecule) as an example that the conformation is different. (Table 7) (c) Half-normal probability plot for the anthraquinone skeletons of versicolorin A-versicolorin C including all data, and (d) that excluding the data of interatomic distances greater than 3.0 Å.

unequivalence of bond lengths in the anthraquinone skeleton is also found in 1,5-dianilinoanthraquinone and 1,8-dianilinoanthraquinone.[20] As expected from the chemical structure, however, the symmetry of the dimensions of the skeleton about the vector O(2)–

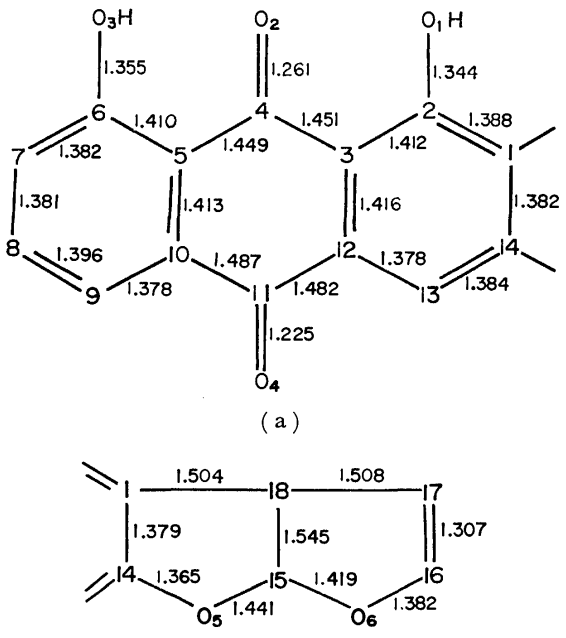

Fig. 3. Averaged dimensions of (a) anthraquinone skeleton and (b) dihydrofuro[2,3-*b*]furan moiety. Taking account of the underestimation of e.s.d. of bond length of individual molecule, the e.s.d. of the mean length may be about 0.004 Å for both anthraquinone skeleton and dihydrofuro[2,3-*b*]furan moiety.

O(4) is excellent.

The computations were performed, using programs written by the authors, on a TOSBAC-3400 computer at the Tottori University Computing Center, and on a NEAC2200-N700 computer at the Computation Center of Osaka University.

The authors wish to thank Professor Yuichi Hatsuda and Dr. Takashi Hamasaki for supplying the samples.

References

1) T. C. van Soest and A. F. Peerdeman, *Acta Crystallogr., Sect. B*, **26**, 1940 (1970); T. C. van Soest and A. F. Peerdeman, *ibid.*, **26**, 1947 (1970).

2) K. K. Cheung and G. A. Sim, *Nature*, **201**, 1185 (1964).

3) E. Bullock, J. C. Roberts, and J. G. Underwood, *J. Chem. Soc.*, **1962**, 4179.

4) K. Fukuyama, K. Hamada, T. Tsukihara, Y. Katsube, T. Hamasaki, and Y. Hatsuda, *Bull. Chem. Soc. Jpn.*, **49**, 1153 (1976); K. Fukuyama, K. Hamada, T. Tsukihara, and Y. Katsube, *Bull. Chem. Soc. Jpn.*, **51**, 37 (1978).

5) G. C. Elsworthy, J. S. E. Holker, (Mrs) J. M. McKeown, J. B. Robinson, and L. J. Mulheirn, *J. Chem. Soc., Chem. Commun.*, **17**, 1069 (1970).

6) T. Hamasaki, Y. Hatsuda, N. Terashima, and M. Renbutsu, *Agric. Biol. Chem.*, **29**, 166 (1965).

7) M. Biollaz, G. Büchi, and G. Milne, *J. Am. Chem. Soc.*, **92**, 1035 (1970); D. P. H. Hsieh, R. C. Yao, D. L. Fitzell, and C. A. Reece, *J. Am. Chem. Soc.*, **98**, 1020 (1976); K. G. R. Pachler, P. S. Steyn, R. Vleggaar, P. L. Wessels, and D. B. Scott, *J. Chem. Soc., Perkin Trans. 1*, **1976**, 1182.

8) R. Huber, in "Crystallographic Computing," ed by F. R. Ahmed, Munksgaard, Copenhagen (1970).

9) T. Ashida, HBLS-V, The Universal Crystallographic Computing System-Osaka, The Computation Center, Osaka University (1973). pp. 55—60.

10) G. Germain, P. Main, and M. M. Woolfson, *Acta Crystallogr., Sect. A*, **27**, 368 (1971).

11) "International Tables for X-Ray Crystallography," Kynoch Press, Birmingham (1974), Vol. IV, pp. 72—73.

12) C. A. Bear, J. M. Waters, and T. N. Waters, *J. Chem. Soc., Chem. Commun.*, **1970**, 1705.

13) S. C. Abrahams and E. T. Keve, *Acta Crystallogr., Sect. A*, **27**, 157 (1971).

14) W. H. De Camp, *Acta Crystallogr., Sect. A*, **29**, 148 (1973).

15) K. Fukuyama, T. Tsukihara, Y. Katsube, T. Hamasaki, Y. Hatsuda, N. Tanaka, T. Ashida, and M. Kakudo, *Bull. Chem. Soc. Jpn.*, **48**, 1639 (1975).

16) G. D. Smith and W. L. Duax, *Cryst. Struct. Commun.*, **4**, 697 (1970).

17) O. Yoshida, N. Tanaka, T. Ashida, M. Kakudo, K. Fukuyama, and Y. Katsube, *Acta Crystallogr.*, in press.

18) Y. Katsube, T. Tsukihara, N. Tanaka, K. Ando, T. Hamasaki, and Y. Hatsuda, *Bull. Chem. Soc. Jpn.*, **45**, 2091 (1971).

19) K. Fukuyama, T. Tsukihara, Y. Katsube, T. Hamasaki, and Y. Hatsuda, *Bull. Chem. Soc. Jpn.*, **48**, 2648 (1975).

20) M. Bailey and C. J. Brown, *Acta Crystallogr.*, **22**, 488 (1967); M. Bailey and C. J. Brown, *ibid.*, **22**, 493 (1967).

Transport of Picrate Anion against Its Concentration Gradient through a Dichloroethane Membrane

Masaaki SUGIURA* and Toshio SHINBO
National Chemical Laboratory for Industry, Nishiyawata, Hiratsuka 254
(Received August 9, 1978)

The rate of picrate transport coupled to a diffusion of potassium ions through a bulk 1,2-dichloroethane membrane has been measured. The membrane, containing a potassium ionophore separated two aqueous phases, one containing picrate and potassium salt and the other containing picrate and lithium salt. The picrate anion was accumulated against the concentration gradient in the aqueous phase containing the lithium salt. The rate of picrate transport incrased with increasing ionophore concentration and in the absence of the ionophore, the transfer of picrate did not occur. The effect of potassium and lithium counter-ions such as chloride, nitrate and sulfate on the transport of picrate has been examined. The combination of potassium sulfate and lithium nitrate showed the highest rate of transport. In the potassium nitrate–lithium nitrate system, the transport of picrate was appreciably depressed by the transfer of nitrate ions across the membrane. The decrease in concentration of potassium ion in the aqueous phase brought about a lowering of the rate of picrate transport. The rate of picrate transport rose according to the following order of ionophore : dicyclohexyl-18-crown-6 > dicyclohexyl-24-crown-8 > dibenzo-18-crown-6 > dibenzo-24-crown-8 > valinomycin.

When the chemical potential difference of ions is imposed across an oil membrane, a lipophilic ion or a specific ion which binds to a transport carrier can be moved against the concentration gradient to one side of the membrane. The uphill transport of alkaline cations[1,2] and amino acids[3] through bulk organic liquid membranes has been reported and in these systems, the energy for transport was the chemical potential difference of the protons across the membrane. Kusaka *et al.*[4] have observed the accumulation of alanine and proline into phospholipid vesicles containing hydrohobic proteins as transport carriers, in response to a membrane potential introduced by the diffusion of potassium ions *via* valinomycin.

In the present paper, the uphill transport of picrate anion through the bulk 1,2-dichloroethane membrane has been investigated. In this system, the transport of picrate has been coupled to a diffusion of potassium ions *via* various potassium ionophores.

Experimental

Apparatus. The apparatus used for measuring the transport of picarte is shown in Fig. 1. It is a modification of the apparatus described by Behr and Lehn.[3] The cell consisted of a cylindrical glass vessels (7 cm i.d.; height 7 cm) containing a central glass wall which separated the two aqueous phases (50 ml each). The dichloroethane phase (phase III, 100 ml) lay under these aqueous phases and bridged across the central separation. The aqueous phase I in the cell contained initially 10^{-4} M potassium picrate, a 0.01 M Tris-H_2SO_4 buffer of pH 8.3 and a 0.1 M potassium salt (the experiment on the effect of potassium ion concentration was different) while phase II contained 10^{-4} M potassium picrate, a 0.01 M Tris-H_2SO_4 buffer and a 0.1 M lithium salt. To the dichloroethane phase, an appropriate quantity of potassium ionophore was added. The cell was placed in a water bath adjusted to 25±0.1 °C. All three phases were agitated at 180 r.p.m. with a pair of glass stirrers.

Materials. The potassium ionophores, dicyclohexyl-18-crown-6 and dicyclohexyl-24-crown-8 were commercial products from Nihon Soda Co., dibenzo-18-crown-6 and dibenzo-24-crown-8 from Aldrich Chemical Co. and valinomycin from Sigma Chemical Co. All other chemicals were reagent grade and not subsequently purified.

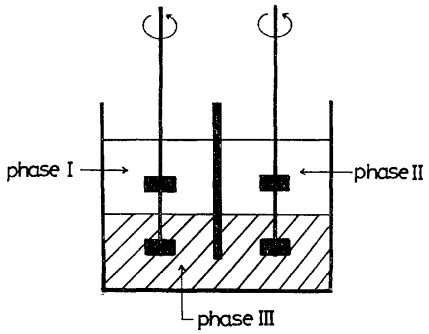

Fig. 1. Apparatus for measuring the transport of picrate. Initial composition of each phase;
phase I : aqueous solution (50 ml) containing 10^{-4} M K-picrate, 0.01 M Tris-H_2SO_4 buffer (pH 8.3) and 0.001—0.1 N K-salt,
phase II : aqueous solution (50 ml) containing 10^{-4} M K-picrate, 0.01 M Tris-H_2SO_4 buffer (pH 8.3) and 0.1 N Li-salt,
phase III : 1,2-dichloroethane (100 ml) containing 0—10^{-3} M ionophore.

Procedure. The dichloroethane used for phase III was pre-equilibrated with 10^{-4} M potassium picrate solution containing a Tris-H_2SO_4 buffer and potassium and lithium salts, whose concentrations were equal to those in the aqueous phases I and II. 1,2-Dichloroethane (100 ml) containing an appropriate quantity of ionophore was shaken with the above-mentioned picrate solution(250 ml) for *ca.* 6 h at 25 °C. During this treatment, the picrate solution was occasionally renewed until the picrate concentration in the aqueous solution became constant. After attainment of equilibrium, the picrate solution was removed, after which dichloroethane (100 ml) was placeed in the cell. Two kinds of aqueous solution used for phases I and II were subsequently poured into either side, as shown in Fig. 1. The transport of picrate was initiated by the addition of the aqueous solutions. The concentration of picrate in both the aqueous phases and the membrane potential were measured at regular time intervals, the determination being conducted on a Hitachi Model 100-10 spectrophotometer at 420 nm and that of the membrane potential using a Keithley Model

Table 1. Initial concentration of picrate in the 1,2-dichloroethane phase and concentration 7 h after the start of picrate transport for various membrane systems

K, Li salts Phase I-Phase II	Ionophre (Concn, M)	Picrate concentration (M) Initial	After 7 h
0.1 M KCl-0.1 M LiCl	Dicyclohexyl-18-crown-6 (10^{-5})	0.9×10^{-5}	0.8×10^{-5}
0.1 M KCl-0.1 M LiCl	Dicyclohexyl-18-crown-6 (10^{-4})	9.0×10^{-5}	7.2×10^{-5}
0.1 M KCl-0.1 M LiCl	Dicyclohexyl-18-crown-6 (10^{-3})	9.2×10^{-4}	8.2×10^{-4}
0.1 M KNO_3-0.1 M $LiNO_3$	Dicyclohexyl-18-crown-6 (10^{-4})	9.9×10^{-5}	9.3×10^{-5}
0.05 M K_2SO_4-0.05 M Li_2SO_4	Dicyclohexyl-18-crown-6 (10^{-4})	8.3×10^{-5}	6.1×10^{-5}
0.05 M K_2SO_4-0.1 M $LiNO_3$	Dicyclohexyl-18-crown-6 (10^{-4})	9.1×10^{-5}	6.6×10^{-5}
0.1 M KCl-0.05 M Li_2SO_4	Dicyclohexyl-18-crown-6 (10^{-4})	8.8×10^{-5}	6.5×10^{-5}
0.05 M KCl, 0.05 M LiCl-0.1 M LiCl	Dicyclohexyl-18-crown-6 (10^{-4})	8.2×10^{-5}	7.1×10^{-5}
0.01 M KCl, 0.09 M LiCl-0.1 M LiCl	Dicyclohexyl-18-crown-6 (10^{-4})	7.9×10^{-5}	6.8×10^{-5}
0.005 M KCl, 0.095 M LiCl-0.1 M LiCl	Dicyclohexyl-18-crown-6 (10^{-4})	7.4×10^{-5}	6.8×10^{-5}
0.001 M KCl, 0.099 M LiCl-0.1 M LiCl	Dicyclohexyl-18-crown-6 (10^{-4})	5.3×10^{-5}	5.2×10^{-5}
0.1 M KCl-0.1 M LiCl	Dicyclohexyl-24-crown-8 (10^{-4})	8.9×10^{-5}	7.4×10^{-5}
0.1 M KCl-0.1 M LiCl	Dibenzo-18-crown-6 (10^{-4})	2.6×10^{-5}	1.1×10^{-5}
0.1 M KCl-0.1 M LiCl	Dibenzo-24-crown-8 (10^{-4})	2.4×10^{-5}	2.1×10^{-5}
0.1 M KCl-0.1 M LiCl	Valinomycin (10^{-4})	8.9×10^{-5}	8.7×10^{-5}

610C or a Toadenpa Model PM-19A electrometer, with calomel electrodes connected to the aqueous phase, *via* salt bridges made of polyethylene tubing containing agar saturated with potassium chloride. The picrate concentrations in the dichloroethane phase before and after the measurement of picrate transport were also determined spectrophotometrically.

Results

Effect of Ionophore Concentration. The picrate concentrations in both aqueous phases and the membrane potential against time curves for various concentration of dicyclohexyl-18-crown-6 are shown in Fig. 2. The polarity of the membrane potential was positive in phase II with respect to phase I. In these systems, phase I contained 0.1 M potassium chloride and phase II 0.1 M lithium chloride. The picrate concentration in phase I decreased with time [dotted line in Fig. 2 (a)], while that in phase II increased [solid line in Fig. 2 (a)]. Thus the picrate anion was transferred from phase I to phase II against the concentration gradient through the dichloroethane membrane. The increment of picrate in phase II however was larger than the decrement in phase I attributable to the liberation of picrate from the dichloroethane phase into phase II. The initial concentrations of picrate in the dichloroethane phase and the concentrations 7 h after the start of picrate transport are listed in Table 1, together with those for the other transport systems.

The rate of picrate transport increased with increasing ionophore concentration. In the absence of ionophore, the transfer of picrate was not observed. In this case, the membrane potential was about 25 mV.

Effect of Potatsium and Lithium Counter-ions. When the nitrates and sulfates of potassium and lithium were added in the aqueous phases in place of the chlorides, the transport of picrate was affected by the counter-ions, the effect of which is shown in Fig. 3.

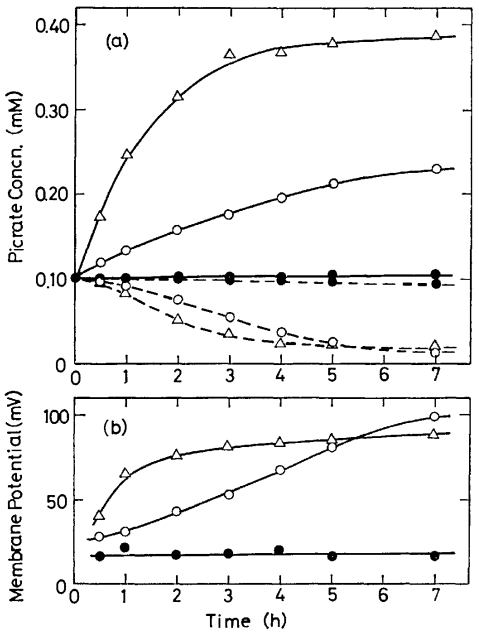

Fig. 2. Effect of ionophore concentration on the transport of picrate.
(a) Picrate concentrations in both aqueous phases against time curves.
The dotted and solid lines represent the picrate concentrations in phases I and II respectively.
(b) Membrane potential against time curves. Ionophore concentration;
● : 10^{-5} M, ○ : 10^{-4} M, △ : 10^{-3} M.
Ionophore; dicyclohexyl-18-crown-6, K, Li salts; phase I : 0.1 M KCl, phase II : 0.1 M LiCl.

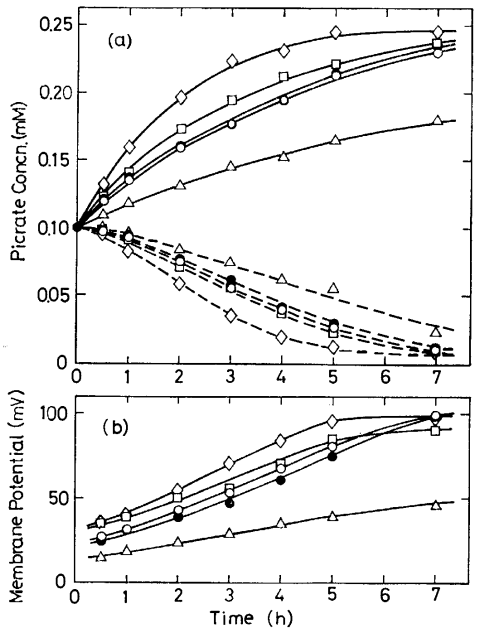

Fig. 3. Effect of potassium and lithium counter-ions on the transport of picrate.
The curves have the same meanings as in Fig. 2. K and Li salts in phases I and II; ○: 0.1 M KCl (I)–0.1 M LiCl (II), △: 0.1 M KNO_3 (I)–0.1 M $LiNO_3$ (II), □: 0.05 M K_2SO_4 (I)–0.05 M Li_2SO_4 (II), ◇: 0.05 M K_2SO_4 (I)–0.1 M $LiNO_3$ (II), ●: 0.1 M KCl (I)–0.05 M Li_2SO_4 (II). Ionophore; 10^{-4} M dicyclohexyl-18-crown-6.

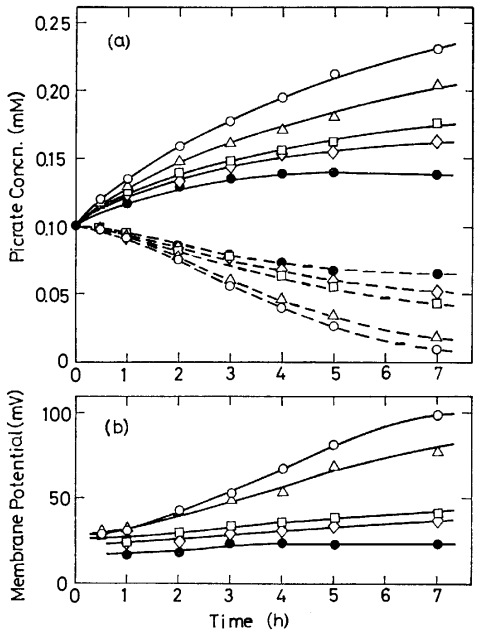

Fig. 4. Effect of potassium ion concentration on the transport of picrate.
The curves have the same meanings as in Fig. 2. K and Li salts in phases I and II; ○: 0.1 M KCl (I)–0.1 M LiCl (II), △: 0.05 M KCl, 0.05 M LiCl (I)–0.1 M LiCl (II), □: 0.01 M KCl, 0.09 M LiCl (I)–0.1 M LiCl (II), ◇: 0.005 M KCl, 0.095 M LiCl (I)–0.1 M LiCl (II), ●: 0.001 M KCl, 0.099 M LiCl (I)–0.1 M LiCl (II). Ionophore; 10^{-4} M dicyclohexyl-18-crown-6.

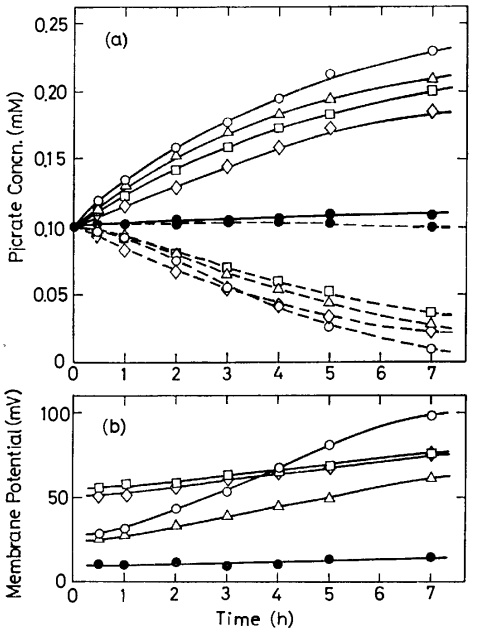

Fig. 5. Effect of ionophores on the transport of picrate.
The curves have the same meanings as in Fig. 2. Ionophore; ○: dicyclohexyl-18-crown-6, △: dicyclohexyl-24-crown-8, □: dibenzo-18-crown-6, ◇: dibenzo-24-crown-8, ●: valinomycin.
Ionophore concentration; 10^{-4} M, K, Li salts; phase I: 0.1 M KCl, phase II: 0.1 M LiCl.

In these systems, dicyclohexyl-18-crown-6 was used as an ionophore at a concentration in dichloroethane of 10^{-4} M.

In the potassium sulfate–lithium nitrate system, the highest rate of picrate transport was observed. On the contrary, a considerable decrease in the rate of picrate transport occurred in the potassium nitrate–lithium nitrate system.

Effect of Potassium Ion Concentration. The effect of varying the concentration of potassium chloride in phase I from 0.001 to 0.1 M on the transport of picrate is shown in Fig. 4. In this system, lithium chloride was added to compensate for the lack of chloride ion in phase I. The ionophore used was dicyclohexyl-18-crown-6 and the concentration in the dichloroethane phase was 10^{-4} M.

The rate of picrate transport decreased with decreasing potassium ion concentration. The change in membrane potential with time also decreased according to the reduction of the rate of picrate transport.

Effect of Ionophores. The picrate concentrations in the aqueous phases and the membrane potential against time curves for various ionophores are shown in Fig. 5. In these systems, phase I contained 0.1 M potassium chloride and phase II 0.1 M lithium chloride. The concentrations of ionophores in the dichloroethane phase were 10^{-4} M in all cases.

The rate of picrate transport increased according in the following order of ionophore; dicyclohexyl-18-crown-6 > dicyclohexyl-24-crown-8 > dibenzo-18-crown-6 > dibenzo-24-crown-8 > valinomycin. This order, with the exception of valinomycin, agreed with that for

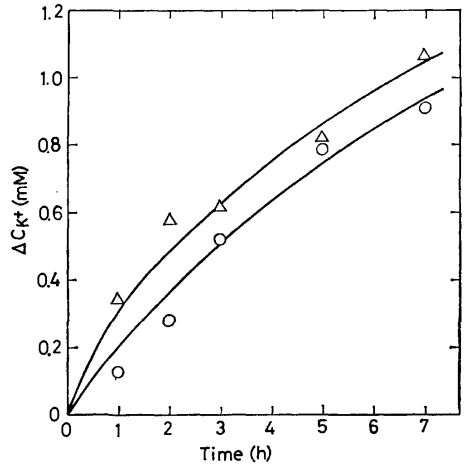

Fig. 6. Increment of potassium ion concentration (ΔC_{K^+}) in phase II against time curves.
○: 0.1 M KCl (phase I)–0.1 M LiCl (phase II) system, △: 0.1 M KCl (phase I)–0.05 M Li_2SO_4 (phase II) system. Ionophore; 10^{-4} M dicyclohexyl-18-crown-6.

the permeability ratio of potassium ion to sodium ion across the liqiud membrane consisting of dioleyl phosphate and oleyl alcohol.[5]

Discussion

It has been reported that picrate is a lipophilic anion and that it permeates the phospholipid membrane electrophoretically.[6] In the present experiments, however, the transport of picrate through the dichloroethane membrane containing no ionophore was not observed: picrate was transferred only in the presence of potassium ion and potassium ionophore. The rate of picrate transport increased with increasing ionophore concentration suggesting that the picrate anion in phase I was dissolved in the dichloroethane phase forming an ion-pair with a complexed cation consisting of ionophore and potassium ion and then liberated into phase II by the dissociation of the ion-pair.

The rate of picrate transport depended on various factors such as the concentration of ionophore and potassium ion and the type of potassium and lithium counter-ions and ionophore. To investigate the mechanism of this transport system, the change in potassium ion concentration in phase II with time was measured by means of flame analysis, the results of which for the potassium chloride–lithium chloride and potassium chloride–lithium sulfate systems are shown in Fig. 6. The change in chloride ion concentration in phase II for the potassium chloride–lithium sulfate system was also determined by a titrimetric method. It was found that increment of potassium ion concentration in phase II was approximately 10^{-3} M for 7 h and that for chloride ion concentration also approximately 10^{-3} M indicating that approximately 1% of the potassium chloride in phase I was transferred to phase II across the membrane. Using the assumption of electroneutrality, the number of moles of potassium ions diffusing into phase II must equal the sum

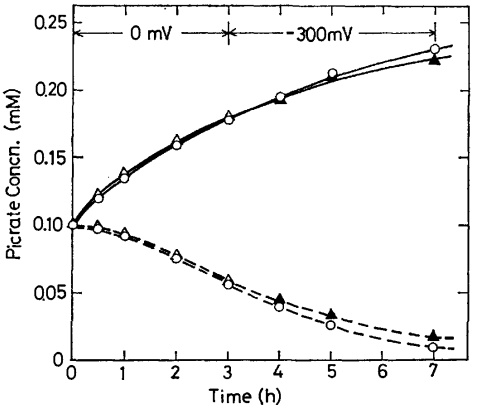

Fig. 7. Examination for the influence of membrane potential on the transport of picrate.
○: Usual transport, △: the potential difference between both aqueous phases was clamped at 0 mV, ▲: a potential difference of 300 mV was applied between both aqueous phases in the reverse direction of the membrane potential.
The dotted and solid lines represent the picrate concentrations in phases I and II respectively. Ionophore; 10^{-4} M dicyclohexyl-18-crown-6, K, Li salts; phase I : 0.1 M KCl, phase II : 0.1 M LiCl.

of those of chloride and picrate ions transferred into phase II. The effect of potassium and lithium counter-ions on the transport of picrate can be explained by the difference in permeability across the membrane. To obtain the order of permeability for the counter-ions, the membrane potential of the dichloroethane membrane in the absence of picrate and Tris-H_2SO_4 buffer was measured. The membrane potentials for the potassium chloride–lithium chloride, potassium nitrate–lithium nitrate, potassium sulfate–lithium sulfate and potassium sulfate–lithium nitrate systems were found to be approximately 70, 50, 80, and 160 mV, respectively. The polarity of the potential was positive in phase II with respect to phase I. Using the relationship between the membrane potential and permeability coefficient derived by Hodgkin and Katz,[7] the following order of permeability for the counter-ions was established: $NO_3 > Cl > SO_4$— in fact, the rate of picrate transport decreased according to the same order for the potassium counter-ions. In the case of the potassium nitrate–lithium nitrate system, the liberation of picrate from the ion-pair at the phase II-dichloroethane interface was depressed by the co-transport of nitrate with potassium ion, whereas, in the case of the potassium sulfate–lithium nitrate system, the transfer of nitrate from phase II to phase I facilitated the transport of picrate.

In general , the membrane potential has been shown to be important in transport across the membrane. In the present experiments, the membrane potential gradually increased with time attaining a steady value. To examine the role of the membrane potential, the potential difference between phases I and II was set 0 mV by a short circuit method.[8] No difference in the results was observed , as shown in Fig. 7. Furthermore, only a slight decrease in the rate of picrate

transport occurred, even when a potential difference of 300 mV was applied between both the aqueous phases in the reverse direction of the membrane potential (Fig. 7), *i.e.* the transport of picrate is largely unaffected by the membrane potential. The explanation for this is that the transport of picrate occurs only by the diffusion of potassium ions across the membrane and therefore, the decrease in concentration gradient of the potassium ion across the membrane brings about a lowering of the rate of picrate transport, as seen from Fig. 4.

The effect of ionophores on the transport of picrate is associated with the permeability ratio of the potassium ion to the lithium ion for the dichloroethane membrane. This permeability ratio depends on the ionic selectivity of ionophore, the mobility of the potassium– and lithium–ionophore complexes in the dichloroethane membrane and the partition coefficient of the complexes.[9] It is thought that the behavior of the above-mentioned crown compounds for the dichloroethane membrane system is similar to that for the dioleyl phosphate–oleyl alcohol membrane system previously described.[5] In that system, the oleyl phosphate–oleyl alcohol membrane in the presence of valynomycin showed the highest permeability ratio of potassium ion to sodium ion. In the present experiment, the rate of picrate transport was extremely small in the presence of valinomycin and bearing in mind that the membrane potential is very samll in the presence of valinomycin, this may be attributed to a lowering of the potassium-ion selectivity of valinomycin, based on the interaction between valinomycin and picrate.

References

1) J. H. Moore and R. S. Schechter, *Nature*, **222**, 476 (1969).
2) E. M. Choy, D. F. Evans, and E. L. Cussler, *J. Am. Chem. Soc.*, **96**, 7085 (1974).
3) J. P. Behr and J. M. Lehn, *J. Am. Chem. Soc.*, **95**, 6108 (1973).
4) I. Kusaka, K. Hayakawa, K. Kanai, and S. Fukui, *Eur. J. Biochem.*, **71**, 451 (1976).
5) M. Sugiura and T. Shinbo, *Nippon Nogei Kagaku Kaishi*, **50**, 547 (1976); M. Sugiura and T. Shinbo, *ibid.*, **50**, 91 (1976).
6) L. L. Grinius, A. A. Jasaitis, Yu. P. Kadziauskas, E. A. Liberman, V. P. Skulachev, V. P. Topali, L. M. Tsofina, and M. A. Vladimirova, *Biochem. Biophys. Acta*, **216**, 1 (1970).
7) A. L. Hodgkin and B. Katz, *J. Physiol.*, **108**, 37 (1949).
8) "Seitaimaku Jikken-gijutsu," ed by T. Onishi, Nankodo, Tokyo (1967), p. 301; H. H. Ussing and K. Zerahn, *Acta Physiol. Scand.*, **23**, 110 (1951).
9) "Membrane," ed by G. Eisenman, Marcel Dekker, New York (1973), Vol. 2, p. 190.

Phase Transition and Electronic States of Solid Ion Radical Salts

Yôichi IIDA

Department of Chemistry, Faculty of Science, Hokkaido University, Sapporo 060

(Received August 16, 1978)

Such crystalline ion radical salts as Würster's Blue perchlorate and K^+ *p*-Chloranil$^-$ are known to undergo phase transitions in the solid state. There are distinct differences in their optical and magnetic properties between the low- and high-temperature phases. Using Hubbard Hamiltonian, the electronic states of the high-temperature phases of those solid ion radical salts were explained in terms of an infinite non-alternant linear chain model, while those of the low-temperature phases, in terms of a dimer model.

The prominent magnetic, electrical and optical properties of a number of solid ion radical salts have been the subject of many theoretical and experimental investigations over the past fifteen years.[1-17] In such ion radical salts, the planar ion radical molecules are known to form, in themselves, a segregated stacking into columns so as to make a large overlap between their half-occupied molecular orbitals.[11-13] There have been known several crystalline ion radical salts that undergo solid-state phase transitions. For example, a stable cation radical salt of Würster's Blue (*N,N,N',N'*-tetramethyl-*p*-phenylenediamine) perchlorate undergoes a phase transition at 186 K,[1-3] while an anion radical salt of K^+ *p*-Chloranil$^-$, around 210—260 K.[4,8,9] In both of these salts, because of the structural change in the phase transition, the optical and magnetic properties of the high-temperature phases differ distinctly from those of the low-temperature phases.[1-10]

In previous papers,[14-17] we applied half-filled Hubbard model to the segregated stack of ion radical molecules and investigated the optical and magnetic properties of a number of crystalline ion radical salts. In the present paper, we shall apply this method to Würster's Blue perchlorate and K^+ *p*-Chloranil$^-$ crystals and explain the electronic states and the optical and magnetic properties of their high- and low-temperature phases. This kind of approach will be very important to investigate the mechanism of the phase transitions of those ion radical salts.

Würster's Blue Perchlorate

At room temperature the crystal is known to be orthorhombic and to be built up from non-alternant one-dimensional columns composed of equivalent Würster's Blue cation radicals along the a-axis, the intermolecular spacing between nearest neighbor cation radicals being 3.550 Å.[11] A phase change into the monoclinic form occurs at 186 K, and in the monoclinic phase the a- and c-axes are almost doubled in length in comparison with the orthorhombic modification.[11]

The magnetic susceptibility of Würster's Blue perchlorate and its temperature dependence were measured by Duffy and by Okumura.[1,2] In the region above the transition temperature, the salt had been considered to be a normal paramagnet. The paramagnetic susceptibility above the transition temperature has been reported to be consistent with a Curie-Weiss law with a Curie constant C=0.325 emu deg/mol and a Curie temperature $\theta = -23 \pm 5$ K.[2] However, the observed paramagnetism is often short of the expected 100% free radical value. For example, Duffy found it to be 94%, and Okumura, as low as 81%.[1,2] The reason for this is that, although the cation radicals have almost free spins, there may act weak antiferromagnetic exchange interaction between the cation radicals. Soos and Hughes considered the salt of the high-temperature phase to be non-alternant one-dimensional antiferromagnet with exchange interaction $2J\sum_i \boldsymbol{S}_i \cdot \boldsymbol{S}_{i+1}$, ($S$= 1/2).[10] They used their pseudo-spin method to derive theoretical magnetic susceptibility *versus* temperature curve. The pseudo-spin result with J=70 cm^{-1} gave excellent agreement between the observed and theoretical magnetic susceptibility curves in the high-temperature phase.

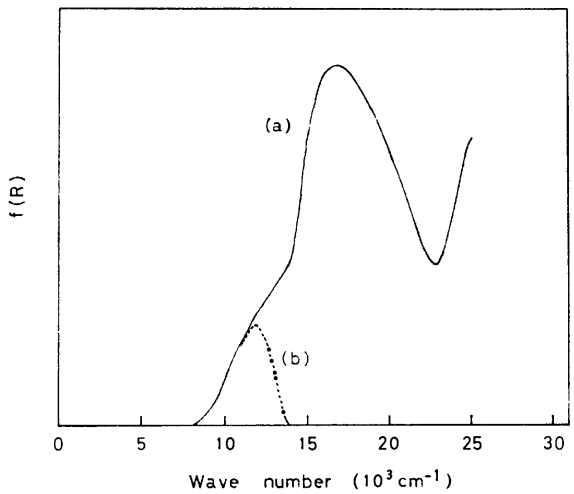

Fig. 1. (a) The observed diffuse reflection spectrum of solid Würster's Blue perchlorate salt at room temperature. The value of Kubelka-Munk function, $f(R) = (1-R)^2/2R$, was plotted *versus* wave number. (b) The intermolecular charge-transfer band of the salt. It was obtained by subtraction of the monomer absorption of the cation radical. See text and Ref. 5.

Earlier, we measured the electronic spectrum of Würster's Blue perchlorate crystal at room temperature (*i.e.*, the high-temperature phase) by means of diffuse reflection method.[5] The observed spectrum is reproduced in Curve (a) of Fig. 1, where we note a strong absorption at 16700 cm^{-1} and a weak shoulder around 12000 cm^{-1}. The strong absorption at 16700 cm^{-1} corresponds well to the 16400 cm^{-1} band of the monomer spectrum of Würster's Blue cation radical,

while the shoulder around 12000 cm^{-1} was assigned to the charge-transfer transition between the cation radicals in the solid state.[5-7,9] By subtracting the 16700 cm^{-1} monomer absorption from the observed solid-state spectrum, the intermolecular charge-transfer band of the high-temperature phase is given by Curve (b) of Fig. 1, and its peak position appears to be at 11900 cm^{-1}.

In order to understand those optical and magnetic properties of the high-temperature phase of Würster's Blue perchlorate crystal, we consider the system of non-alternant one-dimensional stack of Würster's Blue cation radicals in terms of Hubbard Hamiltonian, which can be written by[14,16]

$$\mathscr{H} = \sum_{i,j,\sigma} T_{ij} C_{i\sigma}^{+} C_{j\sigma} + I \sum_{i} n_{i\uparrow} n_{i\downarrow}, \tag{1}$$

where $n_{i\sigma}=C_{i\sigma}^{+}C_{i\sigma}$, and $C_{i\sigma}^{+}$ and $C_{i\sigma}$ are the creation and annihilation operators of an electron with σ-spin at the i-th site, respectively, and where $T_{ij}(<0)$ is the transfer matrix element between the i-th and j-th sites. The Coulomb repulsion potential, I, appears only when two electrons with up and down spins are at the same site. For non-alternant one-dimensional column of ion radicals, we consider the half-occupied molecular orbital of the unpaired electron as one site of ion radical molecule, and only take into account the transfer matrix element between the nearest neighbor sites. Hereafter, it is simply denoted by T (<0). We consider a paramagnetic state for our system, and further assume a δ-function for each elementary transition in which the spin and the wave vector of an electron are conserved. The intermolecular charge-transfer absorption of this system, $\sigma(\omega)$, is then given by[14]

$$\sigma(\omega) \propto \frac{e^2}{4} \frac{I^2}{\omega^2\sqrt{\omega^2-I^2}} \sqrt{4T^2-\omega^2+I^2}. \tag{2}$$

A schematic representation of the absorption line shape has been given in Fig. 1 of Ref. 14. The theoretical charge-transfer absorption has a sharp divergent peak at $\omega=I$, and has a band width of $\sqrt{I^2+4T^2}-I$ in the region of $\omega>I$. On the other hand, we examine the magnetic properties of the same system. In a region of small $|T|$ limit, the Hubbard model leads to a stabilization of the antiferromagnetic state between ion radical molecules.[16,17] For a pair of nearest neighbor ion radicals, if the small direct exchange is neglected, the energy gap between the parallel and antiparallel spin states is given by $2J=4T^2/I$. Therefore, we can well consider our solid Würster's Blue perchlorate salt as one-dimensional antiferromagnet with an exchange interaction, J. In this respect, Soos and Hughes' treatment of regular one-dimensional antiferromagnetic model is quite adequate. Therefore, if we combine the experimental data on the peak energy of the observed charge-transfer absorption and the exchange interaction parameter derived from the magnetic susceptibility measurement, we can uniquely determine the magnitudes of I and T of Eq. 1 for our system.

We apply this approach to the high-temperature phase of the Würster's Blue perchlorate crystal. The observed peak energy of the charge-transfer absorption, 11900 cm^{-1}, thus corresponds to $I=11900$ cm^{-1}. As for the magnitude of the transfer matrix element, by putting the estimated $I=11900$ cm^{-1} and $J=70$ cm^{-1} values into $J=2T^2/I$, we obtain $T=-650$ cm^{-1} for the one-dimensional system of the Würster's Blue perchlorate salt. The $|T|$ value thus estimated is found to be much smaller than the $|T|$ values estimated with a number of other ion radical salts,[14-17] indicating weak intermolecular interaction between the Würster's Blue cation radicals.[18] This is supported by the fact that the intermolecular distance between the cation radicals in the perchlorate salt is as large as 3.550 Å and also by the spectroscopic features that the 16700 cm^{-1} band of the solid salt corresponds well to the monomer spectrum of the Würster's Blue cation radical and that the intermolecular charge-transfer band appears very weakly as a shoulder in the solid-state spectrum.

Next, we consider the low-temperature phase of the same salt. As the phase transition occurs, the non-alternant one-dimensional stack of Würster's Blue cation radicals alternates strongly in the low-temperature phase.[11] The Würster's Blue cation radicals stack predominantly in a pair-by-pair manner, so that the crystal system can be practically confined to a dimer of the cation radicals. In fact, Thomas *et al.* observed the triplet-state fine structures in the ESR spectrum below the transition temperature and determined the energy gap between the ground singlet state and the excited triplet state to be 246 cm^{-1}.[3] On the other hand, Sakata *et al.* and Ishii *et al.* measured the crystal electronic spectrum of the perchlorate salt below the transition temperature.[6,9] With decreasing temperature, they found marked increase in intensity of the low-energy charge-transfer absorption, whose peak position was at 12100 ± 400 cm^{-1}. This absorption was assigned to the charge-transfer transition between the Würster's Blue cation radicals in the dimer.

On the basis of these experimental results, we consider the electronic state of the low-temperature phase of the Würster's Blue perchlorate salt in terms of a dimer model of Hubbard Hamiltonian, which can be written by[16]

$$\mathscr{H} = \sum_{\sigma} T(C_{1\sigma}^{+}C_{2\sigma} + C_{2\sigma}^{+}C_{1\sigma}) + I(n_{1\uparrow}n_{1\downarrow} + n_{2\uparrow}n_{2\downarrow}), \tag{3}$$

where the notations are common to those in Eq. 1. The suffixes, 1 and 2, denote two sites of ion radicals in a dimer, and $T(<0)$ is the transfer matrix element between ion radicals in the dimer. If we only take the half-occupied molecular orbital of ion radical for each site, there are six bases of the wave functions for the dimer. After solving the eigenvalue problem, we have three singlet states and one triplet state. A detail of the wave functions and the energy levels was described in a previous paper.[16] The energy of the charge-transfer absorption, $h\nu_{CT}$, and the singlet-triplet energy separation, δ, are given by

$$h\nu_{CT} = \left\{\left(\frac{1}{2}I\right)^2 + (2T)^2\right\}^{1/2} + \frac{1}{2}I, \tag{4}$$

$$\delta = \left\{\left(\frac{1}{2}I\right)^2 + (2T)^2\right\}^{1/2} - \frac{1}{2}I. \tag{5}$$

This dimer model was then applied to the above experimental results of the low-temperature phase of

the Würster's Blue perchlorate salt. By putting the observed values of $h\nu_{CT}=12100\pm400\ cm^{-1}$ and $\delta=246\ cm^{-1}$ into Eqs. 4 and 5, we obtain $I=h\nu_{CT}-\delta=11900\pm400\ cm^{-1}$ and $T=-865\pm15\ cm^{-1}$, respectively. The I value thus estimated almost coincides with the $I=11900\ cm^{-1}$ value of the high-temperature phase, while the $|T|$ value of the dimer is found to be appreciably larger than the $|T|=650\ cm^{-1}$ value of the high-temperature phase. In view of these results, the 186 K phase transition associated with slight crystal structure modification scarcely changes the magnitude of Coulomb repulsion energy, but increases significantly the magnitude of transfer matrix element of the dimer in the low-temperature phase.

K^+ *p*-Chloranil$^-$

At room temperature, although there are several polymorphs, in the structure of the orthorhombic α-form the *p*-chloranil anion radicals are stacked with equal intervals, forming non-alternant one-dimensional columns parallel to the c-axis, the interplanar spacing being 3.47 Å.[12] The optical and magnetic properties and the electronic state of the room-temperature (high-temperature) phase of the K^+ *p*-Chloranil$^-$ salt have been already discussed in a previous paper.[16] The Hubbard Hamiltonian of Eq. 1 was applied to the non-alternant one-dimensional column of the *p*-chloranil anion radicals, and the values of $I=11800\ cm^{-1}$ and $T=-820\ cm^{-1}$ were obtained.

As temperature is lowered, the K^+ *p*-Chloranil$^-$ salt undergoes a phase transition at 210 K.[4] With increasing temperature, however, a large hysteresis occurs and the low-temperature phase changes into the high-temperature phase around 260 K. The magnetic susceptibility and its temperature dependence in the low-temperature phase were measured by Andre *et al.* and were well explained in terms of an equilibrium between ground singlet state and excited triplet state lying $\delta=400\ cm^{-1}$ above the singlet state.[4] In the low-temperature phase, although there have been no crystal structure data, the magnetic behavior strongly suggests a dimeric structure of the *p*-chloranil anion radicals. The electronic spectrum of the solid salt below the transition temperature was measured by Hiroma and Kuroda.[8] With decreasing temperature, they found marked increase in intensity of the low-energy charge-transfer absorption, whose peak position was reported to be at $11500\ cm^{-1}$. This absorption was assigned to the charge-transfer transition in the dimer. In order to explain those optical and magnetic properties, the dimer model of Hubbard Hamiltonian of Eq. 3 was again applied. By taking the same procedure as described in the preceding section, together with Eqs. 4 and 5, the values of $I=11100\ cm^{-1}$ and $T=-1070\ cm^{-1}$ were estimated for the low-temperature phase of the K^+ *p*-Chloranil$^-$ salt. We can also see that the $|T|$ value of the low-temperature phase is larger than the $|T|$ value of the high-temperature phase. The phase change causes a slight decrease of the I value in the low-temperature phase.

Concluding Remarks

In both of the Würster's Blue perchlorate and K^+ *p*-Chloranil$^-$ crystals, the high-temperature phases correspond to non-alternant one-dimensional stacks of ion radical molecules, while the phase transitions cause alternate stacks of ion radicals in the low-temperature phases. In the present paper, we cannot explain the detailed mechanism of these phase transitions, but can understand the electronic states of both high- and low-temperature phases in terms of Hubbard Hamiltonian. The motive force of the phase changes probably comes from Peierls instability in one-dimensional system of segregated stacks of ion radical molecules.

As for the transfer matrix element of the high-temperature phase, the $|T|$ value of Würster's Blue perchlorate is found to be smaller than that of K^+ *p*-Chloranil$^-$. In this respect, the intermolecular interaction between Würster's Blue cation radicals appears to be weaker than that between *p*-chloranil anion radicals. We can understand this difference, because the intermolecular distance between Würster's Blue cations, 3.550 Å, is longer than that between *p*-chloranil anion radicals, 3.47 Å.

In the low-temperature phases, alternate stacks of ion radical molecules cause shorter intermolecular distance in a dimer and longer distance between dimers, compared to the intermolecular distance in non-alternant stacks. On this basis, it is reasonable that, in both of the Würster's Blue perchlorate and K^+ *p*-Chloranil$^-$ salts, the $|T|$ values estimated with the low-temperature phases are appreciably larger than those of the high-temperature phases. Concerning the magnitude of the $|T|$ values in the low-temperature phases, the $|T|$ value of K^+ *p*-Chloranil$^-$ is larger than that of Würster's Blue perchlorate, so that the singlet-triplet energy separation of the former salt is wider than that of the latter. Although we have no structural information, the *p*-chloranil anion radicals may stack in the dimer more closely than do the Würster's Blue cation radicals.

The theoretical consideration made in the present paper will be useful to investigate the mechanism of the phase transitions of those solid ion radical salts.

References

1) W. Duffy, Jr., *J. Chem. Phys.*, **36**, 490 (1962).
2) K. Okumura, *J. Phys. Soc. Jpn.*, **18**, 69 (1963).
3) D. D. Thomas, H. Keller, and H. M. McConnell, *J. Chem. Phys.*, **39**, 2321 (1963).
4) J. J. Andre, J. Clementz, R. Jesser, and G. Weill, *C. R. Acad. Sci., Ser. B*, **266**, 1057 (1968).
5) Y. Iida and Y. Matsunaga, *Bull. Chem. Soc. Jpn.*, **41**, 2615 (1968).
6) T. Sakata and S. Nagakura, *Bull. Chem. Soc. Jpn.*, **42**, 1497 (1969).
7) J. Tanaka and M. Mizuno, *Bull. Chem. Soc. Jpn.*, **42**, 1841 (1969).
8) S. Hiroma and H. Kuroda, *Bull. Chem. Soc. Jpn.*, **46**, 3645 (1973).
9) K. Ishii, K. Kaneko, and H. Kuroda, *Bull. Chem.*

Soc. Jpn., **49**, 2077 (1976).
10) Z. G. Soos and R. C. Hughes, *J. Chem. Phys.*, **46**, 253 (1967).
11) J. L. DeBoer and Aafje Vos, *Acta Crystallogr., Sect. B*, **28**, 835, 839 (1972).
12) M. Konno, H. Kobayashi, F. Marumo, and Y. Saito, *Bull. Chem. Soc. Jpn.*, **46**, 1987 (1973).
13) J. Tanaka, M. Tanaka, T. Kawai, T. Takabe, and O. Maki, *Bull. Chem. Soc. Jpn.*, **49**, 2358 (1976), and the references cited therein.
14) Y. Iida, *Bull. Chem. Soc. Jpn.*, **50**, 1445 (1977), and the references cited therein.
15) Y. Iida, *Bull. Chem. Soc. Jpn.*, **50**, 2481 (1977); **51**, 631 (1978).
16) Y. Iida, *Bull. Chem. Soc. Jpn.*, **51**, 2523 (1978).
17) Y. Iida, *Bull. Chem. Soc. Jpn.*, **51**, 3637 (1978).
18) J. Tanaka, M. Inoue, M. Mizuno, and K. Horai, *Bull. Chem. Soc. Jpn.*, **43**, 1998 (1970). In this paper, they discussed the interaction parameter between the ground and charge-transfer configurations in terms of dimer model of Würster's Blue cation radicals. Although their dimer model was not applied directly to the high-temperature phase of Würster's Blue perchlorate, they estimated the magnitude of the interaction parameter as 645 cm^{-1}, which should approximately correspond to $2|T|$ of our Hubbard model. Their value is somewhat smaller than the 1300 cm^{-1} value derived from our one-dimensional Hubbard model, thus giving a J value much smaller than the observed $J=70$ cm^{-1}.

Delayed Excimer Fluorescence of Acridine Orange Bound to DNA

Yuko MOTODA and Yukio KUBOTA*

Department of Chemistry, Faculty of Science, Yamaguchi University, Yamaguchi 753

(Received August 23, 1978)

The temperature dependence of long-lived emissions of Acridine Orange bound to DNA has been investigated. Only phosphorescence with a maximum close to 620 nm is observed in the range 77—*ca.* 150 K. With a rise in temperature, the delayed thermal fluorescence around 530 nm is observed in addition to phosphorescence at a high ratio of DNA phosphate to dye (P/D). With a decrease in P/D value, the delayed thermal fluorescence is replaced by a new delayed emission band around 640 nm. Its maximum wavelength is very close to that of dimer fluorescence of Acridine Orange in water. It has been shown that the emission results from two processes: (1) thermal excitation of the triplet state of the dimer to the excimer state and (2) excimer formation after the thermal excitation of the triplet state of the monomer to the first excited singlet state.

The binding of Acridine Orange (AO) to DNA has been extensively studied because of its biological effects.[1,2] Like many acridine derivatives, AO binds to DNA to form two types of complexes; one (Complex I) results from external binding where electrostatic forces play an important role,[3,4] while the other (Complex II) occurs at high DNA phosphate/dye (P/D) ratios, generally considered as an intercalation process.[5,6] As compared to other related dyes, the binding of AO presents a particularly complex aspect due, in part, to its high tendency to dimerize.[7,8] It is well known that fluorescence spectra of AO in aqueous solutions at room temperature strongly depend on its concentration.[9] With increasing concentration of the dye, its green fluorescence with a maximum near 540 nm is replaced by a red fluorescence with a maximum close to 650 nm.[9] AO, especially when bound to single-strand polynucleotides or denatured DNA at a low P/D value, also shows red fluorescence.[10-13] Such emission properties of the dye have been applied to studies of the conformational change of DNA and the nearest neighbor dye-dye interactions.[10-13]

In order to understand biological action of AO, it is of significance to clarify the nature of its excited state and the character of the interaction of the dye with the binding site, as well as the nearest neighbor dye-dye interactions. In previous papers,[14,15] reports were given on the phosphorescence, the delayed fluorescence due to triplet-triplet annihilation and the sensitized delayed fluorescence in the DNA–acridine dye complexes at 77 K. A study at low temperatures is of particular interest, since the radiationless processes which compete with the radiative processes (fluorescence and phosphorescence) are largely suppressed. Further, it is of interest to investigate the temperature dependence of the emission properties in order to elucidate the excited states of the bound dye.

The present paper describes the emission properties of AO bound to DNA over a wide temperature range and the newly-observed delayed emission.

Experimental

AO (Chroma) was purified by the method of Zanker.[9] No trace of impurity was detected by thin-layer chromatography on silica gel. Calf thymus DNA was obtained from Worthington Biochemical Corporation. The concentration of DNA was determined spectrophotometrically at 260 nm with the extinction coefficient per mole of DNA phosphate ($\varepsilon_p = 6600\ M^{-1}\ cm^{-1}$).[16] The thermal denaturation of DNA was performed by heating the DNA solution for 20 min in boiling water and then rapidly cooling in ice water. The solutions of the complexes were made up in 5 mM phosphate buffer at pH 6.9.

All the solutions were degassed by freezing, pumping, and thawing under a high vacuum. The solutions were placed in a quartz tube (inner diam. 1 mm) mounted in a Dewar flask with provision for the excitation and detection of the delayed emissions at right angles. For studies at 77 K the sample tube was immersed in liquid nitrogen. For measurements at various temperatures the temperature was controlled by a constant flow of cold nitrogen gas through the Dewar. The temperature was monitored by a copper-constantan thermocouple attached to the outside of the sample tube. The precision of the quoted values is $\pm 1°$.

The emission and excitation spectra were measured with a Hitachi MPF-2A fluorescence spectrophotometer; the detector was a red-sensitive photomultiplier tube, R446-UR (Hamamatsu Television Co.). Both spectra are given with corrections on the quantum response of detecting and exciting systems. A rotating-shutter phosphoroscope was used to separate the delayed emissions from normal fluorescence. The intensity of the exciting light was varied by introducing calibrated wire screens.

The absorption spectra at 77 K and at room temperature were measured with a Shimadzu MPS spectrophotometer with a 0.1 cm quartz cell.

Results and Discussion

Absorption Spectra of the Complexes. First, absorption spectra of the complexes were measured at room temperature and at 77 K in order to confirm the binding states of AO. It was found that the bound dye molecules predominantly exist as the monomeric species at a sufficiently high P/D value, tending to associate with a decrease in the P/D value. The association tendency is more remarkable in the denatured DNA and at 77 K than in the native one and at room temperature. Typical absorption spectra at 77 K are shown in Fig. 1. They exhibit a red shift of about 5 nm, being well resolved as compared with those at room temperature.[7,8,17] The 0-1 band around 470 nm in the monomer absorption spectrum generally overlaps the dimer absorption band.[7,9,18] As the P/D value decreases ($P/D<50$), the band around 470 nm becomes marked, while the 0-0 band around 500 nm is suppressed. This is ascribed to the formation of dye dimers. In the case $P/D<20$, the absorption

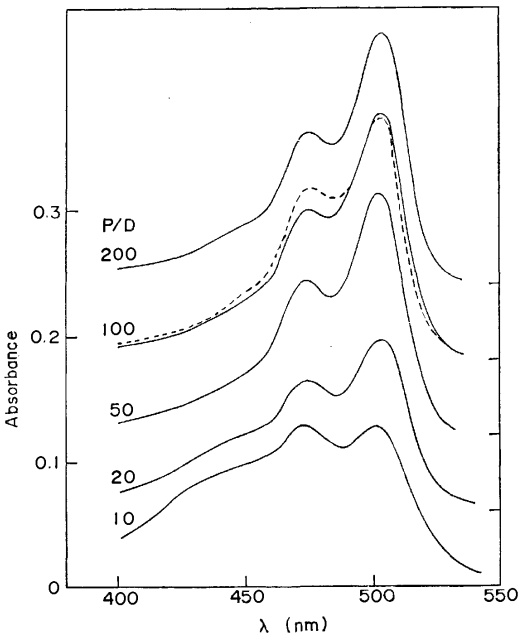

Fig. 1. Absorption spectra of DNA-AO complexes in 5 mM phosphate buffer at 77 K. The light-path length of the cell was 0.1 cm. For clarity of presentation the upper curves are displaced by a constant amount. Each line on the right ordinate corresponds to a base line. AO: 5.0×10^{-5} M, ——: native DNA, ----: denatured DNA.

band due to higher aggregates of the dye develops at wavelengths shorter than the 0-1 band around 470 nm.

Delayed Emission Spectra of the Complexes. Total emission and delayed emission spectra obtained under various temperatures are shown in Figs. 2A, 2B, and 2C. The spectral distribution of total emission shows little dependence on the temperature except that its maximum is slightly shifted to longer wavelength with increasing temperature. Total emission seems to be mainly composed of normal fluorescence, since its intensity is several ten times that of the delayed emission.

The delayed emission of the complexes consists only of phosphorescence with a maximum close to 620 nm in the range 77—*ca.* 150 K. With an increase in temperature, another delayed emission appears in addition to the phosphorescence; this phenomenon depends on the *P/D* value.

At a high *P/D* value (*P/D*>100), the delayed emission peaking at 530 nm becomes remarkable above *ca.* 200 K (Fig. 2A). The spectral distribution of delayed emission is very similar to that of normal fluorescence. The intensity of the delayed emission was found to be proportional to the first power of the intenisty of the exciting light, decaying exponentially with a lifetime equal to that of the phosphorescence. Thus, the delayed emission around 530 nm is due to the mechanism in which there is thermal activation from the lowest triplet state to the first excited singlet state followed by radiative transition from there to the ground state.[19,20] In the present study the delayed emission is called delayed thermal fluorescence

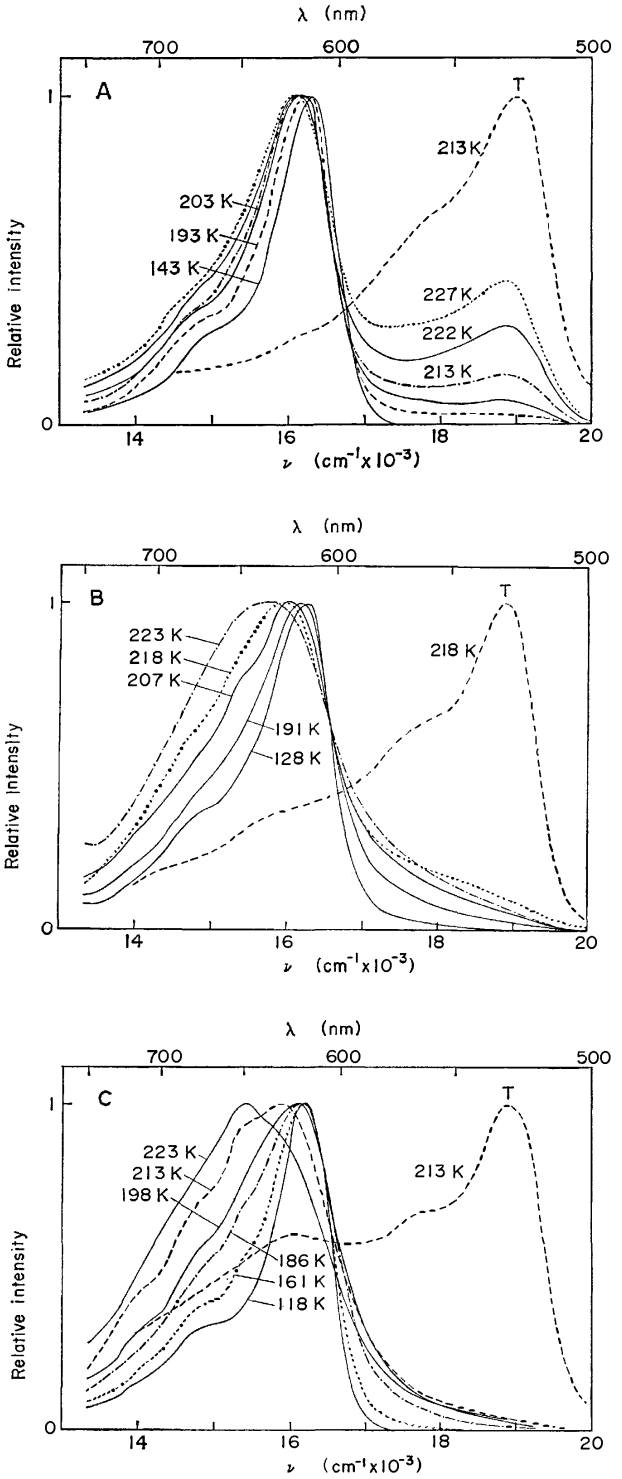

Fig. 2. (A) Normalized delayed emission spectra of DNA-AO complex (*P/D*=302) as a function of temperature. Excitation wavelength: 470 nm, AO: 5.0×10^{-5} M, T: total emission spectrum. (B) Same, *P/D*=100. (C) Same, *P/D*=50.

according to the terminology of McGlynn *et al.*[20] The Arrhenius plot of ϕ_f/ϕ_p against $1/T$ were linear and the activation energy was obtained as 7.1 kcal mol^{-1}; here, ϕ_f and ϕ_p are the efficiencies of the delayed thermal fluorescence and phosphorescence, respectively. On the other hand, the peak-to-peak

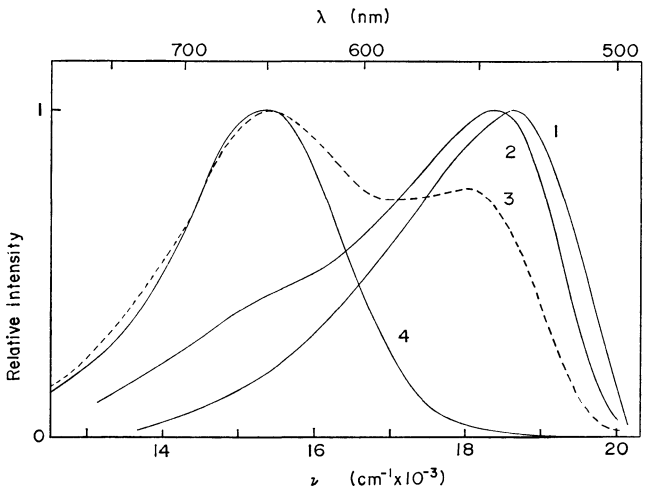

Fig. 3. Normalized fluorescence spectra of AO in 5 mM phosphate buffer at 25 °C. Excitation wavelength: 400 nm, AO: (1) 1.1×10^{-6} M, (2) 2.1×10^{-4} M, (3) 1.0×10^{-3} M, (4) 1.1×10^{-2} M.

separation between the delayed thermal fluorescence and the phosphorescence was 7.5 kcal mol^{-1}. Both values agree within experimental error, confirming the proposed mechanism.

With a decrease in P/D value ($P/D<120$), two interesting effects are observed (Figs. 2B and 2C): (1) a marked decrease in the intensity of the delayed thermal fluorescence as compared with the results at a high P/D value (Fig. 2A), and (2) appearance of a new emission band around 640 nm at elevated temperatures. AO easily associates to form a dimer or higher aggregates.[9] As shown in Fig. 3, fluorescence spectra of AO in aqueous solution highly depend on its concentration. With an increase in the concentration of dye, the green fluorescence with a maximum near 540 nm is replaced by a red fluorescence with a maximum close to 650 nm. The former is due to the dye monomer and the latter to the dye dimer or higher aggregates.[9] It should be noted that the shape of the delayed emission spectra peaking around 640 nm is very similar to that of a red fluorescence of the dye itself (Figs. 2B, 2C, and 3).

Excitation Spectra of the Delayed Emissions. Figure 4 shows typical results obtained with $P/D=50$. The excitation spectra of both the phosphorescence at 77 K and the delayed thermal fluorescence at 213 K ($\lambda_{max}=$ 530 nm) are almost the same as the absorption spectrum at 77 K. On the other hand, the excitation spectrum of the delayed emission observed at 640 nm and at 213 K differs from that of the delayed thermal fluorescence at 530 nm. The excitation spectrum of the delayed emission at 640 nm shows an increase of the band at 470 nm, accompanied by the corresponding decrease of the band at 500 nm. This shape of the excitation spectrum is similar to that of the absorption spectrum at a low P/D value (Fig. 1).

Delayed emission around 640 nm was observed more remarkably in the case of denatured DNA and at lower P/D values where the absorption band due to the dye dimer becomes pronounced (Fig. 1).

Mechanism of the Newly-observed Delayed Emission.

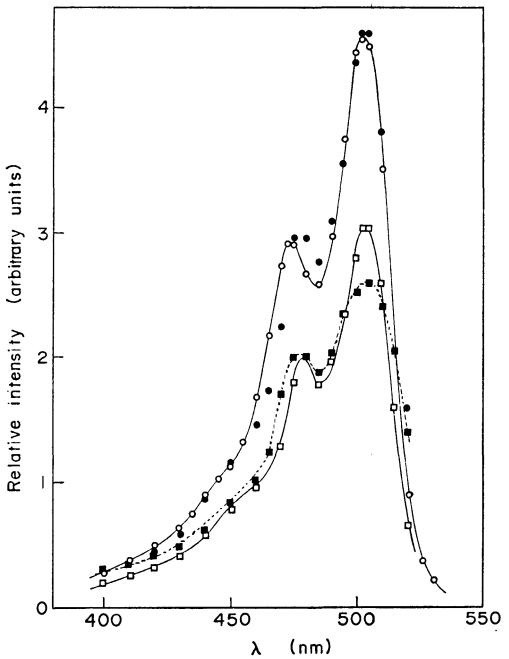

Fig. 4. Excitation spectra of delayed emissions of DNA–AO complex ($P/D=50$). ○: Absorption spectrum at 77 K, ●: excitation spectrum of phosphorescence observed at 610 nm and at 77 K, □: excitation spectrum of delayed thermal fluorescence observed at 530 nm and at 213 K, ■ : excitation spectrum of delayed emission observed at 640 nm and at 213 K.

A comparison of absorption, total emission and excitation spectra of the delayed emissions suggests that the dye dimer formed in the ground state may contribute to the newly-observed delayed emission. However, even at $P/D=100$ and $P/D=50$ where the monomeric form of the dye predominates, there is an intense delayed emission around 640 nm (Figs. 2B and 2C). This indicates that the newly-observed delayed emission can not be explained only by ground-state dimerization of the dye. An alternative explanation is that the newly-observed band is due, in part, to another type of dimeric species, known as excimer.

In the present case, the intensity of the delayed emission around 640 nm varies not with the second power but with the first power of the intensity of the exciting light. Thus, it seems that the delayed emission observed anew in this study is not due to triplet-triplet annihilation.[19]

It has been shown that the dimerization of AO leads to a red shift of *ca.* 30 nm in the peak of phosphorescence.[21] If we compare the phopshorescence spectra at 77 K, the shoulder around 660 nm becomes manifest at a low P/D value and in the case of denatured DNA where ground-state dimerization becomes significant; this is due to the dimer phosphorescence.[21]

In view of these findings, a mechanism similar to that of delayed thermal fluorescence may provide a good explanation for the above results.[22,23] The delayed emission around 640 nm can be interpreted as a result of two processes: 1. The thermal excitation from the triplet state of the dimer (D^t) to the excimer

state (E), followed by an emission. 2. The excimer formation, $M_1+M_0 \rightarrow E$, after the thermal excitation of the triplet state of the monomer (M^t) to the first excited singlet state (M_1), followed by an emission; here, M_0 is the monomer in the ground state. The delayed emission due to this mechanism is then called delayed thermal excimer fluorescence. Because of the very small energy gap between D^t and E, the delayed thermal excimer fluorescence according to process 1 is expected to show up at considerably lower temperatures than the delayed thermal fluorescence (Figs. 2A, 2B, and 2C).

Formation of the Excimer. The bound dye is not uniformly distributed in DNA, but has a tendency to form clusters.[12] The freezing of the DNA–dye solutions may accelerate the formation of clusters.[12] The dye molecules in clusters exist closely and thus seem to be responsible for the dimer formation both in the ground and excited states.

In general, the bound dye molecules are considered to be intercalated between adjacent DNA base pairs at a high P/D value. Two models for the intercalation process have been proposed: complete intercalation model[5,6] and partial intercalation model in which partly intercalated dye molecule is a possible binding site for additional, non-intercalated dye molecule.[7] In the case of the former, the closest distance between bound dye molecules could be 10.2 Å assuming the exclusion of adjacent intercalation sites,[7,24] while the closest distance could be 3.4 Å in the case of the latter. The mutual orientation and extent of overlap of adjacent dye molecules might be very important for the formation of the excimer. Observation of triplet-singlet and triplet-triplet energy transfers between DNA bases and dyes at 77 K shows that the structure of complexes at low temperatures is very similar to that at room temperature.[25,26] If we judge from the distance between two bound dye molecules, the partial intercalation model seems favorable for the formation of the excimer.

In conclusion, it is evident that the nearest neighbor dye-dye interactions produce the excimer state of the dye. Such interactions may play an important role in the biological actions of AO.

This work was supported in part by a Grant-in-Aid for Scientific Research from the Ministry of Education.

References

1) A. R. Peacocke, "Acridines," 2nd ed, ed by R. M. Acheson, Interscience Publishers, New York (1973), pp. 723—757.
2) E. R. Lochmann and A. Micheler, "Physico-Chemical Properties of Nucleic Acids," ed by J. Duchesne, Academic Press, New York (1973), Vol. 1, pp. 223—267.
3) D. F. Bradley and M. K. Wolf, *Proc. Natl. Acad. Sci. U.S.A.*, **45**, 944 (1959).
4) A. L. Stone and D. F. Bradley, *J. Am. Chem. Soc.*, **83**, 3627 (1961).
5) L. S. Lerman, *J. Mol. Biol.*, **3**, 18 (1961).
6) L. S. Lerman, *Proc. Natl. Acad. Sci. U.S.A.*, **49**, 94 (1963).
7) R. W. Armstrong, T. Kurucsev, and U. P. Strauss, *J. Am. Chem. Soc.*, **92**, 3174 (1970).
8) E. Fredericq and C. Houssier, *Biopolymers*, **11**, 2281 (1972).
9) V. Zanker, *Z. Phys. Chem. Leipzig.*, **199**, 225 (1952).
10) O. F. Borisova and L. A. Tumerman, *Biofizika*, **9**, 537 (1964).
11) O. F. Borisova and L. A. Tumerman, *Biofizika*, **10**, 32 (1965).
12) R. F. Steiner, I. Weinryb, and R. Kolinski, *Biochim. Biophys. Acta*, **209**, 306 (1970).
13) S. Ichimura, M. Zama, and H. Fujita, *Biochim. Biophys. Acta*, **240**, 485 (1971).
14) Y. Kubota, *Bull. Chem. Soc. Jpn.*, **43**, 3121 (1970).
15) Y, Kubota, *Bull. Chem. Soc. Jpn.*, **43**, 3126 (1970).
16) H. R. Mahler, B. Kline, and B. D. Mehrotra, *J. Mol. Biol.*, **9**, 801 (1964).
17) G. Weill and M. Calvin, *Biopolymers*, **1**, 401 (1963).
18) T. Kurucsev and U. P. Strauss, *J. Phys. Chem.*, **74**, 3081 (1970).
19) C. A. Parker, "Photoluminescence of Solutions," Elsevier, Amsterdam (1968), pp. 86—125.
20) S. P. McGlynn, T. Azumi, and M. Kinoshita, "Molecular Spectroscopy of the Triplet State," Prentice-Hall, Englewood Cliffs (1969), pp. 27—29.
21) R. W. Chambers, T. Kajiwara, and D. R. Kearns, *J. Phys. Chem.*, **78**, 380 (1974).
22) M. Sato, T. Azumi, and H. Azumi, *Bull. Chem. Soc. Jpn.*, **39**, 857 (1966).
23) M. Sato, T. Azumi, and H. Azumi, *Bull. Chem. Soc., Jpn.*, **40**, 1031 (1967).
24) D. M. Crothers, *Biopolymers*, **6**, 575 (1968).
25) I. Isenberg, R. B. Leslie, S. L. Baird, Jr., R. Rosenbluth, and R. Bersohn, *Proc. Natl. Acad. Sci. U.S.A.*, **52**, 379 (1964).
26) W. C. Galley, *Biopolymers*, **6**, 1279 (1968).

Heterogeneous Catalysis in the Liquid-phase Oxidation of Olefins. III. Activity of Supported Vanadium–Chromium Binary Oxide Catalyst for the Oxidation of Cyclohexene

Katsuomi TAKEHIRA,* Takashi HAYAKAWA, and Toshio ISHIKAWA
Catalysis Division, National Chemical Laboratory for Industry, Mita, Meguro-ku, Tokyo 153

(Received August 24, 1978)

The liquid-phase oxidation of cyclohexene has been conducted in benzene using a vanadium–chromium binary oxide supported on γ-Al_2O_3 or SiO_2 as the catalyst. Three series of catalysts have been prepared by a kneading method using the following combinations of raw materials; NH_4VO_3+$Cr(NO_3)_3\cdot 9H_2O$+alumina hydrate (Catalyst G), NH_4VO_3+$(NH_4)_2CrO_4$+alumina hydrate (H), and NH_4VO_3+$Cr(NO_3)_3\cdot 9H_2O$+silica sol (I). It has been found that the activity of the supported binary system is due to the interactions between the metal oxides and the carrier. The contributions of compounds such as the chromium isopolyvanadates appear to add to the above activity. The order of catalytic activity has been established as : I>H>G. The V_2O_5–SiO_2 system in the I series showed the highest activity, but rapidly became depleted in the course of reaction. The second highest activity was given by Cr_2O_3–SiO_2 system, on which Cr^{5+} species was observed. In both cases, the vanadium and chromium metal ions may be coordinated tetrahedrally on SiO_2. The Cr_2O_3–Al_2O_3 in the H series contained Cr^{5+} ions and exhibited high activity which may be attributed to the tetrahedral configuration. It is thought that the tetrahedral complexes catalyze the autoxidation of cyclohexene by decomposing 1-cyclohexenyl hydroperoxide.

Vanadium–chromium binary oxides (V–Cr) have shown activities in the liquid-phase oxidations of acrylaldehyde[1] and cyclohexene.[2,3] The activities were found to be largely influenced by the method of catalyst preparation, *i.e.*, the use of a more acidic medium promoted the formation of chromium isopolyvanadate which contained a more condensed vanadate anion, resulting in the increase in catalytic activity.[3]

With practical catalysts, the active components are generally supported on carriers such as silica and alumina which possess a high surface area; that the carriers have a profound effect on the activity of catalyst has been demonstrated. A one component system, *i.e.*, supported V_2O_5 or Cr_2O_3, has been extensively used as a catalyst for example in gas-phase oxidation of hydrocarbons and in the polymerization of ethylene, respectively. The dependency of the activity of γ-Al_2O_3- or SiO_2-supported one component systems on the surface structure has been investigated in detail.[4-10] In the present work, the liquid-phase oxidation of cyclohexene has been conducted using γ-Al_2O_3- or SiO_2-supported V–Cr system as the catalyst. The effects of the carriers and the methods of preparation on the activity have been discussed.

Experimental

Catalysts. The supported binary system catalysts were prepared by the kneading method as follows; aqueous solutions of the raw materials of vanadium and chromium oxide components were poured into alumina hydrate (Shokubai Kasei Co., Ltd.) or silica sol (Snowtex, Kokusan Kagaku Co., Ltd.), and the mixture kneaded at 80 °C for 6 h, dried at 100 °C for one day, and calcined at 450 °C for 5 h in air. The resulting catalyst was pulverized and used (30—40 mesh particle size powder). NH_4VO_3, $Cr(NO_3)_3\cdot 9H_2O$, and $(NH_4)_2CrO_4$ were used as the raw materials for the metal oxide components. The symbol, concentration (calculated as V_2O_5+Cr_2O_3 (wt %)) and composition of supported metal oxides (in terms of atomic % of Cr/(V+Cr)), and specific surface area (S_s) are given in Tables 1 and 2.

Apparatus and Procedure. The oxidation was conducted at 60 °C for 4 h under 1 atm of O_2 using the batch system.[2] Cyclohexene (20.0 ml, purified by passing it over activated alumina to eliminate the hydroperoxide), benzene as solvent (50.0 ml), *t*-butyl hydroperoxide (BHPO) (0.1 ml), and the catalyst (50.0 mg) were used in each reaction. BHPO purified by distillation (40.0 °C/25 mmHg) was added such that reproducible results of oxidation were obtained.

Analyses of Reaction Products and Catalysts. The reaction products; 1-cyclohexenyl hydroperoxide (HPO), 2-cyclohexen-1-one (ONE), 2-cyclohexen-1-ol (OL), and cyclohexene oxide (OXIDE) were determined by the iodometric method and gas chromatography.[2]

The surface area of the catalyst was measured by the BET method, the structure being studied by means of X-ray diffraction and infrared absorption.[2] X-Ray photoelectron spectroscopy (XPS) measurements were carried out on a Du Pont ESCA 650 B using monochromatic Al $K\alpha$ radiation in order to clarify the surface properties of the catalyst. The power of X-ray radiation was 300 W (7.5 kV, 40 mA) in all measurements. All binding energy values were referred to the contamination C 1s line (285.0 eV).

Results and Discussion

Surface Area of Catalyst. Both γ-Al_2O_3 and SiO_2 prepared in the present work gave similar values of S_s. This value increased by supporting metal oxides on γ-Al_2O_3, and decreased on SiO_2 (Table 1). On the γ-Al_2O_3 carrier, the use of $(NH_4)_2CrO_4$ caused a small increase in S_s, compared with that of $Cr(NO_3)_3\cdot 9H_2O$ (Table 2).

Addition of BHPO. The results of using the G-5 catalyst are shown in Table 3 (Run Nos. 6 and 7). In the absence of BHPO, the induction period of oxygen uptake showed no fixed value, resulting in no reproducibility for the conversion. By adding a small amount of BHPO, reproducible results were obtained (Run No. 7). No oxygen absorption was observed for 5 h in the absence of catalyst and BHPO; the addition of 1 ml of BHPO caused a small amount of oxygen

Table 1. Concentration of supported metal oxides, symbol, and specific surface area of catalyst

Concentration $V_2O_5+Cr_2O_3$ (wt %)	γ-Al_2O_3-series[a]		SiO_2-series[b]	
	Symbol	S_s, (m^2/g)	Symbol	S_s, (m^2/g)
0	γ-Al_2O_3	220	SiO_2	210
1	V–Cr-γ-Al_2O_3-(1)	246	V–Cr–SiO_2-(1)	202
5	V–Cr-γ-Al_2O_3-(5)	277	V–Cr–SiO_2-(5)	181
10	V–Cr-γ-Al_2O_3-(10)	293	V–Cr–SiO_2-(10)	160
20	V–Cr-γ-Al_2O_3-(20)	270	V–Cr–SiO_2-(20)	142

a) Cr/(V+Cr): 50 atom %. b) Cr/(V+Cr): 70 atom %. Both series were prepared from NH_4VO_3 and $Cr(NO_3)_3\cdot 9H_2O$.

Table 2. Composition of supported metal oxides, symbol, and specific surface area of catalyst

Composition Cr/(V+Cr) (atom %)	G-Series[a]		H-Series[b]		I-Series[c]	
	Symbol	S_s, (m^2/g)	Symbol	S_s, (m^2/g)	Symbol	S_s, (m^2/g)
0	G-0	261	H-0	255	I-0	109
20	G-2	274			I-2	105
30			H-3	268		
40	G-4	282			I-4	124
50	G-5	265	H-5	249		
60	G-6	260			I-6	132
70			H-7	232	I-7	138
80	G-8	252			I-8	131
100	G-10	244	H-10	212	I-10	136

a) Prepared from NH_4VO_3, $Cr(NO_3)_3\cdot 9H_2O$, and alumina hydrate. b) Prepared from NH_4VO_3, $(NH_4)_2CrO_4$, and alumina hydrate. c) Prepared from NH_4VO_3, $Cr(NO_3)_3\cdot 9H_2O$, and silica sol. Concentration of metal oxides (calculated as $V_2O_5+Cr_2O_3$) was 20 wt % in each series.

Table 3. Oxidation of cyclohexene[a]

Run No.	Catalyst	Amount of BHPO added (ml)	Induction period (min)	R_{max} (mol/l·s)	Conversion of cyclohexene (%)	Selectivity			
						HPO (%)	ONE (%)	OL (%)	OXIDE (%)
1	—	1	110	3.13×10^{-6}	3.7	—	—	—	—
2	γ-Al_2O_3	1	240	—	—	—	—	—	—
3	SiO_2	1	179	3.36×10^{-6}	3.8	—	—	—	—
4	V–Cr–D-5[b]	—	110—120	3.24×10^{-5}	10.1	40.3	10.5	25.2	20.3
5	V–Cr–D-5[b]	0.1	10	3.31×10^{-5}	25.0	38.5	9.7	24.5	21.0
6	G-5	—	150—300	1.03×10^{-4}	c)	16.9[c]	30.5[c]	35.3[c]	15.1[c]
7	G-5	0.1	4	1.06×10^{-4}	30.1	15.2	31.3	36.0	12.6

a) Cyclohexene (20.0 ml), benzene (50.0 ml), and catalyst (50.0 mg) were used. The reaction temperature was 60 °C, the reaction time 4 h, and the oxygen pressure 1 atm. b) V–Cr–D-5 is the unsupported catalyst reported in a previous paper.[3] Cr/(V+Cr); 50 atom %, and S_s; 8.3 m^2/g. c) The value of conversion was not precisely obtained, as the induction period was not constant. The values of selectivity are average values.

absorption (Run No. 1). Both γ-Al_2O_3 and SiO_2 showed no activity. V–Cr–D-5 is the unsupported binary oxide catalyst which showed high activity in a previous report[3] (Run Nos. 4 and 5, S_s 8.3 m^2/g). The activity of the V–Cr system of G-5 showing a S_s of 265 m^2/g may be attributed to the large surface area.

The effect of the addition of BHPO is shown in Fig. 1. The induction period was greatly reduced by the addition of a small amount of BHPO, producing an almost constant induction period when the amount of BHPO exceed 0.1 ml. There is the possibility that the BHPO affects the reaction reults, *e.g.*, the product distribution may be changed by a stoichiometric epoxidation of cyclohexene with BHPO, *etc.* In order to avoid such possibilities, the amount of BHPO was fixed at 0.1 ml (9.2×10^{-4} mol) which is extremely small compared with the amount of cyclohexene (20 ml; 1.97×10^{-1} mol). The values of selectivity were not affected as shown in the two pairs of reaction (Run Nos. 4 and 5 and Run Nos. 6 and 7). BHPO appears to work mainly as an initiator by way of its decomposition on the catalyst. In all subsequent reactions, 0.1 ml of BHPO was added to obtain reproducible results.

Oxygen Uptake. The curves of oxygen uptake

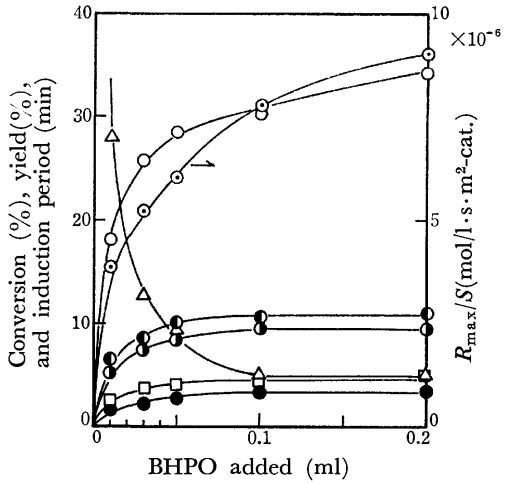

Fig. 1. Effect of the addition of BHPO. 20.0 ml of cyclohexene, 50.0 ml of benzene, and 50.0 mg of G-5 catalyst were used. The reaction temperature was 60 °C, the reaction time was 4 h, and the O_2-pressure was 1 atm.
⊙ R_{max}/S, ○ conversion of cyclohexene, □ yield of HPO, ◑ yield of ONE, ◑ yield of OL, ● yield of OXIDE, △ induction period.

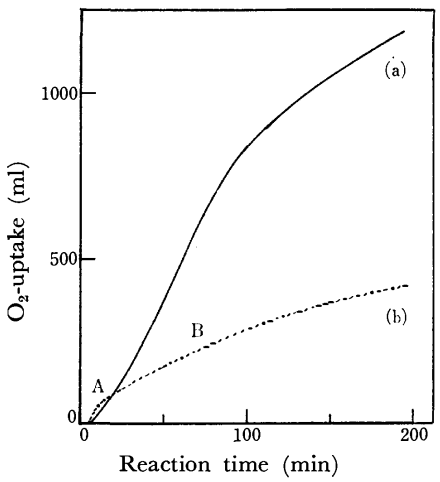

Fig. 2. Oxygen absorption.
(a) Catalyst: G-5, (b) catalyst: I-0. 20.0 ml of cyclohexene, 50.0 ml of benzene, and 50.0 mg of the catalyst were used. The reaction temperature was 60 °C, and the O_2-pressure was 1 atm.

are shown in Fig. 2. Most of the catalysts used gave a typical S-shaped oxygen absorption curve (a); I-0, I-2, and I-4 show different types of absorption (b). In the latter type, rapid absorption was observed immediately after the induction period (A), followed by a linear decrease in the rate of oxygen uptake (B). As the V_2O_5–SiO_2 system illustrates the high activity for the decomposition of BHPO into radicals[11] (Eq. 1), the rapid reaction at A may be due to a chain reaction (Eqs. 2, 3, and 4) induced by the radicals formed from BHPO.

$$\text{BHPO} \xrightarrow{M^{n+}/M^{(n+1)+}} \text{RO}\cdot \text{ and } \text{RO}_2\cdot \quad (1)^{12}$$

$$\text{RO}\cdot \text{ or } \text{RO}_2\cdot + \bigcirc \rightarrow \text{ROH or } \text{RO}_2\text{H} + \bigcirc\cdot \quad (2)$$

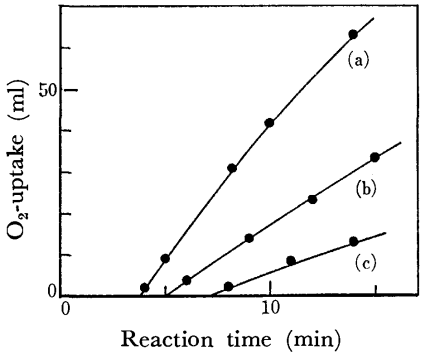

Fig. 3. Effect of the amount of BHPO added on the oxygen absorption.
BHPO added; (a) 0.1 ml (b) 0.05 ml (c) 0.03 ml
20.0 ml of cyclohexene, 50.0 ml of benzene, and 50.0 mg of I-0 catalyst were used. The reaction temperature was 60 °C, and the O_2-pressure was 1 atm.

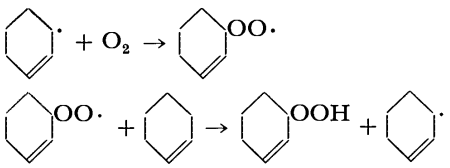
(3)

(4)

M indicates the metal on the catalyst. Evidence for such an induction period was conducted with several oxidations with a I-0 catalyst and a changing amount of BHPO, the results of which are given in Fig. 3 (A is magnified). As can be seen, the maximum rate of O_2-uptake at A (R_{max}-A) showed a first order dependency on the amount of BHPO added, supporting the above mechanism. The rate at B, which suggests a steady state in the oxidation, was independent of the amount of BHPO added. As BHPO was decomposed rapidly on V_2O_5–SiO_2,[11] the O_2-uptake at B may be uniquely due to the radical chain of cyclohexene oxidation, the rate of which is shown by R_{max}-B. The specific activity, *i.e.*, the maximum rate per unit surface area of the catalyst, and the induction period of O_2-uptake are shown in Figs. 4 and 5.

Effect of Amount of Metal Oxides Supported. Figure 4 illustrates the effect of the amount of metal oxides supported on γ-Al_2O_3 or SiO_2. It is of interest that the activity on SiO_2 increased rapidly when a small amount (about 1 wt %) of metal oxides was supported, and remained almost constant with further additions. On γ-Al_2O_3, however, high acitivity was obtained only when a sufficient amount of metal oxides was supported. The product distributions are shown in Figs. 6 and 7. The formations of the two types of active site, *i.e.*, one effective for the autoxidation and another for the selective epoxidation of cyclohexene with HPO, on V–Cr system catalyst have been reported.[2,3] For the present catalysts, two types of active site appear to form, because the OXIDE formation was accompanied with that of OL, suggesting selective epoxidation. The autoxidation which produces HPO and ONE appears to be well catalyzed on the catalyst including a small amount of metal oxides.

Effect of Composition of Metal Oxides. Figure 5 shows the influence of the composition of metal

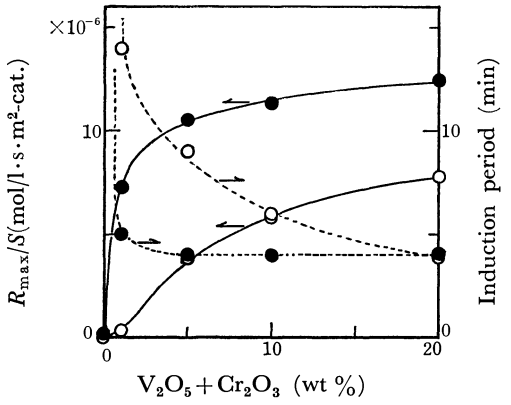

Fig. 4. Effect of the concentration of metal oxides supported.
20.0 ml of cyclohexene, 50.0 ml of benzene, and 50.0 mg of the catalyst were used. The reaction temperature was 60 °C, and the O_2-pressure was 1 atm. Catalyst; ● V-Cr-SiO_2 (Cr/(V+Cr)=70 atom%), ○ V-Cr-γ-Al_2O_3 (Cr/(V+Cr)=50 atom%).

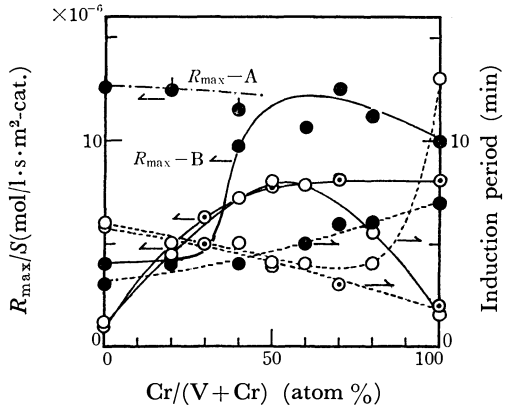

Fig. 5. Effect of the composition of metal oxides supported.
20.0 ml of cyclohexene, 50.0 ml of benzene, and 50.0 mg of the catalyst were used. The reaction temperature was 60 °C, and the O_2-pressure was 1 atm. Catalyst; ● I-series, ⊙ H-series, ○ G-series. Concentration of metal oxides supported, $V_2O_5+Cr_2O_3$: 20 wt %.

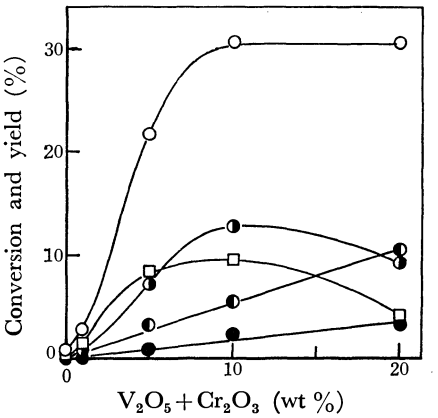

Fig. 6. Effect of the concentration of supported metal oxides on γ-Al_2O_3.
20.0 ml of cyclohexene, 50.0 ml of benzene, 50.0 mg of the catalyst, and 0.1 ml of BHPO were used. The reaction temperature was 60 °C, the reaction time was 4 h, and the O_2-pressure was 1 atm.
○ Conversion of cyclohexene, □ yield of HPO, ◑ yield of ONE, ◐ yield of OL, ● yield of OXIDE.

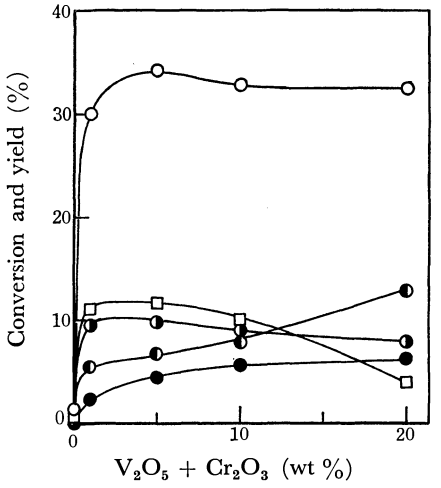

Fig. 7. Effect of the concentration of supported metal oxides on SiO_2
20.0 ml of cyclohexene, 50.0 ml of benzene, 50.0 mg of the catalyst, and 0.1 ml of BHPO were used. The reaction temperature was 60 °C, the reaction time was 4 h, and the O_2-pressure was 1 atm.
○ Conversion of cyclohexene, □ yield of HPO, ◑ yield of ONE, ◐ yield of OL, ● yield of OXIDE.

oxides supported. In the case of the I-series catalyst, the two types of reaction rate, *i.e.*, R_{max}-A and R_{max}-B, are shown together. The activity of the binary system on SiO_2 was higher than that on γ-Al_2O_3, when adopting the value of R_{max}-A/S. According to the oxygen uptake in B, the activities (R_{max}-B/S) of only two catalysts I-0 and I-2 showed similar values to those of the γ-Al_2O_3-supported system, *i.e.*, the two catalysts exhibited high activities at the start of oxygen uptake, being largely deactivated during the oxidation. It is noteworthy that V_2O_5–SiO_2 (I-0) showed a high activity (R_{max}-A/S) in comparison with V_2O_5–Al_2O_3. In the activity of the γ-Al_2O_3-supported systems, clear difference between the G- and H-series catalysts including the large amount of Cr was observed, H-series prepared from $(NH_4)_2CrO_4$ being more active than the G-series from $Cr(NO_3)_3 \cdot 9H_2O$. The difference was observed in both the R_{max}/S and the induction period.

Reaction Scheme. The product distributions obtained with the three series of catalysts are shown in Figs. 8, 9, and 10. The results can be interpreted by the following reaction scheme which has been proposed in the literatures.[2,13-18]

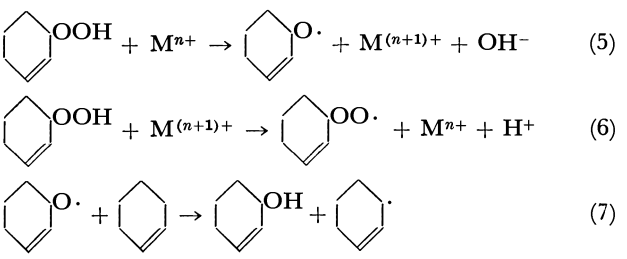

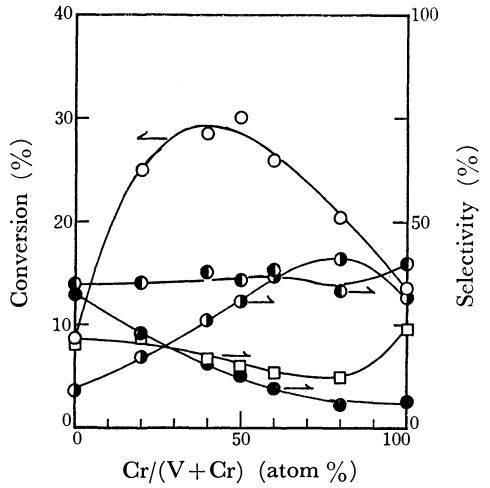

Fig. 8. Product distributions in the oxidation with G-series catalysts.
20.0 ml of cyclohexene, 50.0 ml of benzene, 50.0 mg of the catalyst, and 0.1 ml of BHPO were used. The reaction temperature was 60 °C, the reaction time was 4 h, and the O_2-pressure was 1 atm.
○ Conversion of cyclohexene, □ selectivity of HPO, ◑ selectivity of ONE, ◐ selectivity of OL, ● selectivity of OXIDE.

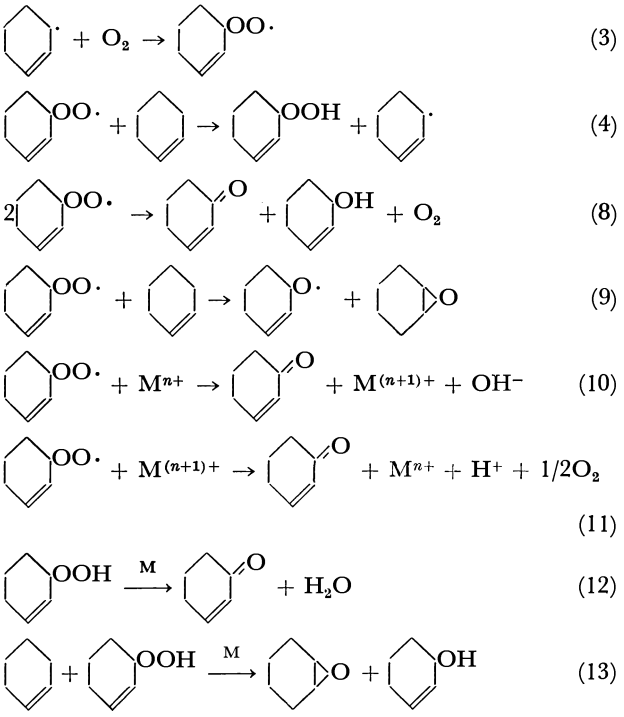

For the purpose of studying the action of the catalysts on hydroperoxide, the decomposition of BHPO was conducted at 60 °C in a N_2 atmosphere. All the catalysts used except I-0—I-6** gave *t*-butyl alcohol (85%), di-*t*-butyl poerxide (10%), and acetone (5%), showing that the decomposition of BHPO proceeds *via* a homolytic mechanism.[12] The homolytic decomposition of

** When using these catalysts, isobutylene and di-*t*-butyl ether were formed together with three products mentioned above. The details of the decomposition of BHPO will be reported in a later paper.

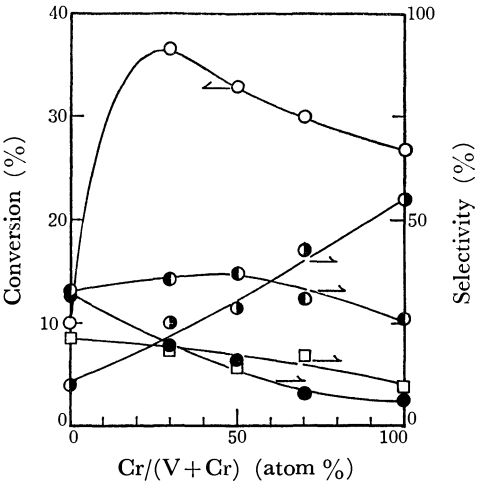

Fig. 9. Product distributions in the oxidation with H-series catalysts.
20.0 ml of cyclohexene, 50.0 ml of benzene, 50.0 mg of the catalyst, and 0.1 ml of BHPO were used. The reaction temperature was 60 °C, the reaction time was 4 h, and the O_2-pressure was 1 atm.
○ Conversion of cyclohexene, □ selectivity of HPO, ◑ selectivity of ONE, ◐ selectivity of OL, ● selectivity of OXIDE.

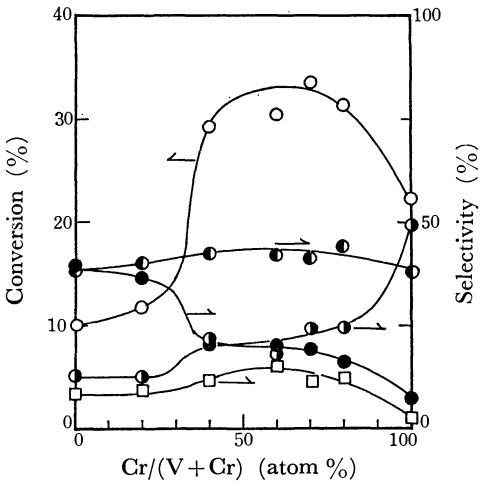

Fig. 10. Product distributions in the oxidation with I-series catalysts.
20.0 ml of cyclohexene, 50.0 ml of benzene, 50.0 mg of the catalyst, and 0.1 ml of BHPO were used. The reaction temperature was 60 °C, the reaction time was 4 h, and the O_2-pressure was 1 atm.
○ Conversion of cyclohexene, □ selectivity of HPO, ◑ selectivity of ONE, ◐ selectivity of OL, ● selectivity of OXIDE.

HPO (Eqs. 5 and 6) must also be considered. Reactions 3 and 4 are chain propagating and Reaction 8 is a biradical termination, by which equimolar amounts of ONE and OL are formed. Reaction 9 is the addition of the peroxyl radical to cyclohexene, although the contribution is very small.[13] Reactions 10 and 11 are an adaptation of the mechanism recently proposed by Mizukami *et al.* in the oxidation of tetralin.[18] The dehydration of HPO on the catalyst

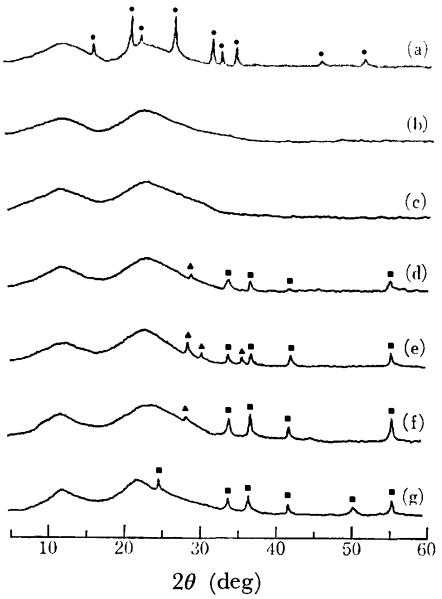

Fig. 11. X-Ray diffraction diagrams of I-series catalysts (Cu $K\alpha$).
a : I-0, b : I-2, c : I-4, d : I-6, e : I-7, f : I-8, g : I-10.
● : V_2O_5, ▲ : $Cr_4(V_2O_7)_3$, ■ : Cr_2O_3.

(Eq. 12) must also be considered as reported by Neuburg *et al.*[17] and Reaction 13 is the selective epoxidation already reported.[2] It may be easily understood that the selective epoxidation proceeded well on the catalyst containing large amount of vanadium. On γ-Al_2O_3, a higher value of conversion was obtained with the H-series , the G- and H-series showing a similar pattern of product distribution up to a Cr content of about 70 atom %. Beyond this value, ONE increased in the H-series and the formation of HPO and OL took precedence over the G-series. Thus, a higher ratio of ONE/OL and simultaneously higher activity (Fig. 5) given by the H-series at higher Cr content, suggests that Reactions 10, 11, and 12 may be useful together with the biradical termination (Eq. 8) as the mechanism for ONE formation. On the other hand, OL is considered to form mainly by Reactions 7 and 8 and the selective epoxidation when using catalysts containing a lot of vanadium. The stabilities of ONE and OL under reaction conditions were examined: separate solutions with 10 ml of ONE and OL in benzene (50 ml containing BHPO (0.1 ml)) were prepared and oxidized at 60 °C with G-5 catalyst (50 mg). ONE did not show any conversion to further oxidized products after 4 h of reaction, whilst an extremely small amount (about 0.8 mol %) of OL was converted into the ketone after 4 h.

I-0 and I-2 showing the high activities at the beginning were deactivated quickly as described above, resulting in low conversion. This suggests the instability of the active species on I-0 and I-2.

Structure of Catalysts. It has already been reported[1-3] that several chemical compounds, *e.g.*, chromium divanadate ($Cr_4(V_2O_7)_3$), chromium metavanadate ($Cr(VO_3)_3$), and chromium polyvanadates, together with V_2O_5 and Cr_2O_3 form in the catalysts of the V–Cr system. These species largely influence catalytic activity. In the present binary system supported on γ-Al_2O_3 or SiO_2, the contributions of the species formed by the interaction between metal oxides and carrier may be reasonably expected together with those of the above chemical compounds. The former contributions have been extensively studied by many researchers.[4-10] When each of V_2O_5 andCr_2O_3 was supported on γ-Al_2O_3 or SiO_2 by impregnation, various problems were encountered, among which one can quote the stabilization and the role of different valency states of metals. The system under study appears to show further complexity due to the binary oxide being supported on γ-Al_2O_3 or SiO_2 by the kneading method.

X-Ray diffraction diagrams of the I-series catalysts are shown in Fig. 11. Several weak diffraction lines of V_2O_5, $Cr_4(V_2O_7)_3$, and Cr_2O_3 were observed together with two broad lines of fine SiO_2 crystals. The γ-Al_2O_3 supported systems (G- and H-series) did not exhibit any lines other than the broad lines of γ-Al_2O_3. The indication is that the crystal of the metal oxides developed better on SiO_2 than on γ-Al_2O_3, the interspacing of the lattice planes of each metal oxide being the same as that of each pure oxide. Yoshida *et al.*[5] reported that γ-Al_2O_3 interacts with V_2O_5 more strongly than SiO_2 as a carrier of the impregnated catalyst. In the system here, prepared by the kneading method, further interaction may be expected as observed in the case of the coprecipitated Cr_2O_3–Al_2O_3 (Cr_2O_3; 19.6 mol %) system, in which the only structure detected by X-ray diffraction measurement was γ-Al_2O_3.[9] Infrared absorption spectra of the γ-Al_2O_3-supported system showed a strong broad band of γ-Al_2O_3 below 1000 cm^{-1} which covered the characteristic absorption bands of V_2O_5, Cr_2O_3, and chromium isopolyvanadates.[3] The binary systems supported on SiO_2; I-0—I-7, exhibited weak absorption bands centered at about 950 and 870 cm^{-1}, together with the strong absorption bands at 1100 and 800 cm^{-1} of SiO_2. The weak bands may be assigned to the vibrations of VO_3 in $Cr_4(V_2O_7)_3$,[3] the formation of $Cr_4(V_2O_7)_3$ together with V_2O_5 and Cr_2O_3 being thus clarified in the binary system of I-series. Such formation need not be excluded from the γ-Al_2O_3-supported system, though it may not be detected.

Recently, XPS studies have been conducted to elucidate the surface properties of γ-Al_2O_3-[7] or SiO_2-[6] supported chromia systems. The advantages of the XPS technique are its ability in simultaneously detemining the valencies of metal ions on the surface layer (−10 Å) of the catalyst and the interaction between the catalyst and the support. The first XPS spectra of Cr^{5+} were observed by Okamoto *et al.*[7] who emphasized that the spin-orbit splitting of the Cr 2p level (ΔE) is useful together with the binding energy for discriminating the valence states of chromium. Moreover, it was pointed out that the chromium species on the catalyst surface can readily be photo-reduced by X-ray radiation during XPS measurements.[6,7] In order to avoid surface reduction, all spectra of the Cr 2p level were measured within 10 min exposure to X-ray flux, in which the photo-reduction

Table 4. Binding energy of Cr 2p3/2 and V 2p3/2, spin-orbit splitting of Cr 2p level, and assignment of valency of chromium

Catalyst or compound	Cr 2p3/2 (eV)	V 2p3/2 (eV)	ΔE (eV)	Assignment of Cr valency[a]
V_2O_5	—	515.9	—	—
$VO(acac)_2$	—	516.0	—	—
Cr_2O_3	576.7	—	9.8	3+
K_2CrO_4	579.6	—	9.1	6+
V-Cr-D-5	577.5	517.5	9.7	3+
G-0	—	517.4	—	—
G-4[b]	577.6	517.4	9.7	3+ (5+)
G-6	578.0	517.5	9.5	5+ (3+)
G-10	577.5	—	9.8	3+ (5+)
H-3[b]	577.5	517.4	9.7	3+ (5+)
H-5	577.8	517.4	9.5	5+ (3+)
H-7[c]	579.3	517.3	9.0	6 & 5+ (3+)
H-10[c]	579.7	—	9.1	6 & 5+
I-0	—	516.6	—	—
I-4	577.4	516.7	9.8	3+
I-6	577.6	516.5	9.1	5+ (3+)
I-10	577.9	—	9.1	5+ (3+)

a) Valence state in parentheses indicates minor one. b) This peak has a weak shoulder at higher binding energy. c) This peak shows a large broadening at lower binding energy.

Table 5. Comparison of the activities of several chromium system catalysts[a]

Catalyst[b]	Induction period (min)	R_{max} (mol/l·s)	Conversion of cyclohexene (%)	Selectivity HPO (%)	ONE (%)	OL (%)	OXIDE (%)
V-Cr-γ-Al_2O_3	5	8.6×10^{-5}	29.0	20.1	22.2	35.0	18.5
Mo-Cr-γ-Al_2O_3	11	7.8×10^{-5}	28.8	11.5	20.5	37.1	30.3
W-Cr-γ-Al_2O_3	8	5.2×10^{-5}	20.2	17.6	45.0	28.3	7.3
Co-Cr-γ-Al_2O_3	8	6.5×10^{-5}	23.2	17.4	51.4	23.6	5.6
Mn-Cr-γ-Al_2O_3	5	5.8×10^{-5}	26.7	19.6	41.5	32.3	3.5

a) Cyclohexene (20.0 ml), benzene (50.0 ml), the catalyst (50.0 mg), and BHPO (0.1 ml) were used. The reaction temperature was 60 °C, the reaction time 4 h, and the O_2-pressure 1 atm. b) The catalysts (Me-Cr-γ-Al_2O_3) were prepared from the following raw materials; NH_4VO_3, $(NH_4)_6Mo_7O_{24}\cdot4H_2O$, $5(NH_4)_2O\cdot12WO_3\cdot5H_2O$, $Co(NO_3)_3\cdot6H_2O$, $Mn(NO_3)_3\cdot xH_2O$, $Cr(NO_3)_3\cdot9H_2O$, and alumina hydrate by the kneading method. The concentration of metal oxides supported on each catalyst was 20 wt % when calculated as V_2O_5, MoO_3, WO_3, Co_2O_3, Mn_2O_3, and Cr_2O_3. The composition of the binary system (Cr/(Me+Cr)) was 30 atom %.

was found to be negligible. The results of XPS measurements are shown in Table 4, the assignment of the valence states of chromium being done according to the results by Okamoto *et al.*[7] In the valence state of vanadium, Larrson *et al.*[19] observed a shift of the V 2p3/2 binding energy between V_2O_5 (516.6 eV) and $VO(acac)_2$ (515.1 eV), but it was not observed here (Table 4). Valdelievre *et al.*[20] obtained the V 2p3/2 values of 515.5 eV for V_2O_5 and 516.0 eV for V_2O_4 when studying the V_2O_5 catalyst in the oxidation of propylene. Therefore, it may be difficult to determine the valence state of vanadium, importance being given to the fact that the V 2p3/2 binding energy is lower on SiO_2 than on γ-Al_2O_3.

Active Sites. The active sites on the supported V–Cr binary oxide catalyst may be classified into two types; autoxidation and selective epoxidation.[2] The latter site may consist mainly of vanadium species, although the details have not been clarified. The activities of several Me–Cr systems, when Me is V, Mo, W, Co, and Mn, have been compared (Table 5), exhibiting the following order of activity for selective epoxidation; Mo–Cr-γ-Al_2O_3>V–Cr-γ-Al_2O_3>W–Cr-γ-Al_2O_3. The order of metals, *i.e.*, Mo>V>W, agrees well with that observed in the selective epoxidation of olefins with organic hydroperoxide using soluble metal complexes.[21] Co, Mn, and Cr species did not contribute to the epoxidation but accelerated the autoxidation. Thus, the Mo–Cr or V–Cr binary system showed a high yield of OXIDE whose formation may

have been aided by the dual functions of the systems, as observed in the homogeneous mixed catalyst system by Fusi *et al.*[22] and Arzoumanian *et al.*[23]

The former site appears more complex than the latter since the the value of R_{max}/S depends largely on the carrier (Figs. 4 and 5) and the composition of the binary system (Fig. 5). The activity of the G-series showed a maximum value at a composition of 50 atom % Cr, which may be due to the formation of chromium isopolyvanadates, as reported in the unsupported system.[3] Such an increase in the activity due to chemical compound formation may be also expected in the H-series and especially in the I-series, in which the formation of $Cr_4(V_2O_7)_3$ was clearly observed. A more important problem, however, appears to be the effect of the carrier on the activity. At high Cr content on γ-Al_2O_3, the H-series gives a higher rate and a simultaneously higher valence state of chromium (Table 4) than the G-series, suggesting the active species of highly charged chromium ions. The high valence state of chromium (Cr^{5+}) was also observed in the I-series supported on SiO_2 which showed high activity. One of the active species for autoxidation appears, therefore, to be the Cr^{5+} ions which form on the catalyst during preparation. The role of the Cr^{6+} species which still remains in the H-series (prepared from $(NH_4)_2CrO_4$) after calcination can not be ignored, but it is not so clear. The Cr^{5+} ions observed on G-4 and G-6 catalysts may mainly form in the interaction between the catalyst and carrier, since the unsupported system (V–Cr–D-5) does not show such evidence.

Van Reijen *et al.*[4] reported that Cr^{5+} is coordinated mainly tetrahedrally when supported on SiO_2 and square-pyramidally on γ-Al_2O_3, and that the tetrahedral complex (CrO_4) is more reactive than the squarepyramidal one (CrO_5). Such phenomena has also been confirmed in the literature.[8,10] Also the vanadium (V^{4+}) species is coordinated in (VO_4) on SiO_2 and in (VO_5) on γ-Al_2O_3,[4,5,24] and the (VO_4) on SiO_2 is highly reactive towards, *e.g.*, C_2H_4, being subsequently transformed into the stable (VO_5).[4] By contrast, the (VO_5) is more stable than the corresponding configuration of Cr^{5+}, *i.e.*, (CrO_5).[4] Moreover, when considering the coordination state in aqueous solution of the catalyst preparation, the tetrahedral $(CrO_4)^{3-}$ ion may be preferentially found in highly alkaline solution[25] whereas the coordination is square-pyramidal in acid solution, as well known for V^{4+} in many vanadyl complexes.[26] A part of the Cr^{5+} ions on H-10 and H-7 can be reasonably coordinated in the tetrahedral configuration, whereas those on G-8 in the square-pyramidal configuration. The order of reactivity of these configurations has been given by van Reijen *et al.*[4] as follows; (VO_4)>(CrO_4)>(CrO_5)>(VO_5), in which only the (VO_4) is unstable. This order appears to explain the activity of the supported V–Cr binary system catalyst, when the configurations of vanadium and chromium complexes might be allowed on the carriers as described above. On SiO_2, the catalyst abundant in vanadium exhibited high activity (Fig. 5, R_{max}-A/S) at the beginning of reaction, which decreased (R_{max}-B/S) in the course of reaction. This may be due to the high reactivity and instability of the (VO_4) complex. The subsequently high activity of the chromium abundant catalyst on SiO_2 may be due to the (CrO_4) species which is reactive and simultaneously stable. When supported on γ-Al_2O_3, the catalysts of the H-series expected to contain the (CrO_4) complex in abundance exhibited higher activities than those of the G-series rich in chromium. It has been reported that the (CrO_4) complex was formed on SiO_2 even when small amounts of chromia was supported,[6] and therefore, the rapid increase in activity of the V–Cr–SiO_2 systems (Fig. 4) may be due to the (CrO_4) species formed. The tetrahedral complexes are thought to catalyze the autoxidation of cyclohexene through HPO decomposition (Reactions 5 and 6) which proceeds *via* coordination of HPO to a vacant site in the complex. The low activities of the G- and H-series of high vanadium content and also of the G-series of high chromium content may be attributed to the (VO_5) and (CrO_5) species, respectiviely, on γ-Al_2O_3 (Fig. 5). Thus, the activity of the supported V–Cr binary catalyst can be thought principally due to the formation of the two types of configuration; tetrahedral on SiO_2 and square-pyramidal on γ-Al_2O_3. It is supposed that the two modes of configuration are performed against the surroundings of the carrier, *i.e.*, the tetrahedral structure of SiO_2 and the spinel structure of γ-Al_2O_3.[10] The contribution of chemical compounds, such as chromium isopolyvanadates, appear to overlap the principal contribution of the two configurations, as observed in the G-series (Fig. 5).

References

1) K. Takehira, T. Nishimura, M. Araki, T. Hayakawa, and T. Ishikawa, *Nippon Kagaku Kaishi*, **1974**, 652.
2) K. Takehira and T. Ishikawa, *Bull. Chem. Soc. Jpn.*, **49**, 2351 (1976).
3) K. Takehira, T. Hayakawa, and T. Ishikawa, *Bull. Chem. Soc. Jpn.*, **51**, 1685 (1978).
4) L. L. van Reijen and P. Cossee, *Discuss. Faraday Soc.*, **41**, 277 (1966).
5) S. Yoshida, T. Iguchi, S. Ishida, and K. Tarama, *Bull. Chem. Soc. Jpn.*, **45**, 376 (1972).
6) A. Cimino, B. A. de Angelis, A. Luchetti, and G. Minelli, *J. Catal.*, **45**, 316 (1976).
7) Y. Okamoto, M. Fujii, T. Imanaka, and S. Teranishi, *Bull. Chem. Soc. Jpn.*, **49**, 859 (1976).
8) Yu. I. Pecherskaya and V. B. Kazanskii, *Kinet. Katal.*, **8**, 401 (1967).
9) C. P. Poole, Jr., W. L. Kehl, and D. S. MacIber, *J. Catal.*, **1**, 407 (1962).
10) V. B. Kazanskii, *Kinet. Katal.*, **11**, 455 (1970).
11) K. Takehira and T. Ishikawa, presented at the 9th Symposium on Oxidation, Tokyo, Japan, November 25, 26 (1975).
12) R. Hiatt, K. C. Irwin, and C. W. Gould, *J. Org. Chem.*, **33**, 1430 (1968).
13) D. E. van Sickle, F. R. Mayo, and R. M. Arluck, *J. Am. Chem. Soc.*, **87**, 4824 (1965).
14) C. Meyer, G. Clement, and J. C. Balaceanu, *Proc. Int. Congr. Catal., 3rd*, 1964, **1**, 184 (1965).
15) E. S. Gould and M. Rado, *J. Catal.*, **13**, 238 (1969).
16) H. J. Neuburg, J. M. Basset, and W. F. Graydon,

J. Catal., **25**, 425 (1972).
17) H. J. Neuburg, M. J. Phillips, and W. F. Graydon, *J. Catal.*, **38**, 33 (1975).
18) F. Mizukami and J. Imamura, *Bull. Chem. Soc. Jpn.*, **51**, 1404 (1978).
19) R. Larsson, B. Folkesson, and G. Schon, *Chemica Scripta*, **3**, 88 (1973).
20) M. Valdelièvre, H. Baussart, R. Delobel, and J. M. Leroy, *Bull. Soc. Chim. Fr.*, **1975**, 2467.
21) N. Indictor and W. F. Brill, *J. Org. Chem.*, **30**, 2074 (1965).
22) A. Fusi, R. Ugo, and G. M. Zanderighi., *J. Catal.*, **34**, 175 (1974).
23) H. Arzoumanian, A. Blanc, U. Hartig, and J. Metzer, *Tetrahedron Lett.*, **1974**, 1011.
24) T. Suzuki, S. Yoshida, and K. Tarama, presented at the 37th National Meeting of the Chemical Society of Japan, Tokyo, April 1978.
25) N. Bailey and M. C. R. Symons, *J. Chem. Soc.*, **1957**, 203.
26) H. B. Gray and C. R. Hare, *Inorg. Chem.*, **1**, 363 (1962).

Population Analysis of (*R*)-Thiazolidine-4-carboxylic Acid

Jun KAMO,† Nobuo TANAKA,* Yoshiki MATSUURA, Tamaichi ASHIDA,††
and Masao KAKUDO

Institute for Protein Research, Osaka University, Suita 565

(Received August 31, 1978)

The structure of (*R*)-thiazolidine-4-carboxylic acid was refined at 111 and 293 K, respectively. Population analysis, which refines the population of the electrons in the molecule, was carried out, the result being compared with that of theoretical calculation.

In studies on structure by means of X-ray diffraction, the recent development of the diffractometer has afforded intensity data accurate enough for discussion of the distribution of the electron cloud. The population analysis[1] deals with the observed electron density distribution quantitatively. The number of electrons in each non-bonded and bonded orbital is derived from the refinement, from which bond orders and charge distribution of the molecule can be discussed.

(*R*)-Thiazolidine-4-carboxylic acid is an analogue of the proline and cysteine, and the structure was determined by Chacko.[2] In this paper, the structure of this molecule at both 293 and 111 K was refined by the population analysis method, the electronic structure being discussed in comparison with the theoretical one.

Experimental

Two sets of intensity data were measured at 293 and 111 K with a four circle diffractometer. Each set has 4 octants of the reciprocal space measured in 2θ-θ mode. The crystal data and experimental conditions are given in Tables 1 and 2, respectively. The crystal was treated with liquid nitrogen before the data collection in order to prevent from suffering of the extinction effect. The average structure amplitudes among the equivalent reflections in each set was used for further calculations. The estimated standard deviations, $\sigma(|F_o|)$ of the amplitudes are given by

$$\sigma(|F_o|) = \sqrt{\sum_i \sigma_i(|F_i|)^2/N},$$

where σ_i denotes the e.s.d. of i-th equivalent reflection.

Structure

The structure was determined independently with the program of automatic structure determination.[3] The conventional refinement of the structure was carried out by the full matrix least squares method, applying the following weighting scheme.

$$\text{wt} = c \text{ when } |F_o| = 0$$

$$\text{wt} = 1.0/(\sigma(|F_o|)^2 + a|F_o| + b|F_o|^2) \text{ when } |F_o| > 0$$

a, b, and c were adjusted in such a way that the differences between the calculated and observed structure amplitudes are uniform in any region of the reciprocal space. The absolute configuration of the molecule was also determined to be the *R*-configuration from the anomalous scattering of the sulfur atom (Table 3).

After the refinement with all reflections, the structure was refined using the higher order reflections only at 111 K ($\sin\theta/\lambda \geqq 0.65$, hereafter HOR) to reduce the effect of the bonding electrons. In comparison with the case of the low-temperature refinement based on all the reflections, all the positional parameters showed no significant shifts , the values of the temperature factors becoming smaller than those of all the reflections as expected (Table 5).

The bond lenghts and angles, shown in Fig. 1, are essentially the same as those reported by Chacko.

Table 1. Crystal data

Space group	$P2_12_12_1$	
Z	4	
Lattice constant	293 K	111 K
a	9.929±0.002 Å	9.813±0.002 Å
b	9.936±0.002 Å	9.885±0.002 Å
c	5.664±0.001 Å	5.663±0.001 Å
d_{calcd} (g/cm^3)	1.58	1.61
d_{obsd} (g/cm^3)	1.57	
Linear absorption coefficient μ (cm^{-1})	4.947	4.855

Table 2. Experimental conditions

Crystal size	0.1×0.1×0.2 mm^3	0.2×0.2×0.4 mm^3
Source	Mo $K\alpha$	Mo $K\alpha$
Scan speed (2θ deg./min)	2	4
Background (s)	10	10
$2\theta_{max}$ (deg.)	70	70
Monochromator	Graphite (0 0 2) plane	
Temperature	111±3 K	293±3 K

Table 3. Determination of the absolute configuration (293 K)

	R config.	*S* config.
f''	−0.16	+0.16
R (%)	3.95	4.06
R_w (%)	2.27	2.35

Difference Fourier Synthesis

The difference Fourier synthesis was carried out with the low and high temperature data phased by the

† Present address; Mitsubishi Rayon Co., Ltd. Central Research Laboratory, Otake, Hiroshima 739-06.

†† Present address; Department of Engineering, Nagoya University, Chikusa, Nagoya 464.

Table 4. Atomic coordinates (e.s.d. in parentheses)

(a)	293 K		
	x/a	*y/b*	*z/c*
S	−0.17160 (6)	0.11728 (5)	0.10730 (11)
O_1	0.0093 (2)	0.3874 (2)	−0.2755 (3)
O_2	−0.1531 (2)	0.4960 (2)	−0.0683 (3)
N	−0.1200 (2)	0.3510 (2)	0.3193 (3)
C_1	−0.0590 (2)	0.4126 (2)	−0.0924 (4)
C_2	−0.0147 (2)	0.3329 (2)	0.1295 (4)
C_3	0.0008 (2)	0.1821 (2)	0.0864 (4)
C_4	−0.1947 (2)	0.2206 (2)	0.3656 (4)
H_1	0.0706	0.3682	0.1849
H_2	0.0375	0.1651	−0.0666
H_3	0.0585	0.1406	0.2028
H_4	−0.2910	0.2356	0.3944
H_5	−0.1565	0.1876	0.4972
H_6	−0.1823	0.4211	0.2760
H_7	−0.0696	0.3881	0.4858
(b)	HOR		
	x/a	*y/b*	*z/c*
S	−0.17148 (7)	0.11733 (5)	0.10759 (11)
O_1	0.0094 (2)	0.3872 (2)	−0.2755 (3)
O_2	−0.1530 (2)	0.4963 (2)	−0.0687 (4)
N	−0.1203 (2)	0.3510 (2)	0.3184 (3)
C_1	−0.0589 (2)	0.4124 (2)	−0.0912 (4)
C_2	−0.0589 (2)	0.3327 (2)	0.1304 (3)
C_3	0.0011 (2)	0.1820 (2)	0.0863 (4)
C_4	−0.1940 (2)	0.2208 (2)	0.3661 (4)
(c)	111 K		
	x/a	*y/b*	*z/c*
S	−0.17212 (7)	0.11696 (6)	0.10868 (12)
O_1	0.0048 (2)	0.3834 (2)	−0.2772 (3)
O_2	−0.1558 (2)	0.4908 (2)	−0.0733 (3)
N	−0.1226 (2)	0.3506 (2)	0.3175 (3)
C_1	−0.0620 (2)	0.4089 (2)	−0.0956 (4)
C_2	−0.0184 (2)	0.3322 (2)	0.1282 (4)
C_3	−0.0020 (3)	0.1818 (2)	0.0881 (5)
C_4	−0.1975 (3)	0.2215 (3)	0.3636 (5)
H_1	0.0648	0.3688	0.1812
H_2	0.0296	0.1613	−0.0829
H_3	0.0534	0.1421	0.2063
H_4	−0.2909	0.2373	0.3826
H_5	−0.1555	0.1834	0.5056
H_6	−0.1843	0.4214	0.2683
H_7	−0.0777	0.3819	0.4866

The average standard deviation of the positional parameters of the hydrogen atoms is 0.025 Å.

final parameters of HOR (Figs. 2 and 3). Some density humps probably due to the bonding electrons are found on the C_3–S–C_4 plane. Peaks A and B are situated off the bonds S–C_3 and S–C_4, respectively, in particular deviating from the S–C_4 bond direction. This was found in both the high and low temperature maps, the angles of A–S–B being 105 and 97°, respectively. This indicates that the 3p atomic orbital of the sulfur atom is hybridized with the 3s orbital, the humps due to the bonding electrons deviating from the interatomic vectors as seen in cyclopropane.[5] The

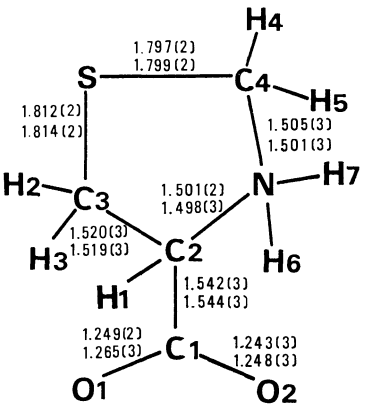

Fig. 1(a). Bond lengths(Å) at 293 K(upper) and 111 K (lower) along with their e.s.d. (in parentheses).

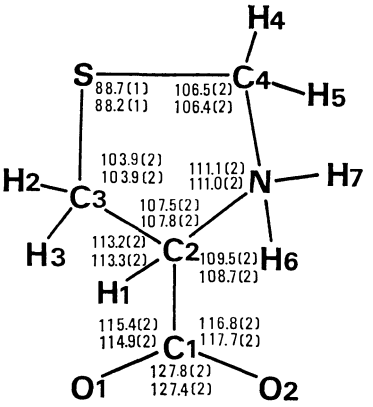

Fig. 1(b). Bond angles(degree) at 293 K(upper) and 111 K(lower) along with their e.s.d. (in parentheses).

Table 5. Equivalent isotropic temperature factors

	293K	111K	HOR
S	1.97	0.802	0.677
O_1	2.17	0.709	0.556
O_2	2.20	0.992	0.817
N	1.19	0.605	0.424
C_1	1.33	0.674	0.428
C_2	1.02	0.502	0.341
C_3	1.68	0.760	0.606
C_4	1.81	0.782	0.603

Each value was estimated from the anisotropic temperature factors.[4]

difference maps contain some peaks at the center of each atom. This might be caused by the poor accuracy of reflections intensities of high order. This is verified by the difference Fourier synthesis shown in Fig. 4 which was carried out by means of the reflections of $\sin\theta/\lambda<0.65$. No peaks were observed at the atomic positions. The three maps (Figs. 2, 3, and 4) contain peak D which may be assigned to the lone pair electrons of the sulfur atom.

Population Analysis

The distribution of electron density is defined as a sum of the square of the absolute value of the occupied molecular orbitals.

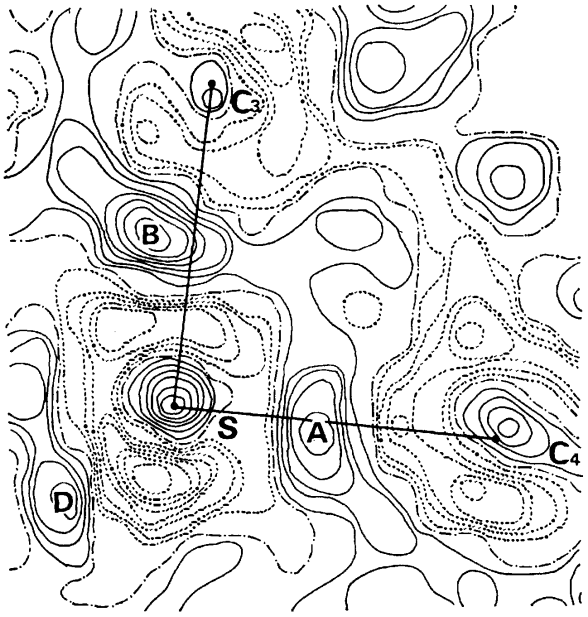

Fig. 2. Difference electron density map in the C_3–S–C_4 plane (111 K). Contours are drawn at the interval of 0.05 e/Å^3. The solid lines are above 0 e/Å^3 and the broken lines are below 0 e/Å^3.

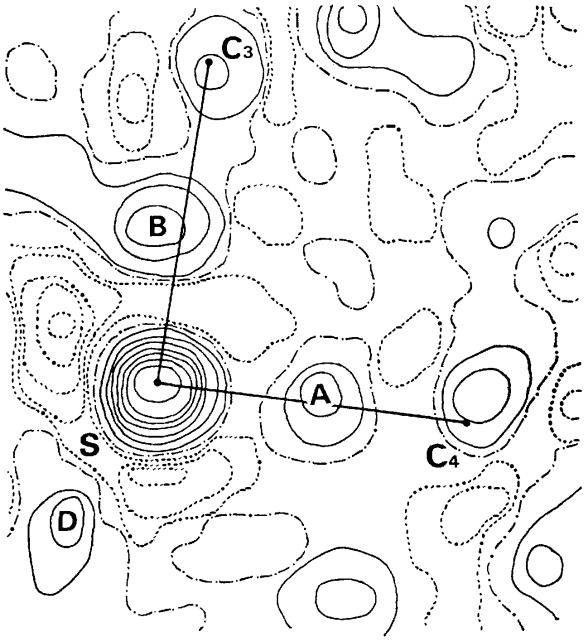

Fig. 3. Difference electron density map in the C_3–S–C_4 plane(293 K).

$$\rho = \sum_{i}^{\text{occupied}} \Psi_i^* \Psi_i \tag{1}$$

The molecular orbital is represented as a liner combination of the atomic basis function ϕ_μ

$$\Psi_i = \sum_{\mu} C_{\mu i} \phi_\mu \tag{2}$$

Substituting Eq. 2 into Eq. 1, we have

$$\rho = \sum_{i}^{\text{occupied}} \sum_{\mu,\nu} C_{\mu i}^* C_{\nu i} \phi_\mu^* \phi_\nu = \sum_{\mu,\nu} P_{\mu\nu} \phi_\mu^* \phi_\nu \tag{3}$$

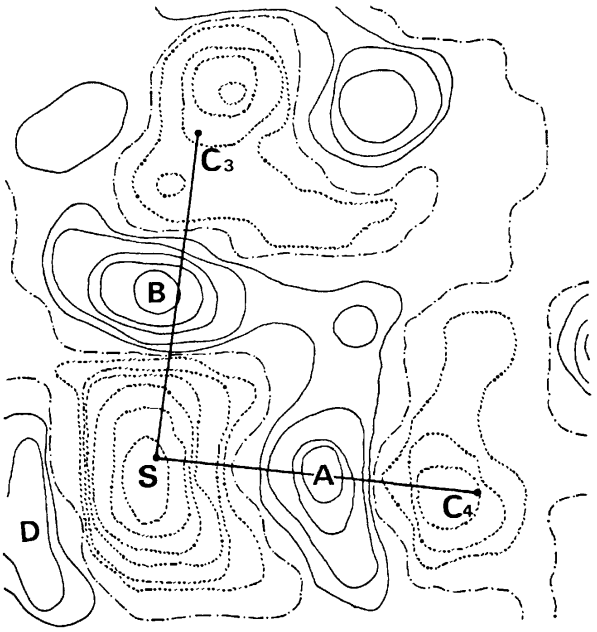

Fig. 4. Difference electron density map in the C_3–S–C_4 plane using only low order reflections($\sin\theta/\lambda < 0.65$) at 111 K.

$$P_{\mu\nu} = \sum_{i}^{\text{occupied}} C_{\mu i}^* C_{\nu i} \tag{4}$$

where $P_{\mu\nu}$ is a population parameter. The structure factor of the crystal is represented by

$$F_h = \sum_{j,k} \boldsymbol{F}[\rho_k] \cdot T_{kj} \cdot \exp(i\boldsymbol{s} \cdot \boldsymbol{r}_{kj}) \tag{5}$$

j: atom
k: symmetry operation
$\boldsymbol{F}[\rho_k]$: molecular transform
T_{kj}: temperature factor

where

$$\begin{aligned} \boldsymbol{F}[\rho] &= \sum_{\mu,\nu} P_{\mu\nu} \boldsymbol{F}[\phi_\mu^* \phi_\nu] \\ &= \sum_{\mu,\nu} P_{\mu\nu} \int \phi_\mu^* \phi_\nu \exp(i\boldsymbol{s} \cdot \boldsymbol{r}) d\boldsymbol{r} \\ &= \sum_{\mu,\nu} P_{\mu\nu} X_{\mu\nu} \end{aligned} \tag{6}$$

$X_{\mu\nu}$ is called the generalized structure factor. In the population analysis developed by Stewart,[1] the structure factor, F_h, is separated into two parts, F_h(atom) and F_h(bond), the former consisting of the atomic orbitals from one atom only, and the latter showing the effect of the overlap between orbitals of the bonded atoms. As a whole, considering the anomalous effects, F_h is written as follows.

$$F_h = F_h(\text{atom}) + F_h(\text{bond}) = A + iB, \tag{7}$$

$$\begin{aligned} A = \sum_{j,k} [&(f_{\text{core},j} + f_j' + P_{vj} f_{vj} - 3 f_{np,np,j} Q_{kj}) \cdot \\ &\cos(2\pi h r_{kj}) \cdot T_{kj} - (f_j'' + \sqrt{3} f_{ns,np,j} D_{kj}) \cdot \\ &\sin(2\pi h r_{kj}) \cdot T_{kj}] + \sum_m b_m f_{\text{bond},m} \sum_k \cos(2\pi h r_{km}) \cdot T_{km}, \end{aligned}$$

$$\begin{aligned} B = \sum_{j,k} [&(f_{\text{core},j} + f_j' + P_{vj} f_{vj} - 3 f_{np,np,j} Q_{kj}) \cdot \\ &\sin(2\pi h r_{kj}) \cdot T_{kj} - (f_j'' + \sqrt{3} f_{ns,np,j} D_{kj}) \cdot \\ &\cos(2\pi h r_{kj}) \cdot T_{kj}] + \sum_m b_m f_{\text{bond},m} \sum_k \sin(2\pi h r_{km}) \cdot T_{km}, \end{aligned}$$

$$f_{\text{core}} = 2X_{1s,1s} \text{ or } 2X_{1s,1s} + 2X_{2s,2s} + 6X_{2p,2p},$$

$f_v = aX_{ns,ns} + bX_{npx,npx} + cX_{npy,npy} + dX_{npz,npz}$,

a, b, c, d: the scattering of electrons in each orbital

$f_{ns,np}$: the scattering effect due to the overlap between ϕ_{ns} and ϕ_{np}

$f_{np,np}$: the scattering effect due to the overlap between ϕ_{npx} and ϕ_{npy}, or ϕ_{npy} and ϕ_{npz}, or ϕ_{npz} and ϕ_{npx}

f_{bond}: the scattering factor of the postulated orbital at the center of the bond (r_m)

Table 6. Population analysis refinement (111K)

	R_w[a)]	Scale of $\|F_o\|$
ELS	2.28	0.839
OCR	2.07	0.841
TCR	2.06	0.841
b)	2.76	0.819
HOR	5.26	0.895

a) $R_w = (\sum w \| |F_o| - |F_c| \| / \sum |F_o|) \times 100.0$. b) Value obtained by the usual refinement.

Table 7. Experimental and theoretical population parameters

	111 K			293 K				111 K			293 K		
	ELS	OCR	TCR	ELS	OCR	CNDO		ELS	OCR	TCR	ELS	OCR	CNDO
Sp_v	6.908	6.990	7.174	6.233	6.202	6.011	C_2p_v	3.794	3.783	3.792	3.872	3.839	4.008
d_x		−0.817	−0.607		1.006	−0.211	d_x		−0.063	0.094		0.311	0.022
d_y		−0.042	0.159		0.486	−0.269	d_y		0.556	0.709		0.375	0.073
d_z		−0.444	−0.842		−0.703	−0.232	d_z		−0.362	−0.573		−0.207	−0.196
q_1		−0.112	−0.095		0.015		q_1		−0.015	−0.046		0.052	
q_2		−0.287	−0.210		0.015		q_3		−0.199	−0.170		0.143	
q_3		0.008	−0.069		−0.014	−0.159	q_3		−0.109	−0.143		0.345	−0.013
q_4		0.049	0.016		0.143	0.172	q_4		−0.114	−0.113		−0.206	0.227
q_5		0.232	0.194		0.122	−0.424	q_5		−0.304	−0.289		0.032	−0.116
O_1p_v	6.158	6.139	5.935	6.247	6.245	6.492	C_3p_v	3.818	3.744	3.624	3.806	3.775	3.956
d_x		−0.023	−0.049		0.159	0.231	d_x		−0.121	−0.050		0.239	0.053
d_y		0.114	0.171		0.244	−0.086	d_y		0.143	0.192		0.377	−0.018
d_z		−0.322	−0.415		−0.137	−0.361	d_z		−0.245	−0.436		−0.183	−0.024
q_1		0.083	0.158		0.007		q_1		−0.109	−0.052		−0.002	
q_2		0.061	0.084		0.021		q_2		−0.047	−0.024		0.084	
q_3		−0.176	−0.035		−0.029	−0.085	q_3		−0.996	−0.006		0.183	−0.051
q_4		−0.283	−0.428		0.030	0.249	q_4		−0.295	0.145		−0.019	−0.004
q_5		−0.181	−0.215		0.078	−0.162	q_5		0.219	0.093		0.060	0.012
O_2p_v	6.121	6.066	5.967	6.258	6.240	6.519	C_4p_v	3.501	3.458	3.558	3.596	3.635	3.927
d_x		0.020	0.070		0.107	−0.324	d_x		−0.093	0.005		0.128	−0.056
d_y		0.115	0.136		0.278	0.287	d_y		0.034	0.124		0.156	−0.115
d_z		−0.369	−0.536		−0.154	0.039	d_z		−0.170	−0.350		0.033	−0.005
q_1		0.086	0.082		0.083		q_1		−0.002	−0.038		0.067	
q_2		0.012	0.105		0.103		q_2		0.209	0.131		0.194	
q_3		−0.043	−0.033		0.120	0.193	q_3		−0.141	−0.057		0.209	−0.094
q_4		−0.207	−0.258		−0.143	−0.005	q_4		−0.161	−0.034		−0.075	0.007
q_5		−0.108	−0.084		0.071	0.083	q_5		0.128	0.092		−0.078	0.004
Np_v	5.077	5.009	5.092	5.079	5.040	4.978	H_1	1.039	1.046	1.044	1.083	1.105	0.963
d_x		−0.274	−0.235		0.047	0.039	H_2	1.038	1.078	1.048	1.047	1.076	0.941
d_y		−0.077	−0.043		0.223	−0.019	H_3	1.010	0.999	1.006	1.074	1.067	0.990
d_z		−0.241	−0.362		−0.265	−0.055	H_4	1.118	1.152	1.158	1.119	1.133	0.962
q_1		−0.010	0.029		0.074		H_5	0.959	0.957	0.975	1.054	1.016	0.973
q_2		0.054	0.124		0.066		H_6	0.967	0.990	1.026	0.940	0.992	0.805
q_3		−0.146	−0.310		0.010	0.002	H_7	0.862	0.962	0.903	0.972	0.998	0.860
q_4		−0.084	−0.175		−0.136	−0.088	S-C_3			−0.664			0.559
q_5		0.171	0.132		0.104	0.004	S-C_4			−0.279			0.588
C_1p_v	3.626	3.627	3.343	3.622	3.637	3.615	C_1-O_1			1.131			0.841
d_x		0.155	0.220		0.269	−0.026	C_1-O_2			0.768			0.771
d_y		−0.236	−0.243		0.377	−0.051	C_1-C_2			0.781			0.563
d_z		−0.318	−0.570		−0.479	−0.094	C_2-N			−1.057			0.547
q_1		−0.174	−0.063		−0.060		C_4-N			1.320			0.562
q_2		0.328	0.358		0.174		C_2-C_3			0.615			0.726
q_3		−0.827	−0.671		0.343	−0.060							
q_4		0.056	−0.095		0.107	−0.066							
q_5		0.580	0.514		−0.219	0.041							

D_{kj} and Q_{kj} in Eqs. are expressed in terms of parameters d and q in this table.

$D_{kj} = d_{xj}S_{xsj} + d_{yj}S_{ysj} + d_{zj}S_{zsj}$

$Q_{kj} = q_{1j}(S_{xsj}^2 - S_{ysj}^2) + q_{2j}(S_{zsj}^2 - 1/3) + q_{3j}S_{xsj}S_{ysj} + q_{4j}S_{xsj}S_{zsj} + q_{5j}S_{ysj}S_{zsj}$

S_{xsj}, S_{ysj}, and S_{zsj} are direction consines of the scattering vector to the principal axes of the p_x, p_y, and p_z orbitals of the j-th atom, respectively.

TABLE 8. EXPERIMENTAL AND THEORETICAL CHARGES

Atom	111 K	293 K	CNDO	EN[a)]
S	−0.990	−0.202	−0.011	0.00
O_1	−0.139	−0.245	−0.492	—
O_2	−0.066	−0.240	−0.519	—
N	−0.009	−0.040	0.022	0.48
C_1	0.373	0.363	0.385	0.40
C_2	0.217	0.161	−0.008	0.02
C_3	0.256	0.225	0.044	−0.14
C_4	0.542	0.365	0.073	−0.03
H_1	−0.046	−0.105	0.037	0.07
H_2	−0.078	−0.076	0.059	0.07
H_3	0.001	−0.067	0.010	0.07
H_4	−0.152	−0.133	0.038	0.07
H_5	0.043	−0.016	0.027	0.07
H_6	0.010	0.008	0.195	0.17
H_7	0.038	0.002	0.141	0.17

a) Calculated from the differences in electronegativity of the neighboring atoms with Mulliken's equation.

The parameter P_v is the number of valence electrons associated with the j-th atom. A dipole distortion of these spherical valence electrons is described by D and a quadrupole distortion by Q. The extended L-shell method(ELS) refines P_v after the usual refinement of the positional and thermal parameters. P, Q, and D are treated as adjustable parameters in the one-center refinement(OCR). The two-center refinement (TCR) includes the b_{mk} term as variables in addition to those of OCR.

In the present calculation, the $f_{core,j}$'s of the carbon and nitrogen atoms are taken from those calculated by use of Clementi's analytical SCF atomic orbitals.[6] f_{vj}'s of these atoms being taken from these calculated by use of the Slater-type atomic orbitals.[7] f_v of the hydrogen atom is taken from Stewart-Davidson-Simpson's value,[8] f_{core} and f_v of the sulfur atom are from the Roothaan-Hartree-Fock wave function by Fukamachi[9] and $f_{ns,np}$ and $f_{np,np}$ are those of Stewart.[10] In the case of TCR, f_{bond} is taken as $\overline{X_{ns,ns}(s\cdot r)}$ at the center of each bond where $\overline{X_{ns,ns}(s\cdot r)}$ is a spherically averaged value of the overlapping function between the ns-orbital. The population analysis of the present molecule at 111 and 293 K was carried out after the usual refinement, using ELS, OCR, and TCR, successively. The computer program was written by one of the authors (J.K.). The positional and thermal parameters of OCR and TCR are fixed to the values of ELS. The R factors and scale factors after the refinement are given in Table 6. The R factor decreased from that of the usual refinement, the scale factor of $|F_o|$ becoming close to that of HOR.

The population parameters, thus refined, are compared with the theoretical values calculated by the CNDO method (Table 7). Experimental and theoretical charges are given in Table 8. The experimental values show as a whole the same distribution as the theoretical values except for the hydrogen atoms. However, the charge of the sulfur atom in the low-temperature data deviates considerably from that of CNDO and EN, because of errors in $|F_o|$'s and inaccuracy in the scattering factor of the sulfur atom.

The dipole moment of the molecule can be calculated from the charge distribution in the density map. The absolute values of the dipole moment of the molecule, 11.4 Debye at 111 K and 9.3 Debye at 293 K are roughly in line with the theoretical value (13.2 Debye). However, their directions do not agree with each other.

Discussion

In the present work, we used the higher order reflections refinement to reduce the effect of the spread of the electron cloud. The effect, however, still remains in the parameters, in spite of the considerable depression of the temperature factor (Table 5). The population analysis seems to refine the electronic structure of the molecule; the overall scale factor is improved so as to become close to the value of the HOR, the R factor decreasing significantly from the usual refinement. Some discrepancy in distribution is found between the X-ray and theoretical results. In particular, the sulfur atom at 111 K has a more negative charge than that at 293 K and CNDO. This may be explained as follows:

1) The population analysis treats the small differences between the conventionally calculated structure factors and the observed. The data at 111 K have four times weaker intensities than those at 293 K, depending on the size of the crystal used. Though the smaller crystal gives less systematic errors due to absorption and extinction in the data, the experimental errors in the weaker intensities at 111 K may give rise to some discrepancies.

2) The discrepancy may be due to the neglect of the d-orbital of the sulfur atom and the different character between the L- and M-shell orbitals which are not distinguished in the present analysis.

In spite of these discrepancies we can say that the population analysis throws light on the character of the molecule.

The authors wish to express their thanks to Professor Nobutami Kasai and Dr. Noritake Yasuoka for the use of their diffractometer equipped with a crystal cooling system.

References

1) R. F. Stewart, *J. Chem. Phys.*, **51**, 4569 (1969).
2) K. K. Chacko, *Cryst. Struct. Commun.*, **3**, 561 (1974).
3) N. Tanaka, Y. Matsuura, Y. Kai, N. Yasuoka, N. Kasai, and M. Kakudo, *Acta Crystallogr., Sect. A*, **30**, S10 (1975).
4) W. C. Hamilton, *Acta Crystallogr.*, **12**, 609 (1959).
5) A. Hartman and F. L. Hirshfeld, *Acta Crystallogr.*, **20**, 80(1966).
6) D. T. Cromer and A. C. Larson, *J. Chem. Phys.*, **53**, 205(1970).
7) R. F. Stewart, *J. Chem. Phys.*, **53**, 205 (1970).
8) R. F. Stewart, E. R. Davidson, and W. T. Simpson, *J. Chem. Phys.*, **42**, 3175 (1965).
9) T, Fukamachi, *Technical Report of ISSP, Ser. B*, **12** (1971).
10) R. F. Stewart, *J. Chem. Phys.*, **51**, 4569 (1969).

Molecular Structure and Internal Rotation of Trimethylamine-Boron Trifluoride. A Combination of Electron Diffraction and Spectroscopic Data

Kinya IIJIMA and Shuzo SHIBATA*

Department of Chemistry, Faculty of Science, Shizuoka University, Oya, Shizuoka 422

(Received September 7, 1978)

The molecular structure of trimethylamine-boron trifluoride $(CH_3)_3N \cdot BF_3$ was determined from gas electron-diffraction data with vibrational and rotational spectroscopic data. The geometric parameters of the molecule were found to be very close to those inferred from the preliminary analysis of the diffraction data alone. The structural parameters and uncertainties were r_g(N–B)=1.674(4) Å, r_g(B–F)=1.374(2) Å, r_g(C–N)=1.485 (2) Å, r_g(C–H)=1.100(3) Å, r_g(F···F)=2.288(2) Å, and r_g(C···C)=2.420(4) Å. The potential barrier about the N–B axis was estimated to be 4.3±0.3 kcal/mol in the gas phase; this value is much larger than that from NMR spectra.

Several studies have recently been carried out on the gas-phase structure of trimethylamine-boron trifluoride $(CH_3)_3N \cdot BF_3$,[1-3] which is a representative of donor-acceptor molecular complexes, in order to clarify the difference in the molecular structure between the gas and the solid. However, there are considerable discrepancies among the results from electron diffraction[2,3] and microwave spectra:[1] *e.g.*, the N–B distance determined by microwave spectroscopy is about 0.03 Å shorter than that from electron diffraction. The electron diffraction study by Hargittai and Hargittai[3] also gave different results from ours,[2] especially for the B–F and C–N distances, though the rotational constant calculated using their results did not agree well with the observed one. On the other hand, this molecule has an internal rotation about the N–B bond, and the rotational barrier was found to be 1.7 kcal/mol from the NMR study in the solid phase.[4] The height of the barrier seems to be too small, compared with those in other ethane-like molecules.[5] The height of the potential barrier about the N–B bond cannot be estimated from IR or Raman vibrational spectroscopic studies, because the torsional vibration is inactive in these spectra. It is therefore very desirable to estimate it from a combined analysis of electron diffraction intensities with spectroscopic data. Thus, the molecular structure of $(CH_3)_3N \cdot BF_3$ was reinvestigated in order to determine more accurate molecular parameters as well as the height of the potential barrier about the N–B bond, by means of a joint analysis of gas-electron diffraction and spectroscopic data.

Experimental

Trimethylamine and boron trifluoride gases, which were prepared by the procedures described in the literature,[6,7] were condensed in a flask cooled by liquid air and were allowed to react while being warmed slowly to room temperature. A white product was purified by sublimation under vacuum, and its infrared spectrum[8,9] revealed no impurities. In the electron-diffraction experiment the sample was vaporized at about 130 °C by means of a high tepmerature nozzle, and photographs were taken with an r^3-sector at the camera distances of 144 and 294 mm. The accelerating voltage was 40 kV. The exposure time at the short camera distance was 60 s, using an electron-beam current of 0.8 μA, and that at the long camera distance was 20 s, using a beam current of 0.6 μA. The pressure of the diffraction chamber was below 1×10^{-5} Torr during the experiment. The electron wavelength was measured using diffraction patterns of thallium chloride powder.[10] Photographs were recorded on Fuji spectroscopic plates, and the optical densities of four short and three long camera distance plates were measured at 0.4 mm intervals by means of a digital microphotometer. The electron-diffraction unit and digital microphotometer used in the present study were described elsewhere.[11]

Analysis and Results

Molecular Intensity and Radial Distribution. The scattering intensities were obtained in the range of s=2.5—17.3 and 5.0—33.0 Å^{-1} from the photographic plates at long and short camera distances, respectively. They were leveled by the theoretical backgrounds, and then the leveled intensities of several plates for each camera distance were averaged. The background curves were drawn smoothly by hand for the long distance data and were fitted by a polynomial of 7th degree[12] for the short distance data, and then the molecular intensities for each camera distance were joined at s=14.8 Å^{-1}. Figure 2 shows the observed intensities and Fig. 3 shows the experimental radial distrubution curve. The elastic and inelastic scattering factors were taken from the tables prepared by Kimura *et al.*[13] and Cromer and Mann,[14] respectively. The inelastic scattering factor for the hydrogen atom was taken from Ref. 15.

Mean Amplitude of Vibration and Shrinkage Effect. Several workers have measured the vibrational spectra of $(CH_3)_3N \cdot BF_3$ in the solid phase and calculated the force field.[9,16] However, these calculations seem not to be reasonable because a large number of

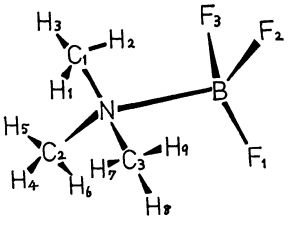

Fig. 1. Numbering of atoms in trimethylamine-boron trifluoride (symmetry C_{3v}).

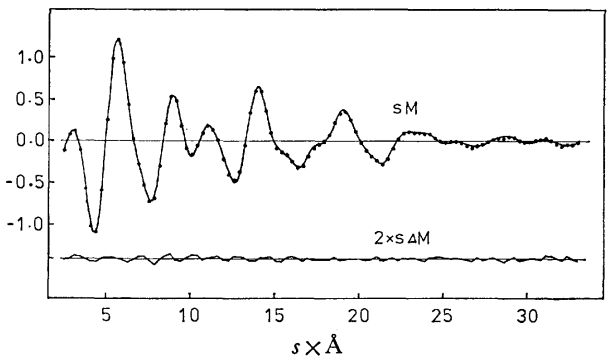

Fig. 2. Molecular intensities for trimethylamine-boron trifluoride. Solid curve, calculated; dotted curve, experimental. Lower curve, two times the residuals with respect to the experimental curve.

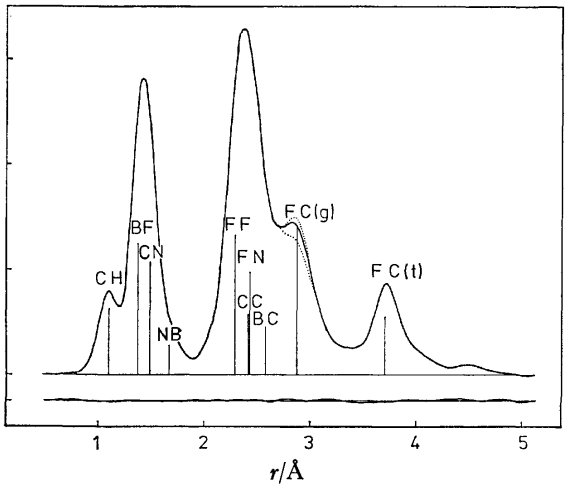

Fig. 3. Radial distribution curve for trimethylamine-boron trifluoride. Solid curve, experimental; lower curve, the residual curve; dotted curves, calculated using V_0=6.0 kcal/mol (upper) and V_0=3.0 kcal/mol (lower).

unknown parameters were used; *e.g.*, Laswick and Taylor obtained forty force constants on the basis of twenty wave numbers measured for each of five isotopic species.[9] In the present study, a modified Urey-Bradley force field was adopted in order to reduce the variable parameters. The force constants used are shown in Table 1, and the calculated wave numbers are listed in Table 2, where the spectra were assigned according to the notation suggested by Laswick and Taylor.[9] The mean amplitudes of vibration and shrinkage effects,[17] r_a-r_α, at 130 °C, which were calculated using the above force constants, are shown in Table 3. The calculated mean amplitudes of most atomic pairs agreed well with the observed ones, but the observed mean amplitude of the N–B bond is significantly larger than the calculated one. The reason for this disagreement is that the calculation was carried out on the basis of the vibrational spectra observed in the solid state, where the N–B bond strength is probably enhanced.

Torsional Vibration and Height of Potential Barrier. Torsional vibrations around the N–B and C–N bonds

Table 1. Force constants for $(CH_3)_3N\cdot BF_3$

K(B-F)	2.8	H(CNC)	0.36
K(N-B)	1.5	H(CNB)	0.65
K(C-N)	3.3	H(HCH)	0.35
K(C-H)	4.5	H(NCH)	0.33
p_1	0.6	F(FF)	0.70
p_2	−0.02	F(FN)	0.70
Y(N-B)	0.134	F(CC)	0.05
Y(C-N)	0.18	F(CB)	0.50
H(FBF)	0.38	F(HH)	0.20
H(FBN)	0.42	F(HN)	0.40

K, p, H, F: mdyn/Å unit; Y: mdyn·Å unit. p_1: cross term between Δr(N-B) and Δr(B-F). p_2: cross term between Δr(N-B) and Δr(C-N).

Table 2. Observed and calculated wave numbers for $(CH_3)_3N\cdot BF_3$[a] (cm^{-1} unit)

		Obsd	Calcd	$\Delta\nu/\nu$
A_1	ν_3	1486	1488	−0.1%
	ν_4	1453	1453	0.0
	ν_5	1271	1269	0.2
	ν_6	843	844	−0.1
	ν_7	694	696	−0.3
	ν_8	330	319	3.3
	ν_9	929	931	−0.2
E	ν_{19}	1478	1491	−0.9
	ν_{20}	1469	1454	1.0
	ν_{21}	1412	1438	−1.8
	ν_{22}	1255	1351	−7.6
	ν_{23}	1105	1064	3.7
	ν_{24}	990	990	0.0
	ν_{25}	1144	1129	1.3
	ν_{26}	432	431	0.2
	ν_{27}	343	343	0.0
	ν_{28}	300	275	8.3
	ν_{29}	520	521	−0.2
	ν_{30}	323	321	0.6

a) Assignment is according to the notation in Ref. 9.

Table 3. Mean amplitudes and shrinkage effects for $(CH_3)_3N\cdot BF_3$ (in 10^{-4} Å)

	l	r_a-r_α		l	r_a-r_α
B-F_1	528	86	N-C_1	501	81
B-N	589	−6	N···H_1	1041	171
B···C_1	714	39	C_1···C_2	807	113
B···H_1	1030	108	C_1-H_1	778	238
B···H_2	1632	86	C_1···H_4	1620	128
F_1···F_2	681	140	C_1···H_5	1635	137
F_1···N	665	39	C_1···H_6	1071	227
F_1···C_1	717	−1	H_1···H_2	1262	362
F_1···C_2	1532	12	H_1···H_4	2399	98
F_1···H_1	1109	48	H_1···H_5	2476	72
F_1···H_2	1669	12	H_1···H_6	1700	236
F_1···H_4	1653	85	H_2···H_5	1778	246
F_1···H_5	2682	−97	H_2···H_6	1408	299
F_1···H_6	2387	60	H_2···H_9	2384	92

The numbering of the atoms is shown in Fig. 1.

TABLE 4. MOLECULAR PARAMETERS

	$(CH_3)_2N \cdot BF_3$					$(CH_3)_3N$[f]	BF_3[g]	$(CH_3)_3N \cdot BF_3$[h]
	r_α[a]	r_α^0[b]	r_g[c]	r_g[d]	r_0[e]	r_α^0	r_α^0	(solid)
B-F	1.363 (2)	1.370 (2)	1.374	1.356 (6)	1.387 (5)		1.311 (1)	1.39
N-B	1.669 (6)	1.669 (4)	1.674	1.666(11)	1.636 (4)			1.585
C-N	1.476 (3)	1.481 (2)	1.485	1.470(10)	1.476 (5)	1.458 (2)		1.50
C-H	1.072 (3)	1.081 (3)	1.100	1.104 (8)	1.10 (3)	1.100 (5)		
F···F	2.272 (3)	2.285 (2)	2.288	2.261 (6)	2.305(10)		2.271	2.24
C···C	2.407 (5)	2.417 (4)	2.420	2.383(12)	2.400(10)	2.401 (6)		
∠NCH	110.0 (8)	110.2 (6)	110.2	106.3(18)	109 (2)	110.2(13)		
∠FBF	113.0 (3)	113.1 (3)	112.6	113.1 (9)	112.4 (2)		120	107
∠CNC	109.3 (4)	109.4 (4)	109.2	108.5 (7)	108.6 (2)	110.9 (6)		114

Bond distance: Å unit; bond angle: degree unit. a) Results from electron diffraction data. b) Results from the joint analysis of electron diffraction data and rotational constant. c) r_g parameters transformed from r_α^0 parameters.[17] The limits of error are equal to those in the r_α^0 parameters. d) Results reported by Hargittai and Hargittai.[3] r_a parameters given by them are transformed to r_g parameters by the relation of $r_g = r_a + l^2/r_a$. e) Results from microwave spectroscopic study. Ref. 1. f) Ref. 24. g) Ref. 25. The F···F distance was calculated by the relation of $r_\alpha^0(F \cdots F) = \sqrt{3} \cdot r_\alpha^0(B\text{-}F)$. h) Ref. 26. Limits of error are not clear.

TABLE 5. ROOT-MEAN-SQUARE AMPLITUDES FOR $(CH_3)_3N \cdot BF_3$ (IN Å UNIT)

	l_{obsd}[a]	l_{calcd}
B-F	0.051 (3)	0.053
N-B	0.083 (9)	0.059
C-N	0.054 (3)	0.050
C-H	0.074 (3)	0.078
F···F	0.064 (2)	0.068
F···N	0.066 (2)	0.067
trans F···C	0.081 (3)	0.072
gauche F···C	0.154 (3)	0.153

a) Results from joint analysis of electron diffraction data and rotational constant.

were treated in a high barrier approximation.[18] However, the torsional vibration around the N–B axis which was completely isolated from other vibrations contributes greatly to the *gauche* F···C mean amplitude. The mean amplitude of the *gauche* F···C calculated without consideration of this motion resulted in 0.099 Å. The electron diffraction experiment gave the mean amplitude of 0.154±0.003 Å, as listed in Table 5. The difference between the two values suggests a significant contribution of the torsional vibration around the N–B bond. Therefore, the force constant Y in the formula $V=(1/2)Y\Delta t^2$, where V is a potential energy and Δt is an internal coordinate in the torsional vibration, was chosen so that the calculated mean amplitude of the *gauche* F···C was in agreement with the observed one. Thus the force constant Y and the wave number of the vibration were estimated to be 0.134±0.010 mdyn·Å and 67±3 cm^{-1}, respectively. The errors were estimated from that of the observed *gauche* F···C mean amplitude. If the potential function around the N–B bond is assumed to be $V(t)=(1/2)V_0(1-\cos 3t)$, where V_0 is the height of the potential barrier, V_0 can be estimated to be 4.3±0.3 kcal/mol using the relation $V_0=(2/9)Y$.

On the other hand, the torsion around the N–B bond was also treated in a low barrier approximation,[18] and then the molecular intensities were calculated by the average over the torsional angle at 5° intervals, using the weight of the Boltzmann factor $\exp(-V/kT)$. The *gauche* F···C mean amplitude was assumed to be 0.099 Å at each torsional angle. Thus radial distributions were obtained from the molecular intensites calculated using assumed values of V_0, as shown in Fig. 3. The radial distribution obtained from $V_0=$ 4.5 kcal/mol gave the same shape of the *gauche* F···C peak as in the experimental radial distribution, and the value of V_0 was consistent with that obtained from the analysis of a high barrier approximation.

Analysis of Electron Diffraction Intensities and Rotational Constants. Shrinkage effects were considered and the molecular parameters in the r_α structure were determined by the least-squares analysis of the molecular intensities; these are shown in Table 4. It is assumed that the molecule of $(CH_3)_3N \cdot BF_3$ has a staggered form with C_{3v} symmetry, and that the methyl group also has local C_{3v} symmetry in the staggered form with respect to the C–N axis. The mean amplitudes (except those listed in Table 5) were fixed as shown in Table 3, and the asymmetry parameters κ for the C–H, B–F, N–B, and C–N bonds were estimated to be 12, 2.4, 11, and 2.5×10^{-6} Å^3, respectively, by a diatomic approximation.[19] The κ parameters for other atomic pairs were ignored.

Bryan and Kuczkowski obtained the rotational constant B_0 value of 1756.073±0.01 MHz for the normal species of $(CH_3)_3N \cdot BF_3$.[1] The vibrational correction for the rotational constant[20] was made by the library program in the Computer Center of the University of Tokyo; B_z was 1756.17 MHz. The uncertainty in the vibrational correction was tentatively assumed to be 80%. The r_α parameters in Table 4 was transformed to r_α^0 parameters by extrapolating $r_a - r_\alpha$ to zero kelvin.[17] Here the anharmonic contributions were estimated by a diatomic approximation. The rotational constant calculated from the r_α^0 parameters was 1758±12 MHz, which was in good agreement with the experimental B_z. Although the parameters obtained from the above electron diffraction analysis

TABLE 6. CORRELATION MATRIX FOR MOLECULAR PARAMETERS OF $(CH_3)_3N\cdot BF_3$[a]

	r(BF)	r(NB)	r(CN)	r(CH)	r(FF)	r(CC)	∠NCH	l(BF)	l(CN)	l(FF)	l(FN)	l(FC(t))	l(FC(g))	l(NB)	l(CH)	R_1[b]	R_2[b]
r(BF)	1.0																
r(NB)	−0.59	1.0															
r(CN)	−0.31	−0.03	1.0														
r(CH)	−0.07	−0.01	0.33	1.0													
r(FF)	0.41	0.38	−0.10	0.04	1.0												
r(CC)	−0.27	0.29	0.87	0.31	0.19	1.0											
∠NCH	0.34	0.01	−0.35	−0.22	0.43	−0.04	1.0										
l(BF)	0.33	−0.14	−0.59	−0.38	0.02	−0.55	0.16	1.0									
l(CN)	0.48	−0.24	−0.53	−0.33	0.10	−0.50	0.21	0.92	1.0								
l(FF)	0.15	−0.19	−0.20	−0.12	0.07	−0.33	0.04	0.39	0.36	1.0							
l(FN)	0.23	−0.09	−0.17	−0.08	0.23	−0.25	−0.02	0.30	0.30	0.79	1.0						
l(FC(t))	−0.04	−0.01	0.03	−0.08	−0.07	−0.01	−0.08	0.24	0.22	0.14	0.09	1.0					
l(FC(g))	0.08	−0.02	−0.06	−0.02	0.14	0.08	0.52	−0.06	−0.03	−0.09	−0.15	−0.07	1.0				
l(NB)	0.36	−0.18	−0.37	−0.24	0.11	−0.30	0.33	0.54	0.67	0.17	0.11	0.10	0.09	1.0			
l(CH)	0.06	−0.23	0.29	−0.03	−0.13	0.19	−0.09	0.26	0.29	0.15	0.05	0.25	−0.06	0.19	1.0		
R_1	−0.26	0.18	0.04	−0.14	−0.18	−0.03	−0.38	0.35	0.26	0.35	0.35	0.25	−0.23	−0.05	0.16	1.0	
R_2	0.02	−0.20	0.13	−0.14	−0.19	0.03	−0.10	0.60	0.57	0.30	0.15	0.36	−0.11	0.33	0.76	0.38	1.0

a) Matrix elements are defined as $\rho_{ij}=B_{ij}^{-1}/(B_{ii}^{-1}\times B_{jj}^{-1})^{1/2}$. b) R_1 and R_2 are indices of resolution for the long and short camera-distance data, respectively.

TABLE 7. OBSERVED AND CALCULATED ROTATIONAL CONSTANTS FOR $(CH_3)_3N\cdot BF_3$ (IN MHz UNIT)

B_0[a]	1756.073 ± 0.01
B_z[b]	1756.17 ± 0.08
B_α^0[c]	1758 ± 12
B_{av}[d]	1756.17 ± 0.08

a) Observed rotational constant for the ground vibrational state. Ref. 1. b) Rotational constant corrected for vibrational effects. c) Rotational constant calculated from the parameters obtained by the analysis of electron diffraction data. See text. d) Best-fit rotational constant obtained by the joint analysis.

TABLE 8. ROTATIONAL CONSTANTS OF $(CH_3)_3N\cdot BF_3$ (IN MHz UNIT)

	B_0[a]	B_0^a[b]
$(^{13}CH_3)_3N\cdot{}^{11}BF_3$	1706.100	1706 (2)
$(^{13}CH_3)_3N\cdot{}^{10}BF_3$	1709.884	1710 (2)
$(CD_3)_3N\cdot{}^{11}BF_3$	1546.799	1545 (2)[c]
$(CD_3)_3N\cdot{}^{10}BF_3$	1550.445	1548 (2)[c]
$(CH_3)_3N\cdot{}^{10}BF_3$	1759.780	1760 (2)
$(CH_3)_3{}^{15}N\cdot{}^{11}BF_3$	1751.630	1752 (2)

a) Observed rotational constants, Ref. 1; the vibrational corrections, $\Delta B=B_0-B_\alpha^0$, are adout 0.1 MHz. b) Rotational constants caluculated from the r_α^0 parameters in Table 4. The correlations between the parameters were taken into consideration in calculating the errors. c) The C–D distance and NCD angle were assumed to be equal to r(C–H) − 0.0015 Å and ∠NCH − 0.16°, respectively.[21]

were quite compatible with the rotational constant determined by the microwave experiment, the joint analysis of electron diffraction intensities and rotational constant was performed. The relative weight for the observed rotational constant in the least-squares calculation was estimated to be 6×10^8, in such a way that 2.5 times the standard deviation of the rotational constant obtained from the least-squares calculation is nearly equal to the uncertainty in B_z. The r_α^0 parameters and mean amplitudes determined by the joint analysis are given in Tables 4 and 5, together with the r_g parameters and their associated errors. The errors were estimated from random errors in the least-squares calculations and systematic errors originating from the measurements of camera distance and electron wavelength. The correlation matrix is listed in Table 6. The results from the joint analysis were the same as those obtained from the preliminary analysis.[2] The errors for the molecular parameters were much smaller than those from the study by Hargittai and Hargittai,[3] though there seems to be systematic devitation between the two sets of data. The calculated rotational constants were in quite good agreement with the observed ones, as listed in Table 7. Recently, the microwave spectra of deuterium and carbon-13 enriched samples of $(CH_3)_3N\cdot BF_3$ have been studied.[1] The rotational constants for these isotopic species were calculated using the parameters obtained by the above joint analysis, and their calculated values are also in agreement with the observed values, as shown in Table 8. The best-fit theoretical intensity curve is shown in Fig. 2.[22]

Discussion

The joint analysis of electron diffraction and vibrational spectra gave the result that the height of the potential barrier hindering the internal rotation of $(CH_3)_3N\cdot BF_3$ is 4.3 kcal/mol in the gas phase. This corresponds to that of Cl_3CSiCl_3.[18] The height of the potential barrier of $(CH_3)_3N\cdot BF_3$ is considerably larger than that of $H_3P\cdot BH_3$, 2.47 kcal/mol, which was obtained from microwave spectroscopy.[23] The increase of the potential barrier can be attributed to the large size of fluorine atoms and methyl groups and the smaller N–B distance in $(CH_3)_3N\cdot BF_3$. A wide line NMR study of $(CH_3)_3N\cdot BF_3$ in the solid phase showed that the barrier around the N–B axis was rather small, 1.7 kcal/mol.[4] The reason for this discrepancy is unknown, though one should be careful in comparing the values obtained by the two different methods.

Comparing the molecular structure of $(CH_3)_3N \cdot BF_3$ with those of the component molecules of $(CH_3)_3N$ and BF_3[24,25] (Table 4), the C–N and B–F distances increase by the complex formation by 1.6 and 4.5%, respectively, and the CNC and FBF angles decrease by 1.4 and 5.8%, respectively. This shows that the changes in the molecular parameters of the acceptor are much larger than those of the donor. In the solid phase, the molecule takes the same configuration as in the vapor phase, but the bond distances and the angles in the crystal[26] are considerably different from those in the vapor phase (Table 4). The C–N and B–F bond distances are longer and the N–B bond distance is shorter than those in the vapor phase. These changes indicate that the donor-acceptor bonding is enhanced in the solid state. The increments of the C–N and B–F bond distances are 2.9 and 6.0%, respectively, and the rate of the decrease of the FBF angle is 10.8%; these results are obtained by comparing the structural data from X-ray with those for the gaseous component molecules.

The authors are indebted to Dr. Tsutomu Fukuyama of the University of Tokyo for his advice in the computer calculation.

References

1) P. S. Bryan and R. L. Kuczkowski, *Inorg. Chem.*, **10**, 200 (1971); P. Cassoux, R. L. Kuczkowski, and A. Serafini, *Inorg. Chem.*, **16**, 3005 (1977).
2) S. Shibata and K. Iijima, *Chem. Lett.*, **1977**, 29.
3) M. Hargittai and I. Hargittai, *J. Mol. Struct.*, **39**, 79 (1977).
4) C. T. Yim and D. F. R. Gilson, *Can. J. Chem.*, **48**, 515 (1970).
5) "Kagaku Binran," 2nd ed, ed by The Chemical Society of Japan, Maruzen, Tokyo (1975), p. 1330.
6) H. S. Booth and K. S. Willson, *Inorg. Synth.*, Vol. I, 21 (1939).
7) R. Adams and B. K. Brown, *Org. Synth.*, Coll. Vol. I, 528 (1941).
8) R. L. Amster and R. C. Taylor, *Spectrochim. Acta*, **20**, 1487 (1964).
9) P. H. Laswick and R. C. Taylor, *J. Mol. Struct.*, **34**, 197 (1976).
10) W. Witt, *Z. Naturforsch., Teil A*, **19**, 1363 (1964).
11) S. Shibata, K. Iijima, R. Tani, and I. Nakamura, *Rep. Fac. Sci. Shizuoka Univ.*, **9**, 33 (1974).
12) S. Shibata, *Bull. Chem. Soc. Jpn.*, **45**, 1631 (1972).
13) M. Kimura, S. Konaka, and M. Ogasawara, *J. Chem. Phys.*, **46**, 2599 (1967); M, Ogasawara, S. Konaka, and M. Kimura, *ibid.*, **50**, 1488 (1969).
14) D. T. Cromer and J. B. Mann, *J. Chem. Phys.*, **47**, 1892 (1967); D. T. Cromer, *ibid.*, **50**, 4857 (1969).
15) C. Tavard, D. Nicolas, and M. Rouault, *J. Chim. Phys.*, **64**, 540 (1967).
16) W. Sawodny and J. Goubeau, *Z. Phys. Chem.*, **44**, 227 (1965).
17) K. Kuchitsu and S. J. Cyvin, "Molecular Structures and Vibrations," ed by S. J. Cyvin, Elsevier, Amsterdam (1972). Chap. 12.
18) Y. Morino and E. Hirota, *J. Chem. Phys.*, **28**, 185 (1958).
19) K. Kuchitsu, *Bull. Chem. Soc. Jpn.*, **40**, 505 (1967).
20) M. Toyama, T. Oka, and Y. Morino, *J. Mol. Spectrosc.*, **13**, 193 (1964).
21) T. Iijima, *Bull. Chem. Soc. Jpn.*, **45**, 3526 (1972).
22) Numerical experimental data of the leveled total intensity and background have been deposited with the Chemical Society of Japan (Document No. 7907).
23) J. R. Durig, Y. S. Li, L. A. Carreira, and J. D. Odom, *J. Am. Chem. Soc.*, **95**, 2491 (1973).
24) B. Beagley and A. R. Medwid, *J. Mol. Struct.*, **38**, 229 (1977).
25) K. Kuchitsu and S. Konaka, *J. Chem. Phys.*, **45**, 4342 (1966).
26) S. Geller and J. L. Hoard, *Acta Crystallogr.*, **4**, 399 (1951).

High-resolutional Calorimetric Study on Solid Solutions $SnCl_2(H_2O)_x(D_2O)_{2-x}$

Masami TATSUMI,† Takasuke MATSUO, Hiroshi SUGA, and Syûzô SEKI*

Department of Chemistry, Faculty of Science, Osaka University, Toyonaka, Osaka 560

(Received September 4, 1978)

Heat capacities of the system of solid solutions $SnCl_2$ $(H_2O)_x(D_2O)_{2-x}$ (x=2.00, 1.97, 1.75, 0.96, 0.50, 0.25, and 0.03) were measured by an adiabatic calorimeter capable of determinations of heat capacity with the temperature step of 5—10 mK. The heat capacity peak due to order-disorder change of hydrogens becomes broader and its transition temperature rises as the deuteron concentration is increased. A small first-order component was found in the crystals of x=2.00, 1.97, and 1.75. Measurements were repeated for aged crystals of x=0.96, 0.50, and 0.03. Nature of the phase transition has been discussed in analogy with the liquid-vapor critical point. From the heat capacity data around the glass transition it is concluded that the motion of the hydrogen atoms is strongly correlated with each other over a range whose size is large enough that fluctuation of the local isotopic composition from the average is negligible.

The phase transition in tin(II) chloride dihydrate $SnCl_2 \cdot 2H_2O$ (abbreviated as TCD) was discovered by Kiriyama *et al.*[1] The complete crystal structure was determined by them by using the X-ray[2] and the neutron diffraction[3] techniques. The crystal consists of layers of tin(II) chloride molecule alternating with layers of water molecules. There are two types of water molecules in the layers. One of them, designated as H_2O (1), is coordinated to the tin(II) ion and the other, H_2O (2), is a water of crystallization. Each type of water molecules is hydrogen-bonded to three others of different type in the same layer parallel to the (100) plane. In the hydrogen bonding network, there are seven kinds of positions which deuterons can occupy and the three types of hydrogen bond with different bond length.[4-7] The O(2)···O(1′) hydrogen bond differs from the other two in that its bond length increases anomalously below T_c, in contrast to the other two which contract as the temperature is lowered.

An unusual property of the phase transition in TCD is that there occurs no change of symmetry of the crystal at the transition, including that pertaining to the hydrogen atom. The space group is $P2_1/c$ both below and above the transition. No symmetry elements are lost or gained on passing through the transition. It is generally assumed that a phase transition of any substance is accompanied by a change of symmetry of the substance. The symmetry in question may be that of the distribution function of the atoms in the crystals or that of the average spin orientation in magnetic substances. More abstract symmetry of wave function is relevant to superconductivity and the λ-transition of liquid helium. It is generally observed that one or more of the symmetry elements disappear as the substance undergoes the phase transition. The symmetry change is thus a general characteristic of phase transitions.[8] In fact, Landau theory of the phase transitions of the second kind connects the symmetry change with the thermodynamics of the phase transition through appropriate definition of the order parameters. If there is no change in the symmetry of the crystal, how can one distinguish one phase from the other? One cannot tell one phase from the other from the atomic distribution function alone because there is no qualitative difference between the distribution functions of the two phases. A question thus arises as to whether the two phases are really different from each other.

From the calorimetric point of view, the phase transition in TCD is characterized by a sharp peak of the heat capacity.[9,10] The anomalous heat capacity increases symmetrically from both sides of the transition point. This has been recognized as a distinguishing feature of the two-dimensional phase transition. A small isothermal increment of the enthalpy (33.0 J mol^{-1} or 3.5% of the total transition enthalpy) was observed at the very transition temperature of x=2.00.[9] Thus, the phase transition occurs gradually but is of the first-order nature. These observations suggest formal similarity of the transition in TCD with vaporization of a typical liquid. Thus the liquid and vapor have the same continuous translational symmetry. Below the critical pressure, the vaporization is, of course, a first-order transition. Far below the critical point, there is no gradual increase of enthalpy in the isobaric process both below and above the vaporization temperature. Only the latent heat of vaporization dominates in that process. However, gradual increase of the enthalpy appears as the critical pressure is approached. At the critical point the isothermal change of enthalpy disappears and the heat capacity at the critical pressure diverges strongly. The region beyond the critical point is called supercritical. Here, the heat capacity as a function of temperature will be still large but remains finite. If the analogy between the phase transition in TCD and vaporization of liquid is something more than superficial, one should expect existence of a critical point at an appropriate value of some external parameter of the TCD crystal. In the present study, we have chosen the hydrogen-deuterium isotopic composition as the adjustable "external" parameter and made heat capacity measurement of the mixed crystals of $SnCl_2(H_2O)_x(D_2O)_{2-x}$ for x=2.00, 1.97, 1.75, 1.50, 0.96, 0.50, 0.25, and 0.03.

High resolution measurements of the heat capacity including that of the crystals aged for four years have established that the critical composition does really exist near x=1.50. The phase transition in TCD provides thus an example of a new class of solid state phase transition for which there is no concomitant

† Present address: Sumitomo Electric Industries Ltd., Osaka 541.

change of the symmetry of the crystal. It should be mentioned that the dimer model of Salinas and Nagle[11] which gives a logarithmic singularity of heat capacity at the transition point T_c seems to have a similar property in that the symmetry of the dimer distribution is the same for $T>T_c$ as for $T<T_c$. A relevant problem of the difficulty of defining the order parameter for a certain class of the dimer lattice was first pointed out by Kasteleyn.[12]

Another aspect of interest of TCD crystal is that the anomalous heat capacity has an appreciable magnitude even at a lower temperature where the motion of the hydrogen atom is so slow that it falls out of thermal equilibrium when the temperature is varied at a typical rate of the calorimetric experiment.[10] The temperature at which the average lifetime of the proton (or deuteron) configuration is equal to the time required for the heat capacity measurement, *i.e.*, the temperature where the calorimetric Deborah number[13] is equal to unity, is called the glass transition temperature T_g. Below T_g only the vibrational degree of the crystal is active and contributes to the observed heat capacity. This is a particularly fortunate property of the crystal, because it leads to unambiguous determination of the lattice heat capacity. Occurrence of the glass transition in TCD is intimately related to the structure of the hydrogen-bond network of the crystal. The network structure is such that the hydrogen atoms can change their positions without violating the ice conditions if eight of them move in unison.[10,14] A very different behavior is observed in copper formate tetrahydrate, a similar hydrate crystal with layer structure, in which the ice condition prohibits redistribution of finite number of the hydrogen atoms in the low-temperature phase. The anomalous heat capacity is essentially zero below T_c because the ordering is complete in the whole range of the low-temperature phase. It has been pointed out previously that Bjerrum and ionic defects can have only minor effect that scarcely affects the bulk thermodynamic properties of the copper formate tetrahydrate crystal, although they may be responsible to the dielectric dispersion in the low temperature phase.[15] In the present study the isotope effect on the glass transition in TCD has also been investigated by the heat capacity measurement. It will be shown that the relaxational properties depend on the isotopic composition in a monotonous way. The experimental result presented in this paper will be analysed in the subsequent paper[16] in terms of the general consideration discussed above.

Experimental

Sample Preparation. The single crystals of solid solution of TCD and DTCD were prepared in the following manner. Commercial TCD (extra pure grade from Wakō Pure Chemical Co., Ltd.) was first dehydrated by evacuation for a week. The extent of dehydration was determined by measurement of the weight loss. An appropriate amount of mixture of normal and 99.75% heavy water (E. Merck) having desired composition was added to the dehydrated crystal together with a small quantity of normal or deuterated hydrochloric acid. The slurry was heated to about 45 °C in a closed glass vessel giving a clear solution and cooled slowly after addition of a small piece of single crystal. The crystal was grown in the water bath thermostatted by the proportional controller (within ± 10 mK) for a month. The sample for the calorimetry was cut from a large single crystal, shaped into a cylinder with 25 mm diameter and 40 mm height, and enclosed in a calorimeter cell under atmosphere of helium. All the six single crystals having different isotopic composition were prepared in the same manner.

Determination of the Isotopic Composition. The H_2O concentration in $SnCl_2(H_2O)_{0.96}(D_2O)_{1.04}$ was determined by means of the quantitative absorption intensity measurements of the proton magnetic resonance by use of the high resolution NMR spectrometer (Varian 60). Several mixtures of D_2O and H_2O having different compositions were used as standards for making the calibration curve. The isotopic mixture of water was collected into the NMR tube by vacuum distillation from the calorimetric crystal after completion of the heat capacity measurement. The error in the determination of the deuterium content was estimated to be $\pm 2\%$ from the scatter in the calibration. The mole ratio of H_2O and D_2O in solid solution thus determined agreed with that of the initial mixture. The other solid solutions were assumed to have the same isotopic composition as the slurry.

Calorimeter. The design and construction of the high resolution calorimeter used in the present work was described in detail elsewhere.[17] One of the feature of the adiabatic calorimeter is that it is equipped with two thermometers, that is, a platinum resistance thermometer and a thermistor-thermometer. The former is employed to determine heat capacity with ordinary resolution ($\Delta T \approx 1-2$ K) and the inaccuracy and the imprecision of the heat capacity measurement by use of the platinum resistance thermometer is less than ± 0.1 and $\pm 0.05\%$,[18] respectively, between 50 and 275 K. The latter, the thermistor-thermometer, is essential for high resolution measurement with the temperature step of 10—20 mK. The temperature resolution attained by this thermometer was about 3 μK at 220 K. Meticulously careful attention had to be paid to the adiabatic control in order to exploit the good temperature resolution of the thermistor-thermometer. When the control was left undisturbed, the cell temperature remained constant within 0.3 mK over a period of 24 h. Temperature steps as small as 5 mK could be attained without introducing unduely large imprecision in the result. The performance of the calorimeter was improved by several modifications made since the previous publication of the apparatus. Some of them are briefly described here.

i) Use of an indium O-ring facilitates the vacuum-tight closure of the calorimeter cell.

ii) In order to ease the procedure of assembling the calorimeter cell especially in the dry-box, two gold electric contacts were attached to the hermetic seal as the terminal for the calorimeter-heater-leads.

iii) In order to decrease the heat transfer to the calorimeter cell by conduction along the electrical leads, one of the thermocouple junctions, which was previously located between the calorimeter cell and bottom cone, was fixed to the inner jacket. The copper leads of the two thermometers were replaced by the constantan leads with smaller thermal conductivity.

iv) The significant temperature drift was caused by the stray E.M.F. induced at the terminal of the thermocouple-lead in the previous high resolution measurement. The stray E.M.F. was reduced by decreasing the number of binding-post between the calorimeter and the microvolt amplifier.

TABLE 1. SUMMARY OF SOLID SOLUTIONS AND AGING PERIOD

Abbreviation	Formula	t/month[a)]
$x=2.00$	$SnCl_2(H_2O)_{2.00}$	3
$x=1.97$	$SnCl_2(H_2O)_{1.97}(D_2O)_{0.03}$	4
$x=1.75$	$SnCl_2(H_2O)_{1.75}(D_2O)_{0.25}$	4
$x=1.50$	$SnCl_2(H_2O)_{1.50}(D_2O)_{0.50}$	7
$x=0.96$	$SnCl_2(H_2O)_{0.96}(D_2O)_{1.04}$	1
$x=0.96$(II)	$SnCl_2(H_2O)_{0.96}(D_2O)_{1.04}$	24
$x=0.50$	$SnCl_2(H_2O)_{0.50}(D_2O)_{1.50}$	4
$x=0.50$(II)	$SnCl_2(H_2O)_{0.50}(D_2O)_{1.50}$	10
$x=0.25$	$SnCl_2(H_2O)_{0.25}(D_2O)_{1.75}$	1
$x=0.03$	$SnCl_2(H_2O)_{0.03}(D_2O)_{1.97}$	1
$x=0.03$(II)	$SnCl_2(H_2O)_{0.03}(D_2O)_{1.97}$	48

a) Time elapsed before starting the measurement after the preparation of the crystal.

v) The ASL AC double bridge works adequately when the resistance ratio (n_A) is between 0.2 and 0.8. Previously, we used two home-made standard resistors (6.238453 and 0.390430 Ω) and a commercial one of 100 Ω (Shimadzu Electrical Measuring Instruments Co., Ltd.). The first resistors were replaced by three card-type precision resistors (10, 1, 0.1 Ω, General Radio Company) resulting in ample overlap between the intervals of the recommended ratio value. This modifications did not influence the temperature scale because the new resistors were calibrated against the 100 Ω resistor which remained as before.

vi) The maximum temperature coefficient of the card-type standard resistor has been stated ±20 ppm/K by the manufacturer. The improved thermostat was constructed, which consisted of the double-walled-aluminium box temperature-regulated by proportional controllers. The temperature was kept constant within ±50 mK.

vii) The effect of the self-heating is corrected more reproducibly by monitoring the accurate power dissipated in the thermometer. For this purpose the bridge carrier voltage was measured by an AC voltmeter (Yokogawa Electric Works Ltd.).

viii) Temperature constancy of the bridge components was found to be essential for the high resolution measurement especially in the vicinity of critical points where thermal equilibrium is reached very sluggishly. In order to stabilize the temperature of the bridge components (two 1 kΩ resistors for the fixed arms and a seven-decade 111.11110 kΩ variable resistor) against the change of the room temperature, they were housed in an air thermostat. The temperature of the thermostat was regulated within ±0.1 K by a controller equipped with a thermistor throughout a series of heat capacity measurements. Temperature gradient in the air thermostat was minimized by a fan driven by a remote motor through a flexible torque transmitter.

Heat Capacity Measurements. The heat capacity measurements were performed on crystals of seven different compositions in addition to $x=2.00$ already reported. Table 1 summarizes the isotopic composition of the samples and the time elapsed between preparation of the crystal and the heat capacity measurement. The abbreviatiated designation for each of the solid solutions is also given there.

In all of the isotopic compositions studied, the heat capacity behaved anomalously in two temperature regions. One is around 220—230 K region and is due to the order-disorder change of proton (deuteron) in the hydrogen bonding network. The other is a relaxational anomaly (glass transition) around

TABLE 2. MOLAR HEAT CAPACITY OF $SnCl_2(H_2O)_{2.00}$

T/K	C_p / J K^{-1} mol^{-1}	T/K	C_p / J K^{-1} mol^{-1}	T/K	C_p / J K^{-1} mol^{-1}
216.009	149.79	217.866	182.97	218.886	155.67
216.081	149.89	217.885	186.93	218.911	155.33
216.152	150.23	217.903	191.27	218.965	154.78
216.224	150.51	217.921	197.99	218.988	154.62
216.295	150.78	217.938	208.20	219.014	154.31
216.354	151.06	217.955	224.55	219.042	153.99
216.402	151.15	217.970	253.90	219.070	153.71
216.438	151.48	217.984	305.39	219.098	153.53
216.467	151.53			219.126	153.38
216.499	151.62	1st order region		219.154	153.23
216.531	151.79			219.182	153.08
216.563	151.97	218.022	236.73	219.210	152.94
216.595	152.11	218.038	216.23	219.238	152.72
216.627	152.22	218.055	204.46	219.266	152.58
216.659	152.58	218.072	196.40	219.294	152.61
216.691	152.64	218.090	190.49	219.322	152.43
216.723	152.79	218.108	186.12	219.350	152.28
216.755	152.99	218.127	182.72	219.378	151.93
216.786	153.19	218.146	179.78	219.406	151.94
216.818	153.41	218.165	177.52	219.438	151.88
216.850	153.74	218.184	175.40	219.473	151.77
216.881	153.69	218.203	173.65	219.508	151.41
216.913	154.17	218.222	172.03	219.542	151.40
216.945	154.28	218.241	170.61	219.577	151.21
216.976	154.66	218.261	169.14	219.613	151.13
217.008	154.95	218.280	168.34	219.650	150.78
217.039	155.09	218.300	167.30	219.690	150.68
217.071	155.07	218.321	166.64	219.730	150.55
217.102	155.58	218.342	165.78	219.772	150.39
217.134	155.85	218.362	165.06	219.814	150.25
217.165	156.22	218.382	164.15	219.858	150.19
217.197	156.65	218.402	163.55	219.904	149.77
217.228	156.90	218.422	162.88	219.951	149.98
217.259	157.38	218.442	162.49	220.140	149.32
217.291	157.68	218.462	161.83	220.490	148.56
217.322	158.19	218.482	161.32	220.885	147.72
217.353	158.54	218.502	160.93	221.309	147.11
217.384	159.11	218.522	160.38	221.734	146.62
217.415	159.64	218.543	160.28	222.159	146.19
217.446	160.21	218.563	159.93	222.585	146.09
217.477	160.79	218.583	159.93	223.012	145.57
217.507	161.20	218.603	159.47	223.440	144.79
217.537	162.14	218.624	158.99		
217.566	163.07	218.644	158.63		
217.596	163.90	218.665	158.24		
217.625	164.94	218.686	157.94		
217.653	165.26	218.707	157.60		
217.705	168.28	218.729	157.31		
217.729	169.63	218.750	156.85		
217.753	171.31	218.772	156.65		
217.778	173.02	218.794	156.33		
217.803	175.10	218.817	156.22		
217.826	177.86	218.840	155.86		
217.847	180.27	218.863	155.76		

TABLE 3. MOLAR HEAT CAPACITY OF $SnCl_2(H_2O)_{1.50}(D_2O)_{0.50}$

T/K	C_p/J K^{-1} mol^{-1}	T/K	C_p/J K^{-1} mol^{-1}	T/K	C_p/J K^{-1} mol^{-1}	T/K	C_p/J K^{-1} mol^{-1}	T/K	C_p/J K^{-1} mol^{-1}
198.46	136.63	163.05	121.20	220.445	156.75	221.785	221.11	222.494	165.36
199.70	137.64	164.14	121.69	220.476	157.03	221.796	229.21	222.509	165.34
200.95	138.03	165.23	122.19	220.512	156.72	221.807	238.83	222.525	164.46
202.34	138.98	166.31	122.61	220.548	157.48	221.818	250.57	222.540	164.57
203.83	139.63	167.40	123.09	220.584	157.46	221.828	266.17	222.556	163.99
205.26	140.29	168.46	123.63	220.619	157.86	221.838	284.06	222.572	163.70
206.69	141.08	169.54	124.12	220.653	157.78	221.847	306.45	222.588	163.98
208.15	141.87	170.81	124.65	220.687	158.27	221.856	344.73	222.603	163.24
209.59	142.72	172.38	125.35	220.721	158.46	221.863	396.40	222.619	162.81
210.99	143.60	174.00	125.99	220.755	158.64	221.870	465.68	222.635	162.57
212.38	144.47	175.63	126.95	220.789	159.01	221.876	571.29	222.651	162.27
213.76	145.53	173.43	125.82	220.823	159.39	221.881	459.08	222.667	162.10
215.15	146.67	175.28	126.63	220.852	159.26	221.888	422.80	222.684	161.89
216.53	148.09	177.12	127.45	220.884	159.72	221.895	382.22	222.700	161.38
217.93	149.86	178.95	128.24	220.917	160.07	221.903	357.60	222.716	161.48
219.42	153.64	180.77	129.07	220.950	160.23	221.912	329.33	222.732	161.22
220.68	159.19	182.68	129.91	220.983	161.01	221.921	304.43	222.748	161.04
221.94	202.54	184.69	130.77	221.015	161.29	221.930	287.57	222.765	160.98
223.17	158.24	186.68	131.68	221.047	161.60	221.940	268.62	222.781	160.80
224.49	153.40	188.67	132.61	221.077	162.00	221.951	255.16	222.797	160.15
225.77	151.26	190.63	133.44	221.106	162.60	221.961	242.62	222.814	160.05
227.13	149.98	192.59	134.25	221.135	162.85	221.973	232.62	222.830	161.44
228.48	149.32	194.54	135.37	221.163	163.44	221.982	223.67	222.847	160.60
229.84	149.05	196.48	136.11	221.191	163.81	221.993	218.73	222.864	159.53
		198.40	136.95	221.219	164.27	222.006	214.50	222.882	159.62
		200.16	137.86	221.247	164.70	222.018	208.52	222.899	159.49
		201.74	138.73	221.273	165.54	222.030	203.10	222.917	159.00
125.50	101.07	203.15	139.34	221.297	166.06	222.043	200.24	222.935	159.19
126.55	101.57	204.40	139.93	221.314	165.84	222.056	195.20	222.953	159.09
127.64	102.12	205.64	140.54	221.334	166.39	222.069	193.12	222.967	158.42
128.82	102.67	206.79	141.30	221.353	167.38	222.082	190.70	222.986	158.40
130.19	103.27	207.85	141.89	221.372	167.75	222.096	188.47	223.004	158.39
131.36	103.96	208.89	142.43	221.390	168.63	222.109	186.51	223.023	158.24
132.60	104.52	209.87	143.09	221.409	169.32	222.123	185.04	223.042	157.63
133.83	105.09	210.78	143.45	221.426	169.89	222.133	182.32	223.058	157.84
135.06	105.66			221.444	170.50	222.147	181.06	223.078	157.88
136.28	106.25	215.583	147.06	221.461	171.10	222.161	179.74	223.098	157.97
137.50	106.78	216.128	147.60	221.478	172.00	222.175	178.39	223.118	157.91
138.71	107.39	216.593	148.11	221.495	172.80	222.189	178.27	223.139	157.53
139.91	108.38	217.046	148.62	221.512	173.89	222.202	176.64	223.162	157.25
141.12	108.59	217.470	149.16	221.528	175.26	222.217	175.98	223.184	157.52
142.32	109.13	217.845	149.39	221.543	176.12	222.231	174.95	223.206	157.16
143.50	109.43	218.144	150.07	221.559	176.07	222.245	174.39	223.228	157.15
144.70	110.21	218.399	150.52	221.573	177.77	222.259	173.32	223.252	157.00
145.89	110.77	218.640	150.96	221.588	178.44	222.273	172.35	223.278	156.75
147.08	111.28	218.867	151.46	221.602	179.83	222.288	171.91	223.303	156.68
148.25	111.80	219.075	151.83	221.616	181.38	222.302	171.58	223.329	156.51
149.44	112.26	219.276	152.36	221.630	183.55	222.317	170.58	223.355	156.61
150.62	112.83	219.468	152.83	221.644	183.52	222.331	170.10	223.382	156.06
151.81	113.27	219.652	153.42	221.658	185.32	222.346	169.22	223.409	156.25
152.98	113.77	219.813	153.90	221.671	187.52	222.360	169.08	223.438	155.86
154.15	114.31	219.950	154.27	221.685	189.57	222.375	168.17	223.468	155.97
155.30	115.45	220.062	154.74	221.698	192.24	222.390	167.94	223.498	155.63
156.42	117.98	220.141	155.12	221.711	194.54	222.404	167.49	223.528	155.85
157.54	118.87	220.205	155.43	221.724	197.79	222.419	167.25	223.558	155.30
158.64	119.21	220.260	155.57	221.736	200.65	222.434	166.41	223.588	155.43
159.75	119.71	220.311	155.94	221.749	204.78	222.449	166.43	223.619	155.28
160.86	120.38	220.357	156.20	221.761	212.19	222.464	166.04	223.650	155.15
161.96	120.74	220.402	156.51	221.773	214.91	222.479	165.03	223.682	155.15

TABLE 3. Continued

T/K	C_p/J K^{-1} mol^{-1}	T/K	C_p/J K^{-1} mol^{-1}	T/K	C_p/J K^{-1} mol^{-1}	T/K	C_p/J K^{-1} mol^{-1}
223.714	155.00	58.99	55.72	238.93	149.63	26.73	20.17
223.748	154.87	60.35	56.99	240.23	149.82	27.80	21.49
223.783	154.73	61.80	58.30	241.51	150.13	28.81	22.71
223.819	154.46	63.35	59.68	242.87	150.22	29.75	23.85
223.855	154.39	64.87	61.00	244.29	150.70	30.74	25.04
223.891	154.44	66.32	62.28	245.71	150.83	31.86	26.40
223.931	154.24	67.85	63.56	247.13	151.25	32.96	27.76
223.976	153.88	69.42	64.92	248.54	151.52	33.96	28.94
224.020	153.77	70.97	66.21	250.05	151.91	34.92	30.06
224.065	153.81	72.49	67.47	251.68	152.33	35.88	31.22
224.111	153.92	73.96	68.69	253.31	152.80	36.79	32.24
224.158	153.79	75.54	69.90	254.92	153.20	37.74	33.32
224.213	153.45	77.21	71.21	256.54	153.46	38.71	34.42
224.274	153.50	78.84	72.45	258.15	153.94	39.64	35.44
224.335	153.28			259.85	154.40	40.62	36.55
224.397	153.40			261.46	154.81	41.67	37.74
224.457	152.72	80.44	73.67	263.24	155.32	42.69	38.87
224.522	152.92	82.01	74.70	265.03	155.82	43.77	40.07
224.591	153.01	83.56	75.96			44.92	41.31
224.662	152.67	84.98	77.00			46.01	42.54
224.731	152.76	86.57	78.08	266.81	156.35	47.08	43.67
224.805	152.44	88.17	79.12	268.59	156.87	48.15	44.82
224.880	152.40	89.86	80.27	270.47	157.37		
224.931	152.69	91.52	81.42	272.53	158.08		
224.981	152.44	93.18	82.45	274.64	158.61		
225.081	152.30	94.79	83.56	276.75	159.30		
225.203	152.17	96.36	84.52	278.85	160.06		
225.325	152.10	97.92	85.58	280.93	160.56		
225.473	152.08	99.45	86.48	283.01	161.16	49.22	46.00
225.643	151.48	101.03	87.51	285.08	161.77	50.48	47.31
225.861	151.60	102.63	88.45	287.15	162.55	51.91	48.84
226.166	151.01	104.22	89.41	289.21	163.21	53.31	50.20
226.517	150.16	105.78	90.37	291.23	164.07	54.75	51.68
226.868	150.00	107.34	91.23	293.28	164.41	56.23	53.10
227.219	149.90	108.88	92.17	295.39	165.01	57.67	54.48
227.661	149.72	110.41	93.01	297.60	165.80	59.06	55.77
228.193	149.44	111.91	93.81	299.88	166.63		
228.771	149.27	113.42	94.71	302.24	167.64		
229.385	148.74	114.95	95.52				
229.992	148.95	116.54	96.28			130.04	103.22
230.608	148.95	118.09	97.24			131.70	104.06
231.240	148.89	119.63	98.04	13.14	4.87	133.51	104.89
231.967	148.85	121.18	98.83	13.75	5.48	135.41	105.80
232.774	148.89	122.70	99.66	14.32	6.00	137.29	106.67
233.581	149.00	124.22	100.38	15.18	6.88	139.22	107.53
234.388	148.99	125.72	101.20	16.35	7.97	141.19	108.43
235.195	149.04			17.18	8.94	143.15	109.37
236.001	149.21			18.00	9.85	145.15	110.38
236.801	149.22			18.77	10.74	147.08	111.26
237.605	149.36	227.43	149.82	19.46	11.54	148.99	112.08
238.409	149.62	228.84	149.34	20.19	12.40	150.84	112.96
		230.27	149.09	20.94	13.25	152.60	114.84
239.33	149.27	231.45	148.99	21.75	14.20	154.40	117.15
240.38	149.78	232.63	148.98	22.62	15.23	156.24	117.95
241.49	150.00	233.81	148.95	23.42	16.17	158.07	118.62
242.70	149.71	235.05	149.11	24.18	17.07	159.98	119.73
243.90	150.81	236.34	149.33	24.96	18.05	162.03	120.61
		237.64	149.38	25.77	19.07	164.24	121.63

TABLE 4. MOLAR HEAT CAPACITY OF $SnCl_2(H_2O)_{0.03}(D_2O)_{1.97}$

T/K	C_p/J K^{-1} mol^{-1}	T/K	C_p/J K^{-1} mol^{-1}	T/K	C_p/J K^{-1} mol^{-1}	T/K	C_p/J K^{-1} mol^{-1}
232.482	172.83	234.646	231.07	236.497	174.39	234.550	225.42
232.541	173.06	234.668	230.04	236.564	174.19	234.582	229.23
232.596	173.28	234.694	229.89	236.641	173.90	234.602	230.67
232.651	173.52	234.720	228.70	236.719	173.61	234.618	228.64
232.705	173.71	234.746	227.18	236.799	173.35	234.634	227.56
232.755	173.94	234.774	224.62	236.871	173.14	234.651	228.42
232.804	174.16	235.043	198.62	236.933	172.94	234.668	230.76
232.853	174.54	235.012	200.17	237.042	172.76	234.684	231.73
232.899	174.60	234.981	203.45	237.196	172.41	234.785	221.27
232.946	174.77	234.950	206.25	237.350	172.01	234.809	215.92
232.993	175.07	234.920	209.37	237.505	171.68	234.838	213.97
233.040	175.16	234.890	212.23	237.661	171.40	234.871	208.12
233.086	175.64	234.861	215.70	237.817	171.11	234.904	203.25
233.133	177.64	234.832	219.13	237.972	170.95	234.944	200.52
233.178	176.21	234.803	221.90	238.128	170.64	234.997	195.44
233.223	176.39	235.074	196.48	238.283	170.43	235.066	190.00
233.267	176.58	235.106	194.70	238.574	170.22	235.143	185.95
233.312	177.16	235.137	192.90	239.053	169.78	235.222	182.63
233.356	177.57	235.169	191.69	239.586	169.37	235.319	177.05
233.400	177.86	235.201	190.38			235.403	179.21
233.444	178.36	235.233	189.46			235.505	177.80
233.488	178.69	235.265	188.06			235.616	174.81
233.529	179.19	235.298	187.22	222.69	156.27	235.756	173.59
233.566	179.85	235.330	186.29	223.56	156.87	235.925	172.50
233.604	179.80	235.363	185.46	224.44	157.48	236.122	170.64
233.641	180.55	235.395	184.73	225.30	157.36	236.350	169.41
233.678	182.07	235.428	183.97	226.21	158.70	236.578	168.45
233.715	181.70	235.462	183.31	227.15	159.51	236.858	167.49
233.751	182.05	235.495	182.74			237.213	166.53
233.788	182.57	235.529	182.20			237.686	165.76
233.825	183.36	235.562	181.47			238.254	164.95
233.861	183.89	235.595	181.01	225.11	157.55	238.822	164.41
233.898	184.50	235.628	180.66	226.48	158.59		
233.935	185.07	235.661	180.19	227.84	159.69		
233.969	186.47	235.694	179.87	229.19	161.03		
234.006	187.27	235.728	179.65	230.40	162.60		
234.040	188.57	235.761	179.15	231.33	163.97		
234.072	189.70	235.794	178.44	231.901	165.76		
234.104	191.03	235.828	178.40	232.248	166.37		
234.136	192.35	235.861	178.04	232.535	167.79		
234.168	193.82	235.896	177.82	232.764	168.50		
234.199	195.66	235.931	177.47	232.993	169.60		
234.231	197.06	235.967	177.21	233.220	170.33		
234.262	199.05	236.002	177.10	233.447	172.78		
234.293	201.43	236.038	176.94	233.615	174.66		
234.323	204.00	236.073	176.65	233.728	175.78		
234.354	206.89	236.110	176.41	233.842	177.46		
234.384	209.89	236.147	176.22	233.939	179.46		
234.413	213.06	236.185	176.10	234.032	182.74		
234.443	216.19	236.223	175.79	234.120	186.51		
234.472	219.35	236.260	175.56	234.202	189.36		
234.501	222.41	236.298	175.36	234.278	194.13		
234.529	225.09	236.336	175.16	234.353	200.52		
234.558	227.13	236.374	174.94	234.419	210.12		
234.595	229.34	236.413	174.76	234.463	216.12		
234.628	230.27	236.451	174.50	234.514	221.63		

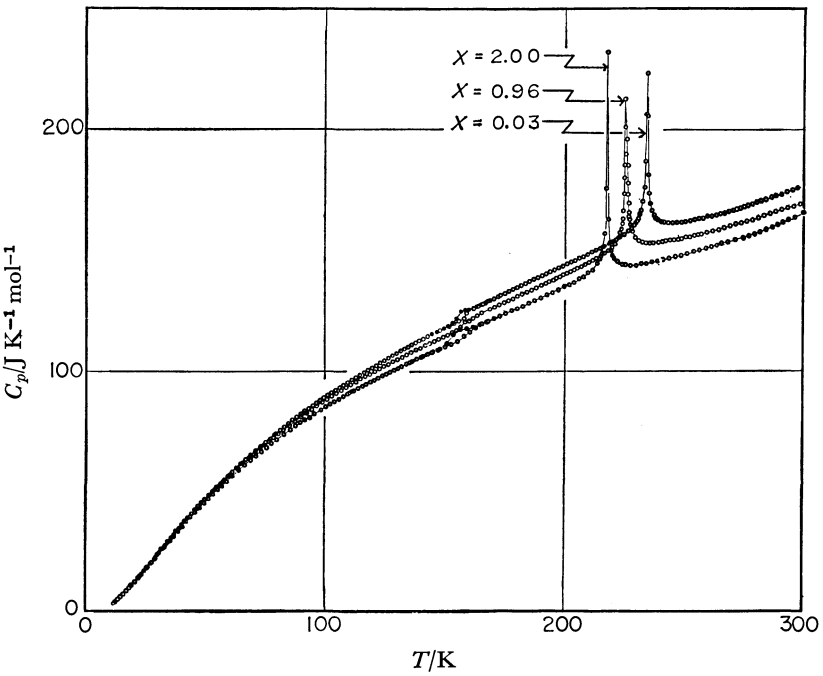

Fig. 1. Heat capacity curves for the samples of $x=2.00$, $x=0.96$, and $x=0.03$.

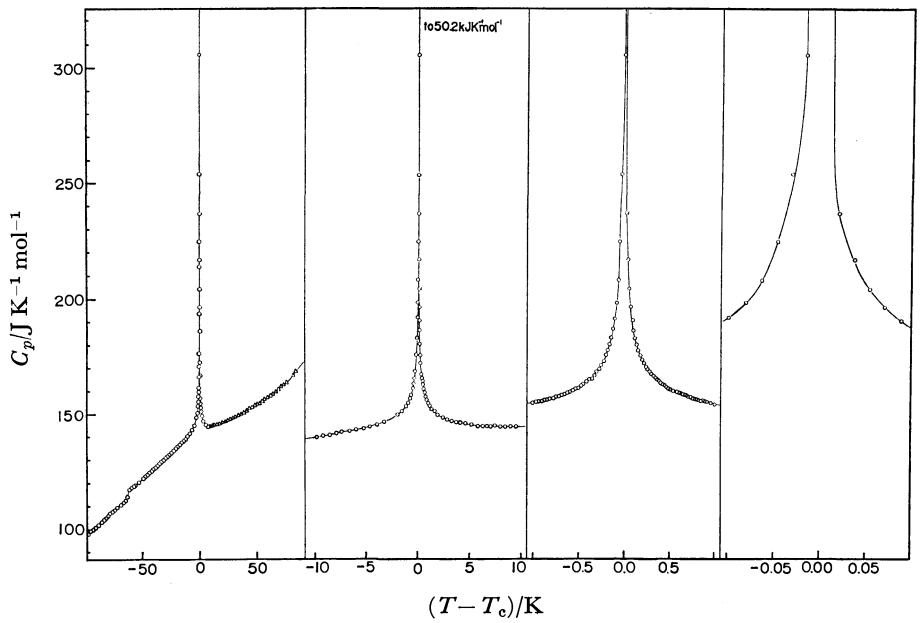

Fig. 2. Heat capacity curves of $x=2.00$ as a function of $(T-T_c)$ in successively expanded scales.

150 K due to loss of equilibrium in rearrangement of protons in that network at the lower temperature. Both anomalies change smoothly with the isotopic composition in their characters including the temperature and the interval of their occurrence. Each measurement was carried out both with ordinary resolution ($\Delta T \approx 1$—3 K) from 11 to 300 K and with high resolution ($\Delta T \approx 10$—50 mK) in the vicinity of the transition temperature. Prior to the high resolution measurement, the transition temperature was located by the measurement with ordinary temperature step. It took about fifteen minutes for all crystals to attain thermal equilibrium after switching off the heater current. Longer time was required to determine the final temperature in the high resolution measurement. Calorimetric operations around the glass transition were performed according to the procedure already reported.[10] Thus the calorimeter was first cooled rapidly to 130 K, some 25 K below the anomalous region. The cooling rate was about 2 K min^{-1}. In the measurements in the exothermic region, temperature drifts were followed for 30—60 min after the energy input for heat capacity measurements. These periods were kept constant for a series of measurement. In the endothermic region, heat capacities were measured in the same way as in normal region but by following temperature drift for longer time (2—3 h). Details of the heat capacity measurement for each of the samples are described in the following. The numerical values of the heat capacity are given in Tables 2, 3, and 4 for $x=2.00$, $x=1.50$, and $x=0.03$, respectively. The

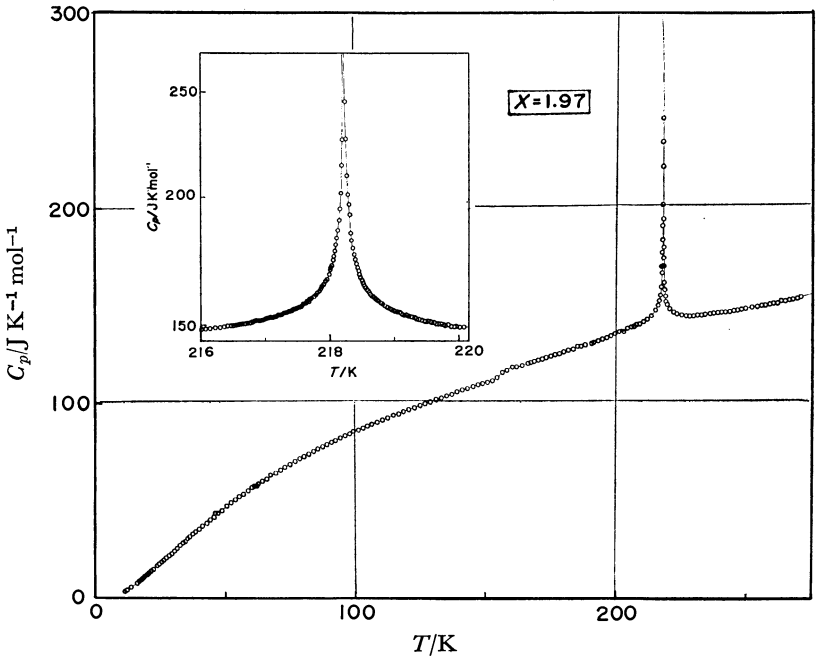

Fig. 3. Heat capacity of $x=1.97$. The inset shows an expanded view close to T_c.

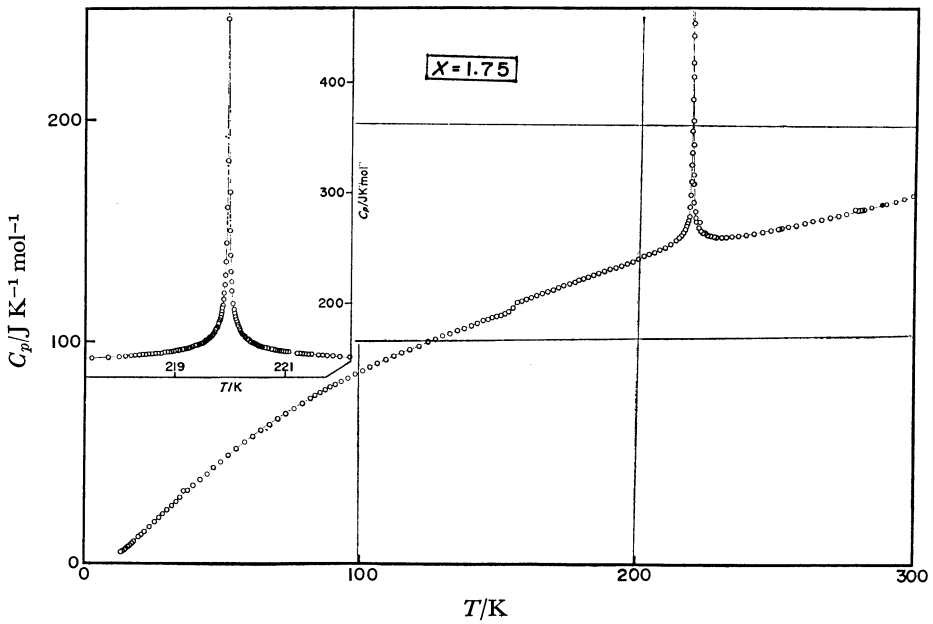

Fig. 4. Heat capacity of $x=1.75$. The inset shows an expanded view close to T_c.

complete data of other crystals amounting in number to 2096 are all kept as Document No. 7913 at the Chemical Society of Japan. Figure 1 shows the results of heat capacity measurements of $x=2.00$, $x=0.96$, and $x=0.03$ with ordinary resolutions.

(i) $x=2.00$: The highly symmetrical shape of the anomaly was observed at 218.01 K with a quasi-isothermal absorption of energy amounting to 32.4 J mol^{-1}. It is somewhat difficult to distinguish experimentally the small isothermal enthalpy increase (*i.e.* the first-order component) from the very large heat capacity. The first-order component is calorimetrically detected by abrupt increase of large endothermic drift with longer equilibration time and by the steep rise in the enthalpy or entropy curve plotted against temperature (see Ref. 16). The present measurements are precise enough to detect the quasi first-order component. In Fig. 2 the heat capacities are plotted as a function of $(T-T_c)$ in successively expanded scales.

(ii) $x=0.03$: This crystal exhibited no first-order component. The heat capacity curve is rounded at the peak temperature (234.64 K). The anomalous heat capacity was broader than those found in any other crystal and the maximum value of the peak, 220 J K^{-1} mol^{-1}, is the smallest in the series of the mixed crystals.

(iii) $x=1.97$: The phase transition occurred at 218.22 K. A quasi-isothermal absorption of energy was found around ± 15 mK of the peak temperature. In this region the equilibration time increased by a factor of 4—6 with a sudden increase

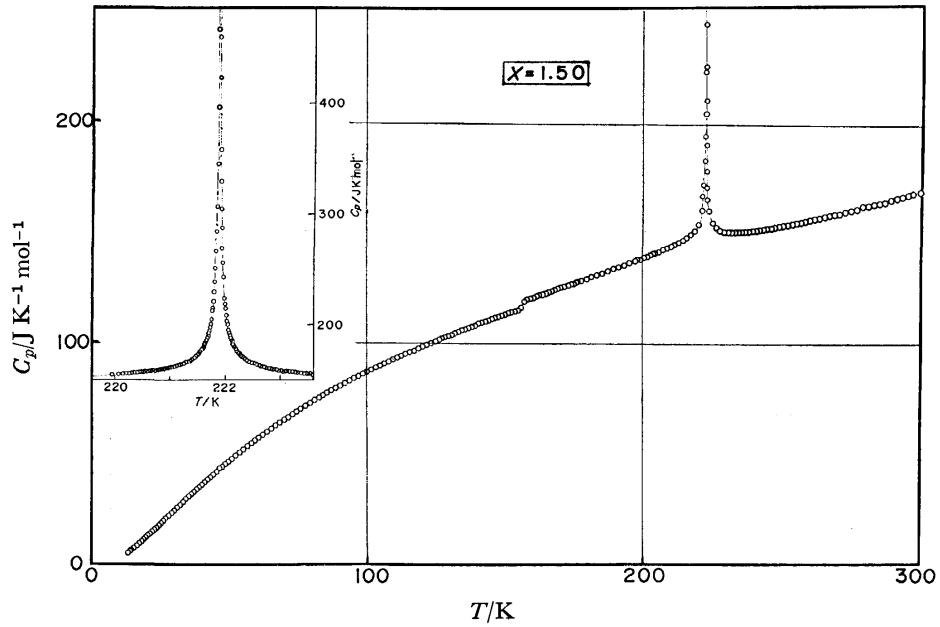

Fig. 5. Heat capacity of $x=1.50$. The inset shows an expanded view close to T_c.

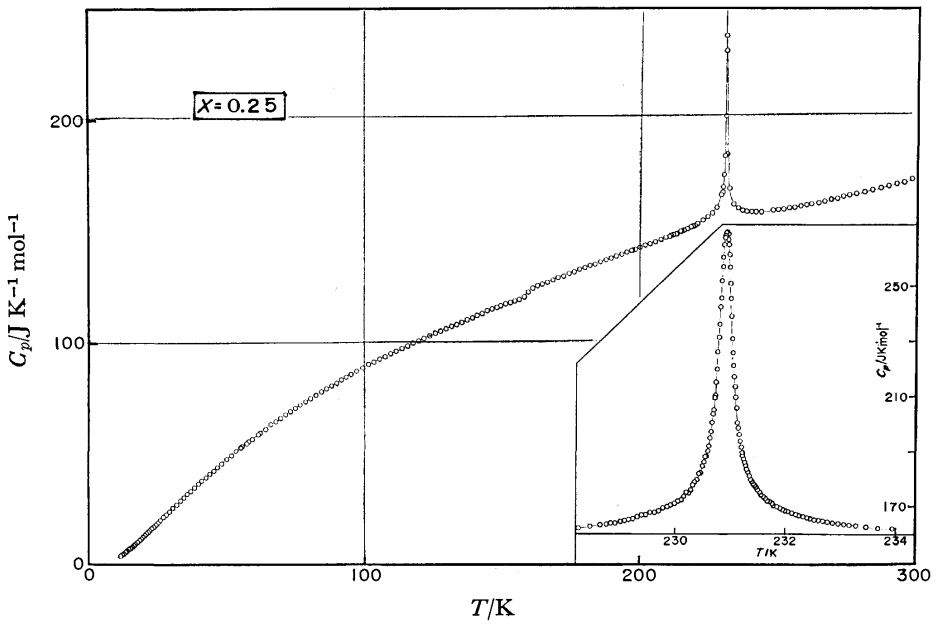

Fig. 6. Heat capacity of $x=0.25$. The inset shows an expanded view close to T_c.

of the apparent heat capacity. The latent heat absorbed quasi-isothermally was 33.12 J mol^{-1}. These behaviorsare similar to those observed for $x=2.00$. The heat capacity curve is given in Fig. 3.

(iv) $x=1.75$: Figure 4 shows the results of heat capacity measurements on this crystal. The transition temperature was 219.96 K. The first-order component was again observed at the transition temperature. The latent heat of transition is 29.24 J mol^{-1}. In the first measurement a small hump was observed around 224 K, some 4 K above the phase transition temperature. In view of the reproducibility of the small peak, presence of impurity in the calorimetric specimen was suspected. Therefore, the heat capacity was measured on a crystal having the same composition but prepared from TCD of a different commercial source. However, in the newly prepared crystal the shoulder appeared at the same temperature. Consequently it was concluded that this phenomenon was intrinsic in the crystal with the composition of $x=1.75$. In the temperature region of this anomally, it took longer time (about 100 min) for the equilibrium with the endothermic temperature drift of 0.3—0.6 mK during the drift period (about 1 h). The phenomenon was reproducible and depended on the pre-cooling condition. It was observed repeatedly when the crystal was cooled below the transition temperature prior to the measurement. When the measurement was started after coolling the sample crystal just 1 K above the transition temperature, the hump in the heat capacity and the associated endothermic effect were not observed.

(v) $x=1.50$: Although latent heat was not observed around the phase transition temperature 221.88 K, the crystal exhibited the highest peak of anomalous heat capacity (500

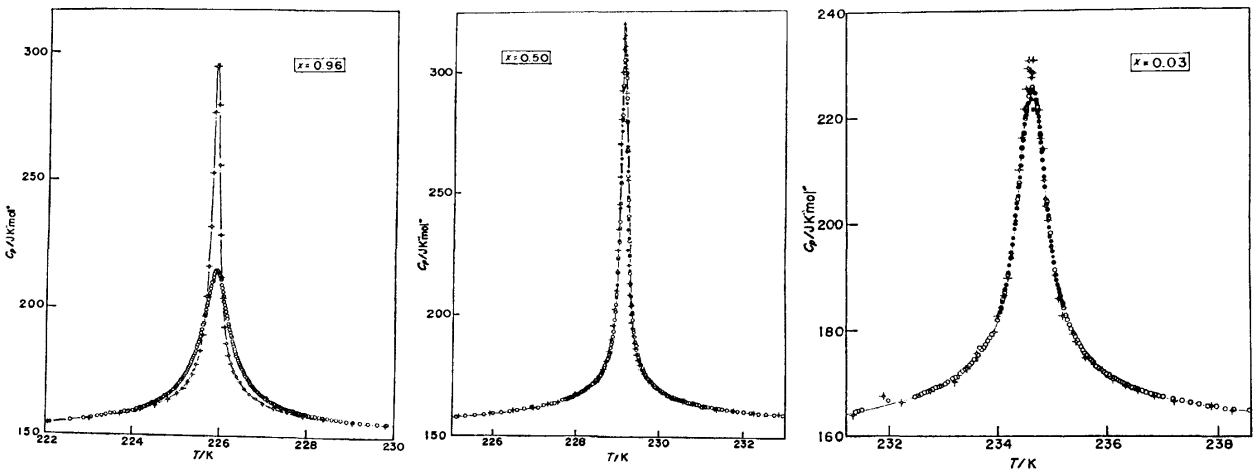

Fig. 7. Aging effect on heat capacity of (a) $x=0.96$, (b) $x=0.50$ and (c) $x=0.03$.
○ and ● : first measurement, -○- : measurement for aged crystals.

J K^{-1} mol^{-1}) among the crystals having no distinguishable first-order component. However, the equilibration time increased gradually up to 90 min with increase of the heat capacity. Rounding of the heat capacity peak was not observed. At 3 K above the peak temperature, the same phenomena as that found for $x=1.75$ appeared in the temperature drift but the heat capacity hump was not observed. The heat capacity curve is given in Fig. 5.

(vi) $x=0.96$: The anomalous heat capacity due to phase transition is located at 225.92 K and its maximum value is 220 J K^{-1} mol^{-1} which is smaller than those of any other crystal though the annealed crystal shows higher and sharper peak (see below). The peak was rounded within +0.2 K of the transition temperature. The rounding region is slightly wider than those of other crystals. The magnitude and the shape of the heat capacity are similar to those of $x=0.03$.

(vii) $x=0.50$: In this crystal the high resolution measurements were carried out twice before and after the cooling of the crystal down to nitrogen temperature, in order to check the effect of thermal history. Reproducibility of the heat capacity was excellent in all respects including the transition temperature, the maximum value of heat capacity and the rounding region. Rounding phenomenon was found within ±20 mK of the transition temperature (229.15 K) but the maximum of the heat capacity reached 290 J K^{-1} mol^{-1} and is larger than that of $x=0.96$. This corresponds to the narrower region of the peak rounding at this composition of the crystal.

(viii) $x=0.25$: The transition temperature is 230.92 K and the maximum of the peak is 260 J K^{-1} mol^{-1} which is intermediate between those of $x=0.96$ and $x=0.50$ (see Fig. 6). The rounding region is nearly the same as the case of $x=0.50$, and outside of this region the heat capacity due to phase transition is similar to that of $x=0.50$ in respect to the peak width and the sharpness. The measurements of $x=0.03$, $x=0.25$, $x=0.50$, and $x=0.96$ were performed within one month after the preparations of the single crystals. In order to study any effect of aging of the crystals we repeated high resolution measurements for these compositions near the transition temperatures. The sample crystal that had been measured before was used in the renewed measurement for $x=0.50$ and new single crystals of $x=0.03$ and $x=0.96$ were cut from the same ingot from which single crystals used in the earlier measurements were prepared. The time elapsed between the first and the second measurements were four years, ten months, and two years for the $x=0.03$, $x=0.50$, and $x=0.96$, respectively. The crystals had been kept in closed glass jars separately during these periods. For $x=0.96$ and $x=0.50$, the transition temperatures decreased by 30 and 10 mK. In view of the stability of the thermometers discussed earlier,[17] one can attribute the shifts of the transition temperatures to change in the isotopic compositions. The amount of the normal water that had replaced the heavy water during the aging was estimated from the change of the transition temperatures. They are 14 mg in the 47 g crystal of $x=0.96$ and 6 mg in the 60 g crystal of $x=0.50$. It would be reasonable to assume that water of these amount might well had been absorpted on the inner surface of the glass jars when the ingots of the crystal were placed in them and equilibrated with the mixed crystal during the storage. Figure 7 shows the aging effects in anomalous heat capacity of $x=0.96$, $x=0.50$, and $x=0.03$. The anomalous heat capacity in crystal $x=0.96$ increased by a factor of two and became sharper with accompanying the decrease of the rounding region. The peak height of $x=0.50$ increased 3% in the rounding region but the heat capacity was in agreement with the previous results within 0.1% outside the rounding region. In the crystal $x=0.03$ the anomalous heat capacity was reproduced (to 0.1%) in both the temperatures as well as the shape of peak.

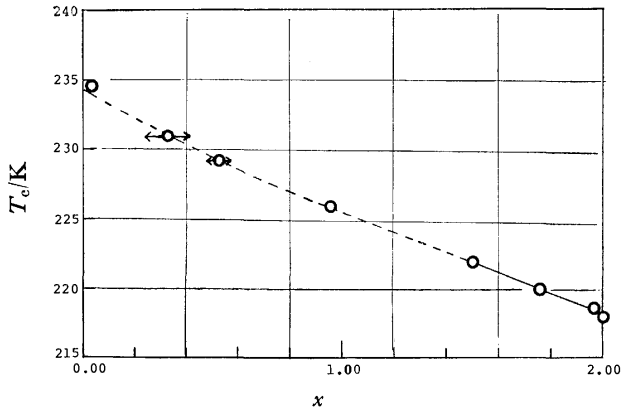

Fig. 8. Transition temperature *vs.* composition of the solid solution. The horizontal arrows indicate the ambiguity of estimation. Meaning of dashed line will be given in the forthcoming paper.

Dependence of Transition Temperature upon the Composition of Solid Solution. The isotope effect on the transition

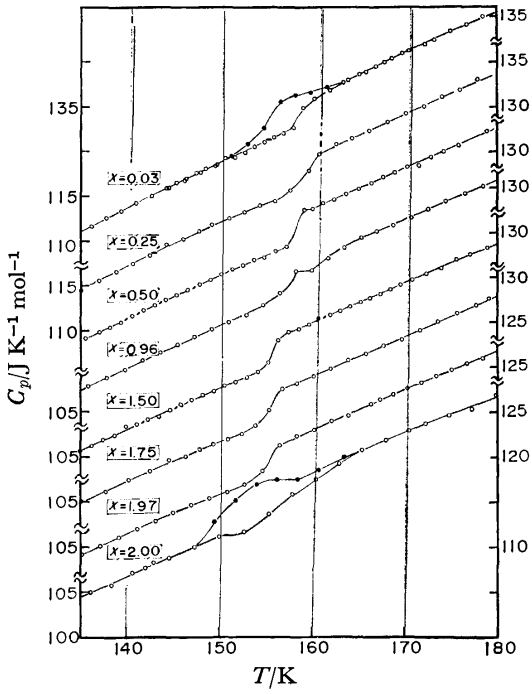

Fig. 9. Heat capacity curves in the region of glass transitions.
Cooling rate; —○— 1.7 K min^{-1}, —●— 0.01 K min^{-1}.

temperature of the present substance ($T_c^D/T_c^H=1.076$) is of the same order of magnitude as that of a group of hydrogen-bonded ferro- and antiferroelectrics such as $Cu(HCO_2)_2\cdot 4H_2O$,[14] $K_4Fe(CN)_6\cdot 3H_2O$,[19] TGS,[20] TGSe,[21] and Rochelle salt.[22] The relatively small change of T_c on deuteration suggests that the transition is associated with the ordering of the protonic position but is not related to the tunneling motion as in KDP.[23] Figure 8 shows a dependence of transition temperature upon the composition of solid solutions. The observed behavior of T_c against x for the present system is similar to that reported for TGS–DTGS[20] and TGSe–DTGSe[21] systems, where the transition temperature increases monotonously with increasing x.

Glass Transition. Figure 9 shows the heat capacities in the region of the glass transition for each of the crystals in which those of $x=2.00$ and $x=0.03$ are the results by Matsuo *et al.*[10] The glass transition temperature was found to depend on the isotopic composition (Fig. 10). Here, the glass transition temperature was defined as the temperature where the temperature drift changed from the exothermic to the endothermic.

Conclusion

We have thus shown that the heat capacities of the mixed crystals $SnCl_2(H_2O)_x(D_2O)_{2-x}$ exhibit two thermal anomalies for the entire range of the isotopic composition. The small isotope effect on the temperature of the relaxational anomaly ($T_g(H_2O)=152.9$ K and $T_g(D_2O)=158.8$ K) may be understood in terms of the smaller vibrational frequency of the deuterium atoms in comparison with the hydrogen. It is important to recognize that glass transition region of the mixed crystals does not split into two. This means that the motions of the hydrogenic atoms are strongly correlated with each other. They migrate in the

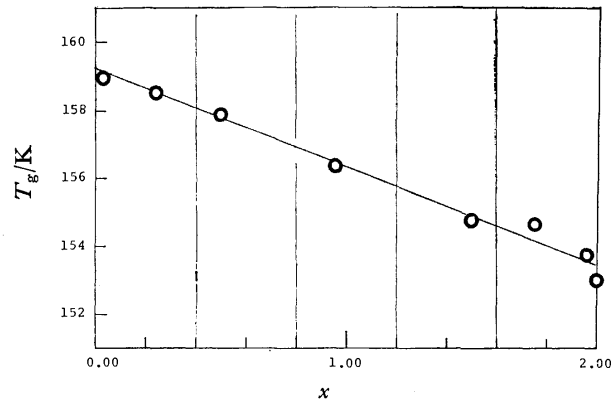

Fig. 10. Concentration dependence of the glass transition temperature.

crystal as a unit whose mobility depends on the local isotopic composition. It appears that the size of the correlation region is large enough that the local composition can be approximated well by the average composition. The smallest unit, and as such the most probable one, is the eight-membered ring of the hydrogen-bonded water molecules, as pointed out previously in relation to the ice condition.[10] The molecular model proposed earlier for the pure $SnCl_2\cdot 2H_2O$ and $SnCl_2\cdot 2D_2O$ thus fits in with the present result on the mixed crystals. Probably the most interesting property of the phase transition in the solid solution is that the first-order component disappears at the composition of 25% deuterium. The disappearance of the first-order nature is not due to inhomogeneity of the isotopic concentration. For, if this were the case, we would have observed the first-order transition also in the D_2O-rich crystals because the compositional inhomogeneity is small here again. The experimental fact is that the rounding of the anomalous heat capacity of $x=0.03$ is most extensive. Aging of the crystal for four years did not alter this result. The glass transition at 150 K indicates that the motion of the hydrogen atoms at the transition temperature, ≈ 220 K, is rapid enough that they find the equilibrium distribution during the experimental time scale, provided that possible nonuniformity in the initial isotopic distribution has been homogenized by the aging. The existence of the first-order component in the H_2O-righ crystals, its disappearance around $\approx 25\%$ D_2O concentration and the gradual increase of rounding of the anomalous heat capacity in the D_2O-rich region are the principal results of the present high resolutional measurements. The correspondence between the liquid-vapor critical point and the phase transition in TCD discussed above has been hinted upon from the structural data. The thermodynamic measurement presented in this study give strong support to the analogy. In the subsequent paper the experimental result will be analysed and discussed in terms of this correspondence.

References

1) H. Kiriyama and R. Kiriyama, *J. Phys. Soc. Jpn.*, **28**, Suppl., 114 (1970).

2) H. Kiriyama, K. Kitahama, O. Nakamura, and R. Kiriyama, *Bull. Chem. Soc., Jpn.*, **46**, 1389 (1973).
3) R. Kiriyama, H. Kiriyama, K. Kitahama, and O. Nakamura, *Chem. Lett.*, **1973**, 1105.
4) H. Morisaki, H. Kiriyama, and R. Kiriyama, *Chem. Lett.*, **1973**, 1061.
5) C. H. Wang, M. Tatsumi, T. Matsuo, and H. Suga, *J. Chem. Phys.* **67**, 3097 (1977).
6) H. Kiriyama, O. Nakamura, and R. Kiriyama, *Chem. Lett.*, **1976**, 689.
7) K. Kitahama and H. Kiriyama, *Bull. Chem. Soc. Jpn.*, **50**, 3167 (1977).
8) R. Brout, "Phase Transitions," Benjamin Inc., (1965).
9) T. Matsuo, M. Tatsumi, H. Suga, and S. Seki, *Solid State Commun.*, **13**, 1829 (1973).
10) T. Matsuo, M. Oguni, H. Suga, S. Seki, and J. F. Nagle, *Bull. Chem. Soc. Jpn.*, **47**, 57 (1974).
11) S. R. Salinas and J. F. Nagle, *Phys. Rev.*, **B9**, 4920 (1974).
12) P. W. Kasteleyn, *J. Math. Phys.*, **4**, 287 (1963).
13) M. Reiner, *Physics Today*, **17**, 62 (1964).
14) T. Matsuo, M. Kume, H. Suga, and S. Seki, *J. Phys. Chem. Solids*, **37**, 499 (1976).
15) K. Hamano, K. Ema, and Y. Iwana, *J. Phys. Soc. Jpn.*, **44**, 933 (1978).
16) M. Tatsumi, T. Matsuo, H. Suga, and S. Seki, Subsequent paper.
17) M. Tatsumi, T. Matsuo, H. Suga, and S. Seki, *Bull. Chem. Soc. Jpn.*, **48**, 3060 (1975).
18) M. Tatsumi, T. Matsuo, H. Suga, and S. Seki, *J. Phys. Chem. Solids*, **39**, 427 (1978).
19) M. Oguni, T. Matsuo, H. Suga, and S. Seki, *Bull. Chem. Soc. Jpn.*, **48**, 379 (1975).
20) B. Brezina and F. Smutny. *Czech, J. Phys.*, **B18**, 393 (1968).
21) K. Gesi, *J. Phys. Soc. Jpn.*, **41**, 565 (1976).
22) J. Habluetzel, *Helv. Phys. Acta*, **12**, 489 (1939).
23) B. A. Strukov, A. Baddur, V. A. Koptsik, and I. A. Velichko, *Sov. Phys. Solid State*, **14**, 885 (1972).

Phase Transition of $SnCl_2(H_2O)_x(D_2O)_{2-x}$ as Studied by High Resolution Heat Capacity Measurement

Masami TATSUMI, Takasuke MATSUO, Hiroshi SUGA, and Syûzô SEKI*
Department of Chemistry, Faculty of Science, Osaka University, Toyonaka, Osaka 560
(Received September 28, 1978)

The previously published heat capacity data on $SnCl_2(H_2O)_x(D_2O)_{2-x}$ (x=2.00, 1.97, 1.75, 1.50, 0.96, 0.50, 0.25, 0.03) were analyzed to derive anomalous contribution due to the phase transitions that occur between 218 and 235 K depending on the isotopic composition. The phase transition is of the first-order for x=2.00, 1.97, and 1.75. The entropy discontinuities at the transitions are (0.149±0.005), (0.152±0.005), and (0.133±0.010) J K^{-1} mol^{-1}, respectively, out of the total transition entropies of 3.98, 3.90, and 3.89 J K^{-1} mol^{-1}. The first-order transition does not occur for the other crystals for which the heat capacity anomaly is rounded. Apparent critical exponent α of the heat capacity was calculated for all of the crystals. They are in the range from 0.43 to 0.80 and have the same value below and above the transition temperature for each of the crystals in agreement with the spatial two dimensionality of the crystal structure. No evidence was found for crossing-over to the three dimensional ordering. Change of the transitional behavior with the isotopic composition was discussed in analogy with the liquid-vapor critical phenomenon. An argument based on the crystallographic symmetry of the actual crystal and the corresponding dimer lattice was advanced for this interpretation of the unusual isotope effect.

In the previous paper[1] we reported on the high resolution measurement of the heat capacity of the solid solution system $SnCl_2(H_2O)_x(D_2O)_{2-x}$ in which the heat capacity was measured from 10 to 300 K with an adiabatic calorimeter that is capable of measurement with a temperature step smaller than 10 mK. We obtained the following result from the measurement. The phase transition temperature defined as the temperature of the entropy discontinuity or, in case of absence of the discontinuity, as the temperature of the maximum of the heat capacity, increased smoothly from 218.0 to 234.6 K as the deuterium content increased from the natural abundance to 98.5%. The anomalous heat capacity became broader at the same time. Small first-order transition portion was found in the hydrogen-rich solid solutions, x=2.00, x=1.97, and x=1.75. In order to reveal their differences, the anomalous heat capacities are displayed in Fig. 1 as a function of reduced temperature T/T_c. Increasing the proton concentration x tends to increase sharpness of the anomalous heat capacity. The heat capacities of x=2.00 and x=1.97 and also x=1.50, x=0.96, x=0.50, and x=0.25 lie on the same smooth curves, respectively.

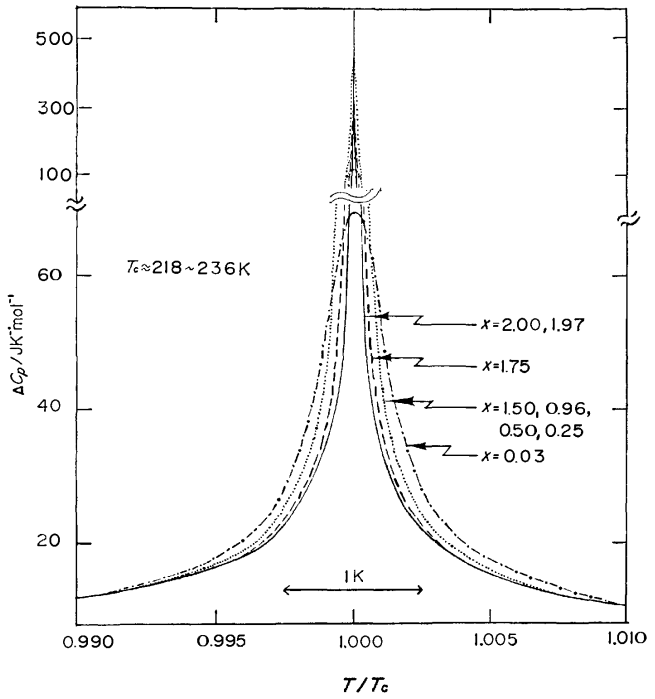

Fig. 1. Anomalous heat capacity (ΔC_p) *versus* reduced temperature (T/T_c).

Annealing effect was found in the crystal with x=0.96 (annealing period; two years), but not for x=0.50 (ten months) and x=0.03 (four years). The difference in the annealing behavior is due partly to the difference in the time intervals between the crystal preparation and the first measurement and partly to the difference in the isotopic composition. Naturally one does not expect much inhomogeneity in the x=0.03 crystal because only 1.5% of the deuterium is replaced by hydrogen. It will be significant that this crystal exhibits extensive rounding while the conjugate crystal (x=1.97) has a first-order transition without any rounding. Thus, inhomogeneous distribution of the isotopes did contribute to the rounding but it was removed by annealing.

It was concluded that the first-order transitions in the hydrogen-rich crystals and the rounded heat capacity in the deuterium-rich ones are genuine equilibrium properties of the solid solutions. This conclusion will be corroborated later by the smooth and regular behavior of the entropy surface as a two-dimensional function of the temperature and the isotope composition. It is to be noticed in particular that the behavior of the crystal is asymmetric with respect to the substitution of deuterium for hydrogen. In this paper, we will analyse the heat capacity data with an emphasis on the isotope effect on the phase transition.

We showed in earlier papers[2-4] that the first-order transition in $Cu(HCO_2)_2\cdot 4H_2O$ remains of the first-order when the H_2O is replaced by D_2O, and the second-order transition in $K_4Fe(CN)_6\cdot 3H_2O$ remains to be second-order after similar substitution. The isotope effects on the transition temperature are of the same magnitude for these three substances and are much

smaller than in *e.g.* KH_2PO_4 where tunneling motion of the proton is incorporated. Disappearence of the first-order transition is thus the most unique aspect of the isotope effect in this solid solution system.

Salinas and Nagle[5] reported a statistical mechanics of the phase transition of $SnCl_2 \cdot 2H_2O$ (TCD), using the isomorphism between the proton distribution allowed by the Bernal-Fowler ice condition and close-packed dimer distribution on the 4—8 lattice. The theory succeeded in predicting the correct ground state configuration of the proton arrangement and reproducing the symmetrical heat capacity anomaly characteristic of the two-dimensional system. However, quantitative prediction of the theory—logarithmic divergence of the heat capacity— was not supported by the experiment.

Determination of the Critical Parameters. The heat capacity C is assumed to have the asymptotic form near the critical temperature T_c,

$$C = (A/\alpha)(|t|^{-\alpha}-1)(1+D|t|^{\beta}) + B + Et, \qquad (1)$$

where

$$t = (T-T_c)/T_c$$

is the reduced temperature. The parameters A, B, D, E, α, β are allowed to take different values above and below T_c. In the latter case, the primed notations are used. The term $(A/\alpha)|t|^{-\alpha}$ represents the leading contribution to the singularity of C. The positive value of α corresponds to a heat capacity diverging to infinity. The smaller the magnitude of α, the sharper the heat capacity becomes and it is called weaker divergence. Negative value of α corresponds to a cusped singularity where the heat capacity curve has an infinite slope but finite value. In the case of $\alpha=0$, there are two possibilites. One is the logarithmic divergence and the other a finite discontinuity. $D|t|^{\beta}$ is the correction term which represents a singular contribution that vanishes at T_c. The lattice contribution to the heat capacity is expressed by the last two terms, $B+Et$, where the constant B may contain a contribution associated with the phase transition.

We calculated the critical exponents from the experimental data in the range of $|t| \leq 10^{-2}$. The first-order phase transition and rounding were excluded from the fitting. The discontinuous increase of the entropy at the first-order transition is about 4% of the total transition entropy and was disregarded for this purpose.

To simplify the fitting procedure, we imposed several constraints. We assumed that the correction term is negligible, $D=D'=0$. The lattice contribution in Eq. 1 was assumed to be smooth through the transition. This assumption should be more legitimate for this crystal than is usual for other crystal because there is no major change in the crystal structure at the transition.[6] We put $E=E'$ and $B=B'$. The latter term includes the quantity $-A/\alpha$. Thus the final form used in the fitting is

$$C = (A/\alpha)|(T-T_c)/T_c|^{-\alpha} + B + ET. \qquad (2)$$

The terms B and E in this equation have slightly different meaning from that in Eq. 1. Determination

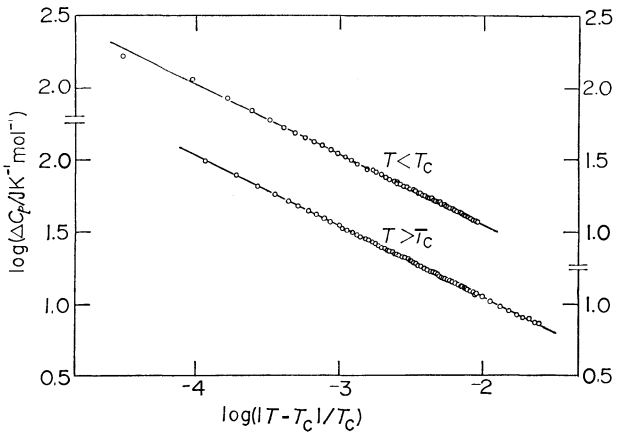

Fig. 2. Logarithmic plot of the anomalous heat capacity of $SnCl_2(H_2O)_{2.00}(D_2O)_0$.

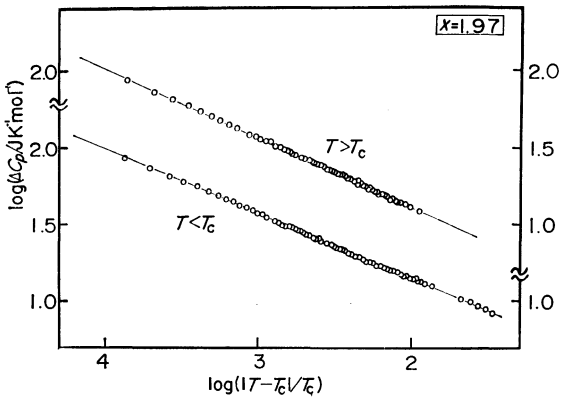

Fig. 3. Logarithmic plot of the anomalous heat capacity of $SnCl_2(H_2O)_{1.97}(D_2O)_{0.03}$.

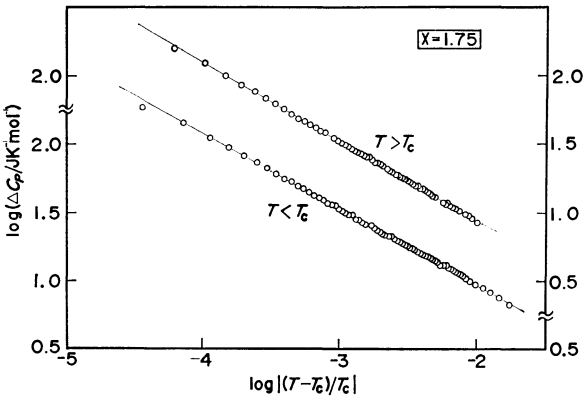

Fig. 4. Logarithmic plot of the anomalous heat capacity of $SnCl_2(H_2O)_{1.75}(D_2O)_{0.25}$.

of the lattice terms $B+ET$ is discussed in appendix II.

The $\log\{C_p-(B+ET)\}$ was plotted as a function of $\log|(T-T_c)/T_c|$ for various values of T_c and B. The best combination was chosen with the linearity of the plot as the measure of the good fit. Combined uncertainty in α due to uncertainty in determining T_c and the lattice heat capacity would be about 5% of its value.

For $|t|>10^{-2}$, the plot deviated from Eq. 2. This may imply that contribution from the higher

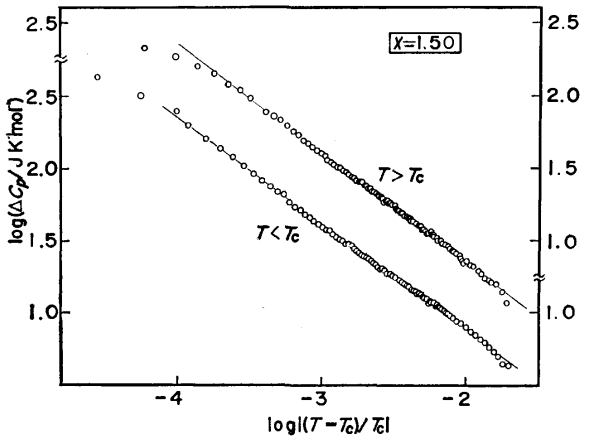

Fig. 5. Logarithmic plot of the anomalous heat capacity of $SnCl_2(H_2O)_{1.50}(D_2O)_{0.50}$.

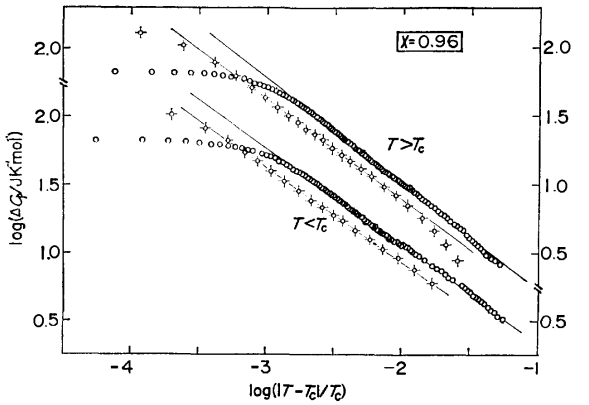

Fig. 6. Logarithmic plot of the anomalous heat capacity of $SnCl_2(H_2O)_{0.96}(D_2O)_{1.04}$. ○: $x=0.96$, -○- : $x=0.96$(II).

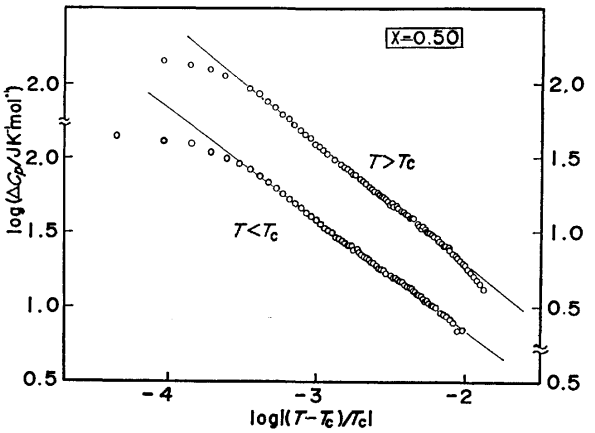

Fig. 7. Logarithmic plot of the anomalous heat capacity of $SnCl_2(H_2O)_{0.50}(D_2O)_{1.50}$.

order correction terms is significant and/or that the lattice heat capacity deviates from the assumed linearity in T. This is not a serious problem as far as determination of α is concerned. Figures 2—9 show the logarithmic plots for the crystals $x=2.00$ to 0.03. The plot for $x=2.00$ is reproduced here for the sake of completeness.[7]

Rounding of the anomalous heat capacity and hence deviation of the logarithmic plot from the linearity in

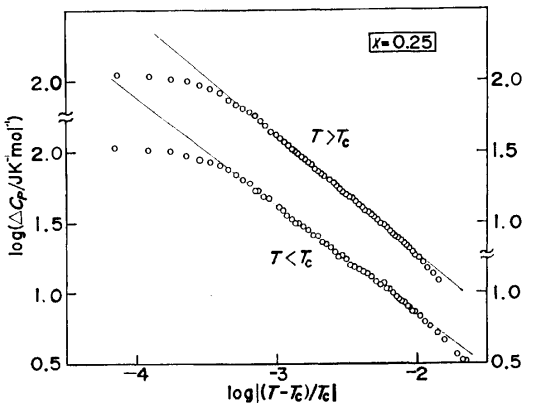

Fig. 8. Logarithmic plot of the anomalous heat capacity of $SnCl_2(H_2O)_{0.25}(D_2O)_{1.75}$.

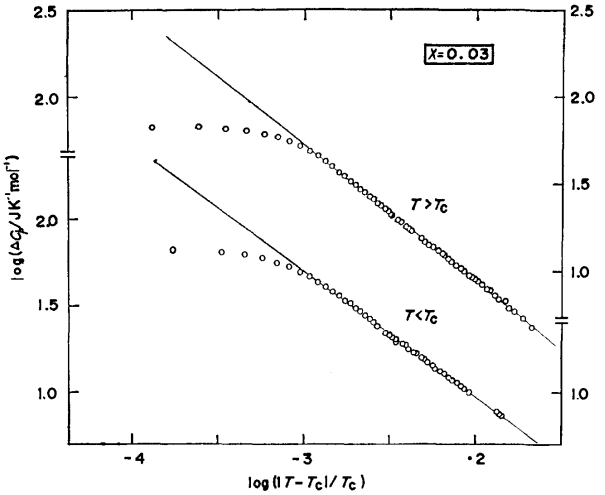

Fig. 9. Logarithmic plot of the anomalous heat capacity of $SnCl_2(H_2O)_{0.03}(D_2O)_{1.97}$.

the small $|t|$ region occurs for the crystals $x=1.50$, 0.96, 0.50, 0.25, and 0.03. The rounding of the first crystal is limited to $|t|<10^{-4}$ and those of the second, third, and fourth were to $|t|\leq 3\times 10^{-4}$. The last crystal had a wider rounding region $|t|\leq 10^{-3}$. It is interesting to remember that in most magnetic transitions a larger rounding region occurs below T_c than above. Heller[8] pointed out that this may be an intrinsic effect related with the formation of domain structure. The rounding in the present crystal occurs in the same temperature interval on both sides of the transition temperature and cannot be due to a domain structure.

We attempted to interpret the rounding on an assumption that the crystal behaves as if it were composed of microcrystals which have distributed transition temperatures.[9] The heat capacity of the entire crystal is then given by

$$C(T,\ T_c) = \sum_i C(T,\ T_{ci}) f(T_c,\ T_{ci}) / \sum_i f(T_c,\ T_{ci}), \qquad (3)$$

where $C(T,T_{ci})$ is the heat capacity at T of a microcrystal having the transition temperature T_{ci}. This is assumed to have the form of Eq. 2. $f(T_c,T_{ci})$ is the distribution function of the critical temperature T_{ci} and assumed to be gaussian centering at T_c.

TABLE 1. SUMMARY OF CRITICAL PARAMETERS

	T_c/K	α'	α	α'/α	A' / J K^{-1} mol^{-1}	A / J K^{-1} mol^{-1}	A'/A	$C_{p_{max}}$ / J K^{-1} mol^{-1}	S_∞ / J K^{-1} mol^{-1}
$x=2.00$	218.01	0.492	0.492	1.000	0.568	0.565	1.005	∞	3.98
$x=1.97$	218.22	0.434	0.451	0.962	0.793	0.720	1.101	∞	3.90
$x=1.75$	219.96	0.573	0.579	0.990	0.389	0.354	1.099	∞	3.89
$x=1.50$	221.88	0.731	0.757	0.966	0.200	0.168	1.192	571	4.02
$x=0.96$	225.92	0.720	0.765	0.941	0.287	0.233	1.228	214	—
$x=0.96$(II)	225.89	0.696	0.733	0.950	0.238	0.194	1.225	295	4.05
$x=0.50$	229.15	0.747	0.785	0.952	0.165	0.134	1.230	306	3.86
$x=0.50$(II)	229.14	—	—	—	—	—	—	316	—
$x=0.25$	230.92	0.753	0.754	0.999	0.168	0.134	1.251	269	3.95
$x=0.03$	234.64	0.730	0.778	0.938	0.228	0.170	1.341	226	4.02
$x=0.03$(II)	234.64	—	—	—	—	—	—	231	—

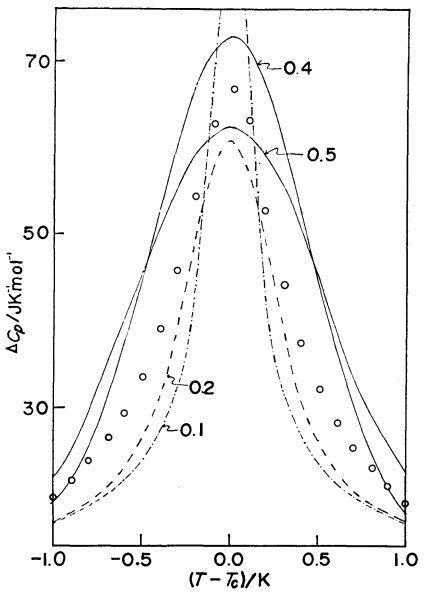

Fig. 10. Comparison of the experimental heat capacity with the model calculation assuming gaussian distribution of T_c. The numbers are the values of adjustable parameter corresponding to the half-width d of the gaussian distribution.

Some of the results for $x=0.96$ are shown in Fig. 10. Evidently the fit is very poor. A similar attempt[10] on KDP was also reported to be unsuccessful. If one wishes to save the model of the distributed transition temperature, one would have to modify Eq. 2 and/or Eq. 3. Modification of Eq. 2 is not acceptable because it describes the heat capacity of the $x=2.00$ crystal accurately. On the other hand, it is impossible to refute every modification of the distribution function in Eq. 3. However, so far as the model was applicable at all, it was applicable with the gaussian distribution.[11]

It will not be fruitful to look for the distribution function that reproduces the experimental result. Distributed T_c implies, as an underlying picture, quenched distribution of chemical or physical impurities and inhomogeneities in the crystal. In view of the manner in which the eight crystals were prepared, the only possibility is the inhomogeneity of the isotope distribution. This inhomogeneity was leveled off

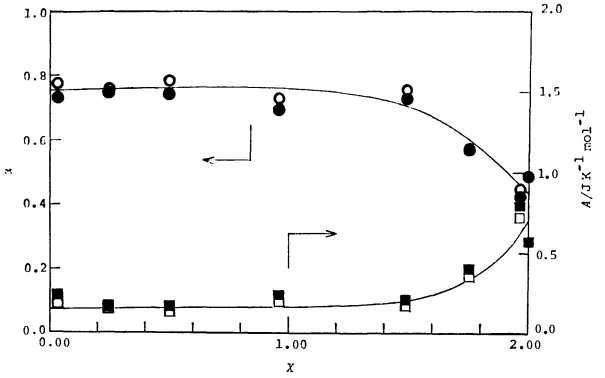

Fig. 11. Composition dependence of the critical parameters. ●: α', ○: α, ■: A', □: A.

by annealing (see Ref. 1). It is important to note that occurrence of the phase transition contradicts the assumption of quenched distribution of the isotopes. The phase transition occurs because the protons (or deuterons) jump around in the hydrogen bonded layer, not just among a few localized states. We conclude that the model of distributed transition temperature is not appropriate for the present crystal.

Recently, it was suggested from dielectric measurement[12,13] that TCD shows a cross-over from two to three dimensional ordering around $t=10^{-3}$. However, the logarithmic plot of the heat capacity is smooth without any irregularity. This is true not only for the $x=2.00$ crystal but also for all of the other crystals except the $x=0.03$ crystal for which the rounding extends out to this region.

The critical parameters thus determined are given in Table 1 and Fig. 11. The critical exponent has the same value below and above T_c as expected from the symmetric shape of the heat capacity curves. In the region where the rounding is appreciable, physical meaning of the critical exponent is not clear because the region of small t where Eq. 2 is expected to be most appropriate is excluded from the fitting. However, the logarithmic plot is on a straight line over more than a decade of $|t|$ even for the most rounded case. Its physical meaning will be hopefully understood in future. The α values are in the range 0.43—0.8. They are much larger than typical value for magnetic systems. Comparable magnitude of α are

TABLE 2. SOME GRADUAL PHASE TRANSITIONS

Substance	T_c/K	ΔS/J K^{-1} mol^{-1}	ΔS_{jump}/J K^{-1} mol^{-1}	$\Delta S_{jump}/\Delta S$	Ref.[a]
KH_2PO_4	121.71	3.33	0.379	0.114	(a)
KD_2PO_4	219.62	3.80	2.001	0.527	(b)
TlH_2PO_4	229.76	1.80	0.25	0.14	(c)
KH_2AsO_4	96.15	4.2	3.1	0.75	(d)
KD_2AsO_4	161.02	4.2	3.5	0.84	(d)
CsH_2AsO_4	146.23	4.4	2.7	0.61	(e)
NH_4HgCl_3	54.97	5.6	1.1	0.20	(f)
ND_4HgCl_3	58.26	5.7	1.2	0.21	(f)
$SnCl_2 \cdot 2H_2O$	218.01	3.98	0.149	0.0374	present study
$SnCl_2(H_2O)_{1.97}(D_2O)_{0.03}$	218.22	3.90	0.152	0.0390	present study
$SnCl_2(H_2O)_{1.75}(D_2O)_{0.25}$	219.96	3.89	0.133	0.0342	present study
$SnCl_2(H_2O)_{1.50}(D_2O)_{0.50}$	221.88	4.02	0.00	0	present study

a) (a) Ref. 10, (b), Ref. 14, (c) T. Matsuo and H. Suga, *Solid State Commun.*, **13**, 1829 (1973), (d) C. W. Fairall and W. Reese, *Phys. Rev. B*, **6**, 193 (1972), (e) M. Deutsch and E. Litov, *Ferroelectrics*, **7**, 209 (1974), (f) H. Kitano, Master's Thesis; Osaka University (1977).

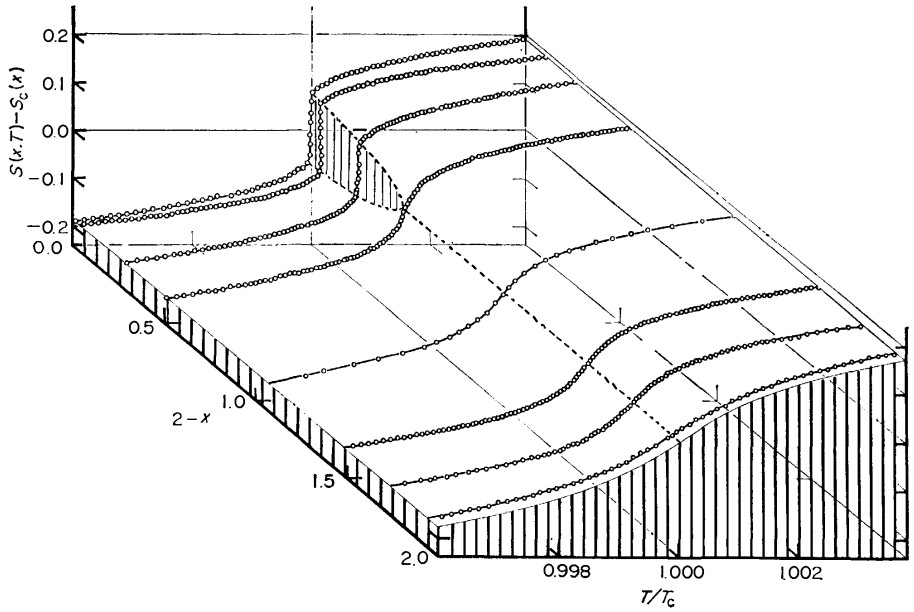

Fig. 12. Anomalous entropy of $SnCl_2(H_2O)_x(D_2O)_{2-x}$ *versus* temperature and isotopic composition.

found in KDP,[10] DKDP,[14] NH_4Cl,[15] NH_4Br,[16] and $NaNO_2$.[17] The crystals with $x=2.00$ and $x=1.97$ resemble KDP with respect to the value of α and occurrence of the first-order phase transition, but do not exhibit the logarithmic singularity which KDP[18] does. This indicated that dominant interaction in TCD is strong short-range forces that express themselves as the ice condition.

Order of the Phase Transition and Entropy Change near the Transition Temperature. It is often noticed that thermal equilibrium in the crystal is attained very slowly at a first-order transition. This is usually attributed to slow progress of the first-order transition. In the present study, slow equilibration was observed in the crystals with high hydrogen content. At the transition temperature of the crystals of $x=2.00$, 1.97, and 1.75, the equilibration time was 5—7 times as long as those in the normal temperature region. Such anomalous equilibration behavior was not found in the crystals with $x=0.96$, 0.50, 0.25, and 0.03. The crystal $x=1.50$ was the boundary case where the long equilibration time was observed only at one point of the measurement at the peak of the transition. A more quantitative evidence of the change in character of the phase transition with increasing deuterium content is shown in Fig. 12 as the anomalous entropy plotted as a function of the temperature and the isotopic composition. The surface was calculated by integration of the anomalous heat capacity divided by T. Evidently the transition is of the first-order for $x=2.00$, 1.97, and 1.75. The entropy discontinuities for these three crystals are (0.149±0.005), (0.152±0.005), and (0.133±0.010) J K^{-1} mol^{-1}, respectively. The crystal with $x=1.50$ did not show distinct jump, but as noted above its equilibration behavior was similar to that of the crystal with the first-order transition. Thus $x=1.50$ corresponds to the critical composition where the first-order transition disappears.

We shall change subject for a while to the problem of classification of phase transitions. A phase transition

is of the n'th order if the n'th derivative of the free energy is discontinuous at the phase transition. This is the classification due to Ehrenfest. Discontinuity in the higher-order derivative is not easy to detect experimentally. Therefore, phase transitions which are not of the first-order are classified collectively as the higher-order. This classification is not general enough to be applicable to all of the phase transitions, since it does not contain the divergent anomalies.

In another classification, a phase transition is called isothermal if it occurs at a fixed temperature, and gradual if the anomaly occurs over a range of temperature. An isothermal transition is of the first-order, but gradual transition can be of the first-order, higher-order or divergent type. This classification is more convenient than the first classification, because gradual first-order transitions are more closely related to higher-order and divergent transitions than to the strictly first-order transitions. The first-order transitions are divided into strongly first-order and weakly first-order.

As a quantitative measure of the strength of the "first-orderedness," we propose the entropy discontinuity divided by the total transition entropy. Thus the fusion of a pure substance is a strongly first-order transition because all of the entropy change occurs at the melting temperature. In Table 2 we collected some of the weakly first-order transitions of ferroelectric and related substances including the present crystals. It is interesting that, so far as is known, magnetic transitions are rarely of weakly first-order. It should be added that we singled out the entropy from among other thermodynamic quantities that may possibly behave anomalously at the transition. This is because this quantity is amenable to direct experimental measurement irrespective of the atomic mechanism of the transition so far as we choose the temperature as the independent variable.

Comparison with the Dimer Model Calculation. Salinas and Nagle[5] gave an expression for the internal energy of the dimer model. We calculated the heat capacity C from the energy U,

$$C=\mathrm{d}U/\mathrm{d}T. \tag{4}$$

The explicit expression is too lengthy to be reproduced here. For the sake of checking the calculation, we computed S_∞ numerically from the equation

$$S_\infty=\int_0^\infty (C/T)\mathrm{d}T, \tag{5}$$

using the heat capacity given above. The result agreed with the direct calculation[19] given earlier, $S_\infty/R=0.3769956\cdots$. Figure 13 compares the experimental heat capacity with the dimer model calculation. The calculated heat capacity is too sharp, corresponding to the logarithmic divergence as noted by Salinas and Nagle.[5] However, agreement between the experiment and the theory is excellent at 150 K where the glass transition (see Appendix I) allowed determination of the lattice heat capacity without ambiguity. The experimental entropy at $T=T_c$ and $T=2T_c$ are (3.00 ± 0.12) and (3.94 ± 0.23) J K^{-1} mol^{-1}, respectively, for the $x=2.00$ crystal. These are compared with the dimer model calculation $S(T_c)=2.34$ and $S(2T_c)=3.02$ J K^{-1} mol^{-1}.

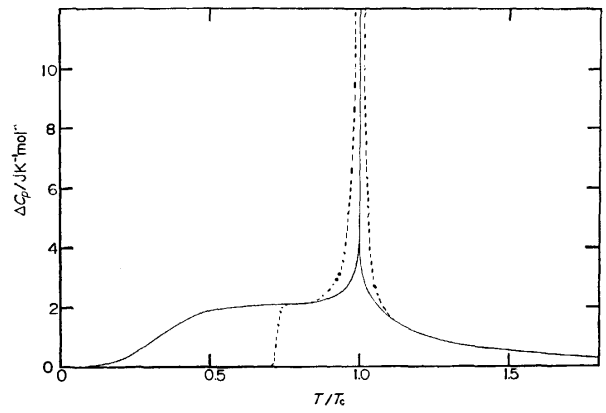

Fig. 13. Comparison of the heat capacity of $SnCl_2\cdot 2H_2O$ with the dimer model calculation.

Problem of Tricritical or Bicritical Phenomenon. In this section we are concerned with interpretation of the disappearance of the first-order transition in the deuterium-rich crystals. In order to be sufficiently general, we consider a phase diagram in three dimensions.[20] A first-order phase transition is described by a coexistence surface in the space. The coexistence surface may terminate in following ways. i) The coexistence surface intersects another coexistence surface in a triple line at which three phases are in equilibrium. ii) The coexistence surface passes into another surface which continues to separate two phases but which has the property that all extensive variables are continuous at the surface. iii) The coexistence surface terminates in a line of critical point. In the two dimensional phase diagram, these three correspond to i) triple point, ii) tricritical point and iii) bicritical point. Our result corresponds to ii) or iii).

a) Tricritical Point: The three axes in the phase diagram are temperature T, the field η conjugate to the order parameter and a secondary variable ζ. η is often a fictious field uncontrollable in the laboratory. For instance we have no direct means of controlling the orientational order of the ammonium ion in NH_4Cl crystal. ζ is taken as a controllable variable such as pressure, magnetic field or chemical potential. The phase diagram looks schematically like Fig. 14. The three curves meeting at the tricritical point represent

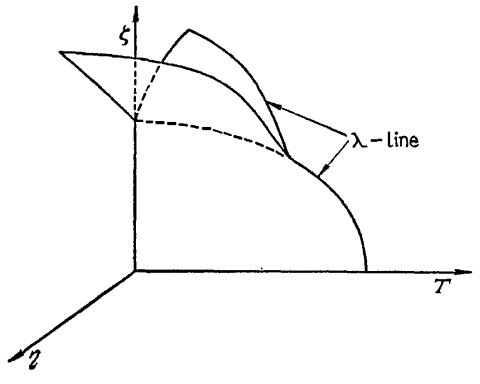

Fig. 14. Schematic phase diagram of a system with a tricritical point.

lines of the critical point. The three coexistence surfaces meets in a line of triple point represented by the broken line. The surface at $\eta=0$ is the coexistence surface of the positively and negatively ordered phases.

The behavior of $SnCl_2(H_2O)_x(D_2O)_{2-x}$ appears to fit in well with the phase diagram if one identifies the ζ axis with the isotopic concentration. The first-order transition line (the broken line) disappears as the tricritical point is approached by changing the ζ value.

However, there is a difficulty in this correspondence arising from the peculiarity of this crystal. We cannot define order parameters because the symmetry of the two phases involved are the same. Therefore, it is impossible to define its conjugate field η.

In order to illustrate the point, we shall take NH_4Cl as an example. The two phases coexisting on the surface $\eta=0$ are related with each other by changing the orientation of all the ammonium ions by 90° relative to the crystal axis. In the disordered phase this produces an equivalent state. Such an operation is not possible in TCD. A proton in the crystal occupies one of the seven sites but none of them are equivalent with each other. Tricritical points have been discussed in NH_4Cl,[21] ND_4Cl,[22] NH_4Cl–NH_4Br,[23] and other systems where a first-order transition changes to a higher-order one as an external parameter changes. The same argument can not be applied in the present case in spite of the similarity of the thermodynamic behavior.

b) Bicritical Point and Super Critical State: This type of critical point always exists in a simple liquid-vapor system. If one chooses an appropriate path in the pressure-temperature plane, one can obtain vapor phase from the liquid phase without discontinuity. This is possible because the vapor and liquid have the same spatial symmetry.[24] The same would be true in the crystalline state. Non-existence of the critical point between liquid and crystal was rationalized by the same argument.[24] In the case of TCD, Kiriyama *et al.*[25] showed that the space group $P2_1/c$ and the unit cell size remain the same as the crystal undergoes the phase transition. This is a very peculiar property of this crystal, since change of symmetry is believed to be the most essential characteristic of solid state phase transitions in general. On the other hand, thermodynamic property of this phase change is also unusual. As shown in Fig. 12 the first-order transition disappears at $x\simeq 1.5$, beyond which the heat capacity is rounded and genuine singularity does not occur any more. This behavior is similar to that of a simple liquid-vapor system at least qualitatively. The region $x\geq 1.5$ where the first-order transition occurs corresponds to subcritical region and the region $x<1.5$ to the supercritical region.

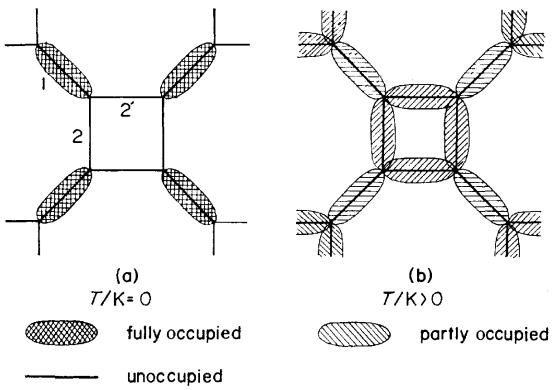

Fig. 15. Dimer distribution at $T=0$ K (a) and $T>0$ K (b) on the 4—8 lattice.

Thus, two peculiarities of the phase transition in TCD, one crystallographic and the other thermodynamic, are interpreted coherently by an analogy with the liquid-gas critical point. At present, however, how the correspondence comes about between the isotope concentration in TCD and pressure in the liquid-vapor system is not understood.

It will be pertinent here to point out that a phase transition is possible at all between two phases of the same spatial symmetry. As an example we show in Fig. 15 a part of the dimer lattice studied by Salinas and Nagle.[5] Figure 15(a) shows the distribution of the dimers at 0 K where all of the dimer sites (1) and none of the (2) and (2′) are occupied. Two dimensional space group of this distribution is P4mm. At higher temperature, some of the dimers occupy the sites (2) and (2′) as shown in Fig. 12(b). This dimer distribution has the space group P4 mm again. Salinas and Nagle showed there is a phase transition between (a) and (b) in the sense that the thermodynamic function behaves singularly at a temperature determined by the energy of the dimer site (2) and (2′). It is evident that the low-temperature-phase is more ordered than the high-temperature-phase because it has a lower entropy. However we cannot define the order parameter for this lattice, since there is no symmetry breaking coordinate. Difficulty of defining order parameters in some dimer lattices was discussed also by Kasteleyn.[26] Thus, the dimer model gives some theoretical credential to the isomorphous transition found experimentally.

It is not clear how the nuclear mass influences the critical behavior of the hydrogen bonded system. It has been known that thermodynamic property of Ising model changes substantially if one assumes a distance-dependent coupling between the spins on a compressible lattice. Specifically, a first-order phase transition is possible if the lattice is sufficiently compressible.[27] It will be extremely interesting to investigate a compressible dimer lattice on the 4—8 lattice of Salinas and Nagle.

Conclusion

The heat capacity data discussed in the present paper was obtained with an adiabatic calorimeter using platinum and thermistor thermometers. High sensitivity of the thermistor allowed the heat capacity measurement close to the transition temperature without distorting the true temperature dependence of the anomalous heat capacity. Long term stability of the platinum thermometer and the resistance measuring apparatus enabled us to measure the heat capacity reproducibly over many years, which was essential for the investigation of the annealing effect. Adiabatic calorimetry rather than transient and temperature

oscillation method was particularly suitable for studying the phase transition where thermal equilibration time was long at the transition temperature as in the present case. Use of the single crystals is also believed to be of essential importance not only in the thermal aspect but also for the homogeneity of the solid solutions. With these experimental set-up we believe that we have established the occurrence of a liquid-vapor type critical point in a crystalline substance for the first time.

Several problems are yet to be studied. We do not know physical meaning of the formal correspondence between the isotopic concentration in the present solid solution and pressure in the liquid-vapor system. This will be related to an equally interesting problem of phase transition in isotopic mixture in general. How can a phase transition temperature be defined accurately in the isotopically impure system? Position-exchangeability of the different isotopic atoms must be involved in this problem.

Finally, calorimetric and dielectric measurements at higher pressure will be informative for investigation of the critical behavior of the present system and are now in progress at the laboratory.

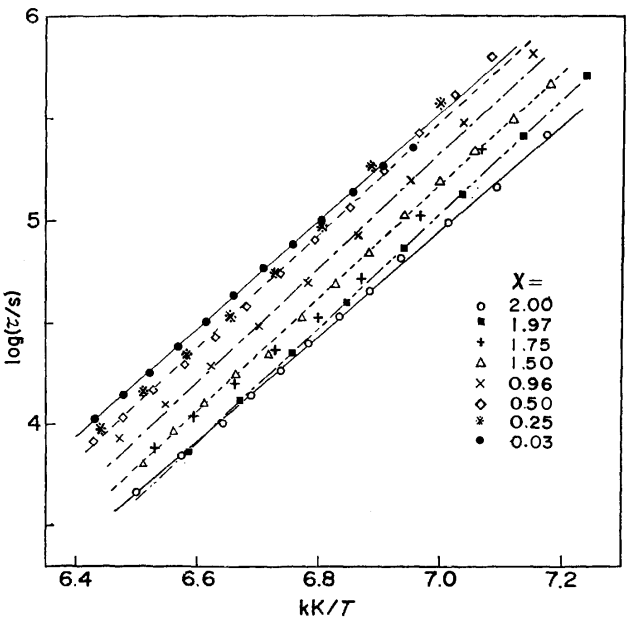

Fig. A1. Arrhenius plot of the enthalpy relaxation time of $SnCl_2(H_2O)_x(D_2O)_{2-x}$.

Appendix I. The Glass Transition

The glass transition is not a phase transition. It is a change from a non-equilibrium to equilibrium state. The glass transition in TCD occurs when, around 150 K, positional change of the protons (or deuterons) becomes so slow that they cannot find the equilibrium distribution within the experimental time. The glass transitions in normal and deuterated TCD were discussed in an earlier paper.[19] In this appendix we add some comments on the glass transition of the solid solutions.

Occurrence of the glass transition in TCD is a fortunate phenomenon for interpretation of the phase transition in two respects. First, we can be sure that the motion of the protons (or deuterons) at the phase transition temperature is rapid enough for their equilibrium distribution to be attained within the experimental time. For the phase transition occurs at much higher temperature than the glass transition. This is particularly important for the solid solutions because we can be sure that we are dealing with an annealed system rather than quenched one. Second, the glass transition allows experimental determination of the vibrational heat capacity below the glass transition temperature. This is a useful piece of information for separating the anomalous heat capacity from the total experimental heat capacity. Appendix II deals with this problem.

As the glass transition *per se*, the relaxational behavior deserves a comment. The heat capacity of the solid solutions around the glass transition and the glass transition temperature as a function of the composition were given in the previous paper. From the exothermic drift rate the relaxation time was determined by the method described previously[19] and plotted in Fig. A1. These figures show that the glass transition in $SnCl_2 \cdot 2D_2O$ occurs at ≈ 5 K higher than in $SnCl_2 \cdot 2H_2O$ and that the glass transition interval in the solid solutions is not broader than in the hydrate or deuterate crystal. This means that correlation region of the atomic motion is so large that the local isotopic concentration does not deviate from the average concentration. This supports the earlier discussion based on the structure of the hydrogen bond network that the smallest unit of the atomic motion consists of eight hydrogen atoms.

Appendix II. Determination of the Lattice Heat Capacity

It was found that the heat capacity jump at the glass transition is reproduced correctly by the dimer model using the experimental transition temperature as the only adjustable parameter. The dimer model calculation was assumed to be correct up to 190 K and above 250 K where the anomalous heat capacity is small again. The dimer model gave too small a heat capacity in the intermediate region involving the phase transition. Interpolation of the normal heat capacity into this region was facilitated by spectroscopic data.[28,29] The vibrational frequencies used are as follows. Internal vibration of the two water molecules: 3125, 2975, 1545, and 3505, 3375, 1610 cm^{-1}, librational modes of the two water molecules: 945, 853, 542, and 710, 486 and 415 cm^{-1}, internal and external vibrations of $SnCl_2 \cdot H_2O$: 323, 198, 134, 101, 67, 58, and 254, 250, 164, 139, 121, and 111 cm^{-1}.

References

1) M. Tatsumi, T. Matsuo, H. Suga, and S. Seki, *Bull. Chem. Soc. Jpn.*, **52**, 716 (1979).
2) T. Matsuo, Y. Kume, H. Suga, and S. Seki, *J. Phys. Chem. Solids*, **37**, 499 (1977).
3) M. Oguni, T. Matsuo, H. Suga, and S. Seki, *Bull. Chem. Soc. Jpn.*, **48**, 379 (1975).
4) T. Matsuo, M. Oguni, H. Suga, and S. Seki, *Proc. Jpn. Acad.*, **48**, 237 (1972).
5) S. R. Salinas and J. F. Nagle, *Phys. Rev. B*, **9**, 4920 (1974).
6) K. Kitahama and H. Kiriyama, *Bull. Chem. Soc. Jpn.*, **50**, 3167 (1977).
7) T. Matsuo, M. Tatsumi, H. Suga, and S. Seki, *Solid State Commun.*, **13**, 1829 (1973).
8) P. Heller, *Rep. Progr. Phys.*, **30**, 731 (1967).

9) T, Yamamoto, O. Tanimoto, Y. Yasuda, and K. Okada, "Critical Phenomena," Proceedings of a Conference (Natl. Bur. Standards Misc. Publications), No. 273, Washington D. C. (1966), p. 86.
10) W. Reese and L. F. May, *Phys. Rev.*, **162**, 510 (1967).
11) J. J. White, H. I. Song, J. A. Reves, and D. P. Landau, *Phys. Rev. B*, **4**, 4605 (1971).
12) E. R. Mognashi and A. Rigamonti, *Phys. Rev. B*, **14**, 2005 (1976).
13) S. R. Salinas and J. F. Nagle, *J. Phys. Soc. Jpn.*, **41**, 1643 (1976).
14) W. Reese and L. F. May, *Phys. Rev.*, **167**, 504 (1968).
15) P. Schwartz, *Phys. Rev.*, **4**, 920 (1971).
16) E. N. Kostina and G. A. Milńor, *Sov. Phys., Solid State*, **14**, 2923 (1973).
17) I. Hatta and A. Ikushima, *J. Phys. Chem. Solids*, **34**, 57 (1973).
18) W. Reese and L. F. May, *Phys. Rev.*, **181**, 905 (1969).
19) T. Matsuo, M. Oguni, H. Suga, S. Seki, and J. F. Nagle, *Bull. Chem. Soc. Jpn.*, **47**, 57 (1974).
20) R. B. Griffith and J. C. Wheeler, *Phys. Rev. A*, **2**, 1047 (1970).
21) C. W. Garland and B. B. Weiner, *Phys. Rev. B*, **3**, 1634 (1971); C. W. Garland and B. B. Weiner, *J. Chem. Phys.*, **56**, 155 (1972).
22) W. B. Yelon, D. E. Cox, and P. J. Daniels, *Phys. Rev. B*, **9**, 4843 (1974).
23) I. R. Jahn and E. Neumann, *Solid State Commun.*, **12**, 721 (1973).
24) L. D. Landau and E. M. Lifshitz, "Statistical Physics," 2nd ed, Pergamon Press, Oxford (1969).
25) H. Kiriyama, K. Kitahama, O. Nakamura, and R. Kiriyama, *Bull. Chem. Soc. Jpn.*, **46**, 1389 (1973).
26) P. W. Kasteleyn, *J. Math. Phys.*, **4**, 287 (1963).
27) G. A. Baker, Jr., and J. W. Essam, *J. Chem. Phys.*, **55**, 861 (1971).
28) C. H. Wang, M. Tatsumi, T. Matsuo, and H. Suga, *J. Chem. Phys.*, **67**, 3097 (1977).
29) H. Koseko (private communication, 1977).

The Crystal and Molecular Structure of (Carboxymethyl)(pyridine)-(triphenylphosphine)palladium(II) Dichloromethane Solvate, $[Pd(C_2H_2O_2)(PPh_3)(py)]\cdot 0.6\,CH_2Cl_2$

Yasushi KAI, Noritake YASUOKA, and Nobutami KASAI*

Department of Applied Chemistry, Faculty of Engineering, Osaka University, Yamadakami, Suita, Osaka 565

(Received October 2, 1978)

The molecular structure of carboxymethylpalladium(triphenylphosphine)pyridine has been determined by X-ray crystal structure analysis of its dichloromethane solvate, $[Pd(C_2H_2O_2)(PPh_3)(py)]\cdot 0.6\,CH_2Cl_2$. The crystal belongs to the monoclinic system, space group $P2_1/c$, with four formula units in a cell with dimensions of $a=8.791(4)$, $b=14.623(7)$, $c=19.862(5)$ Å, and $\beta=101.53(4)°$. $R=0.091$ for 2806 non-zero reflections. The feature of the structure is that the palladium atom is C,O-chelated by an acetic acid to form a four-membered ring [Pd–C=2.004 (16) and Pd–O=2.093 (11) Å], and the palladium atom has approximately square-planar geometry.

In a series of palladium complexes (Scheme) prepared by the reaction of ketene and triphenylphosphine with bis(acetylacetonate)palladium(II),[1] the molecular structures of I,[2] II,[3] IV,[4] and VII[5] have been determined by means of X-ray diffraction. The crystal structure analysis of V has been first attemped, however, all the crystals examined were decomposed by X-ray irradiation. Therefore, the more stable crystals of Vb, which is also a palladium C,O-chelate of acetic acid, has been selected. This paper deals with the structure of Vb, of which preriminary result has been reproted briefly.[6]

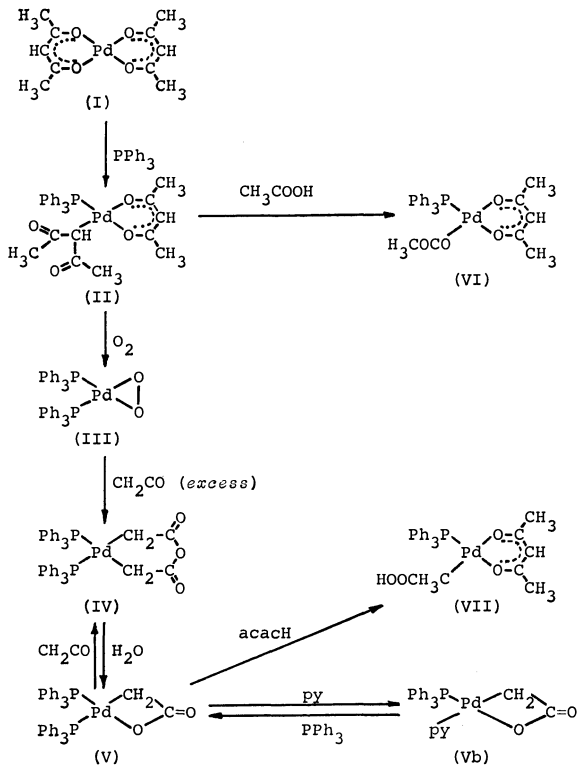

Experimental

Pale yellow, polyhedral crystals of $[Pd(C_2H_2O_2)(PPh_3)(py)]\cdot 0.6\,CH_2Cl_2$ were kindly supplied by Professor S. Kawaguchi and his coworkers of Osaka City University. Preliminary X-ray work showed that the crystals belong to the monoclinic system and that the space group is $P2_1/c$ (No. 14, absent reflections, $h0l$; $l=2n+1$ and $0k0$; $k=2n+1$). Unit-cell dimensions were determined by 2θ values of 12 strong reflections measured on a Rigaku automated, four-circle single crystal diffractometer.

Crystal Data. $(C_{25}H_{22}NO_2PPd+0.6\,CH_2Cl_2)$, $F.W.=556.8$, monoclinic, space group, $P2_1/c$, $a=8.791(4)$, $b=14.623(7)$, $c=19.862(5)$ Å, $\beta=101.53(4)°$, $D_m=1.474$ g cm^{-3} (by flotation in aqueous solution of zinc bromide), $Z=4$, $D_c=1.478$ g cm^{-3}.

For the intensity measurement, a crystal with approximate dimensions of $0.20\times 0.175\times 0.15$ mm was used. Intensity data were collected on the Rigaku diffractometer using Zr-filtered Mo $K\alpha$ radiation. All data within a 2θ sphere of 44° ($\sin\theta/\lambda=0.527$) were measured using the θ-2θ scan technique. The integrated intensity was determined by scanning over the peak at a rate of 4° min^{-1} and subtracting the background obtained by averaging the two values measured for 10 s at both ends of a scan; the scan width of each reflection was $\Delta(2\theta)=(2.0+0.7\tan\theta_c)°$, where θ_c is the calculated Bragg angle for Mo $K\alpha_1$ ($\lambda=0.70926$ Å). The intensities of two standard reflections (080 and 300) were measured after every 25 reflections. After about 2400 reflections with lower Bragg angles were measured, these standard reflections showed a sudden drop down in their intensities. Therefore, the second crystal with approximately the same dimensions was cut out from the same mother crystal as the first, which was then used to collect about 900 more reflections with high angles. A total of 3053 independent reflections was collected of which the number of non-zero reflections was 2806. Usual Lorentz and polarization corrections were made, but the absorption correction was ignored ($\mu=6.37$ cm^{-1} for Mo $K\alpha$).

Solution and Refinement of the Structure

The structure was solved by the heavy atom method. The palladium and phosphorus atoms were located from a three-dimensional Patterson function. The remaining non-hydrogen atoms of the $[Pd(C_2H_2O_2)(PPh_3)(py)]$ molecule were located by succesive Fourier syntheses. However, three low and broad peaks remained undefined, which could be assigned as non-hydrogen atoms of dichloromethane, the recrystallization solvent. The structure was then refined by the block-diagonal least-squares procedure. The HBLS-V program[7] was used, the function minimized being $\Sigma(|F_o|-k|F_c|)^2$, where k is a single scale factor. Several cycles of isotropic refinement followed by the several more cycles of anisotropic refinement reduced

TABLE 1. FRACTIONAL ATOMIC COORDINATES OF NON-HYDROGEN ATOMS
(estimated standard deviations in parentheses)

Atom	x	y	z	Atom	x	y	z
Pd	0.19485 (12)	0.03753 (7)	0.09744 (5)	C(34)	0.3170 (20)	−0.1962 (11)	0.3413 (8)
P	0.1323 (4)	0.0470 (2)	0.2006 (2)	C(35)	0.1806 (20)	−0.1513 (11)	0.3504 (8)
C(11)	−0.0730 (14)	0.0613 (8)	0.1991 (6)	C(36)	0.1196 (17)	−0.0797 (11)	0.3066 (8)
C(12)	−0.1302 (16)	0.0906 (10)	0.2558 (7)	N	0.1548 (13)	−0.1053 (8)	0.0765 (6)
C(13)	−0.2918 (17)	0.0961 (11)	0.2545 (9)	C(42)	0.0435 (17)	−0.1575 (10)	0.0950 (7)
C(14)	−0.3925 (16)	0.0693 (11)	0.1934 (9)	C(43)	0.0193 (19)	−0.2488 (11)	0.0777 (9)
C(15)	−0.3352 (15)	0.0423 (9)	0.1352 (8)	C(44)	0.1233 (19)	−0.2889 (10)	0.0450 (8)
C(16)	−0.1817 (16)	0.0380 (9)	0.1375 (8)	C(45)	0.2437 (20)	−0.2395 (12)	0.0251 (8)
C(21)	0.2196 (14)	0.1393 (8)	0.2564 (6)	C(46)	0.2532 (19)	−0.1491 (11)	0.0427 (8)
C(22)	0.1680 (18)	0.2294 (10)	0.2409 (7)	C(1)	0.3245 (17)	0.1515 (10)	0.0323 (8)
C(23)	0.2312 (21)	0.3029 (10)	0.2819 (8)	C(2)	0.2465 (17)	0.1702 (11)	0.0907 (8)
C(24)	0.3449 (19)	0.2869 (11)	0.3394 (8)	O(1)	0.4102 (14)	0.1994 (8)	0.0078 (6)
C(25)	0.3968 (18)	0.1999 (11)	0.3550 (8)	O(2)	0.2874 (12)	0.0673 (7)	0.0107 (5)
C(26)	0.3346 (16)	0.1264 (10)	0.3147 (8)	Cl(1S)	0.2649 (13)	0.4770 (6)	−0.0273 (4)
C(31)	0.1930 (14)	−0.0525 (9)	0.2546 (6)	Cl(2S)	0.2314 (14)	0.4312 (6)	0.1077 (5)
C(32)	0.3235 (16)	−0.0999 (10)	0.2439 (7)	C(S)	0.3304 (35)	0.4110 (17)	0.0462 (15)
C(33)	0.3822 (20)	−0.1719 (11)	0.2872 (8)				

TABLE 2. ANISOTROPIC THERMAL PARAMETERS ($\times 10^4$) EXPRESSED IN THE FORM:
$\exp\{-(\beta_{11}h^2+\beta_{22}k^2+\beta_{33}l^2+\beta_{12}hk+\beta_{13}hl+\beta_{23}kl)\}$
(estimated standard deviations in parentheses)

Atom	β_{11}	β_{22}	β_{33}	β_{12}	β_{13}	β_{23}
Pd	117.6 (16)	39.1 (6)	20.5 (3)	−2.6 (15)	19.2 (11)	−3.3 (7)
P	95.5 (51)	32.1 (18)	19.0 (10)	7.0 (49)	12.4 (36)	−5.1 (22)
C(11)	94 (19)	28 (7)	20 (4)	9 (18)	28 (14)	−5 (8)
C(12)	125 (22)	42 (8)	25 (4)	29 (22)	20 (16)	0 (10)
C(13)	103 (22)	60 (10)	40 (6)	68 (24)	50 (18)	11 (12)
C(14)	79 (20)	47 (9)	51 (7)	24 (22)	40 (19)	12 (12)
C(15)	84 (20)	29 (7)	42 (6)	16 (19)	26 (17)	−8 (10)
C(16)	120 (22)	32 (7)	31 (5)	−7 (21)	11 (17)	10 (10)
C(21)	99 (19)	28 (6)	17 (4)	−10 (18)	29 (13)	−13 (8)
C(22)	158 (25)	47 (9)	24 (4)	4 (24)	11 (17)	−6 (10)
C(23)	241 (33)	35 (8)	33 (5)	18 (27)	70 (22)	−4 (11)
C(24)	187 (28)	57 (10)	27 (5)	−45 (27)	22 (19)	−55 (12)
C(25)	150 (26)	59 (10)	31 (5)	−31 (19)	−11 (19)	−16 (12)
C(26)	93 (20)	44 (8)	31 (5)	−15 (21)	1 (16)	−1 (10)
C(31)	98 (19)	34 (7)	17 (4)	−8 (19)	14 (14)	3 (8)
C(32)	132 (23)	39 (8)	24 (4)	29 (21)	34 (16)	−12 (9)
C(33)	210 (31)	49 (9)	31 (5)	85 (28)	33 (21)	−6 (11)
C(34)	209 (30)	43 (9)	27 (5)	46 (26)	−2 (19)	20 (11)
C(35)	210 (31)	50 (9)	26 (5)	−50 (27)	31 (20)	10 (11)
C(36)	124 (23)	53 (9)	26 (5)	−6 (24)	−3 (17)	5 (11)
N	137 (19)	39 (6)	21 (3)	−8 (18)	33 (13)	−1 (8)
C(42)	142 (24)	47 (9)	24 (5)	−4 (23)	16 (17)	−19 (10)
C(43)	175 (28)	41 (8)	36 (6)	−32 (25)	3 (20)	−10 (11)
C(44)	186 (28)	33 (8)	37 (6)	6 (24)	32 (20)	−8 (11)
C(45)	184 (29)	69 (11)	30 (5)	103 (30)	34 (20)	−6 (12)
C(46)	171 (27)	55 (9)	28 (5)	29 (26)	50 (19)	7 (11)
C(1)	155 (25)	40 (8)	28 (5)	13 (23)	39 (18)	9 (10)
C(2)	145 (25)	50 (9)	26 (5)	5 (24)	29 (17)	3 (10)
O(1)	231 (22)	64 (7)	35 (4)	−53 (21)	77 (15)	15 (9)
O(2)	196 (19)	52 (6)	19 (3)	19 (17)	54 (12)	6 (7)
Cl(1S)	512 (27)	62 (5)	26 (2)	162 (19)	121 (13)	33 (5)
Cl(2S)	486 (27)	78 (6)	42 (3)	168 (20)	204 (16)	27 (7)
C(S)	241 (56)	36 (14)	37 (10)	71 (46)	42 (38)	38 (19)

Table 3. Atomic parameters of hydrogen atoms (estimatimated standard deviations in parentheses)

	x	y	z	B[a]
H(12)	−0.055(14)	0.096(8)	0.299(6)	3.6
H(13)	−0.327(15)	0.114(9)	0.303(7)	4.8
H(14)	−0.506(15)	0.076(9)	0.188(7)	4.4
H(15)	−0.459(14)	0.035(9)	0.093(6)	3.7
H(16)	−0.115(14)	0.030(8)	0.100(6)	3.7
H(22)	0.096(14)	0.241(9)	0.199(6)	4.0
H(23)	0.191(16)	0.382(10)	0.263(7)	4.9
H(24)	0.397(15)	0.338(9)	0.373(7)	4.7
H(25)	0.497(15)	0.178(9)	0.397(7)	4.8
H(26)	0.356(14)	0.057(8)	0.325(6)	3.7
H(32)	0.368(14)	−0.089(8)	0.206(6)	3.5
H(33)	0.500(15)	−0.206(9)	0.282(7)	4.7
H(34)	0.369(15)	−0.251(9)	0.377(7)	4.3
H(35)	0.113(15)	−0.164(9)	0.379(7)	4.6
H(36)	0.031(14)	−0.034(9)	0.313(6)	4.1
H(42)	−0.025(14)	−0.118(9)	0.120(6)	3.9
H(43)	−0.060(15)	−0.296(9)	0.090(7)	4.6
H(44)	0.103(15)	−0.355(9)	0.040(7)	4.3
H(45)	0.316(16)	−0.268(10)	0.009(7)	5.0
H(46)	0.344(15)	−0.117(9)	0.029(7)	4.5
H(2A)	0.313(15)	0.195(9)	0.127(6)	4.3
H(2B)	0.158(15)	0.209(9)	0.078(6)	4.3

a) The isotropic temperature factors of each hydrogen atom is taken equal to that of equivalent temperature factor of its parent atom.

the R_1 factor ($R_1=\Sigma||F_o|-|F_c||/\Sigma|F_o|$) to 0.090 for non-zero reflections. The difference Fourier synthesis, based on the atomic parameters at this stage, revealed all the hydrogen atoms except those of dichloromethane. Three cycles of refinement including those 22 hydrogen atoms gave $R_1=0.082$. However, equivalent isotropic thermal parameters of non-hydrogen atoms of the solvent molecule were exceptionally large, and the calculated density for four formula weights of [Pd-$(C_2H_2O_2)(PPh_3)(py)$, CH_2Cl_2] per unit-cell [1.56 g cm^{-3}] is much larger than the observed value of 1.474 g cm^{-3}. These facts suggested a lower occupancy of dichloromethane than unity. Assuming the occupancy as 0.6. which gives the calculated density of 1.478 g cm^{-3} and a good fit with the observed values, the refinement converged: R_1 being 0.091 ($R_2=\Sigma||F_o|-|F_c||^2/\Sigma|F_o|^2=0.106$) for non-zero reflections. The atomic scattering factors used in the calculations were taken from International Tables for X-Ray Crystallography, Vol. IV.[8] The final atomic parameters of non-hydrogen atoms are listed in Tables 1 and 2, and those of hydrogen atoms in Table 3.†

Description of the Structure

Molecular Structure. The perspective view of the $[Pd(C_2H_2O_2)(PPh_3)(py)]$ and CH_2Cl_2 molecules are given in Fig. 1, with the numbering scheme of

† The tables of observed and calculated structure factors are kept as Document No. 7914 at the Chemical Society of Japan.

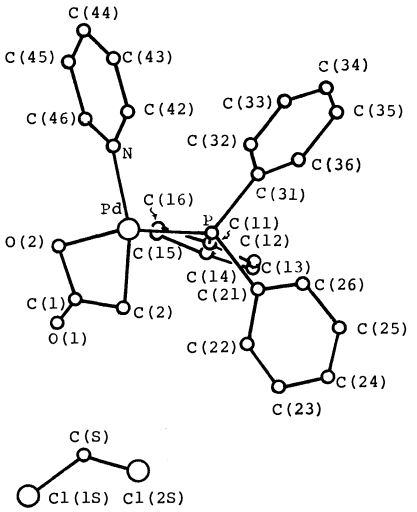

Fig. 1. Perspective view of the $[Pd(C_2H_2O_2)(PPh_3)-(py)]$ and CH_2Cl_2 molecules with the numbering scheme of atoms.

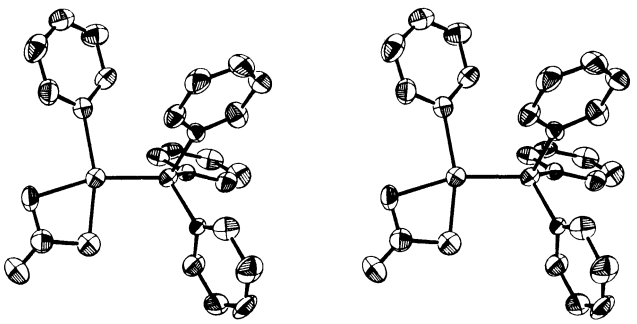

Fig. 2. A stereoscopic view of the $[Pd(C_2H_2O_2)-(PPh_3)(py)]$ molecule. Non-hydrogen atoms are represented by the thermal ellipsoids at 50% probability level.

atoms. The stereoscopic drawing of the $[Pd(C_2H_2-O_2)(PPh_3)(py)]$ molecule is given in Fig. 2. Bond lengths and bond angles are given in Table 4. Least-squares planes of some groups of atoms, deviations of atoms from, and dihedral angles between these planes are listed in Table 5.

The remarkable feature of the molecular structure is that this complex contains a C,O-chelate ring of acetic acid (Fig. 1). The palladium atom has an approximately square-planar geometry coordinated by an oxygen and an sp^3 carbon atoms of the chelate ring and a phosphorus and a nitrogen stoms; the mean and maximum deviations of atoms from the best plane being 0.057 and 0.078 Å, however, the planarity is not so good as that of IV, a C,C′-chelate of acetic anhydride.[4]

The Pd–C(2) bond lengths [2.004(16) Å] is much shorter than those in IV [2.141(13) and 2.124(11) Å], which is probably the shortest of the observed Pd–C σ-bond. The Pd–O(2) length [2.093(11) Å] is longer than those of O,O′-chelate of acetylacetone [1.989(2) and 1.986(2) Å],[2b] which is considered as due to trans-influence of the pyridine ligand. The C(2)–Pd–O(2) angle [67.3(5)°] is much smaller than 90°.

The Pd–P bond [2.230(4) Å] is equal in length to that of 2.235(1) Å in VII,[5] and this is shorter than that

TABLE 4. BOND LENGTHS AND BOND ANGLES (estimated standard deviations in parentheses)

Bond length [l/Å]			
Pd-P	2.230(4)	Pd-N	2.144(12)
C(1)-C(2)	1.487(22)	C(1)-O(2)	1.322(19)
C(1)-O(1)	1.201(20)		
Pd-O(2)	2.093(11)	Pd-C(2)	2.004(16)
P-C(11)	1.811(13)	P-C(21)	1.816(13)
P-C(31)	1.822(13)		
C(11)-C(12)	1.376(19)	C(11)-C(16)	1.435(20)
C(12)-C(13)	1.421(22)	C(13)-C(14)	1.409(25)
C(14)-C(15)	1.405(24)	C(15)-C(16)	1.343(22)
C(21)-C(22)	1.408(20)	C(21)-C(26)	1.389(20)
C(22)-C(23)	1.396(24)	C(23)-C(24)	1.380(25)
C(24)-C(25)	1.367(24)	C(25)-C(26)	1.385(23)
C(31)-C(32)	1.392(19)	C(31)-C(36)	1.383(20)
C(32)-C(33)	1.392(23)	C(33)-C(34)	1.361(25)
C(34)-C(35)	1.410(25)	C(35)-C(36)	1.398(23)
N-C(42)	1.349(19)	N-C(46)	1.358(20)
C(42)-C(43)	1.384(23)	C(43)-C(44)	1.356(24)
C(44)-C(45)	1.402(25)	C(45)-C(46)	1.365(24)
C(S)-Cl(1S)	1.749(33)	C(S)-Cl(2S)	1.661(33)
Bond angle [ϕ/°]			
P-Pd-N	100.2(3)	P-Pd-C(2)	95.8(4)
P-Pd-O(2)	162.1(3)	N-Pd-C(2)	163.9(5)
N-Pd-O(2)	96.8(4)	C(2)-Pd-O(2)	67.2(5)
Pd-C(2)-C(1)	91.1(9)	C(2)-C(1)-O(1)	129.3(15)
Pd-O(2)-C(1)	92.2(9)	C(2)-C(1)-O(2)	107.6(13)
O(1)-C(1)-O(2)	123.1(14)		
Pd-P-C(11)	114.8(4)	Pd-P-C(21)	117.1(4)
Pd-P-C(31)	113.2(4)	C(11)-P-C(21)	102.9(6)
C(11)-P-C(31)	106.0(6)	C(21)-P-C(31)	101.3(6)
P-C(11)-C(12)	123.1(10)	P-C(11)-C(16)	118.6(10)
C(12)-C(11)-C(16)	118.3(12)	C(11)-C(12)-C(13)	122.6(14)
C(12)-C(13)-C(14)	116.4(15)	C(13)-C(14)-C(15)	121.4(16)
C(14)-C(15)-C(16)	120.6(15)	C(11)-C(16)-C(15)	120.7(14)
P-C(21)-C(22)	118.9(10)	P-C(21)-C(26)	123.8(10)
C(22)-C(21)-C(26)	117.3(12)	C(21)-C(22)-C(23)	121.3(14)
C(22)-C(23)-C(24)	119.5(16)	C(23)-C(24)-C(25)	119.9(16)
C(24)-C(25)-C(26)	121.1(15)	C(21)-C(26)-C(25)	120.9(14)
P-C(31)-C(32)	117.5(10)	P-C(31)-C(46)	123.0(11)
C(32)-C(31)-C(36)	119.5(13)	C(31)-C(32)-C(33)	119.9(14)
C(32)-C(33)-C(34)	121.5(16)	C(33)-C(34)-C(35)	118.9(16)
C(34)-C(35)-C(36)	119.9(16)	C(31)-C(36)-C(35)	120.2(14)
N-C(46)-C(45)	124.8(15)	C(42)-C(43)-C(44)	116.9(15)
C(43)-C(44)-C(45)	122.1(16)	C(44)-C(45)-C(46)	116.0(16)
N-C(42)-C(43)	124.2(14)	C(42)-N-C(46)	115.8(13)
Cl(1S)-C(S)-Cl(2S)	112.5(18)		

of 2.267(1) Å in $[PdCl(CH_2SCH_3)(PPh_3)]$.[9] The Pd-N bond length [2.144(12) Å] is comparable to those in $[PdCl(CH_2COCH_2COOCH_2Ph)(py)_2]$ [2.027(6) and 2.120(6) Å]. The P-Pd-N angle of 100.2(3)° is much larger than 90° because of steric interaction between the triphenylphosphine and pyridine ligands.

In the C,O-chelate ring of acetic acid, the C(1)-C(2) bond length of 1.487(22) is equal to those in IV of 1.473(18) and 1.479(19) Å, which can be compared with those observed in C-C=O moieties in many organic compounds [av 1.506(5) Å]. The C(1)-O(2) bond length [1.322(19) Å] is shorter than those in IV [1.412(16) and 1.386(17) Å]. The C(1)=O(1) double bond length of 1.201(20) is equal to those of 1.192(18) and 1.202(17) Å in IV, which is normal value in aldehydes and ketones [av 1.215(5) Å],[10] and α-oxalic acid [1.207(1) Å].[11] Both the Pd-C(2)-C(1) and Pd-O(2)-C(1) angles are around 90° [91.1(9) and 92.9(9)°, respectively]. The C(2)-C(1)-O(2) angle [107.6(13)°] is much smaller, whereas the C(2)-C(1)-O(1) angle [129.3(15)°] is much larger than 120°. However, the sum of the three angles around

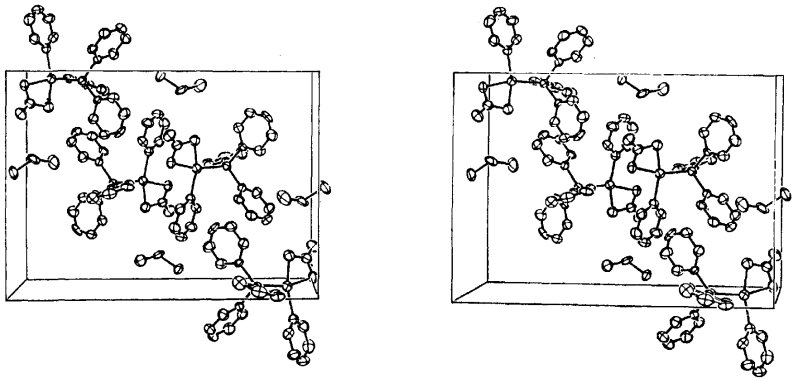

Fig. 3. A stereoscopic drawing of the molecular packing in the unit cell.

TABLE 5. LEAST-SQUARES PLANES, DEVIATIONS (l/Å) OF ATOMS FROM THE PLANE, AND DIHEDRAL ANGLES [ϕ/°]

Equation of the plane is of the form: $AX+BY+CZ+D=0$, where X, Y, Z, and D are measured in Å units: $X=ax+cz\cos\beta$, $Y=by$, $Z=cz\sin\beta$. (Atoms marked by * are not in the least-squares plane calculation.)

(a) Coordination plane
$-0.8594X+0.1982Y-0.4714Z+1.959=0$

Pd	0.035	P	−0.060	N	0.045
C(2)	0.068	O(2)	−0.078	C(1)*	−0.239
O(1)*	−0.606				

(b) Plane defined by C(1), C(2), O(1), and O(2)
$-0.6749X+0.3618Y-0.6431Z+1.451=0$

C(1)	0.010	C(2)	−0.003	O(1)	−0.004
O(2)	−0.003	Pd*	−0.465		

(c) Plane defined by Pd, C(2), and O(2)
$-0.8326X+0.1707Y-0.5270Z+2.010=0$

Dihedral angle between (a) and (b):	17.3
Dihedral angle between (b) and (c):	15.7

the C(1) atom is 360.0°; the planarity around the C(1) being good (Table 5). The dihedral angle between the planes defined by Pd, C(2), and O(2) and C(1), C(2), O(1), and O(2), is 15.7°.

Similar to those in IV the phosphorus atom show a deviation from the tetrahedral geometry: the C(11)–P–C(21), C(11)–P–C(31), and C(21)–P–C(31) [102.9(6), 106.0(6), and 101.3(6)°] being much smaller, whereas Pd–P–C(11), Pd–P–C(21) and Pd–P–C(31) [114.8(4), 117.1(4), and 113.2(4)°] being larger than th tetrahedral angle. Three P–C bond lengths are equal [1.811(13), 1.816(13), and 1.822(13) Å]. Three phenyl rings in triphenylphosphine group have normal structure [C–C(av)=1.392 Å and C–C–C(av)=120.0°]. The pyridine ring coordinated to palladium atom also has normal geometry [C–C(av)=1.377, C–N(av)=1.354 Å, C–N–C=115.8°, and C–C–C(av)=120°].

Crystal Structure. Figure 3 shows a stereoscopic drawing of the molecular packing in the unit-cell along the c axis. All intermolecular atomic contacts are considered to be normal van der Waals distances, the shortest contact being 3.285(21) Å (C(24)(x, y, z)··· O(1)(x, 0.5−y, 0.5+z)).

Computations throughout the present study were carried out on a NEAC 2200-700 computer at the Osaka University. Figures 2 and 3 were drawn on the NUMERICON 7000 system at Osaka University with a local version of ORTEP.[12]

The authors wish to express their deep thanks to Professor Shinichi Kawaguchi and coworkers of the Osaka City University for supplying crystals and helpful discussions. The authors are also indebted to Mr. Kunio Miki who helped the computations and ORTEP drawings.

References

1) S. Baba, T. Ogura, and S. Kawaguchi, *Bull. Chem. Soc. Jpn.*, **47**, 665 (1974); S. Baba, T. Sobata, T. Ogura, and S. Kawaguchi, *ibid.*, **47**, 2792 (1974).

2) a) A. N. Knyazeva, E. A. Shugam, and L. M. Shkol'nikova, *Zh. Strukt. Khim.*, **11**, 938 (1970); b) M. Sato, K. Miki, Y. Kai, N. Yasuoka, and N. Kasai, unpublished work.

3) M. Horike, Y. Kai, N. Yasuoka, and N. Kasai, *J. Organomet. Chem.*, **72**, 441 (1974).

4) Y. Zenitani, H. Tokunan, Y. Kai, N. Yasuoka, and N. Kasai, *Bull. Chem. Soc. Jpn.*, **51**, 1730 (1978).

5) Y. Zenitani, K. Inoue, Y. Kai, N. Yasuoka, and N. Kasai, *Bull. Chem. Soc. Jpn.*, **49**, 1531 (1976).

6) S. Baba, T. Ogura, S. Kawaguchi, H. Tokunan, Y. Kai, and N. Kasai, *J. Chem. Soc., Chem. Commun.*, **1972**, 910.

7) T. Ashida, "The Universal Crystallographic Computing System-Osaka," The Computation Center, Osaka University (1973), p. 55.

8) "International Tables for X-Ray Crystallography," The Kynoch Press, Birmingham (1974), Vol. IV, pp. 71—98.

9) K. Miki, Y. Kai, N. Yasuoka, and N. Kasai, *J. Organomet. Chem.*, **135** (1977).

10) "Tables of Interatomic Distances and Configuration in Molecules and Ions, Supplement 1956—1959," ed by L. E. Sutton, The Chemical Society (1965), pp. S15s and S22s.

11) J. L. Derissen and P. H. Smit, *Acta Crystallogr., Sect. B*, **30**, 2240 (1974).

12) C. K. Johnson, "ORTEP-II, Report ORNL-5138," Oak Ridge National Laboratory, Tennessee (1976).

Absorption and Fluorescence Spectra of Anthracenecarboxylic Acids. II. 1- and 2-Anthroic Acids

Satoshi SUZUKI,* Tsuneo FUJII, Shigeru YAMANAKA, Nobuyuki YOSHIIKE,† and Zenro HAYASHI††

Department of Industrial Chemistry, Faculty of Engineering, Shinshu University, Wakasato, Nagano 380

(Received October 9, 1978)

The absorption and fluorescence spectra of 1- and 2-anthroic acids (1- and 2-anthracenecarboxylic acids) in alcoholic solvents have been observed as a function of solute concentration. It was revealed that 1- and 2-anthroic acids form hydrogen-bonded dimers in their ground states. The equilibrium constants for dimer formation are : 1.2×10^4 mol^{-1} l for 1-anthroic acid in methanol and 2.0×10^4 mol^{-1} l for 2-anthroic acid in ethanol. Owing to dimer formation, the lowest frequency absorption band of 1-anthroic acid was uniformly displaced to the red, while that of 2-anthroic acid was distinctly resolved into two bands. The band assignment was confirmed by the method of photoselection. No excimer-type fluorescence was observed in 1- and 2-anthroic acids. The lack of mirror-symmetry relationship between the absorption and fluorescence spectra of 1-anthroic acid is explained by the geometrical relaxation in its excited state.

The fluorescence spectrum of 9-anthroic acid (9-anthracenecarboxylic acid) in ethanol shows a remarkable concentration dependence. At a concentration below 10^{-5} mol/l the spectrum has an anthracene-like structure, while at a concentration above 10^{-3} mol/l it largely shifts to the red, turning into a broad structureless band. Some attempts to elucidate the origin of this spectral change have been made.[1-5] In connection with this, the electronic spectra of 1- and 2-anthroic acids (1- and 2-anthracenecarboxylic acids) were also investigated.[6]

In the preceding paper[4] of this series, an excimer-type mechanism was presented for the broad fluorescence of 9-anthroic acid. In alcoholic solvents, 9-anthroic acid forms a hydrogen-bonded dimer in its ground state. The hydrogen-bonded dimer is excited and then associates with an unexcited hydrogen-bonded dimer to form an excited tetramer from which the broad fluorescence occurs. A polarization study also supports the excimer mechanism.[5]

This paper presents the concentration and temperature dependence of the absorption and fluorescence spectra of 1- and 2-anthroic acids. In the ground state, 1- and 2-anthroic acids form hydrogen-bonded dimers as does 9-anthroic acid. They do not, however, show any excimer-type fluorescence in contrast to 9-anthroic acid.

Experimental

1-Anthroic acid was prepared from benzanthrone[7,8] and was purified by repeated recrystallization. 1-Anthroic acid from K & K Laboratories was purified by repeated recrystallization . Methanol (Wako fluorometric grade) was used without further purification. Ethanol (Wako super special grade) and propylene glycol (1,2-propanediol, Wako JIS S grade) were stored over molecular sieves 3A and passed through a silica gel column. The absorption spectra were recorded on a Hitachi EPS-3 recording spectrophotometer. The fluorescence and excitation spectra were obtained by means of a Hitachi MPF-2A fluorescence spectrophotometer and are given without corrections on the quantum response of the detecting and exciting systems and on reabsorption. The degree of polarization, P, was measured by the method of photoselection.[9-12]

Results and Discussion

Absorption Spectra and Dimer Formation. The absorption spectra of 1-anthroic acid in methanol are shown in Fig. 1 as a function of concentration. The absorption spectrum of 1-anthroic acid has an anthracene-like structure at lower concentration. The spectra become less sharp on increasing the concentration. Several isosbestic points appear in the spectra. The most probable origin of the isosbestic points in the absorption specta of 1-anthroic acid may be monomer-dimer equilibrium in consideration of the results of 9-anthroic acid. When one ascribes the spectral changes to monomer-dimer equilibrium, the equilibrium constant of dimer formation, K_D, can be determined by the usual procedure.[13] The K_D of 1-anthroic acid was 1.2×10^4 mol^{-1} l in methanol at 290 K.

The concentration dependence of the absorption spectra of 2-anthroic acid in ethanol is given in Fig. 2. The absorption spectrum of 2-anthroic acid has four

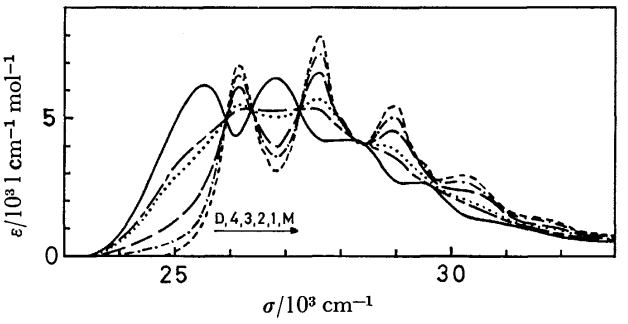

Fig. 1. The absorption spectra of 1-anthroic acid in methanol at various concentrations and the estimated monomer and dimer absorption spectra. 1 : 9.0×10^{-6} mol/l, 2 : 3.0×10^{-5} mol/l, 3 : 1.5×10^{-4} mol/l, 4 : 4.0×10^{-4} mol/l, M : the estimated monomer spectra, D : the estimated dimer spectra.

† Present address: Central Research Laboratory, Matsushita Electric Co., Ltd., Kadoma, Osaka 571.

†† Present address: Catalysis Project, Matsushita Industrial Equipment Co., Ltd., Toyonaka, Osaka 561.

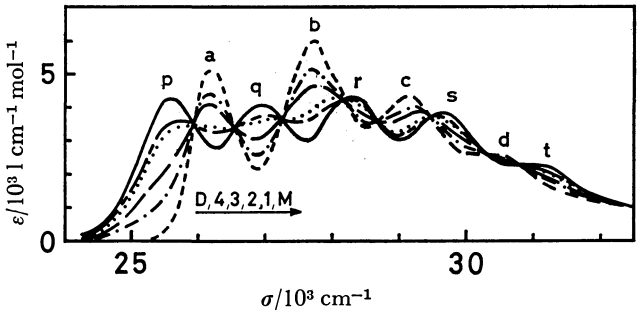

Fig. 2. The absorption spectra of 2-anthroic acid in ethanol at various concentrations and the estimated monomer and dimer absorption spectra. 1 : 2.0×10^{-5} mol/l, 2 : 4.0×10^{-5} mol/l, 3 : 9.9×10^{-5} mol/l, 4 : 2.0×10^{-4} mol/l, M : the estimated monomer spectra, D : the estimated dimer spectra.

vibrational peaks at lower concentration, while it has five vibrational peaks at higher concentration. From an analysis of the data on the concentration dependence of the absorption spectra, the K_D of 2-anthroic acid was determined to be 2.0×10^4 mol^{-1} l in ethanol.

By using the observed spectral data at various concentrations and the K_D value, we can estimate the monomer and dimer absorption spectra.[13] The estimated monomer and dimer absorption spectra of 1- and 2-anthroic acids are included in Figs. 1 and 2.

Figure 1 shows that the monomer absorption spectrum of 1-anthroic acid has an anthracene-like progression spaced by 1400 cm^{-1}. The dimer absorption spectrum is displaced to the red with keeping the vibrational structure. The monomer absorption band of 1-anthroic acid in this region may safely be assigned to the ^1L_a transition.

The monomer absorption spectrum of 2-anthroic acid has four vibrational peaks in the region of the lowest-frequency absorption band, while the dimer absorption spectrum has five vibrational peaks. It has well been established that the ^1L_b and ^1L_a bands of 2-anthrol lie closely in this region.[14–16] The lowest-frequency absorption band of 2-anthrol was assigned to the ^1L_b transition and the next one to the ^1L_a transition. The ^1L_a band of 2-anthrol holds an anthracene-like vibrational structure which is characterized by equal spacings of about 1300 cm^{-1}. The ^1L_b band of 2-anthrol is greatly displaced to the red due to hydrogen bonding, while the ^1L_a band is slightly displaced to the blue. As a consequence of this, the ^1L_b and ^1L_a bands are resolved distinctly. The assignment of the absorption bands of 2-anthroic acid can be made as follows, by reference to that of 2-anthrol. Band b of the monomer absorption spectrum is composed of two vibrational bands, one of which belongs to the ^1L_b transition and the other to the ^1L_a transition. Owing to dimer formation, the ^1L_b band is greatly displaced to the red yielding Bands p and q, while the ^1L_a band is displaced to the blue yielding Bands r, s, and t. Band a and a part of Band b of the monomer absorption band may reasonably be assigned to the ^1L_b and a part of Band b and Bands c and d to the ^1L_a transition. This assignment was confirmed

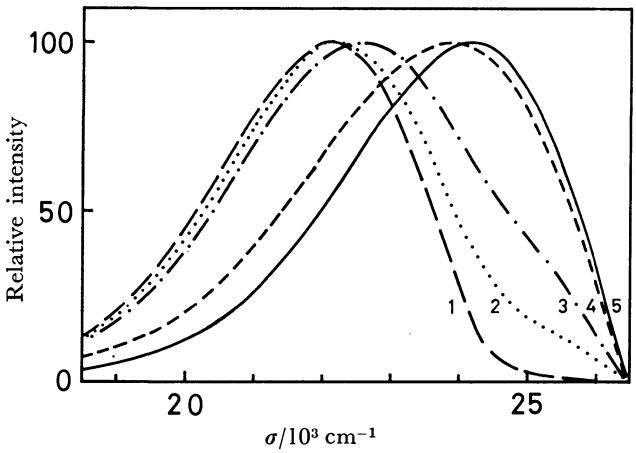

Fig. 3. The fluorescence spectra of 1-anthroic acid in methanol at various concentrations. 1 : 8.8×10^{-4} mol/l, 2 : 4.4×10^{-5} mol/l, 3 : 2.2×10^{-5} mol/l, 4 : 1.1×10^{-5} mol/l, 5 : 4.4×10^{-7} mol/l. Excitation wavelength : 360 nm.

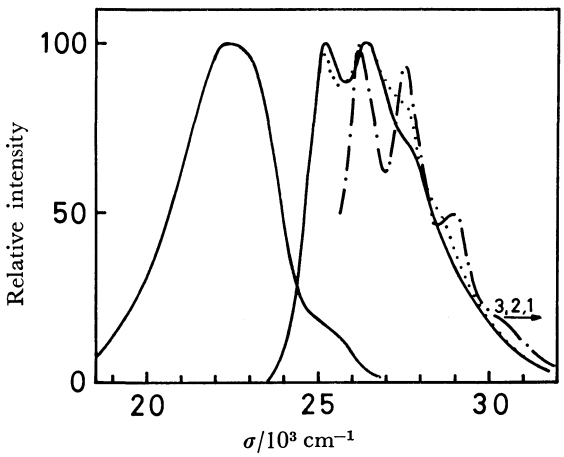

Fig. 4. The fluorescence and excitation spectra of 1-anthroic acid in methanol at 181 K. Solute concentration : 5.0×10^{-6} mol/l. 1 : Observed at 396 nm, 2 : observed at 440 nm, 3 : observed at 490 nm.

by the polarization study (see below).

It has well been established that carboxylic acids have pK_a values in ethanol larger by about 5.8 than in water.[17–19] The reported pK_a's are 3.7[20] and 3.69[21] for 1-anthroic acid and 4.2[20] and 4.18[21] for 2-anthroic acid. The pK_a's of 1- and 2-anthroic acids in ethanol are estimated to be 9.5 and 10.0, respectively. Proton dissociation can, therefore, be ruled out as the origin of the spectral changes in these solvents.

Fluorescence Spectra. Figure 3 shows the concentration dependence of the fluorescence of 1-anthroic acid in methanol. The fluorescence of 1-anthroic acid exhibits no vibrational structure at lower concentration and the mirror-image relationship between the absorption and fluorescence spectra is lost. A large Stokes shift is observed on increasing the concentration.

The excitation spectra of 1-anthroic acid in methanol at 181 K are shown in Fig. 4. The excitation spectrum monitored at the maximum of the fluorescence band

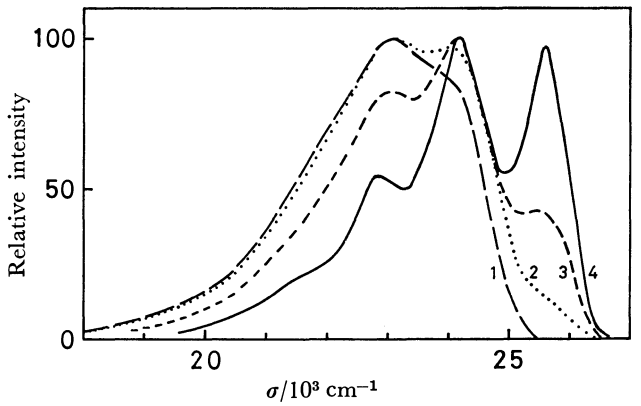

Fig. 5. The fluorescence spectra of 2-anthroic acid in ethanol at various concentrations. 1 : 4.0×10^{-4} mol/l, 2 : 9.9×10^{-5} mol/l, 3 : 4.0×10^{-5} mol/l, 4 : 4.0×10^{-6} mol/l. Excitation wavelength : 354 nm.

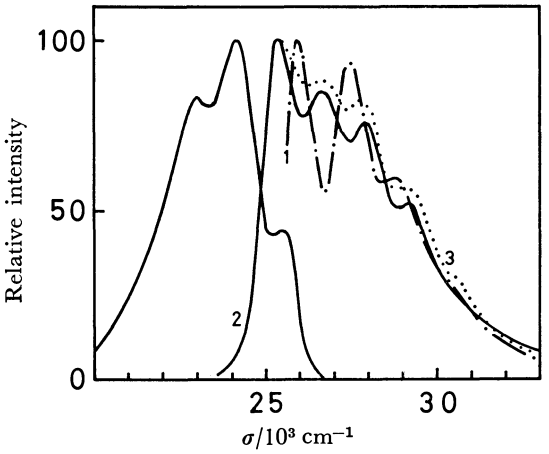

Fig. 6. The fluorescence and excitation spectra of 2-anthroic acid in ethanol at room temperature. Solute concentration : 4.0×10^{-5} mol/l. 1 : Observed at 395 nm, 2 : observed at 430 nm, 3 : observed at 460 nm.

corresponds to the dimer absorption spectrum. On the other hand, the excitation spectrum monitored at 396 nm corresponds to the monomer absorption spectrum. This indicates that the fluorescence observed at higher concentration is attributed to the dimer species.

The spectral dependence of the fluorescence of 2-anthroic acid on concentration is given in Fig. 5. The fluorescence of 2-anthroic acid has a vibrational structure at lower concentration. An approximate mirror-image relation of the fluorescence spectrum to the ^1L_b absorption band is observed. The fluorescence observed at lower concentration may therefore be assigned to the ^1L_b transition. On increasing the concentration, the fluorescence spectrum shifts to the red and becomes structureless. Figure 6 shows the excitation spectra of 2-anthroic acid in ethanol. The excitation spectrum corresponds to the monomer absorption band when monitored at 395 nm, while it corresponds to the dimer one when monitored at 430 nm. These findings indicate that the broad fluorescence can be assigned to the dimer fluorescence.

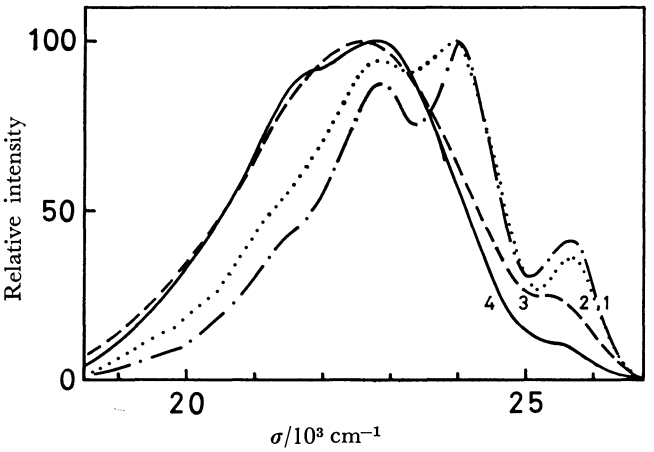

Fig. 7. The fluorescence spectra of 2-anthroic acid in ethanol at various temperatures. Solute concentration : 5.0×10^{-6} mol/l. Excitation wavelength : 360 nm. 1 : 293 K, 2 : 141 K, 3 : 109 K, 4 : 77 K.

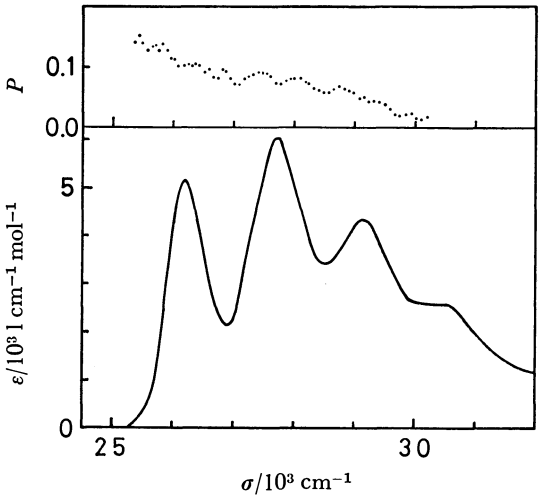

Fig. 8. The fluorescence excitation polarization spectra of 2-anthroic acid in ethanol at 152 K (upper) and the estimated monomer absorption spectrum (lower). Solute concentration : 6.8×10^{-6} mol/l. Observation wavelength : 420 nm.

Figure 7 shows the temperature dependence of the fluorescence of 1-anthroic acid in ethanol. Below the temperature at which the solvent freezes, the fluorescence of 1-anthroic acid has a vibrational structure. A mirror-image relationship between the absorption and fluorescence spectra is observed at lower temperature, although it is lost at room temperature. On the contrary to this, a mirror-image relation between the absorption and fluorescence spectra is observed in 2-anthroic acid at room temperature. These indicate that some geometrical relaxation occurs in 1-anthroic acid during its fluorescence lifetime.

X-Ray analysis of 1-naphthoic acid shows that the angle between the planes of the naphthalene ring and carboxyl group is 11°.[22] Steric hindrance in 1-anthroic acid to coplanarity of the carboxyl group and an aromatic ring should be similar to that of 1-naphthoic acid. An excited-state rotation of the carboxyl group into the plane of the anthracene ring may occur and

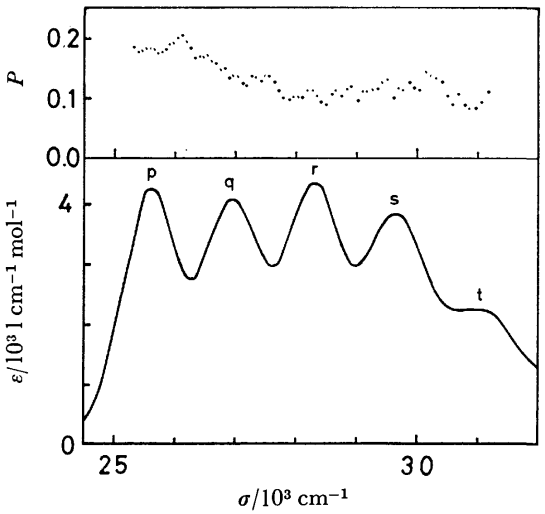

Fig. 9. The fluorescence excitation polarization spectra of 2-anthroic acid in ethanol at 156 K (upper) and the estimated dimer absorption spectrum (lower). Solute concentration : 4.7×10^{-5} mol/l. Observation wavelength : 480 nm.

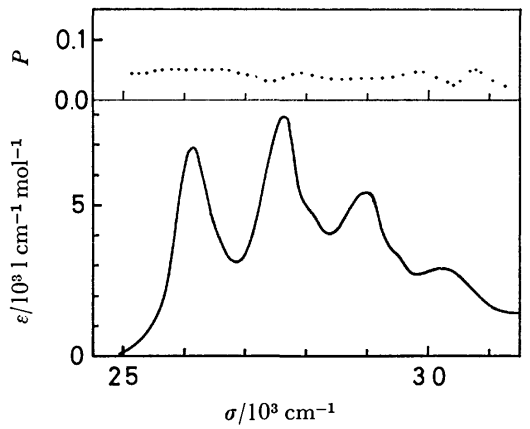

Fig. 10. The fluorescence excitation polarization spectra of 1-anthroic acid in methanol at 171 K (upper) and the estimated monomer absorption spectrum (lower). Solute concentration : 4.4×10^{-5} mol/l. Observation wavelength : 425 nm.

a structureless fluorescence is observed. Steric hindrance in 2-anthroic acid seems to be negligible and no geometrical relaxation upon excitation is expected to occur in 2-anthroic acid. Indeed, a mirror-symmetry relationship is observed in 2-anthroic acid even at room temperature. Any geometrical relaxation is impossible at sufficiently low temperature and, consequently, a mirror-symmetry relationship is observed in 1-anthroic acid at low temperature.

Figure 8 shows the fluorescence excitation polarization spectrum of 2-anthroic acid in ethanol at a concentration of 6.8×10^{-6} mol/l, together with the estimated monomer absorption spectrum. At such a low concentration, 2-anthroic acid exists substantially in the monomer form. The degree of polarization, P, decreases with increasing excitation energy. This suggests that two different electronic bands lie in this region. Figure 9 shows the fluorescence excitation spectrum of 2-anthroic acid at a concentration of 4.7×10^{-5} mol/l, together with the estimated dimer absorption spectrum. It appears from Fig. 2 that the 4.7×10^{-5} mol/l solution contains considerable amounts of dimer species. Furthermore, a 480-nm observation predominantly detects the fluorescence from dimer species. The polarization spectrum indicates that Bands p and q and Bands r, s, and t belong to different transitions.

The fluorescence excitation polarization spectrum of 1-anthroic acid in methanol is given in Fig. 10, together with the estimated monomer absorption spectrum. The concentration of the sample solution was 4.4×10^{-5} mol/l; 1-anthroic acid predominantly exists in monomer form. The value of P is relatively small, since the temperature is high compared with the freezing point of the solvent. The polarization spectrum has almost the same P values over the whole region of the lowest-frequency absorption band. The lowest-frequency absorption band appears to consist of a single electronic transition. The ^1L_a and ^1L_b bands of 1-derivatives of anthracene, in general, lie closely, the ^1L_b band being found at the lower energy side of the ^1L_a band.[13-15] There is no evidence of the ^1L_b band lying under the ^1L_a band in 1-anthroic acid. The ^1L_b band of 1-anthroic acid seems to have a very small oscillator strength owing to the steric hindrance described above. The same situation was encountered in 9-anthroic acid.

Kinetic Consideration. An excimer mechanism has been presented for the pronounced concentration dependence of 9-anthroic acid in alcoholic solvents.[4] 9-Anthroic acid forms a hydrogen-bonded dimer in its ground state. The monomer species show the structured fluorescence. The red-shifted broad fluorescence was assigned to the excimer which is formed by the association of the excited and unexcited hydrogen bonded dimers. It was shown that the ratio of the intensity of the excimer fluorescence to that of the monomer fluorescence, $R=I_E/I_M$, is proportional to $[D]^{3/2}$ at low dimer concentrations, where I_E and I_M refer to the fluorescence intensity of the excimer and the monomer, respectively.[4] When the broad fluorescence is attributed to the dimer, on the other hand, it can easily be shown that the ratio R is proportional to [D].

The corrected fluorescence spectra at various concentrations were divided into the monomer and dimer components, the spectral shapes of which are assumed to be the same as the corrected fluorescence spectra observed at the lowest and the highest concentration. Figure 11 gives the log R plots *vs.* log [D] for 1- and 2-anthroic acids. It is seen from the figures that the slope of the plots is 1 for both 1- and 2- anthroic acids. These observations indicate that no excimer-type fluorescence is observed in 1- and 2-anthroic acids in contrast to 9-anthroic acid.

The sufficient overlap of the two anthracene rings constituting the hydrogen-bonded dimers is essential to the formation of stable excimers. The hydrogen-bonded dimers of 1- and 2-anthroic acids may have two types of conformations which are *cis-* and *trans-*

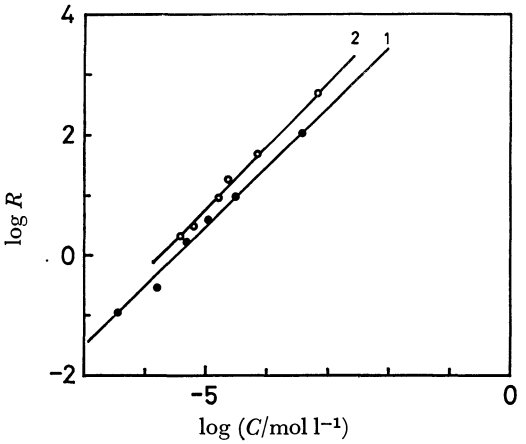

Fig. 11. The log R plots *vs.* log [D]. 1 : 1-Anthroic acid in methanol, 2 : 2-anthroic acid in ethanol.

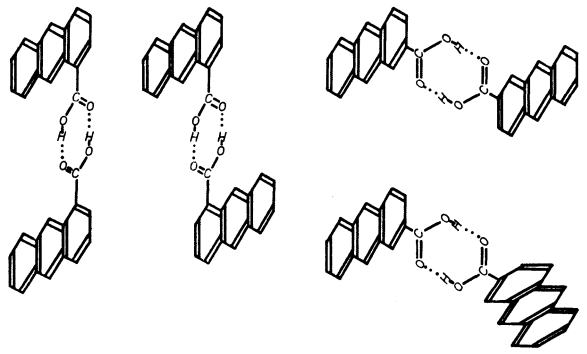

Fig. 12. The types of dimer conformations.

forms relative to $-C\begin{matrix}\diagup O\cdots HO\diagdown \\ \diagdown OH\cdots C\diagup\end{matrix}C-$ linkages, while 9-anthroic acid forms a single type of dimers (see Fig. 12). This decreases the possibilities of excimer formation in 1- and 2-anthroic acids compared with 9-anthroic acid, because the presence of two types of dimer conformations decreases the possibility for encounter of the same type of dimers. Furthermore, the molecular rotation necessary for the two pairs of anthracene rings to overlap sufficiently is generally greater in 1- and 2-anthroic acids than in 9-anthroic acid. For example, when the planes of two dimers are parallel, the complete overlap of two anthracene rings can be realized by the in-plane rotation less than 45° with respect to the other in 9-anthroic acid. In the case of 1- and 2-anthroic acids, on the other hand, the complete overlap is not always realized by the in-plane rotation; sometimes it is necessary to reverse one dimer molecule with respect to the other. This further decreases the possibility of excimer formation in 1- and 2-anthroic acids than in 9-anthroic acid.

The ground-state dimer formation in alcoholic solvents is confirmed in 1- and 2-anthroic acids as well as in 9-anthroic acid. No excimer-type fluorescence is observed in 1- and 2-anthroic acids in contrast to 9-anthroic acid. This is interpreted by the variety of dimer conformations in 1- and 2-anthroic acids. The lack of mirror-symmetry relationship between the absorption and fluorescence spectra of 1-anthroic acid is explained by the geometrical relaxation in its excited state.

References

1) N. S. Bazilevskaya and A. S. Cherkasov, *Opt. Spectrosc.*, **18**, 30 (1965).
2) N. S. Bazilevskaya and A. S. Cherkasov, *Zh. Prikl. Spektrosk., Akad. Nauk Berlorussk, SSR* **3**, 548 (1965).
3) T. C. Werner and D. M. Hercules, *J. Phys. Chem.*, **73**, 2005 (1969).
4) S. Suzuki, T. Fujii, N. Yoshiike, S. Komatsu, and T. Iida, *Bull. Chem. Soc. Jpn.*, **51**, 2460 (1978).
5) S. Suzuki, T. Fujii, and N. Yoshiike, *Chem. Phys. Lett.*, in press.
6) T. C. Werner and D. M. Hercules, *J. Phys. Chem.*, **74**, 1030 (1970).
7) E. B. Barvett, J. W. Cook, and H. H. Graingen, *Chem. Ber.*, **57**, 1775 (1924).
8) E. A. Coulson, *J. Chem. Soc.*, **1930**, 1931.
9) A. C. Albrecht, *J. Mol. Spectrosc.*, **6**, 84 (1961).
10) A. K. Kalantar and A. C. Albrecht, *Ber. Bunsenges. Phys. Chem.*, **68**, 361 (1964).
11) F. Dörr, *Angew. Chem.*, **78**, 457 (1966).
12) F. Dörr in "Creation and Detection of the Excited States," ed by A. A. Lamola, Marcel Dekker, New York, N. Y. (1971), Vol. 1, Part A, Chap. 2.
13) H. Hosoya, J. Tanaka, and S. Nagakura, *J. Mol. Spectrosc.*, **8**, 257 (1962).
14) H. Baba and S. Suzuki, *J. Chem. Phys.*, **35**, 1501 (1961).
15) H. Baba and S. Suzuki, *Bull. Chem. Soc. Jpn.*, **35**, 684 (1962).
16) S. Suzuki and H. Baba, *J. Chem. Phys.*, **38**, 349 (1963).
17) G. Charlot and B. Trémillon, "Les Reactions Chimiques dans les Solvants et les Sels Fondus," Gauthier-Villars and Cie, Paris (1963), Chap. 10.
18) R. B. Heslop and P. L. Robinson, "Inorganic Chemistry," 3rd ed, (1967), p. 242.
19) B. W. Clare, D. Cook, E. C. F. Ko, Y. C. Mac, and A. J. Parker, *J. Am. Chem. Soc.*, **88**, 1911 (1966).
20) E. Vander Donckt and G. Proter, *Trans. Faraday Soc.*, **64**, 3218 (1968).
21) K. Lauer, *Ber. B*, **70**, 1288 (1937).
22) J. Trotter, *Acta Crystallogr.*, **13**, 732 (1962).

The Formation of Mg-bearing Ferrite by the Air Oxidation of Aqueous Suspensions

Ken KANEKO* and Takashi KATSURA

Department of Chemistry, Tokyo Institute of Technology, Ookayama, Meguro-ku, Tokyo 152

(Received June 21, 1978)

When the Mg^{2+}/Fe_{total} molar ratio in the initial aqueous suspension is below 0.1 at pH 9.0 and 65 °C, almost all Mg^{2+} is incorporated into the spinel type ferrite by the air oxidation of $Fe(OH)_2$. The chemical composition of the Mg-bearing ferrite thus obtained is not stoichiometric, and is expressed as the $MgFe_2O_4$–Fe_3O_4–γ-Fe_2O_3 system. When the Mg^{2+}/Fe_{total} ratio exceeds 0.1, the excess Mg^{2+} produces a basic magnesium sulfate which has a composition of $[Mg^{2+}_{1.00}, Na^{+}_{0.64}]\,[OH^{-}_{1.36}, (SO_4^{2-})_{0.64}]$. At pH 8.0, a small amount of the Mg^{2+} is incorporated into the ferrite, between pH 9.0 and 10.0 only the Mg-bearing ferrite is formed, and at pH 11.0, the α-FeOOH type compound is formed together with the Mg-bearing ferrite.

Recently, the formation of the spinel type ferrites from aqueous suspensions have been extensively studied.[1–5] Mn and Co ferrites have been synthesized by the air oxidation of the $Fe(OH)_2$ aqueous suspensions containing these metal ions by Kiyama.[5]

Feitknecht[6] studied in detail the formation of the iron oxides and presented the optimum conditions to form magnetite (Fe_3O_4) from the aqueous suspension of $Fe(OH)_2$. Kiyama[7] clarified the temperature dependence of the formation of Fe_3O_4 and pointed out that higher temperatures are more favorable. Recently, more favorable reaction conditions for the formation of Fe_3O_4 have been studied using some weak dispersing reagents.[8] The optimum conditions for the formation of the spinel type ferrites containing various heavy elements from aqueous suspensions appears to differ from those of Fe_3O_4, and are dependent on the pH value, temperature and the concentration of the metal ions in the $Fe(OH)_2$ aqueous suspension.

The complete removal of the heavy metal ions by means of the ferrite formation process is important not only for the basic study but also for the treatment of the concentrated waste water by the "Ferrite Process."[9]

In this study, the formation of the Mg-bearing ferrite from the aqueous suspension of $Fe(OH)_2$ by air oxidation has been investigated in the presence of various concentrations of magnesium at pH values ranging from 8 to 11 at 65 °C. On the basis of these results, the most favorable conditions for the formation of the Mg-bearing ferrite are presented.

Experimental

Reagents. Chemical reagents of analytical grades were used. A 2 mol/dm³-NaOH solution was prepared by dissolving NaOH in distilled water free from CO_2 and O_2. A 0.863 mol/dm³ of $MgSO_4$ solution was prepared using $MgSO_4 \cdot 7H_2O$.

Apparatus. The Dewar reaction vessel used is shown in Fig. 1. The temperature of the vessel was kept constant at 65 °C by circulating warm water at just 65 °C through the outer jacket. The inner flask with a semi-spherical bottom (300 cm³) was closed with a silicone-rubber stopper incorporating a stirring apparatus(A), a N_2- or air-introducing tube (B), a condenser(C), a platinum electrode(D), a glass electrode (E), a calomel electrode with double junction(F) and a buret(G).

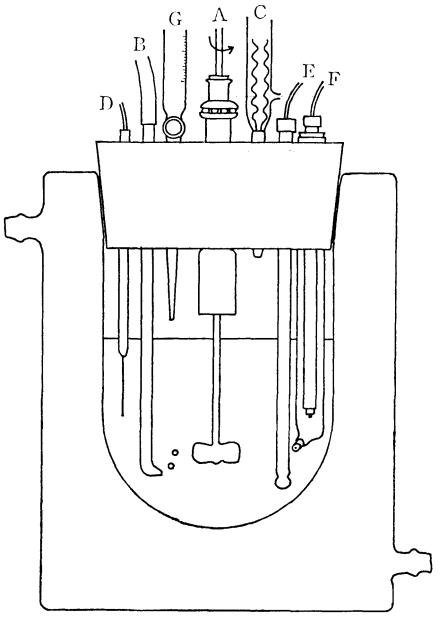

Fig. 1. The reaction vessel with a silicone stopper. A : Stirring apparatus, B : N_2- or air-introducing tube, C : reflux condenser, D : platinum electrode, E : glass electrode, F : calomel electrode(double junction type), G : buret.

Procedure. After addition of the distilled water and the solutions of $MgSO_4$ and Na_2SO_4, nitrogen gas was bubbled into the solution with stirring at 1000 r.p.m. for 1 h to remove the dissolved gases of carbon dioxide and oxygen. Then, $FeSO_4 \cdot 7H_2O$ (12 g) was added to the solution and dissolved completely. The resultant volume of the solution was 200 cm³, and the total concentration of SO_4^{2-} was fixed at 65 mmol/200 cm³ (this solution is termed the initial solution). The pH was adjusted using 2 mol/dm³ NaOH solution. After standing for 1 h with stirring under nitrogen 65 °C, the oxidation of the ferrous ion was initiated by passing air into the suspension instead of nitrogen at the rate of 0.20 dm³/min. During the oxidation, the pH value was kept constant by the addition of 2 mol/dm³ NaOH or 0.5 mol/dm³ H_2SO_4 solution, and the oxidation potential(ORP) was measured. At the end of the oxidation reaction, the ORP value increased rapidly from about −800 mV to nearly 0 mV (measured by Pt-calomel electrodes). Figure 2 illustrates the relationship between the Fe^{2+}/Fe_{total} value and the oxidation time (min). As seen the rapid increase of the ORP indicates an abrupt change in the oxidation rate. The detailed study of the ORP change will be reported in the near future. In

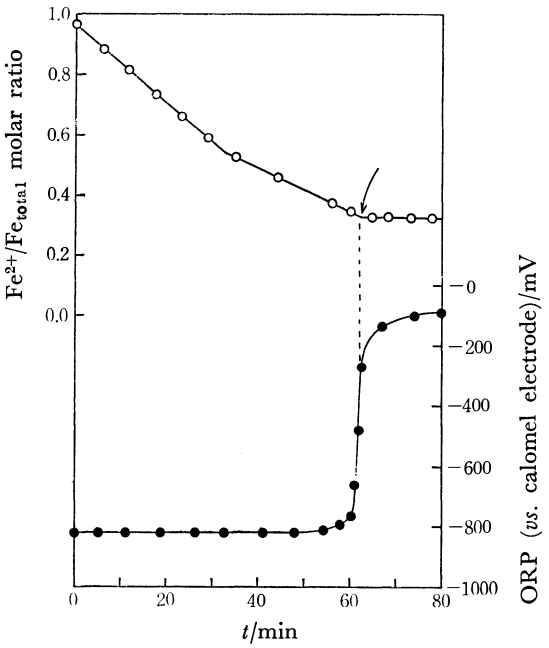

Fig. 2. The relationship between the Fe^{2+}/Fe_{total} molar ratio in suspension (the initial solution contains $Fe(OH)_2$ alone). An arrow means the end point of the formation of ferrite.

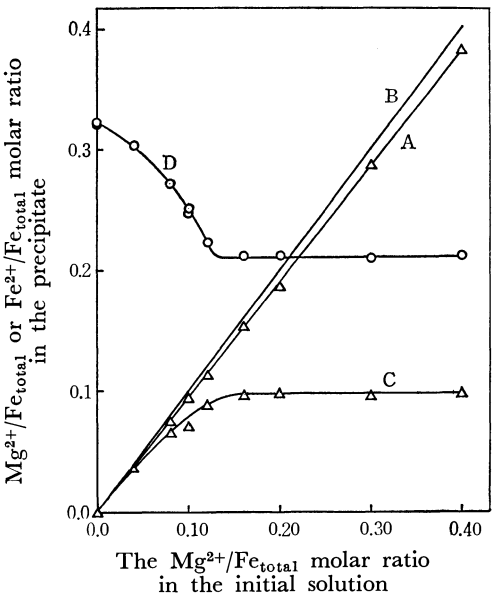

Fig. 3. The relationship between the Mg^{2+}/Fe_{total} molar ratio in the initial solution and the Mg^{2+}/Fe_{total} or Fe^{2+}/Fe_{total} molar ratio in the Precipitates A and B. Curve A: The Mg^{2+}/Fe_{total} molar ratio in the Precipitate A, Curve B: the Mg^{2+}/Fe_{total} molar ratio in the initial solution, Curve C: the Mg^{2+}/Fe_{total} molar ratio in the Precipitate B, Curve D: the Fe^{2+}/Fe_{total} molar ratio in the Precipitate B.

the present study, the air oxidation was stopped 10 min after the abrupt change in the ORP value and then nitrogen gas was passed through the suspension in place of the air. An aliquot of the suspension was removed and immediately centrifuged (3000 r.p.m.). The precipitate thus obtained is referred to as Precipitate A in this paper. The suspension containing Precipitate A was treated with 0.5 mol/dm^3-H_2SO_4 solution to lower the pH value of the suspension to 5.0. At this time, 0.5 mol/dm^3 H_2SO_4 solution was added very slowly at the rate of 0.1—1.0 cm^3/15 min. The obtained suspension was then centrifuged (3000 r.p.m.). The precipitate thus obtained is referred to as Precipitate B. Precipitates A and B were dried *in vacuo* at room temperature.

Chemical Analysis. The Fe^{2+} and Fe^{3+} contents in the Precipitates A and B were determined by the method described by Katsura.[10] When necessary, the spectrophotometric method using 2,2′-bipyridyl[11] or the gravimetric method was applied. The magnesium content was determined by EDTA titration after removal of iron from solution as tris(8-quinolinolato)iron(III) or iron(III) hydroxide. Sodium and sulfate ions were determined by flame-photometry and gravimetry(as $BaSO_4$), respectively.

Precipitates A and B were examined by the X-ray powder diffraction method using Fe *Kα* radiation. The Curie point of Precipitate B was measured *in vacuo*, and the saturation magnetization was measured at room temperature in comparison with Ni as standard.

Results and Discussion

The Oxidation Products at pH *9.0.* Mg-bearing ferrites were prepared at pH 9.0 and at 65 °C by varying the Mg^{2+}/Fe_{total} molar ratio, the results of which are shown in Fig. 3. As shown by Curve A in Fig. 3, the Mg^{2+} content in Precipitate A increases linearly with increasing concentration of Mg^{2+} in the initial solution. The initial concentration of Mg^{2+} before the air oxidation is also given by Curve B in Fig. 3, and Curve B is very similar to Curve A, indicating that almost all the Mg^{2+} added to the initial solution was incorporated into Precipitate A. The Mg^{2+}/Fe_{total} ratio in Precipitate B is also given by Curve C in Fig. 3. As seen in Curve C, the concentration of Mg^{2+} in Precipitate B increases with increasing concentration of Mg^{2+} in the initial solution when the Mg^{2+}/Fe_{total} ratio in the initial solution is sufficiently low. However, when the Mg^{2+}/Fe_{total} ratio is higher than 0.1, the ratio in Precipitate B gives a constant value of about 0.1, suggesting that Precipitate A is composed of a heterogeneous mixture of a soluble and an insoluble Mg compound at pH 5.0.

The X-ray diffraction patterns of Precipitates A and B at conditions below the Mg^{2+}/Fe_{total} ratio of 0.15 were almost identical and all peaks corresponded to those of the spinel type structure. An example is given by A in Fig. 4. In the patterns of Precipitate A which has a Mg^{2+}/Fe_{total} ratio of 0.3, there are two distinct additional peaks other than those of the Mg-bearing ferrite. An example is given by B in Fig. 4. These small and broadened peaks could not assigned, but in the patterns of Precipitate B having the same Mg^{2+}/Fe_{total} ratio, these two peaks disappeared as shown by C in Fig. 4. This suggests that Precipitate A contains some Mg-bearing compound which is soluble at pH 5.0. In addition, the amount of iron dissolved from Precipitate A was negligibly small at pH 5.0, indicating the absence of iron-bearing compounds in Precipitate A other than Mg-bearing ferrite. The chemical composition of the soluble Mg-bearing compound was determined to be $[Mg^{2+}_{1.00}, Na^{+}_{0.64}][OH^{-}_{1.36}, (SO_4^{2-})_{0.64}]$ on the basis of the differences between the

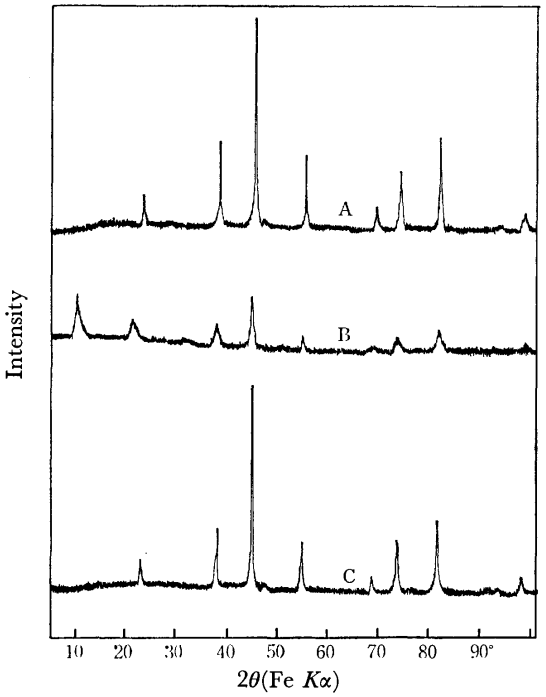

Fig. 4. The X-ray powder diffraction patterns of the Precipitates A and B. Pattern A : For the Precipitate A obtained at the Mg^{2+}/Fe_{total} molar ratio of 0.1, Pattern B : for the Precipitate A at the ratio of 0.3, Pattern C : for the Precipitate B obtained at the ratio of 0.3.

chemical compositions of Precipitates A and B. Here the number of hydroxy entities has been estimated based on the electrical neutrality. This estimation will be discussed in a later section of this paper.

The relationship between the Fe^{2+}/Fe_{total} molar ratio in Precipitate B and the Mg^{2+}/Fe_{total} ratio in the initial solution is given by Curve D in Fig. 3. As seen the amount of Fe^{2+} relative to the total concentration of iron in Precipitate B decreases with increasing concentration of Mg^{2+} in the initial solution becoming constant at approximately 0.21 of the Fe^{2+}/Fe_{total} ratio. Thus, Curves C and D are in good agreement with each other. Moreover, the fall in concentration of Fe^{2+} is approximately equal to the rise in concentration of Mg^{2+}. These results indicate the high possibility that the Mg-bearing ferrite is formed during the course of the air oxidation and that the Mg^{2+} replaces the Fe^{2+} in the crystal lattice of the spinel structure. The formation of the solid solution between Fe_3O_4 and $MgFe_2O_4$ is narrowly limited to below 0.1 measured by the Mg^{2+}/Fe_{total} ratio. It is easy however to synthesize the complete solid solution at high temperatures above 1000 °C.[12] In addition, the composition of Fe_3O_4 (magnetite), formed from the $Fe(OH)_2$ suspended solution by air oxidation, is usually non-stoichiometric, tending to form the γ-Fe_2O_3 component with a spinel structure. Thus, it is necessary to analyze Fe^{2+}, Fe^{3+}, and Mg^{2+} in solid solution to obtain the composition as a ternary system. In the present work, the maximum solid solubility of the component $MgFe_2O_4$ has been caluculated to be 0.249 $MgFe_2O_4 \cdot 0.541$ $Fe_3O_4 \cdot 0.210$ γ-Fe_2O_3 implying that the solid solution is appreciably non-stoichiometric in

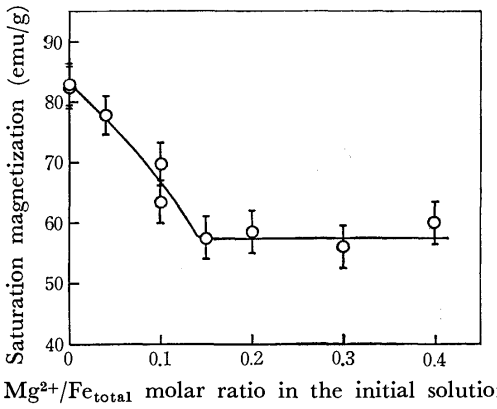

Fig. 5. The magnetization of the Precipitate B with various amounts of Mg^{2+} (at room temperature).

composition.

Saturation Magnetization. Precipitate B is a ferromagnet at room temperature. The temperature dependence of the magnetization of Precipitate B obtained at the Mg^{2+}/Fe_{total} ratio of 0.3 was measured under 4000 Oe of the external magnetic field(1 Oe= $(1000/4\pi)$A/m) and *in vacuo*. The Curie temperature was found to be approximately 568 °C. The magnetization of Precipitate B formed from the initial solution with varying Mg^{2+}/Fe_{total} ratios was also measured at room temperature, the results of which are shown in Fig. 5. As seen the magnetization at room temperature decreases with increasing concentration of Mg^{2+} in the initial solution, but in the range of Mg^{2+}/Fe_{total} ratio from 0.1 to 0.4, the magnetization becomes constant at about 60 emu/g(1 emu/g=10^{-7} Tm^3/kg). This value is intermediate between those of $MgFe_2O_4$ (27 emu/g at 20 °C), Fe_3O_4(92 emu/g at 20 °C), and γ-Fe_2O_3(82.5 emu/g at 0 K). The results obtained from the magnetic properties are in good agreement with those obtained from chemical analysis and the X-ray analysis previously described. It may thus be concluded that at the Mg^{2+}/Fe_{total} ratio below 0.1, almost all Mg^{2+} in the initial solution is incorporated into the spinel type structure by replacement of Fe^{2+}. Above 0.1, the excess Mg^{2+} does not replace the Fe^{2+} which is constructing the spinel type structure.

Non-stoichiometry in the Mg-bearing Ferrite Composition. It is convenient to illustrate the non-stoichiometry in the Mg-bearing ferrite using three components as the Fe_3O_4–Fe_2O_3–$MgFe_2O_4$ system. The results are shown in Fig. 6. The letter at each point in Fig. 6 corresponds to the Mg^{2+}/Fe_{total} in the initial solution, and the broken line indicates an oxygen reaction lines as an example. When the stoichiometric composition of the Fe_3O_4–$MgFe_2O_4$ solid solution was obtained, the composition of the product must be on the Fe_3O_4–$MgFe_2O_4$ line. As clearly seen in Fig. 6, the Mg-bearing ferrite is appreciably oxidized while maintaining a spinel type structure, and the degree of oxidation increases with increasing $MgFe_2O_4$ component.

pH *Change during Reaction.* In general, as indicated by Katsura *et al.*,[9] the pH of the suspension decreases with air oxidation. However, when the initial solution contains Mg^{2+}, the pH increases gradually in the early stages of the air oxidation and then falls.

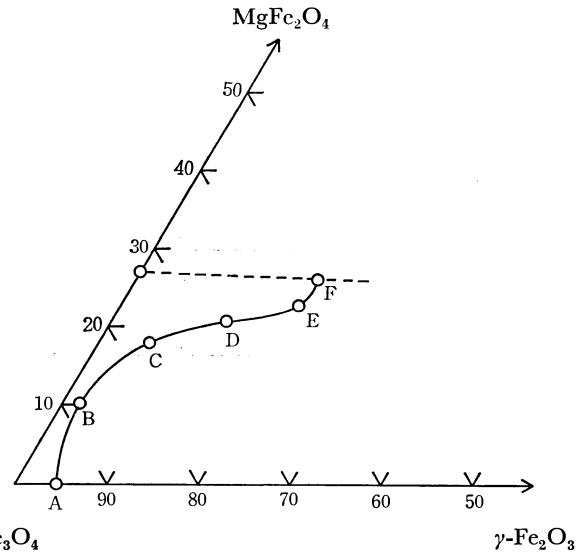

Fig. 6. The chemical compositions of the Precipitates B expressed as the Fe_3O_4–Fe_2O_3–$MgFe_2O_4$ system. Points A, B, C, D, E, and F were obtained at the Mg^{2+}/Fe_{total} molar ratios of 0.00, 0.04, 0.08, 0.10, 0.12, and above 0.15, respectively. The broken line shows *the oxygen reaction line.*

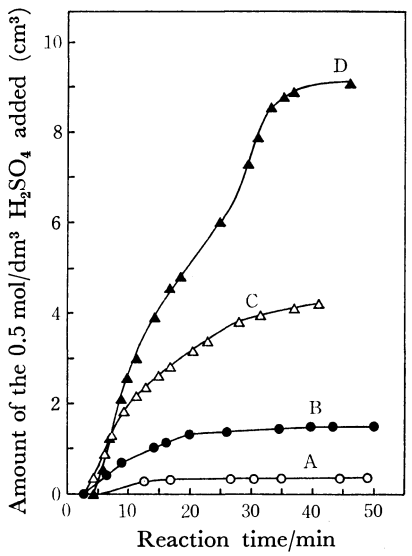

Fig. 7. The relationship between the reaction time and the amount of 0.5 mol/dm³ H_2SO_4 solution added to the suspension to keep the pH value of the initial solution constant at pH 9.0. Curves A, B, C, and D were obtained at the Mg^{2+}/Fe_{total} molar ratios of 0.1, 0.2, 0.3, and 0.4, respectively.

In this study, a 0.5 mol/dm³ H_2SO_4 solution was added at an early stage in the reaction to maintain the pH at 9.0. Figure 7 illustrates the relationship between the reaction time and the amount of 0.5 mol/dm³ H_2SO_4 solution necessary to maintain the pH at 9.0. The amount of 0.5 mol/dm³ H_2SO_4 solution in Fig. 7 indicates the total amount of solution added at each reaction time. The curves A, B, C, and D show the results corresponding to varying the Mg^{2+}/Fe_{total} ratios; 0.1, 0.2, 0.3, and 0.4, respectively. As seen in Fig. 7, the pH did not change for about 4 min from the starting time irrespective of the Mg^{2+}/Fe_{total} ratio. However, when the Mg^{2+}/Fe_{total} ratio exceeded 0.1, rapid increases in the 0.5 mol/dm³ H_2SO_4 solution were necessary to maintain the pH at 9.0, and the amount of 0.5 mol/dm³ H_2SO_4 solution added depended on the Mg^{2+}/Fe_{total} ratio in the initial solution. In the case of A, the amount of the H_2SO_4 solution added was very small (0.36 cm³), and the addition of H_2SO_4 solution ceased at about 15 min after the reaction was initiated. In a previous section, it was suggested that Precipitate A contains a basic Mg-bearing sulfate with the composition of $[Mg^{2+}_{1.00}, Na^{+}_{0.64}][OH^{-}_{1.36}, (SO_4^{2-})_{0.64}]$ (hereafter compound A). On the basis of these experimental results, the following schematic equation has been postulated for the change in pH of the suspension in the early stages of oxidation,

$$3Fe(OH)_2 + 3x\cdot Mg(OH)_2 + 1.92(x-y)\cdot Na_2SO_4 + \frac{1+y}{2}\cdot O_2 \rightarrow (1+y)\cdot[Mg^{2+}_{3y/(1+y)}Fe^{2+}_{(1-2y)/(1+y)}Fe^{3+}_2O_4] + 3(1-y)\cdot A + 1.92(x-y)\cdot NaOH + 3(1+x-0.64)\cdot H_2O \quad (x>0.1), \quad (1)$$

where x and y are the Mg^{2+}/Fe_{total} ratios in the initial solution and the spinel type Mg-bearing solid solution, respectively. It is evident from Eq. 1 that some amount of Na_2SO_4 in the initial solution should be consumed to form compound A. The calculated amount of 0.5 mol/dm³ H_2SO_4 solution was obtained on the basis of Eq. 1 at the molar ratios of 0.2, 0.3, and 0.4 and the values obtained are summarized in Table 1. As seen in Table 1, the calculated values are in reasonable agreement with the experimental values within experimental error strongly supporting the validity of Eq. 1 in representing the oxidation process occurring in the suspension at the early stage when the Mg^{2+}/Fe_{total} ratio in the solution exceeds 0.1.

TABLE 1. TOTAL AMOUNTS OF THE 0.5 mol/dm³ H_2SO_4 SOLUTION CONSUMED TO KEEP THE pH CONSTANT IN THE COURSE OF THE OXIDATION REACTION

Amount of Mg^{2+} in the initial solution (Mg^{2+}/Fe_{total})	Experimental value (cm³)	Theoretical value evaluated from Eq. 1 (cm³)
0.20	1.5	2.42
0.30	4.15	5.33
0.40	9.10	7.89

As previously reported when the Mg^{2+}/Fe_{total} ratio in the initial solution is below 0.1, all the Mg^{2+} is completely incorporated into the spinel type structure to form Mg-bearing ferrite solid solution. Consequently there is no need to consume H_2SO_4 solution to maintain the pH in the suspension, and no magnesium basic sulfate A is formed. Thus, the oxidation reaction may be represented as the following when the Mg^{2+}/Fe_{total} ratio in the initial solution is below 0.1.

$$3Fe(OH)_2 + 3x\cdot Mg(OH)_2 + \frac{(x+1)}{2}\cdot O_2 \rightarrow (x+1)\cdot[Mg^{2+}_{3x/(x+1)}Fe^{2+}_{(1-2x)/(x+1)}Fe^{3+}_2O_4] + 3(x+1)\cdot H_2O \quad (x<0.1). \quad (2)$$

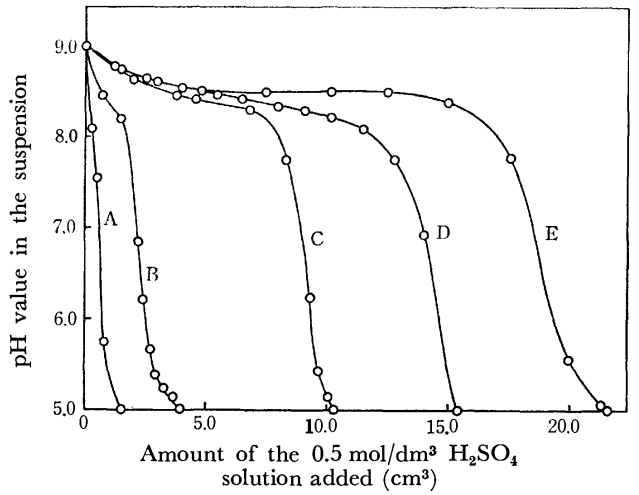

Fig. 8. The relationship between the pH changes of the suspensions containing the Precipitate A and the amount of 0.5 mol/dm³ H_2SO_4 solution. Curves A, B, C, D, and E were obtained at the Mg^{2+}/Fe_{total} molar ratios of 0.04, 0.1, 0.2, 0.3, and 0.4, respectively.

Dissolution of Compound A. Figure 8 demonstrates the relationship between the change in pH of the suspended solution containing Precipitate A and the added amount of 0.5 mol/dm³ H_2SO_4 solution. The curves A, B, C, D, and E show the pH change curves at Mg^{2+}/Fe_{total} ratios of 0.04, 0.1, 0.2, 0.3 and 0.4 at pH 9.0, respectively. As seen in Fig. 8, a smooth plateau exists in the pH range from 8.0 to 8.5 when the Mg^{2+}/Fe_{total} ratios are above 0.2. These results may indicate that compound A is formed at higher concentrations of Mg^{2+} and that compound A appears to consist of one phase considering the smooth plateau at pH 8.5. It is reasonable to assume that the amounts of 0.5 mol/dm³ H_2SO_4 solution consumed to lower the pH of the suspension to 5.0 correspond to the amounts of OH^- of compound A. Consequently the OH^-/Mg^{2+} ratio has been determined in each suspension for Mg^{2+}/Fe_{total} ratios of 0.2, 0.3, and 0.4, and 1.30 obtained as an average value. This ratio is in good agreement with that estimated by chemical analysis, $[Mg^{2+}_{1.00}, Na^{+}_{0.64}][OH^{-}_{1.36}, (SO_4^{2-})_{0.64}]$.

The pH Dependence of Precipitate A. In the preceding sections, the properties of Precipitate A formed at pH 9.0 and 65 °C have been discussed. In subsequent experiments the pH was changed from 8.0 to 11.0 at constant temperature. The Mg^{2+}/Fe_{total} ratio in the initial solution was fixed at 0.1. Curve A in Fig. 9 illustrates the relationship between the Mg^{2+}/Fe_{total} ratio in Precipitate A and the pH value of the suspension, and Curve B that for Precipitate B. As seen in Curves A and B in Fig. 9, the Mg^{2+}/Fe_{total} ratio in Precipitates A and B is almost constant (0.1 to 0.095) in the pH range 9.0 to 11.0, but at pH 8.0 the ratio was lowered to 0.02 and 0.01 in Precipitates A and B, respectively. The implication is that the incorporation of Mg^{2+} into Precipitate B having a spinel type structure is strongly influenced by a lowering of the pH. Some appreciable but small differences in composition are seen between Precipitates A and B, even in the high pH range 9.0 to 11.0. This small

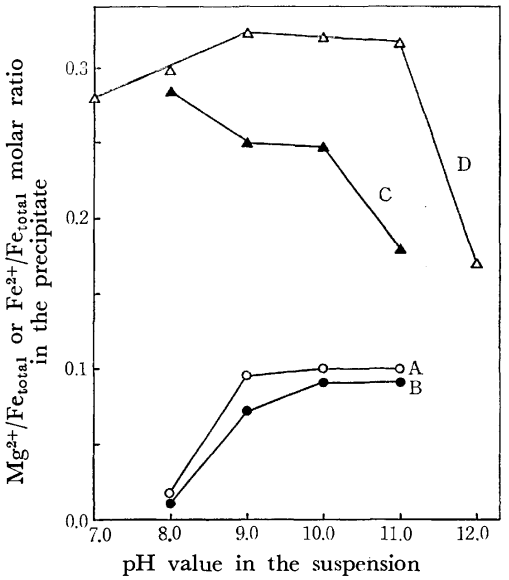

Fig. 9. The relationship between the pH value of the suspension and the chemical composition of the Precipitates A and B. The Mg^{2+}/Fe_{total} molar ratio in the initial solution is fixed to 0.1. Curve A : The ratio in the Precipitate A, Curve B : the ratio in the Precipitate B, Curve C : the Fe^{2+}/Fe_{total} molar ratio in the Precipitate B, Curve D : the Fe^{2+}/Fe_{total} molar ratio in the precipitate formed by the air oxidation of the $Fe(OH)_2$ suspension without Mg^{2+}.

difference may be attributed to the presence of small amounts of compound A included in Precipitate A.

Curve C in Fig. 9 illustrates the relationship between the Fe^{2+}/Fe_{total} ratio in Precipitate B and the pH value in the suspension. At pH 8.0 the Fe^{2+}/Fe_{total} ratio was 0.285. This means that the $(Mg^{2+}+Fe^{2+})/(Mg^{2+}+Fe_{total})$ ratio for this sample is 0.292 which is close to that for the Fe_3O_4 compound. In the case of pH 11.0, the Mg^{2+}/Fe_{total} ratio was 0.1 and the Fe^{2+}/Fe_{total} ratio 0.180, and so the $(Mg^{2+}+Fe^{2+})/(Mg^{2+}+Fe_{total})$ ratio becomes 0.254. This decrease in value is caused by the oxidation of Precipitate B with or without change in crystal structure. Thus, it is evident from Curve C in Fig. 9 that Precipitate B, prepared at relatively high pH is oxidized.

According to the powder X-ray diffraction patterns, the peaks were all of the spinel type when Precipitate B was prepared in the pH range 8.0 to 10.0. Precipitate B prepared at pH 11.0 however contained the α-FeOOH type together with the spinel type compound. Thus it is evident that when Precipitate A is prepared at relatively high pH, such as 11 or greater, then the Fe^{2+} in the Precipitate A is oxidized to form the α-FeOOH type but not the γ-Fe_2O_3 type compound.

As a comparison, the results shown in Curve C in Fig. 9, the Fe^{2+} content in the precipitate formed by the air oxidation of the $Fe(OH)_2$ suspension without magnesium at various values of pH(7 to 12) and at 65 °C were determined, the results of which are shown by Curve D in Fig. 9. As seen the Fe^{2+}/Fe_{total} ratio in the precipitates gradually increased with increasing pH of the suspension (from 7 to 9), after which the ratio remained constant (0.323) in the pH interval

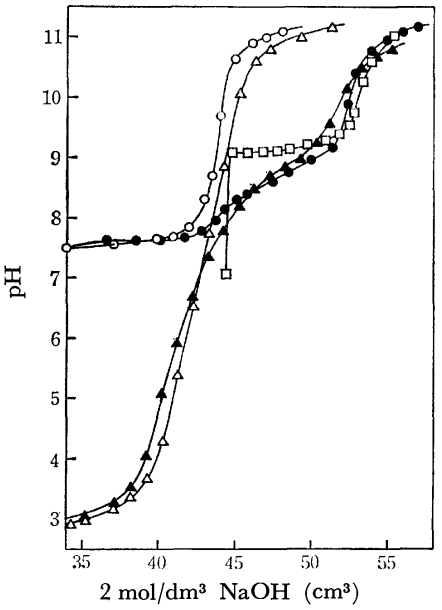

Fig. 10. Titration curves of Fe(II), Fe(II)+Mg(II), Fe(III), Fe(III)+Mg(II) and Mg(II) solutions by the 2 mol/dm³-NaOH solution. Open circle: 4.31×10^{-2} mol of Fe(II), Closed circle : 4.31×10^{-2} mol Fe(II)+ 8.63×10^{-3} mol Mg(II), Open triangle : 2.88×10^{-2} mol Fe(III), Closed triangle : 2.88×10^{-2} mol Fe(III) $+8.63\times10^{-3}$ mol Mg(II) and Open square : 8.63×10^{-3} mol Mg(II). The titration curve of Mg-(II) solution is shown from the titer of 44.3 cm³ to compare with the others. The initial volume of the solutions was fixed to 200 cm³.

from 9 to 11. At pH 12.0 however the ratio sharply decreased to 0.170. From a comparison of Curve C and Curve D, it may be concluded that the α-FeOOH type compound is liable to form in the presence of Mg^{2+}.

Hydrolysis of Magnesium in $Fe(OH)_2$ Suspension. The hydrolysis of Mg^{2+} in the course of formation of Precipitate A, was studied using the titration curves of the solution containing only Mg^{2+} and $Mg^{2+}+Fe^{2+}$ at 65 °C. The hydrolysis may enable an interpretation of the low concentration of Mg^{2+} in the Precipitates A and B when the precipitates were prepared at relatively low pH, the results of which are shown in Fig. 10. As evident from Fig. 10, Mg^{2+} was titrated at pH 9.1 to 9.3, but when the solution contained Fe^{2+} together with Mg^{2+}, both ions were titrated at 8.0 to 9.0. This lowering of the pH value is due to the co-precipitation of Mg^{2+} with Fe^{2+}. In the presence of Fe^{2+}, the hydrolysis of Mg^{2+} is therefore completed at pH 9.0, but not at 8.0, suggesting that the unhydrolyzed Mg^{2+} is not incorporated into the spinel type ferrite structure.

Feitknecht[6] demonstrated that Fe_3O_4 is formed *via* the intermediate "green rust" in neutral solution, but in slightly alkaline solutions, Fe_3O_4 is formed directly from the $Fe(OH)_2$ suspension. In the present experiments, greenish precipitates were seen in the early stages of the oxidation in the presence of the Mg^{2+} at pH 8.0. No incorporation of Mg^{2+} into the ferrite structure at pH 8.0 may, therefore, account for the formation of the "green rust" in the course of reaction.

Conclusion

From the experimental results, several conditions concerning the formation of Mg-bearing ferrite by the air oxidation of the $Fe(OH)_2$ aqueous suspension may be drawn:

1. At pH 9.0 and at 65 °C, almost all Mg^{2+} is incorporated into the spinel type ferrite when the Mg^{2+}/Fe_{total} ratio in the initial solution is less than 0.1. The chemical composition thus obtained may be expressed as the $MgFe_2O_4$–Fe_3O_4–γ-Fe_2O_3 ternary system, implying that the Mg-bearing ferrite which is a ferromagnet is not stoichiometric in its composition. The degree of oxidation increases with increasing Mg^{2+}/Fe_{total} ratio while the spinel type structure is maintained.
2. When the Mg^{2+}/Fe_{total} ratio exceeds 0.1 at pH 9.0 and 65 °C, the excess Mg^{2+} produces a basic magnesium sulfate which readily dissolves at pH 5.0. The chemical composition of this compound has been estimated as $[Mg^{2+}_{1.00}, Na^{+}_{0.64}][OH^{-}_{1.36}, (SO_4^{2-})_{0.64}]$.
3. At pH 8.0, a small amount of Mg^{2+} is incorporated into the ferrite, attributed to the formation of "green rust" in the course of reaction, indicating an absence of interaction between Mg^{2+} and the "green rust." In connection with this, the Mg^{2+} incorporated must be hydrolyzed before producing the ferrite.
4. Between pH 9.0 and 10.0, only the Mg-bearing ferrite is formed, but at pH 11.0, the α-FeOOH type compound is formed together with the Mg-bearing ferrite. Thus, the pH interval for Mg-bearing ferrite formation is limited from 9.0 to 10.0.

The authors would like to express their thanks to Drs. T. Kanzaki, Y. Tamaura, and T. Sugihara, Tokyo Institute of Technology, for the kind advice and helpful cooperation throughout the study.

References

1) H. Yasuoka, A. Hirai, T. Shinjo, M. Kiyama, Y. Bando, and T. Takada, *J. Phys. Soc. Jpn.*, **22**, 174 (1967).
2) T. Akashi, I. Sugano, Y. Kenmoku, Y. Shimada, and T. Tsuji, "Proc. Intern. Conf. Ferrites," Univ. Tokyo Press, Japan (1971). p. 183.
3) H. Takei, T. Kanzaki, Y. Tamura, and T. Katsura, Meeting of the Chemical Society of Japan in Tohoku District, Akita, October 1977, Abstr. No. 1B02.
4) K. Kaneko, T. Kanzaki, Y. Tamaura, and T. Katsura, Meeting of the Chemical Society of Japan in Tohoku District, Akita, October 1977, Abstr. No. 1B03.
5) M. Kiyama, *Bull. Chem. Soc. Jpn.*, **51**, 134 (1978).
6) W. Feitknecht, *Z. Electrochem.*, **63**, 34(1959).
7) M. Kiyama, *Bull. Chem. Soc. Jpn.*, **47**, 1646(1974).
8) Y. Tamaura, G. S. Chyo, and T. Katsura, *Water Res.*, **13**, 21 (1979).
9) T. Katsura, Y. Tamaura, and H. Terada, *Kogyo Yosui*, **223**, 16 (1977).
10) T. Katsura, "Zikken Kagaku Koza," ed by the Chemical Society of Japan, Maruzen (1958), No. 15, pp. 272—275.
11) I. Iwasaki, T. Katsura, T. Ozawa, M. Mashima, H. Hamamura, and B. Iwasaki, *Bull. Volc. Soc. Jpn., Ser. II*, **5**, 75 (1960).
12) T. Katsura and S. Kimura, *Bull. Chem. Soc. Jpn.*, **38**, 1664 (1965).

Preparation and Characterization of *uns-cis*-Trimethylenediamine-*N,N'*-diacetato Cobalt(III) Complexes with Several L-Amino Acids

Minahiro OKABAYASHI,* Kozo IGI,† and Jinsai HIDAKA*
Department of Chemistry, University of Tsukuba, Ibaraki 300-31
(Received May 26, 1978)

Five *uns-cis-mer* and two *uns-cis-fac* complexes of (trimethylenediamine-*N,N'*-diacetato)(L-amino carboxylato)cobalt(III) were prepared, where L-amino carboxylate denotes L-alaninate, L-valinate, L-prolinate, L-hydrogen aspartate, or L-hydrogen glutamate ion. The complexes were separated into the fourteen isomers, *Δ*-, *Λ-uns-cis-mer* for the L-alaninato, L-valinato, and L-prolinato complexes, and *Δ*-, *Λ-uns-cis-mer* and *Δ*-, *Λ-uns-cis-fac* for the L-hydrogen aspartato and L-hydrogen glutamato complexes. They were characterized by their proton magnetic resonance, absorption and circular dichroism spectra. Each of the *uns-cis-mer* and *uns-cis-fac* isomers showed the characteristic CD behavior in the second absorption band region. The *Λ-uns-cis-mer* and *Δ-uns-cis-fac* isomers of the L-aspartato and L-glutamato complexes were stereoselectively formed, the formation ratios of the isomers being estimated spectrophotometrically.

Cobalt(III) complexes with the trimethylenediamine-*N,N'*-diacetate ion (tmdda) have been investigated in the past few years.[1,2] The trimethylenediamine-*N,N'*-diacetate ion is an O–N–N–O type ligand and similar to the ethylenediamine-*N,N'*-diacetate ion (edda) except that the former has a longer diamine moiety. The tmdda complexes were obtained only in *uns-cis* geometry except the ethylenediamine complex[3] while the edda complexes have been isolated in both geometries, *uns-cis* and *s-cis*.[4-16] In these circumstances, a synthetic work of the complexes containing tmdda, which forms a six-membered diamine backbone, and an L-amino carboxylate ion is significant for the stereoselective formation of the complexes[17] and CD behavior in the d-d transition band region.[18,19]

In the present study, the *uns-cis*-tmdda-Co(III) complexes containing the L-aspartate, L-glutamate, L-prolinate, L-valinate, or L-alaninate ion in the remaining two coordination sites were prepared and their isomers, *Δ*-, *Λ-uns-cis-mer* and *Δ*-, *Λ-uns-cis-fac* types for L-aspartato and L-glutamato complexes and *Δ*-, *Λ-uns-cis-mer* types for L-alaninato, L-valinato and L-prolinato complexes were chromatographically separated. The stereoselectivity of the complex with the L-aspartate or L-glutamate ion is discussed on the basis of the formation ratios of their isomers. Absorption and proton magnetic resonance spectra of the complexes are discussed in relation to their structures. The configurational CD contribution of the isomers was separated from the vicinal CD contribution due to the optically active ligand and the CD spectra are discussed in relation to their configurations.

Experimental

Preparation and Separation of Isomers of uns-cis-*(Trimethylenediamine-*N,N'*-diacetato) (L-hydrogen aspartato)cobalt(III)*, [*Co(tmdda)(L-aspH)*]. A solution containing 1.00 g (3.05 $\times 10^{-3}$ mol) of hydrogen dichloro(trimethylenediamine-*N,N'*-diacetato)cobaltate(III) hemihydrate,[1] H[Co(tmdda)Cl_2]·0.5H_2O in 50 cm^3 of water was heated at *ca.* 65 °C for 20 min. The color of the solution turned from green to blue and finally violet. To the solution was added a solution containing 0.50 g (3.79$\times 10^{-3}$ mol) of L-aspartic acid in 100 cm^3 of water. The pH of the solution was adjusted to 8.0 by addition of 1 mol dm^{-3} NaOH aqueous solution. After 0.5 g of activated charcoal had been added to the solution, the mixture was mechanically stirred at *ca.* 65 °C for 20 min. The charcoal and insoluble material were removed by filtration and washed with hot water until the washings became colorless. The combined filtrate and washings were concentrated to *ca.* 50 cm^3 with a rotary evaporator. The resulting violet solution was poured into a column (50 mm$\times$450 mm) containing anion-exchange resin (Dowex 1-X8, 200—400 mesh, CH_3COO^- form). The adsorbed band was separated into three bands (violet, violet, and red in the order of elution) by elution with *ca.* 0.05 mol dm^{-3} CH_3COOK solution. From their absorption and CD spectra, it was found that the first and second violet bands consist of *Λ*- and *Δ-mer*-[Co(tmdda)(L-asp)]$^-$, respectively, and the third band consists of *Δ-fac*-[Co(tmdda)(L-asp)]$^-$. The yield of each of the three isomers being very small, the chromatographic separation was repeated several times in order to store up the same eluates.

Each of the stored eluates was concentrated to a small volume with a rotary evaporator and the precipitated CH_3COOK was removed by filtration. The filtrate was then poured into a column (30 mm$\times$530 mm) packed with Sephadex G-10 resin and the adsorbed band was eluted with water in order to remove the residual CH_3COOK in the filtrate. The eluate was passed through a column (30 mm$\times$100 mm) containing cation-exchange resin (Dowex 50W-X8, 200—400 mesh, H^+ form). The passed solution was concentrated and kept in a refrigerator for two or three days after the addition of ethanol and ether. The resulting crystals were collected, washed with ethanol and then ether and dried in the air. The crystals were recrystallized from an ethanol–water (5:1) mixture by addition of acetone. Potassium salt of the *Λ-uns-cis-mer* isomer for the PMR measurement was isolated before being passed through a column containing cation-exchange resin.

The fourth isomer, *Λ-uns-cis-fac*-[Co(tmdda)(L-aspH)], not formed by the above procedure, was obtained in the following way. A reaction solution was prepared from a solution containing 2.6 g (7.93$\times 10^{-3}$ mol) of H[Co(tmdda)Cl_2]·0.5H_2O in 100 cm^3 of water and a solution containing 1.4 g (1.05$\times 10^{-2}$ mol) of L-aspartic acid in 150 cm^3 of water. The solution was mechanically stirred at *ca.* 65 °C for 60 min, no activated charcoal being used. After a small amount of insoluble material had been filtered off, the filtrate was concentrated to *ca.* 50 cm^3 with an evaporator. The solution was chromatographed on an anion-exchange column (Dowex 1-X8, 200—400 mesh, CH_3COO^- form). A large amount

† Present address: Department of Chemistry, Washington State University, Pullman, Washington 99164.

Table 1. Elemental analyses for *uns-cis*-[Co(tmdda)(L-am)] complexes

Complex	Found (%)			Calcd (%)		
	C	H	N	C	H	N
Λ-mer-[Co(tmdda)(L-aspH)]·2.5H_2O	30.95	5.48	9.88	31.15	5.47	9.90
Δ-mer-[Co(tmdda)(L-aspH)]·H_2O·0.5C_2H_5OH	34.26	5.42	10.12	34.29	5.52	10.00
Δ-fac-[Co(tmdda)(L-aspH)·3H_2O	30.90	5.58	9.84	30.49	5.58	9.70
Λ-mer-[Co(tmdda)(L-gluH)]·H_2O	34.89	5.46	9.99	35.05	5.39	10.22
Δ-mer-[Co(tmdda)(L-gluH)]·2H_2O	33.59	5.63	9.59	33.58	5.64	9.79
Λ-fac-[Co(tmdda)(L-gluH)]·1.5H_2O	34.06	5.47	9.99	34.30	5.52	10.00
Δ-fac-[Co(tmdda)(L-gluH)]·1.5H_2O·0.5C_2H_5OH	34.91	5.93	9.18	35.22	5.92	9.48
Λ-mer-[Co(tmdda)(L-ala)]	32.30	6.02	11.38	32.35	5.97	11.32
Δ-mer-[Co(tmdda)(L-ala)]·2H_2O	35.95	5.53	12.30	35.83	5.42	12.54
Λ-mer-[Co(tmdda)(L-val)]	39.53	6.15	11.45	39.67	6.12	11.57
Δ-mer-[Co(tmdda)(L-val)]·2H_2O	36.31	6.74	10.22	36.10	6.56	10.52
Λ-mer-[Co(tmdda)(L-pro)]·0.5H_2O·0.5C_2H_5OH	40.10	5.92	10.78	39.69	6.16	10.69
Δ-mer-[Co(tmdda)(L-pro)]·2.5H_2O	35.06	5.91	10.35	35.47	6.21	10.34

of complex unreacted, presumably $[Co(tmdda)(OH_2)_2]^+$, was swept out with water. The adsorbed band was separated into four bands, violet, violet, red, and red, by elution with *ca.* 0.05 mol dm^{-3} CH_3COOK solution. It was confirmed from the absorption and CD spectra that the red band eluted last contains *Λ-uns-cis-fac*-[Co(tmdda)(L-asp)]$^-$. The last eluate was desalted and passed through a cation-exchange column (Dowex 50W-X8, 200—400 mesh, H^+ form). After the eluate had been concentrated, the solution was applied to the Sephadex G-10 column once again. This eluate was used for the absorption and CD measurements. The concentration of the eluate was determined with a Hitachi 208 atomic absorption spectrophotometer.

Preparation and Separation of Isomers of uns-cis-*(Trimethylenediamine-*N,N′*-diacetato)(*L*-hydrogen glutamato)cobalt(III)*, [*Co(tmdda)(*L*-gluH)*]. The complex was prepared and separated into four isomers in the same procedure as that for [Co(tmdda)(L-aspH)] using L-glutamic acid instead of L-aspartic acid. The reaction solution was concentrated and chromatographed on an anion-exchange column. The adsorbed band was separated into four bands (violet, violet, red, and red in the order of elution). From their absorption and CD spectra, the first and second violet bands turned out to be *Λ-* and *Δ-mer* isomers, respectively, and the third and fourth red bands *Δ-* and *Λ-fac* isomers, respectively. The four isomers have been isolated in the same procedure as that for L-aspartato complex. Since the yield of each isomer was very small, the isomers were treated in the same way as in the case of [Co(tmdda)(L-aspH)].

Preparation and Separation of Isomers of uns-cis-*(Trimethylenediamine-*N,N′*-diacetato)(*L*-prolinato)cobalt(III)*, [*Co(tmdda)(*L*-pro)*]. The complex was prepared in the same way as that for [Co(tmdda)(L-aspH)] using 0.05 g (1.52×10^{-3} mol) of H[Co(tmdda)Cl_2]·0.5H_2O[1] and 0.22 g (1.89×10^{-3} mol) of L-proline. The separation of the diastereomers was carried out by use of a column (QAE-Sephadex A-25, Cl^- form). The adsorbed band was progressively separated into three bands by elution with water. It was shown, from the absorption and CD spectra, that the first and second violet bands contain *Λ-mer* and *Δ-mer* isomers, respectively. A trace amount of the third red band was confirmed to be *fac* isomers. The two *mer* isomers have been isolated as follows.

Λ-uns-cis-mer-[*Co(tmdda)(*L*-pro)*]: The first eluate was concentrated to a small volume with a rotary evaporator and the violet complex was deposited by adding ethanol to the concentrated solution. The complex was recrystallized from an ethanol-water (3:1) mixture by adding acetone. Yield: 0.06 g.

Δ-uns-cis-mer-[*Co(tmdda)(*L*-pro)*]·*2.5H$_2$O*: The second eluate was concentrated and the violet crystals were deposited by adding ethanol and acetone to the solution. The crystals were recrystallized from an ethanol-water mixture and dried in a desiccator. Yield: 0.33 g.

Preparation and Separation of Isomers of uns-cis-*(Trimethylenediamine-*N,N′*-diacetato)(*L*-valinato)cobalt(III)*, [*Co(tmdda)(*L*-val)*]. The complex was prepared in the same way as that for [Co(tmdda)(L-aspH)] using 2.6 g (7.93×10^{-3} mol) of H[Co(tmdda)Cl_2]·0.5H_2O[1] and 1.2 g (1.00×10^{-2} mol) of L-valine. The reacted solution was evaporated to *ca.* 20 cm^3 with a rotary evaporator. The resulting violet solution was chromatographed on a column (30 mm×850 mm, QAE-Sephadex A-25, Cl^- form). The adsorbed band was separated into two bands. It was confirmed from absorption and CD spectra that the first violet band contains *Δ-mer* and *Λ-mer* isomers, and the second red band *Λ-fac* and *Δ-fac* isomers. The two *mer* isomers were isolated as follows. The first violet eluate was concentrated and the solution was kept at room temperature overnight after the addition of ethanol and ether to the concentrated solution. The purple precipitate (F 1) was separated by filtration and washed with acetone and then ether and dried in the air. Further fractions (F2—7) were obtained from the mother liquor by further addition of ethanol and ether and subsequent cooling. It was found from absorption and CD spectra that F 1, F 5, and F 6 contain both *Δ-mer* and *Λ-mer* isomers, F 2 *Λ-mer* isomer, and F 3, F 4, and F 7 *Δ-mer* isomer. Yield: 0.25 g for *Λ-mer* isomer, 1.11 g for *Δ-mer* isomer. The *Λ-mer* isomer is less soluble in water or ethanol than the *Δ-mer* isomer. The *Δ-uns-cis-mer* isomer was recrystallized from an ethanol–water (10:1) mixture and *Λ-uns-cis-mer* isomer from an ethanol–water (5:2) mixture by adding a small amount of acetone. The CD intensities of the isomers were unchanged by repeated recrystallization.

Preparation and Separation of Isomers of uns-cis-*(Trimethylenediamine-*N,N′*-diacetato)(*L*-alaninato)cobalt(III)*, [*Co(tmdda)(*L*-ala)*]. The complex was prepared by the same procedure as that for the L-valinato complex using 0.89 g (1.00×10^{-2} mol) of L-alanine in 100 cm^3 of water. Two *mer* isomers were isolated as follows. Separation of the *mer* isomers from a trace amount of *fac* isomers was carried out using a QAE-Sephadex column. The first eluate containing *Λ-mer* and *Δ-mer* isomers was concentrated and the solution

was kept at room temperature overnight, after the addition of ethanol and ether. The purple precipitate (F 1) was separated by filtration and washed with ethanol and then ether. F 2 and F 3 were obtained from the mother liquor by further addition of ethanol and ether and subsequent cooling. It was found from absorption and CD spectra that F 1 contains *Λ-mer* isomer, F 2 *Δ-mer* isomer, and F 3 both *Δ-mer* and *Λ-mer* isomers. Yield: 0.60 g for *Δ-mer* isomer, 0.60 g for *Λ-mer* isomer. Recrystallization was carried out twice for the *Δ-mer* isomer and three times for the *Λ-mer* isomer, giving no change in CD intensity from a mixture of ethanol and water by adding a small amount of acetone.

Measurements. Electronic absorption spectra were recorded with a JASCO UVIDEC-1 spectrophotometer and CD spectra with a JASCO J-20 spectropolarimeter. PMR spectra were recorded on a JEOL JNM-MH-100 NMR spectrometer at probe temperature in D_2O as solvent. Sodium 2,2-dimethyl-2-silapentane-5-sulfonate (DSS) was used as an internal reference. For determination of the concentration of *Λ-uns-cis-fac*-[Co(tmdda)(L-aspH)] aqueous solution, a Hitachi 208 atomic absorption spectrophotometer was used. The formation ratios for the L-aspartato and L-glutamato complexes were evaluated on the basis of the absorption measurements of the bands separated chromatographically.

Results and Discussion

Structural Assignments for Isomers of [Co(tmdda)(L-am)]. Three geometrical isomers, *uns-cis-mer*, *uns-cis-fac*, and *s-cis*, are possible for the [Co(tmdda)(L-am)] type complex as shown in Fig. 1. Only the *uns-cis* isomers were obtained for the $[Co(tmdda)(N\text{–}N)]^+$ and $[Co(tmdda)(O\text{–}O)]^-$ type complexes except for the ethylenediamine complex in which the *s-cis* isomer was obtained as a minor product.[1-3] It is presumed that the *uns-cis* isomers would be dominantly formed in the present series unless there is any special interaction between the L-amino carboxylate ion and tmdda.

The CD and absorption spectra of the complexes obtained are shown in Figs. 2—6. Of the *uns-cis-mer*, *uns-cis-fac*, and *s-cis* isomers of [Co(tmdda)(L-am)] complex, the *s-cis* isomer should take only *mer* configuration with respect to the coordination atoms because of the regulated coordination of tmdda (Fig. 1). The *mer* and *fac* isomers can be easily assigned from their d-d electronic absorption spectra; the holohedrized symmetry[20] of the *fac* isomer is cubic, whereas that of the *mer* isomer is rhombic. The former can be expected to show a sharp first absorption band and the latter a broad one[19] (Figs. 2—6). The two *mer* isomers, the *s-cis* and the *uns-cis*, can not be distinguish-

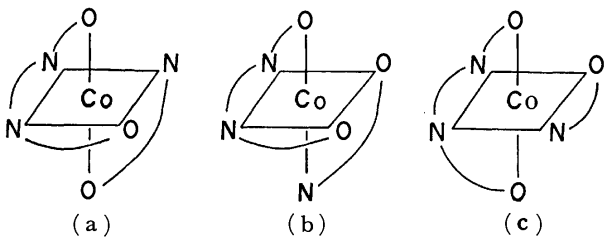

Fig. 1. Three geometrical isomers of [Co(O-N-N-O)-(L-am)] type complexes, (a) *uns-cis-mer*, (b) *uns-cis-fac*, and (c) *s-cis*.

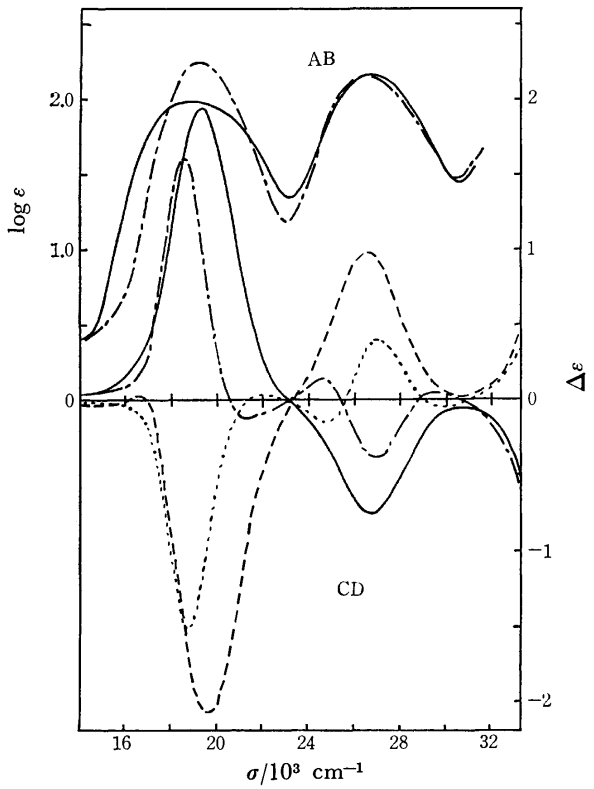

Fig. 2. Absorption and CD spectra for the isomers of *uns-cis*-[Co(tmdda)(L-aspH)], *Λ-mer* (——), *Δ-mer* (----), *Λ-fac* (——), and *Δ-fac* (·····).

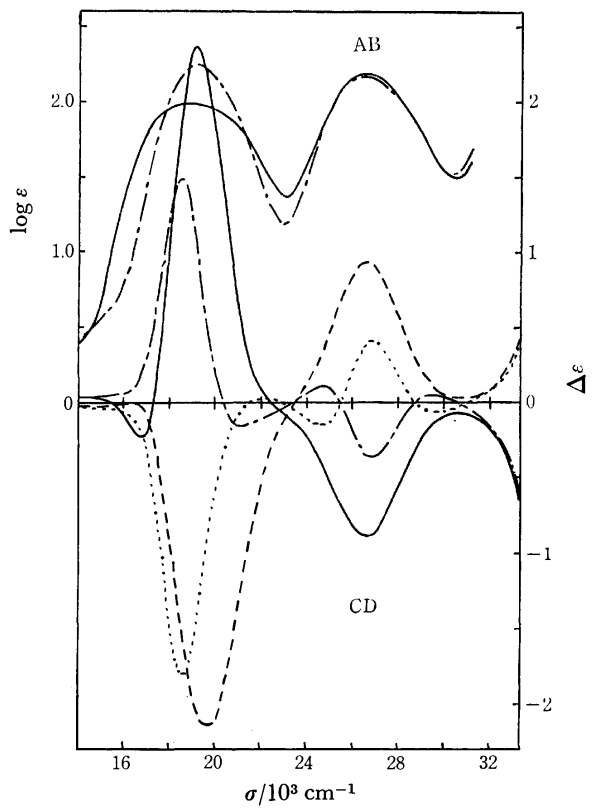

Fig. 3. Absorption and CD spectra for the isomers of *uns-cis*-[Co(tmdda)(L-gluH)], *Λ-mer* (——), *Δ-mer* (----), *Λ-fac* (——), and *Δ-fac* (·····).

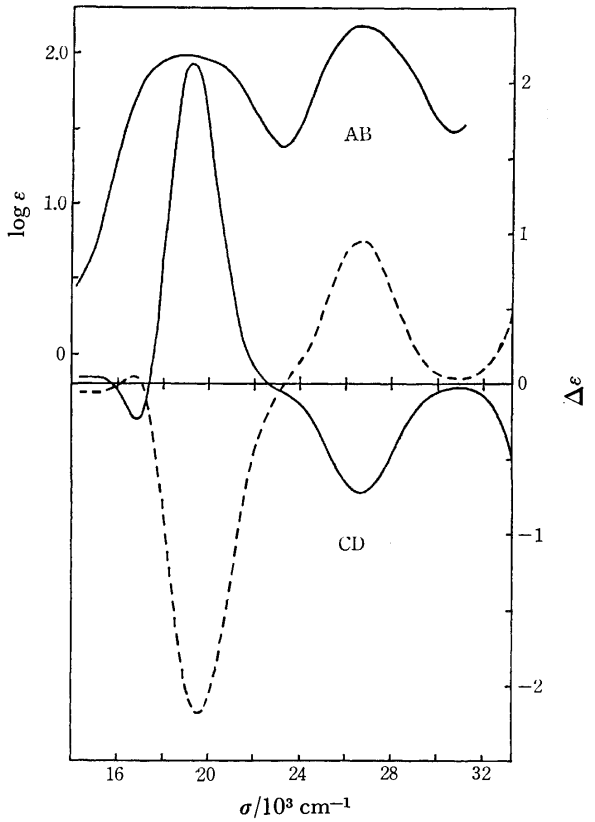

Fig. 4. Absorption and CD spectra for the isomers of *uns-cis*-[Co(tmdda)(L-ala)], *Λ-mer* (——) and *Δ-mer* (----).

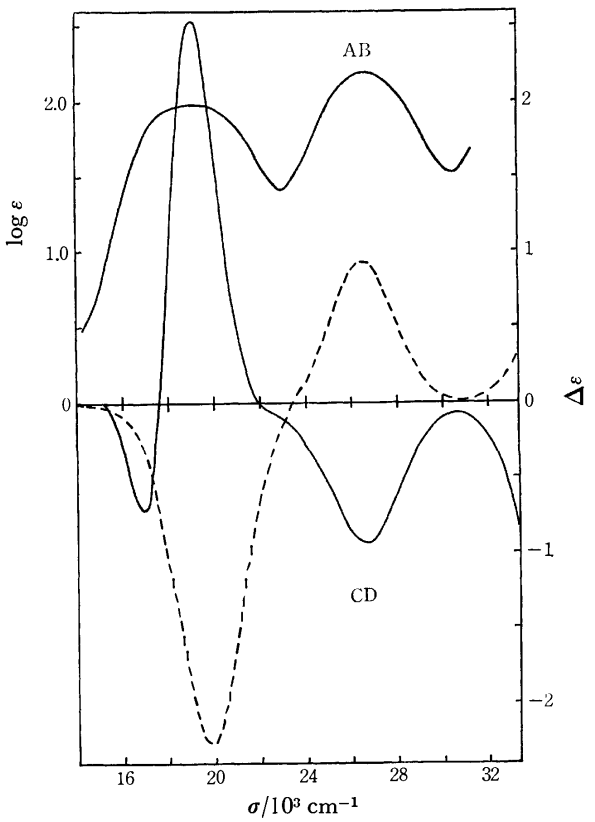

Fig. 5. Absorption and CD spectra for the isomers of *uns-cis*-[Co(tmdda)(L-val)], *Λ-mer* (——) and *Δ-mer* (----).

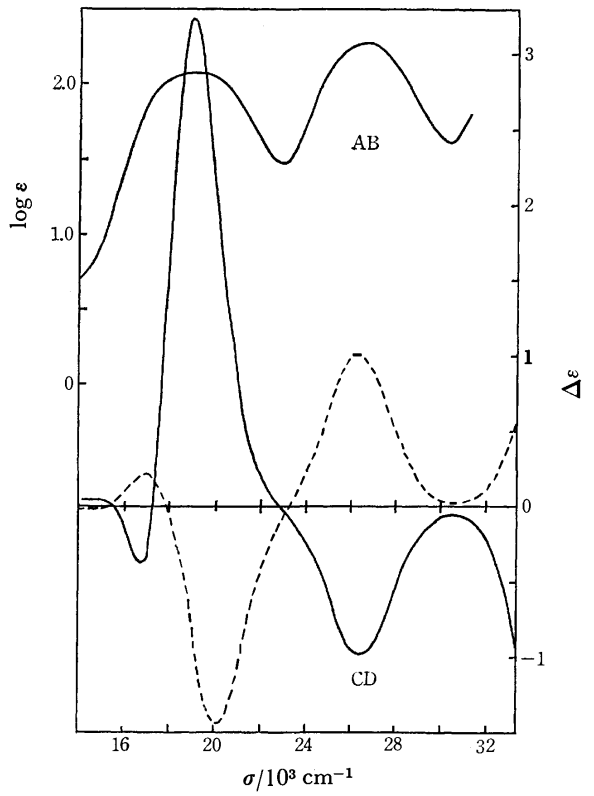

Fig. 6. Absorption and CD spectra for the isomers of *uns-cis*-[Co(tmdda) (L-pro)], *Λ-mer* (——) and *Δ-mer* (----).

ed from the patterns of their first absorption bands. Therefore, each was investigated on the basis of their PMR spectra.

The geminal proton coupling constants (J_{AB}) for (amino carboxylato)cobalt(III) complexes are classified into two groups, those in the vicinity of 16 Hz for in-plane (G) rings and those of 18 Hz for out-of-plane (R) rings.[27] This was also investigated for the *s-cis* and *uns-cis* isomers of edda Co(III) complexes.[9,11,16] Coleman *et al.*[9] and Kuroda[11] reported that *s-cis*-[Co(edda)A_2] complex shows only one AB pattern (J_{AB}=*ca.* 18 Hz) due to the R rings, and *s-cis*-[Co(edda)AB] complex two AB patterns (J_{AB}=*ca.* 18 Hz) due to two different unidentate ligands, A and B, in contrast to which the *uns-cis* isomers of [Co(edda)A_2] show a single intense peak due to the G ring protons superimposed on one AB pattern of the R ring protons. The singlet was considered to be an extreme case of an AB pattern in which the environments of the two protons are very similar.[9] A similar spectral behavior was also observed for the *uns-cis* isomer of [Co(tmdda)$(NH_3)_2$]Cl.[3] PMR data we obtained for tmdda Co(III) complexes are given in Table 4. All the *mer* isomers show two four-line AB patterns with J_{AB}, 16.0—16.5 Hz and 18.0—18.5 Hz for the glycinate protons. As an example, the spectrum of *mer*-K[Co(tmdda)(L-asp)] is shown (Fig. 7a). The resonance line with J_{AB}=*ca.* 18 Hz is assigned to the R ring protons and that with J_{AB}=*ca.* 16 Hz to the G ring protons. Thus it is concluded that the *mer* isomers obtained are all *uns-cis* one (Table 4). For the *fac*

Table 2. Absorption data of *uns-cis*-[Co(tmdda)(L-am)] complexes

Complex	First band		Second band	
Λ-mer-[Co(tmdda)(L-aspH)]·2.5H_2O	18.69	(1.99)	26.67	(2.19)
Δ-mer-[Co(tmdda)(L-aspH)]·H_2O·0.5C_2H_5OH	18.69	(2.00)	26.53	(2.19)
Λ-fac-[Co(tmdda)(L-aspH)]	19.08	(2.31)	26.46	(2.23)
Δ-fac-[Co(tmdda)(L-aspH)]·3H_2O	19.19	(2.25)	26.53	(2.15)
Λ-mer-[Co(tmdda)(L-gluH)]·H_2O	18.80	(1.99)	26.60	(2.20)
Δ-mer-[Co(tmdda)(L-gluH)]·2H_2O	18.83	(2.01)	26.60	(2.20)
Λ-fac-[Co(tmdda)(L-gluH)]·1.5H_2O	19.16	(2.25)	26.39	(2.17)
Δ-fac-[Co(tmdda)(L-gluH)]·1.5H_2O·0.5C_2H_5OH	19.16	(2.25)	26.39	(2.17)
Λ-mer-[Co(tmdda)(L-ala)]	18.94	(1.98)	26.67	(2.18)
Δ-mer-[Co(tmdda)(L-ala)]·2H_2O	18.80	(2.00)	26.60	(2.17)
Λ-mer-[Co(tmdda)(L-val)]	18.90	(1.99)	26.60	(2.20)
Δ-mer-[Co(tmdda)(L-val)]·2H_2O	18.73	(2.01)	26.60	(2.19)
Λ-mer-[Co(tmdda)(L-pro)·0.5H_2O·0.5C_2H_5OH	19.08	(2.08)	26.39	(2.29)
Δ-mer-[Co(tmdda)(L-pro)]·2.5H_2O	18.66	(2.03)	26.32	(2.20)

Wave numbers and log ε values (in parentheses) are given in 10^3 cm^{-1} and mol^{-1} dm^3 cm^{-1}, respectively.

Table 3. Observed CD data of *uns-cis*-[Co(tmdda)(L-am)] complexes

Complex	First band region		Second band region	
Λ-mer-[Co(tmdda)(L-aspH)]·2.5H_2O	19.34	(+1.95)	26.81	(−0.76)
Δ-mer-[Co(tmdda)(L-aspH)]·H_2O·0.5C_2H_5OH	16.67	(+0.05)	26.60	(+0.99)
	19.69	(−2.08)		
Λ-fac-[Co(tmdda)(L-aspH)]	18.52	(+1.61)	24.63	(+0.14)
	21.28	(−0.13)	26.88	(−0.39)
			29.41	(+0.04)
Δ-fac-[Co(tmdda)(L-aspH)]·3H_2O	18.73	(−1.52)	24.81	(−0.15)
	21.93	(+0.03)	27.10	(+0.40)
			29.76	(−0.05)
Λ-mer-[Co(tmdda)(L-gluH)]·H_2O	16.86	(−0.23)	26.74	(−0.88)
	19.19	(+2.37)		
Δ-mer-[Co(tmdda)(L-gluH)]·2H_2O	19.69	(−2.13)	26.60	(+0.95)
Λ-fac-[Co(tmdda)(L-gluH)]·1.5H_2O	18.52	(+1.50)	24.69	(+0.12)
	21.05	(−0.15)	26.88	(−0.36)
			29.50	(+0.06)
Δ-fac-[Co(tmdda)(L-gluH)]·1.5H_2O·0.5C_2H_5OH	18.62	(−1.80)	24.69	(−0.15)
	22.12	(+0.03)	26.88	(+0.41)
			29.76	(−0.05)
Λ-mer-[Co(tmdda)(L-ala)]	16.89	(−0.24)	26.88	(−0.73)
	19.23	(+2.14)		
Δ-mer-[Co(tmdda)(L-ala)]·2H_2O	16.72	(+0.05)	26.67	(+0.96)
	19.61	(−2.18)		
Λ-mer-[Co(tmdda)(L-val)]	16.89	(−0.73)	26.74	(−0.94)
	19.08	(+2.54)		
Δ-mer-[Co(tmdda)(L-val)]·2H_2O	19.88	(−2.26)	26.60	(+0.93)
Λ-mer-]Co(tmdda)(L-pro)]·0.5H_2O·0.5C_2H_5OH	16.78	(−0.39)	26.53	(−0.98)
	19.01	(+3.24)		
Δ-mer-[Co(tmdda)(L-pro)]·2.5H_2O	16.92	(+0.22)	26.39	(+1.01)
	20.12	(−1.46)		

Wave numbers and $\Delta\varepsilon$ values (in parentheses) are given in 10^3 cm^{-1} and mol^{-1} dm^3 cm^{-1}, respectively.

isomers of [Co(tmdda)(L-am)] assigned from the first absorption band pattern, one AB pattern (J_{AB}=*ca.* 18 Hz) and a single intense peak superimposed on an AB pattern are observed. The spectrum of *fac*-[Co(tmdda)(L-aspH)] is shown as an example in Fig. 8. The singlet intense peak is assigned to the G ring and the AB pattern to the R ring (Table 4). It is concluded that the *fac* isomers are also *uns-cis*. The information from the PMR spectrum is consistent with the consideration based on the molecular model construction that the *fac* isomer takes an *uns-cis* arrangement (Fig. 1). Another support for the assignments of *uns-cis* isomers is based on the selective deuteration of R ring proton.[9,28-31] H_A (the less sterically hindered proton) of the R ring protons is selectively deuterated in the course of heating of the sample solution. The PMR spectra of *mer*-K[Co(tmdda)(L-asp)] are shown in Fig. 7 (7a is the spectrum of a freshly prepared D_2O solution and 7b the spectrum of the sample solution after being heated in boiling water for 30 min). In

Table 4. Chemical shifts of the glycinate ring methylene protons in *uns-cis*-[Co(tmdda)(L-am)] complexes[a)]

Complex	R ring[b,d)]				G ring[c,d)]			
	H_A		H_B		H_A		H_B	
Λ-mer-K[Co(tmdda)(L-asp)]	3.84	3.66	3.38	3.20	3.94	3.78	3.68	3.52
Λ-mer-[Co(tmdda)(L-aspH)]	3.82	3.65	3.47	3.29	3.98	3.82	3.72	3.55
Δ-mer-[Co(tmdda)(L-aspH)]	3.80	3.63	3.46	3.27	3.96	3.79	3.71	3.55
Δ-fac-[Co(tmdda)(L-aspH)]	4.00	3.82	3.49	3.31		3.65		
Λ-mer-K[Co(tmdda)(L-glu)]	3.80	3.62	3.41	3.22	3.93	3.77	3.69	3.52
Λ-mer-[Co(tmdda)(L-gluH)]	3.81	3.63	3.42	3.24	3.93	3.76	3.69	3.53
Δ-mer-[Co(tmdda)(L-gluH)]	3.80	3.62	3.44	3.26	3.97	3.81	3.71	3.54
Λ-fac-[Co(tmdda)(L-gluH)]	3.93	3.74	3.43	3.25		3.61		
Λ-mer-[Co(tmdda)(L-ala)]	3.81	3.63	3.42	3.24	3.93	3.77	3.70	3.54
Λ-mer-[Co(tmdda)(L-ala)]	3.82	3.63	3.43	3.25	3.96	3.79	3.71	3.54
Δ-mer-[Co(tmdda)(L-val)]	3.78	3.60	3.48	3.30	3.95	3.78	3.70	3.53
Δ-mer-[Co(tmdda)(L-val)]	3.80	3.62	3.43	3.25	3.97	3.80	3.71	3.54
Λ-mer-[Co(tmdda)(L-pro)]	3.85	3.67	3.50	3.31	3.92	3.75	3.69	3.52
Δ-mer-[Co(tmdda)(L-pro)]	3.85	3.67	3.47	3.28	3.96	3.79	3.70	3.53

a) Values in ppm from DSS. b) $J_{AB}=18.0$—18.5 Hz. c) $J_{AB}=16.0$—16.5 Hz. d) Where an AB quartet was observed for the glycinate ring protons, the low field proton has been designated H_A in accordance with nomenclature already devised.[9)]

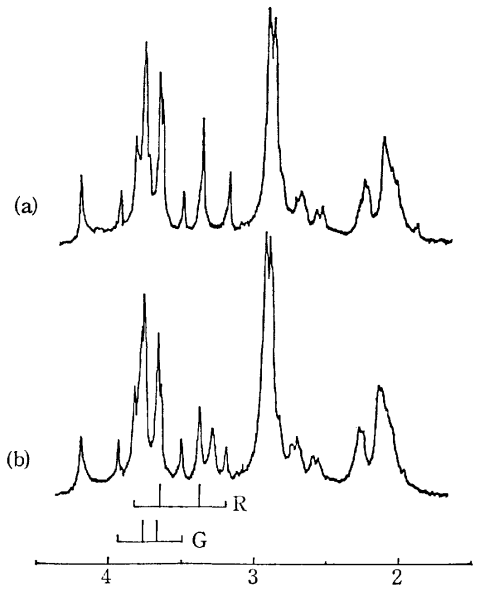

Fig. 7. Proton magnetic resonance spectra of *Λ-uns-cis-mer*-K[Co(tmdda)(L-asp)] in D_2O solution. (a) The spectrum of a freshly prepared D_2O solution. (b) The spectrum of the solution after being heated in boiling water for 30 min.

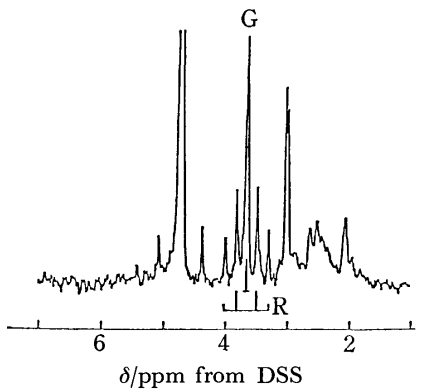

Fig. 8. Proton magnetic resonance spectra of *Δ-uns-cis-fac*-[Co(tmdda)(L-aspH)] in D_2O solution (after heating the sample in boiling water for 30 min).

the spectrum, the AB pattern ($J_{AB}=16.0$ Hz) due to the G ring protons is observed at 3.94, 3.78, 3.68, and 3.52 ppm, and another AB pattern ($J_{AB}=18.0$ Hz) due to the R ring protons is observed at 3.84, 3.66, 3.38, and 3.20 ppm. On the other hand, the 7b spectrum shows a new peak at 3.30 ppm, the intensity of the AB pattern due to the R ring protons decreasing drastically. The new peak increases to an integrated value equivalent to one proton, the AB pattern due to the R ring disappearing completely after being heated in boiling water for 2.5 h. The new peak is assigned to the resonance for decoupled H_B. The AB pattern due to the G ring protons ($J_{AB}=16.0$ Hz) is not deuterated under the same conditions. This indicates that *mer*-K[Co(tmdda)(L-asp)] takes the *uns-cis* configuration. The same behavior is also observed for *mer*-K[Co(tmdda)(L-glu)]. From the results of absorption and PMR measurements, all of the complexes obtained can be assigned to the *uns-cis* configuration.

Stereochemistry of the Isomers. On the basis of the CD spectra in the first absorption band region, the absolute configurations of *uns-cis*-$[Co(tmdda)A_2]^+$ ($A_2=(NH_3)_2$, en, and tn) and *uns-cis*-$[Co(edda)A_2]^+$ were discussed in the same category, though the difference in the backbone diamine ring of the quadridentate ligands gives rise to a slight change in the shape of CD curves.[1)] Thus, the absolute configurations of the isomers are assigned tentatively from the sign of a major CD band in the first absorption band region as shown in Table 3 and Figs. 2—6.

A remarkable CD difference between the *mer* and

Table 5. Calculated configurational CD data of *Λ-uns-cis*-[Co(tmdda)(L-am)] complexes

Complex	First band region		Second band region	
mer-[Co(tmdda)(L-aspH)]	19.53	(+2.00)	26.60	(−0.87)
fac-[Co(tmdda)(L-aspH)]	18.66	(+1.56)	24.75	(+0.15)
	21.65	(−0.07)	27.03	(−0.39)
			29.76	(+0.05)
mer-[Co(tmdda)(L-gluH)]	16.72	(−0.12)	26.74	(−0.91)
	19.31	(+2.21)		
fac-[Co(tmdda)(L-gluH)]	18.52	(+1.65)	24.75	(+0.13)
	21.55	(−0.08)	26.88	(−0.39)
			29.59	(+0.05)
mer-[Co(tmdda)(L-ala)]	16.84	(−0.15)	26.60	(−0.84)
	19.38	(+2.14)		
mer-[Co(tmdda)(L-val)]	16.67	(−0.23)	26.60	(−0.93)
	19.38	(+2.28)		
mer-[Co(tmdda)(L-pro)]	16.67	(−0.30)	26.60	(−1.00)
	19.38	(+2.11)		

Wave numbers and $\Delta\varepsilon$ values (in parentheses) are given in 10^3 cm^{-1} and mol^{-1} dm^3 cm^{-1}, respectively.

Table 6. Formation ratios (percent compositions) of reaction mixture

Complex	Isomer			
	Λ-mer	*Δ-mer*	*Λ-fac*	*Δ-fac*
uns-cis-[Co(tmdda)(L-asp)]$^-$	81%	6%	0%	13%
uns-cis-[Co(tmdda)(L-glu)]$^-$	51%	40%	3%	6%

fac isomers appears in the second absorption band region. The *uns-cis-fac*-[Co(tmdda)(L-aspH)] shows three CD bands (+, −, and + from the lower energy side) for the *Λ* isomer, while the *uns-cis-mer* isomer shows a negative band for the *Λ* isomer (Fig. 2). The CD difference substantiates the configurational CD curves estimated from the observed CD curves of *Λ-* and *Δ-uns-cis-fac*-[Co(tmdda)(L-aspH)] and the observed CD curves of *Λ-* and *Δ-uns-cis-mer*-[Co(tmdda)(L-aspH)] (Table 5). A similar CD behavior in the second absorption band region is also observed for the isomers of *uns-cis*-[Co(tmdda)(L-gluH)] (Table 5). The behavior seems to be a characteristic pattern reflecting the arrangement of ligands. A similar behavior was pointed out for the CD spectra of the C_1-*cis* and C_2-*cis* isomers of $[Co(am)_2ox]^-$ or $[Co(am)_2en]^+$.[26] However, no CD difference in the second absorption band region is observed for the CD spectra of the *mer* and *fac* isomers of *uns-cis*-[Co(edda)(L-am)]. The CD difference in the present isomers is not due to the difference of the *mer* and *fac* arrangements, but can be attributed to the chelate ring conformations of the backbone diamine of the coordinated tmdda.

It was suggested that the tmdda Co(III) complexes prefer the *uns-cis* configuration to the *s-cis* one and the backbone diamine chelate ring of tmdda has a marked effect on the distribution of geometrical isomers.[1] This is also applicable to the present work. Of the *uns-cis-mer* and *uns-cis-fac* configurations, the *uns-cis-mer* isomer was formed dominantly. For the L-alaninato, L-valinato, and L-prolinato complexes, the *uns-cis-mer* isomer was easily formed, while the *uns-cis-fac* isomer was hardly formed. The reason for the *uns-cis-mer* configuration dominancy is unknown at present. In the case of the L-aspartate and L-glutamate ions which have three functional groups, both the *uns-cis-mer* and *uns-cis-fac* isomers were obtained, though the *uns-cis-mer* isomers were also formed dominantly. The formation ratios (percent compositions) of their possible isomers are given in Table 6. A marked stereoselectivity was found for the *Λ* configuration of *uns-cis-mer*-[Co(tmdda)(L-asp)]$^-$ (*Λ-mer* : *Δ-mer*=81 : 6) and for the *Δ* configuration of the *uns-cis-fac* isomer (*Λ-fac* : *Δ-fac*=0 : 13). A similar trend was also observed for the isomers of the L-glutamato complex, though it was to a much smaller extent (Table 6). The stereoselectivities might be explained on the basis of the enhanced stabilization of *Λ-uns-cis-mer* and *Δ-uns-cis-fac* isomers caused by the formation of interligand hydrogen-bond in the isomer.[17,21-24] In the alkaline condition employed for the preparation of the complexes, the dangling *β*-carboxylato group of the coordinated L-aspartate ion is deprotonated. As a result, the *β*-carboxylato group can form a hydrogen-bond with the imino group of tmdda in the case of *Λ-uns-cis-mer* and *Δ-uns-cis-fac* isomers of L-aspartato complexes. The same consideration can be applied to the isomers of L-glutamato complex. The selectivity of L-glutamato complex is lower than that of L-aspartato one (Table 6). It can be presumed that the lower selectivity in comparison to that of L-aspartato complex is due to the longer dangling group of the coordinated L-glutamate ion.[21,24]

References

1) K. Igi and B. E. Douglas, *Inorg. Chem.*, **13**, 425 (1974).
2) K. Igi and B. E. Douglas, *Inorg. Chim. Acta*, **10**, 109 (1974).
3) K. D. Gailey, K. Igi, and B. E. Douglas, *Inorg. Chem.*, **14**, 2956 (1975).

4) M. Mori, M. Shibata, E. Kyuno, and F. Maruyama, *Bull. Chem. Soc. Jpn.*, **35**, 75 (1962).
5) J. I. Legg and D. W. Cooke, *Inorg. Chem.*, **4**, 1576 (1965).
6) J. I. Legg, D. W. Cooke, and B. E. Douglas, *Inorg. Chem.*, **6**, 700 (1967).
7) J. I. Legg and B. E. Douglas, *Inorg. Chem.*, **7**, 1452 (1968).
8) C. W. Van Saun and B. E. Douglas, *Inorg. Chem.*, **8**, 115 (1969).
9) P. F. Coleman, J. I. Legg, and J. Steele, *Inorg. Chem.*, **9**, 937 (1970).
10) K. Kuroda and K. Watanabe, *Bull. Chem. Soc. Jpn.*, **44**, 1034 (1971).
11) K. Kuroda, *Bull. Chem. Soc. Jpn.*, **45**, 2176 (1972).
12) W. T. Jordan and B. E. Douglas, *Inorg. Chem.*, **12**, 403 (1973).
13) K. Kuroda, *Chem. Lett.*, **1974**, 17.
14) W. T. Jordan and J. I. Legg, *Inorg. Chem.*, **13**, 955 (1974).
15) L. J. Halloran and J. I. Legg, *Inorg. Chem.*, **13**, 2193 (1974).
16) P. J. Garnett and D. W. Watts, *Inorg. Chim. Acta*, **8**, 293 (1974).
17) K. Kawasaki, J. Yoshii, and M. Shibata, *Bull. Chem. Soc. Jpn.*, **43**, 3819 (1970).
18) C. T. Liu and B. E. Douglas, *Inorg. Chem.*, **3**, 1356 (1964).
19) B. E. Douglas and S. Yamada, *Inorg. Chem.*, **4**, 1561 (1965).
20) C. J. Hawkins, "Absolute Configuration of Metal Complexes," Wiley-Interscience, N. Y. (1971).
21) K. Kawasaki and M. Shibata, *Bull. Chem. Soc. Jpn.*, **45**, 3100 (1972).
22) T. Matsuda, T. Okumoto, and M. Shibata, *Bull. Chem. Soc. Jpn.*, **45**, 802 (1972).
23) T. Matsuda and M. Shibata, *Bull. Chem. Soc. Jpn.*, **46**, 3104 (1973).
24) M. Takeuchi and M. Shibata, *Bull. Chem. Soc. Jpn.*, **47**, 2797 (1974).
25) N. Matsuoka, J. Hidaka, and Y. Shimura, *Inorg. Chem.*, **9**, 719 (1970).
26) N. Matsuoka, J. Hidaka, and Y. Shimura, *Bull. Chem. Soc. Jpn.*, **48**, 458 (1975).
27) J. L. Sudmeier, A. J. Senzel, and G. L. Blackmer, *Inorg. Chem.*, **10**, 90 (1971).
28) D. H. Williams and D. H. Busch, *J. Am. Chem. Soc.*, **87**, 4644 (1965).
29) J. B. Terrill and C. N. Reilley, *Inorg. Chem.*, **5**, 1988 (1966).
30) J. L. Sudmeier and G. Occupati, *Inorg. Chem.*, **12**, 2524 (1968).
31) G. L. Blackmer and J. L. Sudmeier, *Inorg. Chem.*, **10**, 2019 (1971).

Preparation and Resolution of a Series of Chromium(III) Complexes Containing 2,2′-Bipyridyl *N,N′*-Dioxide and Ethylenediamine

Hideaki KANNO, Kazuo KASHIWABARA, and Junnosuke FUJITA*

Department of Chemistry, Faculty of Science, Nagoya University, Chikusa, Nagoya 464

(Received September 11, 1978)

A series of chromium(III) complexes of the type, $[Cr(bpdo)_n(en)_{3-n}]^{3+}$ was obtained by preparing two new complexes, $n=1$ and 2, where bpdo denotes 2,2′-bipyridyl *N,N′*-dioxide. Each of the bpdo complexes gave only one pair of enantiomers, which were resolved by an SP-Sephadex column chromatographic or a chemical method. The circular dichroism spectra of the resolved complexes were compared with those of the related complexes of the known absolute configuration. The $[Cr(bpdo)_3]^{3+}$ complex in water racemizes spontaneously in dark. The rate is independent of the concentrations of the complex, acid, and the free ligand, and an intramolecular racemization mechanism is suggested.

Although a number of metal complexes with 2,2′-bipyridyl *N,N′*-dioxide(bpdo) have been known,[1] no optically active complexes have ever been obtained. This paper is concerned with the preparation and properties of optically active chromium(III) complexes containing bpdo.

The ligand bpdo forms a skew seven-membered chelate ring upon coordination. The skew conformer can exist in a pair of enantiomers which can be designated by δ and λ, as shown in Fig. 1. Simpson *et al.*[2] and Vinciguerra *et al.*[3] prepared first bpdo complexes with a variety of metal ions including chromium(III) and suggested that the bpdo moiety in metal complexes takes the skew conformation on the basis of IR spectra. ^{1}H-NMR spectra of $[M(bpdo)_3]^{2+}$ ($M=Co^{2+}$ and Ni^{2+}) were also best interpreted by assuming the skew conformation of the ligand.[4] A tris-type complex with the chiral conformers of bpdo results theoretically in four diastereomers, each of which has a pair of enantiomers. In this paper, we describe such optical isomerism in the chromium(III) complexes on the basis of the circular dichroism (CD) spectra.

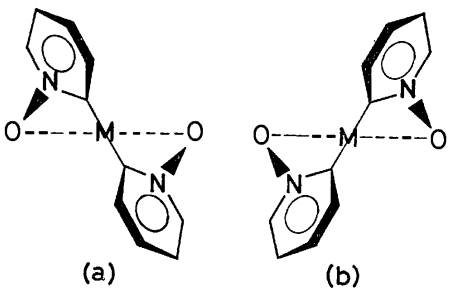

Fig. 1. The conformation of bpdo, (a) δ- and (b) λ-skew form.

Experimental

Preparation and Resolution of the Complexes. The chromium(III) complexes containing ethylenediamine (en) are photo-sensitive to occur hydrolysis. The $[Cr(bpdo)_3]^{3+}$ complex in solution does not hydrolyze in light, but its active isomer racemizes by exposure of ultraviolet light. Hence the following procedures should be done in dark, if necessary.

(1) $[Cr(bpdo)_3]^{3+}$: The racemic complex was prepared by a method similar to those of Simpson *et al.*[2] and Madan and Bull.[5] The solid of bpdo·H_2O[6] (3.5 g, 17 mmol) was dissolved in an aqueous solution (20 cm^3) of $Cr(NO_3)_3\cdot 9H_2O$ (2.0 g, 5 mmol). The solution was adjusted to pH *ca.* 2 with hydrochloric acid to avoid the formation of hydroxo complexes, kept at 90 °C for 1 h, and cooled to room temperature. Sodium perchlorate was then added to the solution to yield green precipitate, which was recrystallized from hot water and air-dried. Yield: 4 g (88%). Found: C, 37.78; H, 2.73; N, 9.53%. Calcd for $C_{30}H_{27}N_6O_{19.5}Cl_3Cr=[Cr(bpdo)_3](ClO_4)_3\cdot 1.5H_2O$: C, 38.25; H, 2.89; N, 8.92%.

The complex was resolved with $(+)_{589}$-Ag_3[Co(L-cysteinesulfinato(2−)-SN)$_3$].[7] The resolving agent (0.9 g, 1.1 mmol) was added to an aqueous solution (20 cm^3) of $[Cr(bpdo)_3]Cl_3$ which was prepared from the perchlorate (1.0 g, 1.1 mmol) and the anion exchanger, Dowex 1X8 in the chloride form. White precipitate of AgCl was filtered off and a small amount of ethanol was added to the filtrate to yield greenish orange precipitate, which was recyrstallized from water by adding ethanol. The product was dissolved in water and sodium perchlorate was added to the solution to give green crystals, which were filtered, washed with cold water and then ethanol, and air-dried. The crystals showed positive rotation at 589 nm in water. This complex loses gradually its optical activity in water. Found: C, 37.69; H, 2.58; N, 9.55%. Calcd for $C_{30}H_{27}N_6O_{19.5}Cl_3Cr=(+)_{589}$-$[Cr(bpdo)_3](ClO_4)_3\cdot 1.5H_2O$: C, 38.25; H, 2.89; N, 8.92%.

Attempts to separate possible diastereomers were all unsuccessfull by SP-Sephadex column chromatography. The column gave only one band of $[Cr(bpdo)_3]^{3+}$, all fractions of which showed the same pattern in the absorption spectra. The resolution was not achieved by the column chromatography because of racemization of the complex (*vide infra*).

(2) $[Cr(bpdo)_2en]^{3+}$: To an aqueous solution (10 cm^3, pH *ca.* 2) of $[CrCl_2(H_2O)_2(en)]Cl$[8] (1.1 g, 4 mmol) was added bpdo·H_2O (1.7 g, 8.2 mmol) and the solution was stirred at 50 °C for 4 h. Sodium perchlorate was then added to the solution to yield violet crystals, which were filtered. Yield: 1.1 g (34%). The product was contaminated with a small amount of $[Cr(bpdo)_3](ClO_4)_3$, and purified by SP-Sephadex column chromatography. The crude product dissolved in water was poured on an SP-Sephadex column, and the adsorbed band was eluted with a 0.3 mol dm^{-3} Na_2SO_4 solution. The violet fractions were collected, concentrated under reduced pressure to a small volume, and mixed with sodium perchlorate to yield violet crystals. They were washed with a mixture of water and ethanol (1:1), then ethanol and air-dried. Yield: 0.7 g (20%). Found: C, 32.46; H, 2.89; N, 10.11%. Calcd for $C_{22}H_{27}N_6O_{17.5}Cl_3Cr=[Cr(bpdo)_2en](ClO_4)_3\cdot 1.5H_2O$: C, 32.46; H, 3.35; N, 10.33%.

The resolution was achieved by use of the complex chloride and $(-)_{589}$-$K[As(cat)_3]$[9] (cat=1,2-benzenediolate ion). An aqueous solution (20 cm^3) of the chloride which was

prepared from the perchlorate (1.2 g, 1.5 mmol) and a Dowex 1X8 anion exchanger in the chloride form was adjusted to pH 7—8 with potassium carbonate. To this solution was added an aqueous solution (30 cm^3) of the resolving agent (0.66 g, 1.5 mmol) to yield violet precipitate, which was filtered off. The filtrate was stirred for a while with a Dowex 1X8 anion exchanger in the chloride form to remove the resolving agent remained. The resulting solution gave positive rotation at 589 nm and was used for the CD measurement. The absorption spectrum of the solution was identical with that of the racemic complex and remained constant, but the optical activity was lost gradually at room temperature. Hence the procedure of resolution was carried out at a temperature as low as possible. The violet precipitate obtained above by the addition of the resolving agent was quite insoluble in water and the resolving agent could not be removed by usual methods. The optically active complex was isolated as perchlorate by the addition of sodium perchlorate to the filtrate obtained above. Found: C, 32.95; H, 2.94; N, 10.51%. Calcd for $C_{22}H_{26}N_6O_{17}Cl_3Cr=(+)_{589}$-$[Cr(bpdo)_2en](ClO_4)_3\cdot H_2O$: C, 32.83; H, 3.26; N, 10.44%. The resolution by SP-Sephadex column chromatography was not achieved and the column showed only one band of racemic $[Cr(bpdo)_2en]^{3+}$.

(3) $[Cr(bpdo)(en)_2]^{3+}$: To an aqueous solution (30 cm^3) of *cis*-$[CrCl_2(en)_2]Cl$[10] (1.5 g, 5 mmol) was added bpdo·H_2O (1.7 g, 8.2 mmol) and the solution was stirred at 50 °C for 1 h. Sodium perchlorate was then added to the solution to yield red orange crystals, which were filtered and recrystallized from warm water (50 °C). Yield: 1.7 g (50%). Found: C, 24.21; H, 3.88; N, 12.39%. Calcd for $C_{14}H_{28}N_6O_{16}Cl_3Cr=[Cr(bpdo)(en)_2](ClO_4)_3\cdot 2H_2O$: C, 24.20; H, 4.07; N, 12.10%.

The complex was resolved completely by SP-Sephadex column chromatography. The complex perchlorate (*ca.* 0.35 g) was loaded on a column (ϕ 2.7×80 cm) of SP-Sephadex C-25 in the sodium form and the adsorbed red orange band was eluted with a 0.2 mol dm^{-3} sodium $(+)_{589}$-tartratoantimonate(III) solution. When the band was separated into two, the column was washed with water to remove the eluent. Two parts of the resin adsorbed the complex were separately taken out from the column and poured into small columns (ϕ 2.7×30 cm). Each of the adsorbed complexes (a pair of enantiomers) was eluted with a 3 mol dm^{-3} lithium chloride solution and the eluate was mixed with sodium perchlorate to give red orange precipitate. The isomer obtained from the fast eluted band showed positive rotation at 589 nm. The optical activity of this complex remains unchanged in dark at room temperature. Found: C, 24.37; H, 3.51; N, 12.01%. Calcd for $C_{14}H_{28}N_6O_{16}Cl_3Cr=[Cr(bpdo)(en)_2](ClO_4)_3\cdot 2H_2O$: C, 24.20; H, 4.07; N, 12.10%.

(4) $[Cr(en)_3]^{3+}$: This complex was prepared by the method described previously[11] and resolved by an SP-Sephadex column chromatographic method similar to that for $[Co(en)_3]^{3+}$.[12] The complex chloride (*ca.* 0.5 g) was loaded on a column (ϕ 2.7×50 cm) of SP-Sephadex C-25 resin in the sodium form and the complex was eluted with a 0.3 mol dm^{-3} sodium $(+)_{589}$-tartratoantimonate(III) solution. Each eluate of the two separate bands was collected and diluted with water. The solution was poured on a small column of SP-Sephadex C-25 in the hydrogen form. The adsorbed complex was eluted with a 3 mol dm^{-3} lithium chloride solution and the eluate was concentrated under reduced pressure to yield orange crystals of the active chloride. The isomer obtained from the fast moved band showed positive rotation at 589 nm.

Kinetic Runs. Decrease in the CD strength of $(+)_{589}$-$[Cr(bpdo)_3]^{3+}$ at the CD peak (485 or 575 nm) was continuously recorded on a JASCO model J-20 spectropolarimeter with a cell jacket to keep the temperature constant within ±0.1 °C using a Haake thermostat Type FSe. A Takara Thermister Type SPD-10 thermometer was placed inside the CD cell. The pH and ionic strength of the solution were adjusted with an aqueous solution of $NaClO_4$–$HClO_4$. The rate of decrease obeyed the first order kinetic law and the observed rate constant (k_{obsd}) is expressed as follows: $k_{obsd}=-\ln[(\alpha_t-\alpha_\infty)/(\alpha_0-\alpha_\infty)]/t$ where α's are CD strengths at the time denoted by the suffixes.

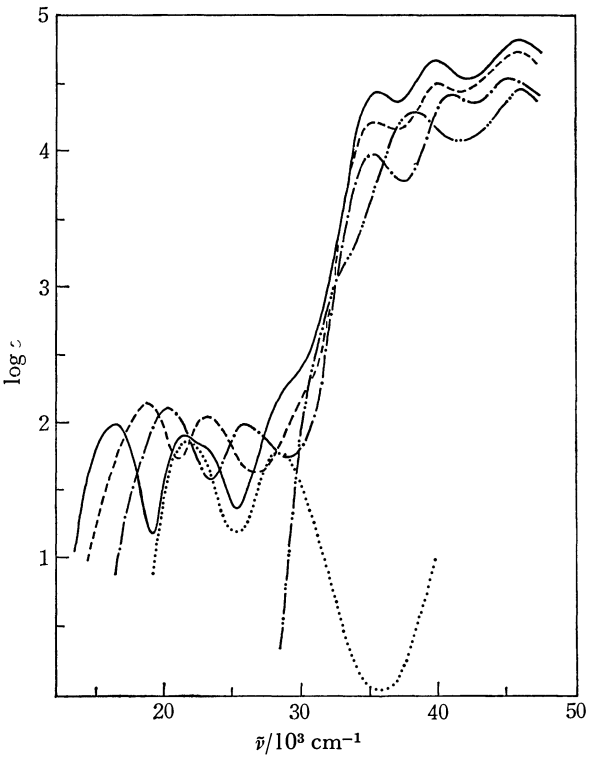

Fig. 2. Absorption spectra of $[Cr(bpdo)_3]^{3+}$ (——), $[Cr(bpdo)_2en]^{3+}$ (----), $[Cr(bpdo)(en)_2]^{3+}$ (—·—), $[Cr(en)_3]^{3+}$ (·····), and bpdo (—··—) in water.

Absorption and circular dichroism spectra were recorded on a HITACHI 323 spectrophotometer and a JASCO model J-20 spectropolarimeter, respectively.

Results and Discussion

Two new complexes, $[Cr(bpdo)_n(en)_{3-n}]^{3+}$ (n=1 and 2) were prepared from *cis*-$[CrCl_2(en)_2]^+$ and $[CrCl_2(H_2O)_2en]^+$, respectively, by replacing the chloride ions and water molecules with bpdo. The reactions should be carried out at below *ca.* 50 °C to reduce the formation of $[Cr(bpdo)_3]^{3+}$. The pure complexes were easily isolated from the crude products by SP-Sephadex column chromatography using a 0.3 mol dm^{-3} Na_2SO_4 solution as an eluent. The tris- and bis-en complexes were resolved by SP-Sephadex column chromatography, while the tris- and bis-bpdo complexes were not done by this method, but achieved by the chemical method with $(+)_{589}$-[Co(L-cysteinesulfinato-(2−)-SN)$_3$]$^{3-}$ and $(-)_{589}$-$[As(cat)_3]^-$, respectively. The former two complexes are optically stable in water at room temperature in dark, while the latter two complexes lose slowly the optical activity under

Table 1. Absorption and CD spectral data

	Absorption $\tilde{\nu}/10^3$ cm^{-1} (log ε)	CD $\tilde{\nu}/10^3$ cm^{-1} ($\Delta\varepsilon$)
bpdo	38.4 (4.30)	
	46.0 (4.45)	
$(+)_{589}$-$[Cr(en)_3]^{3+}$	21.8 (1.89)	21.9 (+1.64)
	28.6 (1.80)	26.5 (+0.07)
		30.4 (+0.08)
$(+)_{589}$-$[Cr(bpdo)(en)_2]^{3+}$	20.4 (2.11)	18.9 (+3.25)
	26.0 (1.99)	24.7 (+0.43)
	35.2 (3.96)	27.0 (+0.43)
	40.8 (4.43)	31.6 (+0.20)
	45.1 (4.55)	34.4 (−7.76)
		37.8 (+24.8)
		40.9 (−86.3)
		45.0 (+77.7)
$(-)_{589}$-$[Cr(bpdo)_2(en)]^{3+}$	18.8 (2.15)	17.5 (+3.75)
	23.2 (2.06)	22.9 (+2.08)
	35.5 (4.21)	29.4 (−0.72)
	40.0 (4.52)	34.5 (−46.5)
	45.5 (4.73)	37.5 (+13.4)
		40.0 (−81.0)
		43.5 (+67.4)
$(+)_{509}$-$[Cl(bpdo)_3]^{3+}$	16.3 (2.01)	15.2 (−2.66)
	21.4 (1.94)	17.6 (+0.46)
	22.5^{sh} (1.88)	20.6 (−0.52)
	35.7 (4.46)	23.3 (+0.08)
	40.0 (4.67)	29.0 (+0.62)
	45.8 (4.83)	34.7 (+56.5)
		38.0 (+59.3)
		40.8 (−80.0)

sh: shoulder.

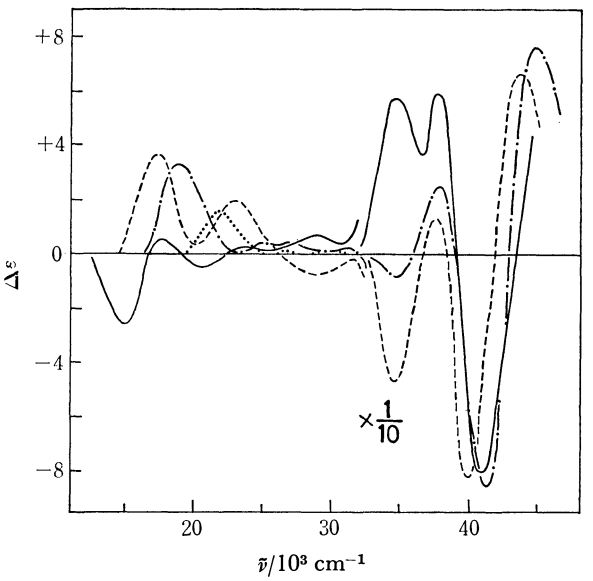

Fig. 3. CD spectra of $(+)_{589}$-$[Cr(bpdo)_3]^{3+}$ (——), $(-)_{589}$-$[Cr(bpdo)_2en]^{3+}$ (----), $(+)_{589}$-$[Cr(bpdo)(en)_2]^{3+}$ (—·—), and $(+)_{589}$-$[Cr(en)_3]^{3+}$ (·····) in water.

the same conditions (*vide infra*).

The bpdo ligand forms a skew seven-membered chelate ring upon coordination. The skew conformation is chiral and can exist in a pair of enantiomers which are designated by δ and λ, as shown in Fig. 1. The δ-(or λ-)skew conformers in the Λ- and Δ-configurations form the *lel*(or *ob*) and *ob*(or *lel*) structures, respectively, as seen in $[Co(en)_3]^{3+}$ which is constituted by the gauche conformers of en.[13] For $[Cr(bpdo)_3]^{3+}$, therefore, there are four possible diastereomers, each of which has a pair of enantiomers (lel_3 : $\Lambda(\delta\delta\delta)=\Delta(\lambda\lambda\lambda)$, lel_2ob : $\Lambda(\delta\delta\lambda)=\Delta(\lambda\lambda\delta)$, $lelob_2$: $\Lambda(\delta\lambda\lambda)=\Delta(\lambda\delta\delta)$, and ob_3 : $\Lambda(\lambda\lambda\lambda)=\Delta(\delta\delta\delta)$). Similarly, $[Cr(bpdo)_2en]^{3+}$ and $[Cr(bpdo)(en)_2]^{3+}$ have three (lel_2 : $\Lambda(\delta\delta)=\Delta(\lambda\lambda)$, *lelob* : $\Lambda(\delta\lambda)=\Delta(\lambda\delta)$, and ob_2 : $\Lambda(\lambda\lambda)=\Delta(\delta\delta)$) and two (*lel* : $\Lambda(\delta)=\Delta(\lambda)$ and *ob* : $\Lambda(\lambda)=\Delta(\delta)$) diastereomers, respectively. However, each of the bpdo complexes gave only one diastereomer. These results suggest that the bpdo chelate ring changes easily its conformation ($\delta\rightleftharpoons\lambda$) in solution, and that each complex crystallizes in a particular diastereomer. The structures of the diastereomers are not certain at present. However, molecular models indicate that the *lel* isomers are always less crowded than the *ob* isomers. The tris-, bis- and mono-bpdo complexes isolated will have the lel_3, lel_2 and *lel* structures, respectively in the solid state, but will be in equilibrium among the isomers involving the *ob* conformation in solution. The bis-(ethylenediamine)cobalt(III) complex containing 2,2′-diaminobiphenyl which forms a similar seven-membered chelate ring is also known to yield only one pair of enantiomers, $\Lambda(\delta)$ and $\Delta(\lambda)$.[14,15]

Figure 2 shows the absorption spectra of the complexes and the free ligand. Table 1 gives the spectral data. The first and the second absorption bands shift to lower wave numbers by replacing en with bpdo, but the magnitudes of the shift are not proportional to the number of the bpdo ligand, the first absorption

TABLE 2. KINETIC DATA FOR RACEMIZATION

Complex	Temp (°C)	pH (Ionic strength)	k / 10^{-4} s^{-1}	E_a / kJ mol^{-1}	ΔS^* / J K mol^{-1}	Ref.
$(+)_{589}$-$[Cr(bpdo)_3]^{3+}$	26.9	7 (2.1×10^{-2})	1.40±0.04			
	36.3	7 (2.3×10^{-2})	3.72±0.12	81.3±4.4	−49±14	
	47.5	7 (2.4×10^{-2})	10.6±0.1			
	28.0	2 (2.1×10^{-2})	1.54±0.06			
	36.5	2 (2.1×10^{-2})	3.54±0.09	80.2±5.0	−51±17	
	47.5	2 (2.0×10^{-2})	10.0±0.1			
$[Cr(phen)_3]^{3+}$	25	6	0.005	98.7	−46	22)
$[Cr(ox)_3]^{3-}$	18.2	7	1.75	66.2	−100	23)

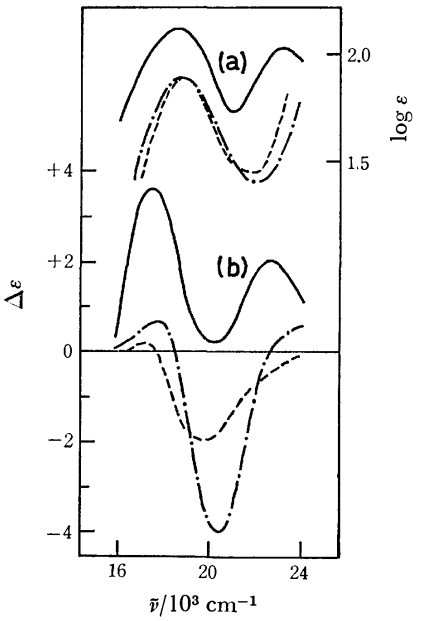

Fig. 4. Absorption (a) and CD (b) spectra of $[CrO_4N_2]$ complexes in the region of the first absorption band, $(-)_{589}$-$[Cr(bpdo)_2en]^{3+}$ (——), Λ-$[Cr(acac)_2en]^+$ (—·—), and Λ-$[Cr(ox)_2en]^-$ (----).

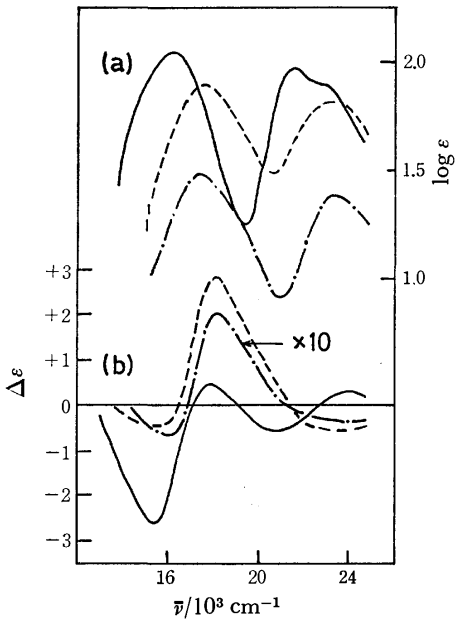

Fig. 5. Absorption (a) and CD (b) spectra of $[CrO_6]$ complexes in the region of the first absorption band, $(+)_{589}$-$[Cr(bpdo)_3]^{3+}$ (——), Λ-$[Cr(mal)_3]^{3-}$ (—·—), and Λ-$[Cr(ox)_3]^{3-}$ (----).

band of $[Cr(bpdo)_3]^{3+}$ being at lower wave numbers by 1000 cm^{-1} than those expected from other complexes of the present series. In a series of complexes, $[Cr(ox)_{3-n}(en)_n]^{2n-3}$ (ox=oxalate ion),[16,17] the first absorption bands shift regularly with nearly the same interval. In the ultraviolet region, the bpdo complexes exhibit three strong absorption bands, while the free ligand two bands, the lower wave number band of which seems to split into two in the complexes. The intensities of the bands in the complexes are nearly proportional to the number of the bpdo ligand.

Figure 3 compares the CD spectra of $(+)_{589}$-$[Cr(bpdo)_{3-n}(en)_n]^{3+}$ (n=0, 2, and 3) and $(-)_{589}$-$[Cr(bpdo)_2en]^{3+}$. The last isomer is opposite to that used for the measurement. The tris- and bis-bpdo complexes racemize spontaneously in solution so that the spectral variations with time are corrected at each wave number (*vide infra*). Since $(+)_{589}$-$[Cr(en)_3]^{3+}$ has been assigned to the Λ-configuration,[18] $(+)_{589}$-$[Cr(bpdo)(en)_2]^{3+}$ which gives a similar positive CD band in the region of the first absorption band can be assigned to the same Λ-configuration. The analogous complexes of the type, $[CrO_2N_4]$ such as Λ-$(+)_{589}$-$[Cr(acac)(en)_2]^{2+}$[19] (acac=acetylacetonate ion) or Λ-$(+)_{589}$-$[Cr(ox)(en)_2]^+$[20] also give a positive CD band in this region. The CD patterns of $(-)_{589}$-$[Cr(bpdo)_2en]^{3+}$ and $(+)_{589}$-$[Cr(bpdo)_3]^{3+}$ isomers in the region of the first absorption band are quite different from those of complexes of the type, $[CrO_4N_2]$ and $[CrO_6]$, respectively, whose absolute configurations have been known, as shown in Figs. 4 and 5. However, these isomers show the same CD pattern in the ultraviolet region as that of $(+)_{589}$-$[Cr(bpdo)$-

$(en)_2]^{3+}$ except the positive band at 34700 cm^{-1} of $(+)_{589}$-$[Cr(bpdo)_3]^{3+}$. Therefore, both $(-)_{589}$-$[Cr(bpdo)_2en]^{3+}$ and $(+)_{589}$-$[Cr(bpdo)_3]^{3+}$ may be assigned to the Λ-configuration. In Fig. 5 is compared the CD spectrum of $(+)_{589}$-$[Cr(bpdo)_3]^{3+}$ in the region of the first absorption band with those of Λ-$[Cr(ox)_3]^{3-}$[17,20] and Λ-$[Cr(mal)_3]^{3-}$[17,20] (mal=malonate ion). All of the isomers show a negative and a positive CD band from the smaller wave number side. The CD strength of the malonato complex is extremely weak and the sign of the main CD band of the bpdo complex is negative and opposite to that of the oxalato complex. Such a change in the CD spectra among the complexes of five-, six-, and seven-membered chelate rings is very similar to that observed for a series of complexes, $[Co(NH_2(CH_2)_nNH_2)_3]^{3+}$ (n=2, 3, and 4).[21] On the other hand, the CD pattern of $(-)_{589}$-$[Cr(bpdo)_2en]^{3+}$ is quite different from those of analogous complexes and is not given any plausible discussion at present.

As stated previously, the optically active $[Cr(bpdo)_3]^{3+}$ and $[Cr(bpdo)_2en]^{3+}$ lose their activity in solution. The rates of decrease in the optical activity for $(+)_{589}$-$[Cr(bpdo)_3]^{3+}$ were obtained under the conditions described in Experimental part in dark so as to avoid photo-induced reactions. During the loss of optical activity, the absorption spectrum of the complex was unchanged. The rates obeyed the first order kinetic law and the rate constants (k_{obsd}) were calculated from the slopes of time *vs.* $\Delta\varepsilon$. The data are given in Table 2 together with the activation parameters, and with data for other chromium(III) complexes for comparison. The loss of optical activity should be caused by racemization of the complex, and the racemization will involve both inversions of the complex ion and the ligand, $\Delta \rightleftharpoons \Lambda$ and $\delta \rightleftharpoons \lambda$. The rates were independent of the concentrations of the complex, acid, and the free ligand. Hence, the racemization is suggested to proceed by an intramolecular twist mechanism.[22] The activation parameters are similar to those of other complexes given in Table 2, for which intramolecular mechanisms have been postulated.[23]

The authors wish to thank the Ministry of Education for Scientific Research Grant-in-Aid (No. 243013) and the Kurata Research Grant.

References

1) N. M. Karayannis, A. N. Speca, D. E. Chasan, and L. L. Pytlewski, *Coord. Chem. Rev.*, **20**, 37 (1976).
2) P. G. Simpson, A. Vinciguerra, and J. V. Quagliano, *Inorg. Chem.*, **2**, 282 (1963).
3) A. Vinciguerra, P. G. Simpson, Y. Kakiuti, and J. V. Quagliano, *Inorg. Chem.*, **2**, 286 (1963).
4) I. Bertini, D. Gatleschi, and J. Wilson, *Inorg. Chim. Acta*, **4**, 629 (1970).
5) S. K. Madan and W. E. Bull, *J. Inorg. Nucl. Chem.*, **26**, 2211 (1964).
6) I. Murase, *Nippon Kagaku Zasshi*, **77**, 682 (1956).
7) L. S. Dollimore and R. D. Gillard, *J. Chem. Soc., Dalton Trans.*, **1973**, 933.
8) D. A. House, *Inorg. Chem.*, **5**, 840 (1966).
9) G. E. Pyschkewitsh and J. M. Garrett, *J. Am. Chem. Soc.*, **90**, 7234 (1968).
10) E. Pedersen, *Acta Chem. Scand.*, **24**, 3362 (1970).
11) *Inorg. Synth.*, **2**, 196 (1946).
12) Y. Yoshikawa and K. Yamasaki, *Inorg. Nucl. Chem. Lett.*, **6**, 523 (1970).
13) E. J. Corey and J. C. Bailar, Jr., *J. Am. Chem. Soc.*, **81**, 2620 (1959).
14) T. Tanimura, H. Ito, J. Fujita, K. Saito, S. Hirai, and K. Yamasaki, *J. Coord. Chem.*, **3**, 161 (1973).
15) W. T. Jordan, C. Y. Lin, and B. E. Douglas, *J. Coord. Chem.*, **3**, 1 (1973).
16) S. Kaizaki, J. Hidaka, and Y. Shimura, *Inorg. Chem.*, **12**, 142 (1973).
17) A. J. McCaffery, S. F. Mason, and R. E. Ballard, *J. Chem. Soc.*, **1965**, 2883.
18) Y. Kushi, M. Kuramoto, and H. Yoneda, *Chem. Lett.*, **1976**, 339.
19) S. Kaizaki, J. Hidaka, and Y. Shimura, *Inorg. Chem.*, **12**, 135 (1973).
20) K. R. Butler and M. R. Snow, *J. Chem. Soc., Dalton Trans.*, **1976**, 251.
21) M. Kojima, H. Yamada, H. Ogino, and J. Fujita, *Bull. Chem. Soc. Jpn.*, **50**, 2325 (1977).
22) N. A. Kane-Maguire and S. A. Edwards, *J. Inorg. Nucl. Chem.*, **38**, 1037 (1976).
23) E. Bushra and C. H. Johnson, *J. Chem. Soc.*, **1939**, 1937; K. V. Krishnamurty and G. M. Harris, *Chem. Rev.*, **61**, 213 (1961).

Thermochromism of Metal Chelates with Triphenylmethane Complexons in Aqueous Solutions. I. Copper(II)–Xylenol Orange System†

Shoji NAKADA, Mutsuo YAMADA, Tasuku ITO,†† and Masatoshi FUJIMOTO*

Department of Chemistry, Faculty of Science, Hokkaido University, Sapporo 060

(Received September 18, 1978)

Reversible thermochromisms are found for about thirty kinds of metal complexes of triphenylmethane complexons in aqueous solutions. The thermochromism observed in the aqueous solution of copper(II) complex with 3,3′-bis[*N*,*N*-bis(carboxymethyl)aminomethyl]-*o*-cresolsulfonphthalein (Xylenol Orange, XO) was primarily ascribed to the temperature-dependence of the protolytic equilibria between a complex species AH having an uncoordinated free phenolic hydroxyl group and a complex species A having a coordinated phenolate group: $AH \rightleftarrows A + H$. The equilibrium constant K of the reaction was determined to be $p(K/\text{mol dm}^{-3}) = 4.40$ at 25 °C. The thermodynamic parameters ΔH and ΔS for the reaction were calculated to be 26 ± 2 kJ mol^{-1} and 1 ± 3 J mol^{-1} K^{-1} (298 K), respectively. The rate constant of the proton dissociation of the phenolic hydroxyl group in the complex AH was estimated to be *ca.* 2×10^5 s^{-1}.

In the course of a series of research works on the complexation reactions of metal ions with the multidentate ligands of triphenylmethane complexon††† type, Yamada discovered a phenomenon of thermochromism in the aqueous solution of copper(II)–XO complex.[1] In the previous communication, we reported that the complexes of other triphenylmethane complexons with some bivalent metal ions are also thermochromic.[2]

In the present paper, we report the thermochromism of the complexes of bivalent metal ions with various triphenylmethane complexons in aqueous media. We studied in detail the mechanism of the thermochromic change for the copper(II)–XO complex by means of the spectrophotometric and the temperature-jump method.

The mechanism was found to be quite different from that of the thermochromisms observed so far in the metal complexes in solutions, which were ascribed to the change in the configurational requirements on the central metal ions or the change in the ligand-field stabilization energies.[3,4]

Experimental

Materials. All chemicals used were of analytical grade, unless otherwise specified. Water was deionized and distilled. Xylenol Orange was synthesized by Mannich condensation from *o*-Cresol Red, iminodiacetic acid (IDA), and formaldehyde.[5] The crude sample of the synthesized XO was purified beforehand by means of cellulose column chromatography and finally by means of high-performance liquid chromatography.[6] The purity of the specimen of XO was confirmed by elemental analyses and melting point measurements.[6] Melting point was measured with a Rigaku Denki Differential Scanning Calorimeter Model 8001 SL/C. The purified XO was used as a free acid form. A 1.0×10^{-3} mol dm^{-3} stock solution of XO was prepared by dissolving a desired amount of XO in water.

The perchlorates of bivalent metals were prepared by heating the chlorides with small excess of perchloric acid until no trace of chloride ion was detected. The perchlorate was recrystallized from water. The stock solution was standardized titrimetrically with EDTA.

The pre-purified sodium perchlorate[7] was heated in an oven at *ca.* 200 °C to prepare an anhydrous salt. A desired amount of the anhydrous perchlorate was dissolved in water to prepare a stock solution. Buffer solutions were prepared from 0.1 mol dm^{-3} acetic acid and 0.1 mol dm^{-3} sodium acetate.

Measurements. The equilibria were measured with Hitachi recording spectrophotometers Model EPS-3T and Model 323 equipped with a cell thermostated at high temperatures. A 1 cm quartz cell was used. The kinetic measurements were carried out with a Union Giken co-axial-cable temperature-jump apparatus Model RA-105.[8] The pH values of the solutions were adjusted with acetate buffers and measured with a Hitachi-Horiba pH-meter Model F-7SS. For the pH measurements at high temperatures a glass electrode 1027-05T and a saturated calomel electrode 2631-05T were used. Temperature of the solution was measured with a copper-constantan thermocouple and a millivoltmeter. The ionic strength of the solution was adjusted to 0.1 mol dm^{-3} with sodium perchlorate.

Results and Discussion

Equilibria. In Table 1 are summarized the results of the thermochromism observed for the metal complexes of triphenylmethane complexons, which include both sulfonphthalein complexons and phthalein complexons. The structures and the abbreviated nomenclatures of the ligands are shown in Fig. 1(a) and Table 2. The results observed for the complexes of bivalent metal ions, Mg^{2+}, Ca^{2+}, Mn^{2+}, Co^{2+}, Ni^{2+}, Cu^{2+}, and Zn^{2+}, were included in the table. Color changes of the aqueous solutions containing triphenylmethane complexons and 10—100 fold excess of metal ions have been studied at various buffered pH as a function of temperature by the measurements of visible absorption spectra as well as by visual observation. The thermochromic changes were observed only in the narrow pH range characteristic of the individual system.

The systems No. 1—29 in Table 1 include the com-

† Presented in part at the 27th Annual Meeting on Coordination Chemistry, Matsumoto, September 28, 1977, Abstracts, pp. 263 and 265.

†† Present address: Institute for Molecular Science, Okazaki 444.

††† Triphenylmethane complexons denote a series of multidentate ligands derived from the triphenylmethane dyes and iminodiacetic acid or other amino acids.

TABLE 1. THERMOCHROMISMS OF SOME METAL CHELATES WITH TRIPHENYLMETHANE COMPLEXONS[a)]

No.	Ligand	Metal ion	pH[b)] at 25 °C	Color (λ_{max}/nm[c)]) at room temperature	Color (λ_{max}/nm[c)]) at 60 °C	Remark[d)]
1	XO	Mg^{2+}	5.90	yellow (435)	reddish violet (575)	vs
2		Ca^{2+}	5.90	yellow (435)	reddish violet (580)	vs
3		Mn^{2+}	4.92	orange (440)	reddish violet (583)	vs
4		Co^{2+}	3.99	orange (452)	reddish violet (584)	s
5		Ni^{2+}	3.64	orange (452)	reddish violet (584)	s
6		Cu^{2+}	4.21	orange (450)	reddish violet (574)	vs
7		Zn^{2+}	3.97	orange (448)	reddish violet (572)	vs
8	MXB[e)]	Mg^{2+}	6.72	pale blue (450)	blue (606)	s
9		Ca^{2+}	5.90	green (440)	bluish green (590)	s
10		Mn^{2+}	5.04	yellow (446)	blue (615)	vs
11		Co^{2+}	3.81	pale yellow (468)	blue (618)	s
12		Ni^{2+}	3.80	yellow (456)	blue (618)	s
13		Cu^{2+}	4.34	yellow (460)	dark blue (600)	s
14		Zn^{2+}	4.06	dark yellow (464)	blue (610)	vs
15	MTB[e)]	Mg^{2+}	5.75	yellow (438)	yellow green (600)	s
16		Ca^{2+}	5.85	yellow green (438)	green (600)	s
17		Mn^{2+}	5.85	yellow (438)	green (605)	vs
18		Co^{2+}	3.67	yellow (460)	dark green (615)	vs
19		Ni^{2+}	3.67	yellow (446)	yellow green (618)	vs
20		Cu^{2+}	5.19	brown (444)	brown violet (600)	s
21		Zn^{2+}	3.80	yellow (454)	dark blue (598)	vs
22	CO[f)]	Cu^{2+}	4.38	orange (460)	pink (563)	s
23	GCR[e)]	Co^{2+}	5.24	dark yellow (438)	reddish violet (579)	s
24		Cu^{2+}	3.46	dark yellow (440)	reddish violet (576)	s
25	SCR[g)]	Co^{2+}	4.45	yellow (434)	reddish violet (578)	vs
26		Ni^{2+}	4.47	yellow (438)	reddish violet (578)	vs
27		Cu^{2+}	3.50	pale yellow (444)	reddish violet (572)	s
28		Zn^{2+}	4.82	yellow (444)	reddish violet (570)	vs
29	SXO[g)]	Cu^{2+}	5.46	orange (464)	reddish violet (570)	s
30	PC[h)]	Mg^{2+}	6.42	colorless (——)	violet (574)	vs
31		Mn^{2+}	5.27	pale violet (——)	violet (578)	vs
32		Ni^{2+}	4.82	colorless (——)	violet (580)	vs
33	PPC[h)]	Mg^{2+}	6.90	pale pink (——)	reddish violet (556)	vs
34	TPC[h)]	Mg^{2+}	7.11	colorless (——)	pale blue (608)	vs
35		Mn^{2+}	6.41	colorless (——)	blue (614)	s
36		Ni^{2+}	5.15	pale blue (——)	blue (618)	vs

a) Observed for the solutions containing $(1—5)\times10^{-5}$ mol dm^{-3} ligand and 10—100 fold excess of metal perchlorate. b) The pH, at which the remarkable thermochromic change was observed. Acetate buffer (CH_3COOH-CH_3COONa) and phosphate buffer (NaH_2PO_4-Na_2HPO_4) were used for the pH adjustment. c) λ_{max}'s represent the positions of the absorption maxima of the shorter- or the longer-wavelength absorptions. — denotes no, weak, or broad absorption. d) s: strong, vs: very strong. e) Purified by preparative thin-layer chromatography. See Ref. 9. f) Kindly supplied by Professor H. Nakayama, Kagawa Nutrition College. g) Purified by cellulose column chromatography. h) The commercial specimens of PC, PPC, and TPC (Dojindo, Kumamoto) were used.

TABLE 2. TRIPHENYLMETHANE COMPLEXONS LISTED IN TABLE 1 (See Fig. 1(a))

Ligand	R_1[a)]	R_2[a)]	R_3	R_4	R_5
Xylenol Orange (XO)	A	A	CH_3	H	SO_3H
Methylxylenol Blue (MXB)	A	A	CH_3	CH_3	SO_3H
Methylthymol Blue (MTB)	A	A	$CH(CH_3)_2$	CH_3	SO_3H
Cresol Orange (CO)	A	A	H	H	SO_3H
Glycine Cresol Red (GCR)	B	B	CH_3	H	SO_3H
Sarcosine Cresol Red (SCR)	C	C	CH_3	H	SO_3H
Semi-Xylenol Orange (SXO)	A	H	CH_3	H	SO_3H
Phthalein Complexon (PC)	A	A	CH_3	H	COOH
Phenolphthalein Complexon (PPC)	A	A	H	H	COOH
Thymolphthalein Complexon (TPC)	A	A	$CH(CH_3)_2$	CH_3	COOH

a) A=$CH_2N(CH_2COOH)_2$, B=CH_2NHCH_2COOH, C=$CH_2N(CH_3)CH_2COOH$.

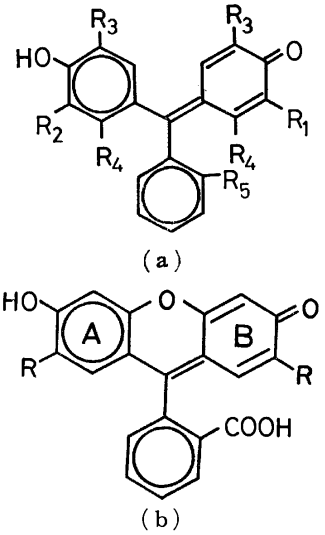

Fig. 1. The structures of the triphenylmethane complexons used. (a) Sulfonphthalein and phthalein complexons listed in Table 2. (b) Phthalein complexons with an ether linkage between two benzene rings. Calcein ($R=CH_2N(CH_2COOH)_2$) and Methyl Calcein ($R=CH_2N(CH_3)CH_2COOH$).

plexes of sulfonphthalein complexons. The absorption spectra of these complexes in visible region consist of two absorption bands. Temperature-dependencies of the spectra of these complexes were similar to the dependency shown in Fig. 2(a), *i.e.*, with a temperature-rise, the absorptions at longer wavelength increased, whereas those at the shorter wavelength decreased. The absorption spectra of the systems No. 30—36, which include the complexes of phthalein complexons, have only one absorption band in the visible region; The absorptions in the region 550—620 nm increased in intensities with a temperature-rise. The high-temperature color of the metal complexes of these one-color complexons strongly resembles the alkaline color of the corresponding parent phthalein dyes. The positions of the visible absorption bands suggest that the complexes responsible for the absorptions at high temperatures have a coordinated phenolate group. In order to clarify the mechanism of the thermochromism, the quantitative measurements have been carried out for the copper(II)–XO system.

It should particularly be emphasized that for the quantitative studies the use of the highly purified specimen of the ligand was essential. The use of commercial crude specimens of the triphenylmethane complexons, which are available only as metallochromic indicators or as colorimetric reagents, gave no definite quantitative results, though the qualitative observations of the thermochromic changes were still possible.

Figure 2(a) shows the visible absorption spectra at various temperatures of an aqueous solution containing 3.0×10^{-5} mol dm^{-3} XO and 1.2×10^{-4} mol dm^{-3} Cu^{2+} ion, the pH of the solution being adjusted at 3.94± 0.05. The most remarkable thermochromic change was observed in the pH region 3.8—4.5. In this pH region the solutions are orange at lower temperatures

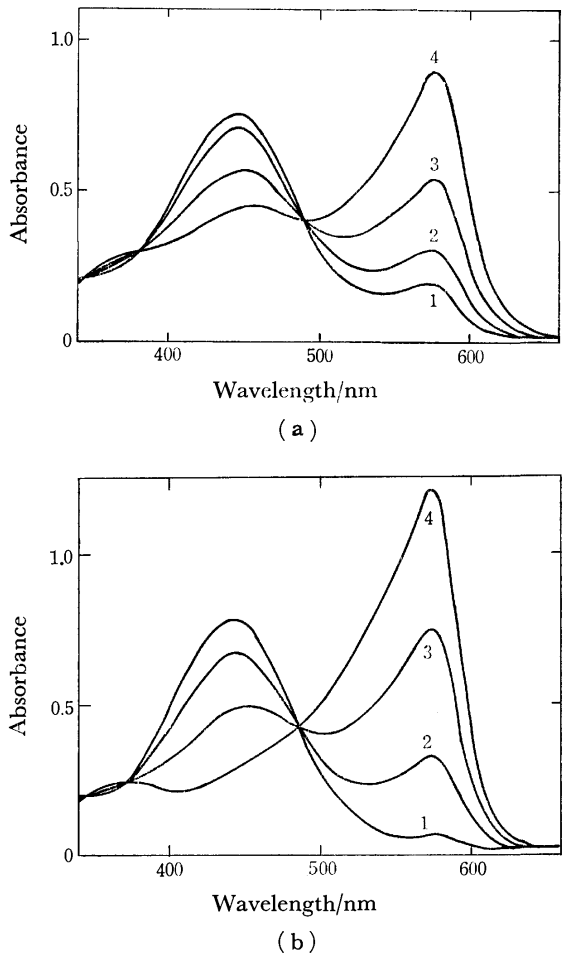

Fig. 2. Absorption spectra of the Cu(II)-XO. (a) Temperature-dependence. At 7 (1), 20 (2), 48 (3), and 78 °C (4). [Cu]$=1.2\times10^{-4}$ mol dm^{-3}; [XO]$=3.0\times10^{-5}$ mol dm^{-3}. I=0.1 mol dm^{-3} ($NaClO_4$). At pH$=3.94\pm0.05$. (b) pH-Dependence. At pH 2.99 (1), 3.93 (2), 4.49 (3), and 5.04 (4). [Cu]$=1.2\times10^{-4}$ mol dm^{-3}; [XO]$=3.0\times10^{-5}$ mol dm^{-3}. I=0.1 mol dm^{-3} ($NaClO_4$). At 25 °C. Cell length=1 cm.

and reddish violet at higher temperatures. The absorption spectrum changes reversibly with a distinct isosbestic point at 491 nm, showing the existence of an equilibrium between two chemical species. As the temperature rises the absorbance at 450 nm decreases accompanied with a large increase in the absorbance at 574 nm. The absorbance at 574 nm increases about 4.5-fold for the temperature-rise from 7 to 78 °C.

Figure 3 shows the results of the molar-ratio method for the Cu(II)–XO complex measured at 574 nm, at various temperatures, and at pH 4.58±0.02. The metal-to-ligand ratio of the complex species formed in the solution was found to be invariably 2 : 1 irrespective of the temperature. For the solutions containing more than two-fold excess of Cu^{2+} ion over XO, the absorbance at a constant temperature increases only slightly even with the large increase in the concentration of Cu^{2+} ion, whereas for the solution at an arbitrary definite [Cu(II)] to [XO] ratio the absorbance increases markedly with the rise of temperature. This

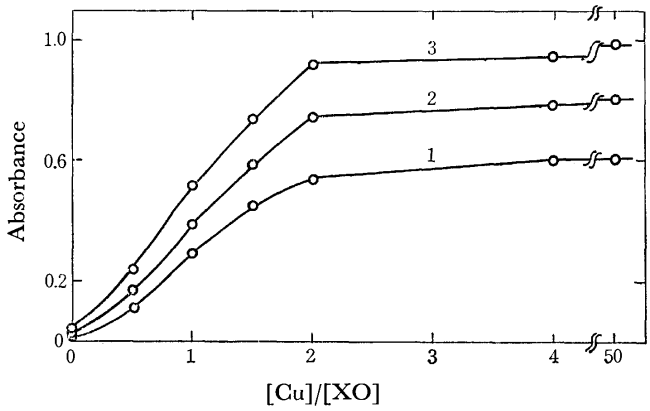

Fig. 3. Molar-ratio method at 574 nm for the Cu(II)-XO at various temperatures. At 25 (1), 50 (2), and 80 °C (3). $[XO]=3.0\times10^{-5}$ mol dm^{-3}. pH=4.58±0.02. I=0.1 mol dm^{-3} ($NaClO_4$). Cell length=1 cm.

fact indicates that the observed thermochromism should be ascribed to the temperature-dependence of an equilibrium between two 2 : 1 complex species, *i.e.*, between the low-temperature and the high-temperature form of a 2 : 1 complex species, but not to the step of complex formation between Cu^{2+} ion and the free ligand. In fact, the absorption maximum at the shorter wavelength observed in the presence of a large excess of Cu^{2+} ion (λ_{max}=450 nm) distictly differs from that of the free ligand in the given pH region (λ_{max}=434 nm).

The feature of the temperature-dependence of the absorption spectrum at a constant pH (Fig. 2(a)) was quite similar to that of the pH-dependence of the spectrum at a constnat temperature as depicted in Fig. 2(b). For the increase in the pH value of the solution from 3.93 to 5.04 the absorbance at 574 nm considerably increased about 3.7-fold accompanied with the corresponding decrease in the absorbance at 450 nm, and with a distinct isosbestic point at 491 nm. The observed wavelengths for the absorption maxima and the isosbestic point were found to be all the same as those for the temperature-dependence of the spectra at constant pH (Fig. 2(a)). It should be noted in this connection that the pH value of the acetate buffer solution used changed only slightly upon heating, *e.g.*, the solution of pH 4.55 at 20 °C shows the pH 4.62 even upon heating at 70 °C. The similarity of the temperature- and the pH-dependencies of absorption spectra suggests that the effect of heating of the solution essentially corresponds to the effect of the increase in pH of the same solution.

These facts indicate clearly that the observed thermochromism is primarily due to the temperature-dependence of the protolytic equilibria between the complex AH having an uncoordinated phenolic hydroxyl group and the complex A having a coordinated phenolate group

$$\underset{\text{(at lower temperatures)}}{AH} \overset{K}{\rightleftharpoons} \underset{\text{(at higher temperatures)}}{A + H.} \quad (1)$$

The complex A is predominant at higher temperatures.

When the experiments were carried out in unbuffered aqueous solutions of the complex, the pH of the solution decreased with the rise of temperature. For example, if the pH of the solution containing 1.6×10^{-2} mol dm^{-3} $Cu(ClO_4)_2$ and 4.0×10^{-3} mol dm^{-3} XO (I=0.1 mol dm^{-3} ($NaClO_4$)) was adjusted at 4.53 at 25 °C only with $HClO_4$ and NaOH, the pH of the solution did decrease to 4.20 by heating the solution to 70 °C. The value of the pH at 70 °C accorded approximately with the calculated value of pK based on the ΔH and ΔS (see below). The same color change of the solution was observed as in the case of the buffered solution. These results directly confirm the dissociation of the proton from the species AH upon heating, which forms the hydrated proton in the unbuffered aqueous solution to lower the pH value of the solution as to be expected from the reaction mechanism (1).

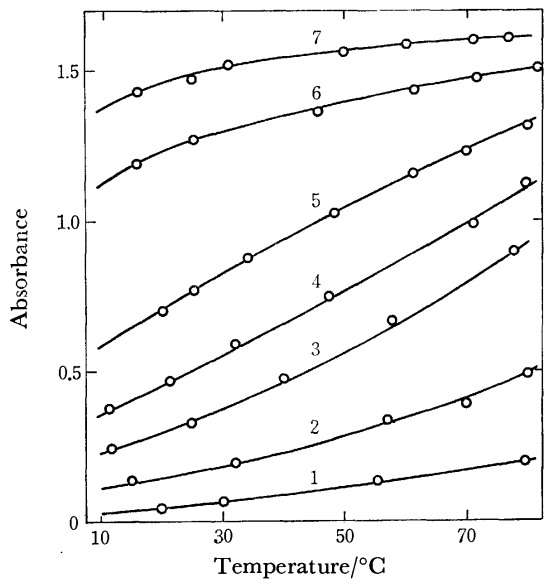

Fig. 4. The temperature-dependence of the absorbance at 574 nm of the Cu(II)-XO at various pH. At pH 2.99 (1), 3.53 (2), 3.94 (3), 4.21 (4), 4.49 (5), 5.04 (6), and 5.58 (7). $[Cu]=1.2\times10^{-4}$ mol dm^{-3}; $[XO]=3.0\times10^{-5}$ mol dm^{-3}. I=0.1 mol dm^{-3} ($NaClO_4$). Cell length=1 cm.

Figure 4 shows the temperature-dependence of the absorbance at 574 nm of the solution of the 2 : 1 Cu(II)-XO chelate at various buffered pH values. Upon heating the solution at pH higher than 5.0 or lower than 3.5 the absorbance increases only slightly. The largest increase in the absorbance was observed only in a narrow pH range between 3.9 and 4.5. This tendency suggests the existence of an optimum pH range for the given thermochromism. From the given temperature-dependence of the absorbance we can derive the pH-dependence of the absorbance at various temperatures as reproduced in Fig. 5. From the pH-dependences of the absorbance we calculated the values of pK for the equilibrium (1) at 15, 25, 35, 50, and 70 °C, which are listed in Table 3.

The uncomplexed free ligand XO did not show a thermochromic behavior at all around the pH region where its metal complexes are strongly thermochromic. However, in neutral or weakly basic media, *i.e.*, at

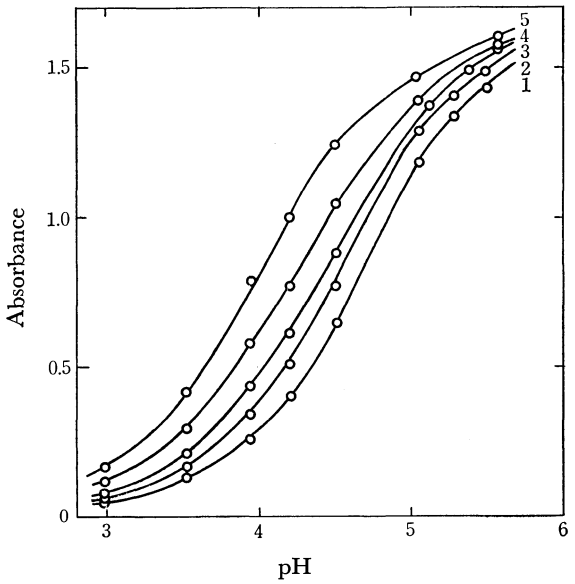

Fig. 5. The pH-dependence of the absorbance at 574 nm of the Cu(II)–XO at various temperatures. At 15 (1), 25 (2), 35 (3), 50 (4), and 70 °C (5). [Cu]= 1.2×10^{-4} mol dm^{-3}; [XO]$=3.0\times10^{-5}$ mol dm^{-3}. I=0.1 mol dm^{-3} ($NaClO_4$). Cell length=1 cm.

Table 3. Temperature-dependence of the acid-dissociation constants for the Cu(II)–XO and the free XO at I=0.1 mol dm^{-3} ($NaClO_4$)

Temperature °C	p(K/mol dm^{-3}) for Cu(II)–XO	p(K_a/mol dm^{-3}) for free XO
15	4.62	6.66
25	4.40, 4.55[a)]	6.57, 6.70[b)]
35	4.27	6.50
50	4.11	—
70	3.83	—

a) See Ref. 10. b) See Ref. 11.

pH in the vicinity of the pK_a value of the phenolic proton, the free ligand XO were weakly thermochromic. Figure 6 shows the absorption spectra of the solution of the free ligand XO at two different temperatures and at three pH values. The temperature-dependence of the spectra was similar to the pH-dependence also in this case, the isosbestic point being identical in both cases. However, the thermochromic effect in the free ligand XO was much weaker compared with that in the Cu(II)–XO complex. Whereas upon heating from 15 to 35 °C the absorbance at 574 nm of a solution of the free ligand at pH 6.40, *viz.*, near the pK_a value of the phenol protons of the free ligand XO, increased only by 19%, the absorbance at 574 nm of the Cu(II)–XO system at pH 4.50 increased by so large as 36% for the same temperature-rise. The values of pK for the reaction AH$\rightleftarrows$A+H between two 2 : 1 Cu(II)–XO chelates decreases remarkably with the rise of temperature, whereas pK_a value of the phenol proton in the free ligand does not decrease so remarkably (Table 3).

The thermodynamic parameters ΔH and ΔS for the Reaction 1 and for the acid-dissociation of the phenol

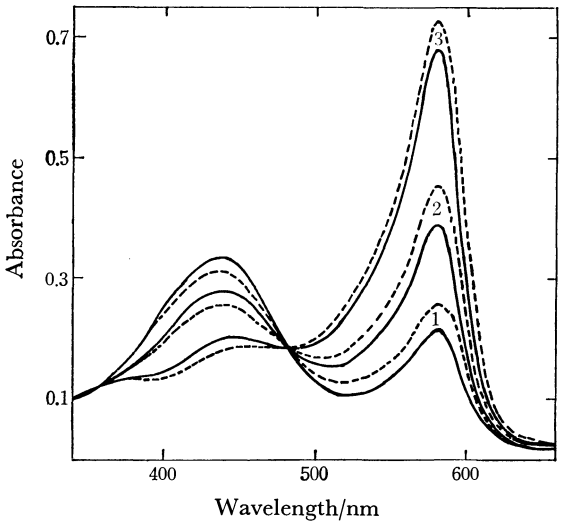

Fig. 6. Absorption spectra of the free ligand XO at various pH and temperatures. At pH 6.27 (1), 6.67 (2), and 7.14 (3). Temperature : 15 (—) and 35 °C (---). [XO]$=3.0\times10^{-5}$ mol dm^{-3}. I=0.1 mol dm^{-3} ($NaClO_4$). Cell length=1 cm.

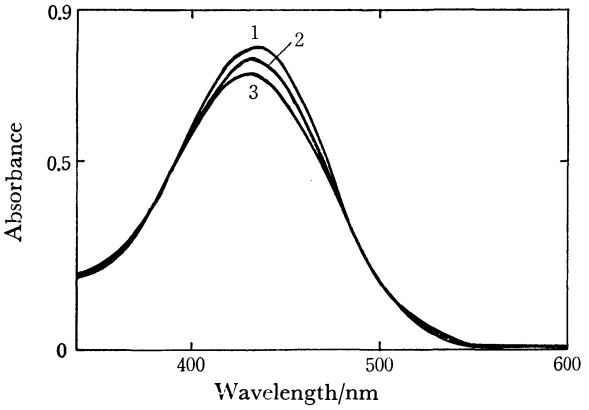

Fig. 7. Temperature-dependence of the absorption spectra of the free ligand XO at pH 3.47—3.97. [XO]$=3.0\times10^{-5}$ mol dm^{-3}. I=0.1 mol dm^{-3} ($NaClO_4$). At 6 (1), 25 (2), and 63 °C (3). Cell length=1 cm.

proton in the free ligand were graphically determined by plotting the values of log K and log K_a against $1/T$ to be 26±2 and 14±1 kJ mol^{-1} and 1±3 and −78±1 J mol^{-1} K^{-1} (298 K), respectively. The positive values of the enthalpy show that the observed thermochromic changes are endothermic. The value of the enthalpy for the Cu(II)–XO complex is about twice as large as that for the free ligand. These results correspond to the fact that the more remarkable thermochromism is observed for reaction (1) than for the protolytic equilibrium of the free ligand. A small value of ΔS obtained for Eq. 1 would be due to the compensation of the increase in the entropy by a water molecule released from the coordination sphere of the metal ion upon coordination of the phenolate oxygen and the decrease in the entropy by the hydration of a dissociated proton. The values of ΔH and ΔS obtained for the free ligand are reasonable as the values for the usual proton-transfer reactions of the phenolic

groups in aqueous media.[12]

In addition, molar absorptivity of the free ligand XO were found to depend on the temperature. In the pH region between 3.47 and 3.97 corresponding to the pK_a of the carboxyl proton of the free ligand[11] where the absorption spectra show no pH-dependency, the definite temperature-dependence of the spectra was clearly observed (see Fig. 7). This would be attributed to the change in molar absorptivity of the free ligand. Therefore, the temperature-dependency of the molar absorptivity might also contribute to the thermochromic behavior of the present complexes, though the effect is not so strong.

It is interesting to note that the metal complexes of the triphenylmethane complexons with the two benzene rings A and B tightly linked together, say, *e.g.*, through an ether linkage as shown in Fig. 1(b), were not thermochromic. This fact shows the possibility that the change in resonance structure of the π-system of the triphenylmethane skeleton could also contribute to the thermochromic changes.

Kinetics. The temperature-jump studies were carried out for the thermochromic changes of the Cu(II)–XO complex together with the Co(II), Ni(II), and Zn(II) complexes of XO, and also for the acid-dissociation of the free ligand in the pH range where the thermochromic changes were observed. The relaxation times τ observed in 5 μs region can be expressed as

$$\tau^{-1} = k_1 + k_{-1}([\overline{H}]+[\overline{A}]). \quad (2)$$

As regards the acid-dissociation of phenolic proton in the free ligand in aqueous media, we obtained the values of the rate constants for the deprotonation and for the protonation $k_1=(1.0\pm0.6)\times10^4\ s^{-1}$ and $k_{-1}=(3.0\pm0.1)\times10^{10}\ mol^{-1}\ dm^3\ s^{-1}$, respectively (Fig. 8). The value of k_1 lies in the same order of magnitude as the values of the rate constants reported for the acid-dissociation of the phenolic ligands of similar structure[13] and the quotient $k_1/k_{-1}=10^{-6.5}\ mol\ dm^{-3}$ is in good agreement with the acid-dissociation constant, K_a, of the phenolic proton of XO.[11] However, from the signals of the temperature-jump observed for the thermochromic changes of the metal chelates we could evaluate only the approximate values of the rate constants for reaction (1), since the values of τ as derived from the exponential signals (see Table 4) lie just near the time constant τ_c for the temperature-rise of our apparatus. The value of k_1 estimated for reaction (1) was *ca.* $2\times10^5\ s^{-1}$. Similar temperature-jump studies were also carried out preliminarily for the Co(II)–XO, Ni(II)–XO, and Zn(II)–XO systems. The corresponding k_1 values for these systems were found to be *ca.* $2\times10^5\ s^{-1}$, essentially independent of the metal ion involved. Thus the kinetic measurements also suggest that the phenomena of the thermochromism observed in the presence of a large excess of metal ions are primarily due to the process involving a protonation-deprotonation in the coordinated ligand. The quantitative studies for other thermochromic systems are now in progress and will be reported elsewhere.

For the kindness in the DSC measurements, the authors thank Professor Yoshio Matsunaga. They also thank Professor Mitsuo Shimoji and Professor Yoshio Nakamura for aid in the use of a spectrophotometer for the measurements at high temperatures.

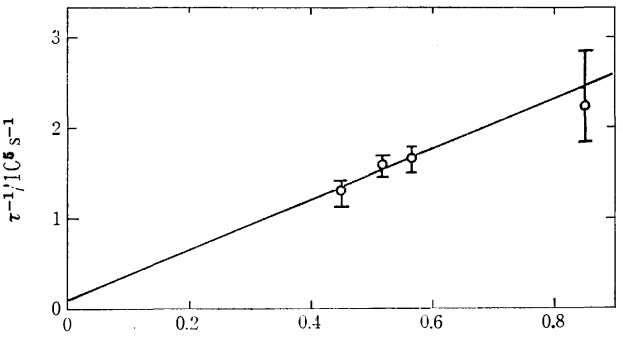

Fig. 8. Plot of τ^{-1} *vs.* $([\overline{H}]+[\overline{XO}])$ at 25 °C for the acid-dissociation of the free ligand XO. $[XO]=3.0\times10^{-5}$ mol dm^{-3}. $I=0.1$ mol dm^{-3} ($NaClO_4$).

Table 4. The reciprocal of the relaxation times for the deprotonation-protonation of the $Cu_2(XO)$, $AH \rightleftharpoons A+H$ at 25 °C and $I=0.1$ mol dm^{-3} ($NaClO_4$)

$[\overline{A}]+[\overline{H}]$ / 10^{-4} mol dm^{-3}	τ^{-1} / $10^5\ s^{-1}$
0.32	2.8
0.37	2.6
0.70	2.7
1.28	2.9
1.33	2.4

References

1) M. Yamada, *Bull. Chem. Soc. Jpn.*, **49**, 1023 (1976).
2) S. Nakada, M. Yamada, T. Ito, and M. Fujimoto, *Chem. Lett.*, **1977**, 1243.
3) J. H. Day, *Chem. Rev.*, **63**, 65 (1963); **68**, 649 (1968).
4) K. Sone and S. Utsuno, *Kagaku No Ryoiki*, **22**, 222 (1968).
5) J. Körbl and R. Přibil, *Chem. Ind. (London)*, **1957**, 233.
6) S. Nakada, M. Yamada, T. Ito, and M. Fujimoto, *Bull. Chem. Soc. Jpn.*, **50**, 1887 (1977).
7) Y. Kawai, T. Takahashi, K. Hayashi, T. Imamura, H. Nakayama, and M. Fujimoto, *Bull. Chem. Soc. Jpn.*, **45**, 1417 (1972).
8) N. Yoshida and M. Fujimoto, *Bull. Chem. Soc. Jpn.*, **50**, 1328 (1977).
9) M. Yamada, Doctor Thesis, Hokkaido University, 1975; M. Yamada and M. Fujimoto, *Bull. Chem. Soc. Jpn.*, **49**, 693 (1976).
10) H. Wada, T. Ishizuki, and G. Nakagawa, The 36th National Meeting of the Chemical Society of Japan, Osaka, April 2, 1977, Abstract Vol. 1, p. 22.
11) M. Murakami, T. Yoshino, and S. Harasawa, *Talanta*, **14**, 1293 (1967).
12) J. J. Christensen, L. D. Hansen, and R. M. Izatt, "Handbook of Proton Ionization Heats and Related Thermodynamic Quantities," John Wiley & Sons, New York (1976).
13) M. Eigen, W. Kruse, G. Maass, L. De Maeyer, *Progr. React. Kinet.*, **2**, 287 (1964).

Circular Dichroism Spectra of Cobalt(III) Complexes of the Type, *trans*-[CoX_2(1,3-Diamine)$_2$]$^{n+}$ (X=Cl^-, CN^-, or NH_3)

Kazuo KASHIWABARA, Masaaki KOJIMA, and Junnosuke FUJITA*

Department of Chemistry, Faculty of Science, Nagoya University, Chikusa, Nagoya 464

(Received September 27, 1978)

Four new complexes of the type, *trans*-[$Co(CN)_2$(1,3-diamine)$_2$]$^+$ were prepared, where 1,3-diamine is (*S,S*)-1,3-diphenyl-1,3-propanediamine, (*R,R*)-2,4-pentanediamine, (*S*)-1,3-butanediamine, or (*S*)-1-phenyl-1,3-propanediamine. Two diammine complexes of the same type with (*S*)-1,3-butanediamine and (*S*)-1-phenyl-1,3-propanediamine, and *trans*-[$Co(CN)_2$((*R,R*)-1,2-diphenyl-1,2-ethanediamine)$_2$]$^+$ were also newly prepared. The circular dichroism(CD) spectra of the new complexes measured in several solvents were compared with those of the corresponding dichloro and diammine complexes. The CD spectra of the dicyano complexes of (*S*)-1,3-butanediamine and (*S*)-1-phenyl-1,3-propanediamine showed remarkable solvent dependence, while those of the other complexes small or little dependence.

Bosnich and Harrowfield[1] found that the sign of circular dichroism(CD) under the $^1A_{2g}\leftarrow{}^1A_{1g}$ transition in the first absorption band of *trans*-[$CoCl_2$(*R*-pn)$_2$]$^+$ (*R*-pn=(*R*)-1,2-propanediamine) is negative in methanol, but positive in dimethyl sulfoxide(DMSO), and suggested that the effects of chiral distortions of the donor atoms and of chiral arrangements of the amino hydrogen atoms caused by solvation are important for such solvent dependence. Recently, Hawkins *et al.*[2] reported by both CD and PMR studies of the same complex and its related complexes in various solvents that the solvent dependence of the CD will be cussed by stereoselective solvation at the equatorial amino hydrogen atoms of the diamines, rendering the donor nitrogens chiral. This paper is concerned with the CD spectra of complexes of the type, *trans*-[CoX_2(1,3-diamine)$_2$]$^{n+}$ (X=Cl^-, CN^-, or NH_3) in several solvents, the abbreviations and the absolute configurations of the 1,3-diamines being shown in Fig. 1. The flexibility of six-membered chelate rings formed with the 1,3-diamines will affect the CD spectra of their complexes in a different way from that of the complexes of five-membered chelate rings. The *R*-pn and (*R,R*)-1,2-diphenyl-1,2-ethanediamine (*R,R*-dpen) complexes of the same type were also prepared to compare their CD spectra with those of the 1,3-diamine complexes.

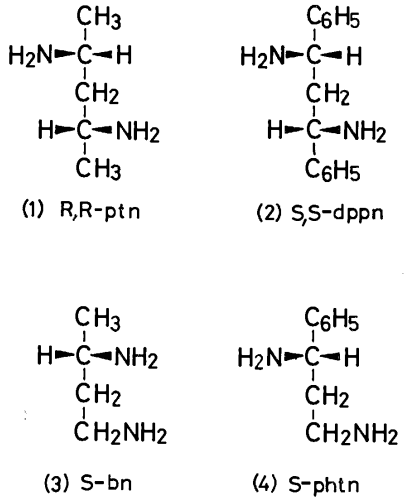

Fig. 1. Absolute configurations of the 1,3-diamines, (1) (*R,R*)-2,4-pentanediamine(*R,R*-ptn), (2) (*S,S*)-1,3-diphenyl-1,3-propanediamine(*S,S*-dppn), (3) (*S*)-1,3-butanediamine(*S*-bn), and (4) (*S*)-1-phenyl-1,3-propanediamine(*S*-phtn).

Experimental

Preparation of Ligands. Optically active diamines were prepared according to the references reported previously; *S,S*-dppn,[3] *R,R*-ptn,[4] *S*-phtn,[5] *S*-bn,[6] *R*-pn,[7] and *R,R*-dpen.[8]

Preparation of Complexes. *1)* The following complexes were prepared by the methods described previously; *trans*-[$CoCl_2$(*S,S*-dppn)$_2$]Cl·HCl·H_2O,[3] *trans*-[$CoCl_2$(*R,R*-ptn)$_2$]ClO_4,[9] *trans*-[$CoCl_2$(*S*-phtn)$_2$]Cl·H_2O,[5] *trans*-[$CoCl_2$(*R*-pn)$_2$]ClO_4,[1] *trans*-[$CoCl_2$(*R,R*-dpen)$_2$]ClO_4,[1] *trans*-[$Co(CN)_2$(*R*-pn)$_2$]Cl·1.5H_2O,[10] *trans*-[$Co(NH_3)_2$(*S,S*-dppn)$_2$]$(ClO_4)_3$·3H_2O,[11] and *trans*-[$Co(NH_3)_2$(*R,R*-ptn)$_2$]$(ClO_4)_3$·H_2O.[12]

2) trans-[*$CoCl_2$*(S-*bn*)$_2$]*ClO_4*: This complex was prepared by adding sodium perchlorate to an aqueous solution of the complex chloride.[13] Found: C, 23.88; H, 6.19; N, 13.56%. Calcd for [$CoCl_2(C_4H_{12}N_2)_2$]ClO_4 : C, 23.69; H, 5.98; N, 13.82%.

3) trans-[*$Co(CN)_2$*(S,S-*dppn*)$_2$]*Cl*·*2H_2O*: To sodium cyanide (30 mg) in 12 cm^3 of DMSO was added *trans*-[$CoCl_2$-(*S,S*-dppn)$_2$]ClO_4 (140 mg) with stirring at 40 °C. The solution changed from green to orange instantly and was kept at 40 °C for 10 min. After cooling to room temperature, the solution was poured into a column (ϕ3×60 cm) of an SP-Sephadex C-25 ion exchanger and then the column was washed with water to remove DMSO. The adsorbed orange product was eluted with 0.1 mol/dm^3 sodium chloride in a mixture of methanol and water (1:4). The column showed only one orange yellow band. The eluate was concentrated under reduced pressure to give orange yellow crystals, which were recrystallized from a small amount of water. The yield was almost quantitative. Found: C, 60.36; H, 6.19; N, 13.15%. Calcd for [$Co(CN)_2(C_{15}H_{18}N_2)_2$]Cl·2$H_2O$: C, 60.51; H, 6.35; N, 13.23%.

4) trans-[*$Co(CN)_2$*(R,R-*ptn*)$_2$]*ClO_4*·*H_2O*: This complex was prepared from *trans*-[$CoCl_2$(*R,R*-ptn)$_2$]ClO_4 and sodium cyanide by the same method as that for *trans*-[$Co(CN)_2$-(*S,S*-dppn)$_2$]Cl·2H_2O except that the eluent was an aqueous solution of 0.05 mol/dm^3 sodium perchlorate. The yield was almost quantitative. Found: C, 33.62; H, 7.10; N, 19.65%. Calcd for [$Co(CN)_2(C_5H_{14}N_2)_2$]ClO_4·H_2O: C, 33.30; H, 6.94; 19.42%.

5) trans-[*$Co(CN)_2$*(S-*bn*)$_2$]ClO_4·H_2O: This complex was prepared from *trans*-[$CoCl_2$(*S*-bn)$_2$]ClO_4 and sodium cyanide according to the same method as described for the above *R,R*-ptn complex. Found: C, 29.94; H, 6.63; N, 20.80%.

Calcd for $[Co(CN)_2(C_4H_{12}N_2)_2]ClO_4\cdot H_2O$: C, 29.67; H, 6.49; N, 20.76%.

6) trans-$[Co(CN)_2(S\text{-}phtn)_2]ClO_4\cdot H_2O$: The procedure was the same as that for the *R,R*-ptn complex. However, two light yellow bands (probably the *cis*-Δ and *cis*-Λ isomers on the basis of the absorption spectra) followed after an orange band (*trans* isomer) by eluting with a 0.05 mol/dm^3 aqueous solution of sodium perchlorate. Yield: about 40%. Found: C, 45.65; H, 5.34; N, 15.69%. Calcd for $[Co(CN)_2(C_9H_{14}N_2)_2]ClO_4\cdot H_2O$: C, 45.42; H, 5.72; N, 15.89%.

7) trans-$[Co(CN)_2(R,R\text{-}dpen)_2]ClO_4\cdot 2H_2O$: To a DMSO solution (20 cm^3) of sodium cyanide (60 mg) was added *trans*-$[CoCl_2(R,R\text{-dpen})_2]ClO_4\cdot H_2O$ (180 mg) at 50 °C with stirring. The solution changed from green to orange instantly and was kept at 50 °C for 10 min. After cooling to room temperature, the solution was poured into a column ($\phi 3\times$ 90 cm) of an SP-Sephadex C-25 ion exchanger. DMSO in the column was washed out with water. The adsorbed orange product was eluted with an aqueous solution of 0.1 mol/dm^3 sodium acetate. An orange yellow band (the *trans* isomer) was eluted first and then two light yellow bands (the *cis* isomers) followed. The orange yellow eluate was mixed with a small amount of sodium perchlorate and concentrated under reduced pressure to give crystals. Yield: 50 mg. Found: C, 53.98; H, 5.39; N, 12.67%. Calcd for $[Co(CN)_2(C_{14}H_{16}N_2)_2]ClO_4\cdot 2H_2O$: C, 53.70; H, 5.41; N, 12.52%.

8) trans-$[Co(NH_3)_2(S\text{-}bn)_2](ClO_4)_3$: When *trans*-$[CoCl_2(S\text{-bn})_2]ClO_4$ (100 mg) was dissolved in liquid ammonia (20 cm^3), the solution changed from green to orange instantly. After removal of liquid ammonia at room temperature, the residue was mixed with 2 mol/dm^3 hydrochloric acid (5 cm^3). The solution was diluted with water (500 cm^3) and passed through a column ($\phi 3\times 120$ cm) of an SP-Sephadex C-25 ion exchanger. The adsorbed orange product was eluted with a 0.15 mol/dm^3 aqueous solution of sodium $(+)_D$-tartratoantimonate(III), yielding two orange yellow bands. The first eluting orange yellow band appeared to consist of one isomer because the CD patterns of all the fractions remained constant. On the other hand, the initial and final fractions of the second orange band gave different CD patterns, suggesting the presence of more than two isomers in this band. The fractions of the first orange yellow band were collected and concentrated to give crystals. Yield: 40 mg. Found: C, 16.94; H, 5.40; N, 14.67%. Calcd for $[Co(NH_3)_2(C_4H_{12}N_2)_2](ClO_4)_3$: C, 16.93; H, 5.33; N, 14.80%. The ^{1}H-NMR spectrum of the crystals in D_2O showed only one kind of methyl signal. Thus, we tentatively assigned this complex to the *trans* isomer. The chromatographic behavior that this isomer was eluted faster than did the other isomer(s) will support this assignment.[11,12]

9) trans-$[Co(NH_3)_2(S\text{-}phtn)_2](ClO_4)_3\cdot 0.5H_2O$: This complex was prepared by the same method as that for the above *S*-bn complex. By eluting the product, the column gave five orange bands. The complex isolated from the first eluted orange band was tentatively assigned to the *trans* isomer, although no definite evidence for this structure was obtained from ^{1}H-NMR spectroscopy. Found: C, 30.82; H, 5.23; N, 11.67%. Calcd for $[Co(NH_3)_2(C_9H_{14}N_2)_2](ClO_4)_3\cdot 0.5H_2O$: C, 30.84; H, 5.03; N, 11.99%.

Measurements. Visible and ultraviolet absorption spectra were recorded on a HITACHI 323 spectrophotometer. CD spectra were obtained with JASCO J-20 and J-40 spectropolarimeters and ^{1}H-NMR spectra with a JEOL PMX-60 spectrometer. All the solvents for optical measurements are of spectroscopic grade and used without further purification.

Results and Discussion

Figure 2 shows the absorption spectra of ptn and dppn complexes of the type, *trans*-$[CoX_2(diamine)_2]^+$ ($X=Cl^-$ or CN^-). Except the absorptions due to the phenyl group in the near ultraviolet region, the ptn and dppn complexes with the same X ligand show the same spectral pattern. The first absorption band ($^1T_{1g}\leftarrow{}^1A_{1g}$) in an octahedral field, CoN_6^{3+} splits into two components, $^1A_{2g}+{}^1E_g\leftarrow{}^1A_{1g}$ in a tetragonal field, *trans*-$CoX_2N_4^+$. According to Yamatera's theory,[14] the ^1E_g component should have lower energy than the $^1A_{2g}$ component when the axial ligand, X is lower than the ligating N atoms in the spectrochemical series, and inversely the ^1E_g component should be at higher energy for a complex in which the X ligand has a higher position than N in the series. All the complexes studied here obey this prediction as seen in Table 1. In the present paper, the CD spectra in this region are discussed . The CD spectra in the ultraviolet region are not described, because the spectra are complicated and no significant discussion can be made at present. The absorption and CD data of all the complexes are summarized in Table 1.

For the complexes of the present type with *R*-pn, *S*-bn, and *S*-phtn, there are two possible geometrical isomers, *cis* and *trans* with respect to the alignment of the substituents. The experiments gave neither the indication for the presence of these isomers nor the information for assigning such geometrical isomerism of the complexes obtained. The structure of *trans*-$[CoCl_2(R\text{-pn})_2]Cl\cdot HCl\cdot 2H_2O$ was determined by X-ray work to have a *trans*(CH_3, CH_3) configuration.[15] On the other hand, Boucher and Bosnich[16] reported that the *trans*-$[CoCl_2(R,S\text{-ptn})_2]^+$ complex prepared by oxidizing an aqueous solution containing cobalt(II) chloride and *R,S*-ptn with air consists mainly (>95%) of the *cis*(*R,R*) isomer (C_{2h}). The stable conformer of the *R,S*-ptn chelate ring is expected to be the *chair* form with the equatorially disposed methyl groups. In the crystals, *trans*-$[CoX_2(trimethylenediamine)_2]^+$ ($X=Cl^-$ [17] and NO_3^- [18]) also have the same skeletal structure as that of the *cis*(*R,R*) isomer. The *trans*-dichloro complexes of *S*-bn and *S*-phtn were prepared from cobalt(II) chloride and the diamines by air-oxidation. The stable conformations of these diamine chelate rings will be the *chair* form. (*vide post*) Therefore, these complexes may be assigned to the *cis*(CH_3,CH_3) and *cis*(phenyl, phenyl) isomers which correspond to the *cis*(*R,R*) isomer of the *R,S*-ptn complex. The corresponding dicyano and diammine complexes which were derived from the dichloro complexes may also have the same geometrical arrangement.

(1) Complexes of Five-membered Chelate Diamines. As Fig. 3 shows, the dichloro complex of *R*-pn in methanol gives a positive and a negative CD band in the ^1E_g and $^1A_{2g}$ transitions, respectively, while the *R,R*-dpen complex in the same solvent two positive CD bands in these transitions. Other dichloro complexes of *R*-1- or *R,R*-1,2-dialkyl-substituted 1,2-diamines

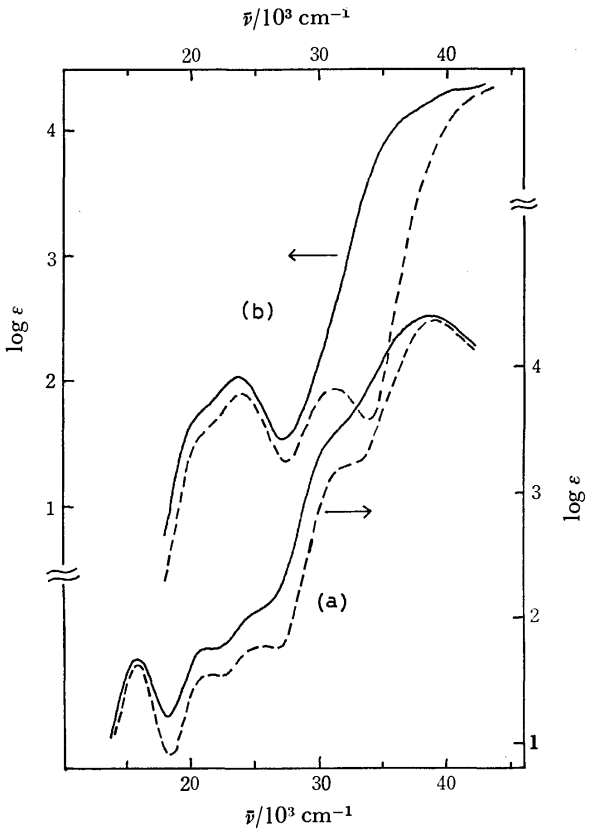

Fig. 2. Absorption spectra, (a) *trans*-$[CoCl_2(R,R\text{-ptn})_2]^+$ in methanol (— — —) and *trans*-$[CoCl_2(S,S\text{-dppn})_2]^+$ in methanol (——), (b) *trans*-$[Co(CN)_2(R,R\text{-ptn})_2]^+$ in water (— — —), and *trans*-$[Co(CN)_2(S,S\text{-dppn})_2]^+$ in methanol (——).

TABLE 1. ABSORPTION AND CD SPECTRAL DATA IN THE FIRST ABSORPTION BAND IN METHANOL

	Absorption $\bar{\nu}/10^3$ cm^{-1} (ε)	CD $\bar{\nu}/10^3$ cm^{-1} ($\Delta\varepsilon$)
trans-$[CoCl_2(R,R\text{-ptn})_2]$-$ClO_4$[9]	15.75 (43) 21.37 (37)	16.00 (+0.48) 20.92 (−0.58)
trans-$[CoCl_2(S,S\text{-dppn})_2]$-$Cl\cdot HCl\cdot H_2O$	15.70 (46) 21.16 (60)	15.57 (+0.70) 20.62 (−0.83)
trans-$[CoCl_2(S\text{-bn})_2]ClO_4$	15.70 (42) 21.10 (34)	15.87 (−0.04) 20.41 (−0.02)
trans-$[CoCl_2(S\text{-phtn})_2]Cl\cdot H_2O$	15.67 (47) 21.01 (46)	15.39 (−0.08) 20.62 (+0.30)
trans-$[Co(CN)_2(R,R\text{-ptn})_2]$-$ClO_4\cdot H_2O$[a]	21 (sh) 23.84 (82)	20.41 (−1.17) 24.10 (+2.44)
trans-$[Co(CN)_2(S,S\text{-dppn})_2]$-$Cl\cdot 2H_2O$	21 (sh) 23.53 (108)	20.10 (−1.69) 23.53 (+2.38)
trans-$[Co(CN)_2(S\text{-bn})_2]$-$ClO_4\cdot H_2O$[a]	21 (sh) 23.80 (78)	20.62 (+0.03) 24.10 (−0.11)
trans-$[Co(CN)_2(S\text{-phtn})_2]$-$ClO_4\cdot H_2O$	21 (sh) 23.58 (103)	20.83 (+0.14) 26.32 (−0.02)
trans-$[Co(CN)_2(R,R\text{-dpen})_2]$-$ClO_4\cdot 2H_2O$	21 (sh) 24.39 (120)	21.3 sh (+1.3) 24.00 (+1.95)

a) Solvent: water. sh: shoulder.

show the same CD patterns as that of the *R*-pn complex, and the CD pattern of the *R*-1-phenyl-1,2-ethanediamine(*R*-pen) complex is the same as that of the *R,R*-dpen complex.[19] The absolute configurations of *R,R*-dpen[20] and *R*-pen[21] have been determined

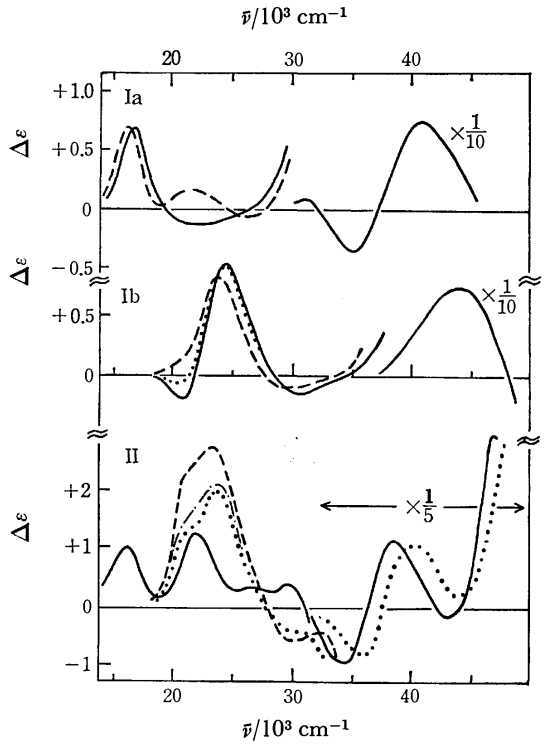

Fig. 3. CD spectra, (Ia) *trans*-$[CoCl_2(R\text{-pn})_2]^+$ in methanol (——) and in DMSO (— — —), (Ib) *trans*-$[Co(CN)_2(R\text{-pn})_2]^+$ in methanol (——), in DMF (·····), and in DMSO (— — —), (II) *trans*-$[CoCl_2(R,R\text{-dpen})_2]^+$ in methanol (——) and *trans*-$[Co(CN)_2(R,R\text{-dpen})_2]^+$ in methanol (·····), in DMF (—·—·—), and in DMSO (— — —).

by the X-ray and chemical methods, respectively, and these diamines will form chelate rings with the same λ-gauche conformation as that of *R*-pn upon coordination. Nevertheless, the *R,R*-dpen and *R*-pen complexes give the positive CD sign in the $^1A_{2g}$ band opposite to that of the *R*-pn complex. The corresponding dicyano complex of *R*-pn in methanol also exhibits a negative and a positive CD band in the $^1A_{2g}$ and ^1E_g transitions, respectively, and that of *R,R*-dpen two positive CD bands. Bosnich and Harrowfield,[1] however, found that in DMSO, the CD sign of the $^1A_{2g}$ band in *trans*-$[CoCl_2(R\text{-pn})_2]^+$ changes to positive, and the corresponding CD band of the dichloro *R,R*-dpen complex increases in the strength. The same phenomena are observed for the dicyano complexes as seen in Fig. 3. The weak negative CD band at 20410 cm^{-1} of *trans*-$[Co(CN)_2(R\text{-pn})_2]^+$ in methanol decreases its strength in *N,N*-dimethylformamide (DMF), and changes to positive sign in DMSO. The *R,R*-dpen complex shows the same trend. This fact suggests that the variations in CD sign or pattern with changes in solvent will be little related to the axial ligands in the complexes. As suggested by Bosnich and Harrowfield,[1] such solvent effect on CD spectra of the *trans*-bis(diamine) complexes may be caused by solvation of solvent molecules in chiral arrangements to the complex ions. Recently, Hawkins *et al.*[2] claimed that the solvation occurs stereoselectively at the equatorial amino hydrogens, rendering the donor nitrogens chiral. The new

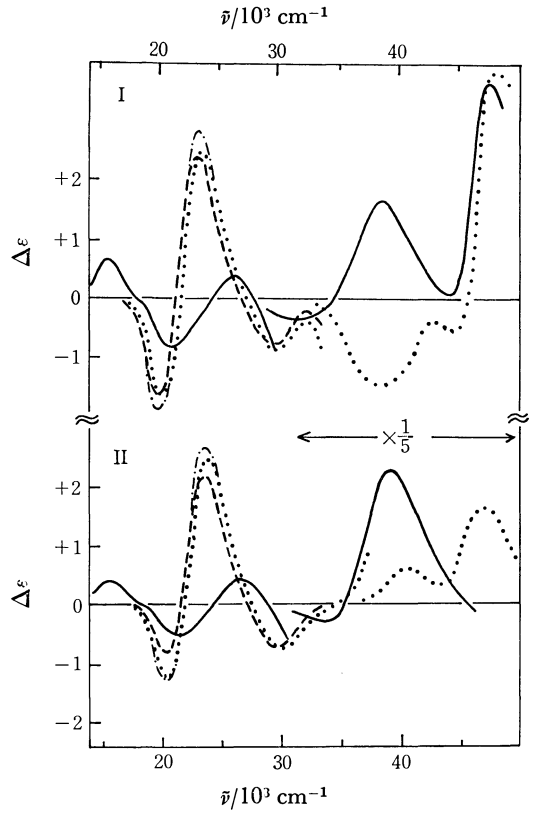

Fig. 4. CD spectra, (I) *trans*-$[CoCl_2(S,S\text{-dppn})_2]^+$ in methanol (——), and *trans*-$[Co(CN)_2(S,S\text{-dppn})_2]^+$ in methanol (·····), in DMF (—·—·—), and in DMSO (— — —). (II) *trans*-$[CoCl_2(R,R\text{-ptn})_2]^+$ in methanol (——), and *trans*-$[Co(CN)_2(R,R\text{-ptn})_2]^+$ in methanol (·····), in DMF (—·—·—), and in DMSO (— — —).

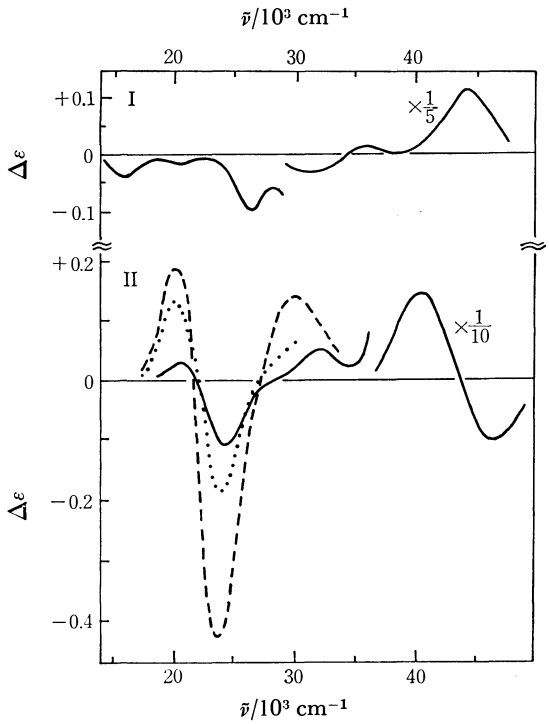

Fig. 5. CD spectra, (I) *trans*-$[CoCl_2(S\text{-bn})_2]^+$ in methanol (——), (II) *trans*-$[Co(CN)_2(S\text{-bn})_2]^+$ in water (——), in DMF (·····), and in DMSO (----).

chiral nitrogen atoms will affect the CD spectra of the diamine complexes. The dicyano complexes are probably the same case, since the variations in their CD spectra with changes in solvent quite resemble those in the CD spectra of the dichloro complexes.

(2) Dichloro and Dicyano Complexes of Six-membered Chelate Diamines. A 1,3-diamine chelate ring is known to take either the *chair* or the *skew* (δ or λ) conformation. When the chelate ring has substituent(s) attached to the skeletal carbon atom(s) of the ring, the conformation with the equatorially oriented substituent(s) will be more stable than the other. Thus the *R,R*-ptn and *S,S*-dppn chelate rings will be the most stable in the λ-*skew* conformation. The designation (*R* or *S*) of dppn which forms a chelate ring with the same conformational chirality as that of the ptn chelate ring is opposite to that of ptn according to the sequence rule.[22] The λ-*skew* form of the *R,R*-ptn chelate ring has been confirmed by X-ray crystallographic studies on $(-)_{546}$- and $(+)_{546}$-$[Co(R,R\text{-ptn})_3]^{3+}$.[23] On the other hand, the *S*-bn and *S*-phtn chelate rings can take the equatorially disposed substituent both in the *chair* and *skew* conformations. The δ-*skew* of the former diamine and the λ-*skew* of the latter diamine have the equatorial substituent on the basis of the sequence rule. Since a diamine chelate ring in the *chair* form is achiral in the skeleton, its vicinal effect should be much weaker than that of a diamine ring in the *skew* form.

Figure 4 shows the CD spectra of the dichloro and dicyano complexes of *R,R*-ptn and *S,S*-dppn. The dichloro complexes of all the 1,3-diamines studied here are stable in methanol, but unstable in DMF and DMSO to change the CD spectra during the measurement. The CD patterns of the dichloro complexes of *R,R*-ptn and *S,S*-dppn are very similar to each other and also to that of the *R*-pn complex, indicating the λ-chirality of the chelate rings, although the negative CD bands ($\approx$21000 cm^{-1}) assignable to the $^1A_{2g}$ transition are much stronger than that of the *R*-pn complex. The positive CD bands ($\approx$16000 cm^{-1}) can be assigned to the ^1E_g transition. The sign of the $^1A_{2g}$ band of the *S,S*-dppn complex is opposite to that of the *R,R*-dpen complex which gives the $^1A_{2g}$ band with the same sign as that of the ^1E_g band. The dicyano complexes of *R,R*-ptn and *S,S*-dppn also give a similar CD pattern to each other in the region of the first absorption band. The spectra show little variations with changes in solvent. The negative ($\approx$20000 cm^{-1}) and positive ($\approx$24000 cm^{-1}) CD bands can be assigned to the $^1A_{2g}$ and ^1E_g transitions, respectively, and these signs coincide with those of the corresponding CD bands of the dichloro complexes.

On the other hand, the dichloro complexes of *S*-bn and *S*-phtn give quite different CD spectra from each other, and from those of the *R,R*-ptn and *S,S*-dppn complexes, as seen in Figs. 5 and 6. The CD intensities of these complexes are very weak. The weakness suggests that the predominant conformations of the *S*-bn and *S*-phtn chelate rings are in the *chair* form. The CD pattern of the *S*-bn complex, however, is nearly enantiomeric to that of the *R*-pn complex in

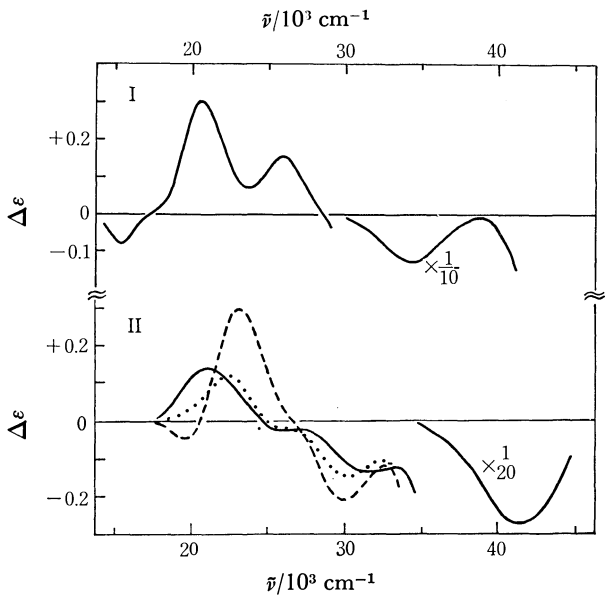

Fig. 6. CD spectra, (I) *trans*-$[CoCl_2(S\text{-phtn})_2]^+$ in methanol (——), (II) *trans*-$[Co(CN)_2(S\text{-phtn})_2]^+$ in water (——), in DMF (·····), and in DMSO (— — —).

DMSO. Hence the *S*-bn chelate ring will be in equilibrium between the *chair* and *δ-skew* forms in solution, the former being predominant. As stated previously, the *S*-bn chelate ring can have the equatorial methyl group in both the *δ-skew* and the *chair* conformations. The CD pattern of the *S*-phtn complex is nearly enantiomeric to that of the *S,S*-dppn complex, although the positive CD band at 20620 cm^{-1} ($^1A_{2g}$) is strong relative to the negative one at 15390 cm^{-1} (^1E_g). Such a pattern suggests the *δ-skew* conformation for the *S*-phtn chelate ring. This suggestion, however, is very unlikely, because the big phenyl group disposed axially interacts strongly with the apical ligand, Cl^-. The absolute configuration of *S*-phtn was confirmed by preparing an authentic sample from (*S*)-3-amino-3-phenyl propionic acid of known absolute configuration.[24] The reason for the anomalous CD of the *S*-phtn complex remains unknown. The vicinal effect of the asymmetric carbon atom, which has never been made clear but recognized to be weak, may appear on CD spectra explicitly to vary CD patterns of weak intensity.

The dicyano complexes of *S*-bn and *S*-phtn in water also show weak CD in the region of the first absorption band, indicating that the predominant conformations of these diamine chelate rings are the *chair* form. However, the CD patterns of the *S*-bn and the *R,R*-ptn complexes are nearly enantiomeric to each other, and it is concluded that the chelate rings will be in equilibrium between the *chair* and *δ-skew* conformations. The *S*-phtn complex gives again an anomalous pattern of only one CD band, although the positive sign of the band indicates the *λ-skew* conformation which is expected for the *S*-phtn chelate ring. The CD patterns of the *S*-bn complex in DMF and DMSO are the same as that in methanol, but the CD strengths increase to a large extent. Such variations in CD may be attributed to that the conformational equilibrium between the two forms, *chair* and *δ-skew* shifts toward the latter in these solvents. The *S*-phtn complex decreases the CD strength of smaller wave number side of the band in DMF, and exhibits a negative CD band in DMSO. The pattern in DMSO resembles that of the *S,S*-dppn complex, and suggests that the stability of the *λ-skew* conformer increases in such organic solvents.

The variations in CD for the dicyano complexes with changes in solvent seem to depend on the kind of diamines. In general, six-membered chelate rings formed with 1,3-diamines will be more flexible than five-membered ones with 1,2-diamines. Therefore, if the conformational change of a chelate ring is responsible for such variations in CD, the spectra of 1,3-diamine complexes should vary more remarkably than those of 1,2-diamine complexes. The dicyano complexes of *S*-bn and *S*-phtn will be this case. As stated previously, these chelate rings can have two stable conformations, the *chair* and the *skew* forms. The energy difference between these conformers has been calculated to be very small, the *chair* form being a little more stable than the other.[25] Hence, the relative stability of these conformers will be affected by many factors involving interactions with solvent molecules. The solvent dependence of the CD of the dicyano complexes of *S*-bn and *S*-phtn may be caused by such conformational changes of the chelate rings. In fact, the complexes of *R,R*-ptn and *S,S*-dppn which are expected to form less flexible six-membered chelate rings than those diamines show little solvent dependence in the CD spectra.

However, the solvent dependence of the *R,R*-ptn and *S,S*-dppn complexes seems to be even smaller than that of the complexes of 1,2-diamines, *R*-pn and *R,R*-dpen, although the chelate rings of the former 1,3-diamines may be more flexible than those of the latter 1,2-diamines. As suggested by Hawkins *et al.*,[2] if the variation in CD is caused by the stereoselective solvation of solvent molecules at the equatorial amino-hydrogens of diamines, the little solvent dependence of the *R,R*-ptn and *S,S*-dppn complexes indicates the followings; weak solvation, no stereoselective solvation, or weak contribution of new chiral nitrogen atoms introduced by stereoselective solvation to the CD. Details are not clear at present. However, molecular models indicate that in a *trans*-bis(1,3-diamine) complex, the distance between two equatorial amino-hydrogens in the *cis*-positions from each diamine chelate becomes much shorter than that in the corresponding 1,2-diamine complex. The crowded structure resulted from the shortening of distance between these hydrogen atoms may prevent them from strong interactions with solvent molecules. The little solvent dependence in the CD spectra of the *R,R*-ptn and *S,S*-dppn complexes may be interpreted by such a weak solvation effect.

(3) Diammine Complexes of Six-membered Chelate Diamines. Figures 7 and 8 show the CD spectra of diamine complexes of *R,R*-ptn and *S,S*-dppn, and *S*-bn and *S*-phtn, respectively. The *S,S*-dppn and *S*-phtn complexes were only stable in acidic solution, so that all

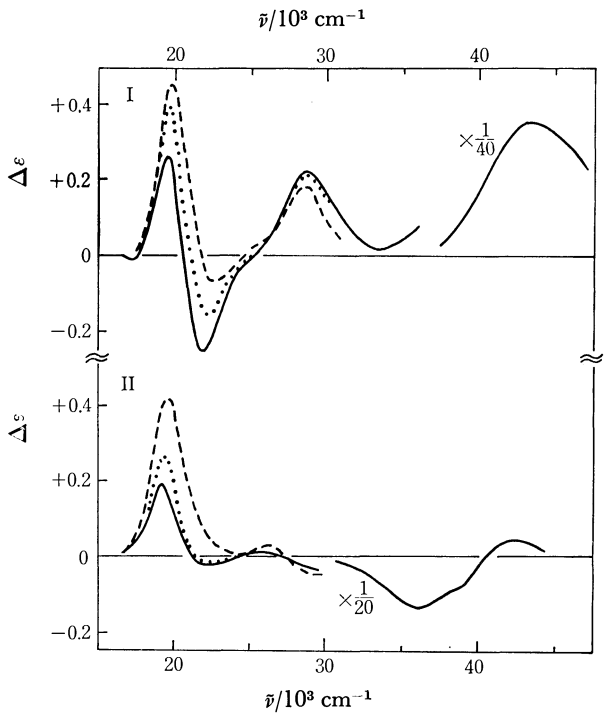

Fig. 7. CD spectra, (I) *trans*-$[Co(NH_3)_2(R,R\text{-ptn})_2]^{3+}$ in water (——), in DMF (·····), and in DMSO (- - - -). (II) *trans*-$[Co(NH_3)_2(S,S\text{-dppn})_2]^{3+}$ in methanol (——) in DMF (·····), and in DMSO (- - - -).

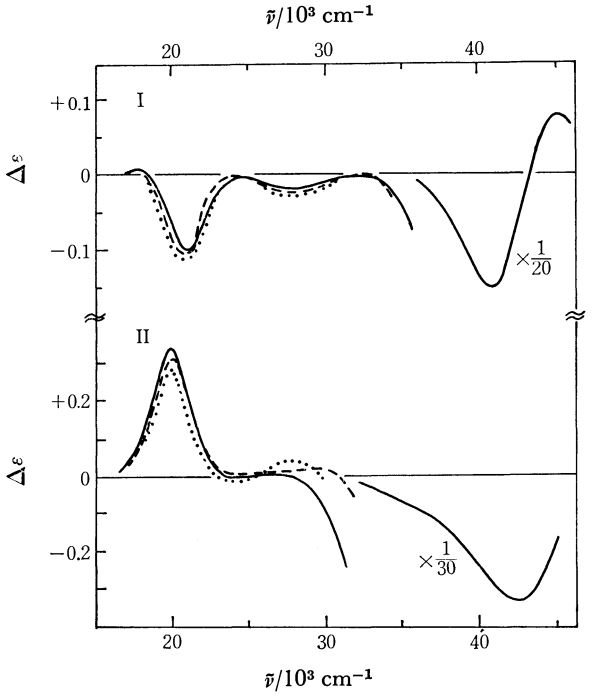

Fig. 8. CD spectra, (I) *trans*-$[Co(NH_3)_2(S\text{-bn})_2]^{3+}$ in water (——), in DMF (·····), and in DMSO (- - - -). (II) *trans*-$[Co(NH_3)_2(S\text{-phtn})_2]^{3+}$ in water (——), in DMF (·····), and in DMSO (- - - -).

the solutions were acidified with perchloric acid. The signs of the main CD bands or the patterns of CD spectra in the region of the first absorption band of these complexes suggest the *skew* conformation of the chirality expected from the equatorial preference of the substituent for the chelate rings, as stated previously. The CD strength of the *S*-bn complex is smaller than those of the other diamine complexes, indicating that the chelate rings are in equilibrium between the *chair* and the *δ-skew* conformations. In contrast to the cases of the *trans*-dicyano complexes, the CD spectra of the *S*-bn and *S*-phtn complexes show little solvent dependence, while those of the *R,R*-ptn and *S,S*-dppn complexes change the strength fairly remarkably with changes in solvent. Hawkins *et al.*[2] measured the CD spectra of *trans*-$[Co(NH_3)_2(R\text{-pn})_2]^{3+}$ in various solvents and concluded that for such a tri-positive complex ion, ion-association with its counter anions is more important for the solvent dependence in CD rather than the stereoselective solvation as seen in the dichloro complexes. The *R,R*-ptn and *S,S*-dppn complexes increase the strengths of the positive CD components in DMF and DMSO compared with those in water or methanol. Since the vicinal effect due to a chiral chelate ring in the *λ*-conformation is known to exhibit positive CD in the region of the first absorption band, these rings may be more stabilized in the *λ-skew* form by ion-association in the former solvents.[13] The ion-association should be facilitated in organic solvents compared with that in water. However, the *S*-bn and *S*-phtn complexes show little solvent dependence, as seen in Fig. 8. Neither the ion-association nor the stereoselective solvation appears to operate in the CD spectra of these complexes. These systems should not be greatly different from those of *R,R*-ptn and *S,S*-dppn. The reason why these complexes show little solvent dependence is unknown at present.

The authors wish to thank the Ministry of Education for Scientific Research Grant-in-Aid No. 243013 and the Kurata Research Grant.

References

1) B. Bosnich and J. MacB. Harrowfield, *J. Am. Chem. Soc.*, **94**, 3425 (1972).
2) C. J. Hawkins, G. A. Lawrance, and R. M. Peachey, *Aust. J. Chem.*, **30**, 2115(1977).
3) S. Arakawa, K. Kashiwabara, J. Fujita, and K. Saito, *Bull. Chem. Soc. Jpn.*, **50**, 2103 (1977).
4) F. Mizukami, H. Ito, J. Fujita, and K. Saito, *Bull. Chem. Soc. Jpn.*, **44**, 3051 (1971).
5) M. Kojima, to be published.
6) E. Strack and H. Schwaneberg, *Ber.*, **67**, 39(1934); E. Balieu, P. M. Boll, and E. Larsen, *Acta Chem. Scand.*, **23**, 2191 (1969).
7) F. P. Dwyer, F. L. Garvan, and A. Schulman, *J. Am. Chem. Soc.*, **81**, 290 (1959).
8) O. F. Williams, and J. C. Bailar, Jr., *J. Am. Chem. Soc.*, **81**, 4464 (1959).
9) F. Mizukami, H. Ito, J. Fujita, and K. Saito, *Bull. Chem. Soc. Jpn.*, **45**, 2129(1972).
10) K. Kashiwabara, T. Yamanaka, K. Saito, N. Komatzu, N. Hamada, H. Nishikawa, and M. Shibata, *Bull. Chem. Soc. Jpn.*, **48**, 3631 (1975).
11) S. Arakawa, K. Kashiwabara, J. Fujita, and K. Saito, *Bull. Chem. Soc. Jpn.*, **50**, 2331 (1977).
12) M. Kojima, M. Fujita, and J. Fujita, *Bull. Chem.*

Soc., Jpn., **50**, 898 (1977).
13) M. Kojima and J. Fujita, *Bull. Chem. Soc. Jpn.*, **50**, 3237(1977).
14) H. Yamatera, *Bull. Chem. Soc. Jpn.*, **31**, 95(1958).
15) Y. Saito and H. Iwasaki, *Bull. Chem. Soc. Jpn.*, **35**, 1131(1962).
16) H. Boucher and B. Bosnich, *Inorg. Chem.*, **15**, 2364, (1976).
17) K. Matsumoto, S. Ooi, and H. Kuroya, *Bull. Chem. Soc. Jpn.*, **43**, 1903 (1970).
18) E. Yasaki, I. Oonishi, H. Kawaguchi, and Y. Komiyama, *Bull. Chem. Soc. Jpn.*, **43**, 1354 (1970).
19) S. Yano, M. Saburi, S. Yoshikawa, and J. Fujita, *Bull. Chem. Soc. Jpn.*, **49**, 101(1976).
20) R. Kuroda and S. F. Mason, *J. Chem. Soc., Dalton Trans.*, **1977**, 1016.
21) J. P. Greenstein and M. Winitz, "Chemistry of Amino Acids," John-Wiley & Sons, New York, N. Y. (1961), p. 69.
22) R. S. Cahn, C. K. Ingold, and V. Prelog, *Angew. Chem., Int. Ed. Engl.*, **5**, 385 (1966).
23) A. Kobayashi, F. Marumo, and Y. Saito, *Acta Crystallogr., Sect. B*, **28**, 3591(1972), **29**, 2443(1973).
24) S. G. Cohen and S. Y. Weinstein, *J. Am. Chem. Soc.*, **86**, 725 (1964).
25) L. J. DeHayes and D. H. Busch, *Inorg. Chem.*, **12**, 1505(1973).

The Acid-catalyzed Reaction of Alicyclic Ketones with Formaldehyde. III.[1] The Reaction of 3- and 3,5-Methyl-substituted Cyclohexanones with Formaldehyde

Fukumi HIRANO* and Shoji WAKABAYASHI

Department of Chemistry, Faculty of Science, Okayama College of Science, 1-1 Ridai-cho, Okayama 700

(Received December 20, 1977)

The reaction of 3- and 3,5-methyl-substituted cyclohexanones with formaldehyde in acid media has been studied. The acid-catalyzed reaction gave 2,4,12,14-tetraoxatricyclo[8.4.0.0^{1,6}]tetradecane, 2,4-dioxaspiro-[5.5]undecan-7-one, and 2,4,8,10-tetraoxatricyclo[4.4.4.0^{1,6}]tetradecane derivatives. The effect of the methyl groups on the product distribution has been discussed.

In previous papers,[1,2] the acid-catalyzed reaction of cycloalkanones or alkyl-substituted cycloalkanones with formaldehyde has been reported. The reaction involved an aldol condensation analogous to the Prins reaction to afford spiro mono(1,3-dioxanes), fused di-(1,3-dioxanes), and hydroxymethyl derivatives. The yield and distribution of the products were strongly influenced by the ring-size of the cycloalkanones, the alkyl-substituents on the alicyclic ketones and the reaction conditions. This paper deals with the reaction of 3- and 3,5-methyl-substituted cyclohexanones with formaldehyde, together with the effect of the methyl substituent affecting the distribution of the products in the acid-catalyzed reaction.

Results and Discussion

Reaction of Methylcyclohexanones with Formaldehyde. The reaction of 3-methylcyclohexanone(**1a**) with formaldehyde has been conducted in a mixture of acetic acid and acetic anhydride in the presence of phosphoric acid at 60—65 °C for 10 h. The resulting products were isolated by column chromatography over silica gel and purified by preparative gas chromatography. The reaction of **1a** gave 7-methyl-2,4,12,14-tetraoxatricyclo[8.4.0.0^{1,6}]tetradecane(**2a**), 9-methyl-2,4-dioxaspiro[5.5]undecan-7-one (**3a**), 14-methyl-2,4,8,10-tetraoxatricyclo[4.4.4.0^{1,6}]tetradecane (**4a**), 11-methyl-2,4-dioxaspiro[5.5]undecan-7-one (**5a**), and 12-methyl-2,4,8,10-tetraoxatricyclo[4.4.4.0^{1,6}]tetradecane (**6a**). 3,3-Dimethylcyclohexanone (**1b**), *cis*-3,5-dimethylcyclohexanone(**1c**), *trans*-3,5-dimethylcyclohexanone (**1d**), 3,3,5-trimethylcyclohexanone (**1e**) and 3,3,5,5-tetramethylcyclohexanone(**1f**) were similarly treated with formaldehyde to give the same type of products as those of the reaction of **1a**. The yields are summarized in Table 1.

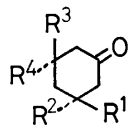

1

1a: R^1=Me, R^2=R^3=R^4=H
1b: R^1=R^2=Me, R^3=R^4=H
1c: R^1=R^3=Me, R^2=R^4=H
1d: R^1=R^4=Me, R^2=R^3=H
1e: R^1=R^2=R^3=Me, R^4=H
1f: R^1=R^2=R^3=R^4=Me

Fig. 1.

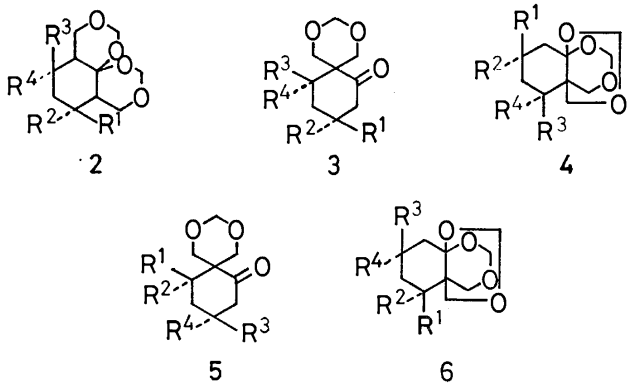

2 3 4 5 6

Fig. 2.

Structures of Reaction Products. The structure of the spiro mono(1,3-dioxane) (**3a**) has been identified by the synthesis of an authentic specimen from 2,4-dioxaspiro[5.5]undecan-7-one.[2] The structure of **3b** or **3e** has also been confirmed by direct comparison with an authentic specimen prepared from **3a** or **3d** (see Experimental). The spiro mono(1,3-dioxanes) (**5**) have been characterized as the structural isomers of **3**, which differ only from the substituted position of a spiro(1,3-dioxane) ring, on the basis of similar spectral data and elemental analyses.

The acid-catalyzed hydrolysis of fused di(1,3-dioxanes) (**4** or **6**) quantitatively afforded the corresponding spiro mono(1,3-dioxanes) (**3** or **5**), respectively (see Experimental). On this basis, the structure of the fused di(1,3-dioxanes) (**4** or **6**) has been characterized. Fused di(1,3-dioxanes) (**2**) were presumed to be the structural isomers of **4** or **6**, on the basis of similar spectral data and elemental analyses.

Methyl-substituent Effect. As seen in Table 1, the methyl groups adjacent to the reaction points (C_2- and C_6-positions in methyl-substituted cyclohexanones) play an important role in the individual reactions. When the C_5-position of cyclohexanone has no methyl groups, *e.g.*, **1a** or **1b**, the reactivity is the largest in the reactions studied. When both C_3- and C_5-positions are substituted by a methyl group, *e.g.*, **1c** or **1d**, the reactivity decreases to one-half of that of **1a** or **1b**. As the methyl group is further introduced, *e.g.*, **1e** or **1f**, the reactivity becomes very poor.

The substituent also influences the product distribution. The reaction of **1a** or **1c**, which has no C_3-

TABLE 1. ACID-CATALYZED REACTION OF 3- AND 3,5-METHYL-SUBSTITUTED CYCLOHEXANONES (**1a**—**1f**) WITH FORMALDEHYDE

Alicyclic ketone **1**	Isolated yield (%)					Total yield (%)	Recovered **1** (%)
	2	**3**	**4**	**5**	**6**		
3-Methylcyclohexanone (**1a**)	2	4	83	1	2	92	3
3,3-Dimethylcyclohexanone (**1b**)	—	30	59	6	—	95	3
cis-3,5-Dimethylcyclohexanone (**1c**)	3	5	42	—	—	50	48
trans-3,5-Dimethylcyclohexanone (**1d**)	26	25	3	—	—	54	41
3,3,5-Trimethylcyclohexanone (**1e**)	—	4	1	2	—	7	89
3,3,5,5-Tetramethylcyclohexanone (**1f**)	—	3	—	—	—	3	95

or C_3,C_5-axial substituents, mainly affords **4**; **1b**, which has two C_3-substituents, chiefly affords **4**, accompanied by **3**; **1d**, which has an axial and an equatorial substituent at each of the C_3- and C_5-positions, chiefly yields **2**, together with **3**, and very little **4**; **1e** or **1f** mainly affords **3**, although the yield is very low.

These results have been interpreted as follows; (i) The first step in the acid-catalyzed reaction is the enolization of the cyclic ketone, followed by the axial attack of a hydroxymethyl cation ($^+CH_2OH$) on the enolic double bond. The attack takes place predominantly at the α-methylene position where the steric interference caused by the C_3- or C_5-methyl substituent is very small (steric approach control). (ii) The resulting intermediate, a *cis* fused hemiacetal, attains equilibrium with the *trans* fused isomer as shown below. The hemiacetal is dehydrated preferentially according to the Sayzeff rule to give an olefin. The olefin is again attacked by the cation in an antiparallel attack[3] to give the fused di(1,3-dioxane) (**4**).

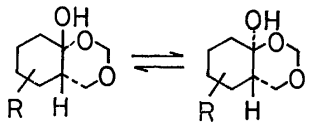

Fig. 3.

(iii) The axial methyl groups at C_3- or C_3,C_5-positions interfere with the formation of **4** and promote that of **3**, because of the 1,3-diaxial interactions between a 1,3-dioxane ring and the axial methyl groups (product development control). (iv) The formation of **5** is more unfavored than that of **3**. However, the reaction of **1e** affords **5e** in a fairly high ratio. This may be explained by the steric approach control and product development control described above, that is, there is no remarkable differences between the two controls on the formation of **3e** or **5e**. (v) In a series of this reaction, the fused di(1,3-dioxane) (**2**) is produced in only small quantities and has been attributed to the fact that **2** is more thermodynamically unstable than **4**, in addition to the reasons given in (ii). However, the reaction of **1d** gave **2d** in an exceptionally good yield but the explanation for this remains unknown.

Experimental

All the boiling and melting points are uncorrected. PMR spectra were taken with a JEOL LMN-MH-60 II spectrometer (60 MHz) with tetramethylsilane as an internal reference. IR spectra were recorded with a Japan Spectroscopic IR-A spectrophotometer. The molecular weight was determined by Rast's method. Preparative GLPC was performed with a Shimadzu GC-3AH using a 3 m×3 mmφ column with 30% diethylene glycol succinate polyester on 60/80 kamelite operating at 160 °C with a H_2 pressure of 0.2 kg/cm². Preparative column chromatography was conducted over silica gel (Wakogel C-200) with a mixture of hexane and ether (5:1 v/v) as an eluent.

Materials. Commercial 3-methylcyclohexanone(**1a**) of analytical grade was used. 3,3-Dimethylcyclohexanone(**1b**),[4] *cis*-3,5-dimethylcyclohexanone(**1c**),[5] *trans*-3,5-dimethylcyclohexanone(**1d**),[5] 3,3,5-trimethylcyclohexanone(**1e**),[6] and 3,3,5,5-tetramethylcyclohexanone(**1f**)[7] were prepared according to reported methods. **1c** and **1d** were obtained as a mixture of their isomers and each isomer was isolated by preparative GLPC. **1b**: bp 51—52 °C/4 mmHg, n_D^{25} 1.4460. **1c**: n_D^{25} 1.4400. **1d**: n_D^{25} 1.4456 (mixture of **1c** and **1d**: bp 174—176 °C). **1e**: bp 72—73 °C/8 mmHg, n_D^{25} 1.4426. **1f**: bp 196—197 °C, n_D^{25} 1.4512.

*Reaction of Methylcyclohexanones(**1a**—**1f**) with Formaldehyde.* A mixture of methylcyclohexanone(10 mmol) and acetic anhydride (1.02 g, 10 mmol) was added to a stirred solution of 95% paraformaldehyde (1.58 g, 50 mmol) and 85% phosphoric acid (0.58 g, 5 mmol) in glacial acetic acid(10 ml) at room temperature, stirring being continued at 60—65 °C for 10 h. After the usual work-up, each product was isolated by column chromatography and subsequent preparative GLPC.

*Hydrolysis of Fused Di(1,3-dioxanes)(**4** or **6**).* A solution of the fused di(1,3-dioxane)(**4** or **6**) (10 mmol) in 10% aqueous hydrochloric acid(10 ml) and cyclohexane(10 ml) was stirred under reflux for 5 h. The mixture was extracted with ether (20 ml×3), the combined extracts washed with 5% aqueous sodium carbonate and saturated brine (10 ml×2), and dried. Removal of the solvent gave crude spiro mono(1,3-dioxane) (**3** or **5**), which was isolated by preparative GLPC. The yields of hydrolyzed products are given in Table 6.

*Authentic Sample of **3a**.* A solution of 2,4-dioxaspiro-[5.5]undecan-7-one(**7**) (1.07 g, 10 mmol) in ethylene glycol (20 ml) was treated with bromine(1.60 g, 20 mg atom) according to the method of Garbisch Jr.[8] The work-up gave crude crystals of 8-bromo-2,4-dioxaspiro[5.5]undecan-7-one ethylene acetal(**8**), which were recrystallized from benzene-petroleum ether to give white crystals of **8**(2.87 g, 98%); mp 110.5—111.5 °C. PMR[C_6H_6–CCl_4(4 : 1 v/v)]: δ 1.1—2.7(br m, 6H), 3.2—4.2(m, 9H), 4.64 (AB-q, J=5.8 Hz, 2H). IR(Nujol): 2764(w), 1153(s), 1027(s), 748(w), 680(m) cm^{-1}. Found: C, 45.41; H, 5.84%; mol wt: 295. Calcd for $C_{11}H_{17}O_4Br$: C, 45.06; H, 5.85%; mol wt: 293.3. Ethylene acetal (**8**) (2.93 g, 10 mmol) was stirred with sodium methoxide(1.62 g, 30 mmol) in dimethyl sulfoxide(30 ml)

Table 2. Physical properties of fused di(1,3-dioxanes) (**2**, **4**, and **6**)

Compd	n_D^{25} (mp)	Molecular formula	Found %		Calcd %		Molecular weight	
			C	H	C	H	Found	Calcd
2a	(82—84 °C)[a]	$C_{11}H_{18}O_4$	61.82	8.41	61.66	8.47	216	214.3
2c	(76—78 °C)[a]	$C_{12}H_{20}O_4$	63.02	8.85	63.13	8.83	231	228.3
2d	1.4887	$C_{12}H_{20}O_4$	63.41	8.87	63.13	8.83	229	228.3
4a	(73—74 °C)[a]	$C_{11}H_{18}O_4$	61.27	8.43	61.66	8.47	218	214.3
4b	(86—88 °C)[a]	$C_{12}H_{20}O_4$	63.55	8.91	63.13	8.83	227	228.3
4c	1.4874	$C_{12}H_{20}O_4$	63.40	8.68	63.13	8.83	228	228.3
4d	1.4887	$C_{12}H_{20}O_4$	63.38	8.87	63.13	8.83	224	228.3
4e	1.4862	$C_{13}H_{22}O_4$	64.80	9.38	64.44	9.15	245	242.3
6a	1.4926	$C_{11}H_{18}O_4$	61.95	8.46	61.66	8.47	215	214.3

a) Recrystallized from 2-propanol.

Table 3. Physical properties of spiro mono(1,3-dioxanes) (**3** and **5**)

Compd	n_D^{25} (mp)	Molecular formula	Found %		Calcd %		Molecular weight	
			C	H	C	H	Found	Calcd
3a	1.4791	$C_{10}H_{16}O_3$	65.02	8.68	65.19	8.75	181	184.2
3b	(76—77 °C)[a]	$C_{11}H_{18}O_3$	66.73	9.36	66.64	9.15	194	198.3
3c	1.4829	$C_{11}H_{18}O_3$	66.88	9.10	66.64	9.15	201	198.3
3d	1.4822	$C_{11}H_{18}O_3$	66.89	9.32	66.64	9.15	200	198.3
3e	(53—54 °C)[a]	$C_{12}H_{20}O_3$	67.42	9.13	67.89	9.50	210	212.3
3f	(87—88 °C)[a]	$C_{13}H_{22}O_3$	68.63	9.76	68.99	9.80	227	226.3
5a	1.4890	$C_{10}H_{16}O_3$	65.18	8.82	65.19	8.75	183	184.2
5b	(80—81 °C)[a]	$C_{11}H_{18}O_3$	66.73	9.36	66.64	9.15	194	198.3
5e	1.4880	$C_{12}H_{20}O_3$	67.88	9.47	67.89	9.50	212	212.3

a) Recrystallized from 2-propanol.

Table 4. IR and PMR spectral data of fused di(1,3-dioxanes) (**2**, **4**, and **6**)

Compd	IR (cm^{-1})	PMR (ppm in CCl_4)
2a[a]	2779(w), 1164(s), 1064(s), 997(s)	0.77 (d, J=5.3 Hz, 3H), 0.9—2.5 (m, 7H), 3.14—4.07 (m, 4H), 4.60 (AB-q, J=6.0 Hz, 2H), 4.66 (AB-q, J=6.0 Hz, 2H)
2c[a]	2766(w), 1163(s), 1063(s), 995(s)	0.82 (d, J=6.3 Hz, 3H), 1.01 (d, J=6.9 Hz, 3H), 1.2—2.7 (m, 6H), 3.4—4.3 (m, 4H), 4.86 (AB-q, J=5.3 Hz, 2H), 4.88 (AB-q, J=5.3 Hz, 2H)
2d	2769(w), 1172(s), 1153(s), 1092(s), 1044(s)	1.04 (d, J=7.2 Hz, 3H), 1.07 (d, J=7.2 Hz, 3H), 1.2—2.3 (m, 6H), 3.63 (s, 2H), 3.73 (AB-q, J=12 Hz, 2H), 4.87 (AB-q, J=6.0 Hz, 2H), 4.92 (AB-q, J=6.0 Hz, 2H)
4a[a]	2770(w), 1160(s), 1040(s), 992(s)	0.93 (d, J=7.2 Hz, 3H), 1.0—2.7 (m, 7H), 3.39 (AB-q, J=11 Hz, 2H), 3.66 (AB-q, J=11 Hz, 2H), 4.78 (AB-q, J=5.7 Hz, 2H), 4.83 (s, 2H)
4b[a]	2774(w), 1160(s), 1046(s), 953(s)	1.05 (s, 6H), 1.1—2.0 (m, 6H), 3.18—3.90 (br, 4H), 4.73 (AB-q, J=6.0 Hz, 4H)
4c	2769(w), 1161(s), 1041(s), 940(s)	0.72 (d, J=7.5 Hz, 3H), 0.94 (d, J=7.5 Hz, 3H), 1.1—2.8 (m, 6H), 3.50 (AB-q, J=12 Hz, 2H), 3.96 (AB-q, J=12 Hz, 2H), 4.91 (AB-q, J=6.0 Hz, 2H), 4.93 (s, 2H)
4d	2767(w), 1173(s), 1044(s), 946(s)	1.04 (d, J=6.9 Hz, 3H), 1.06 (d, J=7.2 Hz, 3H), 1.2—2.4 (m, 6H), 3.63 (s, 2H), 3.74 (AB-q, J=11 Hz, 2H), 4.88 (AB-q, J=6.0 Hz, 2H), 4.92 (AB-q, J=6.0 Hz, 2H)
4e	2766(w), 1164(s), 1044(s), 952(s)	0.82 (d, J=6.5 Hz, 3H), 0.97 (s, 3H), 1.15 (s, 3H), 1.3—2.9 (m, 5H), 3.49 (AB-q, J=12 Hz, 2H), 3.98 (AB-q, J=12 Hz, 2H), 4.93 (s, 2H), 4.95 (AB-q, J=5.6 Hz, 2H)
6a	2760(w), 1160(s), 1036(s), 936(s)	0.81 (d, J=7.5 Hz, 3H), 1.0—2.8 (m, 7H), 3.43 (AB-q, J=12 Hz, 2H), 3.83 (AB-q, J=12 Hz, 2H), 4.75 (AB-q, J=6.0 Hz, 2H), 4.80 (s, 2H)

a) IR spectrum was measured in Nujol.

TABLE 5. IR AND PMR SPECTRAL DATA OF SPIRO MONO(1,3-DIOXANES) (**3** AND **5**)

Compd	IR (cm^{-1})	PMR (ppm in CCl_4)
3a	2751(w), 1696(s), 1159(s), 1032(s)	1.02 (m, 3H), 1.2—2.7 (m, 7H), 3.67 (AB-q, J=11 Hz, 4H), 4.48 (AB-q, J=5.6 Hz, 2H)
3b[a]	2754(w), 1699(s), 1157(s), 1035(s)	0.97 (s, 6H), 1.3—2.2 (m, 6H), 3.70 (s, 4H), 4.53 (AB-q, J=5.6 Hz, 2H)
3c	2751(w), 1703(s), 1164(s), 1034(s)	1.02 (m, 3H), 1.24 (d, J=6.0 Hz, 3H), 1.4—2.4 (m, 6H), 3.92 (AB-q, J=12 Hz, 4H), 4.62 (AB-q, J=6.0 Hz, 2H)
3d	2758(w), 1704(s), 1150(s), 1032(s)	0.93 (d, J=7.5 Hz, 3H), 1.02 (d, J=4.5 Hz, 3H), 1.3—2.9 (m, 6H), 3.80 (AB-q, J=11 Hz, 2H), 3.90 (AB-q, J=11 Hz, 2H), 4.60 (AB-q, J=6.0 Hz, 2H)
3e[a]	2757(w), 1703(s), 1169(s), 1036(s)	0.90 (s, 3H), 1.07 (s, 3H), 1.22 (d, J=6.3 Hz, 3H), 1.4—2.5 (m, 5H), 3.97 (AB-q, J=12 Hz, 4H), 4.70 (AB-q, J=5.7 Hz, 2H)
3f[a]	2777(w), 1684(s), 1144(s), 1036(s)	1.06 (s, 12H), 1.55 (s, 2H), 2.18 (s, 2H), 3.91 (AB-q, J=11 Hz, 4H), 4.54 (s, 2H)
5a	2751(w), 1698(s), 1150(s), 1034(s)	0.98 (d, J=7.5 Hz, 3H), 1.3—2.9 (m, 7H), 3.84 (s, 2H), 3.92 (AB-q, J=11 Hz, 2H), 4.63 (AB-q, J=6.0 Hz, 2H)
5b[a]	2776(w), 1700(s), 1160(s), 1045(s)	0.97 (s, 6H), 1.2—2.1 (m, 4H), 2.13 (s, 2H), 3.78 (AB-q, J=12 Hz, 4H), 4.62 (AB-q, J=6.0 Hz, 2H)
5e	2754(w), 1711(s), 1175(s), 1041(s)	0.87 (s, 3H), 1.03 (m, 3H), 1.18 (s, 3H), 1.3—2.5 (m, 5H), 3.97 (AB-q, J=12 Hz, 4H), 4.68 (s, 2H)

a) IR spectrum was measured in Nujol.

TABLE 6. ACID-CATALYZED HYDROLYSIS OF FUSED DI(1,3-DIOXANES) (**4** OR **6**)

Reactant	Product	Isolated yield (%)
4a	**3a**	98
4b	**3b**	95
4c	**3c**	97
4d	**3d**	94
4e	**3e**	98
6a	**5a**	97

at room temperature for 15 h. The mixture was then acidified with 10% aqueous hydrochloric acid and stirred at 50 °C for 1 h. The work-up gave crude crystals of *2,4-dioxaspiro[5.5]undec-8-en-7-one(**9**)*, which were recrystallized from benzene to give white crystals of **9**(1.53 g, 91%); mp 77.5—78.0 °C. PMR(CCl_4): δ 2.1—2.6(m, 4H), 3.80(s, 4H), 4.70 (AB-q, J=6.0 Hz, 2H), 5.82(d, J=10.2 Hz, of t, J=1.8 Hz, 1H), 6.91(m, 1H). IR(Nujol): 2762(w), 1654(s), 1610(w), 1153(s), 1054(s), 1027(s), 931(s), 924(s) cm^{-1}. Found: C, 64.38; H, 7.17%; mol wt: 168. Calcd for $C_9H_{12}O_3$: C, 64.27; H, 7.19%; mol wt: 168.2. A solution of α,β-unsaturated ketone(**9**) (1.68 g, 10 mmol) in absolute ether (50 ml) was treated with methylmagnesium iodide prepared from the reaction of magnesium turnings (0.48 g, 20 mg atom) and methyl iodide(2.84 g, 20 mmol) in absolute ether (20 ml) in the presence of anhydrous copper(I) bromide(0.29 g, 1 mmol) below −10 °C. The work-up gave crude *9-methyl-2,4-dioxaspiro[5.5]undecan-7-one(**3a**)* which was isolated by preparative GLPC as a colorless oil (1.80 g, 96%). The physical constants of the compound were consistent with those of **3a**, produced by the acid-catalyzed reaction of **1a** with formaldehyde.

*Authentic Sample of **3b**.* By a procedure similar to that for the preparation of **8**, **3a**(1.84 g, 10 mmol) reacted with bromine (1.60 g, 20 mg atom) to afford crystals of *8-bromo-9-methyl-2,4-dioxaspiro[5.5]undecan-7-one ethylene acetal (**10**)*, which was recrystallized from methanol to give white crystals of **10**(2.92 g, 95%); mp 135—136 °C. PMR(CCl_4): δ 1.03(d, J=6.5 Hz, 3H), 1.2—2.5(br m, 5H), 3.43—4.22 (m, 9H), 4.50(AB-q, J=5.7 Hz, 2H). IR(Nujol): 2769(w), 1166(s), 1117(s), 1085(s), 1025(s), 748(m), 680(m) cm^{-1}. Found: C, 46.77; H, 6.02%; mol wt: 306. Calcd for $C_{12}H_{19}O_4Br$: C, 46.92; H, 6.24%; mol wt: 307.2. Ethylene acetal(**10**)(3.07 g, 10 mmol) reacted with sodium methoxide (1.62 g, 30 mmol) by the same procedure as that for the preparation of **9** to afford crystals of *9-methyl-2,4-dioxaspiro[5.5]undec-8-en-7-one(**11**)*, which were recrystallized from methanol to give white needles of **11** (1.46 g, 80%); mp 102.0—102.5 °C. PMR(C_5H_5N): δ 1.73(s, 3H), 2.23(s, 4H), 3.95 (AB-q, J=12 Hz, 4H), 4.82(AB-q, J=6.0 Hz, 2H), 5.76(br s, 1H). IR(Nujol): 2773(w), 1638(s), 1624(s), 1154(s), 1025(s), 920(s) cm^{-1}. Found: C, 66.18; H, 7.68%; mol wt: 181. Calcd for $C_{10}H_{14}O_3$: C, 65.91; H, 7.74%; mol wt: 182.2. α,β-Unsaturated ketone(**11**) (1.82 g, 10 mmol) reacted with methylmagnesium iodide (20 mmol) to give crude crystals of *9,9-dimethyl-2,4-dioxaspiro[5.5]undecan-7-one(**3b**)*, which were recrystallized from 2-propanol to give white crystals of **3b**(1.92 g, 97%). The physical constants of the compound were identical with those of **3b**, produced by the acid-catalyzed reaction of **1b** with formaldehyde.

*Authentic Sample of **3e**.* By a procedure similar to that for the preparation of **8**, **3c**(1.98 g, 10 mmol) reacted with bromine (1.60 g, 20 mg atom) to afford crude crystals of *8-bromo-9,11-dimethyl-2,4-dioxaspiro[5.5]undecan-7-one ethylene acetal(**12**)*, which were recrystallized from methanol to give white crystals of **12**(3.08 g, 96%); mp 115.0—122.0 °C. PMR(CCl_4): δ 0.98(dd, J=3.0, 6.0 Hz, 3H), 1.25(d, J=6.8 Hz, 3H), 1.4—2.3(m, 4H), 3.60—4.18(m, 8H), 4.42(d, J=6.0 Hz, 1H), 4.58 (AB-q, J=6.0 Hz, 2H). IR(Nujol): 2760(w), 1184(s), 1160(s), 1114(s), 1034(s), 686(m) cm^{-1}. Found: C, 48.73; H, 6.62%. Calcd for $C_{13}H_{21}O_4Br$: C, 48.61; H, 6.59%. Ethylene acetal(**12**)(3.21 g, 10 mmol) reacted with sodium methoxide (1.62 g, 30 mmol) to give a dark brownish mixture. Column chromatographic separation (silica gel with a 3:1 mixture of hexane and chloroform) of the mixture gave crude *9,11-dimethyl-2,4-dioxaspiro[5.5]-*

*undec-8-en-7-one(**13**)* which was purified by preparative GLPC to give a colorless oil(1.63 g, 83%); n_D^{25} 1.5083. PMR (CCl_4) : δ 1.07(d, J=7.1 Hz, 3H), 1.92(s, 3H), 2.1—3.1 (m, 3H), 3.72(AB-q, J=12 Hz, 2H), 3.90(AB-q, J=12Hz, 2H), 4.68(AB-q, J=6.0 Hz, 2H), 5.64(m, 1H). IR(neat): 2751(w), 1652(s), 1146(s), 1026(s), 920(s) cm^{-1}. Found: C, 67.58; H, 8.20% ; mol wt: 200. Calcd for $C_{11}H_{16}O_3$: C, 67.32; H, 8.22%; mol wt: 196.2. α,β-Unsaturated ketone (**13**) (1.96 g, 10 mmol) reacted with methylmagnesium iodide(20 mmol) to give crude crystals of *9,9,11-trimethyl-2,4-dioxaspiro[5.5]undecan-7-one(**3e**)*, which were recrystallized from 2-propanol to give white crystals of **3e**(2.08 g, 98%). The physical constants of the compound were identical with those of **3e**, produced by the acid-catalyzed reaction of **1e** with formaldehyde.

The authors wish to thank Prof. K. Harada, Tsukuba University, for his valuable discussions and suggestions.

References

1) Part II; F. Hirano and S. Wakabayashi, *Bull. Chem. Soc. Jpn.*, **50**, 3059 (1977).
2) F. Hirano and S. Wakabayashi, *Bull. Chem. Soc. Jpn.*, **48**, 2579 (1975).
3) J. Valls and E. Toromanoff, *Bull. Soc. Chim. Fr.*, **1961**, 758.
4) W. von E. Doering and F. M. Beringer, *J. Am. Chem. Soc.*, **71**, 2225 (1949).
5) H. E. Ungnade and D. V. Nightingale, *J. Am. Chem. Soc.*, **66**, 1218 (1944).
6) E. L. Eliel and H. Haubenstock, *J. Org. Chem.*, **26**, 3504 (1961).
7) S. M. Kharasch and O. P. Tawney, *J. Am. Chem. Soc.*, **63**, 2308 (1941).
8) E. W. Garbisch Jr., *J. Org. Chem.*, **30**, 2109 (1965).

Glucosidation of Tetra-*O*-benzyl-α-D-glucose with Chlorosilane and Silver Sulfonate

Shinkiti KOTO,* Naohiko MORISHIMA, and Shonosuke ZEN
School of Pharmaceutical Sciences, Kitasato University, Shirokane, Minato-ku, Tokyo 108
(Received February 7, 1978)

Glucosidation of 2,3,4,6-tetra-*O*-benzyl-α-D-glucopyranose with methanol or cyclohexanol in the presence of chlorosilane and silver sulfonate is described. As by-products, octa-*O*-benzyl-α,α- and -α,β-trehaloses are also formed. Possible reaction pathways are discussed.

The development of methods for the synthesis of glycosides has always been very important in carbohydrate chemistry.[1] The Fischer method[1] appears to have the methodological advantage that it can be performed by a direct dehydration between glycose and alcohol in the presence of an acid catalyst. Modified methods[2-4] using acid with a dehydrating agent have been developed for the glycosidation of appropriately protected precursors having a reducing hydroxyl group. Such methods suggested a novel glucosidation of a stable precursor, 2,3,4,6-tetra-*O*-benzyl-α-D-glucopyranose (**1**), with alcohol by using strongly dehydrating chlorosilanes,[5-7] which was investigated[8] as a part of our continuing studies.[9]

Results and Discussion

On treating **1** with methanol at 0 °C in dichloromethane containing dichlorodiphenylsilane (DCPS) and methanesulfonic acid as catalyst, methyl glucosides (**2a** and **2b**) of **1** were formed with a moderate efficiency. As the dehydration with DCPS and methanesulfonic acid was insufficient, the reaction was carried out with DCPS and silver methanesulfonate, from which more reactive bis(methylsulfonyloxy)diphenylsilane[10] was expected to be formed. The reaction proceeded well without addition of the acid.

A series of experiments were then done using stoichiometric amounts of **1** (αGOH), aglucon (methanol or cyclohexanol), chlorosilane, and silver sulfonate according to Eq. 1, where *n* denotes the number of chlorine atom(s) in the silanes and G represents a tetra-*O*-benzyl-D-glucopyranosyl moiety.

$$\alpha\mathrm{GOH} + \mathrm{ROH} + \frac{2}{n}\mathrm{R'_{4-n}SiCl_n} + 2\mathrm{R''SO_3Ag} \longrightarrow \mathrm{GOR} + \frac{2}{nx}\text{-}\left[\mathrm{R'_{4-n}SiO_{n/2}}\right]_x\text{-} + 2\mathrm{R''SO_3H} + 2\mathrm{AgCl} \quad (1)$$

The results are shown in Table 1 and Fig. 1. Yields are based on the amounts of the products obtained on column chromatography, in reference to the amount of **1** charged. In every case, self-condensation products identified as octa-*O*-benzyl-α,α- and -α,β-trehaloses (**3a** and **3b**) and unchanged **1** were obtained on chromatography.

Treatment of **1** with DCPS and silver sulfonate without alcohol led to efficient self-condensations which can be described by Eq. 2, where GOG expresses the trehalose derivatives (**3a** and **3b**).

$$2\alpha\mathrm{GOH} + (\mathrm{C_6H_5})_2\mathrm{SiCl_2} + 2\mathrm{R''SO_3Ag} \longrightarrow \mathrm{GOG} + \frac{1}{x}\text{-}\left[(\mathrm{C_6H_5})_2\mathrm{SiO}\right]_x\text{-} + 2\mathrm{R''SO_3H} + 2\mathrm{AgCl} \quad (2)$$

Results are shown in Table 2.

As shown in Fig. 1, DCPS was almost exhausted within 1 h and the amount of dimethoxydiphenylsilane (DMPS)[11] hardly exceeded 6%. Siloxanes[12] such as **4** and **5**[8,13] were detected by TLC throughout the reaction.

A filtrate of the reaction mixture of DCPS and silver methanesulfonate was able to condense **1** with methanol to give **2a** and **2b** as well as by-products **4** and **5**. Treatment of **4** with methanesulfonic acid in dichloromethane gave **2a** and **2b** in 78% yield, and **5** treated similarly gave **3a** and **3b** in 74% yield. DMPS with methanesulfonic acid in dichloromethane also transformed **1** into **2a** and **2b** in 63% yield. Consequently, the scheme of glucosidation of **1** with methanol in the presence of DCPS and silver methanesulfonate can be postulated as in Fig. 2, the bis(methylsulfonyloxy)-diphenylsilane formed reacts with methanol and **1** to

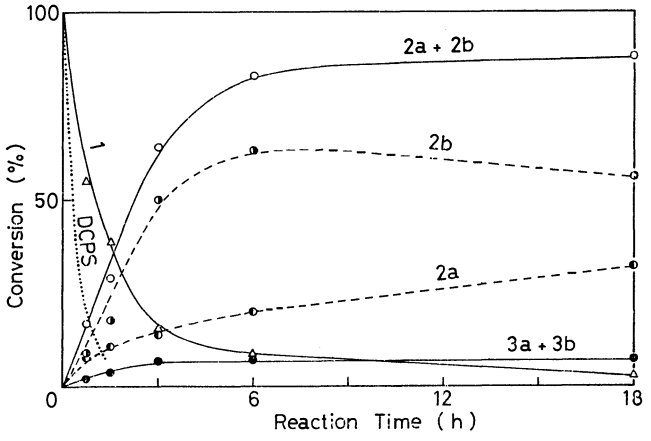

Fig. 1. Time-dependence of glucosidation of **1** with methanol in the presence of DCPS and silver methanesulfonate at 0 °C, plotted from the data of runs 1—5 in Table 1 except the GC data for DCPS (·····).

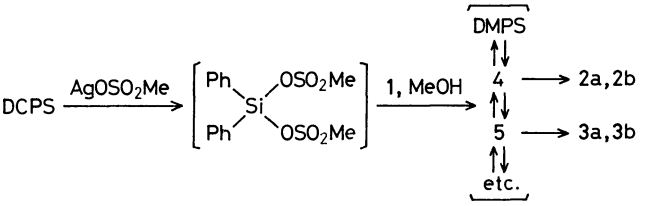

Fig. 2. A scheme of glucosidation of **1** with methanol in the presence of DCPS and silver methanesulfonate.

Table 1. Glucosidation[a] of tetra-*O*-benzyl-α-D-glucopyranose (**1**)

Run	R	*n*	R′	R″	Reaction time (h)	Yield (%) 2(2′)**a**+2(2′)**b**	(α/β)	**3a**+**3b**	**1**
1	Me	2	Ph	Me	0.5	17	(8/ 9)	2	55
2	Me	2	Ph	Me	1.5	29	(11/18)	4	39
3	Me	2	Ph	Me	3.0	64[b]	(14/50)[b]	8[b]	15[b]
4	Me	2	Ph	Me	6.0	83	(20/63)	7	8
5	Me	2	Ph	Me	18.0	88	(32/56)	7	3
6	Me	2	Me, Ph[c]	Me	3.0	43	(9/34)	8	45
7	Me	2	Me	Me	3.0	36	(10/26)	6	51
8	Me	1	Ph	Me	3.0	21	(9/12)	—[d]	58
9	Me	3	Ph	Me	3.0	75	(21/54)	8	8
10	Me	4	—	Me	3.0	73	(23/50)	7	11
11	Me	2	Ph	Tol[e]	3.0	44	(13/31)	2	26
12	Me	2	Ph	Pnp[f]	2.0	73	(18/55)	18	8
13	Ch	2	Ph	Me	3.0	55	(18/37)	28	10
14	Ch	2	Ph	Tol[e]	3.0	31	(12/19)	21	34
15	Ch	2	Ph	Pnp[f]	3.0	70	(54/16)	21	8

a) Reactions were carried out in dichloromethane at 0 °C according to Eq. 1. b) Revised data of Ref. 6. c) Dichloromethylphenylsilane. d) Not determined. e) $C_6H_4CH_3(p)$. f) $C_6H_4NO_2(p)$.

Table 2. Self-condensation[a] of tetra-*O*-benzyl-α-D-glucopyranose (**1**)

R″	Temp (°C)	Time (h)	Yield (%) **3a**+**3b**	(αα/αβ)	**1**
CH_3	0	6.5	68	(23/45)	15
$C_6H_4NO_2(p)$	0	4.5	80	(39/41)	12
CF_3	−20	0.33	70	(26/44)	16

a) Reactions were carried out in dichloromethane according to Eq. 2.

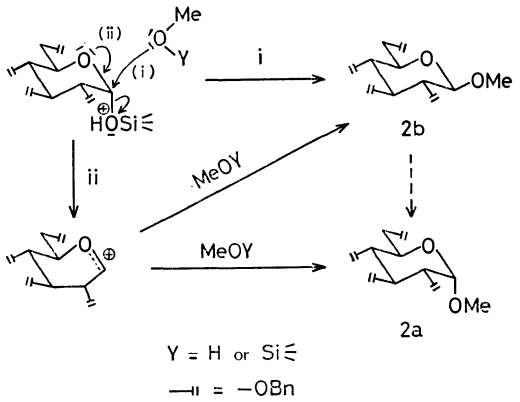

Fig. 3. Pathways of glucosidation of **1** with methanol in the presence of chlorosilane and silver sulfonate.

generate a mixture of methanesulfonic acid and siloxanes, such as DMPS, **4**, and **5**, the latters of which eventually produce the glucosides. Dimeric 1,3-dichloro-1,1,3,3-tetraphenyldisiloxane was also effective for the glucosidation of this kind. This suggests that a part of the glucosidation is likely to proceed by way of oligosiloxanes structurally related to **4** and **5**, which were actually detected in the reaction mixture.

The role of the liberated acid is essential for the glucosidation, since no glucosides, but only siloxanes **4** and **5**, formed when a base such as pyridine was first added to the reaction mixture.

An inefficient condensation of **1** and methanol with methanesulfonic acid alone proceeded to give **2a** and **2b** in 12 and 13% yields, respectively, indicating that the condensation of **1** and methanol with DCPS and silver methanesulfonate goes partly at least through a pathway i leading directly to **2b**, as shown in Fig. 3. Tables 1 and 2 show that ratios of **2a** to **2b** are mostly smaller than those of **3a** to **3b**, reflecting the idea that the less bulky methanol has more chances to take pathway i than the bulky **1** does.[14] The decrease of the amount of **2b** which accompanied the increase of that of **2a** occurred during a longer reaction period, as seen in Fig. 1, obviously indicating that a part of **2b** is isomerized into **2a** by the methanesulfonic acid generated. Actually, about 10% of **2b** was anomerized with two equivalents of methanesulfonic acid in dichloromethane at 0 °C within 3 h. No appreciable amount of the β,β-isomer[4] formed in the self-condensation reaction of **1**, suggesting that the α-configuration of **1** was mostly retained during the condensation reaction.

The results thus summarized in Table 1 allow the following remarks. Of the dichlorosilanes so far examined, DCPS was best for the glucosidation. The trends in the efficiency of the reaction appear to follow the order of stability of the siloxane[15] to be formed.

The efficiency of the reaction was also affected by the number, *n*. The order of the efficiency, 3—4> 2≫1, roughly correlates with the relative ease of the hydrolytic formation of polysiloxanes.[16] The high efficiencies favoring **2b** in the cases where $n \geqslant 2$ could partly be attributable to the direct pathway i in Fig. 3. The ratios of **2a** to **2b** increased progressively with the larger *n*; this seems to imply a generation of the glucosyl cation as indicated by pathway ii. The remarkably low yield of the glucosides with a fair increase of the anomer ratio in Run 8 may be due to

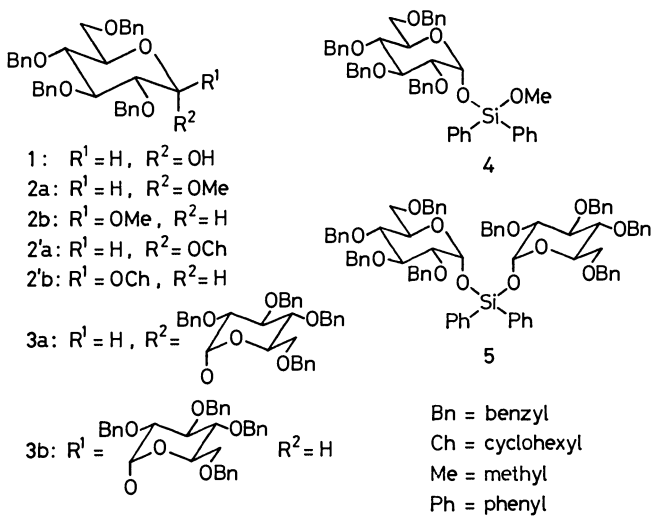

a steric effect caused by three phenyl groups on the silicon atom retarding the formation of the intermediary glucosylsiloxane which would afford the glucosides.

Silver arenesulfonates were also of use. The stronger liberated acid gave the greater efficiency. This was also observed in the self-condensation of **1**, as seen in Table 2. When silver trifluoromethanesulfonate was used, the self-condensation reaction had practically finished after 20 min at −20 °C.

As might be expected, the formation of self-condensation products became significant in the glucosidation of **1** with less reactive cyclohexanol, as shown in Table 1. Treatment with silver *p*-nitrobenzenesulfonate and DCPS yielded mostly **2'a**, agreeing with the fact that **2'b** is less resistant than **2b** to anomerization by acid.[17]

Finally, it should be mentioned that crystalline bis(*p*-nitrophenylsulfonyloxy)diphenylsilane (**6**) was successfully used as a reagent for glucosidation of **1** in a direct fashion :[18] a mixture of **1**, methanol, and **6** in dichloromethane furnished the glucosides, **2a** and **2b**, in 71% yield, favoring the latter.

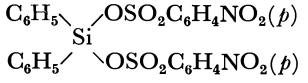

6

Experimental

Instruments used are the same as those previously described,[9] except for a DIP-180 (Japan Spectr.) for optical rotation.

Each aliquot of the reaction mixture was diluted with benzene, and powdered $NaHCO_3$ was added before application to TLC (silica gel No. 7731 (Merck)). Two kinds of solvent systems, consisting of benzene and butanone (solvent A) and of hexane and ethyl acetate (solvent B), were used for column chromatography (silica gel (Kanto Kagaku)), and each fraction was examined by TLC. GLC was carried out by a F6-D (Hitachi Perkin-Elmer): 10% Silicone SE-30 on Chromosorb W AW HMDS (80—100 mesh), 3 mm × 1 m (U-tube), 165 °C, 30 ml/min N_2.

Predistilled solvents and alcohols were stored over molecular sieves (Linde 3A). Silanes were distilled before use. Compound **1**,[19] whose C-13 NMR in $CDCl_3$ showed a single peak at 91.2 ppm, and silver sulfonate prepared from silver carbonate (Wako) and an appropriate sulfonic acid (Tokyo Kasei) were kept *in vacuo* over P_2O_5. Experiments were carried out at 0 °C, unless otherwise stated.

A General Procedure for the Preparation of 2(2')a and 2(2')b (Eq. 1). To a mixture of **1** (0.33 mmol) with alcohol (0.33 mmol) and silver sulfonate (0.67 mmol) in dichloromethane (0.9 ml), chlorosilane (0.67/*n* mmol, stated by Eq. 1) was added with stirring at 0 °C. The mixture was then diluted with benzene and an excess of $NaHCO_3$ was added with stirring. The filtrate was evaporated and chrmatographed over silica gel. Yields were based on the weight of fractions after removing the solvent and were reproducible within 5%. Reaction conditions and results are summarized in Table 1.

Methyl 2,3,4,6-Tetra-O-benzyl-α- and -β-D-glucopyranosides (2a and 2b). A mixture of **1** (180 mg), methanol (14 μl), silver methanesulfonate (136 mg), and DCPS (69 μl) in dichloromethane (0.9 ml) was stirred for 3 h. The processed mixture of products was chromatographed. After elution of **4** and **5** (R_f=0.75 and 0.67, solvent A (40 : 1), respectively) with solvent A (80 : 1), **2b**, **2a**, and then **3a** (R_f=0.55, 0.45, and 0.40, solvent A (40 : 1)) were eluted with solvent A (40 : 1), followed by the elutions of **3b** (R_f=0.30, solvent A (40 : 1)) with solvent A (20 : 1) and of **1** with solvent A (10 : 1). On recrystallization from hexane, **2b** was obtained as colorless needles : 92 mg (50%), mp 74—75 °C, $[\alpha]_D^{20}$ +14° (*c* 1.0, dioxane) [lit,[20] mp 68—69 °C, $[\alpha]_D^{20}$ +11° (*c* 5.3, dioxane)]. Found: C, 75.20; H, 6.92%. Calcd for $C_{35}H_{38}O_6$: C, 75.79; H, 6.90%. Syrupy **2a** (26 mg, 14%) had a NMR spectrum ($CDCl_3$)[21] identical with that of **2a**[20] prepared from methyl α-D-glucopyranoside. Syrupy **3a** (6 mg, 3%) had an R_f value identical with that of **3a** prepared from α,α-trehalose. On recrystallization from hexane, **3b** was obtained as colorless needles : 9 mg (5%), mp 100—101 °C, with an IR spectrum (KBr) identical with that of **3b** prepared as noted below. Crystalline **1** (27 mg, 15%) was recovered.

Glucosidation by the Filtrate of the Reaction Mixture of DCPS and Silver Methanesulfonate. A mixture of silver methanesulfonate (149 mg, 2.2 eq.) and DCPS (76 μl, 1.1 eq.) in dichloromethane (1.8 ml) was stirred for 2 h. Then the resulting mixture was filtered onto **1** (180 mg) kept in a cooling bath. Methanol (14 μl, 1 eq.) was immediately added and the resulting mixture was stirred for 3 h to give **2a** (28 mg, 15%) and **2b** (23 mg, 17%). Fractions containing **4** and **5** were eluted prior to the appearance of **2a** and **2b** on the chromatography.

Evaporation of the solvent from the above-mentioned filtrate (NMR(CH_2Cl_2)δ=3.05 (s, CH_3SO_3Si)[22]) gave a clear syrup, which rapidly turned into a white paste in air.

Glucosidation with DCPS and Methanesulfonic Acid. Treatment of a mixture of **1** (180 mg), methanol (14 μl, 1 eq.), and DCPS (69 μl, 1 eq.) in dichloromethane (0.9 ml) with methanesulfonic acid (1.0—2.0 eq.) for 3 h gave **2a** and **2b**. The following data were obtained : [the acid used, **2a**, **2b**] 22 μl (1.0 eq.), 13 mg (7%), 24 mg (13%); 33 μl (1.5 eq.), 22 mg (12%), 37 mg (20%); and 44 μl (2.0 eq.), 32 mg (17%), 46 mg (25%).

Glucosidation with DMPS and Methanesulfonaic Acid. A mixture of **1** (180 mg) and DMPS (38 μl, 1 eq.) in dichloromethane (0.9 ml) was treated with methanesulfonic acid (44 μl, 2 eq.) to afford **2a** (44 mg, 24%) and **2b** (72 mg, 39%), after 3 h.

Glucosidation with Methanesulfonic Acid. A solution of **1** (180 mg) in dichloromethane (0.9 ml) containing methanol (14 μl, 1 eq.) was treated with methanesulfonic acid (44 μl, 2 eq.) for 3 h to give **2a** (22 mg, 12%) and **2b** (24 mg, 13%).

*Glucosidation with Bis(p-nitrophenylsulfonyloxy)diphenylsilane (**6**).* A mixture of silver *p*-nitrobenzenesulfonate (51.5 mg) and DCPS (18 μl) in acetone (0.5 ml) was stirred at 27 °C for 1 h. Filtration and evaporation gave **6** : hygroscopic prisms, mp 98—101 °C, IR (KBr) 1435 (C_6H_5Si),[23] 1520, 1365 cm^{-1} (NO_2). Found: N, 4.44%. Calcd for $C_{24}H_{28}N_2O_{10}S_2Si$: N, 4.77%.

A mixture of **1** (90 mg) and **6** (98 mg) in dichloromethane (0.9 ml) and methanol (7 μl) was stirred. *p*-Nitrobenzenesulfonic acid soon deposited. After 3 h, the reaction mixture was diluted with benzene, filtered, and chromatographed to give **2a** (11.1 mg, 14%), **2b** (54.2 mg, 57%), **3a**+**3b** (14.3 mg, 16%), and **1** (8.5 mg, 9%).

Glucosidation with 1,3-Dichloro-1,1,3,3-tetraphenyldisiloxane[24] and Silver p-Nitrobenzenesulfonate. A mixture of **1** (90 mg), the siloxane (75 mg), and silver *p*-nitrobenzenesulfonate (103 mg) in dichloromethane (0.45 ml) and methanol (7 μl) was stirred for 3 h to give **2a** (17 mg, 18%), **2b** (35 mg, 38%), **3a**+**3b** (18 mg, 20%), and **1** (4 mg, 5%).

*Conversion of **4** into **2a** and **2b** with Methanesulfonic Acid.* A solution of **4** (47 mg) in dichloromethane (0.24 ml) was treated with methanesulfonic acid (8.2 μl, 2 eq.) for 3 h to give **2a** (8.3 mg, 24%) and **2b** (19 mg, 54%).

*Anomerization of **2b** with Methanesulfonic Acid.* A mixture of **2b** (46 mg) and methanesulfonic acid (11 μl, 2 eq.) in dichloromethane (0.23 ml) was stirred for 3 h to give **2a** (4.7 mg, 10%) and **2b** (36.5 mg, 79%).

*Cyclohexyl 2,3,4,6-Tetra-O-benzyl-α- and -β-D-glucopyranosides (**2'a** and **2'b**).* A mixture of **1** (180 mg), cyclohexanol (35 μl), silver methanesulfonate (136 mg), and DCPS (69 μl) in dichloromethane (0.9 ml) was stirred for 3 h. The processed mixture of products was chromatographed. After elution with the solvent A (80 : 1), a mixture of **2'a** and **2'b** appeared with solvent A (40 : 1), followed by **3a** and **3b** (49 mg, 28%) with solvent A (20 : 1), and unchanged **1** (18 mg, 10%) with solvent A (10 : 1). The mixture of **2'a** and **2'b** was separated by chromatography with solvent B (3 : 1) to afford **2'b** and then **2'a**. On recrystallization from diisopropyl ether, **2'b** was obtained as colorless needles : 77 mg (37%), mp 104—105 °C, $[\alpha]_D^{20}$ +8°(*c* 1.0, $CHCl_3$). Syrupy **2'a** (38 mg, 18%), $[\alpha]_D^{20}$ +43°(*c* 1.0, $CHCl_3$), showed a NMR spectrum identical with that of **2'a** prepared in the alternative fashion described below. Found: for **2'a**, C, 76.74; H, 7.25%. For **2'b**, C, 77.17; H, 7.64%. Calcd for $C_{40}H_{46}O_6$: C, 77.14; H, 7.45%.

*Alternative Synthesis of **2'a**.* A mixture of cyclohexyl 2,3,4,6-tetra-*O*-acetyl-α-D-glucopyranoside[25] (92 mg), KOH (260 mg), and benzyl chloride (3 ml) was heated at 110 °C for 5.5 h. Filtration and evaporation gave a yellow syrup which was chromatographed over silica gel. After one elution with solvent A (100 : 1), another with solvent A (40 : 1) furnished **2'a** (73 mg, 60%), $[\alpha]_D^{20}$ +41° (*c* 2.3, $CHCl_3$). Found: C, 76.14; H, 7.25%. Calcd for $C_{40}H_{46}O_6$: C, 77.14; H, 7.45%.

*Octa-O-benzyl-α,α- and -α,β-trehaloses (**3a** and **3b**).* To a stirred mixture of **1** (180 mg, 0.33 mmol) and silver methanesulfonate (64 mg, 0.03 mmol) in dichloromethane (0.9 ml), DCPS (35 μl, 0.17 mmol) was added; the resulting mixture was stirred for 6.5 h. The processed mixture of products was chromatographed. After one elution with solvent A (80 : 1), **3a** was eluted again with solvent A (40 : 1). Further elution with solvent A (20 : 1) gave **3b**. **3a** was colorless syrup, 41 mg, (23%), $[\alpha]_D^{20}$ +84° (*c* 1.0, $CHCl_3$), having a NMR spectrum identical with that of the sample prepared as given below. On recrystallization from hexane, **3b** was obtained as colorless needles : 80 mg (45%), mp 100—101 °C, $[\alpha]_D^{20}$ +52° (*c* 1.0, $CHCl_3$); its IR and NMR spectra were identical with those of the sample prepared as given below.

Hydrogenation of syrupy **3a** over Pd-black in a mixture of aq ethanol and dioxane containing acetic acid, followed by heating with acetic anhydride and sodium acetate, gave octa-*O*-acetyl-α,α-trehalose: mp 94—97 °C, $[\alpha]_D^{20}$ +163° (*c* 1.0, $CHCl_3$) [lit,[26] mp 98—100 °C, $[\alpha]_D^{23}$ +160° (*c* 1.0, $CHCl_3$)]. Found: C, 49.26; H, 5.57%. Calcd for $C_{20}H_{38}O_{19}$: C, 49.56; H, 5.60%. Similar treatment of **3b** gave octa-*O*-acetyl-α,β-trehalose: mp 138—140 °C, $[\alpha]_D^{20}$ +78° (*c* 1.0, $CHCl_3$) [lit,[26] mp 140—142 °C, $[\alpha]_D^{22}$ +84.5° (*c* 0.68, $CHCl_3$)]. Found: C, 49.54; H, 5.65%. Calcd for $C_{20}H_{38}O_{19}$: C, 49.56; H, 5.60%.

Reaction conditions and results of analogous self-condensations of **1** stated by Eq. 2 using other silver sulfonates are shown in Table 2.

*Conversion of **5** into **3a** and **3b** with Methanesulfonic Acid.* A solution of **5** (156 mg) in dichloromethane (0.78 ml) was treated with methanesulfonic acid (19 μl, 1 eq.) for 4 h to afford **3a** (20 mg, 22%) and **3b** (67 mg, 51%).

*Alternative Synthesis of **3a**.* Crystalline α,α-trehalose dihydrate (Wako, 96.3 mg) was dried *in vacuo* at 90 °C and then heated with benzyl chloride (0.9 ml), crushed KOH (0.71 g), and Drierite (0.7 g) in *N*,*N*-dimethylformamide (1 ml) at 60 °C for 5 h. After filtration and evaporation, chromatography over silica gel with solvent A (gradient, 80 : 1→40 : 1) afforded **3a** (151 mg, 56%), $[\alpha]_D^{20}$ +88° (*c* 1.3, $CHCl_3$). Found; C, 76.42; H, 6.61%. Calcd for $C_{68}H_{70}O_{11}$: C, 76.81; H, 6.64%.

*Alternative Synthesis of **3b**.* A mixture of acetobromoglucose (94 mg), **1** (108 mg), $Hg(CN)_2$ (50 mg), and $HgBr_2$ (72 mg) in nitromethane (1 ml) was stirred at room temperature for 70 h. The product (132 mg) was treated with sodium methoxide (10 ml, 0.02 M) and then benzylated with benzyl bromide (0.25 ml) in *N*,*N*-dimethylformamide (0.5 ml) in the presence of BaO (0.2 g) and $Ba(OH)_2 \cdot 8H_2O$ (0.1 g).[27] After removal of insoluble material by filtration and evaporation *in vacuo* at 98 °C, the residue obtained was chromatographed over silica gel with solvent A (gradient, 100 : 1→30 : 1) to give **3b** (69 mg, 32%). Recrystallization from hexane afforded **3b** : Colorless needles, mp 100—101 °C, $[\alpha]_D^{20}$ +53° (*c* 1.4, $CHCl_3$). Found: C, 76.93; H, 6.62%. Calcd for $C_{68}H_{70}O_{11}$: C, 76.81; H, 6.64%.

*Methoxydiphenyl(2,3,4,6-tetra-O-benzyl-α-D-glucopyranosyloxy)silane (**4**) and Bis(2,3,4,6-tetra-O-benzyl-α-D-glucopyranosyloxy)diphenylsilane (**5**).* A mixture of **1** (180 mg, 0.33 mol), pyridine (93 μl, 0.67 mmol), silver *p*-toluenesulfonate (186 mg, 0.67 mmol), and DCPS (69 μl, 0.33 mmol) in 1,2-dichloroethane (0.9 ml) was stirred at 0 °C for 1 h. Methanol (14 μl, 0.33 mmol) was then added to the mixture. After stirring for 3 h, the mixture was treated with an excess of sodium acetate, filtered, evaporated, and then chromatographed over silica gel. After one elution with benzene, another with solvent A (100 : 1) gave **4** as a syrup: 53 mg (24%), $[\alpha]_D^{20}$ +47° (*c* 0.9, $CHCl_3$), IR (film) 1422 cm^{-1} (C_6H_5Si),[23] NMR ($CDCl_3$) δ=3.61 (3H, s, OCH_3), 5.48 (1H, d, anomeric H, J=3.2 Hz), 7.1—7.5 (phenyl), and 7.6—7.8 (4H, m, H's β to Si in $=Si(C_6H_5)_2$.[28] Found: C, 74.86; H, 6.44%. Calcd for $C_{47}H_{48}O_7Si$: C, 74.97; H, 6.43%.

Elution with solvent A (80 : 1) gave **5** as a syrup: 74 mg (35%), $[\alpha]_D^{20}$ +64° (*c* 1.0, $CHCl_3$), IR(film) 1432 cm^{-1} (C_6H_5Si),[23] NMR($CDCl_3$) δ=5.54 (1H, d, anomeric H, J=3.0 Hz), 7.0—7.4 (phenyl), and 7.6—7.8 (2H, m, H's β to Si in $=Si(C_6H_5)_2$[28]). Found: C, 75.55; H, 6.34%. Calcd for $C_{80}H_{80}O_{12}Si$: C, 76.16; H, 6.39%.

Isolation of Hexaphenylcyclotrisiloxane. The mixture of

Run 3 was poured onto a column of silica gel, and eluted with benzene. On evaporation, crystals were obtained (28 mg, 43%), mp 188—189 °C, [lit,[29] 190 °C], whose IR(KBr)[30] was identical with that of a sample prepared by the known procedure.[29]

Examination of Volatile Components in the Reaction Mixture of Run 3. Aliquots of the supernatant were injected into the GLC-apparatus without quenching to give the data: ([reaction time, DMPS (3.8 min), DCPS(4.4 min)] 8 min, 3%, 74%; 15 min, 5%, 48%; 45 min, 6%, 20%, and 60 min, 4%, 10%.

Examination of the Fractions Containing Siloxanes.[31] The reaction mixture of Run 2 (**1**, 180 mg) quenched with excess benzene and powdered $NaHCO_3$ was poured onto a column of silica gel, which was eluted with solvent A (100 : 1) to give a syrup (94 mg). Rechromatography with solvent B (gradient, 100 : 1→10 : 1) afforded three fractions: A, B, and C. The fastest-moving fraction A (19 mg) was a mixture (*ca.* 1 : 2) of **4** (NMR(CCl_4) δ=3.57 (s, OCH_3)) and 1-methoxy-3-(2,3,4,6-tetra-*O*-benzyl-α-D-glucopyranosyloxy)-1,1,3,3-tetraphenyldisiloxane (NMR(CCl_4) δ=3.45 (s, OCH_3), 5.40(d, anomeric H, J=4 Hz), overlapping to that of **4**). Fraction B (23 mg) had a NMR spectrum consistent with the structure of 1,5-bis(2,3,4,6-tetra-*O*-benzyl-α-D-glucopyranosyl)-1,1,3,3,5,5-hexaphenyl trisiloxane (NMR(CCl_4) δ= 5.23 (d, anomeric H, J=4 Hz), 7.5—7.7 (6H, m, H's β to Si in $=Si(C_6H_5)_2$[28]). The slowest-moving fraction C (13 mg) was a mixture of (1 : 1) of **5** (NMR(CCl_4) δ=5.47 (d, anomeric H, J=4 Hz)) and 1,3-bis(2,3,4,6-tetra-*O*-benzyl-α-D-glucopyranosyloxy)-1,1,3,3-tetraphenyldisiloxane (NMR (CCl_4) δ=5.23 (d, anomeric H, J=2 Hz), 7.5—7.7 (m, H's β to Si in $=Si(C_6H_5)_2$[28]).

We thank the Toray Silicone Co. for the gifts of silanes.

References

1) W. G. Overend, "The Carbohydrates, Chemistry and Biochemistry," ed by W. Pigman and D. Horton, Academic Press (1972), Vol. IA, Chap. 9.
2) F. Micheel and A. Böckmann, *Makromol. Chem.*, **51**, 97 (1962).
3) A. Klemer and B. Kraska, *Carbohydr. Res.*, **32**, 400 (1974).
4) F. Micheel and E.-D. Pick, *Tetrahedron Lett.*, **1969**, 1695.
5) V. Bažant, V. Chevlovski, and J. Rathousky, "Organosilicon Compounds," Academic Press (1965), Chaps. 3 and 4.
6) W. Noll, "Chemistry and Technology of Silicones," Academic Press (1968), Chaps. 4, 5, and 6.
7) B. Helferich and J. Hausen, *Ber.*, **57**, 795 (1924).
8) S. Koto, N. Morishima, and S. Zen, *Chem. Lett.*, **1976**, 61.
9) S. Koto, Y. Takebe, and S. Zen, *Bull. Chem. Soc. Jpn.*, **45**, 291(1972); S. Koto, T. Uchida, and S. Zen, *ibid.*, **46**, 2520 (1973).
10) M. Schmidt and H. Schmidbaur, *Angew. Chem.*, **70**, 469 (1958).
11) M. Čerńy, *Collect. Czech. Chem. Commun.*, **41**, 110 (1976).
12) S. A. Barker and M. R. Harnden, *J. Chem. Soc., C*, **1968**, 644.
13) The earlier mentioned IV and V in Ref. 8 were mixtures composed of silanes such as **4**, **5**, and related oligosiloxanes.
14) L. J. Sargent, J. G. Buchanan, and J. Baddiley, *J. Chem. Soc.*, **1962**, 2184; F. E. Hardy, J. G. Buchanan, and J. Baddiley, *ibid.*, **1963**, 3361.
15) B. Csákvári, L. Fábry, P. Gömöry, and K. Ujszászy, *Acta Chim. Acad. Sci. Hung.*, **90**, 213 (1976).
16) J. Pola, M. Jakoukove, and V. Chevlovsky, *Collect. Czech. Chem. Commun.*, **39**, 1169 (1974).
17) S. Koto, N. Morishima, and S. Zen, unpublished results.
18) S. Koto, N. Morishima, Y. Hamada, T. Sato, Y. Miyata, and S. Zen, The 8th International Symposium on Carbohydrate Chemistry, Kyoto, 1976, 1D-4.
19) S. Koto, N. Morishima, Y. Miyata, and S. Zen, *Bull. Chem. Soc. Jpn.*, **49**, 2639 (1976).
20) P. W. Austin, F. E. Hardy, J. G. Buchanan, and J. Baddiley, *J. Chem. Soc.*, **1964**, 2128.
21) F. J. Kronzer and C. Schuerch, *Carbohydr. Res.*, **34**, 71 (1974).
22) H. Schmidbaur, L. Sechser, and M. Schmidt, *J. Organomet. Chem.*, **15**, 77 (1968).
23) Y. Nakaido and T. Takiguchi, *J. Org. Chem.*, **26**, 4144 (1961).
24) Compagnie Francaise, Thomson-Houston, Fr. Patent 1440923; *Chem. Abstr.* **66**, 19074 m (1967).
25) E. Pacsu, *J. Am. Chem. Soc.*, **52**, 2568 (1930).
26) G. J. F. Chittenden, *Carbohydr. Res.*, **9**, 323 (1969).
27) S. Koto, T. Tsumura, Y. Kato, and S. Umezawa, *Bull. Chem. Soc. Jpn.*, **41**, 2765 (1968).
28) P. N. Preston, L. H. Sutcliffe, and B. Taylor, *Spectrochim. Acta, Part A*, **28**, 197 (1972).
29) C. A. Burkhard, *J. Am. Chem. Soc.*, **67**, 2173 (1945).
30) R. E. Richards and H. W. Thompson, *J. Chem. Soc.*, **1949**, 124.
31) Estimations of structure of oligosiloxanes and composition of mixtures were based on NMR spectra measured in CCl_4, using signals of anomeric H's and aromatic H's β to Si, with reference to the spectra of **4** and **5**.

Photolysis of Organic Azides. IV.[1] Formation of *o*-Xylylene Derivatives from 2,3-Diazidonaphthalenes. Direct Observation by Low-temperature and Flash Photolysis

Akira YABE

National Chemical Laboratory for Industry, Hiratsuka Branch, Nishiyawata 1-3-4, Hiratsuka, Kanagawa 254

(Received June 3, 1978)

The photolysis of 2,3-diazidonaphthalene (**3a**) in a rigid matrix at 77 K gave the product having absorption bands in the 400—500 nm region, which has been assigned as α,ω-dicyano-*o*-xylylene (**2a**) by use of another precursor 1,2-dicyano-1,2-dihydrobenzocyclobutene. **2a** has been also observed by the flash photolysis of **3a** in fluid solution at room temperature, and the lifetime in methanol at 20 °C was 62 s. The dominating factor in the lability of **2a** was the rigidity of the medium rather than the temperature. The reaction mechanism for the formation of **2a** from **3a** has been proposed as a monophotonic process involving the attack of the nitreno group on the azido group at the *ortho* position. Similarly, direct observations of α,ω-dimethoxy- and α,ω-diacetoxy-α,ω-dicyano-*o*-xylylenes have been given from 1,4-dimethoxy- and 1,4-diacetoxy-2,3-diazidonaphthalenes respectively.

o-Xylylene (*o*-quinodimethane, **1**) and the wide variety of derivatives have evoked theoretical and experimental interest.[2–13] The reactive species have been proposed as intermediates in a number of re-

1

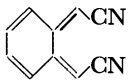

2

actions. In the thermal decomposition of 2,3-diazidonaphthalenes (**3**) to give 1,2-dicyano-1,2-dihydrobenzocyclobutenes (**4**), the α,ω-dicyano-*o*-xylylenes (**2**) have been considered intermediates. Flash pyrolysis in the vapor phase of **3a** has been reported to yield *trans*-1,2-dicyano-1,2-dihydrobenzocyclobutene in 55% yield,[14] and the thermolysis of **3b** in refluxing *o*-dichlorobenzene has given the *trans*- and *cis*-1,2-diacetoxy-1,2-dicyano-1,2-dihydrobenzocyclobutenes (23% and less than 3% yields, respectively),[15] possibly through the intermediate **2**.

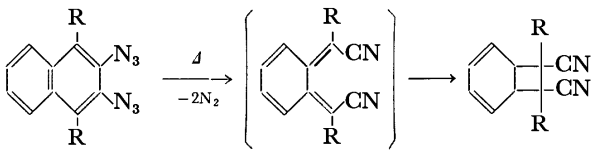

3 **2** **4**

a: R=H
b: R=OCOCH$_3$
c: R=OCH$_3$

The α,ω-dicyano-*o*-xylylene (**2a**), which is a simple derivative of **1**, would itself be of interest since it has not been observed directly and there is the possibility that the dicyano substituents might stabilize the *o*-xylylene system sufficiently to allow isolation. In the course of the work on the low-temperature photochemistry of aromatic diazido compounds, the formation of **2a** was observed in the photolysis of **3a** in rigid matrices at low temperatures. The present paper reports the direct observation of **2a** by matrix isolation and flash photolysis, and the mechanism of the low-temperature photochemical reaction of **3a**, together with two derivatives 1,4-diacetoxy-2,3-diazidonaphthalene (**3b**) and 2,3-diazido-1,4-dimethoxynaphthalene (**3c**).

Results and Discussion

Low-temperature Photolysis. In the thermal reactions of **3** mentioned above, the evidence for dicyano-*o*-xylylene had been indirect, based on speculation from the final products. No study on the photolysis of 2,3-diazidonaphthalenes has been reported. The photolysis of **3a** in methanol or hexane at room temperature did not yield any trace of the expected 1,2-dicyano-1,2-dihydrobenzocyclobutenes, as distinct from the thermolysis. In view of the reactivity of *o*-xylylenes, matrix isolation and flash photolysis techniques appeared appropriate for the direct observation of **2**.

A rigid glassy solution of **3a** in EPA was irradiated at 77 K with a high-pressure mercury lamp with a Toshiba UV-D2 filter (transmission in the 300—400 nm region), and the low-temperature photochemical reaction was followed by absorption spectroscopy. With an increase in irradiation, new absorption bands in the 400—500 nm region were observed as shown in Fig. 1. The melting of the glassy solution containing the photoproduct having the new absorption bands to room temperature resulted in the disappearance of the absorption bands. The photoproduct showed strong fluorescence (λ_{max} 485 and 506 nm) similar to the parent *o*-xylylene and the spectral shape was independent of the excitation wavelength. The excitation spectrum followed the shape of the absorption band and was independent of the monitoring wavelength. Therefore, it has been suggested that all of the absorption curve, at least below 35000 cm^{-1}, belongs to one photoproduct.

On the prolonged irradiation of **3a**, the corresponding 1,2-dihydrobenzocyclobutene derivatives were not obtained, while Flynn and Michl[2] reported that upon strong irradiation the 373 nm band of the photoproduct **1** was replaced by the UV absorption spectrum of 1,2-dihydrobenzocyclobutene. After melting of the glassy solution containing the 400—500 nm bands, no azido group was detected among the reaction products while cyano groups were detected by IR spectroscopy.

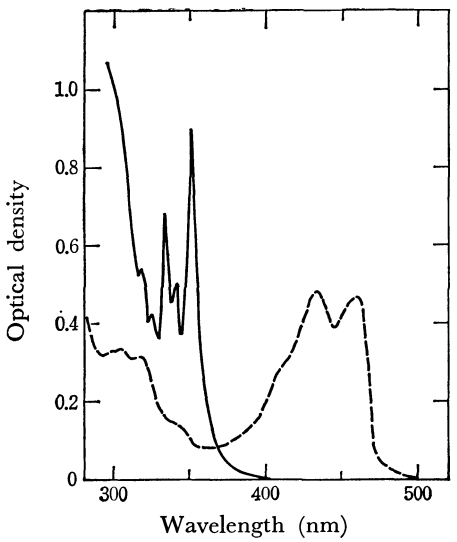

Fig. 1. Absorption spectrum of **3a** in EPA at 77 K before (——) and after (– – –) irradiation.

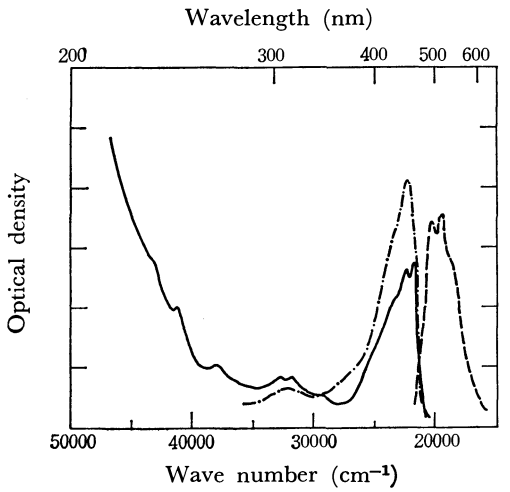

Fig. 2. Absorption (——), excitation (—·—), and emission (– – –) spectra of **2a** in EPA at 77 K. Excitation and emission spectra are not corrected for instrument response (arbitary scale).

The identity of **2a** for the transient absorption was shown by the photolysis of another precursor. The irradiation of *trans*-1,2-dicyano-1,2-dihydrobenzocyclobutene (**5**) with a low-pressure mercury lamp (253.7 nm) in EPA at 77 K gave a spectrum similar to that obtained in the low-temperature photolysis of **3a**.[16] Moreover, the behavior on warming to room temperature and the fluorescence spectrum were consistent with that observed for **3a**. Thus, the transient absorption has been assigned to the expected **2a**.

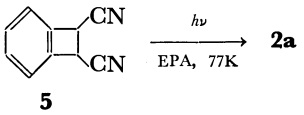

5

The conversion of **5** to **2a** was considerable compared with that of 1,2-dihydrobenzocyclobutene to **1**.[17] Upon irradiation of a rigid solution of **5** (10^{-4} M) in EPA at 77 K (15 W low-pressure mercury lamp), the conversion to **2a** was virtually complete after 1 h.

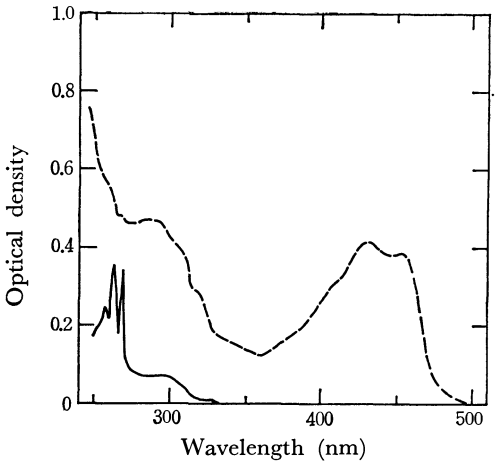

Fig. 3. Absorption spectra of **5** in EPA at 77 K before (——) and after (– – –) irradiation.

These results which have been attributed to the dicyano substituents are consistent with the fact that **2a** was not converted to **5** in the matrices upon continued irradiation, as mentioned previously.

The spectral shifts compared with **1** can be explained in terms of the substitution of the two cyano groups conjugated with the *o*-xylylene system. The absorption of **2a** is shifted by about 50 nm to a wavelength longer than that of the parent *o*-xylylene, which absorbs at 313—417 nm.[2] In the case of *cis,cis*-1,4-dicyano-1,3-butadiene (λ_{max} 258, 268 nm) and butadiene (λ_{max} 217 nm), a similar shift was observed.

The assignment for **2a** is further supported by the following results. Previously the formation of *cis,cis*-1,4-dicyano-1,3-butadiene (**7**) by the photolysis of 1,2-diazidobenzene (**6**) as well as the results of thermal reactions has been established,[18,19] the photolysis of

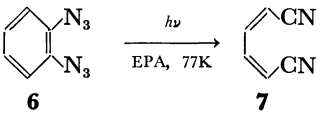

6 **7**

6 in a rigid matrix at 77 K being quantitative. In a low-temperature matrix **7** was not converted to cyclobutenes on prolonged irradiation, whereas the cyclization of **7** proceeded readily in fluid solution at room temperature.

In the case of the two derivatives **3b** and **3c**, the appearance of photoproducts could also be observed by the absorption spectra in the 400—500 nm region. Furthermore, the photoproduct from **3c** exhibited strong fluorescence in the 500—600 nm region (λ_{max} 540 nm), such as **2a**. In the low-temperature photolysis of **3b** in a rigid matrix the photolysis differed from the others. After the expected **2b** was generated as a primary photoproduct, some secondary reactions proceeded at considerable rate as shown in Fig. 4. Among the secondary photoproducts the corresponding 1,2-dihydrobenzocyclobutene derivatives (**4b**) were not detected. Details of the secondary reactions will be reported in a separate paper.

Although the stereochemical constitutions of **2** have not been unambigously established, three stereoisomers **2**(*Z,Z*), **2**(*E,E*), and **2**(*Z,E*) of α,ω-dicyano-*o*-xylylenes

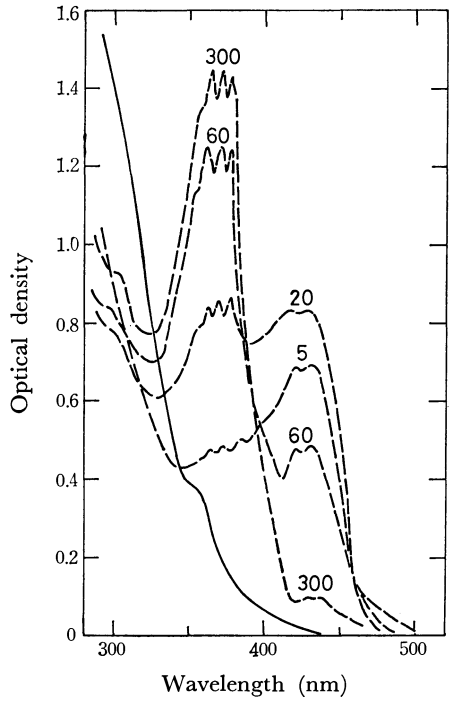

Fig. 4. Absorption spectra of **3b** in EPA at 77 K before (——) and after (– – –) irradiation. Numbers refer to irradiation time in second.

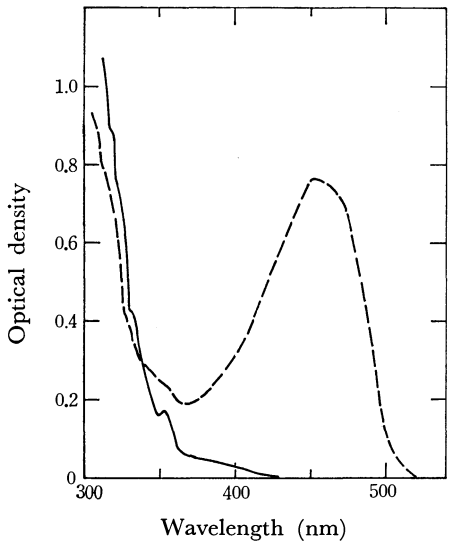

Fig. 5. Absorption spectra of **3c** in 3MP–IP (1 : 4) at 77 K before (——) and after (– – –) irradiation.

need consideration. One would predict that the

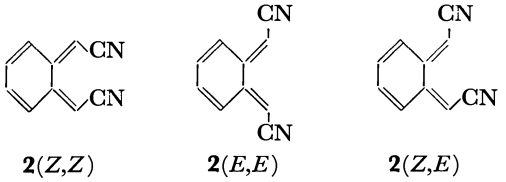

2(*Z*,*Z*) **2**(*E*,*E*) **2**(*Z*,*E*)

isomer generated in the photolysis of **3a** was exclusively **2**(*Z*,*Z*), from an analogy to the photolysis of **6** where the photoproduct **7** was assigned as the *cis*,*cis*-isomer by comparison with an authentic sample. The isomer of **2a** generated in the photolysis of **5** is presumed to be **2**(*Z*,*E*) from a consideration of the orbital symmetry. The whole spectra of **2a** generated from **3a** and **5** are consistent with each other

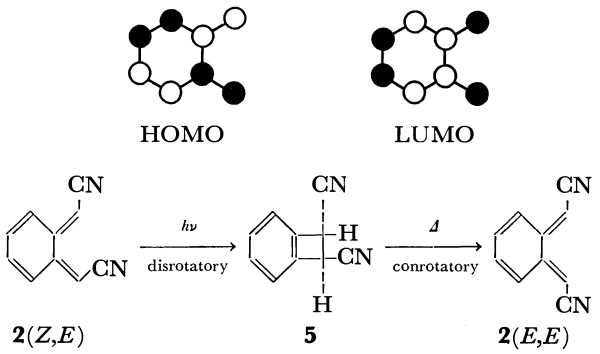

2(*Z*,*E*) **5** **2**(*E*,*E*)

as shown in Figs. 1 and 3. However, there is a slight difference observed in the longest absorption maxima, *i.e.*, the isomers generated from **3a** and **5** have absorption bands at 458 and 454 nm respectively (Table 1). This spectral shift could be explained in terms of the different configurations, as reported in the case of α,ω-diphenyl-*o*-xylylenes by Quinkert and coworkers.[9e]

Table 1. Absorption maxima of α,ω-dicyano-*o*-xylylenes by photolysis at 77 K

Reactant	Solvent	Absorption maxima (nm) (>400 nm)
3a	EPA (5:5:2)	432, 458
	3MP–IP (1:4)	427 (broad)
5	EPA (5:5:2)	432, 454
	3MP–IP (1:4)	427 (broad)
3b	EPA (5:5:2)	425, 448
	3MP–IP (1:4)	425
3c	EPA (5:5:2)	452
	3MP–IP (1:4)	450

Temperature and Rigidity Dependence of the Stability of **2**. The dicyano-*o*-xylylenes formed in rigid matrices at 77 K are indefinitely stable under these conditions but as yet have been isolated at room temperature. In order to study the stability and the conditions for the isolation of **2a**, the photolyses of **3** were conducted in media of different viscosities at various temperatures. In the photolysis at 77 K the matrices dependence was not observed in such glassy solvents as ether–isopentane–ethanol (EPA, 5 : 5 : 2), isopentane–3-methylpentane (IP–3MP, 4 : 1, 3 : 1, 1 : 1, 1 : 3, 1 : 4), 3-methylpentane (3MP), or methylcyclohexane–isopentane (MCH–IP, 1 : 3) matrix, which showed a viscosity ranging from 10^2 to 10^{10} Pa s.[20] Although the shape of the absorption bands in the 400—500 nm region was slightly different, the rates of formation of **2a** were virtually similar.

Figure 6 shows the absorption spectra of **3a** irradiated in 3MP–IP (1 : 4) (8 min, 500 W high-pressure mercury lamp, Toshiba UV-D2 filter, several temperatures). At 100 K, although the spectral shape was considerably different from that generated at 77 K, the concentration of **2a** was deduced to be 60—70% compared with that generated at 77 K. At 170 K, **2a** was no longer detect-

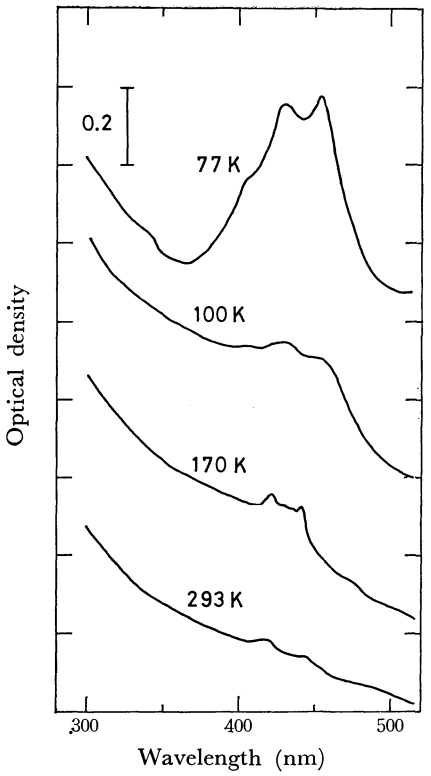

Fig. 6. Absorption spectra of the photoproducts of **3a** in 3MP–IP (1 : 4) by irradiation at several temperatures.

able by fluorescence spectroscopy and therefore the small peaks of the absorption spectra at 170 and 293 K in the 400—500 nm region are not ascribable to **2a**.

The photolysis of **3a** in a glycerol matrix at 180 K (viscosity; 10^{12} Pa s[20]) gave **2a** quantitatively and it was indefinitely stable in this medium. Figure 7 shows the libility of **2a** plotted against the rise in temperature. The change in the absorbance of **2a**, formed by the photolysis in rigid matrices (3MP and MCH–IP) at 77 K, was monitored at 432 nm with an increase in temperature allowing the matrices to grow warmer. The difference in lability of **2a** on 3MP and MCH–IP (1 : 3) matrices may be explained in terms of the rigidity of the medium, since the former had a higher viscosity than the latter (3MP : 9.4×10^{10} Pa s at 77 K, 3.0×10^{9} Pa s at 87 K; MCH–IP : 1×10^{2} Pa s at 89.5 K).[20] The appreciable decrease in absorbance began at 100 K in MCH–IP and at 120 K in 3MP, and the viscosities at these temperatures were estimated to be about 1 Pa s in both media from the literature.[21] Thus, it has been concluded that the rigidity of the medium is a dominating factor for the isolation of **2a**.

Flash Photolysis. Flash photolysis showed the presence of **2** in fluid solution at room temperature. The absorption spectra of **3a** (4×10^{-5} M) in methanol after flash photolysis at 293 K are shown in Fig. 8. These spectra are consistent with those obtained by low-temperature photolysis although the fine structures have disappeared. The lifetimes of **2a** and **2c** in methanol at 293 K were 62 s (monitored at 432 nm) and 33 s (monitored at 455 nm) respectively. The final photoproducts by room-temperature photolysis

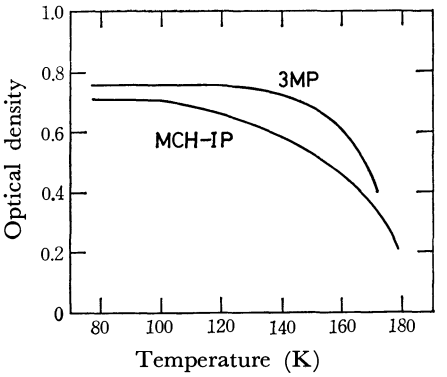

Fig. 7. Change in the absorbance at 432 nm of **2a** with temperature. Temperature-rise time : *ca.* 5 min (77—110 K) and *ca.* 4 min (110—180 K).

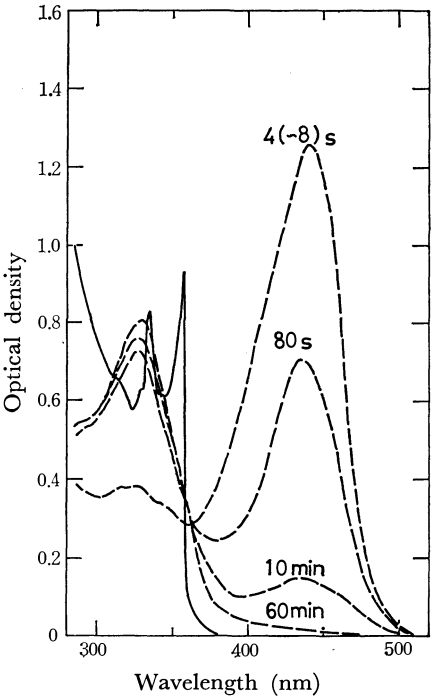

Fig. 8. Absorption spectra of **3a** in methanol at 20 °C before (——) and after (——) flash photolysis.

were not 1,2-dicyano-1,2-dihydrobenzocyclobutenes as reported above, and the decay of **2a** did not exhibit first-order kinetics. A detailed description of the kinetic study of **2** will be presented in a separate paper together with the reactivity of **2**. The decay of **2b** after the flash photolysis of **3b** was complicated, and the monitoring of the transient (**2b**) was difficult since the absorption bands of the secondary photoproducts interfered with those of **2b**.

Reaction Mechanism. Although the photochemistry of azido compounds has been the subject of considerable interest, little is known about the photochemical reactions of vicinal diazido compounds. In the photolysis of **3** which results in the formation of **2**, it is of interest to examine whether the two neighboring azido groups participate with each other, whether the two azido groups are decomposed by a single quantum or the photolysis proceeds in two separate steps, and

whether the mononitrene and/or the dinitrene are included as intermediates. The low-temperature reaction mechanism of **3** has been investigated by a comparison with the preliminary results of 1,2-diazidobenzene.[18]

The photolysis of **6** in a rigid matrix at 77 K yielded 1,4-dicyano-1,3-butadiene (**7**) in one step, *i.e.* no intermediate was observed in the process from **6** to **7** by the absorption spectra. The spectral change by irradiation at low temperature was quite similar to that in the fluid solution at room temperature. Moreover, the dependence of the formation rate of **7** on the incident-light intensity showed a monophotonic process. These results exclude the following reaction mechanism which is a biphotonic process involving the stepwise loss of nitrogen. This is distinct from the mechanism which is a biphotonic process involving the mononitrene and the dinitrene as in the case of 1,4-diazidobenzene.[22,23]

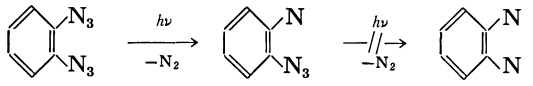

The possibility that the two azido groups were simultaneously decomposed by a single photon was excluded by comparison with the results of 1,4-diazidobenzene[22,23] and 2,2′-diazidobiphenyls.[24] Only one of the two azido groups was decomposed by a single photon. It is well known that nitreno groups located *ortho* to groups with α,β-unsaturation undergo cyclization to give five-membered hetero cyclic rings, as observed in the decompositions of 2-azidonitrobenzene[25] and *o,o′*-diazidoazobenzene.[26,27] Thus, the intermediate such as **9** appears to be the result of nitreno groups on azido groups. The intermediate **9** would be readily converted to **7** *via* **10** at room

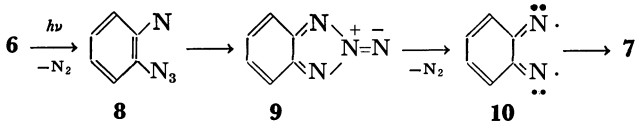

8 **9** **10**

temperature or 77 K by the consecutive homolytic cleavage of the nitrogen–nitrogen bonds and the carbon–carbon bond in a nonphotonic process, since the elimination of nitrogen from **9** is exothermic.[28]

An attempt has been made to establish the spin states of the intermediates. In the room-temperature photolysis of methanol solutions of **6** (2×10^{-4} M) involving 1,3-pentadiene (2×10^{-4}—10^{-3} M) or oxygen saturated by bubbling as a triplet quencher, the rate of formation of **7** was not affected. Hence, it may be considered that the azidonitrene **8** is produced in the singlet state from the excited singlet **6**, as reported in the direct photolysis of phenyl azide.[29,30] However, it is still uncertain that the participation of triplet states is excluded, since each process in the formation of **7** from **6** might be much faster than the energy transfer, and since the photochemical reaction from **6** to **7** occurs by triplet sensitization. Moreover, it is possible that the actual precursor of **9** is the triplet **8**, although it may be transferred from the singlet **8** by intersystem crossing. The multiplicity of the diradical (**10**) which was produced by nitrogen elimination would

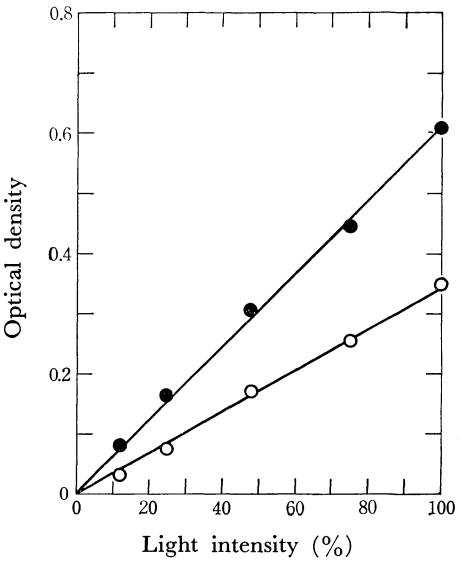

Fig. 9. Dependence of the formation rates of **2a** (○) and **2c** (●) on the light intensity by the photolyses of **3a** and **3c** in 3MP–IP (1 : 4), respectively. The yields of **2a** and **2c** correspond the optical densities at 432 and 452 nm respectively.

be the singlet state, since the energy required to break the carbon–carbon bond of **10** would be lost if the triplet nitrogen, which is 590 kJ/mol above the ground state, were produced by the decomposition of **9**. That is to say, since the elimination of nitrogen in the singlet ground state is an energetically favored process, **10** must be produced in the singlet state from the spin conservation rule.

The preceding mechanism for 1,2-diazidobenzene may be adapted to the photolysis of **3** in rigid matrices at low-temperature and in fluid solutions at room temperature. In the photolysis of **3** in a rigid matrix at 77 K, no intermediate was observed by absorption spectroscopy. The dependence of the formation rates of **2a** and **2c** on the light intensity is shown in Fig. 9 and as good linearity was obtained in the both cases, it was concluded that the formation of **2** from **3** was a monophotonic process similar to that for **7** from **6**. In an attempt to establish the spin state, the flash photolysis of the solutions of **3** involving 1,3-pentadiene or oxygen were studied. The absorbance belonging to the formed **2**, that is, the yield of **2**, was not affected. Although the spin states of the intermediates were not established by this quenching experiment alone, the pathway from **3** to **2** will be given below.

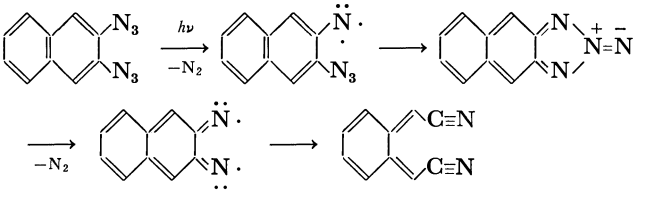

Experimental

IR and UV absorption spectra were recorded on JASCO IR-S and Shimadzu UV-300 spectrophotometers respectively.

Fluorescence and excitation spectra were recorded on a Hitachi MPF-1 spectrophotometer. In the above measurements, optical densities were uncorrected for volume contraction accompanied by the variation in temperature. NMR spectra were recorded on a Hitachi R-24A spectrometer at 60 MHz using TMS as an internal standard. Mass spectra were recorded on a Shimadzu GCMS-9000 spectrometer. The microanalyses were performed at the Institute of Physical and Chemical Research.

Materials. *2,3-Diazidonaphthalene (**3a**)*,[14] *1,4-diacetoxy-2,3-diazidonaphthalene (**3b**)*,[15] *1,2-diazidobenzene (**6**)*,[19b] and trans-*1,2-dicyano-1,2-dihydrobenzocyclobutene (**5**)*[14] were prepared according to the literature. The crude materials were purified by column chromatography on silica gel and recrystallized.

*2,3-Diazido-1,4-dimethoxynaphthalene (**3c**)* : **3c** was prepared from 2,3-diazido-1,4-naphthoquinone[15] through 2,3-diazido-1,4-naphthalenediol, which was not isolated. A solution of sodium dithionite (12 g; 0.069 mol) in water (20 ml) was added to a well-stirred suspension of the quinone (8 g; 0.033 mol) in ether (200 ml) and methanol (50 ml) at room temperature under an atmosphere of nitrogen. The mixture was vigorously stirred until the color stopped fading after about 30 min. The organic layer containing the 1,4-naphthalenediol was separated and the aqueous layer washed quickly several times with ether. The combined organic layers were then cooled in an ice bath and the cooled solution added dropwise to a cooled ether solution containing diazomethane (about 3 g) prepared from *p*-tolylsulfonylmethylnitrosamide (21.5 g). The reaction mixture was stirred for 1 h in an ice bath and for 1 h at ambient temperature. The solvent was evaporated under vacuum to afford purple crystallites, which were purified by column chromatography on silica gel. Elution with petroleum ether–ether (9 : 1) gave 2.4 g (26.9%) of **3c**: mp 54—55 °C; UV_{max} (CH_3OH) 300 sh, 260 nm (ε 49000); IR(KBr) 2130 cm^{-1} (N_3); NMR ($CDCl_3$) δ=8.2—7.3 (m, 4H, aromatic), 3.95 (s, 6H, OCH_3); MS, *m/e* 270 (M^+), 242 ($M-N_2$), 220, 214($M-2N_2$), 199. Found : C, 53.79; H, 3.75; N, 30.03%. Calcd for $C_{12}H_{10}N_6O_2$: C, 53.33; H, 3.73; N, 31.10%.

The solvents used in the spectroscopic study and in the low-temperature photolysis were dried over sodium wire or a molecular sieve and finally passed through a column of alumina.

Irradiation at Low-temperatures. The light sources were an Ushio USH-500D 500 W high-pressure mercury lamp equipped with a Nikon G-250 monochromator and a Toshiba GL-15 15 W low-pressure mercury lamp. The quartz cells of 10 mm path length were immersed in a quartz Dewar vessel equipped with optical windows containing liquid nitrogen and used for absorption and emission spectroscopy at 77 K. Instead of the quartz Dewar vessel, an Oxford Instrument DN-704 liquid nitrogen cryostat was used for spectroscopy at variable low-temperatures. It was equipped with an Oxford Instrument DTC-2 digital temperature controller, and temperatures in the range from 77 K to room temperature could be controlled and measured by a cryogenic linear temperature sensor and carbon resistor.

Flash Photolysis. All flash measurements were made using cylindrical, jacketed quartz cells of 10 cm path length and 25 ml capacity. The flash photolysis system consisted of an Applied Photophysics K-10 flash equipment, a M-300 monochromator, and a Textronix T-912 storage oscilloscope. The two 12 cm length flash lamps fitted in the K-10 equipment are rated at a maximum energy of 1000 J, corresponding to a maximum charged voltage of 22.4 kV. In these experiments, the lamps were discharged at 20 kV and had a half-life of 10 μs. The absorbance and the decay of the transients were followed quantitatively by monitoring the transmittance of the light with the oscilloscope through the monochromator from a tungsten iodine lamp (Osram A 1/125, 12 V/100 W). The absorption spectra of the transient **2a** generated by the flash photolysis of **3a** were recorded on the Shimadzu UV-300 spectrophotometer, after the cell was immediately transferred from the flash cavity to the sample bench of the spectrophotometer (Fig. 8).

References

1) Part III : A. Yabe and K. Honda, *Chem. Lett.*, **1976**, 827.

2) a) C. R. Flynn and J. Michl, *J. Am. Chem. Soc.*, **95**, 5802 (1973); b) C. R. Flynn and J. Michl, *ibid.*, **96**, 3280 (1974), and references cited therein.

3) K. L. Tseng and J. Michl, *J. Am. Chem. Soc.*, **99**, 4840 (1977).

4) N. C. Baird, *J. Am. Chem. Soc.*, **94**, 4941 (1972).

5) E. Migirdicyan and J. Baudet, *J. Am. Chem. Soc.*, **97**, 7400 (1975).

6) J. J. McCullough and A. J. Yarwood, *J. Chem. Soc., Chem. Commun.*, **1975**, 485.

7) R. D. Miller, J. Kolc, and J. Michl, *J. Am. Chem. Soc.*, **98**, 8510 (1976).

8) W. R. Dolbier, Jr., K. Matsui, J. Michl, and D. V. Horák, *J. Am. Chem. Soc.*, **99**, 3876 (1977).

9) a) G. Quinkert, K. Opitz, W.-W. Wiersdorff, and J. Weinlich, *Tetrahedron Lett.*, **1963**, 1863; b) G. Quinkert, K. Opitz, W.-W. Wiersdorff, and M. Finke, *ibid.*, **1965**, 3009; c) G. Quinkert, W.-W. Wiersdorff, M. Finke, K. Opitz, and F.-G. von der Haar, *Chem. Ber.*, **101**, 2302 (1968); d) G. Quinkert, M. Finke, J. Palmowski, and W.-W. Wiersdorff, *Mol. Photochem.*, **1**, 433 (1969); e) K. H. Grellmann, J. Palmowski, and G. Quinkert, *Angew. Chem.*, **83**, 209 (1971); f) G. Quinkert, J. Palmowski, H.-P. Lorenz, W.-W. Wiersdorff, and M. Finke, *ibid.*, **83**, 210 (1971).

10) a) M. P. Cava and D. R. Napier, *J. Am. Chem. Soc.*, **79**, 1701 (1957); b) M. P. Cava and A. A. Deana, *ibid.*, **81**, 4266 (1959); c) M. P. Cava, A. A. Deana, and K. Muth, *ibid.*, **81**, 6458 (1958); d) M. P. Cava, M. J. Mitchell, and A. A. Deana, *J. Org. Chem.*, **25**, 1481 (1960).

11) L. A. Errede, *J. Am. Chem. Soc.*, **83**, 949 (1961).

12) J. R. du Manoir, J. F. King, and R. R. Fraser, *J. Chem. Soc., Chem. Commun.*, **1972**, 541.

13) a) K. K. de Fonseka, J. J. McCullough, and A. J. Yarwood, *J. Chem. Soc., Chem. Commun.*, **1977**, 721; b) K. K. de Fonseka, C. Manning, J. J. McCullough, and A. J. Yarwood, *J. Am. Chem. Soc.*, **99**, 8257 (1977).

14) M. E. Peek, C. W. Rees, and R. C. Storr, *J. Chem. Soc., Chem. Commun.*, **1974**, 1260.

15) D. S. Pearce, M.-S. Lee, and W. Moore, *J. Org. Chem.*, **39**, 1362 (1974).

16) *cis*-1,2-Dicyano-1,2-dihydrobenzocyclobutene was not available by literature method (Ref. 14), although it is an important precursor for the elucidation of the configurational isomers of **2a**.

17) Flynn and Michl (Ref. 2) reported that 2.9×10^{-2} M 1,2-dihydrobenzocyclobutene solution in EPA was converted to **1** in 2% yield after irradiation for 3 h. Quinkert and coworkers (Ref. 9d) reported that the matrix photolysis of 1,2-dihydrobenzocyclobutene proceeded with no reaction.

18) Presented in part at the 32nd National Meeting of the Chemical Society of Japan, Tokyo, April 1975, 3A16.

19) a) J. H. Hall, *J. Am. Chem. Soc.*, **87**, 1147 (1965); b) J. H. Hall and E. Patterson, *ibid.*, **89**, 5856, 1967.

20) W. G. Herkstroeten, "Creation and Detection of

the Excited State," ed by A. A. Lamola, Marcel Dekker, New York, N. Y. (1971), p. 43.
21) H. Geenspan and E. Fischer, *J. Phys. Chem.*, **69**, 2466 (1965).
22) a) A. Reiser, H. M. Wagner, R. Marley, and G. Bowes, *Trans. Faraday Soc.*, **63**, 2403 (1967); b) A. Reiser and R. Marley, *ibid.*, **64**, 1806 (1968).
23) a) B. Singh and J. S. Brinen, *J. Am. Chem. Soc.*, **93**, 540 (1971); b) J. S. Brinen and B. Singh, *ibid.*, **93**, 6623 (1971).
24) a) A. Yabe and K. Honda, *Tetrahedron Lett.*, **1975**, 1079; b) A. Yabe and K. Honda, *Bull. Chem. Soc. Jpn.*, **49**, 2495 (1976).
25) T. F. Fagley, J. R. Sutter, and R. L. Oglukian, *J. Am. Chem. Soc.*, **78**, 5567 (1956).
26) R. A. Carboni and J. E. Castle, *J. Am. Chem. Soc.*, **84**, 2453 (1962).
27) J. H. Hall, J. G. Stephanie, and D. K. Nordstrom, *J. Org. Chem.*, **33**, 2951 (1968).
28) C. D. Campbell and C. W. Rees, *J. Chem. Soc., C*, **1969**, 742.
29) A. Reiser and L. J. Leyshon, *J. Am. Chem. Soc.*, **93**, 4051 (1971).
30) M. Sumitani, S. Nagakura, and K. Yoshihara, *Bull. Chem. Soc. Jpn.*, **49**, 2995 (1976).

Syntheses of *N*-Acyl Dipeptide Derivatives by Metalloproteinases†

Yoshikazu Isowa and Tetsuya Ichikawa*
Sagami Chemical Research Center, Sagamihara, Kanagawa 229
(Received May 10, 1978)

X–Dipeptides (X=Z, Z(OMe), or Z(3Me)) have been catalytically synthesized by several microbial metalloproteinases. Among the enzymes used, Thermolysin showed the most remarkable ability in the coupling reactions of the esters or the amides of phenylalanine, leucine, isoleucine, and valine (and methionine in the case of the amide) with various X–amino acids. This method has been applied to the syntheses of ZPhePheOMe and ZPheIleOMe on a practical scale. Ammonium sulfate and sodium chloride had a marked effect on the condensed products, increasing the yield.

Since Bergmann and Fraenkel-Conrat[1] first demonstrated the papain catalyzed amide-bond formation between an acylamino acid and an amino acid anilide, the enzymatic syntheses of peptides have received much attention. However, only a few papers have appeared in which the substrates had the proper protecting groups for the elongation of the peptide chains, for example Z, Z(OMe), BOC, the methyl or ethyl ester, the non-sustituted amide, *etc.*[2,3] There appears to be two reasons for this. Firstly, the most investigations have used papain (thiol proteinase) or α-chymotrypsin (serineproteinase), both of which catalyze the hydrolysis of carboxylic esters comprising the primary alcohol or the non-substituted amide. Consequently the peptides containing those groups are not easily obtainable in high yields except the peptides which show extremely low solubilities in buffer solution.[2] When those peptides are once formed, they are barely subjected to hydrolysis of the C-terminal protecting groups. Secondly, many *N*-acylamino acid derivatives (acyl= Z, Z(OMe), BOC, *etc.*) are almost insoluble in water and troublesome on operating the enzymatic reaction. Recently, it has been reported that the peptides whose N- and C-terminal groups were protected by such groups were readily obtained in certain cases by several enzymes.[4]

In the course of the current study to extend the enzymatic syntheses of peptides, it has been found that several microbial metalloproteinases catalyze the formation of X–dipeptide methyl esters or amides (X=Z, Z(OMe), or Z(3Me)). The C-terminal groups in these dipeptides are not hydrolyzed by metalloproteinases, so it is anticipated that the syntheses of these peptides would be smoother using metalloproteinases than by thiol- or serineproteinases.

For inhibiting the action of serineproteinase contained in the crude metalloproteinases, potato inhibitor was used as reported previously.[4c]

Materials and Methods

Thin layer chromatography was performed on precoated TLC plates Silica Gel F_{254} (Merck) using the following solvent systems : AcOEt–$CHCl_3$ (10 : 1), AcOEt, *s*-BuOH–3% aqueous ammonia (8 : 3) (see Ref. 4c for other analytical procedures). Protease activity was assayed by the method of Tsuru *et al.*[5]

Potato Inhibitor. See Ref. 4c.

Proteinases. See Ref. 4c for Prolisin A (*Bacillus subtilis var. amyloliquefacience*), Thermolysin (*Bacillus thermoproteoliticus*), Thermoase (*Bacillus thermoproteoliticus*), and Tacynase N (*Streptomyces caespitosus*). Dispase I (*Bacillus polymyxa*, Godo Shusei Co., Tokyo, Japan, 4.93×10^6 PU/g) had little esterase action and was used without further purification. The partially purified metalloproteinase of *Bacillus subtilis* was obtained by treating Prolisin A with DEAE-Sephadex A-50[6] and freeze-drying. The protease activity was 5.3×10^6 PU/g and the esterase action was almost completely inhibited by the potato inhibitor in one tenth the weight of enzyme. Commercial Thermoase was purified by dissolving it in 0.01 M $Ca(OAc)_2$ aqueous solution, removing the insoluble materials and precipitating from acetone. The protease activity was 1.0×10^7 PU/g and the esterase action was suppressed almost completely by the potato inhibitor in one tenth the weight of enzyme.

Reagents. Z– or Z(OMe)–amino acids, amino acid methyl ester hydrohalogenides were all prepared by the ordinary methods. Z(3Me)–His(Bzl)–OH was prepared by the method previously reported.[4b]

Enzymatic Syntheses of Peptides (General Procedures). An enzyme and potato inhibitor, if necessary, were dissolved in a buffer solution and the insoluble materials filtered off. In a mixture of this solution, two appropriate substrates and 4 M NaOH aqueous solution were incubated and the product collected on a suction filter, washed thoroughly in succession with 1 M aqueous ammonia, 1 M HCl, and water, and dried *in vacuo* over P_2O_5 at room temperature. The product was recrystallized, if necessary, from organic solvents and weighed.

Results

Enzymatic reactions between X–AA_1–OH (X=Z, Z(OMe), or Z(3Me); AA_1=Ala, Val, Leu, Ile, Phe, Glu(OBzl), Asp(OBzl), Gln, Asn, Lys(Z), His(Bzl), Met, Cys(Bzl), Tyr, Trp, and Pro) and H–AA_2–OMe·HCl or H–AA_2–NH_2·HX (X=Cl or Br; AA_2=Ala, Val, Leu, Ile, Phe, Met, Cys(Bzl), Tyr, Trp, and Ser) have been investigated, although all combinations of both components were not examined for each enzyme. In many cases the high purity of the product from the reaction mixture was assured by physical constants and elemental analysis without further purification (Table 1). If necessary, the product was recrystallized

† All amino acids are of L configuration. Symbols and abbreviations are in accordance with the recommendations of the IUPAC-IUB Commission on Biochemical Nomenclature, *J. Biol. Chem.*, **247**, 977 (1971). Other abbreviations used are : PU=protease unit; *B. sub.*=*Bacillus subtilis*; Tris=tris(hydroxymethyl)methanamine; Z(3Me)=2,4,6-trimethylbenzyloxycarbonyl.

Table 1. Physical constants and elemental analyses of X-AA_1-AA_2-OMe and X-AA_1-AA_2-NH_2

Peptide	Mp (°C)	$[\alpha]_D^{25}$ a) (°)	Found (Calcd), % C	H	N	S
X-AA_1-AA_2-OMe						
ZPhePhe-	143—145	−18.0	70.21 (70.41)	6.12 (6.14)	6.09 (6.08)	
ZLeuPhe-	86—90	−22.2	67.47 (67.57)	7.03 (7.10)	6.74 (6.57)	
ZCys(Bzl)Phe-	96—100	−29.2	65.94 (66.37)	5.90 (5.98)	5.36 (5.53)	6.66 (6.33)
ZAlaPhe-	95—96	−12.0	65.69 (65.59)	6.17 (6.30)	7.53 (7.29)	
PGlnPhe-	179—180.5	−11.0	62.41 (62.56)	6.12 (6.18)	9.63 (9.52)	
ZCys(Bzl)Ile-	77—79	−24.2	63.29 (63.52)	6.74 (6.84)	5.62 (5.93)	6.88 (6.78)
ZPheIle-	100—101	−8.4	67.55 (67.57)	7.06 (7.10)	6.56 (6.57)	
Z(OMe)MetIle-	88—92	−9.8	57.12 (57.24)	7.29 (7.34)	6.38 (6.36)	7.32 (7.28)
ZLeuIle-	70—71	−24.0	64.18 (64.58)	8.17 (8.28)	7.13 (7.17)	
ZLys(Z)Ile-	120—122	−11.0	64.11 (64.41)	7.21 (7.28)	7.78 (7.77)	
Z(3Me)His(Bzl)Ile-	135—137	+6.0	67.05 (67.38)	7.18 (7.18)	10.23 (10.48)	
Z(OMe)Glu(OBzl)Ile-	70—71	−10.6	63.48 (63.61)	6.79 (6.88)	5.28 (5.30)	
ZSer(Bzl)Ile-	74—78.5	0	65.47 (65.76)	7.02 (7.08)	6.10 (6.14)	
ZAsnIle-	177—179	−12.8	57.20 (58.00)	7.00 (6.92)	10.61 (10.68)	
ZGlnIle-	154—155	−15.4	58.40 (58.94)	7.24 (7.19)	10.36 (10.31)	
ZCys(Bzl)Val-	70—72	−30.0	62.55 (62.85)	6.53 (6.61)	6.18 (6.11)	7.07 (6.99)
ZPheVal-	107—108	−16.0	66.57 (66.96)	6.79 (6.86)	6.70 (6.79)	
Z(OMe)Glu(Bzl)Val-	88—89	−17.9	63.06 (63.02)	6.67 (6.66)	5.44 (5.45)	
ZPheLeu-	111—113	−24.4	67.53 (67.57)	7.06 (7.10)	6.57 (6.57)	
Z(OMe)Glu(OBzl)Leu-	85—87	−21.5	63.69 (63.61)	6.83 (6.88)	5.30 (5.30)	
Z(OMe)Asp(OBzl)Leu-	76—78	−20.3	62.85 (63.01)	6.55 (6.67)	5.34 (5.44)	
X-AA_1-AA_2-NH_2						
ZAlaLeu-	186.5—187.5	−16.0	60.99 (60.87)	7.46 (7.51)	12.47 (12.53)	
ZPheLeu-	184—186	−19.5	66.93 (67.13)	7.00 (7.10)	10.40 (10.21)	
Z(OMe)Glu(OBzl)Leu-	141—142	−9.0	63.24 (63.14)	6.84 (6.87)	8.06 (8.18)	
Z(OMe)MetLeu-	195.5—196	−17.4	56.08 (56.45)	7.23 (7.34)	9.61 (9.86)	7.84 (7.54)
ZCys(Bzl)Leu-	169—170.5	−25.4	63.00 (62.99)	6.83 (6.83)	9.12 (9.18)	7.06 (7.01)
ZLys(Z)Leu-	183—185	−13.6	63.78 (63.86)	7.22 (7.27)	10.58 (10.64)	
ZProLeu-	185—186	−56.4	63.03 (63.14)	7.42 (7.53)	11.60 (11.63)	
ZSer(Bzl)Leu-	142—143	−3.4	65.43 (65.28)	7.11 (7.08)	9.67 (9.52)	
Z(OMe)LeuMet-	194.5—196	−14.5	56.47 (56.45)	7.42 (7.34)	9.61 (9.88)	7.49 (7.54)
Z(OMe)Glu(OBzl)Met-	153—155	−5.6	58.85 (58.74)	6.20 (6.26)	7.65 (7.90)	5.95 (6.03)
Z(OMe)MetMet-	183—184	−13.6	51.39 (51.44)	6.55 (6.59)	9.43 (9.47)	14.49 (14.46)
ZAlaPhe-	215—216	−19.9	64.82 (65.02)	6.24 (6.28)	11.49 (11.38)	
ZPhePhe-	232—235	−30.3	69.81 (70.09)	6.05 (6.11)	9.51 (9.43)	
Z(OMe)Glu(OBzl)Phe-	165—167	−18.0	65.24 (65.08)	5.97 (6.07)	7.60 (7.67)	
Z(OMe)MetPhe-	205—207	−24.7	59.87 (60.11)	6.30 (6.36)	9.27 (9.14)	
ZCys(Bzl)Phe-	181—182.5	−37.3	65.88 (65.96)	5.93 (5.95)	8.53 (8.55)	6.55 (6.52)
ZAlaVal-	258—263	+11.9	59.47 (59.79)	7.14 (7.21)	12.93 (13.08)	
ZPheVal-	243—246	−1.6	65.86 (66.48)	6·74 (6.85)	10.52 (10.57)	
Z(OMe)Glu(OBzl)Val-	190—197	+6.9	62.29 (62.51)	6.53 (6.66)	6.14 (6.53)	
Z(OMe)MetVal-	233—235	+2.2	55.30 (55.45)	7.07 (7.10)	10.31 (10.21)	7.82 (7.79)
ZCys(Bzl)Val-	117—118	−16.5	62.30 (62.28)	6.56 (6.59)	9.56 (9.47)	7.29 (7.23)
ZLeuVal-	233—235	+24.0 b)	62.28 (62.79)	7.91 (8.04)	11.37 (11.56)	

a) Conditions: for X-AA_1-AA_2-OMe; *c* 0.5, MeOH; for X-AA_1-AA_2-NH_2; *c* 1, DMF. b) *c* 1, AcOH.

from ethyl acetate and petroleum ether.††

Dipeptide Syntheses with Thermolysin. As shown in Table 2, the methyl esters of amino acids such as Phe, Val, Leu, and Ile condensed with various amino acids of the type X-AA_1-OH to give the desired products in good yields. Interestingly, the yields often increased, in some cases to a great extent, by the addition of 20% (wt/v) ammonium sulfate or sodium chloride (*vide infra*). In the cases of the methyl esters of tryptophan, tyrosine, and other amino acids the

†† The raw products were sufficiently pure in most cases, and if further purification was required, the simple removal of the materials insoluble in organic solvents was sufficient to give the pure products. However, the yields of the pure products were often considerably reduced by this procedure.

Table 2. Synthesis of X-AA_1-AA_2-OMe with thermolysin[a]

X-AA_1-AA_2-OMe	Yield (%)	X-AA_1-AA_2-OMe	Yield (%)
ZPhePhe-	76	Z(OMe)Glu(OBzl)Ile-	91.1[b]
ZLeuPhe-	47[b,c]	ZSer(Bzl)Ile-	87.4[b]
ZCys(Bzl)Phe-	65.6	ZAsnIle-	62.5[d]
ZAlaPhe-	61[d]	ZGlnIle-	65.0[d]
ZGlnPhe-	32.9[b,c]	ZCys(Bzl)Val-	80.7[b]
ZCys(Bzl)Ile-	84.7	ZPheVal-	75.0[b]
ZPheIle-	65.4[c]	Z(OMe)Glu(OBzl)Val-	80.2[b]
Z(OMe)MetIle-	78.2[b]	ZPheLeu-	56.8[b,c]
ZLeuIle-	82.8[b]	Z(OMe)Glu(OBzl)Leu-	71.6[b]
ZLys(Z)Ile-	51.7[b]	Z(OMe)Asp(OBzl)Leu-	70.6[b]
Z(3Me)His(Bzl)Ile-	53.9[b]		

a) A mixture of substrates (1 mmol each), Thermolysin (10 mg), 4 M NaOH aqueous solution (0.25 ml), and 0.2 M Tris·HCl (pH 8, containing 5×10^{-2} M $Ca(OAc)_2$, 10 ml) was incubated at 38—40 °C for 15 h. b) Ammonium sulfate (2 g) was added. c) After recrystallization from AcOEt-petroleum ether. d) Sodium chloride (0.8 g) was added and the buffer (4 ml) was used.

Table 3. Synthesis of X-AA_1-AA_2-NH_2 with thermolysin[a]

X-AA_1-AA_2-NH_2	Yield (%)	X-AA_1-AA_2-NH_2	Yield (%)
ZAlaLeu-	61.4[b]	ZAlaPhe-	78.2[c]
ZPheLeu-	86.0[c]	ZPhePhe-	90.7[c]
Z(OMe)Glu(OBzl)Leu-	81.6[c]	Z(OMe)Glu(OBzl)Phe-	84.6[c]
Z(OMe)MetLeu-	84.6[c]	Z(OMe)MetPhe-	79.4[c,d]
ZCys(Bzl)Leu-	68.8[c,d]	ZCys(Bzl)Phe-	90.7[c]
ZLys(Z)Leu-	77.3	ZAlaVal-	59.4[e]
ZProLeu-	52.8[c]	ZPheVal-	84.0[c]
ZSer(Bzl)Leu-	66.4	Z(OMe)MetVal-	79.7[c]
Z(OMe)Glu(OBzl)Met-	83.7[c]	Z(OMe)Glu(OBzl)Val-	66.3[c]
Z(OMe)MetMet-	81.8[c]	ZCys(OBzl)Val-	81.8[c]
Z(OMe)LeuMet-	82.0[c]	ZLeuVal-	79.8[c]

a) A mixture of substrates (1 mmol each), Thermolysin (10 mg), 4 M NaOH aqueous solution (0.25 ml), and 0.2 M Tris·HCl (pH 8, containg 5×10^{-2} M $Ca(OAc)_2$, 10 ml) was incubated at 38—40 °C for 16 h. b) Ammonium sulfate (0.8 g) was added and the buffer (4 ml) was used. c) Ammonium sulfate (2 g) was added. d) After recrystallization. e) The buffer (4 ml) was used.

condensed products were not produced even in the presence of ammonium sulfate or sodium chloride. Similarly the X–dipeptide amides were obtained in higher yields than those of the corresponding esters (Table 3). The amide of methionine, in contrast with the ester, also gave various dipeptides, except those of alanine and proline.

Effect of Ammonium Sulfate on the Yield of Peptides with Thermolysin. The effect of ammonium sulfate described above was examined in the following two cases. The reaction of Z–Phe–OH with either H–Leu–OMe·HCl or H–Val–OMe·HCl gave the expected products in 40 and 29% yields, respectively; in contrast, the yields of both reactions were increased by the addition of ammonium sulfate in 5—30% (wt/v), especially in the case of 20% (Fig. 1).

Dipeptide Syntheses with Metalloproteinases Other than Thermolysin. The peptides given by these proteinases in Table 4 were highly limited and other peptides were hardly obtained by each enzyme. These results demonstrate that Dispase I, Prolisin A, and Tacynase N are not such effective catalysts in the coupling reactions as Thermolysin. The amino acids appropriate for the amine components are all hydrophobic for the synthesis of peptides by using those proteinases.

Syntheses on a Practical Scale. The method was examined as to its suitability for practical peptide syntheses of the two peptides with two proteinases (Table 5). The Table shows that both peptides are easily obtained in good yields. Moreover, it was found that aqueous ammonium sulfate solution can be substituted for the buffer in the reaction with Thermoase and that the reaction can be conducted at room temperature (20 °C).

Discussion

In general, microbial metalloproteinases specifically catalyze the "hydrolysis" of the peptide bond with a hydrophobic amino acid residue at the amino side of the linkage.[7] However, the "hydrolysis" of the bond with tyrosine or tryptophan is catalyzed at rather a slow rate.[8] In the present study, all the amino acids of the amine components which readily formed the peptide bond with various X–amino acids were

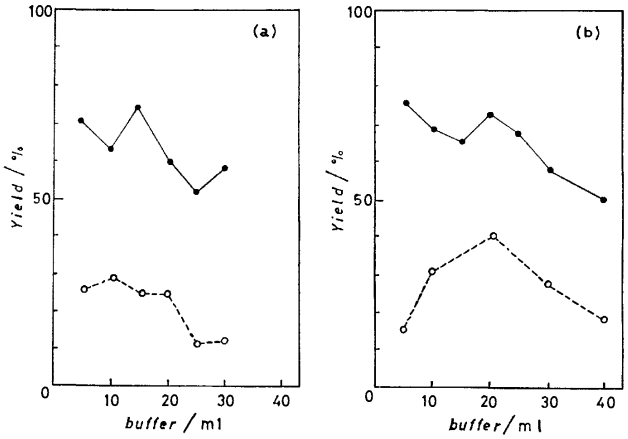

Fig. 1. The effect of ammonium sulfate on the yield of peptide synthesis with Thermolysin. a) ZPheOH+HValOMe·HCl; b) ZPheOH+HLeuOMe·HCl. A mixture of substrates (1 mmol each), Thermolysin (10 mg), 0.2 M Tris·HCl (pH 8, containing 5×10^{-2} M $Ca(OAc)_2$, 5—40 ml), ammonium sulfate (20% wt/v for the buffer), and 4 M NaOH aqueous solution (0.25 ml) was incubated at 40 °C for 16 h and treated under the general procedures. $(NH_4)_2SO_4$: ●—● present; ○--○ absent.

hydrophobic, while the derivatives of tyrosine or tryptophan were practically inert to the coupling reaction. Consequently, the most scissile bond is the most suitable point for the condensation. It is clearly seen in Table 2 that the isoleucine methyl ester in its amine component is the most suitable, and the susceptibility of the methyl esters of phenylalanine, valine, and leucine are successively decreasing in that order. For the carboxyl component, various amino acid derivatives except those of valine, isoleucine, proline, and tryptophan are applicable and there appears to be no difference in susceptibility towards the metalloproteinases used. Better results were obtained in the syntheses of the *N*-acyl dipeptide amides (Table 3) and the methionine amide was also found appropriate to this reaction. The different sensitivity of the enzymes towards the ester or the amide is attributed to the properties of the enzymes as endopeptidases.†††

Table 4. Synthesis of Z-AA_1-AA_2-OMe with several enzymes[a]

AA_1AA_2	Enzyme	Yield (%)	Mp (°C)
PheLeu	Dispase I	37.5	105—107
PhePhe	Dispase I	62	134—137
Cys(Bzl)Leu	Dispase I	94[b]	69—71
PheIle	Prolisin A	72.7	99—102
Cys(Bzl)Ile	Prolisin A	78	72—74
PheTyr	Tacynase N	44[c]	131—132

a) A mixture of substrates (1 mmol), enzyme, and 0.2 M Tris·HCl (pH 8, containing 5×10^{-2} M $Ca(OAc)_2$, 10 ml) was incubated at 38—40 °C for 15 h; each enzyme used: Dispase I (15 mg); Prolisin A (20 mg) with potato inhibitor (60 mg); Tacynase N (20 mg) with potato inhibitor (20 mg). b) Elemental analysis, Found: C, 63.23; H, 6.71; N, 5.81; S, 6.70%. Calcd for $C_{25}H_{28}N_4O_5S$: C, 63.52; H, 6.84; N, 5.93; S, 6.78%. c) Elemental analysis, Found: C, 67.77; H, 6.04; N, 6.16%. Calcd for $C_{27}H_{28}N_2O_6$: C, 68.04; H, 5.93; N, 5.88%.

The dissimilarities in catalytic ability in the syntheses of dipeptides by Thermolysin and the other enzymes are interesting when compared to those in the hydrolysis of the peptide bond.[9] Morihara *et al.*[9b] reported that Z-Gly-Leu-NH_2 is hydrolyzed by Thermolysin and also by *B. sub.* metalloproteinase at approximately the same rate and that Z-Gly-Phe-NH_2 is hydrolyzed by Thermolysin 10 times faster than by *B. sub.* metalloproteinase. Feder and Shuck[9d] reported that the most pronounced difference between Thermolysin and *B. sub.* metalloproteinase at the dipeptide level was observed when phenylalanine is the amino acid donating the amino group to the cleaved bond. Accordingly, in the "hydrolysis" of the peptide bond, there is only

††† An endopeptidase catalyzes the hydrolysis of the peptide bond containing the C-terminal residues (whose carboxyl group is free or protected by the ester group) either very slowly or not at all.

Table 5. Synthesis in large scale[a]

Peptide (mmol)	Enzyme (mg)	Solvent (ml)	Additive (g)	Yield (%)	Mp (°C)
ZPhePheOMe (30)	Th[b] (600)	buffer[d] (600)	—	73	133—135
	Th[b] (600)	buffer[d] (600)	$(NH_4)_2SO_4$ (120)	70	133—135
	Th[b] (600)	H_2O[e] (450)	—	(60)[f]	110—119
	Th[b] (600)	H_2O[e] (450)	$(NH_4)_2SO_4$ (120)	80	133—135
ZPheIleOMe (50)	*B. sub.*[c] (700)	buffer[d] (500)	—	76	96—98

a) A mixture of substrates, enzyme, solvent, additive, and 4 M NaOH aqueous solution of equimolar quantity with the amine component was stirred in a three-necked flask at 20 °C for 16 h and treated under the general procedures. b) Partially purified Thermoase and the potato inhibitor (60 mg). c) Partially purified metalloproteinase of *B. sub.* and the potato inhibitor (70 mg). d) 0.2 M Tris·HCl (pH 8, containing 5×10^{-2} M $Ca(OAc)_2$). e) With continuous control of the pH at 7.2 by the addition of 4 M NaOH. f) Pure product was not obtained.

a slight difference in efficiency between the two enzymes. As shown *B. sub.* metalloproteinase (Prolisin) was far less capable of catalyzing the peptide "synthesis" than Thermolysin.

An examination of the variation of the Thermolysin activity caused by ammonium sulfate or sodium chloride, shows an increment in the peptidase activity,[10] in contrast to the remarkable decrease in protease activity.[10] This effect, coupled with the salting out effect of the salt, seems to play a major role in the increased yield of the product.

The authors wish to express their thanks to Mr. Masanari Satoh for the enzyme purification and to Miss Reiko Matsumoto and Miss Noriko Shutoh for technical assistance.

References

1) M. Bergmann and H. Fraenkel-Conrat, *J. Biol. Chem.*, **119**, 707 (1937).
2) K. Morihara and T. Oka, *Biochem. J.*, **163**, 531 (1977).
3) a) P. L. Luisi, R. Saltman, D. Vlach, and R. Guarnaccia, *J. Mol. Catal.*, **2**, 133 (1977); b) R. Saltman, D. Vlach, and P. L. Luisi, *Biopolymers*, **16**, 631 (1977).
4) a) Y. Isowa, M. Ohmori, T. Ichikawa, H. Kurita, M. Satoh, and K. Mori, *Bull. Chem. Soc. Jpn.*, **50**, 2762 (1977); b) Y. Isowa, M. Ohmori, M. Satoh, and K. Mori, *ibid.*, **50**, 2766 (1977); c) Y. Isowa, T. Ichikawa, and M. Ohmori, *ibid.*, **51**, 271 (1978).
5) D. Tsuru, T. Yamamoto, and J. Fukumoto, *Agric. Biol. Chem.*, **6**, 651 (1966).
6) J. Fukumoto, T. Yamamoto, and D. Tsuru, Japan Patent 7009230 (1970); *Chem. Abstr.*, **73**, 43922b (1971).
7) H. Matsubara and J. Feder, "The Enzymes," 3rd ed, ed by P. D. Boyer, Academic Press, New York, N. Y. (1971), Vol 3, p. 765.
8) a) K. Morihara and H. Tsuzuki, *Eur. J. Biochem.*, **15**, 374 (1970); b) W. R. Tester and B. W. Matthews, *Biochem.*, **16**, 2506 (1977).
9) a) K. Morihara, *Biochem. Biophys. Res. Commun.*, **26**, 656 (1967); b) K. Morihara, H. Tsuzuki, and T. Oka, *ibid.*, **123**, 572 (1968); c) K. Morihara and H. Tsuzuki, *Arch. Biochem. Biophys.*, **146**, 291 (1971); d) J. Feder and J. M. Schuck, *Biochem.*, **9**, 2784 (1970).
10) T. Ichikawa and Y. Isowa, to be published.

Photoisomerization and Photodimerization of 3-(1- and 2-Naphthyl)acrylate in Bichromophoric Systems

Hideaki TANAKA,* Setsuo TAKAMUKU,† and Hiroshi SAKURAI†

National Chemical Laboratory for Industry, Hiratsuka, Kanagawa 254

† *The Institute of Scientific and Industrial Research, Osaka University, Suita, Osaka 565*

(Received June 19, 1978)

The photochemical *trans-cis* isomerization of methyl 3-(1- and 2-naphthyl)acrylate (**1Me** and **2Me**) and the intramolecular (2+2) cycloaddition of ethylene bis[3-(1- and 2-naphthyl)acrylates] (**1E** and **2E**) have been studied in cyclohexane and methanol. The quantum yield of the *trans-cis* isomerization of **2Me** and **2E** in methanol was larger than that in cyclohexane, while the yield of the cyclization of **2E** showed the reverse. The isomerization is thought to occur *via* the triplet state, while the cyclization is *via* the singlet excited state. The triplet yield of **2Me** in the polar solvent has been estimated to be larger than in nonpolar solvent. The cyclization of **1E** was much slower than that of **2E**, and the quantum yield of the reaction of **1Me** and **1E** did not appreciably depends on the polarity of the solvent.

The Photodimerization of cyclic α,β-unsaturated carbonyl compounds has been studied extensively, but the acyclic ones have not, due to the rapid *trans-cis* isomerization making quantitative analysis of the dimerization impossible.[1-4] The quantum yield of dimerization is usually very small compared with that of the isomerization, and most of the dimerization occurs from the equilibrium mixture of *trans* and *cis* isomers.[5,6] In the crystalline state or in the solid monolayer assemblies the *trans-cis* isomerization is greatly diminished and the dimerization proceeds more efficiently.[7,8] In solution, however for example, methyl cinnamate or ethyl cinnamylideneacetate does not dimerize but rapidly isomerizes.[9] In dimerization, the distance between the chromophores is an important factor. If two cinnamate groups are incorporated in the same molecule, namely, in the bichromophoric system, the cinnamate groups dimerize intramolecularly in solution.[10,11] Bichromophoric systems are recently attracting wide interest because they provide a method for controlling bimolecular reactions—model systems for polymer photochemistry such as DNA, and give information on chain dynamics.[12] Several bichromophoric systems bearing photodimerizable chromophores have been reported recently and most of them are cyclic compounds such as coumarin,[13] anthracene,[14] maleimides,[15] and thimine.[16]

In this study, the photoisomerization and photodimerization of 3-(1- and 2-naphthyl)acrylate have been studied in bichromophoric systems; ethylene bis[3-(1-naphthyl)acrylates] (**1E**) and ethylene bis[3-(2-naphthyl)acrylates] (**2E**) have been studied along with methyl 3-(1-naphthyl)acrylate (**1Me**) and methyl 3-(2-naphthyl)acrylate (**2Me**).

Results and Discussion

trans-cis *Isomerization.* In a previous paper, the solvent effect on the *trans-cis* isomerization and fluorescence of **2Me** was reported.[17] The quantum yield of the *trans-cis* isomerization, ϕ_{t-c} of **2Me** increased with increase in the solvent polarity, while the fluorescence quantum yield, ϕ_f decreased remarkably.

Table 1 shows the ϕ_{t-c} for **1Me** and **2Me** in cyclohexane and methanol. The ϕ_{t-c} of **1Me** in methanol is only slightly larger than that in cyclohexane and the dependency on solvent polarity for **1Me** is much smaller than that for **2Me**.

Table 2 shows the quantum yield of the fluorescence in cyclohexane and methanol where solvent dependency was observed for **2Me**, but not for **1Me**.

The solvent polarity effect on *trans-cis* isomerization has been demonstrated for stilbenes having electron-withdrawing and electron repelling groups.[18-22] For molecules having large dipole moments in the ground state, the quantum yield of the *trans* to *cis* isomerization was small in polar solvents due to stabilization of the excited trans isomer. Here the opposite tendency was observed— the quantum yield of the *trans* to *cis* isomerization of **2Me** was large in polar solvents and small in nonpolar solvents.

The isomerization was little affected by aerobic oxygen but enhanced by pure oxygen. The enhancement of the isomerization by oxygen has been observed

Table 1. The quantum yield of isomerization and cyclization

		In cyclohexane			In methanol			In methanol–*n*-PrBr
		Argon	Air	Oxygen	Argon	Air	Oxygen	Air
1E	ϕ_{cy}	0.0075	0.010		0.0085	0.013		0.001
	ϕ_{t-c}	0.19	0.18		0.22	0.22		0.19
trans-**1Me**	ϕ_{t-c}	0.19	0.18		0.22	0.22		0.19
2E	ϕ_{cy}	0.22	0.17	0.08	0.11	0.10	0.09	0.01
	ϕ_{t-c}	0.09	0.09	0.09	0.25	0.26	0.23	0.21
trans-**2Me**	ϕ_{t-c}	0.22	0.24	0.31	0.37	0.37	0.37	0.40
cis-**2Me**	ϕ_{c-t}	0.16			0.14			

TABLE 2. THE QUANTUM YIELD OF THE FLUORESCENCE

	In cyclohexane		In methanol		In methanol–*n*-PrBr
	Argon	Air	Argon	Air	Air
1E	0.021	0.015	0.0090	0.0083	
trans-**1Me**	0.052	0.043	0.052	0.038	0.028
2E	0.22	0.13	0.17	0.17	0.094
trans-**2Me**	0.61	0.25	0.39	0.38	0.097
cis-**2Me**	0.041		0.030		

more remarkably in the case of styrylnaphthalenes.[23,24] The explanation for this has been that $O_2(^3\Sigma_{-g})$ increased the population of the triplet state by quenching the excited singlet state which has been attributed to direct intermolecular exchange interaction or the inhomogeneous field of the O_2 triplet ground state. As shown in Table 2, oxygen and heavy atom solvents, *e.g.*, propyl bromide strongly quenched the fluorescence. The heavy atom solvent remarkably increased the ϕ_{t-c} and the intensity of the phosphorescence of **2Me** by quenching the fluorescence suggesting that the isomerization takes place from the triplet state. The corrected fluorescence spectra for **2Me** in cyclohexane and methanol are shown in Fig. 1.

The fluorescence spectrum of **2Me** in cyclohexane is a good mirror image of the absorption spectrum and therefore, the lowest singlet excited state is thought to lie near 355 nm (28169 cm^{-1}). This resembles the ^1L_b state of naphthalene in the weakness of the absorption and the long-lifetime of the fluorescence (107 ns in cyclohexane from the quenching of the fluorescence by aerobic oxygen). In methanol and in other polar solvents, a large Stokes' shift is observed and the maximum of the fluorescence shifts to 400 nm indicating that the dipole moment of the fluorescence state in polar solvents is larger than in cyclohexane. The separation between the singlet and triplet state may be small in polar solvent. The above solvent effects lead to the conclusion that the isomerization occurs from the triplet state, and that the triplet yield in polar solvents may be larger than in nonpolar solvents due to the small separation between the singlet and triplet states. The enhancement of ϕ_{t-c} by oxygen has been observed only in nonpolar solvents; in polar solvents, the triplet yield is sufficiently large before enhancement by oxygen.

Phosphorescence of **2Me** was too weak to be observed in EPA [ether–isopentane–ethanol (5 : 5 : 2) mixed solvent] at 77 K, but was observed in propyl bromide–ethanol (1 : 1 mixed solvent). The phosphorescence spectrum has three peaks at 544, 593, and around 650 nm as shown in Fig. 1, the first peak rising from 533 nm (53.5 kcal/mol).

For *cis*-**2Me** the fluorescence was very weak and the measurement was always interfered from by the strong fluorescence of the *trans*-**2Me** which was produced during the measurement. No phosphorescence was observed in the heavy atom solvent.

That the fluorescence yield of the *cis*-**2Me** is markedly smaller than the *trans* form (Table 2) implies that the singlet excited state of the *trans* and *cis* form may be different from each other, *i.e.* there may exist an energy barrier between the two excited singlet states.

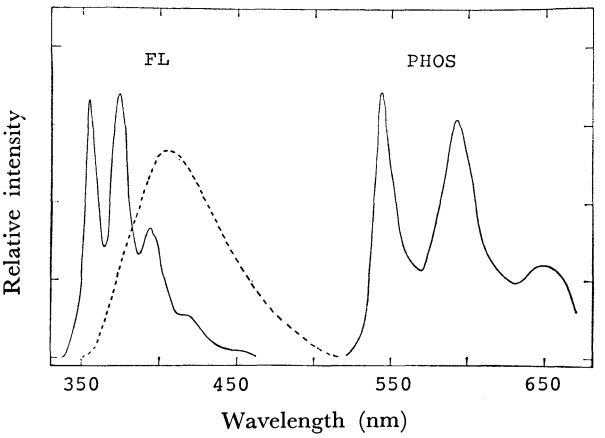

Fig. 1. Corrected fluorescence (—— in cyclohexane, ---- in methanol) and phosphorescence (in propyl bromide–ethanol 1:1 mixed solvent) spectra of **2Me**.

If the *trans* to *cis* isomerization of **2Me** occurs only from the triplet state, the triplet yield can be estimated using the following equation:

$$\frac{\phi_{isc}}{\phi^s_{isc}} = \frac{\phi_{t-c}}{\phi^s_{t-c}}, \quad (1)$$

where ϕ^s_{t-c} is the quantum yield of the *trans* to *cis* isomerization for sensitized reaction and ϕ^s_{isc} is the triplet yield of the sensitizer. (ϕ^s_{isc} is known for Michler's ketone in several solvents.[25]) The triplet energy of Michler's ketone is 72 kcal/mol in cyclohexane, 61 kcal/mol in ethanol.[26] Since the triplet energy of **2Me** has been estimated to be 53.6 kcal/mol from the phosphorescence spectrum, the energy transfer from Michler's ketone to **2Me** is considered to be a diffusion controlled process. The concentration of **2Me**, 5×10^{-4} mol/l is sufficiently large to completely accept the energy from Michler's ketone within the lifetime (20—40 μs). Therefore, under the experimental conditions, the energy transfer from Michler's ketone to **2Me** occurs with an efficiency of nearly unity. Thus the ϕ_{isc} of **2Me** has been estimated to be 0.41 in cyclohexane and 0.81 in ethanol by measuring ϕ_{t-c}/ϕ^s_{t-c}. The radiationless deactivation of the singlet excited state cannot be ignored, and consequently the sum of ϕ_f and ϕ_{isc} should be less than unity, but here the sum becomes 1.02 in cyclohexane, 1.06 in ethanol. This may be caused by an impurity or incomplete degassing which would decrease ϕ^s_{isc}, and thus ϕ_{isc} of **2Me** might have been overestimated. The value obtained however are thought to be qualitatively reliable.

The quantum yield of the *cis* to *trans* isomerization, ϕ_{c-t} of *cis*-**2Me** is small as shown in Table 1.

The fluorescence yield of **1Me** is far smaller than that of **2Me** and is not appreciably diminished by aerobic oxygen as found for **2Me**, suggesting that the lifetime of the excited state of **1Me** is much shorter than that of **2Me** and that the triplet yield does not depend on solvent polarity.

The difference in oxygen effect between **1Me** and **2Me** is analogous to the results between 1- and 2-styrylnaphthalene. The ϕ_f of 2-styrylnaphthalene

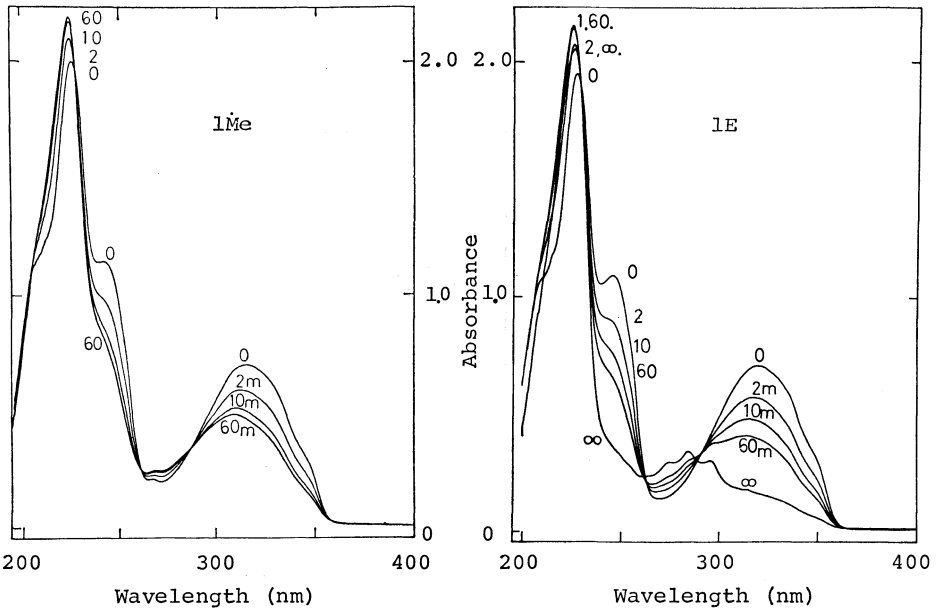

Fig. 2. UV absorption spectral change of **1Me** (0.31×10^{-4} mol/l) and **1E** (0.15×10^{-4} mol/l) in cyclohexane on the irradiation with 313 nm light.

decreased to one third, and ϕ_{t-c} doubled when aerobic oxygen was used, while ϕ_f and ϕ_{t-c} of 1-styrylnaphthalene changed very little.[24] The lifetime of the fluorescence of the former is 20 ns and that of the latter is 2 ns.[27]

*Photochemical Reactions of **1E** and **2E**.* The photochemical reaction of **1E** in solution was a rapid *trans-cis* isomerization followed by a slow intramolecular (2+2) cycloaddition giving *cis,cis*-**1E** (18%) and **1ED** (53%) as final products. The photoproduct *cis,cis*-**1E** was assinged on the basis of the NMR spectrum and **1ED** on the basis of the NMR, UV, and IR spectra.

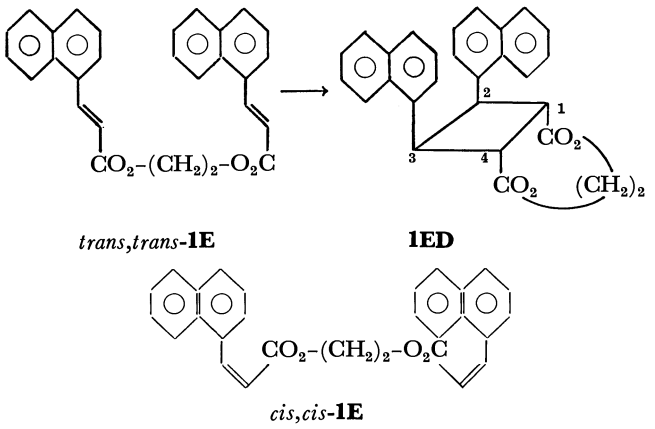

Figure 2 shows that UV absorption spectral change of *trans,trans*-**1E** and -**1Me** when irradiated with 313 nm light. A rapid *trans-cis* isomerization occurs and isosbestic points are observed at 260 and 290 nm until the equilibrium state is attained since cyclization proceeds very slowly. In the equilibrium state, the *cis* isomers predominate (approximately 70% *cis*, 30% *trans*) under the irradiation conditions since the *cis* isomer has an absorption maximum at a shorter wavelength (296 nm) and a smaller extinction coefficient. In the ^{1}H NMR spectrum, the peak for the methylene protons of *cis,cis*-**1E** shift to a higher field (3.58 ppm) compared with 4.54 ppm for *trans,trans*-**1E** suggesting that the methylene chain of the *cis,cis*-**1E** is more strongly affected by the naphthalene nuclei than the *trans,trans*-**1E**. The Stuart molecular model shows that the double bond of the *cis* isomer is twisted out of the two naphthalene nuclei and therefore the methylene chain may possibly interfere in the accessability of the two double bonds on dimerization. A further consequence of the steric hindrance, is that *cis,cis*-**1E** is considered to be poorly photocyclizable. In the photo-stationary mixture, the *cis,cis*-**1E** probably photocyclizes *via* the *trans,trans*-**1E**. Thus **1ED** may be largely formed from the photo-stationary mixture.

The photochemical reaction of **2E** was a slow *trans-cis* isomerization followed by a rapid intramolecular (2+2) cycloaddition of 3-(2-naphthyl)acrylate giving a single product, **2ED**. The structure of **2ED** was assinged by the method analogous with that for **1ED**. Figure 3 shows the UV absorption spectral changes of **2E** and **2Me** on irradiation with 313 nm light. The cyclization is so rapid that the reaction is considered to take place from the original *trans,trans*-**2E**.

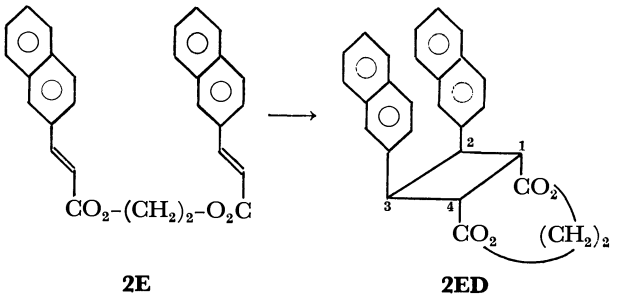

The quantum yield of the cyclization, ϕ_{cy}, and the isomerization, ϕ_{t-c}, of **1E** and **2E** are shown in Table 1. Taking into consideration the large triplet yield of **2Me** in methanol, the fact that **2E** in cyclohexane cyclized with a larger quantum yield than in methanol

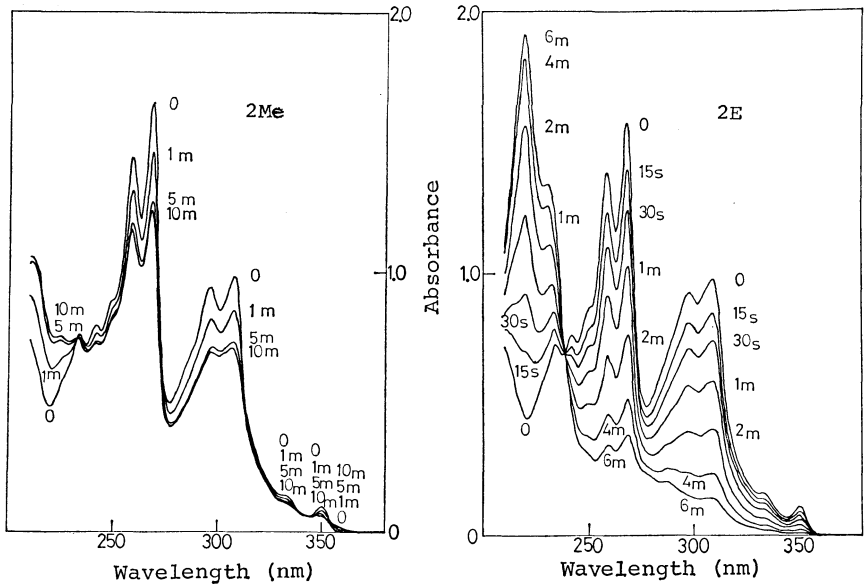

Fig. 3. UV absorption spectral change of **2Me** (0.39×10^{-4} mol/l) and **2E** (0.20×10^{-4} mol/l) in cyclohexane on the irradiation with 313 nm light.

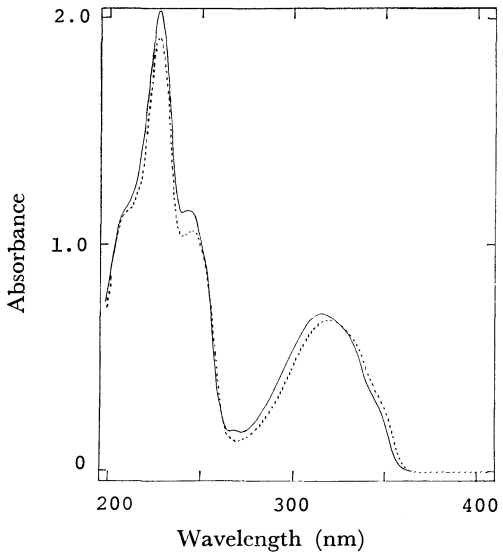

Fig. 4. UV absorption spectra of **1Me** (——, 0.29×10^{-4} mol/l) and **1E** (----, 0.14×10^{-4} mol/l) in cyclohexane.

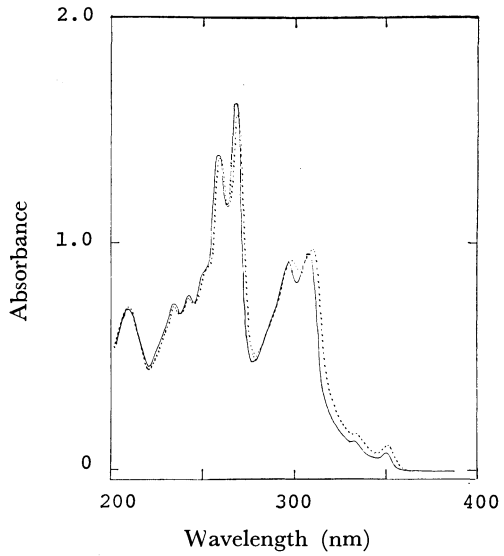

Fig. 5. UV absorption spectra of **2Me** (——, 0.39×10^{-4} mol/l) and **2E** (----, 0.20×10^{-4} mol/l) in cyclohexane.

suggests that the reactive state for the cyclization is the excited singlet state. Accordingly the cyclization was depressed while the *trans-cis* isomerization was accelerated by the heavy atom solvent which strongly quenches the fluorescence and accelerates intersystem crossing of the excited singlet state of **2Me**

In the case of **1E**, the solvent dependency of ϕ_{cy} is very small. The difference in the reactivity between **1E** and **2E** has been interpreted as follows : firstly, in the bichromophoric system, the quantum yield of the fluorescence was reduced to about half that of the corresponding methylesters and the amount of the decreased fluorescence is attributed to the cyclization. From Table 2, the difference in ϕ_f between **1Me** and **1E** is 0.03, while that between **2Me** and **2E** is 0.39 in cyclohexane the former being one tenth of the latter coinciding with the difference in the quantum yield of the cyclization. Secondly the lifetime of the fluorescence of **2Me** has been estimated from the quenching by aerobic oxygen to be much longer than that of **1Me** and because of this it is thought the two chromophores of **2E** cyclize more rapidly than **1E,** and the *trans-cis* isomerization proceeds slowly. A further consequence of the long-lifetime is that the cyclization of **2E** is susceptible to quenching by oxygen, while **1E** is not. In methanol, the lifetime of the fluorescence of **2Me** has been estimated to be shorter than in cyclohexane and consequently, the cyclization in methanol is not appreciably quenched by oxygen.

The above discussion demonstrates that the difference in reactivity between **1E** and **2E** can be explained by the difference in quantum yield and lifetime of the

fluorescence between **1Me** and **2Me**. The excited state of **1Me** is considered to be more rapidly deactivated by radiationless transitions than that of **2Me**. 1-Substituted naphthalene derivatives are considered to be sterically hindered owing to the protons at the 8 position in the naphthalene nucleus, which causes the rapid radiationless deactivations resulting in the short lifetime of the fluorescence.

The absorption spectra of the bichromophoric molecules, **1E** and **2E**, are shifted slightly into the red compared to the corresponding monochromophoric molecules as shown in Figs. 4 and 5 indicating the existence of a slight interaction between the chromophores in the ground state. The fluorescence spectra of **1E** and **2E** were accordingly shifted slightly into the red from those of **1Me** and **2Me**. Excimer fluorescence in the long wavelength side of the fluorescence spectra, frequently observed for aromatic bichromophoric molecules, was not observed for **1E** and **2E**.[14]

Experimental

Instrumentation. IR spectra were recorded on a JASCO model IR-S using KBr discs and UV absorption spectra on a Shimadzu model UV-300 and UV-200. NMR spectra were measured in $CDCl_3$ (otherwise indicated) with tetramethylsilane as an internal standard on a Hitachi model R-24A for ^1H, and a varian model NV-14 for ^{13}C. Emission spectra were recorded on a Hitach model MPF-1, and corrected for the photomultiplier (Hamamatsu TV Co. R446) response. Mass spectra were recorded on a Shimdzu model LKB-9000. High speed liquid chromatography was performed on a Waters Associate model equipped with a column, Michrobonda pack C-18 and a UV detector.

For the photolysis on a preparative scale, an immersion well type photoreactor was used. A naphthalene–ethanol solution ($\lambda>320$ nm) or cinnamylideneacetic acid–ethanol solution ($\lambda>360$ nm) was used as a filter.

For the photolysis on a analytical scale, a 4 ml rectangular cell equipped with an inlet tube about 10 cm was used. Pure argon or oxygen was bubbled through the tube for 5 min and immediately bottled. The period of bubbling (5 min) has been shown to be sufficient to change the air in the solution by measuring the intensity of the fluorescence. The light source was a 500 W high pressure mercury arc lamp (Ushio Electric Co.) with a monochromator (Nikon G250). Potassium ferioxalate system was used for actinometry.

Materials. 3-(1- and 2-Naphthyl)acrylic Acid: 3-(1- and 2-Naphthyl)acrylic acid were synthesized by the Knoevenagel condensation from the corresponding naphthaldehyde and recrystallized from methanol. 3-(1-Naphthyl)-acrylic acid, mp 206.0 °C (lit, 205.0 °C[21]). 3-(2-Naphthyl)-acrylic acid, mp 189.5 °C (lit, 196.0 °C[21])

*Methylesters (**1Me** and **2Me**)*: The acrylic acids were esterified in refluxing dry methanol with a trace of *p*-toluenesulfonic acid. Methyl 3-(2-naphthyl)acrylate (**2Me**), mp 91.0 °C. Methyl 3-(1-naphthyl)acrylate (**1Me**) was an oil at room temperature.

*Ethylene Bis[3-(1-naphthyl)acrylates] (**1E**) and Ethylene Bis-[3-(2-naphthyl)acrylates] (**2E**)*: **1E** and **2E** were synthesized from the corresponding acid chloride and ethylene glycol by heating in benzene with a trace amount of pyridine. ***1E***, mp 114—115 °C. ^1H NMR (ppm), 4.54(s, 4H, methylene), 6.51 (d, $J=5.6$, 2H, vinyl), 8.53 (d, $J=15.6$, 2H, benzyl), 7.2—8.2 (m, 14H, aromatic). IR (cm^{-1}), 1700 (s, carbonyl), 1620 (s, double bond), 1296, 1245, 1160, 1350, 770, 795, UV, $\lambda_{max}=323$ nm, $\varepsilon=4.80\times10^4$. MS, 422.

Found : C, 79.96; H, 5.2%. Calcd for $C_{28}H_{22}O_4$: C, 79.60; H, 5.21%.

2E, mp 148.0 °C. ^1H NMR (ppm), 4.60 (s, 4H, methylene), 6.60 (d, $J=16.0$, 2H, vinyl), 7.3—8.1 (m, 16H, aromatic and benzyl). IR (cm^{-1}), 1700 (s, carbonyl), 1630 (s, double bond), 1360, 1290, 1250, 1170, 1180, 860, 820. UV, $\lambda_{max}=307$ nm, $\varepsilon=5.00\times10^4$. MS, 422.

Found : C, 79.24, H, 5.25%. Calcd for $C_{28}H_{22}O_4$: C, 79.60; H, 5.21%.

*Photolysis of **1E***: **1E** (0.9 g) in acetone (990 ml) was irradiated with light ($\lambda>320$ nm) under nitrogen for 11 h and the solution concentrated in a rotary evaporator. On adding hexane, crystals precipitated out from the solution which were recrystallized from acetone–hexane to give **1ED**. 0.48 g, 53%. Concentration of the filtrate gave 0.16 g (18%) of *cis,cis*-**1E**.

1ED, mp 205—210.5 °C. ^1H NMR (ppm), 4.64 (s, 4H, methylene) 4.15—4.30 (d, 2H, cyclobutane), 5.45—5.65 (d, 2H, cyclobutane), 7.0—8.2 (m, 14H, aromatic). ^{13}C NMR (ppm), 65.20 (methylene C), 49.28 (carbon 1 and 4 on cyclobutane), 41.18 (carbon 2 and 3 on cyclobutane). IR (cm^{-1}), 1750 (s, carbonyl), 1603, 1250, 1225, 777. UV, λ_{max} 220 and 285 nm. MS, 422.

Found : C, 79.20; H, 5.30%. Calcd for $C_{28}H_{22}O_4$: C, 79.60; H, 5.21%.

cis,cis-***1E***, mp 107.0—108.0 °C ^1H NMR (ppm), 3.85 (s, 4H, methylene), 6.05 (d, $J=11.7$, 2H, vinyl), 7.0—8.5 (m, 16H, aromatic and benzyl). IR(cm^{-1}), 1723 (s, carbonyl), 1635 (s, double bond), 1180, 1214, 1420, 829, 814, 790. UV, $\lambda_{max}=296$ nm $\varepsilon=2.32\times10^4$. MS 422.

*Anhydride of **1ED** (**1EA**)*: **1ED** (0.21 g) was heated in 1M aqueous sodium hydroxide (50 ml) for 3 h at 60—70 °C. After filtration the filtrate was acidified. The precipitate (0.17 g 81%) was dried over P_2O_5 and refluxed in acetyl chloride (20 ml) for 3 h. Concentration of the solution gave crystals of **1EA** 0.10 g (48%). ***1EA***, mp 214.0—215.0 °C. ^1H NMR (ppm) in C_5D_5N, 4.63 (d, 2H, cyclobutane), 5.97 (d, 2H, cyclobutane), 7.0—8.0 (m, 14H, aromatic). IR (cm^{-1}), 1870 and 1795 (five membered ring anhydride), 1603, 1245, 1214, 1065, 903, 780, MS, 378.

Found : C, 78.35; H, 4.93%. Calcd for $C_{26}H_{18}O_3$: C, 80.53; H, 4.79%.

*Photolysis of **2E***: **2E** (1 g) was irradiated in the same way as **1E** for one hour and the reactant solution concentrated in a rotary evaporator. The addition of hexane precipitated crystals of **2ED**, 0.75 g in 75% yield. **2ED**, mp 190.0 °C. ^1H NMR (ppm), 4.62 (s, 4H, methylene), 4.1—4.8 (m, 4H, cyclobutane), 6.85 and 7.0, 7.2—8.2 (m, 14H, aromatic). ^{13}C NMR (ppm), 65.03 (methylene C), 49.02 (carbon 1 and 4 on cyclobutane), 44.63 (carbon 2 and 3 on cyclobutane).

*Anhydride of **2ED**, (**2EA**)*: **2ED** was converted into the anhydride (**2EA**) in the same way as **1ED**. **2EA**, mp 165.0—168.0 °C. ^1H NMR (ppm), 4.1 and 4.6 (m, 4H, cyclobutane), 6.84 and 6.97, 7.20—8.00 (14H, aromatic). IR(cm^{-1}), 1855 and 1775 (five-membered ring anhydride), 1235, 1210, 1060, 900. MS, 378.

Found : C, 79.45; H, 4.82%. Calcd for $C_{26}H_{18}O_3$: C, 80.53; H, 4.79%.

*Dimethyl Ester of **2ED** (**2EM**)*: The dicarboxylic acid of **2ED** was esterified by diazomethane. **2EM** mp 108.0—109.0 °C. ^1H NMR (ppm), 3.80 (s, 6H, methyl), 4.10 and 4.80 (m, 4H, cyclobutane), 6.90 and 7.07, 7.2—8.0 (14H, aromatic). IR (cm^{-1}), 1730 (s, carbonyl), 1600, 1430, 1270, 1200. MS, 378.

*Photolysis of a Concentrated Solution of **2Me***. **2Me** (1 g)

in 50 ml of benzene was irradiated with light ($\lambda > 320$ nm) for 24 h. After irradiation, evaporation of the solvent gave crystals. Thin layer chromatography and NMR methyl signals showed the presence of at least two kind of products and HLC retention times indicated that one product was **2EM**.

*Identification of **1ED** and **2ED*** : The compound **1ED** was assigned the proposed cyclobutane structure based on NMR, UV, and IR spectra. ^{13}C NMR spectrum of **1ED** showed a single peak at 65.20 ppm for the methylene carbons, 49.29 ppm for carbons 1 and 4, 41.18 ppm for carbons 2 and 3 on the cyclobutane ring. The hydrolyzed product of **1ED** gave an acid anhydride (**1EA**) in boiling acetyl chloride. **1EA** has IR peaks at 1795 and 1870 cm^{-1}, characteristic of a five-membered ring anhydride. The all-*cis* structure presumably can be neglected since the hydrolyzed product of **1ED** gave *trans*-3-(1-naphthyl)acrylic acid upon irradiation with 253.7 nm light. The structure of **2ED** was assigned by an analogous method. The ^{13}C NMR spectrum has a peak at 65.03 ppm for the methylene carbons, 49.02 ppm for carbons 1 and 4, 44.63 ppm for carbons 2 and 3 on the cyclobutane ring. The hydrolyzed product of **2ED** gave an anhydride (**2EA**) in boiling acetyl chloride. **2EA** has IR peaks at 1780 and 1855 cm^{-1}, characteristic of a five-membered ring anhydride. Photolysis of **2EM** by 253.7 nm light or thermolysis above 250 °C in a gas chromatograph gave *trans*-**2Me**. These facts support the proposed structure for **2ED**.

Quantum Yield Measurements. A) The quantum yield of *trans* to *cis* isomerization of **1Me** and **2Me** was calculated from the decrease in the UV absorbance. Molar extinction coefficients used are shown below.

	In methanol			In cyclohexane
trans-**1Me**	$\lambda_{max}=323$ nm	$\varepsilon=2.40$ ($\times 10^4$)	$\varepsilon_{313}=2.36$ ($\times 10^4$)	$\varepsilon_{313}=2.36$ ($\times 10^4$)
cis-**1Me**	$\lambda_{max}=296$ nm	$\varepsilon=1.16$	$\varepsilon_{313}=0.933$	$\varepsilon_{313}=0.933$
trans-**2Me**	$\lambda_{max}=307$ nm	$\varepsilon=2.52$	$\varepsilon_{313}=1.80$	$\varepsilon_{313}=1.48$
cis-**2Me**	$\lambda_{max}=298$ nm	$\varepsilon=1.11$	$\varepsilon_{313}=0.779$	$\varepsilon_{313}=0.967$

B) The quantum yield of the cyclization and *trans-cis* isomerization of **1E** and **2E** was calculated from the peak area in the HLC chart. Usually a 2×10^{-5} mol/l reactant solution in 4 ml rectangular cell was irradiated for 30 or 60 s with 313 nm light.

C) The fluorescence quantum yield was calculated by using 2-(1-naphthyl)-5-phenyloxazole (α**NPO**) in cyclohexane as standard,[22] $\phi_f=0.70$.

D) Michler's ketone photosensitized isomerization of **2Me**. A solution of Michler's ketone (1.1×10^{-3} mol/l) and **2Me** (5×10^{-4} mol/l) in cyclohexane or ethanol was purged with argon for 10 min and irradiated with light of wavelength 365 nm or 405 nm respectively. A solution of **2Me** of the same concentration without Michler's ketone was irradiated with 313 nm light. The ratio of *trans*- and *cis*-**2Me** was measured by HLC.

The authors wish to thank Dr. H. Nakanishi of this laboratory for the ^{13}C NMR measurements and Dr. K. Honda for his useful discussions.

References

1) N. Sugiyama, K. Yamada, Y. Watari, and T. Koyama, *Nippon Kagaku Zasshi*, **87**, 737 (1966).
2) T. Ishigami, T. Murata, and T. Endo, *Bull. Chem. Soc. Jpn.*, **49**, 3578 (1976).
3) G. Hammond, C. A. Stout, and A. A. Lamola, *J. Am. Chem. Soc.*, **86**, 3103 (1964).
4) H. Morrison, H. Curtis, and T. McDowell, *J. Am. Chem. Soc.*, **88**, 5415 (1966).
5) J. R. Scheffer and A. Bire, *J. Am. Chem. Soc.*, **93**, 5490 (1971).
6) J. R. Scheffer and R. A. Wostradowski, *J. Org. Chem.*, **37**, 4317 (1972).
7) M. D. Cohen, G. M. J. Schmidt, and F. I. Sonntag, *J. Chem. Soc.*, **1964**, 2000.
8) F. H. Quina and D. G. Whitten, *J. Am. Chem. Soc.*, **99**, 877 (1977).
9) H. Tanaka, M. Tsuda, and H. Nakanishi, *J. Polym. Sci., Part A-1*, **10**, 1729 (1972).
10) B. S. Green, Y. Rabinsohn, and M. Rejto, *J. Chem. Soc., Chem. Commun.*, **1975**, 313.
11) J. Rennert, S. Soloway, I. Waltcher, and B. Leong, *J. Am. Chem. Soc.*, **94**, 7242 (1972); M. Freedman, Y. Mohadger, J. Rennert, S. Soloway, and I. Waltcher, *Org. Prep. Proced.*, **1**, 267 (1969).
12) The chemistry of bichromophore systems is reviewed by F. C. De Schryver, N. Boens, and J. Put in "Advances in Photochemistry," John Wiley & Sons, Inc. (1977), Vol. 9 pp. 359—465.
13) L. Leenders, E. Schoutenden, and F. C. De Schryver, *J. Org. Chem.*, **38**, 957 (1973); F. C. De Schryver, J. Put, L. Leenders, and H. Loos, *J. Am. Chem. Soc.*, **96**, 6994 (1974).
14) F. C. De Schryver, M. De Brackeleire, S. Toppet, and M. Van Schoor, *Tetrahedron Lett.*, **1973**, 1253. N. Boens, M. De Brackeleire, J. Huybrechts, and F. C. De Schryver, *Phys. Chem. NF*, **101**, 417 (1976).
15) J. Put and F. C. De Schryver, *J. Am. Chem. Soc.*, **95**, 137 (1973).
16) M. W. Logue and N. J. Leonard, *J. Am. Chem. Soc.*, **94**, 2843 (1972); N. J. Leonard, R. S. McCredie, M. W. Logue, and R. Cundal, *ibid.*, **95**, 2320 (1973); N. J. Leonard and R. L. Cundal, *ibid.*, **96**, 5904 (1974).
17) H. Tanaka, K. Honda, and N. Suzuki, *J. Chem. Soc., Chem. Commun.*, **1977**, 506.
18) D. S-Frohlinde, H. Blume, and H. Gusten, *J. Phys. Chem.*, **66**, 2486 (1962).
19) D. Gegiou, K. A. Muszkat, and E. Fischer, *J. Am. Chem. Soc.*, **90**, 3907 (1968).
20) D. V. Bent and D. S-Frohlinde, *J. Phys. Chem.*, **78**, 446, 451 (1974).
21) D. S-Frohlinde and D. V. Bent, *Mol. Photochem.*, **6**, 315 (1974).
22) E. Lippert and W. Luder, *J. Phys. Chem.*, **66**, 2430 (1962).
23) G. G. Aloisi, U. Mazzucato, J. B. Birks, and L. Minuti, *J. Am. Chem. Soc.*, **99**, 6340 (1977).
24) P. Bortolus and G. Galiazzo, *J. Photochem.*, **2**, 361 (1973/74).
25) D. I. Schster, M. D. Goldstein, and Bane, *J. Am. Chem. Soc.*, **99**, 187 (1977).
26) R. G. Brown and G. Porter, *J. Chem. Soc., Faraday Trans. 1*, **73**, 1569 (1977).
28) Beilstein Handbuch der Organic Chemie, 9—672.

The Reaction of Group V Metal Alkoxides with Sulfur Dioxide and Selenium Dioxide

Fumio Ando, Jugo Koketsu,* and Yoshio Ishii

Department of Industrial Chemistry, Chubu Institute of Technology, 1200 Matsumoto, Kasugai 487

(Received June 22, 1978)

Trialkoxyarsines (I) and -stibines (II) react with sulfur dioxide to give the corresponding dialkyl sulfites and arsenic trioxide or polymeric residues containing antimony. The reactivity of the compounds (I) is very low, and the yield is poor. Reactions of I and II with selenium dioxide afford dialkyl selenites together with arsenic trioxide or the same polymeric residues containing antimony as in the case of the reaction with sulfur dioxide. The reaction followed a stoichiometry of three moles of trialkyl phosphites (III) and one mole of selenium dioxide yields a 2 : 1 molar ratio of the phosphates : the phosphoroselenoates. A similar reaction of the phosphites with selenium dioxide in a 2 : 1 stoichiometry gives the phosphates and red selenium quantitatively. The rate of oxidation of the phosphorus compounds by selenium dioxide decreases in the order $Bu_3P > BuP(OEt)_2 > P(OEt)_3$. Based on these results, the possible mechanisms have been discussed.

In a previous paper,[1] the reaction of group V metal amides with sulfur dioxide was reported. In the reaction of phosphorus amide, the phosphorus atom is oxidized giving P=O, and P=S compounds. Tris-(dialkylamino)arsine and stibine, however, add across the S=O bond of sulfur dioxide and deoxygenation by the metal atom occurs giving the tetraalkylsulfurous diamides.

Selenium dioxide, a white crystalline solid, has been used as a selective oxidizing agent of organic compounds.[2] There are, however, few reports concerning the reaction of selenium dioxide with the group V metal compounds. Triaryl phosphines, arsines, and stibines react with selenium dioxide to give the corresponding oxides and selenides.[3,4] Esters of arsinous acids $R_2As(OR')$[5] and arsonous acids $RAs(OR')_2$[6] are also oxidized with selenium dioxide to arsinic acid esters $R_2As(O)OR'$ and arsonic acid esters $RAs(O)(OR')_2$, respectively. The oxidation of the cyclic esters of arsonous acid with selenium dioxide however, yields the spirocyclic esters of orthoarsonic acids instead of the normal arsonic acid esters.[7]

Trialkoxyarsines and -stibines are very reactive compounds and react with acetic anhydride[8] and heterocumulenes such as phenylisocyanate[9] and ketene.[10] However no study concerning the reaction between group V metal alkoxides and selenium dioxide has been found except for Dubrovia's report[11] concerning the reaction between triethoxystibine with selenium dioxide. Equally there are no reports of the reactions between group V metal alkoxides and sulfur dioxide. In this paper, the reactions between group V metal alkoxides and sulfur dioxide and selenium dioxide will be reported and discussed.

Results and Discussion

Trialkoxyarsines react very slowly with sulfur dioxide to give a precipitate of arsenic trioxide and dialkyl sulfites in low yields. The reaction was incomplete and large amounts of the starting materials were recovered, even on heating at 100 °C for several months.

The reaction of trialkoxystibines with sulfur dioxide proceeded more readily than that of the arsines to give the corresponding dialkyl sulfites and polymeric residues in place of antimony trioxide. The polymeric residues, which were formulated as $(ROSbO)_n$ on the basis of the elemental analysis showed infrared absorption bands assignable to the Sb–O–Sb[12–14] group (745, 618, and 540 cm^{-1} for $R=Pr^n$) and alkoxyl group. The residues were insoluble in many organic solvents and hydrolyzed in hot water to give antimony trioxide (identified by X-ray powder diffraction). It is interesting to note that the As–O bond is less reactive to sulfur dioxide than Sb–O, and this may be due to improved matching of the sizes of the reaction centers and also to the ionic properties of metal oxygen bonds. As the degree of ionic character in the metal oxygen bond increases when the central metal changes from arsenic to antimony, it appears that the nucleophilic property of the oxygen atom of antimony alkoxide is much greater than that of arsenic alkoxide.

The affinity of the metal atom for oxygen decreases in the order : As>Sb>Bi,[1] and therefore trialkoxystibine is more reactive than trialkoxyarsine, but the poor affinity for the oxygen atom results in the failure of Sb_2O_3 formation. Based on these considerations, one of the possible mechanisms consists of the nucleophilic attack by a alkoxyl group on the sulfur atom rather than the electrophilic attack by the metal on the oxygen atom of sulfur dioxide, to form an insertion product, and the reaction proceeds as follows :

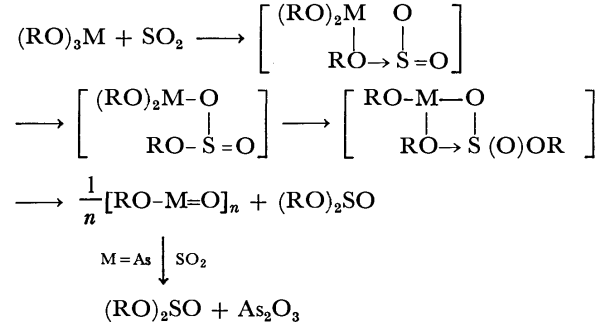

Trialkoxyarsines reacted completely with selenium dioxide in boiling benzene to give arsenic trioxide and the corresponding selenites in poor yield due to the thermal decomposition of the selenites.[15] The reaction of the trialkoxystibines with selenium dioxide also gave the selenites and the polymers, which showed the same physical and spectral properties as those observed in the reaction with sulfur dioxide. An

Table 1. Products of the reaction of trialkoxystibine with sulfur dioxide

$(RO)_2S=O$	Bp (°C/mmHg)	Yield (%)	n_D^{20}	IR ν(S=O)cm^{-1} a)	NMR (δ) ppm b)
R=Et	53—55/16	45	1.4142	1205	1.34 (3H, t) 4.05 (2H, q)
n-Pr	78—79/13	41	1.4236	1208	0.98 (3H, t) 1.70 (2H, m) 3.95 (2H, m)
i-Pr	60.5—62/15	44	1.4150	1200	1.34 (6H, d) 4.78 (H, m)
n-Bu	87—90/5	56	1.4290	1208	0.94 (3H, t) 1.56 (4H, m) 3.97 (2H, m)

a) Coated on KBr plate. b) In CCl_4.

Table 2. Oxidation products of trialkyl phosphites with selenium dioxide in the ratio of 3 : 1

$(RO)_3P$	$(RO)_3P=O$ compound		$(RO)_3P=Se$ compound		
	Yield (%)	IR ν(P=O) cm^{-1}	Yield (%)	IR ν(P=Se) cm^{-1}	NMR (δ) ppm a)
$(MeO)_3P$	49	1275	27	557, 502	3.90 (d, J=14.6)
$(EtO)_3P$	62	1270	18	568, 525	1.35 (t, 3H) 4.20 (dq, 2H, J=10.0)
$(i\text{-}PrO)_3P$	47	1274	21	570, 534	1.34 (d, 6H) 4.83 (m, 1H, J=10.5)
$(n\text{-}BuO)_3P$	50	1277	26	585, 548	0.95 (t, 3H) 1.10—1.88 (m, 4H) 4.20 (dt, 2H, J=9.8)
$(i\text{-}BuO)_3P$	39	1284	12	572, 545	0.97 (d, 6H) 2.00 (m, 1H) 3.88 (dt, 2H, J=8.8)

a) In $CHCl_3$, the J value is J_{POCH} (Hz).

analytical pure sample $(ROSbO)_n$ could not be obtained since it was impossible to completely remove the unreacted selenium dioxide. The structure was however shown to be the same as the product in the reaction of trialkoxystibine with sulfur dioxide. The stoichiometric results of the reactions studied with selenium dioxide are shown in the following equations :

$$2As(OR)_3 + 3SeO_2 \longrightarrow 3(RO)_2SeO + As_2O_3,$$

$$Sb(OR)_3 + SeO_2 \longrightarrow (RO)_2SeO + \frac{1}{n}(ROSbO)_n.$$

The reaction of trialkoxyarsines and -stibines with selenium dioxide may proceed *via* an identical pathway to that of sulfur dioxide.

The reaction of trialkyl phosphites with excess sulfur dioxide was performed at room temperature to yield trialkyl phosphates and trialkyl phosphorothioates in the ratio of 2 : 1, the results of which agree with those reported by Fluck and Binder.[16] The reaction of trialkyl phosphites with selenium dioxide, however, gave different products, depending on the proportions of the reagents used.

The reaction followed a stoichiometry of 3 mol of trialkyl phosphite and 1 mol of selenium dioxide yields a 2 : 1 molar ratio of trialkyl phosphate : trialkyl phosphoroselenoate. The phosphoroselenoates were identified by comparing the spectral data with those of authentic samples[17-19] prepared by the reaction between phosphite and selenium. Ethyl dibutylphosphinite was also oxidized with selenium dioxide to give ethyl dibutylphosphinate and ethyl dibutylphosphinoselenoate. The products from the oxidation in the 3 : 1 stoichiometric ratio are listed in Table 2.

Similar reactions of the phosphites with selenium dioxide in a 2 : 1 stoichiometry gave the phosphates and selenium in quantitative yields.

Trialkyl phosphoroselenoates reacted readily with selenium dioxide to yield the corresponding phosphites and selenium in good yields, the reactions of which are summarized in the following equations :

$$3(RO)_3P + SeO_2 \longrightarrow 2(RO)_3PO + (RO)_3PSe$$

$$2(RO)_3P + SeO_2 \longrightarrow 2(RO)_3PO + Se,$$

$$2(RO)_3PSe + SeO_2 \longrightarrow 2(RO)_3PO + 3Se.$$

The reactivity of trivalent phosphorus compounds toward selenium dioxide has been compared by means of GLC analysis by the same method used in a previous paper[1] and found to decrease in the order, $Bu_3P > BuP(OEt)_2 > P(OEt)_3$. This order is parallel with the order of electron density on the phosphorus atom, and consistents with the order found in the reaction of phosphorus compounds with sulfur dioxide.[1] It may be reasonable to consider the nucleophilic attack by the phosphorus atom on selenium occurs as the first step in the formation of cyclic intermediates followed by the formation of phosphoryl bonds to give trialkyl phosphates and selenium monoxide, which disproportionates into selenium and selenium dioxide. The selenium reacts with unreacted phosphites to provide phosphoroselenoates.

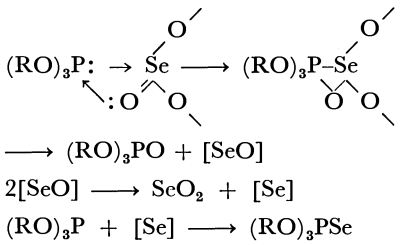

$$\longrightarrow (RO)_3PO + [SeO]$$

$$2[SeO] \longrightarrow SeO_2 + [Se]$$

$$(RO)_3P + [Se] \longrightarrow (RO)_3PSe$$

Experimental

All the reactions as well as preparations of trialkoxyarsines and stibines were conducted under an atmosphere of argon or nitrogen. The IR spectra were taken with a Shimadzu IR-430 spectrometer. The NMR spectra were run on a JEOL-C60 HL spectrometer in CCl_4 or $CHCl_3$ using TMS as internal standard. The analytical GLC was conducted with a Shimadzu GC 6A gas chromatograph using a 3 m glass column packed with 10% PEG 6000.

Materials. Trialkoxyarsines were prepared according to the method described by Brill and Campbell;[20] $As(OMe)_3$; bp 90—96 °C/35 mmHg, $As(OEt)_3$; bp 120—126 °C/18 mmHg, $As(OPr^n)_3$; bp 107—108 °C/43 mmHg, $As(OPr^i)_3$; bp 92—94 °C/12 mmHg, $As(OBu^n)_3$; bp 60—72 °C/0.05 mmHg. The preparation of the trialkoxystibines was conducted by the reaction between antimony trichloride and 3 mol of lithium alkoxide. $Sb(OEt)_3$; bp 89—96 °C/0.08 mmHg, $Sb(OPr^n)_3$; bp 70—74 °C/0.05 mmHg, $Sb(OPr^i)_3$; bp 39—44 °C/0.03 mmHg, $Sb(OBu^n)_3$; bp 81—89 °C/0.15 mmHg.

Triisopropyl phosphite,[21] triisobutyl phosphite,[21] diethyl butylphosphonite,[22] ethyl dibutylphosphinite,[23] and tributyl phosphine[24] were prepared by the methods previously reported. The other phosphorus compounds were obtained commercially and distilled prior to use.

Reaction of Trialkoxyarsines with Sulfur Dioxide. The triisopropoxyarsine (1.56 g, 6.24 mmol) was dissolved in an excess of liquid SO_2 and heated in sealed tube at 100 °C for 4 months during which time white precipitates of arsenic trioxide (0.20 g, 33% yield) were formed. The liquid part of the reaction mixture gave the fraction (0.76 g, bp 40—52 °C/50 mmHg) by distillation under reduced pressure. GLC analysis showed the presence of diisopropyl sulfite together with the starting material. These two compounds were identified by comparing the GLC retention times with those of authentic samples.

Reaction of Trialkoxystibines with Sulfur Dioxide. A mixture of triethoxystibine (2.76 g, 10.7 mmol) and excess sulfur dioxide was heated at 100 °C for 3 d in a sealed tube. After removal of the white precipitates and the excess sulfur dioxide, diethyl sulfite (1.00 g, 45%) was obtained by distillation under reduced pressure; bp 53—55 °C/16 mmHg, IR ν(S=O) 1205 cm^{-1}, NMR (CCl_4) δ=1.34 (3H, t), 4.05 (2H, q). The precipitates had strong infrared bands assignable to the Sb–O–Sb group (745, 618, 585 cm^{-1}) and the alkoxyl group (2980, 2940, 2900, 1225, 1170, 1120, 1065. 1015, and 920 cm^{-1}). Found; C, 13.8; H, 2.65%. Calcd for $C_2H_5O_2Sb$; C, 13.14; H, 2.76%. The reactions of other trialkoxystibines with sulfur dioxide were performed in the same way, the results of which are shown in Table 1. The white precipitates in each reaction also showed the same IR spectra as reported above and identified to be $(ROSbO)_n$.

Reaction of Trialkoxyarsines with Selenium Dioxide. A mixture of trimethoxyarsine (1.2 g, 7.20 mmol) and selenium dioxide (1.20 g, 10.8 mmol) in benzene (10 ml) was heated in a sealed tube at 100 °C for 2 d. The As_2O_3 precipitate was then filtered and the solvent removed using a rotary evaporator. The remaining product was distilled under vacuum to yield dimethyl selenite (1.41 g, 83%); bp 64—65 °C/15 mmHg, IR (neat) ν(Se=O) 926 cm^{-1}, ν(Se–O) 632 cm^{-1}; NMR (CCl_4) δ=3.70 (S).

Similar treatment of triethoxyarsine (1.45 g, 6.90 mmol) with selenium dioxide (1.15 g, 10.4 mmol) gave diethyl selenite (1.19 g, 62%); bp 76—76.5 °C/15 mmHg; IR (neat) ν(Se=O) 934 cm^{-1}, ν(Se–O) 632 cm^{-1}, NMR (CCl_4) δ=1.27 (3H, t), 4.03 (2H, m). The reaction of tri-*n*-propoxyarsine (1.90 g, 7.53 mmol) with selenium dioxide (1.26 g, 11.3 mmol) gave di-*n*-propyl selenite (1.58 g, 65%); bp 77—78 °C/2.5 mmHg; IR (neat) ν(Se=O) 930 cm^{-1}, ν(Se–O) 634 cm^{-1}; NMR (CCl_4) δ=0.98 (3H, t), 1.65 (2H, m), 3.94 (2H, m). The reaction of triisopropoxyarsine (1.76 g, 6.99 mmol) and tributoxyarsine (1.71 g, 5.80 mmol) with selenium dioxide gave the following products, respectively; diisopropyl selenite (1.08 g, 51%); bp 78—81 °C/14 mmHg; IR (neat) ν(Se=O) 940 cm^{-1}, ν(Se–O) 640 cm^{-1}; NMR (CCl_4) δ=1.30 (6H, m), 4.85 (1H, m), and dibutyl selenite (0.85 g, 41%); bp 127—129 °C/12 mmHg; IR (neat) ν(Se=O) 924 cm^{-1}, ν(Se–O) 635 cm^{-1}; NMR (CCl_4) δ=0.96 (t, 3H), 1.50 (m, 4H), 3.97 (m, 2H).

Reaction of Trialkoxystibines with Selenium Dioxide. A mixture of triethoxystibine (2.13 g, 8.29 mmol) and selenium dioxide (1.31 g, 11.8 mmol) was allowed to react at 100 °C for 3 d. After removal of the precipitates by filtration, the filtrate was distilled under vacuum to give diethyl selenite (0.76 g, 33%). Under similar conditions, tri-*n*-propoxystibine (2.09 g, 6.98 mmol) reacted with selenium dioxide and gave di-*n*-propyl selenite (0.76 g, 34%). Also diisopropyl selenite (0.88 g, 41%) and di-*n*-butyl selenite (0.52 g, 53%) were obtained by the reaction of selenium dioxide with triisopropoxystibine (1.99 g, 6.72 mmol) and tri-*n*-butoxystibine (1.15 g, 3.36 mmol), respectively.

The white precipitates obtained in each reaction exhibited the same IR absorptions as those obtained in the reaction of the corresponding trialkoxystibine with sulfur dioxide.

Reaction of Trialkyl Phosphites with Sulfur Dioxide. When an excess of dry sulfur dioxide was bubbled through trimethyl phosphite (2.20 g, 17.7 mmol) at −78 °C, an exothermic reaction took place which gave a colorless solution after standing for 30 min at room temperature. The reaction mixture was distilled to give a distillate (2.28 g) of boiling point range bp 71—78 °C/14 mmHg . From the mixture, trimethyl phosphate (1.35 g, 63%) and trimethyl phosphorothioate (0.75 g, 31%) were obtained by column chromatography (silica gel–chloroform). In a similar manner, triethyl phosphite (1.96 g, 11.8 mmol) reacted with sulfur dioxide to yield triethyl phosphite (1.14 g, 53%) and triethyl phosphorothioate (0.68 g, 29%). Triisopropyl phosphite (2.50 g, 11.7 mmol) also underwent a similar reaction to give triisopropyl phosphate (1.42 g, 54%) and triisopropyl phosphorothioate (0.76 g, 27%). These compounds were identified by comparing the physical (bp) and spectroscopic (IR and NMR) data with those of the authentic samples.[17]

Reaction of Trialkyl Phosphites with Selenium Dioxide in the Molar Ratio 3 : 1. Trimethyl phosphite (2.48 g, 20.0 mmol) was added slowly with stirring to selenium dioxide (0.74 g, 6.66 mmol) suspended in benzene (5 ml) at room temperature, and the solution stirred for 2 h. After removal of the solvent, the reaction mixture was distilled under reduced pressure. The distillate (3.04 g, bp 84—90 °C/15 mmHg) was subjected to column chromatography (silica gel–chloroform) to give trimethyl phosphate (1.39 g, 49%), and trimethyl phosphoroselenoate (1.10 g, 27%), IR (neat) ν(P=Se) 557, 502 cm^{-1}, NMR ($CHCl_3$) δ=3.74 (d, J_{POCH}=

14.4 Hz.

Further oxidations of phosphites with seleniium dioxide were conducted according to the same procedure as reported above, the results of which are shown in Table 2.

Reaction of Trialkyl Phosphites with Selenium Dioxide in the Molar Ratio 2 : 1. Trimethyl phosphite (1.77 g, 14.3 mmol) was added to selenium dioxide (0.79 g, 7.12 mmol) in benzene (5 ml) at room temperature. An exothermic reaction took place giving a red precipitate. The mixture was stirred overnight and the red selenium (0.47 g, 84%) was then filtered and the solvent removed from the filtrate using a rotary evaporator. The remaining product was distilled under reduced pressure to yield trimethyl phosphate (1.68 g, 84%); bp 77—78 °C/13 mmHg. Similar treatment of triethyl phosphite (1.94 g, 11.6 mmol) with selenium dioxide (0.65 g, 5.82 mmol) gave triethyl phosphate (1.89 g, 89%); bp 94—95 °C/12 mmHg and selenium (0.38 g, 82%).

Reaction of Trialkyl Phosphoroselenoates with Selenium Dioxide. The reaction of trimethyl phosphoroselenoate (0.87 g, 5.26 mmol) with selenium dioxide (0.24 g, 2.15 mmol) was conducted in benzene (5 ml) to produce trimethyl phosphate (0.46 g, 76%) and selenium (0.46 g, 91%). From triethyl phosphoroselenoate (1.29 g, 5.26 mmol) and selenium dioxide (0.29 g, 2.63 mmol) were obtained triethyl phosphate (0.92 g, 96%) and selenium (0.62 g, 100%).

Effect of Substituent on the Reactivity. A reactivity comparison of trivalent phosphorus compounds towards selenium dioxide was performed by mixing each reagent (0.05 mmol/l) in ethanol at −78 °C and determining by GLC analysis the remaining amount of trivalent phosphorus compound under the same conditions used in a previous paper.[1] The following figures show the remaining amounts of phosphorus compounds (mmol/l) after 30 min; Bu_3P : (0), $BuP(OEt)_2$: (0.0182), $P(OEt)_3$: (0.0485).

References

1) F. Ando, J. Koketsu, and Y. Ishii, *Bull. Chem. Soc. Jpn.*, **51**, 1481 (1978).
2) N. Rabjohn, *Org. React.*, **24**, 261 (1976).
3) N. N. Melnikov and M. S. Rokistskaya, *Zh. Obshch. Khim.*, **8**, 1834 (1938).
4) S. I. A. El Sheikh, M. S. Patel, B. C. Smith, and C. B. Waller, *J. Chem. Soc., Dalton Trans.*, **1977**, 641.
5) L. M. Werbel, T. D. Dawson, J. R. Hooton, and T. E. Dalbey, *J. Org. Chem.*, **22**, 452 (1957).
6) G. Kamai and B. D. Chernokal'skii, *Zh. Obshch. Khim.*, **33**, 2904 (1960).
7) M. Wierber, B. Eichhorn, and J. Gotz, *Chem. Ber.*, **106**, 2738 (1973).
8) J. Koketsu, F. Ando, and O. Kato, *Nippon Kagaku Kaishi*, **1977**, 1669.
9) R. C. Mehrotra, A. K. Rai, and R. Bohra, *Syn. React. Inorg. Metal-org. Chem.*, **5**, 289 (1975).
10) V. L. Foss, E. A. Basolova, and I. F. Lutsenko, *J. Gen. Chem. USSR*, **35**, 764 (1965).
11) O. D. Dubrovina, Uchenye. Zapiski, *Kazan. Gosudarst. Univ. im. V. I. Ul'yanova-Lenina*, **116**, 3 (1956), *Chem. Abstr.*, **51**, 6534i (1957).
12) D. L. Venzky, C. W. Sink, B. A. Nevett, and W. F. Fortescue, *J. Organomet. Chem.*, **35**, 131 (1972).
13) W. Levason, C. A. McAuliffe, and S. G. Murray, *J. Organomet. Chem.*, **88**, 171 (1975).
14) G. Chremos and R. Zingaro, *J. Organomet. Chem.*, **22**, 637 (1970).
15) N. Sonoda, *Yuki Gosei Kagaku Kyokai Shi*, **30**, 739 (1972).
16) E. Fluck and H. Binder, *Z. Anorg. Allg. Chem.*, **354**, 139 (1967).
17) G. M. Kosolapoff and L. Maier, "Organic Phosphorus Compound," Wiley-Interscience (1976), Vol. 7, Chap. 19, and references cited therein.
18) L. C. Thomas and R. A. Chittenden, *Spectrochim. Acta*, **20**, 31 (1964).
19) W. McFarlance and D. S. Rycroft, *J. Chem. Soc., Dalton Trans.*, **1973**, 2162.
20) T. B. Brill and N. C. Campbell, *Inorg. Chem.*, **12**, 1884 (1973).
21) A. H. Ford-Moore and B. J. Perry, *Org. Synth.*, Coll. Vol. **4**, 955 (1963).
22) A. K. Kazuonov and O. A. Mukhacheva, *Zh. Obsch. Khim.*, **26**, 1436 (1956), *Chem. Abstr.*, **50**, 14325g (1956).
23) M. Sander, *Chem. Ber.*, **93**, 1220 (1960).
24) G. B. Kauffman and L. A. Teter, *Inorg. Synth.*, **6**, 87 (1960).

Synthesis of Decachloro-4-allylidenecyclopentene and Its Chemistry[1)]

Kousuke KUSUDA* and Alfred ROEDIG†

Research Institute for Atomic Energy, Osaka City University, Sugimoto-cho, Sumiyoshi-ku, Osaka 558
† *Institut für Organische Chemie, Universität Würzburg, 87 Würzburg, Am Hubland, West Germany*

(Received June 23, 1978)

Decachloro-4-allylidenecyclopentene (**6**) was synthesized by the reaction of pentachlorocyclopentadiene with hexachloropropene in the presence of anhydrous aluminium chloride. Hexachloro-2-allylidene-4-cyclopentene-1,3-dione (**11**), prepared from **6** by treatment with concd nitric acid, cyclized to hexachloro-2,5-dihydrocyclopenta[*b*]pyran-5-one (**14**) on heating. In a solvent such as acetone and acetonitrile, **14** rearranged to hexachloro-2,5-dihydrocyclopenta[*b*]pyran-2-one (**18**) at room temperature. The mechanism of this rearrangement is discussed. Hydrolysis of **14** by 90% sulfuric acid afforded tetrachloro-2,5-dihydrocyclopenta[*b*]pyran-2,5-dione (**15**), which was obtained directly from **6** by treatment with sulfuric acid. The reactions of **11** with anhydrous methanol, and of **15** with diazomethane were investigated.

As a part of our study to synthesize new cyclic conjugated chlorocarbons, we have investigated the reaction of 1,1,2,3-tetrachloropropenium cation (**2**) with hexachlorocyclopentadiene (**1**) at 80 °C, obtaining decachlorobicyclo[3.3.0]octa-2,6-diene (**3**).[2)] The reaction of pentachloropropenium cation (**5**)[3)] with 1,2,3,4,5-pentachlorocyclopentadiene (**4**) has similarly attracted our interest.

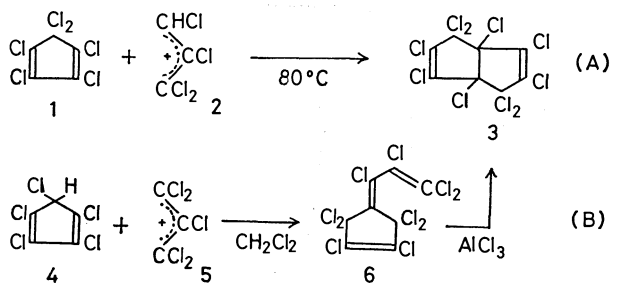

The reaction of **4** with **5** at 80 °C gave a mixture of **3** and a small amount of white crystals of unknown structure (**6**). When the reaction was carried out in refluxing dichloromethane, **6** was obtained in a 87% yield. Treatment of **6** with a catalytic amount of anhydrous aluminium chloride in refluxing carbon tetrachloride afforded **3** quantitatively. This cyclization suggests that **6** is a stable intermediate of reaction B. The mechanism of reaction A seemed to differ from that of B, because **6** could not be detected in the products of reaction A carried out in refluxing dichloromethane. The infrared spectrum of **6** shows three absorptions in the double bond region. Two peaks at 1207 and 1195 cm^{-1} are suggestive of polychlorinated five membered ring, and a peak at 810 cm^{-1} is seemingly due to a double allylic dichloromethylene.[5)] The UV spectrum of **6** (Fig. 1) shows that the three double bonds are not fully conjugated. The ^{13}C NMR spectrum of **6** (Table 1) shows the presence of six sp^2 carbons and two doubly allylic dichloromethylene carbons,[6)] both of which are under similar circumstances in the molecule.

Although chlorination of **6** in carbon tetrachloride was uncuccessful, treatment in liquid chlorine with irradiation by sunlight gave octachloro-4-methylenecyclopentene (**10**).[7)] Dechlorination of **6** with copper powder gave brownish red crystals of (**9**), which was identified with an authentic sample of the dimer of hexachloropentalene[3a,8)] by their IR spectra. This transformation is well interpreted by assuming intermediary formation of octachloro-6-vinylfulvene (**7**) followed by ring closure and dechlorinative dimerization. Structure **6** is fully consistent with the beforementioned spectral data and its chemical transformations.

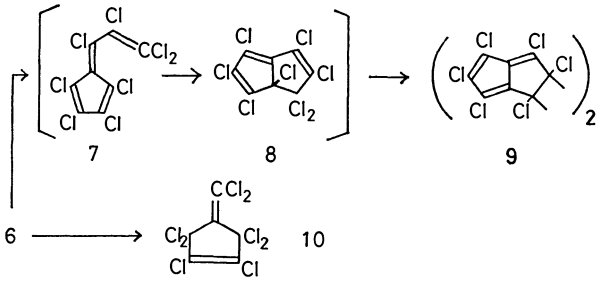

When 1,2,3,4-tetrachlorocyclopentadiene was allowed to react with **5** in refluxing dichloromethane, a small amount of octachlorobicyclo[3.3.0]octa-1,4,6-triene[4)] was the only product isolated.

Treatment of **6** with 20% fuming nitric acid gave pale yellow crystals. Assignment of the structure (**11**) to the product follows from the elemental analysis, spectroscopic data, and the analogous reaction of **10** to give tetrachloro-2-methylene-4-cyclopentene-1,3-dione.[7)] In the reaction of this 1,3-dione with ethanol, an exocyclic dichloromethylene group is eliminated to give (**13**).[9)] Therefore, a similar reaction could be expected for **11**, which also has carbonyl groups on both sides of the exocyclic group. By heating 2 h in refluxing methanol, **11** was converted to the compound $C_{11}H_{10}Cl_4O_5$, the spectral data of which point to a monoketalized triketone (**12**) as shown. An attempted hydrolysis of the ketal group with hydrochloric acid in refluxing methanol gave a cyclopentenedione **13**.[10)] Identification of the product with an authentic sample was carried out by measurement of the mixed melting point and comparison of their IR spectra. The results suggests intermediary formation of an unstable triketone. When **11** was heated in refluxing carbon tetrachloride under anhydrous conditions, deep red crystals of (**14**) were formed in high yield. Assignment of the structure **14** was based on its IR, UV, and ^{13}C NMR spectra as well as on its formation from **11** and the conversion to (**15**) by 90% sulfuric acid.

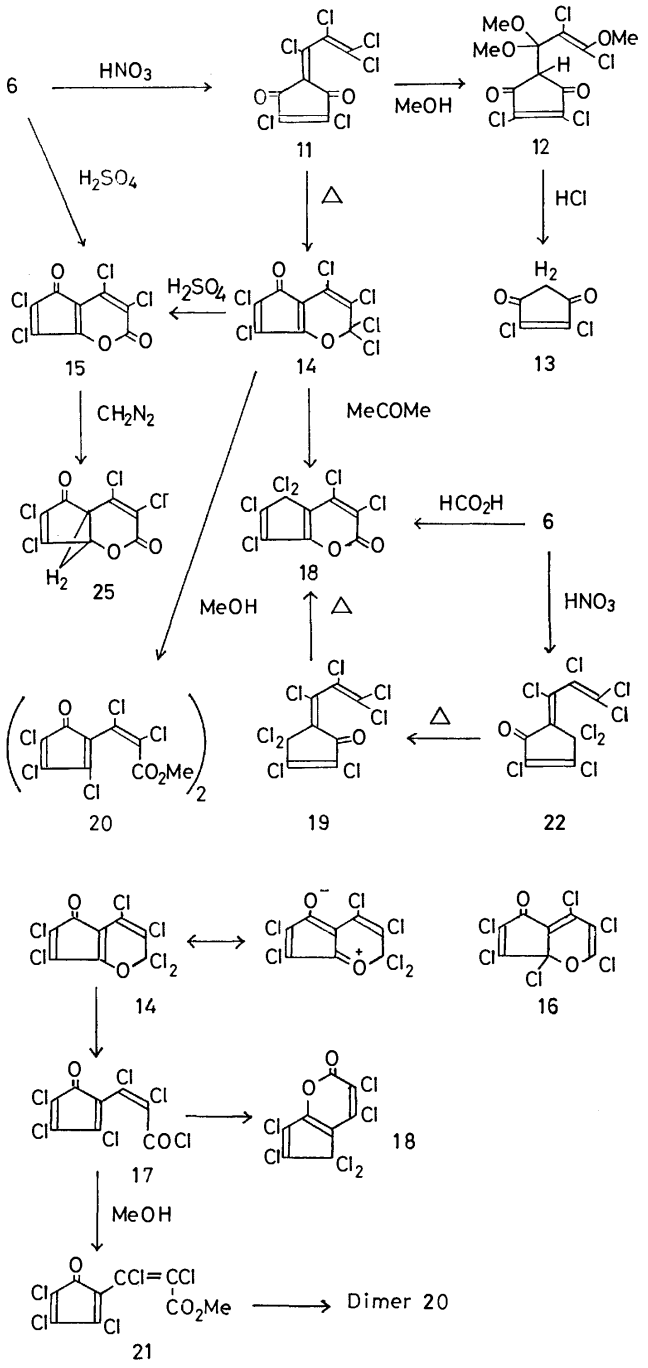

The formation of **14** is significant in view of the mechanism of 1,5-pentadiene-oxygen rearrangements.[12] Because the pyran **14** is stabilized by mesomerism,[1] 1,5-sigmatropic chlorine shift followed by ring opening of the second pyran intermediate (**16**) to an acyl chloride (**17**) is not so favored.

Crystalline **14** decomposed slowly in the air with evolution of hydrogen chloride; however, the solution of **14** in a nonpolar solvent was stable in a dark place. In a polar solvent such as acetone, ethyl acetate, and acetonitrile, an unexpected rearrangement occurred leading to (**18**) at room temperature. Figure 2 shows UV spectra of these compounds. The longest wavelength maxima of both **14** and **15** seem to be due to a cyclopentadienone chromophore.[13] The broad

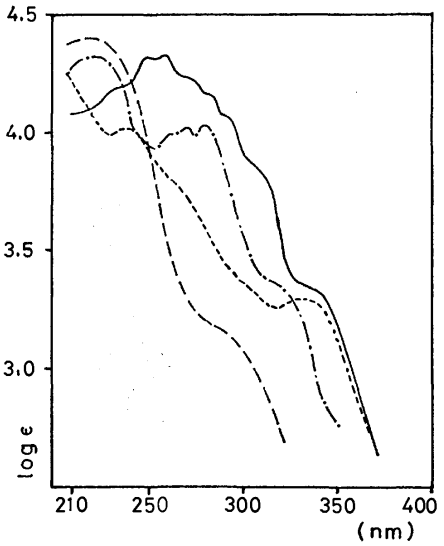

Fig. 1. Ultraviolet spectra of **6**, **11**, **19**, and **22**: — — — **6**; —— **11**; ------ **19**; —·—·— **22**.

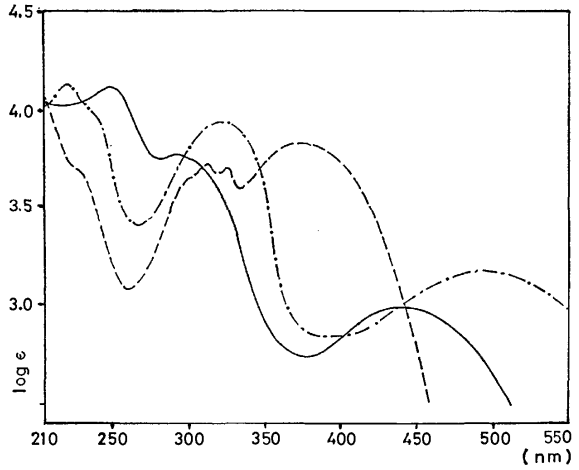

Fig. 2. Ultraviolet spectra of **14**, **15**, and **18**: —— **14**; —·—·— **15**; ———— **18**.

maximum of **18** at 380 nm is due to polychlorinated α-pyrone.[14] Cyclization of (**19**) under mild conditions, resulting in the formation of **18**, and the spectral data indicated the double bond location and the presence of α-pyrone ring in **18**.

When anhydrous methanol was added to **14**, a moderate exothermal reaction took place to afford white crystals, $C_{18}H_6Cl_{10}O_6$ (**20**). Although the structure is unknown, the high resolution mass spectrum of **20** indicates that it is a dimer of (**21**), $C_9H_3Cl_5O_3$, which corresponds to the base peak of the mass spectrum. Plausible mechanisms for the formation of **18** and **20** could be outlined as follows. In a polar solvent, a chlorine migration followed by ring opening takes place, giving an acid chloride **17**, which either reacts with methanol and dimerizes to **20** or, without any reactive materials in the reaction medium, cyclizes to **18**.

On the other hand, the reaction of **6** with dilute nitric acid yielded a pale yellow monoketone (**22**). The transformation is similar to that of **10** with nitric

Table 1. ^{13}C data of selected compounds[a,b]

Compound No.	>C=O	>=<	Saturated
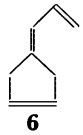 **6**	c)	139.8 137.8 135.5 135.3 128.1 122.1	80.9 82.0
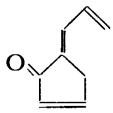 **22**	d) 174.4	158.5 141.6 137.6 135.4 126.8 123.4	80.7
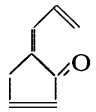 **19**	e) 162.0	138.9 137.6 134.2 132.4 128.9 128.0	83.0
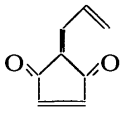 **11**	c) 180.2 179.3	153.7 151.4 140.7 128.2 127.3 124.6	
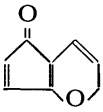 **14**	f) 180.3	163.4 149.3 143.8 131.6 130.8 122.6	121.7
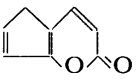 **18**	c) 156.9	155.5 144.2 143.8 126.9 121.1 119.5	80.4
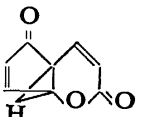 **25**	g) 185.0 155.3	144.4 129.6 123.7	70.0 43.9 34.4
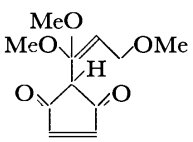 **12**	h) 179.5 164.6	156.1 143.3 137.6 128.9	103.4 77.2 54.5 53.7 51.8
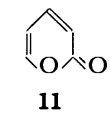 **11**	i) 153.3	146.6 144.8 120.2 112.4	

a) All positions are substituted by chlorine unless indicated. b) Spectra were run in the solvent cited and the data reported in ppm downfield from external TMS converted from the solvent internal standand using (CD_3COCD_3) methyl carbon 29.7, (dioxane) 67.4, (CCl_4) 94.0, ($CDCl_3$) 76.9, (CH_3COCH_3) methyl carbon 30.4, ($CHCl_3$) 77.2, (C_6D_6) 128.0 (Ref. 25, p. 23); accuracy ±0.1 ppm. c) CD_3COCD_3. d) Neat sample; dioxane was used as an external standard. e) CCl_4. f) $CDCl_3$. g) CH_3COCH_3. h) $CHCl_3$. i) C_6D_6.

acid or sulfuric acid.[7] Although **22** was stable at room temperature or during the chromatographic separation, vacuum distillation at 180 °C or heating in refluxing carbon tetrachloride promoted an (*E*)-(*Z*) rearrangement to **19**. In contrast to the (*E*)-ketone **22**, **19** cyclized to **18** during chromatographic separation on silica gel or in the air with the gradual liberation of hydrogen chloride. These chemical behavior as well as the IR, UV, and ^{13}C NMR spectra of both monoketones support the proposed structures. Reaction of **6** with fuming sulfuric acid yielded **15** and two kinds of dimers $C_{16}Cl_8O_6$, (**23**) and (**24**) of unknown structure, which could be distinguished by the IR spectra. It is interesting that **15** gave **23** in ether, while it gave **24** in acetone-d_6 at room temperature.

Since the 1,3-dipolar cycloaddition of diazomethane to tetraphenylcyclopentadienone has been reported,[16] we wanted to compare the reactivity of the two double bonds in the cyclopentadienone moiety of **15**. The structure (**25**) was assigned on the basis of its high resolution mass, IR, ^1H NMR, ^{13}C NMR, and UV spectra. The latter shows one absorption maximum at 257 nm, indicating the existence of α,β-unsaturated carbonyl chromophore. Addition of diazomethane[17] preferentially at the middle double bond of **15** may be explained in terms of the cationic quasi-aromatic character of the α-pyrone moiety.

Experimental

General. The melting points were determined on a Yanagimoto micro melting point apparatus and were uncorrected. Elemental analyses of carbon, hydrogen, and nitrogen were performed by Mr. J. Goda of Osaka City University. Chlorine analyses, when required, were carried out according to the combustion method by use of a modified flask.[18] IR spectra were recorded on a Perkin-Elmer Model 337 spectrophotometer as mulls in Nujol betweeen NaCl disks or as a solution of carbon tetrachloride. Only significant absorptions are reported. UV spectra were recorded on a Hitachi EPS-20 spectrophotometer as solutions in hexane. Nuclear quadrupole resonance spectra were recorded on a Decca Radar NQR spectrometer at 77 K. Both proton and ^{13}C NMR spectra were recorded on a JEOL FX-60 Fourier transform NMR spectrometer. Gas chromatographic analyses were performed on a Nikki Model G-77 gas chromatograph using a 2 m 10% SE-30 column with helium flow. Mass spectra were recorded on a JEOL JMS-D 300 high resolution mass spectrometer.

*Decachloro-4-allylidenecyclopentane (**6**).* To a solution of 50.3 g(0.211 mol) of hexachloropropene[20] in 50 ml of dried dichloromethane was added 2.0 g of powdered anhydrous aluminium chloride,[21] and the mixture was stirred at room temperature. Owing to an exothermal reaction, the mixture began to reflux after several minutes with the evolution of hydrogen chloride.[22] After the exothermal reaction had come to an end, the mixture was heated to reflux for 2 h with mechanical stirring . After having been kept at room temperature over night, the reaction mixture was poured into ice–water to decompose the complex. The organic layer was separated and the water solution was extracted with carbon tetrachloride. The combined solution was dried over anhydrous sodium sulfate and filtered, and evaporation of the solvent under reduced pressure afforded sludge. Crystals precipitated from the sludge by the

addition of ethanol were collected by vacuum filtration. Yield: 71.1 g. After the mother solution was evaporated under reduced pressure, the residue was distilled at 150 °C under 30—36 mmHg to collect a mixture of the starting materials (44.7 g). Crude **6**(13.4 g) was obtained from the crystalline residue by washing with ethyl alcohol. Total yield was 84.5 g(89%). Recrystallization from ethyl acetate gave an analytical sample. Mp 108 °C;[23] IR: 1648, 1620, 1565(-C=C-); UV: λ_{max} (nm, log ε) 221(4.41), 285(3.09); NQR: (MHz) (77 K) 37.220, 37.607. 37.618, 38.026, 38.100, 38.262, 38.520, 38.733, 38.854, 38.975; (Found: C, 21.47; Cl, 78.45%).

Chlorination of ***6*** *in Liquid Chlorine.* In an annealed glass tube (wall thickness: 4 mm, outside diameter: 19 mm × 180 mm), 10.0 g(2.22×10^{-2} mol) of **6** and about 10 ml of liquid chlorine were sealed at −70 °C. The mixture was exposed to the sunlight for two weeks at Osaka in May, giving a transparent liquid chlorine solution. Having been chilled in a Dry Ice–acetone bath, the tube was opened. The chlorine was allowed to evaporate at room temperature under atmospheric pressure and finally under reduced pressure by using an aspirator, and the light yellow residue was distilled at 150 °C(bath)/0.5 mmHg. The crystals which appeared in the distillate on standing at room temperature were collected by filtration, and washed with a small amount of ethanol. Yield : 3.9 g. The product was identified as octachloro-4-methylenecyclopentene by comparison of the IR spectrum with that of an authentic sample.[7]

Dechlorination of ***6*** *with Copper Powder.* A mixture of 5.0 g(8.0×10^{-2} g·atom) of copper powder and 9.0 g(2.0×10^{-2} mol) of **6** in petroleum ether (bp: 30—50 °C) was heated to gentle refluxing with brisk mechanical stirring for 4 days. Insoluble materials were removed by filtration and washed with hot petroleum benzine (bp : 100—140 °C). The solvent was evaporated under vacuum and the residue was triturated with a mixture of petroleum benzine and ethyl alcohol, giving 4.6 g of brown powder. The crude product was dissolved in chloroform and then the small amount of insoluble materials was removed by filtration. After the red solution had been concentrated, petroleum ether was added to precipitate orange crystals. The mother solution was cooled in an ice-bath, and the crystals which precipitated from the solution were collected by filtration. The product was identified as a dimer of hexachloropentalene by means of its IR spectra.

Isomerization of ***6*** . To a solution of 3.22 g(1.6×10^{-2} mol) of **6** in 10 ml of carbon tetrachloride was added a catalytic amount of anhydrous aluminium chloride. The greenish color of a complex appeared immediately. The mixture was heated to gentle reflux with mechanical stirring for 6 h. The reaction mixture was treated in the usual way, giving 3.60 g of light brown crystals of **3**, from which a pure sample was obtained by washing with methanol.

*(E)-Octachloro-5-allylidene-2-cyclopenten-1-one (****22****).* A mixture of 5.0 g(11 mmol) of **6** and 15.0 mol of the nitric acid solution prepared by mixing 50 ml of fuming nitric acid (d=1.52) and 10 ml of nitric acid (d=1.38) was stirred for 40 min at room temperature(19 °C). The reaction mixture was poured into ice–water and the organic products were extracted with carbon tetrachloride. The solution was dried over sodium sulfate and evaporated under reduced pressure, giving 5.2 g of a yellow oily product. Addition of petroleum ether to the product precipitated 1.8 g of **6**, which was removed by means of vacuum filtration. The mother solution was chromatographed on a 22 mm × 35 cm column of silica gel (Mallinckrodt, 100 mesh) by use of petroleum ether at the beginning, followed by 5% acetone in petroleum benzine as an eluent. Unreacted **6** (0.52 g) was obtained from the first band. The second fraction, containing **6** and **22** was followed by a band containing 2.2 g of pure **22**. Evaporation of the solvent under reduced pressure at room temperature gave an analytical sample. IR: 1735 (>CO), 1640, 1590, 1570 (-C=C-), 1240, 1190, 800, 720, 710; UV: λ_{max} 224(4.30), 262 sh(3.91), 272(3.98), 281(3.99), 290sh(3.86), 310sh(3.39), 322sh(3.30); ^{13}C NMR : see Table 1. Found: C, 23.92; H, 0.16%. Calcd for C_8Cl_8O: C, 24.28%.

*(Z)-Octachloro-5-allylidene-2-cyclopentene-1-one (****19****).* 518 mg of **22** that had been purified by column chromatography on silica gel was sealed in a small glass tube. The tube was heated to 100 °C for 6 h in a water bath. The ampoule was opened and the oily product was taken up in petroleum ether. This solution was chromatographed on a column (13 mm × 10 cm) of silica gel by use of 50 ml of petroleum ether and then 40 ml of 3% acetone in petroleum ether as eluent. Pure **22** (180 mg) was recovered by evaporation of the first yellow eluate (25 ml). The second (20 ml) and the third(25 ml) fractions afforded small amounts of oily materials. A subsequent fraction, obtained from the deep yellow band, afforded 318 mg of **19**. Monoketone **22** isomerized to **19** on distillation at 170—180 °C(bath) under a pressure of 2 mmHg. IR: 1760(>CO), 1630, 1590, 1545 (-C=C-), 1230, 1155, 1105, 800, 710; UV: λ_{max} 240(4.00), 330(3.30); ^{13}C NMR: see Table 1. Found: C, 24.76; H, 0.12; Cl, 71.89%. Calcd for C_8Cl_8O: C, 24.28; Cl, 71.68%.

Reaction of ***22*** *with Anhydrous Aluminium Chloride.* A mixture of 50 mg of **22** and 50 mg of anhydrous aluminium chloride in 5 ml of dried carbon tetrachloride was refluxed for 4.5 h. The reaction complex was quenched by pouring into ice–water. The product, isolated by conventional extraction procedures, was crude **18**, which was purified by recrystallization from petroleum ether.

Reaction of ***6*** *with 89% Formic Acid; Hexachloro-2,5-dihydrocyclopenta*[b]*pyran-2-one (****18****).* A mixture of 5.0 g (1.1×10^{-2} mol) of **6** and 20 ml of commercially available formic acid(98%) was heated to gentle reflux with stirring for 3 h. The deep yellow reaction mixture was cooled to room temperature, precipitating black materials. The oily black mateirals separated from the formic acid solution by decantation, were triturated in a small amount of methanol to give 1.1 g of slightly gray crystals of **3**. The formic acid solution was diluted with 150 ml of water, and extracted 4 times with chloroform. The extract(50 ml) was washed with water, dried over anhydrous sodium sulfate, and evaporated *in vacuo*. The oily residue (1.77 g) solidified on standing at room temperature. The water layer was further extracted twice with ether, and the solvent was evaporated to yield 0.67 g of **18**. The combined crystals were recrystallized twice from a mixture of benzene and petroleum ether and once from benzene ; mp 117 °C. The mother solution containing crude product was chromatographed on a silica gel column by using chloroform as an eluent. The crystals obtained from the first fraction were recrystallized from petroleum ether to give an analytical sample, mp 118—120 °C. IR: 1745 broad(CO), 1610, 1560, 1500(-C=C-), 1405, 1360, 1188, 1178, 1132, 895, 883, 805; UV: λ_{max} 230 sh(3.75), 305sh(3.66), 317(3.74), 330(3.71), 380(3.85); ^{13}C NMR: see Table 1. Found: C, 28.30; H, 0.07%. Calcd for $C_8Cl_6O_2$: C, 28.20%.

Reaction of ***6*** *with Fuming Nitric Acid; Hexachloro-2-allylidene-4-cyclopentene-1,3-dione (****11****).* A mixture of 10 g (2.2×10^{-2} mol) of **6** and 30 ml of fuming nitric acid(d=1.53) was placed in a 100 ml Erlenmeyer flask equipped with a

magnetic stirring bar and a thermometer. The stirred mixture was heated on a hot plate. The temperature went up to 55 °C after 5 min, and the nitric acid began to reflux after 10 min. The homogeneous reaction mixture obtained by heating for 12 min was poured onto ice–water to precipitate a light yellow oily product. The organic materials were taken up in carbon tetrachloride and dried over sodium sulfate, and the solvent was evaporated on a rotary evaporator at room temperature. The residue (7.1 g) crystallized on standing at room temperature. Washing twice with methanol gave an analytical sample. Mp 88—92 °C; IR: 1710 (>CO), 1630, 1590 (–C=C–); UV: λ_{max} 230sh (4.16), 248(4.32), 255.5(4.32), 267sh(4.21), 277sh(4.16), 288sh(4.05), 300sh(3.84), 330sh(3.33); ^{13}C NMR: see Table 1. Found: C, 27.93; Cl, 61.66%. Calcd for $C_8Cl_6O_2$: C, 28.20; Cl, 62.42%.

Reaction of ***11*** *with Methanol.* A mixture of 4.03 g (1.18×10^{-2} mol) of **11** and 15.0 ml of anhydrous methanol was heated to gentle reflux for 2 h. The solution was concentrated under vacuum, affording a mixture of sticky oily substance and crystals. Washing the mixture with methanol yielded 0.82 g of white crystals of **12**. Recrystallization twice from petroleum benzine gave an analytical sample. Mp 110—111.5 °C; IR; 1740, 1710(>CO), 1640, 1595(–C=C–), 1450, 1310, 1250; UV: λ_{max} 218—220 (4.13), 285(4.06); ^{13}C NMR: see Table 1. Found: C, 36.55; H, 2.75%. Calcd for $C_{11}H_{10}Cl_4O_5$: C, 36.30; H, 2.70%.

Reaction of ***12*** *with Methanolic Hydrochloric Acid.* A mixture of 3 ml of methanol, 3 ml of concd hydrochloric acid, and 0.264 g (7.95×10^{-4} mol) of **12** was heated to reflux with stirring for 2 h. The reaction mixture was allowed to stand at room temperature, giving colorless needles, which were collected by filtration. Sublimation under reduced pressure gave 81 mg of a pure sample of **13**, mp 167—168 °C, which was identified as the authentic sample by means of infrared spectra.

Thermal Reaction of ***11*** *: Hexachloro-2,5-dihydrocyclopenta*[b]*pyran-5-one (****14****).* A solution of 2.5 g (7.3×10^{-3} mol) of **11** in 25 ml of carbon tetrachloride was heated to reflux for 1.25 h, to give a deep red solution. Evaporation of the solvent and recrystallization of the residue from petroleum benzine afforded an analytical sample. Mp 96.5—100 °C; IR: 1745(>CO), 1620, 1575, 1510(–C=C–), 1250, 1180, 1145, 1100; UV: λ_{max} 254 (4.11), 302 (3.76), 445 (2.97); ^{13}C NMR: see Table 1. Found: C, 28.51; H, 0.15; Cl, 62.40%. Calcd for $C_8Cl_6O_2$: C, 28.20; Cl, 62.42%.

Reaction of ***12*** *with Anhydrous Methanol.* When 10 ml of absolute methanol was added to 2.053 g of **12**, an exothermal reaction took place immediately, giving a yellow precipitate. The crude product (0.20 g) was separated by filtration and recrystallized from ethyl acetate. Mp 245—246 °C; IR : 1755, 1730, 1725 sh (>CO), 1645, 1575 (–C=C–), 1445, 1390, 1290, 1270; Mass: *m/e* 667.7243 (M^+, 31.4), 333.8522 (100); Found: C, 32.13; H, 0.92%. Calcd for $C_9H_3Cl_5O_3$: C, 32.14; H, 0.90%.

Reaction of ***14*** *with Concd Sulfuric Acid.* To a solution of 100 mg (2.93×10^{-4} mol) of **14** in 1 ml of carbon tetrachloride was added 4 ml of 90% sulfuric acid, and the mixture was vigorously stirred with a magnetic stirrer for 6 h at room temperature. After the addition of water, the organic product was separated and extracted with carbon tetrachloride. The combined solution was washed with water and dried over sodium sulfate. Evaporation of the solvent left 96 mg of crude **15**, which gave 45 mg of pure **15** by washing with a small amount of petroleum ether.

Reaction of ***6*** *with Sulfuric Acid : Hexachloro-2,5-dihydrocyclopenta*[b]*pyran-2,5-dione (****15****).* To a mixture of 20 ml of 98% sulfuric acid and 90 g of 20% fuming sulfuric acid was added 32.0 g (7.1×10^{-2} mol) of powdered **6**, whereupon a mild exothermal reaction took place and the mixture changed from dark green to brownish red during 3 h stirring. The mixture was stirred for an additional 45 h at room temperature, and poured onto ice. The precipitated brown solid was isolated by vacuum filtration and washed with water. After being dried overnight, the crude product was 25.5 g in weight. Carbon tetrachloride (200 ml) was added to the powdered product and the suspension was heated to reflux for a short time. Insoluble white crystals were separated by vacuum filtration, and the mother solution was concentrated. The addition of petroleum ether to the solution afforded dark reddish-brown crystals of **15**. Compound **15** dimerizes at approximately 180 °C without melting. IR : 1750 sh, 1730 (>CO), 1625, 1570, 1510 (–C=C–), 1390, 1340, 1160, 1130; UV: λ_{max} 228 (4.16), 332 (3.93), 240 sh (4.04), 488 (2.72); Mass: *m/e* 284 (M^+, 16.2), 256 (19.9), 221 (18.0), 200 (3.9), 193 (4.5), 165 (20.6), 87 (54.4), 43 (100); Found: C, 33.33; H, 0.23; Cl, 49.12%. Calcd for $C_8Cl_4O_3$: C, 33.61; Cl, 49.60%.

The product, which was insoluble in hot carbon tetrachloride, was extracted with 300 ml of benzene by the use of Soxhlet apparatus. The crystals which appeared in the benzene extract were removed by filtration and separated into two parts, powdery crystals **23** and rather big crystals **24**, according to their crystal shape. Compound **23**; mp 337 °C dec; IR: 1788, 1735, 1612, 1535, 1380, 1312, 1195; Found: C, 33.69; H, 0.37; Cl, 50.48%. Calcd for $C_8Cl_4O_3$: C, 33.61; Cl, 49.60%. Compound **24**; 335 °C dec; IR: 1790, 1750, 1617, 1532, 1380, 1310, 1195; Found: C, 33.04; H, 0.22; Cl, 49.60%. Calcd for $C_8Cl_4O_3$: C, 33.61; Cl, 49.60%. Mass: *m/e* 568 (M^+, 5.3), 533 (5.3), 505 (8.6), 371 (18.0), 343 (18.4), 284 (100), 256 (15.8).

Thermal decomposition of **23** was carried out under vacuum in a sublimation apparatus, and reddish brown crystals of **15** were collected on the cold finger condenser. Recrystallization of the product from a mixture of chloroform and petroleum benzine gave a mixture of **23** and **15**.

Reaction of ***15*** *with Diazomethane: 4,5,8,9-Tetrachloro-2-oxatricyclo*[$4.3.1.0^{1,6}$]*deca-4,8-diene-3,7-dione (****25****).* The ether solution of diazomethane, which had been prepared from 5.0 g of *N*-methyl-*N*-nitroso-*p*-toluenesulfonamide according to the conventional method,[24] was added to a suspension of 0.5 g (1.75×10^{-4} mol) of **15** in 5 ml of ether until the red solution became orange. About 1/3 of the diazomethane solution was needed. Excess diazomethane was decomposed with acetic acid, and the reaction mixture was worked up in the usual way. Evaporation of the solvent left a sticky light brown material, which was taken up in 3 ml of benzene, and the solution was chromatographed on a column (12 mm × 12 cm) of silica gel by using benzene. The benzene of the eluate was evaporated under vacuum, and the residue was recrystallized twice from a benzene-petroleum ether mixture. Yield: 0.22 g; IR: 3085 (–CH_2–), 1760, 1730(>CO), 1610, 1590(–C=C–), 1360, 1310, 1030; UV: λ_{max} 257 (4.08); ^{13}C NMR: see Table 1. ^{1}H NMR: ($CDCl_3$) 2.23 (d), 2.70 (d), $|J_{AB}|$=6.1 Hz. Mass: *m/e* 297.8749 (M^+, 34.0), 269.8806 (M^+—CO, 32.5), 262.9078 (M^+—Cl, 49.3), 51 (100); Found: C, 35.83; H, 0.90%. Calcd for $C_9H_2Cl_4O_3$: C, 36.04; H, 0.67%.

The authors wish to express their thanks to Dr. Takashi Tokuyama of Osaka City University for obtaining the mass spectra. We also would like to thank Mr. Junichi Goda for the elemental analysis

of carbon, hydrogen, and nitrogen. The present work was partially supported by a Grant-in-Aid for Public Universities from the Ministry of Education.

References

1) A preliminary report of this work was presented at the 26th IUPAC Congress, Tokyo, 1977; Abstracts of Papers, Sections 4 and 5, p. 1001; see also K. Kusuda, A. Roedig, and G. Bonse, *Chem. Lett.*, **1977**, 819.

2) K. Kusuda, M. Endo, R. West, and V. N. M. Rao, *J. Org. Chem.*, **39**, 1641 (1974).

3) R. West and P. T. Kwitowski, *J. Am. Chem. Soc.*, **88**, 5280 (1966).

4) a) A. Roedig, G. Bonse, and R. Helm, *Chem. Ber.*, **106**, 2156 (1973); b) K. Kusuda and N. Osaka, *J. Chem. Soc., Chem. Commun.*, **1972**, 508.

5) V. Mark and E. D. Weil *J. Org. Chem.*, **36**, 676 (1971).

6) R. C. Griffith, D. M. Grant, and J. D. Roberts, *J. Org. Chem.*, **40**, 3726 (1975).

7) A. Roedig, *Ann.*, **569**, 161 (1950); E. T. McBee, H. E. Ungnade, H. Rakoff, and K. Dinbergs, *J. Am. Chem. Soc.*, **77**, 4379 (1955).

8) K. Kusuda and M. Endo, unpublished work.

9) E. T. McBee, C. W. Roberts, and K. Dinbergs, *J. Am. Chem. Soc.*, **78**, 491 (1956).

10) T. Zinke and A. Rhode, *Ann.*, **299**, 371 (1897); A. Roedig and L. Hörnig, *Chem. Ber.*, **88**, 2003 (1955).

11) A. Roedig and G. Märkl, *Ann.*, **636**, 1 (1960); A. Roedig and G. Märkl, *Chem. Ber.*, **95**, 2852 (1962).

12) A. Roedig, H. Göpfert, and A. A. Renk, *Chem. Ber.*, **111**, 860 (1978); and the references cited therein.

13) E. W. Garbish, Jr., and R. F. Sprecher, *J. Am. Chem. Soc.*, **91**, 6785 (1969).

14) A. Roedig, G. Märkl, and V. Schaal, *Chem. Ber.*, **95**, 2844 (1962); A. Roedig, G. Märkl, and H. Schaller, *Chem. Ber.*, **103**, 1101 (1970).

15) X-Ray crystallographical structural determination of **18** was unsuccessful because the crystal surface quickly became clouded after the crystals were separated from the mother solution. The authors express their sincere thanks to Dr. Tai-ichi Higuchi for the X-ray crystallographic study.

16) B. Eistert and A. Langbein, *Ann.*, **678**, 78 (1964).

17) R. Huisgen, *Angew. Chem.*, **75**, 604 (1963).

18) S. Oota, *Bunseki Kagaku*, **15**, 689 (1966); **17**, 1322 (1968); **18**, 1257 (1969).

19) Freshly distilled pentachlorocyclopentadiene should be used; otherwise a dimer of pentachlorocyclopentadiene will contaminate the product.

20) When an equimolar amount of hexachloropropene was used, the yield of the product was decreased, but the method of purification was simpler. Washing the crude product with a 1 : 1 mixture of ethyl acetate and methanol was enough for the synthesis. The yield was 78%.

21) The reaction catalyzed by antimony pentachloride under similar conditions yielded much unreacted materials.

22) For a large scale reaction, it is recommended that the pentachlorocyclopentadiene be introduced into the mixture of hexachloropropene and anhydrous aluminium chloride at a slow speed so as to maintain gentle refluxing of dichloromethane.

23) Compound **6** is identical with the substance of unknown structure (mp 108 °C), which was obtained by the reaction between perchlorocyclopentadiene and perchlorocyclopropene at 180 °C in low yield : D. C. F. Low and S. W. Tobey, *J. Am. Chem. Soc.*, **90**, 2376 (1968). We wish to thank Dr. Tobey for supplying us with the IR and UV spectra of the sample.

24) L. F. Fieser and M. Fieser, "Reagents for Organic Synthesis," John & Wiley Sons, Inc., New York (1967), p. 191.

25) G. C. Levy and G. L. Nelson, "Carbon-13 Nuclear Magnetic Resonance for Organic Chemists," Wiley-Interscience, New York (1972).

Nitrogen Compounds in Petroleum. IV. Distribution Profiles of Nitrogen Compounds in Petroleum by Solid-Liquid Chromatography†

Akira NOMURA,* Yazaemon MORITA, and Yukitoshi KOGURE

Department of Analytical Chemistry, National Chemical Laboratory for Industry, Honmachi, Shibuya-ku, Tokyo 151

(Received July 7, 1978)

A simple method for the characterization of nitrogen compounds in petroleum products by the investigation of the distribution profiles of nitrogen compounds using stepwise gradient elution on silica gel has been conducted. Samples were charged onto a $8\phi \times 150$ mm glass column containing 3 g of silica gel for column chromatography, followed by 15 ml of hexane to remove the non-polar bulk hydrocarbons from the sample. The eluate collected was removed from the solvent and analyzed for nitrogen, wt % yield and UV absorbance at 220 nm. The same procedure was followed by each 15 ml of 1, 3, 5, 10, 30, 60, 100%(v/v)-THF in hexane eluents. Plots of the nitrogen contents *vs.* the concentration of eluents gave characteristic patterns for petroleum distillates. The crude and residual oils from different geological sources exhibit similar nitrogen distribution profiles. There are two peak values; the peak at 3%-THF increases and that at 30%-THF decreases as the boiling range of the distillate decreases. Nitrogen compounds are distributed uniformly in a wide range of polar components with regard to adsorptivity on silica gel. The method was further applied to the reaction products of quinoline and indole by irradiation with UV light in isooctane (2,2,4-trimethylpentane) solution.

Organic nitrogen compounds in petroleum distillates poison many of the catalysts used in refining processes and cause undesirable deposits, color formation, odor, and poor storage properties. In addition, the nitrogen compounds produce on combustion fairly large amounts of nitrogen oxides (fuel NO_x), one of the sources of air pollution. Further knowledge of these nitrogen compounds should prove useful for the development of processes for their removal and of additives for their control.

Several studies have been made on the nature of nitrogen compounds in petroleum and several separation and identification schemes have been reported. Recently Snyder *et al.*[1-4] systematically studied nitrogen compounds in various petroleum distillates using liquid-solid chromatography combined with UV, IR, and mass spectrometry. Although it is desirable to isolate individual nitrogen compounds from petroleum distillates for the necessary identification by UV, IR, mass spectrometry *etc.*, the isolation is quite difficult in the cases of heavy oils, residual oils, and crude oils, since many nitrogen compounds are present and in small amounts. Therefore it is useful in practice to characterize and classify the nitrogen compounds, not each of them, in crude oil or high-boiling petroleum distillates. Potentiometric titration using perchloric acid has been applied in the characterization of basic nitrogen compounds in petroleum products.[5-8] Linear elution adsorption chromatography[9-12] has been investigated for both basic and non-basic nitrogen compounds by Snyder and Buell, and has proved a useful method for the characterization of nitrogen compounds. In previous papers, a concentration method for nitrogen compounds in various petroleum distillates using a silica gel adsorption technique and a method for the determination of trace nitrogen by Dumas method combined with a silica gel adsorption technique have been presented.[13,14]

This paper describes a simple method for the characterization of nitrogen compounds in petroleum distillates by distribution profiles of nitrogen contents in various petroleum distillates or crude oils using stepwise gradient elution, hexane–tetrahydrofuran (THF) as the eluent on a column of silica gel. The profiles of wt % yield and UV absorbance of eluate have also been determined and compared with the nitrogen contents. This method has been applied in the identification of the reaction products of quinoline and indole by the irradiation with UV light in isooctane solution. The method applies to the analysis of the mechanism in the denitrogenation[16] and characterization of coal liquefaction products and shale oils.

† A preliminary report of this work was presented at the 36th National Meeting of the Chemical Society of Japan, Osaka, April 1977.

Experimental

Reagents. Wako's hexane for liquid chromatography was used. Silica gel used was Wako C-200 for column chromatography (pore diameter : 70 Å). Other reagents were of reagent grade.

Apparatus. Hitachi type 356 double beam spectrophotometer was used to obtain UV absorbance. Nitrogen contents were obtained by either Kjeldahl method[15] or microcoulometric titration (Mitsubishi Kasei Model TN-01). Toshiba H400-PQ high pressure mercury lamp was used for the UV irradiation.

Procedure. Silica gel (3 g) for column chromatography was packed in a $8\phi \times 150$ mm glass column with a quartz wool plug at one end by the dry packing technique in tapping manner. The filled column (approximately 10 cm in length) was capped with quartz wool. The sample containing the nitrogen compounds (approximately 1 mg as N), diluted with isooctane, if necessary, was added into a separating funnel used as both a sample and eluent reservoir which was attached to the top of the column. A vacuum was applied and the sample was charged into the column by opening the stopcock of the reservoir. After loading of the sample, 15 ml of hexane was added to remove the non-polar bulk hydrocarbons from the sample, leaving all polar components including the nitrogen compounds adsorbed on the silica gel. An eluent flow rate of 5 ml/min or less was maintained through the elution. The eluate was collected in a suction bottle and solvent removed over a water bath. Quartz wool with solid components (asphaltenes) was removed from the column. The eluent was changed from hexane to 1%(v/v)-THF in hexane (15 ml) and the same procedure performed, followed

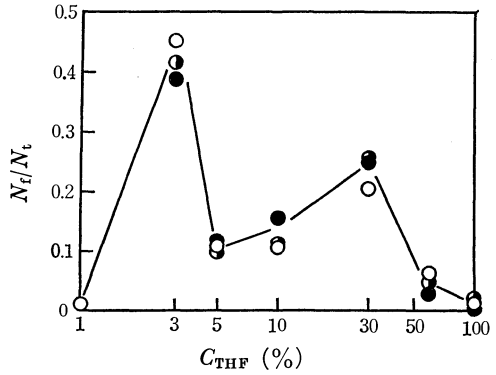

Fig. 1. Distribution profiles of nitrogen contents in crude oils. C_{THF}: Concentration of THF in hexane, N_f/N_t: relative nitrogen ratio (N_f: nitrogen in fraction, N_t: total nitrogen), ○: Kurokawa (Japan), ●: Duri (Indonesia), ◑: Shori (China).

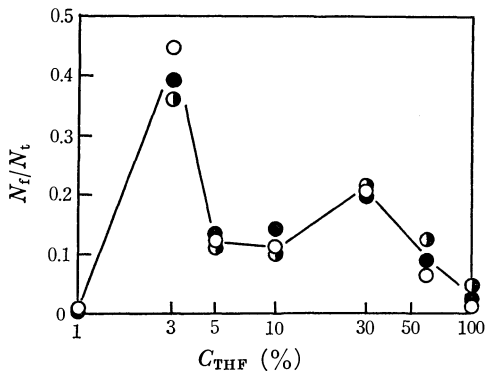

Fig. 2. Distribution profiles of nitrogen contents in residual oils. ○: Kurokawa (Japan), ●: Iranian light (Iran), ◑: Arabian heavy (Saudi Arabia).

by 15 ml of 3, 5, 10, 60, 100% (v/v)-THF in hexane eluents. Each fraction removed from the solvent was weighed and a portion used for the determination of the nitrogen content and another dissolved in THF for the determination of UV absorbance.

Results and Discussion

The silica gel pore diameter used for adsorption and separation of petroleum distillates with a wide boiling range has been investigated in detail previously.[13] A pore diameter ranging from 60 to 100 Å proved to be suitable. The silica gel used here was Wako gel C-200 with a pore diameter of 70 Å. The hexane–THF eluent system was selected because THF is one of the best solvents for petroleum and also the low boiling temperature enables simpler fractionation.

Distribution Profiles of Crude and Residual Oils. The distribution profiles for the nitrogen contents in three different geological crude and residual oils are shown in Figs. 1 and 2, respectively. The three different oils, both crude and residual, show almost the same patterns with regard to nitrogen content, and the patterns of the crude and residual oils are also the same, while the absolute nitrogen contents for each petroleum differ. The similarity in pattern between the crude and residual oils is expected since most nitrogen compounds exist in high-boiling distillates.

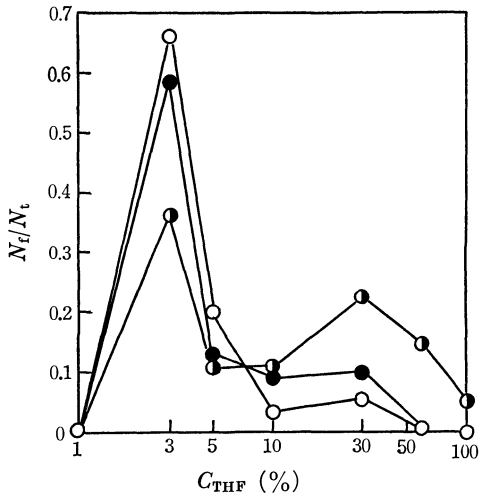

Fig. 3. Distribution profiles of nitrogen contents in different distillates.
Boiling range; ○: 170—340 °C, ●: 340—520 °C, ◑: 520 °C— tower bottom.

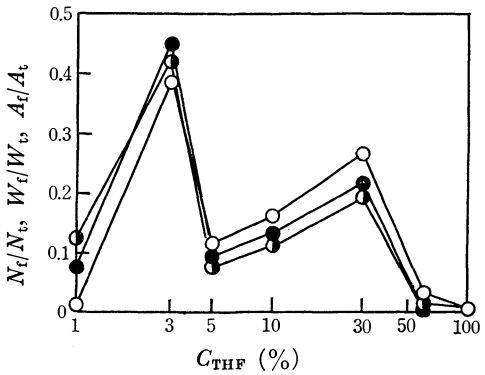

Fig. 4. Distribution profiles of polar components in crude oil. W_f/W_t: Relative weight ratio (W_f: weight of fraction, W_t: total weight), A_f/A_t: relative absorbance ratio (A_f: absorbance of fraction, A_t: total absorbance), ○: nitrogen, ●: weight, ◑: UV absorbance at 220 nm.

The two peak values (at 3 and 30%-THF eluents) are characteristic of crude and residual oils and the pattern is thought characteristic of all high-boiling distillates regardless of the fact that they come from different geological sources.

Distribution Profiles of Different Distillates. Distribution profiles for the nitrogen contents in three different distillates (boiling range : 170—340 °C, 340—520 °C, 520 °C— tower bottom) from the same sample of crude oil are shown in Fig. 3. As the boiling range of the distillate decreases, the nitrogen content at 3%-THF increases and that at 30%-THF decreases. This tendency is similar to the distillates from other crude oils. By examining the distribution profiles, the approximate boiling range can be estimated.

Distribution Profiles of Polar Components. Polar components in petroleum such as oxygen and sulfur compounds (except nitrogen compounds) are also adsorbed on silica gel and eluted with hexane–THF eluent. The relationship between the nitrogen compounds and polar compounds was investigated with

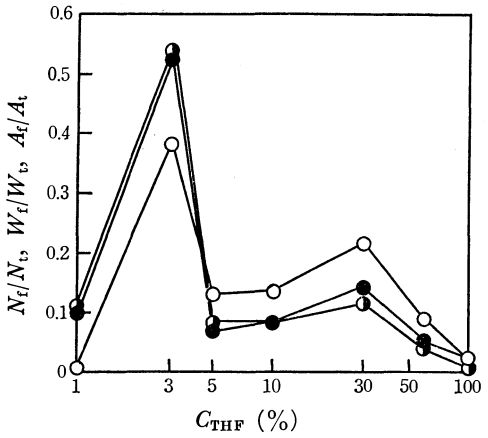

Fig. 5. Distribution profiles of polar components in residual oil. ○: Nitrogen, ●: weight, ◑: UV absorbance at 220 nm.

regard to nitrogen content, wt % yield and UV absorbance in THF at 220 nm. Since practically all fractions eluted with more than 3% THF concentration have a UV absorbance plateau between 215 and 230 nm, the absorbance at 220 nm was selected to characterize the polar components. Figures 4 and 5 indicate the relationship for crude and residual oils, respectively. The other crude and residual oils investigated exhibited similar relationships. Nitrogen compounds are considered to be distributed rather uniformly in a wide range of polar components with regard to adsorptivity on silica gel because of the good correlation among the three distribution profiles.

Application to Irradiated Products. The proposed method for the characterization of petroleum distillates was applied to the reaction products of quinoline and indole by irradiation with UV light in isooctane solution. Many reagents involving nitrogen have been examined in order to obtain standard samples for the calibration of the instrument determining nitrogen in petroleum. During the process heterocyclic nitrogen compounds were irradiated with UV light and the distribution profiles of nitrogen contents in the products were examined, the results of which are shown in Figs. 6 and 7 for quinoline and indole, respectively. Before irradiation most quinoline and indole are eluted with 10%- and 5%-THF, respectively, so the profiles are represented by single peak without a shoulder. The pattern of quinoline changed as the time of irradiation increased, and after 3 h the pattern of the products became similar to that for a typical crude oil. The pattern for indole remained rather unchanged after irradiation. It should not be concluded from the results that nitrogen compounds in crude oil are similar to the irradiated products of quinoline but the proposed method has been shown useful for the characterization of complicated products.

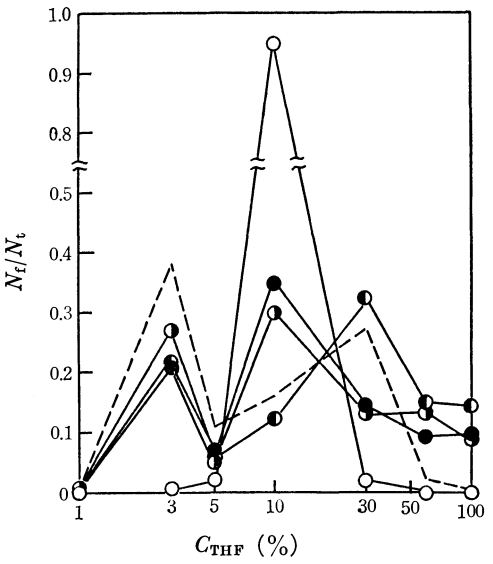

Fig. 6. Distribution profiles of nitrogen contents in quinoline irradiated with UV light.
Irradiating time; ○: 0 h, ●: 0.5 h, ◑: 1 h, ◐: 3 h, ——: distribution profile of typical crude oil.

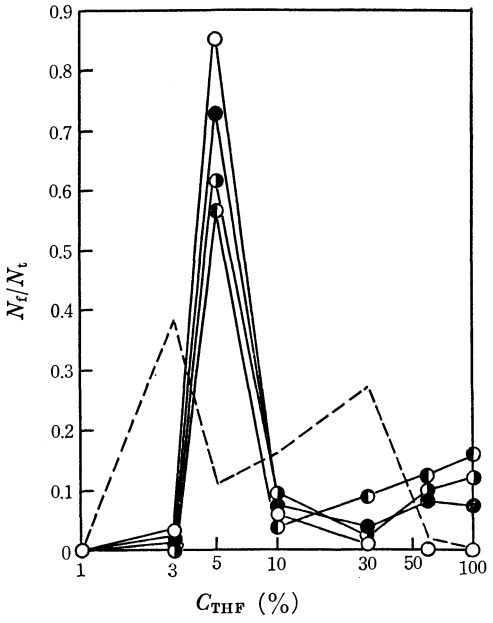

Fig. 7. Distribution profiles of nitrogen contents in indole irradiated with UV light.
Irradiating time; ○: 0 h, ●: 0.5 h, ◑: 1 h, ◐: 3 h, ——: distribution profile of typical crude oil.

References

1) L. R. Snyder and B. E. Buell, *Anal. Chem.*, **40**, 1295 (1968).
2) L. R. Snyder, B. E. Buell, and H. E. Howard, *Anal. Chem.*, **40**, 1303(1968).
3) L. R. Snyder, *Anal. Chem.*, **41**, 314 (1969).
4) L. R. Snyder, *Anal. Chem.*, **41**, 1084 (1969).
5) F. P. Richter, P. D. Caesar, S. L. Meisel, and R. D. Offenhauer, *Ind. Eng. Chem.*, **44**, 2601 (1952).
6) I. Okuno, D. R. Latham, and W. E. Haines, *Anal. Chem.*, **37**, 54 (1965).
7) B. E. Buell, *Anal. Chem.*, **39**, 756 (1967).
8) J. F. Mckay, J. H. Weber, and D. R. Latham, *Anal. Chem.*, **48**, 891 (1976).
9) L. R. Snyder and B. E. Buell, *Anal. Chem.*, **34**, 689 (1962).

10) L. R. Snyder and B. E. Buell, *Anal. Chem.*, **36**, 767 (1964).
11) L. R. Snyder and B. E. Buell, *Anal. Chem. Acta*, **33**, 285 (1965).
12) L. R. Snyder, *Anal. Chem.*, **38**, 1319 (1966).
13) Y. Morita, A. Nomura, and Y. Kogure, *Sekiyu Gakkai Shi*, **21**, 391 (1978).
14) Y. Kogure, Y. Morita, and A. Nomura, *Sekiyu Gakkai Shi*, **21**, 395 (1978).
15) Y. Morita, Y. Kogure, and A. Nomura, *Sekiyu Gakkai Shi*, **21**, 387 (1978).
16) Y. Morita, A. Nomura, and Y. Kogure, 37th National Meeting of the Chemical Society of Japan, Yokohama, April 1978, Abstr. No. 3T08.

Dechlorination of Polychlorinated Biphenyls by UV-irradiation. V. Reaction of 2,4,6-Trichlorobiphenyl in Neutral and Alkaline Alcoholic Solution

Tohru NISHIWAKI,* Masao USUI, Kinji ANDA, and Mitsuhiko HIDA†

Organic Division, Tokyo Metropolitan Industrial Technology Center, Nishigaoka, Kita-ku, Tokyo 115

† *Department of Industrial Chemistry, Faculty of Technology, Tokyo Metropolitan University, Fukazawa, Setagaya-ku, Tokyo 158*

(Received July 11, 1978)

2,4,6-Trichlorobiphenyl and seven other chlorobiphenyls have been photolyzed in both alkaline and neutral 2-propanol in order to investigate the reactivity and selectivity towards dechlorination. Predominant dechlorination at the 2-position has been confirmed for all PCBs in neutral solution and interpreted in terms of the steric and electronic effects of the phenyl group. In the presence of alkali, however, competitive elimination between the ortho and para chlorine atoms of 2,4-dichlorobiphenyl and 2,4,6-trichlorobiphenyl occurred. The photo-dechlorination of 2,3- and 2,5-dichlorobiphenyls took place however only at the ortho position. The dechlorination ratios (ortho/para) were 7.5 and 0.8 for 2,4-dichlorobiphenyl and 2,4,6-trichlorobiphenyl, respectively. This characteristic of the ortho chlorine atom has been elucidated assuming the steric and electronic effects of the phenyl group in the radical anion. A correlation has been found between the reduction potential and the reactivity of PCB in alkaline solution. The differences in reactivity among the chlorobiphenyls has been attributed to the electron acceptabilities in the ground states.

The authors have reported that a commertial PCB mixture (KC-300) dissolved in 2-propanol was successfully decomposed by ultraviolet radiation to biphenyl in the presence of sodium hydroxide,[1] the reaction proceeding rapidly by the chain degradative mechanism.[2–4] Some chlorobiphenyls, however, *e.g.* 2-chlorobiphenyl and 2,6-dichlorobiphenyl (2-CB and 2,6-DCB),[5] decomposed only slightly by the photolysis in alkaline solution and were detected in solution after other chlorobiphenyls had been completely decomposed to biphenyl.[4] In neutral alcoholic solutions the chlorine atom at the ortho position of tetrachlorobiphenyls was much more readily eliminated than at other positions.[6,7] No investigation has been undertaken on the difference in reactivities found among chlorobiphenyl homologues.

In the present study eight chlorobiphenyls (2-CB, 3-CB, 4-CB, 2,3-DCB, 2,4-DCB, 2,5-DCB, 2,6-DCB, and 2,4,6-TCB) have been photolyzed in both alkaline and neutral 2-propanol solutions in order to investigate the behavior of the ortho chlorine atom in detail.

Experimental

GLC analysis was conducted on a JEOL 20-K gas chromatograph with a flame ionization detector employing a 2 m × 3 mmϕ stainless steel column packed with 10% SE30 on 80—100 mesh chromosorb A (HMDS) or 15 m × 1 mmϕ glass capillary column with OV-101 (Chromato Research Co.). Preparative liquid chromatography was performed with a JAI LC-08 employing a 600 mm × 20 mmϕ stainless steel column packed with JAIGEL-1H; chloroform was used as the eluting solvent. Infrared spectra were obtained on a JASCO DS-701G spectrometer and mass spectra recorded at 24 eV on a JEOL Model D-100 mass spectrometer equipped with a gas chromatograph. UV spectra were taken with a Union Giken SM-401 spectrophotometer and melting points determined on a Yanagimoto micro melting apparatus.

Materials. The following reagents of special and guaranteed grade were used without further purification: 2,6-DCB (Nihon Chromato Co.), chloroanilines, 2-propanol and benzene (Wako Junyaku Co.). Isopentyl nitrite (Tokyo Kasei Co.) was distilled under a nitrogen atmosphere. 2-CB, 3-CB, 4-CB, 2,3-DCB, 2,4-DCB, 2,5-DCB, and 2,4,6-TCB were prepared by a modification of Cadogan's method,[8] the crude CBs being chromatographed over a silica-gel column using hexane as an eluent, and recrystallized from ethanol, ethanol-water, or petroleum ether. The melting points and UV spectra showed good agreement with the literature.[9] The purity was further checked by gas chromatography (>98%).

Irradiation Experiments. A solution of chlorobiphenyl (15 mmol/dm^3) and sodium hydroxide (30 mmol/dm^3) if necessary, in 2-propanol was photolyzed under the following conditions:

Procedure 1: After the solution (4.5 ml) in a quartz reaction cell was bubbled with purified nitrogen for 5 min, the cell was sealed and placed in a water bath kept at 30 °C. The solution was then irradiated through an interference filter (Nihon Shinku S50ϕ, 298 nm) with a 250 W high pressure mercury lamp (Ushio USH-250).

Procedure 2: A solution (400 ml) was photolyzed in a photochemical reaction vessel with an immersed 100 W high pressure mercury lamp (Ushio UM-102) without a filter under a stream of nitrogen at 30 °C.

Dechlorination Products. Irradiation of chlorobiphenyls gave low chlorinated biphenyls and biphenyl in both neutral and alkaline 2-propanol. 2,4,6-TCB gave, however, a biphenyl derivative having an alcoholic hydroxyl group together with the ordinary dechlorinated products in the alkaline solution. After evaporation of the solvent the residue was dissolved in chloroform. Preparative column chromatography and subsequent recrystallization from ethanol gave white needle crystals (mp 160—161 °C). NMR ($CDCl_3$), phenyl protons (δ 7.5—7.2, 7H, m), hydroxyl proton (δ 1.80, 1H, s), methyl protons (δ 1.60, 6H, s); IR (KBr), hydroxyl group (ν_{OH}, 3300 cm^{-1}, polymeric; ν_{C-O}, 1157 cm^{-1}, tertiary), methyl group (δ_{CH_3}, 1380, 1365 cm^{-1}; $\nu_{(CH_3)_2C}$, 1195 cm^{-1}, skelctal); MS (*m/e*), 282 (M^++2), 280 (M^+), 267 (M^+-CH_3), 262 (M^+-H_2O). On the basis of this data the compound has been identified as *xx'*-dichloro-*y*-(1-hydroxy-1-methylethyl)biphenyl. The substituted position in

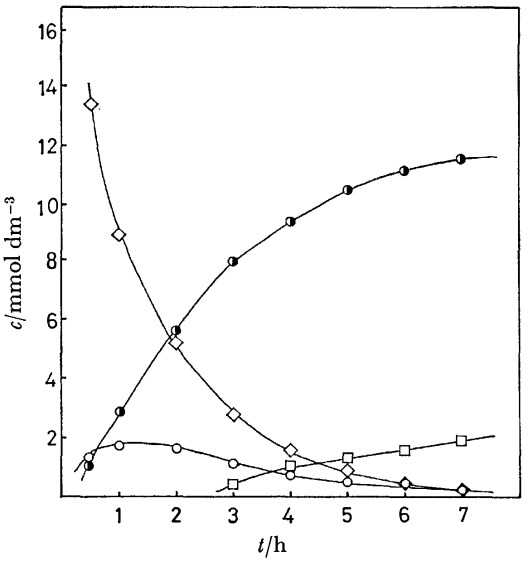

Fig. 1. Decomposition of 2,4,6-TCB in neutral 2-propanol ◇: 2,4,6-TCB, ○: 2,4-DCB, ◑: 4-CB □: biphenyl.
Initial concentration of 2,4,6-TCB: 16.2 mmol/dm³.
Photolysis was carried out by Procedure 2 (no filter).

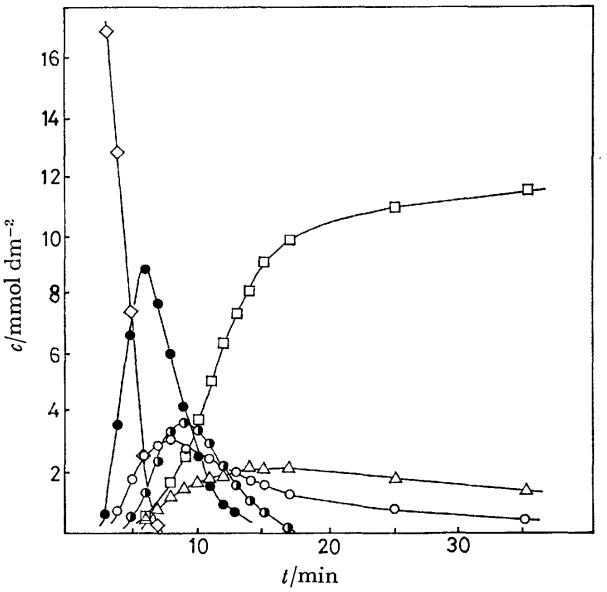

Fig. 2. Decomposition of 2,4,6-TCB in alkaline alcoholic solution
◇: 2,4,6-TCB, ●: 2,4-DCB, ◑: 4-CB, ○: 2,6-DCB, △: 2-CB, □: biphenyl.
Initial concentration of 2,4,6-TCB: 17.9 mmol/dm³.
Photolysis was carried out by Procedure 2 (no filter).

the phenyl ring cannot be clarified from this data. When the alkaline solutions of 2,6- and 2,4-DCB were photolyzed, however, 2,4-DCB afforded an alcohol in a small amount while 2,6-DCB did not and from this, 2,6-dichloro-4-(1-hydroxy-1-methylethyl)biphenyl (**1**) was considered to be formed in the photolysis of 2,4,6-TCB. On irradiation in alkaline solution **1** was both dechlorinated and dehydrated and gave the following compounds; 2-chloro-4-isopropenylbiphenyl (**2**), MS (*m/e*), 230 (M^++2), 228 (M^+), 193 (M^+−Cl); 4-isopropenylbiphenyl (**3**), MS (*m/e*), 194 (M^+), 179 (M^+-CH_3), 153 ($M^+-C(CH_3)=CH_2$).

Results and Discussion

Dechlorination of CBs in Neutral Solution. The photolysis of 2,4,6-TCB in 2-propanol gave 2,4-DCB, 4-CB, and biphenyl as shown in Fig. 1. Elimination occurred predominantly at the ortho position, and indeed no para dechlorinated products, *e.g.* 2,6-DCB or 2-CB, were found in the photolyzed solution. This prominent feature of the ortho chlorine atom was also observed in the photolysis of other chlorobiphenyls as follows. The photo-products of 2,3-DCB, 2,4-DCB, and 2,5-DCB were 3-CB, 4-CB, and 3-CB, respectively. 2-CB showed an outstanding reactivity among the monochlorobiphenyls and all results indicate a preference for elimination at the ortho chlorine atom in the neutral solution. The selectivities of the dechlorination are summarized in Table 1. The results in neutral solution are understandable bearing in mind the steric and the electronic effects of the phenyl group. Since biphenyl is known to have a planar structures in the excited state,[10] involving a high degree of conjugation between the two phenyl rings, the ortho chlorinated biphenyl would be largely unstable in the excited state. Therefore, the departure of the chlorine atom from the ortho position stabilizes the conjugation system. Ruzo *et al.*,[6,7] on the basis of the photolysis of tetrachlorobiphenyls in neutral solution, concluded that the marked elimination of the ortho chlorine atom was caused by both electronic and steric effects of the phenyl group, especially the latter.

Table 1. Dechlorination of CBs[a]

Compound	Positional selectivity (%)		
	Neutral	Alkaline	
2,3-DCB	100 (ortho)	100 (ortho)	
2,4-DCB	100 (ortho)	88 (ortho)	12 (para)
2,5-DCB	100 (ortho)	100 (ortho)	
3,4-DCB	100 (meta)	100 (para)	
2,4,6-TCB	100 (ortho)	44 (ortho)	56 (para)

a) Photolysis was carried out by Procedure 1.

Dechlorination of CBs in the Presence of Alkali. In the presence of alkali the competitive elimination of the ortho and para chlorine atoms of 2,4,6-TCB occurred as indicated in Fig. 2. The primary products were 2,4-DCB and 2,6-DCB, and further irradiation resulted in the formation of 4-CB and 2-CB from 2,4-DCB. The photo-dechlorination of 2,3- and 2,5-DCBs took place only at the ortho position, even in the presence of alkali. The reactivities of 2,6-DCB and 2-CB were, however, much lower than that of 2,4-DCB and 4-CB. The selectivities of the dechlorination reaction in the presence of alkali are compared in Table 1. Thus the ortho chlorine atom was not predominantly eliminated, in contrast to the prominent feature in the neutral solution.

The following chain mechanism, proposed for the photoreaction of PCBs,[2-4] appears to help the understanding of the reactivity of ortho chlorinated biphenyls.

$$PCB(n) \xrightarrow{h\nu} PCB(n-1,j)\cdot + Cl\cdot \quad (1)$$

$$Cl\cdot + (CH_3)_2CHOH \longrightarrow HCl + (CH_3)_2\dot{C}OH \quad (2)$$

$$(CH_3)_2\dot{C}OH + (CH_3)_2CHO^- \longrightarrow (CH_3)_2CO^{\cdot-} + (CH_3)_2CHOH \quad (3)$$

$$(CH_3)_2CO^{\cdot-} + PCB(n) \xrightarrow{k_{red}} (CH_3)_2CO + PCB(n)^{\cdot-} \quad (4)$$

$$PCB(n)^{\cdot-} \xrightarrow{k_{el}(i)} PCB(n-1,i)\cdot + Cl^- \quad (5)$$

$$PCB(n-1,i)\cdot + (CH_3)_2CHOH \longrightarrow PCB(n-1,i) + (CH_3)_2\dot{C}OH \quad (6)$$

$$2(CH_3)_2\dot{C}OH \longrightarrow \text{Termination} \quad (7)$$

$PCB(n)$; n is the number of chlorine atoms substituted in the phenyl ring.
$PCB(n-1,i)\cdot$; CB radical formed by the chlorine elimination at the i-position.
$k_{el}(i)$; the rate constant of the chlorine elimination at the i-position of $PCB(n)^{\cdot-}$.

The radical anion of PCB would afford $PCB(n-1,i)\cdot$ by elimination of the chloride ion. Assuming steady state conditions for the CB radical $PCB(n-1,i)\cdot$, the rate of dechlorination may be written:

$$d[PCB(n-1,i)]/dt = k_{el}(i)[PCB(n)^{\cdot-}], \quad (8)$$

where, Reaction 1[11] is assumed negligible compared with Reaction 5, since the chain length is expected to be large in alkaline solution : the quantum yield at 298 nm for KC-300 has been determined to be 36 in alkaline solution and 0.09 in neutral solution.[12] Then the relative rate constant for dechlorination at the i-position to that at the j-position is given by

$$[PCB(n-1,i)]/[PCB(n-1,j)] = k_{el}(i)/k_{el}(j). \quad (9)$$

The value $k_{el}(i)/k_{el}(j)$ can be evaluated by the amount of two daughter CBs derived from the parent PCB. As considered above the chlorine atom at the ortho position was selectively eliminated in the photolysis. Therefore similar acceleration due to the steric effect of the phenyl group as observed in the neutral solution can be expected in the dechlorination of $PCB(n)^{\cdot-}$ to yield $PCB(n-1, i)\cdot$.

Photolysis of 2,4-DCB in Alkaline Solution: 2,4-DCB produced 2-CB and 4-CB by photolysis followed by degradation to biphenyl as shown in Table 2. These reactions proceeded simultaneously so that the concentration ratio [2-CB]/[4-CB] in the photolyzed solution did not give the true ratio of daughter CBs derived from 2,4-DCB. Therefore, in order to obtain the true value of $k_{el}(i)/k_{el}(j)$ it is necessary to find the respective rates of 4-CB and 2-CB to yield biphenyl. Assuming steady state conditions for $[2\text{-}CB^{\cdot-}]$, $[4\text{-}CB^{\cdot-}]$, [Biph(2-CB)$\cdot$], and [Biph(4-CB)$\cdot$], the rate of biphenyl formation attributed to 4-CB is given by

$$\frac{d[Biph(4\text{-}CB)]}{dt} = -\frac{d[4\text{-}CB]}{dt}, \quad (10)$$

$$\frac{d[Biph(4\text{-}CB)]}{dt} = \frac{d[Biph]}{dt}\cdot\frac{(k_{red}(4)/k_{red}(2))[4\text{-}CB]}{(k_{red}(4)/k_{red}(2))[4\text{-}CB]+[2\text{-}CB]}, \quad (11)$$

Table 2. Decomposition of 2,4-DCB in alkaline alcoholic solution[a,b]

Conversion of 2,4-DCB %	Biph	2-CB	4-CB	Biph+4-CB	(Biph+4-CB)/2-CB[c]
		c/mmol dm^{-3}			
6.4	0.14	0.13	0.70	0.84	6.5
7.0	0.17	0.17	0.76	0.93	6.1
16.5	0.94	0.25	1.32	2.25	9.0
39.3	1.97	0.77	3.23	5.20	6.8
49.3	3.70	0.93	2.87	6.57	7.1
61.4	5.23	1.13	2.98	8.21	7.3
72.0	8.02	1.17	1.75	9.78	8.4
72.2	8.40	1.16	1.42	9.82	8.5

a) Initial concentration of 2,4-DCB; 15.2 mmol/dm^3. b) Photolysis was carried out by Procedure 1. c) $((Biph+4\text{-}CB)/2\text{-}CB)_{av} = 7.5\pm1.0$.

where, [Biph(4-CB)] and [Biph] represent the concentration of biphenyl derived from 4-CB and the biphenyl concentration in the photolyzed solution, respectively. The formation rate of Biph(2-CB) can also be written by similar equations. Combination of these four equations results in Eq. 12, by which the $k_{red}(4)/k_{red}(2)$ can be determined.

$$\frac{\ln([4\text{-}CB]_0/[4\text{-}CB])}{\ln([2\text{-}CB]_0/[2\text{-}CB])} = k_{red}(4)/k_{red}(2) \quad (12)$$

4-CB and 2-CB were consequently decomposed competitively in alkaline solution in order to evaluate the left hand side of Eq. 12, the results of which are summarized in Table 3. The average value of 17.2± 4.5 suggests that 4-CB is far more reactive than 2-CB. Table 2 indicates that the concentration of 4-CB is always higher than that of 2-CB by a factor of 1.2 to 5.1. Consequently the following inequality can be assumed:

$$(k_{red}(4)/k_{red}(2))[4\text{-}CB] \gg [2\text{-}CB].$$

Resolving Eq. 11 under these conditions gives the simple relation ; [Biph(4-CB)]=[Biph]. This indicates that all biphenyl can be assumed to be derived from 4-CB, and that 2-CB makes a negligible contribution to the biphenyl formation. Thus the true amounts of 4-CB and 2-CB produced by the dechlorination of the radical anion $2,4\text{-}DCB^{\cdot-}$ are [Biph]+[4-CB] and [2-CB], respectively. These concentrations were then utillized to calculate the value of $k_{el}(2)/k_{el}(4)$ using Eq. 9. As Table 2 shows, in the dechlorination of $2,4\text{-}DCB^{\cdot-}$ the chlorine at the ortho position is more easily eliminated by a factor of 7.5± 1.0 than that at the para position, a result explainable on the assumption of the steric acceleration effect of the phenyl group.

Photolysis of 2,4,6-TCB in Alakline Solution: 2,4,6-TCB gave 2,4-DCB, 2,6-DCB, and compound **1**. These compounds were negligibly dechlorinated during the photolysis so that any further reduction of the compounds was neglected in the calculation of Eq. 9. As compound **1** has a 1-hydroxy-1-methylethyl group at position 4, the true ratio of daughter compounds derived from 2,4,6-TCB will be given by [2,4-DCB]/([2,6-

Table 3. Competitive dechlorination of 2-CB and 4-CB in alkaline alcoholic solution[e]

Conversion %	2-CB	4-CB	$k_{red}(4)/k_{red}(2)$[d]
	c/mmol dm^{-3}		
2.4[a]	3.74	3.55	17.5
6.9[b]	3.52	3.23	24.9
8.4[c]	3.47	2.84	15.0
22.8[a]	3.59	2.18	12.3
35.1[a]	3.58	1.27	23.2
55.7[c]	2.83	0.22	12.7
58.2[a]	2.99	0.14	14.5

Initial concentration of 2-CB and 4-CB: a) 3.75, 3.72; b) 3.54, 3.37; c) 3.51, 3.37 mmol/dm^3, respectively. d) $(k_{red}(4)/k_{red}(2))_{av}=17.2\pm4.5$. e) Photolysis was carried out by Procedure 1.

Table 4. Decomposition of 2,4,6-TCB in alkaline alcoholic solution[a,b]

Conversion %	2,6-DCB	2,4-DCB	**1**	2,4-DCB/(2,6-DCB+**1**)[c]
	c/mmol dm^{-3}			
5.5	0.13	0.50	0.20	1.52
7.5	0.18	0.58	0.27	1.29
9.3	0.23	0.87	0.31	1.61
9.8	0.28	0.91	0.35	1.44
20.1	0.48	1.62	0.48	1.69
27.2	0.84	2.66	0.72	1.70
43.7	1.13	4.14	1.10	1.86
44.1	1.03	4.14	1.10	1.94

a) Initial concentration of 2,4,6-TCB were 15.7—13.7 mmol/dm^3. b) Photolysis was carried out by Procedure 1. c) $(2,4\text{-DCB}/(2,6\text{-DCB}+\mathbf{1}))_{av}=1.6\pm0.1$.

DCB]+[**1**]), the experimental results of which are shown in Table 4. The value of 1.6±0.1 was obtained as the average ratio from eight measurements. The $k_{el}(2)/k_{el}(4)$ is thus 0.8 since the elimination at the 2-, and 6-position of 2,4,6-TCB are equivalent. Contrary to expectations this indicates that the para chlorine atom is more active than the ortho chlorine atom. The explanation for this result is as follows. Since the presence of the chlorine atom at position 6 disturbs the release of the dihedral angle between the two phenyl rings by the dechlorination at position 2, the steric acceleration effect by the phenyl group cannot markedly affect the dechlorination.

Photolysis of 3,4-DCB. 3,4-DCB was dechlorinated exclusively at position 4 in the presence of alkali. Since this elimination cannot be explained only by the steric effect of the phenyl group, the electronic effect must be considered. As shown in Table 1 the elimination of para chlorine atom was also observed in the alkaline solution of 2,4-DCB and 2,4,6-TCB. From these results it has been assumed that the para position of PCB$^{\cdot-}$ is activated by the electronic effect.

In neutral solution 3,4-DCB did not eliminate the para chlorine atom and similar inactivity in the para position has been observed in 2,4-DCB and 2,4,6-TCB. This shows a remarkable contrast to the alkaline reaction. In the photolysis of 3,4-DCB only the meta chlorine atom was eliminated but 2,3-DCB and 2,5-DCB did not eliminate the meta chlorine. This suggests that the para chlorine atom may be stabilized by the electronic effect of the phenyl group in the photo-excited state, but that the steric acceleration effect is far more important than the electronic effect in the dechlorination at the ortho position from the photo-excited CB.

Relative Reactivities of PCBs in the Presence of Alkali. Successive dechlorination of 2,4,6-TCB produced 2,4-DCB, 2,6-DCB, 4-CB, and finally biphenyl in the presence of alkali as shown Fig. 2. Consequently the ease of dechlorination is expected to increase in the order : 2,4,6-TCB > 2,4-DCB > 4-CB > 2,6-DCB ≈ 2-CB. This reaction scheme suggests that the relative reactivities of PCBs in the presence of alkali will be determined by the k_{red} value. As described above the value of $(k_{red})_{4\text{-CB}}/(k_{red})_{2\text{-CB}}$ has been evaluated as 17.2±4.5 from Eq. 12. This shows 4-CB is more readily dechlorinated than 2-CB by a factor of 17.2. For di-, and poly-CBs, however, k_{red} is not easy to estimate experimentally due to further reaction of the daughter CBs. Since Reaction 4 is an electron transfer step from the radical anion $(CH_3)_2CO^{\cdot-}$ to PCB(n), the reactivity k_{red} will depend on the reduction potential of PCB(n). The reduction potentials of 2-CB, 4-CB, 2,6-DCB, 2,4-DCB, 2,4,6-TCB, and biphenyl have been reported[13] as −2.097, −2.056, −2.107, −1.983, −1.966, and −2.411 E/V *vs.* SCE, respectively. These reduction potentials are reasonably correlated with the ease of dechlorination of CBs. It was thus considered that the reactivities of the CB homologues largely depend on the electron acceptabilities in the ground state.

The authors wish to express their thanks to Mr. Haruo Inoue of Tokyo Metropolitan University for his valuable suggestions, and to Mr. Tsutomu Shinoda for his help in the preparation of this paper.

References

1) T. Nishiwaki, A. Ninomiya, S. Yamanaka, and K. Anda, *Nippon Kagaku Kaishi*, **1972**, 2225.
2) S. Arai, M. Matsui, J. Moriguchi, and M. Imamura, *Reports Inst. Phys. Chem. Res.*, **48**, 185 (1972).
3) T. Sawai and Y. Shinozaki, *Chem. Lett.*, **1972**, 865.
4) T. Nishiwaki, A. Ninomiya, S. Yamanaka, and K. Anda, *Nippon Kagaku Kaishi*, **1973**, 2326.
5) CB denotes chlorobiphenyl; *e.g.*, dichlorobiphenyl and 2,4,6-trichlorobiphenyl are abbreviated to DCB and 2,4,6-TCB, respectively.
6) L. O. Ruzo, M. J. Zabic, and R. D. Schuetz, *J. Agric. Food Chem.*, **22**, 2, 199 (1974).
7) L. O. Ruzo, M. J. Zabik, and R. D. Schuetz, *J. Am. Chem. Soc.*, **96**, 3809 (1974).
8) J. I. G. Cadogan, *J. Chem. Soc.*, **1967**, 4257.
9) O. Hutzinger, S. Safe, and V. Zitko, "The Chemistry of PCBs," CRC Press (1974), Chap. 3.
10) Peter J. Wagner, *J. Am. Chem. Soc.*, **89**, 2820 (1967).
11) As Ohashi *et al.* reported the decomposition of 4-CB *via* the encounter complex of the singlet excited 4-CB with

triethylamine (M. Ohashi, K. Tsujimoto, and K. Seki, *J. Chem. Soc., Chem. Commun.*, **1973**, 384.) the following electron transfer reaction, besides the direct photo-dissociation shown in the Reaction 1, may be considered in alkaline solution.

$PCB(n)^* + (CH_3)_2CHO^-$ or $OH^- \rightarrow PCB(n)^- + (CH_3)_2CHO\cdot$ or $OH\cdot$

Even if this reaction takes place in the dechlorination reaction, this will be disregarded for similar reasons that Reaction 1 was neglected.

12) T. Nishiwaki, M. Usui, M. Tsuda, and K. Anda, *Nippon Kagaku Kaishi*, **1975**, 2132.

13) S. O. Farwell, F. A. Blend, and R. D. Geer, *J. Electroanal. Chem. Interfacial Electrochem.*, **61**, 315 (1975).

Electrochemical Synthesis and Reactivity of α-Alkoxy α-Amino Acid Derivatives[1,2]

Tameo IWASAKI,* Hiroshi HORIKAWA, Kazuo MATSUMOTO, and Muneji MIYOSHI

Department of Synthetic Chemistry, Research Laboratory of Applied Biochemistry, Tanabe Seiyaku Co., Ltd., 16-89 Kashima-3-chome, Yodogawa-ku, Osaka 532

(Received September 22, 1978)

α-Alkoxy α-amino acid derivatives were synthesized in good yields by anodic oxidation of acylaminomalonic acid monoesters in alcohols. Transformation of ethyl *N*-acetyl-α-methoxyalaninate into ethyl *N*-acetyl-α,β-dehydroalaninate was achieved in an excellent yield by thermal treatment of the former amino acid with a catalytic amount of ammonium bromide. Substitution of the α-alkoxy group of the α-alkoxy amino acids with nucleophiles was effected by tin tetrachloride to afford the α-substituted α-amino acids.

α-Functionalized α-amino acids such as α-methoxy or α-acetoxy α-amino acids[3a,b] have been found to be useful for the preparation of physiologically important amino acids. Some remarkable examples have been shown by Ben-Ishai *et al.*;[4] α-methoxyglycine derivatives undergo the reaction with a variety of nucleophiles to afford a novel class of α-substituted α-amino acids. However, the synthetic versatility of the α-methoxy α-amino acids other than the α-methoxyglycines in amino acid chemistry has not yet been explored.

Several α-methoxy α-amino acids were prepared by the addition reaction to α,β-dehydro amino acids,[5a,b] oxidation of *N*-acylamino acid derivatives with *t*-BuOCl,[6a-d] or oxidation of α-methylthio *N*-acylamino acids.[7] However, difficulty is still encountered in these reactions in which the starting materials and/or the reagents are not readily available, and the experimental procedures are often tedious. In the course of our synthetic studies by electrochemical method, Kolbe type oxidation has been found to be a suitable method for a selective replacement of carboxylic acid group with acetoxyl[3a] or olefinic functional group.[8] In the present paper, we wish to report a convenient synthesis of various types of α-alkoxy α-amino acid derivatives by anodic oxidation of substituted and nonsubstituted acylaminomalonic acid monoesters. Transformation of the α-alkoxy amino acids into α,β-dehydroalaninate and α-substituted α-amino acids is also described, the synthetic potentiality of the α-alkoxy amino acids in amino acid chemistry, being taken into account.

Results and Discussion

Electrochemical Synthesis. Synthesis of α-alkoxy amino acid derivatives **3** was carried out according to the reaction Scheme 1. Substituted acylaminomalonic acid monoesters **2b—f** were synthesized in good yields by the reaction of acylaminomalonates **1a, b** with alkyl halides in ethanol–sodium ethoxide, followed by the saponification of the coupling products with potassium hydroxide in ethanol. α-Acetamido-α-cyano-β-phenylpropionic acid (**2g**) was similarly prepared from **1c** in 68% overall yield. Anodic oxidation was carried out at 10—15 °C with use of a graphite anode-graphite cathode in a non-divided cell. On electrolysis of **2a** in methanol containing 1/20 molar equivalent of sodium methoxide to that of **2a**, ethyl *N*-acetyl-α-methoxyglycinate (**3a**) was obtained in 89% yield. The monoesters **2b—f** were also oxidized under the same conditions as above to afford the corresponding α-methoxy α-amino acid derivatives **3b—f** in 80—97% yield. The presence of the cyano group in electrolysis of **2g** did not obstruct methoxylation. In these reactions, the starting materials were consumed completely by passing a theoretical amount of current which is calculated as a two-electron

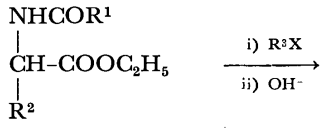

1a—c

a, $R^1=CH_3$; $R^2=COOC_2H_5$
b, $R^1=OCH_2Ph$; $R^2=COOC_2H_5$
c, $R^1=CH_3$; $R^2=CN$

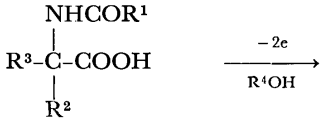

2a—g

a, $R^1=CH_3$; $R^2=COOC_2H_5$; $R^3=H$
b, $R^1=CH_3$; $R^2=COOC_2H_5$; $R^3=CH_3$
c, $R^1=CH_3$; $R^2=COOC_2H_5$; $R^3=C_2H_5$
d, $R^1=CH_3$; $R^2=COOC_2H_5$; $R^3=CH_2Ph$
e, $R^1=CH_3$; $R^2=COOC_2H_5$; $R^3=CH_2CH=CH_2$
f, $R^1=OCH_2Ph$; $R^2=COOC_2H_5$; $R^3=H$
g, $R^1=CH_3$; $R^2=CN$; $R^3=CH_2Ph$

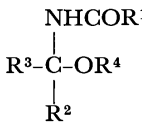

3a—i

a, $R^1=CH_3$; $R^2=COOC_2H_5$; $R^3=H$; $R^4=CH_3$
b, $R^1=CH_3$; $R^2=COOC_2H_5$; $R^3=R^4=CH_3$
c, $R^1=CH_3$; $R^2=COOC_2H_5$; $R^3=C_2H_5$; $R^4=CH_3$
d, $R^1=CH_3$; $R^2=COOC_2H_5$; $R^3=CH_2Ph$; $R^4=CH_3$
e, $R^1=CH_3$; $R^2=COOC_2H_5$; $R^3=CH_2CH=CH_2$; $R^4=CH_3$
f, $R^1=OCH_2Ph$; $R^2=COOC_2H_5$; $R_3=H$; $R^4=CH_3$
g, $R^1=CH_3$; $R^2=COOC_2H_5$; $R^3=C_2H_5$; $R^4=C_2H_5$
h, $R^1=CH_3$; $R^2=COOC_2H_5$; $R^3=CH_3$; $R^4=CH(CH_3)_2$
i, $R^1=CH_3$; $R^2=CN$; $R^3=CH_2Ph$; $R^4=CH_3$

Scheme 1.

Table 1. Yields and characterization of electrolysis products

Compd	Yield (%)	Mp [Bp] (°C)	IR (cm^{-1})	NMR (δ, in $CDCl_3$)	Formula	Analysis (%)[a]		
						C	H	N
3a	89	[85—6/0.3 mmHg]	3300, 1750, 1670, 1520	1.33 (t, 3H), 2.12 (s, 3H), 3.49 (s, 3H), 4.29 (q, 2H), 5.56 (d, 1H), 7.12 (broad d, 1H)	$C_7H_{13}NO_4$	47.99 47.63	7.48 7.21	8.00 8.10
3b	97	40—42	3270, 1750, 1665, 1550	1.35 (t, 3H), 1.77 (s, 3H), 2.09 (s, 3H), 3.32 (s, 3H), 4.32 (q, 2H), 6.97 (broad s, 1H)	$C_8H_{15}NO_4$	50.78 50.55	7.99 7.94	7.40 7.51
3c	91	80—81	3270, 1755, 1650, 1545	0.83 (t, 3H), 1.36 (t, 3H), 2.10 (s, 3H), 1.6—2.9 (m, 2H), 3.28 (s, 3H), 4.32 (q, 2H), 6.68 (broad s, 1H)	$C_9H_{17}NO_4$	53.19 52.91	8.43 8.21	6.89 6.78
3d	96	97—98	3300, 1743, 1685, 1527	1.33 (t, 3H), 2.04 (s, 3H), 3.29 (s, 3H), 3.22 and 3.87 (AB q, 2H, J=13 Hz), 4.26 (q, 2H), 6.58 (broad s, 1H), 7.23 (s, 5H)	$C_{14}H_{19}NO_4$	63.38 63.11	7.22 6.99	5.28 5.28
3e	83	63—65	3300, 1740, 1670, 1530	1.33 (t, 3H), 2.09 (s, 3H), 2.4—3.3 (m, 2H), 3.30 (s, 3H), 4.26 (q, 2H), 4.9—6.0 (m, 3H), 6.9 (broad s, 1H)	$C_{10}H_{17}NO_4$	55.80 55.65	7.96 8.01	6.51 6.77
3f	93	[138—9/0.5 mmHg]	3300, 1725, 1520	1.30 (t, 3H), 3.44 (s, 3H), 4.24 (q, 2H), 5.17 (s, 2H), 5.31 (d, 1H), 6.00 (broad d, 1H), 7.30 (s, 5H)	$C_{13}H_{17}NO_5$	58.42 58.12	6.41 6.51	5.24 5.29
3g	79	102—104	3330, 1740, 1680, 1550	0.32 (t, 3H), 1.21 (t, 3H) 1.32 (t, 3H), 1.7—2.8 (m, 2H), 2.08 (s, 3H), 3.47 (q, 2H), 4.28 (q, 2H), 6.83 (broad s, 1H)	$C_{10}H_{19}NO_4$	55.28 55.31	8.82 8.80	6.45 6.35
3h	80	71—73	3330, 1738, 1685, 1536	1.15 (d, 6H), 1.32 (t, 3H), 1.78 (s, 3H), 2.03 (s, 3H), 3.83 (m, 1H), 4.26 (q, 2H), 6.73 (broad s, 1H)	$C_{10}H_{19}NO_4$	55.28 55.39	8.82 8.62	6.45 6.51
3i	80	68—70	3200, 1660, 1540	1.96 (s, 3H), 3.39 (s, 2H), 3.50 (s, 3H), 7.03 (broad s, 1H), 7.31 (s, 5H)	$C_{12}H_{14}N_2O_2$	66.03 65.85	6.47 6.67	12.84 12.53

a) Upper lines show calculated values and lower lines found values.

transfer. Furthermore, the use of ethanol or 2-propanol as an electrolysis solvent resulted in the formation of the corresponding alkoxylated products **3g,h** in excellent yields despite rather poor current efficiency (60—70%). No Kolbe dimer was observed throughout the alkoxylation. Furthermore, no elimination and rearrangement products were detected. Meanwhile, in the hope of preparing ethyl *N*-acetyl-α-hydroxyphenylalaninate (**4**), the electrolysis of **2d** was carried out in aqueous tetrahydrofuran. However, **4** was extremely unstable under the reaction conditions, and carbon–nitrogen bond cleavage ocurred to give ethyl phenylpyruvate (**5**) and acetamide[9] (Scheme 2).

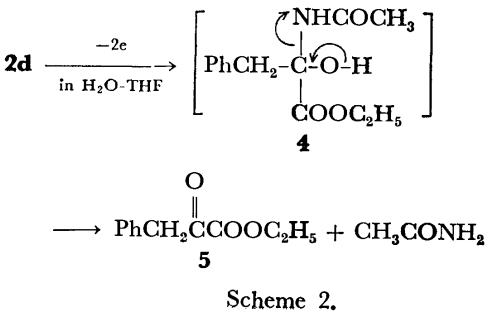

Scheme 2.

The structural elucidation was carried out based on the spectral data and elemental analyses. The results are summarized in Table 1.

The electrode reaction in the alkoxylation is thought to be a typical abnormal Kolbe reaction in which the carbonium ion is generated *via* a two-electron transfer[3a,8,10a-c] (Scheme 3). The delocalization

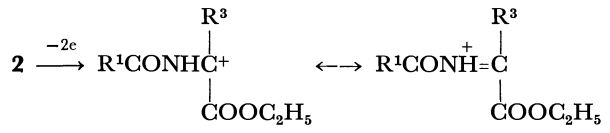

Scheme 3.

of the carbonium ion character onto the neighboring nitrogen atom would make the lifetime longer enough to be susceptible of nucleophilic attack of the solvent, though the inductive effect of both the *N*-acyl and the ethoxycarbonyl groups destabilizes the carbonium ion. Participation of the neighboring acylamino group in the anodic replacement of carboxylic acid group by methoxyl or acetoxyl group has been described by us[3a] and other workers.[11a,b]

The α-methoxy amino acid derivative **3d** was saponified with potassium hydroxide in methanol to afford *N*-acetyl-α-methoxyphenylalanine in 51% yield.

Conversion into α,β-Dehydroalanine Derivative. α,β-Dehydro amino acids, especially α,β-dehydroalanine derivatives, are used as important intermediates in the synthesis of natural peptides possessing antibacterial activity.[12] α,β-Dehydroalanine derivatives have hitherto been prepared by the methods involving the following: thermal condensation of primary amines with pyruvic acid;[13] base-catalyzed elimination of *N*-acyl-α-methoxyalanines,[5a] *N*-acyl-*N*-chloroalaninates prepared *in situ*,[5a] and *N*-acylserine derivatives.[14] These methods, however, are not suitable for large scale production[15] of α,β-dehydroalanine.

In order to develop a method for a convenient and large scale preparation of the α,β-dehydroalanines, thermal conversion of α-methoxyalaninate into α,β-dehydroalaninate was carried out. Ethyl *N*-acetyl-α-methoxyalaninate (**3b**) was heated at 120 °C for 20 min in the presence of a catalytic amount of ammonium bromide to afford the corresponding α,β-dehydro-

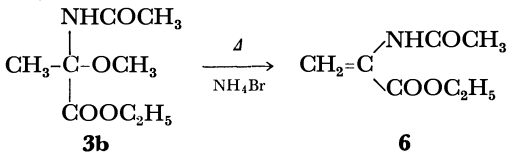

Scheme 4.

alaninate **6b** in 76% yield (Scheme 4). Prolonged heating or the use of a greater amount of ammonium bromide than that employed here resulted in a low yield, owing to the thermal polymerization of the product.

Reaction with Nucleophiles. *N*-Acyl-α-methoxyglycines have been reported to amidoalkylate olefins,[16a,b] active methylene compounds,[17] and aromatic compounds[18a-c] through *N*-acylimine intermediates in the presence of Lewis acid catalyst. The acylamino group functions to stabilize the carbonium ion generated at the α-carbon, thus providing enhanced reactivity toward nucleophiles. In α-amidoalkylation on tertiary carbon atom of the α-methoxy α-amino acids, however, the substitution as well as competitive elimination reactions should be considered. Thus, the reactions of the methoxy amino acids with typical nucleophiles have been investigated in the presence of Lewis acid, in order to examine the scope and limitation of amidoalkylation using the amino acids.

First of all, the reactions of the α-methoxy amino acid derivatives with thiols were carried out. Ethyl *N*-acetyl-α-methoxyalaninate (**3b**) was subjected to react with phenylmethanethiol in acetonitrile in the presence of $SnCl_4$ to afford ethyl *N*-acetyl-α-benzylthioalaninate (**7b**) in 92% yield. **3d** was similarly treated with phenylmethanethiol to give **7d** in 84% yield (Scheme 5). Careful analysis of the reaction mixture by liquid chromatography indicated no formation of the elimination and rearrangement products. Furthermore, α-amidoalkylation of aromatic compounds was carried out by using anisole as a typical example. Treatment of **3b** with anisole using a molar equivalent of $SnCl_4$ to that of **3b** gave the α-substituted product **8b** (para isomer) in 58% yield along with the ortho isomer **9b** (29%). In this case, α,β-dehydro amino acid **6b** was obtained in 5% yield. Furthermore, **3d** was allowed to react with anisole to afford a mixture

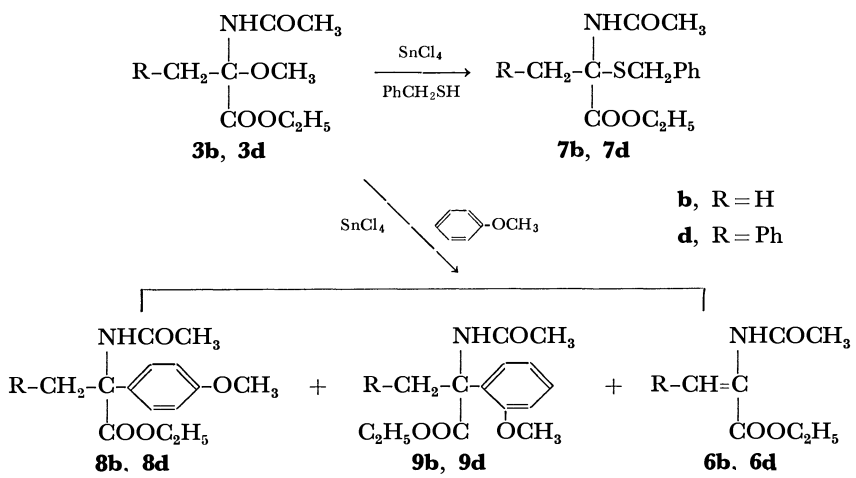

Scheme 5.

of **8d** and **9d** in 70% yield in a 4 : 1 ratio determined by NMR spectrum of the crude products. The α,β-dehydro amino acid derivative **6d** was detected.

Efforts to amidoalkylate benzene or toluene, a less reactive nucleophile, were made under the Lewis acid-catalyzed conditions. However, though no substitution product was detected, formation of the elimination product was observed. The reaction of **3j** with toluene gave the same result as above. Treatment of **3b** or **3d** with active methylene compounds such as diethyl malonate and ethyl acetoacetate did not lead to the formation of any substitution products. The results are in sharp contrast with those reported by Ben-Ishai *et al.*[16–18] in which α-methoxyglycine derivatives react easily with benzene as well as active methylene compounds to afford the α-substituted α-amino acids derivatives.

It may be concluded that the α-methoxy α-amino acid derivatives can be used as reagents for α-amidoalkylation by which various types of amino acid skeletons are introduced to afford α-substituted amino acids. However, formation of α,β-dehydro amino acids becomes overwhelming when a feeble nucleophile such as toluene is employed.

Experimental

Equipment. Melting points were measured with a Yamato melting point apparatus and are uncorrected. IR spectra were recorded on a Shimadzu IR-27G infrared spectrophotometer, and NMR spectra on a Hitachi Perkin-Elmer R-20 high resolution NMR spectrometer with tetramethylsilane as an internal standard. High performance liquid chromatography was taken by Waters ALC-GPC-244. The electrolyses were carried out with use of a Hokuto Potentio-Galvanostat HA 104 (1A-55V), PGS 2500 (2.5 A-60V) or PGS 2000 (2A-100V) equipped with a Hokuto HA 108A coulomb meter.

*Preparation of the Starting Materials **2a—g**.* **2a—f** were prepared according to the method reported previously.[3a] **2g**: Sodium hydride (65%) (4.4 g, 0.12 mol) was suspended in 100 ml of tetrahydrofuran. To this was added **1c** (17 g, 0.1 mol) dissolved in 30 ml of tetrahydrofuran at 10—15 °C under vigorous stirring. Stirring was continued for additional 1 h at the same temperature. To the mixture was added dropwise benzyl bromide (17 g, 0.1 mol) at 10—30 °C. After being stirred overnight, the reaction mixture was neutralized with acetic acid and the solvent was evaporated to dryness *in vacuo*. The residue was dissolved in ethyl acetate, and the solution was washed with water, dried over magnesium sulfate, then evaporated to dryness *in vacuo*. The resulting crystals were recrystallized from ethyl acetate–hexane to afford 22 g (90%) of ethyl α-acetamido-α-cyano-β-phenylpropionate as colorless needles: mp 111—113 °C; IR (Nujol) 3330, 1748, 1670, 1510 cm^{-1}; NMR ($CDCl_3$) δ 1.15 (t, 3H), 2.05 (s, 3H), 3.39 (s, 2H), 4.16 (q, 2H), 7.3 (m, 6H); Found: C, 64.61; H, 6.35; N, 10.48%. Calcd for $C_{14}H_{16}N_2O_3$: C, 64.60; H, 6.20; N, 10.76%.

Ethyl α-acetamido-α-cyano-β-phenylpropionate (10 g, 0.04 mol) obtained above was dissolved in **20** ml of ethanol. To this was added dropwise potassium hydroxide (2.3 g, 0.04 mol) dissolved in 5 ml of water at 5—10 °C under vigorous stirring. The reaction mixture was allowed to stand at room temperature for 3 days, and then concentrated to dryness *in vacuo* below 30 °C. The residue was dissolved in 10 ml of water and the solution was shaken once with ethyl acetate. The aqueous layer was acidified to Congo Red with 12 M hydrochloric acid. The acidified solution was shaken with three 50 ml portions of ethyl acetate, and the combined ethyl acetate layer was washed twice with 10 ml of brine, dried over magnesium sulfate, then evaporated to dryness *in vacuo* below 30 °C. The resulting crystals were recrystallized from ethyl acetate–hexane to afford 6.5 g (75%) of **2g** : mp 140—141 °C; IR (Nujol) 3350, 1730, 1630, 1540 cm^{-1} ; NMR ($CDCl_3$+DMSO-d_6) δ 2.02 (s, 3H), 3.43 (s, 2H), 7.30 (s, 5H), 8.17 (s, 1H); Found: C, 61.81; H, 5.35; N, 12.22%. Calcd for $C_{12}H_{12}N_2O_3$: C, 62.06; H, 5.21; N, 12.06%.

General Electrolysis Procedure. The general electrolysis procedure is the same as reported previously.[2] In the electrolysis in 2-propanol, a 50 mA of current was passed. For large scale (1 mol) electrolysis, electrodes of an area of 40 cm^2 were used in a non-divided cell.

*Electrolysis of **2d** in Aqueous Tetrahydrofuran.* **2d** (2.8 g, 0.01 mol) was electrolyzed in a mixture of 25 ml of water and 6 ml of tetrahydrofuran containing 0.38 ml of 1 M potassium hydroxide. The other electrolysis conditions were the same as those described above. The electrolyzed solution was evaporated to dryness *in vacuo* and the resulting residue was extracted with ethyl acetate, washed once with brine, dried over magnesium sulfate, then evaporated to dryness *in vacuo*. Extraction of the resulting residue with 100 ml of hexane gave 1.8 g (93%) of ethyl phenylpyruvate (**5**). The derivative of the 2,4-dinitrophenylhydrazone showed mp 130—131 °C (lit,[19] mp 132—133 °C).

*Saponification of Compound **3d**.* Compound **3d** (2.65 g, 0.01 mol) was dissolved in 30 ml of methanol. To this was added potassium hydroxide (0.56 g, 0.01 mol) dissolved in 3 ml of water under vigorous stirring at room temperature. The reaction mixture was allowed to stand at room temperature for 24 h, and then concentrated to dryness *in vacuo*. The residue was dissolved in 10 ml of water and the solution was shaken once with ethyl acetate. The aqueous layer was acidified to Congo Red with 6 M hydrochloric acid. The acidified solution was shaken with three 30 ml portions of ethyl acetate, and the combined ethyl acetate layer was washed once with brine, dried over magnesium sulfate, then concentrated to dryness *in vacuo*. The resulting crystals were recrystallized from ethyl acetate–hexane to afford 1.2 g (51%) of *N*-acetyl-α-methoxyphenylalanine: mp 133—135 °C; IR (Nujol) 3290, 1760, 1633, 1564 cm^{-1}; NMR (DMSO-d_6) δ 1.90 (s, 3H), 3.17 (s, 5H), 7.17 (s, 5H), 8.18 (broad s, 1H); Found: C, 60.77; H, 6.36; N, 6.01%. Calcd for $C_{12}H_{15}NO_4$: C, 60.75; H, 6.37; N, 5.90%.

*Conversion to **6b**.* Compound **3b** (80 g, 0.42 mol) and ammonium bromide (80 mg) were put into a distillation apparatus. The mixture was heated at 120 °C for 20 min at 70—100 mmHg under nitrogen atmosphere, methanol being distilled off. Subsequent distillation at 5 mmHg afforded 50 g (76%) of **6b**: bp 100—103 °C (5 mmHg). IR and NMR spectra of **6b** were identical with those of an authentic sample.[13]

*Reactions of **3b** and **3d** with Phenylmethanethiol.* Ethyl *N*-acetyl-α-methoxyalaninate (**3b**) (0.95 g, 5 mmol) and phenylmethanethiol (0.62 g, 5 mmol) were dissolved in 5 ml of acetonitrile. To this was added dropwise $SnCl_4$ (0.58 ml, 5 mmol) at 0—5 °C under vigorous stirring . Stirring was continued for 1 h at the same temperature and the reaction was quenched by addition of 5 ml of saturated aqueous sodium hydrogencarbonate solution. The insoluble materials were filtered off and the filtrate was evaporated to dryness *in vacuo*. The residue was dissolved in ethyl acetate and the solution was washed with brine, dried over

magnesium sulfate, and then evaporated to dryness *in vacuo*. The resulting syrup was treated with silica gel chromatography using bezene–acetone (5 : 1) as eluent to afford 1.29 g (92%) of ethyl *N*-acetyl-α-benzylthioalaninate (**7b**). Recrystallization from ethyl acetate–hexane gave colorless needles: mp 79—80 °C; IR (Nujol) 3230, 1739, 1637, 1528 cm^{-1}; NMR ($CDCl_3$) δ 1.28 (t, 3H), 1.73 (s, 3H), 1.86 (s, 3H), 3.82 (s, 2H), 4.18 (q, 2H), 6.37 (broad s, 1H), 7.27 (s, 5H); Found: C, 59.61; H, 6.79; N, 4.69%. Calcd for $C_{14}H_{19}NO_3S$: C, 59.76; H, 6.81; N, 4.98%.

3d was also allowed to react with phenylmethanethiol under the same conditions as above to afford the substitution product **7d** in 84% yield. **7d**: mp 103—104 °C ; IR (Nujol) 3230, 1728, 1640, 1534 cm^{-1}; NMR ($CDCl_3$) δ 1.33 (t, 3H), 1.68 (s, 3H), 3.43 and 3.98 (AB q, 2H, J=13 Hz), 3.75 (s, 2H), 4.25 (q, 2H), 6.20 (broad s, 1H), 7.14 (s, 5H), 7.25 (s, 5H); Found: C, 67.37; H, 6.52; N, 3.90%. Calcd for $C_{20}H_{23}NO_3S$: C, 67.20; H, 6.49; N, 3.92%.

*Reactions of **3b** and **3d** with Anisole.* To a stirred solution of ethyl *N*-acetyl-α-methoxyalaninate (1.0 g, 5.3 mmol) dissolved in anisole (10 ml) was added dropwise $SnCl_4$ (0.61 ml, 5.3 mmol) at 0—5 °C. The reaction mixture was stirred for 1 h at the same temperature and the reaction was quenched by addition of 10 ml of saturated aqueous sodium hydrogencarbonate solution. The insoluble materials were filtered and washed thoroughly with acetonitrile. The filtrate was evaporated to dryness *in vacuo* and the residue was extracted with ethyl acetate. The extract was washed with water, dried over magnesium sulfate, and then concentrated to dryness *in vacuo*. The resulting syrup was treated with silica gel chromatography using chloroform as an eluent to afford 0.82 g, (58%) of **8b** (para isomer), 0.41 g (29%) of **9b** (ortho isomer), and 0.04 g (5%) of ethyl *N*-acetyl-α,β-dehydroalaninate **6b**. **8b**: mp 108—109 °C; IR (Nujol) 3240, 1736, 1632, 1560, 1513 cm^{-1}; NMR ($CDCl_3$) 1.17 (t, 3H), 1.96 (s, 3H), 2.01 (s, 3H), 3.77 (s, 3H), 4.14 (q, 2H), 6.75 (broad s, 1H), 6.83 (d, 2H), 7.34 (d, 2H); Found: C, 63.27; H, 7.01; N, 5.33%. Calcd for $C_{14}H_{29}NO_4$: C, 63.38; H, 7.22; N, 5.28%. **9b** : syrup; IR (film) 3410, 1730, 1660, 1600, 1490 cm^{-1}; NMR ($CDCl_3+D_2O$) δ 1.14 (t, 3H), 1.87 (s, 3H), 2.02 (s, 3H), 3.73 (s, 3H), 4.15 (q, 2H), 6.7—7.7 (m, 4H); MS (30 eV), *m/e* (rel intensity), 265 (M^+, 10), 192 (73), 150 (100), 133 (32), 118 (32), 105 (47), 43 (36). The physical constants of **6b** were identical with those of an authentic sample.

3d was also treated with anisole in the presence of $SnCl_4$. The work-up was the same as that described above. TLC of the reaction mixture showed the presence of the substitution products **8d** and **9d** and the elimination product **6d**. The resulting residue was treated with silica gel chromatography using benzene–acetone (5 : 2) as an eluent to afford a mixture of **8d** and **9d** as syrup in 70% yield, the ratio of **8d** to **9d** being 4:1, based on the NMR spectrum. Elemental analysis of the mixture showed a reasonable result. Found: C, 70.12; H, 6.80; N, 4.11%. Calcd for $C_{20}H_{23}NO_4$: C, 70.36; H, 6.79; N, 4.10%. We failed in separating each isomer by liquid chromatography under various conditions. As an example, liquid chromatography of the mixture by use of μ Porasil as resin (column: 4 mm × 30 cm; flow rate : 1 ml/min) showed a single peak at retention time of 10.5 min. The mixture was crystallized from ethyl acetate–hexane to afford **8d** as needles: mp 95—96 °C; IR ($CHCl_3$) 3420, 1726, 1675, 1608, 1593 cm^{-1} ; NMR ($CDCl_3$) δ 1.19 (t, 3H), 1.95 (s, 3H), 3.78 (s, 3H), 3.74 and 4.10 (AB q, 2H, J=14 Hz), 4.13 (q, 2H), 6.83 (d, 2H), 6.6—7.4 (m, 6H), 7.33 (d, 2H). **9d** could not be isolated as a pure form. The structure of **9d** was assigned by the NMR spectrum of the mixture of **8d** and **9d**. **9d**: NMR ($CDCl_3$) δ 1.17 (t, 3H), 1.88 (s, 3H), 3.65 (s, 3H), 3.32 and 4.50 (AB q, 2H, J=14 Hz), 4.13 (q, 2H), 6.6—7.4 (m, 10H).

We thank Prof. Mitsuyoshi Kawanishi, Kyoto University, for his valuable suggestion. We are also grateful to Dr. Ichiro Chibata, Director of our Research Laboratory, for his encouragement.

References

1) Synthetic Electroorganic Chemistry. VIII. Part VII: see Ref. 8.

2) Preliminary report : H. Horikawa, T. Iwasaki, K. Matsumoto, and M. Miyoshi, *Tetrahedron Lett.*, **1976**, 191.

3) a) T. Iwasaki, H. Horikawa, K. Matsumoto, and M. Miyoshi, *J. Org. Chem.*, **42**, 2419 (1977) and references cited therein; b) R. K. Olsen and A. J. Kolar, *Tetrahedron Lett.*, **1975**, 3579.

4) D. Ben-Ishai, R. Moshenberg, and J. Altman, *Tetrahedron*, **33**, 1533 (1977).

5) a) G. Lucente and D. Rossi, *Chem. Ind. (London)*, **1973**, 324 ; b) C. Gallina, M. Maneschi, and A. Romeo, *J. Chem. Soc., Perkin Trans. 1*, **1973**, 1134.

6) a) H. Poisel and U. Schmidt, *Chem. Ber.*, **108**, 2547 (1975); b) Chung-gi Shin, Y. Sato, and J. Yoshimura, *Bull. Chem. Soc. Jpn.*, **48**, 2891 (1975); c) U. Schmidt and E. Ohler, *Angew. Chem. Int. Ed. Engl.*, **15**, 42 (1976); d) H. Poisel and U. Schmidt, *ibid.*, **15**, 294 (1976).

7) K. Ogura, J. Yoshimura, N. Katoh, and G. Tsuchihashi *Chem. Lett.*, **1975**, 803.

8) H. Horikawa, T. Iwasaki, K. Matsumoto, and M. Miyoshi, *J. Org. Chem.*, **43**, 335 (1978).

9) *N*-Benzyloxycarbonyl-α-methylphenylalanine was electrolyzed under similar conditions to afford phenylacetone in 68% yield.

10) a) L. Eberson in "The Chemistry of Carboxylic Acids and Esters," ed by S. Patai, Interscience, New York, N. Y. (1969), p. 53; b) J. T. Keating and P. S. Skell in "Carbonium Ions," ed by G. A. Olah and P. v. R. Schleyer, Wiley-Interscience, New York, N. Y. (1970), Vol. II, p. 573; c) S. D. Ross. M. Finkelstein, and E. J. Rudd, "Anodic Oxidation," Academic Press, New York, N. Y. (1975), p. 134.

11) a) R. P. Linstead, B. R. Shephard, and B. C. L. Weeden, *J. Chem. Soc.*, **1951**, 2854; b) M. Finkelstein and S. D. Ross, *Tetrahedron*, **28**, 4497 (1972).

12) B. W. Bycroft, *Nature*, **224**, 595 (1969) and references cited therein.

13) D. Hale, P. Mamalis, and J. Green, *J. Chem. Soc.*, **1960**, 2847 and references cited therein.

14) N. J. Leonard and R. Y. Ning, *J. Org. Chem.*, **31**, 3928 (1966).

15) A. J. Kolar and R. K. Olsen, *Synthesis*, **1977**, 457.

16) a) D. Ben-Ishai, G. Ben-Et, and A. Warshavski, *J. Heterocycl. Chem.* **7**, 1289 (1970); b) J. Altman, R. Moshenberg, and D. Ben-Ishai, *Tetrahedron Lett.*, **1975**, 3737.

17) D. Ben-Ishai, Z. Berler, and J. Altman, *J. Chem. Soc., Chem. Commun.*, **1975**, 905.

18) a) D. Ben-Ishai, I. Satati, and Z. Bernstein, *Tetrahedron*, **32**, 1571 (1976); b) D. Ben-Ishai, I. Satati, and Z. Berler, *J. Chem. Soc., Chem. Commun.*, **1975**, 349; c) J. E. Barry, E. A. Mayeda, and S. D. Ross, *Tetrahedron*, **33**, 369 (1977).

19) H. O. House, J. W. Blaker, and D. A. Madden, *J. Am. Chem. Soc.*, **80**, 6386 (1958).

S_N2 Reactions in Dipolar Aprotic Solvents. VII. Kinetic and Equilibrium Secondary α-Deuterium Isotope Effects in Chlorine Isotopic Exchange Reactions of Substituted Chloromethanes in Acetonitrile[1)]

Jun-ichi HAYAMI,*,[2)] Nobuhisa HIHARA, Nobuo TANAKA, and Aritsune KAJI

Department of Chemistry, Faculty of Science, Kyoto University, Kyoto 606

(Received August 11, 1978)

Secondary α-deuterium isotope effects were studied in the symmetrical nucleophilic substitution of the substituted chloromethanes in acetonitrile. The apparent second order rate coefficients show a significant isotope effect for chloromethyl aryl ethers and sulfides (1.11—1.14 per D), and an intermediate value of 1.05 for cinnamyl chlorides. 2-Arylethyl chlorides were shown to give an appreciable isotope effect of 1.03—1.04, and arylchloromethanes to give varying amount of the isotope effect from 1.006 to 1.050 depending upon the ring substituent. The deuterium label also gave rise to a significant equilibrium isotope effect on the substrate-nucleophile association in the reaction mixture. The observation of an equilibrium isotope effect suggested a possibility that an apparent isotope effect was a composite of the thermodynamic and the kinetic isotope effects. Thus the dissection resulted in a uniform and a fairly large kinetic isotope effect for all the activated substrates studied and in a small kinetic isotope effect for 2-arylethyl chloride. The results are explained in a framework of loose-tight transition state.

In the studies of the Hammett type analysis of the Finkelstein reaction in a dipolar aprotic solvent acetonitrile, the present authors proposed the rate accelerating effect by the conjugative stabilization of the S_N2 transition state.[3)]

When a hetero atom[3a)] or an unsaturated linkage[3b,c)] adjacent to the reaction center is available, the conjugative stabilization may be operative, superposing upon the nucleophilic approach of the attacking nucleophile, in the displacement reaction that proceeds through a loose transition state. The looseness or the tightness of the transition state has often been postulated. A successful example is found in the study of the solvent effect on the rate of the bimolecular reactions.[4)]

Another approach to verify such a spectrum of the transition state may be tenable by the study of the secondary hydrogen isotope effect. The method, which was awarded with success, has mainly applied to the unimolecular solvolytic reactions.[5)]

Formerly, the rate ratio k_2^H/k_2^D of unity has been believed to be a criterion of the S_N2 reaction and the secondary isotope effect has been considered not existent in this class of reactions.[6)] Recent works show that the isotope effect is observable in some examples of the S_N2 reactions, and that the typical observed value is in the range of 0.95—1.06 per one α-deuterium atom.[7,8)] However, the study with a systematic variation in the substrate reactivity was scarcely undertaken in the study of bimolecular substitutions.

In the present work, the substituted chloromethanes with the deuterium label at the reacting carbon were subjected to the chlorine-chlorine isotopic exchange reaction. The deuterium label also affected substrate-nucleophile interaction which accompanied with the symmetrical exchange reaction.[9)] The kinetic deuterium isotope effect was discussed in relation to the reactivity of these model compounds and in relation to the potential role of the substrate-nucleophile association complex.

Results and Discussion

Substituted chloromethanes which have a variety of substituents adjacent to the reaction center were subjected to the chlorine isotopic exchange reaction in dry acetonitrile as shown in Scheme 1.

$$X\text{-}C_6H_4\text{-}Y\text{-}CZ_2Cl + Et_4N^*Cl \rightleftharpoons X\text{-}C_6H_4\text{-}Y\text{-}CZ_2{}^*Cl + Et_4NCl$$

X; H and other substituent
Y; O, S, CH^t=CH, none(benzyl), and CH_2
Z; H and D

Scheme 1.

The incorporation of the radioactive chlorine from the reagent tetraethylammonium chloride-^{36}Cl followed first-order kinetics and the plausible second-order rate coefficients were obtained as reported earlier.[3)] This result definitely shows that the rate determining transition state should involve both the organic chloride and the nucleophile, chloride ion.

The results of the exchange reactions with the deuterated substrates as well as that with the unlabeled substrates are given in Table 1. As shown in Table 1, normal isotope effect was observed in every case. The magnitude of the effect was about 11—14% for chloromethyl aryl ethers and chloromethyl aryl sulfides. 2-Arylethyl chlorides gave about 3—4% of the effect while arylchloromethanes gave diverse normal effect of 0.6—5.0%. Cinnamyl chloride gave an intermediate value of 5%.

The constancy of the secondary deuterium isotope effect for chloromethyl aryl sulfides is excellent and possibly indicates an operation of a single mechanism for all these sulfides as are also indicated by the establishment of the good linear free energy relationship for exchange reactions.[3a,10)]

The equilibrium constants for the formation of substrate-nucleophile complex were determined with deuterated substrates, as well as with unlabeled substrates. The formation of such a complex in the Finkelstein reaction mixture was already reported.[9)] Equilibrium deuterium isotope effects were observed for the representative substrates and the results are shown in Table 2. Except for 2-(*p*-nitrophenyl)ethyl chloride, which shows essentially the absence of equilibrium

TABLE 1. RATE CONSTANTS AND ISOTOPE EFFECTS OF CHLORINE ISOTOPIC EXCHANGE REACTIONS OF SUBSTITUTED CHLOROMETHANES [X-C_6H_4-Y-CZ_2Cl]

Y	X	t °C	k_{obsd}[a] l/mol·min ×10^2 Z;H	Z;D	k_H/k_D[b]
O	*p*-Cl	−20	20.0	16.2[c]	1.112
	m-Cl		11.6	9.46[c]	1.108
S	*p*-OCH_3	20	6.49	5.27	1.120
	H		3.10	2.44	1.128
	p-Cl		1.99	1.57	1.124
	m-Cl		1.60	1.23	1.141
	p-NO_2		0.652	0.519	1.121
CH=CH	H	20	2.54	2.30	1.050
None	*p*-OCH_3	20	4.52	4.13	1.046
	p-CH_3		1.83	1.66	1.050
	m-CH_3		1.25	1.23	1.006
	H		1.23	1.17	1.026
	p-Cl		1.81	1.72	1.025
	m-NO_2		2.46	2.38	1.017
	p-NO_2		3.47	3.28	1.028
CH_2	H	60	0.523	0.489	1.035
	p-Cl		0.889	0.836	1.031
	p-NO_2		1.92	1.78	1.039

a) [Substrate]=[*Cl^-]=0.10 M. b) Per one D atom. c) 98% isotopic purity.

TABLE 2. EQUILIBRIUM CONSTANTS AND ISOTOPE EFFECTS OF THE FORMATION OF COMPLEX [X-C_6H_4-Y-CZ_2Cl]

Y	X	t °C	$K_{Z;H}$[a] M^{-1}	$K_{Z;D}$[a] M^{-1}	K_H/K_D[b]
S	*p*-NO_2	30.0	0.348	0.365	0.976
CH=CH[d]	H	30.0	0.0964	0.104[c]	0.928
None	*p*-NO_2	19.7	0.365	0.400[c]	0.913
		27.2	0.303	0.322[c]	0.913
		31.0	0.277	0.308[c]	0.901
		32.7	0.266	0.322	0.909
CH_2[e]	*p*-NO_2	20.0	0.202	0.199	1.007

a) Errors estimated to be within 2% or better. b) Per one D atom. c) For X-C_6H_4-Y-CHDCl. d) At 30 °C, $\rho_K=0.40\pm0.1$. For *p*-NO_2-C_6H_4-CH=CH-CH_2Cl, at 20 °C, $\Delta H^\circ=(-1.52\pm0.5)$ kcal/mol, $\Delta S^\circ=(-8.2\pm2)$ eu. e) At 30°C, $\rho_K=0.65\pm0.1$. For *p*-NO_2-C_6H_4-CH_2CH_2Cl, at 20 °C, $\Delta H^\circ=(-1.22\pm0.5)$ kcal/mol, $\Delta S^\circ=(-7.3\pm2)$eu.

isotope effect, chloromethyl *p*-nitrophenyl sulfide, cinnamyl chloride, and (*p*-nitrophenyl)chloromethane all show an inverse equilibrium isotope effect. The observation of the inverse equilibrium isotope effect is not unexpected.[11]

The data of substrate-nucleophile association allow one to calculate the intrinsic second order rate coefficient corrected for the change of the concentration of both the substrate and the reagent upon complex formation (*vide infra*). In Table 3, the corrected isotope effects are summarized for the representative classes of the compounds. Table 3 also contains the results of the Hammett type analyses of the corresponding unlabeled substrates.

TABLE 3. SUMMARY OF THE α-SUBSTITUENT EFFECTS AND THE KINETIC ISOTOPE EFFECTS [X-C_6H_4-Y-CZ_2Cl]

Y	Rel rate[a]	ρ (σ, r)[b]	k_2^H/k_2^D[c] (X)	t °C
O	400000	−1.56(σ, 0.997)	1.112[d](*p*-Cl)	−20
S	1020	−0.92(σ, 0.997)	1.119(*p*-NO_2)	20
CH=CH	680	−0.19[e](σ, 0.962)	1.048(H)	20
None	330	— —	1.024(*p*-NO_2)	20
CH_2	1	0.57(σ°, 0.991)	1.039(*p*-NO_2)	60

a) Ref. 3b. X; H, at 20 °C. b) Ref. 3. c) k_{obsd} was corrected for the formation of substrate-nucleophile complex. d) Uncorrected valuc. e) Obtained for *m*-substituted compounds.

The inspection of the results in Table 3 is quite intuitive. The spectrum of the secondary deuterium isotope effect obtained in the present study seems to have a parallelism to the degree of the electron-donating conjugative stabilization of the transition state. As suggested from the Hammett type analysis, and from the relative rate of the substituted chloromethanes studied, such a stabilization is most prevailing in the ethers ($\rho=-1.56$, $k_{rel}=400000$) and in sulfides ($\rho=-0.92$, $k_{rel}=1020$), less effective but still significant in cinnamyl chlorides ($\rho^m=-0.19$, $k_{rel}=680$), and is apparently not operating in 2-arylethyl chlorides ($\rho=+0.57$, $k_{rel}=1$).

The difficulty is encountered for arylchloromethanes. The observed isotope effects in the Table 1 seem too small for these activated Finkelstein substrates. This is also the case with cinnamyl chlorides (*cf.* Table 3).

The behavior of the arylchloromethanes is often a matter of controversy.[12] The significant change from tight transition state (*p*-NO_2) into loose transition state (*p*-OCH_3 or *p*-CH_3) was suggested by the studies of the substituent effect upon the rate of the Finkelstein reaction[3b] and upon the solvent activity coefficient of the reaction.[4]

Table 1 shows the small and varying extent of the isotope effect. Thus (*p*-nitrophenyl)chloromethane, the transition state of which is considered to be tighter than that of (*m*-methyl- or unsubstituted phenyl)chloromethane, gives an appreciable isotope effect of about 3%. While (*m*-methylphenyl)chloromethane shows the isotope effect close to unity and phenylchloromethane shows a fair isotope effect of 2.6% contrary to the expectation from the looseness-tightness approach (*cf.* Table 1).

These findings seem to suggest that the (overall) isotope effect should tell something that is different from the implication of the rate studies.

A clue to answer this difficulty is found in an observation of an association complex in the Finkelstein reaction. The present authors have reported the presence of the substrate-reagent complex which possesses a structure quite similar to the traditional S_N2 transition state.[9] There are indications that the nucleophilic anion coordinates at the rear side of the potential leaving group resulting in the freezing of the intramolecular rotation, which is the necessary condition for the operation of an electron-donating *p*-π and(or) *p*-*p*

interaction by the neighboring functionality.

Such a complex can play one of the two quite distinct roles in the bimolecular reaction. One is the direct precursor that intervenes before the rate determining unimolecular scrambling (Scheme 2).

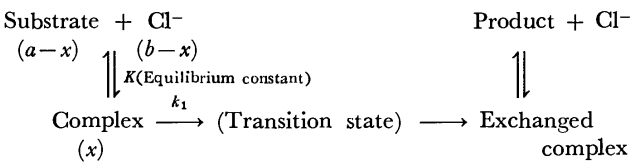

$$\text{Rate} = k_1 K(a-x)(b-x)$$

Scheme 2.

The other is the indifferent entity in the subsidiary or parasitic equilibrium with the free substrate and the free nucleophile (Scheme 3).

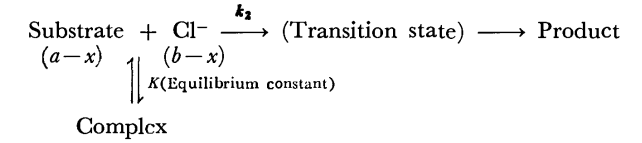

$$\text{Rate} = k_2(a-x)(b-x)$$

Scheme 3.

The equilibrium isotope effect in Table 2 seems to support the operation of the association mechanism (Scheme 2), giving the more comprehensive picture of the observed kinetic isotope effect. When one postulates an operation of the mechanism in Scheme 2, the observed second order rate coefficient k_2 can be separated into the equilibrium constant K for the substrate-nucleophile association, and the rate constant k_1 for the unimolecular scrambling, as is shown in Eq. 1.

$$k_2 = k_1 \cdot K \tag{1}$$

Accordingly the kinetic isotope effect observed can be dissected into the equilibrium isotope effect of bimolecular association(K_H/K_D) and the kinetic isotope effect of unimolecular scrambling (k_1^H/k_1^D, Eq. 2).

$$k_2^H/k_2^D = k_1^H/k_1^D \cdot K_H/K_D \tag{2}$$

Combining the data from Table 1 and Table 2, the kinetic isotope effect k_1^H/k_1^D can be calculated postulating the intervention of the substrate-nucleophile complex. Results are shown in Table 4.

For the activated substrates, reflecting the inverse equilibrium isotope effects, the kinetic isotope effects calculated (that correspond to the rate determining unimolecular scrambling of the complex) are now close to that of the limiting solvolysis.[13] For 2-(*p*-nitrophenyl)ethyl chloride, the equilibrium isotope effect of about unity substantiates the figure of the isotope effect observed (k_2^H/k_2^D) is essentially intrinsic.

Thus the explanation in the framework of the looseness of the transition state seems to hold for the whole classes of the compounds studied. In a significantly loose transition state, the carbon under attack has essentially little difference from the carbonium ion having negligible nucleophilic attachment to both the leaving and the incoming group (chloride ion).[14] Thus 15.7% might be the limiting value for the secondary deuterium isotope effect in S_N2 reactions as it is the case with the unimolecular limiting solvolysis of organic chlorides.[15]

Table 4. Dissection of the isotope effect
[X-C_6H_4-Y-CZ_2Cl]

Y	X	k_2^H/k_2^D a)	K_H/K_D a)	k_1^H/k_1^D a)
S	*p*-NO_2	1.119	0.976	1.147
CH=CH	H	1.048	0.928	1.129
None	*p*-NO_2	1.024	0.909	1.127
CH_2	*p*-NO_2	1.039	1.007	1.032

a) Per one D atom. There are some differences between the temperature for the kinetic measurement and that for the equilibrium measurement. However, the change of temperature in the range studied gave negligiblly small effect upon the equilibrium isotope effect, and an example is shown in Table 2 for (*p*-nitrophenyl)-chloromethane.

The S_N1 like behavior of the chloromethyl aryl ether was suggested in the nucleophilic displacement reaction of chloromethyl methyl ether.[16]

In the loose transition state, the change of the out-of-plane bending motion, caused by the bond breaking, may hardly be compensated by the bond formation with the incoming nucleophile.

The largest kinetic isotope effect observed in the present study, for chloromethyl aryl sulfides and ethers, is still smaller than the limiting value of S_N1 reactions. This is the indication of a nucleophilic interaction in the transition state.[7] The magnitude of the isotope effect seems to be smaller as the transition state becomes tighter. 2-(*p*-Nitrophenyl)ethyl chloride shows a small kinetic isotope effect which seems to be compatible with the implication from ρ_{k_1} (and with ρ_{k_2}).[17]

The nature of the unimolecular scrambling of the complex suggests that the nucleophile assists the expulsion of the leaving group. A quite similar suggestion was made by Schleyer as "nucleophilically assisted ion pair formation."[18]

Another explanation in a framework of traditional nucleophilic substitution may be pursued. The operation of an S_N2-C^+ or of the rate determining nucleophilic attack upon an ion pair may be one of the possibilities. The absence of a very high ρ value in the Hammett relationship[17] and the absence of k_Δ process[19] in the case of 2-arylethyl chlorides (and probably cinnamyl chloride) are the evidences against the classical S_N2-C^+ route.[3a]

As long as an S_N2-C^+ or an ion pair mechanism is operative, one should postulate a spontaneous ionization of the substrate.[20] Bearing in mind the existence of the substrate-nucleophile complex in the Finkelstein reaction mixture studied, and the feature of the complex which shows interesting similarities to the traditional S_N2 transition state, one can hardly imagine a spontaneous ionization without help of the nucleophile that locates at the rear side of the potential leaving group. The absence of the inert salt effect is also against the operation of S_N2-C^+ and(or) ion pair intervention.[3a] In addition, the classical explanation necessitates a significant attachment of the nucleophile for arylchloromethanes or cinnamyl chlorides, one of the classes of the activated substrates.

Table 5. Protic–aprotic solvent effects on the rate of the chlorine exchange and the formation of complex in acetonitrile [p-NO_2-C_6H_4-CH_2Cl + Et_4N^*Cl]

[MeOH] / M	k_{obsd} [a] / l/mol min $\times 10^2$	K [b] / M^{-1}
0	10.8	0.287
0.0493	8.16	0·242
0.0985	6.90	0.219
0.197	4.55	0.181
0.296	3.27	0.138
0.493	1.90	0.110

a) At 30 °C. Errors estimated to be within 1.5%.
b) At 30 °C. Errors estimated to be within 0.005.

Table 6. Physical constants of substituted chloromethanes [X-C_6H_4-Y-CZ_2Cl]

Y	X	Bp °C/mmHg (Mp °C) Z; D	Z; H[a]
O	p-Cl	74.0—74.5/3.5	87.0—88.0/6
	m-Cl	71.0—71.5/3.5	82.0—83.0/6
S	p-OCH_3	109.0—109.5/1.0	105.0/0.7
	H	117.5—118.0/24	115.5—116.0/20
	p-Cl	98.0—99.0/1.0	109—111/4
	m-Cl	94.0/0.6	94.5/0.7
	p-NO_2	(62.5—63.0)	(63.5—64.0)
CH=CH	H	76.0/3 65.0/0.7[b]	116—118/16
None	p-OCH_3	82.0—82.5/3	70.5/0.5
	p-CH_3	99.5/30	88.5/17
	m-CH_3	97.0/26 45.5/0.8[b]	56.5—57.0/2.5
	H	77.5—78.0/26	76.8—77.0/24.5
	p-Cl	110.5—111.5/28	108.5/28
	m-NO_2	(45.0)	(45.0)
	p-NO_2	(72.0—72.5) (73.0) [b]	(72.5—73.0)
CH_2	H	93.0—94.0/26	86.0/18
	p-Cl	128.5—129.0/27	84.0/4
	p-NO_2	(48.8)	(49.0)

a) Ref. 3. b) X-C_6H_4-Y-CHDCl.

Thus the postulation of the substrate-nucleophile complex as the "intermediate" of the Finkelstein reaction opens up the new possibility to have a unified view of the behavior of the variety of the substrate. There is hardly available a good means to examine the possible equilibrium isotope effects of the substrate-nucleophile association in a protic medium. At present it is an open question if the present postulation can become a general proposal.

The preliminary result of the protic-aprotic solvent effect is also compatible with the association mechanism. Successive additions of the small amount of methanol to solvent acetonitrile give rise to the decrease in the equilibrium constant of the complex formation as well as the decrease in the rate of symmetrical exchange reactions (Table 5). However the decrease of the second order rate coefficient is much more profound than that of the equilibrium constant. According to the association mechanism (Scheme 2), the nucleophilic displacement reaction in the presence of methanol added should contain "deactivated anionic nucleophile"[4] both at the preliminary association and at the unimolecular scrambling, thus the overall rate should be doubly affected by the deactivation of the anionic nucleophile, as is envisaged by Eq. 1.

Experimental

Instruments. The radioactivity was measured with a Nuclear Chicago Model-6801 liquid scintillation counter. The PMR spectra were obtained on a JEOL JNM-PS-100 NMR spectrometer equipped with a Hetero Spin Decoupler JNM-SD-HC 1. The melting points were measured with a Yanagimoto Micro Melting Point Apparatus and were uncorrected.

Materials. Aryloxymethane-α,α-d_2-sulfonates were obtained as follows. Sodium p-chlorophenoxymethanesulfonate(8g) was dissolved in 10 ml of 1M-NaOD/D_2O (99.75% isotopic purity). The mixture was maintained at about 100 °C in a Teflon tube for four days. After cooling the solution was acidified with 1M-HCl and evaporated. The residue was subjected to the exchange once again according to the above procedure. Recrystallization from aqueous ethanol gave pure p-chlorophenoxymethane-α,α-d_2-sulfonate. The sulfonate was converted to p-chlorophenyl chloromethyl-d_2 ether with phosphorous pentachloride.[21]

Methyl-d_3 aryl sulfides were prepared from the corresponding thiophenols and CD_3I (99% isotopic purity) in ethanol in the presence of KOH. Chlorination of these sulfides with sulfuryl chloride gave chloromethyl-d_2 aryl sulfides.

(p-Nitro- and m-nitrophenyl)methan-α,α-d_2-ols were prepared from the corresponding methyl nitrobenzoates by mixed hydride reduction.[22] $LiAlD_4$(Merck, 99% isotopic purity, 0.75 g) was stirred in 40 ml of ether. To the solution anhydrous $AlCl_3$(2.5 g) in 40 ml of ether was added dropwise, and the solution was stirred for another few minutes. The methyl p-nitrobenzoate (3.2 g) in 20 ml of ether was added slowly. After stirring for an hour under reflux, the mixture was worked up as usual. The alcohols were purified by recrystallization or distillation after chromatographic purification on alumina.

(p-Nitrophenyl)methan-α-d-ol was prepared from p-nitrobenzaldehyde by mixed hydride reduction. (m-Methylphenyl)methan-α-d-ol was prepared from m-methylbenzaldehyde with $LiAlD_4$ as usual. Other arylmethan-α,α-d_2-ols were prepared from the corresponding methyl benzoates with $LiAlD_4$. Arylchloromethanes-α-d, and -α,α-d_2 were prepared from these alcohols by standard method.[23]

Cinnamyl-1,1-d_2 and cinnamyl-1-d derivatives were obtained by mixed hydride reduction from ethyl cinnamate and cinnamaldehyde, respectively.[24] Cinnamyl chlorides were proved to be trans isomers by PMR spectra and physical constants.

2-(p-Nitrophenyl)ethan-1,1-d_2-ol was prepared from ethyl (p-nitrophenyl)acetate by mixed hydride reduction. Other 2-arylethan-1,1-d_2-ols were obtained from the corresponding ethyl arylacetates by the reaction with $LiAlD_4$ as usual. The alcohols were subjected to the reaction with thionyl chloride which gave 2-arylethyl-1,1-d_2 chlorides.

After purification all these chlorides showed satisfactory NMR and IR spectra. Physical constants are listed in Table 6.

Kinetic Measurements. Batch method was undertaken as reported previously.[3a,b] In order to ensure the accuracy of the isotope effect measurement, the parallel reaction was always run with unlabeled compounds simultaniously in the same bath. The reproducibility of the isotope effect was within 0.01 for duplicate runs, though the difference in rate constants was within the range of 1.5% for independent series of measurements.

Equilibrium Measurements. Proton chemical shift measurements were undertaken as reported previously.[9] The shifts of α-proton of (*p*-nitrophenyl)chloromethane-α-*d*, (*m*-methylphenyl)chloromethane-α-*d*, and cinnamyl-α-*d* chloride were measured under the irradiation of D-frequences at 23000 G (15.349404, 15.349408, and 15.349589 MHz, respectively), noise-modulation was applied when necessary (white noise band width; 50 Hz).[25]

Some troubles are encountered in the preparation of chloromethyl-*d* *p*-nitrophenyl sulfide and of 2-(*p*-nitrophenyl)-ethyl-1-*d* chloride. Accordingly α,α-d_2 labeled substrates were utilized to measure the equilibrium isotope effect observing the chemical shift of ortho hydrogens on the phenyl ring. The control experiment with (*p*-nitrophenyl)chloromethane-α-*d*, and -α,α-d_2 resulted essentially the identical equilibrium isotope effect. In the case of 2-(*p*-nitrophenyl)-ethyl chloride two independent analyses from α- and *o*-proton(s) gave rise to the identical association constant.

Scott-Benesi-Hildebrand analyses for cinnamyl chlorides and 2-arylethyl chlorides were difficult because of their small low field shifts at the chloride concentrations studied.[26] However, the repeated measurements of the line position (up to 30 times and to the reproducibility of ±0.05 Hz or better) gave a reliable association constant.

Tracer experiments were undertaken at Radioisotope Research Center of Kyoto University. The authors are grateful to the staff of the institution. Supports by the Ministry of Education (No. 83151, 84076, 748167), Saneyoshi Shogakkai, and Ito Kagaku Shinkokai are gratefully acknowledged.

References

1) Part of this work was presented before the 2nd IUPAC Conference on Physical Organic Chemistry(Noordwijkerhout, 1974), and before the 33th National Meeting of the Chemical Society of Japan(Invited lecture, Fukuoka, 1975, abstract III p1314), and was reported in a preliminary form by N. Tanaka, A. Kaji, and J. Hayami, *Chem. Lett.*, **1972**, 1223.

2) Address correspondence to the Department of Chemistry, College of Liberal Arts and Science, Kyoto University.

3) a) J. Hayami, N. Tanaka, S. Kurabayashi, Y. Kotani, and A. Kaji, *Bull. Chem. Soc. Jpn.*, **44**, 3091 (1971); b) J. Hayami, N. Tanaka, and A. Kaji, *ibid.*, **46**, 954 (1973); c) J. Hayami, N. Tanaka, and N. Hihara, *Bull. Inst. Chem. Res., Kyoto Univ.*, **50**, 354 (1973).

4) A. J. Parker, *Chem. Rev.*, **69**, 1 (1969).

5) a) V. J. Shiner, Jr., W. E. Buddenbaum, B. L. Murr, and G. Lamaty, *J. Am. Chem. Soc.*, **90**, 418 (1968); b) V. J. Shiner, Jr., "Isotope Effects in Chemical Reactions," ACS Monograph No. 167, ed by C. J. Collins and N. S. Bowman, Van Nostrand Reinhold Co., New York, N. Y. (1970), pp. 90—159.

6) a) R. R. Johnson and E. S. Lewis, *Proc. Chem. Soc.*, **1958**, 52; b) L. Melander, "Isotope Effects on Reaction Rates," Ronald Press Co., New York, N. Y. (1960), p. 90.

7) a) V. J. Shiner, Jr., and R. D. Fisher, *J. Am. Chem. Soc.*, **93**, 2553 (1971); b) K. T. Leffek and A. F. Matheson, *Can. J. Chem.*, **50**, 986 (1972); c) S. Seltzer and A. A. Zavitsas, *ibid.*, **45**, 2023 (1967).

8) Willi reported about 14% of secondary kinetic deuterium isotope effect in the nucleophilic displacement reaction. *Cf.* A. V. Willi, C. Ho, and A. Ghanbarpour, *J. Org. Chem.*, **37**, 1185 (1972).

9) a) J. Hayami, N. Tanaka, N. Hihara, and A. Kaji, *Tetrahedron Lett.*, **1973**, 385; b) J. Hayami, T. Koyanagi, N. Hihara, and A. Kaji, *Bull. Chem. Soc. Jpn.*, **51**, 891 (1978).

10) H. H. Jaffé, *Chem. Rev.*, **53**, 191 (1953).

11) S. N. Vinogradov, R. H. Linnell, "Hydrogen Bonding," Van Nostrand Reinhold Co., New York, N. Y. (1971), p. 124.

12) Ref. 3b, 3c and references cited therein.

13) Beside *p*-nitrophenyl derivatives, the substrates give only a small low field shift upon complexing, thus one is not allowed to determine equilibrium isotope effect accurately. However, after repeated measurements, (*m*-methylphenyl)-chloromethane gave K_H/K_D of about 0.91 (with fair error of ±5%). Dissection of k_2^H/k_2^D suggests a loose transition state for this arylchloromethane.

14) A. Streitwieser, Jr., "Solvolytic Displacement Reactions," McGraw-Hill Book Co., Inc., New York, N. Y. (1962), p. 5.

15) V. J. Shiner, Jr., and W. Dowd, *J. Am. Chem. Soc.*, **93**, 1029 (1971).

16) T. C. Jones and E. R. Thornton, *J. Am. Chem. Soc.*, **89**, 4863 (1967).

17) As a corollary, the ρ_{k_2} obtained can be split into ρ_K and ρ_{k_1}, provided the linear free energy relationships hold for both K and k_2.

$$\log(k_2/k_2^\circ) = \log(Kk_1/K^\circ k_1^\circ) = \log(K/K^\circ) + \log(k_1/k_1^\circ)$$
$$= \rho_K\sigma + \rho_{k_1}\sigma = (\rho_K + \rho_{k_1})\sigma = \rho_{k_2}\sigma$$

For 2-arylethyl chlorides; $\rho_K = 0.65$, $\rho_{k_2} = 0.57$, $\therefore \rho_{k_1} = 0.57 - 0.65 = -0.08$. For chloromethyl aryl sulfides; $\rho_K = 0.59$, $\rho_{k_2} = -0.92$, $\therefore \rho_{k_1} = -0.92 - 0.59 = -1.51$. The value of ρ_K for the equilibrium of the complex formation between modified methyl chlorides and chloride ion was found essentially constant.[9] Using the average value of $\rho_K = 0.57$, for chloromethyl aryl ethers; $\rho_{k_2} = -1.56$, $\therefore \rho_{k_1} = -1.56 - 0.57 = -2.13$.

18) J. M. Harris, F. L. Schadt, P. von R. Schleyer, and C. J. Lancelot, *J. Am. Chem. Soc.*, **91**, 7508 (1969).

19) D. J. Raber, J. M. Harris, and P. von R. Schleyer, *J. Am. Chem. Soc.*, **93**, 4829 (1971).

20) Acetonitrile with the very low nucleophilicity and with a dielectric constant of about 30 seems not to be a good ionizing solvent. There is a report that the dissociation of 1,1-dimethyl-2-methylsulfonylhydrazine is quite facile in water but essentially absent in acetonitrile. *Cf.* D. M. Lemal, C. D. Underbrink, and T. W. Rave, *Tetrahedron Lett.*, **1964**, 1955.

21) H. J. Barber, R. F. Fuller, M. B. Green, and H. T. Zwartouw, *J. Appl. Chem.*, **1953**, 266.

22) R. F. Nystrom, *J. Am. Chem. Soc.*, **77**, 2544 (1955).

23) M. G. Darzens, *Compt. Rend.*, **152**, 1314 (1911).

24) M. J. Jorgenson, *Tetrahedron Lett.*, **1962**, 559.

25) The line position of the proton in question did not change with or without the irradiation for heteronuclear decoupling. (*p*-Nitrophenyl)chloromethane-α-d_1 gave rise to a beautiful 1 : 1 : 1 triplet on ^1H spectra, which, on heteronuclear decoupling, coalesced to a sharp singlet centering at the center of the triplet mentioned above. The successful heteronuclear decoupling was experienced in every case.

26) The low field shift of α-proton at the concentration, [substrate] = 0.1 M, [Et_4NCl] = 1.0 M, at 30 °C, was 0.079 ppm for cinnamyl chloride, 0.085 ppm for 2-(*p*-nitrophenyl)-ethyl chloride, whereas 0.398 ppm for chloromethyl *p*-nitrophenyl sulfide, 0.199 ppm for (*p*-nitrophenyl)chloromethane.

Photo-induced Transformation of Polyalkylbenzyl Thiocyanates into Polyalkylbenzyl Isothiocyanates. A Synthesis of Some Bis- and Tris(isothiocyanatomethyl)polymethylbenzenes by Multiple Thiocyanate Isomerization[1]

Hitomi SUZUKI,* Michiyo USUKI, and Terukiyo HANAFUSA
Department of Chemistry, Faculty of Science, Hiroshima University, Higashi-sendamachi, Hiroshima 730

(Received August 21, 1978)

Polyalkylbenzyl thiocyanates, upon irradiation in acetic acid, readily undergo reversible photoisomerization, giving an equilibrium mixture composed mostly of the corresponding isothiocyanates. Several new bis- and tris(isothiocyanatomethyl)polymethylbenzenes have been prepared by utilizing the photoinduced multiple thiocyanate isomerization.

In connection with our studies on the *ipso*-thiocyanation of arenes, we needed several polyalkylbenzyl isothiocyanates as reference compounds for comparison. The classical synthesis of alkyl isothiocyanates[2] has been based on the reaction of alkyl halides with alkali thiocyanates,[3] thermal isomerization of thiocyanates,[4] and treatment of dithiocarbamate derivatives with heavy metal salts,[5] ethyl chloroformate,[6] aqueous potassium hydroxide,[7] sodium hypochlorite or chlorite,[8] and iodine.[9] Other methods of limited generality include the reaction of primary amines with thiophosgen,[10] action of sulfur and alkali cyanide upon alkyl halides,[11] addition of thiocyanic acid to olefins,[12] reaction of carbon disulfide and carbodiimide at high temperatures,[13] and treatment of isocyanates with phosphorus pentasulfide under pressure.[14] Recent proposals involve the reaction of primary amines with bis(trichloromethyl)pentathiodiperoxycarbonate,[15] treatment of dithiocarbamate derivatives with butyllithium,[16] phenylpropiolamidines,[17] phosphoryl chloride,[18] cyanuric chloride,[19] or dicyclohexylcarbodiimide,[20] pyrolysis of alkyldithiourethanes,[21] reaction of phosphoramidate anions with carbon disulfide,[22] and cleavage of secondary carboxamides by successive treatment with sodium hydride and carbon disulfide.[23] Many of these, however, suffer from either the lack of wide applicability, or the use of less common starting materials, and often require relatively tedious manipulative procedures.

Of the various methods previously reported, the isomerization of thiocyanates appeared attractive for our purpose, since the starting materials are easily accessible from aromatic hydrocarbons by chloromethylation and subsequent treatment with potassium thiocyanate. However, mild heating of polyalkylbenzyl thiocyanates in *N*,*N*-dimethylformamide (DMF) with or without potassium thiocyanate does not bring about isomerization; forced thermal isomerization under drastic conditions is accompanied by extensive decomposition. Conversions are generally slow and incomplete, rendering the reaction unfeasible for preparative purposes. Irradiation of benzyl thiocyanates in inert solvents in the absence of oxygen has been known to give a photo-stationary mixture of thiocyanate and isothiocyanate,[24] although the photoisomerization itself is not a general process for alkyl thiocyanates. In order to examine the synthetic potentials of obtaining polyalkylbenzyl isothiocyanates by a photochemical process, a series of polyalkylbenzyl thiocyanates were prepared from the corresponding chlorides and irradiated in dry acetic acid with a high-pressure mercury lamp. Solutions of 1.0—0.1 mM in compounds **1a**—**1d** afforded upon irradiation photo-equilibria which were composed mostly of the corresponding isothiocy-

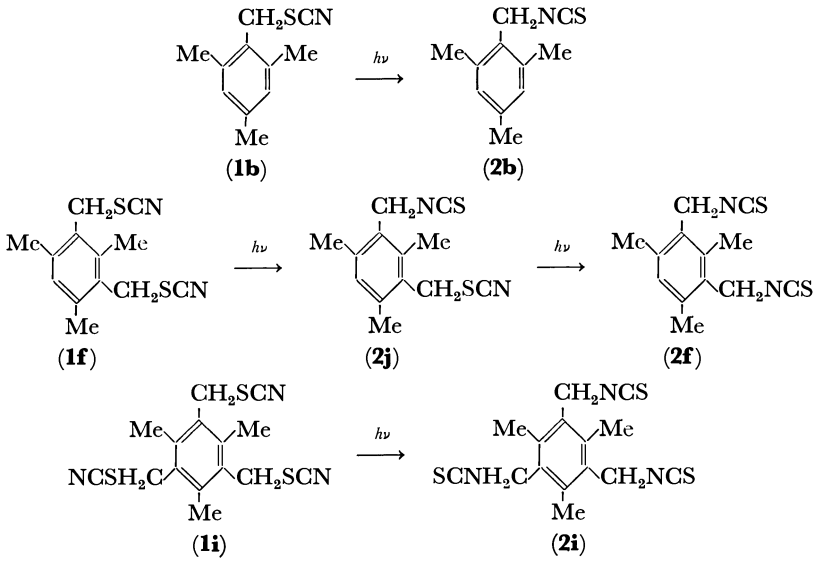

Scheme 1.

Table 1. Physical properties of some polyalkylbenzyl thiocyanates and poly(thiocyanatomethyl)polyalkylbenzenes

Compound	Mp (°C)	Yield[a] (%)	PMR spectra (δ, ppm)	IR spectra (cm^{-1})	Elemental analysis (%) Found	Calcd
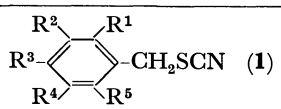 (**1**)						
a: R^1, R^4=Me; R^2, R^3, R^5=H	49—50	74	2.37 (Me), 2.40 (Me), 4.22 (CH_2), 7.10 (3 aromatic H)	2150, 1500, 880, 805, 725	C: 67.6 H: 6.3 N: 7.8	67.7 6.3 7.9
b: R^1, R^3, R^5=Me; R^2, R^4=H	81—82	88	2.23 (Me), 2.36 (2Me), 4.23 (CH_2), 6.83 (2 aromatic H)	2140, 1605, 1225, 1195, 845	C: 69.0 H: 6.9 N: 7.2	69.1 6.9 7.3
c: R^1, R^2, R^3, R^4, R^5=Me	122—124	70	2.22 (3Me), 2.33 (2Me), 4.40 (CH_2)	2150, 1225, 1055, 1010, 795	C: 71.1 H: 7.8 N: 5.9	71.2 7.8 6.4
d: R^1, R^3, R^5=*i*-Pr R^2, R^4=H	113—114	68	1.24 (2Me, d; J=7 Hz), 1.29 (4Me, d; J=7 Hz), 2.7—3.6 (3CH, m), 4.48 (CH_2), 7.05 (2 aromatic H)	2140, 1605, 1225, 935, 870	C: 74.0 H: 9.2 N: 5.0	74.1 9.2 5.1
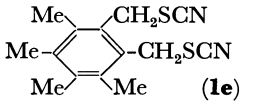 (**1e**)	155—156	77	2.27 (2Me), 2.37 (2Me), 4.47 ($2CH_2$)	2150, 1285, 1220, 805, 710	C: 60.5 H: 5.8 N: 9.9	60.8 5.8 10.1
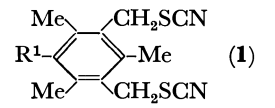 (**1**)						
f: R^1=H	110—111	69	2.40 (2Me), 2.47 (Me), 4.37 ($2CH_2$), 6.97 (aromatic H)	2140, 1230, 1020, 875, 790	C: 59.4 H: 5.3 N: 10.6	59.5 5.4 10.7
g: R^1=Me	128—130	75	2.23 (Me), 2.37 (2Me), 2.48 (Me), 4.40 ($2CH_2$)	2155, 1230, 1000, 800, 760	C: 61.1 H: 5.9 N: 9.9	60.8 5.8 10.1
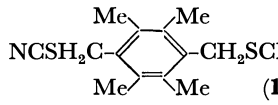 (**1h**)	205—207 (lit,[27] 199—201)	84	2.35 (4Me), 4.42 ($2CH_2$)	2145, 1220, 1005, 800, 765		——
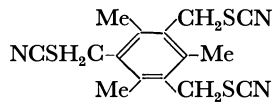 (**1i**)	143—145	76	2.52 (3Me), 4.40 ($3CH_2$)	2150, 2140, 1235, 1000, 785, 755	C: 54.2 H: 4.5 N: 12.3	54.0 4.5 12.6

a) Based on the isolated pure product.

anates **2a**—**2d**. Photo-equilibrium was reached within 1 h when these dilute solutions were used. Longer irradiations were not advantageous, since the formation of tarry substances began to occur. Acetic acid was apparently a solvent of choice; in hexane an insoluble polymeric solid deposited, while in ethanol the formation of side products was prominent. Ordinary work-up of the reaction mixture gave a light brown solid or oily substance, which was chromatographed on a short silica gel column using hexane as eluant, giving the isothiocyanates as an early eluate. Unchanged material and small amounts of benzyl acetate were retained on the column or eluted quite slowly.

In order to ascertain the scope of photochemical isothiocyanate synthesis, we extended the present procedure to some poly(thiocyanatomethyl)benzenes. Upon irradiation in acetic acid, bis(thiocyanatomethyl)-polymethylbenzenes **1e**—**1h** likewise underwent isomerization, giving the corresponding bis(isothiocyanatomethyl)polymethylbenzenes **2e**—**2h** in fair to moderate yields (Table 2). The two vicinally disposed thiocyanatomethyl groups did not seem to interfere with each other during isomerization, since **1e** was smoothly transformed into **2e**. When the reaction was interrupted at early stages, (isothiocyanatomethyl)(thiocyanatomethyl)benzenes were obtained as intermediates along with the expected diisothiocyanates. Until now, no direct method was available for the preparation of such mixed benzylic thiocyanate–isothiocyanates.

Under similar irradiation, tris(thiocyanatomethyl)-benzene **1i** readily isomerized to tris(isothiocyanatomethyl)benzene **2i**. A patent description claims that

Table 2. Physical properties of some polyalkylbenzyl isothiocyanates and poly(isothiocyanatomethyl)polyalkylbenzenes

Compound	Mp (°C)	Yield[a] (%)	PMR spectra (δ, ppm)	IR spectra (cm^{-1})	Elemental analysis (%) Found	Calcd
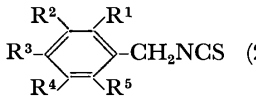 (**2**)						
a: R^1, R^4=Me; R^2, R^3, R^5=H	oil[b]	51	2.30 (Me), 2.33 (Me), 4.60 (CH_2), 6.97 (3 aromatic H)	2160, 2100, 2050, 1505, 1335, 1155	C: 67.5 H: 6.3 N: 7.6	67.8 6.3 7.9
b: R^1, R^3, R^5=Me; R^2, R^4=H	33—34	54	2.27 (Me), 2.37 (2Me), 4.60 (CH_2), 6.87 (2 aromatic H)	2150, 2070, 2040, 1610, 1330, 845	C: 68.8 H: 6.9 N: 7.0	69.1 6.9 7.3
c: R^1, R^2, R^3, R^4, R^5=Me	116—117	45	2.23 (3Me), 2.30 (2Me), 4.67 (CH_2)	2180, 2090, 1380, 1055, 1025, 795	C: 71.1 H: 7.9 N: 6.2	71.2 7.8 6.4
d: R^1, R^3, R^5=*i*-Pr; R^2, R^4=H	oil[b]	61	1.26 (2Me, d; J=7 Hz), 1.29 (4Me, d; J=7 Hz), 2.6—3.4 (3CH, m), 4.65 (CH_2), 6.90 (2 aromatic H)	2140, 2070, 2040, 1605, 1330, 870	C: 74.6 H: 9.3 N: 4.8	74.1 9.2 5.1
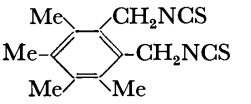 (**2e**)	147—149	20	2.27 (2Me), 2.35 (2Me), 4.73 ($2CH_2$)	2160, 2100, 1335, 1235, 700	C: 61.1 H: 6.0 N: 9.6	60.9 5.8 10.1
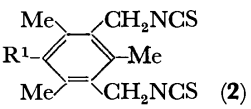 (**2**)						
f: R^1=H	99—100 (lit,[26] 92—95)	27	2.35 (2Me), 2.42 (Me), 4.65 ($2CH_2$), 6.91 (aromatic H)	2130, 2050, 1320, 805	——	
g: R^1=Me	141—143	55	2.27 (Me), 2.37 (2Me), 2.43 (Me), 4.72 ($2CH_2$)	2155, 2070, 1325, 1010, 810	C: 61.0 H: 5.9 N: 9.8	60.8 5.8 10.1
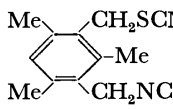 (**2j**)	80—82	27	2.38 (Me), 2.42 (Me), 2.46 (Me), 4.37 (CH_2), 4.67 (CH_2), 6.98 (aromatic H)	2150, 2070, 1330, 860, 805	C: 59.5 H: 5.4 N: 10.6	59.5 5.4 10.7
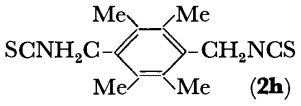 (**2h**)	153—155	18	2.35 (4Me), 4.70 ($2CH_2$)	2170, 2075, 2045, 1335, 790	C: 61.0 H: 6.1 N: 9.2	60.8 5.8 10.1
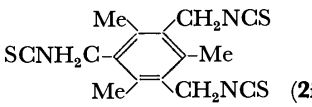 (**2i**)	137—139	24	2.48 (3Me), 4.73 ($3CH_2$)	2175, 2090, 1335, 790, 760	C: 54.2 H: 4.7 N: 12.3	54.0 4.5 12.6

a) Based on the isolated pure product. b) The PMR spectra were measured in carbon tetrachloride.

the reaction of poly(chloromethyl)benzenes with potassium thiocyanate in the presence of potassium iodide in *N*,*N*-dimethylformamide under reflux gives the corresponding poly(isothiocyanatomethyl)benzenes in high yields.[25] This procedure was carefully repeated using several poly(chloromethyl)polymethylbenzenes as substrate, and the products obtained were shown by TLC and PMR analyses to be a mixture of various benzylic compounds. Although polyisothiocyanates could be isolated pure by preparative thick-layer chromatography, this method was unsuitable for laboratory purposes, especially when pure compounds were needed. The photochemical conversion of polythiocyanates into polyisothiocyanates represents, to our knowledge, the first example of a multiple thiocyanate isomerization and the results summarized in Table 2 indicate the general character of this reaction. All the polyisothiocyanates obtained are colorless fine needles, slightly soluble in hexane, benzene, and carbon tetrachloride, and soluble in dichloromethane and hot

ethanol. They can be recrystallized without alteration from ethanol and stored indefinitely, without appreciable deterioration, when kept in a dessicator protected against the daylight.

Although yields were only fair to modest (no attempt was made to optimize the reaction conditions), the easy availability of the starting compounds, the ease of performance, and the mild reaction conditions render this procedure quite useful for the laboratory-scale preparation of various poly(isothiocyanatomethyl)-benzenes, which are otherwise only laboriously accessible.

Experimental

The melting points were taken on a hot-stage apparatus and are uncorrected. The IR spectra were determined in Nujol mulls on a Hitachi 215 spectrophotometer. The PMR spectra were obtained on a Varian T-60 spectrometer, using deuteriochloroform as solvent and TMS as internal standard, unless otherwise stated. The UV spectra were recorded on a Hitachi 124 spectrophotometer in 95% ethanol solutions. All photochemical reactions were conducted using a Halōs PlH 100 high-pressure mercury lamp in a water-cooled quartz immersion well. The solution was flushed with dry nitrogen prior to irradiation and was stirred during the reaction by a magnetic stirring bar.

The benzyl thiocyanates and poly(thiocyanatomethyl)-benzenes were prepared by the reaction of the corresponding chlorides with potassium thiocyanate and recrystallized from ethanol or hexane prior to use. All the new thiocyanates were characterized by elemental analyses as well as by the IR and PMR spectral data summarized in Table 1. The following is a typical experimental procedure.

*2,4,6-Tris(thiocyanatomethyl)-1,3,5-*trimethylbenzene (**1i**). A solution of 2,4,6-tris(chloromethyl)-1,3,5-trimethylbenzene (2.0 g (7.5 mM)) and potassium thiocyanate (15.0 g (156 mM)) in DMF (100 ml) was allowed to stand at room temperature for 4 h and then diluted with water (200 ml). The precipitated solid was filtered off and recrystallized from ethanol to give **1i** as white needles, mp 143—145 °C. Yield, 1.90 g (76%).

The general procedure of photo-induced transformation of thiocyanates into isothiocyanates is illustrated below with the representative preparation of two isothiocyanates. Other isothiocyanates obtained are shown in Table 2, along with the corresponding isolation yields as well as IR and PMR spectral data.

2,4,6-Trimethylbenzyl Isothiocyanate (**2b**). A solution of 2,4,6-trimethylbenzyl thiocyanate (**1b**; 100 mg (0.524 mM)) in acetic acid (40 ml) was irradiated with a high-pressure mercury lamp for 0.5 h in an atomosphere of nitrogen at room temperature. Thin-layer chromatography showed that the conversion to a single photo-product was nearly complete within this period of time, with only a little starting material recovered. A pale yellow photo-equilibrium mixture was diluted by the addition of water (200 ml) and the product was extracted with ether. The ethereal extract was washed successively with water, aqueous sodium hydrogencarbonate, and water again, dried over anhydrous magnesium sulfate, and evaporated to dryness on a rotary evaporator. The residue was placed on a top of a short silica gel column and eluted with hexane. Evaporation of early eluates followed by recrystallization of the residue from ethanol gave isothiocyanate **2b** as colorless needles, mp 33—34 °C. Yield, 54 mg (54%).

4,6-Bis(isothiocyanatomethyl)-1,2,3,5-tetramethylbenzene (**2g**). A solution of 4,6-bis(thiocyanatomethyl)-1,2,3,5,-tetramethylbenzene (**1g**; 100 mg (0.362 mM)) in dry acetic acid (100 ml) was irradiated under nitrogen for 0.5 h at room temperature and worked up in a manner similar to the above. The solid residue obtained after removal of the solvent was chromatographed on a short column of silica gel; evaporation of the early eluates gave bis(isothiocyanatomethyl) compound **2g** as fine needles, 55 mg (55%). Mp 110—111 °C (ethanol).

2-(Isothiocyanatomethyl)-4-(thiocyanatomethyl)-1,3,5-trimethylbenzene (**2j**). The photoisomerization was carried out essentially as described for **2b**, using 2,4-bis(thiocyanatomethyl)-1,3,5-trimethylbenzene (**1f**; 300 mg (1.1 mM)) and acetic acid (70 ml). After 15 min the reaction was stopped and the solution was diluted with water, extracted with ether, and the solvent removed *in vacuo*. The crude product mixture was separated by silica gel chromatography and further purified by preparative thin-layer chromatography to give **2j** (80 mg (27%)), mp 80—82 °C, and **2f** (57 mg (19%)), mp 99—100 °C.

References

1) The reaction of polysubstituted aromatics. Part LIII. Part LII: H. Suzuki, T. Mishina, and T. Hanafusa, *Bull. Chem. Soc. Jpn.*, **52**, 191 (1979).

2) For a general survey of the chemistry of isothiocyanates, see M. Bögemann, S. Petersen, O. E. Schultz, and H. Söll, in "Houben-Weyl Methoden der Organischen Chemie," 4th ed, ed by E. Müller, Georg Thieme Verlag, Stuttgart (1955), Vol. IX, p. 867.

3) E. Schmidt, W. Striewsky, M. Seefelder, and F. Hitzler, *Justus Liebigs Ann. Chem.*, **568**, 192 (1950).

4) O. Mumm and H. Richter, *Chem. Ber.*, **73**, 843 (1940); P. A. S. Smith and D. W. Emerson, *J. Am. Chem. Soc.*, **82**, 3076 (1960); J. Kalamar, J. Hrivnak, A. Kovac, and J. Obertas, Czech. Patent, 131547 (1969); *Chem. Abstr.*, **72**, 100264u (1970).

5) M. Delépine, *Bull. Soc. Chim. Fr.*, [**4**], **3**, 642 (1908).

6) M. L. Moore and F. S. Crossley, *Org. Synth.* Coll. Vol. III, 599 (1955).

7) J. E. Hodgkins and M. G. Ettlinger, *J. Org. Chem.*, **21**, 404 (1956).

8) E. Schmidt, F. Zaller, F. Moosmüller, and E. Kammerl, *Justus Liebigs Ann. Chem.*, **585**, 230 (1954); E. Schmidt, E. Kammerl, D. Ross, and F. Zaller, *ibid.*, **594**, 233 (1955).

9) J. von Braun and H. Deutsch, *Chem. Ber.*, **45**, 2188 (1912).

10) A. Rathke, *Justus Liebigs Ann. Chem.*, **167**, 218 (1873).

11) N. E. Searle, U. S. Patent, 2462433 (1946); *Chem. Abstr.*, **43**, 3843d (1949).

12) M. S. Kharasch, E. M. May, and F. R. Mayo, *J. Am. Chem. Soc.*, **59**, 1580 (1937).

13) W. Weith, *Chem. Ber.*, **7**, 1303 (1874).

14) A. Michael and G. M. Palmer, *Am. Chem. J.*, **6**, 258 (1884); W. V. Wirth, U. S. Patent, 2681358 (1954); *Chem. Abstr.*, **49**, 6303f (1955).

15) R. Gottfried, *Angew. Chem. Int. Ed. Engl.*, **5**, 963 (1966).

16) S. Sakai, T. Aizawa, and T. Fujinami, *J. Org. Chem.*, **39**, 1970 (1974).

17) H. Fujita, R. Endo, and K. Murayama, *Chem. Lett.*, **1973**, 883.

18) D. Martin, E. Beyer, and H. Gross, *Chem. Ber.*, **98**, 2425 (1965).

19) W. Schwarze and W. Weigert, Ger. Patent, 1935302, 2002903 (1971); *Chem. Abstr.*, **74**, 87457d (1971), **75**, 88101r

(1971).
20) J. C. Jochims and A. Seeliger, *Angew. Chem. Int. Ed. Engl.*, **6**, 174 (1967).
21) Y. E. Moharir, *J. Indian Chem. Soc.*, **58**, 148 (1975).
22) W. S. Wadsworth, Jr. and W. D. Emmons, *J. Org., Chem.*, **29**, 2816 (1964).
23) I. Shahak and Y. Sasson, *J. Am. Chem. Soc.*, **95**, 3440 (1973).
24) U. Mazzucato, G. Beggiato, and G. Favaro, *Tetrahedron Lett.*, **1966**, 5455; T. E. Parks and L. A. Spurlock, *J. Org. Chem.*, **38**, 3922 (1973).
25) E. J. Tarlton and A. F. McKay, Ger. Patent, 1148540 (1963); *Chem. Abstr.*, **60**, 2825 g (1964).
26) H. Teubner, W. Weuffen, and H. Höppe, *Arch. Exper. Vet. Med.*, **29**, 621 (1975).
27) I. Rosen, U. S. Patent, 3109015 (1963); *Chem. Abstr.*, **60**, 2827a (1964).

Preparation of *S*-Vinylsulfilimines

Tamotsu YAMAMOTO,*,† Masa-aki KAKIMOTO, and Makoto OKAWARA
Research Laboratory of Resources Utilization, Tokyo Institute of Technology, Nagatsuta-cho, Midori-ku, Yokohama 227
(Received August 24, 1978)

For the preparation of *S*-vinylsulfilimines (**1**), mainly *S*-phenyl-*N*-tosyl-*S*-vinylsulfilimine, three routes were examined, *viz.*, (A) the reaction of vinyl sulfide with chloramine T, (B) that of 2-haloethyl phenyl sulfide with chloramine T followed by dehydrohalogenation, and (C) that of 2-hydroxyethyl sulfide with chloramine T followed by acetylation of the hydroxyl group and deacetoxylation. Route A has disadvantages of troublesome preparation of vinyl sulfides and low yield. Route B gives the precursor sulfilimine to **1** in good yield only by use of anhydrous chloramine T. Route C gives the best results in view of starting material and yield.

For the preparation of common *N*-tosylsulfilimines such as *S,S*-dialkyl-, *S,S*-diaryl-, and *S*-alkyl-*S*-aryl-*N*-tosylsulfilimines, the reaction of the corresponding sulfides with chloramine T is known to be a convenient method.[1]

However, only a few reports have appeared on the preparation of *S*-vinylsulfilimines (**1**) which exhibit interesting behavior, *i.e.*, *S,S*-divinyl-*N*-tosylsulfilimine[2] prepared for the structural confirmation of divinyl sulfide and 2-substituted vinylsulfilimines, RS(CH=CHSO$_n$Ar)=NTs (n=0—2) prepared for antibiotics.[3] The sulfilimines have been prepared by the reaction of the corresponding vinyl sulfides with chloramine T (route A).

Recently, it was reported that *S*-phenyl-*N*-tosyl-*S*-vinylsulfilimine (**1a**) reacts with several protonic compounds to give the Michael-type adducts in good yields[4] and with Grignard reagents to give 2-substituted vinyl sulfides,[5] for the preparation of which the method *via* the reaction of 2-bromoethyl phenyl sulfide (**2a**) with chloramine T followed by dehydrobromination was employed (route B).

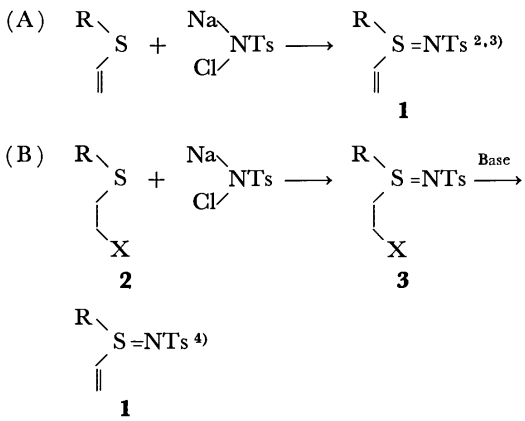

However, route A has such disadvantages as troublesome preparation of vinyl sulfide and low yield of *S*-vinylsulfilimine, and route B the unavoidable use of toxic (dermatitis) 2-bromoethyl sulfide (**2**) and anhydrous chloramine T. Since **2** can be prepared by the reaction of 2-chloroethanol with thiolate followed by the bromination of hydroxyl group, an alternative route to *S*-vinylsulfilimine (route C) *via* the reaction of 2-hydroxyethyl sulfide (**4**) with chloramine T followed by dehydration seems to be promising.

In the present paper we describe the results obtained by examination of the three routes A, B, and C mainly for the preparation of *S*-phenyl-*N*-tosyl-*S*-vinylsulfilimine (**1a**).

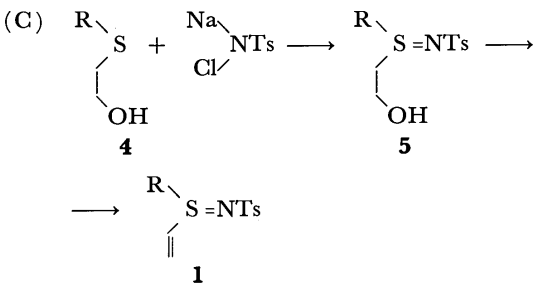

Results and Discussion

Method Using Vinyl Sulfide (Route A). Route A was first examined for the preparation of *S*-phenyl-*N*-tosyl-*S*-vinylsulfilimine (**1a**). Phenyl vinyl sulfide was allowed to react with an equimolar amount of chloramine T ($3H_2O$) in ethanol to give the corresponding sulfilimine **1a** in 44% yield. In this reaction, a by-product confirmed to be a Michael-type adduct, *S*-phenyl-*N*-tosyl-*S*-(2-tosylaminoethyl)sulfilimine (**6**), was obtained. The yield of **6** could be reduced by the addition of a trace amount of acetic acid. The structures of the compounds were confirmed by IR and NMR spectra and elemental analyses.

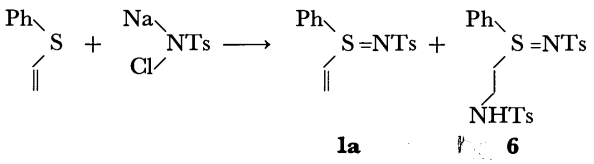

Method Using 2-Haloethyl Sulfide (Route B). Preparation of S-*(2-Bromoethyl)*-S-*phenyl*-N-*tosylsulfilimine (**3a**)*: 2-Bromoethyl phenyl sulfide (**2a**) and a slight excess of chloramine T ($3H_2O$) were allowed to react in methanol at 0 °C. After the reaction, the sulfilimine (**3a**) was isolated as white crystals in a 74% yield. The structure of **3a** was confirmed by IR and NMR spectra and elemental analysis.

The semi-solid compound (**7**) having the following structural characteristics was isolated besides **3a**. From the IR spectrum, **7** was assumed to have NH groups, two kinds of SO_2 groups, and S–N bond. From its NMR as well as IR spectra **7** was shown to

† Present address: Faculty of Engineering, Kanto Gakuin University, Mutsuura, Kanazawa-ku, Yokohama 236.

be formed from sulfide **2a** and chloramine T in the ratio 2 : 3.

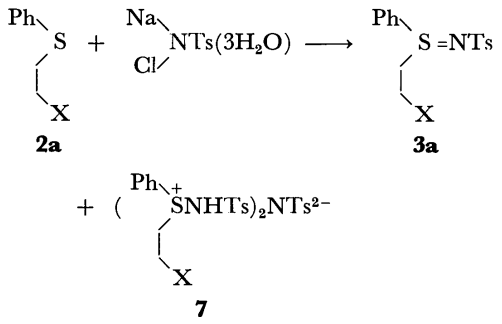

In this case, the starting sulfide **2a** was not recovered.

When the anhydrous chloramine T (dehydrated over phosphorus pentaoxide) was used, **3a** was obtained in a 62% yield and the starting sulfide **2a** was recovered in a 33% yield. Thus, the yield of **3a** based on reacted **2a** amounted to 93%.

The formation of **7** is attributable to the presence of water. This was also observed by Mann and Chaplin : triphenylphosphine reacts with anhydrous chloramine T to give the corresponding phosphine imide, while with hydrated chloramine T it gives a compound with the composition $(Ph_3\overset{+}{P}\text{–NHTs})_2NTs^{2-}$.[6]

In a similar manner, other *S*-(2-haloethyl)-*N*-tosylsulfilimines (**3**) were prepared. *S*-(2-Bromoethyl)-*S*-*p*-tolyl-*N*-tosylsulfilimine (**3a**) was prepared in a good yield from the corresponding starting materials. The reacation of *t*-butyl 2-chloroethyl sulfide with chloramine T($3H_2O$) is complicated. When the reaction was carried out at room temperature (20—25 °C), *S*-(2-chloroethyl)-*N*-tosylsulfenamide (**8**) was obtained quantitatively, while when carried out below 0 °C, *S*-*t*-butyl-*S*-(2-chloroethyl)-*N*-tosylsulfilimine (**3c**) was obtained in an 80% yield. The duality of the reaction seems to be caused by competition between nucleophilic substitution and elimination.

The structures of **3b**, **3c**, and **8** were confirmed by IR and NMR spectra and elemental analyses.

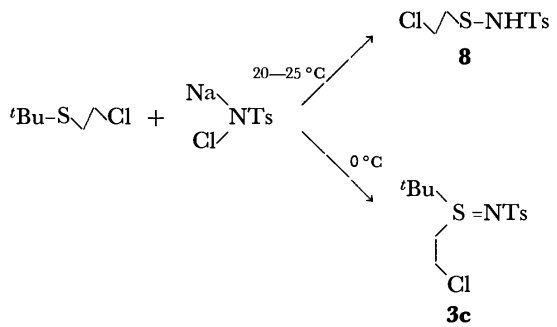

Dehydrohalogenation of S-*(2-Haloethyl)*-N-*tosylsulfilimines*: Dehydrobromination of *S*-(2-bromoethyl)-*S*-phenyl-*N*-tosylsulfilimine (**3a**) to *S*-phenyl-*N*-tosyl-*S*-vinylsulfilimine (**1a**) in dichloromethane was accomplished quantitatively by treatment with a slight excess of triethylamine at room temperature.

Similarly, dehydrobromination of **3b** gave the corresponding *S*-vinylsulfilimine (**1b**) almost quantitatively. However, dehydrochlorination of *S*-*t*-butyl-*S*-(2-chloroethyl)-*N*-tosylsulfilimine (**3c**) with triethylamine was not successful. In this case, a stronger base, DBU (1,8-diazabicyclo[5.4.0]undec-7-ene), acted to cause dehydrochlorination to *S*-*t*-butyl-*N*-tosyl-*S*-vinylsulfilimine (**1c**).

The structures of the *S*-vinylsulfilimines obtained, **1a, 1b**, and **1c** were confirmed by IR and NMR spectra and elemental analyses.

Method Using 2-Hydroxyethyl Sulfide (Route C). Routes A and B have some disadvantages : troublesome preparation of vinyl sulfide and low yield of *S*-vinylsulfilimine **1a** in route A, preparation of anhydrous chloramine T and toxicity of 2-haloethyl sulfide in route B.

2-Hydroxyethyl sulfide, which is an accessible and non-toxic sulfide source, was found to react with chloramine T ($3H_2O$) to give the corresponding sulfilimine, *S*-(2-hydroxyethyl)-*S*-phenyl-*N*-tosylsulfilimine (**5**), in a good yield. We examined a route to *S*-vinylsulfilimine from **5**.

The reaction of 2-hydroxyethyl phenyl sulfide with a slight excess of chloramine T ($3H_2O$) in methanol was carried out at 40 °C for 2 h to give the corresponding sulfilimine **5** in a 74% yield. The structure of **5** was confirmed by IR and NMR spectra and elemental analysis (Table 2). 2-Hydroxyethyl phenyl sulfoxide (**9**) was obtained in a 20% yield as a by-product, but no starting sulfide was recovered.

As a route to *S*-vinylsulfilimine **1a**, direct dehydration of **5** by use of *p*-toluenesulfonic acid (acidic catalyst) or phosphorus pentaoxide (dehydrating agent) was unsuccessful. **5** was found to undergo acetylation followed by deacetoxylation to give **1a**. Thus, acetylation of **5** with acetic anhydride was accomplished quantitatively in dichloromethane at room temperature. The acetylated compound (**10**) was deacetoxylated quantitatively with sodium hydride in THF. The structure of **10** was confirmed by spectral comparison with the authentic sample prepared from 2-acetoxyethyl phenyl sulfide and chloramine T ($3H_2O$) in 48% yield.

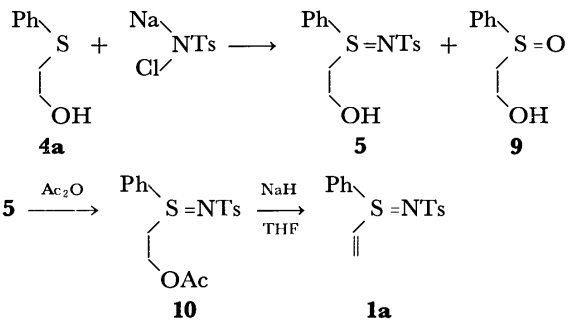

The results obtained from examination of the three routes together with those from the preparation of the starting sulfides are summarized in Scheme 1 and Table 1. The route starting from 2-chloroethanol gives the best result *via* path P–C, P–H, P–M, and P–N.

Experimental

General. All the melting and boiling points were uncorrected. The IR spectra were recorded on a Hitachi

Table 1. Preparation of *S*-vinylsulfilimines (**1**)
(R-S(CH=CH_2)=NSO_2Ar)

	R	Ar	Method	Y (%)	Mp (°C)
a	C_6H_5	4-$CH_3C_6H_4$	(P-B)→(P-C)	62 (93) [a]	111—113
			(P-E)	54 [b]	
			(P-H)→(P-M)→(P-N)	74 [b]	
b	4-$CH_3C_6H_4$	4-$CH_3C_6H_4$	(P-B)→(P-C)	46 [b]	127—129
c	$(CH_3)_3C$	4-$CH_3C_6H_4$	(P-B)→(P-C)	73 [b]	91—93
d	C_6H_5	C_6H_5	(P-B)→(P-C)	46 [b]	93.5—94.5
e	C_6H_5	4-ClC_6H_4	(P-B)→(P-C)	41 [b]	111—114
f	C_6H_5	2,4,6-$(CH_3)_3C_6H_2$	(P-B)→(P-C)	34 [b]	124.5—126

a) Anhydrous chloramine T used (value in parentheses shows the yield based on reacted sulfide). b) Hydrated chloramine T used.

Table 2. Spectral and analytical data of the sulfilimines

	IR (KBr) cm^{-1}	NMR ($CDCl_3$) δ ppm	Elementary analysis (%)
1a	3080(=CH_2); 1285, 1140(SO_2); 1085; 958(S=N); 810(*p*-C_6H_4); 748, 685(C_6H_5)	2.37 s 3H; 6.04 q 1H, 6.26 q 1H, 6.45 q 1H(J_{AB} 0.3, J_{AX} 14, J_{BX} 7); 7.15 d 2H(J_{AB} 8.4); 7.4—7.7 m 5H; 7.72 d 2H(J_{AB} 8.4)	C, 59.66; H, 4.97; N, 4.50 Calcd for $C_{15}H_{15}NO_2S_2$ C, 58.99; H, 4.97; N, 4.59
1b	3080(=CH_2); 1298, 1280, 1135 (SO_2); 1084; 965(S=N); 810 (*p*-C_6H_4)	2.28 s 3H; 2.33 s 3H; 5.8—6.4 m 3H; 7.10 d 2H(J_{AB} 8); 7.20 d 2H (J_{AB} 7); 7.45 d 2H(J_{AB} 7); 7.65 d 2H(J_{AB} 8)	C, 60.10; H, 5.33; N, 4.23 Calcd for $C_{15}H_{17}NO_2S_2$ C, 60.15; H, 5.37; N, 4.39
1c	3080(=CH_2); 1298, 1282, 1143 (SO_2); 1088; 972(S=N); 812 (*p*-C_6H_4)	1.30 s 9H; 2.37 s 3H; 6.0—6.4 m 3H; 7.27 d 2H(J_{AB} 8.4); 7.82 d 2H(J_{AB} 8.4)	C, 54.59; H, 6.81; N, 5.03 Calcd for $C_{13}H_{19}NO_2S_2$ C, 54.70; H, 6.72; N, 4.91
1d	3080(=CH_2); 1275, 1135(SO_2); 1085; 970(S=N); 748, 680 (C_6H_5)	6.08 q 1H, 6.30 q 1H, 6.51 q 1H (J_{AB} 0.3, J_{AX} 14, J_{BX} 7); 7.32—7.95 m 10H	C, 57.80; H, 4.40; N, 4.82 Calcd for $C_{14}H_{13}NO_2S_2$ C, 57.70; H, 4.51; N, 4.81
1e	3060(=CH_2); 1273—1298, 1140 (SO_2); 1080; 990(S=N); 818 (*p*-C_6H_4); 748, 680(C_6H_5)	6.08 q 1H, 6.28 q 1H, 6.49 q 1H (J_{AB} 0.3, J_{AX} 14, J_{BX} 7); 7.38 d 2H(J_{AB} 9); 7.5—7.9 m 5H; 7.84 d 2H(J_{AB} 9)	C, 51.63; H, 3.59; N, 4.42 Calcd for $C_{14}H_{12}ClNO_2S_2$ C, 51.60; H, 3.72; N, 4.30
1f	3080(=CH_2); 1290, 1136(SO_2); 1052; 944(S=N); 848(C_6H_2)	2.26 s 3H; 2.67 s, 6H; 6.04 q 1H, 6.27 q 1H, 6.46 q 1H(J_{AB} 0.3, J_{AX} 14, J_{BX} 7); 6.84 s 2H; 7.4—7.6 m 5H	C, 61.31; H, 5.83; N, 4.04 Calcd for $C_{17}H_{19}NO_2S_2$ C, 61.22; H, 5.72; N, 4.20
3a	1293, 1280, 1138(SO_2); 985 (S=N); 812(*p*-C_6H_4); 750, 685(C_6H_5)	2.36 s 3H; 3.2—3.7 m 4H; 7.16 d 2H(J_{AB} 8); 7.4—7.8 m 5H; 7.71 d 2H(J_{AB} 8)	C, 46.82; H, 4.11; N, 3.51 Calcd for $C_{15}H_{10}BrNO_2S_2$ C, 46.63; H, 4.18; N, 3.63
3b	1298, 1285, 1140(SO_2); 1086; 990(S=N); 815(*p*-C_6H_4)	2.36 s 3H; 2.40 s 3H; 3.0—3.7 m 4H; 7.13 d 2H(J_{AB} 7.8); 7.25 d 2H(J_{AB} 6); 7.53 d 2H(J_{AB} 6); 7.68 d 2H(J_{AB} 7.8)	C, 47.85; H, 4.50; N, 3.38 Calcd for $C_{16}H_{18}BrNO_2S_2$ C, 48.00; H, 4.54; N, 3.50
3c	1285, 1140(SO_2); 1087; 972 (S=N); 818(*p*-C_6H_4)	1.28 d 9H; 2.40 s 3H; 2.8—3.8 m 4H; 7.19 d 2H(J_{AB} 8); 7.73 d 2H (J_{AB} 8)	C, 48.33; H, 6.20; N, 4.34 Calcd for $C_{13}H_{20}ClNO_2S_2$ C, 48.50; H, 6.28; N, 4.35
5	3400—3250(OH); 1280, 1138 (SO_2); 956—938(S=N); 811(*p*-C_6H_4); 748, 685(C_6H_5)	2.39 s 3H; 3.2—3.4 m 2H; 3.6—4.3 m 2H; 7.20 d 2H(J_{AB} 8); 7.5—7.8 m 5H; 7.73 d 2H(J_{AB} 8)	C, 55.29; H, 5.42; N, 4.29 Calcd for $C_{15}H_{17}NO_3S_2$ C, 55.70; H, 5.31; N, 4.33
10	1738(COO-); 1295, 1148(SO_2) 1223(COO-); 968—950(S=N); 810(*p*-C_6H_4); 750, 685(C_6H_5)	1.97 d 3H; 2.37 s 3H; 3.33 t 2H; 4.27 t 2H; 7.20 d 2H(J_{AB} 8); 7.5—7.8 m 5H; 7.47 d 2H(J_{AB} 8)	C, 58.46; H, 5.55; N, 3.90 Calcd for $C_{17}H_{19}NO_4S_2$ C, 58.42; H, 5.49; N, 4.01

EPI-S2 spectrophotometer and NMR spectra on a JNM-C-100 spectrometer of Japan Electron Optics Lab.

Materials. Sodium Salts of N-*Chloroarenesulfonamides*: Chloramine T and chloramine B of reagent grade were used. Sodium salts of *N*-chloro-*p*-chlorobenzenesulfonamide and *N*-chloromesitylenesulfonamide were prepared by treatment of the corresponding free amide with aq solution of sodium hypochlorite (7%).

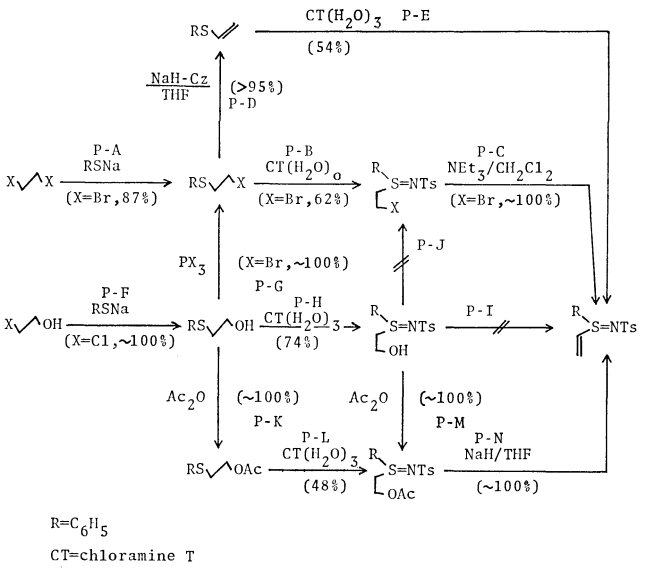

Scheme 1.

Sulfides: 2-Bromoethyl phenyl sulfide was prepared by the reaction of sodium benzenethiolate with 1,2-dibromoethane[7] or 2-chloroethanol followed by bromination with PBr_3.[8] Bp 106 °C/4 Torr (132—136 °C/13 Torr).[7] 2-Bromoethyl *p*-tolyl sulfide was prepared by the reaction of sodium *p*-toluenethiolate with 1,2-dibromoethane. Yield 65%; bp 135—136 °C/6 Torr. *t*-Butyl 2-chloroethyl sulfide was prepared by the reaction of sodium 2-methyl-2-propanethiolate with 2-chlroroethanol followed by chlorination with thionyl chloride. Yield(overall) 77%; bp 79—82 °C/30 Torr (81—82 °C/30 Torr).[9] 2-Hydroxyethyl phenyl sulfide was prepared by the reaction of sodium benzenethiolate with 2-chloroethanol.[10] Yield 99%; bp 115—118 °C/3 Torr (115—116 °C/2 Torr).[10] 2-Acetoxyethyl phenyl sulfide was prepared by acetylation of 2-hydroxyethyl phenyl sulfide with acetic anhydride. Yield 20% (rt, 24 h) and 99% (160 °C, 3 h); bp 111—112 °C/1 Torr; NMR($CDCl_3$): δ 1.96 (s, 3H), 3.09 (t, 2H), 4.18 (t, 2H), 7.1—7.4 (m, 5H). Phenyl vinyl sulfide was prepared by dehydrobromination of **2a** with sodium hydride (more than equimolar amount) in THF in the presence of carbazole (1/10 mol to sulfide). Yield 90%; bp 75—77 °C/12 Torr (66—68 °C/6 Torr).[11]

*Preparation of **1a** from Vinyl Sulfide and Chloramine T.* To a stirred solution of chloramine T($3H_2O$)(2.82 g, 10 mmol) in EtOH (20 ml) was added phenyl vinyl sulfide (1.36 g, 10 mmol) and then 0.05 ml of acetic acid. After the reaction mixture had been stirred at 40 °C for 1 h, the mixture was stirred at room temperature for one day. The solution obtained was concentrated under reduced pressure and added to ice water to precipitate a white solid of **1a**. The solid was collected by filtration, washed with Et_2O–MeOH (1:1) and dried. Yield of **1a**: 1.65 g (54%). When this reaction was carried out without acetic acid, a mixture of **1a** and *S*-(2-tosylaminoethyl)-*S*-phenyl-*N*-tosylsulfilimine (**6**) was obtained which were separated by treatment with benzene. **1a** (1.34 g, 44%) was obtained from sparingly soluble part in benzene and **6** (1.7 g, 10%) from the soluble part. **1a**: mp 111—113 °C (CH_2Cl_2–Et_2O). **6**: mp 124—125.5 °C (CH_2Cl_2–Et_2O); IR(KBr): 3230 (NH), 1338 and 1282 ($\nu_{as}SO_2$), 1160 and 1140 (ν_sSO_2), 970 (S=N), 815 (*p*-C_6H_4), 748 and 688 cm^{-1} (C_6H_5); NMR($CDCl_3$): δ 2.40 (s, 3H), 2.48 (s, 3H), 3.0—3.7 (m, 4H), 5.9 (s, 1H), 7.19 (d, 2H, J=8 Hz), 7.4—7.8 (m, 5H), 7.31 (d, 2H, J=8 Hz), 7.69 (d, 4H, J=8 Hz). Found: C, 55.18; H, 5.20; N, 5.65%. Calcd for $C_{22}H_{24}N_2O_4S_3$: C, 55.43; H, 5.09; N, 5.88%.

*Preparation of **3a**.* [A] To a stirred solution of chloramine T($3H_2O$)(6.19 g, 22 mmol) in MeOH (50 ml) was added dropwise a solution of **2a** (4.34 g, 20 mmol) in MeOH (10 ml) at 20 °C. After 3 h stirring, the resulting mixture was evaporated to dryness under reduced pressure. The residue obtained was extracted with $CHCl_3$ (50 ml), washed with saturated aq solution of NaCl and dried over anhydrous Na_2SO_4. The dried $CHCl_3$ solution was evaporated to dryness under reduced pressure and the resulting oily residue was triturated with Et_2O (50 ml) until solid of **3a** was deposited. The white solid was collected by filtration and recrystalized from CH_2Cl_2–Et_2O. Yield of **3a**: 3.63 g (47% based on **2a**).

To the ethereal filtrate was added hexane (20 ml) to deposit 2.79 g (30% based on **2a**) of **7** which has low melting point. **7**: IR (neat): 3220 (NH), 1330 and 1280 ($\nu_{as}SO_2$), 1158 and 1140 (ν_sSO_2), 970 cm^{-1} (S=N); NMR($CDCl_3$): δ 2.33 (s, 6H), 2.37 (s, 3H), 3.1—3.7 (m, 8H), 7.15 (d, 4H, J=8 Hz), 7.25 (d, 2H, J=8 Hz), 7.3—7.8 (m, 16H); MS: *m/e* 605 and 601 (metastable ion), 388 and 386, 279, 278, 169.

[B] To a stirred solution of chloramine T (anhydrous, 5.01 g, 22 mmol) in absolute ethanol (50 ml) was added a solution of **2a** (4.34 g, 20 mmol) in absolute ethanol (10 ml) at 20 °C. The reaction mixture was worked up in a similar manner to that in [A]. By trituration with Et_2O followed by filtration, 4.79 g (62% based on **2a**) of **3a** was obtained. 1.43 g of **2a** (33%) was recovered from the filtrate. **3a**: mp 98—98.5 °C (CH_2Cl_2–Et_2O). The spectral and analytical data are given in Table 2.

*Preparation of **3b**.* **3b** was obtained in a similar manner to that for **3a**. Yield: 50%. Mp: 127—129 °C. The spectral and analytical data are given in Table 2.

*Preparation of **3c**.* To a solution of chloramine T ($3H_2O$) (987 mg, 3.5 mmol) in EtOH(30 ml) was added dropwise *t*-butyl 2-chloroethyl sulfide (458 mg, 3 mmol) in EtOH (10 ml) at 0 °C for 1 h. After 10 h stirring at 0 °C, the reaction mixture was concentrated to 10 ml under reduced pressure. The solution was added to 200 ml of ice water to precipitate white solid of **3c**, which was collected by filtration, washed with MeOH–Et_2O (1 : 1) and dried. Yield : 775 mg (80%). **3c**: mp 102—104 °C (CH_2Cl_2–Et_2O). When the reaction was carried out at room temperature, a white precipitate of *S*-(2-chloroethyl)-*N*-tosylsulfenamide (**8**) was obtained. The precipitate was collected by filtration and dissolved in ether (50 ml) followed by drying over anhydrous Na_2SO_4. The ethereal solution was concentrated to reprecipitate by addition of hexane. Yield 12.0 g (90%). **8**: mp 92—94 °C (Et_2O–hexane); IR(KBr): 3280 (NH), 1370 ($\nu_{as}SO_2$), 1160 (ν_sSO_2), 868 (S=N), 818 cm^{-1} (*p*-C_6H_4); NMR($CDCl_3$) : δ 2.44 (s, 3H), 3.02(t, 2H, J=7 Hz), 3.78 (t, 2H, J=7 Hz), 6.48 (s, 1H), 7.33 (d, 2H, J=8 Hz), 7.81 (d, 2H, J=8 Hz). Found: C, 41.00; H, 4.67; N, 5.26%. Calcd for $C_9H_{12}ClNO_2S_2$: C, 40.67; H, 4.56; N, 5.27%. MS: *m/e* 267 and 265 (M^+), 155 ($SO_2C_7H_7$).

*Dehydrohalogenation of **3**. General Procedure*: To a solution of **3** (3 mmol) in CH_2Cl_2 (30 ml) was added NEt_3 or DBU in more than an equimolar amount at room temperature. After 2—10 h stirring the reaction mixture was washed with brine and dried over anhydrous Na_2SO_4. The dried solution was evaporated to dryness under reduced pressure. The residue was triturated with ether (30 ml) to deposit the solid of *S*-vinylsulfilimine (**1**).

*Preparation of S-(2-Hydroxyethyl)-S-phenyl-N-tosylsulfilimine (**5**).* To a stirred solution of chloramine T ($3H_2O$) (3.10 g, 11 mmol) in MeOH (20 ml) was added a solution

of 2-hydroxyethyl phenyl sulfide (1.54 g, 10 mmol) in MeOH (10 ml) at room temperature. After the mixture was stirred at 40 °C for 2 h, the resulting solution was worked up as described above to give 2.38 g (74%) of **5** as white solid. **5**: mp 95—96 °C (CH_2Cl_2–Et_2O). The ethereal solution obtained by filtration of **5** gave 687 mg (20%) of 2-hydroxyethyl phenyl sulfoxide (**9**) after evaporation followed by chromatography (silica gel–CH_2Cl_2 followed by acetone). **9**: oil; IR(neat) : 3400—3300 (OH), 1040—1020 (S=O), 758 and 690 cm^{-1} (C_6H_5); NMR ($CDCl_3$): δ 2.9—3.4 (m, 2H), 3.9—4.4 (m, 3H), 7.5—7.8 (m, 5H); MS: *m/e* 171 (M^+), 170 (M^+-H), 126 ($M^+-CH_2CH_2OH$).

*Acetylation of **5** to **10**.* To a solution of **5** (3.23 g, 10 mmol) in CH_2Cl_2 (50 ml) was added 2 ml of acetic anhydride at room temperature. The mixture was stirred at room temperature for 24 h. The resulting solution was evaporated to dryness under reduced pressure. The residue was triturated with Et_2O (50 ml) to give 3.47 g (95%) of white solid **10**. **10**: mp 95—96 °C (CH_2Cl_2–Et_2O). The spectral and analytical data are given in Table 2.

*Authentic Sample of **10**.* To a solution of chloramine T ($3H_2O$) (3.10 g, 11 mmol) in MeOH (20 ml) was added 2-acetoxyethyl phenyl sulfide (1.96 g, 10 mmol) in MeOH (10 ml) at room temperature. The mixture was stirred at 40—50 °C for 2 h. The resulting solution was worked up in similar manner to that for **3a** to give 1.93 g (48%) of **10**.

*Deacetoxylation of **10** to **1a**.* To a solution of **10** (3.65 g, 10 mmol) in THF (50 ml) was added sodium hydride (0.5 g) at room temperature under nitrogen atmosphere. The mixture was stirred at room temperature for 24 h. The resulting mixture was filtrated, evaporated and triturated with ether (50 ml) to give 3.60 g (99%) of **1a**.

References

1) For example : F. G. Mann and W. J. Pope, *J. Chem. Soc.*, **121**, 1052 (1922).
2) J. S. H. Davis and A. E. Oxford, *J. Chem. Soc.*, **1931**, 224.
3) H. O. Bayer, U. S. Patent 3542865 (1970).
4) T. Yamamoto and M. Okawara, *Chem. Lett.*, **1975**, 581.
5) T. Yamamoto, M. Kakimoto, and M. Okawara, *Tetrahedron Lett.*, **1977**, 1659.
6) F. G. Mann and E. J. Chaplin, *J. Chem. Soc.*, **1937**, 527.
7) H. Hahl, *Chem. Zent.*, **1925**, **I** 1533.
8) S. M. Scherlin and A. I. Jakukowitch, *J. Prakt. Chem.*, **138**, 23 (1933).
9) T. P. Dawson, *J. Am. Chem. Soc.*, **69**, 1211 (1947).
10) W. R. Kirner and G. H. Richter, *J. Am. Chem. Soc.*, **51**, 3409 (1929).
11) W. Wücherpfennig and C. Kresze, *Tetrahedron Lett.*, **1966**, 1871.

Syntheses of Polymerizable Acetals. II. Readily Hydrolyzable Acetals from Citronellol and Vitamins

Hiroyoshi KAMOGAWA,* Yuichiro HARAMOTO, and Masato NANASAWA
Department of Applied Chemistry, Yamanashi University, Takeda, Kofu 400
(Received August 31, 1978)

Three perfume acetals and four vitamin acetals have been synthesized by the acid-catalyzed reactions of vinylbenzyloxy- and methoxy-substituted benzaldehydes with citronellol and the reactions of vinylbenzaldehyde with vitamins B_6, C, B_1, and B_2, respectively. The acid hydrolyses of these novel acetals readily released citronellol and vitamins under mild conditions, some accelerations of the hydrolysis rate by the electron-donating para substituents being observed in the case of the perfume acetals.

The controlled release of functional compounds by means of the hydrolytic cleavage of chemical bonds is interesting since the susceptibility to cleavage is dependent upon chemical structure, thereby assuring a variety of release rates.

Some instances of the controlled release taking advantage of the ready hydrolysis of an ester linkage are known.[1,2] In a previous paper,[3] the syntheses of the polymerizable vinylbenzaldehyde acetals with perfume alcohols, which provided, by polymerization, the pendant polymers possessing the ability of the ready release of pendant portion (perfume) by acid hydrolysis, were reported.

The present paper is intended to cover three perfume acetals synthesized from the benzaldehyde substituted with electron-donating groups and citronellol as well as four vinylbenzaldehyde acetals with vitamin alcohols, all acetals synthesized being novel.

Acetals of substituted benzaldehyde with citronellol have been synthesized *via* the following route.

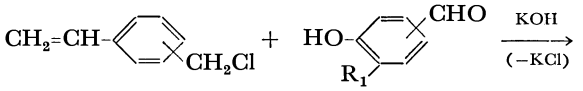

I: $m/p = 60/40$

IIa: R_1 = H (CHO, para to OH)
IIb: $R_1 = OCH_3$ (CHO, meta to OH and para to R_1)
IIc: $R_1 = OCH_3$ (CHO, para to OH)

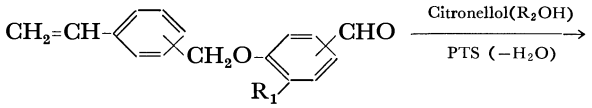

IIIa: R_1 = H (CHO, para to OCH_2)
IIIb: $R_1 = OCH_3$ (CHO, meta to OCH_2)
IIIc: $R_1 = OCH_3$ (CHO, para to OCH_2)

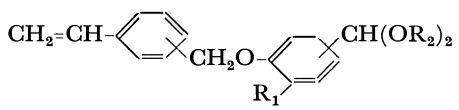

IVa: R_1 = H ($CH(OR_2)_2$, para to OCH_2)
IVb: $R_1 = OCH_3$ ($CH(OR_2)_2$, meta to OCH_2)
IVc: $R_1 = OCH_3$ ($CH(OR_2)_2$, para to OCH_2)

Vinylbenzaldehyde acetals with vitamin alcohols have been prepared from vinylbenzaldehyde (m/p= 60/40) and the corresponding vitamin alcohols in the same manner as that for IVa—c. The structures of the acetals conforming to the experimental data are as follows.

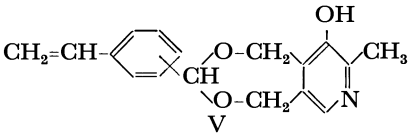

V
Acetal with vitamin B_6

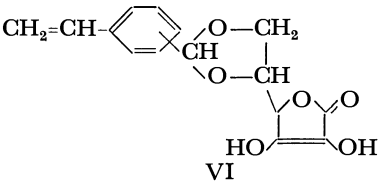

VI
Acetal with vitamin C

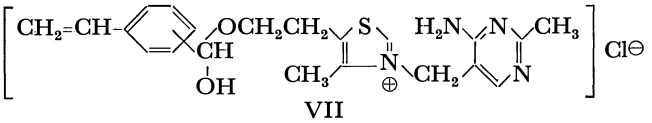

VII
Hemiacetal with vitamin B_1

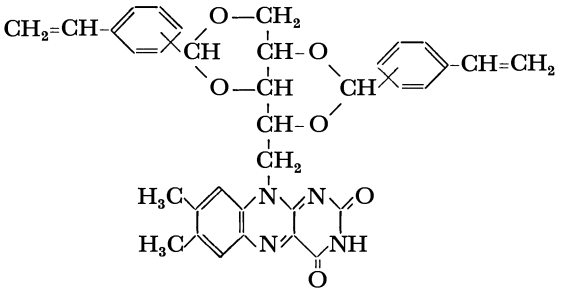

VIII
Acetal with vitamin B_2

The ring structure of acetal VIII is uncertain, due to insufficient analytical data sufficient to exactly determine the structures of the dioxa rings. Vinylbenzyl chloride (I) and vinylbenzaldehyde,[3] both of which were 60/40 mixtures of the meta and para isomers, were chosen as starting materials from the stand-point of availability, such that the acetals made should also be mixtures of the meta and para isomers. The isomers, however, could not be separated by chromatographic means; all attempts to determine the m/p ratios in the acetals isolated also failed. These problems, however, are not thought to pose any practical troubles.

Benzaldehyde acetals with citronellol, bearing two electron-donating alkoxyl substituents at both the para and meta positions (IVa—c), were synthesized smoothly. Despite the poor stabilities and limited solubilities of the vitamins employed, the vitamin acetals and a hemiacetal were isolated in low yields. Vitamin B_1

provided only a hemiacetal (VII), presumably due to the steric hindrance exerted by the bulky vitamin B_1 molecule and the electrostatic repulsion of the VII cation produced against the attack of another vitamin B_1 cation.

The ring structure of the acetal V involving a seven-membered dioxa ring appears to be correct, since a phenolic hydroxyl singlet (δ=5.9 ppm) exists in the NMR. The poor reactivity of the phenolic hydroxyl group in the acetalization also supports this structure.

The ring structure of acetal VIII with two six-membered dioxa rings, as presented here, is thought to represent the most strain-free structure. However, five-membered and seven-membered dioxa rings may also be possible, since it appears that little differences exist in the reactivity of acetalization among the three secondary hydroxyl groups in riboflavin and that the main factor determining the ring structure is a steric one.

In vitamin acetal syntheses, the poor solubilities of the vitamins employed in solvents appear to be the principal causes of the low yields found for VI, VII, and VIII. In the case of acetal V, the basicity of the ring nitrogen lowered the acidity of the reaction medium, thereby causing a low yield. However, a large amount of unreacted vitamin was recovered making recycling possible.

The hydrolytic behavior of the acetals has also been investigated. Thus, when subjected to acid hydrolysis with *p*-toluenesulfonic acid in water–tetrahydrofuran (1:2 vol/vol) at 20 °C, monomers IVa—c with electron-donating para substituents hydrolyzed more rapidly than vinylbenzaldehyde dicitronellyl acetal, indicating the resonance stabilization of the intermediate carbocation (IX) and the resulting acceleration of hydrolysis.

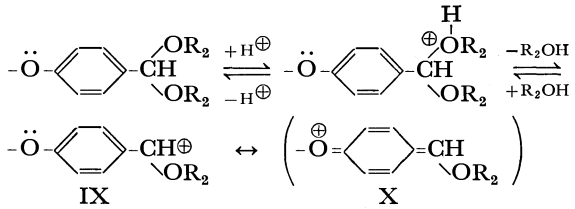

It appears reasonable that a more electron-donating *p*-methoxyl substituent (IVb) provides a higher rate than the *p*-benzyloxyl substituent (IVa and IVc).

Since the hydrolysis of acetals from aromatic aldehydes is generally rapid,[4] the differences observed in the rate of hydrolysis were small and all acetals synthesized underwent complete hydrolysis under mild acidic conditions, thereby assuring the controlled release of the functional portions (perfumes and vitamins).

The acetals and the hemiacetal synthesized possess polymerizable styrenic double bonds which, on polymerization, afford the vinyl polymers containing functional portions as pendant.

Experimental

IR, ^{1}H-NMR, and mass spectra were obtained with a Hitachi EPI-G spectrophotometer, a JNM-PMX 60 spectrometer, and a Hitachi RMU-6 MG spectrometer, respectively. Elemental analyses were conducted using a Perkin-Elmer 240.

4-(Vinylbenzyloxy)benzaldehyde (IIIa). A solution of 4-hydroxybenzaldehyde (IIa) (12.2 g, 100 mmol) in methanol (60 ml) containing potassium hydroxide (6.6 g, 100 mmol) was evaporated *in vacuo* at 50 °C to dryness. The residue was dissolved in *N,N*-dimethylformamide (60 ml). vinylbenzyl chloride (15.3 g, 100 mmol)(I ; Seibi Chem. Co., 60/40 mixture of meta and para isomers) and phenothiazine (0.1 g) added, and the solution kept at 90 °C for 2 h under nitrogen. The reaction mixture was then poured into a large quantity of water and the resulting oily mass extracted with ether. The extract was washed with dilute aqueous sodium hydroxide, then with water, dried over anhydrous sodium sulfate, and evaporated *in vacuo* at 50 °C. The oily mass was washed with a large amount of petroleum ether and dried *in vacuo* to give a yellowish compound in 60% yield. Oxime: mp 95—96 °C (colorless crystals). This product was pure by TLC and all attempts to separate the meta and para isomers failed.

Found: C, 80.53; H, 6.00%. Calcd for $C_{16}H_{14}O_2$: C, 80.68; H, 5.88%. IR (CCl_4) 2840, 2740 (CHO), 1695 (C=O), 1600 (aryl), 990, 910 (vinyl) cm^{-1}. NMR (CCl_4) δ 5.1 (s, 2H, CH_2), 5.2 (d, 1H, $C\underline{H}_2$=CH–), 5.7 (d, 1H, $C\underline{H}_2$=CH–), 6.6 (q, 1H, CH_2=C$\underline{H}$–), 7—8 (m, 8H, ArH), 9.9 (s, 1H, CHO) ppm. Mass (*m/e*) 283 (M^+, 3), 117 (100).

3-Vinylbenzyloxy-4-methoxybenzaldehyde (IIIb). Following the same procedure as for IIIa, a light brown viscous liquid was obtained in 50% yield. Oxime: oily.

Found: C, 76.04; H, 6.08%. Calcd for $C_{17}H_{16}O_3$: C, 76.12; H, 5.97%. IR (CCl_4) 2840, 2720 (CHO), 1690 (C=O), 1600 (aryl), 990, 910 (vinyl) cm^{-1}. NMR (CCl_4) δ 3.8 (s, 3H, OCH_3), 5.0 (s, 2H, CH_2), 5.2 (d, 1H, $C\underline{H}_2$=CH–), 5.7 (d, 1H, $C\underline{H}_2$=CH–), 6.6 (q, 1H, CH_2=C$\underline{H}$–), 6.7—7.4 (m, 7H, ArH), 9.8 (s, 1H, CHO) ppm. Mass (*m/e*) 268 (M^+, 54), 117 (100).

4-Vinylbenzyloxy-3-methoxybenzaldehyde (IIIc). Following the same procedure as that for IIIa, a light brown solid was obtained in 40% yield. Oxime: mp 82—83 °C (white powder).

Found: C, 76.04; H, 6.06%. Calcd for $C_{17}H_{16}O_3$: C, 76.12; H, 5.97%. IR (CCl_4) 2830, 2720 (CHO), 1680 (C=O), 1590 (aryl), 990, 910 (vinyl) cm^{-1}. NMR (CCl_4) δ 3.8 (s, 3H, OCH_3), 5.1 (s, 2H, CH_2), 5.2 (d, 1H, $C\underline{H}_2$=CH–), 5.7, (d 1H, $C\underline{H}_2$=CH–), 6.6 (q, 1H, CH_2=C$\underline{H}$–), 6.5—7.3 (m, 7H, ArH), 9.7 (s, 1H, CHO) ppm. Mass (*m/e*) 268 (M^+, 3), 117 (100).

4-(Vinylbenzyloxy)benzaldehyde Dicitronellyl Acetal (IVa). A solution of IIIa (3.0 g, 13 mmol), citronellol (3.9 g, 25 mmol), *p*-toluenesulfonic acid (PTS) (0.4 g), and phenothiazine (0.1 g) in chloroform (100 ml) was refluxed for 6 h in a flask fitted with a Soxhlet extractor charged with 3 A molecular sieves (1/16). The chloroform solution was then washed with aqueous sodium carbonate, dried over anhydrous sodium sulfate, and evaporated *in vacuo* at 50 °C to leave an oil. The oil was subjected to alumina column chromatography to collect petroleum ether eluates. Upon evaporation of the solvent, a pale yellow liquid, pure by VPC, was obtained. This could not be separated into the meta and para isomers (31% yield).

Found: C, 81.65; H, 9.24%. Calcd for $C_{36}H_{52}O_3$: C, 81.20; H, 9.77%. IR(CCl_4) 2960—2850 (alkyl), 1600 (aryl), 990, 910 (vinyl) cm^{-1}. NMR(CCl_4) δ 0.8—3.6 (m, 38 H, citronellyl), 5.1 (s, 2H, $ArCH_2O$), 5.1—5.6 (m, 2 H, $C\underline{H}_2$=CH–+–CH$\begin{matrix}\diagup O- \\ \diagdown O-\end{matrix}$), 5.7 (d, 1H, $C\underline{H}_2$=CH–), 6.5—7.6 (m, 9H, CH_2=C$\underline{H}$–+ArH) ppm. Mass (*m/e*) 377 ($M^+ - OC_{10}H_{19}$).

3-Vinylbenzyloxy-4-methoxybenzaldehyde Dicitronellyl Acetal (IVb). Following the same procedure as that for IVa, a pale yellow liquid was obtained in 27% yield.

Found: C, 79.16; H, 9.24%. Calcd for $C_{37}H_{54}O_4$: C, 79.00; H, 9.61%. IR(CCl_4) 2960—2860 (alkyl), 1600 (aryl), 990, 910 (vinyl) cm^{-1}. NMR(CCl_4) δ 0.8—3.5 (m, 38 H, citronellyl), 3.8 (s, 3 H, OCH_3), 5.0 (s, 2 H, Ar–CH_2O), 5.3 (s, 1H, $-\underset{}{\overset{\diagup O-}{CH}}\underset{\diagdown O-}{}-$), 5.2 (d, 1H, $C\underline{H}_2$=CH–), 5.7 (d, 1H, $C\underline{H}_2$=CH–), 6.3—7.5 (m, 8H, CH_2=C$\underline{H}$–+ArH) ppm. Mass (*m/e*) 407 ($M^+-OC_{10}H_{19}$).

4-Vinylbenzyloxy-3-methoxybenzaldehyde Dicitronellyl Acetal (IVc). Following the same procedure as that for IVb, a pale yellow liquid was obtained in 28% yield.

Found: C, 79.17; H, 9.35%. Calcd for $C_{37}H_{54}O_4$: C, 79.00; H, 9.61%. IR(CCl_4) 2970—2850 (alkyl), 1600 (aryl), 990, 910 (vinyl) cm^{-1}. NMR(CCl_4) δ 0.8—3.5 (m, 38H, citronellyl), 3.8 (s, 3H, OCH_3), 5.0 (s, 2H, $ArCH_2O$), 5.1 (d, 1H, $C\underline{H}_2$=CH–), 5.3 (s, 1H, $-\underset{}{\overset{\diagup O-}{CH}}\underset{\diagdown O-}{}-$), 5.7 (d, 1H, $C\underline{H}_2$=CH–), 6.5—7.6 (m, 8H, CH_2=C$\underline{H}$–+ArH) ppm. Mass (*m/e*) 563 (M^+, 6), 286 (100).

Vinylbenzaldehyde Acetal with Vitamin B_6 (V). A mixture of vinylbenzaldehyde (3.0 g, 23 mmol) (*m/p*= 60/40),[3] pyridoxine (9.3 g, 45 mmol)(vitamin B_6), PTS (0.5 g), phenothiazine (0.1 g), and chloroform (100 ml) was stirred at 70 °C for 6 h under nitrogen in the presence of 3A molecular sieves (1/16). The reaction mixture was washed with aqueous sodium carbonate, dried over anhydrous sodium sulfate, filtered, and evaporated to dryness *in vacuo* at 50 °C. The brown mass was purified by alumina column chromatography and the methanol eluates collected. Upon evaporation of the solvent, a brownish oily mass, which was pure by TLC, was obtained in 4% yield.

Found: C, 72.16; H, 6.28; N, 4.51%. Calcd for $C_{17}H_{16}NO_3$: C, 72.08; H, 6.01; N, 4.95%. IR(CCl_4) 3600 (OH), 1600 (aryl), 1120 (ether), 990, 910 (vinyl) cm^{-1}. NMR(CCl_4+DMSO-d_6) δ 2.4 (s, 3H, CH_3), 4.5(s, 1H, $-\underset{}{\overset{\diagup O-}{CH}}\underset{\diagdown O-}{}-$), 4.6—5.1 (m, 4H, CH_2), 5.2 (d, 1H, $C\underline{H}_2$=CH–), 5.8 (d, 1H, $C\underline{H}_2$=CH–), 5.9 (s, ArOH), 6.5—6.8 (b, 1H, $-\underset{}{\overset{\diagup O-}{CH}}\underset{\diagdown O-}{}-$), 7.0—8.0 (m, ArH) ppm. Mass (*m/e*) 283 (M^+, 4), 43 (100).

Vinylbenzaldehyde Acetal with Vitamin C (VI). A mixture of vinylbenzaldehyde (3.0 g, 23 mmol), L-ascorbic acid (4.0 g, 23 mmol)(vitamin C), PTS (0.4 g), phenothiazine (0.1 g), and dioxane (50 ml) was stirred at room temperature for 24 h under nitrogen in the presence of 3A molecular sieves with the exclusion of light. Dioxane was then removed by freeze-drying, the residue extracted with ether, and the extract evaporated *in vacuo* at 50 °C. The oily mass, which was washed with petroleum ether, afforded a colorless sticky mass, which was pure by TLC, in 13% yield.

Found: C, 61.27; H, 5.60%. Calcd for $C_{15}H_{14}O_6$: C, 62.07; H, 4.83%. IR ($CHCl_3$) 3580 (OH), 1680 (C=O), 1120 (C–O–), 990, 910 (vinyl) cm^{-1}. NMR(CCl_4+DMSO-d_6) δ 3.4—3.5 (t, 2H, CH_2), 4.1 (b, 1H, $-O\underset{|}{C}\underline{H}CH_2-$), 4.8—4.9 (s, 1H, $-\underset{|}{CH}\underline{C}\underset{|}{H}O-$), 5.3 (s, 1H, $-\underset{}{\overset{\diagup O-}{CH}}\underset{\diagdown O-}{}-$), 5.2 (d, 1H, $C\underline{H}_2$=CH–), 5.8 (d, 1H, $C\underline{H}_2$=CH–), 6.7 (b, 1H, CH_2=C$\underline{H}$–), 7.0—7.8 (m, 4H, ArH) ppm.

Vinylbenzaldehyde Hemiacetal with Vitamin B_1 (VII). A mixture of vinylbenzaldehyde (1.5 g, 11 mmol), thiamine hydrochloride (3.8 g, 11 mmol), PTS (0.5 g), phenothiazine (0.1 g), and acetonitrile (50 ml) was stirred at room temperature for 72 h under nitrogen in the presence of 3A molecular sieves (1/16). The reaction mixture was evaporated in vacuo at 50 °C to dryness and washed with petroleum ether and ether. The residue was thoroughly shaken with a mixture of aqueous sodium carbonate and sodium chloride and chloroform and the chloroform layer dried over anhydrous sodium sulfate. The sodium sulfate was filtered and extracted with acetonitrile to afford a white powder (mp 138—140 °C) in 10% yield upon evaporation of solvent.

Found : C, 56.77; H, 5.95; N, 12.99%. Calcd for $C_{20}H_{24}N_4O_2SCl$: C, 57.14; H, 5.73; N, 13.33%. IR(KBr) 3300 (OH+NH_2), 1650 (C=$\overset{+}{N}$<), 1000, 920 (vinyl) cm^{-1}. NMR ($CDCl_3$+DMSO-d_6) δ 2.3—2.6 (d, 6H, $2CH_3$), 2.9—3.2 (t, 2H, 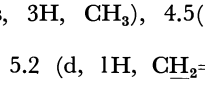), 3.4 (s, 1H, OH), 3.6—3.8 (t, 2H, $OC\underline{H}_2CH_2$), 5.2 (d, 1H, $C\underline{H}_2$=CH–), 5.5 (s, 3H, $-C\underline{H}O-+-\overset{\overset{\|}{N}}{\underset{\oplus}{}}-CH_2$), 5.8 (d, 1H, $C\underline{H}_2$=CH–), 6.6—7.0 (b, 1H, CH_2=C$\underline{H}$–), 7.0—7.6 (m, 4H, ArH), 7.6—7.8 (b, 2H, NH_2), 8.1 (s, 1H, 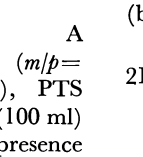), 9.8 (s, 1H, 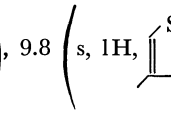) ppm.

Vinylbenzaldehyde Acetal with Vitamin B_2 (VIII). A mixture of vinylbenzaldehyde (2.0 g, 15 mmol), riboflavin (2.9 g, 7.6 mmol)(vitamin B_2), PTS (0.4 g), phenothiazine (0.1 g), and dioxane (50 ml) was stirred at 50 °C for 5 h under nitrogen in the presence of 3A molecular sieves (1/16), followed by stirring at room temperature for 20 h. The dioxane was then removed by freeze-drying and the residue washed with petroleum ether and aqueous sodium hydrogen carbonate and extracted with chloroform. The chloroform extract was dried over anhydrous sodium sulfate, evaporated *in vacuo* at 50 °C to leave a reddish brown powder (mp 110—113 °C) in 8% yield.

Found: C, 70.62; H, 5.33 ; N, 8.09%. Calcd for $C_{35}H_{32}N_4O_6$: C, 69.54; H, 5.30; N, 9.27%. IR($CHCl_3$) 3380 (NH), 1680 (C=O), 990, 910 (vinyl) cm^{-1}. NMR($CDCl_3$+DMSO-d_6)δ 2.2—2.5 (s, 6H, $2CH_3$), 3.0—5.0 (m, 7H, $3CH+2CH_2$), 5.1—5.3 (d, 3H, $C\underline{H}_2$=CH–+$-\underset{}{\overset{\diagup O-}{CH}}\underset{\diagdown O-}{}-$), 5.8 (d, 2H, $C\underline{H}_2$=CH–), 6.5—7.7 (m, 12H, ArH), 8.3 (b, 1H, NH) ppm. Mass (*m/e*) 604 (M^+, 2), 18 (100).

Hydrolyses of Acetals. A solution of the acetal (1 mmol), PTS (0.05 g), and *t*-butylcatechol (0.001 g) in 30 ml of H_2O–THF (1 : 2 v/v) was stirred at 20 °C under nitrogen. The reaction mixture was neutralized with solid sodium carbonate and evaporated *in vacuo* at 50 °C to remove THF, followed by extraction with a mixture of aqueous sodium carbonate and chloroform. The chloroform layer was dried over anhydrous sodium sulfate and evaporation *in vacuo* at 50 °C afforded the sample for analysis. NMR-determinations using either methoxyl or aryl signals provided the degree of hydrolysis. Typical data are as follows.

IVa: 72.8% in 2 h and 100% in 10 h; IVb: 82.9% in 2 h and 100% in 10 h; IVc: 74.6% in 2 h and 100% in 10 h; V; 62.8% in 2 h and 100% in 10 h; vinylbenzaldehyde dicitronellyl acetal:[3] 64.0% in 2 h and 100% in 10 h.

References

1) Tanabe Pharmaceutical Co., JP 38-25392 (1965).
2) F. W. Harris, *Polym. Lett.* **13**, 225 (1975).
3) H. Kamogawa, S. Okabe, and M. Nanasawa, *Bull. Chem. Soc. Jpn.*, **49**, 1917 (1976).
4) M. S. Newman, "Steric Effects in Organic Chemistry," Wiley, New York (1956), p. 637.

Preparation of Diphenyl(tricyclohexylphosphine)manganese(II) and Its Reactions with Carbon Dioxide and Organic Carbonyl Compounds

Kazunori MARUYAMA, Takashi ITO, and Akio YAMAMOTO*

Research Laboratory of Resources Utilization, Tokyo Institute of Technology, Nagatsuta, Midori-ku, Yokohama 227

(Received September 9, 1978)

Treatment of $Mn(acac)_3$ (acac=acetylacetonato ligand) with $AlPh_3 \cdot Et_2O$ in the presence of PCy_3 (Cy=*cyclo*-C_6H_{11}) gave a new diphenylmanganese(II) complex, Ph_2MnPCy_3 (**1**). Complex **1** reacted with allylic compounds, $CH_2=CHCH_2X$ (X=Br, OPh, $OCH_2CH=CH_2$, and $OCOCH_3$), to give allylbenzene. Carbon dioxide was found to be inserted into the phenyl-manganese σ-bond of **1** to give bis(benzoato)manganese complex, $(PhCOO)_2MnPCy_3$, **2**, which on successive treatment with HCl and diazomethane produced methyl benzoate. Complex **1** reacted with aldehydes, ketones, and esters having no active α-hydrogen atom to give alkoxomanganese species in solution, indicating that the insertion of C=O double bond into the phenyl-manganese σ-bond occurred. On the other hand, acetone and acetophenone reacted with Ph_2MnPCy_3 to give benzene and 2-oxoalkyl complexes, $(RCOCH_2)_2Mn(PCy_3)_m$ (R=Me, Ph), **3**. Reaction of alcohols with **1** afforded alkoxomanganese compounds which catalyze the Tishchenko type and Meerwein-Pondorf type reactions as well as transesterification reactions at room temperature.

Employment of alkylaluminium compounds in combination with transition metal acetylacetonates in the presence of stabilizing ligands has provided useful means in giving alkyl-, hydrido- and low valent transition metal complexes.[1] Extension of the method to the preparation of phenyl-transition metal complexes using triphenylaluminium etherate, $AlPh_3 \cdot Et_2O$, proved successful as well affording new phenyl-nickel,[2] chromium,[3] cobalt,[4] and iron[4] complexes. We now report the preparation of diphenylmanganese(II) complex having tricyclohexylphosphine (PCy_3) from a reaction system composed of $Mn(acac)_3$, $AlPh_3 \cdot Et_2O$ and PCy_3. Although there are many reports concerning organomanganese complexes, isolated examples of organomanganese complexes having other ligand than cyclopentadienyl and carbonyl are quite scarce. As a homoleptic phenylmanganese complex without stabilizing ligand, preparation of somewhat impure diphenylmanganese in 1956 presents the sole example,[5] but characterization of the complex and study of its chemical properties are by no means satisfactory.[6,7] We have found that binding of tricyclohexylphosphine ligand confers a considerable stability on the diphenylmanganese. Treatment of the new diphenylmanganese complex with various reagents, particularly organic carbonyl compounds, produced hitherto unknown new types of organic manganese complexes, some of which show catalytic activities for various reactions.

Results and Discussion

Preparation and Characterization of Ph_2MnPCy_3. Treatment of $Mn(acac)_3$ with $AlPh_3 \cdot Et_2O$ in the presence of PCy_3 in a mixture of diethyl ether and toluene at −50 °C gave a yellow complex of Ph_2MnPCy_3, **1**, in a good yield.

$$Mn(acac)_3 + PCy_3 + 3AlPh_3 \cdot Et_2O \xrightarrow{-50\,^\circ C} Ph_2MnPCy_3 \quad (1)$$

The complex is recrystallizable from hot toluene to give yellow-brown crystals which decompose under vacuum at 160—165 °C. Since the micro-analysis of Ph_2MnPCy_3 was not feasible due to its high sensitivity to air, characterization of this paramagnetic complex (μ_{eff}=2.73 B. M.) was achieved by means of macroscopic analysis of manganese content, infrared spectroscopy and some chemical reactions. The characteristic IR bands of **1** were assigned as follows: 3040 cm^{-1}, ν(C–H) of the phenyl group; 2925 and 2850 cm^{-1}, $\nu_{as}(CH_2)$ and $\nu_s(CH_2)$ of PCy_3; 1445 cm^{-1}, δ(C–H) of PCy_3; 430 cm^{-1}, ν(Mn–C). Treatment of Ph_2MnPCy_3 with gaseous HCl in diethyl ether gave 1.92 mol of benzene per manganese. Treatment of **1** with an excess amount of methyl iodide gave toluene (0.32 mol per mol of complex) and biphenyl (0.74 mol). A quantitative amount of tricyclohexylphosphine oxide was isolated on decomposition of **1** with aqueous H_2O_2. Pyrolysis of **1** at 220 °C under vacuum gave benzene (0.57 mol per mol of complex) and biphenyl (0.63 mol). The Mn^{2+} content in complex **1** determined by a chelate titration method was 11.4% (Calcd for $C_{30}H_{43}PMn$: Mn, 11.2%).

The reaction of $Mn(acac)_3$ and $AlPh_3 \cdot Et_2O$ without tertiary phosphine gave Ph_2Mn in a yield of 23%, which was already prepared from MnI_2 and PhLi by Beerman and Clauss.[5] Addition of PCy_3 in ether to the isolated Ph_2Mn also led to Ph_2MnPCy_3, **1**. However, less basic tertiary phosphines such as PPh_3, PPh_2Me and $Ph_2PCH_2CH_2PPh_2$ did not give isolable adducts of the phosphines with Ph_2Mn. It is noteworthy that the sensitivity of Ph_2MnPCy_3, **1**, towards air is considerably reduced as compared with that of Ph_2Mn which ignites spontaneously on contact with air.

Reaction of Ph_2MnPCy_3 with Allylic Compounds. Ph_2MnPCy_3, **1**, reacted with allylic compounds, $CH_2=CHCH_2X$ (X=Br, OPh, $OCH_2CH=CH_2$, and $OCOCH_3$), to give allylbenzene in fairly high yields (Table 1). Cleavage of C–X bond in $CH_2=CHCH_2X$ on reactions with transition metal complexes have been reported in the cases of *e.g.*, $PhNi(acac)PPh_3$,[8] $Ni(cod)_2$,[9,10] (cod=1,5-cyclooctadiene), and $RuH_2(PPh_3)_4$.[11] The reaction of Ph_2MnPCy_3 with $(CH_2=CHCH_2)_2O$ liberated mainly allylbenzene with small amounts of benzene and biphenyl, and gave a pale

Table 1. Reactions of Ph_2MnPCy_3 **1** with allyl compounds

Allyl compound	Reaction condition (Solvent)	Products (mol/mol of **1**)		
		Ph-H	Ph-$CH_2CH{=}CH_2$	Ph-Ph
$CH_2{=}CHCH_2Br$	r. t., 1 d (Et_2O)	trace	2.00	trace
$CH_2{=}CHCH_2OPh$	45 °C, 1 h (Et_2O)	0.20	1.60	0.03
$(CH_2{=}CHCH_2)_2O$	80 °C, 2 h (neat)	0.20	1.34	0.11
$CH_3COOCH_2CH{=}CH_2$	r. t., 1 d (neat)	0.57	1.17	trace

Table 2. Reactions of Ph_2MnPCy_3, **1**, with aldehydes and ketones[a)]

Aldehyde or ketone (mmol)	Amount of **1** (mmol)	Solvent	Product (mol/mol of **1**)
Ph_2CO[b)] (2.26)	0.204	toluene	Ph-H (0.07)[c)], Ph_3COH (0.49)[c)], Ph-Ph (0.05)[c)]
MeCHO (0.72)	0.290	Et_2O	Ph-H (0.79)[c)], $PhCH{=}CH_2$ (0.21)[c)], Ph(Me)C(H)OH (0.40)[c)]
EtCHO (0.56)	0.230	Et_2O	Ph-H (0.80), PhCOEt (0.09), Ph(Et)C(H)OH (0.45), Ph-Ph (0.05)
PhCHO (neat) (14.7)	0.194	none	Ph-H (0.21), Ph_2CO (1.33), $PhCH_2OH$ (1.36), $PhCOOCH_2Ph$ (67.4)[d)]

a) Reactions were carried out at room temperature for 1 d. b) Reaction was carried out at 70 °C for 1 h. c) Yields after treating the reaction mixture with PhOH or HCl gas. d) Conversion of PhCHO into benzyl benzoate was 89%.

yellow powder, which on treatment with acetyl chloride yielded allyl acetate, suggesting that it contains the allyloxomanganese bond.

Two alternative mechanisms are conceivable in accounting for the products. One involves the insertion of $CH_2{=}CHCH_2X$ into the Ph–Mn bond followed by β-elimination of X, not of hydrogen as one usually encounters in the decomposition of alkyltransition metal complexes carrying a β-hydrogen:

$$\underset{\mathbf{1}}{Ph_2MnPCy_3} \xrightarrow[\text{insertion}]{CH_2{=}CHCH_2X} \left[\begin{array}{ccc} CH_2 & -CH & -CH_2 \\ | & | & | \\ Ph & Mn & X \\ & | & \end{array}\right] \xrightarrow[\beta\text{-elimination}]{} PhCH_2CH{=}CH_2 + \text{-Mn-X} \qquad (2)$$

Similar mechanisms have been proposed in accounting for the reaction products of allylic compounds with $PhNi(acac)PPh_3$ and $RuH_2(PPh_3)_4$.[8,11] The alternative mechanism involves the oxidative addition of $CH_2{=}CHCH_2X$ to Ph_2MnPCy_3 with cleavage of the C–X bond followed by reductive elimination to give allylbenzene. Although a similar oxidative addition has been observed in the reactions of bis(cyclooctadiene)nickel(0) with phenyl carboxylate, alkenyl acetate[10] and allylic ethers,[9,12] it seems somewhat less likely that the manganese(II) complex attacks these allyl compounds to cause oxidative addition. In fact **1** did not react with benzyl phenyl ether and dibenzyl ether even by heating at 100 °C for 10 h, whereas under similar conditions the C–O bond in these ethers has been reportedly cleaved in the presence of $Ni(cod)_2$.[9]

Reaction of Ph_2MnPCy_3 with Carbon Dioxide. Carbon dioxide reacted with Ph_2MnPCy_3 at ambient conditions in toluene or diethyl ether at room temperature to give a dark brown precipitate. This precipitate, after isolation, turned to a white powder on drying *in vacuo*. The infrared spectrum of the complex was identical with that of $(PhCOO)_2MnPCy_3$, **2**, prepared by the reaction of Ph_2MnPCy_3 with PhCOOH. The result suggests that insertion of carbon dioxide into the phenyl-manganese σ-bond took place to give benzoatomanganese species. Formation of benzoate derivative of rhodium(I), $(PhCOO)Rh(PPh_3)_3$, has been reported by a similar insertion reaction of CO_2 into the Rh–C bond.[13] The characteristic IR bands of $(PhCOO)_2MnPCy_3$ were observed at 1550 and 1400 cm^{-1} which may be assigned to $\nu_{as}(CO_2)$ and $\nu_s(CO_2)$, respectively. Although $(PhCOO)_2MnPCy_3$, **2**, did not react with methyl iodide at room temperature, treatment of **2** (0.17 g, 0.35 mmol) with gaseous HCl in diethyl ether followed by methylation with diazomethane gave methyl benzoate (0.43 mmol).

$(PhCOO)_2MnPCy_3$, **2**, is thermally very stable and liberates PCy_3 and only trace amounts of CO and CO_2 on heating at 200 °C *in vacuo* for 40 min. The residue is a dark brown powder, which was judged as $(PhCOO)_2Mn$ on the basis of its IR spectrum.

Although the insertion of carbon dioxide into the carbon-manganese σ-bond has been briefly reported for Me_2Mn,[7] the present result exhibits the first example of the isolation of the carboxylato manganese complex as a result of the CO_2 insertion reaction.

Reactions of Ph_2MnPCy_3 with Aldehydes and Ketones. Anionic nature of the phenyl ligand in Ph_2MnPCy_3, **1**, was demonstrated through its reactions with organic carbonyl compounds such as aldehydes, ketones and esters, where secondary alcohols from the first compound

Table 3. Reactions of Ph_2MnPCy_3 **1** with esters[a]

Ester ($PhCOOCH_2R$)	Products (mol/mol of **1**)							
	PhH	RCH_2OH	Ph-Ph	PhCOPh	Ph_3COH	Others		
$PhCOOCH_2$-H	b)	b)	0.11	0.26	0.35			c)
	b)	b)	0.11	0.20	0.74			d)
$PhCOOCH_2Me$	0.35	0.18	0.06	0.07	0.75			c)
	0.35	0.52	0.05	0.10	0.70			d)
$PhCOOCH_2Ph$	0.23	0.11	0.07	0.11	0.36	PhCHO, 0.17		c)
	0.28	0.51	0.04	0.09	0.56	PhCHO, 0.07		d)
	PhH	EtOH	Ph-Ph	PhCOPh	Ph_3COH	Ph_2CHOH	PhCOOEt	
HCOOEt	0.34	0.54	0.00	0.08	trace	0.46	trace	d)

a) Reactions were carried out at 70 °C for 10 minutes in toluene solution. b) Not measured. c) Yield before treating the reaction system with PhOH. d) Yield after treating the reaction system with PhOH.

and tertiary alcohols from the last two compounds were detected as the main products (*vide infra*). The results indicate that the chemical property of phenylmanganese complex **1** resembles considerably to that of a phenyl Grignard reagent especially in respect of the stoichiometric reactions with carbonyl compounds.

Complex **1** reacted with benzophenone, acetaldehyde and propionaldehyde to give, after treatment with gaseous HCl or phenol, triphenylmethanol, 1-phenylethanol and 1-phenyl-1-propanol, respectively (Table 2). These results suggest the existence of alkoxomanganese intermediates in the reaction mixtures as shown in Eq. 3.

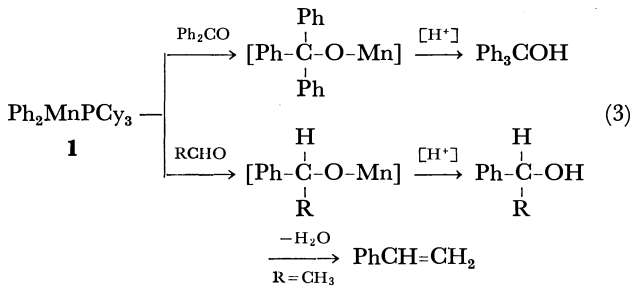

(3)

The formation of styrene after treatment of the reaction mixture of **1** and acetaldehyde with phenol is considered to be the result of dehydration of 1-phenylethylalcohol catalyzed by phenol which is a weak acid (Eq. 3). The acid-catalyzed dehydration reaction of alcohol is well known.[14]

The reaction of **1** with a large excess of acetaldehyde without solvent at −50 °C to room temperature afforded polyether of the type $-[CH(CH_3)-O]_n-$ probably as a result of consecutive insertion of acetaldehyde into Mn–O bond.[15]

Ph_2MnPCy_3, **1**, was found to convert benzaldehyde catalytically into benzyl benzoate at room temperature. The reaction was accompanied by formation of 0.21 equiv. of benzene, 1.33 equiv. of benzophenone and 1.36 equiv. of benzyl alcohol as Table 2 shows. The pale brown powder, isolated from this reaction system, liberated benzyl acetate on the reaction with acetyl chrolide. The result suggests that the powder contains benzyloxo group bonded to manganese. The reaction of **1** with benzaldehyde may be, again, explained by the insertion of the C=O double bond into the Ph–Mn σ-bond as shown in Eq. 4.

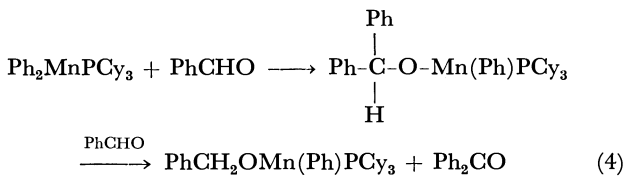

(4)

The benzyloxomanganese thus produced is considered to be responsible for the catalytic Tischchenko type reaction converting benzaldehyde into benzyl benzoate. A Tischchenko type reaction catalyzed by ruthenium complexes has been recently reported.[16]

The insertion of aldehydes and ketones into the metal-carbon σ-bond, a quite common reaction observed in the reactions of non-transition metal alkyls and aryls such as Grignard reagents, has some precedents also among the reactions involving organo-transition metal compounds.[3,17]

Formation of benzene in the reactions of **1** with benzaldehyde, acetaldehyde, and propionaldehyde may be accounted for by assuming a β-hydrogen elimination from the presumed intermediate, alkoxomanganese complex bearing a β-hydrogen, followed by reductive elimination with the remaining phenyl group bonded to manganese. The alternative to the above mechanism is the abstraction of protonic α-hydrogen at the α-carbon of aliphatic aldehydes. This type of reaction may be predominantly taking place in the reactions of **1** with acetone and acetophenone which carry active α-hydrogens. In these cases about two moles of benzene were liberated to leave white complexes. The IR spectrum of the complex derived from acetone showed the ν(C=O) band at 1690 cm^{-1} with a shift of 30 cm^{-1} from that of free acetone. Although insolubility of the complex in common organic solvents hindered its purification, this complex is considered to be (2-oxopropyl)manganese, since treatment of the complex with methyl iodide gave methyl ethyl ketone and acetonylacetone.

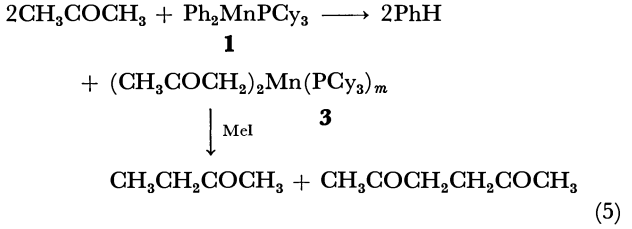

(5)

TABLE 4. REACTION OF SECONDARY ALCOHOLS WITH BENZALDEHYDE AND ACETOPHENONE IN THE PRESENCE OF ALKOXOMANGANESE COMPOUND[a)]

Reactant (mmol)	Product (mol/mol of complex **1**)			
Ph_2CHOH (2.16) PhCHO (4.95)	$PhCH_2OH$ (8.6)	Ph_2CO (9.3)	PhH (1.9)	$PhCOOCH_2Ph$ (6.2)
Me_2CHOH (12.8) PhCHO (9.90)	$PhCH_2OH$ (8.2)[b)]	Me_2CO (3.5)[b)]	PhH (1.7)[b)]	$PhCOOiPr$ (0.9)[b)]
Ph(Me)CHOH (2.91) PhCHO (4.95)	$PhCH_2OH$ (4.9)	Ph(Me)CO (2.0)	PhH (1.5)	
Ph_2CHOH (5.76) MeCOPh (8.60)	Ph(Me)CHOH (trace)	Ph_2CO (trace)		
Me_2CHOH (7.85) MeCOPh (5.16)	Ph(Me)CHOH (0.4→0.7[b)])	Me_2CO (0.4)	PhH (1.6)	

a) Reactions were carried out at room temperature for 1 d. The amount of Ph_2MnPCy_3 **1** used for each reaction was about 0.1 g (0.22 mmol). b) The yield after heating the system at 70 °C for 9 h.

A similar β-oxo-alkyl type compound of gold has been reported.[18)]

Reactions of Ph_2MnPCy_3 with Esters. The insertion reaction of the C=O double bond into Ph–Mn σ-bond was similarly observed when alkyl and benzyl benzoates, $PhCOOCH_2R$ (R=H, CH_3, Ph) were allowed to react with **1**. In these cases, benzophenone, triphenylmethanol, benzene, biphenyl, primary alcohols (RCH_2OH) and benzaldehyde (when R=Ph) were yielded as organic products (Table 3). Treatment of the reaction mixture with phenol caused the significant increase in the yields of alcohols indicating the existence of an alkoxomanganese intermediate (Ph_3COMn– and RCH_2OMn–) in the reaction mixtures as is assumed in the preceding section. Thus, the reaction between Ph_2MnPCy_3 and alkyl benzoate seems to proceed through an alkoxomanganese intermediate produced by the insertion of C=O double bond of the ester into the Ph–Mn σ-bond followed by β-alkoxy-elimination as shown in eq. 6.

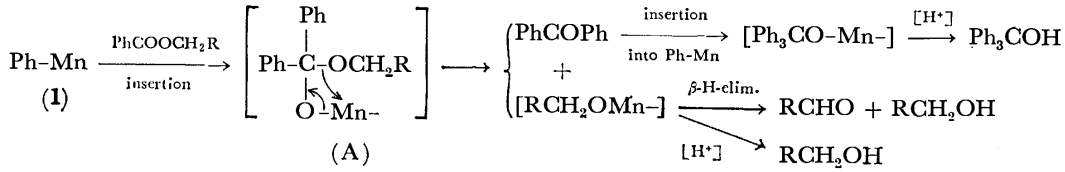

(6)

The acetal type intermediate (A) in Eq. 6 may decompose to alkoxomanganese and benzophenone, the latter of which may react further with Ph–Mn species to give triphenylmethyloxomanganese compound, Ph_3C–O–Mn– (*vide supra*). These alkoxomanganese species may liberate the corresponding alcohols on treatment with phenol. Provided the reaction proceeds according to Eq. 6, the ratio of the products (PhCOPh+Ph_3COH)/(RCH_2OH+RCHO) (=γ), whould be 1.0. In fact experimental values of γ=1.5 for R=Me and γ=1.1 for R=Ph have been obtained supporting the validity of the proposed reaction scheme.

The reaction of ethyl formate with complex **1** proceeded similarly to those of alkyl benzoates.

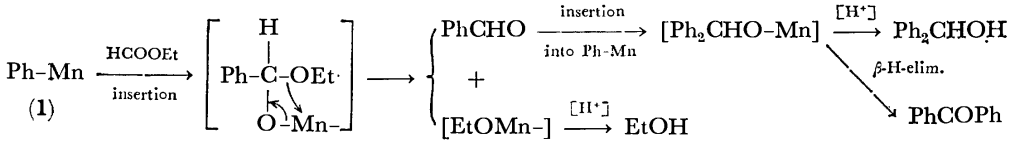

(7)

In this case, also, the observed value of the ratio, γ=(PhCOPh+Ph_2CHOH)/(EtOH) was 1.0 in accordance with the expected value of 1.0 for the assumed mechanism.

Reactions of Secondary Alcohols and Benzaldehyde or Acetophenone in the Presence of Alkoxomanganese. The above results of conversion of benzaldehyde with Ph_2MnPCy_3, **1**, into benzophenone and benzyloxomanganese (Eq. 4) prompted us to investigate the possibility of catalytic Meerwein-Pondorf type reaction in the presence of alcohol promoted by the manganese complex.

As Table 4 shows, the catalytic Meerwein-Pondorf type reaction did take place when the mixtures of benzaldehyde and diphenylmethanol and of benzaldehyde and 2-propanol were allowed to react in the presence of **1**.

$$PhCHO + Ph_2CHOH \xrightarrow{1} PhCH_2OH + Ph_2CO \quad (8)$$

$$PhCHO + Me_2CHOH \xrightarrow{1} PhCH_2OH + Me_2CO \quad (9)$$

In each case about two moles of benzene was produced per mol of **1** indicating the conversion of the diphenylmanganese into the alkoxomanganese species. The reaction path might be similar to that proposed for the Meerwein-Pondorf reaction using isopropoxoaluminium[19)] as shown below :

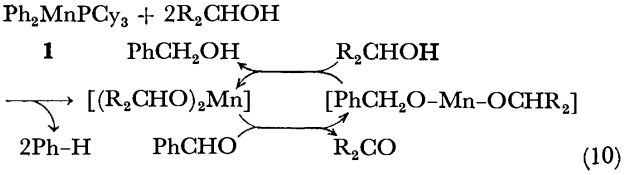

(10)

Table 5. Transesterification reactions using alkoxomanganese compound[a)]

Ester (PhCOOR)	Alcohol (R'OH)	Products, mol/mol of compound		
		PhCOOR'	ROH	PhH
$PhCOOCH_2Ph$ (5.3 mmol)	EtOH (34.7 mmol)	18.7 (0.63)[c)]	17.1	1.7
$PhCOOCH_2Ph$ (5.9 mmol)[d)]	EtOH (34.7 mmol)[d)]	8.7 (0.98)[c)]	8.3	—[d)]
$PhCOOCH_2Ph$ (5.3 mmol)	Me_2CHOH (13.1 mmol)	1.2	0.4	1.6
$PhCOOCH_2Ph$ (5.3 mmol)	Me_3COH (5.2 mmol)[e)]	0.0	0.0	1.4
PhCOOPh (1.1 mmol)	MeOH (71.4 mmol)	6.7 (1.0)[c)]	5.8	1.7
PhCOOPh (2.6 mmol)	Me_2CHOH (22.7 mmol)	3.2→7.4[b)] (0.73)[c)]	0.9→5.4[b)] (0.53)[c)]	1.6
PhCOOPh (2.0 mmol)	Me_3COH (5.0 mmol)[e)]	0.3	0.0	1.8
PhCOOMe (4.0 mmol)	PhOH (4.1 mmol)[e)]	0.0	0.0	1.8
$PhCOOCHMe_2$ (3.1 mmol)	PhOH (5.3 mmol)[e)]	0.0	0.0	1.6
$PhCOOCMe_3$ (2.8 mmol)	PhOH (3.6 mmol)[e)]	0.2	0.0	1.8

a) Reactions were carried out at room temperature for 1 d. The amount of Ph_2MnPCy_3, **1** used for each reaction was about 0.1 g (0.22 mmol). b) The yields were measured after heating the system at 70 °C for 15 h. c) Yields calculated on the basis of mol of PhCOOR used. d) This reaction was carried out using isolated $(PhO)_2Mn$ (0.16 g, 0.66 mmol) as catalyst at room temperature for 2 d. e) Diethyl ether was used as solvent.

Table 6. Reactions of benzaldehyde and primary alcohols in the presence of alkoxomanganese compound[a)]

PhCHO (ml)	ROH (ml)	Products (mol/mol of complex)			
		PhCOOR	$PhCH_2OH$	$PhCOOCH_2Ph$	PhH
(2.1)	MeOH (0.8)[b)]	1.6	1.2	0	1.7
(0.2)	EtOH (0.2)[b)]	1.4	1.2	0	1.7
(1.5)	EtOH (0.6)[c)]	14.3	—	14.2	1.8

a) Reactions were carried out at room temperature for 1 d. The amount of complex **1** used for each reaction was about 0.1 g (0.22 mmol). b) Diethyl ether was used as solvent. c) 0.5 ml of $PhCH_2OH$ was added together with EtOH.

By-products of the present reaction system such as benzyl benzoate and isopropyl benzoate might be produced by Tishchenko type reaction (*vide supra*) and that followed by transesterification (alcoholysis) (*vide infra*), respectively.

When acetophenone was used in place of benzaldehyde, on the other hand, only minimal amounts of Meerwein-Pondorf type reaction products were obtained (Table 4). Even when the system which contains acetophenone and isopropyl alcohol was heated at 70 °C for 9 h in the presence of alkoxomanganese, only 0.7 mol of 1-phenylethanol per mol of Ph_2Mn-PCy_3 was produced. A steric hindrance in the transition state may affect the reactivity of the present system as was proposed for the Meerwein-Pondorf reaction using isopropoxoaluminium.

Transesterification Reactions Using Alkoxomanganese Compounds. The transesterification reactions between alkyl benzoate and various alcohols were examined using dialkoxomanganese compounds prepared *in situ* from Ph_2MnPCy_3, **1**, and alcohols.

$$PhCOOR + R'OH \xrightarrow{(R'O)_2Mn} PhCOOR' + ROH \quad (11)$$

As Table 5 shows, the catalytic reactions of the transesterification reactions proceed at room temperature when primary alcohols were used. The ease of transesterification reactions of alcohols decreased in the order of prim. alcohol≫sec. alcohol≫tert. alcohol≈phenol. This tendency corresponds to the order of the ester yields in the acid catalyzed ester formation reaction from carboxylic acid and alcohols.[20)] The isolated $(PhO)_2Mn$, which was prepared by the reaction of Ph_2MnPCy_3 with phenol, was found also to catalyze the transesterification reaction between benzyl benzoate and ethanol (Table 5, line 2). Catalyst $(PhO)_2Mn$ used in this reaction was recovered without suffering from alcoholysis with ethyl alcohol. This suggests that the reaction mechanism for the present transesterification reaction may be manganese-assisted replacement of alkoxyl group as shown below.

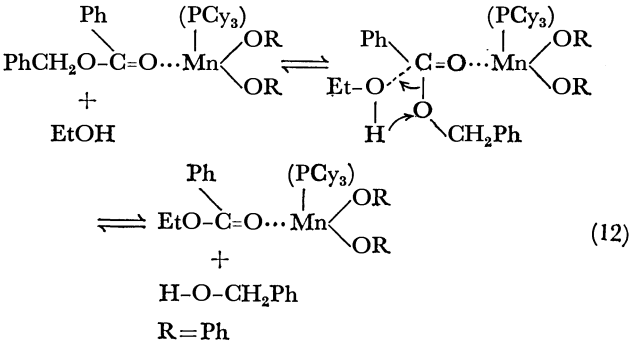

(12)

The transesterification reaction using transition metal compounds such as described here and that with alkoxocopper compounds[21)] have some advantages in that they act under neutral and mild conditions.

The reaction between benzaldehyde and primary alcohols to give alkyl benzoate directly through the combination of the catalytic Tishchenko type reaction and transesterification reaction was attempted and the

results are summarized in Table 6.

$$2PhCHO \xrightarrow{(RO)_2Mn} PhCOOCH_2Ph \xrightarrow[ROH]{(RO)_2Mn} PhCOOR + PhCH_2OH \quad (13)$$

Although the yield of methyl benzoate or ethyl benzoate was not high when methanol or ethanol alone was used, a high yield of ethyl benzoate was obtained when ethanol was allowed to react in the presence of benzyl alcohol. The result suggests that the (benzyloxo)manganese species have higher activity towards Tishchenko type reaction than methoxo- or ethoxomanganese species.

Some alkoxomanganese compounds which are analogous to those prepared *in situ* in the present work have been isolated, for example $(MeO)_2Mn$,[22] $(EtO)_2Mn$[23] and $(i\text{-}PrO)_2Mn$,[23] although none of their reactions has been examined.

Experimental

All reactions and manipulations were carried out under dry, oxygen-free nitrogen or *in vacuo* using Schlenk-type flasks.

Solvents were dried and purified in the usual manner and stored under an atmosphere of nitrogen. Carbon dioxide was dried by passing the gas through columns containing $CaCl_2$ and P_2O_5. Allylic compounds and esters were distilled over calcium hydride *in vacuo* and stored under nitrogen atmosphere. Aldehydes and ketones were purified by distillation under reduced pressure. Methanol and ethanol were purified by distilling over magnesium turnings. Other liquid alcohols were dried by Drierite and degassed under vacuum. $AlPh_3 \cdot Et_2O$ was prepared from PhMgBr and $AlCl_3$ according to the reported method.[24] Tris(acetylacetonato)manganese(III) (Tokyo Kasei Industrial Co.) was used as purchased without further purification. Tricyclohexylphosphine was prepared according to the literature method.[25]

Infrared spectra were recorded on a Hitachi model 295 spectrometer using KBr disks prepared under inert atmosphere. The magnetic susceptibility was measured by Gouy method using Shimadzu MB-100 apparatus at 23 °C and the diamagnetic corrections for the coordinated ligands were made on the basis of the Pascal's constants. The organic products formed in the various reactions were quantitatively analyzed by GLC using internal standard. GLC was recorded on a Shimadzu GC-3BT or GC-6A gas chromatography using SDC-550, SDC-410 and/or PEG-20M columns and helium as a carrier gas.

*Preparation of Ph_2MnPCy_3, **1**.* To the mixture of $Mn(acac)_3$ (2.1 g, 6.0 mmol), PCy_3 (2.0 g, 7.1 mmol), diethyl ether (20 ml) and toluene (5 ml) cooled at −50 °C, $AlPh_3 \cdot Et_2O$ (6.1 g, 18.3 mmol) was added. On stirring the mixture, the initial black suspension turned to a yellow suspension. After raising the temperature of the system to room temperature, the precipitate was filtered, washed with diethyl ether and dried *in vacuo*. The yellow powder thus obtained weighed 2.8 g (93% of the theoretical amount based on $Mn(acac)_3$ used). The crude product (2.0 g) was recrystallized from hot toluene (95 °C) to give yellow brown crystals of Ph_2MnPCy_3 (1.3 g, recrystallization yield, 65%). Analytical data and physical properties of **1** are mentioned in the text.

*Reaction of Ph_2MnPCy_3, **1**, with Allylic Compounds.* To a flask containing Ph_2MnPCy_3 (0.246 g, 0.502 mmol), dialkyl ether (2 ml) was added and heated at 70—80 °C for 2 h. The initial yellow suspension turned to a deep yellow solution. Allylbenzene (0.675 mmol), benzene (0.097 mmol) and biphenyl (0.057 mmol) were formed, as judged by GLC analysis. Hexane (5 ml) was added to the solution to give a pale yellow precipitate which was filtered and dried *in vacuo*. The pale yellow powder thus obtained was allowed to react with acetyl chrolide at room temperature to give allyl acetate. The other reactions of Ph_2MnPCy_3 with allylic compounds were carried out in a similar fashion.

Reaction of Ph_2MnPCy_3 with Carbon Dioxide. On bubbling carbon dioxide into the toluene suspension of Ph_2MnPCy_3 for one day at room temperature, the initial yellow suspension turned to a dark brown suspension. The precipitate was filtered and dried *in vacuo* to give a white powder of $(PhCOO)_2MnPCy_3$ **2**. Characterization of this compound was achieved as mentioned in the text.

Reactions of Ph_2MnPCy_3 with Esters, Aldehydes, and Ketones. Since the method is general, some typical reactions are described here, the organic reaction products are being listed in Tables 2 and 3.

a) Reaction with Benzyl Benzoate : To a flask containing Ph_2MnPCy_3 (0.094 g, 0.191 mmol), toluene (1 ml) and benzyl benzoate (1 ml) were added. On heating the system at 70 °C for ten minutes, the initial yellow suspension turned to a yellow solution. Formation of benzene (0.021 mmol), benzaldehyde (0.032 mmol), benzyl alcohol (0.021 mmol), biphenyl (0.013 mmol), benzophenone (0.020 mmol) and triphenylmethanol (0.068 mmol) were observed by GLC analysis. The amounts of these reaction products changed on treatment with phenol as follows : benzene (0.053 mmol), benzaldehyde (0.013 mmol), benzyl alcohol (0.098 mmol), benzophenone (0.018 mmol) and triphenylmethanol (0.107 mmol).

b) Reaction with Benzaldehyde: To a flask containing Ph_2MnPCy_3 (0.095 g, 0.194 mmol), benzaldehyde (1.5 ml, 15 mmol) was added and stirred at room temperature for one day. A dark brown solution thus formed contained benzene (0.04 mmol), benzyl alcohol (0.264 mmol), benzophenone (0.258 mmol) and benzyl benzoate (13.1 mmol) as analyzed by GLC.

c) Reaction with Acetone: To a flask containing Ph_2MnPCy_3 (0.137 g, 0.279 mmol) and diethyl ether (2 ml), acetone (75 μl, 1.02 mmol) was added and stirred for one day. A pale yellow suspension thus obtained was analyzed by GLC and found to contain benzene (0.447 mmol) and unreacted acetone (0.38 mmol). White powder (0.027 g, 0.060 mmol calculated as $(CH_3COCH_2)_2MnPCy_3$) isolated from this reaction system, reacted with methyl iodide to give ethyl methyl ketone (0.7 μl, 0.008 mmol) and acetonyl acetone (0.6 μl, 0.005 mmol).

Reactions between Alcohols and Aldehydes or Ketones in the Presence of Alkoxomanganese Compound Prepared in situ. To a flask containing Ph_2MnPCy_3 (0.099 g, 0.202 mmol) and diphenylmethanol (0.40 g, 2.16 mmol), was added diethyl ether (2 ml) to give a white suspension. Benzaldehyde (0.5 ml) was added to this system which was stirred for one day at room temperature. Benzene (0.39 mmol), benzyl alcohol (1.74 mmol), benzophenone (1.88 mmol) and benzyl benzoate (1.26 mmol) were formed, as analyzed by GLC.

The reactions listed in Tables 4 and 6 carried out similarly.

Transesterification Reactions Using Alkoxomanganese Compound Prepared in situ. To a flask containing Ph_2MnPCy_3 (0.087 g, 0.178 mmol) ethanol (1.0 ml) was added to give a pale brown suspension. Benzyl benzoate (1.0 ml, 5.3 mmol) was added to this system and the mixture was stirred for one day at room temperature. The GLC analysis of the reaction mixture revealed the formation of benzene

(0.30 mmol), benzaldehyde (0.047 mmol), benzyl alcohol (3.05 mmol) and ethyl benzoate (3.05 mmol).

The other transesterification reactions listed in Table 5 were carried out in a similar fashion.

References

1) (a) References cited in A. Yamamoto and S. Ikeda, *J. Macromol. Sci., Chem.*, **9**, 931 (1975); (b) T. Ito, H. Tsuchiya, and A. Yamamoto, *Bull. Chem. Soc. Jpn.*, **50**, 1319 (1977) and references cited therein.

2) K. Maruyama, T. Ito, and A. Yamamoto, *J. Organomet. Chem.*, **90**, C28 (1975).

3) K. Maruyama, T. Ito, and A. Yamamoto, *Chem. Lett.*, **1978**, 479.

4) K. Maruyama, T. Ito, and A. Yamamoto, unpublished results.

5) C. Beerman and K. Clauss, *Angew. Chem.*, **71**, 627 (1956).

6) K. Clauss and H. Bestian, *Justus Liebigs Ann. Chem.*, **656**, 8 (1962).

7) Y. Inoue and H. Hashimoto, 30th National Meeting of the Chemical Society of Japan, Osaka, April, 1974, Abstr. p. 1715.

8) K. Maruyama, T. Ito, and A. Yamamoto, *J. Organomet. Chem.*, **155**, 359 (1978).

9) J. J. Eish and K. R. Im, *J. Organomet. Chem.*, **139**, C45 (1977).

10) J. Ishizu, T. Yamamoto, and A. Yamamoto, *Chem. Lett.*, **1976**, 1091.

11) S. Komiya and A. Yamamoto, *J. Organomet. Chem.*, **87**, 333 (1975).

12) J. Ishizu, T. Yamamoto, and A. Yamamoto, unpublished results.

13) I. S. Kolomnikov, A. D. Gusev, T. B. Belopotapova, M. Kh. Grigoryan, T. V. Lysyak, Yu. T. Struchkov, and M. E. Vol'pin, *J. Organomet. Chem.*, **69**, C10 (1974).

14) R. H. Boyd, R. W. Taft, Jr., A. P. Wolf, and D. R. Christman, *J. Am. Chem. Soc.*, **82**, 4729 (1960).

15) J. Furukawa, T. Saegusa, and H. Fujii, *Makromol. Chem.*, **44-6**, 398 (1961) ; T. Yamamoto, S. Konagaya, and A. Yamamoto, *J. Polym. Sci., Polym. Lett. Ed.*, **15**, 729 (1977).

16) H. Horino, T. Ito, and A. Yamamoto, *Chem. Lett.*, **1978**, 17.

17) R. P. A. Sneeden, T. F. Burger, and H. H. Zeiss, *J. Organomet. Chem.*, **4**, 397 (1965) ; D. G. H. Ballard, W. H. Janes, and T. Medinger, *J. Chem. Soc., B*, **1968**, 1168; L. Cassar and G. P. Chiusoli, *Chim. Ind. (Milan)*, **48**, 323 (1966); S. Sakai, Y. Kawashima, Y. Takahashi, and Y. Ishii, *Chem. Commun.*, **1967**, 1073; R. M. Manyik, W. E. Walker, K. E. Atkins, and E. S. Hammack, *Tetrahedron Lett.*, **1970**, 3813; K. Ohno, T. Mitsuyasu, and J. Tsuji, *Tetrahedron*, **28**, 3705 (1972).

18) A. N. Nesmeyanov, *J. Organomet. Chem.*, **100**, 161 (1975).

19) See for example, J. B. Hendrickson, D. J. Cram, and G. S. Hammond, "Organic Chemistry," McGraw-Hill, Kogakusha, Tokyo (1970), p. 460—461.

20) For example, L. F. Fieser and M. Fieser, "Textbook of Organic Chemistry," Maruzen (1952), p. 169.

21) M. Kubota, T. Yamamoto, and A. Yamamoto, *Bull. Chem. Soc. Jpn.*, **52**, 146 (1979).

22) R. W. Adams, E. Bishop, R. L. Martin, and G. Winter, *Aust. J. Chem.*, **19**, 207 (1966).

23) J. G. F. Druce, *J. Chem. Soc.*, **1937**, 1407.

24) T. Mole, *Aust. J. Chem.*, **16**, 794 (1963).

25) K. Issleib and A. Brack, *Z. Anorg. Allg. Chem.*, **227**, 258 (1954).

Synthesis and Properties of Bis(cyclopropylphenyl)cyclopropenones and the Tris(*p*-cyclopropylphenyl)cyclopropenium Ion

Koichi KOMATSU, Isao TOMIOKA, and Kunio OKAMOTO*

Department of Hydrocarbon Chemistry, Faculty of Engineering, Kyoto University, Sakyo-ku, Kyoto 606

(Received September 13, 1978)

The reaction of trichlorocyclopropenium tetrachloroaluminate with cyclopropylbenzene has been found to readily afford the disubstitution products, bis(*p*-cyclopropylphenyl)- (**1a**), (*p*-cyclopropylphenyl) (*o*-cyclopropylphenyl)-, and bis(*o*-cyclopropylphenyl)cyclopropenones, each of which has been separated and fully characterized spectroscopically. The tris(*p*-cyclopropylphenyl)cyclopropenium ion (**2**) could not be obtained by the direct trisubstitution of the trichlorocyclopropenium ion with cyclopropylbenzene, but has been synthesized *via* two other routes starting from cyclopropenone **1a**. The UV and ^{13}C NMR spectral data of the cation **2** indicated the conjugative interaction of the *para*-cyclopropyl group with the cyclopropenium ring. However, the cation-stabilizing effect of the *para*-cyclopropyl group, as shown by the pK_{R^+} value (3.23 in 23% ethanol) for **2**, is much smaller than in the case of the tris(*p*-cyclopropylphenyl)methyl cation. This has been interpreted in terms of the decrease in delocalization of the positive charge to the *para*-position of the cation **2**, when compared with the triarylmethyl analogue.

The smallest-ring member of the aromatic halocarbon, the trichlorocyclopropenium ion ($C_3Cl_3^+$), was first synthesized by Tobey and West,[1a] and found to react with various aromatic rings resulting in stepwise electrophilic substitution.[1b] Recently this reaction was successfully applied to the syntheses of new cyclopropenium ions stabilized by non-benzenoid- or heteroaromatic substituents such as ferrocene,[2] azulene,[3] and thiophene rings.[4] Among the substituted benzenes, those carrying the strongly activating groups such as methoxyl, hydroxyl, and dialkylamino groups react with $C_3Cl_3^+AlCl_4^-$ to give the trisubstituted product, *i.e.* the triarylcyclopropenium ion,[1b,5] whereas the unsubstituted and weakly activated benzenes such as fluorobenzene and toluene give only the disubstituted cyclopropenones.[6]** Since the cyclopropyl group is expected to exert conjugative stabilization upon the cationic intermediate formed during the reaction,*** it was of interest to establish whether such an effect could lead to the trisubstitution of $C_3Cl_3^+$ with cyclopropylbenzene. Also having been interested in the stabilizing effect of the cyclopropyl group upon the triarylcyclopropenium ion which may be prepared by this reaction, we examined the reaction of $C_3Cl_3^+$-$AlCl_4^-$ with cyclopropylbenzene.

Results and Discussion

Bis(cyclopropylphenyl)cyclopropenones. The reaction of $C_3Cl_3^+AlCl_4^-$ with cyclopropylbenzene was examined in dichloromethane in the temperature range −60 to 40 °C. When two molar equivalents of cyclopropylbenzene were employed the disubstitution reaction occurred smoothly at −10 °C yielding a mixture of the isomeric bis(cyclopropylphenyl)cyclopropenones (**1a**, **1b**, and **1c**) after hydrolysis. Complete separation of the isomers was effected by the use of thin-layer

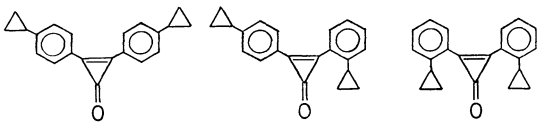

1a **1b** **1c**

chromatography. The R_f values of each component (**1a**, 0.14; **1b**, 0.34; **1c**, 0.64 : over silica gel developed with benzene–ether (4 : 1)) reflect the extent of molecular polarization, the *p,p*-isomer (**1a**) being the least developed due to the greatest polarization with two cyclopropyl groups located farthest away from the carbonyl group. In a representative run, the yield of the cyclopropenones was 31.2% for **1a**, 47.2% for **1b**, and 7.4% for **1c**. Assuming that the *ortho*/*para* reactivity ratio does not change between the first and the second substitutions of $C_3Cl_3^+$, it has been estimated from the yields of **1a** and **1b** that the *para*-position of cyclopropylbenzene is approximately 2.6 times more reactive to the electrophilic attack of $C_3Cl_3^+$ than the *ortho*-position. The decrease in the yield of **1c** (7.4%) to approximately half the calculated value (18%) is

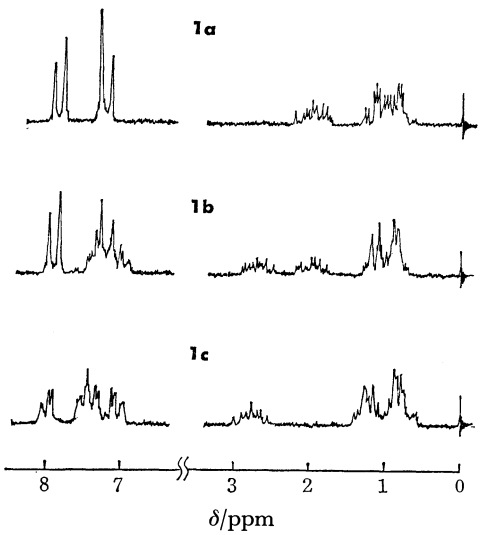

Fig. 1. ^1H NMR Spectra of the cyclopropenones **1a**, **1b**, and **1c**.

** The σ_p^+ values, which express the ability of the substituent to stabilize the cationic intermediate, are −0.778 for OCH_3, −0.92 for OH, −1.7 for NMe_2, −0.073 for F, and −0.311 for CH_3.[7]

*** The σ_p^+ value for the cyclopropyl group has been reported as −0.462.[8]

Table 1. Physical and spectral properties of the bis(cyclopropylphenyl)-cyclopropenones, **1a**, **1b**, and **1c**

Compd	Mp °C	IR ν(KBr) cm^{-1}	UV λ_{max}^{EtOH} nm (log ε)	^1H NMR δ ($CDCl_3$) ppm
1a	142.6—144.5	1850 1610	277 sh(4.45), 295 (4.59), 301 sh(4.50), 313 (4.52),	7.83 (d, 4H, *o*-H), 7.22 (d, 4H, *m*-H), 2.00 (m, 2H, methine), 1.3—0.8 (m, 8H, CH_2)
1b	83.5— 85.0	1845 1605	294 sh(4.30), 307 (4.40), 325 (4.38), 337 sh(4.32)	7.88 (d, 2H, *o*-H), 7.20 (m, 6H, aromatic), 2.70 (m, 1H, methine), 1.95 (m, 1H, methine), 1.3—0.7 (m, 8H, CH_2)
1c	120.0—121.0	1850 1600	289 (4.23), 312 (4.17), 324 (4.15), 341 sh(4.08)	8.0—7.0 (m, 8H, aromatic), 2.77 (m, 2H, methine), 1.3—0.7 (m, 8H, CH_2)

Table 2. Physical and spectral properties of the tris- (**2**) and the bis(*p*-cyclopropylphenyl)cyclopropenium ions (**3**)

Compd	Mp °C	IR ν(KBr)cm^{-1}	UV λ_{max}^{EtOH} nm (log ε)	^1H NMR δ ($CDCl_3$) ppm
2	>250	1410 1050	230 (4.33), 285 sh(4.25), 343 (4.84), 359 (4.84)	8.32 (d, 6H, *o*-H), 7.53 (d, 6H, *m*-H) 2.17 (m, 3H, methine), 1.30 (m, 6H, (*E*)-CH_2), 1.03 (m, 6H, (*Z*)-CH_2)[a]
3	169.0—171.0 (dec)	1415 1050	220 (4.17), 279 (4.10) 343 (4.63)	10.40 (s, 1H, C^+-H), 8.25 (d, 4H, *o*-H) 7.39 (d, 4H, *m*-H), 2.02 (m, 2H, methine), 1.25 (m, 4H, (*E*)-CH_2), 0.93 (m, 4H, (*Z*)-CH_2)

a) Taken in CD_2Cl_2.

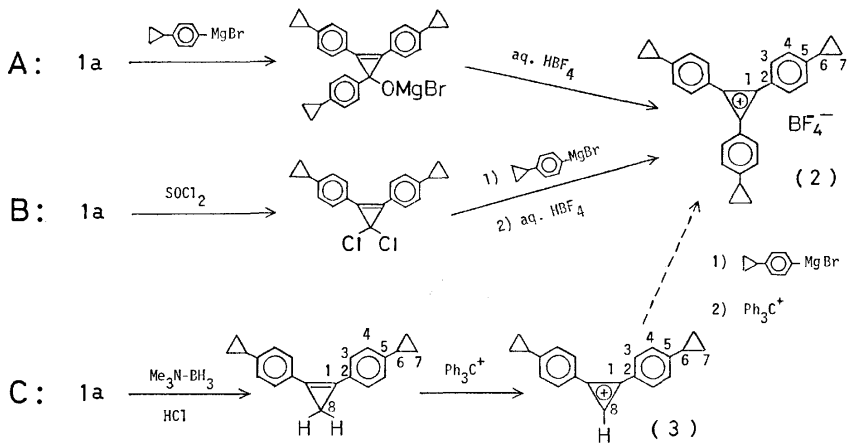

Scheme 1.

thus ascribed to steric inhibition which operates more strongly at the second substitution step.

The physical properties of the cyclopropenones, **1a**, **1b**, and **1c**, are given in Table 1. The compounds all exhibit two broad and strong IR absorption bands at 1850 and $\approx$1610 cm^{-1}, which are diagnostic for the cyclopropenone system. The higher mp's for **1a** and **1c** are consistent with the symmetrical positions of the substituents, but stronger evidence for structure **1a**, **1b**, and **1c** is given by the ^1H NMR spectra. As is shown in Fig. 1 compound **1a** exhibits an AB quartet for the aromatic protons indicating substitution only at the *para*-position, while compound **1b** has an AB quartet plus a multiplet in the aromatic region. Furthermore, in the spectrum of **1b** one of the two cyclopropyl methine multiplets is shifted downfield, presumably due to the deshielding effect of the carbonyl group, to the same position as that of the compound **1c**, which is consistent with the assignment of **1b** and **1c** to the *o*,*p*- and *o*,*o*-isomers respectively.

*Tris(*p*-cyclopropylphenyl)cyclopropenium Ion.* In contrast to the ready formation of diarylcyclopropenones, the reaction of $C_3Cl_3^+AlCl_4^-$ with three molar equivalents of cyclopropylbenzene at low (—60 °C) or ambient temperature did not produce any evidence for trisubstitution. The reaction conducted at higher temperature (40 °C) for a prolonged time merely resulted in the formation of intractable polymeric material. Thus, attempts were made to synthesize the tris(*p*-cyclopropylphenyl)cyclopropenium ion (**2**) from cyclopropenone **1a** following the three synthetic routes shown in Scheme 1.† Methods A and B gave the tetrafluoroborate salt of the cation **2** in a low yield. On the other hand, method C afforded the bis(*p*-

† The reaction of 1,2-bis(*p*-cyclopropylphenyl)-3,3-dichlorocyclopropene with cyclopropylbenzene in the presence of silver triflate according to the method reported by Weiss *et al.*[9] afforded an inseparable mixture of the triflate (32% yield) of the cation **2** and 1,2-bis(*p*-cyclopropylphenyl)-3-(*o*-cyclopropylphenyl)cyclopropenium ion.

Table 3. ^{13}C NMR data for the triphenylcyclopropenium ion (**4**) and the tris- (**2**) and the bis(*p*-cyclopropylphenyl)cyclopropenium ions (**3**)

Cation	Chemical shift δ (CD_3CN), ppm from TMS[a]							
	C-1	C-2	C-3	C-4	C-5	C-6	C-7	C-8
4[b]	156.7 s	121.0 s	137.0 d	131.5 d	139.6 d	—	—	—
2	152.9 s [c]	118.0 s	136.8 d	128.0 d	158.6 s	17.5 d	12.9 t	—
3	161.1 s [c]	117.0 s	137.6 d	127.9 d	160.0 s	17.6 d	13.1 t	151.6 d

a) The peak multiplicity of the off-resonance spectrum is indicated by s (singlet), d (doublet), and t (triplet). b) The numbering system is similar to that used in the cation **2**. The reported values obtained in $ClSO_3H$ are 155.4(C-1), 120.1(C-2), 135.9(C-3), 131.2(C-4), and 139.2(C-5) ppm from TMS.[10] c) The assignment of these signals to C-1, not to C-5, is made based on the fact that in the proton-coupled spectra the signals are distinctly more narrow and sharp compared with those for C-5 carbons which are apparently broadened by the long-range coupling with protons attached to the C-4 and C-6 carbons.

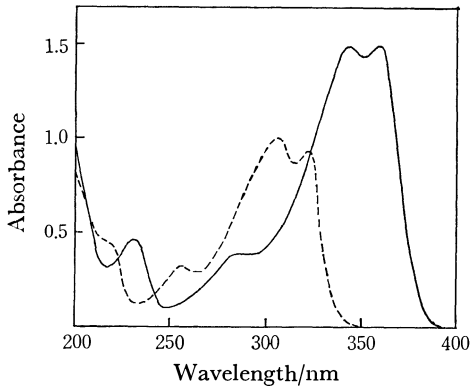

Fig. 2. UV Spectra of the tris(*p*-cyclopropylphenyl)-cyclopropenium ion (**2**, ——) and the triphenylcyclopropenium ion (**4**, – – –), 2.1×10^{-5} M in CH_3CN.

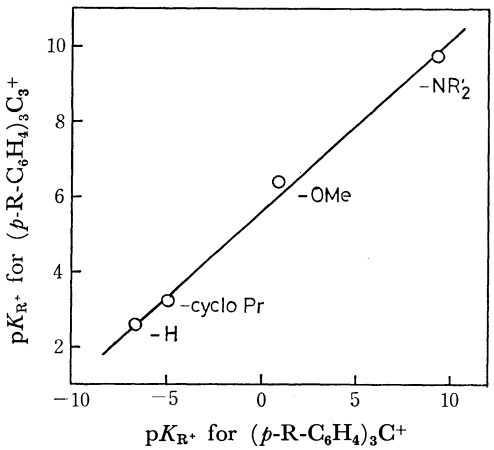

Fig. 3. Plot of the pK_{R^+} values for the *para*-substituted triarylcyclopropenium ions against those for the corresponding triarylmethyl cations. The alkyl group R′ in "$-NR'_2$" is methyl for $(p\text{-R-}C_6H_4)_3C^+$ and isopropyl for $(p\text{-R-}C_6H_4)_3C_3^+$.

cyclopropylphenyl)cyclopropenium ion (**3**) in a 59.1% overall yield, but the presence of many unfavorable side reactions in the subsequent reaction-step rendered this route impractical as a synthetic route for the cation **2**.

The spectral properties of the cations **2** and **3** are shown in Table 2. For both cations, the IR spectra exhibit broad and strong absorptions at $\approx 1410\ cm^{-1}$, which is assigned to the cyclopropenium ring stretching, and at $1050\ cm^{-1}$ due to the tetrafluoroborate anion, while the AB quartets of the aromatic protons in the ^1H NMR spectra illustrate the presence of all the cyclopropyl substituents at the *para*-position. As shown in Fig. 2 the UV spectrum of cation **2** is quite similar to that of the unsubstituted triphenylcyclopropenium ion (**4**) in general absorption pattern, but the longer-wave absorptions of the former are bathochromically shifted by *ca.* 40 nm with an apparent increase in the absorption coefficient. This shift is regarded as a result of conjugative interaction of the *para*-cyclopropyl group with the cationic central ring. The ^{13}C NMR data shown in Table 3 allow a more quantitative estimation of the conjugative effect of the *para*-cyclopropyl group : from the difference in chemical shift for the C-1 signal between the cyclopropylsubstituted cation **2** and the unsubstituted cation **4** and the Spiesecke-Schneider correlation $\Delta\delta = 160\Delta q$, the amount of the positive charge withdrawn from the cyclopropenium ring has been calculated as +0.071 or 7.3% of the amount of the positive charge (+0.969)[10] assumed to be originally present in the three-membered ring of cation **4**.

Stabilization of cation **2** resulting from the conjugative effect of the cyclopropyl group is demonstrated by the pK_{R^+} value of 3.23 (spectrophotometrical method in 23% aqueous ethanol at 25 °C) as compared with the value of 2.60[11] determined for the unsubstituted cation **4** in our laboratory. In the case of the triphenylmethyl cation system, substitution with three *para*-cyclopropyl groups has been reported to raise the pK_{R^+} value from −6.6 for the unsubstituted cation to −4.9.[12] Thus, in order to compare the effectiveness of various *para*-substituents on the stability of the triarylcyclopropenium ions with that for the triarylmethyl cations, the reported pK_{R^+} values[5,13] for the triarylcyclopropenium ions together with the present data were plotted against those[12,14] for the corresponding triarylmethyl cations. As shown in Fig. 3 there exists a reasonable linear free-energy relationship for the pK_{R^+} values between the two systems. However, the slope (0.46) is much smaller than unity, *i.e.*, the conjugative interaction of the substituent to stabilize the cationic center is apparently smaller in the triarylcyclopropenium system than in the triarylmethyl sys-

tem. This phenomenon is consistent with the results of the ^{13}C NMR measurements,[5,10] which implies that the positive charge in the triphenylcyclopropenium ion (**4**) resides mostly in the central three-membered ring to retain the "aromatic" 2π-electron ring system so that less of the charge is delocalized to the *para*-position to interact with the substituents than in the case of the triarylmethyl system, even though the coplanarity of the whole π-system is more favored in the triarylcyclopropenium system.

Experimental

General. The melting points are uncorrected. The elemental analyses were performed by the Microanalytical Center, Kyoto University, Kyoto. The IR and UV spectra were recorded on Hitachi 215 and Hitachi 200-10 spectrometers, respectively. The ^1H NMR spectra were taken with a Hitachi R-24 spectrometer with tetramethylsilane as the internal standard. The ^{13}C NMR spectra were recorded on a JEOL FX-100 spectrometer operated in the Fourier transform mode.

Materials. All the reagents employed were of reagent grade quality except when otherwise stated. Tetrachlorocyclopropene (C_3Cl_4) was supplied by Aldrich Chemical Co. Cyclopropylbenzene[15] and *p*-bromocyclopropylbenzene[16] were prepared according to the literature.

Bis(cyclopropylphenyl)cyclopropenones ***1a***, ***1b***, *and* ***1c***. To a stirred suspension of $C_3Cl_3^+AlCl_4^-$, prepared from C_3Cl_4 (1.12 g; 6.29 mmol) and $AlCl_3$ (0.67 g, 5.0 mmol) in dichloromethane (CH_2Cl_2 ; 2.5 ml), was added dropwise a solution of cyclopropylbenzene (1.32 g; 11.2 mmol) in CH_2Cl_2 (5 ml) at -60 °C under an atmosphere of nitrogen. When the temperature was raised slowly to -10 °C, rapid evolution of HCl took place accompanied by a sudden color change to dark red. The mixture was further stirred at 0 °C for 1 h and then hydrolyzed with cold water (10 ml). The aqueous layer was extracted with CH_2Cl_2 (5 ml×3). The combined organic solution was washed with 10% NaCl, dried ($MgSO_4$), and evaporated *in vacuo* to give 2.016 g of the crude product, from which was separated the cyclopropenone **1a** (0.216 g) as a white powder by washing with ether (3 ml). The remaining mixture was separated by the use of preparative TLC over SiO_2 (Merck, PF_{254}) developed with benzene–ether(4 : 1). The fraction with an R_f 0.14 afforded an additional amount of **1a** (0.231 g; total yield 31.2%). Purification was effected by recrystallization from benzene. Found: C, 88.35; H, 6.25%. Calcd for $C_{21}H_{18}O$: C, 88.08; H, 6.33%. The next TLC fraction with an R_f 0.34 gave the cyclopropenone **1b** (0.675 g; 47.2%) as a white powder from benzene. Found: C, 88.09; H, 6.25%. Calcd for $C_{21}H_{18}O$: C, 88.08; H, 6.33%. The last fraction with an R_f 0.64 afforded the cyclopropenone **1c** (0.106 g; 7.4%) as a white powder from benzene–hexane. Found: C, 88.31; H, 6.63%. Calcd for $C_{21}H_{18}O$: C, 88.08; H, 6.33%. The yields for the cyclopropenone isomers in duplicate runs were 29.8 and 23.8% for **1a**, 57.2 and 45.2% for **1b**, and 7.4 and 8.9% for **1c**.

*Tris(*p*-cyclopropylphenyl)cyclopropenium Tetrafluoroborate (***2*** BF_4^-). Method A*:[17] To a stirred solution of *p*-cyclopropylphenylmagnesium bromide, prepared from *p*-bromocyclopropylbenzene (0.592 g; 3.00 mmol) and magnesium (0.081 g; 3.3 mg atom) in dry ether (10 ml), was added a solution of the cyclopropenone **1a** (0.231 g; 0.808 mmol) in dry benzene (20 ml) during a 25-min period at 0 °C. After stirring for 1.5 h at 0 °C, the mixture was hydrolyzed with 0.2 M KH_2PO_4 (30 ml) and worked up in the usual manner. Addition of 42% aq HBF_4 (1 ml) to the stirred solution of the crude product in ether (30 ml) gave a white precipitate, which was collected, washed with ether, and vacuum-dried to give the tetrafluoroborate salt of the cation **2** as a white powder (0.006 g; 2%). Found: C, 75.88; H, 5.59%. Calcd for $C_{30}H_{27}BF_4$: C, 75.96: H, 5.74%.

Method B: A solution of the cyclopropenone **1a** (0.169 g; 0.590 mmol) and thionyl chloride (0.334 g; 2.81 mmol) in dry benzene was stirred at room temperature for 30 min and then refluxed for 15 min. Evaporation of the mixture *in vacuo* left crude 1,2-bis(*p*-cyclopropylphenyl)-3,3-dichlorocyclopropene as a brownish sludge. The dichlorocyclopropene was dissolved in dry ether (2 ml) and added to a stirred solution of *p*-cyclopropylphenylmagnesium bromide, prepared from *p*-bromocyclopropylbenzene (0.299 g ; 1.51 mmol) and magnesium (0.041 g; 1.7 mg atom) in dry ether (2 ml), at 0 °C. After stirring at 0 °C for 30 min and at room temperature for 24 h, the mixture was hydrolyzed with 0.2 M KH_2PO_4 (20 ml) and worked up. The crude product was dissolved in ether (2 ml) and treated with 1 ml of a solution of acetic anhydride–42% aq HBF_4 (10 : 1) to give the cation salt **2** BF_4^- (0.005 g; 2%).

Method C: *Synthesis of Bis(*p*-cyclopropylphenyl)cyclopropenium Tetrafluoroborate (***3*** BF_4^-)*. Following the method reported by Perkins and Wadsworth[18] for the reduction of diphenylcyclopropenone, the cyclopropenone **1a** was converted to 1,2-bis(*p*-cyclopropylphenyl)cyclopropene by reaction with borane–trimethylamine complex and HCl; mp 75.5—78.0 °C; IR ν(KBr) 1825 cm^{-1} (C=C stretching in the cyclopropene ring); ^1H NMR δ ($CDCl_3$) 7.64 (d, 4H, *o*-H), 7.14 (d, 4H, *m*-H), 1.95 (m, 2H, methine), 1.50 (s, 2H, CH_2-(cyclopropene)), 1.1—0.7 (m, 8H, CH_2(cyclopropane)); ^{13}C NMR δ 144.5 (s, C-5), 129.8 (d, C-3), 127.8 (s, C-2), 126.0 (d, C-4), 110.4 (s, C-1), 15.8 (d, C-6), 9.9 (t, C-7), 6.5 (t, C-8).

Into a refluxing solution of triphenylmethyl tetrafluoroborate[19] (1.532 g; 4.64 mmol) in CH_2Cl_2 (7 ml) was added dropwise during a 1.5-h period with stirring a solution of 1,2-bis(*p*-cyclopropylphenyl)cyclopropene (0.421 g; 1.55 mmol) in CH_2Cl_2 (10 ml). The solution was further refluxed for 10 min, and then concentrated to *ca.* 8 ml. Addition of ether (50 ml) produced a yellow precipitate, which was collected and washed with ether to give the tetrafluoroborate salt of the cation **3** as a brownish yellow powder (0.336 g; 60.6%). Found: C, 70.27; H, 5.48%. Calcd for $C_{21}H_{19}BF_4$: C, 70.42; H, 5.35%.

Determination of pK_{R^+}. The pK_{R^+} value was determined in 23% aqueous ethanol at 25 °C following the spectrophotometric method described by Breslow and Chang.[13] The cationic solution was found to be stable over the whole pH range examined. The pH values were read on a Horiba model H pH meter precalibrated with standard buffers.

References

1) a) S. W. Tobey and R. West, *J. Am. Chem. Soc.*, **86**, 1459 (1964); b) R. West, D. C. Zecher, and W. Goyert, *ibid.*, **92**, 149 (1970), and the references cited therein.

2) I. Agranat and E. Aharon-Shalom, *J. Am. Chem. Soc.*, **97**, 3829 (1975).

3) I. Agranat and E. Aharon-Shalom, *J. Org. Chem.*, **41**, 2379 (1976).

4) K. Komatsu, I. Tomioka, and K. Okamoto, *Tetrahedron Lett.*, **1978**, 803.

5) K. Komatsu, R. West, and D. Stanislawski, *J. Am. Chem. Soc.*, **99**, 6286 (1977).

6) S. W. Tobey and R. West, *J. Am. Chem. Soc.*, **86**,

4215 (1964).
7) H. C. Brown and Y. Okamoto, *J. Am. Chem. Soc.*, **80**, 4979 (1958).
8) R. C. Hahn, T. F. Corbin, and H. Shechter, *J. Am. Chem. Soc.*, **90**, 3404 (1968).
9) R. Weiss, H. Kölbl, and C. Schlierf, *J. Org. Chem.*, **41**, 2258 (1976).
10) G. J. Ray, A. K. Colter, and R. J. Kurland, *Chem. Phys. Lett.*, **2**, 324 (1968).
11) K. Okamoto, K. Komatsu, and A. Hitomi, *Bull. Chem. Soc. Jpn.*, **46**, 3881 (1973).
12) T. Sharpe and J. C. Martin, *J. Am. Chem. Soc.*, **88**, 1815 (1966).
13) R. Breslow and H. W. Chang, *J. Am. Chem. Soc.*, **83**, 2367 (1961).
14) N. C. Deno and A. Schriesheim, *J. Am. Chem. Soc.*, **77**, 3051 (1955).
15) H. E. Simmons and R. D. Smith, *J. Am. Chem. Soc.*, **81**, 4256 (1959).
16) R. T. LaLonde, P. B. Ferrara, and A. D. Debboli, Jr., *J. Org. Chem.*, **37**, 1094 (1972).
17) The method is essentially the same as the one reported by Breslow *et al.* for the preparation of the cation **4** from diphenylcyclopropenone : R. Breslow, T. Eicher, A. Krebs, R. A. Peterson, and J. Posner. *J. Am. Chem. Soc.*, **87**, 1320 (1965).
18) W. C. Perkins and D. H. Wadsworth, *J. Org. Chem.*, **37**, 800 (1972).
19) H. J. Dauben, Jr., L. R. Honnen, and K. M. Harmon, *J. Org. Chem.*, **25**, 1442 (1960).

Functionalization of *trans*-Decalin. II. A Synthesis of *dl*-Isopetasol from *trans*-5-Oxodecalin-8a,2-carbolactone

Sigeru Torii,* Tsutomu Inokuchi, and Kiyoto Kawai

Department of Industrial Chemistry, School of Engineering, Okayama University, Okayama 700

(Received September 21, 1978)

A stereocontrolled synthesis of *dl*-isopetasol (**1a**) from *trans*-5-oxodecalin-8a,2-carbolactone (**2a**) is described. The key intermediate, *trans*-5,5-ethylenedioxy-1β,8aβ-dimethyldecalin-2-one (**7b**) was prepared by reductive methylation of *trans*-5,5-ethylenedioxydecahydrocyclopropa[*d*]naphthalen-2-one (**5**) for introducing the vicinal two methyl groups at C-1 and C-8a carbon atoms. The cyclopropyl ketone **5** was obtained by reduction of the acetal of **2a** followed by (1) tosylation of the primary alcohol, (2) oxidation of the secondary alcohol with Corey's NCS–DMS reagent, and (3) cyclization with *t*-BuOK. Reduction of **5** with lithium in liquid ammonia provides initially the corresponding enolate anion, which can be trapped with methyl iodide to give *trans*-5,5-ethylenedioxy-1α,8aβ-dimethyldecalin-2-one (**7a**), smoothly. Epimerization of **7a** with MeONa in MeOH gave the desired intermediate **7b**. Reduction of **7b** with lithium in liquid ammonia gives the 2α-alcohol **8b**, stereoselectively. The conversion of **8b** into **1a** was carried out as follows: (1) deacetalization of **8b** followed with acetylation, giving *trans*-6α-acetoxy-4aβ,5β-dimethyldecalin-1-one (**9b**); (2) reduction of **9b** with $NaBH_4$ and subsequent dehydration affording the olefinic acetate **11**; (3) oxidation of **11** with CrO_3–pyridine complex, giving the enone **12**; (4) aldol condensation of **12** with acetone followed by dehydration, isomerization of double bond, and hydrolysis, providing the desired **1a**.

Previous paper from our laboratory has presented a convenient preparative method of *trans*-5-oxodecalin-8a,2-carbolactone (**2a**), provided by iodo–lactonization of *trans*-1-oxo-$\Delta^{6,7}$-octalin-4a-carboxylic acid and subsequent reduction of the carbon–iodine bond with tri-*n*-butyltin hydride.[1] As an extensible use of the intermediate **2a**, we describe here a stereocontrolled synthesis of *dl*-isopetasol (**1a**),[2] an eremophilane type sesquiterpene, isolated from *Petasites officinalis*[2a,b] and *P. japonicus* Maxim,[2c] whose carbon skeleton coincides with that of biologically active phomenone.[3]

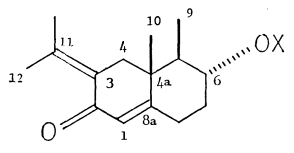

1a: X = H
1b: X = Ac
1c: X = CCH=CMe$_2$ (O)

The key starting material in our attempt is *trans*-5,5-ethylenedioxydecalin-8a,2-carbolactone (**2b**), prepared by acetalization of **2a**. The lactone function of **2b** is expected to be used for the construction of the substituents at C-4a, C-5, and C-6 carbons of **1**. In particular, the stereocontrolled formation of vicinal *cis* two methyl groups at the C-4a and C-5 carbons as well as stereoselective introduction of the α-hydroxyl group at the C-6 carbon is of interest.

Reduction of **2b** with lithium aluminum hydride (LAH) affords the acetal diol **3a** in 85% yield. Selective tosylation[4] of the primary alcohol of **3a** provides smoothly **3b** in 92% yield. The formation of cyclopropyl ketone **5** can be achieved by heating the tosylated ketone **4**, prepared from **3b** by oxidation with NCS–DMS,[5] with potassium *t*-butoxide in *t*-butyl alcohol at 78 °C. In contrast, LAH-induced reaction of either **3b** or **4** affords the corresponding etherated compound **6** as a sole product.

Reductive cleavage of the cyclopropyl ring of **5** with lithium metal in liquid ammonia and subsequent methylation of the carbanion *in situ*[6] gives the desired intermediate **7a** in 76% yield. Epimerization[7] of the C-1 axial methyl of **7a** provides **7b** exclusively after

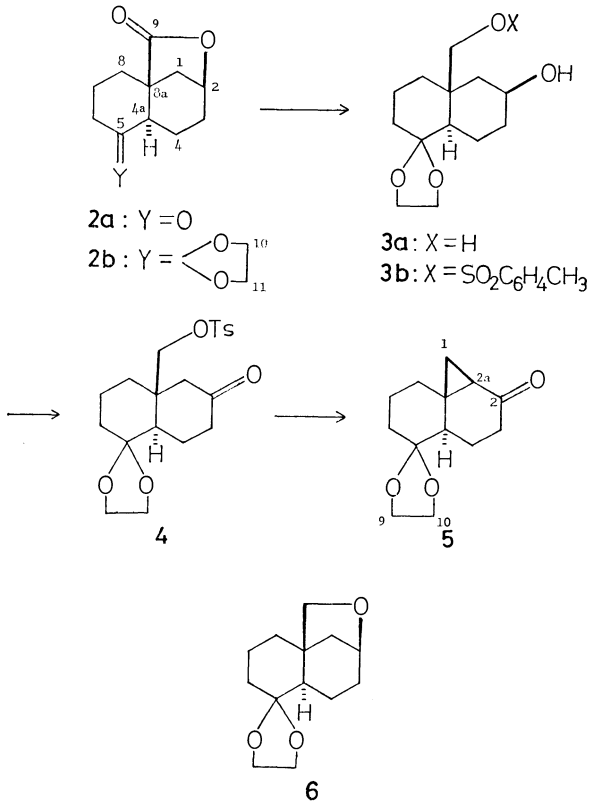

2a: Y = O
2b: Y = ethylenedioxy
3a: X = H
3b: X = $SO_2C_6H_4CH_3$
4
5
6

treatment with sodium methoxide at room temperature for 24 h. The reference compound **7c** can be easily obtained by the reduction of **5**.

The epimerized product **7b** is apparently homogeneous by NMR spectroscopy and is assigned the equatorial stereochemistry at the C-5 methyl group based on the comparison of ^{13}C NMR results of **7a**, **7b**, and **7c** with calculated values from Crews's substituent increment parameter[8] (Table 1). Direct evidence for the assigned structure **7b** is presented by ^{13}C NMR chemical shifts of C-1 and C-8a methyl groups appearing at 5.8 and 7.8 ppm higher fields than those of **7a**, due to steric compression effect.

Table 1. The shielding effect of ^{13}C NMR spectra of the C-8a (C-1) methyl groups of **7a**, **7b**, and **7c**

Compound	^{13}C Chemical shift, ppm		
	Obsereved		Calculated[a]
	C-8a Me	(C-1 Me)	C-8a Me
7a (*anti*-axial)	21.1	(12.9)	20.4
7b (equatorial)	13.3	(7.1)	13.1±0.5
7c	18.7		

a) Based on the Crews's substituent increment parameter as follows: the increment of the chemical shift of methyl (ax) group, being affected by the vicinal methyl groups (equatorial and *anti*-axial) is given as follows: the shielding effect of methyl (ax) with methyl (eq): +5.6±0.5 ppm; the shielding effect of methyl (ax) with *anti*-methyl (ax): −1.7 ppm.

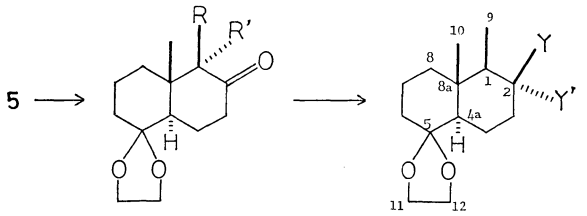

7a: R=H, R'=Me
7b: R=Me, R'=H
7c: R=R'=H

8a: Y=OH, Y'=H
8b: Y=H, Y'=OH

Stereospecific reduction of the carbonyl group of **7b** was achieved as follows. Treatment of **7b** with lithium metal in liquid ammonia with a trace of ethanol affords the thermodynamically stable equatorial alcohol **8a**[9] (92%), whereas the bulky reducing reagent such as lithium tri-*t*-butoxyaluminum hydride[10] gives the corresponding axial alcohol **8b** (98%), selectively.

The ^{13}C NMR spectra of **8** reveal that the marked downfield shifts of the C-8a methyl signals of **8a**, δ_{ax-eq} +1.4 ppm, due to 1,3-*syn*-axial interaction[11] between C-8a methyl and C-2 hydroxyl groups would account for the stereochemistry assigned to the structures of **8a** and **8b**. In addition, the structures of **8** can be rationally interpreted on the basis of 1,3-diaxial downfield shift[12] of ^1H NMR signals due to C-8a methyl protons of **8a** (δ 1.09), comparing to **8b** (δ 0.87).

The conversion of **8b** into the alcohol **10** *via* **9a** and **9b** was carried out in 91% overall yield by deacetalization with perchloric acid and subsequent reduction with sodium borohydride after treatment with acetic anhydride–pyridine. The tentative assignment of the *syn*-axial hydroxyl group of **10** is based on 1,3-diaxial downfield shift of ^1H NMR signals due to C-4a methyl protons at δ 1.01, contrasting to that of **9b** at δ 0.71.

Dehydration of the hydroxyl group of **10** attached to the C-1 carbon *via* the corresponding mesylate affords the olefin **11** in quantitative yield. Allylic oxidation of **11** with a slurry of anhydrous chromium trioxide–pyridine complex (Sarett reagent)[13] gives the promising intermediate **12** in 85% yield. Kinetically controlled aldol condensation[14] of the enone **12** with

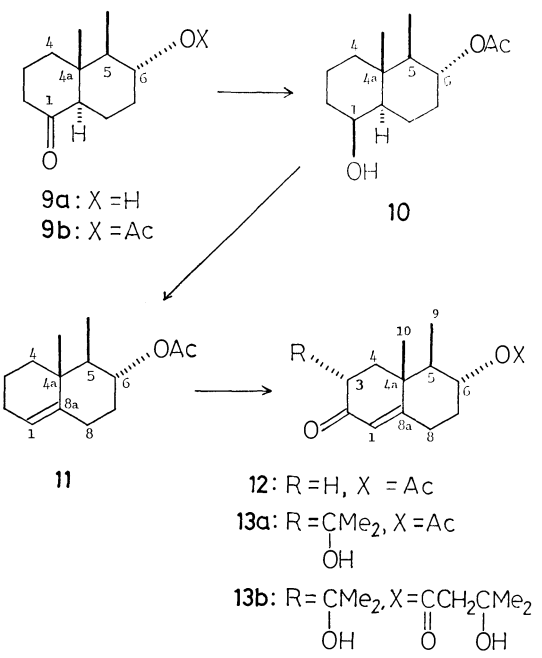

9a: X=H
9b: X=Ac

10

11

12: R=H, X=Ac
13a: R=CMe$_2$(OH), X=Ac
13b: R=CMe$_2$(OH), X=CCH$_2$CMe$_2$(O, OH)

acetone can lead smoothly to **13a** (38%) as well as **13b** (38%). Thermal decomposition of the mesylates of **13** giving the corresponding *exo* and *endo* double bond isomers **14** and subsequent isomerization from isopropenyl group to the corresponding isopropylidene group on treatment with rhodium(III) chloride[15] in ethanol at 110 °C and/or by passing an activated alumina column affords a mixture of **1b** and **1c**, precursors of *dl*-isopetasol, whose hydrolysis gives the desired *dl*-isopetasol (**1a**)[16] (46—51% from **13**).

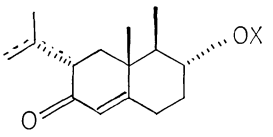

14a: X=Ac
14b: X=CCH=CMe(O)

Experimental

Melting points and boiling points are uncorrected. Column chromatography was carried out using silica gel (100—200 mesh) unless otherwise noted. IR spectra were determined with a JASCO IRA-1 grating spectrometer. ^1H NMR spectra were determined at 60 MHz with a Hitachi Model R-24 or at 100 MHz with a JEOL Model MH-100, and ^{13}C NMR spectra were measured at 25.05 MHz with a JEOL Fourier transform spectrometer, Model FX-100. Samples were dissolved in $CDCl_3$ containing TMS as an internal standard and signals are reported in parts per million (δ) downfield from the internal standard. Elemental analyses were performed in our laboratory.

*trans-5,5-Ethylenedioxydecalin-8a,2-carbolactone (**2b**).* A solution of **2a** (388 mg, 2.0 mmol), ethylene glycol (1.2 g, 19 mmol) and *p*-toluenesulfonic acid (50 mg) in benzene (40 ml) was refluxed for 12 h using a Dean-Stark apparatus

and most of water was removed azeotropically. The mixture was washed with aqueous 5% $NaHCO_3$, dried (Na_2SO_4), and concentrated to give 369 mg (77%) of **2b** as a white solid : mp 128.5 °C (benzene); IR (Nujol) 1777 cm^{-1} (lactone) ; ^1H NMR (60 MHz) δ 0.90—2.55 (m, 13, CH_2, CH), 3.85—3.91 (m, 4, CH_2O), 4.60 (t, 1, J=5 Hz, CH-O) ; ^{13}C NMR δ 17.6 (t), 19.3 (t), 27.9 (t), 30.9 (t, C-8), 35.0 (t, C-6), 45.0 (s, C-8a), 45.6 (t, C-1), 48.2 (d, C-4a), 64.6, 66.1 (t, C-10, C-11), 74.8 (d, C-2), 108.6 (s, C-5), 178.2 (s, C-9). Found : C, 65.71; H, 7.78%. Calcd for $C_{13}H_{18}O_4$: C, 65.53; H, 7.61%.

trans-*5,5-Ethylenedioxy-8aβ-(hydroxymethyl)decalin-2β-ol (**3a**)*. To a stirred suspension of $LiAlH_4$ (230 mg, 6.1 mmol) in dry ether (10 ml) was added dropwise a solution of **2b** (720 mg, 3.0 mmol) in THF (5 ml) with cooling. After being stirred for 1 h at room temperature, the mixture was quenched with AcOEt. After workup in the usual manner, there was obtained 620 mg (85%) of **3a** as a white solid : mp 112.5—114.0 °C (hexane–benzene, 1:1); IR (Nujol) 3300 cm^{-1} (OH); ^1H NMR (60 MHz) δ 0.80—2.15 (m, 13, CH_2, CH), 3.12 (s, 2, OH), 3.87 (AB_q, 2, J=10 Hz, CH_2O), 3.65—4.07 (m, 5, CH_2O, CH-O); ^{13}C NMR δ 15.1 (t), 19.2 (t), 33.5 (t), 35.7 (t), 36.0 (t), 39.0 (s, C-8a), 43.5 (t, C-1), 51.8 (d, C-4a), 64.4, 64.7, 65.7 (t, C-9, C-10, C-11), 66.1 (d, C-2), 109.9 (s, C-5). Found: C, 64.40; H, 9.33%. Calcd for $C_{13}H_{22}O_4$: C, 64.44; H, 9.15%.

trans-*5,5-Ethylenedioxy-8aβ-(*p*-tolylsulfonyloxymethyl)decalin-2β-ol (**3b**)*. To a cold solution of **3a** (242 mg, 1.0 mmol) in pyridine (13 ml) was added *p*-toluenesulfonyl chloride (250 mg, 1.3 mmol) with stirring. The mixture was stirred for 36 h at 5 °C, taken up in AcOEt, and washed with cold aqueous 5% $NaHCO_3$. The organic phase was washed with aqueous 2% $NaHCO_3$, dried (Na_2SO_4), and rotoevaporated at 30 °C. The residue was chromatographed (hexane–AcOEt, 3 : 1) to give 364 mg (92%) of **3b** as an oil, slowly crystallized on standing: mp 97.0—98.0 °C (dec, benzene–hexane, 1 : 1); IR (Nujol) 3550 (OH), 1598 cm^{-1} (C=C); ^1H NMR (60 MHz) δ 0.85—2.35 (m, 13, CH_2, CH), 1.68 (s, 1, OH), 2.43 (s, 3, CH_3), 3.84 (broad complex 4, CH_2O), 4.06 (br s, 1, CH-O), 4.67 (AB_q, 2, J=10 Hz, CH_2O), 7.26 (d, 2, J=8 Hz, HC=C), 7.75 (d, 2, J=8 Hz, HC=C); ^{13}C NMR δ 14.4 (t), 18.1 (t), 21.6 (q, aromatic C-Me), 32.6 (t), 34.5(t, C-8), 35.6 (t, C-6), 38.4 (s, C-8a), 41.0 (t, C-1), 52.1 (d, C-4a), 64.6, 65.5 (t, C-10, C-11), 66.4 (d, C-2), 71.7 (t, C-9), 109.2 (s, C-5), 127.7 (d, 2C), 129.6 (d, 2C), 133.3 (s), 144.3 (s). Found: C, 60.58; H, 7.22%. Calcd for $C_{20}H_{28}O_6S$: C, 60.59; H, 7.12%.

trans-*5,5-Ethylenedioxy-8a-(*p*-tolylsulfonyloxymethyl)decalin-2-one (**4**)*. To a stirred suspension of *N*-chlorosuccinimide (843 mg, 6.3 mmol) and Me_2S (429 mg, 1.26 mmol) in toluene (10 ml) was added a solution of **3b** (500 mg, 1.26 mmol) in CH_2Cl_2 (7 ml) in a 15 min at −25 °C. After being stirred for 12 h at −25 °C and for 1.5 h at 5 °C, the mixture was treated with Et_3N (708 mg, 7.0 mmol), then taken up in CH_2Cl_2, washed with water, dried (Na_2SO_4), and rotoevaporated. The residue was chromatographed (hexane–AcOEt, 3 : 1) to give 415 mg (84%) of **4** as an oil, slowly crystallized on standing : mp 132.0—133.0 °C (hexane–benzene); IR (Nujol) 1708 (C=O), 1595 cm^{-1} (C=C); ^1H NMR (60 MHz) δ 1.30—2.70 (m, 13, CH_2, CH), 2.45 (s, 3, CH_3), 3.88 (br s, 4, CH_2O), 4.15 (AB_q, 2, J=10 Hz, CH_2O), 7.28 (d, 2, J=8 Hz, HC=C), 7.72 (d, 2, J=8 Hz, HC=C); ^{13}C NMR δ 18.8 (t), 19.8 (t), 21.7 (q, aromatic C-Me), 34.5 (t, C-8), 35.4 (t, C-6), 40.4 (t, C-3), 42.2 (s, C-8a), 49.9 (d, C-4a), 51.0 (t, C-1), 64.6, 65.6 (t, C-10, C-11), 69.5 (t, C-9), 109.0 (s, C-5), 127.9 (d, 2C), 129.8 (d, 2C), 132.8 (s), 144.6 (s), 208.8 (s, C-2). Found: C, 61.01; H, 6.90%. Calcd for $C_{20}H_{26}O_6S$: C, 60.90; H, 6.64%.

trans-*5,5-Ethylenedioxydecahydrocyclopropa*[d]*naphthalen-2-one (**5**)*. To a suspension of **4** (86 mg, 0.22 mmol) in *t*-BuOH (3 ml) was added a solution of *t*-BuOK (286.7 mg, 2.56 mmol) in *t*-BuOH (7 ml). The stirred mixture was heated at 75—78 °C for 20 min and then allowed to cool to room temperature. The mixture was poured into cold water (*ca.* 100 ml) and extracted with benzene–ether. The extracts were worked up in the usual manner to give 38 mg (79%) of **5** : bp 99.0—102.0 °C/0.003 Torr (Kugelrohr); IR (neat) 1690 (shoulder), 1682 cm^{-1} (C=O); ^1H NMR (60 MHz) δ 0.74—1.04 (m, 2, CH_2), 1.25—2.35 (m, 12, CH_2, CH), 3.92 (br s, 4, CH_2O), ^{13}C NMR δ 15.9 (t), 16.0 (t), 22.3 (t), 28.7 (s, C-8a), 32.1 (d, C-2a), 35.4 (t), 35.6 (t), 36.0 (t), 42.9 (d, C-4a), 64.9, 65.3 (t, C-9, C-10), 109.7 (s, C-5), 208.4 (s, C-2). Found: C, 70.19; H, 8.12%. Calcd for $C_{13}H_{18}O_3$: C, 70.24; H, 8.16%.

4,4-Ethylenedioxy-9-oxatricyclo[*8.2.1.0*^{5,11}]*dodecane (**6**)*. To a refluxing suspension of $LiAlH_4$ (50 mg, 1.32 mmol) in THF (3 ml) was added a solution of **3b** (32 mg, 0.08 mmol) in THF (1 ml) and stirring was continued for 3 h. After being cooled, the mixture was quenched with AcOEt and aqueous 5% $NaHCO_3$ and the organic layer was decanted. Removal of the solvent and following chromatography (hexane–AcOEt, 4 : 1) gave 14 mg (77%) of **6** as a white solid : mp 86.5—87.5 °C; IR (Nujol) 1143, 1090, 1041, 1005, 886 cm^{-1}; ^1H NMR (100 MHz) δ 1.12—1.90 (m, 13, CH_2, CH), 3.86 (AB_q, 2, J=8 Hz, CH_2O), 3.76—4.02 (m, 4, CH_2O), 4.24 (t, 1, J=5 Hz, CH-O). Found: C, 69.71; H, 9.21%. Calcd for $C_{13}H_{20}O_3$: C, 69.61; H, 8.99%.

Similarly, **6** was obtained in 71% yield by the reaction of **4** (37 mg, 0.094 mmol) and $LiAlH_4$ (70 mg, 1.84 mmol) in THF (3 ml) at reflux for 5 h.

trans-*5,5-Ethylenedioxy-1α,8aβ-dimethyldecalin-2-one (**7a**)*. A solution of **5** (265 mg, 1.19 mmol) and *t*-BuOH (88 mg, 1.19 mmol) in DME (5 ml) was added to a blue solution of lithium (40 mg, 5.7 mmol) in liquid NH_3 (*ca.* 40 ml). After being stirred for 30 min at −70 °C and for 10 min at −33 °C, the blue solution was quenched with an excess amount of MeI (0.75 ml, 12.1 mmol) and allowed to stand at room temperature in order to dispel most of liquid NH_3. To the residue, DME (5 ml) and HMPA (1 ml) was added and the mixture was stirred for 1 h, washed with a cold aqueous NH_4Cl, and taken up in ether–benzene. The organic phase was washed with aqueous 5% $NaHCO_3$, dried (Na_2SO_4), and concentrated. The residue was chromatographed (hexane–ether, 4 : 1) to give 216 mg (76%) of **7a** as a white solid: mp 47.5—48.5 °C; IR (Nujol) 1698 cm^{-1} (C=O); ^1H NMR (60 MHz) δ 0.98 (s, 3, CH_3), 1.09 (d, 3, J=7.5 Hz, CH_3), 0.80—2.55 (m, 12, CH_2, CH), 3.80—3.96 (m, 4, CH_2O); ^{13}C NMR δ 12.9 (q, C-9), 19.1 (t, C-7), 20.6 (t, C-6), 21.1 (q, C-10), 35.1 (t, C-4), 35.7 (t, C-8), 36.9 (t, C-3), 39.6 (s, C-8a), 42.9 (d, C-4a), 57.1 (d, C-1), 64.1, 65.5 (t, C-11, C-12), 110.3 (s, C-5), 215.8 (s, C-2). Found : C, 70.56; H, 9.35%. Calcd for $C_{14}H_{22}O_3$: C, 70.56; H, 9.30%.

trans-*5,5-Ethylenedioxy-1β,8aβ-dimethyldecalin-2-one (**7b**)*. A solution of **7a** (280 mg, 0.85 mmol) and MeONa (658.8 mg, 12.2 mmol) in MeOH (12 ml) was stirred for 24 h at room temperature. The mixture was poured into cold water and extracted with ether–benzene. The organic phase was worked up to give 269 mg (96%) of **7b** as a white solid : mp 41.0—42.0 °C; IR (Nujol) 1708 cm^{-1}; ^1H NMR (60 MHz) δ 0.81 (s, 3, CH_3), 0.89 (d, 3, J=7.0 Hz, CH_3), 0.90—2.50 (m, 12, CH_2, CH), 3.87—4.07 (m, 4, CH_2O); ^{13}C NMR δ 7.1

(q, C-9), 13.3 (q, C-10), 19.6 (t, C-7), 21.1 (t, C-6), 35.3 (t, C-4), 38.0 (t, C-3), 40.9 (t, C-8), 42.2 (s, C-8a), 51.7 (d, C-4a), 56.7 (d, C-1), 64.1, 65.5 (t, C-11, C-12), 109.8 (s, C-5), 212.3 (s, C-2). Found : C, 70.37; H, 9.38%. Calcd for $C_{14}H_{22}O_3$: C, 70.56; H, 9.30%.

trans-*5,5-Ethylenedioxy-8a-methyldecalin-2-one (**7c**)*. To a stirred solution of **5** (30 mg, 0.135 mmol) in *t*-BuOH (10 mg, 0.135 mmol), ether (4 ml), and liquid NH_3 was added a piece of lithium (14 mg, 2.0 mmol). After being stirred for 30 min at −33 °C, the solution was cooled to −70 °C and quenched all at once with NH_4Cl (500 mg). The mixture was worked up in the usual manner to give 28 mg (92%) of **7c** as a white solid : mp 66.0—67.5 °C; IR (Nujol) 1715 cm^{-1} (C=O); ^1H NMR (60 MHz) δ 1.00 (s, 3, CH_3), 1.10—2.50 (m, 13, CH_2, CH), 3.78—3.93 (m, 4, CH_2O); ^{13}C NMR δ 18.7 (q, C-9), 19.5 (t, C-7), 20.7 (t, C-6), 35.7 (t, C-4), 39.0 (s, C-8a), 40.6 (t, C-8), 41.1 (t, C-3), 50.1 (d, C-4a), 57.5 (t, C-1), 64.2, 65.5 (t, C-10, C-11), 109.7 (s, C-5), 211.2 (s, C-2). Found : C, 69.53 ; H, 9.03%. Calcd for $C_{13}H_{20}O_3$: C, 69.61 ; H, 8.99%.

trans-*5,5-Ethylenedioxy-1β,8aβ-dimethyldecalin-2β-ol (**8a**)*. To a stirred slurry of $LiAl(t\text{-}BuO)_3H$ (610 mg, 2.4 mmol) in THF (3 ml) was added a solution of **7b** (115 mg, 0.48 mmol) in THF (7 ml) at 0—5 °C under N_2. After being stirred for 12 h at room temperature, the mixture was quenched with cold aqueous 5% $NaHCO_3$ and worked up in the usual manner to give 113 mg (98%) of **8a** as a white solid : mp 82.5—83.5 °C; IR (Nujol) 3340 cm^{-1} (OH); ^1H NMR (60 MHz) δ 0.98 (d, 3, J=7 Hz, CH_3), 1.09 (s, 3, CH_3), 0.80—2.10 (m, 13, CH_2, CH, OH), 3.73 (m, 1, CH-O), 3.75—4.00 (m, 4, CH_2O); ^{13}C NMR δ 11.7 (q, C-9), 14.3 (q, C-10), 15.0 (t), 18.9 (t), 34.2 (t), 35.6 (t), 38.3 (s, C-8a), 38.3 (t, C-8), 47.3 (d, C-4a), 53.6 (d, C-1), 64.0, 65.4 (t, C-11, C-12), 72.2 (d, C-2), 110.2 (s, C-5). Found: C, 70.02; H, 10.10%. Calcd for $C_{14}H_{24}O_3$: C, 69.96; H, 10.07%.

trans-*5,5-Ethylenedioxy-1β,8aβ-dimethyldecalin-2α-ol (**8b**)*. To a blue solution of lithium (8.9 mg, 1.27 mmol) in liquid NH_3 (6 ml) was added a solution of **7b** (30 mg, 0.126 mmol) in EtOH (7.2 μl), ether (3 ml), and dioxane (1 ml). After being stirred for 10 min at −70 °C and for 1 h at −33 °C, the solution was quenched with aqueous saturated NH_4Cl and worked up to give 28 mg (93%) of **8b** as an oil : bp 139.0—142.0 °C/0.1 Torr (Kugelrohr); IR (neat) 3360 cm^{-1} (OH); ^1H NMR (60 MHz) δ 0.87 (s, 3, CH_3), 0.95(d, 3, J=2 Hz, CH_3), 0.90—2.30 (m, 12, CH_2, CH), 2.25 (br, s, 1, OH), 3.38 (m, 1, CH-O), 3.75—3.98 (m, 4, CH_2O); ^{13}C NMR δ 10.3 (q, C-9), 12.9 (q, C-10), 18.8 (t), 19.2(t), 35.4(t), 35.7 (t), 38.1 (t, C-8), 38.8 (s, C-8a), 51.3 (d, C-4a), 52.5 (d, C-1), 64.0, 65.4 (t, C-11, C-12), 72.0 (d, C-2), 110.3 (s, C-5). Found : C, 70.12 ; H, 10.13%. Calcd for $C_{14}H_{24}O_3$: C, 69.96; H, 10.07%.

trans-*6α-Hydroxy-4aβ,5β-dimethyldecalin-1-one (**9a**)*. A cold solution (0—5 °C) of **8b** (24 mg, 0.1 mmol) and 3 drops of 70% $HClO_4$ in THF (2 ml) and water (1 ml) was stirred for 12 h. The organic layer was taken up in benzene and washed with brine, dried (Na_2SO_4), and concentrated to give 18 mg (92%) of **9a** as an oil : bp 77.0—78.0 °C/0.007 Torr (Kugelrohr); IR (neat) 3360 (OH), 1700 cm^{-1} (C=O) ; ^1H NMR (60 MHz) δ 0.66 (s, 3, CH_3), 0.97 (d, 3, J=6 Hz, CH_3), 0.90—2.45 (m, 12, CH_2, CH), 2.05 (s, 1, OH), 3.36 (d, d, d, 1, J=10, 5, 5 Hz, CH-O); ^{13}C NMR δ 11.0 (q, C-9), 13.3 (q, C-10), 19.6 (t), 22.1 (t), 34.5 (t), 37.5 (t, C-4), 41.0 (t, C-2), 43.4 (s, C-4a), 50.1 (d, C-5), 58.1 (d, C-8a), 71.5 (d, C-6), 212.6 (s, C-1). Found : C, 73.65 ; H, 10.25%. Calcd for $C_{12}H_{20}O_2$: C, 73.43 ; H, 10.27%.

trans-*6α-Acetoxy-4aβ,5β-dimethyldecalin-1-one (**9b**)*. A cold solution (5 °C) of **9a** (70 mg, 0.357 mmol) in pyridine (1.2 ml) and Ac_2O (0.5 ml, 5.29 mmol) was stirred for 12 h at room temperature. The mixture was poured into cold water and extracted with ether–benzene. The extracts were worked up to give 85 mg (100%) of **9b** as a white solid : mp 88.0—89.5 °C; IR (Nujol) 1724 (ester C=O), 1709 cm^{-1} (C=O); ^1H NMR (60 MHz) δ 0.71 (s, 3, CH_3), 0.85 (d, 3, J=7 Hz, CH_3), 1.00—2.45 (m, 12, CH_2, CH), 2.02 (s, 3, $COCH_3$), 4.63 (d, d, d, 1, J=10, 5, 5 Hz, CH-O); ^{13}C NMR δ 10.9 (q, C-9), 13.3 (q, C-10), 19.4 (t), 21.3 (q, acetyl CH_3), 22.1 (t), 30.7 (t), 37.5 (t, C-4), 40.9 (t, C-2), 43.4 (s, C-4a), 47.0 (d, C-5), 57.8 (d, C-8a), 74.2 (d, C-6), 170.6 (s, acetyl C=O), 211.9 (s, C-1). Found: C, 70.56; H, 9.28%. Calcd for $C_{14}H_{22}O_3$: C, 70.56; H, 9.30%.

trans-*6α-Acetoxy-4aβ,5β-dimethyldecalin-1β-ol (**10**)*. A solution of **9b** (37 mg, 0.155 mmol) in MeOH (1.5 ml) was treated with a solution of $NaBH_4$ (19 mg, 0.5 mmol) in water (0.3 ml) at 0—5 °C for 30 min. The mixture was quenched with cold AcOH (0.15 ml) and water (1.35 ml), and extracted with ether–benzene. The extracts were worked up to give 37 mg (99%) of **10** as a white solid : mp 87.5—89.0 °C; IR (Nujol) 3540 (OH), 1715 cm^{-1} (ester C=O); ^1H NMR (60 MHz) δ 0.75 (d, 3, J=6 Hz, CH_3), 1.01 (s, 3, CH_3), 0.80—2.42 (m, 12, CH_2, CH), 1.69 (s, 1, OH), 2.02 (s, 3, $COCH_3$), 3.88 (br s, 1, CH-O), 3.75 (d, d, d, 1, J=10, 5, 5 Hz, CHO); ^{13}C NMR δ 9.7 (q, C-9), 14.0 (q, C-10), 16.3 (t), 21.3 (q, acetyl CH_3), 24.6 (t), 32.3 (t), 33.8 (t), 37.0 (s, C-4a), 38.5 (t, C-4), 48.4, 48.8 (d, C-5, C-8a), 71.5 (d, C-1), 75.1 (d, C-6), 170.8 (s, acetyl C=O). Found: C, 70.02; H, 10.07%. Calcd for $C_{14}H_{24}O_3$: C, 69.96; H, 10.07%.

*6α-Acetoxy-4aβ,5β-dimethyl-$\Delta^{1,8a}$-octalin (**11**)*. To a stirred, cold solution (0—5 °C) of **10** (28 mg, 0.117 mmol) in pyridine (0.5 ml) was added methanesulfonyl chloride (148 mg, 1.29 mmol). After being stirred for 30 min at 0—5 °C and for 30 min at 40—50 °C, the mixture was quenched with water and extracted with ether–benzene. The organic phase was washed with cold aqueous 5% tartaric acid, aqueous 5% $NaHCO_3$, and brine, dried (Na_2SO_4), and concentrated. The residue was chromatographed (hexane–ether, 5 : 1) to give 26 mg (100%) of **11** as an oil : bp 99.0—101.0 °C/0.1 Torr (Kugelrohr); IR (neat) 1735 cm^{-1} (ester C=O); ^1H NMR (60 MHz) δ 0.86 (d, 3, J= 6 Hz, CH_3), 0.99 (s, 3, CH_3), 1.06—2.45 (m, 11, CH_2, CH), 2.03 (s, 3, $COCH_3$), 4.80 (d, d, d, 1, J=10, 5, 5 Hz, CH-O), 5.39 (t, 1, J=3 Hz, HC=C); ^{13}C NMR δ 10.8 (q, C-9), 18.7 (t), 19.2 (q, C-10), 21.3 (q, acetyl CH_3), 25.6 (t), 30.7 (t), 33.1 (t), 37.5 (t, C-4), 37.8 (s, C-4a), 47.3 (d, C-5). 75.1 (d, C-6), 120.6 (d, C-1), 142.1 (s, C-8a), 170.8 (s, acetyl C=O). Found: C, 75.69; H, 10.01%. Calcd for $C_{14}H_{22}O_2$: C, 75.63; H, 9.97%.

*6α-Acetoxy-4aβ,5β-dimethyl-$\Delta^{1,8a}$-octalin-2-one (**12**)*. To a solution of **11** (22 mg, 0.1 mmol) in dry CH_2Cl_2 (5 ml) was added in one portion a slurry of anhydrous CrO_3-(pyridine)$_2$ complex (800 mg, 31 mmol) in CH_2Cl_2 (5 ml) under argon. After being stirred for 24 h at room temperature, the mixture was filtered off and the solid in the flask was washed with ether. The combined filtrate and washings were washed with aqueous 5% $NaHCO_3$, cold aqueous 5% HCl, and brine, dried (Na_2SO_4), and concentrated. The residue was chromatographed (hexane–ether, 4 : 1) to give 20 mg (85%) of **12** as a solid : mp 69.0—70.5 °C; IR (Nujol) 1731 (ester C=O), 1676 (C=O), 1618 cm^{-1} (C=C); ^1H NMR (60 MHz) δ 0.82 (d, 3, J=6.5 Hz, CH_3), 1.15 (s, 3, CH_3), 1.00—2.65 (m, 9, CH_2, CH), 2.04 (s, 3, $COCH_3$), 4.71 (d, d, d, 1, J=10, 5, 5 Hz, CH-O), 5.72 (br s, 1, HC=C);

^{13}C NMR δ 10.5 (q, C-9), 17.1 (q, C-10), 21.2 (q, acetyl CH_3), 30.9 (t, C-8), 31.5 (t, C-7), 33.3 (t, C-4), 35.7 (t, C-3), 39.3 (s, C-4a), 46.7 (d, C-5), 73.4 (d, C-6), 124.6 (d, C-1), 167.6 (s, C-8a), 170.6 (s, acetyl C=O), 198.9 (s, C-2). Found: C, 71.06; H, 8.60%. Calcd for $C_{14}H_{20}O_3$: C, 71.16; H, 8.53%.

6α-Acetoxy-3α-(1-hydroxy-1-methylethyl)-4aβ,5β-dimethyl-$\Delta^{1,8a}$*-octalin-2-one (**13a**)* and *3α-(1-Hydroxy-1-methylethyl)-6α-(3-hydroxy-3-methylbutyryloxy)-4aβ,5β-dimethyl-*$\Delta^{1,8a}$*-octalin-2-one (**13b**).* To a stirred solution of *i*-Pr_2NLi (246.1 mg, 2.3 mmol) in THF (4 ml) was added dropwise a solution of **12** (115 mg, 0.49 mmol) in THF (4 ml) at −78 °C under argon. After being stirred for 1 h at −78 °C, $ZnCl_2$[17] (133 mg, 0.98 mmol) in ether (5 ml) was added and stirred for 10 min and to this mixture acetone (300 mg, 5.2 mmol) was added. The mixture was quenched with cold aqueous 5% tartaric acid and extracted with ether–benzene. The organic phase was worked up in the usual manner and the crude product was chromatographed (hexane–AcOEt, 4 : 1) to give 55 mg (38%) of **13a** and 65 mg (38%) of **13b** as an oil. Physical constants along with elemental analyses of **13a** and **13b** are as follows : **13a**; IR (neat) 3440 (OH), 3020, 1735 (ester C=O), 1650 cm^{-1} (C=O); ^1H NMR (60 MHz) δ 0.94 (d, 3, J=7 Hz, CH_3), 1.19 (s, 3, CH_3), 1.22 (s, 6, CH_3), 1.10—2.70 (m, 8, CH_2, CH), 4.83 (d, d, d, 1, J=10, 5, 5 Hz, CH-O), 5.01 (br s, 1, OH), 5.73 (br s, 1, HC=C); ^{13}C NMR δ 10.5 (q, C-9), 17.1 (q, C-10), 21.2 (q, acetyl CH_3), 24.6 (q, C-13), 28.3 (q, C-12), 30.5 (t, C-8), 31.3 (t, C-7), 38.7 (t, C-4), 40.0 (s, C-4a), 47.1 (d, C-5), 50.6 (d, C-3), 72.4 (s, C-11), 73.1 (d, C-6), 125.1 (d, C-1), 168.2 (s, C-8a), 170.6 (s, acetyl C=O), 202.8 (s, C-2). Found: C, 69.44; H, 8.92%. Calcd for $C_{17}H_{26}O_4$: C, 69.36; H, 8.90%.

13b: IR (neat) 3440 (OH), 3020, 1720 (ester C=O), 1660 cm^{-1} (C=O); ^1H NMR (60 MHz) δ 0.85 (d, 3, J= 7 Hz, CH_3), 1.00 (s, 3, CH_3), 1.21 (s, 6, CH_3), 1.20—2.75 (m, 8, CH_2, CH), 1.29 (s, 6, CH_3), 2.02 (s, 2, CH_2), 4.93 (d, d, d, 1, J=10, 5, 5 Hz, CH-O), 4.96 (br s, 1, OH), 5.31 (br s, 1, OH), 5.73 (br s, 1, HC=C). Found: C, 68.31; H, 9.11%. Calcd for $C_{20}H_{32}O_5$: C, 68.15; H, 9.15%.

Independently, the compound **13a** was prepared as follows: To a stirred solution of lithium *N*-isopropylcyclohexylamide (73.6 mg, 0.5 mmol) in THF (3 ml) was added dropwise a solution of **12** (24 mg, 0.1 mmol) in THF (3 ml) at −78 °C. After being stirred for 2.5 h at −78 °C, $ZnCl_2$ (13.6 mg, 0.1 mmol) in ether (3 ml) was added and stirred for 10 min and to this mixture acetone (0.1 ml, 13.6 mmol) was added. The mixture was quenched with cold aqueous 5% tartaric acid and worked up to give 20 mg (68%) of **13a**.

6α-Acetoxy-3-isopropylidene-4aβ,5β-dimethyl-$\Delta^{1,8a}$*-octalin-2-one (**1b**).* To a solution of **13a** (21 mg, 0.071 mmol) in pyridine (1.5 ml) was added MsCl (29.6 mg, 0.26 mmol) at 0 °C under N_2. After being stirred for 1 h at 20 °C and 2 h at 40—42 °C, the mixture was quenched with cold water and taken up in ether–benzene. The organic layer was washed with brine, dried (Na_2SO_4), and concentrated. The residue was chromatographed (hexane–AcOEt, 4 : 1) to give 3 mg of **12** and 13 mg (66%) of an *exo* and *endo* double bond mixture **14a**: IR (neat) 3070, 1735 (ester C=O), 1675 (C=O), 1630 cm^{-1} (C=C); ^1H NMR (60 MHz) δ 4.80, 4.96 (br s, H_2C=C). Without further purification, **14a** was passed through an activated alumina 300 (Nakarai Chemicals) column (hexane–AcOEt, 3 : 1) to give **1b** in a quantitative yield as a white solid : mp 78.0—79.0 °C (lit,[18] 86.0—87.0 °C); IR (Nujol) 1735 (ester C=O), 1665 (C=O), 1635 (C=C), 1242, 1030 cm^{-1}; ^1H NMR (100 MHz) δ 0.99 (d, 3, J=6 Hz, CH_3), 1.04 (s, 3, CH_3), 1.10—2.60 (m, 6, CH_2, CH), 1.85 (s, 3, CH_3), 2.07 (s, 3, $COCH_3$), 2.09 (s, 3, CH_3), 2.94 (d, 1, J=14 Hz, C=CCH), 4.88 (d, d, d, 1, J=10, 5, 5 Hz, CH-O), 5.82 (br s, 1, HC=C); ^{13}C NMR δ 10.7 (q, C-9), 17.1 (q, C-10), 21.2 (q, acetyl CH_3), 22.1 (q, C-12), 22.6 (q, C-13), 30.1 (t, C-8), 31.5 (t, C-7), 41.1 (t, C-4), 42.2 (s, C-4a), 46.0 (d, C-5), 73.6 (d, C-6), 126.7 (d, C-1), 127.0 (s, C-3), 143.4 (s, C-11), 165.0 (s, C-8a), 170.7 (s, acetyl C=O), 191.6 (s, C-2).

6α-(3,3-Dimethylacryloyloxy)-3-isopropylidene-4aβ,5β-dimethyl-$\Delta^{1,8a}$*-octalin-2-one (**1c**)* was obtained in 72% yield by dehydration with MsCl and isomerization with activated alumina 300 column of **13b** : bp 129.0—131.0 °C/0.01 Torr (Kugelrohr); IR (neat) 3020, 1712 (ester C=O), 1665 (C=O), 1630 (C=C), 1620 cm^{-1} (C=C); ^1H NMR (100 MHz) δ 0.98 (d, 3, J=7 Hz, CH_3), 1.04 (s, 3, CH_3), 1.10—2.59 (m, 6, CH_2, CH), 1.85, 1.91, 2.10, 2.18 (s, 12, CH_3), 2.92 (d, 1, J=13 Hz, C=CCH), 4.86 (d, d, d, 1, J=10, 5, 5 Hz, CH-O), 5.65 (complex s, 1, HC=C), 5.75 (d, 1, J=1 Hz, HC=C); ^{13}C NMR δ 10.7 (q, C-9), 17.2 (q, C-10), 20.3 (q, 3,3-dimethylacryl γ-CH_3), 22.1 (q, C-13), 22.6 (q, C-12), 27.5 (q, 3,3-dimethylacryl γ-CH_3), 30.2 (t, C-8), 31.8 (t, C-7), 41.2 (t, C-4), 42.2 (s, C-4a), 46.2 (d, C-5), 72.4 (d, C-6), 116.0 (d, acryl α-CH), 126.6 (d, C-1), 127.1 (s, C-3), 143.2 (s, C-11), 157.2 (s, acryl β-C), 165.3 (s, C-8a), 166.3 (s, acryl C=O), 191.6 (s, C-2). Found: C, 75.93; H, 8.97%. Calcd for $C_{20}H_{28}O_3$: C, 75.91; H, 8.92%.

*Conversion of **14a** into **1b** with $RhCl_3 \cdot 2H_2O$.* A solution of **14a** (19 mg, 0.069 mmol) and $RhCl_3 \cdot 2H_2O$ (2 mg, 0.008 mmol) in EtOH (2 ml) was heated for 12 h at 110 °C in a sealed tube. After being cooled, the mixture was filtered and the filtrate was concentrated. The residue was chromatographed (hexane–AcOEt, 4 : 1) to give 14 mg (84%) of **1b** as a white solid.

Similarly, **1c** was obtained by the reaction of **14b** and $RhCl_3 \cdot 2H_2O$ in EtOH at 110 °C for 12 h in 82% yield.

*dl-Isopetasol (**1a**).* To a solution of **1b** (21 mg, 0.076 mmol) in MeOH (2 ml) was added a solution of KOH (95 mg, 17 mmol) in H_2O (0.3 ml) at 5 °C. The mixture was stirred for 2 h at 10 °C and taken up in ether–benzene. The extract was worked up in the usual manner to give 13 mg (73%) of **1a** as white solid : mp 104.0—105.5 °C (lit,[2c] 124.0—125.0 °C, lit,[2d] 105.0—106.0 °C); IR (Nujol) 3390 (OH), 1652 (C=O), 1628 (C=C), 1608 (C=C), 1380, 1298, 1230, 1217, 1048, 890, 858 cm^{-1}; ^1H NMR (100 MHz) δ 0.99 (s, 3, CH_3), 1.12 (d, 3, J=6.5 Hz, CH_3), 1.10—1.67 (m, 3, CH_2, CH), 1.79 (s, 1, OH), 1.87 (s, 3, C=CCH_3), 2.03—2.50 (m, 3, CH_2), 2.11 (s, 3, C=CCH_3), 2.93 (d, 1, J=14 Hz, C=CCH), 3.60 (d, d, d, 1, J=10, 5, 5 Hz, CH-O), 5.82 (br s, 1, HC=C); ^{13}C NMR δ 10.8 (q, C-9), 17.3 (q, C-10), 22.1 (q, C-13), 22.6 (q, C-12), 30.5 (t, C-8), 35.3 (t, C-7), 41.2 (t, C-4), 42.0 (s, C-4a), 49.1 (d, C-5), 71.3 (d, C-6), 126.5 (d, C-1), 127.2 (s, C-3), 143.2 (s, C-11), 166.1 (s, C-8a), 191.7 (s, C-2).

Similarly, *dl*-isopetasol (**1a**) was obtained in 71% yield by hydrolysis of **1c** at room temperature for 2 h with KOH in aqueous MeOH. IR and ^1H NMR spectra data were identical with those of an authentic sample.[13]

References

1) S. Torii, T. Kunitomi, and T. Okamoto, *Bull. Chem. Soc. Jpn.*, **47**, 2349 (1974).

2) Isolation and elucidation : (a) A. Aebi and C. Djerassi, *Helv. Chim. Acta*, **42**, 1785 (1959); (b) D. Herbst and C. Djerassi, *J. Am. Chem. Soc.*, **82**, 4337 (1960); (c) K. Naya, I. Takagi, Y. Kawaguchi, Y. Asada, Y. Hirose, and N. Shinoda, *Tetrahedron*, **24**, 5871 (1968); Synthesis; (d) K.

Yamakawa, I. Izuta, H. Oka, and R. Sakaguchi, *Tetrahedron Lett.*, **1974**, 2187.

3) C. Riche, C. Pascard-Billy, M. Devys, A. Gaudemer, M. Barbier, and J.-F. Bousquet, *Tetrahedron Lett.*, **1974**, 2765.

4) W. S. Johnson, J. C. Collins, Jr., R. Pappo, M. B. Rubin, P. J. Kropp, W. F. Johns, J. E. Pike, and W. Bartmann *J. Am. Chem. Soc.*, **85**, 1409 (1963).

5) E. J. Corey and C. U. Kim, *J. Am. Chem. Soc.*, **94**, 7586 (1972).

6) (a) G. Stork, S. Uyeo, T. Wakamatsu, P. Grieco, and J. Labovitz, *J. Am. Chem. Soc.*, **93**, 4945 (1971); (b) P. A. Grieco, Y. Masaki, and D. Boxler, *J. Org. Chem.*, **40**, 2261 (1975); (c) W. G. Dauben and E. J. Deving, *ibid.*, **31**, 3794 (1966).

7) I. Nagakura, S. Maeda, M. Ueno, M. Funamizu, and Y. Kitahara, *Chem. Lett.*, **1975**, 1143.

8) P. Crews and E. Kho-Wiseman, *Tetrahedron Lett.*, **1978**, 2483.

9) J. W. Huffman and J. T. Charles, *J. Am. Chem. Soc.*, **90**, 6486 (1968).

10) D. Taub, R. D. Hoffsommer, C. H. Kuo, H. L. Slates, Z. S. Zelawski, and N. L. Wendler, *Chem. Commun.*, **1970**, 1258.

11) S. H. Grover and J. B. Stothers, *Can. J. Chem.*, **52**, 870 (1974).

12) R. B. Miller and E. S. Behare, *J. Am. Chem. Soc.*, **96**, 8102 (1974).

13) W. D. Dauben, M. Lorber, and D. S. Fullerton, *J. Org. Chem.*, **34**, 3587 (1969).

14) The reaction of the kinetical enolate anion of α,β-enone with methyl iodide : (a) M. Tanabe and D. F. Crowe, *Chem. Commun.*, **1973**, 564; The reaction of the kinetical enolate anion of β-alkoxy-α,β-enones with carbonyl compounds; (b) G. Stork and G. A. Kraus, *J. Am. Chem. Soc.*, **98**, 2351 (1976); (c) S. Torii, T. Okamoto, and S. Kadono, *Chem. Lett.*, **1977**, 495.

15) P. A. Grieco, M. Nishizawa, N. Marinovic, and W. J. Ehmann, *J. Am. Chem. Soc.*, **98**, 7102 (1976).

16) We are gratefull to Professor K. Naya, Kwansei Gakuin University, for providing ^{1}H NMR and IR spectra of natural isopetasol (**1a**).

17) H. O. House, D. S. Crumrine, A. Y. Teranishi, and H. D. Olmstead, *J. Am. Chem. Soc.*, **95**, 3310 (1973).

18) I. Takagi, Y. Tazuke, and K. Naya, *Bull. Chem. Soc. Jpn.*, **50**, 3320 (1977).

Imidazopteridines. II.[1] Synthesis of Imidazo[1,2-*c*]pteridines with a Functional Group at the 6-Position

Takashi SUGIMOTO,* Keiko SHIBATA, and Sadao MATSUURA

Department of Chemistry, College of General Education, Nagoya University, Chikusa-ku, Nagoya 464

(Received September 28, 1978)

Several imidazo[1,2-*c*]pteridines with a functional group such as amino, alkylamino, alkoxyl, or hydroxyl group at the 6-position were synthesized by a nucleophilic replacement of 6-methylthioimidazo[1,2-*c*]pteridine with an appropriate nucleophile. The key intermediate methylthio compound was synthesized by condensation of 4-amino-2-methylthiopteridine with chloroacetaldehyde. Similarly, 4-amino-6,7-dimethyl-2-methylthiopteridine and chloroacetaldehyde gave 2,3-dimethyl-6-methylthioimidazo[1,2-*c*]pteridine, which was also used as a precursor to synthesize several imidazopteridines analogous to above.

In the course of our research programs on tricyclic imidazoazines,[1-4] we previously reported the synthesis of the parent imidazo[1,2-*c*]pteridine and its *C*-alkyl derivatives.[1] These compounds were found to be susceptible to ring-opening reaction into an 2-amino-3-(2-imidazolyl)pyrazine *via* a nucleophilic addition of water at the 6-position. This ring-opening reaction proceeded easily even in the presence of a blocking methyl group[5] at the site of addition. All these results indicated a high reactivity of the ring system toward various nucleophiles at the 6-position. This paper reports the synthesis of some 6-methylthio derivatives of the ring system and their easy derivation into a variety of imidazo[1,2-*c*]pteridines with a functional group at the 6-position.

Condensation of 4-amino-2-methylthiopteridine(**1a**) with chloroacetaldehyde at pH 6—7 gave intensive blue fluorescent 6-methylthioimidazo[1,2-*c*]pteridine-(**2a**) in about 45% yield. When the reaction was carried out at the pH values out of the above range, either higher or lower, the yield of **2a** lowered significantly, probably due to instability of **2a** under such conditions. The structure of the product was confirmed from the elemental analyses, pK_a values, and UV spectra (Table 1) which showed a characteristic bathochromic shift when the molecule was doubly protonated. The ^1H NMR spectrum of **2a** showed two singlets at δ 2.68 for the methyl group and at δ 7.86 for the imidazole ring protons and a pair of doublets at δ 8.82 and 8.92 (J=2 Hz) representing the pyrazine ring protons. Analogous treatments of 4-amino-6,7-dimethyl-2-methylthiopteridine(**1b**) with chloroacetaldehyde furnished 2,3-dimethyl-6-methylthioimidazo[1,2-*c*]-pteridine(**2b**).

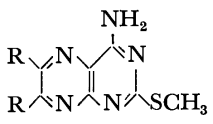

1

a: R=H
b: R=CH_3

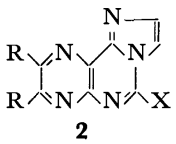

2

a: R=H, X=SCH_3
b: R=CH_3, X=SCH_3
c: R=H, X=NH_2
d: R=CH_3, X=NH_2
e: R=H, X=$NHCH_3$
f: R=CH_3, X=$NHCH_3$
g: R=H, X=$NHCH_2CH_3$
h: R=CH_3, X=$NHCH_2CH_3$
i: R=H, X=$NHCH_2CH_2OH$
j: R=CH_3, X=$NHCH_2CH_2OH$
k: R=H, X=OH
l: R=CH_3, X=OH
m: R=H, X=OCH_2CH_3
n: R=CH_3, X=OCH_2CH_3
o: R=H, X=OCH_3
p: R=CH_3, X=OCH_3

These methylthioimidazopteridines(**2a** and **2b**) were found to be highly reactive toward various nucleophiles and proved to be useful precursors for the synthesis of many other imidazo[1,2-*c*]pteridines with a functional group such as amino, alkylamino, hydroxyl, or alkoxyl group at the 6-position. Aminolysis of **2a**, carried out by heating with ethanolic ammonia, gave 6-aminoimidazo[1,2-*c*]pteridine(**2c**) in a high yield. A similar aminolysis of the methylthio compound (**2a**) with methylamine, ethylamine, or 2-aminoethanol gave 6-methylamino-(**2e**), 6-ethylamino-(**2g**), and 6-(2-hydroxyethylamino)imidazo[1,2-*c*]pteridines (**2i**), respectively. The basic characters of these amino compounds were fairly strenghened compared to that of the precursor (see Table 1) on replacement of the methylthio group by an amino group. All of these aminoimidazopteridines (**2e**, **2g**, and **2i**) were of very similar UV spectra, which also showed a large bathochromic shift on double protonation. Similarly, 2,3-dimethyl-6-methylthioimidazo[1,2-*c*]pteridine (**2b**) gave the 6-amino and 6-alkylamino analogues (**2d**, **2f**, **2h**, and **2j**) on aminolysis with the corresponding amine. Conversion of the methylthio compounds (**2a** and **2b**) into 6-hydroxyimidazo[1,2-*c*]pteridines (**2k** and **2l**) was achieved by heating either in dilute aqueous sodium hydroxide or in dilute hydrochloric acid. On the other hand, 6-ethoxyimidazo[1,2-*c*]pteridine (**2m**) and its 2,3-dimethyl derivative (**2n**) were obtained in a rather unusual way from the corresponding methylthio precursors (**2a** and **2b**) by heating in ethanol with silver oxide, a reagent recently reported useful for an exchange of alkoxyl groups in several heterocyclic systems.[6] Treatment of **2a** with sodium ethoxide or hydrogen chloride in ethanol gave no ethoxy compound (**2m**); the sole product was 6-hydroxyimidazopteridine(**2k**). Similar treatments of **2a** and **2b** with silver oxide in methanol gave the corresponding 6-methoxyimidazo[1,2-*c*]pteridines (**2o** and **2p**).

Experimental

The elemental analyses were carried out at the Analytical Section, Meijo University and at the Analytical Section,

Table 1. The pK_a values and UV spectra of imidazo[1,2-*c*]pteridines

Compound	pK_a	Ionic species[a]	λ_{max} (log ε)[b]	pH of buffer[c]
2a	2.20±0.02	○	232 (4.29), 255 (4.30), *292 (3.76)*, 303 (3.78), 350 (4.09)	4.5
	−2.62±0.02	+	225 (4.21), 253 (4.23), *287 (4.03)*, 294 (4.04), 343 (4.06), *355 (4.00)*	0.0
		++	241 (4.19), *270 (4.03)*, 290 (4.00), 386 (4.09)	−4.0
2b	2.60±0.02	○	232 (4.38), 252 (4.24), *294 (3.81)*, 304 (3.82), 351 (4.19)	5.0
	−1.50±0.02	+	226 (4.25), 248 (4.24), *288 (4.05)*, 296 (4.07), 342 (4.17) 353 (4.14)	0.5
		++	242 (4.28), *265 (3.97)*, *297 (3.98)*, 310 (4.03), 384 (4.20)	−3.5
2c	2.71±0.02	○	228 (4.43), 255 (3.96), *280 (3.58)*, 357 (4.13)	5.0
	−0.96±0.04	+	214 (4.32), 251 (4.11), 273 (3.91), 354 (4.01)	1.0
		++	224 (4.37), 270 (4.01), *337 (3.68)*, 354 (3.82), 392 (4.08)	−3.0
2d	3.19±0.03	○	227 (4.54), 255 (4.00), 282 (3.73), 358 (4.22)	5.5
	−0.18±0.04	+	219 (4.41), 251 (4.17), 275 (3.99), *285 (3.96)*, 356 (4.12)	1.5
		++	224 (4.46), 270 (4.06), *290 (3.91)*, 396 (4.25)	−2.5
2e	2.71±0.02	○	228 (4.44), *260 (3.97)*, *290 (3.72)*, 361 (4.14)	5.0
	−0.81±0.03	+	217 (4.32), *230 (4.20)*, 259 (4.12), 277 (4.07), 364 (4.01)	0.5
		++	228 (4.37), 278 (4.07), *295 (3.92)*, 402 (4.15)	−3.0
2f	3.38±0.02	○	227 (4.55), 257 (4.01), 284 (3.88), 362 (4.23)	5.5
	0.03±0.05	+	220 (4.40), 254 (4.16), 279 (4.15), 286 (4.15), 365 (4.11)	1.5
		++	227 (4.44), *280 (4.10)*, 296 (4.12), 406 (4.28)	−2.5
2g	2.91±0.02	○	228 (4.42), *260 (4.01)*, *285 (3.76)*, 362 (4.13)	5.0
	−0.72±0.03	+	217 (4.30), *230 (4.17)*, 260 (4.13), 279 (4.09), *282 (4.08)*, 367 (4.00)	1.0
		++	228 (4.35), 279 (4.08), *293 (3.97)*, 403 (4.15)	−3.0
2h	3.42±0.02	○	227 (4.51), 257 (3.99), 283 (3.87), *290 (3.86)*, 363 (4.20)	5.5
	0.31±0.05	+	219 (4.39), 255 (4.14), 279 (4.14), 286 (4.15), 367 (4.07)	1.5
		++	226 (4.37), 280 (4.06), 296 (4.08), 407 (4.22)	−3.0
2i	2.76±0.02	○	228 (4.43), *260 (4.00)*, *285 (3.75)*, 361 (4.14)	5.0
	−0.86±0.03	+	217 (4.31), 258 (4.14), 278 (4.08), *283 (4.06)*, 363 (4.01)	1.0
		++	228 (4.37), 277 (4.09), *293 (3.94)*, 399 (4.17)	−3.0
2j	3.32±0.02	○	228 (4.53), 257 (4.01), 284 (3.89), *290 (3.87)*, 362 (4.21)	5.5
	0.00±0.05	+	220 (4.38), 255 (4.16), 279 (4.15), 286 (4.14), 364 (4.10)	1.5
		++	228 (4.43), 279 (4.10), 297 (4.11), 404 (4.27)	−2.5
2k	7.39±0.02	−	223 (4.42), 256 (3.99), *283 (3.58)*, 363 (4.16)	9.5
	2.08±0.05	○	218 (4.16), 240 (3.89), 278 (3.38), 343 (4.21)	5.0
		+	230 (4.02), 262 (3.60), 337 (4.19), 350 (4.15)	−0.5
2l	7.79±0.02	−	222 (4.48), 254 (3.99), *280 (3.71)*, 365 (4.20)	10.0
	2.34±0.02	○	217 (4.29), 241 (3.93), *270 (3.51)*, 346 (4.26)	4.5
		+	209 (4.22), 232 (4.11), 262 (3.75), *270 (3.67)*, 341 (4.25), 354 (4.22)	−0.5
2m	2.28±0.02	○	220 (4.34), *250 (3.82)*, 278 (3.37), 342 (4.01)	4.5
	−2.60±0.02	+	215 (4.14), *235 (3.97)*, 263 (3.56), 330 (4.00), *345 (3.90)*	0.0
		++	218 (4.31), *255 (3.82)*, 354 (4.05)	−4.0
2n	2.85±0.02	○	223 (4.37), *245 (3.87)*, 279 (3.51), 287 (3.51), 344 (4.12)	5.0
	−1.29±0.03	+	213 (4.42), *235 (4.03)*, 265 (3.74), *273 (3.66)*, 333 (4.12) 347 (4.08)	0.5
		++	220 (4.36), 258 (3.86), *277 (3.57)*, *360 (4.16)*, 369 (4.17)	−3.4
2o	2.20±0.04	○	220 (4.19), *247 (3.75)*, 289 (3.27), 343 (3.93)	4.5
	−2.54±0.03	+	215 (4.19), *235 (3.90)*, 263 (3.46), 329 (3.93), *342 (3.83)*	0.0
		++	215 (4.22), *255 (3.71)*, 352 (3.97), *365 (3.92)*	−4.0
2p	2.83±0.02	○	223 (4.24), *243 (3.74)*, 286 (3.38), 343 (3.98)	5.0
	−1.42±0.04	+	213 (4.28), *235 (3.89)*, 265 (3.60), *273 (3.51)*, 332 (3.98) 346 (3.95)	0.5
		++	218 (4.24), 255 (3.74), *277 (3.44)*, 360 (4.05), *365 (4.04)*	−3.5

a) Ionic species in an aqueous buffer of the indicated pH are shown by −(anion), ○(neutral molecule), +(monocation), and ++(dication). b) Wavelength in nm and inflexions or shoulders in italics. c) Negatives figures are H_0 values.

Faculty of Agriculture, Nagoya University. The pK_a values were determined by a spectroscopic method. The UV spectra were measured on a Shimadzu UV-300 spectrophotometer and NMR spectra on a JEOL JNM-NH-100 spectrometer in TFA-*d* with TMS as an internal standard.

*6-Methylthioimidazo[1,2-c]pteridine(**2a**) and Its 2,3-Dimethyl Derivative(**2b**).* 4-Amino-2-mercaptopteridine[7] was methylated with dimethyl sulfate in an alkaline solution to give 4-amino-2-methylthiopteridine(**1a**) in 80% yield, mp 210.5—211.5 °C (from water) (Found: C, 43.69; H, 3.56%. Calcd for $C_7H_7N_5S$: C, 43.50; H, 3.66%). A solution of **1a** (10 g) and chloroacetaldehyde (40 g) in 50% aqueous methanol (1500 ml) was heated at 65 °C for 20 h, during which time the pH of the solution was maintained at pH 6—7 by addition of sodium acetate. The solution was evaporated to dryness under reduced pressure and the residue was extracted with hot acetone (500 ml). The extract, after evaporation to dryness, was chromatographed on a silica gel column (Wako Gel C-100, 4×40 cm) eluted first by a mixture of ethyl acetate and benzene (1 : 4) to remove a small amount of fluorescent impurities. The column was then eluted by a 1 : 1 mixture of the two solvents. The eluate was evaporated to dryness and the residue was crystallized from ethyl acetate to give ivory needles (4.9 g) of **2a**, mp 195—196 °C (Found: C, 49.81; H, 3.11; N, 32.00%. Calcd for $C_9H_7N_5S$: C, 49.75; H, 3.25; N, 32.24%).

By using 4-amino-6,7-dimethyl-2-methylthiopteridine (**1b**)[8] in stead of **1a** in the above reaction, **2b** was obtained in 36% yield as ivory needles, mp 216—216.5 °C (from ethyl acetate)(Found : C, 53.69; H, 4.40; N, 28.46%. Calcd for $C_{11}H_{11}N_5S$: C, 53.85; H, 4.53; N, 28.55%); NMR: three singlets at δ 2.50(3H), 2.56(6H), and 7.70 (2H).

*6-Aminoimidazo[1,2-c]pteridine(**2c**) and Its 2,3-Dimethyl Derivative(**2d**).* A suspension of **2a** (300 mg) in a saturated ethanolic ammonia (50 ml) was heated in a sealed tube at 100 °C for 5 h. After cooling, the solid was collected and crystallized from methanol to give colorless needles (200 mg) of **2c**, mp>300 °C (Found: C, 50.68; H, 2.92; N, 43.93%. Calcd for $C_8H_6N_6 \cdot 0.2\,H_2O$: C, 50.84; H, 3.40; N, 44.29%).

Its 2,3-dimethyl derivative(**2d**) was synthesized from **2b** in a similar way in 70% yield, mp>300 °C (Found: C, 55.78; H, 4.76; N, 39.23%. Calcd for $C_{10}H_{10}N_6$: C, 56.07; H, 4.71; N, 39.23%).

*6-Methylamino- and 6-Ethylaminoimidazo[1,2-c]pteridines (**2e** and **2g**) and Their 2,3-Dimethyl Derivatives(**2f** and **2h**).* A solution of **1a** (500 mg) and methylamine (40% aqueous solution, 10 ml) in ethanol (100 ml) was heated under reflux for 5 h. The solution was evaporated to dryness in vacuo and the residue was fractionated on a Florisil column (3.5×40 cm) eluted gradiently by 0—3% ammonia (2 l). The eluate, after evaporation and crystallization from water, gave ivory needles (280 mg) of **2e**, mp 296—297 °C (Found: C, 53.62; H, 3.96; N, 41.53%. Calcd for $C_9H_8N_6$: C, 53.98; H, 4.04; N, 41.98%).

Heating of **2a** with ethylamine as above, followed by chromatographic separation on a silica gel column eluted by ethanol–ethyl acetate (1 : 9) gave **2g** as colorless needles (75% yield), mp 211—211.5 °C (from acetone)(Found: C, 55.90; H, 4.56; N, 38.84%. Calcd for $C_{10}H_{10}N_6$: C, 56.07; H, 4.71; N, 39.23%).

Similarly, **2b** was treated with methylamine or ethylamine to give, without using chromatography, **2f** (50% yield), mp>300 °C (from ethanol)(Found : C, 57.93; H, 5.29; N, 36.63%. Calcd for $C_{11}H_{12}N_6$: C, 57.87; H, 5.31; N, 36.82%) and **2h** (65% yiled), mp 295—296 °C (from ethanol)(Found: C, 59.69; H, 5.97; N, 34.59%. Calcd for $C_{12}H_{14}N_6$: C, 59.48; H, 5.84; N, 34.69%), respectively.

*6-(2-Hydroxyethylamino)imidazo[1,2-c]pteridine (**2i**) and Its 2,3-Dimethyl Derivative(**2j**).* A solution of **2a** (500 mg) and 2-aminoethanol (2 g) in water (20 ml) was heated under reflux for 5 h. The solution was adjusted at pH 2—3 with hydrochloric acid and chromatographed on a Florisil column in a similar way to that used for **2e**. Evaporation of the eluate to dryness and crystallization of the residue from water gave colorless needles (200 mg) of **2i**, mp 244—244.5 °C(Found: C, 51.62; H, 4.33; N, 36.02%. Calcd for $C_{10}H_{10}N_6O \cdot 0.1H_2O$: C, 51.75; H, 4.44; N, 36.22%). In a similar way, **2b** and 2-aminoethanol gave **2j** (60% yield), mp 266—267 °C (from ethanol)(Found: C, 55.98; H, 5.60; N, 32.43%. Calcd for $C_{12}H_{14}N_6O$: C, 55.80; H, 5.47; N, 32.54%).

*6-Hydroxyimidazo[1,2-c]pteridine(**2k**) and Its 2,3-Dimethyl Derivative(**2l**).* A solution of **2a** (1.0 g) in 0.1 M sodium hydroxide (20 ml) was heated at 60 °C for 1.5 h. The solution was adjusted at pH 2—3 with formic acid and chilled. The solid was collected and crystallized from water to give colorless needles (0.35 g) of **2k**; the compound darkened above 205 °C without melting (Found: C, 51.03; H, 2.47; N, 37.39%. Calcd for $C_8H_7N_5O$: C, 51.33; H, 2.70; N, 37.42%). The same compound(**2k**) was obtained from **2a** by heating in 0.1 M hydrochloric acid at 60 °C, by treatment with sodium ethoxide or hydrogen chloride in ethanol at 25 °C, or by heating in 50% aqueous methanol with silver oxide.

Heating of **2b** (280 mg) in 0.2 M hydrochloric acid at 70 °C for 20 h and evaporation to dryness in vacuo gave a solid, which was dissolved in water (10 ml). The solution was adjusted at pH 3—4 with ammonia and chilled to give colorless needles (200 mg) of **2l**, mp 294—295.5 °C (from water)(Found: C, 54.30; H, 4.60; N, 31.73%). Calcd for $C_{10}H_9N_5O \cdot 0.3H_2O$: C, 54.43; H, 4.39; N, 31.75%).

*6-Ethoxy- and 6-Methoxyimidazo[1,2-c]pteridines(**2m** and **2o**) and Their 2,3-Dimethyl Derivatives(**2n** and **2p**).* A mixture of **2a** (400 mg) and silver oxide (2 g) in ethanol (150 ml) was heated under reflux for 7 h. After filtration, the filtrate was evaporated to dryness and the residue was chromatographed on a silica gel column eluted by ethanol–ethyl acetate(1 : 9). Evaporation of the eluate and crystallization from ethyl acetate gave colorless needles (200 mg) of **2m**, mp 143—143.5 °C (Found: C, 56.00; H, 4.18; N, 32.61%. Calcd for $C_{10}H_9N_5O$: C, 55.81; H, 4.22; N, 32.54%).

By using methanol in place of ethanol in the above reaction, the 6-methoxy compound(**2o**) was obtained in 30% yield, mp 238—239 °C (from ethyl acetate)(Found: C, 53.53; H, 3.33; N, 34.39%. Calcd for $C_9H_7N_5O$: C, 53.72; H, 3.51; N, 34.81%).

Similar treatments of **2b** with silver oxide in ethanol or methanol gave the ethoxy compound(**2n**) in 50% yield, mp 184—185 °C (from benzene)(Found: C, 59.22; H, 5.39; N, 28.51%. Calcd for $C_{12}H_{13}N_5O$: C, 59.24; H, 5.40; N, 28.79%), and the methoxy compound (**2p**) in 55% yield, mp 216—216.5 °C (from toluene)(Found: C, 56.13; H, 4.78; N, 29.64%. Calcd for $C_{11}H_{11}N_5O \cdot 0.3H_2O$: C, 56.29; H, 4.86; N, 29.85%), respectively.

We thank Dr. Y. Yokoyama for measuring the NMR spectra and Mrs. N. Nishioka for determining the pK_a values.

References

1) Part I: T. Sugimoto, K. Shibata, and S. Matsuura, *Bull. Chem. Soc. Jpn.*, **50**, 2744 (1977).

2) H. Kasai, M. Goto, S. Takemura, T. Goto, and S. Matsuura, *Tetrahedron Lett.*, **1971**, 2725.
3) H. Kasai, M. Goto, K. Ikeda, M. Zama, Y. Mizuno, S. Takemura, S. Matsuura, T. Sugimoto, and T. Goto, *Biochemistry*, **15**, 898 (1976).
4) T. Sugimoto and S. Matsuura, *Bull. Chem. Soc. Jpn.*, **50**, 1359 (1977).
5) A. Albert and W. L. F. Armarego, *Adv. Heterocyclic Chem.*, **4**, 1(1965).
6) D. J. Brown and T. Sugimoto, *J. Chem. Soc., C*, **1970**, 2661.
7) E. M. Gal, *J. Am. Chem. Soc.*, **72**, 3532 (1950).
8) E. C. Taylor and C. K. Cain, *J. Am. Chem. Soc.*, **74**, 1644 (1952).

Stereochemistry of Elimination Reactions of Halohydrin Derivatives and Related Compounds with Butyllithium[1)]

Toshio SUGITA,* Junichi NAKAGAWA, Kazuhito NISHIMOTO, Yasuhiro KASAI, and Katsuhiko ICHIKAWA

Department of Hydrocarbon Chemistry, Faculty of Engineering, Kyoto University, Sakyo-ku, Kyoto 606

(Received May 24, 1978)

The *erythro* and *threo* isomers of 1-bromo-2-methoxy-1,2-diphenylethane (**1**), 1-bromo-2-acetoxy-1,2-diphenylethane (**2**), 1-bromo-2-methylsulfonyloxy-1,2-diphenylethane (**3**), 1-bromo-2-methylthio-1,2-diphenylethane (**4**), stilbene dibromide (**6**), and stilbene dichloride have been prepared. These compounds were allowed to react with butyllithium in various solvents to give *cis*- and *trans*-stilbenes. Depending on the solvent, the stereochemistry of the elimination of **1** changed from a complete *syn*-type (in nonpolar solvents) to a less-selective type. The same tendency was observed in the cases of **2** and **3**. In contrast, *anti*-elimination was favored for **4** and **6**, and a different type of solvent effect was observed. Elimination reactions with lithium metal and pentylmagnesium bromide were also carried out. Possible mechanisms for eliminations are discussed.

Results of extensive studies on the bimolecular elimination of halohydrin derivatives and *vicinal* dibromides with metal or metal salts have shown that the reactions display a variable stereoselectivity, depending on the nature of the metals used.[2-5)] The effects of the structure of substrates and the solvent, however, remain ambiguous. This paper reports the results of studies on the stereochemistry of the elimination of stilbene halohydrin derivatives and related compounds; in particular, the effects of the leaving group and the solvent were probed.

House and Ro have shown that the treatment of β-halo ethers and esters with zinc in aqueous ethanol or with sodium in tetrahydrofuran gave nonstereospecific elimination products.[2)] They postulated that the organometallics formed by halogen–metal exchanges give olefins by the mechanism of ElcB but not by that of E2, because OR and OCOR are poor leaving-groups. However, since the reactions of metals such as magnesium[6)] and lithium[7)] with alkyl halides to form Grignard and organolithium reagents result in the loss of stereochemical integrity, it is not clear whether the loss of stereospecificity in the reaction of halohydrin derivatives with metal occurs during the halogen–metal exchange or in the subsequent elimination process.

When the halide is treated with an alkyllithium reagent instead of lithium metal, the lithium compound formed is capable of maintaining its configuration, although the degree of retention of configuration is both solvent- and temperature-dependent.[8)] In order to preclude the loss of stereospecificity in the halogen–metal exchange stage, our eliminations were carried out by the use of butyllithium.

Results

The *erythro* and *threo* pairs of 2-substituted 1-bromo-1,2-diphenylethanes were chosen as the substrates because of their accessibility in pure form and the accuracy with which analysis of the products is possible. The *erythro* (**e**) and *threo* (**t**) isomers of 1-bromo-2-methoxy-1,2-diphenylethane (**1**), 1-bromo-2-acetoxy-1,2-diphenylethane (**2**), 1-bromo-2-methylsulfonyloxy-1,2-diphenylethane (**3**), and 1-bromo-2-methylthio-1,2-diphenylethane (**4**) have been prepared. Each compound was allowed to react with butyllithium in various kinds of solvents. The organic products were analyzed by GLPC. *cis*- (**5c**) and *trans*-Stilbenes (**5t**) produced were isolated and identified by means of GLPC, IR, and NMR. The results are summarized in Table 1.

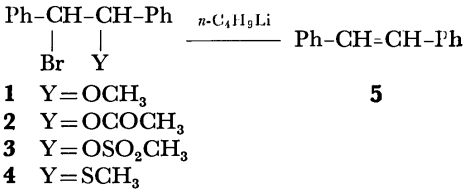

In any attempt to account for stereoselectivity, we must remember that **5t** is much more stable than **5c** under the reaction conditions: the thermodynamical isomer ratio of *trans* to *cis* is 500 at 25 °C.[9)] The exclusive formation of **5c** from **1e** as well as **5t** from **1t** in nonpolar solvents such as diethyl ether and benzene indicates that the stereospecific *syn* elimination occurred in the reaction of **1** with butyllithium in nonpolar solvents. Although the stereospecificities were diminished, the same tendency of *syn* elimination was clearly observed in the cases of **2** and **3**.

The solvent study was limited by the insolubility of the substrates in hydrocarbon solvents. Within the limited range of solvents, however, it was observed that changing the solvent from nonpolar to better solvating ones, such as tetrahydrofuran (THF) or bis(2-methoxyethyl) ether (diglyme), diminished the stereospecificity. The addition of a cation complexing reagent, *N,N,N,N*-tetramethylethylenediamine (TMEDA), also reduced the stereospecificity. The fact that only **5c** was formed, even in the elimination reaction using an excess amount of butyllithium, can eliminate the possibility of isomerization of **5c** to **5t** in nonpolar solvents. In a separated experiment, in which **5c** was treated with an equivalent amount of butyllithium in diglyme under the reaction condition, the recovered **5** was exclusively *cis* isomer. Thus the possibility of isomerization can also be eliminated in a better solvating medium.

When **1e** in diethyl ether was treated with butyllithium at −72 °C and the reaction was quenched

Table 1. Elimination reactions of stilbene halohydrin derivatives with butyllithium

Run	Substrate (mmol)	n-C_4H_9Li (mmol)	Solvent (ml)	Additive (mmol)	React. condition		5		
					Time (min)	Temp (°C)	Yield (%)	*cis* : *trans*	
1	**1e** (1.01)	1.0	Et_2O (50)		30	0	42	100	trace
2	**1e** (1.00)	2.3	Et_2O (50)		30	0	48	100	trace
3	**1e** (1.00)	5.3	Et_2O (50)		30	0	44	100	trace
4	**1e** (1.00)	1.2	Benzene (50)		30	r. t.	22	100	trace
5	**1e** (1.00)	2.0	Benzene (50)		30	r. t.	32	100	trace
6	**1e** (1.05)	2.4	THF (50)		15	0	59	52	48
7	**1e** (1.34)	3.5	Diglyme (50)		10	0	76	22	78
8	**1t** (1.11)	3.5	Et_2O (50)		10	0	53	trace	100
9	**1t** (1.02)	2.4	THF (50)		15	0	48	trace	100
10	**1t** (1.41)	3.5	Diglyme (50)		10	0	93	trace	100
11	**2e** (0.31)	1.48	Hexane (25)		30	0	30	37	63
12	**2e** (0.31)	1.48	Benzene (25)		30	r. t.	28	48	52
13	**2e** (0.31)	1.48	Et_2O (25)		30	0	46	12	88
14	**2e** (0.31)	1.48	THF (25)		30	0	52	12	88
15	**2e** (0.31)	1.48	Diglyme (25)		30	0	84	8	92
16	**2e** (0.31)	1.48	Hexane (25)	TMEDA (1.5)	30	0	13	11	89
17	**2t** (0.31)	1.48	Hexane (25)		30	0	18	8	92
18	**2t** (0.31)	1.48	Benzene (25)		30	r. t.	29	9	91
19	**2t** (0.31)	1.48	Et_2O (25)		30	0	34	4	96
20	**2t** (0·31)	1.48	THF (25)		30	0	5	trace	100
21	**2t** (0.31)	1.48	Diglyme (25)		30	0	23	3	97
22	**3e** (0.28)	2.08	Benzene (25)		30	r. t.	56	57	43
23	**3e** (0.28)	2.08	Et_2O (25)		30	0	49	21	79
24	**3e** (0.28)	2.08	THF (25)		30	0	52	7	93
25	**3e** (0.28)	2.08	Diglyme (25)		30	0	38	7	93
26	**3t** (2.08)	2.08	Benzene (25)		30	r. t.	53	3	97
27	**3t** (0.28)	2.08	Et_2O (25)		30	0	54	4	96
28	**3t** (0.28)	2.08	THF (25)		30	0	22	8	92
29	**3t** (0.28)	2.08	Diglyme (25)		30	0	18	3	97
30	**4e** (0.33) [a]	2.08	Benzene (25)		30	r. t.	37	3	97
31	**4e** (0.33) [a]	2.08	Et_2O (25)		30	0	42	2	98
32	**4e** (0.33) [a]	2.08	THF (25)		30	0	40	trace	100
33	**4e** (0.33) [a]	2.08	Diglyme (25)		30	0	36	2	98
34	**4t** (0.33) [a]	2.08	Benzene (25)		30	r. t.	59	trace	100
35	**4t** (0.33) [a]	2.08	Et_2O (25)		30	0	43	trace	100
36	**4t** (0.33) [a]	1.50	Et_2O (25)		30	0	54	2	98
37	**4t** (0.33) [a]	2.08	THF (25)		30	0	56	6	94
38	**4t** (0.33) [a]	2.08	DME (25)		30	0	49	9	91
39	**4t** (0.33) [a]	2.08	Diglyme (25)		30	0	67	86	14
40	**4t** (0.33) [a]	2.08	Et_2O (25)	TMEDA (2.1)	30	0	10	6	94
41	**4t** (0.32) [a]	1.15	Et_2O (25)	TMEDA (6.5)	30	0	65	20	80
42	**4t** (0.33) [a]	1.50	Et_2O (25)	TMEDA (8.8)	30	0	56	33	67
43	**4t** (0.33) [a]	1.50	Et_2O (25)	CE (1.85) [b] DME (9.2)	30	0	60	19	81
44	**4t** (0.35) [a]	1.15	Et_2O (25)	DME (6.7)	30	0	72	5	95

a) The substrate contained a small amount (less than 5%) of **6**, and the product ratio is uncorrected for the contamination. b) Dicyclohexyl-18-crown-6.

with methanol after 0.5—3 min, small amounts of 1-methoxy-1,2-diphenylethane were detected by GLPC, together with **5c** and unreacted **1e**. This GLPC peak could not be detected any more when the reaction was completed after 30 min.

As can be seen from Table 1, the stereochemical feature of elimination of 1-bromo-2-methylthio derivative (**4**) were quite different from the above-mentioned oxygen analogue (**1**). Recently Trost and Ziman reported that the elimination of 2-bromo-3-ethylthio- and 2-bromo-3-phenylthiobutanes with butyllithium proceeded with a moderate to high degree of *anti* stereoselectivity in THF solution.[10] In our case, the stereospecificity of the elimination was completely lost in nonpolar solvents such as benzene or diethyl ether, while a high *anti* stereoselectivity was observed in a

Table 2. Elimination reactions of stilbene dihalides with butyllithium

Run	Substrate (mmol)	n-C_4H_9Li (mmol)	Solvent (ml)	React. condition		5	
				Time (min)	Temp (°C)	Yield (%)	*cis* : *trans*
45	**6e** (1.21)	1.2	Et_2O (50)	10	0	43[a)]	trace 100
46	**6e** (1.20)	2.4	Et_2O (50)	10	0	95	trace 100
47	**6e** (1.05)	3.6	Et_2O (50)	60	−59	35[a)]	trace 100
48	**6e** (1.03)	5.5	Diglyme (50)	10	0	99	trace 100
49	**6t** (1.53)	4.4	Et_2O (50)	15	0	100	19 81
50	**6t** (1.54)	4.8	Et_2O (50)	120	−58	100	21 79
51	**6t** (1.53)	5.5	Diglyme (50)	15	0	99	20 80
52	**7e** (1.02)	3.6	Et_2O (80)	10	0	99	trace 100
53	**7t** (1.14)	3.6	Et_2O (50)	10	0	62[a)]	3 97

a) Unreacted substrate was recovered.

Table 3. Elimination reactions with lithium metal[a)]

Run	Substrate (mmol)	Li (mg-atom)	Reaction time (h)	8	5	
				Yield (%)	Yield (%)	*cis* : *trans*
54	**1e** (2.11)	24	30	9.1	67	13 87
55	**1e** (2.10)	17	50	7.7	79	11 89
56	**1t** (2.17)	17	15	18	18	0 100
57	**1t** (2.10)	26	30	11	6	0 100
58	**1t** (1.74)	16	50	20	trace	

a) The reactions were carried out under reflux in 100 ml of diethyl ether.

highly cation solvating medium such as diglyme. By increasing the cation solvating ability of the solvent, the *anti* elimination was increased. When 5 equivalents of TMEDA or 1 equivalent of crown ether accompanied with 5 equivalents of 1,2-dimethoxyethane (DME) was added, moderate *anti* stereoselectivities were observed even in the diethyl ether medium.

In a similar study by Winkler on phenyllithium-induced debromination of *dl*- and *meso*-2,3-dibromobutanes, an almost exclusive *anti* elimination has been demonstrated.[11] In order to compare with these data, we investigated the stereochemistry of elimination with butyllithium on *vicinal* dibromide as well as dichloride in the present stilbene system. The results are summarized in Table 2.

The debromination of *meso*-stilbene dibromide (**6e**) produced only **5t**, but a mixture of 20% of **5c** and 80% of **5t** was obtained from the *dl*-isomer (**6t**). By the fact that the thermodynamically unstable **5c** was obtained from **6t**, it is apparent that the reaction proceeds by *anti* fashion, but the stereospecificity is considerably lower than in the case of 2,3-dibromobutane. In this case, no solvent effects on the stereochemistry were observed when the solvent was changed from diethyl ether to diglyme.

In the case of *vicinal* dichloride (**7**), the elimination was no longer stereoselective, and **5t** was virtually exclusively obtained from both the *dl* and *meso* isomers.

The present stereochemical results of elimination of bromohydrin derivatives with butyllithium markedly contrast with those using metals such as zinc and sodium, which resulted in nonstereospecific eliminations.[2] There have also been indications that certain metal debrominations may display a variable stereoselectivity, and a surface radical process has been suggested for the debromination reaction of **6** with metals.[4] In order to learn more about the discrepancy of the stereochemistry of elimination with butyllithium and with metal, we undertook the elimination reaction using lithium metal.

The β-bromo ether **1** was refluxed with lithium metal in diethyl ether. The amounts of **5** and 1,2-diphenylethane (**8**) produced were determined by GLPC analysis and are summarized in Table 3. As the IR spectra of the unreacted **1** recovered from the reaction mixture were superimposable with those of each starting material, the possibility of isomerization during the reaction process could be eliminated.

Since the formation of dilithio compounds from **5** and the other arylated alkenes has been reported,[12] **5t** was allowed to react with lithium metal under the reaction conditions, **8** was obtained after the work-up, as shown in Table 4. These results indicate that **8** was produced by addition of the excess lithium metal to **5** of the elimination product, followed by hydrolysis in the work-up process. Since the relative rate of formation of the dilithio compounds from **5c** and **5t** is not clear, the ratios of **5c** and **5t** in Table 3

Table 4. Reactions of **5** with lithium metal[a)]

5t (mmol)	Li (mg-atom)	Reaction time (h)	Yield of **8** (%)
2.04	18	5	37
2.04	16	30	70

a) Reactions were carried out under reflux in 100 ml of diethyl ether.

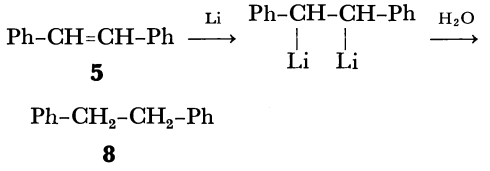

may not reflect the actual ratios of the elimination process. However, the result that **5c** was obtained only from **1e**, though the yield was not so high, indicates that *syn* elimination has occurred at least partly in the reaction using lithium metal.

Dehydrohalogenation of alkyl halide[13] and debromination of *vicinal* dibromide[4] with Grignard reagents have been investigated in only a few instances. Furthermore, β- and γ-haloalkyl phenyl ethers gave olefin and cyclopropane respectively by the reaction with Grignard reagents in the presence of cobaltous bromide.[14] On the other hand, halogen–metal interchange reactions with Grignard reagents have been established.[15] Zakharkin and his coworkers have made extensive studies of the exchange of Grignard reagents with ordinary alkyl and aryl halides.[16] Highly solvating ethers such as THF and DME favor the exchange. The rate of exchange is dependent on the polarizability of the halogens in the alkyl halides. On the basis of these studies, they have concluded that the mechanism of halogen–metal interchange reaction is the same for both organomagnesium and organolithium compounds. We thus undertook an investigation of the stereochemistry of elimination promoted by pentylmagnesium bromide. The results are given in Table 5.

TABLE 5. ELIMINATION REACTIONS OF **1** WITH PENTYLMAGNESIUM BROMIDE[a]

Substrate (mmol)	n-$C_5H_{11}MgBr$ (mmol)	Reaciton time (min)	**5** Yield (%)	*cis*	: *trans*
1e (1.05)	2.0	90	27	0	100
1e (1.01)	2.0	180	49	0	100
1e (1.05)	2.0	360	34	0	100
1t (1.04)	2.0	180	31	0	100
1t (1.04)	2.7	360	33	0	100

a) Reactions were carried out in 50 ml of diethyl ether at 0 °C.

As can be seen from Table 5, **5t** was an exclusive product from both **1e** and **1t**. As the IR spectra of substrates recovered from the reaction mixtures were completely identical with that of the respective starting materials, isomerization of the substrates during the reaction process can be eliminated. The isomerization of **5** also could not be detected under the experimental conditions. The present results indicate the elimination reaction of β-halo ethers promoted by a Grignard reagent to be nonstereospecific.

Discussion

Although a number of mechanistic implications have been reported for the base-catalyzed bimolecular elimination reactions, two possible routes may be considered for the butyllithium-induced *syn* elimination of halohydrin derivatives. One is the process *via* a cyclic transition state such as **9**, and the other is a mechanism which involves a carbanion or the equivalent organolithium reagent (**10**). In both cases, the factor which forces the production of **5c** from the *erythro* isomers of substrates, even against the large thermodynamical instability of the product, is expected to be the coordination between lithium and oxygen atoms. This is proved by the fact that the stereospecificity of *syn* elimination decreased by increasing the cation complexing ability of solvents. The cation complexing ability of the medium increases in the order: hexane < benzene < diethyl ether < THF < DME < diglyme,[17] and is also enhanced by the addition of cation-coordinating reagents such as TMEDA and crown ethers.[18,19]

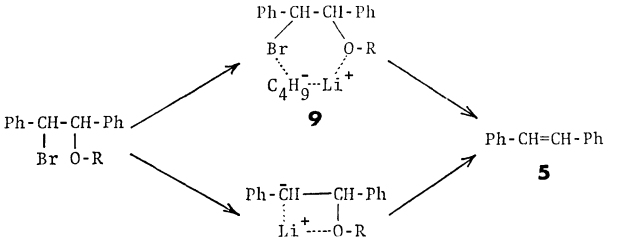

Scheme 1.

The cyclic transition state (**9**) is similar to that postulated by Letsinger to explain the more rapid *syn* elimination of the elements of methanol when *cis*- and *trans*-1-methoxy-2-phenylcyclohexanes are heated under reflux with butyllithium in a mixture of pentane and diethyl ether.[20] The coordination between lithium and oxygen should be stronger in a nonpolar solvent such as hexane, benzene, or diethyl ether, and weaker in the coordinating solvents. Thus the reduction of stereospecificity in THF or diglyme solvent would seem to occur as a matter of course. However, the fact that considerable lower stereospecificity was observed in the reactions of **2** and **3** in nonpolar solvents in comparison with the reaction of **1** is not conceivable from a concerted mechanism *via* such a cyclic transition state, because it was recently reported by Staley and Beauchamp that the binding energy of an ester to a lithium cation is much stronger than that of an ether.[21]

The alternative mechanism involving a carbanion intermediate (**10**) appears to be more plausible, because of the poor leaving group ability of OR and OCOR. The formation of the carbanion intermediate is also evidenced by the fact that 1-methoxy-1,2-diphenylethane was detected when the reaction of **1** at −72 °C was quenched by methanol. House and Ro postulated a similar intermediate for the nonstereospecific elimination of β-halo ethers and esters with zinc and sodium.[2]

It has been demonstrated that metal–halogen exchange with butyllithium occurs with a high degree of retention of configuration.[8] While spectroscopic studies indicate a polar covalent character for the

carbon–lithium bonds in alkyllithiums, it has also been revealed that alkyllithiums exist in solution in equilibrium with different types of ion pairs: tight, solvent separated, and free ion-pairs, and that such equilibria are affected not only by the structure of the carbanion but also by the solvent polarity, temperature, and the presence of gegenion-coordinating additives.[18] Thus the *erythro*- and *threo*-carbanions (**10**) are expected to be produced from the corresponding isomers of **1**, **2**, and **3**. These carbanions will form tight ion-pairs with lithium cation in nonpolar solvents. A lithium cation, on the other side, may coordinate with the substituent oxygen. The interaction between the metal cation in a tight ion-pair and the substituent oxygen makes it a better leaving group, and appears to force *syn* elimination.

As the coordinating-ability of an OAc group to a lithium cation is stronger than that of a methoxyl group, and a stronger ability is also expected for the OSO_2CH_3 group, higher *syn* selectivities are expected for **2** and **3** than for **1**. The results summarized in Table 1 are, however, inconsistent with this expectation. These results seems to reflect the ease with which the leaving group Y are eliminated. Although there is no exact data to indicate the departing tendencies of various groups, it would be expected by analogy with the behavior of various groups in nucleophilic displacement reactions to decrease in the following order: $OSO_2CH_3 > OAc \gg OR$.[22] The weakening of the bond to the leaving group makes the carbanionic intermediate **10** unstable, so the elimination mechanism is expected to have an E2 character. The *syn* selectivities of the eliminations of **2** and **3** would thus be lower than that of **1**.

In contrast with the bromohydrin derivatives, the *vic*-dibromide (**6**) indicated *anti*-fashion stereoselectivity ; in this reaction no solvent effect was observed in the stereochemistry of elimination. Stereospecific *anti*-debromination has been reported by Winkler in the reaction of 2,3-dibromobutane with phenyllithium.[11] In the present case, due to a very weak binding energy of bromine to a lithium cation, it is expected to be much weaker than that between a phenyl group of the substrate and a lithium cation,[21] and also due to the easily-departing tendency of bromine, an intermediate such as **10** is not conceivable for the debromination of *vic*-dibromide. The fact that changing the solvent from diethyl ether to diglyme has no effect on the stereochemistry of elimination suggests that a lithium cation should not play an important role on the intermediate or the transition state for butyllithium-catalyzed debromination, and that the reaction proceeds through a concerted process.

Although a number of authors have likened dehalogenation to a base-promoted E2 reaction on the basis of stereochemistry, a more detailed approach have been recently outlined by Miller and his coworkers.[23] We believe that an analogous mechanism can be applied to the present butyllithium-induced debromination, as indicated in Scheme 2. The present results indicated lower stereospecificity than Winkler's results, but this is ignorable if the large differences of the configurational stability between the transition states

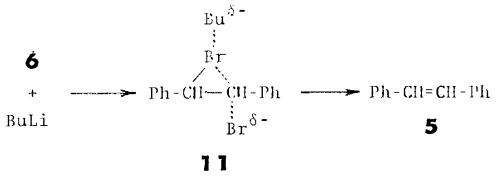

Scheme 2.

derived from **6e** and **6t** as well as the products are taken into consideration.

The nonstereospecific results obtained in the butyllithium-induced dechlorination of **7** do not conflict with the above mechanism, because it is well-known that neighboring group participation by chlorine is much weaker than that of bromine; thus the formation of a cyclic transition state such as **11** is difficult for the *vic*-dichloride.

The results of the elimination of **4** contrast markedly with those of the oxygen analogue (**1**), as well as those of the dihalides. In diethyl ether and benzene solvents, the elimination is nonstereospecific, *e.g.*, both *threo* and *erythro* isomers gave thermodynamically stable **5t** exclusively. In diglyme, where the oxygen analogue indicates loss of stereospecificity, however, the elimination converts **4e** into **5t**, and **4t** into 86% of **5c** and 14% of **5t**. The *anti* selectivity is increased by increasing the cation complexing ability of the solvents: THF < DME < diglyme. The addition of cation complexing reagents such as TMEDA and crown ether facilitated the *anti*-elimination. Recently, Panek reported that the rate of geometric isomerization of 1-lithio-1-phenyl-1-butene in hexane solution was enhanced by the addition of cation complexing reagents; the following order was observed: TMEDA > DME > THF > diethyl ether.[19] Furthermore, Walborsky reported that the addition of 1 equiv. dicyclohexyl-18-crown-6 with 5 equiv. of DME was very effective for complexing the lithium cation and making a free carbanion.[24]

A methylthio group may be considered as one of the groups with a lower departing tendency, similar to the methoxyl group. The butyllithium-induced elimination of **4** is thus considered to proceed *via* a carbanion intermediate.

The solvent study indicates that a nonstereospecific elimination results from the tight ion-pair intermediate derived from **4**, and the free ion or the solvent separated ion-pair provides an *anti*-elimination. The coordinating bond strength between a lithium cation and a sulfide sulfur is reported to be very weak, weaker than that between lithium cation and phenyl group.[21] Therefore, there is little effect to force the lithium cation and methylthio group into a *s-cis* conformation. The elimination reaction in nonpolar solvents proceeds *via* a carbanion intermediate (**12**) and the stereochemistry is not specific (Scheme 3, path a).

On the other hand, at present, it appears to be difficult to find a good reason why an *anti* fashion elimination resulted from the free ion of **12**. Although considerable experimental data have been accumulated which indicate that carbanions are stabilized by the adjacent sulfur atom,[25] the participation of sulfur-

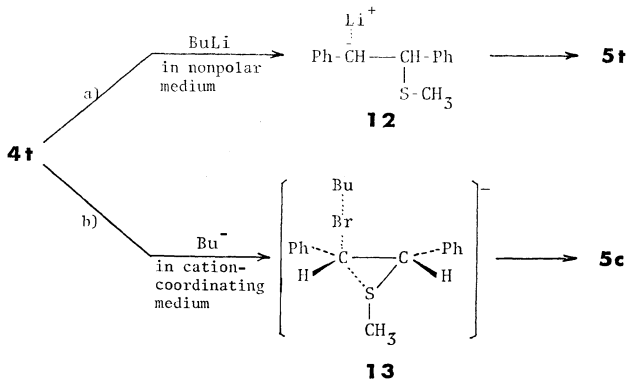

Scheme 3.

containing substituents at the β-position with carbanion has rarely been reported. Recently, Kaji and his co-workers reported that the rate of base-catalyzed H–D exchange reactions of substituted cyclopropanes was enhanced by the substitution of a phenylthio group at β-position.[26] They suggested the neighboring sulfur participation in stabilization of the carbanion. Yano and Oae have shown that the rates of the base-catalyzed elimination of a series of γ-(p-substituted phenylthio)propyl bromides are slower than that of the corresponding oxygen analogues and that the ρ value obtained for the sulfur compounds is larger than that for the oxygen compounds.[27] They have suggested the non-bonding participation of a vacant d-orbital of the sulfur atom for the developing double bond to elucidate this phenomena. Furthermore, Howard has proposed a three-membered ring anion involving sulfur, in which the charge of the carbanion is delocalized to the neighboring sulfur atom, as an intermediate of the base-promoted rearrangement of diethyl dithiodiacetate.[28]

In the present case, when a 1-butanide anion pulls bromine off the substrate at the initial stage of the reaction, a vacant 3d-orbital of the sulfur atom assists the developing carbanion at the opposite side from the leaving bromine to form a three-membered ring transition state or an intermediate (**13**). Stereospecific elimination from such an intermediate has been proposed by Trost and Ziman. The desulfurization of *cis*- and *trans*-2-butene episulfides with butyllithium to the corresponding butenes proceeds stereospecifically. They suggested a three-membered ring anion similar to **13** as one of the possible transition state.[10] Thus it is conceivable that the stereospecific *anti* elimination would occur if a neighboring participation of sulfenyl group against the carbanion is taken into account.

When **1** was treated with lithium metal instead of butyllithium, the elimination proceeded with *syn* selectivity, but the selectivity was much lower than the case of organolithium reagent. It has been reported that the reaction of lithium metal with alkyl halides, in which the halogen atom is attached to a tetrahedrally hybridized carbon atom, results in the formation of lithium reagents along with much racemization.[7] Recently a more detailed discussion on the stereochemistry of halogen–lithium exchange reaction with lithium metal has been reported by Walborsky and Aronoff.[7b] Moderate retention of configuration resulted in the reaction of substituted cyclopropyl halide with very finely divided lithium metal, but the optical purity of the produced organolithium compound decreased by increasing the particle size of lithium. It has also been pointed out that the halogen–lithium exchange reaction involves a surface radical process. Thus the loss of stereospecificity in the elimination of **1** with lithium metal is considered to occur during the bromine–lithium exchange process on a lithium metal surface. The nonstereospecific results of House[2] for the use of sodium and zinc metals fit into these considerations.

Halogen–metal exchange reactions involving Grignard reagents have been reported, and it has been found that there is no fundamental difference between exchange reactions in the series of organolithium and magnesium compounds.[16] However, the stereochemistry of the exchange reaction between alkylmagnesium and an alkyl halide is not yet clear. The present result that the Grignard reagent-promoted elimination reaction proceeds nonstereospecifically would imply that the exchange proceeds with racemization. Examinations on these subjects are in progress.

Experimental

IR spectra were obtained using a Hitachi EPI-G2 spectrophotometer. NMR spectra were recorded as $CDCl_3$ solutions on a JEOL PMX-60 spectrophotometer; chemical shifts are reported in parts per million relative to TMS as an internal standard.

Solvents. GR grade diethyl ether was dried over sodium metal and distilled. GR grade THF was distilled from lithium aluminum hydride under nitrogen and stored over 4A molecular sieves. Diglyme was passed through activated alumina, and distilled before use. Bulk solvents were distilled before use.

Reagents. Butyllithium (*ca.* 20% in hexane) was purchased from Merck Co., Inc. and Aldrich Chemical Co. Inc., and titrated before use.[29] Pentylmagnesium bromide in ether was purchased from the Alfa Division of Ventron Corp. and titrated before use.[30] TMEDA was kept over solid sodium hydroxide and used with no further purification. DME was passed through activated alumina before use. Crown ether was purchased from Nippon Soda Co., and was used without further purification. Commercially available GR grade *trans*-stilbene was used without further purification. *cis*-Stilbene, bp 108.5—112.0 °C/2 mmHg, was prepared by the literature procedure.[31]

Preparations of 1-Bromo-2-methoxy-1,2-diphenylethanes (1). Following the procedure developed by House,[2] a solution of 5.4 g (0.03 mol) of **5t**, 10.8 g (0.06 mol) of *N*-bromosuccinimide, 3 ml of acetic acid, and 30 ml of acetone in 300 ml of methanol was allowed to stand for 5 h and then concentrated, diluted with water, and extracted with ether. The ether extract was washed first with water and then with aqueous sodium hydrogencarbonate solution and then dried over sodium sulfate. After removal of ether, petroleum ether was added to the residual oil. The crude bromo ether deposited was recrystallized twice from hexane, giving pure **1e**, mp 120—121 °C (lit,[2] mp 117—118 °C), yield 6.2 g (71%); NMR δ=3.20 (s, 3, OCH_3), 4.63 (d, 1, CHBr), 5.06 (d, 1, J=7 Hz, CHOR), 7.28 (s, 10, C_6H_5). Found: C, 62.12; H, 5.20; Br, 27.43%. Calcd for $C_{15}H_{15}OBr$:

C, 61.86; H, 5.19; Br, 27.45%.

In a similar manner, 5.4 g (0.03 mol) of **5c** afforded 3.7 g (42%) of **1t**, mp 85.5—86.5 °C (lit,[2] mp 86—87.5 °C), NMR δ=3.33 (s, 3, OCH_3), 4.50 (d, 1, CHBr), 5.00 (d, 1, J=8 Hz, CHOR), 7.14 (s, 10, C_6H_5). Found: C, 62.10; H, 5.11; Br, 27.52%. IR of the *threo*-isomer (**1t**) was similar to that of the *erythro*-isomer (**1e**) except for a band at 1215 cm^{-1}, where **1t** exhibited an absorption.

Preparations of 2-Bromo-1,2-diphenylethanols. *erythro*- and *threo*-2-Bromo-1,2-diphenylethanols were prepared by the method of House[32] from **5t** and *cis*-stilbene oxide respectively. The *erythro*-isomer, mp 83.5—85.0 °C (lit,[32] mp 83.5—85.0 °C), and the *threo*-isomer, mp 51.0—52.0 °C (lit,[32] mp 51—52 °C) were used for the following preparations.

Preparations of 1-Bromo-2-acetoxy-1,2-diphenylethanes (2). To 6.8 g (45 mmol) of *erythro*-2-bromo-1,2-diphenylethanol was added 6.0 ml (64 mmol) of freshly distilled acetic anhydride over a period of 10 min at room temperature. The mixture was stirred at 70 °C for 2 h. 200 ml of water was added to the cooled mixture, which was then extracted with 100 ml of ether three times. The ether extract was washed with water and dried over magnesium sulfate. After removal of ether, the residual product was recrystallized from hexane–petroleum ether, giving **2e**, mp 100.0—100.7 °C (lit,[33] mp 102 °C), yield 6.8 g (87%); NMR δ=1.89 (s, 3, $OCOCH_3$), 5.15 (d, 1, CHBr), 6.50 (d, 1, J=7.5 Hz, CHOAc), 7.23 (s, 10, C_6H_5). Found: C, 60.38; H, 4.61%. Calcd for $C_{16}H_{15}O_2Br$: C, 60.20; H, 4.74%.

In a similar manner, 3.95 g (14.2 mmol) of the *threo*-bromohydrin was treated with 4.0 ml (42.6 mmol) of acetic anhydride to give **2t**, mp 79.5—81.0 °C, yield 3.44 g (70.7%); NMR δ=2.14 (s, 3, $OCOCH_3$), 5.15 (d, 1, CHBr), 6.20 (d, 1, J=4.6 Hz, CHOAc), 7.10 and 7.15 (ds, 10, C_6H_5). Found: C, 60.02; H, 4.62%.

Preparations of 1-Bromo-2-methylsulfonyloxy-1,2-diphenylethanes (3). To a stirred solution of *erythro*-2-bromo-1,2-diphenylethanol (2.5 g, 9.0 mmol) in 25 ml of pyridine, 1.14 g (10 mmol) of methanesulfonyl chloride was added dropwise at −5 °C. After the mixture had been stirred at 0 °C for 24 h, 5 ml of water was added; then it was extracted with 50 ml each of chloroform three times. The extracts were combined and washed first with dil. sulfuric acid and then with aqueous sodium hydrogencarbonate solution, and dried over sodium sulfate. After removal of chloroform, the residual product was recrystallized from chloroform–petroleum ether. An additional crystallization afforded the pure **3e**, mp 113.5—114.0 °C, yield 1.6 g (50%). NMR δ=2.48 (s, 3, CH_3), 5.15 (d, 1, CHBr), 5.93 (d, 1, J=4.0 Hz, $CHOSO_2$), 7.37 (s, 10, C_6H_5). Found: C, 50.56; H, 4.30; S, 9.11%. Calcd for $C_{15}H_{15}O_3BrS$: C, 50.71; H, 4.26; S, 9.03%.

In a similar manner, 2.5 g of *threo*-2-bromo-1,2-diphenylethanol gave 2.0 g (62.5%) of **3t**, mp 107.0—108.0 °C, NMR δ=2.82 (s, 3, CH_3), 5.17 (d, 1, CHBr), 5.83 (d, 1, J=4.3 Hz, $CHOSO_2$), 7.13 (s, 10, C_6H_5). Found: C, 50.42; H, 4.18; S, 8.62%.

Preparations of 1-Bromo-2-methylthio-1,2-diphenylethanes (4). The method of Helmkamp[34] was applied to **5**. A solution of 5.0 g (53 mmol) of dimethyl disulfide in 120 ml of dry dichloromethane was placed in a 200 ml four-necked flask protected from moisture. The flask was kept in a cold bath at −20 to −25 °C and was protected from light during the subsequent reaction. A solution of 8.0 g (50 mmol) of bromine in 60 ml of dichloromethane was added dropwise over a period of 2 h with stirring. The mixture was allowed to warm to −15 °C during a 1 h period, then 18.1 g (100 mmol) of **5t** in 140 ml of dichloromethane was added dropwise over a period of 1 h. The mixture was allowed to stand at 0 °C for 24 h. The solvent was stripped off under a reduced pressure; the residual product was recrystallized twice from ligroin to give **4e**, mp 126—127 °C (dec), yield 15.3 g (50%), NMR δ=1.60 (s, 3, SCH_3), 4.20 (d, 1, CHS), 5.10 (d, 1, J=10 Hz, CHBr), 7.28 (s, 10, C_6H_5). Found: C, 58.88; H, 5.15; Br, 27.01; S, 10.30%. Calcd for $C_{15}H_{15}BrS$: C, 58.63; H, 4.92; Br, 26.01; S, 10.44%. Found: *m/e* 306.0085, 308.0095. Calcd for $C_{15}H_{15}BrS$: M, 306.0078; M+2, 308.0059. MS indicated that the sample contained less than 5% of **6**.

In a similar manner, 9.1 g (50.5 mmol) of **5c** gave 9.6 g (61.9%) of **4t**, mp 63 °C, NMR δ=1.91 (s, 3, SCH_3), 4.40 (d, 1, CHS), 5.28 (d, 1, J=9 Hz, CHBr), 7.13 (s, 10, C_6H_5). Found: C, 58.42; H, 4.84; Br, 26.25; S, 10.42%. Found: *m/e* 303.9932, 305.9981, 308.0025. Calcd for $C_{15}H_{15}BrS$: M−2H, 303.9922; M, 306.0078; M+2, 308.0059. MS indicated that the sample contained less than 2% of **6**.

Preparations of Stilbene Dibromides (6). The *meso*- (**6e**) and *dl*-isomers (**6t**) were prepared according to the procedures developed earlier by the addition of bromine to **5t** in diethyl ether[35] and to **5c** in carbon tetrachloride[36] respectively. The *meso*-isomer (**6e**): mp 237 °C (dec) (lit,[36] mp 237—239 °C (dec)), (Found: C, 49.41; H, 3.32%). The *dl*-isomer (**6t**): mp 110.5—111.5 °C (lit,[36] mp 110— 111 °C), NMR δ=5.44 (s, 2, CHBr), 7.13 (s, 10, C_6H_5), (Found: C, 49.01; H, 3.26%).

Preparations of Stilbene Dichlorides (7). *meso*- (**7e**) and *dl*-Stilbene dichlorides (**7t**) were prepared according to the procedure developed by Buckles[37] by treating **5t** and **5c** respectively with tetrabutylammonium iodotetrachloride. The *meso*-isomer (**7e**) : mp 190.0—190.5 °C (lit,[37] mp 191—192 °C), NMR δ=5.19 (s, 2, CHCl), 7.36 (s, 10, C_6H_5), (Found: C, 66.79; H, 4.92%). The *dl*-isomer (**7t**): mp 90.0—90.5 °C (lit,[37] mp 91—92 °C), NMR δ=5.20 (s, 2, CHCl), 7.13 (s, 10, C_6H_5), (Found: C, 66.90; H, 4.94%).

A Typical Procedure for the Elimination Reaction with Butyllithium. Reactions were done in a four-necked flask fitted with a reflux condenser, a thermometer, a gas inlet tube, a rubber septum, and a magnetic stirrer. The flask was protected from moisture. All experiments were carried out under nitrogen, passed through a Fieser's solution[38] to remove traces of oxygen, or under argon. *erythro*-1-Bromo-2-methoxy-1,2-diphenylethane (**1e**, 293 mg, 1.01 mmol) in 50 ml of diethyl ether was placed in the flask and cooled in a Dry-Ice bath. The system was flushed with argon gas for 2 h. The solution of butyllithium in hexane (3.0 ml, 1.0 mmol) was added *via* a syringe and the mixture was stirred for 30 min at 0 °C. By the addition of butyllithium, the mixture was turned pale red, but this color disappeared if the solution was flushed with air. The mixture was poured into ice-water, extracted with ether, and dried over sodium sulfate. When excess butyllithium was used, a small amount of methanol was added *via* a syringe to decompose it before treating with water. To the concentrated product, 100 mg of diphenyl ether was added as an internal standard. The mixture was analyzed by GLPC using a silicone OV-17 3% on Chromosorb-W 2 m column at column temperature 160 °C.

In a separate experiment, the reaction product was chromatographed with silica gel (Wako-gel C-200) column using hexane as an elutant, giving **5c**, bp 96—102 °C/3 mm, (Found: C, 93.08; H, 6.91%). It was identified by the comparisons of its GLPC, IR, and NMR data with those of an authentic sample.

A Typical Procedure for the Elimination Reaction with Pentylmagnesium Bromide. The equipment used in these reactions is the same as that used in the butyllithium reactions.

A solution of 295 mg (1.01 mmol) of **1e** in 50 ml of diethyl ether was placed in the flask and cooled in a Dry-Ice bath. The system was flushed with nitrogen. A solution of pentylmagnesium bromide in ether (5.0 ml, 2.0 mmol) was added *via* a syringe and the solution was stirred for 180 min at 0 °C. The reaction mixture was poured into ice-water, extracted with ether, and dried over sodium sulfate. After removal of ether, 107 mg of diphenyl ether was added as an internal standard. The products were analyzed by GLPC; decane, **5t**, and the unreacted substrate were identified. The yield of **5t** was 49%.

Separation of the products was carried out by column chromatography using neutral alumina (W-200) and petroleum ether. The obtained **5t** was contaminated with **1e**, as identified by comparing its NMR spectrum with that of a mixture of **5t** and **1e**. The recovered **1e** has a mp of 110—114 °C; its IR spectrum was superimposable with that of an authentic sample. When **1t** was used as a substrate, the recovered **1t** had a mp of 69—73 °C and its IR spectrum was superimposable with that of an authentic sample. Thus the isomerization of substrates during the reaction process could be eliminated.

In a separate experiment, 219 mg (1.22 mmol) of **5c** was stirred with pentylmagnesium bromide (5.0 ml, 2.0 mmol) for 3 h under the reaction conditions. No **5t** but **5c** alone was detected in the reaction product by means of GLPC.

A Typical Procedure for the Elimination Reaction with Lithium Metal. To a solution of 613 mg (2.11 mmol) of **1e** in 100 ml of diethyl ether was added 164 mg (24 mg-atom) of lithium metal (a lithium wire 3 mm in diameter cut into 1—2 mm lengths). The stirred mixture was refluxed for 30 h under a nitrogen atmosphere. Excess lithium metal was filtered off, and the filtrate was poured into a cold aqueous ammonium chloride solution and extracted with ether. The ether extract was dried over sodium sulfate and concentrated. After adding 108 mg of diphenyl ether as an internal standard, the product was analyzed by GLPC, giving the following yields: **8**, 9.1; **5c**, 8.7; **5t**, 58.3%; a trace of a peak expected to be diphenylacetylene. The product was chromatographed by the use of alumina (W-200) and petroleum ether, giving three fractions: the 1st fraction was **8**, which was identified by means of GLPC, NMR, and IR; the 2nd fraction, mp 124—125 °C, was **5t**, which was identified by means of GLPC and IR; the 3rd fraction was a mixture of **5c** and a trace amount of diphenylacetylene, identified by the retention times of GLPC.

The authors wish to express their thanks to Dr. Tokio Yamabe of this department for his helpful discussion. We also would like to thank Messrs. Hiroyasu Furukawa and Yukio Ueda for their assistance in the preliminary experiments of this work. This work was supported in part by a Scientific Research Grant from the Ministry of Education, Japan (No. 110305).

References

1) A part of this work has been presented as a preliminary communication: T. Sugita, K. Nishimoto, and K. Ichikawa, *Chem. Lett.*, **1973**, 607.

2) H. O. House and R. S. Ro, *J. Am. Chem. Soc.*, **80**, 182 (1958).

3) J. K. Kochi and D. M. Singleton, *J. Am. Chem. Soc.*, **90**, 1582 (1968); D. M. Singleton and J. K. Kochi, *ibid.*, **89**, 6547 (1967); C. L. Stevens and J. A. Valicenti, *ibid.*, **87**, 838 (1965); J. Sicher, M. Havel, and M. Svoboda, *Tetrahedron Lett.*, **1968**, 4269.

4) I. M. Mathai, K. Schug, and S. I. Miller, *J. Org. Chem.*, **35**, 1733 (1970).

5) W. K. Kwok, I. M. Mathai, and S. I. Miller, *J. Org. Chem.*, **35**, 3420 (1970).

6) H. M. Walborsky and M. S. Aronoff, *J. Organomet. Chem.*, **51**, 31 (1973).

7) a) W. H. Glaze and C. M. Selman, *J. Org. Chem.*, **33**, 1987 (1968); D. E. Applequist and G. N. Chmurny, *J. Am. Chem. Soc.*, **89**, 875 (1967); b) H. M. Walborsky and M. S. Aronoff, *J. Organomet. Chem.*, **51**, 55 (1973).

8) a) R. L. Letsinger, *J. Am. Chem. Soc.*, **72**, 4842 (1950); b) H. M. Walborsky, F. J. Impastato, and A. E. Young, *ibid.*, **86**, 3283 (1964).

9) G. Fischer, K. A. Muszkat, and E. Fischer, *J. Chem. Soc., B*, **1968**, 1156.

10) B. M. Trost and S. Ziman, *Chem. Commun.*, **1969**, 181; *J. Org. Chem.*, **38**, 932 (1973).

11) H. J. S. Winkler and H. Winkler, *Justus Liebigs Ann. Chem.*, **705**, 76 (1967).

12) E. A. Braude, "Progress in Organic Chemistry," ed by J. W. Cook, Butterworths, London (1955), Vol. 3, p. 209; A. G. Brook, H. L. Cohen, and G. F. Wright, *J. Org. Chem.*, **18**, 447 (1953).

13) M. S. Kharasch, F. Engelmann, and W. H. Urry, *J. Am. Chem. Soc.*, **66**, 365 (1944).

14) M. S. Kharasch, G. Stampa, and W. Nudenberg, *J. Org. Chem.*, **18**, 575 (1953).

15) W. Reeve and L. W. Fine, *J. Am. Chem. Soc.*, **86**, 880 (1964); O. R. Pierce, A. F. Meiners, and E. T. McBee, *ibid.*, **75**, 2516 (1953); R. D. Chambers, W. K. R. Musgrave, and J. Savory, *Proc. Chem. Soc.*, **1961**, 113; R. Sullivan, J. R. Lacher, and J. D. Park, *J. Org. Chem.*, **29**, 3664 (1964).

16) L. I. Zakharkin, O. Yu. Okhlobystin, and K. A. Bilevitch, *J. Organomet. Chem.*, **2**, 309 (1964); *Tetrahedron*, **21**, 881 (1965).

17) T. E. Hogen-Esch and J. Smid, *J. Am. Chem. Soc.*, **88**, 307 (1966); J. B. Grutzner, J. M. Lawlor, and L. M. Jackman, *ibid.*, **94**, 2306 (1972); H. O. House, A. V. Prabhu, and W. V. Phillips, *J. Org. Chem.*, **41**, 1209 (1976); E. S. Gore and H. S. Gutowsky, *J. Phys. Chem.*, **73**, 2515 (1969).

18) J. Smid, *Angew. Chem.*, **84**, 127 (1972).

19) E. J. Panek, B. L. Neff, H. Chu, and M. G. Panek, *J. Am. Chem. Soc.*, **97**, 3996 (1975).

20) R. L. Letsinger and E. Babko, *J. Am. Chem. Soc.*, **75**, 2649 (1953).

21) R. H. Staley and J. L. Beauchamp, *J. Am. Chem. Soc.*, **97**, 5920 (1975).

22) See, for example, E. S. Gould, "Mechanism and Structure in Organic Chemistry," Henry Holt Co., New York (1959), p. 261.

23) C. S. Tsai Lee, I. M. Mathai, and S. I. Miller, *J. Am. Chem. Soc.*, **92**, 4602 (1970); for a detailed discussion of the intermediates and transition states of base-induced dehalogenation see W. H. Saunders, Jr. and A. F. Cockerill, "Mechanisms of Elimination Reactions," John Wiley & Sons, New York (1973), p. 336.

24) M. P. Periasamy and H. M. Walborsky, *J. Am. Chem. Soc.*, **99**, 2631 (1977).

25) See, for example, D. J. Cram, "Fundamentals of Carbanion Chemistry," Academic Press, New York (1965), p. 71.

26) T. Koyanagi, J. Hayami, and A. Kaji, *Bull. Chem. Soc. Jpn.*, **50**, 763 (1977).

27) Y. Yano and S. Oae, *Tetrahedron*, **26**, 67 (1970).

28) E. G. Howard, *J. Org. Chem.*, **27**, 2212 (1962).

29) H. Gilman, *Org. React.*, Vol. 8, 285 (1954).

30) H. Gilman, E. A. Zoellner, and J. B. Dickey, *J. Am. Chem. Soc.*, **51**, 1576 (1929).
31) R. E. Buckles and N. G. Wheeler, *Org. Synth.*, Coll. Vol. IV, 857 (1963).
32) H. O. House, *J. Am. Chem. Soc.*, **77**, 3070 (1955).
33) G. Heublein, H. Schütz, and A. Zschunke, *Tetrahedron*, **25**, 4225 (1969).
34) G. K. Helmkamp and D. J. Pettitt, *J. Org. Chem.*, **29**, 3258 (1964).
35) L. I. Smith and M. M. Falkof, *Org. Synth.*, Coll. Vol. III, 350 (1955).
36) R. E. Buckles, J. M. Bader, and R. J. Thurmaier, *J. Org. Chem.*, **27**, 4523 (1962).
37) R. E. Buckles and D. F. Knaack, *J. Org. Chem.*, **25**, 20 (1960).
38) L. F. Fieser and M. Fieser, "Reagents for Organic Synthesis," John Wiley, Inc., New York (1967), Vol. 1, p. 393.

Polyelectrolyte Complexes of [2-(Diethylamino)ethyl]dextran Hydrochloride with Sodium Carboxymethylcellulose

Yasuo KIKUCHI* and Takashi KODA

Department of Materials Science and Engineering, Faculty of Engineering, Ōita University, 700-Dannoharu, Ōita 870

(Received July 24, 1978)

Sodium carboxymethylcellulose(*anti*-thrombogenic material)(CMC) reacted with [2-(diethylamino)ethyl]-dextran hydrochloride(*anti*-cancer material)(EA) having an opposite charge and three groups of different basicity at different hydrogen ion concentrations to form novel water-insoluble precipitates, the so-called polyelectrolyte complex(PEC) comprised of both biomedical materials, focusing on the coagulation of precipitate(PEC) produced. The mole ratio N(EA)/Na(CMC) of the reaction mixture in solution at the start coagulation increased with a lowering of hydrogen ion concentration. This depended on the change of the degree of dissociation of EA and CMC with changing hydrogen ion concentration. The nitrogen contents which describe the mole ratios of EA/CMC in each PEC thus prepared were determined to range from 1.75 to 4.51. It was established that the hydrogen ion concentration and mixing mole ratio of N/Na in solution play an important role in determining the composition ratio of EA/CMC in the PEC. The results of IR, elemental analyses, solubility measurements, degree of swelling in water, color reaction with Toluidine Blue, and blood clotting test for PEC, revealed that the molecular structure of the various PEC's differed according to the hydrogen ion concentration and the mole ratio of reaction mixture in solution, though all PEC's were prepared from the same starting materials. It appears that the degree of dissociation and conformation of EA and CMC change with hydrogen ion concentration. The blood clotting tests were performed on a slightly swelled tablet of PEC where it was found that the PEC suppressed coagulation of the blood.

The mixing of oppositely charged polyelectrolytes give rise to the formation of a polyelectrolyte complex whose properties, conformations, and biomedical characters, in general, are sensitive to such reaction conditions as the composition of the reaction mixture, the hydrogen ion concentration, the order of mixing, and the polyion concentration at which the reaction is conducted.[1,2]

The mechanism of polyion interaction, the probable structures of the PEC, and properties have been investigated in detail by Michels *et al.*[3,4]

To date, however, few papers[5] have dealt with the polyion interaction between polysaccharide, or polysaccharide and synthetic macromolecules of importance becasue of the similarities to biological systems, membranes, and industrial and biomedical applications.[6] In a previous paper[7] the chemical reaction of EA and sodium dextran sulfate (*anti*-thrombogenic material) which is a biomedical material was reported.

This paper deals with a novel chemical reaction of [2-(diethylamino)ethyl]dextran hydrochloride with sodium carboxymethylcellulose, focusing on the coagulation of the PEC produced, the general characteristics, and the process of clot formation.

Experimental

Sodium carboxymethylcellulose(*anti*-thrombogenic material, weak acid polyelectrolyte, intrinsic viscosity 0.401 dl/g in 1 M NaCl at 25 °C, sodium content 7.79%) and [2-(diethylamino)ethyl]dextran hydrochloride(*anti*-cancer material, weak basic polyelectrolyte, nitrogen content 4.97%, degree of substitution 1.11 mol/A.G.U.†) prepared by molecular weight 250000 of dextran(described later in detail), were obtained from Wako Junyaku Co., Ltd., and from Meito Sangyo Co., Ltd., Japan, respectively.

CMC and EA were highly-purified and used without further purification. CMC and EA (2 g/1000 ml) were dissolved in aqueous solution. The reaction were conducted at pH 3.0, 7.0, and 11.0, the pH of solution being adjusted to 7.0 and 11.0 with sodium hydroxide and to 3.0 with hydrochloric acid. The EA solutions were added dropwise to the CMC solutions, adjusted to the same pH as those of the EA solutions at a rate of 50 ml/30 min with stirring. The water-insoluble precipitate, the so-called PEC comprised of both biomedical materials, were thus obtained. After aging for a half hour, the precipitate was washed with water and methanol, centrifuged, and dried in vacuo at 50 °C to constant weight.

The blood clotting test was conducted according to the procedure of Imai and Nose;[8] PEC 200 mg was pressed (8 t/4.9 cm^2) in a vacuum for 10 min to make a sample tablet. The ACD blood of type A (Red Cross Hospital Blood Center) was kept in a thermostat at 4—6 °C for 3 days. The ACD blood was prepared by adding the blood to an anticoagulant citrate dextrose solution consisting of sodium citrate, citric acid and dextrose.

Elemental analyses of the PEC were performed at the Institute of Physical and Chemical Research.

The structures of **1** and **2** of EA have been proposed by Meito Sangyo Co., Ltd., Japan:

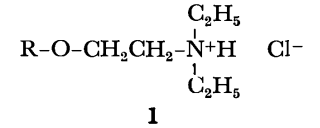

1

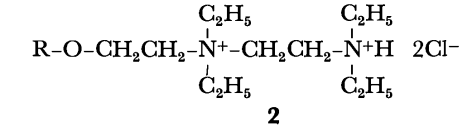

2

R: dextran residue.

Both groups are present in each molecule of EA *i.e.* three groups of different basicity, are reflected in the form of the titration curves in a previous paper,[7] quarternary (strong basic) and two tertiary ammonium groups in **1** and **2**, respectively.[9] Potentiometric titration studies of polybases for

† Determined at Meito Sangyo Co., Ltd., Japan.

EA have supplied information regarding the properties of the substances in solution.[10] The titration curves obtained in these experiments have been reported in a previous paper.[7] The ratio of groups **2** to group **1** was approximately 0.78 : 1. On the basis of the inflection points in the potentiometric titrations and the start, before and after of coagulation of PEC in the reaction system, subsequent experiments were conducted at pH 3.0, 7.0, 11.0, and a mole ratio N/Na of the reaction mixture in solution in Table 1.

The purple coloration is due to the reaction of CMC with a solution containing Toluidine Blue, utilized to demonstrate the CMC elution from PEC and the change of structure produced.

Results and Discussion

Experimental conditions, yields and elemental analyses for the PEC prepared at the beginning and end point, and before and after coagulation of PEC in the reaction system are given in Table 1, respectively.

The nitrogen contents which describe the molar ratios of EA/CMC in each PEC increased with an increased in the mole ratio of N/Na of the reaction mixture in solution and with a decrease in hydrogen ion concentration a direct consequence of the fact that the degree of dissociation of CMC and EA are dependent on the hydrogen ion concentration, *i.e.* the composition ratio of EA/CMC in the PEC was sensitive to the reaction conditions. Thus, the pH as well as the mole ratio of EA to CMC in the reaction mixture, played an important role in changing the ratio of the reactive group of CMC to that of EA in the PEC produced.

As seen in Fig. 1, the mole ratios N/Na of the reaction mixture in solution at the beginning point of coagulation increase with an increase in pH, *i.e.* a larger amount of EA is necessary to coagulate the CMC solution containing PEC with a lowering of hydrogen ion concentration. The reason for this is that the degree of dissociation of EA decreases and that of CMC increases with a lowering of hydrogen ion concentration, *i.e.* the decreasing of the positive net charge of EA and the increasing of the negative charge of CMC.

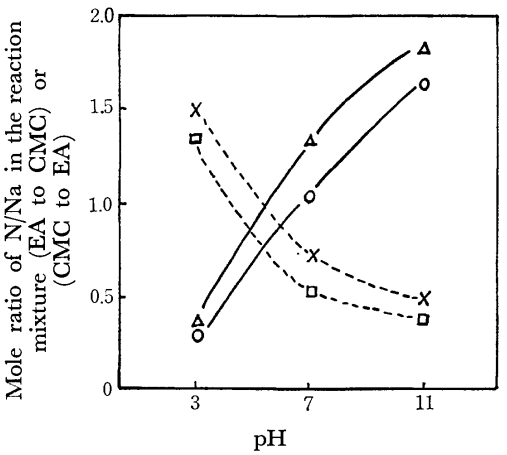

Fig. 1. Beginning and end points of coagulation. ○: Beginning point of coagulation, △: end point of coagulation (EA to CMC, N/Na).
×: Beginning point of coagulation, □: end point of coagulation (CMC to EA, Na/N).

The IR spectrum of PEC is similar to that of a mixture of CMC and EA, differing only in detail. How-

Table 1. Experimental conditions,[a] polymer yield and elemental analyses of polyelectrolyte complexes[b]

Sample code	Amount of EA or CMC solution (ml EA or ml CMC / 100 ml CMC or EA)	Mole ratio of N/Na in solution	Yield of polymer (g)	Nitrogen content (%)	Sodium content (%)	Chlorine content (%)
A-1[c]	19.1	0.20	0.09	2.05	—	—
A-2[c,f]	29.5	0.31	0.18	1.75	—	—
A-3[c,g]	34.0	0.36	0.21	1.83	—	—
A-4[c]	200.0	2.10	0.24	2.27	0.02	0.08
B-1[d]	76.5	0.80	0.20	3.74	—	—
B-2[d,f]	99.5	1.04	0.26	3.84	—	—
B-3[d,g]	128.0	1.34	0.37	3.80	—	—
B-4[d,h]	200.0	2.10	0.37	4.10	0.05	0.77
C-1[e]	76.5	0.80	0.17	4.14	—	—
C-2[e,f]	155.0	1.62	0.38	4.34	—	—
C-3[e,g]	176.0	1.84	0.44	4.42	—	—
C-4[e]	200.0	2.10	0.45	4.51	0.19	0.13
D-1[c]	188.5	0.56	0.47	2.43	0.11	0.0
D-2[d,i]	188.5	0.56	0.30	3.82	0.06	0.07
D-3[e]	188.5	0.56	0.26	3.99	0.14	0.0

a) Concentration of EA and CMC, 2.0 g/l. A, B, C series: EA solution was added dropwise to CMC solution. Amount of CMC solution was 100 ml. D series: CMC solution was added dropwise to EA solution. Amount of EA solution was 100 ml. b) The analyses were performed at the Institute of Physical and Chemical Research. c) Both CMC and EA solutions were adjusted to pH 3.0. d) Both CMC and EA solutions were adjusted to pH 7.0. e) Both CMC and EA solutions were adjusted to pH 11.0. f) Coagulation just occured. g) End point of coagulation. h) Carbon content, 50.67%, hydrogen content, 7.77%. i) Carbon content, 50.59%, hydrogen content, 7.79%.

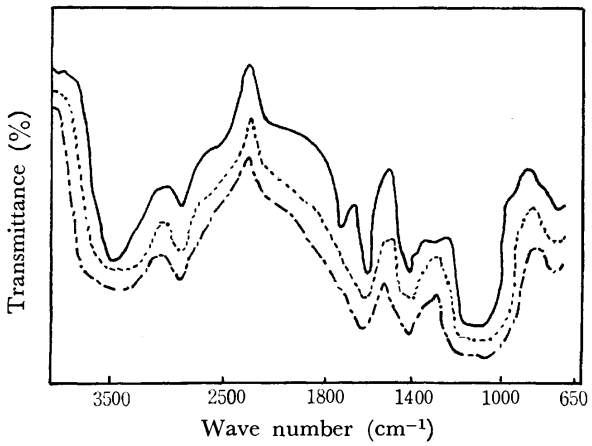

Fig. 2. IR spectra of polyelectrolyte complexes.
—— : Polyelectrolyte complex prepared at pH 3.
---- : Polyelectrolyte complex prepared at pH 7.
—·— : Polyelectrolyte complex prepared at pH 11.

ever, the PEC prepared at pH 3 had an absorption band at 1740 and 1240 cm^{-1}, which appeared neither in the PEC prepared at pH 7 and 11.0 nor in the mixture of EA and CMC. These absorption bands had been assigned to COOH group.[11] Furthermore, the absorption band at 3500 cm^{-1} (assigned to the OH group) of PEC prepared at pH 3 shifted to a higher wave number. In consideration hydrogen bond of formation between the OH group and other reaction groups, it is reasonable to expect shifts in frequency. In addition, the sodium and chlorine contents in the PEC are smaller than those in CMC or EA, and the nitrogen content distinctly different (Table 1). The results suggest that the amino groups in EA participate in the binding with CMC, probably through the $-COO^-$ groups, and that the molecular structures of PEC are different from one another. Actually, the PEC prepared at low hydrogen ion concentration differed appreciably from the PEC prepared at higher hydrogen ion concentration in such properties as the degree of swelling and the color reaction with Toluidine Blue as described later.

Table 2. Color reaction with Toluidine Blue[a]

Sample code	Color of solution	Color of PEC
EA	blue green	—
CMC	blue purple	—
A-1	blue purple	blue
A-2	blue purple	blue
A-3	blue purple	blue
A-4	blue purple	blue
B-1	blue green	white
B-2	blue green	white
B-3	blue green	white
B-4	blue green	white
C-1	blue green	white
C-2	blue green	white
C-3	blue green	white
C-4	blue green	white
D-1	blue purple	blue
D-2	blue green	white
D-3	blue green	white

a) Sample code corresponds to that in Table 1.

The resulting purple stain with Toluidine Blue provides a very sensitive test for CMC. Only the PEC of series A prepared at pH 3 gave a blue coloration, but not a blue purple coloration with Toluidine Blue as shown in Table 2.

The *anti*-thrombogenic CMC in the PEC produced did not elute into the solution except for PEC of series A as shown in Table 2.

PEC's are insoluble or only partially soluble in dimethyl sulfoxide or *N*,*N*-dimethylformamide on heating, partially soluble in a ternary solvent mixture (acetone/KBr/H_2O=20 : 20 : 60 wt %) on heating, and soluble in formic acid or a ternary solvent mixture (HCl/dioxane/H_2O=48 : 47 : 5 wt %) on heating. The difference in solubility however, is in discernible. The PEC's prepared at low hydrogen ion concentration are however, more soluble than those prepared at high hydrogen ion concentration.

Table 3. Swelling with water

Sample code	Degree of swelling
A-1	No swelling
A-2	No swelling
A-3	No swelling
A-4	No swelling
B-1	Slight swelling
B-2	Slight swelling
B-3	Slight swelling
B-4	Fairly large swelling
C-1	Slight swelling
C-2	Slight swelling
C-3	Slight swelling
C-4	Fairly large swelling
D-1	No swelling
D-2	Slight swelling
D-3	Fairly large swelling

a) Sample code corresponds to that in Table 1.

Swelling tests were performed with all PEC listed in Table 3. All the PEC prepared at pH 3 did not swell entirely. The degree of swelling of PEC became larger with decreasing hydrogen ion concentration and increasing mole ratio N/Na of the reaction mixture.

These experimental results support the differences in molecular structure according to the experimental conditions of hydrogen ion concentration and mole ratio of the reaction mixture, although the PEC have common constituents. It appears that the degree of dissociation and conformation of EA and CMC changes with hydrogen ion concentration.

The blood clotting tests were performed on a PEC tablet (A-4, B-3, C-2, D-1, D-2) prepared in solution (Table 1) by gravimetric measurement[8] of the amount of clot formed at the appropriate time intervals, after the addition of calcium chloride solution (0.1 M, 0.015 ml) to ACD blood (0.15 ml, A type, storage time 3 d) which had been in contact with the ma-

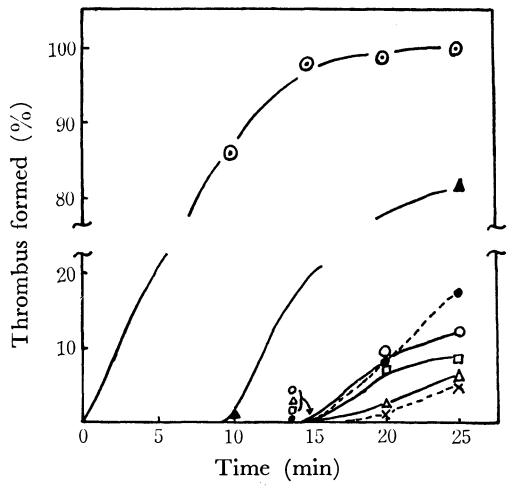

Fig. 3. Percentage of the thrombus formed on polyelectrolyte complexes compared with that on glass.
⊙: Glass, ▲: polyvinyl chloride, ●: C-2, ○: B-3, □: D-1, △: A-3, ×: D-2.
Sample codes C-2, B-3, D-1, A-3, and D-2 correspond to those in Table 1.

terials. The lightly swelled PEC could not perform the blood clotting test because of the soaking of blood into the tablet and therefore, the tests were performed on a PEC tablet with a small degree of swelling in A, B, C, and D series. The quantities of the clot formed on the PEC tablet are smaller than those formed on glass or PVC tablets. The PEC has an *anti*-thrombogenic character and supresses the coagulation of blood. Differences in *anti*-thrombogenic behavior among them is however, hardly discernible.

References

1) E. Tsuchida and T. Osada, *Kobunshi Kagaku*, **22**, 384 (1973).
2) H. Noguchi, *Kobunshi Kagaku*, **22**, 402 (1973).
3) A. S. Michels and R. G. Miekka, *J. Phys. Chem.*, **65**, 1765 (1961).
4) A. S. Michels, L. Mir, and N. S. Schneider, *J. Phys. Chem.*, **69**, 1447 (1965).
5) K. Shinoda and A. Nakajima, "Summary of Paper of 23th Polymer Symposium (Tokyo, Japan)," 1974, p. 21.
6) A. Nakajima, *Kagaku To Kogyo*, **27**, 88 (1974).
7) Y. Kikuchi and H. Fukuda, *Nippon Kagaku Kaishi*, **1977**, 1051.
8) Y. Imai and Y. Nose, *J. Biomed. Mater. Res.*, **6**, 165 (1972).
9) *Cf.* Sephadex Ion Exchange Pharmacia, Uppsala.
10) S. A. Rice and M. Nagasawa, "Polyelectrolyte Solutions," Academic Press, New York (1961).
11) K. Nakanishi, "IR Absorption Spectroscopy," Nankodo, Tokyo (1960), p. 49.

Photoinduced Dechlorination of β-Benzene Hexachloride in Alkaline Alcohols[1)]

Yoshiro OGATA,* Katsuhiko TAKAGI, and Yasuharu SASOH
Department of Applied Chemistry, Faculty of Engineering, Nagoya University, Furo-cho, Chikusa-ku, Nagoya 464

(Received August 9, 1978)

Photo-induced dechlorination of β-benzene hexachloride(β-BHC) in alkaline alcohols has been studied. Benzene is a major product accompanying other minor products such as chlorobenzene, alkoxybenzene, and benzyl alcohols. Their yields vary a great deal depending on the kind of alcohol. The efficiency of reaction and the selectivity of benzene increase in the order : methanol<ethanol<2-propanol. The reaction may go by way of dechlorination of β-BHC with base in the dark giving trichlorobenzenes(predominantly 1,2,4-isomer) followed by its photochemical dechlorination. The radical chain mechanism involving H-abstraction by Cl· atom is presented, since the efficiency is raised *ca.* 8 times as much as that in the dark.

Attention has recently been centered upon the photochemical decomposition of organic chlorine-containing compounds as pollutants. Several reports have appeared on the photodechlorination of polychlorinated biphenyl(PCB) in either neutral or alkaline media,[2-8)] since PCB has high stability and high resistance against thermolysis.

On the other hand, the photochemical decomposition of aliphatic chlorine-containing compounds used as insecticides, *e.g.*, Aldrin, Deldrin, Endrin or γ-BHC, is difficult on account of their transparency towards UV light over 230 nm,[9,10-12)] so that few attempts have been made to decompose the aliphatic chlorine-containing compounds. Only a qualitative study on photoinduced decomposition of γ-BHC with sodium hydroxide in 2-propanol was reported, but no attempt was made for identification of the photoproducts and no mechanistic study carried out.[12)]

The present work was undertaken to elucidate photoproducts and to present the mechanism for photoinduced decomposition of β-BHC in various alkaline alcohols.

Results and Discussion

Photodecomposition of β-BHC in Alkaline Alcohols. Irradiation of 0.01 M β-BHC in *ca.* 0.3 M alkaline alcohols with a 300 W high pressure Hg lamp (wavelength 360—600 nm) results in the decomposition of β-BHC with efficiency depending on the kind of alcohol used (Fig. 1). The efficiency increases with the change of alcohol in the order: MeOH<EtOH<2-PrOH. β-BHC is transparent at wave length over 200 nm, but on addition of alkali, a dark reaction occurs forming aromatics, so that the solution absorbs the 270—280 nm light.

The decomposition rate in 2-propanol is *ca.* 8 times as high as that in methanol, all β-BHC being completely consumed within 2 h. However, the yield of benzene still increased even after 100% consumption of β-BHC, reaching a maximum value after 6 h, implying the intervention of precursors to benzene. A slight decrease in the yield of benzene after reaching its maximum can be attributed to further degradation, *e.g.*, benzene reacts with chlorobenzene to give biphenyl.[12)]

The extent of dechlorination of β-BHC was estimated to be 4.89 of Cl atoms per one molecule of β-BHC

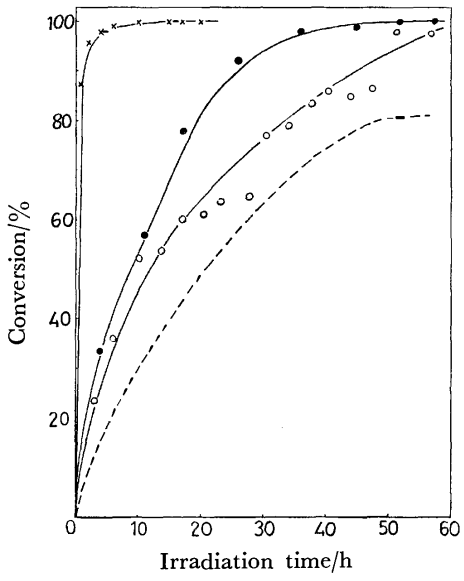

Fig. 1. Irradiation time-conversion curve of photodecomposition of β-BHC in various alkaline alcohols: methanol (—○—○—), ethanol(—●—●—), and 2-propanol(—×—×—). A curve (----) obtained on the basis of chloride ion at 15—20 °C.

decomposed (or 81% Cl^- production), indicating the formation of chlorine-containing substances in yields of 19% based on the decomposed β-BHC. Most of them could not be identified except for chlorinated benzenes such as mono-, di-, and trichlorobenzenes which appeared in the initial stage of the decomposition of β-BHC.

Scheme 1 represents the isolated and/or characterized photoproducts in various alkaline alcohols. Their yields after almost complete decomposition of β-BHC are summarized in Table 1.

Products were identified and estimated by means of GLC and GLC-MS in comparison with the corresponding authentic samples.

Formation of the corresponding carboxylic acids was observed by further oxidation of **7**'s in an aerated solution. They were characterized as their corresponding esters by addition of excess HCl to the reaction mixture; *e.g.*, methyl formate from formaldehyde.

Benzene was obtained as the major non-chlorine containing product in yields of 23.5, 37, and 48% in alkaline methanol, ethanol, and 2-propanol, re-

Table 1. Products from photolysis of β-BHC in alkaline alcohols[a)]

$[\beta\text{-BHC}]_0$	$[R^1R^2CHONa]_0$ in R^1R^2CHOH	Irrad. time (h)	Conv. (%)	Yield (%) PhH (1)	PhCl (2)	$PhOCR^1R^2$ (3)	$PhCR^1R^2$ OH (4)	Ph_2 (5)
0.02	0.36 ($R^1=R^2=H$)	50	91	23.6	3.5	2.3	2.3	0.5
0.017	0.28 ($R^1=H$, $R^2=CH_3$)	17	78	21	12.1	3.8	12.3	2.5
0.017	0.28 ($R^1=H$, $R^2=CH_3$)	56	100	37	1.0	—b)	—b)	—b)
0.011	0.19 ($R^1=R^2=CH_3$)	2	96	14	20	—b)	—b)	—b)
0.011	0.19 ($R^1=R^2=CH_3$)	6	100	48	11	—b)	—b)	—b)

a) Conversion and yields were measured by means of GLC using bromobenzene and/or diphenylmethane as internal standard reagents. b) Not determined.

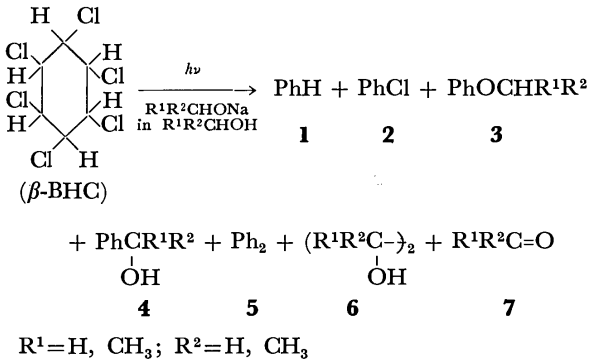

Scheme 1.

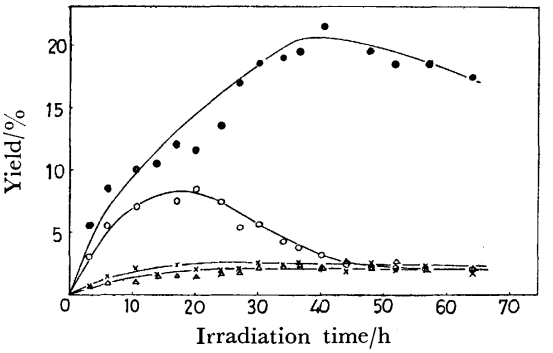

Fig. 2. Irradiation time-conversion curve of photodecomposition of β-BHC to give benzene (—●—●—), chlorobenzene (—○—○—), anisole (—×—×—), and benzyl alcohol (—△—△—) in alkaline methanol at 15—20 °C.

spectively.

Although 81% of chlorine of β-BHC was liberated as chloride ion, the material balance calculated by means of the chloride formed deviates significantly from that on the basis of cyclic six-membered carbon compounds which comprise benzene, chlorobenzene, alkoxybenzene, benzyl alcohols, and bibenzyl. Total yields of the aromatic compounds are at most as follows: 45.5% for the case in metanol, 50% in ethanol, and 60% in 2-propanol. The loss of Cl content can be attributed to the formation of ring-ruptured chlorine-containing fragments and/or polymerized β-BHC which cannot be detected by GLC up to 250 °C. Detection of fragments or oligomers derived from β-BHC was unsuccessful even by careful GLC analysis.

Effect of Irradiation Time on Photoproducts. A typical example of photolysis of β-BHC in alkaline methanol is shown in Fig. 2. Apparently no substantial amounts of di- and trichlorobenzenes were formed even at the initial stage

Independent photolysis of 1,2,4-trichlorobenzene in alkaline ethanol generated 74% of chloride ion. It is assumed that three atoms of chlorine are liberated from one molecule of the trichlorobenzene, thus yielding benzene, chlorobenzene and phenetole (33, 45, and 22%, respectively).

Competitive dechlorination with a mixture of 1,2,4-trichloro-, 1,2-dichloro-, 1,4-dichloro-, and monochlorobenzenes showed that the 1,2,4-isomer is the most unstable towards UV light and monochlorobenzene the most stable; 1,2,4- and 1,2-halides are almost photodecomposed within 1.5 h irradiation, whereas the mono- and 1,4-dihalides require over 6 h for almost complete decomposition. This suggests that the trichlorobenzene is formed at the earliest stage, but it does not accumulate on account of its instability towards UV light in the presence of alkali.

Progressive Dechlorination of β-BHC. β-BHC is stable under UV irradiation because of its transparency to UV light over 230 nm. The initiation

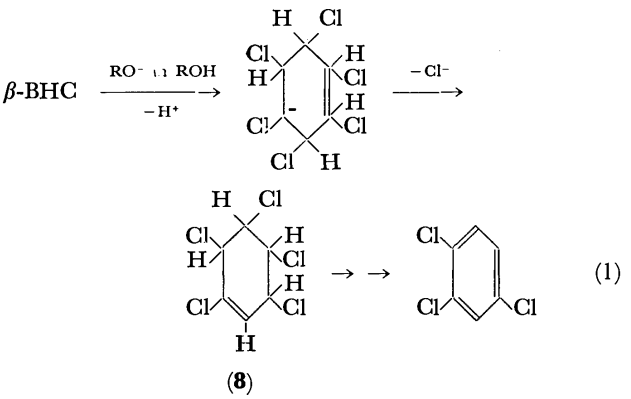

(1)

necessitates UV-absorbing species. Trichlorobenzenes containing 87% of the 1,2,4-isomer are formed in the dark by treatment of β-BHC in alkaline methanol.[13] The reaction is explained by a mechanism involving a carbanion formed by deprotonation of β-BHC with alkoxide.[13] Trichlorobenzenes, however, do not undergo dechlorination with alkali in the dark, but they are easily decomposed into benzene, chlorobenzene, and alkoxybenzene on irradiation as described above.

Hence, the photolysis of β-BHC is apparently initiated by the trichlorobenzenes. Nevertheless, the photoinduced dechlorination of β-BHC cannot be explained only by the photodecomposition of trichlorobenzenes, since the photoinduced decomposition of β-BHC is *ca.* 8 times as fast as that in the dark (Fig. 3).

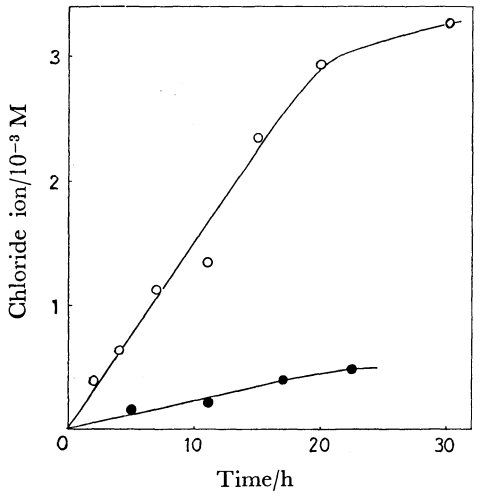

Fig. 3. The time dependence of the formation of chloride ion at 25 °C (a) on photolysis of an ethanol solution of β-BHC (0.0014 M) and sodium hydroxide (0.028 M) (—○—○—) and (b) on standing it in the dark (—●—●—) at 15—20 °C.

If only the above carbanionic dechlorination of β-BHC with alkali is operating, the efficiency of photoinduced consumption of β-BHC would not exceed that in the dark. A radical chain mechanism is conceivable in which dechlorination of β-BHC occurs mainly via a hydrogen abstraction by chlorine atom generated by photolysis of trichlorobenzenes.

$$\beta\text{-}C_6H_6Cl_6 + 3RO^- \xrightarrow[\text{dark}]{ROH} C_6H_3Cl_3 + 3ROH + 3Cl^- \quad (2)$$

$$C_6H_3Cl_3 \xrightarrow{h\nu} C_6H_3Cl_2\cdot + \cdot Cl \quad (3)$$

$$Cl\cdot + \beta\text{-}C_6H_6Cl_6 \longrightarrow HCl + C_6H_5Cl_6\cdot \quad (4)$$

$$C_6H_5Cl_6\cdot \longrightarrow C_6H_5Cl_5 + Cl\cdot \quad (5)$$

(**8**)

$$\mathbf{8} \longrightarrow C_6H_3Cl_3 + 2HCl \quad (6)$$

$$C_6H_3Cl_2\cdot + R^1R^2CHOH \longrightarrow C_6H_4Cl_2 + R^1R^2\dot{C}OH \quad (7)$$

$$R^1R^2\dot{C}OH + Cl\cdot \longrightarrow R^1R^2C{=}O + HCl \quad (8)$$

$$2R^1R^2\dot{C}OH \longrightarrow (R^1R^2C(OH)-)_2 \quad (9)$$

(pinacol)

Analogously,

$$C_6H_4Cl_2 + R^1R^2CHOH \xrightarrow{h\nu} C_6H_5Cl + R^1R^2\dot{C}OH + Cl\cdot \quad (10)$$

$$C_6H_5Cl + R^1R^2CHOH \xrightarrow{h\nu} C_6H_6 + R^1R^2\dot{C}OH + Cl\cdot \quad (11)$$

Pinacol was accumulated during the course of irradiation, especially in 2-propanol, 2,3-butanediol being rapidly accumulated even after 100% decomposition of β-BHC. The pinacol is derived by photoreduction of acetone in 2-propanol. The formation of biphenyl is explained by the reaction of chlorobenzene with benzene.

$$C_6H_5Cl + C_6H_6 \xrightarrow{h\nu} Ph_2 + HCl \quad (12)^{12}$$

Chlorobenzene is known to be easily photodecomposed to give alkoxybenzene or phenol by photosubstitution along with benzene.[14–17] In our photoreaction, anisole (in methanol) and phenetole (in ethanol) were observed (see Table 1). However, careful analysis by GLC and GLC-MS revealed no formation of tri- or dialkoxybenzenes, and/or alkoxychlorobenzenes, suggesting that tri- or dichlorobenzenes are very rapidly dechlorinated rather than undergoing nucleophilic substitution under these conditions.

It is of interest that aromatic radical substitution occurs; *i.e.*, benzyl alcohol and 1-phenylethanol are formed during photolysis. Independent photolysis of trichlorobenzenes, or chlorobenzene under similar conditions did not afford such products; hence the substitution may originate at the stage of dechlorination of β-BHC. They may be formed as follows.

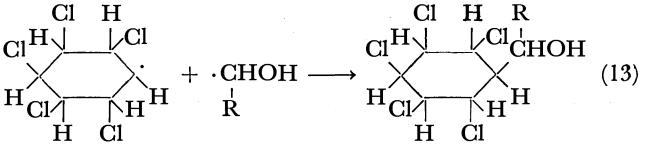

(13)

(R=H, or CH_3)

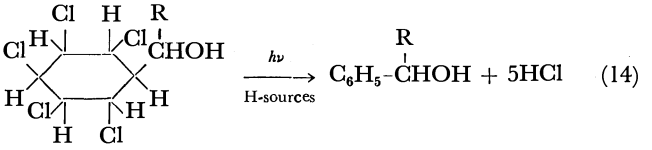

(14)

This is an evidence for the homolytic dechlorination of β-BHC to the radical $\cdot C_6H_6Cl_5$ through a radical chain mechanism involving chlorine atom as a chain carrier.

Experimental

Materials. β-BHC(extra pure grade, Tokyo Kasei Co.) was used without further purification. 2,3-Butanediol was synthesized by photolysis of acetone in 2-propanol.[18] *o*-(and *p*-)Chlorophenetoles were prepared by treatment of *o*-(and *p*-)chlorophenols with ethyl bromide in the presence of potassium carbonate.[19]

General Procedures. A Halos high-pressure 300 W Hg lamp with a water-cooling quartz jacket was used as a light source immersed in a reaction solution in a reactor (1000 ml

volume) equipped with a thermometer and a condenser. The reaction solution was adjusted to contain 0.01 M β-BHC and 0.3 M sodium alkoxide in alcohol. The reaction mixture was irradiated until the starting β-BHC disappeared. Aliquots were taken out at appropriate intervals of time, yields being estimated by means of titration and GLC technique.

Analysis of Products. Identification of products was carried out by means of GLC with a Yanagimoto gas chromatograph, Model GCG-550F operated with columns packed with either PEG 20 M (4 mm × 1.2 m) or Porapak QS (4 mm × 0.7 m) using N_2 as a carrier gas. Low-boiling products such as benzene, chlorobenzene, aldehyde, and esters were identified and estimated by means of GLC with a Porapak QS column using bromobenzene as an internal standard in comparison with the corresponding authentic specimen. High-boiling products such as polychlorobenzenes (*e.g.*, 1,2,4-trichlorobenzene), alkoxybenzene, benzyl alcohol, 1-phenylethanol, and β-BHC were identified and estimated by GLC with the PEG 20 M column using diphenylmethane as an internal standard.

The other products such as 1,2-ethanediol were characterized by means of GLC-MS with a Shimadzu GLC-MS Model 7000 as follows : *m/e* (relative yield); benzene, 78(M^+) (100); methyl formate, 60(M^+) (56), 32(100), 31(100); methyl acetate, 74(M^+) (32), 43(100); acetic acid, 60(M^+) (100), 58(13), 44(100), 43(15), 31(100), 32(69), 33(28); benzyl alcohol, 108(M^+) (100), 107(33), 79(50); ethylene glycol, 60(M^+) (25), 45(5), 44(12), 43(10), 33(75), 32(12), 31(100); 1-phenylethanol, 122(M^+) (66), 108(10), 107(100), 79(56), 78(12); butanediol, 90(M^+) (9), 75(10), 68(12), 47(12), 46(8), 45(100), 44(8), 43(8); benzene, 78(M^+) (100); chlorobenzene, 113(M^++1) (30), 112(M^+) (100), 77(45), 51(10), 50(10).

The analysis of chloride ion was carried out by addition of excess silver nitrate (10 ml × 0.016 M) to the above aliquot (10 ml), followed by titration with aqueous thiocyanate (0.016 M) after acidification by addition of excess nitric acid. The concentration of the appropriate sodium alkoxide was measured with 0.0662 M HCl using phenolphthalein as an indicator. A control experiment indicated that the covalent-bonded chlorine cannot be detected as chloride ion in the stage of titration.

References

1) Contribution No. 251.
2) V. Zitko, O. Hutzinger, and S. Safe, *Bull. Environ. Contam. Toxicol.*, **6**, 160 (1971); *Chem. Abstr.*, **75**, 19113j (1971).
3) S. Safe and O. Hutzinger, *Nature*, **232**, 641 (1971).
4) L. O. Ruzo, M. J. Zabik, and R. D. Schuetz, *Bull. Environ. Contam. Toxicol.*, **8**, 217 (1972); *Chem. Abstr.*, **78**, 28825g (1973).
5) L. O. Ruzo, M. J. Zabik, and R. D. Schuetz, *J. Agric. Food Chem.*, **22**, 199 (1974); *Chem. Abstr.*, **81**, 24693b (1974).
6) L. O. Ruzo, M. J. Zabik, and R. D. Schuetz, *J. Am. Chem. Soc.*, **96**, 3809 (1974).
7) T. Nishiwaki, M. Usui, K. Anda, and M. Hida, The 36th National Meeting of the Chemical Society of Japan, Osaka, April 1977, Abstr. No. 2G22.
8) T. Nishiwaki, T. Shinoda, K. Anda, and M. Hida, The 37th National Meeting of the Chemical Society of Japan, Tokyo, April 1978, Abstr. No. 3M27.
9) R. D. Ross and D. G. Crossby, *Chemosphere*, 277 (1975); *Chem. Abstr.*, **84**, 55026c (1976).
10) K. Raghu and I. C. McRae, *Science*, **154**, 263 (1966).
11) T. Kawahara, *Nogyo Kensasho Hokoku*, **12**, 49 (1972).
12) Y. Matsui, M. Eto, and K. Maekawa, *Nippon Nogei Kagaku Kaishi*, **47**, 599 (1973).
13) (a) J. Hine, R. D. Weimer, Jr., P. B. Longford, and O. B. Ramsay, *J. Am. Chem. Soc.*, **88**, 5522 (1966); (b) D. J. Cram, "Steric Effects in Organic Chemistry," ed by M. S. Newman, John Wiley and Sons, Inc., New York, N. Y. (1956), p. 319.
14) For a comprehensive review, see J. Cornelisse and E. Havinga, *Chem. Rev.*, **75**, 353 (1975).
15) M. A. Fox, W. C. Nichols, and D. M. Lemal, *J. Am. Chem. Soc.*, **95**, 8164 (1973).
16) D. R. Arnold and P. C. Wong, *J. Am. Chem. Soc.*, **99**, 336 (1977).
17) N. J. Bunce and L. Ravanal, *J. Am. Chem. Soc.*, **99**, 4150 (1977).
18) A. Schönberg, "Preparative Organic Photochemistry," Spring-Verlag New York Inc. (1968), p. 203.
19) D. M. Birosel, *J. Am. Chem. Soc.*, **53**, 1408 (1931).

On the Effects of Crystalline Planes and Purities on Working States of Vanadium Oxide Catalysts in CO-oxidation

Yoshiya KERA

Department of Chemistry, Faculty of Science, Osaka University, Toyonaka, Osaka 560

(Received July 1, 1977)

It was confirmed that the kinetics of CO-oxidation over powdered V_2O_5 under the condition of (P_{CO}/P_{O_2}) more than 2 differed clearly from that under the (P_{CO}/P_{O_2}) less than 2 at 450 °C. The activation energies were 5.6 kcal/mol at 250—410 °C and 13 kcal/mol at 410—490 °C under a reductive condition of $(P_{CO}/P_{O_2})=4.4$, and on the other hand 5.9 kcal/mol at 250—490 °C under an oxidative condition of $(P_{CO}/P_{O_2})=0.43$. On a thin crystalline sample, in which the (010) plane was exposed extensively to the surface, a very rapid process appeared at the initial stage but was soon followed by a steady process. The rapid process was explained well by the Elovich law. On the thin crystalline, cautiously purified, the Elovich process did not appear, but the initial rapid process was kept steadily for 10—20 min and then followed by the other steady process. Accompanied by the change in the kinetics during the reaction, the activation energy changed from 2.3 kcal/mol at 271—410 °C and 17 kcal/mol at 410—480 °C to 29 kcal/mol at 271—480 °C under the $(P_{CO}/P_{O_2})=2.1$. Based on these results, the effects of the crystalline planes and the purities on the working states of V_2O_5 crystal in CO-oxidation are discussed.

Many investigators have devoted themselves to the discussions on the working states of vanadium oxide catalysts-especially as to whether oxygen in the catalyst takes part directly in the catalysis or only adsorbed oxygen and which phases of vanadium oxide play an important role in the working state.[1–13] A unified understanding of the problem, however, has not yet been established fully for the differences from author to author in the biography of the catalysts (purity, carrier *etc.*), in the reaction systems, and in the reaction conditions. By the same reason, divergence is seen in the proposed kinetics even in such a simple reaction as CO-oxidation on vanadium oxide catalysts.[14–18]

Previously, CO-oxidation on crystalline powder of V_2O_5 has been studied by using ^{18}O-tracer[19] and the rates of isotopic exchange between the surface oxygen and ^{18}O-carbon dioxide on the crystalline powder and on the thin plate crystalline, in which the (010) plane was highly exposed to the surface, were compared with each other.[20] These results suggested clearly an important role and a high activity of the (010) plane to CO-oxidation.

In this paper, in order to obtain further information on the effects of the crystalline planes and also the purities of V_2O_5 on the catalytic activity and the working states, the rates of CO-oxidation over various kinds of V_2O_5 crystalline- powdered and thin plate, and unpurified and purified- were investigated under various reaction conditions: temperature, pressure and the ratio of CO to O_2. From the results it was deduced that the catalytic properties of the surface, especially the (010) plane, changed remarkably only by the elimination of a very little amount of impurities.

Experimetnal

Materials. V_2O_5 obtained by thermal decomposition of NH_4VO_3 (special grade, Wako Pure Chem. Co.) at 600 °C in air stream for 3 h was used as the powdered catalyst. Thin plate crystallines were prepared by a soft touched pulverization of single crystals of V_2O_5 with an agate mortar and then sieving. The single crystals, unpurified and purified, were made from the unpurified V_2O_5 and cautiously purified V_2O_5 powder, respectively, by a zone-melting method.[24] The purification was done chemically according to the methods of McCarely *et al.*[21] and Haemers.[22] The BET surface areas of the V_2O_5 catalysts are summarized in Table 1. In the unpurified single crystal, S_s-u, ESR signals ascribed to V^{4+} ions and Fe^{3+} ions[23] were found. According to a chemical analysis, the content of Fe was 0.005% (Fe/V). On the other hand, in the purified single crystal, S_s-p, no ESR signal was detected.[24]

Table 1. V_2O_5 catalysts and BET surface area

V_2O_5 catalyst			Surface area (m^2/g)
Powdered V_2O_5 (commercial, special grade)		S_p-c	2.5
Powdered V_2O_5 (dec. of NH_4VO_3, special grade)		S_p-d	8.0
Thin plate crystallines (unpurified V_2O_5)	20—42 mesh	S_s-u-1	0.09
	80—100 mesh	S_s-u-2	0.3
	170—200 mesh	S_s-u-3	1.2
Thin plate crystallines (purified V_2O_5)	20—42 mesh	S_s-p	0.09

The preparations and purifications of CO and O_2 gases were done by usual methods. In the reactants no impurity was detected mass-spectrometrically.

Apparatus and Procedures. The reaction was done statically with a cylindrical glass vessel (diameter=8 cm, length=6 cm). In the reaction apparatus, the dead volume of the trap and the manometer, V_D($\approx$25 cm^3), was kept as small as possible compared with the reaction volume, V_R ($\approx$310 cm^3). The catalysts were dispersed widely on the side wall. The changes in the pressures during the reaction were determined by reading the level of the Hg-manometer with a cathetometer. Reaction temperature were controlled within $\pm$1 °C.

For the measurement of a very rapid rate at the initial stage on S_s-u and S_s-p, a small trap, inserted between the manometer and the reaction vessel, was cooled with liq.N_2. For the measurements of a steady rate it was not cooled. The catalysts were previously heated in air and then *in vacuo* at 490 °C for 1 h. Activities of the catalysts were almost recovered by such a pretreatment. Thus, for a series of determinations of the temperature- and pressure-dependences of the rates, the same catalyst was used repeatedly.

Results

Effects of the Sizes, the Shapes, and the Purities of V_2O_5 Catalysts on the Rate of the Catalytic Oxidation of CO-a Survey of the Kinetics. CO-oxidation on the Unpurified V_2O_5- the Powdered (S_p-d) and the Thin Plate Crystalline(S_s-u): In the catalytic oxidation of carbon monoxide over the unpurified V_2O_5 catalyst, S_p-d and S_s-u, a very rapid process appeared at the initial stage but was soon followed by a slow steady process. The period of the appearance of the initial process was prolonged on a small amount of the catalysts and at a low temperature, as illustrated in Fig. 1. The rapid process, which is almost invisible at 450 °C on S_p-d of 0.122 g (Fig. 1-a), appears clearly at 450 °C on that of 0.03 g (Fig. 1-b) and at 256 °C on that of 0.116 g (Fig. 1-c).

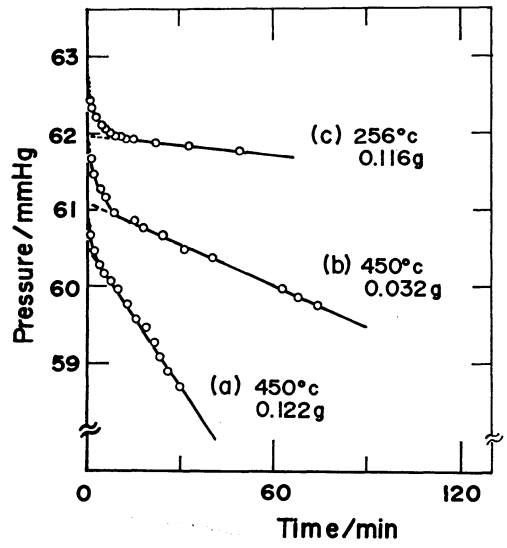

Fig. 1. Appearence of an initial fast process in CO-oxidation at a decreased temperature by use of a reduced amount of V_2O_5 catalyst.

The rapid process was recovered easily by the evacuation at 10^{-5} mmHg above 450 °C for 1 h. When the temperature of the trap, inserted between the reaction vessel and the manometer, was suddenly changed from 195 to 77 K in the steady state, the rapid process seems to be recovered again for a while. The results obtained at 434 °C on S_s-u-3 of 0.027 g are illustrated in Fig. 2. Under the condition that the produced CO_2 was always removed from the gaseous phase by the liq. N_2 trap, the period of the appearance of the process was further prolonged. The result obtained on S_s-u-1 of 0.121 g at 410 °C under the total pressure of 42 mmHg and the ratio (P_{CO}/P_{O_2}) of 2.1 is given in Fig. 3-a as an example. The analysis of the process by the "Elovich equation,"[25] $(P_0-P)/(P_0-P_\infty)=\log(t_0+t)$, is shown in Fig. 3-b, where P is the total pressure and t_0 is a parameter assumed as 5 min. The initial rapid process seems to be described well by the Elovich law. This feature of the kinetics suggests that the surface is gradually deactivated, accompanied by adsorption of the produced CO_2. However,

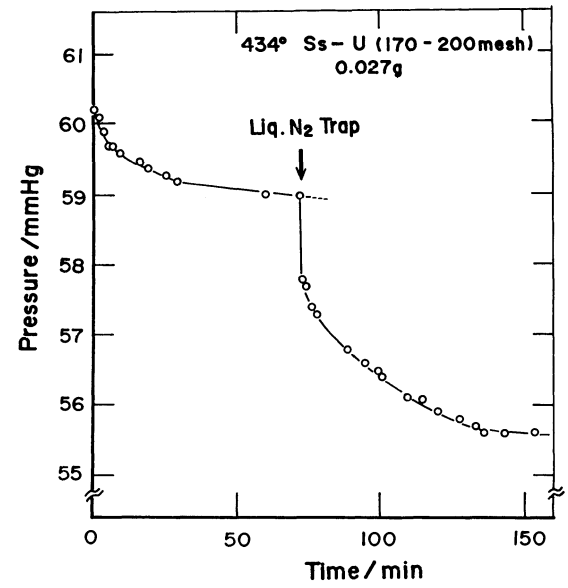

Fig. 2. Effect of elimination of produced CO_2 from gaseous phase and surface after a steady state was reached on the initial fast process.

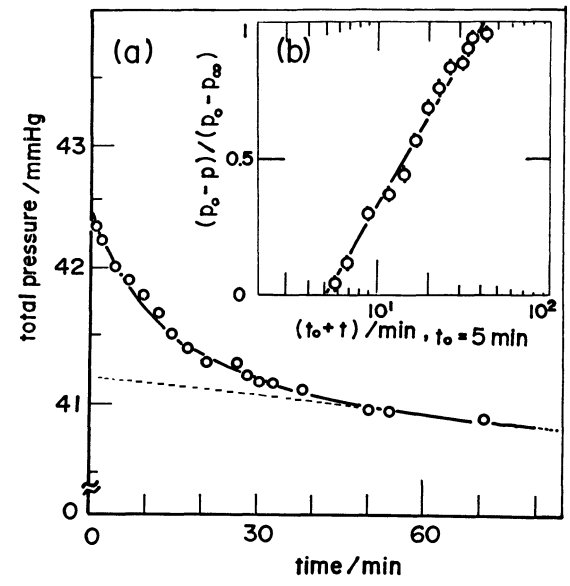

Fig. 3. A kinetical treatment of the initial fast process. (a) reaction curve of CO-oxidation on thin crystallines of V_2O_5 at initial. (b) analysis of the initial process according to Elovich low; $(P_0-P)/(P-P_\infty)=\log(t_0+t)$, where P is total pressure, P_0 and P_∞ are given by the cross point between the vertical axis and the reaction curve and the points on the dotted line at each time, respectively, t is reaction time, and t_0 is a parameter, assumed as 5 min.

no further discussion on the kinetics is done. Only the mean rates for 5 min at the start of the rapid process, measured repeatedly on S_s-u-1 of 0.121 g at various temperatures from 210 to 490 °C under the total pressure of 20 mmHg and the $(P_{CO}/P_{O_2})=2.1$, are evaluated. The results are discussed below.

The rates of the steady process were evaluated from the slope at the steady state of the reaction curves

on the catalysts of S_p-c, S_p-d, and S_s-u. The rates are summarized in Fig. 4 for comparison. In spite of the rather large differences in the particle sizes, the shapes, and the surface areas, the rates per unit surface area were very similar, especially at the lower pressures. The difference in the rates between the fresh and the repeated runs is seen in Fig. 4. The steady rate on S_p-d at 450 °C changed linearly with the increase in the amount of the catalyst from 0.03 to 0.3 g, as is shown in Fig. 5. The contribution of the diffusion process to the rate may, therefore, be ignored for the steady process.

CO-oxidation on the Purified V_2O_5-the Thin Plate Crystalline, S_s-p: CO-oxidation on the thin plate crystalline, S_s-p, of 0.075 g was examined in the temperature range from 271 °C to 480 °C under the total pressure ($(P_{CO}/P_{O_2})=2.1$) of 23 mmHg. The results are illustrated in Fig. 6. The features of the kinetics seem to be completely different from that on the unpurified catalyst, S_s-u, except for the run at 271 °C. The total pressures decrease linearly and it is noted that the slopes in the reaction curves change abruptly at 10—20 min : from given values to smaller values in the runs at 330 and 370 °C and on the contrary to larger values in the runs at 410—480 °C. The temperature dependences of the rates of the first and the second processes are discussed quantitatively below.

Pressure Dependences of the Steady Rate. The Steady Rate on S_p-d: The steady rates on S_p-d, determined

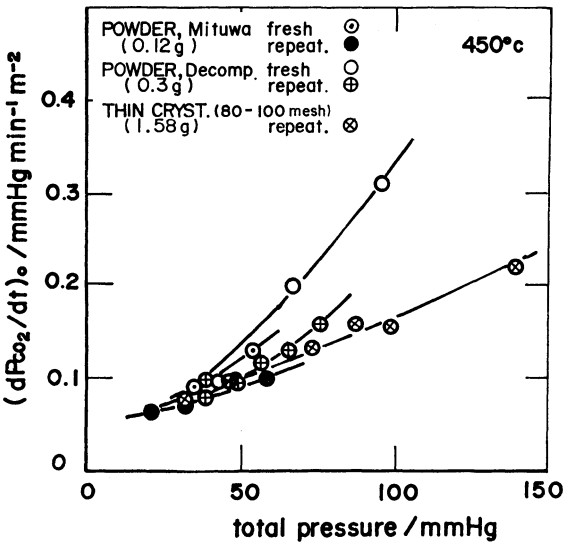

Fig. 4. Comparisons of activities of CO-oxidation among some kinds of powdered and thin crystalline V_2O_5 catalysts at 450 °C.

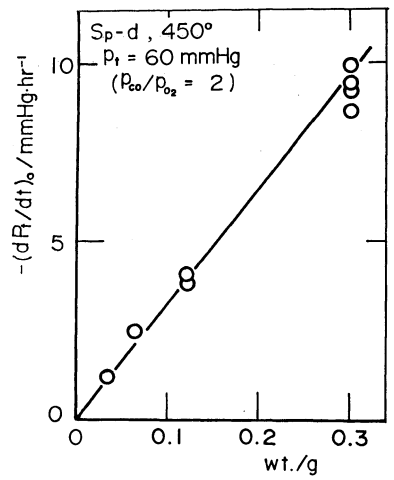

Fig. 5. Verification of linear relation of the steady rate of CO-oxidation with used amount of powdered V_2O_5, S_p-d, at 450 °C.

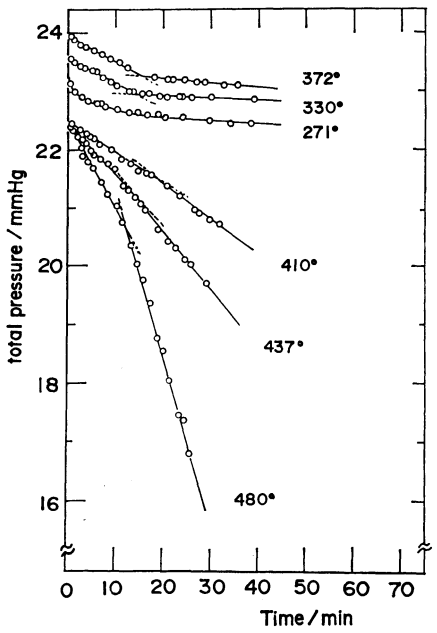

Fig. 6. Reaction curves of CO-oxidation on highly purified V_2O_5 crystallines, S_s-p. Changes in kinetical feature with reaction temperatures.

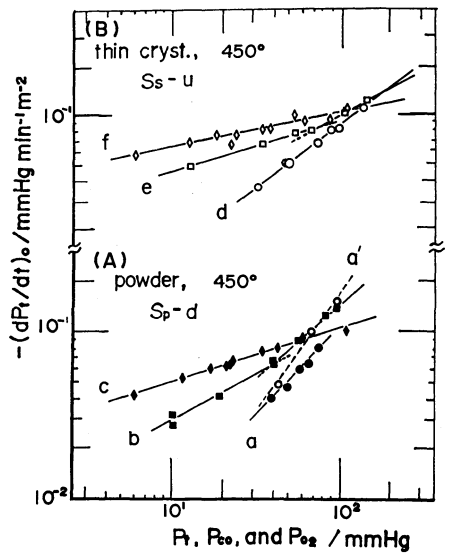

Fig. 7. Pressure dependences of the steady rate at 450 °C on unpurified powdered V_2O_5, S_p-d, (A), (a; the rate *vs.* total pressure, a'; *vs.* total pressure on fresh catalyst, b, *vs.* partial pressure of CO and c; *vs.* partial pressure of O_2) and on unpurified thin crystallines of V_2O_5, S_s-u, (B), (d; the rate *vs.* total pressure, e; *vs.* CO and f; *vs.* O_2).

at 450 °C under various pressures, are summarized in Fig. 7(A). On the vertical axis, the total pressure change (mmHg) per unit time (min) and per unit surface area (m^2) are given in a common logarithm scale. On the abscissa, the total pressure and the partial pressures of CO and O_2 (mmHg) are given in a common logarithm scale, corresponding to the curves a, b, and c, respectively. In curve a, the ratio of CO to O_2, $(P_{CO}/P_{O_2})\equiv r$, was fixed at 2 and the total pressure, P_t, was varied from 39 to 75 mmHg. The curve a′ indicates the rate on the fresh catalyst. It is known from the comparison between the curves a and a′ that the reaction order for P_t is higher on the fresh catalyst than on the catalysts used repeatedly. In the curve b, P_{O_2} was fixed at 20 mmHg and P_{CO} was varied from 10 to 95 mmHg. It should be noted that when P_{CO} exceeded 40 mmHg, that is, the ratio (P_{CO}/P_{O_2}) exceeded 2, the reaction order for P_{CO} changed at once from a given value to a larger one. In the curve c, P_{CO} was fixed at 40 mmHg and P_{O_2} was varied from 6 to 109 mmHg. The reaction order for P_{O_2} was kept constant over all the pressure ranges.

The reaction rates of the steady state can be described by an empirical equation:

$$V_{steady} = k(r)\cdot P_{CO}^{n}\cdot P_{O_2}^{m}. \quad (1)$$

In the case of the stoichiometric mixture of the reactant, $r=2$, Eq. 2 is available:

$$V_{steady} = k(2)\cdot 2^{n}\cdot 3^{-(n+m)}\cdot P_t^{(n+m)}. \quad (2)$$

The reaction orders and the apparent rate constants, evaluated by Eqs. 1 and 2, are summarized in Table 2. It is seen in the table that as soon as r exceeds 2, n increases from 0.57 to 1.0 and at the same time $k(r)$ decreases to one-fifth. The changes in the reaction order and $k(r)$ suggest a change in the working state of the catalyst from V_2O_5 to some lower oxides.

The Steady Rate on the Thin Crystalline, S_s-u: Pressure dependences of the steady rate on the thin crystallines, S_s-u-2 of 1.58 g, were examined at 450 °C. The results are also given in log-log plots in Fig. 7(B). In the curve d, the (P_{CO}/P_{O_2}) was kept constant as 2 and P_t was varied from 32 to 139 mmHg. In the curve e, P_{O_2} was fixed at 30 mmHg and P_{CO} was varied from 12 to 143 mmHg. In the curve f, P_{CO} was fixed at 60 mmHg and P_{O_2} was varied from 6 to 108 mmHg. By the repetition the activity decreased more or less. The activity for the curve d at $P_t=60$ mmHg ($r=2$) was selected as a standard. The activities for the curves e and f at the same condition as $P_t=60$ mmHg ($r=2$) were compared with the standard to estimate the correction factors. The activities of the other points in the curves e and f were evaluated by the use of the correction factors. The reaction orders and the apparent rate constants are also given in Table 2. In the case of S_s-u the changes in n and $k(r)$ are also seen at $r=2$, as shown in Fig. 7 and in Table 2.

The data on the thin plate crystallines are scattered, but the general feature of the kinetics agrees fairly well with that on the powder. The value of $k(r)$ in the former is about 10 times as large as that in the latter. On the other hand, the reaction order for P_{CO}, n, on the former was below one-half of the value on the latter, while the order for P_{O_2}, m, is nearly the same for the two cases. These differences might be caused by the difference in the extent of the (010) plane exposed to the surface between the powder and the thin plate crystalline.

Temperature Dependences of the Rates. The Steady Rates on S_p-d: The steady rates on S_p-d of 0.116 g were measured in the temperature range from 250 to 490 °C under an oxidative ($r=0.43$) and a reductive ($r=4.4$) condition; the total pressures were 70 mmHg. Arrhenius plots of the overall rates (per min and per m^2) are given in Fig. 8. The curve a indicates the

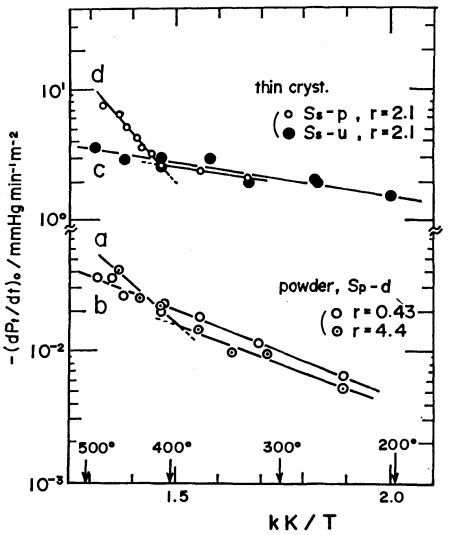

Fig. 8. Arrhenius plots of overall rates of various processes of CO-oxidation. curve-a and -b indicate the run on unpurified powdered V_2O_5, S_p-d, under $P_{CO}/P_{O_2}=4.4$ and 0.43, respectively, curve-c on unpurified thin crystallines, S_s-u, under $P_{CO}/P_{O_2}=2.1$, and curve-d on purified thin crystallines, S_s-p under $P_{CO}/P_{O_2}=2.1$.

Table 2. Changes in the reaction orders on S_p-d and S_s-u with mixing ratios of the reactant

Sample	Temp °C	The ratio P_{CO}/P_{O_2}	$m+n$	m	n	$k(r)$ molecules·cm^{-2}·s^{-1}·P_{CO}^{-n}·$P_{O_2}^{-m}$
Powdered V_2O_5		$r>2$	1.30	0.30	1.00	0.93×10^{-2}
S_p-d, 0.122 g	450	$r<2$	0.87	0.30	0.57	$4.5_4\times10^{-2}$
(0.98 m^2)		$r=2$	1.10 (1.48)[a]			
Thin plate crystallines		$r>2$	0.78	0.25	0.53	1.1×10^{-1}
S_s-u, 1.58 g	450	$r<2$	0.54	0.25	0.29	3.1×10^{-1}
(0.48 m^2)		$r=2$	0.75			

a) The value on the fresh catalyst.

TABLE 3. COMPARISON OF THE ACTIVATION ENERGIES AMONG VARIOUS PROCESSES AND CATALYSTS

Total pressure/mmHg (P_{CO}/P_{O_2} ratio)	Catalyst (process)	E_{ex}/kcal·mol^{-1}	Temp ranges/°C	Reference
70 (r=4.4)	S_p-d (at steady process)	5.6 13	250—400 400—460	Fig. 8
70 (r=0.43)	S_p-d (at steady process)	5.9	250—490	Fig. 8 curve b
20 (r=2.1)	S_s-u (at the initial stage of Elovich's process)	2.3	210—490	Fig. 8 curve c
23 (r=2.1)	S_s-p (1st process up to initial 10—20 min)	2.3 17	330—410 410—480	Fig. 8 curve d and Fig. 9
	S_s-p (2nd process after 10—20 min)	29	330—480	Fig. 9

run of r=4.4 and the curve b the run of r=0.43. Although the data are rather scattered for repeated measurements, the apparent activation energy clearly increased above 400 °C in the run of r=4.4 but was constant over all the temperature range in the run of r=0.43. The activation energies are summarized in Table 3.

Mean Rates at the Start of the Elovich Process on S_s-u: The mean rates for 5 min at the initial stage of the Elovich process on S_s-u-1 of 0.121 g (*cf.* Fig. 3), which were measured repeatedly at various temperatures from 210 to 490 °C under the pressure of 20 mmHg and the (P_{CO}/P_{O_2}) of 2.1, are plotted in Fig. 8(c). The values seem to correspond to the rates on the (010) plane without poisoning by the produced CO_2. The activation energy is as low as 2.3 kcal/mol over all the range of the temperature.

The Rates on S_s-p: The reaction rates were evaluated from the slope of the reaction curves in Fig. 6. The Arrhenius plots of the overall rates are given in Fig. 9. The circles (○) and the squares (□) denote the rates of the first and the second process, respectively. The sequence of the repetition of the measurements is indicated by the numbers given in the upper part of Fig. 9. The number 5 is missing in Fig. 9, because the run was done at 271 °C and the reaction curve did not give a linear change but seemed to correspond to the Elovich equation, as mentioned above. The number 1 indicates the run on the fresh catalyst. By comparison of the activities between the numbers 1 and 11, it is known that the activity decreases only 20—30% even after the catalyst was used eleven times insuccession. Such as extent of deactivation is inessential to the discussion given below.

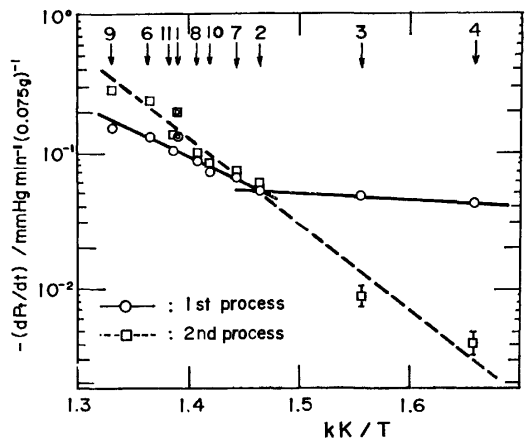

Fig. 9. Arrhenius plots of the first and second processes of CO-oxidation on highly purified thin crystallines, S_s-p. The numbers of the upper part of the Figure indicate sequence of repetition of the measurements.

It should be noted that the experimental points for the second process in the temperature regions above and below 410 °C can be connected with each other by the dotted line in Fig. 9. On the other hand, the Arrhenius plot of the first process consists of two lines crossing each other— the line above 410 °C shows a considerably larger slope than that below the temperature. The temperature dependence of the first process is also given in Fig. 8(d), for comparison.

Discussion

Hughes and Hill[14] have suggested for CO-oxidation over vanadium pentoxide catalyst that a high activation energy is required in the process in the elimination of surface oxygen by carbon monoxide and on the other hand the process in the re-oxidation by oxygen occurs easily. Boreskov *et al.*[17] have indicated that the rates of the reduction of vanadium pentoxide by carbon monoxide and the re-oxidation by oxygen largely depends upon the extent of reduction and oxidation of the surface. Based on their results, the activation energy of 13 kcal/mol, obtained on the unpurified powder above 400 °C under a reductive condition (r=4.4) (*cf.* Fig. 8 and Table 3), would arise from the process on the surface reduced to some extent. On the other hand, at the temperatures below 400 °C, even under such a reductive condition (r=4.4) the surface would be kept in an oxidative state, since the activation energy is as low as 5.6 kcal/mol and is almost the same as 5.9 kcal/mol obtained for the process under an oxidative condition (r=0.43) (*cf.* Fig. 8 and Table 3).

The change in the kinetics, which appeared as soon as the (P_{CO}/P_{O_2}) became larger than 2 with the increase

in the CO partial pressure (*cf.* Fig. 7), would also be understood favorably as corresponding to the changes in the surface state on working. That is, the surface of the powder and the thin plate crystalline, unpurified, is kept in the reduced state on working to some extent at 450 °C under the condition that the (P_{CO}/P_{O_2}) is larger than 2. The differences in the kinetic parameters, $k(r)$ and n, however, are not so small between the powder and the thin plate crystalline (*cf.* Table 2). These differences would arise from the difference in the extent of the (010) plane exposed to the surface. In the thin plate crystalline, the extent of the (010) plane was estimated roughly to be higher by about 38 times than the other planes. In the estimation it was assumed that each crystalline is a square plate with mean sides of 160 μm (*cf.* the sizes of sieves of 80 and 100 meshes, which correspond to 177 and 149 μm, respectively), and the values of 0.31 m^2/g and 3.3 g/cm^3 were used as the surface area of S_s-u-2 and as the density, respectively.

In this work, if the measurements of the oxidation rate of CO over V_2O_5 had been carried out without special attention, only the steady process could be found. On the reduced amount of the catalyst at a low temperature, a very rapid process appeared at the initial stage, as was shown in Fig. 1. On the thin plate crystalline, in which the (010) plane was highly exposed to the surface compared to the other planes, the rapid process was completely differentiated from the steady process and was analyzed well with an Elovich equation, as was shown in Fig. 3. The rapid process could occur mainly on the (010) plane, because in the thin plate crystalline the (010) is exposed to the surface much more than the other planes. Furthermore, from the fact that the rapid process is recovered easily by the evacuation at 450 °C and is prolonged on the elimination of the produced CO_2 from the gaseous phase by the insertion of the liq. N_2 trap, the initial rapid process may be attributed to a process accompanied by the poisoning of the surface by the produced CO_2. Such a process is really consistent with the physical content of the Elovich law.

On the thin plate crystalline, purified carefully, such Elovich kinetics have never been found, and inversely the rapid rate was kept for a while at the beginning but was soon followed by the second rapid process with a very high activation energy (29 kcal/mol), as is shown in Figs. 6, and 9 and Table 3. The initial mean rate for 5 min on the unpurified thin crystalline was almost the same as the rate of the first process on the purified thin crystalline and its temperature dependence was also the same as that on the latter at the temperatures lower than 410 °C (*cf.* Fig. 8). Those consistencies suggest that the active site for CO-oxidation is the same for the thin plate crystallines, unpurified and purified, at least at the start. The sites for the subsequent process, however, differ largely among the crystallines, unpurified and purified, depending upon whether there are very small amounts of impurities. That is, the site on the unpurified seems to be inhibited by the produced CO_2 mentioned above; on the other hand, the sites on the purified seem to vary easily into other sites during the oxidation, as is suggested by Figs. 6 and 9. Such a low activation energy as 2.3 kcal/mol was reported by Kazanskii *et al.*,[18] who obtained the value of 1.6 kcal/mol for a radical process on a vanadium oxide catalyst, $CO + O^-_{ads} \rightarrow CO_2$, below room temperature. From comparison of the activation energies, the very initial process on the thin plate crystallines, unpurified and purified, could be ascribed to a small cycle of reduction and oxidation on the (010) plane. Such a large activation energy as 29 kcal/mol may arise from the process on a considerably reduced surface, according to the indication by Hughes *et al.*[14] and Boreskov *et al.*[17] Thus, the large changes in the activation energies from 2.3 kcal/mol below 410 °C and 17 kcal/mol above 410 °C in the first process to 29 kcal/mol in the second process during the oxidation (*cf.* Fig. 9 and Table 3) suggest clearly the changes in the surface state on working in the purified thin plate crystalline.

In TGA of V_2O_5 in an SO_2 stream, clear-cut and stepwise weight losses were found by Kawashima *et al.*[26] Each step corresponds to a phase change from a given oxide to a different lower one. The clear-cut transitions were explained favorably on the basis of the fact that each vanadium oxide phase has a shear structure and belongs to the Magnéli phase.[27] On the other hand, the recent studies on vanadium bronzes[28] would suggest that such clear-cut transitions between the vanadium oxides are inhibited by the existence of metal impurities, even if the amount is very little. Based on these references, the clear-cut changes in the activation energies, seen only on the highly purified crystalline, could be related to a phase transition of the surface from V_2O_5 to a given lower oxide. However, the question still remains as to which states or phases of the surface are realized on working, depending upon the reaction condition.

The high activity of the (010) plane to CO-oxidation, obtained in this work, is fairly consistent with the results of the previous paper on the isotopic exchange[20] and gives support to the suggestion by Hirota[29] that the pure vanadium oxides themselves without carrier and impurity would play an important role in catalysis. The steady rate on the unpurified powder or thin plate crystalline was slower by one or two orders than the rate on the purified thin crystalline, but the former seemed to be more stable than the latter. Those features of vanadium(V) oxide should also be discussed in view of the stabilities and activities of vanadium bronzes.[28]

The author wishes to express his appreciation to Mr. Michihisa Kyoto for his help in the determination of the surface area of the V_2O_5 catalysts, and Professor Keiji Kuwata for his continued interest in this work and for his valuable suggestions.

References

1) P. Mars and D. W. Krevelen, *Chem. Eng. Sci. (Spec. Suppl.)*, **3**, 41 (1954).
2) G. L. Simard, J. F. Steger, R. J. Arnott, and L. A. Siegel, *Ind. Eng. Chem.*, **47**, 1424 (1955).
3) V. A. Roiter, *Kinet. Katal.*, **1**, 63 (1960).
4) L. Ya. Margolis, *Adv. Catal.*, **14**, 429 (1963).
5) V. Ya. Vol'fson, L. N. Ganyuk, and E. F. Totskaya,

Kinet. Katal., **5**, 1100 (1964); V. Ya. Vol'fson, Ya. V. Zhigailo, E. F. Tatskaya, and V. V. Raksha, *ibid.*, **6**, 162 (1965).
6) T. Vrbaski, *J. Phys. Chem.*, **69**, 3092 (1965).
7) T. Seiyama, A. Suenaga, and W. Sakai, *Nippon Kagaku Zasshi*, **82**, 292 (1966).
8) H. Schaefer, *Ber. Bunzenges. Phys. Chem.*, **71**, 222 (1967).
9) G. K. Boreskov, *Kinet. Katal.*, **8**, 1020 (1967); **13**, 543 (1972).
10) G. L. Ross and P. H. Calderbank, *Chem. Eng. Sci.*, **26**, 2003 (1971).
11) W. M. H. Sachtler, *Catal. Rev.*, **4**, 27 (1971).
12) P. H. Emmett, *Catal. Rev.*, **7**, 1 (1973).
13) E. I. Andreikov, Yu. A. Sveshnikov, and N. D. Rusyanova, *Kinet. Katal.*, **15**, 1207 (1974); **16**, 919 (1975).
14) M. F. Hughes and G. R. Hill, *J. Phys. Chem.*, **59**, 388 (1955).
15) K. Tarama, S. Teranishi, and A. Yasui, *Nippon Kagaku Zasshi*, **81**, 1034 (1960); K. Tarama, S. Teranishi, S. Yoshida, and N. Tamura, *Proc. Int. Congr. Catal. 3rd, Amsterdam*, **1964**, 262 (1963); K. Tarama, S. Yoshida, S. Ishida, and H. Kakioka, *Bull. Chem. Soc. Jpn.*, **41**, 2840 (1968).
16) K. Hirota, Y. Kera, and S. Teratani, *J. Phys. Chem.*, **72**, 3133 (1968).
17) G. K. Boreskov, V. I. Marsheva, V. D. Solovskii, *Dokl. Akad. Nauk SSSR*, **199**, 1091 (1971); G. K. Boreskov and V. I. Marshneva, *ibid.*, **213**, 112 (1973); V. I. Marshneva, G. K. Boreskov, and V. D. Sokolovskii, *Kinet. Katal.*, **13**, 1209 (1972).
18) M. Ya. Koń, V. A. Shets, and V. B. Kazanskii, *Dokl. Akad. Nauk SSSR*, **203**, 624 (1972); *Kinet. Katal.*, **13**, 735 (1972); *ibid.*, **14**, 403 (1973).
19) Y. Kera, S. Teratani, and K. Hirota, *Bull. Chem. Soc. Jpn.*, **40**, 2458 (1967); Y. Kera and K. Hirota, *J. Phys. Chem.*, **73**, 3973 (1969).
20) Y. Kera, *Bull. Chem. Soc. Jpn.*, **50**, 2841 (1977).
21) R. E. McCarley and J. W. Roddy, *J. Less-Common Met.*, **2**, 29 (1960).
22) J. Haemers, *Bull. Soc. Chim. Belg.*, **79**, 473 (1970).
23) Y. Kera and K. Kuwata, unpublished data; see the following references : a) V. A. Ioffe and I. B. Patrina, *Soviet Phys.-Solid States*, **6**, 2425 (1965), b) K. Janzen and G. Sperlich, *Phys. Stat. Sol.*, **55(b)**, 495 (1973).
24) Y. Kera and K. Kuwata, *Bull. Chem. Soc. Jpn.*, **50**, 2438, 2831 (1977).
25) M. J. D. Low, *Chem. Rev.*, **60**, 267 (1960); G. C. Bond, "Catalysis by Metals," Acad. Pres. (1962), p. 108.
26) K. Kawashima, K. Kosuge, and S. Kachi, *Chem. Lett.*, **1975**, 1131.
27) a) A. Magnéli, *Acta Crystallogr.*, **6**, 495 (1953); b) A. D. Wadsley, *ibid.*, **10**, 261 (1957); c) J. S. Anderson and B. G. Hyde, *J. Phys. Chem. Solids*, **28**, 1393 (1967); J. S. Anderson, "Reaction Kinetics in Heterogeneous Chemical Systems," ed by P. Barret, Elsev. (1975), p. 713; d) K. Kosuge and S. Kachi, *Chemica. Scripta.*, **8**, 70 (1975).
28) a) P. Hagenmuller, "Chem. Extend. Defects in Non-Metal. Solids," Amsterdam (1970), pp. 91—108; *Prog. Solid State Chem.*, **5**, 71 (1971); b) M. Nygren, *Chem. Commun. Univ. Stockholm*, 1 (1973).
29) K. Hirota, *Kagaku No Ryoiki*, **25**, 513 (1971); *Chem. Abstr.*, **75**, 122465z (1971).

Molecular Dynamics in Lyotropic Mesophases Studied by ^{23}Na NMR and ESR

Yoko KANAZAWA* and Hirotake KAMEI†

Faculty of Pharmaceutical Sciences, Kyushu University, Maidashi, Higashi-ku, Fukuoka 812

†*Electrotechnical Laboratory, Mukodai-machi, Tanashi, Tokyo 188*

(Received June 19, 1978)

The hexagonal phases of sodium octadecanoate–water system NaS and sodium hexadecanoate–sodium tetradecanoate–water system Na(P+M) were studied by sodium-23 NMR and spin label ESR in the temperature range 40—100 °C, covering the transition temperature of isotropic-liquid crystal T_{I-L} and that of liquid crystal-gel T_{L-G}. The ESR spectrum of liquid crystal systems aligned by the magnetic field and the center line of ^{23}Na NMR spectrum were analyzed. The motions of the alkyl chain and sodium ion are reflected on the ESR and NMR spectral shape and width. The NMR line width is predominantly determined by the local motion of the cation attached on the hydrocarbon rod. During the phase separation region its correlation time $\tau_c \simeq 10^{-10}$ s is constant, comparable to that of chain motion. The change in the local motions of these two species is similar, being continuous across T_{I-L} but drastic across T_{L-G}.

Many studies on the lyotropic liquid crystal including biological systems have been carried out by spectroscopic measurements. For example, the properties of the hydrocarbon chain have been studied by ^{1}H, ^{2}H NMR, and spin label ESR.[1a-1l] NMR of sodium-23 and other alkali metal ions has been utilized for the analysis of cation binding in soap–water systems.[2a-f] Most works have been performed by changing the concentration of components. For the study of molecular dynamics in lyotropic systems around the phase transition or phase separation point, a continuous observation through the transition point is important and variable temperature measurement is essential. Furthermore, a comparison between the dynamical properties of hydrophobic and hydrophilic parts of the amphiphile molecules especially near these transition points will give important information on the mechanisms of biological phenomena. In the present work the dynamical properties of hydrocarbon chain and counter ion in hexagonal phase of lyotropic systems have been studied through phase transition points by means of magnetic resonance.

We have observed the temperature dependence of sodium-23 NMR and spin label ESR of lyotropic liquid crystals, sodium octadecanoate–water (NaS) and sodium hexadecanoate–sodium tetradecanoate–water (Na(P+M)) systems, in the range covering the isotropic liquid-liquid crystal and liquid crystal-gel transition temperatures, T_{I-L} and T_{L-G}, respectively. Choice of the soap systems and their phases is made in order to make stable lyotropic liquid crystals of low transition temperatures. The concentrations of the soaps are adjusted to form hexagonal liquid crystals of T_{I-L} below 90 °C so that the liquid crystals can be aligned under the static magnetic field below 100 °C. The use of the systems of low transition temperatures enables us to measure the spin label ESR throughout the transition temperatures including even the liquid crystal alignment by magnetic field with no noticeable label decomposition. Otherwise, the label is rapidly lost in the slightly alkaline medium above 100 °C. The ^{23}Na NMR and spin label ESR of the system through the transition points were observed continuously.

Experimental

Samples. The soaps (sodium octadecanoate, hexadecanoate, and tetradecanoate) were prepared from reagent grade acids (purity 99%, Wako Chemicals Co.) by NaOH titration and reprecipitated from hot water. The sodium octadecanoate mixture used for NMR measurement was obtained as sodium salt (Kishida Chemicals, Co.) the purity being determined by gas chromatography : 70% octadecanoic, 27% hexadecanoic, and 3% of tetradecanoic and eicosanoic acids.

The sample for NMR measurement was prepared in a 10 mm OD tube with a silicone rubber stopper, being made homogeneous by repeated cooling and heating. The space between the sample mixture and stopper was kept small in order to prevent the evaporation of water. In the case of sodium octadecanoate system, the space above the sample mixture was not small as compared with sample volume so that the homogeneity of the sample might not be satisfactory. The concentration of the mixture was determined by weighing before and after each NMR measurement.

The sample for ESR measurement was prepared in a similar way with appropriate spin probe molecules, **I**, **I′**

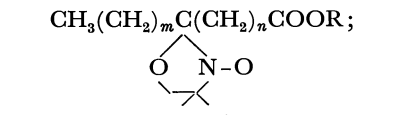

I: $(m, n) = (12, 3)$, $R = CH_3$
I′: $(m, n) = (m, n)$, $R = H$

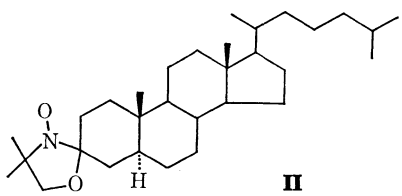

II

(12,3), **I′**(5,10), **I′**(1,14), and **II** (Syva), then sucked up in a capillary tube of about 1 mm diameter, both ends of capillary being sealed. Only the tubes with good sample homogeneity were used. The concentration was determined by means of isotropic-liquid crystal transition points.

The phase transition temperatures T_{I-L} and T_{L-G} were determined by laser light depolarization and scattering. The temperature for both NMR and ESR measurements was initially set above T_{I-L} in order to bring the sample to com-

plete isotropic solution, then slowly changed downwards and spectra were taken 30—60 min after each temperature setting.

NMR Measurement. For the measurement of ^{23}Na NMR signals, a JEOL PS-100 electromagnet with ^{1}H external field lock system was used with 26.45 MHz home made detector systems. Free induction decay (FID) signals were averaged 1000 times and subjected to Fourier transformation with a JEOL EC-6 or EC-100 computer. An average of three observations was taken for each temperature setting. The uncertainty in the shift data for continuous observation was within ± 0.012 ppm over a period of three days. The temperature was controlled by heated air flow (*ca.* 20 l min^{-1}). The temperature distribution across the sample was within ± 0.2 °C.

The half full width of the Fourier transformed signal was taken as the line width and the half full width times the peak height as the measure of intensity. No correction was made for intensity due to the change in the sample density at various temperature nor for the delay time (200 μs) of FID sampling. The maximum line width observable by the present instrumental setting is 500 Hz which has ample allowance for the observed width of the center line of up to 60 Hz. No ^{23}Na satellite for oriented molecules is to be detected under these experimental conditions. ^{23}Na signals of 1.1 M NaCl and 0.8 M sodium acetate aqueous solutions were taken as references.

ESR Measurement. The X-band ESR spectra of nitroxide spin probes were taken with a JEOL JES ME-X spectrometer with temperature control system JEOL JES VT-3. The variation in temperature at each setting was within ± 1 °C. The sample capillary was set perpendicular to the magnetic field so that it can easily be rotated around its axis for observation of the effect of magnetic field alignment of the amphiphile systems. Microwave power of 1.0—1.5 mW and 100 kHz field modulation of 1.0 G amplitude were used.

Results

The phase diagram of Na(P+M) system is constructed by laser light depolarization and ESR and NMR spectra (Fig. 1). It is similar to that of NaS system and its analogs such as NaP, NaM, NaL(sodium dodecanoate–water) systems with some depression in

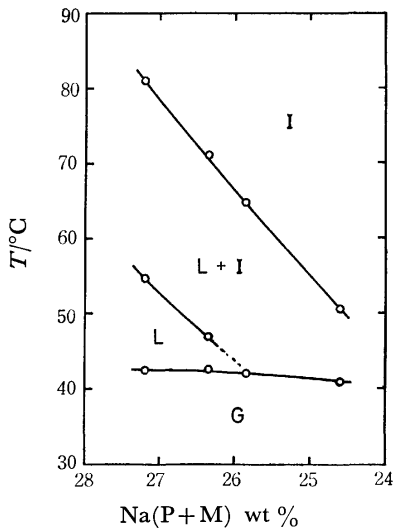

Fig. 1. Phase diagram of Na(P+M) system.

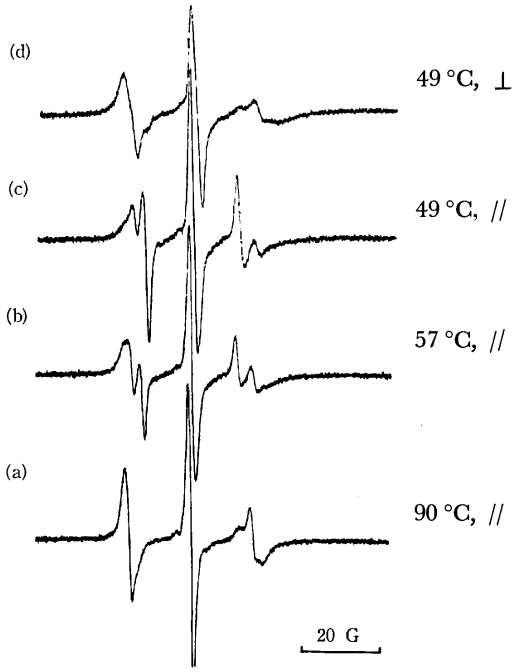

Fig. 2. ESR spectra of label **I** in Na(P+M) 27% system.

the transition point T_{I-L} as compared with that of the corresponding carbon number.

The ESR spectra of label **I** in the system of 27 weight percent aqueous solution of the equal weight mixture of sodium hexadecanoate and sodium tetradecanoate (abbreviation Na(P+M) 27% likewise will be used hereafter) is shown in Fig. 2. The spectrum above T_{I-L} consistes of one triplet due to ^{14}N hyperfine coupling constant of 14.9 G. The spectrum below T_{I-L} seems to be a superposition of two triplets: one with the coupling constant A_{iso} of 14.9 G arising from the isotropic phase and the other with a smaller coupling constant of 11.8 G from oriented molecules. The order parameter of the z axis, the direction of the largest hyperfine splitting (radical axis), for the oriented label **I** can be given by

$$S = (1/2)\langle 3\cos^2\theta - 1\rangle = (A_{//} - A_{\perp})/(A_{zz} - A_{xx})$$
$$= (3A_{//} - 2A_{xx} - A_{zz})/2(A_{zz} - A_{xx}) = -0.19,$$

where $A_{//}$(11.6 G) is the observed coupling constant, A_{xx}=6.1 G, A_{zz}=32.4 G,[1f] and θ is the angle between the radical axis and the static magnetic field. The spectral intensity of the oriented molecules increases and that of the isotropic phase decreases towards T_{L-G}. The line widths of these signals seems to be constant throughout the liquid crystal region. Below T_{L-G}, a sudden signal broadening is observed and the spectrum changes gradually to that of solid towards lower temperature.

The spectrum of label **I** in Na(P+M) 27% system with the sample capillary rotated by 90° in the magnetic field under the conditions of fixed molecular alignment below T_{I-L} shows a larger coupling constant $A_{\perp}$ than isotropic ones (Fig. 2d).

Because of high T_{I-L} of NaS system, the spin labeled compounds decompose when the sample preheating is sufficient enough to equilibrate the system in the

isotropic phase. The ESR experiment of NaS system was carried out only for the purpose of confirming whether the molecular arrangement is of similar type to that of Na(P+M) system in liquid crystal region.

The line widths, intensities, and chemical shifts of ^{23}Na NMR signals of Na(P+M) 25.9, 26.4, and 27.2% systems and NaS 17.1% and 20.0% systems were observed at various temperatures. The results of Na(P+M) 26.4, 27.2, and NaS 20.0% systems are shown in Figs. 3, 4, and 5. The temperature dependence of linewidths and intensities of these five samples are of the same type.

The linewidth in the isotropic region increases towards T_{I-L} with fall in temperature. The Arrhenius plot of the width gives the activation energy for the reorientational motion of ion or the fluctuational motion of the environment of the sodium ion provided that the motional narrowing condition is satisfied in the isotropic region. The activation energie is 18.0—20.0 kJ mol^{-1} for NaS systems and 14.6—16.8 kJ mol^{-1} for Na(P+M) systems. The signal intensity is constant in this region.

In the liquid crystal region, $T_{I-L} > T > T_{L-G}$, the line width remains constant till it starts to increase at T' ($T' > T_{L-G}$). The signal intensity decreases distinctly between T_{I-L} and T' and approaches asymptotically to about 40% of its isotropic value, while the width remains constant, keeping the 40% value till the phase transition temperature T_{L-G} is reached. The effect of sample rotation on the center line width

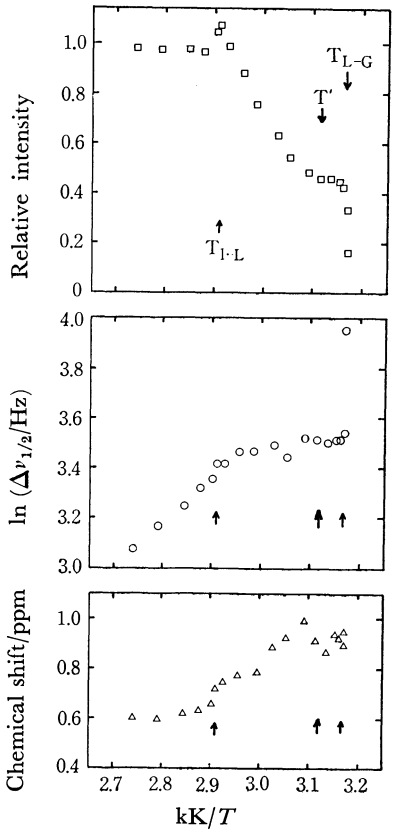

Fig. 3. ^{23}Na NMR parameters plotted against $1/T$ for Na(P+M) 26.4% system. The chemical shift is measured from an arbitrary point and its increasing number means an high field shift.

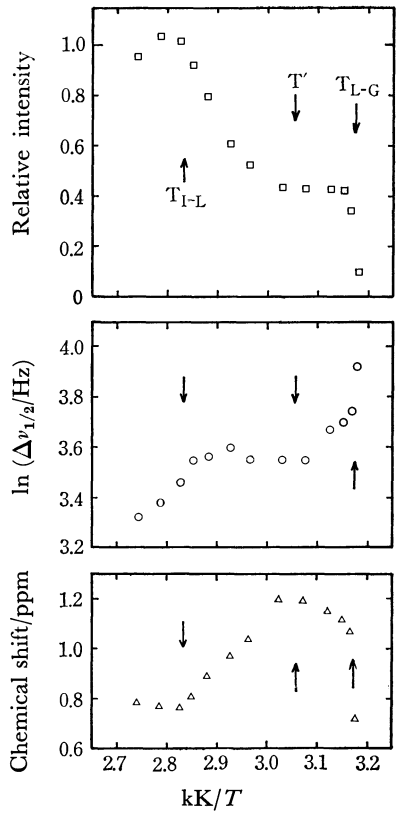

Fig. 4. ^{23}Na NMR parameters plotted against $1/T$ for Na(P+M) 27.2% system.

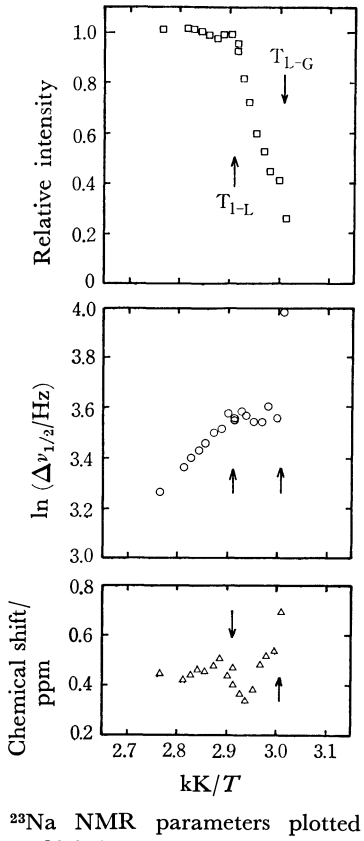

Fig. 5. ^{23}Na NMR parameters plotted against $1/T$ for NaS 20.0% system.

is expected to be negligible, neither linewidth change nor line distortion being observed.

When the temperature is set at T_{L-G}, the line width increases abruptly and the signal becomes undetectable within a few hours as the sample solidifies. No signal in the gel state could be observed.

The temperature dependence of the chemical shift of NaS system and that of Na(P+M) system are not alike. However the data within each system has a similar aspect.

Discussion

ESR Spectrum. The label **I** ESR signal in the isotropic phase is a triplet with the coupling constant A_{iso} of 14.9 G. However, the peak heights of the three lines are not the same, indicating that the phase is a micellar solution as expected. An extra small signal observed at 90 °C in the high field region is probably due to the molecules near the air- and/or glass-sample interface which tends to align while the bulk is still in isotropic state.

Two sets of triplets observed between T_{I-L} and T', one with the coupling constant of isotropic and the other of oriented state, indicates that the system is in the coexistence region of isotropic and liquid crystal phases. The variation in their relative intensities with temperature between T_{I-L} and T' is a further indication of the two phase region. The spectrum of the oriented label is comparable to that of a spin label in shear oriented hexagonal rods observed by Seelig and Limacher.[11] The order parameter S found for the oriented radical axis -0.19 is also that of the molecular axis since the direction of p electrons on N atom in the molecule **I** is parallel to the long axis of the molecule in all its trans configuration. The value $S=-0.19$ can be easily interpreted in terms of the hexagonal phase in which molecules aggregate to form rods with the rod axis parallel to the static magnetic field. The order parameter of a fictitious molecule, with the arrangement $\theta=\pi/2$ and no fluctuational motion of the molecular axis, should be -0.5. The difference between -0.5 and -0.19 is presumably due to the fluctuational motion of the chain and to a slight tilt of the radical axis or that of the molecular axis itself from the normal of the rod surface. The evidence for a magnetic field alignment of rods is obtained from the coupling constant. (1) The coupling constant $A_\perp$ of label **I** observed with sample rotated by 90° is large; $A_\perp(\text{obsd}) > A_{iso} = 14.9\text{ G} > A_{//}(\text{obsd}) = 11.8$ G. The spectrum is consistent with the calculated coupling constant $A_\perp = 16.5$ G for the rod structure with the rod axis perpendicular to the static magnetic field. (2) The spectrum of label **II** whose radical axis is perpendicular to the molecular axis is also consistent. The order parameter of the molecular axis in Na(P+M) calculated from the observed coupling constant 17.5 G and known constants $A_{xx}=6.1$ and $A_{zz}=32.1$ G[1f] is -0.3. The higher order found for molecular axis of label **II** than for label **I** is probably due to more rigid nature of the labeled molecule **II** itself.

The orders observed for the label **I**′(5, 10) and **I**′(1, 14) are lower than that of **I** and **I**′(12, 3), decreasing with the increasing distance between nitroxide group and the carboxyl group. Such a tendency is in line with the liquid crystal structure where the polar group is fixed at the surface of the rods, and resembles that observed in the chain motion in parallel bilayers of lyotropic systems.[1d,g]

The ESR line width is narrow, not changing with temperature in the liquid crystal region. A reasonable interpretation is that the motion of the chain in amphiphilic molecules is rapid enough[3] to average out the θ distribution, leaving only the effective $\langle\cos^2\theta\rangle$ in the spectrum. The increase in line width below T_{L-G} is due to that in rigidity of the chain and in the restriction of molecular rotation around its molecular axis.

No attempt was made to evaluate the equilibrium proportion of liquid crystal *vs.* isotropic liquid in the phase separation region from the apparent intensity of oriented molecules by two reasons. (1) A rather high proportion of molecules is in glass-sample interface of the capillary where the effect of the glass surface on the liquid crystal orientation should be considerable. (2) It is probable that the molecules turning into liquid crystal when their large porportion is already in an array of liquid crystal might not find ample space to form the rod in its preferred orientation along the magnetic field. The following result supports the above argument. No signal for reoriented molecule is detected 1 h after the sample capillary rotation by 90° in the static field at 55 °C while the molecular reorientation is confirmed 10 minutes after the sample rotation at 67 °C, 4 degrees below T_{I-L}, where the liquid crystal is only partly formed.

NMR Spectrum. The factor which determines the NMR line shape and relaxation times of spin 3/2 nucleus ^{23}Na is mainly the interaction between nuclear quadrupole moment Q and the electric field gradient at the nucleus expressed by a tensor $\boldsymbol{q}$.[4] The spin dipolar interaction between ^{23}Na and ^{1}H in the nearby water is negligible unless the system is almost rigid. The following discussion is based on the predominant contribution of the quadrupole interaction to the ^{23}Na spectrum.

Signal Intensities: The constant signal intensity in the isotropic phase has a value similar to that of the free ions in NaCl and in sodium acetate aqueous solutions of corresponding concentrations. No signal intensity is lost in satellites (*vide infra*).

In the liquid crystal region, the signal intensity decreases to 4/10 of isotropic value towards T' ($T' > T_{L-G}$). The phase of isotropic and liquid crystal coexistence has been known for NaS, NaP, and NaM systems in between isotropic and pure liquid crystal phases. The presence of such a phase is also demonstrated for Na(P+M) system by our ESR experiment. Gradual decrease in the NMR intensity is also an evidence of this phase. The loss of intensity is caused by the quadrupole splitting of the signal components m_s: $3/2 \rightarrow 1/2$ and m_s: $-1/2 \rightarrow -3/2$ with 3/10 of total intensity for each by the frequency $\pm\nu_Q S$, where $\nu_Q = e^2qQ/2h$, q is the principal value of the electric field gradient tensor $\boldsymbol{q}$ at the ^{23}Na nucleus, and S is the

order parameter for the principal axis of **q**, when the correlation time for the rod tumbling motion becomes longer than $(2\pi\nu_Q S)^{-1}$ by the liquid crystal formation.[4] The satellite would be out of our experimental frequency range. Evaluation of micelle tumbling rate necessary to collapse the quadrupole splittings may be helpful. The observed quadrupole splittings $\nu_Q S$ for lamellar NaL[2f] and NaP[2e] systems are 25—30 KHz. The splitting for hexagonal phase can be a half of these values[2c] or less, since the area per polar group is larger in hexagonal phase than in lamellar phase, suggesting a lower ordering. Thus $\nu_Q S$ can be estimated to be 15 kHz or less. The calculated correlation time for tumbling motion $\tau_\perp$[5] of a rod with its short axis $a=20$ Å[6] at 60 °C is 5×10^{-6} s, if the long to short axis ratio $b/a=25$, which is just short enough to average out the splitting of 30 kHz. A rod motion under the same conditions except for $b/a=50$ gives $\tau_\perp=4\times10^{-5}$ s, which satisfies $2\pi\nu_Q S\tau_\perp\simeq1$ for $\nu_Q S=4$ kHz. The rotational motion of a rod around the rod axis is also effective to collapse the splitting if the rod is not aligned parallel to the magnetic field, the motion being faster than the tumbling motion. Therefore, Na ion attached to the rod in free state, *i.e.* in the isotropic part, has a motion sufficiently fast to give a single signal even below T_{I-L}, while the ion on the rod in the aligned domain gives satellite signals.

The constant intensity 4/10 of the total in the range $T'>T>T_{L-G}$ indicates that the phase is purely liquid crystalline.

Spectrum Analysis: The line width remains constant while the liquid crystal is equilibrated with isotropic liquid($T_{I-L}>T>T'$). The intrinsic widths of both liquid crystal and isotropic parts should be indistinguishable since the width of the superposed signal is constant irrespective of a drastic composition change. A rapid local motion[2d] should be effective for determining the line width in both cases in order to meet the requirement that the width is the same regardless of the presence of a rod motion. In this case the line width is determined by the relation[1d,4]

$$\begin{aligned}1/T_2 &= (8\pi^2\nu_Q^2/5)f(\tau_c)\\ &= (8\pi^2\nu_Q^2/5)[\tau_c+(5/3)\tau_c(1+\omega_0^2\tau_c^2)^{-1}\\ &\qquad +(2/3)\tau_c(1+4\omega_0^2\tau_c^2)^{-1}],\end{aligned}\tag{1}$$

where τ_c is the correlation time for the local motion which changes the direction of the principal axis of **q**. The estimated value $\nu_Q=100$ kHz[7] is used to evaluate $f(\tau_c)$ for the observed width of 25—40 Hz. The result of $f(\tau_c)=1.4$—2.5×10^{-10} s and $\omega_0=1.6\times10^6$ s^{-1} leads to the extreme narrowing condition $f(\tau_c)=\tau_c$. The rapid local motion seems to be a wobbling motion of the principal axis of **q** for the following reasons. First, the correlation time for the local chain motion is of the same order as determined by deuterium NMR of β-CD_2 group in potassium hexadecanoate-water lamellar phase[1d] ($\tau_c\simeq10^{-10}$ s) and by the present ESR experiment ($10^{-10}\simeq\tau_c<10^{-9}$ s). Second, the observation that the order parameters and their temperature dependence of chain part and of Na^+ ion are comparable[2e,f] suggests that the Na^+ ion whose hydrated water is hydrogen bonded to carboxyl group moves as the chain moves around its equilibrium direction. The reported values of the quadrupole splittings 28—36 kHz for α-CD_2 deuterium NMR and 18—27 kHz for ^{23}Na NMR of unoriented lamellar NaL[2f] and NaP[2e] systems give the order parameters 0.11—0.14 with $\nu_Q(D)=(3/2)e^2qQ/h=250$ kHz[1d] for α-CD_2 and 0.18—0.27 with $\nu_Q(Na)=100$ kHz for Na^+. The former is about 1/3 of calculated value 1/2—1/3[2e] and the latter is about 1/4 of the calculated maximum value 1. The values of order parameters for D and Na are comparable and the observed to calculated ratios for both cases can be regarded to be similar.

The ion exchange phenomenon between rod sites or between a rod site and free state can also be considered as a mechanism of nuclear relaxation.[2a] However, the same ion exchange rate should be assumed for free and aligned rods in the liquid crystal domain in order to explain the common width for both states. This is not appropriate. The exchange phenomena, although not completely ruled out, can not be taken as an important mechanism.

Before concluding that the fast local motion contributes to the line width of the center line predominantly, it should be pointed out that the comparison of T_2 with T_1(Na) would confirm this point since the contribution of local motion to T_1 is dominant.

The broadening of the center line in the region $T'>T>T_{L-G}$ may be caused by the decreased local motion and to a certain extent by the onset of second order shift of the center line expressed by

$$\nu^{(2)} = (3/16)(\nu_Q^2/\nu_L)(\cos^2\theta-1)(9\cos^2\theta-1),\tag{2}$$

where ν_L is the Larmor frequency and θ is the angle between the principal axis of **q** and the direction of static magnetic field. The second order shift can contribute to the line width when there is appreciable distribution in θ. The constant term of (2) is 70 Hz when ν_Q is 100 and 1.8 kHz when it is 500 kHz.[2b] Since there is no observable line distortion, the signal must be the results of a time average of $\nu^{(2)}$ under the decreased local motion of **q** principal axis around θ_0, the ensemble average of θ, which is 90° for hexagonal phase unless the ion binding is in bridged form or there is some chain tilt. The average value of $\nu^{(2)}$ should appear on the chemical shift. A simple trial calculation of the θ dependent term of (2) under the conditions of uniform θ distribution[8] around θ_0 (90°) in the range between $\theta_0-\alpha$ and $\theta_0+\alpha$ shows that $\nu^{(2)}$ is a sharp function of ordering:

$$\delta(\alpha) = \langle(\cos^2\theta-1)(9\cos^2\theta-1)\rangle_\alpha,\tag{3}$$

$\delta(0)=1$(distribution around θ_0 is 0), $\delta(37°52')=0$, and $\delta(90°)=-0.53$, as shown in Fig. 6. The observed temperature dependence of chemical shift of Na(P+M) and NaS systems are not monotonous, showing no resemblance to each other at low temperature. A possible explanation for the different behavior in the two systems can be found in a slight difference in the ordering. At $T\simeq T_{L-G}$, where the local motion started to be highly restricted, the difference in shift behavior shoud be amplified. The equilibrium position $\theta_0=90°$, which gives the highest order for the hexagonal phase, takes $\nu^{(2)}=(3/16)\nu_Q^2/\nu_L$ giving rise to a low field shift. The present result

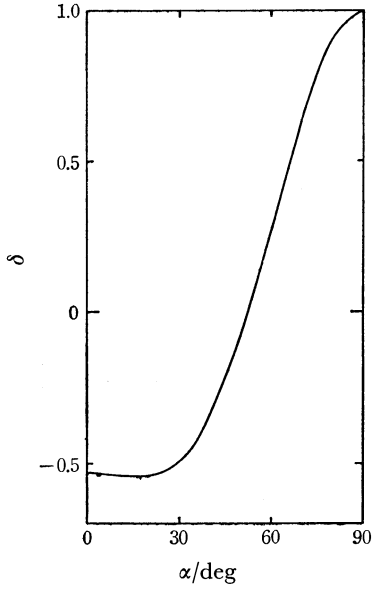

Fig. 6. Plot of $\delta(\alpha)$ against α.

	observed shift near T_{L-G}	ordering detected by ESR
Na(P+M)	low field shift	good
NaS	high field shift	poor

is explained by the difference in the ordering.

It is of importance to point out the possibility of evaluation of $\langle\cos^4\theta\rangle$ from shift data since a comparison of $\langle\cos^4\theta\rangle$ and $\langle\cos^2\theta\rangle$ can give information on the orientational direction θ_0 and the amplitude of orientational fluctuation separately, while $\langle\cos^2\theta\rangle$ available from the first order splitting of ^{23}Na satellite lines or from ESR parameter, alone gives the combined effect of these two factors.

In the gel phase, $T_{L-G} > T$, the θ distribution in (2) may be effective under the diminished time averaging effect of local motion, a contribution of the dipolar interaction bringing about further broadening.

The behavior of Na^+ ions in the Na(P+M) and NaS systems is obviously different from that of free ions even in the isotropic region, $T > T_{I-L}$. The widths of hydrated free Na^+ ions in 1.2 M NaCl and 0.8 M sodium acetate solutions are 3 and 4 Hz at 70 °C, respectively, being much narrower than those of Na(P+M) and NaS systems, 22—30 Hz (70—92 °C) and 26—36 Hz (72—89 °C), respectively. The apparent activation energies obtained by simple Arrhenius plots of these widths are 8 and 11 kJ mol^{-1} for NaCl and sodium acetate solutions while they are 16 and 19 kJ mol^{-1} for Na(P+M) and NaS systems, respectively. It is thus not probable that all or even the large portion of the counter ion is free in the isotropic region. Since there is no jump in the width at T_{I-L} in changing from isotropic to liquid crystal region, the origin of the line width and its temperature dependence should be found in the model in which all or most of the cations are attached to the micelles. The tensor q of hydrated Na^+ is not susceptible to an appreciable change in this narrow temperature range because of the high charge density at Na^+ ion.[9] The local molecular motion as in the liquid crystal region together with some contribution from a micelle tumbling motion should be responsible for the width. The increasing exchange rate (exchange between micelle sites and between micelle and free ion) at higher temperature might contribute to the apparent activation energy.

Concluding Remarks. The phase diagram of Na(P+M) system, which has not been given so far, is found to be similar to that of NaS, NaP, NaM in the concentration 26—28%. It is shown that the motions of the individual molecules and ions are reflected on the magnetic resonance spectra, and their motions change similarly across the phase trnasition points: the cation has fluctuational motions as the chain in the liquid crystal region. This observation is consistent with that of Abdolall *et al.* observed in the lamellar phase of NaP system.[2e]

The models we present for the observed phases are not completely based on concrete evidence, but they give the only interpretation consistent with both NMR and ESR data. It is desirable to have a better signal to noise ratio for further argument of line widths and shapes. T_1 data and the observation of the satellite signals are also important.

References

1) a) K. D. Lawson and T. J. Flautt, *Mol. Cryst.*, **1**, 241 (1966); b) J. Charvolin and P. Rigny, *J. Chem. Phys.*, **58**, 3999 (1977); c) B. Mely, J. Charvolin, and P. Keller, *Chem. Phys. Lipids*, **15**, 161 (1975); d) J. H. Davis, K. R. Jeffrey, and M. Bloom, *J. Magn. Reson.*, **29**, 191 (1978); e) W. L. Hubbell and H. M. McConnell, *Proc. Natl. Acad. Sci. U. S. A.*, **64**, 20 (1969); f) J. Seelig, *J. Am. Chem. Soc.*, **92**, 3881 (1970); g) J. Seelig, *ibid.*, **93**, 5017 (1971); h) J. M. Boggs and J. C. Hsia, *Proc. Natl. Acad. Sci. U. S. A.*, **70**, 1406 (1973); i) J. Seelig and H. Limacher, *Mol. Cryst. Liq. Cryst.*, **25**, 105 (1974).

2) a) B. Lindman and P. Ekwall, *Mol. Cryst.*, **5**, 79 (1968); b) D. M. Chen and L. W. Reeves, *J. Am. Chem. Soc.*, **94**, 4384 (1972); c) G. Lindblom, *Acta Chem. Scand.*, **26**, 1745 (1972); d) H. Gustavsson and B. Lindman, *J. Am. Chem. Soc.*, **97**, 3923 (1975); e) K. Abdolall, E. E. Burnell, and M. I. Valic, *Chem. Phys. Lipids*, **20**, 115 (1977); f) K. Abdolall, A. L. MacKay, and M. Bloom, *J. Magn. Reson.*, **29**, 309 (1978).

3) H. Schindler and J. Seelig, *J. Chem. Phys.*, **59**, 1841 (1973) : The motion of the radical axis may be estimated by the comparison with their spectra to be the order of $\tau_c = 10^{-9}$—10^{-10} s. Their simulated spectra with a similar label under various conditions show as narrow widths by $\tau_c = 2\times10^{-10}$ s, and much broader widths by $\tau_c = 2.8\times10^{-9}$ s as compared with the present data.

4) A. Abragam, "The Principles of Nuclear Magnetism," Oxford (1961).

5) These calculations are based on the Stokes-Einstein model for spherical particles, $\tau = 4\pi a^3\eta/3kT$, where τ is the reorientational correlation time of the sphere, a is the radius, and η is the viscosity, which is used in approximating a rod by an ellipsoid following the Perrin treatment : H. Shimizu, *J. Chem. Phys.*, **40**, 754 (1964); U. Henriksson *et al.*, *J. Phys. Chem.*, **81**, 76 (1977) where $\ln x$ in Eq. 22 should be $\ln 2x$.

6) The observed radii of the rods are 16.2 Å for NaM, 18.6 Å for NaP, and 21.0 Å for NaS. V. Luzzati, H. Mustacchi, and A. Scoulios, *Discuss. Faraday Soc.*, **25**, 43 (1958).

7) The value of ν_Q is given for Na ion in γ-alum $NaAl(SO_4)_2 \cdot 12H_2O$ to be of order 100 kHz where the octahedron $Na^+ \cdot 6H_2O$ is regular : N. Weiden and A. Weiss, *J. Magn. Reson.*, **20**, 279 (1975). This is a good or lower estimation for hydrated sodium ion in an asymmetric environment. The value $\nu_Q = 500$ kHz is used by Chen and Reeves[2b] and that of a single crystal $NaNO_3$ is 167 kHz,[4] but they must be too large since the data are obtained from non-hydrated ions.

8) The time average of $\cos^n\theta$ is better represented by the form $\int \cos^n\theta \cdot \exp[-V(\theta-\theta_0)/RT]\sin\theta d\theta$ where the potential function $V(\theta-\theta_0)$ takes its minimum value at the equilibrium position θ_0.

9) G. Lindblom and B. Lindman, *J. Phys. Chem.*, **77**, 2531 (1973).

The Relative Rate Constants of Reactions of Oxygen Atoms with Several Olefins in Liquid Carbon Dioxide

Hidetoshi KARASAWA, Tai SASAMOTO, Rei YUGETA, and Shin SATO*

Department of Applied Physics, Tokyo Institute of Technology, Ookayama, Meguro-ku, Tokyo 152

(Received August 19, 1978)

The relative rate constants of reactions of oxygen atoms with several olefins and 2-methylpropane have been determined in liquid carbon dioxide at −18 °C, using the γ-radiolysis of carbon dioxide in the presence of these hydrocarbons. They are : 1-butene, 1.0; *cis*-2-butene, 2.3; *trans*-2-butene, 3.0; 2-methylpropene, 2.9; 2,3-dimethyl-2-butene, 2.0; 2-methylpropane, 0.07. These relative values are very different from those obtained in the gas phase. A possible reason is discussed and a simple theoretical treatment is proposed for the competition between diffusion and reaction on the basis of the idea of a "collision set" in the liquid phase. The reaction of oxygen atoms with paraffin in liquid carbon dioxide seems to be faster than that in the gas phase. The reason is not clear at present.

The γ-radiolysis of liquid carbon dioxide is now believed to be a convenient source of oxygen atoms.[1] When an olefin is present in the γ-irradiated liquid carbon dioxide, the main products are the same compounds as those observed in the reaction of oxygen atoms with the olefin in the gas phase. By measuring the relative yields of products from a γ-irradiated liquid carbon dioxide solution in which two kinds of olefins are present, one can estimate the relative rate constants of reaction of oxygen atoms with olefins. According to Sakurai and his coworkers,[2] the relative rate constants of reaction of oxygen atoms with four olefins in liquid carbon dioxide at room temperature are 1.0 : 1.3 : 1.7 : 1.3 in the order of *cis*-2-butene, 2-methyl-2-butene, 2,3-dimethyl-2-butene, and cyclohexene. These relative values are different from those reported for the reaction of oxygen atoms in the gas phase (1.0 : 3.34 : 4.28 : 1.14).[3] This discrepancy is probably due to the fact that the diffusion process plays a role in determining the rate of reaction in the liquid phase.

The present experiment was attempted to confirm and explain this discrepancy and to gain an insight into the γ-ray-induced oxidation of olefins in liquid carbon dioxide.

Experimental

The carbon dioxide and hydrocarbons used were all purchased from the Takachiho Shoji Co. and were used after thorough degassing and distillation. No detectable impurities were observed by the gas chromatograph equipped with a 5 m dimethyl sulfolane column of 20% w/w on celite.

The sampling tube with a breakable seal attached was made of Pyrex glass, 10 mm in diameter. After a known amount of a hydrocarbon mixture had been condensed in the sampling tube at 77 K, carbon dioxide was introduced. The electron fraction of carbon dioxide in the solution was controlled at 0.98. After having been sealed, the sampling tube was transferred in a Dewar flask containing ice–sodium chloride slush at −18 °C and was shaken so as to homogenize the solute concentration in the solution.

The γ-irradiation was carried out at −18 °C at the dose rate of 1.1×10^{6} R h^{-1}, usually for two hours. After irradiation, the sampling tube was immersed into a Dewar flask containing petroleum ether slush at −80 °C and then the seal was broken. It took about one hour for the vaporization of carbon dioxide. The products thus obtained were subjected to gas chromatographic analysis after a known amount of cyclohexane or ethanol was added as the standard. The column used was 2 m polyethylene glycol 1500 of 15% w/w on Uniport B and was operated at room temperature. The products were identified by the retention time of the authentic sample.

Results

In every experiment, 1-butene was used as the competitive reactant, so that the relative rate constants were obtained against the rate constant of reaction of 1-butene with oxygen atoms. Since the gas chromatographic analysis of products was not very reproducible, as can seen from the figures, the following procedure was used for the determination of the relative rate constants and of the formation ratios of products.

The competition of two olefins A and B for oxygen atoms produced in the radiolysis of carbon dioxide may be described as follows:

$$CO_2 \rightsquigarrow CO + O \tag{1}$$

$$\left.\begin{aligned} O + A &\xrightarrow{\alpha} P_\alpha \\ &\xrightarrow{1-\alpha} P_{1-\alpha} \end{aligned}\right\} \tag{2}$$

$$\left.\begin{aligned} O + B &\xrightarrow{\beta} Q_\beta \\ &\xrightarrow{1-\beta} Q_{1-\beta} \end{aligned}\right\} \tag{3}$$

Then the G-value of the P_α product can be expressed by this equation:

$$G(P_\alpha) = G_0\frac{\alpha k_a[A]}{k_a[A]+k_b[B]}. \tag{4}$$

Here, G_0 is the total G-value of products of the reaction of oxygen atoms with two olefins, A and B, and k_a and k_b are the rate constants of reaction of oxygen atoms with two olefins. If $k_b/k_a>1$, the plots of $G(P_\alpha)$ as a function of the mole fraction of [B] give a concave curve, while if $k_b/k_a<1$, a convex curve is found.

Now let us introduce a weighted mole fraction:

$$X = \frac{f[B]}{[A]+f[B]}, \tag{5}$$

where f is a factor to be estimated. If the f factor is equal to the ratio k_b/k_a, the plots of $G(P_\alpha)$ as a

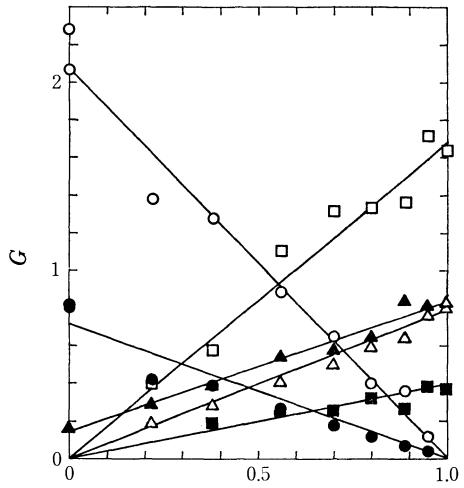

Fig. 1. The G-values of products from the mixture of 1-butene and *cis*-2-butene in carbon dioxide solution as a function of the weighted mole fraction of *cis*-2-butene. The value of f is taken as 2.3.
○ 1-Butene oxide; ● butanal; □ *cis*-2-butene oxide; △ *trans*-2-butene oxide; ■ 2-methylpropanal; ▲ 2-butanone.

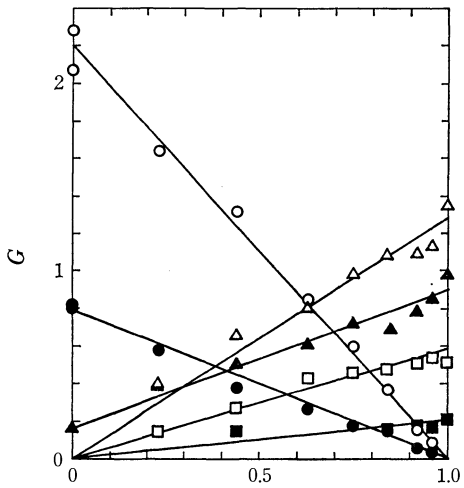

Fig. 2. The G-values of products from the mixture of 1-butene and *trans*-2-butene in carbon dioxide solution as a function of the weighted mole fraction of *trans*-2-butene. The value of f is taken as 3.0.
○ 1-Butene oxide; ● butanal; □ *cis*-2-butene oxide; △ *trans*-2-butene oxide; ■ 2-methylpropanal; ▲ 2-butanone.

function of X will give a straight line:

$$G(\mathrm{P}_\alpha) = G_0\alpha(1-X). \quad (6)$$

A similar linearity can be obtained for the products of the reaction with B olefin:

$$G(\mathrm{Q}_\beta) = G_0\beta X. \quad (7)$$

Consequently, once an appropriate value of f is obtained, all of the addition products formed in Reactions 2 and 3 should give straight lines when the G-values

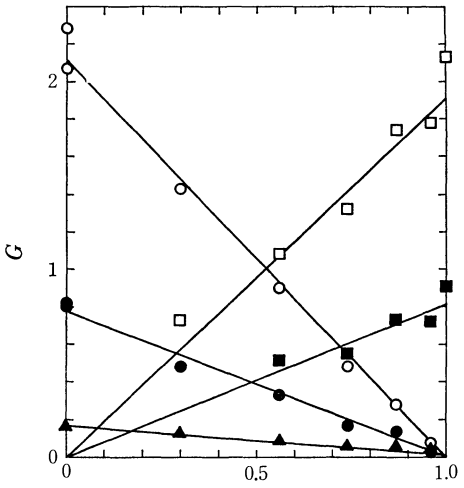

Fig. 3. The G-values of products from the mixture of 1-butene and 2-methylpropene in carbon dioxide solution as a function of the weighted mole fraction of 2-methylpropene. The value of f is taken as 2.9.
○ 1-Butene oxide; ● butanal; □ 2-methylpropene oxide; ■ 2-methylpropanal; ▲ 2-butanone.

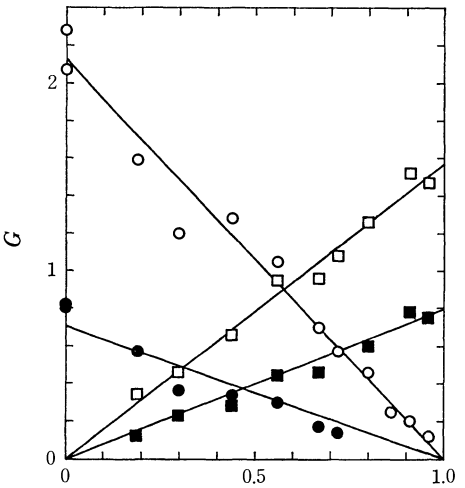

Fig. 4. The G-values of products from the mixture of 1-butene and 2,3-dimethyl-2-butene in carbon dioxide solution as a function of the weighted mole fraction of 2,3-dimethyl-2-butene. The value of f is taken as 2.0.
○ 1-Butene oxide; ● butanal; □ 2,3-dimethyl-2-butene oxide; ■ 3,3-dimethyl-2-butanone.

are plotted as a function of the weighted mole fraction X.

Figure 1 shows such plots for the competition of 1-butene and *cis*-2-butene. Calculations with trial and error showed that the error introduced in the estimation of f was less than 10% in all cases examined except for the mixture of 1-butene and 2-methylpropane.

When more than two addition products are formed in the reaction of oxygen atoms with olefin, the ratio

TABLE 1. FRACTIONAL YIELDS OF THE ADDITION PRODUCTS FORMED IN THE REACTION OF OXYGEN ATOMS WITH FIVE OLEFINS

Olefin	Product	Liquid phase in CO_2 −18 °C (This work)	Liquid phase in N_2[5] 77 K	Gas phase[4]
1-Butene	1-Butene oxide	0.70	0.58	0.53
	Butanal	0.25	0.41	0.43
	2-Butanone	0.05	0.01	0.04
cis-2-Butene	*cis*-2-Butene oxide	0.46		0.25
	trans-2-Butene oxide	0.21		0.26
	2-Methylpropanal	0.10		0.23
	2-Butanone	0.23		0.26
trans-2-Butene	*cis*-2-Butene oxide	0.20		0.15
	trans-2-Butene oxide	0.43		0.33
	2-Methylpropanal	0.07		0.21
	2-Butanone	0.30		0.31
2-Methylpropene	2-Methylpropene oxide	0.70	0.55	0.54
	2-Methylpropanal	0.28	0.45	0.43
	2-Butanone	0.02	0.001	0.03
2,3-Dimethyl-2-butene	2,3-Dimethyl-2-butene oxide	0.66		0.52
	3,3-Dimethyl-2-butanone	0.34		0.48

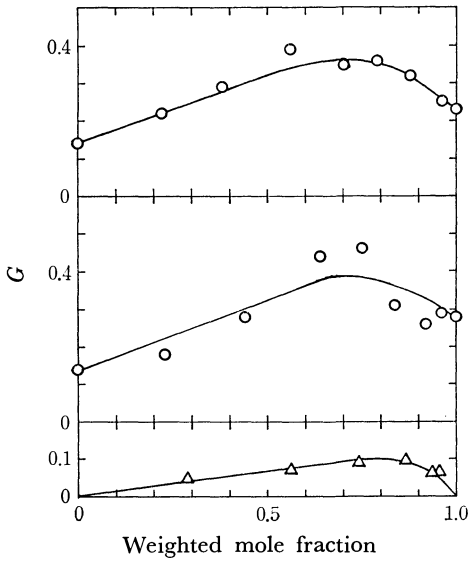

Fig. 5. The *G*-values of the largest minor products from the mixtures of 1-butene and *cis*-2-butene, 1-butene and *trans*-2-butene, and 1-butene and 2-methylpropene, respectively, from the top to the bottom, as a function of the weighted mole fraction of the competitive reactant for 1-butene. ○ Propanal; △ acetone.

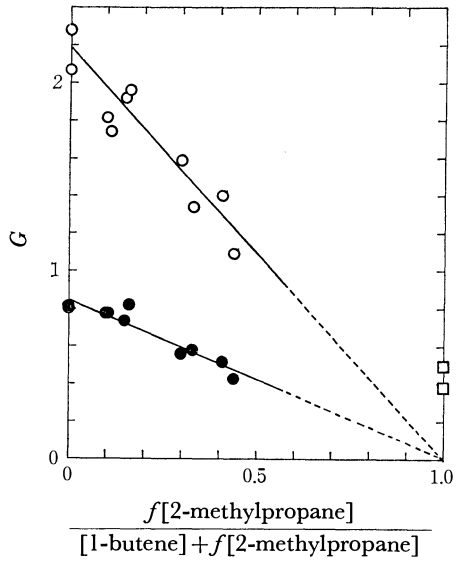

Fig. 6. The *G*-values of products from the mixture of 1-butene and 2-methylpropane in carbon dioxide solution as a function of the weighted mole fraction of 2-methylpropane. The value of f is taken as 0.07. ○ 1-Butene oxide; ● butanal; □ 2-methylpropene oxide after 2 hour-irradiation, see text for the detail.

of the slopes of the two straight lines obtained from the plots of $G(P_{\alpha 1})$ and $G(P_{\alpha 2})$ corresponds to the formation ratio of the two products, $P_{\alpha 1}$ and $P_{\alpha 2}$. In the case of the mixture of 1-butene and *cis*-2-butene (Fig. 1), 2-butanone is a common product from two olefins. In such a case, the formation ratio was estimated from the intercepts of the linear relations at $X=0.0$ and 1.0.

Figures 2, 3, and 4 show the results obtained with the mixtures of 1-butene and *trans*-2-butene, 1-butene and 2-methylpropene, and 1-butene and 2,3-dimethyl-2-butene, respectively. In every case, several minor products were observed, the total yield of which was estimated as about 10% of the main addition products by measuring the peak areas in the gas chromatograms. In the case of 2,3-dimethyl-2-butene, the total *G*-value of the addition products is about 10% smaller than those obtained with other olefins. This fact is consistent with the observation that the fraction of the fragmentation products in the gas phase reaction of oxygen atoms with 2,3-dimethyl-2-butene is larger than those obtained with other olefins.[4] Figure 5 shows the largest amounts of minor products observed

Table 2. The relative rate constants of reaction of oxygen atoms with several hydrocarbons in liquid carbon dioxide and in the gas phase[3)]

Hydrocarbon	Relative rate	
	In CO_2 at -18 °C (This work)	In the gas phase at room temp[a)]
1-Butene	1.0	1.00
cis-2-Butene	2.3	4.13
trans-2-Butene	3.0	4.91
2-Methylpropene	2.9	4.35
2,3-Dimethyl-2-butene	2.0[b)]	13.8
2-Methylpropane	0.07	0.015[c)]

a) Because of the low activation energies, the relative rates shown in this Table are almost the same as those at the temperature of -18 °C. b) This value is somewhat smaller than that expected from the previous work.[2)] The explanation of the discrepancy is not yet clear. c) Calculated on the basis of $k_{\text{butane}}/k_{\text{2-methylpropene}}=0.0018$[3)] and $k_{\text{2-methylpropane}}/k_{\text{butane}}\simeq 2$.[6)]

with three different mixtures which did not show the linear relationship with X. This is probably due to the fact that these minor products are formed in the reaction of radicals produced in fragmentation processes with hydrocarbons.

Figure 6 shows the competition between 1-butene and 2-methylpropane. Since the value of f was very small, the error introduced in its estimation was probably about 20%.

The formation ratios and the relative rate constants thus obtained are summarized in Tables 1 and 2, together with those obtained in the gas phase and in liquid nitrogen.[4–6)]

Discussion

Reaction Mechanism. As Table 1 shows, the main addition products obtained in the present experiment are the same as those obtained by Cvetanović for the gas phase reaction of oxygen atoms.[4)] The difference in their formation ratios may be explained in terms of the solvent effect.

According to the Cvetanović mechanism, oxygen atoms in the ^3P state mainly add to the less substituted of the two doubly bonded carbon atoms and the initial adduct rearranges to the final products by ring closure (to form epoxide) and by migration of an H atom or alkyl group, from the C atom to which the oxygen atom becomes attached to the other C atoms of the original bond (to form carbonyl compounds). In the present reaction system, the migration of an H atom or an alkyl group may be somewhat restricted by the solvent, carbon dioxide. This effect seems to correspond with the observation that the fraction of epoxide is larger than that of carbonyl compounds, compared with that in the gas phase, in every olefin. Exactly the same effect can interpret the difference in the *cis-trans* ratio of the two 2-butene oxides produced in the reaction of 2-butene ; *i.e.*, the rotation around the C–C axis in the initial adduct is more restricted in liquid carbon dioxide than in the gas phase. In the liquid nitrogen solution, however, Hirokami and Cvetanović found that the formation ratios of epoxide/carbonyl compounds obtained with propylene, 1-butene, and 2-methylpropene are consistent with those obtained in the gas phase at room temperature.[5)] This discrepancy seems to suggest that there is a small but definite interaction between the initial adduct and carbon dioxide.

Moreover, the comparison of the formation ratios listed in Table 1 suggests that the ratio between the addition of oxygen atoms to the less substituted and that to the more substituted of the two doubly bonded carbon atoms is not dependent upon the phase but on the temperature at which the reaction occurs ; *i.e.*, the yields of 2-butanone, which is the product formed through the addition reaction of oxygen atom to the more substituted carbon atom in the reactions of 1-butene and of 2-methylpropene, are very small in liquid nitrogen compared with those obtained in the gas phase and in the carbon dioxide solution -18 °C.

The quantitative analysis of the fragmentation products could not be carried out because of the experimental difficulty of the measurement of the small peaks appearing in the gas chromatogram. Only the largest minor products obtained with three systems are shown in Fig. 5. The formation of propanal from the solution containing 2-butene and of acetone from the solution containing 2-methylpropene may be explained by the decomposition of the initial adduct followed by the radical-radical reactions.

When 2-methylpropane was used as the solute, the main products observed were alcohols: 2-methyl-1-propanol and 2-methyl-2-propanol. With the increase in irradiation time, 2-methylpropene oxide and 2-methylpropanal became important products. These compounds must be formed through a secondary reaction: *i.e.*, the reaction of oxygen atoms with 2-methylpropene eventually produced in the system. A similar observation can always be made when paraffin molecules are used as the solute.[7)]

Relative Rate Constants. As Table 2 shows, the differences in relative rate constants obtained with six hydrocarbons in liquid carbon dioxide are much smaller than those obtained in the gas phase, which suggests that the diffusion process plays a role. However, the difference between 1-butene and other butenes in the relative rate constants cannot simply be explained by the assumption that all of the reactions of oxygen atoms with olefins in the liquid phase are diffusion-controlled.

It is well known that collisions between two species A and B in a solvent occur in sets. Therefore, the total collision frequency, Z_{AB}, may be expressed as the product of the average collision number, n, in a collision set and the diffusion-controlled collision frequency, k_D.

$$Z_{AB} = n\,k_D \tag{8}$$

$$k_D = 4\pi(D_A+D_B)(r_A+r_B) \tag{9}$$[8)]

Here D is the diffusion coefficient and r is the collision radius.

Now let us assume that the p fraction of the collision is effective ; then the rate constant of the reaction

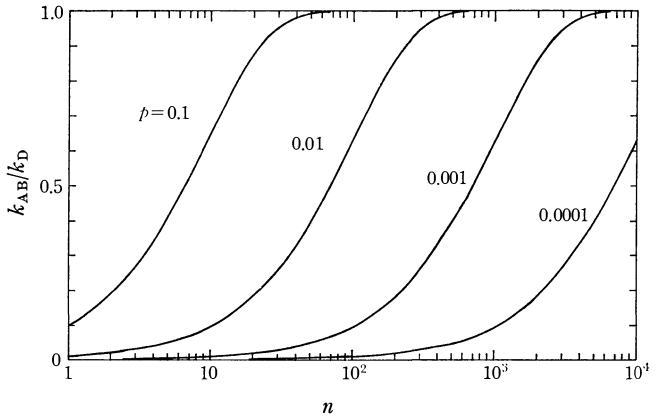

Fig. 7. The ratio of k_{AB}/k_D as a function of the average collision number n in a collision set at different values of effective collision fractions.

between A and B may be expressed as follows:

$$k_{AB} = k_D[1-(1-p)^n]. \quad (10)$$

Here, $(1-p)^n$ corresponds to the fraction of collisions which do not lead to the reaction. At the two extreme cases, $p \ll 1$ and $p \approx 1$, Eq. 10 is converted into Eqs. 11 and 12, respectively.

$$k_{AB} = npk_D = pZ_{AB} \quad (11)$$

$$k_{AB} = k_D \quad (12)$$

The former is the usual expression for the reaction-controlled reaction and the latter for the diffusion-controlled reaction. Figure 7 shows the k_{AB}/k_D ratio as a function of the average collision number in a collision set at several p values.

Recent measurements of the absolute rate constants and of the activation energies for the reaction of oxygen atoms with olefins in the gas phase[9,10] allowed us to estimate the p values. By taking 2.0×10^{11} l mol^{-1} s^{-1} as the collision frequency between oxygen atoms and olefins in the gas phase at -18 °C (the collision diameter was assumed to be 4.0 Å), we estimated the following p values : 0.01 for 1-butene, 0.05 for other butenes, and 0.3 for 2,3-dimethyl-2-butene.

On the other hand, the estimation of n is a very difficult problem. Several theoretical treatments have been proposed[11,12] and have suggested $n=10$—100 in the solutions which are not too viscous. We calculated the n values so as to satisfy the following equation:

$$\frac{k}{k_{1\text{-butene}}} = \frac{1-(1-p)^n}{1-(1-p_{1\text{-butene}})^n}. \quad (13)$$

The values obtained were 30—50 for butenes and 70 for 2,3-dimethyl-2-butene. The fact that a somewhat larger n value was obtained for 2,3-dimethyl-2-butene may be due to the fact that the value of k_D for this compound is smaller than that for butenes because of the large molecular dimension. If k_D for 2,3-dimethyl-2-butene is assumed to be 10% smaller than that for butenes, the number of 50 can be obtained for n. As the conclusion of this calculation, we may state that the reactions of oxygen atoms with *cis*-, *trans*-2-butenes, 2-methylpropene, and 2,3-dimethyl-2-butene in liquid carbon dioxide are almost diffusion-controlled.

The relative rate constant of reaction of oxygen atoms with 2-methylpropane obtained in liquid carbon dioxide was five times that obtained in the gas phase when the rate constant of 1-butene was taken as unity in both phases, as is shown in Table 2. We have recently measured the competition of cyclohexane and cyclohexene for oxygen atoms, by using a method similar to that described in the present paper, and found that k(O+cyclohexane)/k(O+cyclohexene)$=$0.03.[7] This value conforms to the present result, k(O+2-methylpropane)/k(O+1-butene)$=$0.07, because the ratio of k(O+2-methylpropane)/k(O+cyclohexane) can be estimated as about unity in the gas phase,[6] and k(O+cyclohexene) in liquid carbon dioxide is 1.3 times k(O+*cis*-2-butene).[2]

In order to apply Eq. 13 to the competition between 2-methylpropane and 1-butene, however, we have to assume that $n \approx 700$. If $n=700$ is correct, the difference between 1-butene and other olefins in relative rate constant cannot be explained. We have no proper interpretation for this discrepancy at present.

Reacting Species. In the foregoing discussion, all of the addition products are treated as the products of the reaction of oxygen atoms in the ^{3}P state with olefins. In the radiolysis of carbon dioxide, however, active species other than oxygen atoms in the ^{3}P state can be expected to be formed, such as oxygen atoms in the ^{1}D state, CO_3, and ionic species.

The present analysis is based on the experimental fact that the observed addition products are very similar to those obtained in the gas phase reaction of oxygen atoms with olefins. Consequently, if active species other than oxygen atoms in the ^{3}P state should react with olefins exactly in the same manner as do oxygen atoms, we cannot discriminate these species from the ^{3}P oxygen atoms. The species CO_3 might be a candidate.

The participation of ^{1}D oxygen atoms may be ignored because of the high quenching efficiency of carbon dioxide.[13] In the present experiment, we often observed the formation of various alcohols, the formations of which were not reported in the gas phase reaction of oxygen atoms with olefins. This fact suggests that ionic species such as O^- ions are produced in the present system, although they cannot be major reacting species.[14]

References

1) L. Wojnarovits, S. Hirokami, and S. Sato, *Bull. Chem. Soc. Jpn.*, **49**, 2956 (1976).
2) H. Sakurai, K. Akimoto, S. Toki, and S. Takamuku, *Chem. Lett.*, **1975**, 469.
3) R. J. Cvetanović, *Adv. Photochem.*, **1**, 115 (1963).
4) R. J. Cvetanović, *Can. J. Chem.*, **36**, 623 (1958).
5) S. Hirokami and R. J. Cvetanović, *J. Am. Chem. Soc.*, **96**, 3738 (1974).
6) J. T. Herron and R. E. Huie, *J. Phys. Chem.*, **73**, 3327 (1969).
7) R. Yugeta, A. Matsumoto. H. Karasawa. and S, Sato, unpublished data.

8) M. V. Smoluchowski, *Z. Phys. Chem.*, **92**, 129 (1917).
9) D. L. Singleton and R. J. Cvetanović, *J. Am. Chem. Soc.*, **98**, 6812 (1976).
10) R. Atkinson and J. N. Pitts, Jr., *J. Chem. Phys.*, **67**, 38 (1977).
11) E. Rabinowitch and W. C. Wood, *Trans. Faraday Soc.*, **32**, 1381 (1936).
12) G. M. Barrow, "Physical Chemistry for Life Sciences," McGraw-Hill Kogakusha Ltd., Tokyo (1974), p. 336.
13) P. Warneck and J. O. Sullivan, International Conference on Photochemistry, München, 1967, part 1, p. 94.
14) S. Hirokami, L. Wojnarovits, and S. Sato, *Bull. Chem. Soc. Jpn.*, **52**, 299 (1979).

Electrochemical Behavior of the Oxygen Radical. IV. The Reaction Mechanism of the Electrogenerated Hyperoxide Ion with Bis(acetylacetonato)cobalt(II) in Dimethyl Sulfoxide and Acetone†

Setsuko KUDO†† and Akio IWASE*

Department of Chemistry, Faculty of Science, Yamagata University, Yamagata 990

(Received March 27, 1978)

The reaction mechanism of the electrogenerated hyperoxide ion with bis(acetylacetonato)cobalt(II) in dimethyl sulfoxide and acetone has been investigated. The reaction was conducted in a 0.05 mol dm^{-3} TBAP solution at 20 °C in an open system. $Co(acac)_2$ reacted with the hyperoxide ion which was generated by the controlled potential electrolysis of dissolved oxygen to afford the following product, $[(acac)_2\ Co{-}O_2{-}Co(acac)_2]^{2-}$. The complex was separated in solution by column chromatography using alumina as the adsorbent. The electronic spectrum and oxidation state are discussed.

In Part III of this series,[1] the mechanism of the polarographic catalytic reduction of disso'ved oxygen in dimethyl sulfoxide in the presence of bis(1,3-diketonato)cobalt(II) complexes was discussed. In this paper, the reaction mechanism of bis(acetylacetonato)-cobalt(II) complex, $Co(acac)_2$ with electrogenerated hyperoxide ion in dimethyl sulfoxide (DMSO) and acetone will be reported in more detail. Moreover, the reaction product, μ-peroxo-dicobalt(II) complex, has been separated by column chromatography using alumina as an adsorbent.

Experimental

Apparatus and Reagents. D.c. polarograms were recorded with a PA 101 Yanagimoto Polarograph and a PT-P8 Yanagimoto Potentiostat, by the same procedures as described in a preceding paper.[1] The capillary used had an m value of 1.057 mg/s and drop time of 5.1 s/drop at -1.0 V *vs.* SCE when measured in an air-free 0.05 mol dm^{-3} TBAP(tetrabutylammonium perchlorate)–DMSO solution at 49 cm of effective height of mercury ($m^{2/3}\ t^{1/6} = 1.364\ mg^{2/3}\ s^{-1/2}$).

Cyclic voltammetric measurements were made with a three-electrode potentiostat constructed with a LS-LC Hokuto Denko Linear Scanner and a PT-P8 Yanagimoto Potentiostat. The voltammograms were recorded on a F-32 Riken Denshi X-Y plotter. The working electrode for cyclic voltammetry was a hanging mercury drop electrode (surface area : 0.033 cm^2).

A VE-8 Yanagimoto Controlled Potential Electrolyser was used for the controlled potential electrolysis of dissolved oxygen, at -1.15 V *vs.* SCE at room temperature (*ca.* 20 °C). For the controlled potential electrolyses, a mercury pool electrode was used as cathode. The electrolytic cell was the same as reported previously.[2]

The electronic spectra were measured with a Spectronic 88-UV Shimadzu-Bausch & Lomb spectrophotometer.

All voltammetric measurements were conducted at (25± 0.2) °C.

Bis(acetylacetonato)cobalt(II) and tris(acetylacetonato)-cobalt(III) complexes of reagent grade were obtained from Dojin Yakukagaku Kenkyusho. DMSO(Wako Pure Chemical) and acetone (Koso Chemical), guaranteed reagents were used without further purification (water contents were below 0.2%). TBAP for polarography from Nakarai Chemicals was used as the supporting electrolyte.

The alumina used for the chromatographic separation of the reaction product was Alumina 60(Merk). The separation of reaction product was carried out by using an alumina column of diameter 1.2 cm and height 30 cm.

Procedure. The solution for controlled potential electrolysis (40 cm^3), containing 2×10^{-3} mol dm^{-3} $Co(acac)_2$ and 0.05 mol dm^{-3} TBAP in DMSO(B) or acetone(A), was placed in an electrolytic cell and electrolyzed for 18 min on a mercury pool electrode. Subsequently the electrolyzed solution was transferred to a clean flask and allowed to stand overnight at room temperature. This solution (30 cm^3) was fed into the top of the column bed, which had been washed with acetone or DMSO. The column was operated by the usual chromatographic procedures. In the case of solution A, one of the green complexes, A-1, was eluted with acetone and the other green complex, A-2, was eluted with DMSO. In the case of solution B, the major part of the green complex, B-1, was eluted with DMSO. In both cases, some original complex remained on top of the column under these conditions.

The eluates were used for the polarographic and the spectrophotometric measurements because of the difficulty of preparing crystals.

Results and Discussion

The typical cyclic voltammograms of dissolved oxygen in acetone and DMSO with 0.05 mol dm^{-3} TBAP are shown in Fig. 1. The rate of voltage change was 0.05 V/s. The experimental results were very similar to that reported by earlier investigators.[3] Curve 2 and curve 4 represent cyclic voltammograms for oxygen in the presence of $Co(acac)_2$. It is clear that the heights of cathodic peaks in both cases are larger than those of curves 1 and 3. This catalytic current is clearly based on the reduction of oxygen which is reproduced from the reaction of hyperoxide ion with $Co(acac)_2$ complex at the electrode surface. Conversely, the heights of the anodic peaks decreased by the addition of the complex.

For the controlled potential electrolysis in acetone and DMSO, the reaction was followed by taking the visible spectrum of the solution at different times. Those spectra are shown in Figs. 2 and 3. In Fig. 2, curve 1 was obtained from a solution containing 2×10^{-3} mol dm^{-3} $Co(acac)_2$ and 0.05 mol dm^{-3} TBAP in DMSO before electrolysis. The spectrum consists of

† A preliminary report of this work was presented at the 36th National Meeting of the Chemical Society of Japan, Osaka, April 1977.

†† Present address : Chemical Laboratories, Yamagata Building Service Co., Ltd., Yamagata 990.

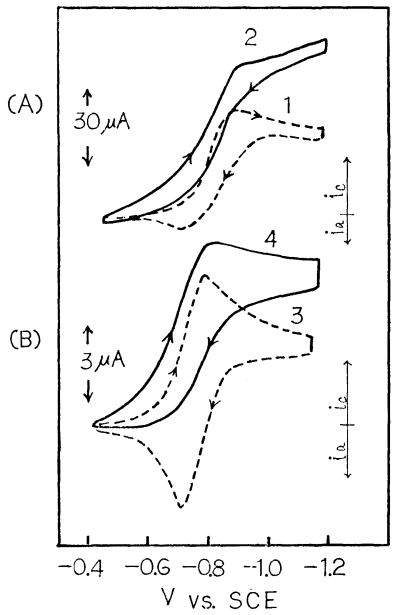

Fig. 1. Cyclic voltammograms of dissolved oxygen in (A) acetone and (B) DMSO.
The concentration of $Co(acac)_2$ added : (1) and (3), 0; (2), 1.5×10^{-3} mol dm^{-3}; (4), 1.9×10^{-3} mol dm^{-3}.

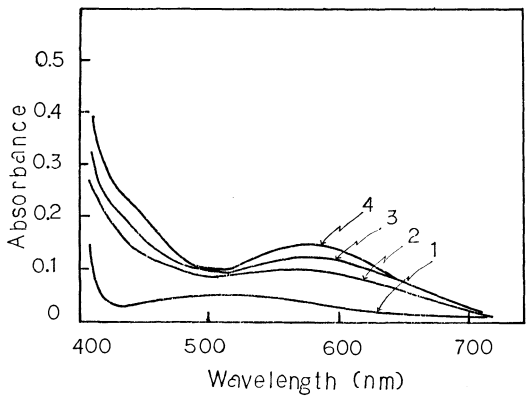

Fig. 2. Electronic spectra of Co(II) complexes in DMSO.
1: 2×10^{-3} mol dm^{-3} $Co(acac)_2$,
2: solution (1) electrolyzed for 20 min at −1.15 V *vs.* SCE,
3: solution (2) after 5 h at room temperature,
4: solution (2) after 6 d at room temperature.

a peak split at 520 and 510 nm (molar absorption coefficient : $\varepsilon=30$ dm^3 mol^{-1} cm^{-1}), which corresponds to $^4T_{1g}(F)\rightarrow{}^4T_{1g}(P)$.[4] For curves 2, 3, and 4 a new strong peak appeared in the neighbourhood of 590 nm with a shoulder at 440 nm, and the intensity increased with respect to the time after electrolysis. In the case of acetone, the spectrophotometric profile of the solution after electrolysis also showed a similar tendency (Fig. 3). The new absorption band in Figs. 2 and 3 can be attributed to the absorption of the μ-peroxo-dicobalt(II) complex, formed by the disproportionation of the $Co(acac)_2O_2^-$ complex in acetone or DMSO (Scheme 1).

In Fig. 4, curves 1 and 2 are shown for complexes A-1 and B-1. In curve 1, the absorption peak appeared

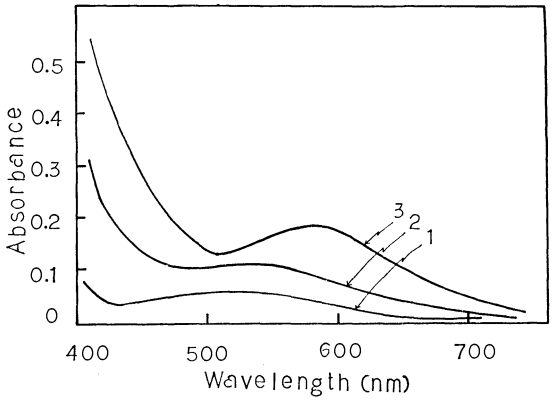

Fig. 3. Electronic spectra of Co(II) complexes in acetone.
1: 2×10^{-3} mol dm^{-3} $Co(acac)_2$,
2: solution (1) electrolyzed for 18 min at −1.15 V *vs.* SCE,
3: solution (2) after 17 h at room temperature.

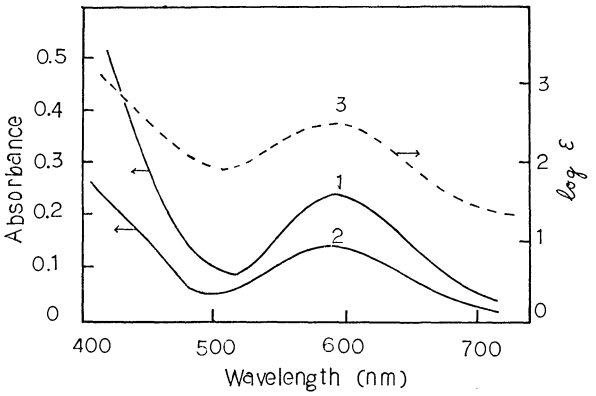

Fig. 4. Electronic spectra of Co(II) complexes.
1: $[(acac)_2Co{-}O_2{-}Co(acac)_2]^{2-}$ in acetone,
2: $[(acac)_2Co{-}O_2{-}Co(acac)_2]^{2-}$ in DMSO,
3: $[(dpm)_2\ Co{-}O_2{-}Co(dpm)_2]^{2-}$ in acetone.

at 597 nm in acetone and in curve 2, at 590 and 440 nm (shoulder) in DMSO. The band widths were usually about 110 nm. The molar absorption coefficients are unknown since it is difficult to obtain the solids. Attempts to isolate the μ-peroxodicobalt(II) complex as crystals were unsuccessful for two reasons: (1) increasing the time of electrolysis did not change the yield and (2) the complex was contaminated by TBAP and consequently difficult to crystallize under the experimental conditions. In the case of the $Co(dpm)_2$ complex, however, the $[(dpm)_2Co{-}O_2{-}Co(dpm)_2]^{2-}$ complex was isolated as crystals[5] (dpm represents an anion of dipivaloylmethane). The molar absorption coefficient and band width of the peak at 588 nm was 410 dm^3 mol^{-1} cm^{-1} and 110 nm respectively (curve 3 in Fig. 4).

It is well documented that the most common geometry of ligands around the cation in the high spin state cobalt(II) complex are octahedral, square pyramidal, and tetrahedral. Generally in an octahedral field, there are two d-d absorption bands at approximately 500 and 1200 nm. The intensity of this band is always low in octahedral complexes and it is

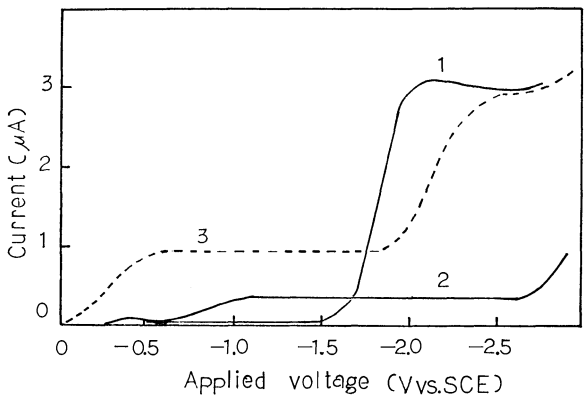

Fig. 5. D.c. polarograms of Co(II) and Co(III) complexes in DMSO.
1 and 2: $[(acac)_2Co–O_2–Co(acac)_2]^{2-}$,
3: 9×10^{-4} mol dm^{-3} $Co(acac)_3$.

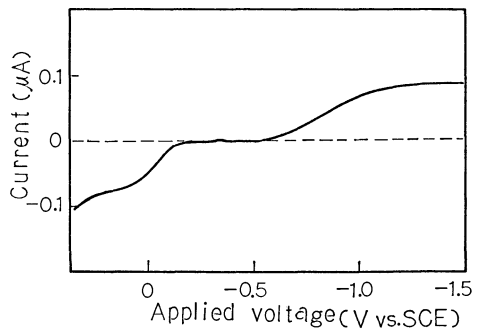

Fig. 6. D.c. polarogram of Co(II) complex in DMSO. Solution containing 0.05 mol dm^{-3} TBAP and μ-hyperoxo-dicobalt(II) complex.

not known where the molar absorption coefficient exceeds 50 dm^3 mol^{-1} cm^{-1}.[6] It is known that the intensity in tetrahedral field is usually close to the molar absorption coefficient of 700 dm^3 mol^{-1} cm^{-1}.[6] On the other hand, the intensity at 588 nm for the $[(dpm)_2Co–O_2–Co(dpm)_2]^{2-}$ complex which has a square pyramidal structure[5,7] shows an intermediate intensity between that of tetrahedral and octahedral cobalt(II). The spectrophotometric profiles of the complexes A-1 and B-1 in the visible region are similar to the spectrum of the Co(II)-dpm complex(curve 3 in Fig. 4). Consequently, it appears that the two absorption bands at 17000 and 23000 cm^{-1} for the Co(II)-acac complexes in Fig. 4 are associated with a square pyramidal structure. From these results, we can consider A-1 and B-1 complexes as the same.

Typical polarograms of the above complex and tris(acetylacetonato)cobalt(III) complex are shown in Fig. 5. In Fig. 5, curves 1, 2, and 3 were obtained from a solution of the complexes, A-1, B-1, and Co(acac)$_3$ containing about 0.05 mol dm^{-3} TBAP. In a DMSO medium, the Co(acac)$_3$ complex undergoes stepwise reduction to Co(II) and Co(O). The half-wave potentials of the first Co(III)→Co(II) and the second Co(II)→Co(O) waves are −0.29 and −2.13 V *vs.* SCE. On the other side, for curve 1, the reduction wave at −1.8 V was caused by the reduction of aldol condensation products of acetone[8] in A-1. The complex did not show a reduction wave under these conditions. For curve 2, the reduction wave at −0.85 V can be attributed to the presence of other complexes produced during the electrolysis, namely, the μ-peroxo-dicobalt(II) complex is unreducible.

In Fig. 6, the polarogram of the complex, A-2, is shown. This complex gives two waves in DMSO containing 0.05 mol dm^{-3} TBAP, the first half-wave potential at −0.05 V corresponding to oxidation to the +3 cobalt state and the second at −0.85 V probably corresponding to the reduction to the $[Co–O_2–Co]^{2-}$ state. The limiting currents of both waves were almost equal to each other and diffusion controlled. The second wave was characteristically irreversible and the half-wave potential was the more negative side than that of the oxygen molecule under the same conditions, thought to be due to the reduction of the bridging group, $–O_2–$, in the μ-hyperoxide-dicobalt(II) complex. Recently, it has become apparent that the catalytic electrode reaction consists of two distinct simultaneous chemical reactions. Accordingly, the μ-hyperoxo-dicobalt(II) complex may also be formed simultaneously. There is no doubt that such a reaction results in a lowering of the rate of the oxygen regeneration.

The catalytic electrode reaction mechanism has been estimated as follows:

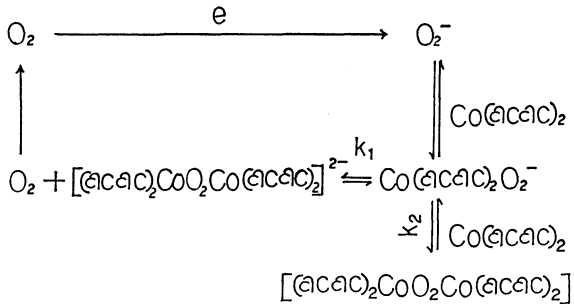

Scheme 1.

In this scheme, the k_1 path ocurred through a six coordinate intermediate, $[Co(acac)_2O_2^-]_2$. Moreover, the k_1 path was easier than the k_2 path in aprotic solvents. Thus, in the k_2 path the releasing process of the solvent molecule in a solvated complex, $Co(acac)_2(sol)_2$ is the rate-determining step.

References

1) A. Iwase and S. Kudo, *Nippon Kagaku Kaishi*, **1976**, 42.
2) A. Iwase and S. Tada, *Nippon Kagaku Kaishi*, **1972**, 1828.
3) C. K. Mann and K. K. Barnes, "Electrochemical Reactions in Nonaqueous Systems," Marcel Dekker (1970), p. 497.
4) W. L. Jolly, *Inorg. Synth.*, **11**, 84 (1968).
5) A. Iwase and S. Kudo, Paper 9A714, 26th International Congress of Pure and Applied Chemistry, Tokyo, September 1977.
6) R. L. Carlin, "Transitional Metal Chemistry," Marcel Dekker (1966), Vol. 2, p. 149.
7) F. Lions, I. G. Dance, and J. Lewis, *J. Chem. Soc., A*, **1967**, 565.
8) J. Riddick and W. B. Bunger, "Techniques of Chemistry," Organic Solvents, Wiley-Interscience (1970), Vol. 2, p. 722.

Gas-Chromatographic Studies of the Thermal Decomposition of Nitropentaammine-, Dinitrotetraammine-, Trinitrotriammine-, Tetranitrodiammine-, and Pentanitroamminecobalt(III) Complexes in the Solid State

Sukeo ONODERA*

Department of Chemistry, Faculty of Science, Tokyo University of Science, Kagurazaka, Shinjuku-ku, Tokyo 162

(Received July 24, 1978)

The gas-chromatographic study of the thermal decompositions of the complexes, $[Co(NO_2)(NH_3)_5]Cl_2$ (I), *cis*- (II) and *trans*-$[Co(NO_2)_2(NH_3)_4]Cl$ (III), $[Co(NO_2)_3(NH_3)_3]$ (IV), $K[Co(NO_2)_4(NH_3)_2]$ (V), and $K_2[Co(NO_2)_5NH_3]$ (VI) are reported. The EGA curves for these complexes show that the compounds decompose in two or three stages. In the first stage (*ca.* 140—240 °C), all complexes evolve nitrogen with the evolution of ammonia and/or nitrogen monoxide. The second stage (*ca.* 210—300 °C) has been ascribed to the evolution of ammonia from the intermediate dissociation products of compound I, II, and III. The third stage (*ca.* 275—350 °C) has been ascribed to the evolution of nitrogen monoxide from the solid residue with the exception of IV.

The thermal decomposition of the cobalt(III) nitroammine complexes in the solid state are usually studied by thermogravimetry (TG)[1-3] and differential thermal analysis (DTA).[2-5] The various steps in the decomposition often overlap and a mixture of gases is evolved, the composition of the mixture and the residual product depending upon temperature. In TG and DTA, these aspects are often not revealed and consequently the complexity of the decomposition is overlooked. Thus evolved gas analysis (EGA) is required in order to obtain more exact information on the decomposition processes of the compounds.

Although gas-chromatographic (GC) analysis may be expected to be useful in determining the composition of the gaseous decomposition products of the metal ammine complexes, few papers have been published on the GC study of the thermal dissociation, even in simple metal complexes.[6-8] The present work illustrates the applicability of pyrolysis-gas chromatography in elucidating the mechanism of the cobalt(III) nitroammine complexes.

Experimental

Materials. The complexes, $[Co(NO_2)(NH_3)_5]Cl_2$, *cis*- and *trans*-$[Co(NO_2)_2(NH_3)_4]Cl$, $[Co(NO_2)_3(NH_3)_3]$, $K[Co(NO_2)_4(NH_3)_2]$, and $K_2[Co(NO_2)_5NH_3]$ were prepared according to the methods given in the literature[9] and identified by infrared analysis. Samples ranging in particle size from 100 to 200 mesh were used.

Apparatus and Procedure. The EGA apparatus employed has been described previously.[8a] The procedure used for the pyrolysis of the sample and the analysis of the gaseous products are essentially the same as reported previously.[8a] The GC patterns for the various pure substances are shown in Fig. 1.

Results and Discussion

The EGA curves for the cobalt(III) nitroammine complexes in the 25 to 400 °C temperature range under helium are given in Figs. 2 and 3. The curves of water evolved have not been drawn since it was impossible to exactly determine the water in the gaseous products by means of the GC techniques employed in the present work. Although the chemical analysis of the gaseous products evolved from nitropentaammine- and trinitrotriamminecobalt(III) complexes *in vacuo* have been conducted by Clark *et al.*[10] and the EGA curves of some halogenopentaamminecobalt(III) complexes reported by Wendlandt and Smith[2] and Smith,[5] the EGA curves for *cis*- and *trans*-$[Co(NO_2)_2(NH_3)_4]Cl$, $[Co(NO_2)_3(NH_3)_3]$, $K[Co(NO_2)_4(NH_3)_2]$, and $K_2[Co(NO_2)_5NH_3]$ seem to be the first to appear. The EGA curves of the cobalt (III) nitroammine complexes were reproducible under the experimental conditions employed in the present work.

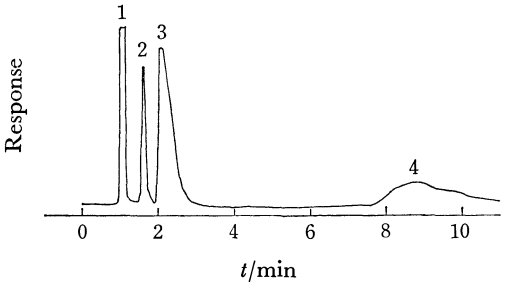

Fig. 1a. Gas chromatogram of nitrogen (1), nitrogen-(II) oxide (2), ammonia (3), and water (4) using 20% Silicon SF-96 on Fluoro Pack-80.

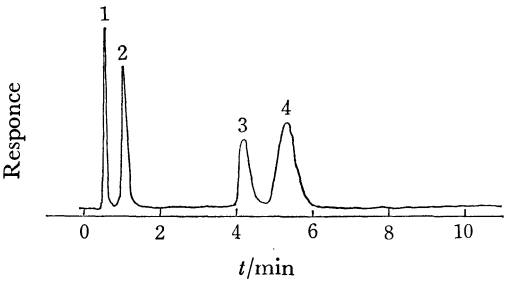

Fig. 1b. Gas chromatogram of nitrogen (1), nitrogen-(II) oxide (2), nitrous oxide (3), and nitrogen dioxide (4) using chromatographic silica gel.

The EGA curves for the cobalt(III) nitroammine complexes given in Figs. 2 and 3 show that the compounds decomposed in two or three stages. In the first stage (*ca.* 140—240 °C), all complexes evolved

* Present address: Faculty of Pharmaceutical Science, Tokyo University of Science, Ichigaya-funagawara, Shinjuku-ku, Tokyo 162.

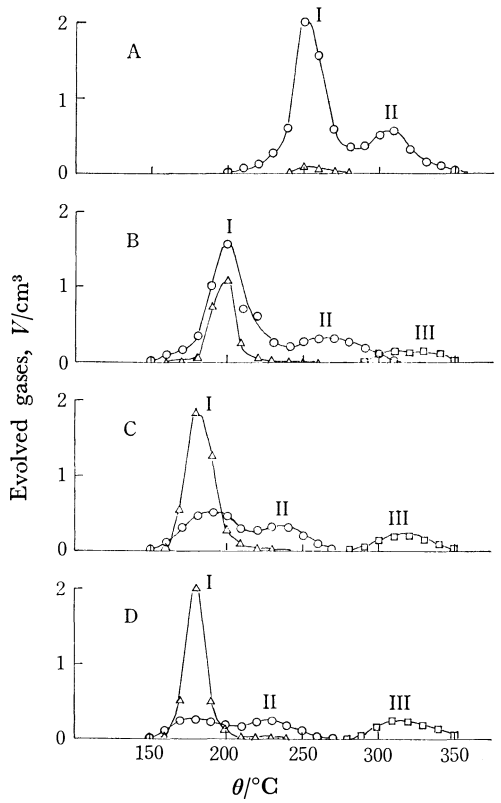

Fig. 2. EGA curves for $[Co(NH_3)_6]Cl_3$ (A), $[Co(NO_2)(NH_3)_5]Cl_2$ (B), *trans*-$[Co(NO_2)_2(NH_3)_4]Cl$ (C), and *cis*-$[Co(NO_2)_2(NH_3)_4]Cl$ (D) in a helium atmosphere.
NH_3; —○—, N_2; —△—, NO; —□—.

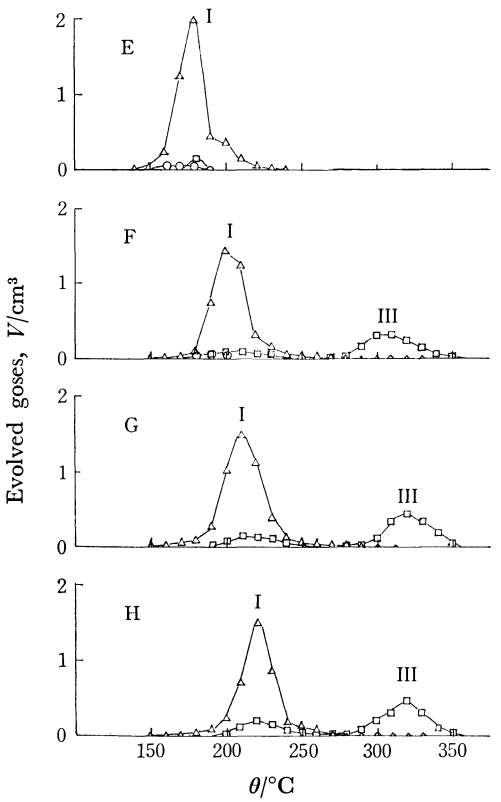

Fig. 3. EGA curves for $[Co(NO_2)_3(NH_3)_3]$ (E), $K[Co(NO_2)_4(NH_3)_2]$ (F), $K_2[Co(NO_2)_5NH_3]$ (G), and $K_3[Co(NO_2)_6]$ (H) in a helium atmosphere.
NH_3; —○—, N_2; —△—, NO; —□—.

nitrogen with the evolution of ammonia and/or nitrogen monoxide. The second stage (*ca.* 210—300 °C) has been ascribed to the evolution of ammonia from the intermediate dissociation products for $[Co(NO_2)(NH_3)_5]Cl_2$ and $[Co(NO_2)_2(NH_3)_4]Cl$. The third stage (*ca.* 275—350 °C) has been ascribed to the evolution of nitrogen monoxide from the solid residue with the exception of $[Co(NO_2)_3(NH_3)_3]$. The temperature ranges and the number of peaks are in agreement with those from the DTA curves reported by earlier workers,[3-5] except that the third peak can not be found in the case of DTA.

Decomposition of the Complexes (Stage I). Upon heating the cobalt(III) nitroammine complexes under helium, the yellow-brown compounds, especially $K[Co(NO_2)_4(NH_3)_2]$ and $K_2[Co(NO_2)_5NH_3]$, changed to orange-red in the 130 to 150 °C temperature range prior to the evolution of gas. Beattie and Sathell[11] and Doron[12] concluded that this phenomenon indicates that most of the nitro-form in the complexes is thermally converted to the nitrito-form.

Upon heating the complexes to temperatures higher than 150 °C, the yellow-brown compounds, $[Co(NO_2)(NH_3)_5]Cl_2$ and $[Co(NO_2)_2(NH_3)_4]Cl$, changed to greenish yellow ones, while the orange-red compounds, $[Co(NO_2)_3(NH_3)_3]$, $K[Co(NO_2)_4(NH_3)_2]$, and $K_2[Co(NO_2)_5NH_3]$, changed to black-brown ones, with the evolution of gas. In addition, thin layer chromatograms for the greenish yellow compounds, developed by a mixed solution, $HClO_4$–DMSO–CH_3OH (0.3 : 60 : 40), on Merck's silica gel G, were characterized by the appearance of new spots, which have been attributed to the tetraamminedianiono- and triammine-trianiono-complexes.[13]

The polarograms for the greenish yellow compounds, recorded in a 0.5 mol dm^{-3} K_2SO_4 containing 0.005% gelatin by use of a Yanagimoto KM-85-3 pen recording polarograph, showed that the limiting diffusion currents of the first wave, attributed to the reduction of cobalt(III) to cobalt(II) for the nitroammine-complexes,[14] decreased in comparison with the original compound. The polarograms for the black-brown compounds were characterized by a decreasing of the limiting diffusion currents of the first wave and a slight decreasing of the second wave, which has been attributed to the reduction of cobalt(II) to cobalt(0) for the nitroammine-complexes,[14] in comparison with those of both for the original complexes.

These results described together with earlier data,[2,16,17] suggest that the thermal decomposition of cobalt(III) nitroammine complexes under helium as:

$[Co(NO_2)(NH_3)_5]Cl_2$

$\xrightarrow{150\text{—}240\,^\circ C}$ $[CoCl(NO_2)(NH_3)_4]Cl + NH_3$

$\xrightarrow{150\text{—}240\,^\circ C}$ $[CoCl_2(NO_2)(NH_3)_3] + NH_3$

$\xrightarrow{150\text{—}240\,^\circ C}$ low ammine cobalt(II) complexes

$[Co(NO_2)_2(NH_3)_4]Cl$

$\xrightarrow{150\text{—}220\,^\circ C}$ $[CoCl(NO_2)_2(NH_3)_3] + NH_3$

$\xrightarrow{150\text{—}220\,^\circ C}$ low ammine cobalt(II) complexes

for other complexes,

$$[Co(NO_2)_3(NH_3)_3] \xrightarrow{140-210\,^\circ C} Co_2O_3 + N_2 + H_2O$$

$$K[Co(NO_2)_4(NH_3)_2] \xrightarrow{150-225\,^\circ C} \begin{cases} Co_3O_4 + KNO_3 + \text{gaseous products} \\ \text{low nitro cobalt(II) complexes} \end{cases}$$

$$K_2[Co(NO_2)_5NH_3] \xrightarrow{150-230\,^\circ C} \begin{cases} Co_3O_4 + KNO_3 + \text{gaseous products} \\ \text{low nitro cobalt(II) complexes} \end{cases}$$

Since large quantities of water and nitrogen were evolved in this stage, it has been concluded that ammonium nitrite was an intermediate dissociation product.

The decomposition temperatures at which the first maximum peaks observed on the EGA curves for the cobalt(III) nitroammine complexes in Figs. 2 and 3 are in the same order as the minimum temperatures where the color changes as observed by Matsui and Nakanishi.[15] This order for the cobalt(III) nitroammine complexes in Figs. 2 and 3 is related to the polarographic reduction potentials of cobalt(III) to cobalt(II) for the complex ions reported by Willis, Friend, and Mellor.[14] Plots of the above temperatures *versus* the potentials did not however give a strick linear relationship. Since the polarographic reduction potentials of the complex ions are considered to measure the relative electron affinities of the central metal ions, it has been concluded that the thermal stability of the cobalt(III) nitroammine complexes is dependent upon the electron affinity of the central cobalt(III) ion.

Subsequent Decomposition (Stage II). Upon heating $[Co(NO_2)(NH_3)_5]Cl_2$ and $[Co(NO_2)_2(NH_3)_4]Cl$ to temperatures higher than 230 °C, it was observed that the greenish yellow compounds, formed at the first stage, subsequently changed to grayish blue ones with the evolution of gas. In addition, the polarograms for the grayish blue compounds showed that the limiting diffusion currents of the first wave disappeared and those of the second wave decreased slightly in comparison with those of the both waves for the original complexes. These results appear to indicate that the greenish yellow compounds, probably $[CoCl(NO_2)(NH_3)_4]Cl$, $[CoCl_2(NO_2)(NH_3)_3]$, and $[CoCl(NO_2)_2(NH_3)_3]$, decomposed to form Co_2O_3, which has poor solubility in water.

The second EGA peaks of $[Co(NH_3)_6]Cl_3$, $[CoCl(NH_3)_5]Cl_2$, and *trans*-$[CoCl_2(NH_3)_4]Cl$ in a previous paper[8a] were obtained in the same temperature range (280—350 °C), although the numbers of coordinated-chloride ions are different, while, the second EGA peaks of $[Co(NO_2)(NH_3)_5]Cl_2$ and $[Co(NO_2)_2(NH_3)_4]Cl$ shifted to lower temperatures with the increase in the numbers of coordinated-nitrite ions. These results indicate that $[CoCl_3(NH_3)_3]$ is an intermediate dissociation product for the above three compounds, while $[CoCl_2(NO_2)(NH_3)_3]$, is for the nitropentaammine-complex, and $[CoCl(NO_2)_2(NH_3)_3]$, is for the dinitrotetraamine-complex.

Subsequent Decomposition (Stage III). When the complexes were heated to temperatures higher than 275 °C, it was observed that the grayish blue compounds, formed by heating $[Co(NO_2)(NH_3)_5]Cl_2$ and $[Co(NO_2)_2(NH_3)_4]Cl$ in stage II, changed to blue-black ones while the black-brown compounds, formed by heating $K[Co(NO_2)_4(NH_3)_2]$ and $K_2[Co(NO_2)_5NH_3]$ in stage I, changed to black ones with the evolution of nitrogen(II) oxide. In addition, the polarograms for the above solid residues were characterized by a decrease or the complete disappearance of the limiting diffusion currents of the second wave in comparison with that in the original compounds. These results suggest that the grayish blue and black-brown compounds, may be Co(ONO)Cl, $KCo(ONO)_3$, and KNO_3, decomposed with the evolution of nitrogen(II) oxide from the compounds to form cobalt oxides, which have poor solubility in water.

Although the exact nature of the solid residues, Co(ONO)Cl and $KCo(ONO)_3$, is not known, Devrainne and Belsot[3] demonstrated that the decomposition products up to 250 °C of $K[Co(NO_2)_4(NH_3)_2]$ consisted of Co_3O_4 and KNO_3.

The author wishes to thank Professor Masaakira Iguchi, Tokyo University of Science, for his interest in this work, and also Mr. Katsumi Kimura for his polarographic and thin-layer chromatographic analyses.

References

1) E. Kyuno, *Nippon Kagaku Zasshi*, **78**, 1494 (1957).
2) W. W. Wendlandt and J. P. Smith, *J. Inorg. Nucl. Chem.*, **26**, 445 (1964).
3) P. Devrainne and B. Belsot, *C. R. Acad. Paris*, **267**, 648 (1968).
4) N. I. Lobanov, I. R. Rassonskaya, and A. V. Ablov, *Zh. Neorg. Khim.*, **3**, 1335 (1958).
5) J. P. Smith, Ph. D. Thesis, Texas Technological College, Lubbock, Texas, Jun 1966.
6) K. Nagase, *Bull. Chem. Soc. Jpn.*, **46**, 144 (1973).
7) T. S. Rao and B. R. Gandhe, *J. Chromatogr.*, **88**, 407 (1974).
8) a) S. Onodera, *Bull. Chem. Soc. Jpn.*, **50**, 123 (1977); b) S. Onodera, *ibid.*, **51**, 1889 (1978).
9) M. Shibata, M. Mori, and E. Kyuno, *Inorg. Chem.*, **3**, 1573 (1964); S. M. Jorgensen, *Z. Anorg. Chem.*, **17**, 469 (1898).
10) G. L. Clark, A. J. Quick, and W. D. Harkins, *J. Am. Chem. Soc.*, **42**, 2483 (1920).
11) I. R. Beattie and D. P. N. Sathell, *Trans. Fraday. Soc.*, **52**, 1590 (1956).
12) V. Doron, *Inorg. Nucl. Chem. Lett.* **4**, 601 (1968).
13) L. F. Druding and R. B. Hazel, *Anal. Chem.*, **38**, 478 (1966).
14) J. B. Willis, J. A. Friend, and D. P. Mellor, *J. Am. Chem. Soc.*, **67**, 1680 (1945).
15) M. Matsui and T. Nakanishi, *J. Sci. Res. Inst.*, **51**, 159 (1957).
16) A. V. Ablov and N. I. Lobanov, *Zh. Obschex. Khim.*, **25**, 648 (1955).
17) N. Tanaka and M. Nanjo, *Bull. Chem. Soc. Jpn.*, **37**, 1330 (1964); N. Tanaka and K. Nagase, *ibid.*, **40**, 546 (1967).

The X-Ray Structure of Bis((*S,S*)-2,4-pentanediamine)platinum(II) Ion, $[Pt(SS\text{-ptn})_2]^{2+}$

Yasuji NAKAYAMA, Shun'ichiro OOI,* and Hisao KUROYA

Department of Chemistry, Faculty of Science, Osaka City University, Sumiyoshi-ku, Osaka 558

(Received September 2, 1978)

The bis((*S,S*)-2,4-pentanediamine)platinum(II) chloride monohydrate crystallizes in the space group $P2_12_12_1$ with four formula units in a unit cell of dimensions $a=12.089(3)$, $b=13.547(3)$, $c=10.697(2)$ Å. The crystal structure has been determined from diffractometer data and refined to $R=0.052$ for 1903 independent reflections. The Pt atom has a square planar coordination by four N atoms, the average value of the Pt–N distance being 2.05 Å. The complex has a pseudo two-fold axis which is perpendicular to the coordination plane defined by the four N atoms. The 6-membered chelate ring is of a chair conformation and one methyl group is axial with respect to the chelate ring, while the other is equatorial. From a comparison of the circular dichroism spectra of the diammine-(*S,S*)-2,4-pentanediamineplatinum(II) and the bis((*S,S*)-2,4-pentanediamine)platinum(II) ions, the effect of the (*S,S*)-2,4-pentanediamine on the rotatory strength of the Pt(II) complex has been found to be not additive.

The (*S,S*)-2,4-pentanediamine (*SS*-ptn) can coordinate to a metal ion yielding the 6-membered chelate ring with a skew or chair conformation, and it has been utilized in the studies of circular dichroism (CD) exhibited by the Co(III) complexes with 6-membered rings. In the crystal structure analyses made for some octahedral Co(III) chelates, the *RR*-ptn ring has been found usually to be of the λ skew conformation,[1] although a recent CD study for $[Co(NH_3)_{2n}(RR\text{-ptn})_{3-n}]^{3+}$ ($n=0$, 1, or 2) gave evidence for interconversion between the λ skew and the chair conformations in solution.[2] Appleton and Hall concluded, on the basis of the PMR study on Pt(II) chelates, that the *SS*-(or *RR*-)ptn ring in the planar complexes preferentially assumes the chair conformation.[3] The present work is an attempt to confirm their view and to study the structural parameters of the *SS*-ptn ring.

Experimental

Preparations of Complexes. *SS*-ptn·2HCl was purchased from Tokyo Kasei Co., Ltd. and used for the preparation of the complexes without further purification. $PtCl_2(SS\text{-ptn})$ was prepared by the method of Appleton and Hall[4] using the *SS*-ptn instead of *rac*-ptn.

$[Pt(NH_3)_2(SS\text{-ptn})]Cl_2$: The $PtCl_2(SS\text{-ptn})$ was suspended in water and concentrated aqueous ammonia added to the suspension at 80 °C until the dichloro complex was completely dissolved. The resulting solution was rotary evaporated. The colorless crystals were obtained by recrystallization from water–1-propanol.

Found: C, 14.75; H, 5.12; N, 13.84%. Calcd for $[Pt(NH_3)_2(C_5H_{14}N_2)]Cl_2$: C, 14.92; H, 4.97; N, 13.93%.

$[Pt(SS\text{-ptn})_2]Cl_2\cdot H_2O$: $K_2[PtCl_4]$ (1.27 g) and *SS*-ptn·2HCl (1.50 g) were dissolved in water. The solution was heated to 80 °C with stirring and then KOH solution (0.96 g in 10 ml of water) was added dropwise. The resulting solution was rotary evaporated to dryness. The separation of the Pt(II) complex from the residue was effected by extraction with methanol, the process being repeated two times to complete separation and the crystals were recrystallized from water–1-propanol.

Found: C, 24.75; H, 6.24; N, 11.59%. Calcd for $[Pt(C_5H_{14}N_2)_2]Cl_2\cdot H_2O$: C, 24.59; H, 6.15; N, 11.48%.

Spectral Measurements. Electronic spectrum was measured in aqueous solution on a Hitachi EPS-3T Recording Spectrometer. The CD spectrum in aqueous solution was obtained using a JASCO J-20 Automatic Recording Spectrometer. The FT ^{13}C NMR spectra were obtained in D_2O at 15.04 MHz with broad band proton decoupling and off-resonance proton decoupling on a JEOL JNM-FX-60 Spectrometer. Dioxane was used as an internal reference but the chemical shifts are given based on the TMS scale. In every ^{13}C NMR spectrum 4096 data points were taken over a 1-kHz spectral width. All measurements were conducted at room temperature.

Measurement of X-Ray Data of $[Pt(SS\text{-ptn})_2]Cl_2\cdot H_2O$.

Crystal Data: $C_{10}Cl_2H_{30}N_4OPt$, $F.W.=488.1$, orthorhombic, $a=12.089(3)$, $b=13.547(3)$, $c=10.697(2)$ Å, $D_m=1.85$, $D_c=1.85$ g/cm^3, $Z=4$, space group $P2_12_12_1$, $\mu(Mo\,K\alpha)=87.3$ cm^{-1}. The space group and the approximate unit cell dimensions were determined from Weissenberg photographs taken with Cu $K\alpha$ radiation. The unit cell dimensions were refined by the least-squares analysis of 15 θ values measured on a Philips PW1100 four circle diffractometer, Mo $K\alpha$ radiation being employed.

Data Collection: Diffraction intensities were measured by ω-2θ scan method on the diffractometer using graphite-monochromated Mo $K\alpha$ radiation. The crystal size was $0.28\times0.26\times0.25$ mm. The scan speed and scan width in ω were 0.017° s^{-1} and $(0.8+0.2\tan\theta)$°, respectively. Background was counted for 20 s at each end of the scan range. A total of 1903 independent reflections for which $I_t-2\sqrt{I_t}>I_b$ were collected in the $2\theta\geq55°$ range (I_t=intensity at the top of peak; I_b=mean background intensity obtained from preliminary background measurements for 5 s on both sides of the peak). A spherical absorption correction ($r=0.13$ mm) was applied. During the data collection no appreciable variations were observed in the intensities of three standard reflections (200,020,002) monitored every 2 h.

Structure Determination and Refinement. The crystal structure of $[Pt(SS\text{-ptn})_2]Cl_2\cdot H_2O$ was solved by the Patterson and Fourier method. The positional and thermal parameters were refined by a block-diagonal least-squares method, the minimized function being $\sum w(F_o-|F_c|)^2$. The weighting scheme, $w=1.0$ for $F_o\leq100.0$ and $w=(100.0/F_o)^2$ for $F_o>100.0$, were found to be optimum conditions to make the average values of $w|\Delta F_o|^2$ relatively constnat over ranges of F_o. The final R value was 0.052. In the final cycle of the refinement all parameter shifts were less than 0.2σ. Positional and thermal parameters are listed in Table 1.

Atomic scattering factors of Pt^0, Cl^-, N, C, O were taken from Ref. 5. Anomalous dispersion corrections were made for Pt^0 and Cl^-. The absolute crystal structure was determined on the basis of the configuration (*S*) of asymmetric carbon atoms. The observed and calculated structure factors are preserved at the Chemical Society of Japan (Docu-

Table 1. Positional and thermal parameters

	x	y	z	B/Å^2		x	y	z	B/Å^2
Pt	0.15536(4)	0.24402(3)	0.20000(4)	a)	C(3)	0.406(2)	0.244(1)	0.057(2)	4.1(3)
Cl(1)	0.3336(5)	0.4345(3)	0.6707(7)	a)	C(4)	0.356(2)	0.345(1)	0.089(2)	4.1(3)
Cl(2)	0.2726(6)	0.0639(3)	0.8223(5)	a)	C(5)	0.391(2)	0.380(2)	0.222(2)	5.0(4)
N(1)	0.256(1)	0.134(1)	0.133(1)	3.1(2)	C′(1)	−0.020(2)	0.456(1)	0.440(2)	4.3(4)
N(2)	0.230(1)	0.339(1)	0.079(1)	2.8(2)	C′(2)	0.056(1)	0.368(1)	0.410(2)	3.1(3)
N′(1)	0.056(1)	0.355(1)	0.266(1)	3.1(2)	C′(3)	0.013(2)	0.277(1)	0.470(2)	3.8(3)
N′(2)	0.080(1)	0.147(1)	0.321(1)	2.8(2)	C′(4)	0.081(1)	0.184(1)	0.459(2)	3.2(3)
C(1)	0.448(2)	0.065(1)	0.111(2)	4.8(4)	C′(5)	0.202(2)	0.195(2)	0.501(2)	5.2(4)
C(2)	0.378(1)	0.157(1)	0.147(2)	3.4(3)	O_w	0.188(2)	0.284(1)	−0.176(2)	6.6(4)

a) Anisotropic temperature factors ($\times 10^4$) in the form $\exp[-(B_{11}h^2+B_{22}k^2+B_{33}l^2+B_{12}hk+B_{13}hl+B_{23}kl)]$.

	B_{11}	B_{22}	B_{33}	B_{12}	B_{13}	B_{23}
Pt	37.9(3)	33.1(2)	48.3(4)	−3.9(6)	−5.1(6)	−1.4(6)
Cl(1)	64(4)	49(2)	225(9)	5(5)	−6(10)	−6(7)
Cl(2)	114(5)	54(2)	87(4)	35(6)	−13(8)	−17(5)

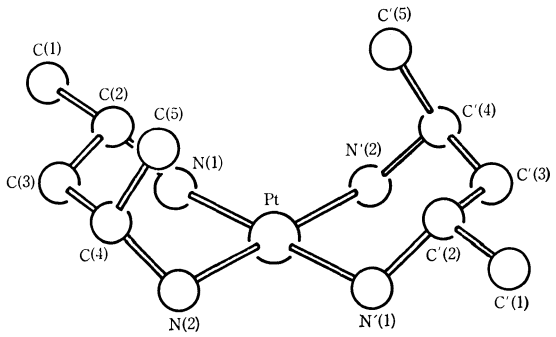

Fig. 1. The structure of $[Pt(SS\text{-ptn})_2]^{2+}$.

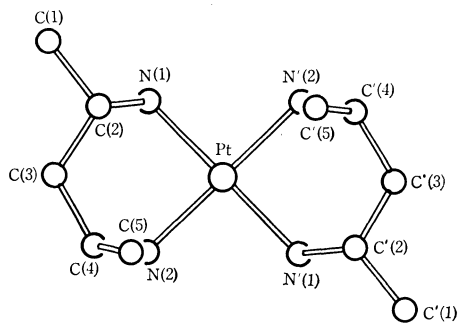

Fig. 2. The projection of complex on the coordination plane.

ment No. 7909). All computations were conducted on a FACOM 270-30 computer of Osaka City University, using RSSFR-5, HBLS-IV, and DAPH programs in the UNICS.[6]

Results and Discussion

The perspective drawing and projection of the complex are shown in Figs. 1 and 2, respectively. The complex has a pseudo two-fold axis which runs through Pt and is perpendicular to the coordination plane defined by N(1), N(2), N′(1), and N′(2). The disposition of these atoms is completely planar (±0.005 Å) and the Pt atom lies on the plane, the deviation being 0.003 Å.

Each chelate ring is of a chair conformation. One methyl group is equatorial with respect to the chelate ring, while the other is axial. The interplanar angle between the coordination plane and the mean plane of N(1), C(2), C(4), and N(2) is 130°, whereas that between the coordination plane and [N′(1), C′(2), C′(4), N′(2)] plane is 133°. These values are generally smaller than those (136.3—158.6°) of the 6-membered ring of tn (=1,3-propanediamine) with a chair conformation in octahedral complexes.[7] The larger interplanar angle in the octahedral complexes could be ascribed to interligand interactions within the complex, while the smaller interplanar angle in the present complex indicates that the extent of the interaction is smaller in spite of the presence of the methyl substituents in the ring. The Pt···C(5) and Pt···C′(5) distances are 3.40 and 3.34 Å, respectively. Bond lengths and angles are given in Table 2.

Table 2. Bond lengths (l/Å) and bond angles (ϕ/°)

Pt-N(1)	2.05(1)	C(1)-C(2)	1.56(3)
Pt-N(2)	2.04(1)	C(2)-C(3)	1.55(3)
Pt-N′(1)	2.05(1)	C(3)-C(4)	1.53(3)
Pt-N′(2)	2.06(1)	C(4)-C(5)	1.56(3)
N(1)-C(2)	1.52(2)	C′(1)-C′(2)	1.53(3)
N(2)-C(4)	1.53(2)	C′(2)-C′(3)	1.48(3)
N′(1)-C′(2)	1.55(2)	C′(3)-C′(4)	1.52(3)
N′(2)-C′(4)	1.56(2)	C′(4)-C′(5)	1.54(3)
N(1)-Pt-N(2)	88.6(5)	N′(1)-Pt-N′(2)	89.5(5)
Pt-N(1)-C(2)	113(1)	Pt-N′(1)-C′(2)	115(1)
Pt-N(2)-C(4)	115(1)	Pt-N′(2)-C′(4)	113(1)
N(1)-C(2)-C(1)	110(1)	N′(1)-C′(2)-C′(1)	107(1)
N(1)-C(2)-C(3)	108(1)	N′(1)-C′(2)-C′(3)	110(1)
N(2)-C(4)-C(3)	110(1)	N′(2)-C′(4)-C′(3)	109(1)
N(2)-C(4)-C(5)	110(2)	N′(2)-C′(4)-C′(5)	109(1)
C(1)-C(2)-C(3)	110(2)	C′(1)-C′(2)-C′(3)	110(1)
C(2)-C(3)-C(4)	117(2)	C′(2)-C′(3)-C′(4)	118(2)
C(3)-C(4)-C(5)	112(2)	C′(3)-C′(4)-C′(5)	114(2)

In the chelate ring the N–Pt–N coordination angle is significantly greater than those (81.9—87.4°) in the 5-membered ring,[8] but slightly less than 90°. The Pt–N–C bond angles are small compared with

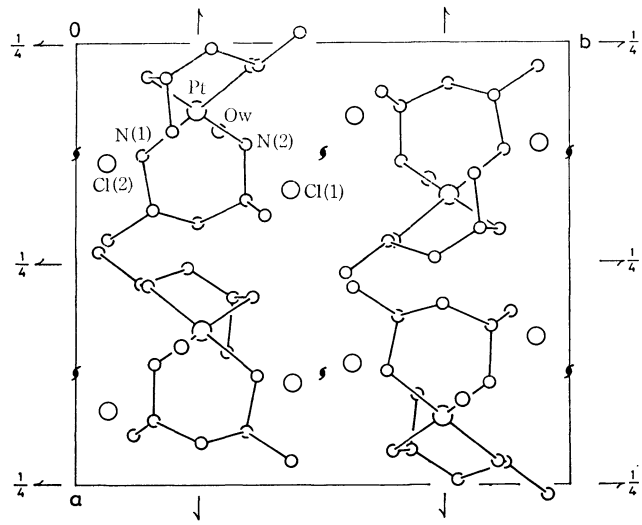

Fig. 3. The crystal structure viewed down the c axis.

TABLE 3. POSSIBLE HYDROGEN BONDS

X-H[a)]···Y	X···Y(*l*/Å)	H···Y(*l*/Å)	X-HY(*φ*°)
N(1)-H···Cl(2^{I})	3.46(2)	2.50	156
N(1)-H···Cl(2^{II})	3.38(2)	2.37	168
N(2)-H···O_w[b)]	2.87(2)	1.84	174
N(2)-H···Cl(1^{III})	3.31(2)	2.31	164
N′(1)-H···Cl(1^{III})	3.31(2)	2.29	168
N′(2)-H···Cl(2^{II})	3.37(2)	2.35	173
N′(2)-H···Cl(1^{IV})	3.18(2)	2.26	148
O_w-H···Cl(1^{I})[b)]	3.15(2)		
O_w-H···Cl(2^{I})[b)]	3·16(2)		

Roman numeral superscripts refer to the atoms in the following equivalent positions:
I $x, y, -1+z$ II $(1/2)-x, -y, -(1/2)+z$
III $(1/2)-x, 1-y, -(1/2)+z$
IV $-(1/2)+x, (1/2)-y, 1-z$

a) The positions of amino H atoms have been calculated on the assumption that the N-H distance is 1.03 Å. b) N(2)···O_w···Cl(1^{I})=103(1)°, N(2)···O_w···Cl(2^{I})=101(1)°, Cl(1^{I})···O_w···Cl(2^{I})=115(1)°.

those (116.5—121.3°) in the octahedral tn complexes.[7] This is also in harmony with the smaller interligand interaction in the planar complex, since the decrease in the interplanar angle is related to the decrease in the Pt–N–C angle. Both of C(2)–C(3)–C(4) angle and its primed analogue are significantly larger than those (111.3—116.0°) in the tn complexes[7] and this is thought due to steric repulsion between the axial methyl group and C(2)–H(axial) segment.

The crystal structure viewed down the c axis is shown in Fig. 3. Except for the axial H atom bonded to N′(1) all remaining amino H atoms participate in N–H···Cl^- or N–H···O(H_2O) hydrogen bonding, the data of which are given in Table 3.

In the ^{13}C NMR spectrum of [Pt(NH_3)$_2$(*SS*-ptn)]Cl_2 three signals, each of which is accompanied with satellites due to paltinum coupling, appear at 46.6 ($^2J_{Pt-C}$=25 Hz), 40.6 ($^3J_{Pt-C}$=21 Hz), and 21.9 ppm ($^3J_{Pt-C}$=31 Hz). These signals have been assigned

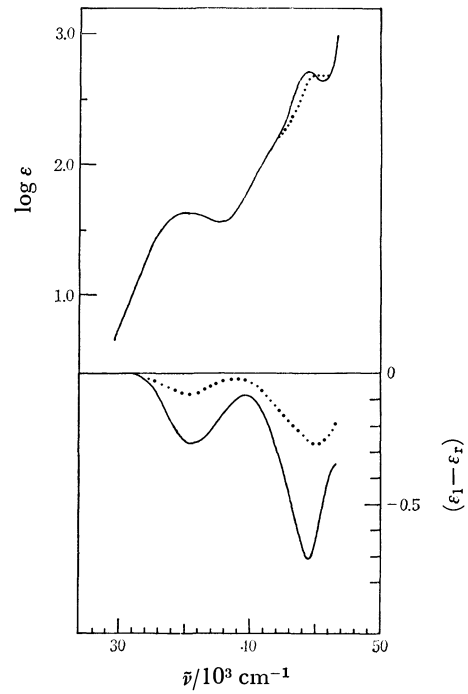

Fig. 4. The absorption (top) and CD (bottom) spectra of [Pt(NH_3)$_2$(*SS*-ptn)]Cl_2 (·····) and [Pt(*SS*-ptn)$_2$]Cl_2·H_2O (——) in aqueous solution.

to the resonances due to CH, CH_2, and CH_3 carbons, respectively, on the basis of the spectrum with off-resonance proton decoupling. The corresponding resonances appeared at 46.8, 40.7, and 21.8 ppm in [Pt(*SS*-ptn)$_2$]Cl_2·H_2O. Appleton and Hall reported that the Pt—*SS*-ptn chelate ring makes rapid chair-to-chair interconversion in solution.[3] The feature of ^{13}C NMR spectrum is compatible with this conclusion, since five carbon signals should be observed if the chelate ring is fixed in the chair conformation. According to the conformational analysis of the planar Mb_2(tn) type complex (b=a monodentate ligand), the interconversion occurs *via* a skew intermediate.[9] However, the intermediate conformer is small in population at room temperature, as the free energy difference (ΔG) between the skew and chair conformers has been estimated to be 1.6 kcal/mol.[9] In Mb_2(*SS*-ptn) both methyl groups are equatorial in the δ skew conformer, whereas they are axial in the λ one. Conformational analysis of [$CoCl_4$(*S*(or *R*-)-1,3-butanediamine)]$^-$ showed that in the case of the skew ring the chelate ring with axial methyl group has greater atom overcrowding than that with equatorial one.[10] This may also be the case for planar Mb_2(*SS*-ptn). The ΔG(chair, δ skew) value in Mb_2(*SS*-ptn) may not be very different from that in Mb_2(tn) but the ΔG(chair, λ skew) may be larger in magnitude than the ΔG(chair, δ skew).

Figure 4 shows the absorption and CD spectra of [Pt(NH_3)$_2$(*SS*-ptn)]Cl_2 and [Pt(*SS*-ptn)$_2$]Cl_2·H_2O in aqueous solution. The absorption spectra are very similar to those of the corresponding 1,2-propanediamine complexes.[11] Since the populations of the skew conformers are small as inferred from the free energy differences, the CD spectrum of the diammine

complex can be regarded as virtually arising from the vicinal effect due to the *S* asymmetric carbons.

The effect of the *SS*-ptn ligand on the CD spectra of $[Pt(NH_3)_2(SS\text{-ptn})]^{2+}$ and $[Pt(SS\text{-ptn})_2]^{2+}$ is not additive as seen in Fig. 4, indicating that the vicinal effect of the asymmetric carbons is not the only source of the CD of bis(*SS*-ptn) complex. In general the asymmetry factors responsible for the optical activity of the Pt(II) chelates of *SS*-ptn are the chirality of the asymmetric carbon in the chelate ring and the chelate ring in the skew conformation. The non-additivity suggests that the CD spectrum of the bis-chelate comprises the conformational contribution from the conformers with skew ring.

This research was supported by Grant-in-Aid from the Ministry of Education.

References

1) A. Kobayashi, F. Marumo, and Y. Saito, *Acta Crystallogr., Sect. B*, **28**, 3591 (1972) ; A. Kobayashi, F. Marumo, and Y. Saito, *ibid., Sect. B*, **29**, 2443 (1973).

2) M. Kojima, M. Fujita, and J. Fujita, *Bull. Chem. Soc. Jpn.*, **50**, 898 (1977).

3) T. G. Appleton and J. R. Hall, *Inorg. Chem.*, **9**, 1807 (1970).

4) T. G. Appleton and J. R. Hall, *Inorg. Chem.*, **9**, 1800 (1970).

5) "International Tables for X-Ray Crystallography," Kynoch Press, Birmingham (1962), Vol. 3, pp. 202, 215.

6) "The Universal Crystallographic Computation Program System," Crystallographic Society of Japan, (1969).

7) F. A. Jurnak and K. N. Raymond, *Inorg. Chem.*, **13**, 2387 (1974).

8) K. Yokoho, K. Matsumoto, S. Ooi, and H. Kuroya, *Bull. Chem. Soc. Jpn.*, **49**, 1864 (1976); K. Matsumoto, S. Ooi, M. Sakuma, and H. Kuroya, *ibid.*, **49**, 2129 (1976); Y. Nakayama, K. Matsumoto, S. Ooi, and H. Kuroya, *ibid.*, **50**, 2304 (1977); R. G. Ball, N. J. Bowman, and N. C. Payne, *Inorg. Chem.*, **15**, 1704 (1976); W. A. Freeman, *Inorg. Chem.*, **15**, 2235 (1976).

9) J. R. Gollogly and C. J. Hawkins, *Inorg. Chem.*, **11**, 156 (1972); C. J. Hawkins, R. M. Peachey, and C. L. Szoredi, *Aust. J. Chem.*, **31**, 973 (1978).

10) L. J. DeHyes and D. H. Busch, *Inorg. Chem.*, **12**, 1505 (1973).

11) H. Ito, J. Fujita, and K. Saito, *Bull. Chem. Soc. Jpn.*, **40**, 2584 (1967).

Emission Spectra and Luminescence Life Times of Uranium-Mica Type Compounds

Yoshinori SUGITANI,* Kenji KATO, and Kozo NAGASHIMA

Department of Chemistry, The University of Tsukuba, Sakura-mura, Ibaraki 300-31

(Received September 7, 1978)

A series of uranium–mica type compounds $M(UO_2)_2(XO_4)_2 \cdot nH_2O$, where M=Ca, Sr, Ba, Mg, Na_2, K_2, and $(H_3O)_2$; X=P and As, as well as the doped samples of $Mg(UO_2)_2(PO_4)_2 \cdot nH_2O$: Mn(0.03 mol %) and $Zn(UO_2)_2(PO_4)_2 \cdot nH_2O$: Cu(0.1 mol %), have been prepared and measured for emission spectra under the UV-(365 nm) excitation and decay times. Some of these samples, *e.g.*, $(H_3O)_2(UO_2)_2(AsO_4)_2 \cdot nH_2O$, have been found to give weak shoulders and a separated band, in addition to the six bands so far reported for other uranyl(VI) compounds. Samples containing AsO_4^{3-} ions in place of PO_4^{3-} gave emission spectra, where the main bands shifted by approximately 100 cm^{-1} to lower energy also giving shorter life times. The decay times of the six emission bands of $Mg(UO_2)_2(PO_4)_2 \cdot nH_2O$ have been found to have the same value of 2.5×10^{-4} s.

Uranyl(VI) compounds exhibit a highly characteristic luminescence both in the solid state and in solution. The spectral properties of uranyl(VI) compounds have been studied in great detail, since Stokes gave the first systematic investigation on light-emission and absorption in the middle of the nineteenth century.[1-4] The theoretical basis, however, for understanding the spectroscopic properties of the UO_2 group has been established only in the last two or three decades and remain incomplete.[5,6] The luminescence, which is assigned to emission from the lowest excited $^3\Pi_u$ state displays considerable sub-structure probably due to vibrational effects. Bell and Biggers,[6] who gave possibly the most comprehensive analysis of Uranyl(VI) salts, resolved the six emission bands in the luminescence spectrum of uranyl(VI) perchlorate in water. Iimori and Iwase resolved the sixteen bands of the fluorescence spectrum of natural autunite, a hydrous phosphate of uranyl (VI) and calcium, by photo techniques.[7] No further description has, however, been published on the luminescence spectrum of this mineral. In the present paper, the emission spectra and the decay times for a series of uranium–mica compounds including the synthetic and natural autunites are reported. In addition to the conventional decay time measurement, the life times of the six resolved bands have been measured separately for a sample of Mg-containing uranium–mica.

Experimental

Samples. Samples were prepared according to the literature.[8,9] The general formula of uranium–micas is given[10] as $M(UO_2)_2(XO_4)_2 \cdot nH_2O$, where M is an univalent metal ion (M^{I}) or a bivalent metal ion (M^{II}), XO_4 is a phosphate PO_4^{3-} or arsenate AsO_4^{3-}. The prepared samples are those with M=Na_2, K_2, $(H_3O)_2$, Ca, Mg, Sr, Ba, and Zn. The number of water molecules n varies according to the condition of the samples; natural autunites with bivalent metal ions have values of ranging from 8 to 12, while those with univalent ions have, to some extent, a lower value of n.

The samples were prepared by mixing the solutions containing the component ions and adjusting the temperature and pH at the appropriate values. The procedure for the preparation of $Ca(UO_2)_2(PO_4)_2 \cdot nH_2O$ is given here as an example. The reagents used were of guaranteed grade. Diluted (1.48 mol/l) phosphoric acid (5 ml) was added to a solution of $CaCl_2$ (s.g.=1.25, 500 ml), followed by boiling and the slow addition of about 10 ml of uranyl solution containing 3.7 g of $UO_2(NO_3)_2 \cdot 6H_2O$. The resultant solution was kept warm on a water bath, and the required precipitate was obtained at the bottom of a beaker in approximately 1 h. The samples were confirmed by X-ray diffractometry.

Apparatus. A block diagram for the measurement of the luminescence decay time is shown in Fig. 1. The main part of the system is composed of a microcomputer (TK-80, NEC Japan, 8080 type) and digital counters. All interface units including the digital counters have been hand-made in this laboratory within the expense of one hundred and sixty thousands yen. The microcomputer system with peripheral interfaces is connected on line to the optical system, for which some units of the multi-purpose spectrometer (SS-25, JASCO Japan) are employed. The apparatus is able to measure a wide range of decay times at weak intensity. More details of the system, especially concerning the hardware will be reported later. The measurement of emission spectra and decay times were made at room temperature.

Results and Discussion

According to McGlynn and Smith,[5] the ground state configuration of the UO_2^{2+} molecule is expressed as $(1\sigma_u^+)^2(1\sigma_g^+)^2(1\pi_u)^4(1\pi_g)^4$, leading to a totally symmetric singlet ground state $^1\Sigma_g^+$. The resolved absorptions between 20500 and 30000 cm^{-1} (visible to near UV) occur because of transitions from the ground state to the lowest excited state $^3\Pi_u$, which is split into twelve sublevels due to the symmetric stretching in the excited state (Fig. 3). The luminescence appears to occur from the lowest one or two sublevels to the ground state which is also further split due to the symmetric stretching in the ground state.[4] Figure 2 shows the emission spectra of a synthetic sample of $Mg(UO_2)_2(PO_4)_2 \cdot nH_2O$, which gives a typical spectral pattern for a series of uranium–micas prepared here. Excitation by UV light of 365 nm was found more efficient for the measurement of luminescence than 254 nm, which is understood since the closely separated sublevels arising from the triplet $^3\Pi_u$ efficiently absorb the exciting energy of 365 nm (27400 cm^{-1}), while there is not any appropriate absorbing level for 254 nm (39400 cm^{-1}) (Fig. 3).

The spectra is apparently composed of six bands with an appoximate intensity ratio of 3 : 13 : 45 : 100 : 95 : 8. Peak positions for all the prepared samples are listed in Table 1, together with the life time data. The average spacing of the five lowest energy bands

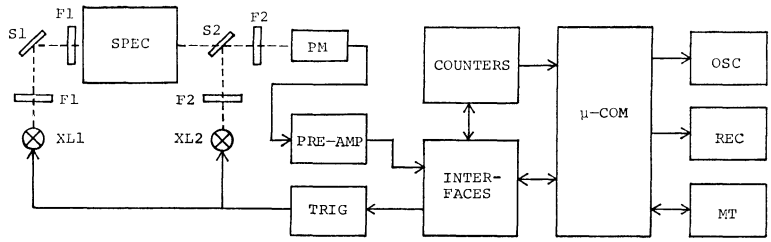

Fig. 1. Block diagram showing the measuring system of luminescence life time. Either the combination of (XL1, F1, S1, F1) or (XL2, F2, S2, F2) is used in the actual measurement.
XL1, XL2 : Xenon lamps, F1, F2 : filters, S1, S2 : samples, SPEC : spectrometer, PM : photomultiplier, TRIG : trigger circuit, μ-COM : microcomputer, OSC : XY-oscilloscope, REC : XY-recorder, MT : magnetic tape.

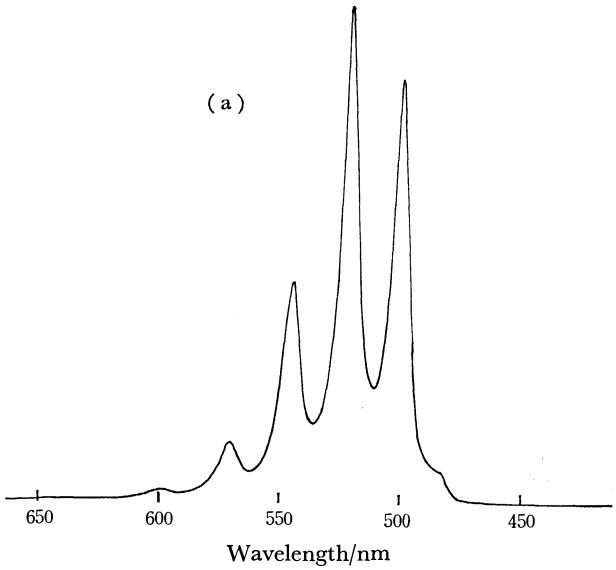

Fig. 2. Emission spectra at the excitation of UV (365 nm) light for $Mg(UO_2)_2(PO_4)_2 \cdot nH_2O$ (a), and for $(H_3O)_2(UO_2)_2(AsO_4)_2 \cdot nH_2O$ (b), where the additional bands are observed.

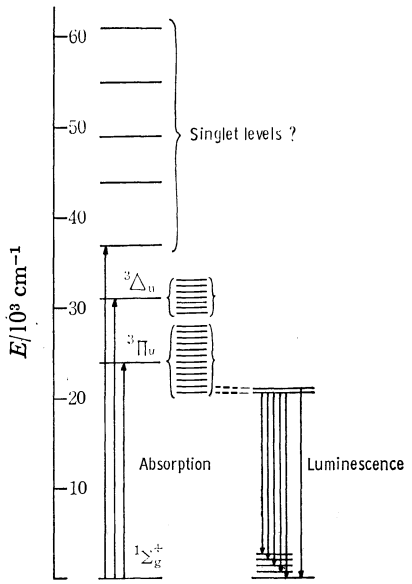

Fig. 3. Energy level diagram for uranyl(VI) ion based on Bell and Biggers' paper.[6]

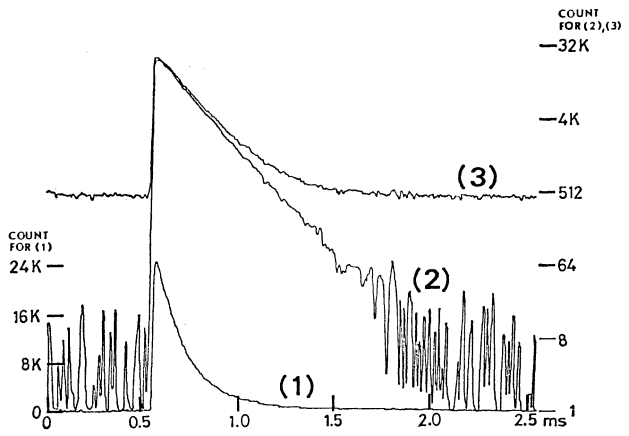

Fig. 4. Decay curve of $Mg(UO_2)_2(PO_4)_2 \cdot nH_2O$ (1) and it's logarithmic conversions with (2) and without (3) background subtraction.

is 840±20 cm^{-1}, while the band at the highest energy is spaced only 710±40 cm^{-1} from the next lower energy band. Bell and Biggers reported the same spectral feature for the emission bands of uranyl(VI) perchlorate in water.[6] In that case the average spacing for the five lowest energy bands was 855±20 cm^{-1}, while another band was spaced 768 cm^{-1} from its neighbor. They suggested that the latter band is probably from a different origin to the other five emission bands, that is, from the second absorption level. The smaller spacings of the uranium–mica

Table 1. Emission band position and life time of uranium-micas

Sample	Life time $\tau/10^{-4}$ s		ν_1[a]	ν_2	ν_3		ν_4			ν_5			ν_6
$Ca(UO_2)_2(PO_4)_2\cdot nH_2O$	1.9, 2.1[b]		604	576	550		527			505			488
$Sr(UO_2)_2(PO_4)_2\cdot nH_2O$	3.5, 3.6	(633)[c]	602	575	549		527			506			488
$Ba(UO_2)_2(PO_4)_2\cdot nH_2O$	2.8, 2.9		604	576	551	545	527			504		(494)	486
$Ba(UO_2)_2(AsO_4)_2\cdot nH_2O$	1.9	(638)	608	579	554		531			509	(500)		(493)
$Mg(UO_2)_2(PO_4)_2\cdot nH_2O$	2.5		600	572	544		523			500			484
$Mg(UO_2)_2(AsO_4)_2\cdot nH_2O$	0.57, 0.7	(636)	603	575	550		526			504			(488)
$Mg(UO_2)_2(PO_4)_2\cdot nH_2O$: Mn(0.03 mol %)	1.3	(631)	599	571	547		523			501			483
$Zn(UO_2)_2(PO_4)_2\cdot nH_2O$: Cu(0.1 mol %)	0.81		602	575	549		525			503			487
$Na_2(UO_2)_2(PO_4)_2\cdot nH_2O$	1.6, 2.2		604	575	549		526			504			486
$Na_2(UO_2)_2(AsO_4)_2\cdot nH_2O$	0.87		607	578	552	546	528	523		506	500		(490)
$K_2(UO_2)_2(PO_4)_2\cdot nH_2O$	2.7, 2.9		603	575	549		526			504			487
$K_2(UO_2)_2(AsO_4)_2\cdot nH_2O$	0.95, 1.1		607	579	553		529			507	(499)		491
$(H_3O)_2(UO_2)_2(PO_4)_2\cdot nH_2O$	—	(636)	602	573	547		523			500			481
$(H_3O)_2(UO_2)_2(AsO_4)_2\cdot nH_2O$	1.3	(640)	609	580	553	537	528	521	514	506	499	495	489
Natural autunite	2.5, 2.6, 2.8		605	575	550		527			505			488

a) ν_1 to ν_6 correspond to the six emission bands after Bell and Biggers.[6] b) Data obtained at a different run of measurement on the some sample. c) Data in the parentheses are less reliable than others.

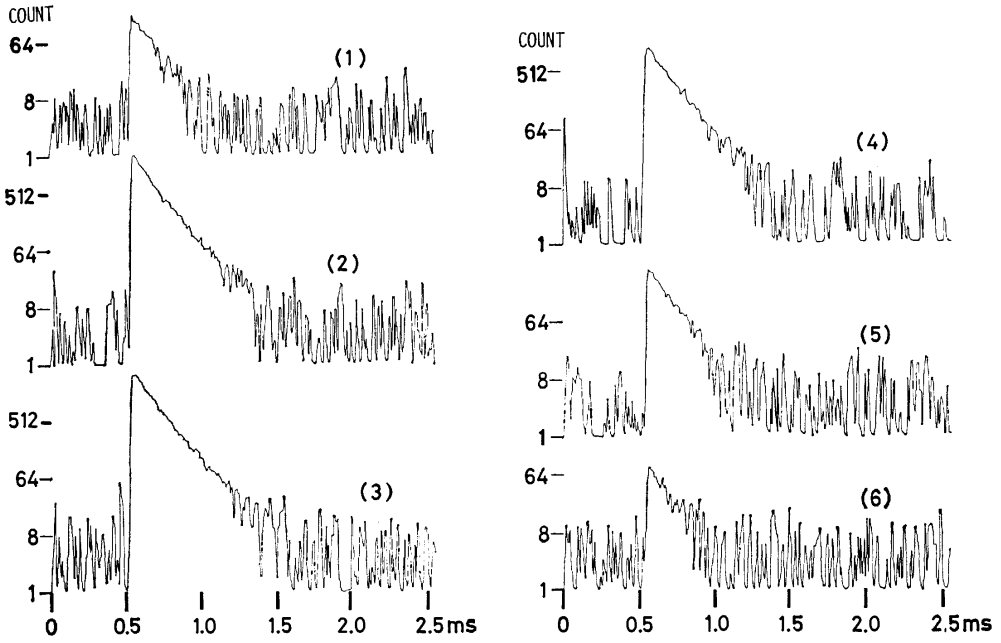

Fig. 5. Logarithmic converted decay curves for bands at 484 nm (1), 500 nm (2), 523 nm (3), 544 nm (4), 572 nm (5), and 600 nm (6) of $Mg(UO_2)_2(PO_4)_2\cdot nH_2O$.

samples compared to those of uranyl(VI) perchlorate in water may be considered as reflecting the geometry of coordination of ligand molecules around the uranyl-(VI) ion.[11]

Decay curves for the six emission bands have been recorded as shown in Fig. 5, where the logarithmic converted lines instead of the direct decay curves are given for convenience. Life time data obtained for the most intense band at 19011 cm^{-1} have the value of 2.5×10^{-4} s, which agrees with the five others within experimental error suggesting that the six emission bands emerge from the same transition mechanism.

As seen in Table 1, some of the samples have additional weak bands besides the six main bands, one of which was observed as a very weak band at the low energy side with the same spacing as the five bands. The others were observed either as shoulders or as asymmetrics of the main bands. Iimori and Iwase[7] found sixteen emission bands for a natural autunite using a photo technique in almost the same energy region as that of the six bands found here. The sixteen bands were arranged into three series, E(seven bands, very intense), B(five bands, dim), and H(four bands, very dim), each of which has the same wave-number interval of 800 cm^{-1}. The six highest energy bands in the E series coincided well with the six bands reported here.

The remaining band in the E series at the lowest energy (635 nm) found its counterpart only as a very weak and broad band in the spectra recorded here (Table 1). The shoulder bands which were found, for instance, in the spectra of $(H_3O)_2(UO_2)_2(AsO_4)_2 \cdot nH_2O$ could be related to some bands in the B or H series. However, the imprecise energy position and the limited number of shoulder bands do not allow a precise comparison between the bands. The presence of the additional bands, however, is thought to necessitate a more rigorous discussion concerning the origin of the emission bands than has hitherto appeared.[5,6]

The value of n and the changes found during measurement were not recorded however in the present study, since no significant changes were observed in the spectral patterns and in the life times during repeated measurements. The reason for this is presumably that the water molecules in the uranium–micas are located in the cavities in the $[(UO_2)(XO_4)]_n$ layer structure and having a zeolitic water character, they exert only a small influence on the UO_2 energy levels as perturbing ligands.[9]

The replacement of PO_4 by AsO_4 causes a shortening of the life time as well as a shift of the emission bands to low energy about 100 cm^{-1} in the uranium–micas of Ba, Mg, Na_2, and K_2 but the explanation of this remains unknown. It does not seem, however, to be due to paramagnetic impurities contained, for instance, in aresenic acid used in the experiment, since the doped sample of Mg-containing uranium–mica (Mn 0.03 mol %) shows a shortening in life time as a result of the transfer of the absorbed energy to the paramagnetic ion Mn^{2+}, while it does not show any band shift with respect to the sample without paramagnetic impurities.

References

1) G. G. Stokes, *Phil. Trans. Roy. Soc. London*, **142**, 518 (1852).
2) S. G. Gordon, *Am. Mineral.*, **14**, 363 (1929).
3) H. D. Burrows and T. J. Kemp, *Chem. Soc. Rev.*, **1974**, 139.
4) E. Rabinowitch and R. L. Belford, "Spectroscopy and Photochemistry of Uranyl Compounds," Macmillan, New York (1964).
5) S. P. McGlynn and J. K. Smith, *J. Mol. Spectrosc.*, **6**, 164 (1961).
6) J. T. Bell and R. E. Biggers, *J. Mol. Spectrosc.*, **18**, 247 (1965); **22**, 262 (1967); **25**, 312 (1968).
7) S. Iimori and E. Iwase, *Sci. Papers Inst. Phys. Chem. Res. (Tokyo)*, **34**, 372 (1938).
8) J. G. Fairchild, *Am. Mineral.*, **14**, 265 (1929).
9) Y. Sugitani, H. Kasuya, K. Nagashima, and S. Fujiwara, *Nippon Kagaku Zasshi*, **90**, 52 (1969).
10) For instance, H. Strunz, "Mineralogische Tabellen," Akad. Verlag., Leipzig (1957).
11) C. Göller-Walrand and S. De Jaegere, *Spectrochim. Acta, Part A*, **28**, 257 (1972); C. Göller-Walrand and S. De Jaegere, *J. Chim. Phys.*, **69**, 726 (1972).

Formation of Micelles of Hexadecyltrimethylammonium Bromide in Water–*N,N*-Dimethylformamide Solutions

Lavinel G. Ionescu,*,† Tadashi Tokuhiro, and Benjamin J. Czerniawski
Department of Chemistry, University of Detroit, Detroit, Michigan 48221, U.S.A.
(Received July 7, 1978)

The critical micellar concentration of aqueous solutions of hexadecyltrimethylammonium bromide (HTAB) containing various amounts of *N,N*-dimethylformamide (DMF) has been determined at 25 and 40 °C by means of surface tensiometric measurements. The standard free energy ($\Delta G_m°$), enthalpy ($\Delta H_m°$), and entropy ($\Delta S_m°$) of micellization were also determined. The experimental results indicate that: (1) micelle formation is somewhat hindered by a raise in temperature, and (2) DMF has an inhibitory effect on the formation of micelles of HTAB. This effect is relatively small at low DMF concentrations, but it increases drastically as the mole fraction of DMF approaches 0.33. The changes in the $\Delta G_m°$, $\Delta H_m°$, and $\Delta S_m°$ values indicate that the formation of HTAB micelles in the water–DMF mixtures is an entropy directed process at lower concentrations of DMF and the inhibitory effect of DMF on micelle formation is attributed to an increase in the orderliness of this system with increasing DMF concentration.

N,N-Dimethylformamide (DMF) is a common dipolar aprotic solvent often used as a medium for many organic reactions. Other common dipolar aprotic solvents are dimethyl sulfoxide (DMSO), *N,N*-dimethylacetamide, acetone, tetrahydrofuran, sulfolane, and dioxane. They are usually weak hydrogen bond donors and very weakly acidic. On the contrary, they may often act as strong bases. Usually aprotic solvents contain hydrogen attached to carbon and are generally dipolar in nature.[1-3] Most of them are relatively miscible with water.

As part of our study of the effect of polar solvents on the formation of micelles in aqueous solutions, we decided to also investigate the effect of DMF on the micellization of hexadecyltrimethylammonium bromide (HTAB). Our previous studies of the HTAB–H_2O–DMSO system have revealed that the addition of DMSO has an inhibitory effect on the formation of micelles in aqueous solutions.[4-6] Surface tensiometric experiments indicated that DMSO increased the critical micellar concentration of HTAB in water at low concentrations.[4] At mole fractions of DMSO higher than 0.33 micelle formation did not appear to take place. The results of spin-lattice relaxation measurements for the terminal methyl, *N*-methyl, and methylene groups of hexadecyltrimethylammonium bromide substantiated these results and showed that when the DMSO concentration is equal to a mole fraction of 0.366 the surfactant monomer molecules are essentially isolated from each other by the increased "structuring" of the water–DMSO liquid system.[5-6] Spin-lattice relaxation and chemical shift measurements performed in our laboratory also indicated that this liquid system is in its most structured state through hydrogen bonding between water and DMSO molecules when the mole fraction of DMSO is about 0.35.[7]

The mixing of DMF with water is a strongly exothermic process with a maximum value at the mole fraction of 0.66 for H_2O, while the activity coefficients for water and DMF are relatively near unity.[8] In addition, a variety of other physical properties of water–DMF solutions exhibit extrema at a mole fraction of 0.66 for water.[9-11] On the basis of cryoscopic and calorimetric measurements of aqueous solutions of *N,N*-dimethylformamide, Bougard and Jadot[8] have concluded that DMF forms both the monohydrate ($DMF \cdot H_2O$) and the dihydrate ($DMF \cdot 2H_2O$) and that the association is probably mainly through hydrogen bonding.

We have decided to study in some detail the HTAB–H_2O–DMF system because of the vast information available in the literature for the surfactant and in order to compare it to the HTAB–H_2O–DMSO system that we have previously studied. The present work essentially involved the experimental evaluation of thermodynamic functions such as the free energy, enthalpy, and entropy of micellization from the critical micellar concentration (CMC) of HTAB in various water–DMF mixtures at 25 and 40 °C determined by means of surface tensiometry.

Experimental

The DMF used was of spectro quality and was obtained from Eastman Organic Chemicals, Cleveland, Ohio 44114. It was employed without any additional treatment or purification. Hexadecyltrimethylammonium bromide (HTAB), $CH_3(CH_2)_{15}N^+(CH_3)_3Br^-$, was purchased from Aldrich Chemical Company, Milwaukee, Wisconsin 53233. It was recrystallized twice from 95% ethyl alcohol and dried under vacuum for two days. Doubly distilled water was used in the preparation of all the solutions.

The surface tension of HTAB–H_2O–DMF solutions was measured at 25 and 40 °C by means of a Fisher Model 21 Semi-Automatic Tensiometer. The solutions were prepared gravimetrically at the following mole fractions of DMF: 0.000, 0.025, 0.055, 0.091, 0.134, 0.188, 0.258, and 0.351. All of them contained at least fifteen different concentrations of HTAB. Ten milliliter aliquots of the solutions were measured in a Petri dish with a diameter of 6 cm. The tensiometer was set at a constant height. The final surface tension of any solution was the average of at least three measurements.

The CMC's were determined from plots of the surface tension of the solutions *versus* the logarithm of the concentration of HTAB. The marked change in the plots is taken as an indication of micelle formation and the inflection

† Present address: Departamento de Química, Universidade Federal de Santa Catarina, Florianópolis S.C. 88000 Brasil.

Table 1. Critical micellar concentration of hexadecyltrimethylammonium bromide in aqueous solutions containing different mole fractions of *N*,*N*-dimethylformamide

Mole fraction of DMF	Critical micellar concentration at 25 °C ($M\times10^3$)	Critical micellar concentration at 40 °C ($M\times10^3$)
0.0	0.92	1.00
0.025	2.00	2.24
0.055	3.55	3.98
0.091	6.31	7.08
0.134	10.0	11.5
0.188	12.6	20.0
0.258	29.5	—
0.351	—	—

Table 2. Some thermodynamic properties for the formation of micelles of hexadecyltrimethylammonium bromide in water-*N*,*N*-dimethylformamide solutions

Mole fraction of DMF	$\Delta H_m°$ kcal mol^{-1}	$\Delta G_m°$ at 25 °C kcal mol^{-1}	$\Delta S_m°$ at 25 °C e.u.
0.0	—	−4.12	—
0.025	−1.37	−3.68	+7.75
0.055	−1.37	−3.34	+6.61
0.091	−1.49	−3.00	+5.06
0.134	−1.73	−2.73	+3.35
0.188	−5.73	−2.59	−10.6
0.258	—	−2.09	—

point in the curve is considered to correspond to the CMC. Linear plots are taken as an indication that micelle formation does not occur.

Results and Discussion

Some representative experimental results obtained for the surface tension of different HTAB solutions in various water–DMF mixtures at 25 °C are given in Fig. 1. Most plots of surface tension *versus* the logarithm of the concentration of HTAB exhibit an initial marked drop and subsequently level off. Similar results have been obtained for the same solutions at 40 °C. The CMC values thus determined for the different H_2O–DMF mixtures are summarized in Table 1.

As can be seen from Table 1, the effect of DMF on micelle formation is relatively small at low concentrations of DMF, but it increases drastically as the mole fraction of DMF approaches 0.33. This mole fraction corresponds to the formation of the stoichiometric hydraote DMF·2H_2O.[8] At mole fractions of DMF higher than 0.33, the formation of HTAB micelles does not appear to take place in similarity to the HTAB–H_2O–DMSO system.[4–6] We have shown conclusively by means of proton spin-lattice relaxation measurements that this was true for the latter system.[4–6]

The thermodynamics of micelle formation has been discussed and treated extensively in the literautre.[12–14] One approach assumes that the process of micellization involves the formation of a distinct micellar phase at the CMC and that the concentration of monomers in solution is constant, once micelles are formed. Then, the standard free energy of micellization, $\Delta G_m°$, is given by the following equation to a good approximation:

$$\Delta G_m° = RT \ln \text{CMC}. \quad (1)$$

If one assumes that the aggregation number and the degree of ionization of the surfactant are temperature independent, the standard enthalpy ($\Delta H_m°$) and entropy ($\Delta S_m°$) of micellization can be evaluated by temperature dependence of the CMC and the Gibbs-Helmholtz relationship. The values thus determined for $\Delta G_m°$ for the fomation of HTAB micelles in variuos water–DMF solutions at 25 °C are given in Table 2. The more approximate $\Delta H_m°$ and $\Delta S_m°$ quantities, calculated on the basis of the measurements at two temperatures only, are also shown in the same table. The experimental results show that micelle formation is slightly hindered by increasing the temperature from 25 to 40 °C. The results also indicate that the addition of DMF has an inhibitory effect on the formation of micelles of HTAB in aqueous solutions. This effect due to the cosolvent is more pronounced than the one that we have observed for dimethyl sulfoxide.[4–6] Figure 2 illustrates a comparison of the effects of DMF and DMSO at 25 °C in terms of $\Delta G_m°$.

The $\Delta G_m°$ values determined for micelle formation in the water–DMF mixed solvent system vary almost linearly from −3.68 to −2.09 kcal/mol with increasing concentration of DMF and are always less negative than those determined for the formation of HTAB micelles in pure water (Table 2). The approximate enthalpy of micellization calculated, $\Delta H_m°$, is exothermic and almost constant at concentrations of DMF betweeen 0.025 and 0.134 mole fractions. The corresponding values of the entropy of micellization,

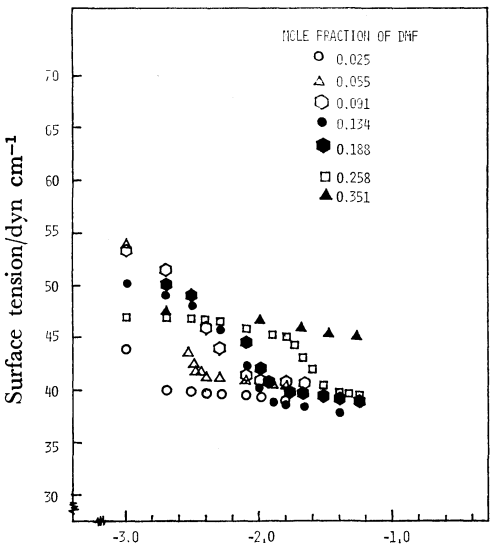

Fig. 1. Dependence of surface tension on the logarithm of the concentration of hexadecyltrimethylammonium bromide in water-*N*,*N*-dimethylformamide solutions at 25 °C.

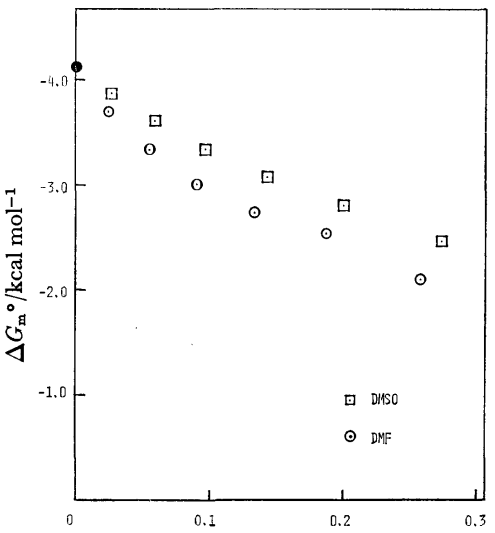

Fig. 2. Depence of the free energy of Micellization of hexadecyltrimethylammonium bromide at 25 °C on the composition of the water-dimethyl sulfoxide and water-*N*,*N*-dimethylformamide binary liquid systems.

$\Delta S_m°$, decrease gradually from 7.75 to 3.35 e.u. This means that the negative free energy of micellization is mainly due to the contribution of the entropy term in the H_2O–DMF mixed solvent system at low concentrations of DMF. This is in agreement with the general concept that micelle formation in aqueous solutions is an entropy directed process and arises mainly from the break-up of the "Frank-Evans microcrystals" of the ordered water structure by the surfactant molecules, even though the formation of aggregates by surfactant molecules is an entropy decreasing process. Since the $\Delta S_m°$ values decrease with increasing concentration of DMF (Table 2), an increase in the orderliness of the HTAB–H_2O–DMF system takes place as the mole fraction of DMF is increased. This is consistent with a strong interaction, such as hydrogen bonding, between water and DMF. As already mentioned, Bougard and Jadot[8] have confirmed the existence of the stoichiometric hydrate DMF·$2H_2O$ and suggested the presence of hydrogen bonding.

A further addition of DMF caused a significant change in the relative contributions from enthalpy and entropy, *i.e.*, at 0.188 mole fraction of DMF $\Delta H_m°$ and $\Delta S_m°$ become −5.73 kcal/mol and −10.6 e.u., respectively. A change similar to this was also observed in the water–DMSO mixed solvent system when the DMSO mole fraction was 0.275. This change implies that the driving force for micellization in both the H_2O–DMF and H_2O–DMSO mixed solvent systems containing higher concentrations of DMF or DMSO must be attributed to the enthalpic term. Why this change occurs at lower concentrations of DMF than DMSO may be explained by the fact that DMF has a more pronounced effect on the disruption of the water structure through hydrogen bonding, even though DMF is less polar than DMSO[15] (the dielectric constant of DMF at 25 °C is 36.7 while that of DMSO is 46.4). Altogether, the inhibitory effect of *N*,*N*-dimethylformamide on micelle formation can be explained in terms of a decrease of hydrophobic forces in the ternary system due to interactions between water and the cosolvent.

References

1) A. J. Parker, *Quart. Rev.*, **16,** 163 (1962).
2) A. J. Parker, *Chem. Rev.*, **69**, 1 (1969).
3) B. Tchoubar, *Bull. Soc. Chim. Fr.*, **1964** 2069.
4) L. G. Ionescu, T. Tokuhiro, B. J. Czerniawski, and E. S. Smith, Proceedings of the 52nd ACS Colloid and Surface Science Symposium, Knoxville, Tennessee, 1978.
5) T. Tokuhiro, L. G. Ionescu, and D. S. Fung, Abstracts, 174th American Chemical Society National Meeting, Chicago, Illinois, August 28 — September 2, 1977, PHYS 39.
6) T. Tokuhiro, L. G. Ionescu, and D. S. Fung, submitted to *J. Chem. Soc. Faraday Trans. 2.*
7) T. Tokuhiro, L. Menafra, and H. H. Szmant, *J. Chem. Phys.*, **61**, 2275 (1974).
8) J. Bougard and R. Jadot, *J. Chem. Thermodyn.*, **7**, 1185 (1975).
9) K. Quitzsch, H. P. Hofmann, R. Pfestorf, and G. Geiseler, *J. Prakt. Chem.*, **34**, 145 (1966).
10) I. Geller and T. M. Ivanova, *Zh. Fiz. Kim.*, **35**, 1105, 1221 (1961).
11) F. Blankenship and B. Clampitt, *Proc. Oklahoma Acad. Sci.*, **31**, 106 (1952).
12) N. Muller, *J. Phys. Chem.*, **76**, 3017 (1972).
13) D. G. Hall, *Trans. Faraday Soc.*, **66**, 1351, 1359 (1970).
14) N. Muller, in "Reaction Kinetics in Micelles," ed by E. H. Cordes, Plenum Press, New York (1973).
15) C. Agami, *Bull. Soc. Chim. Fr.*, **1965**, 1021.

Chemistry of Organo Halogenic Molecules. XLVIII. Stereochemistry of Halofluorination of 1,2- and 1,4-Dihydronaphthalene

Stojan STAVBER and Marko ZUPAN*

Department of Chemistry and "J. Stefan" Institute, University of Ljubljana, Yugoslavia

(Received April 3, 1978)

Halofluorination of 1,2-dihydronaphthalene with a mixture of *N*-chlorosuccinimide or *N*-bromosuccinimide or *N*-iodosuccinimide–hydrogen fluoride–pyridine in ether proceeds with Markovnikov type regioselectivity. The reaction is stereospecifically anti, the anti adduct isomerizing to syn products under the reaction conditions. The elimination of hydrogen halide under basic conditions occurs only from the syn adduct, thus forming 1-fluoro-3,4-dihydronaphthalene. Halofluorinations of 1,4-dihydronaphthalene also occur stereospecifically anti, and elimination under basic conditions gives naphthalene.

The mechanism of electrophilic addition has been widely investigated, both from the kinetic and stereochemical points of view.[1] Apart from the relative importance of the various kinetically significant processes, it is now known that the nature of the intermediates of the addition depends on the structure of the substrate, on the halogen and on the reaction medium, ranging from strongly bridged ions (type **C**), to weakly bridged species (type **B**) or open ions like **A**.

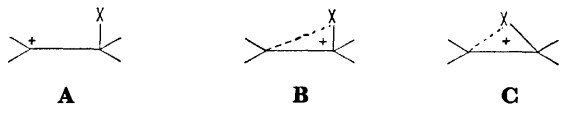

Scheme 1.

If the cation is of the open structure (**A**, X=F), a mixture of syn and anti adducts is generally expected. However, ion pairing phenomena can cause preferential formation of the syn adduct and electronic, steric or conformational effects can cause attack at one or other side of the carbonium p-orbital of **A** to be favoured. On the other hand, the intermediate can have a bridged structure (**C**, X=Br), which will presumably be opened to form an anti adduct. Available data on the addition of "BrX" species to olefins are sparse. In the steroid series,[2,3,4] stereospecific anti addition with Markovnikov type regioselectivity is observed; on the other hand, the bromofluorination of carbohydrates[5,6] is stereospecifically syn. Using hydrogen fluoride–pyridine in conjunction with *N*-bromosuccinimide for fluorination of aliphatic olefins, Olah and his coworkers[7] observed typical Markovnikov type regioselectivity. Bromofluorination of phenyl substituted olefins proceeds with Markovnikov type regioselectivity and the reaction is stereospecifically anti for trans and nonstereospecific for cis olefins.[8] The bromofluorination of 1-phenylcyclohexene also proceeds with Markovnikov type regioselectivity and is stereospecifically anti.[9] The halofluorinations of norbornene[10] and norbornadiene[11] with a mixture of *N*-halosuccinimide–hydrogen fluoride–pyridine have also been studied. Recently we found that fluorination of 1,2-dihydro- and 1,4-dihydronaphthalene occurs in different ways,[12] which stimulated us to investigate the reaction pathways involved in halofluorination of these systems.

Results and Discussion

The preparation of fluoroalkanes presents a different problem from that of other halogenoalkanes, and necessitates a specific method of fluorination.[13] Difficulties involve the handling of anhydrous hydrogen fluoride on the laboratory scale, the need for pressure equipment and low temperatures, and the ease of polymerisation of alkenes. Bromofluorination with hydrogen fluoride–pyridine–NBS avoids some experimental difficulties,[7] *e.g.* low temperature, high pressure techniques, and polymerisation of olefins.

Halofluorination of 1,2-Dihydronaphthalene. The 3 h reaction of 1,2-dihydronaphthalene (**1**), with a mixture of *N*-chlorosuccinimide–hydrogen fluoride–pyridine in ether at room temperature resulted in the formation of a crude reaction mixture, which showed two signals in its ^{19}F NMR spectrum: $\delta F = -158.5$ and -176 in the ratio 1.78:1.

Reduction of the reaction time from 3 to 1.5 h resulted in the formation of only one product, which showed one signal in its ^{19}F NMR spectrum at $\delta F =$

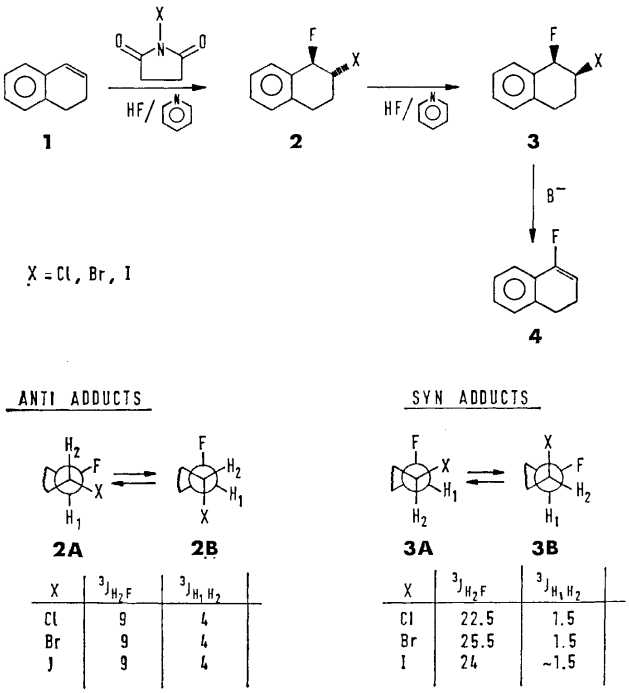

X	$^3J_{H_2F}$	$^3J_{H_1H_2}$
Cl	9	4
Br	9	4
I	9	4

X	$^3J_{H_2F}$	$^3J_{H_1H_2}$
Cl	22.5	1.5
Br	25.5	1.5
I	24	~1.5

Scheme 2.

−158.5. Treatment of the reaction mixture formed in a 3 h halofluorination reaction with K–O-*t*-Bu in *t*-BuOH at T=50 °C resulted in the formation of a crude reaction mixture which showed a new signal at $\delta F = -123.75$, besides the signal at $\delta F = -158.5$, with the signal ratio of 1.7:1. Separation of the reaction mixture by TLC gave two products. The major product formed showed a doublet of multiplet signal at $\delta F = -158.5$ ($^2J_{FH}$=56 Hz), in its ^{19}F NMR spectrum and in its proton spectrum two signals at lower field: $\delta H_1 = 5.4$, $\delta H_2 = 4.6$. The mass spectrum showed the following signals: *m/e*: 186 (M^++2, 20%), 184 (M^+, 60%), 148 (60), 129 (50), 122 (100), 115 (15). The second product showed a doublet signal at $\delta F = -123.75$, ^3J=15 Hz in its ^{19}F NMR, and in its mass spectrum the following signals: *m/e*: 148 (M^+, 63%), 147 (65), 146 (38), 133 (44). On the basis of the spectroscopic data we established that the crude reaction mixture formed under basic conditions contained 1-fluoro-2-chloro-1,2,3,4-tetrahydronaphthalene, and as the minor product, 1-fluoro-3,4-dihydronaphthalene (**4**). We were unable to separate the two products formed by the 3 h chlorofluorination reaction. However, on the basis of differences in their NMR spectra, which are shown in Scheme 2, and in the stability of the products under basic conditions, we have established that the major product formed (**2**) was *trans*-1-fluoro-2-chloro-1,2,3,4-tetrahydronaphthalene, while the second product, which was not formed in the case of the 1.5 h reaction, and which transformed under basic conditions to 1-fluoro-3,4-dihydronaphthalene, was found to be *cis*-1-fluoro-2-chloro-1,2,3,4-tetrahydronaphthalene (**3**).

A 3 h reaction of 1,2-dihydronaphthalene with a mixture of NBS–hydrogen fluoride–pyridine resulted in a crude reaction mixture, which showed two signals in its ^{19}F NMR spectrum: $\delta F = -149$ and -169 in the ratio 1.5:1, while reduction of the reaction time to 0.5 h resulted in the formation of only one product with the ^{19}F NMR signal at $\delta F = -149$. Under basic conditions, heating (T=50 °C) the mixture obtained in the 3 h bromofluorination reaction resulted in a mixture containing 1-fluoro-2-bromo-1,2,3,4-tetrahydronaphthalene and 1-fluoro-3,4-dihydronaphthalene (**4**) in the ratio 1.5:1. We were unable to separate the two products formed by the 3 h bromofluorination reaction. However, on the basis of differences in their NMR spectra, which are shown in Scheme 2, and in the stability of the products under basic conditions, we established that the major product formed (**2**) was *trans*-1-fluoro-2-bromo-1,2,3,4-tetrahydronaphthalene, while the second product, which was not formed in the case of a 0.5 h reaction and which was transformed under basic conditions to 1-fluoro-3,4-dihydronaphthalene, was found to be *cis*-1-fluoro-2-bromo-1,2,3,4-tetrahydronaphthalene (**3**).

Fifteen minutes iodofluorination with a mixture of *N*-iodosuccinimide–hydrogenfluoride–pyridine of 1,2-dihydronaphthalene resulted in the formation of a crude reaction mixture which showed two signals in its ^{19}F NMR spectrum, $\delta F = -139$ and -157, in the ratio 1.5:1. On the basis of a comparison (Scheme 2) of the NMR data of the products to those formed by chloro and bromofluorination, we established that the major product formed was *trans*-1-fluoro-2-iodo-1,2,3,4-tetrahydronaphthalene (**2**), and that the minor product formed was *cis*-1-fluoro-2-iodo-1,2,3,4-tetrahydronaphthalene (**3**). Reduction of the reaction time to 5 minutes resulted in the formation of product (**2**), while treatment of the reaction mixture obtained by 15 minutes iodofluorination under basic conditions resulted in a mixture containing products (**2**) and (**4**) in the ratio 1.5:1.

Halofluorination of 1,4-Dihydronaphthalene. A 5 h reaction of the mixture *N*-chlorosuccinimide–hydrogen fluoride–pyridine with 1,4-dihydronaphthalene at room temperature resulted in the formation of one product (**6**), which showed one signal in its ^{19}F NMR spectrum at $\delta F = -177.5$ (dtd, $^2J_{FH_2}$=51 Hz, $^3J_{FH_1}$=25.5 Hz, $^3J_{FH_3}$=5 Hz), and in its ^1H spectrum two signals at lower field. $\delta H_2 = 4.7$ (ddd, $^2J_{H_2F}$=51 Hz, $^3J_{H_2H_3}$= 10 Hz, $^3J_{H_1H_2}$=5 Hz), $\delta H_3 = 4.3$ (ddd, $^3J_{H_3F}$=5 Hz, $^3J_{H_3H_2}$=10 Hz, $^3J_{H_3H_4}$=5 Hz). In its mass spectrum the product showed the following signals: *m/e*: 186 (M^+ +2, 33%), 184 (M^+, 100%), 148 (53), 147 (43), 129 (85), 104 (45). 3 h heating (T=50 °C) of the adduct **6** resulted, under basic conditions, in the formation of naphthalene (**8**).

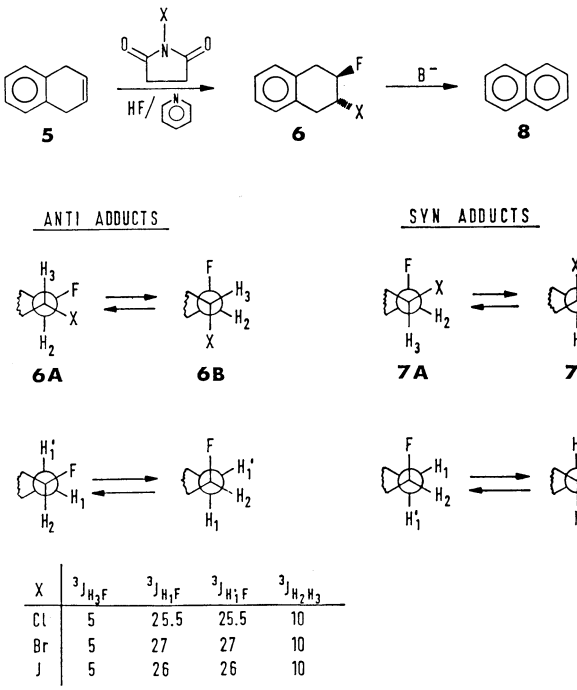

X	$^3J_{H_2F}$	$^3J_{H_1F}$	$^3J_{H_1'F}$	$^3J_{H_2H_3}$
Cl	5	25.5	25.5	10
Br	5	27	27	10
J	5	26	26	10

Scheme 3.

On the basis of the spectroscopic data and chemical transformation, we established that 2-fluoro-3-chloro-1,2,3,4-tetrahydronaphthalene was formed. The Newman projection formulae of two possible isomers are shown in Scheme 3. On the basis of coupling constants we have established that the trans adduct was formed and that conformation **6A** is the favoured one.

A 3 h reaction of the mixture *N*-bromosuccinimide–hydrogenfluoride–pyridine with 1,4-dihydronaphthalene resulted in the formation of one product (**6**), which

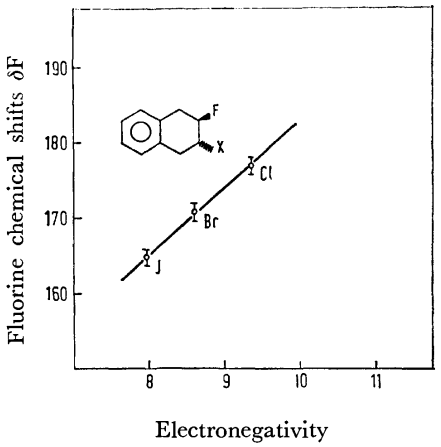

Fig. 1. Dependence of δF on electronegativity of the halogen atom.

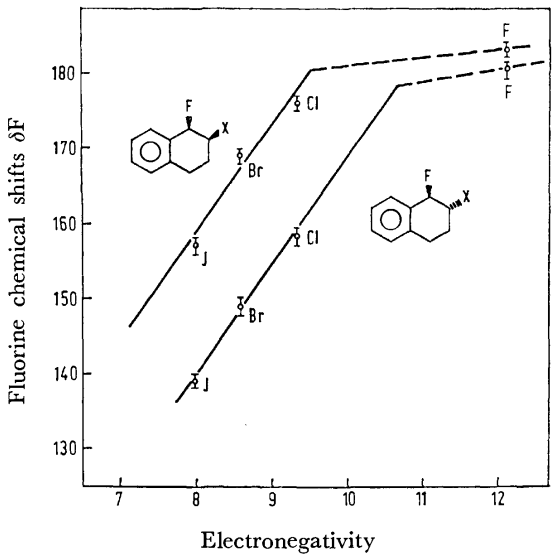

Fig. 2. Dependence of δF on electronegativity of the halogen atom.

showed one signal in its ^{19}F NMR at δF=−171 (dtd, $^{2}J_{FH_2}$=51 Hz, $^{3}J_{FH_1}$=27 Hz, $^{3}J_{FH_3}$=5 Hz) and in its proton spectrum two signals at lower field: δH_2=4.9 (ddd, $^{2}J_{H_2F}$=51 Hz, $^{3}J_{H_2H_1}$=5 Hz, $^{3}J_{H_2H_3}$=10 Hz), δH_3=4.3 (ddd, $^{3}J_{H_3F}$=5 Hz, $^{3}J_{H_3H_2}$=10 Hz, $^{3}J_{H_3H_4}$=5 Hz). In its mass spectrum, product **6** showed the following signals: *m/e*: 230 (M^++2, 60%), 228 (M^+, 60), 129 (100), 128 (50), 104 (16). Adduct **6** was also converted under basic conditions to naphthalene (**8**). On the basis of the spectroscopic data and the chemical transformation we established that *trans*-2-fluoro-3-bromo-1,2,3,4-tetrahydronaphthalene was formed. In this case also the preferential conformation is **6A**.

A 15-minute reaction of the mixture *N*-iodosuccinimide–hydrogenfluoride–pyridine with 1,4-dihydronaphthalene resulted in the formation of one product which showed one signal in its ^{19}F NMR spectrum at δF=−165 (dtd, $^{2}J_{FH_2}$=52 Hz, $^{3}J_{FH_1}$=26 Hz, $^{3}J_{FH_3}$=5 Hz), and in its proton spectrum two signals at lower field δH_2=5 (ddd, $^{2}J_{H_2F}$=52 Hz, $^{3}J_{H_2H_3}$=10 Hz, $^{3}J_{H_2H_1}$=5 Hz), δH_3=4.5 (ddd, $^{3}J_{H_3F}$=5 Hz, $^{3}J_{H_3H_2}$=10 Hz, $^{3}J_{H_3H_4}$=5 Hz). In its mass spectrum the product **6** showed the following signals: *m/e*: 276 (M^+, 45%), 149 (80), 130 (33), 129 (85), 128 (100), 127 (35), 115 (23). Product **6** was also converted under basic conditions to naphthalene. On the basis of the spectroscopic data and the chemical transformation, we established that *trans*-2-fluoro-3-iodo-1,2,3,4-tetrahydronaphthalene was formed. Again the preferential conformation was found to be **6A**.

The dependence of fluorine chemical shifts in *trans*-2-fluoro-3-halo-1,2,3,4-tetrahydronaphthalene on the Mulliken electronegativity of the halogen atom is presented in Fig. 1, while in Fig. 2 the influence of Mulliken electronegativity on chemical shifts of the fluorine atom in cis and trans 1-fluoro-2-halo-1,2,3,4-tetrahydronaphthalene is shown.

The correlation is good in the case of *trans*-2-fluoro-3-halo-1,2,3,4-tetrahydronaphthalene and *trans*-2-fluoro-3-halo-1,2,3,4-tetrahydronaphthalene, while in the case of cis adducts the correlation is worse. From Figs. 1 and 2 it can also be seen that the influence of different electronegativities of the halogen atom on fluorine chemical shifts is greater in the case of *trans*-1-fluoro-2-halo-1,2,3,4-tetrahydronaphthalene ($\Delta\delta$F/Δelectronegativity=13.4) than in the case of *trans*-2-fluoro-3-halo-1,2,3,4-tetrahydronaphthalene ($\Delta\delta$F/Δelectronegativity =9.4). Introduction of the values of fluorine chemical shifts[12] for cis and trans 1,2-difluoro-1,2,3,4-tetrahydronaphthalene into Figure 2 shows that these values strongly deviate from the straight line connecting the values for chloro, bromo and iodo derivatives, which could be ascribed to the different conformation of the difluoride and, or, through space interaction between fluorine atoms.

For bromofluorination with *N*-bromosuccinimide in the presence of hydrogen fluoride, reaction sequences involving a cyclic bromonium ion have been suggested.[3,4,14] In general, one can suggest a reaction between *N*-halosuccinimide and hydrogen fluoride, resulting "XF" species which can then react with the double bond, following Markovnikov type regioselectivity.

However, it is known that β-chlorocarbonium ions have only partly bridged structures, while the strongly

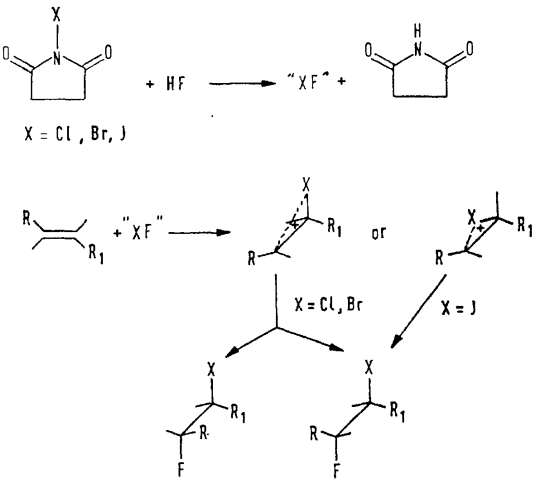

Scheme 4.

bridged halonium ions can be expected only in the case of iodofluorination with "IF" species. So, in the case of chlorofluorination and bromofluorination with "XF" species, syn and anti adducts should be observed, while in the case of iodofluorination only an anti-adduct is to be expected. We suggest a reaction pathway (Scheme 5), which can better explain the anti stereoselectivity. We propose the formation of a polarized *N*-halosuccinimide–hydrogen fluoride complex (**D**), which reacts in a reversible step with 1,2-dihydro- or 1,4-dihydronaphthalene to form a complex (**F**), decomposing in the next step to halofluorides. The reversible step, leading to complex (**F**), could explain the high degree of isomerization of cis alkenes.[8] The formation of "XF" species could be involved only in iodofluorination with the mixture of *N*-iodosuccinimide–hydrogen fluoride–pyridine.

A complex similar to (**F**) was suggested for bromination of 1-phenylcyclohexene with bromine–pyridine complex[15] and has also been proposed for E2Hal elimination of bromine from *trans*-1,2-dibromocyclohexane with benzenethiolate as base.[16] A polarized complex of NBS with olefins has been suggested in the bromination of styrene and cyclohexene with NBS in the presence of dimethylsulfoxide and methanol.[17]

A third interpretation presents the halofluorination reaction as involving the formation of the pyridinium–halide complex (**E**), reacting with 1,2- or 1,4-dihydronaphthalene with high stereoselectivity. *trans*-1-Fluoro-2-halo-1,2,3,4-tetrahydronaphthalenes, the only products formed in shorter reaction times, are unstable under the reaction conditions and isomerize to cis adducts.

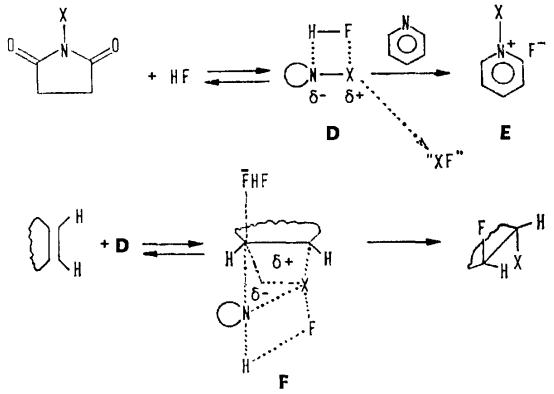

Scheme 5.

Experimental

Procedure. IR spectra were recorded with a Perkin-Elmer 257 spectrometer, ^1H and ^{19}F NMR spectra with a JEOL JNM-PS-100 (CCl_4 or $CDCl_3$ as solvent and Me_4Si or CCl_3F as internal reference). Mass spectra, including high resolution measurements, were carried out on a CEC-21-110 spectrometer. GLPC was carried out with a Varian Aerograph 1800 instrument and TLC with Merck chromatoplates (PSC-Fertig-platten silica gel F-254, activated for 2 h at 120 °C before use).

Materials. A solution of pyridine–hydrogen fluoride was prepared according to Olah's procedure.[7] The pyridine used was predistilled, while hydrogen fluoride (Fluka, Purum) was used without prior purification. *N*-halosuccinimides (Fluka, Purum) were crystallised and dried (P_2O_5) before use. Diethyl ether was purified by standard methods and distilled before use. 1,2- and 1,4-dihydronaphthalene were prepared by known methods from naphthalene[18] and purified before use.

Addition and Isolation Procedures. In a mixture of hydrogen fluoride in pyridine (70% solution, 2 ml) and ether (2 ml), *N*-halosuccinimide (1.2 mmol) was dissolved with stirring at 0 °C for 10 min, and then the olefin (1 mmol) was added. The mixture was left at room temperature for various reaction times with stirring, then poured into ice-water and extracted with ether. The ether layer was washed with water, aqueous sodium hydrogencarbonate, then water again, dried (Na_2SO_4) and evaporated. The NMR spectra of crude reaction mixtures were recorded and then the pure products were obtained by preparative TLC or by crystallisation from the corresponding solvent. The structure of pure products were established from ^{19}F and ^1H NMR mass and IR spectral data.

trans-*1-Fluoro-2-chloro-1,2,3,4-tetrahydronaphthalene (**2a**)*: **2a** is an oily product (48%) (purified by preparative TLC, SiO_2; cyclohexane:chloroform:triethylamine 95:4.5:0.5). NMR: $\delta F = -158.5$ (dm), $\delta H_1 = 5.40$ (dd), $\delta H_2 = 4.60$ (m), δCH_2-$CH_2 = 2$ to 3 (m), δPh (m) $= 7.30$ $^2J_{FH_1} = 56$ Hz, $^3J_{FH_2} = 9$ Hz, $^3J_{H_1H_2} = 4$ Hz. MS: calcd for $C_{10}H_{10}ClF$ *m/e* 184.0449, found 184.0448 *m/e*: 186 ($M^+ + 2$, 20%), 184 (M^+, 60), 149 (20), 148 (60), 147 (20), 129 (50), 128 (35), 122 (100), 115 (15), 104 (10).

trans-*1-Fluoro-2-bromo-1,2,3,4-tetrahydronaphthalene (**2b**)*: White crystals (52%), mp=29—30 °C, (purified by preparative TLC under conditions mentioned below). NMR: $\delta F = -149$ (dm), $\delta H_1 = 5.60$ (dd), $\delta H_2 = 4.60$ (m), δCH_2—$CH_2 = 2.2$ to 2.8 (m), $\delta Ph = 7.30$ (m), $^2J_{FH_1} = 54$ Hz, $^3J_{FH_2} = 9$ Hz, $^3J_{H_1H_2} = 4$ Hz. MS: calcd for $C_{10}H_{10}BrF$ *m/e* 227.9964, found 227.9966, *m/e* 230 ($M^+ + 2$; 35%), 228 (M^+, 35%), 210 (16), 208 (16), 149 (40), 148 (48), 147 (25), 146 (15), 129 (100), 128 (60), 127 (24), 115 (21), 104 (10), 102 (10).

trans-*1-Fluoro-2-iodo-1,2,3,4-tetrahydronaphthalene (**2c**)*: White crystals (75%) (from ethanol) decomposing at room temperature. NMR: $\delta F = -139$ (dm), $\delta H_1 = 5.60$ (dd), $\delta H_2 = 4.60$ (m), $\delta CH_2 - CH_2 = 2.2$ to 2.8 (m), $^2J_{FH_1} = 54$ Hz, $^3J_{FH_2} = 9$ Hz, $^3J_{H_1H_2} = 4.5$ Hz. MS: calcd for $C_{10}H_{10}FJ$ *m/e* 275.9813, found 275.9816 *m/e* 276 (M^+, 28%), 149 (100), 129 (75), 128 (81), 127 (25), 115 (20), 102 (11).

trans-*2-Fluoro-3-chloro-1,2,3,4-tetrahydronaphthalene (**6a**)*: White crystals (60%), mp=29—30 °C, (purified by preparative TLC), NMR: $\delta F = -177.5$ (dtd), $\delta H_2 = 4.9$ (ddd), $\delta H_3 = 4.3$ (ddd), $\delta H_1 = 2.9$ (m), $\delta H_4 = 3.7$ (m), $\delta Ph = 7.1$ (m), $^2J_{FH_2} = 51$ Hz, $^3J_{FH_3} = 5$ Hz, $^3J_{FH_1} = 25.5$ Hz, $^3J_{FH_1'} = 25.5$ Hz, $^3J_{H_2H_3} = 10$ Hz, $^3J_{H_1H_2} = 5$ Hz, $^3J_{H_3H_4} = 5$ Hz. MS: calcd for $C_{10}H_{10}ClF$ *m/e* 184.0449, found 184.0449, *m/e*: 186 ($M^+ + 2$; 33%), 184 (M^+, 100), 149 (34), 148 (54), 147 (43), 146 (21), 129 (85), 128 (43), 127 (16), 115 (18), 104 (45), 103 (10).

trans-*2-Fluoro-3-bromo-1,2,3,4-tetrahydronaphthalene (**6b**)*: White crystals (68%), mp=35—37 °C, (purified by preparative TLC), NMR: $\delta F = -171$ (dtd), δ $H_2 = 4.9$ (ddd), δ $H_3 = 4.3$ (ddd), δ $H_1 = 2.9$ (m), δ $H_4 = 3.7$ (m), δ Ph=7.1, $^2J_{FH_2} = 54$ Hz, $^3J_{FH_3} = 5$ Hz, $^3J_{FH_1} = 27.0$ Hz, $^3J_{FH_1'} = 27.0$ Hz, $^3J_{H_2H_3} = 10$ Hz, $^3J_{H_1H_2} = 5$ Hz, $^3J_{H_3H_4} = 5$ Hz. MS: calcd for $C_{10}H_{10}BrF$ *m/e* 227.9964, found 227.9940, *m/e*: 230 ($M^+ + 2$; 60%), 228 (M^+, 60), 149 (31), 148 (35), 147 (28), 146 (17), 129 (100), 128 (50), 115 (20), 104 (16).

trans-*2-Fluoro-3-iodo-1,2,3,4-tetrahydronaphthalene (**6c**)*: White crystals (70%) (from ethanol), mp=57—58 °C.

NMR: $\delta F = -165$ (dtd), $\delta H_2 = 5.0$ (ddd), $\delta H_3 = 4.5$ (ddd), $\delta H_1 = 3.2$, $\delta H_4 = 3.7$ (m), $\delta Ph = 7.1$, $^2J_{FH_2} = 52$ Hz, $J_{FH_3} = 5$ Hz, $^3J_{FH_1} = 26$ Hz, $^3J_{FH_1'} = 26$ Hz, $^3J_{H_2H_3} = 10$ Hz, $^3J_{H_1H_2} = 5$ Hz, $^3J_{H_3H_4} = 5$ Hz. MS: calcd for $C_{10}H_{10}FJ$ *m/e* 275.9813, found 275.9825, *m/e*: 276 (M^+, 45%), 149 (80), 148 (7), 147 (14), 146 (14), 129 (85), 128 (100), 127 (35), 126 (13), 102 (20).

Treatment of the Mixture of trans- *and* cis-*1-Fluoro-2-halo-1,2,3,4-tetrahydronaphthalene with Base.* To a crude reaction mixture obtained by halofluorination of 1,2-dihydronaphthalene (longer reaction time), a solution of 1.3 mmol of potassium *t*-butoxide in *t*-butylalcohol (2 ml) was added, and the mixture heated for 3—4 h at $T = 50$ °C, then poured into water (10 ml), exacted with ether, the ether layer washed with water (5 ml twice), dried and evaporated. NMR spectra of the crude reaction mixture were recorded to obtain the product distribution, and then it was separated by preparative TLC (SiO_2, cyclohexane: chloroform: triethylamine 95:4.5:0.5). Products (**2**), and 1-fluoro-3,4-dihydronaphthalene (**4**) were isolated. Spectroscopic data for **4** were in agreement with those already published.[12]

Treatment of trans-*2-Fluoro-3-halo-1,2,3,4-tetrahydronaphthalene with Base.* To a solution of 1.5 mmol of potassium *t*-butoxide in *t*-butyl alcohol (2 ml), 1 mmol of product **6** was added and the mixture heated for 3—4 hours at 50 °C. The reaction mixture was poured into water (10 ml), extracted with ether, the ether layer washed with water (5 ml, twice), dried (Na_2SO_4) and evaporated. NMR spectra of the crude reaction mixture were recorded, showing that naphthalene (**8**) was the only product formed.

The financial assistance of the Boris Kidric Foundation is acknowledged.

References

1) R. C. Fahey in "Topics in Stereochemistry," ed by E. L. Eliel and N. L. Allinger, Interscience, New York (1968), Vol. 3, p. 280; P. B. D. de la Mare and R. Bolton, "Electrophilic Additions to Unsaturated Systems," Elsevier, New York (1966); P. B. D. De La Mare, "Electrophilic Halogenation," Cambridge University Press, Cambridge (1976); G. A. Olah, "Halonium Ions," Wiley, New York (1975).
2) A. Bowers, *J. Am. Chem. Soc.*, **81**, 4107, (1959).
3) A. Bowers, L. C. Ibanez, E. Denat, and R. Becerra, *J. Am. Chem. Soc.*, **82**, 4001 (1960).
4) A. Bowers, E. Denot, and R. Becerra, *J. Am. Chem. Soc.*, **82**, 4007 (1960).
5) P. W. Kent and M. R. Freeman, *J. Chem. Soc., C*, **1966**, 910.
6) K. R. Wood, P. W. Kent and D. Fisher, *J. Chem. Soc., C*, **1966**, 912.
7) G. A. Olah, M. Nojima, and I. Kerekes, *Synthesis*, **1973**, 780.
8) M. Zupan and A. Pollak, *J. Chem. Soc., Perkin Trans. 1*, **1976**, 971.
9) M. Zupan, *J. Fluorine Chem.*, **9**, 177 (1977).
10) A. Gregorcic and M. Zupan, *Coll. Czechoslov. Chem. Commun.*, **42**, 3192, (1977).
11) A. Gregorcic and M. Zupan, *Tetrahedron*, **33**, 3243 (1977).
12) B. Šket and M. Zupan, *J. Chem. Soc., Perkin Trans. 1*, **1977**, 2169.
13) For a review see: W. A. Sheppard, C. M. Sharts "Organic Fluorine Chemistry," W. A. Benjamin, Inc. New York (1969).
14) R. D. Chambers, "Fluorine in Organic Chemistry," John Wiley & Sons, New York (1973), p. 57.
15) P. L. Barili, G. Bellucci, F. Marioni, I. Marelli, and V. Scartoni, *J. Org. Chem.*, **38**, 3472 (1973).
16) E. C. F. Ko, and A. J. Parker, *J. Am. Chem. Soc.*, **90**, 6447 (1968).
17) V. L. Haesley, and R. A. Skidgel, *J. Org. Chem.*, **39**, 3953 (1974).
18) F. Straus and L. Lemmel, *Ber.*, **46**, 232, 1051 (1913).

Spirans. 16. 3,3′-Spirobi[3,4-dihydro-2*H*-[1,3]oxazino[3,2-*a*]benzimidazole] and Its Thia Analogue†

Stefan Smoliński* and Agnieszka Czarny

Stereochemical Laboratory, Institute of Chemistry, Jagellonian University, 30-060 Kraków, Krupnicza 41, Poland

(Received November 10, 1977)

In order to obtain spiran the sodium derivative of *o*-phenylenediamine was subjected to reaction with 1,3-dibromo-2,2-bis(bromomethyl)propane in *N,N*-dimethylformamide. The compound was also synthesized by the reaction of the sodium derivative of 2,3-dihydro-1*H*-benzimidazol-2-one with 1,3-dibromo-2,2-bis(bromomethyl)propane. By this procedure the thia analogue of the spiran was obtained. In both cases the condensation route was unexpected. This is due to the fact that the solvent (DMF) takes part in the reaction and a stereo-electronic situation occurs, which is similar to that covered by Bredt's exclusion rule.

In order to obtain suitable tetraazaspirans the condensation of two moles of the sodium derivative of *o*-phenylenediamine, obtained by treating *o*-phenylenediamine in the presence of sodium hydride in dry dioxane with 1,3-dibromo-2,2-bis(bromomethyl)-propane in *N,N*-dimethylformamide was carried out. After heating for 100 h under reflux a product melting at 385—390 °C (with decomposition) was obtained. From elemental analysis and the molecular weight estimated from mass spectra it was found necessary to ascribe the structure of the required spiran enriched with two CO groupings to the product. Under the above conditions, it can be assumed that *N,N*-dimethylformamide reacts most likely with *o*-phenylenediamine yielding its monoformyl derivative, which gives with the other molecule of *N,N*-dimethylformamide 2,3-dihydro-1*H*-benzimidazol-2-one. Consequently it was established that spiran is formed in the condensation of the sodium derivative of 2,3-dihydro-1*H*-benzimidazol-2-one with 1,3-dibromo-2,2-bis(bromomethyl)propane in cellosolve. We have also found that 2,3-dihydro-1*H*-benzimidazol-2-one is obtained when *o*-phenylenediamine is heated with sodium hydride in dioxane with *N,N*-dimethylformamide. We have proposed two structures for the spiran compound obtained:

(**1**) a structure containing the urea grouping that has the CO group bridging in a 7-membered ring,

(**2**) a constitutionally symmetrical spiro compound of six rings containing the dihydrooxazine-benzimidazole arrangement.

In order to determine which structure is correct, the IR, UV, mass and NMR spectra were obtained. In the IR spectra the band at 1625 cm^{-1} indicates

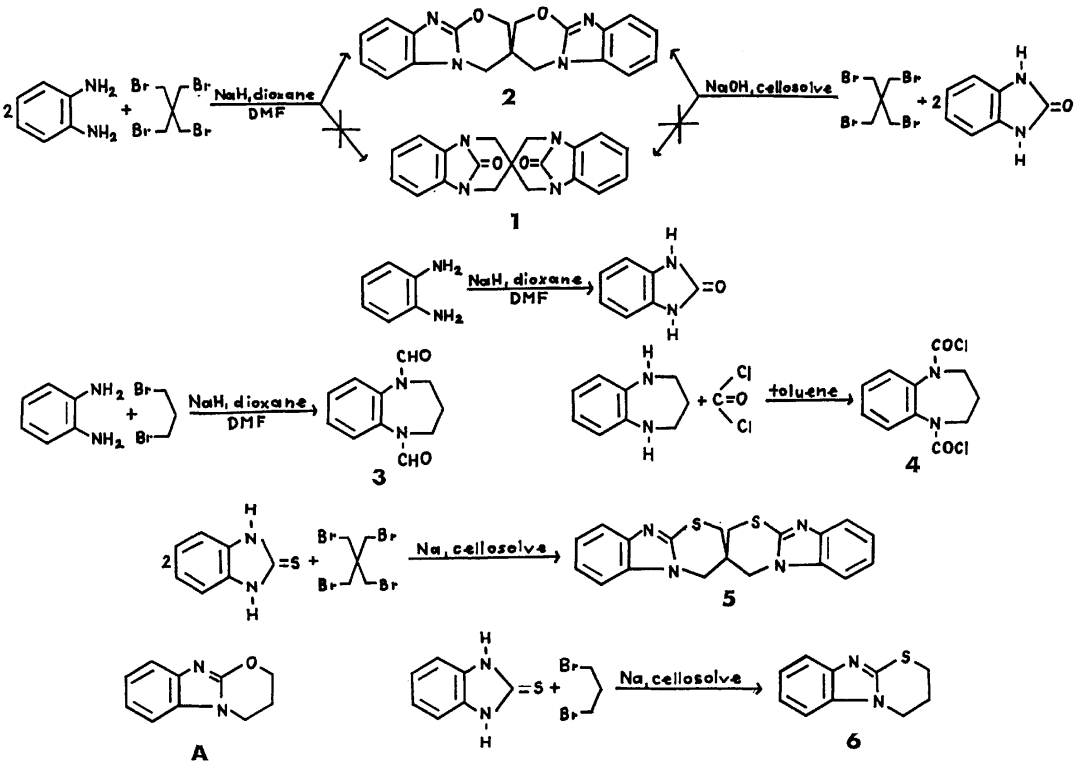

Fig. 1.

† Presented at the 26th IUPAC Congress, Tokyo (September 1977).

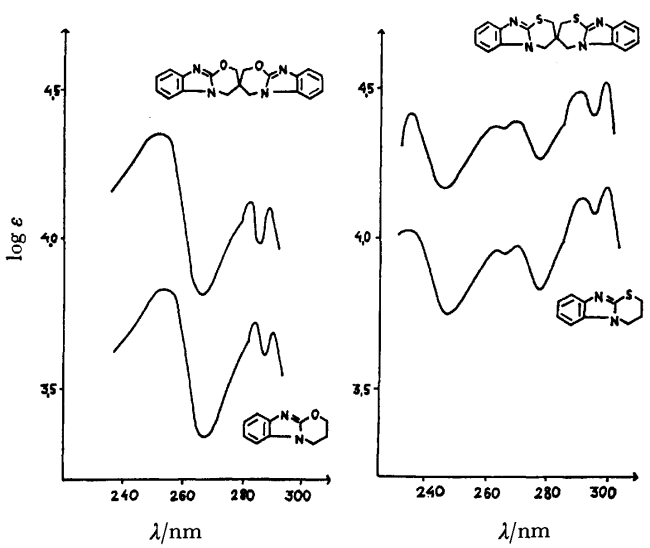

Fig. 2. UV-absorption spectra of compounds **2**—A and **5**—**6** in CH_2Cl_2.

the presence of the C=N group but not C=O; absorption bands indicate the presence of amine, methylene and aromatic groups. The NMR spectrum also suggests that structure (**2**) is correct. It was thus decided that the reported method of comparison[1-5] could be used and that the "half-compound" of the spiran obtained should be synthesized. The UV curves of the spiran and the "half-compound" could then be measured and compared. We expect them to have an analogous shape, the λ_{max} having different value in the extinction coefficient of λ_{max}. In spite of attempts, no "half-compound" of structure (**1**) could be obtained. Only compound **3** was obtained by treating 1,3-dibromopropane with *o*-phenylenediamine in the presence of sodium hydride in dioxane and *N*,*N*-dimethylformamide. 2,3,4,5-Tetrahydro-1*H*-1,5-benzodiazepine was treated with phosgene in toluene. Only product **4** was obtained. The structures of compounds **3** and **4** were confirmed by IR, NMR, and mass spectra.

2,3,4,5-Tetrahydro-1*H*-1,5-benzodiazepine was heated with *N*,*N*-dimethylformamide, but it remained unchanged. We followed the method of Htay and Meth-Cohn[6] to get the "half-compound" of the spiran **2** (structure A) by condensing the sodium derivative of 2,3-dihydro-1*H*-benzimidazol-2-one with 1,3-dibromopropane. By measuring the UV-absorption spectra of spiran **2** and compound A, low hyperchromism was found (at λ_{max}=250 nm the ratio of extinction coefficients was 1:3.25; at λ_{max}=282 nm 1:2.57; 288 nm 1:2.64) indicating that the dominant conformation of spiran **2** is as shown in Fig. 3a.

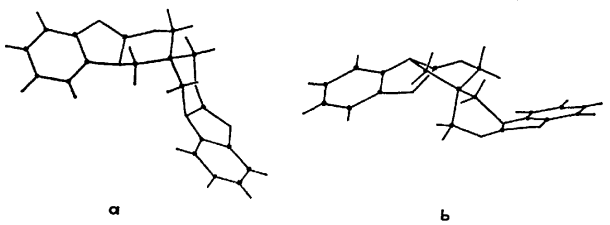

Fig. 3. The possible conformations of spiran **2**.

In conformation 3a the benzimidazole components are placed nearly orthogonally whereas the dihydrooxazine rings possess a chair conformation. Conformation 3b can be represented by two nearly parallel planes of the benzimidazole components annulated with dihydrooxazine rings in the biplanar conformation. Such geometry would have caused a higher hyperchromism.[5] Thus it is assumed that, in the reaction to obtain spiran **2**, 2,3-dihydro-1*H*-benzimidazol-2-one undergoes reaction in the tautomeric form, which in the presence of 1,3-dibromo-2,2-bis(bromomethyl)propane, forms the *O*-derivative from which spiran **2** resulted. Some analogy can be found with the experiments and results obtained by Htay and Meth-Cohn.[6]

In order to confirm the assumption we obtained the sulfur analogue of spiran **2**. 2,3-Dihydro-1*H*-benzimidazol-2-thione was heated with 1,3-dibromo-2,2-bis(bromomethyl)propane in the presence of metallic sodium in cellosolve; spiran **5**, mp 365—370 °C (with decomposition) and its dipicrate were obtained. Its "half-compound" (**6**) was synthesized in a similar way.[6] The measurement of UV-absortpion of spiran **5** and "half-compound" **6** revealed a hyperchromism of nearly the same magnitude as in the former case (at λ_{max}=235 nm the ratio of extinction coefficients was 1 : 1, 99; at λ_{max}=264 nm 1 : 2.6; 271 nm 1 : 2.6; 291 nm 1 : 2.25; 299 nm 1 : 2.2).

Considering the reactions, the following conclusion has been reached: Formation of structure (**2**) neglecting structure (**1**), is a result of the stereo-electronic effect. Structure (**1**) is inherently improbable, being of high energy due to steric inhibition of resonance the N lone pair and CO π-orbitals become necessarily orthogonal. The geometrical aspect is responsible for the case discussed being analogous with the arrangements covered by Bredt's rule concerning monocarbocyclic bridged ring system. The case is therefore considered to be included in Bredt's rule (whose nature is of stereo-electronic character), since there is no steric hindrance involved in the formation of spiran **1**.

It seems that failure[7,8] in obtaining 2-quinuclidinone and its 2-thione analogue (system [2.2.2]) which differs from the system considered here [3.2.1] but in which a similar stereo-electronic effect can be expected, confirms the assumption.

Experimental

IR spectra were measured with a Zeiss UR-10 spectrometer, UV-absorption spectra with a Unicam SP-1800, NMR spectra with a Tesla BS 487 at 80 MHz using TMS as a standard, and mass spectra with a LKB 9000 S apparatus at 70 eV.

*3,3'-Spirobi[3,4-dihydro-2*H*-[1,3]oxazino[3,2-a]benzimidazole] (**2**) from o-Phenylenediamine.* In a three necked flask 9.6 g of sodium hydride (0.2 m) in a 50% oil suspension were washed with dry benzene. 10.8 g (0.1 m) of *o*-phenylenediamine in 150 ml of dry dioxane was then added. The mixture was heated with stirring under reflux until no further hydrogen was evolved (3—4 h). A solution of 19.4 g (0.05 m) of 1,3-dibromo-2,2-bis(bromomethyl)propane in 150 ml of DMF was then added dropwise and the mixture refluxed for 100 h. The NaBr precipitate was separated and the

solvents removed by evaporation. The residue was treated with dilute hydrochloric acid (2:1). After filtering off the unreacted 1,3-dibromo-2,2-bis(bromomethyl)propane (10%) and resinous substances the spiran was precipitated from the acidic filtrate by addition of concentrated sodium hydroxide solution. The crude product was purified by sublimation at 320 °C in a high vacuum (0.1 mmHg); 510 mg (3%) of a colourless, crystalline product, mp 385—390 °C with decomposition.

From 2,3-Dihydro-1H-benzimidazol-2-one. In a thick glass tube a suspension of 4.5 g (0.025 m) of the sodium salt 2,3-dihydro-1*H*-benzimidazol-2-one in 100 ml cellosolve was prepared and 9.7 g (0.025 m, excess) of 1,3-dibromo-2,2-bis(bromomethyl)propane was added. The glass tube was sealed and heated at 120 °C for 100 h. The cellosolve was then distilled off and the spiran was purified as above; 680 mg (16%). IR(KBr): 1010, 1050 (C–O–C); 2940 (C–H aliph.); 770, 3060 (C–H arom.); 1625 cm^{-1} (C=N); UV (CH_2Cl_2): λ (logε)=250 (4.45), 282 (4.22), 288 nm (4.21); NMR(CF_3COOH): δ 4.75 (s, 4H, $-CH_2-N$), 5.2 (s, 4H, $-CH_2-O$), 7.5—7.7 (m, 8H, arom.); mass spectrum: *m/e*= 332. Found: C, 68.65; H, 4.96; N, 16.61%. Calcd for $C_{19}H_{16}N_4O_2$: C, 68.66; H, 4.85; N, 16.86%.

Dipicrate of Spiran **2**: 40 mg of the spiran **2** was treated with 10 ml of saturated picric acid solution in ethanol and refluxed for 1 h. A yellow, crystalline product (cellosolve) with a mp 235—237 °C was obtained. Found: N, 17.60%. Calcd for $C_{31}H_{32}N_{10}O_{16}$: N, 17.71%.

3,3'-Spirobi[3,4-dihydro-2H-[1,3]thiazino[3,2-a]benzimidazole] (5). 0.46 g (0.02-g atom) of metallic sodium was introduced into a thick glass tube containing 50 ml of cellosolve and then 1.5 g (0.01 m) of 2,3-dihydro-1*H*-benzimidazol-2-thione and 3.9 g (0.01 m, excess) of 1,3-dibromo-2,2-bis(bromomethyl)propane were added. The tube was sealed and heated at 120 °C for 50 h. The cellosolve was then distilled off and the spiran separated and purified as above. 880 mg (48%) of a colourless, crystalline product, mp 365—370 °C (with decomposition) were obtained. IR (KBr): 2935 (C–H aliph.); 770, 3055 (C–H arom.); 1610 cm^{-1} (C=N); UV(CH_2Cl_2): λ(log ε)=235 (4.41), 264 (4.37), 271 (4.38), 291 (4.48), 299 nm (4.50); NMR (CF_3COOH): δ 3.9 (s, 4H, $-CH_2-S$), 4.8 (s, 4H, $-CH_2-N$), 7.5—7.85 (m, 8H, arom.); mass spectrum *m/e*=364. Found: C, 62.45; H, 4.39; N, 15.13%. Calcd for $C_{19}H_{16}N_4S_2$: C, 62.61; H, 4.43; N, 15.37%.

Dipicrate of Spiran **5**: This was prepared according to the procedure for the previously described dipicrate. A yellow, crystalline product (cellosolve), mp 215—217 °C was obtained. Found: N, 16.84%. Calcd for $C_{31}H_{22}N_{10}O_{14}S_2$: N, 17.02%.

1,5-Diformyl Derivative of 2,3,4,5-Tetrahydro-1H-1,5-benzodiazepine (3). In a three necked flask, 9.6 g (0.2 m) of sodium hydride in a 50% oil suspention were washed with dry benzene, 10.8 g (0.1 m) of *o*-phenylenediamine in 150 ml of dry dioxane was then added. The mixture was heated with stirring under reflux until no further hydrogen was evolved (3—4 h). A solution 20.2 g (0.1 m) of 1,3-dibromopropane in 150 ml of DMF was then added dropwise and the mixture refluxed for 50 h. The NaBr precipitate was separated and the solvents removed by evaporation. The residue was treated with dilute hydrochloric acid (2:1). After filtration, the filtrate was treated with concentrated sodium hydroxide solution and decanted off, leaving oily impurities, and extracted with butanol. From the extract, 150 mg (0.7%) of a colourless, crystalline product (1-butanol) were recovered, mp 170—172 °C. IR(KBr): 1670 (C=O), 790, 3040 (C–H arom.), 2950 cm^{-1} (C–H aliph.); NMR ($CDCl_3$): δ 2.0 (q, 2H, $-CH_2-$), 3.8 (t, 4H, $-CH_2-N$), 7.1—7.5 (m, 4H, arom.), 8.25 (s, 2H, H–C=O); mass spectrum: *m/e*=204. Found: C, 64.58; H, 6.13; N, 13.56%. Calcd for $C_{11}H_{12}N_2O_2$: C, 64.72; H, 5.93; N, 13.74%.

1,5-Bis(chloroformyl) Derivative of 2,3,4,5-Tetrahydro-1H-1,5-benzodiazepine (4). A solution of 0.75 g (0.005 m) of 2,3,4,5-tetrahydro-1*H*-1,5-benzodiazepine in 120 ml of dry toluene was prepared in a three necked flask fitted with a reflux condenser and stirrer. While being mixed 4.2 g of a 12% solution of phosgene in toluene (0.005 m) was added and the reaction mixture stirred for 3 h. After amine hydrochloride had been removed and toluene distilled off, the solid residue was purified chromatographically on an Alox column in benzene. 120 mg (8.8%) of a colourless, crystalline product, mp 165—166 °C were obtained. IR(KBr): 2965 (C–H aliph.), 785, 3050 (C–H arom.), 675 (C–Cl), 1725 cm^{-1} (C=O); mass spectrum: *m/e*=272. Found: C, 48.46; H, 3.75; N, 10.27%. Calcd for $C_{11}H_{10}N_2O_2Cl_2$: C, 48.37; H, 3.69; N, 10.29%.

3,4-Dihydro-2H-[1,3]thiazino[3,2-a]benzimidazole (6). 0.92 g (0.04 g-atom) of metallic sodium was introduced into 50 ml of cellosolve in a three necked flask equipped with reflux condenser and stirrer and then 1.5 g (0.02 m) of 2,3-dihydro-1*H*-benzimidazol-2-thione and 4 g (0.02 m) of 1,3-dibromopropane were added. The mixture was refluxed for 3 h. The cellosolve was distilled off and the product was purified chromatographically on an Alox column in benzene. 120 mg (6.3%) of a colourless, crystalline (benzene) product, mp 133—135 °C were obtained. IR (KBr): 2935 (C–H aliph.), 775, 3040 (C–H arom.), 1610 cm^{-1} (C=N); UV (CH_2Cl_2): λ(log ε)=235 (4.12), 264 (3.95), 270 (3.97), 292 (4.13), 300 nm (4.16); NMR ($CDCl_3$): δ 2.2—2.5 (m, 2H, $-CH_2-$), 3.1 (t, 2H, $-CH_2-S$), 4.0 (t, 2H, $-CH_2-N$), 7.0—7.7 (m, 4H, arom.); mass spectrum: *m/e*=190. Found: C, 62.97; H, 5.22; N, 14.66%. Calcd for $C_{10}H_{10}N_2S$: C, 63.12; H, 5.29; N, 14.73%.

References

1) S. Smoliński, *Tetrahedron*, **22**, 199 (1966).
2) S. Smoliński and G. Kinyua, *Tetrahedron*, **27**, 265 (1971).
3) S. Smoliński and J. Jamrozik, *Tetrahedron*, **27**, 4977 (1971).
4) S. Smoliński, I. Deja, and J. Nowicka, *Tetrahedron*, **31**, 1527 (1975).
5) S. Smoliński, J. Nowicka, J. Mokrosz, M. Jamrozik, M. Jaworski, and E. Wiekiera, *Tetrahedron*, **33**, 1219 (1977).
6) M. M. Htay and O. Meth-Cohn, *Tetrahedron Lett.*, **1976**, 79.
7) L. N. Yakhontov and M. V. Rubtsov, *Zh. Obshch. Khim.*, **27**, 72 (1957).
8) H. Pracejus, M. Kehlen, H. Kehlen, and H. Matschiner, *Tetrahedron*, **21**, 2257 (1965).

NOTES

BULLETIN OF THE CHEMICAL SOCIETY OF JAPAN, VOL. 52 (3), 933—934 (1979)

Promoting Action of Inorganic Gases on the Rate of Dehydration of 2-Propanol over Ca-Y Zeolite

Yoshio ISHINAGA, Kiyoshi OTSUKA,* and Akira MORIKAWA

Department of Chemical Engineering, Tokyo Institute of Technology, Ookayama, Meguro-ku, Tokyo 152

(Received July 28, 1978)

Synopsis. The dehydration of 2-propanol over Ca-Y zeolite has been enhanced in the presence of NO_2, SO_2, and Cl_2 at 100 °C. This promoting action has been ascribed to the formation of acidic hydroxyl groups resulting from the reaction of the inorganic gases with zeolitic water or basic hydroxyl groups attached to the metal cations.

The promoting action of inorganic gases on the rate of dehydration of alcohol or hydrocarbon conversion, such as cracking, alkylation or isomerization has been recognized specifically on zeolites.[1-3] The favorable action of gases which contain hydrogen atom or atoms in their structure, such as H_2O, HCl, or H_2S, has been ascribed to their ability to generate protonic sites by the dissociation of the hydrogen atoms as follows:[4-9]

$$M^{2+} + H_2O \rightleftharpoons M(H_2O)^{2+} \rightleftharpoons M(OH)^{+} + H^{+} \quad (1)^{4,10,11}$$

$$M^{2+}Z^{2-} + HCl \rightleftharpoons \overset{Cl^- \; H^+}{\underset{|}{M^{2+}}\underset{|}{Z^{2-}}} \quad (2)^{6,7,12,13}$$

$$M^{+}Z^{-} + H_2S \rightleftharpoons \overset{SH^- \; H^+}{\underset{|}{M^{+}}\underset{|}{Z^{-}}} \quad (3)^{14}$$

where, M^{2+} or M^{+} and Z^{2-} or Z^{-} represent the exchange-able cation and the anionic framework of the zeolite, respectively. The promoting action of compounds possessing no hydrogen atoms, such as NO_2, SO_2, or Cl_2, has however not satisfactorily been interpreted.

In this work, the promoting action of NO_2, SO_2, Cl_2, CO_2, HCl, and H_2S on the dehydration of 2-propanol over Ca-Y zeolite has been studied in connection with the formation of acidic hydroxyl groups by the foreign gases. The dehydration of 2-propanol is a typical reaction catalyzed by protonic sites over zeolites[2] and consequently has been used as a test reaction.

Results and Discussion

The effect of the gases on the rate of propylene and diisopropyl ether formation, denoted by R_{prp} and R_{ether}, over Ca-Y zeolite is shown in Fig. 1, where the initial rate has been plotted as a function of the amount of adsorbed gases measured during the course of reaction. The reaction was conducted at 100 °C under 24 Torr of 2-propanol using a conventional gas circulation system. Prior to each run, the Ca-Y zeolite (79% exchanged) was calcined at 500 °C in dried oxygen and degassed for 2 h at the same temperature. After the adsorption of the foreign gas

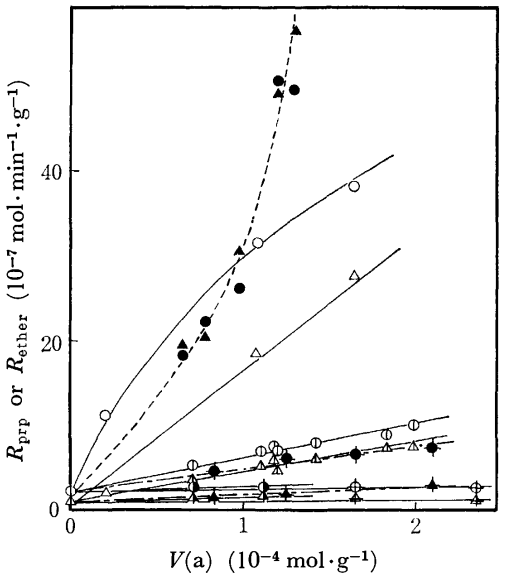

Fig. 1. Effect of inorganic gases on the rate of dehydration of 2-propanol over Ca-Y zeolite : Circle; propylene, triangle; diisopropyl ether, ●, ▲; NO_2, ○, △; Cl_2, ◑, ◭; SO_2, ◑, ◭; CO_2, ⊕, ⊕; HCl, ⊕, ⊕; H_2S.

at 100 °C for 20 min, 2-propanol was fed into the system thereby initiating reaction. The amount of gas adsorbed during the course of the reaction was calculated by measuring the amount of foreign gas in the gas-phase by gas-chromatography. The pressure of the foreign gas under the reaction conditions was less than 1.5 Torr. The Ca-Y was prepared from Na-Y (Linde SK-40) by a conventional ion-exchange method using an aqueous solution of $CaCl_2$ at 25 °C. The 2-propanol (spectro grade) and the inorganic gases (purity>99%) were purified by trap to trap distillation *in vacuo*. The results illustrated in Fig. 1 indicate that NO_2, Cl_2, SO_2, and HCl considerably enhance the dehydration of 2-propanol over Ca-Y zeolite. In the case of CO_2, the promoting action developed when the gas was pre-adsorbed at temperatures in excess of 300 °C up to 500 °C.

The formation of acidic hydroxyl groups after adsorption of the six inorganic gases onto the zeolite has been examined as follows. A wafer of the zeolite (3—4 mg/cm^2) was calcined in dried oxygen at 450 °C for 1 h, and degassed for 2 h at the same temperature. The wafer was then allowed to come into contact with D_2O vapour 9 Torr for 4 h at 200 °C in order to exchange OH by OD groups since the broad OH stretching band around 3600 cm^{-1}, probably due to

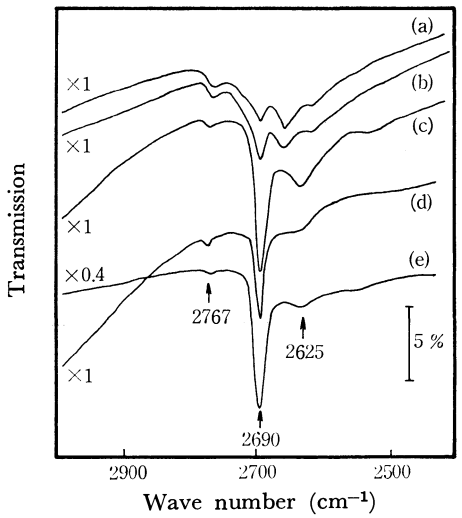

Fig. 2. Spectra of the deuteroxyl stretching vibrations of Ca-Y zeolite : (a) evacuated for 1 h at 450 °C after D_2O treatment, (b) exposed to SO_2 after (a), (c) exposed to NO_2 after (a), (d) exposed to Cl_2 after (a), (e) exposed to DCl after (a). The bands at 2767, 2690, and 2625 cm^{-1} are due to silica-type deuteroxyl groups, acidic deuteroxyl groups in supercages, and those in hexagonal prisms or sodalite cages, respectively.

strongly held water molecules on the zeolite, and the absorption of infrared beam by water in the air make it difficult to identify the different kinds of OH group. After the exchange, the wafer was degassed again for 1 h at 450 °C. Figure 2 shows the spectra of the OD stretching vibrations of Ca-Y zeolite after adsorption of NO_2, Cl_2, SO_2, and DCl for 20 min at 100 °C (16 Torr for each compound; 9 Torr for NO_2). The spectra have been measured at 100 °C after condensing the adsorbate in the gas phase in a liquid nitrogen trap. For these four compounds, it is clear that the intensity of the 2690 cm^{-1} band due to the acidic deuteroxyl groups[12] increases greatly after the adsorption of the gas. This band corresponds to the band at 3640 cm^{-1} attributed to the acidic hydroxyl groups in the supercages for the undeuterated Ca-Y zeolite.[11,15]

The high promoting action of NO_2, Cl_2, and SO_2 indicated in Fig. 1 can be ascribed to the newly formed acidic hydroxyl groups. The lower promoting action of H_2S and CO_2 can be accounted for by the low ability to generate acidic hydroxyl groups, substantiated by a very small increase in intensity of the acidic OD band after adsorption of the gas. In the case of CO_2, a much higher temperature was needed for the generation of the acidic hydroxyl groups.[2,16] The promoting action of HCl was not as large as anticipated from the evidence in Fig. 2.

The following schemes are proposed for the generation of protonic sites after the adsorption of NO_2, SO_2, and Cl_2 from an analogy to the mechanisms suggested in the case of CO_2:[2,16]

$$Ca^{2+}(H_2O)_x + A \longrightarrow Ca^{2+}[B]^{2-} + 2H^+ + (H_2O)_{x-1} \quad (4)$$

where, A is NO_2, SO_2, or Cl_2 and B is $O{\diagdown}N{=}O{\diagup}O$, $O{\diagdown}S{=}O{\diagup}O$, or $OCl{\diagup}Cl$, respectively, or

$$Ca(OH)^+ + A \longrightarrow Ca^+B^- + H^+ \quad (5)$$

where, A is NO_2, SO_2, or $1/2Cl_2$ and B is $-O-N{\diagup}{\diagdown}O$, $-O-S{\diagup}{\diagdown}O$, or OCl, respectively. $Ca^{2+}(H_2O)_x$ is the divalent cation coordinated by water, and $Ca(OH)^+$ is the basic species formed through the dissociation of hydrating water during the pretreatment of the zeolite. Further infrared spectroscopic studies on this point are in progress.

References

1) Kh. M. Minachev and Ya. I. Isakov, *Adv. Chem. Ser.*, **121**, 451 (1973).
2) P. A. Jacobs, "Carboniogenic Activity of Zeolites," Elsevier, North-Holland Inc., New York (1977).
3) K. Otsuka and A. Morikawa, *Hyomen(Surface)*, **16**, 12 (1978).
4) P. B. Venuto and P. S. Landis, *Adv. Catal.*, **18**, 259 (1968).
5) E. A. Lombardo, G. A. Sill, and W. K. Hall, *Adv. Chem. Ser.*, **102**, 346 (1971).
6) H. Matsumoto and Y. Morita, *Kogyo Kagaku Zasshi*, **70**, 1674 (1967).
7) H. Matsumoto, K. Yasui, and Y. Morita, *J. Catal.*, **12**, 84(1968).
8) M. Sugioka, T. Hosotsubo, and K. Aomura, *J. Chem. Soc., Chem. Commun.*, **1976**, 54.
9) H. Matsumoto, H. Futami, M. Tokuno, and Y. Morita, *Kogyo Kagaku Zasshi*, **73**, 841 (1970).
10) A. E. Hirschler, *J. Catal.*, **2**, 428 (1963).
11) J. W. Ward, *Adv. Chem. Ser.*, **101**, 380 (1971).
12) C. L. Angell and P. C. Schaffer, *J. Phys. Chem.*, **69**, 3463(1965).
13) C. L. Angell and M. V. Howell, *J. Phys. Chem.*, **74**, 2737(1970).
14) H. G. Karge and J. Rasko, *J. Colloid Interface Sci.*, **64**, 522(1978).
15) J. W. Ward, *J. Phys. Chem.*, **72**, 4211 (1968).
16) C. Mirodatos, P. Pichat, and D. Barthomeuf, *J. Phys. Chem.*, **80**, 1335(1976).

BULLETIN OF THE CHEMICAL SOCIETY OF JAPAN, VOL. 52 (3), 935—936 (1979)

Fluorescence from Bound Ionic States of Neat Molecular Crystals: *p*-Substituted *N,N*-Dimethylanilines[1)]

Kotaro ARAYA and Jun-ichi AIHARA*

Department of Chemistry, Faculty of Science, Hokkaido University, Sapporo 060

(Received May 24, 1978)

Synopsis. Fluorescences were detected from bound ionic states (*i.e.*, charge-transfer exciton states) of two neat molecular crystals, each formed by a single molecular component. These fluorescent compounds are *p*-(2,2-dicyanovinyl)-*N,N*-dimethylaniline and *p*-(2-nitrovinyl)-*N,N*-dimethylaniline. They are dimorphic in the solid state.

Interest in charge-transfer (CT) properties of molecular solids[2)] has increased greatly due to the recent observation of a high conductivity anomaly in a mixed molecular crystal TTF-TCNQ.[3)] It is now well-known that transitions to bound ionic states (*i.e.*, CT exciton states) are observed in the optical spectra of such mixed crystals.[4,5)] Here, a CT exciton means an intermolecular CT excitation in the solid.[2)] However, the corresponding states of neat molecular crystals had long eluded direct observation, until in 1968 Tanaka and Shibata detected a CT excitation in the 9,10-dichloroanthracene crystal.[6)] One of the most serious difficulties in studying CT excitons has been heavy interference from neutral Frenkel excitons (*i.e.*, excitons caused by the intramolecular excitations) energetically degenerate with them.[7)]

In previous papers,[8)] we showed that a CT exciton band can be shifted to the low energy side, lower than any Frenkel exciton band, if one uses an appropriate aromatic compound with a strong electron-attracting chromophore. This idea was verified by a recent X-ray crystallographic analysis of 2-(*p*-methoxyphenyl)-*p*-benzoquinone crystals.[9)] Component molecules are therein arranged so as to promote intermolecular CT interactions. In this note we report the first observation of fluorescence from the bound ionic states of neat molecular solids of this type.[10)]

Results and Discussion

After an extensive search two aromatic compounds, each with a strong electron-attracting chromophore, were found to be fluorescent in the solid state.[11)] They are *p*-(2,2-dicyanovinyl)-*N,N*-dimethylaniline (I) and *p*-(2-nitrovinyl)-*N,N*-dimethylaniline (II). Figures 1

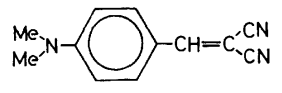

I

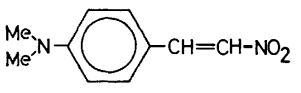

II

and 2 show electronic spectra of these two compounds both in chloroform solution and in the solid state. Fluorescence spectra were recorded on a Hitachi MPA-2A fluorescence spectrophotometer, and were corrected for the spectral response of the analyzing system, unless otherwise stated. All absorption spectra were measured with a Beckman DK-2A spectrophotometer with reflectometric equipment. Solid-state absorption spectra were derived from diffuse reflection spectra of the solids dispersed in the powdered sodium chloride.

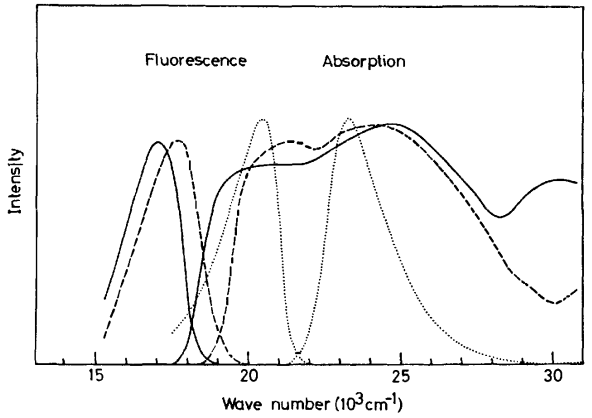

Fig. 1. Electronic spectra of Compound I in two solid states (—— and ----) and in chloroform solution (……).

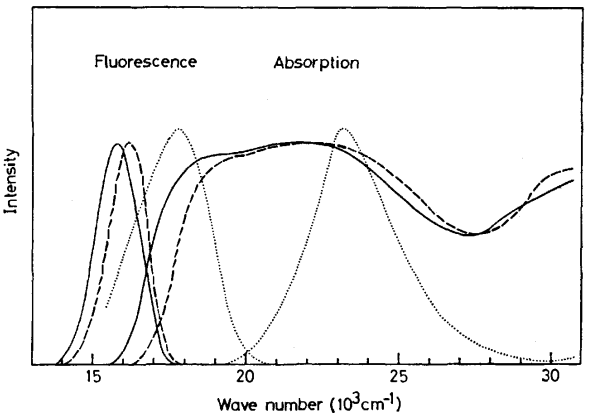

Fig. 2. Electronic spectra of Compound II in two solid states (—— and ----) and in chloroform solution (……).

Interestingly, Compound I was dimorphic. The yellow crystal was obtained from a benzene solution, whereas the orange crystal was obtained by recrystalization from methanol. The visible spectra of these solids consist of two broad absorption bands, one around 20000 cm^{-1} and one around 24000 cm^{-1}. As before,[8,12)] the first absorption band of each crystalline form can be assigned to the transition to the bound ionic state, *i.e.*, an intermolecular CT transition, because of the dual charge-transfer properties of the component molecule.[13)] The second absorption band has a counterpart in the solution absorption spectrum, and should hence be a neutral Frenkel exciton band.

The difference in color between the two crystalline forms is evidently related to a considerable shift of the CT exciton band. The spectral shift amounts to about 1000 cm^{-1}.

Here, one should note that a remarkable red shift in the fluorescence maximum of Compound I occurs on going from solution to solids. The fluorescent levels of the solids are obviously different from that of the solution. By inspection of the spectra, the fluorescence of each solid can naturally be identified as arising from the bound ionic state (*i.e.*, CT exciton state). The fluorescence maxima are located at 17700 cm^{-1} for the yellow crystal and 17000 cm^{-1} for the orange crystal. The energy difference between the two fluorescence bands is comparable to that between the corresponding CT exciton bands. In contrast to the spectral behavior, the structural difference between the two crystalline forms is too small to discern by means of the X-ray powder patterns.

Compound II also exists in two different crystalline forms. They are red and red-violet crystals obtained from the methanol and benzene solutions, respectively. As shown in Fig. 2, a CT absorption band of the red-violet crystal is about 700 cm^{-1} shifted to the low energy side compared with that of the red one. The shift of the fluorescence band due to dichromism appears to be in the same direction and of the same amount as that of the absorption edge, although these solid-state fluorescence spectra are uncorrected. The spectral shift of the bound ionic state suggests a change in the intermolecular interactions in the solid.

The importance of these bound ionic states mostly stems from their involvement in electron transfer and electron-hole recombination processes in neat molecular crystals.[2,3,13] The existence of the CT exciton level may also be responsible for the shifts of local excitation bands in the solid-state spectrum.[5] In this sense, the present finding of fluorescent CT exciton bands provides an important clue to a substantial characterization of the CT exciton state, and might help to clarify its role in electron and energy transfers in the neat molecular crystals.

The authors are grateful to the Ministry of Education for a Scientific Research Grant-in-Aid.

References

1) Part V of "Organic Charge-Transfer Self-Complexes;" Part IV : J. Aihara, *Bull. Chem. Soc. Jpn.*, **47**, 2899 (1974).

2) F. Gutman and L. E. Lyons, "Organic Semiconductors," Wiley, New York, N. Y. (1967), Chap. 5; M. Pope and H. Kallmann, *Discuss. Faraday Soc.*, **51**, 7 (1971).

3) "Low-Dimensional Cooperative Phenomena," ed by H. J. Keller, Plenum, New York, N. Y. (1975); "Chemistry and Physics of One-Dimensional Metals," Plenum, New York, N. Y. (1977).

4) D. B. Tanner, C. S. Jacobsen, A. F. Garito, and A. J. Heeger, *Phys. Rev. B*, **13**, 3381 (1976); J. B. Torrance, B. A. Scott, and F. B. Kaufman, *Solid State Commun.*, **17**, 1369 (1975).

5) J. Tanaka, M. Tanaka, T. Kawai, T. Tanabe, and O. Maki, *Bull. Chem. Soc. Jpn.*, **49**, 2358 (1976).

6) J. Tanaka and M. Shibata, *Bull. Chem. Soc. Jpn.*, **41**, 34 (1968); S. C. Abbi and D. M. Hanson, *J. Chem. Phys.*, **60**, 319 (1974).

7) J. Tanaka, *Bull. Chem. Soc. Jpn.*, **36**, 1237 (1963); **38**, 86 (1965); J. Tanaka, T. Kishi, and M. Tanaka, *ibid.*, **47**, 2376 (1974).

8) J. Aihara, G. Kushibiki, and Y. Matsunaga, *Bull. Chem. Soc. Jpn.*, **46**, 3584 (1973); J. Aihara, *ibid.*, **47**, 2063 (1974).

9) G. R. Desiraju, I. C. Paul, and D. Y. Curtin, *J. Am. Chem. Soc.*, **99**, 1594 (1977).

10) It goes without saying that not a few charge-transfer complexes are fluorescent in the solid state. See, *e.g.*, S. Iwata, J. Tanaka, and S. Nagakura, *J. Am. Chem. Soc.*, **89**, 2813 (1967).

11) Unfortunately, fluorescence of the solid 2-(*o*- or *p*-methoxyphenyl)-*p*-benzoquinone could not be detected. Fluorescences of many tricyanovinyl aromatics and several *p*-substituted *N*,*N*-dimethylanillines were not appreciable in the solid state, either.

12) R. L. Hansen and J. J. Neumayer, *J. Phys. Chem.*, **71**, 3047 (1967).

13) R. L. Hansen, *J. Phys. Chem.*, **70**, 1646 (1966).

14) See, *e.g.*, M. Pope, J. Burgos, and J. Giachino, *J. Chem. Phys.*, **43**, 3367 (1965); M. Pope and J. Burgos, *Mol. Cryst.*, **1**, 395 (1966); G. T. Pott and D. F. Williams, *J. Chem. Phys.*, **51**, 203 (1969); H. P. Schwob and D. F. Williams, *ibid.*, **58**, 1542 (1973).

BULLETIN OF THE CHEMICAL SOCIETY OF JAPAN, VOL. 52 (3), 937—938 (1979)

Solvent Isotope Effect of H_2O and D_2O on the Partition Coefficient of 1,3-Di-*n*-alkyl-1,3-propanedione

Hitoshi WATARAI, Motoya MURAKAMI, and Nobuo SUZUKI*

Department of Chemistry, Faculty of Science, Tohoku University, Sendai 980

(Received July 1, 1978)

Synopsis. The apparent partition coefficients of seven 1,3-di-*n*-alkyl-1,3-propanediones have been determined in dodecane/H_2O and dodecane/D_2O systems. From the results, the transfer free energies of β-diketones from H_2O to D_2O, $\Delta G_{H_2O\rightarrow D_2O}$, have been calculated and are discussed in terms of the cavity formation energy.

In solvent extraction, the partition process of a metal chelate formed in an aqueous phase is one of the most important processes governing the distribution ratio of a metal ion. The partition coefficient of a metal chelate is primarily determined by the hydrophobic character which is a substantial part of the chelate formed by the reaction of a metal ion with a hydrophobic extractant. A quantitative discussion of the hydrophobicity of the extractant, however, is not thoroughly recognized. In this study the interaction between water and 1,3-di-*n*-alkyl-1,3-pentanediones has been examined, the latter compounds being well-known as extractants, by partition experiments in the dodecane/H_2O and dodecane/D_2O systems. The reason for employing β-diketones is that the size of the hydrophobic part of the reagent can be varied stepwise by changing the chain length of the *n*-alkyl group. D_2O is considered to be more structured than H_2O,[1] so that partition experiments in the two systems will provide useful information on the hydrophobic interaction between water and the reagents.

Experimental

Materials. Reagent grade acetylacetone (2,4-pentanedione) was purified by fractional distillation. Other normal chain β-diketones were synthesized by the Claisen acylation.[2] The crude products were purified by the copper salt method[3] and subsequently distilled under reduced pressure. Dodecane (Tokyo Kasei G. R.) was agitated twice with a mixture of fuming sulfuric acid and sulfuric acid (1 : 4) overnight, washed with water and distilled under reduced pressure. Redistilled water was used throughout the experiments and heavy water (Merk 99.7%) used as purchased.

Partition Experiments. A certain volume (5 ml or 4 ml) of the dodecane solution of the β-diketone (below 10^{-2} M) and an equal volume of H_2O (5 ml) or D_2O (4 ml) were stirred by a magnetic stirrer for 6 h in a thermostated glass vessel at 25±0.05 °C. After being allowed to stand for 1 h, an aliquot of the aqueous phase was pipetted into a quartz cell and the transmittance at the absorption maximum recorded for each β-diketone on a Hitachi 356 spectrophotometer. Partition coefficients were obtained from the initial concentration and the concentration in the aqueous phase determined photometrically. Partition experiments were repeated a minimum of three times.

Results and Discussion

The observed partition coefficients (P_{H_2O} and P_{D_2O}) are listed in Table 1 and as can be seen the partition coefficients appear to increase with the carbon numbers of the *n*-alkyl group. P_{D_2O} values appear to be slightly less than the P_{H_2O} values for the smaller diketones, but slightly greater for the larger diketones. The ratios of P_{D_2O}/P_{H_2O}, which are shown in Table 1, differ from unity revealing the solvent isotope effect on the partition coefficient.

From the partition coefficient data, the transfer free energy of the β-diketone from H_2O to D_2O ($\Delta G_{H_2O\rightarrow D_2O}$) has been estimated using,

$$\Delta G_{H_2O\rightarrow D_2O} = RT\ln\left(\frac{P_{D_2O}}{P_{H_2O}}\cdot\frac{V_{H_2O}}{V_{D_2O}}\right), \quad (1)$$

where V is the molar volume of the solvent. The results are also listed in the last column of Table 1. Since the diketones are in the keto and enol forms in solution and possess reactive protons, *viz.* an enol proton and a methyne proton for the enol form and methylene protons for the keto form, a change in the keto-enol equilibrium will be the result of H–D exchange and/or by the solvent effect of H_2O and D_2O. The PMR spectra of acetylacetone in D_2O provides that all the reactive protons are replaced by deuteron in D_2O. However, since the ratio of the molar ex-

TABLE 1. THE PARTITION COEFFICIENTS[a] AND THE FREE ENERGIES OF TRANSFER FROM H_2O TO D_2O AT 25 °C

β-Diketone	P_{H_2O}	P_{D_2O}	P_{D_2O}/P_{H_2O}	$\Delta G_{H_2O\rightarrow D_2O}$ (cal mol^{-1})
2,4-Pentanedione	0.69±0.04	0.64±0.03	0.93	−47±30
2,4-Hexanedione	2.41±0.14	2.27±0.25	0.94	−40±7
2,4-Heptanedione	11.7±0.2	10.9±0.4	0.93	−44±10
2,4-Octanedione	43.5±0.3	48.7±6.6	1.12	63±6
3,5-Octanedione	37.5±0.4[b]	43.8±1.6[b]	1.17	89±28
2,4-Nonanedione	194±29	253±5	1.30	157±6
4,6-Nonanedione	144±2[b]	198±2[b]	1.38	187±12

a) Partition coefficients are shown with the standard deviation at 95% confidence level.
b) An average value of two experiments. The precision refers to the range of the two values.

tinction coefficients in H_2O and D_2O, which is thought to reflect the difference in the keto-enol equilibrium constant in the two solvent,[4] is constant (*ca.* 1.03) for most diketones, it is to be expected that the transfer free energies of the enol and keto forms will show a similar trend to the observed transfer free energy including those of the keto and enol forms. Hence, in this study the apparent transfer free energy of β-diketones will be discussed.

From Table 1, it may be seen that $\Delta G_{H_2O\to D_2O}$ is approximately zero for smaller compounds but positive for larger β-diketones. A large compound, however, does not always show a positive value of transfer free energy, *e.g.*, Jolicoeur *et al.*[5] have reported a negative value for 3-decanone (-270 ± 36 cal mol^{-1}).

The free energy of transfer can conveniently be divided into three contributions;[6]

$$\Delta G_{H_2O\to D_2O} = \Delta G(\mathrm{CAV}) + \Delta G(\mathrm{SOL}) + \Delta G(\mathrm{STR}), \quad (2)$$

where the terms on the righthand side of Eq. 2 represent the solvent isotope effect on the free energy due to CAV, the process of cavity formation in the solvent; SOL, the solvation of the polar group of the molecule; STR, the structural rearrangement of the solvent around the cavity enclosing the solute. ΔG(SOL) is expected to reflect the interactions between the solvent and both the carbonyl group of the keto form and the hydroxyl group of the enol form. Dahlberg[7] reported that the transfer free energy for acetone is close to zero and consequently there will be no serious difference between the free energies of the H-bond and D-bond to the carbonyl oxygen. Dahlberg furthermore reported the transfer free energy of benzene (0 ± 15 cal mol^{-1}) and benzyl alcohol (-9 ± 20 cal mol^{-1}) and from these data, it is expected that ΔG(SOL) for β-diketones is slightly negative and is not the dominant factor in the present situation.

The hydrogen bonding energy in D_2O is thought to be larger than that in H_2O in consideration of the greater cohesive energy density of D_2O than H_2O, and consequently the structural change around the solute molecule will be more extensive in D_2O. Hence, ΔG(STR) will show a negative value with increasing carbon number in the *n*-alkyl chain due to hydrophobic hydration around the group. This factor may be important in the case of decanone, but is not dominant here. Dahlberg reported that $\Delta G_{H_2O\to D_2O}$ for 3-methylacetylacetone showed a fairly large value ($+200$ cal mol^{-1}) and interpreted this result from the general tendency that a solute which possesses both ring and branches shows a positive value.[7] The present results appear to support this hypothesis.

Since the amount of void is greater in D_2O than in H_2O, the small solute molecules which can occupy void without excessive disruption of the hydrogen bonds in the solvent will be better accommodated in D_2O (negative ΔG(CAV)). The bulky molecules which disrupt a significant number of hydrogen bonds will show a positive ΔG(CAV). This hypothesis appears to be supported by the recent solution theory, *viz.* the scaled particle theory amended by Stillinger.[8] Lucas and Bury[9] have computed $\Delta G_{H_2O\to D_2O}$ for a nonpolar solute using this theory and plotted the result as a function of solute hard sphere diameter, a_2. The plot of the transfer free energy is slightly negative for $a_2 < \approx 3.0$ Å and positive for $a_2 > 3.0$ Å. This is consistent with the trend observed in this study.

From the above discussion, it has been concluded that the positive transfer free energy observed for the larger β-diketones is attributable to the contribution from the cavity formation work. Since the most important process in solvent extraction is the partition of the metal chelate coordinated by a hydrophobic ligand, more attention needs to be focused on the cotribution of cavity formation in the extraction process.

References

1) D. P. Wilson and W. Y. Wen, *J. Phys. Chem.*, **79**, 1527 (1975).
2) F. W. Swamer and C. R. Hauser, *J. Am. Chem. Soc.*, **72**, 1352 (1950).
3) J. T. Adams and C. R. Hauser, *J. Am. Chem. Soc.*, **66**, 1220 (1944).
4) D. W. Thompson and A. L. Allred, *J. Phys. Chem.*, **75**, 433 (1971).
5) C. Jolicoeur and G. Lacroix, *Can. J. Chem.*, **51**, 3051 (1973).
6) C. V. Krishnan and H. L. Friedman, *J. Phys. Chem.*, **73**, 1572 (1969).
7) D. B. Dahlberg, *J. Phys. Chem.*, **76**, 2045 (1972).
8) F. H. Stillinger, *J. Solution Chem.*, **2**, 141 (1973).
9) M. Lucas and R. Bury, *J. Phys. Chem.*, **80**, 999 (1976).

BULLETIN OF THE CHEMICAL SOCIETY OF JAPAN, VOL. 52 (3), 939—940 (1979)

Electronic Properties and π-π^* Absorption Spectra of 1- and 2-Methyl-4-amino-5*H*-[1]benzopyrano[3,4-*c*]pyridin-5-one

Kozo INUZUKA* and Akira FUJIMOTO

Department of Applied Science, Faculty of Technology, Tokyo Denki University, Kanda, Chiyoda-ku, Tokyo 101

(Received August 7, 1978)

Synopsis. The tautomerization of 4-amino-5*H*-[1]-benzopyrano[3,4-*c*]pyridin-5-one (BPP) in the ground state has been briefly discussed by the CNDO/2 method. The π-π^* absorption spectra of 1-methyl-4-amino-5*H*-[1]benzo-pyrano[3,4-*c*]pyridin-5-one (1-MBPP) and 2-methyl-4-amino-5*H*-[1]benzopyrano[3,4-*c*]pyridin-5-one (2-MBPP) in solution have been obtained. Based on the MO calculations of BPP, assignment of the observed π-π^* absorption bands of 1-MBPP and 2-MBPP have been made.

Recently, the thermodynamic properties of the hydrogen bond of 1- and 2-alkyl-4-amino-5*H*-[1]benzo-pyrano[3,4-*c*]pyridin-5-one with alcohols have been studied both experimentally and theoretically.[1] Also, the fluorescence of the proton-transferred excited species (tautomer) between 2-MBPP and acetic acid has been investigated,[2] but as yet the absorption spectra of 1-MBPP and 2-MBPP have not been discussed. In this paper, the possibility of tautomerization of BPP in the ground state and the π-π^* absorption spectra of 1-MBPP and 2-MBPP are reported.

Results and Discussion

Electronic Properties in the Ground State. Dipole moments, charge densities, and π-bond orders of BPP, 1-MBPP, and 2-MBPP in the ground state have already been discussed in a previous paper.[1] In this paper the calculation of the total energies of the following three kinds of the models **1**, **2**, and **3** were conducted to clarify the tautomerization from **1** to **2** and **3** in the ground state by the CNDO/2 method using the parameters of Pople, Santry, and Segal.[3] The calculated total energies (a. u.) and dipole moments are as follows: **1**: −151.47204 (3.735 D); **2**: −151.42766 (9.483 D); **3**: −151.42170 (8.043 D).

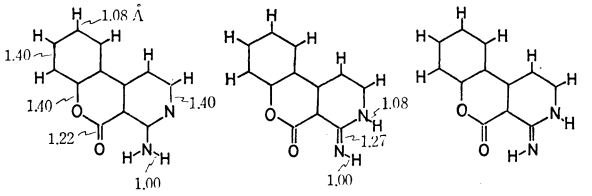

1 **2** **3**

The energy differences between **1** and **2**, and **1** and **3** are 27.84 and 31.58 kcal/mol suggesting that the tautomerization from model **1** to **2** and **3** may be difficult in the ground state. Therefore, the most stable structure corresponds to model **1** with an intramolecular hydrogen bond between the carbonyl and amino groups as discussed in a previous paper.[1]

π-π^* Absorption Spectra of 1-MBPP and 2-MBPP. 1-MBPP, 2-MBPP, isooctane (2,2,4-trimethylpentane), and ethanol were the same as reported previously.[1]

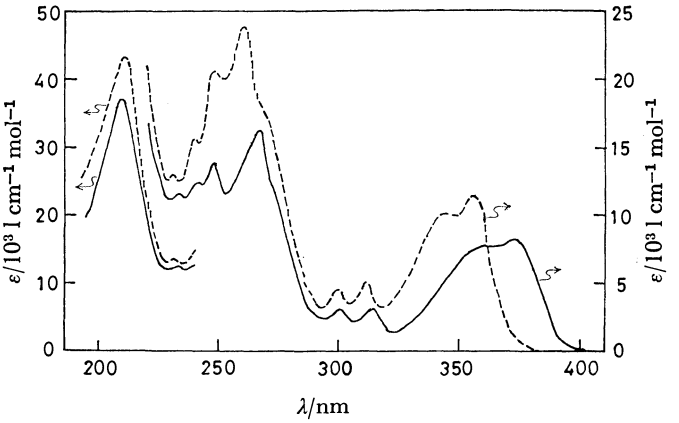

Fig. 1. Absorption spectra of 1-MBPP (——) and 2-MBPP (----) in isooctane solution.

TABLE 1. CALCULATED TRANSITION ENERGIES (E) AND OSCILLATOR STRENGTHS (f) OF THE SINGLET π,π^* EXCITED STATES OF BPP AND THE CORRESPONDING OBSERVED π,π^* BANDS OF 1-MBPP AND 2-MBPP

No.	BPP			1-MBPP		2-MBPP	
	E/eV	λ/nm	f	λ/nm	f	λ/nm	f
1	3.631	342	0.213	374	0.122	356	0.135
2	3.892	319	0.082	315	0.015	311	0.026
3	4.137	300	0.186	303	0.017	299	0.020
4	4.633	268	0.522	266	0.267	263	0.391
5	4.915	252	0.446	248	0.143	243	0.184
6	5.162	240	0.431	242		240	
7	5.284	234	0.411	232		231	
8	5.596	222	0.002				
9	5.699	218	0.095				
10	5.793	214	0.244				
11	5.944	209	0.085	209		210	
12	6.046	205	0.032				
13	6.135	202	0.175				
14	6.198	200	0.141				

The absorption spectra of 1-MBPP and 2-MBPP in isooctane at room temperature are shown in Fig. 1, and the band maxima and corresponding oscillator strengths are listed in Table 1. The first absorption band of 1-MBPP appears at a wavelength longer than that of 2-MBPP. A trend is found in other alkyl compounds (alkyl group: *n*-pentyl-, *n*-nonyl-).[1]

It was necessary to establish whether (1) the first excited state was of π,π^* character or not, and (2) the first absorption band of 1-alkyl compounds appeared at a wavelength longer than that of the 2-alkyl compounds or not. To this end the energies of the

Table 2. The energies of the next highest occupied molecular orbital (NHOMO), the highest occupied molecular orbital (HOMO), and the lowest unoccupied molecular orbital (LUMO) of 1-MBPP, 2-MBPP, and BPP (in a. u.)

MO	1-MBPP	2-MBPP	BPP
NHOMO	−0.4091 (n)	−0.4178 (n)	−0.4238 (n)
HOMO	−0.3930 (π)	−0.4026 (π)	−0.4040 (π)
LUMO	0.0496 (π^*)	0.0522 (π^*)	0.0498 (π^*)

highest occupied and lowest unoccupied π-molecular orbitals and the n-orbitals of BPP, 1-MBPP, and 2-MBPP[1b] were calculated using the CNDO/2 method,[3] results of which are shown in Table 2. It may be seen that the highest occupied MO is of π-character and the next occupied MO is of n-character for the three molecules. These results suggest that the lowest excited state is of π,π^* character and that the n,π^* state may be higher than the first excited π,π^* state.

The absorption spectra of 1- and 2-alkyl benzopyranopyridines are displaced to a wavelength longer by the addition of ethanol[1] and this suggests that the absorption bands may be assigned to the π-π^* transition.

The energy gap between the highest occupied and the lowest unoccupied orbitals of 2-MBPP is larger than that of 1-MBPP and BPP and indicates qualitatively that the lowest π,π^* state of 2-MBPP is higher than that of 1-MBPP, as shown in the absorption spectra in Fig. 1.

The P-P-P SCF-MO-CI method[4-6] was applied to calculate the π-π^* transition energies and corresponding oscillator strengths of BPP. The following empirical parameters were used for the present calculation:

Atom, μ	I_μ/eV	A_μ/eV
C	11.42	0.578
–N=	14.12	1.78
NH_2	27.525	13.435
=O	17.32	2.649
-O-	33.50	11.97

The value −2.10 eV was used for all the resonance integrals, and the Mataga-Nishimoto approximation[6] was adopted for the two-center Coulomb integral. The 36 singly excited configurations were built into the configuration interaction matrix elements. In the present calculation the effect of the intramolecular hydrogen bond was not taken into account.

The calculated transition energies and corresponding oscillator strengths of BPP are listed in Table 1. The calculated directions of the transition moment are shown in Fig. 2 in which the length of the transition moment is proportional to the magnitude of the oscillator strength. Referring to the calculated results in Table 1 and Fig. 2 the assignment of the absorption bands for 1-MBPP and 2-MBPP were made. The band assignments are given in Table 1.

The first band of BPP calculated at 342 nm is mainly polarized along the x axis. The second and third bands are weak and their transition moments are mainly polarized along the y axis as shown in Fig. 2. The bands near 266 nm for 1-MBPP and 263 nm for 2-MBPP correspond to the fourth band of BPP calculated at 268 nm which is polarized along the x axis, and with a relatively strong oscillator strength. The fourth band has a shoulder on the longer-wavelength side, which disappears in alcoholic solution. 2-MBPP has two bands at 240 and 231 nm in isooctane solution. These bands are observable at 241 and 233 nm in ethanol solution. The behavior of the two bands in polar solvents suggests that they belong to the different electronic states. These bands were assigned to the bands calculated at 240 and 234 nm. For 1-MBPP, the corresponding bands at 240 and 231 nm were observed at 242 and 232 nm. The strongest bands of 1-MBPP and 2-MBPP at 209 and 210 nm were tentatively assigned to the remaining transition bands from the eighth to the fourteenth transition band. The total oscillator strengths thus become equal to 0.774.

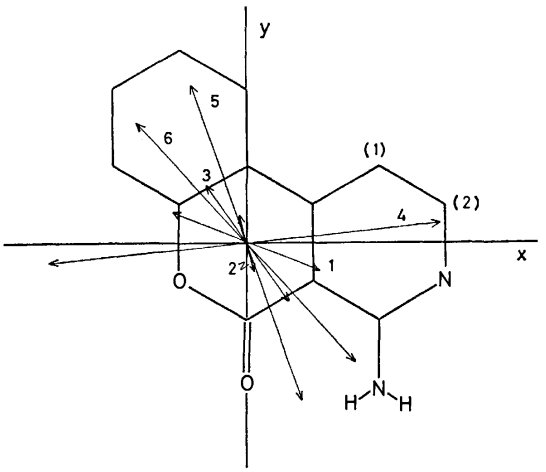

Fig. 2. Polarization directions of six π-π^* transitions in BPP predicted by the P-P-P SCF-MO-CI method.

The authors acknowledge the assistance of the staff of Tokyo Denki University Computing Center in the present work.

References

1) a) A. Fujimoto and K. Inuzuka, *Bull. Chem. Soc. Jpn.*, **51**, 2781 (1978); b) K. Inuzuka and A. Fujimoto, *Bull. Chem. Soc. Jpn.*, **51**, 2786 (1978).

2) a) A. Fujimoto, A. Sakurai, H. Midorikawa, and E. Iwase, *Nippon Kagaku Kaishi*, **1974**, 1; b) A. Fujimoto and H. Hirose, *Bull. Chem. Soc. Jpn.*, **51**, 3377 (1978).

3) J. A. Pople, D. P. Santry, and G. A. Segal, *J. Chem. Phys.*, **43**, 129 (1965); J. A. Pople and G. A. Segal, *ibid.*, **43**, 136 (1965); **44**, 3289 (1966).

4) R. Pariser and R. G. Parr, *J. Chem. Phys.*, **21**, 466, 767 (1953).

5) J. A. Pople, *Trans. Faraday Soc.*, **49**, 1375 (1953).

6) N. Mataga and K. Nishimoto, *Z. Phys. Chem.*, **13**, 140 (1957).

BULLETIN OF THE CHEMICAL SOCIETY OF JAPAN, VOL. 52 (3), 941—942 (1979)

Mechanism of the Ferroelectric Phase Transition in $K_4[Fe(CN)_6]\cdot 3H_2O$ and $K_4[Fe(CN)_6]\cdot 3D_2O$

Masaharu OGUNI, Takasuke MATSUO, Hiroshi SUGA, and Syûzô SEKI*
Department of Chemistry, Faculty of Science, Osaka University, Toyonaka, Osaka 560
(Received September 4, 1978)

Synopsis. Mechanism of the ferroelectric phase transition in potassium hexacyanoferrate trihydrate is discussed from static and dynamic points of view, and a new model is proposed. The model takes into account four states as accessible for a water trimer, instead of two in the earlier model. If the four states were equally probable in the disordered phase, the predicted transition entropy is R ln 4 compatible with the experimental value. It is expected that a glass transition, if possible, occurs at 50—60 K for the model. Since the anomalous heat capacity in this temperature region is effectively zero, the model is consistent with absence of a glass transition. Occupancy fractions of hydrogen sites are given for the earlier and the present models.

There are three aspects of interest in the property of orientationally disordered crystals. First, what is the molecular unit of disorder in the crystal? Second, is the disorder static or dynamic? and if dynamic, how rapid is the molecular reorientation? And third, at what temperature does the disorder change to order? The first and third are equilibrium aspects and can be studied by structural and thermodynamic methods. The second is the kinetic property and has been studied rather independently of the other two by NMR, dielectric and other spectroscopic methods. However, it has been shown recently that precise measurement of the heat capacity, a typical equilibrium property, can be used for study of molecular motion in a number of orientationally disordered crystals including molecular, ionic and hydrogen-bonded crystals.[1] The principle involved here is simple and may be summarized as follows. A relaxational heat-capacity anomaly occurs at the temperature at which the molecular relaxation time becomes comparable with the time required for a single heat-capacity measurement, typically 10^2—10^5 s. An important proviso for the anomaly, glass transition, to be observed is that orientational heat capacity has to be appreciable at that temperature. When such a situation prevails in a stable (as opposed metastable) crystal, formation of a glassy state is an unescapable result. If one does not find a glass transition in a careful measurement of the heat capacity of a substance, one can conclude that molecular reorientation is sufficiently rapid in the relevant temperature range. In this note we shall supplement the previous paper on the calorimetric study[2] of the phase transition in potassium hexacyanoferrate trihydrate $K_4[Fe(CN)_6]\cdot 3H_2O$ and the deuterate analogue in the light of above argument.

Figure 1 reproduces the anomalous heat capacity of $K_4[Fe(CN)_6]\cdot 3H_2O$ and $K_4[Fe(CN)_6]\cdot 3D_2O$. The anomaly extends from the transition temperature (250 K (H_2O), 255 K (D_2O)) down to 110 K. The entropy of transition is 12.4 J K^{-1} mol^{-1} (H_2O) and 14.3

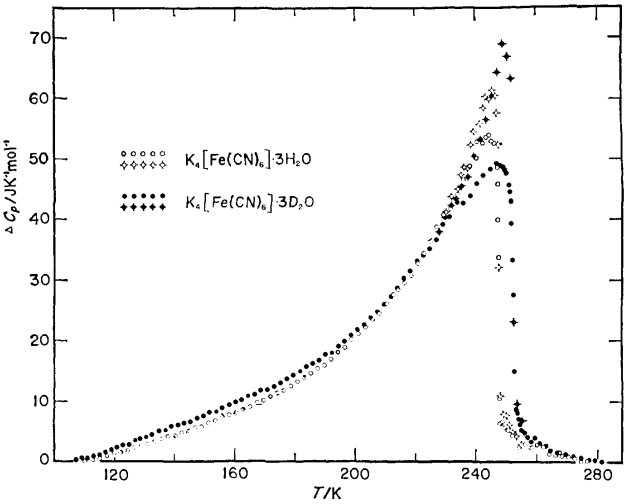

Fig. 1. Anomalous part of heat capacity of $K_4[Fe(CN)_6]\cdot 3H_2O$ and $K_4[Fe(CN)_6]\cdot 3D_2O$.

J K^{-1} mol^{-1} (D_2O) ($\approx R$ ln 4 or more). According to the neutron diffraction,[3] the crystal contains trimers of water molecules. The trimer itself is polar as shown in Fig. 2. It has been suggested that the ferroelectricity originated from the parallel alignment of the polar trimer. This model leads to the transition entropy of R ln 2 ($=5.76$ J K^{-1} mol^{-1}) because there are two orientations for each of the trimer as shown schematically in Figs. 2(a) and (d). The predicted entropy is too small to account for the experimental value.

An alternative model proposed here assumes four states per water trimer. The two states (b) and (c) of Fig. 2 are assumed in addition to the states (a) and (d). The state (a) is symmetry-related to (d) and (b) to (c), but states (a), (d) are not equivalent to (b) or (c). However, all of hydrogen atoms are engaged in hydrogen bonding in any of the four arrangements. Therefore we may neglect difference in their energy for the moment. The transition entropy is Rln4 for this model in agreement with the experiment.

The kinetic aspect of the model is considered next. Clearly the rearrangement from one state to the other proceeds through the reorientation of water molecules, and as such it is related to librational mode of water molecule. The relaxation time of such rearrangement is usually described by Arrhenius expression $\tau=\tau_0\exp(\Delta H_a/RT)$. The pre-exponential factor τ_0 will be of the order of magnitude 10^{-14}—10^{-15} s, since it may be equated to $1/(2\pi\nu)$ where ν is the vibrational frequency of the librational mode. Similar situations were found to be adequate for relaxation times in the glass transitions of orthoboric acid and stannous chloride

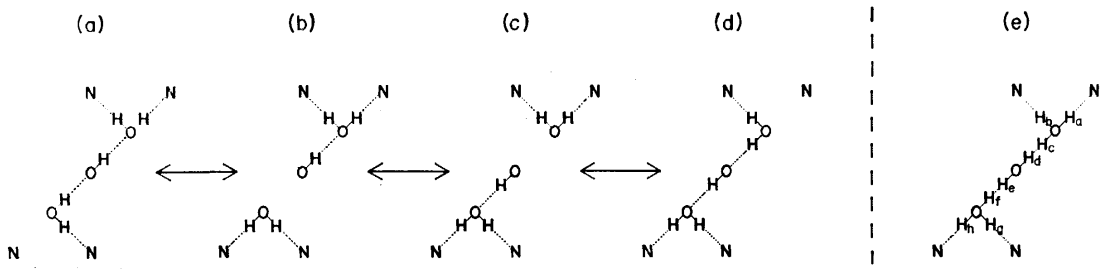

Fig. 2. Arrangements of hydrogen atoms in the hydrogen-bonded system composed of three water molecules and the surrounding nitrogen atoms.

dihydrate crystals.[4,5] The activation enthalpy may be equated to the order of the energy for breaking of the hydrogen bond. The energy of relatively long hydrogen bonds is 15—25 kJ mol^{-1}.[6] Waldstein *et al.*[7] estimated 15 kJ mol^{-1} per bond for the potential barrier hindering the reorientational motion of the molecule in ice. The same value was also found from the thermodynamic study of the glass transition in orthoboric acid crystal.[4] Therefore the activation enthalpy per bond is estimated to be 15—20 kJ mol^{-1} for the present crystals.

If the rearrangement from (a) to (d) in Fig. 2 proceeded through the simultaneous reorientation of three water molecules, then the activation enthalpy for the process would be estimated to be 45—60 kJ mol^{-1}. Since the glass transition takes place when the relaxation time becomes the order of 1 ks, this activation enthalpy corresponds to the glass transition temperature of 140—190 K. Here we took $\tau_0=8\times10^{-15}$ s from experimental value for $SnCl_2\cdot2H_2O$. If this were really the case, the glass transition would have been observed because the configurational contribution to the heat capacity is large enough in this temperature region as shown in Fig. 1. The glass transition, however, was not observed in the actual calorimetric measurement.[2] This indicates that the process assumed above is incorrect.

Next, the alternative model including states (b) and (c) is examined. The process (a)↔(b), (b)↔(c), or (c)↔(d) may be interpreted as the transfer of a Bjerrum L defect. In this case the activation enthaply will be 15—20 kJ mol^{-1} because it involves disruption of only one hydrogen bond. Using the same τ_0 as above one obtains 50—60 K for the glass transition temperature. The glass transition will not be observed in this case because the configurational heat capacity is practically zero at this temperature. This agrees with the experimental result that the glass transition does not occur in this crystal.

At the same time, the assumption that the four states (a)—(d) occur equally probably in the high temperature disordered phase would be reasonable because they all involve one L defect in common. Thus, by allowing the intermediate states (b) and (c) as well as the states (a) and (d) in the disordered phase, one can interpret consistently both the observed entropy of transition and absence of glass transition in this compound. A direct test of the model proposed here, including the validity of the energetical equivalence of the four arrangements, may be obtained from precise determination of the occupancy fraction of the hydrogen sites at different temperatures by neutron diffraction. The symbols H_a, H_b··· in Fig. 2(e) represent hydrogen sites in a water trimer. Now let α, β, γ, δ, ε, ζ, η, and θ denote the occupancy fraction for H_a, H_b, H_c, H_d, H_e, H_f, H_g, and H_h, respectively. If the energy of states (b) and (c) in Fig. 2 were higher in the disordered phase by E than that of (a) and (d), the fraction would be given as follows; $\alpha=\theta=(1/2)[1+2\exp(-E/RT)]\cdot[1+\exp(-E/RT)]^{-1}$, $\beta=\eta=1$, $\gamma=\zeta=(1/2)[1+\exp(-E/RT)]^{-1}$, and $\delta=\varepsilon=1/2$. In the earlier model taking only the states (a) and (d) as accessible into account, $\alpha=\theta=1/2$, $\beta=\eta=1$, $\gamma=\zeta=1/2$, and $\delta=\varepsilon=1/2$ in the disordered phase. In the limiting case of $E=0$, where the four states (a)-(d) in Fig. 2 are allowed equally probably, we obtain $\alpha=\theta=3/4$, $\beta=\eta=1$, $\gamma=\zeta=1/4$, and $\delta=\varepsilon=1/2$. Thus the two models predict different occupation fractions of proton or deuteron in each site. The earlier neutron diffraction data have been analysed *a priori* with $\alpha=\theta=1/2$, $\beta=\eta=1$, $\gamma=\zeta=1/2$, and $\delta=\varepsilon=1/2$. New diffraction experiment as well as reinvestigation of the earlier neutron diffraction data will be interesting because the proposed model is a modification of the half-hydrogen model of hydrogen bonding that has been used so extensively.

References

1) H. Suga and S. Seki, *J. Non-Cryst. Solids*, **16**, 171 (1974).
2) M. Oguni, T. Matsuo, H. Suga, and S. Seki, *Bull. Chem. Soc. Jpn.*, **48**, 379 (1975).
3) J. C. Taylor, M. H. Mueller, and R. H. Hitterman, *Acta Crystallogr., Sect. A*, **26**, 559 (1970).
4) M. Oguni, T. Matsuo, H. Suga, and S. Seki, *Bull. Chem. Soc. Jpn.*, **50**, 825 (1977).
5) T. Matsuo, M. Oguni, H. Suga, and S. Seki, *Bull. Chem. Soc. Jpn.*, **47**, 57 (1974).
6) G. C. Pimentel and A. L. McClellan, "The Hydrogen Bond," W. H. Freeman and Company, San Francisco, (1960) p. 213.
7) P. Waldstein, S. W. Rabideau, and J. A. Jackson, *J. Chem. Phys.*, **41**, 3407 (1964).

Note added in proof

Helwig, Klöpperpieper, and Müser measured recently the spontaneous polarization and heat capacity of $K_4[Fe(CN)_6]\cdot3H_2O$ in a limited temperature range covering the transition point) (*Ferroelectrics*, **18**, 257 (1978)). Their data support our conclusion on a phenomenological level.

BULLETIN OF THE CHEMICAL SOCIETY OF JAPAN, VOL. 52 (3), 943—944 (1979)

Separation of Barium and Radium as Their TTA-complexes by Extraction Chromatography

Kazuo JIN*,† and Toshiyasu KIBA

Department of Chemistry, Faculty of Science, Kanazawa University, Kanazawa, Ishikawa 920

(Received May 26, 1978)

Synopsis. Satisfactory separation of a trace amount of radium from miligram amount of barium was attained on a column of 1.5 M TTA–MIBK (Daiflon) system. An HETP value as low as 0.47 mm was obtained with a column $0.98\phi \times 30$ cm at flow rate of 0.17 cm³ per minute. Distribution ratio of radium estimated from this column technique was compatible with the liquid-liquid extraction data.

Solvent extraction of radium has been investigated in several extraction systems in view of synergistic effect.[1-3] However, no report seems to have appeared on the separation of radium from barium matrix, because of their similar chemical properties. The separation of tracer level radium from barium matrix is desirable in view of not only analytical chemistry but also geochemistry.

Akaza studied the extraction of barium, strontium, calcium, and magnesium with 2-thenoyltrifloworoacetone (TTA)–methyl isobutyl ketone (MIBK),[4,5] the results being extended to extraction chromatography.[5,6] In this note, a further application of the same TTA–MIBK extraction system to radium(II), the extraction chromatographic separation of radium from miligram amounts of barium, and separation of alkaline earth metal ions involving radium are described.

Experimental

Radioactive Tracers. ^{140}Ba ($t_{1/2}=12.8$ d) was used as a tracer of barium. ^{223}Ra ($t_{1/2}=11.68$ d) was obtained from ^{227}Ac by milking.

Batch Extraction of Radium(II) in TTA–MIBK. A buffer solution consisting of 0.5 M ammonium acetate–aqueous ammonia–acetic acid was employed to adjust the pH of the aqueous solution. The final pH of extraction was measured immediately after the two phases had been separated, whereas γ-activity of ^{223}Ra in each phase was counted with a NaI(Tl) scintillation counter 6 h after the separation.

Column Preparation. The column was prepared by the method previously reported.[6] A glass chromatographic column with water jacket was employed to keep the column temperature constant.

Test Solutions and Eluting Solutions. Fifty milliliters of the test solution which has a similar composition to that of eluting solution was used for the column experiment. Eluting solutions were prepared by the method reported.[6]

A fraction collector was employed to collect an adequate fraction of the eluate. In some cases, a microtube pump, Tokyo Rikagakukikai Co., Model MP-11, was used to feed a solution on the column. Tigon tube was employed for solution transport.

† Present address: Department of Chemistry, Faculty of Science, Hokkaido University, Nishi 8-chome, Kita 10-jo, Kita-ku, Sapporo, Hokkaido 060.

Results and Discussion

The extraction of radium as TTA-complex into MIBK was carried out with TTA in various concentrations. The results are shown in Fig. 1. Quantitative extraction was attained at pH 6.5< in 1.5 M TTA–MIBK, these conditions being preferable for the separation of relatively large amounts of alkaline earth metal ions from each other. The half extraction pH ($pH_{1/2}$) of radium(II) could be estimated as 6.0 in the same system, and that of barium as 5.2 from the previous data.[4] Thus, the difference between $pH_{1/2}$ values suggests the possibility of the separation of barium and radium as their TTA-complexes by extraction chromatography.

The separation of alkaline earth metal ions involving radium(II) was carried out on a 1.5 M TTA–MIBK column ($0.98\phi \times 19$ cm). The results are shown in Fig. 2. First, radium and barium were eluted with a solution of pH 6.5, giving some overlapping of two elution curves, secondly, strontium and calcium were eluted with a solution of pH 5.5, and finally magnesium with 0.1 M hydrochloric acid. The concentration of each metal ion in each fraction was determined by γ-counting for radium and barium and by atomic absorption spectrophotometry for strontium, calcium and magnesium, respectively. The results, except for radium, are in line with those reported.[5] ^{140}La was caught firmly on the column and eluted down together with magnesium (Fig. 2).

In order to achieve complete separation between radium and barium, the column was replaced by a longer one ($0.98\phi \times 30$ cm, $0.98\phi \times 40$ cm, and $0.97\phi \times 42$ cm). Figure 3 shows the results obtained.

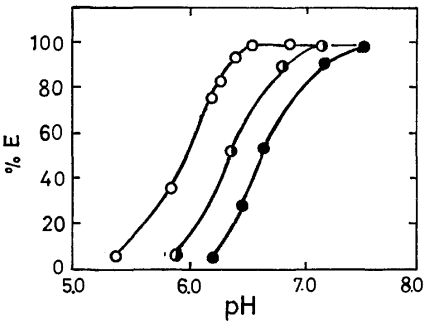

Fig. 1. Extraction curves of radium(II) with TTA in MIBK.
Aqueous phase: 10 cm³ of 0.5 M buffer solution, organic phase: 10 cm³, 1.5 M TTA-MIBK —○— 0.5 M TTA-MIBK —◑— 0.2 M TTA-MIBK —●—, shaking time: 30 min.

Table 1. Performance of the 1.5 M TTA-MIBK column

Column	Column size		D(pH 6.7)	N	HETP (mm)
(a)	0.98ϕ×30 cm	Ra	51±3	650±30	0.47±0.02
		Ba[a)]	126±5	840±40	0.36±0.03
(b)	0.98ϕ×40 cm	Ra	44±2	675±30	0.59±0.02
		Ba[a)]	93±5	773±40	0.52±0.03
(c)	0.97ϕ×42 cm	Ra	48±2	560±30	0.75±0.02
		Ba[b)]	105±5	815±40	0.52±0.03

Void volum; (a) 9±2 cm³, (b), (c) 12±2 cm³. a) Ba 0.5 mg. b) Ba 5.0 mg.

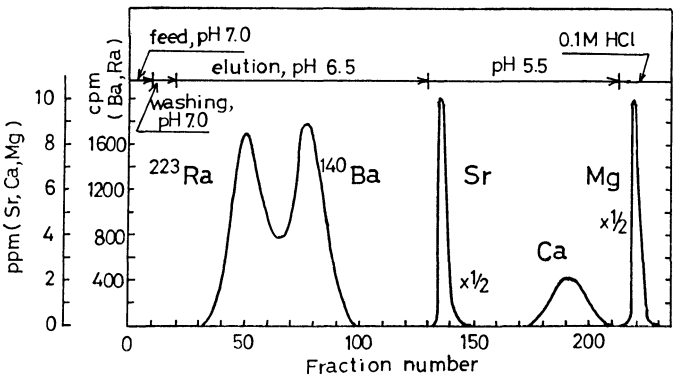

Fig. 2. Separation of alkaline earth metal ions on 1.5 M TTA-MIBK column.
Metal, loaded: 0.5 mg each (except radium), Daiflon: 5.5 g, one fraction: 5.0 g stationary phase: 7.8 cm³, temp: 20±1 °C column size: 1.0ϕ×19 cm flow rate; feed and washing: 0.2—0.3 cm³·min⁻¹ elution: 0.5 cm³·min⁻¹.

A test solution of pH 7.5 and an eluting solution of pH 6.7 were used, the flow rate of elution being 0.17-cm³ min⁻¹. Under these conditions excellent separation of trace radium(II) could be achieved from 0.5 mg, of barium(II) (Figs. 3 (a) and (b)), and also from 5.0 mg of barium(II) (Fig. 3 (3)). From these column experiments, distribution ratios of radium and barium ions were estimated (Table 1) by the well-known relation of $D=(E-F)/B$, where E is the volume of effluent in relation to the maximum of the eluted metal concentration, F the void volume of the column, and B the volume of the stationaly phase. The distribution ratio of radium shown as 44, 48, and 51 in Table 1 is somewhat large, but roughly compatible with the value 30 obtained in the liquid-liquid extraction under the same extraction pH. In order to elucidate the performance of extraction column in Fig. 3, a number of theoretical plates of column (N) and height equivalent to a theoretical plate (HETP) were estimated. N is given by the equation $N=E(E-F)/S^2$, where S is half width (ml) at 0.607 peak maximum. HETP is given by the column length divided by N. Thus the HETP value as low as 0.47 mm could be maintained on the column 0.98ϕ×30 cm long.

The elution of alkaline earth metal ions proceeds in the order of light element in conventional cation-exchange chromatography. However, elution takes place in the reversed order in extraction chromatography. Thus, the latter is appropriate for a precise

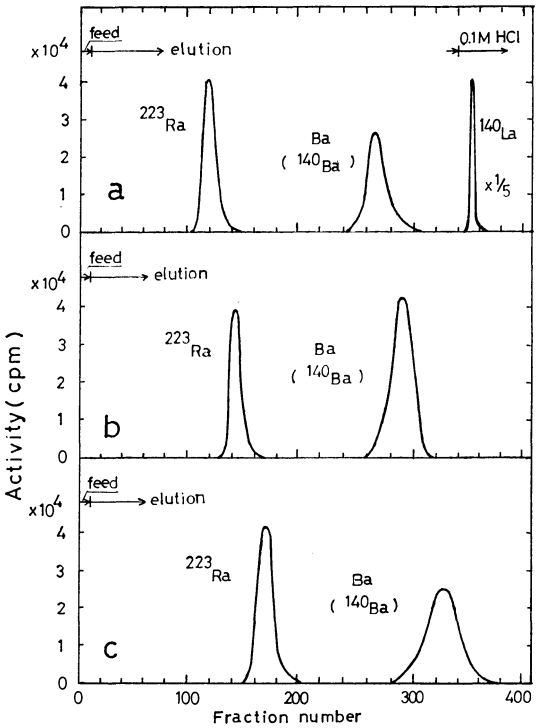

Fig. 3. Separation of barium and radium on 1.5 M TTA-MIBK column.
One fraction: 5.0 cm³, temp: 18±1 °C flow rate; feed: 0.1 cm³·min⁻¹, pH 7.5 elution: 0.17 cm³·min⁻¹, pH 6.7
(a) Column size: 0.98ϕ×30 cm, barium loaded: 0.5 mg Daiflon: 9.0 g, stationary phase 10.4 cm³,
(b) column size: 0.98ϕ×40 cm, barium, loaded: 0.5 mg Daiflon: 12.0 g, stationary phase 15 cm³,
(c) column size: 0.97ϕ×42 cm, barium loaded: 15.0 mg Daiflon: 12.0 g, stationary phase 15 cm³.

and delicate separation of trace amount of radium from other alkaline earth metals or barium matrix.

References

1) T. Sekine, Y. Kawashima, T. Unnai, and M. Sakairi, *Bull. Chem. Soc. Jpn.*, **41**, 3013 (1968).
2) F. Sebesta and B. Havilik, *J. Radioanal. Chem.*, **24**, 337 (1975).
3) A. F. Ghose, F. Sevesta, and J. Stary, *J. Radioanal. Chem.*, **24**, 337 (1975).
4) I. Akaza, *Bull. Chem. Soc. Jpn.*, **39**, 971 (1966).
5) I. Akaza, *Bull. Chem. Soc. Jpn.*, **39**, 980 (1966).
6) I. Akaza, T. Tajima, and T. Kiba, *Bull. Chem. Soc. Jpn.*, **46**, 1199 (1973).

BULLETIN OF THE CHEMICAL SOCIETY OF JAPAN, VOL. 52 (3), 945—946 (1979)

Super High Sensitivity of CuSe–Ag_2S Solid Membrane Copper(II) Ion Selective Electrode in Several Metal Buffer Solutions

Yoshio UMEZAWA,* Yuichiro IMANISHI, Katsuhiko SAWATARI, and Shizuo FUJIWARA

Department of Chemistry, Faculty of Science, The University of Tokyo, Hongo, Tokyo 113

(Received July 11, 1978)

Synopsis. A CuSe–Ag_2S solid membrane Cu(II) ion electrode in certain metal buffer solutions gave detection limit of free Cu(II) ion as low as 10^{-18}M.

Nakagawa and his coworkers observed extremely high sensitivity of copper(II) ion selective electrodes-(ISE) in metal buffer solutions with the use of a CuS–Ag_2S solid membrane.[1] Similar phenomena have also been observed with the same type of electrodes by Ishibashi and Jyo.[2] It has been believed that the actual sensitivity of a cupric ion selective electrode is determined by the residual concentration of Cu(II) and Ag(I) ions at the interface.[3] Therefore, if we can lower this residual concentration as low as possible by complex formation of Cu(II) and Ag(I) ions with added ligand species, the concentration of the detection limit of the electrode may possibly be descreased. However, an inherent reaction of solid membrane itself with ligand species was found to be taken into consideration.[1] Unwanted reactions between the solid membrane and solution species may cause slow and unstable response of the ISE.

In the present study, the effect of several ligand species on the response of a CuSe–Ag_2S solid membrane Cu(II) ISE was studied with a view to examine whether or not similar phenomenon to CuS–Ag_2S is observed even with the different solid membrane material in order to generalize the behavior of the ISE in metal buffer solutions.

Experimental

The solid membrane used for a Cu(II) ISE is of CuSe–Ag_2S, where the ratio of CuSe to Ag_2S is several %. A reference used is an Ag/AgCl electrode of TOA Dempa Co. Water used is deionized and distilled. Chemicals were of analytical reagent grade. The electrochemical cell assembly employed is as follows:

$$\text{CuSe–Ag}_2\text{S} \;\Big|\; \begin{matrix}\text{Test solution}\\ \mu=0.1(\text{NaNO}_3)\end{matrix} \;\Big|\; \text{KCl(sat.)} \;\Big|\; \text{AgCl} \;\Big|\; \text{Ag}$$

Potential-time profiles of the ISE were recorded using an on-line computer controlled ISE measuring system described elsewhere,[4] where the potential from the electrode is first converted into frequency in order to increase the precision of the voltage measurement. The response time for the electrode is slowed down appreciably upon addition of certain types of ligand species in aqueous Cu(II) solution. Therefore, we employed 30 minutes waiting time for the measurement of an equilibrium potential. By doing so, the equilibrium is nearly attained in most cases except for the case of EDTA. The measurement was performed in a room thermostated at 20±0.5 °C. The solution was stirred with a magnetic stirrer.

Procedure

The procedure employed is as follows : First of all, an empirical relation between the Cu(II) concentration and the observed frequency (potential) is obtained through the calibration curve in standard Cu(II) solution,

$$f = 3.16461 \log[\text{Cu}] + 39.7125 \quad (\text{kHz}), \qquad (1)$$

where f is the frequency which is one to one equivalent to the observed potential, and [Cu] the activity of Cu(II) solution. With the use of Eq. 1, the activity of Cu(II) ion [Cu] was calculated from the observed potential values of the Cu(II) ISE in each ligand solution. Values thus obtained are compared with the theoretical one, where the latter is simply calculated from β_n through the relations as follows :

$$\frac{[\text{CuL}_n]}{[\text{Cu}][\text{L}]^n} = \beta_n,$$

$$p[\text{Cu}] = \log\beta_n + n\log[\text{L}] - \log[\text{CuL}_n],$$

$$[\text{L}] = \frac{C_\text{L}}{\alpha_{\text{L(H)}}},$$

where [L] is a function of pH and is obtained using the total concentration of the ligand C_L, and the side reaction coefficient $\alpha_{\text{L(H)}}$ which is calculated from the concentration of proton ion in the solution and the acid dissociation constants of the ligand(1,5).

Results and Discussion

In Table 1, the extremely low activity of Cu(II) ions determined by the response of a CuSe–Ag_2S Cu(II) ISE is compared with those calculated using the reported data of stability constants of Cu(II) complexes in each ligand. In most cases except EDTA, the agreement is fairly well indicating that the copper(II) ISE of the present study is actually responding to such low activities as 10^{-15} M, for example, of free Cu(II) ions. This result is to be compared with similar results obtained by Nakagawa *et al.*, where CuS–Ag_2S is used instead of CuSe–Ag_2S for the cupric ion selective electrode. In the case of EDTA as a ligand, the agreement is not good, probably due to some unknown reactions between the CuSe–Ag_2S solid membrane itself and EDTA molecules. This is partly supported by the result in Fig. 1 where the potential-time profile for the copper(II) ISE in 1×10^{-3} M Cu(II) aqueous solution is extremely slowed down by the addition of certain amount of EDTA, indicating the non-equilibrium reaction, if any, between EDTA and solid membrane material itself. Appa-

Table 1. Extremely low activities of Cu(II) ions obtained by CuSe-Ag_2S solid membrane Cu(II) ion selective electrode

	C_{Cu}	C_L	pH	Cu(II) calculated from $\beta_n(\mu=0.1)$	$\log \beta_n$[a)]	Cu(II) observed
en	1.01×10^{-3} M	4.24×10^{-3} M	10.47	8.5×10^{-19} M	19.72 (β_2)	5.4×10^{-18} M
NH_3	1.01×10^{-3} M	6.8×10^{-1} M	11.41	2.9×10^{-16} M	13.23 (β_4)	4.6×10^{-16} M
bpy	9.94×10^{-4} M	1.00×10^{-3} M	5.47	1.0×10^{-5} M	8.00 (β_1)	1.4×10^{-5} M
bpy	1.01×10^{-3} M	4.30×10^{-3} M	6.30	4.1×10^{-12} M	17.08 (β_3)	1.1×10^{-13} M
edta2Na	1.02×10^{-3} M	2.01×10^{-3} M	3.08	2.4×10^{-19} M	18.80 (β_1)	7.5×10^{-9} M

a) Taken from Ref. 5. Abbreviations: en; ethylenediamine, NH_3; ammonia, bpy; α,α'-bipyridine, edta; ethylenediaminetetraacetic acid.

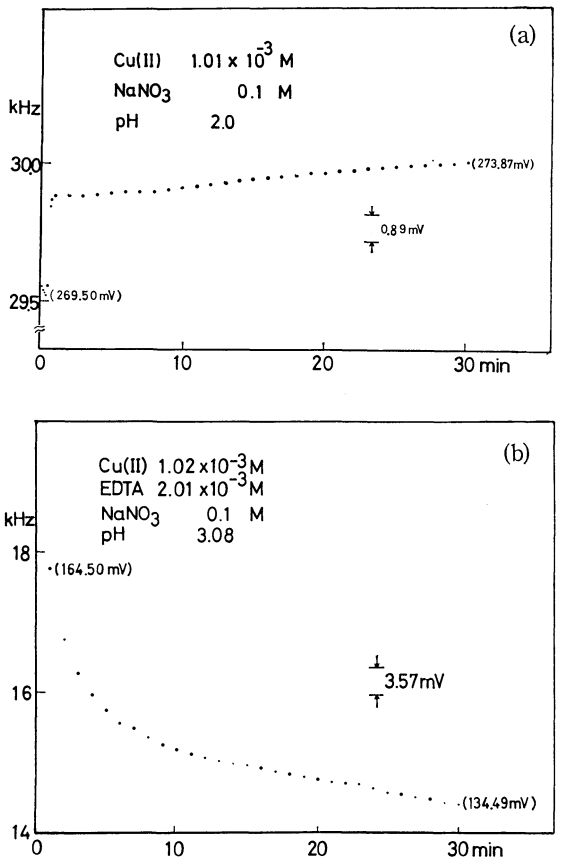

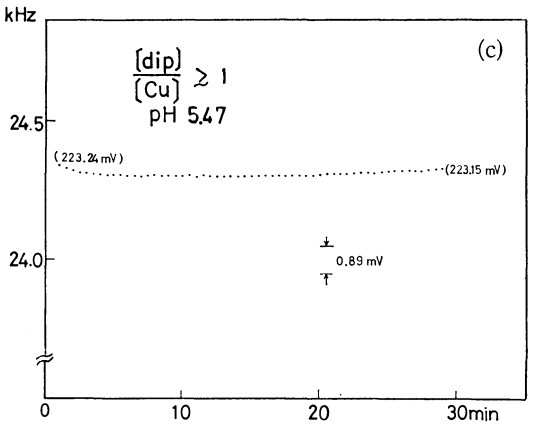

Fig. 1. Potential(Frequency)-time profiles of a CuSe-Ag_2S solid membrane Cu(II) ion selective electrode in different buffer solutions.
(a) Cu(II) ion 1.01×10^{-3} M, $NaNO_3$ 0.1 M, pH 2.0.
(b) Cu(II) ion 1.02×10^{-3} M, edta·2Na 2.01×10^{-3} M, $NaNO_3$ 0.1 M, pH 3.08.
(c) Cu(II) ion 0.99×10^{-3} M, bpy 1.00×10^{-3} M, $NaNO_3$ 0.1 M, pH 5.47.
Frequency f in kHz is equivalent to the potential E in mV as the following : $E=8.9287f+5.9184\pm2.679\times10^{-1}$.

rently, this reaction does not seem to have reached equilibrium during 30 min waiting time (Fig. 1). Also, it is interesting to note that although the activity of Cu(II) ion is generally decreased with the addition of any ligand species, the resulting response time is not necessarily slowed down and is specific to the kind of ligand species as shown in Fig. 1. Therefore, the reason why the response time is slowed down only in certain types of ligand species is attributed to some specific interaction of unknown nature between the ligand species and solid membrane materials rather than simply being due to the decrease in the activity of Cu(II) ions.

In conclusion, the CuSe–Ag_2S solid membrane electrode responds similar manner to the CuS–Ag_2S electrode in that both electrodes have the detection limit well lower than 10^{-15} M of Cu(II) ion activity in certain metal buffer solutions. Also, the response time in extremely low activity solution is not necessarily slow and is dependent on some specific chemical interaction between the ligand species and the solid membrane materials.

The authors thank Kayoko Umezawa for calculating the data.

References

1) G. Nakagawa, H. Wada, and T. Hayakawa, *Bull. Chem. Soc. Jpn.*, **48**, 424 (1975).
2) N. Ishibashi and A. Jyo, Private communication.
3) A. Jyo, *Bunseki*, **12**, 849 (1976).
4) K. Sawatari, Y. Imanishi, Y. Umezawa, and S. Fujiwara, *Bunseki Kagaku*, **27**, 180 (1978).
5) L. G. Sillen and A. E. Martell, "Stability Constants of Metal Ion Complexes," The Chemical Society, London (1964).

BULLETIN OF THE CHEMICAL SOCIETY OF JAPAN, VOL. 52 (3), 947—948 (1979)

Crystallographic Properties of $Ca_2Fe_2O_5$. Difference in Crystallographic Properties of Brownmillerite-like Compounds, $Ca_2Fe_2O_5$ and $Sr_2Fe_2O_5$, at Elevated Temperatures

Shigemitsu SHIN,* Michiko YONEMURA, and Hiroyuki IKAWA†

National Chemical Laboratory for Industry, Mita, Meguro-ku, Tokyo 153

†*Faculty of Technology, Tokyo Institute of Technology, O-okayama, Meguro-ku, Tokyo 152*

(Received September 27, 1978)

Synopsis. High-temperature X-ray diffraction analysis has revealed that $Ca_2Fe_2O_5$ remains in the original brownmillerite-like form up to *ca.* 1100 °C, whereas $Sr_2Fe_2O_5$ changes in crystal structure from brownmillerite to anion-deficient perovskite, without a change in oxygen content, above 700 °C.

It has been reported that $Sr_2Fe_2O_5$ has a cubic perovskite structure, without any change in the oxygen content, above 700 °C, whereas at room temperature this compound has an orthorhombic brownmillerite(Ca_2AlFeO_5)-like structure.[1] It has also been reported that the calcium analogue, $Ca_2Fe_2O_5$, is another brownmillerite-like compound at room temperature.[2] The crystallographic affinity between both compounds at room temperature has assumed that $Ca_2Fe_2O_5$ also has a cubic perovskite structure with the oxygen vacancies statistically disordered at elevated temperature. In this paper the existence of an oxygen-deficient perovskite phase for $Ca_2Fe_2O_5$ at elevated temperature has been examined by means of high-temperature X-ray diffraction techniques. The results have been discussed in connection with the oxygen pressure effect on the preparation of Fe^{4+}-bearing perovskites, $CaFeO_3$ and $SrFeO_3$.

Experimental

Dicalcium diiron(III) pentoxide $Ca_2Fe_2O_5$ was prepared by firing the appropriate mixture of $CaCO_3$ and α-Fe_2O_3 in air at 1200 °C, with intermediate regrinding and refiring until a single phase product was obtained. Subsequently, the powder sample of composition $Ca_2Fe_2O_5$ was mounted on a platinum specimen holder in a high-temperature X-ray diffractometer. The X-ray measurement conditions and the calculation of the lattice parameters were the same as described in Ref. 1.

Results and Discussion

The brownmillerite-like structure is referred to as an "ordered" oxygen-deficient perovskite structure.[3] Therefore, there is a crystallographic relation between the orthorhombic brownmillerite-like structure and an ideal perovskite structure with cubic symmetry as follows : $a \simeq \sqrt{2}\,a_0$, $b \simeq 4a_0$, and $c \simeq \sqrt{2}\,a_0$, where a, b, and c are the lattice constants of a brownmillerite-like phase and a_0 that for an ideal perovskite phase. On this basis new lattice parameters can be defined, a', b', and c', for the dample $Ca_2Fe_2O_5$, where the three lattice constants have such a crystallographic relationship with the original orthorhombic cell constants, a, b, and c, as $a'=a/\sqrt{2}$, $b'=b/4$, and $c'=c/\sqrt{2}$.

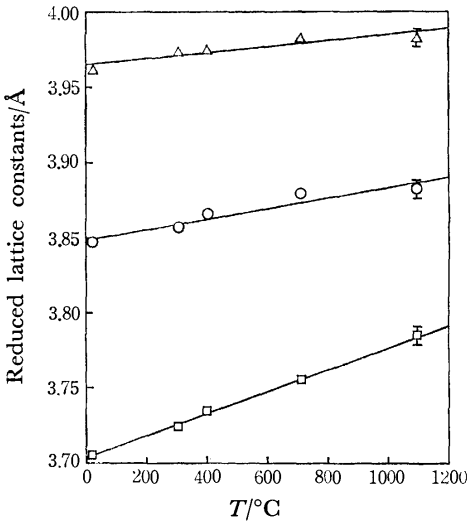

Fig. 1. Plots of reduced orthorhombic lattice constants *vs.* temperature for $Ca_2Fe_2O_5$.
△ : a′-axis, □ : b′-axis, ○ : c′-axis.

Figure 1 illustrates the reduced lattice constants of the sample of composition $Ca_2Fe_2O_5$ as a function of temperature. It may be seen that the three axes, a', b', and c', expand linearly with increase in temperature in the range of temperature from 20 to 1093 °C, and that the three lines do not intersect. In other words, $Ca_2Fe_2O_5$ does not exist as a statistically disordered oxygen-deficient perovskite structure, but remains as a brownmillerite-like phase even at elevated temperatures. This result is quite different from that of $Sr_2Fe_2O_5$ obtained in a previous work.[1]

For diiron(III) distrontium pentoxide, the a'-axis of the reduced cell begins to shrink at around 335 °C, and at 700 °C the three axes of the reduced orthorhombic cell meet, and consequently, the compound transforms to a cubic anion-deficient perovskite phase at temperatures above 700 °C (see Fig. 2, Ref. 1). From this it has been concluded that the oxygen atoms arranged regularly in the brownmillerite-like lattice begin abnormal thermal movement at around 335 °C. At 700 °C, a complete phase transition takes place as a result of the random displacement of the oxygen atoms or the vacancies throughout the oxygen lattice sites in the perovskite structure.

It is evident that the difference in movement of the oxygen ions at elevated temperatures between dicalcium and distrontium diiron(III) pentoxides is caused by differences in chemical composition between the double oxides, although the essential reason remains unclarified. The calcium ion has a smaller ionic radius

than the Sr ion, so that the electrostatic binding energy must be higher in the Ca–O bonds than in the Sr–O bonds, as implied by the melting point of CaO. This assumption may be valid for the brownmillerite-like structure. In the brownmillerite-like structure, complete rows of oxygens are regularly missing from the ideal perovskite structure, and the accompanying movements of atoms result in tetrahedral coordination of the Fe atoms, and eight- or ninefold coordination about the alkaline-earth metal atoms, not twelvefold as in perovskite.[3] Consequently, the transition of $A_2Fe_2O_5$ (A=Ca or Sr) from brownmillerite-like structure to perovskite structure must be accompanied by a breaking of the A–O bonds and rearrangement of the component atoms. Therefore, it is reasonable to speculate that the binding energy of the Ca–O bonds in $Ca_2Fe_2O_5$ is so high that cleavage is difficult, so that $Ca_2Fe_2O_5$ is not transformed to an anion-deficient perovskite structure.

The experimental results and conclusions obtained in this work may explain why $CaFeO_3$ can only be synthesized under ultra high oxygen pressures[4] whereas $SrFeO_3$ can be readily prepared under less rigorous conditions,[5,6] *i.e.*, the energy necessary to break the Ca–O bonds in $Ca_2Fe_2O_5$ to yield $CaFeO_3$ by oxidizing the iron atoms from Fe^{3+} up to Fe^{4+} is higher than that which is necessary for $Sr_2Fe_2O_5$.

The authors wish to express their thanks to Professor S. Udagawa at Tokyo Institute of Technology for his interest and support in this work.

References

1) S. Shin, M. Yonemura, and H. Ikawa, *Mater. Res. Bull.*, **13**, 1017 (1978).

2) E. F. Bertaut, P. Blum, and A. Sagnières, *Acta Crystallogr.*, **12**, 149 (1959).

3) A. D. Wadsley, "Non-stoichiometric Compounds," ed by L. Mandelcorn, Academic Press, New York and London (1964), p. 135.

4) F. Kanamaru, H. Miyamoto, Y. Mimura, M. Koizumi, M. Shimada, S. Kume, and S. Shin, *Mater. Res. Bull.*, **5**, 257 (1970).

5) J. B. MacChesney, R. C. Sherwood, and J. F. Potter, *J. Chem. Phys.*, **43**, 1907 (1965).

6) S. Shin, F. Kanamaru, S. Kume, and M. Koizumi, "Reactivity of Solids," ed by J. W. Mitchell, R. C. DeVries, R. W. Roberts, and P. Cannon, Wiley Interscience, New York (1969), p. 837.

BULLETIN OF THE CHEMICAL SOCIETY OF JAPAN, VOL. 52 (3), 949—950 (1979)

Stereospecific Synthesis of D-Isothreonine from L-Threonine[1)]

Yasuyuki SHIMOHIGASHI, Michinori WAKI, and Nobuo IZUMIYA*

Laboratory of Biochemistry, Faculty of Science, Kyushu University 33, Higashi-ku, Fukuoka 812

(Received December 23, 1977)

Synopsis. D-Isothreonine, (2*R*,3*S*)-3-amino-2-hydroxybutanoic acid (**4**), was readily prepared by the ammonolysis of optically active 2-bromo-3-hydroxybutanoic acid derived from L-threonine. The configuration of **4** was deduced from the shift of molecular rotation, Cotton effect in ORD curve of **4**, and NMR measurement of its oxazolidone derivative.

In recent years α-hydroxy β-amino carboxylic acids have been found in nature as constituent amino acids of biologically active peptides; L-isoserine[2)] in an antibiotic, edeine, and (2*S*,3*R*)-3-amino-2-hydroxy-4-phenylbutanoic acid[3)] in an aminopeptidase B inhibitor, bestatin. However, the syntheses of these optically active α-hydroxy β-amino carboxylic acids are tedious. L-Isoserine was prepared by optical resolution[4)] or through three steps starting from L-asparagine.[5)]

This paper deals with a convenient method of preparation of such optically active α-hydroxy β-amino carboxylic acids as exemplified by the first synthesis of (2*R*,3*S*)-3-amino-2-hydroxybutanoic acid (D-isothreonine)[6)] (**4**) through two steps starting from L-threonine (**1**).

It is known that racemic α-halo β-hydroxy carboxylic acids are converted by the action of ammonia into racemic α-hydroxy β-amino carboxylic acids, α-amino β-hydroxy carboxylic acids, or a mixture of the two.[7–9)] For the amination reactions Carter and Zirkle[8)] and Neuberg and Mayer[10)] proposed possible α,β-epoxy carboxylic acid intermediates. In fact, Liwschitz *et al.*[11)] prepared DL-*threo*-2-hydroxy-3-aminobutanoic acid without formation of *erythro* form by the reaction of racemic *cis*-2,3-epoxybutanoic acid with amine. The closure and opening of epoxide ring accompany an inversion of the configuration of carbon atom attacked by nucleophiles.[12,13)] Thus we assumed that optically active α-hydroxy β-amino carboxylic acids could be stereospecifically prepared from optically active α-halo β-hydroxy carboxylic acids. In order to confirm the prediction we attempted a simple preparation of **4** through the amination reaction of (2*S*,3*R*)-2-bromo-3-hydroxybutanoic acid (**2**) derived from **1** (Scheme 1).

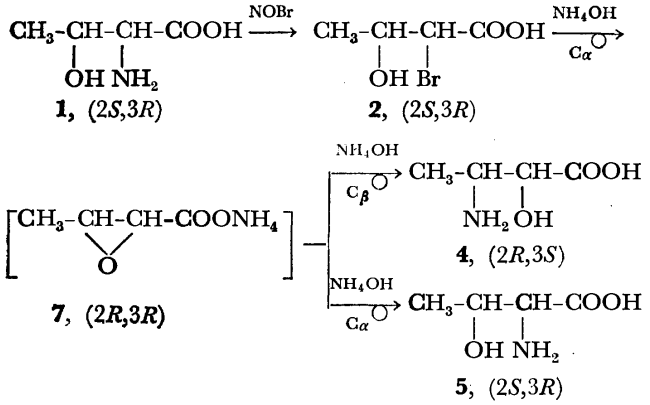

Scheme 1. Stereochemical reaction route.

Compound **2** was prepared by the action of nitrosyl bromide on **1**. This reaction is known to proceed with retention of the configuration of C_α.[14)] Treatment of **2** with 28% aqueous ammonia afforded a mixture of isothreonine and threonine (92 : 8). The mixture was separated into each component by column chromatography on Dowex 50X8 (NH_4^+ form).

The configuration of C_α atom of isolated isothreonine (**4**) was confirmed to be 2*R* by the negative shift in molecular rotation on acidification[15)] and the negative Cotton effect in the region 200—240 nm.[16)] In order to determine the configuration of C_β atom of **4**, we measured the ^{1}H-NMR spectrum of 2-oxazolidone derivative (**6**) of **4**. The coupling constants ($J_{\alpha\beta}$) between the vicinal methine protons of the oxazolidone derivatives of α-amino β-hydroxy carboxylic acids are reported to be 5.0±1.0 Hz for *threo* and 9.6±0.6 Hz for *erythro* isomers in CD_3OD.[17)] Those of α-hydroxy β-amino carboxylic acids are also reported to be 4.0 Hz for *threo* and 9.0 Hz for *erythro* isomers in CD_3OD.[3)] NMR spectrum of **6** was recorded in DMSO-d_6 because of its insolubility in CD_3OD, $J_{\alpha\beta}$ value of **6** being 5.0 Hz. $J_{\alpha\beta}$ values of reference oxazolidone derivatives of L-threonine (*threo*) and L-allothreonine (*erythro*) were 4.8 and 8.5 Hz in DMSO-d_6, respectively. The values in DMSO-d_6 are almost equal to those for *threo* and *erythro* in CD_3OD, respectively. These results suggest that the configuration of **4** should be *threo* form (2*R*, 3*S*). Thus the prediction (Scheme 1) was confirmed by the first synthesis of optically active isothreonine **4**.

In a similar manner D-isoserine, (2*R*)-3-amino-2-hydroxypropanoic acid (**8**), was prepared from L-serine in optically pure state. On the basis of this fact and the result obtained by Liwschitz *et al.*,[11)] we assume that **4** should be optically pure as regards both C_α and C_β.

Experimental

The following solvent systems were used: R_f^1, pyridine–H_2O (65 : 35, v/v) for TLC and R_f^2, cyclohexylamine–H_2O–methyl ethyl ketone–*n*-BuOH (2 : 5 : 10 : 10, v/v) for paper chromatography. ^{1}H-NMR spectra were measured with a Hitachi R-20B spectrometer (60 MHz), using sodium 3-trimethylsilyl-1-propanesulfonate in D_2O or tetramethylsilane in DMSO-d_6 as an internal standard.

Synthesis of D-*Ith* (**4**). *(2S,3R)-2-Bromo-3-hydroxybutanoic Acid* (**2**): This was prepared from L-Thr (5.95 g, 50 mmol), KBr (20.9 g, 175 mmol) and sodium nitrite (5.58 g, 80 mmol) in 1.25 M H_2SO_4 (105 ml) according to the procedure of Izumiya;[18)] yield of an oil, 8.27 g (90%); R_f^1 0.64.

Mixture (**3**) *of Ith and Thr*: Compound **2** (8.20 g, 45 mmol) was dissolved in 28% aqueous ammonia (82 ml) at

0 °C. After being left to stand for 10 d at 0 °C, the solution was evaporated and the residual solid was dissolved in a small amount of water. The solution was applied on a column (2.2×20 cm) of Dowex 50X8 (H^+ form), and the column was washed with water and eluated with 2 M NH_4OH (100 ml). The eluate was evaporated and the yellowish residue was collected; yield, 2.40 g (45%); R_f^1 0.43 (major) and 0.70 (minor); R_f^2 0.40 (major), 0.56 (minor) and 0.45 (faint). R_fs of reference compounds: L-Thr, R_f^1 0.70, R_f^2 0.56; L-aThr, R_f^1 0.70, R_f^2 0.45. The ratio of major to minor component in **3** was determined as 92 : 8 based on the chromatogram of **3** on an amino acid analyzer.

D-*Ith* (*4*): The mixture (**3**) (1.0 g) was chromatographed with Dowex 50X8 (NH_4^+ form) under the following conditions: column, 1.8×80 cm; buffer, 0.2 M ammonium acetate in 40% MeOH at pH 3.50; flow rate, 14 ml/h. The eluate (340—580 ml) was collected and evaporated to a small volume. The solution was applied on a column (1.0×10 cm) of Dowex 50X8 (H^+ form). The column was washed with water and eluated with 2 M NH_4OH (30 ml). The eluate was evaporated and the residue was crystallized from H_2O–EtOH; yield, 0.69 g (31% from **1**); mp 215—216 °C (dec); $[\alpha]_D^{20}$ +23.5° (*c* 2, H_2O), +5.5° (*c* 2, 5 M HCl). NMR (D_2O) δ: 4.01 (1H, d, J=5.0 Hz, H-2), 3.54 (1H, m, H-3), 1.31 (3H, d, J=6.7 Hz, CH_3).

Found: C, 40.12; H, 7.53; N, 11.67%. Calcd for $C_4H_9NO_3$: C, 40.33; H, 7.62; N, 11.76%.

Determination of the Configuration of ***4***. *Configuration of* C_α: The molecular rotation values of **4** were calculated as +6.6° (5 M HCl) and +28.0° (H_2O) based on the observed optical rotation values at D-line. Thus the shift value in the molecular rotation of **4** on acidification is −21.4°. ORD spectrum of **4** was obtained with a JASCO spectropolarimeter model ORD-CD/UV-5 in 0.5 M HCl. The value of the specific rotation at minimum absorption (220 nm) was −900°.

Configuration of C_β: According to the procedure of Futagawa *et al.*[17] **4** (100 mg) was converted into its 2-oxazolidone derivative (**6**) by treatment with phosgene. The obtained oil (**6**) was dissolved in DMSO-d_6 and the solution was directly analyzed by NMR. The coupling constant of the vicinal methine protons was 5.0 Hz. Those of the oxazolidones derived from L-Thr and L-aThr were 4.8 Hz and 8.5 Hz in DMSO-d_6, respectively.

Synthesis of D-*Ise* (*8*). Compound **8** was prepared from L-Ser after bromination, ammonolysis and chromatographic separation in a similar manner to that used for **4**; yield, 58% from L-Ser; mp 197—199 °C (dec); $[\alpha]_D^{20}$ +32.0° (*c* 2, H_2O), +17.6° (*c* 2, 5 M HCl). NMR(D_2O) δ: 4.24 (1H, dd, J=7.6, 4.8 Hz, H-1), 3.40 (1H, dd, J=13.0, 4.8 Hz, H-2), 3.08 (1H, dd, J=13.0, 7.6 Hz, H-2). R_fs on TLC and paper chromatography of **8** were identical with those of DL-Ise prepared by the procedure of Gundermann and Holtmann.[19] Reported values for D-Ise;[4] mp 199—201 °C (dec); $[\alpha]_D$ +32.4° (*c* 10, H_2O).

Found: C, 34.03; H, 6.83; N, 13.21%. Calcd for $C_3H_7NO_3$: C, 34.28; H, 6.72; N, 13.33%.

We thank Prof. T. Yoshino and Mr. T. Shinmyozu, Kyushu University, for their ^{1}H-NMR measurements.

References

1) Presented at the 30th National Meeting of the Chemical Society of Japan, Osaka, April 1974.
2) G. Roncari, Z. Kurylo-Borowska, and L. C. Craig, *Biochemistry*, **5**, 2153 (1963).
3) H. Suda, T. Takita, T. Aoyagi, and H. Umezawa, *J. Antibiot.*, **29**, 100 (1976).
4) E. Fischer and W. A. Jacobs, *Chem. Ber.*, **40**, 1057 (1907).
5) T. Miyazawa, E. Akita, and T. Ito, *Agric. Biol. Chem.*, **40**, 1651 (1976).
6) Abbreviations for amino acids follow the rules of the IUPAC-IUB commission on Biochemical Nomenclature. Other abbreviations: Ise, isoserine; Ith, isothreonine, which is used for *threo*-2-hydroxy-3-aminobutanoic acid analogously to that of isoserine.
7) P. Melikoff, *Chem. Ber.*, **13**, 956, 1265 (1880).
8) H. E. Carter and C. L. Zirkle, *J. Biol. Chem.*, **178**, 709 (1949).
9) W. J. N. Burch, *J. Chem. Soc.*, **1930**, 310.
10) C. Neuberg and P. Mayer, *Biochem. Z.*, **3**, 116 (1907).
11) Y. Liwschitz, A. Singerman, and M. Luwish, *Israel J. Chem.*, **1**, 441 (1963).
12) S. Winstein and R. B. Henderson, "Heterocyclic Compounds," John Wiley & Sons Inc., New York (1950), Vol. 1, Chap. 1.
13) R. E. Parker and N. S. Isaacs, *Chem. Rev.*, **59**, 737 (1959).
14) P. Brewster, E. Hiron, E. D. Hughes, C. K. Ingold, and P. A. D. S. Rao, *Nature*, **166**, 179 (1950).
15) J. P. Greenstein and M. Winitz, "Chemistry of the Amino Acid," John Wiley & Sons, Inc., New York (1961), Vol. 1, pp. 83, 157.
16) F. W. Bachelor and G. A. Miana, *Can. J. Chem.*, **47**, 4089 (1969).
17) S. Futagawa, T. Inui, and T. Shiba, *Bull. Chem. Soc. Jpn.*, **46**, 3308 (1973).
18) N. Izumiya, *Bull. Chem. Soc. Jpn.*, **26**, 53 (1953).
19) K-D. Gundermann and G. Holtmann, *Chem. Ber.*, **91**, 160 (1958).

BULLETIN OF THE CHEMICAL SOCIETY OF JAPAN, VOL. 52 (3), 951—952 (1979)

Electrochemical Vicinal Addition of Two Alkyl Groups to Phenyl Substituted Olefins and Diethyl Fumarate

Shōhei SATOH, Tōru TAGUCHI, the late Mitsuomi ITOH, and Masao TOKUDA*

Department of Chemical Process Engineering, Hokkaido University, Sapporo 060

(Received June 26, 1978)

Synopsis. Electrochemical reactions of styrene, 1-phenyl-1-propene, 2-phenyl-1-propene, stilbene, and diethyl fumarate with alkyl halides in hexamethylphosphoric triamide containing lithium chloride produce the corresponding vicinal adducts of two alkyl groups of alkyl halides.

Electrochemical reduction of an alkyl halide produces a radical or a carbanion intermediate, these have been employed as an useful species for a carbon-carbon bond formation. Alkyl halides also work as efficient trapping agents for the anionic intermediate generated by the electrochemical reduction of neutral organic compounds, although relatively few reports on such trapping reactions are available.[1] The work reported here was carried out to explore a carbon-carbon bond formation reaction using alkyl halide or trialkylborane by an electrochemical method.[2] In the present paper we wish to report that the electrolysis of alkyl halides with phenyl substituted olefins or diethyl fumarate produces the corresponding vicinal addition products in which two alkyl groups from alkyl halides were introduced to the double bond carbons. This reaction is of synthetic interest because an introduction of two identical alkyl groups to a carbon-carbon double bond in one step is very difficult.

Electrolysis of a mixture of styrene (**1a**) and excess methyl iodide in hexamethylphosphoric triamide (HMPA) containing lithium chloride as a supporting electrolyte produced 2-phenylbutane (**3a**) in a good yield. Phenylpropenes **1b** and **1c**, *trans*-stilbene (**1d**), and diethyl fumarate (**2**) were found to undergo similar dialkylation reactions. These representative results are summarized in Table 1. In the electrochemical reaction of **1b** with methyl iodide, 3-methyl-3-phenylpentane (**7**) was also produced in a 11% yield along with 2-methyl-2-phenylbutane (**3b**). Alkyl benzene with a chain length of C_7 was also detected by GC-mass spectroscopy. The reactions of **1a** and **1b** using a nickel cathode produced almost the same yields of **3a**, **4a**, **5a**, and **3b** as those using a platinum cathode, while diethyl fumarate (**2**) did not produce **6**. The reaction of **2** was successfully carried out by using a mercury pool as a cathode.

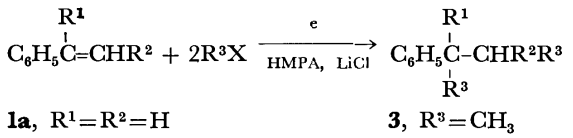

1a, $R^1=R^2=H$ — **3**, $R^3=CH_3$
1b, $R^1=CH_3$, $R^2=H$ — **4**, $R^3=C_2H_5$
1c, $R^1=H$, $R^2=CH_3$ — **5**, $R^3=n\text{-}C_4H_9$
1d, $R^1=H$, $R^2=C_6H_5$

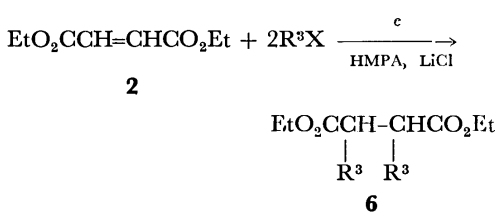

2 **6**

A detailed understanding of the electrode processes seems very difficult, since HMPA adsorption at the electrode surface sometimes prevented a direct electron transfer to substrates.[3] Hence, a voltammetric study or a controlled potential electrolysis in HMPA solution could not be carried out successfully. However, several points must be noted. First, the electrolysis using a divided cell showed that all products obtained were formed at a cathode. Second, from the fact that the reduction potential of **1** is more negative than those of alkyl halides while that of **2** is slightly more positive,[4,5] it may be said that the reaction mechanism of phenyl substituted olefins **1** is different from that of diethyl fumarate (**2**). At the same time, the difference of the reaction mechanisms between **1** and **2** may be also substantiated from the results in Table 1 in which nickel and mercury cathodes are used. Third, formation of **7** from **1b** may be elucidated by further electrochemical dialkylation of 2-phenyl-1-butene (**8**) which may be produced as the intermediate, since the electrochemical reaction of **8** with methyl iodide was found to produce **7** as a main product. Consequently, two pathways may be involved in these reactions. (a) Electron transfer to alkyl halide directly from a cathode, from a solvated electron,[3,6] or from lithium metal formed by reduction of lithium chloride[3,6b,7] produced an alkyl radical or a carbanion. Addition of these species to the olefin provided the intermediate radical or carbanion, the former of which may be further reduced to the latter. These carbanions are trapped by an excess of alkyl halide to produce the dialkylation product. (b) Electron transfer to olefin produced an anion radical,[8] which was trapped by alkyl halide to produce the intermediate radical. The resulting radical is reduced to the corresponding carbanion, which may be trapped again by alkyl halide to produce the dialkylation product. The former pathway (a) may be predominant in phenyl-substituted olefins and the latter (b) in diethyl fumarate.

A similar dialkylation reaction using an alkali metal was reported by Scilly *et al.*[9]

Experimental

All materials were distilled before use. HMPA was dried over calcium hydride and distilled before use. Quantitative GLPC analyses (SE-30, 15% on Uniport B) were carried out by an internal standard method.

General Procedure for Electrolysis. The electrolysis was carried out in the usual undivided cell equipped with two platinum plate electrodes (1×1 or 2×2 cm^2), a magnetic

Table 1. Electrochemical dialkylations of phenyl-substituted olefins and diethyl fumarate[a)]

Substrate	RX	Cathode	LiCl (M)	Product	Conversion of **1** or **2** (%)	Yield[b)] of product (%)
1a	CH_3I[c)]	Pt	0	**3a**	59	33
	CH_3I	Pt	0.3	**3a**	28	96
	CH_3I[d)]	Pt	0.3	**3a**	98	43
	CH_3I	Ni	1.5	**3a**	47	73
	C_2H_5I	Pt	0.3	**4a**	57	69
	C_2H_5Br	Pt	0.3	**4a**	68	35
	C_4H_9Br	Pt	1.5	**5a**	84	42
	C_4H_9Br	Ni	1.5	**5a**	83	48
1b	CH_3I	Pt	1.5	**3b**	49	23
	CH_3I	Ni	1.5	**3b**	58	33
	CH_3I	Hg	1.5	**3b**	5	0
1c	CH_3I	Pt	1.5	**3c**	42	32
	CH_3I	Pt	0.2[e)]	**3c**	21	45
1d	CH_3I	Pt	1.5	**3d**	—	trace
2	CH_3I	Pt	0.3	**6**	39	51
	CH_3I	Pt	0.1[f)]	**6**	66	36
	CH_3I	Ni	1.5	**6**	—	trace
	CH_3I	Hg	1.5	**6**	100	63

a) Current density: 0.5 A/cm^2; electricity passed: 20 F/mol. b) Yields are based on **1** or **2** comsumed. c) 0.1 A/cm^2; 20 F/mol. d) 100 F/mol. e) Instead of LiCl, tetrabutylammonium iodide was used. f) Instead of LiCl, $LiClO_4$ was used.

stirring bar, and a reflux condenser. A divided cell, when needed, was used. Olefin **1** or **2** (1 mmol) and excess alkyl halides (20—30 mmol) were dissolved in 8 ml of HMPA containing 0.1—0.5 g of LiCl. The solution was electrolyzed at a constant current (0.5 A/cm^2) with the passage of electricity of approximately 20 F/mol.

*Electrochemical Reaction of Styrene (**1a**) with Alkyl Halides.* Electrolysis of **1a** and excess methyl iodide produced 2-phenylbutane (**3a**) : NMR (CCl_4) δ 0.83 (t, 3H), 1.24 (d, 3H), 1.59 (qi, 2H), 2.55 (m, 1H), 7.08 ppm (m, 5H); m/e= 134 (M^+). Spectral data of **3a** were fully identical to those of an authentic sample. A similar electrolysis of **1a** and excess ethyl iodide or ethyl bromide produced 3-phenylhexane (**4a**): NMR (CCl_4) δ 0.75 (t, 3H), 0.84 (t, 3H), 1.15 (m, 2H), 1.56 (m, 4H), 2.36 (qi, 1H), 7.06 ppm (m, 5H); m/e=162 (M^+). Electrolysis of **1a** and excess butyl bromide produced 5-phenyldecane (**5a**): NMR (CCl_4) δ 0.83 (t, 6H), 1.20 (m, 10H), 1.55 (m, 4H), 2.47 (m, 1H), 7.10 ppm (m, 5H); m/e=218 (M^+). Spectral data of **5a** were fully identical to those of an authentic sample prepared from **1a** and butyl bromide using lithium metal.[9)]

*Electrochemical Reaction of 2-Phenyl-1-propene (**1b**) with Methyl Iodide.* Electrolysis of **1b** and methyl iodide produced 2-methyl-2-phenylbutane (**3b**) [NMR (CCl_4) δ 0.67 (t, 3H), 1.27 (s, 6H), 1.64 (q, 2H), 7.16 ppm (m, 5H); m/e=148 (M^+)] and 3-methyl-3-phenylpentane (**7**) [NMR (CCl_4) δ 0.67 (t, 6H), 1.23 (s, 3H), 1.65 (m, 4H), 7.19 ppm (m, 5H); m/e=162 (M^+)]. Spectral data of the latter product **7** were identical to those of the product obtained by electrochemical reaction of 2-phenyl-1-butene (**8**) with methyl iodide.

*Electrochemical Reaction of 1-Phenyl-1-propene (**1c**) with Methyl Iodide.* Electrolysis of **1c** and methyl iodide produced 2-methyl-3-phenylbutane (**3c**): NMR (CCl_4) δ 0.75 (d, 3H), 0.94 (d, 3H), 1.23 (d, 3H), 1.79 (m, 1H), 2.38 (qi, 1H), 7.13 ppm (m, 5H); m/e=148 (M^+).

Electrochemical Reaction of trans-*Stilbene (**1d**) with Methyl Iodide.* Electrolysis of **1d** and methyl iodide produced a trace of 2,3-diphenylbutane (**3d**). The retention time and mass spectrum of **3d** were identical to those of an authentic sample prepared from **1d** and methyl iodide using lithium metal.[9)] Spectral data of **3d** are as follows: NMR (CCl_4) δ 1.02 (d, 6H, *meso*), 1.27 (d, 6H, *dl*), 2.88 (m, 2H), 6.9—7.2 ppm (m, 10H); m/e=210 (M^+).

*Electrochemical Reaction of Diethyl Fumarate (**2**) with Methyl Iodide.* Electrolysis of **2** and methyl iodide produced diethyl 2,3-dimethylbutanedioate (**6**): NMR (CCl_4) δ 1.11 (d, 6H), 1.25 (t, 6H), 2.59 (m, 2H), 4.08 ppm (q, 4H); IR (CCl_4) 1735, 1160 cm^{-1}; m/e=157 (M^+-45).

References

1) a) S. Wawzonek, E. W. Blaha, R. Berkey, and M. E. Runner, *J. Electrochem. Soc.*, **102**, 235 (1955); b) S. Wawzonek and A. Gundersen, *ibid.*, **107**, 537 (1960); c) T. Shono and M. Mitani, *Nippon Kagaku Kaishi*, **1972**, 2370; d) M. M. Baizer and J. L. Chruma, *J. Org. Chem.*, **37**, 1951 (1972); e) F. J. Goodman and J. Q. Chambers, *ibid.*, **41**, 626 (1976).

2) a) Y. Takahashi, M. Tokuda, M. Itoh, and A. Suzuki, *Chem. Lett.*, **1975**, 523; b) Y. Takahashi, M. Tokuda, M. Itoh, and A. Suzuki, *Synthesis*, **1976**, 616; c) M. Tokuda, T. Taguchi, O. Nishio, and M. Itoh, *J. Chem. Soc., Chem. Commun.*, **1976**, 606; d) Y. Takahashi, K. Yuasa, M. Tokuda, M. Itoh, and A. Suzuki, *Bull. Chem. Soc. Jpn.*, **51**, 339 (1978); f) S. Satoh, M. Itoh, and M. Tokuda, *J. Chem. Soc., Chem. Commun.*, **1978**, 481.

3) H. W. Sternberg, R. E. Merkby, I. Wender, and D. M. Mohilner, *J. Am. Chem. Soc.*, **91**, 4191 (1969).

4) H. Siegerman, "Technique of Electroorganic Synthesis," ed by N. L. Weinberg, John Wiley and Sons, New York (1975), Part II, p. 667.

5) T. Iwasaki and K. Harada, *J. Chem. Soc., Perkin Trans. 1*, **1977**, 1730.

6) a) M. R. Rifi, "Organic Electrochemistry," ed by M. M. Baizer, Marcel Dekker, New York, N. Y. (1973), p. 842; b) H. W. Sternberg, R. E. Markby, I. Wender, and D. M. Mohilner, *J. Am. Chem. Soc.*, **89**, 186 (1967); c) H. Normant, *Angew. Chem., Int. Ed. Engl.*, **6**, 1046 (1967).

7) R. A. Benkeser, E. M. Kaiser, and R. F. Lambert, *J. Am. Chem. Soc.*, **86**, 5272 (1964).

8) D. A. Tyssee and M. M. Baizer, *J. Org. Chem.*, **39**, 2819 (1974).

9) A. Davis, M. H. Morgan, D. H. Richards, and N. F. Scilly, *J. Chem. Soc., Perkin Trans. 1*, **1972**, 286.

BULLETIN OF THE CHEMICAL SOCIETY OF JAPAN, VOL. 52 (3), 953—954 (1979)

The Modified Wurtz Reaction Using Tetrakis(*p*-dimethylaminophenyl)ethylene

Yuji MIYAHARA,* Takanari SHIRAISHI, Takahiko INAZU, and Tamotsu YOSHINO

Department of Chemistry, Faculty of Science, Kyushu University 33, Hakozaki, Higashi-ku, Fukuoka 812

(Received September 4, 1978)

Synopsis. The Wurtz reaction has been found to be catalyzed by easily removable tetrakis(*p*-dimethylaminophenyl)ethylene. This modification facilitated the separation of products in the syntheses of [2.1.2.1.]-, [2.2.2.2]-, and [3.2.3.2]paracyclophanes, the isolated yields of which were better than in the case of tetraphenylethylene.

The Müller-Röscheisen modification of the Wurtz reaction using tetraphenylethylene(TPE)[1] has been used extensively, especially in the synthesis of cyclophanes.[2] Although the reaction has been claimed to be catalytic, TPE is gradually consumed and 1,1,2,2-tetraphenylethane **1** is formed as a reduction product. Separation of the desired cyclophanes from TPE and **1** is often troublesome owing to a similarity in properties. For the practical synthesis of cyclophanes an easily removable substitute for TPE is desirable[3] and the acid-soluble tetrakis(*p*-dimethylaminophenyl)ethylene (TDAPE) has been found suitable for the purpose.

TDAPE was readily prepared by the reductive dimerization of 4,4'-bis(dimethylamino)benzophenone with tin powder in concentrated hydrochloric acid.[4] In spite of the electron-rich nature as evidenced by the fact that in chloroform it is easily oxidized to a violet pigment, it is known to react with sodium in ether yielding a bluish green powder of the disodium adduct.[5] In tetrahydrofuran (THF) TDAPE and sodium reacted smoothly to afford a wine-colored solution which was similar in reactivity to a solution of the TPE-disodium adduct. Thus, the Wurtz reaction was catalyzed effectively by TDAPE (0.05 mol per mol of benzyl halide was sufficient) as shown in Table 1.

$$2\,PhCH_2X \xrightarrow[TDAPE,\ THF]{Na\ or\ Na\text{-}K} PhCH_2CH_2Ph$$

Table 1. The Wurtz reaction of benzyl halides

Reactant	Yields of 1,2-diphenylethane (%) TDAPE		TPE
	ca. −40 °C	Room temp	Room temp
$PhCH_2Cl$, Na-K	87	46	78[80(Na)][1]
$PhCH_2Br$, Na	77	66	(78)[1]

Although the reactions at room temperature were less fruitful compared with the corresponding TPE-catalyzed reactions, especially in the case of the chloride (see Experimental), the yields were improved by lowering the reaction temperature. The use of a liquid sodium–potassium alloy (Na–K) enabled a large metallic surface to be established and, thus, facilitated adduct formation especially at low temperatures.

To demonstrate the applicability of the modified Wurtz reaction to cyclophane synthesis several paracyclophanes have been synthesized. The cyclization was conducted by the addition over 24 h of a dihalide to a solution of the TDAPE–Na (or K) adduct at *ca.* −40 °C for the chloride **6** or, for convenience, at room temperature for the bromides **2** and **4**. Separation of the products from TDAPE was readily effected by acid-washing. The yields of **3** and **5** were satisfactory compared with those reported using TPE. The simplicity of separation without loss of yield in the Wurtz reaction will also be valuable in the synthesis of other systems.

Experimental

All the melting points are uncorrected. The PMR spectra were recorded at 60 MHz with a Hitachi R-20B spectrometer. The ^{13}C-NMR spectra were obtained at 22.6 MHz using a Hitachi R-22 spectrometer equipped with FT accessories. The mass spectra were obtained on a JEOL 01 SG mass

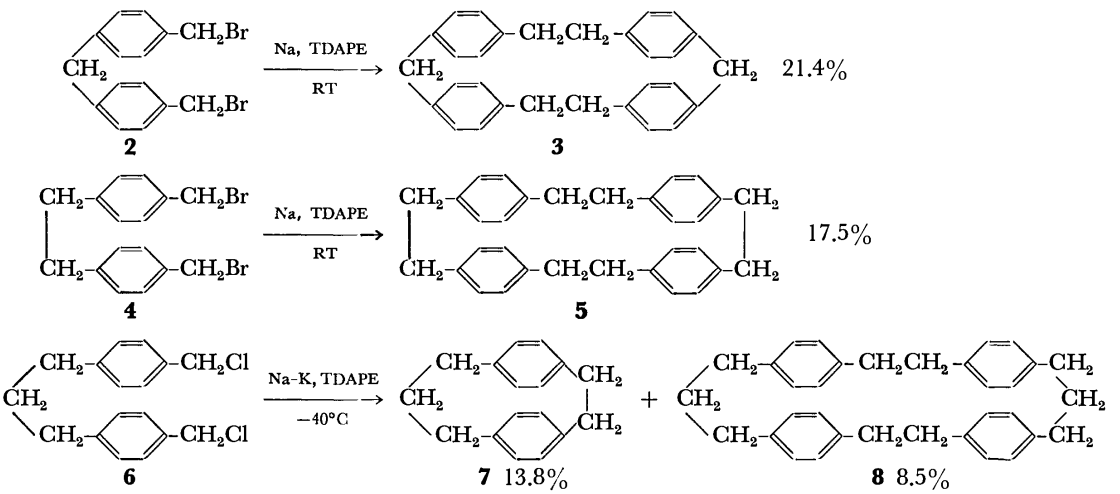

spectrometer.

Tetrakis(p-dimethylaminophenyl)ethylene, TDAPE.[4] To a stirred solution of 4,4'-bis(dimethylamino)benzophenone (50 g) in concd HCl (750 ml) was added tin powder (90 g) in small portions over a 3 h period at 90—100 °C. After stirring for 6 h the solution was allowed to cool and the precipitate formed was collected by filtration and treated with excess aq NaOH. The precipitate was extracted with warm benzene, washed with water, dried over Na_2SO_4, and concentrated. TDAPE was obtained as a 1/2 benzene solvate (35.5 g, 70%). Rapid crystallization of TDAPE from benzene–hexane gave yellow needles free from benzene but on standing in the solution the crystals turned gradually into prisms. The PMR spectrum(C_6D_6) and analyses indicate that the prisms are a 1/2 benzene solvate. TDAPE: yellow needles, mp 321—323 °C (sealed tube, lit,[6] mp 310—314 °C) Found: C, 80.83; H, 8.09; N, 11.17%. Calcd for $C_{34}H_{40}N_4$: C, 80.91; H, 7.99; N, 11.10%. TDAPE.1/2 benzene: greenish yellow prisms, mp 318—323 °C. Found: C, 81.67; H, 8.05; N, 10.40%. Calcd for $C_{37}H_{43}N_4$: C, 81.73; H, 7.97; N, 10.30%. A solution of TDAPE in $CDCl_3$, yellow at first, turned rapidly to violet with precipitation exibiting broad PMR peaks and a strong ESR signal, indicating the presence of radical cationic species formed by air oxidation. Therefore chloroform which was originally used for extraction is not suitable as the solvent.

The Wurtz Reaction of Benzyl Halide. To a solution of TDAPE (2.5 g, 0.005 mol) in THF (freshly distilled from sodium–benzophenone, 400 ml) was added a Na–K alloy (1 : 2 by weight, 6 ml) or sliced sodium (6 g) with stirring under nitrogen. After stirring for 30 min, to the deep wine-colored solution was added a solution of benzyl halide (0.1 mol) in THF (200 ml) at room temperature of at *ca.* −40 °C. Care was taken to prevent complete disappearance of the color of the adduct. After the addition the solution was filtered and evaporated. The residue was taken up in benzene and washed with dil HCl and water and the solution dried ($MgSO_4$), concentrated and distilled under reduced pressure yielding 1,2-diphenylethane. In the reaction of benzyl chloride at room temperature a considerable amount of residue remained after distillation, which gave, after purification through a silica gel column(chloroform), colorless prisms of high melting point and low solubility in common solvents in 8% yield. This product shows complex PMR signals at δ 6.6—7.5 and 2.3—3.3 ppm ($CDCl_3$), but MS (M^+ 362) and ^{13}C-NMR data [δ_{TMS} ($CDCl_3$) 41.0, 54.3, 125.4, 126.3, 127.7, 128.2, 128.6, 128.8, 130.7, and 133.3 ppm] indicate that it is 1,2,3,4-tetraphenylbutane **9**. The structure was confirmed by comparison with a sample of meso-**9** prepared by the reduction of tetraphenylthiophene.[7] Mp 182—183 °C (lit,[7a] 181—182 °C). Found: C, 92.65; H, 7.24%. Calcd for $C_{28}H_{26}$: C, 92.77; H, 7.23%. The formation of this product may be explained in terms of the incipient proton abstraction from benzyl chloride as follows:[8]

$$\underset{\mathbf{10}}{PhCH_2Cl} \longrightarrow PhCH^-Cl \xrightarrow{10} \underset{\mathbf{11}}{PhCHClCH_2Ph}$$

$$\xrightarrow{11} PhCH_2\overset{Ph}{\overset{|}{C}}H-\overset{Ph}{\overset{|}{C}}HCH_2Ph$$

$$\mathbf{9}$$

Synthesis of Paracyclophanes. [2.1.2.1]Paracyclophane **3** was prepared as follows. To a solution of TDAPE (2.5 g, 0.005 mol) in THF (400 ml) was added sliced sodium (11.5 g, 0.5 mol) under argon. After stirring for 30 min, to the deep wine-colored solution was added dropwise a solution of bis(*p*-bromomethylphenyl)methane **2** (17.7 g, 0.05 mol) in THF (500 ml) over a period of 24 h. The reaction mixture was decanted and evaporated and the residue dissolved in benzene, washed with dil HCl and water, dried over $MgSO_4$, and passed through a short column of silica gel to ensure removal of TDAPE. After evaporation of the solvent the residue was sublimed (230—240 °C at 0.03 Torr) and the sublimate recrystallized from benzene–hexane to give **3** as colorless prisms (2.08 g, 21.4%), mp 198—199 °C (lit,[9b] mp 199 °C, 14% yield from the corresponding chloride).

[2.2.2.2]Paracyclophane **5** was prepared analogously from 1,2-bis(*p*-bromomethylphenyl)ethane **4** in 17.5% yield, mp 179—181 °C (lit,[10] mp 185 °C, 7% yield from the corresponding chloride).

The reaction of 1,3-bis(*p*-chloromethylphenyl)propane **6** with Na–K at *ca.* −40 °C over a period of 24 h yielded **7** and **8**, the separation of which was readily effected by fractional sublimation. [3.2]Paracyclophane **7** : sublimed at 200—220 °C at atmospheric pressure, recrystallized from ethanol, colorless needles, mp 146—147 °C (lit,[11] mp 148—149 °C), 1.57 g (13.8%). MS: M^+ 222. PMR($CDCl_3$): δ 6.15, 6.39 (AA'BB' doublets, J=8 Hz, 8H), 2.95 (s, 4H), 2.9—2.5 (m, 4H), and 2.4—1.8 (m, 2H) ppm. [3.2.3.2]-Paracyclophane **8**: sublimed at 200—220 °C at 0.1 Torr, recrystallized from benzene, colorless prisms, mp 223—224 °C, 967 mg (8.5%). The compound had different properties from those reported (mp 61—62 °C[9a]) but the structure was confirmed by the following data. MS: *m/e* 444(M^+, 64), 222 (67), 131 (56), and 118 (100). PMR($CDCl_3$): δ 6.80, 6.72 (AA'BB' doublets, J=9 Hz, 16H), 2.86 (s, 8H), 2.6—2.2 (m, 8H), and 2.1—1.5 (m, 4H) ppm. Found: C, 91.64; H, 8.25%. Calcd for $C_{34}H_{36}$: C, 91.84; H, 8.16%.

References

1) E. Müller and G. Röscheisen, *Chem. Ber.*, **90**, 543 (1957).

2) T. Kawato, T. Inazu, and T. Yoshino, *Bull. Chem. Soc. Jpn.*, **44**, 200 (1971).

3) Several catalysts for the Wurtz reaction have been tested to make chromatographic separation efficient: K. Burri and W. Jenny, *Helv. Chim. Acta*, **50**, 1978 (1967).

4) R. Willstätter and M. Goldmann, *Ber.*, **39**, 3765 (1906).

5) W. Schlenk and E. Bergmann, *Justus Liebigs Ann. Chem.*, **493**, 1 (1928).

6) R. Foster and T. J. Thomson, *Trans. Faraday Soc.*, **59**, 1059 (1963).

7) a) E. Bergmann, *J. Chem. Soc.*, **1936**, 505; b) D. P. Wyman, *J. Org. Chem.*, **27**, 3712 (1962).

8) R. Koppang, *Acta Chem. Scand.*, **25**, 3067 (1971).

9) a) H. Steinberg and D. J. Cram, *J. Am. Chem. Soc.*, **74**, 5388 (1952); b) C. Sergheraert, P. Marcincal, and E. Cuingnet, *Tetrahedron Lett.*, 2879 (1977).

10) I. Tabushi, H. Yamada, K. Matsushita, Z. Yoshida, H. Kuroda, and R. Oda, *Tetrahedron*, **28**, 3381 (1972).

11) D. J. Cram and H. Steinberg, *J. Am. Chem. Soc.*, **73**, 5671 (1951).

BULLETIN OF THE CHEMICAL SOCIETY OF JAPAN, VOL. 52 (3), 955—956 (1979)

Modifiction of Aminocyclitol Antibiotics. 7. Preparation of 5-Epikanamycin B

Tetsuo SUAMI* and Katsumi NAKAMURA

Department of Applied Chemistry, Faculty of Engineering, Keio University, Hiyoshi, Yokohama 223

(Received September 9, 1978)

Synopsis. A configuration of the OH group on C-5 of 2-deoxystreptamine moiety of kanamycin B has been epimerized. 5-Epikanamycin B thus obtained was tested against several microorganisms. The structure of the antibiotic was elucidated by ^1H and ^{13}C NMR spectrometry.

In connection with the preceding paper of this series,[1] we have attempted to prepare 5-epikanamycin B (**4**), since 5-epineamine[2] showed an improved activity against a resistant strain of bacteria, compared to the parent neamine.

When 3′,4′,2″,4″,6″-penta-*O*-benzoyl-1,3,2′,6′,3″-pentakis-*N*-(ethoxycarbonyl)kanamycin B[1] (**1**) was treated with methanesulfonyl chloride in pyridine, a 5-*O*-mesyl derivative (**2**) was obtained. Nucleophilic substitution of **2** with an acetate ion in DMF, followed by purification afforded 5-*O*-acetyl-3′,4′,2″,4″,6″-penta-*O*-benzoyl-1,3,2′,6′,3″-pentakis-*N*-(ethoxycarbonyl)5-epikanamycin B (**3**). Hydrolysis of **3** in barium hydroxide solution, followed by purification on a CG-50(NH_4^+) resin column gave **4**, which was converted to a penta-*N*-acetyl derivative (**5**).

The ^1H NMR spectrum of **3** revealed acetoxyl methyl protons at δ 2.20 as a singlet, indicating an existence of an axial acetoxyl group, since the corresponding 5-*O*-acetylkanamycin B derivative revealed an equatorial acetoxyl methyl signal at δ 2.07.[3]

The structure of **4** was confirmed by ^{13}C NMR spectrometry. The spectrum of **4** was determined at pD above 11, showing 18 carbon signals which are assigned in accordance with the data for kanamycin B.[1,4] When the spectrum of **4** is compared with that of kanamycin B, it is obvious that the epimerization causes no appreciable shift of the signals of carbons in the aminosugar moieties, except that of C-1′, *i.e.*, the signal of C-1′ shifts to a higher field by 4.5 ppm, and analogous shifts have been described in the cases of 5-deoxykanamycin B[1] and 5-deoxyneamine.[7] While, the signals of carbons in the 2-deoxystreptamine moiety are shifted more or less to a higher field, except

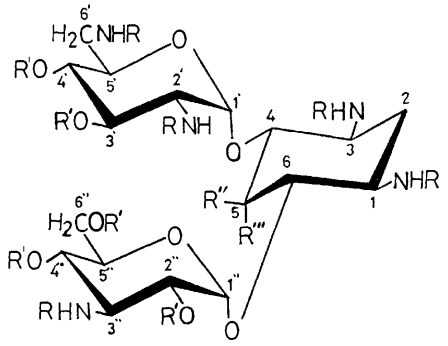

1 R=C_2H_5OCO, R′=C_6H_5CO, R″=OH, R‴=H
2 R=C_2H_5OCO, R′=C_6H_5CO, R″=OSO_2CH_3, R‴=H
3 R=C_2H_5OCO, R′=C_6H_5CO, R″=H, R‴=CH_3COO
4 R=R′=R″=H, R‴=OH
5 R=CH_3CO, R′=R″=H, R‴=OH

TABLE 2. ANTIMICROBIAL ACTIVITY OF 5-EPIKANAMYCIN B (**4**) AND KANAMYCIN B

Test organisms	Compound **4** MIC (mcg/ml)	Kanamycin B MIC (mcg/ml)
Staphyloccocus aureus ATCC 6538P	1.56	0.39
Staphyloccoccus epidermidis ATCC 12228	0.77	0.2
Diplococcus pneumoniae Type 3	0.39	0.1
Bacillus subtilis ATCC 6633	0.39	0.1
Escherichia coli NIH JC-2	6.25	1.56
Klebsiella pneumoniae 602	3.12	0.78
Pseudomonas aeruginosa IAM 1007	100	12.5
Proteus vulgaris OX-19	0.78	0.2
Salmonella paratyphi A 1015	1.56	0.39
Salmonella paratyphi B	3.12	1.56
Shigella flexneri 2a·SH-74-1	12.5	3.12

TABLE 1. THE ^{13}C NMR CHEMICAL SHIFTS[a] OF 5-EPIKANAMYCIN B AND KANAMYCIN B

	5-Epikanamycin B (**4**)		Kanamycin B[1]	
	pD 11	pD 1	pD 11	pD 1
C-1	48.0	48.2	50.5	50.5
C-2	36.6	28.8	36.5	28.6
C-3	47.3	47.6	50.3	49.3
C-4	79.9	73.8[c]	87.4	77.5
C-5	68.4	65.7	75.2[d]	75.1
C-6	86.1	81.0	88.6	84.5
C-1′	96.0	91.3	100.5	96.2
C-2′	55.2	54.1	56.3	54.4
C-3′	74.8	69.5	74.9[d]	69.0
C-4′	72.9[b]	71.5	73.3[e]	71.8
C-5′	73.9	69.9	74.7	70.1
C-6′	42.6	41.0	42.8	41.2
C-1″	101.9	100.8	101.4	101.4
C-2″	72.4[b]	68.8	73.0[c]	69.0
C-3″	55.8	55.7	56.5	55.8
C-4″	71.1	66.4	71.3	66.3
C-5″	73.5	73.7[e]	74.0	73.7
C-6″	62.1	61.3	62.0	60.8

a) In parts per million downfield from tetramethylsilane. b—e) The signals may be reversed.

that of C-2. That is, the signal of C-5 shifts by 6.8 ppm, and this is coincident with the fact that a shift of the signal of C-3 was observed between β-D-gluco and β-D-allopyranoses.[5] The signals of C-4 and 6 shift by 7.5 and 2.5 ppm, owing to a shielding effect of an adjacent axial OH group on C-5. Also, the signals of C-1 and 3 shift by 2.5 and 3.0 ppm, respectively. An analogous shielding effct of an axial OH group was described in a literature.[5,6]

When ^{13}C NMR spectrum of **4** was determined at pD 1 to find out a *N*-protonation effect,[4,8] a β-shielding effect is observed as was described in the case of kanamycin B.[1] Therefore, the inversion of the configuration has been confirmed.

Antimicrobial activities of **4** were determined against several microorganisms. The MIC (minimum inhibition concentration) values are listed in Table 2. No improvement of the activity was achieved by the epimerization of the OH group on C-5 in kanamycin B.

Experimental

General Methods. The same method was used as described in the preceding paper.[1]

3′,4′,2″,4″,6″-Penta-O-benzoyl-1,3,2′,6′,3″-pentakis-N-(ethoxycarbonyl)-5-O-mesylkanamycin B (2). To a stirred solution of 3′,4′,2″,4″,6″-penta-*O*-benzoyl-1,3,2′,6′,3″-pentakis-*N*-(ethoxycarbonyl)kanamycin B[1] (**1**, 311 mg) in pyridine (3 ml), mesyl chloride (0.5 ml) was added. After 160 h, the solution was quenched into ice–water (50 ml), and precipitates were collected by filtration. The precipitates were dissolved in $CHCl_3$, and the solution was passed through a short alumina column and evaporated. The residue was dissolved in benzene, and hexane was added to the solution to give 232 mg (71%) of **2** as amorphous powder, mp 121—126 °C, $[\alpha]_D^{21}$ +76.8° (*c* 0.5, chloroform), R_f 0.37 on TLC in 7 : 1 (v/v) benzene–methanol ^1H NMR: δ 3.32 (s, 3, SO_2CH_3).

Found: C, 57.80; H, 5.54; N, 4.90; S, 1.92%. Calcd for $C_{69}H_{79}N_5O_{27}S$: C, 57.45; H, 5.52; N, 4.86; S, 2.22%.

5-O-Acetyl-3′,4′,2″,4″,5″-penta-O-benzoyl-1,3,2′,6′,3″-pentakis-N-(ethoxycarbonyl)-5-epikanamycin B (3). A mixture of **2** (1.0 g) and sodium acetate (622 mg) in DMF (16 ml) was heated at 100 °C with agitation. After 68 h, the mixture was poured into ice–water (80 ml), and precipitates were collected by filtration. The precipitates were dissolved in chloroform, and the solution was washed with water, dried over Na_2SO_4 and evaporated. The residue was purified on a silica gel column with 20 : 1 (v/v) benzene–methanol. Fractions homogeneous on TLC (R_f 0.43) in 7 : 1 (v/v) benzene–methanol were combined and concentrated. The residue was dissolved in benzene and hexane was added to the solution to give 571 mg (54%) of **3**, mp 132—138 °C, $[\alpha]_D^{21}$ +100.6° (*c* 1.03, chloroform). ^1H NMR: δ 2.20 (s, 3, OAc).

Found: C, 59.45; H, 5.59; N, 4.70%. Calcd for $C_{70}H_{79}N_5O_{26}$: C, 59.78; H, 5.66; N, 4.98%.

5-Epikanamycin B (4). To a stirred solution of $Ba(OH)_2 \cdot 8H_2O$ (4 g) in water (14 ml), a solution of **3** (518 mg) in methanol (6 ml) was added. The mixture was heated at 100 °C for 15 h, and CO_2 was bubbled into the mixture. The precipitates were filtered off and the filtrate was concentrated. The residue was purified on a column of Amberlite CG-50 (NH_4^+) resin as described in the preceding paper[1] to give 20 mg (11%) of **4**, mp 172—178 °C (dec), $[\alpha]_D^{21}$ +159° (*c* 0.6, water).

A part of **4** (11 mg) was acetylated with acetic anhydride in methanol to give 15 mg (93%) of the penta-*N*-acetyl derivative (**5**), mp 217—223 °C (dec).

Found: C, 45.69; H, 6.88; N, 9.36%. Calcd for $C_{28}H_{47}N_5O_{15} \cdot 2H_2O$: C, 46.08; H, 7.04; N, 9.59%.

The authors wish to express their sincere thanks to Dr. Shyoji Omoto for determination of ^{13}C NMR spectra and to Mr. Saburo Nakada for elemental analyses. This work has been supported by a grant of the Asahi Glass Foundation to Industrial Technology.

References

1) T. Suami, S. Nishiyama, Y. Ishikawa, and E. Umemura, *Bull. Chem. Soc. Jpn.*, **51**, 2354 (1978).
2) T. Suami, S. Nishiyama, Y. Ishikawa, and S. Katsura, *Carbohydr. Res.*, **65**, 57 (1978).
3) F. W. Lichtenthaler, *Chem. Ber.*, **96**, 2047 (1963).
4) G. Kotowycz and R. U. Lemieux, *Chem. Rev.*, **73**, 669 (1973).
5) A. S. Perlin, B. Casu, and H. J. Koch, *Can. J. Chem.*, **48**, 2596 (1970).
6) S. Hanessian, R. Massié, and T. Nakagawa, *Can. J. Chem.*, **56**, 1509 (1978).
7) T. Suami, S. Nishiyama, Y. Ishikawa, and S. Katsura, *Carbohydr. Res.*, **53**, 239 (1977).
8) K. F. Kocv, J. A. Rhoades, E. W. Hagaman, and E. Wenkert, *J. Am. Chem. Soc.*, **96**, 3300 (1974).

BULLETIN OF THE CHEMICAL SOCIETY OF JAPAN, VOL. 52 (3), 957—958 (1979)

Reaction of Optically Active 1-Dimethylaminoethylferrocene Palladium Complexes

Akira KASAHARA,* Taeko IZUMI, and Hiroyuki WATABE
Department of Applied Chemistry, Faculty of Engineering, Yamagata University, Yonezawa 992

(Received September 21, 1978)

Synopsis. *ortho*-Palladation products of optically active 1-dimethylaminoethylferrocene were treated with phenyl vinyl ketone and carbon monoxide and a variety of optically active 1,2-disubstituted ferrocene derivatives were obtained.

Recently, the reactions of *ortho*-palladation products from aromatic nitrogen derivatives with various reagents have been reported.[1] The carbonylation of *ortho*-palladation products of azobenzene, Schiff bases, and tertiary benzylamines usually give a variety of heterocyclic compounds.[2] The reaction of *ortho*-palladated benzylamine-type complexes with enones result in the formation of aryl-substituted enone derivatives.[3] On the other hand, it has been reported that stereoselective metallation of optically active α-ferrocenyl tertiary amines produce lithio amines with a high degree of asymmetric induction.[4] Sokolov *et al.*[5] described the *ortho*-palladation of optically active 1-dimethylaminoethylferrocene [(+)-**1** and (−)-**1**] with sodium tetrachloropalladate(II) in methanol in the presence of sodium acetate and found it to proceed with moderate stereoselectivity. For example, the *ortho*-palladation of (+)-**1** with sodium tetrachloropalladate(II) produced a mixture of two diastereoisomers [(−)-**2a** (major product) and (+)-**2b** (minor product)].[5a] The *ortho*-palladation products [(+)-**3a** and (−)-**3b**] were similarly obtained from (−)-**1**.[5b] In this paper, the reactions of optically active dimeric 2-chloropalladio-1-(1′-dimethylaminoethyl) ferrocene [(−)-**2a** and (+)-**3a**] with phenyl vinyl ketone and carbon monoxide, affording optically active 1,2-disubstituted ferrocene derivatives with a plane of chirality will be reported.

In the presence of triethylamine, the (−)-**2a** complex reacted with phenyl vinyl ketone in benzene, leading to the formation of (−)-1-(2′-benzoylvinyl)-2-(1″-dimethylaminoethyl)ferrocene (**4**). Treatment of (−)-**4** with methyl iodide resulted in the formation of (−)-1-(2′-benzoylvinyl)-2-vinylferrocene (**5**). In the presence of triphenylphosphine in ethanol, (−)-**2a** was carbonylated under carbon monoxide pressure, affording (+)-1-(1′-dimethylaminoethyl)-2-ethoxycarbonylferrocene (**6**). Elimination of the chiral center from (+)-**6** by the treatment with methyl iodide led to the formation of (+)-1-ethoxycarbonyl-2-vinyl-ferrocene (**7**).

On the other hand, the reaction of the (+)-**3a** complex with phenyl vinyl ketone, gave (+)-1-(2′-benzoylvinyl)-2-(1″-dimethylaminoethyl)ferrocene (**8**), and subsequent elimination of a chiral carbon center of (+)-**8** with methyl iodide afforded (+)-1-(2′-benzoylvinyl)-2-vinylferrocene (**9**). The carbonylation of the (+)-**3a** complex in ethanol also led to the formation of (−)-1-(1′-dimethylaminoethyl)-2-ethoxycarbonylferrocene (**10**), and subsequent treatment with methyl iodide afforded (−)-1-ethoxycarbonyl-2-vinylferrocene (**11**).

The structures of these compounds were identified by elemental analyses, IR, NMR, and MS spectra. There is no rapid interconversion (−)-**2a**⇌(+)-**2b** or (+)-**3a**⇌(−)-**3b**, the reaction of (−)-**2a** or (+)-**3a** with phenyl vinyl ketone is not the stereoselectivity determining process for (−)-**2a**→(−)-**4** or (+)-**3a**→(+)-**8** in the sence of the Curtin-Hammett principle,[6] and the carbonylation of σ-bonded palladium complexes proceeds with retention of configuration.[7] On the basis of the work of Uri,[4c] Sokolov *et al.*[5] suggested (*R*)-(*S*)-configuration to (−)-**2a** (the major product of the direct palladation of (+)-**1**). Consequently, one may assign a (*R*)-(*S*)-configuration to (−)-**4** and (+)-**6**; and *S*-configuration to (−)-**5** and (+)-**7**. It is similarly inferred that (*S*)-(*R*)-configuration to (+)-**3a** (the major product of the palladation of (−)-**1**), (+)-**8**, and (−)-**10**; and *R*-configuration to (+)-**9** and (−)-**11** were assigned.

Experimental

Materials. All melting points are uncorrected. The optically pure (1*R*)-(1*S*)-di-μ-chlorobis[2-(1′-dimethylaminoethyl)ferrocenyl]dipalladium(II) ((−)-**2a**) (mp 146 °C (dec), $[\alpha]_D^{20}$ −435.5° (*c* 0.053, $CHCl_3$)) and (1*S*)-(1*R*)-di-μ-chlorobis[2-(1′-dimethylaminoethyl)ferrocenyl]dipalladium-(II) ((+)-**3a**) (mp 145—146 °C (dec), $[\alpha]_D^{20}$ +438.1° (*c* 0.041, $CHCl_3$)) were synthesized by the methods in the literature.[5]

The Reaction of ortho-*Palladated Complexes with Phenyl Vinyl Ketone.* A mixture of complex ((1*R*)-(1*S*)-**2a** or (1*S*)-(1*R*)-**3a**) (2.0 g; 2.3 mmol), phenyl vinyl ketone (0.6 g; 4.6 mmol), and triethylamine (0.45 g; 4.6 mmol) in benzene (50 ml) was heated at 75 °C under nitrogen. The reaction mixture was then cooled and filtered to remove the precipitated palladium, benzene (100 ml) was added, and the mixture washed with water, dried over anhydrous magnesium sulfate, filtered, and concentrated under reduced pressure. The residue was then purified by column chromatography (Al_2O_3–benzene).

(1*R*)-(1*S*)-**4**: yield 90%, reddish viscous oil, $[\alpha]_D^{20}$ −1982° (*c*, 0.045, $CHCl_3$). IR: 1660 (C=O), 1600 and 970 (*trans* –CH=CH–), 1100. 1000, and 908 cm^{-1} (1,2-disubstituted Fc ring). NMR: δ 1.44 (d, 3H, $-CH_3$), 2.05 (s, 6H, $-N-(CH_3)_2$), 3.85 (q, 1H, –CH–), 4.07, 4.44, and 4.67 (m, 8H, Fc protons), 7.14 (d, 1H, –C=CH–CO–), 7.45 (m, 5H, Ph), and 7.87 ppm (d, 1H, –CH=C–CO–). MS: *m/e* 387 (M^+). Found: C, 70.93; H, 6.58; N, 3.55%. Calcd for $C_{23}H_{25}FeNO$: C, 71.07; H, 6.53; N, 3.61%; mol wt, 387.

(1*S*)-(1*R*)-**8**: yield 92%, reddish viscous oil, $[\alpha]_D^{20}$ +1972° (*c* 0.043, $CHCl_3$). IR: 1660 (C=O), 1600 and 970 (*trans* –CH=CH–), 1100, 1000, and 910 cm^{-1} (1,2-disubstituted Fc ring). NMR: δ 1.45 (d, 3H, $-CH_3$), 2.06 (s, 6H, $-N-(CH_3)_2$), 3.85 (q, 1H, –CH–), 4.06, 4.44, and 4.67 (m, 8H, Fc protons), 7.13 (d, 1H, –C=CH–CO–), 7.45 (m, 5H, Ph), and 7.86 ppm (d, 1H, –CH=C–CO–). MS: *m/e* 387 (M^+).

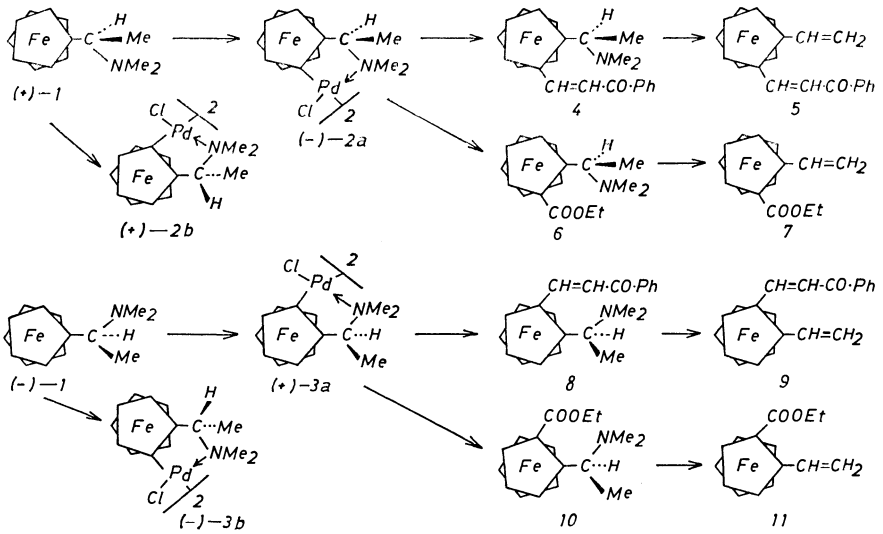

Fig. 1.

Found: C, 71.18; H, 6.55; N, 3.61%. Calcd for $C_{23}H_{25}FeNO$: C, 71.07; H, 6.53; N, 3.61%; mol wt, 387.

Synthesis of (1S)-5 and (1R)-9 Compounds. In acetone (15 ml), the (1*R*)-(1*S*)-**4** or (1*S*)-(1*R*)-**8** compound (1.00 g), and methyl iodide (10.0 g) were refluxed for 20 min; the solution was then diluted with ether (30 ml), washed with 8% aqueous phosphoric acid and saturated sodium hydrogencarbonate solution, dried over anhydrous magnesium sulfate, and evaporated. The residue was purified by column chromatography (silica gel-benzene).

(*1S*)-**5**: yield 34%, mp 91—92 °C, $[\alpha]_D^{20}$ −2229° (*c* 0.084, $CHCl_3$). IR: 1660 (C=O), 1600 and 980 (*trans* –CH=CH–), 1100, 1000, and 910 (1,2-disubstituted Fc ring), 990 and 900 cm^{-1} (–C=CH_2). NMR: δ 4.08, 4.53, and 4.73 (m, 8H, Fc protons), 5.18 and 5.43 (m, 2H, Fc–C=CH_2), 6.85 (m, 1H, Fc–CH=C–), 7.16 (d, 1H, –C=CH–CO–), 7.45 (m, 5H, Ph), 7.92 ppm (d, 1H, –CH=C–CO–). MS: *m/e* 342 (M^+). Found: C, 73.58: H, 5.22%. Calcd for $C_{21}H_{18}FeO$: C, 73.70; H, 5.30%; mol wt, 342.

(1*R*)-**9**: yield 40%, mp 91—92 °C, $[\alpha]_D^{20}$ +2238° (*c*, 0.082, $CHCl_3$). IR: 1660 (C=O), 1600 and 980 (*trans* –CH=CH–), 1100, 1000, and 910 (1,2-disubstituted Fc ring), 990 and 900 cm^{-1} (–CH=CH_2). NMR: δ 4.08, 4.53, and 4.72 (m, 8H, Fc protons), 5.18 and 5.43 (m, 2H, Fc–C=CH_2), 6.85 (m, 1H, Fc–CH–C–), 7.16 (d, 1H, –C=CH–CO–), 7.45 (m, 5H, Ph), 7.92 ppm (d, 1H, –CH=C–CO–). MS: *m/e* 342 (M^+). Found: C, 73.61; H, 5.18%. Calcd for $C_{21}H_{18}FeO$: C, 73.70; H, 5.30%; mol wt, 342.

Synthesis of (1R)-(1S)-6 and (1S)-(1R)-10. In the presence of triphenylphosphine (1.2 g; 4.6 mmol) in ethanol (70 ml), (1*R*)-(1*S*)-**2a** or (1*S*)-(1*R*)-**3a** (2.0 g, 2.3 mmol) was carbonylated with shaking at 100 °C under carbon monoxide at 70 atm for 10 h. The reaction mixture was filtered to remove precipitated palladium and evaporated to dryness and the residue purified by column chromatography (silica gel-benzene).

(1*R*)-(1*S*)-**6**: yield 20%, reddish viscous oil, $[\alpha]_D^{20}$ +141.0° (*c* 0.85, $CHCl_3$). IR: 1705 (ester), 1100, 1000, and 910 cm^{-1} (1,2-disubstituted Fc ring). NMR: δ 1.24 (t, 3H, -O-C-CH_3), 1.35 (d, 3H, $-CH_3$), 2.08 (s, 6H, $-N(CH_3)_2$), 3.78 (q, 1H, -CH-), 4.22 (q, 2H, $-CH_2-$), 4.12, 4.52, and 4.84 ppm (m, 8H, Fc protons). MS: *m/e* 329 (M^+). Found: C, 61.93; H, 6.88; N, 4.07%. Calcd for $C_{17}H_{23}FeNO_2$: C, 62.02; H, 7.03; N, 4.25%; mol wt, 329.

(1*S*)-(1*R*)-**10**: yield 25%, reddish viscous oil, $[\alpha]_D^{20}$ −137.0° (*c* 0.85, $CHCl_3$). IR: 1705 (ester), 1100, 1000, and 910 cm^{-1} (1,2-disubstituted Fc ring). NMR: δ 1.24 (t, 3H, -O-C-CH_3), 1.35 (d, 3H, $-CH_3$), 2.08 (s, 6H, $-N(CH_3)_2$), 3.78 (q, 1H, –CH–), 4.22 (q, 2H, $-CH_2-$), 4.12, 4.52, and 4.84 ppm (m, 8H, Fc protons). MS: *m/e* 329 (M^+). Found: C, 61.90; H, 6.93; N, 4.11%. Calcd for $C_{17}H_{23}FeNO_2$: C, 62.02; H. 7.03; N, 4.25%; mol wt, 329.

Synthesis of (1S)-7 and (1R)-11. In acetone (15 ml), (1*R*)-(1*S*)-**6** or (1*S*)-(1*R*)-**10** (1.00 g), and methyl iodide (10.0 g) were refluxed for 20 min; then the solution was diluted with ether (30 ml), washed with 8% aqueous phosphoric acid and saturated sodium hydrogencarobonate solution, dried over anhydrous magnesium sulfate, and evaporated. The residue was purified by column chromatography (silica gel-benzene).

(1*S*)-**7**: yield 40%, reddish viscous oil, $[\alpha]_D^{20}$ +179.8° (*c* 0.26, $CHCl_3$). IR: 1710 (ester), 1100, 1000, and 910 (1,2-disubstituted Fc ring), 1410, 995, and 900 cm^{-1} (–CH=CH_2). NMR: δ 1.28 (t, 3H, –O–C–CH_3), 4.27 (q, 2H, $-CH_2-$), 4.13, 4.41, and 4.76 (m, 8H, Fc protons), 5.15 and 5.44 (m, 2H, Fc–C–CH_2), and 7.23 ppm (m, 1H, Fc–CH=C–). MS: *m/e* 284 (M^+). Found: C, 63.33; H, 5.58%. Calcd for $C_{15}H_{16}FeO_2$: C, 63.40; H, 5.67%; mol wt, 284.

(1*R*)-**11**: yield 35%, reddish viscous oil, $[\alpha]_D^{20}$ −175.5° (*c* 0.182, $CHCl_3$). IR: 1710 (ester), 1100, 1000, and 910 (1,2-disubstituted Fc ring), 1410, 995, and 900 cm^{-1} (–CH=CH_2). NMR: δ 1.28 (t, 3H, –O–C–CH_3), 4.27 (q, 2H, $-CH_2-$), 4.13, 4.41, and 4.75 (m, 8H, Fc protons), 5.15 and 5.44 (m, 2H, Fc–C–CH_2), and 7.23 ppm (m, 1H, Fc–CH=C–). MS: *m/e* 284 (M^+), Found: C, 63.26; H, 5.61%. Calcd for $C_{15}H_{16}FeO_2$: C, 63.40; H, 5.67%; mol wt, 284.

References

1) J. Tsuji, *Yuki Gosei Kagaku Kyokai Shi*, **35**, 10 (1977).

2) H. Takahashi and J. Tsuji, *J. Organomet. Chem.*, **10**, 511 (1967); J. M. Thompson and R. F. Heck, *J. Org. Chem.*, **40**, 2667 (1975).

3) R. A. Holton, *Tetrahedron Lett.*, **1977**, 355.

4) a) T. Aratani, T. Gonda, and H. Nozaki, *Tetrahedron*, **26**, 5453 (1970); b) D. Marquarding, H. Klusacek, G. Gokel, P. Hoffmann, and I. Ugi, *J. Am. Chem. Soc.*, **92**, 5389 (1970); c) L. F. Battelle, R. Bau, G. W. Gokel, R. T. Oyakawa and I. Ugi, *ibid.*, **95**, 482 (1973).

5) a) V. I. Sokolov, L. L. Troitskays, and O. A. Reutov, *J. Organomet. Chem.*, **133**, C28 (1977); b) V. I. Sokolov, L. L. Troitskays, and O. A. Reutov, *Dokl. Akad. Nauk SSSR*, **236**, 371 (1977).

6) E. L. Eliel, "Stereochemistry of Carbon Compounds," McGraw-Hill, New York (1962), p 151.

7) L. F. Hines and J. K. Stille, *J. Am. Chem. Soc.*, **94**, 485 (1972); Y. Becker and J. K. Stille, *ibid.*, **100**, 838 (1978).

BULLETIN OF THE CHEMICAL SOCIETY OF JAPAN, VOL. 52 (3), 959—960 (1979)

Photochemical Formation of Tetrahydro-2-furyl Ether in Alcohol–Tetrahydrofuran–Iron(III) Chloride System

Hideo KUROKAWA, Tatsuzo ISHIGAMI, Katsuaki MORIMOTO, and Akira SUGIMORI*

Department of Chemistry, Faculty of Science and Technology, Sophia University, Kioi-cho 7, Chiyoda-ku, Tokyo 102

(Received October 12, 1978)

Synopsis. Primary and secondary alcohols are converted into the corresponding tetrahydro-2-furyl ethers upon UV- and solar irradiation of alcohol and tetrahydrofuran in the presence of iron(III) chloride.

Preparative organic chemists have expressed increasing interest in the photoreactions which can occur in the presence of metal ions. As for the catalysis of iron(III) under illumination, methoxylation of styrene[1] and coupling of toluene[2] have been reported. Kochi reported the formation of 2-(4-chlorobutoxy)tetrahydrofuran in the photolysis of tetrahydrofuran–copper(II) system.[3] We report here the photochemical formation of tetrahydro-2-furyl ether catalyzed by iron(III) chloride. Several interesting photosubstitution reactions of tetrahydrofuran by sulfur dioxide[4] and 1,2,4,5,-tetracyanobenzene[5] have also been reported. As the method for the preparation of tetrahydro-2-furyl ethers, the reaction of alcohol with 2,3-dihydrofuran,[6] the reaction of alcohol, tetrahydrofuran, and *t*-butyl perbenzoate in the presence of copper(I) chloride[7] and the reaction of 4-formyloxybutyraldehyde with trialkyl orthoformate[8] have been reported.

Experimental

Materials. Tetrahydrofuran(THF) was purified according to Zweifel.[9] When THF was not treated with $LiAlH_4$, a small amount of tetrahydrofuryl ether was formed without irradiation. This is probably due to the reaction induced by peroxides contained in the non-purified THF, similar to the reaction induced by *t*-butyl perbenzoate in the presence of copper(I) chloride.[7] Commercially available alcohols were used after the purification by distillation or by recrystallization.

Irradiation. The general procedure is as follows. A solution containing alcohol(1.0 mmol) and iron(III) chloride (1.0 mmol) in 40 cm^3 of THF is irradiated with a low or a high pressure mercury lamp or with sunlight under nitrogen at room temperature. Quartz and glass vessels were employed in UV and sunlight irradiation, respectively.

Products. After irradiation, the reaction mixture was washed with sodium hydrogencarbonate solution and extracted with diethyl ether. The products were separated by means of thin layer chromatography. Tetrahydro-2-furyl ethers were identified on the basis of IR, NMR, and mass spectra.

Cinnamyl tetrahydro-2-furyl ether (liquid): IR 3030 (aromatic C–H), 2940, 2880 (aliphatic C–H), 1180, 1080 cm^{-1} (ether C–O) No absorption which can be assigned to O–H was observed. NMR(CCl_4) δ=1.84(4H, m, $C\underline{H}_2$ in THF moiety), 3.81(2H, t, J=3 Hz $C\underline{H}_2$ in THF moiety), 4.14 (2H, d, J=6 Hz, $C\underline{H}_2$–O in alcohol moiety), 5.06(1H, t, J=4.5 Hz, O–C$\underline{H}$–O), 6.28(2H, m, olefinic), 7.20(5H, m, phenyl). The NMR spectra are very similar to those of cinnamyl tetrahydro-2-pyranyl ether prepared from 3,4-dihydro-2*H*-pyran and cinnamyl alcohol. MS (70 eV), *m/e*(relative intensity), 204(2), 160(3), 132(4), 131(5), 118(11), 117(23, $[C_6H_5CH{=}CH_2]^+$),116(3), 115(3), 106(7), 105(7), 77(4), 72(5), 71(100, [tetrahydrofuryl]$^+$), 70(3), 57(3), 43(12). Found: C, 75.57; H, 7.94%; M^+, 204. Calcd for $C_{13}H_{16}O_2$: C, 76.44; H, 7.90%; M, 204. By refluxing the ether with hydrochloric acid, cinnamyl alcohol was obtained.

Cholesteryl tetrahydro-2-furyl ether(liquid): IR 2940, 2900, 2860(aliphatic C–H), 1090, and 1040 cm^{-1}(ether C–O); NMR(CCl_4) δ=0.7—2.3, 3.30(O–C$\underline{H}$ of cholesteryl moiety), 3.73($C\underline{H}_2$–O of THF moiety), 5.10(O–C$\underline{H}$–O), and 5.22(olefinic); Found: C, 81.03; H, 12.07%, Calcd for $C_{31}H_{54}O_2$: C, 81.16; H, 11.86%. Reflux of the ether (0.2 mmol) in aqueous ethanol in the presence of *p*-toluenesulfonic acid gave cholesterol (yield by TLC, 62%).

Other tetrahydro-2-furyl ethers were identified by the comparison of their IR and NMR spectra with those of tetrahydro-2-pyranyl ethers prepared by 3,4-dihydro-2*H*-pyran with alcohols. NMR spectra of tetrahydro-2-furyl ethers have a good correspondence with those of methyl and ethyl tetrahydro-2-furyl ether reported by Frehel and Delongchamps.[8] Hexyl,[7] cyclohexyl,[6] and benzyl[6] tetrahydro-2-furyl ethers are described in the literature.

Butyl tetrahydro-2-furyl ether (liquid): IR 2990, 2950, 2870 (aliphatic C–H), 1460, 1440 (CH_2 and CH_3), 1195, and 1040 cm^{-1} (ether C–O); NMR(CCl_4) δ=0.87(3H, t, J=6.8 Hz, $C\underline{H}_3$), 1.36(4H, m, $C\underline{H}_2$ of alcohol moiety), 1.80 (4H, m, $C\underline{H}_2$ of THF moiety), 3.1—3.9 (4H, m, $C\underline{H}_2$–O of alcohol and THF moieties), 4.92 (1H, t, J=4 Hz, O–C$\underline{H}$–O).

s-Butyl tetrahydro-2-furyl ether(liquid): IR 2950, 2900 (aliphatic C–H), 1090, and 1030 cm^{-1} (ether C–O); NMR (CCl_4) δ=0.9—1.6 (8H, ethyl and methyl of alcohol moiety), 1.80 (4H, $C\underline{H}_2$ of THF moiety), 3.5—3.7(3H, m, O–$C\underline{H}_2$ of THF moiety and O–C$\underline{H}$ of alcohol moiety), 5.08 (1H, t, J=4 Hz, O–C$\underline{H}$–O).

Hexyl tetrahydro-2-furyl ether (liquid): IR 2950, 2920, 2850 (aliphatic C–H), 1450 (CH_2 and CH_3) 1100. 1090, and 1040 cm^{-1} (ether C–O); NMR(CCl_4) δ=0.88 (3H, t, J=5.7, CH_3), 1.32 (8H, m, CH_2 of alcohol moiety), 1.80-(4H, m, $C\underline{H}_2$ of THF moiety), 3.61 (4H, m, $C\underline{H}_2$–O of alcohol and THF moieties), 4.94 (1H, t, J=4 Hz, O–C$\underline{H}$–O).

Cyclohexyl tetrahydro-2-furyl ether (liquid): IR 2930, 2850 (aliphatic C–H), 1450(CH_2), 1090, and 1040 cm^{-1} (ether C–O); NMR(CCl_4) δ=1.2—1.8 (14H, CH_2 in cyclohexyl and THF moieties), 3.2—3.8(3H, m, C$\underline{H}$–O of cyclohexyl moiety and $C\underline{H}_2$–O of THF moiety), 5.10(1H, t, J=4.5 Hz, O–C$\underline{H}$–O).

Benzyl tetrahydro-2-furyl ether(liquid) : IR 3030(aromatic C–H), 2970, 2940, 2880,(aliphatic C–H) 720, and 690 cm^{-1} (monosubstituted benzene); NMR(CCl_4) δ=1.89 (4H, m, $C\underline{H}_2$ in THF moiety), 3.82(2H, $C\underline{H}_2$–O in THF moiety), 4.55 (2H, CH_2–O of alcohol moiety), 5.10 (1H, t, J=4.5 Hz,

Table 1. Photochemical formation of tetrahydro-2-furyl ether in alcohol–tetrahydrofuran–iron(III) chloride system

Alcohol	Light source[a]	Irradiation time (h)	Yield of ether (%)	Recovered starting material (%)
Butyl alcohol[b]	LP	24	86	
	HP	24	97	
	Solar	6	46	
Hexyl alcohol[b]	LP	24	40	
	HP	16	70	
	Solar	6	46	
s-Butyl alcohol[b]	LP	24	66	
	HP	24	43	
	Solar	6	26	
Cyclohexanol[b]	LP	24	51	
	HP	24	43	
	Solar	6	37	
Benzyl alcohol[c]	LP	16	48	
	HP	16	46	
	Solar	6	24	
Cinnamyl alcohol[c]	LP	24	36	
	HP	24	27	
	Solar	6	18	
Cholesterol[c]	LP	24	15	53
	HP	24	14	39
	Solar	6	14	61

a) LP=low pressure mercury lamp, HP=high pressure mercury lamp. b) Yield was determined gas-chromatographically. c) Yield was determined by means of thin layer chromatography.

O–CH–O), 7.28 (5H, phenyl). Found: C, 73.18; H, 7.37%.

Gas-Chromatographic Analysis. Gas-chromatographic analysis was performed with a Shimadzu GC-6A equipped with 2 m column of Carbowax 20M at about 100 °C.

Results and Discussion

Primary and secondary alcohols react with tetrahydrofuran (THF) under irradiation in the presence of iron(III) chloride to give the corresponding tetrahydro-2-furyl ether of alcohols.

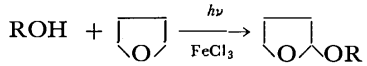

The results are shown in Table 1. Both aliphatic and aromatic alcohols give photochemically tetrahydrofuryl ether, but *t*-butyl alcohol does not undergo the photoetherification. Tetrahydro-2-furyl ethers are formed upon irradiation not only with a low or a high pressure mercury lamp, but also with sunlight. The presence of iron(III) chloride as the catalyzer in the reaction is essential, since no reaction took place in the absence of iron(III) chloride. These facts suggest that the photoreaction has a possibility for synthetic utilization of sunlight catalyzed by metal ions.[10]

The formation of tetrahydro-2-furyl ether is accompanied by that of iron(II). In the initial stage, the consumption of iron(III) is nearly twice as much as the formation of tetrahydro-2-furyl ether : in hexyl alcohol–THF–$FeCl_3$ system(hexyl alcohol : $FeCl_3$ = 1 : 1) the ratio of iron(II) to hexyl tetrahydro-2-furyl ether at 1 and 2 hours' irradiation were 2.5 and 1.8, respectively. The formation of $CH_3\dot{C}HOCH_2CH_3$ was reported in the UV-irradiation of the diethyl ether–iron(III) system.[11] One mole of iron(III) is consumed for the generation of tetrahydro-2-furyl radicals, probably *via* the electron transfer from THF to iron(III).

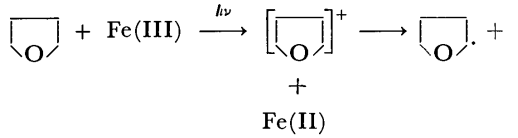

The second step in which iron(III) participates would be the oxidation of tetrahydro-2-furyl radicals to give tetrahydro-2-furyl cations, which react with alcohol in the following scheme.

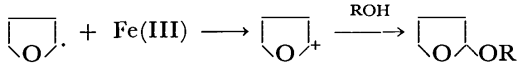

The present work was partially supported by a Grant-in-Aid for Scientific Research from the Ministry of Education, Science and Culture (No. 147026).

References

1) S. A. Ivanitskaya, V. K. Pogorelyi, and A. I. Kryukov, *Dokl. Akad. Nauk. SSSR*, **206**, 140 (1972).
2) H. Inoue, M. Izumi, and E. Imoto, *Chem. Lett.*, **1973**, 571.
3) J. K. Kochi, *J. Am. Chem. Soc.*, **84**, 2121 (1962).
4) H. Takeuchi, T. Nagai, and N. Tokura, *Bull. Chem. Soc. Jpn.*, **46**, 695 (1973).
5) M. Ohashi and K. Tsujimoto, *Chem. Lett.*, **1975**, 829.
6) E. L. Eliel, B. E. Nowak, R. A. Daignault, and V. G. Badding, *J. Org. Chem.*, **30**, 2441 (1965).
7) S. -O. Lawesson and C. Berglund, *Acta Chem. Scand.*, **14**, 1854 (1960); *Arkiv Kemi*, **17**, 475 (1961).
8) D. Frehel and P. Delongchamps, *Can. J. Chem.*, **50**, 1783 (1972).
9) L. F. Fieser and M. Fieser, "Reagents for Organic Synthesis," John Wiley, N. Y. (1967), Vol. 1, p. 1140.
10) Tetrahydro-2-furyl ether is easily hydrolyzed by refluxing with acid to give the starting alcohol. Like tetrahydro-2-pyranyl ether, tetrahydro-2-furyl ether can be used for the protection of the hydroxyl group.
11) S. A. Ivanitskaya, A. N. Korol, and A. I. Kryukov, *Ukr. Khim. Zh.*, **39**, 1248 (1973).

BULLETIN OF THE CHEMICAL SOCIETY OF JAPAN, VOL. 52 (3), 961—962 (1979)

Nature of Bonding in Pyrazine-2,3-dicarboxamide Complexes of Copper(II), Cobalt(II), and Nickel(II)

G. S. SANYAL* and S. K. MONDAL†

Department of Chemistry, University of Kalyani, Kalyani, West Bengal, India

† *Department of Inorganic Chemistry, Indian Association for the Cultivation of Science, Calcutta 700032, India*

(Received August 8, 1977)

Synopsis. Pyrazine-2,3-dicarboxamide complexes with the perchlorates of copper(II), cobalt(II), and nickel(II) have been prepared and characterised, copper having a square planar configuration and cobalt and nickel an octahedral geometry. Bonding takes place through a ring nitrogen and the oxygen atom of the adjacent amide group.

Heterocyclic carboxamides are known to possess powerful antitubercular activity.[1] During the course of the investigation on metal ion-assisted hydrolysis of pyrazine-2,3-dicarboxamide (pzda), a paper[2] was published on several cobalt and nickel(II) complexes with both ring nitrogens of the ligand bonded to the same metal without participation of the amide groups. The structure seemed untenable to us. Since delineation of the above mentioned reaction requires knowledge of the bonding in metal complexes, this problem has been reinvestigated. In this study perchlorate has been chosen as the anion since the stereochemistry will not be affected by the anion participation.

Experimental

Preparation. To the ligand (0.2 g) dissolved in water (30 ml) on a steambath, was added the metal perchlorate (1 g). The copper compound which separated as bluish violet crystals when cooled to room temperature, was washed with cold water and recrystallised from hot water. Large orange-red crystals of the cobalt(II) complex and greenish crystals of the nickel(II) complex, however, separated on slow evaporation of the solution over concentrated H_2SO_4. The crystals were filtered, washed with dry ethanol, dried in air. The analytical data (Table 1) confirms the complexes to be $[Cu(pzda)_2](ClO_4)_2$ (I), $[Co(pzda)_2(H_2O)_2](ClO_4)_2$-(II), and $[Ni(pzda)_2(H_2O)_2](ClO_4)_2$ (III) respectively.

Results and Discussion

The preparation of pyrazine-2,3-dicarboxamide complexes possessed difficulties because of the poor solubility of the ligand in common organic solvents including 1-butanol used by Singh *et al.*,[2] consequently an aqueous solution of the ligand was used for preparation of the complexes. Since the copper(II) complex, cobalt(II) and nickel(II) compounds decomposed on dissolution in water, an excess of the metal perchlorates which consumed the ligand totally and hindered any dissociation was used.

Table 2 shows the important IR bands of the ligand, its deuterated form, and the metal complexes. The assignments of these bands can readily be made by comparing them with the 2-pyridine carboxamide (pya) and 2-pyrazine carboxamide (pza) complexes,[3,4] and by taking into considerations the pyrazine ring vibrations.[5] In all the complexes the asymmetric and symmetric OCN stretching bands are shifted to lower and higher frequencies respectively relative to the free ligand, indicating that coordination takes place through the oxygen atom of the amide group. Similar shifts describing coordination through amide oxygen have been observed for complexes of 2-pyridine carboxamide,[3,6,7] 2-pyridine acetamide,[8] 2-pyrazine carboxamide[9] and 8-quinoline carboxamide.[10]

The room temperature magnetic moments and electronic spectra (Table 1) are indicative of the square planar configuration of the copper complex and the octahedral geometry of the cobalt(II) and nickel(II) complexes.[11] In an aqueous solution the copper(II) complex shows only a single broad band (10520—

Table 1. Elemental analysis,[a] magnetic moments, and electronic spectra of metal complexes of pyrazine-2,3-dicarboxamide

Compound	%C	%H	%N	%M	%ClO_4	μ_{eff} in B. M. (27 °C)	$\frac{\nu_{max}}{cm^{-1}}$	Transition	$\frac{10\,Dq}{cm^{-1}}$
I	24.42	1.95	18.64	10.61	33.42	2.01	12100[b]	$^2B_{1g}$-$^2A_{1g}$	
	(24.23)	(2.02)	(18.64)	(10.69)	(33.46)		18180 sh	$^2B_{1g}$-^2E_g	
II	23.14	2.54	17.74	9.53	31.70	3.48	10100	$^4T_{1g}$-$^4T_{2g}$	11120
	(23.00)	(2.55)	(17.88)	(9.39)	(31.79)		17530	?	
							20850	$^4T_{1g}$-$^4T_{1g}^{(P)}$	
III	23.32	2.53	17.76	9.28	31.68	4.74	10160	$^3A_{2g}$-$^3T_{2g}$	10160
	(23.00)	(2.55)	(17.88)	(9.41)	(31.78)		11770 sh	$^3A_{2g}$-^1E_g	
							17400	$^3A_{2g}$-$^3T_{1g}$	

a) Calculated values in parenthesis. Electronic spectra in Nujol mulls. b) This band is observed both in aqueous solutions and in Nujol mulls.

Table 2. Infrared spectra of pyrazine-2,3-dicarboxamide and of its metal complexes in KBr discs, cm^{-1}

pzda		Cu	Ni	Co	Assignment
H	D[a]				
3430(s)	2580(s)	3440(m)	3420(s, b)[b]	3430(s, b)[b]	NH_2 antisym. stretch
3310(s)	2540(s)	3380(w)	3320(m)	3320(m)	NH_2 sym. stretch
3205(m)	2410(m)	3290(m)			
1695(sh)	1660(s)	1690(sh)	1670(s)	1695(s)	OCN antisym. stretch
1680(sh)		1660(s)		1670(sh)	(mainly C=O stretch)
1615(m)	1170(m)				NH_2 scissoring
	1140(m)				
1565(m)	1565(m)	1565(m)	1565(m)	1560(m)	Pyrazine ring
1445(w)	1440(m)	1530(w)	1535(sh)	1540(sh)	vibration
		1425(m)	1425(w)	1420(w)	
1395(m)	1410(m)	1405(w)	1400(w)	1400(w)	OCN sym. stretch
1348(m)	1355(m)	1365(m)	1365(w)	1360(w)	(mainly C-N stretch)

a) D stands for the deuterated ligand. Bands occuring at lower frequencies are not shown. b) Broadening of this band indicates its merger with OH stretching of water molecules.

14300 cm^{-1}). The mull spectrum, however, shows the presence of a shoulder in addition to that observed in solution. It is expected that due to the absence of Jahn-Teller distortion more bands should appear in the visible range,[12] Ferguson has shown[13] that distinct bands observed in the polarised spectra of square planar copper(II) complexes are considerably broadened in solution. It has therefore been concluded that the square planar geometry of the copper(II) complex is retained in solution.

Regarding the nature of bonding in pyrazine-2,3-dicarboxamide complexes support is given by the X-ray crystallographic study of $[Cu(pzda)_2]$ $(ClO_4)_2$.[14]

Thanks are due to Dr. K. Nag, Department of Inorganic Chemistry, Indian Association for the Cultivation of Science, Calcutta-32 for his helpful discussions.

References

1) S. Kushner, H. Dallalian, J. L. Senjurjo, F. L. Bach Jr., S. R. Safir, V. K. Smith Jr., and J. H. Williams, *J. Am. Chem. Soc.*, **74**, 3617 (1952).
2) P. P. Singh and J. N. Seth, *J. Inorg. Nucl. Chem.*, **37**, 593 (1975).
3) M. Sekizaki and K. Yamasaki, *Spectrochem. Acta, Part A*, **25**, 475 (1969).
4) M. Mikami, I. Nakagawa, and T. Shimanouchi, *Spectrochim. Acta, Part A*, **25**, 365 (1969).
5) C. N. R. Rao, "Chemical Applications of Infrared Spectroscopy," Academic Press, New York (1963), p. 325.
6) M. Sekizaki and K. Yamasaki, *Nippon Kagaku Zasshi*, **87**, 1053 (1966).
7) M. Sekizaki, M. Tanase, and K. Yamasaki, *Bull. Chem. Soc. Jpn.*, **42**, 399 (1969).
8) M. Sekizaki and K. Yamasaki, *Inorg. Chim. Acta*, **4**, 296 (1970).
9) M. Sekizaki and K. Yamasaki, *Rev. Chim. Miner.*, **6**, 255 (1969).
10) M. Noji, Y. Kidani, and H. Koike, *Bull. Chem. Soc. Jpn.*, **48**, 2274 (1975).
11) A. B. P. Lever, "Inorganic Electronic Spectroscopy," Elsevier, Amsterdam (1968), p. 318.
12) D. W. Smith, *Inorg. Chem.*, **5**, 2236 (1966).
13) J. Ferguson, *J. Chem. Phys.*, **54**, 1609 (1961).
14) M. Mondal and S. Ray, *Acta Crystallogr., Sect. B*, **33**, 2297 (1977).

Intercalation Compounds FeOCl(Pyridine derivatives)$_{1/n}$ and FeOCl(*n*-Propylamine)$_{1/4}$

Shinichi KIKKAWA, Fumikazu KANAMARU,† and Mitsue KOIZUMI*

The Institute of Scientific and Industrial Research, Osaka University, Suita, Osaka 565

†*Research Institute for Non-crystalline Materials, School of Engineering, Okayama University, Okayama 700*

(Received April 24, 1978)

Some pyridine derivatives were intercalated into the van der Waals gap of layered compound FeOCl. Pyridine, 2,6-dimethylpyridine, 4-aminopyridine, 2,4,6-trimethylpyridine, and *n*-propylamine were used as intercalates having different Lewis basicities. X-Ray diffraction, Mössbauer effect, electrical resistivity, ESR and electronic spectra were studied, some correlations being found between the measured parameters of these complexes and the basicities of organic intercalates. It is assumed that organic intercalates transfer their lone pair electrons on the nitrogen atom to FeOCl layers.

Iron oxychloride is a layered compound belonging to an orthorhombic space group Pmnm with $a=3.780$, $b=7.917$, $c=3.302$ Å, and $Z=2$.[1] The crystal structure consists of a stack of double layer sheet of *cis*-$FeCl_2O_4$ octahedra linked together with shared edges. The outermost atoms at each side of the layers are Cl ions. The interlayer bonding between adjacent layers is van der Waals interaction. Hagenmüller *et al.* found that FeOCl reacts with ammonia and some amine molecules.[2] Kanamaru *et al.* reported the intercalation of pyridine into FeOCl, and observed remarkable changes in electrical and magnetic properties.[3-5] The changes can be attributed to charge transfer from the nitrogen atom of the intercalated pyridine molecule to the FeOCl layer.

Transition metal dichalcogenides (MX_2) intercalate some organic bases. Their superconducting transition temperatures (T_c) change with organic intercalation. Bray and Sauer measured the lone pair electron densities on nitrogen atoms of organic bases by means of nuclear quadrupole resonance.[6] The electron densities were correlated with T_c of the intercalated MX_2. Lewis basicity of organic base is a measure of the ability to donate electrons to acids. pK_a value would be qualitatively related to the change of the property of host caused by intercalation if charge-transfer interaction is significant in the bonding between host layer and guest molecule.

Effect of pK_a on the properties of FeOCl-organic complexes can be checked by use of some pyridine derivatives having different basicities. Pyridine derivatives can act as either n- or π-donor.[7] Study on aliphatic amine is useful to distinguish the effects of these two kinds of electrons in comparison with pyridine intercalated complexes.

The present report deals with intercalation of some pyridine derivatives and *n*-propylamine into FeOCl. Electrical resistivity, Mössbauer effect, ESR and electronic spectrum were studied for these intercalated compounds. Some correlations were found between basicities of the intercalate and properties of the products. The possibility of charge transfer is discussed on FeOCl (organic compound)$_{1/n}$.

Experimental

Preparation. Iron oxychloride was prepared by heating a mixture of α-Fe_2O_3 and $FeCl_3$ with mole ratio 1 : 4/3 in a sealed Pyrex glass tube at 370 °C for two days. The product was washed with water and dried. Reddish violet and thin blade-like FeOCl crystals were obtained.

The reactions with pyridine (Py) and its derivatives, 2,6-dimethylpyridine (DMP), 4-aminopyridine (AP), and 2,4,6-trimethylpyridine (TMP), were conducted at 100 and 40 °C, respectively, in a closed system for about a week. Intercalation of *n*-propylamine (PA) was completed within 1 h at room temperature. Since Py, DMP, TMP, and PA are liquid at room temperature, FeOCl was directly soaked into these liquids. The acetone solution of AP was used for solid AP. The intercalated compounds obtained were black crystals. X-Ray diffractometry showed no unreacted FeOCl. Chemical analyses of C, H, and N showed that each intercalated compound has a stoichiometric composition. If the complex is represented by FeOCl(organic compound)$_{1/n}$, *n*-values are four for Py, DMP, AP, and PA, and six for TMP, respectively

Measurement. X-Ray analysis was carried out with a Rigaku-Denki diffractomer using Fe-filtered Co $K\alpha$ radiations. The electrical resistivities of FeOCl and its complexes were measured in the temperature range 373—200 K using carbon electrodes. The Mössbauer spectra were measured at room temperature and at liquid nitrogen temperature using radiation from ^{57}Co in Pd metal with a 200 channel multichannel analyzer. Samples were dispersed with silicon grease, the thickness being *ca.* 30 mg/cm^2. Calibration was based on the Mössbauer spectrum of Fe metal. The ESR measurements of FeOCl and its complexes were carried out on a JES-ME-2X spectrometer at 77 K and at room temperature. Ultraviolet spectra of FeOCl and the intercalated complexes were obtained by the diffuse reflectance method. Samples were dispersed in MgO. Transmission method was used for the intercalates themselves, which were diluted with cyclo hexane.

Results

The *b*-values corresponding to the interlayer distances are summarized in Table 1. Each *b*-value for the complexes is much larger than 7.92 Å for FeOCl. The expansion is explained by the insertion of organic intercalates into the van der Waals gap of FeOCl.

FeOCl is a semiconductor with resistivity of 10^6 Ω cm at room temperature. The intercalated complexes are still semiconductive, but exhibit improved electrical conductivities along their c-axis. Their electrical resistivities are 10—10^3 Ω cm at room temperature. The values are smaller than that of FeOCl by a factor of

10^{3-5}. The electrical activation energy also changes from 0.6 eV to 0.2—0.3 eV for the complexes.

Mössbauer spectra were obtained as shown in Fig. 1. The pertinent parameters at room temperature obtained with a least-squares fit computer program are summarized in Table 1. Isomer shifts of the intercalated pyridine derivative complexes are 0.40—0.44 mm/s. The values seem to increase with pK_a of organic intercalates, and are larger than 0.40 mm/s for FeOCl. Isomer shifts of Py- and PA-FeOCl complexes are also larger than that of FeOCl. Quadrupole splittings are 0.67—0.92 mm/s for the intercalated complexes, being smaller than 0.93 mm/s for pure FeOCl. Q.S. tends to decrease with increase in I.S.

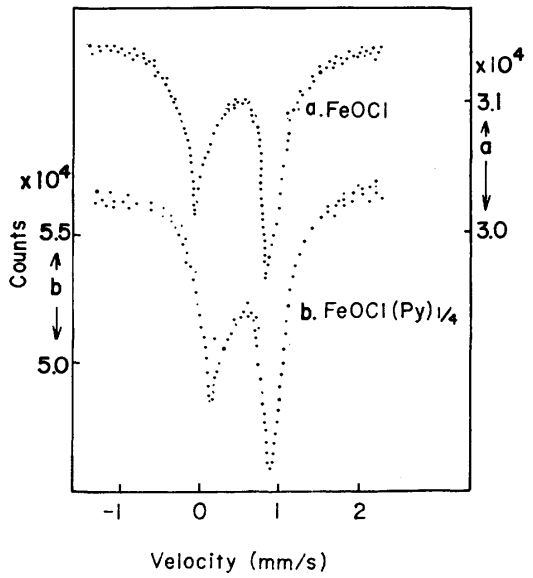

Fig. 1. Mössbauer spectra of FeOCl and FeOCl(Py)$_{1/4}$.

TABLE 1. PARAMETERS FOR FeOCl AND FeOCl(ORGANIC COMPOUND)$_{1/n}$

	pK_a	b(Å)	ρ (Ω cm)	E_a (eV)	I.S. (mm/s)	Q.S. (mm/s)	$\Delta H_{1/2}$ (G)
FeOCl		7.92	10^6	0.6	0.40	0.93	
FeOCl-(Py)$_{1/4}$	5.2	13.27	10	0.2	0.45	0.67	200
FeOCl-(DMP)$_{1/4}$	6.8	14.98	10^2	0.3	0.40	0.92	600
FeOCl-(AP)$_{1/4}$	9.2	13.57	10^3	0.2	0.42	0.84	1000
FeOCl-(TMP)$_{1/6}$	9.6	11.79	10^3	0.2	0.44	0.81	—
FeOCl-(PA)$_{1/4}$	10.5	11.89	10^2	0.2	0.44	0.68	900

The ESR spectra of FeOCl(pyridine derivative)$_{1/n}$ were recorded at room temperature and at 77 K. Except for TMP, broad singlet spectra were observed at g=2.003, their line shapes being almost Lorentzian. Neither FeOCl nor pyridine derivatives show any signals by themselves. The linewidth $\Delta H_{1/2}$ shows no change with temperature but changes with the kind of intercalate (Table 1). No signal was detected for TMP complex. In order to avoid the skin effect, some samples were dispersed in γ-alumina. Neither linewidths nor g-values were affected by dilution. Anisotropic effects were checked on highly preferred oriented samples. Signals did not change with directions of the samples to magnetic field.

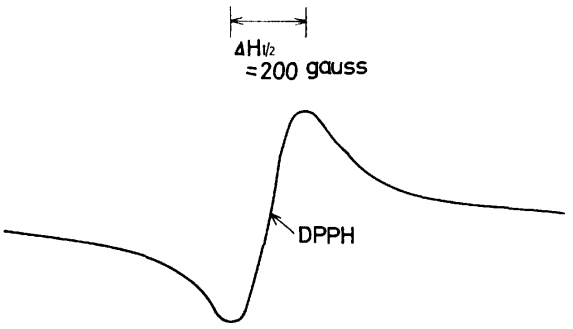

Fig. 2. ESR signal obtained for FeOCl(Py)$_{1/4}$.

Iron oxychloride shows no absorption in its ultraviolet spectrum. Pyridine has an intense $\pi \rightarrow \pi^*$ absorption at 250 nm, and a weak $n \rightarrow \pi^*$ one at 285 nm.[8] FeOCl-(Py)$_{1/4}$ complex has a broad and asymmetric absorption at about 270 nm, and FeOCl(pyridine derivative)$_{1/n}$ have absorptions around 265 nm. The latter absorptions are in almost the same regions as those of pyridine derivatives. n-Propylamine without π-electrons has an absorption at 261 nm with a shoulder at around 252 nm, but complex FeOCl(PA)$_{1/4}$ has a weak absorption at 248 nm. Furthermore, very broad absorptions around 310 nm were observed for both FeOCl(Py)$_{1/4}$ and FeOCl(PA)$_{1/4}$. Neither FeOCl nor the intercalates show any absorptions in this region; DMP, TMP, and AP complexes have no prominent absorptions.

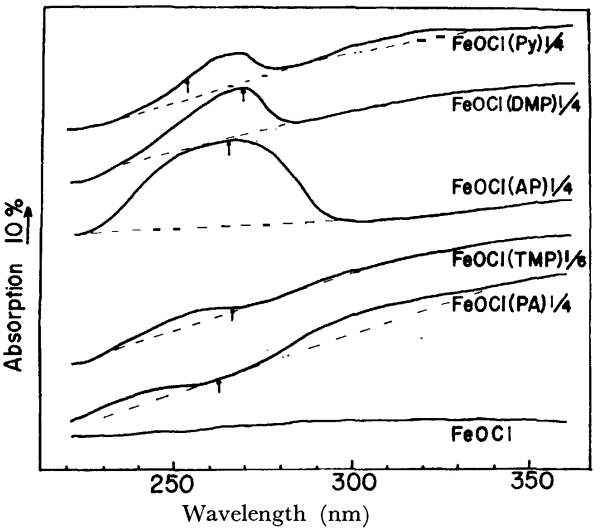

Fig. 3. Ultraviolet spectra of FeOCl and FeOCl(organic compound)$_{1/n}$. (Solid line).
Arrows show the positions of absorption maxima of organic compounds.

Discussion

Layered inorganic compound FeOCl intercalates some organic molecules. Each intercalated compound

has an expanded spacing between 11.79 and 14.98 Å (Table 1). The expanded spacings are explained by the insertion of organic intercalates into the van der Waals gap of FeOCl. Kanamaru *et al.* showed that planes of pyridine rings are perpendicular to the host layers so that nitrogen atoms face the layers in the pyridine complex.[4] However, FeOCl(PA)$_{1/4}$ seems to be in a different situation from pyridine complex since no more than approximately 4.0 Å is available between the layers. One of the sp^3 hybridized orbitals of terminal nitrogen atom, which contains lone pair electrons, faces the FeOCl layer, but the alkyl chain is nearly parallel to the host layer. For FeOCl(DMP)$_{1/4}$, FeOCl(AP)$_{1/4}$, and FeOCl-(TMP)$_{1/6}$, molecular orientations of pyridine derivatives in the interlayer space of FeOCl have been estimated using the results of one-dimensional electron density projections based on X-ray diffractions.[9] The pyridine ring of DMP is perpendicular to the host layer, but rotates a little around the center of the ring due to the steric effect of methyl groups. For FeOCl(AP)$_{1/4}$, the pyridine ring tilts slightly from a plane perpendicular to the layer. The inclination arises from a steric effect and the hydrogen bond between the amino group and the host layer. The pyridine ring of TMP is more tilted than that of DMP because of the larger steric effect of methyl groups of the former. However, in all cases, organic molecules are in the van der Waals gap so that their nitrogen atoms are as close to FeOCl layer as possible.

Parameters for FeOCl and FeOCl(organic compound)$_{1/n}$ are summarized in Table 1 with pK_a values of organic intercalates, which are values for pure organic compounds and not for the intercalated ones.[10] Formation of the complexes caused much reduction in electrical resistivity in the direction parallel to the host layer. The improved electrical conductivity can be explained by increased number of charge carriers. Mössbauer parameters change with intercalation. Isomer shifts of the complexes are slightly larger than that of FeOCl, but they are still those for ferric ions. The observed increase in I.S. values suggests the increased d-electron density around Fe atom in the intercalated FeOCl layer. However Fe^{2+} is not detected above liquid nitrogen temperature. A correlation between pK_a and I.S. is observed for pyridine derivative complexes. But FeOCl-(Py)$_{1/4}$ has the largest I.S., pyridine having the smallest pK_a. This suggests the importance of the effect of interaction between the side groups and Cl ions on the surface of FeOCl layer as well as that of pK_a. With increase of interaction between host and guest, charge carriers in the complexes tend to localize, electrical conductivity decreasing with increase in pK_a. The reduction of electrical resistivity and the increase of the isomer shift are explained by assuming the charge transfer from the nitrogen atoms of the intercalated organics to the FeOCl layer. The assumption seems to be supported by the molecular arrangements of intercalated organics in the interlayer region of FeOCl. ESR and UV spectroscopy were used in order to obtain direct evidences of the charge transfer.

Charge transfer interactions which involve formation of unpaired electrons were observed on ESR spectroscopy.[11,12] Very broad signals are detected on the intercalated FeOCl except for TMP complex. These signals are Lorentzian. They show no hyperfine, fine structures and anisotropic effects to magnetic field. *g*-Values are 2.003. Conduction electrons in metals and semiconductors sometimes show resonance of Lorentzian shape at around $g=2.003$, the linewidth becoming broader with increase of electrons.[13] ESR signal of charge transfer complex in solid state often loses its fine structure because of delocalization of the transferred electrons. In the case of FeOCl(organic compound)$_{1/n}$, the very broad ESR signal may be attributed to the conduction electrons formed in the host layer due to intercalation.

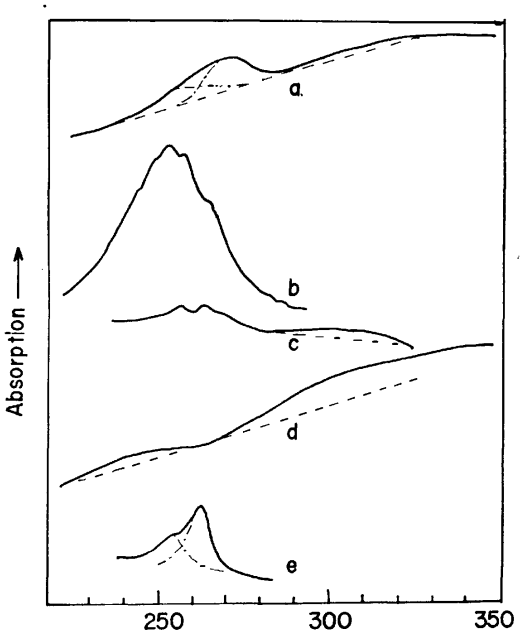

Fig. 4. Ultraviolet spectra of FeOCl(organic compound)$_{1/n}$.
a: FeOCl(Py)$_{1/4}$, b: pyridine c: $[IrOH(py)_2(NH_3)_3]^{2+}$
d: FeOCl(PA)$_{1/4}$, e: PA.

Figure 4 (a) and (d) show ultraviolet spectra of FeOCl-(Py)$_{1/4}$ and FeOCl(PA)$_{1/4}$, respectively. They have very broad absorptions around 310 nm observed in neither FeOCl nor the intercalates. These absorptions may be assigned to charge transfer bands as compared with that of $[IrOH(py)_2(NH_3)_3]^{2+}$ in which a similarly broad charge transfer band is observed at around 300 nm (Fig. 4 (c)).[14] For DMP-, AP-, and TMP-complexes, however, no clear C.T. absorptions are found in ultraviolet and visible regions. On the other hand, absorptions of the intercalates are perturbed by the intercalation into FeOCl. The pyridine $\pi \rightarrow \pi^*$ absorption in FeOCl(Py)$_{1/4}$ shifts to longer wavelength by 20 nm, turning asymmetric. Red shift of pyridine absorption is also observed on Ir–Py complexes.[14] Absorptions of the pyridine derivatives do not clearly shift by intercalation, the peaks being broad and asymmetric in the respective FeOCl complexes. The asymmetric absorption can be divided into two or more components (Fig. 4(a)). Further

analysis is difficult, since pyridine and pyridine derivatives have both lone pair and π-electrons. These two kinds of electrons can contribute to charge transfer. In order to observe the absorption of lone pair electron which is in non-bonding orbital, aliphatic amine is more suitable than pyridine derivatives. *n*-Propylamine shows an absorption from non-bonding orbital to σ^* one at 261 nm. A broad blue shifted absorption is observed at around 248 nm on the spectrum of $FeOCl(PA)_{1/4}$. Since chlorine is the outermost ion in each FeOCl layer and the nitrogen atoms of the intercalates are very close to FeOCl layer, it is reasonable to assume a certain interaction between the non-bonding orbital of the intercalated donor and the σ orbital of chlorine. The amount of blue shift of $n \rightarrow \sigma^*$ absorption is 13 nm on PA. The present value for the Cl···N pair is in the range of blue shifts of other n-donor and iodine pairs. Thiourea and thioacetoamide show blue shifts of 10 and 21 nm, respectively.[15] This suggests that the bonding between FeOCl and PA is similar to that of other n-donor and I_2 molecular complexes. A similar blue-shift of lone pair electron absorption might also contribute to the asymmetric absorption observed on FeOCl(pyridine derivative)$_{1/n}$.

$FeOCl(PA)_{1/4}$ is similar to FeOCl(pyridine derivative)$_{1/n}$ as regards electrical resistivity, Mössbauer effect and ESR. This suggests that FeOCl(pyridine derivative)$_{1/n}$ having lone pair electrons has almost the same bonding character between host and guest as $FeOCl(PA)_{1/4}$.

The charge-transfer interaction has been confirmed in the intercalated FeOCl complexes. In Mulliken's charge-transfer formulation of donor-acceptor systems, pyridine can work as either a π-donor or an n-donor.[7] Correlations are found between pK_a and properties of the obtained complexes. Thus, we assume that lone pair electrons of the nitrogen atom are involved in the donor-acceptor interactions, and pK_a values of the respective compounds can be used as a measure of n-ionization potential. A similar speculation was made by Chaudhuri and Basu for the system of iodine and many aza-aromatics.[16] They found the proportionality between the logarithm of equilibrium constants for charge transfer type interaction and pK_a values.

In conclusion, pyridine, pyridine derivatives, and propylamine molecules having nitrogen atoms are intercalated into the van der Waals gap of FeOCl. The properties of the products are explained by means of a charge-transfer model. It is assumed that lone pair electrons on the nitrogen atoms of the organic molecules transfer to FeOCl layer in the intercalated complexes.

We are grateful for the help given by Dr. R. Kikuchi and Mr. T. Sawai in the measurement of the Mössabuer effect, by Dr. T. Fujino in the C, H, and N elementary analysis, and by Mr. H. Miyamoto in the ESR measurements. A part of this research was defrayed by a Grant-in-Aid for Special Research Project from the Ministry of Education.

References

1) M. D. Lind, *Acta Crystallogr., Sect. B*, **26**, 1058 (1970).
2) P. Hagenmüller, J. Portier, B. Barbe, and P. Bouclier, *Z. Anorg. Allg. Chem.*, **355**, 209 (1967).
3) F. Kanamaru, M. Shimada, M. Koizumi, M. Takano, and T. Takada, *J. Solid State Chem.*, **7**, 1 (1973).
4) F. Kanamaru, S. Yamanaka, M. Koizumi, and S. Nagai, *Chem. Lett.*, **1974**, 373 (1974).
5) F. Kanamaru and M. Koizumi, *Jpn. J. Appl. Phys.*, **13**, 1319 (1974).
6) P. J. Bray and E.G. Sauer, *Solid State Commun.*, **11**, 1239 (1972).
7) R. S. Mulliken, *J. Am. Chem. Soc.*, **74**, 811 (1952).
8) H. P. Stephensen, *J. Chem. Phys.*, **22**, 1077 (1954).
9) S. Kikkawa, F. Kanamaru, and M. Koizumi, "Reactivity of Solids," Plenum Press (1977), p. 725.
10) "Constants of Organic Compounds," ed by M. Kotake, Asakura Publishing Co., Tokyo (1963), p. 597.
11) D. Biji, H. Kainer, and A. C. Rose-Innes, *J. Chem. Phys.*, **30**, 765 (1959).
12) Y. Matsunaga and C. A. McDowell, *Nature*, **185**, 916 (1960).
13) G. Feher and A.F. Kip, *Phys. Rev.*, **98**, 337 (1955).
14) D. Sutton, "Electronic Spectra of Transition Metal Complexes," McGraw-Hill Publishing (1968), Chap. 1.
15) R. P. Lang, *J. Am. Chem. Soc.*, **84**, 1185 (1962).
16) J. N. Chaudhuri and S. Basu, *Trans. Faraday Soc.*, **55**, 898 (1959).

Studies on the Aqueous Solutions of Guanidinium Salts. IX. Activity Coefficients of Biguanide Hydrochloride and Sucrose in Aqueous Ternary Solutions at 25 °C

Koichiro MIYAJIMA,* Shigeo NAKANISHI, and Masayuki NAKAGAKI

Faculty of Pharmaceutical Sciences, Kyoto University, Yoshida-shimoadachi-cho, Sakyo-ku, Kyoto 606

(Received June 29, 1978)

Activity coefficients for the ternary system biguanide·HCl–sucrose–water were determined by the isopiestic vapor pressure method at 25 °C. Biguanide hydrochloride (Bg·HCl) and sucrose each decreased the activity coefficient of the other solute, showing a mutual salting-in effect. The excess free energy of mixing was negative and its magnitude was about twice as large as that of the system urea–sucrose–water. The pair interaction parameter $\{Bg\cdot HCl\text{–sucrose}\}_g$ was calculated to be -89.2 (cal mol^{-2} kg). Thermodynamic properties of this system were found to be similar to those of the system urea–sucrose–water, indicating that Bg·HCl exerted a structure breaking effect on the aqueous solutions of sucrose as urea did.

Biguanide (guanylguanidine) derivatives have been widely used as hypoglysemic agents. Though the direct interaction of the drugs with sugars is questionable, the physicochemical study of the ternary system Bg·HCl–sucrose–water seems to be important, especially concerning the denaturation of protein and the structure of water, because biguanide halides are known as strong protein denaturants and their effectiveness is known to be stronger than that of urea or guanidinium halides.[1] On the other hand, sugars and polyalcohol are known to stabilize the native conformation of protein.[2,3] In the urea–sucrose–water system, which contained two solutes with opposite effects for the denaturation of protein and the structure of water, each solute decreased the activity coefficient of the other.[4] In the mannitol–sucrose–water system, which has two solutes with similar stabilizing action for the conformational change of protein, each solute increased the activity coefficient of the other.[5] Uedaira reported that in the ternary system which contained two structure maker, mutual salting-out was observed, while in the system with a structure maker and a structure breaker, mutual salting-in was found.[6] From these points of view, we measured the activity coefficients of Bg·HCl and sucrose in mixed solutions. The results are interpreted in terms of the structural change of water.

Experimental

Materials. The free biguanide was prepared from biguanide sulfate dihydrate[7] (Aldrich Co., Ltd.). This was neutralized with hydrochloric acid solution and was concentrated under reduced pressure. The crude Bg·HCl was recrystallized twice from aqueous ethanol solution and dried *in vacuo* at room temperature. Sucrose (Wako Chemical Co., Ltd. reagent grade) was used without further purification and dried *in vacuo* at 90 °C. Analytical grade sodium chloride (Matsunaga Chemical Co., Ltd.) was dried *in vacuo* at 110 °C. These salts were dissolved in redistilled and deionized water.

Method. Osmotic and activity coefficients were determined by the isopiestic vapor pressure method.[8] About 1 ml of each sample solution was placed in a silver dish with dimensions $2\times2\times2$ cm^3. Similar quantities of the reference solutions were placed on a flat copper block containined in a vacuum desiccator, which was evacuated to a pressure of approximately 25 mmHg. The solutions were then allowed to equilibrate under reduced pressure for 3—10 d in a large thermostat bath, controlled to approximately 25 ± 0.05 °C. A total of 10 dishes were usually equilibrated together at once. The concentrations of sample and reference solutions were adjusted initially so as to be fairly close to the desired equilibrium values. The solutions were regarded to have reached the equilibria if the molalities of the two reference solutions differed by not more than 0.1%. Bacterial activity in dilute sucrose solutions was not experienced. The equilibrium concentrations were determined by weighing the dishes. Buoyancy corrections were made by using the densities of sodium chloride, sucrose and Bg·HCl: 2.165, 1.588, and 1.25 g cm^{-3}, respectively, while the corresponding molecular weight used were 58.443, 342.303, and 137.573.

After the equilibrium concentrations were measured, all solutions were diluted by adding several drops of water and reequilibrated in order to attain another equilibrium at more diluted concentrations. Several dilution treatments were carried out and then a new set of solutions was prepared.

Theory

Consider an aqueous ternary solution containing two solutes, 1 (1:1 electrolyte) and 2 (nonelectrolyte), and let m_s and ϕ_s be the molality and the osmotic coefficients of the solute s ($s=1$ and 2); then it is convenient to define a quantity[6,9]

$$\Delta = \nu_R m_R \phi_R - 2m_1\phi_1 - m_2\phi_2, \qquad (1)$$

where m_R and ϕ_R are the molality and the osmotic coefficient of the reference solution which is in vapor equilibrium with the ternary solution, and ν_R is the number of moles of ions or molecules produced by the dissolution of 1 mol of the reference solute.

The value of Δ/m_1m_2 is given Eq. 2.

$$\Delta/m_1m_2 = \sum_{i=0}^{3}\sum_{j=0}^{3} A_{ij}m_1^i m_2^j \quad (i+j\leq 3) \qquad (2)$$

The Δ/m_1m_2 was obtained experimentally and the coefficients A_{ij} in Eq. 2 were determined by the least-squares method.

The activity coefficients of the solute 1 and 2 in the ternary solution are given by Eqs. 3 and 4.

$$\begin{aligned}\ln\gamma_1 = \ln\gamma_1^0 &+ (1/2)A_{00}m_2 + (1/2)A_{10}m_1m_2 + (1/4)A_{01}m_2^2 \\ &+ (1/2)A_{20}m_1^2m_2 + (1/3)A_{11}m_1m_2^2 + (1/6)A_{02}m_2^3 \\ &+ (1/2)A_{30}m_1^3m_2 + (3/8)A_{21}m_1^2m_2^2 \\ &+ (1/4)A_{12}m_1m_2^3 + (1/8)A_{03}m_2^4, \qquad (3)\end{aligned}$$

and

$$\ln\gamma_2 = \ln\gamma_2^0 + A_{00}m_1 + (1/2)A_{10}m_1^2 + A_{01}m_1m_2 + (1/3)A_{20}m_1^3 + (2/3)A_{11}m_1^2m_2 + A_{02}m_1m_2^2 + (1/4)A_{30}m_1^4 + (1/2)A_{21}m_1^3m_2 + (3/4)A_{12}m_1^2m_2^2 + A_{03}m_1m_2^3, \quad (4)$$

where γ_s^0 ($s=1$ or 2) are the molal activity coefficients of binary solutions containing only solute s at molality m_s. The relation among the coefficients A_{ij} in Eqs. 2, 3, and 4 was derived by using the Gibbs-Duhem equation and the cross differential relation between solute 1 and 2. Thus the concentration dependencies of γ_1 and γ_2 for the ternary systems (Eqs. 3 and 4) can be obtained if γ_1^0 and γ_2^0 have already been measured as functions of m_1 and m_2, respectively.

The excess free energy of mixing $\Delta\ \mathrm{P}_mG^{ex}$ is the sum of the contributions from each component of the ternary solution.

$$\Delta_mG^{ex} = \Delta_mG_w^{ex} + \Delta_mG_1^{ex} + \Delta_mG_2^{ex}, \quad (5)$$

where $\Delta_mG_w^{ex}$, $\Delta_mG_1^{ex}$, $\Delta_mG_2^{ex}$, are the excess free energy of mixing for water and solute 1 and 2, respectively. $\Delta_mG_w^{ex}$ is directly related to Δ as

$$\Delta_mG_w^{ex} = -RT\Delta = -RT(A_{00}m_1m_2 + A_{10}m_1^2m_2 + A_{01}m_1m_2^2 + A_{20}m_1^3m_2 + A_{11}m_1^2m_2^2 + A_{02}m_1m_2^3 + A_{30}m_1^4m_2 + A_{21}m_1^3m_2^2 + A_{12}m_1^2m_2^3 + A_{03}m_1m_m^4), \quad (5)$$

$$\Delta_mG_1^{ex} = 2m_1RT\ln(\gamma_1/\gamma_1^0) = RT(A_{00}m_1m_2 + A_{10}m_1^2m_2 + (1/2)A_{01}m_1m_2^2 + A_{20}m_1^3m_2 + (2/3)A_{11}m_1^2m_2^2 + (1/3)A_{02}m_1m_2^3 + A_{30}m_1^4m_2 + (3/4)A_{21}m_1^3m_2^2 + (1/2)A_{12}m_1^2m_2^3 + (1/4)A_{03}m_1m_2^4), \quad (6)$$

and

$$\Delta_mG_2^{ex} = m_2RT\ln(\gamma_2/\gamma_2^0) = RT(A_{00}m_1m_2 + (1/2)A_{10}m_1^2m_2 + A_{01}m_1m_2^2 + (1/3)A_{20}m_1^3m_2 + (2/3)A_{11}m_1^2m_2^2 + A_{02}m_1m_2^3 + (1/4)A_{30}m_1^4m_2 + (1/2)A_{21}m_1^3m_2^2 + (3/4)A_{12}m_1^2m_2^3 + A_{03}m_1m_2^4). \quad (7)$$

Hence Δ_mG^{ex} is expressed as

$$\Delta_mG^{ex} = RT(A_{00}m_1m_2 + (1/2)A_{10}m_1^2m_2 + (1/2)A_{01}m_1m_2^2 + (1/3)A_{20}m_1^3m_2 + (1/3)A_{11}m_1^2m_2^2 + (1/3)A_{02}m_1m_2^3 + (1/4)A_{30}m_1^4m_2 + (1/4)A_{21}m_1^3m_2^2 + (1/4)A_{12}m_1^2m_2^3 + (1/4)A_{03}m_1m_2^4). \quad (8)$$

Cassel and Wood[10] showed that Δ_mG^{ex} was related to the interaction parameters between solute molecules, as shown in Eq. 9.

$$\Delta_mG^{ex} = 2\{AB\}_gm_1m_2 + 3\{AAB\}_gm_1^2m_2 + 3\{ABB\}_gm_1m_2^2 + \cdots, \quad (9)$$

where $\{AB\}_g$ is a pair interaction parameters, and $\{AAB\}_g$ and $\{ABB\}_g$ are triplet interaction parameters. Comparing the coefficients of Eq. 8 with those of Eq. 9, we obtain

$$2\{AB\}_g = RTA_{00}, \quad (10)$$

$$3\{AAB\}_g = RTA_{10}, \quad (11)$$

$$3\{ABB\}_g = RTA_{01}. \quad (12)$$

Results

Bg·HCl–Water System. The activity coefficients of Bg·HCl in water at 25 °C are shown in Table 1. The solubility of Bg·HCl was determined to be 2.8 mol kg^{-1}, and the values of ϕ_1^0 and γ_1^0 at higher concentrations than 2.8 mol kg^{-1} were obtained from the extrapolation.

Table 1. Osmotic and activity coefficients of Bg·HCl at 25 °C

m_1	ϕ_1^0	γ_1^0
0.1	0.919	0.760
0.2	0.891	0.693
0.3	0.871	0.647
0.4	0.855	0.613
0.5	0.843	0.585
0.6	0.831	0.561
0.7	0.821	0.541
0.8	0.813	0.523
0.9	0.804	0.508
1.0	0.797	0.493
1.2	0.783	0.468
1.4	0.770	0.446
1.6	0.758	0.427
1.8	0.748	0.411
2.0	0.739	0.396
2.5	0.722	0.367
3.0	0.701	0.341

Sucrose–Water System. Accurate isopiestic data for the sucrose–water system were reported by Robinson and Stokes[5] in the form

$$\phi_2^0 = 1 + 0.07028m_2 + 0.01847m_2^2 - 0.004045m_2^3 + 0.000228m_2^4, \quad (13)$$

$$\ln\gamma_2^0 = 0.14056m_2 + 0.02770m_2^2 - 0.00539m_2^3 + 0.000285m_2^4. \quad (14)$$

The solubility of sucrose at 25 °C is 6.053 mol kg^{-1}. In the ternary system where sucrose dissolved above this concentration, Eqs. 13 and 14 were also used for the determination of ϕ_2^0 and γ_2^0.

Bg·HCl–Sucrose–Water System. The isopiestic molalities of solute 1 (Bg·HCl) and 2 (sucrose) in the ternary solutions and of the reference solute (sucrose or sodium chloride) in reference solutions are shown in Table 2, together with the values of the experimental quantities Δ/m_1m_2. The values of osmotic coefficients for reference sodium chloride were taken from the values given by Robinson and Stokes.[12] In order to fit the experimental values of Δ/m_1m_2 to a power series of m_1 and m_2 in the form of Eq. 2, polynomials involving terms up to cubic in m_1 and m_2 were examined with a FACOM M190 computer by the least-squares method. The values of coefficients A_{ij} are shown in Table 3.

From Eqs. 3 and 4 and Table 3, we obtain

$$\ln\gamma_1 = \ln\gamma_1^0 - 0.150519m_2 + 0.057513m_1m_2 + 0.014594m_2^2 - 0.012850m_1^2m_2 - 0.005573m_1m_2^2 - 0.000844m_2^3 + 0.001518m_1^3m_2 + 0.000497m_1^2m_2^2 + 0.000166m_1m_2^3 + 0.000023m_2^4,$$

TABLE 2. ISOPIESTIC DATA FOR THE TERNARY SYSTEM Bg·HCl–SUCROSE–WATER AT 25 °C

m_1 (mol·kg^{-1})	m_2 (mol·kg^{-1})	m_R (mol·kg^{-1})	$-(\Delta/m_1m_2)$ exptl	$-(\Delta/m_1m_2)$ calcd[c]	Diff. %[d]
0.05125	0.44633	0.52863[a]	0.3493	0.2705	0.33
0.09410	0.37719		0.3132	0.2697	0.28
0.16787	0.25950		0.3576	0.2683	0.71
0.27505	0.07148		0.1352	0.2675	−0.47
0.06692	0.48847	0.59265[a]	0.3531	0.2666	0.46
0.11661	0.40963		0.3174	0.2657	0.40
0.18375	0.30251		0.3152	0.2645	0.45
0.21618	0.24627		0.2522	0.2641	−0.10
0.26665	0.16068		0.2209	0.2636	−0.29
0.06613	0.57591	0.67956[a]	0.2363	0.2622	−0.14
0.12326	0.49407		0.3458	0.2606	0.72
0.21960	0.33946		0.2733	0.2590	0.15
0.27610	0.24631		0.2520	0.2582	−0.06
0.36503	0.09487		0.1992	0.2574	−0.28
0.08830	0.64448	0.78010[a]	0.1949	0.2564	−0.42
0.15491	0.54419		0.2022	0.2549	−0.53
0.24708	0.40679		0.2449	0.2528	−0.10
0.29134	0.33189		0.1901	0.2524	−0.73
0.36208	0.21819		0.1919	0.2514	−0.57
0.10955	0.95406	1.10572[a]	0.1997	0.2392	−0.34
0.20721	0.83062		0.2615	0.2359	0.36
0.37821	0.58464		0.2280	0.2321	−0.07
0.47963	0.42788		0.2055	0.2306	−0.43
0.50605	0.38406		0.1900	0.2304	−0.65
0.64511	0.16766		0.2420	0.2288	0.12
0.18358	1.33989	1.55353[a]	0.2278	0.2150	0.18
0.33136	1.16404		0.2187	0.2102	0.18
0.54510	0.89742		0.2194	0.2046	0.41
0.65547	0.74673		0.2140	0.2025	0.32
0.82410	0.49919		0.2007	0.2004	0.01
1.01030	0.21266		0.2443	0.1990	0.55
0.20127	1.60477	1.82934[a]	0.1833	0.2025	−0.29
0.38180	1.40643		0.1875	0.1963	−0.22
0.52305	1.24547		0.1891	0.1922	−0.09
0.80741	0.89867		0.1929	0.1857	0.24
0.98600	0.65720		0.1966	0.1832	0.41
1.15852	0.40633		0.2115	0.1817	0.66
0.19982	1.68604	1.90277[a]	0.1888	0.1993	−0.16
0.43311	1.43575		0.1925	0.1913	0.03
0.64720	1.19202		0.1933	0.1855	0.27
0.86460	0.92716		0.1966	0.1809	0.56
1.10781	0.59178		0.1967	0.1780	0.55
1.24031	0.38816		0.1963	0.1773	0.41
0.35433	1.88226	2.23550[a]	0.1728	0.1802	−0.18
0.65058	1.57988		0.1714	0.1711	0.01
0.96128	1.23235		0.1661	0.1643	0.08
1.18273	0.96389		0.1659	0.1607	0.22
1.44098	0.61050		0.1654	0.1585	0.23
1.61377	0.34319		0.1637	0.1581	0.11
0.37646	1.99981	2.36382[a]	0.1687	0.1744	−0.15
0.69346	1.68399		0.1642	0.1649	−0.03
1.02946	1.31975		0.1597	0.1576	0.10
1.26958	1.03466		0.1583	0.1539	0.20
1.55189	0.65749		0.1586	0.1514	0.26
1.73970	0.36998		0.1619	0.1509	0.25
0.41550	2.20725	2.59749[a]	0.1475	0.1648	−0.49
0.76993	1.86970		0.1450	0.1545	−0.42
1.14835	1.47217		0.1369	0.1467	−0.51
1.42212	1.15898		0.1339	0.1427	−0.45
1.74763	0.74042		0.1335	0.1398	−0.25
1.96358	0.41759		0.1269	0.1391	−0.31
0.43102	2.28965	2.68865[a]	0.1426	0.1611	−0.54
0.80049	1.94391		0.1399	0.1505	−0.49
1.19858	1.53656		0.1338	0.1424	−0.47
1.48711	1.21195		0.1311	0.1383	−0.39
1.83098	0.77574		0.1306	0.1352	−0.19
2.05814	0.43770		0.1230	0.1344	−0.30
0.43969	2.56177	2.94235[a]	0.1454	0.1520	−0.20
0.90728	2.14972		0.1393	0.1391	0.01
1.37327	1.69596		0.1315	0.1304	0.07
1.60576	1.44086		0.1256	0.1274	−0.11
1.75691	1.27543		0.1285	0.1256	0.17
1.89795	1.10968		0.1293	0.1241	0.29
2.06525	0.89179		0.1267	0.1229	0.19
2.19493	0.71577		0.1270	0.1220	0.21
0.19637	2.98982	3.15484[a]	0.1503	0.1537	−0.05
0.39316	2.82352		0.1370	0.1468	−0.27
0.59547	2.66469		0.1427	0.1404	0.09
0.82959	2.46366		0.1354	0.1343	0.05
1.02635	2.29264		0.1329	0.1299	0.17
1.22738	2.10435		0.1267	0.1262	0.03
1.49757	1.84546		0.1234	0.1219	0.10
1.67646	1.66549		0.1218	0.1195	0.16
0.51537	3.00267	3.41628[a]	0.1304	0.1352	−0.16
1.07504	2.54720		0.1174	0.1216	−0.26
1.64595	2.03271		0.1122	0.1126	−0.03
1.93574	1.73695		0.1068	0.1093	−0.18
2.12656	1.54378		0.1075	0.1070	0.04
2.30321	1.34663		0.1055	0.1051	0.03
2.51754	1.08709		0.1029	0.1028	0.01
2.68195	0.87456		0.1008	0.1011	−0.01
0.21395	3.25754	3.42810[a]	0.1467	0.1446	0.03
0.42925	3.08275		0.1318	0.1375	−0.17
0.65122	2.91415		0.1336	0.1309	0.11
0.91009	2.70270		0.1271	0.1246	0.13
1.12790	2.51947		0.1235	0.1202	0.20
1.35304	2.31979		0.1172	0.1165	0.05
1.65652	2.04134		0.1131	0.1121	0.07
1.85800	1.84585		0.1120	0.1096	0.18
0.53858	3.13791	3.56127[a]	0.1267	0.1305	−0.13
1.12650	2.66913		0.1172	0.1169	0.02
1.72993	2.13643		0.1078	0.1079	0.00
2.03788	1.82860		0.1012	0.1044	−0.25
2.24094	1.62681		0.1012	0.1020	−0.06
2.42925	1.42032		0.0991	0.0999	−0.05
2.65797	1.14773		0.0954	0.0972	−0.12
2.83350	0.92401		0.0915	0.0950	−0.19
0.57673	3.36020	3.79900[a]	0.1212	0.1232	−0.07
1.21143	2.87036		0.1104	0.1097	0.05
1.86966	2.30898		0.1007	0.1008	0.00
2.20873	1.98191		0.0938	0.0970	−0.27
2.43050	1.76443		0.0924	0.0943	−0.16
2.63879	1.54283		0.0897	0.0917	−0.16
2.88907	3.24753		0.0830	0.0882	−0.36

TABLE 2. (Continued)

m_1 (mol·kg^{-1})	m_2 (mol·kg^{-1})	m_R (mol·kg^{-1})	$-(\Delta/m_1m_2)$ exptl	$-(\Delta/m_1m_2)$ calcd[c]	Diff. %[d]	m_1 (mol·kg^{-1})	m_2 (mol·kg^{-1})	m_R (mol·kg^{-1})	$-(\Delta/m_1m_2)$ exptl	$-(\Delta/m_1m_2)$ calcd[c]	Diff. %[d]
0.62554	3.64454	4.10355[a]	0.1145	0.1146	0.00	3.50942	4.15077		0.0527	0.0499	0.42
1.32052	3.12884		0.1031	0.1014	0.12	0.97713	5.83307	4.34053[b]	0.0704	0.0709	−0.03
2.04855	2.52991		0.0921	0.0927	−0.06	1.59954	5.46115		0.0681	0.0680	0.01
2.42682	2.17760		0.0846	0.0886	−0.37	1.91644	5.26714		0.0665	0.0672	−0.06
2.67867	1.94458		0.0835	0.0851	−0.15	2.25506	5.05461		0.0640	0.0660	−0.23
2.91409	1.70379		0.0798	0.0815	−0.15	2.91370	4.61804		0.0579	0.0608	−0.38
0.28236	4.29907	4.48911[a]	0.1343	0.1147	0.37	3.09869	4.49024		0.0573	0.0582	−0.12
0.56914	4.08737		0.1097	0.1074	0.08	3.53523	4.18130		0.0520	0.0491	0.43
0.86770	3.88291		0.1057	0.1011	0.24	0.48941	6.19602	4.36719[b]	0.0827	0.0750	0.59
1.22259	3.63074		0.0992	0.0955	0.26	1.01231	5.88899		0.0797	0.0698	−0.05
1.52538	3.40736		0.0941	0.0917	0.19	1.60978	5.49608		0.0671	0.0677	−0.05
1.84334	3.16040		0.0888	0.0885	0.03	1.92893	5.30145		0.0656	0.0668	−0.13
2.27787	2.80703		0.0820	0.0841	−0.21	2.26886	5.08554		0.0626	0.0657	−0.36
2.57299	2.55616		0.0788	0.0806	−0.19	2.93066	4.64491		0.0564	0.0604	−0.54
0.70820	4.12615	4.61751[a]	0.1057	0.1017	0.18	3.13238	4.53906		0.0583	0.0574	0.14
1.50577	3.56778		0.0934	0.0898	0.29	3.55823	4.20849		0.0510	0.0484	0.39
2.35440	2.90763		0.0809	0.0814	−0.05	0.98860	5.90156	4.38777[b]	0.0691	0.0700	−0.05
2.80080	2.51318		0.0723	0.0759	−0.39	1.61896	5.52745		0.0672	0.0674	−0.01
3.09782	2.24887		0.0717	0.0708	0.09	1.94053	5.33334		0.0660	0.0665	−0.06
0.93703	4.01266	3.15085[b]	0.1001	0.0967	0.19	2.28361	5.11861		0.0634	0.0654	−0.23
1.12081	3.88576		0.0975	0.0939	0.24	2.95100	4.67715		0.0573	0.0600	−0.37
1.34149	3.72974		0.0938	0.0910	0.21	3.13739	4.54633		0.0552	0.0572	−0.29
1.60752	3.53836		0.0903	0.0881	0.18	3.58314	4.23796		0.0517	0.0476	0.62
1.81854	3.38120		0.0879	0.0861	0.17	0.49655	6.25591	4.42531[b]	0.0647	0.0741	−0.29
1.92148	3.30148		0.0861	0.0851	0.09	0.99853	5.96085		0.0697	0.0692	0.03
2.12140	3.14686		0.0835	0.0832	0.02	1.63494	5.58201		0.0671	0.0668	0.02
2.37680	2.93997		0.0812	0.0807	0.06	1.95910	5.38437		0.0652	0.0661	−0.09
1.09132	4.67339	3.64444[b]	0.0885	0.0830	0.36	2.30554	5.16754		0.0626	0.0650	−0.27
1.30777	4.53392		0.0859	0.0808	0.38	2.98094	4.72460		0.0568	0.0593	−0.35
1.56844	4.36074		0.0825	0.0787	0.33	3.16994	4.59349		0.0549	0.0564	−0.22
1.88461	4.14827		0.0796	0.0765	0.30	3.61665	4.27760		0.0506	0.0465	0.63
2.13604	3.97152		0.0762	0.0748	0.15	1.00006	5.96997	4.43227[b]	0.0694	0.0691	0.01
2.26022	3.88349		0.0747	0.0739	0.09	1.64395	5.61274		0.0715	0.0665	0.45
2.49981	3.70819		0.0718	0.0718	0.00	1.96338	5.39614		0.0656	0.0660	−0.04
2.80791	3.47319		0.0673	0.0683	−0.12	2.31920	5.19837		0.0662	0.0647	0.18
0.45303	5.70759	4.05774[b]	0.0770	0.0828	−0.16	2.98794	4.73570		0.0571	0.0592	−0.29
0.90958	5.42982		0.0791	0.0766	0.13	3.17614	4.60247		0.0549	0.0563	−0.20
1.48676	5.07608		0.0753	0.0724	0.23	3.62910	4.29232		0.0516	0.0461	0.84
1.77964	4.89116		0.0730	0.0711	0.18	1.81341	6.19400	4.83866[b]	0.0630	0.0617	0.12
2.09114	4.68785		0.0700	0.0697	0.02	2.17493	5.98008		0.0606	0.0616	−0.11
2.69805	4.27624		0.0624	0.0654	−0.39	2.56216	5.74548		0.0581	0.0603	−0.29
2.86787	4.15577		0.0618	0.0635	−0.23	3.31829	5.26135		0.0518	0.0514	0.07
3.26741	3.86453		0.0573	0.0570	0.04	3.53545	5.12522		0.0508	0.0465	0.68
0.46128	5.81154	4.12858[b]	0.0742	0.0811	−0.20	1.82277	6.22329	4.86871[b]	0.0598	0.0615	−0.17
0.92601	5.52792		0.0761	0.0751	0.05	2.18781	6.01297		0.0586	0.0613	−0.32
1.51434	5.17026		0.0731	0.0713	0.15	3.33898	5.29207		0.0504	0.0509	−0.07
1.81318	4.98333		0.0711	0.0701	0.11	3.55590	5.15277		0.0464	0.0459	0.08
2.13930	4.79515		0.0717	0.0686	0.35	2.23699	6.21949	4.99141[b]	0.0559	0.0601	−0.49
2.74990	4.35842		0.0618	0.0643	−0.32	2.70121	5.94570		0.0538	0.0583	−0.62
2.92300	4.23565		0.0596	0.0622	−0.34	3.07387	5.71521		0.0513	0.0545	−0.48
3.33362	3.94284		0.0558	0.0551	0.09	3.25850	5.59872		0.0500	0.0516	−0.24
0.48349	6.09139	4.31565[b]	0.0718	0.0766	−0.14	3.61768	5.36642		0.0476	0.0436	0.66
0.97156	5.79982		0.0737	0.0713	0.14	2.32294	6.45848	5.15367[b]	0.0574	0.0586	−0.15
1.59001	5.42859		0.0702	0.0684	0.16	2.80514	6.17446		0.0544	0.0564	−0.29
1.90488	5.23537		0.0684	0.0675	0.10	3.19428	5.93910		0.0521	0.0518	0.05
2.24050	5.02198		0.0653	0.0663	−0.11	3.38685	5.81925		0.0507	0.0482	0.40
2.89489	4.58822		0.0592	0.0612	−0.27	2.49878	6.86764	5.41611[b]	0.0576	0.0559	0.22
3.07762	4.45972		0.0571	0.0586	−0.21	2.94947	6.61109		0.0547	0.0531	0.24

a) Reference solute: sucrose. b) Reference solute: sodium chloride. c) Calculated by Eq. 2 using the values in Table 3. d) Percentage error defined by Kelly.[9]

Table 3. The values of coefficients in Eq. 2 for the system Bg·HCl–sucrose–water

Coefficient		Coefficient	
A_{00}	−0.301038	A_{02}	−0.005065
A_{10}	0.115026	A_{30}	0.003036
A_{01}	0.058376	A_{21}	0.001324
A_{20}	−0.025700	A_{12}	0.000664
A_{11}	−0.016720	A_{03}	0.000187

$$\ln \gamma_2 = \ln \gamma_2^0 - 0.301038m_1 + 0.058377m_1m_2 + 0.057513m_1^2 - 0.005065m_1m_2^2 - 0.011146m_1^2m_2 - 0.008567m_1^3 + 0.000187m_1m_2^3 + 0.000498m_1^2m_2^2 + 0.000662m_1^3m_2 + 0.000759m_1^4,$$

for the system Bg·HCl–sucrose–water.

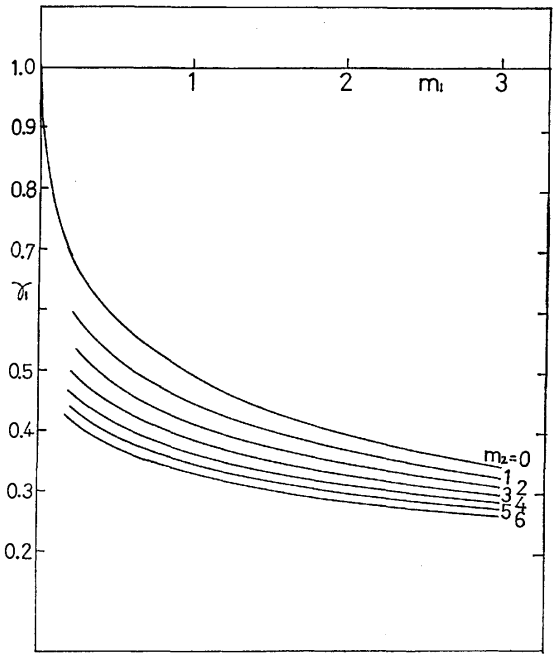

Fig. 1. Activity coefficients of Bg·HCl in sucrose solutions of various concentrations.
m_1; Molality of Bg·HCl, m_2; molality of sucrose.

The activity coefficients for Bg·HCl in binary and ternary solutions are shown in Fig. 1 and the activity coefficients of sucrose in binary and ternary solutions are given in Fig. 2. The activity coefficient of each solute decreased in the presence of the other solute.

Discussion

Bg·HCl–Water System. Biguanide is the condensed compound of two guanidine molecules and, structurally, guanidine corresponds to urea and biguanide to biuret.

Urea is known as a protein denaturant and affects the hydrophobic hydration, as in the system urea–tetrabutylammonium bromide–water,[13] and also the hydrophilic hydration, as in the system urea–sucrose–water.[4] These influences of urea on the hydrophobic and hydrophilic hydration play an important role in protein denaturation.

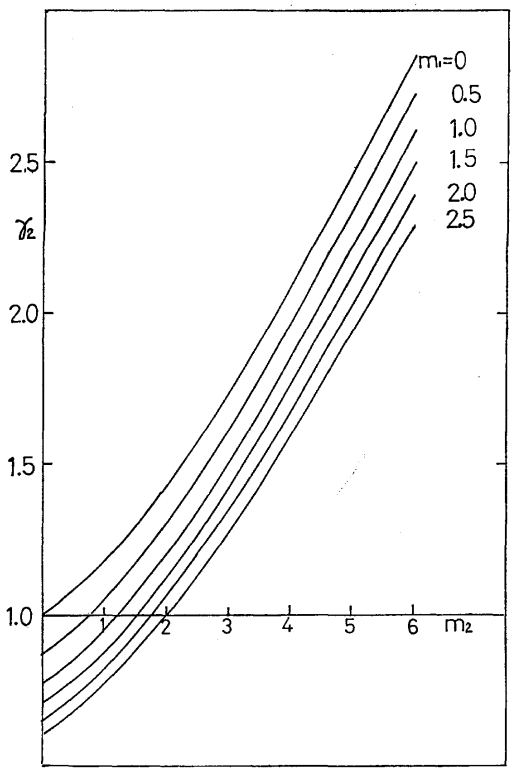

Fig. 2. Activity coefficients of sucrose in Bg·HCl solutions of various concentrations.
m_1; Molality of Bg·HCl, m_2; molality of sucrose.

Guanidinium halides are also known as protein denaturants. The properties of the guanidinium ion in aqueous solutions were studied in our laboratory and the guanidinium ion was concluded to be a strong structure breaker ion.[14–16] Biguanide halides are strong protein denaturants and their effectiveness is stronger than urea and guanidinium halides.[1] The effects of the biguanide ion on the structure of water have been studied in our laboratory. The viscosity *B*-coefficient of the biguanide ion showed no temperature dependence and the increment of the ionic *B*-coefficient arising from the change in the water structure was nearly zero, indicating the biguanide ion to be neither structure maker nor structure breaker.[17] But the temperature dependence of the Walden product obtained from the conductivity measurement was positive, indicating the biguanide ion to be a weak structure maker.[18] The activity coefficients of the biguanide salts in the aqueous solutions obtained from the isopiestic measurement were somewhat lower than those of guanidinium salts with the same counter anions. The activity coefficients of biguanide salts decreased in the order $OAc^- > Cl^- > Br^-$, as in the case of guanidinium salts, when the anion was changed.[19] These results indicate that the biguanide ion is thermodynamically a structure breaker.[15]

Bg·HCl–Sucrose–Water System. As shown in Figs. 1 and 2, the mutual salting-in was observed in this system. The free energy of transfer of trace sucrose from water to various binary solutions are shown in Fig. 3. Mannitol is regarded as a hydrophilic structure maker[5] and its structure of hydration may be similar to that of sucrose. 2-Aminobutyric acid (2-ABA) is

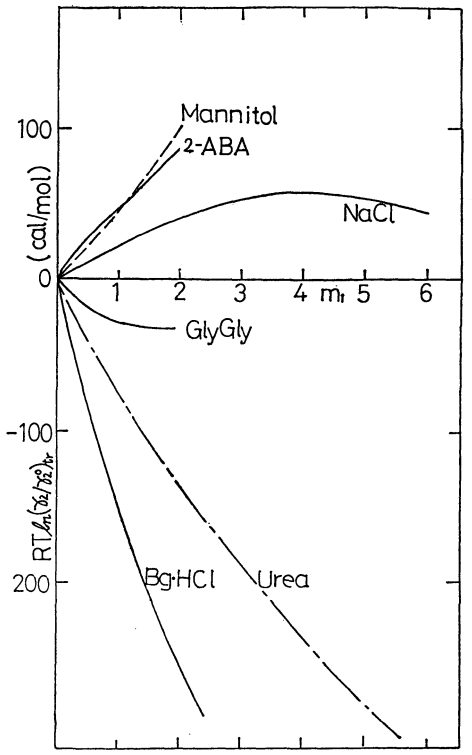

Fig. 3. Free energy of transfer of trace sucrose (solute 2) from water to aqueous solute 1 solutions at 25 °C.
m_1; Molality of solute 1 as indicated in the figure.

considered to be a weak structure maker.[6] On the other hand, glycylglycine (GlyGly)[6] and urea are regarded as structure breakers. Uedaira suggested that the mixing of two kinds of structure making solutes caused the positive free energy change of transfer, while the mixing of the structure making and the breaking solutes caused the negative free energy change of transfer for each solute in aqueous solutions.[6] As seen in Fig. 3, Bg·HCl is more structure breaking than urea and GlyGly, if Uedaira's postulation is applied to the system Bg·HCl–sucrose–water.

On the other hand, Bg·HCl is an electrolyte and its interaction with sucrose is the sum of the electrostatic and the non-electrostatic terms. Therefore it is meaningful to compare the system Bg·HCl–sucrose–water with the system NaCl–sucrose–water,[20] because the interaction involved in the system NaCl–sucrose–water may be considered to represent the electrostatic interaction for the system Bg·HCl–sucrose–water. In Fig. 4, the excess free energy of mixing for the system Bg·HCl–sucrose–water are compared with those of the system urea–sucrose–water and NaCl–sucrose–water. The excess free energy of mixing $\Delta_m G^{ex}$ is the sum of each component $\Delta_m G_w^{ex}$, $\Delta_m G_1^{ex}$, and $\Delta_m G_2^{ex}$. Figure 4 shows $\Delta_m G^{ex}$, $\Delta_m G_w^{ex}$, $\Delta_m G_1^{ex}$, and $\Delta_m G_2^{ex}$ at a total molality of 6 mol kg^{-1}. For the system urea–sucrose–water, $\Delta_m G^{ex}$, $\Delta_m G_1^{ex}$, and $\Delta_m G_2^{ex}$ are negative and $\Delta_m G_w^{ex}$ is positive, indicating a strong inter-

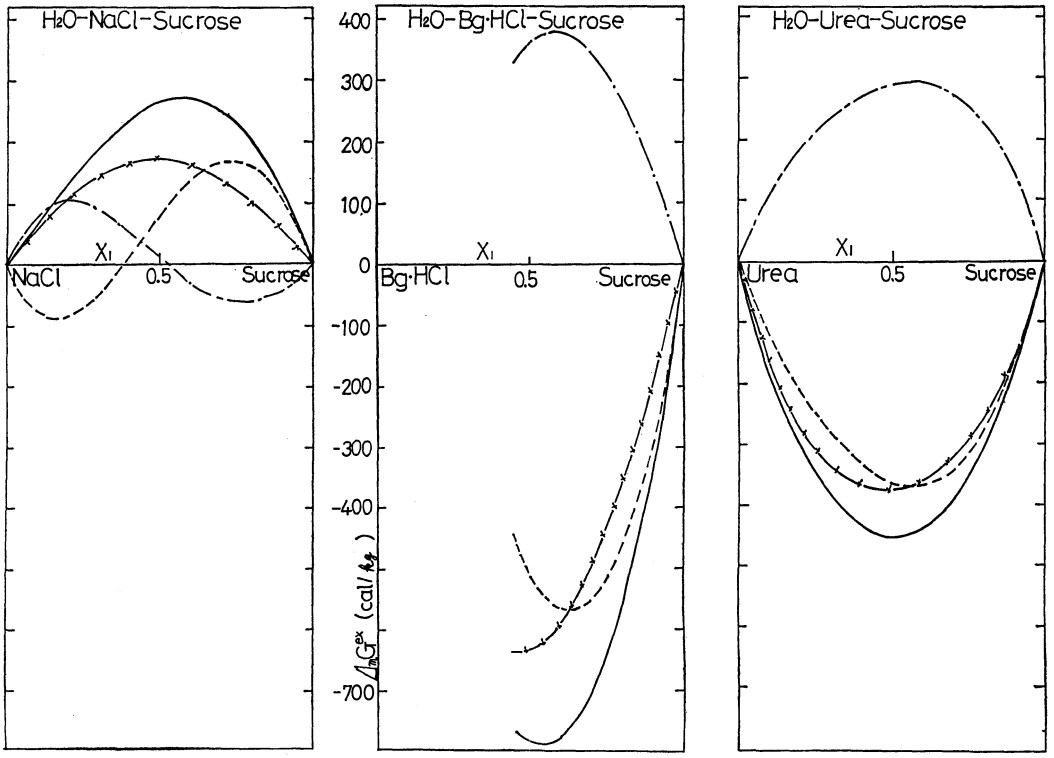

Fig. 4. Excess free energy changes of mixing for ternary systems containing sucrose as a component at 6 mol·kg^{-1} of total molality.
—·—·— $\Delta_m G_w^{ex}$ (excess free energy of mixing for water),
———— $\Delta_m G_1^{ex}$ (excess free energy of mixing for Bg·HCl or urea or NaCl),
—×—×— $\Delta_m G_2^{ex}$ (excess free energy of mixing for sucrose),
———— $\Delta_m G^{ex}$ (total excess free energy of mixing),
X_1; mole fraction of solute 1 (NaCl, Bg·HCl, Urea).

TABLE 4. FREE ENERGY OF TRANSFER OF Bg·HCl FROM WATER TO SUCROSE SOLUTIONS AT 25 °C (cal/mol)

m_{10}[a]	m_2[b] 0.5	1	2	3	4	5	6
0	−74.4	−140.9	−253.2	−341.9	−411.3	−465.1	−506.3
0.2	−69.4	−131.6	−236.6	−319.9	−385.8	−437.6	−478.3
0.5	−61.9	−117.3	−211.0	−285.9	−345.9	−394.2	−433.3
1.0	−51.1	− 97.0	−175.2	−239.0	−291.8	−336.5	−375.0
1.5	−42.6	− 81.0	−147.7	−203.9	−252.6	−295.9	−335.3
2.0	−35.3	− 67.7	−126.4	−174.9	−220.1	−262.1	−301.5
2.5	−29.4	− 56.5	−105.7	−150.1	−191.7	−231.3	−269.0

a) The molality of Bg·HCl in a binary solution. The molalities in ternary solutions are slightly larger than m_{10}, as the transfer is carried out at constant mole fraction.[19] b) The molality of sucrose.

action between urea and sucrose. The system Bg·HCl–sucrose–water showed a similar tendency to that for the system urea–sucrose–water, though the values of $\Delta_m G^{ex}$, $\Delta_m G_w{}^{ex}$, $\Delta_m G_1{}^{ex}$, and $\Delta_m G_2{}^{ex}$ were much larger than those of the system urea–sucrose–water. There may be two kinds of interactions between sucrose and Bg·HCl, that is, the direct interaction (the formation of water soluble complex) and the interaction through the change of water structure. The free energy data do not inform us which interaction is really working. But if we take into account that both solutes are hydrophilic and that the interaction takes place in water, the possibility of the direct interaction may be small. For the system NaCl–sucrose–water, $\Delta_m G^{ex}$ and $\Delta_m G_2{}^{ex}$ were positive, while $\Delta_m G_1{}^{ex}$ changed sign as the mole fraction changed. The relation between the excess free energy changes and the mole fraction of the system Bg·HCl–sucrose–water resembled those of the system urea–sucrose–water rather than those of the system NaCl–sucrose–water. This means that a large organic salt, such as Bg·HCl, is more likely to act as a non-electrolyte like urea rather than as an inorganic electrolyte like NaCl in such a ternary system in the high concentration region. Therefore we applied Eq. 10 to the electrolyte–non-electrolyte system. The pair interaction parameter $\{AB\}_g$ of the system Bg·HCl–sucrose–water was calculated to be −89.2 and that of the system urea–sucrose–water was −37.3 in cal kg mol^{-2}.

Table 4 shows the free energy of transfer $\Delta G^t(N)$ (mole fraction scale)[21] of Bg·HCl from water to sucrose solutions of various concentrations. The trace free energy of transfer is the most negative and its magnitude is twice as large as that of urea.

As shown in Figs. 3 and 4 and Table 4, Bg·HCl exerts a more significant effect on the hydrophilic hydration than urea does. This result is consistent with the fact that Bg·HCl is a stronger denaturant than urea.

It is interesting to investigate the effect of biguanide salts on the hydrophobic hydration as observed in aqueous tetraalkylammonium salts solutions. We are currently working in this direction.

References

1) F. J. Castellino and R. Barker, *Biochemistry*, **7**, 4135 (1968).
2) C. D. Ball, D.H. Hardt, and W. J. Duddles, *J. Biol. Chem.*, **151**, 163 (1943).
3) S. Y. Gersma and E. R. Stuur, *Int. J. Pept. Protein Res.*, **4**, 377 (1972).
4) H. D. Ellerton and P. J. Dunlop, *J. Phys. Chem.*, **70**, 1831 (1966).
5) R. A. Robinson and R. H. Stokes, *J. Phys. Chem.*, **65**, 1954 (1961).
6) H. Uedaira, *Bull. Chem. Soc. Jpn.*, **50**, 1298 (1977).
7) S. N. Holter and W. C. Fernelius, *Inorg Synth.*, **7**, 58 (1968).
8) W.-Y. Wen and S. Saito, *J. Phys. Chem.*, **69**, 3569 (1965).
9) V. E. Bower and R. A. Robinson, *J. Phys. Chem.*, **67**, 1524 (1963).
10) R. B. Cassel and R. H. Wood, *J. Phys. Chem.*, **78**, 2460 (1974).
11) F. J. Kelly, R. A. Robinson, and R. H. Stokes, *J. Phys. Chem.*, **65**, 1958 (1961).
12) R. A. Robinson and R. H. Stokes, "Electrolyte Solutions," 2nd ed, Butterworths, London (1959).
13) W.-Y. Wen and Chun-meei Lee, *J. Phys. Chem.*, **73**, 2895 (1969).
14) K. Miyajima, K. Inari, and M. Nakagaki, *Nippon Kagaku Kaishi*, **1974**, 2031.
15) K. Miyajima, K. Inari, N. Hamaguchi, H. Yoshida, and M. Nakagaki, *Nippon Kagaku Kaishi*, **1975**, 1447.
16) K. Miyajima, K. Kitamura, K. Inari, and M. Nakagaki, *Nippon Kagaku Kaishi*, **1975**, 2060.
17) K. Miyajima, S. Nakanishi, and M. Nakagaki, *Nippon Kagaku Kaishi*, **1976**, 205.
18) Unpublished data.
19) Unpublished data.
20) R. A. Robinson, R. H. Stokes, and K. N. Marsh, *J. Chem. Thermodynamics*, **2**, 745 (1970).
21) H. Uedaira, *Bull. Chem. Soc. Jpn.*, **48**, 2006 (1975).

Polarity of Free Radicals in Hydrogen Abstraction Reactions

Hiroyuki SHINOHARA,* Akira IMAMURA,† Takahiro MASUDA,†† and Masaharu KONDO††

Department of Radiology, Fujigaoka Hospital, Showa University, Fujigaoka, Midori-ku, Yokohama 227

†*Shiga University of Medical Science, Seta, Otsu, 520-21*

††*Department of Chemistry, Faculty of Science, Tokyo Metropolitan University, Fukasawa, Setagaya-ku, Tokyo 158*

(Received July 3, 1978)

The electrophilicity of the CF_3 radical in hydrogen abstraction reactions was studied theoretically by the CNDO/2 method. The activation energy for hydrogen abstraction by the CF_3 radical from aliphatic hydrocarbons decreases with an increase in the electron density on the hydrogen atom to be abstracted. The origin of the electrophilicity of the CF_3 radical can be well understood by the stabilization energy due to delocalization of electrons (SEDE) between the radical and substrate. The electrophilic stabilization energy defined by the SEDE from substrate to the radical governs the relative reactivities of aliphatic hydrocarbons, $CH_4 < CH_3CH_3 < CH_3CH_2CH_3 < (CH_3)_3CH$, which corresponds to the order of the increase in the electron density. The results indicate that the radical is an electrophile if the relative reactivities of substrates are governed by the electrophilic stabilization energy, and a nucleophile when the reactivities are governed by the nucleophilic stabilization energy (the SEDE from the radical to substrate). SEDE was calculated for the reactions of the OH and the CH_3 radicals with CH_4 and CH_3CN; the results indicated that the OH radical is electrophilic and the CH_3 radical nucleophilic. These polarities of radical reagents are discussed in connection with their physicochemical properties such as ionization potentials and electron affinities.

The reactions of free radicals often show substituent effects[1-5] which resemble those of ionic reactions. A number of radical reactions can be correlated with the Hammett or Taft equation[1,2,5,6] and the polarity of a radical (nucleophilicity or electrophilicity) has been investigated. In rationalizing the observed trends, the polar effects concept[1,2,7] (substituent effect on the transition state) has been widely accepted for a hydrogen abstraction reaction (Eq. 1), which can be described by the three resonance structures shown in Eq. 2[8] (RH: hydrogen donor, X: radical):

$$RH + X \longrightarrow R + HX, \tag{1}$$

$$\underset{1}{[R\cdot \dot{H}\cdot X} \longleftrightarrow \underset{2}{R^{-}\!:\dot{H}^{+}X} \longleftrightarrow \underset{3}{R^{+}\dot{H}\,\ddot{:}X^{-}}] \tag{2}$$

According to Pryor *et al.*,[8] if R^+ is more stable than X^+ and X^- is more stable than R^-, then the structure 3 makes a more important contribution to the stability of the transition state than does the structure 2 and the electrophilicity would be expected. The negative ρ values were obtained for reactions of hydrogen abstractions with substituted toluenes by the radicals that were thought to be electrophilic, such as CH_3, C_6H_5, Br, and Cl, and this result has supported the polar effects concept. Moreover, Sakurai *et al.*[9] reported a linear relationship of negative ρ values for CH_3, C_6H_5, *t*-BuO, and Cl (for these radicals, HX bonds formed in Eq. 1 have nearly equal bond dissociation energies) and the electron affinities of the radicals. This evidence supports the importance of the structure 3 in the transition state. In connection with the polarity of a radical, however, quantitative investigation of structures 2 or 3 has not yet been made. Imamura has recently developed a molecular orbital (MO) method[10] which determines the polarity of a radical on the basis of the stabilization energy due to delocalization of electrons (SEDE) between a substrate and a radical. This method was applied to the reaction of OH and H radicals with benzene derivatives, and OH and H radicals were found to behave as electrophiles, in good correspondence with the experimental facts.[10] Moreover, the polarities of various radical reagents in the reaction of hydrogen and chlorine abstractions were studied by using SEDE; the interesting conclusion was reached that a radical reagent with an electrophilic nature changes its SEDE for the electrophilicity from substrate to substrate remarkably, while a radical reagent with a nucleophilic nature changes its SEDE for the nucleophilicity. That is, the electrophilicity or the nucleophilicity can be determined not by the absolute value of SEDE but by the change in SEDE from substrate to substrate.[11,12]

In the present work, along the above-mentioned line, we calculated the SEDE in hydrogen abstraction by CF_3 radical from aliphatic hydrocarbons by the MO method and attempted to clarify the factors determining the polarity of the radical. This radical is interesting from a theoretical point of view since the fluorine atoms have large electronegativity, leading to the strong electrophilicity of the radical reagent. The calculations of SEDE correspond to the evaluation of the contribution of the structure 2′ or 3′ to the stabilization of the reacting system. That is, the structure 2′ or 3′ correlates with the nucleophilicity or the electrophilicity of the radical.

$$\underset{2'}{[R\cdots H\cdots \overset{\delta-}{X}} \longleftrightarrow \underset{3'}{R\cdots H\cdots \overset{\delta-}{X}}] \tag{2'}$$

If the relative reactivities of RH are governed by the SEDE corresponding to the structure 3′, the radical is an electrophiles; it is a nucleophile when the reactivities are governed by the SEDE corresponding to the structure 2′.

Method of Calculation

The total energies for the reacting system were calculated by the UHF method[13] in the CNDO/2 approximation.[14,15] The values of the parameters included in the method are the same as those used in the original papers.[14,15]

Geometries used for calculation are as follows: for CH_4,[16] r(C–H)=1.09 Å; for CH_3CN,[17] r(C–H)=1.107, r(C–C)=1.468, and r(C–N)=1.159 Å; for CH_3CH_3, $CH_3CH_2CH_3$, and $(CH_3)_3CH$, r(C–H)=1.09 and r(C–C)=1.54 Å. The bond angle HCH for these compounds is assumed to be 109.47°.

Procedure of Analysis. The magnitude of the contribution of 2 in Eq. 2 to the reacting system is evaluated by the SEDE from a radical to substrate. This energy is a measure for the nucleophilic character of the radical, so it is defined as the nucleophilic stabilization energy. Similarly, the contribution of 3 in Eq. 2 is evaluated by the electrophilic stabilization energy (the SEDE from substrate to the radical). Here, we may mention the method of calculating the SEDE in connection with hydrogen abstraction:

$$R\uparrow\downarrow H + \uparrow X \longrightarrow [R\cdots\uparrow\downarrow\cdots H\cdots\uparrow X] \longrightarrow R\uparrow + HX,$$

where RH and X denote a substrate (hydrogen donor) and a radical, respectively. The SEDE (ΔE) is defined by Eq. 3;

$$\Delta E = E(R\cdots\uparrow\downarrow\cdots H \quad \uparrow X) - E(R\cdots\uparrow\downarrow\cdots H\cdots\uparrow X), \quad (3)$$

where the first term on the right in Eq. 3 denotes the energy of the reacting system in which the delocalization of electrons between RH and X is forbidden (absence of the dotted line between H and X). The second term includes the delocalization of electrons. The first term is obtained by the SCF calculation after dropping the resonance integrals I_{rs} between atomic orbitals (AO's) of RH, χ_r, and AO's of X, χ_s, given by Eq. 4:

$$I_{rs} = \frac{1}{2}(\beta_r+\beta_s)S_{rs}, \quad (4)$$

β denotes the bonding parameter in the CNDO/2 method.[11,13] The MO's of the reacting system (R···H··· X) thus obtained are classified into the MO's localized on R···H and the ones localized on X in Eqs. 5 and 6, respectively:

$$\psi_{RHi} = \sum_r C_{RHi,r}\chi_r, \quad (5)$$

$$\psi_{Xj} = \sum_s C_{Xj,s}\chi_s, \quad (6)$$

ψ_{RHi} is the i-th MO localized on R···H and $C_{RHi,r}$ is the coefficient of AO in the i-th MO, and ψ_{Xj} and C_{Xj}'s are for the radical X.

From Eq. 5, one obtains

$$\sum_i^{all} C_{RHi,r_1}\psi_{RHi} = \sum_r\sum_i^{all} C_{RHi,r_1}C_{RHi,r}\chi_r = \sum_r \chi_r \sum_i^{all} C_{RHi,r_1}C_{RHi,r}. \quad (7)$$

Since a set of ψ_{RHi}'s is orthonormal,

$$\sum_i^{all} C_{RHi,r_1}C_{RHi,r} = \delta_{rr_1}. \quad (8)$$

Namely

$$\chi_r = \sum_i^{all} C_{RHi,r}\psi_{RHi}, \quad (9)$$

$$\chi_s = \sum_j^{all} C_{Xj,s}\psi_{Xj}. \quad (10)$$

From Eqs. 9 and 10, one obtains the relation between the I_{rs} represented by the AO basis (χ_r, χ_s) and the I_{ij} by the MO basis (ψ_{RHi}, ψ_{Xj}):

$$I_{rs} = \int\chi_r h^\circ\chi_s d\tau = \sum_i^{all}\sum_j^{all} C_{RHi,r}C_{Xj,s}\int\psi_{RHi}h^\circ\psi_{Xj}d\tau = \sum_i^{all}\sum_j^{all} C_{RHi,r}C_{Xj,s}I_{ij}. \quad (11)$$

Instead of Eq. 11, the modified resonance integrals between AO's. I'_{rs} in Eq. 12 are used in the SCF calculation in order to include the delocalization of electrons between a particular orbital set (i_1, j_1).

$$I'_{rs} = \sum_{(i_1-j_1)} C_{RHi_1,r}C_{Xj_1,s}I_{i_1j_1}, \quad (12)$$

where $(\Sigma_{i_1-j_1})$ denotes the summation over the set. From Eq. 12, it is easily proved that the modified resonance integrals between MO's, I'_{ij}, reduces to zero except for the $I_{i_1j_1}$, which has the same value as that obtained by using Eq. 11 (I_{ij}). The proof is as follows.

$$\begin{aligned} I'_{ij} &= \sum_r\sum_s C_{RHi,r}C_{Xj,s}I'_{rs} \\ &= \sum_r\sum_s C_{RHi,r}C_{Xj,s}\sum_{(i_1-j_1)} C_{RHi_1,r}C_{Xj_1,s}I_{i_1j_1} \\ &= \sum_{(i_1-j_1)} I_{i_1j_1}\sum_r C_{RHi,r}C_{RHi_1,r}\sum_s C_{Xj,s}C_{Xj_1,s} \\ &= \sum_{(i_1-j_1)} I_{i_1j_1}\delta_{ii_1}\delta_{jj_1}. \end{aligned} \quad (13)$$

The procedure of the calculation is written as follows. (i) The total energy of the reacting system without the delocalization of electrons is calculated with the unrestricted SCF method in the CNDO/2 approximation after dropping all the resonance integrals between AO's on the fragment RH and those on the fragment X. Thus we obtain the value for the first term in Eq. 3, as well as the MO's localized on the fragments given by Eqs. 5 and 6. (ii) By using the MO's obtained in step (i), the modified resonances integrals between AO's are calculated according to Eq. 12 in order to take the delocalization of electrons between particular MO's into account. (iii) The modified resonance integrals are employed to calculate the total energy of the reacting system with the delocalization of electrons, which corresponds to the nucleophilic or the electrophilic nature of the radical reagent in question. (iv) A measure of the nucleophilicity or the electrophilicity of the radical reagent can be obtained by calculating the difference between the two energies obtained in the steps (i) and (iii), as is shown in Eq. 3.

When the vacant MO's of the substrate and the

Table 1. The schematic representation of the orbital interaction between substrate RH and radical X[a)]

Interaction	α-spin			β-spin		
Electrostatic (Zero)	RH	Occ	Vac	RH	Occ	Vac
	X	Occ	Vac	X	Occ	Vac
Nucleophilic (N)	RH	Occ	Vac	RH	Occ	Vac
	X	Occ	Vac	X	Occ	Vac
Electrophilic (E)	RH	Occ	Vac	RH	Occ	Vac
	X	Occ	Vac	X	Occ	Vac

a) The orbital interaction which includes the $I_{i_1j_1}$ is represented by a solid line. The symbol for the interaction used in the text is given in the parentheses.

occupied MO's of the radical are chosen for i_1 and j_1, respectively, in Eq. 12, ΔE in Eq. 3 corresponds to the SEDE from radical to substrate. Thus, ΔE should be the nucleophilic stabilization energy; it is represented by the symbol N. When the occupied MO's of the substrate and the vacant MO's of the radical are chosen for i_1 and j_1, respectively, ΔE is the electrophilic stabilization energy; it is represented by the symbol E. Table 1 shows the schematic representation of intermolecular interaction between the MO's of RH and X obtained by dropping the resonance integrals I_{rs} (they interact electrostatically with each other but the delocalization of electrons is prohibited).

Results and Discussion

The coordinate system assumed for a hydrogen abstraction reaction by the CF_3 radical from aliphatic hydrocarbons is shown in Fig. 1. In a previous paper,[11] we examined the reaction path of the CH_4–OH system by the INDO method, and the geometry in Fig. 1 might

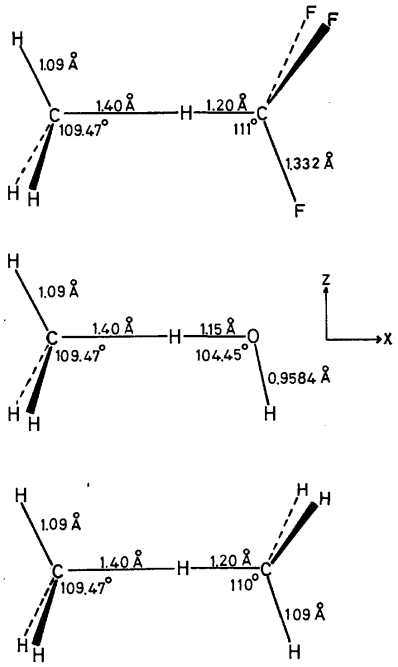

Fig. 1. The coordinate system assumed for hydrogen abstraction by the CF_3 radical from methane.

be roughly approximated as the transition state. Moreover, the electrophilicity of the OH radical in the reaction with methane deduced from the SEDE was not dependent on the reaction paths: A(1.09, 1.46), B(1.20, 1.35), C(1.30, 1.25), D(1.40, 1.15) which are specified respectively by the sets of C^1–H^5 and H^5–O distances indicated in the parenthesis. For the OH and the CH_3 radicals, therefore, we used the same geometries as in the previous paper to determine the polarity in the reaction with a series of substrates. Although the geometry in Fig. 1 is tentatively chosen for the reaction of the CF_3 radical, we believe that the result need not be revised when the geometry is changed slightly.

We may assume here without loss of generality that

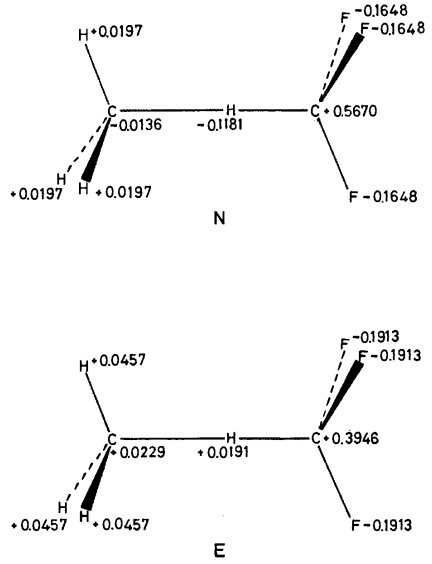

Fig. 2. The electron distribution of CH_4–CF_3 system by the orbital interaction corresponding to the nucleophilic (N) and the electrophilic (E) stabilization energy.

the CF_3 radical has thirteen valence electrons with α-spin and twelve valence electrons with β-spin. It is noticed from the electron distribution shown in Fig. 2 that the delocalization of electrons occurs from the CF_3 radical to methane by the orbital interaction N, while it occurs from methane to the CF_3 radical by the interaction E. Thus the stabilization energy defined by N or E corresponds to the direction of the delocalization of electrons occurring between a substrate and a radical. The structure 2′ or 3′ in Eq. 2′ is considered to correspond to N or E. Figure 3a shows the correlation of the activation energy[18] and the electron density on the hydrogen atom. The activation energy decreases with an increase in the electron density. The origin of the electrophilicity of the CF_3 radical can be understood by N and E, as summarized in Table 2. E increases with the increasing

Table 2. The electrophilicity of the CF_3 radical in hydrogen abstraction with aliphatic hydrocarbons

Substrates	Orbital interaction[a]	Total energy[b]	SEDE[b]	ET[c]
	Zero	−100.0340	0	0
CH_4(11.3)[d]	N	−100.0845	0.0505	0.0726
	E	−100.1534	0.1194	−0.1793
	Zero	−108.7335	0	0
CH_3CH_3 (7.5)	N	−108.7827	0.0492	0.0711
	E	−108.8568	0.1233	−0.1927
	Zero	−117.4275	0	0
CH_3CH_2 CH_3(5.1)	N	−117.4758	0.0483	0.0708
	E	−117.5540	0.1265	−0.2035
	Zero	−126.1176	0	0
$(CH_3)_3$ CH(3.6)	N	−126.1652	0.0476	0.0702
	E	−126.2469	0.1293	−0.2141

a) See the notes in Table 1. b) Atomic units. c) Electron transfer quantities due to delocalization of electrons. Positive values correspond to those from the radical to substrate and negatives, *vice versa*. d) Activation energy (kcal/mol).[18]

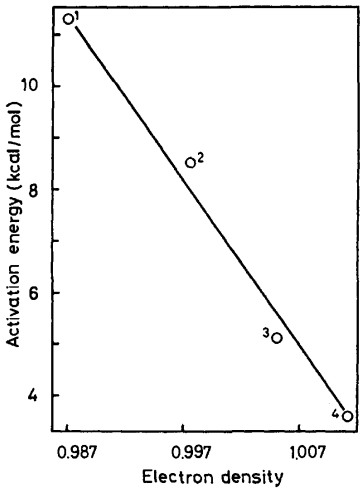

Fig. 3a. The correlation of the activation energy and the electron density for hydrogen abstraction by the CF_3 radical from aliphatic hydrocarbons. 1: CH_4, 2: CH_3CH_3, 3: $CH_3CH_2CH_3$, 4: $(CH_3)_3CH$.

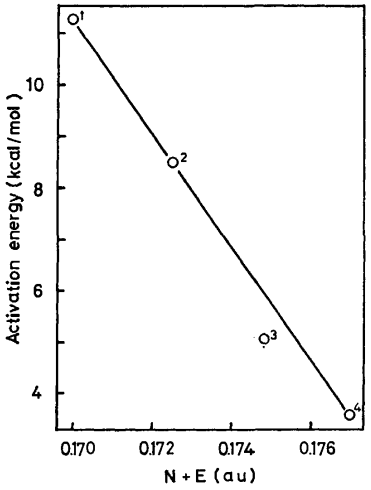

Fig. 3b. The correlation of the activation energy and the sum of the nucleophilic and the electrophilic stabilization energy ($N+E$). 1—4, see the caption in Fig. 3a.

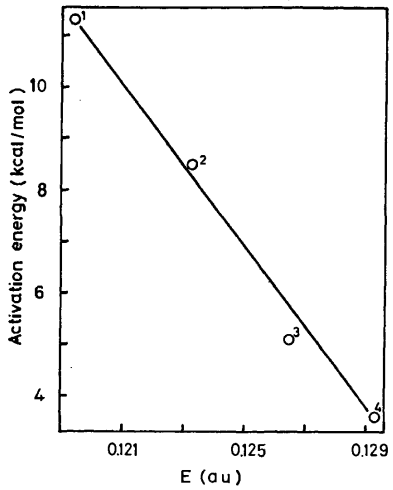

Fig. 3c. The correlation of the activation energy and the electrophilic stabilization energy E. 1—4, see the caption in Fig. 3a.

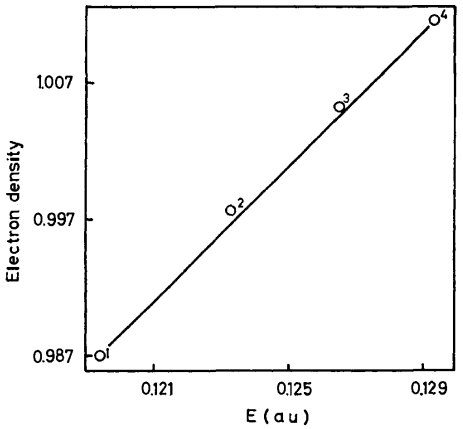

Fig. 3d. The correlation of the electron density and the electrophilic stabilization energy E. 1—4, see the caption in Fig. 3a.

number of electron-donating CH_3 groups, while N decreases. The reactivities of aliphatic hydrocarbons correlate linearly with the sum of N and E, as is shown in Fig. 3b. It should be pointed out that both N and E contribute in determining the reactivity, but the increase of E from molecule to molecule is much larger than the decrease of N. Hence E governs the relative reactivities, as is shown in Fig. 3c. The electrophilicity of the CF_3 radical suggested by the electron density is ascribable to the correlation of the electron density and E shown in Fig. 3d. The electrophilic stabilization energy is closely related with the electron affinity of a radical. Therefore the linear relationship of the negative ρ values and the electron affinities of the radical[9] supports the present conclusion that the radical is an electrophile if the relative reactivities of the substrates are governed by E.

For the study of factors which determine the polarity of radical reagents, the polarities of the OH and CH_3 radicals were subjected to the analysis by the above-mentioned procedure for the reaction with CH_4 and CH_3CN. Fig. 4 shows the difference in the polarity

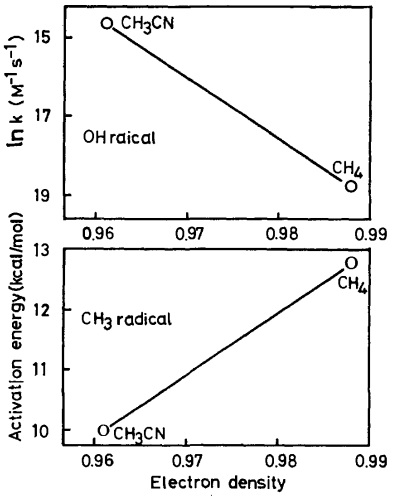

Fig. 4. The difference in the polarity between the OH and the CH_3 radicals.

TABLE 3. THE DIFFERENCE IN THE POLARITY BETWEEN THE OH AND THE CH_3 RADICALS

	Substrates	Orbital interaction[a]	Total energy[b]	SEDE[b]	ET[c]
OH radical	CH_3CN (0.0212)[d]	Zero	−46.6568	0	0
		N	−46.7480	0.0912	0.1067
		E	−46.6616	0.0048	−0.0093
	CH_4 (1.43)[d]	Zero	−28.8765	0	0
		N	−28.9422	0.0657	0.0527
		E	−28.9445	0.1180	−0.1253
CH_3 radical	CH_3CN (10.0)[e]	Zero	−36.7689	0	0
		N	−36.8312	0.0623	0.1038
		E	−36.9112	0.1423	−0.2029
	CH_4 (12.8)[e]	Zero	−18.9882	0	0
		N	−19.0441	0.0559	0.0892
		E	−19.1339	0.1457	−0.2048

a), b), c) See the notes in Table 2. d) Rate constant (10^8 M^{-1} s^{-1}).[6e] e) Activation energy (kcal/mol).[19]

between the OH and the CH_3 radicals in hydrogen abstraction.[19] Although only two points are available, a distinct tendency is observed: the OH is electrophilic while the CH_3 radical is nucleophilic. This result is in good agreement with our previous studies on the polarity of the OH and the CH_3 radicals in the reaction with methane and a series of chloromethanes, respectively.[12] It is evident that the correlation in Fig. 4 is not explained by the bond dissociation energy of the C–H bond broken, D_{C-H}, only (D_{C-H} in CH_3CN: 86 kcal/mol,[9] CH_4: 104 kcal/mol[20]) but by the significant contribution of the polar effects. As Table 3 shows, the relative reactivities are interpreted by the sum of *N* and *E*. For the OH radical, the increase of *E* is larger than the decrease of *N* when the substrate changes from CH_3CN to CH_4, so that *E* governs the reactivities. This tendency is consistent with that of the CF_3 radical. The electrophilicity of the OH radical determined by the SEDE is in agreement with the one reported by Anbar *et al.*[6e] on the basis of the Hammett equation. For the CH_3 radical, on the other hand, the increase of *E* is smaller than the decrease of *N*, hence *N* governs the reactivities. As the difference of the ionization potential between the

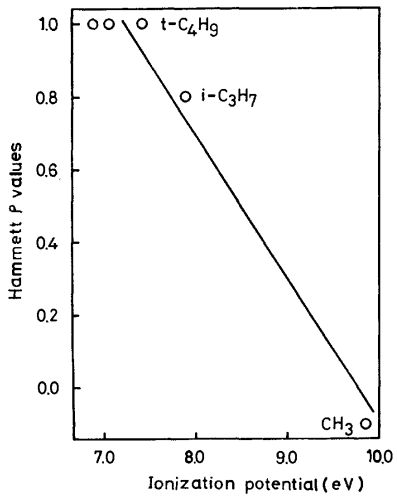

Fig. 5. The correlation of the Hammett ρ values and the ionization potentials of alkyl radicals.

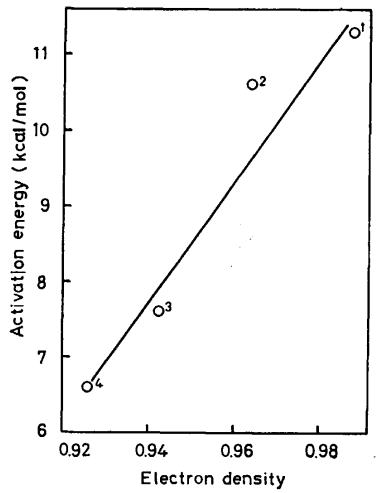

Fig. 6a. The correlation of the activation energy and the electron density for hydrogen abstraction by the CF_3 radical from chloromethane. 1: CH_4, 2: CH_3Cl, 3: CH_2Cl_2, 4: $CHCl_3$.

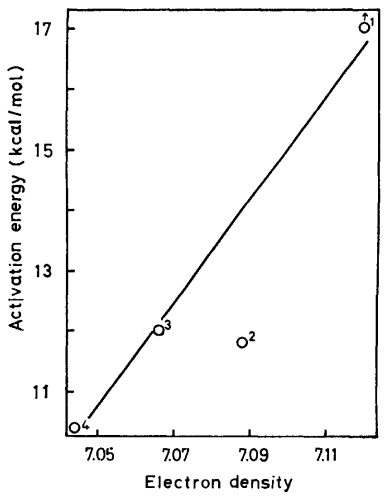

Fig. 6b. The correlation of the activation energy and the electron density for chlorine abstraction by the CF_3 radical from chloromethanes. 1: CH_3Cl, 2: CH_2Cl_2, 3: $CHCl_3$, 4: CCl_4.

OH and the CH_3 radicals (OH: 13.18,[21] CH_3: 9.86 eV[21]) is larger than that of the electron affinity[22] (OH: 1.83, CH_3: 1.4 eV), the former seems to play a dominant role in determining the polarity of the radical. The nucleophilicity of the CH_3 radical is based on its low ionization potential. In fact, i-C_3H_7 and t-C_4H_9 radicals having low potentials[21] (i-C_3H_7: 7.90, t-C_4H_9: 6.90, 7.07, 7.42 eV) have recently been found by Pryor *et al.*[8c] to react as nucleophiles in hydrogen abstractions from substituted toluenes. As Fig. 5 shows, the positive ρ value increases with a decrease in the ionization potential of a radical. This supports the conclusion that the radical is a nucleophile if the relative reactivities of the substrates are governed by N.

According to Pryor *et al.*, the CH_3 radical is slightly electrophilic in hydrogen abstraction with substituted toluenes ($\rho=-0.1$[23]), while it abstracts electron deficient α hydrogen 7.8-fold faster than β hydrogen in the reaction with propionic acid.[24] Similarly, the CF_3 radical is nucleophilic in hydrogen abstraction or chlorine abstraction with chloromethanes, as is shown in Figs. 6a and 6b.[25] The electron affinity of the CF_3 radical is nearly equal to that of the electrophilic OH radical (CF_3: 1.85, OH: 1.83 eV),[22] while its ionization potential (10.18, 8.90 eV)[21] is lower than that of the OH radical (13.18 eV[19]) and approximately the same as that of the CH_3 radical (9.86 eV).[21] This may account for the two different behaviors of the CF_3 radical in the polarity. These results show that the polarity of a radical seems to be primarily determined by its physicochemical properties (ionization potential or electron affinity), but also to depend on the nature of the substrate.

We would like to express our gratitude to the Computer Center, Tokyo University, for its generous permission to use the HITAC 8700/8800 computer.

References

1) C. Walling, "Free Radicals in Solution," Wiley, New York, N. Y. (1957), pp. 132—140, 365—369, 375—376, 474—491.

2) W. A. Pryor, "Free Radicals," McGraw-Hill, New York, N. Y. (1966), p. 170 ff.

3) K. U. Ingold and B. P. Roberts, "Free Radical Substitution Reactions," Wiley-Interscience, New York, N.Y. (1971), p. 158.

4) E. S. Huyser, "Free Radical Chain Reactions," Wiley-Interscience, New York, N. Y. (1970), pp. 70, 143, 346, 358.

5) J. E. Leffler and E. Grunwald, "Rates and Equilibria of Organic Reactions," Wiley, New York, N. Y. (1963), pp. 177 ff.

6) (a) J. A. Howard and K. U. Ingold, *Can J. Chem.*, **41**, 1744 (1963); (b) G. A. Russel and R. C. Williamson, *J. Am. Chem. Soc.*, **86**, 2357 (1964); (c) M. A. DaRooge and L. R. Mahoney, *J. Org. Chem.*, **32**, 1 (1967), and references cited therein; (d) ρ values for hydrogen abstractions by radicals from substituted toluenes are summarized by W. A. Pryor, T. H. Lin, J. P. Stanley, and R. W. Henderson, *J. Am. Chem. Soc.*, **95**, 6993 (1973); (e) M. Anbar, D. Meyerstein, and P. Neta, *J. Chem. Soc., B*, 742 (1966); (f) Y. Nagai, K. Yamazaki, I. Shiojima, N. Kobori, and M. Hayashi, *J. Organomet. Chem.*, **9**, 21 (1967); (g) H. Sakurai and K. Mochida, *J. Organomet. Chem.*, **42**, 339 (1972).

7) J. M. Hay, "Reactive Free Radicals," Academic Press, London (1974), pp. 135—145.

8) W. A. Pryor, W. H. Davis, Jr., and J. P. Staley, *J. Am. Chem. Soc.*, **95**, 4754 (1973); (b) W. H. Davis, Jr., J. H. Gleaton, and W. A. Pryor, *J. Org. Chem.*, **42**, 7 (1977); (c) W. H. Davis, Jr., and W. A. Pryor, *J. Am. Chem. Soc.*, **99**, 6365 (1977).

9) H. Sakurai and K. Tokumaru, *Kagaku No Ryoiki, Zokan*, **81**, 355 (1967).

10) A. Imamura and K. Hirao, to be published.

11) H. Shinohara, A. Imamura, T. Masuda, and M. Kondo, *Bull. Chem. Soc. Jpn.*, **51**, 1917 (1978).

12) H. Shinohara, A. Imamura, T. Masuda, and M. Kondo, to be published.

13) J. A. Pople and R. K. Nesbet, *J. Chem. Phys.*, **33**, 571 (1954).

14) J. A. Pople, D. P. Santry, and G. A. Segal, *J. Chem. Phys.*, **43**, s129 (1965); J. A. Pople and G. A. Segal, *ibid.*, **43**, s136 (1966).

15) J. A. Pople and G. A. Segal, *J. Chem. Phys.*, **44**, 3289 (1966).

16) H. C. Allen and E. K. Plyler, *J. Chem. Phys.*, **26**, 972 (1957).

17) "Molecular Structures and Dimensions," ed by O. Kennard and D. G. Watson, Crystallographic Data Centre Cambridge, International Union of Crystallography, N. V. A. Oosthoek's Uitegevers Mij Utrecht (1972), Vol. A1.

18) The activation energy for CH_4 is cited from W. G. Alcock and E. Whittle, *Trans. Faraday Soc.*, **61**, 244 (1965); for C_2H_6 and $CH_3CH_2CH_3$, G. O. Pritchard, H. O. Pritchard, H. I. Schiff, and A. F. Trotman-Dickenson, *Trans. Faraday Soc.*, **52**, 849 (1956); for $(CH_3)_3CH$, R. E. Dodd and J. W. Smith, *J. Chem. Soc.*, 1465 (1957). These values are cited by R. R. Baldwin and R. W. Walker, *J. Chem. Soc., Perkin Trans. 2*, **1973**, 362.

19) The activation energy for CH_4 is cited from A. F. Trotman-Dickenson, "An Introduction To Free Radicals," Methuen, London (1959), p. 34; for CH_3CN, A. F. Trotman-Dickenson, "Tables of Bimolecular Gas Reactions," NSRDS-NBS 9, USA (1967).

20) G. A. Russell in "Free Radicals," ed by J. K. Koichi, Wiley-Intersceince, New York, N. Y. (1970), Vol. 1, p. 284.

21) "Mass Spectrometry of Organic Ions," ed by F. W. McLatterty, Academic Press, N. Y. (1963), Chap. 5.

22) F. M. Page in "Handbook of Chemistry and Physics," 53rd, ed, CRC Press (1972—1973).

23) W. A. Pryor, U. Tonellato, D. L. Fuller, and S. Jumonville, *J. Org. Chem.*, **34**, 2018 (1969).

24) (a) Ref. 20, p. 293; (b) Ref. 2. p. 171.

25) W. G. Alcock and E. Whittle, *Trans. Faraday Soc.*, **62**, 664 (1966).

Electron Spin-Spin Interaction and Translational Diffusion of Nitroxide Radicals in Sodium Dodecyl Sulfate Micelles

Masayuki AIZAWA,* Tsuyoshi KOMATSU, and Tsurutaro NAKAGAWA

Department of Polymer Science, Faculty of Science, Hokkaido University, Sapporo 060

(Received August 9, 1978)

The line width measurements of ESR spectra of 2,2,6,6-tetramethyl-4-benzoyloxypiperidinyl-1-oxyl (BzONO) in sodium dodecyl sulfate (SDS) micelles have been carried out at various concentrations of BzONO. The plot of the line width against the concentration of BzONO shows a line with a break at mole fraction *ca.* 0.05, as opposed to the theoretical prediction that the plot would give a straight line. In order to explain this anomalous behavior, three models for the solubilization of BzONO are considered. On the basis of two of these models, spin exchange rates of BzONO in the micelles are estimated. Translational diffusion coefficients of BzONO in the SDS micelles at 20, 31, and 38.5 °C are calculated by using the spin exchange rate constants and an appropriate diffusion model. The obtained values are of the order of 10^{-7} cm²/s.

Magnetic resonance methods have been used to study both microscopic and dynamical aspects of the solubilization of hydrophobic substances into surfactant micelles.

In the NMR method,[1] the change in chemical shifts caused by aromatic solubilizates is utilized to know a solubilizing site and its environment. Fendler and coworkers[2] have reported that benzene is mainly solubilized in the interior of sodium dodecyl sulfate (SDS) micelles, but it is located near the surface of hexadecyltrimethylammonium bromide (CTAB) micelles.

By means of another NMR technique utilizing the line broadening caused by paramagnetic counter ions, Fox and coworkers[3] have found that *p*-xylene as a solubilizate is distributed uniformly throughout the hydrophobic region of SDS micelles.

By the ESR method, besides the solubilizing site and its environment,[4] dynamical quantities such as rotational correlation times[4,5] in micelles and exchange rates[6] between micellar environment and bulk water have been obtained for nitroxide radical molecules as hydrophobic solubilizates. The values reported so far are of the order of 10^{-10} s/rad for the former and 10^4—10^5/s for the latter.

Recently, the measurement of spin exchange interaction has been applied to the study of translational diffusion in fluid media,[7] and has given very interesting results. In a fluid medium, the spin exchange is accompanied by the molecular collision between dissolved radicals. The exchange rate, therefore, can be connected with their translational diffusion coefficient.[8]

By means of this technique, McConnell and coworkers[9] have estimated that the translational diffusion coefficient of spin-labeled phospholipid molecules in lipid membranes is 6×10^{-8} cm²/s at 37 °C. Ablett and coworkers[10] have studied the hydrophobic interaction by the measurement of spin exchange rate of nitroxide radicals in both water and various organic solvents.

The purpose of the present study is to determine the translational diffusion coefficients of solubilizates in surfactant micelles by this technique, which utilizes the electron spin exchange broadening. The information about this quantity may lead to a further understanding of the solubilization phenomena and the chemical reaction in micellar environments.

Experimental

The synthesis of 2,2,6,6-tetramethyl-4-benzoyloxypiperidinyl-1-oxyl (BzONO, Fig. 1) was reported elsewhere.[11] Sodium dodecyl sulfate (SDS) of specially prepared reagent was recrystallized several times from ethanol-acetone solutions. Its CMC is 8.3×10^{-3} mol/dm³ at 25 °C.

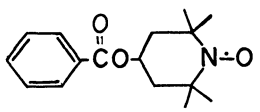

Fig. 1. BzONO.

ESR spectra were recorded on a JEOL model ME-3X spectrometer equipped with a variable temperature accessory. The accuracy of temperature measurements is ±1 K.

The concentration of aqueous SDS solutions ranges from 4 to 7 wt %. In this concentration range, the ESR spectra come only from BzONO in SDS micelles; the fraction of BzONO in bulk water is very small.

Results and Discussion

As unpaired electron spin concentration increases in a system, the electron spin-spin interaction becomes more and more important in the electron magnetic relaxation mechanism.[12] This interaction consists of two parts; one is the spin exchange interaction and the other is the dipolar interaction. The former is a contact interaction which occurs only on overlapping of the wave functions of the electron spins. In a solution, therefore, this interaction accompanies the collisional process between paramagnetic species. The latter is a classical magnetic interaction which depends on the distance between paramagnetic species.

From theoretical and experimental studies,[13] both interactions increase linearly with the spin concentration. However, in regard to an increase in T/η where T is the absolute temperature and η is the environmental viscosity, the two interactions behave differently.[14] The spin exchange interaction is proportional to the increase, and, on the other hand, the dipolar interaction is inversely proportional to it. That is to say, the electron spin relaxation rate of spin exchange interaction T_{2E}^{-1} and that of dipolar interaction T_{2D}^{-1} are given by the following formulae, respectively:

$$T_{2E}^{-1} = k_E C \propto T/\eta, \quad (1)$$

$$T_{2D}^{-1} = K_D C \propto \eta/T, \quad (2)$$

where k_E is the second order rate constant for the exchange process, C the spin concentration, and K_D is a proportionality constant.

In the case of nitroxide radicals, the net spin-spin relaxation rate T_2^{-1} takes the following form:

$$T_2^{-1} = T_{20}^{-1} + T_{2E}^{-1} + T_{2D}^{-1} = T_{20}^{-1} + (k_E + K_D)C, \quad (3)$$

where T_{20}^{-1} is the relaxation rate when no electron spin-spin interaction occurs. Thus, Eq. 3 predicts that a plot of T_2^{-1} against C will give a straight line.

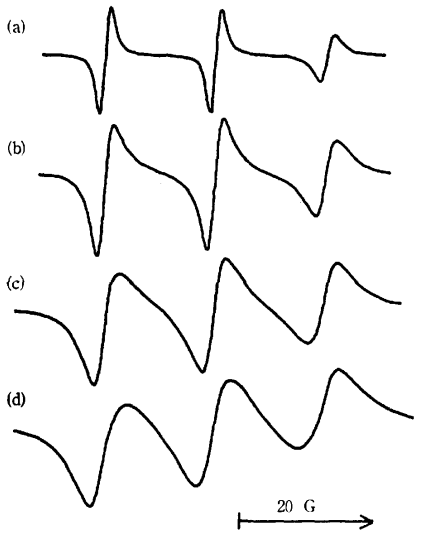

Fig. 2. ESR spectra of BzONO in 4.75 wt % aqueous SDS solutions at 20 °C. Mole fraction of BzONO in micelles: (a) 0.009, (b) 0.037, (c) 0.065, (d) 0.090.

Figure 2 shows ESR spectra of BzONO in 4.75 wt % aqueous SDS solutions at 20 °C. At this SDS concentration, the spectra can be assigned only to BzONO in the SDS micelles. The spectra consist of three lines owing to the contact interaction between an electron spin ($S=1/2$) and an ^{14}N nuclear spin ($I=1$). The three lines correspond to ^{14}N nuclear spin quantum numbers $M_I=+1$, 0, and -1, toward the high field direction. Each line width of the spectra increases with the concentration of BzONO. The broadening is due to the electron spin-spin interaction.

Figure 3 shows the plots of each line width W, equal to $(2/\sqrt{3})T_2^{-1}$, against the mole fraction X of BzONO in micelles. The obtained plots were not represented by straight lines, contrary to the foregoing theoretical consideration. Each line breaks at mole fraction *ca.* 0.05.

Recently, Barratt and coworkers[15] have reported similar results from the study of electron spin exchange of 2,2,6,6-tetramethylpiperidinyl-1-oxyl in glycerol-water mixed solvent; they give no interpretation. We will give our opinion later, though it is an open question whether the nature of their results is the same as in the present study.

The results of line width measurement with two SDS concentrations were on the same lines, as is shown in

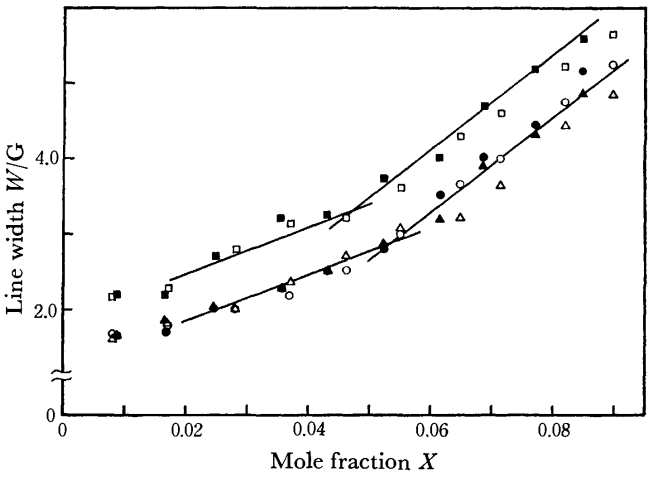

Fig. 3. Plots of W against X at 20 °C in 4.75 wt % aqueous SDS solutions (○: $M_I=+1$, △: $M_I=0$, and □: $M_I=-1$); in 7.01 wt % aqueous SDS solutions (●: $M_I=+1$, ▲: $M_I=0$, and ■: $M_I=-1$).

Fig. 3. This fact guarantees that the ESR spectra observed involve no signal from BzONO in bulk water, and indicates that the presence of the break is not caused by the interaction between electron spins belonging to different micelles.

Figures 4 and 5 show the results at 31 and 38.5 °C, respectively. At these temperatures, it was also observed that the linear plots of W against X fail. The gradients of these lines above and below mole fraction of *ca.* 0.05 are listed in Table 1. It is observed that the gradient decreases with an increase in temperature in the mole fraction range below *ca.* 0.05, whereas it increases in the higher mole fraction range. This finding can be interpreted by suggesting that below *ca.* 0.05 of X the dipolar interaction is predominant and, on the contrary, above *ca.* 0.05 of X the electron spin exchange interaction is predominant. (*cf.* Eqs. 1 and 2)

In order to understand the above-stated anomalous spin concentration dependence of the line width, three models for the solubilized state may be considered, as follows.

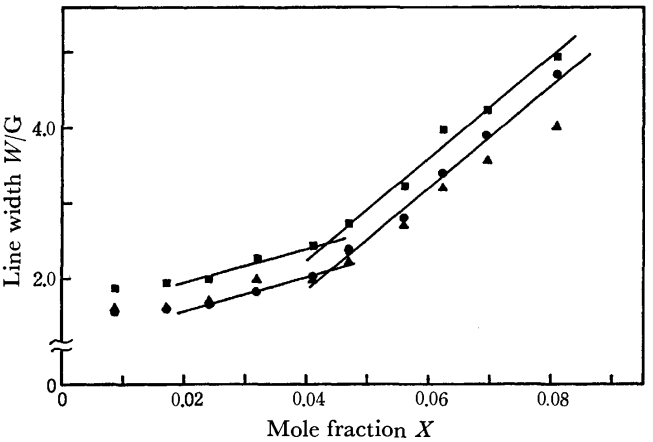

Fig. 4. Plots of W against X in 5.71 wt % aqueous SDS solutions at 31 °C (●: $M_I=+1$, ▲: $M_I=0$, and ■: $M_I=-1$).

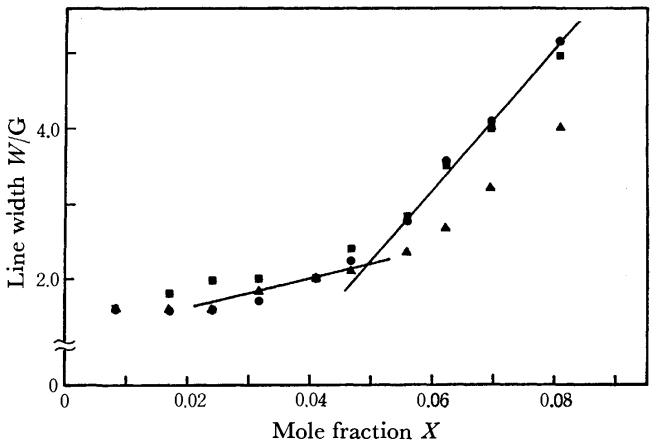

Fig. 5. Plots of W against X in 5.71 wt % aqueous SDS solutions at 38.5 °C (●: $M_I=+1$, ▲: $M_I=0$, and ■: $M_I=-1$).

TABLE 1. GRADIENTS OF W-X LINES IN TWO MOLE FRACTION RANGES

Temp (°C)	Gradient/G	
	$X<0.05$	$X>0.05$
20	30.4	62.4
31	22.4	67.2
38.5	19.2	92.8

Model 1. In this model it is considered that one SDS micelle consists of several clusters containing some SDS molecules. It is, moreover, assumed that a solubilizate molecule is bound in one of these clusters and cannot transfer from one to another. In a cluster, however, a solubilizate molecule can move easily. On this assumption, the occurrence of a break in the W-X plot can be explained as follows.

With an increase in the concentration of BzONO in SDS micelles, the number of BzONO in each cluster increases. When the number of BzONO in one micelle exceeds one, the dipolar interaction takes place, and as long as the number of BzONO in each cluster does not exceed one, only this interaction is present. The reason for this is that BzONO molecules in different clusters cannot collide with each other. When the number in one cluster exceeds one, the spin exchange interaction is superimposed to the dipolar interaction.

Thus, in the plot of line width against BzONO mole fraction, a break may occur and this point corresponds to the concentration where one cluster solubilizes just one BzONO molecule.

Since the values of mole fraction at the break in Figs. 3, 4, and 5 are almost equal to 0.05, the number N^c_{mo} of the SDS molecules constituting one cluster is estimated to be 19, satisfying $1/(1+N^c_{mo})=0.05$. Considering that the aggregation number of the SDS molecules in one SDS micelle is equal to 62,[16] it can be derived that three clusters exist in one SDS micelle.

Accoridng to the studies[17] concerning the micellar structure of ionic surfactants, the micelles at low concentration have spherical or ellipsoidal shape with a single hydrophobic core and a continuous surface. On the other hand, at high concentration (more than 10 wt %), some surfactants form a bilayer structure. Since the concentration of SDS solutions used in the present study ranges from 4 to 7 wt %, it is supposed that the micellar structure in the solutions is similar to that at low SDS concentration. In these micellar models, a continuous structure is assumed in the micelle. Therefore, the nature of the cluster proposed in this model 1 remains unexplained.

Model 2. In this model, the occurrence of spin exchange interaction above the mole fraction *ca* 0.05 is explained by a structural change in micelles caused by the solubilization of BzONO. The structural change assumed here is one which makes the hydrophobic portion of micelles more fluid-like. As was stated above, the dipolar interaction predominates over the spin exchange interaction at lower radical concentration, so that the change into fluid-like structure weakens the former and strengthens the latter. Thus, the plots of line width against BzONO concentration produce a break at the concentration of the structural change.

In the NMR study[18] on mixed solutions of a nonionic surfactant, hexa(oxyethylene)dodecyl ether, and a fluorescent dye, it was found that the line width of alkyl methylene protons decreases with an increase in the concentration of the dye and remains constant above 0.05 of the mole fraction of the dye. These findings have been explained on the basis of a change in the micelle structure caused by the electrical charge of the dye molecules trapped in the poly(oxyethylene) shell of the micelle.

Fendler and coworkers[2] found that plots of chemical shifts of a zwitterionic surfactant, 3-(*N*,*N*-dimethyldodecylammonio)-1-propanesulfonate, against the concentration of solubilizate, benzene, or nitrobenzene, exhibit a break in the region of mole fraction from 0.04 to 0.12. This break has been ascribed to an alteration in the micelle structure.

These results may support this model 2, if one assumes that the aromatic solubilizates including BzONO cause the structural change in micelle.

Model 3. In this model the occurrence of the break in the W-X curves is ascribed to a clustering of BzONO themselves in SDS micelles. The clustering, which occurs at some BzONO content, makes its local concentration higher in the micelle. Therefore, the dependence of electron spin-spin interaction on the BzONO concentration changes, producing a break. Recently, in the case of some nitroxide biradicals in lipid membranes, a clustering of radicals was observed by Rey and McConnell.[19] It is a disadvantage of this model that, in the ESR spectra in the present study, there is no signal corresponding to monomeric BzONO molecules which should exist in equilibrium with BzONO clusters.

All three models can explain, in any event, the occurrence of the breaks on the lines in Figs. 3—5. The determination of the most favorable model remains a further problem, and the simulation of the experimental spectra which will serve to solve the question is now being carried out.

On the basis of model 1 and model 2, the spin exchange rate of BzONO in SDS micelles are determined, and then the translational diffusion coefficients of BzONO in the micelles are calculated. The tanslational diffusion coefficient cannot be defined in model 3, since the spin exchange rate in this model does not reflect the diffusion process of BzONO in SDS micelles.

According to studies[20] on the relationship between the spin exchange interaction and the molecular collision process, the rate f_c of the bimolecular collision between radicals has the following relationship with the spin exchange rate T_{2E}^{-1} ($=f_E$) in a relatively viscous medium ($\eta>3$—4 cp):

$$f_c = 3T_{2E}^{-1} = 3f_E. \quad (4)$$

Since $f_E=k_EC$ in Eq. 1,

$$f_c = 3k_EX \quad (5)$$

is derived, if C is defined as the mole fraction X.

On the other hand, assuming that the surfactant molecules and solubilizate, BzONO, constitute a two-dimensional hexagonal structure in the micelle, the average number[8,21] of new solubilizate molecules encountered by a solubilizate molecule in one diffusion step is equal to $3X$, where X is the mole fraction of the solubilizate in micelles. Thus, f_c is represented by

$$f_c = 3nX, \quad (6)$$

where n is an average rate of diffusion step.

A two-dimensional diffusion coefficient D_{tr} can be written as

$$D_{tr} = n\lambda^2/4 \quad (7)$$

where λ is a mean length in one diffusion step. Substituting Eqs. 5 and 6 into Eq. 7, D_{tr} is rewritten as

$$D_{tr} = k_E\lambda^2/4. \quad (8)$$

Therefore, if k_E can be estimated from Figs. 3—5, and an appropriate diffusion model is assumed, the translational diffusion coefficient of BzONO in SDS micelles can be reasonably determined.

In model 1, k_E corresponds to a difference between the two gradients (below and above mole fraction *ca.* 0.05). Strictly speaking, the value does not correspond to k_E, since the magnitude of intra-cluster dipolar interaction may not be equal to that of inter-cluster dipolar interaction.

In model 2, k_E corresponds to the gradient above mole fraction *ca.* 0.05.

λ^2 was estimated to be 5.8×10^{-15} cm^2 from the results[22] of the surface area occupied by one polar head group in SDS micelles.

Table 2. Translational diffusion coefficents of BzONO in sodium dodecyl sulfate micelles

Temp (°C)	Model 1 $D_{tr}/10^{-7}$cm^{2}s^{-1}	Model 2 $D_{tr}/10^{-7}$cm^{2}s^{-1}
20	1.1	2.2
31	1.6	2.4
38.5	2.6	3.3

Substituting the values of k_E and λ^2 into Eq. 8, the translational diffusion coefficients of BzONO in SDS micelles were obtained. The results at 20, 31, and 38.5 °C are listed in Table 2. The increasing tendency of D_{tr} with temperature is more reasonable in model 1 than in model 2.

The translational diffusion coefficient of low-molecular weight substances in ordinary solutions is of the order of 10^{-5} cm^2/s, and that of phospholipid[21] or steroid[23] molecules in lipid membranes is of the order of 10^{-8} cm^2/s. The values obtained in the present system fall between these two.

References

1) T. Nakagawa and F. Tokiwa, *Surf. Colloid Sci.*, **1976**, 69.
2) E. J. Fendler, C. L. Day, and J. H. Fendler, *J. Phys. Chem.*, **76**, 1460 (1972).
3) K. K. Fox, I. D. Robb, and R. Smith, *J. Chem. Soc., Faraday Trans. 1*, **68**, 445 (1972).
4) A. S. Waggoner, O. H. Griffith, and C. R Christensen, *Proc. Natl. Acad. Sci. U.S.A.*, **57**, 1198 (1967).
5) M. Aizawa, T. Komatsu, and T. Nakagawa, *Bull. Chem. Soc. Jpn.*, **50**, 3107 (1977).
6) T. Nakagawa and H. Jizomoto, *Colloid Polym. Sci.*, **252**, 482 (1974).
7) T. Sridhar and O. E. Potter, *J. Phys. Chem.*, **81**, 2679 (1977).
8) G. E. Pake and T. R. Tuttle, Jr., *Phys. Rev. Lett.*, **3**, 423 (1959).
9) C. J. Scandella, P. Devaux, and H. M. McConnell, *Proc. Natl. Acad. Sci. U.S.A.*, **69**, 2056 (1972).
10) S. Ablett, M. D. Barratt, and F. Franks, *J. Solution Chem.*, **4**, 797 (1975).
11) E. G. Rozantzev, V. A. Golubev, and M. B. Neiman, *Bull. Acad. Sci. USSR*, **1965**, 379.
12) A. Carrington and A. D. McLachlan, "Introduction to Magnetic Resonance," Harper and Row, New York, N. Y. (1967).
13) M. T. Jones, *J. Chem. Phys.*, **38**, 2892 (1963).
14) Y. Ayant, R. Besson, and A. Salvi, *J. Physique*, **36**, 571 (1975).
15) M. D. Barratt, F. Franks, and P. N. Robinson, *J. Solution Chem.*, **6**, 625 (1977).
16) J. H. Fendler and E. J. Fendler, "Catalysis in Micellar and Macromolecular Systems," Academic Press, New York, N. Y. (1975), p. 20.
17) C. Tanford, "The Hydrophobic Effect," John Wiley and Sons, New York, N. Y. (1973).
18) I. Homma, F. Tokiwa, and J. Mino, *Nippon Kagaku Kaishi*, **1976**, 1349.
19) P. Rey and H. M. McConnell, *J. Am. Chem. Soc.*, **99**, 1637 (1977).
20) N. Edelstein, A. Kwok, and A. H. Maki, *J. Chem. Phys.*, **41**, 3473 (1964).
21) P. Devaux, C. J. Scandella, and H. M. McConnell, *J. Magn. Reson.*, **9**, 474 (1973).
22) H. V. Tartar, *J. Phys. Chem.*, **59**, 1195 (1955).
23) H. Träuble and E. Sackmann, *J. Am. Chem. Soc.*, **94**, 4499, (1972).

The H/D Isotope Effect in the Reaction of Hydrogen Atoms with Olefins

Yo-ichi Ishikawa and Shin Sato*

Department of Applied Physics, Tokyo Institute of Technology, Ookayama, Meguro-ku, Tokyo 152

(Received August 14, 1978)

The absolute rate constants of reaction of deuterium atoms with seven simple olefins at room temperature have been measured by using the pulse-radiolysis technique. The comparison with the rate constants of reaction of hydrogen atoms previously obtained shows that the ratios of k(D+olefin)/k(H+olefin) are in the range of 0.7—0.8. This isotope effect is theoretically discussed.

The H/D isotope effect has widely been used for the elucidation of the reaction mechanism of a complex reaction;[1] however, reliable absolute rate constants which can be utilized for the analysis of the isotope effect in an elementary reaction are not abundant. In 1975, Mihelcic *et al.* measured the absolute rate constants of the reactions between H or D atoms and C_2H_4, C_2D_4, or C_3H_6 and discussed the kinetic isotope effects.[2]

In a previous paper,[3] we obtained the absolute rate constants of reaction of hydrogen atoms with seven simple olefins by using a pulse-radiolysis technique and found that the relative rate constants obtained are in good agreement with those reported as reliable values in the literature. Since the method we used can easily be extended to the reactions of deuterium atoms, we have attempted to measure the absolute rate constants of reaction of deuterium atoms with the same seven olefins and to discuss the H/D isotope effect.

Experimental

The technique used in this study consists of that of pulse radiolysis coupled with the time resolved detection of the resonance absorption of deuterium atoms. The apparatus and procedure used are similar to those previously described for the reaction of hydrogen atoms,[3] except for the detection system. A photomultiplier tube for the vacuum ultraviolet region (Hamamatsu TV Co., R976) was mounted for the detection of Lyman-α line of D atoms. The signal/noise ratio was improved to about 20. The photomultiplier output was amplified by an operational amplifier (Harris HA-2625) and monitored by a Tektronix 475 oscilloscope.

The deuterium gas, whose nominal purity was 99.5% (Showa Denko Co.), was used after having been passed through a molecular sieve 4A at the temperature of liquid nitrogen. The research grade olefins supplied by the Takachiho Shoji Co. were used after thorough degassing.

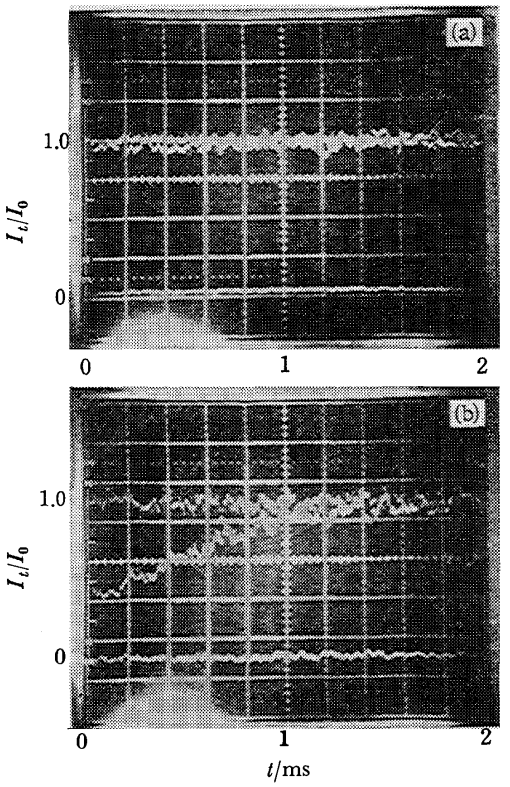

Fig. 1. a) The pulse-irradiated H_2 gas at 500 Torr was detected by the Lyman-α of D atoms. No absorption can be observed. b) Under the same condition of the lamp, the D_2 gas at 500 Torr containing 74 mTorr trans-2-butene was pulse-irradiated.

In order to ascertain the separation of Lyman-α's of H and D atoms, 500 Torr H_2 gas was pulse-irradiated and the absorption of the product at the wavelength of Lyman-α was pursued

Table 1. The absolute rate constants of reaction of hydrogen and deuterium atoms with simple olefins at room temperature

Olefin	Mihelcic *et al.*[2]			Present authors		
	k_H	k_D	k_D/k_H	k_H[3]	k_D	k_D/k_H
	10^{-12} cm^3 molecule^{-1} s^{-1}			10^{-12} cm^3 molecule^{-1} s^{-1}		
Ethylene	1.25±0.03	0.87±0.03	0.70	1.1±0.1	0.8±0.1	0.73
Ethylene-d_4	1.15±0.03	0.85±0.03	0.74			
Propylene	1.68±0.05	1.14±0.02	0.68	1.7±0.1	1.3±0.2	0.76
1-Butene				2.0±0.5	1.6±0.1	0.80
trans-2-Butene				1.1±0.1	0.8±0.1	0.73
cis-2-Butene				1.0±0.1	0.8±0.1	0.80
2-Methylpropene				5.2±0.6	3.8±0.3	0.73
2-Methyl-2-butene				2.4±0.3	2.0±0.3	0.83

by using a lamp in which D_2 gas was made to flow. As Fig. 1a shows, pratically no absorption could be observed. On the other hand, when the reactant was replaced by D_2 gas under the same condition of the lamp, a strong absorption could be observed. Figure 1b shows the decay of deuterium atoms obtained with 500 Torr D_2 and 74 mTorr *trans*-2-butene.

Results

Figure 2 shows the decay rates of deuterium atoms as functions of the concentration of olefins. From the slopes of the linear relations, the rate constants of reaction of deuterium atoms with olefins can be calculated. The results are summarized in Table 1, together with the rate constants previously obtained for hydrogen atoms and with the results obtained by Mihelcic *et al.*[2] All of the ratios k(D+olefin)/k(H+olefin) are in the range of 0.7—0.8. The experimental errors prevent us from determining whether the ratios are dependent upon the kind of olefins.

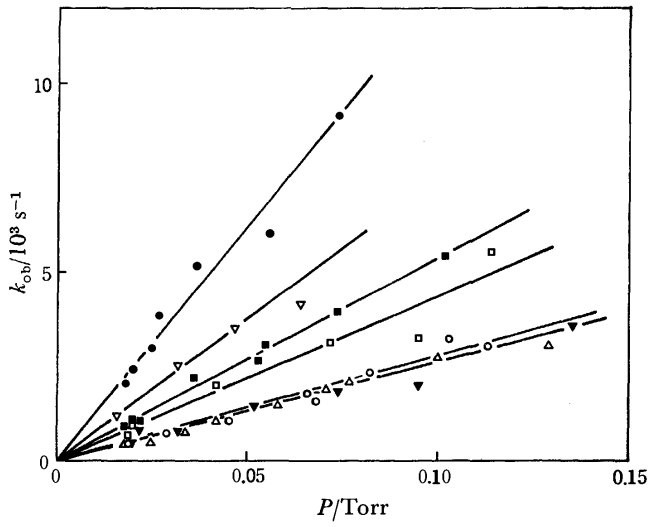

Fig. 2. Plots of the decay rates of D atoms against the olefin pressures. The deuterium pressure is around 500 Torr. ○: Ethylene, □: propylene, ■: 1-butene, △: *trans*-2-butene, ▼: *cis*-2-butene, ●: 2-methylpropene, ▽: 2-methyl-2-butene.

Discussion

Correlations between the Rate Constants and the Reaction Index Calculated by the Semi-empirical MO Method for Olefins. When Jennings and Cvetanović measured the relative rate constants of reaction of hydrogen atoms with several olefins,[4] they correlated their data with the reaction index calculated by the simple Hückel method including hyperconjugation and found a linear relationship between the logarithm of the relative rate constants and the atom localization energies of olefins.[5] Since symmetric olefins such as ethylene and *cis*- and *trans*-2-butenes have two reactive sites for the addition reaction of a hydrogen atom, the rate constants might have to be divided by two when such a correlation is examined; however, the division by two does not lead to the linear relationship.

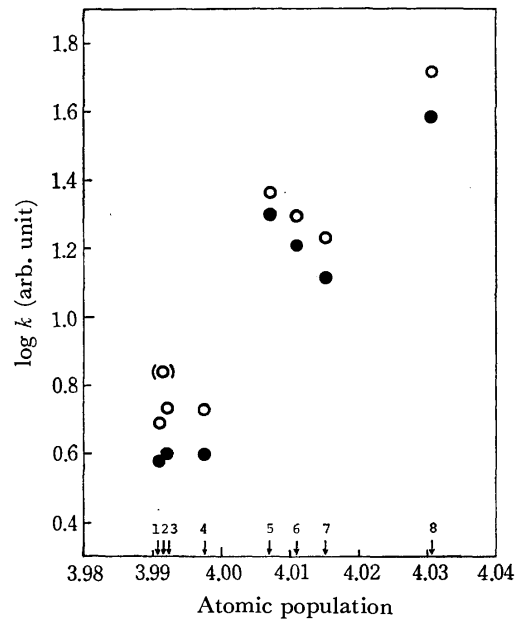

Fig. 3. The logarithm of the rate constants against the atomic populations calculated by the INDO method. 1: *cis*-2-Butene, 2: 2,3-dimethyl-2-butene (estimated from the data in Ref. 4), 3: *trans*-2-butene, 4: ethylene, 5: 2-methyl-2-butene, 6: 1-butene, 7: propylene, 8: 2-methylpropene. ○: For hydrogen atoms and ●: for deuterium atoms.

Recently Koda *et al.* showed a linear relationship between the logarithm of the relative rate constants of reaction of hydrogen atoms with simple olefins and the atomic population on the less substituted of the doubly bonded carbon atoms calculated by the CNDO/2 method.[6] In this case, they divided the relative rate constants for symmetric olefins by two. In their plots, however, 2-methyl-2-butene was not included. We, therefore, have calculated the atomic populations using the INDO method. As Fig. 3 shows, we could not find a linear relationship between the logarithm of the rate constants we obtained and the atomic population calculated.

A Simple Interpretation of the H/D Kinetic Isotope Effect. According to the recent *ab initio* calculation using STO 3G basis set for the reaction path of the addition of a hydrogen atom to ethylene, a hydrogen atom approaches one of the doubly bonded carbon atom perpendicularly to the plane of the ethylene molecule and there is no energy barrier on the reaction path.[7]

In the present experiment, however, we have found that k(H+2-methylpropene)/k(H+ethylene)=4.7 at room temperature. This large ratio cannot easily be explained by the difference in the preexponential factor of the Arrhenius equation. Moreover, recent measurements suggest that the apparent activation energy for the reaction between hydrogen atoms and ethylene is in the range of 1—3 kcal mol^{-1}.[8-10]

In the present treatment, we tentatively assume that there is a small energy barrier, E_0, on the reaction path for the approach of a hydrogen atom to ethylene and also that this type of addition reaction may be treated as a bimolecular association between an atom (H or D) and a radical (A). Then the activated complex theory

predicts the rate constant of reaction between H and A as follows:[11]

$$k_H = \kappa \frac{kT}{h} \frac{\frac{[2\pi(m_H+m_A)kT]^{3/2}}{h^3}}{\frac{(2\pi m_H kT)^{3/2}}{h^3}\frac{(2\pi m_A kT)^{3/2}}{h^3}} \frac{8\pi^2 I_{HA} kT}{\sigma h^2} e^{-E_0/RT} \quad (1)$$

Here, m_H and m_A stand for the atomic weight of hydrogen and the molecular weight of ethylene, respectively, and I_{HA} for the moment of inertia of the activated complex. Using this equation, we can easily calculate the isotope effect for k_D/k_H.

$$\frac{k_D}{k_H} = \left[\frac{m_H}{m_D}\right]^{3/2}\left[\frac{m_D+m_A}{m_H+m_A}\right]^{3/2}\left[\frac{I_{DA}}{I_{HA}}\right]$$
$$= \left[\frac{m_H}{m_D}\frac{m_D+m_A}{m_H+m_A}\right]^{1/2}$$
$$= 0.72 \quad (2)$$

Almost the same value can be obtained for k_D/k_H for other olefins. As Table 1 shows, all of the values of k_D/k_H obtained in these experiments are a little larger than the calculated one. This is probably due to the simplification made for the calculation. However, in order to make a more detailed analysis, we have to wait for the detailed calculation of the potential energy surface.

The authors wish to express their thanks to Dr. Kazuo Shimokoshi of this Institute for the use of the program of INDO calculation.

References

1) L. Melander, "Isotope Effects on Reaction Rates," The Ronald Press Co., New York (1960).
2) D. Mihelcic, V. Schubert, F. Hölfer, and P. Potzinger, *Ber. Bunsen Phys. Chem.*, **79**, 1230 (1975).
3) Y. Ishikawa, M. Yamabe, A. Noda, and S. Sato, *Bull. Chem. Soc. Jpn.*, **51**, 2488 (1978).
4) K. R. Jennings and R. J. Cvetanović, *J. Chem. Phys.*, **35**, 1233 (1961).
5) S. Sato and R. J. Cvetanović, *J. Am. Chem. Soc.*, **81**, 3223 (1959).
6) S. Koda, K. Nakamura, T. Hoshino, and T. Hikita, *Bull. Chem. Soc. Jpn.*, **51**, 957 (1978).
7) C. S. Sloane and W. L. Hase, *Faraday Discuss. Chem. Soc.*, **62**, 210 (1977).
8) J. H. Knox and D. G. Dalgleish, *Int. J. Chem. Kinet.*, **1**, 69 (1969).
9) R. D. Penzhorn and B. deB. Darwent, *J. Chem. Phys.*, **55**, 1508 (1971).
10) J. H. Lee, J. V. Michael, W. A. Payne, and L. J. Stief, *J. Chem. Phys.*, **68**, 1817 (1978).
11) S. Glasstone, K. J. Laidler, and H. Eyring, "The Theory of Rate Processes," McGraw-Hill Book Co. Inc., New York (1941).

An UV-Visible Spectrophotometer Provided with a Photon Counting System for the Studies of Very Weak Absorption Spectra

Naoto YAMAMOTO,* Takanori SAWADA, and Hiroshi TSUBOMURA

Department of Chemistry, Faculty of Engineering Science, Osaka University, Toyonaka, Osaka 560

(Received September 7, 1978)

An ultrasensitive UV-visible spectrophotometer, of a single-beam type provided with a photon counting system having a time resolution of 10 ns has been constructed. It has been shown that absorption spectra can be measured to within an error of 10^{-5} in optical density with this instrument. Noise levels, measured as a function of the photon count numbers, are found to agree with the theoretically expected statistical fluctuation of the photons. Absorption spectra of thin naphthacene films, 32 nm or below in thicknesses, deposited on a quartz plate, were obtained with this instrument, and found to change with the film thickness.

Most of the commercial UV-visible spectrophotometers employ a double-beam optical system. They can be used to measure absorption spectra of very weak absolute intensities or small changes in absorption, with the aid of a digital memory background corrector, for example. An absorption spectrum of a material in a cell or on a transparent substrate is obtained as a difference in optical densities of a sample containing the material and a proper reference. The optical density, d, is expressed as

$$d = \log (I_R/I_S), \quad (1)$$

where I_S and I_R indicate light intensities through the sample and the reference, respectively.

It is interesting to pursue how weak absorption is measurable spectroscopically throughout the near UV and the visible region. In the case of the double-beam spectrophotometers, the limit of exact measurement is set by the difficulty of providing highly equivalent double beams throughout the UV-visible region and from the instability of the analog amplifiers equipped. As the sample absorption becomes less and less, the requirements for a proper reference and a good alignment of the sample-reference system along the monitoring optical path in addition to the instrumental accuracy get more and more severe. Kuhn *et al.* reported on an instrument employing a single beam system and a lock-in-amplifier to measure the absorption spectra of monomolecular layers of organic dyes, and *suggested* the possibility that absorbing species of 10^{-5} in optical density was detected.[1] However, they did not give any result showing the limit of detection they reached.

We have constructed an ultrasensitive UV-visible spectrophotometer of a single-beam type having a photon counting system, in which the optical density can be represented by the following relation,

$$d = \log (N_R/N_S) = \log (T_S/T_R), \quad (2)$$

where N_S and N_R are the photon numbers passing through the sample and the reference, respectively, and T_S and T_R stand for the times required to count a given photon number for the sample and the reference. In this paper, the details of the instrument and a few experimental results obtained with it are described.

Experimental

The block diagram of the spectrophotometer is shown in Fig. 1. The light from a 25 W deuterium arc lamp or a 20 W tungsten-halogen lamp is focused with a spherical mirror onto the entrance slit of a 25 cm monochromator. The monochromatic light from it is approximately focused through a quartz lens on to the sample. The light is introduced alternately onto the sample and the reference by moving the sample-reference holder, and the intensity of the light passing through the sample or the reference is monitored with a Hamamatsu R818 photo-multiplier, a Princeton Applied Research (PAR) 1120-02 discriminator, and a PAR 1109 photon counter. The overall photon monitoring system has an 100 MHz count rate. The entrance and exit slit widths of the monochromator are manually controlled so as to set the count rate below 10^7 pps. The operation of the photon counter, the wavelength driving and the moving of the sample-reference holder are controlled by a 24 K microcomputer. The optical density was calculated using the digital data sent out from the photon counter into the computer, and then displayed on an X-Y recorder versus wavelength.

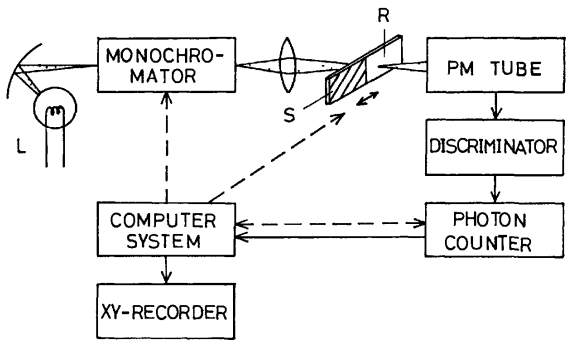

Fig. 1. Diagram of the spectrophotometer.
L: Light source, S: sample, and R: reference.

The monochromator and the sample-reference system are precisely driven with two step-motors sequentially as described below: The wavelength is set to λ_1. The sample is set into the position of light beam. Photon counting is started, and stopped when the number reaches a fixed value, say 10^7. The time required, T_S, is measured. The reference is moved into the beam position. Time, T_R required for a counting of the same number, is measured. Optical density at λ_1 is calculated from T_S and T_R and the value displayed. The wavelength is set to λ_2, different from λ_1 by a given interval, and the optical density for λ_2 is obtained by the same operation sequence as above. The spectrum can be measured in the range from 195 to 900 nm by a repetition of such procedures. The precision in the positioning of sample and reference is 1 μm or less.

Naphthacene from Wako Chemicals Co. was purified by vacuum sublimation. Naphthacene film was deposited on one

half of the surface of an optically flat 26 mm×76 mm Suprasil quartz plate by vacuum evaporation, leaving the other half as the reference.

Results and Discussion

In order to show the limit of absorbances measurable with the instrument, an absorbance measurement was run using a clean Suprasil quartz plate, half of which is regarded as a sample and the other half as a reference. The measurements were performed by sampling from 195 to 900 nm at an interval of 1.0 nm. The result gave actually the magnitude of noise, or fluctuation. It was confirmed that the noise levels, in the whole wavelength region were essentially the same as in the small region in Fig. 2, as an example. The base line was flat throughout the whole wavelength range.

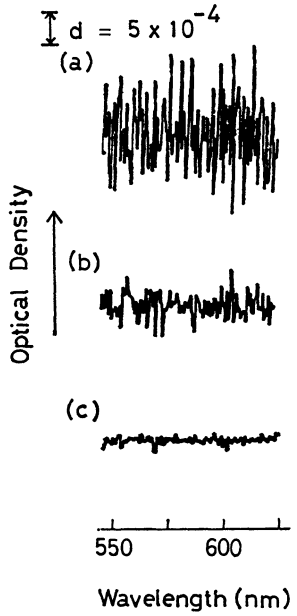

Fig. 2. Noise levels shown in an OD scale for operation between 550 and 625 nm at the photon count numbers of 10^6 for (a), 10^7 for (b) and 4×10^8 for (c), respectively.

The statistical fluctuation of the photons, ΔN, at the count number, N, is theoretically given by the following equation,

$$\Delta N/N = N^{-1/2}. \quad (3)$$

The magnitude of fluctuation in optical density, Δd, due to the statistical error can be given from Eqs. 2 and 3 as $\Delta d=(1/2.303)(\Delta N_S/N_S+\Delta N_R/N_R)$. The theoretical Δd values for the count numbers at which the noise curves (a), (b), and (c) in Fig. 2 were taken are 8.6×10^{-4}, 2.7×10^{-4}, and 4.3×10^{-5}, respectively. Comparison of these theoretical Δd values with the experimental noise levels shows that the fluctuations shown in Fig. 2 agree with the statistical fluctuations of the light intensity itself. It is, therefore, realized that all possible sources of error in our instrument, for instance, the fluctuation in the light source, the distortion and vibration of optical alignment, the sample-reference positioning imprecision, and the fluctuation of light monitoring system are not significant for the measurement of optical density of 10^{-5}.

The present instrument takes a count time of about 10 s or more for obtaining the optical density with an accuracy of the order of 10^{-5} at each of the wavelength, so that 2 h is at least necessary to get a spectrum over the region 200 to 900 nm with an interval of 1.0 nm. It is, of course, not difficult to detect absorption spectra less intense than the noise level by adopting an appropriate smoothing technique. In addition, the improvement of the time resolution of the counting system makes our absorption spectra measurements more accurate or speedy.

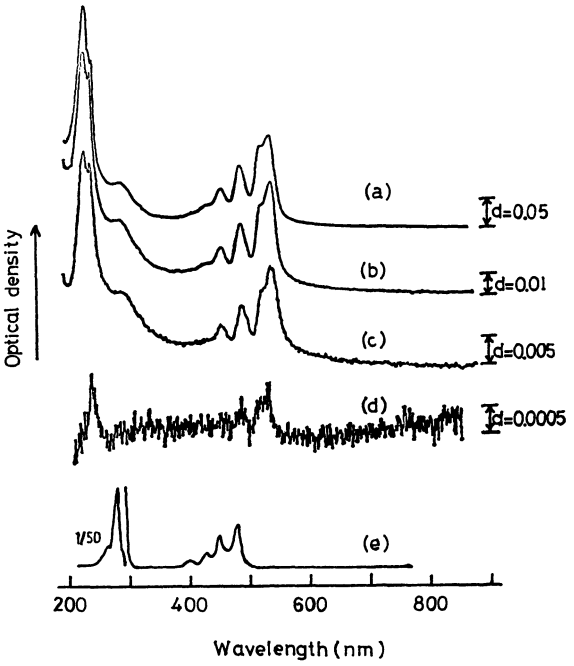

Fig. 3. Absorption spectra of naphthacene deposited on quartz plates measured at the photon count numbers of 10^7 for (a), (b) and (c), and 4×10^7 for (d), in the order of decreasing thickness. (e) is the absorption spectrum of naphthacene in an ethanol solution in an arbitrary unit.

Figure 3 shows the absorption spectra obtained for naphthacene films with various thicknesses, together with that taken in an ethanol solution with a Cary 15 spectrophotometer. The absorption in the visible region, ascribable to the ^1L_a band, of the films is largely red-shifted compared with that obtained in the solution. The spectra of the films, in the UV region, in (a), (b), and (c) have several absorption bands, presumably formed as a result of Davydov splitting of the ^1B_b band at 274 nm in the solution. The spectra of (a), (b), and (c) are essentially the same as those obtained for a naphthacene single crystal by Bree and Lyons[2] and for naphthacene films, 0.05—1 μm thick, by Maruyama and Iwasaki[3] and by us[4] at room temperature. However, there are some differences between the present spectra and others. For example, the peaks at 527 and 504 nm by Maruyama and Iwasaki are located at around 522 and 504 nm in (a), (b), and (c) in Fig. 3.

Though there is no marked shift in peak positions, the intensity ratio of the 504 peak to the 522 peak becomes small with the decreasing film thickness, (a) to (c). Similar change of the absorption intensity ratio on thickness is also found between the bands at 220 and 232 nm. These results suggest that the films are too thin to have the usual bulk properties.

The film thicknesses are roughly estimated from the peak absorption values at aroung 522 nm, assuming that the films produced are uniform in thickness. Taking the molar extinction coefficient at the peaks to be 1.0×10^4 and the density of the film to be 1.29,[2] the thicknesses are derived to be 32 nm for (a), 8.9 nm for (b), 3.3 nm for (c), and 0.13 nm for (d). The absorption spectrum of the thinnest film (d), though similar to (a), (b), and (c) in the visible region, is considerably different from them in the near UV region. It seems to lack the bands found for the thicker films at around 220 and 280 nm, and its absorption intensity in the near UV region is considerably smaller as compared to the visible band intensity. These suggest that, in the thinnest film, naphthacene molecules are separately deposited on the substrate surface: that is to say, a sub-monomolecular layer is formed. Though the reason for the decrease of the UV band intensity is not clear at present, such data for the very thin layers on solid surfaces will contribute to the elucidation of electronic structures of materials on solid surfaces.

We are also studying the absorption spectra of Langmuir films of fatty acids mixed with some organic dyes using this spectrophotometer.

In addition to the spectroscopy of thin films, this instrument will serve extensively for the accurate spectroscopy of very small quantities of materials in gaseous and liquid phases, or the spectroscopy of very weak bands arising from forbidden transitions.

The present results have shown that the optical density measurements can be performed in an accuracy of the order of 10^{-5} or better with our instrument. The limit of accuracy depends only on the performance of the photomultiplier, and the time resolution of the photon counter.

References

1) H. Kuhn, D. Möbius, and H. Bücher, "Techniques of Chemistry," ed by A. Weissberger and B. W. Rossiter, Wiley, New York (1972), Vol. 1, Part 3B, p. 577; G. R. Bird, G. Debuch, and D. Möbius, *J. Phys. Chem.*, **81**, 2657 (1977).
2) A. Bree and L. E. Lyons, *J. Chem. Soc.*, **1960**, 5206.
3) Y. Maruyama and N. Iwasaki, *Chem. Phys. Lett.*, **24**, 26 (1974).
4) M. Matsumura, H. Uohashi, M. Furusawa, N. Yamamoto, and H. Tsubomura, *Bull. Chem. Soc. Jpn.*, **48**, 1965 (1975).

Energy Levels and g Values of Some Rare Earth Crystals with f^2 Configuration

Yoshifumi KATO* and Hirokazu TAKADA

Department of Chemistry, Faculty of Science, Kobe University, Nada-ku, Kobe 657

(Received September 28, 1978)

The energy levels of the rare earth ions in praseodymium ethyl sulfate, magnesium praseodymium nitrate, and thulium ethyl sulfate crystals are calculated by using an extended Hamiltonian for $4f^2$ configuration. The Hamiltonian includes two-body electrostatic interactions, spin-other-orbit interactions and two-body pseudo-magnetic interactions as configuration-mixing parameters in addition to the Slater, spin-orbit coupling and crystal-field parameters. The standard deviations for praseodymium ethyl sulfate, magnesium praseodymium nitrate and thulium ethyl sulfate are respectively 10.1 cm^{-1} for 25 observed levels by using 13 parameters, 3.8 cm^{-1} for 12 observed levels by using 11 parameters, and 8.9 cm^{-1} for 32 observed levels by using 13 parameters. These results are consistent with similar studies of rare earth ions doped in the $LaCl_3$ and LaF_3 crystals. Most of the calculated Zeeman splitting factors (g value) parallel to the principal axis of the crystals also are in fairly good agreement with the experimental values. Some discussion is given as to the effect of configuration interactions, the accuracy of wave functions obtained and the discrepancy between some of the calculated g values and the observed ones.

Most of early studies regarding the energy calculation of rare earth crystals were carried out by fitting both the intermediate coupling parameters (the Slater integrals F_k and spin-orbit coupling constant ζ) and the crystal-field parameters B_q^k to observed energy levels. Recently it has been recognized that the configuration interaction (CI) effects characteristic of the "free ion" levels (the center of gravity of a multiplet) of rare earth crystals is more important than those arising from the crystal-field potential. Some attempts[1-3] have been made to identify such effective interactions operating within $4f^N$ configuration that reproduce the observed electronic structure of crystals. The basic theory consists of simultaneously diagonalizing (J-mixing) both ion and crystal parts of an extended Hamiltonian matrix which involves several additional parameters introduced from the second-order perturbation theory. In recent analyses, the least-squares fits of 20 parameters to over 100 observed levels resulted in a mean error of less than 10 cm^{-1} for the energy levels of rare earth ions doped into $LaCl_3$[4-6] and that of about 20 cm^{-1} or less for the energy levels of rare earth ions doped into LaF_3.[7]

In this paper, the energy levels of praseodymium ethyl sulfate, $Pr(C_2H_5SO_4)_3 \cdot 9H_2O$ (Pr(ES)), magnesium praseodymium nitrate, $Mg_3Pr_2(NO_3)_{12} \cdot 24H_2O$ (Pr(DN)), and thulium ethyl sulfate, $Tm(C_2H_5SO_4)_3 \cdot 9H_2O$ (Tm(ES)), are calculated by the aforementioned extended Hamiltonian. The purpose of the present calculations is to determine the wavefunctions giving good agreement of both the calculated energy levels and Zeeman splitting factors (*i.e.*, g values) with the observed ones.

Calculational Procedure

Hamiltonian Structure. The theoretical formulation of electronic structures of rare earths by the tensor operator method has first been developed by Racah[8] and several authors have expanded this method to introduce the configuration mixing effects by using the second-order perturbation theory. Rajnak and Wybourne gave a detailed treatment for the second-order effect of electrostatic interactions[9] and also investigated the combined effects between spin-orbit and electrostatic interactions.[10] Furthermore Rajnak[3] discussed the relative roles of various mechanisms of CI by the application of this theory to the $4f^3$ configuration of the Pr^{2+} ion. Judd *et al.*[11,12] independently treated the intra-atomic magnetic interactions due to relativistic correction, and introduced several new parameters for spin-other-orbit interactions and electrostatically correlated spin-orbit interactions as main effects of these magnetic interactions. Here, an extended Hamiltonian on the basis of such refined tensorial method will briefly be given, especially for the second-order perturbation terms.

When we expand the wavefunction of a rare earth ion in crystals under the intermediate coupling scheme, a basis function is given as

$$|\Psi\rangle = \sum_i^N a_i \varphi_i | f^N;\ q, S, L, J, M\rangle, \tag{1}$$

where q is an additional quantum number introduced to distinguish the electronic states. The total Hamiltonian of $4f^N$ configuration can be written as

$$H = H_{\text{ion}} + H_{\text{cry}}, \tag{2}$$

where H_{ion} and H_{cry} are the ion and crystal-field parts of interactions respectively. H_{ion} for an N-electron system of rare earth ions with appreciable spin-orbit interaction may be given as

$$H_{\text{ion}} = \sum_i^N h_i + \sum_{i>j}^N e^2/r_{ij} + \sum_i^N \zeta_{4f}(\boldsymbol{s}_i \cdot \boldsymbol{l}_i), \tag{3}$$

where
$$h_i = -(\hbar^2/2m)\Delta_i - Ze^2/r_i. \tag{4}$$

The Hamiltonian may be divided into $H_{\text{ion}} = H_0 + H_1$ such that

$$H_0 = \sum_i^N (h_i + v_i), \tag{5}$$

and
$$H_1 = -\sum_i^N v_i + \sum_{i>j}^N e^2/r_{ij} + \sum_i^N \zeta_{4f}(\boldsymbol{s}_i \cdot \boldsymbol{l}_i)$$
$$= -V + G + A, \tag{6}$$

where v_i is an average potential that acts on the ith electron, while

$$V=\sum_i^N v_i,\quad G=\sum_{i>j}^N e^2/r_{ij},\quad \text{and}\quad \Lambda=\sum_i^N \zeta_{4f}(\boldsymbol{s}_i\cdot\boldsymbol{l}_i). \tag{7}$$

Within the first-order perturbation, the V term in Eq. 6 is purely radical and contributes energy shifts that are the same for all the levels belonging to a given configuration, while the G and Λ terms are different for different states of the same configuration. Hereafter, the perturbing terms, that are the same for all the levels belonging to a given configuration without affecting the energy-level structure of the configuration, are neglected because we are interested only in relative energy shift due to various interactions in the configuration. When a nonperturbing basis of $4f^N$ configuration and a perturbing basis belonging to a particular perturbing configuration are designated by $\langle\psi J|$ or $|\psi' J\rangle$ and $|mJ\rangle$ respectively, the perturbation energy E' due to the second-order perturbation theory may be expressed as

$$E'=\langle\psi J|H_1|\psi' J\rangle - \sum_m \langle\psi J|H_1|mJ\rangle\langle mJ|H_1|\psi' J\rangle/\Delta E_m. \tag{8}$$

The first-order perturbation energy in Eq. 8 is described in terms of the intermediate coupling parameters; *i.e.*, the Slater integrals $F_k(4f,4f)$ (or the equivalent E^k of Racah[8d]) and the spin-orbit coupling constant ζ_{4f}, and the reduction formula involving these parameters by the tensor method is given in a previous paper.[13]

The second-order perturbation energy in Eq. 8, exhibiting CI effects owing to the mixing levels from interacting configuration $|mJ\rangle$, consists of six distinct terms arising from substituting V, G, or Λ into the H_1 operators of matrix elements. The following three parts of them give rise to the dominant contribution:

$$-\sum_m \langle\psi J|G|mJ\rangle\langle mJ|G|\psi' J\rangle/\Delta E_m, \tag{9a}$$

$$-\sum_m \langle\psi J|\Lambda|mJ\rangle\langle mJ|\Lambda|\psi' J\rangle/\Delta E_m, \tag{9b}$$

$$-\sum_m \langle\psi J|G|mJ\rangle\langle mJ|\Lambda|\psi' J\rangle/\Delta E_m. \tag{9c}$$

Here, the terms, which may be absorbed as screening effects in the intermediate coupling parameters (F_k and ζ), are excluded. The tensorial reduction of Eq. 9a is given as[3,9]

$$\sum_{t\,\text{odd}} P(t)\langle\psi J|\sum_{i>j}(\boldsymbol{U}_i^{(t)}\cdot\boldsymbol{U}_j^{(t)})|\psi' J\rangle + \sum_{k,k'} X(kk',l')\,Y(kk',l'), \tag{10}$$

where the coefficient $X(kk',l')$ is given by

$$X(kk',l')=\sum_{k''\,\text{even}}(2k''+1)\begin{Bmatrix}k & k' & k''\\ l & l & l'\end{Bmatrix} \times\langle\psi\|\sum_{h\neq i\neq j}(\{\boldsymbol{U}_h^{(k)}\cdot\boldsymbol{U}_i^{(k'')}\}^{(k')}\cdot\boldsymbol{U}_j^{(k')})^{(0)}\|\psi'\rangle. \tag{11}$$

The first term in Eq. 10 is the same scalar two-body electrostatic interactions as those arising from the linear theory,[14,15] and, by using the properties of the Casimir operators,[16] is further simplified to the following expression,

$$\delta(\psi,\psi')[\alpha L(L+1)+\beta G(G_2)+\gamma G(R_7)], \tag{12}$$

where $G(G_2)$ and $G(R_7)$ are the eigenvalues of Casimir's operators for the group G_2 and R_7 used to classify the states of $4f^N$ configuration, and α, β, and γ are new parameters involving the radial factors and excitation energies. The second term in Eq. 10 represents effective three-body electrostatic interactions which are the nonlinear effects arising from interactions with $l^{N-1}l'$ configurations. The triple-tensor matrix elements in the coefficient $X(kk',l')$ expressing the angular dependence can be evaluated by a general expression of Rajnak.[3] $Y(kk',l')$ is a new parameter which depends on the radial integrals, excitation energies and the one-electron quantum numbers. Since there are ten distinct combinations of k, k', and k'' regarding the summation of the triple scalar product in Eq. 11 and the number of parameters is equal to the number of terms, then the number of independent $Y(kk',l')$ becomes to be ten. The combined reduction formula of Eqs. 9b and 9c by use of the algebra of tensor operators is given as

$$(-1)^{S'+L+J}\begin{Bmatrix}S' & L' & J\\ L & S & 1\end{Bmatrix}\langle qSL\|\boldsymbol{T}^{(11)}+\boldsymbol{t}^{(11)}\|q'S'L'\rangle. \tag{13}$$

In Eq. 13, the first term represents the spin-other-orbit magnetic interaction and is reduced to the form involving the Marvin integrals[17] M^k (k=0, 2, 4) as parameters, while the second term expresses the electrostatically correlated spin-orbit interaction and reduced to the form involving P^k(k=2, 4, 6) as pseudomagnetic parameters.[11]

The crystal-field potential H_{cry} in Eq. 2 may be expanded by the irreducible tensor $\boldsymbol{C}_q^{(k)}$ to give

$$H_{\text{cry}}=\sum_i^N\sum_k\sum_q B_q^k(\boldsymbol{C}_q^{(k)})_i, \tag{14}$$

where the summation including i is over all the electrons of the ion of interest and B_q^k is the crystal-field parameter to be determined from the experimental data. The reduction formula of the matrix element of H_{cry} is given in the previous paper.[13] The number of crystal-field parameters is restricted depending on the symmetry of the crystal-field potential and the maximum number of them does not exceed 27 even when an ion is at a site of no symmetry; the number is, in general, only a few for crystals with appropriate symmetry.

Within the above-mentioned framework for an effective Hamiltonian of $4f^N$ configuration, the total number of parameters necessary for energy-level fitting is less than 50; three Slater integrals F^k (k=2, 4, 6), one spin-orbit interaction ζ_{4f}, three two-body electrostatic interactions α, β, γ, ten three-body electrostatic interactions $Y(kk',l')$, three spin-other-orbit magnetic interactions M^k (k=0, 2, 4), three two-body pseudomagnetic configuration-mixing interactions P^k (k=2, 4, 6), and less than 27 crystal-field parameters B_q^k. In such semi-empirical approach, it will be seen later that the interaction energies as large as 10 cm^{-1} are taken into account for the energy fitting.

Application. The Pr^{3+} and Tm^{3+} ions have $4f^2$ and $4f^{12}$ configurations respectively. Since $4f^{12}$ configuration is complementary to $4f^2$, the Tm^{3+} ion has the same number and kind of levels as those of the Pr^{3+} ion, for which there are 13 different free-ion levels $|q,S,L,J\rangle$ under intermediate coupling. From the results of X-ray analyses, the space group and site symmetry at a rare earth ion are $P6_3/m$ (C_{6h}^2) and D_{3h} for ES,[18] and $R\bar{3}$ (C_{3i}^2) and C_{3v} for DN[19] respectively. The crystal fields of D_{3h} and C_{3v} symmetries are expanded as

TABLE 1. PARAMETERS AND ROOT MEAN SQUARE DEVIATIONS FOR $Pr(C_2H_5SO_4)_3 \cdot 9H_2O$[a]

Parameter	Present work				Gruber[b]	Hüfner[c]
	I	II	III	IV		
F_2	310.93	310.53	310.17	309.76	307.4	
F_4	48.53	48.87	48.74	48.72	49.44	
F_6	4.857	4.866	4.856	4.856	5.138	
ζ_{4f}	749.8	739.1	736.2	737.3	727.9	
α	22.33	20.89	21.10	20.67		
β	−609	−644	−583	−536		
γ	453	636	643	612		
M^0		1.13	1.09	1.18		
P^2		34	54	70		
B_0^2			51.30	63.05	30.62	46.0
B_0^4			−745.3	−654.6	−706.6	−640
B_0^6			−877.2	−892.9	−780.2	−704
B_6^6			675.4	838.8	577.4	732
rms deviation						
For total 25 levels			7.8	10.1		
For 9 ion levels	25.1	5.0	4.4	5.2	212.5	
For 24 cryst. levels			7.0	9.1	7.7	10.8
$\|g\|$ value[d]			1.12	0.86	1.18	0.89

a) Energy units in cm^{-1}. The ion level and the rms deviation for crystal levels denote the center of gravity in a manifold and the rms deviation from the center respectively. b) Data from Ref. 23. Although he reported to be an average deviation of 3 cm^{-1} for total levels and that of 10.2 cm^{-1} for 9 ion levels with a slight change of the parameters, the details of calculations are not given explicitly. c) Data from Ref. 24. He obtained an average deviation of 5.9 cm^{-1} for 11 crystal levels. d) The absolute value of the ground state $^3H_4(\eta=\pm 2)$. The experimental g value is 0.775 (Ref. 25).

$$H_{cry}(D_{3h}) = B_0^2 C_0^{(2)} + B_0^4 C_0^{(4)} + B_0^6 C_0^{(6)} + B_6^6 (C_6^{(6)} + C_{-6}^{(6)}), \quad (15a)$$

$$H_{cry}(C_{3v}) = H_{cry}(D_{3h}) + B_3^4 (C_{-3}^{(4)} - C_3^{(4)}) + B_3^6 (C_{-3}^{(6)} - C_3^{(6)}). \quad (15b)$$

Each free-ion level under a crystal symmetry may be classified several irreducible representations designated by the crystal quantum number (η) following Hellwege;[20] *i.e.*, $\eta=0$, ± 1, ± 2, and 3 for ES, and $\eta=0$ and ± 1 for DN, where the levels with double signs are twofold degenerate. Any three-body interaction in Eq. 10 is not necessary to be taken into account in the case of f^2 configuration. For f^2 configuration, the reduced matrix elements of the magnetic interaction $\boldsymbol{T}^{(11)}$ and pseudomagnetic interaction $\boldsymbol{t}^{(11)}$ are already given in the explicit expressions involving M^k and P^k.[11] In practice, only M^0 and P^2 were freely varied and M^k and P^k were constrained to the following ratios proposed by Crosswhite *et al.*;[4] *i.e.*, $M^2=0.56M^0$, $M^4=0.38M^0$, and $P^4=0.75P^2$, $P^6=0.50P^2$. Other reduced matrix elements of various tensor operators with respect to f^N configuration are also tabulated by Nielson and Koster.[21] The procedure to determine the parameters by an iterative method is described in the previous paper.[13]

Once the eigenvectors are determined by diagonalizing the Hamiltonian, we can evaluate the parallel component of g values as

$$g_z = \langle\phi|\mu_z|\phi\rangle = \sum_i a_i^2 M g_i(qSLJ), \quad (16)$$

where μ_z is the z component of the magnetic dipole operator along the principal axis of a crystal and $g_i(qSLJ)$ denotes the Lande g factor for an ion level. The g value defined by Eq. 16 is half the Zeeman splitting in Lorentz units $\beta_e H$ (β_e=Bohr magneton). Then the total Zeeman splitting is expressed as $2g\beta_e H$.

Results and Discussion

The final parameters determined and the standard

TABLE 2. PARAMETERS AND ROOT MEAN SQUARE DEVIATIONS FOR $Mg_3Pr_2(NO_3)_{12} \cdot 24H_2O$[a]

Parameter	Present work	Judd[b]	Tinsley[c] in Nd (DN)
F_2	315.17		
F_4	51.38		
F_6	5.079		
ζ_{4f}	746.4		
α	22.81		
B_0^2	−158.9	−140	200
B_0^4	−0.7	−160	−166
B_3^4	−47.2	±140	±302
B_0^6	31.3	−800	1440
B_3^6	575.6	∓1800	±1760
B_6^6	−427.7	740	−1790
rms deviation			
For total levels	3.8(12)		
For ion levels	1.5(5)		
For cryst. levels	3.6(11)	6.1(8)	11.3(18)

a) See the footnote (a) in Table 1. The number of energy fitted is given in parentheses. b) Data from Ref. 29. c) Data from Ref. 30.

Table 3. Parameters and root mean square deviation for $Tm(C_2H_5SO_4)_3 \cdot 9H_2O$[a]

Parameter	Present work	Gruber-Conway[b]	Wong-Richman[c]	Krupke-Gruber[d]
F_2	454.23	450.0		449.2
F_4	66.31	62.1		64.57
F_6	7.006	6.80		7.065
ζ_{4f}	2636.9	2700.0		2667.9
α	15.52			
β	−629.0			
γ	1962			
M^0	5.11			
P^2	1010.0			
B_0^2	277.1	26.0	259.6	270.6
B_0^4	−547.9	−640	−568.0	−570.8
B_0^6	−492.2	−512	−457.6	−460.8
B_6^6	394.8	316.0	455.6	450.7
rms deviation				
For total 32 levels	8.9			
For 10 ion levels	9.0	134.4[e]		58.4[e]
For 31 cryst. levels	4.7	25.6	8.2	7.1

a) See the footnote (a) in Table 1. b) Data from Ref. 35. c) Data from Ref. 33. They reported to be an average deviation of 5 cm^{-1} for 21 crystal levels. d) Data from Ref. 34. They reported that all the observed crystal levels were fitted within 4 cm^{-1}. e) The ion level $^1I_6$ is excluded. Both the deviation of this level by Gruber and Conway, and that by Krupke and Gruber are over 1000 cm^{-1}. Then the rms deviations for both cases are over 300 cm^{-1}, if the $^1I_6$ level is included.

Table 4. Experimental and calculated values of the energy levels and g values for $Pr(C_2H_5SO_4)_3 \cdot 9H_2O$[a]

Term	η	Energy level			$\lvert g \rvert$ (calcd)	Term	η	Energy level			$\lvert g \rvert$ (calcd)
		Exptl	Calcd	Diff				Exptl	Calcd	Diff	
$^3H_4$	±2	0	0	0	0.86	$^3F_4$	3		6720.4		
	3	12.2	9.6	−2.6			3		6802.4		
	±1		196.7		0.79		±2	6830.8	6821.4	−9.4	1.39
	±2		212.0		2.49		±1	6862.8	6861.2	−1.6	1.15
	3		245.6				0	6872.0	6857.4	−14.6	
	0		324.1				±2	6896.0	6904.4	8.4	3.73
$^3H_5$	3		2083.9			$^1G_4$	3		9478.4		
	±2		2127.5		0.04		0	9793.6	9791.4	−2.2	
	3		2211.2				±2	9811.0	9789.4	−21.6	0.98
	±1		2232.2		4.69		3		9808.3		
	±2		2250.8		2.02		±1	9862.8	9879.5	16.7	1.07
	±1		2290.4		0.59		±2		10052.7		1.18
	0		2333.2			$^1D_2$	0	16709.3	16715.4	6.1	
$^3H_6$	3		4087.3				±2	16857.7	16870.3	12.6	2.07
	±2		4183.2		2.04		±1	16955.0	16935.0	−20.0	1.03
	0		4319.9			$^3P_0$	0	20687.0	20691.3	4.3	
	0		4366.0			$^3P_1$	±1	21276.1	21260.0	−16.1	1.50
	±1		4373.3		3.78		0	21289.6	21279.3	−10.3	
	3		4373.6			$^1I_6$	0	21398.5	21391.8	−6.7	
	±2		4434.1		0.26		0	21407.6	21407.9	0.3	
	±1		4545.0		0.59		±1	21447.4	21449.3	1.9	0.28
	0		4555.6				0	21456.2	21440.7	−15.5	
$^3F_2$	±1		4988.0		0.44		±2		21542.8		1.00
	±2		5011.2		1.36		±1		21559.4		4.23
	0		5041.9				3		21601.2		
$^3F_3$	3		6309.9				±2		21674.7		2.98
	0	6310.4	6311.4	1.0			3		21700.2		
	±2	6330.7	6323.0	−7.7	2.14	$^3P_2$	0	22424.8	22425.6	0.8	
	±1	6382.6	6385.2	2.6	1.02		±2	22440.5	22448.5	8.0	2.90
	3		6425.9				±1	22447.6	22443.3	−4.3	1.42
						$^1S_0$	0		48995.8		

a) Energy units in cm^{-1}. Diff=Calcd−Exptl.

TABLE 5. EXPERIMENTAL AND CALCULATED VALUES OF THE ENERGY LEVELS AND g VALUES FOR $Mg_3Pr_2(NO_3)_{12}\cdot 24H_2O$[a)]

Term	η	Energy level			$\lvert g\rvert$ (calcd)
		Exptl	Calcd	Diff	
$^3H_4$	±1	0	0	0	0.67
	0	37.7	37.1	−0.6	
	0		48.8		
	±1	95.8	96.9	1.1	0.80
	±1		167.9		2.55
	0		174.5		
$^3H_5$	±1		2129.5		1.53
	0		2130.4		
	±1		2143.8		0.59
	0		2147.7		
	±1		2197.1		2.52
	0		2224.6		
	±1		2249.5		3.64
$^3H_6$	0		4242.6		
	±1		4269.3		0.66
	0		4270.9		
	±1		4300.1		0.33
	0		4328.8		
	±1		4366.5		2.94
	±1		4464.8		0.39
	0		4477.2		
	0		4550.6		
$^3F_2$	±1		4653.3		1.07
	±1		4684.7		0.31
	0		4689.8		
$^3F_2$	0		5978.2		
	±1		6008.7		0.54
	0		6054.4		
	0		6060.2		
	±1		6087.8		0.56
$^3F_4$	0		6668.3		
	±1		6679.3		3.79
	±1		6688.8		0.09
	0		6692.9		
	±1		6704.8		0.17
	0		6705.2		
$^1G_4$	0		9717.1		
	±1		9797.1		2.77
	±1		9815.0		0.93
	0		9956.3		
	0		9977.5		
	±1		10023.8		1.35
$^1D_2$	±1	16872.2	16868.2	−4.0	1.91
	±1	16920.0	16918.6	−1.4	0.88
	0	16933.6	16930.6	−3.0	
$^3P_0$	0	20845.9	20847.5	1.6	
$^3P_1$	0	21421.8	21417.3	−4.5	
	±1	21461.4	21463.8	2.4	1.50
$^1I_6$	0		21691.4		
	±1		21712.6		0.15
	±1		21742.4		0.30
	0		21753.4		
	0		21773.8		
	±1		21811.0		3.21
	±1		21851.6		4.76
	0		21909.6		
	0		21910.7		
$^3P_2$	±1	22630.1	22633.7	3.6	2.91
	±1	22693.3	22685.2	−8.1	1.45
	0	22695.8	22701.6	5.8	
$^1S_0$	0		50464.1		

a) See the footnote (a) in Table 1.

TABLE 6. EXPERIMENTAL AND CALCULATED VALUES OF THE ENERGY LEVELS AND g VALUES FOR $Tm(C_2H_5SO_4)_3\cdot 9H_2O$[a)]

Term	η	Energy level			$\lvert g\rvert$ (calcd)
		Exptl	Calcd	Diff	
$^3H_6$	0	0	0	0	
	±1	32.2	35.5	3.3	0.67
	±2	111.5	122.3	10.8	1.13
	3	176.9	176.1	−0.8	
	±1	198.9	200.2	1.3	5.33
	0		226.3		
	0		230.8		
	±2	273.4	272.4	−1.0	3.46
	3	302.5	300.1	−2.4	
$^3F_4$	±2		5729.9		3.16
	±1		5779.7		1.14
	0		5799.2		
	±2		5809.7		0.87
	3		5842.1		
	3		5944.8		
$^3H_5$	0		8191.7		
	±1		8227.4		0.95
	±2		8298.6		1.40
	3		8348.2		
	±1		8363.8		5.08
	±2		8378.5		3.47
	3		8396.5		
$^3H_4$	0		12517.4		
	3	12585.8	12573.0	−12.8	
	±1	12627.0	12603.9	−23.1	0.95
	±2	12648.7	12636.8	−11.9	1.82
	3	12704.4	12707.9	3.5	
	±2	12763.3	12754.3	−9.0	0.07
$^3F_3$	3	14406.6	14407.2	0.6	
	±1	14466.0	14455.6	−10.4	1.08
	±2	14485.7	14484.4	−1.3	2.16
	3	14487.3	14488.2	0.9	
	0		14508.5		
$^3F_2$	±2	15078.8	15090.8	12.0	1.51
	±1	15106.1	15111.1	5.0	0.76
	0		15175.2		
$^1G_4$	±2	21170.6	21176.5	5.9	1.36
	±1	21194.0	21198.1	4.1	0.96
	0		21214.0		
	±2	21279.5	21282.4	2.9	0.56
	3	21343.5	21340.6	−2.9	
	3		21477.5		
$^1D_2$	±2	27906.6	27894.2	−12.4	2.28
	0		27961.4		
	±1	27977.1	27961.7	−15.4	1.14
$^1I_6$	3		34816.2		
	±2	34843.6	34850.9	7.3	0.89
	3	34870.0	34868.4	−1.6	
	±2	34899.7	34897.9	−1.8	1.12
	±1		34919.1		0.83
	0		34940.7		
	±1		35014.1		4.83
	0		35220.4		
	0		35228.1		
$^3P_0$	0	35436.9	35448.9	12.0	
$^3P_1$	0	36400.9	36390.4	−10.5	
	±1	36484.2	36473.5	−10.7	1.50
$^3P_2$	±2	38144.9	38158.5	13.6	2.55
	±1	38184.9	38196.0	11.1	1.28
	0		38344.6		
$^1S_0$	0		74880.2		

a) See the footnote (a) in Table 4.

deviations are given in Tables 1—3 for Pr(ES), Pr(DN) and Tm(ES) respectively, together with those obtained by other authors. Now, the root mean square (rms) deviation is defined as

$$\sigma = [\sum_i \Delta_i^2/N]^{1/2}, \quad (17)$$

where Δ_i is the difference between the observed and calculated values of the ith level, and N is the number of observed levels. The calculated numerical results are given in Tables 4—6 for Pr(ES), Pr(DN), and Tm(ES) respectively.

Energy Levels for Pr(ES). The energy levels of Pr(ES) have been investigated by several authors.[22-24] We have used 25 crystal levels assigned by experiments. As seen in Table 1, the inclusion of three two-body electrostatic interactions (case I) considerably reduces the rms deviation for 9 ion levels except the $^3H_5$, $^3H_6$, $^3F_2$, and $^1S_0$ levels from 213 to 25 cm^{-1}, when compared to the result without CI parameters by Gruber. Further improvement of the rms deviation of 20 cm^{-1} for ion levels is achieved by including one magnetic interaction M^0 and one pseudomagnetic interaction P^2 parameter (case II). This fact evidently exhibits that the CI effects arising from magnetic interactions as well as electrostatic interactions play highly important role in giving ion levels. The fit for 25 observed levels by 13 adjustable parameters (case III) yields an rms deviation of 7.8 cm^{-1}. This deviation is the same order of magnitude as that in rare earth crystals.[4-7] The parameter values in case IV are determined so as to fit both the calculated energy levels and the g value of the ground state with the observed values. Although the rms deviation of 10 cm^{-1} for all the 25 levels in case IV is slightly larger than that in case III, the former g value is only 10% larger than the value (=0.775)[25] observed by paramagnetic resonance, whereas the latter g value is 1.45 times as large as the experimental one. As to the rms deviation for 24 crystal levels given in Table 4 (deviation from the center of gravity in a manifold) and the g value of the ground state, the results in cases III and IV is rather similar to those by Gruber and by Hüfner respectively. It is easily supposed that this fact arises from the difference of the crystal-field parameters B_q^k used.

In order to make this point further clear, the main terms of the eigenvectors for the ground state, $^3H_4$ ($\eta=\pm2$), are given in Table 7, together with the ground state eigenvector determined only within the ground state manifold to fit the experimental g value by Abragam and Bleaney.[26] As seen in Table 7, the coefficients of two dominant bases, $|^3H_4(M=2)>$ and $|^3H_4(M=-4)>$, in case IV are evidently different from those by Gruber: the ours are rather close to the coefficients estimated by Abragam and Bleaney. As seen in Eq. 16, a basis function with negative M makes the g value decrease against functions with positive M. Then a slight difference of coefficients between $|^3H_4(M=2)>$ and $|^3H_4(M=-4)>$ results in fairly large difference in calculated g values. The ground state manifold with $J=4$ is split into six crystal levels owing to the D_{3h} crystal symmetry; one $\eta=0$ level, one $\eta=\pm1$ level, two $\eta=\pm2$ levels and two $\eta=3$ levels. Thus a level to be mixed predominantly in the ground state, $^3H_4(\eta=\pm2)$, should be the other $\eta=\pm2$ level in the same manifold because the lowest $^3H_4$ ion level is separated far away from other ion levels. The mixing between two crystal levels with $\eta=\pm2$ in the ground state manifold is taken into account reasonably in case IV by fitting to the observed g value of the ground state, but this mixing is not taken in other energy fits, because there is no experimental value of this level to be available. Therefore, the crystal-field parameters in case IV is considered to be more reliable than those in other cases, even though the result in case IV is not so good as that in case III. In determination of a set of crystal-field parameters, the information of the experimental levels as many as possible within a given manifold is considered to be substantially more important than performing complete J-mixing. Furthermore it is dangerous to conclude simply that in energy-level fitting by restricted experimental data the wavefunction giving better rms deviation is immediately more accurate wavefunction.

Energy Levels for Pr(DN). From the spectral analysis of Pr(DN) by Hellwege and Hellwege,[27] 12 levels of 61 crystal levels and 5 levels of 13 ion levels have only been established experimentally.

Before a definitive X-ray diffraction analysis of Ce(DN),[19] Judd[28] developed a theory for the effect of the crystalline electric field on rare earth double nitrates. The crystal field potential may be regarded as having two components; the first is a dominating potential corresponding to icosahedral symmetry and the second is a weaker residual C_{3v} symmetry potential. In pure icosahedral symmetry,

$$B_0^2 = B_0^4 = B_3^4 = 0, \quad B_3^6 = \pm 1.5275 B_0^6,$$
$$\text{and} \quad B_6^6 = -0.9211 B_0^6. \quad (18)$$

Using this icosahedral approximation, Judd[29] estimated the crystal parameters of Pr(DN) with the rms deviation of 6.1 cm^{-1} for 8 crystal levels, and Tinsley[30] obtained the rms deviation of 11.3 cm^{-1} for 18 crystal levels of Nd(DN) (Table 2). The present calculation yields the rms deviation of 1.5 cm^{-1} for 5 ion levels and that of

Table 7. Coefficients of the eigenvectors for the ground state $^3H_4(\eta=\pm2)$ of $Pr(C_2H_5SO_4)_3 \cdot 9H_2O$[a]

Author	$\|^1G_4(2)>$	$\|^1G_4(-4)>$	$\|^3H_4(2)>$	$\|^3H_4(-4)>$	$\|^3H_5(-4)>$	$\|g\|$ value
Present work	0.1408	−0.0553	0.9077	−0.3835	0.0612	0.86
Gruber[b]	0.1429	−0.0405	0.9430	−0.2899	0.0469	1.18
Abragam-Bleaney[c]			0.9135	−0.4067		0.775

a) The basis functions with coefficients over 0.05 only are given. Values in parentheses are the z component of total angular momentum J. b) Data from Ref. 23. c) Data from Ref. 26.

3.6 cm^{-1} for 11 crystal levels. The result exhibits unexpectedly good agreement between the calculated and experimental values, but does not satisfy the relation predicted by Judd (Eq. 18).

According to the crystal structure of Ce(DN),[19] 12 oxygen atoms being the nearest-neighbors of the Ce atom must be moved distances of the order of 0.5 Å to make the icosahedron regular and most of 20 triangle on the surface of an icosahedron are also considerably irregular. Therefore the icosahedral model for rare earth double nitrates should be allowed only as the first approximation. Thus the three crystal parameters, B_0^2, B_0^4, and B_3^4, might be not necessary to be small compared to the six-order parameters. However, it is not adequate to conclude immediately that the crystal parameters obtained by us are reasonable because of the lack of experimental values to be fitted.

Energy Levels for Tm(ES). The observed energy levels have been reported by several authors[31-34] and some parameter analyses[33-35] have been carried out. Here, we have adopted the quantum numbers and wavenumbers by Johnsen,[31] and by Krupke and Gruber.[34] As seen in Table 3, when the present result for ion levels is compared to previous studies, the inclusion of CI parameters reduces the rms deviation of 58 or 134 cm^{-1} for the ion levels to 9 cm^{-1}. This remarkable improvement for Tm(ES) is the same degree as that for Pr(ES). For the assignment of ion levels with $J=4$, of which eigenvectors are given in Table 8, there is a substantial discrepancy between the present result and previous ones. The ion level at 5635 cm^{-1} and that at 12475 cm^{-1} are designated respectively to $^3F_4$ and $^3H_4$ unlike all previous assignments as far as the present parameters are appropriate.

TABLE 8. EIGENVECTORS OF THE ELECTRONIC TERMS WITH $J=4$ OF $Tm(C_2H_5SO_4)_3 \cdot 9H_2O$

Energy (cm^{-1})	Coefficients of basis			Assignment
	$\|^3H_4\rangle$	$\|^1G_4\rangle$	$\|^3F_4\rangle$	
5635	−0.2799	0.5348	0.7973	$^3F_4$
12475	0.7766	−0.3621	0.5155	$^3H_4$
21089	0.5644	0.7635	−0.3140	$^1G_4$

For crystal levels, our result yielding an rms deviation of 4.7 cm^{-1} improves fairly previous results[33-35] which were obtained only within a given manifold by using the first-order perturbation theory. This improvement might simply be considered to be due to complete J-mixing. However, it is seen by examining the present result in somewhat details as well as previous results of crystals with f^3 configuration[13,36] that the mixing of an ion level into other ion levels of different J through crystal field perturbation is still fairly small. This will be plausible when we consider that the energy separation between most of lower excited ion levels well established by experiments is of the order of 10^3—10^4 cm^{-1}, whilst the interaction energy due to crystal field perturbation is of the order of 10—100 cm^{-1} and do not exceed 300 cm^{-1} at most, although the admixing due to crystal fields are, in principle possible for the most part of levels with different J. Thus if all the crystal levels within a manifold with relatively large J value are known completely from the experiments, the crystal-field parameters determined only within this manifold may be fairly reliable. This fact is obviously seen in Er(ES),[13] in which the energy calculation by complete J-mixing does not bring any improvement of the rms deviation when compared to that by crystal-field parameters determined only from the ground state manifold, where all of 8 crystal levels are known by experiments.

From the above consideration, it is more important than a least-squares fit including complete J-mixing for determination of reliable crystal parameters that there exists at least one manifold with J value as large as possible, of which most of the crystal levels are settled by experiments.

TABLE 9. COMPARISON OF ABSOLUTE g VALUES

Level	Energy (cm^{-1})	Exptl $\|g\|$		Calcd $\|g\|$	
		Zeeman[a]	MCD[b]	Present	W-R[c]
Pr(ES)					
$^3H_4(\pm2)$	0	0.85 (0.775)	0.77	0.86	
$^1D_2(\pm2)$	16858	1.30	1.30	2.07	
(±1)	16955		1.09	1.03	
$^3P_1(\pm1)$	21276	1.39	1.61	1.50	
$^3P_2(\pm1)$	22448	1.58		1.42	
Pr(DN)					
$^3H_4(\pm1)$	0	0.72 (0.725)	0.79	0.67	
$^1D_2(\pm1)$	16872	1.67		1.91	
$(\pm1')$	16920	1.12		0.88	
$^3P_1(\pm1)$	21461	1.17	1.24	1.50	
Tm(ES)					
$^3H_6(\pm1)$	32	0.57[d]	1.11	0.67	0.55
$^3H_4(\pm2)$	12649	1.57		1.82	1.85
$(\pm2')$	12763	0.0		0.07	0.06
$^3F_3(\pm2)$	14486	1.88	1.45	2.16	2.17
$^3F_2(\pm2)$	15079	1.46	1.34	1.51	1.51
$^1G_4(\pm2)$	21171	1.80	1.89	1.36	1.52
$(\pm2')$	21280	0.0	0.11	0.56	0.40
$^1D_2(\pm2)$	27907		1.99	2.28	2.27
(±1)	27977		1.23	1.14	1.14
$^3P_1(\pm1)$	36484		1.48	1.50	

a) Values in parentheses are those from paramagnetic resonances. See Refs. 25 and 38 for Pr(ES) and Pr(DN) respectively. b) See Refs. 40 and 39 for Pr(ES) and Pr(DN), and Tm(ES) respectively. c) Values by Wong and Richman. See Ref. 33. d) The value that Wong and Richman (Ref. 33) recalculated using the datum of the Zeeman splitting obtained by Johnsen (Ref. 31). Johnsen reported for this g value to be 1.0 ± 0.2.

Estimate of g Values. The experimental g values of Pr(ES), Pr(DN), and Tm(ES) have been obtained by the Zeeman effects,[22,31,37] paramagnetic resonances,[25,38] and recently magnetic circular dichroisms (MCD).[39,40] The comparison of the calculating g values to these experimental values are tabulated in

Table 10. Summary of calculated g values for crystals with f^3 configuration[a)]

Crystal	No. of fitted level	rms dev. (cm^{-1})	No. of g with dev. over 35%
Nd(ES)[b)]	43	3.6	1(7)
Er(ES)[b)]	50	3.6	2(14)
Nd: $LaCl_3$[c)]	66	4.9	4(33)
Nd(DN)[d)]	18	10.9	12(34)

a) Values in parentheses are total number of calculated g values compared to the observed ones. b) Data from Ref. 13. c) Data from Ref. 36. d) Data from Ref. 30.

Table 9. The calculated g values except those of the $^1D_2(\eta=\pm 2)$ level in Pr(ES) and the $^1G_4(\eta=\pm 2')$ level in Tm(ES) are in good agreement within 30% with the experimental values. Similar situation is found in rare earth crystals with f^3 configuration as shown in Table 10, where some of g values are very different from the experimental values.

It is not easy to find why only some of calculate g values involve large discrepancy although almost all of those are fairly consistent with experimental values. Undoubtedly, one of the origins may still be in experimental errors due to the misclassification of observed crystal levels, the broadening of the Zeeman lines and the overlap of the MCD curves. The other may arise from the inadequacy of crystal parameters due to the lack of energy levels to be available as pointed out in Pr(ES). Obviously the theoretical evaluation of some physical quantities, such as g value, exclusively depends on the accuracy of wavefunctions used. The present semiempirical procedure by the tensor method turns out to get a set of wavefunctions which are in good agreement with the average value of r^{-1}, because the main part of the Hamiltonian consists of the Coulomb interactions and the radial integrals as parameters contained in the Hamiltonian are determined to reproduce the experimental energy levels. On the other hand, the evaluation of g value given in Eq. 16 comes to estimate the average value of r^0; *i.e.*, a sum of overlap-type integrals. A basis $|J,M>$ under intermediate coupling is transformed to $|J',M'>$ on operation of the magnetic dipole moment operator $\mu=\beta_e(L+2S)$, where J' and M' are respectively equal to J and M or different from J and M by one unit, since both orbital and spin operators are a tensor operator of rank one. Consequently, the operation of magnetic dipole moment on a ket vector is to yield a new ket vector, then the average value of the magnetic dipole moment is reduced to a sum of several overlap-type integrals. Thus the wavefunction being fitted to energy levels may be better charge density in the region of r^{-1}, but it is not assured to give also better charge density in the region of r^0. In principle, exact wave function should give exact value for physical quantities as well as for the energy. However, an approximate wave function which is better regarding the energy levels does not necessarily yield better physical quantities. Such circumstances are, of course, manifested already for theoretical estimate of physical quantities of a number of simple molecules.[41] Such disadvantage is considered to be impossible to avoid in semiempirical method depending on solely energy level fitting. In practical purpose, it will be desirable that there are fairly amount of experimental energy levels to be available. However, it might be stated that the calculated g value can, at least, be taken as a reference when no experimental value is available.

The present work was partially supported by a Grant-in-Aid for Scientific Research (No. 139012) from the Ministry of Education.

References

1) J. S. Margolis, *J. Chem. Phys.*, **35**, 1367 (1961).
2) K. Rajnak, *J. Chem. Phys.*, **43**, 847 (1965).
3) K. Rajnak, *J. Opt. Soc. Am.*, **55**, 126 (1965).
4) H. M. Crosswhite, H. Crosswhite, F. W. Kaseta, and R. Saup, *J. Chem. Phys.*, **64**, 1981 (1976).
5) W. T. Carnall, H. Crosswhite, H. M. Crosswhite, and J. G. Conway, *J. Chem. Phys.*, **64**, 3582 (1976).
6) H. M. Crosswhite, H. Crosswhite, N. Edelstein, and K. Rajnak, *J. Chem. Phys.*, **67**, 3002 (1977).
7) W. T. Carnall, H. Crosswhite, and H. M. Crosswhite, Argonne National Lab., Chem. Division Report, "Energy Level Structure and Transition Probabilities of the Trivalent Lanthanides in LaF_3," Appendix II, Argonne, Illinois (1977).
8) G. Racah, (a) *Phys. Rev.*, **61**, 186 (1942); (b) *ibid.*, **62**, 438 (1942); (c) *ibid.*, **63**, 367 (1943), (d) *ibid.*, **76**, 1352 (1949).
9) K. Rajnak and B. G. Wybourne, *Phys. Rev.*, **132**, 280 (1963).
10) K. Rajnak and B. G. Wybourne, *Phys. Rev.*, **134**, A596 (1964).
11) B. R. Judd, H. M. Crosswhite, and H. Crosswhite, *Phys. Rev.*, **169**, 130 (1968).
12) H. Crosswhite, H. M. Crosswhite, and B. R. Judd, *Phys. Rev.*, **174**, 89 (1968).
13) Y. Kato, T. Nagai, and A. Saika, *Bull. Chem. Soc. Jpn.*, **50**, 862 (1977).
14) R. E. Trees, *Phys. Rev.*, **83**, 756 (1951).
15) G. Racah, *Phys. Rev.*, **85**, 381 (1952).
16) B. R. Judd, "Operator Techniques in Atomic Spectroscopy," McGraw-Hill Book Co., New York (1963).
17) H. H. Marvin, *Phys. Rev.*, **71**, 102 (1947).
18) D. R. Fitzwater and R. E. Rundle, *Z. Kristallogr.*, **112**, 362 (1959). Although the site symmetry about a rare earth ion in the ethylsulfate crystals is C_{3h}, usually this site symmetry is taken as D_{3h} by most of authors. This adequacy has been discussed by Margolis (Ref. 1). In practice, this site symmetry is D_{3h} as far as the nearest neighbor oxygen atoms of 9 crystalline waters are concerned.
19) A. Zalkin, J. D. Forrester, and D. H. Templeton, *J. Chem. Phys.*, **39**, 2881 (1963).
20) K. H. Hellwege, *Ann. Physik*, **4**, 95 (1949).
21) C. W. Nielson and G. F. Koster, "Spectroscopic Coefficients for the p^n, d^n, and f^n Configurations," M. I. T. Press, Cambridge, Mass. (1963).
22) K. H. Hellwege, G. Hess, and H. G. Kahle, *Z. Physik*, **159**, 333 (1960).
23) J. B. Gruber, *J. Chem. Phys.*, **38**, 946 (1963).
24) S. Hüfner, *Z. Physik*, **169**, 417 (1963).
25) H. Meyer, *J. Phys. Chem. Solids*, **9**, 296 (1959).
26) A. Abragam and B. Bleaney, "Electron Paramagnetic Resonance of Transition Ions," Clarendon Press, Oxford (1970), p. 313.
27) A. M. Hellwege and K. H. Hellwege, *Z. Physik*, **130**,

549 (1951).
28) B. R. Judd, *Proc. R. Soc. London, Ser. A*, **241**, 122 (1957).
29) B. R. Judd, *Proc. R. Soc. London, Ser. A*, **232**, 458 (1955).
30) B. M. Tinsley, *J. Chem. Phys.*, **39**, 3503 (1963).
31) U. Johnsen, *Z. Physik*, **152**, 454 (1958).
32) J. B. Gruber and J. G. Conway, *J. Chem. Phys.*, **32**, 1178 (1960).
33) E. Y. Wong and I. Richman, *J. Chem. Phys.*, **34**, 1182 (1961).
34) W. F. Krupke and J. B. Gruber, *Phys. Rev.*, **139**, A2008 (1965).
35) J. B. Gruber and J. G. Conway, *J. Chem. Phys.*, **32**, 1531 (1960).
36) J. C. Eisenstein, *J. Chem. Phys.*, **39**, 2134 (1963). Eisenstein has reported that the standard deviation for 31 crystal levels is 0.91 cm^{-1}. However, the rms deviation defined in Eq. 13 for 66 crystal levels being represented as calculated values in Table II of his article becomes to be 4.9 cm^{-1}.
37) J. Brochard and K. H. Hellwege, *Z. Physik*, **135**, 620 (1953).
38) (a) A. H. Cooke and R. J. Duffus, *Proc. R. Soc. London, Ser. A*, **229**, 407 (1955); (b) B. J. Judd, *ibid., Ser. A*, **232**, 458 (1955).
39) Y. Kato, T. Nakaya, and T. Nagai, *Bull. Chem. Soc. Jpn.*, **50**, 589 (1977).
40) Y. Kato and M. Asano, *Bull. Chem. Soc. Jpn.*, **52**, 999 (1979).
41) For example, see (a) Y. Kato, *J. Chem. Phys.*, **34**, 619 (1961) for electricfield gradient; (b) Y. Kato and A. Saika, *J. Chem. Phys.*, **46**, 1975 (1967) for nuclear spin coupling constants; (c) F. Grimaldi, A. Lecourt, and C. Moser, *Intern. J. Quantum Chem.*, **1S**, 153 (1967) for molecular electric dipole moment.

Magnetic Circular Dichroism of Praseodymium Ethyl Sulfate and Praseodymium-Magnesium Double Nitrate

Yoshifumi KATO* and Motoshi ASANO

Department of Chemistry, Faculty of Science, Kobe University, Nada-ku, Kobe 657

(Received October 7, 1978)

The magnetic circular dichroism of praseodymium ethyl sulfate and praseodymium–magnesium double nitrate was measured in the visible wave number region at low temperatures down to 17 K. Analysis was carried out for six absorption bands of praseodymium ethyl sulfate and three bands of praseodymium–magnesium double nitrate. With available information on energy levels, the g values of the crystal-field levels relevant to absorptions were derived from the MCD parameters obtained. These values are in good agreement with those from other methods.

During the passed ten years the utility of magnetic circular dicroism (MCD) studies has been presented by many authors,[1] especially for clarifying spectroscopic assignments and characterizing the symmetry and angular momentum properties of both ground and excited states of molecules and ions. However, there are only a few evidences to judge the reliability of the results. It was pointed out that MCD provides fairly reliable spectroscopic splitting factors (g value) of some rare earth crystals with the aid of well-established energy levels even when no direct Zeeman components of a transition are resolved.[2–4]

We have measured the MCD spectra of praseodymium ethyl sulfate, $Pr(C_2H_5SO_4)_3\cdot 9H_2O$ (Pr(ES)), and praseodymium–magnesium double nitrate, $Mg_3Pr_2(NO_3)_{12}\cdot 24H_2O$ (Pr(DN)) at low temperatures, and obtained the g values for several crystal-field levels of these crystals.

Results and Discussion

The preparation of the Pr(ES) crystal has been reported.[2] Pr(DN) was prepared by the method described by Jantsch.[5] An aqueous solution of stoichiometric amount of $Pr(NO_3)_3\cdot 6H_2O$ and $Mg(NO_3)_2\cdot 6H_2O$ was allowed to evaporate slowly. After a month, a transparent single crystal of double nitrate grew in the form of a thick hexagonal plate $30\times 30\times 8$ mm^3, with a well-developed face perpendicular to the principal axis of the crystal. The details of absorption and MCD measurements at low temperatures with use of a metal Dewar vessel have been reported.[2,3] The temperature of crystals cooled by thermal conduction was measured with an Au–Co *versus* chromel thermocouple with one junction pressed directly against the crystal and found to be 80 ± 1 and 17 ± 1 K at liquid nitrogen and helium temperatures, respectively.

The general expression for the MCD of an absorption[6,7] can be applied to a uniaxial crystal such as Pr(ES) and Pr(DN). The ellipticity accompanied by an electronic transition is given by

$$\theta = -\frac{4}{3}\gamma N_a[Af_1/\hbar + (B+C/kT)f_0]H. \qquad (1)$$

The explicit expressions for the MCD parameters A, B, and C are given elsewhere.[1,2] The condition assumed in the derivation of Eq. 1 (the Zeeman energy is less than the zero-field state separation, line width and kT) are still satisfied in the present measurements. The ratios of the MCD parameters to the dipole strength D $(=(1/d_a)|\langle a|\boldsymbol{m}|j\rangle|^2)$ are related to the g values of the ground a and excited j states in a transition as[8]

$$|A/D| = |g_j - g_a|, \quad |C/D| = |g_a|, \qquad (2)$$

where the Zeeman splitting is taken as $2g\beta H$ since there are no multiplets except for the doublet in both Pr(ES) and Pr(DN). We see that term C can arise only when the ground state is degenerate, whereas term A has the value when the ground and/or excited states are degenerate.

There are 13 ion levels for a trivalent Pr ion with $4f^2$ configuration in the aforementioned crystals, an ion level placed in a crystal-field splitting into several crystal-field levels designated by the crystal quantum number η after Hellwege.[9] From the results of X-ray analyses,[10] the site symmetries around a Pr^{3+} ion in the ethyl sulfate and double nitrate crystals are known to be D_{3h} and C_{3v}, respectively. Thus the crystal-field levels in Pr(ES) and Pr(DN) are classified by $\eta=0, \pm 1, \pm 2$, and 3, and $\eta=0$ and ± 1 respectively, where the levels with double signs are twofold degenerate. The crystal levels in the visible region of Pr(ES)[11,12] and Pr(DN)[13,14] have been determined. The energy level diagrams of these crystals relevant to the present analysis are shown in Fig. 1, in which σ-transitions observed in the present experiments are indicated by lines with arrow. The absorption and MCD spectra

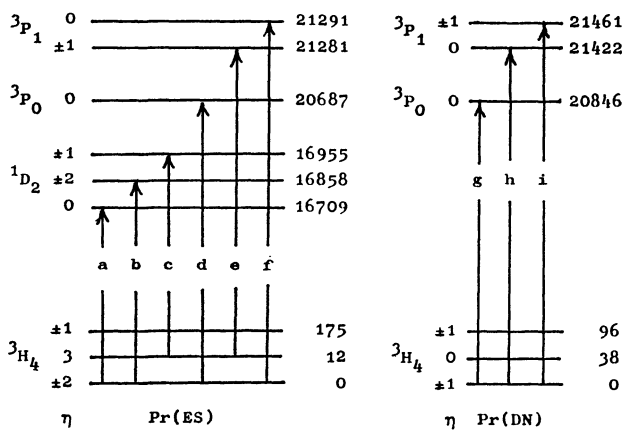

Fig. 1. Energy level diagrams of Pr(ES) and Pr(DN). The units of energy are in cm^{-1}. Allowed σ-transitions are indicated by arrows.

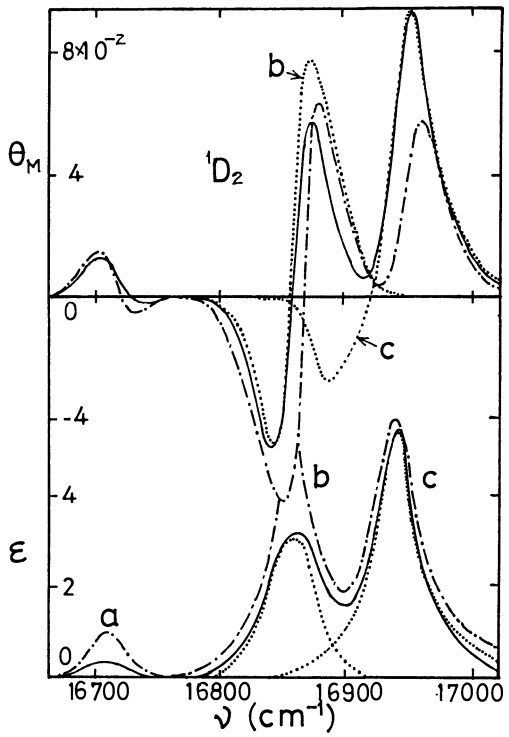

Fig. 2. Absorption and MCD spectra for the $^3H_4 \rightarrow {}^1D_2$ transition of Pr(ES) at 17 (solid line) and 80 K (chain line). The curves shown by dotted lines are those resolved into the constituent curves at 17 K. θ_M and ε are the MCD in molar ellipticity units (K dl dm^{-1} mol^{-1}) per unit gauss and molar extinction coefficient respectively.

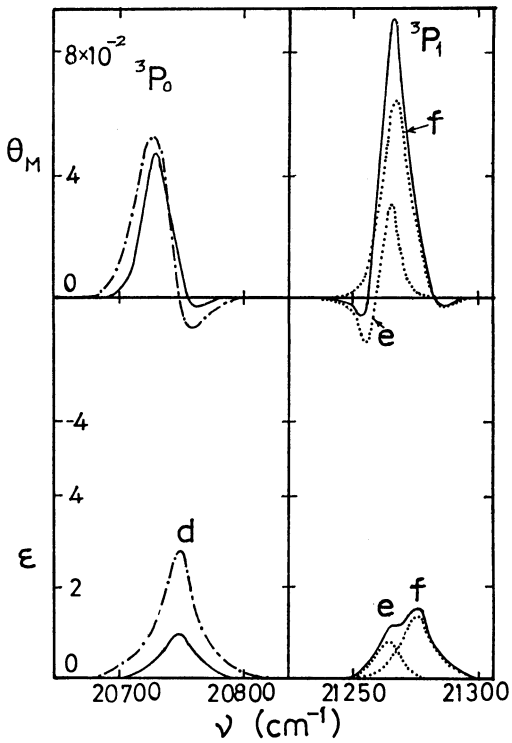

Fig. 3. Absorption and MCD spectra for the $^3H_4 \rightarrow {}^3P_0$, $^3P_1$ transitions of Pr(ES) at 17 (solid line) and 80 K (chain line). See the note in Fig. 2.

observed are shown in Figs. 2—4, where molar extiction coefficient ε and molar ellipticity θ_M in terms of K dl dm^{-1} mol^{-1} G^{-1} are used for the sake of convenience. The lowest crystal-field level of the $^3H_4$ state of Pr(ES) is doubly degenerate ($\eta=\pm 2$), and the population of the next level ($\eta=3$), which is 12 cm^{-1} higher than the lowest level, is 36% that of the latter at 17 K. Thus it is necessary to take account of σ-transitions from these two levels for Pr(ES) (Fig. 1). On the other hand, all the absorption bands of Pr(DN) at 17 K might arise from only the lowest crystal-field level $^3H_4$ ($\eta=\pm 1$), since the population of the next level ($\eta=0$), 38 cm^{-1} higher than the lowest level, is 4% that of the latter at 17 K.

A summary of the MCD parameters derived from the method of moments[7,15] is given in Table 1. Separation of term C from term B can be performed by means of the temperature dependence of θ_M as shown in Fig. 5. The A/D value for a transition should be independent

TABLE 1. MCD PARAMETERS DIVIDED BY DIPOLE STRENGTH D, CENTRAL FREQUENCY ν_0 AND HALF-WIDTH Γ AT $1/e$ OF THE MAXIMUM ABSORPTION IN Pr(ES) AND Pr(DN). VALUES IN PARENTHESES ARE ASSUMED ONES

Transition	T (K)	ν_0 (cm^{-1})	Γ (cm^{-1})	D (10^{-4}D^2)	A/D (β)	$(B+C/kT)/D$ (β/cm^{-1})	B/D (β/cm^{-1})	C/D (β)
Pr(ES)								
(a) $^3H_4(\pm 2) \longrightarrow {}^1D_2(0)$	80	16708	24	0.225	−0.751	−0.0360	−0.0225	−0.75
	17	16709	20	0.080	−0.801	−0.0861		
(b) $^3H_4(\pm 2) \longrightarrow {}^1D_2(\pm 2)$	80	16858	26	1.401	2.02	0.0128	0.0262	(−0.77)
	17	16858	31	0.905	2.09	−0.0371		
(c) $^3H_4(3) \longrightarrow {}^1D_2(\pm 1)$	80	16941	26	1.470	1.04	−0.0209	−0.0244	0
	17	16942	26	1.599	1.13	−0.0278		
(d) $^3H_4(\pm 2) \longrightarrow {}^3P_0(0)$	80	20686	21	0.508	−0.796	−0.0419	−0.0286	−0.74
	17	20687	21	0.173	−0.771	−0.0913		
(e) $^3H_4(3) \longrightarrow {}^3P_1(\pm 1)$	17	21269	14	0.092	1.61	−0.0527	−0.0527	0
(f) $^3H_4(\pm 2) \longrightarrow {}^3P_1(0)$	17	21291	19	0.219	−0.791	−0.112	−0.0477	(−0.77)
Pr(DN)								
(g) $^3H_4(\pm 1) \longrightarrow {}^3P_0(0)$	80	20847	43	0.055	−0.775	−0.0165	−0.0017	−0.82
	17	20845	43	0.087	−0.791	−0.0719		
(h) $^3H_4(\pm 1) \longrightarrow {}^3P_1(0)$	17	21421	24	0.256	0.800	−0.0780	−0.0120	(−0.79)
(i) $^3H_4(\pm 1) \longrightarrow {}^3P_1(\pm 1)$	17	21461	29	0.197	2.05	−0.0666	−0.0016	(0.79)

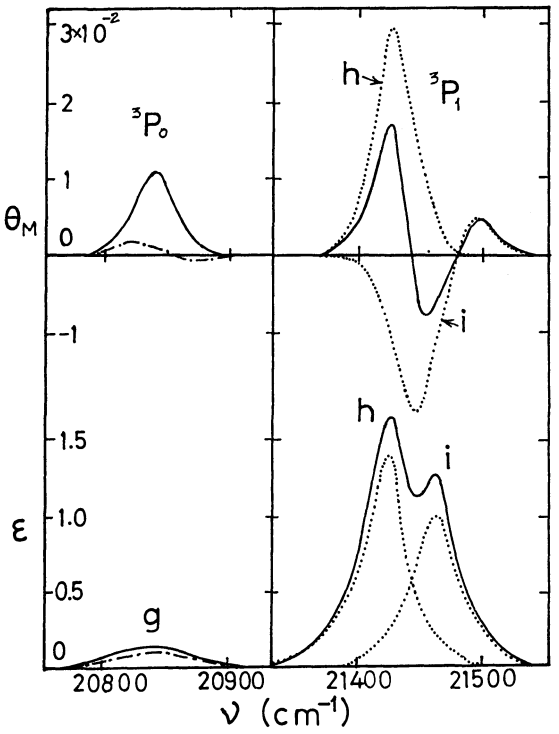

Fig. 4. Absorption and MCD spectra of Pr(DN) at 17 (solid line) and 80 K (chain line). See the note in Fig. 2.

of temperature. This is satisfied for both Pr(ES) and Pr(DN) (Table 1). Absolute C/D values for various transitions from the same lower level should be identical, indicating the $|g|$ value of this level. Although the absorption bands (b) and (c) in Pr(ES) overlap each other (Fig. 2), separation of the experimental MCD into the MCD's corresponding to these absorption bands is possible when we take the $|C/D|$ values of the $\eta=\pm 2$

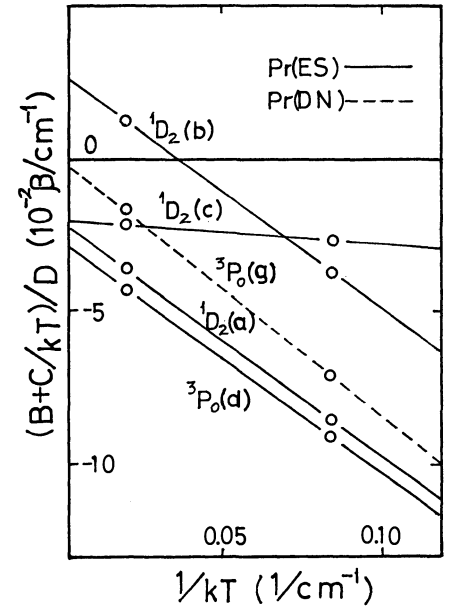

Fig. 5. Temperature dependence of $(B+C/kT)/D$ of Pr(ES) (solid line) and Pr(DN) (broken line) obtained by the moment analysis.

and 3 levels of the $^3H_4$ state to be 0.77 β and 0 β, respectively. The former is the average value obtained from the band (a) and (d), for which all the $|A/D|$ and $|C/D|$ values should be equal since both bands correspond to the transitions from the lowest crystal-field level $^3H_4$ ($\eta=\pm 2$) to non-degenerate excited levels. The latter value should, in principle, be zero since the lower level $^3H_4(\eta=3)$ is non-degenerate. The absorption and MCD curves for each of the bands (b) and (c) (dotted lines, Fig. 2) originate from a curve fitting by using the values given in Table 1 for central frequencies, half-widths and dipole strengths, and by adopting the above values for $|C/D|$ values, the Gaussian form for the shape function f_0 and then the rigid shift model[7] ($f_1=df_0/d\nu$) in Eq. 1. For both absorption and MCD, the sum of two constituent curves reproduces satisfactorily the experimental curve. A similar treatment is applied to the separation of other overlapping absorption and MCD curves into the constituent curves; *i.e.*, the (e) and (f) bands in Pr(ES), and the (h) and (i) bands in Pr(DN). Thus all the MCD parameters for observed bands can be determined. As expected, B terms due to higher-order perturbation are small as compared to the other terms, the contribution of B terms to θ_M not being sizable for paramagnetic salts. Ultimately the absolute g value of the ground state of Pr(ES) and that of Pr(DN) are estimated to be 0.77 β and 0.79 β, respectively. The g values for excited crystal-field levels can be evaluated by using Eq. 2. The absolute g values thus obtained are compared with other experimental values by the Zeeman splittings[13,14] and paramagnetic resonances,[16,17] and theoretical values[18] in Table 2. The g values from MCD are in good agreement with the other experimental ones within the experimental error (*ca.* 15%). The theoretical values also agree with the experimental ones except for the g value of the $^1D_2(\eta=\pm 2)$ level in Pr(ES), which is 1.6 times larger than the experimental value. For theoretical g values of rare earth crystals by the wavefunctions determined so as to get the best agreement of calculated energies

Table 2. Comparison of the g values in Pr(ES) and Pr(DN)

Level	Energy (cm^{-1})	Absolute value of g		
		MCD[a]	Zeeman[b]	Calcd[c]
Pr(ES)				
$^3H_4(\pm 2)$	0	0.77	0.85(0.775)	0.86
$^1D_2(\pm 2)$	16858	1.30	1.30	2.07
(± 1)	16955	1.09		1.03
$^3P_1(\pm 1)$	21281	1.61	1.39	1.50
Pr(DN)				
$^3H_4(\pm 1)$	0	0.79	0.72(0.725)	0.67
$^3P_1(\pm 1)$	21461	1.24	1.17	1.50

a) As the g value of an excited level, two kinds of values are derived from Eq. 2, the value close to those by the other methods being adopted. b) The values from Refs. 13 and 14 for Pr(ES) and Pr(DN), respectively. The values by paramagnetic resonances are given in parentheses. See Refs. 16 and 17 for Pr(ES) and Pr(DN), respectively. c) The values from Ref. 18.

with the observed values obtained from crystal spectra, it frequently occurs that only for few specific crystal-field levels the calculated g values differ considerably from the observed ones, although there is good agreement between both values for most crystal-field levels.[19,20] This problem is further discussed elsewhere.[18] The present analysis has confirmed previous results,[2-4] *viz.*, with available information on energy levels, the g values obtained from the MCD measurement of Pr crystals as well as those from the Zeeman effects and paramagnetic resonances are reliable.

References

1) For references up to 1973, see the tables cited in; (a) P. N. Schatz and A. J. McCaffery, *Quart. Rev.*, **23**, 552 (1969); (b) P. J. Stephens, *Ann. Rev. Phys. Chem.*, **25**, 201 (1974).
2) Y. Kato, T. Nagai, and T. Nakaya, *Chem. Phys. Lett.*, **39**, 183 (1976).
3) Y. Kato, T. Nakaya, and T. Nagai, *Bull. Chem. Soc. Jpn.*, **50**, 589 (1977).
4) Y. Kato and I. Nakano, *Chem. Phys. Lett.*, **45**, 359 (1977).
5) G. Jantsch, *Z. Anorg. Chem.*, **76**, 303 (1912).
6) A. D. Buckingham and P. J. Stephens, *Ann. Rev. Phys. Chem.*, **17**, 399 (1966).
7) P. J. Stephens, *J. Chem. Phys.*, **52**, 3489 (1970).
8) J. Badoz, M. Billardon, A. C. Boccara, and B. Briat, *Symp. Faraday Soc.*, **3**, 27 (1969).
9) K. H. Hellwege, *Ann. Physik*, **4**, 95 (1949).
10) For Pr(ES), D. R. Fitzwater and R. E. Rundle, *Z. Kristallogr.*, **112**, 362 (1959); for Pr(DN), A. Zalkin, J. D. Forrester, and D. H. Templeton, *J. Chem. Phys.*, **39**, 2881 (1963).
11) K. Hellwege, G. Hess, and H. G. Kahle, *Z. Physik*, **159**, 333 (1960).
12) B. Gruber, *J. Chem. Phys.*, **38**, 946 (1963).
13) A. M. Hellwege and K. H. Hellwege, *Z. Physik*, **130**, 549 (1951).
14) J. Brochard and K. H. Hellwege, *Z. Physik*, **135**, 620 (1953).
15) P. J. Stephens, *Chem. Phys. Lett.*, **2**, 241 (1968).
16) H. Meyer, *J. Phys. Chem. Solids*, **9**, 296 (1959).
17) A. H. Cook and R. J. Duffus, *Proc. R. Soc. London, Ser. A*, **229**, 407 (1955); B. R. Judd, *ibid.*, **232**, 458 (1955).
18) Y. Kato and H. Takada, *Bull. Chem. Soc. Jpn.*, **52**, 990 (1979).
19) J. C. Eisenstein, *J. Chem. Phys.*, **39**, 2134 (1963).
20) Y. Kato, T. Nagai, and A. Saika, *Bull. Chem. Soc. Jpn.*, **50**, 862 (1977).

Metachromasy. V.† The Effect of the Chain Length of Polyphosphate on the Metachromatic Behavior of Crystal Violet and Trypaflavine with Emphasis on the Binding Curve and the Spectra of Bound Dyes

Mineo TAKATSUKI and Kiwamu YAMAOKA*

Faculty of Science, Hiroshima University, Higashisenda-machi, Hiroshima 730

(Received October 6, 1978)

Absorption spectra of two metachromatic dyes, Crystal Violet, CV, and Trypaflavine, TF, were measured in the presence of three sodium polyphosphates, NaPP, of different chain lengths. The optical titrations of these systems were performed at the phosphate residue-to-dye ratios, P/D, between 0: 1 and about 1: 1, where isosbestic points are present in the absorption spectra. The apparent molar absorption coefficients of the two dyes in each system changed sigmoidally with the increase in P/D. The extended principal component analysis was applied to the observed spectra of each dye–NaPP system in order to determine both the equilibrium constant for the binding reaction between the dye and the polymer and the pure spectra of the bound dyes. An empirical parameter α was introduced into the expression for the equilibrium constant, $K=$[complex]/[free dye][unoccupied binding site]$^{\alpha}$, to reproduce the sigmoidal titration curve ($\alpha>1$). The amount of the bound CV and TF increased with the increase in the chain length of NaPP at a given P/D, although the pure spectra of those bound dyes were independent of the chain length for low P/D values. The binding behavior of those dyes for high P/D values was also discussed by comparing the previous data with the binding curves calculated in this work.

The striking change in the absorption spectrum of a metachromatic dye in the presence of polyelectrolyte is generally characteristic of the specific nature of the polymer. For example, such a change has been related to the chain length,[1-3] overall or local conformation,[4-8] and functional or ionizable group of individual polymers.[4,9,10] The interaction between dye and polymer is effected by adjusting the experimental conditions such as pH, temperature, ionic strength, and the molar mixing ratio of polymer residues to dye, P/D. Therefore, detailed studies which take into account these factors quantitatively are necessary for full understanding of both the metachromatic behavior of dyes and the dye–polymer interaction.

The method of extended principal component analysis, the PCA method,[11] was successfully applied to the complicated equilibrium systems of cationic dyes (Crystal Violet, CV, and Trypaflavine, TF) and various polyanions, in order to determine the number of dye species in equilibrium, the equilibrium constants, and the absorption spectra of the bound-dye species.[4] Experimentally, the successive titration method was employed in a series of measurements to ensure the accuracy of the dye concentration within 1%. Since the metachromatic behavior of CV and TF has been shown to depend on the number-average degree of polymerization, $\bar{n}$, of sodium polyphosphate over a wide P/D range of 0—2000,[2,3] the purpose of this article is to apply the extended PCA method to the CV– and TF–NaPP ($\bar{n}=11$, 24, and 64) systems in order to clarify the relationship between the metachromatic behavior of these dyes and the chain length of NaPP.

In this work, the equilibrium constants and the pure absorption spectra of the bound-dye species could be determined for those systems. The optical titration curves of all the systems were sigmoidal within the P/D range from zero to about one. In order to analyze the sigmoidal titration behavior, an equilibrium expression with an empirical parameter α was utilized in the same manner as in the previous work.[4] The present results clearly indicate that the equilibrium constant and the value of α both depend on the combination of dyes and NaPP samples. On the contrary, the pure spectra of the bound-dye species are independent of the chain length of NaPP in the low P/D range. The fraction of the bound dye was calculated against P/D by using the equilibrium constant and the parameter α obtained for each dye–NaPP system. By comparing the binding fraction *vs.* P/D curves with previous data,[2,3] it was concluded that two or more bound-dye species should be present over the entire P/D range. The mechanism of the chain-length dependence on the metachromasy was also discussed quantitatively in terms of the amount of the bound dye and its absorption spectrum. Lastly, the empirical parameter α was qualitatively related to the cooperative parameter q which was defined by Schwarz.[12]

Experimental

Materials. All the NaPP samples ($\bar{n}=11$, 24, and 64) used in this work are the same refractionated preparations as described elsewhere.[2,3] The cationic dyes, CV ($\varepsilon=9.20\times10^4$ at 592 nm) and TF ($\varepsilon=4.67\times10^4$ at 452 nm), are also those used in the previous work.[4]

Procedures and Measurements. A Hitachi EPS-3T recording spectrophotometer was used together with a matched pair of 1 and 2 cm long quartz cells. The temperature was set at 25 °C by circulating regulated water through a cell holder. Procedures of the optical titration and other precautions for measurements were described in Ref. 4. The observed data were analyzed by the extended PCA method, which was described in detail in the previous papers.[4,11]

Results

Absorption Spectra and Optical Titration Curves. The absorption spectra were measured at the different stages of titration with a titrant NaPP solution up to a P/D

† For the preceding paper of this series, see Ref. 4.

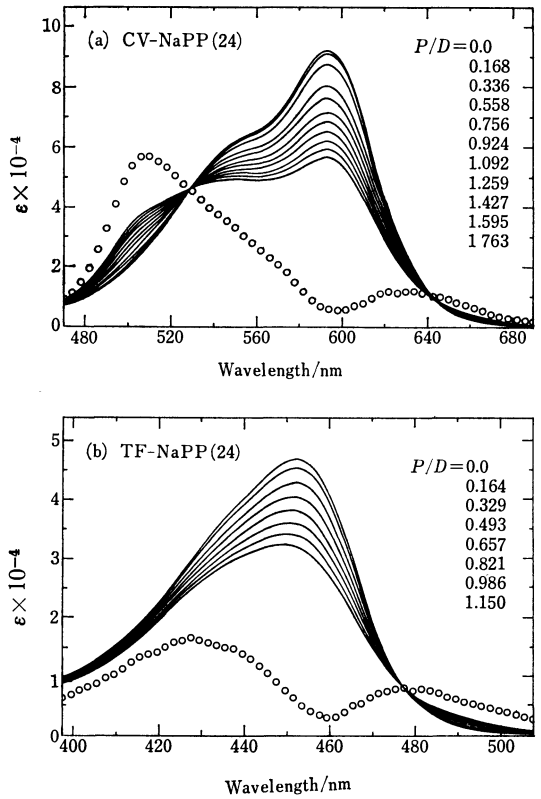

Fig. 1. Absorption spectra of CV (a) and TF (b) in the presence and absence of NaPP(24) and the pure absorption spectra of bound dyes (open circles). The initial concentrations of CV and TF are 8.86 and 11.0 μM (1μM=1×10⁻⁶ mol dm⁻³) respectively. The concentrations of NaPP are given in the respective figures in terms of *P/D*, the order of which corresponds to the order of the decrease in the maximum absorbance.

value near one. Figures 1(a) and (b) show the absorption spectra of CV and TF in the presence of NaPP whose $\bar{n}$ is 24 (hereafter denoted as NaPP (24)). For other CV- and TF-NaPP (11 and 64) systems, the series of absorption spectra were similarly obtained. Since the observed spectrum of a dye-NaPP solution is a composite of the component spectra of the known free and unknown bound dyes, the apparent molar absorption coefficients, ε, were calculated on the basis of the analytical concentration of the dye in solution. The spectra of CV-NaPP (24) show only a shoulder at 510 nm, as is shown in Fig. 1(a), although the metachromasy band was clearly observed at 510 nm for NaPP(64) and NaPP(154). (The absorption spectra for CV-NaPP(154) and for TF-NaPP(216) and TF-NaPP(154) were shown in Refs. 2 and 4, and Refs. 3 and 4, respectively. They will hereafter be quoted without the references.) In the TF-NaPP(24) system which is shown in Fig. 1(b), the maximum absorption band at 452 nm is shifted gradually with increasing *P/D* toward the shorter wavelength with no explicit metachromasy band.

Three and two isosbestic points are observed at 460, 529, and 639 nm and at 371 and 476 nm for the CV- and TF-NaPP(11, 24, 64, and 154) systems, respectively. These isosbestic points predict the presence of two absorbing components in each system, free dye and a bound-dye species, between the *P/D* values of zero and about one. It should also be noted that the ε and position of those isosbestic points remain unchanged regardless of the chain length of NaPP. These findings suggest that the pure spectra of the bound-dye species may not depend on the chain length of NaPP for low *P/D* values.

The optical titration curves are plotted against *P/D* at 592 nm for CV and at 450 nm for TF in the presence of NaPP with the varying degree of polymerization in Figs. 2(a) and (b). All the titration curves change sigmoidally, but not monotonously, with *P/D* in a manner similar to the NaPP(154) systems. The values of the apparent ε at a given *P/D* (*e.g.*, *P/D*=1) decrease with the increase in the chain length of NaPP for both CV- and TF-NaPP systems.

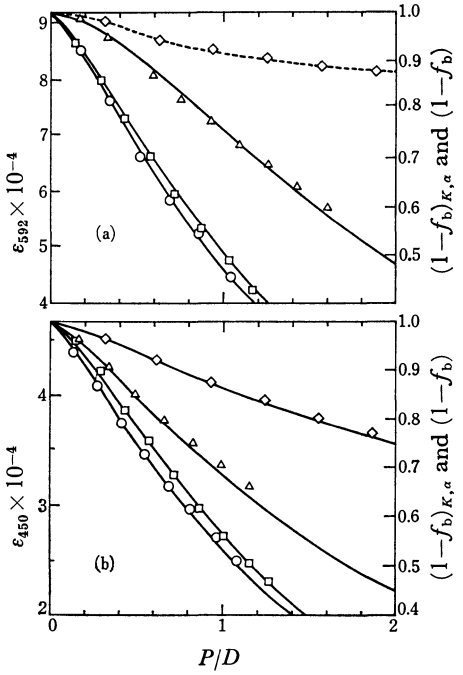

Fig. 2. Optical titration data and calculated binding curves for CV (a) and TF (b). The optical titration data (open symbols) are plotted against *P/D* in terms of ε_λ at 592 nm for CV and 450 nm for TF (left ordinate). The fractions of free dyes calculated from those data (open symbols) are also indicated in terms of $(1-f_b)$ (right ordinate). □: NaPP(64), △: NaPP (24), ◇: NaPP(11), and ○: NaPP(154). The calculated binding curves (solid lines) are shown in terms of $(1-f_b)_{K,\alpha}$ (right ordinate). The dashed line for the CV-NaPP(11) indicates that the $(1-f_b)_{K,\alpha}$ curve could not be calculated by the PCA method (see text for detail).

Pure Spectra of Bound-dye Species and Equilibrium Constants. The extended PCA method is especially useful for the determination of the equilibrium scheme for binding of dye to polyelectrolyte of relatively low molecular weight which cannot be retained by a semipermeable membrane in equilibrium dialysis.[4,11] Therefore, the absorption spectra of all dye-NaPP systems obtained in this work were analyzed by the same method. The number of the absorbing components was first deter-

mined to be two, free and bound dyes, for all the systems which are expected from the presence of isosbestic points. In order to reproduce the observed sigmoidal and monotonous titration curves, an empirical parameter α was introduced into the equilibrium equation for a dye–NaPP system consisting of such two absorbing components as follows:[4]

$$K = \frac{[DP^*]}{[D][P]^{\alpha}}. \quad (1)$$

In this expression D is the free, unbound dye; P means the unoccupied binding site of NaPP; DP* is the bound dye which gives rise to an absorption spectrum different from that of the free dye; the brackets denote the equilibrium concentration. When the value of α is greater than one, the sigmoidal titration curve can be obtained. The pure spectrum of the bound-dye species, equilibrium constant, and empirical parameter were all determined simultaneously from a series of absorption spectra of a particular dye–NaPP system.[4]

Figure 3(a) shows the pure spectra of the CV bound

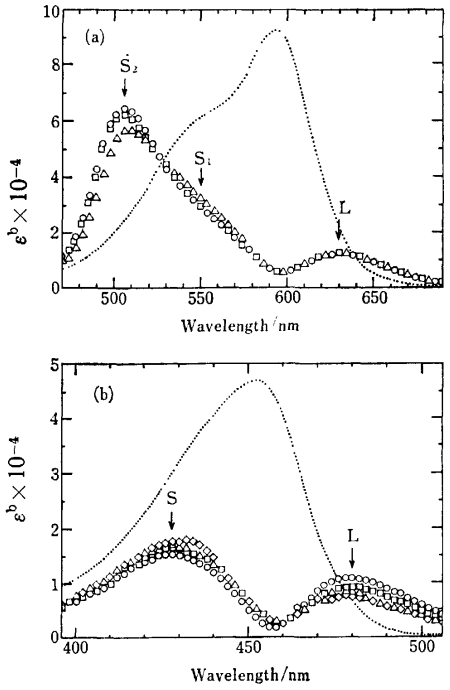

Fig. 3. Pure absorption spectra of CV (a) and TF (b) bound to NaPP's with different chain lengths. □: NaPP(64), △: NaPP(24), ◇: NaPP(11), and ○: NaPP(154). The spectra of free dyes (……) are also shown.

to NaPP(24), NaPP(64), and NaPP(154), thus obtained by the PCA method, together with the free CV for comparison. The pure spectrum of the bound CV for CV–NaPP(11) system could not be obtained from a set of the absorption spectra because their variation was only slight. For all the CV–NaPP systems, the spectra of bound CV exhibit three metachromasy bands: they are designated as the Meta S_2, S_1, and L bands which are located at 506, 550, and 630 nm, respectively, and are indicated by arrows in Fig. 3(a). (The Meta S_1 and S_2 bands are for the short-wavelength ones relative to the peak of the free CV, while the Meta L band is for the long-wavelength one; the numbering is from the one closest to the peak position of the free dye.) The pure spectra of TF bound to NaPP(11), NaPP(24), NaPP(64), and NaPP(154) are shown in Fig. 3(b). They exhibit two metachromasy bands: the Meta S band at 428 nm and the Meta L band at 480 nm. The pure spectra of the bound-dye species show pronounced metachromasy bands (or peaks), in spite of the fact that such bands have not been observed in the spectra for the CV–NaPP(24) or for all of the TF–NaPP systems. Furthermore, the spectral profiles of the bound dyes and the positions of the Meta bands are all independent of the chain length of NaPP bound by either CV and TF. It should be noted that the pure spectra of the bound-dye species have been unraveled in detail by the extended PCA method.

The values of α and of the equilibrium constant K in Eq. 1 were calculated from the series of the absorption spectra of CV– and TF–NaPP systems and are listed in Table 1. It should be noted that the values of α are always greater than one for the sigmoidal titration curves (Figs. 2(a) and (b)). Furthermore, the values of α depend on the combination between dyes and NaPP's with varying $\bar{n}$ values. The binding of dye to NaPP may be affected by the chemical structure of the dye and by the chain length of NaPP with the identical residue structure. Since the chain length may affect the electrostatic potential field of NaPP, the parameter α may be considered as an indicator which reflects the binding mode of dyes. The values of equilibrium constant listed in Table 1 vary widely, because the dimension of K ($=[dm^3\ mol^{-1}]^{\alpha}$) now depends on α. Therefore, the values of K of the different dye–NaPP systems cannot be readily compared with each other to characterize them. However, the equilibrium constant K defined in Eq. 1 may be related to the frequently postulated equilibrium constant K' in such that $K' = [DP^*]/[D][P] = K[P]^{\alpha-1}$. The values of K' were calculated at a representative P/D of 1 and are listed

Table 1. Empirical parameters, α, and equilibrium constants, K and K' at 25 °C for CV– and TF–NaPP systems

$\bar{n}$ of NaPP	CV			TF		
	α	K[a]	K'[b]	α	K[a]	K'[b]
154	1.5	1.0×10^8	2.1×10^5	1.5	5.1×10^7	1.3×10^5
64	1.5	0.98×10^8	2.1×10^5	1.3	7.7×10^6	1.1×10^5
24	1.9	2.2×10^9	0.49×10^5	1.3	2.3×10^6	0.66×10^5
11	—	—	—	1.2	2.1×10^5	0.20×10^5

a) The dimension is given by $[dm^3\ mol^{-1}]^{\alpha}$. b) $K' = K[P]^{\alpha-1}$ at $P/D = 1$.

in Table 1. For both CV and TF, the values of K' increase with the increase in the chain length of NaPP. Thus, the greater part of either dye should be bound to the longer chain of NaPP (*vide infra*).

Binding Curves. The fraction of bound dye, f_b, defined as the ratio of the concentration of bound dye, C_b, to the sum total of the concentrations of the bound and free dyes in solution, C_0, can be calculated at a given P/D in three ways. First, the f_b is obtained with the values of K and α by solving the following equation, which is derived from Eq. 1, for f_b by the Newton method:

$$(1-f_b) = \frac{f_b}{K\{C_0(P/D-f_b)\}^\alpha}. \quad (2)$$

The $(1-f_b)$, *i.e.*, the fraction of free dye, calculated from Eq. 2 is denoted as $(1-f_b)_{K,\alpha}$. The values of $(1-f_b)_{K,\alpha}$ for CV and TF are shown with solid curves in Figs. 2(a) and (b) respectively.

Figures 2(a) and (b) show an excellent agreement between the calculated curve $(1-f_b)_{K,\alpha}$ and the observed points of ε_λ for each dye–NaPP system. Secondly, the fraction of bound dye, f_b, can be calculated from the observed ε_λ at a selected wavelength, according to Lambert-Beer's law, as follows:

$$(1-f_b)_\lambda = \frac{\varepsilon_\lambda - \varepsilon_\lambda{}^b}{\varepsilon_\lambda{}^f - \varepsilon_\lambda{}^b}, \quad (3)$$

where $\varepsilon_\lambda{}^b$ and $\varepsilon_\lambda{}^f$ are the molar absorption coefficients of bound and free dyes at the wavelength λ respectively. Thirdly, the mean value of $(1-f_b)_\lambda$ (*cf.* Eq. 6 in Ref. 4) may be defined as follows:

$$(1-f_b) = \frac{1}{n}\sum_{i=1}^{n}(1-f_b)_{\lambda_i} \quad (n=56), \quad (4)$$

where n denotes the number of selected wavelengths. The $(1-f_b)$ is determined for a given absorption spectrum at a given P/D by the PCA method.[11] The calculated $(1-f_b)_{K,\alpha}$ agrees with the $(1-f_b)$ at all P/D values in Figs. 2(a) and (b). It should be noted that the sigmoidal decrease of the observed ε_λ can be reproduced by $(1-f_b)_{K,\alpha}$ for each system with the value of α larger than one. Hence, the α should be a useful parameter to represent the binding of dye to polyelectrolyte.

The binding curves (solid lines) calculated with the aid of Eq. 2 together with the appropriate α and K in Table 1 are plotted against P/D in Figs. 4(a) and (b). In these figures, the open symbols indicate the points of $(1-f_b)$ which were obtained by analyzing the present optical titration data by the PCA method, while the closed symbols represent the points of $(1-f_b)_\lambda$, $\lambda=592$ and 450 nm for CV and TF respectively, which were calculated from the previous data over a wide P/D range[2,3] with the aid of Eq. 3 together with the values of ε_λ, $\varepsilon_\lambda{}^f$, and $\varepsilon_\lambda{}^b$ (the last was determined in this work by the PCA method). The points of $(1-f_b)_\lambda$ and $(1-f_b)$ obtained from the observed spectra of dye–NaPP fall on the binding curves $(1-f_b)_{K,\alpha}$, which were calculated from Eq. 2, in the P/D range between 0 and 2—3. The $(1-f_b)_{K,\alpha}$ curves approach the limiting value of zero, as the P/D values further increase.

On the contrary, the points of $(1-f_b)_\lambda$ deviate from the $(1-f_b)_{K,\alpha}$ curves and gradually ascend back to the original value of unity[2,3] passing through the minima in the P/D ranges of 2—8 for CV–NaPP and 3—10 for TF–NaPP. (The P/D values for the minima slightly depend on the chain length of NaPP). In addition, the isosbestic points remaining at the low P/D values of less than *ca.* 2 tend to disappear gradually in those intermediate P/D ranges. Both the deviation of the $(1-f_b)_\lambda$ points from the calculated binding curve (solid line) and the concurrent disappearance of the isosbestic points strongly indicate that some unknown bound-dye species are being formed in the dye–NaPP solution with the increase in P/D. These results also eliminate the possibility that the bound dye begins to dissociate from the polymer site. (If this were the case, the isosbestic points should remain.) Thus, it is most reasonable to conclude that two or more of the bound-dye species are present in the dye–NaPP solution in the intermediate P/D range 2—30. Since the pure spectrum of one of them has already been determined in the previous section (Fig. 3), it is worth now finding out the pure spectrum of the other bound-dye species.

At present, the pure spectrum of the unknown bound-dye species cannot be determined uniquely, because both the number of the bound-dye species and the fraction of each bound-dye species are not available yet in the intermediate P/D range. The sum total of the bound-dye species, however, can be estimated from the calculated binding curve. Therefore, the apparent spectrum of the mixture of bound-dye species, *i.e.*, the mixed spectrum of the bound dyes, may be calculated by using the f_b value, which is obtained from the calculated binding curve, $(1-f_b)_{K,\alpha}$, (solid line in Fig. 4), and the observed spectrum of the dye–NaPP solution, ε_λ, at a given P/D value as follows:

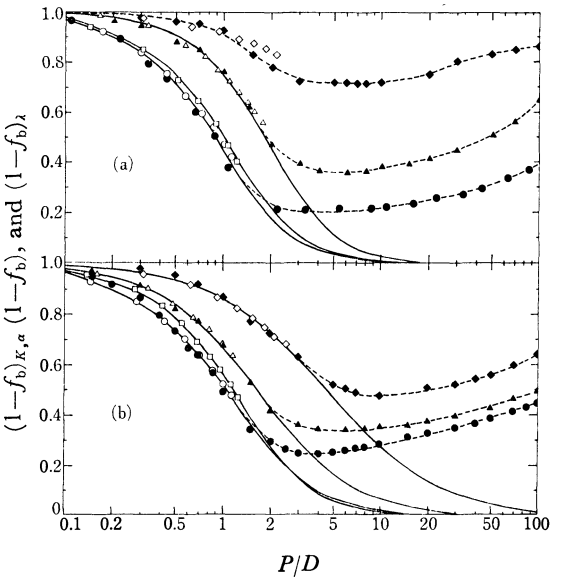

Fig. 4. Binding curves of CV (a) and TF (b) to NaPP's with different chain lengths. The binding curves were calculated in three ways: solid lines for $(1-f_b)_{K,\alpha}$, open symbols for $(1-f_b)$; and closed symbols with dashed lines for $(1-f_b)_\lambda$ ($\lambda=592$ nm for CV and 450 nm for TF). For details, see text. □: NaPP(64), △: NaPP-(24), ◇: NaPP(11), and ○: NaPP(154) for CV and NaPP(216) for TF.

$$\varepsilon_\lambda^{mb} = \varepsilon_\lambda^{f} + \frac{\varepsilon_\lambda - \varepsilon_\lambda^{f}}{f_b} \quad (5)$$

where ε_λ^{mb} is the apparent molar absorption coefficient of the mixture of bound-dye species at a wavelength of λ. For each dye–NaPP system, the mixed spectrum of bound dyes, ε_λ^{mb}, was calculated at the minimum point of the observed $(1-f_b)_\lambda$ *vs.* P/D curve (dashed line in Fig. 4), where no isosbestic point exists. The results are shown for the bound CV and TF in Figs. 5(a) and (b), respectively. Figure 5 shows that the separation between the Meta S and L bands of the mixed spectrum of multiple bound-dye species is apparently narrower than that of the corresponding pure spectrum of a single bound-dye species obtained in the low P/D range (*cf.* Fig. 3), and that the values of ε_λ^{mb} are generally greater than those of ε_λ^{b} in the wavelengths where the peak of the spectrum of free dye is located.

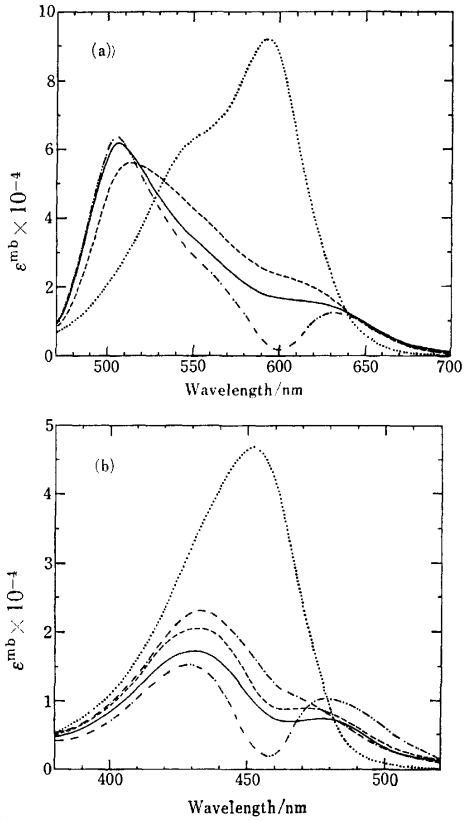

Fig. 5. The mixed bound-spectra of CV (a) and TF (b) calculated at the minimum values of P/D in the $(1-f_b)_\lambda$ *vs.* P/D curves in Fig. 4. CV–NaPP(154) and TF–NaPP(216) at $P/D=3$ (——), CV- and TF–NaPP(24) at $P/D=4$ (– – –), and CV- and TF–NaPP(11) at $P/D=10$ (–·–·–). Pure absorption spectra of a single bound-dye species obtained in the low P/D region (–··–··–) and the respective free dyes (·····) are also shown.

Discussion

Absorption Spectra of Bound CV and TF. The peaks or shoulders of the pure spectra of the bound CV or TF (at 506, 550, and 630 nm for CV, and at 428 and 480 nm for TF) are independent of the chain length of NaPP (Figs. 3(a) and (b)). On the other hand, the values of ε_λ^{b} for the metachromasy bands vary slightly with the chain length of the NaPP to which CV or TF is bound. However, their difference is probably due to the experimental errors, which include the readout of a series of overlapping spectra.[11] Hence, together with the fact that the isosbestic points exist at the constant wavelengths for all the families of the absorption spectra of either CV or TF in the presence of NaPP with the varying value of $\bar{n}$, the spectrum of bound CV or TF can now be concluded to be independent of the chain length of the NaPP samples ($\bar{n}=11$—154) in the low P/D range of 0—*ca.* 2. This conclusion excludes, at least in the low P/D range, one of two possible hypotheses: that the "flexibility" of the polymer backbone, to which dyes are bound, is responsible for the origin of metachromasy.[2]

Shirai *et al.*[9] investigated the metachromasy of Methylene Blue in the presence of potassium poly(ethylene sulfate)s which were different in the degree of sulfation. The metachromasy band of Methylene Blue shifted to the longer wavelength region with the decrease in the degree of sulfation of the polyanion. In the previous report,[4] the position of the metachromasy band was shown to vary considerably with the conformation of polyanion, even if their residue structures are identical or closely related. This situation is especially remarkable in the dye–NaPP and –DNA systems in which the peak positions of the metachromasy bands of bound CV (and also TF) are different, although both NaPP and DNA have the ionized phosphate residues as the binding site for those dyes. On the other hand, the positions of the metachromasy bands of bound CV and TF do not vary with the chain length of NaPP's, each of which has the identical backbone structure and binding site for dyes (Fig. 3). These results all lead to the conclusion that the peak positions of the metachromasy bands of a metachromatic dye depend on the local conformation of the binding site of polymers. It is also reasonable to conclude that the configuration of the π electrons of the bound dye may be affected by the mean distance between the binding sites of a particular polyanion.

Empirical Parameter α and Sigmoidal Titration Curve. As shown in Figs. 2(a) and (b), the ε_λ and $(1-f_b)_{\kappa,\alpha}$ decrease sigmoidally with the increase in P/D from zero to about one in all cases. The empirical parameter α was introduced to reproduce a sigmoidal or monotonous titration curve.[4] Schwarz[12] proposed a theory for the binding of a dye to a linear lattice in which cooperative interaction is restricted to the nearest neighbor binding sites. Subsequently, Schwarz *et al.*[15,16] applied the theory to the monotonous titration curves of some Proflavine-polyanion systems and determined the cooperative binding constant and the parameters, g (the number of the binding sites per segment of polymer) and q (a factor measuring the strength of cooperativity). However, it is obvious that the sigmoidal titration curve cannot be reproduced by using those parameters q and g, which are assumed to be constant for a given dye–polyanion system. The sigmoidal titration curve means that the binding of dye is inhibited near the limiting P/D value ($P/D=0$), and gradually

accelerated with the increase in P/D, whereas a monotonous one means that the binding of dye is either independent of P/D or retarded with the increase in P/D. In Schwarz's theory, the titration curves with $q>1$ indicate positive cooperativity, while those with $q<1$ indicate negative cooperativity. Therefore, the following qualitative relations may be summarized between the empirical parameter α and Schwarz's cooperative parameter q: (i) for $\alpha>1$ (sigmoidal), the parameter q increases continuously with increasing P/D, which contradicts Schwarz's assumption that q is a constant; (ii) for $\alpha=1$ (monotonous), the q is constant; and (iii) for $\alpha<1$ (monotonous), the q decreases continuously with increasing P/D, which also contradicts his assumption.

Binding Curves. The binding curves (solid lines) shown in Figs. 2(a) and (b) reveal that the fraction of the bound dye increases at a low P/D value with the increase in the chain length of NaPP. On the other hand, the spectra of bound CV and TF are independent of the chain length of NaPP in the same low P/D range ($P/D<ca.$ 2) where a single bound-dye species exists. Since the ε_λ is related to the fraction of bound dye by Eq. 3, the dependence of the observed metachromasy on the chain length of NaPP in the low P/D range can be attributed to the difference in the fraction of CV (or TF) bound to the NaPP with different chain lengths. This view is supported from the fact that the $(1-f_b)_{\kappa,\alpha}$ *vs.* P/D curves coincide with the points of various symbols in Figs 4(a) and (b).

The result that the fraction of bound CV and TF varies with the chain length of NaPP is an interesting problem. Schindewolf[13] reported that the degree of dissociation of the Na^+ counter-ion from NaPP decreases sharply with the increase in the chain length in aqueous solution. Kielman and Leyte[14] measured the longitudinal relaxation time, T_1, of the $^{23}Na^+$ ion in NaPP solution by NMR. Since the value of $(T_1)^{-1}$ can be related to the amount of the bound and free Na^+ ions, its sharp increase clearly indicates that the amount of the bound Na^+ ions increases with the increasing chain length of NaPP up to $\bar{n}\approx 60$. Two alternative views on the binding mechanism of a dye to NaPP are considered below.

The first view is that the dye competes with the Na^+ ion upon binding to NaPP. The aforementioned results suggest that larger amounts of both the dye and Na^+ ion are bound to the NaPP with the longer chain length. If both the dye and Na^+ ion are bound to NaPP by the electrostatic force, and if the force becomes stronger with the increase in the chain length of NaPP, the dye would compete with the Na^+ ion in binding to the ionized group of NaPP in the low P/D range. In order to examine the competitive binding between the dye and Na^+ ion to NaPP, the concentration of the free counter-ion has to be measured in the presence of dye. The second view is that the counter-ion Na^+ participates in the formation of a dye–polymer site complex directly, as is described by Eq. 13 of Ref. 4, or indirectly, as is indicated by Eq. 1 in this work. The direct participation of the Na^+ ion in the binding between a cationic dye and an ionized phosphate residue of NaPP may be examined by means of electrophoresis of the dye–NaPP solution. On the other hand, the indirect participation of the Na^+ ion (*e.g.*, the charge neutralization of the nearest neighbor phosphate residue) may be studied by the potentiometric[17] and conductometric[2,3] measurements. Certainly these are the interesting subjects to be investigated in detail.

The experimental points (various symbols) in Figs. 4(a) and (b) begin to deviate from the calculated binding curves (solid lines), as the P/D value reaches about 2 to 3. When the curves approach zero, the points ascend again in the higher P/D range, as if the dye were dissociating from NaPP. Concurrently the isosbestic points disappear in the absorption spectra as the P/D becomes larger than about 2—3; that is, there are three or more dye species in a dye–NaPP solution. The ultrafiltration of TF–NaPP(216) has verified that TF is still bound to NaPP at a high P/D value of 1000.[3] Furthermore, the new isosbestic points appear at 636 nm for CV and at 374 and 479 nm for TF in the P/D range higher than *ca.* 30. Thus, it is concluded that there are probably two kinds of bound-dye species in this P/D range. As a consequence, the experimental binding curves (dashed lines) may be classified into three P/D ranges: (i) the low P/D range of 0—near 2 where free dye and only one type of the bound-dye species are present, (ii) the intermediate P/D range of 2—30 where the free and two or more types of bound-dye species are present, and (iii) the high P/D range where two or more types of bound-dye species are present probably without the free dye.

The change of the absorption spectrum with P/D in the high P/D range may be due to the redistribution of the bound-dye species on polymer sites as the sites increase relative to the bound dye. Although many authors[12,18-20] have treated statistically the redistribution of bound dyes on a polyelectrolyte chain assuming an infinitely long chain length, there remain many questions to be answered, *e.g.*, the number and absorption spectra of bound-dye species and the scheme for the redistribution of the bound-dye species on a single (or multiple) polymer chain of finite length. The application of the extended PCA method to the precise experimental data covering a wide P/D range will shed light on these problems.

The Mixed Bound-spectrum. The mixed spectrum of bound-dye species (Figs. 5(a) and (b)) may be composed of two or more absorbing components, one of which is present in the low P/D range. The bound-dye species newly appearing in the intermediate and high P/D ranges should show an absorption spectrum in which the separation between the Meta S and L bands is small. If the energy separation between the two bands is directly proportional to the perturbation of the π electronic system of bound CV or TF resulting from the interaction between the dye and the polymer site or between the bound dyes themselves, such perturbation may be smaller in the intermediate and high P/D ranges than in the low P/D range possibly because of the redistribution of the bound dyes on the polymer.

From the fact that the pure spectra of a single CV or TF species in the low P/D range are independent

of the chain lengths of NaPP (Fig. 3), the difference in the mixed spectra of the multiple CV or TF species (Fig. 5) should result from the polyelectrolyte property of NaPP. In other words, the chain lengths of those NaPP samples ($\bar{n}$=216, 154, 64, 24, and 11) may be responsible for the formation of the bound dye species with the varying types upon the possible redistribution on the polymer sites with the increase in P/D. The effect of the chain length of NaPP on the metachromatic behavior of CV and TF[2,3] is now confirmed quantitatively to originate from a complicated interplay between the free dye and two or more bound-dye species. That is, the pronounced changes in the ε_λ *vs.* P/D curves given in Figs. 3 and 5 of Ref. 1, in Fig. 3 of Ref. 2, and in Fig. 3 of Ref. 3, and the $(1-f_b)_\lambda$ *vs.* P/D curves in Fig. 4 of this work should result from the variation of the relative amounts not only between free and a single bound-dye species (P/D=0—*ca.* 2) but also between multicomponent bound-dye species ($P/D \geq 2$) themselves. Since the extended PCA method is powerful in the multicomponent system,[4] its application to the series of the absorption spectra of the metachromatic dye–polyelectrolyte system over an entire P/D range should yield information leading to the fuller understanding of metachromasy.

Conclusion

The dependence of the chain length of NaPP on metachromasy of CV and TF was quantitatively clarified for the first time. The equilibrium constant, an empirical parameter, α, and the pure absorption spectra of the bound CV and TF species were determined by the PCA method. Both the equilibrium constant and the value of α depend on the chain length of NaPP, while the pure spectra of bound CV and TF are independent of it. Two or more of the bound-dye species should exist over the entire P/D range. From the profiles of the mixed spectra of the multiple bound-dye species, the effect of the chain length of NaPP on metachromasy was concluded to be such that the redistribution of the bound dyes would be promoted with the increase in the chain length.

References

1) K. Yamaoka, T. Suenaga, A. Fujita, and M. Miura, *J. Sci. Hiroshima Univ., Ser. A*-II, **34**, 1 (1970).
2) K. Yamaoka, M. Takatsuki, K. Yaguchi, and M. Miura, *Bull. Chem. Soc. Jpn.*, **47**, 611 (1974).
3) K. Yamaoka, M. Takatsuki, and M. Miura, *Bull. Chem. Soc. Jpn.*, **48**, 2739 (1975).
4) K. Yamaoka and M. Takatsuki, *Bull. Chem. Soc. Jpn.*, **51**, 3182 (1978).
5) B. C. Myhr and J. G. Foss, *Biopolymers*, **10**, 425 (1971).
6) W. H. J. Stork, J. A. M. Van Boxsel, A. F. P. M. De Goeij, P. L. De Haseth, and M. Mandel, *Biophys. Chem.*, **2**, 127 (1974).
7) V. Vitagliano, L. Costantino, and R. Sartorio, *J. Phys. Chem.*, **80**, 959 (1976).
8) J. S. Tan and R. L. Schneider, *J. Phys. Chem.*, **79**, 1380 (1975).
9) M. Shirai, T. Nagatsuka, and M. Tanaka, *Chem. Lett.*, **1976**, 291.
10) M. Shirai, T. Nagatsuka, and M. Tanaka, *Makromol. Chem.*, **178**, 37 (1977).
11) M. Takatsuki and K. Yamaoka, *J. Sci. Hiroshima Univ., Ser. A*, **40**, 387 (1976).
12) G. Schwarz, *Eur. J. Biochem.*, **12**, 442 (1970).
13) U. Schindewolf, *Z. Phys. Chem.*, **1**, 134 (1954).
14) H. S. Kielman and J. C. Leyte, *J. Phys. Chem.*, **77**, 1593 (1973).
15) G. Schwarz, S. Klose, and W. Balthasar, *Eur. J. Biochem.*, **12**, 454 (1970).
16) G. Schwarz and S. Klose, *Eur. J. Biochem.*, **29**, 249 (1972).
17) F. Watanabe, *Bull. Chem. Soc. Jpn.*, **49**, 1465 (1976).
18) D. F. Bradley and M. K. Wolf, *Proc. Natl. Acad. Sci. U.S.A.*, **45**, 944 (1959).
19) V. Vitagliano, L. Costantino, and A. Zagari, *J. Phys. Chem.*, **77**, 204 (1973).
20) T. Soda and K. Yoshioka, *Nippon Kagaku Zasshi*, **87**, 22 (1966).

Dual Fluorescence and Excited-state Double Proton Transfer in the Dimer of 3,5-Dialkyl-4-hydroxybenzylidenemalononitrile

Michiya Itoh,* Kenji Inoue, Tomoko Kuzuhara, and Tomoko Kusui
Faculty of Pharmaceutical Sciences, Kanazawa University, Takara-machi, Kanazawa 920
(Received October 24, 1978)

Dual fluorescence of the dimer of 3,5-dialkyl-4-hydroxybenzylidenemalononitrile (HO-BMN) was investigated by steady-state and nanosecond fluorescence spectroscopies. The dimerization of the compounds in 3-methylpentane (MP) solution was confirmed by concentration dependence of absorption and fluorescence spectra at low temperature (<150 K). While the MP solutions of the compounds are almost non-fluorescent at room temperature, the dimer exhibits a short-lived fluorescence (τ=4—9 ns) at 450—520 nm and a long-lived fluorescence (τ=21—34 ns) at 490—550 nm. The short-lived fluorescence was ascribed to a sandwich type dimer (D*) with a center of symmetry. An orientational relaxation leading to the double proton transfer reaction seems to occur in the excited state of the dimer. The long-lived fluorescence in the dimer was tentatively ascribed to the excited species (T*) generated by the double proton transfer reaction in D*. The excited-state proton transfer is discussed in terms of the effect of deuterium substitution of a 4-hydroxyl hydrogen upon fluorescence lifetimes of the dimer.

Taylor *et al.*,[1] and Ingham and El-Bayoumi[2] reported extensive studies of the hydrogen-bonded dimer formation in 3-methylpentane (MP) of 7-azaindole and the photoinduced double proton transfer reaction in the excited state of the dimer at low temperature. They observed a weak dimer fluorescence and a strong tautomer fluorescence generated by the double proton transfer reaction in the excited state. On the other hand, numerous investigations of dual fluorescence of aromatic hydrocarbons in nonpolar solvents consisting of the dimer and excimer fluorescence were reported.[3-5]

Recently, 3,5-dialkyl-4-hydroxybenzylidenemalononitrile (HO-BMN) was reported to be an active uncoupler of the oxidative phosphorylation,[6] and to show a remarkable pH dependence of absorption spectra.[7] The HO-BMN molecule exhibits an absorption band at 350—360 nm and a very weak fluorescence (almost non-fluorescent) in such a nonpolar solvent as MP. In strong hydrogen-bonding solvents, however, a proton transfer occurs from 4-hydroxy group to a proton acceptor to form an anion form of HO-BMN which reveals an absorption band at 450—460 nm and a corresponding fluorescence at 480—500 nm. Similar highly polar molecule, 3,5-dialkyl-4-methoxybenzylidenemalononitrile (MO-BMN) in MP solution exhibits very similar absorption band at 330—350 nm to that of the corresponding HO-BMN (a neutral form).[8] In MO-BMN, however, neither absorption (450—460 nm) nor fluorescence (480—500 nm) due to the anion form of HO-BMN was detected in such a highly polar solvent as alcohol. Recently, Itoh, *et al.*[9] reported the crystal structure of 3,5-di-*t*-butyl-4-hydroxybenzylidenemalononitrile (*t*-Bu_2-HO-BMN), and the excited-state proton transfer in the crystals. The crystalline *t*-Bu_2-HO-BMN exhibits a strong green fluorescence at 490—500 nm at low temperature, which was ascribed to the excited-state proton transfer between *t*-Bu_2-HO-BMN molecules in the crystals.

This paper describes the dimer formation of HO-BMN in the ground state in MP solution at low temperature, and dual fluorescence consisting of a short-lived fluorescence at 450—520 nm and a long-lived one at 490—550 nm. The former fluorescence in HO-BMN is ascribed to the dimer (D*) of the compound. The latter fluorescence is attributable to the excited species (T*) generated by the double proton transfer reaction in the excited state of the dimer,[10] while in MO-BMN to the excimer-type dimer by an orientational relaxation in D* as reported previously.[8] By taking account of the crystal structure, the structure of the dimer is proposed to be a sandwich-type dimer with a center of symmetry as follows:

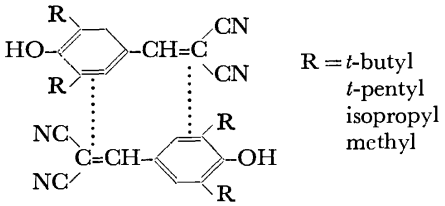

The dimer formation of these compounds seems to be attributable to an exciton interaction as well as a charge-transfer (CT) interaction between two component molecules in the dimer. Here, an orientational relaxation leading to the double proton transfer reaction maybe occur in the excited state of the dimer. In the HO-BMN dimer, the effect of deuterium substitution of a 4-hydroxyl hydrogen upon fluorescence lifetimes of the dimer (D*) was observed. The excited-state double proton transfer in the HO-BMN dimer is discussed in comparison with the orientational relaxation in the excited state of the MO-BMN dimer.

Experimental

At the initial stage of the experiment, 3,5-di-*t*-butyl-4-hydroxybenzylidenemalononitrile was given by Prof. Y. Anraku (Department of Botany, The University of Tokyo). All of 3,5-dialkyl-4-hydroxybenzylidenemalononitrile were prepared by known procedures.[11] Pure samples were obtained by chromatography and recrystallization before use. Deuterium substitution of 4-OH hydrogen was performed by CH_3OD (CEA, deuterium grade 99.0%) in a vacuum system. After removing CH_3OD, 3-methylpentane was added through a vacuum system. Proton NMR gave an isotope purity of approximately 85—90%.

Solutions of samples were contained in rectangular quartz cells (1 cm) equipped with graded seals, and degassed by freeze-thaw cycles (several times) at 10^{-5} Torr. All of the

optical absorption and fluorescence spectra were recorded by Hitachi 323 and MPF-4 spectrophotometers. Determination of their spectra at several temperatures was carried out by the method described previously.[12] The fluorescence lifetimes were determined by analyzing exponential decay curves measured by an oscilloscope, and by a coaxial N_2 laser as described previously,[13] and analyzed by a deconvolution method.[14]

Results and Discussion

Dimer Formation in the Ground State. The MP solution of *t*-Bu_2-HO-BMN shows an absorption band in the 340—360 nm region at room temperature, while shows considerable red-shift at low temperature (<150 K) as shown in Fig. 1. Figure 2 shows concentration dependence of absorption spectra of MP solutions of *t*-Bu_2-HO-BMN at 77 K. Here, a monomer-dimer equilibrium of *t*-Bu_2-HO-BMN in MP solution is assumed, and an association constant (K) can be written as follows:

$$K = [D]/([C]-2[D])^2,$$

where [C] and [D] are concentrations of the monomer and dimer. If an absorption band at 400 nm is assumed to be owing to the dimer as shown in Fig. 2, an absorbance (A) at 400 nm is expressed as $A=\varepsilon[D]l$, where ε is a molar extinction coefficient at this wavelength, and l is a light-path length. The following equation is obtained;[2,15]

$$[C]/A = 2/\varepsilon + (1/\varepsilon K)^{1/2}(1/A)^{1/2}.$$

An MP solution of considerable concentration of *t*-Bu_2-HO-BMN exhibits a strong green fluorescence at 77 K as shown in Fig. 1, while the solution is almost non-fluorescent at room temperature. Figure 1 also shows the fluorescence spectrum of this compound in 2-methyltetrahydrofuran (MTHF) at 77 K. The MTHF solution exhibits no significant temperature dependence of fluorescence and absorption spectra.[16] The green fluorescence in the MP solution markedly increases and a fluorescence spectrum at 400—430 nm decreases in intensity with increasing concentration of *t*-Bu_2-HO-BMN, as shown in Fig. 3. The excitation spectrum of the former fluorescence corresponds to an absorption band at 390 nm, while that of the latter to a band at 350—360 nm. Then, the fluorescence at 400—430 nm is tentatively ascribed to the monomer and the green one to the dimer of *t*-Bu_2-HO-BMN.[17] Intensity (I) of the green fluorescence may be proportional to the concentration of the dimer [D], though the green fluorescence consists of a short-lived fluorescence (D*) and a long-lived one (T*) as will be mentioned later. Therefore, the following equation is obtained for the monomer-dimer equilibrium;

$$[C]/I = 2/q + (1/qK)^{1/2}(1/I)^{1/2},$$

where q is a constant including several experimental factors. Plots of [C]/A and [C]/I exhibit linear relationship against $(1/A)^{1/2}$ and $(1/I)^{1/2}$, respectively, as

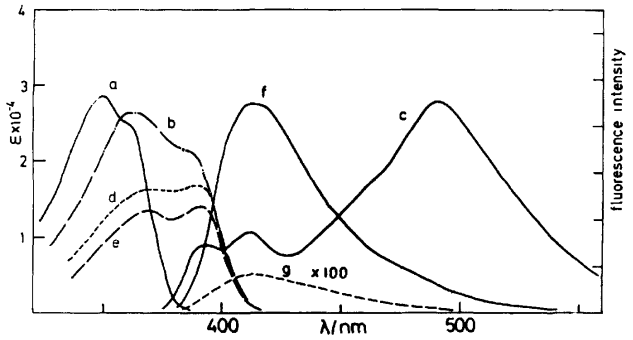

Fig. 1. Absorption spectra of an MP solution (concentration, 6×10^{-5} M) of *t*-Bu_2-HO-BMN at room temperature (a) and at 77 K (b). Fluorescence spectra of an MP solution (concentration, 2×10^{-6} M) of *t*-Bu_2-HO-BMN at 77 K excited at 360 nm (c) and the excitation spectra monitored at 455 nm (d) and at 530 nm (e). Fluorescence spectra of an MTHF solution of *t*-Bu_2-HO-BMN at 77 K (f) and at room temperature (g) (concentration, 2×10^{-6} M).

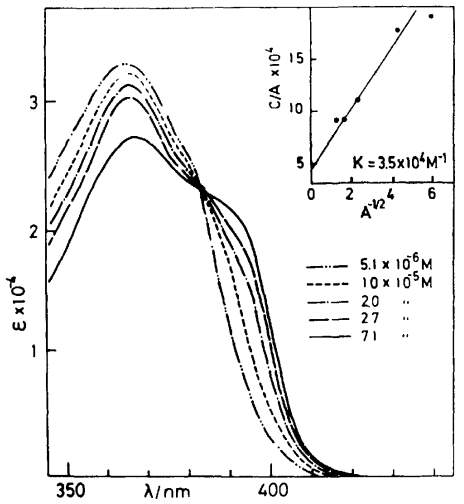

Fig. 2. Concentration dependence of absorption spectra of MP solutions of *t*-Bu_2-HO-BMN at 77 K, and plots of [C]/A *vs.* $A^{-1/2}$ (A, monitored at 400 nm).

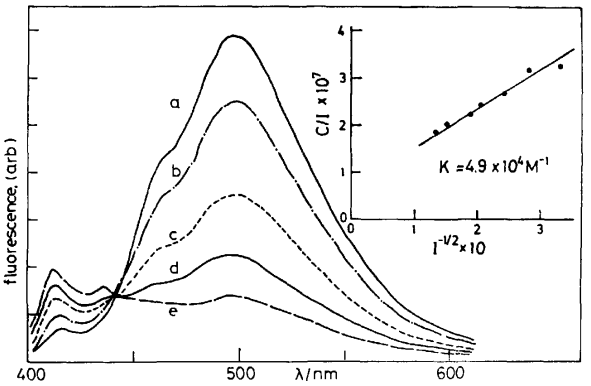

Fig. 3. Concentration dependence of fluorescence spectra of MP solutions of *t*-Bu_2-HO-BMN at 77 K (excited at 360 nm); concentrations of the compound are 9.6×10^{-6} (a), 8.5×10^{-6} (b), 5.1×10^{-6} (c), 3.6×10^{-6} (d), and 2.4×10^{-6} M (e). Plots of [C]/I *vs.* $I^{-1/2}$ at 77 K (I, monitored at 520 nm).

Table 1. Fluorescence maxima and lifetimes of D* and T*, and the effect of deuterium substitution of a 4-OH hydrogen at 77 K
Equilibrium constants for the dimerization of dialkyl HO-BMN (MO-BMN) in MP at 77 K.

Dialkyl HO-BMN	λ_{max}/nm[a]		τ/ns[b]		K/M^{-1}
	D*	T*	D*	T*	
t-Pe$_2$-HO-BMN	470	510	6(9)	34(34)	5.1×10^{4}[c]
t-Bu$_2$-HO-BMN	470	500	6(7—8)	32(32)	3.5×10^{4}[c]
i-Pr$_2$-HO-BMN	510	530	8(9)	25(25)	4.9×10^{4}[d]
Me$_2$-HO-BMN	515	547	7(8)	34(34)	1.6×10^{5}[e]
Me$_2$-MO-BMN[f]	490	505	4	21	4.8×10^{4}

a) Determined by time-resolved fluorescence spectra, error approximately ±5 nm. b) Determined by a computer deconvolution. Data in parenthese are those of the deuterium substituted samples of HO-BMN, error approximately ±5%. c) Determined by absorption spectra, monitored at 400 nm. d) Determined by absorption spectra, monitored at 410 nm. e) Determined by fluorescence spectra, monitored at 520 nm. f) Ref. 9.

shown in Figs. 2 and 3. Two straight lines confirm an assumption of the monomer-dimer equilibrium, and afford equilibrium constants; $K=4.9\times10^{4}$ M^{-1} from plots of the fluorescence spectra and $K=3.5\times10^{4}$ M^{-1} from those of the absorption spectra. Concentration dependence of absorption and fluorescence spectra of other alkyl HO-BMN in MP solutions also reveals the dimer formation at low temperature, whose equilibrium constants are summarized in Table 1. The absorption spectra of several concentrations of 3,5-dimethyl-4-methoxybenzylidenemalononitrile (Me$_2$-MO-BMN) in MP solutions at 77 K were reported to indicate the dimer formation of this compound. The equilibrium constant is also shown in Table 1 in comparison. An MP solution of Me$_2$-MO-BMN exhibits a strong green fluorescence in 460—500 nm at 77 K consisting of short and long components of decay. The former and the latter were ascribed to the dimer and the excimer fluorescence, respectively, as reported in the previous paper.

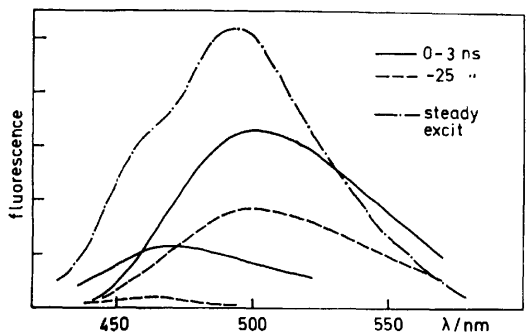

Fig. 4. A steady-state fluorescence and time-resolved fluorescence spectra of an MP solution of t-Bu$_2$-HO-BMN (3×10^{-5} M) at 77 K, which were depicted by a deconvolution method. The time indicated is virtually after a signal maximum of the fluorescence.

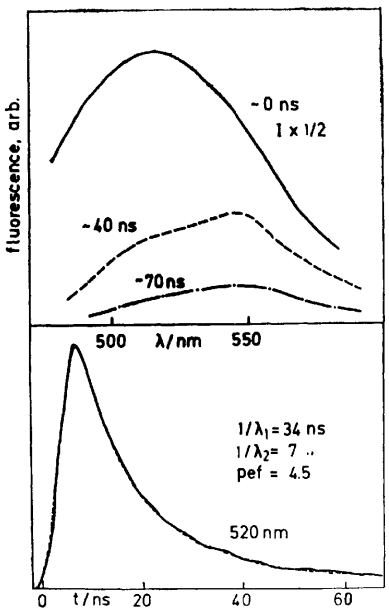

Fig. 5. Time-resolved fluorescence spectra and time evolution of fluorescence (at 520 nm) of an MP solution of Me$_2$-HO-BMN at 77 K; (——) and (– – –) are observed and simulated decay curves based on the obtained time constants and pre-exponential factor (pef), respectively. The time indicated in the time-resolved fluorescence spectra is virtually after a signal maximum of the fluorescence.

Excited-state Double Proton Transfer in HO-BMN Dimer. Nanosecond time-resolved fluorescence spectra of an MP solution of t-Bu$_2$-HO-BMN at 77 K shown in Fig. 4 demonstrate that the green fluorescence consists of two fluorescence spectra; a short-lived fluorescence ($\tau_D=6$ ns, $\lambda_{max}=470$ nm) and a long-lived fluorescence ($\tau_T=32$ ns, $\lambda_{max}=500$ nm). The dual fluorescence of the dimer was also observed in other dialkyl HO-BMN (3,5-di-t-pentyl, 3,5-diisopropyl- and 3,5-dimethyl HO-BMN). Figure 5 shows time-resolved fluorescence spectra and decay curve of an MP solution of Me$_2$-HO-BMN at 77 K. Table 1 summarizes the fluorescence maxima determined by time-resolved fluorescence spectra and lifetimes in the dimers of these compounds at 77 K. The excitation spectra of the short-lived and long-lived fluorescence are identical each other, and corresponding to the dimer absorption band. The spectral behavior in the case of t-Bu$_2$-HO-BMN is shown in Fig. 1. From the large Stokes shift of the long-lived fluorescence, the fluorescence may be tentatively ascribed to the excited species (T*) generated from the excited state of the HO-BMN dimer (D*), while the short-lived one to the dimer.

The photochemical reaction scheme of the excited state of the dimer (D*), and the excited species T* generated from D* is as follows:

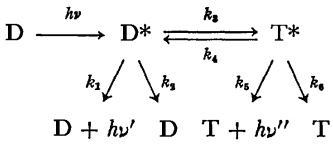

Time-depedent concentrations of D* and T* are ex-

pressed by the following equations;[18,19]

$$[D^*] = c_1 \exp(-\lambda_1 t) + c_2 \exp(-\lambda_2 t), \quad (1)$$

$$[T^*] = c_3 \exp(-\lambda_1 t) - c_3 \exp(-\lambda_2 t), \quad (2)$$

$$\lambda_{1,2} = \frac{1}{2}[k_1+k_2+k_3+k_4+k_5+k_6 \mp (\{k_1+k_2+k_3-(k_4+k_5+k_6)\}^2+4k_3k_4)^{1/2}].$$

Since two fluorescence decay curves of D* and T* at a certain wavelength overlap each other, actual decay curves at several wavelengths were analyzed by the following equation:

$$[D^*] + [T^*] \propto \exp(-\lambda_1 t) + (c_2-c_3)\exp(-\lambda_2 t)/(c_1+c_3).$$

Here, if $k_3 \gg k_4$, and k_4 is negligible, fluorescence lifetimes of D* and T* were determined to be 6 ns and 32 ns from λ_2 and λ_1, respectively. If a pre-exponential factor (pef), $(c_2-c_3)/(c_1+c_3)$ is obtained to be negative, T* should show the fluorescence rise. Unfortunately, the fluorescence rise of T* was not significant as shown in Fig. 6, because the D* fluorescence overlaps on the decay curve of T* even at 600 nm.

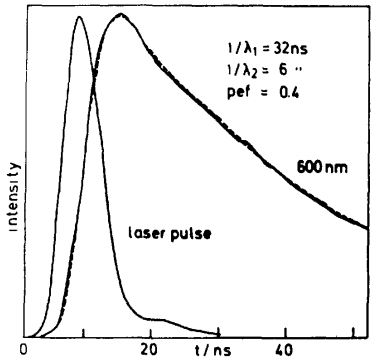

Fig. 6. Time evolution of fluorescence observed at 600 nm of an MP solution of *t*-Bu_2-HO-BMN at 77 K, and a computer simulation (-----) from time constants and pre-exponential factor obtained (concentration, 2×10^{-5} M).

The crystal structure of *t*-Bu_2-HO-BMN demonstrated that the molecule is almost planar and packed along the b axis with a spacing of 3.69 Å in a monoclinic unit cell, as reported in a previous paper.[9] Two molecules packed along the b axis are considered to be a sandwich-type dimer with a center of symmetry. Therefore, the structure of the dimer in solution may be similar to that in the crystals. In the excited state of the dimer, an orientational relaxation maybe occur eeading to the formation of the excited species T*. Here, it is likely that the double proton transfer reaction is involved in the orientational relaxation in the excited state of the dimer. On the other hand, there seems to be a possibility that the excited species T* might be ascribed to an ordinary excimer-type dimer, where no proton transfer is involved. However, this was excluded by the effect of deuterium substitution of a 4-OH hydrogen of HO-BMN upon fluorescence lifetimes of D*. Fluorescence lifetimes of D* and T* in several dialkyl HO-BMN and their deuterium substituted HO-BMN at 77 K were determined and analyzed by computer simulation mentioned above. The results are summarized in Table 1. All of fluorescence lifetimes of D* somewhat increase by deuterium substitution of 4-OH protons, while those of T* remain almost unaltered. The significant effects of deuterium substitution upon fluorescence quantum yield or proton transfer rate in 2-naphthol,[20] 2-naphthylamine, and carbazol[21] were reported by several investigators. El-Bayoumi and his coworkers[2,22] reported that the rate constant (k_3) of the double proton transfer in 7-azaindole dimer was decreased by deuterium substitution. In the excited-state proton transfer reaction reported here, increases of fluorescence lifetimes and pre-exponential factor (pef) mentioned above may be attributable to the effect of the deuterium substitution upon the proton transfer rate constant k_3.

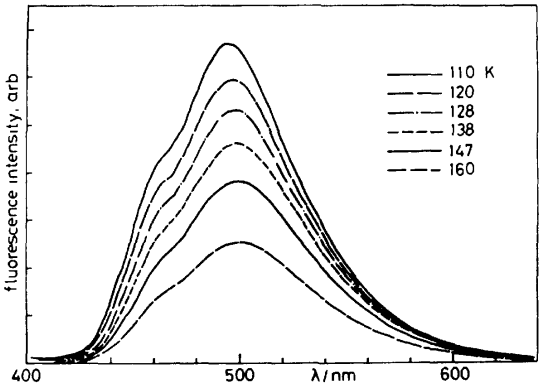

Fig. 7. Temperature dependence of fluorescence spectra of an MP solution of *t*-Bu_2-HO-BMN (concentration, 5×10^{-5} M) excited at 390 nm.

On the other hand, an MP solution of considerable concentration of *t*-Bu_2-HO-BMN reveals temperature dependence of fluorescence spectra, as shown in Fig. 7. The D* fluorescence at 450—490 nm decreases in intensity slightly more than the T* fluorescence at 480—550 nm with increasing temperature (77 K to 150 K). Since most of molecules are virtually present as dimers trapped in the MP matrix, and since no monomer fluorescence is detected under these conditions, the temperature dependence suggests that there seems to be very small activation barrier between these two fluorescent states. However, the energy was too small to be estimated from the fluorescence spectra. The fact is compared with the results in Me_2-MO-BMN (0.9 kcal mol^{-1}) reported previously.

The structure of the dimers of dialkyl-HO-BMN is conclusively considered to be a sandwich type with a center of symmetry from the crystal structure reported previously. The dimer formation of nonpolar molecules such as anthracene and tetracene may be attributable to the exciton interaction as well as the charge transfer (or charge resonance) interaction. In the highly polar molecules reported here, the charge transfer character between two component molecules in the dimer seems to increase in the excited state. Further, it is likely that an orientational relaxation from the short-lived dimer state to the fluorescent excimer occurs in the excited state. Here, the simultaneous double

proton transfer reaction leading to the formation of T* may occur in the orientational relaxation process in the excited state dimer of HO-BMN as follows:

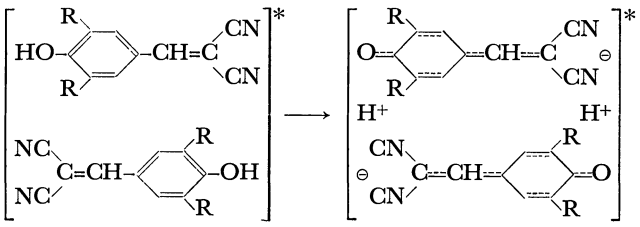

The effect of deuterium substitution of the 4-hydroxyl hydrogen upon fluorescence lifetimes of D* confirms the excited-state proton transfer reaction. On the other hand, the difference of fluorescence band maxima between D* and T* (E*) was observed to be somewhat greater in the HO-BMN dimer than in the MO-BMN dimer as seen in Table 1. Further, the activation barrier of D* to T* seems to be smaller in the HO-BMN system than that of D* to E* in the MO-BMN system, as mentioned above. These results of the fluorescence behavior are instructive for understanding of the electronic structure of T* as well as E*, though it is not obvious at this stage.

The authors wish to express their thanks to Professor S. Nagakura, The Institute for Solid State Physics, The University of Tokyo, for valuable discussion, and to Professor Y. Anraku, Department of Botany, The University of Tokyo, for samples of *t*-Bu_2-HO-BMN at the early stage of this work. They are also indebted to Drs. Y. Tanimoto and K. Fuke for valuable discussions and for computer deconvolutions. The work was partly supported by the Grant-in-Aid (#221611) of the Ministry of Education.

References

1) C. A. Taylor, M. A. El-Bayoumi, and M. Kasha, *Proc. Natl. Acad. Sci. U.S.A.*, **63**, 253 (1969).
2) K. C. Ingham and M. A. El-Bayoumi, *J. Am. Chem. Soc.*, **96**, 1674 (1974), and references therein.
3) J. Tanaka, *Bull. Chem. Soc. Jpn.*, **36**, 1237 (1963).
4) J. Ferguson, *J. Chem. Phys.*, **43**, 306 (1965).
5) N. Mataga and T. Kubota, "Molecular Interactions and Electronic Spectra," Marcel Dekker, New York, N. Y. (1970).
6) S. Muraoka and H. Terada, *Biochim. Biophys. Acta*, **275**, 271 (1972).
7) H. Terada, *Biochim. Biophys. Acta*, **387**, 519 (1975).
8) K. Inoue and M. Itoh, *Bull. Chem. Soc. Jpn.*, **52**, 45 (1979).
9) M. Itoh, Y. Tanimoto, and Y. Iitaka, *J. Chem. Phys.*, **69**, 816 (1978).
10) Preliminary results were presented in the 26th IUPAC Congress (Tokyo) Sept. 1977.
11) F. Horiuchi, K. Fujimoto, T. Ozaki, and Y. Nishizawa, *Agric. Biol. Chem.*, **35**, 2003 (1971).
12) M. Itoh, T. Mimura, H. Usui, and T. Okamoto, *J. Am. Chem. Soc.*, **95**, 4388 (1973); M. Itoh, *ibid.*, **96**, 7390 (1974).
13) T. Mimura and M. Itoh, *J. Am. Chem. Soc.*, **98**, 1095 (1976).
14) P. R. Berington, "Data Reduction and Error Analysis for the Physical Sciences," McGraw-Hill, New York (1969).
15) R. S. Mulliken and W. B. Person, "Molecular Complexes, A Lecture and Reprint Volume," Wiley-Interscience, New York (1970).
16) Although the complex formation in the weak electron donor-acceptor system was observed in such a nonpolar solvent as MP and methylcyclohexane, no complex formation was detected in MTHF and in acetonitrile (see Ref. 12).
17) Dialkyl HO-BMN in the MP solution exhibits very weak fluorescence at low temperature, while almost no fluorescence at room temperature.
18) J. B. Birks, "Photophysics of Aromatic Molecules," Wiley-Interscience, New York (1970).
19) W. R. Ware, D. Watt, and J. D. Holmes, *J. Am. Chem. Soc.*, **96**, 7853 (1974).
20) T. Kishi, J. Tanaka, and T. Kouyama, *Chem. Phys. Lett.*, **41**, 497 (1976); **46**, 383 (1977).
21) L. Stryer, *J. Am. Chem. Soc.*, **88**, 5708 (1966).
22) M. A. El-Bayoumi, P. Avouris, and W. R. Ware, *J. Chem. Phys.*, **62**, 2499 (1975).

Far-infrared Spectra of Low- and High-temperature Phases of $CsCuCl_3$

Kenji AKIYAMA, Yoshiyuki MORIOKA, and Ichiro NAKAGAWA*

Department of Chemistry, Faculty of Science, Tohoku University, Aoba, Aramaki, Sendai 980

(Received November 1, 1978)

Polarized far-infrared reflection spectra of the $CsCuCl_3$ single crystal have been recorded with the electric vector parallel and perpendicular to the c axis at room temperature. Polarized far-infrared transmission spectra have been measured at liquid-nitrogen temperature. The observed spectra have been interpreted using the factor group analysis based on the space group D_6^2. Far-infrared transmission spectra of the powder sample have also been measured over the temperature range from 175 °C to liquid-nitrogen temperature. The spectrum at 175 °C consists of five bands and reveals a typical feature characteristic of the $CsNiCl_3$ structure (D_{6h}^4). The spectral change due to the phase transition has been interpreted based on the structural distortion of the crystal.

A number of double salts of the AMX_3 type, where A and M are univalent and divalent metal ions, respectively, and X is a halogen ion, crystallize in a hexagonal $CsNiCl_3$ structure with the space group D_{6h}^4-($P6_3/mmc$).[1] Almost all of these crystals do not undergo a phase transition down to liquid helium temperature, with the exception of $CsCuCl_3$. $CsCuCl_3$ transforms from the high-temperature $CsNiCl_3$ structure to a more complex one around 423 K[2-4]. According to the crystal structural analysis of the low-temperature phase of $CsCuCl_3$, the displacement of the atoms caused by the phase transition at 423 K can be expressed as the helical distortion around the c axis of the high-temperature structure. In relation to that remarkable structural change of $CsCuCl_3$, the studies on the optical activity, the X-ray and neutron scattering, the dielectric constant and the sound velocity have been made.[5]

From the vibrational spectroscopic point of view, the spectral change at the transition temperature and the relation between the high- and low-temperature spectra are interesting. The infrared spectrum of $CsCuCl_3$ reported so far has been limited to the transmission spectrum of the polycrystalline sample at room temperature by McPherson and Chang.[6] In their study the high-temperature spectrum and the spectral change due to the phase transition have not been remarked. The present paper reports the results of the polarized far-infrared transmission and reflection spectra of a single crystal for the low-temperature phase. The Raman spectrum at low temperature is given as complementary data. The far-infrared transmission spectra of the powder sample have been measured at various temperatures in the range from 175 °C to liquid-nitrogen temperature in order to persue the spectral change due to the structural phase transition.

Crystal Structure and Factor Group Analysis

The structure of the high-temperature phase of $CsCuCl_3$ is the $CsNiCl_3$ type, for which the details of the structure and the factor group analysis are described in our previous paper.[7] The structure of the low temperature phase is a helically distorted structure of the $CsNiCl_3$ structure, with the space group D_6^2 ($P6_122$) or its enantiomorph D_6^3 ($P6_522$), with six formula units in a Bravais primitive cell, as shown in Fig. 1.[8] The factor group for both of the D_6^2 and D_6^3 groups is isomorphous to the point group D_6 and the result of the factor group analysis is summarized in Table 1.

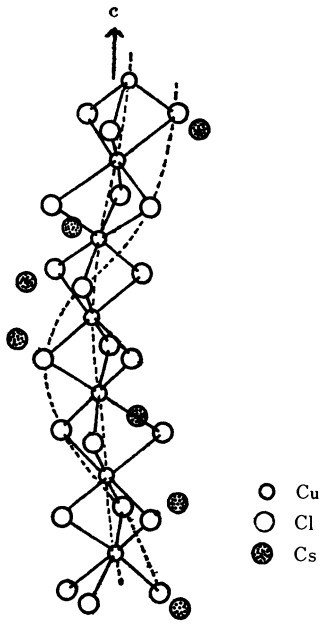

Fig. 1. Crystal structure of the low-temperature phase of $CsCuCl_3$.

TABLE 1. FACTOR GROUP ANALYSIS FOR THE LOW-TEMPERATURE PHASE OF $CsCuCl_3$

D_6	N[a]	T[b]	$N-T$[c]	Activity[d]
A_1	6	0	6	r(XX+YY, ZZ)*
A_2	9	1	8	ir(Z)
B_1	7	0	7	
B_2	8	0	8	
E_1	15	1	14	r(XZ, YZ), ir(X, Y)
E_2	15	0	15	r(XX−YY, XY)

a) Total freedom. b) Acoustic modes. c) Optically active modes. d) r: Raman active modes, ir: infrared active modes.
* X and Y axes are perpendicular, and a Z axis is parallel to the crystallographic c axis, respectively.

Experimental

The powder sample of $CsCuCl_3$ was obtained by evaporation of the hot concentrated aqueous solution of CsCl and

$CuCl_2 \cdot 2H_2O$ in a 1 : 1 mole ratio or in a slight excess of $CuCl_2 \cdot 2H_2O$. The single crystal was grown from a saturated aqueous solution by the temperature difference method. The hexagonal bipyramidal crystal about $7 \times 7 \times 15$ mm^3 in size was obtained after 2 weeks. The plane including the c axis was polished and used for the reflection measurement. The specimen for the transmission measurement is about 0.1 mm thick.

Far-infrared spectra were recorded using a Hitachi 070 far-infrared interferometer equipped with a wire-grid polarizer. For the measurement below 50 cm^{-1}, a high-sensitive liquid-helium cooled germanium bolometer was used as a detector. A Raman spectrum was obtained with a Spex 401 double monochromator using 647.1 nm excitation from a Kr ion laser.

Results and Discussion

Spectra of the Low-temperature Phase. The polarized far-infrared transmission spectra of a single crystal at liquid-nitrogen temperature are shown in Fig. 2. The polarized far-infrared reflection spectra at room temperature are shown in Fig. 3a. The $\varepsilon'(\nu)$ and $\varepsilon''(\nu)$ curves obtained by the Kramers-Kronig analysis are shown in

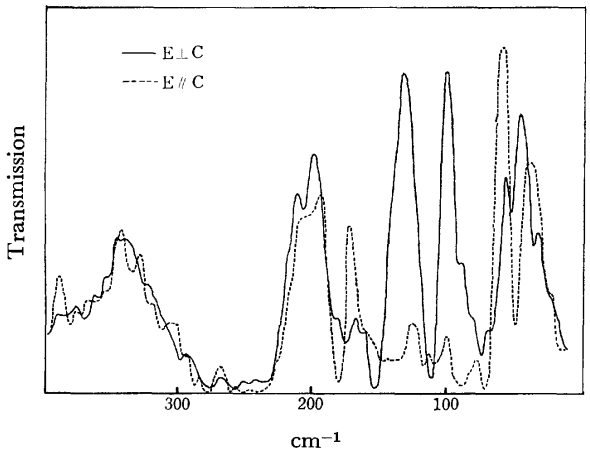

Fig. 2a. Single crystal far-infrared transmission spectra of $CsCuCl_3$ (400—20 cm^{-1}).

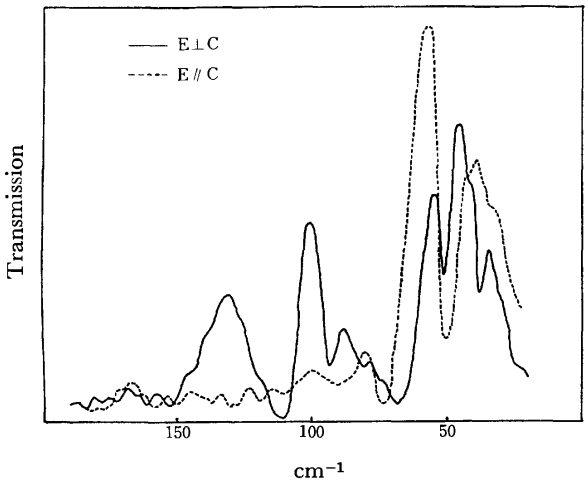

Fig. 2b. Single crystal far-infrared transmission spectra of $CsCuCl_3$ (200—20 cm^{-1}).

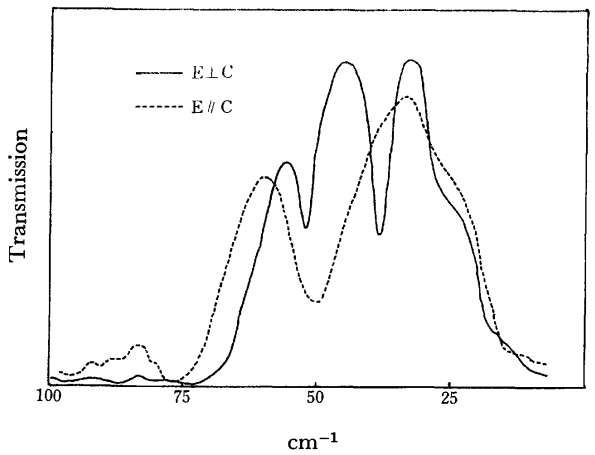

Fig. 2c. Single crystal far-infrared transmission spectra of $CsCuCl_3$ (100—10 cm^{-1}).

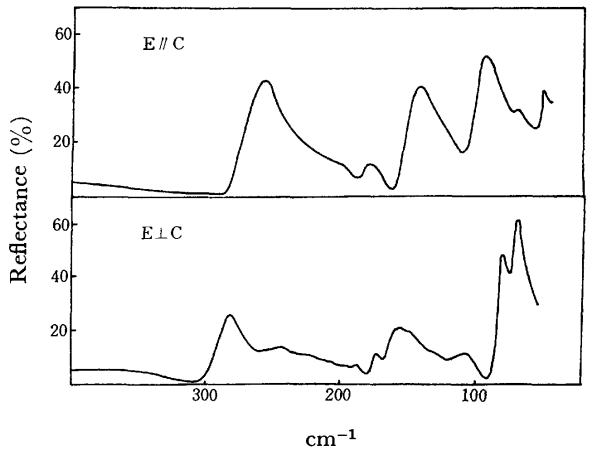

Fig. 3a. Single crystal far-infrared reflection spectra of $CsCuCl_3$.

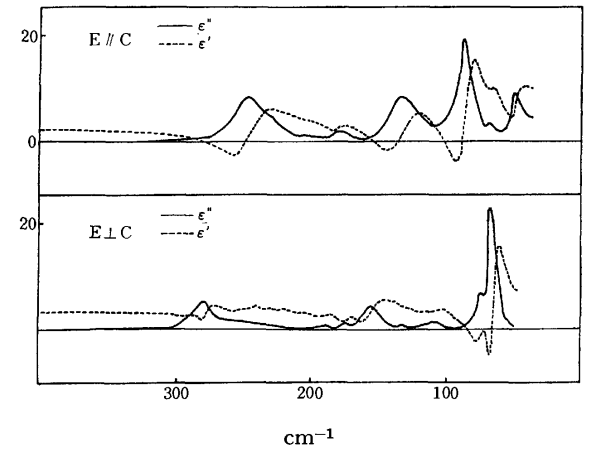

Fig. 3b. $\varepsilon'(\nu)$ and $\varepsilon''(\nu)$ obtained from reflection spectra of $CsCuCl_3$.

Fig. 3b, where the maxima of $\varepsilon''(\nu)$ give the transverse frequencies. The transmission spectra above 200 cm^{-1} are uninformative, since the absorptions are too strong and saturated. From the maxima of $\varepsilon''(\nu)$ in Fig. 3b, 247 and 279 cm^{-1} are assigned to the A_2 and E_1 modes,

Table 2. Vibrational frequencies (cm^{-1}) of the low-temperature phase of $CsCuCl_3$

Polarized single crystal spectra				Powder sample spectra Trans.[a]
A_2 species Trans.[a]	(E//C) Ref.[b]	E_1 species Trans.[a]	(E⊥C) Ref.[b]	
*	247	*	279	287
				256
		187	187	188
179	180			180
		174	173	175
		163	157	163
		152		146
140	135			
119				119
		111	111	114
		94		96
90	88			82
		80	76	
72	69			76
		68	68	
		54		52
51	50			
		39		

a) Transmission. b) Reflection.
* Too strong absorption and the frequencies may not be determined.

respectively. In the frequency region below 200 cm^{-1}, the absorption bands at 179, 140, 119, 90, 72, and 51 cm^{-1} are attributed to the A_2 modes, and those at 187, 174, 163, 152, 111, 94, 80, 68, 54, and 39 cm^{-1} to the E_1 modes as shown in Figs. 2a—2c. The $7A_2$ modes and $11E_1$ modes are now determined, while a factor group analysis predicts $8A_2$ and $14E_1$ modes. Table 2 summarizes the observed frequencies obtained from the single crystal transmission and reflection spectra. The frequencies determined by the two different methods agree well, as a whole, with each other.

The frequencies at which $\varepsilon'(\nu)$ changes the sign from negative to positive, *i.e.* 278, 154, and 102 cm^{-1} for E//C, and 85 and 73 cm^{-1} for E⊥C, correspond to the longitudinal frequencies. However, it is difficult to determine all the longitudinal frequencies, because of the complex structure of the crystal and the fairly large damping at room temperature. Therefore, no further discussion will be done on the longitudinal frequencies.

Figure 4 shows the transmission spectra of the powder sample at room and liquid-nitrogen temperatures. The room temperature spectrum is essentially the same as the spectrum reported by McPherson and Chang. With lowering the temperature, the absorption bandwidth becomes narrower considerably. In the spectrum at liquid-nitrogen temperature 13 absorption bands are observed, and the vibrational assignment of each band is definitely determined as listed in Table 2, on referring to the single crystal spectra described before.

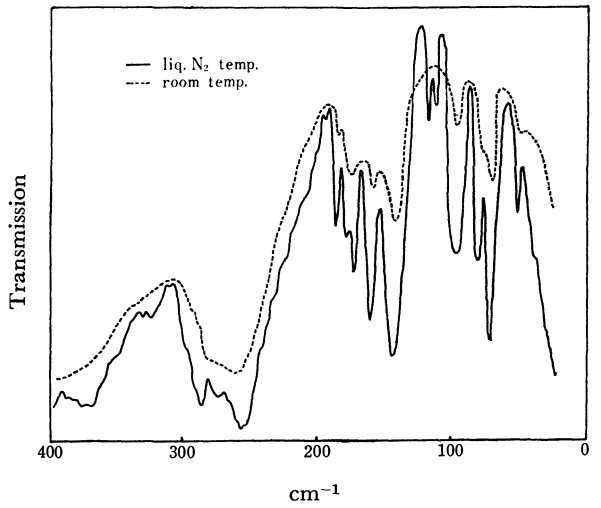

Fig. 4. Far-infrared transmission spectra of the powder sample of $CsCuCl_3$ at room and liquid-nitrogen temperatures.

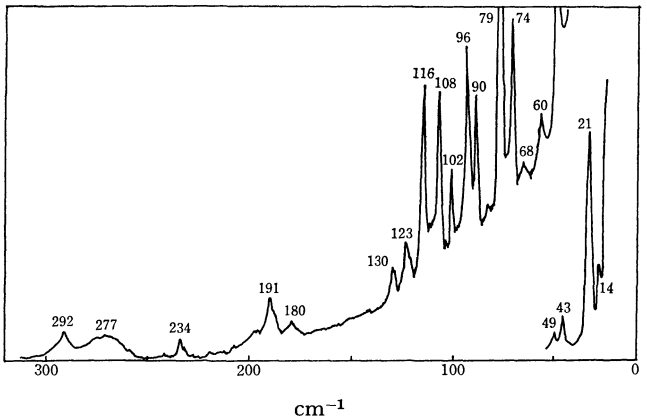

Fig. 5. Raman spectrum of the powder sample of $CsCuCl_3$ at 30 K.

The Raman spectrum of the powder sample observed at 30 K are shown in Fig. 5. Twenty Raman lines are observed, while 35 ($6A_1+14E_1+15E_2$) are expected from the factor group analysis. The E_1 modes are active both in the infrared and Raman spectra. However, a definite assignment of the Raman lines is difficult from this powder Raman spectrum only.

Spectra of the High-temperature Phase and Spectral Change Due to the Phase Transition. Figure 6 shows the far-infrared transmission spectrum of the powder sample at 175 °C. This spectrum which consists of five bands is attributable to the high-temperature phase of $CsCuCl_3$ and reveals a typical feature characteristic of the $CsNiCl_3$ type structure. The band assignment to the symmetry species is possible, on referring to the results of the polarization measurements for the $CsNiCl_3$ type crystals by Adams and Smardzewski,[9] and by the present authors.[7,10] (See Table 3.)

Figure 7 shows the far-infrared transmission spectra of the powder sample at various temperatures. The absorption bands at 52 and 39 cm^{-1} of the low-temperature phase decrease their intensities with raising temperature and disappear above 140 °C, and the new band at 42 appears in the temperature range from 140 to 150 °C. The two bands at 82 and 76 cm^{-1} in the low-temperature phase are shifted to the

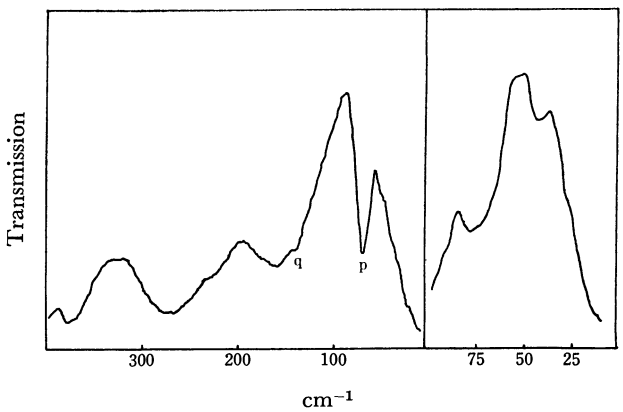

Fig. 6. Far-infrared transmission spectrum of the powder sample of $CsCuCl_3$ at 175 °C. (q and p are the absorptions by quartz and polyethylene, respectively.)

Table 3. Vibrational frequencies (cm^{-1}) of the high-temperature phase of $CsCuCl_3$

270	E_{1u}
220	A_{2u}
160	E_{1u}
70	E_{1u}
42	A_{2u}

lower frequency side and merged into one at 70 cm^{-1} on transition to the high-temperature phase. The strong absorption band at 146 cm^{-1} also disappears around 140 °C and the four bands at 188, 180, 175, and 163 cm^{-1} become unresolved and are replaced by a single broad band centered at 160 cm^{-1}. The lower frequency side of the broad bands around 280—250 cm^{-1} loses its intensity, and above 140 °C only one band around 270 cm^{-1} with an unresolved shoulder around 220 cm^{-1} is observed.

Among the five bands of the high-temperature phase the 270, 220, and 160 cm^{-1} bands are rather broad, comparing with the corresponding bands of $CsNiCl_3$ crystal,[7] which is isomorphous to the high-temperature phase of $CsCuCl_3$. This fact supports the presence of a local tetragonal distortion of $CuCl_6$-octahedra suggested based on the EPR study.[3] It might be noted that the other two bands at 70 and 42 cm^{-1}, associated with the Cs^+ ion displacements, are not so broad.

The authors wish to express their sincere thanks to Dr. Issei Harada of the University of Tokyo for his kind guidance in the measurement of Raman spectrum. A part of this work was supported by Kurata Science Foundation.

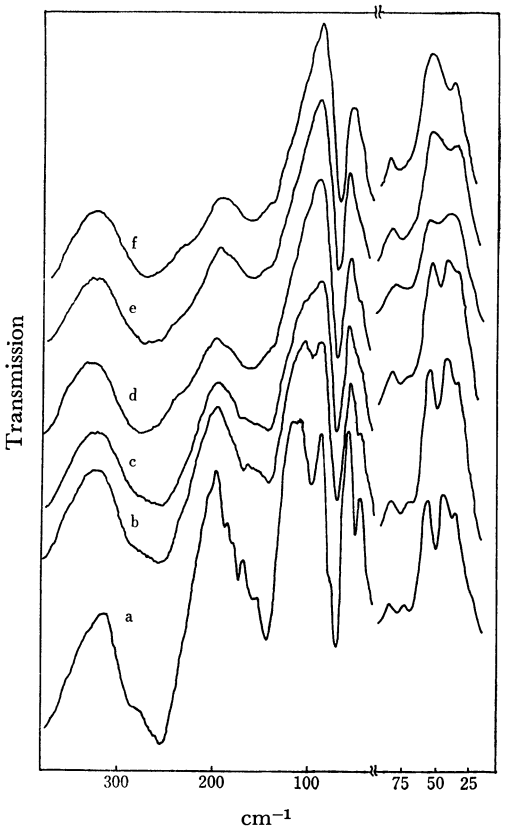

Fig. 7. Far-infrared transmission spectrum of the powder sample of $CsCuCl_3$ at various temperatures.
a: Room temperature, b: 118 °C, c: 131 °C, d: 138 °C, e: 140 °C, f: 148 °C.

References

1) N. Achiwa, *J. Phys. Soc. Jpn.*, **27**, 561 (1969).
2) C. J. Kroese, J. C. M. Tindemans-van Eyndhoven, and W. J. A. Maaskant, *Solid State Commun.*, **9**, 1707 (1971).
3) S. Hirotsu, *J. Phys. C: Solid State Phys.*, **8**, L12 (1975); *ibid.*, **10**, 967 (1977).
4) C. J. Kroese and W. J. A. Maaskant, *Chem. Phys.*, **5**, 224 (1974).
5) As for a summary of these studies, see Ref. 3.
6) G. L. McPherson and Jin Rong Chang, *Inorg. Chem.*, **12**, 1196 (1973).
7) K. Akiyama, Y. Morioka, and I. Nakagawa, *Bull. Chem. Soc. Jpn.*, **51**, 103 (1978).
8) A. W. Schlueter, R. A. Jacobson, and R. E. Rundle, *Inorg. Chem.*, **5**, 277 (1966).
9) D. M. Adams and R. R. Smardzewski, *Inorg. Chem.*, **10**, 1127 (1971).
10) Y. Morioka and I. Nakagawa, *Bull. Chem. Soc. Jpn.*, **51**, 2467 (1978).

Thermodynamics of the Redox Equilibria and the Site Preference in $(Fe_{1-y}Al_y)_{3-\delta}O_4$

Akio NAKAMURA,** Shigeru YAMAUCHI,* Kazuo FUEKI, and Takashi MUKAIBO

Department of Industrial Chemistry, Faculty of Engineering, The University of Tokyo, Hongo, Bunkyo-ku, Tokyo 113

(Received May 18, 1978)

In order to elucidate the defect model in the spinel ferrites, the nonstoichiometry in magnetite and its solid solutions, $(Fe_{1-y}Al_y)_{3-\delta}O_4$, ($y$=0.0, 0.25, 0.33), was determined at temperatures between 1300 and 1550 °C. The redox equilibria between Fe^{2+} and Fe^{3+} and the site preference of Fe^{2+}, Fe^{3+}, and Al^{3+} ions and cation vacancies were investigated and sixteen kinds of models were examined. The "best" model was chosen using the criteria that the dependence of the equilibrium constant on δ and y should be as small as possible. In the selected model, Fe^{2+} ions on B-sites are regarded as electron donors in a narrow 3-d band formed by Fe ions in B-sites. The following expression for the defect equilibrium was found:

$$\frac{2}{3(1-y)}Fe_A^{2+} + \frac{2(2-3y)}{3(1-y)}e_B^- + \frac{1}{2}O_2(g) \rightleftarrows \frac{2}{3(1-y)}Fe_A^{3+} + \frac{1}{4}V_A + \frac{1}{2}V_B + O_L^{2-}.$$

The thermodynamic properties of the Fe–O system have been studied in relation to the metallurgy and corrosion of steels. Among the oxides of iron, magnetite (Fe_3O_4) has a wide nonstoichiometric range; this attracted much attention in the field of solid state chemistry.[1-3] Magnetite is also regarded as a model compound of spinel-type ferrites, which are industrially important as magnetic oxide materials.

Electrical and magnetic properties of ferrites are largely affected by the charge and distribution of cations and lattice defects, which can be controlled during fabrication processes. Therefore, information about lattice defects in magnetite and ferrites is necessary for the production of ferrites with desired properties.

Magnetite and its solid solutions with $FeAl_2O_4$ have a wide nonstoichiometric composition with cation deficiency at high oxygen pressures.[4] Al^{3+} ions are stable in the spinel structure, so the charge distribution among cations in the spinel ferrite is simpler than in the other ferrites, such as manganese or copper ferrites.

The purpose of this paper is to determine the nonstoichiometry of spinel-type solid solutions of Fe_3O_4 and $FeAl_2O_4$, and to interpret the result on the basis of statistical thermodynamics.

Experimental

Materials. Magnetite was prepared by heating the cold-pressed hematite of 99.99% purity at 1500 °C in air. Solid solutions $(Fe_{1-y}Al_y)_3O_4$ (y=0.25 and 0.33) were formed by heating the cold-pressed powder mixtures of 99.99% pure hematite and alumina in a platinum crucible at 1500 °C in air for 12 h. The X-ray powder diffraction study revealed that the resulting materials were spinel-type solid solutions in a single phase. The weight increase observed when the ferrite specimens were oxidized into alumina and hematite coincided with the values calculated from the composition, within experimental error. The compacts were crushed to grains, 1—2 mm in diameter, and used as samples for the nonstoichiometric measurement.

Measurement of Nonstoichiometry. The apparatus for thermogravimetric measurement has been described elsewhere.[5] About 1 g of crushed oxide sample was placed in a platinum basket suspended from the balance to the furnace heated by a silicon carbide tubular heater. The temperature of the furnace was controlled within ±0.5 °C and the partial pressure of oxygen was controlled within 1—10^{-4} atm by mixing purified oxygen and argon gases.

For the determination of δ-values in $(Fe_{1-y}Al_y)_{3-\delta}O_4$, it was assumed that δ is zero at the phase boundary between wüstite and the ferrites.[5] Such a condition was realized by adjusting the ratio of CO to CO_2 in CO–CO_2 gas mixtures. The nonstoichiometry δ was calculated from the difference in weight.

Corrections for bouyancy, thermomolecular force, and evaporation of platinum were made, based on the results of preliminary experiments.

Results

Nonstoichiometric data of $(Fe_{1-y}Al_y)_{3-\delta}O_4$ (y=0.25, 0.33) obtained in this research are shown in Figs. 1 and 2 as the isothermal curves of log δ *versus* log P_{O_2}. Nonstoichiometric data of magnetite have already been reported,[5] so they are not presented here again. At a constant oxygen partial pressure, the nonstoichiometry decreased with the increase in temperature. The same tendency was observed for Fe_3O_4. The value of δ increased with the increase in aluminum content at an oxygen partial pressure. The slope $(\partial \ln\delta/\partial \ln P_{O_2})$ seems

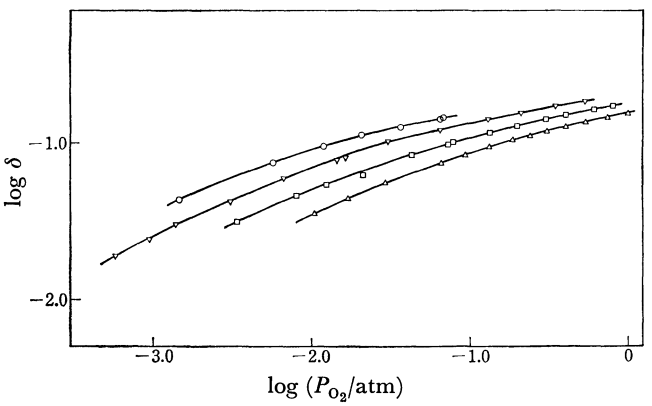

Fig. 1. Nonstoichiometric Data of $(Fe_{0.75}Al_{0.25})_{3-\delta}O_4$.
○: 1350 °C, ▽: 1400 °C, □: 1450 °C, △: 1500 °C.

** Present address: Center for Solid State Science, Arizona State University, Tempe, Arizona 85281, U. S. A.

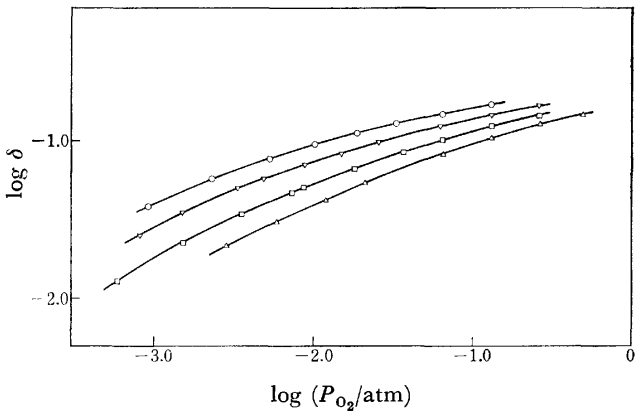

Fig. 2. Nonstoichiometric Data of $(Fe_{0.67}Al_{0.33})_{3-\delta}O_4$.
○: 1400 °C, ▽: 1450 °C, □: 1500 °C, △: 1550 °C.

to decrease slightly with the increase in aluminium content. Thus the same defect model as was suggested for magnetite can perhaps interpret the nonstoichiometry of these solid solutions.

Defect Model

Nonstoichiometry. In the spinel structure, the anion sublattice forms the fcc lattice; thirty two oxide ions are contained in an unit cell. The unit cell also has sixty four tetrahedral cation sites (A-sites) and thirty two octahedral cation sites (B-sites). These cation sites are not completely occupied: only eight A-sites and sixteen B-sites are occupied.[6]

Magnetite is a metal-deficient type oxide. According to Roiter,[4] $Fe_{3-\delta}O_4$ and $FeAl_2O_4$ form a solid solution, which would be a metal-deficit type oxide, in analogy with magnetite. Effective negative charges created by cation vacancy formation are compensated by the conversion of Fe^{2+} ions into Fe^{3+} by the reaction

$$2Fe^{2+} + \frac{1}{2}O_2(g) \longrightarrow 2Fe^{3+} + \frac{3}{4}V_C + O_L^{2-}, \quad (1)$$

where V_C denotes a vacancy on a cation lattice site (A site or B site) and O_L^{2-} denotes an oxide ion on an anion sublattice site.

The mass action law for equilibrium (1) is given by

$$K_1 = \frac{[Fe^{3+}]^2[V_C]^{3/4}}{[Fe^{2+}]^2 P_{O_2}^{1/2}}. \quad (2)$$

Equation 2 implies that δ is proportional to $P_{O_2}^{2/3}$ as δ is proportional to V_C. The nonstoichiometric data reported so far[1-3] indicate the 2/3 power dependence on P_{O_2} in a small δ range. However, the exponent of P_{O_2} decreases with the increase in δ and reaches 0.33 for magnetite and 0.25 for spinel ferrites. Although Eq. 1 can interpret the nonstoichiometry in magnetite and spinel ferrites qualitatively, internal equilibria and site preference of cations and vacancies have to be taken into account to establish the defect equilibria in spinel ferrite. Thus the analysis was made considering the distribution of cations on A and B sublattices.

Site Preference and Random Distribution of Cations. As mentioned above, the solid solutions have two kinds of cation sites, A-sites and B-sites, on which Fe^{2+}, Fe^{3+}, Al^{3+}, and V_C are distributed. The numbers of Fe^{2+}, Al^{3+}, and V_C on the sublattice are regarded as independent variables. As a pliausble approximation, it can be assumed that the above cations and cation vacancies are distributed either preferentially on A-sites or B-sites or randomly on both sites. The combination of these three kinds of cations and vacancy and the three ways of distribution yields $27(=3^3)$ defect models. Investigations reported so far have elucidated the site preference of each kind of cation in spinel lattices. These results reduce the number of possible defect models. In the following the observed site preference is briefly reviewed.

A recent Mössbauer spectroscopy study by Daniels and Rosencweig[7] has shown that magnetite has an inverse spinel type crystal structure and Fe^{2+} and V_C has a B-site preference at room temperature. On the other hand, Takeuchi and Furukawa[8] suggested that Fe^{2+} is randomly distributed on A- and B-sites at high temperatures. Flood and Hill[9] also assumed a random distribution of Fe^{2+} ions. Dieckmann and Schmalzried[10] have recently analysed the nonstoichiometric data of magnetite based on their tracer diffusion data of Fe and concluded that Fe^{2+} is randomly distributed over A- and B-sites. Although a definite conclusion was not given on the site preference of cation vacancies, they have pointed out that the random distribution of cation vacancies is the most reasonable one to presume.

Trivalent aluminum ions have relatively strong B-site preference, as shown by the normal spinel structure of $FeAl_2O_4$. From his neutron diffraction study and magnetic susceptibility measurements on $FeAl_2O_4$, Roth[11] stated that the structure of $FeAl_2O_4$ can be expressed as $Fe_{0.923}Al_{0.077}(Fe_{0.077}Al_{1.923})O_4$.

Navrotsky and Kleppa[12] reviewed site preference in spinel lattice and evaluated the enthalpy change associated with the reaction:

$$Fe_A^{2+} + Al_B^{3+} \rightleftarrows Fe_B^{2+} + Al_A^{3+}$$

as 9.2 kcal mol^{-1}. They also evaluated the site preference energy of various kinds of cations in the spinel lattice and concluded that Al^{3+} ions have the strongest B-site preference among Fe^{2+}, Fe^{3+}, and Al^{3+} ions.

In summarizing the above investigations, it is concluded that Fe^{2+} and Al^{3+} ions and vacancies prefer B-sites at low temperatures and both ions and vacancy are likely to be distributed randomly at high temperatures. Thus, the twenty seven defect models are reduced to eight defect models. Table 1 shows the description of these eight defect models and the expressions of concentrations of Fe^{2+}, Fe^{3+}, Al^{3+} ions and vacancies V_C on A- and B-sites in terms of moles per mole of $(Fe_{1-y}Al_y)_{3-\delta}O_4$. Notations R and B designate the random distribution and the B-site preference, respectively. Details of the assignment of the concentration are given in Appendix A.

Equilibrium Constants. To determine which one of the eight models listed in Table 1 best interprets the observed nonstoichiometric data, we employed two methods of calculation, the quasi-chemical model (Q.C. model) and the band electron model (B.E. model).

Calculation by the Q.C. Model: In this model Fe^{2+}, Fe^{3+}, and Al^{3+} ions and vacancies are assumed to form an ideal solution in the cation sublattice.

TABLE 1. DESCRIPTION OF POSSIBLE MODELS AND CONCENTRATIONS OF CATIONS AND VACANCIES

Model No.	Distribution of cations[a]			C_i^j		
	Fe^{2+}	V_C	Al^{3+}	Fe_A^{2+}	Fe_A^{3+}	V_A
1	R	R	R	$\frac{1-3\delta}{3}$	$\frac{2(1+\delta)-y(3-\delta)}{3}$	$\frac{\delta}{3}$
2	R	R	B	$\frac{1-3\delta}{3(1-y)}$	$\frac{2(1+\delta)-y(3-\delta)}{3(1-y)}$	$\frac{\delta}{3}$
3	R	B	R	$\frac{1-3\delta}{3-\delta}$	$\frac{2(1+\delta)-y(3-\delta)}{3-\delta}$	0
4	R	B	B	$\frac{1-3\delta}{(1-y)(3-\delta)}$	$\frac{2(1+\delta)-y(3-\delta)}{(1-y)(3-\delta)}$	0
5	B	R	R	0	$\frac{(3-\delta)[2(1+\delta)-y(3-\delta)]}{6(1+\delta)}$	$\frac{\delta}{3}$
6	B	R	B	0	$\frac{3-\delta}{3}$	$\frac{\delta}{3}$
7	B	B	R	0	$\frac{2(1+\delta)-y(3-\delta)}{2(1+\delta)}$	0
8	B	B	B	0	1	0

Model No.	C_i^j				
	Al_A^{3+}	Fe_B^{2+}	Fe_B^{3+}	V_B	Al_B^{3+}
1	$\frac{y(3-\delta)}{3}$	$\frac{2(1-3\delta)}{3}$	$\frac{2[2(1+\delta)-y(3-\delta)]}{3}$	$\frac{2\delta}{3}$	$\frac{2(3-\delta)y}{3}$
2	0	$\frac{(2-3y)(1-3\delta)}{3(1-y)}$	$\frac{(2-3y)[2(1+\delta)-y(3-\delta)]}{3(1-y)}$	$\frac{2\delta}{3}$	$y(3-\delta)$
3	y	$\frac{(2-\delta)(1-3\delta)}{3-\delta}$	$\frac{(2-\delta)[2(1+\delta)-y(3-\delta)]}{(3-\delta)}$	δ	$y(2-\delta)$
4	0	$\frac{[2-\delta-y(3-\delta)](1-3\delta)}{(1-y)(3-\delta)}$	$\frac{[2-\delta-y(3-\delta)][2(1+\delta)-y(3-\delta)]}{(1-y)(3-\delta)}$	δ	$y(3-\delta)$
5	$\frac{y(3-\delta)^2}{6(1+\delta)}$	$1-3\delta$	$\frac{(3+7\delta)[2(1+\delta)-y(3-\delta)]}{6(1+\delta)}$	$\frac{2\delta}{3}$	$\frac{y(3-\delta)(3+7\delta)}{6(1+\delta)}$
6	0	$1-3\delta$	$\frac{3+7\delta-3y(3-\delta)}{3}$	$\frac{2\delta}{3}$	$y(3-\delta)$
7	$\frac{y(3-\delta)}{2(1+\delta)}$	$1-3\delta$	$\frac{(1+2\delta)[2(1+\delta)-y(3-\delta)]}{2(1+\delta)}$	δ	$\frac{y(3-\delta)(1+2\delta)}{2(1+\delta)}$
8	0	$1-3\delta$	$1+2\delta-y(3-\delta)$	δ	$y(3-\delta)$

a) R designates random distribution and B designates localization on B-sites.

The chemical potential of the oxygen equilibrated with the oxide can be obtained by the following equation:

$$\frac{1}{2}(\mu_{O_2}^{\circ}+kT\ln P_{O_2}) = \frac{\partial G(N_1, N_2, N_3, N_4, N_5)}{\partial N_5}, \quad (3)$$

where N_i's with subscripts 1, 2, 3, 4, and 5 are numbers of Fe^{2+}, Fe^{3+}, V_C, Al^{3+}, and O^{2-} in the crystal, respectively, and G is the Gibbs energy of the crystal. The number of sites to be occupied by vacancies is given by the equation

$$N_3 = \frac{3}{4}N_5 - (N_1+N_2+N_4) \equiv \frac{3}{4}(N_5-N_5^{\circ}), \quad (4)$$

where N_5° is the number of oxide ions at the stoichiometric composition. If cations and vacancies form an ideal solution, the Gibbs energy is expressed as follows:

$$G = \frac{N_5^{\circ}}{4}G^{\circ}(N_3=0) + N_3 g_V - TS_{config}, \quad (5)$$

where g_V is the Gibbs energy of forming a cation vacancy, G° is the Gibbs energy of the crystal when $\delta=0$. S_{config} is expressed by

$$S_{config} = k\ln W_A W_B = k\ln \frac{(N_5/4)}{N_1^A!N_2^A!N_3^A!N_4^A!}\frac{(N_5/2)}{N_1^B!N_2^B!N_3^B!N_4^B!}, \quad (6)$$

where superscripts A and B designate A- and B-sites.

Substituting Eqs. 4, 5, and 6 into Eq. 3, the following expression is obtained by a standard calculation:

$$\frac{1}{2}(\mu_{O_2}^{\circ}+kT\ln P_{O_2}) = \frac{3}{4}g_V - kT\sum_{i=1}^{4}\left[\left(\frac{\partial N_i^A}{\partial N_5}\right)\ln\left(\frac{4N_i^A}{N_5}\right) - \left(\frac{\partial N_i^B}{\partial N_5}\right)\ln\left(\frac{2N_i^B}{N_5}\right)\right]. \quad (7)$$

If we express the concentration, the number of moles in one of $(Fe_{1-y}Al_y)_{3-\delta}O_4$, by the notation C_i^j, using a meaning similar to N_i^j, C_i^j can be related to N_i^j and N_5 as follows:

$$C_i^j = 4N_i^j/N_5 \quad (j=A, B;\ i=1, 2, 3, 4). \quad (8)$$

The differentials $(\partial N_i^j/\partial N_5)$ can be expressed by C_i^j

and as follows:

$$\left(\frac{\partial N_i^{\mathrm{j}}}{\partial N_5}\right) = \frac{1}{4}\left(\frac{\partial C_i^{\mathrm{j}} N_5}{\partial N_5}\right) = \frac{1}{4}\left(C_i^{\mathrm{j}} + N_5\frac{\partial C_i^{\mathrm{j}}}{\partial N_5}\right)$$
$$= \frac{1}{4}\left(C_i^{\mathrm{j}} + \frac{3}{4}N_5\frac{\partial C_i^{\mathrm{j}}}{\partial N_3}\right)$$
$$= \frac{1}{4}\left(C_i^{\mathrm{j}} + 3N_5\frac{N_5^\circ}{N_5^2}\frac{\partial C_i^{\mathrm{j}}}{\partial\delta}\right)$$
$$= \frac{1}{4}\left[C_i^{\mathrm{j}} + \frac{3\left(N_5 - \frac{4}{3}N_3\right)}{N_5}\left(\frac{\partial C_i^{\mathrm{j}}}{\partial\delta}\right)\right]$$
$$= \frac{1}{4}\left[C_i^{\mathrm{j}} + (3-\delta)\left(\frac{\partial C_i^{\mathrm{j}}}{\partial\delta}\right)\right]. \quad (9)$$

In the above calculations the following relations are used, besides Eqs. 4 and 8:

$$\delta = \frac{4N_3}{N_5} = \frac{4N_3}{N_5^\circ + \frac{4}{3}N_3},$$

$$\mathrm{d}\delta = \frac{4N_5^\circ}{N_5^2}\mathrm{d}N_3.$$

Substituting Eqs. 8 and 9 into Eq. 7, we obtain the following expression:

$$\frac{1}{2}(\mu_{\mathrm{O}_2}^\circ + kT\ln P_{\mathrm{O}_2}) = \frac{3}{4}g_{\mathrm{V}} - kT\sum_{i=1}^{4}\left[\left(C_i^{\mathrm{A}} + (3-\delta)\frac{\partial C_i^{\mathrm{A}}}{\partial\delta}\right)\right.$$
$$\left.\times\ln C_i^{\mathrm{A}} + \left(C_i^{\mathrm{B}} + (3-\delta)\frac{\partial C_i^{\mathrm{B}}}{\partial\delta}\right)\ln(C_i^{\mathrm{B}}/2)\right].$$

Putting

$$\nu_i^{\mathrm{j}} \equiv \left(\frac{\partial N_i^{\mathrm{j}}}{\partial N_5}\right) = \frac{1}{4}\left[C_i^{\mathrm{j}} + (3-\delta)\frac{\partial C_i^{\mathrm{j}}}{\partial\delta}\right] \quad (10)$$
$$i = 1, 2, 3, 4;\ \mathrm{j} = \mathrm{A}, \mathrm{B},$$

we obtain

$$\prod_{i=1}^{4}(C_i^{\mathrm{A}})^{-\nu_i^{\mathrm{A}}}\prod_{i=1}^{4}(C_i^{\mathrm{B}}/2)^{-\nu_i^{\mathrm{B}}}P_{\mathrm{O}_2}^{-1/2}$$
$$= \exp\left[\left(\frac{1}{2}\mu_{\mathrm{O}_2}^\circ - \frac{3}{4}g_{\mathrm{V}}\right)\Big/kT\right].$$
$$\equiv K(\mathrm{QC}) \quad (11)$$

Equation 11 is the mass action law for the following defect equilibrium:

$$\nu_1^{\mathrm{A}}\mathrm{Fe_A}^{2+} + \nu_2^{\mathrm{A}}\mathrm{Fe_A}^{3+} + \nu_3^{\mathrm{A}}\mathrm{V_A} + \nu_4^{\mathrm{A}}\mathrm{Al_A}^{3+} + \nu_1^{\mathrm{B}}\mathrm{Fe_B}^{2+}$$
$$+ \nu_2^{\mathrm{B}}\mathrm{Fe_B}^{3+} + \nu_3^{\mathrm{B}}\mathrm{V_B} + \nu_4^{\mathrm{B}}\mathrm{Al}^{3+} + \frac{1}{2}\mathrm{O_2(g)} = 0. \quad (12)$$

By using the expressions for C_i^{j} in Table 1, the stoichiometric coefficient ν_i^{j} is calculated by Eq. 10. The results are given in Table 2. Details are given in Appendix B. Let us term the defect models described by Eq. 12 as QC-1, QC-2, ···, QC-8 models.

Thus the defect equilibrium equations and the mass action laws can be written explicitly. For example, the equilibrium for model QC-3 is

$$\frac{1}{4}\frac{7+3\delta}{3-\delta}\mathrm{Fe_A}^{2+} + \frac{17-11\delta}{4(3-\delta)}\mathrm{Fe_B}^{2+} + \frac{y}{4}\mathrm{Al_B}^{3+} + \frac{1}{2}\mathrm{O_2(g)}$$
$$\rightleftarrows \left[\frac{5+\delta}{2(3-\delta)} - \frac{y}{2}\right]\mathrm{Fe_A}^{3+} + \left[\frac{7-5\delta}{2(3-\delta)} + \frac{y}{2}\right]\mathrm{Fe_B}^{3+}$$
$$+ \frac{3}{4}\mathrm{V_B} + \frac{y}{4}\mathrm{Al_A}^{3+} + \mathrm{O_L}^{2-}.$$

In this equation the stoichiometric coefficients depend on δ. When equilibrium constants are calculated using Eq. 11 and the expressions of concentration listed in Table 1, δ is canceled in the powers of concentrations and simple expressions are obtained. For example, the equilibrium constant for model QC-3 can be expressed as

$$K(\mathrm{QC\text{-}3}) = \left(\frac{2}{2-\delta}\right)^{1/4}\left(\frac{2+2\delta-(3-\delta)y}{1-3\delta}\right)^2\left(\frac{\delta}{2}\right)^{3/4}P_{\mathrm{O}_2}^{-1/2}$$

Thus equilibrium constants are easily calculated using observed values of δ and P_{O_2}.

Equilibrium Constants Calculated by the B. E. Model: In the band electron model, Fe^{2+} ions on B-sites are regarded as electron donors in a 3-d band. This is a consequence of the observation that the electric conduction in magnetite and spinel ferrites is caused by the electron movements in a narrow 3-d band formed by Fe ions on B-sites.[13]

TABLE 2. STOICHIOMETRIC COEFFICIENTS FOR VARIOUS MODELS

Model No.	$-\nu_i^{\mathrm{j}}$							
	$\mathrm{Fe_A}^{2+}$	$\mathrm{Fe_A}^{3+}$	$\mathrm{V_A}$	$\mathrm{Al_A}^{3+}$	$-\mathrm{Fe_B}^{2+}$	$\mathrm{Fe_B}^{3+}$	$\mathrm{V_B}$	$\mathrm{Al_B}^{3+}$
1	$\frac{2}{3}$	$-\frac{2}{3}$	$-\frac{1}{2}$	0	$\frac{4}{3}$	$-\frac{4}{3}$	$-\frac{1}{2}$	0
2	$\frac{2}{3(1-y)}$	$-\frac{2}{3(1-y)}$	$-\frac{1}{4}$	0	$\frac{2(2-3y)}{3(1-y)}$	$-\frac{2(2-3y)}{3(1-y)}$	$-\frac{1}{2}$	0
3	$\frac{7+3\delta}{4(3-\delta)}$	$-\frac{2(5+\delta)-2y(3-\delta)}{4(3-\delta)}$	0	$-\frac{y}{4}$	$\frac{17-11\delta}{4(3-\delta)}$	$-\frac{2(7-5\delta)+2y(3-\delta)}{4(3-\delta)}$	$-\frac{3}{4}$	$\frac{y}{4}$
4	$\frac{7+3\delta}{4(1-y)(3-\delta)}$	$-\frac{2(5+\delta)-2y(3-\delta)}{4(1-y)(3-\delta)}$	0	0	$\frac{17-11\delta-8y(3-\delta)}{4(1-y)(3-\delta)}$	$-\frac{2(7-5\delta)+2y(3-\delta)}{4(1-y)(3-\delta)}$	$-\frac{3}{4}$	0
5	0	$-\frac{y(3-\delta)^2}{24(1+\delta)^2}$	$-\frac{1}{4}$	$\frac{y(3-\delta)^2}{24(1+\delta)^2}$	2	$-\left[2-\frac{y(3-\delta)^2}{24(1+\delta)^2}\right]$	$-\frac{1}{2}$	$-\frac{y(3-\delta)^2}{24(1+\delta)^2}$
6	0	0	$-\frac{1}{4}$	0	2	-2	$-\frac{1}{2}$	0
7	0	$-\left[\frac{1}{4}+\frac{y(3-\delta)^2}{32(1+\delta)^2}\right]$	0	$\frac{y(3-\delta)^2}{32(1+\delta)^2}$	2	$-\left[\frac{7}{4}-\frac{y(3-\delta)^2}{32(1+\delta)^2}\right]$	$-\frac{3}{4}$	$-\frac{y(3-\delta)^2}{32(1+\delta)^2}$
8	0	$-\frac{1}{4}$	0	0	2	$-\frac{7}{4}$	$-\frac{3}{4}$	0

Samokhvalov and his co-investigators[14] have measured the electrical conductivity and thermoelectric power of solid solutions of the zinc ferrite-magnetite and nickel ferritemagnetite systems and derived the following expression for the chemical potential of an electron on a B-site:

$$\mu_{e_B^-} = E_C - kT\ln\frac{1}{2}\left[\frac{N_O}{N_D} - 1 + \sqrt{\left(1-\frac{N_O}{N_D}\right)^2 + 4\left(\frac{N_O}{N_D}\right)\exp(E_D/kT)}\right], \quad (13)$$

where E_D is the difference in energy level between the bottom of the conduction band and the donor level, and N_O and N_D are the densities of state of the conduction band and the donor level, respectively. In the present system, N_O and N_D are given as follows:

$$N_O = [Fe_B^{2+}] + [Fe_B^{3+}],$$
$$N_D = [F_Be^{2+}].$$

At high temperatures, the second term in the square root in Eq. 13 can be eliminated and Eq. 13 can be reduced to

$$\mu_{e_B^-} = E_C + kT\ln\frac{N_D}{N_O} = E_C + kT\ln\frac{C_1^B}{C_1^B+C_2^B}. \quad (14)$$

As Fe^{2+} is regarded as $e_B^- + Fe_B^{3+}$, the defect equilibrium is expressed by replacing Fe_B^{2+} in Eq. 12 by $e_B^- + Fe_B^{3+}$. Thus,

$$\nu_1^A Fe_A^{2+} + \nu_2^A Fe_A^{3+} + \nu_3^A V_A + \nu_4^A Al_A^{3+} + \nu_1^B e_B^- + (\nu_1^B+\nu_2^B)Fe_B^{3+} + \nu_3^B V_B + \nu_4^B Al_B^{3+} + \frac{1}{2}O_2 = 0. \quad (15)$$

The mass action law for Eq. 15 is

$$K(BE) = \prod_{i=1}^{4}(C_i^A)^{-\nu_i^A}\prod_{i=1}^{4}(C_i^B/2)^{-\nu_i^B}\left(\frac{C_2^B}{C_1^B+C_2^B}\right)^{-\nu_1^B} = K(QC)\left(\frac{C_2^B}{C_1^B+C_2^B}\right)^{-\nu_1^B}. \quad (16)$$

Fundamental aspects of Eqs. 15 and 16 are described in Appendix B. Let us term the defect models described by Eq. 16 as BE-1, BE-2, ···, and BE-8 models.†

The defect equilibrium equation and mass action law for model BE-3 are, for example,

$$\frac{7+3\delta}{4(3-\delta)}Fe_A^{2+} + \frac{17-11\delta}{4(3-\delta)}e_B^- + \frac{1}{4}(1-2y)Fe_B^{3+} + \frac{y}{4}Al_B^{3+} + \frac{1}{2}O_2 \rightleftarrows \frac{5+\delta}{2(3-\delta)}Fe_A^{3+} + \frac{y}{4}Al_A^{3+} + \frac{3}{4}V_B + O_L^{2-}$$

and

$$K(BE\text{-}3) = \left(\frac{2}{2-\delta}\right)^{1/4}\left(\frac{2+2\delta-y(3-\delta)}{1-3\delta}\right)^2\left(\frac{\delta}{2}\right)^{3/4} \times\left[\frac{2(1+\delta)-y(3-\delta)}{(3-\delta)(1-y)}\right]^{17-11\delta/4(3-\delta)} P_{O_2}^{-1/2}.$$

In this way equilibrium constants for each respective model can be easily calculated by using Eq. 16, using the expressions of ν_i^j and C_i^j in Tables 1 and 2, and the experimental values of δ and P_{O_2}.

† There may arise a question about applying Eq. 14 to models 5—8, where $C_2^B \leq C_1^B$. As no observation has been reported as to the characteristics of an electron band on B-sites if $[Fe_B^{3+}] \lesssim [Fe_B^{2+}]$, Eq. 14 was provisionally assumed to work for models 5—8.

Discussion

Criteria for the Selection of the "best" Model. In order to select the best one of these sixteen defect models, some criteria are necessary. Usually the slope of the log δ *vs.* log P_{O_2} plot is used for the selection. However, the slopes are 2/3 at small values of δ for several models, and also vary with δ. Thus this simple criterion is inadequate for the present purpose. Since the equilibrium constant K should be constant if the model is appropriate, the criteria that the dependence of ln$K$ on δ, as well as the dependence of ln$K$ on y, should be smallest for the "best" model were adopted for the selection. The advantage of this criteria is that one can easily detect the differences among the defect models.

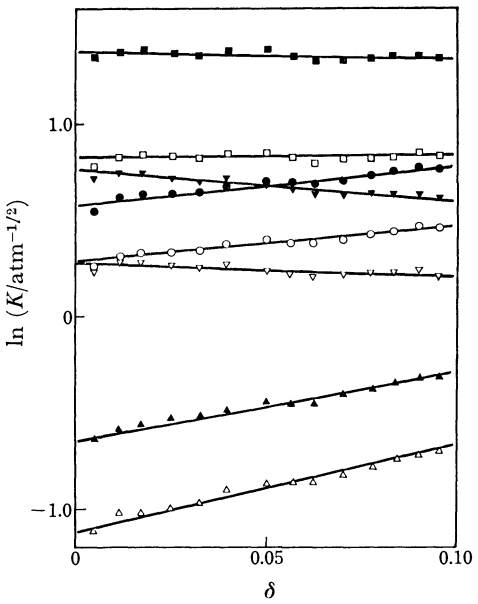

Fig. 3. Values of ln$K$ for respective defect model of $Fe_{3-\delta}O_4$.
○: QC-1, ●: QC-3, △: QC-5, ▲: QC-7, □: BE-1, ■: BE-3, ▽: BE-5, ▼: BE-7.

Analysis of Nonstoichiometric Deta. The equilibrium constants for equilibria 1 to 8 were calculated using Eqs. 11 and 16 and the observed values of δ and P_{O_2}. Figure 3 illustrates the dependence of ln$K$ on δ for $Fe_{3-\delta}O_4$ at 1400 °C. As $y=0$ for magnetite, only the eight equilibrium constants given in this figure were calculated. As is easily seen, ln$K$ changes almost linearly with δ for all the models. The equilibrium constants changed similarly with δ for solid solutions with aluminum ferrite. Thus the relationship between ln$K$ and δ can approximately be represented by the equation

$$\ln K = \alpha\delta + \beta. \quad (17)$$

The value α gives the slope of the ln$K$-δ plot and, according to the critetia adopted above, the model with the samllest absolute value of α is the "best" one.

Figure 4 illustrates the values of α for $(Fe_{0.75}Al_{0.25})_{3-\delta}$-

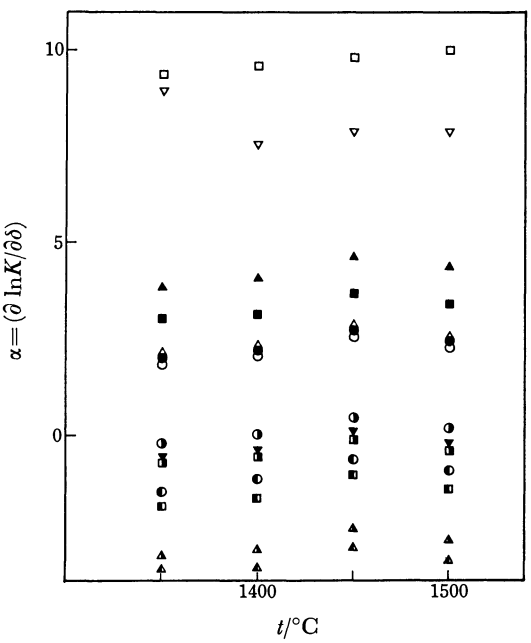

Fig. 4. Values of α for respective defect model of $(Fe_{0.75}Al_{0.25})_{3-\delta}O_4$.
○: QC-1, ●: QC-3, △: QC-4, ▲: QC-5, □: QC-6, ■: QC-7, ▽: QC-8 ▼: BE-1, ◑: BE-2, ◐: BE-3, ◨: BE-5 ◧: BE-6, ◭: BE-7, ◮: BE-8.

O_4. Those for model QC-2 are not given because K(QC-2) has the same value as K(QC-1). Those for model BE-4 are also excluded, since their absolute values are too large. As is easily seen in this figure, the value for QC-1 was the smallest among the QC models, although the differences from those for the QC-3 and QC-4 models. are small. A Similar conclusion has been reached by Dieckmann and Schmalzried[10] in their analysis of the tracer diffusion and nonstoichiometry of magnetite.

The α values for the BE-1 and BE-2 models are very small. They are smaller then those for the QC-1 model and it is concluded that the "best" model would be either the BE-1 or the BE-2 model. But it is difficult to choose the better one of the two only from this figure. A similar calculation was made for $Fe_{3-\delta}O_4$ and $(Fe_{0.67}Al_{0.33})_{3-\delta}O_4$. Figure 5 shows the values of α for K(BE-1)

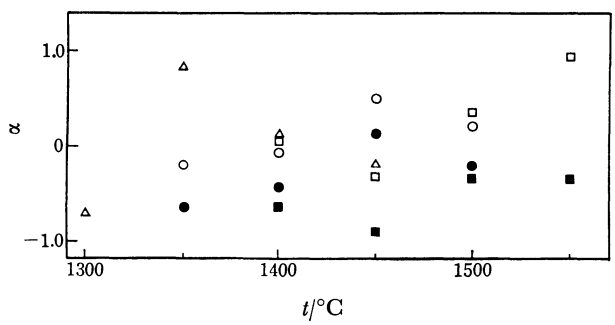

Fig. 5. Values of α for BE-1 and BE-2 models. The open and the solid marks denote the values for BE-1 and BE-2 models, respectively.
△ and ▲: $Fe_{3-\delta}O_4$, ○ and ●: $(Fe_{0.75}Al_{0.25})_{3-\delta}O_4$, □ and ■: $(Fe_{0.67}Al_{0.33})_{3-\delta}O_4$.

and K(BE-2). As is seen from Table 2, values of ν_i^j are the same for models 1 and 2 if $y=0$: Thus the values of α of the BE-1 and BE-2 models are the same for $Fe_{3-\delta}O_4$.

Except for some cases (1500 °C for $y=0.25$, and 1500 and 1550 °C for $y=0.33$), the absolute values of α are smaller for the BE-2 model than for the BE-1 model. This preference for the BE-2 model is also supported by the dependence of $\ln K$ on y. Figure 6 shows the plot of $\ln K$ against y. Clearly equilibrium constants for the BE-2 model depend less on y than those for the BE-1 model. The result indicates that the BE-2 model is better than the BE-1 model and, therefore, the BE-2 model was chosen as the "best" model in this investigation.

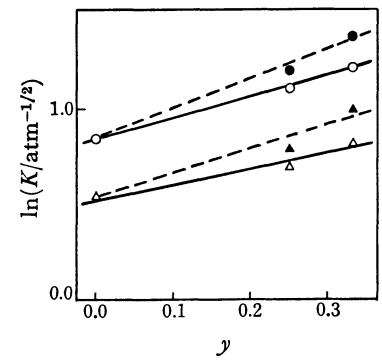

Fig. 6. Dependence of $\ln K$ on y.
●: 1400 °C, BE-1 model, ○: 1400 °C, BE-2 model, ▲: 1450 °C, BE-1 model, △: 1450 °C, BE-2 model.

BE-2 Model and Equilibrium Constant. The BE-2 model which has been chosen as the "best" model can be characterized as follows:
(1) Fe^{2+}, Fe^{3+} ions, and vacancies distribute randomly on A- and B-sites.
(2) Al^{3+} ions are localized on B-sites.
(3) Fe^{2+} and Fe^{3+} ions on B-sites provide a narrow d-band whose Fermi level can be approximated by Eq. 14.
The explicit expression of the defect equilibrium and

Table 3. Values of $\ln K$(BE-2)

T/°C	$\ln(K/\mathrm{atm}^{-1/2})$		
	$y=0$	$y=0.25$	$y=0.33$
1300	1.767± 0.007		
1350	1.219± 0.002	1.493± 0.006	
1400	0.833± 0.01	1.11± 0.01	1.231± 0.002
1450	0.547± 0.003	0.709± 0.01	0.843± 0.008
1500		0.305± 0.0002	0.463± 0.007
1550			0.110± 0.004
$\Delta H°$/kcal mol^{-1}	−43.7± 3.6	−45.3± 1.3	−45.7± 0.9
$\Delta S°$/cal K^{-1} mol^{-1}	−24.4± 2.2	−24.9± 0.8	−24.9± 0.5

Figures after ± signs are standard deviations.

the equilibrium constant are given as follows:

$$\frac{2}{3(1-y)}Fe_A^{2+} + \frac{2(2-3y)}{3(1-y)}e_B^- + \frac{1}{2}O_2(g) \rightleftarrows \frac{2}{3(1-y)}Fe_A^{3+} + \frac{1}{4}V_A + \frac{1}{2}V_B + O_L^{2-}, \quad (18)$$

$$K(\text{BE-2}) = \left[\frac{(3-\delta)(1-y)}{1-3\delta}\right]^{2(2-3y)/3(1-y)} \times \left[\frac{2+2\delta-y(3-\delta)}{1-3\delta}\right]^{2/3(1-y)} \left(\frac{\delta}{3}\right)^{3/4} P_{O_2}^{-1/3}. \quad (19)$$

Table 3 gives the values of $\ln K(\text{BE-2})$ together with values of $\Delta H°$ and $\Delta S°$ for Reaction 18. It is noteworthy that $\Delta H°$ and $\Delta S°$ are negative and almost independent of y.

The large negative values of $\Delta S°$ would be due to the disappearance of $O_2(g)$ and e_B^- in Reaction 18. The large negative value of $\Delta H°$ comes mainly from the negative partial molar enthalpy of oxygen in magnetite and its solid solutions with $FeAl_2O_4$.

Appendix

A. Assignment of Concentration of Ions and Vacancy. The concentrations of ions and vacancies for respective model are given in Table 1 in terms of moles in one mole of $(Fe_{1-y}Al_y)_{3-\delta}O_4$. One mole of $(Fe_{1-y}Al_y)_{3-\delta}O_4$ has 1 and 2 mol of A- and B-sites, respectively. Over these 3 mol of cation sites, $1-\delta$, $[2(1+\delta)-y(3-\delta)]$, $y(3-\delta)$, and δ mol of Fe^{2+}, Fe^{3+}, Al^{3+} ions, and vacancies, respectively, are distributed.

To elucidate the concentrations on the A- and B-sites the following procedure was adopted.

1) First, the concentration of vacancies was assigned. In the case of random distribution vacancies were assumed to be distributed in the ratio of 1:2 over A and B sites. If the vacancy is localized on a B-site, the concentration of the B-site is δ and that on the A-site is 0.

2) Concentrations of localized Fe^{2+} and/or Al^{3+} ions are assigned in the second step. When they are localized on a B-site, the concentrations on the B-site are $1-3\delta$ and $y(3-\delta)$ for Fe^{2+} and Al^{3+} ions, respectively. Concentrations on an A-site are 0 when they are localized on a B-site.

3) Concentrations of randomly distributed Fe^{2+} and/or Al^{3+} ions are determined in the third step. In this calculation, it was assumed that the concentration on A- or B-site is proportional to the number of sites still remaining at this step. For example, in model 5 the concentrations of Fe^{2+} and V_C are already assigned and the numbers of remaining sites are $1-\delta/3$ and $(3+7\delta)/3$ for A- and B-sites, respectively. Thus the concentration of Al^{3+} on A-site is calculated as

$$y(3-\delta) \times \frac{(1-\delta/3)}{(1-\delta/3)+(3+7\delta)/3} = \frac{y(3-\delta)^2}{6(1+\delta)}.$$

4) Finally the concentration of Fe^{3+} ion is assigned by allotting them on the remaining cationic sites.

B. Stiochiometric Coefficients and Equilibrium Conditions.

Equation 11 implies that a mass action law holds between the defects in the crystal of $(Fe_{1-y}Al_y)_{3-\delta}O_4$. The stoichiometric coefficients can be calculated by using Eq. 10. An illustration is given below for model 2.

The expressions for stoichimetric coefficients, ν_i^j's are calculated by using the expressions in Table 1 for C_i^j's. For example, ν_1^A is calculated as follows:

$$\nu_1^A = \frac{1}{4}\left[C_1^A + (3-\delta)\frac{\partial C_1^A}{\partial \delta}\right] = \left[\frac{1-3\delta}{3(1-y)} + (3-\delta)\frac{-3}{3(1-y)}\right]\Big/4 = -2/3(1-y).$$

Other coefficients are calculated in the same way; the results are given in Table 2. Using these values of ν_i^j's, Eq. 11 is written as follows:

$$(C_1^A)^{-2/3(1-y)} \cdot (C_2^A)^{2/3(1-y)} \cdot (C_3^A)^{1/4} \cdot (C_1^B/2)^{-2(2-3y)/3(1-y)} \times (C_2^B/2)^{2(2-3y)/3(1-y)} \cdot (C_3^B/2)^{1/2} \cdot P_{O_2}^{-1/2} = \frac{[V_A]^{1/4}[Fe_A^{3+}]^{2/3(1-y)}([V_B]/2)^{1/2}([Fe_B^{3+}]/2)^{2(2-3y)/3(1-y)}}{[Fe_A^{2+}]^{2/3(1-y)}([Fe_B^{2+}]/2)^{2(2-3y)/3(1-y)} P_{O_2}^{1/2}} = \exp\left[\frac{1}{2}\left(\mu_{O_2}^\circ - \frac{3}{4}g_v\right)\Big/kT\right]. \quad (A\text{-}1)$$

Equation A-1 implies that the defect equilibrium for this model can be described by the following chemical equilibrium:

$$\frac{2}{3(1-y)}Fe_A^{2+} + \frac{2(2-3y)}{3(1-y)}Fe_B^{2+} + \frac{1}{2}O_2 \rightleftarrows \frac{2}{3(1-y)}Fe_A^{3+} + \frac{2(2-3y)}{3(1-y)}Fe_B^{3+} + \frac{1}{4}V_A + \frac{1}{2}V_B. \quad (A\text{-}2)$$

The equilibrium condition for Eq. A-2 can also be expressed in terms of chemical potential of defects as follows:

$$\frac{2}{3(1-y)}\mu(Fe_A^{3+}) + \frac{2(2-3y)}{3(1-y)}\mu(Fe_B^{3+}) + \frac{1}{4}\mu(V_A) + \frac{1}{2}\mu(V_B) - \frac{2}{3(1-y)}\mu(Fe_A^{2+}) - \frac{2(2-3y)}{3(1-y)}\mu(Fe_B^{2+}) - \frac{1}{2}\mu_{O_2} = 0. \quad (A\text{-}3)$$

Thus the general expression of the defect equilibria, Eq. 11, implies the equilibrium condition in terms of the chemical potential, μ_i^j, of the i-th ion on the j site.

$$\frac{1}{2}\mu_{O_2} + \sum_{\substack{j=A,B \\ i=1,2,3,4}} \nu_i^j \mu_i^j = 0. \quad (A\text{-}4)$$

The conduction electrons in the BE models are considered to be created by the ionization of Fe_B^{2+} ions and the following virtual equilibrium is conceived.

$$Fe_B^{2+} \rightleftarrows Fe_B^{3+} + e_B^-. \quad (A\text{-}5)$$

For this equilibrium the following expression holds for the chemical potential of Fe_B^{2+} ions:

$$\mu(Fe_B^{2+}) = \mu(Fe_B^{3+}) + \mu_{e_B^-}. \quad (A\text{-}6)$$

Incorporating Eq. A-6 into A-4, an equilibrium conditions for BE modles is obtained:

$$\frac{1}{2}\mu_{O_2} + \nu_{Fe^{2+}}^A\mu(Fe_A^{2+}) + \nu_{Fe^{3+}}^A\mu(Fe_A^{3+}) + \nu_{V_C}^A\mu(V_A) + \nu_{Al^{3+}}^A\mu(Al_A^{3+}) + \nu_{Fe^{2+}}^B[\mu(Fe_B^{3+}) + \mu_{e_B^-}] + \nu_{Fe^{3+}}^B\mu(Fe_B^{3+}) + \nu_{V_C}^B\mu(V_B) + \nu_{Al^{3+}}^B\mu(Al_B^{3+}) = 0. \quad (A\text{-}7)$$

Equation A-7 implies the mass action law, Eq. 16, and the equilibrium equation, Eq. 15, for defect equilibrium, when BE models are adopted.

References

1) L. S. Darken and R. W. Gurry, *J. Am. Chem. Soc.*, **68**, 798 (1946).
2) O. N. Salmon, *J. Phys. Chem.*, **65**, 550 (1961).
3) J. Smiltens, *J. Am. Chem. Soc.*, **79**, 4877, 4881 (1957).

4) B. D. Roiter, *J. Am. Ceram. Soc.*, **47**, 509 (1964).
5) A. Nakamura, S. Yamauchi, K. Fueki, and T. Mukaibo, *J. Phys. Chem. Solids*, **39**, 1203 (1978).
6) R. C. Evans, "An Introduction to Crystal Chemistry," 2nd ed, Cambridge Univ. Press (1964), p. 174.
7) J. M. Daniels and A. Rosencweig, *J. Phys. Chem. Solids*, **30**, 1561 (1969).
8) S. Takeuchi and K. Furukawa, *Sci. Repts. Res. Inst. Tohoku Unive., Ser. A*, **12**, 120 (1960).
9) H. Flood and D. G. Hill, *Z. Elektrochem.*, **61**, 18 (1957).
10) R. Dieckmann and H. Schmalzried, *Ber. Bunsenges. Phys. Chem.*, **81**, 414 (1977).
11) W. W. Roth, *J. Phys.*, **5**, 507 (1964).
12) A. Navrotsky and O. J. Kleppa, *J. Inorg. Nucl. Chem*, **29**, 2701 (1967).
13) C. F. Jefferson and C. K. Barker, *IEEE Trans. Magn.* **4**, 460 (1968).
14) A. A. Samokhvalov and A. G. Rustamov, *Soviet Phys. Solid State*, **7**, 961 (1965).

The Solvent Extraction of Bivalent Metal Picrates by 15-Crown-5, 18-Crown-6, and Dibenzo-18-crown-6

Yasuyuki TAKEDA* and Hisanori KATŌ

Department of Chemistry, Faculty of Science, Chiba University, Yayoi-chō, Chiba 280

(Received August 30, 1978)

The overall extraction equilibrium constants (K_{ex}) for the 1 : 1 : 2 complexes of 15-crown-5 (15C5), 18-crown-6 (18C6), and dibenzo-18-crown-6 (DB18C6) with several bivalent metal picrates between benzene and water have been determined at 25 °C. The K_{ex} sequences of the bivalent metal ions with 15C5, 18C6, and DB18C6 are $Pb^{2+}>Sr^{2+}>Ba^{2+}>Ca^{2+}$, $Pb^{2+}\gg Ba^{2+}=Sr^{2+}>Hg^{2+}>Ca^{2+}$, and $Pb^{2+}>Hg^{2+}>Sr^{2+}>Ca^{2+}$ respectively. To clarify the role of the crown ether in the extraction process, the three constituent equilibria have been investigated: the stability and the extractability of the bivalent metal ion–crown ether complex, and the distribution coefficient of the crown ether. The extractability of the bivalent metal ion–crown ether complex about the same bivalent metal ion increases with increasing size of the crown ether, and appears to be dependent on the chemical nature of the bivalent metal ion trapped in the cavity of the crown ether.

The complex reaction between crown ethers and cations has been widely studied by different methods *e.g.* conductance,[1] calorimetry,[2] potentiometry,[3] spectroscopy,[4] and solvent extraction.[5] It has been found that the crown ether has a remarkable capacity to form stable stoichiometric complexes with certain cations, particularly with the alkali and alkaline earths.

Solvent extraction is a useful method to investigate the complexing power of crown ethers towards cations, though it is not direct. Some solvent extraction studies of crown ether complexes with alkali metal ions have been reported,[5] but there are very little data on bivalent metals. In terms of the analytical application, it is important to investigate the selectivity of crown ethers for various bivalent metal ions in solvent extraction systems. The present study was undertaken to determine the extraction constants for the crown ether–bivalent metal picrate systems between benzene and water, and to clarify the role of the crown ether in the extraction process. The crown ethers included in this work are 15-crown-5 (15C5), 18-crown-6 (18C6), and dibenzo-18-crown-6 (DB18C6). The sizes of these three compounds differ from one another. The cavity size of DB18C6 is equal to that of the 18C6,[3] though the former has two benzo groups. In the cases of DB18C6 and 18C6, it is interesting to investigate the ligand ring substituent effect on the extraction equilibrium. Since a large anion is easily extracted into low dielectric constant solvents,[5d] the picrate anion was used as the counter ion. Benzene was used as the diluent because of its nonpolar nature.

Experimental

Apparatus. Emission and absorption measurements were conducted on Seiko atomic absorption spectrophotometers, models SAS-720 and SAS-725. pH-measurements were made on a Hitachi-Horiba pH meter, model F-5.

Materials. 15C5 and 18C6 were obtained from Nisso Co., Ltd., and DB18C6 from Aldrich Chemical Co., Inc. 15C5 was used without further purification. 18C6 was recrystallized from petroleum ether twice, and dried in a vacuum oven before use. The method of purification of DB18C6 has been described in the literature.[1b] Benzene, HNO_3, $Ca(NO_3)_2\cdot 4H_2O$, $Sr(NO_3)_2$, $Ba(NO_3)_2$, $Hg(NO_3)_2\cdot xH_2O$, and $Pb(NO_3)_2$ were special grade reagents from Wako-Pure Chemicals Ltd., and picric acid from Koso Chemical Co., Ltd. The purity of the bivalent metal nitrates and the concentration of the picric acid solution were determined by EDTA and basic titration, respectively. Benzene was washed twice with distilled water.

Procedure. The organic solution of the crown ether (2×10^{-5}—3×10^{-2} M), the aqueous solution of the bivalent metal nitrate (5×10^{-4}—2.5×10^{-2} M), picric acid (1.5×10^{-4}—1.7×10^{-2} M), and nitric acid (2×10^{-3} M) were placed in stoppered glass tubes (volume 30 ml). The initial volume of each phase was 10 ml in all cases. The two phases in the tubes were shaken in a thermostatted water bath for approx. 30 min at 25±0.2 °C, and centrifuged. An approx. 8 ml portion was removed from the aqueous phase, transferred to a 10 ml beaker and the hydrogen ion concentration determined by a pH meter. All extractions were conducted in the pH range 1.5—3.0. For the systems 15C5–Ca, Sr, Pb, and 18C6–Ca, Sr, Hg, Pb, a 8 ml portion was pipetted from the organic phase, transferred to a 50 ml beaker, and left for several days, until evaporation was complete. The residue was dissolved in 0.01 M nitric acid 8 ml, and the metal concentration determined by atomic absorption. In the 15C5 and 18C6–Ba, and DB18C6–Ca, Sr, Hg, Pb systems, the residue did not dissolve. Consequently, the bivalent metal in the organic phase was back-extracted into 1 M nitric acid 8 ml and the Ba concentration of this aqueous phase determined by flame photometry. For the 15C5–Hg system, it was impossible to extract any Hg into the organic phase. For the DB18C6–Ba system, turbidity was always found in the interface between benzene and water under all experimental conditions.

The Distribution Coefficient of the Crown Ether. A portion of the benzene solution containing the crown ether and an equal volume of distilled water were placed in a stoppered glass tube and shaken under the same conditions as before. The concentration ranges of 15C5 and 18C6 were from 5.1×10^{-2} to 3.3×10^{-1} M, and from 2.8×10^{-2} to 3.1×10^{-1} M, respectively. After the two phases had been separated by centrifuging, a portion of the organic phase 12 ml was transferred to a 10 ml beaker, left for several days until evaporation was complete, and the residue weighed. The average distribution coefficients determined in this way are listed in Table 1, together with the equilibrium constants of the bivalent metal ion–crown ether complexes.

Results

The overall extraction equilibrium between an

aqueous phase containing the bivalent metal cation, M^{2+}, the picrate anion, A^-, and the hydrogen ion, H^+, and an organic phase of the crown ether, L, may be represented by the following equation:

$$M^{2+} + L_0 + 2HA_0 \rightleftarrows MLA_{2,0} + 2H^+$$

$$K_{ex} = \frac{[MLA_2]_0[H^+]^2}{[M^{2+}][L]_0[HA]_0^2}, \quad (1)$$

where MLA_2 represents the ion pair between the bivalent metal–crown ether cation, ML^{2+}, and the picrate anion; the subscript "0" and the absence of subscript denote the organic phase and aqueous phase, respectively. The overall extraction equilibrium is thought to consist of the following equilibria:

○ the distribution of the free crown ether between the two phases

$$L \rightleftarrows L_0 \qquad K_{D,L} = \frac{[L]_0}{[L]}, \quad (2)$$

○ the complex reaction of the bivalent metal ion with the crown ether

$$M^{2+} + L \rightleftarrows ML^{2+} \qquad K_{ML} = \frac{[ML^{2+}]}{[M^{2+}][L]}. \quad (3)$$

Several stability constants of bivalent metal ion–crown ether complexes have been reported.[2a,2b,2c,4] They are listed in Table 1.

○The distribution of picric acid between the two phases

$$HA \rightleftarrows HA_0 \qquad K_{D,HA} = \frac{[HA]_0}{[HA]}, \quad (4)$$

○ the association of picric acid

$$H^+ + A^- \rightleftarrows HA \qquad K_{HA} = \frac{[HA]}{[H^+][A^-]}, \quad (5)$$

○ the association of the complexed cation with the picrate anion

$$ML^{2+} + 2A^- \rightleftarrows MLA_2 \qquad K_{MLA_2} = \frac{[MLA_2]}{[ML^{2+}][A^-]^2}, \quad (6)$$

○ the distribution of the ion pair between the two phases

$$MLA_2 \rightleftarrows MLA_{2,0} \qquad K_{D,MLA_2} = \frac{[MLA_2]_0}{[MLA_2]}. \quad (7)$$

Since benzene is a nonpolar solvent (ε=2.275 at 25 °C[6]), dissociation of the ion pair, MLA_2, has been assumed negligible. Thus,

$$K_{ex} = K_{D.L}^{-1}K_{ML}K_{D.HA}^{-2}K_{HA}^{-2}K_{ex'}, \quad (8)$$

where $$K_{ex'} = K_{MLA_2}K_{D.MLA_2} = \frac{[MLA_2]_0}{[ML^{2+}][A^-]^2}. \quad (9)$$

The all-activity coefficients of the chemical species in this work have been assumed as unity.

The distribution ratio of the bivalent metal has been defined as follows and calculated from the experimental data,

$$D_M = \frac{[M]_{0,total}}{[M]_{total}},$$

where $[M]_{0,total}$ and $[M]_{total}$ are the total bivalent metal concentrations in the organic and aqueous phases, respectively. Assuming that the association between ML^{2+} and A^- is negligible in the aqueous phase;

$$D_M = \frac{[MLA_2]_0}{[M^{2+}]+[ML^{2+}]}. \quad (10)$$

In the case of $[M^{2+}] \gg [ML^{2+}]$, Eq. 10 becomes

$$D_M = K_{ex}K_{HA}^2K_{D.HA}^2[A^-]^2[L]_0, \quad (11)$$

where $K_{HA}K_{D,HA}$ is the extraction equilibrium constant of picric acid. The value of $K_{HA}K_{D,HA}$ in the benzene–water system at 25 °C has been determined to be 247 by spectroscopy using the association constant of picric acid, K_{HA}=1.95.[7] $[A^-]$ in Eq. 11 was calculated from Eq. 12, for the systems of 15C5–Sr, Ba, Pb, and 18C6–Sr, Ba, Hg, Pb, $[L]_0$ in Eq. 11 from Eq. 13 using the stability constants, K_{ML}'[2b] given in Table 2, and for the others $[L]_0$ by Eq. 14.

$$[A^-] = \frac{[HA]_{i.t.}-2[MLA_2]_0}{1+(1+K_{D,HA})K_{HA}[H^+]}, \quad (12)$$

$$[L]_0 = \frac{[L]_{i.t.}-[MLA_2]_0}{1+K_{D.L}^{-1}+K_{ML}K_{D.L}^{-1}[M^{2+}]}, \quad (13)$$

$$[L]_0 = \frac{[L]_{i.t.}-[MLA_2]_0}{1+K_{D.L}^{-1}}, \quad (14)$$

where $[HA]_{i.t.}$ and $[L]_{i.t.}$ are the initial total concentrations of picric acid and crown ether, respectively. $\log(D_M/[A^-]^2)$ *vs.* $\log[L]_0$ plots are illustrated in Figs. 1—3. Figures 1, 2, and 3 correspond to 15C5, 18C6, and DB18C6 respectively. From Figs. 1—3 it may be seen that the plots are linear with a slope of unity. $\log(D_M/[L]_0)$ *vs.* $\log[A^-]$ curves in Fig. 4 are linear with a slope of 2. It has then been concluded that the overall

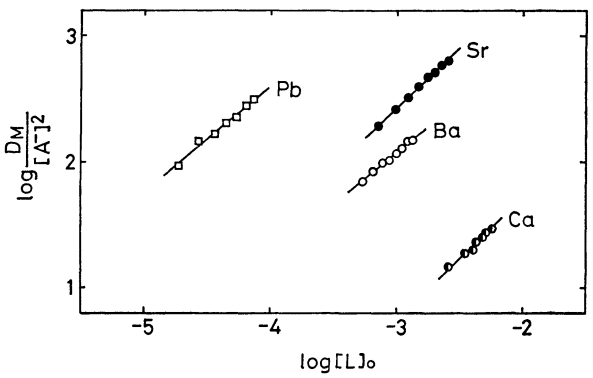

Fig. 1. Plots of $\log(D_M/[A^-]^2)$ *vs.* $\log[L]_0$ for the 15C5 system at 25 °C.

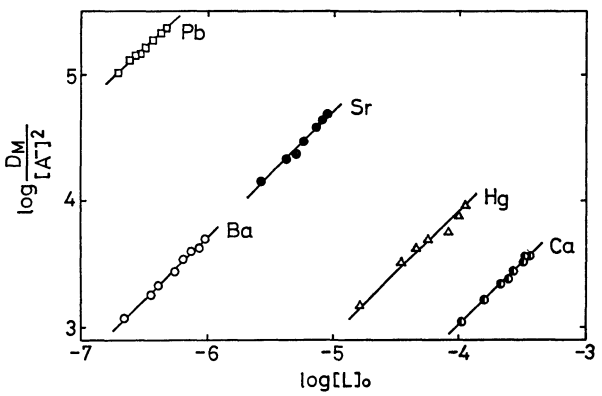

Fig. 2. Plots of $\log(D_M/[A^-]^2)$ *vs.* $\log[L]_0$ for the 18C6 system at 25 °C.

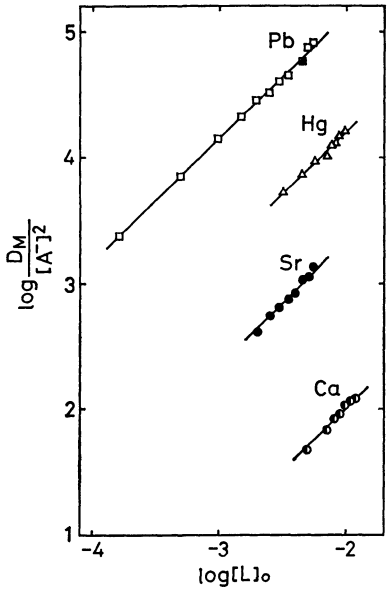

Fig. 3. Plots of $\log(D_M/[A^-]^2)$ *vs.* $\log[L]_0$ for the DB18C6 system at 25 °C.

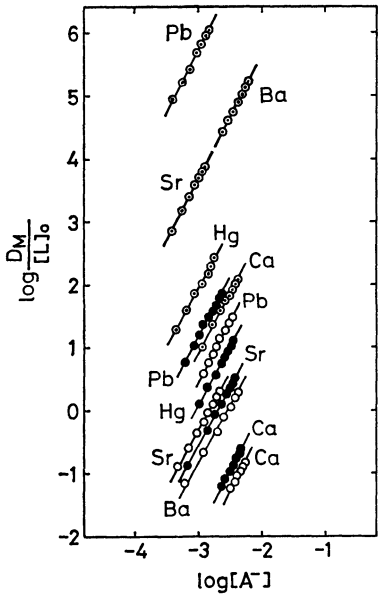

Fig. 4. Plots of $\log(D_M/[L]_0)$ *vs.* $\log[A^-]$ at 25 °C.
○: 15C5, ⊙: 18C6, ●: DB18C6.

extraction equilibrium, K_{ex}, in the present study is described by Eq. 1. For each system the value of the overall extraction equilibrium constant calculated from the data of Figs. 1—3 was found to agree well with that of Fig. 4. The K_{ex} values are given in Table 1.

Discussion

The crystal ionic radii of the bivalent metals and the cavity radii of the crown ethers are listed in Table 2. It may be noted from Tables 1 and 2 that for the 18C6 system $\log K_{ex}$ for Sr^{2+} is identical with that of Ba^{2+} which has a more optimum size for the 18C6 cavity than Sr^{2+}. The $\log K_{ex}$ and $\log K_{ML}$ values have been plotted *vs.* the crystal ionic radius in Fig. 5. As can be

Table 1. Equilibrium constants at 25 °C

Crown ether	$K_{D,L}$	Cation	$\log K_{ex}$	$\log K_{ML}$	$\log K_{ex'}$
15C5	0.15_6	Ca^{2+}	−1.07	—	—
		Sr^{2+}	0.91	1.95[2b]	2.94
		Ba^{2+}	0.41	1.71[2b]	2.68
		Pb^{2+}	1.67	1.85[2b]	3.80
18C6	0.063_4	Ca^{2+}	2.24	<0.5[2b]	>5.33
		Sr^{2+}	4.93	2.72[2b]	5.80
		Ba^{2+}	4.93	3.87[2b]	4.65
		Hg^{2+}	3.18	2.42[2b]	4.34
		Pb^{2+}	6.96	4.27[2b]	6.28
DB18C6	800[5c]	Ca^{2+}	−0.78	<0[4]	>7.39
		Sr^{2+}	0.59	1.00[4]	7.28
		Hg^{2+}	1.43	—	—
		Pb^{2+}	2.37	1.89[4]	8.17

Table 2. Crystal ionic radii of bivalent metals and cavity radii of crown ethers (Å)

Cation	Crystal ionic radius	Crown ether	Cavity radius[3]
Ca^{2+}	0.99[8]	15-crown-5	0.85—1.1
Sr^{2+}	1.13[8]	18-crown-6	1.3 —1.6
Ba^{2+}	1.35[8]		
Hg^{2+}	1.10[8]		
Pb^{2+}	1.20[9]		

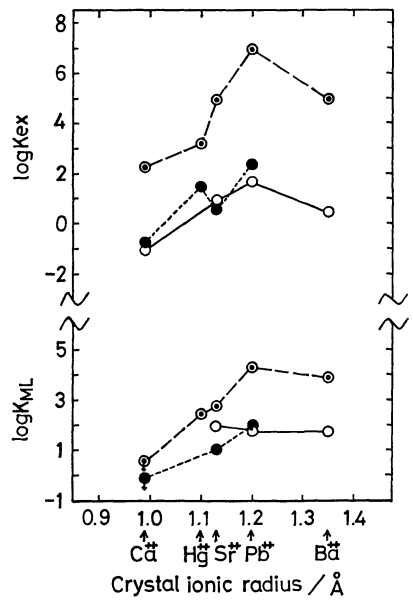

Fig. 5. Plots of $\log K_{ex}$ and $\log K_{ML}$ *vs.* crystal ionic radius of bivalent metal.
○: 15C5, ⊙: 18C6, ●: DB18C6.

seen from Fig. 5, the $\log K_{ex}$ value of Ca^{2+}, whose crystal radius is much smaller than the cavity radius of 18C6 in comparison with the other bivalent metal ions (Table 2), is smallest for the 18C6 and the DB18C6 systems. For the 15C5 system, although the crystal radius of Ca^{2+} is nearly equal to the cavity radius of 15C5 (Table 2), the $\log K_{ex}$ value of Ca^{2+} is also the smallest. The size of Pb^{2+} is larger than the cavity size of 15C5, and Ba^{2+} fits more closely into the 18C6 cavity than Pb^{2+} (Table 2). In Fig. 5 however, 15C5 and 18C6 show the largest

$\log K_{ex}$ value for Pb^{2+}.

The most pronounced substituent effect of the two benzo groups attached to 18C6 on the extractability of Hg^{2+} and Sr^{2+} can be seen in Fig. 5, *i.e.* the $\log K_{ex}$ sequence for Hg^{2+} and Sr^{2+} with 18C6 is $Hg^{2+}<Sr^{2+}$, while that with DB18C6 is $Hg^{2+}>Sr^{2+}$, although the crystal radii of Hg^{2+} (1.10 Å[8]) and Sr^{2+} (1.13 Å[8]) are nearly equal.

From the data it appears that the ratio of the size of the bivalent metal ion to that of the crown ether cavity is not always the dominant factor in the extractability of the bivalent metal-crown ether picrate complex.

Equation 8 shows that the trend for K_{ex} for the same crown ether and different bivalent metal ions reflects the stability and the extractability of the bivalent metal ion–crown ether complex in the aqueous phase. The $\log K_{ex'}$ values calculated from Eq. 8 are given in Table 1. It is interesting that in each crown ether system the largest $\log K_{ex'}$ value is seen for Pb^{2+}. Table 1 shows that in the case of 15C5, the $\log K_{ex}$ sequence of Sr^{2+} and Ba^{2+} is $Sr^{2+}>Ba^{2+}$ and this sequence is determined by both the $\log K_{ML}$ and the $\log K_{ex'}$ sequences, and that the largest $\log K_{ex}$ value for Pb^{2+} is largely attributed to the largest $\log K_{ex'}$ value. In the case of 18C6 the larger $\log K_{ex'}$ value for Sr^{2+} entirely contributes to the larger and equal extractability of Sr^{2+} compared to Hg^{2+} and Ba^{2+}, respectively. It may be noted from Fig. 5 and Table 1 that for the 18C6–all the bivalent metal ions and the DB18C6–Ca^{2+}, Sr^{2+}, and Pb^{2+} systems, the $\log K_{ex}$ sequences largely depend on $\log K_{ML}$. The most remarkable extraction selectivities of 18C6 and DB18C6 for Pb^{2+} are due to the high stability and high extractability of the Pb^{2+}–crown ether complex.

The considerably different $\log K_{ex'}$ values for the bivalent metal ions about the same crown ether can be seen from Table 1, suggesting that the extractability of the bivalent metal ion–crown ether complex is not necessarily independent of the chemical nature of the bivalent metal ion trapped in the cavity of the crown ether.

Among the crown ethers, the $\log K_{ex'}$ value series about Sr^{2+} and Pb^{2+} are in the order 15C5<18C6<DB18C6, and about Ca^{2+} and Ba^{2+} 18C6<DB18C6 and 15C5< 18C6, respectively (Table 1). The size sequences of the crown ethers are 15C5<18C6<DB18C6. These results indicate that the $\log K_{ex'}$ value of the same bivalent metal ion increases with an increase in the size of the crown ether.

The distribution coefficient of the crown ether, $K_{D,L}$, in Eq. 8 is also an important factor which determines the magnitude of K_{ex} for bivalent metal ions. Table 1 shows that about the same bivalent metal ion the difference between the $\log K_{ML}$ value of 15C5 and that of DB18C6 is not great and the difference in $\log K_{D,L}$ values of DB18C6 and 15C5 is comparable to that in $\log K_{ex'}$ value of DB18C6 and 15C5, indicating that the $\log K_{ex}$ values for 15C5 and DB18C6 are nearly identical (Fig. 5). About the same bivalent metal ion, the $\log K_{ML}$ value for 18C6 is larger than the others; the $\log K_{ex'}$ value of 18C6 is much larger than that of 15C5, and moreover the $\log K_{D,L}$ value of 18C6 is smaller than that of 15C5; the $\log K_{ex'}$ value of 18C6 is very small compared with DB18C6, however, the $\log K_{D,L}$ value of 18C6 is exceedingly small compared with DB18C6, indicating that the $\log K_{ex}$ value of 18C6 is consistently much larger than the others (Fig. 5).

References

1) (a) E. Shchori and J. Jagur-Grodzinski, *Isr. J. Chem.*, **11**, 243 (1973); (b) N. Matsuura, K. Umemoto, Y. Takeda, and A. Sasaki, *Bull. Chem. Soc. Jpn.*, **49**, 1246 (1976).

2) (a) R. M. Izatt, D. P. Nelson, J. H. Rytting, B. L. Haymore, and J. J. Christensen, *J. Am. Chem. Soc.*, **93**, 1619 (1971); (b) R. M. Izatt, R. E. Terry, B. L. Haymore, L. D. Hansen, N. K. Dalley, A. G. Avondet, and J. J. Christensen, *ibid.*, **98**, 7620 (1976); (c) R. M. Izatt, R. E. Terry, D. P. Nelson, Y. Chan, D. J. Eatough, J. S. Bradshaw, L. D. Hansen, and J. J. Christensen, *ibid.*, **98**, 7626 (1976).

3) H. K. Frensdorff, *J. Am. Chem. Soc.*, **93**, 600 (1971).

4) E. Shchori, N. Nae, and J. Jagur-Grodzinski, *J. Chem. Soc., Dalton Trans.*, **1975**, 2381.

5) (a) C. J. Pedersen, *Fed. Proc., Fed. Am. Soc. Exp. Biol.*, **27**, 1305 (1968); (b) H. K. Frensdorff, *J. Am. Chem. Soc.*, **93**, 4684 (1971); (c) A. Sadakane, T. Iwachido, and K. Tōei, *Bull. Chem. Soc. Jpn.*, **48**, 60 (1975); (d) P. R. Danesi, H. Meider-Gorican, R. Chiarizia, and G. Scibona, *J. Inorg. Nucl. Chem.*, **37**, 1479 (1975); (e) K. H. Pannell, W. Yee, G. S. Lewandos, and D. C. Hambrick, *J. Am. Chem. Soc.*, **99**, 1457 (1977).

6) "Organic Solvents," ed by A. Weissberger, Techniques of Chemistry, 3rd ed, J. Wiley & Sons, Inc., New York (1970), Vol. 2, p. 108.

7) "Dissociation Constants of Organic Acids in Aqueous Solution," ed by G. Kortün, W. Vogel, and K. Andrussov, Butterworths, London (1961).

8) L. Pauling, "The Nature of the Chemical Bond," 3rd ed, Cornell Univ. Press (1960).

9) R. C. Weast, "Handbook of Chemistry and Physics," 58th ed, CRC Press (1977—1978).

Fluorescence Quenching of Naphthalene and Its Derivatives by Acetyl Chloride

Takashi TAMAKI

Research Institute for Polymers and Textiles, Sawatari 4-1, Kanagawa-ku, Yokohama 221

(Received September 27, 1978)

The fluorescence of naphthalene and its methyl or methoxy derivatives has been found to be quenched by acetyl chloride. The quenching constants, determined by the Stern-Volmer treatment of the emission intensity and lifetime have been found to be in good agreement within experimental error. The quenching rate constants have been correlated with the energy terms of electron-donating forces in the excited states of these naphthalenes. The results suggest that the quenching mechanism involves a charge-transfer stabilized complex, in which the excited naphthyl compounds act as donors. Exciplex formation has been supported by oxygen quenching experiments.

The fluorescence quenching of aromatic molecules by carbonyl compounds is a current topic of research, a special interest of which is that some quenchings occur through non-classical energy transfer to a variety of acids, aldehydes, or ketones, which are of higher singlet excitation energy than those of the fluorescers.[1-3] Although these quenching systems reveal no exciplex emission, studies of the linear-free-energy relationship of the quenching efficiency indicate the validity of an exciplex, formed from excited aromatic compounds (electron donor) and electrophilic carbonyl groups (electron acceptor). This has been related to the anthracene–benzoyl chloride system, which is an example of the Friedel-Crafts-type photoreaction.[4] In addition to the Hammett correlation of the quenching ability of substituted benzoyl chloride, the complete interruption of the photoreaction by oxygen indicated that the exciplex is involved in the fluorescence quenching of anthracene and successive photochemical processes.

This paper reports the fluorescence quenching behavior of naphthalenes by acetyl chloride, based on the Stern-Volmer treatment of the fluorescence intensity and lifetime, and on oxygen quenching experiments, which are method for demonstrating the presence of a non-fluorescent exciplex.[5]

Experimental

All naphthyl compounds examined were purified by recrystallization from benzene or successive vacuum distillation. Distilled acetyl chloride was carefully kept from atmospheric moisture. Acetonitrile was dried and purified by fractional distillation over phosphorus pentoxide.

The fluorescence spectra measurements were made using a Hitachi MPF-2A spectrofluorometer at 21 °C. Samples were prepared in 1 cm square quartz cells with a 5 cm-length cylindrical neck which could be stoppered. The quencher concentrations employed were 0.02—0.4 M and the concentration of naphthalenes was 10^{-5} M. The excitation wavelength was 310 nm, where the absorption of the quencher was negligible. The emission spectra were generally the same both in the absence and presence of quencher and consequently the relative fluorescence intensity was determined by measurements of the height of the peak maxima. The experimental errors were 10%. Unless otherwise reported, the oxygen dissolved in the sample solution was purged by flushing with argon prior to measurement. A time of 10 min was required for complete elimination of oxygen-induced quenching under the conditions.

The fluorescence lifetime measurements were conducted using an ORTEC SP-3 nanosecond spectrometer at 25 °C, the sample preparation being the same as described above. The excitation was made by the 313 nm light and with this instrument, the fluorescence lifetime of quinine sulfate (10^{-5} M) has been estimated to be 20 ns (lit,[6] 19.2 ns).

Results and Discussion

In table 1 the results of the Stern-Volmer treatment for the fluorescence quenching of naphthalene and its methyl and methoxy derivatives by acetyl chloride are listed. The values of K_{sv} have been estimated from the initial slopes of the Stern-Volmer plots, which exhibited upward curvature above 0.1 M. The quenching rate constant, k_q, has been calculated by using the fluorescence lifetime observed.

It appears unlikely that static quenching is important since no new absorption band could be detected for the mixed solutions of naphthalenes and acetyl chloride. This is further supported by the quenching experiments of the fluorescence lifetime. The formation of a non-emissive complex prior to photoexcitation would enable the quenching to affect the fluorescence intensity, but not the fluorescence lifetime. However, this is not the case. As is shown in Table 1, the values of K_{sv} derived from the lifetime measurements are in good agreement with those of the intensity measurements within experimental error. The Stern-Volmer plots found here indicate the formation of the ground-state complex in high quencher concentrations[7] and consequently the dynamic property may be strictly pertinent to the quenching behaviors in low quencher concentrations.

The first excited states of carboxylic acids and derivatives are known to be n-π^* transitions, which are of higher energy than the corresponding transitions of aldehydes and ketones.[8] The singlet n-π^* transition energy of acetyl chloride is 121 kcal/mol (log ε 1.7),[9] which is higher than that of the naphthyl compounds ($<$92 kcal/mol). Thus, there is no region of spectral overlap between the donor fluorescence and the quencher absorption indicating the impossibility of triavial or resonance energy transfer. The quenching data listed in Table 1 reveals that k_q decreases with increase in the excitation energy of the fluorescers, and so endothermic energy transfer through collisional exchanges[10] can be excluded.

TABLE 1. FLUORESCENCE QUENCHING OF NAPHTHYL COMPOUNDS BY ACETYL CHLORIDE IN ACETONITRILE[a)]

	Donor	^1E_D[b)] (eV)	IP_D[c)] (eV)	τ^0 (ns)	Lifetime meas. K_{sv} (M^{-1})	Lifetime meas. $k_q\times10^{-7}$ ($M^{-1}s^{-1}$)	Intensity meas. K_{sv} (M^{-1})	Intensity meas. $k_q\times10^{-7}$ ($M^{-1}s^{-1}$)
1	Naphthalene	3.99	8.07	87	1.0	1.2	1.1	1.3
2	2-Methylnaphthalene	3.89	7.90	51	1.2	2.4	1.1	2.2
3	2,3-Dimethylnaphthalene	3.87	7.85	79	2.0	2.5	1.6	2.0
4	1-Methylnaphthalene	3.91	7.88	71	1.6	2.3	1.7	2.4
5	2,6-Dimethylnaphthalene	3.83	7.74	43	4.6	11	3.1	7.2
6	1,2-Dimethylnaphthalene	3.86	7.74	40	4.5	11	3.8	9.5
7	1,5-Dimethylnaphthalene	3.86	7.74	62	4.5	7.3	3.1	5.0
8	1,4-Dimethylnaphthalene	3.86	7.72	47	6.0	13	5.0	11
9	Acenaphthene	3.86	7.66	49	22	45	18	37
10	2-Methoxynaphthalene	3.78	8.06[d)]	16	7.2	45	5.0	31
11	1-Methoxynaphthalene	3.87	7.85[d)]	18	34	189	28	156

a) Measured under deoxygenated conditions. b) Determined from the absorption and fluorescence spectra.
c) Obtained from Ref. 16. d) Calculated[17] from the polarographic potential.[18]

These cosiderations suggest that the fluorescence quenching is due to exciplex formation, as in the case of the anthracene–benzoyl chloride system.[4] If an exciplex is formed, in which the excited molecules act as the electron donor with the same electron acceptor, the values of $\ln k_q$ should correlate with the energy terms of the electron-donating force, $IP_D-{}^1E_D$,[11] where IP_D and ^1E_D represent the ionization potential and the singlet excitation energy of the donor, respectively. Figure 1 shows the plots of $\ln k_q$ *vs.* $IP_D-{}^1E_D$, calculated for the naphthalenes examined. The linearity of the plots is remarkable, except for Compounds **10** and **11**. The electron transfer in the excited state is then primarily responsible for the fluorescence quenching.

Therefore, the quenching results can be accounted for by the following equations,

$$N \xrightarrow{h\nu} {}^1N^*, \quad (1)$$

$$^1N^* \xrightarrow{k_f} N + h\nu', \quad (2)$$

$$^1N^* \xrightarrow{k_{isc}} {}^3N^*, \quad (3)$$

$$^1N^* \xrightarrow{k_{ic}} N, \quad (3')$$

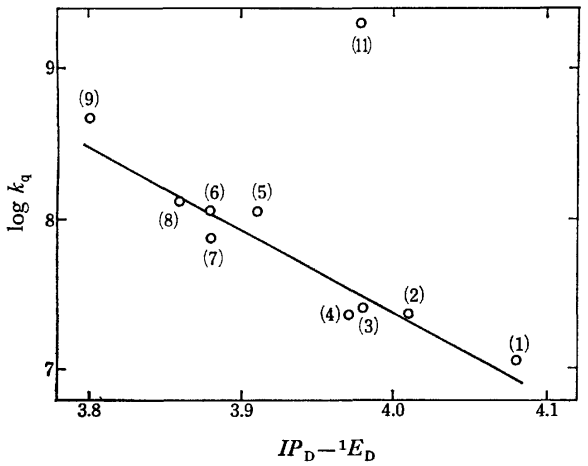

Fig. 1. Plots of log k_q as a function of $IP_D-{}^1E_D$. The values of k_q from the lifetime measurements were used. The numbers in parentheses refer to those in Table 1.

$$^1N^* + A \underset{k_{-e}}{\overset{k_e}{\rightleftharpoons}} [N\cdots A]^* \xrightarrow{k_{de}} N + A \text{ or products}, \quad (4)$$

where N and A represent the naphthyl compounds and acetyl chloride, respectively, $[N\cdots A]^*$ represents an exciplex, and k_q refers to $k_ek_{de}/(k_{-e}+k_{de})$.

If an exciplex is non-fluorescent and its formation is reversible, the oxygen quenching method is convenient for demonstrating the presence of the exciplex.[5] When oxygen is allowed into the sample solutions, both the excited monomer and exciplex are appreciably intercepted with a rate which is diffusion-controlled.

$$^1N^* + O_2 \xrightarrow{k_{qm}} N + O_2, \quad (5)$$

$$[N\cdots A]^* + O_2 \xrightarrow{k_{qe}} N + A + O_2. \quad (6)$$

From Eqs. 1—6, the Stern-Volmer equation is derived.

$$\phi_f^\circ/\phi_f = 1 + k_{qm}\tau^\circ[O_2] + k_ep\tau^\circ[A],$$
$$p = (k_{de}+k_{qe}[O_2])/(k_{-e}+k_{de}+k_{qe}[O_2]),$$

where $\phi_f^\circ=k_f/(k_f+k_{isc}+k_{ic})=k_f\tau^\circ$, ϕ_f represents the fluorescence quantum yield in the presence of the quencher and oxygen, and p is the fraction of the exciplex which does not regenerate an excited monomer. The Stern-Volmer relation of the fluorescence lifetime is the same as that of the fluorescence intensity. If the exciplex formation were irreversible, *i.e.*, $k_{-e}\ll k_{de}$, then the product k_ep approximates to k_q. The oxygen-induced quenching would be strictly competitive with quenching by A and the Stern-Volmer slopes as a function of [A] would be identical, irrespective of oxygen. If the exciplex is reversibly formed, the value of p may increase in the presence of oxygen, resulting in an increase of slope. As shown in Fig. 2, the fluorescence quenching of naphthalene by acetyl chloride is apparently enhanced by dissolved oxygen, strongly supporting the presence of a reversibly formed exciplex. As shown in Table 2, the quenching enhancement decreases with increase in the electron-donating ability of the excited naphthyl compound and consequently the reversibility of exciplex formation becomes less important with electron-rich aromatics.

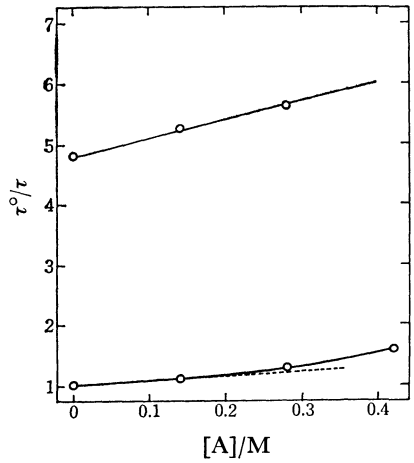

Fig. 2. Fluorescence quenching of naphthalene by acetyl chloride: lower, deoxygenated; upper, aerated.

Table 2. Results of the oxygen quenching experiments

Donor	K_{sv} [a] (M^{-1})	K_{sv} [b] (M^{-1})	$k_e\tau/k_q$
Naphthalene	3.0	3.2	3.0
2-Methylnaphthalene	2.3	1.8	1.8
1-Methylnaphthalene	2.0	2.1	1.2
Acenaphthene	—	21	1.1

a) Determined from lifetime measurements. b) Determined from intensity measurements.

Irradiation of the mixture of naphthalenes and acetyl chloride in benzene with 313 nm light produced an appreciable loss of the starting materials, indicating that the exciplex decays mainly through chemical transformations analogous to the photoreaction of anthracene with benzoyl chloride.[4] Attempts to isolate characterizable products by TLC were, however, unsuccessful. The large k_q values obtained for methoxynaphthalenes are thought due to the increased rates of such chemical changes. Preliminary experiments, in fact, showed that the initial rate of acetyl chloride loss monitored by the iron(III) hydroximate method[12] was larger than that for the methylnaphthalenes, although no precise evaluation of the quantum yield could be made because of the appearance of new intense absorption bands near the excitation wavelength.

Quenching behavior is of interest in view of structure-reactivity relationships. In contrast with the quenching of the excited aromatic hydrocarbons by aromatic ketones or aldehydes,[3] systems involving acyl chlorides as quencher do not necessarily require the assertion that the quencher should have a conjugated system capable of frontier orbital overlap with the aromatic fluorescer. It appears certain that in addition to the electron-withdrawing properties of the carbonyl group of acyl chlorides the chemical reactivity of activated acyl C–Cl bonds play an important role in the quenching processes. This may recall the concept concerned with bimolecular interactions between electron-rich aromatics and chlorinated compounds as the quenching center, *e.g.*, indole–methyl chloroacetate,[13] 1,4-dimethoxybenzene–benzyl chloride,[14] and methoxynaphthalenes–chloroacetonitrile systems.[15] These studies have emphasized that the rate of exciplex decay to chemical transformation is dominant in limiting an overall quenching rate. The CT interaction is of importance, however, giving rise to the association of an exciplex. The quenching mechanism in the present work is related to these instances.

References

1) N. H. C. Cooke and B. S. Solomon, *J. Phys. Chem.*, **76**, 3563 (1972).
2) R. W. Ricci and J. M. Nesta, *J. Phys. Chem.*, **80**, 974 (1976).
3) D. Busch, L. Dahm, B. Siwicke, and R. W. Ricci, *Tetrahedron Lett.*, **51**, 4489 (1977).
4) T. Tamaki, *Bull. Chem. Soc. Jpn.*, **51**, 1145 (1978).
5) J. L. Charton, D. E. Townsend, B. D. Watson, P. Shannon, J. Kowalewska, and J. Saltiel, *J. Am. Chem. Soc.*, **99**, 5992 (1977).
6) L. B. Berlman, "Handbook of Fluorescence Spectra of Aromatic Molecules," Academic Press, New York, N. Y. (1971).
7) C. Lewis and W. R. Ware, *Mol. Photochem.*, **5**, 261 (1973).
8) J. D. Coyle, *Chem. Revs.*, **78**, 97 (1978).
9) H. Baba, *Nippon Kagaku Zasshi*, **72**, 341 (1951).
10) F. D. Lewis and J. C. Dalton, *J. Am. Chem. Soc.*, **91**, 5260 (1969).
11) a) T. R. Evans, *J. Am. Chem. Soc.*, **93**, 2081 (1971); b) G. N. Taylor, *Chem. Phys. Lett.*, **10**, 355 (1971).
12) R. F. Goddu, N. F. LeBlanc, and C. M. Wright, *Anal. Chem.*, **27**, 1251 (1955).
13) M. T. McCall, G. S. Hammond, O. Yonemitsu, and B. Witkop, *J. Am. Chem. Soc.*, **92**, 6991 (1970).
14) F. A. Carroll, M. T. McCall, and G. S. Hammond, *J. Am. Chem. Soc.*, **95**, 315 (1973).
15) F. H. Quina, Z. Hamlet, and F. A. Carroll, *J. Am. Chem. Soc.*, **99**, 2240 (1977).
16) J. B. Birks, "Photophysics of Aromatic Molecules," Wiley-Interscience, London (1970), p. 458.
17) E. S. Pysh and N. C. Yang, *J. Am. Chem. Soc.*, **85**, 2124 (1963).
18) A. Zweig, A. H. Maurer, and B. G. Roberts, *J. Org. Chem.*, **32**, 1322 (1967).

Conditions of the Formation of Rare Earth Phosphates and the Colors of Their Powders

Mitsutomo TSUHAKO,* Sayuri IKEUCHI, Tsuneo MATSUO, Itaru MOTOOKA,** and Masamitsu KOBAYASHI**

Kobe Women's College of Pharmacy, Motoyama, Higashinada-ku, Kobe 658

***Department of Chemistry, Faculty of General Education, Kobe University, Tsurukabuto, Nada-ku, Kobe 657*

(Received July 3, 1978)

Rare earth oxides, such as La_2O_3, Pr_6O_{11}, Nd_2O_3, and Sm_2O_3, can react with phosphoric acid to give four kinds of rare earth phosphates (orthophosphates $LnPO_4 \cdot 0.5H_2O$ and $LnPO_4$, *catena*-polyphosphates $Ln(PO_3)_3$ and ultraphosphates LnP_5O_{14}), while in the reaction of CeO_2 with phosphoric acid there are formed five kinds of phosphates (orthophosphate $CePO_4$, pyrophosphate CeP_2O_7, two types of *catena*-polyphosphate $Ce(PO_3)_3$ and $Ce(PO_3)_4$, and ultraphosphate CeP_5O_{14}). The formation of these products in the CeO_2–H_3PO_4 system are notably different from these in other systems, showing that cerium(III) phosphates as well as cerium(IV) phosphates can exist stably. It can be seen from the X-ray diffraction patterns that each corresponding phosphate (ortho, *catena*-poly, and ultraphosphates) of lanthanum, cerium(III), praseodymium, neodymium, and samarium is isomorphous. This may be caused by the facts that the valencies of all these metals are +3 and that their ionic radii are almost equal to one another (La(III) 1.06 Å—Sm(III) 0.96 Å). The conditions of the formation of each phosphate were investigated, and the colors of the crystals, the densities, and the infrared absorption spectra of various rare earth phosphates were also examined.

The chemistry of rare earth phosphates has developed rapidly in the last few years. Such rapid development may be attributed, first of all, to the use of neodymium ultraphosphate as a laser material.[1-4] Also, it may be attributed to the following circumstances. As for ultraphosphates, the existence of sodium[5,6] and calcium ultraphosphates[7,8] has been hitherto known, but they are unstable structures. However, stable rare earth ultraphosphates were reported by Jaulmes[9] in 1969 and by Bagieu-Beucher and Tranqui[10] in 1970, and their crystallographical interest has occasioned active studies of ultraphosphates.[11,12] Thus, the crystal structures of several rare earth ultraphosphates have been elucidated.[13] However, there have as yet been few systematic studies of rare earth phosphates, various problems regarding their chemical formulae, chemical names, species, methods of preparation, and physical properties remain unsolved. For instance ultraphosphate [$P_5O_{14}^{3-}$] is often called pentaphosphate,[14,15] but this name is unreasonable, for it invites confusion with non-branched chain pentaphosphate [$P_5O_{16}^{7-}$]. In phosphate chemistry, the term "ultraphosphate" is often used as a popular name of phosphates with a net-work structure; therefore, in the present paper [$P_5O_{14}^{3-}$] is designated "ultraphosphate." According to their definition, ultraphosphates, obviously differing from non-branched chain pentaphosphate, are phosphates with P/Ln>3, where Ln=a trivalent rare earth metal, and have some branched P in their structures to form net-work structures.[5,7,16,17] On the other hand, the term "pentaphosphate" usually indicates non-branched chain phosphate [$P_5O_{16}^{7-}$] and not branched phosphate [$P_5O_{14}^{3-}$]. For neodymium *catena*-polyphosphate the chemical formula "NdP_3O_9" is often used,[11] but this formula properly indicates neodymium *cyclo*-triphosphate. Neodymium *catena*-polyphosphate is a long-chain polymer and should be indicated as $[Nd(PO_3)_3]_n$. However, because it is usually indicated as $Nd(PO_3)_3$, in the present study also $Nd(PO_3)_3$ will be used. However, it must be noted that NdP_3O_9 and $Nd(PO_3)_3$ obviously indicate several different compounds. Such being the case, there remain many obscurities regarding rare earth phosphates; moreover, no systematic studies of their preparation have been made at all. Further, it is considered that the establishment of preparation methods for various rare earth phosphates may contribute greatly to the development of the chemistry of rare earth phosphates. Thus, the present authors have investigated in detail the conditions of the formation of orthophosphates, pyrophosphate, *catena*-polyphosphates and ultraphosphates by the reactions of rare earth oxides with phosphoric acid; they have thus established the conditions of the formation of these phosphates.

Experimental

Preparation of Rare Earth Phosphates. In a gold or porcelain crucible, 99.9% portions of rare earth oxides (La_2O_3, CeO_2, Pr_6O_{11}, and Sm_2O_3 made by Shin-etsu Kagaku Co., Ltd.) was mixed with 85% orthophosphoric acid of a special grade in an atomic ratio P/Ln (R)=1—40, where Ln=La, Ce, Pr, and Sm; each mixture was dehydrated by heating with a weak flame. Each mixture gradually became viscous and gave a transparent liquid. However, in the region of R=1—3, an exothermic reaction occurred only by mixing each oxide with phosphoric acid, and the mixture solidified. Lanthanum oxide La_2O_3 reacted especially actively, while CeO_2 was inactive. Transparent liquids and matter obtained by the manner described above were heated in an electric furnace at 300—800 °C for 20 h to obtain rare earth phosphates (this is designated the thermal synthetic method). The color of each product obtained varied according to its metallic ion, its atomic ratio, its heating temperature, and its particle size. Rare earth phosphates prepared by the above method were generally hard, especially those prepared at high temperatures above 500 °C with R=1—5. Thus, these products were roughly crushed in a mortar, pulverized for about 30 min with a grinder, washed with distilled water, dried in a desiccator on silica gel, and then used for the following experiments.

Apparatus and Methods. *X-Ray Analysis*: X-Ray analysis was carried out with a Rigaku Denki Geigerflex X-ray

diffractometer, using Ni-filtered Cu $K\alpha$ radiation. The following conditions were used for the X-ray analysis: voltage 40 kV; current, 7 mA; counter range, 1000 c.p.s; time constant, 1 s, and scanning speed 1, 0.25, and 0.125°/min. The amounts of rare earth orthophosphate $LnPO_4 \cdot 0.5H_2O$ and $LnPO_4$, *catena*-polyphosphate $Ln(PO_3)_3$, ultraphosphate LnP_5O_{14}, cerium(IV) pyrophosphate CeP_2O_7 and *catena*-polyphosphate $Ce(IV)(PO_3)_4$ formed by the thermal synthetic method were determined from the integrated intensities of their characteristic X-ray diffraction peaks; *i.e.*, $LnPO_4 \cdot 0.5H_2O$ was determined by the peak at d=4.46 Å; $LnPO_4$, by that at 3.31 Å; $Ln(PO_3)_3$, by that at 3.43 Å; LnP_5O_{14}, by that at 3.72 Å; CeP_2O_7, by that at 4.33 Å, and $Ce(PO_3)_4$, by that at 4.04 Å.

Colorimetry. Colorimetry was carried out by the use of a color-difference meter (ND-101 type) made by the Nippon Denshoku Kogyo Co., Ltd. By using a halogen lamp as the light source, diffuse reflection light was collected with an integrating sphere and detected. In these experiments, the thickness of the sample layer in the measuring cell was always maintained above 10 mm, so that the reflectivity was not affected by the thickness of the layer. Also, the deviation of the reflectivity caused by the state of the sample layer was negligibly small. All experiments were carried out for samples with a particle size of 250—300 mesh.

Infrared Absorption Spectroscopy: A Hitachi EPI-S2 spectrophotometer was used for the infrared absorption spectroscopy, the spectra being taken by means of a KBr tablet or on Nujol mulls.

The densities of various rare earth phosphates were measured by means of a Beckmann air-comparison pycnometer.

Results and Discussion

Formation of Various Rare Earth Phosphates. In the La_2O_3, Pr_6O_{11}, and Sm_2O_3–H_3PO_4 systems four kinds of phosphates were formed; two kinds of orthophosphate $LnPO_4 \cdot 0.5H_2O$ (hexagonal) and $LnPO_4$ (monoclinic), *catena*-polyphosphate $Ln(PO_3)_3$, and ultraphosphate LnP_5O_{14}, while in the CeO_2–H_3PO_4 system, differing notably from the above systems, five kinds of phosphates —orthophosphate $CePO_4$, pyrophosphate CeP_2O_7, two types of *catena*-polyphosphate $Ce(III)(PO_3)_3$, and $Ce(IV)(PO_3)_4$, and ultraphosphate CeP_5O_{14}—were formed. The difference in the products of the CeO_2 system and those of the other systems may be caused by the fact that cerium can give stable phosphates of both Ce(III) and Ce(IV). On the contrary, lanthanum, praseodymium, neodymium, and samarium give only stable phosphates of La(III), Pr(III), Nd(III), and Sm(III), while no phosphates of Pr(IV) and Sm(II) were formed at all. Figure 1 shows some X-ray diffraction patterns of *catena*-polyphosphates. In this figure, the results for *catena*-polyphosphates of La, Pr, and Sm are shown as examples. However, for *catena*-polyphosphates of other metals (Ce(III) and Nd), X-ray diffraction patterns quite similar to those shown in Fig. 1 were also obtained. As can be seen from this figure, it is obvious that the series of *catena*-polyphosphates of all these rare earth metals are isomorphous, though slight deviations of diffraction peaks caused by the difference in the ionic radii of metals can be observed. That is, the X-ray diffraction peaks shifted toward smaller angles (larger d-values) with the increase in the ionic radii of rare earth metals. It was also proved that crystals of $LnPO_4 \cdot 0.5H_2O$ and $LnPO_4$ as well as crystals of LnP_5O_{14} were isomorphous.

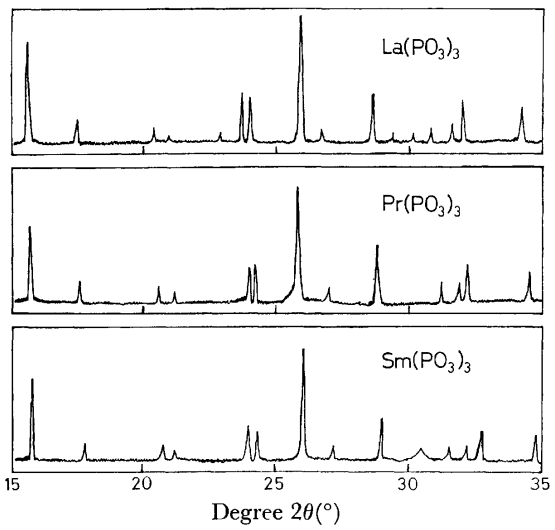

Fig. 1. X-Ray diffraction patterns of $Ln(PO_3)_3$. X-Ray used: Cu $K\alpha$(40 kV, 7 mA).

Relationship between Atomic Ratio P/Ln (R) and the Yields of Products. The reaction products of rare earth oxides with phosphoric acid seem to vary notably with the mixing ratio of the two components. The amounts of samarium ortho, *catena*-poly and ultraphosphates prepared in the Sm_2O_3–H_3PO_4 system at 700 °C for 20 h were determined from the integrated intensities of their characteristic X-ray diffraction peaks; the results are shown as a function of the mixing rate R=P/Sm in

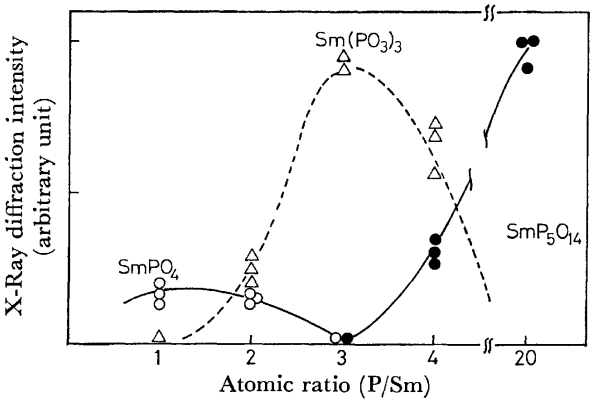

Fig. 2. Relationship between the yields of samarium phosphates and atomic ratio at 700 °C.

Fig. 2. As can be seen, at 700 °C three kinds of phosphates, $SmPO_4$, $Sm(PO_3)_3$, and SmP_5O_{14}, were formed. Orthophosphate $SmPO_4$ was formed in the R=1—2 range, while with R-values above 3 its formation was not observed at all. *catena*-Polyphosphate $Sm(PO_3)_3$ was formed in the range of R=2—8, in especially good yields in the R=3 range. This may be caused by the fact that P/Sm=3 just corresponds to the meta-composition. On the other hand, ultraphosphate began to form with R=4, and with R values above 10 was obtained in a pure form. Further, $SmPO_4 \cdot 0.5H_2O$ was formed with R= 1—2 at relatively low temperatures below 500 °C, while

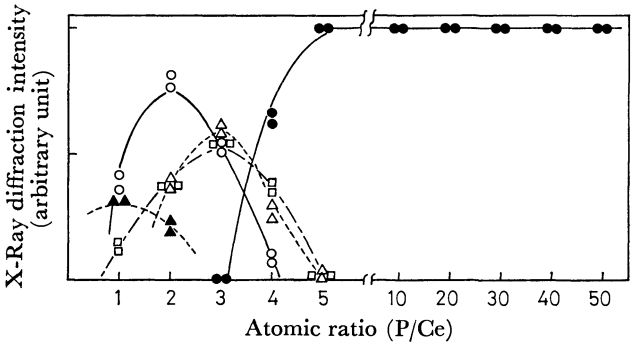

Fig. 3. Relationship between atomic ratio (P/Ce) and the yields of cerium phosphates at 800 °C. --▲--: $CePO_4$, —○—: CeP_2O_7, -—□—; $Ce(PO_3)_3$, --△--: $Ce(PO_3)_4$, —●—: CeP_5O_{14}.

at temperatures above 600 °C its formation could not be observed at all. In the La_2O_3, Nd_2O_3, and Pr_6O_{11}–H_3PO_4 systems, almost the same tendency as that in the Sm_2O_3–H_3PO_4 system was observed. On the other hand, in the CeO_2–H_3PO_4 system a tendency markedly different from that in other systems was found, as is shown in Fig. 3, in which results obtained by heating a mixture of CeO_2 and H_3PO_4 at 800 °C for 20 h are shown. Orthophosphate $CePO_4$ was formed in the R= 1—2 range, CeP_2O_7, in the R=1—4 range, $Ce(PO_3)_3$, in the R=1—4 range, and $Ce(PO_3)_4$, in the R=2—4 range. Thus, in the range of R=1—4 all these compounds were formed as mixtures, and it was impossible to obtain any of them in a pure form. On the other hand, CeP_5O_{14}, which was formed beginning at R=4, could be obtained purely at R above 5. Further, the present authors investigated the formation of cerium phosphates in the range of R=50—200 and at high temperatures (above 600 °C); only ultraphosphate was found to be obtained in all experiments. Also, no formation of $CePO_4 \cdot 0.5H_2O$ could be observed at all in the CeO_2–H_3PO_4 system.

Relationship between Heating Temperature and Products. The relation between the amounts of products and the heating temperature in the CeO_2–H_3PO_4 system with R=4 is shown in Fig. 4. As can be seen, cerium phosphates formed with R=4 were of four kinds: CeP_2O_7, $Ce(PO_3)_4$, $Ce(PO_3)_3$, and CeP_5O_{14}, and the formation of these compounds was strongly affected by the heating

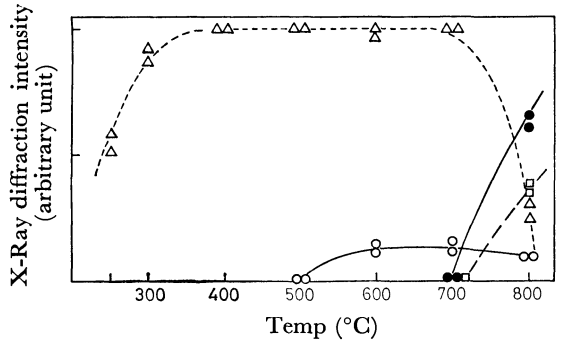

Fig. 4. Relationship between heating temperature and the yields of cerium phosphates in P/Ce=4. —○—: CeP_2O_7, --□--: $Ce(PO_3)_3$, --△--: $Ce(PO_3)_4$, —●—: CeP_5O_{14}.

temperature. Pyrophosphate CeP_2O_7 was formed above 600 °C, but its yield was very small compared with those of the other products. This may be caused by the fact that the amount of phosphoric acid corresponding to R=4 is too much for the preparation of pyrophosphate, but lies in the ultra-component region. *catena*-Polyphosphate $Ce(PO_3)_4$ was formed in a wide temperature range (250—800 °C); especially, it could be obtained purely at 400—500 °C. At 600—700 °C, cerium *catena*-polyphosphate was contaminated with pyrophosphate. Further, at temperatures above 800 °C, the yield of $Ce(PO_3)_4$ decreased rapidly, and corresponding to its decrease, the formation of $Ce(PO_3)_3$ and CeP_5O_{14} was predominant. This phenomenon may be attributed to the transformation of Ce(IV) into Ce(III) through the decomposition of $Ce(PO_3)_4$, accompanied with oxygen evolution. Further studies of the decomposition mechanism and of the effects of the heating temperature and the heating atmosphere are now in progress. The relation between the heating temperature and the product in the R range from 1 to 50 is summarized in Fig. 5, in which the amount of each

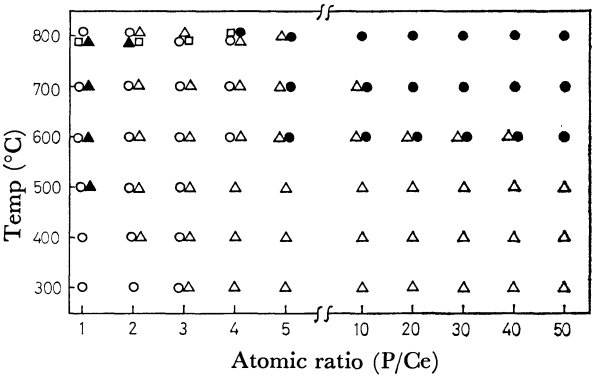

Fig. 5. Relationship of the species of cerium phosphates to heating temperature and atomic ratio. ▲: $CePO_4$, ○: CeP_2O_7, □: $Ce(PO_3)_3$, △: $Ce(PO_3)_4$, ●: CeP_5O_{14}.

cerium phosphate obtained is wholly omitted. Cerium orthophosphate $CePO_4$ was formed with R=1 above 500 °C, while with R=2, it was formed at 800 °C. Pyrophosphate CeP_2O_7 was formed in the range R= 1—3, regardless of the heating temperature, while with R=4, it was formed only at high temperatures (above 600 °C). On the other hand, the region of the formation of $Ce(PO_3)_4$ was wide as compared with those of the other cerium phosphates. It was proved that $Ce(PO_3)_4$ could be obtained in a pure form, especially at low temperatures below 500 °C with a large R, that is, in a much phosphoric acid region. However, with R-values of more than 20, because of the excess phosphoric acid a fairly long time (2—5 weeks) was necessary to form $Ce(PO_3)_4$ crystals; accordingly, the yield was decreased. It was also proved that $Ce(PO_3)_3$ was formed in the R range of 1—4 at high temperatures (above 800 °C) in the CeO_2–H_3PO_4 system; there existed no regions in which $Ce(PO_3)_3$ could be purely synthesized. Also, the formation of this compound could not be observed at all below 700 °C. On the other hand, CeP_5O_{14} was formed above 600 °C and $R \geqq 5$, in an especially large

amount at 700—800 °C with R above 20. As has been reported previously, in the Nd_2O_3–H_3PO_4 system[18] the temperature of the formation of NdP_5O_{14} shifted toward the lower-temperature side with an increase in the P/Nd atomic ratio, that is, with an increase in the amount of phosphoric acid. For instance, with P/Nd= 4—5, the lower-temperature limit of NdP_5O_{14} formation was 500 °C, while with P/Nd above 10, the temperature of the formation has lowered to 400 °C. The temperature of the formation of CeP_5O_{14} in the CeO_2–H_3PO_4 system was quite high (above 600 °C), and no shift toward the lower-temperature side with an increase of R could be observed. This may be caused by the fact that only $Ce(PO_3)_4$ can exist stably at temperatures below 600 °C. It was also found that products in the CeO_2–H_3PO_4 system was notably different from those in the La_2O_3, Pr_6O_{11}, Nd_2O_3, and Sm_2O_3–H_3PO_4 systems. This difference may be explained as follows. In the CeO_2–H_3PO_4 system, both trivalent and quadrivalent cerium phosphates, that is, cerium(III) ortho, *catena*-poly, and ultraphosphates, as well as cerium(IV) pyro and *catena*-polyphosphates, can exist stably. On the other hand, all the phosphates of La, Pr, Nd, and Sm obtained in the present study were trivalent rare earth metal phosphates. The crystal structures (X-ray diffraction patterns and infrared absorption spectra) and properties (thermal change) of Ce(III) ortho, *catena*-poly, and ultraphosphates were

Table 1. Preparation of rare earth phosphates at 300, 500, and 700 °C

Ln	Temp °C	P/Ln = 1	2	3	4	20	40
La	300	$LaPO_4 \cdot 0.5H_2O$(m) + $LaPO_4$(w)	$LaPO_4$(m) + $La(PO_3)_3$(w)	$LaPO_4$(w) + $La(PO_3)_3$(s)	$LaPO_4$(w) + $La(PO_3)_3$(s)	$La(PO_3)_3$(s)	$La(PO_3)_3$(s)
	500	$LaPO_4$(m)	$LaPO_4$(m) + $La(PO_3)_3$(m)	$La(PO_3)_3$(vs)	$La(PO_3)_3$(s) + LaP_5O_{14}(s)	LaP_5O_{14}(vs)	LaP_5O_{14}(vs)
	700	$LaPO_4$(m)	$LaPO_4$(m) + $La(PO_3)_3$(m)	$La(PO_3)_3$(vs)	$La(PO_3)_3$(s) + LaP_5O_{14}(s)	LaP_5O_{14}(vs)	LaP_5O_{14}(vs)
Ce	300	CeP_2O_7(m)	CeP_2O_7(vs)	CeP_2O_7(m) + $Ce(PO_3)_4$(w)	$Ce(PO_3)_4$(m)	$Ce(PO_3)_4$(s)	$Ce(PO_3)_4$(s)
	500	$CePO_4$(vw) + CeP_2O_7(m)	CeP_2O_7(vs) + $Ce(PO_3)_4$(w)	CeP_2O_7(s) + $Ce(PO_3)_4$(m)	$Ce(PO_3)_4$(vs)	$Ce(PO_3)_4$(vs)	$Ce(PO_3)_4$(vs)
	700	$CePO_4$(w) + CeP_2O_7(m)	CeP_2O_7(vs) + $Ce(PO_3)_4$(w)	CeP_2O_7(m) + $Ce(PO_3)_4$(m)	CeP_2O_7(vw) + $Ce(PO_3)_4$(vs)	CeP_5O_{14}(vs)	CeP_5O_{14}(vs)
Pr	300	$PrPO_4 \cdot 0.5H_2O$(w) + $PrPO_4$(w)	$PrPO_4$(m) + $Pr(PO_3)_3$(w)	$Pr(PO_3)_3$(s)	$Pr(PO_3)_3$(s)	$Pr(PO_3)_3$(vs)	$Pr(PO_3)_3$(vs)
	500	$PrPO_4$(m)	$PrPO_4$(m) + $Pr(PO_3)_3$(w)	$Pr(PO_3)_3$(s)	$Pr(PO_3)_3$(s) + PrP_5O_{14}(m)	PrP_5O_{14}(vs)	PrP_5O_{14}(vs)
	700	$PrPO_4$(m)	$PrPO_4$(m) + $Pr(PO_3)_3$(m)	$Pr(PO_3)_3$(s)	$Pr(PO_3)_3$(s) + PrP_5O_{14}(m)	PrP_5O_{14}(vs)	PrP_5O_{14}(vs)
Nd	300	$NdPO_4 \cdot 0.5H_2O$(m)	$NdPO_4$(m) + $Nd(PO_3)_3$(vw)	$NdPO_4$(m) + $Nd(PO_3)_3$(w)	$NdPO_4$(m) + $Nd(PO_3)_3$(m)	$Nd(PO_3)_3$(s)	$Nd(PO_3)_3$(vs)
	500	$NdPO_4$(m)	$NdPO_4$(w) + $Nd(PO_3)_3$(m)	$Nd(PO_3)_3$(s)	$Nd(PO_3)_3$(s) + NdP_5O_{14}(m)	NdP_5O_{14}(vs)	NdP_5O_{14}(vs)
	700	$NdPO_4$(m)	$NdPO_4$(m) + $Nd(PO_3)_3$(m)	$Nd(PO_3)_3$(vs)	$Nd(PO_3)_3$(s) + NdP_5O_{14}(m)	NdP_5O_{14}(vs)	NdP_5O_{14}(vs)
Sm	300	$SmPO_4 \cdot 0.5H_2O$(m)	$SmPO_4 \cdot 0.5H_2O$(m) + $SmPO_4$(w)	$SmPO_4$(m)	$SmPO_4$(m) + $Sm(PO_3)_3$(m)	$Sm(PO_3)_3$(s)	$Sm(PO_3)_3$(s)
	500	$SmPO_4 \cdot 0.5H_2O$(w) + $SmPO_4$(m)	$SmPO_4 \cdot 0.5H_2O$(w) + $SmPO_4$(m) + $Sm(PO_3)_3$(m)	$Sm(PO_3)_3$(s)	$Sm(PO_3)_3$(m) + SmP_5O_{14}(w)	SmP_5O_{14}(vs)	SmP_5O_{14}(vs)
	700	$SmPO_4$(m)	$SmPO_4$(m) + $Sm(PO_3)_3$(m)	$Sm(PO_3)_3$(s)	$Sm(PO_3)_3$(s) + SmP_5O_{14}(m)	SmP_5O_{14}(vs)	SmP_5O_{14}(vs)

X-Ray diffraction intensity: vs: very strong; s: strong; m: medium; w: weak; vw: very weak.

Table 2. Preparation of crystalline rare earth phosphates

	$LnPO_4 \cdot 0.5H_2O$	$LnPO_4$	LnP_2O_7	$LnP_3O_9 \cdot xH_2O$	$Ln_4(P_4O_{12})_3 \cdot xH_2O$	$Ln(PO_3)_3$	$Ln(PO_3)_4$	LnP_5O_{14}
La(III) (1.061 Å)	I, II	I	—	II	II	I	—	I
Ce(III) (1.034 Å)	II	I	—	II	II	I	—	I
Ce(IV) (0.92 Å)	—	—	I	—	—	—	I	—
Pr(III) (1.013 Å)	I, II	I	—	II	II	I	—	I
Nd(III) (0.995 Å)	I, II	I	—	II	II	I	—	I
Sm(III) (0.964 Å)	I, II	I	—	II	II	I	—	I

I: Thermal synthetic method, II: aqueous solution reaction method, —: these phosphates can not be prepared by the methods of I and II.

similar to those of the corresponding phosphates of La, Pr, Nd, and Sm. In the lanthanum, cerium, praseodymium, neodymium, and samarium systems, experimental results on the preparation of the various rare earth phosphates described above are summarized in Table 1.

Results of studies of the formation of various crystalline phosphates prepared by the reactions of La_2O_3, CeO_2, Pr_6O_{11}, Nd_2O_3, or Sm_2O_3 with phosphoric acid (the thermal synthetic method), as well as those prepared by the reactions of aqueous solutions of $LaCl_3$, $CeCl_3$, $Ce(SO_4)_2$, $PrCl_3$, $NdCl_3$, or $SmCl_3$ with orthophosphoric acid or aqueous solutions of various sodium phosphates (this is designated as the aqueous solution reaction method) are summarized in Table 2. The compounds formed by the thermal synthetic method were $LnPO_4 \cdot 0.5H_2O$, $LnPO_4$, $Ln(PO_3)_3$, and LnP_5O_{14} in the lanthanum, praseodymium, neodymium, and samarium systems, and $CePO_4$, CeP_2O_7, $Ce(PO_3)_3$, $Ce(PO_3)_4$, and CeP_5O_{14} in the cerium system. On the other hand, the crystalline compounds formed by the aqueous solution reaction method were $LnPO_4 \cdot 0.5H_2O$, $LnP_3O_9 \cdot xH_2O$, and $Ln_4(P_4O_{12})_3 \cdot xH_2O$.

As La(III), Ce(III), Pr(III), Nd(III), and Sm(III) are almost equal in their ionic radii, they give isomorphic crystals of ortho, *cyclo*-tri, *cyclo*-tetra, *catena*-poly, and ultraphosphates. On the contrary, as crystalline phosphates of Ce(IV) only CeP_2O_7[19] and $Ce(PO_3)_4$[20] are known at present.

Colors of Rare Earth Phosphate Powders. Generally, the colors of rare earth phosphates prepared by the thermal synthetic method vary considerably depending on their preparation conditions (for example, the mixing rate of metallic oxides and phosphoric acid, or the heating temperature) and also on the sizes of their crystalline particles. However, the particle sizes were kept constant (250—300 mesh) in the present study, so the colors of the phosphates may depend strongly on the species of the products. In the lanthanum system, white crystals were obtained regardless of the atomic ratio and the heating temperature. In the cerium system, a light yellow cerium phosphate was obtained at low temperatures (below 500 °C), while above 500 °C with $R \geqq 10$ a white cerium phosphate was formed. In the neodymium system also, the colors of the crystals formed varied in the range from light blue to pink, according to the atomic ratio. In the praseodymium system, dark grey crystals were obtained with a small R, while with an increase in R, *i.e.*, with an increase in the amount of phosphoric acid, more yellowish green crystals were formed. In the samarium system, light yellow crystals were formed regardless of the atomic ratio and the heating temperature. The color changes

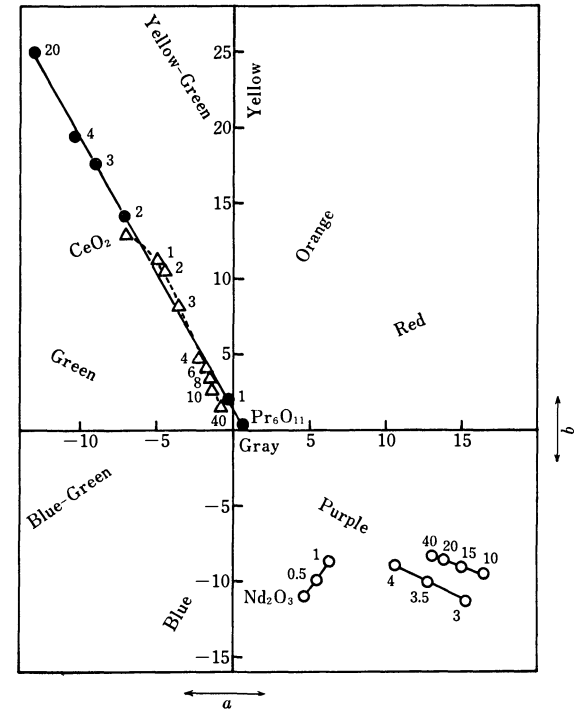

Fig. 6a. Changes of chromaticity coordinates (a and b) of cerium, praseodymium, and neodymium phosphates. --△--: Cerium, —●—: praseodymium, —○—: neodymium.

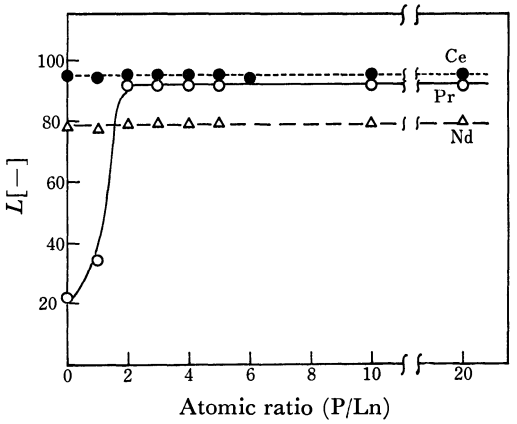

Fig. 6b. Relationship between atomic ratio and the lightness(L) of cerium, praseodymium, and neodymium phosphates.

of these rare earth phosphates will henceforth be expressed with the Lab system,[21,22] which is frequently used in colorimetry. The Lab system has perceptively almost uniform paces, and each color is expressed as a point in a three-dimensional color space. In the Lab system, L shows lightness and a, b show chromaticity coordinates, while a hue is expressed with $\theta=\tan^{-1} b/a$, and saturation, with $\sqrt{a^2+b^2}$. The Lab patterns of the phosphates obtained in the cerium, praseodymium, and neodymium systems are plotted against the atomic ratio in Figs. 6-a, b. The phosphates shown in Fig. 6 were prepared by heating at 700 °C for 20 h. In the cerium system, the product obtained at $R=0$—3 is light yellow, but with the increase in R it gradually becomes whitish. This is also supported by the results of colorimetry. It is found that the starting material (CeO_2) is light yellow, and with the increase in R (in other words, with the increase in the yields of CeP_2O_7, $Ce(PO_3)_4$, and CeP_5O_{14}), cerium phosphate approaches the hue of grey white, that is, to an achromatic color (saturation $\sqrt{a^2+b^2}=0$). However, the lightness, L, depends little on the atomic ratio, R.

In the praseodymium system, the color change is the reverse of that in the cerium system. That is, in the praseodymium system the color of the crystals changes from black (an achromatic color) to yellowish green. With R between 1 and 2, a and b change remarkably, while when R reaches 2, the product begins to turn yellowish green. This result corresponds to the increase in the yield of $Pr(PO_3)_3$, as is shown by the results of X-ray analysis. As the saturation increases with the increase in R, that is, with the successive formation of $PrPO_4 \rightarrow Pr(PO_3)_3 \rightarrow PrP_5O_{14}$, it is understandable that the product gains a brilliant hue. However, as $\theta=\tan^{-1} b/a$ is constant, no change in the hue of the product can be observed at all. On the other hand, as the lightness L varies rapidly in the R range of 0—2, the product obviously turns from black to white.

In the neodymium system, it is clearly observed that, with the increase in R, the color of the neodymium phosphates changes from blue through violet to pink; the results of colorimetry also show the existence of three different types of color changes. It is proved that the color of particles changes from blue to violet in the $R=0$—1 range, while in the $R=3$—4 range the product becomes more purple. However, in the R range from 3 to 4, as the saturation decreases it is apparent that the product approaches an achromatic color. Further, as the straight line on the a—b plane corresponding to $R=10$—40 shifts from that corresponding to $R=3$—4 toward the a-axis, the color of the product obviously changes from purple to red. While L is almost independent of R, the hues of the products with $R=0$—1, 3—4, and 10—40 are quite different from one another. This phenomenon suggests that, in the neodymium system, because of the wide variation in the color tones of the products from blue to red, the color of the particles is strongly affected by the species of neodymium phosphates formed; consequently, three different types of color changes are observed, as is shown in the figure.

Densities of Various Rare Earth Phosphates. The densities of the orthophosphates $LnPO_4$, *catena*-polyphosphates $Ln(PO_3)_3$, and ultraphosphates LnP_5O_{14} of La(III), Ce(III), Pr(III), Nd(III), and Sm(III), as well as of cerium(IV) *catena*-polyphosphate $Ce(PO_3)_4$, prepared by the thermal synthetic method are given in Table 3. The densities of rare earth orthophosphates, reported in detail by Mooney[23] and Weigel *et al.*,[24] are also given in the table for reference. For each metal, the density decreases in this order: $LnPO_4 \rightarrow Ln(PO_3)_3 \rightarrow LnP_5O_{14}$, showing that the P/Ln atomic ratio increases in the same order; the metallic ion content in unit cell of each crystal decreases accordingly.

Table 3. Densities of rare earth phosphates

	La	Ce	Pr	Nd	Sm
$LnPO_4$	5.18	5.30[a]	5.45	5.53	5.92
	5.09[23]	5.23[23]	5.34[23]	5.50[23]	5.82[24]
$Ln(PO_3)_3$	3.46	3.57[a]	3.68	3.63	3.90
$Ce(PO_3)_4$		3.28			
LnP_5O_{14}	3.29	3.43	3.35	3.36	3.45

[a] Cerium orthophosphate, $CePO_4$, and *catena*-polyphosphate, $Ce(PO_3)_4$, were prepared by the reaction of $CeCl_3$ with H_3PO_4.

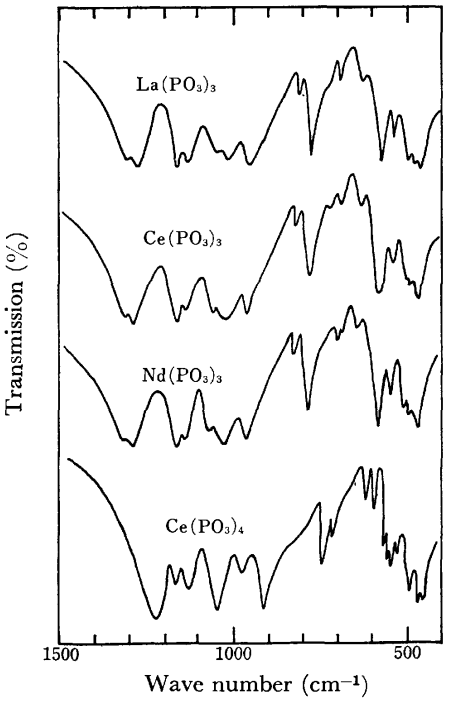

Fig. 7. IRS of $Ln(PO_3)_3$ and $Ce(PO_3)_4$.

Infrared Absorption Spectra (IRS). Figure 7 shows the IRS of $La(PO_3)_3$, $Ce(PO_3)_3$ (prepared by the reaction of $CeCl_3$ with H_3PO_4), $Nd(PO_3)_3$, and $Ce(PO_3)_4$, while Fig. 8 shows those of LaP_5O_{14}, CeP_5O_{14}, and NdP_5O_{14}. As can be seen from Figs. 7 and 8, the IRS of each phosphate is quite similar to those of the others; this fact strongly supports the above-presented conclusion of the X-ray diffraction study that each series of phosphates is crystallographically isomorphous. In the spectra of $Ln(PO_3)_3$, the absorption peaks at 1265—1300 cm^{-1} must be assigned to P=O; those at 1100—1200, 1000, and about 600 cm^{-1} to PO_3, and

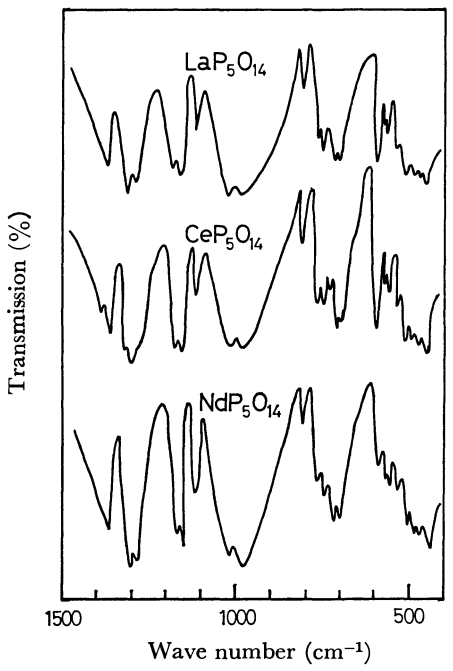

Fig. 8. IRS of LnP_5O_{14}.

those at 970 and about 830—750 cm^{-1}, to the P–O–P linkage. Further, the absorption spectrum of $Ce(PO_3)_4$ differs entirely from that of $Ce(PO_3)_3$, suggesting that the two compounds differ in bonding states from each other. However, for ultraphosphates the assignment of each absorption is not yet clear.

Conclusion

The experimental results can be summarized as follows:

1) In the La_2O_3, Pr_6O_{11}, and Sm_2O_3–H_3PO_4 systems, orthophosphate, *catena*-polyphosphate, and ultraphosphate are obtained.

2) In the CeO_2–H_3PO_4 system, trivalent and quadrivalent cerium phosphates, *i.e.*, cerium(III) ortho, *catena*-poly, and ultraphosphates, as well as cerium(IV) pyro and *catena*-polyphosphates can be prepared. The main products in this system are CeP_2O_7, $Ce(PO_3)_4$, and CeP_5O_{14}.

3) The crystal of each corresponding phosphate (ortho, *catena*-poly, and ultraphosphates) of La, Ce(III), Pr, Nd, and Sm is isomorphous.

4) In the lanthanum, praseodymium, and samarium systems, $LnPO_4 \cdot 0.5H_2O$ is readily formed at 300 °C with an atomic ratio of $R=1$, while $LnPO_4$ is formed at high temperatures (above 600 °C) with $R=1$. *catena*-Polyphosphate $Ln(PO_3)_3$ can be prepared above 500 °C with $R=3$ or by heating at 300 °C for 2—7 d with $R \geqq 10$. Ultraphosphate LnP_5O_{14} is obtained by heating at temperatures above 500 °C with $R \geqq 10$.

5) Cerium pyrophosphate CeP_2O_7 is formed with $R=1$—3, regardless of the heating temperature, while $Ce(PO_3)_4$ is easily obtained at low temperatures (below 500 °C) over a larger R region. Ultraphosphate CeP_5O_{14} can be synthesized purely at 700—800 °C with $R \geqq 20$.

6) Lanthanum phosphates are white, while cerium(IV) and cerium(III) phosphates are yellow and white respectively. Praseodymium phosphates are green, neodymium phosphates with a small R are bluish violet, those with a larger R are pink, and samarium phosphates are light yellow.

The authors wish to express their deep thanks to Assistant Professor Yoshihisa Matsuda of Kobe Women's College of Pharmacy for his many helpful discussions.

References

1) H. G. Danielmeyer and H. P. Weber, *J. Quantum. Electronics*, **8**, 805 (1972).
2) C. Brecher, *J. Chem. Phys.*, **61**, 2297 (1974).
3) T. C. Damen, H. P. Weber, and B. C. Tofield, *Appl. Phys. Lett.*, **23**, 519 (1973).
4) K. -R. Albrand, R. Attig, J. Fenner, J. P. Jeser, and D. Mootz, *Mat. Res. Bull.*, **9**, 129 (1974).
5) S. Ohasi, *Kogyo Kagaku Zasshi*, **66**, 538 (1963).
6) J. W. Gryder, G. Donnay, and H. M. Ondik, *Acta Crystallogr.*, **11**, 38 (1958).
7) Van Wazer, "Phosphorus and Its Compounds," Interscience Publishers, New York (1966), Vol. 1, p. 708.
8) W. L. Hill, G. T. Faust, and D. S. Reynolds, *Am. J. Sci.*, **242**, 457, 542 (1944).
9) S. Jaulmes, *C. R. Acad. Sci.*, **268**, 935 (1969).
10) M. Bagieu-Beucher and D. Tranqui, *Bull. Soc. Fr. Mineral. Cristallogr.*, **93**, 505 (1970).
11) H. Y-P. Hong, *Acta Crystallogr., Sect. B*, **30**, 468 (1974).
12) H. Schulz, K. -H. Thiemann, and J. Fenner, *Mater. Res. Bull.*, **9**, 1525 (1974).
13) H. Y-P. Hong and J. W. Pierce, *Mater. Res. Bull.*, **9**, 179 (1974).
14) B. C. Tofield, H. P. Weber, T. C. Damen, and G. A. Pasteur, *Mater. Res. Bull.*, **9**, 435 (1974).
15) N. Karayianis, C. A. Morrison, and D. E. Wortman, *J. Chem. Phys.*, **64**, 3890 (1976).
16) E. Kobayashi, "Chemistry and Application of Phosphates. Condensed Phosphates," Kagaku, Kogyo-sha, Tokyo (1969), p. 117.
17) P. A. Durif, *Bull. Soc. Fr. Mineral. Cristallogr.*, **94**, 314 (1971).
18) M. Tsuhako, S. Ikeuchi, T. Matsuo, I. Motooka, and M. Kobayashi, *Nippon Kagaku Kaishi*, **1978**, 676.
19) H. Völlenkle, A. Wittmann, and H. Nowotny, *Monatsh. Chem.*, **94**, 956 (1963).
20) M. Tsuhako, S. Ikeuchi, T. Matsuo, I. Motooka, and M. Kobayashi, *Chem. Lett.*, **1977**, 195.
21) Y. Matsuda, S. Shiromoto, Y. Takeda, S. Hayashi, and J. Okada, *Chem. Pharm. Bull.*, **22**, 2803 (1974).
22) Y. Matsuda and Y. Minamida, *Chem. Pharm. Bull.*, **24**, 2229 (1976).
23) R. C. L. Mooney, *J. Chem. Phys.*, **16**, 1003 (1948).
24) F. Weigel, V. Scherer, and H. Henshel, *Radiochim. Acta*, **4**, 18 (1965).

The Chemistry of Americium. IV. The Stability of Am(V) and Am(VI) in Nitric Acid Solutions and in the Solutions Containing Ozone Gas, Fluoride, or Phosphate Ions

Mitsuo HARA* and Shin SUZUKI

The Research Institute for Iron, Steel, and Other Metals, Tohoku University, Katahira 2-chome, Sendai 980

(Received July 31, 1978)

The coprecipitation technique with $BiPO_4$ and ThF_4 was applied to studying the stability of Am(V) and Am(VI) at concentrations lower than 10^{-6} M. It was found that ^{241}Am(V) and ^{241}Am(VI) were rapidly reduced to ^{241}Am(III) in nitric acid solutions at low acidities and at high temperatures, but the reduction was effectively inhibited by the presence of ozone gas or fluoride ions. On the other hand, ^{243}Am(V) and ^{243}Am(VI) were found to be rather stable in nitric acid solutions, while they were readily reduced to ^{243}Am(III) in phosphate solutions in the same manner as ^{241}Am(V) and ^{241}Am(VI).

Most investigations on the chemical properties of Am(V) and Am(VI) have been carried out by the use of an α-emitter ^{241}Am($t_{1/2}$=433 y); its α-decay leads to the radiolytic reduction of Am(V) and Am(VI). In an Am(V) solution, Am(III) is observed as a product. Here the variation of Am(III) and Am(V) concentrations with time is expressed by an empirical equation:

$$-\frac{d[Am(V)]}{dt} = \frac{d[Am(III)]}{dt} = k_1[Am]_T, \quad (1)$$

where k_1 is an apparent rate constant and $[Am]_T$ means the total americium concentration.

In an Am(VI) solution, Am(V) and Am(III) are observed as products. The decrease in the Am(VI) concentration with time can be expressed by an empirical equation:

$$-\frac{d[Am(VI)]}{dt} = k_2[Am]_T, \quad (2)$$

where k_2 is an apparent rate constant. If no reactions other than the radiolytic reduction proceed, the growth of Am(V) can be expressed by an equation:

$$\frac{d[Am(V)]}{dt} = (k_2-k_1)[Am]_T. \quad (3)$$

Values for k_1 and k_2 have been estimated to be 0.01 and 0.03 h^{-1}, respectively, in dilute acid solutions.[1,2]

When the long-lived isotope ^{243}Am($t_{1/2}$=7400 y) is used, the radiolytic reduction is not so remarkable as that in ^{241}Am solutions.[3] On the other hand, ^{241}Am(V) and ^{243}Am(V) disproportionate to Am(VI) and Am(III) in moderately concentrated acids. The rate of disproportionation of ^{241}Am(V) in various media is expressed by the following equation,[4,5] but the rate law is rather complicated when ^{243}Am(V) is used:[3]

$$-\frac{d[Am(V)]}{dt} = k_3[Am(V)]^2[H^+]^4, \quad (4)$$

where k_3 is an apparent rate constant.

This result has been obtained by the application of spectrophotometry to the ^{241}Am and ^{243}Am solutions at concentrations of 10^{-3} M or above. The ^{241}Am and ^{243}Am solutions diluted to about 10^{-7} M and 10^{-6} M, respectively, can be studied by radiometry. In dilute solutions, Am(V) may be free from any disproportionation, while the radiolytic reduction of ^{241}Am(V) and ^{241}Am(VI) may proceed, as suggested by Eqs. 1—4. Furthermore, Am(V) and Am(VI) may be reduced by small amounts of impurities.

The information concerning the instability of Am(V) and Am(VI) at low concentrations is rather poor. Only a little information was obtained by previous works[6,7] in which the instability of Am(V) in several media was studied by means of solvent extraction with 2-thenoyltrifluoroacetone and of column chromatography using bis(2-ethylhexyl) hydrogenphosphate (HDEHP) as an extractant, where the rapid reduction of ^{241}Am(VI) by HDEHP was observed.

When the solutions of Am(V) and Am(VI) were submitted to the coprecipitation method with some fluorides and phosphates at 0—5 °C, no change of oxidation states of americium was observed.[8,9] However, this finding can not always promise the high stability of Am(V) and Am(VI) in fluoride and phosphate solutions at room temperature or above.

In this work, the instability of Am(V) and Am(VI) in nitric acid solutions and in solutions containing ozone gas, fluoride, or phosphate ions was investigated. The change of oxidation state of americium with time was traced by means of the coprecipitation method with bismuth(III) phosphate and thorium(IV) fluoride.

Experimental

Reagents. Nitric acid solutions of ^{241}Am(III) and ^{243}Am(III) were prepared by the manners described before,[6,7] and the concentrations of ^{241}Am and ^{243}Am were determined by α-spectrometry using an Si detector connected to a multichannel pulse-height analyzer. Bismuth(V) sodium oxide was added in quantities of 10 mg/ml to a 0.1 M HNO_3 solution of Am(III), and the mixture was mechanically stirred for 50 min at room temperature and for additional 10 min at 0 °C. An Am(VI) solution was obtained by filtration of the mixture with a glass fibre filter-paper, Whatman GF/A.[10]

An Am(V) solution was prepared at 0 °C by passing the Am(VI) solution through a column of Celite 545 containing HDEHP as an extractant.[7] The solutions of nitric acid and ammonium fluoride or sodium dihydrogenphosphate were added to the Am(V) and Am(VI) solutions, making concentrations up to about 10^{-7} M and 10^{-6} M with respect to ^{241}Am and ^{243}Am, respectively.

Bismuth(V) sodium oxide, min 80 wt %, was used as an oxidant. For the coprecipitation test, bismuth(III) and thorium(IV) nitrates, sodium dihydrogenphosphate, and am-

monium fluoride were used. These and other chemicals were of G.R. grade. Ozone gas, which was bubbled through the required solutions in order to eliminate as many reducing materials as possible, was supplied by an ozone generator.

Procedure. The Am(V) and Am(VI) solutions were stocked in a thermostat at a temperature kept constant with an accuracy of ± 0.5 °C. Appropriate aliquots of the stock solutions were submitted to the coprecipitation test which was carried out under such conditions that Am(III) was quantitatively carried down, while most of Am(V) and Am-(VI) remained in the solution.

Bismuth(III) phosphate and thorium(IV) fluoride were precipitated at 0 °C from the americium solution containing bismuth(III) and thorium(IV) ions, respectively, by the addition of excess precipitants under the following conditions:

Precipitate	$BiPO_4$	ThF_4
Volume	5 ml	3 ml
Acidity	0.5 M	0.1 M
Amounts of metal ion	Bi^{3+} 10 mg	Th^{4+} 1 mg
Time of mixing	7 min	10 min

The mixture was either filtered by glass fibre filter-paper or centrifuged at 6000 rpm for 5 min. The fraction of americium carried, Y, was determined by measuring the γ-activity in the mixture and the filtrate (or the supernatant). The γ-ray assay was performed by the use of a flat-type NaI(Tl) scintillation probe connected to a scaler or by the use of a Ge(Li) detector connected to a multi-channel pulse-height analyzer.

Results and Discussion

Stability of Am(V) and Am(VI) in HNO_3 Solutions. The $BiPO_4$ coprecipitation test was carried out on the nitric acid solutions of ^{241}Am(V) and ^{241}Am(VI) at proper time intervals. The results on the 0.5 M HNO_3 solutions at 0—40 °C and on the (0.125—2 M) HNO_3 solutions at 30 °C are shown in Figs. 1 and 2, respectively. The measured value for Y increased with time of storage, especially at high temperatures and at low acidities. Dependence of the increase in Y on acidity was found only for the Am(VI) solutions at temperatures higher than 20 °C.

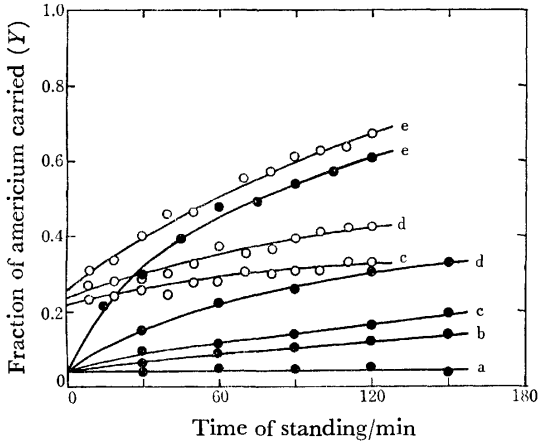

Fig. 1. The result of the $BiPO_4$ coprecipitation test carried out on the 0.5 M HNO_3 solutions of ^{241}Am(V) (○) and ^{241}Am(VI) (●) at 0 °C(a), 10 °C(b), 20 °C(c), 30 °C(d), and 40 °C(e).

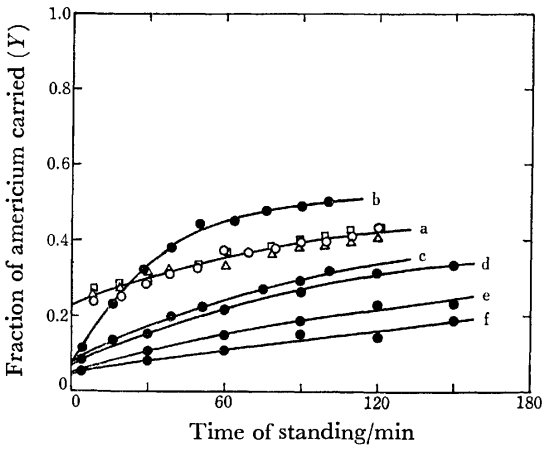

Fig. 2. The result of the $BiPO_4$ coprecipitation test carried out on the ^{241}Am(V) and ^{241}Am(VI) solutions at 30 °C.
a): ^{241}Am(V) solutions at the acidity of 0.125 M(○), 0.25 M(△), and 0.5 M(□). ●: ^{241}Am(VI) solutions at the acidity of 0.125 M(b), 0.25 M(c), 0.5 M(d), 1.0 M(e), and 2.0 M(f).

The increase in Y may be caused by the reduction of Am(V) and Am(VI) to Am(III) in the stock solutions, because Am(III) is more effectively carried by $BiPO_4$ than the others. When the mole fraction of each oxidation state of americium in the stock solution is expressed as f_X(X=III, V, and VI), Y may be given by the equation:[8]

$$Y = f_{III}Y_{III} + f_V Y_V + f_{VI}Y_{VI}, \quad (5)$$

where Y_X(X=III, V, and VI) means the fraction of Am(X) carried, which can be determined by the coprecipitation test on the corresponding single-component solution. The values for Y_X were determined as follows; $Y_{III}=0.99\pm0.01$, $Y_V=0.25\pm0.03$, and $Y_{VI}=0.05\pm0.02$ by the $BiPO_4$ coprecipitation test, and $Y_{III}=0.99\pm0.01$, $Y_V=0.12\pm0.02$, and $Y_{VI}=0.30\pm0.02$ by the ThF_4 coprecipitation test.

If the radiolytic reduction proceeds predominantly in the stock solutions of ^{241}Am, Eq. 5 can be expressed by the following equations, using the solutions of Eqs. 1—3: for the case of ^{241}Am(V) solutions,

$$Y = Y_V + (Y_{III} - Y_V)k_1 t \quad (6)$$

and for the case of ^{241}Am(VI) solutions,

$$Y = Y_{VI} + \{(Y_{III} - Y_{VI})k_1 + (Y_V - Y_{VI})k_2\}t. \quad (7)$$

Unfortunately, the linear relations expected by Eqs. 6 and 7 were valid only for the results on the stock solutions of high acidities and at low temperatures, as are shown in Figs. 1 and 2. It is clear that some reactions other than the radiolytic reduction also proceeded, especially at low acidities and at high temperatures. These reactions are assumed to be first-order reactions such as Am(VI)→Am(V) and Am(V)→Am(III), while the radiolytic reduction of Am(V) and Am(VI) are zero-order reactions with respect to Am(V) and Am-(VI).

In contrast to Eqs. 1—3, the rate law for the above-mentioned reactions can be expressed as follows:
in the case of ^{241}Am(V) solutions,

$$-\frac{d[Am(V)]}{dt} = \frac{d[Am(III)]}{dt} = k_1'[Am(V)] \quad (8)$$

and in the case of ^{241}Am(VI) solutions,

$$-\frac{d[Am(VI)]}{dt} = k_2'[Am(VI)], \quad (9)$$

and $$\frac{d[Am(V)]}{dt} = k_2'[Am(VI)] - k_1'[Am(V)], \quad (10)$$

where k_1' and k_2' are apparent rate constants.

If first-order reactions proceed predominantly in the stock solutions, Eq. 5 can be written as follows, using the solutions of Eqs. 8—10:
for the case of ^{241}Am(V) solutions,

$$Y_{III} - Y = (Y_{III} - Y_V) \exp(-k_1't), \quad (11)$$

and for the case of ^{241}Am(VI) solutions,

$$Y_{III} - Y = \frac{(Y_{III} - Y_V)k_2'}{k_2' - k_1'} \exp(-k_1't) + \left\{(Y_{III} - Y_{VI}) + \frac{(Y_{III} - Y_V)k_2'}{k_1' - k_2'}\right\} \exp(-k_2't). \quad (12)$$

As Y_{III} is nearly equal to unity, Figs. 3 and 4 illustrate the plot of $\log(1-Y)$ *vs.* t, using the data shown in Figs. 1 and 2. The relationship expected by Eqs. 11 and 12 was confirmed for the stock solutions of low acidities and at high temperatures. Thus, it is reasonable to assume that the radiolytic reduction and first-order reactions compete in the dilute ^{241}Am solutions.

The values for k_1' and k_2' were estimated by means of curve-fitting techniques; the results are shown in Table 1. The values for k_1' and k_2' fluctuated, undoubtedly depending upon whether a nitric acid solution had been used to prepare the stock solutions just after or a little after the dilution of concd nitric acid. Therefore, a certain material which induced first-order reaction had been probably introduced into the stock solutions from the nitric acid.

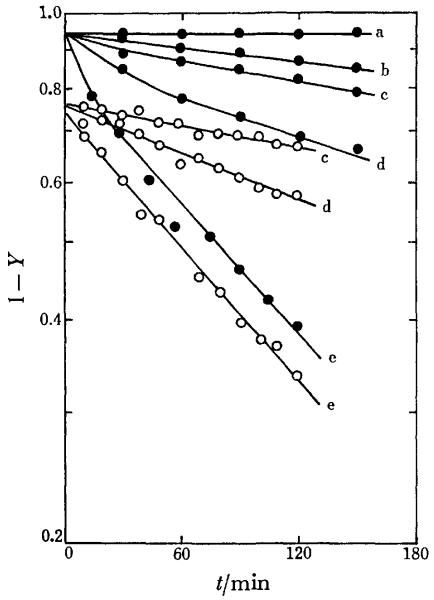

Fig. 3. The plot of $\log(1-Y)$ *vs.* t for the 0.5 M HNO_3 solutions of ^{241}Am(V)(○) and ^{241}Am(VI)(●) at 0 °C(a), 10 °C(b), 20 °C(c), 30 °C(d), and 40 °C(e).

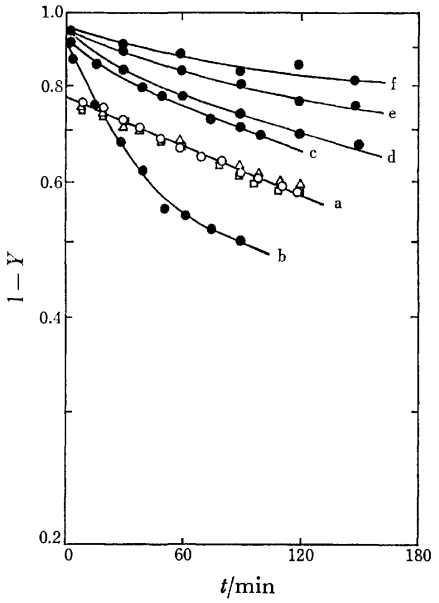

Fig. 4. The plot of $\log(1-Y)$ *vs.* t for the ^{241}Am(V) and ^{241}Am(VI) solutions at 30 °C. a): ^{241}Am(V) solutions at the acidity of 0.125 M(○), 0.25 M(△), and 0.5 M(□). ●: ^{241}Am(VI) solutions at the acidity of 0.125 M(b), 0.25 M(c), 0.5 M(d), 1.0 M(e), and 2.0 M(f).

Table 1. Apparent rate constants for the reduction of ^{241}Am(V) and ^{241}Am(VI) in HNO_3 solutions

$[HNO_3]$ M	Temperature °C	Apparent rate constant/h^{-1}		
		$k_1'^{a)}$	$k_1'^{b)}$	$k_2'^{b)}$
0.125	30	0.14±0.01	0.14±0.02	2.37±0.11
0.25	30	0.12±0.01	0.14±0.02	2.07±0.23
0.5	30	0.13±0.01	0.09±0.02	0.69±0.23
0.5	20	0.06±0.01	—	—
0.5	40	0.40±0.01	0.30±0.05	2.00±0.34

a) Result for Am(V) solutions. b) Result for Am(VI) solutions.

When the 0.05 M HNO_3 solutions of ^{243}Am(V) and ^{243}Am(VI) were investigated, no change in Y with time was observed even on the stock solutions at 30 °C. This finding may be explained only by the serious difference in emission rate of α-particles between ^{241}Am and ^{243}Am. Thus, first-order reactions are considered to be the radiation-induced reactions which may be caused by a product resulting from the interaction between the radiolysis product and the material introduced from the nitric acid.

This assumption was supported by a finding for the ^{241}Am(V) and ^{241}Am(VI) solutions containing ozone gas; that is, Y was constant for the time of storage during which the stimulative smell of ozone gas was still hanging about the vessel of the stock solutions. It can be said that ozone gas effectively eliminates any reducible materials in the same way as chlorine gas does.[4]

Stability of Am(V) and Am(VI) in HNO_3–NH_4F Solutions. The coprecipitation test with ThF_4 was carried out on the 0.05 M HNO_3 solutions of ^{241}Am(V) and ^{241}Am(VI) containing the fluoride at 30 °C, and the result is shown in Fig. 5. The Y for the stock solutions

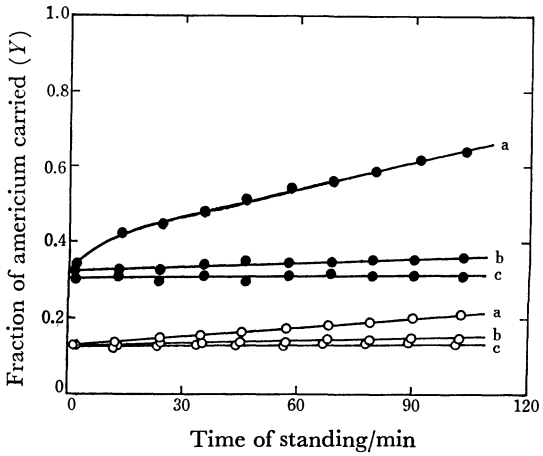

Fig. 5. The result of the ThF_4 coprecipitation test carried out on the 0.05 M HNO_3 solutions of ^{241}Am-(V)(○) and ^{241}Am(VI)(●) at 30 °C. [NH_4F]: a) 0 M, b) 0.05 M, and c) 0.5 M.

containing the fluoride increased more slowly than for the case free from fluoride, and no change in Y was observed for the 0.5 M NH_4F solutions. The stock solutions of acidity higher than 0.05 M called for rather high concentrations of the fluoride in order to minimize the variation in Y.

This finding can be explained by the suggestion that ^{241}Am(V) and ^{241}Am(VI) become free from all reduction reactions if they form fluoro complexes, as in the cases of the acetate[7] and the chloride solutions[11] of ^{241}Am(V). The excellent stability of ^{243}Am(V) and ^{243}Am(VI) in the ozonized fluoride solutions was also confirmed as expected.

Stability of Am(V) and Am(VI) in HNO_3–NaH_2PO_4 Ozonized Solutions. The coprecipitation test with $BiPO_4$ was carried out on the 0.05 M HNO_3–(0—2 M) NaH_2PO_4 and the (0.025—0.2 M) HNO_3–0.5 M NaH_2PO_4 solutions of ^{241}Am(V) and ^{241}Am(VI) at 30 °C.

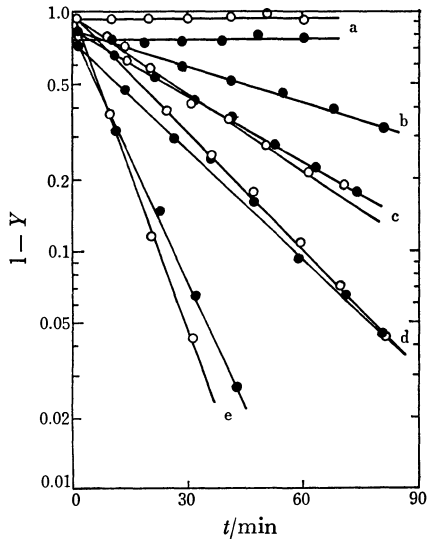

Fig. 6. The plot of $\log(1-Y)$ *vs.* t for the 0.05 M HNO_3 solutions of ^{241}Am(V)(○) and ^{241}Am(VI)(●) at 30 °C. [NaH_2PO_4]: a) 0 M, b) 0.1 M, c) 0.5 M, d) 1.0 M, and e) 2.0 M.

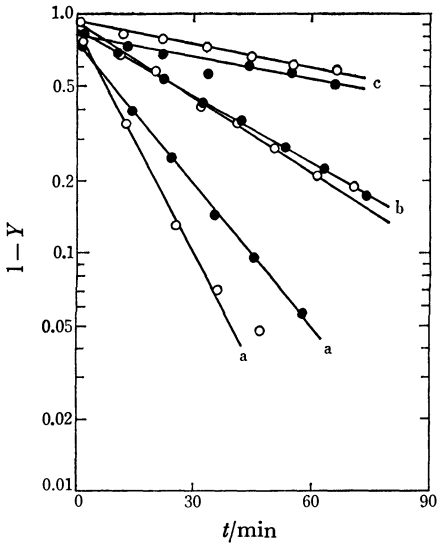

Fig. 7. The plot of $\log(1-Y)$ *vs.* t for the 0.5 M NaH_2PO_4 solutions of ^{241}Am(V)(○) and ^{241}Am(VI)(●) at 30 °C. [HNO_3]: a) 0.025 M, b) 0.05 M, and c) 0.2 M.

The Y for these ozonized solutions increased rapidly with time of storage, especially at low acidities and at high phosphate concentrations. Figures 6 and 7 illustrate the plot of $\log(1-Y)$ *vs.* t; a good linearity was obtained in most cases.

The same result was obtained both for the 0.05 M HNO_3–0.5 M NaH_2PO_4 solutions of ^{241}Am(V) and ^{241}Am(VI) at 0—40 °C and for the (0.05—0.5 M) HNO_3–1 M NaH_2PO_4 solutions of ^{243}Am(V) and ^{243}Am-(VI) at 30 °C. Evidently, the variation in Y with time for the ozonized phosphate solutions of ^{241}Am(VI) and ^{243}Am(VI) can be explained neither by Eq. 7 nor by Eq. 12.

It is known that Am(VI) at such high concentrations as 2×10^{-3} M (^{243}Am 85% and ^{241}Am 15%) is reduced to Am(III) in phosphoric acid.[12] Then, it may be assumed that Am(V) and Am(VI) at low concentrations are also reduced to Am(III) in the ozonized phosphate solutions, and that the reduction rates are given by the following equations:

$$-\frac{d[Am(V)]}{dt} = \frac{d[Am(III)]}{dt} = k_1''[Am(V)], \quad (13)$$

and

$$-\frac{d[Am(VI)]}{dt} = \frac{d[Am(III)]}{dt} = k_2''[Am(VI)], \quad (14)$$

where k_1'' and k_2'' are apparent rate constants. If the change of oxidation states of americium in the ozonized phosphate solutions is predominantly caused by these reactions, Y can be expressed as follows, using the solutions of Eqs. 13 and 14:

for the case of Am(V) solutions,

$$Y_{III} - Y = \exp(-k_1''t) \quad (15)$$

and for the case of Am(VI) solutions,

$$Y_{III} - Y = \exp(-k_2''t). \quad (16)$$

As Y_{III} is nearly equal to unity, Eqs. 15 and 16 can explain the linearity obtained by the plot $\log(1-Y)$ *vs.* t, as are shown in Figs. 6 and 7. Therefore, it seems to be reasonable to assume that Am(V) and Am(VI) are reduced to Am(III) in the ozonized phosphate solutions.

Table 2. Apparent rate constants for the reduction of Am(V) and Am(VI) in HNO_3–NaH_2PO_4 ozonized solutions

$[HNO_3]$ M	$[NaH_2PO_4]$ M	Temperature °C	Apparent rate constant/h^{-1} k_1''[a]	k_2''[a]
0.05	0	30	−0.02±0.03	−0.05±0.02
0.05	0.1	30	—	0.67±0.01
0.05	0.5	30	1.44±0.04	1.28±0.02
0.05	1.0	30	2.32±0.05	2.13±0.04
0.05	2.0	30	6.10±0.04	4.78±0.04
0.05	0.5	0	−0.06±0.03	0.00±0.02
0.05	0.5	15	0.14±0.03	0.12±0.02
0.05	0.5	40	7.63±0.06	6.08±0.06
0.025	0.5	30	4.23±0.04	2.71±0.02
0.1	0.5	30	0.65±0.04	0.55±0.04
0.2	0.5	30	0.40±0.03	0.30±0.05
0.05	0	30	0.02±0.01[b]	0.02±0.02[b]
0.05	0.1	30	1.00±0.02[b]	1.39±0.02[b]
0.05	1.0	30	10.5±0.1[b]	8.98±0.02[b]
0.5	1.0	30	2.89±0.02[b]	5.80±0.03[b]

a) Result for ^{241}Am solutions except as otherwise noted.
b) Result for ^{243}Am solutions.

Values for k_1'' and k_2'' were obtained from the slope of the straight lines. They were found to be rather large for the stock solutions of low acidities, at high phosphate concentrations, and at high temperatures, as are summarized in Table 2. The reduction of ^{243}Am(V) and ^{243}Am(VI) preceeded more rapidly than that of ^{241}Am-(V) and ^{241}Am(VI) because the ^{243}Am concentration was about ten times higher than the ^{241}Am concentration.

The available information concerning the behavior of americium in phosphoric acid[12] and the phosphato-complex formation of neptunium and plutonium[13,14] suggests that Am(V) and Am(VI) may form the phosphato complexes such as $AmO_2H_2PO_4$ and $AmO_2H_2PO_4^+$, respectively, in the phosphate solutions examined. Therefore, the rapid reduction of Am(V) and Am(VI) might result from the intramolecular electron transfer in phosphato complexes.

References

1) G. R. Hall and T. L. Markin, *J. Inorg. Nucl. Chem.*, **4**, 296 (1957).
2) G. N. Yakovlev and V. N. Kosyakov, Proc. 1st Int. Conf. on the Peaceful Uses of Atomic Energy, Geneva (1955), **7**, 363 (1956).
3) J. S. Coleman, *Inorg. Chem.*, **2**, 53 (1963).
4) R. A. Penneman and L. B. Asprey, Proc. 1st Int. Conf. on the Peaceful Uses of Atomic Energy, Geneva (1955) **7**, 355 (1956).
5) G. N. Yakovlev and V. N. Kosyakov, Proc. 2nd Int. Conf. on the Peaceful Uses of Atomic Energy, Geneva (1957), **28**, 373 (1958).
6) M. Hara, *Bull. Chem. Soc. Jpn.*, **43**, 89 (1970).
7) M. Hara and S. Suzuki, *Bull. Chem. Soc. Jpn.*, **47**, 635 (1974).
8) M. Hara and S. Suzuki, *Bull. Chem. Soc. Jpn.*, **48**, 1431 (1975).
9) F. L. Moore, *Anal. Chem.*, **35**, 715 (1963).
10) M. Hara and S. Suzuki, *J. Radioanal. Chem.*, **36**, 95 (1977).
11) M. Kasha, *J. Chem. Phys.*, **17**, 349 (1949).
12) B. F. Myasoedov, V. M. Mikhailov, I. A. Lebedov, O. E. Koiro, and V. Ya. Frankel, *Radiochem. Radioanal. Lett.*, **14**, 17 (1973).
13) A. I. Moskvin and V. F. Peretrukhin, *Radiokhimiya*, **6**, 206 (1964).
14) R. G. Denotkina and U. B. Shevelenko, *Zh. Neorg. Khim.*, **12**, 2345 (1967).

Rate of Ligand Exchange of Tris(acetylacetonato)iron(III) with 2-Thenoyltrifluoroacetone in Organic Solvents

Tatsuya SEKINE,* Hiroshi HONDA, Masakazu KOKISO, and Teruyuki TOSAKA

Department of Chemistry, Science University of Tokyo, Kagurazaka, Shinjuku-ku, Tokyo 162

(Received August 2, 1978)

The rate of exchange of acetylacetonate ions ($acac^-$) in tris(acetylacetonato)iron(III) with 2-thenoyltrifluoroacetonate ions (tta^-) has been measured in several organic solvents. The rate was independent of the concentration of Hacac and Htta and nearly the same in carbon tetrachloride, benzene, acetone, and 4-methyl-2-pentanone. However, the rate was much greater in ethanol. The rate of exchange in carbon tetrachloride, benzene, and acetone was found to be enhanced by water, ethanol, and several acids. The enhancement was smaller in acetone than in nonpolar solvents and the stronger the acid, the greater the catalytic effect. The rate controlling step of the exchange reaction was the rupture of an acetylacetonate ion from iron(III) in the complex. These observations have been discussed and possible mechanisms proposed.

In the course of studies of the chemical equilibria of metal complexes in organic solvents, it was found that exchanging the ligand of tris(acetylacetonato)iron(III) in organic solvents with other chelating ligands proceeded rather slowly. In the present paper, the rate of exchange with 2-thenoyltrifluoroacetonate ions has been studied photometrically.

Experimental

Reagents. All reagents were of reagent grade. The tris(acetylacetonato)iron(III) ($Fe(acac)_3$), acetylacetone (Hacac), 2-thenoyltrifluoroacetone (Htta), and trioctylphosphine oxide (TOPO) were supplied by Dojindo Co., Kumamoto. The organic solvents were also of analytical grade and subsequently passed through a dehydrating column containing an ion-exchanger resin supplied by Mitsubishi Kasei Co., Tokyo, and distilled.

Procedure. The experiments were conducted in a thermostatted room or in a thermostatted bath. A portion of the solvent containing a $Fe(acac)_3$ was added to another portion of the same solvent containing Htta. In several experiments, certain amounts of other materials such as an acid, TOPO, acetone, an alcohol, and/or water were added to the $Fe(acac)_3$ solution. The solution was agitated and transfferred to a glass cell (1 cm path). The change in the optical density of the solution at 550 nm was measured with a spectrophotometer (Hitachi double wavelength double beam spectrophotometer type-556 or Hitachi UV-VIS spectrophotometer type-101 or type-139) as a function of time and the increase in the $Fe(acac)_3$ concentration obtained. The water content was checked by the Karl Fischer titration.

Results

The temperature of the experiments in this study was 25 ± 0.3 °C except when the effect of the temperature was examined. All the data were found to indicate that the reaction was first order with respect to $Fe(acac)_3$ in the initial stage.

Dependence on Hacac Concentration. The rate of exchange of $acac^-$ in $Fe(acac)_3$ with tta^- was measured at several concentrations of Hacac. It was found that the rate was always independent of the co-existing Hacac concentration, at least below 0.1 mol dm^{-3}. When the Htta solution was added to the $Fe(acac)_3$ solution in the absence of Hacac the results were reproducible, at least within 5 min of the dissolution of the $Fe(acac)_3$ crystals. $Fe(acac)_3$ solutions containing no Hacac however were not stable on standing for a long time, especially under light. The addition of, for example, 10^{-3} mol dm^{-3} of Hacac to a solution of 10^{-4} mol dm^{-3} of $Fe(acac)_3$ stabilized the solution. Thus in the present study, ten to hundred times of Hacac to $Fe(acac)_3$ by molar ratio was added to the initial solution.

Dependence on Htta Concentration. The rate was measured in the concentration range of Htta from 10^{-4} to 2×10^{-1} mol dm^{-3} where it was found that the rate was independent of the Htta concentration unless it was below 10^{-3} mol dm^{-3}. This was however found to be an apparent effect; under such conditions the exchange was thermodynamically incomplete and this has been discussed later.

Effect of Solvent. The rate of exchange was measured in carbon tetrachloride and in four other solvents. The rate in ethanol was too high to be measured by the method employed but that in benzene as well as in acetone and 4-methyl-2-pentanone (MIBK) was measurable. No determination was made in water because of low solubilities of the complexes and ligands but the rate in water would be expected to be too high for the measurement as will be seen from the description on the effect of water.

From the experimental results, the rate may be written as

$$v_0 = -d[Fe(acac)_3]/dt = k_0[Fe(acac)_3]. \quad (1)$$

The rate constants in these solvents obtained from the slope of the plot of $\log [Fe(acac)_3]$ *vs.* time are listed in Table 1(a).

Effect of Water. The effect of water in the solvent was examined in carbon tetrachloride, benzene, and acetone and Fig. 1 gives the results. The rates in dehydrated carbon tetrachloride and benzene were identical with each other and increased with increase in the water content and became 2.0 and 3.7 times greater in water-saturated carbon tetrachloride and benzene, respectively. The explanation for this is in terms of the amount of water in the water-saturated solvents. The increase in the rate by water was smaller in acetone than in the two nonpolar solvents. Determination of the water content in the "dehydrated" solvents (experimental section) was not possible but the content was presumed to be lower than 10^{-4} mol dm^{-3}.

TABLE 1. SUMMARY OF CONSTANTS

$v=[Fe(acac)_3](k_0+k_c[C])$. k_c represents k_w, $k_{alc.}$, and k_{acid}, respectively (*cf.* Eqs. 2, 4, and 5).

(a) Rate constant

Solvent	log (k_0/s^{-1})
Carbon tetrachloride	−3.2
Benzene	−3.2
Acetone	−3.5
4-Methyl-2-pentanone	−3.2
Ethanol	too high to be measured
Water	too high to be measured

(b) Catalytic constant

Catalyzer	log $(k_c/s^{-1}\ mol^{-1}\ dm^3)$ Solvent		
	CCl_4	C_6H_6	$(CH_3)_2CO$
Water	−1.2	−1.2	−2.4
Ethanol	−0.8	−0.8	−2.0
Methanol	−0.8	—	—

(c) Catalytic constant in carbon tetrachloride

Acid	pK_a[a]	log $(k_c/s^{-1}\ mol^{-1}\ dm^3)$
Trichloroacetic acid	0.64	1.5
Dichloroacetic acid	1.26	1.2
Chloroacetic acid	2.87	0.6
Bromoacetic acid	2.90	0.6
1-Naphthoic acid	3.70	0.4

a) Taken from L. G. Sillen and A. E. Martell, "Stability Constants," The Chemical Society Spec. Pud., **17** (1964).

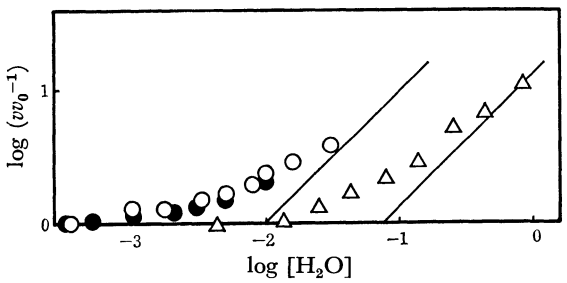

Fig. 1. Effect of water on the rate of exchange with tta^-. v is the rate in the presence of water and v_0 is that in the dehydrated solvent otherwise identical conditions. ●: CCl_4, ○: C_6H_6, △: $(CH_3)_2CO$.

The rate of reaction enhanced by water may be written as

$$v_w = -d[Fe(acac)_3]/dt = k_w[Fe(acac)_3][H_2O]^a. \quad (2)$$

The overall rate is then;

$$v = v_0 + v_w = [Fe(acac)_3](k_0+k_w[H_2O]^a). \quad (3)$$

The plot of log v *vs.* log $[H_2O]$ reached an asymptote and thus log v=log k_w+log $[H_2O]$; "a" was concluded to be unity. The values of k_w are listed in Table 1(b).

Effect of Alcohol. The effect of ethanol was examined in carbon tetrachloride, benzene, and acetone. Some experiments were conducted on the effect of methanol in carbon tetrachloride. The rate of exchange was enhanced by the alcohols and may be written as

$$v_{alc.} = -d[Fe(acac)_3]/dt = k_{alc.}[Fe(acac)_3][alcohol]^a. \quad (4)$$

The results were analyzed and from the analysis, "a" was concluded to be unity. The values for the constant $k_{alc.}$ were determined in a similar manner to that for water and the values are listed in Table 1(b).

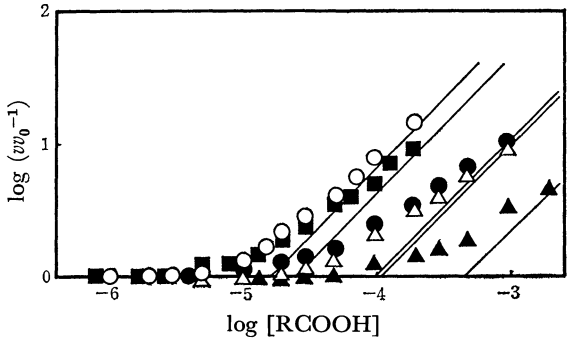

Fig. 2. Enhancement of the rate by acids in CCl_4. v is the rate in the presence of the acid and v_0 is that in the absence otherwise identical conditions. ○: CCl_3COOH, ■: $CHCl_2COOH$, ●: $CH_2ClCOOH$, △: $CH_2BrCOOH$, and ▲: 1-naphthoic acid. The straight lines of slope +1 give the calculated asymptotes, log (vv_0^{-1})=log $k_{acid}k_0^{-1}$[RCOOH] (*cf.* Eq. 6).

Effect of Acids. The rate was enhanced by various carboxylic acids. Figure 2 gives the results in carbon tetrachloride. The rate of reaction catalyzed by acids may be written as

$$v_{acid} = -d[Fe(acac)_3]/dt = k_{acid}[Fe(acac)_3][RCOOH]^a. \quad (5)$$

From an analysis of the results, "a" was concluded to be unity in all cases and the rate may be thus written

$$v = v_0 + v_{acid} = [Fe(acac)_3](k_0+k_{acid}[RCOOH]). \quad (6)$$

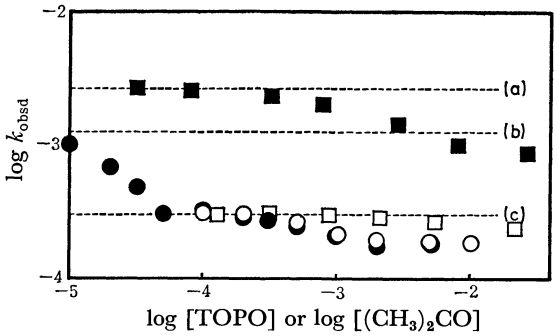

Fig. 3. Effect of TOPO and acetone on the rate. k_{obsd} is $v[Fe(acac)_3]^{-1}=(k_0+k_{acid}[RCOOH])$ (*cf.* Eq. 6). Open symbols give the effect of TOPO (circles) and acetone (squares) on the rate in the absence of any acid in CCl_4. Closed squares give the effect of acetone on the rate in the presence of 2.0×10^{-4} mol dm^{-3} of dichloroacetic acid in CCl_4. Closed circles give the effect of TOPO on the rate in the presence of 4.2×10^{-5} mol dm^{-3} of trichloroacetic acid in CCl_4. Dotted lines show the values of k_{obsd} when the concentration of dichloroacetic acid was 2.0×10^{-4} mol dm^{-3} in the absence of acetone (a), the concentration of trichloroacetic acid was 4.2×10^{-5} mol dm^{-3} in the absence of TOPO (b), and when the solvent contained none of these materials (c). When the molar ratio of TOPO and trichloroacetic acid is 1: 1, the catalysis disappeared.

The values for the constant k_{acid} are given in Table 1(c).

Effect of Temperature. The rate of exchange was also determined at 15 and 35 °C. From these data and that at 25 °C, the activation energies were determined and the values of activation enthalpy (ΔH^*) and entropy (ΔS^*) for k_0 and k_c calculated the values of which given in Table 2.

TABLE 2. SUMMARY OF ACTIVATION PARAMETERS FOR k_c IN CARBON TETRACHLORIDE AT 25 °C[a)]

Catalyzer	ΔH^* (kJ mol^{-1})	ΔS^* (J K^{-1} mol^{-1})
Water	18±3	−223±20
Methanol	23±3	−182±15
Ethanol	23±3	−176±16
Trichloroacetic acid	22±2	−160±14

a) The values of ΔH^* and ΔS^* for k_0 in carbon tetrachloride at 25 °C were found to be 24±3 (kJ mol^{-1}) and −226±20 (J K^{-1} mol^{-1}), respectively.

Effect of TOPO, Acetone, and Water on Acid Catlaysis. The rate in carbon tetrachloride was determined as a function of the concentration of TOPO or acetone, the other concentrations being kept constant. The hydrogen-bond acceptors had little effect on the rate in the absence of acid catalyzers as seen from Fig. 3. However, in the presence of an acid catalyzer, the added TOPO lowered the rate and when the molar concentration of TOPO reached that of the acid catalyzer, the catalytic effect disappeared. Acetone also exhibited such an effect on the acid catalysis although the effect was much smaller than that with TOPO. Figure 3 illustrates the effect of acetone on the acid catalysis. Similar experiments were made on the catalysis by water but the effects of TOPO and acetone were, however, not large even in the water-saturated solvent.

Discussion

As described in a previous paper,[1)] the equilibrium constants for the ligand exchange in a given water-saturated solvent,

$$K_n = ([Fe(acac)_{3-n}(tta)_n]/[Fe(acac)_3]) \times ([Hacac]/[Htta])^n \quad (7)$$

can be calculated from the solvent extraction constants of iron(III) with Hacac and Htta in the same solvent. From separate experiments and previous data[2)] the value for K_3 in carbon tetrachloride was calculated as $10^{4.1}$. From this value it was statistically calculated that more than 99% of iron(III) at equilibrium was in the form of $Fe(tta)_3$ whenever the ratio [Htta]/[Hacac] was higher than 10. No such values for the equilibrium constants are available in the other solvents. However, since the extraction constants are little affected by the solvent if there are no special interactions between the complex and the solvent molecules, similar assumptions may also be possible in the other solvents. The spectra at equilibrium also indicated the complete change of the complex into $Fe(tta)_3$ when the ratio [Htta]/[Hacac] was higher than 10. Furthermore, all the spectra observed during the exchange reactions were found to be expainable in terms of two species, $Fe(acac)_3$ and $Fe(tta)_3$. Thus the correction for mixed complexes should be unnecessary in the data analysis.

Since the rate is independent of the concentrations of both ligands, Hacac and Htta, it is assumed that the rate-determining step is the isolation of the first acetylacetonate ion. The catalytic effect by the acids, alcohols, and water can be explained by both the following two mechanisms, (A) and (B). Since the catalyzers are assumed to be hydrogen-bond donors, they will be denoted as HO–R.

(A) The hydroxyl group of the catalyzer works as a hydrogen-bond donor to one of the oxygens of acetylacetonate ions which are coordinating with the central metal ion and form a hydrogen-bond complex $Fe(acac)_3$(HO–R). This hydrogen-bond formation between the catalyzer and the oxygen of the chelating acetylacetonate ion weakens the coordination bond and thus accelerate ring-opening.

(B) Among the tris(acetylacetonato)iron(III) molecules, a certain fraction is in a five-coordinated state and an equilibrium is established between the six- and five-coordinated complexes (the unidentate acetylacetonate ion will be denoted by an asterisk as $Fe(acac)_2$(acac*)). The hydroxyl group works as a hydrogen-bond donor to the oxygen being octahedral at the free end of the unidentate ligand. The formation of the hydrogen-bond complex in such a way, $Fe(acac)_2$(acac*–HO–R), prevents the recombination of the oxygen at the free end with the central metal ion. Thus the relative concentration of the five-coordinated complex is increased and/or accelerates the isolation of the

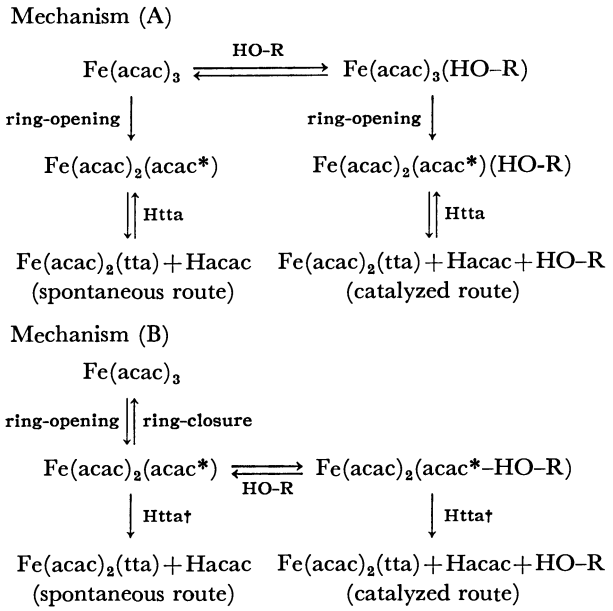

† Addition of tta$^-$ ligand occures after the isolation of the unidentate acac$^-$ ligand which controls the reaction.

Fig. 4. Plausible reaction mechanisms. (acac* denotes unidentate acetylacetonato ligand, HO–R denotes a hydrogen-bond donating catalyzer such as water, alcohol, and carboxylic acid.)

acetylacetonate ion from the complex. The two mechanisms are summarized in Fig. 4.

In both of the mechanisms, the catalytic effect is caused by hydrogen-bond formation and the stronger the acid, the greater the catalytic effect, *i.e.* the greater tendency of a strong acid to form a hydrogen-bond complex than a weak one. A similar tendency was reported in a solvent extraction study where the oxygen in TOPO formed a more stable hydrogen-bond complex in a nonpolar solvent with a strong carboxylic acid as opposed to a weak one.[3] However, the difference in catalysis due to the difference in the acid strength became smaller among the weaker acids; water and alcohols, which are very weak acids catalyze the reaction. This supports the fact that TOPO and various oxygen-containing solvent molecules form hydrogen-bond complexes with water in nonpolar organic solvents. The two β-diketones, Hacac and Htta, have also a hydroxyl group in the enol form and are weak acids (pK_a 9.0 and 6.3 approximately, respectively) but they did not catalyze the exchange reaction as is seen that the rate was not dependent on the concentrations of these materials. This is probably due to the fact that the enolic proton of these materials in nonpolar solvents is hydrogen-bonded with the other oxygen in the same molecule and forms an intramolecular chelate.

In mechanism (A), the rate-determining step is the first ring-opening and in mechanism (B) it is the isolation of the first acetylacetonate ion by breaking the second bond in the chelate. When mechanism (A) operates, the ΔH^* for k_c should be different from that for k_0 and dependent on the catalyzers. When mechanism (B) operates, the ΔH^* for k_c should not be dependent on the catalyzers. However, the experimental errors in the values of ΔH^* are too large to conclude whether mechanism (A) or (B) is operating in the reactions.

The formation of adducts of the $Fe(acac)_3$ chelate with TOPO and various other oxygen-coordinating reagents such as ketones is concluded to be only slight since "synergism" in solvent extraction of tris(β-diketonato)iron(III) is negligible.[4] This is reasonable since TOPO and ketones did not catalyze the reaction by mechanism (A). These reagents could occupy the vacant site of the five-coordinated complex and could accelerate the reaction by preventing the recombination of oxygen at the free end of the unidentate ligand in mechanism (B). However, since no catalytic effect was observed, such an effect would be very slight.

TOPO greatly inhibited the catalysis attributed to the formation of a stable hydrogen-bond complex between TOPO and the catalyzer in the solvent. The catalysis completely disappeared by the addition of TOPO at a 1:1 molar ratio agrees with the previous result that TOPO formed a very stable 1:1 hydrogen-bond complex with carboxylic acids in a nonpolar solvent.[4] Acetone inhibited the catalysis to a much smaller extent than TOPO attributable to the fact that the oxygen of acetone is a much weaker hydrogen-bond acceptor. The limited extent of the catalysis of water and ethanol in acetone may be due to the same reason.

According to the literature,[3,5] the dimerization of the acids is only slight in the solvents when the concentration is lower than 10^{-3} mol dm^{-3}. Such a dimerization effect of the acids on catalysis should be negligible under the conditions of the present study. The intramolecular association of water or alcohol in these solvents is also slight[3,5] and its effect on the catalysis should also be negligible.

When both water and an acid catalyzer co-exist in a solvent, each work as a hydrogen-bond donating catalyzer and, at the same time, as a hydrogen-bond accepting inhibitor for the catalysis. However, as already described, this was not clear in the present study, probably a consequence of the low concentrations.

The isotopic ligand exchange of metal chelates has been studied in several polar solvents and in some nonpolar solvents.[6-16] In the present study, the ligand exchange was not isotopic and no direct comparison with previous results may be possible. However, the following observations in these previous studies may reasonably be compared with the present results.

In nonpolar solvents, especially in the dehydrated ones, the presence of isolated ions should be negligible. Thus the role of protons or hydronium ions in the reaction mechanism should also be negligible and the tendency observed among the catalyzers in the present study that the stronger the acid, the greater the catalytic effect, can be explained only in terms of the higher stabilities of the hydrogen-bond complex by the stronger acids, as already described. Based on this assumption, it can be concluded that water and alcohols are the same type of catalyzers as acids such as trichloroacetic acid although the hydrogen-bonds are weaker. Water was assumed not to assist the acid catalysis. This is quite different from the mechanism proposed for the reactions in polar solvents.[9,10,16]

Solvation of the vacant site of the five-coordinated complex produced by the ring-opening of a chelate ligand was reported to accelerate the reaction by preventing ring closure[10,16] which corresponds to mechanism (B).

In the isotopic exchange reaction of tetrakis(acetylacetonato) or tetrakis(trifluoroacetylacetonato)zirconium(IV) or hafnium(IV) in nonpolar solvents, the rate was dependent on both the metal complex and the free ligand concentration and the presence of an intermediate complex which was coordinated by both the leaving and incoming ligands as unidentate ligands and a transfer of the proton between the two unidentate ligands was assumed.[6] The dependence of the rate on the ligand concentration was also reported in other papers and mechanisms explaining this observation were proposed.[9,13,15]

A kinetic study on the ligand exchange of tris(*N*-benzoyl-*N*-phenylhydroxylaminato)oxovanadium(V) in chloroform or 1,2-dichloroethane with tropolonate ion added as the acid form tropolone was reported.[17] This appears to be the only report of the systematic kinetic study of an exchange reaction of a metal chelate with a different ligand in nonpolar solvents. However, the reaction mechanism was not definitively proposed and a comparative discussion of the results with the present study seems to be difficult.

This work was partly supported by a Grant-in-Aid for scientific research from the Ministry of Education, No. 247042.

References

1) T. Sekine and D. Dyrssen, *J. Inorg. Nucl. Chem.*, **29**, 1489 (1967).
2) T. Sekine and T. Tetsuka, *Bull. Chem. Soc. Jpn.*, **45**, 1620 (1972).
3) M. Niitsu and T. Sekine, *Bull. Chem. Soc. Jpn.*, **51**, 705 (1978).
4) T. Sekine and Y. Hasegawa, "Solvent Extraction Chemistry," Marcel Dekker, New York (1977).
5) G. C. Pimentel and A. L. McClellan, "The Hydrogen Bond," W. H. Freeman, San Francisco (1960).
6) A. C. Adams and E. M. Larsen, *Inorg. Chem.*, **5**, 814 (1966).
7) K. Saito and K. Masuda, *Bull. Chem. Soc. Jpn.*, **41**, 384 (1968).
8) K. Saito, M. Takahashi, Y. Miyakawa, and K. Masuda, *Bull. Chem. Soc. Jpn.*, **41**, 1139 (1968).
9) K. Saito and M. Takahashi, *Bull. Chem. Soc. Jpn.*, **42**, 3462 (1969).
10) K. Saito and K. Masuda, *Bull. Chem. Soc. Jpn.*, **43**, 119 (1970).
11) A. Barabas, *Inorg. Nucl. Chem. Lett.*, **6**, 775 (1970).
12) G. M. Tenner, D. G. Tuck, and E. J. Wells, *Can. J. Chem.*, **50**, 3950 (1972).
13) C. Chetterjee, K. Matsuzawa, H. Kido, and K. Saito, *Bull. Chem. Soc. Jpn.*, **47**, 2809 (1974).
14) S. Wajda and A. Szemik, *Bull. Acad. Pol. Sci., Ser. Sci. Chim.*, **23**, 833 (1975); (*Chem. Abstr.*, **84**, 80349), **24**, 111 (1976); (*Chem. Abstr.*, **84**, 185471).
15) H. Kido and K. Saito, *Inorg. Chem.*, **16**, 397 (1977).
16) A. Nagasawa and K. Saito, *Bull. Chem. Soc. Jpn.*, **51**, 2015 (1978).
17) R. C. Johnson and A. Syamal, *J. Inorg. Nucl. Chem.*, **33**, 2547 (1971).

Preparative Study on Chiral Orthotelluratobis(diamine)cobalt(III) Complexes and Their Condensation Products

Yutaka Hosokawa* and Yoichi Shimura

Department of Chemistry, Faculty of Science, Osaka University, Toyonaka, Osaka 560

(Received November 9, 1978)

Five chiral cobalt(III) complexes coordinating an orthotellurate or a ditellurate ligand have been prepared and their optically active isomers isolated. They belong to one of the three following types: first a "mononuclear" $[Co(TeO_6H_4)(diamine)_2]^+$ type (diamine=ethylenediamine (en) and (*R*)-(−)-1,2-propanediamine); second a "dinuclear" $[Co(diamine)_2(Te_2O_{10}H_4)Co(diamine)_2]^{2+}$ one (diamine=en and (*R,R*)-(−)-*trans*-1,2-cyclohexanediamine); and lastly a "tetranuclear" $[\{Co(diamine)_2\}_2(Te_2O_{10})\{Co(diamine)_2\}_2]^{4+}$ one (diamine=en). The structures of these complexes have been discussed from the visible to ultraviolet absorption and circular dichroism spectra.

Orthotellurate anion $[TeO_6H_{6-n}]^{n-}$ is capable of coordinating with a cobalt(III) center as a bidentate ligand, as was exemplified by the isolation of $K_3[Co(TeO_6H_3)_2(H_2O)_2]$.[1] Also the anion has a tendency to condense easily in solution. One of the condensation products, tetrahydrogenditellurate anion, $Te_2O_{10}H_4^{4-}$, was proved to occur in its potassium salt, in which each tellurium atom is surrounded by six oxygen atoms in an octahedral arrangement, two such octahedra having one edge in common.[2] Thus the anion is a promising ligand for the synthesis of new polynuclear compounds of a hybrid type between metal chelate and heteropoly oxoanion, such as $H_3[Co_4I_3O_{18}(en)_3]\cdot 5H_2O$[3] and $Na_5[Co(Nb_6O_{19})(dien)]$[4]. That is, the mononuclear cobalt(III) complex with the orthotellurate ligand will be able to polymerize into some polynuclear complexes by the dehydration condensation of the coordinated orthotellurate moiety. The present study is concerned with the preparation of such new polynuclear telluratocobalt(III) complexes with configurational and/or vicinal chirality and of their starting mononuclear complex, $[Co(TeO_6H_4)(diamine)_2]^+$, along with electronic absorption and circular dichroism (CD) investigations. The bidentate diamine used are ethylenediamine (en), (*R*)-(−)-1,2-propanediamine (*l*-pn), and (*R,R*)-(−)-*trans*-1,2-cyclohexanediamine (*l*-chxn). This study has been partly reported in a preliminary letter.[5]

Experimental

Preparation, Separation, and Optical Resolution of Complexes.

(1) $[Co(TeO_6H_4)(en)_2]_2SO_4\cdot H_2O$: A solution of 2.3 g (10 mmol) of $Te(OH)_6$ in 25 cm³ of water was added to a solution of 2.9 g (5 mmol) of $[Co(CO_3)(en)_2]_2SO_4$ in 20 cm³ of water. The mixture was stirred mechanically at about 55 °C for an hour, from which a light red product deposited. After the solution had been kept in a refrigerator for a few hours, the product was separated by filtration, washed several times with water, methanol and then acetone, and dried in a desiccator over $CaCl_2$. Found: C, 10.64; H, 4.44; N, 11.99; Co, 12.9; Te, 27.6; SO_4^{2-}, 10.9%. Calcd for $[Co(TeO_6H_4)(en)_2]_2SO_4\cdot H_2O$: C, 10.35; H, 4.57; N, 12.08; Co, 12.7; Te, 27.5; SO_4^{2-}, 10.4%. Cobalt was weighed as Co_3O_4, tellurium as the metal, and sulfate ion as AgCl after being substituted to chloride ion with anion exchange resin (Dowex 1-X8, Cl^- form).

(2) $[Co(TeO_6H_4)(en)_2]Cl\cdot 3H_2O$: A solution of 1.15 g (5 mmol) of $Te(OH)_6$ in 15 cm³ of water was added to a solution of 1.43 g (5 mmol) of *cis*-$[CoCl_2(en)_2]Cl$ in 10 cm³ of water, and to the mixture was added 0.24 g (10 mmol) of LiOH. After stirring mechanically at about 35 °C for an hour, the solution was cooled to room temperature and an appropriate amount of ethanol was gradually added to it. After the solution had been kept in a refrigerator overnight, the light red precipitate deposited was separated by a centrifuge. This was dissolved in a small amount of water and the solution was poured into a column (3 cm×60 cm) of strong acid cation exchanger (SP Sephadex C-25, Li^+ form). The adsorbed band was eluted with 0.25 M LiCl solution, which was adjusted in advance to pH 10 by 1 M LiOH solution. During the elution the column was cooled by flushing ice-water. Two red bands, E_1 and E_2, were eluted in this order. The later eluate (E_2) was treated as in (3) to obtain another complex. The earlier eluate (E_1) was concentrated by freeze-drying method. The product obtained was recrystallized from water (pH 10 by LiOH) at 0 °C by adding ethanol, and washed repeatedly with methanol and acetone. Found: C, 9.49; H, 4.76; N, 11.26%. Calcd for $[Co(TeO_6H_4)(en)_2]Cl\cdot 3H_2O$: C, 9.68; H, 5.29; N, 11.29%. This complex was also obtained predominantly by using DMSO as solvent as follows: A solution of 2.86 g (10 mmol) of *cis*-$[CoCl_2(en)_2]Cl$ in 30 cm³ of DMSO was added with stirring to a solution of 2.30 g (10 mmol) of $Te(OH)_6$ in 40 cm³ of DMSO, and to the mixture was added 0.5 g (20 mmol) of LiOH in 10 cm³ of water. The solution was stirred mechanically at about 35 °C for a few hours. The light red precipitate deposited was separated by filtration. The chromatography of the product showed only one red band (E_1). The absorption spectrum of the eluate was the same as that of the E_1 complex prepared in water.

(3) $[Co(en)_2(Te_2O_{10}H_4)Co(en)_2]Cl_2\cdot CH_3OH\cdot 4H_2O$: The later eluate ($E_2$) from the chromatography in (2) was concentrated at 15 °C in a rotary evaporator, and a large volume of ethanol was added to the concentrated solution. After the solution had been kept in a refrigerator overnight, the red product deposited was collected by a centrifuge. The product was recrystallized from an aqueous LiOH solution of pH 10 at 0 °C by adding acetone–methanol mixture and washed repeatedly with ethanol and acetone. Found: C, 11.28; H, 4.74; N, 11.55%; Co/Te (molar ratio)=1.1. Calcd for $[Co(en)_2(Te_2O_{10}H_4)Co(en)_2]Cl_2\cdot CH_3OH\cdot 4H_2O$: C, 11.34; H, 5.09; N, 11.77%; Co/Te=1.0. Cobalt and tellurium were determined for the eluates from the column. The E_2 complex was also obtained predominantly by raising the reaction temperature to *ca.* 60 °C.

(4) $[\{Co(en)_2\}_2(Te_2O_{10})\{Co(en)_2\}_2]Cl_4\cdot CH_3OH\cdot 12H_2O$: The similar procedure to that for E_1 and E_2 complexes was adopted in water using 1.15 g (5 mmol) of $Te(OH)_6$, 2.86 g

(10 mmol) of *cis*-$[CoCl_2(en)_2]Cl$, and 0.48 g (20 mmol) of LiOH. The reaction was carried out at 60 °C, and the reaction solution was poured into a column directly. The products separated on the column consisted of two red bands, E_2 and a new E_3 in this order, when eluted with 0.35 M LiCl solution (pH 10 by 1 M LiOH). The E_3 complex was purified by the same method as that of E_2 complex. Found: C, 13.58; H,6.07; N, 14.55%; Co/Te (molar ratio)=2.1. Calcd for $[\{Co(en)_2\}_2(Te_2O_{10})\{Co(en)_2\}_2]Cl_4 \cdot CH_3OH \cdot 12H_2O$: C, 13.42; H, 6.10; N, 14.73%; Co/Te=2.0. The metal analyses were carried out using the eluate from the column.

(5) Optical Resolution of E_1, E_2, and E_3 Complexes: Optically active E_1 and E_2 complexes were obtained by the preparation procedure starting from $(+)_{589}$-$[CoCl_2(en)_2]^+$.[7] The $(+)^{CD}_{589}$-E_1 and $(+)^{CD}_{589}$-E_2 complexes have $\Delta\varepsilon=+0.18$ and $+0.44$, respectively, at the Na D line. The optical resolution of E_3 complex was made by the solubility difference between diastereomers: A solution of 0.015 g of $K_2[Sb_2(d\text{-}C_4H_2O_6)_2] \cdot 3H_2O$ in 5 cm^3 of water was gradually added with stirring to a solution of 0.07 g of E_3 complex in 10 cm^3 of LiOH solution of pH 10 on an ice bath. To the mixture was added an appropriate amount of acetone, and the solution was kept in a refrigerator overnight. The light red diastereomer deposited was isolated by a centrifuge and washed with methanol a few times. This less soluble diastereomer was stirred at 0 °C in LiOH solution of pH 10 containing anion-exchange Sephadex (QAE A-25, Cl^- form). The solution was filtered to remove Sephadex, and CD of the filtrate was measured. The $(+)^{CD}_{589}$-E_3 complex has $\Delta\varepsilon=+0.18$ at Na D line.

(6) $[Co(TeO_6H_4)(l\text{-}pn)_2]Cl \cdot 1/2CH_3OH \cdot 3H_2O$: A solution of 0.42 g (2 mmol) of $Te(OH)_6$ in 10 cm^3 of water was added to a solution of 0.63 g (2 mmol) of *cis*-$[CoCl_2(l\text{-}pn)_2]Cl$ in 10 cm^3 of water, and to the mixture was added 0.16 g (4 mmol) of NaOH. After stirring mechanically at about 35 °C for half an hour, the solution was poured into a column (3 cm × 60 cm) of strong acid cation exchanger (SP Sephadex C-25, Li^+ form). The adsorbed band was eluted with 0.25 M LiCl solution, which was adjusted in advance to pH 10 by 1 M LiCl solution. During the elution the column was cooled by flushing ice–water. Two red bands were eluted, and the absorption spectrum of each eluate was similar with that of ethylenediamine E_1 and E_2 complexes, respectively. It was difficult to isolate the crystals from the later eluate. The earlier eluate was poured once more into another similar column and eluted with 0.5 M LiCl solution (pH 10). To the earlier eluate was added a large amount of acetone. After the solution had been kept in a refrigerator overnight, the light red precipitate deposited was separated by a centrifuge. The product was recrystallized from water (pH 10 by LiOH) at 0 °C by adding methanol–acetone mixture and acetone. Found: C, 14.25; H, 5.38; N, 10.28%. Calcd for $[Co(TeO_6H_4)(l\text{-}pn)_2]Cl \cdot 1/2CH_3OH \cdot 3H_2O$: C, 14.45; H, 5.98; N, 10.37%.

Two diastereomeric isomers of this complex were separated also by the column chromatography. When eluted with 0.2 M LiCl solution (pH 10 by 1 M LiOH), the red band further separated gradually into two bands, Pl and P2 (denoted by elution order). Pl and P2 complexes have $\Delta\varepsilon=+0.28$ and -0.20, respectively, at Na D line. These CD values were calculated referring to molar absorption coefficient of the unresolved complex.

(7) $[Co(l\text{-}chxn)_2(Te_2O_{10}H_4)Co(l\text{-}chxn)_2]Cl_2 \cdot 8H_2O$: A solution of 0.57 g (2.5 mmol) of $Te(OH)_6$ in 10 cm^3 of water was added to a solution of 0.98 g (2.5 mmol) of *trans*-$[CoCl_2(l\text{-}chxn)_2]Cl$ in 10 cm^3 of water, and to the mixture was added 0.2 g (5 mmol) of NaOH. After stirring mechanically at about 40 °C for an hour, the solution was cooled in a refrigerator. The red precipitate deposited was separated by filtration, recrystallized from a cold water (pH 10 by LiOH) by adding acetone, and washed with methanol–acetone mixture and ether. Found: C, 24.02; H, 6.52; N, 9.28; Te, 19.9%. Calcd for $[Co(l\text{-}chxn)_2(Te_2O_{10}H_4)Co(l\text{-}chxn)_2]Cl_2 \cdot 8H_2O$: C, 23.85; H, 6.35; N, 9.27; Te, 21.1%.

The filtrate from the red precipitate was poured into a column of SP Sephadex C-25 (Li^+ form) and eluted with 0.225 M LiCl solution (pH 10 by 1 M LiOH). Three red bands, Cl, C2, and C3, were eluted in this order. The absorption spectra of three eluates were similar to that of the corresponding ethylenediamine E_2 complex. Furthermore, the absorption and CD spectra of the first red precipitate, $[Co(l\text{-}chxn)_2(Te_2O_{10}H_4)Co(l\text{-}chen)_2]Cl_2 \cdot 8H_2O$, were the same as those of Cl eluate. Cl, C2, and C3 complexes have $\Delta\varepsilon=-0.90$, -0.41, and -1.42, respectively, at Na D line. These CD values were calculated referring to the molar absorption coefficient of the first red precipitate. In this case, the complex corresponding to E_1 complex of ethylenediamine was not obtained.

Measurements. The visible and ultraviolet absorption measurements were made by a Shimadzu UV-200 spectrophotometer in aqueous solutions. The CD spectra were recoreded on a JASCO MOE-1 spectropolarimeter.

Results and Discussion

The tellurato Co(III) complexes newly obtained are summerized in Tables 1 and 2 with their d-d absorption and CD data. Other highly condensed complexes were observed in trace amounts on the column, but they were too unstable to be isolated. All the complexes obtained are unstable in solution at room temperature, and their solutions were carefully handled below 5 °C. E_1 complex is particularly unstable to reequilibration, and converted rapidly into E_2 complex in aqueous solution at room temperature. This rapid conversion corresponds to the dehydration condensation of the "mononuclear" complex $[Co(TeO_6H_4)(en)_2]^+$ into the "dinuclear" one $[Co(en)_2(Te_2O_{10}H_4)Co(en)_2]^{2+}$. E_1 and E_2 complexes

Table 1. Absorption data of the Tellurato complexes in the d-d transition region

Complex	σ_{max}[a] (log ε)	
	1st band	2nd band
$[Co(TeO_6H_4)(en)_2]^+$	19.2(2.07)	26.7(1.93)
$[Co(en)_2(Te_2O_{10}H_4)Co(en)_2]^{2+}$	19.2(2.41)	26.7(2.38)
$[\{Co(en)_2\}_2(Te_2O_{10})\{Co(en)_2\}_2]^{4+}$	19.2(2.67)	*ca.* 26.5(*ca.* 2.7)
$[Co(TeO_6H_4)(l\text{-}pn)_2]^+$	19.2(2.10)	26.5(1.95)
$[Co(l\text{-}chxn)_2(Te_2O_{10}H_4)Co(l\text{-}chxn)_2]^{2+}$	19.2(2.42)	26.5(2.36)

a) In the unit of 10^3 cm^{-1}.

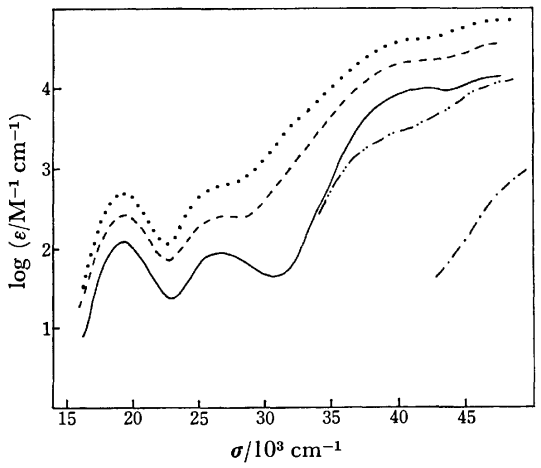

Fig. 1. Absorption spectra of $[Co(TeO_6H_4)(en)_2]^+$ (——), $[Co(en)_2(Te_2O_{10}H_4)Co(en)_2]^{2+}$ (– – –), and $[\{Co(en)_2\}_2(Te_2O_{10})\{Co(en)_2\}_2]^{4+}$ (·····). Absorption spectra of $[TeO_6H_{6-n}]^{n-}$ (—·—) and $[Te_2O_{10}H_{8-n}]^{n-}$ (—··—) are shown for comparison (pH 10—11).

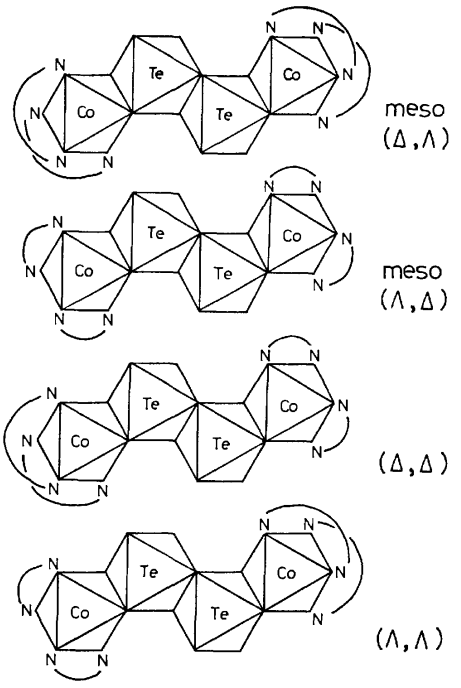

Fig. 2. Proposed structures for the four diastereomeric isomers of $[Co(diamine)_2(Te_2O_{10}H_4)Co(diamine)_2]^{2+}$.

were prepared as their chlorides from the reaction of *cis*-$[CoCl_2(en)_2]^+$ and $Te(OH)_6$ at 35 °C. The formation ratio changed with the reaction temperature. At 60 °C, the former was not obtained at all, and the latter predominantly. The E_1 sulfate $[Co(TeO_6H_4)(en)_2]_2SO_4$ is sparingly soluble in water, but can be converted into the chloride solution by the anion exchange resin Dowex 1-X8 (Cl^- form) at 0 °C. The absorption and CD data of E_1 complex previously reported[5] have been corrected in this paper.

As is seen in Table 1 and Fig. 1, the absorption spectrum of $[Co(TeO_6H_4)(en)_2]^+$ complex shows a characteristic feature of the *cis*-CoN_4O_2 type and is similar to that of $[Co(CO_3)(en)_2]^+$ (σ_{max} = 19500 and 27700 cm^{-1})[6] in the d-d absorption band region. Thus it is concluded that the ligand $TeO_6H_4^{2-}$ stands near after CO_3^{2-} in the spectrochemical series. The second absorption bands of E_2 and E_3 complexes appear as a shoulder because of overlapping with an absorption band at 30000—35000 cm^{-1}. The latter band is assigned to the ditellurate band modified by coordination, since the free ditellurate ion has its longest wavelength absorption band at about 38000 cm^{-1} as a shoulder in contrast to the free orthotellurate ion which scarcely absorbs in the region of 35000—42000 cm^{-1} (Fig. 1). The occurrence of the ditellurate band for E_2 complex and the E_1 to E_2 conversion in solution support that E_2 complex $[Co(en)_2(Te_2-$

Table 2. CD data of the tellurato complexes in the d-d transition region

Complex	σ_{ext}[a] ($\Delta\varepsilon$)	
	1st band	2nd band
$(+)^{CD}_{589}$-$[Co(TeO_6H_4)(en)_2]^+$	19.0(+1.12)	25.0(+0.092)
		27.0(−0.012)
		29.8(+0.023)
$(+)^{CD}_{589}$-$[Co(en)_2(Te_2O_{10}H_4)Co(en)_2]^+$	19.0(+2.63)	25.0(+0.071)
		27.5(−0.071)
$(+)^{CD}_{589}$-$[\{Co(en)_2\}_2(Te_2O_{10})\{Co(en)_2\}_2]^{4+}$ [b]	18.5(+0.83)	24.5(+0.038)
		27.5(−0.023)
$[Co(TeO_6H_4)(l\text{-pn})_2]^+$: P1	19.1(+1.56)	25.1(+0.18)
		29.3(+0.06)
: P2	18.4(−0.79)	25.5(+0.13)
	20.7(+0.38)	
$[Co(l\text{-chxn})_2(Te_2O_{10}H_4)Co(l\text{-chxn})_2]^{2+}$: C1	18.5(−3.03)	26.5(+0.43)
	20.7(+0.84)	
: C2	18.3(−1.36)	26.0(+0.37)
	20.5(+1.44)	
: C3	18.5(−5.24)	26.5(+0.57)
	21.5(+0.26)	

a) In the unit of 10^3 cm^{-1}. b) Partly resolved complex.

$O_{10}H_4)Co(en)_2]^{2+}$ corresponds to the condensation product of E_1 complex $[Co(TeO_6H_4)(en)_2]^+$ (see Fig. 2). Similarly, it is supposed that E_3 complex $[\{Co(en)_2\}_2(Te_2O_{10})\{Co(en)_2\}_2]^{4+}$ is a condensation product of $[Co(en)_2(TeO_6H_2)Co(en)_2]^{2+}$, which has not been isolated in this work.

The optically active forms were obtained for E_1, E_2, and E_3 complexes, and two diastereomeric isomers of $[Co(TeO_6H_4)(l\text{-pn})_2]^+$, P1 and P2, were separated by column chromatography. Furthermore, three diastereomeric isomers of $[Co(l\text{-chxn})_2(Te_2O_{10}H_4)Co(l\text{-chxn})_2]^{2+}$, C1, C2, and C3, were obtained. Among several possible structures for the "dinuclear" complex, $[Co(diamine)_2(Te_2O_{10}H_4)Co(diamine)_2]^{2+}$, the most probable ones are those shown in Fig. 2. In this type of condensation, four diastereomeric isomers are possible, which have *meso*-(Δ,Λ), *meso*-(Λ,Δ), (Δ,Δ), and (Λ,Λ) configurations, respectively, in regard to skew pairs of two diamine chelate rings. Many optical isomers are possible for $[\{Co(en)_2\}_2(Te_2O_{10})\{Co(en)_2\}_2]^{4+}$, but further investigation on this complex has not been intended in the present study, because it seems the optical resolution was successful only partly.

The CD data of the present complexes are summerized in Table 2 and Figs. 3—6. The CD patterns of the $[Co(TeO_6H_4)(en)_2]^+$ and $[Co(en)_2(Te_2O_{10}H_4)Co(en)_2]^{2+}$ complexes are similar to that of Λ-$[Co(CO_3)(en)_2]^+$ ($\Delta\varepsilon = +3.7$ at 18900 cm^{-1})[6] in the d-d absorption band region, and show only one CD band in the first band region (Figs. 4 and 6). Thus, the absolute configurations of $(+)^{CD}_{589}$-E_1 and $(+)^{CD}_{589}$-E_2 complexes are assigned to be Λ and (Λ,Λ), respectively. This corresponds well to the fact that the optically active E_1 and E_2 complexes have been obtained from $(+)_{589}$-$[CoCl_2(en)_2]^+$ (Λ configuration)[6,8]. The CD curves of two diastereomeric isomers, P1 and P2, of $[Co(TeO_6H_4)(l\text{-pn})_2]^+$ are shown in Fig. 3. Their CD patterns somewhat differ from that of $[Co(TeO_6H_4)(en)_2]^+$, because of the presence of vicinal contribution due to the (*R*)-1,2-propanediamine ligand. It has been well known that the configurational and vicinal CD contributions are separable for many kinds of cobalt(III) complexes by utilizing an additivity rule for a pair of CD curves of diastereomeric isomers.[9] When the additivity rule is applied for the CD curves of P1 and P2 isomers, the calculated configurational CD curve agrees well with the observed CD curve of E_1 complex (Fig. 4). Thus the sign pattern of $(+)^{CD}_{589}$-E_1 complex (Λ configuration) suggests that P1 and P2 isomers are Λ and Δ configurations, respectively.

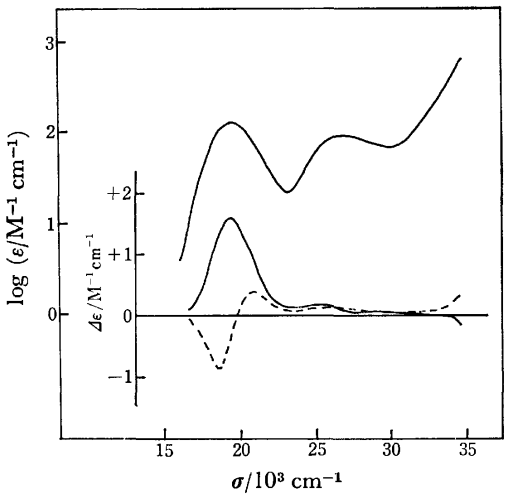

Fig. 3. Absorption and CD spectra of $[Co(TeO_6H_4)(l\text{-pn})_2]^+$: P1 (——) and P2 (– – –) isomers.

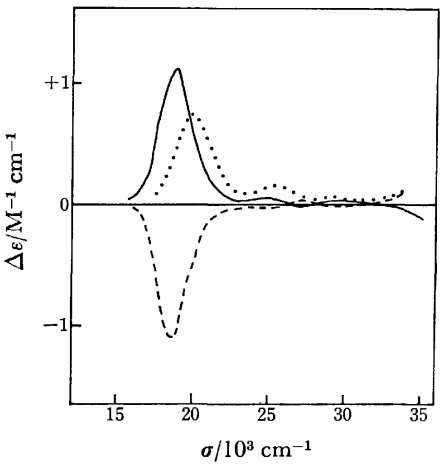

Fig. 4. Calculated configurational (– – –) and vicinal (·····) CD curves of $(-)^{CD}_{589}$-$[Co(TeO_6H_4)(l\text{-pn})_2]^+$, and observed CD curve (——) of $(+)^{CD}_{589}$-$[Co(TeO_6H_4)(en)_2]^+$.

As is seen in Fig. 5, the CD curves of three diastereomeric isomers, C1, C2, and C3, of $[Co(l\text{-chxn})_2(Te_2O_{10}H_4)Co(l\text{-chxn})_2]^{2+}$ differ from that of E_2 complex by the same reason as in the case of P1 and P2 complexes. By the application of the additivity rule for the CD curves of C2 and C3 isomers, the calculated configu-

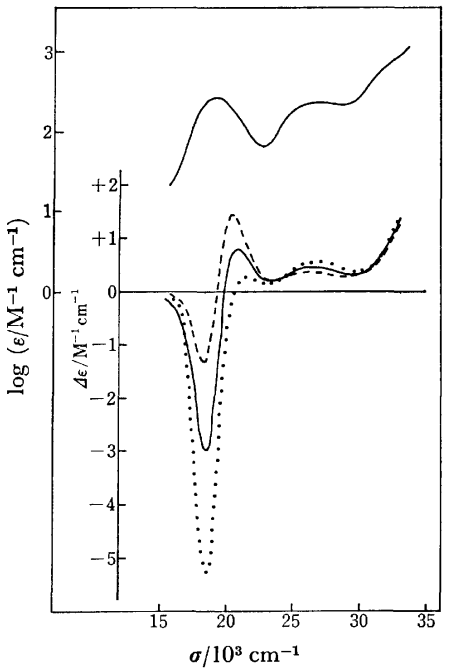

Fig. 5. Absorption and CD spectra of $[Co(l\text{-chxn})_2(Te_2O_{10}H_4)Co(l\text{-chxn})_2]^{2+}$: C1 (——), C2 (– – –), and C3 (·····) isomers.

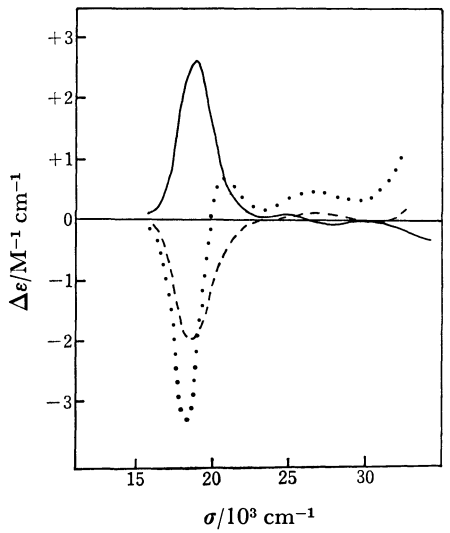

Fig. 6. Calculated configurational (——) and vicinal (……) CD curves of $[Co(l\text{-chxn})_2(Te_2O_{10}H_4)Co(l\text{-chxn})_2]^{2+}$(C3 isomer), and observed CD curve (——) of $(+)^{CD}_{589}$-$[Co(en)_2(Te_2O_{10}H_4)Co(en)_2]^{2+}$.

rational and vicinal CD curves agree well with the observed CD curves of E_2 complex and C1 isomer, respectively (Fig. 6). Thus the CD of C1 isomer is contributed only by the vicinal effect due to the four (*R*,*R*)-*trans*-1,2-cyclohexanediamine ligands; namely C1 isomer corresponds to a *meso* one, (Δ,Λ) or (Λ,Δ) in Fig. 2, or to a mixture of the two *meso* ones. Furthermore, by comparison of the sign patterns of C2 and C3 isomers to that of $(+)^{CD}_{589}$-(Λ,Λ)-$[Co(en)_2(Te_2O_{10}H_4)Co(en)_2]^{2+}$ complex, it is confirmed that C2 isomer has (Λ,Λ) configuration, and C3 isomer (Δ,Δ) one.

References

1) M. W. Lister and Y. Yoshino, *Can. J. Chem.*, **40**, 1490 (1962); Y. Yoshino, T. Takeuchi, and H. Kinoshita, *Nippon Kagaku Zasshi*, **86**, 978 (1965).
2) O. Lindqvist and G. Lundgren, *Acta Chem. Scand.*, **20**, 2138 (1966).
3) T. Ama, J. Hidaka, and Y. Shimura, *Bull. Chem. Soc. Jpn.*, **46**, 2145 (1973).
4) Y. Hosokawa, J. Hidaka, and Y. Shimura, *Bull. Chem. Soc. Jpn.*, **48**, 3175 (1975).
5) Y. Hosokawa and Y. Shimura, *Chem. Lett.*, **1978**, 847.
6) A. J. MacCaffery, S. F. Mason, and B. J. Norman, *J. Chem. Soc.*, **1965**, 5094.
7) F. P. Dwyer, A. M. Sargeson, and I. K. Reid, *J. Am. Chem. Soc.*, **85**, 1215 (1963).
8) K. Matsumoto, S. Ooi, and H. Kuroya, *Bull. Chem. Soc. Jpn.*, **43**, 3801 (1970).
9) N. Matsuoka, J. Hidaka, and Y. Shimura, *Bull. Chem. Soc. Jpn.*, **48**, 458 (1975); *Inorg. Chem.*, **9**, 719 (1970).

Differential Pulse Polarographic Determination of Tellurium by Use of Maximum Wave

Kiyoshi HASEBE

Department of Chemistry, Faculty of Science, Hokkaido University, Sapporo 060

(Received September 7, 1978)

A differential pulse polarographic method for the rapid and simple determination of tellurium by use of maximum wave has been studied. Differential pulse polarographic (DP) peak of tellurium(IV) in 1 mol dm^{-3} phosphoric acid is observed in the potential range −0.7——1.0 V *vs.* SCE. The peak current is very large in comparison with that in d.c. mode, or in normal pulse mode, being proportional to the concentration of tellurium(IV) between 10^{-8} and 10^{-7} mol dm^{-3} contents. The relative standard deviation for 3.94×10^{-8} mol dm^{-3} tellurium(IV) under representative sets of good conditions was 0.0342. The method has been applied to the determination of tellurium in carbon steel.

Tellurium is an important substance in the steel industry and alloy production. However, tellurites and hydrogen telluride are more toxic and dangerous than the corresponding selenium compounds. Thus it is most important to know the tellurium content in the fields of toxicology, industrial hygiene, and environmental pollution. Determination of tellurium can be carried out by the solvent extraction-spectrophotometric[1] and spectrophotometric[2] methods by use of Bismuthiol II (3-phenyl-5-mercapto-1,3,4-thiadiazole-2-thione). However, these methods involve complicated steps for clean-up and color development, requiring much time. On the other hand, differential pulse (DP) polarography as well as atomic absorption spectrometry[3] provide reliable determination of the micro-amount of tellurium.

Since polarographic investigation was carried out in 1935 by Schwaer and Suchy,[4] many reports have appeared on the reduction of tellurium concerning the polarographic maximum wave, mainly in view of establishing reaction mechanisms.[5–14]

For the purpose of working out a reliable analytical method, the author has studied the effect of supporting electrolytes, coexisting ions and surfactants on the DP peak, the effects of instrumental parameters such as modulation amplitude (ΔE) and scan rate (ν) in the DP mode, and also sensitivity and relative standard deviation for tellurium.

Experimental

Reagents. Chemicals used were of reagent grade and dissolved in deionized water. A standard tellurium solution (1.00×10^{-2} mol dm^{-3}) was prepared by dissolving 0.1276 g of tellurium lump (purity 99.999%, Wako Chemical Ind. Ltd.) in 50 cm^3 of 7 mol dm^{-3} nitric acid and diluting to 100 cm^3. All dilute solutions were prepared from a stock solution.

Apparatus. The pulse polarographic determination was carried out with a Model 174A polarographic analyzer and a Model 174/70 drop timer (Princeton Applied Research, U.S.A.) and an Omnigraphic 2000 Recorder (Houston Instrument, U.S.A.). The polarographic solutions were deaerated before and during the course of electrolysis with pure nitrogen by passing through a trap containing a solution of the same supporting electrolyte. Except for temperature dependence studies, all the measurements were carried out at room temperature (21±1) °C. Conditions for the dropping mercury electrode (d.m.e.): drop time t=3.66 s (open circuit in 1 mol dm^{-3} phosphoric acid), rate of mercury flow m=2.156 mg s^{-1}, height of mercury reservoir h=79 cm. The electrolysis circuit was a three electrode system consisting of a d.m.e., a carbon rod as counter electrode and a SCE. Small volumes of tellurium(IV) solutions were supplied from Eppendorf micropipetters.

Results and Discussion

Characteristics of Tellurium(IV) Reduction. Reduction wave or peak of tellurium with catalytic hydrogen evolution was observed in the potential range −0.7—−1.0 V. The mechanism of electrode processes has been discussed by many investigators.[5,6,8,11,12] According to Shinagawa *et al.*,[11] and Volaire *et al.*,[12] the electrode process after the reduction of Te(IV)—Te(0) is as follows:

$$Te^0_{ads} + 2H_{ads} = HTe^-_{ads} + H^+$$
$$HTe^-_{ads} + e = 1/2H_2 + Te^{2-}_{ads}$$
$$Te^{2-}_{ads} + H^+ = HTe^-_{ads}$$

If tellurium undergoes two-electron reduction due to formation of telluride as a whole, we can reexamine the process by means of the dependence of peak half width, $W_{1/2}$, on pulse amplitude, ΔE, for various values of n[15] in order to confirm total number of electrons in electrode reaction, n. The results for the $W_{1/2}$-ΔE dependence are given in Table 1. The values agree with the theoretical ones for n=2. The instantaneous current-time curve of 1×10^{-6} mol dm^{-3} tellurium(IV) in 1 mol dm^{-3} phosphoric acid was observed in the potential in the range −0.70——0.94 V by the potential-step method. The slope of lg i-lg t was 0.480, lying in the range between the maximum of first kind and the kinetic current. No brown mist formed on the d.m.e., convection in the vicinity of the d.m.e., not being observed

Table 1. Dependence of modulation amplitude on DP peak half width for n=2

$W_{1/2}$ (mV)	Modulation amplitude, ΔE (mV)		
	−10	−25	−50
Theoretical	46	50	63
Observed	48	50	70

Concentration: 1.00×10^{-7} mol dm^{-3} Te(IV); scan rate, ν: 5 mV s^{-1}; mechanically controlled drop time, t_d: 1 s.

because of the low concentration of tellurium(IV).[11] The relative temperature coefficient of the DP peak current for tellurium-reduction in the temperature range 1—44 °C was 3.02% K^{-1} at 20 °C, the value being reasonable because of maximum wave. No maximum wave was observed in the potential range −1.0——1.9 V in 1 mol dm^{-3} sodium hydroxide. The reduction is irreversible, the slope of $\lg i/(i_d-i)$ *vs.* potential, E in normal pulse (NP) mode and the peak half width, $W_{1/2}$ in DP mode being 80 and 144 mV, respectively, at $\Delta E=-50$ mV. The peak current in 1 mol dm^{-3} sodium hydroxide is much less than that in 1 mol dm^{-3} phosphoric acid.

Choice of Supporting Electrolyte. Several investigators have recommended alkaline or ammoniacal supporting electrolytes for the determination of tellurium.[6-8,11] Itsuki *et al.*[9] used phosphoric acid for s.w. polarographic determination of tellurium in crude copper, silver and selenium. Maienthal and Taylor[10] determined tellurium in cartridge brass and in white cast iron by cathode-ray polarography in 1.5 mol dm^{-3} phosphoric acid, getting good results. Milner and Slee[16] recommended phosphoric acid as a suitable supporting electrolyte for square wave (s.w.) polarographic determination of heavy metals. Phosphoric acid was thus chosen as the supporting electrolyte. In solutions with phosphoric acid, there was no variation in DP current in the concentration range 0.1—2 mol dm^{-3}.

In a.c. mode, the background current practically does not change because of the irreversible reduction of dissolved oxygen in acid solutions,[17] nevertheless that in DP mode altered remarkably and affected the DP current of tellurium(IV) markedly. Thus it was necessary to monitor the residual current in order to make analytical error minimum. The effects of hydrochloric acid, sulfuric acid and nitric acid were studied. The DP peak for 1×10^{-7} mol dm^{-3} tellurium(IV) remained constant even in the presence of 1 mol dm^{-3} nitric acid in the polarographic solution. The presence of 0.1 mol dm^{-3} hydrochloric acid or 0.1 mol dm^{-3} sulfuric acid in the solution gave practically no influence on the DP peak current.

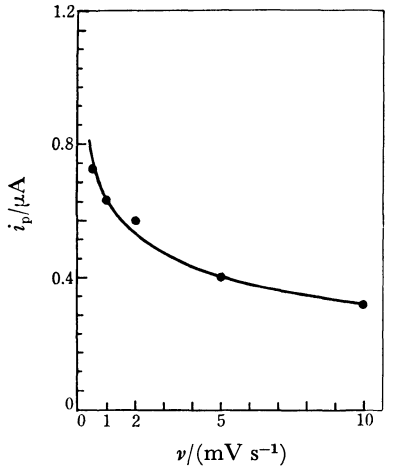

Fig. 1. Effect of scan rate on DP peak of tellurium(IV). Concentration: 1.00×10^{-7} mol dm^{-3} Te(IV); modulation amplitude, ΔE: −50 mV; mechanically controlled drop time, t_d: 1 s.

Effect of Modulation Amplitude and Scan Rate. For the reduction process with catalytic reaction, the peak height-pulse amplitude relationship was found to be linear up to 100 mV pulse amplitude. In general, small pulse amplitude gives better resolution and less instrumental error.[15] However, it is more advantageous to work at larger pulse amplitudes in order to obtain better sensitivity.

Figure 1 shows the effect of scan rate on DP peak height for the reduction of tellurium(IV). It should be noted that the specially slow scan rate for the reduction of tellurium(IV) gives better sensitivity sufficiently reliable for routine analytical operation but its use is time consuming and tedious. However, in the case of lower concentrations as low as 10^{-9} mol dm^{-3} content, it is desirable to use lower scan rates of 0.1—0.5 mV s^{-1}.

Table 2. Effect of maximum suppressor concentration on DP peak

Concentration of Triton X-100(%)	Tellurium concentration (mol dm^{-3})	
	1.00×10^{-7}	1.00×10^{-6}
None	1.00[a]	1.00[a]
5×10^{-4}	0.99	—
1×10^{-3}	0.96	—
5×10^{-3}	0.93	0.99
1×10^{-2}	—	0.60
2×10^{-2}	—	0.31

a) Relative value against the peak current without Triton X-100. Conditions as in Table 1.

Effect of Surfactants. If surfactants are present in the polarographic solution, the current should decrease due to change in interfacial phenomena such as adsorption. Table 2 gives the effect of surfactants on the maximum peak current for the reduction of tellurium(IV). In general, gelatine and Triton X-100 are used for maximum suppressor at concentration lower than 10^{-2}%. These concentrations usually suppress the maximum wave sufficiently. However, none of them affected the current at concentrations less than 10^{-3}% in spite of the fact that the depolarizer concentration was as low as 10^{-7} mol dm^{-3}. In the present method it is not necessary to pay attention to the presence of surfactants. The results of the DP peak current-concentration of Triton X-100 relationship are similar to those obtained in the "suspension polarogram" of tellurium powder in 1 mol dm^{-3} ammonium chloride and in 4×10^{-4} mol dm^{-3} K_2TeO_3.[11]

Calibration Curve. Figure 2 shows typical DP polarograms of tellurium(IV) in 1 mol dm^{-3} phosphoric acid. The DP peak height is proportional to the concentration of tellurium(IV) between 5×10^{-8} and 4×10^{-7} mol dm^{-3} (Fig. 3). The relative standard deviation for 3.94×10^{-8} mol dm^{-3} tellurium(IV) was 0.0342. If the current offset in the instrument, modulation amplitude of −100 mV, and scan rate of 0.5 mV s^{-1} as low as possible are used, detection limits are about 10^{-9} mol dm^{-3} content. The large amount of iron(III) and

Table 3. Contents of constituents of carbon steel specimen

Specimen	Concentration (%)										
No. 1	C	Si	Mn	P	S	Ni	Cr	Cu	Mo	Te	Se
	0.20	0.24	0.59	0.012	0.013	0.15	0.15	0.18	0.05	0.020	0.020

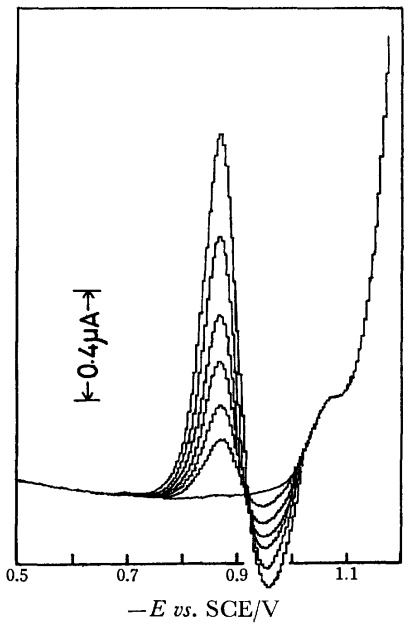

Fig. 2. Differential pulse polarograms of tellurium(IV) in 1 mol dm^{-3} phosphoric acid.
Concentration: 0, 5.00, 10.00, 15.00, 20.00, 30.00, and 40.00×10^{-8} mol dm^{-3} Te(IV); scan rate, v: 5 mV s^{-1}; ΔE: −50 mV; t_d: 1 s.

the elements given in Table 3 did not interfere with the determination of tellurium(IV).

The maximum wave was also observed in NP mode, but it was difficult to measure the wave height accurately.

Analytical Application. An analytical procedure was established from the results. Contents of constituents of carbon steel used as a sample are given in Table 3.

Dissolve *ca.* 0.1 g of the sample weighed accurately in a mixture of 3 cm^3 of nitric acid and 0.1 cm^3 of hydrochloric acid, and keep it in a water-ice bath to prevent fuming. Filter through a No. 5C filter paper when necessary. Wash the paper with a few cm^3 of 4 mol dm^{-3} nitric acid, and dilute to 10 cm^3 accurately with 4 mol dm^{-3} nitric acid. Pipette an adequate amount of the sample solution into the supporting electrolyte solution. After deaeration, measure the tellurium peak in DP mode in the potential range −0.7——1.0 V, and then calibrate the amount by means of a calibration curve or standard addition method. The results of analyses, given in Table 4, are in good agreement with the prescription of sample within experimental error.

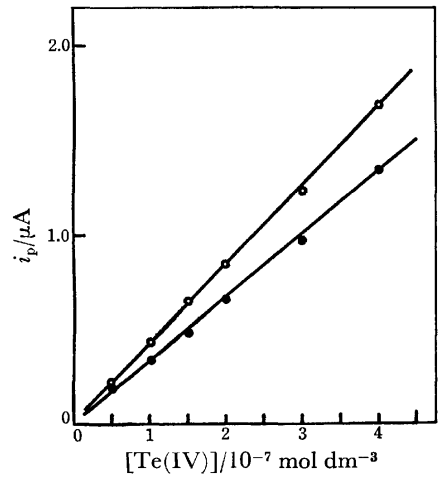

Fig. 3. Calibration curve of tellurium(IV) by DP mode.
Conditions are the same as in Fig. 2.
○: Current measured as a height of peak-to-peak.
●: Current measured as a height of background-to-the peak at more positive potential.

Table 4. Analysis of carbon steel

Method	Found values of tellurium (%), $\times10^2$		
Calibration curve	1.95	1.96	1.95
Standard addition	1.97	1.98	1.96

Conditions are the same as in Fig. 2.

As compared to many analytical procedures the present one was found to be the simplest, giving the highest reliability as the anodic stripping voltammetry for heavy metal determination.

The author is grateful to Profs. S. Hikime, H. Yoshida, and M. Taga for their interest and encouragement, and to Prof. T. Kambara for his comments.

The carbon steel was supplied by Japan Steel Work Co. through Prof. S. Hikime.

References

1) K. Hayashi and T. Ogata, *Bunseki Kagaku*, **15**, 1120 (1966).
2) S. Maekawa and K. Kato, *Bunseki Kagaku*, **19**, 10 (1970).
3) S. Musha, M. Munemori, and T. Nakahara, *Nippon Kagaku Zasshi*, **89**, 495 (1968).
4) L. Schwaer and K. Suchy, *Collect. Czech. Chem. Commun.*, **7**, 25 (1935).
5) J. J. Lingane and L. W. Niedrach, *J. Am. Chem. Soc.*, **70**, 4115 (1948).
6) J. J. Lingane and L. W. Niedrach, *J. Am. Chem. Soc.*, **71**, 196 (1949).
7) Y. Morimoto and F. Suzuki, *Denki Kagaku*, **23**, 544 (1955).
8) G. S. Deshmukh and V. S. Sankara Rao, *Z. Anal. Chem.*, **240**, 322 (1968).
9) K. Itsuki, A. Ide, and A. Minehara, *Bunseki Kagaku*, **9**, 840 (1960).
10) E. June Maienthal and J. K. Taylor, *Anal. Chem.*,

37, 1516 (1965).
11) M. Shinagawa, N. Yano, and T. Kurosu, *Talanta*, **19**, 439 (1972).
12) M. Volaire, O. Vittori, and M. Porthault, *Bull. Soc. Chim. Fr.*, **1974**, 823.
13) M. Volaire, O. Vittori, and M. Porthault, *Anal. Chim. Acta*, **71**, 185 (1974).
14) S. Kim Nuor and O. Vittori, *Anal. Chim. Acta*, **91**, 143 (1977).
15) J. G. Osteryoung and K. Hasebe, *Rev. Polarog. (Kyoto)*, **22**, 1 (1976).
16) G. W. C. Milner and L. J. Slee, *Analyst*, **82**, 139 (1957).
17) H. Shirai, *Bunseki Kagaku*, **8**, 311 (1959).

Color Reactions of Aqua(ethylenediaminetetraacetato)ruthenate(III) with Sulfur Compounds. Kinetic Study of Thiosulfate Anation[1)]

Yukichi Yoshino,* Takashi Uehiro, and Masami Saito

Department of Chemistry, College of General Education, The University of Tokyo, Komaba, Meguro-ku, Tokyo 153

(Received September 18, 1978)

New color reactions of aqua(ethylenediaminetetraacetato)ruthenate(III) with sulfur compounds such as thiols, thiourea and thiosulfate have been found and investigated. It has been established that the coloration is due to the anation of the complex with sulfur compounds. In the case of thiosulfate, the reaction is first order in either reactant and independent of $[H^+]$ in the pH range 4 to 6. The rate constant (k_{AN}) was found to be 2.94 ± 0.11 M^{-1} s^{-1} at 30 °C and $I=0.1$. For a pH>6, the rate decreases with increase in pH due to the formation of a hydroxo complex. In the higher pH region, the reverse reaction, $[Ru(edta)(S_2O_3)]^{3-}+OH^- \rightleftarrows [Ru(edta)(OH)]^{2-}+S_2O_3^{2-}$ takes place. From the value of the equilibrium constant (K_{eq}) for this reaction, the equilibrium constant (K_{AN}) for thiosulfate anation has been estimated as, $\log K_{AN}=5.02$ at 30 °C and $I=0.1$.

In the course of the study on the redox reaction of ethylenediaminetetraacetatoruthenate(III),[2)] it was found that the complex solution gave an intense red color by the addition of sulfur compounds, such as cysteine, thiourea and thiosulfate. Examination revealed that the coloration was due to the substitution of a water molecule in the complex for sulfur-containing anions. The color develops instantaneously, except in the case of thiosulfate where it is rather slow. In order to elucidate the nature of the color reaction, a kinetic examination has been conducted.

Experimental

Preparation of Aquahydrogen(ethylenediaminetetraacetato)ruthenium(III), [Ru(Hedta)(H₂O)]. The method of Mukaida *et al.*[3)] has been modified as follows. Ruthenium(IV) oxide (5 mmol, Japan Engelhard Co., Ltd.) was dissolved in concd HCl and after repeated heating to dryness on a water bath the residue was dissolved in concd HCl (20 ml). To the solution was added EDTA (5.3 mmol, free acid) and the mixture heated to dryness several times. From a 6 M HCl solution of the residue, $H[RuEl_2(H_2edte)]\cdot 5H_2O$ crystallized out. The recrystallized solid was dissolved in water and the solution added with an equimolar amount of NaOH and evaporated to dryness twice. On the addition of ethanol, a yellow solid precipitated which was dissolved in water and the solution repeatedly evaporated. This lead to the crystallization of $[Ru(Hedta)(H_2O)]$ (yield; 60%). The purity of the complex was checked by alkalimetric titration.

Other Chemicals. All chemicals used were "special grade" from Wako Chemicals Co. and purified by recrystallization or distillation when necessary. Twice-distilled water was used throughout the experiments.

Kinetics and Equilibrium Measurements. The majority of the measurements were conducted at 30 °C and an ionic strength of 0.1. Since perchlorate, nitrate and chloride react slowly with $[Ru(Hedta)(H_2O)]$, the pH and ionic strength of the solution were adjusted by adding calculated amounts of buffer solutions (acetate, phosphate, carbonate and borate buffers). Care was taken to avoid the possible photochemical oxidation of the complex solution.[2)]

The buffered solutions of either reactant, thermostated separately in the dark, were mixed together, and the mixture transferred to a 10 mm path quartz cell. The increase in the optical density of the solution at 495 nm was followed on a spectrophotometer at constant temperature. The pseudo-first order rate constant, k_{obsd}, was evaluated by plotting $\log(D_\infty - D_t)$ against time t, where D_t and D_∞ are the optical densities at time t and infinity, respectively.

Physical Measurements. The electronic spectra and the color development were recorded on a Hitachi 124 spectrophotometer with an attached thermostatted cell compartment. CD spectra were obtained by a JASCO J20 recording spectrophotometer and IR spectra on a JASCO 403G infrared spectrophotometer. The magnetic susceptibility was measured on a Gouy magnetic balance and the pH on a Toa Denpa Digital pH meter, Type HM-8 and HM-20B.

Results and Discussion

Color Reaction. Of the sulfur compounds investigated, it was found that alkanethiols, cysteine, phenylmethanethiol, *O*-ethyl dithiocarbonate, diethyldithiocarbamate, thiourea and thiosulfate gave pink to reddish brown colors, while the benzenethiols gave blue colors. Sulfides and disulfides did not react at all. It may be noted that there is a parallel between this color reaction and the iodine-azide reaction of thiols and thiocarbonyl compounds.[4)]

As may be seen from Fig. 1, the mole ratio of the ruthenium(III) complex to sulfur compound was found to be 1 : 1.

The colored mixture of the complex and cysteine gave

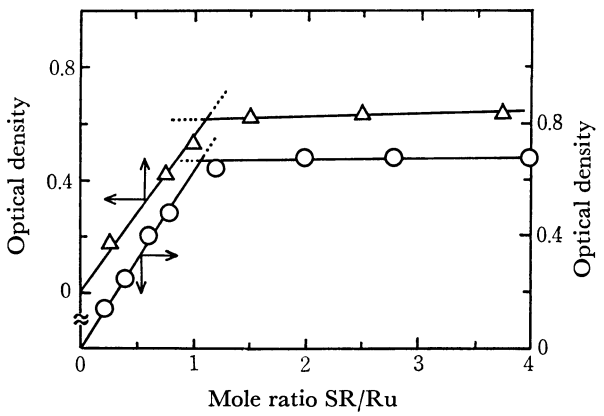

Fig. 1. Mole ratio plot.
$[Ru(Hedta)(H_2O)]$: 2.0×10^{-4} M.
—△—: $S_2O_3^{2-}$; —○—: cysteine.

new CD peaks at 516 nm (+0.64), 436 nm (−0.41), 380 nm (+0.25) and 335 nm (−0.33) where the figures in parentheses represent $\Delta\varepsilon$ values. The reaction products were paramagnetic in both solution and solid states. The magnetic moment of ruthenium in the colored solution (0.1 M Ru) was calculated as; μ_{eff}= 1.91 B.M. at 24.2 °C and therefore it may be said that the +3 state of Ru is retained throughout the reaction. The existence of Ru–carboxylate bonding was confirmed by a strong infrared absorption band at 1620 cm^{-1}. In addition, the elemental analysis of the colored solid gave the atomic ratio C/N as 4.20, which may be compared to the calculated value 4.33 for a 1 : 1 complex of Ru–EDTA and cysteine.

On the basis of these observations, it has been assumed that the color reaction is an anation reaction of the following type;

$$Ru(edta)(H_2O)^- + SR^{n-} \rightleftarrows Ru(edta)(SR)^{(n+1)-} + H_2O, \quad (1)$$

where SR denotes a sulfur-containing compound. The nature of the color change may be a charge transfer between sulfur and ruthenium(III) in the complex.

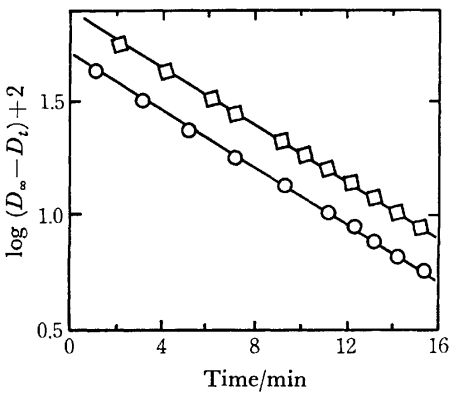

Fig. 2. Pseudo-first-order plot for color reaction of Ru(edta)(H$_2$O)$^-$ with $S_2O_3^{2-}$ at 30 °C, pH 4.7 and I=0.1. [$S_2O_3^{2-}$]$_0$=8.0×10^{-4} M. —◇—: [Ru(edta)(H$_2$O)$^-$]$_0$=2.0×10^{-4} M; —○—: [Ru(edta)(H$_2$O)$^-$]$_0$= 1.2×10^{-4} M.

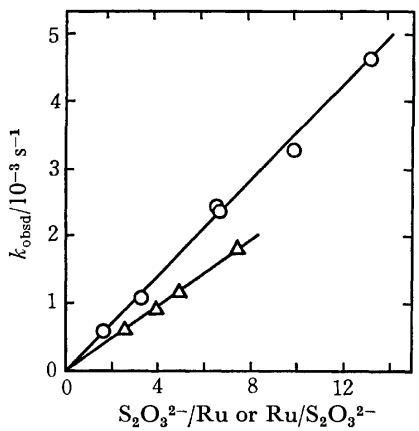

Fig. 3. Dependence of k_{obsd} on the concentration of the excess reactants.
—○—: $S_2O_3^{2-}$ is excess; [Ru(edta)(H$_2$O)$^-$]$_0$=1.2×10^{-4} M; —△—: Ru(edta)(H$_2$O)$^-$ is excess; [$S_2O_3^{2-}$]$_0$= 0.8×10^{-4} M.

Kinetics of Thiosulfate Anation. Of the various sulfur compounds investigated, the color reaction of thiosulfate is relatively slow and the rate could be followed photometrically. The reaction is first order in each reactant (Fig. 2) and the rate is independent of the hydrogen ion concentration in the pH range 4—6. Figure 3 illustrates the dependence of k_{obsd} on the concentration of the excess reactant, thiosulfate or Ru(III)–EDTA complex. A linear relationship is seen to hold in both cases. From the slopes of these straight lines, the rate constant, k_{AN}, of the thiosulfate anation has been evaluated as;

$$k_{AN} = 2.94 \pm 0.11 \text{ M}^{-1} \text{ s}^{-1} \text{ at } 30 \text{ °C and } I = 0.1.$$

In the presence of an excess of thiosulfate ([S_2O_3]/[Ru–EDTA]=6.7), the Arrhenius plot of k_{obsd} at 22, 30, and 40 °C gave the activation energy as, E_a= 37±2 kJ mol^{-1}.

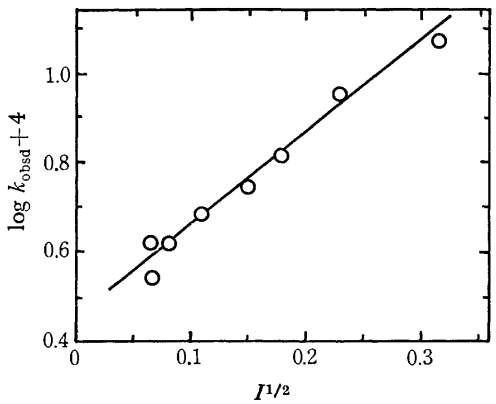

Fig. 4. Dependence of k_{obsd} on the ionic strength.

As illustrated in Fig. 4, a plot of log k_{obsd} *vs.* $I^{1/2}$ gives a straight line with a slope of nearly 2.[5] Taking into consideration the pK values of Ru(Hedta)(H$_2$O) (pK_1=2.75 and pK_2=7.50 at 30 °C and I=0.1) this result is consistent with the reaction of uni-bivalent anions as

$$Ru(edta)(H_2O)^- + S_2O_3^{2-} \rightleftarrows Ru(edta)(S_2O_3)^{3-} + H_2O. \quad (2)$$

The value of the rate constant for this reaction is surprisingly large compared with the halide anation of ruthenium(III)–ethylenediamine and related complexes ($k_{AN}\approx$10^{-3} M^{-1} s^{-1}).[6] However, it has been noted before that substitution reactions at the sixth coordination site of quinquedentate EDTA complexes of Cr(III) and related complexes are remarkably fast.[7,8] Similar labilizing effect due to quinquedentate EDTA may be expected for Ru(edta)(H$_2$O)$^-$.

In the kinetic measurements, k_{obsd} increased linearly with increase in the thiosulfate concentration up to 0.1 M, the concentration range investigated here and no saturation of the rate was observed. Consequently it is not possible to anticipate further the mechanism of the anation.

As reported earlier, the rate of color development is independent of [H$^+$] in the pH range 4—6. However,

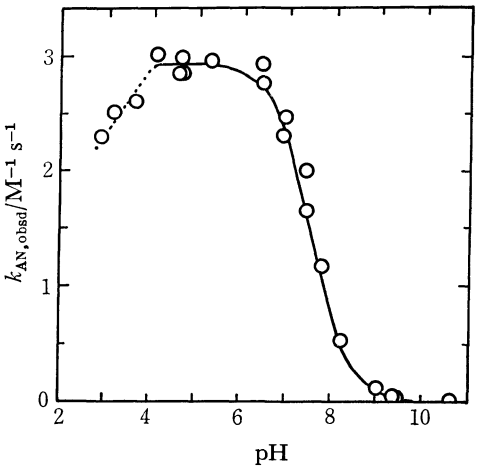

Fig. 5. Dependence of $k_{AN,obsd}$ on pH of the solutions.
○: experimental point; —: calculated curve.

it was found in the region of pH 6—10 that the rate decreases with increase in pH, as illustrated in Fig. 5. (Experimental points are shown by open circles). Since the pK_2 of Ru(Hedta)(H_2O) is known to have the value of 7.50, this result is expected to arise from the decrease in the concentration of the aqua complex with increase in pH. This leads to

$$k_{AN,obsd} = (k_{AN}+k'_{AN}K_2/[H^+])/(1+K_2/[H^+]),$$

where $k_{AN,obsd}$ denotes the observed rate constant in the range pH$>\approx$6 and k_{AN} and k_{AN} are the anation rate constants for Ru(edta)(H_2O)$^-$ and Ru(edta)-(OH)$^{2-}$, respectively. Substituting the values, k_{AN}= 2.94 $M^{-1}\,s^{-1}$, $k'_{AN}\approx 0$ and $K_2=10^{-7.50}$ M, the values of $k_{AN,obsd}$ as a function of pH have been calculated and the results plotted in Fig. 5 (solid line). The agreement between experimental and calculated values is satisfactory.

In the pH range$<$4, $k_{AN,obsd}$ decreases with increase in [H^+]. This may be explained by considering the participation of the less reactive protonated complex, Ru(Hedta)(H_2O) in the reaction, thus

$$k_{AN,obsd} = (k_{AN}+k''_{AN}[H^+]/K_1)/(1+[H^+]/K_1+K_2/[H^+]),$$

where k''_{obsd} refers to the anation rate constant for Ru-(Hedta)(H_2O). The evaluation of k''_{AN} from the rate data in the acidic range (pH$<$4) is, however, difficult owing to the possible decomposition of the thiosulfate in acidic solution.

Equilibrium Study. In the higher pH range (pH$>\approx$8), it was found that the optical densities at infinite time decrease as illustrated in Fig. 6. This may be ascribed to the existence of the following equilibrium;

$$Ru(edta)(S_2O_3)^{3-} + OH^- \rightleftarrows Ru(edta)(OH)^{2-} + S_2O_3^{2-} \quad (3)$$

At 495 nm the only colored species is Ru(edta)(S_2O_3)$^{3-}$ with a molar extinction coefficient, ε, at this wavelength of 3.13×10^3 $M^{-1}\,cm^{-1}$. Using the spectral data of

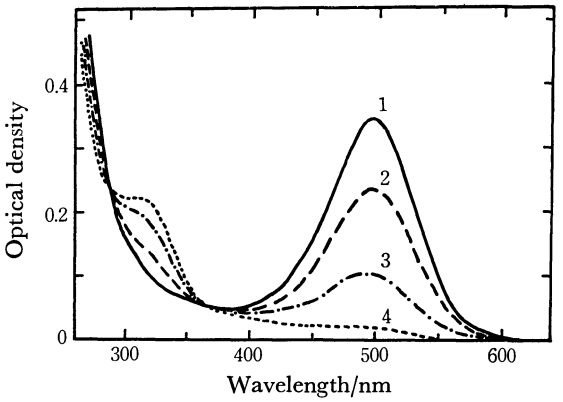

Fig. 6. Change of absorption spectra in the higher pH region.
1: pH 8.57, 2: pH 9.29, 3: pH 9.91, 4: pH 10.81.

Fig. 6, the equilibrium constant (K_{eq}) for Reaction 3 has been calculated as; K_{eq}=19.1 at 30 °C and I=0.1. Since the pK_2 value for Ru(Hedta)(H_2O) is known, the equilibrium constant (K_{AN}) for the thiosulfate anation (Reaction 2) may be calculated using the following relationship:

$$K_{AN} = [Ru(edta)(S_2O_3)^{3-}]/[Ru(edta)(H_2O)^-][S_2O_3^{2-}] = K_2/K_{eq}\cdot K_w,$$

where K_w denotes the ionic product of water. Substituting the values; $K_2=10^{-7.50}$, $K_{eq}=10^{1.28}$ and $K_w=10^{-13.8}$;

$$\log K_{AN} = 5.02 \text{ at } 30\,^\circ C \text{ and } I = 0.1.$$

This value may be compared with that estimated from the spectral data in the mole ratio plot of the optical densities in Fig. 1 (log K_{AN}=5.16).

The authors wish to thank Professor A. Ouchi for his discussion and supply of some sulfur compounds.

References

1) Preliminary paper, Y. Yoshino, T. Uehiro, and M. Saito, *Chem. Lett.*, **1978**, 487.
2) T. Uehiro, Dr. Sc. Thesis, The University of Tokyo, March (1978).
3) M. Mukaida, T. Ishimori, and H. Okuno, *Nippon Kagaku Zasshi*, **86**, 598 (1965).
4) F. Feigl, *Mikrochemie*, **15**, 1 (1934); "Chemistry of Specific, Selective and Sensitive Reactions," Academic Press, New York (1949), p. 145.
5) J. N. Brønsted, *Z. Phys. Chem.* **102**, 169 (1922); N. Bjerrum, *ibid.*, **108**, 82 (1924); V. K. LaMer, *Chem. Rev.*, **10**, 185 (1932).
6) J. A. Broomhead and L. Kane-Maguire, *Inorg. Chem.*, **10**, 85 (1971).
7) H. Ogino, T. Watanabe, and N. Tanaka, *Inorg. Chem.*, **14**, 2093 (1975).
8) Y. Sulfab, R. S. Taylor, and A. G. Sykes, *Inorg. Chem* **15**, 2388 (1976).

Pyrolysis of Tetrasulfur Tetraimide

Shuichi HAMADA* and Yoshiyuki KUDO

Department of Chemistry, Faculty of Science, Science University of Tokyo, Kagurazaka, Shinjuku-ku, Tokyo 162

(Received September 27, 1978)

Tetrasulfur tetraimide was pyrolyzed into sulfur, tetrasulfur tetranitride, tetrasulfur dinitride, ammonia, and nitrogen even below its apparent melting point, 143 °C, under atmospheric pressure; a small amount of heptasulfur imide was also observable. The tetrasulfur dinitride and nitrogen were formed from subsequent reactions between products. The overall pyrolysis consisted of the primary decomposition and the following subsequent ones, as judged from the stoichiometric relationships among the pyrolytic products: $3S_4(NH)_4=4S+2S_4N_4+4NH_3$, $S_4N_4=S_4N_2+N_2$ (in the presence of sulfur), and $S_4N_2=4S+N_2$. Partial pressures of ammonia at the primary pyrolysis were estimated to be 8.5×10^{-2}, 2.1×10^{-1}, 5.2×10^{-1}, and 1.4 Pa at 60, 70, 80, and 90 °C respectively.

Sasaki *et al.*[1] have reported that tetrasulfur tetraimide, $S_4(NH)_4$, melted at 152 °C with an accompanying decomposition on moderately rapid heating, while it was stable in air at room temperature. They have proposed that tetrasulfur tetraimide pyrolyzed as follows over the temperatures from 110 to 135 °C *in vacuo*:

$$3S_4(NH)_4 = 4S + 2S_4N_4 + 4NH_3$$

In this work, the pyrolysis of tetrasulfur tetraimide was studied under atmospheric pressure because there have been few investigations under these conditions.

Experimental

Materials. The tetrasulfur tetraimide was prepared by the method described by Meuwsen[2] as follows: the tetrasulfur tetranitride, S_4N_4,[3] was reduced by adding an ethanolic solution of tin(II) chloride into its benzene solution. A crude product was purified by repeated recrystallization from an acetone and a methanol solution. The tetrasulfur tetraimide thus obtained was confirmed to be pure enough to use in this work by thin-layer chromatography.

Procedures. A differential thermal analysis and a thermal gravimetry of the tetrasulfur tetraimide were carried out at the heating rate of 3 °C/min in an argon atmosphere with a Rigaku Denki Thermoflex, model 8002, differential thermal analyzer. Solid pyrolytic products of the tetrasulfur tetraimide were identified by the TLC as follows: a sample was heated in the argon flow up to the specified temperatures in the DTA equipment, and then was identified by using chlorobenzene, cyclohexane, and carbon tetrachloride as developing solvents. A silver nitrate solution was used as a detecting reagent after quenching. An infrared spectrum of the heat-treated sample was also taken to identify the pyrolytic products, using an IR spectrophotometer, model DS-403G, from the Japan Spectroscopic Co.

The sample was pyrolyzed to identify gaseous products and to estimate their amounts; a glass vessel with a small dead space was employed at the specified temperatures. The gaseous products were identified with a gas chromatograph, model 80, from the Yanagimoto Seisakusho. A silica gel column was used as a stationary phase and helium as a carrier gas. The amount of ammonia, one of the gaseous products, was estimated coulometrically[4,5] during the pyrolysis in the argon and carbon dioxide atmospheres. The amount of nitrogen, another one of the gaseous products, was estimated with an azotometer by using the carbon dioxide as the carrier gas, after removing the accompanying ammonia into diluted perchloric acid.

The partial pressure of ammonia during the pyrolysis was measured over the temperatures from 60 to 90 °C in the argon and the nitrogen atmospheres by a method of transpiration.[6,7] The specified temperature of the sample was kept within a precision of ±0.05 °C. The flow rate of the carrier gas was controlled automatically over the range from 77.4 to 125 cm³/min. The total volume of the carrier gas was measured with a wet-type gas flowmeter, model WK-0.5, from the Shinagawa Seisakusho. The amount of ammonia in the carrier gas was estimated coulometrically after the gas flow was passed through an ice-cold trap to remove volatile solid products.

Results

The Solid Pyrolytic Products of Tetrasulfur Tetraimide. The solid pyrolytic products were identified to be sulfur, tetrasulfur tetranitride, tetrasulfur dinitride, S_4N_2, and heptasulfur imide, S_7NH, by the TLC, as shown in Table 1. Both the tetrasulfur tetranitride[8,9] and the tetrasulfur dinitride[10] were also confirmed by the IR spectrometry, though the heptasulfur imide was unde-

Table 1. Results of TLC on solid pyrolytic products of tetrasulfur tetraimide

Solvent	R_f value				
	S_8	S_4N_4	S_4N_2	S_7NH	$S_4(NH)_4$
Chlorobenzene	1.0 (1.0)[a]	0.61 (0.61)		0.88 (0.88)	0.15 (0.15)
Carbon tetrachloride	0.92 (0.92)	0.47 (0.42)		0.70 (0.68)	0.0 (0.0)
Cyclohexane	0.80 (0.82)	0.16 (0.14)	0.66 (0.67)	0.35 (0.36)	0.0 (0.0)

a) The R_f values in parentheses were previously determined for each species.

Table 2. Solid pyrolytic products at each temperature

t/°C	Species				
90	$S_4(NH)_4$				
100	$S_4(NH)_4$	S_8			
110	$S_4(NH)_4$	S_8	S_4N_4		(S_7NH)[a]
120	$S_4(NH)_4$	S_8	S_4N_4	S_4N_2	(S_7NH)
130	$S_4(NH)_4$	S_8	S_4N_4	S_4N_2	(S_7NH)
140	$S_4(NH)_4$	S_8	S_4N_4	S_4N_2	(S_7NH)
150	$S_4(NH)_4$	S_8	S_4N_4	S_4N_2	(S_7NH)
160		S_8	S_4N_4	S_4N_2	(S_7NH)
170		S_8	S_4N_4	S_4N_2	(S_7NH)
180		S_8			

a) Very small amount.

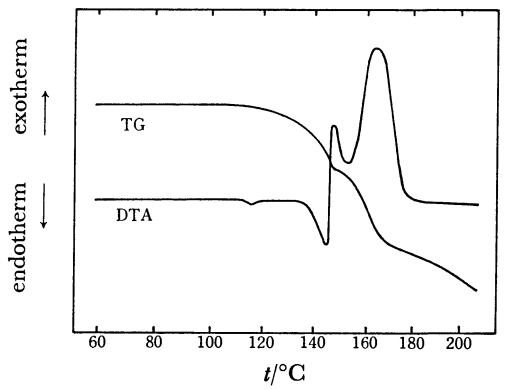

Fig. 1. DTA and TG patterns of tetrasulfur tetraimide.

tectable because of its small amount. The kinds of products at each temperature are shown in Table 2.

Figure 1 shows the DTA and the TG patterns of the tetrasulfur tetraimide taken in the argon atmosphere. An endothermic peak at 143 °C was confirmed to be caused by fusion of tetrasulfur tetraimide,[1] while the apparent melting point increased with increasing the heating rate, *e.g.*, 143, 149, and 152 °C at 3, 5, and 10 °C/min respectively. The tetrasulfur tetraimide was pyrolyzed even below its apparent melting point, judging from a weight loss in the TG and the results in Table 2. The tetrasulfur tetraimide disappeared at 160 °C under these conditions as is shown in Table 2, though it vanished even at 150 °C by heating for 1 h. The sample pre-heated at 150 °C showed only the exothermic peak at 165 °C, besides a small endothermic peak around 115 °C arising from the fusion of sulfur. Judging from these results, the exothermic peaks at 147 and 165 °C were attributable to a vigorous decomposition of tetrasulfur tetraimide and a subsequent decomposition of the pyrolytic products respectively: the contribution of heptasulfur imide to the DTA pattern was obscure because of its small amount.

The weight loss in the TG from about 105 to 147 °C was considered to originate mainly from the primary pyrolysis of the tetrasulfur tetraimide, which was accompanied by evolution of the gas and sublimation of the resulting tetrasulfur tetranitride.[7] The weight loss at the second stage above 147 °C was chiefly attributable to the subsequent decomposition of the pyrolytic products which accompanied the formation of the gas and was followed in turn by vaporization of molten sulfur. Judging from the weight loss, about 30 wt % at 140 °C, at the first stage and the kinds of the pyrolytic products, the subsequent decomposition was also expected to occur even below 147 °C.

Amounts of the tetrasulfur tetranitride and the sulfur in the sample heated at 110 °C for 1.5 h were estimated to be 0.431 and 1.69 respectively, as the molar ratios to the original tetrasulfur tetraimide. A spectrophotometric technique was used after separating the materials chromatographically by using a silica gel column. These values disagreed with those proposed by Sasaki *et al.*[1] The amount of the tetrasulfur dinitride could not be estimated because the tetrasulfur dinitride was easily hydrolyzed in the silica gel column, which contained about 6% water, during the chromatographic separation. Goehring *et al.*[11] have reported that tetrasulfur dinitride produced an equivalent amount of ammonia on its hydrolysis. Therefore, the amount of the tetrasulfur dinitride could be deduced to be 0.257 mol against 1 mol of tetrasulfur tetraimide from a mass balance of nitrogen. The amount of the heptasulfur imide was also estimated to be 0.027 as the molar ratio to the original material: the amount of hydrogen in the observed heptasulfur imide was less than 0.7 mol % against that in the original tetrasulfur tetraimide, so that the formation of heptasulfur imide could be neglected in this case.

The Gaseous Pyrolytic Products of Tetrasulfur Tetraimide. The gaseous products were identified to be ammonia and nitrogen by the gas chromatography on the pyrolysis at 120 °C for 2 h in the argon and the carbon dioxide atmospheres, while neither hydrogen nor hydrogen sulfide was observable. Both ammonia and nitrogen were also detected even at 80 °C in the same atmospheres.

The tetrasulfur tetraimide was pyrolyzed in order to estimate the amount of ammonia over the temperatures from 80 to 160 °C for 1.5—6 h in the argon and the carbon dioxide flows. The molar ratio of the ammonia to the original tetrasulfur tetraimide was estimated to be 1.33 ± 0.008 under these conditions; this value did not depend on the temperature or on the kinds of the carrier gases. Therefore, all the hydrogen atoms in tetrasulfur tetraimide were considered to be released in the form of ammonia by the pyrolysis, though a negligibly small part of the hydrogen was converted into the form of heptasulfur imide. The amount of the nitrogen was estimated with the azotometer over the temperatures from 80 to 170 °C in the carbon dioxide flow, after the accompanying ammonia was absorbed into diluted perchloric acid. Figure 2 shows the molar ratio of the produced nitrogen to the original tetrasulfur tetraimide against the temperature. The molar ratio increased linearly with increasing the temperature up to about 140 °C and then further increased with a steeper slope above 140 °C. This temperature nearly corresponded to the apparent melting point of tetrasulfur tetraimide, so that the increase in the formation of nitrogen above

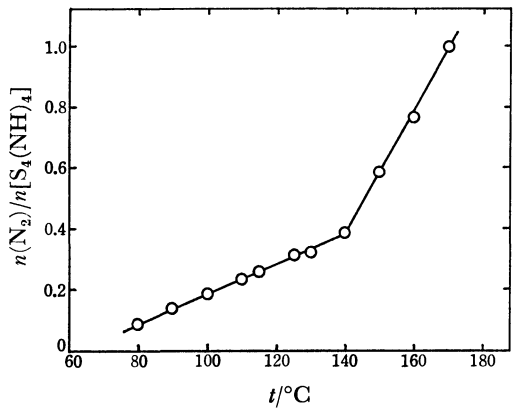

Fig. 2. Molar ratio of produced nitrogen to tetrasulfur tetraimide against temperature.

140 °C was considered to be due to the vigorous decomposition of tetrasulfur tetraimide after fusion and the subsequent decomposition of the pyrolytic products.

The Partial Pressure of Ammonia during the Pyrolysis. In order to estimate apparent partial pressures of ammonia by the method of transpiration,[6,7] the tetrasulfur tetraimide was homogeneously mixed with the tetrasulfur tetranitride to keep proper vapor pressures of tetrasulfur tetranitride at given temperatures[7] in the reaction vessel. A sufficient amount of the ammonia was directly absorbed into an electrolytic solution for the coulometric titration, *i.e.*, 6.5—37.0 μg. The total volume of the carrier gas ranged from 2.4 to 15.0 dm^3 (from 30 to 120 min) as the standard state. The apparent partial pressure, p, of the ammonia was calculated by the following equation, on the assumption that the law of partial pressure was obeyed: $p=nRT(P+p')/[nRT+(P+p''-p_w)V]$. Where P is the atmospheric pressure, p', the excess pressure in the reaction vessel, p'', the excess pressure in the gas flowmeter, p_w, the vapor pressure of water in the gas flowmeter, n, the number of moles of the ammonia, V, the volume of the carrier gas, and R, the gas constant.

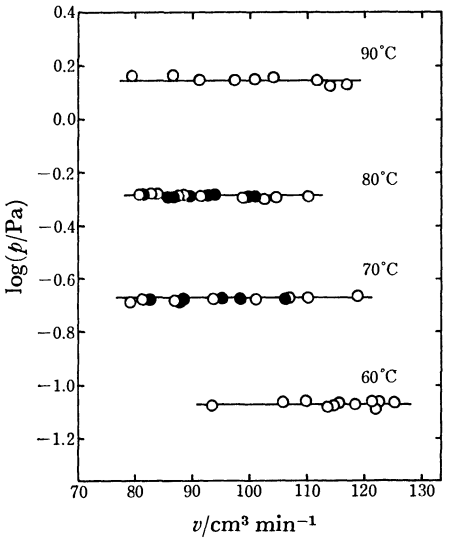

Fig. 3. Relationship between apparent partial pressure of ammonia and flow rate of carrier gas.
○: Estimated in Ar atmosphere, ●: estimated in N_2 atmosphere.

Figure 3 shows the relationship between the apparent partial pressure of the ammonia and the flow rate of the carrier gas. The values of the apparent partial pressures were almost equal at each temperature within these flow rate. Accordingly, it can be concluded that the formation of the ammonia in this system was in an equilibrium state. Therefore, the partial pressures of the ammonia during the pyrolysis were estimated to be 8.5×10^{-2}, 2.1×10^{-1}, 5.2×10^{-1}, and 1.4 Pa at 60, 70, 80, and 90 °C respectively; these are the averages of the apparent values estimated in the argon atmosphere (open circles). The apparent partial pressures estimated in the nitrogen atmosphere (closed circles) agreed with those estimated in the argon atmosphere at 70 and 80 °C, as is shown in Fig. 3. The partial pressures of the ammonia during the pyrolysis were not affected by the kinds of the carrier gases, *i.e.*, argon and nitrogen.

Discussion

The overall pyrolysis of tetrasulfur tetraimide under atmospheric pressure was not so simple as that reported by Sasaki *et al.*[1] All the hydrogen atoms in imide groups of tetrasulfur tetraimide were converted into those in the form of ammonia, judging from their stoichiometric relationship, while a very small part of the imide group remained in the form of heptasulfur imide. On the contrary, the nitrogen atoms were converted into not only the form of tetrasulfur tetranitride but also the forms of nitrogen and tetrasulfur dinitride during the pyrolysis, and a simple stoichiometric relationship could not be obtained among them.

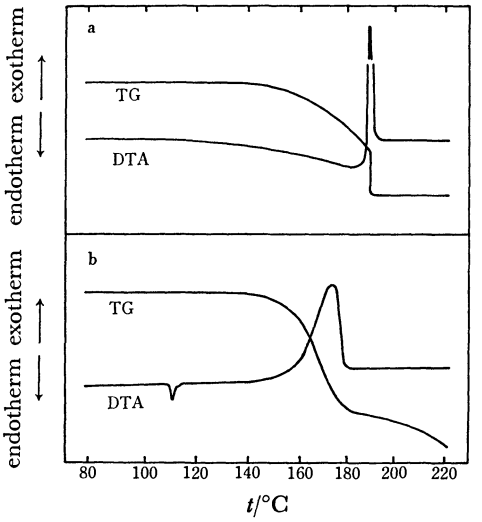

Fig. 4. DTA and TG patterns of tetrasulfur tetranitride
a: S_4N_4, b: $S_4N_4+S_8$ (molar ratio, 4: 1).

The tetrasulfur tetranitride showed a very sharp exothermic peak at 190 °C, along with an abrupt weight loss in the argon atmosphere on its DTA and TG, as is shown in Fig. 4a: it decomposed explosively into its elements at this temperature. No nitrogen could be detected below this temperature, though Goehring *et al.*[12] have reported that it decomposed above 130 °C. Heal[13] has described that tetrasulfur tetranitride decomposed gently above 120 °C when it was mixed with a large amount of sulfur. Figure 4b shows a DTA pattern of the tetrasulfur tetranitride mixed with the sulfur at the molar ratio of 4: 1 in the argon atmosphere. A broad exothermic peak was observed at 174 °C in the DTA instead of the sharp one at 190 °C for the pure tetrasulfur tetranitride, besides a small endothermic peak around 110 °C attributable to the fusion of sulfur. Furthermore, the exothermic peak temperature of the mixed sample decreased from 174 to 165 °C upon increasing the molar ratio of the sulfur from 4: 1 to 1: 4. Backens[14] has reported that tetrasulfur dinitride was produced by the gentle decomposition of tetrasulfur

tetranitride mixed with sulfur above 125 °C. The tetrasulfur dinitride was observed on the pyrolysis of the tetrasulfur tetranitride mixed with the sulfur at 160 °C in the argon atmosphere. An evolution of nitrogen was also confirmed during the pyrolysis of the same sample even at 140 °C. Consequently, the pyrolysis of tetrasulfur tetranitride was concluded to be accelerated in the presence of sulfur. The exothermic peak at 165 °C in Fig. 1 was confirmed to be attributable to this reaction.

It can be concluded that the formations of tetrasulfur dinitride and nitrogen originate from the subsequent pyrolysis of the tetrasulfur tetranitride in the presence of the sulfur, followed by the decomposition of the tetrasulfur dinitride because of its instability,[15] as follows:

$$S_4N_4 = S_4N_2 + N_2 \text{ (in the presence of sulfur)}, \quad (1)$$

$$S_4N_2 = 4S + N_2. \quad (2)$$

This consideration can be supported by the fact that the apparent partial pressures of the ammonia during the pyrolysis were independent of the kinds of the carrier gases, *i.e.*, argon and nitrogen.

TABLE 3. MOLAR RATIOS OF PYROLYTIC PRODUCTS TO TETRASULFUR TETRAIMIDE AT 110 °C

	S	S_4N_4	NH_3	N_2	S_4N_2	S_7NH
Overall reaction	1.69	0.431	1.33	0.235	0.257[a]	0.027
Primary reaction	—[b]	0.666[c]	1.33			
Sasaki *et al.*[1]	1.33	0.667	1.33			

a) Deduced. b) Unestimated. c) Calculated.

The amount of the tetrasulfur tetranitride produced at the primary pyrolysis can be calculated from the estimated amounts of the species and Eqs. 1 and 2, as is shown in Table 3. The amount of the sulfur to be produced at the first stage, however, could not be deduced because of the complicated hydrolysis of tetrasulfur dinitride with respect to sulfur atoms.[11,16] The primary pyrolysis of tetrasulfur tetraimide is considered to be the same as that reported by Sasaki *et al.*,[1] judging from the results in Table 3 and the process of the pyrolysis:

$$3S_4(NH)_4 = 4S + 2S_4N_4 + 4NH_3. \quad (3)$$

The van't Hoff plots of the partial pressure of the ammonia showed a good linear relationship, while the value at 90 °C was overestimated to some degree because of the extra formation of ammonia arising from the reaction between a trace amount of tetrasulfur dinitride and water.[11]

References

1) Y. Sasaki and F. P. Olsen, *Inorg. Nucl. Chem. Lett.*, **3**, 351 (1967).
2) A. Meuwsen and M. Lösel, *Z. Anorg. Allg. Chem.*, **271**, 217 (1953).
3) W. L. Jolly and M. Becke-Goehring, *Inorg. Chem.*, **1**, 76 (1962).
4) G. M. Arcand and E. H. Swift, *Anal. Chem.*, **28**, 440 (1956).
5) T. Yoshimori, S. Ishiwari, Y. Watanabe, T. Harada, and S. Yamada, *Trans. Jpn. Inst. Met.*, **14**, 396 (1973).
6) M. Taniguchi, *Shokubai*, **6**, 202 (1964).
7) S. Hamada, *Bull. Chem. Soc. Jpn.*, **46**, 3598 (1973).
8) E. R. Lippincott and M. C. Tobin, *J. Chem. Phys.*, **21**, 1559 (1953).
9) J. Bragin and M. V. Evans, *J. Chem. Phys.*, **51**, 268 (1969).
10) J. Nelson and H. G. Heal, *J. Chem. Soc., A*, **1971**, 136.
11) M. Becke-Goehring, *Progr. Inorg. Chem.*, **1**, 207 (1959).
12) M. Becke-Goehring and D. Voigt, *Z. Anorg. Allg. Chem.*, **285**, 181 (1956).
13) H. G. Heal, "Advances in Inorganic Chemistry and Radiochemistry," ed by H. J. Emeléus and A. G. Sharpe, Academic Press, New York (1972), Vol. 15, p. 384.
14) A. Backens, Doctoral Thesis, University of Heidelberg, Heidelberg, West Germany.
15) A. Meuwsen, *Z. Anorg. Allg. Chem.*, **266**, 250 (1951).
16) G. W. Donaldson and F. J. Johnston, *J. Phys. Chem.*, **73**, 2064 (1969).

A Rate Study on the Oxidative Addition Reactions of Iodine toward Tetrakis(2,4,6-trimethylphenyl and *t*-butyl isocyanide)-rhodium(I) Perchlorates

Ryosho KUWAE and Toshio TANAKA*

Department of Applied Chemistry, Faculty of Engineering, Osaka University, Suita, Osaka 565

(Received August 31, 1978)

The reaction of $[RhL_4]ClO_4$ (L=2,4,6-$Me_3C_6H_2NC$ and *t*-BuNC) with an equimolar amount of iodine yields a *trans* adduct, $[RhI_2L_4]ClO_4$. The rate of this reaction in acetonitrile was measured employing a stopped-flow technique under pseudo-first-order conditions with excess iodine. The result indicates that the reaction proceeds *via* an intermediate which is presumably assigned to *cis*-$[RhI_2L_4]ClO_4$, followed by intramolecular isomerization to the *trans* adduct.

Kinetics of oxidative addition reactions of various molecules such as hydrogen[1,2] and olefins[2-4] to rhodium(I) substrates have been reported by several research groups. The rate of addition reaction of halogen to rhodium(I) complexes has, however, been little measured, although a number of halogen adducts with Rh(I) are known.[5-7] Our recent kinetic study[8] has shown that the addition of iodine to $Rh(S_2CNMe_2)$-(2,4,6-$Me_3C_6H_2NC)_2$ proceeds *via* a charge transfer complex formed between the sulfur atom of the S_2CNMe_2 ligand (donor) and iodine (acceptor), which is rearranged to *cis*-$RhI_2(S_2CNMe_2)$(2,4,6-$Me_3C_6H_2NC)_2$, followed by isomerization to the *trans* adduct with respect to the iodide anions. It is of interest to examine whether the formation of a *cis* adduct in advance of a *trans* one is general in the addition reaction of iodine to Rh(I) substrates.

This paper reports the rate study on the reactions of tetrakis(2,4,6-trimethylphenyl and *t*-butyl isocyanide)-rhodium(I) perchlorates, $[RhL_4]ClO_4$, with iodine giving *trans*-$[RhI_2L_4]ClO_4$.

Experimental

Materials and Spectra. Iodine was sublimed three times. Acetonitrile and acetone were dried over phosphorus pentaoxide and Drierite, respectively. Dichloromethane was purified by the usual method.[9] $[Rh(2,4,6\text{-}Me_3C_6H_2NC)_4]ClO_4$ was prepared as follows; a methanol (10 ml) solution of 2,4,6-$Me_3C_6H_2NC$ (4 mmol) was added dropwise to a suspension of $[RhCl(1,5\text{-}C_8H_{12})]_2$ (0.5 mmol) in methanol (5 ml). The mixture was stirred for 2 h, followed by the addition of a methanol (10 ml) solution of sodium perchlorate monohydrate (2 mmol). The resulting precipitate was recrystallized from a mixture of dichloromethane with ligroin to give yellowish orange plates in a 73% yield. ν(NC) 2142 cm^{-1}. λ_{max} 402 nm (ε 7500), 339 nm (ε 56300), and 252 nm (ε 66200). Found: C, 61.44; H, 5.74; N, 7.40%. Calcd for $C_{40}H_{44}ClN_4O_4Rh$: C, 61.35; H, 5.66; N, 7.15%. $[Rh(t\text{-}BuNC)_4]ClO_4$ was similarly prepared by the use of *t*-BuNC for 2,4,6-$Me_3C_6H_2NC$, 74% yield. ν(NC) 2156 cm^{-1}. λ_{max} 381 nm (ε 9600) and 309 nm (ε 27900). Found: C, 45.10; H, 6.83; N, 10.37%. Calcd for $C_{20}H_{36}ClN_4O_4Rh$: C, 44.91; H, 6.78; N, 10.47%.

Infrared and electronic spectra were measured with Hitachi-Perkin Elmer 225 and Hitachi 124 spectrophotometers, respectively. ^1H NMR spectra were recorded on a JEOL JNM-PS-100 spectrometer.

Equimolar Reaction of $[RhL_4]ClO_4$ (L=2,4,6-$Me_3C_6H_2NC$ and t-BuNC) with Iodine. An acetonitrile (10 ml) solution of I_2 (0.5 mmol) was added to $[Rh(2,4,6\text{-}Me_3C_6H_2NC)_4]ClO_4$ (0.5 mmol) in acetonitrile (20 ml). After stirred for 1 h, the solution was evaporated to dryness under reduced pressure. The resulting product was recrystallized from dichloromethane–petroleum ether to give orange plates of $[RhI_2(2,4,6\text{-}Me_3C_6H_2NC)_4]ClO_4$ in an 87% yield. ν(NC) 2216 cm^{-1}. λ_{max} 391 nm (ε 9500) and 256 nm (ε 86000). Found: C, 46.44; H, 4.39; N, 5.19%. Calcd for $C_{40}H_{44}ClI_2N_4O_4Rh$: C, 46.33; H, 4.28; N, 5.40%.

$[RhI_2(t\text{-}BuNC)_4]ClO_4$ was similarly obtained by reaction of $[Rh(t\text{-}BuNC)_4]ClO_4$ with an equimolar amount of I_2 in acetonitrile, 68% yield. ν(NC) 2231 cm^{-1}. λ_{max} 384 nm (ε 10000) and 277 nm (ε 42000). Found: C, 30.85; H, 4.70; N, 6.99%. Calcd for $C_{20}H_{36}ClI_2N_4O_4Rh$: C, 30.46; H, 4.60; N, 7.10%.

Reaction of $[RhL_4]ClO_4$ with Excess Iodine. To an acetonitrile (10 ml) solution of $[Rh(2,4,6\text{-}Me_3C_6H_2NC)_4]ClO_4$ (0.3 mmol) was added excess I_2 (3 mmol) in acetonitrile (25 ml). After stirred for 15 h, the solution was evaporated to dryness under reduced pressure. The product obtained was washed with diethyl ether to remove unreacted I_2, followed by recrystallization from dichloromethane–ligroin to give brown plates of $RhI_5(2,4,6\text{-}Me_3C_6H_2NC)_4$ in a 64% yield. ν(NC) 2214 cm^{-1}. Found: C, 36.48; H, 3.28; N, 4.24%. Calcd for $C_{40}H_{44}I_5N_4Rh$: C, 36.45; H, 3.36; N, 4.25%.

$RhI_5(t\text{-}BuNC)_4$ was similarly obtained by reaction of $[Rh(t\text{-}BuNC)_4]ClO_4$ with excess I_2 in acetonitrile, 66% yield. ν(NC) 2227 cm^{-1}. Found: C, 22.43; H, 3.35; N, 5.28%. Calcd for $C_{20}H_{36}I_5N_4Rh$: C, 22.45; H, 3.29; N, 5.24%.

These complexes were also obtained by reaction of $[RhI_2L_4]ClO_4$ with excess I_2.

Kinetic Measurements. Kinetic runs were carried out under pseudo-first-order conditions by mixing an acetonitrile solution of $[RhL_4]ClO_4$ (2.0×10^{-4} M) with excess I_2 in acetonitrile ($2.0-10.0\times10^{-3}$ M). The reaction rate was followed by measuring absorbances of the reaction mixture, using a Union RA-413 stopped flow-rapid scanning spectrophotometer equipped with a 0.2 cm quartz cell in a cell holder thermostated to ±0.2 °C. At least five reaction curves were accumulated by a Union System-71 kinetic data processor and an average curve was recorded on a National VP-6421A X-Y recorder.

Results and Discussion

Characterization of the Iodine Adducts. The four iodine adducts, $[RhI_2L_4]ClO_4$ and RhI_5L_4 (L=2,4,6-$Me_3C_6H_2NC$ and *t*-BuNC), exhibit only a ν(N≡C) band, whose frequency is higher than that of the corresponding

Rh(I) substrate. This confirms the occurrence of oxidative addition reactions[8] of I_2 to Rh(I) with retention of D_{4h} symmetry of the four isocyanide ligands centered at the metal. Thus, $[RhI_2L_4]ClO_4$ (L=2,4,6-$Me_3C_6H_2NC$, *t*-BuNC) assumes an octahedral geometry, in which the two iodide ligands are in mutual *trans* positions. A similar *trans* configuration was reported for $[RhI_2(t\text{-BuNC})_4]PF_6$.[10] Complexes of the RhI_5L_4 type behave as electrolytes in acetonitrile; molar conductivities are 151 (L=2,4,6-$Me_3C_6H_2NC$, 1.0×10^{-4} M) and 176 $cm^2\,ohm^{-1}\,mol^{-1}$ (L=*t*-BuNC, 1.0×10^{-4} M). These complexes may be formulated as *trans*-$[RhI_2L_4]I_3$ since their ν(NC) frequencies were essentially identical with those of the corresponding perchlorate salts and their electronic spectra in acetonitrile appeared as a superposition of the spectrum of the I_3^- anion on that of the *trans*-$[RhI_2L_4]^+$ cation.

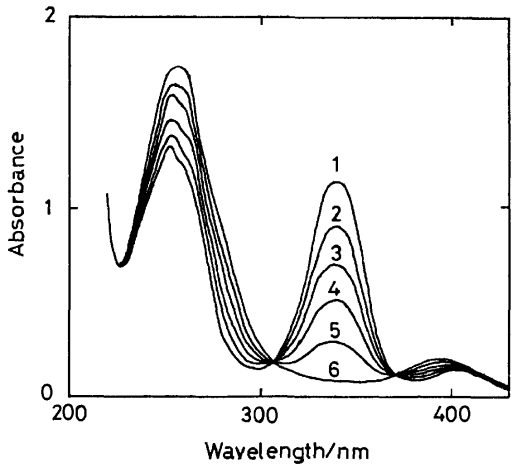

Fig. 1. Electronic spectra of $[Rh(2,4,6\text{-}Me_3C_6H_2NC)_4]ClO_4$ (2.0×10^{-4} M) in acetonitrile containing varying amounts of iodine; (**1**) 0, (**2**) 0.4×10^{-4} M, (**3**) 0.8×10^{-4} M, (**4**) 1.2×10^{-4} M, (**5**) 1.6×10^{-4} M, (**6**) 2.0×10^{-4} M; cell length=0.1 cm.

Stoichiometry. The electronic spectra of $[RhL_4]ClO_4$ in acetonitrile obeyed the Lambert-Beer law over the concentration range from 3×10^{-6} to 4×10^{-4} M. Self-association of these square-planar Rh(I) cations is, therefore, negligible in this range, though such phenomenon has been reported to occur in some Rh(I) complexes at relatively high concentrations.[11] Electronic spectra of acetonitrile solutions containing $[Rh(2,4,6\text{-}Me_3C_6H_2NC)_4]ClO_4$ and varying amounts of I_2 are shown in Fig. 1. The spectrum of a solution containing equimolar amounts of the Rh(I) substrate and I_2 (**6** in Fig. 1) was essentially same as that of an acetonitrile solution of the *trans*-$[RhI_2(2,4,6\text{-}Me_3C_6H_2NC)_4]ClO_4$ adduct. In addition, there was seen no appreciable change in the spectrum even in a solution containing the Rh(I) substrate and I_2 with the mole ratio of 1:2. As shown in Fig. 2, the mole ratio method using the absorbances at 339 and 256 nm indicates the composition of the adduct to be 1:1. The same result was obtained in the $[Rh(t\text{-BuNC})_4]ClO_4$–$I_2$ system. Thus, the stoichiometry for equimolar reaction of I_2 with the Rh(I) substrate is expressed by

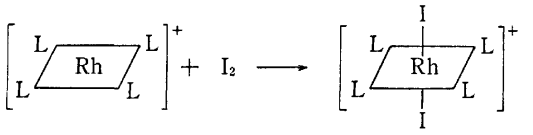

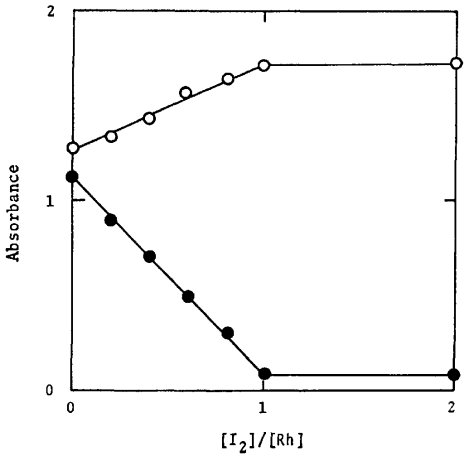

Fig. 2. A plot of the absorbances at 339 (●) and 256 nm (○) *vs.* the mole ratio $[I_2]/[\mathbf{Rh}]$ in acetonitrile; $[\mathbf{Rh}]=2.0\times10^{-4}$ M (**Rh**=$[Rh(2,4,6\text{-}Me_3C_6H_2NC)_4]ClO_4$).

Kinetics and Mechanism. Rapid scanning spectra of the solution after mixing $[Rh(t\text{-BuNC})_4]ClO_4$ (2.0×10^{-4} M) with excess I_2 (2.0×10^{-3} M) in acetonitrile is illustrated in Fig. 3, which shows decay of the absorption maxima at 282 and 376 nm both with half-lives of about 1 s. The spectrum finally obtained shows the absorption maxima at 277 and 384 nm due to *trans*-$[RhI_2(t\text{-BuNC})_4]ClO_4$. As $[Rh(t\text{-BuNC})_4]ClO_4$ and I_2 exhibit no band maximum at 282 and 376 nm, the bands observed at these wavelengths may be associated with a reaction intermediate which is formed during the dead time of the instrument. Similarly, an intermediate

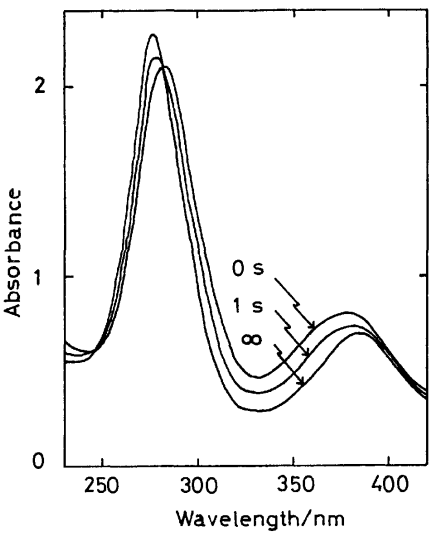

Fig. 3. Rapid scanning spectra after mixing $[Rh(t\text{-BuNC})_4]ClO_4$ (2.0×10^{-4} M) with excess I_2 (2.0×10^{-3} M) in acetonitrile at 25.0 °C, cell length=0.2 cm.

Fig. 4. The ^{1}H NMR spectrum of an equimolar mixture (5.0×10^{-2} M) of [Rh(*t*-BuNC)$_4$]ClO$_4$ and I_2 in acetonitrile-d_3 at −40 °C; the solution was prepared at this temperature.

with absorption maxima at 256 and 375 nm was observed in the reaction of [Rh(2,4,6-$Me_3C_6H_2NC)_4$]-ClO$_4$ with I_2. The discordant wavelengths of the short-lived absorptions observed in the two reaction systems imply that the intermediates are not a common species such as the I_3^- anion.

In order to obtain some knowledge of the intermediate, ^{1}H NMR and infrared spectra were measured for solutions of the mixture of reactants at low temperatures because the intermediate might be stabilized at low temperatures. Figure 4 shows the ^{1}H NMR spectrum of an acetonitrile-d_3 solution containing equimolar amounts (5.0×10^{-2} M) of [Rh(*t*-BuNC)$_4$]ClO$_4$ and I_2 immediately after preparing at −40 °C. There appear two methyl signals, of which the upfield one is ascribed to the intermediate because this signal decreases in intensity with ascending temperature and disappears at −10 °C completely, while the downfield signal assignable to *trans*-[RhI$_2$(*t*-BuNC)$_4$]ClO$_4$ remains unchanged even at room temperature. Figure 5 shows the infrared spectra in the ν(N≡C) region for two acetone solutions both containing equimolar quantities (2.5×10^{-2} M) of [Rh(*t*-BuNC)$_4$]ClO$_4$ and I_2; one was prepared by rapid introduction of the reactant solutions into a cell at −60 °C (solution **a**), and the other was prepared at room temperature, followed by cooling down to −60 °C (solution **b**). The 2231 cm^{-1} band observed in **b** is attributable to *trans*-[RhI$_2$(*t*-BuNC)$_4$]-ClO$_4$ because of its coincidence in position with the band of this compound in acetone at room temperature. The same assignment is given to the high frequency band (2231 cm^{-1}) found in **a**. On the other hand, the low frequency band (2217 cm^{-1}) may be due to the intermediate since it disappeared after solution **a** was allowed to stand at room temperature for more than 20 min and recooled to −60 °C. It is to be noted that the position of the 2217 cm^{-1} band is 61 cm^{-1} higher than that of ν(N≡C) of the starting complex [Rh(*t*-BuNC)$_4$]-ClO$_4$ (2156 cm^{-1}). The magnitude of this high frequency shift is larger than that observed in one electron oxidation (35—50 cm^{-1}) of some Rh(I)–isocyanide complexes, and is close to that in the two electron oxidation (65—80 cm^{-1}).[12] This indicates that the rhodium metal of the intermediate is oxidized with I_2. Thus, two possible configurations, **A** and **B**, are proposed for the intermediate, though the oxidation number of the rhodium metal in **A** is ambiguous. A configuration with metal–iodine interaction like **A** has been suggested as an intermediate in the reactions of I_2 with Pt(acac)$_2$[13] and $Me_3SnCr(CO)_3(\eta\text{-}C_5H_5)$,[14] although no direct spectral evidence for the existence of such an intermediate has been obtained, probably because of its low stability. On the other hand, the half-life of the intermediate (about 1 s) in the present reaction is compared with that of *cis*-[Cr(CO)$_2$($Ph_2PCH_2PPh_2$)$_2$]$^+$ (about 0.6 s) which isomerizes to a *trans* cation.[15] In addition, the electronic spectrum of the present intermediate resembles that of the *trans* adduct (Fig. 3), suggesting that they are at least structurally similar to each other. This is supported from the similarity between the spectra of *cis*- and *trans*-RuCl$_2$(4-$MeC_6H_4NC)_2(PPh_3)_2$ prepared by the literature method,[16] as shown in Fig. 6. In view of these facts, the intermediate is presumably assigned to the *cis* adduct **B** in the present reactions.

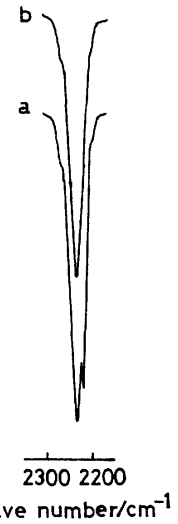

Fig. 5. Infrared spectra of acetone solutions containing equimolar quantities (2.5×10^{-2} M) of [Rh(*t*-BuNC)$_4$]-ClO$_4$ and I_2 at low temperatures; **a** and **b** are the solutions prepared at −60 °C and at room temperature, respectively.

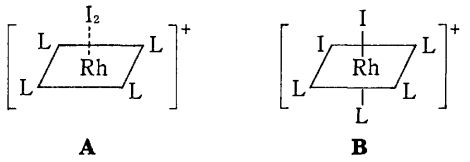

A **B**

Unsatisfactory solubility of [Rh(2,4,6-$Me_3C_6H_2NC)_4$]-ClO$_4$ in polar solvents such as acetonitrile and acetone at low temperatures has prevented ^{1}H NMR and infrared spectral measurements, as described above, for the [Rh(2,4,6-$Me_3C_6H_2NC)_4$]ClO$_4$–I_2 system.

The rate of reaction of [Rh(2,4,6-$Me_3C_6H_2NC)_4$]ClO$_4$ with I_2 was followed by measuring the decay of absorb-

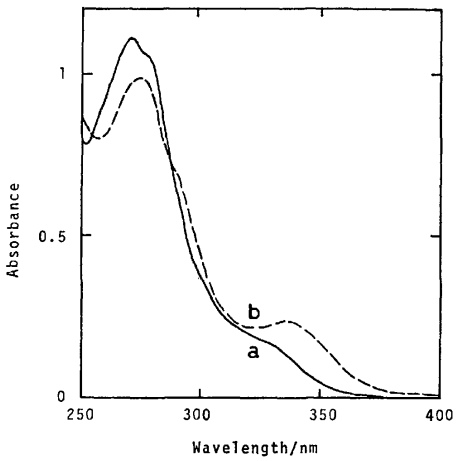

Fig. 6. Electronic spectra of acetonitrile solutions (2.5×10^{-5} M) of *cis*- (**a**) and *trans*-$RuCl_2(4\text{-}MeC_6H_4NC)_2(PPh_3)_2$ (**b**), cell length = 1.0 cm.

TABLE 1. OBSERVED RATE CONSTANTS FOR THE REACTIONS OF $[RhL_4]ClO_4$ (2.0×10^{-4} M) WITH EXCESS I_2 IN ACETONITRILE[a] AT VARIOUS TEMPERATURES

Temp °C	$[I_2]$ 10^{-3} M	k_{obsd}/s^{-1} L=2,4,6-$Me_3C_6H_2NC$ 360 nm	300 nm	k_{obsd}/s^{-1} L=*t*-BuNC 290 nm
15.0	2.0	0.193	0.196	0.206
	4.0	0.191	0.202	0.182
	6.0	0.189	0.201	0.172
	8.0	0.193	0.194	0.170
	10.0	0.208	0.210	0.196
	Mean	0.198±0.005		0.185±0.011
19.9	2.0	0.360	0.327	0.336
	4.0	0.322	0.357	0.331
	6.0	0.343	0.360	0.313
	8.0	0.329	0.379	0.316
	10.0	0.336	0.347	0.325
	Mean	0.346±0.012		0.324±0.007
25.0	2.0	0.604	0.564	0.555
	4.0	0.582	0.641	0.561
	6.0	0.602	0.638	0.549
	8.0	0.581	0.605	0.516
	10.0	0.579	0.606	0.558
	Mean	0.600±0.017		0.548±0.012
30.1	2.0	0.954	0.980	0.916
	4.0	1.001	0.924	0.897
	6.0	0.991	0.988	0.843
	8.0	0.967	0.982	0.873
	10.0	0.926	0.942	0.900
	Mean	0.966±0.019		0.886±0.019

a) In dichloromethane, k_{obsd} values for the reactions of $[RhL_4]ClO_4$ (2.0×10^{-4} M) with I_2 (2.0×10^{-3} M) are $2.98\ s^{-1}$ (L=2,4,6-$Me_3C_6H_2NC$) and $7.08\ s^{-1}$ (L=*t*-BuNC) at 25.0 °C.

ances at both 360 and 300 nm after mixing their acetonitrile solutions. With $[Rh(t\text{-}BuNC)_4]ClO_4$, the reaction was monitored by the absorbance at 290 nm. Plots of $\ln(A_t-A_\infty)$ *vs.* time were found to be linear, where A_t and A_∞ are absorbances at the time "t" and at the end of reaction. Pseudo-first-order rate constants, k_{obsd}, were obtained by the least-squares method. The results are shown in Table 1. The k_{obsd} value in each reaction is essentially independent of the concentration of I_2 at a given temperature. This is consistent with the assumption that the reaction of $[RhL_4]ClO_4$ with I_2 proceeds *via* the *cis* adduct. Furthermore, the formation of the *cis* adduct as an intermediate is compatible with the result that the k_{obsd} value is considerably larger in dichloromethane than in acetonitrile (see the footnote of Table 1), owing to destabilization of the *cis* adduct more polar than the *trans* one in less polar solvent dichloromethane. Thus, the present reaction may be expressed by Eq. 1 which involves *cis-trans* isomerization.

$$[RhL_4]ClO_4 + I_2 \xrightarrow{k} cis\text{-}[RhI_2L_4]ClO_4 \xrightarrow{k'} trans\text{-}[RhI_2L_4]ClO_4 \quad (1)$$

As the first step, though it has not been clarified mechanistically in the present study, is much faster than the second one, k_{obsd} is equal to k'.

The Arrhenius plots gave activation parameters for the *cis-trans* isomerization: $\Delta H^{\ddagger}_{298}=74.0\pm1.3$ kJ mol^{-1}, $\Delta S^{\ddagger}_{298}=-1.3\pm4.2$ J mol^{-1} K^{-1} for the $[Rh(2,4,6\text{-}Me_3C_6H_2NC)_4]ClO_4$–$I_2$ system, and $\Delta H^{\ddagger}_{298}=73.6\pm1.6$ kJ mol^{-1}, $\Delta S^{\ddagger}_{298}=-3.2\pm5.4$ J mol^{-1} K^{-1} for the $[Rh(t\text{-}BuNC)_4]ClO_4$–$I_2$ system. The small negative values of $\Delta S^{\ddagger}_{298}$ in both reactions suggest the isomerization to proceed intramolecularly, probably *via* a twist mechanism. Moreover, the $\Delta H^{\ddagger}_{298}$ values obtained are compared with that of the *cis-trans* isomerization of $RhI_2(S_2CNMe_2)(2,4,6\text{-}Me_3C_6H_2NC)_2$ (75.5 kJ mol^{-1}),[8] reinforcing the assignment of the intermediate as *cis*-$[RhI_2L_4]ClO_4$.

Finally, it should be mentioned that the formation of *trans*-$[RhI_2L_4]ClO_4$ was followed by a much slower reaction which takes about 8 h to completion at 28 °C, giving *trans*-$[RhI_2L_4]I_3$. This reaction, however, has not been kinetically analyzed because we have been interested in the addition reaction.

The authors are grateful to the Ministry of Education for support of this work through Grant-in-Aid for Scientific Research.

References

1) J. Halpern and C. S. Wong, *J. Chem. Soc., Chem. Commun.*, **1973**, 629.
2) Y. Ohtani, M. Fujimoto, and A. Yamagishi, *Bull. Chem. Soc. Jpn.*, **50**, 1453 (1977).
3) M. Haga, K. Kawakami, and T. Tanaka, *Inorg. Chim. Acta*, **12**, 93 (1975).
4) M. Haga, K. Kawakami, and T. Tanaka, *Inorg. Chem.*, **15**, 1946 (1976).
5) J. P. Collman and W. R. Roper, *Adv. Organomet. Chem.*, **7**, 53 (1968), and the references cited therein.
6) A. L. Balch and J. Miller, *J. Organomet. Chem.*, **32**, 263 (1971).
7) J. T. Mague and M. O. Nutt, *Inorg. Chem.*, **16**, 1259 (1977).

8) R. Kuwae, T. Tanaka, and K. Kawakami, *Bull. Chem. Soc. Jpn.*, **52**, 437 (1979).
9) J. A. Riddick and E. E. Toops, Jr., "Technique of Organic Chemistry," Interscience Publishers, New York (1955), Vol. 7, p. 409.
10) J. W. Dart, M. K. Lloyd, J. A. McCleverty, and R. Mason, *Chem. Commun.*, **1971**, 1197.
11) K. R. Mann, N. S. Lewis, R. M. Williams, H. B. Gray, and J. G. Gordon II, *Inorg. Chem.*, **17**, 828 (1978), and the references cited therein.
12) A. L. Balch, *J. Am. Chem. Soc.*, **98**, 8049 (1976).
13) D. Hopgood and R. A. Jenkins, *J. Am. Chem. Soc.*, **95**, 4461 (1973).
14) J. R. Chipperfield, A. C. Hayter, and D. E. Webster, *J. Chem. Soc., Dalton Trans.*, **1975**, 2048.
15) A. M. Bond, B. S. Grabaric, and J. J. Jackowski, *Inorg. Chem.*, **17**, 2153 (1978).
16) B. E. Prater, *J. Organomet. Chem.*, **34**, 379 (1972).

Synthesis and Electrical Resistivity of Bis(dialkyldithiocarbamato)-gold(III) Cation-TCNQ Radical Anion Salts

Yoshiji YUMOTO, Futoshi KATO, and Toshio TANAKA*

Department of Applied Chemistry, Faculty of Engineering, Osaka University, Suita, Osaka 565

(Received November 13, 1978)

Seven simple salts and one complex salt of $TCNQ^{\cdot}$ radical anion with bis(dialkyldithiocarbamato)gold(III) cations, $[Au(S_2CNR_2)_2]^+TCNQ^{\cdot}$ (R=Me, Et, *n*-Pr, *n*-Bu, *n*-C_6H_{13}, *n*-C_8H_{17}, and $CH_2C_6H_5$) and $[Au(S_2CN(CH_2C_6H_5)_2)_2]^+(TCNQ)_2^{\cdot}$, were prepared. The complex salt was also obtained as an acetonitrile solvate, $[Au(S_2CN(CH_2C_6H_5)_2)_2]^+(TCNQ)_2^{\cdot}\cdot MeCN$. The electrical resistivity of the simple salt with R=$CH_2C_6H_5$ (2.9×10^4 ohm cm in compacted sample) is much lower than those of the remaining simple salts (1.1×10^7—2.2×10^{10} ohm cm). The resistivities of two complex salts are in the order of 10^2 ohm cm. Electronic absorption spectra and magnetic susceptibility measurements in the solid state indicate that the simple salts with R=Me, Et, *n*-Pr, *n*-C_6H_{13}, and $CH_2C_6H_5$ involve the $TCNQ^{\cdot}$ radical anion monomer, whereas those with R=*n*-Bu and *n*-C_8H_{17} involve dimeric $(TCNQ)_2^{2-}$. The interaction between $TCNQ^{\cdot}$ radical anion and neutral TCNQ in the complex salts is extremely weak, as suggested from no appreciable absorption band in the near-infrared region.

Much attention has been paid to unusual electrical propeties exhibited by one-dimensional materials in both fields of organic and inorganic chemistry.[1] Up to the present time, the most successful organic materials in this area have been based on the radical anion salts of 7,7,8,8-tetracyanoquinodimethane (TCNQ),[2] while a prominent example in the inorganic field is partially oxidized platinum cyanide complexes ($K_2Pt(CN)_4\cdot X_{0.3}\cdot 3H_2O$, X=Cl, Br).[3] However, only a few $TCNQ^{\cdot}$ radical anion salts containing transition metal complexes have been reported so far.[4]

It is well known that some square-planar d^8 transition metal complexes with 1,1-dithiolato ligands not only assume a columnar structure in the crystalline state, but also undergo reversible oxidation and reduction electrochemically in solution.[5] These facts prompted us to prepare $TCNQ^{\cdot}$ radical anion salts of bis(dialkyldithiocarbamato)gold(III) cations. This paper reports the synthesis and electrical resistivity of some simple and complex salts of $TCNQ^{\cdot}$ with these cations, $[Au(S_2CNR_2)_2]^+TCNQ^{\cdot}$ (R=Me, Et, *n*-Pr, *n*-Bu, *n*-C_6H_{13}, *n*-C_8H_{17}, and $CH_2C_6H_5$), $[Au(S_2CN(CH_2C_6H_5)_2)_2]^+(TCNQ)_2^{\cdot}$ and $[Au(S_2CN(CH_2C_6H_5)_2)_2]^+(TCNQ)_2^{\cdot}\cdot MeCN$. Electronic spectra and magnetic properties of these salts in the solid state are also discussed in terms of the stacking of $TCNQ^{\cdot}$.

Experimental

Bis(dialkyldithiocarbamato)gold(III) chlorides, $[Au(S_2CNR_2)_2]^+Cl^-$ (R=Me, Et, *n*-Pr, *n*-C_6H_{13}, *n*-C_8H_{17}, and $CH_2C_6H_5$), were prepared by the reaction of $NaAuCl_4\cdot2H_2O$ with the appropriate thiuram disulfide, $(R_2NC(S)S)_2$, in a mannar similar to the method[6] for $[Au(S_2CN(n\text{-}Bu)_2)_2]^+Br^-$; an oily product obtained was dissolved in dichloromethane, followed by the addition of diethyl ether to give a yellowish orange precipitate in 78—89% yields.

Bis(dialkyldithiocarbamato)gold(III)-TCNQ Simple Salts, $[Au(S_2CNR_2)_2]^+TCNQ^{\cdot}$ (R=Me (1), Et (2), n-Pr (3), n-Bu (4), n-C_6H_{13} (5), n-C_8H_{11} (6), and $CH_2C_6H_5$ (7)). To a solution of $Li^+TCNQ^{\cdot}$ (0.52 g, 25 mmol) in boiling ethanol (40 ml) was added a hot ethanol (30 ml) solution of $[Au(S_2CNMe_2)_2]^+Cl^-$ (1.1 g, 25 mmol). The mixture was allowed to stand at room temperature. The resulting precipitate was recrystallized from acetonitrile to give **1** in a 56% yield.

TABLE 1. PROPERTIES AND ANALYTICAL DATA OF THE $TCNQ^{\cdot}$ SALTS

No.	Salt	Color	Mp(dec) °C	Found (Calcd) % C	H	N
1	$[Au(S_2CNMe_2)_2]^+TCNQ^{\cdot}$	Dark-green needles	212—213	33.76 (33.70)	2.57 (2.51)	13.27 (13.10)
2	$[Au(S_2CNEt_2)_2]^+TCNQ^{\cdot}$	Dark-green needles	201—202	37.90 (37.87)	3.46 (3.47)	12.05 (12.05)
3	$[Au(S_2CN(n\text{-}Pr)_2)_2]^+TCNQ^{\cdot}$	Dark-green needles	174—177	41.22 (41.43)	4.17 (4.28)	11.05 (11.15)
4	$[Au(S_2CN(n\text{-}Bu)_2)_2]^+TCNQ^{\cdot}$	Violet needles	148—150	44.18 (44.49)	4.90 (4.99)	10.40 (10.38)
5	$[Au(S_2CN(n\text{-}C_6H_{13})_2)_2]^+TCNQ^{\cdot}$	Dark-green needles	86—87	49.40 (49.50)	6.12 (6.25)	9.11 (9.11)
6	$[Au(S_2CN(n\text{-}C_8H_{17})_2)_2]^+TCNQ^{\cdot}$	Black microcrystals	55—57	53.01 (53.42)	7.05 (7.02)	8.20 (8.13)
7	$[Au(S_2CN(CH_2C_6H_5)_2)_2]^+TCNQ^{\cdot}$	Black microcrystals	186—188	53.22 (53.33)	3.40 (3.41)	9.18 (8.88)
8	$[Au(S_2CN(CH_2C_6H_5)_2)_2]^+(TCNQ)_2^{\cdot}$	Dark-blue needles	211—213	56.48 (56.38)	3.15 (3.16)	12.12 (12.18)
9	$[Au(S_2CN(CH_2C_6H_5)_2)_2]^+(TCNQ)_2^{\cdot}\cdot(MeCN)$	Black needles	212—214	56.18 (56.42)	3.22 (3.38)	12.93 (12.93)

Other six simple salts, **2**—**7**, were similarly prepared by the equimolar reaction of TCNQ$^{\cdot}$ in ethanol with the appropriate bis(dialkyldithiocarbamato)gold(III) cation in acetonitrile, 77—90% yields.

Bis(dibenzyldithiocarbamato)gold(III)-TCNQ Complex Salts, $[Au(S_2CN(CH_2C_6H_5)_2)_2]^+(TCNQ)_2^{\cdot}$ (8) and $[Au(S_2CN(CH_2C_6H_5)_2)_2]^+(TCNQ)_2^{\cdot}\cdot MeCN$ (9). To a boiling acetonitrile (60 ml) solution of **7** (0.53 g, 0.56 mmol) was added two equivalent amounts of neutral TCNQ (0.23 g, 1.1 mmol) in boiling acetonitrile (40 ml). After filtration, the mixture was allowed to stand in a refrigerator overnight to afford microcrystals of **8** in a 87% yield. Acetonitrile solvate salt **9** was obtained on recrystallization of **8** from acetonitrile, 57% yield on the basis of **8**.

Physical Measurements. Electrical resistivities, electronic and infrared spectra, and magnetic susceptibilities were measured as described previously.[7]

Results and Discussion

Preparation and Characterization. Simple salt **7** reacted with additional neutral TCNQ in acetonitrile to yield complex salt **8**, while in the reactions of the remaining simple salts (**1**—**6**) with neutral TCNQ in the same solvent the starting materials have only been recovered, respectively. Acetonitrile solvate complex salt **9** was characterized by elemental analysis, infrared spectrum, and differential scanning calorimetry (DSC); **9** in the solid state released acetonitrile on heating to 90 °C in a DSC cell, as confirmed by the fact that the infrared spectrum of **9** after heating coincides with that of **8**.

Electrical Properties. Temperature dependence of electrical resistivities for the simple and complex salts (compacted samples) are illustrated in Fig. 1; the results were satisfactorily reproducible. All the simple and complex salts show typical semiconducting behavior in the temperature range measured. Table 2 summarizes the specific resistivities (ρ) of these salts at 25 °C and the activation energies (E_a) obtained from the Arrhenius plots of the temperature dependence of resistivities, $\rho = \rho_0 \exp(E_a/kT)$, together with the magnetic susceptibility (χ_M). The ρ values of **1**—**6** fall in the range of 10^7—10^{10} ohm cm, which are much larger than the resistivities of alkali metal salts of TCNQ$^{\cdot}$ (10^2—10^5 ohm cm).[8] Simple salt **7** behaves a smaller ρ value by three to six orders of magnitude than **1**—**6**. This is suggestive of the stacking of TCNQ$^{\cdot}$ in **7** being different from those in **1**—**6**.

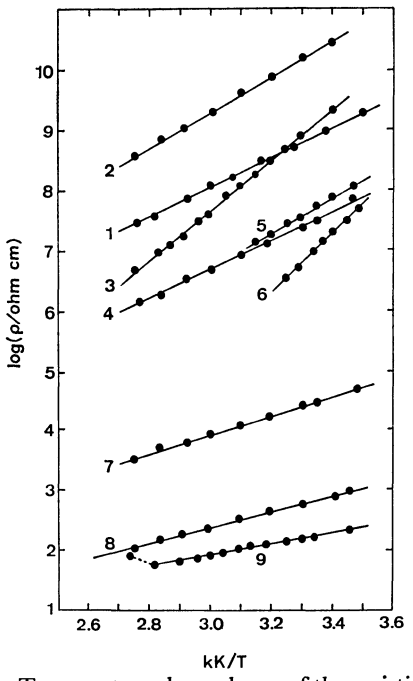

Fig. 1. Temperature dependence of the resistivity of the TCNQ$^{\cdot}$ salts.

Table 2. Electrical resistivity (ρ), activation energy (E_a), and magnetic susceptibility (χ_M) of the TCNQ$^{\cdot}$ salts

Salt	$\rho_{25°C}$ / ohm cm	E_a / eV	χ_M / emu mol^{-1}
Simple salt			
1	8.9×10^{8}	0.50	7.1×10^{-4}
2	2.2×10^{10}	0.58	9.8×10^{-4}
3	1.4×10^{9}	0.83	9.2×10^{-4}
4	3.0×10^{7}	0.43	-3.7×10^{-4}
5	5.4×10^{7}	0.55	8.2×10^{-4}
6	1.1×10^{7}	0.97	-5.2×10^{-4}
7	2.9×10^{4}	0.30	9.3×10^{-4}
Complex salt			
8	6.6×10^{2}	0.26	9.8×10^{-4}
9	1.6×10^{2}	0.13	4.0×10^{-4}

One of the authors has previously reported the preparation of *N,N*-dialkyl-1,3-dithiolan-2-iminium–TCNQ$^{\cdot}$ simple salts, $(CH_2)_2\langle S \rangle C{=}\overset{+}{N}R_2\cdot TCNQ^{\cdot}$ (R=Me, *n*-Pr, *n*-C_6H_{13}, and *n*-C_8H_{17}), whose electrical resistivity (2.2×10^5—1.9×10^9 ohm cm) increases in the order of bulkiness of substituents on the iminium nitrogen atom.[7,9] In contrast to this, the resistivity of the present simple salts seems to decrease as substituents on the carbamato nitrogen atom are bulky. Explanation for this unusual tendency has to await X-ray structure analysis of these simple salts.

The ρ values of complex salts **8** and **9** ($\approx10^2$ ohm cm) are smaller by two orders of magnitude than the corresponding simple salt **7**. Both the resistivity and activation energy of acetonitrile solvate complex salt **9** seem to be smaller than those of **8**, though these values fall in the same order.

Electronic and Magnetic Properties. All the simple salts in acetonitrile exhibited absorption maxima at *ca.* 12000 and 24000 cm^{-1} in the electronic spectra, regardless of the difference of substituents R in the $[Au(S_2CNR_2)_2]^+$ cations. Appearance of the spectra closely resembles that of M$^+$TCNQ$^{\cdot}$ (M=alkali metal or ammonium cation) in acetonitrile, where they are known to dissociate into the monomeric TCNQ$^{\cdot}$ radical anion and the M$^+$ cation.[10] The bands at *ca.* 12000 and 24000 cm^{-1} in acetonitrile have been assigned to locally-excited transitions of the TCNQ$^{\cdot}$ moiety, LE_1 and LE_2, respectively.[11]

Figure 2 illustrates the electronic absorption spectra

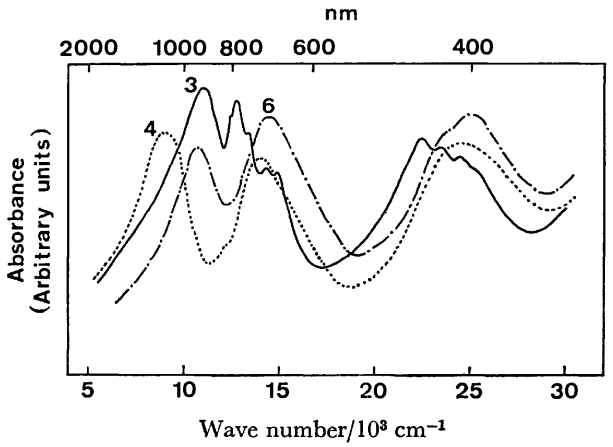

Fig. 2. Electronic absorption spectra of **3**, **4**, and **6** in Nujol mulls.

of **3**, **4**, and **6** in the solid state. The spectrum of **3** is similar in appearance to that of this salt in acetonitrile, indicating that the $TCNQ^{\cdot}$ radical anion in solid **3** may exist as monomeric species. This is compatible with the paramagnetic property of **3** in the solid state at room temperature (Table 2). The presence of the discrete $TCNQ^{\cdot}$ radical anion in the solid state is suggested also for **1**, **2**, and **5** on the basis of their solid state spectra similar to that of **3** and their paramagnetism at room temperature. These assumptions may be consistent with electrically high resistivities and large activation energies of **1**—**3** and **5**, which predict an alternate stacking of the $[Au(S_2CNR_2)_2]^+$ cation and the $TCNQ^{\cdot}$ radical anion ($D^+A^{\cdot}D^+A^{\cdot}\cdots$). Both simple salts **4** and **6** exhibited three absorption maxima at *ca.* 9900, 14000, and 24000 cm^{-1} (Table 3). The spectral patterns closely resemble not only those of simple salts formed between *N*,*N*-dialkyl-1,3-dichalcogenacycloalkan-2-iminium and $TCNQ^{\cdot}$, $(CH_2)_n\langle^{Y}_{Y}\rangle C{=}\overset{+}{N}R_2\cdot TCNQ^{\cdot}$ (n=2, 3; Y=S, Se; R=Me, Et),[7] but also the reflectance spectra of some simple $TCNQ^{\cdot}$ salts with Li^+, NH_4^+, and $MePh_3P^+$,[10] all of which have been reported to involve dimeric $(TCNQ)_2^{2-}$ on the basis of spectral assignments that the lowest energy band may be due to the CT transition between $TCNQ^{\cdot}$ radical anions and that the remaining two to the $(TCNQ)_2^{2-}$ dimer.[10,11] It is therefore suggested that the $(TCNQ)_2^{2-}$ dimer exists in solid **4** and **6**. This is supported also from their diamagnetic properties in the solid state at room temperature (Table 2). Such diamagnetism may confirm that two $TCNQ^{\cdot}$ radical anions are coupled completely with each other. The fact that the CT band of **6** was fairly blue-shifted (*ca.* 2000 cm^{-1}) compared with that of **4** may be correlated with a larger activation energy in **6** than in **4** (Table 1).

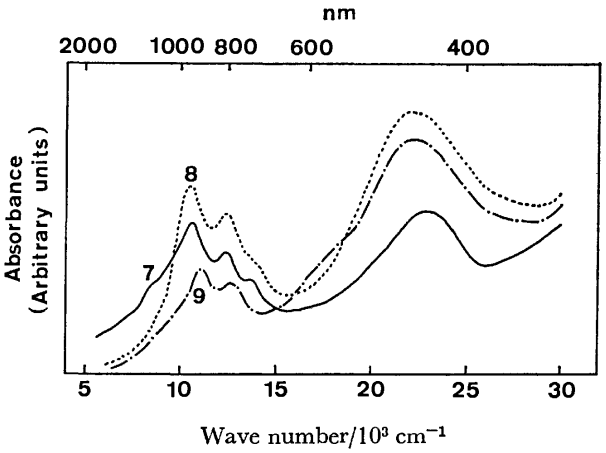

Fig. 3. Electronic absorption spectra of **7**, **8**, and **9** in Nujol mulls.

Figure 3 shows the electronic absorption spectra of simple salt **7** and complex salts **8** and **9** in the solid state. The spectrum of **7** is similar to that of **3**, while no fine structure has been observed in **7**. In fact, **7** exhibited paramagnetic susceptibility at room temperature. Its electrical resistivity, however, is much smaller than those of **1**—**6**, suggesting a segregated columnar stacking of the $TCNQ^{\cdot}$ radical anion in **7**.

The electronic spectra of **8** and **9** show three absorption maxima at *ca.* 11000, 12500, and 22000 cm^{-1} (Table 3). The highest energy band is contributed from the electronic transitions in both the $TCNQ^{\cdot}$ radical anion and neutral TCNQ.[11] The remaining two bands may be due to the $TCNQ^{\cdot}$ monomer, as previously described in the reflectance spectra of some $TCNQ^{\cdot}$ complex salts.[10] The presence of monomeric $TCNQ^{\cdot}$ is consistent with the fact that **8** and **9** exhibited paramagnetic susceptibilities in the solid state at room temperature. In addition, both **8** and **9** have not clearly shown a broad absorption band in the 5000 to 2500 cm^{-1} range; the band has been observed in many $TCNQ^{\cdot}$ complex salts and assigned to the CT transition between

Table 3. Absorption maxima of the electronic spectra of the $TCNQ^{\cdot}$ salts in Nujol mulls

Salt	Wave number/10^3 cm^{-1}								
1		11.0	(12.7)	13.2	14.4		22.5	23.6	25.3
2		11.3	(12.7)	13.1 (13.4)	14.3	14.7	22.5	23.5	25.1
3		11.0	(12.7)	13.1 (13.3)	14.4	14.7	22.4	23.5	24.4 (25.2)
4	8.9				13.9			22.4	
5		11.1	(12.7)	13.0 (13.3)	14.3	14.6	22.6	23.5	24.4 (25.3)
6	10.8				14.5			25.1	
7	(8.8)	10.6	12.4	(13.9)				22.7	
8		10.6	12.4	(14.1)				22.0	
9		11.1	12.7		(17.1)			22.1	

a) Shoulders in parentheses.

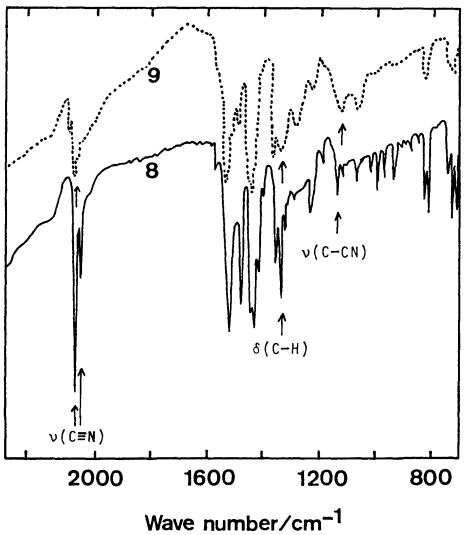

Fig. 4. Infrared spectra of **8** and **9** in Nujol mulls.

TCNQ$^{\tau}$ and neutral TCNQ.[10] It may therefore be concluded that the interaction between TCNQ$^{\tau}$ and neutral TCNQ in **8** and **9** is extremely weak. It should be mentioned, however, that the infrared spectrum of **9** shows considerably broad bands due to ν(C≡N), δ(C–H), and ν(C–CN) compared with that of **8**, as shown in Fig. 4. This sort of broadening observed in the spectra of many TCNQ$^{\tau}$ complex salts has been taken as an evidence for the resonance between TCNQ$^{\tau}$ and neutral TCNQ.[12] Thus, the interaction between TCNQ$^{\tau}$ and neutral TCNQ may be somewhat stronger in **9** than in **8**.

The authors are grateful to the Ministry of Education for support of this work through Grant-in-Aid for Scientific Research.

References

1) A. F. Garito and A. J. Heeger, *Acc. Chem. Res.*, **7**, 232 (1974); "Low-Dimensional Cooperative Phenomena," ed by H. J. Keller, NATO Adv. Study Inst., **7** (1975); E. M. Engler, *Chemtech*, **6**, 274 (1976); "Chemistry and Physics of one-Dimensional Metals," ed by H. J. Keller, NATO Adv. Study Inst., **25** (1977).

2) J. Ferraris, D. O. Cowan, V. Walatka, Jr., and J. H. Perlstein, *J. Am. Chem. Soc.*, **95**, 948 (1973); L. B. Coleman, M. J. Cohen, D. J. Sandman, F. G. Yamagishi, A. F. Garito, and A. J. Heeger, *Solid State Commun.*, **12**, 1125 (1973).

3) J. S. Miller and A. J. Epstein, *Prog. Inorg. Chem.*, **20**, 1 (1976), and the references cited therein.

4) S. Z. Goldberg, R. Eisenberg, J. S. Miller, and A. J. Epstein, *J. Am. Chem. Soc.*, **98**, 5173 (1976); S. Z. Goldberg, B. Spivack, G. Stanley, R. Eisenberg, D. M. Braitsch, J. S. Miller, and M. Abkowitz, *ibid.*, **99**, 110 (1977).

5) J. A. McCleverty, *Prog. Inorg. Chem.*, **10**, 49 (1968); D. Coucouvanis, *ibid.*, **11**, 233 (1970).

6) P. T. Beurskens, H. J. A. Blaauw, J. A. Cras, and J. J. Steggerda, *Inorg. Chem.*, **7**, 805 (1968); P. T. Beurskens, J. A. Cras, and J. G. M. van der Linden, *ibid.*, **9**, 475 (1970).

7) S. Araki, H. Ishida, and T. Tanaka, *Bull. Chem. Soc. Jpn.*, **51**, 407 (1978).

8) L. R. Melby, R. J. Harder, W. R. Hertler, W. Mahler, R. E. Benson, and W. E. Mochel, *J. Am. Chem. Soc.*, **84**, 3374 (1962).

9) S. Araki and T. Tanaka, *Bull. Chem. Soc. Jpn.*, **51**, 1311 (1978).

10) Y. Iida, *Bull. Chem. Soc. Jpn.*, **42**, 71, 637 (1969).

11) J. Tanaka, M. Tanaka, T. Kawai, T. Takabe, and O. Maki, *Bull. Chem. Soc. Jpn.*, **49**, 2358 (1976).

12) T. Kondow and T. Sakata, *Phys. Status Solidi A*, **6**, 551 (1971).

The Synthesis and Crystal Structure of Bis(cyclo-L-histidyl-L-histidyl)copper(II) Perchlorate Tetrahydrate

Fumio Hori, Yoshitane Kojima, Keiji Matsumoto, Shun'ichiro Ooi,* and Hisao Kuroya

Department of Chemistry, Faculty of Science, Osaka City University, Sumiyoshi-ku, Osaka 558

(Received September 16, 1978)

The title compound was prepared, and its structure then determined by X-ray structure analysis. The crystal is trigonal with the space group $P3_221$, $a=8.450(3)$, $c=42.00(6)$Å, and $Z=3$. The crystal structure has been determined from the diffractometer data and refined by a least-squares method to an R value of 0.103 for 1349 independent reflections with $I>3\sigma(I)$. The cyclo-L-histidyl-L-histidyl is coordinated to the Cu atom *via* the N atoms of the respective imidazolyl groups. The coordination of Cu is not planar but distorted toward the tetrahedral configuration, the interplanar angle between $Cu<^{N}_{N}$ planes being 29°. The complex has virtually D_2 symmetry: there are two pseudo two-fold axes and one crystallographically imposed two-fold axis which relates two chelate rings. The chelate rings assume the δ conformation, and the ligating cyclo-L-histidyl-L-histidyl is of a folded form with a bowsprit-boat 2,5-piperazinedione ring. The electronic and circular dichroism spectra in the visible region are presented.

Histidine and its cyclic dipeptide play an important role in biological systems. Langenbeck *et al.* found that these substances catalyze the oxidation of DOPA and that the addition of the Cu^{2+} ion to the reaction system accerelates the oxidation.[1] As structural information is indispensable for an understanding of the function of the L-histidine residue in a biological process, we have attempted to make a structural investigation of cyclo-L-histidyl-L-histidyl [=(3*S*,6*S*)-bis(4-imidazolylmethyl)-2,5-piperazinedione, hereafter abbreviated as cyhis], and

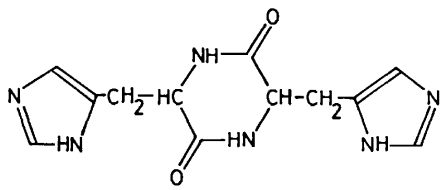

cyhis

its metal chelates. Two of the present authors (Y. K. and K. M.) previously reported the crystal structure of aquabis(cyclo-L-histidyl-L-histidylato)dicopper(II) perchlorate hydrate,[2] which had been obtained from the reaction of $Cu(ClO_4)_2$, cyhis, and LiOH in a 1 : 1 : 1 mole ratio. The reaction of $Cu(ClO_4)_2$ with twice as many moles of the cyhis in methanol yielded a violet compound which was analysed to be $Cu(cyhis)_2(ClO_4)_2\cdot 4H_2O$. This compound has been characterized by means of X-ray structure analysis and its visible and circular dichroism (CD) spectra.

Experimental

Preparation of $Cu(cyhis)_2(ClO_4)_2\cdot 4H_2O$. A suspension of $Cu(ClO_4)_2\cdot 6H_2O$ (0.371 g, 1 mmol) and the cyhis·$2H_2O$ (0.585 g, 2 mmol) in methanol was stirred at room temperature until these compounds were completely dissolved. The violet crystals were then separated out and recrystallized from hot water. Yield, 0.590 g (67%).

Found: C, 32.73; H, 4.11; N, 19.12%. Calcd for $Cu(C_{12}H_{14}N_6O_2)_2(ClO_4)_2\cdot 4H_2O$: C, 32.64; H, 4.11; N, 19.03%.

The compound is different in color from $Cu(cyhis)_2SO_4\cdot 5H_2O$(blue), which was prepared by Losse *et al.*[1]

Spectral Measurements. The absorption and CD spectra in an aqueous solution were recorded at room temperature on a Hitachi EPS 3T Recording Spectrometer and a JASCO J-20 Automatic Recording Spectrometer respectively.

X-Ray Data Measurements. Crystal Data: $C_{24}CuCl_2H_{36}N_{12}O_{16}$, Trigonal, $a=8.450(3)$, $c=42.00(6)$Å, $U=2597.7(2)$ Å^3, $D_m=1.68$, $D_c=1.67$ g/cm^3, $Z=3$, $\mu(Cu\,K\alpha)=32.0$ cm^{-1}, space group $P3_221$. The Laue symmetry, space-group extinctions, and approximate unit-cell dimensions were obtained from Weissenberg and precession photographs. The cell dimensions were refined by the leasts-quares analysis of 22 θ values measured on a Philips PW1100 diffractometer by the use of Cu $K\alpha$ radiation. The space group was determined on the basis of the configuration (*S*) of the asymmetric carbon atom in the cyhis ligand.

Data Collection: The intensity data were collected on the diffractometer using graphite-monochromated Cu $K\alpha$ radiation. The specimen size was $0.20\times 0.20\times 0.18$ mm^3. A scan speed of 0.033 s^{-1} and a scan width of $(0.8+0.2\tan\theta)°$ in ω were chosen. The background was counted for 10 s at each end of scan range. Of the independent reflections collected in the $2\theta\leq 120°$ range, 1349 reflections with $I>3\sigma(I)$ were used for the structure analysis. The number of reflections corresponds to *ca.* 70% of the total number of independent reflections within the range. No appreciable decay was observed in the intensities of the standard reflections monitored every 5 h throughout the data collection. Intensity data were also corrected for Lp factor.[3] A spherical absorption correction ($r=0.10$ mm) was applied.

Structure Determination and Refinement. The crystal structure was solved by the heavy-atom method. The positional and thermal parameters were refined by the block-diagonal least-squares method, anisotropic temperature factors being used for the Cu and Cl atoms. The minimized function was $\sum w(F_o-|F_c|)^2$. The weighting scheme of $w=1.0$ for $F_o\leq F_{max}$ and $w=(F_{max}/F_o)^2$ for $F_o>F_{max}$ was used. The F_{max} value of 30.0 was found to be best for making $w(\Delta F_o)^2$ relatively constant over the whole range of F_o. The final R value was 0.103 ($R'=[\sum w(F_o-|F_c|)^2/\sum wF_o^2]=0.139$). In the final cycle of refinements, all the parameter shifts were less than 0.2σ. The large temperature factors of the O atoms in the ClO_4^- ions are indicative of a disorder in the arrangement of ClO_4^-. The atomic parameters are listed in Table 1. A table of the observed and calculated structure factors is preserved by the Chemical Society of Japan (Document No. 7912). The atomic scattering factors for Cu^0, Cl^-, O, N, and C atoms were taken from Ref. 4, with corrections for

Table 1. Positional and thermal parameters

	x	y	z	B/Å^2
Cu	0.7547(4)	1	2/3	a)
O(1)	0.592(2)	0.344(2)	0.7601(2)	3.4(2)
O(2)	0.562(2)	0.897(2)	0.8161(2)	3.6(2)
N(1)	0.506(2)	0.468(2)	0.6961(3)	3.0(2)
N(2)	0.592(2)	0.747(2)	0.6817(3)	2.5(2)
N(3)	0.422(2)	0.635(2)	0.7880(3)	2.6(2)
N(4)	0.737(2)	0.626(2)	0.7818(3)	3.0(2)
N(5)	0.816(2)	1.153(2)	0.7602(2)	2.3(2)
N(6)	0.835(2)	1.072(2)	0.7110(2)	2.3(2)
C(1)	0.602(2)	0.601(2)	0.6752(3)	2.8(3)
C(2)	0.474(2)	0.701(2)	0.7074(3)	2.5(2)
C(3)	0.419(2)	0.529(2)	0.7173(3)	2.2(2)
C(4)	0.300(2)	0.414(2)	0.7436(3)	2.7(3)
C(5)	0.402(2)	0.467(2)	0.7762(3)	1.7(2)
C(6)	0.591(2)	0.481(2)	0.7731(3)	2.3(2)
C(7)	0.745(2)	0.769(2)	0.8026(3)	2.7(3)
C(8)	0.568(2)	0.774(2)	0.8034(3)	2.5(2)
C(9)	0.903(2)	0.961(2)	0.7934(3)	2.3(2)
C(10)	0.870(2)	1.020(2)	0.7624(3)	1.8(2)
C(11)	0.880(2)	0.975(2)	0.7314(3)	2.0(2)
C(12)	0.795(2)	1.180(2)	0.7288(3)	2.4(2)
Cl(1)	0	0.4811(7)	5/6	a)
Cl(2)	0.2649(8)	1	2/3	a)
O(3)	−0.161(4)	0.333(4)	0.8213(5)	11.7(7)
O(4)	0.058(3)	0.606(3)	0.8071(5)	10.1(5)
O(5)	0.324(2)	0.930(2)	0.6420(3)	5.6(3)
O(6)	0.098(3)	0.855(3)	0.6780(4)	8.8(5)
O(7)	0.087(2)	0.690(2)	0.7430(4)	7.8(4)
O(8)	0.330(2)	0.989(2)	0.7791(3)	5.8(3)

a) Anisotropic thermal parameters ($\times 10^4$) in the form $\exp[-(B_{11}h^2+B_{22}k^2+B_{33}l^2+B_{12}hk+B_{13}hl+B_{23}kl)]$.

	B_{11}	B_{22}	B_{33}	B_{12}	B_{13}	B_{23}
Cu	153(7)	97(6)	1.0(1)	0	0	4(1)
Cl(1)	159(12)	80(10)	2.4(2)	0	9(3)	0
Cl(2)	142(12)	180(13)	4.0(3)	0	0	16(3)

the anomalous scattering for Cu and Cl atoms. All computations were carried out by using programs in the UNICS.[5]

In order to confirm the structure, further least-squares calculations were performed, anisotropic temperature factors being used for all the atoms. The R and R' values reached 0.070 and 0.108 respectively. The difference Fourier map showed no peaks greater than 0.4 e/Å^3.

Results and Discussion

Figures 1a and b show the projection and elevation of the complex. Another elevation (half of the complex) is presented in Fig. 2(a). The complex has a crystallographically imposed two-fold axis; it is parallel to the a axis, runs through the Cu atom, and bisects the N(2)–Cu–N′(2) angle as well as the N(6)–Cu–N′(6) angle. Moreover, there are two pseudo two-fold axes. One bisects the N(6)–Cu–N′(2) (and N(2)–Cu–N′(6)) angle (Fig. 1b), and the other passes through the Cu atom and the center of the 2,5-piperazinedione ring (DKP ring) composed of N(3), C(5), C(6), N(4), C(7), and C(8). These three axes perpendicularly intersect one another at the position of the Cu atom; hence, the complex virtually possesses a D_2 symmetry.

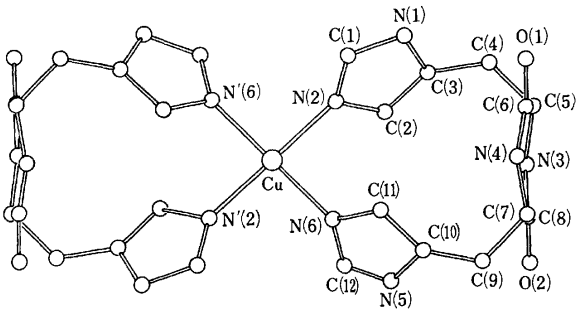

Fig. 1a. The structure of the complex viewed along the a axis.

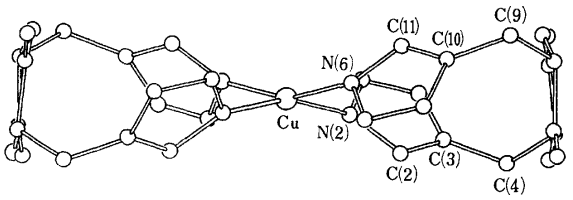

Fig. 1b. An elevation of the complex.

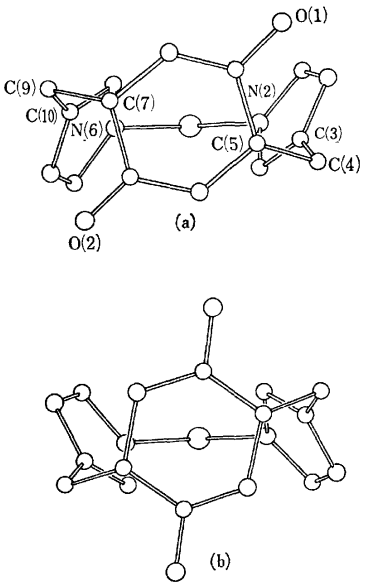

Fig. 2. (a) An elevation of the chelate ring (δ conformation. (b) λ chelate ring.

The Cu atom is surrounded by 4 N atoms of the respective imidazolyl groups. The disposition of the 4 N atoms is not planar, but distorted toward a tetrahedral configuration (Fig. 1b), the interplanar angle between [N(2), Cu, N(6)] and [N′(2), Cu, N′(6)] planes being 29°. The two Cu–N bond lengths are substancially identical and are in agreement with those in the sulfate[6] and perchlorate[7] of tetrakis(imidazole)copper(II), and with the Cu(B)–N(5) distance in the aquabis(cyclo-L-histidyl-L-histidylato)dicopper(II) perchlorate hydrate.[2] Above and below the Cu atom (Fig. 1b) there are no atoms within 3.4 Å. The bond lengths and angles are listed in Table 2.

As has been described above, the chelate ring has a

Table 2. Interatomic distances and bond angles

Bond lengths (l/Å)			
Cu–N(2)	1.98(1)	Cu–N(6)	1.97(1)
N(1)–C(1)	1.34(2)	N(5)–C(12)	1.37(2)
N(1)–C(3)	1.41(2)	N(5)–C(10)	1.41(2)
N(2)–C(1)	1.31(2)	N(6)–C(12)	1.35(2)
N(2)–C(2)	1.39(2)	N(6)–C(11)	1.37(2)
C(2)–C(3)	1.35(2)	C(11)–C(10)	1.37(2)
C(3)–C(4)	1.48(2)	C(10)–C(9)	1.47(2)
C(4)–C(5)	1.56(2)	C(9)–C(7)	1.55(2)
N(3)–C(5)	1.43(2)	N(4)–C(7)	1.46(2)
C(5)–C(6)	1.55(2)	C(7)–C(8)	1.52(2)
C(6)–N(4)	1.28(2)	C(8)–N(3)	1.37(2)
C(6)–O(1)	1.28(2)	C(8)–O(2)	1.20(2)
Cl(1)–O(3)	1.40(3)	Cl(2)–O(5)	1.40(2)
Cl(1)–O(4)	1.43(3)	Cl(2)–O(6)	1.41(3)
Bond angles (ϕ/°)			
N(2)–Cu–N(6)	89(1)		
Cu–N(2)–C(1)	128(1)	Cu–N(6)–C(12)	125(1)
Cu–N(2)–C(2)	125(1)	Cu–N(6)–C(11)	124(1)
N(1)–C(1)–N(2)	111(2)	N(5)–C(12)–N(6)	109(1)
N(2)–C(2)–C(3)	111(2)	N(6)–C(11)–C(10)	110(1)
C(1)–N(1)–C(3)	108(1)	C(12)–N(5)–C(10)	109(1)
N(1)–C(3)–C(4)	122(1)	N(5)–C(10)–C(9)	121(1)
C(2)–C(3)–C(4)	134(2)	C(11)–C(10)–C(9)	134(1)
N(1)–C(3)–C(2)	104(1)	N(5)–C(10)–C(11)	105(1)
C(1)–N(2)–C(2)	106(1)	C(12)–N(6)–C(11)	107(1)
C(3)–C(4)–C(5)	112(1)	C(10)–C(9)–C(7)	111(1)
C(4)–C(5)–N(3)	112(1)	C(9)–C(7)–N(4)	112(1)
C(4)–C(5)–C(6)	110(1)	C(9)–C(7)–C(8)	109(1)
C(5)–N(3)–C(8)	129(1)	C(7)–N(4)–C(6)	126(2)
C(5)–C(6)–O(1)	116(1)	C(7)–C(8)–O(2)	121(2)
C(5)–C(6)–N(4)	120(1)	C(7)–C(8)–N(3)	117(1)
N(3)–C(5)–C(6)	110(1)	N(4)–C(7)–C(8)	113(1)
O(1)–C(6)–N(4)	124(2)	O(2)–C(8)–N(3)	123(2)
Possible hydrogen bonds (l/Å)			
N(1)···O′(5)[a]	3.01(2)	H[N(1)][b]···O′(5)	2.05
N(3)···O(4)	3.07(3)	H[N(3)]···O(4)	2.22
O(1)···O′(8)	2.81(2)		
O(2)···O(8)	2.89(2)		
O(6)···O(7)	3.05(3)		
O(7)···O(8)	2.78(3)		

a) The primed atoms refer to the unprimed ones at the equivalent position ($x, y-1, z$). b) The coordinates of the H atoms were calculated on the assumption that the N–H distance is 1.00 Å.

Table 3. Deviations (Δd) of atoms from least-squares planes and interplanar angles (ϕ)

Plane (1) [Cu,N(2),N(6)]
Plane (2) [N(2), C(1), N(1), C(3), C(2)]
(Δd/Å); N(2) −0.02, C(1) 0.02, N(1) −0.01, C(3) 0.00, C(2) 0.01
Plane (3) [N(6), C(12), N(5), C(10), C(11)]
the d's are less than 0.003 Å.
Plane (4) [C(3), C(4), C(5)]
Plane (5) [C(10), C(9), C(7)]
Plane (6) [C(5), C(6), N(4), C(7), C(8), N(3)]
(Δd/Å); C(5) −0.08, C(6) −0.02, N(4) 0.12, C(7) −0.11, C(8) −0.02, N(3) 0.11, O(1) −0.06, O(2) −0.02

Interplanar angles	ϕ/°
Plane (1)—Plane (2)	58
Plane (1)—Plane (3)	58
Plane (2)—Plane (4)	78
Plane (3)—Plane (5)	75
Plane (6)—Plane (2)	65
Plane (6)—Plane (3)	71

Table 4. Torsion angles (deg) concerning the DKP ring[a]

ϕ_1[C(8), N(3), C(5), C(6)]	−18°
ψ_1[N(3), C(5), C(6), N(4)]	2
ω_1[C(5), C(6), N(4), C(7)]	18
ϕ_2[C(6), N(4), C(7), C(8)]	−23
ψ_2[N(4), C(7), C(8), N(3)]	7
ω_2[C(7), C(8), N(3), C(5)]	13
χ^1_1[N(3), C(5), C(4), C(3)]	74
χ^2_1[C(5), C(4), C(3), N(1)]	101
χ^1_2[N(4), C(7), C(9), C(10)]	68
χ^2_2[C(7), C(9), C(10), N(5)]	105

a) The conventions of the IUPAC-IUB Commission are followed.[b] b) IUPAC-IUB Commission on Biological Nomenclature, *Biochem.*, **9**, 3471 (1970).

pseudo two-fold axis. Every pair of bonds related to each other by the axis agrees well in length. This is also the case for such a pair of bond angles. The bond lengths and angles in the imidazole moieties are comparable to those in the imidazole at −150 °C[8] and the tetrakis(imidazole)copper(II) complexes.[6,7] The Cu–N bond does not lie on the imidazole plane; the Cu–N(2) bond makes an angle of 12° with the [N(2), C(1), N(1), C(3), C(2)] plane, while the Cu–N(6) bond deviates from the [N(6), C(12), N(5), C(10), C(11)] plane by 17°. Several important interplanar angles are listed in Table 3, where the deviations of atoms from least-squares planes are also given.

The DKP ring is slightly buckled toward a boat conformation. The torsion angles (Table 4) rather resemble those of the DKP ring in cyclo(L-alanyl-L-alanyl), which was found to be the bowsprit-boat conformation.[9] The C(5)–C(4) and C(7)–C(9) bonds are quasi-equatorial with respect to the ring. As indicated by χ^1 values, both imidazolylmethyl side chains have a folded conformation. The ligating cyhis molecule thus assumes a folded form with a bowsprit-boat DKP ring. The structural parameters of the DKP ring are comparable to those in cyclo(L-threonyl-L-histidyl) dihydrate.[10]

As may be seen in Fig. 2 (a), the chelate ring has δ chirality. That the crystals comprise solely a (δ,δ)-conformer is indicative of the selective formation of this isomer. The λ chelate ring (Fig. 2 (b)) can be derived from the cyhis ligand of the δ conformation (Fig. 2 (a)) in the following way: i) counter-clockwise rotation (72°)[11] of the C(4)–C(3)–imidazole and C(9)–C(10)–imidazole fragments about the C(5)–C(4) and C(7)–C(9) bonds respectively, followed by ii) the rotation (180°) of the respective imidazole rings about the C(4)–C(3) and C(9)–C(10) bonds, and iii) linking the Cu atom to N(2)

and N(6). These operations can be performed without changing the bond lengths and angles. A comparison of the scaled models of δ and λ chelate rings indicates that there is no appreciable difference between the nonbonded interaction energy in the δ ring and that in the λ ring. However, the δ ring is different from the λ one in the dispositions of the imidazole ring and the polar N(imidazole)–H bond relative to the C=O bond of the DKP ring, which might be partly responsible for the selective formation of the (δ,δ)-conformer.

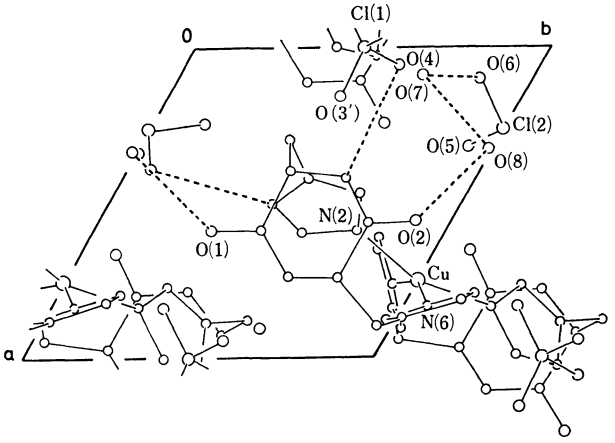

Fig. 3. The bounded projection (z=0.52—0.92) of crystal structure viewed down the c axis. The O(3) at ($-x$, $y-x$, $1\frac{2}{3}-z$) equivalent position is shown by O(3').

A part of the crystal structure is shown in Fig. 3, where the broken lines indicate hydrogen bonds, the data of which are summarized in Table 2.

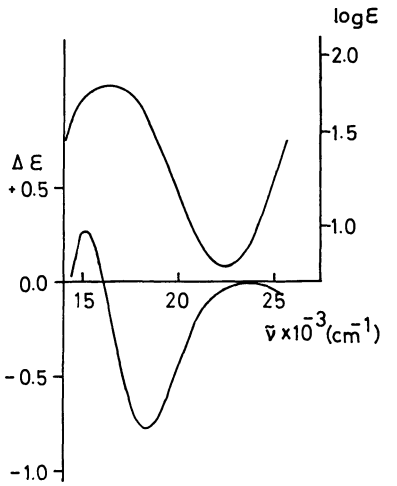

Fig. 4. Absorption (top) and CD (bottom) spectra.

Figure 4 shows the absorption and CD spectra. No appreciable variation in the CD curve was observed within 24 h. The absorption band at 16500 cm^{-1} is assignable to d→d transition. Although, in the crystal structure, the disposition of the 4 N atoms around the Cu atom deviates significantly from a planar configuration toward a tetrahedral one, the intensity and energy of the band are similar to those of tetragonal [Cu(*R*-pn)$_2$](ClO$_4$)$_2$;[12] but different from those of the bis(dipyrromethene)copper(II) complex,[13] in which 4 N donor atoms have a flattened tetrahedral configuration (the interplanar angle between Cu$\langle_{\rm N}^{\rm N}$ planes is 68°).[14] By analogy with the CD of [Cu(*R*-pn)$_2$](ClO$_4$)$_2$ the major CD band at 18300 cm^{-1} may be assigned to d_{xz}, $d_{yz}\rightarrow d_{x^2-y^2}$ transition.[12] The minor band at 15500 cm^{-1} can be regarded as arising from the $d_{xy}\rightarrow d_{x^2-y^2}$ transition, since the $d_{z^2}\rightarrow d_{x^2-y^2}$ transition is magnetically forbidden in D_2 symmetry. As the asymmetric C atoms in the present complex are distant from the Cu atom, the chiral disposition of four imidazolyl groups may be mainly responsible for the d electron optical activity.

This research was supported by Grant-in-Aid from the Ministry of Education.

References

1) G. Losse, A. Barth, and W. Langenbeek, *Chem. Ber.*, **94**, 2271 (1961).
2) Y. Kojima, K. Hirotsu, and K. Matsumoto, *Bull. Chem. Soc. Jpn.*, **50**, 3222 (1977).
3) J. Hornstra and B. Stubbe, PW1100 Data Processing Programs, Philips Research Laboratories, Eindhoven, Holland.
4) "International Tables for X-Ray Crystallography," Kynoch Press, Birmingham (1974), Vol. IV, pp. 71, 148.
5) "The Universal Crystallographic Computation Program System," Crystallographic Society of Japan (1969).
6) G. Fransson and B. K. S. Lundberg, *Acta Chem. Scand.*, **26**, 3969 (1972).
7) G. Ivarsson, *Acta Chem. Scand.*, **27**, 3523 (1973).
8) S. Martinez-Carrera, *Acta Crystallogr.*, **20**, 783 (1966).
9) C. -F. Lin and L. E. Webb, *J. Am. Chem. Soc.*, **95**, 6803 (1973).
10) M. Cotrait, M. Ptak, B. Busetta, and A. Heitz, *J. Am. Chem. Soc.*, **98**, 1073 (1976).
11) In the elevation of the chelate ring (Fig. 2a), the angle between C(5)–C(4) and C(4)–C(3) is 37°, while that between C(7)–C(9) and C(9)–C(10) is 35°. The mean value (36°) corresponds to one-half of the rotation angle (72°) in the text.
12) Y. Nishida and S. Kida, *Bull. Chem. Soc. Jpn.*, **43**, 3814 (1970).
13) J. E. Fergusson and C. A. Ramsay, *J. Chem. Soc.*, **1965**, 5222.
14) M. Elder and B. R. Penfold, *J. Chem. Soc., A*, **1969**, 2556.

The Formation of the Cd-bearing Ferrite by the Air Oxidation of an Aqueous Suspension

Ken KANEKO,* Katsumori TAKEI, Yutaka TAMAURA, Tadao KANZAKI, and Takashi KATSURA

Department of Chemistry, Tokyo Institute of Technology, Meguro-ku, Tokyo 152

(Received October 4, 1978)

When the Cd^{2+}/Fe_{total} ratio in the initial solution is below 0.1, almost all cadmium ions are incorporated into the ferrite with the spinel-type structure by the air oxidation of an aqueous suspension at a pH 9.0 and at 65 °C. The Cd-bearing ferrite thus obtained is a ferromagnet and is oxidized to form a completely oxidized Cd-bearing ferrite at 150 °C in the air; this ferrite is still a ferromagnet and belongs to the Fe_2O_3–$CdFe_2O_4$ binary system, with the same spinel type structure. When the Cd^{2+}/Fe_{total} ratio in the initial solution increases to 0.5, the crystalline phases formed is complicatedly changed; the products are also significantly affected by the pH value of the suspension. The most favorable pH value at 65 °C to form the Cd-bearing ferrite is proposed to be 10.0.

Feitknecht[1] has found that Fe_3O_4 with the spinel-type structure is formed by the air oxidation of the iron(II) hydroxide, $Fe(OH)_2$, in a suspended solution at a pH of about 8.5. Kiyama[2] reported that the temperature increase of the suspension is favorable for the formation of Fe_3O_4. Recently, more favorable conditions for the formation from the suspension have been studied by Tamaura *et al.*[3] by using a dispersing reagent such as sucrose. Ferrite, the solid solution of $(Fe, M)_3O_4$ with a spinel-type structure composed of iron and other metal ions M, was also synthesized at temperature above 60 °C. Yasuoka *et al.*,[4] Hamamura *et al.*,[5] and Kiyama[6] have succeeded in synthesizing Mn- and $ZnFe_2O_4$, $BaFe_2O_4$, and Mn-, Co-ferrites respectively. Katsura *et al.*[7,8] and Kaneko and Katsura[9] have also studied the formation of a solid solution of $FeCr_2O_4$–Fe_3O_4, Fe_2TiO_4–Fe_3O_4, and $MgFe_2O_4$–Fe_3O_4. In their paper, Kaneko and Katsura[9] have clarified that the magnesium ion is incorporated in only a limited amount at 65 °C and pH 9.0, and that no Mg-ferrite is formed at pH values below 8.0. Kiyama[6] has shown that the amount of cobalt ion incorporated into the ferrite structure increases as the R value($NaOH/FeSO_4$) of the suspension increases. The ferrite formation from the suspensions and the content of metals other than iron in the ferrite seem to be influenced by such reaction conditions as the pH value, the temperature, and the metal concentration in the reaction solution.

In this paper, the reaction conditions for the formation of the Cd-bearing ferrite from the suspension are investigated, and the most favorable reaction condition for forming it are discussed. The Cd-bearing ferrite means the ferrite containing the cadmium ions more or less in its crystal structure to form the solid solution between Fe_3O_4 and $CdFe_2O_4$; we will call the Cd-bearing ferrite simply Cd-ferrite; we do not mean the $CdFe_2O_4$ compound.

Experimental

Reagents. Chemical reagents of analytical grades were used. A 2-mol/dm^3 sodium hydroxide solution was prepared by dissolving sodium hydroxide in distilled water free from carbon dioxide and oxygen. A 0.863 mol/dm^3 cadmium sulfate solution was prepared from $CdSO_4 \cdot 7H_2O$.

Apparatus. The reaction vessel of the Dewar type used in this study was the same as that employed in a previous study.[9]

Procedure. After adding the distilled water, cadmium sulfate, and sodium sulfate to the reaction vessel, nitrogen gas was bubbled into the solution while it was being stirred at 1000 r.p.m. for 1 h to remove the dissolved gases of carbon dioxide and oxygen. Then a 12.0-g portion of $FeSO_4 \cdot 7H_2O$ was added to the solution. The resultant volume of the solution was set at 200 cm^3, and the total concentration of the sulfate ion was fixed at 65 mmol/200 cm^3 (we call this solution the initial solution). The subsequent procedures were just the same as those described in the previous paper.[9] The Precipitate A means the product obtained after the air oxidation. The Precipitate B was obtained by lowering the pH value of the suspension containing the Precipitate A to pH 5.0. The procedure was described in detail in the previous report.[9]

Chemical Analysis. The Cd^{2+} content was determined gravimetrically after precipitating bis(8-quinolinolato)Cd(II). The amounts of Fe^{2+} and Fe^{3+} ions were determined by the method described previously.[9]

The Precipitates A and B were examined by the X-ray powder diffraction method by using Fe $K\alpha$ radiation and electron microscopy.

Results and Discussion

The X-Ray Powder Diffraction Data at pH *9.0.* Figure 1 shows the X-ray powder diffraction patterns of the Precipitates A obtained at various concentrations of Cd^{2+} in the initial solutions and at pH 9.0. At the Cd^{2+}/Fe_{total} ratios of 0.03 and 0.1 in the initial solutions, only the peaks corresponding to the compound with the spinel structure are seen (the patterns A and B in Fig. 1). However, at a ratio of 0.2, the peaks of the spinel-type compound become fairly small and the peaks of α-FeOOH are seen (the C pattern in Fig. 1). At a ratio of 0.15 the pattern was the same as that of the ratio of 0.10. At a ratio of 0.30, no peaks were observed in the X-ray powder diffraction pattern; this means that no crystalline compounds are formed. However, at a ratio of 0.40, as may be seen in the D pattern in Fig. 1, cadmium hydroxide was crystallized, together with the spinel-type compound.

Figure 2 shows the X-ray powder diffraction patterns of the Precipitates B. At the ratios of Cd^{2+}/Fe_{total} from

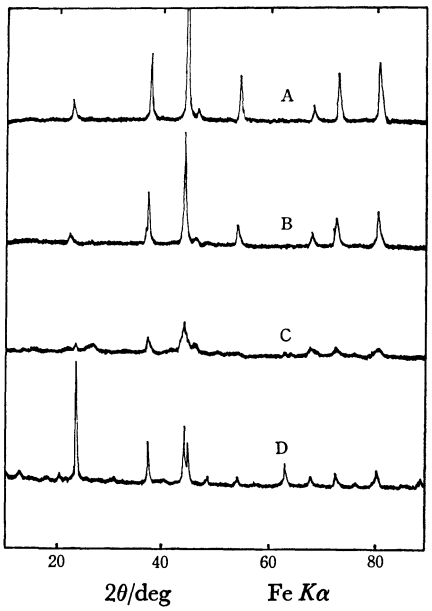

Fig. 1. The X-ray powder diffraction patterns of the Precipitates A obtained at the Cd^{2+}/Fe_{total} molar ratios of 0.03(pattern A), 0.10(pattern B), 0.20(pettarn C), and 0.40(pattern D), respectively.

0.03 to 0.10 in the initial solution, the patterns are similar to those of the Precipitates A (the A and B patterns in Figs. 1 and 2). At the ratio of 0.20, however, the two small peaks due to the presence of the α-FeOOH and the spinel-type compound both seem to be slightly stronger than those of the Precipitate A (the C patterns in Figs. 1 and 2). This indicates that some soluble compounds such as cadmium hydroxide are formed in the Precipitate A, together with α-FeOOH and the spinel-type compounds. At the ratio of 0.40, as may be seen in the D patterns in both Figs. 1 and 2, the cadmium hydroxide in the Precipitate A is completely dissolved by lowering the pH value to 5.0.

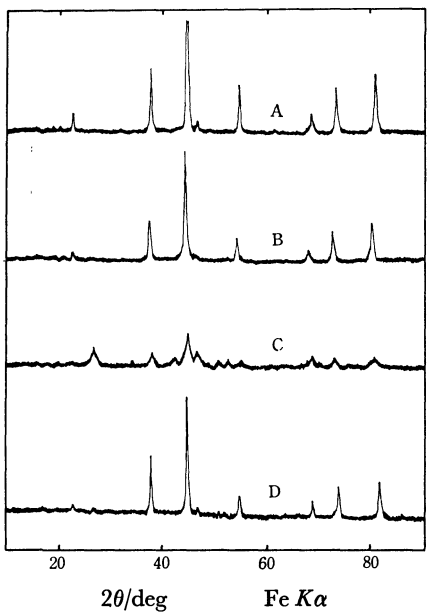

Fig. 2. The X-ray powder diffraction patterns of the Precipitates B obtained at the Cd^{2+}/Fe_{total} molar ratios of 0.03(pattern A), 0.10(pattern B), 0.20(pattern C) and 0.40(pattern D), respectively.

In view of the results presented above, the oxidation reactions of the $Fe(OH)_2$ suspension in the presence of Cd^{2+} at pH 9.0 and at 65 °C may be classified into the four processes: (1) the formation of only the spinel-type compound at the Cd^{2+}/Fe_{total} ratio in the initial solution below 0.10; (2) the formation of α-FeOOH, the spinel compound, and cadmium hydroxide at the ratios from 0.15 to 0.20; (3) the formation of only amorphous materials at the ratio of 0.30, and (4) the formation of the cadmium hydroxide crystal together with the spinel-type compound at the ratios above 0.40.

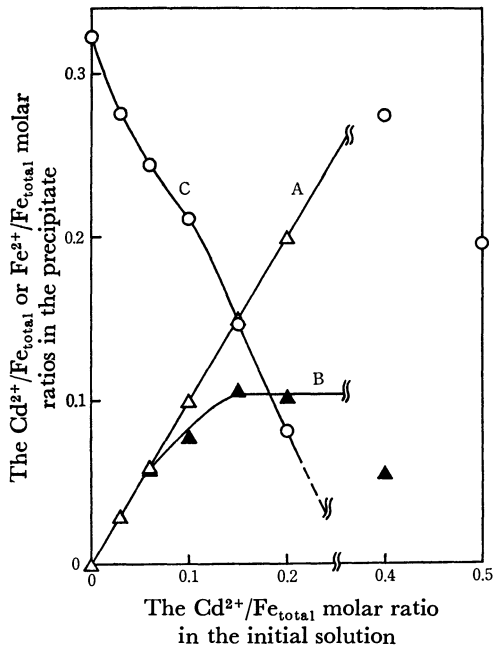

Fig. 3. The relationship between the Cd^{2+}/Fe_{total} molar ratio in the initial solution and the Cd^{2+}/Fe_{total} or the Fe^{2+}/Fe_{total} molar ratio in the Precipitates A and B. The curve A: the Cd^{2+}/Fe_{total} molar ratio in the Precipitate A, the curve B: the Cd^{2+}/Fe_{total} molar ratio in the Precipitate B, the curve C: the Fe^{2+}/Fe_{total} molar ratio in the Precipitate B.

Chemical Composition of the Oxidation Products at pH *9.0.*

Figure 3 shows the relationship between the Cd^{2+}/Fe_{total} molar ratio in the initial solution and the Cd^{2+}/Fe_{total} or Fe^{2+}/Fe_{total} molar ratio in the Precipitates A and B. As may be seen in Fig. 3, Curve A, the Cd^{2+} content in the Precipitate A increases linearly with an increase in the Cd^{2+} concentration in the initial solution. The Cd^{2+} in the initial solution was completely extracted by the Precipitate A over the range from 0 to 0.3 of the Cd^{2+}/Fe_{total} ratio in the initial solution.

As may be seen in Curve B, the Cd^{2+} content in the Precipitate B increases with an increase in the Cd^{2+}/Fe_{total} ratio within a limited range from 0 to 0.1, but approaches a constant Cd^{2+}/Fe_{total} ratio, approximately 0.1, in the range from 0.15 to 0.20 in the initial solution. This suggests that all the Cd^{2+} in the initial solution is taken into the Cd-ferrite at ratios below 0.10. This

process corresponds to the oxidation reaction (1) in the previous section. At the ratios from 0.15 to 0.20, it is likely that some variable amount of the precipitate of cadmium hydroxide which is soluble at pH 5.0 is formed in the Precipitate A. This corresponds to the oxidation reaction (2). At the ratio of 0.30, we could not obtain a constant content of Cd^{2+} after duplicated analyses of the Precipitate B. This may correspond to the oxidation reaction (3). At the ratio of 0.40, the Cd^{2+}/Fe_{total} ratio in the Precipitate B was 0.057, which is smaller than those at the ratios from 0.05 to 0.20. This indicates that the incorporation of the cadmium ion into the Cd-ferrite is rather reduced at ratios above 0.40. This corresponds to the oxidation reaction (4).

Curve C in Fig. 3 shows the Fe^{2+}/Fe_{total} ratio in the Precipitate B. Since no iron ions were detected in the solutions coexisting with both the Precipitate A and B, the iron oxides formed in the Precipitate A seem hardly to be dissolved at all at pH 5.0. As may be seen in Curve C, the Fe(II) content in the Precipitate B decreases with an increase in the Cd^{2+}/Fe_{total} ratio in the initial solution; this may suggest that the cadmium ion replaces the Fe(II) ion in the spinel-type structure at Cd^{2+}/Fe_{total} ratios from 0 to 0.10 in the initial solution. The further decrease in the Fe^{2+}/Fe_{total} ratio at higher ratios of Cd^{2+}/Fe_{total} in the initial solution (0.10 to 0.20) is due to the gradual formation of α-FeOOH, together with the formation of oxidized Cd-ferrite.

Lattice Constant. Figure 4 shows the relationship between the lattice constant of the Cd-ferrite obtained from the Precipitates B and the Cd^{2+}/Fe_{total} ratio in the initial solution at pH 9.0. As may be seen in Fig. 4, Curve A, the lattice constant of the Precipitate B increases almost linearly with an increase in the amount of Cd^{2+} in the initial solution with the Cd^{2+}/Fe_{total} ratios from 0 to 0.15. This shows that the cadmium ion is incorporated into the ferrite. However, at ratios above 0.15 the lattice constant gives a constant value, 0.8510 nm. Curve B in Fig. 4 shows the relationship between the lattice constant of the completely oxidized-Precipitates B obtained by heating at 150 °C in the air and the Cd^{2+}/Fe_{total} ratio in the initial solution. The X-ray diffraction patterns were identical with those of the Precipitates B, but each peak belonging to the spinel-type structure was shifted to a higher angle. The lattice constant of the oxidized-Precipitates B increases with an increase in the Cd^{2+}/Fe_{total} ratios in the initial solution from 0 to 0.20. As has been mentioned before, at the ratio of 0.30 the Precipitate B was composed of only an amorphous product, and even if we heated this at 150 °C for a day, we could not obtain a crystalline phase. At the ratio of 0.40, the lattice constant of the oxidized-Precipitate B was 0.8429 ± 0.0001 nm. This value is somewhat lower than that at 0.20. At present, we are not able to interpret whether or not this difference is significant.

From these experiments, we may say that the Precipitates B obtained from the initial solutions with the Cd^{2+}/Fe_{total} ratios from 0 to 0.20 comprise a limited solid solution between Fe_3O_4 and $CdFe_2O_4$, that the further $CdFe_2O_4$ component is never incorporated in the spinel structure under the present experimental conditions, that this solid solution is unstable at higher temperatures, say, above 100 °C, in the air, and that it is interestingly oxidized completely to form a limited solid solution between γ-Fe_2O_3 and $CdFe_2O_4$. Figure 5 shows the relationship between the lattice constant and the mole fraction x of the $CdFe_2O_4$ component in the solid solution. The lattice constants of γ-Fe_2O_3 and

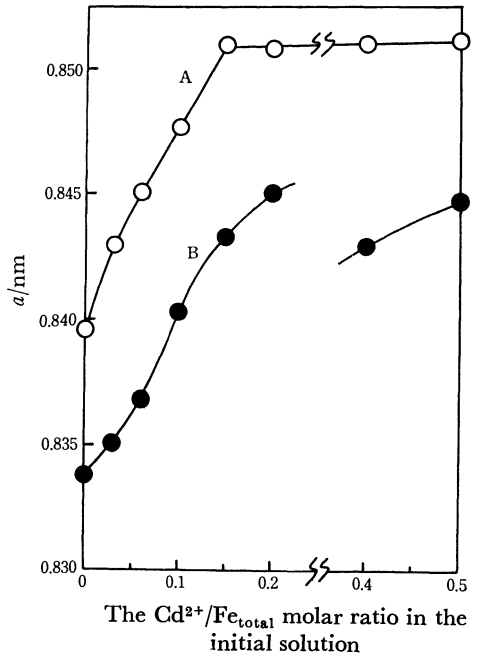

Fig. 4. The relationship between the Cd^{2+}/Fe_{total} molar ratio in the initial solution and the lattice constant of the Precipitate B or the oxidized-Precipitate B. The curve A: Precipitate B, the curve B: the oxidized-Precipitate B. a: Lattice constant.

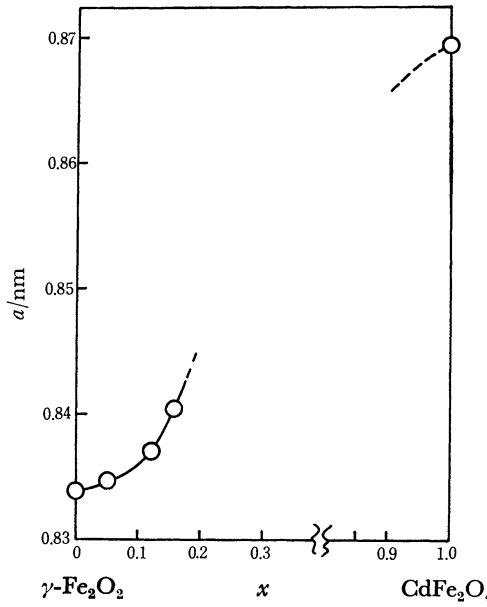

Fig. 5. The relationship between the lattice constant and the x value of the oxidized-Precipitate B. The x represents the molar ratio of $CdFe_2O_4$ to ($CdFe_2O_4$+γ-Fe_2O_3). a: Lattice constant.

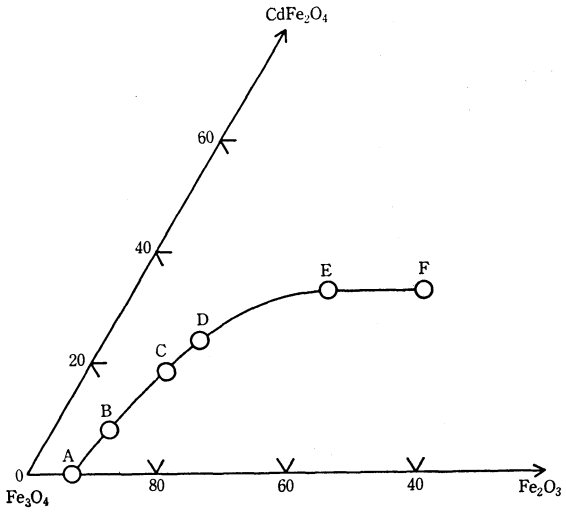

Fig. 6. The chemical compositions of the Precipitate B expressed as the Fe_3O_4–Fe_2O_3–$CdFe_2O_4$ system. Points A, B, C, D, E and F were obtained at the Cd^{2+}/Fe_{total} molar ratios of 0.00, 0.03, 0.06, 0.10, 0.15 and 0.20, respectively.

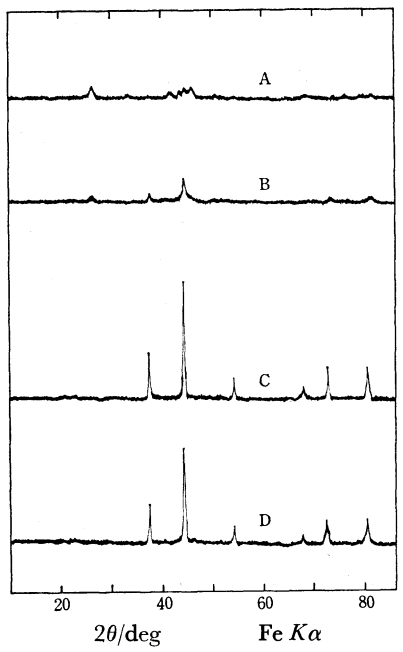

Fig. 7. The X-ray powder diffraction patterns of the Precipitates A obtained at pH 7.0(patternA), 8.0-(pattern B), 10.0(pattern C) and 11.0(pattern D). The Cd^{2+}/Fe_{total} molar ratio was fixed to 0.10.

$CdFe_2O_4$ were determined by Schrader and Buttner[10] and Roberts *et al.*[11] respectively. As may be seen in Fig. 5, the lattice constants of the oxidized-Precipitates B fall between those of γ-Fe_2O_3 and $CdFe_2O_4$.

Composition Diagram for the Precipitates B. Figure 6 shows the composition diagram for the Precipitates B formed at pH 9.0. For convenience, Fe_3O_4, Fe_2O_3 and $CdFe_2O_4$ are selected as the three component systems. As may be seen in Fig. 6, the Precipitates B all significantly deviate from their stoichiometric compositions. Under the present conditions, it seems to be next to impossible to synthesize the stoichiometric solid solution. This was also true for the Fe_3O_4–Fe_2TiO_4 and the Fe_3O_4–$MgFe_2O_4$ systems, which were studied by Katsura *et al.*[8] and by Kaneko and Katsura[9] respectively.

pH *Dependence on the Formation of the Precipitates A and B.* In the preceding section, we discussed the properties of the Precipitates A and B formed at pH 9.0 and at 65 °C. We also studied the pH dependence on the formation of the Precipitates A and B by changing

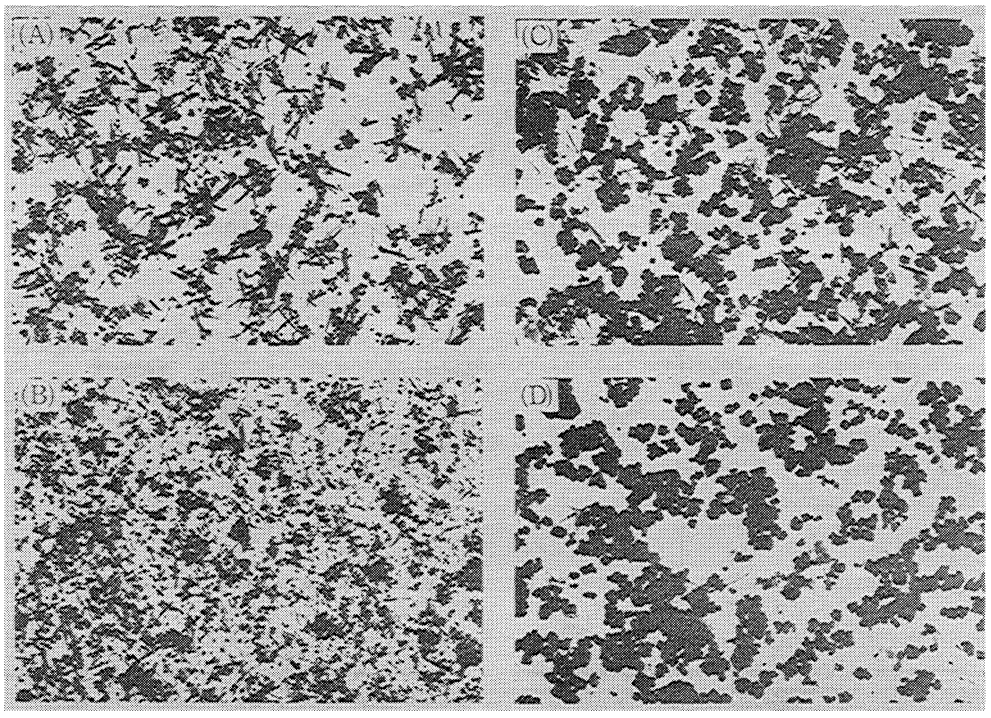

Fig. 8. The electron-micrographs of the Precipitates B obtained at pH 7.0(A), 8.0(B), 10.0(C) and 11.0(D). The Cd^{2+}/Fe_{total} molar ratio was fixed to 0.10.

the pH values from 7.0 to 11.0 at 65 °C. Figure 7 shows the X-ray diffraction patterns of the Precipitates A obtained at pH 7.0, 8.0, 10.0, and 11.0. At pH 9.0 (the patterns B in Fig. 1), 10.0, and 11.0, very sharp peaks caused by the presence of the ferrite structure are seen, while at pH 7.0 and 8.0 the peaks flatten out. It is presumed that the ferrite crystal with a small particle size and the α-FeOOH phase are formed at pH 7.0 and 8.0. The same X-ray patterns were obtained for the Precipitates B. Figure 8 shows the electron micrographs of the Precipitates B obtained at pH 7.0, 8.0, 10.0, and 11.0. As may be seen in Fig. 8, the large-size Cd-ferrite (0.12 μm) is formed together with a little amount of the needle-like crystals. However, the particle of the Cd-ferrite crystal becomes small at pH 7.0 and 8.0, and the amount of the needle-like crystals increases. These needle-like crystals seem to be composed of α-FeOOH. Thus, the results obtained by the electron microscopy agree very well with those obtained from the X-ray diffraction patterns.

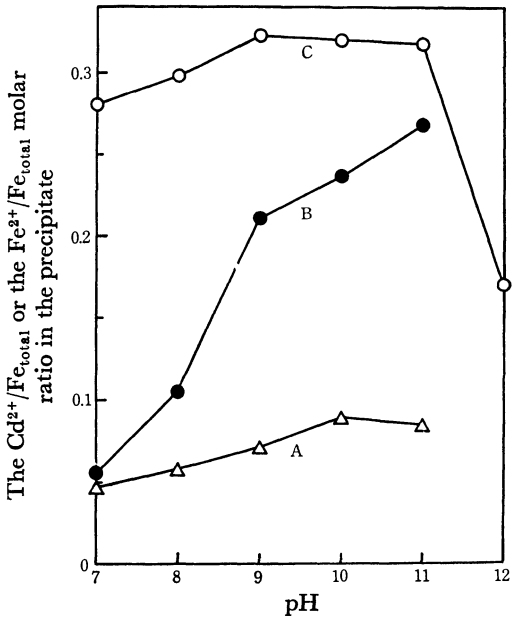

Fig. 9. The relationship between the pH value of the suspension and the chemical composition of the Precipitate B. The Cd^{2+}/Fe_{total} molar ratio in the initial solution is fixed to 0.10. The curve A: the Cd^{2+}/Fe_{total} ratio in the Precipitate B, the curve B: the Fe^{2+}/Fe_{total} ratio in the Precipitate B, the curve C: the Fe^{2+}/Fe_{total} ratio of the Precipitate B formed without Cd^{2+}.

Figure 9 illustrates the relationship between the Cd^{2+}/Fe_{total} or the Fe^{2+}/Fe_{total} ratio in the Precipitate B and the pH value of the suspension. As may be seen in Fig. 9, Curve A, approximately half of the Cd^{2+} added to the initial solution was taken into the Precipitate B at any pH value. However, considering the precision in the present chemical analysis, it is evident that the Cd^{2+}/Fe_{total} ratio in the Precipitate B gives its maximum value at pH 10.0. As seen in Fig. 9, Curve B, the Fe^{2+}/Fe_{total} ratio in the Precipitate B increases abruptly at pH 9.0, and then increases gradually from 9.0 to 11.0. The lower ratio at a lower pH range (from 7.0 to 8.0) is the result of the formation of α-FeOOH, together with the further oxidation of the Cd-ferrite with a small particle size (see Fig. 8). Curve C in Fig. 9 shows the pH dependence of the chemical composition of Fe_3O_4 (Cd=0) for the sake of comparison. As may be seen in Curve C, the Fe^{2+}/Fe_{total} ratios fall in a narrow range from 0.28 to 0.32 (in stoichiometric composition, the ratio is 0.333) at the pH intervals from 7.0 to 11.0. Thus in the presence of Cd^{2+} in the initial solution, α-FeOOH is liable to be formed together with the Cd-ferrite. However, only a small amount of α-FeOOH is crystallized, together with a large amount of the Cd-ferrite, when the pH value increases to 11.0. In addition, we can safely conclude that, at pH 11.0, th e cadmium ion intrinsically replaces the Fe(II) ion in the crystal lattice of the spinel-type structure.

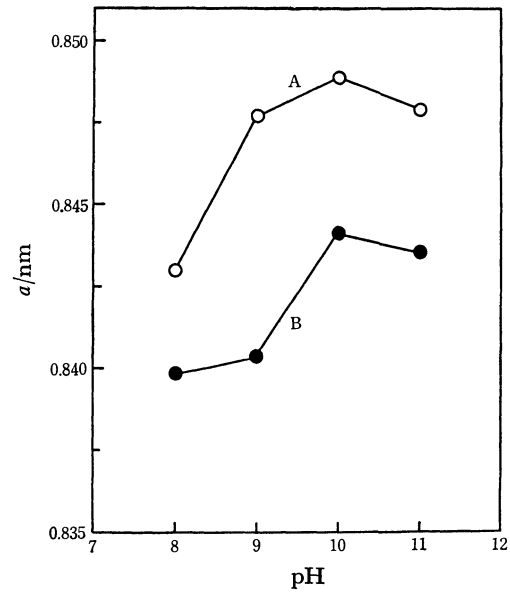

Fig. 10. The relationship between the pH value of the suspension and the lattice constant of the Precipitate B or the oxidized-Precipitate B obtained at the Cd^{2+}/Fe_{total} molar ratio of 0.10. a: Lattice constant.

Figure 10 shows the relationship between the lattice constants of the Precipitate B and the oxidized-Precipitate B and the pH value at which the Precipitate B is formed. As may be seen in Fig. 10, Curve A, the lattice constant of the Precipitate B increases irregularly with an increase in the pH value from 8.0 to 10.0, and attains its maximum value, 0.8489 nm, at pH 10.0. Thereafter, at pH 11.0, the lattice constant decreases slightly. It seems likely that the Cd-ferrite is most favorably formed at pH 10.0, because the more the cadmium ion replaces the Fe(II) ion, the more the lattice constant increases. However, we have to consider also the grades of oxidation of the Cd-ferrite at various pH values in the suspension. As was mentioned in the previous section, the Cd-ferrite formed at low pH values, 7.0 and 8.0, is small in particle size and so is oxidized easily during the air oxidation, while maintaining the spinel-type structure. For example, as may be seen in Fig. 10, the lattice constants of the Cd-ferrites formed

at pH 8.0 and 9.0 are quite different from each other (Curve A). We assume that the Cd-ferrite formed at pH 8.0 is oxidized significantly during the air oxidation. As may be seen in Fig. 10, Curve B, the lattice constants of the completely oxidized-Precipitates B at pH 8.0 and 9.0 are nearly the same amount of cadmium ion is incorporated into the ferrite at both pH values. Furthermore, we have confirmed that the pH value of 10.0 is the most favorable for forming the Cd-ferrite at 65 °C. Here, we should emphasize that the formation of the (Fe, M)$_3$O$_4$ type of ferrite is sensitively affected by the pH value in the suspension.

References

1) W. Feitknecht, *Z. Electrochem.*, **63**, 34 (1959).
2) M. Kiyama, *Bull. Chem. Soc. Jpn.*, **47**, 1646 (1974).
3) Y. Tamaura, G. S. Chyo, and T. Katsura, *Water Res.*, **13**, 21 (1979).
4) H. Yasuoka, A. Hirai, T. Shinjo, M. Kiyama, Y. Bando, and T. Takada, *J. Phys. Soc. Jpn.*, **22**, 174 (1967).
5) A. Hamamura, M. Kiyama, Y. Bando, and T. Takada, *J. Appl. Phys.*, **5**, 1246 (1966).
6) M. Kiyama, *Bull. Chem. Soc. Jpn.* **51**, 134 (1978).
7) T. Katsura, Y. Tamaura, and H. Terada, *Kogyo Yosui*, **223**, 16 (1977).
8) T. Katsura, Y. Tamaura, and G. S. Chyo, *Bull. Chem. Soc. Jpn.*, **52**, 96 (1979).
9) K. Kaneko and T. Katsura, *Bull. Chem. Soc. Jpn.*, **52**, 747 (1979).
10) R. Schrader and G. Büttner, *Z. Anorg. Allgem. Chem.*, **320**, 205 (1963)
11) H. S. Roberts and H. E. Merwin, *Am. J. Sci.*, **21**, 145 (1931).

A Semi-empirical MO Study of Radical-induced Decomposition of Dibenzoyl Peroxide. The Charge-transfer Character and Reaction Mechanism

Osamu KIKUCHI,* Keizo SUZUKI, and Katsumi TOKUMARU
Institute of Chemistry, The University of Tsukuba, Sakura-mura, Ibaraki 300-31
(Received September 30, 1977)

Radical-induced decomposition reactions of diacyl peroxides were investigated on the basis of the electronic structure of the peroxide-radical systems which were calculated using an approximate restricted open-shell SCF MO method in the MINDO/3 approximation, and on the basis of configuration analysis of the transition state of the reaction. For the transition state, (1) the change in peroxy O–O bond length is expected to be small, (2) the odd-electron density on the leaving group of the S_H2 displacement is expected to be very small, although appreciable odd-electron delocalization from the radical to the peroxide was observed, (3) the charge-transfer (CT) interactions which correspond to electron transfer from the radical to the peroxide was found to be important in the transition state. The trends observed in the orbital energies of the LUMO of substituted dibenzoyl peroxides and in the CT character of the transition state, which involves the singly-occupied MO of the radical and the $2p\sigma^*$ MO of the peroxide, agree well with the experimental facts, and strongly support a previous postulate that an important role is played by the $2p\sigma^*$ MO of the peroxy O–O group in the reaction.

Dibenzoyl peroxide (BPO) is one of the most frequently used sources of free radicals,[1] and its various modes of decomposition are an interesting subject of investigation. One typical process involving BPO is redical-induced decomposition:

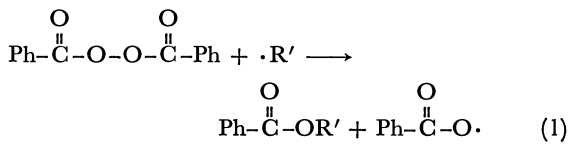

(1)

Extensive experimental studies[1-4] have contributed to the elucidation of the mechanism of this reaction. Step (1) is S_H2 substitution in which the radical attack occurs at the peroxy oxygen atom.[2] An electron-withdrawing substituent in BPO[3] and an electron-donating substituent in the radical[4] both enhance the reaction rate. The ionic character of the transition state of (1) has been pointed out.[3] The mechanism of step (1) has theoretically been considered by Tokumaru and Simamura[5] on the basis of experimental facts regarding the induced decomposition of peroxides by radicals. It has been suggested[5] that an interaction of the charge-transfer (CT) type, involving a singly-occupied MO (SOMO) of the attacking radical and the $2p\sigma^*$ antibonding orbital of the peroxy oxygen atoms, contributes to a lowering of the activation energy of the reaction.

In spite of these extensive experimental studies and qualitative explanations of the mechanism, no MO-theoretical investigations of the interacting BPO-radical system have been reported.[6] The purposes of the present note are: (i) to examine the reaction path of the radical-induced decomposition of BPO by means of a restricted open-shell method in the MINDO/3 approximation; (ii) to clarify the electronic structure of the transition state by means of configuration analysis for the wavefunction of the transition state, and (iii) to elucidate the substituent effect on the induced decomposition of BPO.

Method of Calculation

The electronic structure of the peroxide-radical systems were calculated in an approximate SCF version for open-shell systems which was proposed by Longuet-Higgins and Pople[7] and which has since been applied to all-valence-electron systems by one of the present authors.[8] For evaluating the electron integrals involved, the MINDO/3 approximation[9] was employed. The size of the BPO-radical system is too large to permit solving the problem even if the semi-empirical method is employed. In the present study, the reaction mechanism and the electronic structure of the transition state were considered using rather drastic approximations for the model system and its molecular structure. Diformyl peroxide (FPO), the simplest diacyl peroxide, and the methyl radical were adopted as model substances. The molecular parameters of the –COO group were fixed to those of BPO which were reported in a previous paper,[10] and a value of 90°[11] was used for the dihedral angle between the two RCOO planes. The conformation of C_{3v} CH_3 was optimized during the course of the reaction, the CH bond length being fixed at 1.087 Å, the optimized value for the D_{3h} methyl radical.

The substituent effect on radical-induced decomposition of BPO was elucidated on the basis of the electronic structure of substituted BPO in isolated states and on the basis of the CT character of the transition state of the BPO-methyl system. It is of note that CT from the radical to BPO will be underestimated in the transition state, since the ionization potential of the methyl radical is very large in comparison with those of the radicals currently used in actual experimental studies.

Configuration analysis was performed to clarify the electronic structure of the transition state. The wave function of the transition state (Ψ_T) was expanded in terms of doublet configurations (Ψ°) constructed from reference MO of the peroxide and of the planar methyl radical, thus

$$\Psi_T = C_g\Psi^\circ_g + \sum_i\sum_k C_{ik}\Psi^\circ_{i\to k} + \sum_j\sum_l C_{jl}\Psi^\circ_{j\to l} + \sum_j C_{jm}\Psi^\circ_{j\to m} + \sum_l C_{ml}\Psi^\circ_{m\to l} + \sum_k C_{mk}\Psi^\circ_{m\to k} + \sum_i C_{im}\Psi^\circ_{i\to m} + \sum_i\sum_l C_{il}\Psi^\circ_{i\to l} + \sum_j\sum_k C_{jk}\Psi^\circ_{j\to k}, \quad (2)$$

where Ψ°_g is the slater determinant for the ground-state

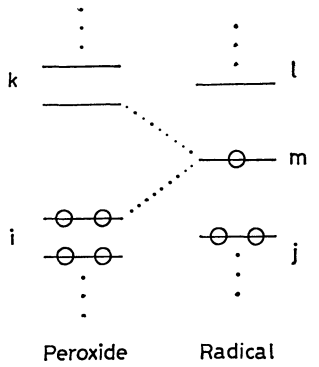

Fig. 1. Orbital interaction between a closed-shell molecule and a radical.

configuration of the peroxide-radical system, $\Psi^{\circ}_{i\to k}$ corresponds to one-electron exitation of the peroxide, $\Psi^{\circ}_{j\to l}$ $\Psi^{\circ}_{j\to m}$, and $\Psi^{\circ}_{m\to l}$ correspond to one-electron excitation of the radical, and the last four terms are CT configurations between the peroxide and the radical. The definition of indices, i, j, k, l, and m is given in Fig. 1. In Eq. 2, $\Psi^{\circ}_{a\to b}$ $(a\neq m,\ b\neq m)$ includes two independent wave functions corresponding to the $a\to b$ excited configuration. Neglecting the overlap between the MO in different molecules, the expansion coefficients in Eq. 2 were calculated using the following equations which were derived from the general formula given by Baba *et al.*,[12]

$$\begin{aligned} C_{a\to m} &= D^{m}_{0}D^{m-1}_{am},\\ C_{m\to b} &= D^{m}_{mb}D^{m-1}_{0}, \quad (a\neq m,\ b\neq m)\\ C_{a\to b} &= (f_1^2+f_2^2)^{1/2}, \qquad (3)\\ f_1 &= \frac{1}{\sqrt{2}}\{D^{m}_{0}D^{m-1}_{ab}+D^{m}_{ab}D^{m-1}_{0}\} \end{aligned}$$

and $$f_2 = \frac{1}{\sqrt{6}}\{D^{m}_{0}D^{m-1}_{ab}-D^{m}_{ab}D^{m-1}_{0}+2D^{m}_{mb}D^{m-1}_{am}\},$$

where $D_0{}^m$ is the determinant derived from the occupied α-spin MO of the interacting and non-interacting peroxide-radical systems, and $D_0{}^{m-1}$ is that derived from the β-spin MO of the systems. The other notations are same as those given in Ref. 12.

Results and Discussion

Reaction Path. The decomposition of FPO induced by the methyl radical was examined. Since the radical attack occurs at one of the peroxy oxygen atoms,[2] several interacting patterns, shown in Fig. 2, were examined. The interaction energy for each pattern was calculated by changing the distance between the peroxy oxygen atom and the methyl carbon atom. The conformation of the methyl radical is fixed for each pattern so that the SOMO of CH_3 is directed toward the oxygen atom to be attacked. The interaction energies at $R_{O\text{-}C}=2.0$ Å are shown in Fig. 2. When the radical attack occurs within the HCOO plane (Fig. 2, A—C), attack from the C direction is the most favorable. However, the C pattern of interaction is not expected in actual systems such as the BPO-triphenylmethyl system, since the large substituents in the peroxide and in the radical make this approach impossible.

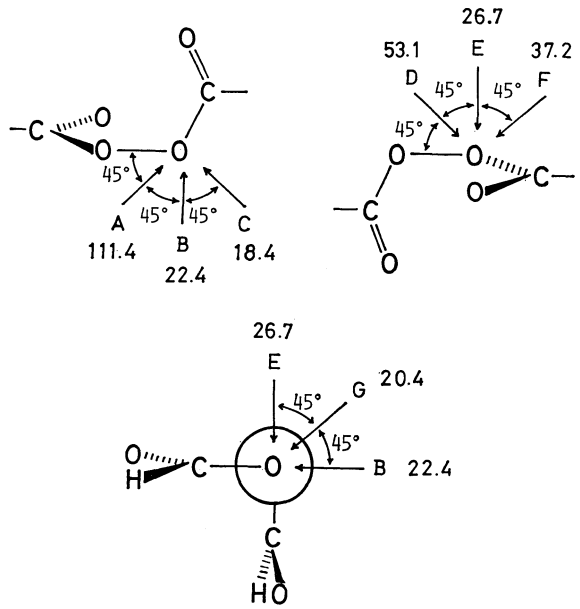

Fig. 2. Several interaction patterns between FPO and the methyl radical, and their interaction energies (kcal/mol) calculated at O–C=2.0 Å.

The G-pattern, for which the radical attack occurs in the plane which bisects the dihedral angle between the two RCOO planes and which is perpendicular to the peroxy O–O bond, may be most favorable in actual BPO-radical systems.

The potential energy surface for the G-approach[13] was calculated as a function of the peroxy O–O distance and of the O–C distance, other molecular parameters in FPO being fixed. The energy map obtained is shown in Fig. 3. For the transition state, the change (0.03 Å)

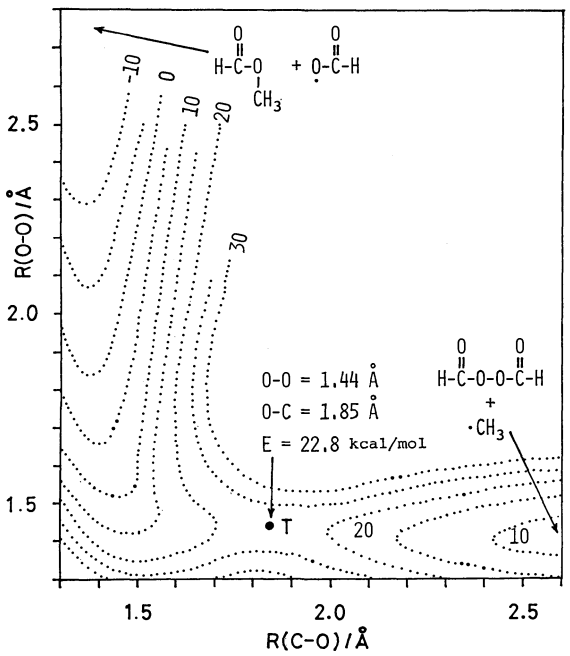

Fig. 3. Energy contours for the FPO–CH_3 system. The zero of energy (kcal/mol) is that of (FPO+CH_3) at infinite distance.

in the peroxy O–O bond length is expected to be small, while the O–C separation is large. The activation energy was estimated to be 23 kcal/mol which is somewhat larger than the observed values ($\simeq$10 kcal/mol, solvent dependent).[1,3]

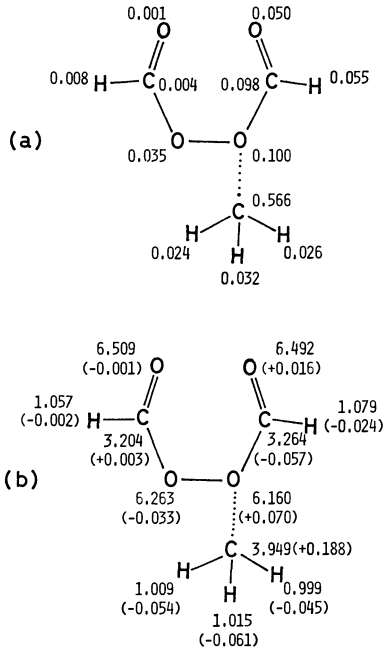

Fig. 4. Atomic spin densities (a) and atomic electron densities (b) of the FPO–CH_3 system in its transition state. The increases of the net charges are shown in parentheses.

Electronic Structure of the Transition State. The odd-electron and atomic electron distributions of the transition state are shown in Fig. 4. The changes in the atomic net charge densities caused by the peroxide-radical interaction are also shown in Fig. 4-b. Although large odd-electron delocalizations (35%) from the methyl radical to FPO are observed in the transition state, the odd-electron density on the leaving HCOO group is very small. This indicates that the contribution of structure III to the transition state is small. The ionic character of the transition state, for which the attacking group acts as an electron-donor, has been pointed out by Suehiro *et al.*[3] From Fig. 4, an ionic character is expected for the transition state, although its magnitude is not large for the present model system. The electronic structure of the transition state can thus be expressed as three structures, I, II, and III, whose contributions are in the order: I$\gg$II$>$III. This does *not* imply that the decomposition of diacyl peroxide by a radical gives the CT intermediate and then the carbonium ion (+R′)

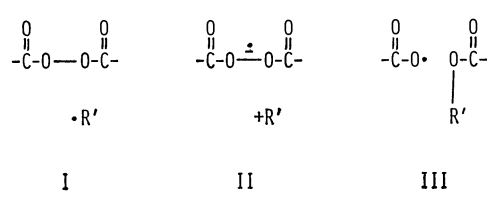

as reaction products. The contribution of II to the electronic structure of the transition state would be larger in actual BPO-radical systems, such as the BPO-triphenylmethyl system, than in the present model system, because the methyl radical is a poorer electron donor than the substituted alkyl radicals.

Configuration Analysis. As may be seen from the general interaction scheme (Fig. 1) between a closed-shell molecule and a radical, the SOMO interactions of CH_3 with both the occupied and unoccupied MO of FPO are expected to be very important for the transition state of the reaction. This was demonstrated by the configuration analysis, in which the wave function of the transition state was expressed in terms of the reference wave functions constructed of the MO of two non-interacting molecules. The electron configurations of the C_2 FPO and D_{3h} CH_3 are:

for FPO (^{1}A), $\cdots(8b)^2(9a)^2(9b)^0(10a)^0\cdots$

and for CH_3 ($^2A_2''$), $\cdots(a_2'')^1(2a_1')^0\cdots$

The qualitative pictures of three MO of FPO are shown in Fig. 5. The a_2'' orbital is the SOMO of the methyl radical. All the "one-electron excited" and "one-electron transfered" configurations of the two reactants were employed in the expansion of the wave function of the transition state. The contributions calculated are listed in Table 1. Since the total contribution accounts for 97%, the contributions of other configurations are small.

The contribution of the ground-state configuration (Ψ_g°) is dominant (48%). The large contribution due to the polarization ($\Psi_{m\to t}^\circ$) of the CH_3 radical comes from the geometrical change of CH_3 from D_{3h} to C_{3v} for the transition state.[14] The CT configurations from FPO to CH_3 (15%) are very important for the transition state, while the polarization interactions for FPO ($\Psi_{i\to k}^\circ$) are relatively small. It is notable that the most important of the CT configurations corresponds to electron transfer from the SOMO of the radical to the LUMO of the peroxide, which has an anti-bonding character with respect to the peroxy O–O bond. This supports the assumption that CT plays an important

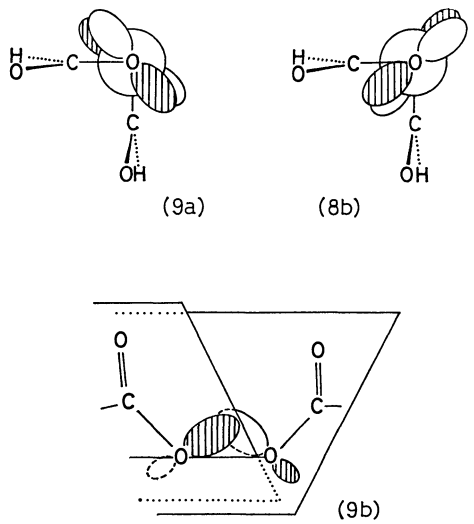

Fig. 5. Qualitative pictures of three MO's of FPO. The shape of each MO is drawn only in the peroxy oxygen region.

Table 1. Configuration analysis of the wave function of the FPO–CH_3 system for the transition state

Character of configurations[a]	Weight	Main configurations	Weight
ground	0.4798	ground	0.4798
$i \rightarrow m$	0.0824	$8b \rightarrow a_2''$	0.0319
		$4a \rightarrow a_2''$	0.0192
		$7a \rightarrow a_2''$	0.0157
$j \rightarrow m$	0.0087	—	—
$m \rightarrow k$	0.1489	$a_2'' \rightarrow 9b$	0.1005
		$a_2'' \rightarrow 10a$	0.0300
$m \rightarrow l$	0.1489	$a_2'' \rightarrow 2a_1'$	0.1487
$i \rightarrow k$	0.0467	$8b \rightarrow 9b$	0.0109
$j \rightarrow l$	0.0041	—	—
$i \rightarrow l$	0.0430	$8b \rightarrow 2a_1'$	0.0169
$j \rightarrow k$	0.0115	—	—
Total	0.9739		

a) i denotes the 17 occupied MO of FPO, j the 3 occupied MO of CH_3, k the 9 unoccupied MO of FPO, l the 3 unoccupied MO of CH_3, and m the singly-occupied MO of CH_3. Thus, $m \rightarrow k$, for example, indicates all the configurations which correspond to charge-transfer configurations from the SOMO of CH_3 to the unoccupied MO of FPO.

role in the induced decomposition of peroxides, as has been suggested by Tokumaru and Simamura.[5]

Substituent Effect on the Induced Decomposition of BPO. The rate constant of the induced decomposition of BPO is enhanced by an electron-withdrawing group in the phenyl group.[3] The important CT interaction at the transition state indicates that the electron-withdrawing group lowers the energy level of the $2p\sigma^*$ orbital of the peroxy O–O bond and increases the CT character of the transition state of the BPO-radical system. The orbital energies of several substituted BPO were calculated for predicted geometries.[10] The results are shown in Table 2. Strictly speaking, the LUMO of BPO is not the $2p\sigma^*$ of the peroxy O–O bond but is an unoccupied MO of the phenyl groups. In Table 2, the unoccupied MO which correspond to the $2p\sigma^*$ MO of FPO are called "LUMO." A very clear correlation between the orbital energies of the LUMO of substituted BPO and the electron-withdrawing character of the substituent is seen in Table 2. The CT character of the transition state was calculated using the geometry estimated for the FPO–CH_3 system. The CT interaction of the *p,p'*-dinitro BPO and CH_3 system is larger than that of unsubstituted BPO, while that for the *p,p'*-dimethoxy BPO–CH_4 system is smaller. This trend is parallel to that observed for the orbital energies of the LUMO of substituted BPO. The trends observed for the orbital energies of the LUMO of substituted BPO and for the CT character of the transition state agree well with the prediction given by Tokumaru and Simamura.[5]

Table 2. Orbital energies of the LUMO and the CT character of the transition state for *p,p'*-di-substituted BPO

Substituents *p-*	Substituents *p'-*	ε(LUMO)[a]	CT character for the transition state $m \rightarrow k$[b]	CT character for the transition state $m \rightarrow \sigma^*$[c]
OCH_3	OCH_3	1.154 eV	10.2%	7.0%
CH_3	CH_3	1.060	—	—
H	H	1.002	10.5	7.1
CN	CN	0.858	—	—
NO_2	NO_2	0.250	11.7	7.9

a) Orbital energies calculated for the equilibrium geometries predicted by MINDO/3.[10] The LUMO corresponds to the 9b orbital of FPO. b) All the configurations corresponding to the CT configurations from the SOMO of CH_3 to the unoccupied MO of BPO. c) All the configurations corresponding to the CT configurations from the SOMO of CH_3 to the unoccupied MO of BPO, which have the anti-bonding character of the peroxy O–O σ bond.

One of the authors, O. K., wishes to express his thanks to Dr. Ken Fujimori for useful discussions.

References

1) R. Hiatt, "Organic Peroxides II," ed by D. Swern,, Wiley-Interscience, New York (1971), p. 799; T. Koenig "Free Radicals I," ed by J. K. Kochi, John Wiley & Sons New York (1973), p. 133; Y. Ogata, "Chemistry of Organic Peroxides," Nankodo, Tokyo (1971), p. 170.

2) D. B. Denney and G. Feig, *J. Am. Chem. Soc.*, **81**, 5322 (1959); W. von E. Doering, K. Okamoto, and H. Krauch, *J. Am. Chem. Soc.*, **82**, 3579 (1960); W. P. Neuman and K. Rubsamen, *Chem. Ber.*, **100**, 1621 (1967).

3) K. F. O'Driscoll and P. J. White, *J. Polym. Sci., Part A*, **3**, 283 (1965); T. Suehiro, A. Kanoya, M. Omori, and T. Komori, *Bull. Chem. Soc. Jpn.*, **40**, 668 (1967).

4) S. Kato and F. Mashio, *Kogyo Kagaku Zasshi*, **59**, 380 (1956).

5) (a) K. Tokumaru and O. Simamura, *Bull. Chem. Soc., Jpn.*, **36**, 333 (1963); (b) K. Tokumaru, *Nippon Kagaku Zasshi*, **92**, 887 (1971).

6) The electronic structures of the peroxy O–O bonds in alkyl peroxides, peroxyacids, and peroxyesters have been investigated using the extended HMO method by T. Yonezawa, O. Yamamoto, H. Kato, and K. Fukui, *Nippon Kagaku Zasshi*, **87**, 26 (1966)) and by T. Yonezawa, H. Kato, and O. Yamamoto (*Bull. Chem. Soc. Jpn.*, **40**, 307 (1967)). The potential curves along the peroxy O-O bond cleavage of H_2O_2 have recently been obtained using CNDO/2-CI calculations by E.M. Evleth (*J. Am. Chem. Soc.*, **98**, 1637 (1976)).

7) H. C. Longuet-Higgins and J. A. Pople, *Proc. Phys. Soc.*, **68**, 591 (1955).

8) O. Kikuchi, *Bull. Chem. Soc. Jpn.*, **42**, 47 (1969).

9) R. C. Bingham, M. J. S. Dewar, and D. H. Lo, *J. Am. Chem. Soc.*, **97**, 1285, 1294, 1302, 1307 (1975).

10) O. Kikuchi, A. Hiyama, H. Yoshida, and K. Suzuki, *Bull. Chem. Soc. Jpn.*, **51**, 11 (1978).

11) X-Ray studies of dibenzoyl peroxide and acetylbenzoyl peroxide indicate a dihedral angle of about 90° (See G. A. Jeffery, R. K. McMullan, and M. Sax, *J. Am. Chem. Soc.*, **86**, 949 (1964), M. Sax and R. K. McMullan, *Acta Crystallogr.*, **22**, 281 (1964) and N. J. Karch, E. T. Koh, B. L. Whitsel, and J. M. McBride, *J. Am. Chem. Soc.*, **97**, 6729 (1975)), while MINDO/3 calculations give a value of 115° (Ref. 10).

12) H. Baba, S. Suzuki, and T. Takemura, *J. Chem. Phys.*, **50**, 2078 (1969).

13) The approach of the methyl radical from the in-plane B-direction gave a similar potential map.

14) The conformation of the FPO fragment for the transition state closely resembles the isolated FPO, while that of CH_3 (C_{3v} with an angle of 109° between the symmetry axis and each C-H bond) differs considerably from the planar CH_3 structure. The large contribution of the $m \rightarrow l$ configurations in Table 1 come from the direct application of configuration analysis[12] to the process accompanied by molecular deformation. When sp^3, instead of planar, conformation, was used as the reference structure of the methyl radical, the contribution of the $m \rightarrow l$ configurations was very small; in this case, all other features appeared in Table 1 and the conclusions obtained here remain unaffected. For a more correct treatment of the configuration analysis for the process accompanied by molecular deformation, see Ref. 15.

15) T. Okada, S. Nagase, K. Yamaguchi, and T. Fueno, *Bull. Chem. Soc. Jpn.*, **49**, 2377 (1976).

Formose Reactions. VI. Formose Synthesis in Methanol

Yoshihiro SHIGEMASA,* Yoshinobu MATSUDA, Chikahiro SAKAZAWA, Ruka NAKASHIMA, and Teruo MATSUURA†

Department of Industrial Chemistry, Faculty of Engineering, Tottori University, Tottori 680
†*Department of Synthetic Chemistry, Faculty of Engineering, Kyoto University, Kyoto 606*

(Received January 6, 1978)

The formose reaction in methanol was compared with that in an aqueous solution. The reaction can occur in aqueous methanol even at a low [CaO]/[HCHO] ratio (0.05), at which the reaction does not take place in an aqueous solution, and the formaldehyde consumption rate decreases with an increase in the methanol concentration. Contrary to the formose reaction in an aqueous solution, the sugar yield in methanol becomes higher with an increase in the formaldehyde concentration. The rates of the sugar degradation and the formaldehyde consumption increase with an increase in the pH. The distribution of products is different from that in an aqueous solution, but both of them are very complex and essentially nonselective.

The formose reaction which forms a complex mixture of sugars from aqueous formaldehyde in the presence of a base, usually $Ca(OH)_2$, has been invesitigated by many workers. Among them, the effects of a nonaqueous solvent, especially methanol, on the reaction have received some attention, mainly in connection with attempts to improve the sugar yield and the selectivity in product formation.[1-4] One significant observation obtained in these studies has been that the sugar yield was found to increase upon the addition of methanol.[2-4] Concerning the effect of methanol on the rate of the formose reaction, two inconsistent experimental results have been reported. Pfeil *et al.*[2] carried out the formose reaction catalyzed by TlOH in aqueous media containing 7—40% of methanol, where the rate of the formaldehyde consumption increased with an increase in the concentration of methanol. Nakai *et al.*[4] reported that the addition of methanol slowed down the rate of the reaction catalyzed by $Ca(OH)_2$ and considered that the accelerating effect of methanol found by Pfeil might be due to impurities in the methanol.

As we have already reported,[5-7] in the formose reaction with $Ca(OH)_2$ in an aqueous solution, the sugar yield varies with the extent of the Cannizzaro reaction occurring, especially during the induction period, and when the ratio $[Ca(OH)_2]/[HCHO]$ is too small (0.05), the formose reaction does not take place. The latter phenomenon has been partly interpreted in terms of pH lowering due to the formation of formic acid by the Cannizzaro reaction. In view of the above results, it seemed interesting to see how the formose reaction is affected by the depression of the Cannizzaro reaction resulting from the addition of methanol. Another aim of the present work is to characterize the formose reaction in a methanol solvent, focussing on the effects of the formaldehyde concentration, the catalyst amount, and the pH on the sugar yield and on the rate of formaldehyde consumption.

Experimental

Materials. The formaldehyde solution in methanol was prepared as follows. After a suspension of 200 g of paraformaldehyde (Merck Co.) in 400 ml of methanol had been refluxed for 7 h, the mixture was filtered. The concentration of formaldehyde in the filtrate was *ca.* 12 M. When the formose reaction was carried out in a 1.0 M formaldehyde solution in methanol in the presence of 0.3 mol/l of a catalyst (CaO, $Ca(OH)_2$, or $CaCO_3$) at 60 °C, the consumption of formaldehyde after 2 h was 67, 41%, or negligible respectively. Thus, the most active CaO was used as the catalyst throughout this work; the catalyst was freshly calcined at 1000 °C for 3 h prior to use to avoid the poor reproducibility caused by the absorption of CO_2 and moisture from air. The methanol was distilled, and the other reagents were of an analytical grade.

Procedure. The reaction was carried out as has been described previously[5,7] and aliquots taken from the reaction mixture at intervals were cooled instantly in a Dry Ice–acetone bath to stop the reaction and were then immediately analyzed. The oxidation-reduction potential (ORP) and pH of the reaction mixture, the formaldehyde consumption, and the sugar yield were measured as has been reported previously.[5,7]

The amount of organic acids (as formic acid) (x M) formed by the Cannizzaro reaction was determined as follows. To a ml of the reaction solution, b ml of 0.05 M HCl was added; after the solution had been back-titrated with 0.05 M KOH (c ml), the amount of calcium ions was determined by titration with 0.01 M EDTA[9] (d ml):

$$x = (0.05c + 2 \times 0.01d - 0.05b)/a.$$

The consumption rate of formaldehyde, $-\mathrm{d[HCHO]}/\mathrm{d}t$ (M/min), was determined from the maximum slope of the formaldehyde consumption curve. The products were trimethylsilylated by Sweeley's method[10] and the TMS derivatives were analyzed by gas chromatography as has been described previously.[8]

Results and Discussion

Effect of Methanol Concentration. Figure 1 shows the effects of the methanol content on the formose reaction which was carried out at [CaO]/[HCHO]= 0.05 in aqueous methanol. As has been reported previously,[5-7] the formose reaction did not proceed at this [CaO]/[HCHO] ratio unless methanol was added, but the Cannizzaro reaction occurred preferentially. Under these conditions, the formaldehyde consumption was found to be approximately equal to the amount of formaldehyde consumed by the Cannizzaro reaction. The addition of methanol brought about the consumption of the formaldehyde resulting from the formation of sugars. When the methanol content varied in the range from 25 to 100%, the amount of formaldehyde consumed by the Cannizzaro reaction became smaller,

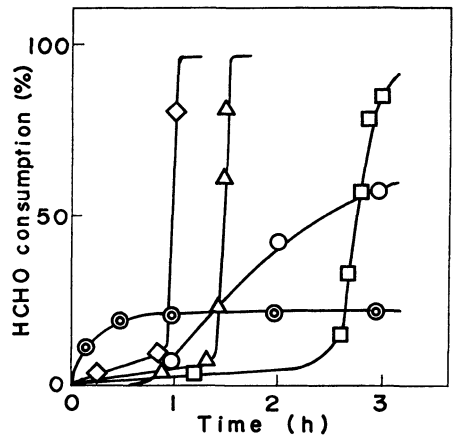

Fig. 1. Effect of methanol concentration on the formose reaction.
[HCHO]=1.0 M; [CaO]=0.05 mol/l; temp, 60 °C; total volume=200 ml. HCHO consumption, [MeOH] (vol %): ◎, 0; ◇, 25; △, 50; □, 75; ○, 100.

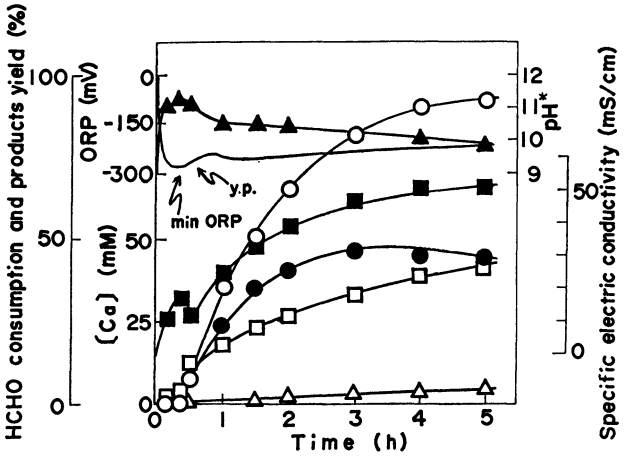

Fig. 2. Potentiometric and products analyses of the formose reaction in methanol.
[HCHO]=1.0 M; [CaO]=0.3 mol/l; temp, 60 °C; total volume=880 ml; ○, formaldehyde; ●, total sugars; △, organic acids; □, [Ca]; ■, electric conductivity; ▲, pH* (apparent pH in methanol); —, ORP.

that is, from *ca.* 12 to 5% for the total formaldehyde consumption. Since methanol obviously prevents the formation of formic acid, the addition of methanol will not appreciably change the pH of the reaction mixture, so the reaction mixture can keep the necessary concentration of $CaOH^+$, which has previously been shown to be the effective catalytic species during the induction period.[6] Figure 1 reveals further that, with an increase in the methanol content, the induction period is prolonged and the formaldehyde consumption rate becomes slower. In 100% methanol, however, the induction period is much more shortened than that in 75% aqueous methanol. This kinetic difference between the reactions in 75 and 100% methanol led us to assume that not only the pH, but also the solvent polarity, may influence the progress of the formose reaction. The solvent-polarity effect on the formose reaction will be reported elsewhere.

The Formose Reaction in 100% Methanol. A typical time-course of the reaction in 100% methanol with respect to physical measures, such as the pH, the oxidation-reduction potential (ORP), and the electric conductivity, and chemical measures, such as the formaldehyde consumption, the sugar yield, the organic acid formation, and the amount of dissolved calcium, is shown in Fig. 2. It has been previously shown that the ORP minimum and maximum indicate the end of the induction period and that of the sugar-forming step respectively in the formose reaction using a $Ca(OH)_2$–H_2O system.[7] The method was found to be applicable to the CaO–MeOH system only for determining the end of the induction period. In an aqueous solution, the yellowing point is observable at the end of the sugar-forming step, where the sugar yield reaches its maximum,[5,7] whereas, in methanol, the end of the sugar-forming step is in accord with neither the yellowing point nor the ORP maximum. As the sugar formation proceeds, the pH of the reaction mixture decreases and the amount of dissolved calcium increases, as was observed in the formose reaction in an aqueous solution.[6] A characteristic change was observed in the electric conductivity with a small drop between the ORP minimum and the yellowing point. Since the electric conductivity increases in parallel with the amount of dissolved calcium ion, it is assumed that the observed drop is due to a change in the dissolved calcium-ion species, such as the formation of a complex between calcium and a product which may be a catalytic species in the formose reaction.[12] This assumption is supported by the fact that the electric conductivity of a 0.1 M methanol solution of calcium chloride decreased from 38 to 23 mS/cm upon the addition of fructose (0.5 M).

As is to be expected from the inhibitory role of methanol on the Cannizzaro reaction, the formation of organic acids (mainly formic acid) is depressed, but the sugar yield does not increase so much as expected. This fact indicates that the sugar yield in methanol would be influenced also by factors other than the Cannizzaro reaction. One such possible factor is a competition between the formation and the degradation of formose sugars. This is supported by the facts that the formaldehyde consumption rate (possibly the formose-forming rate) in methanol is much slower than that in aqueous solution, and that the yellowing point, which implies the degradation of products, appears at an early stage of the total formose reaction in methanol, as is shown in Fig. 2.

In order to obtain further information on the formose-degradation process, the reaction was followed by measuring the ultraviolet spectrum of aliquots. Although no ultraviolet absorption was observed until the yellowing point, a broad absorption maximum at *ca.* 300 nm became observable thereafter and gradually increased. The absorption maximum is shifted from *ca.* 300 to *ca.* 260 nm when the apparent pH (pH*) of the solution is changed from 13.0 to 1.0. The Tilman reagent is reduced strongly by the reaction mixture. On the basis

Table 1. Effects of [HCHO] and [CaO] on the formose reaction in methanol[a)]

[CaO] (mol/l)	[HCHO] (M)	T_{min} (min)	T_{max}[b)] (min)	Sugar yield at T_{max} (%)	r_c (M/min)
0.15	0.2	60	$(17)_{300}$[c)]	13	0.01×10^{-2}
0.15	0.4	20	$(72)_{240}$[c)]	32	0.19×10^{-2}
0.15	1.0	12	240	44	0.55×10^{-2}
0.15	2.0	14	180	52	2.23×10^{-2}
0.15	3.0	22	150	56	2.51×10^{-2}
0.15	5.0	60	$(67)_{300}$[c)]	57	3.16×10^{-2}
0.05	0.5	30	$(59)_{290}$[c)]	36	0.14×10^{-2}
0.2	0.5	20	$(72)_{180}$[c)]	32	0.20×10^{-2}
0.5	0.5	24	180	32	0.79×10^{-2}
0.5	1.0	14	120	40	1.00×10^{-2}
0.5	2.0	12	150	45	2.82×10^{-2}
0.5	3.0	140	220	42	2.41×10^{-2}
0.5	5.0	150	240	50	7.93×10^{-2}

a) Temp, 60 °C; total volume, 200 ml. b) The time when the sugar yield became highest and the HCHO consumption was above 95%. c) The number in parentheses is the HCHO consumption (%) at the time (min) shown by the subscript.

of these results, one of the degradation products is assumed to be a reductone (Triose reductone: λ_{max}, 266 nm (pH, 1.8); 314 (13.5)).[11)] Formose reactions in methanol were carried out with various CaO amounts and formaldehyde concentrations; the results obtained are summarized in Table 1. At a constant formaldehyde concentration ([CaO]/[HCHO]>0.1), the sugar yields are virtually independent of the CaO amount. At a constant CaO amount, the sugar yield increases with an increase in the formaldehyde concentration, but the sugar yield is independent of the formaldehyde concentration when the concentration is high (>2.0 M). These features are significantly different from those in an aqueous solution. The sugar yield in an aqueous solution is known to decrease with an increase in the formaldehyde concentration.[5)] These differences are mainly attributable to an inhibitory effect of methanol on the Cannizzaro reaction.

Since the formaldehyde consumption rate (r_c) in methanol is relatively slow, as has been noted above (Table 1), the product degradation rate (r_d) may appreciably influence the sugar yield. (Because of the complex nature of formose decomposition, the quantitative evaluation of r_d was difficult. Therefore, the decrease in the sugar content analyzed by the known method[13)] was regarded as a rough measure of r_d.) Considering that the observed pH decreases as the formation of sugars progresses (Fig. 2), the high sugar yield at a high level of formaldehyde might be attributable to a slower r_d resulting from the pH lowering, accompanied by the progress of the sugar formation. On the other hand, the sugar yield is rather independent of r_d in an aqueous solution, because the r_c in the formose-forming step is very fast. For example, $r_c=37.5\times10^{-2}$ M/min at [HCHO]=1.0 M and $[Ca(OH)_2]=0.13$ mol/l.[7)] It seems likely that the sugar yield in methanol is also largely dependent on r_c. This idea is supported by the fact that the sugar yield increases with an increase in r_c (Table 1).

Table 2. Effect of the pH on the formose reaction in methanol

[HCHO]=1.0 M; temp, 60 °C

[Ca] (M)	pH*[a)]	T_{min} (min)	T_{max} (min)	Sugar yield at T_{max} (%)	r_c (M/min)
0.05	9.0	84	300	58	0.95×10^{-2}
0.05	9.5	22	150	57	1.58×10^{-2}
0.05	10.0	10	150	50	1.70×10^{-2}
0.05	10.5	8	70	44	2.70×10^{-2}
0.1	8.5	200	600	61	0.34×10^{-2}
0.1[b)]	9.0	52	210	59	1.51×10^{-2}
0.1[b)]	9.5	16	80	56	2.51×10^{-2}
0.1[b)]	10.0	7	60	49	3.98×10^{-2}

a) The apparent pH in methanol measured by electrodes adjusted with aqueous buffers. b) The reaction mixture became heterogeneous near the yellowing point.

In order to examine the effect of the pH on the formose reaction, $CaCl_2$ was used instead of CaO and the pH of the solution was adjusted by methanolic KOH. The results obtained are shown in Table 2. Under the conditions at low calcium concentrations (<0.1 M), the reaction mixture is homogeneous. The sugar yield increases with a decrease in the pH, though r_c slows down at a lower pH. Both r_c and r_d will vary with a change in the pH, and, at a very low pH (pH*=8.5), r_d is assumed to be extremely slow compared with r_c.

The pH and the catalyst concentration were found to affect the induction period in a homogeneous system. As is shown in Table 2, the induction period, T_{min} (the time up to the ORP minimum), becomes shorter with increases in the pH and the calcium concentration. This indicates that the induction step of the formose reaction in methanol may also be catalyzed mainly by $CaOH^+$, as in aqueous media.[6)] Although the sugar yield in an aqueous solution increases as the induction

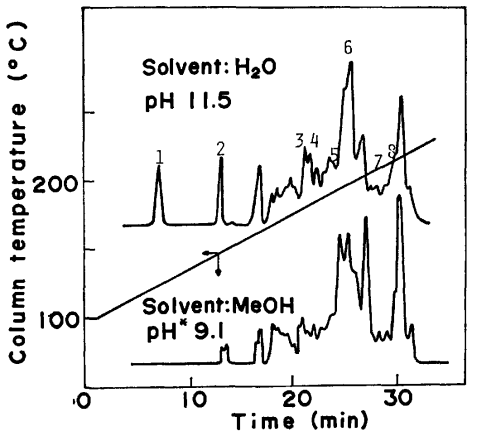

Fig. 3. Gas chromatograms of TMS derivatives of products. Column, SE-30 on Chromosorb W (60—80 mesh); N_2 flow rate, 60 ml/min; [HCHO]=1.0 M; [$CaCl_2$]=0.1 M; temp, 60 °C.
1, Glycerol; 2, 2-hydroxymethylglycerol; 3, xylose; 4, xylitol; 5, fructose; 6, 3-hydroxymethyl-1,2,3,4,5-pentanepentol; 7, solbitol, mannitol; 8, glucose.

period becomes shorter,[5,6] there was no relationship between the sugar yield and the length of the induction step in methanol. Although in an aqueous solution, the sugar yield is greatly affected by the amount of formaldehyde consumed by the Cannizzaro reaction occurring in the induction period, in methanol it is mostly influenced by the difference between r_c and r_d.

In summary, in order to obtain formose in a good yield in methanol, the formose reaction should be carried out under conditions in which the concentrations of formaldehyde and calcium ion are as high as possible and the pH is maintained at low values, such as pH*=8.5 (apparent pH).

Product Distribution. Figure 3 shows gas chromatograms of the TMS derivatives of the products obtained in aqueous and methanol solutions. The identities of some of the peaks were assigned by comparison with the retention times for authentic samples. The formation of sugar alcohols in methanol suggests that methanol strongly depresses the Cannizzaro reaction of formaldehyde, but not the cross-Cannizzaro reaction involving the aldoses formed. A comparison of these gas chromatograms indicates that the reaction in methanol produces a smaller amount of sugar alcohols than those in water, and that the product distribution is quite different, although both cases are essentially nonselective.

References

1) H. Schmalfuss, *Biochem. Z.*, **185**, 70 (1927).
2) E. Pfeil and G. Schroth, *Chem. Ber.*, **85**, 293 (1952).
3) R. Mayer and L. Jäschke, *Ann.*, **635**, 145 (1960).
4) T. Nakai, N. Tsujigado, and S. Sato, *Nippon Nogei Kagaku Kaishi*, **43**, 300 (1969).
5) Y. Shigemasa, T. Fujitani, C. Sakazawa, and T. Matsuura, *Bull. Chem. Soc. Jpn.*, **50**, 1527 (1977).
6) Y. Shigemasa, M. Shimao, C. Sakazawa, and T. Matsuura, *Bull. Chem. Soc. Jpn.*, **50**, 2138 (1977).
7) Y. Shigemasa, M. Shimao, C. Sakazawa, and T. Matsuura, *Bull. Chem. Soc. Jpn.*, **48**, 2099 (1975).
8) Y. Shigemasa, Y. Matsuda, C. Sakazawa, and T. Matsuura, *Bull. Chem. Soc. Jpn.*, **50**, 222 (1977).
9) K. Ueno, "Kireto Tekiteiho," Nankodo, Tokyo (1960), p. 227.
10) C. C. Sweeley, R. Bentley, M. Makita, and W. W. Wells, *J. Am. Chem. Soc.*, **85**, 2497 (1963).
11) H. Euler, *Z. Naturforsch.*, **8b**, 636 (1953).
12) K. Fujino, J. Kobayashi, and I. Higuchi, *Nippon Kagaku Kaishi*, **1972**, 2287, 2292.
13) D. Dubois, K. A. Gilles, J. K. Hamilton, P. A. Revers, and F. Smith, *Anal. Chem.*, **28**, 350 (1956).

Inositol Derivatives. 11. Synthesis of Dianhydroinositols[1]

Seiichiro OGAWA,* Shuichi OKI, and Tetsuo SUAMI

Department of Applied Chemistry, Faculty of Engineering, Keio University, Hiyoshi, Yokohama 223

(Received March 17, 1978)

All the predicted isomers of 1,2: 3,4- and 1,2: 4,5-dianhydrocyclohexanehexols (5 racemates and 6 meso-compounds) were synthesized from appropriate inositol ditosylates and dimesylate by treatment with sodium methoxide.

A diepoxycyclohexane tumor inhibitor, crotepoxide was isolated from *Croton macrostachys*[2] and later from *Piper futokazura*,[3] and an antibiotic LL-Z 1220 was found to contain a *cis*-diepoxycyclohexene structure.[4] Recently, much interest has been taken in the reactivity and stereochemistry of highly mutagenic 7,8-dihydroxy-9,10-epoxide of benzo[*a*]pyrene and analogous substances.[5]

We have studied the structure-activity relationship of diepoxycyclohexanes by preparing diepoxycyclohexanediol as a model compound. We report herewith the details of synthetic studies on all the predicted diastereomers of dianhydrocyclohexanehexol (inositol).[6]

Sixteen isomers (5 racemates and 6 *meso*-compounds) are theoretically possible for dianhydroinositols: 1,2: 3,4-(**1a**, **3a**, **6a**, **7a**, **9a**, and **10a**) and 1,2: 4,5-dianhydrocyclohexanehexols (**2a**, **4a**, **5a**, **8a**, and **11a**), excluding isomers with a 1,3- or 1,4-anhydro ring.

None of these isomers has been described in literature, except for three of their *O*-cyclohexylidene derivatives.[7]

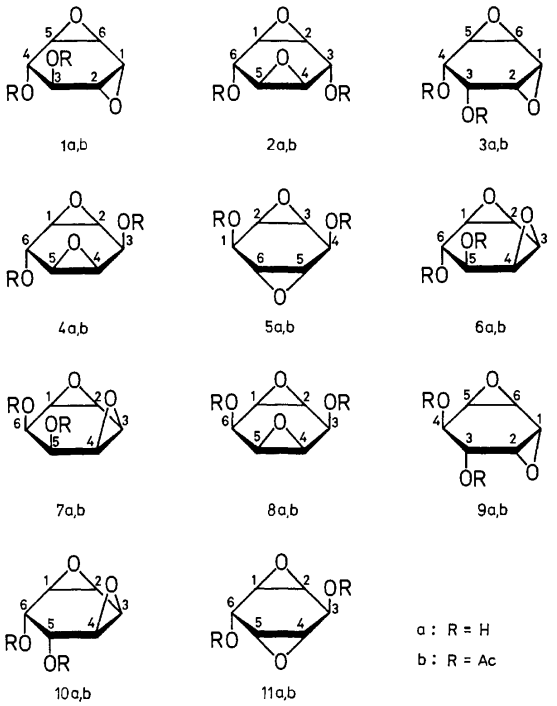

Scheme 1. The sixteen isomers of dianhydroinositol.[a]
a) Isomers **2**, **4**, **5**, **7**, **8**, and **10**, having a plane of symmetry, are meso forms. Of the five racemic diastereomers, **1**, **3**, **6**, **9**, and **11**, the enantiomer is depicted which allows clockwise assignment of positional numbers.

Seven isomers were synthesized from *myo*-inositol ditosylates and other four from *chiro*- and *muco*-inositol ditosylates and dimesylates. Structural elucidation of dianhydroinositols obtained was carried out by means of ^{1}H NMR spectroscopy and consideration of reaction mechanisms.

1,2: 5,6-Dianhydro-chiro- *(1) and 1,2: 4,5-Dianhydro*-muco-*inositols (2).* Treatment of tetra-*O*-acetyl-1, 3-di-*O*-tosyl-*myo*-inositol (**12**)[8] with a slight excess of sodium methoxide in chloroform–methanol at ambient temperature led to the formation of two major and one minor components. The mixture was separated by column chromatography, giving syrupy **1a** and crystalline **2a** in 21 and 15% yields, respectively, which were further characterized by conversion into their crystalline di-*O*-acetyl derivatives (**1b** and **2b**).

We see from the reaction mechanism that the two diepoxy diols can be obtained from **12** through the displacement of tosyloxyl functions with anionic oxygens. Compounds **1a** and **2a** are interconvertible by migration of an oxirane ring in basic media.[9] Structures of the products were determined on the basis of the ^{1}H NMR spectra, taking advantage of the symmetry of molecules. A part

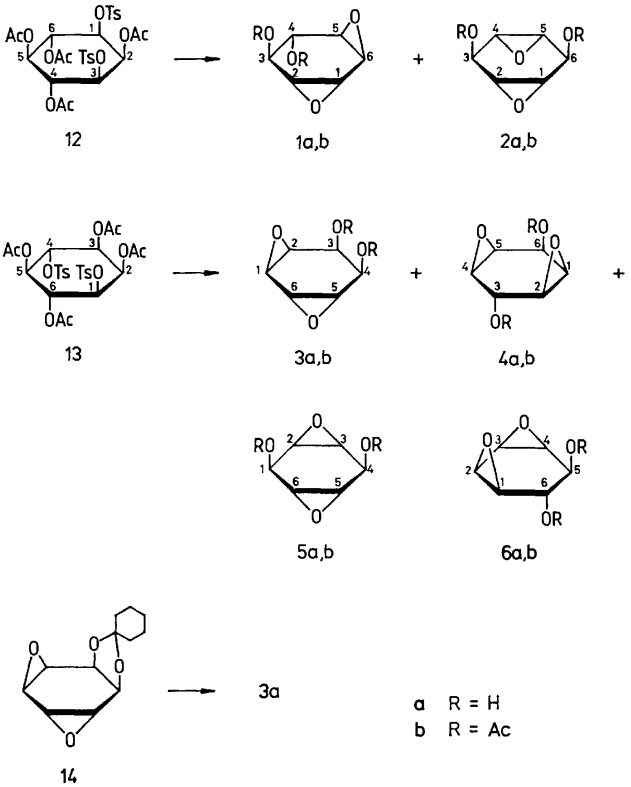

Scheme 2.

of the spectral data are given in Table 1.

In the spectrum of **1b** in deuteriochloroform ($CDCl_3$), a two-proton doublet of triplets at δ 3.18 and a two-proton doublet of doublets at δ 3.58 are attributed to magnetically equivalent H-1 and H-6, and H-2 and H-5, respectively. Appearance of a two-proton relatively narrow triplet at δ 5.11 due to H-3 and H-4 indicates that the acetoxyl and epoxy groups are arranged in trans positions.[10] In the spectrum of **2a** in deuterium oxide (D_2O), the six ring protons appear as a four-proton triplet (δ 3.29) and a two-proton quintet (δ 4.56), showing the presence of magnetically equivalent two epoxy and two hydroxyl groups. The spectral data are consistent with the assigned structures.

A crystalline mixture of the diepoxy diacetates derived by direct acetylation of the intact epoxydation products from **12** was shown to be a 4: 5 mixture of **1a** and **2a** by estimation of the relative intensity of the signals due to each acetoxyl group. On the other hand, when **1b** was *O*-deacetylated with methanolic sodium methoxide, the resulting reaction mixture was found to contain **1a** and **2a** in about 1: 1 ratio by visual observation on TLC. The results give an evidence for the proposed structures of **1a** and **2a**. It is difficult to decide which product is formed first from **12**, because of the ready isomerization resulting from an oxirane ring migration under the conditions in this synthesis.

1,2: 5,6-Dianhydro-allo-*(3)*, *1,2: 4,5-Dianhydro*-epi-*(4)*, *and 2,3: 5,6-Dianhydro*-allo-*inositols (5)*. Under similar conditions with use of sodium methoxide, tetra-*O*-acetyl-1,4-di-*O*-tosyl-*myo*-inositol (**13**)[11] gave, upon separation by column chromatography, three crystalline diepoxy diols **3a** (23%), **4a** (8%), and **5a** (21%). Four diepoxy diols (**3a**, **4a**, **5a**, and **6a**) might be formed from **13**, and two pairs interconvertible in basic media. Both **4a** and **5a** have a plane of symmetry. In the ^1H NMR spectrum of **3a**, two protons on C-3 and C-4 appear as a doublet of doublets and a doublet of doublets of doublets, coupled with each other at δ 4.06 and 4.35, respectively, indicating that **3a** should be a 1,3-diepoxide. The structure of **3a** was confirmed by identification with the compound obtained by a mild acid hydrolysis of 1,2: 5,6-dianhydro-3,4-*O*-cyclohexylidene-*allo*-inositol (**14**).[12] Under these conditions no epoxide group migration occurs. The results also show that **4a**, formed from **3a** by base-catalyzed isomerization, possesses the assigned structure demonstrated by the symmetric pattern of the signals due to the ring protons in its ^1H NMR spectrum. Thus, **4a** shows a four-proton narrow triplet (δ 3.45) and a two-proton broad singlet (δ 4.53), its two hydroxyl groups being found not to be magnetically equivalent by the spectrum of the diacetate **4b**. Compound **5a** exhibits three two-proton narrow multiplets for the methine protons, indicating the presence of a plane of symmetry. Thus, its structure was assigned as 2,3: 5,6-dianhydro-*allo*-inositol. Later, **6a** was found to be transformed completely into **5a** in basic media.

1,2: 3,4- (7) and 1,2: 4,5-Dianhydro-cis-*inositols (8)*. Similar epoxidation of 1,2,5-tri-*O*-acetyl-3-*O*-benzoyl-4,6-di-*O*-tosyl-*myo*-inositol (**15**)[13] gave two diepoxy diols **7a** (4%) and **8a** (37%), together with 2,3-anhydro-6-*O*-tosyl-*epi*-inositol (**17**, 4%).[14] The structure of **17** was

Table 1. ^1H NMR data of dianhydroinositols[a]

Formula	Diol[b]		Diacetate[c]		
	HC(O)CH	HO–C–H	HC(O)CH	AcO–C–H	OAc
1[d]	3.46 (2)	4.13 (2)	3.18 (2)	5.11 (2)	2.13 (6)
	3.66 (2)		3.58 (2)		
2	3.29 (4)	4.56 (2)	3.17 (4)	5.63 (2)	2.17 (6)
3	3.47 (2)	4.06 (1)	3.31 (2)	5.36 (1)	2.07 (3)
	3.72 (1)	4.35 (1)	3.64 (2)	5.72 (1)	2.16 (3)
	3.84 (1)				
4	3.45 (4)	4.53 (2)	3.34 (4)	5.60 (2)	2.16 (3)
					2.22 (3)
5	3.21 (2)	4.31 (2)	3.10 (2)	5.32 (2)	2.17 (6)
	3.51 (2)		3.44 (2)		
6	3.22 (1)	3.69 (1)	3.05 (1)	5.02 (1)	2.09 (3)
	3.46 (1)	4.12 (1)	3.2—3.7 (3)	5.44 (1)	2.12 (3)
	3.70 (2)				
7	3.46 (2)	4.15 (2)	3.31 (2)	5.30 (2)	2.13 (6)
	3.65 (2)		3.47 (2)		
8	3.51 (4)	4.48 (2)	3.50 (4)	5.52 (2)	2.22 (6)
9	3.46 (2)	3.94 (2)	3.39 (2)	5.36 (2)	2.12 (6)
	3.81 (2)		3.65 (2)		
10	3.31 (2)	3.95 (2)	3.22 (2)	5.28 (2)	2.10 (6)
	3.68 (2)		3.56 (2)		
11	3.26 (2)	4.47 (2)	3.13 (2)	5.44 (2)	2.17 (6)
	3.47 (2)		3.42 (2)		

a) Chemical shifts are given in terms of δ-values. Values in parentheses show number of protons. b) Unless otherwise noted, the spectra were measured in D_2O. c) Measured in $CDCl_3$. d) The spectrum of the diol was measured in $CDCl_3$.

confirmed by conversion into **8a** on further treatment with sodium methoxide. Characterization of **7a** and **8a** was carried out by their ^1H NMR spectra. Thus, **8a** shows a four-proton doublet of doublets due to H-1, H-2, H-4, and H-5 appearing at δ 3.51, and a seven-line signal due to H-3 and H-6 at δ 4.48, confirming the assigned structure of **8a**. The spectrum of **7a** exhibits three two-proton narrow multiplets at δ 3.46, 3.65, and 4.15. The A_2B_2 pattern observed for H-1 and H-4, and H-5 and H-6 signals is compatible with the assigned structure of **7a**.

In contrast to the above results, when *O*-deacetylated compound, 1-*O*-benzoyl-4,6-di-*O*-tosyl-*myo*-inositol (**16**)[13] was subjected to epoxidation, **7a** was obtained in 36% yield, together with a trace of **8a**. This might be accounted for by assuming an attack of the C-5 anionic oxygen at C-4 or C-6 giving 1,2-anhydro-6-*O*-tosyl-*epi*-inositol (**18**) as an intermediate for **7a**. In the case of **15**, **17** might be a major intermediate presumably resulting from an attack of the C-1 or C-3 anionic oxygen formed first by *O*-deacylation at C-6 or C-4. The evidence for these assumption was furnished by using tetra-*O*-acetyl-3,6-di-*O*-tosyl-*muco*-inositol (**19**)[15] that would generate only **17** intermediary under the epoxidation conditions. In fact, **19** gave **8a** selectively in 36% yield.

In order to estimate the reactivity of *myo*-inositol ditosylates, we studied the epoxidation of tri-*O*-acetyl-1, 4,6-tri-*O*-tosyl-*myo*-inositol (**20**) and its *O*-deacetylated compound (**21**).[11]

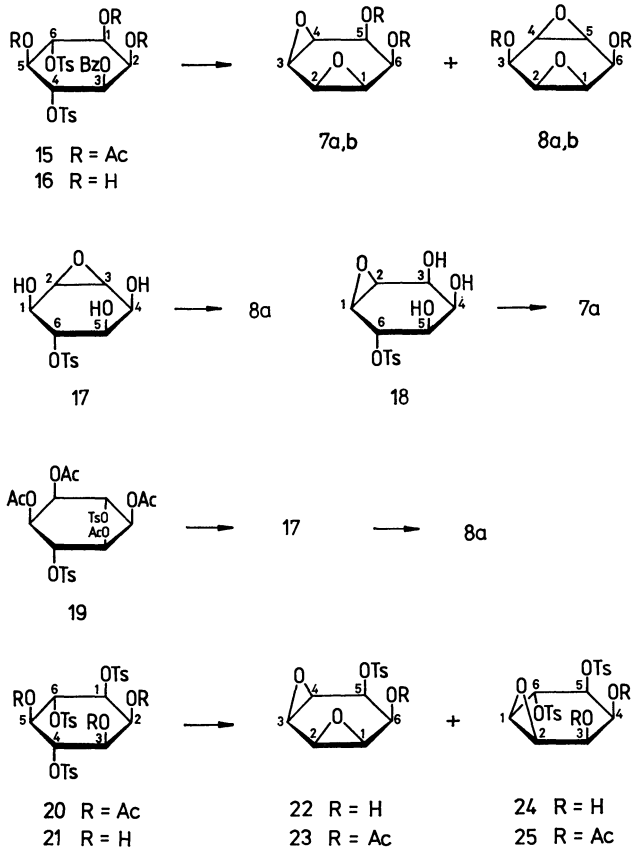

Scheme 3.

Treatment of **20** with an excess of sodium methoxide in chloroform–methanol gave the diepoxide (**22**) preferentially in 50% yield. The corresponding *O*-acetyl derivative (**23**) revealed an ^1H NMR spectrum very similar to that of **7b**, suggesting it to be 1,2: 3,4-dianhydro-5-*O*-tosyl-*cis*-inositol. On the other hand, **21** reacted with sodium methoxide to give the monoepoxide (**24**) in 24% yield, together with a trace of **22**. The di-*O*-acetyl derivative (**25**) of **24** showed, in the ^1H NMR spectrum, a doublet of doublets and a doublet due to two protons on carbon atoms bearing the tosyloxyl functions at δ 4.58 and 4.96, respectively, showing that one of the tosyloxyls is adjacent to the epoxy group in trans orientation. These data allow us to assign the structure of **25** to 3,4-di-*O*-acetyl-1,2-anhydro-5,6-di-*O*-tosyl-*epi*-inositol. In the case of **20**, the C-3 acetoxyl seems to be *O*-deacylated first leading to the 3,4-epoxide, an intermediate for **22**. The preferential formation of the 3,4- or 4,5-epoxide is in line with that observed for **15** and **16**.

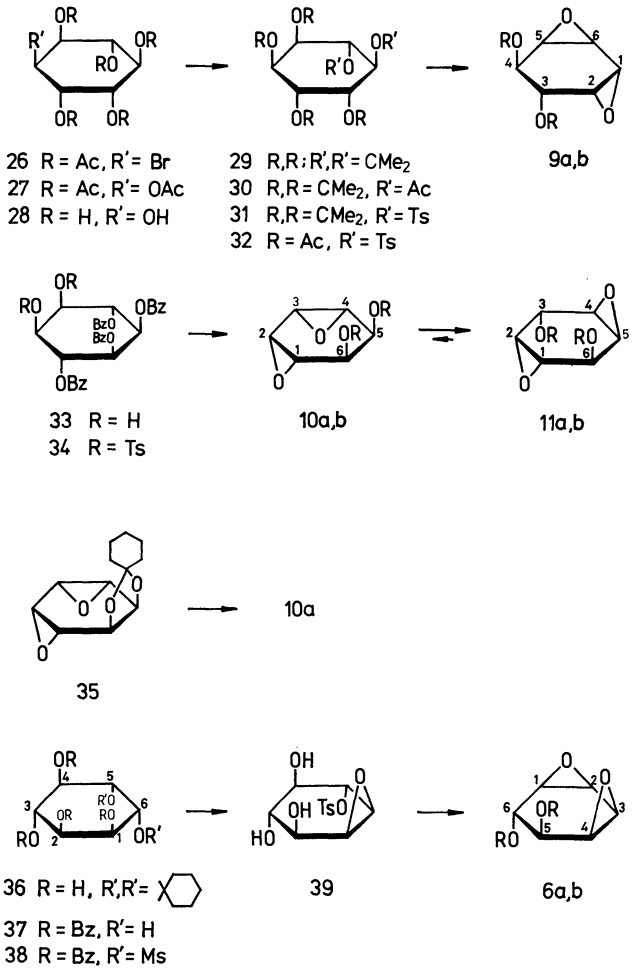

Scheme 4.

1,2: 5,6-Dianhydro-neo-*inositol (9).* Tetra-*O*-acetyl-3,4-di-*O*-tosyl-*chiro*-inositol (**32**), an intermediate compound for **9a**, was synthesized in the following sequences. Penta-*O*-acetyl-1-bromo-1-deoxy-*chiro*-inositol (**26**) derived by bromination of *myo*-inositol with acetyl bromide in acetic anhydride[16] was treated with

sodium acetate in boiling aqueous 2-methoxyethanol to give, after acetylation, hexa-*O*-acetyl-*chiro*-inositol (**27**)[17] in 65% yield. Hydrolysis of **27** with 4 M hydrochloric acid gave *chiro*-inositol (**28**) in 95% yield. Acetonation of **28** by the procedure of Angyal and MacDonald[18] gave the tri-*O*-isopropylidene derivative (**29**) in 30% yield, together with the desired 1,2: 5,6-di-*O*-isopropylidene derivative isolated as the di-*O*-acetyl derivative (**30**) in 18% yield. Compound **30** was *O*-deacylated with sodium methoxide and then tosylated to give the corresponding di-*O*-tosyl derivative (**31**) in 59% yield. On mild acid hydrolysis and successive acetylation **31** gave **32** in 95% yield.

By a similar treatment with sodium methoxide followed by acetylation, **32** gave crystalline di-*O*-acetyl-1,2: 5,6-dianhydro-*neo*-inositol (**9b**) in 48% yield, which was converted into the free diepoxy diol (**9a**) in 35% yield. The ^{1}H NMR spectrum of **9a** contains two-proton doublets of doublets at δ 3.46 and 3.81, and a two-proton singlet at δ 3.94. Characteristic A_2B_2 pattern of the former due to H-1, H-2, H-5, and H-6 supports the assigned structure.

1,2: 3,4-Dianhydro-allo- *(10) and 1,2: 4,5-Dianhydro*-neo-*inositols (11).* A similar epoxidation of tetra-*O*-benzoyl-1,2-di-*O*-tosyl-*muco*-inositol (**34**) derived from the corresponding tetra-*O*-benzoyl derivative (**33**)[19] is considered to afford **10a** and **11a**. However, the equilibrium between **10a** and **11a** in basic media was found to shift almost completely to the latter, **34** giving on epoxidation **11a** as the sole product in 39% yield. The ^{1}H NMR spectrum of **11a** showed three two-proton multiplets at δ 3.26, 3.47, and 4.47.

Preparation of **10a** was accomplished by mild acid hydrolysis of 1,2: 3,4-dianhydro-5,6-*O*-cyclohexylidene-*allo*-inositol (**35**).[11] When **10a** and **11a** were dissolved in 0.1 M methanolic sodium methoxide, respectively, only **10a** was detected in both reaction mixture at ambient temperature. This established the proposed structures of **10a** and **11a**. Compound **10a** showed, in the ^{1}H NMR spectrum, three two-proton multiplets at δ 3.31, 3.68, and 3.95.

1,2: 3,4-Dianhydro-epi-*inositol (6).* Tetra-*O*-benzoyl-1,2-di-*O*-mesyl-*chiro*-inositol (**38**) was prepared from 1,2-*O*-cyclohexylidene-*chiro*-inositol (**36**)[19] by benzoylation and removal of cyclohexylidene group followed by mesylation. Epoxidation between C-1 and C-6 of **38** was assumed to occur first, since the 6-OH and 1-OTs groups are located in diaxial positions in the favored conformation. In order to obtain **6a**, conditions for the next epoxidation should be carefully selected in order to suppress the epoxide migration to **5a**.

First, **38** was treated with 1.1 molar equiv. of sodium methoxide for the conversion into monoepoxide (**39**) which was then, without further purification, passed through a short column of Amberlite IRA-400 (OH^-) in a methanol solution several times until **39** disappeared in the effluent, subjected to monitoring by TLC. The crude product thus obtained consists of **6a** and a trace of **5a**, which were separated by column chromatography to give **6a** in 25% yield. Treatment of **6a** with sodium methoxide gave exclusively **5a**. The ^{1}H NMR spectrum of **6a** revealed two one-proton doublets of doublets at δ 3.69 and 4.12 attributable to H-5 and H-6, indicating that **6a** has an unsymmetric structure.

Experimental

All the compounds treated were racemic except for meso compounds. Diepoxy diols **1**, **3**, **6**, **9**, and **11** were synthesized as racemates. All the formulas depict one enantiomer of the respective racemates.

Unless otherwise stated, melting points were determined on a Mitamura Riken micro hot stage and are uncorrected. Solutions were evaporated under reduced pressure at 40—50 °C. IR spectra were determined for potassium bromide disks with a JASCO IR-E spectrophotometer. ^{1}H NMR spectra were measured at 60 MHz on a Varian A-60D spectrometer in deuteriochloroform ($CDCl_3$) or deuterium oxide (D_2O) with reference to tetramethylsilane or sodium 4,4-dimethyl-4-silapentane-1-sulfonate, respectively, as an internal standard, the peak positions being given in terms of δ. Values given for chemical shifts and coupling constants are of first-order. TLC was performed on silica gel (Wakogel B 10, Wako Pure Chemical Industries, Ltd.) using benzene–ethyl acetate (1: 2, v/v) as an eluent unless otherwise stated. Column chromatography was carried out on Wakogel C-200.

The synthetic reactions were not always conducted under optimum conditions. The isolated yields of the pure diepoxy diols are given for all cases.

1,2: 5,6-Dianhydro-chiro- *(1a) and 1,2: 4,5-Dianhydro*-muco-*inositols (2a).* *a)*: To a solution of tetra-*O*-acetyl-1,3-di-*O*-tosyl-*myo*-inositol (**12**)[8] (5 g) in a mixture of chloroform (50 ml) and methanol (40 ml) was added 1 M methanolic sodium methoxide (24 ml, 3 molar equiv.) and the mixture was allowed to stand at ambient temperature overnight. TLC indicated the formation of two major components (R_f 0.3 and 0.1) and one minor component (R_f 0.15). The reaction mixture was filtered in order to remove sodium *p*-toluenesulfonate precipitated, the filtrate being evaporated to dryness. The syrupy residue was dissolved in methanol (10 ml), mixed with silica gel (5 g), and the mixture was thoroughly dried with a rotary evaporator. The powder obtained was then transfered to the top of a silica-gel column (70 g) packed with benzene–ethyl acetate (1: 2, v/v), which was eluted with the same solvent system. Three fractions were separated according to examination by TLC. The faster-moving component (R_f 0.3) was obtained as a homogeneous syrup (**1a**) by removal of the solvent. The syrupy **1a** was treated with acetic anhydride (5 ml) in pyridine (10 ml) at ambient temperature overnight. The mixture was poured into ice–water (100 ml) and extracted with chloroform (3×20 ml). The extracts were washed with 1M hydrochloric acid, 10% aqueous sodium carbonate, and water, successively, and dried over anhydrous sodium sulfate. The solution was evaporated to give crystals which were recrystallized from chloroform–ethanol to give the diacetate (**1b**, 0.36 g, 21%) as rods, mp 125—127 °C.

Found: C, 52.58; H, 5.14%. Calcd for $C_{16}H_{12}O_6$: C, 52.63; H, 5.30%.

The second fraction consisting mainly of a minor component (R_f 0.15) did not crystallize and its characterization was not attempted.

The third fraction gave crystals which were recrystallized from methanol to give **2a** (0.17 g, 15%) as rods, mp 169—171 °C.

Found: C, 50.17; H, 5.51%. Calcd for $C_6H_8O_4$: C, 50.00; H, 5.60%.

Acetylation of **2a** (60 mg) as described for **1b** gave, after

crystallization from ethanol, the diacetate (**2b**, 58 mg, 76%) as plates, mp 108—109.5 °C.

Found: C, 52.90; H, 5.02%.

b): Compound **12** (2.5 g) was treated with sodium methoxide as described above. The crude product was shown by TLC to be a *ca.* 1:1 mixture of **1a** and **2a**. It was acetylated in the usual manner to give a crystalline mixture (0.33 g, 37%), which was found to be a 4:5 mixture of **1b** and **2b** estimation of the relative intensity of each acetyl signals in the ^{1}H NMR spectrum.

1,2: 5,6-Dianhydro-allo- *(3a)*, *1,2: 4,5-Dianhydro*-epi- *(4a)*, *and 2,3:5,6-Dianhydro*-allo-*inositols (5a)*. To a solution of tetra-*O*-acetyl-1,4-di-*O*-tosyl-*myo*-inositol (**13**)[11] (10 g) in a mixture of chloroform (100 ml) and methanol (80 ml) was added 1 M methanolic sodium methoxide (40 ml, 2.5 molar equiv.), and the mixture was allowed to stand at ambient temperature overnight. TLC showed the formation of three components: R_f 0.18, 0.15, and 0.05. The reaction mixture was processed as described in the epoxidation of **12** and the products were separated in a similar way by chromatography on silica gel with benzene–ethyl acetate (1:1, v/v) as an eluent. Three fractions were obtained. The first fraction gave crystals which were recrystallized from ethanol to give **3a** (0.48 g, 23%) as rods, mp 78—79 °C.

Found: C, 50.38; H, 5.60%.

Compound **3a** (80 mg) was acetylated in the usual way and the product was recrystallized from ethanol to give the diacetate (**3b**, 0.12 g, 90%) as plates, mp 121—121.5 °C.

Found: C, 52.60; H, 5.09%.

The second fraction gave crystals which were recrystallized from ethanol–ether to give **5a** (0.34 g, 15%) as needles, mp 75—76 °C. From the mother liquor, the second crop was obtained as prisms, mp 91—93 °C, weighing 0.13 g (total yield, 21%). These two dimorphic crystals were found to be identical by ^{1}H NMR spectroscopy.

Found: C, 50.16; H, 5.83%.

Acetylation of **5a** (0.18 g) gave, after recrystallization from ethyl acetate, the diacetate (**5b**, 0.22 g, 77%) as rods, mp 110—111.5 °C.

Found: C, 52.66; H, 5.02%.

The third fraction gave crystals which were recrystallized from ethanol to give **4a** (0.18 g, 8%) as plates, mp 124—124.5 °C.

Found: C, 50.42; H, 5.65%.

Acetylation of **4a** (24 mg) gave, after recrystallization from ethanol, the diacetate (**4b**, 28 mg, 73%), mp 136 °C.

Found: C, 52.47; H, 5.07%.

Compound **3a**, as well as **4a**, gave by TLC a *ca.* 3:2 mixture of **3a** and **4a** on treatment with methanolic sodium methoxide. Compound **5a**, however, remained unchanged under similar conditions.

O-Decyclohexylidenation of 1,2: 5,6-Dianhydro-3,4-O-cyclohexylidene-allo-*inositol (14)*.[12] A mixture of **14** (1 g) and 20% aqueous acetic acid (50 ml) was heated under reflux for 0.5 h. After having been cooled, the solution was neutralized with 5% aqueous sodium hydroxide and then evaporated to dryness. The residue was extracted with ethanol (50 ml) and the extract was concentrated to one half volume. TLC indicated the formation of **3a**, together with several minor components, but none of **4a**. The solution was filtered and the filtrate was chromatographed on silica gel (30 g) with benzene–ethyl acetate (1:2, v/v) as an eluent. The main fraction gave a syrup, which crystallized from methanol to give **3a** (0.24 g, 37%), mp 75—77 °C, identical with the compound obtained before.

1,2:3,4- (7a) and 1,2: 4,5-Dianhydro-cis-*inositols (8a)*. *a)*: 1,2,5-Tri-*O*-acetyl-3-*O*-benzoyl-4,6-di-*O*-tosyl-*myo*-inositol (**15**)[13] (3 g) was treated with 1 M methanolic sodium methoxide (11 ml, 2.5 molar equiv.) in a mixture of chloroform (18 ml) and methanol (12 ml) at ambient temperature overnight. TLC showed the formation of three components: one minor (R_f 0.2) and two major components (R_f 0.16 and 0.06). The reaction mixture was processed similarly and the products were fractionated as described in the separation of **1a** and **2a**. The faster-moving component, 2,3-anhydro-6-*O*-tosyl-*allo*-inositol (**17**), was obtained as needles (59 mg, 4.4%), mp 155—156 °C, after crystallization from ethanol–ether. ^{1}H NMR (D_2O): δ 2.47 (3H, s, tosyl CH_3), 3.8—4.4 (6H, m, methine protons).

Found: C, 49.65; H, 5.46%. Calcd for $C_{13}H_{16}O_7S$: C, 49.35; H, 5.11%.

The second fraction was evaporated and the residue was crystallized from ethanol–ether to give **7a** (26 mg, 4.3%) as needles, mp 103—104 °C.

Found: C, 50.00; H, 5.33%.

Acetylation of **7a** (25 mg) gave, after crystallization from ethanol, the diacetate (**7b**, 32 mg, 81%) as needles, mp 142.5—144 °C.

Found: C, 52.89; H, 5.12%.

The third fraction gave crystals which were recrystallized from methanol–ether to give **8a** (0.22 g, 37%) as plates, mp 178—180 °C.

Found: C, 50.39; H, 5.72%.

Acetylation of **8a** (24 mg) gave, after recrystallization from ethanol, the diacetate (**8b**, 24 mg, 63%) as plates, mp 153—154 °C.

Found: C, 52.86; H, 5.14%.

Compound **17** was found by TLC to be selectively converted into **8a** on treatment with methanolic sodium methoxide.

b): 1-*O*-Benzoyl-4,6-di-*O*-tosyl-*myo*-inositol (**16**)[13] (0.8 g) was treated similarly with 1 M methanolic sodium methoxide (3.4 ml, 2.5 molar equiv.) in a mixture of butanone (50 ml) and methanol (50 ml) at ambient temperature overnight. TLC indicated the formation of **7a** (R_f 0.2), together with traces of **8a** and **17**. The products were fractionated by chromatography on silica gel to give **7a** (70 mg, 36%), mp 101.5—103 °C.

The same results as described in (a) were obtained when **15** was treated with methanolic sodium methoxide in the solvent used for the epoxidation of **16**.

Tetra-O-acetyl-3,6-di-O-tosyl-muco-*inositol (19)*. 3,6-Di-*O*-tosyl-*muco*-inositol[15] (0.2 g) was treated with acetic anhydride (2 ml) in pyridine (2 ml) at ambient temperature overnight. The reaction mixture was poured into ice–water and the resulting crystals were recrystallized from chloroform–ethanol to give **19** (0.26 g, 96%) as plates, mp 189—190 °C.

Found: C, 51.41; H, 5.03; S, 9.97%. Calcd for $C_{28}H_{32}O_{14}S_2$: C, 51.20; H, 4.91; S, 9.77%.

Reaction of 19 with Sodium Methoxide. Compound **19** (7 g) was treated with 1 M methanolic sodium methoxide (28 ml, 2.5 molar equiv.) in a mixture of chloroform (100 ml) and methanol (80 ml) at ambient temperature overnight. TLC showed the formation of one major component (R_f 0.06) and one minor one (R_f 0.11). The reaction mixture was processed similarly and the products were separated by chromatography on silica gel to give **8a** (0.55 g, 36%), mp 178—180 °C, as the main product. The minor component was obtained as needles (16 mg), mp 157—159 °C, after crystallization from ethanol; the IR spectrum showed no absorption in the region of tosyloxyl function. No further characterization was carried out owing to a minute amount.

Reaction of Tri-O-acetyl-1,4,6-tri-O-tosyl-myo-*inositol (20)*[11] *and Its O-Deacetylated Derivative (21)*[11] *with Sodium Methoxide.*

a): Compound **20** (0.3 g) was treated with 1 M methanolic sodium methoxide (0.33 ml, 2.5 molar equiv.) in a mixture of chloroform (10 ml) and methanol (2 ml) at ambient temperature overnight. TLC indicated the formation of one major component and one minor one. The reaction mixture was evaporated and the residue was extracted with hot ethyl acetate (3×10 ml). The extracts were evaporated and the residue was crystallized from chloroform–ethanol to give 1,2: 3,4-dianhydro-5-*O*-tosyl-*cis*-inositol (**22**, 59 mg, 50%) as plates, mp 176—177 °C.

Found: C, 52.76; H, 4.99; S, 10.36%. Calcd for $C_{13}H_{14}O_6S$: C, 52.32; H, 4.73; S, 10.75%.

Acetylation of **22** (40 mg) gave, after crystallization from chloroform–ethanol, the acetate (**23**, 36 mg, 79%) as needles, mp 173—174 °C. ^{1}H NMR ($CDCl_3$) δ 2.05 (3H, s, OAc), 2.47 (3H, s, tosyl CH_3), 3.25 (2H, m) and 3.43 (2H, m) (H-1, H-2, H-3, and H-4), 5.12 (2H, m, H-5 and H-6).

Found: C, 52.69; H, 4.74; S, 9.73%. Calcd for $C_{15}H_{16}O_7S$: C, 52.91; H, 4.74; S, 9.42%.

b): Compound **21** (0.5 g) was treated with 1 M methanolic sodium methoxide (1.5 ml, 2.5 molar equiv.) in a mixture of butanone (30 ml) and methanol (10 ml) at ambient temperature overnight. TLC indicated the formation of one major component, together with a trace of **22**. The reaction mixture was worked up as described above and the product was crystallized from ethanol–ether to give 1,2-anhydro-5,6-di-*O*-tosyl-*epi*-inositol (**24**, 90 mg, 25%) as prisms, mp 167—168 °C.

Found: C, 51.29; H, 4.79; S, 13.62%. Calcd for $C_{20}H_{22}O_9S_2$: C, 51.05; H, 4.72; S, 13.64%.

Acetylation of **24** (40 mg) gave, after crystallization from ethanol, the diacetate (**25**, 47 mg, 99%) as plates, mp 159—159.5 °C. ^{1}H NMR ($CDCl_3$) δ 2.05 (6H, s, two OAc), 2.49 (6H, s, two tosyl CH_3), 3.35 (1H, m, H-2), 3.45 (1H, d, $J_{1,2}$=3.5 Hz, H-1), 4.58 (1H, dd, $J_{4,5}$=2.5 Hz, $J_{5,6}$=9 Hz, H-5).

Found: C, 52.00; H, 4.72; S, 11.59%. Calcd for $C_{24}H_{26}O_{11}S_2$: C, 51.97; H, 4.73; S, 11.56%.

chiro-*Inositol (28)*. Penta-*O*-acetyl-1-bromo-1-deoxy-*chiro*-inositol (**26**, 2.3 g), mp 114—116 °C, prepared by the modified method of McCasland and Horswill,[16] was treated with anhydrous sodium acetate (2.3 g) in boiling 90% aqueous 2-methoxyethanol (30 ml) for 18 h. The reaction mixture was evaporated to dryness and the residue was treated with acetic anhydride (10 ml) and pyridine (10 ml) at ambient temperature overnight. The reaction mixture was filtered to remove an insoluble matter. The filtrate was evaporated to give a syrup, which was purified by passing through a short alumina column with ethyl acetate. The eluate was evaporated and the syrupy product was crystallized from ethanol to give hexa-*O*-acetyl-*chiro*-inositol (**27**, 1.43 g, 65%) as crystals, mp 110—112 °C (lit,[16] 110—111 °C).

Compound **27** (5.6 g) was treated with boiling 4 M hydrochloric acid (100 ml) for 2.5 h. The reaction mixture was evaporated and the residue was crystallized from ethanol to give **28** (2.2 g, 95%) as crystals, mp 245—246 °C (lit,[16] 243 °C).

Acetonation of 28. The reaction was carried out following the method of Angyal and MacDonald.[18] A mixture of finely powdered **28** (2 g), anhydrous zinc chloride (10 g), acetic acid (10 ml), and acetone (80 ml) was heated under reflux for 5.5 h. Pyridine (20 ml) was added to the cooled mixture, and the precipitates were removed by filtration and washed with chloroform (30 ml). The filtrate and washings were combined and evaporated to dryness. The residue was treated with acetic anhydride (10 ml) and pyridine (10 ml) and the reaction mixture was worked up by the usual method. The product was crystallized from ethanol to give 1,2: 3,4: 5,6-tri-*O*-isopropylidene-*chiro*-inositol (**29**, 0.99 g, 30%) as plates, mp 140 °C.

Found: C, 60.30; H, 8.05%. Calcd for $C_{15}H_{24}O_6$· C, 60.00; H, 8.05%.

The mother liquor of **29** was evaporated and the residue was crystallized from ethanol to give 3,4-di-*O*-acetyl-1,2: 5,6-di-*O*-isopropylidene-*chiro*-inositol (**30**, 0.69 g, 18%) as needles, mp 111—112 °C. ^{1}H NMR ($CDCl_3$) δ 1.21 (3H, s) and 1.55 (3H, s) (isopropylidene CH_3), 2.06 (6H, s, two OAc), 5.06 (2H, dd, J=3 and 5 Hz, H-3 and H-4).

Found: C, 56.04; H, 6.84%. Calcd for $C_{16}H_{24}O_8$: C, 55.80; H, 7.04%.

Tetra-O-*acetyl-3,4-di*-O-*tosyl*-chiro-*inositol (32)*. Compound **30** (0.65 g) was treated with a catalytic amount of methanolic sodium methoxide in a mixture of chloroform (5 ml) and methanol (5 ml) at ambient temperature overnight. The mixture was evaporated to dryness and the residue was treated with tosyl chloride (2.9 g) in pyridine (10 ml) at 40 °C for four days. The reaction mixture was poured into ice–water, and the resulting crystals were collected and recrystallized from chloroform–ethanol to give 1,2: 5,6-di-*O*-isopropylidene-3,4-di-*O*-tosyl-*chiro*-inositol (**31**, 0.63 g, 59%) as plates, mp 174—176 °C. ^{1}H NMR ($CDCl_3$) δ 1.24 (3H, s) and 1.44 (3H, s) (isopropylidene CH_3), 2.45 (6H, s, two tosyl CH_3), 4.63 (2H, m, J=2.5 and 4 Hz, H-3 and H-4).

Found: C, 54.92; H, 5.86; S, 11.23%. Calcd for $C_{26}H_{32}O_{10}S_2$: C, 54.91; H, 5.68; S, 11.27%.

Compound **31** (0.55 g) was treated with 50% aqueous acetic acid (20 ml) at reflux for 2 h. The reaction mixture was evaporated to dryness and the residue was acetylated in the usual way. The product was recrystallized from chloroform–ethanol to give **32** (0.6 g, 94%) as needles, mp 216—216.5 °C.

Found: C, 51.48; H, 5.12; S, 9.74%. Calcd for $C_{28}H_{22}O_{14}S_2$: C, 51.20; H, 4.91; S, 9.77%.

1,2: 5,6-Dianhydro-neo-*inositol (9a)*. Compound **32** (0.5 g) was treated with 1 M methanolic sodium methoxide (2 ml, 2.5 molar equiv.) in a mixture of chloroform (10 ml) and methanol (5 ml) at ambient temperature overnight. The reaction mixture was evaporated and the residue was acetylated in the usual manner. The product was crystallized from ethanol to give the diacetate (**5b**, 83 mg, 48%), mp 96—97 °C.

Found: C, 52.94; H, 5.47%.

Compound **5b** (80 mg) was treated with a catalytic amount of methanolic sodium methoxide in methanol (4 ml) and the mixture was then treated with Amberlite IR-120 (H^+) and evaporated to dryness. The residue was crystallized from ethanol–ether to give **5a** (18 mg, 35%) as plates, mp 121.5—122.5 °C.

Found: C, 49.88; H, 5.73%.

1,2,3,6-Tetra-O-*benzoyl-4,5-di*-O-*tosyl*-muco-*inositol (34)*. 1,2,3,4,6-Tetra-*O*-benzoyl-*muco*-inositol (**33**)[19] (4 g) was treated with tosyl chloride (6.6 g, 5 molar equiv.) in pyridine (100 ml) at ambient temperature for 2 days. The reaction mixture was poured into ice–water and the precipitates were recrystallized from chloroform–ethanol to give **34** (5.6 g, 93%), mp 194—195 °C. ^{1}H NMR ($CDCl_3$): δ 2.32 (6H, s, two tosyl CH_3).

Found: C, 63.96; H, 4.59; S, 6.69%. Calcd for $C_{48}H_{40}O_{14}S_2$: C, 63.71; H, 4.46; S, 7.09%.

1,2: 4,5-Dianhydro-neo-*inositol (11a)*. Compound **34** (7 g) was treated with 1 M methanolic sodium methoxide (20 ml, 2.5 molar equiv.) in a mixture of chloroform (40 ml) and methanol (50 ml) at ambient temperature overnight. The reaction mixture was worked up similarly and the product was purified by chromatography on silica gel with benzene–

ethyl acetate (1: 1, v/v) as an eluent. The product was crystallized from ethanol to give **11a** (0.44 g, 39%) as plates, mp 150—151 °C. Found: C, 50.30; H, 5.83%.

Compound **11a** (0.1 g) was converted into the diacetate (**11b**, 0.12 g, 83%) as plates, mp 138—139 °C, crystallized from ethanol. Found: C, 52.98; H, 5.14%.

1,2: 3,4-Dianhydro-allo-*inositol (10a)*. 1,2: 3,4-Dianhydro-5,6-*O*-cyclohexylidene-*allo*-inositol (**35**)[12] was prepared in an improved yield (80%) from 1,2-*O*-cyclohexylidene-3,5-di-*O*-tosyl-*myo*-inositol by treatment with 2.5 molar equiv. of methanolic sodium methoxide in boiling 2-methoxyethanol. Compound **35** (1.2 g) was treated with boiling 20% aqueous acetic acid (50 ml) for 45 min. The reaction mixture was then processed as described in the preparation of **3a**. The crude product was purified by chromatography on silica gel with benzene–ethyl acetate (1: 2, v/v) as an eluent and crystallized from ethanol–ether to give **10a** (0.23 g, 30%) as crystals, mp 105—106 °C. Found: C, 50.22; H, 5.53%.

On acetylation, **10a** was converted into the syrupy diacetate (**10b**, 52 mg, 87%). Compound **10a** was found by TLC to give **11a** exclusively on treatment with methanolic sodium methoxide.

1,2,3,4-Tetra-O-*benzoyl*-chiro-*inositol (37)*. 1,2-*O*-Cyclohexylidene-*chiro*-inositol (**36**)[19] (0.1 g) was treated with benzoyl chloride (0.41 ml, 12 molar equiv.) in pyridine (10 ml) at ambient temperature overnight. The reaction mixture was poured into ice–water to give crude tetra-*O*-benzoyl derivative as a white powder. It was treated with boiling 80% aqueous acetic acid (20 ml) for 2 h. The product was purified by chromatography on silica gel with butanone–toluene (1: 5, v/v) as an eluent. The main fraction gave crystals which were recrystallized from ethyl acetate–petroleum ether to give **37** (0.17 g, 72%) as needles, mp 148—150 °C.

Found: C, 68.26%; H, 4.82%. Calcd for $C_{34}H_{28}O_{10}$: C, 68.47; H, 4.73%.

1,2,3,4-Tetra-O-*benzoyl-5,6-di*-O-*mesyl*-chiro-*inositol (38)*.

a): Compound **37** (0.1 g) was treated with mesyl chloride (0.1 ml, 8 molar equiv.) in pyridine (5 ml) at ambient temperature overnight. The reaction mixture was poured into ice–water and the precipitates were crystallized from chloroform–ethanol to give **38** (0.07 g, 55%) as crystals, mp 189—191 °C. ^{1}H NMR ($CDCl_3$): δ 3.04 (3H, s) and 3.36 (3H, s) (mesyl CH_3). Found: C, 57.38; H, 4.35; S, 8.60%. Calcd for $C_{36}H_{32}O_{14}S_2$: C, 57.34; H, 4.29; S, 8.52%.

b): Compound **36** (1.5 g) was treated with benzoyl chloride (8 ml, 12 molar equiv.) in pyridine (120 ml) at ambient temperature overnight and then at 60 °C for 0.5 h. The mixture was poured into ice–water and the resulting gum was extracted with chloroform. The extract was evaporated to give crude **37** (1.5 g), which was treated successively with boiling 80% aqueous acetic acid and with mesyl chloride (1.1 ml) in pyridine (30 ml) to give crude **38** (3.6 g). Recrystallization from chloroform–ethanol gave pure **38** (3.1 g, 72% yield based on **36** used), mp 189—191 °C.

1,2: 3,4-Dianhydro-epi-*inositol (6a)*. A solution of **38** (1.04 g) in a mixture of chloroform (15 ml) and methanol (20 ml) was treated with 1 M methanolic sodium methoxide (1.6 ml, 1.1 molar equiv.) at ambient temperature overnight. TLC showed the formation of one major component (R_f 0.07) and one minor one (R_f 0.12). The reaction mixture was evaporated to dryness and the residue was dissolved in methanol (30 ml) and treated with Amberlite MB-3. The solution was evaporated to give a crude monoepoxide (**39**), which was without further purification dissolved in methanol (30 ml). The solution was passed through a short column of Amberlite IRA-400 (OH^-) several times until **39** disappeared in the effluent subjected to monitoring by TLC. TLC showed the formation of one major component (R_f 0.12) and two minor ones (R_f 0.15 and 0.07). The mixture was fractionated by chromatography on silica gel with benzene–ethyl acetate (1: 2, v/v) as an eluent. The first fraction gave a small amount of syrup, which crystallized to give **5a**, mp 108—110 °C, identical with the compound obtained before. The second fraction gave crystals, which were recrystallized from ethanol to give **6a** (49 mg, 25%) as plates, mp 132—134 °C.

Found: C, 50.14; H, 5.62%.

Acetylation of **6a** gave a syrupy diacetate **6b**.

Compound **6a** was shown by TLC to give **5a** exclusively on treatment with methanolic sodium methoxide.

The authors wish to thank Mr. Shukichi Muto for assistance in preparative experiments. Thanks are due to Mr. Saburo Nakada for elemental analyses.

References

1) For preliminary account see T. Suami, S. Ogawa, and S. Oki, *Chem. Lett.*, **1973**, 901. Part 10 of this series: *Bull. Chem. Soc. Jpn.*, **50**, 1867 (1977).

2) S. M. Kupchan, R. J. Hemingway, P. Coggon, A. T. McPhail, and G. A. Sim, *J. Am. Chem. Soc.*, **90**, 2982 (1968).

3) S. Takahashi, *Phytochemistry*, **8**, 321 (1969).

4) D. B. Border, R. Shu, and J. E. Lancaster, *J. Am. Chem. Soc.*, **94**, 2540 (1972).

5) D. R. Thakker, W. Levin, A. W. Wood, A. H. Conney, T. A. Stoming, and D. M. Jerina, *J. Am. Chem. Soc.*, **100**, 645 (1978) and references cited therein.

6) The nomenclature used in this paper is based on the IUPAC-IUB Tentative Cyclitol Nomenclature Rule [*J. Biol. Chem.*, **22**, 5809 (1968)]. Either the anhydroinositol- or dianhydrocyclohexanehexol-system can designate the configuration of the sixteen isomers of diepoxy diol fairly unambiguously.

7) After the present work had been accomplished, Prinzbach and Schneider reported the synthesis of **6a** from "*cis*-benzene–trioxide:" H. Prinzbach and H-Walter Schneider, *Tetrahedron Lett.*, **35**, 3037 (1975).

8) S. J. Angyal, P. T. Gilham, and G. J. H. Melrose *J. Chem. Soc.*, **1965**, 5252: T. Suami, S. Ogawa, and S. Oki, *Bull. Chem. Soc. Jpn.*, **44**, 2820 (1971).

9) S. J. Angyal and P. T. Gilham, *J. Chem. Soc.*, **1957**, 3691.

10) F. Sweet and R. K. Brown, *Can. J. Chem.*, **46**, 1431 (1968).

11) T. Suami, S. Ogawa, T. Tanaka, and T. Otake, *Bull. Chem. Soc. Jpn.*, **44**, 835 (1971).

12) T. Suami, S. Ogawa, S. Oki, and K. Ohashi, *Bull. Chem. Soc. Jpn.*, **45**, 2597 (1972).

13) T. Suami, S. Ogawa, K. Ohashi, and S. Oki, *Bull. Chem. Soc. Jpn.*, **45**, 3660 (1972).

14) Although **15** was found by TLC to give mainly a *ca.* 2: 3 mixture of **7a** and **8a** on treatment with base, the isolated yield of pure **7a** was comparatively low because of contamination with an unknown by-product showing a similar mobility on TLC.

15) Compound **19** was prepared by acetylation of 3,6-di-*O*-tosyl-*muco*-inositol: T. Suami, S. Ogawa, H. Uchino, and M. Uchida, *Bull. Chem. Soc. Jpn.*, **46**, 3840 (1973).

16) G. E. McCasland and E. C. Horswill, *J. Am. Chem. Soc.*, **75**, 4020 (1953).

17) M. Nakajima, B. Tomida, N. Kurihara, and S. Takei, *Chem. Ber.*, **92**, 173 (1959).

18) S. J. Angyal and C. G. MacDonald, *J. Chem. Soc.*, **1952**, 686.

19) S. Ogawa, S. Oki, H. Kunitomo, and T. Suami, *Bull. Chem. Soc. Jpn.*, **50**, 1867 (1977).

On the Behavior of Sulfonyl Imide as a Reactive Intermediate. The Reaction with Enamines

Toshikazu NAGAI, Tadao SHINGAKI,* Masao INAGAKI, and Tetsuya OHSHIMA

College of General Education, Osaka University, Toyonaka, Osaka 560

(Received March 30, 1978)

The reactions of *N*-alkylsulfamoyl chloride with enamines in the presence of triethylamine showed the presence of *N*-alkylsulfonyl imide ($RN{=}SO_2$) as a reaction intermediate to give either acyclic (sulfonamides) or cyclic products (1,2-thiazetidine 1,1-dioxides), depending upon the enamines used. The enamines leading to the acyclic products possess either a methylene group on the α-carbon or a hydrogen on the β-carbon of the enamine; the enamine leading to the cyclic product has no such available hydrogen atom. It is thought that the products are formed *via* a zwitter ionic intermediate provided by the electrophilic attack of the sulfonyl imide sulfur atom on the β-carbon atom of the enamine.

Sulfonyl imides,[1] $RN{=}SO_2$, are isoelectronic with sulfur trioxide and sulfenes, and are located between sulfenes and sulfur trioxide in regard to the electronegativities of the elements adjacent to the reaction centers. An attractive sulfonyl imide synthesis was

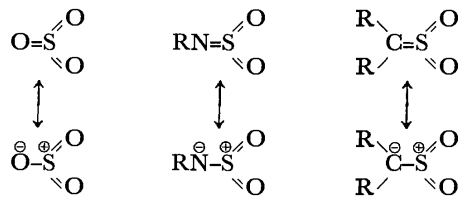

achieved by Burgess[2] in 1967, though the imide had been proposed as an intermediate in the photolysis of benzenesulfonyl azide.[3] Dehydrohalogenation of ethylsulfamoyl chloride by triethylamine at −78 °C led to the generation of *N*-ethylsulfonyl imide, whose interception was accomplished by the addition of aniline to give the sulfamide. *N*-Ethylsulfonyl imide, furthermore, was found to react with strongly nucleophilic olefins such as 2-(dichloromethylene)-1,3-dioxolane[2] and the pyrrolidine enamine of isobutyraldehyde[4] to afford cycloadducts. In this study on sulfonyl imides, the reaction of alkylsulfonyl imides with enamines give acyclic or cyclic adducts depending on the type of the enamine used, and the sulfonyl imides undergo oligomerization in the presence of less nucleophilic olefins or in the absence of the substrates.

Results and Discussion

The reactions of *N*-alkylsulfonyl imide (**2**) with three types of enamines (Types A, B, and C) were conducted.

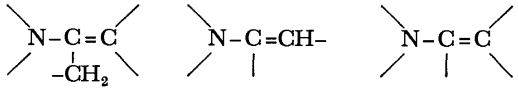

Type A Type B Type C

Reaction of 2 with Type A Enamine. A solution of an alkylsulfamoyl chloride (**1**) in tetrahydrofuran (THF) was added dropwise with stirring to a solution of 1-morpholinocyclohexene (**3**) and triethylamine in THF at −78 °C. Triethylamine hydrochloride was formed nearly quantitatively and removed by filtration. Treatment of the filtrate afforded a colorless crystalline compound characterized not as 1-alkylsulfamoyl-2-morpholinocyclohexene (**4'**) but as the 3-alkylsulfamoyl isomer (**4**) in about 60% yield.

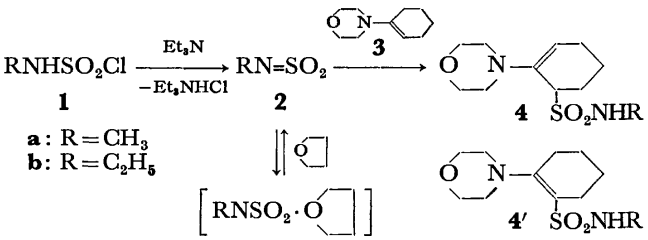

The structure of **4** was established by IR, NMR, and mass spectra analyses (experimental section). Subsequently, a THF solution of triethylamine was added dropwise to a stirred THF solution of **1** at −78 °C. After the removal of the amine hydrochloride at −78 °C, the addition of **3** to the filtrate (maintained at the same temperature) led to **4**, the yield of which varied with the age of the filtrate. These results suggest the intermediacy of *N*-alkylsulfonyl imide (**2**), which may be stabilized in a mode similar to the THF complex of *N*-methoxycarbonyl imide.[5]

The addition of 2-morpholino-1,3-diphenylpropene (**5**) to a THF solution of **2a** at −78 °C produced 3-methylsulfamoyl-2-morpholino-1,3-diphenylpropene (**6a**) rather than the isomeric sulfonamide **6'**, **6a** was isolated in a 26% yield together with *N,N'*-dimethylsulfamide (**7a**) in a 65% yield. When **1a** was added to a mixture of **5** and triethylamine in THF at an elevated temperature, 20 °C, the yield of **6a** increased to 67% and that of **7a** decreased to 7%. In the same manner,

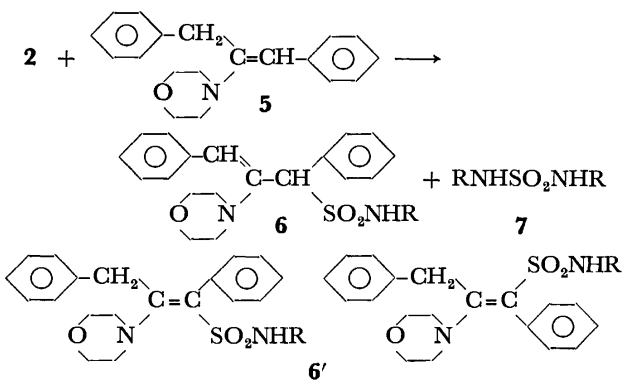

6b was given in a 68% yield from **1b** at 20 °C. That **5** is less reactive than **3** is interpreted in terms of a smaller nucleophilic character due to the phenyl ring on the enamine double bond.

Reaction of 2 with Type B Enamine. The reaction of **2** with either (*E*)-β-morpholinostyrene (**8**) or (*E*)-morpholinostilbene (**10**) provided the 1-alkylsulfamoyl-2-morpholinoethylene derivative (**9** or **11**) in a moderate yield (**9a**: 46%, **9b**: 58%, **11a**: 47%, **11b**: 56%), at 20 °C. The reaction did not take place at −78 °C. In a similar mode as the reaction with the enamines **3** and **5**, the hydrogen atom β to the morpholino moiety served in the formation of the acyclic products:

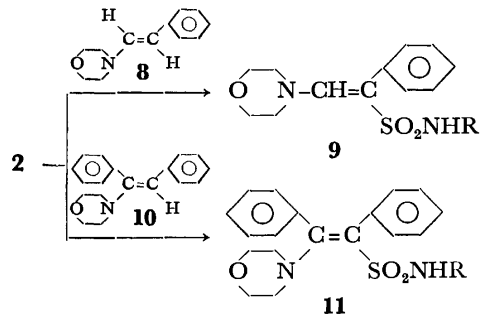

Reaction of 2 with Type C Enamine. From the above results, the cycloadduct formation in reaction of **2** appears to require an enamine having no available hydrogen atom. When **2** was generated at −78 °C in the presence of 2-methyl-1-morpholinopropene (**12**), the expected cycloadduct, 2-alkyl-4,4-dimethyl-3-morpholino-1,2-thiazetidine 1,1-dioxide (**13**) was obtained. Since **13a** and **13b** were very sensitive to moisture,[6] attempts at purification were unsuccessful. The structures of **13** were established on the basis of the IR and NMR spectra and by their subsequent hydrolyses. The IR spectra of **13** showed no ν_{NH} and exhibited ν_{SO_2}

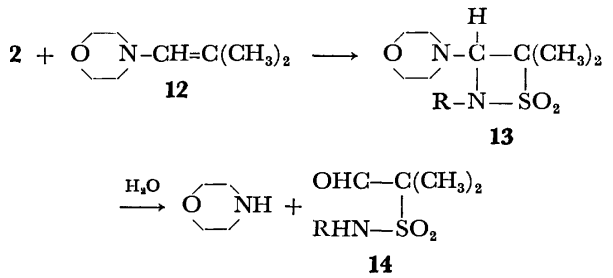

at 1320 and 1125 cm^{-1}. The NMR spectrum ($CDCl_3$, 60 MHz) of **13b** was very similar to that of 4,4-dimethyl-2-ethyl-3-(1-pyrrolidinyl)-1,2-thiazetidine 1,1-dioxide.[4] Chromatographs of **13a** and **13b** over silica gel led to the hydrolyses, giving **14a** and **14b** in 55 and 62% yields respectively.

Reaction Pathway. The reactions of the *N*-alkylsulfonyl imides (**2**) with the enamines provided three kinds of the products, the 3-sulfamoylpropene derivative, the sulfamoylethylene derivative, and the cycloadduct, depending upon the enamine used. The formation of these products can be explained by a mechanism *via* a zwitter ionic intermediate (**15**) shown in Scheme 1.

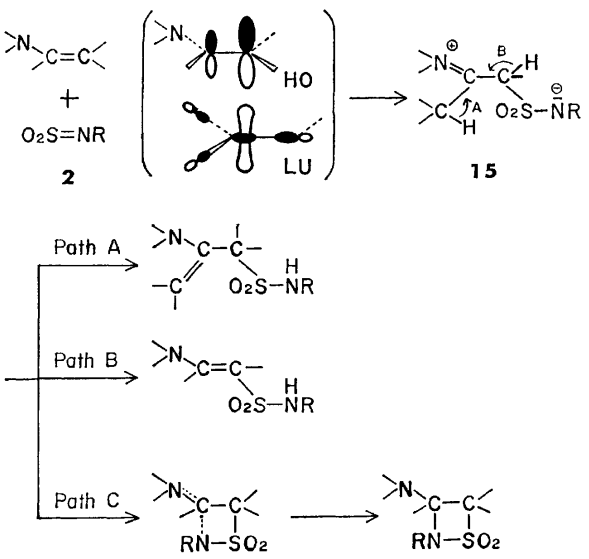

Scheme 1.

The reaction is initiated by an electrophilic attack of the sulfur atom of the sulfonyl imide on the β-carbon of the enamines, leading to **15**. In the cases of Type A and B enamines, prototropy followed by the formation of a new olefinic linkage (Path A) or prototropy followed by the reformation of the olefinic linkage (Path B) takes place to give the corresponding acyclic products. In the reaction with Type A enamine, the exclusive formation of the sulfonamide **4** or **6** which arises from the proton transfer of the methylene, instead of the isomeric sulfonamide **4′** or **6′** ascribable to the transfer of the olefinic proton, may be considered as follows: Both the sulfonamides **4′** and **6′** are destabilized by the steric inhibition of the resonance involving the nitrogen lone pair and the double bond.[9] On the other hand, the zwitter ionic intermediate resulting from the Type C enamine affords the cyclic adduct since there is no mobile proton (Path C).

As an alternative mechanism, the formation of the cycloadduct may be envisaged as resulting from a concerted thermal [$_\pi 2_s + _\pi 2_a$] process.[10] However, in the cycloaddition of *N*-methoxycarbonylsulfonyl imide with variously substituted alkenes to afford the corresponding 1,2-thiazetidines and 2,3-dihydro-1,4,5-oxathiazines, the one-step multi-center cycloaddition has not been accepted on the basis of the adduct distribution with solvent change.[5] Moreover, the addition of sulfene, which closely resembles sulfonyl imide, to enamines has been explained not by a concerted mechanism but by a nonconcerted process on the basis of the stereoselectivity of the cycloaddition and of the product distribution between the cyclic and acyclic adducts.[9]

Oligomerization of 2. The reaction of **2** with the enamine (**5**) possessing a phenyl ring on the double bond gave dimethylsulfamide (**7**) in a significant yield, especially at low temperatures. A dimer of sulfonyl imide which had failed to react with the enamine present might be subjected to hydrolysis to afford **7** with the loss of sulfuric acid. When **1a** was added dropwise to triethylamine in either benzene or ether in the absence

$$2CH_3NSO_2 \longrightarrow (CH_3NSO_2)_2 \xrightarrow[-H_2SO_4]{2H_2O} CH_3NHSO_2NHCH_3$$

2a **7a**

of enamine followed by chromatography, **7a** was isolated in a 90% yield respectively. Furthermore, the reactions of **2a** with less nucleophilic olefins, *e.g. trans*-stilbene and dimethyl fumarate, in THF gave no adduct, affording the amine hydrochloride in the theoretical amount and an unidentified solid which appears to be a polymerization product of **2a**. In addition, the olefins were recovered nearly quantitatively.

The explanation for the favored oligomerization, as well as the preferred tendency of prototropy to form the acyclic compound with enamine, of sulfonyl imide, compared with sulfene, is based on the following consideration: owing to the larger electronegativity of the nitrogen atom than that of the carbon atom, sulfonyl imide and the zwitter ionic intermediate (**15**) are more stabilized and have a longer lifetime than sulfene and the resulting intermediate[9] (like **15**).

Experimental

The IR spectra were recorded on Hitachi EP-S and Hitachi 215 spectrophotometers, and the NMR spectra on a Varian EM-360 (60 MHz) instrument, using tetramethylsilane as an internal standard. The NMR spectra of the products, except for dimethylsulfamide, were measured in chloroform-*d* and all the chemical shifts were given in δ values. The melting points are uncorrected.

Materials. Alkylsulfamoyl chlorides (**1**) were prepared according to the reported method:[13] **1a**; 67 °C/0.03 mmHg, **1b**: 70 °C/0.03 mmHg (lit,[14] 52 °C/0.05 mmHg). All of the enamines, **3**,[15] **5**,[16] **8**,[17] **10**,[18] and **12**[19] were prepared by the respective methods in the literature. *trans*-Stilbene and dimethyl fumarate were commercial materials and used after recrystallizations from 95% ethanol and from methanol respectively. Triethylamine and the solvents were obtained commercially and used after purification by the published direction.[20]

Reactions of 1 with Enamines. Method A: A sulfamoyl chloride (10 mmol) in THF (30 ml) was added dropwise over a period of 1 h to a stirred solution containing an enamine (10 mmol) and triethylamine (10 mmol) in THF (70 ml) at the desired temperature. After the addition, the mixture was stirred for 1 h at that temperature. The precipitates of triethylamine hydrochloride (quantitative amount) were removed by filtration, and the solvent was evaporated under reduced pressure leaving an oily substance tinged with yellow. The addition of methanol to the residue gave the sulfamoyl imide-enamine adduct as a precipitate. The reaction temperatures were maintained at −78 °C in the reactions with enamines **3** and **12**, and at 20 °C for enamines **5**, **8**, and **10**. Method B: A solution of triethylamine (10 mmol) in THF (20 ml) was added dropwise over 15 min to a stirred solution of **1** (10 mmol) in THF (60 ml) at −78 °C. After further stirring for 15 min, to the stirred solution kept at −78 °C was added a solution of the enamine (10 mmol) in THF (20 ml) dropwise over a period of 30 min. After the resulting mixture was stirred for an additional 15 min, the mixture was allowed to attain room temperature. The precipitates of the amine hydrochloride (quantitative amount) were removed by filtration and the solvent evaporated from the filtrate under reduced pressure. Methanol was added to the residual oily substance and the sulfamoyl imide-enamine adduct was obtained as a precipitate.

Reaction with 1-Morpholinocyclohexene (3): By Method A, 3-methylsulfamoyl- and 3-ethylsulfamoyl-2-morpholinocyclohexenes (**4a** and **4b**) were isolated in 1.5 g (58%) and 1.5 g (55%) yields respectively. By Method B, **4a** and **4b** were isolated in 1.3 g (50%) and 1.4 g (51%) yields respectively. As a modification of Method B, when the amine hydrochloride was removed at −78 °C prior to the addition of enamine **3**–THF solution, **4a** and **4b** were obtained in 1.2 g (46%) and 1.1 g (40%) yields respectively. **4a**: mp 120—122 °C. IR (Nujol, cm^{-1}); 3280 (NH), 1645 (C=C), 1315 and 1160 (SO_2). NMR; 1.6—3.2 (m, 10H, NCH_2 and CH_2), 3.65—3.95 (m, 5H, OCH_2 and SO_2CH), 5.05 (bs, 1H, NH), 5.38 (t, 1H, J=4 Hz, vinyl H). MS (70 eV); *m/e* 260 (M^+). Found: C, 50.31; H, 7.72; N, 10.57%. Calcd for $C_{11}H_{20}N_2O_3S$: C, 50.75; H, 7.74; N, 10.76%. **4b**: white crystal, mp 89—90 °C. IR (Nujol, cm^{-1}); 3260 (NH), 1645 (C=C), 1315 and 1160 (SO_2). NMR; 1.22 (t, 3H, J=7 Hz, CH_3), 1.5—3.4 (m, 12H, NCH_2 and CH_2), 3.73 (m, 5H, OCH_2 and SO_2CH), 5.10 (bt, 1H, NH), 5.35 (t, 1H, J=4 Hz, vinyl H). Found: C, 52.84; H, 8.10; N, 10.20%. Calcd for $C_{12}H_{22}N_2O_3S$: C, 52.54; H, 8.08; N, 10.21%.

Reactions with 2-Morpholino-1,3-diphenylpropene (5): The reaction of **1a** was run as in Methods A and B. By Method A, 2.5 g (67%) of 3-methylsulfamoyl-2-morpholino-1,3-diphenylpropene (**6a**) was yielded as the precipitate. The filtrate was evaporated under reduced pressure to give a brownish, oily substance. The residue was chromatographed on silica gel, and 0.04 g (7%) of *N,N'*-dimethylsulfamide (**7a**) was eluted with chloroform. The recrystallization of **6a** from methanol gave colorless needles; mp 153—154 °C. IR (KBr, cm^{-1}): 3200 (NH), 1320 and 1140 (SO_2). NMR: 2.70 (d, 3H, J=5 Hz, CH_3), 2.65—2.90 (m, 4H, NCH_2), 3.55—3.75 (m, 4H, OCH_2), 4.29 (bs, 1H, NH), 5.10 (s, 1H, vinyl H), 6.81 (s, 1H, SO_2CH), 7.2—7.8 (m, 10H, benzene ring). MS (70 eV): *m/e* 372 (M^+). Found: C, 64.23; H, 6.61; N, 7.54%. Calcd for $C_{20}H_{24}N_2O_3S$: C, 64.49; H, 6.49; N, 7.52%. The recrystallization of **7a** from benzene gave colorless leaflets; mp 78—79 °C.[13] IR (KBr, cm^{-1}): 3320 (NH), 1325 and 1160 (SO_2). NMR (DMSO-d_6): 2.47 (d, 6H, J=5 Hz, CH_3), 6.70 (bs, 2H, NH). MS (70 eV): *m/e* 124 (M^+). Found: C, 19.21; H, 6.37; N, 22.97%. Calcd for $C_2H_8N_2O_2S$: C, 19.35; H, 6.49; N, 22.56%. Method B gave **6a** and **7a** in 1.0 g (26%) and 0.4 g (65%) yields respectively. When the reaction of **1b** was run as in Method A, 3-ethylsulfamoyl-2-morpholino-1,3-diphenylpropene (**6b**) was isolated in 2.6 g (68%) yield. The recrystallization from methanol gave colorless needles; mp 133—134 °C. IR (KBr, cm^{-1}): 3250 (NH), 1310 and 1140 (SO_2). NMR: 1.10 (t, 3H, J=7 Hz, CH_3), 2.65—3.30 (m, 6H, NCH_2), 3.60—3.75 (m, 4H, OCH_2), 4.36 (bt, 1H, NH), 5.00 (s, 1H, vinyl H), 6.85 (s, 1H, SO_2CH), 7.3—7.9 (m, 10H, benzene ring). MS (70 eV): *m/e* 386 (M^+). Found: C, 65.15; H, 6.85; N, 7.26%. Calcd for $C_{21}H_{26}N_2O_3S$: C, 65.27; H, 6.78; N, 7.25%.

Reactions with (E)-β-Morpholinostyrene (8): The reactions of **1a** and **1b** gave α-methylsulfamoyl- and α-ethylsulfamoyl-β-morpholinostyrenes (**9a** and **9b**) in 1.3 g (46%) and 1.7 g (58%) yields, respectively, Method A. The recrystallization of **9a** from methanol gave colorless prisms; mp 144—145 °C. IR (KBr, cm^{-1}): 3240 (NH), 1622 (C=C), 1300 and 1130 (SO_2). NMR: 2.62 (d, 3H, J=5 Hz, CH_3), 2.9—3.1 (m, 4H, NCH_2), 3.45—3.65 (m, 4H, OCH_2), 3.65—4.0 (bs, 1H, NH), 7.26 (s, 1H, vinyl H), 7.35 (s, 5H, benzene ring). MS (70 eV): *m/e* 282 (M^+). Found: C, 55.04; H, 6.41; N, 9.90%. Calcd for $C_{13}H_{18}N_2O_3S$: C, 55.31; H, 6.43; N, 9.92%. The recrystallization of **9b** from methanol gave

colorless prisms; mp 117—118 °C. IR (KBr, cm^{-1}): 3260 (NH), 1622 (C=C), 1300 and 1130 (SO_2). NMR: 1.10 (t, 3H, J=7 Hz, CH_3), 2.8—3.1 (m, 6H, NCH_2), 3.45—3.65 (m, 4H, OCH_2), 3.65—3.9 (bs, 1H, NH), 7.22 (s, 1H, vinyl H,) 7.33 (s, 5H, benzene ring). Found: C, 56.45; H, 6.76; N, 9.37%. Calcd for $C_{14}H_{20}N_2O_3S$: C, 56.74; H, 6.80; N, 9.45%.

Reactions with (E)-Morpholinostilbene (10): The reactions of **1a** and **1b** were run as in Method A. Methylsulfamoyl- and ethylsulfamoyl-morpholinostilbenes (**11a** and **11b**) were isolated in yields of 2.6 g (47%) and 2.1 g (56%) respectively. The recrystallization of **11a** gave pale yellow prisms: mp 153—154 °C. IR (KBr, cm^{-1}): 3275 (NH), 1539 (C=C), 1309 and 1140 (SO_2). NMR: 2.46 (d, 3H, J=5 Hz, CH_3), 2.5—2.7 (m, 4H, NCH_2), 3.3—3.5 (m, 4H, OCH_2), 3.7 (bs, 1H, NH), 7.2—7.5 (m, 10H, benzene ring). MS (70 eV): *m/e* 358 (M^+). Found: C, 63.48; H, 6.18; N, 7.74%. Calcd for $C_{19}H_{22}N_2O_3S$: C, 63.67; H, 6.19; N, 7.82%. **11b**: colorless prisms (from methanol), mp 140—142 °C. IR (KBr, cm^{-1}); 3250 (NH), 1545 (C=C), 1297 and 1138 (SO_2). NMR; 0.93 (t, 3H, J=7 Hz, CH_3), 2.5—2.7 (m, 4H, morpholino ring NCH_2), 2.92 (q, 2H, J=7 Hz, NCH_2), 3.33—3.53 (m, 4H, OCH_2), 3.70 (bs, 1H, NH), 7.3—7.5 (m, 10H, benzene ring). MS (70 eV); *m/e* 372 (M^+). Found: C, 64.38; H, 6.50; N, 7.65%. Calcd for $C_{20}H_{24}N_2O_3S$: C, 64.50; H, 6.50; N, 7.52%.

Reactions with 2-Methyl-1-morpholinopropene (12): The reactions of **1a** and **1b** were run as in Method A. The precipitates of triethylamine hydrochloride were removed from the reaction mixture by filtration and the solvent evaporated under reduced pressure, the last traces of solvent being removed at a pressure of 0.1 mmHg. The residual oily, impure 2,4,4-trimethyl-3-morpholino-1,2-thiazetidine 1,1-dioxide (**13a**) displayed the following NMR spectrum: 1.56 (s, 6H, C-CH_3), 2.50—3.13 (m, 4H, NCH_2), 2.76 (s, 3H, NCH_3), 3.31 (s, 1H, CH), 3.60—3.83 (m, 4H, OCH_2). Since attempts to crystallize **13a** were unsuccessful, the oil was chromatographed over silica gel. Elution with benzene gave α-(methylsulfamoyl)isobutyraldehyde (**14a**) as a colorless oil in a yield of 0.9 g (55%). IR (neat, cm^{-1}): 3340 (NH), 1730 (C=O), 1318 and 1130 (SO_2). NMR: 1.53 (s, 6H, CH_3), 2.76 (d, 3H, J=5 Hz, NCH_3), 4.63 (bs, 1H, NH), 9.63 (s, 1H, CHO). From the reaction of **1b**, 2-ethyl-4,4-dimethyl-3-morpholino-1,2-thiazetidine 1,1-dioxide (**13b**) was obtained as an oily residue. IR (neat, cm^{-1}): 1320 and 1122 (SO_2). NMR: 1.26 (t, 3H, J=7 Hz, CH_3), 1.56 (s, 6H, CH_3), 2.50—3.13 (m, 4H, NCH_2), 3.46 (s, 1H, CH), 3.60—3.83 (m, 4H, OCH_2), 3.25 (q, 2H, J=7 Hz, CH_2). The impure **13b** was chromatographed over silica gel to give colorless, oily α-(ethylsulfamoyl)isobutyraldehyde (**14b**): yield 1.1 g (62%). IR (neat, cm^{-1}): 3280 (NH), 1725 (C=O), 1315 and 1130 (SO_2). NMR; 1.17 (t, 3H, J=7 Hz, CH_3), 1.50 (s, 6H, CH_3), 3.18 (q, 2H, J=7 Hz, CH_2), 5.07 (bs, 1H, NH), 9.68 (s, 1H, CHO).

Reaction of 1a in Benzene and in Ether. A benzene (0.5 mol, 39 g) solution of **1a** (20 mmol, 2.6 g) was added dropwise over a period of 1 h to a stirred benzene (0.5 mol) solution of triethylamine (20 mmol, 2.1 g) at 20 °C. The reaction mixture was stirred for a further hour at the temperature and the precipitates of triethylamine hydrochloride were collected by filtration (weighed 2.7 g, 98%). Evaporation of the solvent under reduced pressure gave a yellow oil, which was chromatographed over silica gel. The fraction eluted by chloroform gave 1.05 g (85%) of **7a**, which was recrystallized from benzene. The reaction in ether gave 1.12 g (91%) of **7a**.

Attempted Reactions with trans-*Stilbene and with Dimethyl Fumarate.* The reactions of **1a** were run as in Method A at 20 °C using double the molar quantities of the reactants and the solvent. The reaction with *trans*-stilbene gave 2.64 g (96%) of the amine hydrochloride, and the evaporation of the solvent under reduced pressure gave a yellow solid, which was extracted with benzene. Removal of benzene gave 5.3 g (95%) of the recovered stilbene. Chromatography of the benzene insoluble part on silica gel using chloroform as an eluent gave one gram of a white solid, the NMR of which showed no absorption for protons resulting from the incorporation of stilbene. The reaction with dimethyl fumarate gave 2.5 g (91%) of the amine hydrochloride. Evaporation of the solvent followed by trituration with methanol gave 2.6 g (91%) of the recovered ester. From the methanol solution, the solvent was removed under reduced pressure to give a pale yellow solid, the chromatography of which over silica gel gave 0.8 g of a white product similar to that obtained in the reaction with stilbene.

References

1) According to Chemical Abstracts, $HN{=}SO_2$ is called "sulfimide," but the term is used for $HN{=}SH_2$ in the IUPAC names. The term "sulfonyl imide" will be used in the present paper: J. H. Fletcher, O. C. Dermer, and R. B. Fox, "Nomenclature of Organic Compounds," in "Advances in Chemistry Series," ed by R. F. Gould, American Chemical Society, Washington, D. C. (1974), pp. 304, 308, and 310.

2) G. M. Atkins, Jr. and E. M. Burgess, *J. Am. Chem. Soc.*, **89**, 2502 (1967).

3) W. Lwowski and E. Scheiffele, *J. Am. Chem. Soc.*, **87**, 4359 (1965). Thermolysis of 2,3,5,6-tetramethylbenzenesulfonyl azide also gives a sulfonyl imide intermediate: R. A. Abramovitch, T. Chellathurai, W. D. Holcomb, I. McMaster, and D. P. Vanderpool, *J. Org. Chem.*, **42**, 2920 (1977).

4) G. M. Atkins, Jr. and E. M. Burgess, *J. Am. Chem. Soc.*, **94**, 6135 (1972).

5) E. M. Burgess and W. M. Williams, *J. Am. Chem. Soc.*, **94**, 4386 (1972).

6) The hydrolysis of **13b** in chloroform-*d* in the open system was followed by monitoring the NMR spectrum over 72 h. The lapse of time permitted the disappearance of the peak due to the methylidyne proton (δ 3.46) with the appearances of the two peaks due to the amide proton (δ 5.07)[7] and the aldehyde proton (δ 9.68).

7) Although the amino proton of morpholine is observed at δ 1.92 as a singlet,[8] the NMR spectrum of a mixture of equimolar amounts of **14b** and morpholine has given a broad singlet at δ 5.07 which corresponds to two protons.

8) "Varian NMR Spectra Catalog," ed by N. S. Bhacca, L. F. Johnson, and J. N. Shoolery, Varian Associates, National Press (1962), Vol. 1, Catalog No. 83.

9) T. Tanabe and T. Nagai, *Bull. Chem. Soc. Jpn.*, **50**, 1179 (1977): T. Tanabe, T. Shingaki, and T. Nagai, *Chem. Lett.*, **1975**, 679.

10) The lowest vacant orbital of sulfonyl imide is composed of an orbital heavily localized on sulfur and out-of-plane at the sulfur atom,[11] the antarafacial interaction results from participation of the favorably disposed unoccupied sulfur *d* orbital with the ethylene components.[12]

11) K. N. Houk, R. W. Strozler, and J. A. Hall, *Tetrahedron Lett.*, **1974**, 897.

12) R. B. Woodward and R. Hoffmann, "The Conservation of Orbital Symmetry," Verlay Chemie GmbH, Weinheim West Germany (1970), pp. 68, 69, and 163—168.

13) G. Weiss and G. Schulze, *Ann.* **729**, 40 (1969).
14) N. C. Hansen, *Acta Chem. Scand.*, **17**, 2141 (1963).
15) S. Hünig, E. Lücke, and W. Bernninger, *Org. Synth.*, Coll. Vol. V, 808 (1973).
16) D. Pocar, G. Bianchetti, and P. D. Croce, *Gazz. Chem. Ital.*, **95**, 1220 (1965). K. Kumagaya, K. Suzuki, and M. Seki, *Chem. Pharm. Bull.*, **21**, 1601 (1973).
17) W. Ziegenkein and W. Franks, *Chem. Ber.*, **90**, 2291 (1957).
18) M. E. Munk and Y. K. Kim, *J. Org. Chem.*, **30**, 3705 (1965).
19) E. Benzing, *Angew. Chem.*, **71**, 521 (1959).
20) J. A. Riddic and W. B. Gunger, "Organic Solvents," in "Techniques of Chemistry," ed by A. Weissberger, Wiley-Interscience, New York, N. Y. (1970), Vol. VII.

The Reaction of Vicinal Dinitro Compounds with Tin(II) Chloride

Kimitoshi FUKUNAGA* and Makoto KIMURA

Faculty of Engineering, Yamaguchi University, Tokiwadai, Ube, Yamaguchi 755

(Received April 5, 1978)

The reactions of vicinal dinitro compounds with tin(II) chloride have been studied. The reactions of α,β-diaryl vicinal dinitro compounds and tin(II) chloride in polar solvents gave the corresponding olefins in good yields. The aliphatic vicinal dinitro compounds did not react with tin(II) chloride under the same reaction conditions. A reaction mechanism of elimination involving a radical anion intermediate has been proposed.

The bimolecular removal of two atoms or groups from vicinal dihalides,[1,2] vicinal diols,[3] and vicinal dicarboxylates[4] have been investigated extensively, but there have been few papers on the bimolecular elimination reactions of vicinal dinitro compounds. Kornblum *et al.* reported the denitration of purely aliphatic vicinal dinitro compounds to alkenes with sodium sufide or sodium benzenethiolate.[5]

It has been reported that 1,2-diaryl-1,2-dinitroethanes (**1**) react with tin(II) compounds in ethanol to give 1,2-diarylethylenes (**2**)[6] and this paper will report the reaction in detail.

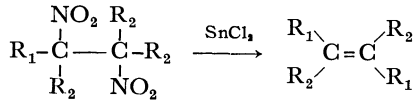

1 (**a**—**g**) **2** (**a**—**g**)

a: R_1, R_2=fluorenyl
b: $R_1=C_6H_5$, R_2=H
c: $R_1=p$-$CH_3C_6H_5$, R_2=H
d: $R_1=o$-$CH_3C_6H_5$, R_2=H
e: $R_1=o$-ClC_6H_5, R_2=H
f: $R_1=\alpha$-naphthyl, R_2=H
g: $R_1=C_6H_5$, $R_2=CH_3$

Scheme 1.

Results and Discussion

Syntheses of **1**. 1,2-Diaryl-1,2-dinitroethane (**1b**—**f**) has been prepared by the reaction of the sodium or potassium salt of α-arylnitromethane with potassium peroxodisulfate. Two isomeric structures are possible for the vicinal dinitro compounds. Figure 1 shows the NMR spectra of the configurationally known *dl*-1,2-dinitro-1,2-diphenylethane (*dl*-**1b**) and *meso*-**1b** pairs.[7] The methine proton of *meso*-**1b** at δ 3.74 is broad compared with that of *dl*-**1b**. These results indicate that the stereochemical assignment can possibly be made for the isomeric **1b**—**f** on the basis of the band width of the methine proton peaks.

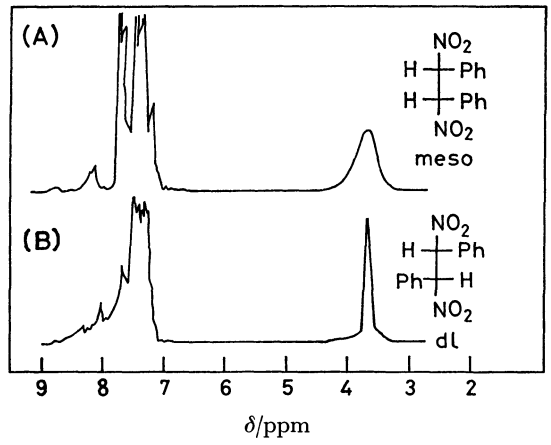

Fig. 1. NMR spectra of **1b** in $(CD_3)_2NCD$; (A): for *meso*-**1b**; (B): for *dl*-**1b**.

2,3-Dinitro-2,3-diphenylbutane (**1g**) was prepared as a mixture of the *dl* and *meso* forms by the reaction of the sodium salt of 1-nitro-1-phenylethane with silver nitrate. The ratio of the stereoisomers in this product has been determined by NMR in $CDCl_3$ which exhibited resonances at δ 2.30 and 2.22 due to two kinds of methyl groups. Other vicinal dinitro compounds (9,9'-dinitro-9,9'-bifluorenyl (**1a**), 2,3-dinitro-2,3-dimethylbutane (**1h**), and 1,1'-dinitrobicyclohexyl (**1i**)) have been prepared by the methods reported in the literature.[6,8]

The analytical data for **1a**—**i** are summarized in Table 1.

Reaction of **1** *with Tin(II) Chloride.* α,β-Diaryl vicinal dinitro compounds (**1a**—**f**) react readily with tin(II) chloride in boiling ethanol to give the corresponding 1,2-diarylethylenes (**2a**—**f**). The products thus obtained were identified with authentic samples by mixed melting point determination and a comparison of IR spectra. The β-elimination products, such as α-nitrostilbenes, were not obtained. Refluxing of the purely aliphatic vicinal dinitro compound, **1h** or **1i** with tin(II) chloride in ethanol gave the starting materials unchanged, even after 48 h. Thus, the presence of the aromatic ring attached to the carbon atom bearing the nitro group is essential for denitration.

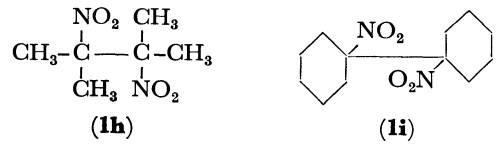

1h **1i**

Scheme 2.

The results of this reaction are shown in Table 2.

The reaction of **1a** with tin(II) chloride has been conducted in various solvents. As shown in Table 3, the reaction is remarkably affected by the polarity of the solvent, and proceeds smoothly with a solvent more polar than ethyl acetate (ε=6.0). In dipolar aprotic solvents, the reaction proceeds more readily, and lower temperature being sufficient for reaction. A vigorous evolution of nitrogen oxide was observed during the reaction employing acetic acid or ethyl acetate as

Table 1. Physical properties and analytical data of vicinal dinitro compounds (**1**)

Compd No.	Mp °C (Recryst solvent)	Formula	Found (Calcd), % C	H	N	IR spectrum, cm^{-1} in KBr NO_2	NMR spectrum, δ in DMF-d_7 CH	CH_3
1a	175 (Benzene)	$C_{26}H_{16}O_4N_2$	—			1550, 1340	—	—
meso-**1b**	230 (AcOH)	$C_{14}H_{12}O_4N_2$	61.83 (61.76)	4.41 (4.44)	10.18 (10.29)	1555, 1380	3.74(bs)	—
dl-**1b**	149—150 (EtOH)	$C_{14}H_{12}O_4N_2$	—			1550, 1360	3.73(s) 6.36(s)[a]	—
dl-**1c**	148 (EtOH)	$C_{16}H_{16}O_4N_2$	63.92 (63.99)	5.26 (5.37)	9.29 (9.33)	1550, 1370	6.36(s)[a]	2.27(d)[a]
dl-**1d**	157—158 (EtOH)	$C_{16}H_{16}O_4N_2$	63.90 (63.99)	5.44 (5.37)	9.24 (9.33)	1560, 1360	4.24(s)	2.31(q)
dl-**1e**	233—234 (AcOH)	$C_{14}H_{16}O_4Cl_2$	49.25 (49.29)	2.88 (2.95)	8.22 (8.21)	1560, 1300	3.46(s)	—
dl-**1f**	141—142 (AcOH)	$C_{22}H_{16}O_4N_2$	70.94 (70.96)	4.30 (4.33)	7.49 (7.52)	1518, 1310	6.89(s)	—
dl-**1g**	139—141 (MeOH–H_2O)	$C_{16}H_{16}O_4N_2$	63.82 (63.99)	5.33 (5.37)	9.32 (9.33)	1550, 1350	—	2.30(s)[a]
1g[b]	118—126 (MeOH–H_2O)	$C_{16}H_{16}O_4N_2$	63.79 (63.99)	5.35 (5.37)	9.34 (9.33)	1550, 1350	—	2.30(s) 2.22(s)[a]
1h	212—213 (EtOH)	$C_6H_{12}O_4N_2$	—			1560, 1360	—	1.75(s)[a]
1i	215—216 (Acetone)	$C_{12}H_{20}O_4N_2$	—			—	—	—

a) Measured in $CDCl_3$. b) The mixture of *dl*-**1g** (73%) and *meso*-**1g** (27%).

Table 2. Reactions of vicinal dinitro compounds (**1a—f**, **1h**, and **1i**) with tin(II) chloride in ethanol[a]

No.	Vicinal dinitro compound	Product	Yield[b] %
1	**1a**	**2a**	94
2	*dl*-**1b**	**2b**[c]	92
3	*dl*-**1c**	**2c**[c]	89
4	*dl*-**1d**	**2d**[c]	83
5	*dl*-**1e**	**2e**[c]	88
6	*dl*-**1f**	**2f**[c]	85
7	**1h**	None	0
8	**1i**	None	0

a) In 15 ml solvent at reflux temp using 1.25 mmol of **1** and 5.0 mmol of tin(II) chloride. b) Isolated yield. c) *trans*-Isomer.

Table 3. Reactions of **1a** with tin(II) chloride in various solvents

Run	Solvent	Dielectric constant (ε)	Yield of **2a**[b] (%)
1	*n*-C_6H_{14}	1.9	0
2	PhH	2.3	2.1
3	EtOEt	4.2	2.0
4	$CHCl_3$	4.9	8.2
5	AcOEt	6.0	89.6
6	AcOH	6.2	90.3
7	THF	7.6	92.4
8	*n*-BuOH	17.1	94.6
9	Me_2CO	20.7	95.8
10	EtOH	23.8	98.1
11	MeOH	33.1	98.5
12	DMF	36.1	97.8
13	MeCN	37.8	98.0

a) In 10 ml solvent at the reflux temp of each solvent for 0.5 h using **1a** (0.625 mmol) and tin(II) chloride (2.50 mmol). b) Yield was determined spectrophotometrically at 453 nm.

solvent. The formation of nitrogen oxide in acidic medium indicates the formation of the nitrite ion during the reaction. In order to find the optimum reaction conditions, several runs were conducted with **1a** and *dl*-**1b** employing ethanol or DMF as the solvent. An solution of ethanol or DMF solution and **2a** had an intense absorption maximum at 453 nm (ε_{max} 2.4×10^4 in EtOH, ε_{max} 3.0×10^4 in DMF). A very small absorption and weak absorption were observed at this wavelength for a solution of tin(II) chloride and **1a** respectively. Therefore, the spectrophotometric determination of **2a** in the reaction mixture from **1a** and tin(II) chloride has been conducted at 453 nm. In the reaction with *dl*-**1b**, the yield of **2b** was determined by GLPC, the results of which are summarized in Tables 4 and 5. As can be seen from the Tables, the best result were obtained with a mole ratio of tin(II) chloride to **1** greater than 4 to 1 was used. Longer reaction time did not significantly increase the yield of elimination product, **2**. It has been reported that a solution of tin(II), except for tin(II) fluoride is oxidized on exposure to air.[9] Consequently an excess of tin(II) chloride has been used.

Stereochemistry of Elimination. Table 6 shows that the product of the reaction of **1b** was solely the *trans* isomer (*trans*-**2b**) regardless of the stereochemical nature of the starting material or the condition of the reaction. The isomerization of *cis*-**2b** to *trans*-**2b** was not observed under these reaction conditions. Similarly a series of *dl*-1,2-diaryl-1,2-dinitroethanes (*dl*-**1c—f**) were treated

Table 4. Reactions of **1a** with tin(II) chloride under various conditions

Run	$SnCl_2$/**1a**[a] (mol/mol)	Solvent (10 ml)	Yield of **2a**[b] (%)
1	0.87	EtOH[c]	18.2
2	0.95	EtOH[d]	19.6
3	1.54	EtOH[d]	48.9
4	1.90	EtOH[d]	50.4
5	3.80	EtOH[d]	97.1
6	4.12	EtOH[d]	100
7	2.00	DMF[e]	51.4
8	2.28	DMF[e]	46.7
9	4.80	DMF[e]	82.8
10	5.20	DMF[e]	98.2

a) **1a**=0.625 mmol. b) Yield was determined spectrophotometrically at 453 nm. c) At reflux temp for 3 h. d) At reflux temp for 0.5 h. e) At room temp for 2 h.

Table 5. Reactions of *dl*-**1b** with tin(II) chloride under various conditions

Run	$SnCl_2$/*dl*-**1b**[a] (mol/mol)	Solvent (10 ml)	Yield of **2b**[b] (%)
1	0.72	EtOH[c]	27.3
2	0.78	EtOH[d]	29.9
3	1.16	EtOH[c]	48.8
4	2.14	EtOH[c]	79.5
5	3.34	EtOH[c]	94.6
6	4.13	EtOH[c]	100
7	4.10	DMF[e]	78.9
8	4.55	DMF[e]	86.2

a) *dl*-**1b**=2.50 mmol. b) Yield was determined by GLPC. c) At reflux temp for 0.5 h. d) At reflux temp for 3 h. e) At room temp for 2 h.

to give *trans*-1,2-diarylethylenes (*trans*-**2c**—**f**), some typical results of which are summarized in Table 2. In the reactions of **1g**, *dl*-**1g** gave a mixture of *cis* and *trans*-2,3-diphenyl-2-butene (*cis* and *trans*-**2g**) in a ratio of 54 to 46, and a mixture of *dl* and *meso*-**1g** in a ratio of 51 to 49, respectively (Table 6). These results suggest that present elimination reaction is not stereospecific.

Table 6. Reactions of *dl*-**1b**, *meso*-**1b**, *dl*-**1g**, and *meso*-**1g** with tin(II) chloride

Run	Substrate[a]	Solvent (10 ml)	Reaction conditions		Yield of olefin	
			Time (h)	Temp (°C)	*cis* (%)	*trans* (%)
1	*dl*-**1b**	EtOH	0.5	reflux	0	97
2	*dl*-**1b**	DMF	2	r.t.	0	69
3	*dl*-**1b**	THF	2	50	0	88
4	*meso*-**1b**	EtOH	0.5	reflux	0	96
5	*meso*-**1b**	DMF	2	r.t.	0	70
6	*dl*-**1g**	EtOH	0.5	reflux	43.2	36.8[b]
7	*dl* and *meso*-**1g**[c]	EtOH	0.5	reflux	41.8	40.2[d]

a) $SnCl_2$/substrate=10 mmol/2.5 mmol. b) *cis*/*trans*=54/46. c) The ratio of *dl*-**1b** and *meso*-**1b** was 73:27. d) *cis*/*trans*=51/49.

Reaction Mechanism. Since no dehydronitration of **1b**—**f** was observed, there appears to be little, if any, formation of an ionic intermediate. On the basis of the stereochemical results, it appears probable that the elimination is not concerted and that a labile mononitro intermediate is involved. Furthermore, the stoichiometric results indicate that the reaction is markedly affected by the concentration of tin(II) chloride. Therefore the carbanion (E1cb), unimolecular (E1), and concerted bimolecular (E2) elimination mechanisms are not possible mechanisms in the elimination.[10] A possible mechanism is Scheme 3:

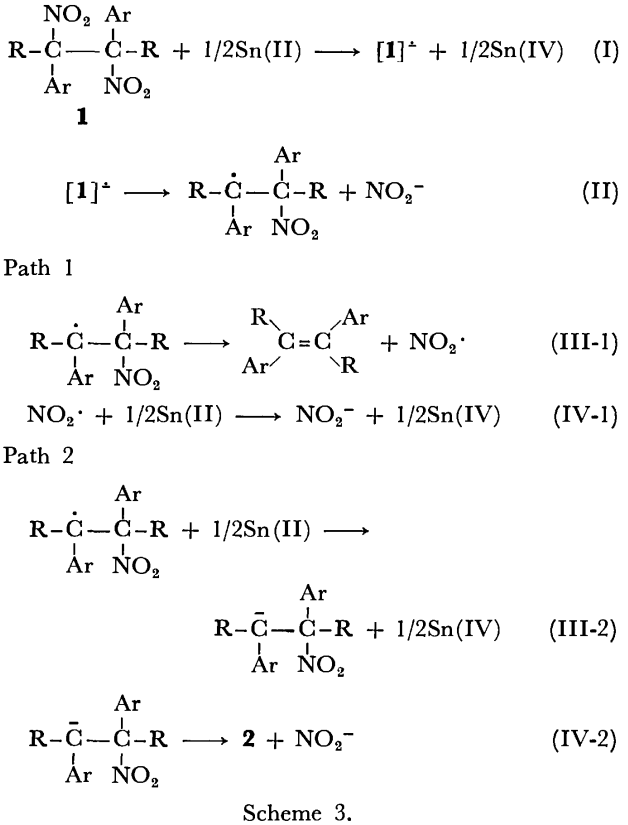

Scheme 3.

The favored coordination numbers for tin(II) are three[11,12] and for tin(IV) four to six,[13] and the tin(II) is coordinated to the oxygen of the nitro group. The first coordination process involving a neutral species should be aided by solvents of high polarity. Under such conditions electron transfer takes place from tin(II) to the nitro group of the vicinal dinitro compounds (Step I), and radical intermediates are formed (Step II). In the thermodynamically controlled conformation, they then react with a second molecule of tin(II) to give the final products (Steps III and IV). In Scheme 3, two mechanisms for the elimination of the second nitro group from the radical intermediate are presented. One is based on the reductive elimination of $\cdot NO_2$, and the other, on the intermediate formation of a carbanion that subsequently loses a nitrite ion. It appears probable that the elimination reaction in Step III proceeds *via* a carbanion mechanism rather than a radical mechanism when the second leaving group is a group such as an acetoxyl group that is not easily lost with its bonding

Table 7. The influence of nitro aromatics and sulfur on the reaction of **1a** with tin(II) chloride

Run	Added inhibitor	mmol	Yield of **2a** (%)[b]
1	None	0	96.2
2	$PhNO_2$	0.125	97.0
3	*m*-DNB	0.063	94.5
4	*m*-DNB	0.250	95.1
5	*p*-DNB	0.125	96.7
6	Sulfur	1.25	97.6

a) In ethanol (30 ml) at reflux temp for 0.5 h using **1a** (1.25 mmol) and tin(II) chloride (5.00 mmol). b) Yield was determined spectrophotometrically.

electron pair.[10] It should be noted here that the reaction of *threo*-1-acetoxy-2-nitro-1,2-diphenylethane with tin(II) chloride afforded no *trans*-**2b** under the same conditions.[14] Therefore, the elimination of the second nitro group proceeds *via* a radical mechanism (Steps III-1 and IV-1 in Scheme 3). Kwok and Miller[15] previously proposed a similar sequence for the reaction of stilbene dibromide with tin(II) chloride. Kornblum *et al.*[5] reported that similar reactions of purely aliphatic vicinal dinitro compounds with sodium sulfide are inhibited by the presence of dinitrobenzene (DNB) or sulfur. In the reactions here of **1a** with tin(II) chloride, however, the presence of DNB or sulfur had no influence on the product yield, as shown in Table 7. Norris and Girdler[16] reported that the reaction of the lithium salt of 2-nitropropane with *p*-nitrobenzylidene diacetate in DMSO was not catalyzed by light, nor was it inhibited by oxygen or *p*-DNB. Presumably the greater stability of the nitroaromatic radical stabilized by α-aromatic substituent allows sufficient time for successful competition between electron transfer and loss of the nitrite ion. Therefore, the difference in the reactivity of α,β-diaryl vicinal dinitro compounds (**1a**—**g**) and purely aliphatic vicinal dinitro compounds (**1h** and **1i**) with tin(II) chloride may be attributed to the stability of the intermediate radical.

Experimental

All melting points are uncorrected. The products were identified, unless otherwise mentioned, by mixed melting point determination and comparing the IR and NMR spectra data with those of authentic samples. The IR, UV, and NMR spectra were measured with a Hitachi Model IR-215 spectrometer, a Shimadzu Model UV-200 spectrometer, and a JNM-MH 100 spectrometer using tetramethylsilane as an internal standard. Gas-liquid partition chromatographic (GLPC) analysis was conducted on a Hitachi Model 063 gas chromatograph.

Materials. Anhydrous tin(II) chloride was prepared from commercial tin(II) chloride dihydrate according to the method of Stephen.[17] Phenylnitromethane, (*o*-chlorophenyl)nitromethane, 1-naphthylnitromethane, and *o*-tolylnitromethane were prepared from corresponding arylacetonitriles[18] with methyl nitrate according to the method of Black and Baker.[19] *p*-Tolylnitromethane was synthesized according to the method previously reported.[20] 1-Nitro-1-phenylethane was prepared from α-methylbenzyl bromide with sodium nitrite in DMSO.[21] 2-Nitropropane, nitrocyclohexane, and diphenylmethane were commercial materials and used without further purification. *cis*-Stilbene and *trans*-2,3-diphenyl-2-butene were prepared from the corresponding diols.[3] Organic solvents were purified by standard methods and the commercial inorganic materials were used without purification.

Preparations of Vicinal Dinitro Compounds (1). Vicinal dinitro compounds, **1b**—**f**, **1h**, and **1i** were prepared according to the method of Dornow *et al.*[8] Each product **1b**—**f** showed a sharp singlet at δ 4.2—3.5 (2H, methine protons) and assigned to the *dl* form. *meso*-1,2-Dinitro-1,2-diphenylethane (*meso*-**1b**) was prepared by the reaction of *trans*-**2b** and dinitrogen tetraoxide in benzene.[22]

The synthesis of **1a** has been described.[6] Compound **1g** was synthesized by the reaction of the sodium salt of 1-nitro-1-phenylethane with silver nitrate, and NMR revealed *dl*- and *meso*-**1g**. The isomer ratio was determined as 73:27 by integration of the NMR spectra on the assumptions that the methyl protons of *dl*-**1g**, being *cis* to the vicinal phenyl group, are shielded by the phenyl group and appear at higher field than that of the *meso* isomer. Pure *dl*-**1g** was separated by repeated fractional recrystallization from methanol-water, and the melting point and IR spectrum were identical with those published.[23] The physical properties and analytical data of **1** are summarized in Table 1.

Reactions of Vicinal Dinitro Compounds (1) with Tin(II) Chloride. General Procedure: The following example shows a typical run. A mixture of *meso*- or *dl*-**1b** (2.50 mmol) and tin(II) chloride (10 mmol) was refluxed in ethanol (10 ml) for 0.5 h. After the solvent had been removed *in vacuo*, the residue was triturated with cold 2 M sodium hydroxide (50 ml) and the resulting organic product extracted with benzene. The extract was washed with water, and dried over anhydrous sodium sulfate, and the solvent removed *in vacuo* to give a crude reaction product. The UV and NMR spectra of this product [UV(EtOH) λ_{max} 295, 308, 320 (shoulder) nm; NMR ($CDCl_3$) δ 7.1 (2H, s, -CH=CH-), 7.2—7.6 (10H, m, $2C_6H_5$)] were characteristic of *trans*-**2b** free of the *cis* isomer. Recrystallization from ethanol afforded colorless fine crystals of *trans*-**2b**, mp 122—123 °C (lit,[24] 123—124 °C). The products obtained by the same procedure were 9,9'-bifluorenylidene (**2a**): Mp 182—183 °C (lit,[25] 189—190 °C); *trans*-4,4'-dimethylstilbene (*trans*-**2c**): Mp 179—180 °C (lit,[26] 179—180 °C); *trans*-2,2'-dimethylstilbene (*trans*-**2d**): Mp 80—81 °C (lit,[26] 82.5—83.5 °C); *trans*-2,2'-dichlorostilbene (*trans*-**2e**): Mp 95—96 °C (lit,[27] 96—97.2 °C); *trans*-1,2-di-(1-naphthyl)ethene (*trans*-**2f**): Mp 160—161 °C (lit,[26] 158—159 °C). The 2,3-diphenyl-2-butene (**2g**) obtained was found to be a *ca.* 1:1 mixture of the *cis* and *trans* isomers from the NMR spectra. In the case of the reaction of **1h** and **1i** the starting material was recovered unchanged.

Reaction of dl-*1b with Tin(II) Chloride in Ethanol*: A mixture of *dl*-**1b** (2.50 mmol) and tin(II) chloride (1.80—10.3 mmol) was refluxed in ethanol (10 ml) for 0.5—3 h. The reaction product, after the usual work up procedure, was analyzed by GLPC with diphenylmethane as an internal standard using a Tenax GC column 2 m long (steel tube) at 245 °C (He as a carrier gas). Retension time: *dl*-**1b**, 7 min; diphenylmethane, 23 min; *trans*-**2b**, 56 min.

Reaction of dl-*1b with Tin(II) Chloride in DMF*: A DMF (10 ml) solution containing *dl*-**1b** (2.50 mmol) and tin(II) chloride (10.25 and 11.4 mmol) was stirred at room temperature for 2 h. The solution was poured into cold 2 M sodium hydroxide (100 ml). After the usual work up, the organic extract was submitted for GLPC analysis.

Isomerization of cis-*Stilbene (*cis-**2b**) *during the Reaction.* A mixture of *cis*-**2b** (2.50 mmol) and tin(II) chloride (10 mmol) in ethanol (10 ml) was refluxed for 0.5 h, and analysis of the product was conducted using GLPC and NMR. *cis*-Stilbene was unchanged under the reaction conditions.

The Influence of Dinitrobenzene or Sulfur on the Reaction of **1a** *with Tin(II) Chloride.* A mixture of **1a** (1.25 mmol) and tin(II) chloride (5.0 mmol) was refluxed in ethanol (30 ml) for 0.5 h in the presence of various amounts of an inhibitor. The yields of **2a** were determined spectrophotometrically employing ethanol as a solvent. The various additives did not affect the yield of **2a** (Table 7).

References

1) C. S. Tsai Lee, I. M. Mathai, and S. I. Miller, *J. Am. Chem. Soc.*, **92**, 4602 (1970).
2) G. A. Olah and G. K. S. Prakash, *Synthesis*, **1976**, 607.
3) J. S. Josan and F. W. Eastwood, *Aust. J. Chem.*, **21**, 2013 (1968).
4) E. J. Corey and J. Casanova, *J. Am. Chem. Soc.*, **85**, 165 (1963).
5) N. Kornblum, S. D. Boyd, H. W. Pinnick, and R. G. Smith, *J. Am. Chem. Soc.*, **93**, 4316 (1971).
6) K. Fukunaga, *Synthesis*, **1975**, 442.
7) The stereochemistry of *dl*-**1b** was demonstrated on the basis that the racemic product is partially resolved by brucine. See, J. J. Gardikes, A. H. Pagano, and H. Shechter, *Chem. Ind. (London)*, **1958**, 632. The NMR spectra of *dl*- and *meso*-**1b** pairs however were unknown.
8) A. Dornow and K. J. Fust, *Chem. Ber.*, **90**, 1774 (1957).
9) J. D. Donaldson, *Prog. Inorg. Chem.*, **8**, 299 (1957).
10) J. Hine, "Physical Organic Chemistry," 2nd ed, McGraw-Hill, New York (1962), p. 186.
11) J. D. Donaldson, *Prog. Inorg. Chem.*, **8**, 287 (1967).
12) R. S. Tobias, *Organomet. Chem. Rev.*, **1**, 93 (1966).
13) M. Gielsen and N. Sprecher, *Organomet. Chem. Rev.*, **1**, 455 (1966).
14) Unpublished data.
15) W. K. Kwok and S. I. Miller, *J. Am. Chem. Soc.*, **92**, 4599 (1970).
16) D. J. Girdler and R. K. Norris, *Tetrahedron Lett.*, **1975**, 431.
17) H. Stephen, *J. Chem. Soc.*, **1930**, 2786.
18) K. Fukunaga, S. Ide, M. Mori, and M. Kimura, *Nippon Kagaku Kaishi*, **1977**, 1379.
19) A. P. Black and F. H. Bakers, *Org. Synth.*, Coll. Vol. II, 512 (1943).
20) K. Fukunaga, *Yuki Gosei Kagaku Kyokai Shi*, **34**, 682 (1976).
21) N. Kornblum and P. A. Wade, *J. Org. Chem.*, **38**, 1418 (1973).
22) J. Schmidt, *Ber.*, **34**, 3536 (1901).
23) A. H. Pagano and H. Shechter, *J. Org. Chem.*, **35**, 295 (1970).
24) R. L. Shrine and A. Berger, *Org. Synth.*, Coll. Vol. III, 786 (1955).
25) D. Bethell, *J. Chem. Soc.*, **1963**, 666.
26) W. Wislicenus and H. Wren, *Chem. Ber.*, **38**, 505 (1905).
27) S. M. Spatz, *J. Org. Chem.*, **26**, 4158 (1961).

Effect of Pressure on the Rates of Solvolysis. Hydrolysis of Some Sterically Hindered Chlorides

Akira SERA,* Shinichi TAKEUCHI, Noboru TACHIKAWA,** and Kazuhiro MARUYAMA**

Department of Chemistry, Faculty of Science, Kobe University, Nada-ku, Kobe 657

***Department of Chemistry, Faculty of Science, Kyoto University, Sakyo-ku, Kyoto 606*

(Received June 3, 1978)

The effect of pressure on the rates of solvolyses of substituted 1-phenylethyl and benzyl chlorides has been investigated in an ethanol–water mixture at 25 °C. The activation volumes have been calculated and the dependence of these values on the number and size of the substituents have been interpreted in terms of the competitive contribution of the steric inhibition of resonance and steric hindrance to solvation in the transition states.

The effect of hydrostatic pressure on the rates of solvolytic displacement reactions have been investigated by many research groups.[1–12] In general, the solvolyses of alkyl halides and arenesulfonates have negative activation volumes ascribable to the electrostriction of solvent molecules by the polar transition states. Attention has also been paid to the substituent dependence of activation volume.[7–12] In most cases, the activation volume was linearly related to the substituent constants, σ^+ and σ^*.[7,8,11] These observations were interpreted in terms of the degree of charge delocalization, taking into account the contribution of electrostrictive volume contraction, *i.e.*, the more the charge delocalizes in the transition state, the less negative the values of activation volume become.[7]

A further characteristic is the rate acceleration of sterically hindered reactions by pressure. It has been said that a more sterically hindered reaction revealed a more negative activation volume.[13,14]

The present investigation concerns the pressure effect on the hydrolysis rates of some substituted 1-phenylethyl and benzyl chlorides in order to elucidate the relationships between steric and pressure effect in solvolytic reactions.

Experimental

The high pressure apparatus has been described elsewhere.[7] The kinetic solvent was ethanol–water (80: 20, v/v) and all reactions were conducted at 25.00±0.02 °C, and followed conductimetrically under pressure. The initial concentration of the kinetic solution was approximately 0.01 mol per liter. Rate constants were calculated by the Guggenheim method[15] or by the first-order rate equation.[16]

Results and Discussion

Solvolyses of the substrates under pressure followed first-order kinetics. In the case of 1-arylethyl chlorides, plots of the logarithm of the rate constants against pressure showed linearity over the range of pressure employed. Accordingly, activation volumes were calculated by the following equation; $RT(\delta \ln k/\delta P)_T = -\Delta V_0^*$, where k is the rate constant and ΔV_0^* is the activation volume at atmospheric pressure and 25 °C. For trialkylbenzyl chlorides, plots of $\ln k$ against pressure revealed curvatures. In these cases the activation volume was calculated assuming the following second-order polynomial equation; $\ln k = a + bP + cP^2$ and the curves fitted using the least-squares method. Since the enthalpies and entropies of activation for the hydrolyses of 1-arylethyl chlorides in 80% ethanol were not available, solvolyses have been conducted at 15.00, 25.00, 35.00, and 45.00±0.01 °C under atmospheric pressure.

For solvolytic reactions, the relationship between steric hindrance and activation volume has not been fully investigated. LeNoble and Shurpic examined the pressure effect on the solvolysis of several sterically hindered cycloalkyl arenesulfonates but unfortunately the difference in the values of the activation volume for hindered and unhindered substrates was small.[4]

TABLE 1. PRESSURE DEPENDENCE OF FIRST-ORDER RATE CONSTANTS FOR THE SOLVOLYSIS OF 1-ARYLETHYL CHLORIDES IN ETHANOL–WATER (80: 20, v/v) AT 25.0 °C

Pressure / kg cm^{-2}	Rate constant/10^{-5} s^{-1} Ar			
	Phenyl	*o*-Tolyl	*p*-Tolyl	2,6-Xylyl
1	1.14	12.8	54.9	26.5
250	1.27	14.9	63.2	30.2
500	1.58	17.6	72.3	34.2
750	1.64	18.6	78.9	38.2
1000	1.87	23.0	85.2	42.5
ΔV_0^* / cm^3/mol	−12.6	−14.1	−11.1	−11.8

The activation volumes for the hydrolyses of 1-arylethyl chlorides are listed in Table 1. The activation volume of the parent 1-phenylethyl chloride was found to be −12.6 cm^3/mol. For 1-(*p*-tolyl)ethyl chloride a rather loose solvation shell might be expected in the transition state where the developing charge is highly delocalized by the resonance effect and hence the activation volume became less negative (−11.4 cm^3/mol). The introduction of one methyl group at the ortho position in the parent chloride showed a rate enhancement of 11 fold, a value lower than expected due to the steric inhibition of resonance (compare to 45 fold by *p*-methyl group). Thus, the activation volume was found to be −14.1 cm^3/mol, more negative than the parent chloride. The volume contraction in this case resulted from a tight transition state solvation shell around the reaction center where some charge localization appears as a result of the steric inhibition of

Table 2. First-order rate constants for the solvolysis of 1-arylethyl chlorides in ethanol–water (80: 20, v/v)

Temperature °C	Rate constant/10^{-5} s^{-1} Ar			
	Phenyl	*o*-Tolyl	*p*-Tolyl	2,6-Xylyl
15.0	—	3.60	15.3	9.00
25.0	1.14	12.1	51.8	25.9
35.0	3.10	43.3	198	98.9
45.0	9.82	—	—	—
$\Delta H^{\ddagger}_{25°C}$ / kcal mol^{-1}	21.3	21.3	21.8	20.5
$\Delta S^{\ddagger}_{25°C}$ / e.u.	−10.2	−4.9	−0.3	−10.2

resonance. This violation of a general understand ing—the more reactive, the less negative,[7,8]—stems from steric reasons.

The additional introduction of the second methyl group at the ortho position revealed a smaller rate enhancement (2 fold); *i.e.* the steric inhibition of resonance operated more strongly making the charge more localized. Consequently, electrostrictive interaction with the solvent molecules should be strong so that a more negative activation volume is expected. However, this was not the case. The observed value was −11.8 cm^3/mol, less negative than that for 1-(*o*-tolyl)-ethyl chloride. A reasonable explanation is that the solvation at the reaction center is strongly restricted by the two ortho substituents and thus the desolvation effect is responsible for the less contracted transition state volume.

Recently, the hydrolyses of 2,4,6-trialkylbenzyl chlorides have been reported,[17] and these chlorides offer a good model to demonstrate sterically hindered solvolysis. As shown in Table 3, the hydrolysis rate of 2,4,6-triisopropylbenzyl chloride was somewhat smaller than that of 2,4,6-trimethylbenzyl chloride. The reason of this rate retardation is complex: the possible operation of steric inhibition of resonance, decreasing hyperconjugative effect, and increasing inductive effect. Considering the bulkiness of the isopropyl groups, the steric effect may predominate. The value of the activation volume for the triisopropyl compound was found as −18.4 cm^3/mol, a value more negative than that for the trimethyl compound (−17.3 cm^3/mol). Again, sterically inhibited resonance is associated with a more negative activation volume. The reactivity of tri-*t*-butylbenzyl chloride was unexpectedly high as shown in Table 3. The presence of steric acceleration in this solvolysis is highly possible,[15] and the value of the activation entropy implies the existence of steric hindrance to solvation. The examination of solvolysis under pressure gave an activation volume of −15.7 cm^3/mol. Thus, as in the case of 1-(2,6-xylyl)ethyl chloride, the presence of bulky substituents near the reaction center results in a less negative activation volume. This observation should be strong evidence for the large steric hindrance by substituents to solvation.

Table 3. Pressure dependence of first-order rate constants for the solvolysis of trialkylbenzyl chlorides in ethanol–water (80: 20, v/v) at 25.0 °C

Pressure bar	Rate constant/10^{-5} s^{-1}		
	2,4,6-Trimethyl-	2,4,6-Triisopropyl-	2,4,6-Tri-*t*-butyl-
1	3.61	0.996	19.8
250	4.29	1.16	24.2
500	5.12	1.42	26.4
750	5.70	1.61	29.7
1000	6.83	1.87	32.8
1250	7.54	2.25	35.7
1500	8.45	2.50	37.3
$\Delta V^{\ddagger}_{0}$ / cm^3 mol^{-1}	−17.3	−18.4	−15.7
$\Delta S^{\ddagger}_{25°C}$ [a] / e.u.	−11.0	−10.4	+0.3

a) See Ref. 17.

Electrostriction is the phenomenon where a strong electrostatic interaction is exerted between a highly polar species and solvent molecules, and consequently the entropy of the system in general decreases. Actually in some reactions which have large negative activation volumes, the activation entropies are large and negative.[1] In some instances, an approximate proportionality between activation volume and activation entropy has been observed.[7] In the present reactions, however, Tables 2 and 3 show that there is no correlation between these two activation parameters.

In conslusion, it appears that the steric inhibition of resonance results in a more negative activation volume. However, with bulkier substituents the steric hindrance to solvation becomes predominant, and consequently a less negative activation volume is observed.

The present work has been supported in part by a Grant-in-Aid for Scientific Research (247021, 1977) from the Ministry of Education and Grants for Fundamental Research in Chemistry (1976).

References

1) W. J. leNoble, *Prog. Phys. Org. Chem.*, **5**, 207 (1967).
2) A. B. Lateef and J. B. Hyne, *Can. J. Chem.*, **47**, 1369 (1969); **48**, 2025, 2416, 2494 (1970); **49**, 2394, 3840 (1971).
3) B. T. Baliga and E. Whalley, *Can. J. Chem.*, **48**, 528, 2021 (1970); *J. Phys. Chem.*, **73**, 654 (1969).
4) W. J. leNoble and A. Shurpik, *J. Org. Chem.*, **35**, 3588 (1970).
5) S. Hariya and S. Terasawa, *Nippon Kagaku Zasshi*, **90**, 765 (1969).
6) D. Buettner and H. Heydtmann, *Ber. Bunsenges. Phys. Chem.*, **73**, 640 (1969).
7) A. Sera, T. Miyazawa, T. Matsuda, Y. Togawa, and K. Maruyama, *Bull. Chem. Soc. Jpn.*, **46**, 3490 (1973).
8) C. Yamagami, A. Sera, and K. Maruyama, *Bull. Chem. Soc. Jpn.*, **46**, 3864 (1973); **47**, 704 (1974).
9) C. Yamagami, A. Sera, and K. Maruyama, *Bull. Chem. Soc. Jpn.*, **47**, 881 (1974).
10) K. R. Brower, *J. Am. Chem. Soc.*, **82**, 4534 (1960).

11) H. Heydtmann and B. Steiger, *Ber. Bunsenges. Phys. Chem.*, **70**, 1095 (1966).
12) K. J. Laidler and R. Martin, *Int. Chem. Kinet.*, **1**, 113 (1969).
13) W. J. leNoble and Y. Ogo, *Tetrahedron*, **26**, 4119 (1970).
14) N. I. Prokhova, B. S. El'anov, and M. G. Gonikberg, *Bull. Acad. Sci. U.S.S.R., Chem. Ser.*; *English Transl.*, 256 (1967).
15) E. A. Guggenheim, *Phil. Mag.*, **2**, 538 (1929).
16) A. A. Frost and R. G. Pearson, "Kinetics and Mechanism," John Wiley & Sons Inc., New York (1953), p. 27.
17) L. R. C. Barklay, H. R. Sonaware, and J. C. Hudson, *Can. J. Chem.*, **50**, 2318 (1972).

The Beckmann Rearrangement in Concentrated Sulfuric Acid. Studies by Means of NMR and Kinetic Isotope Effect

Seung-Geon KIM,† Takeo KAWAKAMI, Takashi ANDO,* and Yasuhide YUKAWA

The Institute of Scientific and Industrial Research, Osaka University, Yamadakami, Suita, Osaka 565

(Received June 14, 1978)

The mechanism of the Beckmann rearrangement of acetophenone (a) and 1-phenyl-2-propanone (b) oximes in concd sulfuric acid was elucidated by means of NMR spectroscopy and the carbon-14 kinetic isotope effect. For (a), the postulated reactive species acetophenone oxime hydrogensulfate was detected, the absence of hydrolysis of the oxime during the course of the reaction being verified. Positive carbon-14 kinetic isotope effect at the phenyl-1, $k^{12}/k^{14}=1.026$ at 40 °C and 1.019 ± 0.005 at 60 °C, confirmed a definite change in bonding of the phenyl-1 carbon in the transition state of the reaction. Concertedness of the rearrangement was thus established. For (b), sulfonation of the benzene ring prior to the rearrangement was observed, kinetic isotope effect study being found to be useless.

The Beckmann rearrangement, the reaction of ketoximes to give amides by the action of many kinds of acidic reagents, has been extensively studied for many years.[1,2] Stereochemical studies showed that the reaction is an intramolecular trans rearrangement. The kinetics of the reaction of *O*-picryl ethers of substituted benzophenone[3] and acetophenone oximes[4] in organic solvents revealed the nucleophilic nature of the rearrangement; electron-donating groups accelerate the reaction. However, the actual rearranging species are still not clear in many cases. Concertedness of the reaction has also not been verified completely. Gregory *et al.* reported a kinetic study on the rearrangement of substituted acetophenone oximes in sulfuric acid.[5] They proposed that the reactive species in concd sulfuric acid (>70%) is an oxime hydrogensulfate and that the transition state has a phenonium ion-like structure in which the leaving hydrogensulfate ion is still partially bonded to the nitrogen atom. This mechanism is substantially similar to the one postulated by Huisgen *et al.*[4] for the rearrangement of acetophenone oxime *O*-picryl ethers in 1,4-dichlorobutane.

On the other hand, studies on kinetic isotope effects give the most decisive information on the structure of transition state. A study on the Beckmann rearrangement along these lines was reported in the reaction of acetophenone and *anti*-1-phenyl-2-propanone oximes labeled with carbon-14 in concd sulfuric acid.[6] However, reverse isotope effects in both cases of acetophenone-*phenyl*-1-^{14}C oxime ($k^{12}/k^{14}=0.893$) and *anti*-1-phenyl-2-propanone-1-^{14}C oxime ($k^{12}/k^{14}=0.951$) were disproved by Glover and Raaen.[7] They claimed that acetophenone oxime is partially hydrolyzed to acetophenone during the course of the reaction, and that kinetic isotope effect study is meaningless under these conditions.

In this paper, evidence for the absence of hydrolysis under the reaction conditions is presented.[8] The mechanism of the rearrangement is discussed using the revised data of carbon-14 kinetic isotope effects.

† Present address: Department of Chemistry, Faculty of Science, Tokai University, Kitakaname, Hirazuka, Kanagawa 259-12.

Results and Discussion

NMR Study. When a solution of acetophenone oxime (**1**) in 99.0% sulfuric acid (210 mg in 6 ml) was placed in a NMR probe preheated at 60 °C, the first change observed was the appearance of a new methyl signal at 3.17 ppm from tetramethylsilane as an external standard, together with that of the oxime at 2.88 ppm (Figs. 1a and b). The signal at 3.17 ppm was neither one of the methyl signals of acetanilide (**4**) nor that of acetophenone (**7**); the spectrum of **4** taken for comparison showed the methyl signals at 2.70 and 2.38 ppm in the same solvent (Fig. 1i). As the reaction proceeded, the signals of the rearranged product **4** appeared as expected but decreased again (Figs. 1c, d, and e). The new signals taking the place of those of **4** had an aromatic AA'BB' pattern (Fig. 1f), which was identified as that of 4-acetylaminobenzenesulfonic acid (**5**) by comparison with the spectrum of the authentic sample (Fig. 1j). It was not the final product, however, slow hydrolysis of **5** to acetic acid and 4-aminobenzenesulfonic acid (**6**)

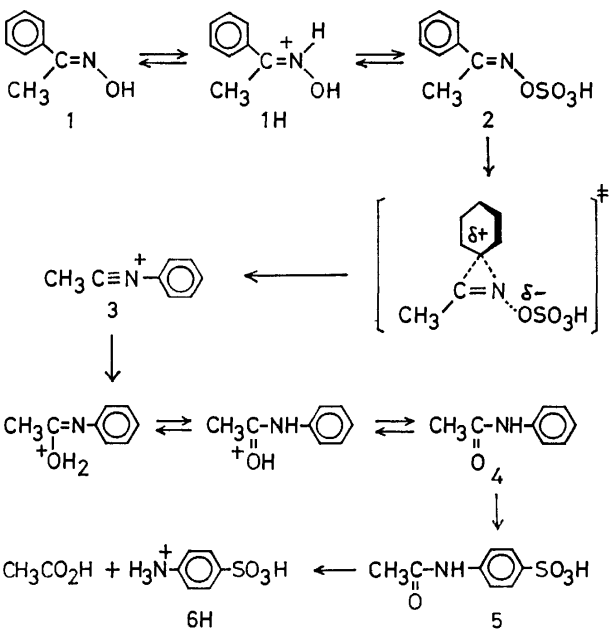

Scheme 1.

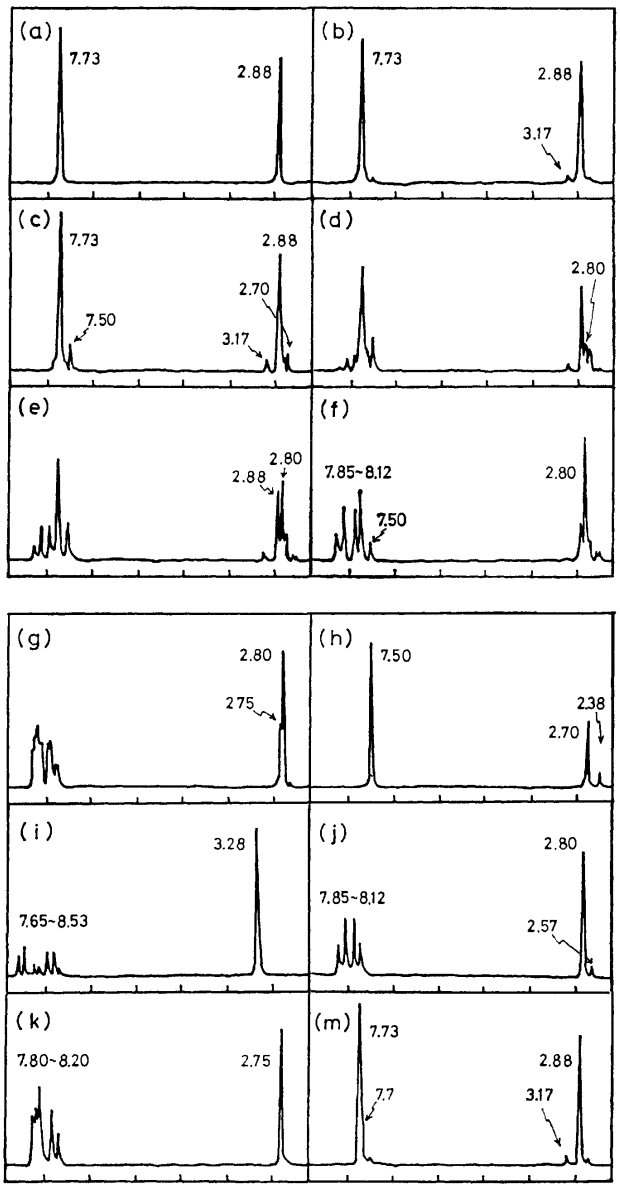

Fig. 1. NMR spectra of the reaction of acetophenone oxime (**1**) in 99.0% sulfuric acid at 60 °C and of reference compounds. (a) Acetophenone oxime (**1**); (b) after 2 min; (c) at 20% reaction; (d) at 40% reaction; (e) at 60% reaction; (f) at 80% reaction; (g) at "infinity"; (h) acetanilide (**4**); (i) acetophenone (**7**); (j) 4-acetylaminobenzenesulfonic acid (**5**); (k) 4-aminobenzenesulfonic acid (**6**) and acetic acid; (m) acetophenone oxime hydrogensulfate (**2**). ppm values from external tetramethylsilane are cited.

being observed later (Figs. 1g and k). The observations lead to a mechanistic scheme (Scheme 1) similar to that of Gregory *et al.*[5]

The structure of the species showing a methyl resonance at 3.17 ppm should be clarified. Gregory *et al.* also detected intermediates spectroscopically in the rearrangement of the oximes of 2-bromo-, 2-iodo-, 2-methyl-, and 2,4,6-trimethylbenzophenone, and 5,6,7,8,-9,10-hexahydrobenzocyclooctene-5-one. From kinetic and spectroscopic evidences, they concluded that the structure of the intermediates should be *N*-arylnitrilium ions. The chemical shifts of the α-methyl groups of these ions were reported to be 3.65—3.85 ppm, which are distinct from 3.17 ppm we observed. The difference of 0.5—0.7 ppm is too large to be attributed to the substituent effect. The species which shows methyl resonance at 3.17 ppm thus would not be *N*-phenylnitrilium ion (**3**). For the sake of comparison, acetophenone oxime hydrogensulfate (**2**) was prepared[9] and dissolved in concd sulfuric acid. The spectrum obtained was similar to that of the reaction solution at an early stage (Fig. 1m); a small methyl signal at 3.17 and a large one at 2.88 ppm, indicating that most of **2** was hydrolyzed to the original oxime in the solution. The intensity ratio of the two peaks remained constant at *ca.* 1 : 10 until 60% of the reaction was completed, after which the peak at 3.17 ppm was too small to be measured accurately. Kinetic treatment of NMR intensities of these methyl signals gave a linear plot with $k=(2.0\pm 0.1)\times 10^{-4}\ s^{-1}$ when the compound showing an absorption at 3.17 ppm was regarded as a species before the rearrangement step. The rate constant agrees fairly well with the value obtained by the gravimetric method, $k=(1.90\pm 0.01)\times 10^{-4}\ s^{-1}$, under the same conditions (*vide infra*). These results indicate that the observed species is acetophenone oxime hydrogensulfate (**2**), which has been postulated to be the reactive species of the rearrangement in concd sulfuric acid.[5]

Throughout the reaction, no signal due to acetophenone (**7**) was detected at all. Furthermore, the reaction solution after 40 h at 60 °C was negative to the 2,4-dinitrophenylhydrazine test. As acetophenone was confirmed to be stable under the reaction conditions, the results prove that acetophenone oxime is not hydrolyzed in 99% sulfuric acid. It is in line with the observations by Gregory *et al.*, who studied the kinetics of the hydrolysis of acetophenone oxime in sulfuric acid of concentration less than 70%.[5,10] Glover and Raaen gave no experimental detail; they might have mistaken the hydrolysis during isolation for that during reaction.[7]

A similar experiment on *anti*-1-phenyl-2-propanone oxime (**8**) at 50 °C showed that the first stage of the reaction in 99.0% sulfuric acid is rapid sulfonation of the benzene ring mainly at the para-position to give 4-(2-hydroxyiminopropyl)benzenesulfonic acid (**9**). The sulfonated benzyl group in **9** rearranges very slowly to 4-(acetylaminomethyl)benzenesulfonic acid (**10**) in the next stage (Scheme 2). Other minor peaks were observed at each stage of the reaction, most of which may be attributed to the presence of isomers other than the para sulfonated ones. Since **9** gave no precipitate of the 2,4-dinitrophenylhydrazone, the gravimetric method followed sulfonation and not rearrangement. Kinetic isotope effect study has no meaning in this case.[6,7]

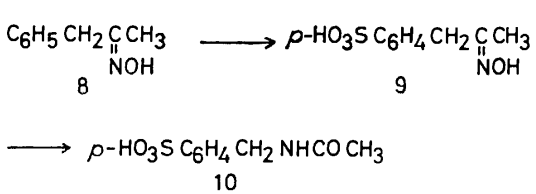

Scheme 2.

Differences in the observations by Gregory *et al.*[5] and by us are interesting; they detected *N*-arylnitrilium ions by UV and NMR and we observed the oxime hydrogensulfate by NMR. However, the two observations do not seem to be in conflict with each other. They recognized that ortho substituents were necessary for the detection of *N*-arylnitrilium ions. On the contrary, oxime hydrogensulfates should have no characteristic absorptions differing from those of oximes in the UV region. We have obtained information that the esterification equilibrium of oximes with sulfuric acid seems to be very sensitive to the concentration of sulfuric acid and the structure of the oximes. NMR spectroscopy is known to be less effective for detecting a small quantity of species present in solution.

Isotope Effect Study. Since the absence of hydrolysis of acetophenone oxime (**1**) under the reaction conditions was established, carbon-14 isotope effects were reexamined. In a previous work, the radioactivity was measured by G. M. counting of barium carbonate disks prepared by wet oxidation of the 2,4-dinitrophenylhydrazone (**11**) derived from the unreacted acetophenone oxime.[6] This is a well-established but old-fashioned method and said to be "the least sensitive and the least precise" one.[11a] In the present reinvestigation, the carbon dioxide gas prepared by wet oxidation of **11** was assayed for radioactivity by the ionization-chamber counting method. The ionization current was measured with a vibrating-reed electrometer by the rate-of-charge method.[11b] By use of this method, the accuracy of the measured radioactivity was much improved.

Acetophenone-*phenyl*-1-^{14}C (**7**-^{14}C) was prepared from benzoyl-*phenyl*-1-^{14}C chloride.[12] Benzoic-*phenyl*-1-^{14}C acid was prepared by the multi-step synthesis from barium carbonate-^{14}C.[13] The overall yield of acetophenone-*phenyl*-1-^{14}C oxime (**1**-^{14}C) from barium carbonate-^{14}C was *ca.* 4.5% (Scheme 3).

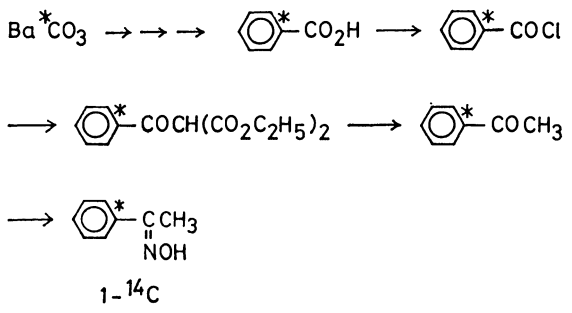

Scheme 3.

In order to measure the rates of rearrangement by the gravimetric method, quantitative isolation of the unreacted **1** as **11** was confirmed under the conditions similar to those applied in the reaction. Yield of **11** were 100.5±0.5% for 40—120 mg of **1**.

The rearrangement of **1** in 99.0% sulfuric acid at 0.25 M concentration was followed at 40 and 60 °C. Aliquots of the reaction solution were pipetted out at appropriate time intervals and poured into 0.4% solutions of 2,4-dinitrophenylhydrazine in 2 M hydrochloric acid. First-order rate plots by the gravimetric method using **11** gave straight lines throughout 85% reaction with correlation coefficients greater than 0.9996. The rate constants obtained were $(1.47\pm0.03)\times10^{-5}$ s^{-1} at 40.00±0.01 °C (average of three runs) and $(1.90\pm0.01)\times10^{-4}$ s^{-1} at 60.00±0.01 °C (average of four runs).

The reaction of the labeled compound (**1**-^{14}C) was carried out in the same way. The rate constants were $(1.42\pm0.01)\times10^{-5}$ s^{-1} and $(1.85\pm0.02)\times10^{-4}$ s^{-1} at 40 and 60 °C, respectively. The radioactivity of the purified samples of **11**-^{14}C was assayed with a Nuclear-Chicago Model 6000 Dynacon electrometer system by the rate-of-charge method using a Model T4 interval timer. Oxidation of the samples to carbon dioxide was performed with a Model GW-1 glassware system by the modified Van Slyke-Folch wet combustion method.[14]

Table 1. Reaction percentage and specific radioactivities in the rearrangement of **1**-^{14}C at 40.00±0.01 °C

No.	t/min	x[a]/%	n[b]	A_x[c]/mCi mol^{-1}
1	0	0	5	1.397
2	240	18.2	2	1.405
3	420	30.4	2	1.410
4	600	40.7	2	1.414
5	780	49.3	2	1.418
6	1020	58.6	2	1.430
7	1320	67.7	2	1.436
8	1740	77.0	2	1.450

a) Fraction of reaction. b) Number of measurements. c) Specific radioactivity.

Table 2. Reaction percentage and specific radioactivities in the rearrangement of **1**-^{14}C at 60.00±0.01 °C

No.	t/min	x[a]/%	n[b]	A_x[c]/mCi mol^{-1}
1	0	0	8	1.300
2	21	18.7	3	1.310
3	31	27.8	3	1.307
4	44	38.2	2	1.307
5	60	48.7	2	1.311
6	78	58.5	3	1.311
7	103	68.3	3	1.332
8	141.5	78.6	2	1.326

a) Fraction of reaction. b) Number of measurements. c) Specific radioactivity.

The results obtained are given in Tables 1 and 2. The specific radioactivities cited are the mean values of two to eight measurements of oxidation analysis for each sample with standard deviations within 0.5%.[15] Kinetic isotope effects were calculated by the linear regression method by means of

$$\log A_x = \log A_0 - [1-(k^{14}/k^{12})]\log(1-x), \quad (1)$$

where x is the fraction of reaction and A_0 and A_x are the specific activities of **11**-^{14}C at $x=0$ and $x=x$, respectively. The calculated isotope effects are given by

$$k^{12}/k^{14} = 1.026 \pm 0.001 \ (40\,^{\circ}C)$$

and

Table 3. Reaction percentage and specific radioactivities in the rearrangement of 1-^{14}C at 59.99±0.01 °C

No.	t/min	$x^{a)}$/%	$n^{b)}$	$A_x^{c)}$/mCi mol^{-1}
1	0	0	1	1.582
2	29	28.5	1	1.594
3	55	48.1	1	1.595
4	80	62.2	1	1.635
5	105	71.8	1	1.655
6	130.5	79.3	1	1.631
7	160	85.4	1	1.647

a) Fraction of reaction. b) Number of measurements. c) Specific radioactivity.

$$k^{12}/k^{14} = 1.014 \pm 0.003 \quad (60\,°C).$$

In order to make the results more reliable, another series of experiment at 60 °C was carried out using another lot of materials. The results are given in Table 3. The calculated isotope effect is given by

$$k^{12}/k^{14} = 1.023 \pm 0.006 \quad (60\,°C).$$

Calculation using the data reported by Glover and Raaen[7] by means of Eq. 1 gave the phenyl-1-^{14}C isotope effect of 1.028±0.006 at 62±1 °C, although the data are scanty. From the results of the present reinvestigation and of Glover and Raaen, all the data reported earlier[6] should have been accompanied by large errors inherent to old techniques and should be retracted.

Carbon-14 kinetic isotope effects of 1.4—2.6% are too large to be classified as secondary effects,[17] and should reflect some change in the bonding of the phenyl-1 carbon in the rate-determining transition state of the rearrangement. As has been verified from the tracer study using ^{18}O that the loss of the oxygen function from an oxime occurs in an irreversible step,[5] the present results of kinetic isotope effects are inconsistent with the stepwise mechanism (path A), giving an evidence for the concerted nature (path B) of the rearrangement (Scheme 4).

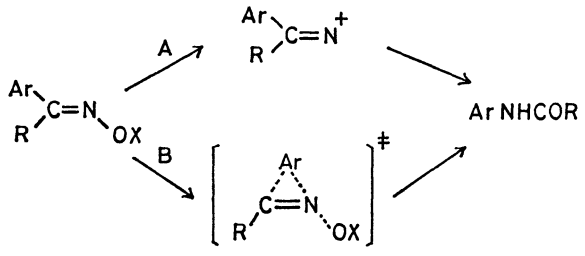

Scheme 4.

The large positive values of the resonance parameter, r, in the LArSR (linear aromatic substituent-reactivity) relationship (Eq. 2) of the Beckmann rearrangement (r=0.60—0.63) also indicate the additional conjugation effect to the reaction center in the transition state.[4,18-20]

$$\log k/k_0 = \rho(\sigma^\circ + r\Delta\bar{\sigma}_R^+) \qquad (2)$$

Thus, the mechanism (Scheme 1) has been further ensured.

The fact that the carbon-14 kinetic isotope effect at the phenyl-1 position is normal (positive) should be discussed. Decrease in force constant in the transition state leads in the direction of a normal isotope effect, an increased one in the direction of an inverse effect.[21,22] Bond formation between the phenyl-1 carbon and the nitrogen may cause an increase in bonding of the carbon. Nevertheless, actual observation of the normal effects at the phenyl-1 carbon can be attributed to a great extent to a decrease in bonding as a result of insulation of the carbon from the aromatic conjugation present at the initial state. Inverse carbon isotope effects caused by the appearance of additional bonding of conjugation have been reported in some cases.[23] Weakening of the bond between the phenyl-1 and carbonyl carbons might make some contribution to the phenomenon. Similar phenomena were observed in some other 1,2-nucleophilic rearrangements as well as in solvolysis with neighboring phenyl participation.[20,24,25] The normal temperature dependence, a larger isotope effect at a lower temperature, though not obvious because of an experimental error, is also considered to be an indication of a decrease in bonding at the transition state. In the case of bond rupture the temperature-dependent factor of the kinetic isotope effect is considered to increase from the higher temperature limit of unity with lowering in temperature.[25,26]

No reexamination was carried out on the kinetic isotope effect at the carbonyl carbon of acetophenone oxime.[6] However, treatment of the data of Glover and Raaen with use of Eq. 1 gave a normal isotope effect at this carbon, k^{12}/k^{14}=1.028±0.004, at 62 °C.[7] This indicates that bonding of this carbon also changes at the transition state of the rearrangement.[25] On the other hand, calculation of the isotope effects using the data of Glover and Raaen on the reaction of *anti*-1-phenyl-2-propanone oxime (**8**) shows that no effects are observed at both the methylene (k^{12}/k^{14}=1.002±0.002) and carbonyl (k^{12}/k^{14}=1.004±0.004) carbons. This is quite natural since the reaction that followed was actually the sulfonation of the benzene ring, and no bonding change at these two carbons is expected for the reaction.

Experimental

Materials. Acetophenone oxime hydrogensulfate (**2**) was prepared according to the procedure of Pearson and Ball[9] and dried over phosphorus pentaoxide in a vacuum at a low temperature. 4-Acetylaminobenzenesulfonic acid (**5**) was dried for many days in a vacuum at 100 °C before the NMR measurement.[27] *Anti*-1-phenyl-2-propanone oxime (**8**) was prepared according to the procedure of Kotera *et al.*:[28] mp 69.5—70.5 °C. All the compounds except **2** were subjected to elemental analysis, giving satisfactory results. Commercial sulfuric acid (99.0%, Wako guaranteed reagent) was used without further purification.

NMR Monitoring of the Reactions. NMR spectra were recorded on a Varian A-60 spectrometer at 60 MHz with tetramethylsilane as an external standard. All the samples were measured in concentrations of 3—5 (w/v)%. Operating temperature was calibrated using ethylene glycol signals. The NMR data are summarized in Table 4.

Table 4. Proton NMR spectroscopic data in concd sulfuric acid

Species	Chemical shifts and assignment[a)]
Acetophenone oxime (**1**)	2.88 (3H, s, CH_3), 7.73 (5H, s, aromatic)
Acetophenone oxime hydrogensulfate (**2**)	3.17 (3H, s, CH_3), 7.7 (5H, s, aromatic)
Acetanilide (**4**)	2.38 and 2.70 (3H, CH_3), 7.50 (5H, s, aromatic)
4-Acetylaminobenzenesulfonic acid (**5**)	2.57 and 2.80 (3H, CH_3), 7.85 and 8.12 (4H, J=7 Hz, aromatic AA'BB')
4-Aminobenzenesulfonic acid (**6**)	7.80 and 8.20 (4H, J=9 Hz, aromatic AA'BB')
Acetic acid	2.75 (CH_3)
Acetophenone (**7**)	3.28 (3H, s, CH_3), 7.65—8.53 (5H, m, aromatic)
1-Phenyl-2-propanone oxime (**8**)	2.50 (3H, s, CH_3), 4.02 (2H, s, CH_2), 7.25—7.45 (5H, m, aromatic)
4-(2-Hydroxyiminopropyl)benzenesulfonic acid (**9**)	2.50 (3H, s, CH_3), 4.15 (2H, s, CH_2), 7.58 and 8.04 (4H, J=8 Hz, aromatic AA'BB')
4-(*N*-Acetylaminomethyl)benzenesulfonic acid (**10**)	2.57 (3H, s, CH_3), 4.80 (2H, d, J=5.5 Hz, CH_2), 7.61 and 8.01 (4H, J=8 Hz, aromatic AA'BB'), 8.90 (1H, broad t, J=5.5 Hz, NH)

a) ppm from external tetramethylsilane.

*Preparation of Acetophenone-*phenyl-*1-*^{14}C *Oxime (1-*^{14}C*).* Benzoic-*phenyl*-1-^{14}*C* acid (4.45 g, 13.6 mCi/mol) was prepared from 7 mCi of barium carbonate-^{14}*C* by the multistep syntheses,[13] radiochemical yield being 7.1%. After dilution with nine times an unlabeled benzoic acid, 15 g of the acid (1.36 mCi/mol) was dissolved in 60 ml of dry ether. After addition of 23 g of thionyl chloride, the mixture was refluxed for 1 h. Benzoyl-*phenyl*-1-^{14}*C* chloride (16.5 g) was isolated by distillation: bp 97—98 °C/30 Torr.

Magnesium ethoxide was prepared from 2.7 g of a magnesium ribbon, 2.5 ml of anhydrous ethanol, and a few drops of carbon tetrachloride in 40 ml of dry ether. Diethyl malonate (17.1 g) in 10 ml each of anhydrous ethanol and ether was added to the above mixture and refluxed until all the magnesium was consumed. The benzoyl-*phenyl*-1-^{14}*C* chloride obtained above was added to this mixture with a small amount of ether and refluxed for 30 min. The reaction mixture was cooled and acidified with 20% sulfuric acid. The ether layer and the ether extract were combined and washed with water, and the solvent was distilled. To the residue was added a mixture of 30 ml of acetic acid, 3.8 ml of concd sulfuric acid, and 30 ml of water, and the mixture was refluxed for several hours until decarboxylation was complete. The reaction mixture was cooled in an ice-bath, made alkaline with 20% sodium hydroxide solution, and extracted with several portions of ether. The ether layer was washed with water and dried with anhydrous sodium sulfate, the solvent being removed. Acetophenone-*phenyl*-1-^{14}*C* (**7**-^{14}*C*: 11.0 g) was obtained by distillation: bp 100.0—101.5 °C/27—28 Torr.

7-^{14}*C* (11.0 g) was treated with 29.7 g of hydroxylamine hydrochloride and 55 g of potassium carbonate in a mixture of 100 ml of water and 500 ml of ethanol in the usual way. Acetophenone-*phenyl*-1-^{14}*C* oxime (**1**-^{14}*C*) obtained (10.8 g) was recrystallized from petroleum ether seven times, when the sample showed a constant radioactivity (1.300±0.003 mCi/mol): mp 60 °C.

Quantitative Isolation of Acetophenone Oxime (1) as the 2,4-Dinitrophenylhydrazone Derivative (11). Forty to 120 mg of **1** was taken in a 150-ml Erlenmeyer flask equipped with a ground glass stopper. Sixty ml of 0.4% 2,4-dinitrophenylhydrazine solution in 2 M hydrochloric acid was added and the resulting solution was kept at 50 °C for 24 h. After addition of 10 ml of distilled water, precipitates of **11** were filtered while warm with a glass filtering crucible, washed thoroughly with warm 2 M hydrochloric acid and then with warm distilled water. The crucible was dried in an oven at 85 °C for 24 h, cooled in a desiccator, and weighed. For repeated measurements, yields of **11** were 100.5±0.5% of the theoretical values.

Gravimetric Rate Measurement. Concd sulfuric acid (*ca.* 30 ml) was added to a weighed sample of **1** (*ca.* 1 g) and weighed. After being thoroughly shaken, the mixture was transferred to a reaction flask which had been heated in a thermostated bath. Aliquots of the solution were pipetted out at appropriate time intervals and poured rapidly into 0.4% solutions of 2,4-dinitrophenylhydrazine in 2 M hydrochloric acid. The quantities of the solutions pipetted out were determined by weighing the flasks before and after the addition. Precipitates of **11** were treated as mentioned above. The fractions of reaction were thus calculated from the observed and theoretical weights of **11**.

Radioactivity Measurement. Samples of the purified **11**-^{14}*C* (7—10 mg) were oxidized to carbon dioxide by the modified Van Slyke-Folch wet combustion method with a Nuclear-Chicago Model GW-1 glassware system. The radioactivities of the carbon dioxide gases collected in an ionization chamber were measured with a Nuclear-Chicago Model 6000 Dynacon electrometer system by the rate-of-charge method using a Model T4 interval timer. The samples were assayed after recrystallization three or four times from ethyl acetate–chloroform (2: 1). For the samples obtained at several stages of the reaction, it was confirmed that further recrystallization does not change the radioactivities beyond experimental errors (±0.5%).

References

1) P. A. S. Smith in "Molecular Rearrangements," ed by P. de Mayo, Interscience, London (1963), Part I, p. 483.
2) L. G. Donaruma and W. Z. Heldt, *Org. React.*, **11**, 1 (1960).
3) A. W. Chapman and F. A. Findler, *J. Chem. Soc.* **1936**, 448.
4) R. Huisgen, J. Witte, H. Walz, and W. Jira, *Justus Liebigs Ann. Chem.*, **604**, 191 (1957).
5) B. J. Gregory, R. B. Moodie, and K. Schofield, *J. Chem. Soc., B*, **1970**, 338.
6) Y. Yukawa and M. Kawakami, *Chem. Ind. (London)*, **1961**, 1401.
7) I. T. Glover and V. F. Raaen, *J. Org. Chem.*, **31**, 1987

(1966).

8) Part of this work appeared in communication form: Y. Yukawa and T. Ando, *J. Chem. Soc., D.*, **1971**, 1601.

9) D. E. Pearson and F. Ball, *J. Org. Chem.*, **14**, 118 (1949).

10) B. J. Gregory and R. B. Moodie, *J. Chem. Soc., B*, **1970**, 862.

11) a) V. F. Raaen, G. A. Ropp, and H. P. Raaen, "Carbon-14," McGraw-Hill, New York (1968), p. 208; b) *ibid.*, pp. 235—240.

12) H. G. Walker and C. R. Hauser, *J. Am. Chem. Soc.*, **68**, 1386 (1946).

13) a) A. Murray, III and D. L. Williams, "Organic Syntheses with Isotopes," Interscience, New York (1958), p. 34; b) *ibid.*, p. 102; c) M. Fields, M. A. Leaffer, S. Rothchild, and J. Rohan, *J. Am. Chem. Soc.*, **74**, 5498 (1952); d) G. A. Ropp, *ibid.*, **72**, 2299 (1950).

14) D. D. Van Slyke, J. Plazin, and J. R. Weisiger, *J. Biol. Chem.*, **191**, 299 (1951).

15) Measurements of the radioactivities were performed in 1965 and 1966. At present we can measure the activities as accurately as with standard deviations of 0.1—0.3% by use of the dry combustion method and with a new electrometer system. Thus, the accuracy of the kinetic isotope effect has been improved.[16] The level of inaccuracy in the present investigation does not affect the conclusion of this paper.

16) For example, see a) T. Ando, H. Yamataka, J. Kuramochi, J. Yamawaki, and Y. Yukawa, *Tetrahedron Lett.*, **1976**, 1879; b) H. Yamataka and T. Ando, *ibid.*, **1975**, 1059.

17) V. F. Raaen, A. K. Tsiomis, and C. J. Collins, *J. Am. Chem. Soc.*, **82**, 5502 (1960); M. Saunders, L. Telkowski, and M. R. Kates, *ibid.*, **99**, 8070 (1977).

18) Y. Yukawa, Y. Tsuno, and M. Sawada, *Bull. Chem. Soc. Jpn.*, **39**, 2274 (1966).

19) P. J. McNulty and D. E. Pearson, *J. Am. Chem. Soc.*, **81**, 612 (1959).

20) T. Imamoto, S.-G. Kim, Y. Tsuno, and Y. Yukawa, *Bull. Chem. Soc. Jpn.*, **44**, 2776 (1971).

21) G. A. Ropp, V. F. Raaen, and A. J. Weinberger, *J. Am. Chem. Soc.*, **75**, 3694 (1953).

22) C. L. Wilkins and T. W. Regulski, *J. Am. Chem. Soc.*, **94**, 6016 (1972); S. -H. Dai and W. R. Dolbier, Jr., *ibid.*, **94**, 3946 (1972).

23) a) Y. Yukawa, T. Ando, and T. Otsubo, *Bull. Chem. Soc. Jpn.*, **45**, 2645 (1972); b) A. J. Kresge, N. N. Lichtin, K. N. Rao, and R. E. Weston, Jr., *J. Am. Chem. Soc.*, **87**, 437 (1965).

24) a) Y. Yukawa and T. Ando, *Mem. Inst. Sci. Ind. Res., Osaka Univ.*, **34**, 39 (1977); b) Y. Yukawa, T. Ando, K. Token, M. Kawada, and S.-G. Kim, *Tetrahedron Lett.*, **1969**, 2367; **1971**, 847; c) Y. Yukawa, S.-G. Kim, and H. Yamataka, *ibid.*, **1973**, 373; d) B. W. Palmer and A. Fry, *J. Am. Chem. Soc.*, **92**, 2580 (1970).

25) A. Fry in "Isotope Effects in Chemical Reactions," ed by C. J. Collins and N. S. Bowman, Van Nostrand Reinhold, New York (1970), Chap. 6.

26) J. Bigeleisen, *J. Chem. Phys.*, **17**, 675 (1949).

27) E. Sakellarios, *Ber.*, **58**, 2286 (1925).

28) K. Kotera, T. Okada, and S. Miyazaki, *Tetrahedron*, **24**, 5677 (1968).

An ESR Study of Polysubstituted *N*-Aryl-*N*-(arylthio)aminyls[1]

Yozo MIURA,* Yosuke KATSURA, and Masayoshi KINOSHITA

Department of Applied Chemistry, Faculty of Engineering, Osaka City University, Sumiyoshi-ku, Osaka 558

(Received June 26, 1978)

An ESR spectroscopic investigation of *N*-(2,4,6-trimethyl-, trimethoxy-, triisopropyl-, and tri-*t*-butylphenyl)-*N*-(arylthio)aminyls (**2**), ArṄSAr′, is described. The aminyls are generated from the corresponding *N*-arylarenesulfenamides, ArNHSAr′, by hydrogen-abstraction, the a_N values of which are 9.10—12.30 G and the *g*-values 2.0056—2.0067. On the basis of the ESR parameters the conformations for **2** have been discussed. Decay kinetic studies on **2** were conducted in benzene, and **2** were found to be persistent aminyls—particularly the *t*-butyl-substituted aminyl, *N*-(2,4,6-tri-*t*-butylphenyl)-*N*-(4-nitrophenylthio)aminyl.

A new family of nitrogen-centered free radicals has been investigated in which one or two divalent sulfur atoms are adjacent to the central nitrogens.[2] In previous ESR studies on *N*-aryl-*N*-(arylthio)aminyls,[3,4] ArṄSAr′, it was established that, in the aminyls, the unpaired electron resides predominantly on the central nitrogen and the *N*-phenyl ring.

The present investigation was directed toward obtaining and isolating persistent *N*-aryl-*N*-(arylthio)-aminyls and for this purpose, several sterically protected thioaminyls have been prepared. In this report the ESR study on *N*-(2,4,6-trimethyl-, trimethoxy-, triisopropyl-, and tri-*t*-butylphenyl)-*N*-(arylthio)aminyls (**2**) is described.

Results and Discussion

Generation of Aminyls. The generation of **2** was achieved through hydrogen-abstraction from the appropriate *N*-arylarenesulfenamides (**1**, Eq. 2). Sulfenamides **1a**—**g** were obtained by the reaction of sulfenyl chlorides with two equivalents of anilines or one equivalent of anilines in the presence of triethylamine (Eq. 1). Sulfenamide **1h** was unobtainable by these procedures.

The hydrogen-abstraction of **1** was performed by two procedures: the photolysis of **1** in the presence of di-*t*-butyl peroxide,[5] and the treatment of **1** with lead dioxide in the presence of potassium carbonate. The ESR parameters obtained for **2** are listed in Table 1, and a typical ESR spectrum is illustrated in Fig. 1.

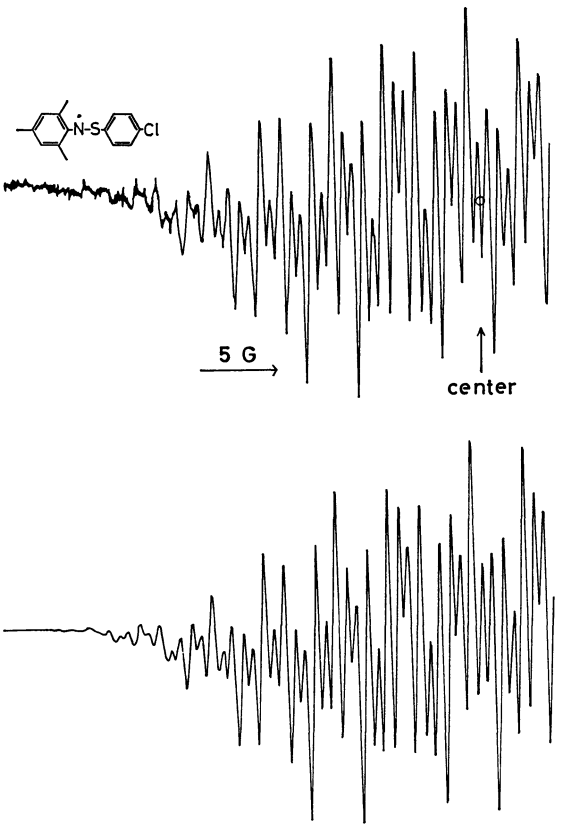

Fig. 1. Experimental ESR spectrum (low-field half) of **2a** in benzene (upper), and computer simulation, using Lorentzian line shapes and a line width of 0.52 G (lower).

Although **1h** could not be isolated as described above, the residue, resulting from filtration and subsequent concentration of the reaction mixture, gave rise to a strong 1:1:1 triplet ESR signal (12.27 G). The a_N value is in good agreement with that for the structurally similar aminyl, **2g** (12.30 G), and is quite different from that for the corresponding nitroxide, **3** (a_N: 16.40

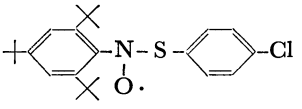

3

a: $R_1=CH_3$, $R_2=R_3=H$, $R_4=Cl$
b: $R_1=OCH_4$, $R_2=R_3=H$, $R_4=Cl$
c: $R_1=R_2=R_4=CH_3$, $R_3=Cl$
d: $R_1=OCH_3$, $R_2=R_4=CH_3$, $R_3=Cl$
e: $R_1=H$, $R_2=R_4=CH_3$, $R_3=Cl$
f: $R_1=i\text{-}C_3H_7$, $R_2=R_3=H$, $R_4=NO_2$
g: $R_1=t\text{-}C_4H_9$, $R_2=R_3=H$, $R_4=NO_2$
h: $R_1=t\text{-}C_4H_9$, $R_2=R_3=H$, $R_4=Cl$
i: $R_1=R_2=R_3=R_4=H$

TABLE 1. THE ESR PARAMETERS FOR *N*-ARYL-*N*-(ARYLTHIO)AMINYLS (**2**)[a]

	Coupling constant (G)									
		N-Phenyl ring			*S*-Phenyl ring				*g*-Value	λ_{max}[f] (nm)
	a_N	$a_{o\text{-H}}$	$a_{m\text{-H}}$	$a_{p\text{-H}}$	$a_{o\text{-H}}$	$a_{m\text{-H}}$	$a_{p\text{-H}}$	a_{other}		
2a[b]	9.32	—	1.29	—	0.79	g	—	3.56(*o*-CH_3), 4.92(*p*-CH_3)	2.0057	574
2b	9.10	—	g	—	g	g	—		2.0056	
2c[b]	9.50	—	1.22	—	—	—	—	3.61(*o*-CH_3),[c] 5.14(*p*-CH_3)[c]	2.0057	
2d	9.36	—	g	—	—	—	—		2.0057	
2e	9.84	4.15	1.30	4.36	—	—	—		2.0057	
2f	9.78	—	g	—	g	g	—		2.0056	
2g	12.30	—	g	—	g	g	—		2.0066	513, 545, 700
2h[d]	12.27	—	g	—	g	g	—		2.0067	
2i[e]	9.59	3.70	1.26	4.18	0.78	0.27	0.84		2.0059	

a) In benzene at room temperature (19 °C). b) The values of coupling constant were determined by computer simulation. c) In the *N*-phenyl ring. d) Ref. 7. e) Ref. 3. f) In benzene. g) Not resolved.

G, *g*-value: 2.0068 in benzene).[6] On the basis of these results, the species has been assigned as **2h**.

In the oxidation of the sulfenamides with lead dioxide, some of them gave purple or brown colored solutions.[7] For example, a benzene solution of **1a** immediately turned purple. Similarly, a solution of **1f** which was pale yellow turned reddish brown, and the pale yellow solution of **1g** turned dark brown. The colorled solutions gave rise to a strong ESR signal due to **2**. In the cases of **2a** and **2f**, the color faded in 10—20 min, and the resulting colorless (**2a**) or light orange solution (**2f**) no longer gave rise to a strong ESR signal. The brown color observed for **2g** persisted for several hours and, under deoxygenated conditions, persisted for several weeks without any apparent fading.

ESR Parameters. As may be seen from Table 1, the a_N values for **2a**—**f** are in the range 9.10—9.84 G, and the *g*-values in the range 2.0056—2.0057, being close to the value for the unsubstituted aminyl, **2i**. Thus, in these aminyls, the unpaired electron resides predominantly on the central nitrogen and the *N*-phenyl ring, as well as in **2i**. The a_N values for the *t*-butyl-substituted aminyls, **2g** and **2h**, are in the range 12.27—12.30 G, being 2.5—3.2 G larger than for the other aminyls, they are rather close to that (11.89 G) observed for *N*-(4-nitrophenylthio)-*t*-butylaminyl (**4**).[8] The

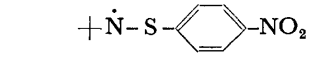

4

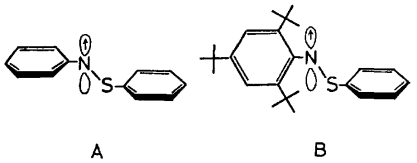

A B

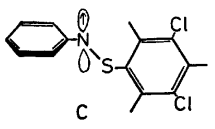

C

Fig. 2.

relatively large a_N values observed for **2g** and **2h** may be explained as follows: in **2i**, the *N*-phenyl ring is probably perpendicular or nearly perpendicular with respect to the nitrogen $2p_z$ orbital containing the unpaired electron (conformation A). The aminyls **2g** and **2h** cannot adopt such a conformation because of the steric repulsion between the two *ortho-t*-butyl groups and the sulfur atom (and/or the ortho-protons in the *S*-pheny ring), as shown by a molecular model (Stuart model). Thus, the steric effect results in the *N*-phenyl ring twisting to be parallel or nearly parallel with respect to the nitrogen $2p_z$ orbital (conformation B). Therefore, in **2g** and **2h**, the unpaired electron is not effectively delocalized onto the *N*-phenyl ring, differing from the other aminyls, leading to an increase in the magnitude of the a_N values. The *g*-values (2.0066—2.0067) observed for **2g** and **2h** are larger than those for the other aminyls (2.0056—2.0059), indicating that the spin density on the sulfur atoms in **2g** and **2h** is greater compared with the other aminyls.[9] Thus, the steric situation assumed for **2g** and **2h** may be also supported by the relatively large *g*-values.

The a_N values for **2a** and **2b** are smaller by 0.3—0.5 G compared with that for **2i**, suggesting that the aminyls adopt conformation A, despite the introduction of methyl or methoxyl groups into the ortho-positions of the *N*-phenyl ring. In a previous report,[10] *N*-aryl-*N*-(phenylthio)aminyls, in terms of Walter's criteria, were classified as class *S*, *i.e.* the magnitude of the a_N values is determined predominantly by the degree of delocalization of the unpaired electron onto the substituents in the *N*-phenyl rings, and the polar effect is of secondary importance (Scheme 1). Therefore, the reduction in the magnitude of the a_N values observed for **2a** and **2b** is interpreted in terms of the delocalization of the unpaired electron onto the methyl and methoxyl groups.

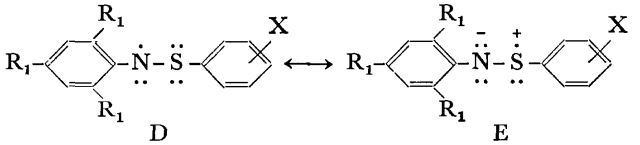

D E

Scheme 1.

The a_N value for **2f** is slightly larger (0.2 G) compared with that for **2i**, suggesting that the *N*-phenyl ring in **2f** is twisted to some extent due to the steric repulsion from the relatively large isopropyl groups in the *N*-phenyl ring.

The a_N values for **2c**, **2d**, and **2e** are larger by 0.18—0.26 G compared with those for the aminyls, **2a**, **2b**, and **2i**. These increases are interpreted in two ways: a) increase in the relative importance of the resonance form D caused by the inductive effect of the substituents in the *S*-phenyl rings, and b) twisting of the *S*-phenyl rings caused by the steric repulsion from the *ortho*-methyl groups in the *S*-phenyl rings. With respect to the inductive effect, the total σ value for the substituents in the *S*-phenyl rings is calculated to be 0.23 ($3\sigma_{p\text{-CH}_3}+2\sigma_{Cl}$),[11] which is identical to the $\sigma_{p\text{-Cl}}$ value. From a comparison of the a_N value for **2k**[12] with that for **2j**,[3] it may be seen that the magnitude of the a_N value for **2k** is little affected by the chlorine atom in the *S*-phenyl ring. Thus, the increases observed for **2c**, **2d**, and **2e** are not due to the inductive effect, but should be interpreted in terms of the twisting of the *S*-phenyl rings (conformation C). Since the spin density on the *S*-phenyl rings of these aminyls is very small, as can be seen from the a_H values due to the *S*-phenyl aromatic protons (0.27—0.84 G), the increase in magnitude of the a_N values caused by the twisting of the *S*-phenyl rings, is not as large as in **2g** and **2h**.

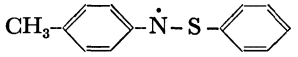

2j: a_N=9.55 G

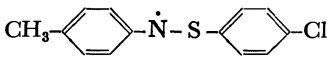

2k: a_N=9.52 G

Decay Kinetics of 2. Decay kinetic studies on **2a**, **2c**, and **2g** were conducted at 19 °C in the dark. A benzene solution containing **1** and di-*t*-butyl peroxide was irradiated with a high-pressure mercury lamp, and the decay rates were followed by measuring the ESR signal intensities. The results are illustrated in Fig. 3. The aminyl **2a** decayed initially at a relatively fast rate which was followed by a slower decay, and persisted for several weeks. Similarly, the aminyl **2c** decayed rapidly for *ca.* 500 min after which the decay slowed down, and persisted for several weeks. The aminyl **2g** decayed very little over several days, even at a relatively high radical concentration. The unsubstituted aminyl, **2i**, on the contrary, decayed immediately and completely upon interruption of the photolysis.[3] From the decay kinetic studies of the aminyls, it has been demonstrated that the polysubstituted aminyls are well protected by the methyl and *t*-butyl groups, **2g** is in particular very interesting.

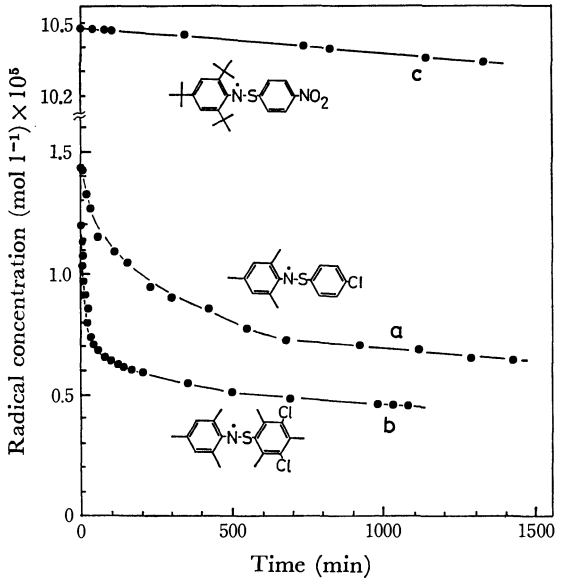

Fig. 3. Decay plots of **2a** (a), **2c** (b), and **2g** (c) in deoxygenated benzene at 19 °C.

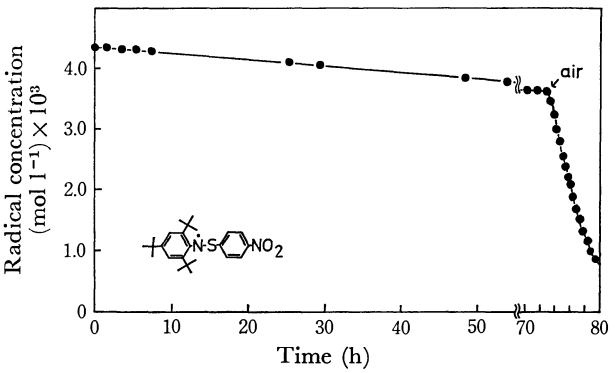

Fig. 4. Decay plots of **2g** in benzene at 19 °C in the absence and presence of oxygen.

Generation of 2g with Lead Dioxide. In order to isolate **2g**, it was generated by oxidation of **1g** with lead dioxide. The procedure was as follows: **1g** (0.10 mmol) was stirred in benzene for 5—15 min in the presence of lead dioxide and potassium carbonate, providing a dark brown solution containing **2g** in a concentration of 4.3 mmol l^{-1}. This value corresponds to 43% based on the **1g** used. On standing for 3 days in a deoxygenated ESR tube, the radical concentration in the solution remained at 3.6 mmol l^{-1} (Fig. 4), indicating little decomposition of **2g**. On the introduction of air, however, the aminyl began to decompose at a relatively fast rate, indicating that **2g** reacts with oxygen. In the range 0.13 to 3.60 mmol l^{-1} of **2g**, the reaction rate with oxygen was measured in benzene saturated with air,[13] and it was found that **2g** decayed with a pseudo first-order kinetics ($k=7.2\times10^{-5}$ s^{-1} at 19 °C).

For the other aminyls, the radical concentrations obtained by oxidation of **1** with lead dioxide were no more than 1% based on the **1** used.

In order to isolate **2g**, benzene was removed from the solution by freeze-drying, affording a dark brown crystalline powder in an almost quantitative yield. The powder gave a strong broad ESR signal (g=2.0068, ΔH=14.7 G) and contained **2g** in a concentration of 40 wt %. When the powder was dissolved in benzene, the resulting brown solution containing **2g** in a concent-

ration of 3.9 mmol l^{-1} (39%), indicating that **2g** was little decomposed during the operation of freeze-drying. The aminyl in the solid was also little decomposed under deoxygenated conditions for one week. On contact with air, however, the solid **2g** was decomposed gradually ($\tau_{1/2}$: half a day) and gave orange decomposition products. From these results, it has been established that **2g** is very stable, even in the solid. The aminyl however has not been isolated as a pure crystal.

Experimental

All melting points are uncorrected. IR spectra were conducted on a JASCO Model IR-G spectrometer. Visible spectra were recorded with a Hitachi recording spectrometer Model ESP-3T and NMR spectra with a Hitachi-Perkin Elmer R-20 spectrometer using TMS as an internal standard.

4-Nitro-[14] and 2,4,6-trimethylbenzenethiols,[15] 2,4,6-trimethoxy-,[16] 2,4,6-triisopropyl-,[17,18] 2,4,6-tri-*t*-butylanilines,[19] and 2,4,6-tri-*t*-butylnitrosobenzene[20] were prepared by reported methods. 2,4,6-Trimethylaniline, 4-chlorobenzenethiol, and di-*t*-butyl peroxide were obtained commercially and used without further purification.

*N-(2,4,6-Trimethylphenyl)-4-chlorobenzenesulfenamide (**1a**).* 4-Chlorobenzenethiol (6.36 g, 0.044 mol) was treated with chlorine gas in dry chloroform (100 ml) at 0 °C. After removal of the solvent, the resulting crude sulfenyl chloride was dissolved in dry ether (100 ml), and the solution was added dropwise to a stirred solution of 2,4,6-trimethylaniline (13.0 g, 0.096 mol) in dry ether (300 ml) at −30——40 °C. After stirring for 30 min, the reaction mixture was filtered and solvent was evaporated to give colorless needles. Recrystallization from hexane afforded colorless needles (11.1 g, 91%) mp 86—87 °C. IR (KBr): 3300 cm^{-1} (NH). NMR ($CDCl_3$): δ 2.15 (s, *o*-CH_3, 6H), 2.22 (s, *p*-CH_3, 3H), 4.76 (br s, NH, 1H), 6.82 (s, C_6H_2, 2H), and 7.29 (s, C_6H_4, 4H). Found: C, 65.02; H, 5.80; N, 5.14%. Calcd for $C_{15}H_{16}NClS$: C, 64.84; H, 5.82; N, 5.04%.

*N-(2,4,6-Trimethoxyphenyl)-4-chlorobenzenesulfenamide (**1b**).* The 4-chlorobenzenesulfenyl chloride, prepared from 4-chlorobenzenethiol (4.60 g, 0.032 mol) as described above, was dissolved in dry ether (80 ml), and the solution was added dropwise to a stirred solution of 2,4,6-trimethoxyaniline (13.1 g, 0.072 mol) in dry ether (300 ml) at −30——40 °C. After stirring for 30 min, the reaction mixture was filtered, and solvent was evaporated to give a light brown crystalline residue. Recrystallization from hexane afforded light brown needles (6.30 g, 60%) with mp 77—78 °C. IR (KBr): 3300 cm^{-1} (NH). NMR ($CDCl_3$): δ 3.70 (s, *o*-CH_3O, 6H), 3.75 (s, *p*-CH_3O, 3H), 5.14 (br s, NH, 1H), 6.19 (s, C_6H_2, 2H), and 7.28—7.32 (m, C_6H_4, 4H). Found: C, 55.20; H, 4.86; N, 4.36%. Calcd for $C_{15}H_{16}NO_3ClS$: C, 55.29; H, 4.95; N, 4.29%.

*N-(2,4,6-Trimethylphenyl)-3,5-dichloro-2,4,6-trimethylbenzenesulfenamide (**1c**).*[21] 2,4,6-Trimethylbenzenethiol (6.00 g, 0.039 mol) was treated with chlorine gas as described for **1a**. After removal of the solvent, the resulting sulfenyl chloride was dissolved in dry ether (100 ml), and the solution was added dropwise to a stirred solution of 2,4,6-trimethylaniline (11.6 g, 0.086 ml) at −30——40 °C. After stirring for 30 min, the reaction mixture was filtered, and solvent was evaporated to give a dark brown oily residue. Repeated recrystallization from hexane afforded colorless prisms (1.30 g, 9.4%) with mp 130—131 °C. IR (KBr): 3300 cm^{-1} (NH). NMR ($CDCl_3$): δ 2.02 [s, *o*-CH_3(*N*-Ph), 6H], 2.19 [s, *p*-CH_3(*N*-Ph), 3H], 2.48 and 2.50 [s, *o*- and *p*-CH_3 (*S*-Ph), 9H], 4.38 (br s, NH, 1H), and 6.72 (s, C_6H_2, 2H). MS (50 eV), *m/e* 353 (M^+). Found: C, 60.90; H, 5.69; N, 3.74; Cl, 20.06; S, 9.26%. Calcd for $C_{18}H_{21}NCl_2S$: C, 61.01; H, 5.97; N, 3.95; Cl, 20.01; S, 9.05%.

*N-(2,4,6-Trimethoxyphenyl)-3,5-dichloro-2,4,6-trimethylbenzenesulfenamide (**1d**).*[21] The sulfenyl chloride, prepared from 2,4,6-trimethylbenzenethiol (5.00 g, 0.033 mol) as described for **1c**, was dissolved in dry ether (100 ml), and the solution was added dropwise to a stirred solution of 2,4,6-trimethoxyaniline (13.3 g, 0.073 mol) in dry ether (400 ml) at −30——40 °C. After stirring for 30 min, the reaction mixture was filtered, and solvent was evaporated to give a dark brown oily residue. Repeated recrystallization from hexane afforded light brown prisms (0.53 g, 4%) with mp 119—120 °C. IR (KBr): 3300 cm^{-1} (NH). NMR ($CDCl_3$): δ 2.45 (s, *p*-CH_3, 3H), 2.54 (s, *o*-CH_3, 6H), 3.58 (s, *o*-OCH_3, 6H), 3.72 (s, *p*-OCH_3, 3H), 4.99 (br s, NH, 1H), and 5.98 (s, C_6H_2, 2H). Found: C, 54.22; H, 5.12; N, 3.55%. Calcd for $C_{18}H_{21}NO_3Cl_2S$: C, 53.73; H, 5.28; N, 3.48%.

*N-Phenyl-3,5-dichloro-2,4,6-trimethylbenzenesulfenamide (**1e**).*[21] The sulfenyl chloride, prepared from 2,4,6-trimethylbenzenethiol (2.00 g, 0.013 mol) as described for **1c**, was dissolved in dry ether (50 ml), and the solution was added dropwise to a stirred solution of aniline (2.50 g, 0.027 mol) in dry ether (200 ml) at −40——50 °C. After stirring for 30 min, the reaction mixture was filtered, and solvent was evaporated to give a dark brown oily residue. Repeated recrystallization from hexane afforded light brown plates (0.15 g, 4%) with mp 110—112 °C. IR (KBr): 3300 cm^{-1} (NH). NMR ($CDCl_3$): δ 2.39 (s, *p*-CH_3, 3H), 2.75 (s, *o*-CH_3, 6H), 4.90 (br s, NH, 1H), and 6.85—7.30 (m, C_6H_5, 5H). Found: C, 58.10; H, 4.76; N, 4.64%. Calcd for $C_{15}H_{15}NCl_2S$: C, 57.69; H, 4.84; N, 4.49%.

*N-(2,4,6-Triisopropylphenyl)-4-nitrobenzenesulfenamide (**1f**).* The sulfenyl chloride, prepared from 4-nitrobenzenethiol (2.02 g, 0.013 mol) as described for **1a**, was dissolved in dry ether (50 ml), and the solution was added dropwise to a stirred solution of 2,4,6-triisopropylaniline (2.80 g, 0.013 mol) and triethylamine (1.94 g, 0.019 mol) in dry ether (250 ml) at −5—0 °C. After addition of the sulfenyl chloride, the reaction mixture was stirred for 5 h at room temperature. Filtration of the reaction mixture, and evaporation of solvent gave a yellow powdery residue, which was chromatographed on alumina [E. Merck, Art 1097, eluent: benzene/hexane (1/4), column size: 3×30 cm]. Recrystallization from hexane afforded light yellow prisms (2.5 g, 53%) with mp 132—133 °C. IR (KBr): 3300 cm^{-1} (NH). NMR ($CDCl_3$): δ 1.18 [d, J=10 Hz, *p*-$CH(C\underline{H}_3)_2$, 6H], 1.25 [d, J=10 Hz, *o*-$CH(C\underline{H}_3)_2$, 12H], 2.75—3.42 [m, $C\underline{H}(CH_3)_2$, 3H], 4.88 (br s, NH, 1H), and 6.99—8.28 (m, C_6H_2 and C_6H_4, 6H). Found: C, 67.28; H, 7.57; N, 7.41%. Calcd for $C_{21}H_{28}N_2O_2S$: C, 67.71; H, 7.58; N, 7.52%.

*N-(2,4,6-Tri-t-butylphenyl)-4-nitrobenzenesulfenamide (**1g**).* The sulfenyl chloride, prepared from 4-nitrobenzenethiol (2.53 g, 0.016 mol) as described for **1a**, was dissolved in dry ether (50 ml), and the solution was added dropwise to a stirred solution of 2,4,6-tri-*t*-butylaniline (4.30 g, 0.016 mol) and triethylamine (2.50 g, 0.025 mol) in dry ether (300 ml) at −5—0 °C. After addition of the sulfenyl chloride, the reaction mixture was stirred for 5 h at room temperature. Filtration of the reaction mixture, and evaporation of solvent gave a yellow powdery residue, which was chromatographed on alumina as described for **1f**. Recrystallization from hexane and then methanol afforded yellow prisms (2.93 g, 46%) with mp 152—153 °C. IR (KBr): 3300 cm^{-1} (NH). NMR ($CDCl_3$): δ 1.30 (s, *p*-*t*-Bu, 9H), 1.50 (s, *o*-*t*-Bu, 18H),

5.20 (br s, NH, 1H), and 7.23—8.23 (m, C_6H_2 and C_6H_4, 6H). Found: C, 69.64; H, 8.27; N, 6.78%. Calcd for $C_{24}H_{34}N_2O_2S$: C, 69.53; H, 8.27; N, 6.76%.

Generation of Aminyls. a) Photolysis: sulfenamide (**1**, 5.0 mg) and a benzene solution (0.20 ml) of di-*t*-butyl peroxide (10% in vol) were placed in an ESR tube and the tube degassed by three freeze-pump-thaw cycles and then sealed. The ESR spectra were recorded during direct irradiation of the solution in the cavity of an ESR instrument with a high-pressure mercury lamp (JES-UV-1, 100W); b) oxidation with lead dioxide: **1** (6.0 mg) was stirred in benzene (3.0 ml) for 1—15 min in the presence of lead dioxide (0.2 g) and potassium carbonate (0.2 g). After filtration, 0.20 ml of the filtrate was placed in an ESR tube and degassed as described above and then sealed.

*Oxidation of **1g** with Lead Dioxide.* Sulfenamide **1g** (42.3 mg) in benzene (10 ml) was stirred for 5—15 min in the presence of lead dioxide (0.5 g) and potassium carbonate (0.5 g). After filtration, the benzene was removed from the filtrate by freeze-drying, giving a dark brown powder in an almost quantitative yield. For measurements of ESR spectra of the filtrate and the powder, 0.20 ml of the filtrate, and 4—5 mg of the powder were used, respectively.

*Generation of Nitroxide **3**.* Nitroxide **3** was generated by the procedure of Konaka *et al.*,[6] *i.e.* 2,4,6-tri-*t*-butylnitrosobenzene (3.0 mg), bis(4-chlorophenyl) disulfide (20.0 mg), and benzene (0.40 ml) were placed in an ESR tube, and degassed as described above, then sealed. ESR spectra were recorded during direct irradiation of the solution with the high-pressure mercury lamp.

*Decay Kinetics of **2**.* Decay kinetic studies on **2** were conducted at 19 °C in the dark. Sample preparation was as follows: **1** (5.0 mg) and a benzene solution (0.20 ml) of di-*t*-butyl peroxide (10% in vol) were placed in an ESR tube, and degassed as described above and then sealed. After the solution was irradiated for 10—20 min in the cavity of an ESR instrument with the high-pressure mercury lamp, the light source was turned off, and the decay rates were measured by monitoring the ESR signal intensities. Integration of the ESR signals was conducted with a Model JES-ID-2 integrator using a benzene solution of 3,4-dihydro-2,4,6-triphenyl-2*H*-1,2,4,5-tetrazin-1-yl (1,3,5-triphenylverdazyl)[22] as a standard.

ESR spectra were recorded at room tempcrature on a JES-ME-3X spectrometer with an X-band microwave unit and a 100 kHz field modulation. Coupling constatns and *g*-values were determined by comparison with the a_N value (13.09 G)[23] and the *g*-value (2.0057)[24] of Fremy's salt.

Computer simulation of spectra was performed using a FACOM 230-60 computer equipped with a FACOM F-6201D plotter.

References

1) Part X of this series, "ESR Studies of Nitrogen-centered Free Radicals." For Part IX, see Y. Miura, H. Asada, and M. Kinoshita, *Chem. Lett.*, **1978**, 1085.

2) For example, Y. Miura, Y. Katsura, and M. Kinoshita, *Bull. Chem. Soc. Jpn.*, **51**, 3004 (1978).

3) Y. Miura and M. Kinoshita, *Bull. Chem. Soc. Jpn.*, **50**, 1142 (1977).

4) H. Sayo and K. Mori, *Chem. Pharm. Bull.*, **25**, 1489 (1977).

5) The aminyls were also detected on the photolysis of the solutions containing arenesulfenamides **1** alone.

6) S. Terabe and R. Konaka, *J. Chem. Soc., Perkin Trans., 2*, **1973**, 369.

7) Y. Miura, Y. Katsura, and M. Kinoshita, *Chem. Lett.*, **1977**, 409.

8) Y. Miura, H. Asada, and M. Kinoshita, *Bull. Chem. Soc. Jpn.*, **50**, 1857 (1977).

9) The spin orbit coupling parameter of the sulfur atom is 382 cm^{-1}; D. S. McClure, *J. Chem. Phys.*, **17**, 905 (1949).

10) R. I. Walter, *J. Am. Chem. Soc.*, **88**, 1923 (1966).

11) For *a* values, see D. H. McDaniel and H. C. Brown, *J. Org. Chem.*, **23**, 420 (1958).

12) The other values of coupling constant and the *g*-value for **2k** are $a_{o\text{-H}(N\text{-Ph})}$: 3.76, $a_{m\text{-H}(N\text{-Ph})}$: 1.16, $a_{o\text{-H}(S\text{-Ph})}$: 0.81, $a_{m\text{-H}(S\text{-Ph})}$: 0.26, and a_{CH_3}: 4.82 G, *g*-value: 2.0059.

13) The concentration of oxygen in benzene saturated with air is 2.0×10^{-3} mol l^{-1} (20 °C); J. Horiuti, *Scientific Papers*, **17**, 125 (1931).

14) C. C. Price and G. W. Stacy, *J. Am. Chem. Soc.*, **68**, 498 (1946).

15) C. H. Wang and S. G. Cohen, *J. Am. Chem. Soc.*, **79**, 1924 (1957).

16) Y. Fukui, Y. Kuwahara, and K. Saeki, and M. Mori, *Yakugaku Zasshi*, **80**, 1472 (1960).

17) A. Newton, *J. Am. Chem. Soc.*, **65**, 2434 (1943).

18) R. G. Wilson and D. H. Williams, *J. Chem. Soc., B*, **1968**, 1163.

19) J. Burgers, M. A. Hoefnagel, P. E. Verkade, H. Visser, and B. M. Wepster, *Recl. Trav. Chim., Pays-Bas*, **77**, 491 (1958).

20) R. Okazaki, T. Hosogai, E. Iwadare, M. Hashimoto, and N. Inamoto, *Bull. Chem. Soc. Jpn.*, **42**, 3611 (1969).

21) Sulfenamides isolated from the reaction mixture were **1c**, **1d**, and **1e**, unchlorinated and monochlorinated sulfenamides could not be isolated.

22) R. Kuhn and H, Trischmann, *Monatsh. Chem.* **95**, 457 (1964).

23) R. J. Faber and G. K. Fraenkel, *J. Chem. Phys.*, **47**, 2462 (1967).

24) J. E. Werz, D. C. Reitz, and F. Dravnieks, "Free Radicals in Biological Systems," Academic Press, New York, N. Y. (1961), p. 186.

Reactions of 2-Chlorothiophene with Cation Exchange Resin and 100% Orthophosphoric Acid. Formation of the Dimer Type Products Containing a Tetrahydro-2-thiophenone Moiety[1)]

Tyo SONE,* Osamu SHIROMARU, Shin-ichi IGARASHI, Eiichi KATO, and Mutsuo SAWARA
Department of Applied Chemistry, Faculty of Engineering, Yamagata University, Yonezawa 992
(Received July 3, 1978)

It has been found that 2-chlorothiophene is converted into the dimer type products by Amberlyst 15 or 100% orthophosphoric acid, the reaction yielding 4- and 5-(5-chloro-2-thienyl)tetrahydro-2-thiophenones and 4-(2-thienyl)-2(5*H*)-thiophenone together with 5-chloro-2,2′-bithienyl. The distribution of the products is considerably affected by the acid used and in the presence of phenol or anisole the reaction affords additionally 4-[5-(*p*-hydroxyphenyl)-2-thienyl]tetrahydro-2-thiophenone or 4-[5-(*p*-methoxyphenyl)-2-thienyl]tetrahydro-2-thiophenone, respectively.

Simple thiophenes have been known to polymerize on treatment with certain acidic materials;[2)] in most cases amorphous, highly insoluble polymers were obtained. Since the products may form a potential source of oligothienylenes, efforts have been made to produce simple oligomers by the use of this type of reaction. Moreover, the oligomerization may supply information regarding the reactivity of thiophene as a conjugated diene which has not been well understood. However, few reports have appeared in the literature, *e.g.*, thiophene reacts with 100% orthophosphoric acid to yield the so-called "thiophene trimers" and "pentamer,"[3)] and with sulfuryl chloride and iron powder to yield the chlorinated bithienyls.[4)]

A novel reaction will be reported here, namely, the reaction of 2-chlorothiophene (**1**) with cation exchange resin and 100% orthophosphoric acid leading to dimer type products containing a tetrahydro-2-thiophenone ring. This result is in contrast to that obtained by the reactions of **1** with sulfuric acid,[5)] and aluminium chloride and copper(II) chloride;[6)] in both cases the major product obtained even under mild conditions was a polymeric material possessing a complicated structure. This reaction also offers a novel example of the conversion of thiophenes to other heterocycles.

2-Chlorothiophene (**1**) was treated with half its own weight of Amberlyst 15 at 120 °C for 4 h. Evolution of hydrogen chloride gas was observed during the reaction. The oily product was shown by thin-layer chromatography (TLC) to consist of two principal components, which were isolated by column chromatography. The component of high R_f value was found to be 5-chloro-2,2′-bithienyl (**4**, 21% based on reacted **1** at 70% conversion) by comparison with the authentic sample. Careful chromatography of the component of low R_f value gave 4-(5-chloro-2-thienyl)tetrahydro-2-thiophenone(**2**, 34%) as a colorless oil together with a small amount of 5-(5-chloro-2-thienyl)tetrahydro-2-thiophenone (**3**, 3.5 %) as colorless crystals. Some 4-(2-thienyl)-2(5*H*)-thiophenone (**5**, 1.5%) was also isolated.

Similar treatment of **1** with an equivalent weight of freshly prepared 100% orthophosphoric acid afforded the same products at 82% conversion. The distribution of products, however, was different from that with Amberlyst 15, *i.e.*, **2** (11.5%), **3** (11%), **4** (7%), and **5** (≈1%), respectively (Scheme 1).

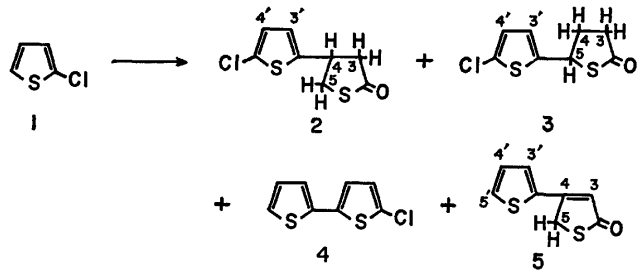

Scheme 1.

The structures of the thiophenones have been assigned on the basis of the following evidence.

The IR spectrum (CCl_4) of **2** indicated carbonyl absorption at 1715 cm^{-1} but no absorption attributable to hydroxyl groups. The UV spectrum [λ_{max}(MeOH) 242 nm (log ε 4.07)] suggested an unconjugated thiophene ring. Compound **2** did not react with ordinary ketonic reagents. When heated with dilute sodium hydroxide solution, it easily dissolved producing a clear solution, but was partially regenerated from the alkaline solution on acidification with hydrochloric acid. The mass spectrum showed the molecular ion at *m/e* 218 (relative intensity 72%) and characteristic M+2 peak (30%) indicative of a structure containing two sulfur atoms and one chlorine atom. Other prominent peaks were *m/e* 144 (base peak; M^+-CH_2SCO) and 109 ($M^+-CH_2SCO-Cl$). These findings suggest a tetrahydro-2-thiophenone substituted by a 5-chloro-2-thienyl moiety. The NMR spectrum (CCl_4) showed, in addition to an AB quartet (J=3.8 Hz) for the two protons of 2,5-disubstituted thiophene ring,[7)] a typical AB octet (centered at approx. δ 2.7) of an ABX spin system for a methylene group, and a three-proton multiplet (δ 3.2—4.1) due to the methine (the X-proton of the ABX system) and a methylene group. The large geminal coupling constant ($J_{a,b}$=16.6 Hz) of the AB octet together with the position indicated that the methylene proton were adjacent to a carbonyl group.[8)] The downfield methylene protons were strongly deshielded indicating that the protons were adjacent to a sulfur atom. Thus the thienyl moiety must be located at the 4-position of the tetrahydro-2-thiophenone ring. A shift reagent [Eu(fod)$_3$] experiment agreed with the assignment; upon addition of the reagent the octet underwent a greater downfield shift and the three-proton multiplet

separated with a smaller shift into a one-proton multiplet for the methine proton and an AB octet for the methylene protons.

The structure assignment was substantiated by the alkaline hydrolysis of **2** followed by reductive desulfurization (Raney nickel) of the resulting mercaptoacid (**6**) which gave 3-methylheptanoic acid (**7**), which was identical with an authentic sample (Scheme 2).

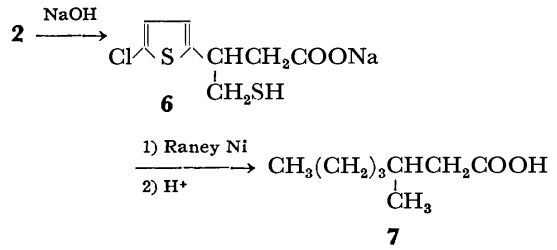

Scheme 2.

Compound **3** had the same molecular weight as that of **2**, and similar IR (CCl_4; ν_{CO} 1715 cm^{-1}), UV [λ_{max} (MeOH) 244 nm (4.09)], and chemical properties, indicating that **3** is an isomer of **2**. The NMR and mass spectra were appreciably different from that of **2**. The mass spectrum showed significant peaks at *m/e* 218 (base peak; M^+), 158 (M^+ — SCO), 157 (M^+ — SCO — H), and 123 (M^+ — SCO—Cl). The NMR spectrum ($CDCl_3$) exhibited, besides the resonance for two protons of a 2,5-disubstituted thiophene ring, a four-proton multiplet (δ 1.9—3.0) due to two adjacent, similarly shielded methylene groups and a multiplet (δ 5.0—5.3) due to a methine proton. The strongly deshielded position of the methine absorption indicates that the methine proton is adjacent to both the sulfur atom and the thienyl group. Upon gradual addition of the shift reagent the four-proton multiplet separated into two methylene multiplets; one (due to the methylene proton α to the carbonyl group) underwent a greater downfield shift relative to the other (due to the β methylene protons) and the methine multiplet. These facts are compatible with structure **3**, which was finally established by comparison of the spectral data and the melting point with those of an authentic sample synthesized according to Scheme

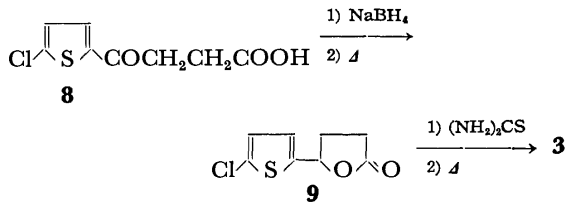

Scheme 3.

The minor product **5** was thought to contain a thiophene ring conjugated with an enone group on the basis of the UV [λ_{max}(MeOH) 277 (3.96), 327 (4.19)] and IR spectra [KBr; $\nu_{C=C}$ 1600, ν_{CO} 1660 cm^{-1}]. The NMR spectrum ($CDCl_3$) displayed significant resonances as follows; signals for three ring protons, a triplet for an olefinic proton at δ 6.49, and a methylene doublet at δ 4.39. Decoupling of the doublet caused the triplet to collapse to a singlet, indicating that the olefinic and the methylene protons were mutually spin-coupled with a coupling constant J=1.5 Hz in an allylic group (–CH=C–CH_2–). These data together with the mass spectrum [*m/e* 182 (base peak; M^+), 154 (M^+— CO), 153 (M^+— CO — H), 108 (M^+— CH_2SCO)] and the elemental analysis confirmed structure **5**.

The formation of **4** can be explained by the mechanism illustrated in Scheme 4 (path A). The entire reaction pathway leading to the thiophenone derivatives is not clear at this stage. Of interest in this regard, however, is the fact that both **2** and **3** were formed in the reaction and the **2**/**3** ratio varied considerably depending upon the acid and the reaction conditions employed. A probable mechanism which is compatible with these facts may involve the intermediacy of 2-thiophenone tautomers,[9] 2(5*H*)-(**11a**) and 2(3*H*)-thiophenones (**11b**), in the reaction: protonation of **11a** and **11b** followed by the reaction of the resulting carbonium ions with **1** and then the loss of a proton affords **2** and **3**, respectively (path B). The reaction of **10b** with **11b** would similarly yield **5**. The tautomers could be produced from **1** by a reaction analogous to hydrolytic conversion of chlorocyclopentadiene to the corresponding cyclopentenone.[10]

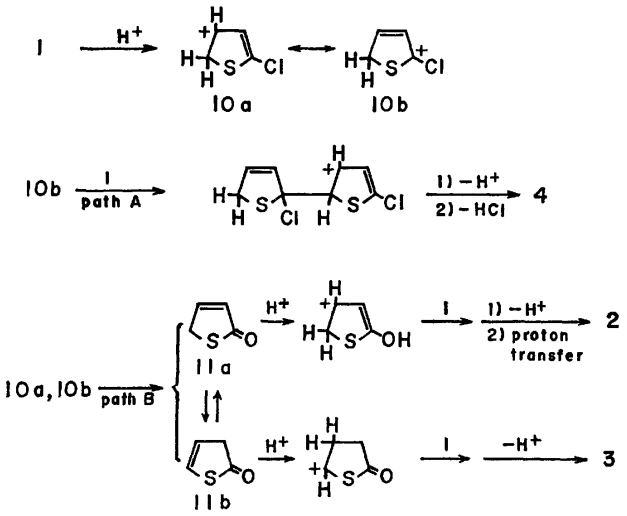

Scheme 4.

It was anticipated from the suggested mechanism that, when the reaction was conducted in the presence of an aromatic compound which is reactive but inert to the resin, the corresponding arylthiophene and/or aryl-substituted tetrahydro-2-thiophenone would be formed. Thus, in the presence of an equimolar amount of phenol the reaction using Amberlyst 15 as an acid resulted in 73% conversion of **1** yielding 4-[5-(*p*-hydroxyphenyl)-2-thienyl]tetrahydro-2-thiophenone (**12**; 28% based on reacted **1**) in addition to **2** (22%) and **4** (7%). The presence of 2-(hydroxyphenyl)thiophene (presumably **13**) and 4-[(*p*-)hydroxyphenyl]tetrahydro-2-thiophenone as the minor products were also detected by mass spectral analysis. Similarly, the reaction in the presence of anisole afforded 4-[5-(*p*-methoxyphenyl)-2-thienyl]tetrahydro-2-thiophenone (**14**; 17% based on reacted **1** at 46% conversion), 2-(*p*-methoxyphenyl)thiophene (**15**;

10%), **2** (20%), and **4** (6%). The structure of **12** and **14** have been assigned on the basis of their mass and NMR spectra, which indicated the presence of one *p*-substituted phenyl, one 2,5-disubstituted thiophene, and one 4-substituted tetrahydro-2-thiophenone ring. The formation of the unexpected tetrahydro-2-thiophenones, **12** and **14**, can be accounted for by a process similar to that of the formation of **2** as shown in Scheme 4. This involves the initial formation of arylthiophene intermediates, **13** and **15**, which react with the protonated **11a** to afford **12** and **14**, respectively.

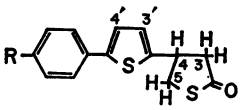

12: R=OH
14: R=OCH_3

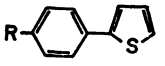

13: R=OH
15: R=OCH_3

In conclusion, it was found that the dimer type products consisting of the unexpected thiophenone derivatives (**2**, **3**, and **5**) and the coupling product (**4**) were formed in the acid-catalyzed reaction of **1** with a cation exchange resin and 100% orthophosphoric acid. In the reaction the thiophene ring clearly behaves as a conjugated diene as well as a heteroaromatic ring. Furthermore, it should be noted that the reaction could be effected with a cation exchange resin. To the authors' knowledge no report in the literature has appeared on the use of cation exchange resins as catalysts for acid-catalyzed oligomerization of aromatic or heteroaromatic nuclei, although the resins have received wide application in organic reactions. It is possible that simple oligomers are formed in the reactions of other properly substituted thiophenes with the resins as well.

Experimental

All melting and boiling points are uncorrected. The NMR spectra were obtained on a Hitachi R-22 spectrometer at 90 MHz, using TMS as an internal reference. The UV, IR, and mass (70 eV) spectra were recorded on Hitachi EPU-2A, Hitachi EPI-S2, and Hitachi UMU-6MG spectrometers, respectively.

2-Chlorothiophene (**1**) was prepared by the method described in the literature.[11] Commercial Amberlyst 15 was used without any treatment. In drying the Amberlyst over phosphorus pentaoxide (115 °C/10—15 mmHg, 24 h), 2—3% weight loss was observed, which was presumably due to loss of water.

*Reaction of **1** with Cation Exchange Resin.* A suspension of Amberlyst 15 (5 g) in **1** (10 g, 0.0843 mol) was stirred at 120 °C for 4 h. Evolution of hydrogen chloride was observed during the reaction. The reaction mixture was extracted with chloroform in a Soxhlet extractor. After the solvent and the unchanged **1** (3.0 g) were distilled off, the residual oil was chromatographed (silica gel, benzene) to give three fractions which are in order of decreasing R_f values: 1) the chlorinated 2,2′-bithienyl, **4**, (1.3 g, 21% based on **1** reacted; contaminated with a small amount of another isomer as shown by GLC), bp 100—110 °C (bath)/3—4 mmHg (lit,[12] 55 °C (bath)/0.05 mmHg); 2) a mixture of the tetrahydrothiophenones, **2** and **3**, (2.4 g, 36%; **2**:**3**=91:9 as determined by NMR analysis); 3) the thiophenone, **5**, (0.08 g, 1.5%), mp 157—159 °C. The spectral and physical properties are described below.

*Reaction of **1** with 100% Orthophosphoric Acid.* A mixture of **1** (10 g) and the phosphoric acid (prepared immediately prior to use by heating a mixture of 85% orthophosphoric acid (7.5 g) and phosphorus pentaoxide (3 g) at 100 °C for 1 h) was stirred at 110 °C for 6 h. Hydrogen chloride gas was evolved throughout the reaction. After cooling, the greenish brown reaction mixture was poured into cold water, and extracted with chloroform. The extract was washed successively with water, 5% sodium hydrogencarbonate solution and again with water, and dried. After the solvent and unchanged **1** (1.8 g) had been removed, the residual oil was chromatographed (silica gel, benzene) to give **4** (0.5 g, 7%; contaminated with a small amount of another isomer), a mixture of **2** and **3** (1.7 g, 22.5%; **2**:**3**=51:49), and **5** (0.05 g, ≈1%).

The isomeric tetrahydrothiophenones were separated by repeated chromatography (silica gel, benzene/ligroin (3:1)).

2: Colorless oil, bp 85—87 °C/5×10^{-4} mmHg. NMR (CCl_4) δ 6.77 (1H, d, $J_{3',4'}$=3.8 Hz, 4′-H), 6.71 (1H, dd, $J_{3',4'}$= 3.8 Hz, $J_{3',4}$=0.7 Hz, 3′-H), 4.1—3.2 (3H, m, 4-H and 5-H_a,H_b), 2.82, 2.62 (2H, ABX octet, $J_{a,b}$=16.6 Hz, $J_{a,4}$=10.1 Hz, $J_{b,4}$=6.6 Hz, 3-H_a,H_b); (CCl_4; in the presence of 0.36 equivalent mol of Eu(fod)$_3$) δ 7.37 (1H, dd, 3′-H), 6.97 (1H, d, 4′-H), 6.76, 6.50 (2H, ABX octet, 3-H_a,H_b), 5.8—5.3 (1H, m, 4-H), 5.06, 4.98 (2H, ABX octet, $J_{a,b}$=11.0 Hz, $J_{a,4}$=8.1 Hz, $J_{b,4}$=6.7 Hz, 5-H_a, H_b). Found: C, 44.05; H, 3.45%. Calcd for $C_8H_7ClOS_2$: C, 43.93; H, 3.23%.

3: Colorless crystals, mp 51.5—52.5 °C (light petroleum ether–ether). NMR ($CDCl_3$) δ 6.83 (1H, dd, $J_{3',4'}$=3.7 Hz, $J_{3',5}$=0.7 Hz, 3′-H), 6.74 (1H, d, $J_{3',4'}$=3.7 Hz, 4′-H) 5.0—5.3 (1H, m, 5-H), 1.9—3.0 (4H, m, 3-H_a,H_b and 4-H_a,H_b); ($CDCl_3$; in the presence of 0.25 equivalent mol of Eu(fod)$_3$ δ 7.20 (1H, dd, 3′-H), 6.91 (1H, d, 4′-H), 5.91 (1H, ABX q, $J_{a,4}+J_{b,4}$=14.4 Hz, 5-H), 5.0—4.3 (2H, m, 3-H_a,H_b), 3.6—2.8 (2H, m, 4-H_a, H_b). Found: C, 43.94; H, 3.03%. Calcd for $C_8H_7ClOS_2$: C, 43.93; H, 3.23%.

5: Pale yellow crystals, mp 165—166 °C (ligroin–benzene). NMR ($CDCl_3$) δ 7.50, 7.39 (2H, ABX octet, $J_{3',5'}$=1.1 Hz, $J_{3',4'}$=3.7 Hz, $J_{4',5'}$=4.8 Hz, 3′-H and 5′-H), 7.11 (1H, ABX q, $J_{3',4'}$=3.7 Hz, $J_{4',5'}$=4.8 Hz, 4′-H), 6.49 (1H, t, $J_{3,5}$=1.5 Hz, 3-H), 4.39 (2H, d, $J_{3,5}$=1.5 Hz, 5-H_2). Found: C, 52.72; H, 3.15%. Calcd for $C_8H_6OS_2$: C, 52.71; H, 3.31%.

*Desulfurization of **2** with Raney Nickel.* The tetrahydrothiophenone **2** (0.93 g, 4.25 mmol) was dissolved in 20% sodium hydroxide solution (50 ml) by heating, and the solution diluted with water (50 ml). W-7 Raney nickel (prepared from 15 g of the alloy) was added to the cooled solution and the mixture stirred at 70 °C for 5 h. The reaction mixture was filtered and the nickel washed with water (300 ml). The filtrate and the washings were combined and evaporated to *ca.* 100 ml. The solution was acidified with hydrochloric acid in the cold to give an oil. Work-up and distillation *in vacuo* afforded 3-methylheptanoic acid (**7**; 0.50 g, 82%) as a colorless liquid, bp 130—140 °C (bath)/15 mmHg (lit,[13] 121 °C/15 mmHg); the IR and NMR spectra were identical with those of the authentic sample.[13]

*5-(5-Chloro-2-thienyl)tetrahydro-2-furanone (**9**).* Sodium borohydride (1.9 g, 0.05 mol) was added with stirring to a mixture of 3-(5-chloro-2-thenoyl)propionic acid[14] (**8**; 10.9 g, 0.05 mol) and sodium hydroxide (1.6 g) in water (80 ml), while the temperature of the reaction mixture being maintained below 40 °C during the addition. The mixture was stirred for 4 h at room temperature, added to water, and acidified with hydrochloric acid. After extraction with ether and the usual work-up, the oily product was distilled under reduced

pressure and the distillate (bp 117—127 °C/1 × 10^{-4} mmHg chromatographed (silica gel, chloroform) to give **9** (4.7 g, 46%) and 4-(5-chloro-2-thienyl)-3-butenoic acid (1.8 g, 17%).

9: Colorless oil, bp 112—114 °C/1 × 10^{-4} mmHg. MS *m/e* 202 (M^+). IR (CCl_4) ν_{CO} 1800 cm^{-1}. NMR ($CDCl_3$) δ 6.83 (1H, d, $J_{3,4'}$=3.8 Hz, thiophene 3'-H), 6.76 (1H, d, $J_{3',4'}$=3.8 Hz, thiophene 4'-H), 5.54 (1H, t, 5-H), 2.9—2.0 (4H, m, 3-H_2 and 4-H_2). Found: C, 47.66; H, 3.48%. Calcd for $C_8H_7ClO_2S$: C, 47.41; H, 3.48%.

4-(5-Chloro-2-thienyl)-3-butenoic Acid: Colorless crystals, mp 84—85 °C (benzene–hexane). MS *m/e* 202 (M^+). IR (KBr) ν_{CO} 1700 cm^{-1}. NMR ($CDCl_3$) δ 9.97 (1H, br s, COOH), 6.71 (1H, d, $J_{3',4'}$=4.0 Hz, thiophene 4'-H), 6.64 (1H, d, $J_{3',4'}$=4.0 Hz, thiophene 3'-H), 6.47 (1H, dd, $J_{3,4}$=15.9 Hz, $J_{2,4}$=1.0 Hz, 4-H), 5.92 (1H, dt, $J_{3,4}$=15.9 Hz, $J_{2,3}$=7.0 Hz, 3-H), 3.19 (2H, dd, $J_{2,3}$=7.0 Hz, $J_{2,4}$=1.0 Hz, 2-CH_2). Found: C, 47.34; H, 3.46%. Calcd for $C_8H_7ClO_2S$: C, 47.41; H, 3.48%.

Preparation of 3 from 9. To a suspension of the lactone **9** (1.0 g, 5 mmol) in 48% hydrobromic acid (2.5 g) was added thiourea (0.4 g, 5 mmol) with shaking. A white solid formed within several minutes and was allowed to stand overnight. A sodium hydroxide solution (0.6 g, in 5 ml of water) was added and the mixture gently refluxed for 70 min. The organic layer was separated, and the aqueous layer acidified and extracted with ether. The organic layer and the ether extracts were combined and dried. After removal of the solvent the residual oil was heated at 160—170 °C under reduced pressure (20 mmHg) for 1 h. The oily product was chromatographed (silica gel, chloroform/benzene (4: 1)) to give **3** (mp 51—52 °C; 160 mg, 15%). The IR and NMR spectra were identical with those of **3** obtained by the acid-catalyzed reaction of **1**, and the mixed melting point exhibited no depression.

Reaction of 1 with Cation Exchange Resin in the Presence of Phenol. A mixture of **1** (4.8 g, 0.04 mol), phenol (3.8 g, 0.04 mol) and Amberlyst 15 (2.4 g) was stirred at 120 °C for 4 h. The dark brown reaction mixture was extracted with aceton in a Soxhlet extractor. After removal of the solvent the unchanged **1** (1.3 g) and phenol (1.9 g) were recovered by distillation under reduced pressure. The residual oil was chromatographed (silica gel, benzene/acetone (9: 1)) to give 4-[5-(*p*-hydroxyphenyl)-2-thienyl]tetrahydro-2-thiophenone (**12**; mp 159—166 °C, 1.1 g, 28% based on reacted **1**), **2** (0.7 g, 22%), **4** (0.2 g, 7%), and polymeric material (0.8 g) Mass spectroscopy suggested the presence of 4-[(*p*-)hydroxyphenyl]tetrahydro-2-thiophenone [*m/e* 194 (M^+), 120 ($M^+ - CH_2SCO$)] and 2-[(*p*-)hydroxyphenyl]thiophene [**13**; *m/e* 176 (M^+), 147 (M^+-CO-H), 131 (M^+-HCS), 115 ($M^+-CO-H-S$)], which were isolated in the impure form by preparative TLC. There was, however, insufficient material for further purification.

12: Pale yellow crystals, mp 171—172 °C (methanol). MS *m/e* 276 (M^+), 202 (M^+-CH_2SCO), 45 (base peak; HCS^+). UV λ_{max}^{MeOH} 304 (4.22). IR (KBr) ν_{CO} 1660, ν_{OH} 3225 cm^{-1}. NMR ($(CD_3)_2CO$): δ 8.46 (1H, s, OH), 7.48, 7.39 (2H, AA'XX' m, *p*-substituted phenyl), 7.10 (1H, d, $J_{3',4'}$=3.8 Hz, 4'-H), 6.96 (1H, dd, $J_{3',4'}$=3.8 Hz, $J_{3',4}$=1.0 Hz, 3'-H), 6.90, 6.80 (2H, AA'XX' m, *p*-substituted phenyl), 4.2—3.2 (3H, m, 4-H and 5-H_a, H_b), 2.92, 2.80 (2H, ABX octet, $J_{a,b}$=16.7 Hz, $J_{a,4}$=10.0 Hz, $J_{b,4}$=7.2 Hz, 3-H_a,H_b). Found: C, 61.01; H, 3.97%. Calcd for $C_{14}H_{12}O_2S_2$: C, 60.84; H, 4.37%.

Reaction of 1 with Cation Exchange Resin in the Presence of Anisole. A mixture of **1** (4.8 g, 0.04 mol), anisole (4.3 g, 0.04 mol) and Amberlyst 15 (2.4 g) was stirred at 120 °C for 4 h and the reaction mixture extracted with chloroform in a Soxhlet extractor. After removal of the solvent, the unchanged **1** (2.6 g) and anisole (3.3 g) were recovered by distillation under reduced pressure. The residual oil was chromatographed (silica gel, hexane/acetone (4: 1)) to afford 4-[5-(*p*-methoxyphenyl)-2-thienyl]tetrahydro-2-thiophenone (**14**; mp 104—107 °C; 0.45 g, 17% based on reacted **1**), 2-(*p*-methoxyphenyl)thiophene (**15**; mp 101—103 °C; 0.35 g, 10%), **2** (0.4 g, 20%), and **4** (0.1 g, 6%). Other traces were detected by TLC but colud not be separated.

15: Colorless crystals, mp 110—111 °C (methanol; lit,[15] 107—108 °C). MS *m/e* 190 (base peak, M^+), 175 (M^+-CH_3), 147 (M^+-CH_3-CO). NMR ($CDCl_3$) δ 7.51, 7.42 (2H, AA'XX' m, *p*-substituted phenyl), 7.2—6.9 (3H, m, monosubstituted thiophene), 6.89, 6.80 (2H, AA'XX' m, *p*-substituted phenyl), 3.79 (3H, s, $-OCH_3$).

14: Pale yellow crystals, mp 115—116 °C (methanol). MS *m/e* 290 (base peak, M^+), 216 (M^+-CH_2SCO), 201 ($M^+-CH_2SCO-CH_3$), 173 ($M^+-CH_2SCO-CH_3-CO$). UV λ_{max}^{MeOH} 300 (4.36). IR (KBr) ν_{CO} 1705 cm^{-1}. NMR ($CDCl_3$) δ, 7.51, 7.41 (2H, AA'XX' m, *p*-substituted phenyl), 7.01 (1H, d $J_{3',4'}$=3.7 Hz, 4'-H), 6.94, 6.84 (2H, AA'XX' m, *p*-substituted phenyl), 6.84 (1H, dd, $J_{3',4'}$=3.7 Hz, $J_{3',4}$=0.9 Hz, 3'-H), 3.80 (1H, s, $-OCH_3$), 4.4—3.3 (1H, m, 4-H and 5-H_a,H_b), 2.92, 2.77 (2H, ABX octet, $J_{a,b}$=16.8 Hz, $J_{a,4}$=11.0 Hz, $J_{b,4}$=6.0 Hz, 3-H_a,H_b). Found: C, 62.28; H, 4.67%. Calcd for $C_{15}H_{14}O_2S_2$: C, 62.03; H, 4.87%.

The authors wish to thank Professor H. Obara, Yamagata University, for his valuable advice. They would also like to thank Dr. J. Onodera, Yamagata University, and Mr. K. Sakai, Hitachi Research Laboratory, Hitachi Ltd., for mass spectral measurements, and Professor K. Takahashi, Nagoya Institute of Technology, and Mr. K. Fujieda, Naka Works, Hitachi Ltd., for NMR spectral measurements.

References

1) Acid-Catalyzed Oligomerization of Thiophene Nuclei. III. For Part II, T. Sone and Y. Abe, *Bull. Chem. Soc. Jpn.*, **46**, 3603 (1973).

2) For references, see R. F. Curtis, D. M. Jones, and W. A. Thomas, *J. Chem. Soc., C*, **1971**, 234.

3) S. L. Meisel, G. C. Johnson, and H. D. Hartough, *J. Am. Chem. Soc.*, **72**, 1910 (1950). The structures of the products were established by Curtis *et al.*[2] Recently, Ishigaki *et al.* also reported the structure of 2-methylthiophene trimer which was obtained in a similar manner; A. Ishigaki and T. Shono, *Bull. Chem. Soc. Jpn.*, **48**, 2977 (1975).

4) T. Sone, K. Sakai, and K. Kuroda, *Bull. Chem. Soc. Jpn.*, **43**, 1411 (1970).

5) T. Sone and E. Kato, *Asahi Garasu Kogyo Gijutsu Shoreikai Kenkyu Hokoku*, **26**, 243 (1975).

6) J. S. Ramsey and P. Kovacic, *J. Polym. Sci., Part. A-1*, **7**, 127 (1969).

7) S. Gronowitz, "Advances in Heterocyclic Chemistry," ed by A. R. Katritzky, Academic Press, New York (1963), Vol. 1, p. 7.

8) M. Barfield and D. M. Grant, *J. Am. Chem. Soc.*, **85**, 1899 (1963).

9) 2-Thiophenones have been prepared by the acid-catalyzed dealkylation of 2-*t*-butoxythiophenes, the hydrogen peroxide oxidation of thiophene boronic acids, or the dealkylative decarboxylation of 2-thienyl isopropyl carbonates with aluminium chloride. 2-Thiophenone has been reported to exist as 2(5*H*)-thiophenone (**11a**). However, two tautomeric forms have been detected in several 5-alkyl- and

5-halogeno-2-thiophenones by NMR spectrometric method; see, for example, A. P. Manzara and P. Kovacic, *J. Org. Chem.*, **39**, 504 (1974), and the references cited therein.
10) Y. Gaoni, *Tetrahedron Lett.*, **1977**, 371.
11) E. Campaigne and W. M. LeSuer, *J. Am. Chem. Soc.*, **70**, 415 (1948).
12) R. F. Curtis and G. T. Phillips, *J. Chem. Soc.*, **1965**, 5134.
13) R. P. Linstead, B. R. Shephard, B. C. L. Weedon, and J. C. Lunt, *J. Chem. Soc.*, **1953**, 1538.
14) Ng. Ph. Buu-Hoi, Ng. Hóan, and Ng. D. Xuong, *Recl. Trav. Chim. Pays-Bas.*, **69**, 1083 (1950); *Chem. Abstr.*, **45**, 7104f (1951).
15) M. Nilsson and C. Ullenium, *Acta Chem. Scand.*, **24** 2379 (1970).

An Improved Synthesis of 3′,4′-Dideoxykanamycin B

Toshio YONETA,* Seiji SHIBAHARA, Tomio MATSUNO, Susumu TOHMA, Shuzo FUKATSU, Shigeo SEKI, and Hamao UMEZAWA†

Central Research Laboratories, Meiji Seika Kaisha, Ltd., Morooka-cho, Kohoku-ku, Yokohama 222

†*Institute of Microbial Chemistry, Shinagawa-ku, Tokyo 141*

(Received July 15, 1978)

A new synthetic route has been exploited for the large scale production of 3′,4′-dideoxykanamycin B starting with kanamycin B. The key stage in the synthesis involves the formation in excellent yield of the 3′,4′-anhydro-4′-*epi* derivative (**5**) followed by convertion to the 3′-*ene* derivative through the iodohydrin. Compound **5** was prepared by the treatment of 3′,2″-di-*O*-benzoyl-4″,6″-*O*-cyclohexylidene-4′-*O*-methylsulfonyl-penta-*N*-*t*-butoxycarbonyl-kanamycin B with sodium methoxide.

The resistance mechanism of most strains resistant to kanamycin has been elucidated by Umezawa *et al.* and attributed to the transphosphorylation from adenosine triphosphate to the 3′-hydroxyl group of kanamycin by intracellular enzymes produced by the resistant organisms.[1-3] 3′-Deoxykanamycin[4] and 3′,4′-dideoxykanamycin B (**15**)[5,6] prepared on the basis of this mechanism have been shown able to inhibit growth of these resistant strains. The latter has already been clinically used for infections of resistant bacteria.

A previous method for the preparation of 3′,4′-dideoxykanamycin B (**15**) involves the treatment of the 3′,4′-di-*O*-sulfonyl derivative with sodium iodide and zinc according to the Tipson-Cohen method.[7] In the present paper, other methods which do not require zinc for the 3′-*ene* formation have been investigated and it has been found that Watanabe's method,[8,9] involving the cleavage of an epoxide ring to iodohydrin followed by *O*-sulfonylation is one method for the large scale preparation of the 3′-*ene* compound.

The five amino groups of kanamycin B were protected by the *t*-butoxycarbonyl (Boc) group using *O*-*t*-butyl *S*-4,6-dimethyl-2-pyrimidinyl thiocarbonate (Boc-*S* reagent)[10] to yield quantitatively the *N*-penta-Boc derivative (**1**). The protecting group can be readily removed under mild acidic conditions without ureide formation[6] at *N*-1 and *N*-3 of the 2-deoxystreptamine, which occured during removal of the *N*-ethoxycarbonyl group. The 4″- and 6″-hydroxyl groups of **1** were selectively protected by the formation of the cyclohexylidene

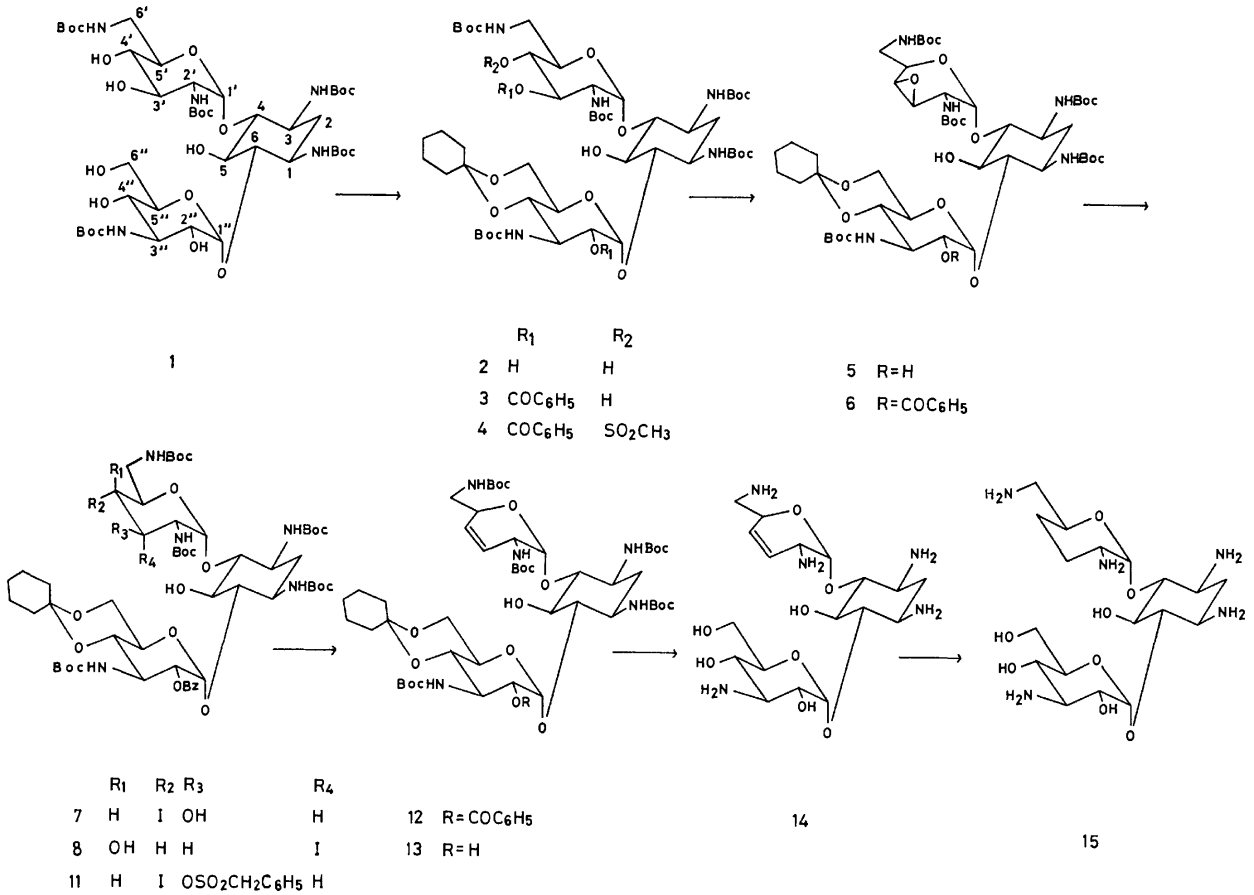

Scheme 1.

derivative in the usual manner.[6] Since the 4-hydroxyl group of hexopyranosides is generally least reactive toward benzoylation with benzoyl chloride in pyridine,[11] the 3′- and 2″-hydroxyl groups of the 4″,6″-*O*-cyclohexylidene derivative (**2**) were preferentially benzoylated with benzoyl chloride (2.7 mol to **2**) in pyridine at 5 °C to give the expected 3′,2″-dibenzoate product (**3**) in 73% yield. The reaction of the dibenzoate **3** with methylsulfonyl chloride gave the 4′-methylsulfonate (**4**) whose NMR spectrum showed the presence of two benzoyl and one methylsulfonyl group. The treatment of **4** with methanolic sodium methoxide gave the desired 3′,4′-anhydro-4′-*epi* derivative (**5**) in a quantitative yield, which was subsequently converted into the 2″-benzoate (**6**) by re-*O*-benzoylation. Successive treatment of **6** with sodium iodide, sodium acetate and acetic acid in acetone[8,9] afforded the iodohydrin (**7**) bearing both iodo and hydroxyl groups in equatorial positions. Formation of the anhydro-ring opening isomer (**8**) was not observed in this reaction.

The structure of **7** was established by conversion into 4′-deoxykanamycin B (**9**). Catalytic hydrogenation of the crude iodohydrin (**7**) followed by successive treatment with methanolic sodium methoxide and 95% trifluoroacetic acid gave **9** and a small amount of less polar compounds. Hydrolysis of **9** with 6 M hydrochloric acid afforded 4′-deoxyneamine (**10**) which was identical with seldomycin factor 2,[12] showing that the hydroxyl and iodo groups of **7** are located at the 3′- and 4′-positions, respectively, in both equatorial positions.

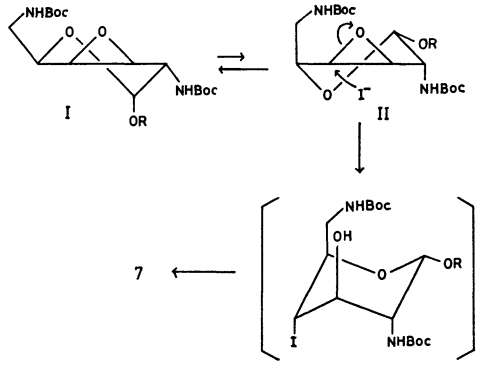

Scheme 2.

The conformation of **6** could be represented as **I** and **II**, as shown in Scheme 2. The trans-diequatorial iodohydrin (**7**) derives from conformer **II** by the attack of the iodide ion and subsequent ring inversion of the product. It has been reported[13] that the direction of the ring opening of 3,4-anhydro-*galacto*-hexopyranosides is controlled by the bulkiness of the entering reagents. In the present case, the attack of the bulky iodide ion is seriously hindered by the anomeric axial group in conformer **I** and hence conformer **II**, with the less-hindered 4′-position is more susceptible to attack although the latter is expected to be less stable than the former.

The iodohydrin (**7**) was treated with α-toluenesulfonyl chloride[6] in pyridine and the resulting 3′-α-toluenesulfonate (**11**) was heated at 90 °C for 20—30 min to give the 3′-*ene*-derivative (**12**) in 76% yield. When the corresponding 3′-methylsulfonate or 3′-*p*-toluenesulfonate was used, only a poor yield of **12** was obtained.

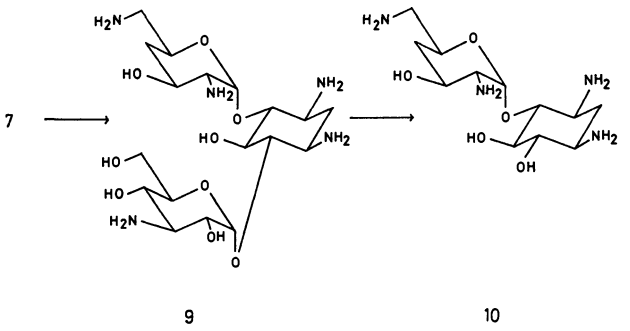

Scheme 3.

Removal of the 2″-*O*-benzoyl group in **12** with methanolic sodium methoxide afforded compound **13**. *N*-*t*-Butoxycarbonyl and 4″,6″-*O*-cyclohexylidene groups of **13** were removed by treatment with 95% trifluoroacetic acid to afford the 3′-*ene*-kanamycin B (**14**). Catalytic hydrogenation of **14** afforded 3′,4′-dideoxykanamycin B (**15**), the NMR, TLC and biological activity of which were identical with that of an authentic sample.[5] The total yield of **15** from kanamycin B was more than 40% on a large scale.[14]

Experimental

All melting points are uncorrected. Optical rotations were measured with a Perkin-Elmer Model 241 polarimeter and NMR spectra with a Varuan XL-100 spectrometer at 100 MHz. Thin-layer chromatography (TLC) was performed on Merck silica gel plate No. 5714.

Penta-N-t-*butoxycarbonylkanamycin B (1).* To a solution of kanamycin B (4.98 g) in aqueous triethylamine (34%, 35 ml), was added Boc-S reagent (18.7 g) in 1,4-dioxane (36 ml) and the mixture stirred for 24 h at room temperature. The syrupy mixture was poured into water (200 ml) and the resulting precipitate filtered, washed successively with 0.1 M-hydrochloric acid and water, and dried to give a white powder of **1** (9.88 g, 97%). The crude product was dissolved in hot ethanol and the solution cooled to give analytically pure **1** as a white powder; mp 253—260 °C (dec), $[\alpha]_D^{25}+70°$ (*c* 1.0, DMF).

Found: C, 52.31; H, 7.62; N, 7.24%. Calcd for $C_{43}H_{77}N_5O_{20}$: C, 52.47; H, 7.90; N, 7.12%.

*4″,6″-*O*-Cyclohexylidene-penta-*N*-t-butoxycarbonylkanamycin B (2).* To a solution of **1** (1.48 g) in *N*,*N*-dimethylformamide (7.4 ml), was added *p*-toluenesulfonic acid hydrate (75 mg) and 1,1-dimethoxycyclohexane (2.1 ml). The mixture was allowed to stand at room temperature overnight. The resulting solution contained three compounds [TLC, chloroform–methanol (15: 1), R_f 0.22 (**2**), R_f 0.35 (trace), R_f 0.07 (starting material)]. After neutralization with triethylamine (0.6 ml), the solution was concentrated to a syrup and water added. The resulting precipitate was filtered, washed with water and dried. The crude product was dissolved in hot methanol and the solution cooled to give pure **2** (1.48 g, 93%); mp 245 °C (dec), $[\alpha]_D^{25}+74°$ (*c* 1.0, DMF).

Found: C, 54.83; H, 8.08; N, 6.24%. Calcd for $C_{49}H_{85}N_5O_{20}$: C, 55.29; H, 8.06; N, 6.58%.

*3′,2″-Di-*O*-benzoyl-4″,6″-*O*-cyclohexylidene-penta-*N*-t-butoxycarbonylkanamycin B (3).* To a solution of **2** (1.63 g) in

dry pyridine (16 ml), was added benzoyl chloride (0.27 ml) and the mixture kept overnight at 5 °C. Benzoyl chloride (0.2 ml) was added dropwise at 5 °C until the starting material disappeared. After the addition of water (0.15 ml), the solution was concentrated to a syrup and water added. The resulting precipitate was filtered, washed with water and dried (2.0 g). Column chromatography over silica gel (50 g) with chloroform–methanol (130: 1) afforded a white powder of **3** (1.42 g, 73%) together with the compound (160 mg) showed a high R_f value. Mp 164—167 °C, $[\alpha]_D^{25}+86°$ (*c* 1.0, $CHCl_3$); NMR (CD_3OD): δ 7.34—8.16 (10H, m, C_6H_5).

Found: C, 59.54; H, 7.20; N, 5.04%. Calcd for $C_{63}H_{93}N_5O_{22}$: C, 59.45; H, 7.38; N, 5.50%.

3′,2″-Di-O-benzoyl-4″,6″-O-cyclohexylidene-4′-O-methylsulfonyl-penta-N-t-*butoxycarbonylkanamycin B (4).* A solution of **3** (966 mg) and methylsulfonyl chloride (0.29 ml) in pyridine (11.3 ml) was kept at 40 °C for 1 h. After the addition of water (0.1 ml), the solution was concentrated to a syrup and water added. The resulting precipitate was filtered, washed with water and dried (1.0 g). Column chromatography over silica gel (30 g) with chloroform–methanol (150: 1) afforded a white powder of **4** (647 mg, 67%); mp 218—221 °C (dec), $[\alpha]_D^{25}+92°$ (*c* 1.0, $CHCl_3$); NMR ($CDCl_3$): δ 2.90 (3H, s, SO_2CH_3), 7.38—8.20 (10H, m, C_6H_5).

Found: C, 56.79, H; 6.93; N, 4.71; S, 2.76%. Calcd for $C_{64}H_{95}N_5O_{24}S$: C, 56.92; H, 7.09; N, 5.18; S, 2.37%.

3′,4′-Anhydro-4″,6″-O-cyclohexylidene-4′-epi-penta-N-t-*butoxycarbonylkanamycin B (5).* To a solution of **4** (1.28 g) in methanol (10.5 ml), was added sodium methoxide (524 mg), and the solution stirred at room temperature for 3 h. After neutralization with concd hydrochloric acid at 0 °C, the resulting suspension was concentrated and precipitated by the addition of water. The resulting precipitate was filtered, washed with water and dried (1.03 g, quantitative). The crude product was dissolved in hot ethanol and the solution cooled to give analytically pure **5** as a white powder; mp 232—234 °C (dec), $[\alpha]_D^{25}+44°$ (*c* 0.5, DMF).

Found: C, 55.93; H, 8.06; N, 6.43%. Calcd for $C_{49}H_{83}N_5O_{19}$: C, 56.24; H, 8.01; N, 6.69%.

3′,4′-Anhydro-2″-O-benzoyl-4″,6″-O-cyclohexylidene-4′-epi-penta-N-t-*butoxycarbonylkanamycin B (6) and the Iodohydrin Formation.* To a solution of **5** (1.28 g) in dry pyridine (20 ml), was added benzoyl chloride (0.5 ml), and the solution kept at 5 °C for 30 min. After the addition of water (0.2 ml), the solution was concentrated to a syrup and water added. The resulting precipitate was filtered, washed with water and dried to give a white powder of **6** (1.39 g, one spot on TLC). A mixture of **6** (1.39 g), sodium iodide (907 mg), sodium acetate (52 mg), acetic acid (0.9 ml) and acetone (39 ml) was refluxed for 6.5 h. The solvent was removed by evaporation under reduced pressure and the residue triturated with water. The resulting precipitate was filtered, washed with water and dried (1.51 g). Column chromatography on silica gel (55 g) with chloroform–methanol (150: 1) gave a white powder (816 mg, 52%) of the crude iodohydrin containing **7**.

Found: I, 10.39%. Calcd for $C_{56}H_{88}IN_5O_{22}$: I, 9.95%.

4′-Deoxykanamycin B (9). The crude iodohydrin (550 mg) in a mixture of methanol (10 ml), 1,4-dioxane (6 ml) and water (5 ml) was hydrogenated for 6 h under atmospheric pressure with Raney nickel (2.3 g). After removal of the catalyst, sodium methoxide (60 mg) was added and the solution kept at room temperature for 2 h. After neutralization with 1 M hydrochloric acid, the solution was concentrated to dryness and the residue triturated with water. The resulting precipitate was filtered, washed with water and dried. The white powder (451 mg) was dissolved in 95% trifluoroacetic acid (4.5 ml) and allowed to stand at room temperature for 30 min. The resulting solution contained three compounds [TLC, 1-butanol–ethanol–chloroform–17% ammonium hydroxide (4: 5: 2: 5), R_f 0.23 (major), R_f 0.21 (minor), R_f 0.17 (minor)] was concentrated to dryness and the residue dissolved in water (13 ml). The aqueous solution was neutralized with 4 M sodium hydroxide and charged onto a column of Amberlite CG-50 (NH_4^+ form, 6 ml). After washing with water, the column was developed with 0.3 M ammonium hydroxide. A mixture of minor components was eluted first (32 mg). From the next fraction 119 mg of the compound **9** was obtained as a colorless solid; mp 227 °C (dec), $[\alpha]_D^{25}+128°$ (*c* 1.3, H_2O); NMR (D_2O): δ 5.83 (1H, d, J=4 Hz, H-1′), 5.55 (1H, d, J=4 Hz, H-1″), 3.45 (1H, q, J=4 and 10.5 Hz, H-2′), 2.38—2.71 and 1.68—2.10 (each 2H, m, H-2 and H-4′).

Found: C, 42.64; H, 7.82; N, 13.41%. Calcd for $C_{18}H_{37}N_5O_9\cdot H_2CO_3$: C, 43.08; H, 7.49; N, 13.23%.

4′-Deoxyneamine (10). A solution of **9** (217 mg) in 6 M hydrochloric acid (4 ml) was kept at 100 °C for 45 min. The solution was concentrated to dryness, water (7 ml) added to the residue followed by neutralization with 1M sodium hydroxide. The solution was charged onto a column of Amberlite CG-50 (NH_4^+ form, 6 ml). The column was washed with water and developed with 0.3 M ammonium hydroxide. The eluate containing **10** was concentrated to give 128 mg of a colorless powder; mp 206 °C (dec), $[\alpha]_D^{25}+80°$ (*c* 0.5, H_2O) [lit,[12] mp 208—209 °C (dec), $[\alpha]_D^{25}+90°$ (*c* 1.0, H_2O)]; NMR (D_2O): δ 5.80 (1H, d, J=4 Hz, H-1′), 3.20 (1H, q, J=4 and 10 Hz, H-2′), 1.85 (1H, q, J=11.2 and 11.6 Hz, H-4′ axial).

Found: C, 44.20; H, 8.05; N, 16.26%. Calcd for $C_{12}H_{26}N_4O_5\cdot\frac{1}{2}H_2CO_3$: C, 44.49; H, 8.08; N, 16.60%.

2″-O-Benzoyl-4″,6″-O-cyclohexylidene-3′,4′-dideoxy-3′-ene-penta-N-t-*butoxycarbonylkanamycin B (12).* To a solution of the crude iodohydrin **7** (954 mg) in pyridine (18 ml), was added α-toluenesulfonyl chloride (643 mg), and the solution kept at 5 °C for 30 min. After the addition of methanol (0.36 ml), the resulting solution was heated at 90 °C for 30 min. The solution was concentrated and mixed with water and the resulting precipitate filtered, washed with water and dried (987 mg). Column chromatography on silica gel (30 g) with chloroform–methanol (150: 1) afforded the pure compound **12** (645 mg, 76%) as a white powder; mp 219 °C (dec), $[\alpha]_D^{25}+32°$ (*c* 0.2, CH_3OH); NMR (C_5D_5N): δ 5.96 (2H, s, olefinic protons).

Found: C, 59.44; H, 7.77; N, 5.90%. Calcd for $C_{56}H_{87}N_5O_{19}$: C, 59.30; H, 7.73; N, 6.17%.

4″,6″-O-Cyclohexylidene-3′,4′-dideoxy-3′-ene-penta-N-t-*butoxycarbonylkanamycin B (13).* To a solution of **12** (397 mg) in methanol (20 ml), was added sodium methoxide (90 mg), and the solution kept at room temperature for 30 min. After neutralization with 1 M hydrochloric acid, the solvent was removed by evaporation and the residue triturated with water. The resulting precipitate was filtered, washed with water and dried (371 mg). Reprecipitation from ethanol–water afforded a white powder (278 mg, 79%) of **13**; mp 215—217 °C, $[\alpha]_D^{25}+30°$ (*c* 1.0, CH_3OH).

Found: C, 57.20; H, 8.07; N, 6.38%. Calcd for $C_{49}H_{83}N_5O_{18}$: C, 57.11; H, 8.14; N, 6.80%.

3′,4′-Dideoxy-3′-enekanamycin B (14). A solution of **13** (398 mg) in 95% trifluoroacetic acid (4 ml) was kept at room temperature for 30 min. The solvent was removed by evaporation and the residue dissolved in water (10 ml). The aqueous solution was neutralized with 1M sodium hydroxide and charged onto a column of Amberlite CG-50 (NH_4^+ form, 9 ml). The column was washed with water and developed

with 0.3 M ammonium hydroxide. The eluate containing **14** was evaporated to give a colorless solid (130 mg, 81%); mp 161—181 °C (dec), $[\alpha]_D^{25}+48.8°$ (*c* 0.9, H_2O); NMR (D_2O): δ 5.55 (1H, d, $J=4$ Hz, H-1″), 5.88 (1H, d, $J=4$ Hz, H-1′), 6.10 (2H, s, olefinic protons).

Found: C, 44.18; H, 7.71; N, 14.52%. Calcd for $C_{18}H_{35}N_5O_8\cdot\frac{1}{2}H_2CO_3\cdot H_2O$: C, 44.57; H, 7.63; N, 14.06%.

3′,4′-Dideoxykanamycin B (15). Compound **14** (114 mg) in water (5 ml), was hydrogenated with platinum oxide (8 mg) under atmospheric pressure overnight. After removal of the catalyst, the solution was charged onto a column of Amberlite CG-50 (NH_4^+ form, 3 ml). After washing with water, the column was eluted with 0.3 M ammonium hydroxide to give a colorless solid (103 mg, 90%) of **15**, $[\alpha]_D^{25}+130°$ (*c* 1.0, H_2O).

This compound was confirmed to be identical with an authentic sample of 3′,4′-dideoxykanamycin B in all respects including biological activity.

The authors wish to thank Dr. Sumio Umezawa of the Institute of Bio-organic Chemistry, for his helpful discussion. We also would like to thank Mr. Katsuyoshi Iwamatsu for the decoupling experiments.

References

1) H. Umezawa, *Adv. Carbohydr. Chem. Biochem.*, **30**, 183 (1974).

2) H. Umezawa, "Drug Action and Drug Resistance in Bacteria. II. Aminoglycoside Antibiotics," Univ. Tokyo Press, Tokyo (1975), p. 211.

3) H. Umezawa, M. Okanishi, S. Kondo, K. Hamana, R. Utahara, K. Maeda, and S. Mitsuhashi, *Science*, **157**, 1559 (1967).

4) S. Umezawa, Y. Nishimura, H. Hineno, K. Watanabe, S. Koike, T. Tsuchiya, and H. Umezawa, *Bull. Chem. Soc. Jpn.*, **45**, 2847 (1972).

5) S. Umezawa, H. Umezawa, Y. Okazaki, and T. Tsuchiya, *Bull. Chem. Soc. Jpn.*, **45**, 3624 (1972).

6) T. Miyake, T. Tsuchiya, S. Umezawa, and H. Umezawa, *Carbohydr. Res.*, **49**, 141 (1976).

7) R. S. Tipson and A. Cohen, *Carbohydr. Res.*, **1**, 338 (1965).

8) R. U. Lemieux, E. Fraga, and K. A. Watanabe, *Can. J. Chem.*, **46**, 61 (1968).

9) K. A. Watanabe, R. S. Goody, and J. J. Fox, *Tetrahedron*, **26**, 3883 (1970).

10) T. Nagasawa, K. Kuroiwa, K. Narita, and Y. Isowa, *Bull. Chem. Soc. Jpn.*, **46**, 1269 (1973).

11) J. M. Williams and A. C. Richardson, *Tetrahedron*, **23**, 1369, 1641 (1970); M. W. Horner, L. Hough, and A. C. Richardson, *J. Chem. Soc., C*, **1970**, 1336.

12) R. S. Egan, A. C. Sinclair, R. L. Vault, J. B. McAlpine, S. L. Meuller, P. C. Goodley, R. T. Mauritz, L. A. Mitscher. K. Shirahata, S. Saito, and T. Iida, *J. Antibiot.*, **30**, 31 (1977),

13) K. Capek, J. Nemec, and J. Jary, *Collect. Czech. Chem. Commun.*, **33**, 1758 (1968).

14) In the case of large scale preparation, all intermediary products were used for subsequent steps without purification except compound **14** which was readily purified by resin column chromatography.

Photochemical Reactions of *N*-Acyl-2,3-dihydrobenzoxazol-2-ones

Sadahiro ISHIDA, Yoji HASHIDA, Haruo SHIZUKA, and Kohji MATSUI*

Department of Chemistry, Faculty of Engineering, Gunma University, Kiryu, Gunma 376

(Received August 2, 1978)

Photo-Fries rearrangements of *N*-acyl-2,3-dihydrobenzoxazol-2-ones are described. Irradiation of *N*-acyl-2,3-dihydrobenzoxazol-2-ones in acetonitrile afforded a mixture of 2-acyl-2,3-dihydrobenzoxazol-2-one and 6-acyl-2,3-dihydrobenzoxazol-2-one together with other minor products. However, 2,3-dihydrobenzoxazol-2-one and *N*-methyl-2,3-dihydrobenzoxazol-2-one were very photostable. The reaction scheme involving Norrish type I dissociation has been discussed.

The photochemical reactions of carbonyl compounds have been extensively studied; among them the photo-Fries rearrangement has been studied in detail for various aryl esters and *N*-arylamides.[1] In the photochemical reactions of acetoanilide[2] and its related compounds,[3] it has been shown that, in the liquid phase, the photo-Fries rearrangement originates from the lowest excited singlet state $S_1(\pi\pi^*)$ forming pair radicals which efficiently recombine in a solvent cage into the original substance, ortho- and para-isomers. The photo-Fries rearrangements of some heteroaromatic compounds, such as aryloxy-1,3,5-triazines,[4] 2-aryloxybenzazoles,[5] and *N*-acetylcarbazole[6] have been reported. The photochemical reactions of imides have been the subject of numerous recent studies; photochemical rearrangements of *N*-alkylphthalimides, which involve ring expansion *via* the Norrish type II process, have been reported by Kanaoka *et al.*,[7] and Mazzocchi *et al.*[8]

This paper will report on the photochemistry of *N*-acyl-2,3-dihydrobenzoxazol-2-ones (**1**) having a semicyclic imide skeleton. The photochemical behavior of these compounds is of interest to ascertain where dissociation occurs upon irradiation and what the photoproducts are.

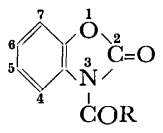

(**1**)

Results and Discussion

Photo-Fries Rearrangement of N-*Acyl-2,3-dihydrobenzoxazol-2-ones.* *N*-Acyl-2,3-dihydrobenzoxazol-2-ones have been prepared by treating 2,3-dihydrobenzoxazol-2-one with acyl halide in pyridine, the details of which are listed in Table 1.

When the substituent at the 3-position is H (**1a**) or CH_3 (**1b**), no photochemical reaction was observed even after prolonged irradiation; this is particularly interesting because ordinary arylamides and arylesters are known to undergo photoreaction involving bond cleavage at –N–CO–[2d] and –O–CO–.[9]

When the substituent is an acyl group, a regular spectral change was observed upon irradiation in every case, a typical example of a spectral change being shown in Fig. 1 for the *N*-benzoyl derivative (**1g**).

In the case of the *N*-benzoyl compound (**1g**), a clean photo-chemical reaction took place to afford five photoproducts (**2g**, **3g**, **4**, **5**, **6**). The two products (**2g** and **3g**) were found to be positional isomers of the starting material (**1g**) which gave aminohydroxybenzophenones on treatment with hydrochloric acid. Spectral data showed that the compounds are benzene-ring-benzoylated products resulting from N→C migration of the benzoyl group, *i.e.* the reaction was a photo-Fries rearrangement. In the ordinary photo-Fries rearrangement of *N*-arylamides, the acyl group migrates to the ortho and para positions relative to the amino group. Therefore, the two isomeric products obtained have been assumed to be the ortho and para benzoylated products.

TABLE 1. 3-SUBSTITUTED 2,3-DIHYDROBENZOXAZOL-2-ONES

No.	3-Substituent	Mp (°C) (Lit)	Solvent for recrystallization	Found (%) C	Found (%) H	Calcd (%) C	Calcd (%) H
1a	H	139—140 (137—138)[a]	Benzene	—	—	—	—
1b	CH_3	84.5—85.5	Cyclohexane	64.31	4.65	64.42	4.73
1c	$COCH_3$	94—95 (95)[b]	Petroleum ether	—	—	—	—
1d	COC_2H_5	92—93	Cyclohexane	62.39	4.71	62.82	4.75
1e	COC_3H_7	82—83	Hexane	64.32	5.38	64.38	5.40
1f	$COCH(CH_3)_2$	47.5—48.5	Petroleum ether	64.61	5.47	64.38	5.40
1g	COC_6H_5	169—170 (174)[c]	Benzene	—	—	—	—
1h	COC_6H_4-(*p*)-CH_3	182.5—183	Benzene	71.35	4.37	71.14	4.37

a) Ref. 12. b) H. Zinner, H. Herbig, and H. Wigert, *Chem. Ber.*, **89**, 2135 (1956).
c) H. Böshagen and W. Geiger, *Chem. Ber.*, **103**, 123 (1970).

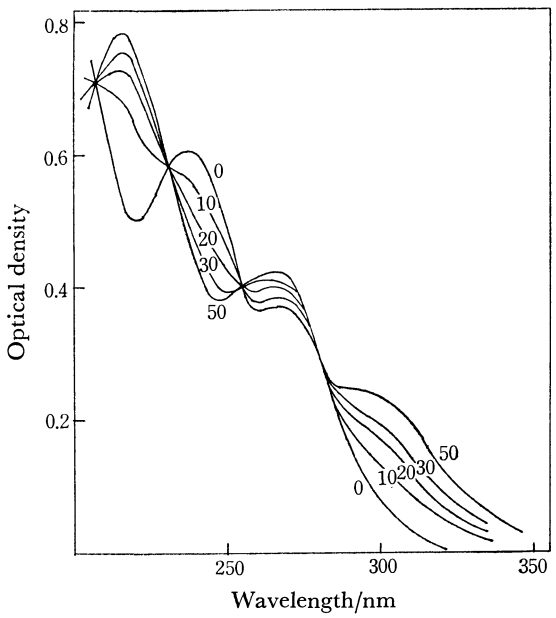

Fig. 1. Spectral change of an ethanol solution of 3-benzoyl-2,3-dihydrobenzoxazol-2-one by irradiation with a low-pressure mercury lamp. Numbers refer to time at a measurement in seconds.

In the ortho rearranged product, the formation of an intramolecular hydrogen bond as shown (**2**) may be possible:

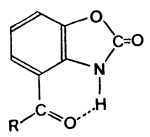

2

One product (**3g**) readily dissociated in the presence of alkali, while the other (**2g**) did not. In addition, the weaker acidic product (**2g**) has a NMR band attributable to an NH proton at a lower magnetic field. On this basis the isomer (**2g**) has been identified as the ortho-rearranged product while the other (**3g**) corresponds to the para-benzoylated product. Other products obtained were benzoic acid (**4**) and 2,3-dihydrobenzoxazol-2-ones (**5**). At the same time a derivative of 2,3-dihydrobenzoxazol-2-one which does not contain benzoyl group was obtained in a low yield. This compound was also obtained in the case of other *N*-acyl derivatives (**1c, 1h**), and was shown to be a dimer (**6**) of benzoxazolin-2-one. It appears that the dimer resulted from the coupling of two benzoxazolonyl radicals. This radical have four reactive positions, *viz*:

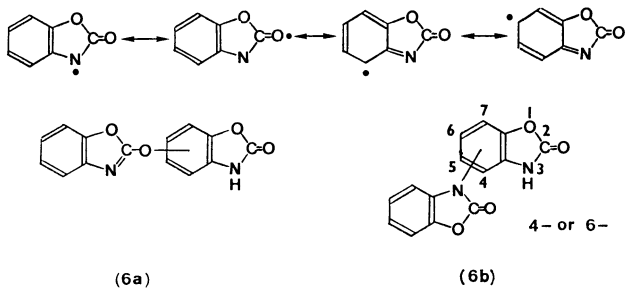

Thus, between the two radicals various types of coupling may be expected resulting in the formation of various dimers. One dimer was however obtained, showing that the coupling was regiospecific. This regiospecific nature of benzoxazolonyl radicals may be ascribed in part to their high selectivity caused by the delocalization as shown above. NMR spectra show that the dimer has seven aromatic protons and one active hydrogen atom, consequently, two possible formulas (**6a** and **6b**) for the dimer have to be considered. However, since 2-aryloxybenzoxazoles readily rearrange to give 2-(2- and/or 4-hydroxyaryl)benzoxazoles upon irradiation,[5] (**6a**) seems less probable than (**6b**). Furthermore, the 6-(2-oxo-2,3-dihydrobenzoxazol-3-yl)-2,3-dihydrobenzoxazol-2-one derivative is preferable to the 4-isomer since there is less steric hindrance and the corresponding odd π-electron density is high at the 6-position.[10] The dimer formation is evidence that the reaction proceeds *via* Norrish type I dissociation in the liquid phase.[11]

Similar photoreactions have been observed for other *N*-acyl derivatives, the yields and products of which are listed in Table 2. Table 2 shows that the ratios of ortho and para rearranged products is about 1. The reaction

Table 2. Photochemical rearrangement of 3-substituted 2,3-dihydrobenzoxazol-2-ones in acetonitrile

Compound	Yield of product (%)			Other compds
	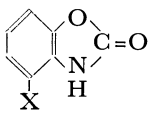 (mp/°C)	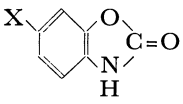 (mp/°C)	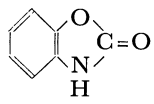	
1c [X: $COCH_3$]	18.8 (208—209)	17.4 (223—225)	19.0	Dimer (trace)
1d [X: COC_2H_5]	14.0 (148—149)	11.5 (203—204)	36.4	—
1e [X: COC_3H_7]	18.2 (136.5—137.5)	14.4 (151—152)	35.5	—
1f [X: $COCH(CH_3)_2$]	15.0 (121—122)	17.7 (192—193)	39.0	—
1g [X: COC_6H_5]	18.4 (197—198)	20.4 (147—148)	28.9	Dimer (6.3), Benzoic acid (17.2)
1h [X: COC_6H_4-(*p*)-CH_3]	19.0 (206—207)	21.5 (203—204)	29.2	Dimer (4.8), *p*-Toluic acid (20.0)

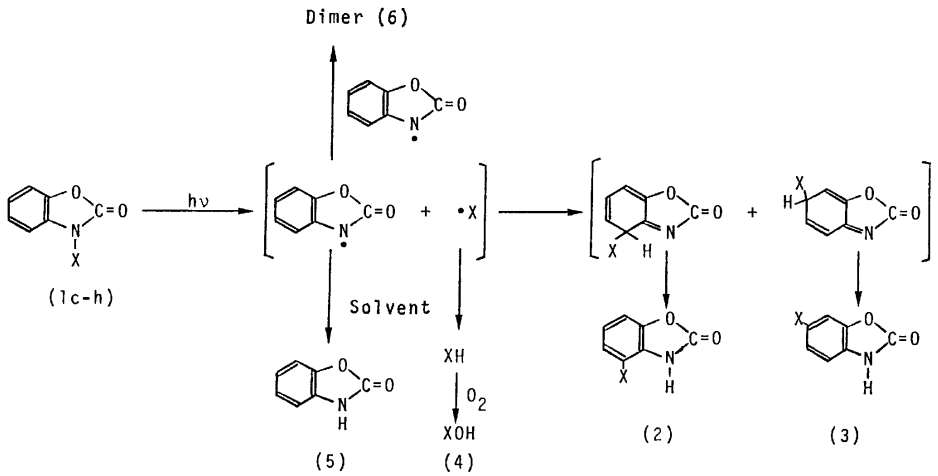

Scheme 1.

appears to proceed *via* the following Scheme *i.e.*, i) a Norrish type I fission of the N–COR bond which may originate from the lowest excited singlet state $S_1(\pi\pi^*)$[2,3] to give benzoxazolonyl and acyl radicals, ii) the attack by the acyl radical upon the 4 and 6 positions in a solvent cage yielding the corresponding products, and iii) the escape of the radicals from the solvent cage reacting differently depending upon the nature of radicals. A part of the benzoxazolonyl radical abstracts hydrogen atoms from the solvent (acetonitrile) resulting in the formation of 2,3-dihydrobenzoxazol-2-one. A part of the benzoxazolonyl radical couples to each other to give the dimer. While the acyl radical gave the corresponding acid, presumably *via* oxidation of the intermediary aldehyde resulted from the hydrogen abstruction of acyl radical from the solvent.

In the photo-Fries rearrangement of aryloxy-1,3,5-triazines,[7a] the viscosity of solvent scarcely affected the ortho-rearrangement, but considerably affected the para-rearrangement. The viscosity dependence of the solvent upon the photochemical rearrangements has been examined in a EtOH–glycerol mixture. In the photolysis of **4f**, the para/ortho (6-/4-) ratios decreased with an increase in the glycerol contents; the ratios were 1.22, 0.88, and 0.55 in zero, 30, 60 glycerol volume percent respectively. This indicates that the dependence of the 6-rearrangement on the stiffness of the solvent cage is larger than that of the 4-rearrangement because the 6-position is separated by a longer path.

In summary, it has been shown that, in *N*-acyl-2, 3-dihydroxybenzoxazol-2-ones, Norrish type I fission takes place at the 3–8 bond to give photo-Fries rearrangement products, demonstrating that the 2,3-dihydrobenzoxazol-2-one skeleton is very photostable. This apparent photostability of 2,3-dihydrobenzoxazol-2-one may be interpreted as follows. If the fission of the 1–2 or 2–3 bond takes place upon irradiation, the free migration of the acyl radical to positions where odd π electron densities are large is hindered by the bond to the benzene nucleus through the hetero atom. Consequently the rate of back reaction to give the starting material would dominate other reactions. The lifetime and fluorescence quantum yield of this molecule **1a** is about 2 ns and $5(\pm 2)\times 10^{-2}$ in ethanol at room temperature respectively, indicating that the radiationless processes in the excited state of **1a**, other than the reaction predominant. The fluorescence quantum yield of **1f** was very small (approx. 10^2 less than that of **1a**), and the lifetime was unobservable.

Experimental

All melting points are uncorrected.

Materials. 2,3-Dihydrobenzoxazol-2-one was prepared according to the literature method.[12] *N*-Methyl-2,3-dihydrobenzoxazol-2-one was prepared by the alkylation of 2,3-dihydrobenzoxazol-2-one with dimethylsulfate, and *N*-acyl-2,3-dihydrobenzoxazol-2-ones by treatment of 2,3-dihydrobenzoxazol-2-one with acyl halide. A typical preparation is shown in the case of *N*-isobutyryl-2,3-dihydrobenzoxazol-2-one (**1f**). Isobutryl chloride (7.46 g, 0.07 mol) was added dropwise into a cold solution of 2,3-dihydrobenzoxazol-2-one (6.76 g, 0.05 mol) in pyridine (50 ml). After stirring for 1 h at room temperature, the mixture was poured into ice water and the resulting precipitate filtered and dried. Recrystallization from petroleum ether gave a pure sample (yield, 90%).

Irradiation. All irradiations were conducted with a low-pressure mercury lamp (30 W×2) and a typical reaction is shown in the case of *N*-benzoyl-2,3-dihydrobenzoxazol-2-one: A solution containing *N*-benzoyl-2,3-dihydrobenzoxazol-2-one (2.00 g, 8.36 mmol) in acetonitrile (100 ml) was irradiated for 48 h and the photochemical reaction monitored by TLC. After removal of the solvent, the residue was chromatographed on a silica gel column using a benzene–acetone mixture (10: 1, v/v) as an eluent and gave the following products: a) starting material (0.30 g, 1.26 mmol) which was identified by a mixed-melting point test with an authentic sample. b) 6-Benzoyl-2,3-dihydrobenzoxazol-2-one (recrystallized from benzene): yield, 0.31 g (18%); MS *m/e* 239 (M^+); PMR ($CDCl_3$), δ 6.93—7.88 (m, 8H), 10.70, (broad, 1H); IR (KBr), 3200 (–NH), 1780 (C=O, ring), 1640 cm^{-1} (C=O). Found: C, 69.92; H, 3.78; N, 5.66%. Calcd for $C_{14}H_9NO_3$: C, 70.29; H, 3.79; N, 5.86%. This compound was decomposed in refluxing hydrochloric acid (20 wt %) for 40 h to give crude 4-amino-3-hydroxybenzophenone. Recrystallization from benzene gave a pure sample: yield, 0.33 g (88%); mp 134—135 °C; MS *m/e* 213 (M^+);

IR (KBr), 3480, 3360 (OH), 3150 cm^{-1} (NH_2). Found: C, 73.35; H, 5.21; N, 6.80%. Calcd for $C_{13}H_{11}NO_2$: C, 73.22; H, 5.20; N, 6.57%. c) 4-Benzoyl-2,3-dihydrobenzoxazol-2-one (recrystallized from benzene): yield, 0.35 g (21%); MS *m/e* 239 (M^+); PMR ($CDCl_3$), δ 6.97—7.85 (m, 8H), 10.00 (broad, 1H); IR (KBr), 3120, 3040 (NH), 1850 (C=O, ring), 1640 cm^{-1} (C=O). Found: C, 70.14; H, 3.83; N, 5.96%. Calcd for $C_{14}H_9NO_3$: C, 70.29; H, 3.79; N, 5.86%. This compound was decomposed in refluxing hydrochloric acid for 10 h to give 2-amino-3-hydroxybenzophenone. Yield, 0.30 g (68%); mp 129.5—130.5 °C; MS *m/e* 213 (M^+). Found: C, 73.29; H, 5.28; N, 6.72%. Calcd for $C_{13}H_{11}NO_2$: C, 73.22; H, 5.20; N, 6.57%. d) Dimer (recrystallized from methanol): yield, 0.069 g (6%); mp 258—259 °C; MS *m/e* 268 (M^+); PMR (*p*-dioxane), δ 7.0—8.0 (m, 7H), 9.97 (broad, 1H); IR (KBr), 3250 (NH), 1780, 1760 cm^{-1} (C=O, ring). Found: C, 62.91; H, 3.11; N, 10.33%. Calcd for $C_{14}H_8N_2O_4$: C, 62.91: H, 3.11; N, 10.45%. e) Benzoic acid (sublimed under reduced pressure) which was identified by a mixed-melting point test with an authentic sample: yield, 0.15 g (17%).

Measurements of the Isomer Ratios. After irradiation in a given solvent, the products were seperated by silica gel TLC using a mixture of benzene and acetone (20: 1 in volume) as the developing solvent. From the chromatogram each isomer was extracted and diluted with ethanol to a fixed volume and the extinction measured spectrophotometrically.

Measurements of Fluorescence Lifetime. The experimental procedure is reported elsewhere.[13]

References

1) D. Bellus, "Advances in Photochemistry," ed by J. N. Pitts, G. S. Hammond, and W. A. Noyes, Jr., Interscience, N. Y. (1971), Vol. 8, p. 109, and references cited therein.

2) a) H. Shizuka and I. Tanaka, *Bull. Chem. Soc. Jpn.*, **41**, 2343 (1968); b) H. Shizuka, *ibid.*, **42**, 52 (1969); c) H. Shizuka, *ibid.*, **42**, 57 (1969); d) H. Shizuka and I. Tanaka, *ibid.*, **42**, 909 (1969).

3) H. Shizuka, T. Morita, Y. Mori, and I. Tanaka, *Bull. Chem. Soc. Jpn.*, **42**, 1831 (1969).

4) a) H. Shizuka, T. Kanai, T. Morita, Y. Ohto, and K. Matsui, *Tetrahedron*, **27**, 4021 (1971); b) Y. Ohto, H. Shizuka, S. Sekiguchi, and K. Matsui, *Bull. Chem. Soc. Jpn.*, **47**, 1209 (1974); c) K. Tsutsumi, K. Matsui, and H. Shizuka, *Mol. Photochem.*, **7**, 325 (1976).

5) T. Nagai, Y. Fukushima, T. Kuroda, H. Shimizu, S. Sekiguchi, and K. Matsui, *Bull. Chem. Soc. Jpn.*, **46**, 2600 (1973).

6) H. Shizuka, M. Kato, T. Ochiai, K. Matsui, and T. Morita, *Bull. Chem. Soc. Jpn.*, **43**, 67 (1970).

7) a) Y. Kanaoka and K. Koyama, *Tetrahedron Lett.*, **1972**, 4517; b) Y. Kanaoka, Y. Migita, Y. Sato, and H. Nakai, *ibid.*, **1973**, 51; c) Y. Kanaoka, Y. Migita, K. Koyama, Y. Sato, H. Nakai, and T. Mizoguchi, *ibid.*, **1973** 1193; d) Y. Saito, H. Nakai, H. Ogiwara, T. Mizoguchi, Y. Migita, and Y. Kanaoka, *ibid.*, **1973**, 4565; e) Y. Kanaoka and Y. Migita, *ibid.*, **1974**, 3693; f) Y. Kanaoka and Y. Hatanaka, *Chem. Pharm. Bull.*, **22**, 2205 (1974); g) Y. Kanaoka, T. Tsuji, K. Itoh, and K. Koyama, *ibid.*, **21**, 453 (1973); h) Y. Kanaoka, K. Koyama, J. L. Flippen, I. L. Karle, and B. Witkop, *J. Am. Chem. Soc.*, **96**, 4719 (1974); i) Y. Sato, H. Nakai, T. Mizoguchi, Y. Hatanaka, and Y. Kanaoka, *ibid.*, **98**, 2349 (1976); j) Y. Kanaoka and Y. Hatanaka, *J. Org. Chem.*, **41**, 400 (1976).

8) P. H. Mazzocchi, M. J. Bowen, and N. K. Narain, *J. Am. Chem. Soc.*, **99**, 7063 (1977).

9) J. W. Meyer and G. S. Hammond, *J. Am. Chem. Soc.*, **92**, 2187 (1970); *ibid.*, **94**, 2219 (1972).

10) Odd π electron densities at positions 4 and 6 were 0.0310 and 0.1384 respectively, calculated by the semi-empirical SCF-MO-CI method. The calculations were conducted by a HITAC 8800 computer (University of Tokyo).

11) In the gas phase, evidence for the fission has been given, see Refs. 2d and 9.

12) H. R. Snyder, C. T. Elston, and D. B. Kellom, *J. Am. Chem. Soc.*, **75**, 2014 (1953).

13) *E.g.*, H. Shizuka, K. Matsui, Y. Hirata, and I. Tanaka, *J. Phys. Chem.*, **81**, 2243 (1977).

Interactions between Sulfur Ylides and Electrophilic Monosulfides[1)]

Haruo MATSUYAMA,* Masae MATSUMOTO, Michio KOBAYASHI, and (the late) Hiroshi MINATO

Department of Chemistry, Faculty of Science, Tokyo Metropolitan University, Fukazawa, Setagaya, Tokyo 158

(Received August 3, 1978)

The catalytic activities of electrophilic monosulfides, Ar–S–R* (R*=CN, CF_3, OMe), for the transylidation reactions of sulfur ylide, $Ph(Me)\overset{\oplus}{S}-\overset{\ominus}{C}(CO_2Me)_2$, with alkyl sulfides and pyridines were investigated. Among these monosulfides, methyl arenesulfenates reacted with dimethylsulfonium phenacylide (or dimethylsulfonium ethoxycarbonylmethylide) to give α-(arylthio)phenacylides (or α-(arylthio)ethoxycarbonylmethylides) and methanol. The ^{13}C-NMR spectra of several sulfur ylides and aryl thiocyanates were investigated in $CDCl_3$, and the presence of *S*-ylide–thiocyanate adduct intermediates was established.

Electrophilic sulfides, $\overset{\delta-}{R}{}^*\leftarrow\overset{\delta+}{S}\rightarrow\overset{\delta-}{R}{}^*$ (R*=electron-withdrawing substituents), are very interesting compounds. We have previously reported that the disulfides containing electron-withdrawing substituents, $\overset{\delta-}{R}\leftarrow\overset{\delta+}{S}-\overset{\delta+}{S}\rightarrow\overset{\delta-}{R}{}^*$ (R*=OMe, CN, CF_3, and COPh), react as novel catalysts in several reactions of sulfur ylides.[2–5)] Particularly, in the presence of dimethoxy disulfide (R*=OMe), transylidation reactions take place smoothly at room temperature, as is shown below:[2)]

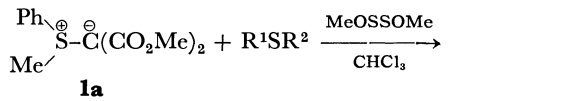

1a

R^1SR^2: Me_2S, MeSEt, MeSBu-*n*, MeSPr-*i*, $MeSC_8H_{17}$-2, $MeSCH_2Ph$, Et_2S, $MeSCH_2SMe$, 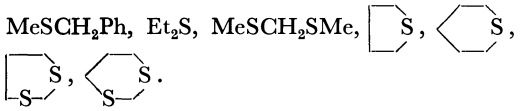

Tamagaki *et al.* reported that carbon disulfide acts as a catalyst for the transylidation reaction of selenonium ylide with alkyl sulfides.[6)] In both reactions, the formation of ylide-catalyst adducts (**2a** and **2b**) and the subsequent nucleophilic attack of alkyl sulfides on the adducts to afford the new ylides were postulated.[2,6)]

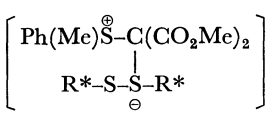

2a

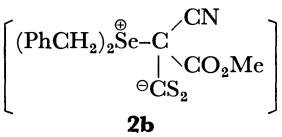

2b

Hitherto, the catalytic ability of the monosulfides for the transylidation reaction of sulfur ylides has not been investigated. Recently, we have found that the monosulfides containing electron-withdrawing substituents, Ar–S–R* (R*=CN, CF_3, and OMe), act as catalysts for the transylidation reaction of sulfur ylide **1a**. In this paper, we wish to report how to produce interaction between sulfur ylides and electrophilic monosulfides which act as catalysts on transylidation reactions.

Results and Discussion

Transylidation. In the presence of aryl thiocyanates (Ar–S–CN), phenylmethylsulfonium bis(methoxycarbonyl)methylide **1a** reacted with 4-methylpyridine to give a new 4-methylpyridinium ylide in chloroform at room temperature.

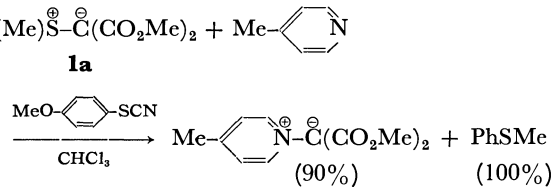

(90%) (100%)

In the absence of aryl thiocyanates, **1a** is very stable and shows no transylidation when it is mixed with pyridine at 35 °C. After the reaction was over, aryl thiocyanates were recovered from its solution by the PLC (preparative layer chromatography) method. The reaction between 4-methylpyridine and ylide **1a** was slow enough for its rate to be determined. The effects of the concentrations of the reactants and the catalyst were examined. The results are summarized in Table 1. The first-order rate constants calculated by assuming $-d[\mathbf{1a}]/dt=k[\mathbf{1a}]$ increased with the initial concentration of 4-methylpyridine; apparently the rate depends on 4-methylpyridine. The rates increased also with the

Table 1. Rates of transylidation between ylide **1a** and 4-methylpyridine in $CDCl_3$ at 35 °C

Reactants (mol/l)			First-order rate constants calcd from $-d[\mathbf{1a}]/dt=k[\mathbf{1a}]$ $10^5\times k$ (s^{-1})
1a			
0.50	0.50	0.50	0.78
0.50	1.00	0.50	2.2
0.50	1.50	0.50	3.4
0.50	1.50	1.00	7.3
0.50	1.50	2.00	10

Table 2. Rates of transylidation of ylide **1a** with methyl sulfide in $CDCl_3$ at 35 °C[a]

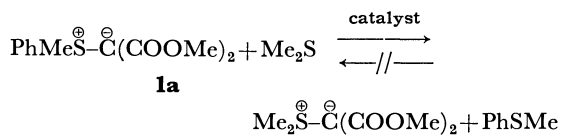

Catalyst		First-order rate constants calcd from $-d[\mathbf{1a}]/dt = k[\mathbf{1a}]$ $10^5 \times k(s^{-1})$
None		No reaction
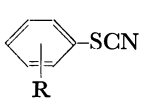	R = *p*-MeO	4.6
	p-Me_2N	0.50
	p-Me	0.50
	p-Cl	0.32
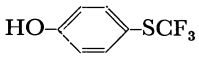		0.73
Cl_3CSOMe		Very fast[b]
CS_2		2.3
PhSOMe		No reaction
PhSC(O)Me		No reaction

a) A mixture consists of **1a** (0.5 M), dimethyl sulfide (1.5 M), and a catalyst (2.0 M). b) 10 min after, the yield of **1b** was 70%.

initial concentration of *p*-methoxyphenyl thiocyanate.

Various monosulfides were examined as regards their catalytic activity in this transylidation. Neither *S*-phenylthioacetate nor methyl benzenesulfenate was effective, methyl trichloromethanesulfenate and *p*-trifluoromethylphenol possessed a catalytic activity similar to that of aryl thiocyanate. Carbon disulfide also acted as catalyst in this transylidation (Table 2). The order of catalytic activity was:

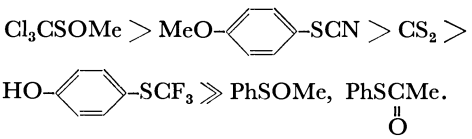

Reactions of Dimethylsulfonium Phenacylide **3** *with Aryl Thiocyanates.* It was found that *p*-chlorophenyl thiocyanate (Ar=*p*-Cl-C_6H_4) reacted very slowly with ylide **3** to give dimethylsulfonium α-(*p*-chlorophenylthio)phenacylide (31%), methyl sulfide (43%), and *p*-chlorophenyl phenacyl sulfide (40%) after 4 days. These reaction products can be explained by assuming the formation of the sulfonium ion **4**.[8]

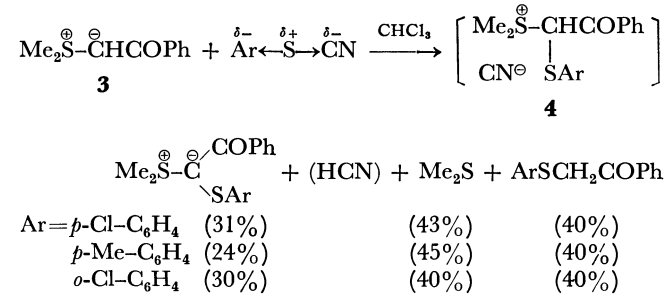

Ar=*p*-Cl-C_6H_4	(31%)	(43%)	(40%)
p-Me-C_6H_4	(24%)	(45%)	(40%)
o-Cl-C_6H_4	(30%)	(40%)	(40%)

Reactions of the **3** *and* **5** *Sulfur Ylides with Methyl Arenesulfenates.* In contrast to aryl thiocyanates, methyl arenesulfenates, ArSOMe, did not act as catalysts for transylidation. However, they reacted instantaneously at room temperature with phenacylide **3** (or ethoxycarbonylmethylide **5**), which contains only one electron-withdrawing substituent, in chloroform and gave the sulfenylated products, dimethylsulfonium α-(arylthio)-phenacylide[19] (or α-(arylthio)ethoxycarbonylmethylide[19]). The results are shown in Table 3.

Table 3. Reactions of sulfur ylides **3** and **5** with methyl arenesulfenates in $CHCl_3$ at room temperature

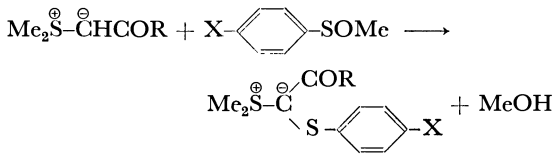

Ylide	R	X	Yield (%)[a]	Mp (°C)	ν_{CO} (cm^{-1})
3	Ph	H	75	138—140	1520
		Me	68	136—138	1520
		Cl	89	148—149	1520
5	OEt	H	42	126—127	1600
		Me	33	114—116	1600
		Cl	87	135—136	1600

a) Isolated yield.

Carbon-13 NMR Spectra of Ylide-catalyst Adducts. In order to obtain spectroscopic evidence for the formation of the sulfur ylide–electrophilic sulfides adducts, we investigated the carbon-13 NMR spectra of solutions of several sulfur ylides and aryl thiocyanates which are active catalysts. Carbon-13 chemical shifts provide some information on the electronic state of carbon atoms in molecules. The chemical shifts of disubstituted sulfur ylides, **1a** and **1b**, are little affected by solvents.[7] On

Table 4. ^{13}C chemical shifts of ylide carbons of some sulfonium ylides[a]

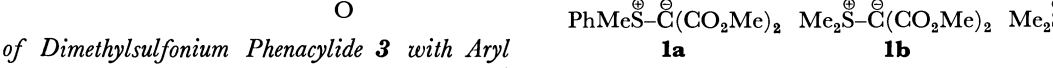

Thiocyanate/Ylide (mol/mol)			$\overset{\ominus}{C}$ or $\overset{\ominus}{C}H$	$\Delta\delta$[b]	Solvent
None	**1a**		59.1	(0)	$CDCl_3$
None	**1a**		59.2	(0.1)	DMSO-d_6
MeO-C_6H_4-SCN	**1a**	(1/1)	59.1	(0)	$CDCl_3$
None	**1b**		58.6	(0)	$CDCl_3$
None	**1b**		58.4	(−0.2)	DMSO-d_6
MeO-C_6H_4-SCN	**1b**	(1/1)	58.7	(0.1)	$CDCl_3$
None	**3**		53.2	(0)	$CDCl_3$
None	**3**		60.6	(7.4)	DMSO-d_6
MeO-C_6H_4-SCN	**3**	(1/1)	54.2	(1.0)	$CDCl_3$
Me_2N-C_6H_4-SCN	**3**	(1/1)	53.8	(0.6)	$CDCl_3$
		(2/1)	54.4	(1.2)	$CDCl_3$
MeSCN	**3**	(1/1)	53.1	(0)	$CDCl_3$
		(5/1)	54.4	(1.2)	$CDCl_3$
		(10/1)	55.5	(2.3)	$CDCl_3$
		(15/1)	56.2	(3.1)	$CDCl_3$
		(23/1)	56.5	(3.3)	$CDCl_3$

a) δ_c, ppm from TMS (accurate to ±0.13).
b) $\Delta\delta = (\delta^{ArSCN}_{CDCl_3} - \delta^{none}_{CDCl_3})$.

the other hand, the chemical shifts of the ylide carbon of dimethylsulfonium phenacylide, **3**, which contains only one electron-withdrawing substituent and which acts as a reactive carbanion, are dependent on the kind of solvent (Table 4).

When ylide **3** and aryl thiocyanate are mixed in chloroform, the downfield shifts (0.6—3.3 ppm) of the ylide carbon of phenacylide **3** were observed. Though the values of the shifts of ylide carbon were small, the NMR data can be explained by assuming that the formation of the adduct **6** from the ylide **3** and aryl thiocyanate is reversible and rapid.

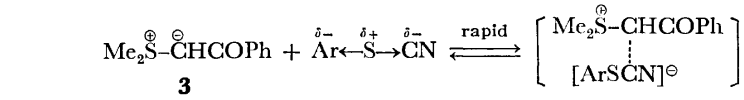

3 **6**

By the formation of the dipole-dipole interaction complex **6**, the negative charge on the ylide carbanion is withdrawn toward the catalytic sulfide, and the nucleophilic attack of a sulfide (or a pyridine) on the sulfonium atom is facilitated.[5] Therefore, monosulfides possessing strongly electronegative substituents can act as the catalysts for transylidation.

Experimental

Materials. Sulfonium bis(methoxycarbonyl)methylide **1a** and **1b** were prepared by the copper sulfate-catalyzed decomposition of dimethyl diazomalonate in a large excess of sulfides.[9] The dimethylsulfonium ylides **3**[10a] and **5**[10b] were prepared by the methods described in the literature. Methyl trichloromethanesulfenate was obtained by the drop-by-drop addition of a CCl_4 solution of trichloromethanesulfenyl chloride (10 mmol; prepared by the reaction of carbon disulfide and chlorine; bp 148 °C) to a CCl_4 solution of methanol (12 mmol) and pyridine (12 mmol) at 0 °C. Cl_3CSOMe, bp 25 °C/5 mmHg; NMR ($CDCl_3$), δ=4.19 (s, OMe). *p*-Methoxyphenyl thiocyanate (mp 33—35 °C (lit,[11] 33—34 °C), IR (KBr), 2180 cm^{-1} (ν_{SCN}); NMR ($CDCl_3$), δ=3.82 (3H, s, OMe) and 6.82—7.55 (4H, q, aromatic-H)), *p*-dimethylaminophenyl thiocyanate (mp 73—74 °C (lit,[12] 73—74 °C); IR (KBr), 2160 cm^{-1} (ν_{SCN}); NMR; ($CDCl_3$), δ=2.96 (6H, s, NMe_2) and 6.55—7.44 (4H, q, aromatic-H)), and *o*-chlorophenyl thiocyanate (bp 98—100 °C/4 mmHg (lit,[13] 160 °C/42 mmHg); IR (neat), 2190 cm^{-1} (ν_{SCN}) were prepared by the methods described in the literature. *p*-Tolyl thiocyanate (bp 92—96 °C/1 mmHg (lit,[14] 117—118 °C/20 mmHg); IR (neat), 2160 cm^{-1} (ν_{SCN})) and *p*-chlorophenyl thiocyanate (bp 101—105 °C/1 mmHg) were prepared by the reaction of formamide and sulfenyl chloride ArSCl (Ar=*p*-Me-C_6H_4, *p*-Cl-C_6H_4) in the presence of $SOCl_2$.[14] Methyl arenesulfenates ArSOMe (Ar-Ph, bp 50 °C/2 mmHg (lit,[15a] 54 °C/10 mmHg); NMR ($CDCl_3$), δ=3.70 (3H, s, OMe) and 7.30 (5H, s, Ph); Ar=*p*-Me-C_6H_4, bp 55 °C/3 mmHg; NMR ($CDCl_3$), δ=2.34 (3H, s, *p*-Me), 3.65 (3H, s, OMe) and 7.28 (4H, s, aromatic-H); and Ar=*p*-Cl-C_6H_4, bp 76—77 °C/3 mmHg; NMR ($CDCl_3$), δ=3.70 (3H, s, OMe) and 7.29 (4H, broad s, aromatic-H) were synthesized by the drop-by-drop addition of an ether solution of the corresponding arenesulfenyl chlorides[15b] to an ether solution of methanol and triethylamine at 0 °C under a nitrogen atmosphere. *p*-(Trifluoromethylthio)phenol (mp 57—58 °C lit,[16] 57—58 °C)) was prepared by the reaction of phenol (0.94 g) and trifluoromethanesulfenyl chloride[17] (in a CCl_4 solution) at 0 °C in the presence of pyridine (0.8 g). *S*-Phenyl thioacetate (bp 82—84 °C/7 mmHg) was obtained by the condensation of thiophenol and acetyl chloride.[18] Carbon disulfide was of reagent grade and was used without purification.

Transylidation. The NMR spectra were determined by means of a Hitachi NMR spectrometer R-20B (60 MHz). A $CDCl_3$ solution of ylide **1a** (0.5 M), dimethyl sulfide (1.5 M), and a catalyst (2.0 M) was placed in an NMR tube at 35 °C, and the intensity changes of the signals of the original ylide, **1a**, the new ylide, **1b**, and the new sulfide, PhSMe, were followed. After the original ylide, **1a**, had completely disappeared, hexane was added to the reaction mixture. The ylide crystals thus precipitated were filtered and recrystallized from methanol. The melting points, IR, and NMR spectra of the ylide obtained were identical with those reported in the literature.[9] The results are listed in Table 2.

Carbon-13 NMR Measurement. The ylide **3** and thiocyanate were dissolved in $CDCl_3$ (usually 100—150 mg/cm^3) containing 1—5% tetramethylsilane as a reference. Solutions were examined in 10-mm tubes using a JEOL-FX-60 NMR spectrometer in the Fourier transform mode. Several hundred transients were typically accummulated with an acquisition time of 3.0 s. The line positions were determined automatically by computer software. The results are shown in Table 4.

*Reactions of Sulfur Ylide **3** with Aryl Thiocyanates in Chloroform.* (a) A chloroform (7 ml) solution of ylide **3** (0.90 g, 5.0 mmol) was mixed with *p*-chlorophenyl thiocyanate (0.86 g, 5.0 mmol) at room temperature. After 90 h the NMR spectra of the reaction mixture showed the presence of dimethyl sulfide (δ=2.10, s; 43%) and $Me_2\overset{\oplus}{S}-\overset{\ominus}{C}$(*p*-Cl-$C_6H_4S$)COPh ($\delta$=2.55, s; 31%). The low-boiling fractions from the mixture were trapped in liquid nitrogen, and the presence of Me_2S was shown by NMR spectroscopy (δ=2.11, s). When CCl_4 was added to the residue, the ylide crystals were precipitated; mp 148—149 °C. The CCl_4 solutions were concentrated *in vacuo*, and the residue was chromatographed by preparative thick-layer chromatography on silica gel, using a 2:1 mixture of hexane–ether as an eluent; the yellowish crystals (R_f=0.41) thus obtained were found to be *p*-Cl-$C_6H_4SCH_2COPh$ (0.52 g, 0.20 mmol; 40%); mp 81—82 °C; IR (KBr), 1680 cm^{-1} (ν_{CO}); NMR ($CDCl_3$), δ=4.25 (2H, s, S-CH_2-CO) and 7.26—8.0 (9H, m, aromatic-H). *p*-Chlorophenyl phenacyl sulfide was prepared independently by the reaction of phenacyl bromide and sodium *p*-chlorophenylmethanethiolate in methanol, and its physical data (mp, NMR and IR spectra) were identified with the above product. (b) Similarly, a chloroform (7 ml) solution of ylide **3** (0.90 g, 5.0 mmol) was mixed with *p*-tolyl thiocyanate (0.75 g, 5.0 mmol) at room temperature. After 6 days, the NMR spectra of the reaction mixture showed the presence of methyl sulfide (δ=2.10, s; 45%) and $Me_2\overset{\oplus}{S}-\overset{\ominus}{C}$(*p*-Me-$C_6H_4S$)COPh ($\delta$=2.54, s; 24%). When CCl_4 was added to the residue, the ylide crystals (mp 136—138 °C) were precipitated. The CCl_4 solutions were concentrated *in vacuo*, and the residue was chromatographed by preparative thick-layer chromatography on silica gel, using a 2:1 mixture of hexane–ether as an eluent; the oil (R_f=0.50) thus obtained was found to be *p*-Me-C_6H_4S-CH_2COPh (0.48 g, 0.20 mmol; 40%); IR (neat), 1680 cm^{-1} (ν_{CO}); NMR ($CDCl_3$), δ=2.28 (3H, s, *p*-Me), 4.20 (2H, s, S-CH_2-CO) and 7.17—8.0 (9H, m, aromatic-H). *p*-Tolyl phenacyl sulfide was prepared independently by the reaction of phenacyl bromide and *p*-tolyl mercaptane sodium salt on methanol, and its spectral data (IR and NMR) were identified with the above product. (c) A chloroform (5 ml) solution of

ylide **3** (1.0 g, 6.6 mmol) was mixed with *o*-chlorophenyl thiocyanate (1.12 g, 6.6 mmol) at room temperature. After 70 h, the NMR spectra of the reaction mixture showed the presence of dimethyl sulfide (δ=2.06, s; 40%) and $\underline{Me_2}\overset{\oplus}{S}-\overset{\ominus}{C}(o\text{-Cl-}C_6H_4\text{-S})COPh$ (δ=2.52, s; 30%). The low-boiling fractions from the mixture were trapped in liquid nitrogen, and the presence of Me_2S was shown by NMR spectroscopy (δ=2.11, s). The high-boiling fractions were chromatographed by preparative thick-layer chromatography on silica gel, using a 2: 1 mixture of hexane–ether as an eluent; the white crystals (R_f=0.25) thus obtained were found to be o-Cl-$C_6H_4SCH_2COPh$ (0.69 g, 2.6 mmol; 40%); mp 91.5—92.5 °C; IR (KBr), 1680 cm^{-1} (ν_{CO}); NMR ($CDCl_3$), δ=4.30 (2H, s, S-CH_2-CO) and 7.0—8.0 (9H, m, aromatic-H). Found: C, 63.26; H, 4.44%. Calcd for $C_{14}H_{11}OClS$: C, 63.99; H, 4.22%.

*Reactions of Sulfur Ylides **3** and **5** with Methyl Arenesulfenates in Chloroform.* (a) A chloroform (5 ml) solution of ylide **3** (0.5 g, 2.8 mmol; $Me_2\overset{\oplus}{S}-$, δ=2.85, s) was mixed with PhSOMe (0.39 g, 2.8 mmol) at room temperature. The NMR spectra of the reaction mixture showed the presence of a new ylide, $Me_2\overset{\oplus}{S}-\overset{\ominus}{C}(SPh)COPh$ (δ=2.54, s), and MeOH (δ=3.38, s). The removal of the solvent *in vacuo* at 25 °C gave white solids. Yield, 0.75 g (75%); recrystallized from benzene; mp 138—140 °C (lit,[19] 136 °C); IR (KBr), 1520 cm^{-1} (ν_{CO}). (b) A chloroform (5 ml) solution of ylide **5** (1.0 g, 6.8 mmol; $Me_2\overset{\oplus}{S}-$, δ=2.74, s) was mixed with PhSOMe (0.95 g, 6.8 mmol) at room temperature. The NMR spectra of the reaction mixture showed the presence of a new ylide, $Me_2\overset{\oplus}{S}-\overset{\ominus}{C}(SPh)CO_2Et$ (δ=2.53), and MeOH (δ=3.40, s). The removal of the solvent *in vacuo* at 25 °C gave white solids. Yield, 0.72 g (42%); mp 126—127 °C (lit,[19c] 126—127 °C); IR (KBr), 1600 cm^{-1} (ν_{OC}). Similarly, various α-(arylthio)phenacylides (or α-(arylthio)ethoxycarbonylmethylides) were obtained by the reactions of ylides **3** (or **5**) with methyl *p*-toluenesulfenate and methyl *p*-chlorobenzenesulfenate. The results are listed in Table 3. The products were identified by means of their NMR and IR spectra.

*The Determination of the Rate of the Transylidation of Ylide **1a** with 4-Methylpyridine (or Dimethyl Sulfide).* A $CDCl_3$ solution of **1a** and a suitable amount of a catalyst and 4-methylpyridine (or dimethyl sulfide) were mixed in a NMR tube. After nitromethane (0.79 mmol; δ=4.33 ppm) had been added as the internal standard, more $CDCl_3$ was added with a microsyringe so that the total volume became 800 μl. The disappearance of **1a** was followed by observing the decrease in $Ph\underline{Me}\overset{\oplus}{S}-$ (δ=3.20 ppm).

This work was supported in part by a Grant-in-Aid for Scientific Research from Ministry of Education (No. 274160).

References

1) Part of this work was presented at the 37th National Meeting of the Chemical Society of Japan, April 1978, Abstracts of Papers, Vol. 2, p. 890: Part VI of this series: H. Matsuyama, H. Minato, and M. Kobayashi, *Bull. Chem. Soc. Jpn.*, **51**, 575 (1978).

2) H. Matsuyama, H. Minato, and M. Kobayashi, *Bull. Chem. Soc. Jpn.*, **46**, 1512 (1973). (Part I).

3) H. Matsuyama, H. Minato, and M. Kobayashi, *Bull. Chem. Soc. Jpn.*, **46**, 2845 (1973). (Part II).

4) H. Matsuyama, H. Minato, and M. Kobayashi, *Bull. Chem. Soc. Jpn.*, **46**, 3158 (1973). (Part III).

5) H. Matsuyama, H. Minato, and M. Kobayashi, *Bull. Chem. Soc. Jpn.*, **46**, 3828 (1973). (Part IV).

6) S. Tamagaki, K. Tamura, and S. Kozuka, *Chem. Lett.*, **1977**, 725.

7) H. Matsuyama, H. Minato, and M. Kabayashi, *Bull. Chem. Soc. Jpn.*, **50**, 3393 (1977). (Part V).

8) Aryl phenacyl sulfides may be formed by the nucleophilic attack of the cyanide ion (CN^-) on the positive sulfur atom of the sulfonium ion and by the subsequent elimination of CH(SAr)COPh groups, since it is known that CN^- attacks the positive sulfur atom of sulfilimines: S. Oae, T. Aida, and N. Furukawa, *Int. J. Sulfur Chem.*, **8**, 73 (1973).

9) W. Ando, T. Yagihara, S. Tozune, S. Nakaido, and T. Migita, *Tetrahedron Lett.*, **1969**, 1979.

10) a) K. W. Ratts and A. N. Yao, *J. Org. Chem.*, **31**, 1185 (1966); b) G. B. Payne, *J. Org. Chem.*, **32**, 3351 (1967).

11) R. G. R. Bacon and R. G. Guy, *J. Chem. Soc.*, **1960**, 318.

12) R. Q. Brewster and W. Schroeder, *Org. Synth.*, Coll. Vol. II, 574 (1943).

13) F. Challenger, C. Higginbottom, and A. Huntington, *J. Chem. Soc.*, **1930**, 26.

14) E. Kuhle, *Chem. Abstr.*, **60**, 6787 (1964).

15) a) D. A. Armitage, M. J. Clark, and A. C. Kinsey, *J. Chem. Soc., C*, **1971**, 3867; b) M. Raban and F. B. Jones, Jr., *J. Am. Chem. Soc.*, **93**, 2692 (1971).

16) S. Andreades, J. F. Harris, Jr., and W. A. Sheppard, *J. Org. Chem.*, **29**, 898 (1964).

17) C. W. Tullock and D. D. Coffman, *J. Org. Chem.*, **25**, 2016 (1960).

18) F. W. Wenzel, Jr., and E. Emmet Reid, *J. Am. Chem. Soc.*, **56**, 1089 (1937).

19) a) Y. Hayashi, M. Takaku, and H. Nozaki, *Tetrahedron Lett.*, **1969**, 3179; b) T. Mukaiyama, K. Hosoi, S. Inokuma, and T. Kumamoto, *Bull. Chem. Soc. Jpn.*, **44**, 2453 (1971); c) L. Field and H. -K. Chu, *J. Org. Chem.*, **42**, 1768 (1977).

Synthesis of Methyl Substituted Chromanol. An Analogue of Vitamin K[1)]

Kazuhiro MARUYAMA,* Takamasa TOBIMATSU, and Yoshinori NARUTA
Department of Chemistry, Faculty of Science, Kyoto University, Kyoto 606
(Received August 7, 1978)

Methylation of 2,2-dimethyl-3,4-dihydro-2*H*-benzo[*h*]chromen-6-ol (**1**) is examined to yield 2,2,3-trimethyl-3,4-dihidro-2*H*-benzo[*h*]chromen-6-ol (**2**). The compound **2** is prepared by Mannich reaction followed by hydrogenative cleavage of the Mannich bases, which are obtained in the reaction with three kinds of amine. Chloromethylation of **1** quantitatively gave a dimer of naphthoquinone methide.

Vitamin K_1 and K_2 are widely distributed in natural products which are contributing in diverse biological processes such as blood clotting, electron transport and oxidative phosphorylation.[2)] Especially an association of vitamin K with the electron transport chain and a coupled phosphorylation in *Mycobacterium phlei* has been reported. The chromanol derivatives of vitamin K, to which noncyclized vitamin is enzymatically cyclized in bacterial system, is the acting vitamin of *M. phlei*.[3)]

We have recently reported the photochemical introduction of 2-alkenoyl group to 1,4-naphthoquinone and the facile preparation of 2,2-dimethyl-3,4-dihydro-2*H*-benzo[*h*]chromen-6-ol **1** ("benzochromanol") by the subsequent reactions (path a).[4)] Introduction of methyl group to the 5-position of **1** is of interest in view of the synthesis of a vitamin K methabolite in bacterial system.

The ortho position of phenol in β- and γ-tocopherols has been methylated by Mannich condensation followed by the successive reduction.[5)] However, in the case of tocopherols high pressure and high temperature were needed in the step of reductive cleavage of the Mannich bases. Therefore, secondary amines liberated from Mannich beses at reduction process were found to induce destruction of tocopherols.

In this paper, we wish to report a successful methylation of benzochromanol **1** *via* the milder hydrogenative cleavage of the Mannich bases.

Result and Discussion

Chromanol **1** was prepared by the following two routes (paths a[4)] and b). With use of three kinds of secondary amine; dimethylamine, piperidine, and morpholine, Mannich beses **6a—c** were prepared in yields of 75, 81, and 84%, respectively. 5-Dimethylaminomethyl derivative **6a** shows chracteristic ^{1}H-NMR signals due to amino benzylic protons at δ 3.70, and IR absorption due to hydrogen bonded hydroxyl group at the region of 3000—2500 cm^{-1}. The corresponding spectra were observed similarly in other Mannich bases, **6b** and **6c**.

Three Mannich bases **6a—c** were catalytically hydrogenated in ethanol similar to that of benzylic amine.[6)] Hydrogenation of these bases at atmospheric pressure and ambident temperature in the presence of 5% Pd–C resulted, however, recovery of the starting chromanol **6** without any hydrogenated products after four days. On the other hand, catalytic hydrogenation under a medium pressure (H_2, 5 kg/cm^2) applying an elevated temperature (80 °C) proceeded smoothly, and after 1 h the reaction was completed to give 2,2,5-trimethyl-3,4-dihydro-2*H*-benzo[*h*]chromen-6-ol **2** in a good yield. (Table 1) Since the obtained chromanol **2** was difficult to purify for its air sensibility, the hydrogenated solution was concentrated directly *in vacuo* and treated with Ac_2O–pyridine solution to give its acetate **7**.

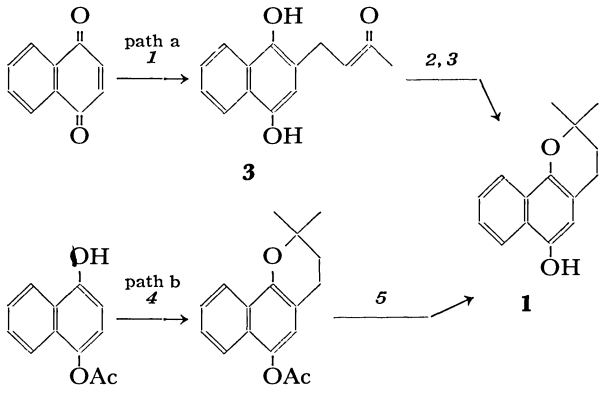

1. $h\nu$, $(CH_3)_2C{=}CHCHO$, C_6H_6
2. HCl, $SnCl_2$, dioxane
3. $LiAlH_4$, $AlCl_3$, ether
4. $(CH_3)_2C{=}CHCH_2Br$, $ZnCl_2$, $CHCl_3$
5. $LiAlH_4$, ether

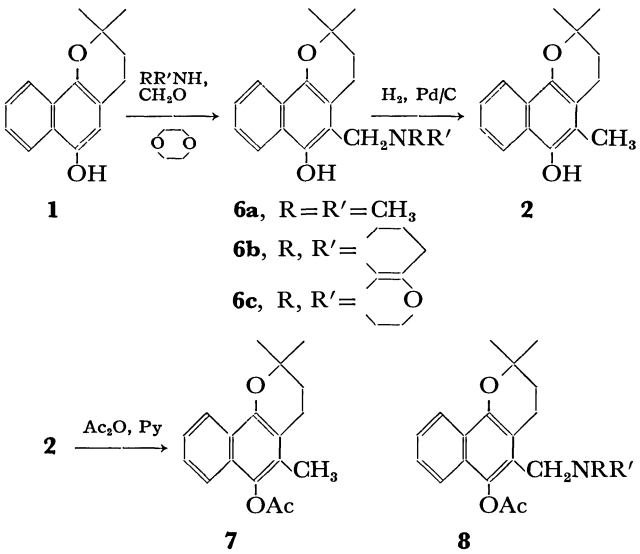

Scheme 1.

Chloromethylation is another useful procedure to introduce a methyl group to phenolic compounds. We tried the procedure to **1** passing dry hydrogen chloride in an ethereal solution of an excess amount of para-

TABLE 1. CATALYTIC REDUCTION OF MANNICH BASES **6a—c** AND ACETYLATION

6	R, R′	7 Yield,[a] %
a	CH_3, CH_3	68
b		83
c		81

a) Isolated yield after purification.

formaldehyde at 0—5 °C. After 2 h a product was isolated in a yield of 78%. The structure was assigned to dimer **11** on the basis of the following spectral and chemical evidences.

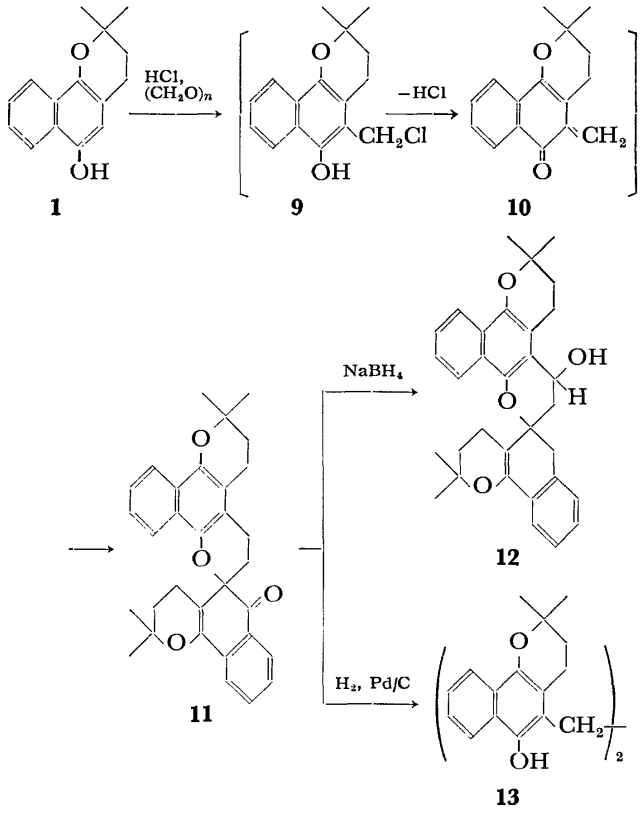

Scheme 2.

The ^{1}H-NMR spectrum of **11** exhibits three singlets at δ 1.32 (6H), 1.37 (3H), 1.38 (3H), representing four methyl groups and multiplets at δ 1.00—2.66, representing twelve methylene protons. The IR spectrum shows an absorption at 1695 cm^{-1} ($\nu_{C=O}$).[7] Mass spectrum and analytical result of **11** were also consistent with the structure of dimer **11**. Reduction of **11** by $NaBH_4$ gave an alcohol **12**. The ^{1}H-NMR of **12** exhibits two singlets at δ 3.62 (1H) and 5.15 (1H), representing a hydroxyl proton and a methine proton, respectively, and the IR spectrum shows an absorption at 3435 cm^{-1} (ν_{OH}). Dimer **11** absorbed equimolecular hydrogen under the conditions of catalytic hydrogenation[7] to give 2,2,2′,2′-tetramethyl-3,4,3′,4′-tetrahydro-5,5′-ethylenedi(2*H*-naphtho[1,2-*b*]pyran)-6,6′-diol (**13**), quantitatively. The ^{1}H-NMR of **13** shows a broad singlet due to phenolic OH at δ 6.32, and the IR spectrum, being compatible with the structure. Thus, the dimeric product **11** obtained by chloromethylation of **1** corresponds to the structure of naphthoquinone methide dimer. The dimer has been prepared independently by oxidizing **2** with potassium hexacyanoferrate(III).[7] Our reaction may be explained taking into consideration of that the 5-chloromethyl-2,2-dimethyl-3,4-dihydro-2*H*-benzo[*h*]chromen-6-ol (**9**) is formed initially and despite in a strong acidic conditions **9** was hydrolized to *o*-naphthoquinone methide **10**.[10] These evidences are also supported by the fact that α-methylenecyclanones and *o*-quinone methides easily dimerize to the corresponding dihydropyran derivatives.[11]

Experimental

All melting points are uncorrected. The elemental analyses were performed at the Microanalysis Center of Kyoto University. ^{1}H-NMR spectra were measured with a JEOL PS-100 with TMS as an internal standard, infrared spectra with a JASCO 402G or a IRA-1, mass spectra with a Hitachi M-52. Analytical gas chromatographs were obtained with a JEOL JGC-20K instrument with a flame ionization detecter using a column (5% SE-30 silicon rubber on 60—80 mesh Celite 545, 3 mm × 1 m).

*2,2-Dimethyl-3,4-dihydro-2*H*-benzo*[h]*chromen-6-ol (1).* was prepared by the photochemical method (path a)[4] and a series of the following reactions (path b). 4-Hydroxy-1-naphthyl acetate **4** was prepared by the similar method to the literature.[8] **4**; Mp 130—131.5 °C. **4** (1.01 g, 5 mmol) and zinc chloride (0.1 g) were dissolved in chloroform (40 ml) under nitrogen. The solution was refluxed and the chloroform solution (5 ml) of 1-bromo-3-methyl-2-butene[9] (745 mg, 5 mmol) was slowly added, after refluxing for thirty minutes the solution was poured into ice water and was washed twice with 2 M hydrochloric acid and once with brine, and dried over Na_2SO_4. The mixture was purified with a use of Wakogel C-200 (30 g) eluted by 4.5% ether–hexane. 6-Acetoxy-2,2-dimethyl-3,4-dihydro-2*H*-benzo[*h*]chromen **5** was obtained (isolated yield; 60%. GLPC yield; 78%); Mp 66.9—67.1 °C. ^{1}H-NMR ($CDCl_3$): δ 1.36 (s, 6H, $2CH_3$), 1.77 (t, 2H, J=7 Hz, O–C–CH_2), 2.34 (s, 3H, $COCH_3$), 2.75 (t, 2H, J=7 Hz, Ar–CH_2), 6.87 (s, 1H, arom. H), 7.28—7.46 (m, 2H, arom. H), 7.57—7.73 (m, 1H, arom. H). IR: ν_{max}^{KBr} 2975 (vs), 1747 (vs), 1367 (vs), and 1189 cm^{-1} (vs).

The ethereal solution (30 ml) of chromanol acetate derivative **5** (2.703 g, 0.01 mol) was treated with lithium aluminum hydride (0.35 g) in ether (30 ml). After usual work-up, the obtained benzochromanol **1** was used without further purification.

*5-Dimethylaminomethyl-2,2-dimethyl-3,4-dihydro-2*H*-benzo*[h]*-chromen-6-ol (6a).* The dioxane solution (25 ml) of benzochromanol **1** (228 mg, 0.01 mol) was cooled in ice water under N_2, and dimethylamine solution (3.7 ml, 40% in water) and formalin solution (2.5 ml, 37% in water) were added and the mixture was stirred for one hour at room temperature and then at gentle refluxing for 4 h. After evaporation of solvent, the residue was extracted with ether, and the ethereal solution was washed several times with brine, dried over Na_2SO_4, and concentrated *in vacuo*. To the residual oil a few ml of ethanol was added, then white crystals of **6a** were obtained (214 mg, 75%): Mp 110.5—113.0 °C (from hexane–ether). ^{1}H-NMR ($CDCl_3$): δ 1.38 (s, 6H, $2CH_3$), 1.88 (t, 2H, J=7 Hz, O–C–CH_2), 2.38 (s, 6H, $N(CH_3)_2$), 2.68 (t, 2H, J=7 Hz, Ar–CH_2–C), 3.70 (s, 2H, Ar–CH_2–N), 7.40 (m, 2H, arom. H), 8.14 (m, 2H, arom. H). IR: ν_{max}^{KBr} 2978(vs), 2830 (bs),

2780 (s), 1592 cm^{-1} (s). MS (20 eV); *m/e* 285 (M^+), 240 ($M^+-NH(CH_3)_2$). Found: C, 75.69; H, 8.26; N, 4.91%. Calcd for $C_{18}H_{23}NO_2$: C, 75.75; H, 8.12; N, 4.91%.

Crude Mannich base **6a** was acetylated with acetic anhydride and pyridine. 6-Acetoxy-5-dimethylaminomethyl-2,2-dimethyl-3,4-dihydro-2*H*-benzo[*h*]chromen **8a**: Mp ≈210 °C (dec) ^{1}H-NMR ($CDCl_3$): δ 1.42 (s, 6H, $2CH_3$), 1.88 (t, 2H, J=7 Hz, O-C-CH_2), 2.17 (s, 6H, $N(CH_3)_2$), 2.36 (s, 3H, $COCH_3$), 2.99 (t, 2H, J=7 Hz, Ar-CH_2-C), 3.31 (s, 2H, Ar-CH_2-N), 7.30—7.52 (m, 3H, arom. H), 8.04—8.20 (m, 1H, arom. H). IR: ν_{max}^{KBr} 2950 (s), 1765 (vs), 1370 (vs), 1208 (vs), 1183 cm^{-1} (s).

2,2-Dimethyl-5-piperidinomethyl-3,4-dihydro-2H-benzo[h]*chromen-6-ol (6b).* To a mixture of benzochromanol **1** (228 mg, 0.01 mol), piperidine (4 ml, 0.04 mol), and dioxane (30 ml), formalin solution (3 ml) was added at 10 °C, and allowed to react as described above. Colorless crystals **6b** (1.311 g, 81%) was obtained: Mp 133.5—134.2 °C (from aceton). ^{1}H-NMR ($CDCl_3$): δ 1.39 (s, 6H, $2CH_3$), 1.40—1.77 (m, 6H, $(CH_2)_3$), 1.86 (t, 2H, J=7 Hz, O-C-CH_2), 2.46—2.68 (m, 4H, $N(CH_2)_3$), 2.70 (t, 2H, Ar-CH_2-C), 3.76 (s, 2H, Ar-CH_2-N), 7.32—7.48 (m, 2H, arom. H), 8.08—8.24 (m, 2H, arom. H). IR: ν_{max}^{KBr} 2940 (vs), 2800 (s), 1593 (s), 1450 (vs), 1381 cm^{-1} (vs). MS (20 eV); *m/e* 325 (M^+). Found: C, 77.41; H, 8.30; N, 4.14%. Calcd for $C_{21}H_{27}NO_2$: C, 77.50; H, 8.36; N, 4.30%. **6b** was acetylated with acetic anhydride and pyridine. 6-Acetoxy-2,2-dimethyl-5-piperidinomethyl-3,4-dihydro-2*H*-benzo[*h*]chromen **8b**: Mp 155—157 °C (from acetone). ^{1}H-NMR ($CDCl_3$); δ 1.26—1.64 (m, 12H, $2CH_3$ and $(CH_2)_3$), 1.88 (t, 2H, J=7 Hz, O-C-CH_2), 2.22—2.44 (m, 7H, $COCH_3$ and $N(CH_2)_2$), 2.95 (t, 2H, J=7 Hz, Ar-CH_2-C), 3.36 (s, 2H, Ar-CH_2-N), 7.22—7.50 (m, 3H, arom. H), 7.94—8.16 (m, 1H, arom. H). IR: ν_{max}^{KBr} 2920 (vs), 1778 (vs), 1369 (vs), 1263 (vs), 1177 cm^{-1} (vs). MS (20 eV); *m/e* 367 (M^+). Found: C, 74.97; H, 8.13; N, 3.68%. Calcd for $C_{23}H_{29}NO_3$: C, 75.17; H, 7.95; N, 3.81%.

2,2-Dimethyl-5-morpholinomethyl-3,4-dihydro-2H-benzo[h]*chromen-6-ol (6c).* To a mixture of benzochromanol **1** (228 mg, 0.01 mol), morpholine (4 ml, 0.046 mol), and dioxane (20 ml), formalin solution (3 ml) was added at 10 °C. After 20 min at room temperature, white precipitate was observed in the reaction mixture. After the solution was stirred for 1 h at room temperature, it was refluxed for 3 h. After solvent was removed *in vacuo*, white crystals **6c** (2.74 g, 84%) were obtained in ethereal solution. **6c**: Mp 149—151 °C from acetone. ^{1}H-NMR ($CDCl_3$); δ 1.35 (s, 6H, $2CH_3$), 1.89 (t, 2H, J=7 Hz, O-C-CH_2), 2.57—2.90 (m, 6H, $N(CH_2)_2$ and Ar-CH_2-C), 3.68—3.84 (m, 6H, Ar-CH_2-N and CH_2-OCH_2), 7.28—7.43 (m, 2H, arom. H), 8.00—8.12 (m, 2H, arom. H). IR; ν_{max}^{KBr} 2960 (vs), 2895 (vs), 2830 (s), 1592 (vs), 1450 (vs), 1380 (vs), 1323 (vs), 1163 (vs), 1111 (vs), 976 cm^{-1} (s). MS (20 eV); *m/e* 327 (M^+), 240 ($M^+-HN\langle\rangle O$). Found: C, 73.21; H, 7.68; N, 4.22%. Calcd for $C_{20}H_{25}NO_3$: C, 73.36; H, 7.70; N, 4.28%.

6-Acetoxy-2,2-dimethyl-5-morpholinomethyl-3,4-dihydro-2*H*-benzo[*h*]chromen **8c**: Mp 151.5—153.0 °C (from acetone). ^{1}H-NMR ($CDCl_3$); δ 1.41 (s, 6H, $2CH_3$), 1.90 (t, 2H, J=7 Hz, O-C-CH_2), 2.36—2.50 (m, 7H, $COCH_3$ and CH_2N-CH_2), 2.98 (t, 2H, J=7 Hz, Ar-CH_2-C), 3.44—3.67 (m, 6H, Ar-CH_2-N and CH_2OCH_2), 7.36—7.60 (m, 3H, arom. H), 8.12—8.24 (m, 1H, arom. H). IR; ν_{max}^{KBr} 2930 (vs), 2865 (vs), 1770 (vs), 1450 (s), 1368 (vs), 1200 (vs), 1180 (vs), 1113 cm^{-1} (vs). MS (20 eV); *m/e* 369 (M^+). Found: C, 71.51; H, 7.44; N, 3.76%. Calcd for $C_{22}H_{27}NO_4$; C, 71.52; H, 7.39; N, 3.79%.

6-Acetoxy-2,2,5-trimethyl-3,4-dihydro-2H-benzo[h]*chromen (7) from 6a—c.* Aminomethylchromanol derivatives **6a—c** (1.7 mmol) were hydrogenated (5% Pd-C, 150 mg in 50 ml ethanol, H_2 5 kg/cm^2 at 80 °C for 2 h) to give **2**. **2**: ^{1}H-NMR ($CDCl_3$); δ 1.38 (s, 6H, $2CH_3$), 1.89 (t, 2H, J=7 Hz, O-C-CH_2), 2.27 (bs, 3H, Ar-CH_3), 2.60—3.00 (m, 2H, Ar-CH_2), 3.80 (bs, 1H, OH), 7.32—7.48 (m, 2H, arom. H), 7.88—8.24 (m, 2H, arom. H). IR; ν_{max}^{KBr} 3250 (vs), 2980 (s), 2920 (s), 1586 (s), 1396 (vs), 1323 (vs), 1161 (vs), 1019 cm^{-1} (vs). MS (20 eV); *m/e* 242 (M^+), 240 (M^+-H_2), 186 ($M^+-C_4H_8$).

Since **2** was very unstable in air, it was directly acetylated in acetic anhydride–pyridene to give **7** in each case of **6a**, **b**, and **c**. After usual work-up, **7** was obtained in the yield of 68, 83, and 81%, respectively (based on **6a**, **b**, and **c**). **7**; Mp 91.4—92.4 °C (from hexane). ^{1}H-NMR ($CDCl_3$) δ 1.39 (s, 6H, $2CH_3$), 1.87 (t, 2H, J=7 Hz, O-C-CH_2), 2.11 (s, 3H, Ar-CH_3), 2.36 (s, 3H, $COCH_3$), 2.71 (t, 2H, J=7 Hz, Ar-CH_2), 7.23—7.56 (m, 3H, arom. H), 8.00—8.14 (m, 1H, arom. H). IR; ν_{max}^{KBr} 2920 (s), 1754 (vs), 1362 (vs), 1206 (vs), 1162 cm^{-1} (vs). MS (20 eV); *m/e* 284 (M^+), 242. Found; C, 76.21; H, 7.04%. Calcd for $C_{18}H_{20}O_3$; C, 76.03; H, 7.09%.

Chloromethylation of 1. The ethereal solution (40 ml) of benzochromanol **1** (1 mmol) and paraformaldehyde (0.8 g) was chilled and dry hydrogen chloride was bubbled into the mixture for 2 h. The reaction mixture was poured into ice (20 g) and ethereal solution was separated, aqueous layer, was extracted with ether. The combined solution was washed with water and dried over Na_2SO_4. Products were separated by Wakogel C-200 column chromatography, dimer **11** was isolated (188 mg, 78%). **11**; Mp 177.5—178.0 °C (lit,[7] 160—161 °C). ^{1}H-NMR (CCl_4); δ 1.32 (s, 6H, $2CH_3$), 1.37 (s, 3H, CH_3), 1.38 (s, 3H, CH_3), 1.60—1.80 (m, 4H), 1.80—2.33 (m, 4H), 2.33—2.66 (m, 4H), 7.19 (m, 4H, arom. H), 7.43, 7.68 (each 1H, m, arom. H), 7.95 (m, 2H, arom. H). IR; ν_{max}^{KBr} 2980 (s), 2930 (s), 1695 (vs), 1658 (m), 1637 (w), 1595 (vs), 1385 (vs), 1162 cm^{-1} (vs). MS (20 eV); *m/e* 480 (M^+), 240 ($M^+/2$), 197 ($M^+/2-C_2H_3O$). Found; C, 79.95; H, 6.76%. Calcd for $C_{32}H_{32}O_4$; C, 79.97; H, 6.71%.

Hydride Reduction of the Dimer (11). The ethanol solution (30 ml) of the dimer **11** (404 mg, 0.92 mmol) and $NaBH_4$ (40 mg) was stirred for 1 h at ambident temperature, and after the usual work-up, **12** was quantitatively obtained. **12**; Mp 169—170 °C (from ether-hexane). ^{1}H-NMR ($CDCl_3$); δ 1.26 (s, 3H, CH_3), 1.35 (s, 6H, $2CH_3$), 1.41 (s, 3H, CH_3), 2.47—2.77 (m, 12H, $6CH_2$), 3.62 (bs, 1H, OH), 5.15 (s, 1H, CH), 7.10—7.56 (m, 6H, arom. H), 7.96—8.12 (m, 2H, arom. H). IR; ν_{max}^{KBr} 3435 (vs), 2935 (vs), 1385 (vs), 1162 cm^{-1} (s). MS (20 eV); *m/e* 482 (M^+). Found: C, 79.64; H, 7.15%. Calcd for $C_{32}H_{34}O_4$; C, 79.64, H, 7.10%.

Catalytic Hydrogenation of the Dimer (11). The dimer **11** (201 mg, 0.42 mmol) was hydrogenated (5% Pd-C 60 mg in 50 ml ethanol, H_2, 4 kg/cm^2 at 50 °C for 4 h) quantitatively to give 2,2,2′2′-tetramethyl-3,4,3′,4′-tetrahydro-5,5′-ethylene-di(2*H*-naphtho[1,2-*b*]-pyran)-6,6′-diol **13**. **13**; Mp >270 °C (dec). ^{1}H-NMR ($CDCl_3$); δ 1.39 (s, 12H, $4CH_3$), 1.92 (t, 4H, J=7 Hz, 2O-C-CH_2), 2.68—3.12 (m, 8H, 4Ar-CH_2), 6.32 (bs, 2H, 2OH), 7.32—7.54 (m, 4H, arom. H), 7.92—8.34 m, 4H, arom. H). IR; ν_{max}^{KBr} 3450 (s), 2995 (s), 1660 (s), 1587 (vs), 1388 cm^{-1} (s). Found; C, 79.46; H, 7.16%. Calcd for $C_{32}H_{34}O_4$; C, 79.64; H, 7.10%.

References

1) Synthesis of naturally occurring quinones. Part 4. Part 3; K. Maruyama and Y. Naruta, *J. Org. Chem.*, **43**, 3796 (1978).

2) For an excellent review of quinones and their chemistry,

see; (a) "Biochemistry of Quinones," ed by R. A. Morton, Academic Press, New York, N. Y. (1965); (b) R. H. Thomson, "Naturally Occurring Quinones," 2nd ed, Academic Press, New York, N. Y. (1971); (c) "The Chemistry of the Quinonoid Compounds," ed by S. Patai, Willy, New York, N. Y. (1974), Part 1 and 2.

3) (a) P. J. Russell and A. F. Brodie, *Biochim. Biophys. Acta*, **50**, 76 (1961); (b) A. F. Brodie, *Federation Proc.*, **20**, 995 (1961).

4) K. Maruyama and Y. Naruta, *Chem. Lett.*, **1977**, 847.

5) T. Nakamura and S. Kijima, *Chem. Pharm. Bull.*, **19**, 2318 (1971).

6) D. L. Fields, J. B. Miller, and D. D. Reynolds, *J. Org. Chem.*, **29**, 2640 (1964).

7) P. Mamont, P. Cohen, R. Azerad, and M. Vilkas, *Bull. Soc. Chim. Fr.*, **1965**, 2513.

8) B. R. Baker, T. H. Davis, L. McElroy, and G. H. Carlson, *J. Am. Chem. Soc.*, **64**, 1096 (1942).

9) J. Tanaka, T. Katagiri, and S. Yamada, *Nippon Kagaku Zasshi*, **87**, 877 (1966).

10) The xylene solution (50 ml) of **6a** (144 mg, 0.51 mmol) and *trans*-stilbene (450 mg, 2.5 mmol) was refluxed for 7 h. An adduct **12** (47 mg, 22%) of *o*-naphthoquinone methide with *trans*-stilbene accompanied with dimer **11** (50 mg, 21%) was obtained. This evidence also supports the generation of *o*-naphthoquinone methide **10** as an unstable intermediate in the course of preparation of the dimer.

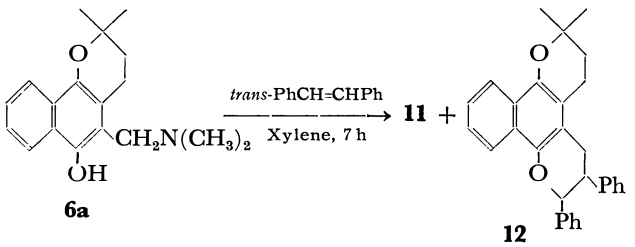

6a **12**

11) J. Colonge and G. Descotes, in "1,4-Cycloaddition Reactions," ed by J. Hamer, Academic Press, New York, N. Y. (1967), p. 217, and references cited therein.

Studies of Polymeric Flocculants. IX.[1] The Formation of Poly(methacrylohydrazide)-Copper(II) Complexes

Takamasa NONAKA,* Eiji MOMONO, and Hiroaki EGAWA

Department of Industrial Chemistry, Faculty of Engineering, Kumamoto University, Kurokami, Kumamoto 860

(Received August 22, 1978)

Formation constants for the complexes of poly(methacrylohydrazide) (PMH) with the copper(II) ion were measured by using a modification of Bjerrum's method proposed by Gregor and his coworkers. The pK_{a1} and pK_{a2} values of PMH determined in an aqueous solution with an ionic strength of 0.1 (KNO_3) at 25 °C were 3.20 and 10.61 respectively. Therefore, when the PMH–copper(II) complexes were formed above pH 7, the average number of ligands combined with one metal ion could be calculated approximately without using the first acid dissociation constant. The pK_{a2} value decreased with an increase in the ionic strength and temperature. The formation curves of the complexes showed that one copper(II) ion formed a coordination compound with six hydrazide groups in a high pH region (about pH 9). The formation constants increased with an increase in T_{Cu}/T_{HL} (the ratio of the total concentration of the copper(II) ion to the total concentration of the ligand) in the range higher than 0.1. The formation constants were unaffected by the degree of polymerization of PMH in the range from 64.1 to 5470, but the formation constants were affected by the kind of anion in copper(II) salts and neutral salts added and they increased in the order of $NO_3^- < SO_4^{2-} < Cl^-$. The thermodynamic parameters for the above reaction were determined by Ringbom's method.

The formation constants for polyelectrolytes–copper(II) complexes have been studied by many investigators.[2-7] However, the formation constants for poly(methacrylohydrazide)–metal(II) complexes had not been studied. In our preceding papers[1,8] we reported that poly(methacrylohydrazide) (PMH) could easily form water-insoluble complexes with heavy metals, especially with mercury(II), over a wide pH region and that mercury(II) could be removed from the solutions containing mercury(II) only or together with other metals. We also reported the formation constants for the complexes of PMH with bivalent transition metal ions and the average number of ligand combined with each metal ion, obtained by using a modification of Bjerrum's method. The formation curves for PMH–copper(II) complexes showed that one copper(II) ion formed a coordination compound with six hydrazide groups in a high pH region. In the present paper, in order to study in detail the formation of PMH–copper(II) complexes, the effect of T_{Cu}/T_{HL} ratio, the degree of polymerization of PMH, and the kind of anion in copper(II) salts and neutral salts added on the formation constants were investigated in an aqueous solution with an ionic strength of 0.1 at 25 °C. The changes in entropy, enthalpy, and free energy for the above reaction were also determined by Ringbom's method.

Experimental

Poly(methyl methacrylate) was prepared by solution polymerization initiated by benzoyl peroxide or α,α'-azobisisobutyronitrile in carbon tetrachloride, 1-dodecanol, and 1-dodecanethiol. Poly(methyl methacrylate) was purified by the conventional method, using acetone and methanol as solvent and precipitant respectively. The number average molecular weight of polymers was calculated by means of the following equation: $[\eta]=K M_n^a$.[9] The intrinsic viscosity was measured in benzene at 30 °C.

PMH was prepared by the hydrazinolysis of poly(methyl methacrylate) (1 g) with hydrazine hydrate (20 ml) at 175 °C for 7 h. The reaction mixture was poured into an excess of methanol in order to precipitate PMH. The PMH was purified by Soxhlet extraction with methanol for 80—100 h. The conversion was calculated on the basis of the nitrogen content of the PMH, itself determined by elemental analysis. Isobutyrohydrazide was selected as a monomeric model of PMH. Isobutyrohydrazide was prepared by treating ethyl isobutylate with anhydrous hydrazine at 90 °C for 6 h. It was purified by recrystallization from benzene. Found: C, 47.43; H, 9.63; N, 26.71%. Calcd for $C_4H_{10}N_2O$: C, 47.06; H, 9.80; N, 27.45%. All the other reagents were of a special reagent grade, and they were used without further purification.

Potentiometric Titration. In spite of the good solubility of PMH in water, the PMH–copper(II) complexes were apparently insoluble in water. Gregor *et al.*[2,3] showed that the binding phenomena are essentially the same whether the polymeric chelates precipitate or not, if the system is in equilibrium. Therefore, potentiometric titration was carried out by a batch method. The procedure was as follows: 5 ml of a 1 g/l PMH solution, 25 ml of a 0.2 mol/l neutral salt solution, and the desired amounts of a 0.005 mol/l potassium hydroxide solution were added into 100 ml stoppered flasks. Water was finally added to each flask until the total volume amounted to 50 ml. After nitrogen had been fully introduced into each flask in order to remove the CO_2, each flask was shaken by means of an incubator at 25 °C for 24 h. After shaking, the pH values of the solutions were measured by means of a Hitachi-Horiba F-7 pH meter at 25 °C under a nitrogen atmosphere. In the case of the complex formation from PMH and the copper(II) ion, a solution of copper(II) nitrate was added to each solution containing PMH and potassium nitrate. Then, the procedure described above was carried out.

Results and Discussion

PMH. The results of the synthesis of PMH are shown in Table 1. When Kern *et al.*[10] reported the synthesis and structure of poly(acrylohydrazide), they considered that each hydrazide group in the polymers contained 2/3 H_2O, even after the polymers had been dried *in vacuo*. It was found by thermo-balance analysis that PMH also contained about 1/3 H_2O per hydrazide group. It was recognized from the IR spectra (C=O, 1720 cm^{-1}) of the polymers obtained that the hydrazino-

TABLE 1. POLY(METHACRYLOHYDRAZIDE)

PMH	$\bar{P}_n$		Elemental analyses C(%)	H(%)	N(%)	O(%)	H_2O Content (wt %)	$(x \cdot H_2O)$	Conv. (%)
PMH-1	5470	Found	47.3	7.5	24.2	21.0	6.3	1/3	91.2
		Calcd	46.5	8.2	24.2	21.1			
PMH-2	991	Found	48.5	8.0	22.4	21.1	5.5	1/3	84.1
		Calcd	47.5	8.2	22.4	21.9			
PMH-3	456	Found	46.6	8.0	22.4	23.0	6.9	1/3	84.1
		Calcd	47.5	8.2	22.4	21.9			
PMH-4	64.1	Found	46.9	8.1	22.0	23.0	6.5	1/3	82.5
		Calcd	47.7	8.1	22.0	22.2			

lysis of poly(methyl methacrylate) did not proceed completely under the present conditions. The calculated values of the elements in PMH shown in Table 1 were determined on the basis of the conversion and water content of PMH.

Acid Dissociation Constants of PMH. Albert *et al.*[11] and Nagano *et al.*[12] reported in detail the acid dissociation constants of hydrazide compound, they reported that the hydrazide compounds had two acid dissociation constants, *i.e.*, K_{a_1} in a low pH region and K_{a_2} in a high pH region. When the acid dissociation constants of PMH were measured in an aqueous solution with an ionic strength of 0.1(KNO_3) at 25 °C, the pK_{a_1} and pK_{a_2} values became 3.20 and 10.61 respectively.

It was proposed by Bjerrum that the average number of ligands combined with one metal ion can be calculated by means of Eq. 1, when the compounds with two acid dissociation constants such as hydrazide compounds form complexes with metal ions:

$$\bar{n} = \frac{[A_t] - ([H^+]^2/K_{a_1}K_{a_2} + [H^+]/K_{a_2} + 1)[A^-]}{[M_t]}, \quad (1)$$

where $[A^-]$, which represents the concentration of the free hydrazide groups in the polymers not combined with metal ions, can be calculated using the following equation:

$$[A^-] = \frac{(2-\alpha)[A_t] - [H^+] + [OH^-]}{2[H^+]^2/K_{a_1}K_{a_2} + [H^+]/K_{a_2}}. \quad (2)$$

$[A_t]$ is the total concentration of hydrazide groups in the polymers added, $[M_t]$ is the total concentration of the metal ions added, and K_{a_1} and K_{a_2} are the first and second acid dissociation constants respectively. α is the degree of neutralization. When the acid dissociation constants of isobutyrohydrazide were measured in an aqueous solution with an ionic strength of 0.1(KNO_3) at 25 °C, the pK_{a_1} and pK_{a_2} values became 3.27 and 10.74 respectively. It was found that the hydrogen ion due to the formation of complexes were released above pH 6.3. Therefore, in a higher pH region than 6.3, Eq. 1 can be approximated by

$$\bar{n} = \frac{[A_t] - ([H^+]/K_{a_2} + 1)[A^-]}{[M_t]}, \quad (3)$$

where

$$[A^-] = \frac{(1-\alpha)[A_t] - [H^+] + [OH^-]}{[H^+]/K_{a_2}}. \quad (4)$$

Thus, it is considered that the average number of ligands combined with one metal ion can be calculated by means of Eq. 3 without using pK_{a_1}. Consequently, the second acid dissociation constant, pK_{a_2}, of PMH was determined in detail.

Katchalsky and many other investigators have studied the potentiometric titration of polyelectrolytes,[13-15] they have shown that the experimental results for titra-

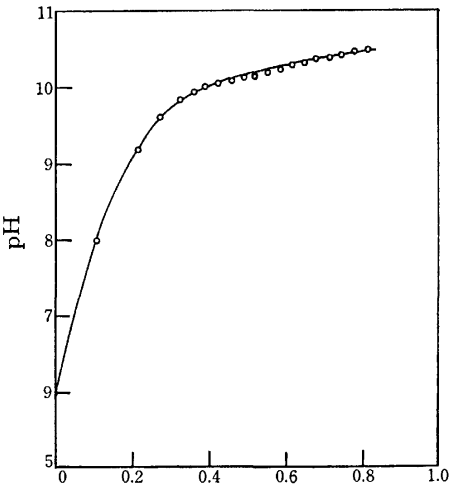

Fig. 1. The pH titration curve of PMH.
PMH ($\bar{P}_n$=5470): 8.64×10^{-4} unit mol/l, 25 °C, μ=0.10(KNO_3).

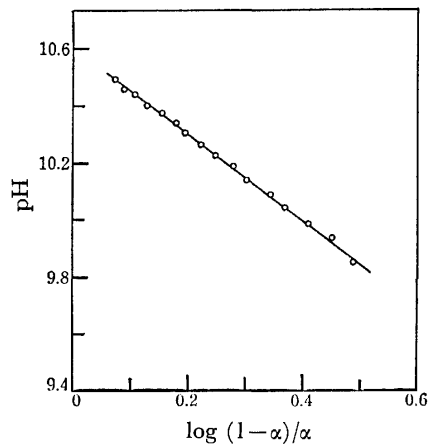

Fig. 2. Henderson-Hassebalch plots of PMH.
PMH ($\bar{P}_n$=5470): 8.64×10^{-4} unit mol/l, 25 °C, μ=0.10(KNO_3).

Table 2. pK_{a2} and n (25 °C, $\mu=0.10$)

Polymer	Neutral salt	pK_{a2}	n
Poly(methacrylohydrazide)	KNO_3	10.61	1.54
	K_2SO_4	10.58	1.48
	KCl	10.45	1.08

tion can be expressed by a modification of the Henderson-Hasselbach equation, $pH=pK_{a_1}-n \log (1-\alpha)$, where n is a constant. The pH titration curve of PMH with KOH in the solution with an ionic strength of 0.1(KNO_3) is shown in Fig. 1, while the Henderson-Hasselbach plots are shown in Fig. 2. The plots of pH *vs.* $\log (1-\alpha)/\alpha$ are linear in the range of the degree of neutralization from 0.3 to 0.8. The pK_{a_1} and n values of PMH were determined in solutions containing different neutral salts at 25 °C; the results are shown in Table 2. In a KCl aqueous solution, the pK_{a_1} and n values determined were smaller than those in the solutions of other neutral salts. Similar phenomena have been observed by Gregor *et al.*[2] for poly(acrylic acid). These pK_{a_1} values show that PMH behaves as a very weak acid, similarly to poly(vinyl alcohol),[4] poly(propenehydraxamic acid),[5] and poly(acrylaldehyde oxime)[6] under the present conditions. Machida *et al.*[16] reported that poly(acrylohydrazide) (conversion *ca.* 50%), which had been prepared by the hydrazinolysis of polyacrylamide with hydrazine hydrate, had a pK_{a_1} value of 10.64 and an n value of 1.36 at the ionic strength of 0.01(KCl) at 25 °C.

Table 3. Effect of the degree of polymerization of poly(methacrylohydrazide) on pK_{a2} and n

Polymer	$\bar{P}_n$	pK_{a2}	n
PMH-1	5470	10.61	1.54
PMH-2	991	10.64	1.55
PMH-3	456	10.60	1.53
PMH-4	64.1	10.61	1.49

Polymer concentration: *ca.* 8×10^{-4} unit mol/l, 25 °C, $\mu=0.1(KNO_3)$.

The pK_{a_1} and n values of PMH with different degrees of polymerization were determined at the ionic strength of 0.1(KNO_3); the results are shown in Table 3. Those results show that the degree of polymerization of PMH, ranging from 64.1 to 5470, did not affect the pK_{a_1} and n values.

The pK_{a_1} and n values of PMH were determined at different temperatures (20—35 °C) and at different ionic strengths (0.01—0.1). The results are shown in Table 4. At the same temperature, the pK_{a_1} values decreased with an increase in the ionic strength, and at the same ionic strength, the pK_{a_1} values decreased with an increase in the temperature. These results suggest that the hydrazide groups of PMH in an aqueous solution are liable to dissociate with increases in the temperature and ionic strength. The n values were unaffected by either the temperature or the ionic strength under the present conditions. The plots of pK_{a_1} *vs.* $\sqrt[3]{\mu}$ at each temperature gave straight lines.[1] The thermodynamic acid dissociation constants, which were determined by an extrapolation of the linear pK_{a_1} *vs.* $\sqrt[3]{\mu}$ plots to the intercept, are shown in Table 5.

Table 5. pK°_{a2} of poly(methacrylohydrazide)

Temp (°C)	20	25	30	35
pK°_{a2}	10.90	10.76	10.62	10.46

Polymer ($\bar{P}_n=5470$): 8.64×10^{-4} unit mol/l.

Calculation of the Formation Constants. The formation constants for PMH–metal(II) complexes were calculated by a modification of Bjerrum's method proposed by Gregor *et al.*[2] It is considered that the hydrazide groups of PMH dissociate as follows in a pH region higher than pH 7:

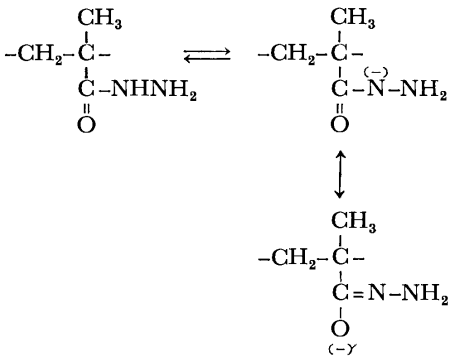

(5)

If the hydrazide groups of PMH are represented by HA, the above equilibrium can be represented by the following simplified equation:

$$HA \rightleftarrows A^- + H^+ \quad (6)$$

and the second acid dissociation constant, K_{a_1} can be represented by the following equation:

$$K_{a_1} = \frac{[A^-][H^+]}{[HA]}. \quad (7)$$

Table 4. Effect of temperature and ionic strength on pK_{a2} and n

Ionic strength	20 °C		25 °C		30 °C		35 °C	
	pK_{a2}	n	pK_{a2}	n	pK_{a2}	n	pK_{a2}	n
0.01	10.83	1.49	10.69	1.56	10.55	1.51	10.39	1.48
0.02	10.80	1.51	10.67	1.53	10.52	1.51	10.36	1.50
0.05	10.77	1.51	10.63	1.52	10.48	1.48	10.33	1.50
0.10	10.74	1.48	10.61	1.54	10.46	1.51	10.30	1.50

Poly(methacrylohydrazide): $\bar{P}_n=5470$, 8.64×10^{-4} unit mol/l.
Neutral salt: KNO_3.

In the case under discussion, the formation of the complexes can be represented by the following equation:

$$HA + MA_{j-1} \rightleftarrows MA_j + H^+. \quad (8)$$

The equilibrium constants, b_j, pertaining to the above equation are represented as:

$$b_j = \frac{[MA_j][H^+]}{[MA_{j-1}][HA]}, \quad (9)$$

$$b_j = K_{a_2}k_j, \quad (10)$$

where K_{a_2} is the second acid dissociation constant of PMH and k_j is the successive formation constant of the complexes. By simple manipulations, Bjerrum formation function can be expressed in terms of the b_j's:

$$\bar{n} = \frac{\sum_{i=1}^{N} iB_i\left(\frac{[HA]}{[H^+]}\right)^i}{1+\sum_{i=1}^{N}B_i\left(\frac{[HA]}{[H^+]}\right)^i}, \quad (11)$$

$$B_i = \prod_{t=1}^{i} B_j. \quad (12)$$

The average number of ligands combined with one copper(II) ion, $\bar{n}$, is given by its definition as:

$$\bar{n} = \frac{[A_t]-[HA]-[A^-]}{[M_t]}. \quad (13)$$

The only unknown $[A^-]$ was calculated from the following equation, Eq. 14, by an iterative procedure for the PMH–copper(II) complexes:

$$K_{a_2} = \frac{[H^+][A^-]}{[HA]}\left(\frac{[A^-]}{[A_t]-[A^-]}\right)^{n-1} \quad (14)$$

where n is the value calculated from the modified Henderson-Hasselbach plots.

From the conservation equations and electroneutrality relation [HA], the concentration of undissociated PMH is found to be:

$$[HA] = [A_t](1-\alpha) + [OH^-] - [H^+] \quad (15)$$

where α is the degree of neutralization. $[H^+]$ and $[OH^-]$ are calculated from the measured pH values and the ionization constant of water, with a correction for the activity coefficients.[17]

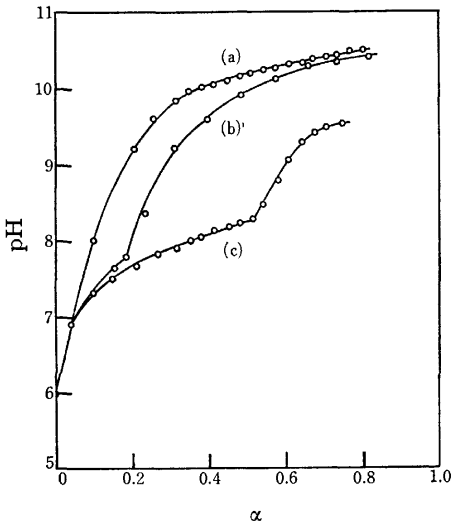

Fig. 3. The pH titration curves.
(a): PMH($\bar{P}_n$=5470) 8.64×10^{-4} unit mol/l, (b): $Cu(NO_3)_2$ 8.00×10^{-5} mol/l, (c): (a)+(b). 25 °C, μ=0.10(KNO_3).

Chelate Formation. Figure 3 shows the titration curves for PMH in the absence and in the presence of copper(II) ions at the ionic strength of 0.1(KNO_3) at 25 °C. PMH–copper(II) complexes precipitated throughout the pH range below about pH 8.5. Above pH 8.5, it was found that the precipitates redissolved into the solution. This shows that the precipitates were not copper(II) hydroxides. It is not always obvious why the precipitates became soluble in water above about pH 8.5. However, it is probably the result of the reversal of the charge of the complexes. From Fig. 3, it may be seen that the release of hydrogen ions caused by the formation of PMH–copper(II) complexes began at about pH 7 and continued up to pH 9, and that the six hydrogen ions per copper(II) ion were released.

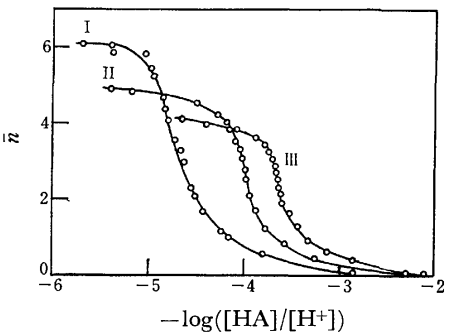

Fig. 4. Effect of T_{Cu}/T_{HL} on modified Bjerrum plots.
PMH($\bar{P}_n$=5470): 8.28×10^{-4} unit mol/l, 25 °C, μ=0.10(KNO_3).
T_{Cu}/T_{HL}; I: 0.024—0.097, II: 0.145, III: 0.193.

The Effect of the T_{Cu}/T_{HL} Ratio on the Modified Bjerrum Plots. The formation of PMH–copper(II) complexes was investigated in the range of the T_{Cu}/T_{HL} values from 0.024 to 0.193. The modified formation curves are shown in Fig. 4. From Fig. 4, it may be seen that the modified Bjerrum plots obtained in the range from 0.024 to 0.097 of the T_{Cu}/T_{HL} values fell on nearly the same curve. The plots show a definite tendency to flatten out toward a value of $\bar{n}$=6 as $-\log([HA]/[H^+])$ becomes more negative. This result suggests that one copper(II) ion forms a coordination compound with six hydrazide groups. However, when the T_{Cu}/T_{HL} values increased above 0.145, the modified formation curves moved to a less negative value of $-\log([HA]/[H^+])$. It was also found that $\bar{n}$ decreased from 6 to 4 with an increase in the T_{Cu}/T_{HL} values. In a previous paper,[1] we also reported that a copper(II) ion formed a coordination compound with six hydrazide groups of isobutyrohydrazide when the formation of isobutyrohydrazide–copper(II) complexes was investigated in the T_{Cu}/T_{HL} value of 0.1. Figure 5 shows the relationship between the successive formation constants and $\log(T_{Cu}/T_{HL})$. The successive formation constants had nearly the same values in the region below $\log(T_{Cu}/T_{HL})$ value of −1, but they increased remarkably in the region above $\log(T_{Cu}/T_{HL})$ value of −1. This suggests that the formation of PMH–copper(II) complexes is favored when the T_{Cu}/T_{HL} values become larger than 0.1.

The Effect of the Degree of Polymerization on the Modified Bjerrum Plots. The formation of PMH–copper(II)

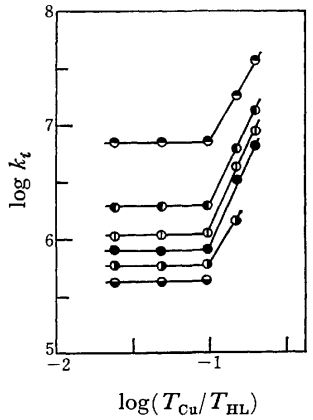

Fig. 5. Relation between formation constants and log-(T_{Cu}/T_{HL}). PMH($\bar{P}_n$=5470): 8.28×10^{-4} unit mol/l, 25 °C, μ=0.10(KNO_3).
◓: log k_1, ◐: lo k_2, ⓘ: log k_3, ●: log k_4, ◑: log k_5, ◒: log k_6.

complexes was investigated for PMH with different degrees of polymerization. The modified Bjerrum plots all fell on nearly the same curve irrespective of the degree of polymerization of PMH. That is, the formation constants for PMH–copper(II) complexes were unaffected by the degrees of polymerization ranging from 64.1 to 5470.

The Effect of the Kind of Anion on the Modified Bjerrum Plots. The formation of PMH–copper(II) complexes was investigated in a solution with the ionic strength of 0.1 by varying the anion (NO_3^-, Cl^-, SO_4^{2-}) in the copper(II) salts and neutral salts added. The modified Bjerrum plots are shown in Fig. 6, while the formation constants are listed in Table 6. It may be seen that the formation constants increased in this order: $NO_3^-<SO_4^{2-}<Cl^-$. As is already known, a complexation reaction in an aqueous solution is a replacement reaction between the ligands in the polymers and aqua-complexes of metals. Therefore, it is considered that the change in the structure of aqua-complexes of metals caused by counter anions and surrounding anions in the solution affected the formation constants. Hojo *et al.*[4] reported analogous phenomena for poly(vinyl alcohol)–copper(II) complexes, but they reported that the formation constants increased in the order of: $SO_4^{2-}<Cl^-<NO_3^-$. The difference in the order of formation constants between poly(vinyl alcohol)–copper(II) complexes and PMH–copper(II) complexes can not be explained at present.

Table 6 also lists the formation constants for isobutyrohydrazide determined in a solution with the ionic strength of 0.1(KNO_3); the data for isobutyrohydrazide were determined in a manner exactly analogous to that used for PMH described above. The data show that the isobutyrohydrazide–copper(II) complexes were more stable than PMH–copper(II) complexes. Such phenomena as that a monomeric analogue forms more stable complexes than its polymer have been observed for poly(acrylaldehyde oxime)[6] or poly(4-pentene-2,3-dione dioxime).[18]

Entropy and Enthalpy for Complexation for PMH–Copper-(II). Entropy and enthalpy changes for the complexation reaction between PMH and copper(II) ions were studied by using Ringbom's method.[19] The formation of PMH–copper(II) complexes was inves-

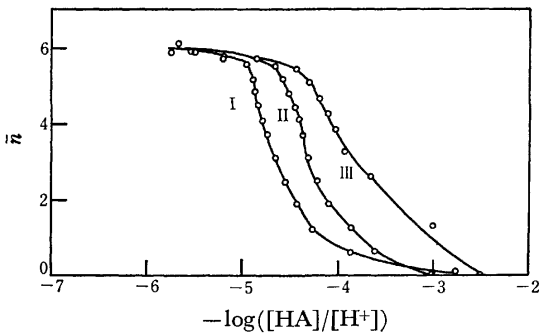

Fig. 6. Effect of the kind of anion on modified Bjerrum plots.
PMH($\bar{P}_n$=5470: 8.28×10^{-4} unit mol/l, $Cu(NO_3)_2$, $CuSO_4$, $CuCl_2$: 8.00×10^{-5} mol/l.
Anion; I: NO_3^-, II: SO_4^{2-}, III: Cl^-.

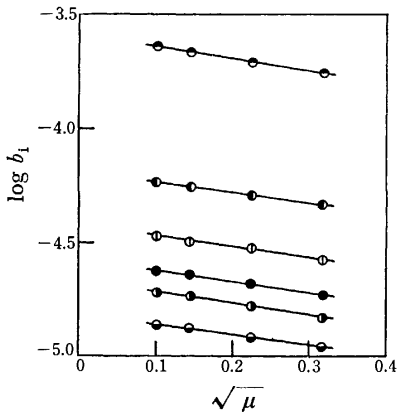

Fig. 7. Relation between log b_i and $\sqrt{\mu}$.
PMH($\bar{P}_n$=5470): 8.64×10^{-4} unit mol/l, $Cu(NO_3)_2$: 8.00×10^{-5} mol/l, 25 °C.
◓: log b_1, ◐: log b_2, ⓘ: log b_3, ●: log b_4, ◑: log b_5, ◒: log b_6.

Table 6. Effect of the kind of anion on the formation constants

Ligand	Anion	log k_1	log k_2	log k_3	log k_4	log k_5	log k_6	log K
PMH[a]	NO_3^-	6.84	6.26	6.04	5.89	5.79	5.67	36.49
	SO_4^{2-}	7.10	6.61	6.38	6.25	6.15	5.71	38.20
	Cl^-	7.73	7.30	6.86	6.52	6.29	5.84	40.54
IBH[b]	NO_3^-	8.52	8.24	8.10	8.04	7.89	7.04	47.83

a) Poly(methacrylohydrazide). b) Isobutyrohydrazide. PMH($\bar{P}_n$=5470): 8.28×10^{-4} unit mol/l, $Cu(NO_3)_2$, $CuSO_4$, $CuCl_2$: 8.00×10^{-5} mol/l, IBH: 1×10^{-3} mol/l, $Cu(NO_3)_2$: 1×10^{-4} mol/l, 25 °C, μ=0.10.

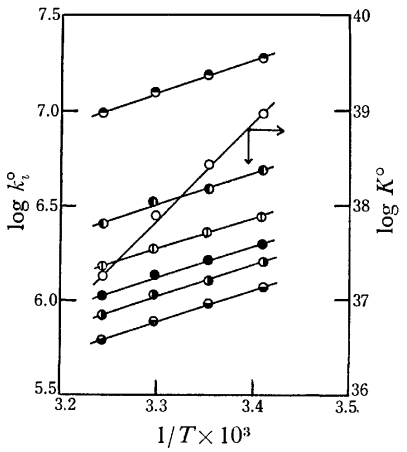

Fig. 8. Formation constants *vs.* $1/T$ plots PMH($\bar{P}_n$= 5470): 8.64×10^{-4} unit mol/l, $Cu(NO_3)_2$: 8.00×10^{-5} mol/l. ◓: log k_1°, ◐: log k_2°, ◑: log k_3°, ●: log k_4°, ◑: log k_5°, ◒: log k_6°, ○: log K°.

tigated at an ionic strength of 0.01—0.1 and a temperature of 20—35 °C. The relationship between the equilibrium constants, b_j, determined from the modified Bjerrum plots and $\sqrt{\mu}$ are shown in Fig. 7. It is found that the plots of log b_j *vs.* $\sqrt{\mu}$ are linear in the range from 0.01 to 0.1 of the ionic strength. The log b_i° was determined by the extrapolation of the linear log b_i *vs.* $\sqrt{\mu}$ plots to the intercept. The plots of log k_i° calculated from Eq. 10 *vs.* $1/T$ are shown in Fig. 8. In all cases, the plots of log k_i° *vs.* $1/T$ gave straight lines.

ΔH°, ΔG°, and ΔS° have the following equations:

$$\Delta G^\circ = -RT\ln K^\circ, \tag{16}$$

$$\ln K^\circ = \frac{-\Delta H^\circ}{RT} + C, \tag{17}$$

$$\Delta G^\circ = \Delta H^\circ - T\Delta S^\circ. \tag{18}$$

Here, from the slope of the plots of log K_i° *vs.* $1/T$, ΔH° for the reaction was obtained, ΔG° was obtained from the value of ln k_i° at 25 °C, and ΔS° was calculated from the difference between ΔH° and ΔG°. The results are shown in Table 7. All the ΔH° values are negative; this suggests that the formation reaction of PMH–copper(II) complexes is an exothermic reaction. Moreover, these values were five times as large as those for poly(vinyl alcohol)–copper(II) complexes.[4] This suggests that the PMH–copper(II) complexes are more stable than the poly(vinyl alcohol)–copper(II) complexes. The ΔS° values are positive, and they decrease as follows: $\Delta S_1^\circ > \Delta S_2^\circ > \cdots > \Delta S_6^\circ$. Generally, entropy increases because of the release of water, which is coordinated with copper(II) ions and polymeric ligands, as a result of the formation of PMH–copper(II) complexes. On the other hand, the degree of freedom of copper(II) ions and polymeric ligands decreases because of the coordination of copper(II) ions with hydrazide groups. Therefore, it is considered that the entropy changes for PMH–copper(II) complexes finally decreased in the order presented above. These phenomena have also been reported for poly(vinyl alcohol)–copper(II) complexes.[4]

Table 7. The thermodynamic parameters of PMH–copper(II) complexes

i	log k_i°	$-\Delta G_i^\circ$ (kcal/mol)	$-\Delta H_i^\circ$ (kcal/mol)	ΔS_i° (cal/deg·mol)
1	7.19	9.81	7.58	7.48
2	6.59	8.99	7.26	5.81
3	6.36	8.67	7.67	3.36
4	6.21	8.47	7.56	3.05
5	6.11	8.33	7.50	2.79
6	5.97	8.14	7.35	2.65
$\sum_{i=1}^{6} i$	38.43	52.41	44.63	26.11

PMH($\bar{P}_n$=5470): 8.64×10^{-4} unit mol/l, $Cu(NO_3)_2$: 8.00×10^{-5} mol/l. 1) HA + $Cu^{2+} \rightleftarrows CuA^+ + H^+$ 2) HA + $CuA^+ \rightleftarrows CuA_2 + H^+$ ……6) HA + $CuA_5^{3-} \rightleftarrows CuA_6^{4-} + H^+$.

From the results described above, it can be seen that one copper(II) ion formed a coordination compound with six hydrazide groups of PMH in a high pH region (about pH 9) when the T_{Cu}/T_{HL} values became less than 0.1. The formation constants were unaffected by the degree of polymerization of PMH, but were affected by the kind of anion of copper(II) salts and neutral salts added. From the thermodynamic data, it was recognized that the formation reaction of PMH–copper(II) was an exothermic reaction.

References

1) Part VIII: T. Nonaka, E. Momono, N. Minari, and H. Egawa, *Nippon Kagaku Kaishi*, **1978**, 1205.
2) H. P. Gregor, L. B. Luttinger, and E. M. Loebl, *J. Phys. Chem.*, **59**, 34 (1955).
3) H. P. Gregor, L. B. Luttinger, and E. M. Loebl, *J. Phys. Chem.*, **59**, 990 (1955).
4) N. Hojo and H. Shirai, *Nippon Kagaku Kaishi*, **1972**, 1316.
5) M. Hatano, T. Nozawa, T. Yamamoto, and S. Kambara, *Makromol. Chem.*, **115**, 1 (1971).
6) N. Muto, T. Kobayashi, and T. Nakagawa, *Nippon Kagaku Zasshi*, **92**, 43 (1971).
7) H. Nishikawa and E. Tsuchida, *J. Phys. Chem.*, **79**, 2702 (1975).
8) T. Nonaka and H. Egawa, *Nippon Kagaku Kaishi*, **1977**, 1722.
9) T. G. Fox, J. B. Kinsinger, H. F. Mason, and E. M. Schuele, *Polymer*, **3**, 71 (1962).
10) W. Kern, Th. Hucke, R. Höllander, and R. Schneider, *Makromol. Chem.*, **22**, 31 (1957).
11) A. Albert, *Nature*, **177**, 525 (1956).
12) K. Nagano, H. Tsukahara, H. Kinoshita, and Z. Tamura, *Chem. Pharm. Bull.*, **11**. 797 (1963).
13) A. Katchalsky and P. Spitnik, *J. Polym. Sci.*, **2**, 432 (1947).
14) R. Arnold and J. T. G. Overbeek, *Recl. Trav. Chim.*, **69**, 192 (1950).
15) A. Oth and P. M. Doty, *J. Phys. Chem.*, **56**, 43 (1952).
16) S. Machida and Y. Takenaka, *Angew. Makromol. Chem.*, **39**, 59 (1974).
17) H. Yoshimura, H. Matsushita, and T. Morimoto, "pH No Riron To Sokuteiho," Maruzen, Tokyo (1968), p. 14.
18) J. B. Andelman, G. K. Hoeschele, and H. P. Gregor, *J. Phys. Chem.*, **63**, 206 (1959).
19) A. Ringbom, "Complexation in Analytical Chemistry," Interscience Pub., New York (1963), p. 24.

New C_{31} Secodammarane-type Triterpenoids, Alnuseric Acid and Alnuselide, in the Male Flowers of *Alnus serrulatoides*

Takayuki SUGA* and Toshifumi HIRATA

Department of Chemistry, Faculty of Science, Hiroshima University, Higashisenda-machi, Hiroshima 730

(Received September 4, 1978)

Two novel C_{31} 3,4-secodammarane-type triterpenoids, alnuseric acid and alnuselide, were isolated from the male flowers of *Alnus serrulatoides* Call. (Betulaceae); their structures were elucidated to be (20*S*,24*R*)-20,24-epoxy-24-methyl-3,4-secodammar-4(28)-en-3-oic acid and (11*R*,20*S*,24*R*)-20,24-epoxy-24-methyl-3,4-secodammar-4(28)-en-3,11α-olactone, respectively, by a combination of chemical and spectroscopic methods.

In connection with the chemical and biochemical studies on pollination of *Alnus* species,[1] we investigated chemical constituents of the male flowers of *Alnus serrulatoides* Call. (Japanese name: Kawara-hannoki) and reported the presence of novel C_{31} dammarane-type dihydroxy keto and 11α-hydroxylated triterpenoids.[2-4] A further investigation on constituents of the male flowers has led to the isolation of two novel triterpenic acid and triterpene lactone, named alnuseric acid and alnuselide, and preliminary accounts of the structural work have been presented in the previous papers, respectively.[5,6] We here wish to report *en bloc* detailed evidence which led to the establishment of the structures of these novel triterpenoids, which are featured in the C_{31} 3,4-secodammarane form.

Results and Discussion

The ether soluble fraction of the male flowers on separation by means of a centrifugal liquid chromatograph and then a preparative TLC gave alnuseric acid (I) and alnuselide (II), along with several dammarane-type triterpenoids, alnincanone,[2,7] alnuserol,[4] and alnuserrudiolone.[2]

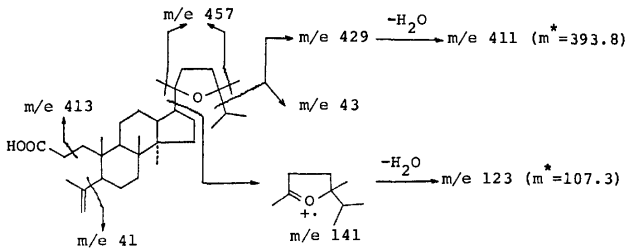

Scheme 1. The mass spectral fragmentation pattern of alnuseric acid (I).

Alnuseric acid (I), $C_{31}H_{52}O_3$, showed IR absorption bands of a terminal methylene and a carboxyl group. The CMR spectrum in $CDCl_3$ also indicated the presence of the terminal methylene, the carboxyl, the ether ring, and eight methyl carbons. The peaks at *m/e* 141 (base), 123, and 43 in the mass spectrum was similar to those in it of alnincanone (III), a naturally occurring dammarane-type triterpenoid with a tetrahydrofuran ring. Ryabinin *et al.*[8] has proved the occurrence of such ions from the tetrahydrofuran ring of alnincanone (III). This has also been established in the mass spectra of alnuserol (IV)[4] and various compounds with a tetrahydrofuran ring.[9,10] Therefore, the occurrence of the peaks in the mass spectrum of alnuseric acid (Scheme 1) indicates clearly that this acid includes a side chain comprised of a tetrahydrofuran ring similarly to III and IV.

The molecular formula indicated that alnuseric acid has four rings, in contrast to alnincanone (III) and alnuserol (IV). Accordingly, alnuseric acid surely contains no ring A located with a carbonyl or hydroxyl group at position 3, though such functional groups appear almost without exception in plant triterpenoids. These structural features of alnuseric acid may result from the cleavage of ring A of a 3-keto triterpenoid having a side chain comprised of a tetrahydrofuran ring as III and IV. To the alnuseric acid, we here propose a biogenetically acceptable structure (I),[11] which is probably formed biologically from alnincanone by ring-cleavage at the 3,4-position.

The structure (I) proposed for alnuseric acid was confirmed by its synthesis starting from alnincanone (III) following the method established for ring-cleavage at the 3,4-position in ring A of β-amyrenone.[12] Alnincanone (III) was transformed to the corresponding ketoxime, which then was treated with *p*-toluenesulfonyl

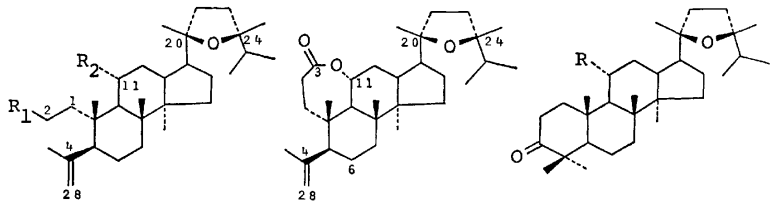

I: R_1=COOH, R_2=H
V: R_1=CN, R_2=H
VI: R_1=COOH, R_2=OH
VII: R_1=COOMe, R_2=OH
VIII: R_1=COOMe, R_2=H
X: R_1=CN, R_2=OAc

II

III: R=H
IV: R=OH
IX: R=OAc

chloride in pyridine to yield an abnormal Beckmann rearrangement product (V) with infrared bands due to a cyano group and a terminal methylene. Alkaline hydrolysis of this product (V) under milder conditions gave (20*S*,24*R*)-20,24-epoxy-24-methyl-3,4-secodammar-4(28)-en-3-oic acid. Identity of this authentic acid with the naturally occurring alnuseric acid was established by comparison of the mixed melting point and spectral data. The structure of alnuseric acid has been elucidated to be in **I**.

Alnuselide (II), $C_{31}H_{50}O_3$, showed IR absorption bands due to a terminal methylene. The CMR spectrum indicated the presence of an ester or a lactone carbonyl, a terminal methylene, and eight methyl carbons in addition to two quaternary carbons bearing an oxygen atom. Appearance of the IR absorption band at 1740 cm^{-1} in CCl_4 suggested the presence of a six- or a seven-membered lactone moiety. This was confirmed by the formation of a hydroxy acid VI from II on hydrolysis with KOH/MeOH and the reproduction of II from VI on acidification with HCl/MeOH. Methylation of VI with CH_2N_2 yielded a hydroxy methyl ester VII, which exhibited the CMR signal at δ 71.2 ppm (d) due to the carbon atom occupied with a secondary hydroxyl group. The mass spectrum of VII (Scheme 2) showed the

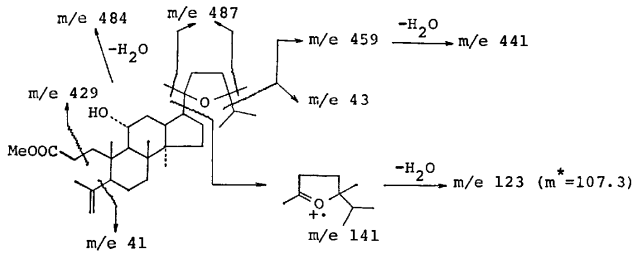

Scheme 2. The mass spectral fragmentation pattern of hydroxy methyl ester VII derived from alnuselide (II).

fragmentation pattern quite similar to that of alnuseric acid methyl ester (VIII). This suggested a secodammarane-type triterpenoid with the side chain comprised of a tetrahydrofuran ring. The seco-form was also indicated by the molecular formula revealing that VII comprises four rings. Accordingly, the hydroxy methyl ester (VII) may be a 6- or a 11-hydroxylated derivative of VIII, because alnuselide (II) is found to involve a six- or a seven-membered lactone comprised of a secondary hydroxyl group as described above. The agreement between the carbon signals due to the C, D, and tetrahydrofuran rings of VII and the signals due to these rings of alnuserol (IV)[4] demonstrated that the secondary hydroxyl group should be located on C-11 of VII. Structure VII is assigned to the hydroxy methyl ester, and structure II is proposed for alnuselide, a novel triterpenoid lactone.

The structure (II) was confirmed by means of its synthesis involving the cleavage of the A-ring of alnuserol (IV)[4] followed by the lactonization of the resulting hydroxy acid. The oxime derivative of alnuseryl acetate (IX) prepared from alnuserol (IV) in the usual manner was treated[12] with *p*-toluenesulfonyl chloride in pyridine to yield a product (X) resulting from the abnormal Beckmann rearrangement. The hydrolysis of the product (X) with KOH/MeOH gave a hydroxy acid. This hydroxy acid on dissolving in ether saturated with 5% hydrochloric acid and then standing at room temperature suffered lactonization to form (11*R*,20*S*,24*R*)-20,24-epoxy-24-methyl-3,4-secodammar-4(28)-en-3,11α-olactone. Identity of naturally occurring alnuselide with this authentic sample was established by comparisons of the mixed melting point, and spectral data. Thus, the structure of alnuselide has been elucidated to be II. Biogenetically, it is fascinating to note that biological cleavage of ring A in alnuserol (IV), similarly to the case of alnuseric acid (I), followed by lactonization between the 3-carboxyl and the 11-hydroxyl groups might result in the formation of alnuselide (II).

Experimental

The mass spectral analyses were performed on a Hitachi RMS-4 mass spectrometer at 70 eV. The PMR spectra were taken with a Varian T-60 spectrometer using TMS as an internal standard. The CMR spectra were determined with a JEOL JNM FX-100 spectrometer operating at 15.1 MHz ($\delta_{TMS}=0$).

Extraction and Isolation. The male flowers (10.3 kg) of *Alnus serrulatoides* Call. grown wildly on a river side in suburbs of Hiroshima city were collected just before the flowering in late February. After minced mechanically, the flowers were immersed in acetone at room temp for 2 months. Removal of the solvent from the acetone solution gave a viscous sirup, which was extracted with ether to give a viscous oil (66.7 g). A part (20.0 g) of the viscous oil was subjected to a centrifugal liquid chromatography (silica gel; 3 mm in thickness) with a hexane–EtOAc mixture with EtOAc increasing 0 to 30% and then to preparative TLC (silica gel; 0.75 mm in thickness) with hexane–EtOAc (7: 3 v/v) to give alnuseric acid (I) (144 mg) and alnuselide (II) (198 mg).

Alnuseric Acid (I). Mp 107—109 °C; $[\alpha]_D^{25}$+24.3° (*c* 0.21, MeOH); IR (KBr) ν_{max} 3300—2800, 1708 (COOH), 3077, 1638, and 888 cm^{-1} (>C=CH$_2$), 1084 (C–O–C); PMR ($CDCl_3$) δ 0.8—1.2 (7×Me), 1.75 (3H, broad s, C(4)–Me), 4.70 and 4.85 (2H, broad s, >C=CH$_2$); CMR ($CDCl_3$) δ 180.2 (s, C-3), 147.4 (s, C-4), 113.4 (t, C-28), 85.8 and 85.3 (s, C-20 and C-24), 25.1, 23.2, 22.9, 20.1, 18.8, 17.6, 16.3, 15.4 (q, 8×Me); MS *m/e* (rel. intensity) 472 (M^+, 1), 457 (3), 429 (20), 411 (8), 141 (100), 123 (61), 43 (63), 41 (52). Found: C, 79.06; H, 11.01%. Calcd for $C_{31}H_{52}O_3$: C, 78.76; H, 11.09%. Methylation of I with CH_2N_2 gave the methyl ester (VIII): IR (liquid film) ν_{max} 1735 (ester), 3078, 1637, and 890 cm^{-1} (>C=CH$_2$); PMR ($CDCl_3$) δ 0.8—1.2 (7×Me), 1.76 (3H, broad s, C(4)–Me), 3.36 (3H, s, OMe), 4.72 and 4.86 (2H, broad s, >C=CH$_2$); MS *m/e* (rel. intensity) 486 (M^+, 2), 471 (3), 141 (100), 123 (60), 43 (65), 41 (59).

Alnuselide (II). Mp 139—140 °C; $[\alpha]_D^{25}$+ 107° (*c* 0.33, MeOH); IR (KBr) ν_{max} 1735 (lactone), 3066, 1635, and 877 cm^{-1} (>C=CH$_2$); UV (MeOH) λ_{max} 220 nm (ε 34.9); PMR ($CDCl_3$) δ 0.8—1.2 (7×Me), 1.79 (3H, broad s, C(4)–Me), 4.73 and 4.88 (2H, broad s, >C=CH$_2$); CMR ($CDCl_3$) δ 176.2 (s, C-3), 146.7 (s, C-4), 114.1 (t, C-28), 85.4 and 84.9 (s, C-20 and C-24), 76.5 (d, C-11), 24.9, 23.7, 22.9, 18.8, 18.7, 17.5, 17.0, and 15.6 (s, 8×Me); MS *m/e* (rel. intensity) 470 (M^+, 2), 426 (60), 408 (18), 141 (100), 123 (62), 43 (60), 41 (67), 28 (83); ORD (*c* 0.33, MeOH) $[\Phi]_{400}$+2090°, $[\Phi]_{219}$ +12300°; CD (*c* 0.33, MeOH) $[\theta]_{219}$+203°. Found: C, 79.01; H, 10.93%. Calcd for $C_{31}H_{50}O_3$: C, 79.10; H, 10.71%.

Preparation of Hydroxy Methyl Ester VII from Alnuselide. A solution of II (20 mg) in 5% NaOH/MeOH (5 ml) was reflux-

ed for 30 min. The reaction mixture, after acidification, was extracted with ether to give a crude product (18 mg), which was then purified by preparative TLC [silica gel; hexane–EtOAc (7:3 v/v)] to afford hydroxy acid VI (15 mg): IR (Nujol) ν_{max} 3350—2500 and 1710 cm^{-1} (OH and COOH). The hydroxy acid (VI) (4.0 mg) was treated for 12 h at room temp with ether (3 ml) saturated with 5% hydrochloric acid to reproduce the original lactone (II) (3.3 mg): mp and mixed mp 139—140 °C. Treatment of the hydroxy acid (VI) (10 mg) with CH_2N_2 gave hydroxy methyl ester VII (10 mg): IR (Nujol) ν_{max} 3350 (OH), 1731 (ester), 3080, 1635, and 883 cm^{-1} (>C=CH_2); MS *m/e* (rel. intensity) 502 (M^+, 0.5), 487 (2), 484 (4), 141 (100), 123 (71), 43 (45), 41 (47); PMR ($CDCl_3$) δ 1.77 (3H, broad s, C(4)–Me), 3.35 (3H, s, OMe), 4.71 and 4.87 (2H, broad s, >C=CH_2); CMR ($CDCl_3$) δ 175.8 (s, C-3), 147.4 (s, C-4), 113.7 (t, C-28), 85.3 (s, C-20 and C-24), 71.2 (d, C-11), 51.4 (q, OMe), 24.6, 23.1, 22.9, 20.4, 18.7, 17.5, 16.4, 16.0 (q, 8×Me). Found: C, 76.69; H, 10.70%. Calcd for $C_{32}H_{54}O_4$: C, 76.45; H, 10.83%.

Synthesis of I. *i) Cleavage of the A Ring of Alnincanone (III)*: According to the previously-described procedure,[12] a mixture of alnincanone oxime (30 mg; prepared from alnincanone (III)[2,7] and hydroxylamine hydrochloride in pyridine) and *p*-toluenesulfonyl chloride (30 mg) in dry pyridine (1.0 ml) was kept for 20 h at room temp. After addition of a few drops of water, the mixture was stirred for 30 min at room temp. The reaction mixture on acidification with 5% hydrochloric acid (10 ml) was extracted with ether to give a solid mass (27 mg), which was subjected to preparative TLC to give 3-cyano-20,24-epoxy-24-methyl-3,4-secodammar-4-(28)-ene (V) (8.2 mg): mp 101—103 °C; IR (Nujol) ν_{max} 2240 (C≡N), 3075, 1632, and 899 cm^{-1} (>C=CH_2); PMR ($CDCl_3$) δ 1.79 (3H, broad s, C(4)–Me) and 4.75 and 4.94 (2H, broad s, >C=CH_2). Found: C, 82.16; H, 11.20%. Calcd for $C_{31}H_{51}ON$: C, 82.06; H, 11.33%. This reaction, as has been described previously,[12] yielded an undesired product, aza-A-homodammarane derivative (12 mg): mp 195—197 °C; IR (Nujol) ν_{max} 1665 cm^{-1} (amide), which was not further investigated.

ii) Hydrolysis of V: A solution of V (5.0 mg) in 20% KOH/EtOH (2 ml) was refluxed for 6 h. The reaction mixture, after acidification was extracted with ether to give 20,24-epoxy-24-methyl-3,4-secodammar-4(28)-en-3-oic acid (I) (3.9 mg): mp 107—109 °C; IR (Nujol) 3300—2800 and 1710 (COOH), 3079, 1638, and 890 cm^{-1} (>C=CH_2); MS *m/e* (rel. intensity) 472 (M^+, 2), 141 (100), 123 (78), 43 (49), 41 (45); PMR ($CDCl_3$) δ 1.75 (3H, broad s, C(4)–Me), 4.70 and 4.85 (2H, broad s, >C=CH_2).

Synthesis of II. *i) Cleavage of the A Ring of Alnuserol (IV)*: By the same procedure as described above, the oxime derivative (228 mg) of alnuseryl acetate (IX)[4] was treated with *p*-toluenesulfonyl chloride (140 mg) in dry pyridine (10 ml) to give 11-acetoxy-3-cyano-20,24-epoxy-24-methyl-3,4-secodammar-4(28)-ene (X) (66 mg): mp 160—162 °C; IR (Nujol) ν_{max} 2245 (C≡N), 1730 (OAc), 3076, 1639, and 890 cm^{-1} (>C=CH_2); PMR ($CDCl_3$) δ 1.77 (3H, broad s, C(4)–Me), 2.07 (3H, s, OAc), 4.72 and 4.92 (2H, broad s, >C=CH_2). Found: C, 77.66; H, 10.51%. Calcd for $C_{33}H_{53}O_3N$: C, 77.45; H, 10.44%. In a similar manner as above, this reaction gave the undesired aza-A-homodammarane derivative (48 mg): mp 225—226 °C; IR (Nujol) ν_{max} 1666 cm^{-1} (amide).

ii) Hydrolysis of X: A solution of X (20 mg) in 20% KOH/MeOH (5 ml) was refluxed for 12 h. The reaction mixture on usual work-up gave 20,24-epoxy-11-hydroxy-24-methyl-3,4-secodammar-4(28)-en-3-oic acid (VI): IR (Nujol) 3350—2500 (OH and COOH), 1708 (COOH), 3080, 1640, and 890 cm^{-1} (>C=CH_2); PMR ($CDCl_3$) δ 1.73 (3H, broad s, C(4)–Me), 4.71 and 4.86 (2H, broad s, >C=CH_2).

iii) Lactonization of VI: Hydroxy acid VI (10 mg) dissolved in ether (5 ml) saturated with 5% hydrochloric acid was left stand for 12 h at room temp to give (11*R*, 20*S*, 24*R*)-20,24-epoxy-24-methyl-3,4-secodammar-4(28)-en-3,11α-olactone (II) (9.0 mg): mp 139—140 °C; IR (Nujol) ν_{max} 1735 (lactone), 3080, 1635, and 890 cm^{-1} (>C=CH_2); MS *m/e* (rel. intensity) 470 (M^+, 2), 141 (100), 123 (68), 43 (59), 41 (67); PMR ($CDCl_3$) δ 1.80 (3H, broad s, C(4)–Me), 4.73 and 4.89 (2H, broad s, >C=CH_2).

We thank Miss Reiko Ideo for having charge of a part of the experiments and JEOL Co., Ltd. for obtaining the ^{13}C-NMR spectra. The present work was partially supported by a Grant-in-Aid for Scientic Research from the Ministry of Education (Nos. 247027 and 234033 to T.S.) and Matsunaga Science Foundation in 1977 (to T.H.).

References

1) J. Heslop-Harrison, "Pollen: Development and Physiology," London Butherworths Ltd., London (1971).
2) T. Suga, T. Hirata, and N. Iwata, *Chem. Lett.*, **1974**, 971.
3) T. Hirata, K. Murai, R. Ideo, and T. Suga, The preprint of The 20th Symposium on the Chemistry of Natural Products, Sendai (1976), p. 273.
4) T. Hirata, K. Murai, T. Suga, and A. Christensen, *Chem. Lett.*, **1977**, 95; T. Hirata and T. Suga, *J. Chem. Soc., Perkin Trans. 2*, **1978**, 347.
5) T. Hirata, R. Ideo, and T. Suga, *Chem. Lett.*, **1977**, 283.
6) T. Hirata, R. Ideo, and T. Suga, *Chem. Lett.*, **1977**, 711.
7) R. Labriola and G. Ourisson, *Tetrahedron*, **29**, 2105 (1973).
8) A. A. Ryabinin, L. H. Matyukhina, I. A. Saltikova, F. Patil, and G. Ourisson, *Bull. Soc. Chim. Fr.*, **1968**, 1089.
9) Q. N. Porter and J. Baldas, "Mass Spectrometry of Heterocyclic Compounds," Wiley-Interscience Inc., New York, N.Y. (1971), p. 39.
10) H. Budzikiewicz, C. Djerassi, and D. H. Williams, "Mass Spectrometry of Organic Compounds," Holden-Day Inc., San Francisco, Calif. (1967), p. 227.
11) A. A. Newman, "Chemistry of Terpenes and Terpenoids," Academic Press Inc., New York, N.Y. (1972), p. 214.
12) G. H. Whitham, *J. Chem. Soc.*, **1960**, 2016.

Reactive Troponoids and *o*-Aminophenol. III. The Reaction of 2-Bromo-7-methoxytropone[1]

Tetsuo NOZOE, Taichi SOMEYA,* and Harue OKAI†

Central Research Laboratory of Takasago Perfumery Co., Ltd., Kamata, Ohta-ku, Tokyo 144

† *Tokyo Research Laboratory of Kao Soap Co., Ltd., Bunka, Sumida-ku, Tokyo 131*

(Received September 9, 1978)

The reaction of 2-bromo-7-methoxytropone with *o*-aminophenol gave 2-bromo-7-(*o*-hydroxyanilino)tropone (**9**), besides small amounts of cyclohepta[*b*][1,4]benzoxazin-6(11*H*)-one (**10**) and 15*H*-[1,4]benzoxazino[3′,2′: 3,4]-cyclohepta[2,1-*b*][1,4]benzoxazine (**11**). The heating of **9** with a strong acid afforded 6-bromocyclohepta[*b*][1,4]-benzoxazine (**13**) quantitatively. On the other hand, the heating of **13** with *o*-aminophenol in ethanol gave **10**, while in acetic acid a mixture of **10** and **11** was obtained. The mechanism of the formation of these products is discussed.

We have previously reported that the reaction of 2-chlorotropone (**1**) with *o*-aminophenol (**2a**) afforded 2-(*o*-hydroxyanilino)tropone (**3**) and cyclohepta[*b*][1,4]-benzoxazine (**4**).[2] The reactions of 4-, 5-, and 6-isopropyl-2-chlorotropones (**5a**—**c**) with *o*-aminophenol gave isopropylcyclohepta[*b*][1,4]benzoxazines (**6a**—**c**), besides a small amount of cyclohepta[*b*][1,4]benzoxazin-10(11*H*)-ones (**7a**—**c**). We also found that, in these reactions, the amino group of *o*-aminophenol attacked the 1- and 2-positions of the tropone ring equally.[3]

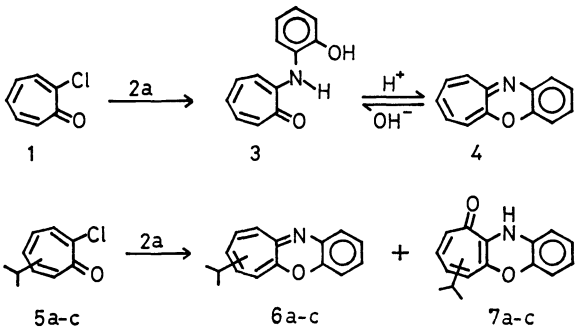

In the present investigation, the reaction of *o*-aminophenol with 2-bromo-7-methoxytropone (**8**), which has two leaving groups, was carried out to find which of two groups, bromo or methoxyl, reacted preferentially and to see if the use of an excess of *o*-aminophenol would give a seven-membered tropylium compound with two oxazine rings.

Results and Discussion

The refluxing of **8** with *o*-aminophenol (**2a**) in acetic acid for 2 h gave yellow prisms (**9**, 82%), orange yellow needles (**10**, 4.7%), and dark violet needles (**11**, 0.5%). The methylation of **9** with diazomethane gave a product which agreed with the 2-bromo-7-(*o*-methoxyanilino)-tropone (**12**) obtained by the reaction of **8** with *o*-methoxyaniline (**2b**) (Scheme 1).

The heating of **9** in acetic acid, in the presence of concd sulfuric acid, resulted in the quantitative formation of **13**, which then easily reverted to **9** on being heated in dilute ethanolic alkali. The catalytic reduction of **13** gave cyclohepta[*b*][1,4]benzoxazine (**4**).[2] These pieces of evidence indicate that **9** is 7-bromo-2-(*o*-hydroxyanilino)tropone and that **13** is 6-bromocyclo-

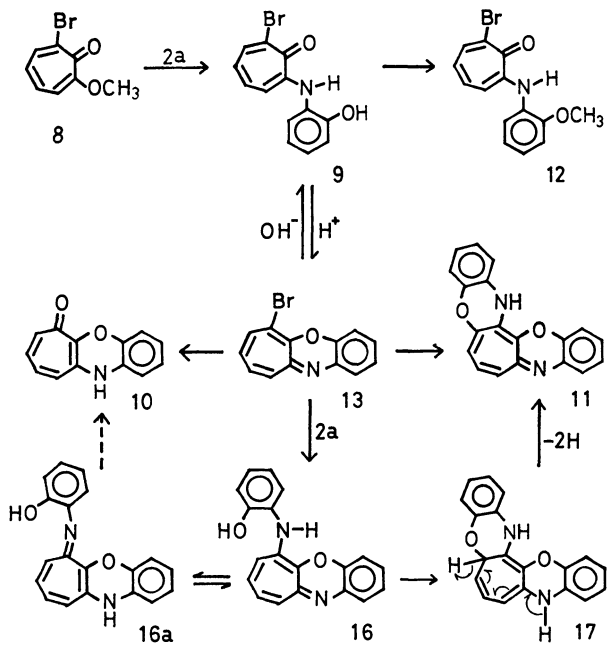

Scheme 1.

hepta[*b*][1,4]benzoxazine. These structures were also supported by the results of the elemental analyses and by the spectral data.

The electronic spectrum of **10** (M^+, 211; $C_{13}H_9NO_2$) is very similar to that of cyclohepta[*b*][1,4]benzothiazin-6(11*H*)-one (**14**).[4] The IR spectrum of **10** shows absorptions at 3300 (NH) and at 1650 cm^{-1} (C=O), which correspond well with those at 3280 (NH) and at 1633 cm^{-1} (C=O) in the IR spectrum of **14**.[4] Consequently, **10** was determined to be cyclohepta[*b*][1,4]-benzoxazin-6(11*H*)-one.

The IR spectrum of **11** (M^+, 300; $C_{19}H_{12}N_2O_2$) shows an absorption at 3250 cm^{-1} (NH). Since the further heating of **13** with **2a** in acetic acid afforded **11** besides **10**, **11** was assumed to be 15*H*-[1,4]benzoxazino[3′,2′: 3,4]cyclohepta[2,1-*b*][1,4]benzoxazine. The visible absorption maximum at 500 nm in **11** corresponds well with that at 490—500 nm in **15**, a tropylium compound with two condensed thiazine rings, which was obtained by the reaction of 3,5-dibromotropolone with *o*-amino-benzenethiol.[4]

The bromo compound **13** was fairly stable on heating in strong acids and did not undergo any change, but the

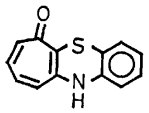

14

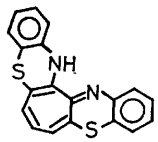

15

refluxing of **13** with **2a** in acetic acid resulted in the formation of **10** and **11**, although it should be noted that the refluxing of **13** with **2a** in ethanol gave mainly **10**, and no **11**. It is interesting to note that, although **13** does not change in strong acids, **13** loses bromine by the reaction with almost neutral **2a** even in ethanol and that the bromine atom is replaced with an oxygen atom. The experiments mentioned above suggest that the saponification of the bromine atom in **13** should be preceded by substitution with **2a**, giving the 6-(*o*-hydroxyanilino) compound (**16**). The Schiff base **16a**, a tautomeric form of **16**, could be saponified under dilute acidic conditions to give the ketone (**10**).

However, since the ketone (**10**) was not obtained by the reaction of **13** with aniline under the same reaction conditions, the hydroxyl group in the substituent at C-6 in **16** seems to participate in the formation of **10**. A study of the mechanism of the ketone (**10**) is now under investigation.

Compound **16** would also be cyclized at the 7-position to form **17**, which then undergoes dehydrogenation to form the more stable **11**.

It is quite notable that the hydroxyanilino group bonded to the seven-membered ring undergoes cyclization on the seven-membered ring not containing a functional group.[3]

Experimental

If not otherwise stated, the instruments and methods are as previously described.[2]

Reaction of 2-Bromo-7-methoxytropone (8) with 2a. A mixture of **8** (1.5 g, 7.0 mmol), **2a** (0.9 g, 8.4 mmol), and acetic acid (4.5 ml) was refluxed for 2 h. After the removal of the acetic acid under reduced pressure, a small amount of ethanol was added to the residue and the precipitate was filtered. The recrystallization of the crude crystals from ethanol gave 1.23 g of **9**. The filtrate and the mother liquor of the recrystallization were chromatographed on a silica gel column. Then, **11** (10 mg, 0.5%), **10** (70 mg, 4.7%), and **9** (370 mg) were obtained from the benzene, benzene–ether (1: 1), and ether fractions respectively.

2-Bromo-7-(o-hydroxyanilino)tropone (9): Yellow prisms; mp 202 °C; λ_{max}^{MeOH} nm (log ε): 205 (4.52), 250 (4.38)^{sh}, 260 (4.39), 346 (3.98), and 418 (4.20); $\lambda_{max}^{MeOH+NaOH}$ nm (log ε): 240 (4.72), 346 (3.98), and 423 (4.20); IR (KBr): 3280 (NH), 3200 (OH), and 1585 cm^{-1} (C=O); NMR (60 MHz in DMSO-d_6): δ 10.0 (s, 1H, OH), 9.25 (s, 1H, NH), 8.24 (dd, 1H, J=10 and 1 Hz, C_3–H), 7.15—7.55 (m, 2H, $C_{5,6}$–H), 6.80—7.15 (m, 4H, benzene ring), and 6.55 ppm (t, 1H, J=10 and 10 Hz, C_4–H). Found: C, 53.40; H, 3.54; N, 4.62%; M$^+$, 293. Calcd for $C_{13}H_{10}NO_2Br$: C, 53.44; H, 3.45; N, 4.80%; M, 293.

Cyclohepta[b][1,4]benzoxazin-6(11H)-one (10): Orange yellow needles; mp 115 °C (from hexane); λ_{max}^{MeOH} nm (log ε): 207 (4.28), 227 (4.43), 275 (3.88), 310 (3.48), and 435 (3.74); IR (KBr): 3300 (NH) and 1650 cm^{-1} (C=O); NMR (60 MHz in $CDCl_3$): δ 9.10 (s, 1H, NH) and 6.30—7.05 ppm (m, 8H). Found: C, 73.64; H, 4.27; N, 6.70%; M$^+$, 211. Calcd for $C_{13}H_9NO_2$: C, 73.92; H, 4.30; N, 6.63%; M, 211.

15H-[1,4]Benzoxazino[3',2': 3,4]cyclohepta[2,1-b][1,4]benzoxazine (11): Dark violet needles; mp 245 °C (from hexane); λ_{max}^{MeOH} nm (log ε): 207 (4.10), 254 (3.99), 350—360 (3.43), and 500 (3.68); $\lambda_{max}^{MeOH+HCl}$ nm (log ε): 207 (4.08), 223 (4.02), 275 (4.00), 325 (3.57)^{sh}, 410 (3.68), and 535 (3.54); IR (KBr): 3250 cm^{-1} (NH); NMR (60 MHz in DMSO-d_6): δ 6.70—6.45 (m, 8H, benzene ring) and 5.72 ppm (m, 3H, cycloheptatriene ring). Found: C, 76.25; H, 4.09; N, 9.38%; M$^+$, 300. Calcd for $C_{19}H_{12}N_2O_2$: C, 75.99; H, 4.03; N, 9.33%; M, 300.

2-Bromo-7-(o-methoxyanilino)tropone (12). a) An ether solution of diazomethane (0.51 mmol) was added to a solution of **9** (0.1 g, 0.34 mmol) in ether (20 ml), and the mixture was stirred for 5 min at room temp. After the removal of the ether, the recrystallization of the residue from benzene gave 0.1 g (95%) of **12**.

b) A mixture of **8** (0.1 g, 0.45 mmol), **2b** (66 mg, 0.54 mmol), and acetic acid (1 ml) was refluxed for 5 h. After the removal of the acetic acid under reduced pressure, the residue was dissolved in benzene. The benzene solution was washed with aq $NaHCO_3$ and water, dried over Na_2SO_4, and evaporated. The residue was chromatographed on a silica gel column; then **12** (61 mg, 91%) and **9** (53 mg) were obtained from the benzene–ether (3: 1) and ether fractions respectively. **12**: Yellow needles; mp 132 °C; λ_{max}^{MeOH} nm (log ε): 205 (4.46), 244 (4.33), 260 (4.34), 348 (4.10), and 420 (4.31); IR (KBr): 3260 (NH) and 1680 cm^{-1} (C=O); NMR (60 MHz in DMSO-d_6): δ 9.25 (s, 1H, NH), 8.20 (d, 1H, J= 10 Hz, C_3–H), 7.20—7.52 (m, 2H, $C_{5,6}$–H), 6.85—7.20 (m, 4H, benzene ring), and 6.57 ppm (m, 1H, C_4–H). Found: C, 55.17; H, 4.07; N, 4.40; Br, 26.16%; M$^+$, 307. Calcd for $C_{14}H_{12}NO_2Br$: C, 54.92; H, 3.95; N, 4.58; Br, 26.10%; M, 307.

6-Bromocyclohepta[b][1,4]benzoxazine (13). A solution of **9** (0.7 g, 2.4 mmol), acetic acid (5 ml), and a small amount of concd H_2SO_4 was refluxed for 1 h. After the removal of the acetic acid under reduced pressure, the residue was dissolved in benzene. The benzene solution was washed with aq $NaHCO_3$ and water, dried over Na_2SO_4, and evaporated. The recrystallization of the residue from hexane gave 0.65 g (98%) of **13** as brown needles; mp 119 °C; λ_{max}^{MeOH} nm (log ε): 208 (4.30), 227 (4.31), 262 (4.43), 268 (4.42), and 410 (4.08); NMR (60 MHz in CCl_4): δ 6.40—6.75 (m, 4H, benzene ring) and 5.30—6.55 ppm (m, 4H, cycloheptatriene ring); NMR (in CF_3COOH): δ 7.75 (d, 1H, J=11 Hz, C_7–H) and 6.45—7.40 ppm (m, 7H). Found: C, 57.08; H, 2.84; N, 5.06; Br, 29.27%; M$^+$, 275. Calcd for $C_{13}H_8NOBr$: C, 56.96; H, 2.94; N, 5.11; Br, 29.15%; M, 275.

The hydrogenation of **13** in ethyl acetate and a small amount of pyridine with palladium carbon (5%) as a catalyst under normal pressure at room temp gave cyclohepta[*b*][1,4]benzoxazine[2] as brown needles; mp 93 °C.

Conversion of 13 into 9. A solution of **13** (50 mg) in EtOH (1 ml) and 1 M NaOH (1 ml) was refluxed for 1 h. After the removal of the ethanol, water (2 ml) was added to the residue, and the mixture was washed with benzene. The water layer was neutralized with 1 M HCl and extracted with benzene. The extract was washed with water, dried, and evaporated to dryness. Recrystallization from hexane gave 45 mg (84%) of **9**.

Reaction of 13 with 2a. A mixture of **13** (55 mg, 0.2 mmol), **2a** (26 mg, 0.24 mmol), and acetic acid (5 ml) was

refluxed for 4 h. After the removal of the acetic acid under reduced pressure, the residue was extracted with benzene. From the extract, 10 mg (17%) of **11** and 15 mg (36%) of **10** were obtained by preparative TLC developed with benzene. On the other hand, a mixture of **13** (85 mg), **2a** (45 mg), and EtOH (5 ml) was refluxed for 3 h. By the method described above, a 50-mg portion (76%) of **10** was obtained.

The authors wish to express their thanks to Dr. Isao Kawamoto and the Sankyo Co., Ltd., for measuring some of the mass spectra and for their elemental analyses.

References

1) A Part of this work was presented at the 34th National Meeting of the Chemical Society of Japan, Kanagawa, April 1976; Abstracts, II, p. 738.

2) T. Nozoe, H. Okai, and T. Someya, *Bull. Chem. Soc. Jpn.*, **51**, 2185 (1978).

3) T. Nozoe and T. Someya, *Bull. Chem. Soc. Jpn.*, **51**, 3316 (1978).

4) T. Nozoe, T. Asao, and K. Takahashi, *Bull. Chem. Soc. Jpn.*, **39**, 1980 (1966).

The Conformation and the Ring Inversion of 8,9,10,11-Tetrahydro-7*H*-cycloocta[*de*]naphthalene

Toshihiro KAMADA* and Osamu YAMAMOTO

National Chemical Laboratory for Industry, Honmachi, Shibuya-ku, Tokyo 151

(Received September 12, 1978)

The ^{1}H-NMR spectra of 8,9,10,11-tetrahydro-7*H*-cycloocta[*de*]naphthalene (**1**) and its 8,8,10,10-tetradeuterio derivative have been studied at various temperatures. The NMR parameters of compound **1** were determined accurately by means of computer analysis of the low-temperature spectrum. It was found that the ground-state conformation of **1** is a boat, which is somewhat in a distorted form (puckering) as a result of the steric repulsion between the interior benzyl protons. Activation parameters $\Delta G^{\ddagger}$, $\Delta H^{\ddagger}$, and $\Delta S^{\ddagger}$, for the boat inversion process in the molecule were obtained by the line-shape analysis method as 14.5, 16.1 kcal/mol and 5.4 e.u., respectively. These results are best explained in terms of a conformational interconversion process in which the pseudorotations of the peri bonds are involved. Some discussion is also made on the conformational properties of compound **1** in comparison with those of the structurally analogous benzocyclic compound 6,7,8,9-tetrahydro-5*H*-benzocycloheptene.

Recently, as parts of our studies on the chemistry of pericyclic naphthalenes, we have studied the conformations of several derivatives of the 8,9,10,11-tetrahydro-7*H*-cycloocta[*de*]naphthalene system.[1,2] In the course of these studies, it was found that the eight-membered peri rings in these compounds are rather strained due to the peri interaction inherent in the peri-substituted naphthalenes.[3] In the present paper, in order to determine accurately the effects of the peri strains on the ring geometry of the 8-membered pericyclized naphthalenic compound and to study in detail the ring inversion of this system, a study has been made on the conformation of the parent compound **1**.

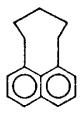

1

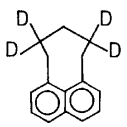

2

Since the knowledge of conformational properties of compound **1** is fundamental and very important for studies of the chemistry of the 8-membered pericyclized naphthalene system, it is worthwhile to discuss fully on the conformation and the ring inversion of this molecule based on the accurate and reliable experimental data, though some brief discussion on these points has already been made by Nelsen and Gillespie[4] using the approximate NMR methods (first order approximation and coalescence temperature method).

In this paper, we study the ^{1}H-NMR spectra of compound **1** and its 8,8,10,10-tetradeuterated derivative **2** at various temperatures. The computer analysis of the low-temperature spectrum is performed to determine the accurate NMR parameters of **1**, from which the precise geometry of the stable ground-state conformation of **1** is defined. Further, we report the results of the complete line shape analysis of the temperature-dependent ^{1}H-NMR spectra of **1** by means of the density matrix method, and present the kinetic parameters of the ring inversion process in **1**. We will also discuss about the ^{1}H-NMR result and the conformational properties of **1** by comparing with those of the structurally analogous 6,7,8,9-tetrahydro-5*H*-benzocycloheptene (**3**).

Results

The room-temperature ^{1}H-NMR spectrum of the alkyl portion of 8,9,10,11-tetrahydro-7*H*-cycloocta[*de*]-naphthalene-8,8,10,10-d_4 (**2**) in *ca.* 10% solution in the deuteriochloroform consists of a singlet at δ 1.24 for the C_9-protons (2H) and a broad hump centered at δ 3.47 for the C_7- and C_{11}-protons (4H). As the temperature of the sample is progressively lowered each methylene signal broadens and then splits into an AB quartet characterized by the chemical-shift difference ($\Delta\delta$) of 0.314 and 1.035 ppm ($J_{AB}=-14.4$ Hz), respectively. The lower-field signal of the benzylic AB pattern can be assigned to the interior protons (H_{in}) on C_7 and C_{11} positions of the peri ring, since these protons are expected to have a large steric interaction owing to their proximity with each other.[1,2,4]

The aromatic region of the spectrum of **2** consists of three quartets of equal intensities (2H) which show almost no change in their appearence on the variation of temperature. From the peak area and the values of the chemical shifts and coupling constants, these signals can be assigned most reasonably as is shown in Table 2.[1]

The room-temperature ^{1}H-NMR spectrum of the aliphatic region of 8,9,10,11-tetrahydro-7*H*-cycloocta-[*de*]naphthalene (**1**) dissolved (*ca.* 10%) in a mixture of deuteriochloroform and carbon disulfide (3: 1) consists of a broad band at δ 2.6—3.2 for the benzylic protons (4H), a somewhat broad quintet at δ 1.86 (4H, J=*ca.* 6.6 Hz) for the C_8- and C_{10}-protons and a multiplet centered at δ 1.30 for the C_9-protons (2H). As the temperature is decreased the spectrum undergoes a change such that at −44.7 °C the benzyl methylene signals are separated into two distinct absorption bands of equal intensities, consisting of eight lines, whereas the signals centered at δ 1.86 and 1.30 are changed into more complex multiplets resonating at δ 1.6—2.2 and 0.8—1.8, respectively. These signals remained unchanged on further decrease in temperature (*ca.* −100 °C).

Figure 1a shows the low-temperature ^{1}H-NMR spectrum of the benzyl methylene groups of **1**, where

TABLE 1. NMR PARAMETERS OF THE BENZYLIC METHYLENE PROTONS OF **1**

	Chemical shifts (ppm)[a]		Coupling constants (Hz)				
	δ_{7in}[d]	δ_{7ex}	J_{7gem}	$J_{7in,8eq}$	$J_{7ex,8ax}$	$J_{7in,8ax}$	$J_{7ex,8eq}$
1[b]	3.9742	2.9406	−14.23	12.88	1.28	6.49	6.82
2[c]	3.975 (4.8)	2.940 (2.9)	−14.4				

a) δ from internal standard TMS. b) Obtained from the computer simulation of the spectrum of **1** at −44.7 °C. c) Obtained by the first order analysis of the spectrum of **2** at −26.7 °C; the figures in the parentheses are the values of the line widths of the signals (in Hz). d) The numbers refer to the carbon position on the ring and the letters are as follows; in (interior), ex (exterior), eq (equatorial) and ax (axial).

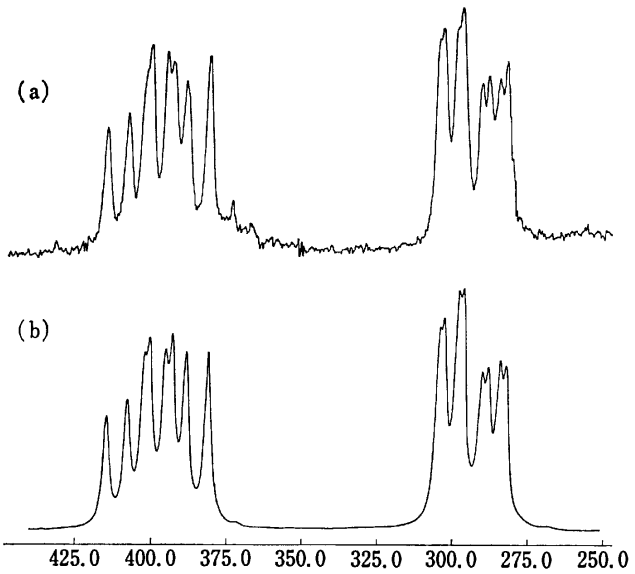

Fig. 1. The observed (a) and the calculated (b) NMR spectra of the benzylic methylene protons of **1** at −44.7 °C.

the low-field signal is assigned to the interior protons and the high-field one to the exterior protons as described above. Analysis of this spectrum as AB part of an ABCD spin system using LAOCOON MBYH program[5] afforded chemical shifts and coupling constants of the benzyl protons of **1** listed in Table 1. The calculated spectrum (Fig. 1b) obtained from these NMR parameters agrees well with the observed one (Fig. 1a). Computer analyses were also attempted for the spectra of the C_8- and C_9-protons but unsuccessful, since these signals are very complex because of their small shift differences.

On the other hand, when the temperature of the sample is elevated, the broad band of the benzylic protons of **1** sharpens and then splits into a triplet (J=6.8 Hz) above 70 °C. The chemical shift (δ=3.45) and coupling constant (J=6.8 Hz) of the benzyl protons of **1** obtained from the high-temperature spectrum are in good agreement with the values (δ=3.46 and J= 6.7 and 7.1 Hz) obtained by averaging the low-temperature data in Table 1.

From the temperature-dependent ^{1}H-NMR spectra of compounds **1** and **2** described above, it is indicated that the 8-membered peri ring of **1** undergoes the conformational change in the temperature range studied, by which the interior and exterior benzyl protons are interchanged. Figure 2a illustrates the gradual spectral changes observed for the benzyl methylene protons of **1** at various temperatures. In order to determine the kinetic parameters for the conformational change of **1**, the complete line shape analysis of the benzyl proton signals of **1** was performed by means of the density

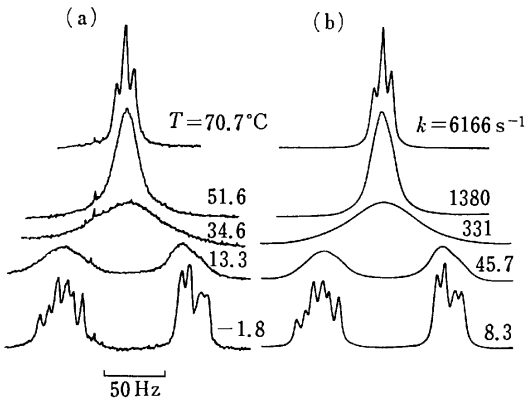

Fig. 2. The observed (a) and the calculated (b) NMR spectra of the benzylic methylene protons of **1** at various temperatures.

TABLE 2. NMR DATA OF THE C_9- AND THE NAPHTHALENE PROTONS OF **1**[a]

	Chemical shifts (ppm)				Coupling constants (Hz)			
δ_{9eq}	δ_{9ax}	$\delta_{1(6)}$	$\delta_{2(5)}$	$\delta_{3(4)}$	J_{9gem}	$J_{1,2}$	$J_{1,3}$	$J_{2,3}$
1.395 (2.8)[b]	1.081 (5.5)	7.186	7.314	7.671	−14.4[c]	7.1	1.9	7.7

a) Obtained from the spectrum of the deuterated derivative **2** at −26.7 °C. b) Values in parentheses are those of the line widths of the peak (in Hz). c) This value is very similar to the value found in the cyclooctane (−14.5 Hz) (Ref. 17) and somewhat larger than the value (−13.9 Hz) observed for the C_7-protons of **3** (Ref. 9).

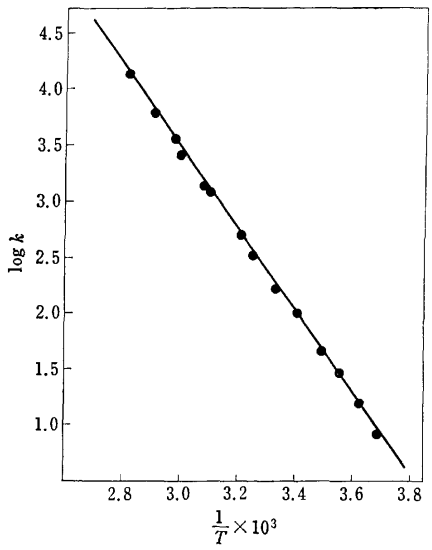

Fig. 3. Arrhenius plot for the ring inversion of **1**.

matrix method[6] using INVERS EX2 program[7] developed by the author (O. Yamamoto) previously. By computer simulation of the temperature-dependent spectra of the benzyl methylene protons, using the NMR parameters given in Table 1, the rate constants (k) for exchanging the benzyl protons of **1** at various temperatures were obtained. Figure 2b shows an example of the best fits between the observed and calculated spectra. The rate constants thus obtained within -10 to 90 °C are then plotted as $\ln k$ *vs.* $1/T$ in Fig. 3, from which the Arrhenius and Eyring activation parameters were calculated through the least-squares method. The results are shown below.

$$E_a = 16.7 \pm 0.5 \text{ kcal/mol}$$
$$\Delta G^{\ddagger} = 14.5 \pm 0.1 \text{ kcal/mol at } 30\,^{\circ}\text{C}$$
$$\Delta H^{\ddagger} = 16.1 \pm 0.5 \text{ kcal/mol}$$
$$\Delta S^{\ddagger} = 5.4 \pm 1.7 \text{ e.u.}$$

Discussion

The relatively simple NMR spectra of 8,9,10,11-tetrahydro-7*H*-cycloocta[*de*]naphthalene (**1**) and its 8,8,10,10-tetradeuterated derivative **2** at low temperatures suggest that, in the ground state, the 8-membered peri ring of compound **1** exists in one conformation, either the boat (**B**) or the chair (**C**), which has a mirror plane (Cs) passing through the C_9 and angular carbon atoms of the naphthalene nucleus.[1] The twist-boat conformation (**TB**) with a C_2 symmetry is excluded from the ground-state conformation of **1**, since the methylene protons on C_9 distinctly show an AB signal in the low-temperature spectrum of **2**.[1]

As can be seen from the Newman projections in Fig. 4, the interior benzyl proton in the boat conformation is situated in a position *trans* to an adjacent equatorial proton, while the exterior proton in the chair has a dihedral angle of about 0° with respect to an adjacent equatrial proton. In light of this and Karplus equation about the dihedral angles and spin coupling constants of

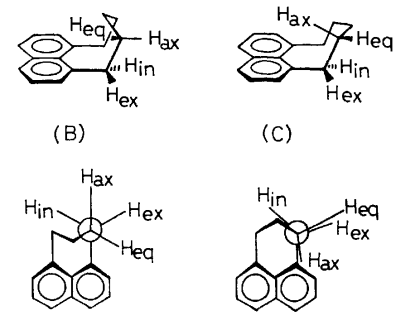

Fig. 4. The boat (**B**) and the chair (**C**) conformations for **1** and their Newman projections about the C_7–C_8 (C_{10}–C_{11}) bonds.

the carbocyclic ring,[8] the fact that the interior benzyl protons of **1** show a considerably large vicinal coupling constant (J=12.88 Hz) clearly suggests that compound **1** assumes the boat (**B**) as the ground-state conformation. This is also indicated from the spectra of the deuterated derivative **2**, where the signal of the interior benzyl proton is much broader (4.8 Hz) than that of the exterior proton (2.9 Hz) in reflection of the strong coupling between the interior proton and the equatorial deuterium which are in *trans* to each other in the boat conformation.

Consequently, the changes in the variable-temperature NMR spectra of **1** are interpreted in terms of the interconverting boat conformations. The predominance of the boat conformation over the chair observed in **1** seems reasonable, since the boat lacks the eclipsing strains about the C_7–C_8 and C_{10}–C_{11} bonds present in the chair.[1,2,4] This is in striking contrast to the case of structurally analogous 6,7,8,9-tetrahydro-5*H*-benzocycloheptene (**3**) which exists only in the chair conformation in the ground state.[9,10]

3

Now that the boat conformation for **1** has been established, the assignment of the C_9–AB signal of **2** is straightforward. That is, the high-field doublet is assigned to the axial proton, H_{9a}, and the low-field one to the equatorial proton, H_{9e}, of the C_9-methylene group of **1**, since the H_{9a}, which lies spatially closer to the naphthalene ring than the H_{9e} proton in the boat conformation, is expected to be more shielded than the H_{9e} proton not only by the effect of the magnetic anisotropies of adjacent C–C bondings but also by the effect of the ring current induced by the naphthalene nucleus.[1] Actually, the H_{9a} proton of **2** resonates at appreciably higher field (δ=1.081) than the corresponding H_{7ax} proton (δ=1.580) on the analogous position of the benzocyclic compound **3**, which exists in the chair conformation.[10] This suggests that the H_{9a} proton of **1** is substantially shielded by the ring current of naphthalene and is a further evidence in

favor of the boat conformation for **1**. The predominance of the boat conformation in **1** is also supported by the line widths of the C_9-protons of **2**, where the signal of the H_{9a} proton is greatly broadened (5.5 Hz) as compared to that of the H_{9e} proton (2.8 Hz) in reflection of the *trans* steric relationship between the H_{9a} and adjacent axial protons (on C_8 and C_{10}) in the boat conformation.

We have already studied the NMR spectra of the boat conformations of several 8,8,10,10-tetrasubstituted 8,9,-10,11-tetrahydro-7*H*-cycloocta[*de*]naphthalenes (**4**).[1]

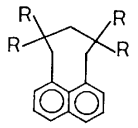

4

Comparing the NMR data of these compounds with those of the unsubstituted compound **1**, the chemical shift of the H_{9a} proton of **1** (δ=1.081) is somewhat larger than those of the substituted compounds (δ=−0.032—1.071).[1] Moreover, the chemical-shift difference ($\Delta\delta$) of the C_9-methylene protons of **1** ($\Delta\delta$=0.314) is small as compared to those of **4** ($\Delta\delta$=0.85—1.2)[1] and also to the $\Delta\delta$ value (1.32—1.92) calculated for the boat conformation of the 8,9,10,11-tetrahydro-7*H*-cycloocta[*de*]naphthalene ring.[1] The shift difference observed between **1** and **4** results possibly from the direct and/or indirect (changes in geometry of the peri ring associated with the introduction of the substituents) effects of the substituting groups, which might cause some differences in the magnetic environments around the C_9-methylene group of the boat conformation between these compounds. Although details are not known at present, the rather large deviation of the $\Delta\delta$ value in **1** from the calculated value might be related partly to the ring distortion inherent in the eight-membered pericyclized naphthalene system as described below.

The chemical shift of the exterior benzyl protons of **1** is almost comparable to those of the benzyl protons (δ=2.827 and 2.721)[10] of the benzocyclic compound **3**, whereas the signal of the interior protons of **1** is shifted markedly (δ=3.9742) to lower field as a result of the steric compression effect. From a calculation similar to that reported by Corey and Sneen,[11] it is revealed that the interatomic distance between the two interior benzyl protons of the boat conformation is 0.652 Å, much smaller than the sum of the van der Waals radii of the two hydrogens (2.4 Å). This suggests that although the boat is the most favored conformation for **1**, it still involves a severe steric repuslion between the two interior protons. Therefore, it is expected that the boat conformation of **1** is somewhat in a distorted form [**B**], in which the two interior protons are pushed apart mutually to avoid the steric interaction between them. This is strongly supported by the observation that the vicinal coupling constant, $J_{7ex,8ax}$ (1.28 Hz) is very small as compared to the value of $J_{7in,8ax}$ (6.49 Hz), since, as is seen in Fig. 5, these couplings are explained much better by the dihedral angles (H_{7ex}/H_{8ax}; $\theta>60°$, H_{7in}/H_{8ax}; $\theta<60°$) in the distorted molecule [**B**] than by the dihedral angles ($\theta\simeq60°$) in the normal boat conformation (**B**).

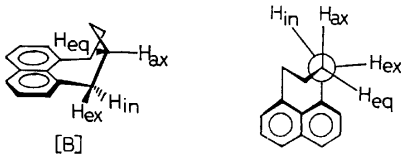

Fig. 5. The distorted boat conformation [**B**] for **1** and its Newman projection about the C_7–C_8 (C_{10}–C_{11}) bond.

Recently, the *R* method has been proposed for the determination of ring geometry in six-membered rings.[12] The *R* value is defined as a ratio of averaged vicinal coupling constants J_{trans}/J_{cis} where $J_{trans}=1/2(J_{aa}+J_{ee})$ and $J_{cis}=1/2(J_{ae}+J_{ea})$ for a $-CH_2CH_2-$ fragment of the ring system. This parameter has not yet been applied or tested for the eight-membered ring.

In order to determine accurately the ring geometry of the 8-membered pericyclic compound **1**, the dihedral arrangement about the C_7–C_8 bond of this molecule was examined by means of the *R* method. For the boat conformation of the 8,9,10,11-tetrahydro-7*H*-cycloocta-[*de*]naphthalene system, the *R* value about the C_7–C_8 bond can be obtained from the expression; $R=J_{trans}/J_{cis}=(J_{7in,8eq}+J_{7ex,8ax})/(J_{7in,8ax}+J_{7ex,8eq})$, using the individual coupling obtained from the low-temperature spectrum. The *R* value can also be obtained from the high-temperature averaged spectrum, where only the time-averaged couplings, $J_{trans}(J_{7in,8eq}\rightleftarrows J_{7ex,8ax})$ and $J_{cis}(J_{7in,8ax}\rightleftarrows J_{7ex,8eq})$ are observed as a result of the rapid boat-boat interconversion.[2]

Thus, from the low-temperature data in Table 1, the *R* value for **1** is calculated to be 1.06, while under the condition of the rapid boat inversion it is calculated to be 1.0 ($J_{trans}=J_{cis}$=6.8 Hz). The two *R* values obtained from the two different temperature spectra agree very well with each other. These values are rather small as compared to the value (2.16) obtained for the cyclohexane chair which has an almost perfect staggered conformation.[12] This suggests that the internal dihedral angle (Ψ) about the C_7–C_8 (and C_{10}–C_{11}) bond of the boat conformation of **1** is appreciably decreased as compared to the case of the cyclohexane ring ($\Psi=58°$).[12]

It is considered that the X–CH_2CH_2–Y fragment in the C_7 and C_8 positions of the 8,9,10,11-tetrahydro-7*H*-cycloocta[*de*]naphthalene ring possesses the pseudo-trigonal projection symmetry as in the six-membered rings.[12] Therefore, the dihedral angles around this bond of compound **1** including Ψ can be estimated from the relationship; $\cos\Psi=(3/(2+4R))^{1/2}$.[12] Using R=1.06, the following angles characterizing the structure of **1** are obtained: $\Psi=46°$, $H_{7in}/H_{8ax}=H_{7ex}/H_{8eq}=46°$, $H_{7ex}/H_{8ax}=74°$, and $H_{7in}/H_{8eq}=166°$.

From this it is apparent that compound **1** exists in the distorted boat [**B**] rather than in the normal boat (**B**) as a result of the steric interaction between the interior benzyl protons. Here, it should be noted that this distortion is puckering, not flattening, in sharp contrast to the cases of the previously studied compounds such

as the six-membered rings[12] or seven-membered rings.[10] This is ascribable to the difference in the ring system, and is a unique feature of the 8-membered pericyclized naphthalene system.

The free energy of activation (ΔG^*) for boat inversion of **1** is 14.5 kcal/mol, which is somewhat higher than the ΔG^* value (12.4 kcal/mol)[2] observed for the boat inversion of the ketone **5**. Since it is known that com-

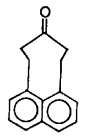

5

pounds **1** and **5** have very similar ring structures in their ground states (based on the discussion similar to that described above, it is clear that compound **5** also exists in the puckered boat in the ground state)[2] and both undergo the ring inversions through the same mechanism,[2] the entropy of activation (ΔS^*) obtained for **1** (5.4 e.u.) can be considered to be also characteristic of **5**.[13] It is therefore justifiable to assume that ΔG^* difference observed between **1** and **5** is entirely enthalpic in origin ($\Delta\Delta G^* = \Delta\Delta H^*$).

It has recently been suggested that the boat-to-boat interconversion of the 8,9,10,11-tetrahydro-7*H*-cycloocta-[*de*]naphthalene ring proceeds by pseudorotations of the peri bonds through the twist-boat (**TB**) as an intermediate,[2,4] the highest energy conformation being possibly (**TS**), which effectively contains six coplanar carbon atoms[2] (Fig. 6). This process involves rotations about the C_8–C_9 and C_9–C_{10} bonds in the conversions of (**B**)⇄(**TS**) and (**TS**)*⇄(**B**)*, respectively.

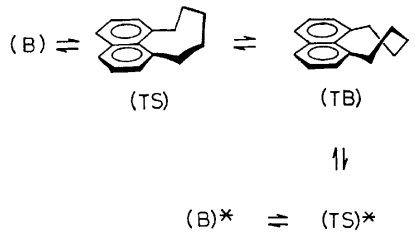

Fig. 6. Pathways for boat inversion of **1** (asterisks* indicate the inverted forms).

Thus, considering the barriers to methyl rotation in propane (3.3 kcal/mol)[14] and acetone (0.8 kcal/mol),[15] it is expected that if the boat inversion of the 8,9,10,11-tetrahydro-7*H*-cycloocta[*de*]naphthalene ring occurs indeed by the pseudorotations of the peri bonds as described above, the energies necessary for reaching the transition states in **5** are smaller than in the case of **1** by the value approximately equal to the difference in the barriers between propane and acetone. Actually, the difference in energy barrier observed between **1** and **5** is almost comparable to that observed in propane and acetone. This strongly supports the idea that the boat inversion is caused by pseudorotations of the peri bonds in the 8-membered pericyclized naphthalene system.

The activation energy for boat inversion of **1** is much higher than the ΔG^* value (10.7 kcal/mol)[16] observed for the chair inversion of **3**. This suggests that although the ground state of **1** is destabilized considerably by the steric interaction between the interior benzyl protons, the transition state of **1** is destabilized to a greater extent because of the peri strains involved.

Experimental

Materials. 8,9,10,11-Tetrahydro-7*H*-cycloocta[*de*]-naphthalene (**1**) was prepared by the Clemmensen reduction of 8,9,10,11-tetrahydro-7*H*-cycloocta[*de*]naphthalen-9-one (**5**) as described previously.[18] 8,9,10,11-Tetrahydro-7*H*-cycloocta[*de*]naphthalene-8,8,10,10-d_4 (**2**) was prepared from the 8,8,10,10-tetradeuterated derivative of **5** using the procedures described below.

Compound **5** (1.5 g) was refluxed with a solution of potassium carbonate (1.5 g) in deuterium oxide (15 ml) and dioxane (25 ml) for 3 days. The mixture was poured into ice-hydrochloric acid, and the resulting crystalline precipitate was collected by filtration, washed with water and dried *in vacuo*. The above deuterium exchange reaction was repeated twice to afford the completely deuterated ketone, 8,8,10,10-tetradeuterio-8,9,10,11-tetrahydro-7*H*-cycloocta[*de*]naphthalen-9-one (1.46 g); mp 193.5—195 °C (**5**; mp 195—196 °C[18]), whose structure was evidenced by the complete absence of the NMR signal due to the α protons.[18] The above deuterated ketone (0.93 g) was stirred overnight with excess sodium borohydride in ethanol (120 ml) at room temperature. The reaction mixture was worked up in the same manner as described above to yield 8,8,10,10-tetradeuterio-8,9,10,11-tetrahydro-7*H*-cycloocta[*de*]naphthalen-9-ol (0.89 g); mp 148—149 °C; IR (Nujol): ν_{max} 3364 and 3284 cm^{-1} due to OH. This alcohol (0.89 g) was then stirred with methanesulfonyl chloride (2.5 ml) in pyridine (9.5 ml) for 4 h at room temperature with an occasional heating on water bath. The mixture was worked up as above to give 9-mesyloxy-8,8,10,10-tetradeuterio-8,9,10,11-tetrahydro-7*H*-cycloocta[*de*]naphthalene (1.2 g); mp 133.5—134.5 °C; IR (Nujol): ν_{max} 1348 and 1173 cm^{-1} (mesyl ester). The mesylate (1.0 g) was then stirred under reflux with lithium aluminum hydride (2.8 g) in ether (250 ml) and benzene (20 ml) for 5 days. The mixture was poured into ice–hydrochloric acid and the mixture was extracted with ethyl acetate. The acetate extracts were worked up as usual to leave a brown paste, which was purified by chromatography on alumina. Elution with hexane gave the hydrocarbon **2** (130 mg), whose structure was confirmed by the TLC (SiO_2–hexane), mp (56.5—57.5 °C, **1**; mp 55—56 °C[4] and 57.5—58 °C[18]) and its spectra (IR, NMR). Further elution with hexane yielded 10,11-dihydro-7*H*-cycloocta[*de*]-naphthalene-8,10,10-d_3 (50 mg; mp 64.5—65.5 °C), details of which will be reported elsewhere. Further elution with ethyl acetate afforded another crystal (104 mg), which, based on the TLC, mp, and IR, was identified to the 8,8,10,10-tetradeuterio-9-ol described above.

Measurements. The IR spectra were determined on a JASCO IR-G spectrometer calibrated with polystyrene. The ^{1}H-NMR spectra were determined on a Varian HA-100D spectrometer (at 100 MHz) in a temperature range between −100—110 °C, using a *ca.* 10% solution in a mixture of deuteriochloroform–carbon disulfide (3:1) (compound **1**) or in deuteriochloroform (compound **2**). The sample temperature was measured by use of the temperature dependent chemical shift of the OH proton of methanol or ethylene glycol.[19] The analysis of the NMR spectra at slow exchange limit and

the calculations of the theoretical line shape were made using a FACOM 270/30 computer.

References

1) T. Kamada, N. Wasada and O. Yamamoto, *Bull. Chem. Soc. Jpn.*, **49**, 275 (1976).
2) T. Kamada and O. Yamamoto, *Chem. Lett.*, **1976**, 843.
3) V. Balasubramanian, *Chem. Rev.*, **66**, 567 (1966).
4) S. F. Nelsen and J. P. Gillespie, *J. Am. Chem. Soc.*, **95**, 2940 (1973).
5) LAOCOON II by Castellano and Bothner-By (*J. Chem. Phys.*, **41**, 3863 (1964)) was modified by the authors.
6) C. S. Johnson, Jr, "Advances in Magnetic Resonance," ed by J. S. Waugh, Academic Press, New York (1965), Vol. 1, p 33.
7) O. Yamamoto and H. Nakanishi, *Tetrahedron*, **29**, 781 (1973).
8) E. W. Garbisch, Jr and M. G. Griffith, *J. Am. Chem. Soc.*, **90**, 6543 (1968).
9) S. Kabuss, H. G. Schmid, H. Friebolin and W. Faisst, *Org. Magn. Res.*, **1**, 451 (1969).
10) M. St-Jacqoues and C. Vaziri, *Org. Magn. Res.*, **4**, 77 (1972).
11) E. J. Corey and R. A. Sneen, *J. Am. Chem. Soc.*, **77**, 2505 (1955).
12) J. B. Lambert, *Acc. Chem. Res.*, **4**, 87 (1971) and references therein.
13) G. Binsch, "Topics in Stereochemistry," ed by E. L. Eliel and N. L. Allinger, Interscience Pubblishers, New York (1968), Vol. 3, p. 97.
14) E. L. Eliel, N. L. Allinger, S. J. Angyal and G. A. Morrison, "Conformational Analysis," Interscience Publishers, New York (1965), p. 9 and references therein.
15) F. A. L. Anet and R. Anet, "Dynamic Nuclear Magnetic Resonance Spectroscopy," ed by L. M. Jackman and F. A. Cotton, Academic Press, New York (1975), p. 584.
16) S. Kabuss, H. Friebolin, and H. Schmid, *Tetrahedron Lett.*, **1965**, 469.
17) F. A. L. Anet and R. Anet, "Determination of Organic Structures by Physical Methods," ed by F. C. Nachod and J. J. Zuckerman, Academic Press, New York (1971), Vol. 3, p. 344 and references therein.
18) T. Kamada, *Bull. Chem. Soc. Jpn.*, **52**, 170 (1979).
19) O. Yamamoto and M. Yanagisawa, *Anal. Chem.*, **42**, 1463 (1970).

Optical Activity and Absolute Configuration of 5,6,11,12-Tetrahydro-2,3,8,9-tetramethoxy-5,11-methanodibenzo[*a*,*e*]cyclooctatetraene†

Fumio OGURA,*,†† Akio NAKAO, and Masazumi NAKAGAWA

Department of Chemistry, Faculty of Science, Osaka University, Toyonaka, Osaka 560

(Received September 20, 1978)

The title compound (VII) was synthesized in an optically active form and the chiroptical properties were recorded. The absolute configuration was determined by chemical correlation method.

The title compound (VII) has a novel type of rigid bicyclo[3.3.1]nonadiene cage skeleton and holds two veratrole chromophores in a twisted spacial position. Formally VII could be transformed to alkaloid argemonine by substituting the methanobridge with an *N*-methyl group. The optical activity of argemonine[1] was discussed in connection with the absolute configuration[2] but not fully understood yet. The perfect C_2-symmetry and pure carbocyclic structure make VII one of the best model for the study of chiroptical properties of organic molecules containing two separate aromatic chromophores.

This paper deals with the synthesis, optical resolution and determination of absolute configuration by chemical means concerning VII and its derivatives.

Synthesis and Optical Resolution. The route of synthesis was outlined in Scheme 1. 3,4-Dimethoxyphenylacetonitrile (I) was allowed to react in THF with diiodomethane in the presence of sodium methoxide to yield 2,4-bis(3,4-dimethoxyphenyl)glutaronitrile (II) which was a mixture of racemic and meso forms. Fractional recrystallization of the crude dinitrile from methanol afforded two kinds of crystals. Higher melting crystals were assigned to the racemate and lower melting ones to the meso form on the basis of splitting patterns of methylene proton singnals in their ^{1}H-NMR spectra.[3] The dicarboxylic acid (III) obtained by alkaline hydrolysis of crude II was cyclized to the diketone (IV) with polyphosphoric acid. Dehydrative cyclization with concd sulfuric acid gave poor results, because of rapid sulfonation to benzene rings activated by two methoxyl groups. The diketone (IV) was reduced to the glycol (VI) with $LiAlH_4$ in THF. The ketol (V) could be obtained along with VI when catalytic reduction of IV over the Adams catalyst was interrupted after one equivalent hydrogen was absorbed.

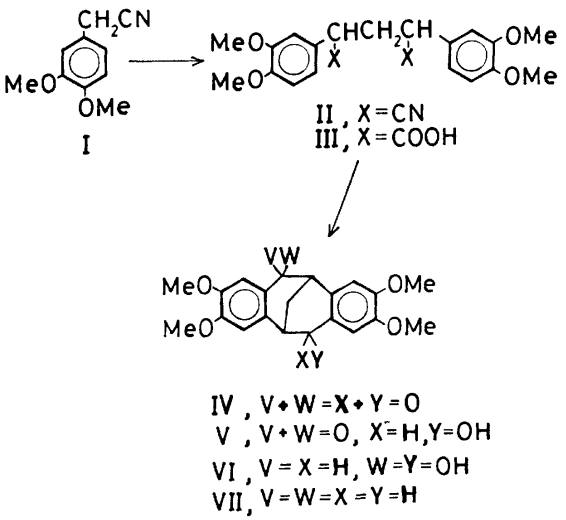

Scheme 1.

Optical resolution was carried out *via* camphanate of the ketol (V) or the glycol (VI). Bis-camphanate prepared from (+)-VI and ω-camphanoyl chloride was fractionally recrystallized eleven times from ethanol to yield optically pure crystals. The camphanate derived from (+)-V could be fractionated more effectively than the bis-camphanate of VI. Thus almost optically pure crystals were obtained after one recrystallization from ethanol. Pure (+)-V and (+)-VI were obtained by alkaline hydrolysis of their camphanates. Catalytic reduction of (+)-V over the Adams catalyst afforded

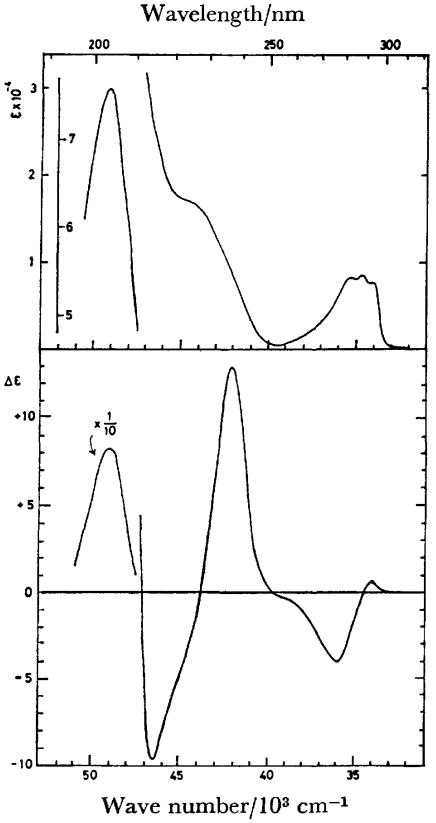

Fig. 1. UV (top) and CD (bottom) spectra of (+)-5,6,11,12-tetrahydro-2,3,8,9-tetramethoxy-5,11-methanodibenzo[*a*,*e*]cyclooctatetraene (VII) in ethanol.

† A preliminary report of this work was presented at the 37th National Meeting of the Chemical Society of Japan, Tokyo, April 1978.

†† Present address: Department of Applied Chemistry, Faculty of Engineering, Hiroshima University, Hiroshima 730.

(+)-VI and (−)-IV was obtained from (+)-VI by the Jones oxidation. All of (−)-IV, (+)-V and (+)-VI could be converted easily to the desired compound, (+)-VII, under condition of the Clemmensen reduction.

Optical Activity and Absolute Configuration. The CD spectra of (+)-VII was shown in Fig. 1. Beautiful positive couplets were observed in both α- and p-band regions and a strong positive band appeared in $^1E_{1u}$ region.

The absolute configuration was estimated to be *R* by usual exciton theoretical CD analysis, in which the transition moments of each band were assumed to lie in the center and in the direction of the short or long axis of benzene rings according to the spectroscopic moments theory.[4] The molecular structural parameters of VII were assumed to be the same as those of 5,6,11,12-tetrahydro-5,11-methanodibenzo[*a*,*e*]cyclooctatetraene, VIII.[5]

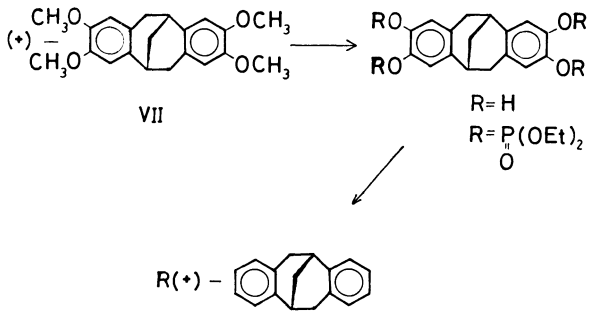

Scheme 2.

The absolute configuration of (+)-VII was determined to be (*R*) by a chemical correlation (Scheme 2). Demethylation of (+)-VII with BBr_3 followed by diethoxyphosphinylation with diethyl phosphonate afforded a tetrakis-phosphate. The phosphate was reduced by sodium metal in liq ammonia to yield (+)-VIII, whose absolute configuration was proven to be *R*.[3,5] Thus the result of CD analysis was in good agreement with that of the chemical correlation.

Experimental

The melting points were measured on a Mettler FP2 apparatus and are uncorrected. Purified and anhydrous solvents were used, unless otherwise stated. The IR spectra were obtained on a Hitachi EPI-2, EPI-G3, and a JASCO DS-301 spectrometers, electronic spectra on a Hitachi EPS-3T and a Zeiss PMQIIM4QIIId spectrometers, ^{1}H-NMR spectra in deuteriochloroform unless otherwise stated on a Varian XL-100, A-60D or Hitachi R-24 spectrometer using TMS as an internal standard and given in δ-unit. The optical rotations were obtained on a Union Giken High Precision polarimeter PM-71 at 20 °C unless otherwise stated. CD spectra were obtained on a JASCO J-20 spectrometer. Shoulders and inflections are denoted by an asterisk.

3,4-Dimethoxybenzyl Cyanide (I): Veratraldehyde (100 g, 0.6 mol) in ether (500 ml) was added dropwise to an ice-cold ether solution (300 ml) of $LiAlH_4$ (13.7 g). Stirring was continued for further 2 h at room temperature. Ethyl acetate (20 ml) and water (20 ml) were added dropwise with stirring and ice-cooling. The resulting mixture was stirred for a while at room temperature. Colorless gelatinous precipitates formed were removed with suction filtration and washed with ethyl acetate (300 ml). Combined filtrate and washings were concentrated and distilled under reduced pressure to afford 3,4-dimethoxybenzyl alcohol as a colorless oil, bp 155 °C/533 Pa (98 g, 96%).

A cold mixture of the alcohol (82.6 g), dichloromethane (100 ml) and concd HCl (100 ml) was stirred vigorously for 20 min at 0—10 °C. Further amount of CH_2Cl_2 (100 ml) was added to the mixture with stirring. The organic layer separated was dried over $CaCl_2$ for 30 min and concentrated under reduced pressure. 3,4-Dimethoxybenzyl chloride obtained was used immediately for further reaction without purification.

Powdered sodium cyanide (48 g) and potassium iodide (6 g) were added to the chloride in acetone (300 ml). The mixture was refluxed for 20 h and filtered with suction after cooling down. The filtrate concentrated under reduced pressure was poured into water and extracted with benzene. The combined extracts were washed with water, dried and concentrated under reduced pressure. Vaccum distillation afforded I as a colorless oil, bp 160 °C/533 Pa (65.0 g, 75%). ^{1}H-NMR (CCl_4): 3.55 (s, 2H, methylene), 3.75 (s, 6H, methoxy), 6.70 (s, 3H, aromatic).

2,4-Bis(3,4-dimethoxyphenyl)glutaronitrile (II): Dry sodium methoxide prepared from sodium (1.8 g, 0.078 g atom) and methanol (100 ml) was suspended in THF (100 ml) and mixed with I (13.5 g, 0.076 mol) and diiodomethane (11.5 g, 0.043 mol). After being refluxed for 1 h with stirring, the mixture was concentrated under reduced pressure and extracted with dichloromethane. After usual work up, the extract was concentrated *in vacuo* to yield a brown oil, which was purified with a column of silica gel (80 g). From benzene–ethyl acetate (1: 1) eluate, II (8.6 g, 61%) was obtained as a diastereomeric mixture of racemic and meso from. Repeated recrystallization of the crude nitrile from methanol gave racemate as colorless needles and meso form as colorless plates.

Racemate: mp 141—142 °C. ^{1}H-NMR: 2.45 (t, J=8 Hz, 2H, methylene), 3.89, 3.91 (two s, 12H, methoxyl), 4.00 (t, J=8 Hz, 2H, methine), 6.80—6.90 (m, 6H, aromatic). Found: C, 68.64; H, 6.11; N, 7.75%. Calcd for $C_{21}H_{22}O_4N_2$: C, 68.83; H, 6.05; N, 7.65%. *meso*-Isomer: mp 101 °C. ^{1}H-NMR: 2.20—2.90 (m, 2H, methylene), 3.91 (br s, 12H, methoxyl), 3.75 (apparent t, 2H, methine), 6.85—6.90 (m, 6H, aromatic). Found: C, 68.77; H, 6.01; N, 7.68%. Calcd for $C_{21}H_{22}O_4N_2$: C, 68.83; H, 6.05; N, 7.65%.

2,4-Bis(3,4-dimethoxyphenyl)glutaric Acid (III) and Its Methyl Ester: The crude dinitrile (II, 1.0 g) dissolved in 95% ethanol (20 ml) was mixed with KOH (5 g) in 50% EtOH (20 ml) and heated to reflux for 20 h. After removal of ethanol under reduced pressure, the mixture was poured into water (100 ml) and washed three times with dichloromethane. Alkaline aqueous layer was decolorized with active charcoal, and acidified with concd HCl. Precipitates formed were extracted with dichloromethane. After usual work up, a colorless solid of III (0.9 g, 81%) was obtained from the extract. Reflux with methanol and concd sulfuric acid gave colorless crystals of dimethyl ester, mp 116—117 °C (from methanol). ^{1}H-NMR: 1.9—2.9 (m, 2H, methylene), 3.4 (t, 2H, methine), 3.65 (s, 6H, methyl), 3.85 (s, 12H, methoxyl), 6.75 (br s, 6H, aromatic). Found: C, 63.84; H, 6.54%. Calcd for $C_{23}H_{28}O_8$: C, 63.88; H, 6.53%.

5,6,11,12-Tetrahydro-2,3,8,9-tetramethoxy-5,11-methanodibenzo-[a,e]cyclooctateraene-6,12-dione (IV): *a) With Polyphosphoric Acid*: Crude dicarboxylic acid (III, 1.8 g, 0.0049 mol) was mixed with polyphosphoric acid (30 g) and stirred for

5 min at 80 °C. The reaction mixture was poured onto ice (100 g) and precipitates separated were extracted with CH_2Cl_2. Combined extracts were washed with brine, 10% aq NaOH, and brine, successively, and dried over $MgSO_4$. Solvent was removed under reduced pressure to yield IV as a colorless solid, which was recrystallized from dichloromethane–ethanol, mp 261—262 °C. ^{1}H-NMR: 3.0 (t, J=3 Hz, 2H, methylene), 3.95, 3.85 (two s, 12H, methoxyl, signals of methine protons (2H) were overlapped with those signals), 6.9, 7.4 (two s, 4H aromatic). IR (Nujol mull): 1670 ($\nu_{C=O}$) cm^{-1}. Found: C, 68.18; H, 5.46%. Calcd for $C_{21}H_{20}O_6$: C, 68.47; H, 5.47%.

b) With Concd Sulfuric Acid: Crude III (0.6 g) was dissolved in concd sulfuric acid and cooled to −15 °C. The mixture was stirred for 2 h at the temperature and mixed with water (30 ml). Precipitated product was extracted with benzene. Combined extracts were washed with water, 5% aq $NaHCO_3$, and water, successively, and dried over Na_2SO_4. Evaporation of solvent *in vacuo* and trituration with ethanol afforded crude crystals (0.15 g, 27%), whose spectroscopic properties were identical with those of the authentic diketone (IV). The acidic component obtained from the above mentioned $NaHCO_3$ washings were converted with a usual procedure to methyl ester, mp 159—160 °C. ^{1}H-NMR: 2.35—2.80 (m, 2H, methylene), 3.75 (s, 3H, methyl), 3.8, 3.9 (two s, 12H, methoxyl), 3.5—4.2 (m, 2H, methine), 6.7—6.8 (m, 4H, aromatic), 7.5 (s, 1H, aromatic). Found: C, 65.77; H, 6.06%. Calcd for $C_{22}H_{24}O_7$: C, 65.99; H, 6.04%. The ester was assigned to methyl 3-(3,4-dimethoxyphenyl)-4-oxo-6,7-dimethoxy-1,2,3,4-tetrahydro-1-naphthoate on the basis of its ^{1}H-NMR spectra.

12-Hydroxy-5,6,11,12-tetrahydro-2,3,8,9-tetramethoxy-5,11-methanodibenzo[a,e]*cyclooctatetraen-6-one (V)*: Diketone IV (2.164 g, 0.0057 mol) dissolved in dichloromethane (70 ml) and ethanol (100 ml) was catalytically reduced over the Adams catalyst at room temperature. In 40 min *ca.* 165 ml of hydrogen was absorbed and the catalyst was removed to stop the reduction.

Evaporation of solvents under reduced pressure yielded a colorless solid, which was chromatographed on a column of silica gel (50 g) with dichloromethane. Recovered IV (0.380 g, 17%), desired ketol (V, 1.28 g, 59%) and the diol (VI, 0.500 g, 23%) were eluted successively. Recrystallization from methanol afforded colorless needles of V, mp 206 °C. ^{1}H-NMR: 1.6 (d, 1H, OH), 2.5 (m, 2H, methylene), 3.6 (m, 2H, bridgehead methine), 3.7—3.9 (four singlets, 12H, methoxyl), 5.0 (q, 1H, methine), 6.7—7.4 (four singlets, 4H, aromatic) IR (Nujol mull): 3400 (ν_{OH}), 1655 ($\nu_{C=O}$) cm^{-1}. Found: C, 67.94; H, 5.94%. Calcd for $C_{21}H_{22}O_6$: C, 68.09; H, 5.99%.

Optical Resolution of 12-Hydroxy-5,6,11,12-tetrahydro-2,3,8,9-tetramethoxy-5,11-methanodibenzo[a,e]*cyclooctatetraen-6-one (V)*: *dl*-Ketol (V, 3.8 g, 0.01 mol) dissolved in pyridine (50 ml) was mixed with freshly prepared ω-camphanoyl chloride (2.40 g) and stirred overnight at room temperature. The mixture was poured into water (100 ml) and extracted with dichloromethane (50 ml) and ether (100 ml). Combined extracts were washed thoroughly with 1 M HCl, brine, saturated aq $NaHCO_3$, and brine, successively. After being dried over Na_2SO_4, solvents were removed under reduceds pressure to yield a colorless solid. The solid was recrystallized four times from ethanol or dichloromethane–ethanol to give (−)-camphanate of V with constant optical rotations as colorless needles (1.68 g). Mp 235—237 °C, $[\alpha]_D^{15}$ − 15.8°, $[\alpha]_{405}^{15}$ − 192.8° (*c* 0.448, $CHCl_3$). Found: C, 67.42; H, 6.32%. Calcd for $C_{31}H_{34}O_9$: C, 67.62; H, 6.22%.

Pure(−)-camphanate (1.68 g) was heated to reflux for 1 h with aq methanolic KOH. Evaporation of methanol afforded crude crystals of (+)-V (1.09 g, 96%). Recrystallization from ethanol yielded colorless needles. Mp 222 °C, $[\alpha]_D^{18}$ + 26°, $[\alpha]_{405}^{18}$ − 258° (*c* 0.270, $CHCl_3$), ^{1}H-NMR: Identical with the racemate, UV: λ_{max}^{EtOH} (ε) 360 (1000), 321 (8200), 280 (11000) 237 (28400), 204.5 (40800) nm, CD: λ_{max}^{EtOH} ($\Delta\varepsilon$) 359 (−1.72), 348 (−1.43), 326 (−3.94), 287 (−6.74), 267 (+11.1), 242 (+26.9), 229 (−18.7), 208 (+45.9) nm. Found: C, 67.82; H, 6.00%. Calcd for $C_{21}H_{22}O_6$: C, 68.09; H, 5.99%.

(+)-5,6,11,12-Tetrahydro-2,3,8,9-tetramethoxy-5,11-methanodibenzo[a,e]*cyclooctatetraene-6,12-diol (VI)*: (+)-Ketol (V, 0.120 g, 0.320 mmol) dissolved in acetic acid (20 ml) and ethanol (30 ml) was catalytically reduced over the Adams catalyst for 3 h under ordinary pressure and temperature. After the catalyst was removed by filtration and the residue was chromatographed on a column of silica gel (20 g) with CH_2Cl_2 and ethyl acetate. Recovered (+)-ketol (0.055 g) and (+)-VI (0.060 g) were eluted successively. (+)-Diol was recrystallized from ethanol. mp 220 °C, $[\alpha]_D^{18}$ + 115,° $[\alpha]_{405}^{18}$ + 327° (*c* 0.163, $CHCl_3$), ^{1}H-NMR: identical with racemate, UV: λ_{max}^{EtOH}(ε) 289 (6600), 284 (6900), 280 (6200), 234 (15300), 207 (70700) nm, CD: λ_{max}^{EtOH} ($\Delta\varepsilon$) 289 (+3.0), 243 (+16.0), 213 (+34.8), 199 (−44.0) nm. Found: C, 67.54: H, 6.42%. Calcd for $C_{21}H_{21}O_3$: C, 67.73: H, 6.50%.

5,6,11,12-Tetrahydro-2,3,8,9-tetramethoxy-5,11-methanodibenzo[a,e]*cyclooctatetraene-6,15-diol (VI)*: A THF solution (150 ml) of the diketone IV (1.5 g, 0.004 mol) was added dropwise to an ice-cold THF solution (120 ml) of $LiAlH_4$ (1.0 g). The mixture was stirred for 3 h at room temperature and decomposed with ethyl acetate (2 ml), water (2 ml) and saturated aq ammonium chloride successively. Gelatinous precipitates formed were removed by suction filtration and the filtrate was concentrated under reduced pressure. The crude product obtained was recrystallized from benzene to yield colorless needles (1.45 g, 95%) of *dl*-VI, mp 210—211 °C, ^{1}H-NMR: 1.6 (d, 2H, OH), 2.4 (t, 2H, methlene), 3.3 (m, 2H, bridgehead methine), 3.8, 3.9 (s, 12H, methoxyl), 4.9 (q, 2H, methine) 6.7, 7.0 (s, 4H aromatic), IR (Nujol mull): 3350 (ν_{OH}) cm^{-1}. Found: C, 67.57; H, 6.51%. Calcd for $C_{21}H_{24}O_6$: C, 67.73; 6.50%.

Optical Resolution of 5,6,11,12-Tetrahydro-2,3,8,9-tetramethoxy-5,11-methanodibenzo[a,e]*cyclooctatetraene-6,12-diol (VI)*: *dl*-Diol (VI, 0.50 g, 1.6 mmol) dissolved in pyridine (3 ml) was mixed with freshly prepared ω-camphanoyl chloride (1.0 g) and the mixture was stirred overnight at room temperature. Water was added to the mixture and extracted with dichloromethane and ether. Combined extracts were washed thoroughly with 1 M HCl and brine. After being dried over magnesium sulfate, solvents were removed under reduced pressure to yield a colorless oil (0.88 g, 90%), which was crystallized by trituration with ethanol.

Repeated fractional recrystallization (11 times) afforded optically pure (−)-bis-camphanate of VI as colorless needles (0.08 g). $[\alpha]_D^{18}$ − 25°, $[\alpha]_{405}^{18}$ − 45° (*c* 0.910, $CHCl_3$). Pure (−)-bis-camphanate obtained was heated to reflux in aq methanolic KOH solution. Crystals appeared on evaporation of methanol were collected by suction filtration and recrystallized from EtOH to yield optically pure (+)-VI (0.030 g), mp 220 °C. $[\alpha]_D^{18}$ + 110°, $[\alpha]_{405}^{18}$ + 330° (*c* 0.370, $CHCl_3$).

(−)-5,6,11,12-Tetrahydro-2,3,8,9-tetramethoxy-5,11-methanodibenzo[a,e]*cyclooctatetraene-6,12-dione (IV)*: Chromium trioxide (0.4 g) in water (2 ml) was added dropwise at room temperature to a well stirred solution of (+)-ketol (VI, 0.430 g, 1.3 mmol) in acetic acid (30 ml). The mixture was diluted with water (50 ml) and extracted with dichloromethane.

Combined extracts were washed with water, saturated aq $NaHCO_3$, and water, successively, and dried over sodium sulfate. On concentration under reduced pressure, a yellow solid was obtained. A dichloromethane solution of the solid was passed through a short column of silica gel (10 g) to remove colored impurities. Recrystallization from ethanol afforded colorless crystals of (−)-IV (0.270 g, 63%). Mp 222—223 °C, $[\alpha]_D^{18}$ − 246°, $[\alpha]_{405}^{18}$ −3290° (*c* 0.06, $CHCl_3$), UV: $\lambda_{max}^{dioxane}(\varepsilon)$ 366* (1050), 348* (3070), 339* (3940), 316 (13600), 284 (19800), 270 (29600), 240 (24700) nm. $\lambda_{max}^{EtOH}(\varepsilon)$ 340* (4700), 315 (12900), 285* (21000), 271 (26900), 238 (23600), 206 (26300) nm. CD: $\lambda_{max}^{dioxane}(\Delta\varepsilon)$ 365 (−13.8), 347 (−50.7), 336.5 (−47.3) 313 (+36.7), 285 (+55.8), 254 (−19.8), 230 (−26.6), 210 (+40.4) nm. λ_{max}^{EtOH} ($\Delta\varepsilon$) 340 (−52.9), 310 (+31.8), 285 (+56.7), 253 (−16.9), 230 (−22.2), 209 (+40.7) nm. Found: C 68.57; H, 5.49%. Calcd for $C_{21}H_{20}O_6$: C, 68.47; H, 5.47%.

(+)-5,6,11,12-Tetrahydro-2,3,8,9-tetramethoxy-5,11-methanodibenzo[a,e]*cyclooctatetraene (VII)*: Granules of zinc (1.0 g) was amalgamated by a standard method[6] and used immediately as follows. A benzene solution of (−)-diketone IV (50 mg) was added to a stirred mixture of the amalgamated zinc, water (0.5 ml), and concd HCl (1 ml). The mixture was refluxed for 4 h, diluted with water, and extracted with dichloromethane and ether. Combined extracts were washed with water, saturated aq $NaHCO_3$ and water, successively, and dried over Na_2SO_4. Solvents were removed under reduced pressure and the residue was passed through a short column of silica gel (10 g) as a CH_2Cl_2 solution. A colorless oil (34 mg, 74%) obtained was crystallized in methanol. Mp 209—210 °C, UV: $\lambda_{max}^{EtOH}(\varepsilon)$ 292 (7700), 288 (8600), 283 (8300), 223* (17300), 204 (76000) nm. CD: $\lambda_{max}^{EtOH}(\Delta\varepsilon)$ 294 (+1.0), 267.5 (−4.0), 237.5 (+13.0), 216 (−9.7), 204 (+82.5) nm. Found: C, 73.66; H, 7.10%. Calcd for $C_{21}H_{24}O_4$: C, 74.09: H, 7.11%.

(R)-(+)-5,6,11,12-Tetrahydro-5,11-metahnodibenzo[a,e]*cyclooctatetraene (VIII)*: As shown in Scheme 2, (+)-VII was converted to (*R*)-(+)-VIII.

Demethylation: A dichloromethane solution (12.5 ml) of (+)-VII (0.431 g, 1.27 mmol) was added with stirring to an ice-cold solution of BBr_3 (1.818 g, 7.26 mmol) in CH_2Cl_2 (15.6 ml). The mixture was stirred overnight at room temperature. Gelatinous precipitates were formed in the case of racemate. After addition of water (30 ml), the reaction mixture was stirred for 30 min and extracted with ether. Combined extracts were washed with saturated aq $NaHCO_3$ and brine, successively, and dried over Na_2SO_4. Upon concentration of the fraction *in vacuo*, the tetrol was obtained as faintly pink powder (0.352 g). Acidification of $NaHCO_3$ washings followed by extraction with ether gave further amount of the tetrol (0.052 g, total 0.404 g quantitative). Alkaline extraction should be avoided because of unstable nature of the phenol. ^{1}H-NMR (acetone-d_6); 2.35—3.27 (m, 8H, methylene and methine), 6.35, 6.62 (two singlets, 4H, aromatic), 7.05 (br s, 4H, OH). The phenol was used directly for further reaction without purification.

Dehydroxylation via *Diethoxyphosphinylation*: The tetrol (0.404 g, 1.421 mmol) was mixed with diethylphosphonate (0.862 g, 8.124 mmol) in CCl_4 (11 ml) and triethylamine (1 ml) and stirred for 48 h at room temperature. Colorless precipitates were formed. The mixture was mixed with water and extracted with chloroform. Combined extracts were washed with 1 M HCl, 5% aq $NaHCO_3$ and water, successively, and dried over Na_2SO_4. Evaporation of solvents under reduced pressure afforded a faintly yellow oil (1.42 g) which showed single spot on a TLC plate. The crude phosphate (1.42 g) dissolved in THF (50 ml) was added to liq NH_3 (50 ml). Sodium metal (0.5 g) was added in small pieces to the solution with stirring until blue color of the solution persisted. Crystals of ammonium chloride were added to the mixture to stop the reaction. Ammonia was evaporated by warming up the solution to room temperature. The residue was diluted with water and extracted with ether. Combined extracts were washed with cold 3% aq KOH and brine successively and dried over Na_2SO_4. On evaporation of solvents *in vacuo*, a light yellow solid was obtained. The crude product was dissolved in benzene and passed through a short column of silica gel (10 g).

The crystals obtained were again purified by high pressure liquid chromatography (machine: Hitachi 635; column: 8 × 500 mm × 2 packed with Merck Lichrosorb S2-100; solvent: hexane; flow rate: 2.6 ml/min; pressure: 110 kg/cm^2; retention time: 45 min) and recrystallized from methanol or pentane. mp 100.5—101.5 °C, ^{1}H-NMR: 2.00 (t, J=3 Hz, 2H, methano-bridge), 2.62—3.52 (m, 6H, methine and benzylic methylene), 6.85—7.22 (m, 8H, aromatic), UV: $\lambda_{max}^{isooctane}(\varepsilon)$: 273 (1500), 266 (1230), 261.5 (800), 259.5 (790), 219 (15500), 214 (17800), 196 (66800) nm. CD: $\lambda_{max}^{isooctane}(\Delta\varepsilon)$: 273 (−1.89), 265.5 (−1.69), 260 (−1.02), 225 (+0.90), 222 (−1.81), 218 (+8.00), 214 (+7.29), 195 (+115.0) nm. Found: C, 92.37; H, 7.33%. Calcd for $C_{17}H_{16}$: C, 92.68; H, 7.32%.

References

1) S. F. Mason, K. Schofield, R. J. Wells, J. S. Whitehurst, and G. W. Vane, *Tetrahedron Lett.*, **1967**, 137; S. F. Mason, G. W. Vane, and J. S. Whitehurst, *Tetrahedron*, **23**, 4086 (1967); R. P. K. Chan, J. Cymerman Craig, R. H. F. Manske, and T. O. Soine, *ibid.*, **23**, 4209 (1967); "Fundamental Aspects and Recent Developments in Optical Rotatory Dispersion and Circular Dichroism," ed by F. Ciardelli and P. Salvadori, Heyden, London (1973), p. 155.

2) A. C. Baker and A. R. Battersby, *Tetrahedron Lett.*, **1967**, 135; A. C. Baker and A. R. Battersby, *J. Chem. Soc., C*, **1967**, 1317; T. Kaneda, N. Sakabe, and J. Tanaka, *Bull. Chem. Soc. Jpn.*, **47**, 1858 (1974).

3) H. Tatemitsu, F. Ogura, Y. Nakagawa, M. Nakagawa, K. Naemura, and M. Nakazaki, *Bull. Chem. Soc. Jpn.*, **48**, 2473 (1975).

4) J. R. Platt, *J. Chem. Phys.*, **19**, 263 (1951); J. Petruska, *ibid.*, **34**, 1111, 1120 (1961).

5) T. Kaneda, C. Katayama, and J. Tanaka, *Bull. Chem. Soc. Jpn.*, **49**, 1709 (1976).

6) "Organic Reactions," ed by R. Adams, Wiley, New York (1942), Vol. 2, p. 163.

The Acid-catalyzed Reactions of 4-Chromanones with Formaldehyde[1)]

Akira NINAGAWA,* Ryoki NOMURA, and Haruo MATSUDA

Department of Petroleum Chemistry, Faculty of Engineering, Osaka University, Yamadakami, Suita, Osaka 565

(Received October 2, 1978)

The reactions of several methyl substituted 4-chromanones, such as 4-chromanone (**1a**), 6-(**1b**), and 8-methyl-(**1c**), as well as 5,7-(**1d**) and 6,8-dimethyl-4-chromanone(**1e**) with formaldehyde were carried out in dioxane or mixed solutions of acetic acid and benzene or cyclohexane in the presence of sulfuric acid as a catalyst. The reactions involved an aldol condensation analogous to the Prins reaction, affording acetoxymethyl derivatives and 1,3-dioxanes. It was found that the formation of products was strongly influenced by the substituents on the 4-chromanones and solvents. In a mixed solution of acetic acid and benzene, **1b** and **1e** gave acetoxymethyl derivatives and 1,3-dioxanes, **1a** and **1c** only 1,3-dioxanes, and **1d** a resinous substance. In a dioxane solution, **1b** and **1e** gave 1,3-dioxanes, while **1c** gave a polymer. Bromination of **1e** in 35 and 96% sulfuric acids gave 3- and 5-bromo-6,8-dimethyl-4-chromanones, respectively. The acid-catalyzed reactions were compared with those in 96% sulfuric acid on the basis of the duterium exchange rates of 4-chromanones.

In previous papers,[2,3)] reports were given on the reactions of 4-chromanones with formaldehyde carried out in the presence of 96% sulfuric acid. The reaction products of 4-chromanone (**1a**), 6-(**1b**) as well as 8-methyl-(**1c**) and 5,7-dimethyl-4-chromanone (**1d**) with formaldehyde were the polymers linked by methylene bridges, while those of 6,8-dimethyl-4-chromanone (**1e**) were 5-hydroxymethyl-6,8-dimethyl-4-chromanone (**4**), along with small amounts of the methylene- and methyleneoxymethylene-bridged dimers.

The present investigation deals with the reactions of 4-chromanones with formaldehyde in dioxane or mixed solutions of acetic acid and benzene or cyclohexane in the presence of sulfuric acids as a catalyst. The reactions in 35% sulfuric acid are compared with those in 96% sulfuric acid.

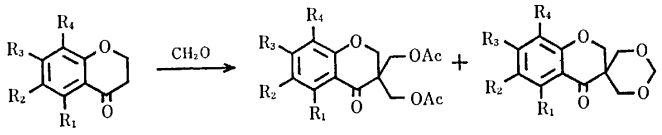

1 **2** **3**

a; $R_1=R_2=R_3=R_4=H$
b; $R_1=R_3=R_4=H$, $R_2=CH_3$
c; $R_1=R_2=R_3=H$, $R_4=CH_3$
d; $R_1=R_3=CH_3$, $R_2=R_4=H$
e; $R_1=R_3=H$, $R_2=R_4=CH_3$
f; $R_1=R_3=R_4=H$, $R_2=CH_2C_6H_5$
g; $R_1=R_3=H$, $R_2=CH_2C_6H_5$, $R_4=CH_3$
h; $R_1=R_3=H$, $R_2=CH_2OAc$, $R_4=CH_3$

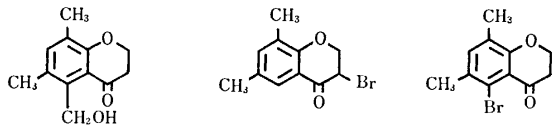

4 **5** **6**

Results and Discussion

Reaction Products of 4-Chromanones with Formaldehyde. The reactions of 4-chromanones with formaldehyde were carried out with different molar ratios of the reactants in a mixture of acetic acid and benzene in the presence of H_2SO_4 as a catalyst. The results are summarized in Table 1.

The reaction of **1a** with formaldehyde in a 1 : 3 molar ratio gave 6-benzylspiro(chroman-3,5′-[1,3]dioxane)-4-one (**3f**), and that in a 1 : 1 molar ratio caused the recovery of **1a** in 68% yield.

The reaction of **1b** with formaldehyde in a 1 : 1 molar ratio gave 3,3-bis(acetoxymethyl)-6-methyl-4-chromanone (**2b**) and that in a 1 : 3.3 molar ratio gave 6-methylspiro(chroman-3,5′-[1,3]dioxane)-4-one (**3b**).

Similarly, the reactions of **1c** in 1 : 3.3 and 1 : 5 molar ratios gave 6-benzyl-8-methylspiro(chroman-3,5′-[1,3]-dioxane)-4-one (**3g**). The reaction in a 1 : 1 molar ratio afforded a small amount of product which was isolated

TABLE 1. REACTION OF 4-CHROMANONES WITH FORMALDEHYDE IN A MIXTURE OF ACETIC ACID AND BENZENE IN THE PRESENCE OF H_2SO_4 AT 60 °C

Run	Chromanone, (mmol)	CH_2O/**1**, mole ratio	Acetic acid, ml	Benzene, ml	H_2SO_4, ml	Time, h	Product, (% yield)
1	**1a** (10)	3.0	15	50	1.0	6	**3f** (11)
2	**1b** (4.2)	1.0	5	30	0.5	4	**2b** (5)[a)]
3	**1b** (10)	3.3	15	50	1.0	16	**3b** (2)
4	**1c** (10)	3.3	15	50	1.0	16	**3g** (9)
5	**1c** (10)	5.0	15	50	1.0	16	**3g** (47)
6	**1d** (10)	1.0	10	50	1.0	5	b)
7	**1d** (10)	3.3	15	50	1.0	16	b)
8	**1e** (10)	1.0	10	50	1.0	6	**2e** (10), **3e** (3)
9	**1e** (100)	3.3	100	450	10.0	16	**3e** (70)

a) Yield determined by the ^{1}H-NMR spectrum. b) Resinous substance obtained (see Experimental).

Table 2. Solvent effect in the reaction of 4-chromanones with formaldehyde in the presence of H_2SO_4 at 60 °C

Run	Chromanone, (mmol)	CH_2O/**1**, mole ratio	Solvent, (ml)	H_2SO_4, ml	Time, h	Product, (% yield)
10	**1e** (50)	3.0	Propionic acid (50) Benzene (225)	5.0	7	**3e** (49)
11	**1e** (10)	3.3	Benzyl acetate (10) Benzene (50)	1.0	17	**3e** (12)
12	**1e** (10)	3.0	Acetic acid (20)	2.0	9	**3e** (32)
13	**1e** (10)	1.0	Acetic acid(6)	34.0	4	**4** (80)
14	**1e** (10)	1.0	Benzene (50)	1.0	4	a)
15	**1e** (10)	3.1	Dioxane (35)	5.0	6	**3e** (51)
16	**1e** (10)	1.0	Dioxane (10)	35.0	4	**4** (33)
17	**1b** (10)	3.1	Dioxane (35)	5.0	6	**3b** (30)
18	**1c** (10)	5.0	Acetic acid (10) Cyclohexane (50)	1.0	6	**3h** (2)
19	**1c** (10)	3.1	Dioxane (35)	5.0	6	b)

a) **1e** recovered in 95% yield. The reaction products were diphenylmethane and its homologues. b) A resinous product was obtained, yield 2.51 g.

with difficulty from the reaction mixture.

The reaction of **1e** with formaldehyde in a 1 : 1 molar ratio gave 3,3-bis(acetoxymethyl)-6,8-dimethyl-4-chromanone (**2e**) and 6,8-dimethylspiro(chroman-3,5′-[1,3]dioxane)-4-one (**3e**), while that in a 1 : 3.3 molar ratio gave **3e** in high yield. **3e** was changed into 6,8-dimethylspiro(chroman-3,5′-[1,3]dioxane)-4-ol (**3e′**) by use of sodium borohydride. The reaction of **1d**, however, gave a resinous substance.

The reactions were examined as regards the effects of the solvents and their acidity. The results are summarized in Table 2.

In the reaction of **1e** with formaldehyde, the use of propionic acid–benzene or benzyl acetate–benzene mixture, acetic acid, or dioxane as solvent gave **3e**, along with resinous substance. When the reaction was carried out in a benzene solution, diphenylmethane and its homologues were obtained, **1e** being recovered in 95% yield. The use of a large amount of H_2SO_4 (Runs 13 and 16) gave **4**, analogous to the case of the use of 96% H_2SO_4.[3]

The reaction of **1b** in dioxane gave only **3b**. The reaction of **1c** in a mixed solution of acetic acid and cyclohexane gave 6-acetoxymethyl-8-methylspiro-(chroman-3,5′-[1,3]dioxane)-4-one (**3h**), and that in dioxane a resinous material.

Bromination of 1e. The bromination of **1e** in acetic acid solution in the presence of H_2SO_4 gave 3-bromo-6,8-dimethyl-4-chromanone (**5**), while that in 96% H_2SO_4 gave 5-bromo-6,8-dimethyl-4-chromanone (**6**).

Deuterium Exchange of 4-Chromanones. Rates of the deuterium exchange of **1e** were observed by means of ^{1}H-NMR spectra. The results obtained in 35% D_2SO_4 (in CH_3CO_2D), 85% D_2SO_4 (in D_2O), and 96% D_2SO_4 are shown in Figs. 1a, 1b, and 1c, respectively. The deuterium atom % was calculated on the basis of the integral value in the C-2 methylene protons of **1e**. There is a clear difference between 1a and 1c. In 35% D_2SO_4, deuterium is incorporated into the C-3 methylene protons faster than the C-5 aromatic proton, while in the case of 96% D_2SO_4, the opposite tendency is

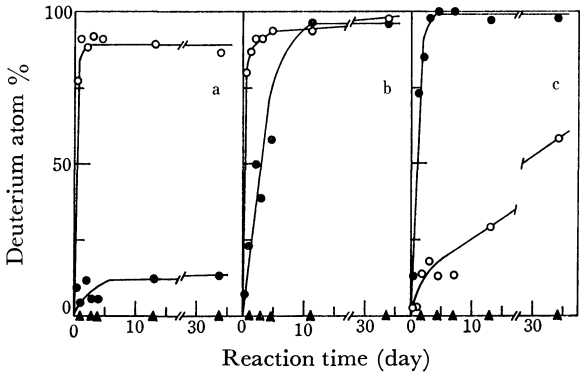

Fig. 1. Deuterium exchange of **1e** in various concentrations of D_2SO_4.
D_2SO_4 concentrations: a, 35% (in CH_3CO_2D); b, 85% (in D_2O); c, 96%. Exchange position: (○), C-3 methylene protons; (●), C-5 aromatic proton; (▲), C-7 aromatic proton.

Table 3. Deuterium exchange of 4-chromanones in 20% D_2SO_4 (in CH_3CO_2D) and 96% D_2SO_4 at 25 °C

Chromanone	Solvent[a]	Concn, wt %	Time	Deuterium atom % 3-,	6-,	8-,
1a	SA	15	3 h	86	0	0
			48 h	87	33	10
	S	15	24 h	5	15	2
			48 h	54	72	44
1b	SA	11	3 h	89	—	0
			48 h	86	—	6
	S	11	24 h	20	—	55
1c	SA	15	3 h	86	0	—
			48 h	89	60	—
	S	15	24 h	49	83	—
1d	SA	12	5 min	77	44[b]	
			3 h	100	73[b]	
			48 h	100	100[b]	
	S	12	3 h	3	91[b]	

a) SA=20% D_2SO_4 (in CH_3CO_2D), S=96% D_2SO_4. b) Signal not resolved to the 6- and 8-protons.

Table 4. ^{13}C-NMR spectra of **1e** in 96% H_2SO_4, 35% H_2SO_4 (in CH_3CO_2H), and $CDCl_3$[a]

Solvent	Concn, wt %	C-2	C-3	C-4	C-5	C-6	C-7	C-8	C-9	C-10	6-CH_3	8-CH_3
96% H_2SO_4	11.9	65.7	31.4	202.7	125.0	133.9	151.9	129.9	168.0	114.6	19.5	14.3
35% H_2SO_4	17.9	67.4	37.4	197.6	125.0	131.1	140.3	128.1	160.2	120.5	20.4	15.5
$CDCl_3$	36.5	66.5	37.2	190.8	123.6	129.1	137.0	126.0	157.6	120.2	19.7	14.9
Δ_1		−0.8	−5.8	11.9	1.4	4.8	14.9	3.9	10.4	−5.6	−0.2	−0.6
Δ_2		0.9	0.2	6.8	1.4	2.0	3.3	2.1	2.6	0.3	0.7	0.6

a) Chemical shifts are reported in ppm relative to Me_4Si. Δ_1=(96% H_2SO_4–$CDCl_3$) and Δ_2=(35% H_2SO_4–$CDCl_3$) are the chemical shift differences.

observed. It was found that the deuterium atom % of the C-5 position in 35% D_2SO_4 is in equilibrium at 10%, but that of the C-3 methylene in 96% D_2SO_4 slowly increases with time. The results of the deuterium exchange of other 4-chromanones are summarized in Table 3. 20% D_2SO_4 preferentially leads to exchange of the C-3 methylene protons, and 96% D_2SO_4 leads to the aromatic protons, but the difference between 20% D_2SO_4 and 96% D_2SO_4 is not as large as in the case of **1e**. The deuterium exchange of **1c** in 20% D_2SO_4 occurred in the order 3>6>8, and that in 96% D_2SO_4 in the order 6>3>8.

^{13}C-NMR Spectra of **1e**. Table 4 gives the carbon-13 chemical shifts obtained in 96% H_2SO_4, 35% H_2SO_4 (in CH_3CO_2H), and $CDCl_3$, as well as the chemical shift differences, Δ_1 and Δ_2, between H_2SO_4 solutions and $CDCl_3$ solution. Assigments of resonance positions to individual carbon atoms were made on the basis of substituent effects,[4] splitting patterns in proton coupled spectra, and internal consistency. A positive Δ indicates that the resonance is deshielded in H_2SO_4 relative to $CDCl_3$. In 96% H_2SO_4, larger deshielding trends of 10—15 ppm are observed for C-4, C-7, and C-9. Deshielding of 6.8 ppm for C-4 is observed in 35% H_2SO_4 solution.

The observed chemical shift trends in 96% H_2SO_4 are interpreted to result predominantly from protonation of the carbonyl oxygen (**7**) (Scheme 1). A deshielding effect is associated with a loss of charge density for carbons of similar hybridization.[5]

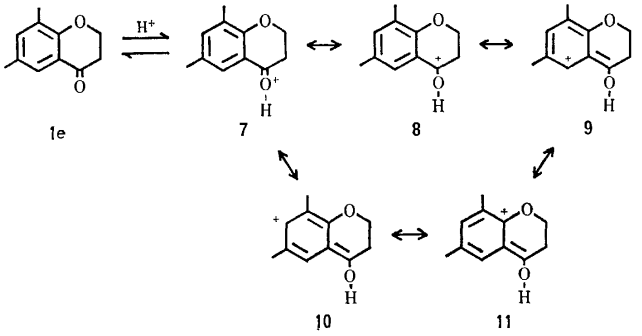

Scheme 1.

Reaction Path. Some papers on the acid-catalyzed condensation of cycloalkanones with formaldehyde[6] have reported the formation of hydroxymethyl derivatives and 1,3-dioxanes.

In the reactions of 4-chromanones with formaldehyde in solvents in the presence of sulfuric acid, the condensation products for the C-3 position were obtained even though **1a**, **1b**, and **1c** gave the aromatic substituted products containing 1,3-dioxanes. The deuterium exchange of 4-chromanones in various concentrations of sulfuric acid suggests that the C-3 methylene protons are more reactive than the aromatic protons.

These results obtained in the low concentrations of sulfuric acid can be explained by the aldol condensation mechanism.[7] The intermediate enol (**12**) is formed by the direct removal of a proton from the protonated intermediate (**8**) by bases (HSO_4^- and/or $CH_3CO_2^-$), reacting with hydroxymethyl cation($\overset{+}{C}H_2OH$)[8] to produce hydroxymethyl derivatives. Diacetates were obtained when the molar quantity of formaldehyde as against that of 4-chromanones was small.

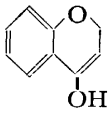

12

Bromination of **1e** in 35 and 96% H_2SO_4 using molecular bromine as an electrophilic substituting agent gave 3- and 5-bromo derivatives, respectively. The different reactivity of 4-chromanones in various concentrations of sulfuric acid might be utilized in synthetic reactions by use of other electrophilic agents.

The aromatic substituted products formed by the addition of formaldehyde to the benzene rings of 4-chromanones proceeds by an electrophilic aromatic substitution.

The results given in Table 1 suggest that the methyl substituents attached to the 6- and/or 8-positions of 4-chromanones play an important role in the formation of aromatic substituted products. **1e** fixed by the two methyl groups gave 3-substituted products only, **1d** containing the reactive 6- and 8-positions a polymer, while **1a** gave the 6-benzyl product. The results are also in line with the rates of deuterium exchange.

Experimental

General. Melting points are uncorrected. IR spectra were obtained on a Hitachi EPI-G2 spectrometer, ^{1}H-NMR spectra on a JEOR Model PS-100 spectrometer with tetramethylsilane(Me_4Si) as an internal standard, and ^{13}C-NMR spectra on a JNM-FX60 spectrometer. Chemical shifts in $CDCl_3$ and 35% H_2SO_4 (in CH_3CO_2H) were measured using Me_4Si as an internal standard. Chemical shifts in 96% H_2SO_4 were obtained relative to external $CDCl_3$ and converted into the Me_4Si scale by the relationship $\delta Me_4Si=\delta CDCl_3+$

77.1. Mass spectra were determined on a Hitachi RUM-6 mass spectrometer operating at 70 eV. Molecular weight was determined with a Mechrolab Model 301A vapor pressure osmometer in *N,N*-dimethylformamide at 65 °C.

Materials. 4-Chromanones were prepared from phenols according to the published procedure.[2,9] Commercial 1,3,5 trioxane, sulfuric acids, and solvents were used.

Reactions of 4-Chromanones with Formaldehyde. The general procedure is as follows. To a mixture of acetic acid and benzene were added 4-chromanones, 1,3,5-trioxane, and H_2SO_4 in this order, and the mixture was stirred at 60 °C. The reaction mixture was poured into cold water, and extracted with benzene. The benzene solution was washed with aqueous sodium hydroxide, aqueous hydrochloric acid, and water successively. After removal of the solvents, the residual oil was separated by column chromatography on silica gel (Wako-gel C-200; developing solvent, chloroform) to some fractions in which the first fractions were starting 4-chromanones, unless otherwise stated. The reaction conditions and products of these reactions are given in Tables 1 and 2.

From ***1a***. The reaction of **1a** with formaldehyde in a 1:3 molar ratio gave a pale yellow oil from the second fraction. The fraction could not be separated further. However, it gave **3f** containing a small amount of **1a**.

3f: IR (neat) 2770, 1670, 1090, 1040, 840, 705 cm^{-1}; ^1H NMR (CCl_4) δ=7.57 (1H, d, J=3.0 Hz, 5-H), 7.10 (5H, m, Ph), 7.06 (1H, dd, 7-H), 6.76 (1H, d, J=9.0 Hz, 8-H), 4.75 (2H, AB-q, J=6.0 Hz, $-OCH_2O-$), 4.53 (2H, s, 2-H), 3.88 (4H, s, $-CH_2O-$), 3.84 (2H, s, 6-CH_2); MS *m/e* 310 (M^+, 60), 211 (100).

From ***1b***. The reaction product obtained in a 1:1 molar ratio was subjected to fractional distillation under reduced pressure. From the first fraction unreacted **1b** was recovered at 86—87 °C/0.5 mmHg, and from the second fraction a yellow viscous oil at 165—166 °C/0.5 mmHg, which was separated by column chromatography to give a mixture of **2b** and **1b**. The distillation residue was a mixture of **3b** and other unknown products. The third fraction of the product obtained in a 1:3.3 molar ratio gave a pale yellow oil, which crystallized after being left to stand overnight. The crystals were recrystallized from cyclohexane to give **3b**.

2b: Oil; IR (neat) 1730, 1680, 1040, 880, 830 cm^{-1}; MS *m/e* 306 (M^+, 5), 174 (100).

3b: Mp 93—94 °C; IR (KBr) 2780, 1680, 1100, 1030, 890, 825 cm^{-1}; ^1H-NMR (CCl_4) δ=7.50 (1H, d, J=2.7 Hz, 5-H), 7.18 (1H, dd, 7-H), 6.80 (1H, d, J=9.1 Hz, 8-H), 4.76 (2H, AB-q, J=6.4 Hz, $-OCH_2O-$), 4.54 (2H, s, 2-H), 3.89 (4H, s, $-CH_2O-$), 2.29 (3H, s, 6-CH_3); MS *m/e* 234 (M^+, 41), 135 (100). Found: C, 66.45; H, 5.97%. Calcd for $C_{13}H_{14}O_4$: C, 66.66; H, 6.02%.

From ***1c***. The yellow oils obtained in 1:3.3 and 1:5 molar ratios in a mixed solution of acetic acid and benzene were separated into three fractions. A crystalline product (**3g**) was isolated from the second fraction, and a small amount of polymer from the third fraction. The first fraction of the product obtained in a 1:5 molar ratio in a mixture of acetic acid and cyclohexane gave **3h**.

3g: Mp 153—154 °C (from ligroin); IR (KBr) 2760, 1670, 1100, 1040, 830, 700 cm^{-1}; ^1H-NMR (CCl_4) δ=7.42 (1H, d, 5-H), 7.04 (1H, d, 7-H), 7.12 (5H, m, Ph), 4.78 (2H, AB-q, J=6.1 Hz, $-OCH_2O-$), 4.58 (2H, s, 2-H), 3.91 (2H, s, $-CH_2O-$), 3.48 (2H, s, 6-CH_2), 2.22 (3H, s, 8-CH_3); MS *m/e* 324 (M^+, 93), 225 (100). Found: C, 74.29; H, 6.32%. Calcd for $C_{20}H_{20}O_4$: C, 74.06; H, 6.22%.

3h: Mp 99—99.5 °C (from ligroin); IR (KBr) 2780, 1680, 1095, 1035, 1025, 820 cm^{-1}; ^1H-NMR (CCl_4) δ=7.52 (1H, d, 5-H), 7.26 (1H, d, 7-H), 4.87 (2H, s, 6-CH_2), 4.75 (2H, AB-q, J=6.0 Hz, $-OCH_2O-$), 4.60 (2H, s, 2-H), 3.89 (4H, s, $-CH_2O-$), 2.26 (3H, s, 8-CH_3), 2.00 (3H, s, $COCH_3$); MS *m/e* 306 (M^+, 77), 207 (100). Found: C, 62.80; H, 5.83%. Calcd for $C_{16}H_{18}O_6$: C, 62.74; H, 5.92%.

From ***1d***. The reaction product obtained in a 1:1 molar ratio gave a resinous substance which could be isolated with difficulty from the reaction mixture: yield 1.5 g; mp 80 °C; molecular weight 420; IR (KBr) 1670, 1100, 1020 cm^{-1}. The absorption due to benzyl group at 3.9 ($C\underline{H}_2Ph$) and 7.2 (Ph) ppm was observed by the ^1H-NMR spectrum. The reaction product obtained in a 1:3 molar ratio gave a resinous substance: yield 2.7 g; mp 100 °C; molecular weight 630; IR (KBr) 1725, 1660, 1095, 1030 cm^{-1}. The absorption due to the benzyl group at 3.9 ($C\underline{H}_2Ph$) and 7.2 (Ph) ppm, and the 1,3-dioxane ring at 5.0 and 4.8 ($-OCH_2O-$) ppm was observed by the ^1H-NMR spectrum.

From ***1e***. The reaction products obtained in Runs 8, 9, 10, 11, and 12 were isolated by column chromatography to three fractions. The second white crystalline fraction and the third yellow oil fraction gave **3e** and **2e**, respectively. The reaction mixtures in Runs 13, 15, and 16 were extracted with chloroform and recrystallized from ligroin to give **3e** or **4**.

2e: Yellow oil; IR (neat) 1730, 1670, 1030, 870 cm^{-1}; ^1H-NMR (CCl_4) δ=7.44 (1H, d, 5-H), 7.04 (1H, d, 7-H), 4.35 (2H, s, 2-H), 4.24 (4H, s, $-CH_2OCO-$), 2.26 (3H, s, 6-CH_3), 2.08 (3H, s, 8-CH_3), 2.00 (6H, s, $-OCOCH_3$); MS *m/e* 320 (M^+, 37), 148 (100). Found: C, 63.98; H, 6.30%. Calcd for $C_{17}H_{20}O_6$: C, 63.74; H, 6.29%.

3e: Mp 146.5—148 °C (from acetone); IR (KBr) 2760, 1660, 1100, 1030, 880 cm^{-1}; ^1H-NMR (CCl_4) δ=7.34 (1H, d, 5-H), 7.08 (1H, d, 7-H), 4.78 (2H, AB-q, J=6.0 Hz, $-OCH_2O-$), 4.56 (2H, s, 2-H), 3.90 (4H, s, $-CH_2O-$), 2.26 (3H, s, 6-CH_3), 2.22 (3H, s, 8-CH_3); MS *m/e* 248 (M^+, 69), 149 (100); ^{13}C-NMR ($CDCl_3$) δ=192.4 (s, 4-C), 157.7 (s, 9-C), 138.5 (d, 7-C), 130.3 (s, 6-C), 127.0 (s, 8-C), 124.3 (d, 5-C), 119.2 (s, 10-C), 94.0 (t, 2′-C), 69.7 (t, 2-C), 67.5 (t, 4′- and 6′-C), 45.2 (s, 3-C), 20.3 (q, 6-CH_3), 15.3 (q, 8-CH_3). The assignments are based on the data of Chauhan and Still,[10] and the procedure of Levy and Nelson.[11] Found: C, 67.61; H, 6.49%. Calcd for $C_{14}H_{16}O_4$: C, 67.73; H, 6.50%.

4: Mp 95—97 °C (lit,[9] mp 95—97 °C). The structure of this product was confirmed by ^1H-NMR and mass spectra.

Reduction of ***3e***. Sodium borohydride (0.14 g, 3.6 mmol) was added to **3e** (1.24 g, 5 mmol) in ethanol (20 ml). The mixture was heated under reflux at 80 °C for 4 h. The reaction mixture was neutralized with acetic acid and then extracted with ether. The ether layer was washed with aqueous sodium hydroxide, aqueous hydrochloric acid, and water and then dried *in vacuo*. The residue was recrystallized from hexane to give **3e′** in a 68% yield: mp 109 °C; IR (KBr) 3400, 2760, 1030, 870 cm^{-1}; ^1H-NMR (CCl_4) δ=6.76 (2H, bd, 5- and 7-H), 4.70 (2H, AB-q, J=6.1 Hz, $-OCH_2O-$), 4.12 (2H, AB-q, J=10.1 Hz, 2-H), 3.67 (4H, AB-q, J=12.1 Hz, $-CH_2O-$), 4.22 (1H, s, OH), 3.80 (1H, s, 4-H), 2.22 (3H, s, 6-CH_3), 2.14 (3H, s, 8-CH_3); MS *m/e* 250 (M^+, 71), 150 (100). Found: C, 66.94; H, 7.39%. Calcd for $C_{14}H_{18}O_4$: C, 67.18; H, 7.25%.

Preparation of ***5***. To a solution of 96% H_2SO_4 (5 ml) and acetic acid (50 ml) was added **1e** (1.76 g, 10 mmol), and the mixture was cooled in an ice-bath. A solution of bromine (0.80 g, 10 mmol) and acetic acid (5 ml) was then added dropwise over a period of 30 min to the mixture with stirring, and the mixture was stirred for 30 min at 0 °C. The reaction mixture was poured into water and extracted with benzene. The organic layer was washed with aqueous sodium hydroxide and water, and dried *in vacuo* to give a yellow oil. The oil

was recrystallized twice from ligroin to give **5**: yield 17%; mp 86—87 °C, IR (KBr) 1680, 1020, 890, 550 cm^{-1}; ^1H-NMR (CCl_4) δ=7.46 (1H, d, 5-H), 7.10 (1H, d, 7-H), 4.54 (2H, d, J=4.5 Hz, 2-H), 4.42 (1H, t, 3-H), 2.27 (3H, s, 6-CH_3), 2.21 (3H, s, 8-CH_3); MS *m/e* 254 (M^+, 31), 148 (100). Found: C, 51.77; H, 4.33; Br, 31.16%. Calcd for $C_{11}H_{11}O_2Br$: C, 51.79; H, 4.35; Br, 31.32%.

Preparation of ***6***. **1e** (3.52 g, 20 mmol) was dissolved in 96% H_2SO_4 (30 ml), and the mixture was cooled in an ice-bath. Bromine (3.2 g, 40 mmol) was added over a period of 30 min to the mixture with stirring, and the mixture was stirred for 30 min at 0 °C. The reaction mixture was treated as described in the preparation of **5**. The product was recrystallized three time from ligroin to give **6**: yield 23%; mp 102—103 °C; IR (KBr) 1680, 1020, 870, 570 cm^{-1}; ^1H-NMR (CCl_4) δ=7.08 (1H, s, 7-H), 4.49 (2H, t, J=6.0 Hz, 2-H), 2.76 (2H, t, 3-H), 2.32 (3H, s, 6-CH_3), 2.14 (3H, s, 8-CH_3); MS *m/e* 254 (M^+, 100), 226 (83). Found: C, 51.63; H, 4.24; Br, 31.23%.

References

1) Formaldehyde polymers Part 24; for Part, 23, see A. Ninagawa and H. Matsuda, *Bull. Chem. Soc. Jpn.*, **51**, 2747 (1978).

2) A. Ninagawa, Y. Oomi, and H. Matsuda, *Nippon Kagaku Kaishi*, **1976**, 1926.

3) A. Ninagawa and H. Matsuda, *Bull. Chem. Soc. Jpn.*, **51**, 1874 (1978).

4) J. B. Sthothers, "Carbon-13 NMR Spectroscopy," Academic Press, New York, N. Y. (1972), p. 197.

5) S. A. Sojka, *J. Org. Chem.*, **40**, 1175 (1975).

6) a) S. Olsen, *Acta Chim. Scand.*, **7**, 1364 (1953); b) W. C. Lumma Jr., and O. H. Ma, *J. Org. Chem.*, **35**, 2931 (1970); c) F. Hirano and S. Wakabayashi, *Bull. Chem. Soc. Jpn.*, **48**, 2579 (1975); d) F. Hirano and S. Wakabayashi, *ibid.*, **50**, 3059 (1977).

7) A. T. Nielsen and W. J. Houlihan, *Org. React.*, **16**, 1 (1968).

8) The active species of formaldehyde might be not only $\overset{+}{C}H_2OH$ but also $\overset{+}{C}H_2OCH_2OH$ or $\overset{+}{C}H_2OCH_2OCH_2OH$.

9) A. Ninagawa, Y. Oomi, H. Matsuda, and S. Matsuda, *Nippon Kagaku Kaishi*, **1973**, 1621.

10) M. S. Chauhan and I. W. Still, *Can. J. Chem.*, **53**, 2880 (1975).

11) G. G. Levy and G. L. Nelson, "Carbon-13 Nuclear Magnetic Resonance for Organic Chemists," Wiley Interscience, New York (1972), p. 81.

Pseudo-sugars. 4. A Facile Synthesis of DL-Validamine and Its Derivative[1]

Seiichiro OGAWA,* Koji NAKAMOTO, Masaaki TAKAHARA, Yoshio TANNO, Noritaka CHIDA, and Tetsuo SUAMI

Department of Applied Chemistry, Faculty of Engineering, Keio University, Hiyoshi, Yokohama 223

(Received October 3, 1978)

Penta-*N,O*-acetyl-DL-validamine was prepared from readily available *endo*-2, *exo*-3-diacetoxy-*endo*-6-acetoxymethyl-7-oxabicyclo[2.2.1]heptane in three steps in an overall yield of 36%.

As a part of a synthetic study of antibiotic validamycins,[2] we wish to report a facile synthesis of DL-validamine, starting from tri-*O*-acetyl-(1,3/2,4,6)-4-bromo-6-bromomethyl-1,2,3-cyclohexanetriol (**7**), which was readily obtained by the bromination of *endo*-2, *exo*-3-diacetoxy-*endo*-6-acetoxymethyl-7-oxabicyclo[2.2.1]-heptane (**4**).[3]

The *exo*-3-acetoxy (**4**), *exo*-3-methoxy (**5**), and *exo*-3-tosyloxy derivatives (**6**) of *endo*-2-acetoxy-*endo*-6-acetoxymethyl-7-oxabicyclo[2.2.1]heptane were prepared in high yields by lithium aluminium hydride (LAH) reduction followed by acetylation of the corresponding lactones (**1**,[3,4] **2**, and **3**). Treatment of **4** with 15% hydrogen bromide in acetic acid in a sealed tube at 75 °C for 24 h led to a cleavage of the anhydro ring to give single crystalline **7** in 70% yield. Under the similar reaction conditions, **5** also gave **7** in 59% yield. The structure of **7** was established on the basis of elemental and ^{1}H NMR analyses, and analogy of the bromination of the corresponding *exo*-3-bromo derivative.[5] Thus, the ^{1}H NMR spectrum contained three singlets (δ 1.99, 2.04, and 2.07) due to the acetoxyl methyl protons and the relatively narrow three-proton multiplet (δ 5.00) due to the protons on the carbon atoms bearing the acetoxyl groups. The one-proton symmetric broad multiplet (δ 3.90) could be attributable to H-4, indicating that the ring bromine atom was in an equatorial position in the favored conformation. The previous results[5] suggested that the anhydro ring of this system would be cleaved by a bromide ion at the carbon atom (C-4) adjacent to the ring methylene group.

The similar bromination of **6** yielded in 62% yield the sole crystalline dibromo diacetate (**8**) which contained a tosyloxyl function. Reaction of **8** with methanolic sodium methoxide followed by acetylation gave the dibromo epoxy acetate (**12**), which was also derived by the same treatment of 1,2-di-*O*-acetyl-(1,3/2,4,6)-3,4-dibromo-6-bromomethyl-1,2-cyclohexanediol.[5] These results allowed to assign **8** as 1,2-di-*O*-acetyl-3-*O*-tosyl-(1,3/2,4,6)-4-bromo-6-bromomethyl-1,2,3-cyclohexanetriol.

Preferential substitution of the primary bromo substituent of **7** by an acetate or an azide ion was effected by treatment with a slight excess of its sodium salt in aqueous 2-methoxyethanol giving the corresponding 7-acetoxy (**9**, 72%) or 7-azido compounds (**11**, 91%). On the other hand, reaction of **7** and **9** with an excess of sodium azide in *N,N*-dimethylformamide resulted in displacement of the C-4 bromine atom by an azido group *via* S_N2 fashion to give selectively the diazido (**13**, 76%) as crystals and the azido compounds (**14**, 96%) as a syrup, respectively. Catalytic hydrogenation of **14** in the presence of Raney nickel[6] in methanol containing acetic anhydride gave the known penta-*N,O*-acetyl-(1,3,4/2,6)-4-amino-6-hydroxymethyl-1,2,3-cyclohexanetriol (DL-validamine) (**16**)[3,5] in 53% yield. Its 7-amino-7-deoxy derivative (**17**) was obtained by the similar hydrogenation of **13** in 51% yield. These data also confirmed the structure of **13** and **14**.

Compound **8** was converted similarly to the corresponding 7-acetoxy derivative (**10**) in 63% yield. On treatment with a slight excess of sodium azide in *N,N*-dimethylformamide **10** gave a syrupy azide tosylate (**15**), which, without further purification, was hydrogenated as described above to the crystalline amide tosylate (**18**) in an over all yield of 35%. In this case, replacement of the C-4 bromine atom by an azide ion seemed to occur faster than that of C-3 tosyloxyl group *via* an anchimeric reaction.[7] Treatment of **18** with methanolic sodium methoxide gave the epoxide, which was directly acetylated by a mixture of acetic anhydride and pyridine followed by the usual work-up giving **16** in 74% yield.

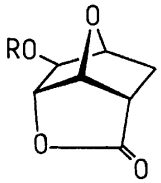

1 R=H
2 R=Me
3 R=Ts

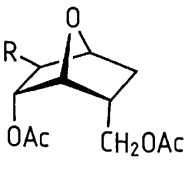

4 R=OAc
5 R=OMe
6 R=OTs

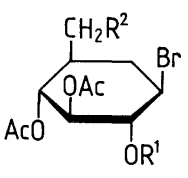

	R^1	R^2
7	Ac	Br
8	Ts	Br
9	Ac	OAc
10	Ts	OAc
11	Ac	N_3

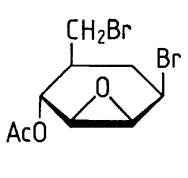

12

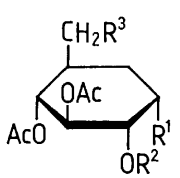

	R^1	R^2	R^3
13	N_3	Ac	N_3
14	N_3	Ac	OAc
15	N_3	Ts	OAc
16	NHAc	Ac	OAc
17	NHAc	Ac	NHAc
18	NHAc	Ts	OAc

Experimental

Melting points were measured in a capillary in a liquid bath and are uncorrected. Solutions were evaporated under diminished pressure at 40—50 °C. ^{1}H NMR spectra were measured at 60 MHz on a Varian A-60D spectrometer in $CDCl_3$ with reference to tetramethylsilane as an internal standard and the peak positions are given in δ-values. Values given for coupling constants are of first-order. TLC was performed on silica gel (Wakogel B-10, Wako Pure Chemical Industries, Ltd.). Elemental analyses were performed by Mr. Saburo Nakada, to whom our thanks are due.

exo-*9-Methoxy-2,7-dioxatricyclo[4.2.1.0^{4,8}]nonan-3-one (2).* A mixture of *exo*-9-hydroxy-2,7-dioxatricyclo[4.2.1.0^{4,8}]nonan-3-one (**1**)[3,4] (5 g), methyl iodide (10 ml), and silver oxide (10 g) in *N,N*-dimethylformamide (20 ml) was vigorously stirred at a room temperature under dark for 20 h. Acetone was added to the reaction mixture, an insoluble material was removed by filtration, and the filtrate was evaporated to give a solid product. Crystallization from ethanol gave **2** (4.2 g, 77%) as needles: mp 85—86 °C; ^{1}H NMR δ 1.86 (1H, dd, $J_{4,5\text{endo}}$=3 Hz, $J_{5\text{gem}}$=12.5 Hz, H-5endo), 2.21 (1H, ddd, $J_{4,5\text{exo}}$=10 Hz, $J_{5\text{exo},6}$=5 Hz, H-5exo), 2.69 (1H, ddd, $J_{4,8}$=5 Hz, H-4), 3.37 (3H, s, OMe), 3.43 (1H, s, H-9), 4.59 (2H, t, $J_{1,8}$=5 Hz, H-1 and H-6), 5.29 (1H, t, H-8).

Found: C, 56.42; H, 5.92%. Calcd for $C_8H_{10}O_4$: C, 56.46; H, 5.92%.

exo-*9-Tosyloxy-2,7-dioxatricyclo[4.2.1.0^{4,8}]nonan-3-one (3).* Compound **1** (1 g) was treated with tosyl chloride (2.5 g, 2 mol equiv) in pyridine (5 ml) at a room temperature overnight. The reaction mixture was poured into ice-water, and the precipitates were collected and recrystallized from ethyl acetate to give **3** (1.4 g, 71%) as needles: mp 174—175 °C. ^{1}H NMR δ 2.48 (3H, s, tosyl Me), 4.51 (1H, s, H-9), 4.60 (1H, d, $J_{1,8}$=5 Hz, H-1), 4.77 (1H, d, $J_{5\text{exo},6}$=5 Hz, H-6), 5.33 (1H, t, $J_{4,8}$=5 Hz, H-8).

Found: C, 53.95; H, 4.56; S, 10.06%. Calcd for $C_{14}H_{14}O_6S$: C, 54.18; H, 4.55; S, 10.33%.

endo-*2*, exo-*3-Diacetoxy*-endo-*6-acetoxymethyl-7-oxabicyclo[2.2.1]heptane (4).* To a stirred mixture of LAH (3 g, 2.5 mol equiv) in dry tetrahydrofuran (THF) (100 ml) was added in several portions pulverized **1** (5 g) under external ice-cooling. The reaction mixture was stirred at this temperature for 15 min and then at a room temperature for 2 h. An excess hydride was destroyed by addition of water (10 ml), and the precipitates were filtered and washed thoroughly with a mixture of acetone and water. The filtrate and washings were combined and evaporated to dryness. The residue was treated with a mixture of acetic anhydride (20 ml) and pyridine (20 ml) at a room temperature overnight. An insoluble material was removed by filtration, and the filtrate was evaporated and co-distilled with toluene to give a syrup, which was dissolved in chloroform and passed through a short alumina column. Evaporation of the solvent gave **4** (8.4 g, 93%) as a practically homogeneous syrup, whose IR and ^{1}H NMR spectra were identical to those of an authentic sample.[3]

endo-*2-Acetoxy*-endo-*6-acetoxymethyl*-exo-*3-methoxy-7-oxabicyclo[2.2.1]heptane (5).* Compound **2** (5 g) was reduced with LAH (1.2 g) in THF (100 ml) similarly as described above and the product was successively acetylated in the usual manner. Crystallization of the crude product from ethyl acetate–hexane gave **5** (5.9 g, 78%) as needles: mp 58—59 °C; ^{1}H NMR δ 1.16 (1H, dd, $J_{5\text{endo},6}$=5 Hz, $J_{5\text{gem}}$=11 Hz, H-5endo), 2.01 (3H, s) and 2.03 (3H, s) (OAc), 3.31 (3H, s, OMe), 3.42 (1H, d, $J_{2,3}$=2 Hz, H-3), 4.22 (2H, dd, C<u>H</u>$_2$OAc), 4.48 (1H, d, $J_{4,5\text{exo}}$=6 Hz, H-4), 4.60 (1H, t, $J_{1,2}$=$J_{1,6}$=4 Hz, H-1), 4.90 (1H, broad d, H-2).

Found: C, 55.89; H, 6.93%. Calcd for $C_{12}H_{18}O_6$: C, 55.80; H, 7.03%.

endo-*2-Acetoxy*-endo-*6-acetoxymethyl*-exo-*3-tosyloxy-7-oxabicyclo[2.2.1]heptane (6).* Compound **3** (5 g) was reduced with LAH (0.67 g) in THF (130 ml) similarly as described in the preparation of **4** and the product was acetylated as usual. Crystallization of the crude product from ethyl acetate gave **6** (4.3 g, 67%) as needles: mp 117—118 °C; ^{1}H NMR δ 1.23 (1H, dd, $J_{5\text{endo},6}$=5 Hz, $J_{5\text{gem}}$=12 Hz, H-5endo), 1.94 (3H, s) and 1.99 (3H, s) (OAc), 2.44 (3H, s, tosyl Me), 4.18 (2H, dd, C<u>H</u>$_2$OAc).

Found: C, 54.37; H, 5.39; S, 7.88%. Calcd for $C_{18}H_{22}O_8S$: C, 54.26; H, 5.57; S, 8.05%.

Tri-O-acetyl-(1,3/2,4,6)-4-bromo-6-bromomethyl-1,2,3-cyclohexanetriol (7). a) A mixture of **4** (2.5 g) and 15% hydrogen bromide in acetic acid (20 ml) was heated in a sealed tube at 75 °C for 24 h. The brown reaction mixture was poured into ice–water (1 l), and the resulting crystals were collected and washed thoroughly with water. The crude crystals were recrystallized from ethanol to give **7** (2.6 g, 70%) as needles or prisms: mp 162—163 °C; ^{1}H NMR δ 1.99 (3H, s), 2.04 (3H, s), and 2.07 (3H, s) (OAc), 3.30 (2H, m, C<u>H</u>$_2$Br), 3.90 (1H, m, H-4), 5.00 (3H, m, H-1, H-2, and H-3).

Found: C, 36.37; H, 4.18; Br, 36.95%. Calcd for $C_{13}H_{18}O_6Br_2$: C, 36.30; H, 4.22; Br, 37.16%.

b) Compound **5** (4.5 g) was treated similarly with 15% hydrogen bromide in acetic acid (35 ml) at 80 °C for 50 h, and the reaction mixture was processed as described above. The crude product was crystallized from isopropyl alcohol to give **7** (4.4 g, 59%) as needles: mp 159—161 °C

1,2-Di-O-acetyl-3-O-tosyl-(1,3/2,4,6)-4-bromo-6-bromomethyl-1,2,3-cyclohexanetriol (8). Compound **6** (1 g) was treated with 15% hydrogen bromide in acetic acid (6 ml) as described in the preparation of **7**. The product was crystallized from ethanol to give **8** (0.85 g, 62%) as needles: mp 161—163 °C; ^{1}H NMR δ 2.03 (6H, s, OAc), 2.42 (3H, s, tosyl Me), 3.85 (1H, m, H-4).

Found: C, 40.05; H, 4.06%. Calcd for $C_{18}H_{22}O_7Br_2S$: C, 39.87: H, 4.09%.

1-O-Acetyl-2,3-anhydro-(1/2,3,4,6)-4-bromo-6-bromomethyl-1,2,3-cyclohexanetriol (12). a) Compound **8** (0.7 g) was dissolved in a mixture of chloroform (3 ml) and methanol (5 ml) and the solution was treated with 1.3 M methanolic sodium methoxide (10 ml) at a room temperature for 3 h. The reaction mixture was evaporated to dryness and the residual product was acetylated in the usual manner. The crude acetyl derivative was crystallized from ethanol to give **12** (0.12 g, 50%) as needles: mp 83—84.5 °C; ^{1}H NMR δ 2.15 (3H, s, OAc), 3.3—3.6 (4H, m, C<u>H</u>$_2$Br, H-2, and H-3), 4.43 (1H, m, H-4), 4.93 (1H, m, H-1).

Found: C, 32.85; H, 3.64; Br, 48.84%. Calcd for $C_5H_{12}O_3Br_2$: C, 32.96; H, 3.69; Br, 48.72%.

b) Treatment of di-*O*-acetyl-(1,3/2,4,6)-3,4-dibromo-6-bromomethyl-1,2-cyclohexanediol[5] (1.35 g) with methanolic sodium methoxide as described above gave **12** (0.76 g, 78%), identical with the compound obtained above.

Tetra-O-acetyl-(1,3/2,4,6)-4-bromo-6-hydroxymethyl-1,2,3-cyclohexanetriol (9). A mixture of **7** (2 g), anhydrous sodium acetate (1.5 g, 3.5 mol equiv), and 90% aqueous 2-methoxyethanol (50 ml) was heated at 80 °C with stirring for 24 h, and evaporated to dryness. The residue was acetylated as usual and the solid product was extracted with chloroform. TLC (1: 15 acetone–benzene, v/v) showed the product to be consist of one major (R_f 0.42) and two minor components (R_f 0.58 and 0.30). The extracts were filtered through a short alumina column and evaporated to give a syrup, which

crystallized from isopropyl alcohol affording **9** (1.4 g, 72%) as needles: mp 119—120 °C; ^{1}H NMR δ 1.97 (3H, s), 2.00 (3H, s), and 2.06 (6H, s) (OAc), 3.8—4.2 (3H, m, C$\underline{H}_2$OAc and H-4), 5.01 (1H, t, $J_{1,2}=J_{1,6}=11$ Hz, H-1), 5.10 (1H, t, $J_{2,3}=J_{3,4}=11$ Hz, H-3), 5.20 (1H, t, H-2).

Found: C, 43.72; H, 5.06; Br, 19.82%. Calcd for $C_{15}H_{21}O_8Br$: C, 44.02; H, 5.17; Br, 19.53%.

1,2,7-Tri-O-*acetyl-3*-O-*tosyl-(1,3/2,4,6)-4-bromo-6-hydroxymethyl-1,2,3-cyclohexanetriol (**10**).* Compound **8** (1 g) was treated with anhydrous sodium acetate (1.2 g) in 90% aqueous 2-methoxyethanol (50 ml) at 90 °C for 2 days. The reaction mixture was processed similarly and the product was acetylated. Crystallization of the acetate from ethanol gave **10** (0.61 g, 63%) as prisms: mp 179—180 °C; ^{1}H NMR δ 2.04 (6H, s) and 2.08 (3H, s) (OAc), 2.45 (3H, s, tosyl Me), 4.00 (2H, broad s, C$\underline{H}_2$OAc).

Found: C, 45.85; H, 4.76%. Calcd for $C_{20}H_{25}O_9BrS$: C, 46.07; H, 4.83%.

Tri-O-*acetyl-(1,3/2,4,6)-6-azidomethyl-4-bromo-1,2,3-cyclohexanetriol (**11**).* A mixture of **7** (1 g), sodium azide (0.45 g), and 90% aqueous 2-methoxyethanol (15 ml) was heated at 95 °C for 2 h, and evaporated to dryness. The residual solid was acetylated as usual and the crude product was purified by passage through a short alumina column with chloroform. Crystallization from ligroin gave **11** (1.7 g, 91%) as needles: mp 136—138 °C; ^{1}H NMR δ 1.95 (3H, s), 2.01 (3H, s), and 2.03 (3H, s) (OAc), *ca.* 3.3 (2H, m, C$\underline{H}_2N_3$), 3.95 (1H, m, H-4).

Found: C, 39.78; H, 4.67; N, 10.85; Br, 20.66%. Calcd for $C_{13}H_{18}N_3O_6Br$: C, 39.81; H, 4.64; N, 10.71; Br, 20.37%.

Penta-N,O-*acetyl-(1,3,4/2,6)-4-amino-6-hydroxymethyl-1,2,3-cyclohexanetriol (**16**).* A mixture of **9** (3 g), sodium azide (1.9 g), and *N,N*-dimethylformamide (100 ml) was heated at 90 °C for 24 h, and evaporated to dryness. The solid residue was extracted with chloroform and the extracts were filtered through a short alumina column. The filtrate was evaporated to give **14** (2.6 g, 96%) as a homogeneous syrup: IR (neat) 2100 (N_3), 1745 cm^{-1} (ester); ^{1}H NMR δ 2.00 (6H, s) and 2.02 (6H, s) (OAc), 5.01 (1H, dd, $J_{1,2}=9.5$ Hz, $J_{1,6}=5.5$ Hz, H-1), 5.39 (1H, t, $J_{2,3}=9.5$ Hz, H-2).

A solution of the crude **14** (2.8 g) in methanol (50 ml) containing acetic anhydride (2 ml) was hydrogenated in a Parr shaker apparatus in the presence of Raney nickel T-4[6] at hydrogen pressure of 3 kg·cm^{-2} at a room temperature overnight. The catalyst was removed by filtration and the filtrate was evaporated to give a crystalline residue. Recrystallization from ethanol gave **16** (1.5 g, 53%) as plates: mp 197—198 °C. This compound was identical with an authentic sample[3] in all respects.

Tri-O-*acetyl-(1,3,4/2,6)-4-azido-6-azidomethyl-1,2,3-cyclohexanetriol (**13**).* Compound **7** (1 g) was treated with sodium azide (0.9 g, 6 mol equiv) in *N,N*-dimethylformamide (40 ml) at 85 °C for 20 h. The reaction mixture was processed similarly as described above and the product was acetylated. Crystallization of the crude acetate from ligroin gave **13** (0.62 g, 76%) as prisms: mp 120—121 °C; ^{1}H NMR δ 2.00 (3H, s), 2.05 (3H, s), and 2.07 (3H, s) (OAc), 3.30 (2H, d, $J=4$ Hz, C$\underline{H}_2N_3$), 4.11 (1H, q, $J=3$ Hz, H-4), 4.82 (1H, t, $J_{1,2}=J_{1,6}=9.5$ Hz, H-1), 4.93 (1H, dd, $J_{2,3}=9.5$ Hz, H-3), 5.37 (1H, t, H-2).

Found: C, 44.23; H, 5.18; N, 23.48%. Calcd for $C_{13}H_{18}N_6O_6$: C, 44.06; H, 5.13; N, 23.72%.

Penta-N,O-*acetyl-(1,3,4/2,6)-4-amino-6-aminomethyl-1,2,3-cyclohexanetriol (**17**).* Compound **13** (0.5 g) was hydrogenated similarly as described in the preparation of **16**. The crude product was crystallized from ethyl acetate to give **17** (0.28 g, 51%) as needles: mp 258—259 °C (lit,[4] 246—248 °C). This compound was identified with an authentic sample[3] by comparison with IR and ^{1}H NMR spectra.

1,2,7-Tri-O-*acetyl-3*-O-*tosyl-(1,3,4/2,6)-4-acetamido-6-hydroxymethyl-1,2,3-cyclohexanetriol (**18**).* Compound **10** (1 g) was treated with sodium azide (0.6 g) in *N,N*-dimethylformamide (20 ml) at 85 °C for 24 h. The product was acetylated and purified by chromatography on alumina with chloroform to give the azide (**15**, 0.9 g, 97%) as a practically pure syrup: ^{1}H NMR δ 1.93 (3H, s), 2.00 (3H, s), and 2.06 (3H, s) (OAc), 2.45 (3H, s, tosyl Me).

The crude **15** (0.78 g) was hydrogenated as described in the preparation of **16**. The product was crystallized from ethanol to give **18** (0.28 g, 34% based on **10** used) as needles: mp 157—158 °C; ^{1}H NMR δ 1.90 (3H, s, NAc), 1.96 (3H, s), 2.00 (3H, s), and 2.06 (3H, s) (OAc), 2.54 (3H, s, tosyl Me), 3.96 (2H, narrow m, C$\underline{H}_2$OAc), 6.38 (1H, d, $J=7$ Hz, N$\underline{H}$).

Found: C, 53.05; H, 5.89; N, 2.62; S, 6.57%. Calcd for $C_{22}H_{29}NO_{10}S$: C, 52.90; H, 5.85; N, 2.80; S, 6.42%.

Compound **18** (0.13 g) was treated with methanolic sodium methoxide as described in the preparation of **12**. The product was treated with acetic anhydride (7 ml) and pyridine (7 ml) at 50 °C for 2 h, and the mixture was worked up in the usual manner. The product was crystallized from ethanol to give **16** (0.073 g, 74%) as prisms: mp 194—196 °C, identical with the compound obtained before in all respects.

The financial support from the Ministry of Education for this work is gratefully acknowledged.

References

1) For paper 3 of this series: *Bull. Chem. Soc. Jpn.*, **52**, 118 (1979). The nomenclature and numbering of cyclitols used in this paper follow IUPAC and IUB tentative rules for cyclitol nomenclature [*J. Biol. Chem.*, **243**, 5809 (1968)]. In this paper, all the compounds are racemic. All the formulas depict only one of the respective racemates.

2) T. Iwasa, H. Yamamoto, and M. Shibata, *J. Antibiot.*, **23**, 595 (1970); S. Horii and Y. Kameda, *J. Chem. Soc., Chem. Commun.*, **1972**, 747.

3) T. Suami, S. Ogawa, K. Nakamoto, and I. Kasahara, *Carbohydr. Res.*, **58**, 240 (1977).

4) M. P. Kunstman, D. S. Tarbell, and R. L. Autrey, *J. Am. Chem. Soc.*, **84**, 4115 (1962).

5) S. Ogawa, I. Kasahara, and T. Suami, *Bull. Chem. Soc. Jpn.*, **52**, 118 (1979).

6) S. Nishimura, *Bull. Chem. Soc. Jpn.*, **32**, 61 (1959).

7) In the case of tri-*O*-acetyl-(1,3/2,4,6)-3,4-dibromo-6-hydroxymethyl-1,2-cyclohexanediol,[5] the displacement of the C-3 bromine atom by an azide ion *via* neighboring group participation of the C-2 acetoxyl group occurred almost simultaneously to give rise to a diazido compound.

Preparation of *N*-Acetylmuramyl-L-[U-^{14}C]alanyl-D-isoglutamine *via* a Novel Synthetic Route[1)]

Shoichi KUSUMOTO, Kazuhiro IKENAKA, and Tetsuo SHIBA*

Department of Chemistry, Faculty of Science, Osaka University, Toyonaka, Osaka 560

(Received October 16, 1978)

For the investigation on the action mechanism of immunoadjuvant active *N*-acetylmuramyl-L-alanyl-D-isoglutamine, its labeled compound, *i.e.*, *N*-acetylmuramyl-L-[U-^{14}C]alanyl-D-isoglutamine was synthesized. For this purpose, an entirely novel synthetic route for the muramyl dipeptide was exploited using cold materials and applied to the preparation of the labeled compound. A convenient synthetic procedure of isoglutamine derivatives is also described.

It has been known that the biologically important immune reactions, which participate in the self-defence mechanisms of living bodies against non-self materials, can be stimulated by immunoadjuvant substances such as bacterial cell walls. The common active structure in the cell walls was recently elucidated to be *N*-acetylmuramyl-L-alanyl-D-isoglutamine (**1**) by the synthetic studies by us[2)] and Merser *et al.*[3)] The muramyl dipeptide (**1**) exhibited remarkable activities not only for antibody production and delayed-type hypersensitivity, but also for so many other immunological systems.[4)]

However, in spite of the current importance of the adjuvant activity in the immunological and therapeutic fields, little has been known about the mechanism for this biological action. This seems to be mainly due to the fact that all the hitherto known natural adjuvants are high molecular materials of unknown or complex structures. Now, we can replace the cell walls with synthetic *N*-acetylmuramyl-L-alanyl-D-isoglutamine (**1**) as an effective adjuvant in many immuno reactions. Therefore, preparation of a labeled compound of the muramyl dipeptide (**1**) has been much urged for investigation of its action mechanism. We thus intended to prepare *N*-acetylmuramyl-L-[U-^{14}C]alanyl-D-isoglutamine (**1a**) of extremely high specific radioactivity, since we aimed a whole body autoradiographic study as a preliminary approach to obtain informations for its local distribution. For this reason, the synthesis must be carried out in μmol scale and preferably in a one-flask system starting from the commercial L-alanine labeled uniformly with ^{14}C with highest specific activity available. Our previous method[2)] can not be applied for this purpose because of several technical disadvantages. Thus, a novel synthetic route to the muramyl dipeptide (**1**) was established in this investigation and the labeled compound (**1a**) was successfully prepared by its application. It should be noted that this new route also serves as an alternative method for a facile and convenient preparation of cold muramyl dipeptide (**1**).

The new synthetic route designed for the preparation of *N*-acetylmuramyl-L-[U-^{14}C]alanyl-D-isoglutamine (**1a**) must fulfil the following requirements. i) The synthesis must be throughout performed in a μmol scale without experimental difficulties. ii) Excess reagents should be used in all reaction steps in order to utilize the radioactive fragments as effective as possible. iii) By-products and excess reagents are better removed by simple procedures such as evaporation or extraction so that the products can be subjected to the successive reactions without transfer into other vessels. Taking account of these principles, the basic strategy of the synthesis was adopted first to prepare a free dipeptide, L-alanyl-D-isoglutamine (**2**), and then to couple it with a muramic acid derivative by means of an active ester method. Only acid-labile protective groups were employed in order to avoid the procedure of hydrogenolysis where an adsorption to the catalyst might occur causing considerable loss of materials.

The synthetic route based on the above principles was first examined with cold materials in preparative scales. The dipeptide, L-alanyl-D-isoglutamine (**2**) was prepared from *t*-butoxycarbonyl(Boc)-L-alanine (**3**) and D-isoglutamine *t*-butyl ester (**5**). To avoid the undesirable dehydration of the isoglutamine moiety by excess condensation reagent, Boc-L-alanine was converted into 1-succinimidyl ester (**4**) in advance and then coupled with **5** giving Boc-L-alanyl-D-isoglutamine *t*-butyl ester (**6**). The product was then treated with trifluoroacetic acid (TFA) to afford pure dipeptide (**2**) TFA salt. This was identified with the authentic sample obtained previously.[2)]

The following alternative pathway for the preparation of the dipeptide (**2**) was also examined. Thus, an isoglutamine derivative in which 4,4′-dimethoxybenzhydryl group[5)] was employed for amide protection, *i.e.*, D-glutamic acid α-4,4′-dimethoxybenzhydrylamide γ-*t*-butyl ester (**7**), was condensed with Boc-L-alanine (**3**) by means of dicyclohexylcarbodiimide (DCC)–*N*-hydroxysuccinimide (HONSu). However, several unknown by-products were formed in this coupling reaction unexpectedly and the pure protected dipeptide, Boc-L-alanyl-D-glutamic acid α-4,4′-dimethoxybenzhydrylamide γ-*t*-butyl ester (**8**), could be obtained only after repeated recrystallization. Although **8** could be converted into the free dipeptide (**2**) by action of dry hydrogen chloride in acetic acid, this second route seemed not to be advantageous for the purpose of preparation of the labeled compound because of the difficulty of purification of **8**.

Nevertheless, the preparative methods of the D-isoglutamine derivatives (**5** and **7**) used in the above syntheses are worthwhile to be described here, since they were both prepared from benzyloxycarbonyl(Z)-D-isoglutamine (**9**) which was obtained *via* a new convenient procedure. Ammonia gas was introduced into a solution of Z-D-glutamic acid anhydride in THF, and the resulting mixture of α- and γ-amide was recrystallized

from methanol–ether. Pure Z-D-isoglutamine (**9**) ammonium salt was readily isolated in 64% yield after this simple recrystallization, while isomeric Z-D-glutamine remained in the mother liquor.[6] Hydrogenolysis of **9** followed by the perchloric acid-catalyzed transesterification with *t*-butyl acetate afforded D-isoglutamine *t*-butyl ester (**5**). D-Glutamic acid α-4,4′-dimethoxybenzhydrylamide γ-*t*-butyl ester (**7**) was also obtained as follows. Condensation of **9** with 4,4′-dimethoxybenzhydrol in the presence of sulfuric acid afforded Z-D-glutamic acid α-4,4′-dimethoxybenzhydrylamide (**10**). Hydrogenolytic removal of Z-group[7] in **10** followed by transesterification with *t*-butyl acetate afforded **7** in a good yield.

For the coupling of the muramic acid moiety with the dipeptide (**2**) obtained by the first method described above, *N*-hydroxy-5-norbornene-2,3-dicarboximide (HONb)[8] was employed as a carboxyl activating agent, which was known to give good condensation yields particularly in aqueous media.[8,9] In order to prevent a formation of the undesirable intramolecular ester in the muramic acid moiety, its 4-hydroxyl group was protected with the *p*-anisylidene group, which can be removed afterward under a very mild acidic conditions. Thus, *N*-acetylmuramic acid was treated with *p*-anisaldehyde dimethyl acetal in *N*,*N*-dimethylformamide (DMF) in the presence of *p*-toluenesulfonic acid to give 4,6-*O*-*p*-anisylidene-*N*-acetylmuramic acid (**11**), which was then converted into HONb ester (**12**) in a usual manner. It was found to be advantageous to transform **11** without isolation directly into the active ester (**12**), since the *p*-anisylidene group was so highly acid-labile that it was slowly but spontaneously cleaved at **11** by action of the free carboxyl group on the own molecule.

The coupling of the muramic acid active ester (**12**) with the peptide moiety and the successive deprotection to the free muramyl dipeptide (**1**) were performed as follows. A solution of L-alanyl-D-isoglutamine (**2**) in aqueous dioxane was treated with an excess of the *p*-anisylidenemuramic acid active ester (**12**) until all the dipeptide was consumed. Evaporation of the solvent afforded a mixture of 4,6-*O*-*p*-anisylidene-*N*-acetylmuramyl-L-alanyl-D-isoglutamine (**13**) and 4,6-*O*-*p*-anisylidene-*N*-acetylmuramic acid (**11**).[10] The mixture was then treated with aqueous acetic acid to remove the anisylidene group. After evaporation of the solvent, the residue was subjected to preparative TLC on silica gel, and the desired *N*-acetylmuramyl-L-alanyl-D-isoglutamine (**1**) was separated from *N*-acetylmuramic acid and other by-products by developing with 1-butanol–acetic acid–butyl acetate–water (80:20:7:40). The final product (**1**) thus obtained was identified with the sample prepared in the previous work[2] in respects of TLC, NMR, and $[\alpha]_D$. In this preparative scale synthesis, the muramyl dipeptide (**1**) was obtained in a fairly good overall yield (41%) from the Boc-L-alanine active ester (**4**).

An application of this novel route to a small scale synthesis was next examined using still cold materials. Thus, a pyrex test tube (15×130 mm) with a standard ground-glass joint was used as a reaction flask. Extraction and evaporation of solvents were carried out by the procedures described in the experimental section.

L-Alanine could be quantitatively converted into the Boc derivative in μmol scale by use of Boc azide. The transformation from Boc-L-alanine (**3**) (1.89 mg, 10 μmol) to L-alanyl-D-isoglutamine (**2**) was then investigated in a one-flask procedure *via* three steps. DCC was also used in this experiment for the preparation of the active ester (**4**). *N*,*N*′-Dicyclohexylurea formed in the reaction course was removed in the final step after deprotection of the dipeptide.[11] The all operations could be carried out without difficulty as described in

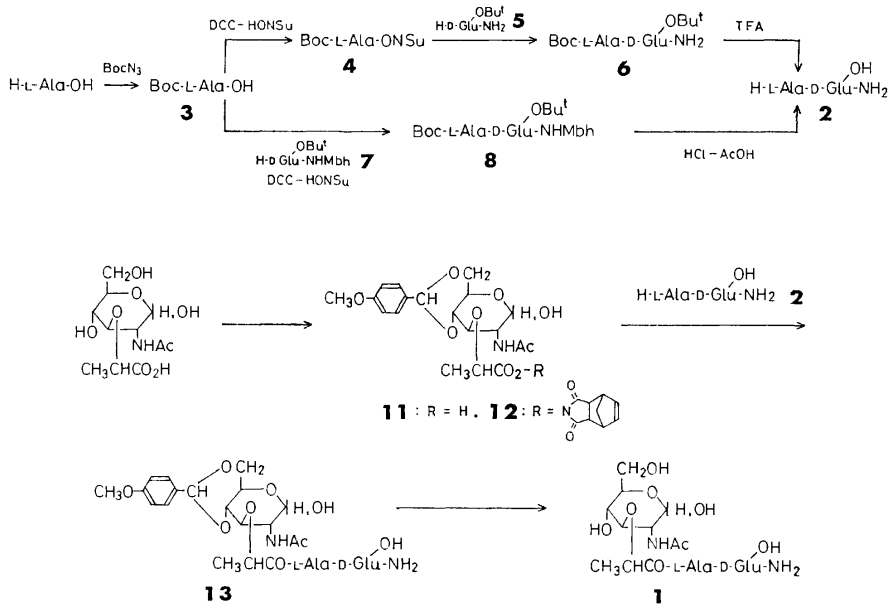

Boc = *t*-butoxycarbonyl
Mbh = 4,4′-dimethoxybenzhydryl
HONSu = *N*-hydroxysuccinimide
Bu^t = *t*-butyl
DCC = dicyclohexylcarbodiimide
Ac = acetyl

the experimental section. The chromatographically pure free dipeptide (**2**) was obtained in a total yield of 90% from Boc-L-alanine as calculated on the basis of amino acid analysis.

TLC examination revealed that the successive steps up to the muramyl dipeptide (**1**) from **2** could be also achieved satisfactorily even in a small scale experiment. Therefore, the new synthetic route became promissing for the preparation of labeled muramyl dipeptide (**1a**) in an extremely small scale. However, in order to apply the new procedure to a radioactive material, one more preliminary experiment prior to the final one was tried starting from diluted labeled L-alanine (10 μmol, 30 μCi) according to the same procedure. In this synthesis, overall 26% (7.7 μCi) of labeled muramyl dipeptide (**1a**) was obtained. The radiochemical purities of **2a** and **1a** were confirmed by a combined technique of TLC and a liquid scintillation counter.

On the basis of the successful results in the series of above experiments, the ultimate synthesis of the strongly labeled compound *via* the novel route was finally carried out. The commercial L-[U-^{14}C]alanine with highest specific activity available[12] was used as a starting material without dilution. All operations except the removal of *N,N'*-dicyclohexylurea were carried out in one test tube without transfer of labeled intermediates to other vessels. The procedures of actual synthesis are described in the experimental section. From 0.97 mCi of L-[U-^{14}C]alanine, *N*-acetylmuramyl-L-[U-^{14}C]alanyl-D-isoglutamine (**1a**) was obtained in a total yield of 46% (0.45 mCi) after purification with TLC.

Experimental

All melting points are uncorrected. TLC was performed on silica gel G, Merck, unless otherwise stated. For each synthesis of the labeled compound as well as the preliminary experiment with cold material in a μmol scale, all operations were carried out in a pyrex test tube (15×130 mm) with a standard ground-glass stopper. Extraction was carried out by mixing two phases in the test tube by means of an electric vibrator and then withdrawing the upper phase with a pipette. The solvent was evaporated by introduction of air stream through a capillary tube on surface of the solution in the tube under reduced pressure.

Boc-L-alanyl-D-isoglutamine t-Butyl Ester (6). *t*-Butoxycarbonyl(Boc)-L-alanine 1-succinimidyl ester (**4**) (0.86 g, 3.0 mmol) was added to an ice-cooled mixture of D-isoglutamine *t*-butyl ester (**5**) perchlorate[13] (0.96 g, 3.0 mmol) and triethylamine (0.42 ml, 3.0 mmol) in THF (20 ml). The mixture was stirred at room temperature overnight and then the solvent was evaporated *in vacuo*. The residue was taken up in ethyl acetate and worked up as usual. The product was crystallyzed from ethyl acetate–ether–hexane; yield, 0.93 g (83%); mp 132—134 °C. A sample for elemental analysis was obtained by further recrystallization from ethyl acetate–hexane; mp 132.5—133.5 °C; $[\alpha]_D^{26}$ −0.23°, $[\alpha]_{365}^{26}$ +3.94° (*c* 2.13, ethyl acetate).

Found: C, 54.75; H, 8.37; N, 11.11%. Calcd for $C_{17}H_{31}O_6N_3$: C, 54.67; H, 8.37; N, 11.25%.

L-Alanyl-D-isoglutamine (2) Trifluoroacetate from 6. Compound **6** (0.186 g, 0.50 mmol) was dissolved in trifluoroacetic acid (1.0 ml) and allowed to stand at room temperature for 30 min. Abs ether was added to the mixture to afford hygroscopic white powder, which was collected by filtration; yield, 166 mg (quantitative); mp 72 °C (dec) (with sintering at around 55 °C and resolidifying thereafter); $[\alpha]_D^{26}$ +18.7° (*c* 1.98, H_2O).[14]

Boc-L-alanyl-D-glutamic Acid α-4,4'-Dimethoxybenzhydrylamide γ-t-Butyl Ester (8). One molar solution of triethylamine in dioxane (0.45 ml, 0.45 mmol) was added to a stirred mixture of Boc-L-alanine (**3**) (0.076 g, 0.40 mmol), D-glutamic acid α-4,4'-dimethoxybenzhydrylamide γ-*t*-butyl ester (**7**) hydrochloride[13] (0.200 g, 0.43 mmol) and *N*-hydroxysuccinimide (HONSu) (0.058 g, 0.50 mmol) in dioxane (10 ml) and tetrahydrofuran (THF) (5 ml). After addition of dicyclohexylcarbodiimide (DCC) (0.103 g, 0.50 mmol) under ice-cooling, the mixture was stirred at room temperature overnight. Usual work-up and crystallization from methanol–acetone–water afforded a crude product, which was recrystallized twice from acetone–water; yield, 0.151 g (63%); mp 146—147 °C. A pure sample was only obtained after two more repetitions of recrystallization from ethyl acetate–hexane; mp 146.5—147.5 °C; $[\alpha]_D^{28}$ −3.3° (*c* 1.94, ethyl acetate).

Found: C, 64.18; H, 7.58; N, 7.01%. Calcd for $C_{32}H_{45}O_8N_3$: C, 64.09; H, 7.56; N, 7.01%.

L-Alanyl-D-isoglutamine (2) from 8. Compound **8** (6.0 mg, 0.01 mmol) was dissolved in 2 M dry HCl in acetic acid (1.0 ml, 2 mmol) and allowed to stand at room temperature for 40 h. After evaporation of the solvent *in vacuo*, the residue was dissolved in water and washed with ether. Evaporation of water *in vacuo* afforded **2** hydrochloride. This was identified with a sample obtained above from **6** by means of TLC (1-butanol–acetic acid–water, 4:1:2) and amino acid analysis.

Z-D-isoglutamine (9). DCC (5.49 g, 26.6 mmol) was added to an ice-cooled solution of Z-D-glutamic acid (6.23 g, 22.2 mmol) in THF (50 ml) with stirring. After the mixture had been stirred in an ice bath for 7 h, *N,N'*-dicyclohexylurea was filtered off. The filtrate was again cooled in an ice-salt bath, and ammonia gas was introduced with stirring for 15 min. After evaporation of the solvent *in vacuo*, the residue was crystallized from methanol–ether to give pure **9** ammonium salt; yield, 4.21 g (64%).

This ammonium salt (4.00 g, 13.5 mmol) was well ground and shaken with ethyl acetate (200 ml) and 1 M HCl (20 ml). The organic layer was washed with 1 M HCl and water, then dried over $MgSO_4$ and concentrated *in vacuo*. The colorless crystals were collected by filtration; yield, 3.29 g (87%); mp 174.5—175.5 °C. These were recrystallized from methanol–ether–hexane; mp 175—176 °C; $[\alpha]_D^{30}$ +5.61° (*c* 2.05, methanol)

Found: C, 55.60; H, 5.74; N, 9.95%. Calcd for $C_{13}H_{16}O_5N_2$: C, 55.71; H, 5.75; N, 10.00%.

D-Isoglutamine t-Butyl Ester (5) Perchlorate. Z-D-isoglutamine (**9**) (3.30 g, 11.8 mmol) was hydrogenolyzed in a mixture of methanol (100 ml) and water (60 ml) in the presence of palladium black catalyst. After usual work-up, recrystallization from water–acetone afforded D-isoglutamine; yield, 1.62 g (94%); mp 188.5—189 °C (dec). This compound (1.62 g, 11.1 mmol) was added to *t*-butyl acetate (150 ml) with stirring in the presence of 70% perchloric acid (1.5 ml, 13 mmol) at room temperature. As the starting material dissolved in about 30 min, another colorless crystals separated out slowly. After 18 h, the crystals were collected by filtration and recrystallized from methanol–ether; yield, 2.93 g (82% from **9**); mp 141—142 °C (dec); $[\alpha]_D^{26}$ −13.6° (*c* 2.00, H_2O).

Found: C, 35.65; H, 6.38; N, 9.17; Cl, 11.65%. Calcd for $C_9H_{18}O_3N_2\cdot HClO_4$: C, 35.71; H, 6.33; N, 9.25; Cl, 11.71%.

Z-D-glutamic Acid α-4,4'-Dimethoxybenzhydrylamide (10). To a solution of **9** (1.40 g, 5.0 mmol) in acetic acid (20 ml) was added 4,4'-dimethoxybenzhydrol (1.22 g, 5.0 mmol) and conc H_2SO_4 (0.02 ml). The mixture was stirred at room temperature overnight. Addition of abs ether afforded a

crystalline material, which was filtered and recrystallized from THF–hexane; yield, 2.04 g (81%); mp 209.5—210.5 °C; $[\alpha]_D^{26}$ −4.6° (*c* 2.05, THF).

Found: C, 66.51; H, 6.01; N, 5.46%. Calcd for $C_{28}H_{30}O_7N_2$: C, 66.39; H, 5.97; N, 5.53%.

D-Glutamic Acid α-4,4'-Dimethoxybenzhydrylamide γ-t-Butyl Ester (7) Hydrochloride. Compound **10** (2.53 g, 5.0 mmol) was suspended in acetic acid (25 ml) and hydrogenolyzed in the presence of palladium black catalyst. After evaporation of the solvent, the residue was crystallized from ethanol–ether to afford D-glutamic acid α-4,4'-dimethoxybenzhydrylamide as hygroscopic powder; yield, 1.55 g (83%).

This compound (0.74 g, 2.0 mmol) was dissolved in *t*-butyl acetate (20 ml) and stirred at room temperature in the presence of 70 % perchloric acid (0.24 ml, 2.1 mmol) for 3 days. After addition of ethyl acetate, the mixture was washed successively with saturated aqueous solution of $NaHCO_3$ and NaCl, dried and evaporated *in vacuo*. The residual syrup was dissolved in abs ether, and 2 M dry HCl in ethyl acetate (1.0 ml, 2.0 mmol) was added. Addition of hexane to the mixture afforded **7** hydrochloride, which was recrystallized from methanol–ether–hexane; yield, 0.31 g (33%); mp 210 °C (dec); $[\alpha]_D^{26}$ −6.0° (*c* 1.01, methanol).

Found: C, 61.37; H, 7.16; N, 5.86; Cl, 7.60%. Calcd for $C_{24}H_{32}O_5N_2 \cdot HCl \cdot 1/4H_2O$: C, 61.40; H, 6.98; N, 5.97; Cl, 7.55%.

4,6-O-p-Anisylidene-N-acetylmuramic Acid (11). *p*-Toluenesulfonic acid (27 mg, 0.14 mmol) was dissolved in a mixture of DMF and benzene (1: 1, 10 ml). From this solution, benzene was evaporated *in vacuo* to remove water completely. To the remaining solution, *N*-acetylmuramic acid[15] (0.40 g, 1.4 mmol) and *p*-anisaldehyde dimethyl acetal (0.95 g, 5.2 mmol) were added. The mixture was kept on a rotary evaporator at 15 mmHg and 40 °C for 2.5 h to remove resulting water, and then most of DMF was evaporated at 3 mmHg. The residue was dissolved in ether, washed with water and dried over $MgSO_4$. After evaporation of the solvent *in vacuo*, benzene was added to the residue. The gelatinous solid formed was filtered and recrystallized from methanol–ether–hexane; yield, 0.31 g (54%); mp 192 °C (dec).

Found: C, 55.65; H, 6.15; N, 3.31%. Calcd for $C_{19}H_{25}O_9N$: C, 55.47; H, 6.13; N, 3.40%.

4,6-O-p-Anisylidene-N-acetylmuramic Acid N-Hydroxy-5-norbornene-2,3-dicarboximide (HONb) Ester (12). DCC (0.17 g, 0.83 mmol) was added to an ice-cooled solution of **11** (0.28 g, 0.68 mmol) and HONb (0.15 g, 0.84 mmol) in THF (10 ml). The mixture was stirred overnight at room temperature. *N,N'*-dicyclohexylurea was filtered off and the solvent was evaporated *in vacuo*. The residue was dissolved in ethyl acetate, washed successively with saturated aqueous solution of $NaHCO_3$ and NaCl, and then dried over $MgSO_4$. After evaporation of the solvent, the residue was subjected to silica gel column chromatography. Elution with $CHCl_3$–acetone (4: 1) and complete evaporation of the solvent afforded pure **12** as white powder; yield, 0.17 g (44%); mp 115 °C.

In an alternative way, the same compound (**12**) was prepared directly from *N*-acetylmuramic acid without isolation of the anisylidene derivative (**11**) as the intermediate. Thus, after formation of **11**, the reaction mixture was neutralized with triethylamine, and then treated with HONb and DCC. In this case, starting from *N*-acetylmuramic acid (0.15 g, 0.51 mmol), **12** was obtained in a rather better yield (0.17 g, 58 %).

N-Acetylmuramyl-L-alanyl-D-isoglutamine (1). L-Alanyl-D-isoglutamine (**2**) trifluoroacetate (54 mg, 0.16 mmol) was dissolved in water (0.5 ml). To this solution were added 1 M triethylamine in dioxane (0.32 ml, 0.32 mmol) and **12** (92 mg, 0.16 mmol) in dioxane (0.6 ml). The mixture was allowed to stand at room temperature for 20 h, then 1 M triethylamine in dioxane (0.30 ml, 0.30 mmol) and **12** (79 mg, 0.14 mmol) in dioxane (0.5 ml) were again added. After the mixture had been allowed to stand at room temperature for further 20 h, the solvent was removed *in vacuo*. The residue was dissolved in a mixture of acetic acid (6 ml) and water (3 ml) and left stand at room temperature for 18 h. After removal of the solvent *in vacuo*, the residue was dissolved in water and washed with ether. Evaporation of the aqueous phase *in vacuo* afforded a pale yellow syrup, which was subjected to preparative TLC; commercial pre-coated silica gel plates were used (seven plates of Wako-gel F_{254}, 0.25 mm thickness, 20×20 cm, Wako Pure Chemicals Co., Ltd.)[16] with a solvent system of 1-butanol–acetic acid–butyl acetate–water (80:20:7:40). The main band was extracted with 80% ethanol, the solvent was evaporated *in vacuo* and the residue was triturated with 99% ethanol. After removal of the insoluble material, ethanol was again evaporated *in vacuo*. The remaining substance was dissolved in water and passed through a short column of Amberlite IRC50 (H^+ form). Lyophilization of the eluate afforded **1**; yield, 39 mg (50% from **2**); $[\alpha]_D^{25}$ +34.4° (*c* 0.550, H_2O after equilibration). This product was identified by TLC and NMR spectrum with the sample ($[\alpha]_D^{15}$ +33.1° (*c* 0.51, H_2O)) obtained previously.[2]

Small Scale Preparation of L-Alanyl-D-isoglutamine (2) from Boc-L-alanine. To a solution of Boc-L-alanine (1.89 mg, 10 μmol) and HONSu (1.96 mg, 17 μmol) in THF (0.27 ml) was added DCC (3.57 mg, 17 μmol) in THF (0.17 ml) under ice-cooling. After the mixture had been allowed to stand overnight, the solvent was evaporated *in vacuo*. The residue was dissolved in $CHCl_3$ (1.5 ml) and the excess DCC was decomposed with acetic acid. The solution was then washed with aqueous $NaHCO_3$ and water. After evaporation of the solvent *in vacuo*, $CHCl_3$ (1 ml) was added to the residue and evaporated again *in vacuo* to remove the remaining water. To the residue were added D-isoglutamine *t*-butyl ester (**5**) perchlorate (5.6 mg, 18.5 μmol) and 0.1 M solution of triethylamine in $CHCl_3$ (0.20 ml, 20 μmol). The mixture was allowed to stand at room temperature for 20 h, then diluted with $CHCl_3$ (1.5 ml) and washed successively with aqueous $NaHCO_3$, 1 M HCl and water. The residue obtained after evaporation of the solvent *in vacuo* was dissolved in TFA (1 ml). After 1.5 h at room temperature, TFA was removed *in vacuo*, the residue was dissolved in water, and insoluble *N,N'*-dicyclohexylurea was removed by filtration through a sintered glass filter. Evaporation of water from the filtrate afforded **2** TFA salt, which showed a single ninhydrin-positive spot on TLC. The yield was deduced to be 90% by means of amino acid analyser.

N-Acetylmuramyl-L-[U-^{14}C]alanyl-D-isoglutamine (1a). To a solution of L-[U-^{14}C]alanine (0.97 mCi, 5.9 μmol)[12] in water (0.5 ml) were added 0.1 M solution of triethylamine in dioxane (0.5 ml, 50 μmol) and Boc azide (10 μl, 74 μmol). While the mixture was allowed to stand at room temperature for 50 h, Boc azide (74 μmol×2) and triethylamine (20 μmol) were again added. After evaporation of the solvent, the residue was dissolved in water (1 ml) and washed with ether. After complete removal of water by coevaporation with ethanol and $CHCl_3$, dry HCl (4.8 μM) in THF (0.12 ml) and HONSu (1.15 mg, 10 μmol) in THF (0.1 ml) were added to the residue. To this mixture was added DCC (2.1 mg, 10 μmol) in THF (0.1 ml) under cooling in an ice bath. Thereafter, the mixture was treated in the same manner as described above for the cold material. Thus, the active ester (**4a**) was coupled with **5** HCl salt (2.4 mg, 10 μmol) in $CHCl_3$ in the presence of triethylamine and the resulting protected dipeptide (**6a**) was

treated with TFA (1 ml). After *N,N'*-dicyclohexylurea had been removed by filtration, the filtrate was condensed to give the free dipeptide (**2a**), which was again dissolved in water (0.3 ml). To this solution were added 4,6-*O*-*p*-anisylidene-*N*-acetylmuramic acid HONb ester (**12**) (3.6 mg, 6.3 μmol) in dioxane (0.3 ml) and triethylamine (60 μmol). During next 26 h, two portions of **12** (6.1 and 3.2 μmol) were added and the final mixture was left to stand overnight. The solvent was then removed by evaporation, and the residue was treated with 66 % aqueous acetic acid (1 ml) for 6 h. After evaporation, the residue was dissolved in water (1 ml), washed with ether and again evaporated. The residue was dissolved in methanol and subjected to preparative TLC as described for the preparation of cold **1** using one 20×20 cm plate. The location of the radioactive substance on the plate was detected with a Geiger-Müller counter and the corresponding band was extracted with 80% ethanol to give chromatographically pure **1a**; total activity 0.45 mCi (overall 46 %).

References

1) This work was presented at the 36th National Meeting of the Chemical Society of Japan, Osaka, April, 1977; cf. Abstract II, p. 1233. It was also reported in a preliminary form; S. Kusumoto, K. Ikenaka, and T. Shiba, *Tetrahedron Lett.*, **1977**, 4055.

2) a) S. Kotani, Y. Watanabe, F. Kinoshita, T. Shimono, I. Morisaki, T. Shiba, S. Kusumoto, Y. Tarumi, and K. Ikenaka, *Biken J.*, **18**, 105 (1975); b) S. Kusumoto, Y. Tarumi, K. Ikenaka, and T. Shiba, *Bull. Chem. Soc., Jpn.*, **49**, 533 (1976).

3) C. Merser, P. Sinaÿ, and A. Adam, *Biochem. Biophys. Res. Commun.*, **66**, 1316 (1975).

4) a) I. Azuma, K. Sugimura, T. Taniyama, M. Yamawaki, Y. Yamamura, S. Kusumoto, S. Okada, and T. Shiba, *Infect. Immun.*, **14**, 18 (1976); b) S. Kotani, Y. Watanabe, T. Shimono, K. Harada, T. Shiba, S. Kusumoto, K. Yokogawa, and M. Taniguchi, *Biken J.*, **19**, 9 (1976); c) A. Tanaka, R. Saito, K. Sugiyama, I. Morisaki, S. Kotani, S. Kusumoto, and T. Shiba, *Infec. Immun.*, **15**, 332 (1977); d) S. Kotani, Y. Watanabe, F. Kinoshita, K. Kato, K. Harada, T. Shiba, S. Kusumoto, Y. Tarumi, K. Ikenaka, S. Okada, S. Kawata, and K. Yokogawa, *Biken J.*, **20**, 5 (1977); e) A. Tanaka, S. Nagao, R. Saito, S. Kotani, S. Kusumoto, and T. Shiba, *Biochem. Biophys. Res. Commun.*, **77**, 621 (1977); f) Y. Nagai, K. Akiyama, K. Suzuki, S. Kotani, Y. Watanabe, T. Shimono, T. Shiba, S. Kusumoto, F. Ikuta, and S. Takeda, *Cellular Immunology*, **35**, 158 (1978).

5) W. König and R. Geiger, *Chem. Ber.*, **103**, 2041 (1970).

6) We also observed a preferential crystallization of Boc-α-glutamylglycine benzyl ester dicyclohexylammonium salt to the corresponding γ-peptide derivative.[9]

7) Almost no transesterification occurred when **10** itself was treated with *t*-butyl acetate and perchloric acid probably due to steric hindrance of the two voluminous protective groups.

8) M. Fujino, S. Kobayashi, M. Obayashi, T. Fukuda, S. Shinagawa, and O. Nishimura, *Chem. Pharm. Bull.*, **22**, 1857 (1974).

9) S. Kusumoto, K. Ikenaka, and T. Shiba, *Bull. Chem. Soc. Jpn.*, submitted.

10) Because of the high acid-lability of the *p*-anisylidene group (see above in the text), attempts to isolate pure **11** led to loss of the material. Separation of the excess muramic acid component was readily accomplished by preparative TLC after deprotection.

11) Preliminary experiments indicated that use of DCC gave the best result for this reaction even though the insoluble *N,N'*-dicyclohexylurea had to be anyhow removed. With the water-soluble carbodiimide, *i.e.*, 1-ethyl-3-(3-dimethylaminopropyl)carbodiimide, the yield of the active ester (**4**) was very low presumably due to the acylurea formation. Other coupling methods such as mixed anhydride were not suitable actually for small scale experiments.

12) 164 mCi/mmol, 87 % isotopic abundance in all carbon atoms; supplied by The Radiochemical Centre, Amersham.

13) Preparation of this compound is described below.

14) The same compound, **2** TFA salt, was obtained by action of TFA on Boc-L-alanyl-D-isoglutamine;[2b] mp 72 °C (dec) (with sintering at 52 °C and resolidifying); $[\alpha]_D^{26}$ +18.4° (*c* 1.96, H_2O).

15) H. M. Flowers and R. W. Jeanloz, *J. Org. Chem.*, **28**, 2983 (1963).

16) Good separation of **1** and *N*-acetylmuramic acid was not achieved with pre-coated silica gel 60 plate, Merck.

Furanoeremophilan-14β,6α-olide. A New Furanosesquiterpene Lactone of an Eremophilane-type from *Ligularia Hodgsoni* Hook, f.[1]

Yoshiaki Ishizaki, Yoshiaki Tanahashi, Takahiko Tsuyuki,
Takeyoshi Takahashi,* and Kazuo Tori**

Department of Chemistry, Faculty of Science, The University of Tokyo, Hongo, Bunkyo-ku, Tokyo 113
***Shionogi Research Laboratory, Shionogi & Co., Ltd., Fukushima-ku, Osaka 553*

(Received October 21, 1978)

A new sesquiterpene lactone of an eremophilane-type was isolated from *Ligularia Hodgsoni* Hook, f., and the structure including the absolute stereochemistry was shown to be furanoeremophilan-14β,6α-olide.

In connection with chemical investigations[2] on plants of the genus *Ligularia* (Compositae), we examined sesquiterpene constituents of *Ligularia Hodgsoni* Hook, f. (Japanese name: Tōgebuki), and isolated a new sesquiterpene lactone together with furanoeremophilane,[3,4] bakkenolide-A[5] (fukinanolide[6]) and eremophilenolide.[4,7] This paper describes the structure determination leading to furanoeremophilan-14β,6α-olide (**1**) for this new sesquiterpene lactone.

A benzene extract of dried roots of the plant was further treated with petroleum ether and the petroleum ether-soluble fraction was subjected to purification by sublimation and recrystallization to afford a furanolactone (**1**) (pink color to the Ehrlich test) as crystals, mp 136—138 °C. Elemental analysis and the mass spectrum indicate the formula $C_{15}H_{18}O_3$. The IR, UV, and ^1H NMR spectra showed the presence of a tertiary methyl, an olefinic methyl, a γ-lactone, and a β-methyl-substituted furan moiety with an α-proton.[8] Signals due to a secondary methyl was absent (*cf.* Table 1 and Experimental).

The lactone (**1**), on reduction with lithium aluminium hydride, gave a diol (**2**), which was readily converted into an ether (**3**) by treatment with *p*-toluenesulfonyl chloride in pyridine. The ^1H NMR spectrum of **3** showed signals due to the AB part of an ABX spin system; this implies the presence of methylene protons in the α-position and of a methine proton in the β-position to the ether oxygen atom. The presence of a tertiary methyl and a proton on a carbon atom bearing the ether oxygen atom was also shown in the NMR spectrum (Table 1).

The carbon skeleton and the absolute configuration of the lactone (**1**) were shown by the following transformation. The lactone (**1**) was subjected to hydrogenolysis in the presence of 10% palladium-charcoal in ethanol to afford a carboxylic acid (**4**). The presence of the carboxyl group and the absence of the hydroxyl group in **4** were suggested by the IR spectrum and the formation of an ester. Reduction of the carboxylic acid

Table 1. Chemical shifts (δ) and coupling constants (Hz) of **1**, **3**, **8**, and **10**

	1		**3**	**8**		**10**	
	$CDCl_3$	$(CD_3)_2CO$	$CDCl_3$	$CDCl_3$	$(CD_3)_2CO$	$CDCl_3$	$(CD_3)_2CO$
5-Me	1.26	1.24	1.16	1.25	1.27	1.12	1.11
11-Me	2.03	2.01	2.03	2.05	2.02	2.02	1.97
9α-H		2.76	2.64	2.45	2.43	2.28	2.28
	2.7						
9β-H		2.62	2.48	2.87	2.90	2.82	2.82
4-H	a)	a)	a)	a)	2.67	a)	a)
6β-H	5.08	5.08	4.63	4.90	4.97	4.17	4.10
14α-H	—	—	3.91	—	—	4.00	3.91
14β-H	—	—	3.53	—	—	3.78	3.75
12-H	7.06	7.19	7.01	7.09	7.21	7.04	7.10
J-values							
9α,9β		−17.3	−16.6		−17.1		−16.9
9α,10		11.3	11.5		1.7		1.9
9β,10		5.9	6.1		6.3		5.6
6,9α		1.8	1.8		0.3		b)
6,9β		1.2	1.3		1.5		1.5
9α,12		b)	b)		0.5		0.5
9β,12		b)	b)		0.9		0.9
11,12		1.0	1.0		1.2		1.1
12,13		1.1	1.1		1.1		1.1
14α,14β		—	−7.4		—		−9.0
4,14α		—	7.3		—		8.6
4,14β		—	11.3		—		3.6

a) Undeterminable. b) Not measured.

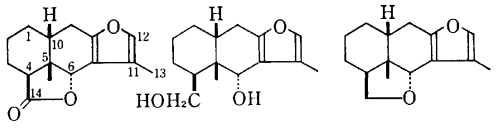

1 2 3

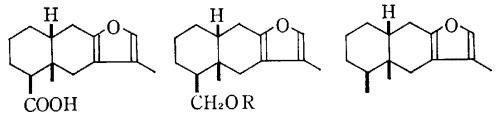

4 5 R=H 6 R=Ts 7

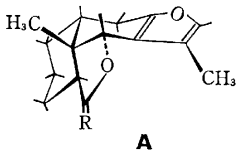

A

1 R = O
3 R = H₂

(**4**) with lithium aluminium hydride gave an alcohol (**5**), which was subsequently converted into a tosylate (**6**). The tosylate (**6**) was treated with lithium aluminium hydride to furnish the known furanoeremophilane (**7**).[3,9]

Since the basic skeleton of the lactone (**1**) was shown to consist of furanoeremophilane, the structure, furanoeremophilan-14β,6ξ-olide, is suggested for this lactone on the basis of the spectral data, showing the absence of the secondary methyl and the presence of the γ-lactone. The structure **3** for the ether is compatible with the spectral data. However, the configuration of the carbon atom in the 6-position bearing the ether-type oxygen atom in the lactone moiety was still obscure. The configuration at C-6 and the stereostructure could be established by the NMR measurement using spin-decoupling experiments and intramolecular nuclear Overhauser effect (NOE) measurements.[10] The result on **1** is shown in Tables 1 and 2. The fact that 6-H is only coupled weakly ($^5J<2$ Hz) to the allylic 9α- and 9β-protons, suggests that the 6-H is adjacent to the furan ring and that the other neighbor, C-5, bears no proton. On saturation of the signals due to the tertiary methyl at C-5β and the β-methyl on the furan ring, the signal due to the 6-H showed increases by 28 and 6% in area, respectively. These observations imply that the 6-H is situated *cis* to the tertiary methyl, indicating 6β-H orientation, and is attached to the other β-position on the furan ring. On triple irradiation at the resonance frequencies of 6-H and 12-H in acetone-d_6, the signals due to 9α-H and 9β-H exhibited the AB part of an ABX spin system, which gave $^2J_{9\alpha,9\beta}=-17.3$, $^3J_{9\alpha,10}=11.3$, and $^3J_{9\beta,10}=5.9$ Hz. Therefore, one of the methylene protons on C-9 was shown to be in *trans* or eclipsed conformation with respect to 10β-H. Triple irradiation on 12-H and 11-methyl signals determined two homoallylic coupling constants, $^5J_{6,9\alpha}=1.8$ and $^5J_{6,9\beta}=1.2$ Hz.[11] These two large ^5J values indicate that the 6-H has a quasi-axial conformation.

Interpretation of the NMR spectrum of **3**, as shown in Table 1, is in full accord with that of the data on the lactone (**1**). This means that no stereochemical change occurred during the transformation of **1** to **3**. The β-configuration of C-14 methylene was supported by the following NOE measurement. On saturation of the signal due to the 5β-methyl by double irradiation, the signal due to one of the methylene protons, 14β-H, at δ 3.53 ($^3J_{4,14\beta}=11.3$ and $^2J_{14\alpha,14\beta}=-7.4$ Hz) showed a substantial increase in area, while 14α-H signal at δ 3.91 ($^3J_{4,14\alpha}=7.3$ and $^2J_{14\alpha,14\beta}=-7.4$ Hz) caused no increase in area (Table 2).

Table 2. Nuclear overhauser effects
(±2%, in $CDCl_3$)

Observed proton	Saturated proton	1	3	8	10
12-H	11-Methyl	22	17	22	16
6β-H	11-Methyl	6	7	4	6
6β-H	5-Methyl	28	23	20	16
14β-H	5-Methyl	—	8	—	8
14α-H	5-Methyl	—	−2	—	0
9β-H	5-Methyl	a)	a)	a)	0
4-H	5-Methyl	b)	b)	≈15	b)

a) Not measured. b) Unobservable.

It is concluded that the structure including the absolute configuration of the new lactone (**1**) should be formulated as furanoeremophilan-14β,6α-olide and the stereostructure could be depicted as shown in **A**.

During the purification of the lactone (**1**), it was shown that the lactone (**1**) isomerizes easily into franoeremophilan-14α,6α-olide (**8**) on treatment with a base. The lactone (**1**) in benzene was kept contacting with basic alumina for 6 h and eluted with benzene. The eluent was examined by GLC and was shown to be a mixture of **1** and **8** in a ratio of 1 : 5. Prolonged contact with alumina resulted in a preferential isomerization into **8** accompanying concomitant hydrolysis of the lactones. Repetition of fractional recrystallization of the isomeric mixture of **1** and **8** gave pure furanoeremophilan-14α,6α-olide (**8**). The isomerized lactone (**8**) showed similar spectral features (Table 1) to those of **1**, and gave an ether (**10**) by the same treatment as in the case of **1**. Reduction of **8** with lithium aluminium hydride gave

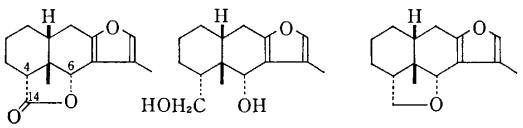

8 9 10

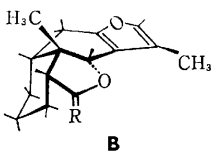

B

8 R = O
10 R = H₂

a diol (**9**; not identical with **2**), which, on dehydration with *p*-toluenesulfonyl chloride in pyridine, afforded the ether (**10**; not identical with **3**). From these observations, the isomerized lactone (**8**) was inferred to be a 4-epimer of **1**.

Proton magnetic double and triple resonance experiments gave the information on the stereochemistry of **8** and **10**. On triple irradiation at the resonance frequencies of 6-H and 12-H in **8**, the signals of 9α-H and 9β-H exhibited the AB part of an ABX spin system, which gave coupling constants, $^2J_{9\alpha,9\beta}=-17.1$, $^3J_{9\alpha,10}=1.7$, and $^3J_{9\beta,10}=6.3$ Hz. Irradiation on 12-H revealed the presence of the two homoallylic coupling constants, $^5J_{6,9\alpha}\leq 0.3$ and $^5J_{6,9\beta}=1.5$ Hz, between 6-H and the methylene protons on C-9. On triple irradiation at the resonance frequencies of 6-H and 11-methyl, the signal due to 12-H showed a quartet as the X part of an ABX spin system. This observation indicates the presence of a long-range coupling between 12-H and the methylene protons on C-9 ($^5J_{9\alpha,12}\leq 0.5$ and $^5J_{9\beta,12}=0.9$ Hz). On saturation of the signal due to the 5-methyl group by double irradiation, a triplet signal at δ 2.67 caused an increase in area (Table 2), indicating that the triplet could be assignable to 4β-H and, therefore, the lactone carbonyl grouping in **8** is oriented in the α-configuration.

The fact that the NMR spectrum of the ether (**10**) is similar to that of the epimerized lactone (**8**) indicates that there is no apparent conformational difference between **10** and **8**. In comparison of the NMR spectra of **1** and **3** with those of **8** and **10**, the following differences are seen: 1) the $^3J_{9\alpha,10}$ values of **8** and **10** (1.7 and 1.9, respectively) are small compared with those of **1** and **3** (11.3 and 11.5 Hz, respectively); 2) the $^3J_{4,14\beta}$ value of **3** (11.3) is larger than that of **10** (3.6 Hz); and 3) in the spectrum of **10**, the 6-H signal is shifted to a higher field by −0.46 ppm in $CDCl_3$ than that of **3**. The NOEs observed for **8** and **10** are quite similar to those observed for **1** and **3**, respectively, except for the data of 4-H (Table 2). From these observations, conformation **B** can be suggested to be the most popular in solution for furanoeremophilan-14α,6α-olide (**8**) and the ether (**10**).

Experimental

General Procedures. All melting points were measured on a hot block, unless otherwise stated, and reported uncorrected. IR spectra were taken on a Hitachi EPI-G2 spectrometer. UV absorption spectra were determined in a methanol solution on a Hitachi EPS-3 spectrometer. ORD curves were measured on a JASCO Model ORD/UV-5 spectrometer. Measurements of optical rotation were carried out using a JASCO-SL polarimeter. ^{1}H NMR spectra were taken on a JNM-3H-60, a JNM-4H-100 spectrometer (JEOL), or a Varian HA-100 spectrometer in the internal TMS-locked mode. Proton magnetic double and triple resonance experiments were performed using the Varian HA-100 spectrometer with two Hewlett-Packerd HP-200 ABR audio-oscillators and an HP-5212A electronic counter. NOEs were measured by % increases in integrated signal intensities with necessary caution.[10] Chemical shifts are expressed in δ (ppm downfield from internal TMS) and coupling constants in Hz. Accuracies are *ca.* ±0.02 ppm for δ and ±0.2 Hz for *J* values. Mass spectra were measured on a Hitachi RMU-6-Tokugata mass spectrometer at 70 eV with a direct inlet system, unless otherwise stated.

GLC analyses were carried out using a Shimadzu GC-4APF equipped with a hydrogen flame ionization detector (column: Diasolid H-523 (2 m), temp 230 °C). Column chromatography was carried out on silica gel (Wakogel C-200) or on activated alumina (Showa Chemicals). Kieselgel G (E. Merck) was used for analytical (in 0.25 mm thickness) and preparative (in 0.5 mm thickness) TLC.

Isolation. Dried roots (1.7 kg) of *Ligularia Hodgsoni* Hook, f. were extracted with benzene (2.5 l) for 4 days. The extraction under the same conditions was repeated three times and the extracts were combined and concentrated to give a dark brown tar (54 g). The residue was dissolved in petroleum ether with warming and insoluble materials were removed by decantation. The organic layer, on evaporation, gave a residue (46 g), which was sublimed under reduced pressure. Recrystallization of the sublimate (11 g), which was obtained at 100—120 °C (bath temperature), from ethyl acetate afforded furanoeremophilan-14β,6α-olide (**1**; *ca.* 10 g) as white needles, mp 136—138 °C (in a sealed tube); $[\alpha]_D$ −45° (*c* 0.45, dioxane); UV λ_{max} 217 nm (ε 8500); IR (Nujol) 3140, 3090, 1767, 1634, 1564, and 1082 cm^{-1}; NMR (Table 1); MS *m/e* (%) 246 (M^+; 41), 202 (100), 187 (72), 173 (36), 159 (88), 145 (85), 131 (20), 115 (22), 95 (48), 91 (44), 79 (25), 77 (35), 67 (23), 65 (21), and 43 (15); ORD (*c* 0.45, dioxane) $[\alpha]^{20}$ (at λ nm) −38° (650), −58° (500), −67° (400), −15° (330), +45° (310), +336° (280), +1000° (260), +4980° (238), +5040° (234), and +4540° (228); Found: C, 73.10; H, 7.35 %. Calcd for $C_{15}H_{18}O_3$: C, 73.14; H, 7.37 %.

The materials sublimed below 100 °C and the mother liquor of the recrystallization were combined (total weight: 11 g) and chromatographed over silica gel (400 g). Elution with petroleum ether gave furanoeremophilane (*ca.* 50 mg).[3,4] Further elution with petroleum ether–benzene (100: 3) provided bakkenolide-A (690 mg),[5,6] additional furanoeremophilan-14β,6α-olide (**1**; 2.9 g), and eremophilenolide (10 mg, after purification by sublimation).[4,7]

Reduction of Furanoeremophilan-14β,6α-olide (1) with Lithium Aluminium Hydride. A mixture of **1** (500 mg) and lithium aluminium hydride (700 mg) in dry ether was heated under reflux for 2 h. Usual treatment and crystallization from ether gave a diol (**2**; 400 mg) as a white powder, mp 197—198 °C; UV λ_{max} 224 nm (ε 7500); IR (Nujol) 3200, 1638, and 1552 cm^{-1}; ^{1}H NMR [$(CD_3)_2CO$] δ 1.16 (3H, s; *t*-Me), 1.97 (3H, d; –C=C–Me), 4.3 and 4.5 (2H, m; –CH–C<u>H</u>$_2$–OH), 4.68 (1H, br s; –C<u>H</u>–OH), 5.55 and 5.72 (each 1H, s; –OH), and 7.11 (1H, t; –C=C–H); Found: C, 71.72; H, 8.64%. Calcd for $C_{15}H_{22}O_3$: C, 71.97; H, 8.86%. The mass spectrum was the same as that of the ether (**3**).

Dehydration of the Diol (2). A mixture of diol (**2**; 200 mg) and *p*-toluenesulfonyl chloride (350 mg) in pyridine (3 ml) was allowed to stand at room temperature overnight. The reaction product was extracted with ether and the extract was evaporated to afford a yellow residue (200 mg), which was chromatographed over silica gel (6 g). Elution with benzene gave an ether (**3**; 110 mg) as white needles, mp 114—115 °C (from petroleum ether); $[\alpha]_D^{21}$ −65° (*c* 0.40, dioxane); UV λ_{max} 218 nm (ε 7000); IR (Nujol) 3140, 3100, 1640, 1567, and 1084 cm^{-1}; NMR (Table 1); MS *m/e* (%) 232 (M^+; 97), 217 (30), 202 (35), 187 (72), 173 (36), 159 (88), 145 (100), 119 (59), 95 (58), 91 (88), 79 (56), 77 (64), 67 (60), 65 (41), and 55 (40); ORD (*c* 0.40, dioxane) $[\alpha]_D^{21.5}$ (at λ nm) −55° (650), −90° (500), −128° (400), −145° (350), −108° (300), +325° (260), +800° (250), +2190°

(240), and +1630° (230); Found: C, 77.64; H, 8.75%. Calcd for $C_{15}H_{20}O_2$: C, 77.55; H, 8.68%.

Acetylation of the Diol (2). Acetic anhydride (0.2 ml) was added to a solution of diol (**2**; 77 mg) in pyridine (3 ml) and the reaction mixture was allowed to stand at room temperature overnight. Methanol (0.2 ml) was added to the mixture and the reaction product was extracted with ether. The ethereal extract was evaporated to afford a residue, which showed three spots on TLC. Only major product (38 mg) was isolated as a colorless oil by column chromatography on alumina (3 g). The structure was revealed to be a 14-acetoxy derivative of the diol (**2**) by the NMR spectrum. IR (neat) 3400, 1740, 1640, and 1560 cm^{-1}; NMR (C_6D_6) δ 0.85 (3H, s; *t*-Me), 2.07 (3H, d, J=1.2 Hz; -C=C-Me), 1.66 (3H, s; -CO-Me), 4.0 and 4.5 (dd, $J_{14\alpha,14\beta}=-11$, $J_{4,14\alpha}=7$, and $J_{4,14\beta}=4$ Hz; -CH-C<u>H</u>$_2$-O-), 4.22 (1H, br s; -C<u>H</u>-OH), and 7.05 (1H, br s; -C=C-H).

Hydrogenolysis of Furanoeremophilan-14β,6α-olide (1). A solution of furanoeremophilan-14β,6α-olide (**1**; 1.16 g) in ethanol (40 ml) was stirred under an atmospheric pressure of hydrogen in the presence of 10% palladium-charcoal (300 mg) at room temperature for 2 h. Usual work-up afforded a residue (1.2 g), which was sublimed under reduced pressure at 80—100 °C to give a crude carboxylic acid (**4**) as a white powder. The crude product was shown to contain unchanged starting material by TLC. Repetition of chromatography on silica gel furnished analytically pure carboxylic acid (**4**) as a colorless glass, UV λ_{max} 221 nm (ε 6800); IR (Nujol) 2900, 1710, 1650, and 1570 cm^{-1}; NMR ($CDCl_3$) δ 1.20 (3H, s; *t*-Me), 1.90 (3H, d, J=1.2 Hz; -C=C-Me), 7.08 (1H, br s; -C=C-H), and 7.37 (1H, s; -COOH); MS *m/e* (%) 248 (M^+; 38), 230 (3), 202 (3), 147 (36), 119 (9), 109 (24), 108 (100), 96 (13), 91 (14), 79 (17), 77 (15), 55 (22), and 43 (37); Found: C, 72.60; H, 7.90%. Calcd for $C_{15}H_{20}O_3$: C, 72.55; H, 8.12%.

Methyl Ester of the Carboxylic Acid (4). Carboxylic acid (**4**; 115 mg) was treated with diazomethane in ether (2 ml). The ether solution was concentrated and subjected to separation by preparative TLC (developed with benzene–chloroform, 1: 1) to afford a methyl ester (60 mg) as a colorless oil, IR (neat) 1735, 1648, 1566, and 1150 cm^{-1}, no absorption band due to hydroxyl group was observed. NMR ($CDCl_3$) δ 1.02 (3H, s; *t*-Me), 1.92 (3H, d, J=1.2 Hz; -C=C-Me), 3.70 (3H, s; -COOMe), and 7.13 (1H, br s; -C=C-H); MS *m/e* (%) 262 (M^+; 26), 231 (3), 215 (4), 198 (6), 170 (12), 155 (25), 147 (37), 142 (35), 141 (100), 128 (19), 115 (25), 108 (70), 69 (20), 57 (40), 55 (34), and 43 (51).

Reduction of the Carboxylic Acid (4) with Lithium Aluminium Hydride. A mixture of carboxylic acid (**4**; 430 mg) and lithium aluminium hydride (600 mg) in ether (30 ml) was heated under reflux for 1 h. The reaction mixture was worked up in usual way and chromatographed on silica gel (15 g). Elution with benzene afforded an alcohol (**5**; 350 mg) as a colorless oil, UV λ_{max} 221 nm (ε 7600); IR (neat) 3350, 1642, and 1562 cm^{-1}; NMR ($CDCl_3$) δ 0.99 (3H, s; *t*-Me), 1.48 (1H, s; -OH), 1.92 (3H, d, J=1.1 Hz; -C=C-Me), 3.7 and 3.9 (dd, $J_{14\alpha,14\beta}=-11$, $J_{4,14\alpha}=5$, and $J_{4,14\beta}=8$ Hz; -CH-C<u>H</u>$_2$-O-), and 7.07 (1H, q; -C=C-H); MS *m/e* (%) 234 (M^+; 20), 218 (6), 138 (5), 122 (8), 109 (25), 108 (98), 74 (40), 59 (65), 45 (60), and 31 (100).

Furanoeremophilane (7) from the Alcohol (5). A mixture of the alcohol (**5**; 250 mg) and *p*-toluenesulfonyl chloride (300 mg) in pyridine (4 ml) was allowed to stand at room temperature overnight. After usual work-up, an orange crude oil (300 mg) was dissolved in benzene and subjected to separation by preparative TLC (developed with chloroform–ether, 5: 1) to afford a tosylate (**6**; 130 mg) as a yellow oil, IR (neat) 1647, 1568, 1600, 1188, and 1176 cm^{-1}.

The tosylate (**6**), above obtained, was reduced with lithium aluminium hydride (500 mg) in ether for 2 h. The reaction mixture was treated as usual and chromatographed on silica gel (4 g). Elution with petroleum ether provided furanoeremophilane (**7**; 53 mg) as a colorless oil, $[\alpha]_D^{23}$ −11° (*c* 0.42, $CHCl_3$); UV λ_{max} 221 nm (ε 7000); IR (neat) 1649, 1568, and 1094 cm^{-1}; NMR ($CDCl_3$) δ 0.95 (3H, s; *t*-Me), 0.99 (3H, d, J=7.0 Hz; *s*-Me), 1.99 (3H, d, J=1.1 Hz; -C=C-Me), and 7.13 (1H, q; -C=C-H); MS *m/e* (%) 218 (M^+; 40), 203 (3), 190 (3), 133 (6), 123 (13), 122 (72), 109 (68), 108 (100), 105 (10), 91 (16), 79 (24), 77 (17), 67 (12), 55 (15), and 53 (13); ORD (*c* 0.42, $CHCl_3$) $[\alpha]^{23}$ (at λ nm) −10° (650), −12° (500), −16° (450), −23° (400), and −32° (350); Found: C, 82.56; H, 10.31%. Calcd for $C_{15}H_{22}O$: C, 82.51; H, 10.16%.

Isomerization of Furanoeremophilan-14β,6α-olide (1) into Furanoeremophilan-14α,6α-olide (8). Furanoeremophilan-14β, 6α-olide (**1**; 900 mg) was dissolved in benzene and adsorbed on basic alumina (15 g) for 6 h. The fraction eluted with the same solvent was shown to be a mixture of furanoeremophilan-14β,6α-olide (**1**) and -14α,6α-olide (**8**) in a ratio of 1: 5 by GLC examination. Repetition of fractional crystallization from ether–petroleum ether afforded **8** (300 mg), mp 124—125 °C, $[\alpha]^{18}$ −147° (*c* 0.33, dioxane); UV λ_{max} 216 nm (ε 7900); IR (Nujol) 3140, 3090, 1759, 1640, 1566, and 1083 cm^{-1}; NMR (Table 1); MS *m/e* (%) 246 (M^+; 48), 202 (64), 187 (62), 173 (24), 159 (56), 145 (64), 124 (32), 115 (34), 95 (100), 77 (54), 67 (40), and 55 (34); ORD (*c* 0.33, dioxane) $[\alpha]^{18.5}$ (at λ nm) −120° (650), −209° (500), −345° (400), −495° (350), −690° (300), −810° (270), −675° (250), and −390° (242); Found: C, 73.08; H, 7.41%. Calcd for $C_{15}H_{18}O_3$: C, 73.14; H, 7.37%.

Reduction of Furanoeremophilan-14α,6α-olide (8) with Lithium Aluminium Hydride. A mixture of furanoeremophilan-14α, 6α-olide (**8**; 240 mg) and lithium aluminium hydride (500 mg) in ether (30 ml) was refluxed for 1 h and the reaction mixture was worked up as usual. The residue (240 mg) was crystallized from petroleum ether to give a diol (**9**; 180 mg) as white wooly crystals, mp 123.5—125 °C; UV λ_{max} 219 nm (ε 9000); IR (Nujol) 3320, 1646, and 1571 cm^{-1}; NMR (DMSO) δ 0.94 (3H, s; *t*-Me), 1.92 (3H, d, J=1.2 Hz; -C=C-Me), 2.3 and 2.8 (dd, $J_{9\alpha,9\beta}$=*ca.* −17, $J_{9\alpha,10}$=*ca.* 1.5, and $J_{9\beta,10}$=*ca.* 5.5 Hz; -C=C-C<u>H</u>$_2$-CH-), 3.78 (2H, m; -C<u>H</u>$_2$-OH), 4.31 (1H, d, J=5.4 Hz; -C<u>H</u>-OH), 4.66 (1H, d, J=5.4 Hz; -CH-O<u>H</u>), 4.85 (1H, t, J=4.8 Hz; -CH$_2$-O<u>H</u>), and 7.17 (1H, br. s; -C=C-H); MS *m/e* (%) (by a direct inlet) 250 (M^+; 6), 232 (4), 159 (3), 149 (5), 123 (100), 91 (4), 67 (7), and 57 (7); (by an indirect inlet) 232 (38), 202 (4), 187 (6), 159 (40), 145 (11), 124 (22), 109 (100), 91 (18), 81 (18), 79 (15), 77 (15), 67 (86), and 55 (32).

Dehydration of the Diol (9). A solution of the diol (**9**; 185 mg) and *p*-toluenesulfonyl chloride (350 mg) in pyridine (5 ml) was heated at 65—70 °C for 1.5 h. Benzene was added to the mixture and the solvents were evaporated under reduced pressure. The residue was dissolved in benzene and chromatographed on silica gel (10 g). 4-Epiether (**10**; 130 mg) was obtained by elution with benzene as a colorless oil, UV λ_{max} 218 nm (ε 6900); IR (neat) 3140, 3090, 1642, 1567, and 1082 cm^{-1}; NMR (Table 1); MS *m/e* (%) 232 (M^+; 100), 217 (7), 202 (5), 199 (16), 187 (7), 159 (40), 145 (8), 124 (13), 109 (40), 91 (6), 85 (19), 83 (29), 67 (16), and 57 (10).

References

1) A part of this work was reported in a preliminary form: Y. Ishizaki, Y. Tanahashi, T. Takahashi, and K. Tori, *Chem. Commun.*, **1969**, 551.

2) T. Takahashi, The 21st Symposium on the Chemistry of Perfumes, Terpenes, and Essential Oils, Tokushima, 1977, Abstract Papers, p. 305, and references cited therein.

3) L. Novotný, V. Herout, and F. Šorm, *Tetrahedron Lett.*, **1961**, 697; J. Hochmannová, L. Novotný, and V. Herout, *Collect. Czech. Chem. Commun.*, **27**, 1870 (1962).

4) Y. Ishizaki, Y. Tanahashi, Y. Moriyama, T. Takahashi, and H. Koyama, *Phytochemistry*, **13**, 674 (1974).

5) N. Abe, R. Onoda, K. Shirahata, T. Kato, M. C. Wood, and Y. Kitahara, *Tetrahedron Lett.*, **1968**, 369; K. Shirahata, T. Kato, K. Kitahara, and N. Abe, *Tetrahedron*, **25**, 3179 (1969).

6) K. Naya, I. Takagi, M. Hayashi, S. Nakamura, M. Kobayashi, and S. Katsumura, *Chem. Ind. (London)*, **1968**, 318.

7) L. Novotný, J. Jizba, V. Herout, F. Šorm, L. H. Zalkow, S. Hu, and C. Djerassi, *Tetrahedron*, **19**, 1101 (1963); L. Novotný, J. Jizba, V. Herout, and F. Šorm, *Collect. Czech. Chem. Commun.*, **31**, 371 (1966).

8) F. Patil, G. Ourisson, Y. Tanahashi, M. Wada, and T. Takahashi, *Bull. Soc. Chim. Fr.*, **1968**, 1047.

9) H. Ishii, T. Tozyo, and H. Minato, *J. Chem. Soc., C*, **1966**, 1545. The authors are grateful to Dr. H. Ishii of Shionogi Research Laboratory for the spectra of authentic furanoeremophilane.

10) J. H. Noggle and R. E. Schirmer, "The Nuclear Overhauser Effect. Chemical Applications," Academic Press, New York (1971).

11) J. T. Pinhey and S. Sternhell, *Tetrahedron Lett.*, **1963**, 275.

Reaction of Coordinated Phosphines. V. Aryl and Alkyl Transfer from Tertiary Phosphine to Transition Metal[1)]

Kiyoshi KIKUKAWA, Toru YAMANE, Yoshihiro OHBE, Makoto TAKAGI, and Tsutomu MATSUDA*

Department of Organic Synthesis, Faculty of Engineering, Kyushu University, Hakozaki, Higashi-ku, Fukuoka 812

(Received October 24, 1978)

A carbon–phosphorus bond cleavage was observed in the reaction of $MCl_2(PR_3)_2$ (M=Ni, Co, or Pd, R=Ph, n-C_8H_{17}) with p-tolyllithium, p-tolylmagnesium halide, lithium aluminum hydride, or magnesium amalgam, and the reactivity was most pronounced with Ni followed by Co and Pd. Reaction of $NiCl_2(PPh_3)_2$ with p-tolyllithium gave biphenyl and 4-methylbiphenyl, along with 4,4′-dimethylbiphenyl. Phenyllithium was formed in the reaction mixture, and the recovered tertiary phosphine contained tri-p-tolylphosphine, di-p-tolylphenylphosphine, and p-tolyldiphenylphosphine as well as triphenylphosphine. 1-Octene was formed in the reaction of $NiCl_2\{P(n\text{-}C_8H_{17})_3\}_2$ with p-tolyllithium. Thermal decomposition of Ni(mesityl)$X(PEt_3)_2$ (X=mesityl or Br) and Co(mesityl)$_2(PPhEt_2)_2$ at 30 °C gave vinyl mesitylene.

Tertiary phosphine is a ligand frequently used in organotransition metal complexes due to its versatility in donor-acceptor properties, and its carbon–phosphorus bonds had been considered to be chemically stable under usual reaction conditions. However, the decomposition of triarylphosphines in which the aryl group transfers from phosphorus to transition metal has become recently known for reactions of palladium,[1,2-4)] nickel,[5-8)] osmium[9)] and other metal complexes.[10)] Low-valent metals are involved in most of them, but there is a case where divalent palladium is undoubtedly responsible for the activation of aryl–P bond.[1,2b,11)] Though a transition metal-assisted C–P bond fission still remains to be rather uncommon reaction in organotransition metal chemistry, it deserves serious attention, not only concerning the basic mechanism involved but also with regards to the scope of the practical occurrence of this type of reaction, since it may have some relevance to the process such as catalyst decay or induction of side reactions in certain catalytic processes. In the present study, a system in which aryl–P bond is cleaved and re-formed under the influence of low-valent Ni, Co, and Pd is described. Evidences are also collected for the alkyl–P bond cleavage facilitated by Ni, Co, and Pd complexes.

Results and Discussion

Reaction of Dichlorobis(triphenylphosphine)metal(II) with p-*Tolyllithium and* p-*Tolylmagnesium Bromide.* The reaction of tertiary phosphine-coordinated transition metal halides with organic derivatives of lithium, magnesium or sodium has been widely used in the synthesis of low-valent transition metal complexes, in which the tertiary phosphines remained on the metal without any chemical transformations in themselves. However, $NiCl_2(PPh_3)_2$ (**1**), $CoCl_2(PPh_3)_2$ (**2**), and $PdCl_2(PPh_3)_2$ (**3**) reacted with p-tolyllithium or p-

TABLE 1. REACTION OF $MCl_2(PPh_3)_2$ WITH p-TOLYLLITHIUM (ArLi)[a)]

Complex	ArLi/M[b)]	Reaction time/h	Product, mol % based on M			Tertiary phosphine recovered, mol % based on PPh_3 in the complex			
			Ph–Ph	Ph–Ar	Ar–Ar	PPh_3	PPh_2Ar	$PPhAr_2$	PAr_3
1	1	40	6.9	8.9	17	—	—	—	—[c)]
	2	40	26	23	46	34	5.1	trace	0
	4	40	86	93	69	16	9.8	3.5	0.14
	8	40	82	210	140	0.7	0.5	0.1	0.4
	2[d)]	35	17	22	58	—	—	—	—[c)]
2	1	35	1.6	3.4	27	—	—	—	—[c)]
	2	35	14	11	59	20	2.9	0	0
	4	35	27	35	79	22	1.5	0.1	0
	2[d)]	35	5.1	10	54	—	—	—	—[c)]
3	1	48	4.9	8.6	34	—	—	—	—[c)]
	2	48	9.3	19	74	45	1.3	0	0
	4	48	2.5	12	150	—	—	—	—[c)]
	20[e)]	48	trace	5	210	—	—	—	—[c)]
PPh_3 only	2[f)]	23	0.04[g)]	0.2[g)]	0[g)]	—	—	—	—[c)]

a) One mmol of complex in ether at room temperature. b) Molar ratio. c) Not determined. d) MCl_2\{1,2-bis(diphenylphosphino)ethane\} was used instead of $MCl_2(PPh_3)_2$. e) A half mmol of **3** was used. Reaction temperature was raised to 25 °C, 3 min afetr the addition of ArLi at −70 °C. f) Molar ratio: (ArLi/PPh_3) × 0.5. g) (mol of biaryl/mol of PPh_3 used) × 0.5 × 100.

Table 2. Reaction of $MCl_2(PPh_3)_2$ with *p*-tolylmagnesium bromide (ArMgBr)[a)]

Complex	Reaction time/h	Product, mol % based on the complex[b)]		
		Ph–Ph	Ph–Ar	Ar–Ar
1	62	8	19	54
2	88	8	16	26
3	153	0.9	2.6	13

a) Five mmol of complex in ether at room temperature. Molar ratio; ArMgBr/M=2.
b) A considerable amount of PPh_2Ar was detected in all cases.

tolylmagnesium bromide at room temperature to give the organic products including biphenyl, 4-methylbiphenyl, tri-*p*-tolylphosphine, di-*p*-tolylphenylphosphine, and *p*-tolyldiphenylphosphine, indicating that the aryl–P bond was cleaved and reformed by the influence of transition metal. Typical results are summarized in Tables 1 and 2. Total yield of biaryls and the amount of phenyl group carried into biaryls are shown in Figs. 1 and 2, respectively. The yield of biaryls increased with the increase of molar ratio of *p*-tolyllithium to $MCl_2(PPh_3)_2$ for all of the three transition metals (Fig. 1). The amount of phenyl group transferred into biaryls increased excepting for Pd as the yield of biaryls increased (Fig. 2). Excess organolithium reagent decreased the amount of recovered tertiary phosphines markedly, only 1 to 2% of triarylphosphines being recovered when 8-fold *p*-tolyllithium over nickel complex was used.

The time course of the reaction was studied for nickel system by direct GLC analysis of the reaction mixture for biaryls. The analysis was also made after the mixture had been treated with excess acetone or iodine to determine the amount of aryllithium present. The results obtained in the reaction at room temperature indicated that most of the biaryls and phenyllithium

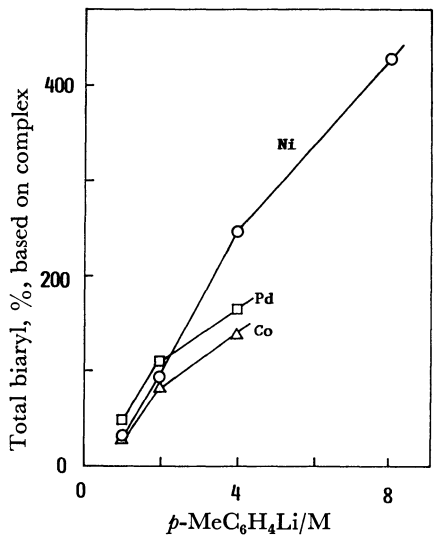

Fig. 1. Reaction of $MCl_2(PPh_3)_2$ with *p*-tolyllithium. Total yield of biaryls as a function of *p*-tolyllithium/M. Ordinate: (total mol of biaryls/mol of $MCl_2(PPh_3)_2$ employed) × 100. See Table 1 for conditions.

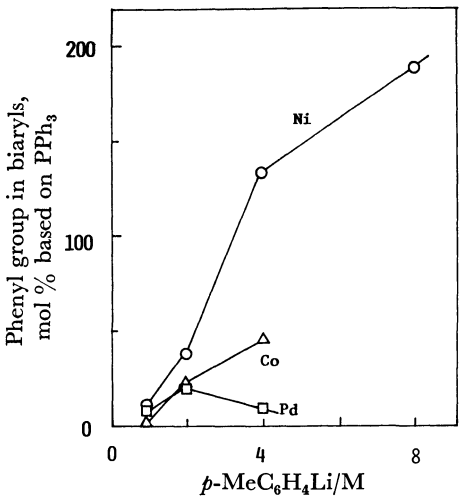

Fig. 2. Reaction of $MCl_2(PPh_3)_2$ with *p*-tolyllithium. Amount of phenyl group found in biaryls. Ordinate: (total mol of phenyl group found in biaryls/mol of PPh_3 employed as metal complex) × 100.

were formed within 10 min after the addition of the lithium reagent to the metal complex. A slow reaction then followed, and the mixture reached an apparent equilibrium after 10 h, which persisted at least for 5 days. The reaction is illustrated by:

$$\mathrm{NiCl_2(PPh_3)_2\ (\mathbf{1})} + 8\mathrm{ArLi} \xrightarrow{\text{ether, r.t., 10 h—4 days}}$$
$$1.0\mathrm{ArLi} + 0.5\mathrm{PhLi} + 0.8\mathrm{Ph\text{–}Ph} + 1.5\mathrm{Ph\text{–}Ar} + 1.9\mathrm{Ar\text{–}Ar} + 0.008\mathrm{PPh_3} + 0.008\mathrm{PPh_2Ar} + 0.004\mathrm{PPhAr_2} \quad (\mathrm{Ar}=p\text{-tolyl}) \qquad (1)$$

The relative yield of each biaryl varied from run to run, but the combined yield remained constant under specified reaction conditions. Similar study at Dry Ice–methanol temperature gave the result:

$$\underset{0.5}{\mathbf{1}} + \underset{4.0\ \mathrm{mmol}}{8\mathrm{ArLi}} \xrightarrow[-70\,^\circ\mathrm{C}]{\text{1) 55 min in ether}} \xrightarrow{\text{2) 5 ml of acetone}} \xrightarrow{\text{3) 16 h, room temp, then aq NH}_4\mathrm{Cl}}$$
$$\underset{0.0}{\mathrm{Ph(CH_3)_2OH}} + \underset{5.5}{\mathrm{ArC(CH_3)_2OH}} + \underset{0.024}{\mathrm{Ph\text{–}Ph}} + \underset{0.032}{\mathrm{Ph\text{–}Ar}} + \underset{1.0\ \mathrm{mmol}}{\mathrm{Ar\text{–}Ar}} \quad (\mathrm{Ar}=p\text{-tolyl}) \qquad (2)$$

GLC analysis of the reaction mixture for sample solutions extracted at earlier reaction stage gave the result illustrated in Fig. 3. The reaction mixture at −70 °C was a yellow-brown solution, and on raising the temperature it quickly darkened to give a blackish, turbid mixture. Since the extracted sample solutions were brought to high temperature during analysis, it was conceivable that the 100% yield of 4,4′-dimethylbiphenyl at 1.5 h reaction in Fig. 3 was an artifact from the thermal decomposition of $Ni(p\text{-tolyl})_2(PPh_3)_2$. It is obvious from Fig. 3 and Reaction 2 that aryl–P bond rearrangement takes place not at −70 °C but only at elevated temperatures around 0 °C or above. The presence of excess lithium reagent is important for this

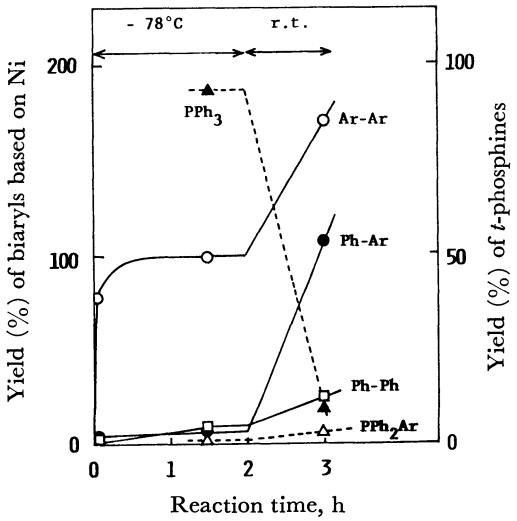

Fig. 3. Time course of the reaction of $NiCl_2(PPh_3)_2$ with *p*-tolyllithium.
Left ordinate: (total mol of biaryls/mol of Ni complex employed) × 100. Right ordinate: (mol of recovered PAr_3/mol of PPh_3 employed as Ni complex) × 100.

process since the yield of biphenyl or 4-methylbiphenyl is low at a low ratio of *p*-tolyllithium to **1**.

Reaction of $MCl_2(PPh_3)_2$ with Magnesium Amalgam and $LiAlH_4$. Similar C–P bond cleavage was observed in the reaction of **1**, **2** and **3** with magnesium amalgam or $LiAlH_4$. The reaction with the amalgam took place in THF but not in ether. Typical results are summarized in Table 3, Ni and Co complexes being much active than Pd complex. A considerable decomposition of triphenylphosphine in the Reaction 1 seem ssomewhat contradictory to the report[12] that reduction of the corresponding bromide complex with sodium amalgam in acetonitrile produced bis(triphenylphosphine)nickel-(0). A difference in solvent combined with a longer reaction time would be responsible for this discrepancy.

Table 3. Reaction of $MCl_2(PPh_3)_2$ with $LiAlH_4$ or magnesium amalgam[a]

	Complex	Solvent	Reaction time/h	Product/% Ph–Ph	Benzene
$LiAlH_4$	**1**	ether	24	trace	31
	2	ether	77	trace	22
	3	ether	24	0	6.1
Mg(Hg)	**1**	ether[b]	42	0	—
	1	THF	25	40	—
	2	THF	19	49	—
	3	THF	43	0.2	—
	PPh_3 only	THF	40	0.4	—

a) To 5 mmol of the complexes in the solvent, 2.5 mmol of $LiAlH_4$ or 14 mg-atom of Mg was used, respectively, at room temperature. b) The complex was scarcely soluble in ether.

Alkyl–P Bond Cleavage of Coordinated Trialkylphosphine. The C–P bond fission is not limited to triarylphosphines but trialkylphosphines, though to a smaller extent.

Table 4. Thermal decomposition of **4**, **5** and **6**[a]

Complex	Solvent	Product, mol % based on complex[b] **7**	**8**	**9**	**10**	**11**
4	ether	trace	8	3	5	—
	benzene	4	40	3	9	—
	CCl_4	trace	5	trace	12	5
5	ether	2	15	2	—	—
	benzene	7	33	9	—	—
	CCl_4	0.2	9	90	—	0
6	ether	0.4	30	36	—	—
	benzene	trace	13	60	—	—
	CCl_4	trace	2	95	—	trace

a) At 30 °C for 3 h. b) Balance was mostly the unreacted complex.

When *trans*-bis(triethylphosphine)mesitylnickel(II) bromide (**4**), *trans*-bis(triethylphosphine)dimesitylnickel-(II) (**5**), and *trans*-bis(diethylphenylphosphine)dimesitylcobalt(II) (**6**) was stirred in ether, benzene or carbon tetrachloride at 30 °C, 2,4,6-trimethylstyrene (**7**) was formed together with mesitylene (**8**), bimesityl (**9**), mesityl bromide (**10**) or mesityl chloride (**11**) (Table 4). The compound **7** presumably resulted *via* ethyl transfer from phosphorus to metal. Reaction of $NiCl_2\{P(n\text{-}C_8H_{17})_3\}_2$ with an 8-fold molar excess of *p*-tolyllithium gave 1-octene (5% on molar basis on the phosphine used) along with 4,4'-dimethylbiphenyl (≈100% on molar basis on the complex used).

Alkyl–P bond fission using Pd complex was not successful under the similar reductive conditions, but had been achieved under oxidative conditions. Thus, simply by heating the equimolar mixture of trialkylphosphine and $Pd(OAc)_2$ in acetic acid at 90 °C, a considerable amount of olefins and carbonyl compounds were formed.[1]

Mechanism. Though the present report concerns with factual description rather than discussion of mechanism operating in the current reactions, some idea on the mechanism is invoked in the following in order to help a correlation among the experimental facts. Typical C–P bond cleavage disclosed in this study is those of $MCl_2(PPh_3)_2$–*p*-tolyllithium system, and seems to be more complicated than that of PAr_3–$Pd(OAc)_2$ system previously reported.[1] The reaction of 1 mol of **1** with 2 mol of *p*-tolyllithium produced nearly stoichiometric amount (0.95 mol) of biaryls on the basis that the diarylnickel compound decomposes into biaryl and zero-valent nickel (Table 1). However, on increasing the ratio of *p*-tolyllithium/**1** more biaryl is formed, the amount exceeding 4 mol per mol of **1** when the ratio is 8, and the recovery of tertiary phosphines decreased concurrently. These observations combined with the results in Reactions 1 and 2 suggest that the Reaction 3 was effected under the catalysis of low (probably zero) valent nickel. The examination of the amount of

$$Ph_3P + ArLi \xrightarrow{Ni(0)} Ph_2PLi + Ar\text{–}Ph \qquad (3)$$

biaryl formed indicates that the resulting Ph_2PLi further reacted with excess ArLi, giving Ph–Ar and

presumably $PhPLi_2$. Direct evidence for the formation of Ph_2PLi or $PhPLi_2$ was not obtained because of its strong tendency to associate with nickel. It should be noted that the reaction like 3 does not proceed in the absence of Ni complex (Table 1, the last low).

It is conceivable that the catalysis of nickel in Reaction 3 resides in the oxidative addition of Ph–P bond to zero-valent Ni (Reaction 4). A further reaction of the resulting Ni complex with ArLi gives Ph_2PLi and ArPhNi, and the decomposition of the latter affords Ar–Ph with reproduction of zero-valent Ni (Reactions 5 and 6). The formation of the mixed tertiary phosphines suggests that the Reactions 4 and 5 are reversible, and phenyllithium may be produced *via* the Reaction 7.

$$Ph_3P + Ni \rightleftarrows Ph_2P\text{–}Ni\text{–}Ph \quad (4)$$

$$Ph_2P\text{–}Ni\text{–}Ph + ArLi \rightleftarrows Ph_2PLi + Ar\text{–}Ni\text{–}Ph \quad (5)$$

$$Ar\text{–}Ni\text{–}Ph \longrightarrow Ar\text{–}Ph + Ni \quad (6)$$

$$Ph_2P\text{–}Ni\text{–}Ph + ArLi \rightleftarrows Ph_2P\text{–}Ni\text{–}Ar + PhLi \quad (7)$$

The oxidative addition of Ar_2P–Ar bond to Ni(0) or Ni(I) has been claimed in the literature.[5,6] Coordinative unsaturation on the metal seems to be one of the essential factors for this type of reactions to take place. The complex $Ni(Ph_3P)_3$ is unstable in solution, and the structure containing Ph_2P–Ni bond has been suggested for the decomposition product.[13] With regard to the use of excess organolithium reagent in our study, a possible involvement of the ate-type complex of Ni(0)[14] may not be overlooked, but its importance in the C–P bond cleavage[7] is yet to be investigated.

Experimental

Materials. Bis(tertiary phosphine) complexes of transition metal dichlorides were prepared by conventional methods from the corresponding metal chlorides and phosphine ligands and characterized by elemental analysis as well as by ordinary spectroscopic methods. Diaryl transition metal complexes; **4**, **5** and **6**, were prepared from the corresponding dichloro complexes according to the literatures.[15,16]

Reaction of $MCl_2(PPh_3)_2$ with p-*Tolyllithium.* An ethereal 0.6—0.7 M organolithium solution was prepared by a conventional method from *p*-tolyl bromide and lithium. The solution was standardized by acid titration, and the amount of by-product (4,4′-dimethylbiphenyl) was determined by GLC with hexadecane as an internal standard. A calculated amount of the organolithium reagent was added under stirring to a suspension of $MCl_2(PPh_3)_2$ (1 mmol) in 10 ml ether containing hexadecane (internal standard). After stirred for several hours under dry nitrogen, the mixture was treated with aqueous ammonium chloride and excess potassium cyanide. The organic layer was worked up in a conventional manner and analyzed by GLC. Since some portion of tertiary phosphines had been converted into the oxides during the work-up, the product was reduced with trichlorosilane–triethylamine in benzene before the analysis for phosphines. Eicosane was employed as an internal standard. All the products were characterized either by direct comparison on GLC with authentic samples or by isolation from a large-scale run followed by a conventional spectroscopic study. By the addition of acetone or iodine to the reaction mixture, aryllithium were converted to 2-aryl-2-propanol or aryl iodides, respectively. They were analyzed by GLC after conventional work-up.

Other Reactions. Reaction of $MCl_2(PPh_3)_2$ with *p*-tolylmagnesium bromide was conducted in a similar manner as with *p*-tolyllithium. The reaction with magnesium amalgam (0.34 g of magnesium in 30 g of mercury) was carried out with 5 mmol of $MCl_2(PPh_3)_2$ in 100 ml of THF or ether. Benzene obtained from the reaction with $LiAlH_4$ was analyzed by GLC with toluene as an internal standard. The thermal decomposition of aryl transition metal complexes **4**, **5**, and **6** was conducted as described in the literature. The products from these reactions were characterized in a usual manner either by comparison with authentic samples or by isolation followed by instrumental study and elemental analysis.

References

1) Part IV, to be published.
2) a) K. Kikukawa, T. Yamane, M. Takagi, and T. Matsuda, *J. Chem. Soc., Chem. Commun.*, **1972**, 695; b) T. Yamane, K. Kikukawa, M. Takagi, and T. Matsuda, *Tetrahedron*, **29**, 955 (1973).
3) D. R. Coulson, *Chem. Commun.*, **1968**, 1530.
4) R. Asano, I. Moritani, Y. Fujiwara, and S. Teranishi, *Bull. Chem. Soc. Jpn.*, **46**, 2910 (1973).
5) D. R. Fahey and J. E. Mahan, *J. Am. Chem. Soc.*, **98**, 4499 (1976).
6) A. Nakamura and S. Otsuka, *Tetrahedron Lett.*, **1974**, 463.
7) M. L. H. Green, M. J. Smith, H. Felkin, and G. Swierczewski, *Chem. Commun.*, **1971**, 158.
8) R. Cramer and D. R. Coulson, *J. Org. Chem.*, **40**, 2267 (1975).
9) a) C. W. Bradford, R. S. Nyholm, G. J. Gainsford, J. M. Guss, P. R. Ireland, and R. Mason, *J. Chem. Soc., Chem. Commun.*, **1972**, 87; b) C. W. Bradford and R. S. Nyholm, *J. Chem. Soc., Dalton Trans.*, **1973**, 529.
10) J. R. Blickensderfer and H. D. Kaesz, *J. Am. Chem. Soc.*, **97**, 2681 (1975).
11) T. Kawamura, K. Kikukawa, M. Takagi, and T. Matsuda, *Bull. Chem. Soc. Jpn.*, **50**, 2021 (1977).
12) R. J. de Pasquale, *J. Organomet. Chem.*, **32**, 381 (1971).
13) P. W. Jolly and G. Wilke, "The Organic Chemistry of Nickel," Academic Press, New York, N. Y. (1974), Vol. 1, p. 129.
14) C. Krüger and Y. H. Tsay, *Angew. Chem.*, **85**, 1051 (1973).
15) J. Chatt and B. L. Shaw, *J. Chem. Soc.*, **1960**, 1718.
16) J. Chatt and B. L. Shaw, *J. Chem Soc.*, **1961**, 285.

Studies on Nucleosides and Nucleotides. VII.[1] Preparation of Pyrimidine Nucleoside 5′-Phosphates and N^3,5′-Purine Cyclonucleosides by Selective Activation of the 5′-Hydroxyl Group

Junji KIMURA, Yoshiyuki FUJISAWA, Toyokichi YOSHIZAWA, Kazuhiro FUKUDA, and Oyo MITSUNOBU*

Department of Chemistry, College of Science and Engineering, Aoyama Gakuin University, Chitosedai, Setagaya-ku, Tokyo 157

(Received November 6, 1978)

The reaction of thymidine or uridine with 1.5 molar equivalents each of dibenzyl hydrogenphosphate, diethyl azodicarboxylate, and triphenylphosphine in HMPT at room temperature for 1 day, followed by debenzylation, afforded dpT and pU in 73 and 78% yields, respectively. Neither nucleoside 3′-phosphate nor 3′,5′-diphosphate was formed. 5′-*O*-Benzoylthymidine 3′-(2-cyanoethyl)phosphate also reacted smoothly with thymidine at room temperature giving d-bzT3′p(CNEt)5′T in a 54% yield. Adenosine and Guanosine gave the corresponding N^3,5′-cyclonucleosides as main products, less than 1% pA and pG being formed.

In relation to biosynthesis and genetic control, there is a need for oligo- and polynucleotides of definite and specific sequences. For the synthesis of oligonucleotides, suitably protected nucleosides and/or nucleotides were condensed with each other to form 3′—5′ phosphodiester bonds.[2] While many organic dehydrating reagents have been developed so far, only a few are effective in nucleotides and oligonucleotides syntheses.[3] Since the condensation of nucleosides with phosphate esters and with nucleotides by these reagents involves initial activation of phosphate components, a side reaction occurs to produce pyrophosphate which in turn afford undesirable by-products.[4] In some cases, undesirable side reactions also take place under the conditions necessary for deprotection.[5] A procedure for selective phosphorylation of unprotected nucleosides would thus be desirable.

Recently, the triester method has been reported to have some advantages over the diester one.[2,6] Because of the lower reactivity of phosphate diesters as compared to phosphate monoesters, only arenesulfonyl chlorides and their derivatives can be utilized in the triester method. In the triester method, however, these reagents, except for arylsulfonyltetrazoles,[7] are slow in completing the condensation reactions.[8]

An alternative route for the preparation of nucleotides is also known in which nucleosides are converted into activated forms at the first stage of the reaction followed by the reaction with phosphate esters. In this case, pyrophosphate formation can, at least in principle, be avoided. Several attempts have been made to synthesize nucleotides by this procedure, the reaction conditions being so drastic as to cause side reactions such as 3′—2′ phosphoryl group migration.[9]

In this paper, we wish to report selective formation of pyrimidine nucleoside 5′-phosphates and cyclization of purine nucleosides by the use of diethyl azodicarboxylate (**1**) and triphenylphosphine (**2**). The reaction proceeds through initial activation of the 5′-hydroxyl group of nucleosides under mild conditions. At the outset of our work,[10] there was only one procedure available for predominant formation of 3′—5′ internucleotidic phosphate linkage from unprotected nucleosides and protected nucleotides.[11] The present method has been worked out on the basis of the following facts.

1) Because of the steric hindrance of three bulky aryl group, the reaction of triarylmethyl chlorides with nucleosides mainly gave 5′-*O*-triarylmethylnucleosides.[12]

2) The reaction of an alcohol with dibenzyl hydrogenphosphate (**3**) in the presence of **1** and **2** at room temperature, followed by debenzylation, resulted in the formation of the corresponding alkyl dihydrogenphosphate in an excellent yield. It was assumed that the 1 : 1 adduct (**4**) of **1** and **2** initially formed was converted into an alkoxyphosphonium salt (**5**) which collapsed to the phosphate triester as shown in Scheme 1.[13]

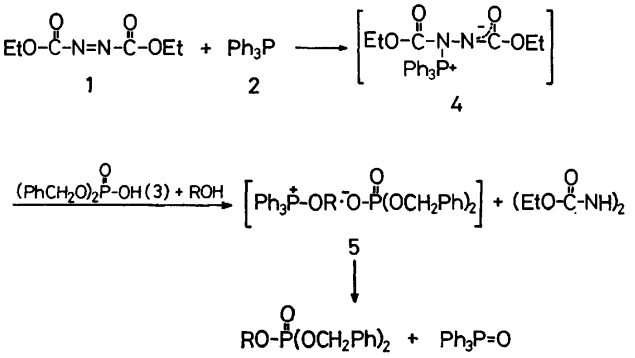

Scheme 1.

When an unprotected nucleoside, instead of an alcohol, is used in this reaction, the nucleophilic attack of the 5′-hydroxyl group of the nucleoside on the sterically crowded phosphorus cation of **4** would be expected to be more favourable than that of 3′- and/or 2′-hydroxyl ones affording the corresponding nucleoside 5′-phosphate. In fact, the reagent formed by combination of **1** and **2** has been found to be effective for the condensation of 5′-hydroxyl group of unprotected thymidine and uridine with **3**.

Thymidine was allowed to react with 1.5 molar equivalents each of **1**, **2**, and **3** in tetrahydrofuran (THF) at room temperature for 1 day, the benzyl group being removed by hydrogenolysis. Examination of the resulting solution by paper chromatography revealed the presence of dpT (47%) and thymidine, with no

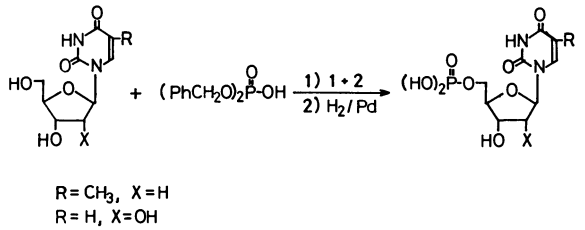

Scheme 2.

formation of dTp and dpTp.[14,15] When the reaction was carried out in dioxane (60 °C) and in hexamethylphosphoric triamide (HMPT; room temperature) for 1 day, followed by debenzylation, dpT was formed in 62 and 73% yields, respectively. Under the same conditions, uridine also reacted smoothly with **3** in dioxane (60 °C) and in HMPT (room temperature) to give pU in 68 and 78% yields, respectively. The analysis of the crude reaction solution obtained after debenzylation was performed by paper chromatography to indicate the absence of by-products derived from the nucleoside (Scheme 2). On the other hand, when thymidine was allowed to react with 3 molar equivalents each of **1**, **2**, and **3** in HMPT at room temperature, followed by hydrogenolysis, the formation of a small amount of a by-product was detected by paper chromatography. The by-product gave a similar UV absorption spectrum, as eluted from paper chromatogram, to that of thymidine, but with twice the electrophretic mobility of dpT at pH 3.2. The by-product was tentatively assigned to be dpTp or 1-(2-deoxy-3,5-bis-*O*-dihydroxyphosphinyl-β-D-xylofuranosyl)thymine. The reaction in pyridine made the solution turn dark, giving dpT in a 19% yield along with several by-products. This would be the result of nucleophilic attack of the solvent to phosphonium salts.[16] The by-products were not characterized.

In order to examine the reactivity of 3′-hydroxyl group of nucleosides, 5′-*O*-benzoylthymidine (dbzT) was allowed to react with **1**, **2**, and **3** in THF at room temperature, a white precipitate being separated from the solution as the reaction proceeded. The precipitate was found to be 5′-*O*-benzoyl-O^2,3′-cyclothymidine (**7**, 46%), 36% of dbzT being recovered.[17] This result indicates that the 3′-hydroxyl group of dbzT can also enter into the reaction to form the corresponding phosphonium salt (**6**), in which an intramolecular displacement leading to **7** takes place more readily than intermolecular phosphate attack on 3′-carbon atom (Scheme 3). The results are summarized in Table 1.

Contrary to the case of pyrimidine nucleosides, purine nucleosides were scarcely converted into 5′-phosphates, the main products being N^3,5′-cyclonucleo-

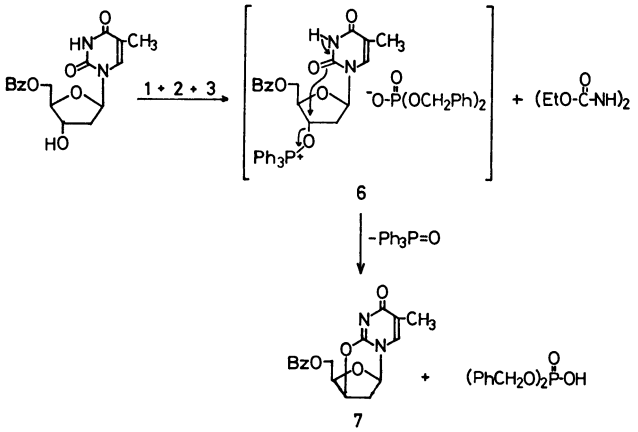

Scheme 3.

Table 1. Reaction of nucleosides with **1**, **2**, and **3**[a]

Nucleoside	Solvent	Product	Yield, %	Recovered nucleoside, %
dT	THF	dpT	47	50
dT	Dioxane[b]	dpT	62	28
dT	HMPT	dpT	73 (77)[c]	25 (8)[c]
dT	Pyridine	dpT	19	22
dbzT	THF	5′-*O*-Benzoyl-O^2,3′-cyclothymidine	46[d]	36
U	THF	pU	42	50
U	Dioxane[b]	pU	68	27
U	HMPT	pU	78	18
U	Trimethyl phosphate	pU	26	63
A	HMPT	pA	0.5	17
		N^3,5′-Cycloadenosine	67	
A	DMF	pA	0.5	10
		N^3,5′-Cycoladenosine	86	
G	HMPT	pG	0.2	50
		N^3,5′-Cycloguanosine	49	
G	DMF	N^3,5′-Cycloguanosine	24	75

a) Unless otherwise stated, nucleoside was allowed to react with 1.5 molar equivalents each of **1**, **2**, and **3** at room temperature, the yields being determined by paper chromatography. b) The reaction was carried out at 60 °C. c) Three molar equivalents of **1**, **2**, and **3** were used; A by-product was formed in a small amount. d) Isolated yields.

sides (**9**). For example, the reaction of adenosine with **1**, **2**, and **3** in HMPT at room temperature resulted in the formation of pA and N^3,5′-cycloadenosine (**9a**) in 0.5 and 67% yields, respectively. The yield of **9a** increased to 86% when the reaction was carriet out in DMF.[18] Similarly guanosine afforded pG and N^3,5′-cycloguanosine (**9b**) in 0.2 and 49% yields. The results are summarized in Table 1.

The formation of **9** can be explained by assuming intermediacy of a quaternary phosphonium salt (**8**), cyclized by nucleophilic attack of the purine base to 5′-carbon atom (Scheme 4, path ii). The predominant formation of the purine cyclonucleoside would be attributed, at least in part, to electrostatic interaction between the phosphorus cation and purine base of **8** which brought the reaction site (5′-*C* and 3-*N*) so close together as to favor cyclization.[19]

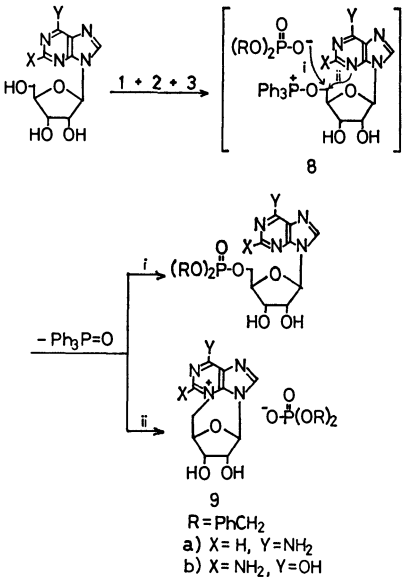

Scheme 4.

Since the intermolecular dehydration described above couples with an oxidation-reduction system,[20] the redox potentials of reagents are expected to play an important role. In order to find the best combination, uridine was allowed to react with **3** in the presence of **2** and various azo compounds for 3 h at room temperature. After hydrogenolysis, the yield of pU was determined by paper chromatography. The results are summarized in Table 2. We see that the combination of **1** and **2** affords the best result. When dibenzoyldiazene was used, 2,5-diphenyl-1,3,5-oxadiazole was isolated in a 50% yield. The formation of the oxadiazole could be explained in terms of the deoxygenation-cyclization process *via* *O*-phosphonium salt (**10**) as shown in Scheme 5.[21] The oxadiazole was also isolated by the reaction of dibenzoyldiazene with **2** in nearly quantitative yield.

Table 2. Reaction of uridine with **3** in the presence of **2** and azo compounds

R–C(=O)–N=N–C(=O)–R	Yield of pU, %	Recovered U, %
EtO	60	27
Ph	3.5	90
	0	94

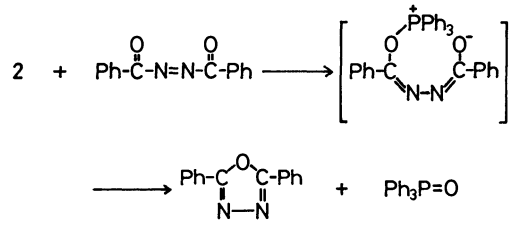

Scheme 5.

In order to cofirm that the present system is applicable to the formation of internucleosidic phosphate linkage, the reaction of 5′-*O*-benzoylthymidine 3′-(2-cyanoethyl)-phosphate [dbzTp(CNEt)] with thymidine was carried out. The dbzTp(CNEt) reacted smoothly with thymidine in the presence of **1** and **2** in HMPT at room temperature. After the solution had been kept stirring overnight, d-bzT3′p(CNEt)5′T was isolated in a 54% yield by column chromatography. Removal of the protecting groups afforded d-T3′p5′T which was completely degraded to dT and dpT by snake venom phosphodiesterase (Scheme 6).

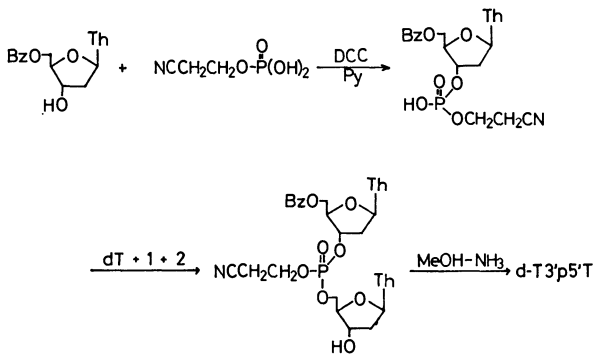

Scheme 6.

The results indicate that the condensation reaction by the use of **1** and **2** proceeds through the initial activation of nucleosides. The system is effective in the selective formation of nucleoside 5′-phosphates and of 3′—5′ internucleotidic linkage by the triester method under mild neutral conditions with the following limitation. 1) Pyrimidine nucleosides selectively give the corresponding nucleoside 5′-phosphates, while purine nucleosides mainly affords N^3,5′-cyclonucleosides. 2) Phosphate diesters can also be activated giving pyrophosphates when hindered nucleosides are used.[22] 3) Since the selectivity originates from the difference in steric requirements between 5′- and 3′(or 2′)-hydroxyl groups, the 3′-hydroxyl group can also enter into the reaction giving nucleoside diphosphates and/or O^2,3′-pyrimidine cyclonucleosides. On hydrolysis, the latter compounds are converted into xylofuranosylnucleoside. 2′-Hydroxy groups would also undergo the same reaction affording O^2,2′-cyclonucleosides which are hydrolyzed to arabino epimers.[23] The use of excess condensing reagent should be avoided.

In spite of several limitations, the selective preparation of pyrimidinenucleoside 5'-phosphates by the use of **1** and **2** was successfully applied to the synthesis of d-T3'p5'T. In order to extend the nucleoside activation process, a method of preventing the intramolecular cyclization of nucleosides should be worked out.[24]

Experimental

Diethyl azodicarboxylate (**1**),[25] dibenzoyldiazene,[26] bis(morpholinocarbonyl)diazene,[27] dibenzyl hydrogenphosphate,[28] and 2-cyanoethyl dihydrogenphosphate[29] were prepared by the known procedure. Unless otherwise stated, the reaction was carried out at room temperature. Paper chromatography was performed by ascending technique using Toyoroshi No. 51A paper. Solvent systems: A, 1-propanol–2 M HCl=5: 1; B, 1-propanol–concd NH_3–H_2O=6: 3: 1; C, 1-butanol–acetic acid–H_2O=5: 2: 3; D, 2-propanol–concd NH_3–H_2O=7: 1: 2. The R_f values of different compounds are given in Table 3. Ultraviolet absorption spectra were obtained on a Hitachi EPS-3T recording spectrometer; the extinction coefficients used in calculating yields are given in Table 3. Tetrahydrofuran (THF) was distilled from Na; stored over Na and distilled from CaH_2 immediately before use. Hexamethylphosphoric triamide (HMPT) was distilled from CaH_2 immediately before use. Dioxane was distilled from Na and stored over Na. It is essential that moisture be excluded from all coupling reaction systems.

Preparation of Pyrimidinenucleoside 5'-Phosphates. A solution of **1** (261 mg, 1.5 mmol) in THF (1 ml) was added dropwise over a period of 1 h to a suspension of nucleoside (1 mmol), **2** (393 mg, 1.5 mmol) and **3** (417 mg, 1.5 mmol) in THF (1 ml).[30] The nucleoside dissolved on addition of **1**. After the solution had been kept stirring overnight, the solvent was removed under reduced pressure. The residue was dissolved in 75 % ethanol (20 ml) and subjected to hydrogenolysis over PdO (200 mg). After the theoretical amount of hydrogen had been absorbed, the catalyst was removed by filtration, the filtrate being made up to 50 ml. A measured volume of the solution was chromatographed for the determination of the amounts of nucleoside 5'-phosphate and the recovered nucleoside. The spots and appropriate blank areas of the paper were eluted after being cut into short pieces by soaking in standard volume of water for about 12 h, and their concentrations were determined spectrophotometrically.

When the reaction was carried out in dioxane, a solution of **1** was added over a period of 1 h to a suspension of nucleoside, **2**, and **3** in dioxane at 60 °C with stirring. Before the work-up, the mixture was held at 60 °C for 2 h and then kept stirring overnight at room temperature.

Thymidine and uridine (1 mmol) nearly completely dissolved in HMPT (1 ml). Triphenylphosphine oxide which separated was removed by filtration before hydrogenolysis. The results are summarized in Table 1.

Comparison of the Combination of Various Azo Compounds with Triphenylphosphine. A solution of azo compound (1.5 mmol) and **3** (1.5 mmol) in HMPT (2 ml) was added dropwise to a solution of uridine (1 mmol) and **2** (1.5 mmol) in HMPT (1 ml) over a period of 2 h at room temperature. After the solution had been kept stirring for 1 h, followed by hydrogenolysis, the yield of pU was determined by paperchromatography. 5 ml of HMPT was required to dissolve bis(morpholinocarbonyl)diazene. The results are summarized in Table 2.

Isolation of 2,5-Diphenyl-1,3,4-oxadiazole. Uridine (1 mmol) was allowed to react with 1.5 molar equivalents each of **2**, **3**, and dibenzoyldiazene. The mixture was poured into water (15 ml) with continuous shaking and left to stand overnight. The aqueous layer was removed by decantation, the residue being washed with water (10 ml). To the residue was added benzene and 4 % aqueous $NaHCO_3$ solution (5 ml), partitioned, and the aqueous phase was extracted with ethyl acetate. The combined extracts were dried, evaporated, and applied to silica gel plates (Merck PF_{254}, 20 cm×20 cm). 2,5-Diphenyl-1,3,4-oxadiazole was isolated by developing the plates with chloroform, 165 mg, 50%, mp 138 °C (ligroin). MS; *m/e* 222 (M^+), 166, 165. The oxadiazole was identified by comparison of its IR spectrum with a standard chart.

Reaction of Dibenzoyldiazene with Triphenylphosphine. A solution of dibenzoyldiazene (238 mg, 1 mmol) in THF (2 ml) was added dropwise to a solution of **2** (262 mg, 1 mmol) in THF (2 ml). After the reaction solution had been kept stirring for 6 h, the solution was chromatographed on silica gel plates (Merck PF_{254}, 20 cm×20 cm, $CHCl_3$) giving 2,5-diphenyl-1,3,4-oxadiazole (214 mg, 96%, mp 136—137.5 °C) and triphenylphosphine oxide (211 mg, 76 %).

Reaction of Purine Nucleosides with 1, 2, and 3. A solution of **1** (270 mg, 1.55 mmol) and **3** (417 mg, 1.5 mmol) in HMPT (1 ml) was added dropwise over a period of 1 h to a suspension

Table 3. R_f values and extinction coefficients used for the calculation of yields

	λ_{max}/nm (Solvent)	$\varepsilon \times 10^{-3}$	R_f value in system[a]			
			A	B	C	D
dT	267 (H_2O)	9.65				0.64
dpT	267 (H_2O)	9.00	0.70			0.17
dTp			0.83			
U	262 (H_2O)	10.1				0.47
pU	262 (H_2O)	10.0		0.22		0.05
Up				0.31		0.12
A	261 (H_2O)	14.9			0.45	
pA	262 (H_2O)	15.0		0.14	0.03	
N^3,5'-Cycloadenosine	273 (0.05 M HCl)	13.6			0.26	
G	256 (0.05 M HCl)	12.3				0.22
pG	256 (0.05 M HCl)	12.2		0.04		
N^3,5'-Cycloguanosine	250 (0.05 M HCl)	11.8				0.11

a) The solvent systems are; A, 1-propanol–2 M HCl=5: 1; B, 1-propanol–concd NH_3–H_2O= 6: 3: 1; C, 1-butanol–acetic acid–H_2O=5: 2: 3; D, 2-propanol–concd NH_3–H_2O=7: 1: 2.

of adenosine (267 mg, 1 mmol) and **2** (393 mg, 1.5 mmol) in HMPT (2 ml). A virtually clear solution was obtained. Precipitation took place shortly afterwards. After the mixture had been kept stirring overnight, triphenylphosphine oxide was removed by filtration and washed with small quantities of HMPT and water successively. The combined filtrate and washing were made up to 25 ml with ethanol and water (solution A). A measured volume was applied to Toyoroshi No. 51A paper which was developed in system C. Two bands corresponding to unchanged adenosine and N^3,5′-cycloadenosine were eluted with water and 0.05 M hydrochloric acid, respectively, and subjected to analysis. The yield of pA was also determined by paper chromatography after the solution A (20 ml) had been subjected to hydrogenolysis over Pd–C (300 mg).

When the reaction was carried out in DMF, no precipitation of triphenylphosphine oxide took place.

In a similar manner, the reactions of guanosine with **1**, **2**, and **3** were carried out in HMPT and in DMF and the yields of products were estimated by paper chromatography. The chromatograms were developed in system D for the estimation of N^3,5′-cycloguanosine and guanosine, and in system B for pG. Respective bands were eluted with 0.05 M HCl. When the reaction was carried out in HMPT, a virtually clear solution was obtained with the progress of reaction. On the other hand, guanosine was hardly soluble in DMF, the undissolved guanosine (65%) being filtered off before analysis.

The results are summarized in Table 1.

Preparation of dbzTp(CNEt). A mixture of 2-cyanoethyl dihydrogenphosphate (10 mmol) and dbzT (692 mg, 2 mmol)[31] was dried by repeated evaporation of added portion of pyridine, dissolved in pyridine (40 ml), and treated with dicyclohexylcarbodiimide (DCC, 30 mmol) for 2 days at room temperature. Water (40 ml) was added and, after allowing the mixture to stand at room temperature for several hours, *N,N′*-dicyclohexylurea was removed by filtration. The filtrate was extracted with petroleum ether (three 40 ml portion) in order to remove DCC. The residual aqueous pyridine solution was passed through a column of Dowex-50 (H^+) ion exchange resine and the column was washed with water. The total effluent was adjusted to pH 7.5 with 0.05 M $Ba(OH)_2$ at 0 °C. The solution was concentrated to *ca.* 5 ml (below 40 °C) and excess 2-cyanoethyl dihydrogenphosphate (barium salt) was removed by precipitation with three volume of ethanol and centrifugation. The supernatant layer was concentrated *in vacuo* (below 30 °C) giving a crystalline product. In order to remove barium ion, the product was applied to Dowex-50 (H^+) ion exchange resin column and effluent was lyophilized affording paper chromatographically homogenious dbzTp(CNEt); 680 mg, 71%, R_f (system C) 0.70.

Preparation of d-bzT3′p(CNEt)5′T. A solution of **1** (174 mg, 1 mmol) in HMPT (1.5 ml) was added dropwise over a period of 1 h to a solution of dbzTp(CNEt) (240 mg, 0.5 mmol), thymidine (242 mg, 1 mmol), and **2** (262 mg, 1 mmol) in HMPT (1.5 ml) at room temperature. After the solution had been kept stirring overnight, triphenylphosphine oxide precipitated was removed by filtration. Solids separated by addition of water (80 ml) to the filtrate. However, on centrifugation followed by removal of the supernatant liquid, the solids became gum which was taken up in THF (3 ml). On addition of ethyl acetate (20 ml), white solids precipitated. They were collected and purified by means of Sephadex LH-20 column (3×40 cm, eluted with THF), giving chromatographically homogenious d-bzT3′p(CNEt)5′T in a 54 % yield; softened at 137 °C, turning a clear melt at 150 °C; R_f (system C) 0.78.

The d-bzT3′p(CNEt)5′T thus obtained was treated with methanol saturated with NH_3 overnight at room temperature. The solution was applied to Toyoroshi No. 51A paper and developed in system C. The band with R_f 0.32 was eluted and the effluent was liophilized giving d-T3′p5′T, which was completely degraded to dT and dpT (1:1 ratio) by snake venom phosphodiesterase (tris buffer, pH 8.1 at 37 °C).

This work was supported financially by the Ministry of Education Japan.

References

1) Part VI: J. Kimura and O. Mitsunobu, *Bull. Chem. Soc. Jpn.*, **51**, 1903 (1978).

2) R. I. Zhdanov and S. M. Zhenodarova, *Synthesis*, **1975**, 222; V. Amarnath and A. D. Broom, *Chem. Rev.*, **77**, 183 (1977); Y. Mizuno, O. Mitsunobu, and T. Hata, "Nukureoshido, Nukureochido no Gosei (Synthesis of Nucleosides and Nucleotides)," Maruzen, Tokyo (1977).

3) T. M. Jacob and H. G. Khorana, *J. Am. Chem. Soc.*, **86**, 1630 (1964); E. Ohtsuka, T. Sugiyama, and M. Ikehara, *Chem. Pharm. Bull.*, **23**, 2257 (1975).

4) E. Ohtsuka, M. W. Moon, and H. G. Khorana, *J. Am. Chem. Soc.*, **87**, 2956 (1965).

5) E. Ohtsuka, *Yuki Gosei Kagaku Kyokai Shi*, **36**, 723 (1978).

6) a) R. L. Letsinger and K. K. Ogilvie, *J. Am. Chem. Soc.*, **91**, 3350 (1969); b) J. C. Catlin and F. Cramer, *J. Org. Chem.*, **38**, 245 (1973).

7) J. Stawinski, T. Hozumi, S. A. Narang, C. P. Bahl, and R. Wu, *Nucleic Acid Res.*, **4**, 353 (1977); T. Hirose, R. Crea, and K. Itakura, *Tetrahedron Lett.*, **1978**, 2449.

8) J. Smrt, *Coll. Czech. Chem. Commun.*, **37**, 1870 (1972).

9) a) E. W. Haeffner, *Biochim. Biophis. Acta*, **212**, 182 (1970); b) J. Zemlicka and J. Smrt, *Tetrahedron Lett.*, **1964**, 2081; c) Y. Mizuno, T. Sasaki, T. Kanai, and H. Igarashi, *J. Org. Chem.*, **30**, 1533 (1965); d) Y. Mizuno and T. Sasaki, *J. Am. Chem. Soc.*, **88**, 863 (1966); e) J. Nagyvary, *Biochemistry*, **5**, 1316 (1966); f) P. C. Srivastava, M. M. Dhar, and K. L. Nagpal, *Indian J. Chem.*, **7**, 1055 (1969), *Chem. Abstr.*, **72**, 13013t (1970).

10) O. Mitsunobu, K. Kato, and J. Kimura, *J. Am. Chem. Soc.*, **91**, 6510 (1969).

11) a) Condensation of d(MeOTr)Tp(CNEt) with thymidine by the use of 2,4,6-triisopropylbenzenesulfonyl chloride afforded d-(MeOTr)T3′p(CNEt)5′T containing 4 % of 3′-3′ linked isomer: R. L. Letsinger and V. Mahadevan, *J. Am. Chem. Soc.*, **87**, 3526 (1965) and Ref. 6a; b) For selective phosphorylation of nucleosides, see J. Hes and M. P. Mertes, *J. Org. Chem.*, **39**, 3767 (1974): Y. Taguchi and Y. Mushika, *Bull. Chem. Soc. Jpn.*, **48**, 1528 (1975); see also Ref 10. By the triester method, fully protected nucleotide monoesters were exclusively condensed with 5′-hydroxyl groups of 2′-*O*-tetrahydropyranylnucleosides or thymidine. T. Neilson and E. S. Werstiuk, *Can. J. Chem.*, **49**, 3004 (1971); M. Sekine and T. Hata, *Tetrahedron Lett.*, **1975**, 1711.

12) a) M. Smith, D. H. Rammler, I. H. Goldberg, and H. G. Khorana, *J. Am. Chem. Soc.*, **84**, 430 (1962); b) H. U. Blank and W. Pfleiderer, *Tetrahedron Lett.*, **1967**, 869.

13) O. Mitsunobu and M. Eguchi, *Bull. Chem. Soc. Jpn.*, **44**, 3427 (1971).

14) Abbreviations used for nucleosides and their derivatives are mostly in line with the principles set up by IUPAC-IUB Commission on Biochemical Nomenclature; *Biochemistry*, **9**, 4022 (1970).

15) Unless otherwise stated, the yields of products were determined by paper chromatography.

16) The amino group has been reported to react with

quaternary phosphonium salts. A. E. Arbuzov and N. N. Sazonova, *Dokl. Akad. Nauk SSSR*, **115**, 1119 (1957), *Chem. Abstr.*, **52**, 6239 (1958); J. P. H. Verheyden and J. G. Moffatt, *J. Org. Chem.*, **37**, 2289 (1972) and references cited therein.

17) 5′-*O*-Benzoyl-O^2,3′-cyclothymidine has the following properties; mp 230—232 °C, λ_{max}^{MeOH} 232, 255 (sh) nm, λ_{min} 215 nm, *cf.* A. M. Michelson and A. R. Todd, *J. Chem. Soc.*, **1955**, 816; J. J. Fox and N. C. Miller *J. Org. Chem.*, **28**, 936 (1963). The formation of cyclonucleosides *via* phosphonium salts has been reported; J. P. H. Verheyden and J. G. Moffatt, *J. Org. Chem.*, **35**, 2319 (1970); M. Wada and O. Mitsunobu, *Tetrahedron Lett.*, **1972**, 1279.

18) The facile cyclization of adenosine in DMF has also been observed in the reaction with *p*-nitrobenzoic acid, **1**, and **2**. S. Shimokawa, J. Kimura, and O. Mitsunobu, *Bull. Chem. Soc. Jpn.*, **49**, 3357 (1976).

19) T. Kurihara, Y. Nakajima, and O. Mitsunobu, *Tetrahedron Lett.*, **1976**, 2455.

20) T. Mukaiyama, *Angew. Chem. Int. Ed. Engl.*, **15**, 94 (1976).

21) The formation of 2,5-diphenyl-1,3,4-oxadiazole through the reaction of tributylphosphine with dibenzoyldiazene in the presence of benzoic acid has also been described. I. Kuwajima, Master of Sc. Thesis, Tokyo Institute of Technology, 1963.

22) No attempt was made to detect tetrabenzyl pyrophosphate in the present system. An evidence of the formation of benzoic anhydride was obtained in the formation of benzoate of a sterically crowded alcohol by means of **1** and **2**. O. Mitsunobu, J. Kimura, K. Iizumi, and N. Yanagida, *Bull. Chem. Soc. Jpn.*, **49**, 510 (1976).

23) a) J. J. Fox, *Pure Appl. Chem.*, **18**, 223 (1969); b) K. K. Ogilvie and D. J. Iwacha, *Can. J. Chem.*, **52**, 1787 (1974) and references cited therein. No detectable evidence of the formation of O^2,3′-pyrimidine cyclonucleoside 5′-phosphate was obtained. However, when thymidine was allowed to react with benzoic acid (1.5 molar equivalent) in the presence of 2.5 molar equivalents each of **1** and **2** at room temperature, **7** and 1-(2-deoxy-3,5-dibenzoyl-β-D-xylofuranosyl)thymine were obtained in 45 and 50 % yields, respectively.

24) Attempts to avoid the intramolecular cyclization of nucleosides have been reported. W. Jahn, *Chem. Ber.*, **98**, 1705 (1965); O. Mitsunobu, S. Takizawa, and H. Morimoto, *J. Am. Chem. Soc.*, **98**, 7858 (1976).

25) J. C. Kauer, *Org. Synth.*, Coll. Vol., IV, 411 (1963).

26) T. Imamoto and Y. Yukawa, *Yuki Gosei Kagaku Kyokai Shi*, **30**, 665 (1972).

27) H. Bock and J. Kroner, *Chem. Ber.*, **99**, 2039 (1966).

28) V. M. Clark and A. R. Todd, *J. Chem. Soc.*, **1950**, 2030.

29) G. M. Tener, *J. Am. Chem. Soc.*, **83**, 159 (1961).

30) Solubility of unprotected nucleosides in organic solvents is usually lower than that of protected nucleosides. In order to increase the yield of the desired product and to avoid the undesirable formation of pyrophosphate, a solution of **1** was added over a long period of time. In the all cases, except for the reaction of guanosine in DMF, virtually clear solution were obtained.

31) O. Mitsunobu, J. Kimura, and Y. Fujisawa, *Bull. Chem. Soc. Jpn.*, **45**, 245 (1972).

Carbon-Carbon Bond Formation by Use of Chloroiodomethane as a C_1 Unit. I. Formation of Chloromethyltriphenylphosphonium Iodide, and Its Application for the Wittig Chloromethylenation of Aldehydes and Ketones[1)]

Sotaro MIYANO,* Yu IZUMI, Katsuo FUJII, Yutaka OHNO, and Harukichi HASHIMOTO
Department of Applied Chemistry, Faculty of Engineering, Tohoku University, Aramaki-Aoba, Sendai 980
(Received September 12, 1978)

Chloromethyltriphenylphosphonium iodide has been prepared by the reaction of chloroiodomethane with triphenylphosphine. Upon treatment with potassium *t*-butoxide in *t*-butyl alcohol, the phosphonium iodide was converted into chloromethylenetriphenylphosphorane; this in turn was used for the Wittig reaction of aldehydes and ketones into the corresponding chloroolefins of the type RCH=CHCl and RR'C=CHCl in good to moderate yields. The configurations of these chloroolefins were assigned on the basis of NMR spectral studies. Direct conversion of benzaldehyde into phenylacetylene was also achieved using the phosphonium salt and excess potassium *t*-butoxide.

Chloroiodomethane can be easily obtained in large quantities from dichloromethane *via* a halogen exchange reaction with sodium iodide in dipolar aprotic media,[2,3)] or under phase-transfer conditions.[4)] It is useful as a methylene source for the cyclopropanation[5)] of olefins as well as for the methylenation[6)] of aldehydes *via* organozinc intermediates.

As is well recognized, the Wittig olefination reaction of carbonyl function is one of the most successful synthetic routes to a wide variety of unsaturated compounds. Chloroolefins are also accessible by the chloromethylenation of carbonyl compounds with chloromethylenetriphenylphosphorane (Ph_3P=CHCl, **2**).[7)] However, the requisite precursor chloromethyltriphenylphosphonium salts ($(Ph_3\overset{+}{P}CH_2Cl)\bar{X}$) have only been prepared by somewhat complicated procedures, such as those described by Seyferth *et al.*,[8)] by Wittig and Schlosser,[9)] and by Appel and Morbach.[10)] Chlorocarbene: CHCl generated from dichloromethane and butyllithium adds to triphenylphosphine to form the phosphorane (**2**),[8,11)] but it is said that troublesome isolation of the phosphorane from residual triphenylphosphine is necessary to obtain chloroolefins in good yields.[8b)] This problem can be avoided to some extent by use of (bromochloromethyl)phenylmercury as the carbene source; nevertheless, the yields are moderate.[12)]

During the course of our investigation on the carbon-carbon bond formation utilizing chloroiodomethane as a C_1 unit, we found that it smoothly reacts with triphenylphosphine to afford chloromethyltriphenylphosphonium iodide (**1**) as a white precipitate.[1)] We report here another convenient method for the conversion of aldehydes and ketones into chloroolefins using the phosphonium iodide (**1**) for the Wittig reaction.**

Results and Discussion

Formation of Chloromethyltriphenylphosphonium Iodide (1) from Chloroiodomethane and Triphenylphosphine. Table 1 shows the results of the reaction of chloroiodomethane and triphenylphosphine in several solvents. When the reaction was carried out in THF, **1** began to precipitate as white solids in the course of the initial 1/2 h heating at reflux. The phosphonium salt amounted to a 60% isolated yield after an 8 h reaction, and to a 70% yield after 20 h (Eq. 1):

Table 1. Preparation of chloromethyltriphenylphosphonium iodide (**1**)

Ph_3P (mmol)	CH_2ClI (mmol)	Solvent	(ml)	Temp (°C)	Time (h)	Yield of **1**[a)] (%)
10	12	Et_2O	20	20—25	20	8
10	11	THF	10	50	20	34
120	150	THF	150	67	8	60
120	150	THF	150	67	20	70
50	70	*t*-BuOH	50	83	6	72
100	110	DMF	120	100	8	0

a) Isolated yield based on Ph_3P.

$$CH_2ClI + Ph_3P \longrightarrow \underset{\mathbf{1}}{(Ph_3\overset{+}{P}CH_2Cl)\bar{I}} \quad (1)$$

This phosphonium salt showed an IR spectrum quite similar to that of chloromethyltriphenylphosphonium chloride over the range from 4000 to 625 cm^{-1}.[13)] It gave satisfactory elemental analysis data, and was converted into the known tetraphenylborate.[8,9)] In refluxing *t*-butyl alcohol, the reaction time was somewhat shortened, probably due to a higher reaction temperature, while the resulting precipitate had to be washed well with THF to remove residual triphenylphosphine. When a mixture of chloroiodomethane and triphenylphosphine in DMF was heated, it turned dark brown, but no precipitate was formed.

Chloromethylenation of Aldehydes and Ketones with Chloromethyltriphenylphosphonium Iodide (1) and Base. Tables 2 and 3 summarize the results of the chloromethylenation of several carbonyl compounds by the Wittig reaction. It can be seen that some aldehydes and ketones can be easily converted into the corresponding chloroolefins of the type RCH=CHCl and RR'C=CHCl in good to moderate yields by use of **1** and potassium *t*-butoxide in *t*-butyl alcohol (Scheme 1).

** After this work had been submitted for publication, the authors learned that fluoromethylenation with $(Ph_3\overset{+}{P}CH_2F)\bar{I}$ had been reported: D. J. Burton and P. E. Greenlimb, *J. Org. Chem.*, **40**, 2796 (1975).

Table 2. Chloromethylenation of ketones[a]

	R–C(=O)–R′	Base	Solvent	Products and yield (%)[b] R–C(R′)=CHCl (3)	E/Z Ratio[c]	R–C(R′)=CH$_2$ (4)
a	–(CH$_2$)$_5$–	*t*-BuOK	*t*-BuOH	94		3.4
		t-BuOLi	*t*-BuOH	58		trace
		EtONa	EtOH	92		0
		t-BuOK	THF	62		7.9
		K_2CO_3[d]	THF	trace		0
b	–(CH$_2$)$_6$–	*t*-BuOK	*t*-BuOH	55		
		t-BuOK	*t*-BuOH	86[e]		
		EtONa	EtOH	56		
c	–CH(CH$_3$)(CH$_2$)$_4$–	*t*-BuOK	*t*-BuOH	89	92/8	
		EtONa	EtOH	49	55/45	
d	–CH(CH$_2$)$_2$CH(CH$_3$)$_2$ CH$_2$CH(CH$_3$)$_2$–[f]	*t*-BuOK	*t*-BuOH	61	72/28	13
		EtONa	EtOH	trace		
e	C$_6$H$_5$– –CH$_3$	*t*-BuOK	*t*-BuOH	75	56/44	13
		EtONa	EtOH	38	68/32	1
f	*p*-ClC$_6$H$_4$– –CH$_3$	*t*-BuOK	*t*-BuOH	59	53/47	13
		EtONa	EtOH	8	75/25	1
g	*p*-CH$_3$C$_6$H$_4$– –CH$_3$	*t*-BuOK	*t*-BuOH	65	57/43	17
		EtONa	EtOH	2		trace

a) Solvent, 50—70 ml; RR′C=O, 20 mmol; **1**, 25 mmol; base, 30 mmol; temp, 20—25 °C; time, 4 h; under a nitrogen atmosphere. b) GLC yield based on RR′C=O. c) Peak area of each isomer on GLC was approximated to the molar ratio. d) The reaction was carried out on the scale of 1/2 using 18-crown-6 (70 mg) as the phase-transfer catalyst under reflux for 9 h. e) Cycloheptanone, 10 mmol. f) Menthone.

Table 3. Chloromethylenation of aldehydes[a]

	RCHO R–	Reaction conditions: Base (mmol)	Reaction conditions: Temp (Time, h)	Products and yield (%)[b]: RHC=CHCl (3)	E/Z Ratio	RC≡CH (5)
h	C$_6$H$_5$–	EtONa 50[c]	Ambient (4)	77	78/22	1
		EtONa 50[c]	Ambient (4), then reflux (3)	60	100/0	16
		EtOK 40[c]	Ambient (4), then reflux (3)	66	100/0	27
		t-BuOK 55	Ambient (1)	81	46/54	7
		t-BuOK 55	Ambient (1), then reflux (2)	20	100/0	71
		t-BuOK 55	Ambient (1), then reflux (8)	trace	—	91
		t-BuOK 30	Ambient (2)	45	62/38	28
i	*p*-ClC$_6$H$_4$–	*t*-BuOK 30	Ambient (4)	69	38/62	3
j	*o*-ClC$_6$H$_4$–	*t*-BuOK 30	Ambient (4)	66	50/50	5
k	*p*-CH$_3$OC$_6$H$_4$–	*t*-BuOK 30	Ambient (4)	60	d)	10
l	*p*-CH$_3$C$_6$H$_4$–	*t*-BuOK 30	Ambient (4)	62	d)	15
m	*n*-C$_8$H$_{17}$–	*t*-BuOK 30	Ambient (4)	45	44/56	trace

a) *t*-BuOH (50—70 ml) was used as solvent unless otherwise noted. RCHO,20 mmol; **1**, 25 mmol. In the case of benzaldehydes (**h**—**l**), the styrene ArCH=CH$_2$ was also detected in 3—5% yield. b) See footnotes b) and c) in Table 2. c) Solvent, EtOH, 50 ml. d) The *E*- and *Z*-isomer could not be sufficiently well separated from each other on GLC (but $E<Z$).

Upon addition of **1** to a potassium *t*-butoxide solution in *t*-butyl alcohol under nitrogen, the orange-red color characteristic of phosphinemethylene reagents developed. To this mixture was added *ca.* 0.8 molar equivalent amount of a carbonyl compound. For example, after 4 h stirring at ambient temperature, all of the cyclohexanone reacted to afford chloromethylenecyclohexane (**3a**) in as high as 94% yield. Small amounts of methylenecyclohexane was also formed a sa by-product, showing some reduction had occurred during the process. The exact nature of the reduction is not yet clear,[14] but the methylenation reaction was dependent

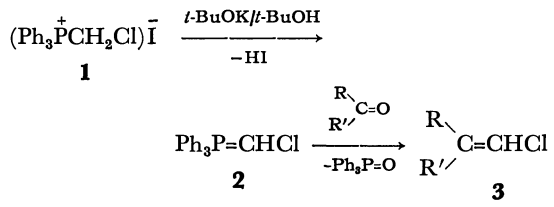

Scheme 1.

on the substrate carbonyl compounds as well as on the reaction medium; menthone and acetophenones gave relatively large amounts of methylenated products, and the EtONa/EtOH system seemed to suppress the reduction.

When the chloromethylenation was carried out in ethyl alcohol using sodium ethoxide as the base, the chloromethylenephosphorane (**2**) showed diminished reactivity. Thus, with this solvent-base combination, reactive substrates such as cyclohexanone and benzaldehyde gave chloroolefins in good yields, but almost all of the menthone was recovered unchanged. A solid-liquid two phase system[16] using 18-crown-6 as the phase-transfer catalyst and sodium carbonate powder as the base did not work well. Organolithium reagents have been used conventionally in the Wittig chloromethylenation reaction under rather severe reaction conditions.[8,9,11] In preliminary experiments, however, chloromethylenation of cyclohexanone with butyllithium was complicated by the occurrence of an alkylation reaction to pentylidenecyclohexane, and no further investigation was conducted.

The Wittig methylenation of cycloheptanone is reported to have resulted in poor yields,[17] but chloromethylenecycloheptane (**3b**) was obtained in a reasonable yield by use of about twice as much of the phosphorane (**2**).

NMR Spectral Studies of 1-Chloroolefins. In the reaction with aldehydes and unsymmetrical ketones, two geometric isomers of 1-chloroolefins were formed in roughly comparable yields, showing that the chloromethylenephosphorane (**2**) is one of the semistabilized ylids.[18] In a given pair of isomeric chloroolefins, the component which eluted first on GLC (Apiezon Grease L column) was assigned to the *Z*-configuration on the

Table 4. NMR spectral data of 1-chloroolefins (**3**)[a]

Compound	Chemical shifts and assignments	
	=CHCl	Other protons
3a	5.63 (m)[b]	1.4—1.8 (6H, br, $-(CH_2)_3-$), 1.8—2.5 (4H, m, $-CH_2$, $-CH_2$, C=C)
3b	5.69 (m)[b]	1.3—1.8 (8H, br, $-(CH_2)_4-$), 2.0—2.5 (4H, m, $-CH_2$, $-CH_2$, C=C)
E-**3d**	5.63 (m)[b]	0.7—1.2 (9H, m, 3-CH_3), 1.2—2.4 (8H, m), 2.4—2.7 (1H, m)
Z-**3e**	5.96 (q, J=1.4)	2.0 (3H, d, J=1.4, $-CH_3$), 7.2 (5H, s, $-C_6H_5$)
E-**3e**	6.15 (q, J=1.3)	2.1 (3H, d, J=1.3, $-CH_3$), 7.2 (5H, s, $-C_6H_5$)
Z-**3f**	5.98 (q, J=1.5)	2.0 (3H, d, J=1.5, $-CH_3$), 7.2 (4H, s, $-C_6H_4$)
E-**3f**	6.19 (q, J=1.4)	2.1 (3H, d, J=1.4, $-CH_3$), 7.1 (4H, s, $-C_6H_4$)
Z-**3g**	5.95 (q, J=1.6)	2.0 (3H, d, J=1.6, =C–CH_3), 2.3 (3H, s, Ph–CH_3), 7.1 (4H, s(br), $-C_6H_4$)
E-**3g**	6.15 (q, J=1.5)	2.1 (3H, d, J=1.5, =C–CH_3), 2.3 (3H, s, Ph–CH_3), 7.0 (4H, s, $-C_6H_4$)
Z-**3h**	6.07 (d, J=8.2)	6.5 (1H, d, J=8.2, =CH–Ph), 7.1—7.6 (5H, m, $-C_6H_5$)
E-**3h**	6.43 (d, J=15)	6.7 (1H, d, J=15, =CH–Ph), 7.1—7.6 (5H, m, $-C_6H_5$)
Z-**3i**	6.11 (d, J=8.2)	6.4 (1H, d, J=8.2, =CH–Ph), 7.1—7.6 (4H, q-like, $-C_6H_4$)
E-**3i**	6.41 (d, J=13.3)	6.7 (1H, d, J=13.3, =CH–Ph), 7.1 (4H, s, $-C_6H_4$)
Z-**3j**	6.28 (d, J=8.0)	6.8 (1H, d, J=8.0, =CH–Ph), 7.0—7.4 (3H, m, $-C_6H_3$), 7.6—7.9 (1H, m, $-C_6H$)
E-**3j**	6.46 (d, J=13.4)	7.0 (1H, d, 13.4, =CH–Ph), 7.0—7.4 (4H, m, $-C_6H_4$)
Z-**3k**	5.98 (d, J=8.0)	3.7 (3H, s, $-OCH_3$), 6.4 (1H, d, J=8.0, =CH–Ph), 6.5—7.6 (4H, m, $-C_6H_4$)
E-**3k**	6.31 (d, J=13.8)	3.7 (3H, s, $-OCH_3$), 6.7 (1H, d, J=13.8, =CH–Ph), 6.6—7.3 (4H, q-like, $-C_6H_4$)
Z-**3l**	5.95 (d, J=8.4)	2.2 (3H, s(br), $-CH_3$), 6.4 (1H, d, J=8.4, =CH–Ph), 6.8—7.5 (4H, m, $-C_6H_4$)
E-**3l**	6.33 (d, J=16)	2.2 (3H, s(br), $-CH_3$), 6.55 (1H, d, J=16, =CH–Ph), 6.8—7.5 (4H, m, $-C_6H_4$)
Z-**3m**	5.91 (dt, J_{cis}=7.2, $J_{H,CH_2}\leq 1$	0.7—1.0 (3H, t, CH_3), 1.0—1.7 (12H, br, $-(CH_2)_6-$), 1.8—2.4 (2H, m, $-CH_2-C=C$), 5.7 (1H, dt, J_{cis}=7.2, J_{vis}=7.2, =CH–Alkyl)
E-**3m**	5.77 (m)[b]	0.7—1.1 (3H, t, $-CH_3$), 1.1—1.6 (12H, br, $-(CH_2)_6-$), 1.7—2.3 (2H, m, $-CH_2-C=C$), 5.8 (1H, br, =CH–Alkyl)

a) CCl_4 (5—10%); chemical shift, δ (ppm) from internal hexamethyldisiloxane; coupling constant, J(Hz).
b) Rather sharp signal.

basis of NMR studies (Table 4). Chemical shifts of vinylic protons of these 1-chloroolefins were correlated well with the known empirical formula of Pascual, Meier, and Simons.[19] In the case of β-chlorostyrenes (**3e**—**3l**), in general, the proton which locates in the *geminal* position to the chlorine atom in the *E*-isomer resonanced at a lower magnetic field than that in the *Z*-isomer. The NMR spectra of (*E*)- and (*Z*)-chloromethylene-2-methylcyclohexane (**3c**) were assigned as summarized in Scheme 2:

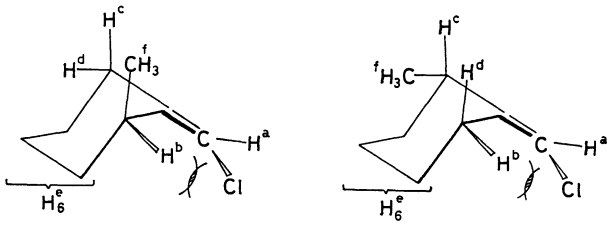

Z-**3c** *E*-**3c**

Z-**3c**	*E*-**3c**
H_a: δ5.63 (d, J_{ac}=1.8 Hz)	H_a: δ5.62 (m, J_{ac}=1.5 Hz)
H_b: 2.9—3.4 (m)	H_b: 2.5—2.9 (m)
H_c+H_d: 1.9—2.4 (m)	H_c: 2.0—2.3 (m)
H_e: 1.3—1.9 (m)	H_d+H_e: 1.2—2.0 (m)
H_f: 1.05 (d, J_{bf}=7 Hz)	H_f: 1.02 (d, J_{cf}=7 Hz)

Scheme 2.

The PCK model shows considerable steric interaction between the Cl and the H_b atom. Thus, the methyl substituent attached to the C_2 atom of the *Z*-isomer seemed to be restrained to the axial position. The remarkable downfield shift of the H_b protons of each isomer can be explained by the steric compression effect (van der Waal's shift) and/or the anisotropic effect of the nearby Cl atom.[20,21] The H_a proton of the *E*-isomer showed a multiplet, but rather narrow signal; this was sharpened by irradiation of the H_c proton, showing a magnetic interaction between H_c and H_a. Similar allylic long-range couplings are documented.[22]

The vinylic protons of (*E*)-1-chloro-1-decene (*E*-**3m**) showed a somewhat confusing NMR spectrum. It can be characterized as shown in the last line of Table 4 on the assumption that each vinylic proton resonanced at almost the same magnetic field, reducing the apparent J_{trans} to zero.[23]

Conversion of Benzaldehyde into Phenylacetylene. From benzaldehydes, phenylacetylenes as well as β-chlorostyrenes were formed in the chloromethylenation reaction (Table 3). From the results of the reaction of benzaldehyde conducted in the presence of excess amounts of alkoxides and employing longer reaction periods, it is concluded that the phenylacetylene was formed *via* dehydrochlorination of the initially formed β-chlorostyrenes, the *Z*-isomer reacting much faster than the *E*-counterpart. The dehydrochlorination with sodium or potassium ethoxide in ethyl alcohol consumed only the *Z*-isomer under the reaction conditions, leaving the other chloride intact, while both were converted to phenylacetylene by refluxing with *t*-butoxide in *t*-butyl alcohol.[24] It is known that dehydrohalogenation from olefinic halides with alkoxides proceeds mainly through an E2 mechanism *via trans*-elimination, and in many instances the relative rate ratio of *Z*- to *E*-isomer ranges from 10^4 to 10^6.[25] On the other hand, Schlosser and Ladenberger reported that (*E*)-β-chlorostyrenes are more sensitive to phenyllithium than the corresponding *Z*-isomer, suggesting an E2cB mechanism for the dehydrochlorination.[26]

Irrespective of the precise mechanism involved, it is noteworthy that the formyl function of benzaldehydes can be converted into the acetylenic grouping in a one-pot reaction. Further studies are now in progress. Multistep formyl to ethynyl conversions have been reported by Villieras *et al.*[27] and by Corey and Fuchs.[28]

Experimental

The IR spectra were recorded on a Shimadzu IR 430 spectrometer. The NMR spectra were determined using a Hitachi R-24A spectrometer (60 MHz), with hexamethyldisiloxane as an internal standard. GLC analyses were carried out with a Shimadzu GC-3AF or a Shimadzu GC-3BT apparatus using a Silicone DC 550 (20%), an Apiezon Grease L (20%), or a Silicone DC 410 (20%) on Diasolid M (60—80 meshes) column. A Shimadzu GC-2C apparatus was used for the preparative GLC using an Apiezon Grease L column.

Materials. Chloroiodomethane was obtained by the procedure described before.[2] Commercial ketones and aldehydes except *p*-chlorobenzaldehyde, which was used as purchased, were dried over magnesium sulfate, and distilled at reduced pressure and stored under nitrogen. Triphenylphosphine (mp 80.5 °C), sodium tetraphenylborate, and 18-crown-6 were used without further purification. Solvents were purified as usual before use.

Preparation of Chloromethyltriphenylphosphonium Iodide (1). Triphenylphosphine (120 mmol) was dissolved in 150 ml of THF in a 500 ml round-bottomed flask equipped with a magnetic stirrer, a pressure-equilibrating dropping funnel, a thermometer, and a Widmer reflux condenser topped with a nitrogen inlet tube. The mixture was stirred rapidly while chloroiodomethane (150 mmol) was added. The flask was immersed in an oil bath and the mixture was heated at reflux for *ca.* 20 h. The resulting white precipitate was filtered, and

Table 5. NMR spectral data of methylenation products (**4**) and acetylenes (**5**)[a]

Compound	Chemical shifts and assignments
4d	0.8—1.1 (9H, m, 3-CH_3), 1.2—2.5 (9H, m), 4.4—4.5 (1H, br), 4.5—4.6 (1H, br)
4f	2.1 (3H, d, $-CH_3$), 5.0 (1H, q, =CH *trans* to Ph), 5.2 (1H, d, =CH *cis* to Ph), 7.2 (4H, s, $-C_6H_4$)
4g	2.0 (3H, dd, =C–CH_3), 2.2 (3H, s, Ph–CH_3), 4.8 (1H, m, =CH *trans* to Ph), 5.2 (1H, m, =CH *cis* to Ph), 6.8—7.3 (4H, q-like, $-C_6H_4$)
4k	3.7 (3H, s, $-OCH_3$), 5.0 (1H, dd, =CH *trans* to Ph), 5.5 (1H, dd, =CH *cis* to Ph), 6.6 (1H, dd, =CH *gem* to Ph), 6.6—7.4 (4H, q-like, $-C_6H_4$), J_{trans}=17.4, J_{cis}=10.4, J_{gem}=1.5
5i	2.9 (1H, s, CH), 7.1—7.4 (4H, m, $-C_6H_4$)
5j	3.1 (1H, s, ≡CH), 6.9—7.6 (4H, m, $-C_6H_4$)
5k	3.7 (3H, s, $-OCH_3$), 2.7 (1H, s, ≡CH), 6.5—7.4 (4H, q-like, $-C_6H_4$)
5l	2.2 (3H, s(br), $-CH_3$), 2.8 (1H, s, ≡CH), 6.8—7.3 (4H, m, $-C_6H_4$)

a) See footnote a) in Table 4.

Table 6. Analytical data

Compound	Molecular formula	C Found(Calcd)	H Found(Calcd)	Cl Found(Calcd)
3a	$C_7H_{11}Cl$	64.67(64.37)	8.92(8.49)	26.58(27.14)
3b	$C_8H_{13}Cl$	66.77(66.43)	8.76(9.06)	24.18(24.51)
E-**3c**	$C_8H_{13}Cl$	66.06(66.43)	9.17(9.06)	24.79(24.51)
3d[a]	$C_{11}H_{19}Cl$	71.23(70.76)	10.60(10.26)	17.41(18.98)
Z-**3e**	C_9H_9Cl	70.90(70.83)	5.69(5.94)	23.64(23.23)
E-**3e**	C_9H_9Cl	70.76(70.83)	5.58(5.94)	23.72(23.23)
3f[a]	$C_9H_8Cl_2$	57.18(57.79)	4.35(4.31)	38.65(37.90)
Z-**3g**	$C_{10}H_{11}Cl$	71.94(72.07)	6.96(6.65)	21.50(21.27)
E-**3g**	$C_{10}H_{11}Cl$	72.29(72.07)	6.68(6.65)	21.04(21.27)
3h[a]	C_8H_7Cl	69.26(69.33)	5.51(5.09)	24.92(25.58)
Z-**3i**	$C_8H_6Cl_2$	55.44(55.53)	3.08(3.49)	41.13(40.98)
E-**3j**	$C_8H_6Cl_2$	55.61(55.53)	3.73(3.49)	41.28(40.98)
Z-**3k**	C_9H_9ClO	63.78(64.11)	5.31(5.38)	20.56(21.02)
3l[a]	C_9H_9Cl	70.44(70.83)	5.85(5.94)	23.73(23.23)
Z-**3m**	$C_{10}H_{19}Cl$	68.71(68.75)	10.59(10.96)	20.65(20.29)
4g	$C_{10}H_{12}$	90.74(90.85)	8.91(9.15)	
5l	C_9H_8	93.18(93.06)	6.53(6.94)	

a) A mixture of *E*- and *Z*-isomer.

the solids were washed thoroughly with 5×50 ml of THF in a nitrogen atmosphere. The phosphonium salt was dried *in vacuo* at 50—60 °C for several hour; it was then stored in a Schlenk tube under nitrogen. The dried product weighed 37 g (70 % yield based on triphenylphosphine). Mp 185—187 °C (dec). Found: C, 51.58; H, 3.82 %. Calcd for $C_{19}H_{17}ClIP$: C, 52.02; H, 3.91 %. IR (KBr, cm^{-1}): 3030 (w), 2890 (m), 2850 (m), 2770 (w, sh), 1580 (m), 1480 (m), 1440 (s), 1350 (w), 1330 (w), 1250 (w), 1170 (m), 1125 (vs), 1005 (m), 940 (w), 920 (w), 880 (m), 820 (w), 770 (s), 750 (m), 740 (m), 730 (m), 705 (s), 545 (s), 530 (s), 505 (m), 506 (w, sh).

Chloromethyltriphenylphosphonium Tetraphenylborate. A sample of the phosphonium iodide (**1**) (1.0 mmol) was placed in 30 ml of water and stirred vigorously. To this suspension was added a solution of sodium tetraphenylborate (1.5 mmol) in 20 ml of 1:1 ethyl alcohol–water. Another 250 ml of ethyl alcohol was added, and then the mixture was stirred at reflux for 2 h. After filtration, the filtrate was kept overnight at −78 °C. The resulting white precipitate was collected, recrystalized from ethyl alcohol (150 ml)–ether (150 ml), washed several times with small portions of alcohol–ether, and dried *in vacuo*. Mp 190—193 °C (dec) (lit, mp 189—192 °C (dec),[8a] 222—223.8 °C[9]). Found: C, 81.85; H, 6.22; Cl, 4.90 %. Calcd for $C_{43}H_{37}BClP$: C, 81.85; H, 5.91; Cl, 5.62 %.

Generation of Chloromethylenetriphenylphosphorane (2) and the Wittig Chloromethylenation of Carbonyl Compounds. The general procedure is described below. Under a nitrogen atmosphere, *t*-butyl alcohol (25 ml) was placed in a 100 ml three-neck round-bottomed flask equipped with a magnetic stirrer, a thermometer, and a Widmer reflux condenser topped with a nitrogen inlet tube. Potassium (30 mg-atom) was added, and the mixture was heated at reflux for *ca.* 1 h to afford a potassium *t*-butoxide solution. The reaction flask was then immersed in a water bath. A powder dropping funnel[29] which contained 25 mmol of **1** was attached to the flask, and the **1** was dropped to the solution over 5 min. The funnel was washed with another 15 ml of *t*-butyl alcohol to bring the residual phosphonium salt into the reaction flask. The mixture was stirred for 1.5 h at ambient temperature; during this time it turned from white to an orange-red slurry. After the formation of **2** was completed, the powder dropping funnel was replaced with a pressure-equilibrating dropping funnel which contained a substrate carbonyl compound (20 mmol) in 10 ml of *t*-butyl alcohol. The carbonyl compound was added over 20 min, while retaining the reaction temperature below 25 °C. The mixture was stirred for another 3 h 40 min at ambient temperature (20—25 °C). At the end of the reaction, the mixture was shaken with 50 ml of pentane and 50 ml of water, filtered, and the layers were separated. The aqueous layer was extracted with 3×50 ml of pentane. The combined organic phase was washed with 3×30 ml of water, and dried over magnesium sulfate. An aliquot of the sample was used for the quantitative determination of the reaction products by GLC, employing experimentally determined calibration curves. After removal of the solvents by distillation *in vacuo*, the volatile products were collected in a cold trap, and subjected to a preparative GLC for the recovery of each component. Reaction products were identified and characterized by means of GLC, NMR (Tables 4 and 5), and IR spectrometry, and elemental analyses (Table 6).

Financial support of this work by a Grant-in-Aid (C-35536) from the Ministry of Education, Japan, is gratefully acknowledged (S. M.).

References

1) Preliminary communication: S. Miyano, Y. Izumi, and H. Hashimoto, *J. Chem. Soc., Chem., Commun.*, **1978**, 446.

2) S. Miyano and H. Hashimoto, *Bull. Chem. Soc. Jpn.*, **44**, 2864 (1971).

3) N. Altabev, R. D. Smith, and S. I. Suratwala, *Chem. Ind.*, **1973**, 331.

4) D. Landini and F. Rolla, *Chem. Ind.*, **1974**, 533.

5) a) S. Miyano and H. Hashimoto, *Bull. Chem. Soc. Jpn.*, **46**, 892 (1973); b) S. Miyano, Y. Izumi, H. Fujii, and H. Hashimoto, *Synthesis*, **1977**, 700.

6) S. Miyano, M. Hida, and H. Hashimoto, *J. Organomet. Chem.*, **12**, 263 (1968).

7) See for example, A. Maercker, "Organic Reactions," (1965), Vol. 14, p. 270.

8) a) D. Seyferth, S. O. Grim, and T. O. Read, *J. Am. Chem. Soc.*, **82**, 1510 (1960); b) D. Seyferth, S. O. Grim, and

T. O. Read, *J. Am. Chem. Soc.*, **83**, 1617 (1961).
9) G. Wittig and M. Schlosser, *Chem. Ber.*, **94**, 1373 (1961).
10) R. Appel and W. Morbach, *Synthesis*, **1977**, 699.
11) G. Wittig and M. Schlosser, *Angew. Chem.*, **72**, 324 (1960).
12) D. Seyferth, J. K. Heeren, G. Singh, S. O. Grim, and W. B. Hughes, *J. Organomet. Chem.*, **5**, 267 (1966).
13) C. J. Pouchert, "The Aldrich Library of Infrared Spectra," Aldrich Chemical Co., Inc., Spectrum No. 867B.
14) *Cf.* Köbrich *et al.* ascribed the formation of the methylenated products to the halogen-metal interconversion on the halomethyltriphenylphosphonium salts by organolithium reagents used as the base for the ylid formation.[15]
15) G. Köbrich, H. Trapp, K. Flory, and W. Drischel, *Chem. Ber.*, **99**, 689 (1966).
16) R. M. Boden, *Synthesis*, **1975**, 784.
17) A. Schriesheim, R. J. Muller, and C. A. Rowe, Jr., *J. Am. Chem. Soc.*, **84**, 3164 (1962).
18) S. Nishida, "Shin Zikken Kagaku Koza," Maruzen, Tokyo (1977), Vol. 14, p. 224.
19) L. M. Jackman and S. Sternhell, "Applications of Nuclear Magnetic Resonance Spectroscopy in Organic Chemistry," 2nd ed, Pergamon Press, London (1969), p. 184.
20) R. C. Fort, Jr., G. W. H. Cheeseman, and E. C. Taylor, *J. Org. Chem.*, **29**, 2440 (1964).
21) Ref. 19), pp. 71, 80.
22) Ref. 19), p. 316.
23) For example, M. Hesse, W. von Philipsborn, D. Schumann, G. Spiteller, M. Spiteller-Friedmann, W. I. Taylor, H. Schmid, and P. Karrer, *Helv. Chim. Acta*, **47**, 878 (1964).
24) *Cf.* L. A. Paquette, L. S. Wittenbrook, and V. V. Kane, *J. Am. Chem. Soc.*, **89**, 4487 (1967).
25) D. V. Banthorpe, "Reaction Mechanisms in Organic Chemistry," ed by E. D. Hughes, Elsevier Publ. Co., New York, N. Y. (1963), Vol. 2, p. 142.
26) M. Schlosser and V. Ladenberger, *Chem. Ber.*, **100**, 3901 (1967).
27) J. Villieras, P. Perriot, and J. F. Normant, *Synthesis*, **1975**, 458.
28) E. J. Corey and P. L. Fuchs, *Tetrahedron Lett.*, **1972**, 3769.
29) T. Suehiro, K. Tokumaru, and M. Yoshida, "Gendai no Yukikagaku Zikken," Gihodo, Tokyo (1971), p. 139.

Synthesis of Some Naturally Occurring Acetylchromenes

Amolak Chand JAIN,* Rajesh KHAZANCHI, and Ashwani KUMAR
Department of Chemistry, Himachal Pradesh University, Summer Hill, Simla 171005, India
(Received December 19, 1977)

2,4-Dihydroxy-5-methoxyacetophenone on treatment with 3-chloro-3-methyl-1-butyne in the presence of K_2CO_3, KI, and DMF yielded its 4-(1,1-dimethyl-2-propynyl) ether (**2**) and the naturally occurring 6-acetyl-5-hydroxy-8-methoxy-2,2-dimethylchromene (**3**). More of the chromene (**3**) could be obtained by the thermal cyclisation of the acetophenone (**2**). Methylation of **3** yielded another natural chromene. 4-Hydroxy-3-methoxyacetophenone, on similar treatment with 3-chloro-3-methyl-1-butyne, gave directly natural 6-acetyl-8-methoxy-2,2-dimethylchromene. 2,3,4-Trihydroxy-5-(3-methyl-2-butenyl)acetophenone, on cyclodehydrogenation followed by methylation with 1 mol of dimethyl sulfate, yielded natural riparіochromene-A. Further methylation provided methylriparіochromene-A.

From a Mexican plant *Ageratina scorodonioides* (Gray) King et Rob., Bohlmann *et al.*[1] isolated 6-acetyl-5-hydroxy-8-methoxy-2,2-dimethylchromene (**3**) and its methyl ether (**4**). The former was also reported to occur in *Flourensia cernua* D.C.[2] Obviously, both seem to be derived in nature from 2,4-dihydroxy-5-methoxyacetophenone (**1**). They are now synthesised from this ketone **1** by heating with 3-chloro-3-methyl-1-butyne in the presence of K_2CO_3, KI, and DMF, when a mixture of two compounds resulted. The major compound proved to be the required natural chromene **3** on the basis of its NMR spectrum and positive ferric chloride reaction. Thus, it showed a characteristic doublet of two olefinic protons at δ 5.50 and 6.70 and a singlet of only one aromatic proton at δ 7.05. Further it was found to be identical in all respects with the description of the natural sample. The minor component was characterised as 2-hydroxy-5-methoxy-4-(1,1-dimethyl-2-propynyloxy)acetophenone (**2**) on the basis of resonance signals of one acetylenic proton at δ 2.70 and of two *para*-coupled aromatic protons at δ 6.88 and 7.20. The yield of the natural chromene **3** was raised by heating **2** with *N,N*-dimethylaniline. When the chromene (**3**) was methylated with excess of dimethyl sulfate in the presence of ignited K_2CO_3 and acetone, the fully methylated chromene **4** identical with the natural sample was obtained.

From *A. scorodonioides*, Bohlmann *et al.*[1] isolated still another chromene to which they gave the constitution of 2,2-dimethyl-6-acetyl-8-methoxychromene (**6**) on the basis of its NMR spectrum. It is now prepared from 4-hydroxy-3-methoxyacetophenone (**5**) by heating it with 3-chloro-3-methyl-1-butyne in the presence of DMF, K_2CO_3, and KI, when the natural chromene (**6**) was straight away obtained identical in all respects with the description of the natural substance.

From *Eupatorium riparium* Regel., Anthonsen[3] isolated two chromenes called riparіochromene-A and methylriparіochromene-A. They were assigned structures as 6-acetyl-7-hydroxy-8-methoxy-2,2-dimethylchromene (**10**) and its methyl ether (**11**) respectively mainly on the basis of their NMR data. More recently, these two compounds have also been isolated from the above mentioned species of *Ageratina*.[1] Methylriparіochromene-A **11** has also been obtained from the dried leaves of *Stevia serrata* by Kohda *et al.*[4] who

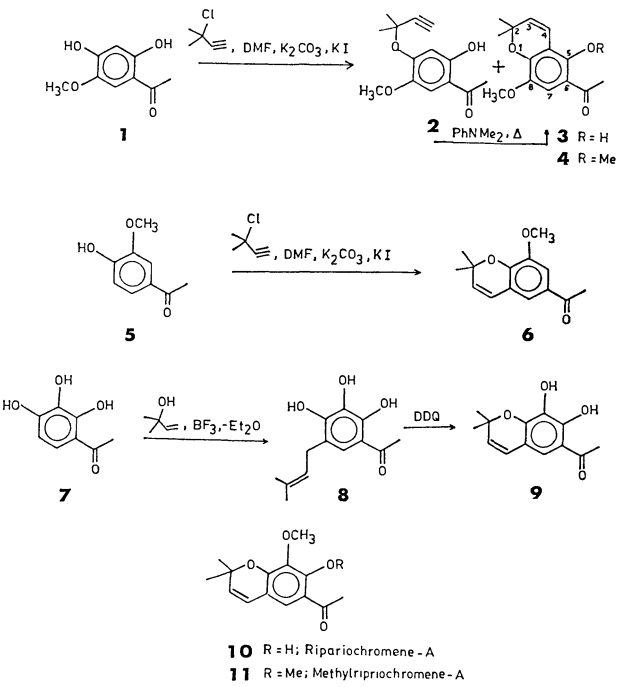

concluded this structure from a study of nuclear Overhauser effect in its PMR spectrum and its ^{13}C NMR spectrum.

These two compounds **10** and **11** have now been synthesised starting from 2,3,4-trihydroxyacetophenone **1** which, on reacting with 2-methyl-3-buten-2-ol in the presence of BF_3-etherate according to the procedure of Bajwa *et al.*,[5] gave 2,3,4-trihydroxy-5-(3-methyl-2-butenylacetophenone (**8**) as the main product. Cyclodehydrogenation of **8** with DDQ afforded 6-acetyl-7,8-dihydroxy-2,2-dimethylchromene (**9**) in nearly quantitative yield. Its structure was established on the basis of its NMR spectrum which showed 2 doublets at δ 5.53 and 6.20 and an aromatic proton at δ 7.25. Partial methylation of **9** with dimethyl sulfate, K_2CO_3 and acetone yielded riparіochromene-A **10**, while complete methylation with excess of dimethyl sulfate afforded methylriparіochromene-A **11** both identical with the natural samples.

Experimental

All melting points are uncorrected. Unless otherwise stated, PMR spectra were determined on a BS 487 C spectrometer (80 MHz) with reference to tetramethylsilane as an

internal standard; the chemical shifts are expressed in δ values; light petroleum used had boiling range 60—80 °C; silica gel was used for column chromatography and silica gel-G for TLC; R_f values refer to TLC using one of the following solvent systems: (A) toluene–ethyl formate–formic acid (5:4:1); (B) benzene; (C) benzene–ethyl acetate (9:1); spraying of TLC plates was carried out with 10% aq H_2SO_4 and/or 1% alcoholic $FeCl_3$.

*Reaction of 2,4-Dihydroxy-5-methoxyacetophenone (**1**) with 3-Chloro-3-methyl-1-butyne.* A mixture of the ketone[6] (**1**, 0.5 g) 3-chloro-3-methyl-1-butyne (0.4 ml), ignited potassium carbonate (2.5 g), anhydrous potassium iodide (1 g) and *N,N*-dimethylformamide (40 ml) was heated at 80—85 °C for 40 h. The solvent was removed *in vacuo*, the residue treated with water (200 ml) and the whole mixture extracted with ether. The ether residue on column chromatography and successive elution with benzene–light petroleum (1:1) and benzene alone gave two fractions A and B.

Fraction-A crystallized from benzene-light petroleum mixture to afford *6-acetyl-5-hydroxy-8-methoxy-2,2-dimethylchromene* (**3**, 200 mg) as yellow needles, mp 87—88 °C (lit,[2] mp 88 °C); R_f 0.45 (solvent B), brown ferric reaction; PMR ($CDCl_3$): 1.48 (6H, s, $(CH_3)_2C\langle$), 2.46 (3H, s, $-COCH_3$), 3.74 (3H, s, $-OCH_3$), 5.50 (1H, d, J=10 Hz, H-3), 6.70 (1H, d, J=10 Hz, H-4), 7.05 (1H, s, H-7) and 12.55 (1H s, chelated OH); UV_{max} (MeOH): 255 nm (log ε 4.31), 320 (3.31), 3.40 (3.74). (Found: C, 68.0; H, 6.2%). These data agree with those of the natural substance.

Fraction-B gave *2-hydroxy-5-methoxy-4-(1,1-dimethyl-2-propenyloxy)acetophenone* (**2**) as a yellow oil (100 mg); R_f 0.4 (solvent B); green ferric reaction; PMR (CCl_4): 1.25; 1.41 (6H, 2s, $(CH_3)_2C\langle$), 2.50 (3H, s, $-COCH_3$), 2.70 (1H, s, $-C\equiv\underline{C}H$), 3.80 (3H, s, $O\underline{C}H_3$), 6.88 (1H, d, J=1.5 Hz, H-3) and 7.20 (1H, d, J=1.5 Hz, H-6); UV_{max} (MeOH): 281 nm (log ε 4.2), 302 (3.9). Found: C, 68.2; H, 6.8. Calcd for $C_{14}H_{16}O_4$: C, 67.7; H, 6.5%.

*6-Acetyl-5-hydroxy-8-methoxy-2,2-dimethylchromene (**3**).* The above acetophenone (**2**) (50 mg) was heated in *N,N*-dimethylaniline at 210—220 °C for 3 h. The mixture was cooled and treated with dil HCl (1:1, 20 ml). The resulting solid crystallized from benzene–light petroleum mixture to give **3** as yellow needles (40 mg), identical in mp and mmp with the sample prepared above.

*6-Acetyl-5,8-dimethoxy-2,2-dimethylchromene (**4**).* A solution of **3** (100 mg) in acetone (20 ml) was refluxed with dimethyl sulfate (0.06 ml) and ignited K_2CO_3 (400 mg) for 4 h. Acetone was evaporated and water added to the residue. The resulting solid crystallised from ether–light petroleum mixture to give **4** as yellow crystals, mp 62—63 °C (lit,[1] mp 63 °C); R_f 0.55 (solvent B); PMR (CCl_4): 1.48 (6H, s, $(CH_3)_2C\langle$), 2.50 (3H, s, $-COC\underline{H}_3$), 3.77 (6H, s, two $-OC\underline{H}_3$), 5.53 (1H, d, J=10 Hz, H-3) 6.48 (1H, d, J=10 Hz, H-4) and 7.22 (1H, s, H-7); UV_{max} (MeOH): 270 nm (log ε 3.2), 281 (3.1), 310 (3.9). (Found: C, 68.8; H, 7.21%). These data agree with those described for the natural sample.

*6-Acetyl-8-methoxy-2,2-dimethylychromene (**6**).* A mixture of 4-hydroxy-3-methoxyacetophenone[7] (**5**, 500 mg), 3-chloro-3-methyl-1-butyne (0.2 ml), K_2CO_3(2 g), KI (1 g), and DMF (20 ml) was heated on a steam bath for 45 h. The product gave **6** as a colourless oil (300 mg), R_f 0.6 (solvent C); PMR ($CDCl_3$): 1.48 (6H, s, $(CH_3)_2C\langle$), 2.57 (3H, s, $-COCH_3$), 3.90 (3H, s, $-OCH_3$), 5.55 (1H, d, J=10 Hz, H-3), 6.30 (1H, d, J=10 Hz, H-4) 7.25 (1H, d, J=2 Hz, H-7), and 7.50 (1H, d, J=2 Hz, H-5); UV_{max} (MeOH): 225 nm (log ε 3.31), 302 (3.90). These data are in accord with those of the natural substance.[1]

*6-Acetyl-7,8-dihydroxy-2,2-dimethylchromene (**9**).* To a solution of 2,3,4-trihydroxy-5-(3-methyl-2-butenyl) acetophenone[5] (**8**, 1 g) in dry benzene (50 ml) was added DDQ (1 g) and the resulting mixture refluxed for 15 min, when colorless hydroquinone separated out. It was filtered while hot and the filtrate after removal of the solvent left a viscous mass which was purified by column chromatography. Elution with benzene–light petroleum (1:1) gave **9** as a dense yellow oil (850 mg); R_f 0.83 (solvent A); dark brown ferric reaction; PMR ($CDCl_3$): 1.47 (6H, s, $(CH_3)_2C\langle$), 2.50 (3H, s, $-COCH_3$), 5.53 (1H, d, J=10 Hz, H-3), 6.20 (1H, d, J=10 Hz, H-4), 7.25 (1H, s, H-5) and 12.30 (1H, s, chelated OH); UV_{max} (MeOH); 230 nm(log ε 4.2), 246 (3.9) and 270 (3.1).

*Riparіochromene-A (**10**).* A solution of the above chromene (**9**, 130 mg) in dry acetone (20 ml) was refluxed with dimethyl sulfate (0.06 ml) and ignited K_2CO_3 for 3 h. The product crystallised from ethyl acetate–light petroleum mixture to give **10** as yellow crystals (100 mg), mp 88—89 °C (lit,[1] mp 88.5 °C); R_f 0.65 (solvent C); brown ferric chloride reaction; PMR ($CDCl_3$): 1.45 (6H, s, $(CH_3)_2C\langle$), 2.58 (3H, s, $COCH_3$), 3.83 (3H, s, $OC\underline{H}_3$), 5.55 (1H, d, J=10 Hz, H-3), 6.30 (1H, d, J=10 Hz, H-4), and 7.20 (1H, s, H-5); UV_{max} (MeOH); 242 nm (log ε 3.2), 292 (3.1). (Found: C, 68.0; H, 6.2%). These data agree with those described for the natural compound.[1]

*Methylriparіochromene-A (**11**).* An acetone solution of the chromene (**9**, 130 mg) was refluxed with dimethyl sulfate (0.15 ml) and ignited K_2CO_3 for 5 h. The product (**11**) was obtained as a light yellow oil (100 mg), R_f 0.75 (solvent A); PMR ($CDCl_3$): 1.45 (6H, s, $(CH_3)_2C\langle$), 2.48 (3H, s, $-COCH_3$), 3.75 (6H, s, two $-OC\underline{H}_3$), 5.55 (1H, d, J=10 Hz, H-3), 6.24 (1H, d, J=10 Hz, H-4) and 7.27 ppm (1H, s, H-5); UV_{max} (MeOH): 255 nm (log ε 3.6), 286 (3.2). (Found: C, 68.8; H, 7.4%). It agreed with the natural substance.[1]

The authors acknowledge with thanks the award of NF to ACJ, and JRF to RK and A.K.

References

1) F. Bohlmann, J. Jakupovic, and M. Lonitz, *Chem. Ber.*, **110**, 301 (1977).
2) F. Bohlmann and M. Grenz, *Chem. Ber.*, **110**, 295 (1977).
3) T. Anthonsen, *Acta Chem. Scand.*, **23**, 3605 (1969).
4) H. Kohda, K. Yamazaki, and O. Tanaka, *Phytochemistry*, **15**, 846 (1976).
5) B. S. Bajwa, P. L. Khanna, and T. R. Seshadri, *Indian J. Chem.*, **9**, 1322 (1971).
6) D. D. Clarke and F. F. Nord, *J. Am. Chem. Soc.*, **77**, 6618 (1955).
7) T. Reichstein, *Helv. Chim. Acta*, **10**, 392 (1927).

NOTES

BULLETIN OF THE CHEMICAL SOCIETY OF JAPAN, VOL. 52 (4), 1205—1206 (1979)

^{14}N Nuclear Quadrupole Relaxation Near the Plastic Transition Point in the Low-temperature Phase of 1,4-Diazabicyclo[2.2.2]octane

Hisao NEGITA,* Michio MAEKAWA, Tsuneo KUBO, and Tsutomu OKUDA
Department of Chemistry, Faculty of Science, Hiroshima University, Hiroshima 730
(Received June 5, 1978)

Synopsis. The relaxation mechanism near the plastic transition in the low-temperature phase of 1,4-diazabicyclo-[2.2.2]octane is attributed to the overall molecular tumbling. The activation energy is 23.0 kJ mol^{-1}, which is nearly equal to the value of 22.2 kJ mol^{-1} in the proton NMR in the plastic phase.

1,4-Diazabicyclo[2.2.2]octane (triethylenediamine), $(CH_2CH_2)_3N_2$, is known as a globular molecule. In the room-temperature phase, the crystal is hexagonal, with two molecule per unit cell.[1] At 351 K it is transformed into a plastic form. Smith[2] studied the proton NMR of 1,4-diazabicyclo[2.2.2]octane and made a few measurements of the spin-lattice relaxation time (T_1) between 77 and 160 K. Soda and Chihara[3] also studied the proton NMR of 1,4-diazabicyclo[2.2.2]-octane and measured the T_1 between 77 K and the melting point. There is no dip of T_1 on approaching the plastic transition point (T_t) from the low-temperature side. The ^{14}N NQR in 1,4-diazabicyclo[2.2.2]-octane was discovered by Haigh and Guibé.[4] Zussman and Alexander investigated this resonance from 77 K to the plastic transition and measured the spin-lattice relaxation time (T_1), the linewidth, and the resonance frequency.[5] According to them, T_1 decreases rapidly towards the plastic transition point, but the behavior near T_t has not been clarified in detail. Therefore, we have measured the T_1 near T_t in detail in order to examine the relaxation mechanism thoroughly.

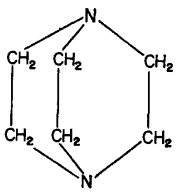

Experimental

The ^{14}N NQR measurements were carried out using a pulsed spectrometer consisting of a Matec gating modulator, Model 5100, a R. F. gated amplifier, Model 515, and a tuned receiver, Model 615, which was designed by Petersen.[6,7] The spin-lattice relaxation times were determined by the repeating 90° pulse method.[8] The pulse width was about 50 μs. The free induction decay signal was averaged in a Nicolet Instrument, Model 527, signal averager. The rf coil containing the sample was enclosed in a cylindrical brass can. This can was placed inside a cylindrical copper container with insulating spacers. The heating wire was wound on this container and connected to a slide-contact voltage regulator. The container was immersed in a large Dewar vessel containing edible oil. The temperature was measured by the use of a copper-constantan thermocouple and stabilized within ±0.1 K.

1,4-Diazabicyclo[2.2.2]octane of an extra pure reagent grade was purchased from the Katayama Chemical Ind. Co. and was purified by sublimation in an evacuated vessel several times. About a 20-g portion of the reagent was used for the measurements.

Results and Discussion

The temperature dependence of the spin-lattice relaxation time (T_1) is shown in Fig. 1. T_1 falls just below the transition point (T_t). The NQR signal becomes progressively weaker as the temperature approaches T_t, and no signal is observed above T_t, presumably because of the "melting" of the molecular orientation, which averages out the electric-field gradients. The relaxation times in our sample are in good agreement with those of Zussman and Alexander throughout the temperature range studied.

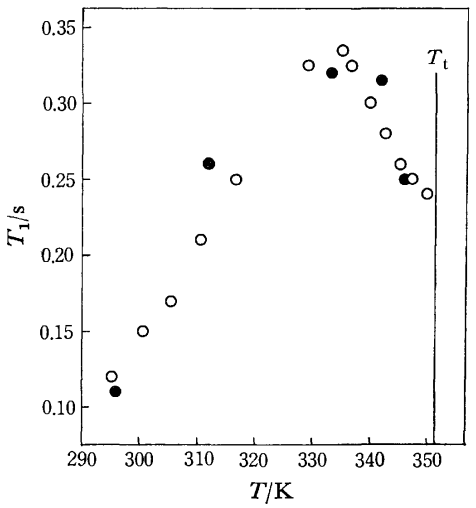

Fig. 1. Temperature dependence of the spin-lattice relaxation times near T_t. Zussman and Alexander's data are shown by the solid circles.

In the room-temperature phase, the N–N axis lies along the hexagonal c axis, and the restricted reorientation of the molecule about the N–N axis is accompanied by a small additional "wobbling" of the N–N axis. In the high-temperature phase above T_t, 351 K, a general molecular reorientation and self-diffusion occur.[2] According to Nimmo *et al.*,[9] molecules at each lattice site undergo hindered reorientations between eight equally weighted orientations at 354 K. It can be said that the "melting" of the molecular orientation or the

overall molecular tumbling occurs at T_t. According to the NMR results in the plastic phase reported by Soda and Chihara,[3] the relaxation mechanism is attributable to the overall molecular tumbling near T_t and to the self-diffusion near the melting point (T_m). As the transition temperature, T_t, is approached, this overall molecular tumbling occurs at an increasing rate, which reduces the T_1 of ^{14}N before it affects the T_1 of ^1H. A similar phenomenon has been found in the temperature dependence of the T_1 and $T_{1\rho}$ of the protons near T_t for $(CH_3)_3CCOOD$.[10] In this case, the relaxation formula is expressed as follows:[5,11]

$$1/T_1 = C\tau/(1+\omega_Q^2\tau^2) \quad (1)$$

and

$$\tau = \tau_0 \exp(E_a/RT), \quad (2)$$

where C is a constant which describes the strength of the interaction, ω_Q is the resonance angular frequency, τ is the correlation time of the motion which changes according to the Arrhenius' relation (2), τ_0 is the inverse frequency factor, and E_a is the activation energy of the motion.

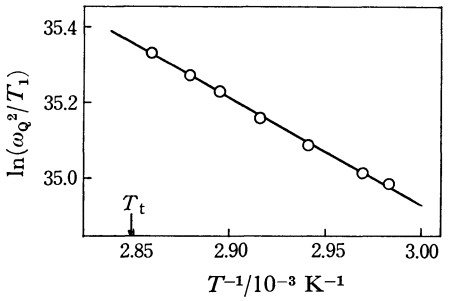

Fig. 2. $\ln(\omega_Q^2/T_1)$ *versus* $10^3/T$.

In the low-temperature region of the T_1 minimum, where $\omega_Q\tau \gg 1$, the following equation is obtained:

$$\ln(\omega_Q^2/T_1) = -E_a/RT + \ln(C/\tau_0) \quad (3)$$

In the plot of $\ln(\omega_Q^2/T_1)$ *versus* $1/T$, seen in Fig. 2, the slope of the straight line gives the activation energy, E_a. This was found to be 23.0 ± 2.3 kJ mol^{-1}. In the plastic phase, the activation energy of the overall molecular tumbling was found by the proton NMR to be 22.2 kJ mol^{-1}.[3] Accordingly, the reduction of T_1 of ^{14}N is attributed to the overall molecular tumbling.

References

1) T. Wada, E. Kishida, Y. Tomiie, H. Suga, S. Seki, and I. Nitta, *Bull. Chem. Soc. Jpn.*, **33**, 1317 (1960).
2) G. W. Smith, *J. Chem. Phys.*, **43**, 4325 (1965).
3) G. Soda and H. Chihara, Abstr. No. 1C08, 26th National Meeting of the Chemical Society of Japan, Hiratsuka, April 1972; G. Soda, private communication.
4) P. J. Haigh and L. Guibé, *C. R. Acad. Sci.*, **261**, 2328 (1965).
5) A. Zussman and S. Alexander, *J. Chem. Phys.*, **48**, 3534 (1968).
6) G. Petersen, Ph. D. thesis, Brown University, 1975.
7) G. Petersen and P. J. Bray, *J. Chem. Phys.*, **64**, 522 (1976).
8) S. Alexander and A. Tzalmona, *Phys. Rev.*, **138**, A845 (1965).
9) J. K. Nimmo and B. W. Lucas, *Acta Crystallogr., Sect. B*, **32**, 597 (1976).
10) S. Albert, H. S. Gutowsky, and J. A. Ripmeester, *J. Chem. Phys.*, **64**, 3277 (1976).
11) Y. Abe, Y. Ohneda, H. Niki, and S. Kojima, *J. Phys. Soc. Jpn.*, **40**, 530 (1976).

BULLETIN OF THE CHEMICAL SOCIETY OF JAPAN, VOL. 52 (4), 1207—1208 (1979)

An Approach to the Interpretation of the Mass Spectra of Aliphatic Acids

Hiroshi NAKASHIMA* and Katsunobu OKAMOTO

Laboratory of Chemistry, School of Paramedicine, Kanazawa University, Kanazawa 920

(Received August 7, 1978)

Synopsis. A method of comparing the sum of the total energies of fragment molecules has been applied to the interpretation of simple cleavage and rearrangement reactions in electron-impact mass spectrometry for the straight chain aliphatic acids.

The quasi-equilibrium theory has been successful in explaining the mass spectra of saturated hydrocarbons.[1] This theory is based on the hypothesis that the active molecular ion is first formed and the energy is distributed throughout the ion. The molecular ion subsequently decomposes when the ion is in the proper configuration and possesses a sufficient amount of vibrational energy. As long as the quasi-equilibrium theory holds in mass spectra, a comparison of the sum of the total energies of the fragments will be able to predict fragmentation. Ichikawa and Ogata used the method to predict the most probable course of bond-scission by comparing the sum of the total energies of the fragments thus produced.[2]

In this paper, the method has been applied to formic, acetic, propionic, and butyric acids. Mass spectrometric studies of those carboxylic acids have been conducted by several investigators, and the fragment ions studied using isotopic labelled compounds and the detection of metastable ion peaks.[3] The total energies of the fragment molecules have been calculated by the CNDO/2 method, the parameters of which were the same as in the paper of Pople and Segal.[4] The total energy may vary with the structure but it is difficult to know the structure of the radical and ionic species. The possible configurational changes were considered to take place to those appropriate forms (*e.g.*, $sp^3 \rightarrow sp^2$), in the cationic and radical molecules and the most stable energy adopted after calculation of the probable configurations. In the present calculation, the following bond lengths (Å) have been assumed: $C(sp^3)$–$C(sp^3)$, 1.54; $C(sp^3)$–$C(sp,sp^2)$, 1.50; $C(sp^2)$–C(sp), 1.45; C=C, 1.35; C–O, 1.32; C=O, 1.25; C≡O, 1.15; C–H, 1.09; O–H, 0.96. Bond angles have been taken to be $109°28'(sp^3)$; $120°(sp^2)$; $110°(<COH)$.

Results and Discussion

The total energies of the molecules, cations and radicals (eV) obtained by the CNDO/2 method are listed in Table 1. Combinations of the fragments listed in Table 1 would give a variety of fragmentation processes. From the point of view of energy comparison, the decomposition reactions appeared to occur more in the production of two fragments than in three fragments. Therefore, only the processes producing two fragments have been discussed here. The difference in energy between molecules and cations indicate the ionization potentials (IP). The IP values obtained were a little greater than that reported in the literature. The CNDO/2 method is not well suited for the estimation of the total energy, but this method proved sufficiently useful for the elucidation of mass spectra. A comparison of the sum of the total energies of the fragments produced and the relative intensities of the peaks are shown in Table 2 where the peak height of the most abundant species has been set at 100. The breakdown patterns of the mass spectra have been classified into simple

TABLE 1. TOTAL ENERGIES OF MOLECULES AND FRAGMENTS (eV)

Compound	Molecule	Ion	Fragment	Radical	Ion
HCOOH	−1232.9	−1220.8	CH_3	−248.1	−235.9
CH_3COOH	−1473.0	−1462.1	C_2H_5	−490.2	−480.7
C_2H_5COOH	−1712.3	−1701.1	C_3H_7	−729.4	−720.7
C_3H_7COOH	−1951.6	−1941.2	HCO	−704.3	−694.1
CO	−681.7	−664.4	CH_3CO	−944.7	−936.6
CO_2	−1187.5	−1173.1	C_2H_5CO	−1185.0	−1176.2
H_2O	−540.5	−525.2	C_3H_7CO	a)	−1415.6
CH_4	−275.2	−256.2	OH	−516.5	−498.9
C_2H_6	−514.5	−498.6	COOH	−1207.3	−1197.8
C_3H_8	−753.7	−738.8	HCOO	−1209.1	−1192.2
CH_3OH	−776.9	−763.8	CH_2COOH	−1449.3	−1436.7
C_2H_5OH	−1016.1	−1003.3	CH_2CH_2COOH	−1687.6	−1679.1
C_3H_7OH	−1255.3	a)	CH_2=COH	−944.6	−934.1
CH_2=CH_2	−469.1	−454.5			
CH_3CH=CH_2	−709.1	−696.0			
CH_2C=$(OH)_2$	−1473.4	−1461.8			
CH_2CO	−922.6	−911.4			
CH_2CH_2CO	−1157.1	−1150.3			

a) The calculation does not show convergence by the SCF method.

Table 2. The sum of the total energies of the produced fragments (eV)

		Fragmentation	
HCOOH		$HCO^+ + OH\cdot = -1210.6$	vs
		$HCO\cdot + OH^+ = -1203.2$	
	R	$H_2O^+ + CO = -1206.9$	w
	R	$H_2O + CO^+ = -1204.9$	
CH_3COOH		$CH_3CO^+ + OH\cdot = -1453.1$	vs
		$CH_3\cdot + COOH^+ = -1445.9$	vs
		$CH_3CO\cdot + OH^+ = -1443.6$	
		$CH_3^+ + COOH\cdot = -1443.2$	m
	R	$CH_2CO^+ + H_2O = -1451.9$	w
	R	$CH_4 + CO_2^+ = -1448.3$	
	R	$CH_2CO + H_2O^+ = -1447.8$	
	R	$CH_3OH^+ + CO = -1445.5$	
	R	$CH_4^+ + CO_2 = -1443.7$	
C_2H_5COOH		$CH_3CH_2CO^+ + OH\cdot = -1692.7$	w
		$CH_3CH_2^+ + COOH\cdot = -1688.0$	s
		$CH_3CH_2\cdot + COOH^+ = -1688.0$	m
		$CH_3^+ + CH_2COOH\cdot = -1685.2$	
		$CH_3\cdot + CH_2COOH^+ = -1684.8$	
		$CH_3CH_2CO\cdot + OH^+ = -1683.9$	
	R	$CH_2{=}CH_2 + HCOOH^+ = -1689.9$	
	R	$CH_3CH_2 + CO_2^+ = -1687.6$	
	R	$CH_2{=}CH_2^+ + HCOOH = -1687.4$	vs
	R	$CH_3CH_3^+ + CO_2 = -1686.1$	
C_3H_7COOH		$CH_3CH_2CH_2CO^+ + OH\cdot = -1932.1$	
		$CH_3CH_2^+ + CH_2COOH\cdot = -1930.0$	w
		$CH_3CH_2CH_2^+ + COOH\cdot = -1928.0$	w
		$CH_3CH_2CH_2\cdot + COOH^+ = -1927.2$	w
		$CH_3\cdot + CH_2CH_2COOH^+ = -1927.2$	m
		$CH_3CH_2\cdot + CH_2COOH^+ = -1926.9$	
	R	$CH_3COOH^+ + CH_2{=}CH_2 = -1931.2$	
	R	$CH_2{=}C(OH)_2^+ + C_2H_4 = -1930.9$	vs
	R	$CH_3CH{=}CH_2 + HCOOH^+ = -1929.9$	
	R	$CH_3CH{=}CH_2^+ + HCOOH = -1928.9$	m
	R	$CH_2{=}C(OH)_2 + C_2H_4^+ = -1927.9$	
$C_2H_5CO^+$		$CH_3CH_2^+ + CO = -1162.4$	s
		$CH_3\cdot + CH_2CO^+ = -1159.5$	
		$CH_3^+ + CH_2CO = -1158.5$	
	R	$CH_2{=}CH_2 + HCO^+ = -1163.2$	s
	R	$CH_2{=}CH_2^+ + HCO\cdot = -1158.8$	vs
$C_3H_7CO^+$		$CH_3CH_2^+ + CH_2CO = -1403.3$	w
		$CH_3CH_2CH_2^+ + CO = -1402.4$	w
		$CH_3CH_2\cdot + CH_2CO^+ = -1401.6$	
		$CH_3\cdot + \cdot CH_2CH_2CO^+ = -1398.4$	
	R	$CH_2{=}CH_2 + CH_2{=}COH^+ = -1403.2$	w
	R	$CH_3CH{=}CH_2 + HCO^+ = -1403.2$	w
	R	$CH_3CH{=}CH_2^+ + HCO\cdot = -1400.3$	m
	R	$CH_2{=}CH_2^+ + CH_2{=}COH\cdot = -1399.1$	m

R indicates rearrangement breakdown. vs, s, m, and w indicate relative intensities as follows: vs; 100—76, s; 75—51, m; 50—26, w; 25—10.

cleavage and rearrangement reactions, the rearrangement processes being denoted by the letter R.

In the mass spectrum of HCOOH, the peak at *m/e* 29 (HCO^+) was predicted as a simple fragment ion. The ion *m/e*=45, as shown in Table 1, $COOH^+$ was calculated to be more stable than $HCOO^+$. Ono *et al.*, however, reported that $HCOO^+$ and $COOH^+$ occurred in equal abundance in the spectrum of HCOOH.[3]

In the mass spectrum of CH_3COOH, the ions CH_3CO^+ (*m/e*=43) and $COOH^+$ (*m/e*=45) were predicted to appear abundantly from simple cleavage, and CH_2CO^+ (*m/e*=42) from rearrangement.

In the mass spectrum of C_2H_5COOH, the ions $C_2H_5CO^+$ (*m/e*=57), $C_2H_5^+$ (*m/e*=29), $COOH^+$ (*m/e*=45) were predicted to appear abundantly as simple fragment ions.

In the mass spectrum of C_3H_7COOH, the following ion peaks were considered as simple fragment ions: $C_3H_7CO^+$ (*m/e*=81), $C_2H_5^+$ (*m/e*=29), $C_3H_7^+$ (*m/e*=43), $COOH^+$ (*m/e*=45), $CH_2CH_2COOH^+$ (*m/e*=73). The ions CH_3COOH^+ (*m/e*=60), $CH_2{=}C(OH)_2^+$ (*m/e*=60) were considered as rearrangement ions. The peak at *m/e* 60 is known as the McLafferty rearrangement ion $CH_2{=}C(OH)_2^+$. Levsen and Schwarz reported that there is no isomerization, or only minor isomerization of $CH_2{=}C(OH)_2^+$ to CH_3COOH^+.[5]

The first process which straight chain aliphatic acids undergo upon electron-impact is the removal of one of the lone pair electron on the oxygen atom. The active molecular ions vibrate and bond-scission occurs statistically in terms of energy. In the mass spectra of the carboxylic acids, $R\text{–}C{\equiv}O^+$, is predicted to appear in appreciable amounts from simple cleavage. The peak heights of $C_2H_5CO^+$ from C_2H_5COOH and $C_3H_7CO^+$ from C_3H_7COOH were, however, not as high as expected. Concerning the $C_2H_5CO^+$ and $C_3H_7CO^+$ ions, the secondary decomposition processes were examined by comparing the sum of the total energies of the fragment molecules, the results of which are shown in Table 2. The probable fragment ions $C_2H_5^+$, HCO^+ (*m/e*=29) from $C_2H_5CO^+$ and $C_2H_5^+$ (*m/e*=29), $CH_2{=}COH^+$ (*m/e*=43) from $C_3H_7CO^+$ were found respectively in the mass spectrum. It is suggested that the $C_2H_5CO^+$, $C_3H_7CO^+$ ions may be unstable, decomposing immediately.

The main peaks in the electron-impact mass spectra are concordant with the results for simple cleavage, but not so good for the rearrangement reactions. The configurational structure may play an important role in the occurrence of rearrangement ions.

The authors thank Dr. Juro Maruha of the Faculty of Liberal Art, Kanazawa University, for his advice in this work. The computations were conducted on a FACOM M-160 computer at the data processing center, Kanazawa University.

References

1) H. M. Rosenstock, M. B. Wallenstein, A. L. Wahrhaftig, and H. Eyring, *Proc. Nat. Acad. Sci.*, **38**, 667 (1952).

2) H. Ichikawa and M. Ogata, *Bull. Chem. Soc. Jpn.*, **46**, 1873 (1973); H. Ichikawa and M. Ogata, *Chem. Pharm. Bull.*, **22**, 1560 (1974).

3) G. P. Happ and D. W. Stewart, *J. Am. Chem. Soc.*, **74**, 4404 (1952); G. A. Ropp and C. E. Melton, *J. Am. Chem. Soc.*, **80**, 3509 (1958); K. Hirota, K. Nagoshi, and M. Hatada, *Bull. Chem. Soc. Jpn.*, **34**, 226 (1961); Y. Ono, T. Makita, and K. Kodera, *Bull. Chem. Soc. Jpn.*, **41**, 1793 (1968).

4) J. A. Pople and G. A. Segal, *J. Chem. Phys.*, **44**, 3289 (1966).

5) K. Levsen and H. Schwarz, *J. Chem. Soc., Perkin Trans. 2*, **1976**, 1231.

BULLETIN OF THE CHEMICAL SOCIETY OF JAPAN, VOL. 52 (4), 1209—1210 (1979)

The X-Ray Structure Determination of Heptaethylene Glycol-$Sr(SCN)_2$

Hideyo OHMOTO, Yasushi KAI, Noritake YASUOKA,† Nobutami KASAI,*
Shozo YANAGIDA, and Mitsuo OKAHARA

Department of Applied Chemistry, Faculty of Engineering, Osaka University, Yamadakami, Suita, Osaka 565

(Received September 12, 1978)

Synopsis. The crystal structure of heptaethylene glycol-$Sr(SCN)_2$ has been determined by X-ray diffraction. The Sr ion is coordinated by eight oxygen atoms arising from the heptaethylene glycol moiety and a nitrogen atom from one of SCN groups. The coordination polyhedron is irregular, Sr–O distances ranging from 2.56 to 2.73 Å.

It is well known that macrocyclic ethers interact with alkali and alkaline earth metal ions to give complexes, some structures of which have been determined by X-ray crystallography.[1-3] On the other hand, linear poly(oxyethylene) (POE) derivatives also have a chelating ability to metal cations.[4] The structures of various glymes with $HgCl_2$ and $CdCl_2$ have been investigated by Iwamoto[5,6] in connection with structural studies of polyethylene glycol–$HgCl_2$ complexes.[7,8] Recently, POE deraviatives with the appropriate number of oxyethylene units have been found to form complexes with alkali and alkaline earth metal thiocyanates.[9] In order to investigate the chlating behavior of POE, X-ray diffraction studies have been made and here the structure of heptaethylene glycol–$Sr(SCN)_2$ is presented.

The crystals, colorless and transparent prisms, were obtained by recrystallization from an acetone solution.

Crystal Data: $(C_{14}H_{30}O_8)\cdot Sr(SCN)_2$, *F.W.*=530.2, monoclinic, space group $P2_1/c$, a=11.368(3), b=14.311(2), c=17.665(6) Å, β=122.13(2)°, V=2434(2) Å^3, D_m=1.45 g cm^{-3} (flotation in dichloromethane–carbon tetrachloride), D_c=1.45 g cm^{-3} for Z=4, μ(Mo $K\alpha$)=23.6 cm^{-1}.

Intensity data were measured on a Rigaku diffractometer with graphite monochromatized Mo $K\alpha$ radiation employing the ω scan technique. The integrated intensity was determined by scanning the peak at a rate of 2°/min along the ω axis. A total of 5313 reflections were obtained, of which 3151 reflections were $F_o > 3\sigma(F_o)$. Lorentz and polarization corrections were made, but no absorption correction was applied, which might limit the accuracy of the present structure determination.

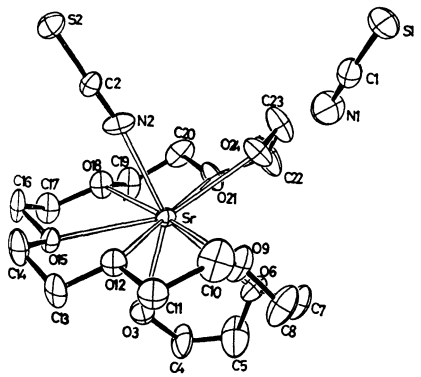

Fig. 1. An ORTEP drawing of the $Sr(SCN)_2$–EO7 molecule together with the numbering scheme.

The structure was solved by the heavy atom method, and refined by the block-diagonal least-squares method with HBLS V[10] program. The atomic scattering factors used in all the computations were taken from the International Tables of X-Ray Crystallography.[11] The refinement was converged to a rather high R value of 0.113 for 3151 reflections and this will be discussed later.

An *ORTEP* drawing of the complex molecule is shown in Fig. 1, together with the numbering system. The bond lengths and bond angles are listed in Table 1.††

Coordination Geometry: Eight oxygen atoms from heptaethylene glycol (EO7) and one nitrogen atom from a SCN anion are coordinated to the Sr ion. The coordination polyhedron is irregular. It is difficult to express the polyhedron in simple terms, although a nine

Table 1. The bond lengths (l/Å) and bond angles (φ/°) in the complex molecule

Sr-O(N) bond		in SCN anion		C-C bond		C-O bond		C-C-O angle		C-O-C angle	
Sr-O(3)	2.56(2)	N(1)-C(1)	1.13(3)	C(4) -C(5)	1.31(5)	O(3) -C(4)	1.41(3)	O(3) -C(4) -O(5)	115(3)	C(5) -O(6) -C(7)	116(2)
Sr-O(6)	2.73(2)	C(1)-S(1)	1.61(2)	C(7) -C(8)	1.42(4)	C(5) -O(6)	1.43(4)	C(4) -C(5) -O(6)	123(3)	C(8) -O(9) -C(10)	120(2)
Sr-O(9)	2.68(2)	N(2)-C(2)	1.15(3)	C(10)-C(11)	1.49(4)	O(6) -C(7)	1.38(3)	O(6) -C(7) -C(8)	117(3)	C(11)-O(12)-C(13)	113(2)
Sr-O(12)	2.72(2)	C(2)-S(2)	1.66(2)	C(13)-C(14)	1.48(4)	C(8) -O(9)	1.36(3)	C(7) -C(8) -O(9)	116(3)	C(14)-O(15)-C(16)	113(2)
Sr-O(15)	2.69(2)	N(1)-C(1)-S(1)	178(2)	C(16)-C(17)	1.50(3)	O(9) -C(10)	1.41(3)	O(9) -C(10)-C(11)	109(2)	C(17)-O(13)-C(19)	110(2)
Sr-O(18)	2.71(2)	N(2)-C(2)-S(2)	179(2)	C(19)-C(20)	1.50(4)	C(11)-O(12)	1.42(3)	C(10)-C(11)-O(12)	109(2)	C(20)-O(21)-C(22)	115(2)
Sr-O(21)	2.66(2)			C(22)-C(23)	1.41(5)	C(12)-C(13)	1.38(3)	O(12)-C(13)-C(14)	108(2)		
Sr-O(24)	2.56(2)					C(14)-O(15)	1.46(3)	C(13)-C(14)-O(15)	108(2)		
Sr-N(2)	2.57(2)					O(15)-C(16)	1.43(3)	O(15)-C(16)-C(17)	109(2)		
						C(17)-O(18)	1.42(3)	C(16)-C(17)-O(18)	107(2)		
						O(18)-C(19)	1.43(3)	O(18)-C(19)-C(20)	107(2)		
						C(20)-O(21)	1.39(3)	C(19)-C(20)-O(21)	109(2)		
						O(21)-C(22)	1.39(4)	O(21)-C(22)-C(23)	116(3)		
						C(23)-O(24)	1.40(4)	C(22)-C(23)-O(24)	111(3)		

† Present address: Institute for Protein Research, Osaka University, Yamadakami, Suita, Osaka 565.

†† The complete F_o-F_c data and the tables of atomic parameters are kept at the Chemical Society of Japan. Document No. 7915.

Table 2. The torsion angles (φ/°) in the heptaethylene glycol chain

O(3) -C(4) -C(5) -O(6)	-15	C(4) -C(5) -O(6) -C(7)	140	C(5) -O(6) -C(7) -C(8)	-107
O(6) -C(7) -C(8) -O(9)	-35	C(7) -C(8) -O(9) -C(10)	179	C(8) -O(9) -C(10)-C(11)	-103
O(9) -C(10)-C(11)-O(12)	-58	C(10)-C(11)-O(12)-C(13)	178	C(11)-O(12)-C(13)-C(14)	168
O(12)-C(13)-C(14)-O(15)	60	C(13)-C(14)-O(15)-C(16)	177	C(14)-O(15)-C(16)-C(17)	-173
O(15)-C(16)-C(17)-O(18)	-60	C(16)-C(17)-O(18)-C(19)	-178	C(17)-O(18)-C(19)-C(20)	173
O(18)-C(19)-C(20)-O(21)	54	C(19)-C(20)-O(21)-C(22)	175	C(20)-O(21)-C(22)-C(23)	115
O(21)-C(22)-C(23)-O(24)	41				

coordinated distorted tricapped trigonal prisms or eight coordinated bicapped trigonal prism have been reported.[12,13] The Sr–O bond lengths range from 2.56 to 2.73 Å. The Sr–O(3) and Sr–O(24) distances are rather short, possibly attributable to the two oxygen atoms at both ends of the EO7 chain being more basic.

Conformations of EO7 Chain: The C–C bond distances found in the EO7 chain are rather short, the mean value being 1.45 Å. The C(4)–C(5) distance of 1.31 Å is abnormally short. The thermal ellipsoids of the atoms are large, and the largest directions are approximately normal to the O(3)–C(4)–C(5)–O(6) plane. Moreover, the torsion angle is −15°, a value which cannot be considered real. It is most probable that partial disorder is present in this part of the chain. Consider a plane made by passing through the Sr, O(3), O(6) atoms and the midpoint between C(4) and C(5). If C(4) lies above the plane, then C(5) must lie below the plane as shown in Fig. 2(a), or *vice versa* (Fig. 2(b)). There may be no energy difference between the two conformations if other conditions are similar. It is most probable that partial disorder, caused by the two conformations is present in the crystal. Some residual peaks were found in the difference map, but attempts to locate the disordered atoms were not successful; possibly real situation is more complex. This may also explain the rather high observed R value. Such apparent bond shortening due to thermal libration and partial disorder has also been discussed by Dunitz, *et al.*[2]

The torsion angles in the EO7 chain are listed in Table 2, and in the central part a TGT–T$\bar{G}$T–TGT conformation is observed. This may be the most stable conformation, a conformation also found in the TGM·$HgCl_2$ complex. Both ends of the chain assume a different conformation, since the TGT–T$\bar{G}$T–TGT conformation results in a helical form of an EO7 chain.

Hydrogen Bonding: Two hydrogen atoms at both ends of the EO7 chain possibly serve as donors to form hydrogen bonding. The N(1) atom in a free SCN group

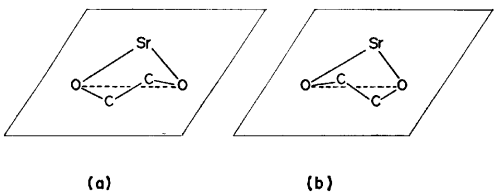

Fig. 2. Two plausible conformations of the –O–CH_2–CH_2–O group.

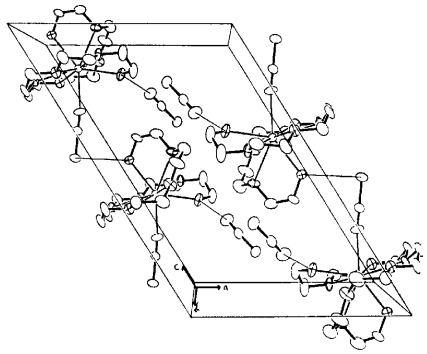

Fig. 3. An ORTEP drawing of the contents of a unit cell.

is located at a distance of 2.73 Å from O(24). Another SCN group is coordinated to the Sr atom *via* N(2) as described above, and S(2) is bonded to the O(3) atom in a neighbouring molecule, the hydrogen bond distance being 3.26 Å. The crystal structure is shown in Fig. 3.

References

1) M. R. Truter, *Struct. Bonding (Berlin)*, **16**, 71 (1973).
2) J. D. Dunitz, M. Dobler, P. Seiler, and R. P. Phizackery, *Acta Crystallogr., Sect. B*, **30**, 2733, 2741, 2746, 2748 (1974).
3) M. R. Truter, "Metal-ligand Interactions in Organic Chemistry and Biochemistry," ed by P. Pullman and M. Goldblum, D. Reidel Publishing Company, Dordrecht-Holland (1977), p. 317.
4) S. Yanagida and M. Okahara, *Kagaku Zokan*, **74**, 149 (1978).
5) R. Iwamoto, *Bull. Chem. Soc. Jpn.*, **46**, 1114, 1118, 1123 (1973).
6) R. Iwamoto and H. Wakano, *J. Am. Chem. Soc.*, **98**, 4777 (1976).
7) R. Iwamoto, Y. Saito, H. Ishihara, and H. Tadokoro, *J. Polym. Sci., Part A-2*, **1968**, 1509
8) M. Yokoyama, H. Ishihara, R. Iwamoto, and H. Tadokoro, *Macromolecules*, **2**, 184 (1969).
9) S. Yanagida, K. Takahashi, and M. Okahara, *Bull. Chem. Soc. Jpn.*, **51**, 3111 (1978).
10) T. Ashida, "The Universal Crystallographic Computing System-Osaka," The Computation Center, Osaka University (1973), pp. 55—60.
11) "International Tables for X-Ray Crystallography," Kynoch Press, Birmingham (1974), Vol. IV, pp. 71—73.
12) B. Briggman and Å. Oskarsson, *Acta Crystallogr., Sect. B*, **33**, 1900 (1977).
13) A. F. Wells, "Structural Inorganic Chemistry," Clarendon Press, Oxford (1975), pp. 556, 562.

BULLETIN OF THE CHEMICAL SOCIETY OF JAPAN, VOL. 52 (4), 1211—1212 (1979)

The Dimorphism and Spectral Properties of 4-Anilino-1,2-naphthoquinones

Yoshio MATSUNAGA* and Nobuhiko MIYAJIMA

Department of Chemistry, Faculty of Science, Hokkaido University, Sapporo 060

(Received September 18, 1978)

Synopsis. On the basis of vibrational spectra, especially in the region from 3050 to 3350 cm^{-1}, solid 4-anilino-1,2-naphthoquinones carrying substituents on the phenyl ring are classified into two groups. The *p*-methyl and *p*-ethyl derivatives are dimorphic and can be members of both the groups.

We have previously examined the vibrational spectra of a number of the derivatives of 2-anilino-1,4-naphthoquinones which carry substituents on the phenyl ring.[1] On the basis of the location and the sharpness of the single band appearing in the region from 3150 to 3350 cm^{-1}, most of the derivatives could be classified into two groups. Furthermore, over ten derivatives were shown to be dimorphic. One of the dimorphic forms exhibits a relatively sharp band near 3300 cm^{-1}; the other, a relatively broad one at a lower wave number. Thus these derivatives can belong to either group. Here, the results of our work extended to the isomeric compounds, the derivatives of 4-anilino-1,2-naphthoquinones, will be presented.

The condensation reaction between 1,2-naphthoquinone and anilines was carried out in warm or boiling ethanol as reported by Zincke or Elsbach.[2,3] The vibrational spectra in the rock-salt region and the electronic spectra in the visible region were measured by the procedures described in the previous paper.[1] The search for dimorphic forms was made by comparing the vibrational spectrum of the crystals deposited from a reaction mixture with that of the sample sublimed in a vacuum. When they were clearly different, recrystallization of the former sample was attempted.

The crystals of the *p*-methyl derivative as deposited from a reaction mixture and also those recrystallized from ethanol are reddish orange. As is shown in Fig. 1a, the vibrational spectrum shows a single band at 3315 cm^{-1}, which may be assigned to the N–H stretching. By sublimation in a vacuum, the color turns deep red and the single vibrational band is replaced by a complicated pattern consisting of at least four bands, appearing at 3070, 3120, 3185, and 3220 cm^{-1}, probably arising from nonequivalent N–H bonds (see Fig. 1b). As the single band and/or the pattern noted here are also observed with the other derivatives, the form giving the former spectrum will be named, for the sake of convenience, form I, and that giving the latter, form II. The spectra of these two in the region below 1700 cm^{-1} are not very different from each other. Therefore, the difference in vibrational spectrum seems to be attributed to a change in the molecular configuration centered round the N–H group, as has been concluded for the case of 2-anilino-1,4-naphthoquinones, rather than the tautomerism involving *o*-quinonoid and *p*-quinonoid forms:

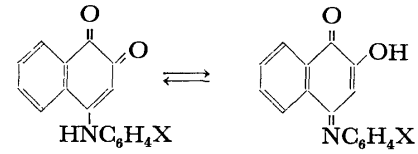

This conclusion seems to be in accordance with the finding by Harmon *et al.* that 4-anilino-1,2-naphthoquinones in aqueous solutions exist predominantly in the aminoquinone form except in strongly acidic solutions, where the hydroxyquinone imine form becomes more stable.[4] Figure 2 presents the Kubelka-Munk plots of the electronic spectra of the dimorphic forms and also the absorption spectrum of the same compound dissolved in chloroform. Form I gives two maxima located at about 515 and 545 nm and form II gives a maximum at 500 nm, with a shoulder around 540 nm.

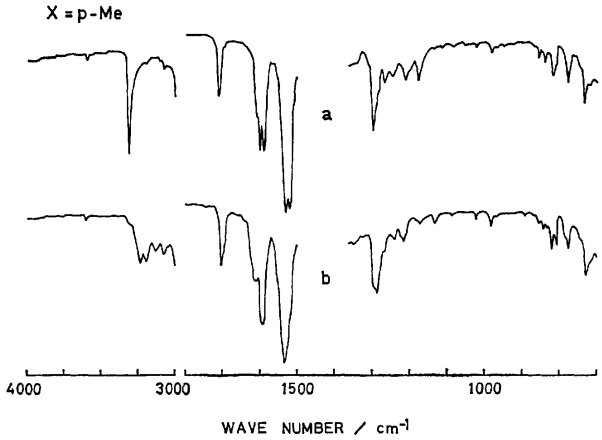

Fig. 1. Vibrational spectra of 4-(*p*-methylanilino)-1,2-naphthoquinone: (a) the form I (recrystallized from ethanol) and (b) the form II (sublimed in a vacuum).

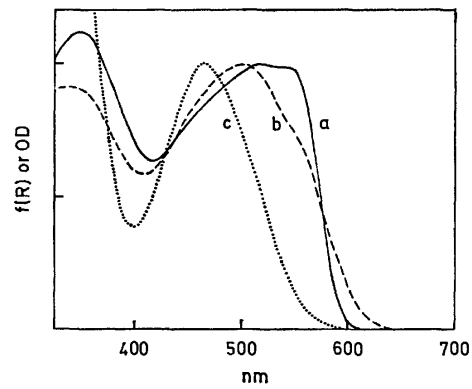

Fig. 2. Electronic spectra of 4-(*p*-methylanilino)-1,2-naphthoquinone: (a) the form I (recrystallized from ethanol), (b) the form II (sublimed in a vacuum), and (c) the compound dissolved in chloroform. The maximum in the visible region was arbitrarily taken as 1.00 in each spectrum.

On the other hand, the maximum of the absorption band is observed at about 463 nm with a chloroform solution. Thus, the band seems to shift to about 500 nm upon the solidification. Since the molecule consists of an electron-donating moiety and an accepting one, this electronic transition is probably of the intramolecular charge-transfer type. The additional bands appearing in the solid-state spectra may be assigned to the intermolecular charge-transfer transition. The location and the intensity of such an absorption are supposed to depend on the mode of molecular stacking in the crystals, as we have reported for a number of cases.[1,5,6]

Form I was found for only three more derivatives: the unsubstituted compound (3320 cm^{-1}), the *p*-ethyl (3310), and the 2,3-dimethyl (3300) derivatives. Among them, the *p*-ethyl derivative was found to be dimorphic, but the other two are not. The *p*-ethyl derivative crystallizes in form I from ethanol and is transformed into form II by vacuum sublimation. The former crystals are reddish brown and the latter are brown. The maxima of the electronic absorption are at about 510 and 500 nm, respectively. In this case too, the intensity in the spectrum of form I changes more steeply in the long-wavelength side than that of form II.

The second group of compounds, obtained only in the form II, consists of a number of derivatives: *o*-methyl, *m*-methyl, *p*-propyl, *m*-chloro, *p*-chloro, *p*-iodo, *m*-methoxy, *p*-methoxy, *m*-ethoxy, *p*-ethoxy, *m*-carboxy, *p*-carboxy, 2,4-dimethyl, 2,5-dimethyl, 3,4-dimethyl, and 2,4,5-trimethyl derivatives. Thus the classification does not seem to be correlated with the electronic nature of the substituents. Their absorption bands are rather broad and the maxima are located around 500 nm. The compounds available in form II are generally darker than those in form I because the absorption bands extend to the longer wavelengths.

References

1) Y. Matsunaga, N. Miyajima, and A. Togashi, *Bull. Chem. Soc. Jpn.*, **50**, 2234 (1977).
2) Th. Zincke, *Ber.*, **14**, 1493 (1881).
3) L. Elsbach, *Ber.*, **15**, 685 (1882).
4) R. E. Harmon, L. M. Phipps, J. A. Howell, and S. K. Gupta, *Tetrahedron*, **25**, 5807 (1969).
5) J. Aihara, G. Kushibiki, and Y. Matsunaga, *Bull. Chem. Soc. Jpn.*, **46**, 3584 (1973).
6) Y. Matsunaga, *Bull. Chem. Soc. Jpn.*, **49**, 1411 (1976).

BULLETIN OF THE CHEMICAL SOCIETY OF JAPAN, VOL. 52 (4), 1213—1214 (1979)

Carbon-13 NMR Spectra of Di-*t*-alkyl Ethers and Related Hindered Ethers

Hiromitsu MASADA* and Yoshiharu MUROTANI

Department of Industrial Chemistry, Faculty of Engineering, Kanazawa University, Kodatsuno, Kanazawa 920

(Received October 12, 1978)

Synopsis. The C-13 NMR spectra of hindered *t*-alkyl ethers and dineopentyl ether have been presented and the electronic and steric effects discussed. The resonances for the α-, methylene β-, and methyl β-carbons of di-*t*-alkyl ethers shifted downfield by +45, +1.2, and −0.2 ppm, respectively, relative to the corresponding alkanes.

The C-13 NMR spectra of primary and secondary alkyl ethers have been investigated in detail.[1,2] However, the spectra of hindered *t*-alkyl ethers except di-*t*-butyl ether[3] have not been reported. This paper deals with the elucidation of the skeletal structures of several hindered ethers together with a spectroscopic study of their electronic and steric effects.

Results and Discussion

Table 1 shows the C-13 NMR chemical shifts of di-*t*-butyl ether (**1**), di-*t*-pentyl ether (**2**), bis(1,1-dimethylbutyl) ether (**3**), bis(1,1-dimethylpentyl) ether (**4**), and bis(1,1-dimethylhexyl) ether (**5**). The values in parentheses indicate the differences in chemical shifts between the di-*t*-alkyl ethers and the corresponding alkanes in which a methyl group has replaced the alkoxyl function. The chemical shifts of the alkanes were the values reported by Lindeman and Adams.[4] The resonance signals for the α-carbons (C-1) of di-*t*-alkyl ethers shifted downfield by 44.8—45.6 ppm relative to the alkanes. The downfield shifts are smaller than in the cases of the corresponding linear and secondary alkyl ethers containing more than eight carbons (48—50 ppm).[2] The difference in the α-effect may be due to steric hindrance of the *t*-alkyl group and variations in the electron density with branching of the alkyl chain. The resonances for the methylene β-carbons of the ethers (C-2) shifted downfield by 0.9—1.5 ppm, while those for the methyl β-carbons (C-2a) shifted upfield by 0.1—0.4 ppm, relative to the alkanes. The chemical shifts of the γ carbons (C-3) and more remote carbons (C-4, C-5, and C-6), in most cases, agreed reasonably with those of the alkanes.

Table 2 shows the C-13 NMR chemical shifts for bis(1-ethyl-1-methylpropyl) ether (**6**), bis(1-ethyl-1-methylbutyl) ether (**7**), *t*-butyl α,α-dimethylbenzyl ether (**8**), and dineopentyl ether (**9**). The resonance shifts of more-crowded di-*t*-alkyl ethers, **6** and **7**, exhibit a similar tendency to those of **1**—**5**. The shielding of a phenyl substituent is observed in **8**. The resonance for the α-carbon attached to the phenyl group (C-1a) moved downfield by 1.2 ppm relative to that for the α-carbon (C-1) in **8**. The effect of the phenyl group was, however, hardly observed on the β-carbon (C-2a). The α-carbon resonance of the hindered primary ether, **9**, shifted by approx. 45 ppm, as much as that of the isomeric di-*t*-pentyl ether. Furthermore, the β- and γ-carbon resonances deviated by +2.1 and −1.9 ppm, respectively, from those of the corresponding alkane. The unusual deviations have been attributed to the steric effect of the neopentyl group, which is also observed to some extent in the case of neopentyl propyl

TABLE 1. C-13 NMR CHEMICAL SHIFTS OF DI-*t*-ALKYL ETHERS[a]

Identification	C-1	C-2	C-2a	C-3	C-4	C-5	C-6
$(C_{2a}-\overset{C_{2a}}{\underset{C_{2a}}{C_1}}-)_2O$ (**1**)	73.6 (+45.6)		31.7 (+0.1)				
$(C_3-C_2-\overset{C_{2a}}{\underset{C_{2a}}{C_1}}-)_2O$ (**2**)	75.4 (+45.1)	38.0 (+1.5)	28.5 (−0.2)	8.7 (+0.2)			
$(C_4-C_3-C_2-\overset{C_{2a}}{\underset{C_{2a}}{C_1}}-)_2O$ (**3**)	75.4 (+44.8)	48.2 (+0.9)	29.1 (−0.4)	17.6 (−0.5)	14.8 (−0.3)		
$(C_5-C_4-C_3-C_2-\overset{C_{2a}}{\underset{C_{2a}}{C_1}}-)_2O$ (**4**)	75.4 (+45.3)	45.4 (+1.3)	29.1 (−0.1)	26.6 (−0.4)	23.5 (−0.2)	14.3 (+0.4)	
$(C_6-C_5-C_4-C_3-C_2-\overset{C_{2a}}{\underset{C_{2a}}{C_1}}-)_2O$ (**5**)	75.4 (+45.2)	45.6 (+1.2)	29.1 (−0.1)	24.0 (−0.4)	32.7 (−0.3)	22.9 (+0.1)	14.1 (+0.3)

a) δ ppm downfield from TMS. $\Delta\delta=(\delta_c^{ROR}-\delta_c^{RCH_3})$ given in parentheses.

TABLE 2. C-13 NMR CHEMICAL SHIFTS OF HINDERED *t*-ALKYL ETHERS AND DINEOPENTYL ETHER[a)]

Identification	C-1	C-1a	C-2	C-2a	C-2b	C-3	C-3a	C-4	Aromatic
$(C_3-C_2-C_1(-C_{2a}))_2O$ (**6**)	78.0 (+45.7)		33.7 (+0.3)	25.5 (−0.1)		8.6 (+0.9)			
$(C_4-C_3-C_2-C_1(-C_{2b}))_2O$ (**7**)	78.0 (+45.2)		44.1 (−0.2)	34.4 (+0.1)	26.0 (−0.5)	17.5 (+0.2)	8.8 (+0.7)	14.9 (+0.1)	
$C_2-C_1(-C_2)(-O-C_{1a}(-C_{2a})-Ph)-C_2$ (**8**)	74.4	75.6	31.4	31.8					150.2, 127.7 126.1, 125.4
$(C_3-C_2(-C_3)-C_1-)_2O$ (**9**)	81.9 (+45.4)		32.4 (+2.1)			26.8 (−1.9)			

a) δ ppm downfield from TMS. $\Delta\delta=(\delta_c^{ROR}-\delta_c^{RCH_3})$ given in parentheses.

ether.[2)]

Experimental

Materials and Preparation. Barium and sodium were commercial extra pure reagents (purity 99%). 2-Chloro-2-phenylpropane was derived from 2-phenylpropene.[5)] Neopentyl tosylate was prepared from neopentyl alcohol and tosyl chloride in pyridine. Organic chemicals were distilled from calcium hydride before use and the purity confirmed by GLPC. Di-*t*-alkyl ethers (**1**—**7**) were prepared from *t*-alkyl chlorides and silver carbonate by the method reported previously.[6)] The ethers, **8** and **9**, were prepared and identified by their physical constants, ^{1}H-NMR, IR, and mass spectra, as described below. Proton NMR spectra were conducted on a JEOL-PS-100 spectrometer operating at 100 MHz using TMS as an internal standard. IR spectra were conducted on a JASCO DS-301 spectrometer and mass spectra on a JEOL-JMS-01SG spectrometer. GLPC analyses were performed on a Shimadzu GC-3AH chromatograph using 3 m×3 mm columns packed with 5 % DNDP and 5 % Silicone DC 550.

t-Butyl α,α-Dimethylbenzyl Ether (8): A mixture of barium (3.30 g, 24 mg-atom) and *t*-butyl alcohol (40 cm^3) was refluxed for 8 h to give barium *t*-butoxide. The solution was cooled to 20 °C and 2-chloro-2-phenylpropane (6.18 g, 40 mmol) added. The mixture was stirred for 6 h, hydrolyzed, and extracted with pentane (30 cm^3×3). The organic layer was washed with water (50 cm^3×8), dried over sodium sulfate, and fractionated *in vacuo* to give 1.29 g (17 %) of pure *t*-butyl α,α-dimethylbenzyl ether: bp 97—98 °C/17 Torr; IR (neat) 1150 (C–O–C) and 768, 702 (aromatic) cm^{-1}; ^{1}H-NMR ($CDCl_3$) δ=1.08 (9H, s, *t*-Bu), 1.56 (6H, s, *gem*-CH_3), and 7.1—7.5 (5H, m, aromatic).

Dineopentyl Ether (9): Prepared by a modification of the literature procedures.[7,8)] A mixture of sodium (0.55 g, 24 mg-atom) and neopentyl alcohol (8.82 g, 0.1 mol) was refluxed for 0.5 h, and a solution of neopentyl tosylate (4.84 g, 20 mmol) in dimethyl sulfoxide (10 cm^3) added. The mixture was stirred for 4 h at 120 °C, cooled, hydrolyzed with 1 M hydrochloric acid, and extracted with pentane (20 cm^3×3). The organic layer was washed with ethylene glycol (20 cm^3×8) and water, dried over sodium sulfate, and fractionated to give 1.96 g (62 %) of pure dineopentyl ether: bp 138 °C; IR (neat) 1126 (C–O–C) cm^{-1}; ^{1}H-NMR ($CDCl_3$) δ=0.91 (18H, s, CH_3) and 3.02 (4H, s, CH_2); MS (75 eV), *m/e* (rel. intensity), 158 (M^+, 7), 101 (15), and 71 (100).

C-13 NMR Spectra. C-13 NMR spectra were conducted on a JEOL model PFT-100 pulse-Fourier transform NMR spectrometer at 25.15 MHz locked on deuterium using 10 mmϕ sample tubes. Data were obtained for 2 M solutions in $CDCl_3$ at 25 °C. Measurement conditions were as follows: pulse width, 12 μs (*ca.* 45°); repetition time, 4 s; spectral width, 5000 Hz; data points, 8191; delay time, 330 μs. The resonance assignments were confirmed by off-resonance decoupling experiments. Chemical shifts are expressed in δ ppm downfield from the internal TMS.

The authors are grateful to Mr. Yoshitaka Itatani of Kanazawa University for the C-13 NMR measurements.

References

1) J. B. Stothers, "Carbon-13 NMR Spectroscopy," Academic Press, New York (1972), pp. 139—144.
2) C. Konno and H. Hikino, *Tetrahedron*, **32**, 325 (1976).
3) G. A. Olah, Y. Halpern, and H. C. Lin, *Synthesis*, **1975**, 315.
4) L. P. Lindeman and J. Q. Adams, *Anal. Chem.*, **43**, 1245 (1971).
5) H. C. Brown and N. H. Rei, *J. Org. Chem.*, **31**, 1090 (1966).
6) H. Masada and T. Sakajiri, *Bull. Chem. Soc. Jpn.*, **51**, 866 (1978).
7) V. W. Gash, *J. Org. Chem.*, **37**, 2197 (1972).
8) R. Davis and J. Hudec, *J. Chem. Soc., Perkin Trans.* **2**, **1975**, 1395.

BULLETIN OF THE CHEMICAL SOCIETY OF JAPAN, VOL. 52 (4), 1215—1216 (1979)

The Extraction Spectrophotometric Determination of Cobalt(II) with 4-(2-Thiazolylazo)resorcinol and Zephiramin

Kazumasa UEDA

Department of Industrial Chemistry, Faculty of Technology, Kanazawa University, Kodatsuno, Kanazawa 920

(Received June 2, 1978)

Synopsis. The cobalt(II)–4-(2-thiazolylazo)resorcinol chelate anion is quantitatively extracted into chloroform with a cation of zephiramin as an ion-pair complex. This process was applied to the spectrophotometric determination of cobalt. The effective separation and the sensitive determination for a trace amount of cobalt could be confirmed even in the presence of high concentrations of masking agents.

There are several ternary chelate extraction systems using *o*-hydroxyphenylazo dyes. Yotsuyanagi and Hoshino[1] systematically studied the 4-(2-pyridylazo)-resorcinol (PAR) chelates and found that the molar absorptivity of the ion-pair chelate increased when the non-coordinative *p*-hydroxyl group dissociated once. The homologous 4-(2-thiazolylazo)resorcinol (TAR) also has a noncoordinative *p*-hydroxyl group. The color reaction of TAR with cobalt[2] and its stability[3] in the aqueous phase have been investigated. The author[4] also studied the solvent extraction of 3d type transition metal–TAR chelate anions with the cation of zephiramin(Z^+Cl^-) and recognized that TAR is superior as an ion-pair extraction reagent, especially for cobalt. In this research, the fundamental conditions for the spectrophotometric determination of cobalt were investigated. The interferences from the other transition metals could be effectively removed.

Experimental

Reagents. TAR (Dojindo Co., Ltd.) was twice recrystallized from a 50 % ethanol–water mixture. Z^+Cl^-(Dojindo Co., Ltd.) was used as obtained. The standard cobalt(II) solution was prepared from cobalt sulfate and was standardized by EDTA titration.

Apparatus. A sample solution was prepared in a 50 ml graduated centrifuge tube with a glass-stopper; the solution was shaken in an Iwaki-KM type reciprocating shaker. A Kubota K-80 type centrifuge with 5000 r.p.m. was used for phase separation. A Hitachi-Horiba model M-5 pH meter equipped with a combined glass electrode was used for pH measurements. Absorption spectra and absorbance were measured with a Hitachi 124 recording spectrophotometer and a Hitachi Perkin Elmer 139 spectrophotometer using 10-mm quartz cells.

Standard Procedure. Transfer the sample solution containing up to 20 μg of cobalt in a centrifuge tube along with 1 ml of 0.05 % TAR, 2 ml of 0.1% Z^+Cl^-, and a suitable masking agent(*e.g.*, 5 ml of 10 % sodium salt of citrate, tartrate, or acetate). Adjust the pH of the solution to 8.0 with 2 ml of 0.05 M borax–phosphate buffer and dilute to 20 ml with redistilled water. Allow the solution to stand for 10 min, and shake it with 10 ml of chloroform for 10 min. After centrifugal separation, transfer the extract into an absorption cell, and measure the absorbance at 550 nm against the reagent blank.

Results and Discussion

Absorption Spectra. The Co–TAR chelate anion and its ion-pair with Z^+Cl^- in the aqueous phase have their absorption maxima at 540 nm; these shift to 550 nm in the chloroform extract.

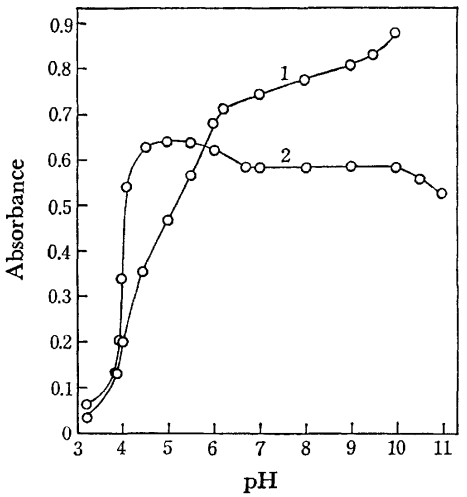

Fig. 1. Effect of pH on the extraction of Co–TAR–Z^+Cl^- chelate.
1: Reagent blank (reference; chloroform), 2: Co; 10.1 μg (reference; reagent blank). 0.05% TAR: 1 ml, 0.1 % Z^+Cl^-: 2 ml. pH 3.5—6.0: 0.025 M succinic acid–borax, pH 6.0—9.2: 0.05 M borax–phosphate buffer.

Effect of pH. The effect of pH on the extraction of the ternary chelate was examined as shown in Fig. 1. The extract shows a constant absorbance at pH 6.7—10.0 with a broad peak at pH 5, where the absorbance of the reagent blank changes remarkably with an increase in pH. When hexamine–nitric acid buffer is used, the extract has a molar absorptivity of about 7×10^4 at 535 nm. An extractable higher order chelate, perhaps the quaternary chelate, may be formed. However, we could not obtain reproducible conditions because the complexation conditions were complicated.

The Effect of TAR Concentration. The effect of TAR concentration was examined and the constant absorbance was obtained by adding from 0.7 to 4 ml of 0.05% TAR solution for 10 μg of cobalt in 20 ml solution.

The Effect of the Z^+Cl^- Concentration. The extract showed a constant absorbance with the addition of 0.1% Z^+Cl^- over the ranges of 0.5—5 ml. The ternary chelate partially dissolved into aqueous phase upon the further addition of Z^+Cl^-.

The Effect of Shaking Time, Color Stability, and the Aqueous Phase Volume. The absorbance of the extract was constant for shaking times from 5 min to one hour. The extracted species was very stable and its absorbance was constant for at least 24 h at room temperature. A constant absorbance was also obtained up to 40 ml of the aqueous phase volume.

Organic Solvents. The chelate was effectively extracted into such polar solvents as chloroform, dichloromethane (2.92×10^4, 552 nm), 1,2-dichloroethane (2.80×10^4, 550 nm), and ethyl acetate (3.27×10^4, 543 nm), but not into such nonpolar solvents as carbon tetrachloride, carbon disulfide, and hexane. The chelate was also extracted into such aromatic hydrocarbons as benzene, toluene, xylene, and chlorobenzene, where the extracts show a brilliant red color, but contain insoluble components. The other ketones and esters formed an emulsion or a third phase at the interface.

Extractability and Molar Absorptivity. The extractability of the ternary chelate was examined by the atomic absorption spectrometry; it was found that 99.6% of cobalt was extracted by a single extraction. The molar absorptivity of the ternary chelate is 3.42×10^4 $l\ mol^{-1}\ cm^{-1}$, which is more sensitive than the ion-pair extraction methods, such as 1-(2-pyridylazo)-2-naphthol–Triton X-100 (1.90×10^4),[5] but less sensitive than that of PAR–Z^+Cl^- (5.9×10^4)[6] methods.

Calibration Curve. A calibration curve for the determination of cobalt was made under the optimum conditions. The curve obeys Beer's law up to 20 μg of cobalt per 10 ml of chloroform, and Sandell's sensitivity for the absorbance of 0.001 is 0.0017 $\mu g\ cm^{-2}$. The variation coefficient of the absorbance is 0.92% for the 8 measurements.

Effect of Masking Agents. A constant absorbance is obtained in the presence of 5 ml each of 10% sodium salt of citrate, tartrate, acetate, oxalate, and thiourea. When the extract is washed with 5 ml of 0.05 M EDTA, the absorbance is constant because the chelate is rather stable once extracted. In the presence of sodium chloride, the extractions of ternary complexes of nickel, copper, and zinc were rapidly decreased as the number of the chloride ions increased, while the extraction of the cobalt complex was scarcely affected.[4] Thus, in the present method, the combined use of high concentrations of various masking agents is possible.

Table 1. Effect of diverse ions

Ions added	Tolerance limit, ppm
Mn(II), Zn(II),[a] Cd(II),[a] Al(III), Ti(IV),[b] Pb(II), Sb(V), Cr(VI), Mo(VI), W(VI), As(V), Se(IV), Rh(III), Ca(II), Mg(II), Sr(II), Ba(II)	100
Fe(II),[a] Fe(III),[a] Ni(II),[a] Cu(II),[c] Hg(II),[a] Cr(III), Sc(III),[d] In(III), Zr(IV), Hf(IV), Sn(IV), Th(IV)	50
Sn(II),[b] Ru(III), CN^-, SCN^-	20
Be(II), Bi(III), Pt(IV)	10

Cobalt taken: 1.01 ppm. a) Extracts were washed with 5 ml of 0.05 M EDTA solution. b), c), and d): Five ml each of 10% citric acid, thiourea, and tartaric acid solution were added, respectively.

Effect of Diverse Ions. The effect of diverse ions was investigated as shown in Table 1, where the tolerance limit was set to ±3% for cobalt recovery. Up to 10-fold amounts of nickel, and 20-fold of iron(II) and iron(III), were also tolerated by the addition of 5 ml each of 1% dimethylglyoxime and 5% sodium pyrophosphate, respectively. Five-fold amounts of nickel, and 2-fold of copper and zinc were left in the aqueous phase in the presence of 1 g of sodium chloride. Of the anions tested, chloride, sulfate, and nitrate did not interfere.

References

1) T. Yotsuyanagi and H. Hoshino, *Bunseki*, **11**, 743 (1976).
2) A. Kawase, *Bunseki Kagaku*, **12**, 817 (1963).
3) R. W. Stanley and G. E. Cheney, *Talanta*, **13**, 1619 (1966).
4) K. Ueda, *Anal. Lett.*, in contribution.
5) H. Watanabe, *Talanta*, **21**, 295 (1974).
6) R. Yamashita, T. Yotsuyanagi, and K. Aomura, *Bunseki Kagaku*, **20**, 1283 (1971).

BULLETIN OF THE CHEMICAL SOCIETY OF JAPAN, VOL. 52 (4), 1217—1218 (1979)

Formation of Vaterite by the Reaction of Calcium Methoxide with Aqueous Sodium Carbonate Solution

Osamu YAMAGUCHI,* Noriyuki TAKASHITA, and Kiyoshi SHIMIZU*

Department of Applied Chemistry, Faculty of Engineering, Doshisha University, Karasuma Imadegawa, Kamigyo-ku, Kyoto 602

(Received July 15, 1978)

Synopsis. A mixture of vaterite and calcite was formed by the reaction of calcium methoxide with aqueous sodium carbonate solutions. The reaction temperature was found to be a dominant factor for the formation of vaterite. The kinetics of the transformation of vaterite into calcite was studied.

Calcium carbonate exists in three polymorphic modifications: calcite(hexagonal), aragonite(orthorhombic) and vaterite(hexagonal). Calcite is stable at ordinary temperature and pressure. Both aragonite and vaterite are transformed into calcite on heating. Although the formation of calcite and aragonite has been studied by many investigators, only a few papers[1-4] have appeared on the formation of vaterite. It was found that the mixture of vaterite and calcite is formed by the reaction of calcium methoxide with aqueous sodium carbonate solution. The present study deals with the conditions on the formation of vaterite and the kinetics of the transformation of vaterite into calcite.

Experimental

The starting material calcium methoxide was prepared by heating calcium metal in an excess dehydrated methanol:

$$Ca + 2CH_3OH \xrightarrow[64\,^\circ C,\ 5\,h]{CH_3OH} Ca(OCH_3)_2 + H_2 \qquad (1)$$

Calcium metal of purity 99 % was used. 20 cm^3 of a methanolic solution containing 1 g calcium methoxide was added rapidly to the stirred 100 cm^3 aqueous sodium carbonate solution, and the resulting colloid was stirred for 5 min. The product was separated immediately from the suspension by filtration, washed repeatedly with hot water, and dried at 40 °C under reduced pressure. The product was examined by means of X-ray diffraction using nickel filtered copper $K\alpha$ radiation and differential thermal analysis.

Results and Discussion

All the products obtained under various conditions were identified as calcium carbonate, which is a mixture of vaterite and calcite. No aragonite was formed. The yield was about 96%. Figure 1 shows the X-ray diffraction patterns of calcium carbonate. No line broadening was observed. The fraction of the two modifications for each calcium carbonate powder is given in Table 1. The fraction was determined from Eqs. 2[4,5] and 3 by measuring the intensity of the (104) reflection of calcite and the intensities of the (110), (112), and (114) reflections of vaterite:

$$f_c = \frac{I_{104(c)}}{I_{110(v)} + I_{112(v)} + I_{104(c)} + I_{114(v)}} \qquad (2)$$

$$f_c + f_v = 1 \qquad (3)$$

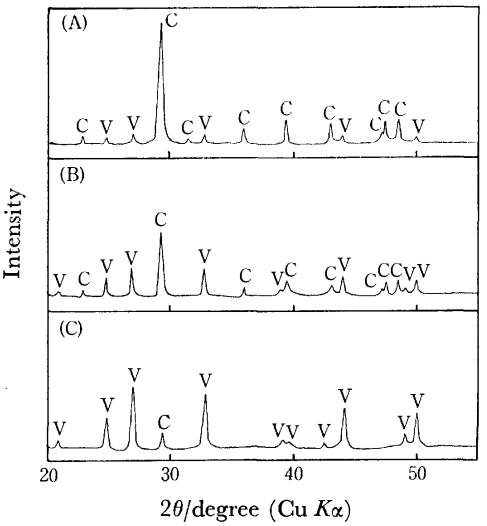

Fig. 1. X-Ray diffraction patterns of $CaCO_3$ prepared from solutions of various temperatures and concentrations. (A): 0.25 N 30 °C, (B): 0.5 N 50 °C, (C): 1 N 90 °C. For Na_2CO_3 solutions, 1 N=0.5 mol/dm^3. V: Vaterite, C: calcite.

Table 1. Fraction of the two modifications for $CaCO_3$ prepared by the reaction of $Ca(OCH_3)_2$ with aqueous Na_2CO_3 solution

Run	Concentration of aq Na_2CO_3 soln/N[a]	Temp/°C	Fraction/%	
			Vaterite	Calcite
1	0.25	30	14	86
2	0.25	50	41	59
3	0.25	70	72	28
4	0.25	90	86	14
5	0.5	30	25	75
6	0.5	50	52	48
7	0.5	70	74	26
8	0.5	90	86	14
9	1	30	40	60
10	1	50	66	34
11	1	70	74	26
12	1	90	87	13

a) 1 N=0.5 mol/dm^3 (for Na_2CO_3 solutions).

where f_c and f_v are the fraction of calcite and vaterite, respectively. For all the concentrations of aqueous sodium carbonate solutions, the fraction of vaterite increased with rise in reaction temperature up to 90 °C, no product consisting of only vaterite being formed. Formation of vaterite at low temperature was promoted with increase in the concentration of aqueous sodium

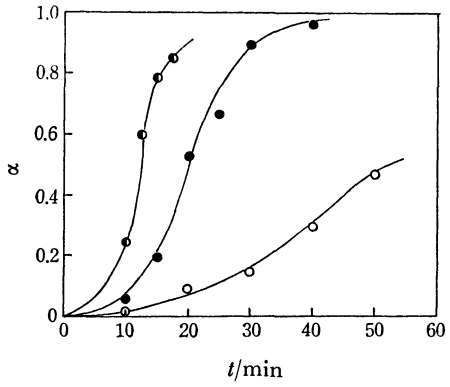

Fig. 2. Phase transformation from vaterite to calcite as a function of time at different temperatures.
○: 360 °C, ●: 380 °C, ◐: 400 °C.

carbonate solution, but not at high temperature. The reaction temperature is a dominant factor in the formation of vaterite. It is important to consider two stages for the formation of calcium carbonate: (a) aggregation velocity of ions; (b) crystallization velocity at which the ions in colloidal state form crystals. The aggregation velocity is considered to be very high. On the other hand, a period of a few seconds to a few minutes is required for crystallization. Increase in the reaction temperature reduces the time of transformation from colloid into crystal. The formation of vaterite seems to be determined by the crystallization velocity which changes with the reaction temperature. Differential thermal analysis was carried out in the air from room temperature to 600 °C. An exothermic reaction was observed in the temperature range 390—430 °C. From the results of X-ray diffraction, the reaction was found to be the transformation of vaterite to calcite. Figure 2 shows the fraction of the transformation of vaterite to calcite (Table 1, run 12) as a function of time at different temperatures. The average particle size of the specimen was 0.14 μm. Transformation isotherms were characterized by sigmoidal shape, the kinetics being best described by the Avrami equation[6] (Fig. 3),

$$\ln(1-\alpha) = -kt^n \quad n = (2.8-3.1) = 3 \qquad (4)$$

where α, t, k, and n are the fraction of transformation, time, rate constant, and proportionality constant, respectively. The activation energy calculated by the

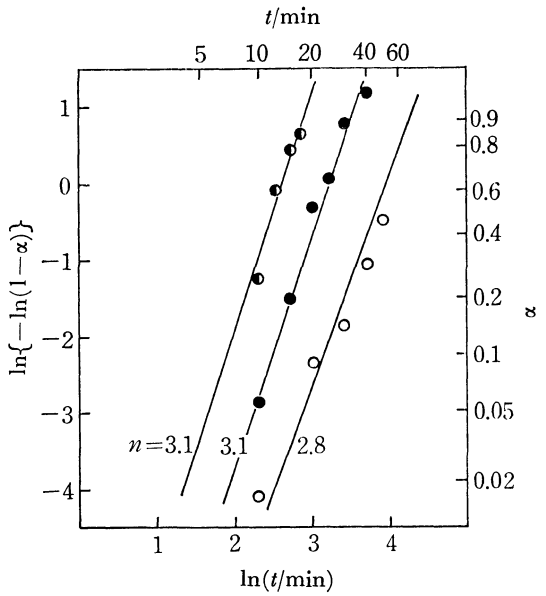

Fig. 3. Plot of $\ln(1-\alpha)$ *vs.* time t.
○: 360 °C, ●: 380 °C, ◐: 400 °C.

Arrhenius plot is *ca.* 130 kJ/mol, representing that of the nucleation growth of calcite. Rao[5] reported that vaterite prepared by the same method as that given by McConnel[1] is transformed into calcite in the temperature range 540—580 °C, the kinetic data being represented by the Avrami equation with $n=4/3$. Higher activation energy 356 kJ/mol was required for the progress of transformation. Our results do not agree with those of Rao.[5] The discrepancy might be attributed to difference in type of impurity and the average particle size of vaterite, which affects the temperature and kinetics of transformation.

References

1) J. D. C. McConnel, *Mineral Mag.*, **32**, 535 (1960).
2) Y. Inoeu, G. Hashizume, Y. Kaneharu, and Y. Ishii, *Nippon Kagaku Zasshi*, **83**, 777 (1962).
3) Y. Kitano, *Bull. Chem. Soc. Jpn.*, **35**, 1973 (1962); **35**, 1980 (1962).
4) Y. Nakahara, T. Tazawa, and K. Miyata, *Nippon Kagaku Kaishi*, **1976**, 732.
5) M. S. Rao, *Bull. Chem. Soc. Jpn.*, **46**, 1414 (1973).
6) M. Avrami, *J. Chem. Phys.*, **7**, 1103 (1939); **8**, 212 (1940).

BULLETIN OF THE CHEMICAL SOCIETY OF JAPAN, VOL. 52 (4), 1219—1220 (1979)

Design and Performance of the Air-Propane Nebulizer Burner for Atomic Absorption Spectrometry

Ryuzo Tsujino,* Akira Ogawa,† and Soichro Musha††

Technical Div., Nippon Jarrell-Ash Co., Ltd., Joshungamae-cho, Shimotoba, Fushimi-ku, Kyoto 612
†*Technical Laboratory, Fujita General Construction Co., Ltd., Otana-cho, Kouhoku-ku, Yokohama 223*
††*Department of Applied Chemistry, College of Engineering, University of Osaka Prefecture, Mozu-umemachi, Sakai 591*

(Received August 16, 1978)

Synopsis. A new air–propane nebulizer burner, by the use of which the sensitivity and precision for atomic absorption measurements was approximately equal to those with an air–hydrogen nebulizer burner, has been developed. The flame with this burner has other characteristic features, such as low auditory noise, high stability, and low radiation noise in the OH band.

Various kinds of chemical flames have been widely used for atomic emission, absorption, and fluorescence spectrometry. There are two types of burners,[1–3] that is, the nebulizer burner and the premix burner. Recently the premix burner has been most often used because it is silent in operation and has a high efficiency[4,5] in atomizing.

However, the nebulizer burner has many merits: less clogging of the burner with high concentrations of various solutes, no necessity to change the burning conditions between aqueous and organic solvents because of the energetic flame, smaller volume of sample consumption for measurement, freedom from flashback, and simplicity in cleaning and use. Another merit is that a strongly acidic or alkaline sample solution can be nebulized directly, without any trouble like corrosion, as the solution passes through only the capillary. The material of the capillary can also be easily changed according to the solution.

It is well known that the exhaust speed of an oxidant of a nebulizer burner is very high. Therefore, some flames with a high burning velocity[2] (*e.g.*, oxygen–acetylene, oxygen–hydrogen, and air–hydrogen flames) have been obtained with the nebulizer burner, while flames of a low burning velocity have blown out.

The maximum temperature of an air–propane flame has been reported to be 2200 K,[1,6] about 100 K lower than that of a relatively low-temperature air–hydrogen flame (*i.e.*, 2300,[1] 2290 K[7]).

In this paper the construction of a new type of nebulizer burner for flames of low-burning velocity, such as an air–propane flame, and its characteristics are reported.

Construction and Experimental

A cross-sectional diagram of the newly constructed nebulizer burner is shown in Fig. 1. By thoroughly mixing propane with air and by equipping the burner with the side cover (H), we prevent the air–propane flame from blowing out. The propane enters from its inlet portion (A) and then passes through a nozzle (D) 0.2 mm in dia., with 12 holes (E) 2 mm in dia. and 16 holes (F) 1.6 mm in dia., into the flame. The propane is concurrently diluted with air from 6 holes (C) 2.5 mm in dia. and thoroughly mixed in the space (G). The side cover (H) has 24 holes 2.5 mm in diameter.

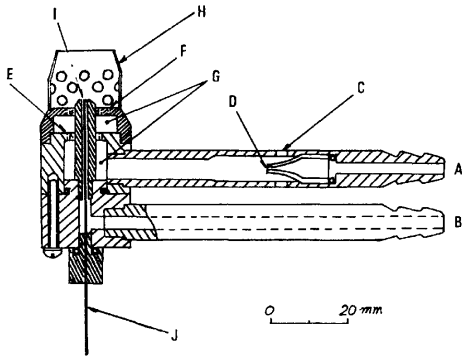

Fig. 1. Cross-sectional diagram of the air–propane nebulizer burner.
A; Fuel inlet, B; air inlet, C; holes, D; nozzle, E; holes, F; holes, G; mixing chamber, H; side cover, I; nozzle, J; capillary.

As an oxidant propane requires about ten times as much air (in volume) than does hydrogen for stoichiometrical burning at its maximum burning velocity. Therefore, we must mix propane with air to a great extent before the propane reaches the flame. The holes of the side cover (H) also serve as a cooler for the sidecover by the stream of entrained air. The burner is made of stainless steel; this makes in significant any contamination in the determination of iron, chromium, and nickel.

The solution passes through a platinum–rhodium capillary (J) 0.55 mm in inside dia. and 0.8 mm in outside dia., and is then sprayed by the air at the nozzle (I) 1.1 mm in diameter. The pressures of air and propane at the inlet ports (B) and (A) are 0.8×10^5 and 2.0×10^5 Pa respectively. The air–propane flame concurrently provides suitable flame conditions in terms of stability and sensitivity for the atomic absorption measurements of several elements.

An atomic absorption and emission spectrophotometer AA-1E (Nippon Jarrell-Ash Co., Ltd.) equipped with a 0.5-m monochromator was used for getting the emission spectra and the other spectra. A photomultiplier, R456 (Hamamatsu T.V. Co., Ltd.), and a grating with 1200 grooves/mm, blazed wavelength 300 nm were used. The voltage applied to the photomultiplier was 500 V. The slit width of the monochromator was 100 μm for both entrance and exit, while the scanning speed of wavelength was 12.5 nm/min. An air–hydrogen flame with a Hetco burner (conventional nebulizer burner, Nippon Jarrell-Ash Co., Ltd.) was used for comparison. The burning gas conditions were 1.0×10^5 Pa and 0.5×10^5 Pa in pressure for air and hydrogen respectively, as usual. Both flames were measured 50 mm above the burner tops, where the highest sensitivities were obtained with both flames for most of the elements listed in Table 1.

Table 1. Sensitivities of several elements with atomizer burners

Element (Wavelength nm)	Sensitivities (ppm/1% absorption)[a]	
	Air–propane	Air–hydrogen
Li (670.8)	0.03	0.04
Na (589.0)	0.01	0.01
K (766.5)	0.02	0.02
Cs (852.1)	0.5	0.2
Mg (285.2)	0.05	0.01
Ca (422.7)	0.5	0.2
Sr (460.7)	1	0.2
Cr (357.9)	2	0.4
Mn (279.5)	0.05	0.1
Fe (248.3)	0.1	0.1
Co (240.7)	0.1	0.2
Ni (232.0)	0.1	0.2
Cu (324.8)	0.05	0.05
Ag (328.1)	0.05	0.05
Zn (213.9)	0.01	0.02
Cd (228.8)	0.04	0.03
Hg (253.7)	2	5
Pb (283.3)	1	0.6
Bi (223.1)	0.2	0.5
Te (214.3)	0.2	0.5

a) Obtained with a single path.

Results and Discussion

The flame emission spectra scanned, originating from the air–hydrogen and the air–propane flames with the nebulizer burners under the same analytical conditions except for the burning-gas conditions, are shown in Fig. 2. The air–propane flame proved relatively smaller in its OH-band spectrum and inversely larger in its swan-band spectra. The spectrum of the oxygen–acetylene flame with the Hetco burner under the same measurement conditions almost scaled out (not shown).

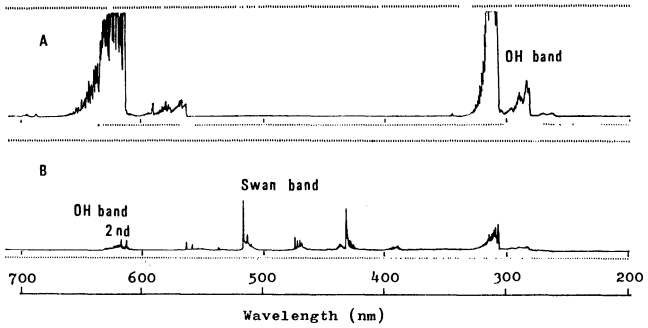

Fig. 2. Emission spectra of (A) air–hydrogen flame and (B) air–propane flame using atomizer burners.
Burning gas conditions: (A) air; 1.0×10^5 Pa, hydrogen; 0.5×10^5 Pa (B) air; 0.8×10^5 Pa, propane; 2.0×10^5 Pa.

The precision and sensitivity were investigated by means of atomic absorption measurements. The coefficient of variation at 4 ppm magnesium in an aqueous solution was 0.9% ($n=10$). Table 1 shows the sensitivities of several elements with the air–propane nebulizer burner (Hetco burner). There was no significant difference in sensitivities for the elements investigated between the two burners. It is apparent that a decrease of about 100 K in the flame temperature, as has been described earlier, leads to something of a loss in sensitivity for magnesium, calcium, strontium, and chromium, which form a relatively stable oxide. A lower sensitivity for cesium was obtained with the air–propane flame than with the air–hydrogen flame, though among the alkali metals cesium was expected to give a higher sensitivity in terms of the ionization potential.

Furthermore, no flashback of the flame occurred at any pressure ratio of air to propane. An air–town gas flame can be obtained by using this burner without holes (C) and nozzle (D). The audible noise of the air–propane and air–town gas flames with this nebulizer burner was much less than that of the air–hydrogen flame with a conventional nebulizer burner. As the background at the OH band is small, this burner can also be used for emission and atomic fluorescence spectrophotometry.

The authors wish to thank Dr. Shohei Tamura of Tokyo University for his helpful discussion.

References

1) R. Mavrodineanu and H. Bocteux, "Flame Spectroscopy," John Wiley & Sons, New York (1965).
2) J. B. Willis, *Appl. Opt.*, **7**, 1295 (1968).
3) J. Stupar, *Spectrochim. Acta, Part B*, **31**, 263 (1976).
4) J. D. Winefordner, C. T. Mansfield, and T. J. Vickers, *Anal. Chem.* **35**, 1607 (1963).
5) R. Püschel, L. Simon, and R. Herrmann, *Optik*, **21**, 441 (1964).
6) C. Woodward, *Spectrosc. Lett.*, **4**, 191 (1971).
7) R. Smith, C. M. Stafford, and J. D. Winefordner, *Anal. Chem.*, **41**, 946 (1969).

BULLETIN OF THE CHEMICAL SOCIETY OF JAPAN, VOL. 52 (4), 1221—1222 (1979)

Dissolution of Metallic Copper in Ethylenediaminetetraacetate Solution in the Presence of Hydrogen Peroxide

Kunio OHZEKI, Koji TAKEUCHI, and Tomihito KAMBARA*

Department of Chemistry, Faculty of Science, Hokkaido University, Sapporo 060

(Received October 5, 1978)

Synopsis. A 50 mg portion of metallic copper (100 mesh) placed in 50 ml of a neutral solution containing 0.1 mol dm^{-3} ethylenediaminetetraacetate (EDTA) was quantitatively dissolved within 20 min at 50 °C after the addition of a small amount of hydrogen peroxide, resulting in blue coloration of the copper(II)–edta complex.

Copper dissolves readily in aqueous ammonia in the presence of oxygen to form copper(II)–ammine complex.[1] A similar reaction is expected in an aqueous solution containing a chelating agent. Quantitative dissolution of copper in EDTA solution in the presence of hydrogen peroxide is reported.

Experimental

Reagents. The following reagents were used. Disodium and tetrasodium salts of ethylenediaminetetraacetic acid (Dotite reagents, Dojindo Laboratories), metallic copper powder of spectrographic standard (99.999 %, 100 mesh, Mitsuwa Pure Chemicals Inc.), and copper(I) oxide (chemically pure grade, Kanto Chemicals Inc.). Other reagents used were of guaranteed grade.

Procedure. A 50 mg portion of copper powder was taken into 50 ml of a 0.1 M (1 M = 1 mol dm^{-3}) EDTA solution in a 100-ml Erlenmeyer flask placed in a thermostat kept at 50 °C, a small amount of hydrogen peroxide being added to the solution with stirring. The course of the reaction was followed by pipetting out a 3-ml portion of the reaction solution at certain time intervals and determining the concentration of copper(II)–edta complex spectrophotometrically at 720 nm with a Shimadzu Spectronic 88 spectrophotometer. The amount of dissolved copper was evaluated from the calibration curve obtained by means of copper sulfate in a solution of the same composition as the reaction solution. After the absorption measurement the solution was returned quickly to the reaction vessel to keep the volume constant.

Results and Discussion

Effect of Hydrogen Peroxide. In the presence of dissolved oxygen, copper reacts slowly with EDTA to form a blue colored copper(II)–edta complex, but no copper dissolves when oxygen is purged by nitrogen. Addition of a small amount of hydrogen peroxide was highly effective in promoting the dissolution (Fig. 1). A 50 mg portion of copper in 50 ml of a 0.1 M Na_2H_2-edta solution (pH 4.8) was quantitatively dissolved within 20 min after the addition of 0.4—2.4 ml of 30% hydrogen peroxide solution when the reaction solution was stirred at 50 °C. At a higher initial concentration of hydrogen peroxide, evolution of oxygen took place in the solution, the dissolution of copper being depressed.

Effect of pH. The pH dependence of the reaction was examined by varying the concentration of hydrogen

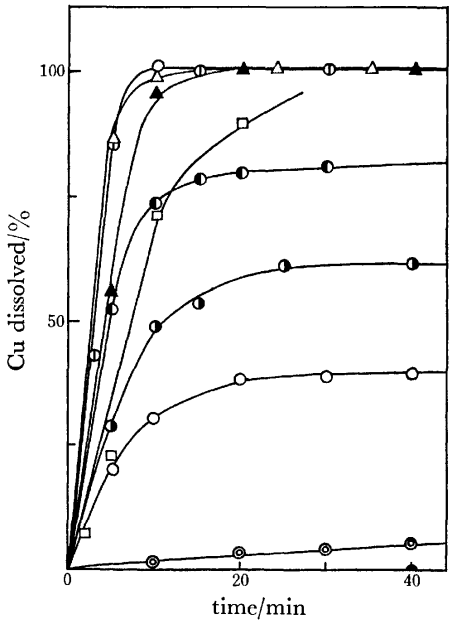

Fig. 1. Effect of hydrogen peroxide on the dissolution of a 50-mg portion of metallic copper in 0.1 M EDTA solution (50 ml, pH 4.8) at 50 °C. Amounts of 30% H_2O_2 solution added; ○: 0.05, ◑: 0.10, ◐: 0.20, ⓘ: 0.5, △: 1.0, ▲: 2.5, □: 5.0 ml, ◎: without H_2O_2, ●: the solution deaerated and without H_2O_2.

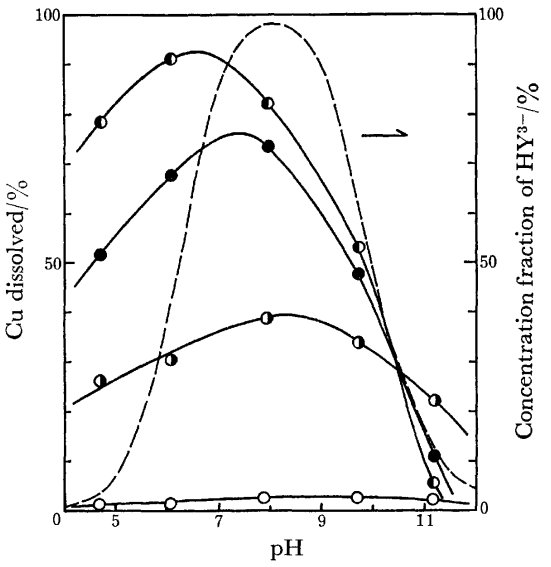

Fig. 2. Effect of pH on the 10-min dissolution of a 50-mg portion of metallic copper. Solution pH was adjusted with mixing 0.1 M EDTA disodium (pH 4.8) and tetrasodium (pH 11.3) salt solutions. Amounts of 30% H_2O_2 solution added; ○: 0, ◑: 0.10, ●: 0.20, ◐: 0.5 ml. The dashed curve indicates the concentration fraction of the HY^{3-} species.

peroxide. The reaction solution was gently shaken in an incubator. Rapid dissolution of copper took place in the pH range 6—8, as shown in Fig. 2, in which the proportion of copper dissolved during the first 10 min is plotted against pH of the initial solution. After quantitative dissolution of copper, the pH of solution was found to increase by *ca.* one unit. The rate of dissolution depends upon the concentration of $Hedta^{3-}$. When the pH was higher than 9, the decomposition of hydrogen peroxide took place with increase in the initial concentration of hydrogen peroxide, no quantitative dissolution of copper taking place.

Dissolution Reaction. The kinetics of the corrosion of copper in aqueous solution was reported by Hill.[2] In the presence of oxygen, copper is oxidized to copper(I) ion, forming copper(I) oxide. The formation of copper-(I) oxide is hindered in the presence of acetate ion owing to the absorption of acetate ion on the copper surface.

Thus the following sequence of reactions is suggested in the presence of hydrogen peroxide and EDTA.

$$2Cu + H_2O_2 + 2H^+ \longrightarrow 2Cu^+ + 2H_2O, \quad (1)$$

$$2Cu^+ + H_2O_2 + 2HY^{3-} \longrightarrow 2CuY^{2-} + 2H_2O, \quad (2)$$

where HY^{3-} denotes EDTA anion predominating near pH 8. The overall reaction is given by

$$Cu + HY^{3-} + H_2O_2 + H^+ \longrightarrow CuY^{2-} + 2H_2O. \quad (3)$$

This indicates the consumption of proton, experimentally confirmed as the increase in pH after the dissolution of copper.

Reaction of Copper Oxide with EDTA. The reactions of copper(I) and copper(II) oxides with EDTA solution were tested. Each sample of the oxides containing 7.89×10^{-4} mol copper was taken into a 0.1 M Na_2H_2-edta solution. Copper(I) oxide reacts readily with EDTA in an air-saturated solution, an appreciable dissolution taking place even in a deaerated EDTA solution. On the other hand, copper(II) oxide dissolves slightly into an EDTA solution even in the presence of hydrogen peroxide.

References

1) J. Halpern, *J. Electrochem. Soc.*, **100**, 421 (1953).
2) G. R. Hill, *J. Electrochem. Soc.*, **100**, 345 (1953).

BULLETIN OF THE CHEMICAL SOCIETY OF JAPAN, VOL. 52 (4), 1223—1224 (1979)

An X-Ray Diffraction Study on the Structure of Hexaamminecadmium(II) Ion in Aqueous Solution

Toshio YAMAGUCHI and Hitoshi OHTAKI*

Department of Electronic Chemistry, Tokyo Institute of Technology at Nagatsuta, Nagatsuta-cho, Midori-ku, Yokohama 227

(Received November 6, 1978)

Synopsis. The structure of the hexaamminecadmium(II) ion in an ammoniacal aqueous solution of cadmium chloride was determined by the X-ray diffraction method at the NH_3/Cd mole ratio of 9.9. The result showed that a cadmium(II) ion is octahedrally surrounded by six ammonia molecules at the distance of (2.37±0.03) Å.

A number of equilibrium studies have been reported[1] for the complex formation between cadmium(II) ion and ammonia molecules, and structures of the complexes have mainly been investigated by spectroscopic ways.[2-5] The structure of the hexaamminecadmium(II) complex in the solid phase has also been studied by the Raman spectroscopy.[3] However, no X-ray crystallographic data are available, because no stable single crystal of the hexaamminecadmium(II) complex, as well as other cadmium ammine complexes, could be prepared. Therefore, we undertook to determine the structure of the hexaamminecadmium(II) complex in an aqueous solution by the X-ray diffraction method. An ammoniacal aqueous solution of $CdCl_2$ at the NH_3/Cd mole ratio of 9.9 has been used as a sample solution. In solutions of the NH_3/Cd mole ratio lower than 9.9, various ammine complexes can coexist, and thus, structural analyses of such solutions are not examined in the present work.

Experimental

The sample solution was prepared as previously described.[6] The solution was almost saturated with both cadmium(II) ion and ammonia. The concentration of cadmium(II) ion in the solution was determined both by EDTA titration using a BT indicator and by electrogravimetry. The results obtained by the two methods agreed each other within 0.2 %. Concentrations of ammonia and chloride ions were determined as described previously.[6] The atomic composition of the sample solution is given in Table 1.

X-Ray scattering data were obtained at (25±1) °C with a θ-θ diffractometer (JEOL Co., Tokyo) equipped with a Philips Mo-tube (Mo $K\alpha$: λ=0.7107 Å). Details of measurements and treatment of data are described elsewhere.[6,7] A Raman spectrum of the sample solution was measured with a JEOL JRS-S1 spectrophotometer using the 4880 Å Ar^+ laser excitation.

TABLE 1. THE ATOMIC COMPOSITION (g-atoms/dm³) AND THE STOICHIOMETRIC VOLUME V PER CADMIUM ATOM FOR THE SOLUTION

Cd	1.336
Cl	2.671
N	12.53
O	36.31
H	110.2
NH_3/Cd	9.9
density/g cm^{-3}	1.112
V/Å³	1243

Results and Discussion

The $(D(r)-4\pi r^2\rho_0)$ and $D(r)$ curves obtained for the solution are shown in Figs. 1a and 1b, respectively. As can be seen from Fig. 1a, five peaks appear around 1.0, 2.4, 2.8, 3.2 and 4.6 Å (indicated by arrows). The small and broad peak at 1.0 Å is due to both O–H and N–H bonds within water and ammonia molecules, respectively. A shoulder locates at *ca.* 2.4 Å, the position being expected from the sum of the sizes of a cadmium(II) ion and an ammonia molecule (0.97 Å[8]+1.40 Å[9]= 2.37 Å). The peak around 3.2 Å can be ascribed to the Cl–O bond within the hydrated chloride ion.[10] The nearest O–O contacts in the bulk water-structure contribute to the shoulder around 2.8 Å.[11] The interatomic N–O distance of the NH_3–H_2O contacts in the ammoniacal aqueous solution[9] is almost the same as the O–O distance of the H_2O–H_2O contacts in the bulk.

In order to deduce the peak due to the Cd–N bond, the contributions of the nearest O–O and N–O contacts in the bulk medium and the Cl–O bonds within the hydrated chloride ions were subtracted from the $D(r)$ curve according to the following procedures. Since the X-ray method could hardly distinguish O from N atoms, the effective scattering factor, $f_X(s)=xf_N(s)+(1-x)f_O(s)$, was introduced in order to calculate the H_2O–H_2O and NH_3–H_2O interactions in the bulk phase (the NH_3–NH_3 contact was neglected because of the relatively low concentration of ammonia compared with the water concentration). The same scattering factor was used for the calculation of theoretical intensities of scattered X-rays from chloride ions solvated with water and, possibly, ammonia molecules. x represents the mole fraction of free ammonia: $x=[NH_3]_F/([NH_3]_F+[H_2O]_T)$, where $[NH_3]_F$ is assumed to be $[NH_3]_T-6[Cd^{2+}]_T$,[12] subscript T denoting the total concentration. f_N and f_O are the scattering factors of nitrogen and oxygen atoms, respectively. The values of 2.78 Å and 0.008 Å² were used as the distance and the temperature factor, respectively, of the H_2O–H_2O interaction in aqueous ammonia solution.[11] The same distance and temperature factor were used for the calculation of the NH_3–H_2O contacts.[9] The result is shown in Fig. 1b. Figure 1c shows the theoretical peak shapes of the atoms pairs which are taken into account in the present consideration. In this picture X means either O or N. A definite peak at 2.4 Å (chain line in Fig. 1b) can be ascribed to the Cd–N bond. The area under the peak

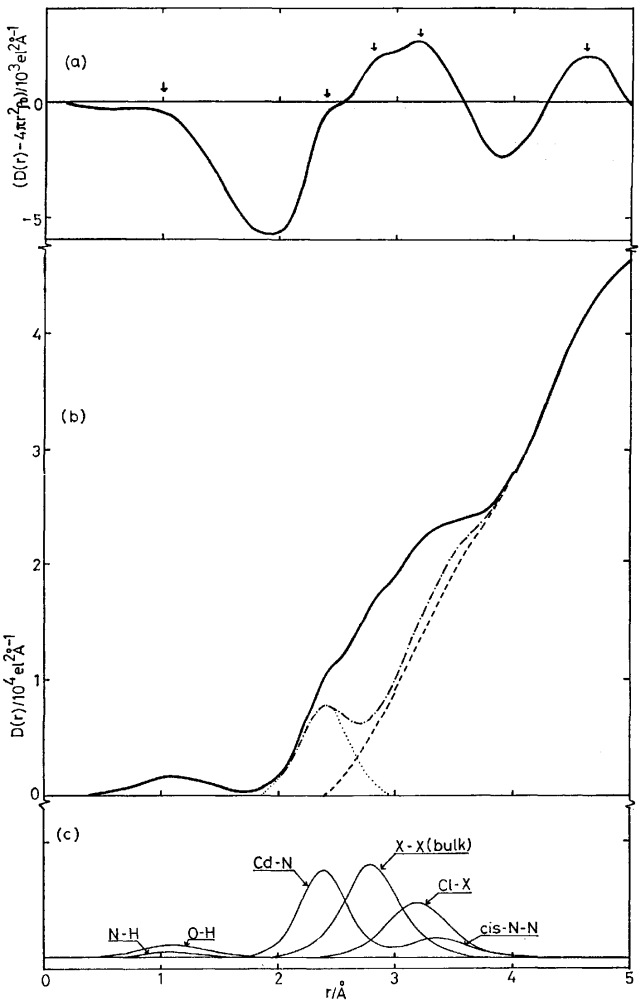

Fig. 1. The radial distribution curve of the sample solution. (a) The $(D(r)-4\pi r^2\rho_0)$ curve. (b) The $D(r)$ curve (solid line). The chain line shows the curve after subtraction of the theoretical peak shapes for the O–H and N–H bonds within H_2O and NH_3 molecules, respectively, the nearest neighbors X–X (*i.e.*, O–O and N–O) interactions in the bulk structure and the Cl–X bonds within the solvated chloride ions from the $D(r)$ curve. The dashed line shows the residual curve after subtraction of the theoretical peak shapes for the Cd–N and *cis*-N–N interactions within the hexaamminecadmium(II) complex. The dotted line is drawn by assuming that the curve having the maximum at 2.4 Å is Gaussian. (c) Theoretical peak shapes for each atom pair.

(dotted line) gave about six ammonia molecules neighboring with the central cadmium(II) ion. The peak can also be explained in terms of the formation of the $Cd(NH_3)_5(OH_2)^{2+}$ complex, because we cannot distinguish $Cd(NH_3)_6^{2+}$ ion from $Cd(NH_3)_5(OH_2)^{2+}$ ion by the present X-ray diffraction technique as far as the Cd–N bond length does not significantly differ from the length of the Cd–O bond. However, the Raman spectrum of the solution revealed a polarized band at (341 ± 2) cm^{-1}, which is assigned to the totally symmetric Cd–N stretching vibration. The frequency agreed well with that of the hexaamminecadmium(II) complex in the solid phase.[3] Therefore, we concluded that the hexaamminecadmium(II) complex is the main species in the present sample solution and that the peak at 2.4 Å is due to six Cd–NH_3 bonds. Subtraction of the theoretical peak due to the Cd–NH_3 bonds, together with the peak due to the *cis*-N–N contacts within the complex, from the residual curve (chain line in Fig. 1b) led to a smooth background curve (dashed line). The Cd–N bond distance finally determined was (2.37 ± 0.03) Å. The bond is slightly longer than the Cd–OH_2 bond (2.31 Å) within the hexaaquacadmium(II) ion.[7]

No other intramolecular interaction could be found, since no appreciable peak was observed in the background curve in the range of $r<4$ Å.

The broad peak around 4.6 Å may be related to the interactions between cadmium(II) ions and ligand molecules (water and ammonia molecules and chloride ions) in the second coordination layer.

The present work has been partially supported by a Grant-in-Aid for Scientific Research from the Ministry of Education.

References

1) L. G. Sillén and A. E. Martell, "Stability Constants," Spec. Publ. No. 17 and Supplement No. 1, Spec. Publ. No. 25, The Chemical Society, London (1964) and (1971).
2) I. Damaschun, *Z. Phys. Chem., Abt. B*, **16**, 81 (1932).
3) K. H. Schmidt and A. Müller, *Inorg. Chem.*, **14**, 2183 (1975); *Coord. Chem. Rev.*, **19**, 41 (1976).
4) I. Sacconi, A. Sabatini, and P. Gans, *Inorg. Chem.*, **3**, 1772 (1976).
5) P. Gans and J. B. Gill, *J. Chem. Soc., Dalton Trans.*, **1976**, 779.
6) T. Yamaguchi and H. Ohtaki, *Bull. Chem. Soc. Jpn.*, **51**, 3227 (1978).
7) H. Ohtaki, M. Maeda, and S. Ito, *Bull. Chem. Soc. Jpn.*, **47**, 2217 (1974).
8) L. Pauling, "The Nature of the Chemical Bonds," Cornell University Press. (1966).
9) A. H. Narten, *J. Chem. Phys.*, **49**, 1962 (1968).
10) A. H. Narten, F. Vaslow, and H. A. Levy, *J. Chem. Phys.*, **58**, 5017 (1973).
11) A. H. Narten, ORNL-4578 (1970).
12) No appreciable difference was observed in calculations of theoretical peak shapes of the X–X and Cl–X interactions when we assume five ammonia and one water molecules, instead of six ammonia molecules, coordinated to a cadmium (II) ion.

BULLETIN OF THE CHEMICAL SOCIETY OF JAPAN, VOL. 52 (4), 1225—1226 (1979)

Studies on 1,2,4-Thiadiazolidine Derivatives. IV.[1] The Isomers of 2,4-Disubstituted 3,5-(Disubstituted imino)-1,2,4-thiadiazolidines

Takeshi KINOSHITA,* Sadao SATO, and Chihiro TAMURA

Central Research Laboratories, Sankyo Co., Ltd., Hiromachi Shinagawa-ku, Tokyo 140

(Received April 21, 1978)

Synopsis. Several 2-alkyl-5-alkylimino-4-aryl-3-arylimino-1,2,4-thiadiazolidines and 4-alkyl-5-alkylimino-2-aryl-3-arylimino-1,2,4-thiadiazolidines were synthesized by the oxidation of 1-alkyl-3-arylthioureas with benzoyl peroxide along with 2,4-dialkyl-3,5-bis(arylimino)-1,2,4-thiadiazolidines.

In a previous paper,[2] we reported that the oxidation of 1-alkyl-3-arylthioureas with benzoyl peroxide (BPO) was found to afford 2,4-dialkyl-3,5-bis(arylimino)-1,2,4-thiadiazolidines (**1**) and their isomers (**2** and **3**), and the three positional isomers of **1**,[2] **2**,[3] and **3**[4] were determined by X-ray analyses.

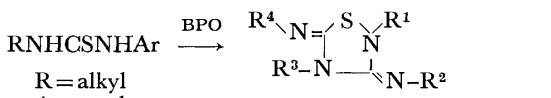

1; $R^1=R^3=$alkyl, $R^2=R^4=$aryl
2; $R^1=R^4=$alkyl, $R^2=R^3=$aryl
3; $R^1=R^2=$aryl, $R^3=R^4=$alkyl

In the course of the studies on 1,2,4-thiadiazolidines, **2** was found to be rearranged into **1** and/or **3** depending on the reaction conditions, whereas **1** and **3** could not be further converted into any of the other type isomers, which are reported herein. When the following solutions of **2** were allowed to stand for a week at room temperature, each solution gave the mixture of 1,2,4-thiadiazolidines (%): **2a** (1.5 mg) in CH_2Cl_2–AcOH (500 μl–50 μl); **1a**: **2a**: **3a**=8: 0: 92, **2a** (1.5 mg) in CH_2Cl_2–AcOH–pyridine (500 μl–50 μl–50 μl); **1a**: **2a**: **3a**=68: 18: 14, **2a** (1.5 mg) in CH_2Cl_2–AcOH–pyridine (500 μl–50 μl–100 μl); **1a**: **2a**: **3a**=53: 44: 3.

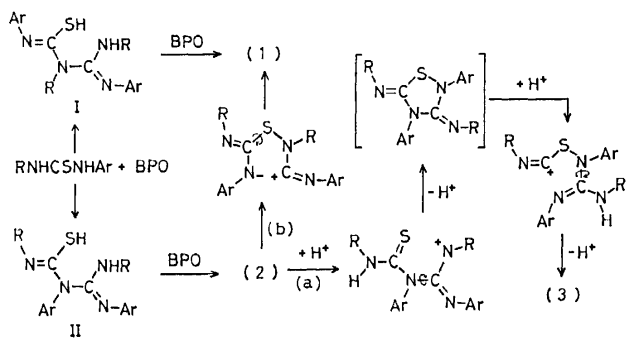

Scheme 1.

From the above results, it may be concluded that the rate of the isomerization of **2** to **3** is accelerated by acid but decelerated by the addition of base. Furthermore the more the base added, the less **3** and the more **1** are produced. However, the total rate of the rearrangement of **2** is reduced when a base is added. Consequently, for the purpose of obtaining **3** from the oxidation of thioureas with BPO, no addition of base is preferable, whereas for the purpose of obtaining the labile isomer **2**, the addition of base to the reaction system is preferable. Table 1 shows the ratio of these products for the oxidation of some thioureas with BPO in dichloromethane–pyridine (8: 1). As shown in Table 1, **2** was gradually converted mainly into **1** in the presence of pyridine, whereas in the acidic medium† converted mainly into **3**. In view of these results the formation of **1** and **2** is expected to proceed through the intermediates I and II,[5] and in the case of **3**, it may be formed through route (a) as shown in Scheme 1. There is no definitive information on a driving force for the isomerization of **2** to **1** (route (b)). The physical properties and analytical data for the 1,2,4-thiadiazolidines (**2** and **3**) are summarized in Table 2.

Table 1. Product ratio of the isomers **1**, **2**, and **3**[a]

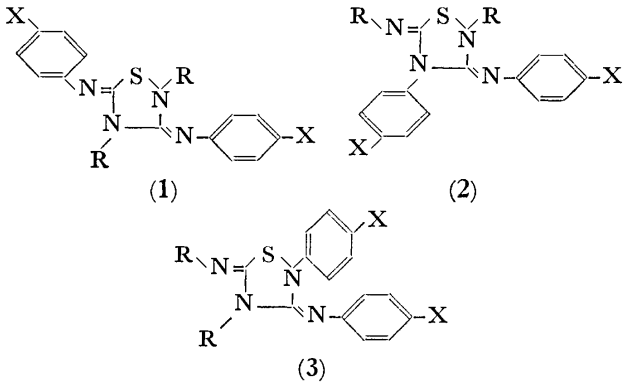

X	R	Ratio,[b] %			Ratio,[c] %		
		1	**2**	**3**	**1**	**2**	**3**
H	Me	53	40	7	69	17	14
(H	Me	55	32	13	59	0	41)[d]
H	Et	28	52	20	39	39	22
OMe	Me	65	26	9	80	6	14
(OMe	Me	65	23	12	67	0	33)[d]
OMe	Et	28	54	18	49	30	21

a) Determined by GLC. b) Reaction time: 1 h at 5—10 °C. c) Reaction time: 1 h at 5—10 °C and 14 days at 15—20 °C. d) Solvent: CH_2Cl_2 only.

Recently Joshua and Rajasekharan have reported 2,4-dialkyl-3,5-bis(arylimino)-1,2,4-thiadiazolidines,[6] which correspond to our **1**, arising from the oxidation of 1-alkyl-3-arylthioureas with hydrogen peroxide in acidic aqueous ethanol. However, it may not be possible to

† Benzoic acid would be produced from BPO as a by-product in this reaction.

Table 2. Physical properties and analytical data of 1,2,4-thiadiazolidines (**2** and **3**)

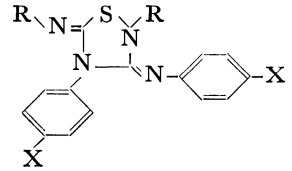

2a—d

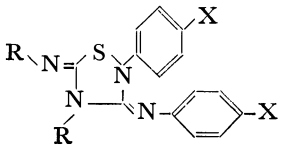

3a—d

Compd	R	X	Yield[a] %	Mp/°C	NMR (δ)[b] N–CH_3	NMR (δ)[b] (N–CH_2–)	IR[c] (cm^{-1}) C=N	Molecular[d] formula	Found (Calcd)% C	H	N	S
2a	Me	H	15	118.5	2.83,	2.86	1615	$C_{16}H_{16}N_4S$	64.63 (64.84	5.33 5.44	18.92 18.90	10.95 10.82)
2b	Me	OMe	7	123	2.85,	2.89	1630	$C_{18}H_{20}N_4O_2S$	60.58 (60.65	5.71 5.66	15.65 15.72	8.96 8.99)
2c	Et	H	28	68	(3.06,	3.19)	1630	$C_{18}H_{20}N_4S$	66.63 (66.64	6.09 6.21	17.43 17.27	10.07 9.88)
2d	Et	OMe	23	75	(3.06,	3.18)	1628	$C_{20}H_{24}N_4O_2S$	62.37 (62.48	6.25 6.29	14.54 14.57	8.35 8.34)
3a	Me	H	38	103.5	2.94,	3.37	1635	$C_{16}H_{16}N_4S$	65.03 (64.84	5.35 5.44	19.07 18.90	10.86 10.82)
3b	Me	OMe	29	oil	2.92,	3.33	1635	$C_{18}H_{20}N_4O_2S$	60.61 (60.65	5.70 5.66	15.68 15.72	9.07 8.99)
3c	Et	H	17	60	(3.07,	4.07)	1630 1640*	$C_{18}H_{20}N_4S$	66.62 (66.64	6.14 6.21	17.18 17.27	10.16 9.88)
3d	Et	OMe	16	91	(3.06,	4.02)	1615 1625*	$C_{20}H_{24}N_4O_2S$	62.40 (62.48	6.23 6.29	14.41 14.57	8.56 8.34)

a) Isolated yields under the following reaction conditions: reaction time; 1 h at 5—10 °C, solvent; CH_2Cl_2–pyridine (8: 1) for **2a—d**, and reaction time; 1 h at 5—10 °C and 14 days at 15—20 °C, solvent; CH_2Cl_2 for **3a—d**. b) Observed in CCl_4. c) Measured in Nujol mulls (*shoulder). d) Determined by high resolution mass spectrometry.

produce the other type isomers (**2** and **3**) under their experimental conditions.

Experimental

Materials. Commercially available benzoyl peroxide of a reagent grade was used. Thiourea derivatives were prepared according to methods in the literature.[7]

Preparation of 2-Alkyl-5-alkylimino-4-aryl-3-arylimino-1,2,4-thiadiazolidines (2). The following procedure illustrates the general method. From a dropping funnel, a solution of BPO (1.4 g, 5.8 mmol) in CH_2Cl_2–pyridine (80 ml: 10 ml) was added to a solution of 1-methyl-3-phenylthiourea (0.83 g, 5 mmol) in CH_2Cl_2–pyridine (80 ml: 10 ml) at 5—10 °C, and the reaction mixture was stirred for 1 h at 5—10 °C. The reaction mixture was washed with an aqueous solution of NaOH to remove benzoic acid, and the solvent was evaporated *in vacuo*, and the residue was subjected to preparative TLC on alumina eluting with ethyl acetate–petroleum ether (1: 3) to give 0.11 g of 2-methyl-5-methylimino-4-phenyl-3-phenylimino-1,2,4-thiadiazolidine (**2a**) along with 0.25 g of **1a** and 0.04 g of **3a**. An analytical sample was recrystallized from ether.

Preparation of 4-Alkyl-5-alkylimino-2-aryl-3-arylimino-1,2,4-thiadiazolidines (3). A typical run is as follows: a solution of BPO (14 g, 58 mmol) in CH_2Cl_2 (200 ml) was added dropwise to a solution of 1-methyl-3-phenylthiourea (8.3 g, 50 mmol) in CH_2Cl_2 (200 ml) at 5—10 °C, and the reaction mixture was stirred for 1 h at 5—10 °C and allowed to stand for 14 days at 15—20 °C. The reaction mixture was washed with an aqueous solution of NaOH, and the solvent was evaporated *in vacuo*, and the residue was dissolved in cold acetone and filtered to remove the insoluble sulfur. The filtrate was subjected to column chromatography on silica gel eluting with ethyl acetate–petroleum ether (1: 6) to give 2.8 g of 4-methyl-5-methylimino-2-phenyl-3-phenylimino-1,2,4-thiadiazolidine (**3a**) along with 4.1 g of **1a**. An analytical sample was recrystallized from ethanol.

References

1) Part III: T. Kinoshita, H. Nagaki, and C. Tamura, *Mass Spectroscopy, Japan*, **25**, 109 (1977).

2) T. Kinoshita, S. Sato, and C. Tamura, *Bull. Chem. Soc. Jpn.*, **49**, 2236 (1976).

3) S. Sato, T. Kinoshita, T. Hata, and C. Tamura, *Acta Crystallogr., Sect B*, **33**, 550 (1977).

4) S. Sato, T. Kinoshita, T. Hata, and C. Tamura, to be published.

5) Using a smaller amount of BPO on the oxidation of 1,3-diethylthiourea, such intermediate could be isolated; see Ref. 2.

6) C. P. Joshua and K. N. Rajasekharan, *Aust. J. Chem.*, **30**, 1819 (1977).

7) E. C. Horning, *Org. Synth.*, Coll. Vol. III, 617 (1955).

BULLETIN OF THE CHEMICAL SOCIETY OF JAPAN, VOL. 52 (4), 1227—1228 (1979)

Asymmetric Synthesis of Alanine by Hydrogenolytic Asymmetric Transamination between (*R*)-2-Amino-2-phenylethanol and Ethyl Pyruvate[1)]

Kaoru HARADA* and Minoru TAMURA

Department of Chemistry, The University of Tsukuba, Niihari-gun, Ibaraki 300-31

(Received August 4, 1978)

Synopsis. Hydrogenolytic asymmetric transamination between (*R*)-2-amino-2-phenylethanol and ethyl pyruvate was studied. The optical purity of the resulting alanine was in the range 10—62 %. The effect of solvents and the asymmetric moieties in the syntheses were explained by the chelation hypothesis based on the substrate-catalyst complex.

In the previous study from this laboratory, hydrogenolytic asymmetric transaminations between optically active α-alkylbenzylamines, (*R*)-phenylglycine, or alkyl (*R*)-phenylglycinate and ethyl pyruvate were studied.[2-5)] The effect of the asymmetric moieties and the solvents used in the asymmetric syntheses was explained by the chelation hypothesis.[2-5)]

In the present study, in order to extend the application of the chelation hypothesis, the asymmetric transamination between optically active amino alcohol (**1**) and ethyl pyruvate was carried out. (*R*)-2-Amino-2-phenylethanol (**1**) was prepared from ethyl (*R*)-phenylglycinate by reduction with lithium aluminium hydride. Alcohol **1** and ethyl pyruvate were dissolved in benzene to form the Schiff base (**2**), which was hydrogenated by the use of palladium on charcoal in various solvents and then hydrogenolyzed with palladium hydroxide on charcoal and the reaction product was hydrolyzed to form alanine. The resulting alanine was purified by the use of a Dowex 50 column; The yield was in the range 46—73%. A part of alanine was converted into DNP-alanine with 2,4-dinitrofluorobenzene and the resulting DNP-alanine was purified by celite column chromatography. The optical purity of DNP-alanine was in the range 10—62%. The results are summarized in Table 1.

In all these kinds of reactions, the configuration of the resulting alanine was (*S*). When a polar solvent was used, the optical purity was lower and when a less polar solvent was used, the optical purity of alanine increased steadily (Fig. 1, R=CH_2OH). The results could be explained by assuming the substrate-catalyst complex as in the previous studies (Fig. 2).[2-5)] In a less polar solvent, the substrate-catalyst complex (**2a**) could be formed prior to hydrogenation. However, in a polar solvent, the amount of **2a** would decrease and the non-chelated structure **2b** would increase because of the

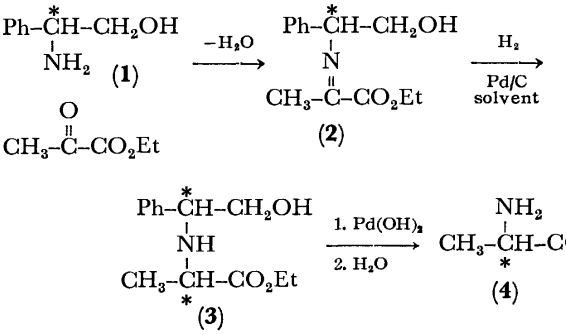

Scheme 1.

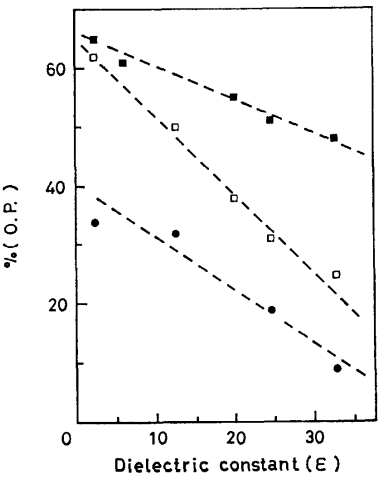

Fig. 1. Optical purities of alanine by hydrogenolytic transamination by using various solvents. ■: R=CH_3,[4)] □: R=CH_2OH, ●: R=$COOCH_3$.[5)]

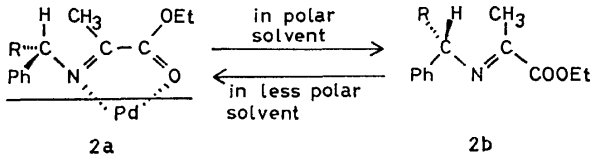

Fig. 2. Conformations of substrate in polar and in less polar solvents.

TABLE 1. OPTICALLY ACTIVE ALANINE SYNTHESIZED BY HYDROGENOLYTIC ASYMMETRIC TRANSAMINATION

Solvent	Yield of Ala[a)]	$[\alpha]_D^{25}$ of DNP-Ala (*c*, 1 M NaOH)	O.P.[b)] (%)	Config. of Ala
PhH	56	+89.6 (1.00)	62	S
t-BuOH	46	+71.3 (1.04)	50	S
i-PrOH	54	+54.8 (0.86)	38	S
EtOH	56	+45.1 (1.38)	31	S
MeOH	73	+36.2 (1.03)	25	S
MeOH-H_2O (2:1 v/v)	67[c)]	+21.8 (1.06)	15	S
H_2O	53[c)]	+15.0 (0.84)	10	S
Hexane	56[c)]	+55.4 (1.14)	39	S

a) Calculation based on ethyl pyruvate. b) Optical purity (O.P.) was difined as ($[\alpha]_D$ obsed/$[\alpha]_D$ in literature) ×100. DNP-(*S*)(+)-alanine, $[\alpha]_D^{25}$ +143.9 °C (1 M NaOH). c) The reaction mixtures were not homogeneous solutions.

stronger solvation of the substrate. In both structures **2a** and **2b**, the substrate would be adsorbed at the less bulky side of the molecules and then the hydrogenation would take place. In the case of **2a**, the adsorption would involve the rotation of the C–N bond. From the structures **2a** and **2b**, (*S*)- and (*R*)-alanine, respectively, were expected to form. The relationship between the R group (Fig. 2) of the asymmetric center and the optical activity was compared with the results obtained from the previous studies using (*S*)-α-methylbenzylamine[4] or methyl (*R*)-phenylglycinate[5] (Fig. 1). As the R group of **2a** becomes small, the difference in bulkiness between phenyl and the R groups increases, the optical purity of the resulting alanine would become higher. When the R group becomes larger, the optical activity would decrease. It was found in the present reactions (R= CH_2OH) that the optical purities were lower than those of the reactions using (*S*)-α-methylbenzylamine (R= CH_3)[4] and were higher than those of the reactions using methyl (*R*)-phenylglycinate (R=$COOCH_3$).[5] This suggests that the hydroxymethyl group would be in the bulkiness between methyl and carboxy methyl groups. These results indicate that the chelation hypothesis could also be applied to the hydrogenolytic transamination between alcohol (**1**) and ethyl pyruvate.

Experimental

The NMR spectra were obtained by using a Hitachi H-60 instrument, and the IR spectra were measured with a Hitachi 215 type grating infrared spectrophotometer. The specific rotations were measured with a JASCO DIP-181 type digital polarimeter using a 50 mm cell.

(R)-2-Amino-2-phenylethanol (1). A mixture of (*R*)-phenylglycine ($[\alpha]_D^{25}$ −163° [*c*=1.13, 5 M HCl])[6] (20 g, 0.133 mol) and absolute ethanol (300 ml) was treated with thionyl chloride at temperatures from −5 to −10 °C for 1 h. The temperature was allowed to rise to 40 °C at which it was kept for 4 h. The resulting mixture was evaporated to dryness. The residual white solid was dissolved in a small amount of water and the solution was made alkaline by adding 3 M NaOH and 50% potassium carbonate with stirring at −10 °C. The separated ethyl (*R*)-phenylglycinate was extracted with ether twice. The ether layer was dried with sodium sulfate in a refrigerator overnight and the ester was distilled under reduced pressure 98—99 °C/2 Torr, yield 18.5 g (77%) $[\alpha]_D^{25}$ −125° (*c*=1.42, EtOH).[7] δ ($CDCl_3$): 1.15 (3H, t, *J*= 6.6 Hz), 1.90 (2H, s), 4.10 (2H, q, *J*=6.6 Hz), 4.50 (1H, s), 7.25 (1H, s). Ethyl-(*R*)-phenylglycinate (14.2 g, 0.08 mol) was dissolved in 100 ml of dry ether and the solution was added dropwise to a mixture of lithium aluminium hydride (9.0 g, 0.24 mol) and 300 ml of dry ether under vigorous stirring. After being stirred for 2 h, the mixture was cooled to −10 °C and a small amount of water was added with stirring. The aluminium hydroxide precipitated was removed by filtration and the precipitate was washed thoroughly with ether three times. The combined ether solution was evaporated to dryness, and the residual oil crystallized by washing with hexane. The slightly yellow crystals (**1**) (yield 9.57 g, 87%) were recrystallized from benzene to yield colorless needles. Mp 75—76 °C, $[\alpha]_D^{25}$ −27.3° (*c*=1.08, methanol).[8] Found: C, 70.17; H, 8.09; N, 10.04 %. Calcd for $C_8H_{11}NO$: C, 70.04; H, 8.08; N, 10.21%. IR(KBr): 3310, 3250, 2900, 2820, 1600, 1490, and 1450 cm^{-1}; δ($CDCl_3$): 2.70 (3H, br, s, NH_2 and OH), 3.3—4.2 (3H, ABC multiplet), 7.2 (5H, s).

Alanine (4). The aminoalcohol **1** (1.0 g, 7.3 mmol) and ethyl pyruvate (0.847 g, 7.3 mmol) were dissolved in 20 ml of dry benzene. The mixture was stirred at room temperature for 4 h with anhydrous sodium sulfate. After separation of sodium sulfate by filtration, the filtrate was evaporated to dryness. The residual light yellow oil (**2**) was dissolved in 20 ml of dry benzene and hydrogenated with 5% palladium on charcoal (1.5 g) for 24 h at 1 atm. After the reaction was over, the catalyst was removed by filtration and washed with 3 M hydrochloric acid. The combined solution was evaporated to dryness under reduced pressure. The residue was dissolved in a small amount of water and the pH was adjusted to about 4.5 with the use of sodium hydrogen carbonate. Palladium hydroxide on charcoal (1.0 g) was added to the solution and hydrogenolysis was carried out for 24 h. After the reaction was completed, the catalyst was removed by filtration and the filtrate was evaporated to dryness. The resulting ethyl alaninate was hydrolyzed with 3 M hydrochloric acid under reflux for 4 h. After evaporation of hydrochloric acid under reduced pressure, the residue was dissolved in a small amount of water and the solution was applied to a Dowex 50 column (H^+ form). The column was eluted with 3 M aqueous ammonia and the solution was evaporated to dryness under reduced pressure. The residue was dissolved in 4% sodium hydrogencarbonate and washed with ethyl acetate three times to remove a small amount of **1**. The aqueous solution was acidified with 3 M hydrochloric acid and evaporated to dryness and the residue was extracted with absolute ethanol. The alcoholic solution was evaporated to dryness *in vacuo* and free alanine was obtained by using a Dowex 50 column. The yield of the resulting alanine[9] was 0.366 g (56 %). The alanine was converted into DNP 2,4-dinitrophenylalanine in the usual way,[2] and the resulting DNP derivative was purified by the use of a celite column treated with pH 6.8 phosphate buffer. The specific rotation of the DNP-(*S*)-alanine was: $[\alpha]_D^{25}$ +89.6° (*c*=1.00, 1 M NaOH); optical purity 62%.

References

1) Sterically Controlled Syntheses of Optically Active Organic Compounds. XXVIII; Part XXVII, *Chem. Lett.*, **1978**, 1171.

2) K. Harada and K. Matsumoto, *J. Org. Chem.*, **33**, 4467 (1968).

3) K. Harada, *J. Org. Chem.*, **32**, 1790 (1967).

4) K. Harada and T. Yoshida, *Bull. Chem. Soc. Jpn.*, **43**, 921 (1970).

5) K. Harada and Y. Kataoka, *Tetrahedron Lett.*, **1978**, 2103, and the references cited therein.

6) (*R*)-α-phenylglycine, $[\alpha]_D^{25}$ −168° (5 M HCl) in Ref. 3.

7) Ethyl (*R*)-phenylglycinate hydrochloride, $[\alpha]_D^{25}$ −119° (*c*=1.45, ethanol), Ref. 5, $[\alpha]_D^{25}$ −115° (ethanol).

8) M. B. Watson and G. W. Youngson, *J. Chem. Soc.*, **1954**, 2145. (I) Mp 75—76 °C, $[\alpha]_D^{25}$ −25.5° (methanol): R. Lukes *et al.*, *Collect. Czech. Chem. Commun.*, **23**, 1367 (1958). (I) $[\alpha]_D^{25}$ −24.5° (methanol).

9) Alanine was confirmed by using an amino acid analyzer and also by the use of thin layer chromatography as the DNP derivative.

BULLETIN OF THE CHEMICAL SOCIETY OF JAPAN, VOL. 52 (4), 1229—1230 (1979)

Liquid Phase Peptide Synthesis by the Fragment Condensation on Soluble Polymer Support. II.[1] The Azide Method

Mitsuaki NARITA

Department of Industrial Chemistry, Tokyo University of Agriculture and Technology, Nakamachi, Koganei, Tokyo 184

(Received August 10, 1978)

Synopsis. Fragment condensation on a soluble polymer support by the azide method gave rise to the efficient coupling (94—99% yield) of an *N*-protected tetrapeptide azide with the amino acid anchored to the soluble polymer support. Bulkiness of amino acid residues on the polymer support did not affect the reactivity toward the peptide azide.

The azide method[2] is one of the most important coupling procedures for the formation of the peptide bond and has been used for over 70 years. The major reason for its wide use in peptide synthesis is the fact that it is free from racemization during the course of coupling reaction, allowing the synthesis of long peptide fragments with minimum protection on the amino acid side chains.[3] However, the method was not extensively used in solid phase peptide synthesis because the procedure involves a process of isolation or the extraction of the azide, and the coupling yield is not very high (about 50—80%).[4-7] We report here an efficient fragment condensation procedure on the soluble polymer support by a modified azide method of Mazur and Schlatter[8] in a nonaqueous system without the extraction of azide.

In order to test the efficiency of the azide coupling reaction on the soluble polymer support, the tetrapeptide azide, Boc–Tyr(Bzl)–Gly–Gly–Phe–N_3 (**1**),[9] was allowed to react with H–Leu–OCH_2–resin, H–Gly–OCH_2–resin, and H–Val–OCH_2–resin (H–A·A–OCH_2–resin) as shown in Scheme 1.

Boc–Tyr(Bzl)–Gly–Gly–Phe–$NHNH_2$

1. HCl–THF, 2. BuONO; −30——40 °C, 40 min, in DMF

Boc–Tyr(Bzl)–Gly–Gly–Phe–N_3

1

1. Neutralization of HCl with Et_3N, 2. H–A·A–OCH_2–resin; −30——35 °C, 1 day; −8——15 °C, 2 days, in DMF

Boc–Tyr(Bzl)–Gly–Gly–Phe–A·A–OCH_2–resin

Scheme 1.

The tetrapeptide hydrazide, Boc–Tyr(Bzl)–Gly–Gly–Phe–$NHNH_2$, was converted into **1** in nonaqueous system (DMF) by treatment with hydrogen chloride followed by butylnitrite at −30——40 °C for 40 min. After neutralization of hydrogen chloride with triethylamine, H–A·A–OCH_2–resin was reacted with **1** at −30——35 °C for 1 day and at −8——15 °C for 2 days. The solution was poured into methanol to precipitate peptide resin. In each case, the recovery of the resulting peptide resin by pouring the reaction mixture into methanol was more than 95% on the assumption that the reaction proceeded quantitatively. Amino acid ratios in acid hydrolysates of the resulting peptide resins are summarized in Table 1. The yields in the coupling reactions of the azide **1** with H–Leu–OCH_2–resin, H–Gly–OCH_2–resin, and H–Val–OCH_2–resin were 95, 99, and 94%, respectively, on the basis of the average values of amino acid ratios.

Table 1. Amino acid analyses[a] of Boc–Tyr(Bzl)–Gly–Gly–Phe–A·A–OCH_2–resins and coupling yields of the azide method

H–A·A–OCH_2–resin	Amino acid content (mmol/g)					Average yield of coupling[b] (%)
	Tyr[c]	Gly	Phe	Leu	Val	
H–Leu–OCH_2–resin	0.37	0.85	0.41	0.44		95
H–Gly–OCH_2–resin	0.31	1.06	0.35			99
H–Val–OCH_2–resin	0.44	0.99	0.49		0.52	94

a) Carried out under the following conditions: resin, 19—23 mg; propionic acid, 4 ml; 12 M HCl, 2 ml; 115 °C; 35 h. b) Determined with use of average values of Gly and Phe contents. c) Acid hydrolysis of tyrosyl peptides usually give low recovery of Tyr.[10]

The results indicate that the azide method enables efficient coupling of the *N*-protected peptide azide with amino free terminals on the soluble polymer support, and that the bulkiness of amino acid residues on amino free terminals does not affect the reactivity of the peptide azide.

Experimental

Soluble chloromethylated polystyrene, H–Leu–OCH_2–resin (Leu content, 0.62 mmol/g), and Boc–Tyr(Bzl)–Gly–Gly–Phe–OMe, prepared previously were used; DMF was purified as reported.[1] Optical rotations were taken in a 1-dm cell on a Jasco Model ORD/UV-5 optical rotatory dispersion recorder. Amino acid analysis was carried out on a Hitachi Liquid Chromatograph, Model 034. Hydrolysis of peptide resins was carried out on 19—23 mg samples of resins with propionic acid–12 M HCl (2: 1 v/v) at 115 °C for 35 h.

H–Gly–OCH_2–resin and H–Val–OCH_2–resin. Esterification of the chloromethylated polystyrene with Boc–Gly–OH and Boc–Val–OH was carried out at room temperature for 5 days. After attachment of Gly and Val to the polymer supports, residual benzylic chlorides were removed by the reaction with sodium acetate in DMF at 105 °C for 24 h. The final chlorine contents were less than 0.02 mmol/g. Removal of Boc group with HCl–THF and neutralization of HCl with triethylamine were performed according to the procedure given by Green and Garson.[11] H–Gly–OCH_2–resin: Gly content, 0.41 mmol/g; H–Val–OCH_2–resin: Val content, 0.69

mmol/g (amino acid analysis).

Boc–Tyr(Bzl)–Gly–Gly–Phe–NHNH$_2$. To Boc–Tyr-(Bzl)–Gly–Gly–Phe–OMe (2.80 g, 4 mmol) in 30 ml of methanol was added 1 ml of 80% hydrazine hydrate and the solution was allowed to stand for 40 h at room temperature. To this was added 100 ml of ether and the solution was kept in a refrigerator overnight. The precipitate was filtered off to give 1.50 g of a substance, the additional hydrazide (0.58 g) being obtained from the mother liquor. Recrystallization from methanol gave the substance: mp 188—190°C, $[\alpha]_D^{21} = +12.4°$ ($c=1.0$, CH_3COOH). Found: C, 62.23; H, 6.31; N, 13.46 %. Calcd for $C_{34}H_{42}N_6O_7$: C, 63.14; H, 6.55; N, 13.00 %. Amino acid ratios: Gly 1.94, Tyr 0.89, and Phe 0.99.

Coupling Reaction of Boc–Tyr(Bzl)–Gly–Gly–Phe–N$_3$ with H–Leu–OCH$_2$–resin, H–Gly–OCH$_2$–resin, and H–Val–OCH$_2$–resin. In a typical experiment, 223 mg (0.36 mmol) of Boc–Tyr(Bzl)–Gly–Gly–Phe–NHNH$_2$ in 20 ml of DMF was cooled to −40 °C with stirring. 565 mg of THF containing 130 mg (3.6 mmol) of hydrogen chloride was added followed by 37 mg (0.36 mmol) of butyl nitrite in 2 ml of DMF. After being kept at −30——40 °C for 40 min, 400 mg (4.0 mmol) of triethylamine in 3 ml of DMF was added. To the peptide azide solution in threefold excess was then added H–Leu–OCH$_2$–resin (200 mg, Leu content: 0.124 mmol). The mixture was stirred at −30——40 °C for 30 min and kept at −30——35 °C for 1 day and −8——15 °C for 2 days. The reaction mixture was poured into 200 ml of methanol followed by the addition of 30 ml of saturated aqueous sodium chloride in order to precipitate the peptide resin. The precipitates were filtered off, and washed successively with water and methanol in order to remove the soluble reactants. The coupling reactions of Boc–Tyr(Bzl)–Gly–Gly–Phe–N$_3$ with H–Gly–OCH$_2$–resin and H–Val–OCH$_2$–resin were carried out in the same manner. Racemization under the reaction conditions mentioned above was tested by the Izumiya method.[12] Less than 0.5 mol % of Gly–D-Ala–L-Leu was detected by ion exchange chromatography.

References

1) Part I of this series: M. Narita, *Bull. Chem. Soc. Jpn.*, **51**, 1477 (1978).
2) T. Curtius, *Ber.*, **35**, 3226 (1902).
3) Y. S. Klausner and M. Bodanszky, *Synthesis*, **1974**, 549.
4) A. M. Felix and R. B. Merrifield, *J. Am. Chem. Soc.*, **92**, 1385 (1970).
5) G. S. Omenn and C. B. Anfinsen, *J. Am. Chem. Soc.*, **90**, 6571 (1968).
6) S. Visser and K. E. T. Kerling, *Rec. Trav. Chim.*, **89**, 880 (1970).
7) G. A. Zheltukhina, M. V. Sidorova, E. I. Filippovich, and R. P. Evstigneeva, *Z. Obsh. Khim.*, **47**, 1208 (1977).
8) R. H. Mazur and J. M. Schlatter, *J. Org. Chem.*, **29**, 3212 (1964).
9) Abbreviations for the amino acids and protecting groups are those recommended by the IUPAC-IUB Commission on Biochemical Nomencalture, *J. Biol. Chem.*, **247**, 977 (1972). Additional abbreviations: DMF, *N*,*N*-dimethylformamide; THF, tetrahydrofuran. Amino acid symbols except Gly denote the L-configuration.
10) B. Iserin, *Helv. Chim. Acta*, **45**, 1510 (1962); K. Watanabe and K. Inouye, *Bull. Chem. Soc. Jpn.*, **50**, 201 (1977).
11) B. Green and L. R. Garson, *J. Chem. Soc., C*, **1969**, 401.
12) N. Izumiya, M. Muraoka, and H. Aoyagi, *Bull. Chem. Soc. Jpn.*, **44**, 3391 (1971).

BULLETIN OF THE CHEMICAL SOCIETY OF JAPAN, VOL. 52 (4), 1231—1232 (1979)

Photolyses of Azidotriazines in Organic Nitro Compounds

Tsuruji GOKA, Yoji HASHIDA, and Kohji MATSUI*

Department of Chemistry, Faculty of Engineering, Gunma University, Kiryu, Gunma 376

(Received August 11, 1978)

Synopsis. Triazinylnitrenes were found to be inert towards nitro compounds. They afforded the products derived from the combination of two molecules of the starting materials.

Nitrene chemistry has been extensively studied and well established.[1] Recently, we reported some photochemical reactions of azidotriazines in aprotic solvents such as nitriles,[2] acetone,[3] and DMSO;[4] triazinyl nitrene reacts with nitriles and acetone to yield a cycloaddition product, while its reaction with DMSO give an ylide. We now wish to report the photochemical reaction of azidotriazines in nitro compounds.

Experimental

Azidotriazines (**1**) were prepared by treating the corresponding chlorotriazines with sodium azide[5] (Table 1).

The experimental produre was almost the same as those described previously.[2-4]

TABLE 1. 4,6-DISUBSTITUTED 2-AZIDO-1,3,5-TRIAZINE[a]

Compound	Substituent 4-	Substituent 6-	Mp(°C)	Solvent for recryst.
1a	OMe	OMe	85—85.5[b]	Ligroin
1b	OEt	OEt	31—32	Petroleum ether
1c	O-*i*-Pr	O-*i*-Pr	30—31	Petroleum ether
1d	OMe	NMe_2	116—117	Ligroin
1e	NMe_2	NMe_2	106—107[b]	Benzene

a) Satisfactory chemical analyses (±0.5%) were obtained for all compounds. b) Ref. 5.

Results and Discussion

*Photolyses of 2-Azido-4,6-dimethoxy-1,3,5-triazine (**1a**) in Nitro Compounds.* When 2-azido-4,6-dimethoxy-1,3,5-triazine (**1a**) was irradiated in several nitro compounds, the same photoproduct (**2a**) was obtained regardless of the solvents employed (Table 2).

TABLE 2. THE PHOTOCHEMICAL REACTIONS OF 2-AZIDO-4,6-DIMETHOXY-1,3,5-TRIAZINE

Solvent	Yield (%) of **2a**
$MeNO_2$	26
$EtNO_2$	32
i-$PrNO_2$	40
$PhNO_2$	23

The mass spectrum of **2a** has a parent peak at *m/e* 311. The PMR spectrum indicates the presence of one active hydrogen atom and 4 kinds of methyl groups, each of which was observed as a singlet.

2g gave a dimethylester (**3**)[6] of dimethyl iminodicarbonate and **4** upon heating in cumene at 190 °C, indicating that **2a** has a skeleton of **4**. The structure of **4** was assigned on the basis of its mass spectrum and by a comparison of its PMR spectrum to those of the known compound (**5**).[2]

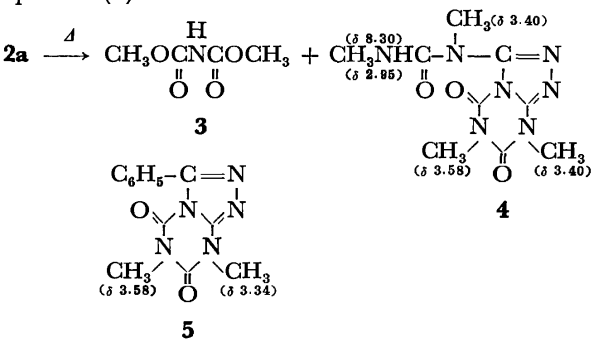

Moreover, **2a** gave **3** as the major product in a very good yield (1 mol of **2a** gave 1.7 mol of **3**) when treated with diluted hydrochloric acid at 40 °C. The results suggest that i) in **2a** the methyl groups in the triazine ring exist as methoxyl groups, and ii) **2a** does not have a aromatic stabilization, because ordinary 1,3,5-triazine derivatives are known to be stable to a treatment with dilute acid.

Effects of Substituents in Triazine Nucleus. Substituents in the triazine nucleus were found to affect the photochemical reactions of azidotriazines in nitro compounds (Table 3). The physical and analytical data of compounds (**2**) are collected in Table 4. In the cases of azidotriazines (**1d** and **1e**), in which the electron-donating NMe_2 groups are found, the corresponding reactions did not take place. In addition, when **1b** was irradiated in the presence of benzophenone, the corresponding aminotriazine was obtained in 18% yield. These results clearly suggest that the reaction to give **2a** involves singlet triazinylnitrene, which has an electrophilic character.[1,4] In the reactions of azidotriazine (**1b**) containing OEt groups, a similar photoproduct was also obtained. On the other hand, the yield

TABLE 3. THE PHOTOCHEMICAL REACTIONS OF AZIDOTRIAZINES

Azidotriazine	Condition	Yield(%) of **2**(product)
1a	a)	26 (**2a**)
1b	a)	19 (**2b**)
1b	b)	6 (**2b**)
1b	c)	26 (**2b**)
1c	a)	15 (**2c**)
1c	b)	5 (**2c**)
1c	d)	2 (**2c**)
1d	a)	—
1e	a)	—

a) Irradiation was performed in nitroethane. b) Neat sample was irradiated. c) Irradiation was performed in water. d) Irradiation was performed in nitroethane under bubbling oxygen.

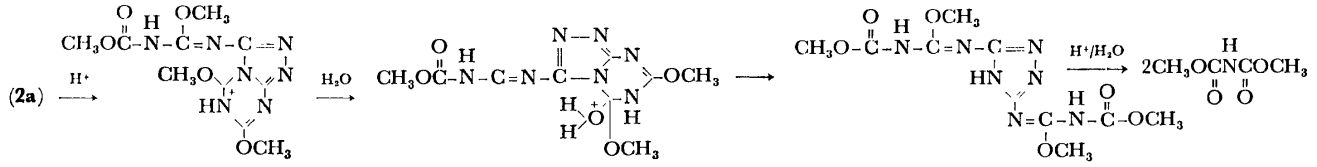

Scheme 1.

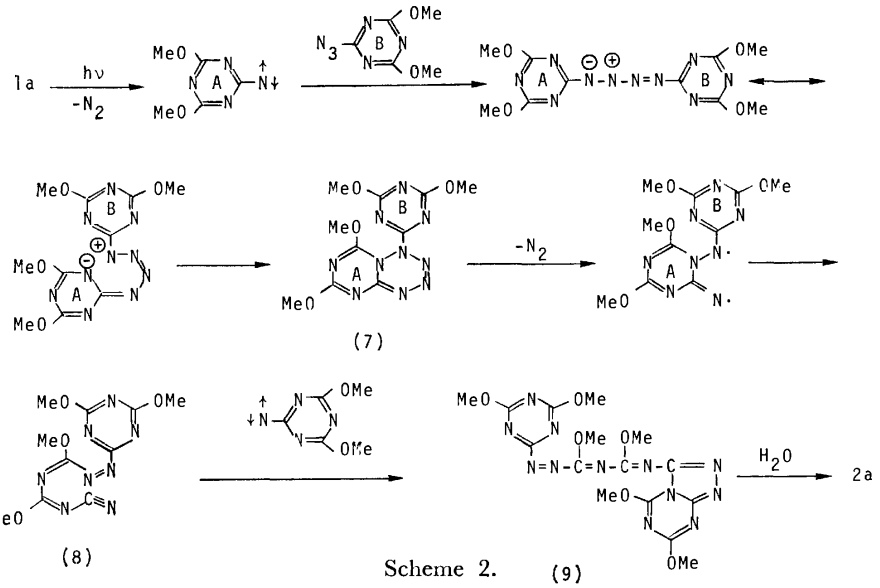

Scheme 2.

Table 4. The physical and analytical data of compounds (**2**)

2	Mp(°C)	Solvent for recryst.	Found (Calcd)% C	H	N	MS *m/e*
2a	198—199	Chloroform	38.65 (38.59	4.55 4.21	31.97 31.50)	311
2b	184—185	Benzene	45.98 (45.77	5.95 5.76	26.91 26.69)	367
2c	162—163	Benzene	51.37 (51.05	7.12 6.90	29.36 23.15)	423

of photoproduct increased considerably when a small amount of water was added into the reaction mixture, showing that water participates in the reaction. From the results described above and a comparison of the PMR data of **2** with those of the known compound (**6**),[2] the constitution of **2a** was assumed to be as shown below:

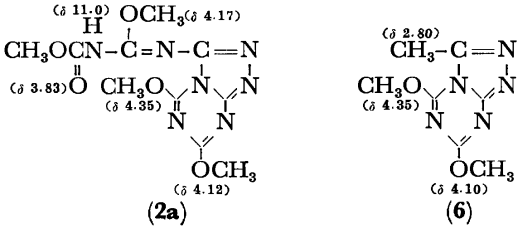

(**2a**)

(**6**)

A probable process of the decomposition of **2a** in the presence of hydrochloric acid is shown in Scheme 1.

On the other hand, in the reactions of azidotriazine (**1c**) in nitroethane in the presence of oxygen, a remarkable decrease in the yield of the photoproduct was observed (Table 3), indicating that the reaction involves the radical process.

Although several pathways could account for the formation of **2**, the most likely one is shown in Scheme 2. That is, singlet triazinylnitrene produced by the photolysis of azidotriazine electrophilically attacks upon the terminal nitrogen of azido group[7] to yield an ylide which cyclizes to give a pentazine (**7**). Then the intermediate (**7**) gives a derivative of nitrile (**8**) under a cleavage of nitrogen and a ring opening of the triazine nucleus (A). Electrophilic attack of singlet triazinylnitrene may occur not only at the azido group but also at the nitrile group of **8**. However, the nucleophilic reactivity of the –CN group in **8** would be much higher than that of the azido group of **1a**, because the –CN group is attached to a conjugated position involving two strong +R(–OCH_3) groups, while the azido group is connected to the electron-withdrawing triazine nucleus. Therefore, electrophilic attack of the singlet triazinyl nitrene should occur upon the –CN group preferentially to give a cycloaddition product (**9**). Finally, the product (**9**) hydrolyzes by water to give the final product (**2a**).

References

1) For example, "The Chemistry of the Azido Group," ed by S. Patai, Wiley, New York (1971).

2) H. Yamada, H. Shizuka, and K. Matsui, *J. Org. Chem.*, **40**, 1351 (1975).

3) R. Kayama, H. Shizuka, S. Sekiguchi, and K. Matsui, *Bull. Chem. Soc. Jpn.*, **48**, 3309 (1975).

4) T. Goka, H. Shizuka, and K. Matsui, *J. Org. Chem.*, **43**, 1361 (1978).

5) R. Kayama, S. Hasunuma, S. Sekiguchi, and K. Matsui, *Bull. Chem. Soc. Jpn.*, **47**, 2825 (1974).

6) R. Stolle and G. Adam, *Ber.*, **57**, 1657 (1924).

7) Electron density at the terminal nitrogen is calculated to be the highest (Ref. 1, Chap. 1).

BULLETIN OF THE CHEMICAL SOCIETY OF JAPAN, VOL. 52 (4), 1233—1234 (1979)

The Cross-Aldol Reaction of 3-Alkoxy-2-cyclohexen-1-ones with α,β-Enals. A Synthesis of 4-(*trans*-2-Butenylidene)-3,5,5-trimethyl-2-cyclohexen-1-ones

Sigeru Torii,* Tsutomu Inokuchi, and Hidenori Ogawa

Department of Industrial Chemistry, School of Engineering, Okayama University, Tsushima, Okayama 700

(Received October 5, 1978)

Synopsis. The cross-aldol reaction of 3-alkoxy-2-cyclohexen-1-ones with α,β-enals afforded the corresponding 3-alkoxy-6-(1-hydroxy-2-alkenyl(or aryl)-2-cyclohexen-1-ones in 78—98 % yields. The condensation of a kinetic enolate anion of 3-ethoxy-5,5-dimethyl-2-cyclohexen-1-one with *trans*-2-butenal, and subsequent dehydration together with methylation, afforded 4-(*trans*-2-butenylidene)-3,5,5-trimethyl-2-cyclohexen-1-ones, one of the most important constituents of tobacco flavour, in a 74% yield.

Vinylogous aldols have recently become available by means of the cross-aldol reaction of α,β-enones[1a] and alkanals[1b] with a kinetic enolate anion of 1,3-diketone enol ether. In this paper, we will describe their reactions with alicyclic 1,3-diketone enol ethers and α,β-enals as well as the preparation of 4-(*trans*-2-butenylidene)-3,5,5-trimethyl-2-cyclohexen-1-ones (**4**),[2] characteristic flavouring components of Burley[2a,b] as well as Greek[2c] and Turkish[2d] tobaccos.

The cross-coupling[3] of a kinetic enolate anion of **1a** with *trans*-2-butenal at −78 °C for 5 min gave the corresponding aldol **2a** (R^1=Me, R^2=Et, R^3=–HC=CHMe) in a 98% yield. The yields and the *threo/erythro* ratios of the cross-aldol condensation of **1** with various α,β-enals are shown in Table 1.

Table 1. Yields of aldols and *threo/erythro* ratios

1,3-Diketone enol ether **1**	α,β-Enal	Product **2**	Yield, %	*threo/erythro* Ratio
1a	*trans*-2-butenal	**2a**	98	93/7[a]
1a	citral	**2b**	98	89/11[a]
1b	*trans*-2-butenal	**2c**	92	90/10[a]
1c	benzaldehyde	**2d**	96	67/33[b]
1c	2-furaldehyde	**2e**	78	67/33[c]

a) The gross ratios of *threo/erythro* were estimated by comparison with the heights of the ^{13}C NMR signals at the carbon of CH–OH of each compound measured in a NNE mode under the conditions of a 60 ° pulse and a 30 s pulse repetition. b) Estimated by the separation of each isomer through column chromatography on SiO_2 on the bases of ^1H NMR signals at δ 4.77 (d, J=9 Hz), and 5.51 (d, J=3Hz). c) Estimated by comparison with the ^1H NMR signals at 4.86 (d, J=9 Hz) and 5.38 (d, J=3 Hz).

The treatment of a *threo/erythro* mixture of **2a** (R^1=Me, R^2=Et, R^3=–HC=CHMe) with methanesulfonyl chloride in pyridine at 0 °C for 1 h, and subsequent heating at 45—50 °C for 2 h, afforded the dehydrated product **3** in an 89% yield. The reaction of the enone **3**, without isolating each geometrical isomer at the C-7 carbon, with methyllithium at 0 °C in ether, followed by stirring at room temperature for 1 h, gave a mixture of **4a** and **4b** in an 85% yield. The gross abundance of the isomers **4a** and **4b**[4] was estimated from the heights of the ^{13}C NMR signals at the C-10 methyl group, giving the ratio of 7 to 4.

We have found that the reaction of the kinetic enolate anion of **1** with α,β-enals is completed within a few minutes at −78 °C without the use of a chelating reagent. It is reasonable to argue that the electron-donating nature of the alkoxyl group for the conjugated enone systems would contribute to the stabilization of lithium alcoholate, which is assumed to be the bidentate chelate **5**, and that this would prevent the progress of the counter-aldol reaction of the condensate **2**. In contrast to the alkoxyl-stabilized enone systems, aldols derived from the reaction of kinetic enolate anions of simple α,β-enones with carbonyl compounds are generally unobtainable without employing a chelating reagent.[5]

We have found that the aldols **2** consist 67—93% of *threo*-rich stereomers (Table 1), which are assumed to suggest a transition state which implies the specified orientation of the enolates of **1** and enals. Therefore, it is necessary to postulate that the favorable attack of the carbanion of **1** would occur on the less hindered side of the carbonyl group of enals.

Experimental

The melting and boiling points are uncorrected. The instruments used in analyses have been described elsewhere.[1b]

*3-Ethoxy-6-(*trans*-1-hydroxy-2-butenyl)-5,5-dimethyl-2-cyclohexen-1-one (**2a**, R^1=Me, R^2=Et, R^3=–HC=CHMe).* To a cold solution (−78 °C) of *i*-Pr_2NLi (578 mg, 5.4 mmol) in THF (6 ml) we added a solution of **1a** (505 mg, 3.0 mmol) in THF (3 ml). After the mixture had been stirred for 6 h, *trans*-2-butenal (316 mg, 4.5 mmol) was added and the solution was stirred for 5 min at −78 °C. The mixture was

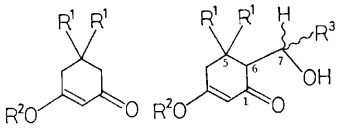

1 **2**

1a: R^1=Me, R^2=Et
1b: R^1=H, R^2=Et
1c: R^1=H, R^2=Me

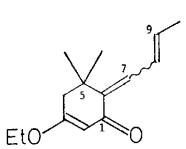

3

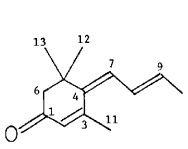

4a

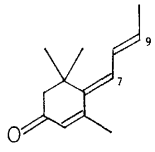

4b

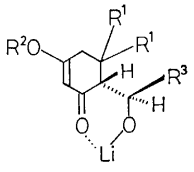

5

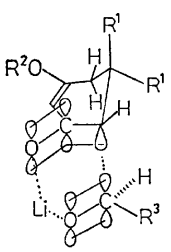

quenched with cold aqueous tartaric acid and extracted with benzene. The extracts were worked up to give 700 mg (98 %) of a *threo/erythro* mixture of **2a** (R^1=Me, R^2=Et, R^3=–HC=CHMe): mp 44.0—45.5 °C; IR (Nujol) 3320 (OH), 1654, 1633 (C=O), 1610 cm^{-1} (C=C); ^1H NMR δ 1.08 (s, 3, CH_3), 1.12 (s, 3, CH_3), 1.37 (t, 3, J=7 Hz, CH_3), 1.68 (d, 3, J=6 Hz, CH_3), 2.27 (br, 2, CH_2), 2.48 (d, 1, J=4 Hz, COCH), 3.73 (br, 1, OH), 3.96 (q, 2, J=7 Hz, OCH_2), 4.32 (d, d, 1, J=8, 4 Hz, CHO), 5.42 (s, 1, HC=C), 5.58—5.82 (m, 2, HC=C); ^{13}C NMR δ 14.1 (q), 17.8 (q), 24.6 (q), 29.8 (q), 34.4 (s, C-5), 43.3 (t, C-4), 60.4 (d, C-6), 64.5 (t), 72.2 (d, C-7), 102.3 (d, C-2), 129.0 (d, C-9), 131.2 (d, C-8), 176.8 (s, C-3), 202.1 (s, C-1). Found: C, 70.53; H, 9.43 %. Calcd for $C_{14}H_{22}O_3$: C, 70.56; H, 9.30 %.

The reaction of 3-alkoxy-2-cyclohexen-1-ones (**1a—c**) with α,β-enals was carried out similarly; the results are listed in Table 1. The physical properties, spectral data, and elemental analyses of **2b—e** are given below.

Compound ***2b*** *(R^1=Me, R^2=Et, R^3=C_9H_{15},* threo-erythro *mixture)*; IR (neat) 3440 (OH), 1640 (C=O), 1610 cm^{-1} (C=C); ^1H NMR δ 1.03, 1.11 (s, 6, CH_3), 1.36 (t, 3, CH_3), 1.59, 1.66, 1.74 (s, 9, CH_3), 2.01—2.19 (m, 4, CH_2), 2.25 (s, 2, CH_2), 2.51 (d, 1, J=4 Hz, COCH), 3.26 (br, 1, OH), 3.92 (q, 2, OCH_2), 4.56 (d, d, 1, J=10, 4 Hz, CHO), 5.05 (m, 1, HC=C), 5.28 (m, 1, HC=C), 5.37 (s, 1, HC=C); ^{13}C NMR δ 14.1 (q), 16.4 (q), 17.6 (q), 24.6 (q), 25.7 (q), 26.1 (t, C-4), 29.8 (q), 34.5 (s, C-5), 39.9 (t), 43.3 (t), 60.5 (d, C-6), 64.5 (t), 67.0 (d, C-7), 102.4 (d, C-2), 124.0 (d), 124.5 (d), 131.6 (s), 139.0 (s), 176.9 (s, C-3), 202.4 (s, C-1). Found: C, 74.66; H, 10.04 %. Calcd for $C_{19}H_{30}O_3$: C, 74.47; H, 9.87 %.

Compound ***2c*** *(R^1=H, R^2=Et, R^3=–HC=CHMe,* threo-erythro *mixture)*; IR (neat) 3400 (OH), 1648, 1639 (C=O), 1609 cm^{-1} (C=C); ^1H NMR δ 1.28—2.36 (m, 4, CH_2), 1.37 (t, 3, J=7 Hz, CH_3), 1.73 (d, 3, J=6 Hz, CH_3), 2.44 (m, 1, COCH), 3.95 (q, 2, J=7 Hz, OCH_2), 4.23 (d, d, 1, J=8 Hz, CHO), 4.40 (br, 1, OH), 5.33—5.95 (m, 2, HC=C), 5.39 (s, 1, HC=C); ^{13}C NMR δ 14.1 (q), 17.7 (q), 24.0 (t, C-5), 28.7 (t, C-4), 49.5 (d, C-6), 64.6 (t), 74.2 (d, C-7), 102.4 (d, C-2), 128.9 (d), 131.0 (d), 178.6 (s, C-3), 203.0 (s, C-1). Found: C, 68.67; H, 8.74%. Calcd for $C_{12}H_{18}O_3$: C, 68.55; H, 8.63 %.

Compound ***2d*** *(R^1=H, R^2=Me, R^3=Ph,* threo*)*; IR (neat) 3400 (OH), 1635 (C=O), 1605 cm^{-1} (C=C); ^1H NMR δ 1.23—1.63 (m, 2, CH_2), 2.00—2.38 (m, CH_2), 2.55 (m, 1, COCH), 3.70 (s, 3, OCH_3), 4.77 (d, 1, J=9 Hz, CHO), 5.33 (br, 1, OH), 5.41 (s, 1, HC=C), 7.32 (br s, 5, Ph); ^{13}C NMR δ 24.3 (t, C-5), 28.5 (t, C-4), 51.0 (d, C-6), 56.0 (q, OMe), 75.9 (d, C-7), 102.1 (d, C-2), 127.1 (d, 2C), 127.9 (d), 128.3 (d, 2C), 141.3 (s), 179.5 (s, C-3), 203.1 (s, C-1). Found: C, 72.51; H, 7.05 %. Calcd for $C_{14}H_{16}O_3$: C, 72.39; H, 6.94 %.

Compound ***2d*** *(R^1=H, R^2=Me, R^3=Ph,* erythro*)*; IR (neat) 3400 (OH), 1635 (C=O) cm^{-1}; ^1H NMR δ 1.48—1.95 (m, 2, CH_2), 2.04—2.40 (m, 2, CH_2), 2.63 (m, 1, COCH), 2.98 (br, 1, OH), 3.67 (s, 3, OCH_3), 5.41 (s, 1, HC=C), 5.51 (d, 1, J=3 Hz, CHO), 7.30 (br s, 5, Ph); ^{13}C NMR δ 20.5 (t, C-5), 28.6 (t, C-4), 52.0 (d, C-6), 55.8 (q, OMe), 71.7 (d, C-7), 102.7 (d, C-2), 125.9 (d, 2C), 127.0 (d), 128.2 (d, 2C), 141.9 (s), 179.1 (s, C-3), 200.5 (s, C-1). Found: C, 72.56; H, 7.09 %. Calcd for $C_{14}H_{16}O_3$: C, 72.39; H, 6.94 %.

Compound ***2e*** *(R^1=H, R^2=Me, R^3=2-furyl,* threo-erythro *mixture)*; IR (neat) 3380 (OH), 1635 (C=O), 1605 cm^{-1} (C=C); ^1H NMR δ 1.32—2.07 (m, 2, CH_2), 2.20—2.49 (m, 2, CH_2), 2.52—2.97 (m, 1, COCH), 3.73 (*erythro*) (s, OCH_3), 3.75 (*threo*) (s, OCH_3), 4.91 (*threo*) (d, J=9 Hz, CHO), 5.33 (*erythro*) (d, J=3 Hz, CHO), 5.41 (s, 1, HC=C), 6.30 (complex, 2, HC=C), 7.37 (complex, 1, HC=C); ^{13}C NMR (*threo*) δ 23.8 (t, C-5), 28.5 (t, C-4), 48.9 (d, C-6), 55.9 (q, OMe), 69.2 (d, C-7), 102.0 (d, C-2), 108.0 (d), 110.0 (d), 142.3 (d), 153.7 (s), 179.5 (s, C-3), 203.5 (s, C-1); (*erythro*) δ 22.0 (t, C-5), 28.5 (t, C-4), 49.2 (d, C-6), 56.0 (q, OMe), 67.8 (d, C-7), 102.5 (d, C-2), 106.8 (d), 110.2 (d), 141.4 (d), 155.2 (s), 179.1 (s, C-3), 200.3 (s, C-1). Found: C, 64.95; H, 6.42 %. Calcd for $C_{12}H_{14}O_4$: C, 64.85; H, 6.35 %.

*6-(*trans*-2-Butenylidene)-3-ethoxy-5,5-dimethyl-2-cyclohexen-1-one (**3**).* A solution of **2a** (R^1=Me, R^2=Et, R^3=–HC=CHMe, 171 mg, 0.72 mmol) and $MeSO_2Cl$ (330 mg, 2.9 mmol) in pyridine (2 ml) was stirred for 1 h at 0 °C and for 2 h at 45—50 °C. The cooled mixture was quenched with cold aqueous tartaric acid. A subsequent work-up gave 141 mg (89 %) of **3**: bp 75.5—76.5 °C/0.015 Torr (Kugelrohr); IR (neat) 1663, 1650 (C=O), 1630, 1615 (C=C) cm^{-1}; ^1H NMR δ 1.20 (s, 6, CH_3), 1.35 (t, 3, CH_3), 1.83 (d, d, J=7, 1 Hz, CH_3), 2.33 (br s, 2, CH_2), 3.92 (q, 2, OCH_2), 5.34 (br s, 1, HC=C), 5.55—7.35 (m, 3, HC=C). Found: C, 76.52; H, 8.88 %. Calcd for $C_{14}H_{20}O_2$: C, 76.33; H, 9.15 %.

*4-(*trans*-2-Butenylidene)-3,5,5-trimethyl-2-cyclohexen-1-one (**4a, 4b**).* To a solution of **3** (122 mg, 0.55 mmol) in ether (9 ml) at 0 °C we added an ether solution of 0.9 M MeLi (0.95 ml, 0.86 mmol). The mixture was stirred for 1 h at room temperature and worked up to give 89 mg (85 %) of a mixture of **4a** and **4b**: bp 85.0—86.0 °C/0.007 Torr(Kugelrohr); IR (neat) 1660 (C=O), 1632, 1584 cm^{-1} (C=C); ^1H NMR δ 1.19, 1.36 (s, 6, CH_3), 1.85 (d, 3, J=7 Hz, CH_3), 2.06—2.36 (m, 2, $COCH_2$), 2.29 (complex, 3, CH_3), 5.72—6.95 (m, 3, HC=C), 5.92 (br s, 1, HC=C); ^{13}C NMR δ 18.7, 18.9 (q, C-10), 22.3, 25.2 (q, C-11), 28.2 (q, C-12), 29.8 (q, C-13), 38.4, 40.5 (s, C-5), 52.5, 54.0 (t, C-6), 125.8, 128.4 (d), 128.6, 128.9 (d), 129.6, 132.6 (d), 134.7, 137.0 (d, C-7), 140.1, 140.7 (s, C-4), 155.2, 155.4 (s, C-3), 198.9, 199.1 (s, C-1).

References

1) (a) G. Stork and G. A. Kraus, *J. Am. Chem. Soc.*, **98**, 2351 (1976); (b) S. Torii, T. Okamoto, and S. Kadono, *Chem. Lett.*, **1977**, 495.

2) Compound **4**, megastigma-4,6,8-trien-3-ones, has been isolated as a mixture of stereoisomers: (a) E. Demole and D. Berthet, *Helv. Chim. Acta*, **55**, 1866 (1972); (b) D. L. Roberts and W. A. Rhode, *Tobacco Science*, **16**, 107 (1972); (c) A. J. Aasen, B. Kimland, S. Almqvist, and C. R.Enzell, *Acta Chem. Scand.*, **26**, 2573 (1972); (d) J. N. Schumacher and L. Vestal, *Tobacco Science*, **18**, 43 (1974). Syntheses: (e) B. M. Trost and J. L. Stanton, *J. Am. Chem. Soc.*, **97**, 4018 (1975) and the literature cited therein.

3) A variety of cross-aldol reactions have been attempted: (a) G. Wittig and A. Hesse, *Org. Synth.*, **50**, 66 (1970); (b) H. O. House, D. S. Crumrine, A. Y. Teranishi, and H. D. Olmstead, *J. Am. Chem. Soc.*, **95**, 3310 (1973); (c) G. Stork, G. A. Kraus, and G. A. Garcia, *J. Org. Chem.*, **39**, 3459 (1974); (d) T. Mukaiyama, K. Banno, and K. Narasaka, *J. Am. Chem. Soc.*, **96**, 7503 (1974); (e) E. J. Corey and D. Enders, *Tetrahedron Lett.*, **1976**, 11; (f) I. Kuwajima, T. Sato, M. Arai, and N. Minami, *ibid.*, **1976**, 1817; (g) T. Mukaiyama, T. Sato, S. Suzuki, T. Inoue, and H. Nakamura, *Chem. Lett.*, **1976**, 95; (h) T. Mukaiyama and T. Inoue, *ibid.*, **1976**, 559; (i) K. Maruoka, S. Hashimoto, Y. Kitagawa, H. Yamamoto, and H. Nozaki, *J. Am. Chem. Soc.*, **99**, 7705 (1977).

4) The stereoisomers **4** at the C-7 and C-9 carbons have been demonstrated: G. Ohloff, "Abstracts of the Scientific Program of 7th International Congress of Essential Oils," Kyoto, Japan, Oct. 7th, p. 201 (1977).

5) The reaction of kinetic enolate anions of α,β-enones with acetone in the presence of $ZnCl_2$ have been described: S. Torii, T. Inokuchi, T. Yamafuji, and K. Kawai, "The Symposium Papers of 21th Symposium on the Chemistry of Natural Products," Sapporo, Japan, Aug. 22th, p. 480 (1978).

BULLETIN OF THE CHEMICAL SOCIETY OF JAPAN, VOL. 52 (4), 1235—1236 (1979)

The Reaction of 3,5-Diphenyl-1,2-dithiolium Perchlorate with Active Methylenes

Isao SHIBUYA

National Chemical Laboratory for Industry, 2-19-19 Mita, Meguro-ku, Tokyo 153

(Received August 21, 1978)

Synopsis. 3,5-Diphenyl-1,2-dithiolium perchlorate (**1**) was synthesized in a new, convenient way, and the reaction of **1** with several active methylene compounds was studied. The compounds possessing no less than one ester group gave novel products, 3-substituted 4,6-diphenyl-2*H*-thiopyran-2-ones, while those possessing a carbamoyl group gave 3-substituted 2-hydroxy-4,6-diphenylpyridines or 3-cyano-1,4,6-triphenyl-2-pyridone. Malononitrile, however, gave 1-mercapto-1,3-diphenyl-4,4-dicyanobutadiene (**10**). On treatment with methyl iodide or *p*-chlorobenzyl chloride, **10** gave 1-methylthio- or 1-(*p*-chlorobenzylthio)-1,3-diphenyl-4,4-dicyanobutadiene, and also led to bis(1,3-diphenyl-4,4-dicyanobutadienyl) disulfide on treatment with hydrogen peroxide.

The reaction of 3-alkylthio-1,2-dithiolium salts or 1,2-dithiol-3-thiones with active methylenes gives 1,2-dithiol-3-ylidene derivatives with the liberation of methanethiol or hydrogen sulfide.[1] However, it is difficult to suppose that 3,5-diaryl- or 3,5-dialkyl-1,2-dithiolium salts give 1,2-dithiol-3-ylidenes by the same reaction course. There is thus an interest in the study of the behavior of these salts toward active methylenes. In this investigation, the reaction of 3,5-diphenyl-1,2-dithiolium perchlorate (**1**) with several active methylenes was checked, and some new information was obtained.

Results and Discussion

The synthesis of **1** has already been done by two methods.[2,3] In this study, another new method was applied: hydrogen sulfide was passed into a dibenzoylmethane–iron bromide(III) mixture in chlorobenzene, and simultaneously bromine was added drop by drop.

Methyl cyanoacetate, dimethyl malonate, ethyl benzoylacetate, ethyl carbamoylacetate, and methyl acetoacetate were refluxed with **1** in methanol to give novel products, **2**—**6** respectively, in good yields. According to their mass spectra, the molecular weights were measured and found to be 289, 322, 368, 307, and 306 respectively. The IR spectra of **2**—**6** resembled each other. The absorption assigned to an ester group was absent in the spectra of **2**, **4**—**6**; this fact suggested that an ester group of these reagents participated in these reactions. On treatment with *p*-toluenesulfonic acid, **4** easily gave 2,4,6-triphenylpyrylium salt, while releasing carbonyl sulfide. These spectral results, the chemical evidence, and their analytical data confirm that **2**—**6** are 3-cyano, 3-methoxycarbonyl, 3-benzoyl, 3-carbamoyl, and 3-acetyl-4,6-diphenyl-2*H*-thiopyran-2-one. The reaction courses seem to be shown in Scheme 1. This recyclization process resembles the reaction of 1,3-diphenyl-2-propyn-1-one with dimethyl malonate, which affords 3-methoxycarbonyl-4,6-diphenyl-2-pyrone.[4]

Cyanoacetamide, benzoylacetamide, or cyanoacetanilide was treated with **1** to give **7**, **8**, or **9** in a good yield. **7** and **8** were identified by direct comparison with the authentic samples and found to be 2-hydroxy-3-cyano- and 2-hydroxy-3-benzoyl-4,6-diphenylpyridines respectively.[5,6] With regard to **9**, its molecular weight was measured as 348. The IR spectrum and the

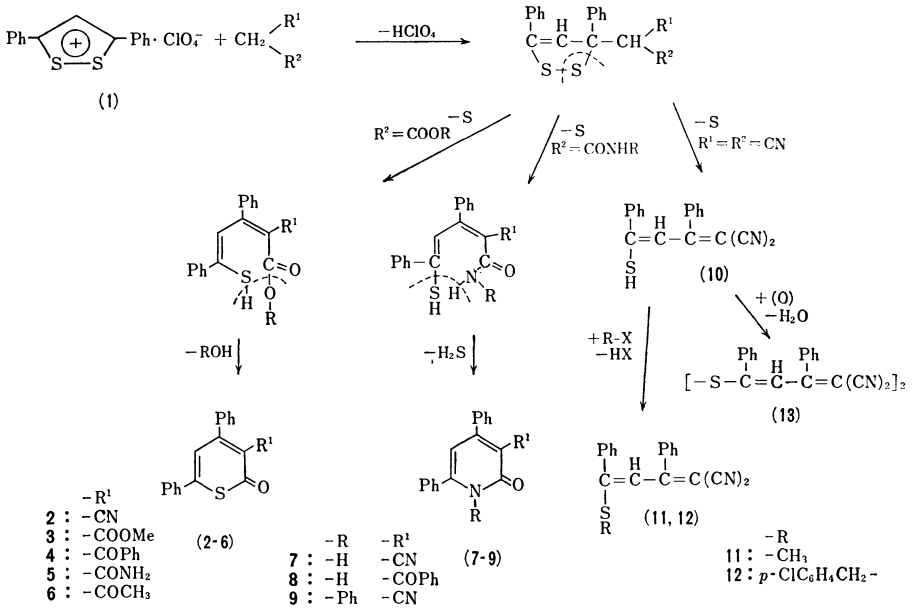

Scheme 1.

Table 1. Data for 2—6, 9—13

Compd	Solv. for recryst.	Mp (°C)	Yield (%)	Formula	Found (Calcd) % C	H	N	S	Cl
2	EtOH	178.0	94	$C_{18}H_{11}NOS$	74.60 (74.71	3.84 3.84	4.79 4.84	11.08 11.08)	
3	EtOH	195.0	61	$C_{19}H_{14}O_3S$	70.81 (70.79	4.35 4.38		9.93 9.94)	
4	MeCN	156.7	65	$C_{24}H_{16}O_2S$	78.29 (78.21	4.39 4.38)			
5	AcOH	270.3	48	$C_{15}H_{13}NO_2S$	70.26 (70.34	4.35 4.26	4.54 4.56	10.56 10.43)	
6	EtOH	179.2	60	$C_{19}H_{14}O_2S$	74.99 (75.11	4.81 4.85)			
9	MeCN	232.6	63	$C_{24}H_{16}N_2O$	82.74 (82.74	4.65 4.63	8.02 8.04)		
10	MeCN	225.3	95	$C_{18}H_{12}N_2S$	74.79 (74.97	4.25 4.20	9.79 9.71	11.12 11.12)	
11	EtOH	159.0	69	$C_{19}H_{14}N_2S$	75.38 (75.47	4.69 4.67	9.29 9.26	10.66 10.60)	
12	EtOH	180.4	61	$C_{25}H_{17}N_2SCl$	72.78 (72.72	4.11 4.15	6.86 6.78	7.48 7.76	8.58 8.58)
13	MeCN	254.1	96	$C_{36}H_{22}N_4S_2$	75.40 (75.23	3.80 3.86	9.68 9.75	11.17 11.16)	

Table 2. The IR and mass spectra for 2—6, 9—13

Compd	IR spectra (cm^{-1})	Mass spectra (m/e)
2	2210(CN), 1633, 1555, 1496, 1487, 1444	289(M), 261(M−CO), 191($C_{13}H_{11}$), 121 (C_6H_5CS), 77(C_6H_5)
3	1727(CO), 1605, 1562, 1509, 1489, 1440	322(M), 294(M−CO), 263(M−$COOCH_3$), 234(263−CO, H), 191, 121, 77
4	1673(CO), 1605, 1556, 1505, 1486, 1439	368(M), 340(M−CO), 263(M−C_6H_5CO), 234, 191, 121, 105(C_6H_5CO), 77
5	3440(NH), 1664(CO), 1603, 1552, 1501, 1486, 1441	307(M), 279(M−CO), 263(M−$CONH_2$), 234, 191, 121, 77
6	1720(CO), 1606, 1563, 1505, 1494, 1446	306(M), 278(M−CO), 263(M−CH_3CO), 234, 121, 77
9	2210(CN), 1650, 1566, 1514, 1486, 1441, 1365, 1201	348(M), 347(M−1), 320(M−CO), 180, 140, 77
10	2160(CN), 1581, 1554, 1528, 1470, 1230, 1207, 1188	288(M), 255(M−SH), 228(255−HCN), 140, 77
11	2216, 1572, 1523, 1492, 1406, 1368, 1261, 1077	302(M), 301(M−1), 255(M−SCH_3), 151 (M/2), 102(C_6H_5CCH), 77
12	2208, 1570, 1524, 1490, 1409, 1367, 1089	414(M+2), 412(M), 411(M−1), 344, 255 (M−$SCH_2C_6H_4Cl$), 125($ClC_6H_4CH_2$)
13	2200, 1570, 1523, 1489, 1409, 1366	576(M+2), 575(M+1), 574(M), 288 (M/2+1), 287(M/2), 255, 140, 77

analytical data confirmed that **9** is 3-cyano-1,4,6-triphenyl-2-pyridone. The reaction course seems to be similar to the course by which thiopyran-2-ones are given; however, hydrogen sulfide is eliminated during the recyclization process.

Malononitrile gave only a thiol, **10**, on treatment with **1**. **10** remained unchanged on treatment because the cyano group of **10** may have no ability of cyclization. The reaction of **10** with methyl iodide or *p*-chlorobenzyl chloride afforded an alkylthiobutadiene, **11** or **12**, with the liberation of a hydrogen halide. **10** was easily oxidized by hydrogen peroxide to give a disulfide, **13**. The structures of **10**—**13** were identified by means of their IR and mass spectra and analytical data. The reaction of **1** with other active methylenes, such as dibenzoylmethane, nitromethane, 1,3-indandione, and benzoylacetonitrile, was also attempted, but it is failed to give any stable products.

Hence, it is proved that the reaction of 3,5-diphenyl-1,2-dithiolium perchlorate, **1**, with active methylenes proceeds as shown in Scheme 1.

Experimental

Preparation of 3,5-Diphenyl-1,2-dithiolium Perchlorate (1). Into a solution of dibenzoylmethane (23 g) and iron bromide-(III) (45 g) in chlorobenzene (175 ml), hydrogen sulfide was passed; simultaneously bromine (20 g) was stirred in, drop by drop, over a 30-min period. After that, the reaction temperature was gradually elevated to 110 °C, and maintained at that point for 2 h; the introduction of hydrogen sulfide was stopped. After having been refluxed for another hour, the reaction mixture was allowed to stand in a refrigerator overnight. The resulting precipitate was filtered, dried *in vacuo*, washed with water, and dissolved again in hot ethanol. The solution was filtered to remove any insoluble substances, poured into an ethanol solution of sodium perchlorate, and allowed to stand overnight. This gave 22 g (61.9 %) of yellow needles of **1** (mp 260.4 °C).

Reaction of 1 with Active Methylenes. Into a mixture of an active methylene (2.4 mmol) and 0.72 g (2 mmol) of **1** in 3 ml of methanol, we stirred 2.5 mol dm^{-3} MeONa–MeOH (2 ml) at room temperature; after a while, the mixture was refluxed for 1 h and poured into dilute hydrochloric acid. The resulting precipitate was filtered and purified by recrystallization from an appropriate solvent. The data of **2**—**6**, **9**, and **10**, are summarized in Table 1, while their IR and mass spectra are shown in Table 2. When the procedure described above has used, cyanoacetamide or benzoylacetamide gave 2-hydroxy-3-cyano-4,6-diphenylpyridine (**7**) or 2-hydroxy-3-benzoyl-4,6-diphenylpyridine (**8**) in a 68.2 or 64.2 % yield respectively. Their IR spectra could be completely superimposed on those of authentic samples.

Conversion of 4 to 2,4,6-Triphenylpyrylium Tetrafluoroborate. A mixture of **4** (0.50 g) and *p*-toluenesulfonic acid (5.00 g) was heated at 140 °C for 2 h, and then poured into 50 ml of 1 mol dm^{-3} tetrafluoroboric acid. The resulting precipitate was collected by filtration to give 2,4,6-triphenylpyrylium tetrafluoroborate almost quantitatively; its IR spectrum completely agreed with that of the authentic sample.[7]

1-Methylthio- or 1-(p-Chlorobenzylthio)-1,3-diphenyl-4,4-dicyanobutadiene (11 or 12). Into a mixture of malononitrile (0.16 g), 0.72 g (2 mmol) of **1**, and 3 mmol of methyl iodide or *p*-chlorobenzyl chloride in 3 ml of methanol we stirred 2.5 mol dm^{-3} MeONa–MeOH (2 ml) at room temperature. The reaction mixture was allowed to stand overnight and then poured into dilute hydrochloric acid. The resulting precipitate was filtered and purified by recrystallization to give **11** or **12**. These results are also shown in Tables 1 and 2.

Bis(1,3-diphenyl-4,4-dicyanobutadienyl) Disulfide (13). Into a solution of **10** (0.58 g) in DMF (5 ml), an aqueous solution of 30 % hydrogen peroxide (1 ml) was stirred drop by drop. The reaction mixture was kept at 50 °C for 2 h and then poured into water. The resulting precipitate was filtered and purified by recrystallization to give **13**. These data are also shown in Tables 1 and 2.

References

1) Y. Mollier and N. Lozac'h, *Bull. Soc. Chim. Fr.*, **1960**, 700; **1961**, 614; **1963**, 157.
2) D. Leaver and W. A. N. Robertson, *Proc. Chem. Soc.*, **1960**, 252.
3) G. Duguay and H. Quiniou, *Bull. Soc. Chim. Fr.*, **1970**, 1918.
4) E. P. Kohler, *J. Am. Chem. Soc.*, **44**, 379 (1922).
5) R. R. Schmidt, *Chem. Ber.*, **98**. 3892 (1965).
6) I. Shibuya and M. Kurabayashi, *Bull. Chem. Soc. Jpn.*, **48**, 73 (1975).
7) K. Dimroth, *Angew. Chem.*, **72**, 331 (1960).

BULLETIN OF THE CHEMICAL SOCIETY OF JAPAN, VOL. 52 (4), 1237—1238 (1979)

The Reductions of Carbonyl Compounds with Sodium 1-Benzyl-3-carbamoyl-1,4-dihydropyridine-4-sulfinate

Hiroo INOUE,* Ichiro SONODA, and Eiji IMOTO

Department of Applied Chemistry, College of Engineering, University of Osaka Prefecture, Sakai, Osaka 591

(Received September 8, 1978)

Synopsis. It is found that sodium 1-benzyl-3-carbamoyl-1,4-dihydropyridine-4-sulfinate reduces α-keto carbonyl compounds to α-hydroxy carbonyl compounds with the assistance of $MgCl_2$ and reacts with 9-fluorenone to give an adduct.

Although sodium 1-benzyl-3-carbamoyl-1,4-dihydropyridine-4-sulfinate (BNA-SO_2Na) is of interest as a reducing agent, not a great deal is yet known about the chemical reactivity of BNA-SO_2Na. Recently we reported that BNA-SO_2Na can undergo reductions of α-halo ketones to the parent ketones[1] and that of acridine to 9,9'-bi(9,10-dihydroacridine)[2] in a protic solvent. In analogy with sodium hydroxymethanesulfinate[3] and thiourea dioxide,[4] the carbon-sulfur bond of BNA-SO_2Na is cleaved in the reduction process. Our interest in the reactivity of BNA-SO_2Na prompted us to examine the capability of BNA-SO_2Na for the reductions of the carbonyl compounds. We now wish to report several results giving information on the reactivity of BNA-SO_2Na caused by its unique structure.

Results and Discussion

Reactions of BNA-SO_2Na with α-Keto Carbonyl Compounds. BNA-SO_2Na reacted under nitrogen with benzil (**1**) in 80 vol % aqueous methanol at 25 °C for 12 min to give α-hydroxydeoxybenzoin (**2**) and a thermally unstable adduct (**3**) in isolated yields of 80 and 19% respectively. In this reaction, BNA-SO_2Na was converted to 1-benzyl-3-carbamoylpyridinium salt[5] in a 92% yield, based on **1**. The amount of the salt produced indicates that BNA-SO_2Na undergoes a two-electron reduction of **1**. When the reaction mixture was allowed to stand at 25 °C for a prolonged reaction

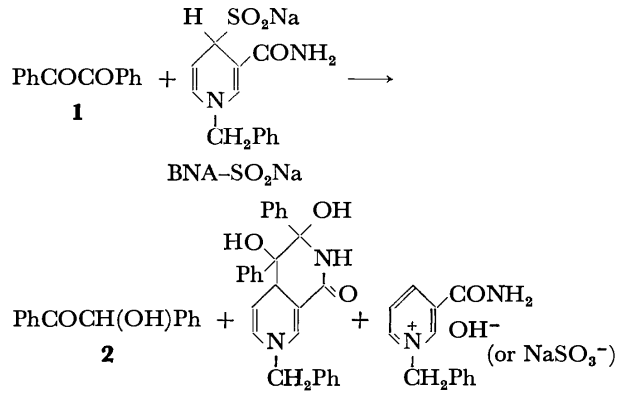

time (20 h), the yield of **2** (88%) increased with a decrease in that of **3** (5%). On the other hand, the reaction of **1** with BNA-SO_2Na in a 0.6 M sodium hydroxide solution (80 vol % aqueous methanol) gave **3** as the only product in a 92% yield.

The addition of $MgCl_2$ to the reaction system containing **1** and BNA-SO_2Na (the molar ratio of $MgCl_2$: BNA-SO_2Na: **1**=5: 2: 1) resulted in the selective formation of **2** in a high yield, as Table 1 shows. Furthermore, **3** reacted with $MgCl_2$ to give **2** in a high yield (87% at 25 °C for 17 h). These facts indicate that **3** is converted to **2** with the assistance of $MgCl_2$. The results of the reductions of the other α-keto carbonyl compounds by the BNA-SO_2Na–$MgCl_2$ system are summarized in Table 1. In the absence of $MgCl_2$, the yields of the α-hydroxy carbonyl compounds became much lower because of the formation of adducts and unproved by-products. Thus, the BNA-SO_2Na–$MgCl_2$ system is effective as a reducing system for the conversion of α-keto carbonyl compounds to α-hydroxy carbonyl compounds.

Table 1. The yields of α-hydroxy carbonyl compounds in the reduction of α-keto carbonyl compounds with the BNA-SO_2Na–$MgCl_2$ system[a]

Substance	Time, h	Product (%)[b]
PhCOCOPh	1	PhCOCH(OH)Ph (92)
PhCOCOOEt	17	PhCH(OH)COOEt (70)
PhCOCHO	18	$PhCOCH_2OH$ (55)
$C_3H_7COCOC_3H_7$	1	$C_3H_7COCH(OH)C_3H_7$ (61)
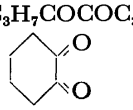	2	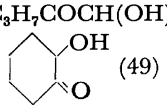 (49)

a) Molar ratio of $MgCl_2$: BNA-SO_2Na: substance= 5: 2: 1. Concentration of the substance: 0.06 mol/l. 80 vol % aqueous methanol. 25 °C. b) Isolated yield.

Reactions of BNA-SO_2Na with Diaryl Ketones. The reaction of BNA-SO_2Na with 9-fluorenone (**4**) in 80 vol % aqueous methanol was carried out under conditions similar to those in the case of **1**. With a BNA-SO_2Na : **4** molar ratio of 2: 1, an adduct (**5**) and

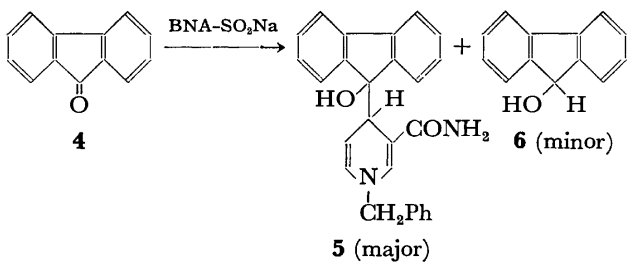

9-fluorenol (**6**) were obtained in 30 and 1% yields respectively, with a 62% recovery of **4**. [9,9'-Bi-9*H*-fluorene]-9,9'-diol (**7**) was not obtained at all. BNA-SO_2Na was converted to 1-benzyl-3-carbamoylpyridinium salt in a 72% yield, based on **4**. The yield of the salt was approximately comparable to the recovery

% of **4**. Even with a BNA-SO_2Na: **4** molar ratio of 5: 1, the yields of **5** and **6** did not increase, as Table 2 shows. These facts suggest that the reaction proceeds through the cleavage of the carbon-sulfur bond of BNA-SO_2Na to give an unstable SO_2Na-adduct (**8**) in addition to **5**. The **8** must be converted to **4** and $NaHSO_3$ by hydrolysis, accompanied by oxidation with air on the separation of the products.

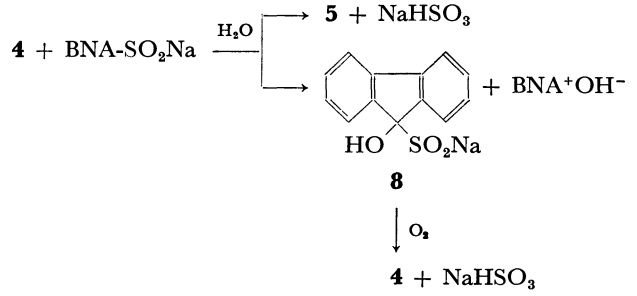

In an alkaline medium, the yield of **5** became better. Furthermore, $MgCl_2$ was ineffective in the reduction of **4** to **6** and **7** by BNA-SO_2Na. When $Mg(OCH_3)_2$ was used with BNA-SO_2Na, **5** was obtained in a good yield (Table 2).

Table 2. The reaction of **4** with BNA-SO_2Na[a]

Additive	Molar ratio Additive/**4**	Yield, %[b]			Recovered **4**, %[b]
		5	**6**	**7**	
None[c]	0	30	1	0	62
NaOH	10	53	0	0	27
$MgCl_2$[d]	5	3	0	4	85
$Mg(OCH_3)_2$[e]	1	75	0	0	21

a) Concentration of **4**: 0.06 mol/l. BNA-SO_2Na: **4** molar ratio=2: 1. 80 vol % aqueous methanol. 1 h. 25 °C. b) Isolated yield. c) In the BNA-SO_2Na: **4** molar ratio of 5: 1, **5** was obtained in a 35% yield, with a 62% recovery of **4**. d) 20 h. e) MeOH solvent.

Benzophenone did not react with BNA-SO_2Na, even in an alkaline medium at 25 °C, and was recovered unreacted. When the temperature was raised to 90 °C, however, benzhydrol was found to be obtained in a 16% yield.[6] Thus, BNA-SO_2Na was not effective as a reducing agent for the reductions of monoketones to alcohols.

$$PhCOPh \xrightarrow[90\,^\circ C]{BNA\text{-}SO_2Na} Ph_2CHOH$$

Experimental

Material. The BNA-SO_2Na was prepared according to the procedures described in our preceding paper.[1]

Reaction of 1 with BNA-SO_2Na. A typical experiment was as follows: to a solution of 3 mmol of **1** in 50 cm^3 of 80 vol % aqueous methanol we added 5.9 mmol of BNA-SO_2Na. The solution was stirred under nitrogen at 25 °C for 12 min. A pale yellow precipitate of **3** was removed by filtration, washed under nitrogen with 80 vol % aqueous methanol, and dried *in vacuo*. The yield of **3** (mp 132—134 °C), was 19%. **3** exhibited NMR (DMSO-d_6) signals at δ=3.9 (d, 1H, H_4), 4.4 (s, 2H, CH_2), 4.7 (d, 1H, H_5), 5.95 (d, 1H, H_6), 7.02 (s, 5H, aromatic protons), 7.23 (s, 10H, aromatic protons), and 7.5 ppm (d, 1H, H_2), and an IR (KBr) peaks at 3450 (OH), 3200—3250 (NH), and 1680 cm^{-1} (CO).

Found: C, 74.51; H, 5.84; N, 6.56%. Calcd for $C_{27}H_{24}N_2O_3$1/2 H_2O: C, 74.78; H, 5.81; N, 6.47 %.

The removal of the methanol from the filtrate gave 80% of **2** (mp 131—132 °C), which was identified by comparing its IR and NMR spectra with those of authentic specimens. After the removal of the methanol, the residual solution was developed on an anion-exchange resin (Amberlite IRA-400) to yield 92% of BNA^+Cl^-, based on **1**. Similar procedures were used for the reaction of **1** with BNA-SO_2Na in an alkaline medium and the reactions of **1** and the other α-keto carbonyl compounds with the BNA-SO_2Na–$MgCl_2$ system.

Reaction of 4 with BNA-SO_2Na. To a solution of 3 mmol of **4** in 50 cm^3 of 80 vol % aqueous methanol we added 5.7 mmol of BNA-SO_2Na. After the solution had been stirred under nitrogen at 25 °C for 1 h, the mixture was neutralized by dilute hydrochloric acid, the methanol was removed *in vacuo*, and the resinous material was extracted with benzene. After the removal of the benzene *in vacuo*, the residue was chromatographed on silica gel. Elution with benzene and then chloroform gave **4**, **5**, and **6** in 62, 30, and 1% yields respectively. The purification of **5** was carried out as follows: a solution of **5** in chloroform was placed on the silica gel column and eluted with 15 % acetone in chloroform to give the purified **5** (mp 88 °C (dec)); **5** exhibited NMR ($CDCl_3$) signals at δ=2.2 (s, 1H, OH), 3.85 (s, 2H, CH_2), 4.2 (d, 1H, H_4), 5.2 (d, 1H, H_5), 6.35 (d, 1H, H_6), 6.5—6.7 (m, 2H, NH_2), and 7.0—7.5 (m, 14H, aromatic protons and H_2), and IR (KBr) peaks at 3300—3350 and 3170—3200 (NH_2) and 1680 cm^{-1} (CO).

Found: C, 78.99; H, 5.75; N, 7.14%. Calcd for $C_{25}H_{22}N_2O_2$: C, 79.14; H, 5.62; N, 7.10 %.

In the reactions of **4** with BNA-SO_2Na in the presence of NaOH, $MgCl_2$, and $Mg(OCH_3)_2$, the procedures of the reactions and the isolation of the products were carried out in a manner similar to that described above.

Reaction of Benzophenone with BNA-SO_2Na. To a solution containing 6 mmol of sodium hydroxide in 100 cm^3 of 80 vol % aqueous methanol we added 2 mmol of benzophenone and then 10 mmol of BNA-SO_2Na. The solution was heated under nitrogen at 90 °C for 2 h. The white precipitate was then removed by filtration, and the methanol was evaporated *in vacuo*. The residual solution, containing a solid, was extracted with benzene. After the removal of the benzene, the residue was placed on the silica gel column and eluted with benzene and then chloroform to give benzophenone (81%) and benzhydrol (16%).

References

1) H. Inoue, N. Inoguchi, and E. Imoto, *Bull. Chem. Soc. Jpn.*, **50**, 197 (1977).

2) H. Inoue, I. Sonoda, N. Inoguchi, and E. Imoto, *Bull. Chem. Soc. Jpn.*, **51**, 3097 (1978).

3) R. Kerber and W. Gestrich, *Chem. Ber.*, **106**, 798 (1973).

4) K. Nakagawa and K. Minami, *Tetrahedron Lett.*, **1972**, 343; J. E. Herz and L. A. Marquez, *J. Chem. Soc., Perkin Trans. 1*, **1973**, 2633.

5) This salt was isolated as 1-benzyl-3-carbamoylpyridinium chloride.

6) It has been reported recently that benzophenone is reduced to benzhydrol by sodium dithionite in an alkaline medium at 90 °C: J. G. de Vries, T. J. van Bergen, and R. M. Kellogg, *Synthesis*, **1977**, 246.

BULLETIN OF THE CHEMICAL SOCIETY OF JAPAN, VOL. 52 (4), 1239—1240 (1979)

Cobalt Metallocycles. VII.[1] η^5-Cyclopentadienyl-η^4-iminocyclopentadienecobalt Complexes from a Reaction of Cobaltacyclopentadienes with Isocyanides

Hiroshi YAMAZAKI* and Yasuo WAKATSUKI
The Institute of Physical and Chemical Research, Wako-shi, Saitama 351

(Received November 22, 1978)

Synopsis. The reaction of (η^5-cyclopentadienyl)(triphenylphosphine)cobaltacyclopentadienes with isocyanides gives η^5-cyclopentadienyl-η^4-iminocyclopentadienecobalt complexes in good yields. Treatment of the product with HBF_4 or CH_3I yields the corresponding aminocobalticinium salt.

Cyclopentadienone–metal complexes have been isolated and characterized from the reactions of metal carbonyls with alkynes and direct reaction with substituted cyclopentadienones.[2] However, few examples of the imino analog *i.e.* iminocyclopentadiene–metal complexes are known. Weiss and Hubel reported that $Fe(CO)_5$ reacts with phenyliminotetraphenylcyclopentadiene to yield an iron tricarbonyl complex.[3] More recently, *t*-butylimino-tetrakis(trifluoromethyl)cyclopentadiene complexes of Mo and W have been reported.[4] Previous work in this laboratory has shown that carbon monoxide reacts with (η^5-cyclopentadienyl)(triphenylphosphine)cobaltacyclopentadienes (**1**) to afford the cyclopentadienone complexes. Consequently it has been predicted that isocyanides would be incorporated into the ring. The synthetic procedure for the preparation of iminocyclopentadienecobalt has the advantage that substituents can be introduced into the iminocyclopentadiene ring, since the parent cobaltacyclopentadienes with corresponding substituents are readily accessible.[5] Some reactions of the obtained iminocyclopentadiene–cobalt complexes are reported, which indicate the strong polarization of the coordinated iminocyclopentadiene ring.

A benzene solution of (η^5-cyclopentadienyl)(triphenylphosphine)tetraphenylcobaltacyclopentadiene (**1a**) and *t*-butyl isocyanide when heated at 70 °C gradually turned dark-brown, and crystals of **2a** (air stable) were isolated in good yield. IR, NMR, and elemental analysis, indicated **2a** to be (η^5-cyclopentadienyl)(η^4-*t*-butyliminotetraphenylcyclopentadiene)cobalt. Other cobaltacyclopentadiene complexes similarly reacted with isocyanides, but higher temperatures were required to complete reaction due to the presence of electron withdrawing substituents in the cobalt metallocycles. The complexes are summarized in Table 1.

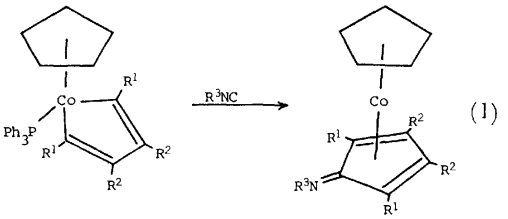

(1)

1a R^1,R^2=Ph **2a—2e**
1b R^1=Ph, R^2=Me
1c R^1=Ph, R^2=CO_2Me

The iminocyclopentadiene ligand in these complexes is strongly coordinated to the cobalt. An attempt to liberate the coordinated iminocyclopentadiene in **2c** by carbon monoxide (40 atm, 120 °C) resulted in the formation of a small amount of the desired product, most of the complex remaining unreacted.

In the iminocyclopentadiene–cobalt complexes, by analogy with the cyclopentadienone analogs,[6] an ionic resonance contribution **2'** may be expected. In agreement with this expectation, the ν(C=N) absorption in 2,6-xylyliminotetraphenylcyclopentadiene (1630 cm^{-1}) was markedly reduced on coordination to cobalt (1575 cm^{-1}).

Furthermore, complex **2** readily forms aminocobalticinium salts (**3**) on protonation and methylation (Eq. 2). The protonation by fluoroboric acid was performed by shaking a benzene solution of **2** with the acid. The ν(C=N) peak was absent in the IR spectrum of the resulting complex while the ν(N–H) appeared at 3300—

TABLE 1. IMINOCYCLOPENTADIENE–COBALT COMPLEXES

	Compound			Yield (%)	Mp (°C)	Found (Calcd) %			NMR[a] δ (ppm)		IR[b] ν(C=N) (cm^{-1})
	R^1	R^2	R^3			C	H	N	η-C_5H_5	CH_3	
2a	Ph	Ph	*t*-Bu	84	213—215	81.26 (80.98	6.12 6.08	2.58 2.49)	4.71	1.27	1580
2b	Ph	Ph	*p*-MeC_6H_4	49	166—168	82.37 (82.40	5.52 5.40	2.24[c] 2.34)	4.60	2.12	1555
2c	Ph	Ph	2,6-$Me_2C_6H_3$	86	250—251	82.75 (82.47	5.46 5.60	2.18 2.29)	4.58	1.88, 2.59 (3H) (3H)	1575
2d	Ph	Me	2,6-$Me_2C_6H_3$	79	211—212	79.36 (78.84	6.44 6.20	2.78 2.87)	4.29	1.69, 1.89, 2.67 (3H) (6H) (3H)	1565
2e	Ph	CO_2Me	2,6-$Me_2C_6H_3$	67	178—179	70.89 (70.95	5.23 5.25	2.38 2.43)	4.97	1.51, 2.47, 3.81[d] (3H) (3H) (6H)	1575

a) In C_6D_6. b) KBr disk. c) Solvated with C_6H_6. d) In $CDCl_3$.

Table 2. Cobalticinium salts

	Compound			Mp (°C)	Found (Calcd) (%)				NMR[a] δ (ppm)				IR[b] ν(N–H) (cm^{-1})
	R^3	R^4	X		C	H	N	I	η-C_5H_5	C–CH_3	N–CH_3	N–H	
3a	*t*-Bu	H	BF_4	277—282	70.25 (70.06	5.40 5.42	2.12 2.15)		5.54	1.08		4.02	3375
3b	2,6-$Me_2C_6H_3$	H	BF_4	290—293	72.08 (72.12	5.08 5.04	1.98 2.00)		5.50	1.82 2.48		6.22	3350
3c	*t*-Bu	Me	I	275—277	66.71 (66.39	5.11 5.29	2.02 1.99	18.05 17.99)	5.78	0.99	2.80		
3d	*p*-Me–C_6H_4	Me	I	303—304	70.65 (70.51	5.07 5.05	1.78 1.71	15.55 15.52)	5.80	2.02	3.33		

a) In $CDCl_3$. b) KBr disk.

3400 cm^{-1}. On shaking the fluoroborate salt with alkali, smooth deprotonation occurred yielding the parent neutral complex (**2**). *N*-Methylated cobalticinium salts were obtained when **2a** and **2b** were treated with iodomethane. **2c** did not react with iodomethane possibly due to steric hindrance around the N atom. The cyclopentadienyl proton resonances shifted from δ 4.58—4.71 in **2a**—**2c** to δ 5.49—5.79 ppm in **3a**—**3d**, in accord with the increase of oxidation number of the cobalt.

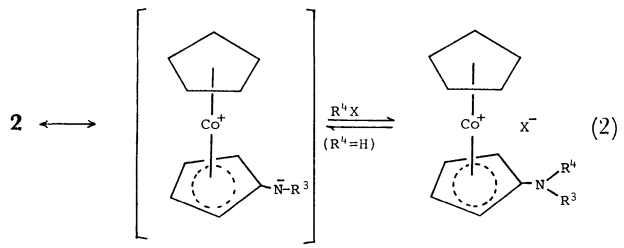

2′ 3

R^4=H or Me
X=BF_4 or I

Experimental

IR spectra were recorded on a Shimadzu IR-27G and NMR spectra on a Varian HA-100 spectrometer. Melting points were determined on a Mitamura micro-melting point apparatus. (η^5-Cyclopentadienyl)(triphenylphosphine)cobaltacyclopentadiene complexes were prepared by the methods reported.[5]

Preparation of (η^5-Cyclopentadienyl)(η^4-iminocyclopentadiene)-cobalt. A solution of **1a** (0.742 g, 1.0 mmol) and *t*-BuNC (0.4 ml) in benzene (10 ml) was heated at 70 °C for 8 h. The volume of the solvent was reduced *in vacuo* and hexane added to give black crystals of **2a** (0.473 g).

Similar treatment of cobaltacyclopentadiene complexes with isocyanides gave the corresponding iminocyclopentadiene–cobalt complexes (Table 1). Preparation of **2e** was conducted at 130 °C.

*Reaction of **2c** with Carbon Monoxide.* A solution of **2c** (0.122 g, 0.2 mmol) in benzene (20 ml) was placed in an autoclave and carbon monoxide introduced (40 atm). After heating at 120 °C for 8 h, the solution was concentrated. The addition of hexane afforded the starting cobalt complex (0.06 g, 49% recovery). The mother liquid was chromatographed on alumina and a red fraction eluted with benzene/hexane (1: 1). Evaporation of the solvent, followed by crystalization from hexane gave dark-red crystals of 2,6-xylyliminotetraphenylcyclopentadiene (0.018 g, 18%), mp 190 °C. Found: C, 91.11; H, 6.03; N, 2.79%; mol wt, 487 (mass spectrum). Calcd for $C_{37}H_{29}N$: C, 91.13; H, 5.99; N, 2.87%; mol wt, 487. NMR ($CDCl_3$): δ 1.99 (s, 9H); 6.5—7.2 (multiplet, Ph protons) ppm. IR (KBr): ν(C=N), 1630 cm^{-1}.

*Reaction of **2** with Fluoroboric Acid.* To a solution of **2a** (0.10 g, 0.18 mmol) in benzene (10 ml) was added a few drops of fluoroboric acid (42 %, aq solution). The mixture turned pale immediately after shaking and an orange-red solid precipitated. Extraction of the solid with a small amount of CH_2Cl_2 followed by the addition of benzene gave red crystals of **3b** (0.083 g, 73%). **3a** was similarly prepared (46%). The physical properties of the complexes are summarized in Table 2.

*Reaction of **2** with Iodomethane.* A solution of **2a** (0.056 g, 0.1 mmol) and iodomethane (0.2 ml) in benzene (10 ml) was left overnight at room temperature. The resulting dark red-brown solution was concentrated *in vacuo* to give dark red brown crystals of **3c** (0.063 g, 89%). **3d** was similarly obtained.

References

1) Part VI, Y. Wakatsuki and H. Yamazaki, *J. Am. Chem. Soc.*, in press.
2) E. O. Fischer and H. Werner, "Metal π-Complexes," Elsevier Pub. Co., Amsterdam (1966), Vol. 1.
3) E. Weiss and W. Hubel, *J. Inorg. Nucl. Chem.*, **11**, 42 (1959).
4) J. L. Davison, M. Green, J. Z. Nyathi, F. G. A. Stone, and A. J. Welch, *J. Chem. Soc., Dalton Trans.*, **1977**, 2246.
5) H. Yamazaki and Y. Wakatsuki, *J. Organomet. Chem.*, **139**, 157 (1977).
6) J. E. Sheats and M. D. Rausch, *J. Org. Chem.*, **35**, 3245 (1970); J. E. Sheats, W. Miller, M. D. Rausch, S. A. Gardner, P. S. Andrews, and F. A. Higbie, *J. Organomet. Chem.*, **96**, 115 (1975).

BULLETIN OF THE CHEMICAL SOCIETY OF JAPAN, VOL. 52 (4), 1241—1242 (1979)

The Silver(I) Salt-promoted Benzylation of Silyl Enol Ethers

Hidetsugu TAKAGAKI, Nobuyoshi YASUDA, Morio ASAOKA, and Hisashi TAKEI*

Department of Life Chemistry, Tokyo Institute of Technology, Nagatsutacho, Midori-ku, Yokohama 227

(Received September 1, 1978)

Synopsis. Various silyl enol ethers gave the corresponding mono benzyl products in moderate to good yields by the reaction with benzyl bromide in the presence of silver perchlorate in dichloromethane at −78—0 °C.

Silyl enol ethers are known to be useful intermediates for the alkylation of carbonyl compounds; the alkylation is usually performed through the enolate anion generated by the treatment with MeLi[1] or $R_4N^+F^-$.[2] On the other hand, the *t*-butylation of silyl enol ethers was recently accomplished by the use of Lewis-acid catalysts.[3]

Silver(I) salts are well known to activate the halogenated compounds. Therefore, it seemed possible to alkylate the silyl enol ethers with alkyl halides activated by silver(I) salt. In this paper, we will describe the silver(I) salt-promoted benzylation of silyl enol ethers.[4]

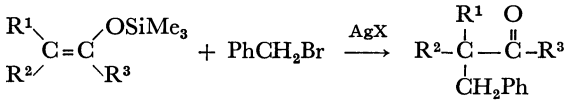

Results and Discussion

First, we examined the reaction of 1-trimethylsiloxycyclohexene and benzyl bromide in dichloromethane as a model reaction. When the reaction was carried out in the presence of silver(I) oxide or silver(I) nitrate, no alkylated product was obtained. However, 2-benzylcyclohexanone was obtained in 9% (Ag_2O) or 15% ($AgNO_3$) yield by the addition of a catalytic amount of zinc chloride to the reaction mixture. Therefore, in order to ascertain the best conditions for the reaction, various silver(I) salts, Lewis acids, and reaction temperatures were examined. These results are summarized in Table 1.

As shown in Table 1, a combination of silver perchlorate and boron trifluoride etherate was the best one. Moreover, it was found that the reaction could proceed without a Lewis-acid catalyst when silver perchlorate or silver tetrafluoroborate was used. In the case of the reaction of 1-phenyl-1-trimethylsiloxyethene and benzyl bromide, silver perchlorate alone gave the best result (44%), although the addition of boron trifluoride etherate, zinc chloride, or magnesium chloride gave the corresponding benzylated product in 21, 41, or 34% yield respectively. The reaction of several silyl enol ethers and benzyl bromide in the presence of silver perchlorate was also examined; the results are listed in Table 2.

Table 1. Reaction of 1-trimethylsiloxycyclohexene with benzyl bromide in dichloromethane

Silver(I) salt (1 equiv)	Catalyst[c]	Temp/°C	Time/h	Isolated yield/%
Ag_2O	$ZnCl_2$	room temp	20	9[a]
$AgNO_3$	$ZnCl_2$	room temp	20	15[a]
$AgClO_4$	$ZnCl_2$	room temp	20	21[a]
$AgNO_3$	$ZnCl_2$	−78—0	14	11[b]
$AgNO_3$	$TiCl_4$	−78—0	14	14[b]
$AgNO_3$	$SnCl_4$	−78—0	14	22[b]
$AgNO_3$	$BF_3\cdot Et_2O$	−78—0	14	49[b]
$AgClO_4$	$BF_3\cdot Et_2O$	−78—0	14	82[b]
$AgClO_4$	—	−78—0	14	64[b]
$AgBF_4$	$BF_3\cdot Et_2O$	−78—0	14	32[b]
$AgBF_4$	—	−78—0	14	51[b]

a) 1-Trimethylsiloxycyclohexene (1 equiv) and benzyl bromide (1.1 equiv) were used. b) 1-Trimethylsiloxycyclohexene (1.2 equiv) and benzyl bromide (1 equiv) were used. c) A catalytic amount of Lewis acid was used.

Table 2. Benzylation of various silyl enol ethers[a]

Silyl enol ether	Product[6]	Isolated yield/%
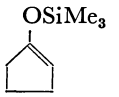	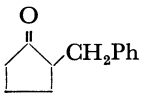	69
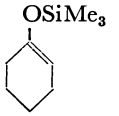	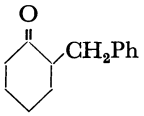	82[b]
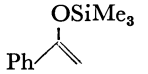	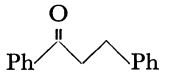	44
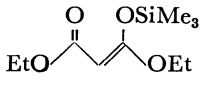	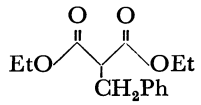	35

a) Silyl enol ether (1.2 equiv) and benzyl bromide (1 equiv) were used in dichloromethane at −78—0 °C for 14 h in the presence of $AgClO_4$ (1 equiv). b) A catalytic amount of $BF_3\cdot Et_2O$ was used.

These yields are well in accordance with the order of the electron density of the carbon-carbon double bond of silyl enol ethers. Therefore, it is reasonable to assume that the reaction is an electrophilic one. Under similar reaction conditions, we examined the alkylation of 1-phenyl-1-trimethylsiloxyethene using other alkyl halides. However, all attempts failed in the cases of isopropyl iodide, allyl brimide, and butyl iodide. The only successful case except for benzyl bromide was that of methyl iodide (51%).

To ascertain the regioselectivity of the reaction, we also examined the reaction of 6-methyl-1-trimethylsiloxycyclohexene with benzyl bromide. However, the reaction was found not to be regioselective even under rather basic conditions.

Table 3. Reaction of 6-methyl-1-trimethylsiloxycyclohexene with benzyl bromide[a)]

Additive	Product[6)] Yield(%)[b)] *cis*	*trans*	Yield/%[b)]	Total yield/%
—	34	14	22	70
2,4,6-Collidine (1 equiv)	28	22	14	64

a) 6-Methyl-1-trimethylsiloxycyclohexene (1.1 equiv) and benzyl bromide (1 equiv) were used in dichloromethane at −78—0 °C for 14 h in the presence of $AgClO_4$ (1 equiv). b) Isolated yield.

Experimental

A typical procedure for the benzylation of silyl enol ethers[5)] was as follows.

2-Benzylcyclohexanone. A dichloromethane solution (2 ml) of 1-trimethylsiloxycyclohexene (204 mg, 1.2 mmol) and benzyl bromide (171 mg, 1 mmol) was added to silver perchlorate (208 mg, 1 mmol) at −78 °C under argon atmosphere. The mixture was then allowed to warm to 0 °C over about 14 h. The silver salts were filtered off, and water was added. The solution was then extracted with ether, and the organic layer was dried over sodium sulfate and evaporated. 2-Benzylcyclohexanone was obtained by using TLC (hexane: ether =10: 1, R_f=0.4); 119 mg (64%).

References

1) G. Stork and P. F. Hudrlik, *J. Am. Chem. Soc.*, **90**, 4462 (1968).

2) I. Kuwajima and E. Nakamura, *J. Am. Chem. Soc.*, **97**, 3257 (1975).

3) T. H. Chan, I. Paterson, and J. Pinsonnault, *Tetrahedron Lett.*, **1977**, 4183; M. T. Reetz and W. F. Maier, *Angew. Chem.*, **90**, 50 (1978).

4) The oxidative coupling reaction of silyl enol ethers using silver(I) oxide in DMSO was previously reported; Y. Ito, T. Konoike, and T. Saegusa, *J. Am. Chem. Soc.*, **97**, 649 (1975).

5) The silyl enol ethers were prepared according to the procedures of H. O. House, L. Czuba, M. Gall, and H. D. Olmstead, *J. Org. Chem.*, **36**, 2361 (1971).

6) These products were confirmed by their spectral data, by elemental analyses, and by comparison with authentic samples prepared according to I. Kuwajima and E. Nakamura, *J. Am. Chem. Soc.*, **97**, 3257 (1975).

Investigation of CdS Photoanode Reaction in the Electrolyte Solution Containing Sulfide Ion

Tooru INOUE,* Tadashi WATANABE, Akira FUJISHIMA, and Kenichi HONDA

Department of Synthetic Chemistry, Faculty of Engineering, The University of Tokyo, Hongo, Bunkyo-ku, Tokyo 113

(Received July 19, 1978)

The study of the photoanodic reaction in the CdS/S^{2-} system was carried out by means of the rotating ring-disk electrode (RRDE) technique. The photoanodic reactions at an n-type CdS electrode are divided into two types; the photoanodic oxidation of redox agents in the electrolyte solution and the photoanodic dissolution of CdS electrode surface. The stabilization of a CdS photoanode could be attained through the preferential progress of the former of these two processes. The ratio between these two processes depends upon the concentration of S^{2-} in the electrolyte solution and the light intensity. Sulfide ion in the electrolyte solution stabilizes CdS photoanode and gives rise to the shift of the flatband potential of CdS electrode by *ca.* −60 mV/log[S^{2-}]. This dependence of the flatband potential on sulfide ions can be explained by an adsorptive dissociation equilibrium at a CdS electrode surface. The results of the photoanodic reaction were disscussed referring to the charge transfer process with the participation of some surface energy state within a bandgap.

The behavior of the reactions at an illuminated semiconductor electrode has been recently drawing attention of a number of investigators primarily in connection with the solar energy conversion into electrical and chemical energy, that is, the electrochemical photocell as a solar energy converting device.[1-24]

At TiO_2 electrode[1-10] and other stable semiconductor electrodes,[11-14] the photosensitized electrolytic oxidation of water[1-14] and various reducing agents such as I^-, Br^-, Cl^-, $Fe(CN)_6^{4-}$, hydroquinone, and Fe^{2+} [15-25] occurs by the action of the excess holes photogenerated at the electrode surface, according to the following reactions.

$$2H_2O + 4h^+ \longrightarrow O_2 + 4H^+ \quad (1)$$

$$Red + n\,h^+ \longrightarrow Ox \quad (2)$$

These semiconductors possess relatively wide bandgaps except WO_3[8] and Fe_2O_3[4,13] and hence can not efficiently utilize the solar energy. In this respect, cadmium sulfide[15-21] seems to be a promising material since it shows a strong absorption in wavelength shorter than 520 nm. However, the anodic reaction at an illuminated CdS electrode is known to be the dissolution[26,27] of the electrode surface, according to

$$CdS + h\nu \longrightarrow CdS(h^+_{val} + e^-_{cond}), \quad (3)$$

$$2h^+_{val} + CdS \longrightarrow S_{ad} + Cd^{2+}, \quad (4)$$

where h^+_{val}, e^-_{cond} and S_{ad} denote a hole in the valence band, an electron in the conduction band, and a sulfur atom deposited on the electrode surface, respectively.

Hence, from the stand-point of practical application of CdS photoanode to the electrochemical photocell, it is desired to stabilize the CdS photoanode. In the previous paper[15] we investigated the suppression of surface dissolution of CdS photoanode by reducing agents through the competitive oxidation between the process (2) and (4).

Some reducing agents had the various efficiencies of the dissolution suppression and especially S^{2-}, SO_3^{2-}, and $S_2O_3^{2-}$ could markedly stabilize the CdS photoanode.[15] Wrighton *et al.*[19] reported that the cadmium calcogenide (CdX) photoanodes are stabilized through the oxidation of the calcogenide ions (S^{2-}, Se^{2-}, and Te^{2-}) in the electrolyte solution and the output power characteristics of the electrochemical photocell can be enhanced by using the CdX/X^{2-} systems.

Miller and Heller[21] also reported the power characteristics of the photocells with CdS and Bi_2S_3 polycrystal photoanodes/sulfide. Minoura *et al.*[16] reported that the dissolved Cd^{2+} and S^{2-} ions cause the shift of the flatband potential of CdS and CdS photoanode is stabilized by the diffusion of S^{2-} to the electrode surface. Memming[20] investigated the oxidation efficiency of a ferrous cyanide at the CdS photoanode surface against pH variation by means of a rotating platinum-semiconductor RRDE technique.

As for the effect of the illumination intensity on the electrochemical photolysis of water at TiO_2 and on the conversion of the light energy to the electricity at CdS, the power charateristics (photovoltages and photocurrents) of the electrochemical photocells were investigated well.[19,28] However, a quantitative dependence of the light intensity on the stability of CdS photoanode has not been investigated in detail.

In this study,[45] we investigated more precisely the dependence of a flat band potential on the dissolved sulfide ion and the dependence of the competitive reaction between the dissolution of CdS photoanode and the oxidation of the dissolved sulfide ions on the light intensity by means of a RRDE technique and others. We show the results that the stabilization of the CdS photoanode can be elucidated based upon the function of the concentration of the sulfide ions and the number of the incident photons. Then we discussed the charge transfer across the semiconductor/electrolyte interface based upon the number of the carriers in both phases.

Experimental

Ring-disk electrode were constructed with single crystal of n-type CdS disk electrode together with Cu(Hg) as the ring electrode. General experimental procedures including electrode pretreatments, establishment of ohmic contacts and RRDE assembly have described elsewhere.[15,29]

The measurement principle of the RRDE method is schematically illustrated in Fig. 1. In the absence of a reducing agent (S^{2-}) in the electrolyte solution (A), Cd^{2+} ion is pro-

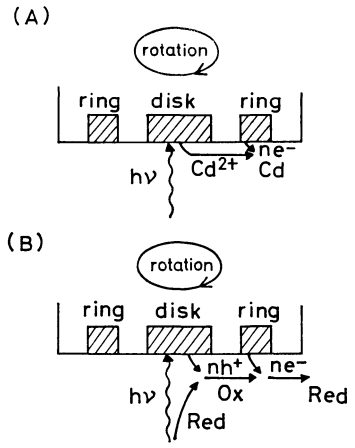

Fig. 1. Schematic diagram of the RRDE system. (A) a detection of the dissolution product of CdS electrode surface, (B) a detection of the oxidation product of a reducing agent.

duced at the disk electrode through the photoelectrochemical process (4), and a part of which, determined by the collection efficiency, is reduced at the Cu(Hg) ring electrode. If a reducing agent is added (B), it undergoes the competitive oxidation of S^{2-} by photogenerated holes, and the oxidized species discharges at the ring electrode.

Dependence of the flatband potential of CdS photoanode on the concentration of the sulfide ion was given by the capacitance measurement of the interface of CdS electrode/electrolyte solution containing sulfide ion, whose method is described in elewhere.[30]

Results and Discussion

Variation of Flatband Potential of CdS Electrode. Figure 2 shows typical $1/C^2$ *vs.* E plots for the CdS electrode in the aqueous electrolyte solution with sulfide ions, obtained by the impedance measurement. The interface capacitance is assumed that the capacitance of a space charge layer is much smaller than any other regions. When a depletion layer is formed for majority carriers (electrons) for n-type semiconductor such a condition can be attained at the anodic polarization. So the determination of the flatband potential of CdS

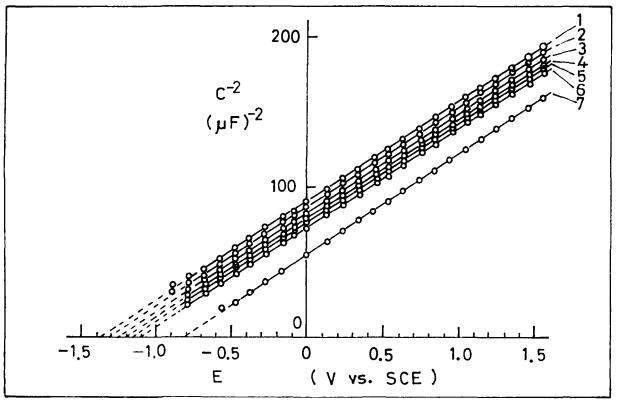

Fig. 2. Mott-Schottky plots for CdS electrode. 1: 1.0 M S^{2-}, 2: 10^{-2} M S^{2-}, 3: 10^{-2} M S^{2-}, 4: 10^{-3} M S^{2-}, 5: 10^{-4} M S^{2-}, 6: 10^{-5} M S^{2-}, 7: 0.0 M S^{2-}. All in 0.2 M Na_2SO_4 aqueous solution.

electrode is based upon the application of Mott-Schottky relationship[31] which is expressed as

$$\frac{1}{C_s^2} = \frac{2}{qee_0N}\left(E - E_{fb} - \frac{kT}{q}\right), \tag{5}$$

where C_s represents the space charge differential capacitance per unit area, q the electric charge, e the dielectric constant of semiconductor, e_0 the permittivity of vacuum, N the carrier concentration (practically equals the donor concentration in the present case (7.4×10^{16} cm^{-3})), E the electrode potential and E_{fb} the flatband potential. Thus the intercept of the E axis of the $1/C^2$ (approximately equals $1/C_s^2$) *vs.* E curves gives a potential differing from the flatband potential by kT/q.

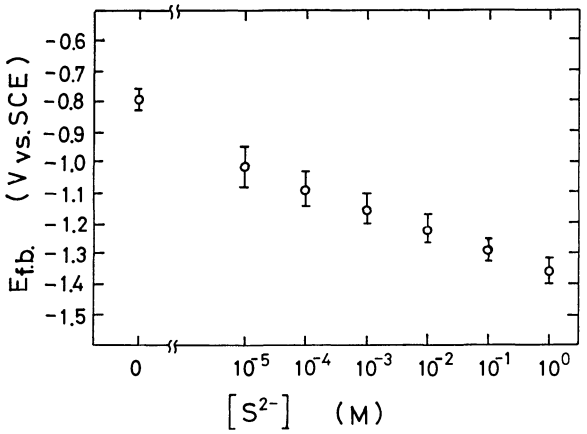

Fig. 3. Dependence of the flatband potential of CdS electrode on the concentration of S^{2-}.

The flatband potentials of CdS electrode thus determined is shown in Fig. 3 as a function of the concentration of S^{2-} with the slope *ca.* -60 mV/log[S^{2-}]. The value of this slope is approximately the same as that reported by others.[32] Otherwise, the flatband potentials of TiO_2 and ZnO depend upon the pH of the electrolyte solution with a slope of -59 mV/pH, which is explained in view of the following dissociation equilibrium established at the semiconductor electrode surface,[33] for example

$$\text{Ti-O}^{2-} + \text{H}^+ \rightleftharpoons \text{Ti-OH}^-, \tag{6}$$

$$\Delta\phi = \text{const} + \frac{RT}{E}\ln\frac{a_{\text{TiO}^{2-}}}{a_{\text{TiOH}^-}} - \frac{2.3RT}{F}\text{pH},$$

where Ti–O^{2-} represents an element of the TiO_2 lattice at the surface, H^+ a proton in the bulk of the electrolyte solution, and Ti–OH^- the lattice element protonated. From the thermodynamic theory, the flatband potential is reasoned with the inner potential difference of the interface between the electrode surface and the electrolyte solution. In the case of CdS electrode in the present study, the same consideration may well be taken.

$$-\text{Cd}_L^{\delta+} + \text{S}^{2-}_{\text{soln}} \rightleftharpoons -\text{Cd}_L^{(\delta-1)+}\rangle\text{S}_{\text{ad}} \tag{8}$$

where $-Cd_L^{\delta+}$ represents the lattice cadmium element of the CdS lattice at the surface, S^{2-}_{soln} a sulfide ion in

the electrolyte solution, $-Cd_L^{\delta(-1)+}\rangle S_{ad}$ the lattice cadmium element adsorbed by a sulfide ion. That is, the interfacial potential difference ($\Delta\phi$) generated by a surface adsorptive dissociation equilibrium of a sulfide ion at the CdS electrode surface depends upon the concentration of the sulfide ion in the bulk of the electrolyte solution and then changes the flatband potential of CdS electrode according to the following equation[34]

$$E_{fb} \simeq \Delta\phi = \text{const} - \frac{RT}{F}\ln\frac{C(N^\circ - N)}{C^\circ N}, \quad (9)$$

where N° and N represent the surface concentrations of adsorbed sulfide ions for maximal coverage and for the equilibrium state, C and C° the concentration of sulfide ions in solution and that in the standard state.

Consequently, the fact that the flatband potential of CdS photoanode shifts to the negative potential implies that the power characteristics, especially the photo-output voltage, of an electrochemical photocell can be increased, because the onset potential of the photocurrent based upon a photoanodic reaction corresponds to the flatband potential of a photoanode.

Current-potential Characteristics of Cu(Hg)/CdS RRDE. An anomalous behavior of the CdS disk photocurrent was observed uniquely on addition of S^{2-} in the electrolyte solution. Figure 4 shows the change of the current-potential characteristics of CdS photoanode with the change in S^{2-} concentration. It is seen that the onset potential for the photocurrent is shifted to more negative potential as S^{2-} concentration increases, corresponding to the flatband potential in Fig. 3, and the photocurrent appears as the twostep wave in lower S^{2-} concentrations. In the dark, the anodic photocurrent does not appear, but under illumination the anodic photocurrents appear at the negative onset potentials. In the absence of the sulfide ion in the electrolyte solution, the limiting anodic photocurrent is controlled by the photogenerated holes at the electrode surface. On the other hand, the first wave of the photocurrent observed in a lower concentration of S^{2-} increases with an increase in the concentration of S^{2-} in the electrolyte solution. In a high concentration of S^{2-}, the photoanodic current becomes one-step wave again. This phenomenon of appearance of a two-step wave photocurrent is considered to be originated from two different reactions at CdS electrode. Minoura and Tsuiki have also reported two- or three-step wave photocurrent in the solution containing S^{2-}, SO_3^{2-}, and $S_2O_3^{2-}$.[35,36] In TiO_2 electrode, a two-step wave photocurrent, it is reported,[37] appears at high pH values of the electrolyte solution, and it is explained that the first wave photocurrent is controlled by the diffusion of a hydroxyl ion (OH^-) to the TiO_2 surface and the second one by that of water (H_2O).

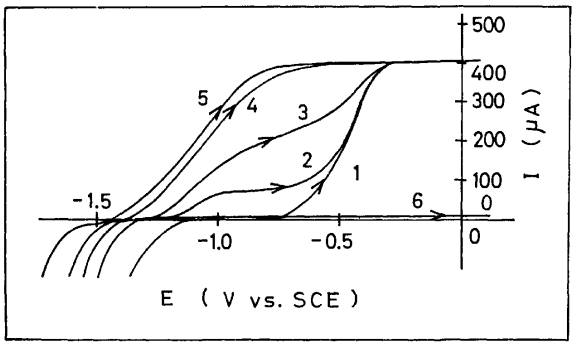

Fig. 4. Current-potential curves of a rotating CdS electrode at 1000 rpm in the electrolyte solution containing various concentrations of S^{2-}.
1: 0.0 M S^{2-}, 2: 7×10^{-4} M S^{2-}, 3: 10^{-3} M S^{2-}, 4: 10^{-2} M S^{2-}, 5: 10^{-1} M S^{2-}, above 1—5; at illuminated, 6: in the dark. All in 0.2 M Na_2SO_4 solution.

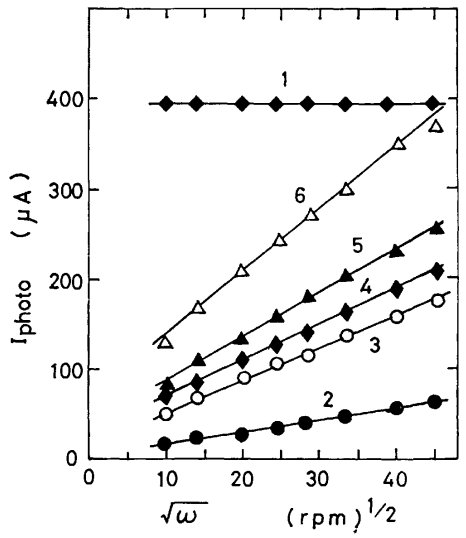

Fig. 5. Dependence of photocurrents on the root of a rotating speed of CdS disk electrode.
1: With and without S^{2-}, potentials at 0.0 V (*vs.* SCE), 2: 10^{-4} M S^{2-}, at −0.8 V, 3: 5×10^{-4} M S^{2-}, at −0.8 V, 4: 7×10^{-4} M S^{2-}, at −0.8 V. 5: 10^{-3} M S^{2-}, at −0.8 V, 6: 1.5×10^{-3} M S^{2-}, at −0.8 V. All in 0.2 M Na_2SO_4 solution.

Concerning the appearance of the two-step wave of an anodic photocurrent, the dependence of the first and the second waves on the rotation speed (ω) was measured and the results are illustrated in Fig. 5. The magnitude of the second wave shows practically no change with ω, which means that the rate-determining step is the formation of photoholes in the valence band. On the contrary, the magnitude, I_{photo}, of the first wave varies linearly with the square root of ω, and increases in an increase of S^{2-} concentration. I_{photo} can be approximated by the following formula,

$$I_{photo} = \text{const} \times [S^{2-}]\omega^{1/2} \quad (10)$$

which, according to the theory of Levich,[38] indicates that the process corresponding to the first wave is controlled by the diffusion of S^{2-} from the solution to the CdS electrode surface. Therefore, the first wave photocurrent is considered to occur from the following reactions

$$nS^{2-} + 2(n-1)h^+ \longrightarrow S_n^{2-} \quad (n=2, 3, 4, 5), \quad (11)$$

or

$$S^{2-} + 2h^+ \longrightarrow S,$$
$$S + S^{2-} \longrightarrow S_2^{2-}. \quad (12)$$

This photoanodic oxidation at CdS photoanode was also reported by Wrighton *et al.*[19] Miller and Heller,[21] and Minoura *et al.*[16]

Figure 6 shows the dependence of the disk (I_D) and ring (I_R) currents on the ring potential (E_R), with or without S^{2-} added in the electrolyte solution. In the dark (curves 1, 3), negligibly small currents are observed at the CdS disk electrode fixed at +1.0 V *vs.* SCE, while hydrogen evolution ($E_R < -1.5$ V) occurs at the Cu(Hg) ring electrode. Illumination of the CdS disk gives rise to an anodic photocurrent (curve 2) and at the same time a reduction current appears at the Cu(Hg) ring electrode in the potential range more negative than −0.6 V *vs.* SCE. The latter current corresponds to the reduction of Cd^{2+} produced by the dissolution reaction of the CdS photoanode (4). Since the ratio of the limiting reduction current at the Cu(Hg) ring electrode to an anodic photocurrent at the CdS disk electrode fairly coincides with the theoretical collection efficiency for the ring-disk electrode employed, it is evident that the process (4) is totally responsible for the anodic photocurrents. By addition of 0.1 M Na_2S in the electrolyte solution, the magnitude of the disk photocurrent undergoes practically no change, while a reduction current of Cd^{2+} disappears and a new ring current (curve 4) appears at potentials more negative than −1.2 V *vs.* SCE, corresponding to the reduction (13) of S_n^{2-} generated by the process (11) or (12).

$$S_n^{2-} + 2(n-1)e^- \longrightarrow nS^{2-} \quad (13)$$

The occurrence of this process can also be verified by the dependence of the disk and ring currents on the disk potential (E_D), with the ring potential fixed at −1.8 V for S_n^{2-} reduction and at −0.8 to −1.1 V for Cd^{2+} reduction, with or without S^{2-} added in the electrolyte solution, as shown in Fig. 7. In Fig. 7(A), in the absence of S^{2-} in the electrolyte solution both reduction currents (curves 1, 2) at the Cu(Hg) ring electrode are corresponding to the reduction of Cd^{2+}. In Fig. 7(B), in the presence of 5×10^{-4} M S^{2-} added in the electrolyte solution the reduction current (curve 1) at the Cu(Hg) ring electrode appears at the same time in occurance of the second wave of the anodic photocurrent at the CdS disk electrode. Then the reduction current (curve 2) at the ring electrode shows a two-step wave similar to the anodic photocurrent at the CdS disk electrode. This first wave of a reduction current is deduced from the reduction of S_n^{2-}. In Fig. 7(C), in the presence of 0.1 M S^{2-} in the electrolyte solution the reduction (curve 1) of Cd^{2+} at the ring electrode disappears, while the reduction current (curve 2) of S_n^{2-} at the ring electrode shows one wave and its value coincides with the theoretical collection of the disk photocurrent for the ring-disk electrode. Therefore, it is evident that the process (11) or (12) is totally responsible for the anodic photocurrent at the CdS electrode.

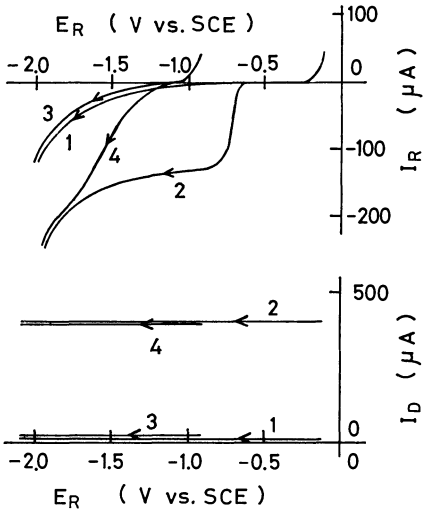

Fig. 6. Current-potential (I_R-E_R, I_D-E_R) curves of Cu(Hg)/CdS RRDE. Potential (E_D) of CdS disk electrode is fixed at 1.0 V vs. SCE.
1: 0.0 M S^{2-}, in the dark, 2: 0.0 M S^{2-}, CdS illuminated 3: 0.1 M S^{2-}, in the dark, 4: 0.1 M S^{2-}, CdS illuminated. All in 0.2 M Na_2SO_4 solution.

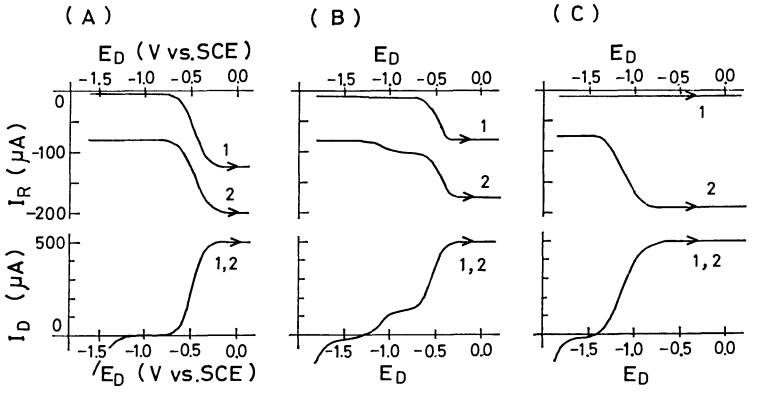

Fig. 7. Current-potential (I_R-E_D, I_D-E_D) curves of Cu(Hg)/CdS RRDE, when CdS disk is illuminated.
(A) With 0.0 M S^{2-}, 1: $E_R = -0.8$ V (*vs.* SCE), 2: $E_R = -1.8$ V. (B) With 5×10^{-4} M S^{2-}, 1: $E_R = -1.0$ V, 2: $E_R = -1.8$ V. (C) With 1×10^{-1} M S^{2-}, 1: $E_R = -1.1$ V, 2: $E_R = -1.8$ V. All in 0.2 M Na_2SO_4 solution.

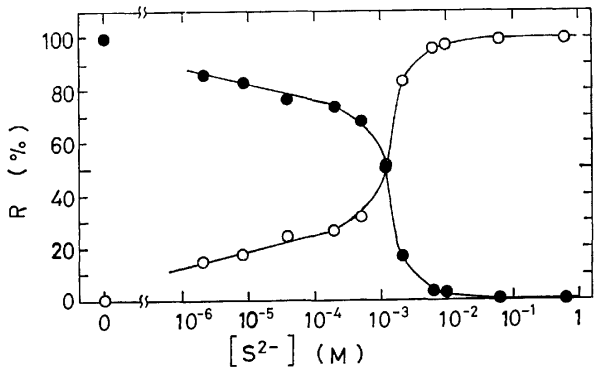

Fig. 8. Dependence of the ratio (R) of a competitive reaction on the concentration of a sulfide ion.
—●—: A dissolution of CdS electrode, —○—: an oxidation of S^{2-} in an electrolyte solution.

If we denote the magnitude of the total ring current by I_R°, that due to Cd^{2+} reduction by $I_{R,Cd}$, and that due to S_n^{2-} reduction by $I_{R,S}$, then $100I_{R,Cd}/I_R^\circ$ and $100I_{R,S}/I_R^\circ$ can be termed as the competition ratio (R) between CdS surface dissolution and oxidation of S^{2-} in the course of the photoelectrochemical process at the CdS photoanode. Figure 8 shows the ratio (R) of the competitive oxidation between CdS photonode and S^{2-} as a function of S^{2-} concentration in the electrolyte solution. It is seen that the value of R for the competitive oxidation of S^{2-} increases with the increase in $[S^{2-}]$ and the value of R for the dissolution of CdS photoanode decreases with the increase in $[S^{2-}]$. This result suggests that in a high concentration of S^{2-} added in the electrolyte solution the dissolution of CdS photoanode can be suppressed, which has been partly reported in a previous paper.[15]

Dependence of Electrode Reactions on Light Intensity. Above results were observed under the constant intensity (*ca.* 3.5×10^{15} photon/s) of illumination (wavelength range from 300 to 410 nm), while the dependence of the two-step wave photocurrent at CdS electrode on the intensity of illumination was observed, as shown in Fig. 9. In Fig. 9(A), with a concentration of 1×10^{-4} M S^{2-} added in the electrolyte solution, in a low intensity of illumination one-step wave photocurrents (curves 1 and 2) appear which are controlled by the number of photoholes formed, and in a high intensity of illumination the two-step wave photocurrents (curves 3 and 4) appear where the first wave photocurrent is constant against the intensity of illumination, however, the second wave photocurrent increases by an increase of the illumination intensity.

In the presence of sufficient sulfide ions in the electrolyte solution, the photocurrent-potential curves become one step waves as shown in Fig. 9(B). In this stage, anodic photocurrents were totally caused by the oxidation of sulfide ions supplied to the CdS electrode surface and the values of photocurrents depend on the number of the incident photons.

The dependence of the two-step wave anodic photocurrents on the intensity of illumination in various concentrations of S^{2-} is shown in Fig. 10. The dots

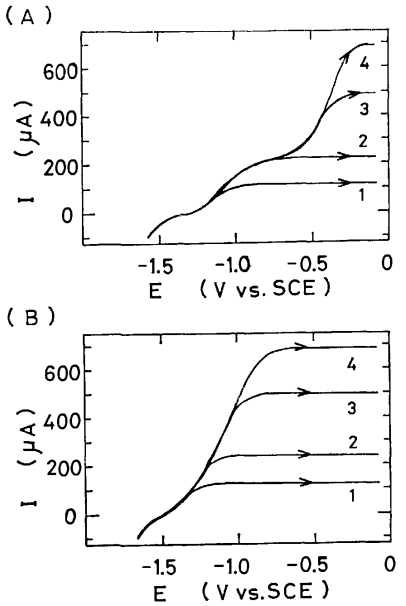

Fig. 9. Dependence of current-potential curves on the intensity (L) of illumination
(A) With 10^{-3} M S^{2-}, 1: L=0.07 a.u., 2: L=0.15, 3: L=0.35, 4: L=0.5. (B) With 10^{-1} M S^{2-}, 1: L=0.07 a.u., 2: L=0.15, 3: L=0.35, 4: L=0.5.

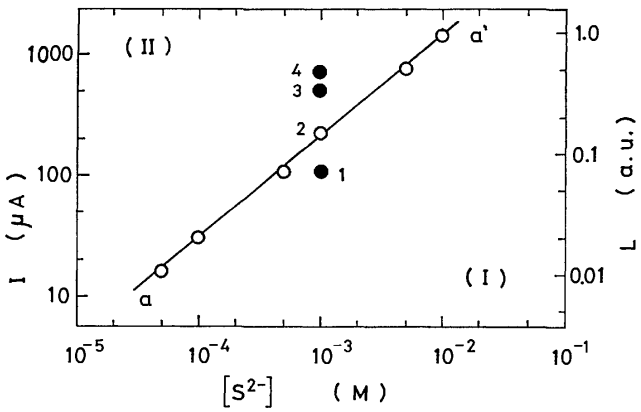

Fig. 10. Dependence of the photocurrents on the illumination intensity (L) and that of the first wave photocurrents on $[S^{2-}]$.

(1, 2, 3, and 4) correspond to the limiting values of the photocurrents in Fig. 9(A), respectively. The curve (a-a') shows the dependence of the limiting photocurrents of the first waves on $[S^{2-}]$. In the region (I) below the curve (a-a'), only a one-step wave photocurrent appears even if the illumination intensity is high, where the oxidation of S^{2-} is controlled by the number of the photogenerated holes. On the contrary, in the region (II) above the curve (a-a'), the second wave photocurrent appears based on the dissolution of CdS photoanode occurs. The oxidation ratio of a sulfide ion depends on the quantitative correlation between the concentration of a sulfide ion and the number of the incident photons.

So we can say that the CdS photoanode can be stabilized when excess sulfide ions are dissolved in the electrolyte solution versus the number of the photo-

TABLE 1. RELATIONS BETWEEN THE THEORETICAL LIMITTING CURRENTS (I_L) AND THE FIRST WAVE-PHOTOCURRENTS (I_P)

$\frac{[S^{2-}]}{mol/l}$	10^{-5}	5×10^{-5}	10^{-4}	5×10^{-4}	10^{-3}	5×10^{-3}	10^{-2}
$\frac{J_L}{mol/s}$	1.80×10^{-11}	8.98×10^{-11}	1.80×10^{-10}	8.98×10^{-10}	1.80×10^{-9}	8.98×10^{-9}	1.80×10^{-8}
$\frac{I_L}{\mu A}$	3.47	17.3	34.7	173	347	1730	3470
$\frac{I_P}{\mu A}$		16.0	29.9	112	211	790	1410
$\frac{[Fe(CN)_6^{4-}]}{mol}$	10^{-5}		10^{-4}		10^{-3}		10^{-2}
$\frac{I_{D,ox}}{\mu A}$	4.0		38.0		310		1760

generated holes at the electrode surface.

Here, we approximate the flow rate (J_L) of the sulfide ion towards the CdS electrode surface and the limiting oxidation current (I_L) of the sulfide ion employing the following equations

$$J_L = 1.95\, D^{2/3}\nu^{-1/6}\omega^{1/2}[S^{2-}]r^2, \quad (14)$$

$$I_L = nFJ_L, \quad (15)$$

where D denotes the diffusion coefficient, ν the dynamic viscosity, r the radius of the rotating disk electrode, n the covalent number, and F Faraday constant, respectively. Substituting the experimental conditions, $D=10^{-5}$ cm^2/s, $\nu=10^{-2}$ cm^2/s, $\omega=1000$ rpm, $r=0.3$ cm, $n=2$, and $F=96500$, into the Eqs. 14 and 15, we obtain the numerical results for the first-wave photocurrents as shown in Table 1. The oxidation currents($I_{D,ox}$) of varous concentration of $Fe(CN)_6^{4-}$ at the ratating Pt disk electrode with the same diameter as the CdS disk electrode are also shown in Table 1 in order to compare with the magnitude of photocurrents (I_P). From the results of Table 1, we can consider that the first wave photocurrents are controlled almost by the limitting diffusion of sulfide ions and increase with the increase of the sulfide concentration. Reflecting the facts that the flatband potential of CdS and the onset potential of the first wave photocurrent make shifts to the negative potential with the increase of the sulfide concentration, the photogenerated holes may transfer to sulfides *via* the active sites which may be caused by the adsorption of sulfides or by the imperfections (for example, kink sites, step sites or dislocations) on the CdS surface.[39]

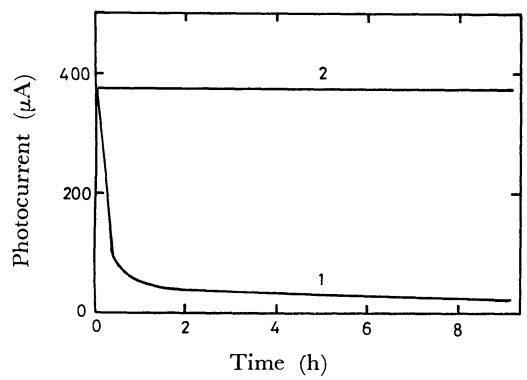

Fig. 11. Time-dependence of photocurrents at CdS electrode. 1: In 0.2 M Na_2SO_4, 2: in 0.2 M Na_2SO_4 +1.0 M Na_2S.

Stabilized CdS Photoanode. From the results in Figs. 8 and 10, we suggest that a stable photocurrent flows at a high concentration of S^{2-} added in the electrolyte solution where the ratio of the competitive oxidation of S^{2-} is almost 100% even if under the high intensity (*ca.* 1×10^{17} photon/cm^2 s) of illumination.

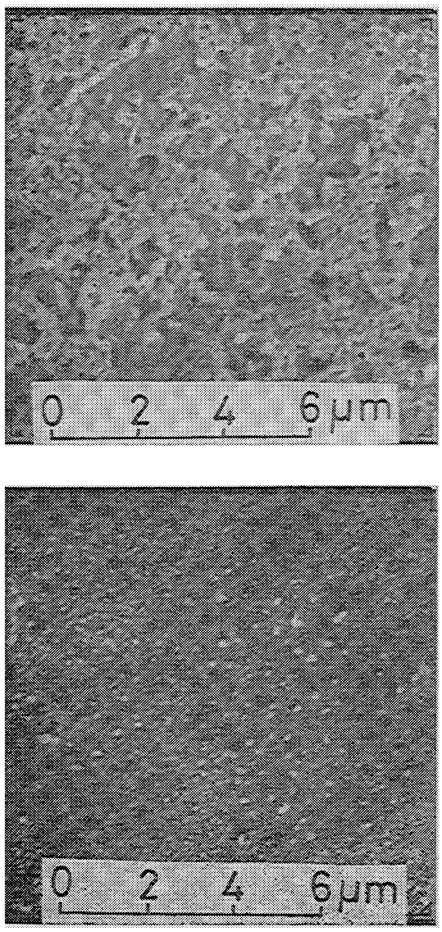

Fig.12. SEM photographs of the CdS electrode surface.
(A) After 2 h photoelectrolysis in 0.2 M Na_2SO_4.
(B) After 2 h photoelectrolysis in 0.2 M Na_2SO_4+ 0.5 M Na_2S.

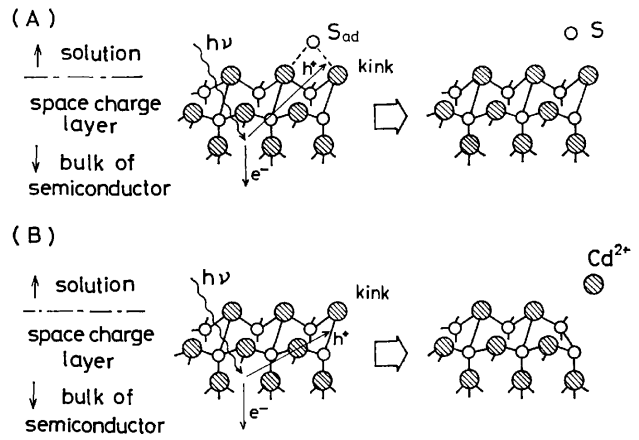

Fig. 13. Schematic diagram of CdS photoanode reactions.
(A) Stabilization of CdS surface with sulfide ions in solution, (B) Oxidation dissolution of CdS surface without sulfide ions in solution.

We show the photocurrent-time characteristics for the electrolyte solution with and without 1.0 M Na_2S in Fig. 11. In the absence of a reducing agent (S^{2-}) in the electrolyte solution, the photocurrent (curve 1) at CdS photoanode usually shows an abrupt decay with time. This phenomenon is attributed to the deposition of sulfur, which acts as a light filter on the electrode surface, produced according to reaction (4). In the presence of a reducing agent (S^{2-}) the photocurrent continues to flow remarkably stably for a long period, as expected above, hence the stabilization of the electrode surface is attained.

The stabilization of CdS photoanode can be visualised by comparing the scanning electron microscopy (SEM) pictures of a CdS surface after photoelectrolysis for 2 hours with (Fig. 12 (B)) and without (Fig. 12(A)) 0.5 M S^{2-} in the electrolyte solution. A rough reticulate structure in (A) might reflect the deposition of sulfur produced by the dissolution reaction (4). The photoanodic reactions at the CdS electrode can be described schematically as shown in Fig. 13, where kink denotes an imperfection site as the example of the active site.

Conclusion

We show in Fig. 14 the schematic diagram of the correlation of the energy levels between a semiconductor (CdS) electrode and reducing agents in the electrolyte solution. E_D in the figure denotes the redox potential of CdS calculated from the thermodynamic data according to the following equation[40]

$$CdS \rightleftharpoons Cd^{2+} + S + 2e^-, \quad E_D = 0.08 \text{ (V } vs. \text{ SCE)}. \quad (14)$$

Concerning the competition ratios[14] of various reducing agents and the values of the reorganization energy (0.7—1.8 eV)[41] of them the charge transfer across the interface is considered to proceed in the participation of some surface energy level.[42]

We propose the schemes in Fig. 15 for the elucidation of the current-potential behaviour of CdS photoanode in contact with an electrolyte solution containing

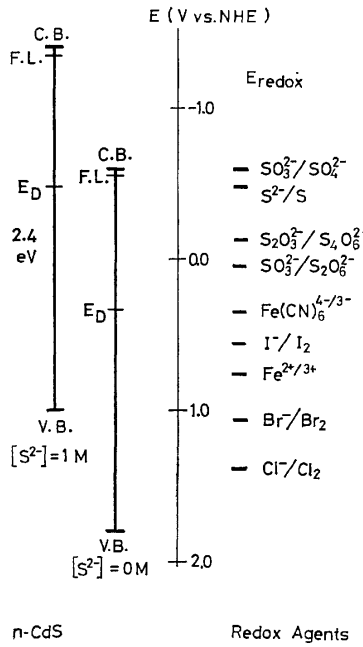

Fig. 14. Schematic diagram of the correlation of the energy levels between a semiconductor (CdS) electrode and reducing agents in the electrolyte solution.

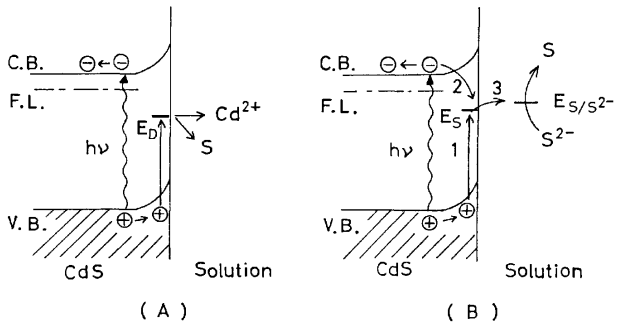

Fig. 15. Schematic diagram of the charge transfer across CdS/electrolyte solution interface.
(A) Dissolution of the CdS electrode surface. (B) Competition between dissolution of the CdS electrode surface and oxidation of S^{2-}.

S^{2-}. Without S^{2-} in solution CdS photoanode can be oxidized by photogenerated holes as shown schematically in Fig. 15(A). In the scheme of Fig. 15(B) it is postulated that a surface state, capable of acting as the recombination center for the photoelectron hole pairs, is induced upon adsorption of S^{2-} on the CdS surface. At potentials differing little from the falt-band potential, both the conduction electron (path 2) and hole (path 1) are easily transferred to such a recombination center. A part of the transferred holes, not undergoing recombination, can oxidize S^{2-} by the path 3 at the rate controlled by the diffusion of S^{2-} to the electrode surface (first wave). When the anodic polarization exceeds a critical value, the probability of the path 2 becomes negligible.[43] At this stage, the excess holes begin to oxidize the electrode itself causing dissolution (second wave), since the rate of oxidation of S^{2-} (path 3) is diffusionally controlled. When the electrolyte solution contains excess sulfide

ions against the incident photons the oxidation of a sulfide ion precedes the dissolution of CdS photoanode through the above competitive reaction scheme, which can elucidate the stabilization of the CdS photoanode.[44]

However, the concrete characteristics of the surface state have not been well known, and are currently under investigation in this laboratory.

References

1) A. Fujishima and K. Honda, *Nature*, **238**, 37 (1972).
2) A. Fujishima, K. Kohayakawa, and K. Honda, *J. Electrochem. Soc.*, **122**, 1487 (1975).
3) H. Yoneyama, H. Sakamoto, and H. Tamura, *Electrochem. Acta*, **20**, 341 (1975).
4) K. L. Hardee and A. J. Bard, *J. Electrochem. Soc.*, **123**, 1027 (1976).
5) K. L. Hardee and A. J. Bard, *J. Electrochem. Soc.*, **124**, 215 (1977).
6) A. J. Nozik, *Nature*, **257**, 383 (1975).
7) N. S. Wrighton, D. S. Ginley, P. T. Wolczanski, A. B. Ellis, D. L. Morse, and A. Linz, *Proc. Natl. Acad. Sci. U.S.A.*, **72**, 1518 (1975).
8) G. Hodes, D. Cahen, and J. Manassen, *Nature*, **260**, 312 (1976).
9) J. O'M. Bockris and K. Uosaki, *J. Electrochem. Soc.*, **124**, 98 (1977).
10) R. H. Wilson, *J. Appl. Phys.*, **48**, 4292 (1977).
11) T. Watanabe, A. Fujishima, O. Tatsuoki, and K. Honda, *Bull. Chem. Soc. Jpn.*, **49**, 355 (1976).
12) J. G. Mavroides, J. A. Kafalas, and D. F. Koleser, *Appl. Phys. Lett.*, **28**, 241 (1976).
13) R. K. Quinn, R. D. Nasby, and R. J. Burghman, *Res. Bull.*, **11**, 1011 (1976).
14) Y. Nakato, T. Ohnishi, and H. Tsubomura, *Chem. Lett.*, **1975**, 883.
15) T. Inoue, T. Watanabe, A. Fujishima, K. Honda, and K. Kohayakawa, *J. Electrochem. Soc.*, **124**, 719 (1977).
16) H. Minoura, M. Tsuiki, and T. Oki, *Ber. Bunsenges. Phys. Chem.*, **81**, 588 (1977).
17) H. Morisaki, M. Haraya, and K. Yazawa, *Appl. Phys. Lett.*, **30**, 7 (1977).
18) H. Gerischer and J. Gobrecht, *Ber. Bunsenges. Phys. Chem.*, **80**, 327 (1976).
19) A. B. Ellis, S. W. Kaiser, J. M. Bolts, and M. S. Wrighton, *J. Am. Chem. Soc.*, **99**, 2839 (1977).
20) R. Memming, *Ber. Bunsenges. Phys. Chem.*, **81**, 732 (1977).
21) B. Miller and A. Heller, *Nature*, **262**, 680 (1976).
22) J. Manassen and G. Hodes, *J. Electrochem. Soc.*, **124**, 583 (1977).
23) J. O'M. Bockris and K. Uosaki, *J. Electrochem. Soc.*, **124**, 1348 (1977).
24) H. Tributsch, *Ber. Bunsenges. Phys. Chem.*, **82**, 169 (1978).
25) T. Inoue, T. Watanabe, A. Fujishima, and K. Honda, *Chem. Lett.*, **1977**, 1073.
26) R. Williams, *J. Chem. Phys.*, **32**, 1505 (1960).
27) D. M. Kolb and H. Gerischer, *Electrochem. Acta*, **18**, 987 (1973).
28) J. H. Carey and B. G. Oliver, *Nature*, **259**, 554 (1976).
29) A. Fujishima, E. Sugiyama, and K. Honda, *Bull. Chem. Soc. Jpn.*, **44**, 304 (1971).
30) T. Watanabe, A. Fujishima, and K. Honda, *Chem. Lett.*, **1974**, 897.
31) H. Gerischer, in "Physical Chemistry: An Advanced Treatise," ed by H. Eyring *et al.*, Academic Press, New York (1970). pp. 467—473.
32) H. Minoura, T. Watanabe, T. Oki, and M. Tsuiki, *Jpn. J. Appl. Phys.*, **16**, 865 (1977).
33) A. Fujishima, A. Sakamoto, and K. Honda, *Seisan Kenkyu*, **21**, 450 (1969).
34) H. Gerischer, in "Physical Chemistry: An Advanced Treatise," ed by H. Eyring *et al.*, Academic Press, New York (1970), pp. 473—478.
35) H. Minoura and M. Tsuiki, *Nippon Kagaku Kaishi*, **1977**, 487.
36) H. Minoura and M. Tsuiki, *Electrochem. Acta*, **23**, 1377 (1978).
37) J. L. Desplat, *J. Appl. Phys.*, **47**, 5102 (1976).
38) V. G. Levich, "Physicochemical Hydrodynamics," Prentice-Hall, Englewood Cliffs, N. J. (1962), pp. 60—72.
39) R. H. Wilson, in a private communication and an abstract at the Electrochemical Society meeting in May, 1978.
40) A. J. Bard and M. S. Wrighton, *J. Electrochem. Soc.*, **124**, 1706 (1977).
41) J. M. Hale, in "Reactions of Molecules at Electrodes," ed by N. S. Hush, Wiley-Interscience, London (1971), pp. 229—257.
42) S. N. Frank and A. J. Bard, *J. Am. Chem. Soc.*, **97**, 7427 (1975).
43) P. A. Kohl and A. J. Bard, *J. Am. Chem. Soc.*, **99**, 7531 (1977).
44) A. Fujishima, T. Inoue, T. Watanabe, and K. Honda, *Chem. Lett.*, **1978**, 357.
45) T. Inoue, T. Watanabe, A. Fujishima, and K. Honda, partly presented in "Semiconductor-Liquid Junction Solar Cells: Proceedings of a Conference on the Electrochemistry and Physics of Semiconductor-Liquid Interfaces under Illumination," 77-3, ed by A. Heller, Electrochem. Soc., Princeton (1977), pp. 210—221.

Study of Metal–Polycarboxylate Complexes Employing Ion-selective Electrodes. III. Complex Formation between Maleic Acid Copolymers and Bivalent Transition Metal Ions

Fumitaka YAMASHITA,* Tsuyoshi KOMATSU, and Tsurutaro NAKAGAWA
Department of Polymer Science, Faculty of Science, Hokkaido University, Sapporo 060
(Received July 27, 1978)

The complex formation of bivalent transition metal ions, Mn(II), Co(II), Ni(II), Cu(II), and Zn(II), with copoly(maleic acid–ethylene) and copoly(maleic acid–styrene) in aqueous solution was studied by potentiometric titration at 25 °C and the ionic strength of 0.1. The systems containing copper(II) ions were investigated by potentiometry employing the copper(II) ion-selective electrode. The titration curves of the bivalent metal–copoly(maleic acid–ethylene) systems were situated in a lower pH region than in the absence of the metal ions. The complex formed involves two carboxylate groups: primary and secondary. The equilibrium constant of the copper(II) complex was estimated to be $10^{-2.6}$. In copoly(maleic acid–styrene) systems, however, the titration curves in the absence and presence of bivalent metal ions overlapped partly in the first neutralization step. From the potentiometric results employing the ion-selective electrode, it was observed that the concentrations of copper(II) ions decrease slightly in the region of overlap. This anomalous behavior is due to the acid dissociation influenced by the conformational transition, including the effect of the side groups of the polymers.

The study of solution properties of the aqueous polyelectrolytes containing various counterions has been well established, especially in the cases of poly(acrylic acid) and poly(methacrylic acid), from the viewpoints of the counterion binding and the conformational transition of polyelectrolytes. Since the various hydrophobic residues of maleic acid copolymers can be relatively easily introduced in polymer chains as comonomers, they are of interest in connection with the short range interaction of the side groups and have been extensively studied.

In addition, the succinic acid residues derived from maleic anhydride units are also of interest as a polymeric ligand consisting of carboxyl pairs, because the acid dissociation constants of these carboxyl groups are found to be quite different. The interaction and complex formation with metal ions, especially with bivalent ones, are important and have been studied by some workers.[1–5]

In our previous papers,[6,7] the systems consisting of copper(II) ions and poly(itaconic acid), whose monomer unit has two carboxyl groups, have been studied by potentiometric titration employing the copper(II) ion-selective electrode. It was concluded that bis(carboxylato)copper(II) complexes are formed and that one of chelating carboxylate groups is the secondary carboxyl group, even in the first neutralization step. In a recent paper,[8] the systems of maleic acid–styrene copolymer were studied and the anomalous overlap of the titration curves in the absence and presence of the bivalent metal ions was observed.

In the present paper, the overlap in maleic acid–styrene copolymer systems was investigated by potentiometry employing an ion-selective electrode, and the maleic acid–ethylene copolymer, in which the hydrophobic side groups are absent, was studied for comparison.

Experimental

Materials. Copoly(maleic acid–ethylene), MAEt, was obtained by hydrolysis of the alternating 1 : 1 copolymer of maleic anhydride with ethylene; this was Monsanto Chemical Co.'s Grade 31. Its characterization was outlined in Technical Bulletin I-261 of the company.

Copoly(maleicanhydride–styrene) was prepared and reprecipitated by the procedures of Ohno and coworkers,[9] and the copolymer was hydrolyzed to obtain copoly(maleic acid–styrene), MASt, in water at 60 °C for 24 h. The aqueous solution of MASt was purified by dialysis using cellophane tubing. The 1 : 1 composition of comonomers was confirmed by elemental analysis, and the molecular weight was found to be 10^5 by viscometry.[9]

The other chemicals and bivalent metal nitrate salts used were guaranteed reagent grade.

Potentiometric Titration. The pH measurements were performed by use of a Yokogawa Model KPH-51A pH meter equipped with Toadenpa Model HG-4005 galss and Model HC-2005 calomel electrodes. The titrations were carried out with about 0.1 mol/l aqueous solution of carbonate-free NaOH at 25±0.05 °C and ionic strength of 0.1(KNO_3) under nitrogen atmosphere.

The activity measurements of free copper(II) ions were carried out by use of an Orion Model 801A digital ion meter equipped with Beckman Model 39612 Cupric and Horiba Model 2010-05T calomel electrodes. The corrections and determination of the concentrations of copper(II) ions were carried out with the calibration curve obtained by potentiometric measurements of the systems free from polymeric ligands.

Each system measured consists of about 5×10^{-3} monomol/l polyacid, 1×10^{-1} mol/l KNO_3, and about 1×10^{-3} mol/l bivalent metal ions.

All the potentiometric measurements were operated in the pH region less than 6.00 because of the precision of pH titration of this weak polyacid and the formation of bivalent metal hydroxides.

Results and Discussion

Titration Behaviors of Copolymers without Complexing Metal Ions. The apparent dissociation constant $pK_{1,app}$ of the primary carboxyl groups is given as

$$pK_{1,app} = pH - \log \alpha_1/(1-\alpha_1),$$

where α_1 is the degree of dissociation of the primary carboxyl groups. The α_1 dependences of $pK_{1,app}$ of MAEt and MASt are shown in Fig. 1. The shapes

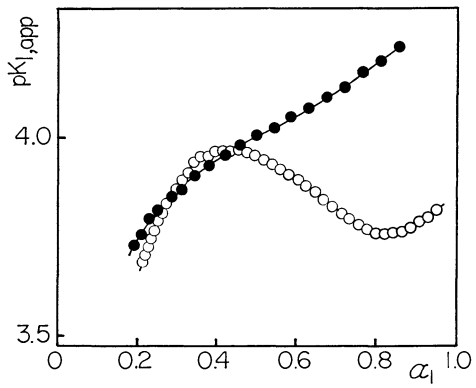

Fig. 1. Apparent dissociation constant, $pK_{1,app}$, as a function of α_1 for MAEt and MASt at the ionic strength of 0.1(KNO_3): (●) MAEt(0.00498 monomol/l); (○) MASt(0.00432 monomol/l).

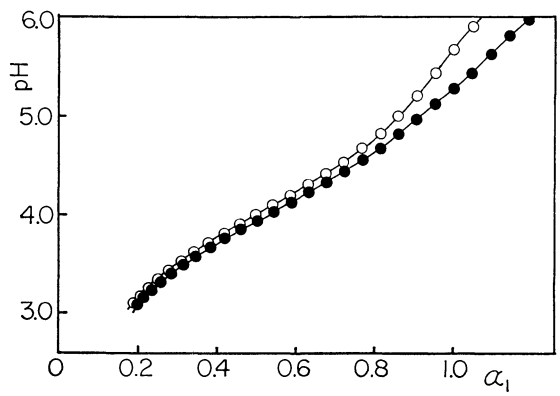

Fig. 2. Titration curves of MAEt(0.00498 monomol/l) in (○) the absence and (●) the presence of zinc(II) ions(1×10^{-3} mol/l $Zn(NO_3)_2$) at the ionic strength of 0.1(KNO_3).

of these curves are similar to those of the same samples observed by some other authors,[9,10] and small discrepancies of $pK_{1,app}$ values may correspond to the difference of concentrations of neutral salts added.

The values of $pK_{1,app}$ of MAEt are linearly dependent on α_1, which shows that the acid dissociation is influenced only by the change of charge density on polyions and that interaction of side groups is absent, as can be concluded from its chemical structure. And the fact that the slope of the $pK_{1,app}$ curve is smaller than that of other homopolymers confirms the dependence on charge density.

In the case of MASt, an anomalous dependence of $pK_{1,app}$ on α_1, the so-called pH-induced conformational transition, is observed. This anomaly was discussed in detail by Ohno and coworkers,[9,11,12] who interpret this anomalous behavior as due to the conformational transition from the compact form, which is stabilized by the hydrophobic interaction between the phenyl groups, to the extended coil form of the copolymer chain. This interpretation is probably reasonable, but it is strange that the decrease of $pK_{1,app}$ with increasing in α_1 is apparently observed in the range from 0.4 to 0.8. This behavior is also observed in the case of poly(methacrylic acid). Such a tendency implies that there occurs some promotion of dissociation with α_1, which is generally improbable. In this dissociation range, the fact that the polymer chain extends suddenly was observed in the viscometric data by Ohno. In such a case, the hydrophobic interaction may decrease, and the local effective dielectric constant may vary; its effect may be reflected in the decrease of the acid dissociation constant, although this point must be confirmed by other experiments.

Titration Behaviors of Systems Containing Bivalent Metal Ions. The titration curves of MAEt in the absence and presence of zinc(II) ions are shown in Fig. 2; the cases of the other bivalent metal ions are similar to this. When complex formation occurs, it is generally observed that the titration curves in the presence of transition metal ions are situated in a lower pH region than in the case of such simple salts as the alkali metal salts. It can be seen from Fig. 2 that a complex is formed between the carboxylate groups of MAEt and zinc(II) ions. In the cases of the other metal ions, the same result was obtained.

Furthermore, the first equivalence point of the titration curve in the presence of the metal ions is observed a little beyond 1.0 of α_1. As is discussed in the previous papers,[7,8] the point at $\alpha_1=1$ corresponds to the end of the titration of the primary carboxyl groups. It is considered that the deviation of the equivalence point from $\alpha_1=1.0$ results from the complex formation including the secondary carboxyl groups.

Thus, it can be concluded that the complex formed involves two carboxylate groups in the same succinic unit : one is a primary carboxylate group and the other a secondary one, even in the first neutralization step; this conclusion agrees with those of Felber[2,3] and Delben.[4,5]

The titration curves of MASt in the absence and presence of zinc(II) ions are shown in Fig. 3. The curves for the other metal ions are similar to this figure, except those of copper(II) ions. Around at $\alpha_1=1.0$, behaviors like those of MAEt systems are observed: there is an apparent shift of the first equivalence point. Thus it can be concluded that bis(carboxylato)zinc(II) complexes which have both the primary and secondary

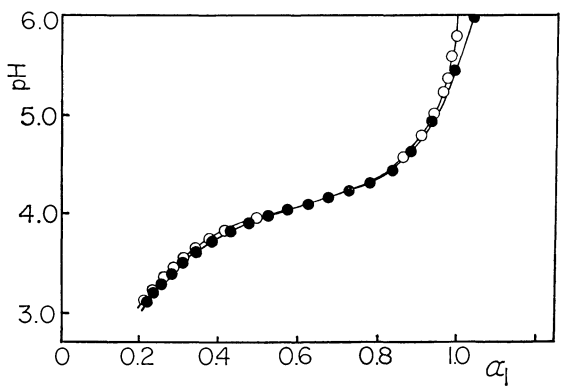

Fig. 3. Titration curves of MASt(0.00432 monomol/l) in (○) the absence and (●) the presence of zinc(II) ions (1×10^{-3} mol/l $Zn(NO_3)_2$) at the ionic strength of 0.1(KNO_3).

carboxylate groups are formed.

In the neighborhood of $\alpha_1=0.7$, a behavior quite different from the case of MAEt is observed; this is shown in Fig. 3. In this region of α_1, the titration curves of MASt in the absence and presence of the metal ions overlap partly, which suggests that the carboxylate groups are released from the metal ions by some effect. However, it is well known that the carboxylate groups produce relatively stable complexes with bivalent transition metal ions. In order to elucidate this point, the results of potentiometry employing the ion-selective electrode were examined.

Titrations Employing a Copper(II) Ion-selective Electrode. Since there is some complexity in the response of this electrode,[6,13] the reproducibility and stability of the response were confirmed again in the present study by measurements of the solutions containing copper(II) ions of known concentrations under similar conditions without the added copolymer.

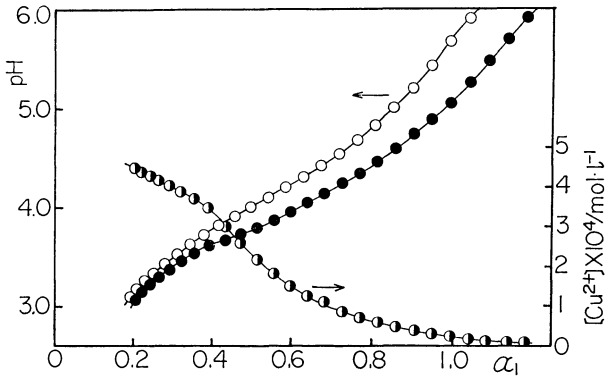

Fig. 4. Dependence of concentration of free copper(II) ions on α_1 (◑), and titration curves of MAEt (0.00498 monomol/l) in (○) the absence and (●) the presence of copper(II) ions (5×10^{-4} mol/l $Cu(NO_3)_2$) at the ionic strength of 0.1(KNO_3).

In Fig. 4, the titration curves of MAEt in the absence and presence of copper(II) ions and the dependence of the concentrations of free copper(II) ions, $[Cu^{2+}]$, on α_1 are shown. In this figure, the initial concentration of copper(II) ions is 5.00×10^{-4} mol/l. The α_1 dependence of the pH difference, ΔpH, between the values in the absence and presence of copper(II) ions at the same value of α_1 corresponds well to the dependence of $[Cu^{2+}]$. This fact shows that the complex formation proceeds along with the increase in α_1. Relatively stable complexes are formed in the α_1 range above 0.35. But when the total concentration of copper(II) ions added is relatively high: more than 10^{-3} mol/l, it was confirmed that the complexes are formed from the first titration step.

Just as in MAEt–zinc(II) systems or poly(itaconic acid)–copper(II) systems,[6] it can be concluded that relatively stable complexes are formed between MAEt and copper(II) ions and that the complex involves both the primary and secondary carboxylate groups in the same succinic acid unit.

In Fig. 5, the dependences of pH and concentrations of free copper(II) ions on α_1 in the case of MASt are

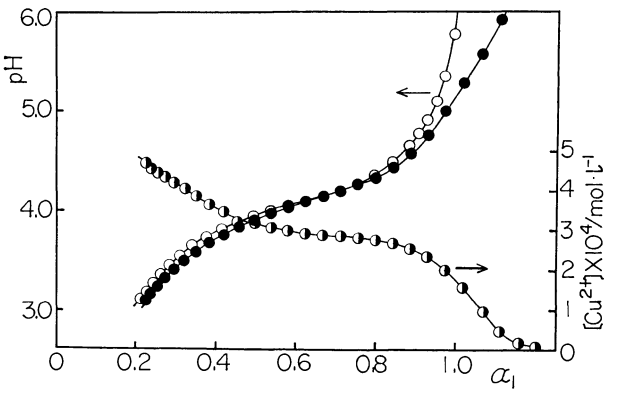

Fig. 5. Dependence of concentration of free copper(II) ions on α_1 (◑), and titration curves of MASt (0.00432 monomol/l) in (○) the absence and (●) the presence of copper(II) ions (5×10^{-4} mol/l $Cu(NO_3)_2$) at the ionic strength of 0.1(KNO_3).

shown. The anomalous overlap of the titration curves, as in MASt–zinc(II) systems, is observed in the α_1 ranging from 0.6 to 0.8, which shows that the complexes once formed are broken. In the same α_1 range, on the other hand, the concentration of free copper(II) ions decreases slightly, which shows that the complexes are not broken and do not change to free copper(II) ions. These two results are incompatible with each other. Considering that rather stable complexes are generally formed between the carboxylate groups of the other polyelectrolytes and copper(II) ions, and that the concentration of carboxylate groups as a ligand increases with α_1, it is difficult to conclude that the complexes once formed may break up.

Thus, one of causes of the anomalous overlap may lie in the character of the dissociation equilibrium of MASt, because this overlap corresponds to the α_1 range where the values of $pK_{1,app}$ are decreasing. The equilibrium constant of the complex formation can be described as the products of the acid dissociation constant, K_a, and the stability constant, β, of the complex; for example:

$$B_2=\frac{[MA_2][H^+]^2}{[M^{2+}][HA]^2}=\frac{[MA_2]}{[M^{2+}][A^-]^2}\frac{[A^-]^2[H^+]^2}{[HA]^2}$$
$$=\beta_2\times(K_a)^2.$$

If the equilibrium constant is only slightly dependent on α_1, the value of β decreases with the decrease in pK_a. In the neighborhood of $\alpha_1=0.7$, where the overlap occurs, such a relation of each constant can be assumed, and the concentration of the complexes scarcely increases, because of the cancelling between the decrease of β and the increase of the concentration of the free carboxylate groups. Such a discussion interprets the variation of the concentration of free copper(II) ions. In order to explain the anomalous overlap of the titration curves sufficiently, it is necessary to have more detailed knowledge of the conformational transition not only of the MASt chain itself but also of the chain which contains the complexing metal ions.

Stability of Complexes. The stability of the

metal complex can be compared by use of the pH difference, ΔpH, between the values in the absence and presence of the bivalent metal ions at the same metal concentration and at the same degree of dissociation. In Table 1, ΔpH of MAEt systems where the initial concentration of each metal ion added is about 1×10^{-3} mol/l are given. The copper(II) complex is much more stable than the others, and the stabilities of each metal complex are roughly in the order of Cu(II)≫Zn(II)>Ni(II)≃Co(II)≃Mn(II). This result agrees approximately with the results for the same systems of Felber[2] and Delben[5] and those for the poly(methacrylic acid) of Sunahara.[14]

In Table 2, the values of ΔpH of MASt systems are given. The stabilities of the MASt complex are in the order of Cu(II)≫Zn(II)≃Ni(II)≃Co(II)>Mn(II). These results are reasonable, except for manganese(II).

TABLE 1. EFFECT OF BIVALENT TRANSITION METAL IONS ON pH TITRATION OF MAEt (polymer concentration= 0.00498 monomol/l) AT THE IONIC STRENGTH OF 0.1 (KNO_3)

α_1	Blank pH	−ΔpH				
		Mn-(II)	Co-(II)	Ni-(II)	Zn-(II)	Cu-(II)
0.0						
0.1						
0.2						
0.3	3.50	0.04	0.03	0.04	0.04	0.17
0.4	3.77	0.05	0.04	0.06	0.06	0.33
0.5	4.02	0.06	0.04	0.06	0.07	0.47
0.6	4.24	0.06	0.05	0.07	0.08	0.54
0.7	4.49	0.08	0.07	0.08	0.10	0.62
0.8	4.79	0.10	0.11	0.11	0.14	0.70
0.9	5.19	0.18	0.20	0.20	0.24	0.84
1.0	5.6_9	0.2_9	0.3_0	0.3_0	0.4_0	1.0_0

TABLE 2. EFFECT OF BIVALENT TRANSITION METAL IONS ON pH TITRATION OF MASt (polymer concentration= 0.00432 monomol/l) AT THE IONIC STRENGTH OF 0.1 (KNO_3)

α_1	Blank pH	−ΔpH				
		Mn-(II)	Co-(II)	Ni-(II)	Zn-(II)	Cu-(II)
0.0						
0.1						
0.2						
0.3	3.51	0.01	0.03	0.05	0.05	0.17
0.4	3.79	0.01	0.02	0.03	0.03	0.16
0.5	3.97	0.02	0.02	0.03	0.03	0.15
0.6	4.08	0.01	0.01	0.02	0.02	0.06
0.7	4.19	0	0	0	0	0.03
0.8	4.36	0	0	0	0.01	0.02
0.9	4.74	0	0.03	0.06	0.04	0.17
1.0	6.0_2	0.2_4	0.3_7	0.4_3	0.4_7	1.1_3

The stability or formation constant of the complex must be estimated for detailed comparison. In the case of the MAEt–copper(II) complex, since the concentration of copper(II) ions can be obtained from potentiometry employing an ion-selective electrode, and since $pK_{1,app}$ of MAEt changes relatively linearly with α_1, the formation constant B_2 can be estimated by the scheme proposed in the previous paper.[6] Here, the constant B_2 is defined as follows:

$$Cu^{2+} + 2HA \rightleftharpoons CuA_2 + 2H^+,\ B_2 = \frac{[CuA_2][H^+]^2}{[Cu^{2+}][HA]^2}.$$

In the α_1 range less than 0.65, the real average coordination number $\bar{n}_x$ of the copper(II)–MAEt system is equal to about two, and each value of $\log B_2$ evaluated from titration is constant and equal to −2.6.

On the other hand, $pK_{1,app}$ of MASt shows a complicated dependence on α_1, so that the reference plot method proposed by Mandel and Leyte[15] cannot be applied. But the value of $\log B_2$ of the copper(II) complex was roughly estimated to be −4.

Thus, it is concluded that the bis(carboxylato) bivalent transition metal complex is formed, in fact, in the first neutralization step of MAEt and MASt, and that the copper(II) complex is the most stable one.

The authors would like to thank Mitsubishi Monsanto Chem. Co., Ltd. and Monsanto Chem. Co. in U. S. A. for a generous supply of MAEt sample.

References

1) H. Morawetz, A. M. Kotlior, and H. Mark, *J. Phys. Chem.*, **58**, 619(1954).
2) B. J. Felber, E. M. Hodnett, and N. Purdie, *J. Phys. Chem.*, **72**, 2496 (1968).
3) B. J. Felber and N. Purdie, *J. Phys. Chem.*, **75**, 1136 (1971).
4) V. Crescenzi, F. Delben, S. Paoletti, and J. Skerjanc, *J. Phys. Chem.*, **78**, 607(1974).
5) F. Delben and S. Paoletti, *J. Phys. Chem.*, **78** 1486 (1974).
6) Part I: F. Yamashita, T. Komatsu, and T. Nakagawa, *Bull. Chem. Soc. Jpn.*, **49**, 2073 (1976).
7) F. Yamashita, T. Komatsu, and T. Nakagawa, *Rept. Probr. Polym. Phys. Jpn*, **20**, 23(1977).
8) F. Yamashita, T. Komatsu, and T. Nakagawa, *Chem. Lett.*, **1978**, 1173.
9) N. Ohno, K. Nitta, S. Makino, and S. Sugai, *J. Polym. Sci., Polym. Phys. Ed.*, **11**, 413 (1973).
10) P. L. Dubin and U. P. Strauss, *J. Phys. Chem.*, **74**, 2842 (1970).
11) T. Okuda, N. Ohno, K. Nitta, and S. Sugai, *J. Polym. Sci., Polym. Phys. Ed.*, **16**, 749 (1977).
12) N. Ohno, T. Okuda, K. Nitta, and S. Sugai, *J. Polym. Sci., Polym. Phys. Ed.*, **16**, 513 (1978).
13) Part II: F. Yamashita, T. Komatsu, and T. Nakagawa, *Bull. Chem. Soc. Jpn.*, **52**, 30(1978).
14) M. Sunahara, N. Muto, T. Komatsu, and T. Nakagawa, *Nippon Kagaku Kaishi*, **1974**, 2414.
15) M. Mandel and J. C. Leyte, *J. Polym. Sci., Part A-2* 2883 (1964).

Perturbation Calculation of Spin Densities in π-Electron Radicals

Hidekazu HAMANO* and Hiroshi KONDO
Department of Chemistry, Ibaraki University, Mito 310
(Received July 31, 1978)

The unrestricted Hartree-Fock perturbation technique was applied to the calculation of spin densities in many hydrocarbon radicals. The method is similar to that of McLachlan but contains partly the SCF and projection procedures. The results agree with the more rigorous SCF ones.

Spin density distributions in conjugated radicals and ions can be successfully explained by the simplified unrestricted McLachlan method.[1] Though approximate UHF functions without projection are used, the spin densities thus obtained are in good agreement with experiment. A discussion on this has been given by Snyder and Amos.[2] They concluded that this might be caused by compensating errors, the use of a single SCF iteration and the failure to project or annihilate. The McLachlan method does not appear to be theoretically well founded. Modified versions of the method have been presented by many authors[3–9] without due attention to theory.

This paper presents an alternative form of the McLachlan method within the perturbed Hückel approximation. Since our approach still contains the SCF and projection procedures, the spin densities in π-electron radicals and ions calculated can be compared with the results obtained by the more rigorous UHF method.

Theory

Let us consider a doublet ground state for a conjugated radical. According to Brickstock and Pople[9] the SCF π-electron Hamiltonian matrix elements are given by

$$\left.\begin{aligned} F^{\alpha(\beta)}_{\mu\mu} &= U_{\mu\mu} + P^{\beta(\alpha)}_{\mu\mu}\gamma_{\mu\mu} + \sum_{\nu\neq\mu}(P_{\nu\nu}-Z_\nu)\gamma_{\mu\nu} \\ F^{\alpha(\beta)}_{\mu\nu} &= \beta_{\mu\nu} - P^{\alpha(\beta)}_{\mu\nu}\gamma_{\mu\nu} \qquad (\mu\neq\nu) \end{aligned}\right\} \quad (1)$$

where

$$P^{\alpha(\beta)}_{\mu\nu} = \sum_{i}^{\text{occ.}} C^{\alpha(\beta)}_{i\mu}C^{\alpha(\beta)}_{i\nu}$$

$$P_{\mu\nu} = P^{\alpha}_{\mu\nu} + P^{\beta}_{\mu\nu}$$

and the superscripts α and β refer to α and β electrons respectively. Throughout this paper, Greek suffixes will be used for atomic orbitals and italics for molecular orbitals. Let us take the arithmetical mean values of the matrix elements given by Eq. 1 as

$$\left.\begin{aligned} \bar{F}_{\mu\mu} &= \frac{1}{2}(F^{\alpha}_{\mu\mu}+F^{\beta}_{\mu\mu}) = U_{\mu\mu} + \frac{1}{2}P_{\mu\mu}\gamma_{\mu\mu} \\ &\quad + \sum_{\nu\neq\mu}(P_{\nu\nu}-Z_\nu)\gamma_{\mu\nu} \\ \bar{F}_{\mu\nu} &= \frac{1}{2}(F^{\alpha}_{\mu\nu}+F^{\beta}_{\mu\nu}) = \beta_{\mu\nu} - \frac{1}{2}P_{\mu\nu}\gamma_{\mu\nu} \\ &\quad (\mu\neq\nu). \end{aligned}\right\} \quad (2)$$

These matrix elements are just those defined by Longuet-Higgins and Pople.[10] From Eqs. 1 and 2 we obtain

$$\left.\begin{aligned} \Delta F^{\alpha}_{\mu\nu} &= F^{\alpha}_{\mu\nu} - \bar{F}_{\mu\nu} = -\frac{1}{2}\rho_{\mu\nu}\gamma_{\mu\nu} \\ \Delta F^{\beta}_{\mu\nu} &= F^{\beta}_{\mu\nu} - \bar{F}_{\mu\nu} = \frac{1}{2}\rho_{\mu\nu}\gamma_{\mu\nu} \end{aligned}\right\} \quad (3)$$

where

$$\rho_{\mu\nu} = P^{\alpha}_{\mu\nu} - P^{\beta}_{\mu\nu}. \quad (4)$$

Equation 3 suggests that the approximate restricted Hartree-Fock method of Longuet-Higgins and Pople[10] is a good starting point for perturbation treatment of the UHF method.

We are now in a position to formulate the spin density by means of perturbation theory. Equation 4 is modified as

$$\begin{aligned} \rho_{\mu\nu} &= (\overline{P^{\alpha}_{\mu\nu}}-\overline{P^{\beta}_{\mu\nu}}) + (\Delta P^{\alpha}_{\mu\nu}-\Delta P^{\beta}_{\mu\nu}) \\ &= \rho^{\circ}_{\mu\nu} + (\Delta P^{\alpha}_{\mu\nu}-\Delta P^{\beta}_{\mu\nu}) \end{aligned} \quad (5)$$

where

$$\overline{P^{\alpha}_{\mu\nu}} - \overline{P^{\beta}_{\mu\nu}} = C_{0\mu}C_{0\nu} = \rho^{\circ}_{\mu\nu}$$

$$\Delta P^{\alpha(\beta)}_{\mu\nu} = P^{\alpha(\beta)}_{\mu\nu} - \overline{P^{\alpha(\beta)}_{\mu\nu}}$$

$\overline{P^{\alpha(\beta)}_{\mu\nu}}$ and $\rho^{\circ}_{\mu\nu}$ stand for the corresponding quantities of $P^{\alpha(\beta)}_{\mu\nu}$ and $\rho_{\mu\nu}$, respectively, within the RHF scheme. We can put

$$\Delta P^{\alpha(\beta)}_{\mu\nu} = \sum_{\kappa\lambda}\Pi^{\alpha(\beta)}_{\mu\nu,\kappa\lambda}\Delta F^{\alpha(\beta)}_{\kappa\lambda} \quad (6)$$

where the polarizability $\Pi^{\alpha(\beta)}_{\mu\nu,\kappa\lambda}$ can be defined as

$$\Pi^{\alpha(\beta)}_{\mu\nu,\kappa\lambda} = \partial\overline{P^{\alpha(\beta)}_{\mu\nu}}/\partial\bar{F}_{\kappa\lambda}.$$

Since

$$\overline{P^{\alpha}_{\mu\nu}} + \overline{P^{\beta}_{\mu\nu}} = \overline{P_{\mu\nu}}$$

we obtain

$$\partial\overline{P_{\mu\nu}}/\partial\overline{F_{\kappa\lambda}} = \Pi^{\alpha}_{\mu\nu,\kappa\lambda} + \Pi^{\beta}_{\mu\nu,\kappa\lambda} \equiv \Pi_{\mu\nu,\kappa\lambda}. \quad (7)$$

Using Eqs. 3, 6, and 7, the resulting expression for the spin density matrix elements is reduced to

$$\rho_{\mu\nu} = \rho^{\circ}_{\mu\nu} - \frac{1}{2}\sum\Pi_{\mu\nu,\kappa\lambda}\rho_{\kappa\lambda}\gamma_{\kappa\lambda}. \quad (8)$$

If we restrict ourselves to the consideration of atom spin densities only, Eq. 8 becomes

$$\rho_{\mu\mu} = \rho^{\circ}_{\mu\mu} - \frac{1}{2}\sum_{\nu}\Pi_{\mu\mu,\nu\nu}\rho_{\nu\nu}\gamma_{\nu\nu}. \quad (9)$$

Since Hückel-type and SCF-type MO's do not differ significantly, according to McLachlan,[1] the Hückel-type MO's can be applied introducing a parameter λ. Thus Eq. 9 can be written as

$$\rho_{\mu\mu} = \rho^{\circ}_{\mu\mu} - \lambda\sum_{\nu}\Pi_{\mu\nu}\rho_{\nu\nu} \quad (10)$$

where the $\Pi_{\mu\nu}$ are dimensionless atom-atom polarizabilities. From Eq. 7, they are defined by

$$\Pi_{\mu\nu} = 4\sum_{i}^{\text{doubly occ.}}\sum_{j\neq i}^{\text{all}}\frac{C_{i\mu}C_{j\mu}C_{i\nu}C_{j\nu}}{\varepsilon_i-\varepsilon_j} + 2\sum_{k\neq 0}^{\text{all}}\frac{C_{0\mu}C_{k\mu}C_{0\nu}C_{k\nu}}{\varepsilon_0-\varepsilon_k} \quad (11)$$

or

$$\Pi_{\mu\nu} = \Pi^{(0)}_{\mu\nu} + \Pi^{(1)}_{\mu\nu} \tag{12}$$

where

$$\left.\begin{aligned}\Pi^{(0)}_{\mu\nu} &= 4 \sum_{i}^{\text{doubly occ.}} \sum_{j}^{\text{vac.}} \frac{C_{i\mu}C_{j\mu}C_{i\nu}C_{j\nu}}{\varepsilon_i - \varepsilon_j} \\ \Pi^{(1)}_{\mu\nu} &= \sum_{i}^{\text{doubly occ.}} \frac{C_{i\mu}C_{0\mu}C_{i\nu}C_{0\nu}}{\varepsilon_i - \varepsilon_0} + 2\sum_{j}^{\text{vac.}} \frac{C_{0\mu}C_{j\mu}C_{0\nu}C_{j\nu}}{\varepsilon_0 - \varepsilon_j}.\end{aligned}\right\} \tag{13}$$

Subscript 0 refers to the odd electron orbital. The polarizability defined by Eq. 11 or 12 is not that for closed shell molecules but is valid for radicals and ions. A similar definition of polarizability has also been proposed by Devolder,[8] but it was incorrect.[7] It is easy to show that the pairing theorem holds for alternant hydrocarbons, even if the polarizability defined above is used in our theory; that is, the spin density distributions in the anion and cation of an even alternant are expected to be identical.

Equation 10 is similar to the McLachlan formula,[1] but is in principle a simultaneous equation. The explicit solution of Eq. 10 can be written as

$$\rho^{\text{UHF}}_{\mu\mu} = \sum_{\nu} X_{\mu\nu}\rho^{\circ}_{\nu\nu} \tag{14}$$

where

$$X_{\mu\nu} = (-1)^{\mu+\nu}\Delta_{\mu\nu}/\Delta$$
$$\Delta = \det\{\delta_{\mu\nu} + \lambda\Pi_{\mu\nu}\}.$$

$\Delta_{\mu\nu}$ is the determinant obtained by striking out the μth column and νth row from the determinant Δ. The equation can be rewritten as

$$\rho^{\text{UHF}}_{\mu\mu} = \rho^{\circ}_{\mu\mu} - \lambda \sum \Pi^{\text{SCF}}_{\mu\nu}\rho^{\circ}_{\nu\nu} \tag{15}$$

where

$$\Pi^{\text{SCF}}_{\mu\nu} = (\delta_{\mu\nu} - X_{\mu\nu})/\lambda. \tag{16}$$

The $\rho^{\text{UHF}}_{\mu\mu}$ thus obtained approximately corresponds to the spin density for the SCF UHF function, though a perturbation theory is used in our approach where the SCF procedure is partly introduced by solving the simultaneous equation instead of iterations. Such an SCF perturbation theory was applied successfully to the bond order problem by Coulson and Golebiewski.[11] Validity of the procedure is confirmed by the numerical results.

In general, UHF spin densities do not agree with experiment because of spin contamination. Let us now introduce the projection procedure to our approach. To the first order of perturbation theory, the spin density for the projected UHF function is given by

$$\rho^{\text{PUHF}}_{\mu\mu} = \rho^{\circ}_{\mu\mu} - \frac{1}{3}\lambda \sum_{\nu} \Pi^{(0)}_{\mu\nu}\rho^{\circ}_{\nu\nu} - \lambda \sum_{\nu} \Pi^{(1)}_{\mu\nu}\rho^{\circ}_{\nu\nu} \tag{17}$$

where the last term comes from the pure doublet configurations, so it is left through a projection.[2,12-15] However, within the SCF perturbation theory, such a procedure as separating the last two terms of Eq. 17 may be cumbersome; our aim is to obtain a simplified formula. Fortunately, Snyder and Amos[2] suggested that the following approximation is practically reasonable.

$$\rho^{\text{PUHF}}_{\mu\mu} \approx \rho^{\circ}_{\mu\mu} - \frac{1}{3}\lambda \sum_{\nu} \Pi^{\text{SCF}}_{\mu\nu}\rho^{\circ}_{\nu\nu} \tag{18}$$

Therefore we may approximate the projected spin density as above.

Let us deal with the next difinition of spin density. If the $\rho_{\nu\nu}$ which appears in the second term of Eq. 10 can be approximated as the $\rho^{0}_{\nu\nu}$, we have

$$\rho^{\text{MMc}}_{\mu\mu} = \rho^{\circ}_{\mu\mu} - \lambda \sum_{\nu} \Pi_{\mu\nu}\rho^{\circ}_{\nu\nu}. \tag{19}$$

The approximation indicates the use of the usual perturbation theory instead of the SCF one. Equation 19 is now formally reduced to the McLachlan formula.[1] However, our formula is different from McLachlan's in the definition of polarizabilities, which is given by Eq. 11 or 12.

Calculations and Results

First let us evaluate the adjustable parameter λ. McLachlan obtained $\lambda = \gamma/2|\beta| \approx 1.2$ using the parameter of Pariser and Parr $\gamma = 10.53$ eV. However, Gutfreund and Little[16] concluded from the consideration of the screened potential that the γ values are of the order of 7—9 eV in most cases for large π-electron systems, depending on the position of the given atomic site in the molecule. To a cruder approximation, we can neglect the small variation of β and position dependence of γ, taking the average value of γ. The λ values then become proportional to the constant γ. It can be inferred that the average value of γ for the anion is smaller than for the corresponding cation and the neutral radical falls into the middle, since the γ values can be considered to be proportional to the screening constants. On this assumption, the spin density distributions for the anion and the corresponding cation differ from each other, indicating a violation of the pairing theorem. However, the pairing theorem should be valid only within certain approximations; a more rigorous theory violates it. For instance, a renouncement of the approximations of zero-differential overlap or an introduction of penetration energies into the term $U_{\mu\mu}$ which appears in Eq. 1 or 2 leads to breakdown of the pairing theorem. Our assumption is thus reasonable.

On the other hand, the experimental fact that the proton hyperfine splittings of the anions and the corresponding cations of even alternants are not identical has so far been accounted for by using the Colpa-Bolton (CB) relationship[17] which includes the charge effect or the Giacometti-Nordio-Pavan (GNP) effect[18] including that of the nearest-neighbor bond spin densities. However, both relations fail to explain the fact that the lower splittings (for example, at the 2 position of anthracene and naphthacene in Tables 1 and 2) for cations are generally smaller in magnitude than for the corresponding anions in contrast to what is found for the higher splititngs.

In view of the discussion above we will introduce partly the small difference between cations and the corresponding anions into our theory by adjusting the parameter λ. Let us take the λ values as $\lambda = 1.1$, 1.0, and 0.9 for cations, neutral radicals and anions, respec-

TABLE 1. PROTON HYPERFINE SPLITTINGS FOR THE ANIONS AND CATIONS OF ANTHRACENE AND NAPHTHACENE (G)[a,b]

Radical	Atom[c]	M[d] PUHF	M[d] MMc	M[d] SA (aa)	M[d] Mc	CB[e] PUHF	CB[e] MMc	CB[e] SA (aa)	CB[e] Mc	GNP[f] PUHF	GNP[f] MMc	GNP[f] SA (aa)	GNP[f] Mc	Expt.[g]
Anthracene∓	1	−2.78	−2.91	−2.83	−3.18	−2.65	−2.77	−2.72	−3.04	−2.52	−2.66	−2.65	−2.93	−2.76
		−2.86	−2.97			−3.00	−3.12	−2.97	−3.33	−3.12	−3.23	−3.03	−3.44	−3.12
	2	−1.11	−1.00	−0.75	−0.86	−1.08	−0.98	−0.73	−0.84	−0.97	−0.85	−0.65	−0.74	−1.53
		−1.02	−0.92			−1.05	−0.94	−0.80	−0.88	−1.17	−1.08	−0.87	−0.99	−1.40
	9	−6.07	−6.59	−7.02	−6.91	−5.48	−5.90	−6.32	−6.28	−5.57	−6.10	−6.40	−6.41	−5.41
		−6.48	−6.89			−7.13	−7.63	−7.74	−7.54	−6.98	−7.38	−7.64	−7.42	−6.65
Naphthacene∓	1	−1.59	−1.62	−1.49	−1.76	−1.55	−1.58	−1.46	−1.71	−1.49	−1.52	−1.33	−1.65	−1.55
		−1.65	−1.65			−1.69	−1.69	−1.53	−1.80	−1.75	−1.75	−1.65	−1.86	−1.72
	2	−0.76	−0.68	−0.43	−0.62	−0.74	−0.66	−0.42	−0.61	−0.70	−0.62	−0.35	−0.56	−1.15
		−0.70	−0.62			−0.71	−0.63	−0.45	−0.64	−0.76	−0.67	−0.51	−0.68	−1.06
	5	−4.56	−4.99	−5.32	−5.10	−4.21	−4.59	−4.91	−4.75	−4.28	−4.71	−4.81	−4.83	−4.25
		−4.83	−5.21			−5.22	−5.65	−5.73	−5.46	−5.12	−5.50	−5.83	−5.37	−5.17

a) Where pairs of members are given, the upper value is for the anion and the lower for the cation. b) Each notation refers to the corresponding spin density listed in Table 2. c) For the numbering see Ref. 2. d) Calculated using the McConnell relationship with the numerical coefficient in Ref. 2. e) Calculated using the CB relationship[16] with the numerical coefficients in Ref. 2. f) Calculated using the GNP relationship[17] with the numerical coefficients in Ref. 2. The bond spin densities are defined in a similar manner to the atomic ones. g) Sources listed in Ref. 2.

tively. The test calculation is carried out for the cations and anions of anthracene and naphthacene. The proton hyperfine splittings and the spin densities calculated are given in Tables 1 and 2, respectively. We see that our calculation gives better agreement with experiment than the others. It should especially be noted that our calculation predicts the relative magnitudes of splittings at the 2 positions of the cations and anions except for the GNP relationship, though the magnitudes are too low. This seems to support our assumption. We will therefore employ the values above throughout this paper.

Secondly, let us see whether the $\rho_{\mu\mu}^{\mathrm{UHF}}$ values defined by Eq. 14 or 15 coincide with the spin densities obtained by means of the more elaborate UHF method. The values of $\rho_{\mu\mu}^{\mathrm{UHF}}$ for a number of hydrocarbon radicals and ions are computed and compared with the spin densities (before annihilation) obtained by Snyder and Amos[2] (Table 2). The spin densities agree reasonably well with each other except for some positions of benzil. This seems to justify our SCF perturbation treatment. Moreover, if it is borne in mind that the perturbed Hückel MO's are used in our treatment, and the SCF MO's in theirs, it may be regarded as an unexpected success.

We have computed the spin densities $\rho_{\mu\mu}^{\mathrm{PUHF}}$ and $\rho_{\mu\mu}^{\mathrm{MMc}}$ defined by Eqs. 18 and 19 respectively, for a number of hydrocarbon radicals and ions in order to compare the results with the ones obtained by Snyder and Amos[2] and by McLachlan[1] (Table 2). A close inspection of Table 2 shows the following :

1) As a whole the values of the four different expressions of spin densities $\rho_{\mu\mu}^{\mathrm{PUHF}}$, $\rho_{\mu\mu}^{\mathrm{MMc}}$, $\rho_{\mathrm{aa}}^{\mathrm{SA}}$, and ρ^{Mc} agree fairly well with each other.

2) In particular agreement between $\rho_{\mu\mu}^{\mathrm{MMc}}$ and ρ^{Mc}, and between $\rho_{\mu\mu}^{\mathrm{PUHF}}$ and $\rho_{\mathrm{aa}}^{\mathrm{SA}}$ is quantitatively good.

3) The values of $\rho_{\mu\mu}^{\mathrm{PUHF}}$ and $\rho_{\mu\mu}^{\mathrm{MMc}}$ are in good agreement with each other in spite of different difinitions.

The discrepancy between the $\rho_{\mu\mu}^{\mathrm{MMc}}$ and ρ^{Mc} spin densities is due to the use of different values of λ and $\Pi_{\mu\nu}$ except for odd alternant hydrocarbon radicals. A similar discussion applies to a comparison of the $\rho_{\mu\mu}^{\mathrm{PUHF}}$ and $\rho_{\mathrm{aa}}^{\mathrm{SA}}$ values.

Let us now compare the $\rho_{\mu\mu}^{\mathrm{PUHF}}$ and $\rho_{\mu\mu}^{\mathrm{MMc}}$ spin densities. The important difference between the two is that the projected UHF functions and the SCF perturbation theory are used for the former, and unprojected ones and a simple perturbation theory for the latter. Nevertheless the two give almost equivalent spin densities. This seems to give numerical evidence of the validity of the McLachlan-type formulas. The theoretical basis of the formulas is not yet established, but agreement between them may probably be due to accidental cancellation in errors when a perturbation method is used. The problem has been discussed by Snyder and Amos.[2]

Discussion

Our theory employs the perturbed Hückel approach with use of the SCF and projection procedures. The McLachlan-type formulas are therefore obtained as a special case. We wish to clarify the correlation between the McLachlan-type formulas and ours.

Since $\lambda \approx 1$ and usually $|\Pi_{\mu\nu}| < 1$, we may expand the SCF polarizability $\Pi_{\mu\nu}^{\mathrm{SCF}}$ as

$$\Pi_{\mu\nu}^{\mathrm{SCF}} = \Pi_{\mu\nu} - \lambda \sum_{\kappa} \Pi_{\nu\kappa}\Pi_{\kappa\nu} + \cdots \tag{20}$$

Substituting Eq. 20 into Eq. 15, we obtain

$$\rho_{\mu\mu}^{\mathrm{UHF}} = \rho_{\mu}^{\circ} - \lambda \sum_{\nu} \Pi_{\mu\nu}\rho_{\nu\nu}^{\circ} + \lambda^2 \sum_{\nu\kappa} \Pi_{\mu\kappa}\Pi_{\kappa\nu}\rho_{\nu}^{\circ} + \cdots \tag{21}$$

By comparing Eq. 21 with Eq. 19 we see that the difference between the UHF spin density $\rho_{\mu\mu}^{\mathrm{UHF}}$ and the modified McLachlan-type one $\rho_{\mu\mu}^{\mathrm{MMc}}$ is the quadratic and higher order terms of polarizabilities. The contributions from these higher order terms to the spin density appear to be rather small. However, the order of magnitude of the $\Pi_{\mu\nu}$ $(\Pi_{\mu\mu}+\Pi_{\nu\nu})$ which appears in the second term of Eq. 20 can be compared with the one of the first term $\Pi_{\mu\nu}$. Actually the order

TABLE 2. SPIN DENSITIES CALCULATED WITH VARIOUS METHODS FOR ALTERNANT AND NON-ALTERNANT HYDROCARBON RADICALS AND IONS[a)]

Radical	Atom	This work			Work of Snyder and Amos		Work of McLachlan
		ρ_{μ}^{UHF}	$\rho_{\mu\mu}^{PUHF}$	$\rho_{\mu\mu}^{MMc}$	ρ_{sd}^{SA} b)	ρ_{aa}^{SA} c)	ρ^{Mc}
Ally	1	0.688	0.563	0.588	0.651	0.547	0.588
	2	−0.376	−0.126	−0.177	−0.302	−0.093	−0.177
Benzyl	1	−0.238	−0.079	−0.102	−0.189	−0.060	−0.102
	2	0.225	0.170	0.161	0.254	0.157	0.161
	3	−0.149	−0.050	−0.063	−0.158	−0.050	−0.063
	4	0.140	0.142	0.137	0.225	0·128	0.137
	7	0.947	0.697	0.770	0.771	0.718	0.770
Butadiene$^-$	1	0.466	0.397	0.416	0.457	0.389	0.442
	2	0.034	0.103	0.084	0.043	0.111	0.058
Naphthalene$^-$	1	0.233	0.200	0.213	0.262	0.215	0.222
	2	0.042	0.059	0.054	0.026	0.048	0.047
	9	−0.050	−0.019	−0.033	−0.076	−0.024	−0.037
Anthracene$^{\mp}$	1	0.117 0.126	0.103 0.106	0.108 0.110	0.138	0.105	0.118
	2	0.027 0.018	0.041 0.038	0.037 0.034	0.014	0.028	0.032
	9	0.289 0.334	0.225 0.240	0.244 0.255	0.319	0.260	0.256
	11	−0.029 −0.050	−0.007 −0.014	−0.017 −0.022	−0.061	−0.014	−0.028
Naphthacene$^{\mp}$	1	0.065 0.071	0.059 0.061	0.060 0.061	0.078	0.055	0.065
	2	0.018 0.012	0.028 0.026	0.025 0.023	0.006	0.016	0.023
	5	0.213 0.243	0.169 0.179	0.185 0.193	0.252	0.197	0.189
	13	−0.018 −0.030	0.002 −0.002	−0.005 −0.009	−0.041	−0.005	−0.010
	17	−0.065 −0.086	−0.019 −0.026	−0.029 −0.036	−0.088	−0.028	−0.033
Azulene$^-$	1	0.008	0.005	−0.019	−0.011	−0.001	−0.027
	2	0.099	0.100	0.111	0.118	0.080	0.120
	4	0.367	0.269	0.276	0.313	0.236	0.292
	5	−0.185	−0.055	−0.058	−0.178	−0.046	−0.081
	6	0.403	0.308	0.327	0.434	0.356	0.368
	9	0.060	0.077	0.082	0.099	0.093	0.071
Fluoranthene$^-$	1	0.200	0.148	0.149	0.189	0.140	0.157
	2	−0.082	−0.013	−0.014	−0.102	−0.020	−0.023
	3	0.279	0.202	0.212	0.304	0.228	0.227
	7	−0.006	0.009	0.004	−0.024	−0.003	0.000
	8	0.036	0.038	0.037	0.041	0.029	0.037
	11	−0.089	−0.030	−0.035	−0.130	−0.041	−0.039
	12	0.015	0.005	−0.012	0.026	0.012	−0.013
	13	0.046	0.067	0.074	0.051	0.070	0.063
	14	0.064	0.061	0.061	0.089	0.070	0.064
Acenaphthylene$^-$	1	0.102	0.103	0.106	0.111	0.097	0.101
	3	0.250	0.184	0.188	0.216	0.158	0.196
	4	−0.115	−0.029	−0.033	−0.123	−0.029	−0.041
	5	0.300	0.219	0.228	0.317	0.236	0.245
	9	−0.101	−0.034	−0.040	−0.138	−0.044	−0.045
	10	0.022	0.007	−0.011	0.050	0.017	−0.012
	11	0.002	0.036	0.036	0.023	0.052	0.027

a) See footnotes a) and c) in Table 1. b) Before annihilation. c) After annihilation.

of magnitude of $\Pi_{\mu\nu}^{SCF}$ is fairly greater than the one of $\Pi_{\mu\nu}$ in many cases. Our result confirms this; the $\rho_{\mu\mu}^{MMc}$ spin density is far from the $\rho_{\mu\mu}^{UHF}$ one at many positions of radicals (Table 2). In the following we will discuss the question why such a crude model as the McLachlan method can successfully interpret experimental results.

Marshall[12] showed that the unprojected spin density should be closer to experimental result than the projected one under certain conditions. On the other hand, Snyder and Amos[2] showed that in first order to Lowdin's extended Hartree-Fock scheme,[19] in terms of our theory, the spin density can be approximated as[20]

$$\rho_{\mu\mu}^{EXT} \approx \rho_{\mu\mu}^{\circ} - K\lambda \sum_{\nu} \Pi_{\mu\nu}^{SCF} \rho_{\nu\nu}^{\circ} \qquad (22)$$

where K is a dimensionless coefficient which can be expressed as some ratio of energy terms; if $K=1$ the $\rho_{\mu\mu}^{EXT}$ is reduced to the $\rho_{\mu\mu}^{UHF}$ and if $K=1/3$ to the $\rho_{\mu\mu}^{PUHF}$. Most radicals fall between these extremes, the conjugated hydrocarbon radicals appearing to approximate the second case. They suggested that the McLachlan spin density, which falls between the unprojected UHF spin densities and projected ones in most cases, can be good approximations to the ones obtained by the extended Hartree-Fock method. Our results also confirm the suggestion; since $|\Pi_{\mu\nu}| \lesssim |\Pi_{\mu\nu}^{SCF}|$ in many cases, if $K \lesssim 1$ the $\rho_{\mu\mu}^{MMc}$ might agree with the $\rho_{\mu\mu}^{EXT}$. This condition is practically satisfied together with that $K \gtrsim 1/3$ in most cases. Harriman and Sando[21] demonstrated explicitly that this is true in many cases by their numerical results, though K is rather closer to unity.

A comparison is given between our approach and that given in other works. Recently Amos *et al.*[22] suggested a method for improving the spin densities obtained from UHF wave functions. Their procedure differs from ours; they have employed the usual perturbation theory, while we take the self-consistency effect into consideration. Nakatsuji and Hirao[23] have proposed a pseudo-orbital theory which corresponds to an extension of UHF and spin-extended HF theories, containing self-consistency terms.

References

1) A. D. McLachlan, *Mol. Phys.*, **3**, 233 (1960).
2) L. C. Snyder and T. Amos, *J. Chem. Phys.*, **42**, 3670 (1965).
3) J. Nowakowski, *Chem. Phys. Lett.* **2**, 289 (1968).
4) J. Nowakowski, *Theor. Chim. Acta (Berl.)*, **18**, 133 (1970).
5) J. C. Bickerton and R. E. Moss, *Mol. Phys.*, **21**, 341 (1971).
6) C. L. Honeybourne, *Mol. Phys.*, **21**, 1057 (1971).
7) C. L. Honeybourne, *Theor. Chim. Acta (Berl.)*, **42**, 87 (1976).
8) P. Devolder, *Theor. Chim. Acta (Berl.)*, **39**, 277 (1975).
9) A. Brickstock and J. A. Pople, *Trans. Faraday Soc.*, **50**, 901 (1954).
10) H. C. Longuet-Higgins and J. A. Pople, *Proc. Phys. Soc. (London)*, *A*, **68**, 591 (1955).
11) C. A. Coulson and A. Golebiewski, *Proc. Phys. Soc. (London)*, *A*, **78**, 1310 (1961).
12) W. Marshall, *Proc. Phys. Soc. (London)*, *A*, **78**, 113 (1961).
13) T. Yonezawa, H. Nakatsuji, T. Kawamura, and H. Kato, *Chem. Phys. Lett.* **2**, 454 (1968); *J. Chem. Phys.*, **51**, 669 (1969).
14) H. Nakatsuji, H. Kato, and T. Yonezawa, *J. Chem. Phys.*, **51**, 3175 (1969).
15) H. Nakatsuji, *J. Chem. Phys.*, **59**, 2586 (1973).
16) H. Gutfreund and W. A. Little, *Phys., Rev.*, **183**, 68 (1969); *J. Chem. Phys.*, **50**, 4468 (1969).
17) J. P. Colpa and J. R. Bolton, *Mol. Phys.*, **6**, 273 (1963).
18) G. Giacometti, C. L. Nordio, and M. V. Pavan, *Theor. Chim. Acta (Berl.)*, **1**, 404 (1963).
19) P. O. Löwdin, *Phys. Rev.*, **97**, 1509 (1955); *Rev. Mod. Phys.*, **34**, 520 (1962).
20) The correct formula, to the first order of perturbation theory, can be obtained by replacing the factor 1/3 in Eq. 17 with K. However, the same approximation as in Eq. 18 is used here. The conclusion obtained is unchanged by using this approximation.
21) J. E. Harriman and K. M. Sando, *J. Chem. Phys.*, **48**, 5138 (1968).
22) A. T. Amos, D. R. Beck, and I. L. Cooper, *Chem. Phys. Lett.*, **56**, 95 (1978).
23) H. Nakatsuji and K. Hirao, *J. Chem. Phys.* **68**, 4279 (1978).

X-Ray Fluorescence Spectroscopy of Inorganic Solids. III. Si K_α and K_β Spectra in Binary Silicates

Niro KIKUCHI, Takashi MAEKAWA, and Toshio YOKOKAWA*

Department of Chemistry, Faculty of Science, Hokkaido University, Sapporo 060

(Received August 15, 1978)

The Si K_α and K_β spectra of several silicates were measured. The K_α spectra showed negative energy shifts referred to SiO_2; these are consistent with the results for the binary silicate glasses. On the other hand, the K_β shifts were positive and the absolute values were about ten times as large as the K_α shifts in each compound. A linear relation was observed between K_α and K_β energy shifts. The Si 1s energy shift for the orthosilicate was estimated from the K_β spectral splitting of $Na_2Si_2O_5$. The stability of the silicon–oxygen bond was discussed with the aid of the shifts in K_β and the Si 1s. The above linear relation suggests that the silicon–oxygen bond strength is lowered (the K_β energy is increased) with decreasing Coulombic interaction (lowering K_α energy) between silicon and oxygen in the silicates.

Recently the chemical state analysis by means of X-ray fluorescence spectroscopy has been extensively developed. In the previous paper, we reported the variations of the Si K_α energy in binary silicate glasses as functions of the concentration and the kind of the basic oxides.[1] However, in order to discuss the nature of the silicon–oxygen bond, it is necessary to investigate further the K_β spectra in these materials. The Si K_β spectra correspond to the transition from Si 3p to 1s and they naturally bring out more valuable information about the electronic states in the silicon–oxygen bond than the K_α spectra do.

Dodd and Glen explained the origin of the Si K_β spectra in silicates by means of an MO theory and defined the destabilization energy of the silicon–oxygen bond.[2] Urch[3] and Tossell[4,5] extended this MO treatment by a more quantitative calculation and discussed the details of the nature of the silicon–oxygen bond. However, they were concerned mainly with SiO_2 and orthosilicates, whose spectra are simple and can be explained by assumming the tetrahedral cluster around silicon atoms. Sakka and Matusita measured the Si K_β spectra of simple binary silicate glasses of different compositions and discussed the chemical shifts and the changes of the band width in terms of the destabilization energy of the silicon–oxygen bond strength and the difference of the state of the silicon atoms, *i.e.* degree of the polymerization.[6] When we applied an improved two-crystal spectrometer to measure the Si K_β spectra of silicates, we found some appreciable changes of the spectral profile, as well as the spectrum width and the frequency, which have not been reported. The Si K_β energy shifts were also measured and discussed in terms of the destabilization of the Si–O bond caused by an introduction of the basic oxides to the silica network.

Experimental

Samples. Commercial α-quartz and other single oxides or carbonates were used to prepare the silicate glasses and crystals. Na_2SiO_3 was prepared by dehydrating a commercial $Na_2SiO_3 \cdot 9H_2O$. These synthesized samples were all checked by the X-ray powder diffraction method. Commercial Na_4SiO_4, $Al_2Si_3O_9$, $Mg_2Si_3O_8 \cdot 5H_2O$, and kaolinite were also used. The crystalline samples were ground and pressed into pellets within a polyvinyl chloride ring. The glassy samples were prepared by melting crystalline compounds or the mixtures of the component oxides and pouring them onto a stainless steel plate. The flat glasses were directly introduced into the spectrometer.

Apparatus. The spectrometer used in this experiment was of the two-crystal type. The analyzing crystal was ADP, and the Cr or Rh X-ray tubes were used for the primary X-ray source. The details of the apparatus were described in previous papers.[1,7]

K_α Chemical Shifts. In a previous paper we employed a fourth order equation for curve fitting to the upper part of the K_α spectra in order to evaluate the chemical shift. However, there is a better way to evaluate the shift than the curve fitting method when the K_α spectra of a series of compounds are different from each other only in absolute energy and are quite similar in their profiles. In this paper the following method was adopted. It consists of 4 steps. (See also Fig. 1.)

(i) The "standard" spectrum with a detailed profile of the reference material is obtained.

(ii) A sandwiched series of a "sample" and the "reference" spectra for the sample and for the reference materials respectively is obtained.

(iii) Both spectra are normalized.

(iv) Both spectra are displaced along the energy abscissa to fit the "standard" spectrum. The difference of the energy displacements evaluated with the least square method gives the chemical shift.

An energy discrepancy between the "standard" and "reference" spectra is usually found, partly because the former is obtained with a much greater number of scan

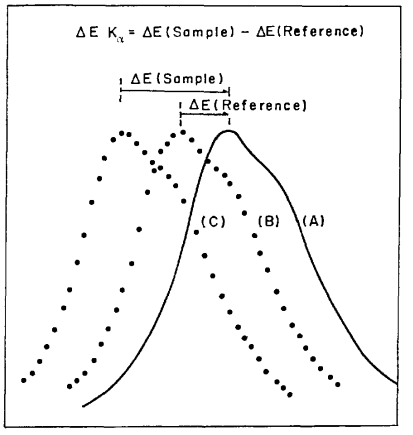

Fig. 1. Determination of the K_α energy shifts.
(A) "Standard" spectrum; (B) "reference" spectrum; (C) "sample" spectrum.

repeats than the "reference" and partly because the performance of the instrument changes from day to day.

K_β Energy Shifts. As the K_β spectra were complex in line shape the shift was evaluated from the energy of the center of gravity of the spectrum. Any complex spectrum was assumed to be composed of two to four Lorentzian curves of various positions and heights. The temperature fluctuation of the analysing crystal(ADP) causes errors of 0.04 eV/deg, which were corrected.

Results

The Si K_α energy shifts of silicates referred to α-quartz are listed in Table 1. All chemical shifts are negative. Generally the absolute values of the chemical shifts are large in samples with high alkali content whenever the comparison is possible. This tendency is in good agreement with the previous findings.[1] Table 1 also shows the K_β energy shifts referred to α-quartz. The shifts are positive and the absolute values are ten times as large as the corresponding K_α energy shifts. These values generally agree well with previous values.[6]

Figure 2 shows Si K_β spectra of several sodium silicates crystals as well as α-quartz and α-cristobalite. No difference between the latter two was detected. The profile becomes complex with Na_2O content and then returns to a single peak of different energy at Na_4SiO_4 composition. Similarly the CaO–SiO_2 system shows a complex profile at intermediate composition, followed by a single peak at the orthosilicate. Table 2 shows the results of Ca K_α, which were also measured for the discussion of ionic charges in silicates.

Table 1. Chemical shifts of Si K_α and K_β energy of silicon compounds

No.	Sample	ΔE K_α/eV	ΔE K_β/eV
1	α-Quartz	—	—
2	α-Cristobalite	−0.002	−0.11
3	SiO_2 (glass)	−0.010	0.0
4	α-$CaSiO_3$	−0.101	1.08
5	β-$CaSiO_3$	−0.066	0.93
6	β-Ca_2SiO_4	−0.107	1.17
7	γ-Ca_2SiO_4	−0.088	1.25
8	$Na_2Si_2O_5$	−0.050	0.56
9	$Na_2Si_2O_5$ (glass)	−0.061	0.68
10	Na_2SiO_3	−0.073	0.81
11	Na_2SiO_3 (glass)	−0.093	0.96
12	Na_4SiO_4	−0.109	1.56
13	$K_2Si_2O_5$ (glass)	−0.070	0.69
14	Mg_2SiO_4	−0.088	1.05
15	$ZrSiO_4$	−0.046	0.45
16	Mn_2SiO_4	−0.082	0.85
17	$Al_2Si_3O_9$	−0.026	0.24
18	$Mg_2Si_3O_8 \cdot 5H_2O$	−0.041	0.51
19	Kaolinite	−0.021	0.08
	Na_2SiF_6	0.364	0.70
	Si_3N_4	−0.161	1.70
	SiC	−0.379	2.60
	Si	−0.607	2.97
	Erros (average)	±0.01	±0.1

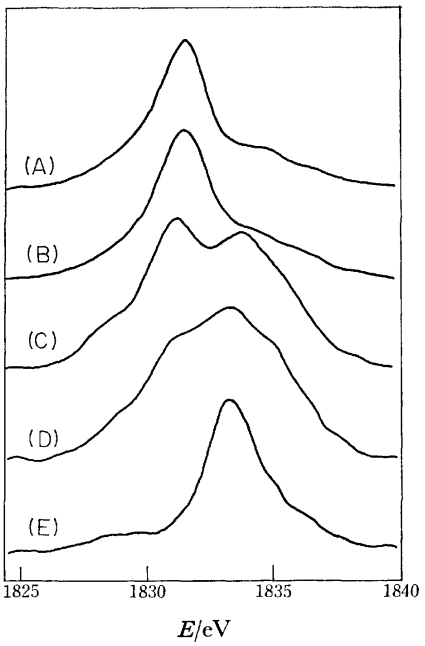

Fig. 2. Si K_β spectra of the Na_2O–SiO_2 system. (A) α-Cristobalite; (B) α-quartz; (C) $Na_2Si_2O_5$; (D) Na_2SiO_3; (E) Na_4SiO_4.

Table 2. Ca K_α energy of some calcium compounds referred to CaF_2

Sample	ΔE K_α/eV
CaF_2	—
α-$CaSiO_3$	0.104
β-Ca_2SiO_4	0.121
CaO	0.161
CaS	0.233
Error (average)	0.008

Discussion

Si–O–Si and Si–O⁻ Bonds in Silicates and the Profiles of the K_β Spectra. The molecular orbital of SiO_4^{4-} ion has been constructed to assign the Si K_β spectra of silicates.[4] The Si K_β spectra involve the transition from Si 3p to Si 1s. According to the selection rule, however, the electrons in the molecular orbital of t_2 symmetry can take part in the transition if the tetrahedral geometry is considered. According to Tossell[4] the main bonding orbital $4t_2$ consists of Si 3p and O 2p atomic orbitals and the transition from this to Si 1s is the origin of the K_β main peak. The peak of higher energy than the main peak, which is shown as a shoulder in SiO_2, corresponds to the transition from $5t_2$ non-bonding orbital, which consists mainly of O 2p with a small mixing of Si 3p, to Si 1s. Further, the transition from $3t_2$ (O 2s+Si 3p) produces the spectrum on the energy side lower than the main peak. This has been called the K_β' satellite peak, but it is out of the spectral range covered by the present study.

It is understood that the silica network is modified by an introduction of a basic oxide, as expressed by the following chemical reaction.[8]

$$\equiv Si\text{-}O\text{-}Si\equiv + M_2O = 2\equiv Si\text{-}O^- + 2M^+$$

Thus there are two types of silicon–oxygen bonds: one is Si–O–Si and the other Si–O$^-$. The oxygen in the former type is called a bridging oxygen and in the latter is called a non-bridging oxygen; these are designated by O^0 and O$^-$ respectively. Considering only the nearest neighbor oxygens, the structure around the silicon atom can be considered as Si[O^0]$_4$ and Si[O$^-$]$_4$ for SiO_2 and orthosilicate respectively. In the compounds of intermediate composition, the general structure around a Si atom can be described as Si[O^0]$_n$[O$^-$]$_{4-n}$, when the chemical formula of the compounds is $M_{4-n}SiO_{4-n/2}$ (M; univalent cation).† The experimental spectra for Na_4SiO_4, Ca_2SiO_4 and SiO_2 can be well understood by the T_d symmetry, while in $Na_2Si_2O_5$ there are two intense peaks. The positions are located near the same positions as those of SiO_2 (Si–O–Si only) and Na_4SiO_4(Si–O$^-$ only). A complex profile is also seen in the spectrum of Na_2SiO_3, which consists of a peak and two or more shoulders. The fact that the higher energy peak increases with the concetration of the basic oxides also suggests that the shape of the K_β spectra could be resolved into two main components, one corresponding to the Si–O–Si type and the other to the Si–O$^-$ type bond.

Shifts of the Si 1s Energy. A discussion of the stability of the silicon–oxygen bond has been developed in terms of energy shifts of the K_β spectra.[2,6] The X-ray spectra do not give an absolute orbital energy, but give only a energy difference among levels. It is necessary to take the energy shift of the 1s level into consideration in order to discuss the stability of a bond from a K_β spectrum. In the following we will show one way of estimation of the 1s level shifts from the X-ray spectra.

In the proceeding section we assummed that the double peaks of Si K_β in $Na_2Si_2O_5$ could be assigned to the transition from Si–O–Si and Si–O$^-$ type bonding orbitals. All silicon atoms in the crystalline materials are identical and they are bound to one non-bridging oxygen and three bridging oxygens in a first coordination shell. The 1s electron of the silicon atom is under the average shielding effects of Si 3p (+O 2s and O 2p) electrons. This implies that the separation of two peaks of K_β spectrum of $Na_2Si_2O_5$ corresponds to the difference of the orbital energies of Si–O–Si and Si–O$^-$ bonds, since the two peaks correspond to the transitions to the same Si 1s level. This energy difference is evaluated to be 2.4 eV.

Thus,

$$E_\sigma(\text{Si-O}^-, Na_2Si_2O_5) - E_\sigma(\text{Si-O-Si}, Na_2Si_2O_5) = 2.4\,\text{eV}. \quad (1)$$

E_σ's are the orbital energies of the bonding orbitals of the two types of Si–O bonds. On the other hand, the K_β energies of SiO_2 and Na_4SiO_4 are given by

$$E_{K_\beta}(\text{Si-O-Si}, SiO_2) = E_\sigma(\text{Si-O-Si}, SiO_2) - E_{1s}(SiO_2) \quad (2)$$

$$E_{K_\beta}(\text{Si-O}^-, Na_4SiO_4) = E_\sigma(\text{Si-O}^-, Na_4SiO_4) - E_{1s}(Na_4SiO_4) \quad (3)$$

† $n/2+(4-n)=4-n/2=$(Total number of oxygen atoms per silicon atom in the compound); for example, $n=2$ and 3 for Na_2SiO_3 and $Na_2Si_2O_5$ respectively.

respectively. If ΔE_{1s} is defined by

$$\Delta E_{1s} \equiv E_{1s}(Na_4SiO_4) - E_{1s}(SiO_2), \quad (4)$$

ΔE_{1s} is the energy difference of the 1s level between SiO_2 and Na_4SiO_4. From Eqs. 2 to 4,

$$\begin{aligned}\Delta E_{K_\beta}(\text{Si-O}^-, Na_4SiO) &\equiv E_{K_\beta}(\text{Si-O}^-, Na_4SiO_4) \\ &\quad - E_{K_\beta}(\text{Si-O-Si}, SiO_2) \\ &= E_\sigma(\text{Si-O}^-, Na_4Si_4) \\ &\quad - E_\sigma(\text{Si-O-Si}, SiO_2) - \Delta E_{1s}.\end{aligned} \quad (5)$$

If the first two terms of the right hand side in Eq. 5 are replaced by Eq. 1,

$$\begin{aligned}\Delta E_{K_\beta}(\text{Si-O}^-, Na_4SiO_4) &= 2.4 - \Delta E_{1s} \\ &= 1.6 \text{ (see Table 1).}\end{aligned} \quad (6)$$

Thus the energy shift of Si 1s of Na_4SiO_4 referred to SiO_2 can be estimated to be about 0.8 eV. In this argument the energies of Si–O in Si–O–Si and Si–O$^-$ are assumed to be constant irrespective of the molecular symmetry. Nefedov *et al.* obtained the binding energy of 2p electrons of silicon of many silicon compounds from ESCA measurement.[9] In the SiO_4^{4-} type silicates, the 2p level is destabilized about 0.5—1.1 eV from that of SiO_2. By combining the X-ray K_α energy shifts of these materials (about −0.1 eV), the 1s level energy shifts are calculated to be 0.6—1.2 eV. The present value of 0.8 eV agrees well with these experimental findings.

Heat of Formation of the Silicates and the Silicon–Oxygen Bond Strength. In alkali silicates and silicate minerals, the Si K_β energy is larger than that of SiO_2. This is interpreted in terms of the destabilization of the silicon–oxygen bond in these materials. White and Gibbs observed a linear relation between K_β energy shifts and the silicon–oxygen bond length.[10] Dodd

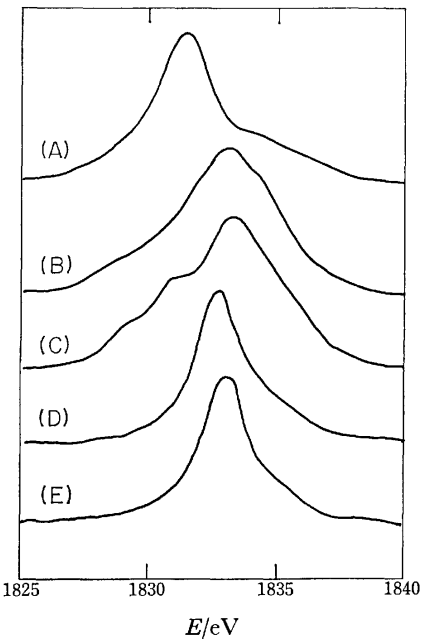

Fig. 3. Si K_β spectra of the CaO-SiO_2 system.
(A) α-Quartz; (B) β-$CaSiO_3$; (C) α-$CaSiO_3$; (D) β-Ca_2SiO_4; (E) γ-Ca_2SiO_4.

and Glen defined the relative destabilization energy of silicon–oxygen bonds from the X-ray K_β energy shifts.[2] However, according to the above argument, the relative destabilization energy of a bonding orbital is better redefined as

$$\Delta \equiv \Delta E_{K_\beta} + \Delta E_{1s}. \quad (7)$$

One obtains a larger destabilization energy for silicates than the previous value deduced only from the K_β chemical shifts.

It is worthwhile to note that when SiO_2 reacts with a basic oxide MO, the Si–O bond becomes weak in spite of the observation that the reaction is usually exothermic. Tossell explained this by an increase of the M–O bond strength.[11] As seen from the Ca K_α sequence measured in the present study (Table 2), the K_α energy shifts to a lower value when the counter F atom is replaced by a less electronegative O and S. In other words, Ca K_α decreases with the decrease of the positive charge on that atom. This means the charge of Ca in silicates $CaSiO_3$ and Ca_2SiO_4 is higher than that of CaO. Therefore the destabilization of the Si–O bond will possibly be counterbalanced by stabilization of the Ca–silicate anion coulombic energy.

Relation between K_α Shifts and K_β Shifts. From the argument that Si K_α energy shifts reflect the degree of the cationic charge on silicon atoms, a relation between Si K_α and K_β energy shifts is expected among silicon compounds. The two quantities are plotted in Fig. 4, whose reference is silicon metal. Except for Na_2SiF_6, which is octahedral in coordination, a quadratic relation was obtained. A linear relation was obtained among silicates where the nearest neighbors are always 4 oxygen atoms and the charges on Si do not change much; this result was independent of the next nearest neighbor cations. (See Fig. 5.)

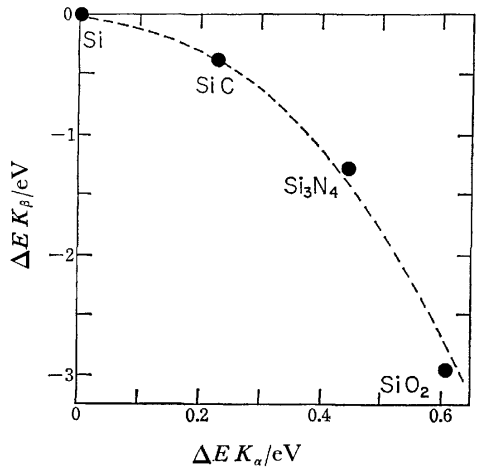

Fig. 4. Relation between Si K_α and K_β energy shifts for the several silicon compounds. The reference material is Si metal.

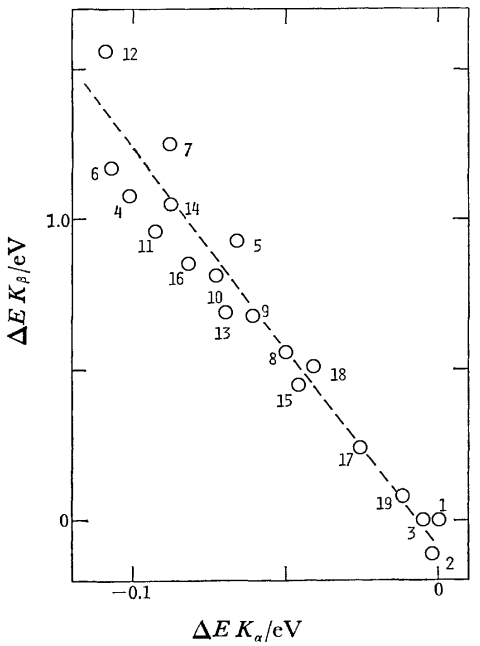

Fig. 5. Relation between Si K_α and K_β energy shifts for the silicates. The reference material is α-quartz. Numbers indicated in the figure correspond to the compounds in Table 1.

References

1) T. Maekawa, N. Kikuchi, S. Sumita, and T. Yokokawa, *Bull. Chem. Soc. Jpn.*, **51**, 780 (1978).
2) C. G. Dodd and G. L. Glen, *J. Appl. Phys.*, **39**, 5377 (1968).
3) D. S. Urch, *J. Phys. C*, **3**, 1275 (1970).
4) J. A. Tossell, *J. Phys. Chem. Solids*, **34**, 307 (1973).
5) J. A. Tossell, *J. Am. Chem. Soc.*, **97**, 4840 (1975).
6) S. Sakka and K. Matusita, *J. Non-Cryst. Solids*, **22**, 57 (1976).
7) T. Maekawa, N. Kikuchi, N. Fukuda, and T. Yokokawa, *Bull. Chem. Soc. Jpn.*, **51**, 777 (1978).
8) See, for example, F. D. Richardson, "Physical Chemistry of Melts in Metallurgy," Academic Press, London (1974), Vol. 1.
9) V. I. Nefedov, V. S. Urusov, and M. M. Kakhana, *Geochem. Int.*, **9**, 7 (1972).
10) E. W. White and G. V. Gibbs, *Am. Mineral.*, **52**, 985 (1967).
11) J. A. Tossell, *Am. Mineral.*, **62**, 136 (1977).
12) S. Sumita, N. Kikuchi, T. Maekawa, M. Shinmei, and T. Yokokawa, *Tetsu To Hagane*, **65**, 107 (1979).

ESR Spectrum of Bis(dibenzoylmethanato)oxovanadium(IV) Dissolved in Molten and Crystalline Charge Transfer Complexes

Kotaro ARAYA, Yoshio MATSUNAGA,* and Eiji OCHI

Department of Chemistry, Faculty of Science, Hokkaido University, Sapporo 060

(Received August 18, 1978)

The ESR spectrum of bis(dibenzoylmethanato)oxovanadium(IV) dissolved in a number of pyrene and fluoranthene complexes with aromatic polynitro compounds just above their melting points indicates that the motion of the spin probe is more or less restricted. In some favorable cases, the high effective viscosity of the melts can be partially attributed to the association of the electron donor and acceptor molecules. No abrupt change in the ESR spectral pattern is noted upon solidification and the motion of the probe gradually ceases upon lowering the temperature. Therefore, the lattice appears to be not rigid in these crystalline complexes. On the other hand, the ESR spectrum observed in the molten naphthalene–dinitrophenol complex is not far from isotropic at the melting point. Because of the segregation of the probe upon solidification, the measurements on this solid complex could not be made.

When a phase diagram indicates the formation of a 1 : 1 complex with a congruent melting point, it does not necessarily follow that the complex is stable in the molten state. The greater the extent of dissociation, the more flat the curve for the region between the eutectic points is expected, in general, to be.[1–3] However, nothing more can be safely inferred in the absence of any definite information regarding the dissociation of the complex in the molten state. As reported by one of the present authors,[4] all the patterns from the isotropic ESR spectrum to the anisotropic one of oxovanadium chelates can be recorded by employing molten *o*-terphenyl as a solvent. The observed anisotropic molecular motion of the spin probe has been speculated to be evidence for the restricted motion of the host molecules, in other words, the formation of clusters. Therefore, one may hope that the ESR spectral measurement of oxovanadium chelates is equally capable of detecting molecular association in molten charge-transfer complexes. The larger the chelate molecule, the more difficult the motion; thus bis(dibenzoylmethanato)oxovanadium(IV) may be the probe which is effective in the widest temperature range among the three chelates examined before. As will be described below, this chelate was found to be incorporated into the crystalline pyrene, fluoranthene, and phenanthrene complexes with aromatic polynitro compounds and to be a probe for the molecular motion in solids as well.

Experimental

Materials. The bis(dibenzoylmethanato)oxovanadium(IV) ($VO(dbm)_2$) was prepared following the procedure reported by Selbin *et al.*[5] The donors employed were pyrene, fluoranthene, phenanthrene, and naphthalene and the acceptors were *m*-dinitrobenzene (DNB), 2,4-dinitrofluorobenzene (DNF), 2,4-dinitrochlorobenzene (DNC), 2,4-dinitrotoluene (DNT), 2,4-dinitrophenol (DNP), 2,4,6-trinitrochlorobenzene (TNC), and 2,4,6-trinitrotoluene (TNT). The pyrene, Eastman white label, and TNT, Eastman yellow label, were recrystallized from appropriate solvents. The phenanthrene, Eastman white label, was boiled with maleic anhydride in xylene to remove any anthracene.[6] The other reagents were used without further purification. The complexes were prepared by melting mixtures of equimolar amounts of the component compounds. Their melting points were read from calorimetric curves recorded on a Rigaku Denki differential scanning calorimeter, Model 8001 SL/C, at a heating rate of 3 °C min^{-1}. As the paramagnetic probe is not very stable above 150 °C, the complexes with relatively low melting points were selected for the present work.

Measurements. The ESR spectra were recorded on a JEOL model JES-ME-3X (X-band) spectrometer with 100 kHz modulation in the range from temperatures well above the melting point of each complex to the temperature where the probe precipitates from the solid complex. The magnetic-field scan was calibrated with Mn^{2+}-doped MgO powder.

Results and Discussion

The ESR spectra of $VO(dbm)_2$ recorded in most of the pyrene complexes kept just above their melting points deviate markedly from the isotropic one. For example, the first derivative of the spectrum in pyrene–DNC (mp 87 °C) recorded at 88.5 °C is shown in Fig. 1. In this spectrum one may locate more lines than the eight expected for the isotropic spectrum. Thus it is apparent that the motion of the probe is restricted. The parameter, S, defined by

$$S = (A_{\parallel}' - a)/(A_{\parallel} - a)$$

will be employed as a measure of the molecular motion of $VO(dbm)_2$. Here, $A_{\parallel}$ is the component parallel to the V=O bond direction of the approximately axial hyperfine tensor of the spin probe, a is the iso-

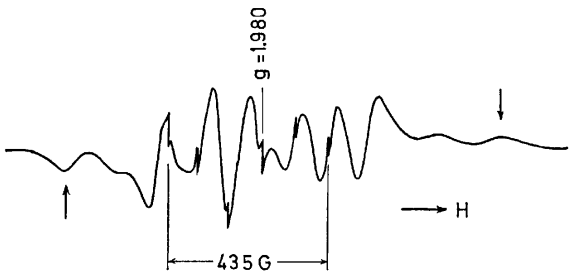

Fig. 1. ESR spectrum of bis(dibenzoylmethanato)-oxovanadium(IV) observed at X-band in pyrene–dinitrochlorobenzene at 88.5 °C. The superimposed small signals are due to the marker, Mn^{2+}-doped MgO powder.

tropic hyperfine constant, and $A_{\parallel}'$ is one-seventh of the separation of the outer hyperfine extrema (these are indicated by arrows in Fig. 1). They are signals from the ensemble of the probe molecules oriented with the applied field, on the average, parallel to the V=O bond direction. The parameter is equal to zero if the probe molecules are tumbling rapidly and unity if they are immobilized in a medium. With the values of $A_{\parallel}$ and a observed in molten *o*-terphenyl, namely, 188 and 108 G (1G=10^{-4} T), the S value for the spectrum in Fig. 1 is estimated to be 0.71. The spectra recorded at higher temperatures indicate a shorter distance for $7A_{\parallel}'$. This means an increased molecular motion. It was not possible to locate the corresponding signals above 114 °C. The probe was found to be dissolved even in the crystalline complex. The spectra recorded below the melting point are still intermediate between the anisotropic and isotropic ones. In this way, the plots given in Fig. 2 were obtained. The open and shaded circles are for two runs with independently-prepared solutions. It must be noted that no discontinuity in the S value is found at the melting point of the complex. This observation may imply that the change of the motional behavior upon solidification is not large or that the motion is slow on an ESR time scale in both the phases. From the macroscopic standpoint, the restriction may be attributed to the high viscosity of the medium, η. Assuming that the η/T value of the medium can be approximated by that of molten *o*-terphenyl at the same S value, the effective viscosity of the molten complex was estimated as 12.2 cP (1cP=10^{-3} Pa s) at the melting point. The viscosity value of *o*-terphenyl required for this estimation was calculated by means of the equation of Greet and Turnbull.[7] It must be added that, if special interactions are conceivable between the probe and solvent molecules, viscosity alone may not account for the deviation from the isotropic ESR spectrum. Therefore, the effective viscosity estimated here may be larger than the actual one.

The S values observed with solidified samples are

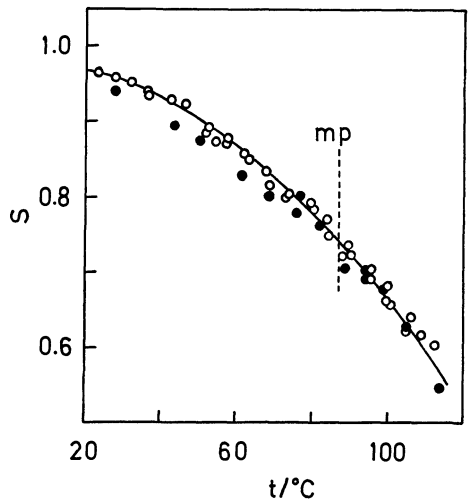

Fig. 2. Temperature dependence of the parameter S in pyrene–dinitrochlorobenzene. The open and shaded circles are for two independent runs.

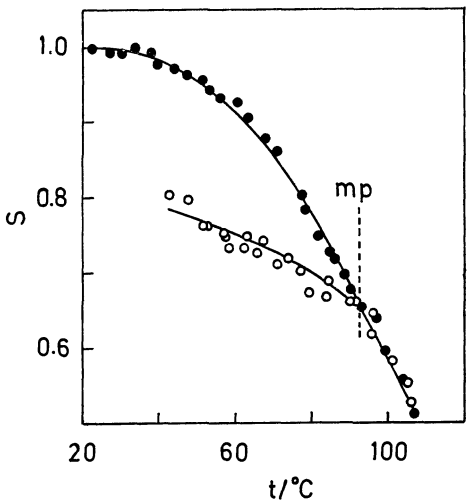

Fig. 3. Temperature dependence of the parameter S in pyrene–dinitrotoluene. The open and shaded circles are for two independent runs.

not very reproducible. In Fig. 3, two independent measurements with the DNT complex are plotted against the temperature. Both the measurements give the same S value, 0.67, at the melting point, 92.5 °C. The open and shaded circles fit on to one curve above this temperature but not below it, suggesting the absence of supercooling of the molten complex. It is unlikely that the difference observed below the melting point arises from a small deviation from the 1 : 1 stoichiometry in the complex for which the lower S values were found. When the complex contains an excess of one of the components, the solid 1 : 1 complex and a liquid coexist in the temperature range from the melting point to the eutectic point. As the probe is generally more soluble in the liquid than in the solid, the observed S value may be largely of the probe in the former phase. If this happens, one expects, in contrast to the observation, that the open circles would lie on the extrapolation of the S-t relation above the melting point. When the temperature is lowered still further, the probe will be more concentrated, eventually leading to the segregation at the eutectic point. As the matter of fact, the segregation was observed at 43 °C, far below the eutectic points, which are 89 °C in the hydrocarbon-rich region and 57.5 °C in the DNT-rich region.[8] Consequently, the large difference in the S values given by these two measurements can be best interpreted in terms of the degree of disorder surrounding the $VO(dbm)_2$ molecules in the solid.

It is well known that dislocations function as a natural haven for solid-state impurities.[9] The large probe molecules may be more satisfactorily accommodated in the expanded region of the dislocation cores and more mobile than elsewhere in the host lattice. On the other hand, Möhwald and Böhm have shown that various guest acceptor molecules can be accommodated in the naphthalene-tetracyanobenzene complex assuming the same very homogeneous orientation as the host donor molecules.[10] In this situation, the motion of the probe molecules does not always occur readily, unless the neighboring host molecules have a large

degree of motion. Thus, the motional behavior of the probe may be dependent upon where the molecules are accommodated which, in turn, may depend on how the melt is quenched.

In addition to the 1 : 1 complex with a congruent melting point, four more pyrene–TNC complexes with mole ratios of 4 : 3, 2 : 1, 3 : 1, and 4 : 1 are known to be formed.[11] The 4 : 3 and 2 : 1 complexes decompose to the solid 1 : 1 complex and a liquid at 136 °C, and the 3 : 1 and 4 : 1 complexes decompose to the solid 2 : 1 complex and a liquid at 126 °C, which is practically the same as the eutectic point. The results obtained with the 1 : 1 and 2 : 1 complexes are illustrated in Fig. 4. The S value at the melting point of the former complex (154.5 °C) is 0.53 and that at the decomposition point of the latter, 0.59. However, the value observed with the 2 : 1 complex at a given temperature above 100 °C is consistently lower than that with the 1 : 1 complex. Thus, the probe molecules are made more mobile as a result of the presence of an excess pyrene in both the molten and solid states. The same tendency was observed with the other TNC complexes containing more pyrene than the 1 : 1 mole ratio. Around 100 °C the S value in the 2 : 1 complex abruptly increases and then becomes almost the same as the value in the 1 : 1 complex. On raising the temperature, a change in the reverse direction occurs between 118 and 125 °C. This change may be associated with the solid-solid transition which was reported earlier to take place at 126 °C.

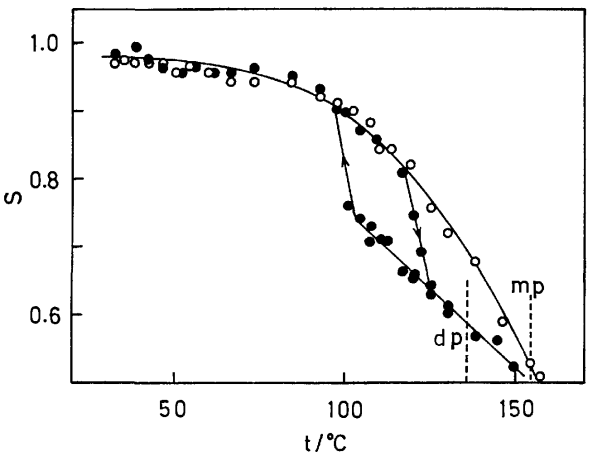

Fig. 4. Temperature dependence of the parameter S in pyrene–trinitrochlorobenzene, the 1 : 1 complex (open circles) and the 2 : 1 complex (shaded circles).

The pyrene complexes with all the aromatic polynitro compounds examined are listed in Table 1 with the S values observed at their melting points. In no case does the value change discontinuously upon solidification. When the molten DNP and TNT complexes are employed as solvents, the outer hyperfine extrema cannot be detected in the ESR spectra near their melting points; however, the extrapolation of the S-t relation obtained with the solid complexes indicates that the required S values are not far from 0.50. Thus, the rapid tumbling of $VO(dbm)_2$ occurs

Table 1. The S values of $VO(dbm)_2$ dissolved in the 1 : 1 molecular complexes at their melting points (Mp), the effective viscosities (η_{eff}) at the same temperatures, and Shinomiya's melting point elevations (τ) (1 cP = 10^{-3} Pa s)

Complex	Mp/K	S	η_{eff}/cP	τ/K
Pyrene-DNB	366	0.68	9.4	−27
Pyrene-DNF	392	0.71	12.1	31
Pyrene-DNC	360	0.73	12.2	−15
Pyrene-DNT	365.5	0.67	9.0	−18
Pyrene-DNP	417	<0.5	5.6	12
Pyrene-TNC	427.5	0.53	6.1	38
Pyrene-TNT	435	<0.5	5.8	46
Fluoranthene-DNB	349.5	0.68	9.0	−23
Fluoranthene-DNF	361	0.71	11.2	9
Fluoranthene-DNC	316	0.90	43.6	−38
Fluoranthene-DNT	346	0.78	15.8	−17
Fluoranthene-DNP	364.5	0.73	12.4	−20
Fluoranthene-TNC	394	0.70	11.1	25
Fluoranthene-TNT	407	<0.5	5.5	39
Phenanthrene-TNC	361	0.78	16.5	−4

in none of these molecular assemblages at their melting points. The parameter S measures the motion around two axes lying in the flat plane including the vanadium atom. When the probe is dissolved in a liquid, this motion is largely governed by the volume of the solvent to be displaced by the probe molecule.[12] The ESR spectrum of $VO(dbm)_2$ dissolved in molten pyrene is essentially isotropic, that is, $S \fallingdotseq 0$. Therefore, the restricted motion in the TNC and TNT complexes, which have melting points a little higher than that of the hydrocarbon, may be considered as evidence for the association of the electron donor and acceptor molecules in the melts. The magnitude of the S value may depend not only on the size of such clusters but also on the concentration. When the melting point of a pyrene complex is much lower than 150 °C, we must deal with the question of how large the temperature dependence of the viscosity is for each complex. As the answer is not available at present, it is difficult to say in such cases whether the effect of cluster formation is really large enough to increase the S value or not. Nevertheless, if two complexes with nearly the same melting points show significantly different S values, the extent of molecular association may be larger in the complex with a larger S value. Three pyrene complexes have their melting points near 90 °C (363 K). Among them the DNC complex exhibits a much larger S value than those of the other two. Furthermore, the viscosity value estimated for the DNF complex is as large as that for the DNC complex, in spite of the melting point being higher by 32 °C. These observations lead qualitatively to the suggestion that the molecular association in these two complexes is considerable.

With the exception of the DNB complex, the pyrene complexes employed here are known to show rather small enthalpies of melting.[13,14] The broad-line NMR measurements clearly indicate the onset of a large degree of thermal motion in the crystalline complexes

upon polymorphic transitions.[14] The motion of $VO(dbm)_2$ observed in these complexes seems to be consistent with these earlier results. The enthalpy of melting for the DNB complex not included in our previous work was determined to be 29 kJ mol^{-1} which is slightly larger than the others.[15] Except in the case of the 2 : 1 TNC complex shown in Fig. 4, the solid-solid transition could not be detected by the variation of S with temperature. This observation is probably due to the fact that the high-temperature forms can be readily supercooled.[13]

The ESR measurements were extended to the fluoranthene complexes where the donor molecule is isomeric to pyrene. Their enthalpies of melting are as low as those of the pyrene complexes; namely, 18 to 35 kJ mol^{-1}.[15] The S values measured at the melting points and the effective viscosities at the same temperatures are summarized in Table 1. The fluoranthene complexes melt at lower temperatures by 16 to 52 °C compared with the corresponding pyrene complexes. The difference in the melting point is especially large when the acceptors are DNC and DNP. Since the DNC complex melts at an exceptionally low temperature and gives an unusually high S value and effective viscosity, measurements can be made over a wide temperature range for this particular melt. The composition of the clusters was assumed to be determined by locating the maximum in the S-composition isotherms; therefore, the mixtures with mole ratios of 3 : 2 and 2 : 3 were also examined for this interesting combination. Unfortunately, no deviation from the curve for the 1 : 1 complex could be established. This complex provides a further clue as to the possible molecular association. Fig. 5 shows a plot of the logarithm of effective viscosity against the reciprocal temperature for the 1 : 1 complex. The exponential temperature dependence can be noted above 60 °C, but the increase of the viscosity is considerably greater on approaching and passing the melting point. This behavior may be considered as an indication that molecules pack into clusters, following the argument by Ubbelohde *et al.* made for molten *o*-terphenyl.[16,17]

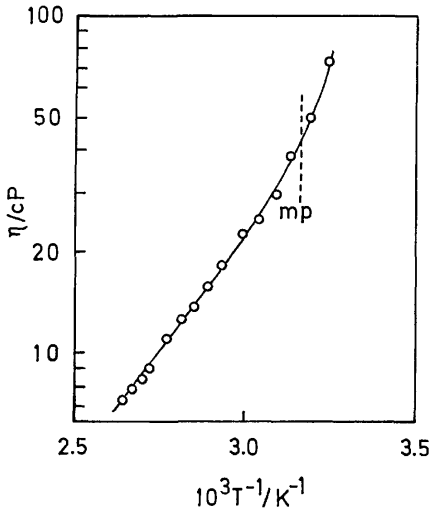

Fig. 5. Temperature dependence of the effective viscosity in fluoranthene-dinitrochlorobenzene.

Nevertheless, it must be emphasized that the high viscosity is largely due to the low melting point and that the value at the melting point may be as large as 36 cP even if the molecular association is absent.

If a complex composed of smaller molecules is selected, the molecular motion above the melting point may be fast enough on an ESR time scale to produce an abrupt increase of the S value upon solidification. With the hope of fulfilling this condition, we examined the ESR spectra of $VO(dbm)_2$ dissolved in the phenanthrene–TNC complex melting at 88 °C and the naphthalene-DNP complex melting at 95 °C. The S value in the former complex varies continuously through the melting point. In the melt of the latter, the ESR spectrum of the probe is essentially isotropic at 106 °C, but slightly deviates from it below this temperature. The value in the crystalline state could not be measured because of the segregation of the probe upon solidification.

As we mentioned already, the congruent melting point of a 1 : 1 complex is expected to be lowered when the association in the melt is less extensive. In order to compare the sequence of the complex formation, Shinomiya defined the melting point elevation for a 1 : 1 complex by

$$\tau = t_C - (t_D + t_A)/2,$$

where t_C is the melting point of the complex and t_D and t_A are the melting points of the donor and acceptor compounds respectively.[18] As we have seen, the large S value of a complex with a low melting point is mostly attributable to the exponential temperature dependence of the viscosity of the medium; therefore, no correlation between the parameters τ and S could be found.

References

1) J. Kendall, A. W. Davidson, and H. Adler, *J. Am. Chem. Soc.*, **43**, 1481 (1921).
2) W. Schottky, H. Ulich, and C. Wagner, "Thermodynamik," Springer, Berlin (1929) pp. 400—402.
3) R. P. Rastogi, *J. Chem. Educ.*, **41**, 443 (1964).
4) Y. Matsunaga, *Bull. Chem. Soc. Jpn.*, **51**, 422 (1978).
5) J. Selbin, G. Maus, and D. L. Johnson, *J. Inorg. Nucl. Chem.*, **29**, 1735 (1967).
6) J. Feldman, P. Pantages, and M. Orchin, *J. Am. Chem. Soc.*, **73**, 4341 (1951).
7) R. J. Greet and D. Turnbull, *J. Chem. Phys.*, **46**, 1243 (1967).
8) C. Shinomiya, *Bull. Chem. Soc. Jpn.*, **15**, 259 (1940).
9) J. M. Thomas, *Chem. Brit.*, **6**, 60 (1970).
10) H. Möhwald and A. Böhm, *Z. Naturforsch.*, **31a**, 1324 (1976).
11) M. Bando and Y. Matsunaga, *Bull. Chem. Soc. Jpn.*, **49**, 3345 (1976).
12) H. J. Stoklosa, H. L. Huffman, and J. R. Wasson, *J. Inorg. Nucl. Chem.*, **35**, 2584 (1973).
13) N. Inoue and Y. Matsunaga, *Bull. Chem. Soc. Jpn.*, **51**, 90 (1978).
14) T. Inabe, Y. Matsunaga, and Y. Yoshida, *Bull. Chem. Soc. Jpn.*, **52**, 615 (1979).
15) M. Nanba, B. Sc. thesis, Hokkaido University (1978).
16) J. N. Andrews and A. R. Ubbelohde, *Proc. R. Soc. London, Ser. A*, **228**, 435 (1955).
17) E. McLaughlin and A. R. Ubbelohde, *Trans. Faraday Soc.*, **54**, 1804 (1958).
18) C. Shinomiya, *Bull. Chem. Soc. Jpn.*, **15**, 92 (1940).

An ESR Study on the Working States of a Pure V_2O_5 Crystal under the CO-oxidation

Yoshiya KERA* and Keiji KUWATA

Department of Chemistry, Faculty of Science, Osaka University, Toyonaka, Osaka 560

(Received August 29, 1978)

The V_2O_5 crystal, prepared from the pure V_2O_5 powder by a zone-melting method in the air, did not show any ESR signal. When the crystal came into contact with a mixture of CO and O_2 ($(CO/O_2)\geq 4$), an ESR spectrum with the hfs of 15-lines ($g_{//}=1.932$, $g_{\perp}=1.978$; $\langle g\rangle=1.963$), which has been previously ascribed to an oxygen defect, was found at the beginning, but after prolonged contact a sharp spectrum ($\langle g\rangle=1.954$) appeared. The intensity of the hf-lines was constant but that of the sharp spectrum increased with the contact time. The *g*-value and line shape of both spectra did not change with the contact time. The same spectra were also found in the crystal grown under a mixture of CO and O_2. On the thermal decomposition of pure NH_4VO_3 *in vacuo* a similar spectrum with a sharp line was found. The *g*-value became lower in the sample reduced further by SO_2 after the thermal decomposition. With reference to the data of TGA, DTA, magnetic susceptibility (χ_{mol}), and X-ray analysis of the vanadium oxides, the sharp spectrum was ascribed to a lower oxide or oxide state such as V_3O_7. Based on the ESR results, the working state of pure V_2O_5 crystal under CO-oxidation and its catalytic property are discussed.

Many phases, described by the general formulas of $V_{2m}O_{5m-2}$ ($m=3$, 4, (5), and 6)[1] and V_nO_{2n-1} ($n=3$—9),[2,3] have been found for the vanadium oxides (V_2O_5–V_2O_3). The phase transitions between them have been well explained by the insertions and eliminations of the oxygen planes through the crystal from one side to the other, that is, by "shear planes."[4,5] The excellent properties of the vanadium oxides as catalysts,[6–8] for instance, high selectivities on the partial oxidations of hydrocarbons and the very long life, have been connected to this feature of the vanadium oxides, that the insertions and the eliminations of the oxygen can occur easily and reversibly during the phase transitions. Many authors[9–20] have discussed the catalytic mechanisms and the working states of vanadium oxide catalysts.

Recently, the X-ray analyses on the crystal structures of V_3O_7[21] and V_4O_9[22] have been accurately done. The crystal structures of the oxides were not so simple as to be induced from that of V_2O_5 based on the idea of the shear plane. The recent TGA and DTA studies on the vanadium–oxygen system have shown that the appearances and disappearances of the intermediate phases depend delicately upon the experimental conditions.[23–25] Furthermore, it has recently been made clear that vanadium oxides easily take several kinds of metals into the lattices and form several types of "vanadium bronzes."[26] The properties of the bronzes complicatedly depend upon the kinds and the contents of metallic impurities. Therefore, catalytic properties of vanadium oxide should be further investigated by taking the results, obtained recently on the oxide, into consideration.

Our kinetic work,[27] which was carried out on several types of the V_2O_5 crystals over wide ranges of the (CO/O_2) ratios, the total pressures, and the temperatures, suggested that even small amounts of metal impurities gave great effects to the catalytic activities and to the working states of the surface. Especially, it was noticed that, during the course of CO-oxidation on the highly purified thin plate crystallines of V_2O_5, the activation energy changed abruptly from a low (2.3 kcal/mol) to a high value (29 kcal/mol) even under the stoichiometric mixture of CO and O_2; the $(CO/O_2)=2.1$. The change in the activation energy suggested the change in the working state from V_2O_5 to some lower oxide.

In the present paper, the working states of the highly purified V_2O_5 crystal during the CO-oxidation was investigated by means of ESR spectroscopy. The problem of which phase or state of vanadium oxides is effective for promoting the catalysis is discussed, especially for the pure crystal.

Experimental

Materials. NH_4VO_3 was chemically purified according to the procedures of McCarley *et al.*[28] and Haemers.[29] Pure V_2O_5 powder was obtained by the thermal decomposition of the purified NH_4VO_3. The single crystals of the pure V_2O_5 were prepared by a zone-melting method, as is mentioned in detail below.

Procedures. The single crystals of V_2O_5 were prepared as follows: a Pt-boat, which contained the purified V_2O_5 powder of about 5.3 g, was placed in a quartz tube (volume, *ca.* 157 cm^3) and then a zone-melting furnance was driven along the quartz tube. The atmosphere in the tube was controlled by varying the ratio and the total pressure of the mixture of CO and O_2. In the preparation under the air, one end of the tube was opened to the air. The width of the melting zone and the maximum temperature in the zone were 1.5 cm and 720 °C, respectively.

The single crystal of V_2O_5, which was prepared in the air and cut down in the proper size, was taken into a quartz tube (0.4 cm in inner diameter) for the measurement of ESR. The tube was gradually jointed with a glass tube (0.8 cm in the inner diameter) for the connection to a vacuum line. After the sample tube was heated preliminarily *in vacuo*, a given amount of the reaction gas was introduced at room temperature, and then the tube was sealed. The reaction tube was heated and was quenched in ice–water just before the ESR measurements. The reaction conditions are summarized in Table 1.

Some purified NH_4VO_3 powder, 0.123 g, was taken in each of the three quartz tubes for the ESR measurements. One of the tubes was opened to the air and the others were connected to a vacuum line. They were heated at 550 °C for 3 h. After heating, both the open tube and one of the

Table 1. The conditions of the contact of the pure V_2O_5 crystals with the reactants of CO and O_2
(Volume of ESR measurement tube sealed: 4 cm^3, temperatures: 460 and 560 °C)

Sample	CO Torr	O_2 Torr	(CO/O_2)	V_2O_5 g	("excess-CO"/V_2O_5)[a] mole ratio
S-S-1	330	20	16	0.182	0.07
S-S-2	352	88	4	0.182	0.04
S-S-3	88	22	4	0.115	0.016
S-S-4	32	8	4	0.115	0.006

a) "excess-CO": the amount of CO which remained after the equilibrium of the CO-oxidation, $CO+O_2/2=CO_2$, was achieved.

evacuated tubes were sealed and then the ESR were measured. The other evacuated tube was filled with SO_2 gas at 724 Torr (1 Torr$=1.333\times10^2$ Pa) after it was cooled down to room temperature and then was sealed. The inner volume of the tube was about 4 cm^3. The sample tube was again heated at 585 °C and, after quenching the tube in ice–water, ESR measurements were done.

ESR Measurements. ESR measurements and the determinations of the spin concentrations were done with the same procedure as was mentioned in the previous papers.[30]

Results

ESR Spectra in the V_2O_5 Crystal Prepared under Various Atmospheres. No ESR spectrum was found for the V_2O_5 crystal prepared in the air. In the V_2O_5 crystal prepared under the mixture of CO and O_2 $(CO/O_2=4)$ at the total pressure of 200 Torr, however, a spectrum with the well-resolved hfs of 15-lines ($A_{//}=8.2$, $A_\perp=4.6$ mT) was found, as was illustrated in Fig. 1(a). On the other hand, in the crystal, prepared under the mixture of CO and O_2 $(CO/O_2=16)$ at the total pressure of 350 Torr, a new sharp line appeared near the center of the hfs of 15-lines, as was shown in Fig. 1(b). In this case, the resolution of the hfs-lines was also good, although the crystallinities seemed to be not so good as for the single crystal.

Those samples showed neither fine structure nor the half resonance in ESR due to the spin-spin interaction for the spin state of $S=1$ or higher. Thus, both spectra could be ascribed to the state of $S=1/2$.

The ESR parameters—the g-values, hf-coupling constants, and the line widths—are given in Table 2. Table 2 indicates that the center of the sharp line differs a little bit from that of the hfs. The relative intensities of the hfs-lines to DPPH in Figs. 1(a) and 1(b) seem to be approximately equal to each other.

Table 2. ESR spectra in the pure V_2O_5 crystals grown under various atmospheres

Conditions of preparation	ESR parameters: g-tensor $\langle g\rangle$	ESR parameters: A-tensor $\langle A\rangle$(mT)	Line widths (mT)[a]: low field	Line widths (mT)[a]: high field
In air	No spectrum			
$CO/O_2=4$, 200 Torr	1.964 ($g_{//}\approx1.939$, $g_\perp\approx1.976$)	5.8 ($A_{//}\approx8.2$, $A_\perp\approx4.6$)	—	—
$CO/O_2=16$ 350 Torr	1.954	—	3.1	4.3

a) The distances from the low field peak of the first derivative curve of the spectrum to the center and from the center to the high field peak were indepently estimated in the estimation of the line width.

The ESR Spectrum for the Highly Purified V_2O_5 Crystal in Contact with the Mixture of CO and O_2. The ESR spectra which appeared for the pure V_2O_5 crystals in contact with the mixture of CO and O_2 are illustrated in Fig. 2. In the Figure, the larger the (CO/O_2) ratio and the total pressure and the longer the contact time, the larger the intensity of the sharp line becomes. In the S-S-4 after the contact of 49 h at 460 °C, only the spectrum with the hfs of 15-lines is seen, but in the S-S-3 after the contact of 49 h, a sharp line appeared together with the hfs-lines, although it is rather weak. In the S-S-2 after the contact of 72 h and in

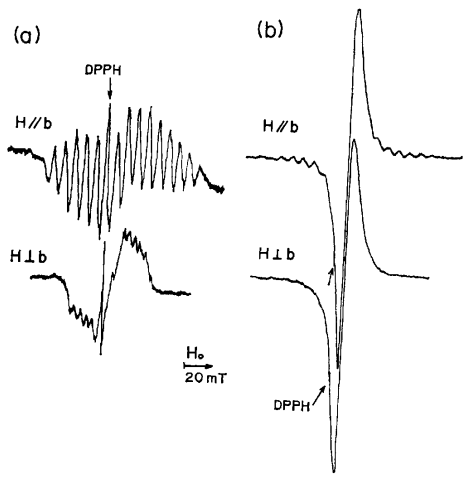

Fig. 1. ESR spectra in the pure V_2O_5 crystals grown under the reactants of CO and O_2. (a) $P_{total}=200$ Torr, $CO/O_2=4$, and the mean composition$=V_2O_{4.975}$ (b) $P_{total}=350$ Torr, $CO/O_2=16$, and the mean composition$=V_2O_{4.90}$.

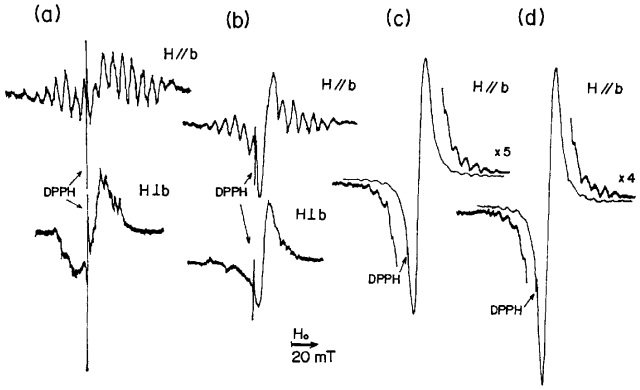

Fig. 2. ESR spectra in the pure V_2O_5 crystal on the contact with the reactants of CO and O_2 at 460 °C; (a) the sample S-S-4 in Table 1 after the contact for 49 h, (b) the sample S-S-3 after the contact for 49 h, (c) the sample S-S-2 after the contact for 71 h, (d) the sample S-S-1 after the contact for 115 h.

TABLE 3. ESR SPECTRA IN THE PURE V_2O_5 CRYSTALS IN CONTACT WITH THE REACTANTS OF CO AND O_2

Sample	Condition of reaction	ESR parameters		Line widths (mT)	
		g-tensor $\langle g \rangle$	A-tensor A(mT)	low field	high field
S-S-4	460 °C 49 h	1.963 $g_{//} \approx 1.932$ $g_{\perp} \approx 1.978$	$A_{//} \approx 8.2$ $A_{\perp}$ —	—	—
S-S-3	460 °C 49 h	1.954	—	37	43
S-S-1 —S-S-4	460 °C 250 h	1.954 ±0.002	—	34	50
S-S-1 —S-S-4	560 °C 240 h	1.954 ±0.002	—	34	47

the S-S-1 after the contact of 115 h, the intensity of the sharp line increased considerably.

Figures 2(a)—2(d) indicate that the intensity of the sharp line increases depending upon contact time and the amount of the excess-CO, and, on the other hand, that of the hfs-lines does not depend on the contact time or on the amount of the excess-CO. This is seen in comparisons of the intensities of the spectra with that of DPPH. During the contact for 250 h an increase in the intensities of the sharp spectrum was found in all samples, S-S-1—S-S-4, but the line shape and the position of the center did not deviate from those at the very start. Even during further contact for 240 h at 560 °C, the intensities of the spectrum in all samples still increased and the shape and the position of the center were also kept constant. The ESR parameters of the spectra are summarized in Table 3.

The line shape of the sharp spectrum varied with the temperature of the measurements : the linewidth became larger at 300 K than that at 77 K. As an example, the spectrum in the S-S-3 after the contact for 240 h at 560 °C is given in Fig. 3. The broadening of the spectrum at room temperature would be caused by the shortening of the spin-lattice relaxation time. The growth of the sharp spectrum in the S-S-1—the S-S-4 at 460 °C and 560 °C are shown in Fig. 4. The growth of the sharp spectrum is seen at 560 °C to be linear against the amount of the excess-CO for

Fig. 3. The changes in the line width of the sharp spectrum with the temperatures of measurement.

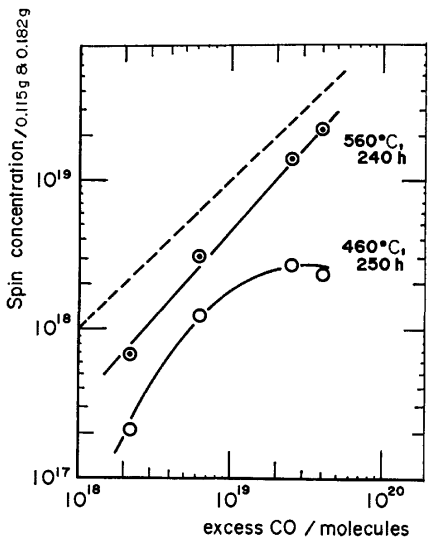

Fig. 4. The relations of the intensities of the sharp spectrum with the excess-CO. The dotted line indicates the spin concentration, expected in the crystal on complete consumption of the excess-CO.

the contact for 240 h, but at 460 °C in the runs with the higher contents of CO (S-S-3 and S-S-4) such linearity is not found. These findings might correspond to the fact that at 460 °C the process in the reduction of the surface is more rapid than the process in the diffusion into the bulk, while at 560 °C both processes are comparable. Table 3 shows that the ESR parameters of the sharp spectrum are constant without regard to the intensity of the spectrum, as was pointed out above.

After the contact with the mixture of CO and O_2 for a long time, the color of the crystal changed from bright brown to dark brown, but the brilliance of the (010) plane exposed to the surface from the start still remained after such treatments. The result was similar to that for the contact with the mixture of SO_2 and O_2.[30]

ESR Spectra in the Vanadium Oxides, Obtained by the Thermal Decomposition of the Highly Purified NH_4VO_3 and Then by the Reduction with SO_2. In the sample obtained by the thermal decomposition of the purified NH_4VO_3 powder in the air, no ESR signal was found, *cf.* Fig. 5(a). After treatment of the sample with SO_2

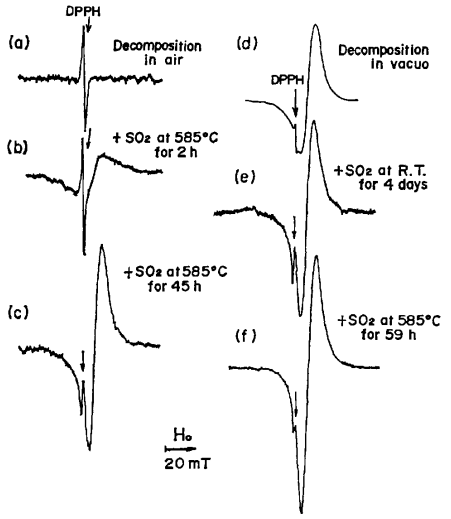

Fig. 5. ESR spectrum found on the thermal decompositions of the pure NH_4VO_3 and then the changes in the spectrum by the contact with SO_2.

at 585 °C, an ESR spectrum grew, as illustrated in Figs. 5(b) and 5(c). In the sample obtained by the thermal decomposition under a vacuum, an ESR spectrum appeared, as is shown in Fig. 5(d). By further treatment of the sample by SO_2, the spectrum changed, as illustrated in Figs. 5(e) and 5(f).

Discussion

The ESR Spectra in the CO–O_2–V_2O_5 System. The ESR spectrum with the hfs of 15-lines was found in the V_2O_5 crystal, which was prepared under the mixture of CO and O_2 (rather weakly reductive), as is shown in Fig. 1(a). After the contact with the mixture of CO and O_2 for a short time, the same spectrum appeared in the crystal in which no ESR signal had been detected initially as is shown in Fig. 2(a). A quite similar spectrum has also been found in the crystal treated with a mixture of SO_2 and O_2 at the initial stage. The spectrum was assigned to a V^{4+}—V^{5+} pair, accompanied by an oxygen defect.[30] On the other hand, in the two cases in which the V_2O_5 crystal was prepared under the mixture of CO and O_2 (rather strongly reductive) and was brought into contact with such a mixture, a new sharp spectrum appeared in the crystal, together with the hf-lines, as shown in Figs. 1(b), 2(c), and 2(d). Since the centers of both spectra were different, the sharp line did not seem to be ascribed simply to the exchange narrowed line of the hfs of 15-lines. The sharp line could be ascribed to a lower oxide phase or a lower oxide state of vanadium oxides, by taking into consideration the results that the ESR parameters of the sharp spectrum are constant without regard to the intensity of the spectrum, as was mentioned above.

According to the phase diagram of the vanadium–oxygen system by Kachi and Kosuge *et al.*,[31] the only phase which can coexist thermodynamically with V_2O_5 is V_3O_7. They[8] also measured the magnetic susceptibility (χ_{mol}) of V_3O_7, V_6O_{13}, and VO_2 and estimated μ_{eff} by using these equations: $\chi_{mol}=C/T-\theta$ and $\mu_{eff}=2.83\sqrt{C}$. The μ_{eff} (=1.32) in V_3O_7 seems to be rather well in accordance with the μ_{calcd} (=1.00), calculated under the assumption that V^{4+} ions were isolated and their concentration was given by the composition of ($V_2O_4 \cdot 2V_2O_5$). In the case of V_6O_{13} the μ_{eff} (=1.92) is not very consistent with the μ_{calcd} (=1.41) calculated using similar procedures, and in the case of VO_2 the μ_{eff} (=2.96) and the μ_{calcd} (=1.73) are quite different from each other. In V_6O_{13} and VO_2, therefore, the spin state of V^{4+} ions in the crystals would not be so simple as that of V_3O_7. From these considerations, the sharp spectrum can be ascribed to the V_3O_7 phase. The slight difference between the μ_{eff} and μ_{calcd} in V_3O_7 suggests that V^{4+} ions are not isolated completely in the V_3O_7 phase. If the V^{4+} ions were isolated completely in the crystal, it should give the hf-coupling with a nuclear spin of ^{51}V ($I=7/2$) and thus the hfs of 8-lines should be found. But infact only a sharp line has been found because of the exchange narrowing.

On heating the pure V_2O_5 crystal at 160 °C and 300 °C under high vacuum (10^{-6} Torr) for a long period, Gillis and Boesman[38] observed the growth of a new sharp spectrum, the center of which was approximately consistent with that of hfs of 15-lines. From the consistency of both centers of the spectra, the growth of the spectrum seems to correspond to a preliminary step before the phase transition, $V_2O_5 \rightarrow V_3O_7$: for instance, the clustering of the oxygen vacancies.

The ESR Spectra Found for the Thermal Decompositions of the Pure NH_4VO_3 and Then for the Reductions by SO_2. In the DTA and TGA studies on NH_4VO_3 by Taniguchi *et al.*,[24] NH_4VO_3 changed to V_2O_5 by the decompositions in the air stream and to V_3O_7 *in vacuo*. Furthermore, their results suggested that the V_3O_7 was reduced to V_6O_{13} by a butadiene stream, and the V_2O_5 was reduced by SO_2 stepwise : $V_2O_5 \rightarrow V_4O_9 \rightarrow V_6O_{13} \rightarrow VO_x$ ($x \fallingdotseq 2$). With reference to these results, the changes in the ESR parameters with the thermal decompositions and then with the reductions by SO_2, as shown in Table 4, might be explained as follows. The spectrum of $\langle g \rangle = 1.956$, obtained on the thermal decomposition *in vacuo*, is ascribed to the V_3O_7 phase and the decrease in the g-value on the reduction by SO_2, $\langle g \rangle = 1.956 \rightarrow 1.947$, is caused by the process, $V_3O_7 \rightarrow$

Table 4. The ESR spectrum found for the thermal decomposition of a pure NH_4VO_3 and the change in the spectrum with the reduction by SO_2

Condition of reaction	ESR parameter g-tensor $\langle g \rangle$	Line widths (mT)	
In air dec	No spectrum		
$+SO_2$ heating for 45 h	1.949	4.9	5.4
Evac. dec	1.956	4.2	6.2
$+SO_2$ at RT standing for 4 days	1.953	4.6	5.3
$+SO_2$ heating for 59 h	1.947	4.5	6.0

V_4O_9 or V_6O_{13}. The decrease in the g-value, accompanied by the appearence of some lower oxides or some lower oxide states, can be understood by taking a change in the symmetry of the crystal field around the vanadium(IV) ion into consideration, as is discussed below.

The V_2O_5 crystal is constructed from a kind of octahedron unit, which distorts quite a bit, as shown in Fig. 6.[32] In VO_2 (rutile type)[33] the octahedron is close to a proper one. In the intermediate phases : V_3O_7,[21] V_4O_9,[22] and V_6O_{13},[34] three or four types of the octahedron unit are contained in the crystals. To show the comparisons of the V–O distances in the octahedron among the phases, Table 6 was prepared. For the intermediate phases, the V–O distances were evaluated as the simple means of those in all octahedrons. In Table 6, the V–O(1) increases gradually, except for the V_6O_{13}, and on the contrary the V–O(6) decreases with the progress in the reduction. This means that the octahedron in the vanadium oxides changes gradually from a highly distorted structure to a proper one with the progress in the reduction, that is, the degree of the deviation of the V(IV) ion from the O(2)–O(3)–O(4)–O(5) plane becomes small, except for V_6O_{13}. The crystal field splittings of V(IV) ions in TiO_2(rutile) and VO_2 crystals have been given by Simizu[36] and Grunin *et al.*,[37] as in Fig. 7(a). In the higher oxides the splittings probably change as in Fig. 7(b), because the V(IV) ion deviates further

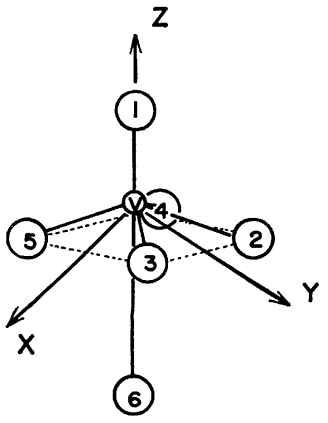

Fig. 6. The VO_6 octahedron unit in V_2O_5 crystal (Ref. 32); small circle: vanadium ion and large circle: oxygen ions.

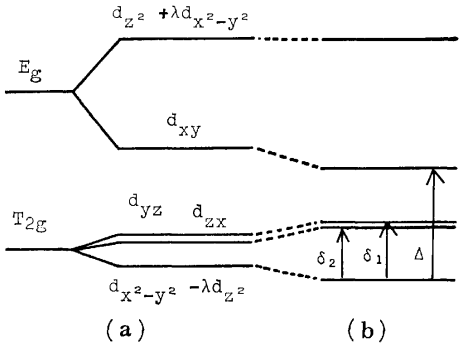

Fig. 7. Schematical view on the changes in the energy diagram for the d-orbitals of the vanadium ion in the VO_6 octahedron with the progress in the oxidation and the reduction of vanadium oxides; (a) the energy diagram for the VO_6 unit in the VO_2 crystal (Refs. 36 and 37) and (b) that in higher oxides than VO_2.

up from the oxygen square plane. The higher the oxidation states, the larger the δ becomes, while the Δ becomes a little smaller (or remains almost constant). The g-value can be roughly estimated by the familiar equations : $g_{zz}=g_0-4\lambda/\Delta$, $g_{xx}=g_0-\lambda/\delta_1$ and $g_{yy}=g_0-\lambda/\delta_2$, where λ is the spin-orbit coupling constant. Therefore, with the progress in the reduction, the following changes in the g-values will be expected : $g_{zz}\rightarrow$increase slightly (or remain constant), and g_{xx} and $g_{yy}\rightarrow$decrease quite a bit.

For the V(IV) ion in the V_2O_5 crystals, $\langle g\rangle \fallingdotseq 1.975$ and g_{xx}, $g_{yy}>g_{zz}$ have been reported.[38] On the other hand, in the V(IV) ion in VO_2 crystal, $\langle g\rangle=1.916$ was given.[37] The g-values of the V(IV) ions deped in TiO_2, SnO_2, and GeO_2 were $\langle g\rangle=1.927$, 1.928, and 1.935, respectively.[39] The tendency of the changes in the g-values is quite consistent with that expected above. The g-value in the spectrum found for the thermal decomposition of NH_4VO_3 *in vacuo*, $\langle g\rangle=1.956$, and also that for the reduction by SO_2, $\langle g\rangle=1.947$, given in Table 4, are also well understood according to the above discussion. That is, the changes in the g-values from 1.975 to 1.956 may correspond to the process, $V_2O_5\rightarrow V_3O_7$, and the change from 1.956 to 1.947, to the process, $V_3O_7\rightarrow V_4O_9$ or V_6O_{13}.

Recently, Kawashima *et al.*[25] examined in detail the process of the reduction of V_2O_5 by SO_2 by means of the TGA and the X-ray analysis. The processes

TABLE 5. THE COMPARISONS OF THE V-O DISTANCES AMONG THE VO_6 OCTAHEDRON UNITS CONTAINED IN THE VANADIUM OXIDES BETWEEN V_2O_5 AND VO_2 (V_3O_7, V_4O_9, and V_6O_{13} are constructed from two or three kinds of the octahedron units. The simple mean values of the octahedrons were given in the oxides.)

Compound	V-O_1	V-O_2	V-O_3	V-O_4	V-O_5	V-O_6	Ref.
V_2O_5	1.595	1.780	1.878	1.878	2.021	2.785	32)
V_3O_7	1.624	1.812	1.946	1.952	1.984	2.690	21)
V_4O_9	1.629	1.891	1.897	1.931	1.974	2.531	22)
V_6O_{13}[a]	1.906	1.835	1.865	1.835	2.086	2.375	34)
VO_2(rutile)	1.76	1.87	1.86	2.01	2.03	2.05	33)

a) Since certain values of the V-O distances have not been given for the V_6O_{13}, the authors estimated roughly, according to the data of Aebi.

in the reduction were found to occur stepwise and the phases described by the general formula of V_nO_{2n-1} appeared successively. However, the appearance and disappearance of the intermediate phases depended delicately and complicatedly upon the experimental conditions: for instance, the flow rates of the reductants, the partial pressures, the temperatures, the states of the pilling of the powder, and so on. According to their results, the present ESR spectra and the parameters found on the thermal decomposition of NH_4VO_3 and then on the reduction, are probably composite values.

The Growth of the V_2O_5 Crystal and Its Coexisting Phase under Oxidative and Reductive Atmospheres. Similar spectra to those shown in Figs. 1(a) and 1(b) have been found in the pure and doped V_2O_5 crystals. Ioffe *et al.*[38] have regarded the spectrum as caused by metal impurities, since the spectrum became more intensive in proportion to the contents of metal impurities. On the other hand, the spectrum was ascribed to the oxygen defect by Gillis *et al.*,[38] as was mentioned above. The fact that no ESR signal was found in the crystal of the V_2O_5 prepared in the tube opened to the air suggests that the concentrations of the impurities and the oxygen defects were below the sensitivity in the detection, that is, the starting material had been fully purified and the growth of the single crystal was accomplished under the condition of equilibrium. It means, furthermore, that the equilibrium pressure of the oxygen at the decomposition of the non-stoichiometric phase ($V_2O_{5-\delta}$) was very low, as compared to the partial pressure of oxygen in the air even at such a high temperature as the melting point of the V_2O_5 (*ca.* 670 °C).

In the case of the crystal prepared under the mixture of CO and O_2 ($CO/O_2=4$) at the total pressure of 200 Torr, only the spectrum ascribed to the oxygen defect was found, as discussed above. Since in the system the (excess-CO/V_2O_5) ratio is estimated to be 0.025, the non-stoichiometric region of V_2O_5 will extend at least up to $V_2O_{4.975}$ near the temperature of 670 °C. On the other hand, in the crystal prepared under the mixture of CO and O_2($CO/O_2=16$) at the total pressure of 390 Torr, a strong sharp spectrum, ascribed to a phase like V_3O_7, appeared in addition to the hfs-lines, as discussed above. In this case, the (excess-CO/V_2O_5) ratio was estimated to be 0.10. Thus the composition of $V_2O_{4.90}$ should be realized, if the equilibrium between the gaseous phase and the solid has been kept fixed throughout the crystal growth. That is, the non-stoichiometric phase of V_2O_5 would not extend up to $V_2O_{4.90}$.

The Change in the Surface States of the Highly Purified V_2O_5 Crystal during the CO-oxidation. The pure V_2O_5 crystal, kept under the conditions of the CO-oxidation (rather reductive atmosphere), showed a sharp spectrum, accompanied with the spectrum with the hfs of 15-lines. The line shape and the *g*-value of the ESR spectra were completely consistent with that in the crystal grown under a similar atmosphere. Both the line shape and the $\langle g \rangle$ were kept constant from the beginning of the appearence without depending on the (CO/O_2) ratio, the partial pressures of CO, the temperatures, or the reaction time. From the beginning the center of the sharp spectrum already differed from that of the hfs-lines, as seen in Fig. 2(b) and Table 3. This finding suggests the coexistence of the non-stoichiometric phase of the V_2O_5 and the V_3O_7 near the surface from the initial stage of the reduction. The intensity of the sharp lines increased gradually with the time, while that of the hfs-lines did not vary, as the comparison of the intensity with DPPH in Figs. 2 and 3 will show. This means probably that the other phases of the lower oxides did not exist in the crystal even locally. This idea will be supported by the fact that, although the color of the crystal varied from bright brown to dark brown, the brilliance of the (010) surface was always kept. The results of the isotopic exchange of oxygen also suggest that the mobility of the lattice oxygen was stimulated abruptly at above 500 °C.[40] Therefore, at least at such a high temperature as 560 °C, the highly purified V_2O_5 crystal is reduced homogeneously and gradually from the surface toward the bulk during the CO-oxidation (under rather reductive atmosphere).

The result obtained in a previous paper,[27] the abrupt change in the activation energy from the lower value to the higher during the CO-oxidation, could be related to the change in the surface states from the nonstoichiometric V_2O_5 to a lower oxides like as V_3O_7. The fact that, on the contrary, such a change in the working state was not seen for the unpurified crystal,[27] suggests that very little amounts of metal impurities play some important roles in preventing the change in working state. This subject is a future problem for the solid state chemistry on vanadium bronzes.

References

1) A. D. Wadsley, *Acta Crystallogr.*, **10**, 261 (1957).
2) S. Andersson and A. Magnéli, *Acta Chem. Scand.*, **8**, 1641 (1957); S. Andersson and L. Jahnberg, *Ark. Kemi.*, **21**, 413 (1966).
3) G. Andersson, *Acta Chem. Scand.*, **8**, 1599 (1954).
4) A. D. Wadslay, "Nonstoichiometric Compounds," ed by L. Mandelcorn, Acad. Press (1964).
5) J. S. Anderson and B. G. Hyde, *J. Phys. Chem. Solids*, **28**, 1393 (1967).
6) G. L. Simard, J. F. Steger, R. J. Arnott, and L. A. Siegel, *Ind. Eng. Chem.*, **47**, 1424 (1955).
7) E. Gillis, *Compt. Rend.*, **258**, 4765 (1964).
8) T. Toda, K. Kosuge, and S. Kachi, *Nippon Kagaku Zasshi*, **87**, 1311 (1966); S. Kachi, K. Kosuge, U. Shiotani, and N. Nakanishi, *Shokubai*, **10**, 1103 (1968); K. Kosuge, *J. Jpn. Soc. Powder and Powder Metal.*, **15**, 400 (1969).
9) P. Mars and D. W. Krevelen, *Chem. Eng. Sci. (Spec. Suppl.)*, **3**, 41 (1954).
10) V. A. Roiter, *Kinet. Katal.*, **1**, 63 (1960).
11) L. Ya Margolis, *Adv. Catal.* **14**, 429 (1963).
12) V. Ya. Vol'fson, L. N. Ganyuk, and E. F. Totskaya, *Kinet. Katal.*, **5**, 1100 (1964); V. Ya. Vol'fson, Ya. V. Zhigailo, E. F. Tatskaya, and V. V. Raksha, *ibid.*, **6**, 162 (1965).
13) T. Vrbaski, *J. Phys. Chem.*, **69**, 3092 (1965).
14) T. Seiyama, A. Suenaga, and W. Sakai, *Nippon Kagaku Zasshi*, **82**, 292 (1966).
15) H. Schaefer, *Ber. Bunzenges. Phys. Chem.*, **71**, 222 (1967).

16) G. K. Boreskov, *Kinet. Katal.*, **8**, 1020 (1967); **13**, 543 (1972).
17) G. L. Ross and P. H. Calderbank, *Chem. Eng. Sci.*, **26**, 2003 (1971).
18) W. M. H. Sachtler, *Catal. Rev.*, **4**, 27 (1971).
19) P. H. Emmett, *Catal. Rev.*, **7**, 1 (1973).
20) E. I. Andreikov, Yu. A. Sveshnikov, and N. D. Rusýanova, *Kinet. Katal.*, **15**, 1207 (1974); **16**, 919 (1975).
21) S. Andersson, J. Galy, and K. Wilhelmi, *Acta Chem. Scand.*, **24**, 1473 (1970); K. Waltersson, B. Forlund, K. Wilhelmi, S. Andersson, and J. Galy, *Acta Crystallogr.*, **30**, 2644 (1974).
22) K. Wilhelmi and K. Waltersson, *Acta Chem. Scand.*, **24**, 3409 (1970).
23) T. Sata, E. Komada, and Y. Ito, *Kogyo Kagaku Zasshi.*, **71**, 643 (1968); T. Sata and Y. Ito, *ibid.*, **71**, 647 (1968).
24) M. Kato, M. Taniguchi, and T. Kubo, *Kogyo Kagaku Zasshi*, **69**, 2102 (1966); M. Taniguchi, A. Miyazaki, and H. Yokomizo, *Shokubai*, **10**, 53 (1968); M. Taniguchi, S. Kato, and T. Nanao, *ibid.*, **14**, 53 (1972); H. Endo, M. Wakihara, and M. Taniguchi, *Chem. Lett.*, **1974**, 905.
25) K. Kawashima, K. Kosuge, and S. Kachi, *Chem. Lett.*, **1975**, 1131.
26) a) P. Hagenmuller, *Chem. Extended Defects in Non-Metallic Solids*, pp. 91—108, Amsterdam (1970); *Prog. Solid State Chem.*, **5**, 71 (1971); b) M. Nygren, *Chem. Commun. Univ. Stockholm*, 1 (1973).
27) Y. Kera, *Bull. Chem. Soc. Jpn.*, **52**, 888 (1979).
28) R. E. McCarley and J. W. Roddy, *J. Less-Common Met.*, **2**, 29 (1960).
29) J. Haemers, *Bull. Soc. Chim. Belg.*, **79**, 473 (1970).
30) Y. Kera and K. Kuwata, *Bull. Chem. Soc. Jpn.*, **50**, 2438, 2831 (1977).
31) K. Kosuge, T. Takada, and S. Kachi, *J. Phys. Soc. Jpn.*, **18**, 318 (1963); K. Kosuge, *J. Phys. Chem. Solids*, **28**, 1613 (1967).
32) a) A. Byström, K. Wilhelmi, and O. Brotzen, *Acta Chem. Scand.*, **4**, 1119 (1950); b) H. G. Bachman, F. R. Ahmed, and W. H. Barnes, *Z. Kristallogr.*, **115**, 110 (1961).
33) G. Andersson, *Acta Chem. Scand.*, **10**, 623 (1956).
34) F. Aebi, *Helv. Chim. Acta*, **31**, 8 (1948).
35) S. Westman, *Acta Chem. Scand.*, **15**, 217 (1961).
36) T. Shimizu, *J. Phys. Soc. Jpn.*, **23**, 848 (1967).
37) V. S. Grunin, V. A. Ioffe, and I. B. Patrina, *Phys. Status Solidi B*, **63**, 629 (1974).
38) a) J. L. Ragle, *J. Chem. Phys.*, **38**, 2020 (1963); b) E. Gillis and E. Boesman, *Phys. Status Solidi*, **14**, 337 (1966); c) V. A. Ioffe and I. B. Patrina, *Soviet Phys. Solid State*, **10**, 639 (1968); d) K. Hirota, K. Kuwata, and Y. Kera, *Bull. Chem. Soc. Jpn.*, **43**, 3017 (1970).
39) a) G. M. Zverev and A. M. Prokhorov, *Soviet Phys. -JETP*, **12**, 160 (1960); b) H. T. Gerritsen and H. R. Lewis, *Phys. Rev.*, **119**, 1010 (1960); c) C. Kikuchi, I. Chen, W. H. From, and P. B. Dorin, *J. Chem. Phys.*, **42**, 181 (1965); d) I. Siegel, *Phys. Rev. A.*, **134**, 193 (1964).
40) a) E. R. S. Winter, *Adv. Catal.*, **10**, 196 (1958); *J. Chem. Soc.*, 2889 (1968); b) G. K. Boreskov, *Adv. Catal.*, **15**, 285 (1964).

Nuclear Magnetic Resonance Studies of the Cu-chlorophyllin Complex with Flavine Mononucleotide

Koe ENMANJI*

Department of Chemistry, Faculty of Science, Kyoto University, Kyoto 606

(Received September 1, 1978)

The NMR relaxation time of the Cu-chlorophyllin (Cu-chln)–flavine mononucleotide (FMN) complex was measured, and its geometrical structure was proposed. The complex has an absorption band at 700 nm which is attributed to complex formation by analogy with the chlorophyll a–FMN complex. Its binding constant is 330 l/mol at 25 °C; this value is larger than those of other Cu-chln complexes. From the analysis of its ESR data, it is clear that the greater part of the electron spin in Cu-chln is distributed on the Cu^{2+} ion. The distance between the nuclear and electron spins was calculated by measuring the spin-lattice relaxation times. From these results, the distance between the porphyrin ring and the isoalloxazine ring in the Cu-chln–FMN complex molecule is found to be 4.2 Å if the two rings are parallel to each other. The chlorophyll a–FMN complex is assumed to have a similar geometrical structure.

There are various kinds of chlorophylls in the lammela structure of the chloroplast. Most of these chlorophylls are called "antana chlorophylls," which harvest solar energy, and part of them exist as P700, which is the reaction center of Photosystem I. It is generally imagined that P700 is formed by interaction between chlorophyll a and an electron acceptor. Tu and Wang[1] have shown that the optical spectrum of the chlorophyll a–flavine mononucleotide (FMN) complex in an acetone–water mixture has a maximum peak at 700 nm and some characteristics of P700. Though the characteristics of this complex are thought to be related to its structure, the structure of the complex was not discussed in their paper. Because the ground state of this complex is not paramagnetic, it is difficult to presume a geometrical arrangement of each constituent molecule in the complex. Cu-chlorophyllin (Cu-chln) is an interesting molecule since the electron magnetism on it will make it easier to study its interaction with itself and with other molecules by means of magnetic resonance methods. Thus, the interaction of chlorophyllin molecules in solution may be studied easily with Cu-chln as a model compound. In the present study, the interaction of Cu-chln with FMN in an aqueous environment was studied in some detail by means of ESR, optical absorption and NMR spectroscopy.

Experimental

Materials. Mg-chlorophyllin was prepared from spinach by the method of Oster and his coworkers.[2] Cu-chln was obtained from Mg-chlorophyllin by the method of Burdick and Carroll.[3]

FMN, reagent grade (Nakarai Chem. Co.), was used without further purification.

Optical Measurement. The optical spectra were measured with a Hitachi PS-3T-type autorecording spectrometer.

NMR Measurement. The proton, phosphorus-31, and carbon-13 NMR spectra were recorded at 100, 40.5, and 25.15 MHz respectively on a JMN PS-100 system equipped with a pulse Fourier transform unit (PFT-100). The sizes of the sample tubes were 5 mm O.D. for ^1H, 8 mm O.D. for ^{31}P. The spin-lattice relaxation time (T_1) was measured by the 180°-τ-90° pulse method. The repetition times were 30 s for both the ^1H and ^{31}P measurements. The spectra were added 16 times for the ^1H and 64 times for the ^{31}P measurements respectively.

Theoretical

For a system containing paramagnetic metal ions and a large excess of free ligands, with magnetic coupling between the metal and a nucleus in the ligand, the following equation holds under appropriate conditions,[4,5]

$$\frac{1}{T_{1P}} = \frac{1}{T_1^*} - \frac{1}{T_1^\circ} = \frac{f}{T_{1M}+\tau_M}, \quad (1)$$

where T_{1M} is the spin-lattice relaxation time of the ligand in the complex, f is the fractional number of the complexed ligand to the total ligand, T_1° is the relaxation time without a paramagnetic substance, T_1^* is that with a paramagnetic substance, and T_{1P} is the apparent relaxation time. If we consider a system consisting of two spins that undergo an isotropic Brownian motion, the nuclear relaxation rate due to magnetic dipolar interaction between the nucleus and the electron spins is given by[5] (for $\omega_s\tau_c \gg 1$),

$$\frac{1}{T_{1M}} = \frac{2}{15}S(S+1)\frac{\gamma_I^2 g^2\beta^2}{r^6}\cdot\frac{3\tau_c}{1+\omega_I^2\tau_c^2}, \quad (2)$$

where ω_I and ω_s are the Larmor angular frequencies of the nucleous and the electron spin respectively. Hence, T_{1M} is proportional to the sixth power of the distance, r, between the unpaired electron and the nuclei. If τ_c is known, T_{1M} can be converted to the electron nuclear distance by means of Eq. 2. The electron-nuclear distance for various neclei in the molecule can give information as to the geometrical arrangement of the intermolecular complex when information about the distribution of the unpaired electron is available.

Results and Discussion

Distribution of the Unpaired Electron in Cu-chln. The ESR spectrum of Cu-chln in an aqueous solution (10 mmol/l) frozen at 77 K shows an almost smeared-out singlet because of the dipolar and the exchange interactions between electron spins on neighboring

* Present address: Central Research Laboratory, Mitsubishi Electric Corp., Amagasaki 661.

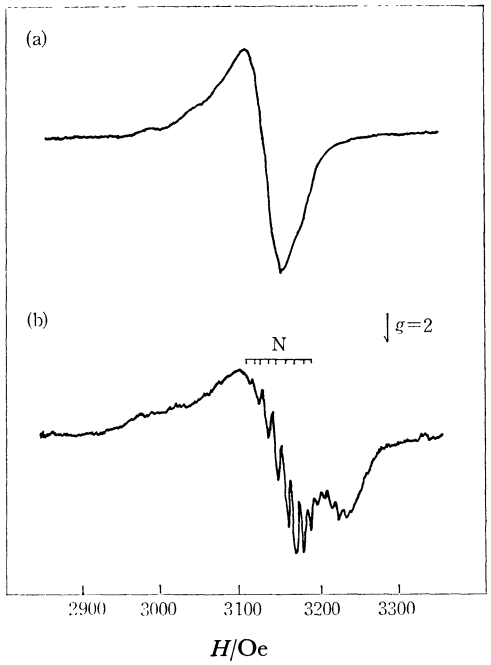

Fig. 1. ESR spectra of Cu-chln at liquid nitrogen temperature a) 0.01 mol/l Cu-chln only, b) 0.01 mol/l Cu-chln plus 0.1 mol/l FMN. Microwave frequency 9.1 GHz, power 2 mW. Modulation width 2.0 G at 100 kHz.

molecules of Cu-chln (Fig. 1(a)), when FMN of 0.1 mol/l is added to this Cu-chln solution and the ESR is measured at 77 K, however a clear superhyperfine structure due to nitrogen atoms is observed, as is shown in Fig. 1(b). The sharpening of the ESR spectrum by the addition of FMN indicates that FMN forms an intermolecular complex with Cu-chln in which the Cu-chln molecules are separated far enough from each other to make the dipolar and exchange interaction between electron spins negligible. The present author previously observed similar effects on the ESR spectrum for Cu-chln with poly(*N*-vinylpyrrolidone) in aqueous solutions and for Cu-chln with Mg-chln in ethanol, both at 77 K.

The hyperfine splitting due to the nitrogen atom is 16.7 G in the Cu-chln–FMN system (Fig. 1(b)). By following the treatment proposed by Koski *et al.*[6] for the ESR spectra of Cu-etioporphyrin and Cu-phthalocyanine, we may conclude that 65% of the unpaired electrons occupy the Cu $d_{x^2-y^2}$ orbital, and while 8.8% occupy each of the four nitrogen atoms, and that the spin density on the pheophytin ring carbons is negligibly small. These findings regarding the spin distribution in Cu-chln and the NMR relaxation measurements to be shown in a later section were used to simulate the structures of the molecular complex between Cu-chln and FMN.

Equilibrium Binding Study between Cu-chln and FMN. The optical difference spectra of the Cu-chln–FMN complex shows a maximum at 700 nm and a minimum at 630 nm. The intensity of the maximum increases with an increase in the concentration of FMN and can be attributed to the complex formation of Cu-chln with FMN. As the change in the concentration of FMN induces no change in the position of the maximum peak, we may assume that the peak height of the difference spectra at 700 nm is proportional to the concentration of the Cu-chln–FMN complex. We further assume this equilibrium:

$$\text{Cu-chln} + n\text{FMN} \rightleftharpoons \text{Complex}, \tag{3}$$

for which the equilibrium constant, K, is given by:

$$K = \frac{C_{\text{chlb}}}{C_{\text{chlf}}} \times \frac{1}{C_{\text{F}}{}^{n}}, \tag{4}$$

where C_{chlb}, C_{chlf}, and C_{F} are the concentration of the bund Cu-chln, that of the free Cu-chln, and that of FMN respectively. Equation 4 can be rewritten as:[7]

$$\log \frac{C_{\text{chlb}}}{C_{\text{chlf}}} = \log C_{\text{F}} + \log K, \tag{5}$$

C_{chlb} can be determined from the ratio of the peak height at 700 nm at a given concentration of FMN to that in the presence of a large excess of FMN at a constant Cu-chln concentration. Thus, the plot of $\log C_{\text{chlb}}/C_{\text{chlf}}$ against $\log C_{\text{F}}$ gives the slope n, *i.e.* the number of FMN molecules bound per Cu-chln; it also gives the equilibrium constant, K. From Fig. 2, we obtain $n=0.91$ and $K=512$ l/mol at 9 °C, $n=0.94$ and $K=330$ l/mol at 25 °C, and $n=1.02$ and $K=101$ l/mol at 84 °C. We may thus conclude that, in this concentration range of FMN ($0—7.0\times10^{-2}$ mol/l), Cu-chln forms a one-to-one complex with FMN in this temperature range. Tsuchida *et al.* measured the Cu-chln–pyridine and poly(4-vinylpyridine) complexes with the same method, thus obtaining values of $K=39$ l/mol and $K=1500$ l/mol at pH 10 respectively.[8] The present author previously measured the Cu-chln–adenosine-5′-monophosphate complex and

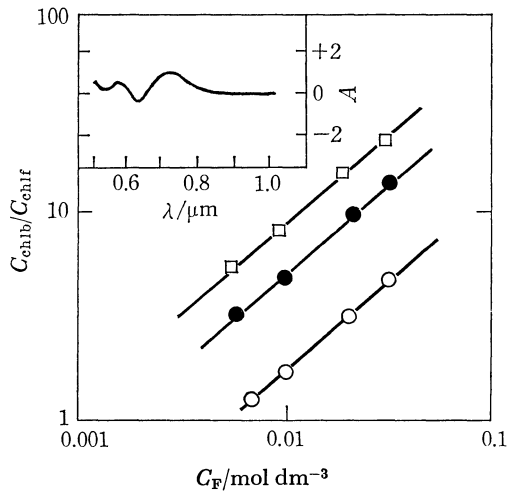

Fig. 2. Optical difference spectrum of Cu-chln–FMN complex and Hill plot for Cu-chln–FMN complex. Reference side: Cell A (Cu-chln 2.99×10^{-4} mol/l, phosphate buffer ,pH 7.0, 0.1 mol/l), Cell B (FMN 7×10^{-2} mol/l, phosphate buffer, pH 7.0, 0.1 mol/l). Sample side: Cell C (Cu-chln 2.99×10^{-4} mol/l, FMN 7×10^{-4} mol/l, phosphate buffer, pH 7.0, 0.1 mol/l), Cell D (phosphate buffer, pH 7.0, 0.1 mol/l) at 25 °C.

obtained $K=19$ l/mol at 30 °C.[9] The view of all these data, it can be said that the Cu-chln–FMN complex has a rather strong binding.

Spin-lattice Relaxation Times of ^1H and ^{31}P Nuclei of FMN. A Probable Structure of the Complex : The detail of the structure may be obtained from studies of FMN and Cu-chln at low concentrations where a one-to-one complex seems to be formed by optical titration. For this purpose, we have measured the spin-lattice relaxation times of nonexchangeable protons, *i.e.*, C(6)–H, C(9)–H, C(7)–CH_3, and C(8)–CH_3 of FMN at 70 mmol/l in the presence (0.9 mmol/l) and the absence of Cu-chln in a neutral D_2O solution (pH 5.8). The results are shown in Fig. 3 (as T_{1P}) as a function of the temperature. The T_1 values vary considerably among different protons, indicating that they are determined by T_{1M} rather than by a common value, τ_M, in Eq. 2. The T_{1P} of each proton shows a minimum at about 30 °C; and according to Eq. 2 we have $\tau_c \approx 1.6\times10^{-9}$ at this temperature. Using this τ_c value and the bound fraction of FMN (f) calculated from the association constant ($K_a=3.3\times10^2$ l/mol) for a one-to-one complex, we obtained the distances from the unpaired electron to the respective protons. The distance from the unpaired electron to the phosphorus atom was similarly calculated using the same τ_c and f value at 30 °C obtained from the T_1 data in Fig. 3. All the results are listed in Table 2.

The long distance obtained for the phosphorus (8.0 Å) indicated that the coordination of the phosphate group to Cu does not occur in the complex formation. The interaction primarily occurs with the known atomic coordinates of FMN and Cu-chln,[11,12] taking the electron-spin distribution of Cu-chln obtained from the ESR study into account.

For this purpose, a computer program developed in our laboratory[13] was applied to this complex. By assuming a parallel arrangement between the two

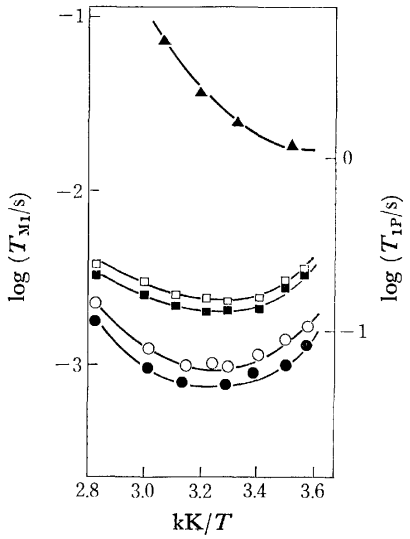

Fig. 3. Temperature dependence of proton and phosphorus relaxation.
FMN (70 mmol/l), Cu-chln (0.9 mmol/l), pH 5.8. C(9)-H: ●, C(6)-H: ○, C(8)-CH_3: ■, C(7)-CH_3: □, phosphorus: ▲.

Table 1. The distances from the electron spin on Cu-chln to the nonexchangeable protons and the phosphorous atom of FMN in the Cu-chln-FMN complex (30 °C, pH 5.8)

	T_{1obsd} [a] / s	R [b] / nm
C(6)-H	8.1×10^{-4}	0.60
C(9)-H	6.1×10^{-4}	0.58
C(7)-CH_3	1.81×10^{-3}	0.69
C(8)-CH_3	1.73×10^{-3}	0.68
P	1.50×10^{-2}	0.80

a) T_{1obsd} is the observed T_{1B}. b) R is the apparent distance between the protons or phosphorus and the electron spin.

planes of FMN and Cu-chln, we find that the central Cu atom is closer to the methylated ring and that the interplane distance is 4.20±0.05 Å. This interplane distance is a little longer than those of the π-π complex consisting of two aromatic compounds with carbon 2pπ orbitals, but considering the involvement of d-orbitals in the present system, the structure is essentially similar to the stacking arrangement of two aromatic compounds.

Barry *et al.* suggested that the family structures of the Co-mesoporphyrin IX dimethyl ester-2,4,7-trinitro-9-fluorenone complex with 4.00±0.02 Å are closely related to those determined for similar complexes in the crystalline state in that the planes of Co^{2+} MPDE and TNF are parallel.[14] We may, therefore, confirm that the interaction between FMN and Cu-chln in an aqueous environment is probably of hydrophobic origin, with the two planes mutually stacked.[15]

From the close similarity in the optical difference spectra between the Cu-chln–FMN system and the chlorophyll a–FMN system, we can expect that chlorophyll a also forms a similar complex with FMN in an aqueous environment.

The author is deeply indebted to Professor Hiroyuki Hatano for his continual encouragement throughout this work, and also to Dr. Kazuyuki Akasaka for his helpful advice and discussions. He also wishes to thank Mr. Hideaki Kusakawa for his advice on the writing of this paper.

References

1) S. Tu and J. H. Wang, *Biochem. Biophys. Res. Commun.*, **36**, 79 (1969).
2) G. Oster, S. B. Bryode, and J. S. Bellin, *J. Am. Chem. Soc.*, **86**, 1313 (1966).
3) E. M. Burdick and R. G. Caroll, *Ind. Eng. Chem. Soc.*, **46**, 2262 (1954).
4) T. J. Swift and R. E. Connick, *J. Chem. Phys. Soc.*, **37**, 307 (1962).
5) N. Bloembergen, E. M. Purcell, and R. M. Pound, *Phys. Rev.*, **73**, 677 (1948).
6) E. M. Roberts and W. S. Koski, *J. Am. Chem. Soc.*, **96**, 103 (1974).
7) E. M. Baker, M. S. Brookhart, and A. H. Corwin,

J. Phys. Chem., **86**, 4587 (1964).
8) E. Tsuchida, K. Shigehara, and K. Miyamoto, *J. Polym. Sci., Polym. Chem. Ed.*, **14**, 911 (1976).
9) K. Enmanji, *Nippon Kogaku Kaishi*, **1978**, 1317.
10) E. Breitmaier and W. Voeltler, *Eur. J. Biochem.*, **31**, 234 (1972).
11) P. Kierkegaard, R. Norrestar, P. Werner, I. Csoregh, M. Glehn, R. Karlsson, M. Leijonmarck, O. Ronnquist, B. Stensland, O. Tillberg, and L. Torbjornsson, "Flavine and Flavoproteins," John Willy & Sons (1972), pp. 1—22.
12) C. J. Brown, *J. Chem. Soc., A*, **1968**, 2494.
13) Y. Nosaka, K. Akasaka, and H. Hatano, *J. Magn. Reson.*, to be published.
14) C. D. Barry, H. A. O. Hill, P. J. Sadler, and R. J. P. Williams, *J. Am. Chem. Soc.*, **95**, 4533 (1973).
15) G. P. Fulton and G.N. La Mar, *J. Am. Chem. Soc.*, **98**, 2124 (1976).

The Vibrational Spectra and Rotational Isomerism of 3-Butenylsilane

Keijiro TAGA, Keiichi OHNO,* and Hiromu MURATA
Department of Chemistry, Faculty of Science, Hiroshima University, Higashisenda-machi, Hiroshima 730
(Received September 9, 1978)

The infrared and Raman spectra of 3-butenylsilane, CH_2=$CHCH_2CH_2SiH_3$ (and $-SiD_3$), were measured for the gaseous, liquid, and solid states. The fundamental vibrations were assigned, and the normal vibrations were calculated in relation to the rotational isomerism. The calculations indicated that the *cis-trans* (CT), *skew-trans* (ST), and *skew-gauche* (SG and SG′) forms coexist in the gaseous and liquid states, while the CT form only persists in the solid state. From the temperature variation in the Raman intensities, the stability of the molecular conformations was found to be in this order: CT≳ST>SG′>SG in the liquid state, indicating that an appreciable interaction between the silicon atom and the C=C bond, such as in the case of allylsilane, is not present for 3-butenylsilane.

The properties of the UV and IR spectra of unsaturated organosilanes have long been investigated and have been commonly cited as evidence of the interaction between vacant 3d-orbitals of the silicon atom and the C=C π electron system, *i.e.*, (p→d)-π-bonding and long (p→d)π-bonding.[1] Recently, however, the bathochromic effect of the UV spectra and the abnormal high reactivity to the C=C bond of β-unsaturated organosilanes have been interpreted in terms of the σ-π hyperconjugation between the C=C π and the Si–C σ bonds.[2] The magnitude of this hyperconjugation varies with the dihedral angle about the axis between the carbon atoms in the α- and β-positions, and it is maximal at 90°,[3] indicating that the *skew* conformation is preferable to the *cis* conformation. Actually, in a previous paper[4] the analysis of the vibrational spectra has confirmed that, for allylsilane, only the form near the *skew* form predominantly exists in the gaseous, liquid, and solid states, although, for methylvinylsilane, the *cis* and *skew* forms coexist in the gaseous and liquid states. The same conclusion as to the molecular conformation of allylsilane has also been drawn from the electron-diffraction study[5] and the microwave spectral analysis.[6]

In the present paper, we will, then, deal with the molecular vibrations and rotational isomerism of 3-butenylsilane in order to obtain information on the interaction between the C=C bond and the silicon atom of the γ-position.

Experimental

The samples of 3-butenylsilane, CH_2=$CHCH_2CH_2SiH_3$, and its deuterated species, CH_2=$CHCH_2CH_2SiD_3$, were prepared as follows. Allyl bromide was converted to 3-buten-1-ol using magnesium and paraform, and the 3-buten-1-ol was then converted to 3-bromo-1-butene using PBr_3, by the method of Linstead *et al.*[7] A Grignard reagent prepared from the 3-bromo-1-butene was added to silicon tetrachloride in dry ether to yield 3-butenyltrichlorosilane. The resulting 3-butenyltrichlorosilane was reduced to 3-butenylsilane with $LiAlH_4$ or $LiAlD_4$ in dry dibutyl ether. The purities of the 3-butenylsilane-d_0 and -d_3 were checked by NMR analysis.[8]

The infrared spectra in the 250—4000 cm^{-1} region and the Raman spectra in the 10—4000 cm^{-1} region were recorded on a Perkin-Elmer instrument (Model 621) and a JEOL Raman spectrometer (Model JRS-400D) with an argon-ion laser respectively. The infrared and Raman spectra were measured for the gaseous, liquid, and solid states and for the liquid and solid states respectively, using the technique described in a previous paper.[4]

Results

Normal Coordinate Treatment. A molecule of 3-butenylsilane has two C–C axes and five possible isomers: *cis-trans* (CT), *cis-gauche* (CG), *skew-trans* (ST), *skew-gauche* (SG: stretched), and *skew-gauche'* (SG′: bent). In order to confirm the molecular forms and the assignments of the observed spectra to rotational isomers, the normal vibrations were calculated using the modified Urey-Bradley force field. The structural parameters used were transferred from those of 1-butene[9] and ethylsilane[10] determined by microwave study. All the valence angles except for the CH_2=CH group were assumed to be tetrahedral, and the dihedral angles were assumed to be 0° for the C form and 120° for the S form about the (CH_2=)CH–CH_2(CH_2) axis, and 60° for the G form and 180° for the T form about the (=CH)CH_2–CH_2-(SiH_3) axis. The force constants used in the present calculation were transferred from those of propylsilane,[11] allylsilane,[4] and olefins,[12] and the torsional force constants[13] of Y(C–C=) and Y(C–Si) were assumed from the barrier heights of 1.7 kcal/mol for 1-butene[9] and 2.04 kcal/mol for ethylsilane[10] respectively. Tables 1 and 2 give the observed and calculated frequencies of 3-butenylsilane-d_0 (BS-d_0) and 3-butenylsilane-d_3 (BS-d_3), together with the assignments based on the predominant potential energy distributions.

Rotational Isomerism. The molecule of 3-butenylsilane has 15 atoms and has the molecular symmetry of C_s for the CT form and that of C_1 for the CG, ST, SG, and SG′ forms. In the C_s symmetry, the 39 normal vibrations are reduced to 24 of the A′ species and 15 of the A″, while in the C_1 symmetry all 39 are of A. All the normal vibrations are infrared and Raman active.

Figures 1 and 2 show that several Raman lines in the liquid state disappear in the solid state, indicating the existence of the rotational isomers in the liquid state. On the other hand, almost all the frequencies observed in the solid state are assigned to the fundamental vibrations for one isomer, as Tables 1 and 2 show.

For such *n*-alkylsilanes as propylsilane and butyl-

TABLE 1. OBSERVED AND CALCULATED FREQUENCIES (cm^{-1}) OF 3-BUTENYLSILANE-d_0[a)]

Gas		Liquid					Solid				Calculated				Assignment[c),d)]
IR		IR		R		ρ	IR		R		CT[b)]	ST	SG′	SG	
							2171 sh	vs	2181	vvs	2174 A′	2174	2174	2174	$\nu_a SiH_3$
2162	vs	2158	vs	2154	vvs	p	2158	vs	2154	vvs	2174 A″	2174	2174	2174	$\nu_a SiH_3$
							2148	vs	2149 sh	vs					
									2127	vvs	2171 A′	2171	2171	2171	$\nu_s SiH_3$
1646	m	1641	w	1640	vvs	p	1639	m	1639	vs	1645 A′	1642	1642	1642	νC=C
1445	w	1444	vw	1447 b	vw	dp							1434	1432	$s SiCH_2$
									1432 sh	w					
1429	w	1432 b	vw	1430 sh	vw		1430	w	1423	m	1430 A′	1427			s=CH_2
1416	w	1415	vw	1416	s	p	1416	vw	1415	w	1426 A′	1424	1422	1424	$s SiCH_2$ (CT, ST), s=CH_2 (SG′, SG)
		1405	vw	1406 sh	w	dp?	1403	vw	1407	s	1404 A′	1406	1405	1405	$s CCH_2$
							1400 sh	vw							
1348	vw	1342	vvw	1345	vvw		1344	vw	1345	vw	1347 A′		1353	1351	$w CCH_2$
1316 b	vw	1314	vvw	1317 sh	vw							1329			$w CCH_2$
				1300 sh	s							1290			$t CCH_2$
		1294	vvw	1295	vs	p	1298 b	vvw	1296	vs	1277 A″		1282	1283	$t CCH_2$
		1262	vvw	1277	m	p	1281 b	vvw	1280	w	1269 A′	1255	1255	1256	δ=CH i.p.
				1193	w	p						1191			$w SiCH_2$
1178 b	w	1181	vw	1184	w	p	1183	w	1181	m	1190 A′				$w SiCH_2$
		1162	vw	1173	w	p								1165	$w SiCH_2$
				1145 b	vvw							1144	1154		ν=C-C
													1145		$w SiCH_2$
1089 sh	w	1095	vw	1087 b	vvw		1087	w	1095	vw	1104 A″			1100	$t SiCH_2$(CT), ν=C-C(SG)
											1093 A′			1092	ν=C-C(CT), $t SiCH_2$(SG)
1057	w	1053	vw	1057 b	vvw							1070	1047		$t SiCH_2$
				1013	w							1008			νC-C
992	s	991	m	992	w	dp?	1000	m	1003	vw	998 A″	997	1004	1003	t=CH_2
							981	vw	985	m	984 A′		995	990	νC-C
				942	vs	dp	939 sh	s	947 sh	vs	950 A″	950	949	950	$\delta_a SiH_3$
									943	vs	947 A′	947	948	948	$\delta_a SiH_3$
936	vs	922 b	vs	931	s	dp?	930	vs	937	m	925 A″	924	927	926	w=CH_2
							917 b	vs	922	w	917 A′	917	917	917	$\delta_s SiH_3$
		908 sh	vs	912	m	dp?			909	w	903 A′	905	904	909	r=CH_2(CT, ST, SG′), $r CCH_2$(SG)
				898	w	p	904	vs	901	m	900 A″	896			$r CCH_2$
				878	vw								887	885	$r CCH_2$(SG′), r=CH_2(SG)
802	m	799	w	800	vw								801		$r SiCH_2$
		789 sh	w	790 sh	vw									787	$r SiCH_2$
753	m	757 b	w	758	s	p	760	m	763	vs	763 A′	758			νC-Si
		749 b	w	745	w	dp?	748	m	746	vw	731 A″	728			$r SiCH_2$
				699 sh	w									696	νC-Si
697	w	692	w	693	m	p							692		νC-Si
				661 sh	w								628	631	δ=CH o. p.
		643	vw	651	w	dp?						623			δ=CH o. p.
		604	vw	610	w	p	601	m	613	s	602 A′				$r_s SiH_3$
									607	m					
582 b	w	578	w	584	vs	p						568	569	574	$r_s SiH_3$
		549	vw	555 b	vw		552	w	554	w	563 A″				δ=CH o. p.
524 b	m	522 b	vw	525	w	dp?	528	w	538	w	538 A″	539	537	537	$r_a SiH_3$ δC=CC
									528	w	525 A′				
				433 sh	w								440		δC=CC
424 b	vw	422	vvw	423	m	p						439		438	δC=CC

TABLE 1. (Continued)

Gas	Liquid			Solid		Calculated				Assignment[c),d)]
IR	IR	R	ρ	IR	R	CT[b)]	ST	SG′	SG	
		332 sh vw						369	371	δCCC=
		305 w	p				321			δCCC=
		261 w	p		264 m	243 A′				δCCSi
		224 b w	dp?					229	219	δCCSi
					208 w					106×2
		179 sh m	dp?		179 w	161 A′	188			δCCC=(CT), δCCSi(ST)
					158 w	162 A″				τC–Si
							156	140	139	τC–Si
		96 sh m	dp?		106 vs	131 A″	95	91	96	τ=C–C
					(92 vs	75 A″				τC–C
					(88 vs					
							78	69	69	τC–C
					79 sh m					Lattice vibrations
					59 s					
					52 vs					
					36 vvs					

a) Frequencies above 2200 cm^{-1} are not included, and infrared spectra below 250 cm^{-1} are not recorded. s: strong, m: medium, w: weak, v: very, sh: shoulder, b: broad, p: polarized, and dp: depolarized. b) A′, A″: A′ and A″ species in the C_s symmetry. c) When molecular symbols are not indicated in parentheses, the band is assigned to each of the existing forms (CT, ST, SG′, and SG). *ν*: stretching, *s*: scissoring, *w*: wagging, *t*: twisting, *r*: rocking, *δ*: deformation, i. p.: in-plane, o. p.: out-of-plane, a: asymmetric mode, and s: symmetric mode. d) A large mixing of the modes occurred. (tCCH$_2$, tSiCH$_2$), (ν=C–C, r=CH$_2$), and (δCCSi, δCCC=) for CT. (r_sSiH$_3$, δ=CH o. p.) for ST, SG′, and SG. (δ=CH i. p., wSiCH$_2$, tCCH$_2$) for SG′ and SG. (δ=CH o. p., w=CH$_2$, t=CH$_2$) and (rCCH$_2$, rSiCH$_2$, w=CH$_2$) for SG.

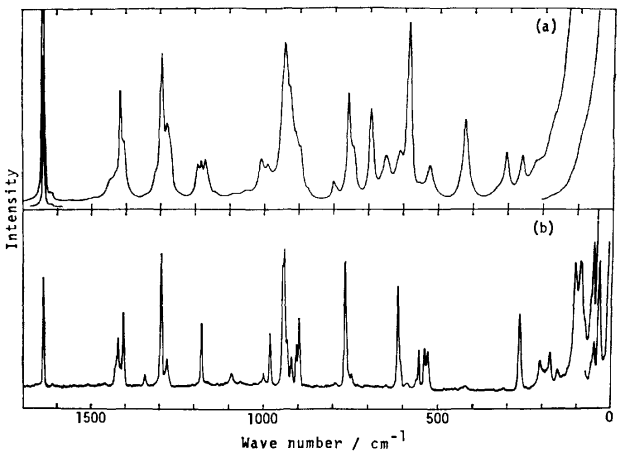

Fig. 1. Raman spectra of 3-butenylsilane-d_0 in the 10—1700 cm^{-1} region.
(a): Liquid state at room temperature, (b): solid state at liquid nitrogen temperature.

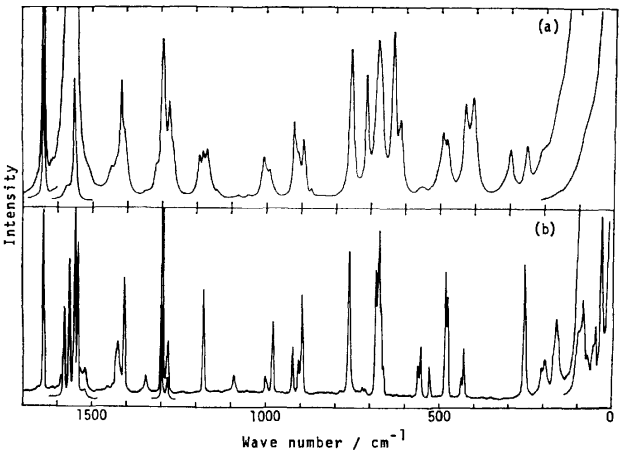

Fig. 2. Raman spectra of 3-butenylsilane-d_3 in the 10—1700 cm^{-1} region.
(a): Liquid state at room temperature, (b): solid state at liquid nitrogen temperature.

silane containing a $-CH_2CH_2SiH_3$ group, only the C–Si stretching and CH_2Si rocking vibrations have been observed in the 650—850 cm^{-1} region.[11] By analogy with the case of the C–Cl stretching vibration in alkyl chlorides,[14] the C–Si stretching vibration for the T form (P_C) has been assigned on a higher-frequency side than that for the G form (P_H), while the reverse is true for the CH_2Si rocking vibration,[15] as is shown in Fig. 3. The CH_2Si rocking vibration, however, is, in general, weak in the Raman scattering and is of medium strength in the infrared absorption. Thus, from a comparison of the spectra of BS-d_0 with those of propylsilane and butylsilane, the stronger Raman lines at 758, 699 (shoulder), and 693 cm^{-1} are assigned to the C–Si stretching vibration, while the Raman lines at 800, 790 (shoulder), and 745 cm^{-1} are assigned to the CH_2Si rocking vibration. The Raman lines at 800, 790, 699, and 693 cm^{-1}, vanishing in the solid state, belong to the G form, and the Raman lines at 758 and 745 cm^{-1}, persisting in the solid state, to the T form.

On the other hand, for 1-butene[12] and allyl chlo-

TABLE 2. OBSERVED AND CALCULATED FREQUENCIES (cm^{-1}) OF 3-BUTENYLSILANE-d_3[a)]

Gas		Liquid				ρ	Solid				Calculated				Assignment[c),d)]
IR		IR		R			IR		R		CT[b)]	ST	SG′	SG	
1646	m	1641	m	1639	vvs	p	1641	s	1640	vs	1645 A′	1642	1642	1642	νC=C
1575	vs	1571	vs	1570	vvs	dp?	1580	vs	1589	vs	1572 A′	1572	1572	1572	$\nu_a SiD_3$
							1565	vs	1564	vs	1572 A″	1572	1572	1572	$\nu_a SiD_3$
1564	vs	1550	vs	1551	vvs	p	1552	vs	1549 1539	vvs vvs	1545 A′	1545	1545	1545	$\nu_s SiD_3$
				1528 sh	w				1521	vw					755×2
1443	w	1445	w	1446	w	dp							1434	1432	$s SiCH_2$
1430	w	1431	w	1432 sh	w		1429	s	1425	w	1430 A′	1427			s=CH_2
1417	w	1415	w	1416	s	p	1418 sh	vw	1416 sh	vw	1426 A′	1424	1422	1424	$s SiCH_2$ (CT, ST), s=CH_2 (SG′, SG)
		1407	w	1407 sh	m	dp?	1406 1401 sh	m vw	1407	s	1404 A′	1406	1405	1405	$s CCH_2$
		1359 sh	vvw												677×2
1356 b	vvw	1345	vvw	1346	vvw		1343	vw	1344	vw	1347 A′		1353	1351	$w CCH_2$
1314 b	vw	1317	vvw	1314	w	p						1329			$w CCH_2$
				1299 sh	s							1290			$t CCH_2$
1299 sh	vw	1295	vvw	1295	vs	p	1299	vw	1296	vs	1277 A″		1282	1283	$t CCH_2$
1260	vvw	1263	vw	1278	m	p	1283	vvw	1280	w	1269 A′	1255	1255	1256	δ=CH i. p.
				1194	w	p						1190			$w SiCH_2$
1170 b	vw	1180	vw	1182	w	p	1180	m	1179	s	1188 A′				$w SiCH_2$
		1161	vw	1171	w	p								1164	$w SiCH_2$
				1142 b	vw							1143	1154		ν=C-C
													1144		$w SiCH_2$
1088 b	vw	1094	vw	1084	vvw		1090	m	1092	vw	1103 A″			1098	$t SiCH_2$(CT), ν=C-C(SG)
											1093 A′			1091	ν=C-C(CT), $t SiCH_2$(SG)
1054	w	1052	vw	1053	vvw							1068	1046		$t SiCH_2$
		1010	w	1007	w							1005	1003	1002	νC-C(ST), t=CH_2(SG′, SG)
999	m	992	m	994	w	dp?	997	m	1002	vw	997 A″	996	993	988	t=CH_2(CT, ST), νC-C (SG′, SG)
				986 sh	vw		983	w	981	m	980 A′				νC-C
918	s	918	s	921	m	p			925	w	924 A″	923	927	925	w=CH_2
912	s			912	w	dp?	903	vs	907	w	903 A′	903	900	905	r=CH_2(CT, ST, SG′), $r CCH_2$(SG)
		901	vs	896	w	p	895 sh	m	896	m	892 A″				$r CCH_2$
				871	vw							887	886	884	$r CCH_2$(ST, SG′), r=CH_2(SG)
760	vs	756	vs	755	vs	p	764	vs	761	s	770 A′	766	785	770	νC-Si(CT, ST), $r SiCH_2$ (SG′, SG)
716	vs	710	vs	713	s	p	727 723	m m	722 714	vvw vvw	718 A″	716	717	715	$r SiCH_2$(CT, ST), νC-Si (SG′, SG)
							688 sh	vw	684	s	681 A″	680	681	681	$\delta_a SiD_3$
676	vs	677 b	vs	678 b	vs	dp?	674	vs	674	vs	680 A′	680 662	680	680	$\delta_a SiD_3$ $\delta_s SiD_3$
							666 662	vs vs	668 661	m vw	664 A′				$\delta_s SiD_3$
635	m	635	w	634	vs	p							638	644	$\delta_s SiD_3$
		610 sh	vw	614	m	p						593	608	613	δ=CH o. p.
		547 b	vw	556	vw	dp?	552	w	562 559	vw w	563 A″				δ=CH o. p.

TABLE 2. (Continued)

Gas IR	Liquid IR	Liquid R	ρ	Solid IR	Solid R	Calculated CT[b]	Calculated ST	Calculated SG′	Calculated SG	Assignment[c),d)]
		520 sh vw		521 vw	529 vw	537 A′				δC=CC
492 b w	489 b w	492 m					492	483	496	$r_s SiD_3$
	477 w	481 w		474 s	482 s 476 m	460 A′				$r_s SiD_3$
424 b w	437 w	428 m	p	434 m	438 vw		424	439	422	$r_a SiD_3$(ST), δC=CC(SG′, SG)
				427 sh w	430 w	419 A″		416	418	$r_a SiD_3$
		406 m	p				409			δC=CC
		319 sh vw						350	351	δCCC=
		300 vw	p				316			δCCC=
		253 w	p		255 s	230 A′				δCCSi
		211 w	dp?					215	207	δCCSi
					206 vw 196 w					102×2
		168 sh w	dp?		165 m	154 A′	175			δCCC=(CT), δCCSi(ST)
						149 A″	129	113	113	τC-Si
		100 sh s	dp?		102 vvs	112 A″	86	80	85	τ=C-C
					88 s	69 A″				τC-C
							76	66	67	τC-C
					73 s 52 vs 35 vs					Lattice vibrations

a), b), c) See a), b), and c) of Table 1. d) A large mixing of the modes occurred. (tCCH$_2$, tSiCH$_2$), (ν=C-C, r=CH$_2$), (δCCSi, δCCC=), and (τC-Si, τ=C-C) for CT. (r_aSiD$_3$, δC=CC) for ST. (wSiCH$_2$, tCCH$_2$, δ=CH i.p.) and (δ=CH o.p., t=CH$_2$, w=CH$_2$) for SG′ and SG. (rCCH$_2$, rSiCH$_2$, w=CH$_2$) for SG.

ride,[16] both containing the CH_2=$CHCH_2$– group, the C=CC skeletal bending vibration can be expected to be in the 400—550 cm^{-1} region; this vibration for the C form has been observed on a higher-frequency side than that for the S form, as is shown in Fig. 3. For BS-d_0, the Raman lines at 525 and 423 cm^{-1} are assigned to the C=CC skeletal bending vibration; the latter (the S form) disappears in the solid state, while the former (the C form) persists. Therefore, for 3-butenylsilane, it is indicated that the CT form persists in the solid state and that the CT and other forms coexist in both the gaseous and liquid states. The above results were confirmed from the normal coordinate treatment. The calculated frequencies of the CT form reproduced well the observed frequencies in the solid state. In the liquid state, the observed spectra were explained by the coexistence of the CT, ST, SG, and SG′ forms. Especially, the Raman lines at 305 cm^{-1} for BS-d_0 and at 300 cm^{-1} for BS-d_3 in the liquid state suggested the existence of the ST form, corresponding to the calculated frequencies of 321 cm^{-1} for BS-d_0 and 316 cm^{-1} for BS-d_3 given in Tables 1 and 2. The Raman lines at 800 and 693 cm^{-1} and the shoulder Raman lines at 790 and 699 cm^{-1} were assigned to the vibrations of the SG′ and SG forms respectively, as Fig. 4 shows. The existence of the CG form was not clear from the comparison of the observed frequencies with the calculated ones. However, this form is unlikely because of its large H···H nonbonded repulsion between the CH_2=CH and SiH_3 or SiD_3 groups.[12]

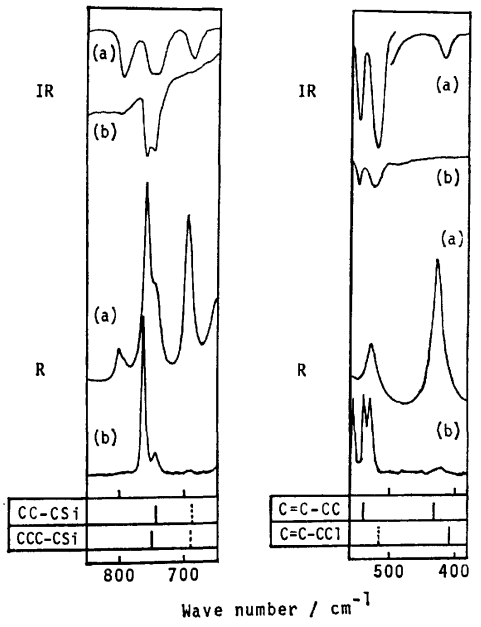

Fig. 3. Comparison of the spectra of 3-butenylsilane-d_0 with those of analogous molecules.
(a): Liquid state at room temperature, (b): solid state at liquid nitrogen temperature.

Stability of the Rotational Isomers. The enthalpy difference can be determined from the intensity ratios

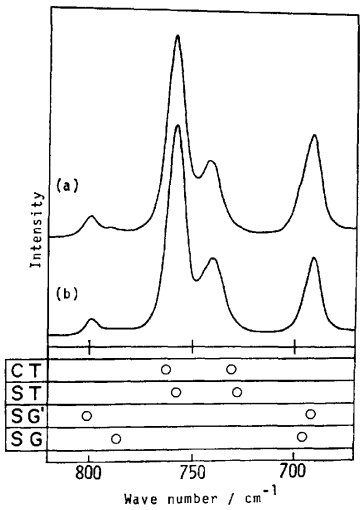

Fig. 4. Observed spectra in the 640—840 cm^{-1} region and calculated frequencies of each molecular form for 3-butenylsilane-d_0.
(a): Liquid state at −84 °C, (b): liquid state at −115 °C, ○: calculated frequency.

of the Raman lines belonging to different isomers.[17] However, only two pairs of the Raman lines were used for the determination because of the requirement that the pair of Raman lines be well separated from each other. The relative intensities were measured in the liquid state at different temperatures between −53 °C and −115 °C. The intensity ratios of the Raman lines at 758 (the CT and ST forms) and 693 cm^{-1} (the SG and SG′ forms) gave the apparent enthalpy difference, $\Delta H[(SG+SG')-(CT+ST)]=0.74\pm0.1$ kcal/mol, and those at 261 (the CT form) and 305 cm^{-1} (the ST form), $\Delta H(ST-CT)=0.22\pm0.2$ kcal/mol. On the other hand, Fig. 4 shows that the 800 and 693 cm^{-1} Raman lines assigned to the SG′ form increase in their relative intensities with a decrease in the temperature, as compared with those of the 790 and 699 cm^{-1} Raman lines assigned to the SG form. Therefore, for 3-butenylsilane, the stability of the rotational isomers is in this order: CT≳ST>SG′>SG in the liquid state.

Discussion

For 3-butenylsilane, it was found that only the CT form persisted in the solid state and that the stability of the rotational isomers was in this order : CT≳ST>SG′>SG in the liquid state. From the intensity ratios of the Raman lines belonging to the isomers, the enthalpy difference between the T and G conformations about the (=CH)CH_2–$CH_2(SiH_3)$ axis was estimated to be *ca.* 0.7 kcal/mol, and that the C and S conformations about the (CH_2=)CH–$CH_2(CH_2)$ axis, 0.22±0.2 kcal/mol. For propylsilane with the (CH_3)CH_2–$CH_2(SiH_3)$ axis, the T form has been found from the Raman spectral analysis[11] to be more stable than the G form by 0.60—0.65 kcal/mol. For 1-butene with the (CH_2=)CH–$CH_2(CH_3)$ axis, the enthalpy difference between the C and S forms has been reported to be ΔH(C–S)=0.15±0.15 kcal/mol from the microwave analysis[9] and ΔH(C–S)=−0.10±0.05 kcal/mol from the NMR analysis.[18] Therefore, 3-butenylsilane has a rough additivity of the enthalpy differences.

On the other hand, Harrah and Mayo[19] have reported, on the basis of their infrared spectral analysis of 1-alkenes, that the isomer with the S conformation persists in the solid state. The molecular form (the CT form) of 3-butenylsilane in the solid state differs from that of 1-pentene. This is, however, not peculiar, for the enthalpy difference about the (CH_2=)CH–$CH_2(CH_2)$ axis is quite small.

For 3-butenylsilane, the most and the least stable isomers in the liquid state were the CT and SG forms respectively. Therefore, the stability of the rotational isomers is mainly interpreted in terms of the steric repulsion between the nonbonded hydrogen atoms. The SG form has a considerable H···H nonbonded repulsion between the =CH– and CH_2Si groups. For the CT form, the silicon atom is more apart from the CH_2=CH group geometrically. Thus, there is no appreciable interaction between the C=C bond and the silicon atom of the γ-position for 3-butenylsilane.

The authors wish to express their thanks to Dr. Hiroatsu Matsuura for his valuable discussion.

References

1) For example, E. A. V. Ebsworth, "Organometallic Compounds of the Group IV Elements," ed by A. G. MacDiarmid, Dekker, New York (1968); J. Nagy and J. Réffy, *J. Organomet. Chem.*, **23**, 79 (1970).
2) For example, C. G. Pitt, *J. Organomet. Chem.*, **23**, C35 (1970).
3) U. Weidner and A. Schweig, *Angew. Chem. Int. Ed. Engl.*, **11**, 146 (1972).
4) K. Ohno, K. Taga, and H. Murata, *Bull. Chem. Soc. Jpn.*, **50**, 2870 (1977).
5) B. Beagley, A. Foord, R. Moutran, and B. Roszondai, *J. Mol. Struct.*, **42**, 117 (1977).
6) M. Hayashi, M. Imachi, and M. Saito, *Chem. Lett.*, **1977**, 221.
7) R. P. Linstead and H. N. Rydon, *J. Chem. Soc.*, **1934**, 1995.
8) R. A. Benkeser, Y. Nagai, J. L. Noe, R. F. Cunico, and P. H. Gund, *J. Am. Chem. Soc.*, **86**, 2446 (1964).
9) S. Kondo, E. Hirota, and Y. Morino, *J. Mol. Spectrosc.*, **28**, 471 (1968).
10) D. H. Petersen, Doctral Thesis, The University of Notre Dame; D. H. Petersen and L. Pierce, *Spectrochim. Acta*, **16**, 1272 (1960—1961).
11) H. Murata, H. Matsuura, K. Ohno, and T. Sato, to be published; Ohno, unpublished work: K(CH; $SiCH_2$)=4.297, K(CC)=2.400, H(HCH; $SiCH_2$)=0.355, H(CCC)=0.320, H(CCSi)=0.083, F(CCC)=0.400 mdyn/Å and Y(CC)=0.100, κ(CH_2)=0.015, t(CH_2, CH_2)=0.104, t(CH_2, SiH_3)=0.067, t(CCSi, SiH_3)=0.125 mdyn·Å.
12) T. Shimanouchi, Y. Abe, and Y. Alaki, *Polym. J.*, **2**, 199 (1971); M. Sakakibara, F. Inagaki, I. Harada, and T. Shimanouchi, *Bull. Chem. Soc. Jpn.*, **49**, 46 (1976). The force constants of olefins were transferred to those for the CH_2=CH–C part except for the cases of K(CH), H(HCH), and F(HCH), but the value of H(C=CH) used was 0.190 mdyn/Å.

13) K. Sera, K. Suehiro, M. Hayashi, and H. Murata, *Bull. Chem. Soc. Jpn.*, **49**, 29 (1976).
14) J. J. Shipman, V. L. Folt, and S. Krimm, *Spectrochim. Acta*, **18**, 1603 (1962).
15) R. G. Snyder and J. H. Schachtschneider, *J. Mol. Spectrosc.*, **30**, 290 (1969).
16) C. Sourisseau and B. Pasquier, *J. Mol. Struct.*, **12**, 1 (1972).
17) S. Mizushima, "Structure of Molecules and Internal Rotation," Academic Press, New York (1954).
18) P. B. Woller and E. W. Garbisch, Jr., *J. Org. Chem.*, **37**, 4281 (1972).
19) L. A. Harrah and D. W. Mayo, *J. Chem. Phys.*, **33**, 298 (1960).

The Visible-UV Absorption and Circular Dichroism Studies of Poly(α-L-glutamic acid)–Copper(II) Complexes with Emphasis on the Extrinsic Cotton Effect†

Kiwamu YAMAOKA* and Tsutomu MASUJIMA

Faculty of Science, Hiroshima University, Higashisenda-machi, Hiroshima, Hiroshima 730

(Received September 20, 1978)

The visible-UV absorption and circular dichroism, CD, of poly(α-L-glutamic acid)–Cu(II) solutions have been measured at 25 °C in the pH range 7 to 3.5 and at the mixing ratio, R, (Glu residues-to-Cu^{2+}) 32 to 4. Complex formation between poly(Glu) and Cu^{2+} was evident from the three absorption bands of bound Cu(II) around 700, 370, and 250 nm. The molar absorption coefficients, ε, varied with pH and R in a complicated but systematic manner. The pH dependence of ε, however, was not in parallel with the helix-coil transition of poly(Glu)–Cu(II) complexes. The extrinsic CD bands of bound Cu(II) have been detected in the three absorption band regions, and found to depend on both pH and R. The optical dissymmetry factor indicated that the 700 and 250 nm absorption bands of bound Cu(II) are associated with multiple CD bands of opposite signs. The intrinsic CD showed that the Cu(II)- and pH-induced helices of the poly(Glu)–Cu(II) complex are alike regarding the polymer backbone.

In order to understand the catalytic function of polypeptide–metal ion complexes, the detailed study of the binding of the transition metal ion to the poly (amino acid) appears to be indispensable. For this purpose, poly(α-L-glutamic acid), poly(Glu), and Cu^{2+} have been extensively utilized as a model system.[1–8] The conformation of the macromolecular complex, *i.e.*, the long-range or overall structure of poly(Glu) bound by Cu(II), and complex formation between Cu(II) and ligands, *i.e.*, the species of the Cu(II)–Glu residue complex, however, remain unclarified. Potentiometric titration is almost powerless from this viewpoint,[1] but optical spectroscopic studies should reveal changes in the configuration of Cu(II) bound by ligands and the conformational transition of poly(Glu) induced by bound Cu(II).

Optical absorption studies on complex formation between Cu(II) and simple polyelectrolytes such as polyacrylate (denoted as poly(Acr)) and polymethacrylate (denoted as poly(Methacr)) are numerous. In the presence of such polyanions, the absorption spectra of Cu(II) show three bands around 700, 360, and 250 nm.[9–15] The interaction between Cu(II) and poly(amino acids) has also been extensively studied, *i.e.*, poly(Glu),[2–4,8] poly(Lys),[16–18] poly(Arg),[19] poly(His),[20] poly(Gly),[21] and poly(Ala).[22,23] The circular dichroism, CD, method is valuable for studies of both complex formation and conformational transition, provided that the intrinsic CD of the chromophore of poly(Glu) and the extrinsic CD of the complex formed between the optically inactive metal ion and the active Glu residue appear separately but simultaneously in the respective wavelength regions. Hence, the conformational change of the macromolecular poly(Glu)–Cu(II) complex can be related to the formation of the ligand complex between Cu(II) and Glu residues. CD studies on the complex formation with Cu(II) have been reported for poly(Glu),[2] poly(Lys),[16–18] poly(Orn),[18] poly(Dbu),[18] poly(Arg),[19] poly(His),[20] poly(Ala),[23] and some Schiff-base derivatives of poly(Lys) and poly(Orn).[24]

† Macromolecule-Metal Ion Complexes. IV. For the preceding papers, see Refs. 5—7.

In the present work, both the absorption and CD spectra of poly(Glu)–Cu(II) solutions have been studied by varying the pH between 7 and 3.5 and the mixing ratio (Glu residues to Cu^{2+}) between 32 and 4. The poly(Glu)–Cu(II) complex exhibited three absorption bands in the 700, 370, and 250 nm regions. The pH dependence of the intensity of each band has been found to be more complicated than previously reported.[2] The extrinsic CD of bound Cu(II) has been observed in all three absorption bands, again contrary to a previous report.[2] The pH dependence of the CD of Cu(II) is not, however, completely in parallel, although closely related, to the helix-coil transition of the macromolecular poly(Glu)–Cu(II) complex. The present absorption and CD data suggest that the variation in the absorption intensity of the bound Cu(II) with pH results not only from the change in amount and species of Cu(II)–Glu ligand complexes but also from the conformational change. Moreover, another conformational transition, possibly helix-to-*aggregate*, has been shown to exist for the poly(Glu)–Cu(II) complex at low pH where the helix is already completed. The present data are discussed in terms of the feedback of the poly(Glu) conformation to the complex formation between Glu ligands and Cu(II), and *vice versa*.

Experimental

Materials. Sodium poly(α-L-glutamate), abbreviated simply as poly(Glu), was kindly supplied from Ajinomoto Co., Ltd. (Tokyo) and purified by dialyzing against redistilled water for 24 h, freeze-drying, and vacuum-drying at 56 °C for 7 h. The weight-average degree of polymerization DP_w was determined to be *ca.* 700 from the intrinsic viscosity in 2 M NaCl solution. The stock poly(Glu) solution was prepared by weighing the anhydrous sample with a mean residue weight of 151. Sodium polyacrylate, abbreviated simply as poly(Acr), was purchased from Nakarai Chemicals Co. (Kyoto) and purified by fractional precipitation,[7] (DP_w 7700). In the CD study the poly(Glu) sample with a DP_w of 610, purchased from Pilot Chemicals, Inc., was exhaustively dialyzed against distilled water and freeze-dried. Reagent grade copper(II) chloride dihydrate was dissolved in distilled water prior to use.

Preparation of the Polymer-Cu(II) Solutions. Typically, a sample solution at the appropriate pH, mixing ratio, R, and ionic strength was prepared by adding appropriate amounts of NaCl, $CuCl_2$, and HCl solutions, in this order, to either poly(Glu) or poly(Acr) solutions. The value of R, defined as the ratio of the molar residue concentration of polymer to the total concentration of added Cu^{2+}, was varied by adjusting the amount of Cu^{2+}. The final concentration of the polymer residue was maintained constant at 8 mM throughout. The salt concentration in the polymer-Cu(II) solution was maintained constant at 7.5 mM in terms of the sum of HCl and NaCl by adjusting either of them. The effect of the mixing order was tested by interchanging the order of addition between $CuCl_2$ and HCl at room temperature. No difference was observed in the absorption and CD spectra, unless the pH of the solution was very low. However, the temperature effect on the absorption spectra of poly(Glu)-Cu(II) solutions was remarkable at low pH in that the temperature cycle between 4 and 70 °C showed irreversible changes. Therefore, the solutions were all prepared and stored at 25 °C.

Measurements of Absorption Spectra and pH. The absorption spectra were measured on a Hitachi Model EPS-3T recording spectrophotometer in the wavelength region 1200—210 nm at 25 °C, temperature-controlled water being circulated through the cell holder. The slit width was set at 0.18 mm at 700 nm. An integrated-sphere attachment was used to minimize the effect of scattered light from poly(Glu)-Cu(II) solutions at low pH (<3.8). The absorption was expressed in terms of the apparent molar absorption coefficient, ε ($cm^{-1}\cdot mol^{-1}\cdot dm^3$), of the total Cu^{2+} added. Matched pairs of quartz cells, 1—50 mm in length were used. The pH of the solutions used for absorption measurements was determined on a Hitachi-Horiba Model N-5 pH meter. A one minute wait preceded by two minutes' stirring was necessary before the reading of the pH, because of a slight time dependence.

Measurements of the CD Spectra and pH. The CD spectra of poly(Glu)-Cu(II) solutions were measured on a Cary Model 60 spectropolarimeter with a Model 6001 CD accessary at 25 °C. The visible and UV CD spectra at 750—240 nm have been expressed in terms of the molar ellipticity, $[\theta]$ ($deg\cdot cm^2\cdot dmol^{-1}$), of the total Cu^{2+} added, the far UV CD spectra at 250—185 nm being expressed in terms of $[\theta]$ of the mean residue concentration of poly(Glu). Quartz cells of 5 cm (700—300 nm), 0.5 and 0.2 cm (340—240 nm), and 0.05 cm (below 250 nm) have been used. The slit width was set manually at 0.3 mm between 750 and 600 nm (the dispersion being 15 nm at 750 nm and 8.5 nm at 600 nm). The slit width was automatically varied at a preset dispersion of 1.7 nm in the visible and UV regions, and was set at 2.4 mm in the far UV region. The pH of the solutions used for CD measurements was determined on either a Radiometer TTT-1 or a Corning Digital Research pH meter in a manner similar to above.

Results

Absorption Spectra of Cu^{2+} in the Presence of Poly(Glu). Figures 1(a—c) and 2(a—c) illustrate the absorption spectra of poly(Glu)-Cu(II) solutions at three values of R. In the presence of poly(Glu), three absorption maxima appear in the spectra of Cu^{2+}: a broad band (ε=40—150) around 700 nm, a weak band (ε=10—50) around 370 nm, and a strong band (ε=3000—5500) around 250 nm. The formation of the complex between poly(Glu) and Cu^{2+} is thus evident. The spectrum of poly(Glu) exhibits only an ascending lobe below 250 nm (Fig. 2(f)). The spectrum of $CuCl_2$ shows a weak and broad peak (ε=10—20) around 800 nm and an ascending lobe below 250 nm (Figs. 1(a) and 2(f)).

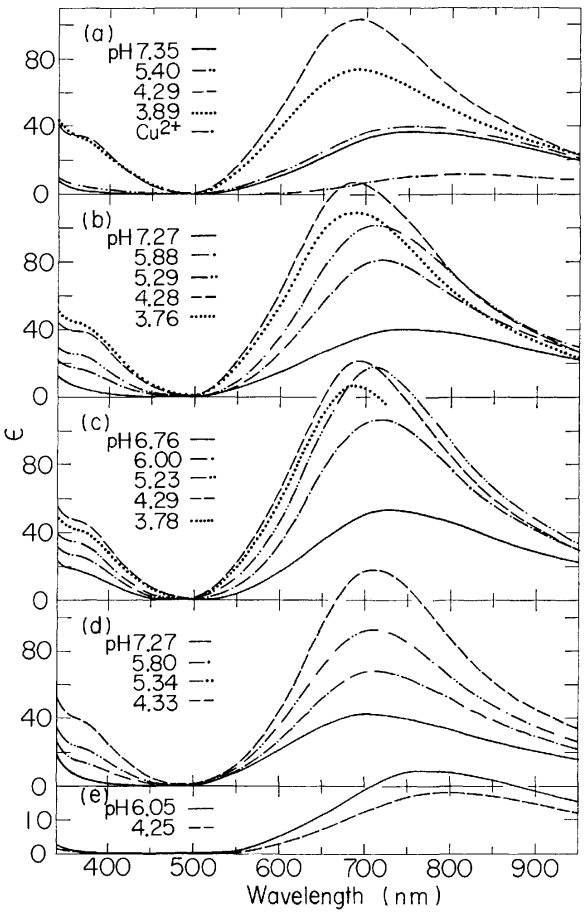

Fig. 1. The visible absorption spectra of Cu^{2+} in the presence of poly(Glu) ((a) R=32, (b) R=16, and (c) R=8), poly(Acr) ((d) R=16), and butyrate ((e) R=16) at various pH. The spectrum of Cu^{2+} at pH=3.81 in the absence of polymer is also shown in (a) for comparison. The pH=3.78 spectrum in (c) was taken with the integrated-sphere attachment which limits the wavelength to 800 nm. The concentration of added HCl plus NaCl is 7.5 mM in terms of the total Cl^- throughout. The molar absorption coefficient, ε, is expressed in terms of the total concentration of Cu^{2+} present in solution.

The 700, 370, and 250 nm bands, in the spectra of poly(Glu)-Cu(II) solutions at R=32 essentially remain unchanged in the pH range 7—5 but become most intense at pH 4.2—4.3 (Figs. 1(a) and 2(a)). In contrast, all the three bands of the R=16 and 8 solutions increase in intensity steadily with decreasing pH (Figs. 1(b—c) and 2(b—c)). The shape of the 700 nm band at each value of R is skewed, tailing towards the long wavelength side. The family of spectra showed no isosbestic point in any of the three absorption bands in the entire pH range 7—3.5.

Absorption Spectra of Cu^{2+} in the Presence of Poly(Acr) and Butyric Acid. The absorption spectra of Cu^{2+} were measured in the presence of either poly(Acr) (polymeric model lacking in the amide group),

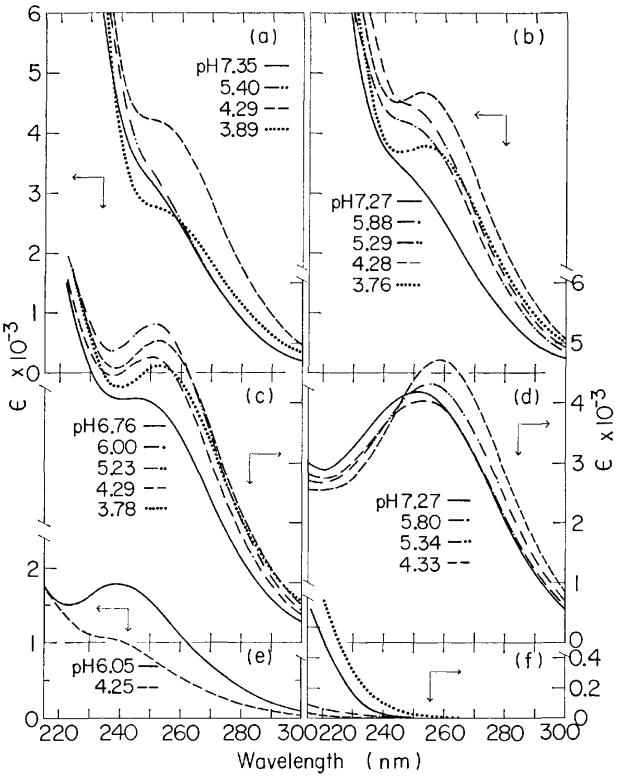

Fig. 2. The UV absorption spectra of Cu^{2+} in the presence of poly(Glu) ((a) R=32, (b) R=16, and (c) R=8), poly(Acr) ((d) R=16), and butyrate ((e) R=16) at various pH. The spectra of poly(Glu) at pH 7.09 (——), poly(Acr) at pH 5.39 (—·—), butyrate at pH 5.25 (----), and $CuCl_2$ at pH 3.81 (·····) are shown in (f) for comparison.

or butyric acid (model of the side-chain carboxylate of poly(Glu)). Figures 1(d) and 2(d) show that the three absorption bands appear again around 710 nm (a broad band ε=40—150), 370 nm (a weak band ε=10—40), and 250 nm (a strong band ε=2000—4500) in the spectra of poly(Acr)–Cu(II) solutions. The 250 nm peak is distinct because of the weaker background absorption of poly(Acr) (Fig. 2(f)). There is no clear isosbestic point in the 250 nm or 700 nm band in the entire pH range 7.3—3.8. The spectrum of Cu^{2+} in the presence of butyric acid shows two bands: one in the region 800—750 nm (ε=12—25) and one around 240 nm (ε=1000—2000) as indicated in Figs. 1(e) and 2(e). In contrast with the two polymer–Cu(II) systems, the spectrum of butyric acid–Cu(II) decreased steadily with decrease in pH, becoming close to that of the Cu(II) aquo-complex. No measurement was carried out at a pH higher than 6.5 because of the secondary reaction of precipitation.

pH *Dependence of the Absorption of Poly(Glu)–Cu(II).* Each spectrum of poly(Glu)–Cu(II) complex may be characterized by three absorption bands, and the variations in ε with pH at four selected wavelengths are shown in Figs. 3(a—d). At R=32 the ε at 680 nm, ε_{680}, is approximately constant in the pH range 7--5.5, but increases sharply attaining a maximum at pH=4.3 and decreasing with a further lowering of pH. At R=16, however, the ε_{680} begins to increase at pH=7 reaching a maximum at pH=4.1 after a marked shoulder near pH=5. At R=8, the ε_{680} becomes still larger between pH=7 and 5 showing a shoulder around pH 5.6, maxima at pH=4.8 and between 4.1—4.3. These peculiar changes in ε have been found for the first time. The intermediate shoulder may have been previously overlooked or mistaken for maxima.[2] It is now clear that the absorption of poly(Glu)–Cu(II) complexes depends on both pH and R in a complicated but systematic manner hitherto unreported.

The pH dependence of ε has also been determined at 880 nm (Fig. 3(b)), because the 700 nm band exhibits a marked skewness. The ε_{880} values generally behave in parallel with the ε_{680} values at R=32 but not at R=16 and 8. This difference may be attributed to the development of a long-wavelength component band around 900 nm with a decrease in R. The ε_{370} *vs.* pH curve at R=8 shows a maximum at pH=4.1 but none at pH=4.8, as illustrated in the ε_{680} *vs.* pH curve. This peculiarity offers two possible explanations, *viz.*, the origin of the 370 nm band differs from that of the remainder, or the maxima in the ε *vs.* pH curves at R=8 are only apparent and actually result from a delicate interplay of two or more processes involved in the formation of Cu(II)–Glu ligand complexes.

Contour Diagram of the Absorption of Poly(Glu)–Cu(II). A typical contour diagram is shown in Fig. 4, where the ε_{710} values for a number of poly(Glu)–Cu(II) solutions are related to pH and R. Similar diagrams may also be drawn for other wavelengths. Figure 4 clearly shows that there are two distinct ridges which lead to two separate summits indicated by X and X′ respectively. The first (AX) is along the R path at a slightly varying value of pH and the second (BX′) is along the pH path at an almost constant R value of approximately 4. In addition, a third, broader and less distinct ridge (CX′) leading to the summit X′ exists. This path depends on both pH and R in clear contrast with the two other paths and represents the marked hump observed in the ε *vs.* pH curves for the R=16 and 8 poly(Glu)–Cu(II) solutions (Figs. 3(a—d)). The slope stretching out between R=50 and 4 and below pH 4.4—4.2 on the left side of the first ridge (AX) is only apparent and should be a plateau with an approximate height of 150 in terms of the ε of the bound Cu(II).[25] The appearance of this slope has been attributed to the dissociation of the bound Cu(II) from the polymer site at low pH.[25]

Extrinsic CD of Bound Cu(II) in the 750—300 nm Region. The appearance of the extrinsic CD of Cu(II) should attest to the formation of Cu(II)–Glu ligand complexes. Two positive extrinsic CD bands are shown in Figs. 5(a—d): the long-wavelength CD band between 750 and 500 nm (designated as the visible CD band) and the short-wavelength band between 500 and 300 nm (designated as the near UV CD band). These CD bands correspond to the broad 700 nm and weak 370 nm absorption bands shown in Figs. 1(a—c) and have not hitherto been reported.

At a high value of R of 32, the peaks of the visible

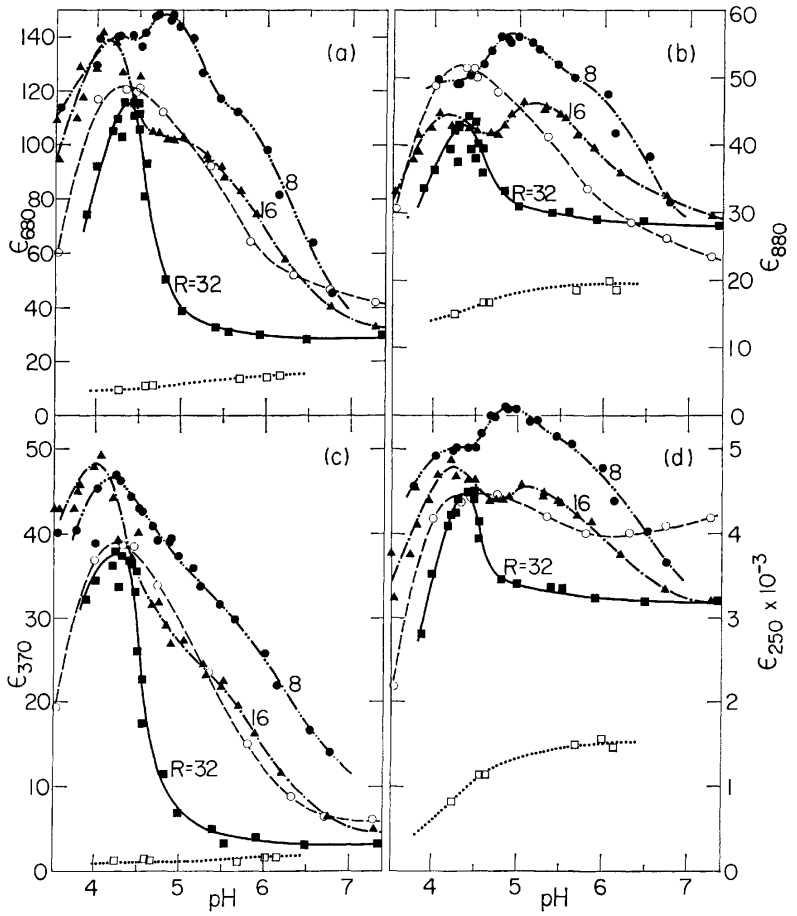

Fig. 3. The variation in the absorption coefficients of Cu^{2+} with pH in the presence of poly(Glu), poly(Acr), and butyrate at various R and at selected wavelengths of (a) 680 nm, (b) 880 nm, (c) 370 nm, and (d) 250 nm. Poly(Glu) (R=32 —■—, 16 —·▲—·, and 8 —··●—··), poly(Acr) (R=16 ——○——), and butylate (R=16 ·····□·····).

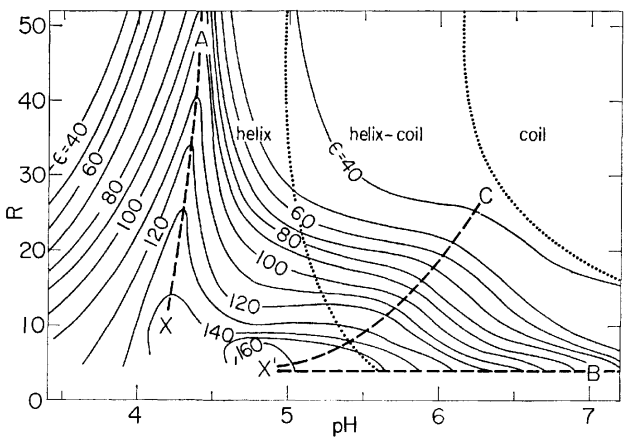

Fig. 4. The contour diagram of absorption intensity of Cu^{2+} at 710 nm in the presence of poly(Glu) at various pH and R. The numerals indicate the apparent molar extinction coefficients of Cu^{2+}. See text for other details.

and near UV CD bands center at 660 and 375 nm (Fig. 5(a)). The intensity increases with a decrease in pH becoming highest at pH 4.60, below which it decreases largely due to dissociation of the bound Cu(II).[25] At R=8, the CD bands have already appeared in the high pH range 6—7. The peak position and intensity depend on pH (Fig. 5(b)). At a value of R=4, CD bands with peaks at 670 nm and *ca.* 365 nm appear in the high pH range (Fig. 5(c)). The effect of R on the extrinsic CD band is shown in Fig. 5(d) at pH 5.75±0.05, which corresponds approximately to the midpoint of the helix-coil transition of poly(Glu) in the absence of Cu^{2+}. The highest value of $[\theta]$ for the visible CD band is approximately 430, when the Glu residues greatly exceed the Cu(II), *i.e.*, R=32 rather than 4, and when the pH of poly(Glu)–Cu(II) solution is low such that the helical structure of poly(Glu) is completed. Hence, the optical activity induced in the Cu(II) bound to poly(Glu) depends on both the backbone conformation of the macromolecular poly(Glu)–Cu(II) complex and the species of the Cu(II)–Glu ligand complex.

Extrinsic CD of Bound Cu(II) in the 310—240 nm Region. Corresponding to the UV absorption band of Cu(II) bound to poly(Glu) (Fig. 2), an extrinsic CD band appears in the 290—250 nm region (designated as the UV CD band) as shown in Fig. 6. The R 32 poly(Glu)–Cu(II) complex is in a helical conformation at pH 5.10 (*vide post*); yet, the negative $[\theta]$ increases only steadily. A shallow minimum and

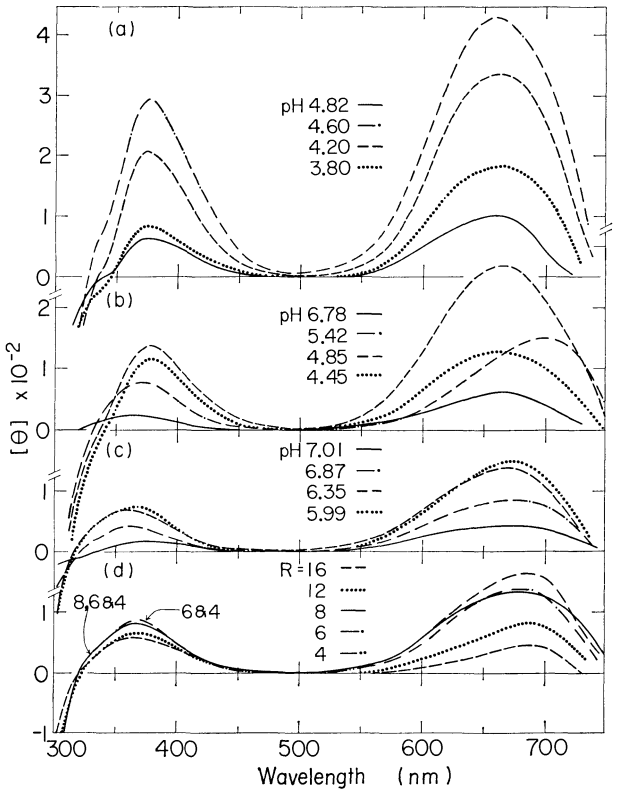

Fig. 5. The visible and near UV extrinsic CD spectra of Cu(II) bound to poly(Glu) at various R and pH. (a) R=32, (b) R=8, (c) R=4, and (d) pH=5.75. The molar ellipticity $[\theta]$ is expressed in terms of the total Cu^{2+} concentration in each poly(Glu)-Cu(II) solution.

maximum appear at 280 and 258 nm with the decrease in pH, respectively, and fully develope at pH 4.60 (Fig. 6(a)). The UV CD band represents a double extrinsic Cotton effect (*cf.* Fig. 10). The UV CD band at R 8 and 4 is shown in Figs. 6(b) and (c). This CD band is not seen at higher pH where the overall conformation is mostly in the random-coil, it however gradually appears as the pH of the solution is lowered. At pH 5.75, where the formation of the helical structure is half completed, the UV CD band becomes discernible as the value of R is decreased (Fig. 6(d)). This is an indication that the helical structure is fostered by the binding of Cu^{2+} to poly(Glu).

Intrinsic CD of the Glu Residue of Poly(Glu)-Cu(II) in the 250—185 nm Region. The conformation of macromolecular poly(Glu)-Cu(II) complexes is reflected in the intrinsic Cotton effect of the peptide chromophore in the far UV CD spectra as shown in Fig. 7. The CD spectra of poly(Glu) are also given as a reference (Fig. 7(a)). An isoelliptic point appears at 203.5 nm in the pH range 7.5—5.1 but deviation occurs at lower pH (<3.8). The intrinsic CD spectra behave essentially the same as the reference poly(Glu) when the Glu residues are in excess (R=32 in Fig. 7(b)). The general shapes of the CD spectra indicate that the helical conformation of poly(Glu)-Cu(II) is not altered by the formation of the Cu(II)-Glu ligand complex.

The intrinsic CD spectra exhibit a pH dependence when the bound Cu(II) is more densely populated on poly(Glu) (R=8 in Fig. 7(c)), indicating the existence of helix-coil transition. The $[\theta]$ values at 192 and 222 nm of a solution containing four peptide residues per Cu^{2+} manifest partial formation of the helix at pH 7 (R 4 in Fig. 7(d)). The R 4 CD spectrum is the largest at pH 5.75 where the reference poly(Glu) is still partly in a random-coil (a further lowering of pH promoted fibrous floats). Deviation from the isoelliptic point at 203.7 nm occurs, however, and does not develop as high as the CD spectra for the complete helical conformation (R ∞ and 32). Induction of the helix by bound Cu(II) is evident from the CD spectra of poly(Glu)-Cu(II) solutions (R 8 at pH 7.10 and R 4 at pH 6.87 in Figs. 7(c) and (d)) to which no proton was added.

Mixing-ratio Dependence of the Far UV CD of Poly(Glu)-Cu(II) and the Visible Absorption of Bound Cu(II). In order to clarify the effect of Cu^{2+} on the conformational changes of poly(Glu)-Cu(II) complexes at various values of R, the far UV CD spectra were measured at a fixed pH of 5.75±0.05 which corresponds approximately halfway to the helix-coil transition of poly(Glu). The results are shown in Fig. 8, where the CD spectra show a typical helix-coil transition pattern. All CD spectra cross at 204 nm with the exception of the R 4 spectrum. The pattern of the spectral change is similar to that of the proton-induced helix-coil transition of poly(Glu) (Fig. 7(a)), indicating that the Cu(II)-induced helix is approximately the same as the proton-induced helix. Hence, the Cu(II) bound to the random-coil or partially helical poly(Glu) probably promotes, but does not alter, the original helical structure in the macromolecular complex assuming the ionizable carboxyls are not completely un-ionized by the protons. This condition is fulfilled even at R 4 and pH 5.75 where approximately 70% of the carboxyls are uncharged.[26]

Corresponding to the increase in CD intensity, the visible absorption band of Cu(II) also steadily develops (inset Fig. 8). The correlation between CD and absorption is, however, not linear as shown in Fig. 9, where the values of $[\theta]$ at the positive and negative maxima (192 and 223 nm) are plotted against R, together with the change in the ε_{710} of the visible band. Both $[\theta]_{192}$ and $-[\theta]_{223}$ run in parallel approaching the limiting values of the complete helix as R becomes less than 4, as indicated by the horizontal line. The curve shows a sharp increment when R is around and below 10, suggesting that the induction of helical structure by the bound Cu(II) is cooperative in nature, *i.e.*, chelation and charge neutralization being responsible.[25,26] The ε_{710} values change almost linearly with R between 25 and 5. Since the amount of unbound Cu^{2+} is very small,[25,26] the ε_{710} *vs.* R curve indicates that complex formation between Cu(II) and the ligands is less cooperative than in helix formation. Thus, the latter may be essentially an overall phenomenon, while the former may be the sum of various local phenomena regarding complex species and binding modes.

Comparison between Electronic Absorption, Extrinsic CD

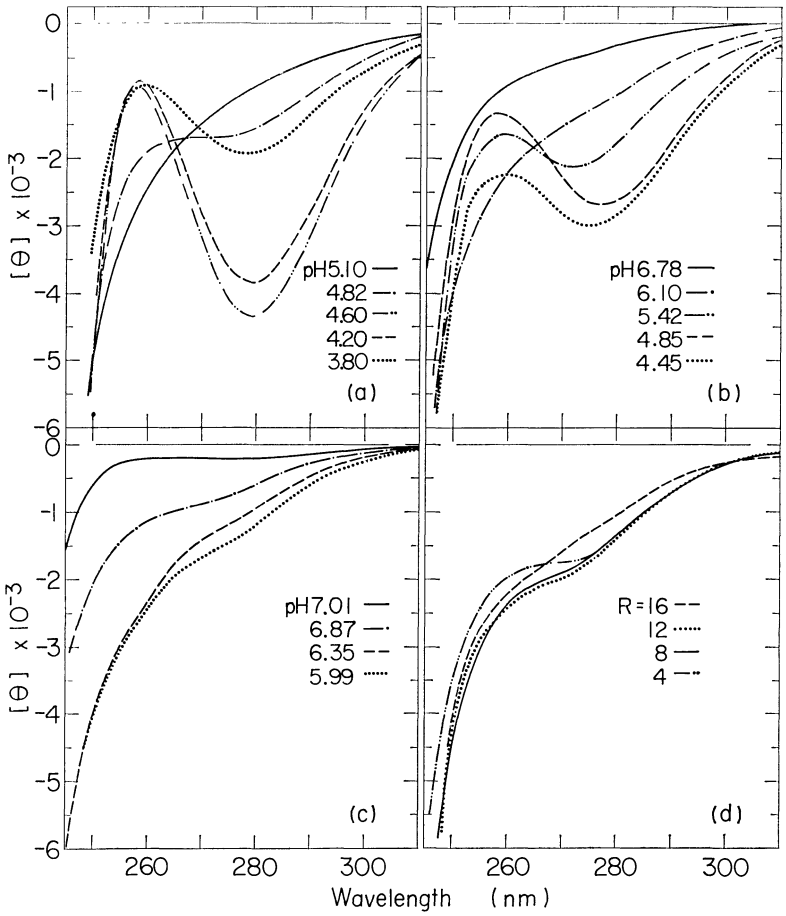

Fig. 6. The UV extrinsic CD spectra of Cu(II) bound to poly(Glu) at various R and pH. Notations are all the same as those in Fig. 5.

and Optical Dissymmetry Factor of Bound Cu(II). In order to realize the spectroscopic property of Cu(II) bound to Glu residues, a typical CD spectrum of Cu(II) bound to the complete helix (R 32 and pH 4.6) is compared with the corresponding absorption spectrum in Fig. 10. The optical dissymmetry factor, g,[27] is expressed as the ratio of the molar CD, $\Delta\varepsilon$, to the molar absorption coefficient, ε. The peak of the visible CD band is at 660 nm, while the absorption band is located at 690 nm, tailing toward the red. This unparalleled situation is reflected on the g-factor which is constant only in the 650—550 nm region descending toward zero around 740 nm. This indicates that the visible absorption band of bound Cu(II) is a composite of two or more optically active component bands. The g-factors of the visible Cu(II) band are generally larger for the R 32 complex than for the R 8 or 4 complex, indicating that optical dissymmetry for the visible band is more pronounced when the bound Cu(II) is less densely populated on the polymer.

Nozawa and Hatano[16] have observed the double CD band for a poly(Lys)–Cu(II) complex in the visible region. Garnier and Tosi[19] have shown that the extrinsic CD of poly(Arg)–Cu(II) is either double or separable into two components in the visible region. The sign, position, and magnitude of the visible CD of Cu(II) bound to poly(Glu) differ from those data previously reported. The difference probably results from the specificity of the ligands participating in complex formation, *i.e.*, γ-carboxylate *vs.* ε-amino or 4-guanidinium, and the stereoselectivity of a particular poly(amino acid) for chelation, but not from the ability of forming helical structures.[19]

It is not self-evident that the near UV CD band is a double type, because the absorption of bound Cu(II) is weak and discernible only as a shoulder so that the wavelength dependence of the g-factor is only apparent. The greater g-value for the 370 nm band may indicate that the contribution of the magnetic transition moment to the rotatory power is greater in the near UV CD band (450—350 nm) than in the visible CD band (700—550 nm). A similar trend has been observed at all values of R and pH. Thus, the near UV CD band is more optically dissymmetric.

The net CD band of bound Cu(II) in the 320—240 nm region may be obtained by subtracting the background intrinsic CD of the Glu residue. The far UV intrinsic CD spectrum of the R 32 poly(Glu)–Cu(II) at pH 4.6 differs from that of the same at pH 5.1 by a constant factor of 1.25 ± 0.05 between 250 and 200 nm. Therefore, the background ellipticity of the pH 4.6 complex is considered to be 1.25 times larger than that of the pH 5.1 complex which shows no extrinsic UV CD band (Fig. 6(a)). The net CD band of the bound Cu(II) thus cleared of background

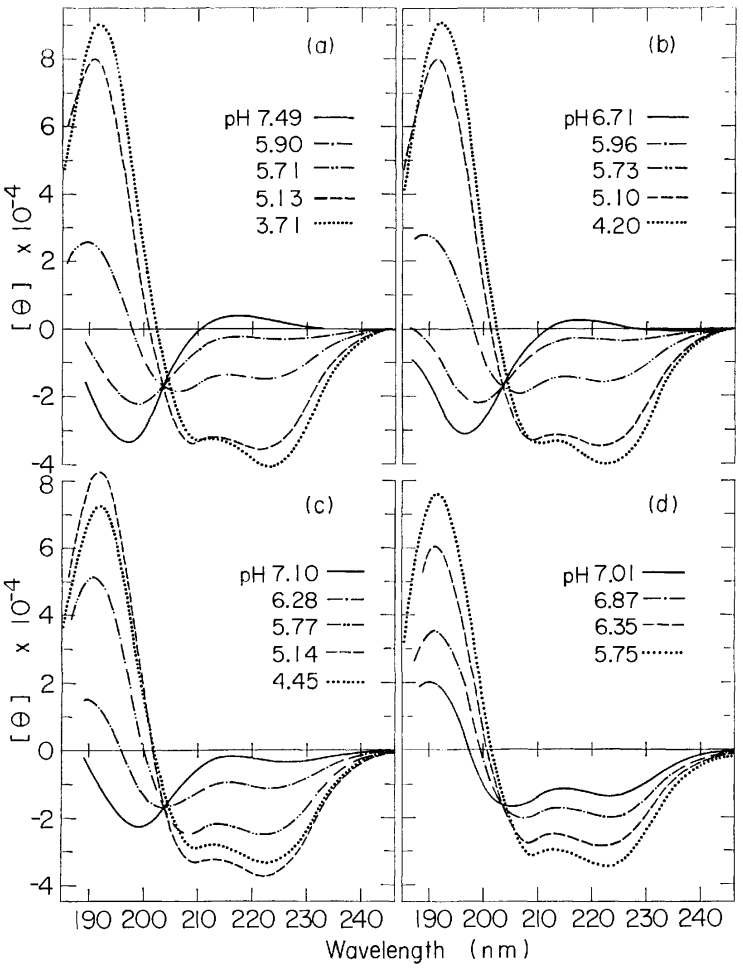

Fig. 7. The far UV intrinsic CD spectra of the peptide chromophore of poly(Glu)-Cu(II) solutions at various R and pH. (a) $R=\infty$ (no Cu^{2+} present), (b) $R=32$, (c) $R=8$, and (d) $R=4$. The molar ellipticity $[\theta]$ is expressed in terms of the mean molar residue concentration of poly(Glu) in the presence and absence of Cu^{2+}.

is double : a negative component with a peak at 280 nm followed by a positive peak around 256 nm. This doublet feature appears to be retained in most of the UV extrinsic CD spectra in Fig. 6. It has also been observed in the poly(Lys)- and poly(Arg)-Cu(II) complexes,[16-18] although the respective signs are probably reversed relative to the poly(Glu)-Cu(II) complex.

Discussion

Conformational Transitions of Poly(Glu)-Cu(II) Complex and the Formation of Cu(II)-Glu Ligand Complex. In order to relate the pH- and Cu(II)-induced conformational transitions of poly(Glu)-Cu(II) to the formation of Cu(II)-Glu ligand complex, the extrinsic CD and absorption data are compared with the far UV intrinsic CD in Fig. 11. The ε_{680}, $[\theta]_{680}$, and $[\theta]_{370}$ values of bound Cu(II) are also plotted against $[\theta]_{223}$ in Fig. 12, which directly shows the dependence of the optical properties of bound Cu(II) on the conformation of macromolecular complexes. For the R 32 complex, both the visible CD ($[\theta]_{680}\approx 0$) and electronic absorption ($\varepsilon_{680}\approx 30$) of bound Cu(II) are weak and remain constant over a wide pH range 7—5 (Fig. 11). The helix-coil transition of the macromolecular complex does occur in the narrow pH range 5.1 and 6.5; however, the bound Cu(II) hardly affects the transition, as clearly seen in Fig. 12. Thus, the feedback-effect of the macromolecular complex on the Cu(II)-Glu ligand complex, and *vice versa*, is weak when the bound Cu(II) is populated sparsely on poly(Glu). This effect however becomes pronounced for the macromolecular complex in which Cu(II) is distributed in a high proportion (R 8 or 4), since both the extrinsic CD and absorption of the bound Cu(II) and the $[\theta]_{223}$ of the Glu residue are already large around pH 7 where the poly(Glu) without Cu(II) is in the extended-coil form (Fig. 11).

As Figs. 11 and 12 indicate, the optical properties of bound Cu(II) for the R 8 and 4 complexes vary together in parallel, but *never* change linearly with respect to the helix content of the poly(Glu) backbone. (It is assumed that $[\theta]_{223}$ is equal to -35400 for a 100% helix.) In fact, the optical properties change with pH (Fig. 11) and helix content (Fig. 12), in a manner which is unexpectedly complicated, in the helix-coil transition, contrary to a previous report.[2] For example, the distinct hump in the ε_{680} curve around

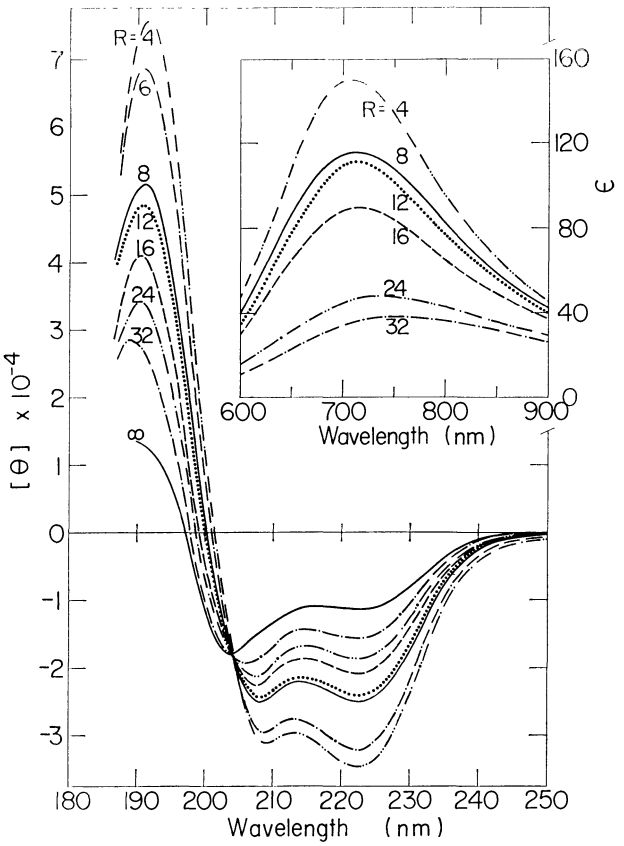

Fig. 8. The variation in the far UV intrinsic CD spectra of poly(Glu)-Cu(II) solutions with R at a pH of 5.75±0.05. The molar ellipticity is expressed as in Fig. 7. The corresponding visible absorption spectra are given in the inset.

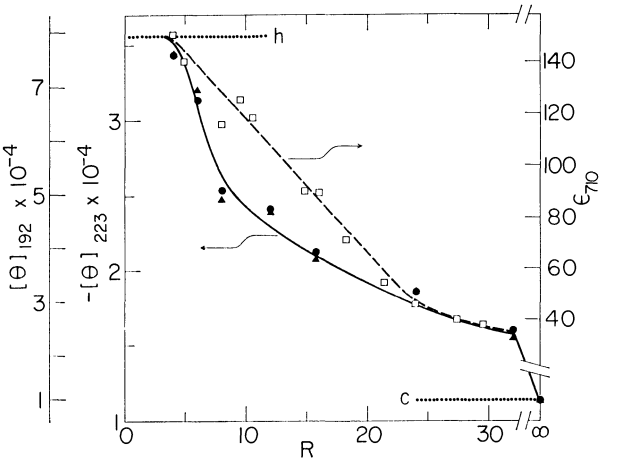

Fig. 9. The effect of added Cu^{2+} on the induction of helical structure in poly(Glu) and the formation of Cu(II)–Glu ligand complex at a constant pH of 5.75. The two horizontal lines (·····h and c·····) indicate the values of $[\theta]_{192}$ (—●—) and $[\theta]_{223}$ (—▲—) for the poly(Glu) solutions without Cu^{2+} ions at pH 5.10 and 7.49, respectively. The molar absorption coefficient ε_{710} (--□--) is the same as plotted in Fig. 4.

pH 5.3—6.0 (Figs. 3, 4, and 11(b)) probably corresponds to the second stage of the helix-coil transition after the midpoint, but not to the completion of the helix or to the midpoint as previously concluded.[2)]

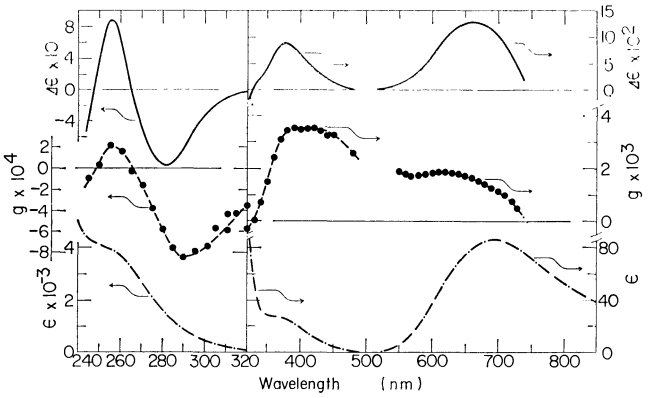

Fig.10. Comparison between extrinsic CD spectrum, $\Delta\varepsilon$, electronic absorption spectrum, ε, and optical dissymmetry factor, g, of a poly(Glu)–Cu(II) solution at R=32 and pH=4.60. The extrinsic CD spectrum is expressed in terms of the molar circular dichroism $\Delta\varepsilon$ (=[θ]/3305).

The most prominent change in the optical properties of the bound Cu(II) probably occurs after completion of the intramolecular helix of poly(Glu)–Cu(II) complex regardless of the amount of the Cu(II) bound to the Glu residues (Figs. 11 and 12). The ascending trend in the visible CD and absorption of Cu(II) is closely related to the second transition in the $[\theta]_{223}$ *vs.* pH curve (Fig. 11). Evidently, the backbone of the macromolecular complex undergoes a further conformational transition, probably, helix to *aggregates*, at low pH 5—4.4.[26,28-31)] It is however undeterminable from optical measurements alone whether or not the changes in optical properties arise from the transition of the intra- or interhelical conformation. In summary, it is probably the dissymmetric conformation of the Cu(II)–Glu ligand complex that is primarily responsible for the induced optical activity. Such a dissymmetry may be conferred on Cu(II) by stereospecific binding (or chelation) to the side-chain carboxylates and backbone amides bi- or tridentately. The overall conformation of a macromolecular complex would promote such binding. These conclusions are new and important.

The processes which are most responsible for the change in optical properties of the Cu(II)–Glu ligand complexes probably belong to two regions: the first half of the helix-coil transition region where the backbone of poly(Glu)–Cu(II) attains a compact-coil form due to the formation of fragmental helices, and the second transition region where the backbone undergoes a further conformational transition, possibly, from helix to *aggregates*. Thus, the species of Cu(II)–Glu ligand complexes are multiple, probably three or more altogether. It is a delicate interplay of these processes and the concentrations of the complex species involved that are responsible for the very involved dependence of the optical properties of poly(Glu)–Cu(II) on both pH and R.

The Cu(II)–Glu Ligand Complex and Its Absorption and CD Spectra. Complex formation between Cu(II) and Glu residues is evident from the absorption

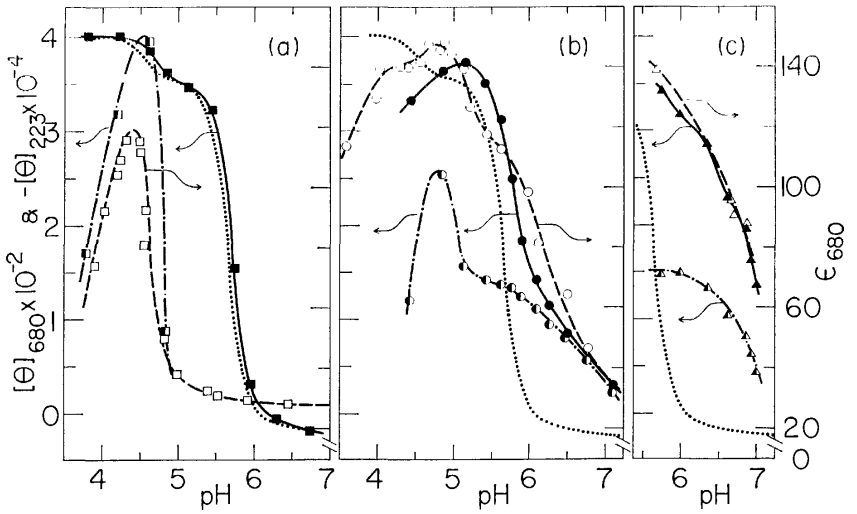

Fig. 11. Comparison of the pH-induced helix-coil transition curves of poly(Glu)–Cu(II) at three values of R (a) 32 (squares), (b) 8 (circles), and (c) 4 (triangles) with the pH variation of the corresponding visible CD and absorption of Cu(II). ε_{680} (——), $[\theta]_{680}$ (—·—), $[\theta]_{223}$ (——), and $[\theta]_{223}$ at $R=\infty$ (·····).

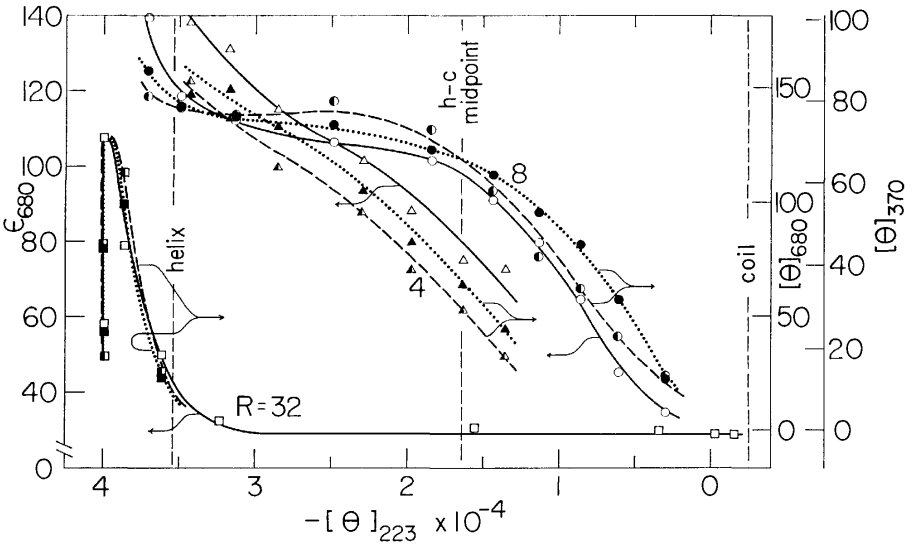

Fig. 12. Correlation between the intrinsic CD of poly(Glu)–Cu(II), $[\theta]_{223}$, and the absorption and extrinsic CD of the Cu(II)–Glu residue complex at three R values of 32 (squares), 8 (circles), and 4 (triangles). ε_{680} (——), $[\theta]_{370}$ (——), and $[\theta]_{680}$ (·····). The actual values of $[\theta]_{370}$ and $[\theta]_{680}$ at $R=32$ should be quadrupled. Regardless of the mixing ratios between Glu residues and Cu^{2+}, the $[\theta]_{223}$ values of +2500, −16500, and −35400 are assumed for the extended-coil, the midpoint of helix-coil transition, and the complete helix, respectively.

and extrinsic CD spectra of Cu(II) (Figs. 1, 2, 5, and 6). The present data manifest that previous reports have unraveled only a part of the whole process involved in the complex formation.[2,3] The absorption band at 700 nm results from the binding of Cu^{2+} by the ionized carboxylate (and possibly amide) groups, as the data of poly(Acr)– and butyrate–Cu(II) solutions (Fig. 1) and poly(carboxylic acid)–Cu(II) complexes have indicated.[9–15] The number of the ligand carboxylates participating in complex formation may range from one to four, most likely two ionized carboxylates.[26] An absorption study is insufficient to ascertain the mechanism of carboxylate neutralization and chelation and the role of the amide group of the Glu residue in chelation. Detailed studies of equilibrium dialysis and electron spin resonance are needed.

The skewed 700 nm band of the poly(Glu)–Cu(II) complex (Figs. 1 and 5) is not simple but composite revealing another component band on the long-wavelength side around 900 nm (Figs. 1 and 3), as reported for the poly(Methacr)–Cu(II) complex.[13] The multiple band structure has also been supported by CD data (Figs. 5 and 10). Hirasawa and Kon[32] analyzed the apparent 700 nm band of Cu(II) doped in L-histidine into three component bands centering at 714, 781, and 901 nm; these component bands may or may not correspond to the 685 and *ca.* 900 nm bands of the Cu(II)–Glu ligand complex. The CD

spectrum of a poly(Glu)–Cu(II) solution at R 32 was scanned to 800 nm with a red-sensitive Hamamatsu R446 photomultiplier. At the longest attainable wavelength, the *negative* CD component was only steadily increasing. Hence, the possibility still exists that the 700 nm absorption band of the bound Cu(II) is a composite of two, instead of three, out of four component bands. The actual situation may be very complicated, since the chemical species of the Cu(II)–Glu ligand complexes would be numerous in the poly(Glu)–Cu(II) macro-complex as indicated by the pH and R dependence of ε (Figs. 3 and 11). For instance, two side-chain carboxylates can chelate to a Cu(II) either in the *cis* or *trans* position. The absorption peaks for these isomers are known to be slightly different in amino acid–Cu(II) complexes.[33]

The origin of the near UV band of the Cu(II)–carboxylic acid complex remains a point of controversy[34] and, therefore, the 370 nm band of the poly(Glu)–Cu(II) complex deserves comment. Leyte *et al.*[13] suggested the presence of binuclear Cu(II) complexes of Cu(II)–acetate type dimeric structure in the poly(Methacr)–Cu(II) complex on the basis of the appearance of the 380 nm band. The optical absorption studies alone however can not resolve the question whether or not the 370 nm band reflects the presence of the binuclear Cu(II) complex in which direct Cu(II)–Cu(II) interaction exists.[34] The 350—380 nm shoulder appears in the absorption spectra of the Cu(II) bound to poly(Lys),[17] poly(Arg),[19] and poly(His),[20] all of which lack the carboxyl side-chain group. It should also be noted that the 370 nm band is associated with Cu(II)–β-diketone complexes which form a monomeric structure in solution.[35] Model buildings with CPK atomic models indicate that the dimer structure of the Cu(II)–acetate type is impossible with four side-chain carboxylates in a single-stranded poly(Glu) which may exist as the α-helix at low pH. The dimer is quite likely to occur if Cu(II) bridges two poly(Glu) strands by binding to two carboxylates of each polymer-chain. Comparative work by ESR and other magnetic methods is necessary here to identify the individual chemical species of Cu(II)–Glu ligand complexes.

The 370 nm CD band shows a slight hump in the shorter wavelength region suggesting a doublet structure (Fig. 5), although the absorption reveals no such feature (Fig. 1). Dubicki[36] reported that the 370 nm band of the Cu(II)–acetate complex is a doublet, assigning it to the charge-transfer transition of ligand-to-metal nature. Graddon[35] considered the 370 nm band of Cu(II)–ethyl acetoacetate complex as originating from the higher energy d-d transition (d_{xz}, $d_{yz} \rightarrow d_{x^2-y^2}$ type). His term-scheme is compatible with the present CD data of poly(Glu)–Cu(II) complexes assuming a weakening of degeneracy of the near UV d-d transition and that the low energy 700 nm band consists of two of the four d-d components. The final assignment of the d-d transition of Cu(II) and, consequently, the most likely coordination of the Cu(II)–Glu ligand complex remains unclear. The detailed CD study of a number of polypeptide–Cu(II) complexes in the near IR region is necessary for solving these problems.

The 250 nm band has been studied because of the high absorption intensity and existence in the spectra of Cu(II) in the presence of polyanions such as poly(Glu),[2,3,8] poly(Methacr)[11–13] and poly(Lys).[17] The band has been assigned to the allowed charge-transfer transition between carboxyl ligands and the metal ion.[2] The 250 nm charge-transfer band is composite, as indicated by the positive and negative CD component bands (Fig. 10). The unambiguous determination of the number and polarization of the optical transition moments involved in the poly(Glu)–Cu(II) complex are important for the understanding of the origin of induced optical activity associated with bound Cu(II). Such studies may be conducted by means of film dichroism.[37]

Conclusion

The Cu^{2+} ion bound to poly(Glu) exhibits the extrinsic Cotton effects of multiple type in three characteristic absorption bands in the visible, near UV, and UV regions. The effect of bound Cu(II) on the polymer conformation induces a helical structure but reduces the cooperative nature of the helix-coil transition. The absorption and CD spectra of bound Cu(II) in this transition region are related but the behavior is not in parallel with the backbone conformation. In addition to the ordinary helix-coil transition, a second conformational transition is involved in the macromolecular poly(Glu)–Cu(II) complex in the pH range <5.3—5.2. Complex formation between Cu(II) and Glu residues is strongly affected by this transition. The pH dependence of absorption and CD intensities results largely from the interplay of the two conformational transitions of the macrocomplex which affect the number of species and stereospecific configurations of the Cu(II)–Glu ligand complexes populated on the poly(Glu).

One of the authors (K. Y.) should like to express his sincere gratitude to Dr. Elliot Charney of the National Institutes of Health, Bethesda, Md. (USA) for his encouragement. The CD measurements were carried out in his laboratory in the summer of 1973 and 1975.

References

1) A. L. Jacobson, *Biopolymers*, **1**, 269 (1963).
2) H. Takesada, H. Yamazaki, and A. Wada, *Biopolymers*, **4**, 713 (1966).
3) Y. Hibino and S. Sugai, *Rep. Res. Group Polymer Phys. Japan*, **11**, 513 (1968).
4) H. Sigel and G. Blauer, *Helv. Chim. Acta*, **51**, 1246 (1968).
5) S. Inoue, K. Yamaoka, and M. Miura, *Bull. Chem. Soc. Jpn.*, **44**, 1443 (1971).
6) S. Inoue, K. Yamaoka, and M. Miura, *Bull. Chem. Soc. Jpn.*, **45**, 1314 (1972).
7) S. Inoue, K. Yamaoka, and M. Miura, *J. Sci. Hiroshima Univ., Ser. A*, **39**, 27 (1975).
8) S. Yamashoji, H. Yoshida, and G. Kajimoto, *Yukagaku*, **25**, 128 (1976).
9) F. T. Wall and S. J. Gill, *J. Phys. Chem.*, **58**, 1128

(1954).
10) A. M. Kotliar and H. Morawetz, *J. Am. Chem. Soc.*, **77**, 3692 (1955).
11) H. Morawetz, *J. Polym. Sci.*, **17**, 442 (1955).
12) M. Mandel and J. C. Leyte, *J. Polym. Sci., A*, **2**, 3771 (1964).
13) J. C. Leyte, L. H. Zuiderweg, and M. van Reisen, *J. Phys. Chem.*, **72**, 1127 (1968).
14) K. Tamaoki, K. Imai, J. Nishino, and Y. Sakaguchi, *Kobunshi Kagaku*, **30**, 608 (1973).
15) J. A. Marinsky and W. M. Anspach, *J. Phys. Chem.*, **79**, 439 (1975).
16) M. Hatano, T. Nozawa, S. Ikeda, and T. Yamamoto, *Makromol. Chem.*, **141**, 1 (1971).
17) T. Nozawa and M. Hatano, *Makromol. Chem.*, **141**, 21 (1971).
18) M. Palumbo, A. Cosani, M. Terbojevich, and E. Peggion, *J. Am. Chem. Soc.*, **99**, 939 (1977).
19) A. Garnier and L. Tosi, *Biopolymers*, **14**, 2247 (1975).
20) A. Levitzki, I. Pecht, and A. Berger, *J. Am. Chem. Soc.*, **94**, 6844 (1972).
21) M. Kawai, T. Hayakawa, and N. Hojo, *Nippon Kagaku Kaishi*, **92**, 617 (1971).
22) N. Hojo, K. Fukatsu, and T. Hayakawa, *Nippon Kagaku Kaishi*, **90**, 823 (1969).
23) N. Hojo, K. Fukatsu, T. Hayakawa, and Y. Kondo, *Nippon Kagaku Kaishi*, **90**, 827 (1969).
24) M. Dentini, P. De Santis, and M. Savio, *J. Chem. Soc., Chem. Commun.*, **1974**, 86.
25) K. Yamaoka and T. Masujima, manuscript in preparation.
26) K. Yamaoka and S. Noji, manuscript in preparation.
27) T. M. Lowry, "Optical Rotatory Power," Dover Publications, Inc., New York, N. Y. (1964) pp. 393—394.
28) T. M. Shuster, *Biopolymers*, **3**, 681 (1965).
29) Y. Tomimatsu, L. Vitello, and W. Gaffield, *Biopolymers*, **4**, 653 (1966).
30) J. Y. Cassim and J. T. Yang, *Biochem. Biophys. Res. Commun.*, **26**, 58 (1967).
31) B. R. Jennings, G. Spach, and T. M. Shuster, *Biopolymers*, **6**, 635 (1968).
32) R. Hirasawa and H. Kon, *J. Chem. Phys.*, **56**, 4467 (1972).
33) T. Yasui and Y. Shimura, *Bull. Chem. Soc. Jpn.*, **39**, 604 (1966).
34) M. Kato, H. B. Jonassen, and J. C. Fanning, *Chem. Rev.*, **64**, 99 (1964).
35) D. P. Graddon, *J. Inorg. Nucl. Chem.*, **14**, 161 (1960).
36) L. Dubicki, *Aust. J. Chem.*, **25**, 1141 (1972).
37) K. Yamaoka and Y. Matsuoka, *J. Sci. Hiroshima Univ., Ser. A*, **40**, 105 (1976).

An Estimation of the Thermodynamic Properties of Organic Compounds in the Ideal Gas State. I. Acyclic Compounds and Cyclic Compounds with a Ring of Cyclopentane, Cyclohexane, Benzene, or Naphthalene**

Yukio YONEDA

Department of Synthetic Chemistry, Faculty of Engineering, The University of Tokyo, Hongo, Bunkyo-ku, Tokyo 113

(Received October 6, 1978)

A new group-contribution method for estimating the standard enthalpy of formation, the standard absolute entropy, and the standard molar heat of organic compounds in the ideal gas state is proposed with tables of the contribution values. This method (the ABWY method) is a completely revised and enlarged version of the Anderson, Bayer, and Watson method, and it can be used with regard to a more diverse variety of compounds with a higher reliability. The neighboring effects in group-contribution methods are introduced to obtain better estimated values. The substitutions of various functional groups on aromatic rings are discriminated. Type-number corrections of the functional groups and multiple-substitution effects of halogens are also introduced; thus even heterofunctional compounds can be processed. A new concept, the quality of contribution values, is proposed to designate the qualitative reliability of the estimated physical properties. The manual procedures and tables of contribution values are given for estimating the thermodynamic properties of the compounds, as mentioned in the title, composed of C, H, O, halogens, S, and N. This method was critically compared with the Benson method in versatility and reliability.

In spite of the tremendous efforts of many scientists, the *observed* values of the fundamental properties of organic compounds, such as the heat of formation in the ideal gas state, are unexpectedly scarce; only around 1600 are known among several million compounds. As for the observed data of IR, already nearly two hundred thousand spectra have been collected by chemists. If we take into account the difficulty in the measurement of thermochemical and thermodynamic data as compared to that of the IR spectra, *e.g.*, the necessary purity of the specimens and the skill in measurement, one can hardly expect rapid increase of the former data within the next few years.

Thus, many investigators have published various methods of estimating the thermodynamic properties of organic compounds in the ideal gas state.[1-2] All of the estimation methods employ the principle of the group contribution; the target molecules are decomposed into atom groups, or functional groups, and the sum of the contributions of these groups makes the estimated values.

Among the group-contribution methods for estimating the standard enthalpy of formation, the standard absolute entropy, and the standard molar heat, the Anderson, Bayer, and Watson method (the ABW method)[3] and the Benson method[4] have been rated as two of the best.[2] The present author has already presented an extended method (the ABWY method)[5] modified from the ABW method. In this paper, a further improved version of the ABWY method and updated tables of contribution values will be reported. The functional groups and correlations due to multiple bonds were much diversified in this version; the concept of quality, or reliability, of the contribution values was also introduced.

The present ABWY method was originally intended to be implemented in computer program packages, EMPRIC[5] and EROICA,[6] the outline of which has been published earlier. These programs permit the CHEMO inputs, *i.e.*, the linear notations of rational formulas also proposed by the present author,[5,6] to accept information on organic compounds. The contribution values were statistically selected from the observed properties with the aid of the method of the least squares with a computer program, THEDES.

In this paper the method is presented for estimating acyclic compounds and cyclic compounds that have only one of four ring compounds, cyclopentane, cyclohexane, benzene and naphthalene, both composed of C, H, O, halogens, N, and S. Even the *heterofunctional* compounds, *i.e.*, compounds with plural kinds of functional groups, can be processed, not to mention the *monofunctional* or the *homofunctional* ones. The estimation method for complex compounds, excluded in this report, will be published in forthcoming papers.

This group-contribution method may be applicable in principle even to properties other than those in the ideal gas state if the properties can be so ingeneously converted that the linear additivity holds in them. The methods of estimating the critical properties, the vapor pressure, the heat of vaporization, and the normal boiling point, as well as the thermodynamic properties in the liquid phase, will also be reported in the forthcoming papers.

Theoretical

Since the thermodynamic properties covered in this paper are those of *ideal gas*, intermolecular forces can play no part in their estimation. Also, by the same reasoning, the law of corresponding states, used so widely in the estimation of other properties such as vapor pressure, is inapplicable. All methods of estimating enthalpy, entropy, and molar heat involve some form of group-contribution method based on the structure of the molecule.[4]

Benson[4] and Benson and Buss[7] pointed out a hierarchy of such methods, in the order of the additivi-

** CHEMOGRAM, a Computer Program Package for Chemical Logic, Part 3.

ties of (i) atom properties, (ii) bond properties, and (iii) group properties. The present author has described the hierarchy in another way.[5] The most successful method assigns the contribution to common groups, for example, $-CH_3$, $-OH$, or $-COO-$; by simple additivity, one can then estimate the ideal-gas properties from tables of the group-contribution values.

Neighboring Effects in Estimation. Allowance is made at least for the next-nearest neighbors to this group in order to proceed to a more complicated and usually more accurate method. In principle, there is no limit to the extension of the neighborhood-environmental concept, although the effect of neighboring groups separated by more than one atom usually becomes so small as to be insignificant. Some exceptions would be the effects of the *cis-trans* isomerism of olefin and the positional isomerism of polysubstituted ring compounds, and the influence of aromaticity; these effects are due to interaction between groups separated by two or more atoms.

Hence, the following classification and nomenclature of neighboring effects are given:

(1) Nearest-neighboring effect: effect from directly bonded atoms.

(2) Geminal effect: effect from atoms separated by one atom.

(3) Vicinal effect: effect from atoms separated by two atoms.

(4) Global effect: effect from atoms separated by more than two atoms.

Examples of these hierarchial effects will be given later.

Definition of Groups. In the ABWY method, a *group* is defined as follows:

(1) Base groups, *i.e.*, methane and ring compounds such as benzene, cyclohexane or naphthalene. Exceptions are the methyl radical, cation, and anion.

(2) Functional groups including $CH_n(n=0—3)$, but excluding H(hydrogen atom). Functional groups usually consist of an atom or an ensemble of atoms. Even when a complicated functional group could be decomposed into simpler or smaller functional groups, the original one should be adopted as a group when its contribution value is available, because complex groups include neighboring effects of a higher order; for example, the chloroformyl group, $-COCl$, should be adopted instead of carbonyl and chlorine. The only two exceptions to this rule are the formyl group, or aldehyde, $-CHO$, and the carbonyl group, $-CO-$, which should be decomposed into carbon and the oxo group, $=O$, as a heritage from the ABW method. Thus, the ligancy of groups may be from one to four, in contrast to two or more in the case of the Benson method.[4]

Linear Additivity of Thermodynamic Properties. The thermodynamic properties[7a] of organic compounds in the ideal gas state can be empirically represented as the sum of group contributions by virtue of the absence of any intermolecular interaction:

$$\Delta H^\circ_{f,298.15}(g)/\text{kcal mol}^{-1} = \sum_j n_{ij}\Delta(\Delta H)_j \quad (1)$$

$$S^\circ_{298.15}(g)/\text{cal mol}^{-1}\,\text{K}^{-1} = \sum_j n_{ij}\Delta S_j \quad (2)$$

$$C_p^\circ(g,T)/\text{cal mol}^{-1}\,\text{K}^{-1} = a + 10^{-3}bT + 10^{-6}cT^2 \quad (3)$$

$$a = \sum_j n_{ij}\Delta a_j,\ b = \sum_j n_{ij}\Delta b_j,\ \text{and}\ c = \sum_j n_{ij}\Delta c_j \quad (4)$$

where $\Delta(\Delta H)_j$, ΔS_j and Δa_j, Δb_j, and Δc_j are the group-contribution values of the j-th group for the standard enthalpy of formation, the standard absolute entropy, and their coefficients of the three-term molar heat equation respectively, where n_{ij} is the contribution count of the j-th contribution in the i-th compound, and where T is temperature in K.

Thermodynamic Properties of Hydrocarbons. In the ABMY method, molecules with hetero atoms are processed by *replacing* CH_n groups in the chain structure of a parent hydrocarbon with functional groups. Hence, the first step is the estimation of the properties of saturated hydrocarbon skeletons. Each compound is considered to be composed of a base group, *i.e.*, methane, or a cyclic compound, which is modified by the *substitution* of the other groups for the atoms composing it. For example, all paraffinic hydrocarbons are considered to be derived from methane by the successive substitution of CH_3 groups for hydrogen atoms. Similarly, any benzene derivatives are regarded as derived from a base group, benzene.

Primary Methyl Substitution: The contributions resulting from the primary substitution of a methyl group for a hydrogen atom in any one of the base groups are the specified ones for the groups concerned. In the cases of ring compounds as base groups, successive substitutions for the different hydrogen atoms on the ring involve different contributions depending on the number and position owing to geminal, vicinal, or global effects.

Secondary Methyl Substitution: A secondary methyl substitution is the substitution of a methyl group with a hydrogen in the methyl group derived by the primary substitution or in recursively substituted methyl groups. Contributions from the secondary substitution depend empirically on the types of both the nearest-neighboring atom and the geminal atoms. The carbon-atom types are defined, on the basis of the number of non-hydrogen atoms attached, as follows:

Type	1	$-CH_3$
	2	$-\overset{\vert}{C}H_2$
	3	$-\overset{\vert}{\underset{\vert}{C}}H$
	4	$-\overset{\vert}{\underset{\vert}{\overset{\vert}{\underset{\vert}{C}}}}-$
	9	C atom in aromatic rings.

Branched hydrocarbons are usually more stable than straight-chain isomers, except for highly branched ones, which suffer from steric hindrance. Hence, the contributions of the secondary substitutions are naturally classified according to A, the type number of the carbon atom on which the substitution is made (the nearest-neighboring effect), and B, the highest type number among adjacent atoms (the geminal effect). The type number 9 of an aromatic ring indicates the strongest geminal effect among them. In the present estimation method, an aromatic ring is limited to a benzene ring or one of the benzene rings in fused-ring compounds.

Multiple Bonds and Corrections due to Their Context: After the properties of saturated-hydrocarbon chain-structure are estimated, some of the single bonds may be replaced with multiple bonds, if any. Contributions for this replacement are classified according to the type numbers of the carbon atoms connected by the multiple bonds. Corrections due to conjugated multiple bonds, conjugation with an aromatic ring, and cumulative double bonds may be added.

Replacement of CH_n Groups with Functional Groups. The implementation of functional groups are made by the *replacement* of CH_n groups with functional groups; three kinds of contribution values, *i.e.*, the *fundamental*, *type-number correction*, and *multiple-substitution correction*, will be described below.

Fundamental Contribution : When one of the CH_n groups is replaced, a fundamental contribution is added. Table 1 shows examples of fundamental contributions, where the global effect of the aromaticity is significant. Therefore, the discriminated values must be given to groups directly connected to aromatic rings. The divalent or trivalent functional groups, such as –O–, –NH–, –N<, or –COO–, have different values from those of the monovalent parent groups, like –OH, $-NH_2$, or –COOH.

Table 1. Global effect of aromatic ring on fundamental contribution values of functional groups.

Replacement of CH_3 with functional group	Change by replacement[a]	
	$\Delta H^\circ_{f,298.15}$ / kcal mol^{-1}	$S^\circ_{298.15}$ / cal mol^{-1} K^{-1}
CH_3-CH_3→CH_3-NH_2	14.74	3.13
C_6H_5-CH_3→C_6H_5-NH_2	8.81	0.36
CH_3-CH_3→CH_3-OH	−27.84	2.44
C_6H_5-CH_3→C_6H_5-OH	−34.98	−1.21

a) 1 cal=4.184 J. Data from SWS.[8]

Type-number Correction for Functional Groups : The geminal effect for functional groups generally may be enhanced by the superconjugation between unshared electrons in functional groups and pseudo-π-orbitals in geminal methyl groups. Table 2 shows the reasonings for the type-number correction. Columns 3 and 6 give, respectively, the increases caused by the replacement in the enthalpy of formation and in entropy, both at the standard state. The fundamental contributions being estimated as −0.39 and 1.19 respectively (line 1), deviations solely due to the geminal effect are seen in Columns 4 and 7. On the other hand, t in Column 2, which is equal to (A-1), denotes the number of geminal methyl groups relative to the chloro group; therefore, the type-number corrections for enthalpy and entropy are derived to be −1.18 and 0.69 respectively, on the assumption that the geminal effect is simply additive regardless of the number of geminal atoms. Finally, Columns 5 and 8 show the calculated geminal effects, which are in good agreement with those observed.

Functional groups directly bonded to aromatic rings have no type-number corrections because these fundamental contributions already include the global effect. The groups directly bonded to non-aromatic rings, however, require the appropriate type-number corrections according to the type number of the methyl-substituted carbon atom in the ring; for example, the twofold corrections to chlorocyclohexane are necessary because the type number, A, of the carbon atom in the ring is three.

Multiple-substitution Correction for Functional Groups: The polar groups bonded to one carbon atom may interact with each other, probably because of electrostatic repulsion or steric hindrance. Therefore, the multiple-substitution correction may be added. Table 3 shows an example of this correction. The quantities in Columns 2, 4, and 7 are the same as the corresponding notations in Table 2. Columns 5 and 8 are the remainders of enthalpy and entropy respectively, after type-number correction by the use of t. The notation m in Column 3 implies the number of geminal Cl–C–Cl effects; its sum is ten. By the use of the averaged correction values of 5.04 and −1.66 derived from the totals in Columns 5 and 8 respectively, the values in Columns 6 and 9 are calculated; again, they are in good agreement with the observed values. The mixed substitutions such as F–C–Cl can be corrected similarly.

Preparation of Contribution Values

Sources of Observed Data. The newest observed values of the standard enthalpy of formation, the absolute entropy at 25 °C, and the molar heat at temperatures from 273 to 1000 K were selected from three major sources: SWS,[8] API,[9] and TRC;[10] the estimated, or correlated, values described very often in the sources were carefully excluded. The observed data thus selected (the molar heats were converted into three coefficients of Eq. 3) were stored in a database, the EROICA database,[6] together with their contribution counts, as prepared by a computer program rigorously following the estimation procedures to be described in the next chapter.

Besides these three sources, three other data sources, PRN[11], BCG,[12] and LBT1,[13] were utilized suplementarily in order to obtain the contribution values of functional groups which could not be retrieved from the former three. The PRN, which was recently published, complies the observed data of enthalpy reported up to early 1976, along with their uncertainties, but this is not yet implemented into the EROICA database. In BCG, Benson *et al.*[8] estimated the enthalpies of formation in the gaseous phase of a wide variety of compounds from those in the liquid phase (even in the solid phase in rare cases) by assuming the heat of evaporation.[14] These estimated values were adopted only when unavoidable. The data of molar heats at temperatures were adopted also from LBT1, which is also not implemented.

Preparation of Contribution Values from the Database. Most of the contribution values were prepared with the aid of a computer program, THEDES, written in FORTRAN IV, on a HITAC 8800/8700 of the University of Tokyo.

Table 2. Type-number correction for replacement by a chloro group[a]

Line	(1) Replacement by a chloro group	(2) t[b]	(3) $\Delta(\Delta H^\circ_f)_{obsd}$[c]	(4) $\Delta(\Delta H)_{t,obsd}$	(5) $\Delta(\Delta H)_{t,calcd}$	(6) $\Delta(S^\circ)_{obsd}$[d]	(7) $\Delta(S)_{t,obsd}$	(8) $\Delta(S)_{t,calcd}$
1	$CH_3CH_3 \rightarrow CH_3Cl$	0	−0.39	—	—	1.19[e]	—	—
2	$CH_3CH_2CH_3 \rightarrow CH_3CH_2Cl$	1	−1.88	−1.49	−1.18	1.42	0.23	0.69
3	$CH_3CH_2CH_2CH_3 \rightarrow CH_3CH_2CH_2Cl$	1	−0.95	−0.56	−1.18	2.15	0.96	0.69
4	$CH_3CH(CH_3)CH_3 \rightarrow CH_3CH(CH_3)Cl$	2	−2.85	−2.46	−2.36	2.28	1.09	1.38
5	$CH_3C(CH_3)_2CH_3 \rightarrow CH_3C(CH_3)_2Cl$	3	−4.13	−3.74	−3.54	3.77	2.58	2.07
6	Total	7	—	−8.25	—	—	4.86	—
7	Mean	—	—	−1.18[e]	—	—	0.69[e]	—

a) 1 cal=4.184 J. Data from SWS.[8] b) Number of geminal methyl groups. c) Unit in kcal mol^{-1}. d) Unit in cal mol^{-1} K^{-1}. e) These contribution values are different from those listed in Tables A5 and A6 in the Appendex, as the latter values were obtained by employing a wider variety of compounds.

Table 3. Multiple substitution correction of replacement by a chloro group[a]

Line	(1) Replacement by a chloro group	(2) t	(3) m[b]	(4) $\Delta(\Delta H^\circ_f)_{obsd}$[c]	(5) $\Delta(\Delta H)_{m,obsd}$	(6) $\Delta(\Delta H)_{m,calcd}$	(7) $\Delta(S^\circ)_{obsd}$[d]	(8) $\Delta(S)_{m,obsd}$	(9) $\Delta(S)_{m,calcd}$
1	$CH_3CH_3 \rightarrow CH_3Cl$	0	0	−0.39	—	—	1.19	—	—
2	$CH_3CH_2CH_3 \rightarrow ClCH_2Cl$	1×2	1	2.02	4.77	5.04	0.08	−2.49	−1.66
3	$\begin{matrix}CH_3\\\vert\\CHCH_3\\\vert\\CH_3\end{matrix} \rightarrow \begin{matrix}Cl\\\vert\\CHCl\\\vert\\Cl\end{matrix}$	2×3	3	7.95	15.42	15.12	−0.24	−5.57	−4.98
4	$\begin{matrix}CH_3\\\vert\\CH_3CCH_3\\\vert\\CH_3\end{matrix} \rightarrow \begin{matrix}Cl\\\vert\\ClCCl\\\vert\\Cl\end{matrix}$	3×4	6	15.67	30.22	30.24	0.89	−8.58	−9.96
5	Total	—	10	—	50.41	—	—	−16.64	—
6	Mean	—	—	—	5.04[e]	—	—	−1.66[e]	—

a) 1 cal=4.184 J. Data from SWS.[8] b) Number of multiple substitutions. c) Unit in kcal mol^{-1}. d) Unit in cal mol^{-1} K^{-1}. e) See footnote e) in Table 2.

Contribution Values in Tables A1 through A4 : Table A1 in the Appendix was prepared from the observed data themselves.

First, all of the paraffins except methane were retrieved from the database, and simultaneous equations of Eqs. 1, 2, and/or 4 were prepared with given contribution counts, n_{ij}'s, as independent variables and observed values minus that of methane as dependent variables; then the parameters, $\Delta(\Delta H)_j$, ΔS_j, and Δa_j, Δb_j, and Δc_j, were calculated by the method of the least squares. The primary substitution to methane in Table A2 and secondary substitutions, except for those related with aromatic rings in Table A3, were thus prepared.

Second, all of the olefins, diolefins and acetylenes were retrieved, and, after the elimination of contributions due to primary and secondary substitutions, multiple-bond contributions and their corrections in acyclic compounds were calculated by the same method; the results are given in Table A4.

Third, all of the hydrocarbon derivatives of cyclopentane and cyclohexane were retrieved, and primary substitutions to these two cycloalkane base groups were estimated; these results are shown in Table A3.

Finally, hydrocarbon derivatives of benzene and naphthalene were processed to estimate the primary substitutions to these two aromatic base groups (Table A2), the secondary substitutions related with the aromatic rings (Table A3), and the conjugation effects of multiple bonds with aromatic rings (Table 4).

Contribution Values in Tables A5 and A6: The fundamental values, type-number corrections, and multiple-substitution corrections were calculated at the same time with the aid of the same procedure, after eliminating the contributions already given in Tables A1 through A4. In practice, compounds with hetero atoms derived from methane or the above-mentioned four cyclic base groups were subdivided, so that compounds containing a specified hetero atom besides carbon and hydrogen were processed to calculate the contribution values for functional groups containing the above-mentioned hetero atom. Following this sequence, the majority of the values in Tables A5 and A6 were statistically estimated.

Illustrations for Tables A1 through A8. In Table A2, several primary methyl substitutions are possible for ring compounds, while only one primary substitution is possible for methane. Each line corresponds to one methyl substitution on the base group; hence the primary methyl substitutions to form 1,2,3-trimethylbenzene, for example, are composed of the first primary (line 23) and two of the second primary substitutions, *i.e.*, 1,2 (line 24) and 1,2,3 (line 27). As for the cyclopentane and cyclohexane derivatives, *cis* or *trans* configuration must be discriminated in polymethyl derivatives, although averaged values without the *cis-trans* notation may be used for an equilibrium mixture. The values designated as *unspecified* may be used to form derivatives which require additive substitutions; 1,2,3,4-tetramethylbenzene may be estimated by adding the unspecified values (line 30) to those of 1,2,3-trimethylbenzene.

In Table A4, the unspecified 2=2 contribution implies that of an equilibrium mixture of *cis* and *trans* configurational isomers. An additional correction to multiple-bond arrangements may be present in lines 12 to 17.

The fundamental contributions of the functional group in Table A5 are arranged in the order of O, F, Cl, Br, I, S, and N. Two single bonds and one double bond should be discriminated; the values of –NH–, secondary amine, should not be used instead of those of =NH, imine. The contribution of functional groups directly connected to an aromatic ring (denoted by @) should be discriminated from the others. The observed values of *o*-difluorobenzene deviate slightly from the ordinarily estimated values because of the vicinal effect.

Corrections due to type numbers are given in lines with one functional-group notation in Table A6. Topologically non-symmetric multivalent groups such as –C(=O)–O– should have two kinds of type-number corrections, for which a percent mark(%) is given to indicate the direction of the bonds to be considered. Corrections due to multiple substitutions are given in lines where two functional-group notations are described.

In addition, Table A7 lists simple substances and Table A8 lists inorganic compounds and a few organic compounds whose properties can not be estimated by the present method, for the convenience of users in calculating the change of properties in reaction, *etc.*

Quality of Contribution Values. The reliability of contribution values given in these tables depends on the reliability and plentifulness of the observed thermochemical and thermodynamic data from which the contribution values are derived. Since the compounds in Table A1 are key compounds, the observed values are highly reliable. The contribution values in Tables A2 to A4, which are employed to form various hydrocarbons, are usually of a high quality because the reliable observed data are available for diversified kinds of hydrocarbons; some minor corrections for the context concerned with multiple bonds are, however, less reliable because of the scarcity of observed data of a high quality. The contribution values for some functional groups are less reliable, because often only one set of observed data even with a low accuracy is available. The assumed contribution values, which could not be otherwise determined because of the lack of observed data, may much diversify the range of organic compounds to be handled, but these assumed values are undoubtedly of less reliability.

Thus, the *quality* given in Table 4 was assigned to each of the contribution values in parentheses following values. The qualities in Table 4 range from 1 (the most reliable) to 6. The reliability of a physical property obtained as a sum of the contribution values may be designated by the worst quality of the contributions.

The uncertainty for quality 1 may be evaluated as 0.5 kcal/mol, except for fluorides and chlorides, for the enthalpies of formation judged from the standard deviations discussed in Results and Discussion, while that for quality 4 may be more than 1 kcal/mol; properties with quality 5 or quality 6 must be used at the

Table 4. Quality of contribution values

Quality	Remarks
1	Calculated values from reliable observed data
2	Approximated values correlated from very similar contributions
3	(Reserved for observed data)
4	Calculated values from less reliable observed data—in the present version, those from observed data rated 'C' in SWS[8]
5	Assumed values by correlation with less reliability
6	Assumed values by decomposing functional groups into their fragments

user's risk.

Contribution Values Manually Selected. In Tables Al through A6 of the Appendix, the values with quality 2 were determined manually, although those from the reliable data in PRN are rated 1; the procedures of estimation are given in the corresponding footnotes of the tables.

As for some primary methyl substitutions (Table A2), the contribution values were assumed from those of the relevant substitutions. The values of the relevant combination of type numbers were also used in place in the secondary methyl substitutions (Table A3). Properties in the gaseous phase were estimated from those in the liquid or even solid phases when the former was unavailable;[12] these values were rated 5.

Fundamental Contribution Values for Functional Groups : It is surprising that no data are available for the entropy and the molar heat of any aromatic ether, a popular homolog, with which the chemical equilibria of its formation at temperatures may be calculated. The contribution values of aromatic ether (@O–) may be assumed by subtraction : $\Delta(@OH)+\{\Delta(-O-)-\Delta(-OH)\}$, where the contributions in the formula stand for phenol, ether, and alcohol, whose values have already been calculated. Supposedly, the entropy and molar heat may be not so seriously affected by the bond to an aromatic ring as enthalpy,[15] because the former is affected by the curvature of the potential surface, whereas the latter is determined by the bond energy itself. Hence, the application of this method to a fundamental contribution was restricted only for entropy and molar heat, although no data is available to verify the above discussion, even for the latter two properties. These methods may give less reliable values, so they were rated 5.

In the cases where the fundamental values of the functional groups could not be estimated by means of any method given above, some of them were assumed by decomposing a group into small fragments. An example is the entropy and molar heat for –COBr, which was decomposed as consisting of –C(=O)– and Br.[16] Table 5 shows the effects of decomposing groups whose contribution values were obtained beforehand from observed data. As regards the entropy and molar heat, the estimation by decomposition may not give bad values, although the agreement between values for enthalpy is untolerably poor; hence, a few values only for the former two properties were estimated by this method, and they were rated 6.

Minor Corrections for Functional Groups : As for the minor corrections in Table A6, the subtraction method was employed even for enthalpy because of their small magnitude. In some cases, values were assumed from those of similar functional groups. One example is that the difference between the values for @COF and –COF is assumed to be equal to that between the values for corresponding COCl groups. Assumption that the type correction of %–COO– is equal to that of –COOH is another example. Some type correction values for the entropy and molar heat, which could not be correlated by these methods, were assumed to be zero because they are usually small; they were rated 5.

Sequence of Manual Operations in Estimation

The following features have been changed from the original ABW method : (1) base groups are limited to methane and ring compounds; (2) functional groups substituted to aromatic rings are discriminated from those substituted to non-aromatic fragments; (3) type corrections are given throughout functional groups; (4) multiple-substitution corrections are also given to some of the functional group; (5) corrections due to the context of multiple bonds are expanded, (6) the *quality* of estimated values is made available in order to make it possible to recognize their reliability, and (7) minor corrections due to the chain length as well as the enlargement of the cyclohexane ring are abolished.

Manual Operation. The suggested sequence of operations in estimating the properties of a complex compound is as follows :

Step 1: Select the base group, and determine its properties from Table A1. In an acyclic compound, yan one of the terminal atom groups may be selected

Table 5. Effects of decomposing functional groups into fragments on their fundamental contribution values

Functional group		Fundamental group-contribution values[a]				
		$\Delta(\Delta H)$	ΔS	Δa	Δb	Δc
-COCl	from observed data	−38.06	12.89	5.41	−5.63	−0.58
	-CO- and -Cl	−32.58	17.07	5.19	−7.29	1.37
$-NHNH_2$	from observed data	40.64	11.76	—	—	—
	-NH- and NH_2	29.13	13.27	—	—	—

a) The units are the same as those given in Table A5.

as the base group. In the case of a cyclic compound, a ring compound should be selected as the base group.

Step 2: Make all the *primary substitutions* before starting the *secondary substitutions*, where *substitution* means an exchange of a hydrogen atom with a methyl group. In the case of methane, only one primary substitution is possible. With ring structures, one primary substitution (the *first* primary substitution) is possible for each hydrogen atom of the base group. If two or more primary substitutions (*second* primary substitutions) are to be made on a base ring, the two substitutions closest together should be made first. If more than one substitution is to be made on a specific carbon atom in the base ring, such additional substitutions are to be treated in the same way. The unspecified contributions may be assigned for substitutions other than those clearly indicated, Table A2 is used to evaluate the group contributions resulting from primary substitutions.

Step 3: Complete the carbon skeleton of the compound by making a series of secondary substitutions, and use Table A3 to obtain the values of group contributions for such substitutions. Each of the multivalent functional groups, *e.g.*, –COO– or –N<, should be regarded as a CH_n group of the carbon skeleton. In order to have the results conform with the procedures used in developing the tables, the following rules should be observed, although the deviations are usually small even if they are violated:

(a) The longest straight chain should be fully developed before any side chains are added.

(b) Side chains are added in the order of their length. However, if the carbon atom with the longest side chain is to have a second side chain, this second side chain should be added before additions are made to other carbon atoms of the straight chain.

Step 4: Make additional secondary methyl substitutions for monovalent functional groups. Allowance for such substitution is made from Table A3. For *multibonded* functional groups in Steps 3 and 4, *e.g.*, =O or =N–, *additional* secondary methyl substitutions should be made; *one* additional substitution for *double* bonds and *two* for *triple* bonds.

Step 5: Add multiple bonds and obtain from Table A4 the contributions resulting from such additions. If required, make the additional corrections indicated by Table A4 for correlations between bonds.

Step 6: Replace CH_n groups by the substitution groups listed in Table A5.

(a) First, add the *fundamental* contributions given in Table A5.

(b) Second, check the types of connecting atom groups, and add contributions for the *type-number correction* from Table A6. In counting the type, assume that all of the functional group(s) were replaced *beforehand*.

(c) Third, check the other substituting groups to the group to which the present group is connected (the geminal effect). Add contributions for *multiple-substitution corrections* from Table A6. Repetition from each substituent should be allowed.

Step 7: Find out the maximum of *quality* associated with the contribution values. This gives the user a measure of the reliability of the estimated values.

Examples of Estimation. Four examples will be illustrated in order to make clear the above-mentioned sequence of manual operations.

Example 1. Enthalpy, Entropy, and Molar Heat of 2-Methyl-1,3-butadiene (Isoprene): The replacement of two single bonds with two double bonds in 2-methylbutane makes this compound. Methane is selected as the base group (Step 1); then a hydrogen atom is substituted by a methyl group as the primary methyl substitution to make ethane (Step 2). The carbon skeleton is completed by the successive secondary substitutions, with consideration paid to the type numbers of the atoms concerned (Step 3). Finally the contribution values due to double bonds as well as the correction for the conjugated double bonds are added to make the given compound (Step 5). The numerals will be given below:

	$\Delta(\Delta H)$ / kcal mol^{-1}	$\Delta(S)$ / cal mol^{-1} K^{-1}
(1) Base group:		
Methane	−17.89 (1)[a]	44.50 (1)[a]
(2) Primary substitution:		
CH_3CH_3	−2.35 (1)	10.35 (1)
(3) Secondary substitutions:		
$CH_3CH_2CH_3$ (1,1)[b]	−5.04 (1)	10.44 (1)
$CH_3CH_2CH_2CH_3$ (1,2)	−4.92 (1)	9.29 (1)
	(−30.20)[c]	(74.58)[c]
$CH_3CH(CH_3)CH_2CH_3$ (2,2)	−6.35 (1)	6.53 (1)
(5) Multiple bonds:		
1=3	27.94 (1)	0.17 (1)
1=2	30.15 (1)	−1.43 (1)
Conjugated double bonds	−3.66 (1)	−4.06 (1)
Total	17.88 (1)	75.79 (1)

where the superscripts a, b, and c indicate the quality, type numbers, and subtotals respectively. The observed values[8] are 18.10 for $\Delta H^\circ_{f,298.15}$ and 75.44 for $S^\circ_{298.15}$, and the quality of the estimates is 1. The molar heats at 298 K and 1000 K were estimated similarly to be 25.43 cal mol^{-1} and 52.68 respectively, while the observed values[9] are 25.00 and 52.90. The agreement among these observed and estimated values is surprisingly good in this case.

The group contributions by the Benson method are composed of $2\times[(C_d\text{-}(H)_2]+[C_d\text{-}(C_d)_2]+[C_d\text{-}(C_d)(H)]+[C\text{-}(C)(H)_3]$; this gives the estimate of enthalpy of 13.7 in the same unit.

Example 2. Enthalpy and Entropy of 2-Butanone: The replacement of two methyl groups with an oxo (=O) group will make this compound. First, 2,2-dimethylbutane will be prepared by Steps 1 through 4; second, two methyl groups will be replaced by a substitution group with the twofold type-number corrections, because the 2-carbon atom *after* substitution is tertiary (Step 6).

	$\Delta(\Delta H)$ / kcal mol^{-1}	$\Delta(S)$ / cal mol^{-1} K^{-1}
(1-3) Methyl substitutions:		
$CH_3CH_2CH_2CH_3$	−30.20 (1)	74.58 (1)

(4) Additional substitutions for functional groups:		
$CH_3CH(CH_3)CH_2CH_3$ (2,2)	−6.35 (1)	6.53 (1)
$CH_3C(CH_3)_2CH_2CH_3$ (3,2)	−6.84 (1)	4.30 (1)
(6) Replacement by functional group:		
$CH_3COCH_2CH_3$		
Fundamental	−7.09 (1)	−20.19 (1)
Type number	−3.30 (1) ×2	7.39 (1) ×2
Total	−57.08 (1)	80.00 (1)

The observed values[9] are −56.97 and 80.81 respectively, whereas the Benson method gives a fairly good value of enthalpy of −56.56.

Example 3. Enthalpy and Entropy of Perfluoroethane: Since fluorine atoms are substituted to ethane by replacing a methyl group for each fluorine atom, the hydrocarbon molecule *before* replacement is 2,2,3,3-tetramethylbutane, as estimated in Steps 1 through 4. In Step 6, the fundamental contributions of fluorine to non-aromatic fragments are added six times at first. As for the type-number correction, threefold corrections for each fluorine atom are necessary because the 2- and 3-carbon atoms are quaternary; hence, altogether 18 corrections are added. Besides, the multiple-substitution corrections must be added six times, because each of the two trifluoromethyl groups has a threefold correction in it.

	$\Delta(\Delta H)$ / kcal mol^{-1}	$\Delta(S)$ / cal mol^{-1} K^{-1}
(1-4) Methyl substitutions:		
$CH_3C(CH_3)_2$-$C(CH_3)_2CH_3$	−53.99 (1)	93.07 (1)
(6) Functional groups:		
(a) Fundamental	−221.10 (1) (−36.85×6)	−23.82 (1) (−3.97×6)
(b) Type number	−26.46 (1) (−1.47×3×6)	17.82 (1) (0.99×3×6)
(c) Multiple substitution	−22.02 (1) (−3.67×3×2)	−5.46 (1) (−0.91×3×2)
Total	−323.57	81.61 (1)

The agreement between the estimated and observed values,[8] −321.00 and 79.37, shall be rated as excellent in the case of rather large numerals. The estimate of enthalpy by the Benson method is −316.8.

Example 4. Enthalpy and Entropy of 1,2,3,4-Tetramethylbenzene: As a matter of course, benzene is selected as the base group (Step 1). The first- and second-primary substitutions will be processed by exactly following the descriptions in Step 2, as is shown below:

	$\Delta(\Delta H)$ / kcal mol^{-1}	$\Delta(S)$ / cal mol^{-1} K^{-1}
(1) Base group:		
Benzene	19.82 (1)	64.34 (1)
(2) Primary substitutions:		
(a) First primary	−8.48 (1)	11.45 (1)
(b) Second primary		
To make 1,2-	−6.64 (1)	8.70 (1)
To make 1,2,3-	−7.26 (1)	10.24 (1)
Unspecified (to make 1,2,3,4-)	−7.61 (1)	4.94 (1)
Total	−10.17 (1)	99.67 (1)

The agreement between the estimated and observed values,[9] −10.02 and 99.55, is again excellent. If one employs the second primary substitution to make 1,2,4- instead of the above one to make 1,2,3-, he may obtain the estimates of −10.19 and 99.85, which are slightly poorer values than the above ones, presumably because of less enhancement of the ortho effect among methyl groups. The contributions by the Benson method, composed of $2\times[C_B\text{-}(C)]+4\times[C_B\text{-}(H)]+4\times[C$-

Table 6. Errors in the estimation of thermodynamic properties

Line	Compound	$\Delta H°_{f,298.15}$ N_d[a]	N_c[b]	N_s[c]	e[d]	σ[e]	$S°_{298.15}$ N_d	N_c	N_s	e[d]	σ[e]
1	Alkanes	51	12	3	0.3	0.4	51	12	3	0.5	0.7
2	Alkenes and alkynes	90	13	3	0.4	0.6	75	13	2	0.5	0.8
3	Cycloalkanes	44	14	12	0.1	0.2	44	14	12	0.1	0.1
4	Aromatics	43	14	4	0.3	0.4	40	13	3	0.3	0.5
5	O[f]	101	34	6	0.9	1.4	49	19	7	1.2	2.0
6	F	30	8	0	2.9	3.5	99	14	1	1.6	2.1
7	Cl	37	5	0	2.2	2.6					
8	Br	21	4	1	0.8	1.1	30	8	0	1.7	2.2
9	I	13	4	1	0.5	0.7					
10	S	49	10	3	0.4	0.6	27	8	2	0.6	1.0
11	N	24	16	7	0.4	0.7	18	12	8	1.3	1.7
Total/mean		503	134	40	0.8[g]	1.4[g]	433	113	38	0.9[g]	1.5[g]

a) Number of compounds employed in calculation. b) Number of contribution values calculated. c) Number of error $=\sum|\text{obsd}-\text{calcd}|/(N_d-N_s)$; kcal mol^{-1} for H, and percentage error for S and C_p. e) Standard deviation; f) For classification of compounds, see text. g) Mean.

(C)(H)$_3$]+3×[ortho correction], give −10.45.

Results and Discussion

In the evaluation of the estimation methods by the use of the correlation of the physical properties of organic compounds, it may be worthwhile to discuss the following four items.

Accuracy or Reliability of the Estimated Values. Table 6 shows the average errors and the standard deviations derived from the differences between the observed data and the calculated data by the use of contribution values; these tables were prepared during the statistical calculations using the program, THEDES.

The errors as well as the number of compounds, N_d, employed for the calculation, the number of contributions, N_c, whose values were found during the calculation, and the number of compounds which contain the unique contributions, N_s, are given for each classification of compounds.

The degree of freedom used for the calculation of errors should not be the number of samples, N_d, but N_d-N_s. Sometimes, it is necessary to determine the value for a specified contribution from one compound, that is, a compound which has a *unique* contribution; for example, the contribution due to the replacement of a single bond in ethane with a triple bond to form acetylene, or Δ(1≡1) in Table A4, is derived solely from the observed value of acetylene. In these cases, the differences between observed and calculated data should be null *by definition*. Hence, the true accuracy must be estimated by excluding the null differences; this consideration suggests the use of N_d-N_s, instead of N_d, for the actual degree of freedom. A high accuracy, including many nulls by definition, in the estimation of thermodynamic values has been reported by the use of group-contribution values, supposedly derived not statistically but by the mere subtraction method;[17] nevertheless, such an unthinkably high accuracy can not be expected throughout a wide variety of compounds other than those cited in their report.

The average errors shown in Table 6 are usually small enough for practical purposes. The standard deviations described there give us the statistical reliability of the estimated values; 95% of the population has a deviation not larger than 2σ, 70% of it, one not larger than σ, and 40% of it, one not larger than $\sigma/2$.

During the processing, however, a number of compounds were excluded because of the poor agreement between the estimated and the observed values, although these compounds very often had observed values measured many years ago and, hence, with less reliability.

A certain monograph[18] presents a comparison between the estimated and the observed values of 29 organic compounds obtained by several methods. The average errors in enthalpy are obtained by excluding the compounds which are outside the scope of each method or which have unique contributions; for the Benson and the ABWY methods, the four compounds described in Examples are added. The average errors are :

Benson: 35.70/27=1.3 kcal mol^{-1}; Verma and Doraiswamy:[19] 50.71/19=2.7; Franklin:[20] 42.28/20=2.1; ABW:[3] 82.8/23=3.6; ABWY: 21.06/27=0.8, where the numerator and the denominator are the sum of errors and the degree of freedom defined above respectively. In conclusion, the ABWY method may exceed the existing methods in accuracy or in the reliability of the estimated values.

Every effort should be made to improve further the reliability of the estimated values; one of such effort may be the experimental determination of the properties of the *key* compounds which contain contributions with poor quality in Table A2 through A6. The endeavors of thermochemists are particularly waited for.

Soundness of the Empirical Rules and Formulations. As has been mentioned earlier, it has been empirically guaranteed that the additivity rule holds for the estimation of the thermodynamic properties of organic compounds in the ideal gas state. Therefore, the soundness of the method may be criticized for its way of incorporating a variety of neighboring effects, especially the global effect. In the present method, the geminal effects includes even the multiple-substitution contributions between different halogen atoms, and the type-number corrections are also incorporated as one of the vicinal effects. The contributions of functional groups to aromatic rings are, as a global effect, discriminated from those to non-aromatic fragments.

The *symmetry number* has been taken into account in the Benson method in order to estimate the values of entropy. In our method, the symmetry number due to the three-dimensional geometry of compounds seems to be implicitly incorporated by adopting the secondary methyl substitution, discriminated from the primary one, which produces the propane skeleton with a higher symmetry number from the ethane skeleton. As for the case of more complicated compounds, the rather small correction due to the symmetry or the existence of optical isomers may be negligible as com-

			C_p°			
			e[d]		σ[e]	
N_d	N_c	N_s	300 K	700 K	300 K	700 K
28	10	3	0.1	0.0	0.3	0.1
119	28	15	0.9	0.3	1.8	0.6
40	13	3	0.5	0.2	1.0	0.3
40	18	9	0.9	0.4	1.5	0.7
60	15	1	2.9	2.5	4.2	4.0
24	7	1	0.8	0.7	1.3	0.9
9	8	5	0.0	0.7	0.2	1.0
320	99	37	1.5[g]	1.0[g]	2.6[g]	2.2[g]

compounds having a unique contribution. d) Average kcal mol^{-1} for H, and percentage error for S and C_p.

pared with the inevitable errors generally associated with the empirical methods.

Variety of Estimable Compounds. The variety of estimable compounds can be judged by the kinds of fundamental, type-number, and multiple-substitution correction contributions and the combinations of them; the present method exceeds others in this respect, because more recent data have been adopted in this method.

The concepts of both the type number and the multiple substitution have been implicitly incorporated in the Benson method. For example, altogether four kinds of carbon atoms are given in the contribution of bromine, although six kinds are logically necessary to process every variety of bromide derivative of paraffinic compounds. The kind of contribution in their method should, however, be surprisingly increased in order to cover mixed halides such as –CFClBr and haloolefins like $=CBr_2$ in contrast to the limited kinds of contributions in the present method. It may be additionally remarked that no compound consisting of one carbon such as CFClBrI can, by definition, be treated with the Benson method.

It should be mentioned, however, that hydrogen is not a functional group in the present method, so HCOOH is not derived from =COOH or HCOO–. Also, compounds that are composed only of functional groups can not be treated; thus, for example, the estimation of oxalic acid, HOOC–COOH, by the ABWY method gives an enthalpy of -193.5 kcal mol^{-1} as compared with the observed value of -174.86.[11] The compounds which are otherwise not processed are listed in Table A8 for convenience.

In conclusion, the ABWY method may be evaluated as having a higher potentiality for estimating a much wider variety of compounds than the existing methods.

Applicability for Computation with the Aid of Computers. As was described in the opening paragraphs, the present method has been already implemented in computer programs including the whole logic. The symmetry number, a stereochemical concept, cannot be determined without the knowledge of the whole geometry of a compound, while the geometry can be estimated with only highly sophisticated computer programs such as a program, STERIC,[5] also prepared by the present author. A logic which requires no symmetry number for estimation may be rated higher for implementation into computer programs.

The author's thanks are due to Dr. Makoto Misono for his helpful discussions. A part of the research expenses was defrayed from the Grant-in-Aid for a Special Project Research, "Chemical Research in the Development and Utilization of Nitrogen-Organic Resources," of the Ministry of Education, Science, and Culture. The clerical work of Miss Masako Oya and the technical aid of Mr. Kiyoshi Arai are highly appreciated.

Appendix

Tables of Contribution Values for the Thermodynamic Properties of Organic Compounds in the Ideal Gas State, A1 through A8. Unit of standard enthalpy of formation(H) in kcal mol^{-1}; unit of standard entropy(S) and three coefficients of molar heat (a, b, and c) in cal mol^{-1} K^{-1}. 1 cal=4.184 J. The abbreviations for the contribution values of the functional groups are: Δ_f: fundamental; Δ_t: type-number correction; Δ_m: multiple substitution correction; @: aromatic ring directly connected; %: direction of extending chain in which the type number may be counted. 'Single data source' in the footnotes implies that the contribution value was derived only from a compound (or a pair of compounds for the contribution of functional groups having type-number correction).

The molar heats can be calculated from three coefficients at 273 through 1000 K.

Table A1. Thermodynamic properties of base groups in ideal gas state

Line	Base group	$\Delta H^\circ_{f,298.15}$	$S^\circ_{298.15}$	a	b	c
1	Methane	−17.89 (1)	44.50 (1)	3.99 (1)	15.68	−2.38
2	Cyclopentane	−18.46 (1)	70.00 (1)	−10.02 (1)	113.22	−43.64
3	Cyclohexane	−29.43 (1)	71.28 (1)	−12.48 (1)	143.35	−55.19
4	Benzene	19.82 (1)	64.34 (1)	−5.38 (1)	96.21	−40.97
5	Naphthalene	36.08 (1)	80.22 (1)	−6.79 (1)	148.96	−64.27

Table A2. Contribution of primary methyl substitution for thermodynamic properties in ideal gas state

Line	Base group	$\Delta(\Delta H)$	ΔS	Δa	Δb	Δc
1	Methane	−2.35 (1)	10.35 (1)	−2.37 (1)	24.81	−10.40
	Cyclopentane					
2	(a) First primary substitution	−8.23 (1)	11.77 (1)	2.09 (1)	16.31	−5.54
	(b) Second primary substitution to form					
3	1,1	−6.36 (1) [a]	4.10 (1) [a]	−1.44 (1) [a]	27.81	−13.28
4	1,2(*cis*)	−4.27 (1) [a]	5.74 (1) [a]	−0.87 (1) [a]	26.40	−12.72
5	1,2(*trans*)	−5.98 (1) [a]	5.90 (1) [a]	−0.59 (1) [a]	25.71	−12.46

TABLE A2. (Continued)

Line	Base group	$\Delta(\Delta H)$	ΔS	Δa	Δb	Δc
6	1,2(unspec.)[h]	−5.12 (2)[b]	5.82 (2)[b]	−0.73 (2)[b]	26.05	−12.59
7	1,3(*cis*)	−5.78 (1)[a]	5.90 (1)[a]	−0.59 (1)[a]	25.71	−12.46
8	1,3(*trans*)	−5.24 (1)[a]	5.90 (1)[a]	−0.59 (1)[a]	25.71	−12.46
9	1,3(unspec.)[h]	−5.51 (2)[b]	5.90 (2)[b]	−0.59 (2)[b]	25.71	−12.46
10	Unspecified locant[i]	−5.97 (2)[c]	6.55 (2)[c]	−0.33 (2)[c]	24.61	−11.49
	Cyclohexane					
11	(a) First primary substitution	−8.04 (1)	11.07 (1)	2.77 (1)	19.41	−9.46
	(b) Second primary substitution to form					
12	1,1	−5.79 (1)[a]	4.89 (1)[a]	−3.23 (1)[a]	26.63	−9.80
13	1,2(*cis*)	−3.68 (1)[a]	7.16 (1)[a]	−1.91 (1)[a]	23.90	−9.25
14	1,2(*trans*)	−5.55 (1)[a]	6.30 (1)[a]	−1.39 (1)[a]	24.69	−10.33
15	1,2(unspec.)[h]	−4.61 (2)[b]	6.73 (2)[b]	−1.65 (2)[b]	24.30	−9.79
16	1,3(*cis*)	−6.69 (1)[a]	6.19 (1)[a]	−1.51 (1)[a]	22.74	−7.89
17	1,3(*trans*)	−4.73 (1)[a]	7.57 (1)[a]	−1.03 (1)[a]	21.13	−7.69
18	1,3(unspec.)[h]	−5.71 (2)[b]	6.88 (2)[b]	−1.27 (2)[b]	21.94	−7.79
19	1,4(*cis*)	−4.75 (1)[a]	6.19 (1)[a]	−1.03 (1)[a]	21.13	−7.69
20	1,4(*trans*)	−6.65 (1)[a]	4.84 (1)[a]	−2.01 (1)[a]	25.72	−10.52
21	1,4(unspec.)[h]	−5.70 (2)[b]	5.51 (2)[b]	−1.52 (2)[b]	23.42	−9.10
22	Unspecified locant[i]	−5.73 (2)[d]	6.77 (2)[d]	−1.17 (2)[d]	23.17	−9.08
	Benzene					
23	(a) First primary substitution	−8.48 (1)	11.45 (1)	1.38 (1)	15.40	−4.66
	(b) Second primary substitution to form					
24	1,2	−6.64 (1)	8.70 (1)	2.98 (1)	11.95	−2.86
25	1,3	−6.96 (1)	9.95 (1)	1.20 (1)	15.48	−4.69
26	1,4	−6.86 (1)	8.65 (1)	1.31 (1)	14.41	−3.86
27	1,2,3	−7.26 (1)	10.24 (1)	3.38 (1)	6.99	2.31
28	1,2,4	−8.00 (1)	10.42 (1)	3.92 (1)	4.45	3.88
29	1,3,5	−8.22 (1)[a]	6.41 (1)[a]	1.48 (1)[a]	13.95	−3.52
30	Unspecified locant[i]	−7.61 (1)	4.94 (1)	1.47 (1)	24.17	−13.81
	Naphthalene					
	(a) First primary substitution to form					
31	1	−8.15 (1)[a]	9.99 (1)[a]	1.52 (1)[a]	8.93	−7.67
32	2	−8.33 (1)[a]	10.61 (1)[a]	2.55 (1)[a]	14.76	−4.82
	(b) Second primary substitution to form					
33	1,2	−6.31 (2)[e]	7.24 (2)[e]	3.12 (2)[c]	15.48	−5.87
34	1,3	−6.63 (2)[e]	8.50 (2)[e]	1.34 (2)[e]	19.01	−7.70
35	1,4	−6.53 (2)[e]	7.19 (2)[e]	1.45 (2)[e]	17.94	−6.87
36	2,3	−6.31 (2)[g]	7.24 (2)[g]	3.12 (2)[g]	15.48	−5.87
37	Unspecified locant[i]	−8.24 (2)[f]	10.30 (2)[f]	2.04 (2)[f]	16.84	−6.24

a) Single data source. b) Average of *cis* and *trans*. c) Average of lines 2, 3, 4, 5, 7, and 8. d) Average of lines 11, 12, 13, 14, 16, 17, 19, and 20. e) Assumed as (values of the position corresponding to benzene) + {Δ(1-naphthalene) − Δ(1-benzene)}. f) Average of Δ(1-) and Δ(2-). g) Assumed to be the same as Δ(1,2-). h) Equilibrium mixture of *cis*- and *trans*-isomers. i) For substitution location not mentioned otherwise.

TABLE A3. CONTRIBUTION OF SECONDARY METHYL SUBSTITUTION FOR THERMODYNAMIC PROPERTIES IN IDEAL GAS STATE

Line	Type number A	Type number B	$\Delta(\Delta H)$	ΔS	Δa	Δb	Δc
1	1	1	−5.04 (1)	10.44 (1)	−0.88 (1)	23.46	−10.10
2	1	2	−4.92 (1)	9.29 (1)	0.35 (1)	19.46	−7.52
3	1	3	−3.67 (1)	8.75 (1)	−0.23 (1)	21.90	−9.31
4	1	4	−3.67 (2)	8.75 (2)	−0.23 (2)	21.90	−9.31
5	1	9	−4.70 (1)	10.83 (1)	0.37 (1)	21.16	−9.00
6	2	1	−6.87 (1)	5.13 (1)	−0.50 (1)	22.87	−9.96
7	2	2	−6.35 (1)	6.53 (1)	−0.15 (1)	21.67	−8.97
8	2	3	−5.31 (1)	6.54 (1)	−1.17 (1) [a]	23.33	−9.95
9	2	4	−4.94 (1)	6.57 (1)	−0.29 (1)	22.00	−9.08
10	2	9	−5.82 (1)	6.71 (1)	−0.76 (1)	21.60	−8.68
11	3	1	−7.52 (1) [a]	2.81 (1) [a]	−0.66 (1) [a]	25.74	−11.77
12	3	2	−6.84 (1)	4.30 (1)	−1.65 (1)	26.70	−12.35
13	3	3	−4.96 (1) [a]	6.20 (1) [a]	−1.65 (2) [b]	26.70	−12.36
14	3	4	−5.66 (1) [a]	1.09 (1) [a]	−1.00 (1) [a]	30.96	−15.85
15	3	9	−6.24 (1) [a]	6.71 (2) [c]	−0.76 (2) [c]	21.60	−8.68

a) Single data source. b) Assumed to be the same as $A(3,2)$. c) Assumed to be the same as $A(2,9)$.

TABLE A4. MULTIPLE-BOND CONTRIBUTION REPLACING SINGLE BOND FOR THERMODYNAMIC PROPERTIES IN IDEAL GAS STATE

Line	Type of bond or correction	$\Delta(\Delta H)$	ΔS	Δv	Δb	Δc
1	1=1	32.74 (1) [a]	−2.40 (1) [a]	0.12 (1)	−7.83	0.89
2	1=2	30.15 (1)	−1.43 (1)	0.91 (1)	−12.17	3.90
3	1=3	27.94 (1)	0.17 (1)	3.06 (1)	−17.06	6.67
4	2=2(unspec.) [f]	27.82 (2) [b]	−2.11 (2) [b]	0.33 (2) [b]	−12.55	4.55
5	2=2(*cis*)	28.30 (1)	−1.51 (1)	−1.53 (1)	−8.98	2.70
6	2=2(*trans*)	27.35 (1)	−2.72 (1)	2.19 (1)	−16.14	6.40
7	2=3	27.40 (1)	0.14 (1)	−0.25 (1)	−12.92	5.07
8	3=3	27.70 (1) [a]	−0.50 (1) [a]	1.41 (1)	−22.91	13.75
9	1≡1	74.43 (1) [a]	−6.85 (1) [a]	4.58 (1)	−23.60	5.49
10	1≡2	69.50 (1)	−4.97 (1)	3.95 (1)	−27.98	9.73
11	2≡2	65.54 (1)	−5.72 (1)	3.07 (1)	−30.36	12.35
12	Adjacent double bonds	9.89 (1)	−3.17 (1)	2.33 (1)	−1.86	0.51
13	Conjugated double bonds	−3.66 (1)	−4.06 (1)	−1.60 (1)	8.91	−6.57
14	Double bond conjugated with aromatic ring	−1.72 (1)	−2.27 (1)	1.28 (1)	−2.17	1.24
15	Triple bond conjugated with aromatic ring	2.1 (4) [a,c]	−4.8 (4) [a,c]	−0.9 (4) [a,c]	1.1	0.1
16	Conjugated triple bonds	4.2 (4) [a,d]	−4.9 (4) [a,d]	0.8 (4) [a,d]	3.5	−3.5
17	Conjugated double and triple bonds	3.3 (4) [a,e]	−1.4 (4) [a,e]	3.0 (4) [a,e]	5.3	2.3

a) Single data source. b) Average of *cis* and *trans*. c) From $CH{\equiv}CC_6H_5$. d) From $CH{\equiv}CC{\equiv}CH$. e) From $CH_2{=}CHC{\equiv}CH$. f) Equilibrium mixture of *cis*- and *trans*-isomers.

TABLE A5. FUNDAMENTAL CONTRIBUTION OF FUNCTIONAL GROUP REPLACING CH_n GROUPS FOR THERMODYNAMIC PROPERTIES IN IDEAL GAS STATE

Line	Functional group	$\Delta(\Delta H)$	ΔS	Δa	Δb	Δc
	Oxygen					
1	=O(aldo)	−2.42 (1)	−13.00 (1)	4.09 (1)	−51.16	20.14
2	=O(keto)	−7.09 (1)	−20.19 (1)	1.51 (1)	−35.49	8.76
3	-OH	−28.44 (1)	2.06 (1)	1.74 (1)	−15.70	5.84
4	@OH	−35.01 (1)	−0.30 (1)	2.87 (1)	−11.90	5.80
5	-O-	−20.43 (1)	−1.26 (1)	3.17 (1)	−20.39 (1)	9.22

TABLE A5. (Continued)

Line	Functional group	$\Delta(\Delta H)$	ΔS	Δa	Δb	Δc
6	@O-	−23.37 (1) [a,b]	−3.6 (5) [h]	4.3 (5) [h]	−16.6	9.1
7	-OOH	−24.7 (4) [a,b]				
8	-OO-	−5.22 (1)				
9	-COOH	−83.69 (1)	12.67 (1)	1.89 (1) [a]	6.98	−6.37
10	@COOH	−80.70 (1) [a]	12.40 (1) [a]	−1.92 (1) [a]	6.02	−1.09
11	-COO-	−73.12 (1) [b,g]	13.1 (5) [i]	−4.2 (5) [i]	0.3	1.9
12	@COO-	−75.93 (1) [a,b]	13.1 (5) [j]	−4.2 (5) [j]	0.3	1.9
12 a	@OOC-	−74.12 (1) [a,b]				
13	-COOCO-	−112.32 (1) [a]	27.93 (1) [a]	−1.26 (1) [a]	29.79	−16.55
14	$-COO_2CO-$	−93.7 (4) [c,g]				
15	HCOO-	−65.93 (1)	17.15 (1) [a]	1.89 (1) [a]	6.98	−6.37
16	$-CO_3-$	−117.17 (1) [a,b]				
	Fluorine					
17	-F	−36.85 (1)	−3.97 (1)	1.01 (1)	−18.30	5.87
18	@F	−39.49 (1)	−4.31 (1)	1.55 (1)	−14.22	4.39
19	@F(ortho)	−34.24 (1)	−3.07 (1)	1.41 (1)	−18.85	7.75
20	-COF	−84.96 (1) [a]	13.7 (6) [k]	3.4 (6) [k]	−4.3	1.1
21	@COF	−84.0 (5) [l]				
	Chlorine					
22	-Cl	0.49 (1)	−1.41 (1)	1.78 (1)	−15.50	3.57
23	@Cl	2.36 (1)	−0.95 (1)	2.56 (1)	−19.92	7.42
24	-COCl	−38.06 (1)	12.89 (1)	5.41 (1) [a]	−5.63	−0.58
25	@COCl	−37.12 (1) [a,b]				
	Bromine					
26	-Br	11.84 (1)	3.13 (1)	2.66 (1)	−11.93	3.12
27	@Br	13.76 (1) [a]	1.74 (1) [a]	2.94 (1) [a]	−16.81	6.91
28	-COBr	−25.27 (1) [a,b]	16.4 (6) [m]	5.0 (6) [m]	−10.4	2.2
29	@COBr	−23.54 (1) [a,b]				
	Iodine					
30	-I	24.17 (1)	3.48 (1)	2.72 (1)	−17.33	4.37
31	@I	27.51 (1) [a]	2.1 (5) [n]	3.0 (5) [n]	−22.2	8.2
32	-COI	−9.09 (1) [a,b]	21.1 (6) [o]	5.6 (6) [o]	−7.9	2.3
33	@COI	−7.4 (5) [p]				
	Sulfur					
34	-SH	14.42 (1)	5.75 (1)	3.44 (1)	−15.76	6.79
35	@SH	15.32 (1) [a]	4.72 (1) [a]	2.90 (1) [a]	−10.14	4.64
36	-S-	16.64 (1)	5.17 (1)	4.09 (1)	−19.98	11.00
37	@S-	16.96 (1)	4.1 (5) [q]	3.6 (5) [q]	−14.4	8.8
38	-SS-	19.08 (1)	15.17 (1)	8.51 (1)	−13.96	4.88
39	-SO-	−10.31 (1)				
40	@SO-	−9.5 (5) [r]				
41	$-SO_2-$	−66.90 (1)				
42	$@SO_2-$	−66.08 (1) [a,b]				
43	$-SO_3H$	−282.7 (5) [s]				
44	$-OSO_2-$	−90.71 (1)				
45	$-OSO_3-$	−139.38 (1) [a,b]				
	Nitrogen					
46	$-NH_2$	14.69 (1)	3.13 (1)	1.79 (1)	−9.00	3.15
47	$@NH_2$	9.42 (1) [a]	0.49 (1) [a]	2.11 (1) [a]	−3.44	1.05
48	-NH-	20.78 (1)	−0.05 (1) [a]	0.33 (1) [a]	−5.88	1.85
49	@NH-	13.76 (1)	−2.7 (5) [ee]	0.6 (5) [ee]	−0.3	−0.2
50	-N<	26.45 (1)	−1.40 (1) [a]	0.01 (1) [a]	−4.44	1.05
51	@N<	19.28 (1) [a]	−4.0 (5) [ff]	0.3 (5) [ff]	1.1	−1.0
52	=N-(keto)	44.7 (5) [c,e,g,t]				

TABLE A5. (Continued)

Line	Functional group	$\Delta(\Delta H)$	ΔS	Δa	Δb	Δc
53	-N=N-	63.6 (5) [a,c,e,u]				
54	-$NHNH_2$	40.64 (1) [a]	11.76 (1) [a]			
55	@$NHNH_2$	36.69 (1) [a,b]				
56	-$N(NH_2)$-	44.87 (1) [a,b]	7.53 (1) [a]			
57	@$N(NH_2)$-	40.9 (5) [v]				
58	-NHNH-	46.78 (1) [a]	9.34 (1)			
59	@NHNH-	42.8 (5) [w]				
60	-CN	41.24 (1)	1.60 (1)	3.42 (1)	−12.76	3.51
61	@CN	40.96 (1) [a]	0.94 (1) [a]	4.25 (1) [a]	−11.37	4.82
62	-NC	56.14 (1) [a]	4.13 (1) [a]	4.2 (5) [x]	−11.4	4.8
63	=NOH	22.0 (4) [c,f,g]				
64	-$CONH_2$	−36.72 (1) [b,g]	18.5 (6) [y]	3.6 (6) [y]	5.7	−3.0
65	@$CONH_2$	−33.73 (5) [z]				
66	-CONH-	−30.6 (5) [a,b,aa]				
67	@NHCO-	−37.83 (1) [a,b]				
68	-CON<	21.00 (1) [a,b]				
69	-NO_2	2.75 (1)	10.88 (1) [a]	1.14 (1) [a]	1.11	−3.48
70	@NO_2	4.30 (1) [b,g]	10.9 (5) [bb]	1.1 (5) [bb]	1.1	−3.5
71	-ONO	4.94 (1)	13.10 (1) [a]	2.47 (1) [a]	1.51	−3.84
72	-ONO_2	−8.77 (1)	17.30 (1)	4.12 (1)	7.61	−6.96
73	-NCS	56.0 (5) [cc]	14.7 (5) [dd]			

a) Single data source. b) Data from PRN.[11] c) Data from BCG.[12] d) Data from LBTI.[13] e) The values of the gaseous state were estimated from those of the liquid phase. f) The values of the gaseous phase were estimated from those of crystal. g) Stasistically calculated with weights reciprocal to errors. h) Assumed as $\Delta_f(@O-) = \Delta_f(@OH) + \{\Delta_f(-O-) - \Delta_f(-OH)\}$. i) From $CH_3COOC_2H_5$, assuming $\Delta_f(\%-OOC-) = \Delta_f(-O-)$. j) Assnmed as $\Delta_f(@COO-) = \Delta_f(-COO-)$. k) Assumed to be composed of -CO- and -F. See text. l) Assumed as $\Delta_f(@COF) = \Delta_f(-COF) + \{\Delta_f(@COCl) - \Delta_f(-COCl)\}$. m) Assumed to be composed of -CO- and -Br. See text. n) Assumed as $\Delta_f(@I) = \Delta_f(-I) + \{\Delta_f(@Br) - \Delta_f(-Br)\}$. o) Assumed to be composed of -CO- and -I. See text. p) Atsumed as $\Delta_f(@COI) = \Delta_f(-COI) + \{\Delta_f(@COBr) - \Delta_f(-COBr)\}$. q) Assumed as $\Delta_f(@S-) = \Delta_f(-S-) + \{\Delta_f(@SH) - \Delta_f(-SH)\}$. r) Assumed as $\Delta_f(@SO-) = \Delta_f(-SO-) + \{\Delta_f(@SO_2-) - \Delta_f(-SO_2-)\}$. s) Assumed as $\Delta_t(-SO_3H) = \Delta_t(-SO_3-)$. t) Assumed as $\Delta_t(\%=N-) = \Delta_t(\%=NOH)$. u) Assumed as $\Delta_t(-N=N-) = \Delta_t(\%-N=)$. v) Assumed as $\Delta_f(@N(NH_2)-) = \Delta_f(-N(NH_2)-) + \{\Delta_f(@NHNH_2) - \Delta_f(-NHNH_2)\}$. w) Assumed as $\Delta_f(@NHNH-) = \Delta_f(-NHNH-) + \{\Delta_f(@NHNH_2) - \Delta_f(-NHNH_2)\}$. x) Assumed as $\Delta_f(-NC) = \Delta_f(-CN)$. y) Assumed to be composed of -CO- and $-NH_2$. See text. z) Assumed as $\Delta_f(@CONH_2) = \Delta_f(-CONH_2) + \{\Delta_f(@COOH) - \Delta_f(-COOH)\}$. aa) From $CH_3CONHC_4H_9$, assuming as $\Delta_t(\%-NHCO-) = \Delta_t(-NH-)$. bb) Assumed as $\Delta_f(@NO_2) = \Delta_f(-NO_2)$. cc) From $CH_2=CHCH_2NCS$, assuming as $\Delta_t(-NCS) = \Delta_t(\%-N=)$. dd) From the same compound, assuming as $\Delta_t(-NCS) = \Delta_t(-NH_2)$. ee) Assumed as $\Delta_f(@NH-) = \Delta_f(-NH-) + \{\Delta_f(@NH_2) - \Delta_f(-NH_2)\}$. ff) Assumed as $\Delta_f(@N<) = \Delta_f(-N<) + \{\Delta_f(@NH_2) - \Delta_f(-NH_2)\}$.

TABLE A6. CORRECTIONS DUE TO TYPE NUMBER AND MULTIPLE SUBSTITUTIONS OF FUNCTIONAL GROUPS FOR THERMODYNAMIC PROPERTIES IN IDEAL GAS STATE

Line	Functional group	$\Delta(\Delta H)$	ΔS	Δa	Δb	Δc
	Oxygen					
1	=O(aldo)	−5.42 (1)	4.50 (1)	−0.86 (1)	1.61	−1.15
2	=O(keto)	−3.30 (1)	7.39 (1)	1.59 (1)	−11.30	8.21
3	-OH	−2.65 (1)	0.20 (1)	0.10 (1)	0.00	−0.10
4	-O-	−2.28 (1)	−0.55 (1)	0.51 (1) [a]	−1.20	0.79
5	@O-	−2.81 (1) [a,b]	−0.6 (5) [h]	0.5 (5) [h]	−1.2	0.8
6	-OOH	2.0 (4) [a,b]				
7	-OO-	−2.50 (1)				
8	-COOH	1.54 (1) [a]	8.58 (1) [a]	0.0 (5) [j]	0.0	0.0
9	%-COO-	−1.21 (1) [b,g]	8.58 (5) [j]	0.0 (5) [j]	0.0	0.0
10	%-OOC-	−2.80 (1) [b,g]	−0.6 (5) [h]	0.5 (5) [h]	−1.2	0.8
11	@COO-	1.79 (1) [b,g]	−0.6 (5) [h]	0.5 (5) [h]	−1.2	0.8
12	-COOCO-	−1.21 (1) [a,b]	8.6 (5) [l]	0.0 (5) [l]	0.0	0.0
13	-COO_2CO-	−5.1 (4) [c,e,g]				

TABLE A6. (Continued)

Line	Functional group	$\Delta(\Delta H)$	ΔS	Δa	Δb	Δc
14	HCOO-	7.99 (1) [a]	−0.6 (5) [m]	0.5 (5) [m]	−1.2	0.8
15	$-CO_3-$	−0.29 (1) [a,b]				
	Fluorine					
16	-F	−1.47 (1)	0.99 (1)	0.38 (1)	−0.13	0.38
17	-F, -F	−3.67 (1)	−0.91 (1)	−0.48 (1)	−0.18	−0.42
18	-F, -Cl	2.63 (1)	−0.16 (1)	1.72 (1) [d,g]	−3.34	4.38
19	-F, -Br	4.19 (1)	1.63 (1)	0.99 (1) [d,g]	−4.01	1.05
20	-F, -I	4.12 (1)	−0.09 (1)	1.68 (1) [a,d]	−1.55	1.01
21	-COF	0.4 (5) [n]				
	Chlorine					
22	-Cl	−0.62 (1)	1.24 (1)	0.90 (1)	−3.00	1.92
23	-Cl, -Cl	4.25 (1)	−1.49 (1)	−0.62 (1)	1.55	−0.90
24	-Cl, -Br	5.14 (1)	1.48 (1)	1.73 (1) [d]	−6.95	3.02
25	-Cl, -I	4.9 (5) [o]	1.24 (1) [a]	1.68 (1) [d]	−6.59	4.52
26	-COCl	0.45 (1)				
	Bromine					
27	-Br	−1.73 (1)	−1.25 (1)	0.39 (1)	−6.35	2.31
28	-Br, -Br	4.21 (1)	2.37 (1)	1.12 (1) [d]	−8.59	4.70
29	-Br, -I	4.9 (5) [p]	1.90 (1) [a]	−0.38 (1) [a,d]	−7.74	3.84
30	-COBr	0.4 (5) [q]				
	Iodine					
31	-I	−1.03 (1)	0.94 (1)	0.66 (1)	−2.42	1.74
32	-I, -I	5.59 (1)	−0.73 (1)	0.12 (1)	0.18	−0.36
33	-COI	0.4 (5) [q]				
	Sulfur					
34	-SH	−0.27 (1)	0.38 (1)	0.35 (1)	−0.29	−0.38
35	-S-	−0.85 (1)	−0.04 (1)	−0.04 (1)	1.08	−0.90
36	@S-	−0.28 (1) [a]	−0.1 (5) [r]	−0.1 (5) [r]	1.1	−0.9
37	-SS-	−0.82 (1)	0.02 (1)	−0.42 (1)	2.66	−2.29
38	-SO-	−1.97 (1)				
39	@SO-	−2.0 (5) [s]				
40	$-SO_2-$	−0.27 (1)				
41	$@SO_2-$	6.18 (1) [b,g]				
42	$-SO_3H$	−2.8 (5) [t]				
43	$-OSO_2-$	−2.81 (1) [b,g]				
44	$-OSO_3-$	−2.57 (1) [b,g]				
	Nitrogen					
45	$-NH_2$	−1.30 (1)	−0.34 (1) [a]	0.16 (1) [a]	0.47	−0.61
46	-NH-	−2.33 (1)	−0.3 (5) [u]	0.2 (5) [u]	0.5	−0.6
47	@NH-	−2.08 (1) [a]	−0.3 (5) [u]	0.2 (5) [u]	0.5	−0.6
48	-N<	−1.70 (1)	−0.3 (5) [u]	0.2 (5) [u]	0.5	−0.6
49	@N<	−1.0 (4) [a,e,v]	−0.3 (5) [u]	0.2 (5) [u]	0.5	−0.6
50	%=N-	0.2 (5) [a,e,w]				
51	%-N=	−0.9 (4) [c,e,g]				
52	-N=N-	−0.9 (5) [x]				
53	$-NHNH_2$	−1.3 (5) [u]	−0.3 (5) [u]			
54	$-N(NH_2)-$	−1.3 (5) [u]	−0.3 (5) [u]			
55	$@N(NH_2)-$	−1.3 (5) [u]				
56	-NHNH-	−1.3 (5) [u]	−0.3 (5) [u]			
57	@NHNH-	−1.3 (5) [cc]				
58	-CN	−3.08 (1)	0.56 (1)	1.02 (1)	−4.88	4.48
59	-NC	−3.1 (5) [y]	0.6 (5) [y]	1.0 (5) [y]	−4.9	4.5
60	=NOH	0.2 (4) [c,f,g]				
61	$-CONH_2$	0.03 (1) [b,g]	8.6 (5) [z]	0.0 (5) [i]	0.0	0.0

Table A6. (Continued)

Line	Functional group	$\Delta(\Delta H)$	ΔS	Δa	Δb	Δc
62	%-CONH-	−1.2 (5) [aa]				
63	%-NHCO-	−2.3 (5) [bb]				
64	@NHCO-	−1.2 (5) [aa]				
65	$-NO_2$	−2.26 (1)	0.0 (5) [i]	0.0 (5) [i]	0.0	0.0
66	-ONO	−6.34 (1)	0.0 (5) [i]	0.0 (5) [i]	0.0	0.0
67	$-ONO_2$	−2.47 (1)	0.66 (1) [a]	−0.37 (1) [a]	0.82	−0.55
68	-NCS	−0.9 (5) [dd]	−0.3 (5) [u]			

a) Single data source. b) Data from PRN.[11] c) Data from BCG.[12] d) Data from LBTl.[13] e) The values of the gaseous phase were estimated from those of the liquid phase. f) The values of the gaseous phase were estimated from those of crystal. g) Statistically calculated with weights reciprocal to errors. h) Assumed to be equal to Δ_t(-O-). i) Assumed as zero. j) Assumed as Δ_t(%-COO-)=Δ_t(-COOH). l) Assumed to be equal to Δ_t(-COOH). m) Assumed as Δ_t(HCOO-)=Δ_t(-O-). n) Assumed as Δ_t(-COF)=Δ_t(-COCl). o) Assumed as Δ_m(-Cl, -I)=$\{\Delta_m$(-Cl, -Cl)+Δ_m(-I, -I)$\}/2$. p) Assumed as Δ_m(-Br, -I)=$\{\Delta_m$(-Br, -Br)+Δ_m(-I, -I)$\}/2$. q) Assumed to be equal to Δ_t(-COCl). r) Assumed as Δ_t(@S-)=Δ_t(-S-). s) Assumed as Δ_t(@SO-)=Δ_t(-SO-). t) Assumed as Δ_t(-SO_3H)=Δ_t(-OSO_2-). u) Assumed to be equal to Δ_t(-NH_2). v) Data of liquid phase from SWS.[8] w) Assumed as Δ_t(%=N-)=Δ_t(=NOH). x) Assumed as Δ_t(-N=N-)=Δ_t(%-N=). y) Assumed as Δ_t(-NC)=Δ_t(-CN). z) Assumed as Δ_t(-$CONH_2$)=Δ_t(-COOH). aa) Assumed as Δ_t(%-CONH-)=Δ_t(%-COO-). bb) Assumed as Δ_t(%-NHCO-)=Δ_t(-NH-). cc) Assumed as Δ_t(@NHNH-)=Δ_t(-NH_2). dd) Assumed as Δ_t(-NCS)=Δ_t(%-N=).

Table A7. Thermodynamic properties of simple substances in standard states[a]

Line	Simple Substance	$\Delta H^\circ_{f,298.15}$	$S^\circ_{298.15}$	a	b	c
1	Br_2(g) [b]	7.47	58.63	8.90	0.14	0
2	Br_2(l) [b]	0	36.80	17.10	0	0
3	C(graphite)	0	1.36	0.33	7.13	−2.19
4	C(diamond)	0.45	0.58	0.01	8.09	−2.45
5	Cl_2(g)	0	53.29	7.59	2.31	−0.89
6	F_2(g)	0	46.80	6.50	1.00	0
7	H_2(g)	0	31.21	6.62	0.81	0
8	I_2(g) [c]	14.88	62.28	9.00	0	0
9	I_2(s) [c]	0	27.90	41.58	−191.00	321.00
10	N_2(g)	0	45.77	6.50	1.00	0
11	O_2(g)	0	49.00	5.21	5.52	−2.26
12	O_3(g)	34.00	57.05	5.68	14.70	−7.42
13	P(yellow)	0	10.60	3.41	7.18	0
14	S(rhombic) [d]	0	7.62	3.63	6.40	0
15	S(monoclinic) [d]	0.07	7.78	4.38	4.40	0

a) Arrangement in alphabetical order. The properties of gases are in the ideal state, regardless of the most stable modifications at 298.15 K. Data are cited from Ref. 5. b) Liquid from 298 K to 332.62 K; ideal diatomic gas state from 332.62 K. c) Crystal from 298 K to 386.75 K; ideal diatomic gas state from 458.39 K. d) Rhombic crystal from 298 K to 368.46 K; monoclinic crystal from 368.46 K to 388.36 K. For those needing more accurate data on liquid and gas states, see W. H. Evans and D. D. Wagman, *J. Res. Natl. Bur. Std.*, **55**, 147 (1955), and D. R, Stull and G. C. Sinke, "Thermodynamic Properties of the Elements," Advances in Chemistry Series No. 18, American Chemical Society, Washington, D. C. (1956).

Table A8. Thermodynamic properties of inorganic compounds and a few organic compounds in standard states[a]

Line	Compound	$\Delta H^\circ_{f,298.15}$	$S^\circ_{298.15}$	a	b	c
1	HBr(aq, 600H_2O)	−28.78				
2	HBr(g)	−8.66	47.44	7.01	−0.53	1.22
3	HCl(aq, 600H_2O)	−39.89				
4	HCl(g)	−22.06	44.64	7.05	−0.66	1.19
5	NOCl(g)	12.57	62.53	8.62	7.95	−3.33
6	NO_2Cl(g)	3.12	65.01	7.54	20.51	−9.94
7	SO_2Cl(g)	−50.60	73.23	12.34	14.43	−7.69

TABLE A8. (Continued)

Line	Compound	$\Delta H^\circ_{f,298.15}$	$S^\circ_{298.15}$	a	b	c
8	$SO_2Cl_2(g)$	−85.40	74.37	13.14	21.38	−11.69
9	$S_2Cl_2(g)$	−4.66	76.35	14.71	11.30	−6.52
10	$HF(aq, 50H_2O)$	−77.03				
11	$HF(g)$	−64.80	41.51	7.06	−0.52	0.66
12	$NOF(g)$	−15.70	59.27	7.34	9.98	−4.59
13	$NOF_2(g)$	−19.00	62.24	6.22	22.62	−10.97
14	$SF_4(g)$	−174.10	69.58	8.74	34.86	−19.26
15	$HI(g)$	6.30	49.35	6.82	0.14	0.99
16	$NH_3(g)$	−10.92	46.03	5.95	8.91	−1.37
17	$N_2H_4(g)$	22.75	57.41	4.91	29.91	−12.67
18	$HNO_3(g)$	−32.02	63.68	4.70	31.90	−14.77
19	$H_2O(g)$	−57.80	45.11	7.56	1.21	1.10
20	$H_2O(l)$	−68.31	16.72	18.00	0	0
21	$H_2O_2(g)$	−32.53	55.66	6.10	16.61	−7.78
22	$H_2SO_4(aq, 115H_2O)$	−212.20				
23	$H_2SO_4(l)$	−194.45	37.49	19.37	58.34	−39.25
24	$H_2S(g)$	−4.82	49.18	7.06	3.53	0.40
25	$NO(g)$	21.60	50.35	6.85	0.66	0.66
26	$NO_2(g)$	8.09	57.35	5.92	11.16	−4.44
27	$N_2O(g)$	19.49	52.56	6.04	12.43	−5.40
28	$SO_2(g)$	−70.95	59.30	6.41	12.16	−5.59
29	$SO_3(g)$	−94.47	61.19	5.34	26.49	−12.19
30	$CNBr(g)$	43.35	59.07	8.98	8.51	−3.90
31	$CNCl(g)$	31.60	56.28	8.82	7.65	−3.10
32	$CNI(g)$	53.80	61.33	9.81	6.84	−2.97
33	$CO(g)$	−26.42	47.30	6.76	0.38	0.82
34	$COCl_2(g)$	−52.80	67.82	9.13	18.77	−9.53
35	$COF_2(g)$	−153.00	61.84	5.23	24.01	−11.56
36	$COS(g)$	−33.08	55.32	6.65	12.94	−6.04
37	$CO_2(g)$	−94.05	51.07	5.54	12.89	−5.51
38	$CS_2(g)$	27.98	56.83	7.83	12.17	−6.04
39	$HCN(g)$	31.20	48.21	6.09	9.56	−3.51
40	$HCOOH(g)$	−90.49	59.49	3.37	28.50	−12.00
41	$(CN)_2(g)$	73.84	57.90	9.96	14.21	−5.98
42	$(COOH)_2(g)$ [b]	−174.86				
43	$(COOH)_2(s)$	−198.36	28.70			
44	$C_3O_2(g)$	−22.38	66.05	9.95	23.66	−10.30

a) Data from Ref. 5 unless otherwise mentioned. b) Data from PRN.[11]

References

1) R. C. Reid and T. K. Sherwood, "The Properties of Gases and Liquids: Their Estimation and Correlation," 2nd ed, McGraw-Hill Book Co., New York (1966).

2) R. C. Reid, J. M. Prausnitz and T. K. Sherwood, "The Properties of Gases and Liquids," 3rd ed, McGraw-Hill Book Co., New York (1977).

3) J. W. Anderson, G. H. Beyer and K. M. Watson, *Natl. Pet. News Tech. Sec.*, **36**, R475 (July 5, 1944).

3a) Also cited in O. A. Hougen, K. M. Watson and R. A. Ragatz, "Chemical Process Principles," 2nd ed, Part II, "Thermodynamics," John Wiley, New York (1959), and Refs. 1 and 2.

4) S. W. Benson, "Thermochemical Kinetics," 2nd ed, John Wiley, New York (1967).

5) Y. Yoneda, "Kemoguramu (CHEMOGRAM)," Maruzen, Tokyo (1972), Vol. 1.

6) Y. Yoneda, "Information Chemistry. Computer Assisted Chemical Research Design," ed by S. Fujiwara and H. B. Mark, Jr., University of Tokyo Press, Tokyo (1975), p. 239.

7) S. W. Benson and J. H. Buss, *J. Chem. Phys.*, **29**, 546 (1958).

7a) Units of thermodynamic properties in cal or kcal were adopted because they are still prevalent in industrial chemistry; the units can be converted into the SI system using the factor described in each table.

8) SWS: D. R. Stull, E. F. Westrum, Jr., and G. C. Sinke, "The Chemical Thermodynamics of Organic Compounds," John Wiley, New York (1969).

9) API: B. J. Zwolinski *et al.*, "Selected Values of Properties of Hydrocarbons and Related Compounds," American Petroleum Institute Research Project 44, Thermodynamics Research Center, Texas A & M University, College Station, Texas.

10) TRC: B. J. Zwolinski *et al.*, "Selected Values of Properties of Chemical Compounds," Thermodynamics Research Center Data Project, Thermodynamics Research Center, Texas A&M University, College Station, Texas.
11) PRN: J. B. Pedley and J. Rylance, "Sussex-N.P.L. Computer Analyzed Thermochemical Data: Organic and Organometallic Compounds," University of Sussex (1977).
12) BCG: S. W. Benson, F. R. Cruickshank, D. M. Golden, G. R. Haugen, H. E. O'Neal, A. S. Rodgers, R. Shaw, and R. Walsh, *Chem. Rev.*, **69**, 279 (1969).
13) LBT1: "Landolt-Börnstein Tabellen," 6 Aufl., II Band, 4 Teil, "Zahlen und Funktionen," Springer-Verlag, Berlin (1961).
14) Benson *et at.*[12] assumed that the heat of evaporation was given by the equation:
$\Delta H_{V,298}=S_T[(1.76\times10^{-3})t_{bp}+0.253]$ (kcal mol^{-1}),
where S_T is the Trouton constant, usually 22 kcal mol^{-1} K^{-1} (in original paper, 22 cal mol^{-1} K^{-1}) and t_{bp}, the normal boiling point in °C.
15) The differences in contribution values for enthalpy between aliphatic and aromatic amines, which reflect the global effect of aromaticity, 5.27 kcal mol^{-1} K^{-1} (primary), 7.22 (secondary), and 7.31 (tertiary), show a fairly good agreement among themselves, whereas those between aliphatic and aromatic hydroxyl, 6.57 for –OH and 2.94 for –O–, may suggest that a subtraction method like this may give a poor estimate of the enthalpy.
16) The values of CH_3COBr are derived from the observed value of CH_3COCH_3 by replacing a methyl group with –Br, with consideration taken of a twofold-type number correction. The subtraction of ethane from acetyl bromide gives the fundamental values for –COBr.
17) T. P. Thinh and T. K. Trong, *Can. J. Chem. Eng.*, **54**, 344 (1976).
18) Tables 7—8 in Ref. 2.
19) K. K. Verma and L. K. Doraiswamy, *Ind. Eng. Chem. Fundam.*, **4**, 389 (1965).
20) J. L. Franklin, *Ind. Eng. Chem.*, **41**, 1070 (1949); *J. Chem. Phys.*, **21**, 2029 (1953).

Electrical Properties of a One-dimensional Conductor, $Na_xV_2O_5$

Hayao KOBAYASHI

Department of Chemistry, Faculty of Science, Toho University, Chiba 274

(Received October 9, 1978)

The resistivity measurement, DTA analysis, refinement of the crystal structure, and examination of the X-ray diffuse scattering have been carried out on the β-phase of the sodium vanadium bronze. A resistivity minimum was observed around 200 K. The peak position of the logarithmic derivative of the resistance and an anomaly in the DTA curvature indicate that a metal-insulator transition occurs at about 130 K. The X-ray diffuse scattering shows a tendency of the sodium atoms toward cluster formation. It is concluded that the β-phase of sodium vanadium bronze is neither a simple one-dimensional metal nor a simple semiconductor, but can behave partly as a one-dimensional metal and partly as an anisotropic semiconductor.

Since the 1960's many investigations have been undertaken by solid state chemists in the field of vanadium oxide bronzes ($M_xV_2O_5$; M=Li, Na, K, Cu, ···). It was at first commonly accepted that the materials lie near the critical donor concentration range required in the Mott theory for semiconductor-metal transitions and that the metal-metal spacing is approximately equal to the critical distance predicted by Goodenough for electron delocalization *via* d-orbital overlap.[1] The early works seemed to established that the charge transfer in vanadium bronzes is realized *via* the auto-localized electrons (polarons).[2,3] However, it has recently suggested that the β-phase vanadium bronzes should be considered as quasi-one-dimensional conductors.[4] Evidence for this view comes from (1) conductivity measurements which show that the anisotropy ($\sigma_{\parallel}/\sigma_{\perp}$) is 130 at room temperature ($\sigma_{\parallel(\perp)}$ is the conductivity parallel (perpendicular) to the b axis) and rises as high as 400 at 125 K;[4] (2) ESR measurements where the lineshape is asymmetric when the electric-field vector is parallel to the b axis, but Lorentzian for $E \perp b$,[5] and (3) optical reflectivity measurements which give a metallic plasma edge with light polarized along the b axis, but a featureless behaviour for perpendicular polarization.[6] In addition, recent investigation by Gunning *et al.*,[7] has shown that the dielectric constant is highly anisotropic and very large parallel to the b axis. This new view appears to conflict with the localization picture of the electron-conduction mechanism.

In this paper, we wish to present the results on our electrical conductivity, DTA measurements, structure refinement, and examination of the X-ray diffuse scatterings of the β-phase of the sodium vanadium bronze (β-NaVB).

Experimental

Preparation of Samples. The samples of the sodium vanadium bronze were prepared in a quartz boat. A 6 : 1 mixture of V_2O_5 and Na_2CO_3 or a 1 : 1 mixture of $NaVO_3$ and V_2O_5 was heated for 17 h at 700 °C in an air atomosphere and then cooled at a rate of 6 °C/h.[1,8] The black needle-shaped crystals were pried out of the quartz boat. Examination by X-ray diffraction revealed that the crystals are monoclinic with the Wadsley β-type structure.[8]

Refinement and Brief Description of the Crystal Structure. The crystal structure of β-NaVB was determined in the 1950's by Wadsley[8] and by Ozerov *et al.*[9] Considering the fundamental significance of the Wadsley β-structure[2] and the relatively large R index (the R indices for $h0l$ and $0kl$ are 0.17 and 0.13 respectively[8]), the crystal structure refinement would be desirable. Since our measurements were made before the publication of the works of Wallis *et al*[4] and [Kaplan and Zylbersztejn,[6] which have first suggested a "one-dimensional metallic character" of this compound, our observation seemed to be inconsistent with the semiconducting behavior previously accepted. At first sight, this discrepancy appears to be attributable to a slight change in the crystalline state, one which might be introduced in the stage of the sample preparation, because our samples were prepared in quartz boats, whereas the other authers used platinum boats or platinum dishes. The purpose of the structure refinement was partly to examine this possibility.

The lattice constants were determined using a computer-controlled four-circle diffractometer. The crystal data are: monoclinic, space group C2/m,[10] $a=16.435(16)$ Å, $b=3.612(1)$, $c=10.086(10)$, $\beta=109.61(15)°$, $D_x=3.55$ gcm^{-3}, $Z=6$ ($Na_xV_2O_5$; $x=0.287$ (see Appendix)).

Some details of the structure refinements, the atomic coordinates, and the bond lengths and angles around the vanadium atoms are given in Appendix. There is no serious difference between the newly refined structure and the previously determined one.

The crystal structure is shown in Fig. 1. The unit cell contains three crystallographycally independent vanadium sites. As was pointed out by Wadsley,[8] the coordination of vanadium is of two kinds. V(1) and V(2) are each linked to six oxygens disposed at the corners of strongly distorted octahedra. The octahedra are associated in pairs, with a shared edge which unites with similar pairs above and below to form a zigzag ribbon extending along the b axis (Fig. 2a). On the other hand, V(3) has five bonds to oxygen to form trigonal bipyramids, which are associated in pairs to form a double chain by each having an edge in common with each V(3) neighbour (Fig. 2b). The short distance between the vanadium ions (Figs. 1 and 2) appears to allow the formation of delocalized states arranged in linear chains along the b axis.[5] The sodium atoms lie at random in two rows in the tunnels formed by the vanadium and oxygen atoms as a whole (Fig. 3). The distance between two sodium sites is only 1.95 Å. With an increase in the sodium content ($Na_xV_2O_5$; $0.2<x<0.33$), the sodium sites are gradually filled; the occupancy probability is 50% if $x=1/3$. Because of the Coulomb interaction, sodium ions will tend to be arrayed regularly. In fact, a tendency for the regular arrangement of sodium atoms has been revealed by the examination of oscillation photographs, which will be described later.

Resistivity Measurements. The d.c. electrical resistivities were measured over the temperature range of 78 K—

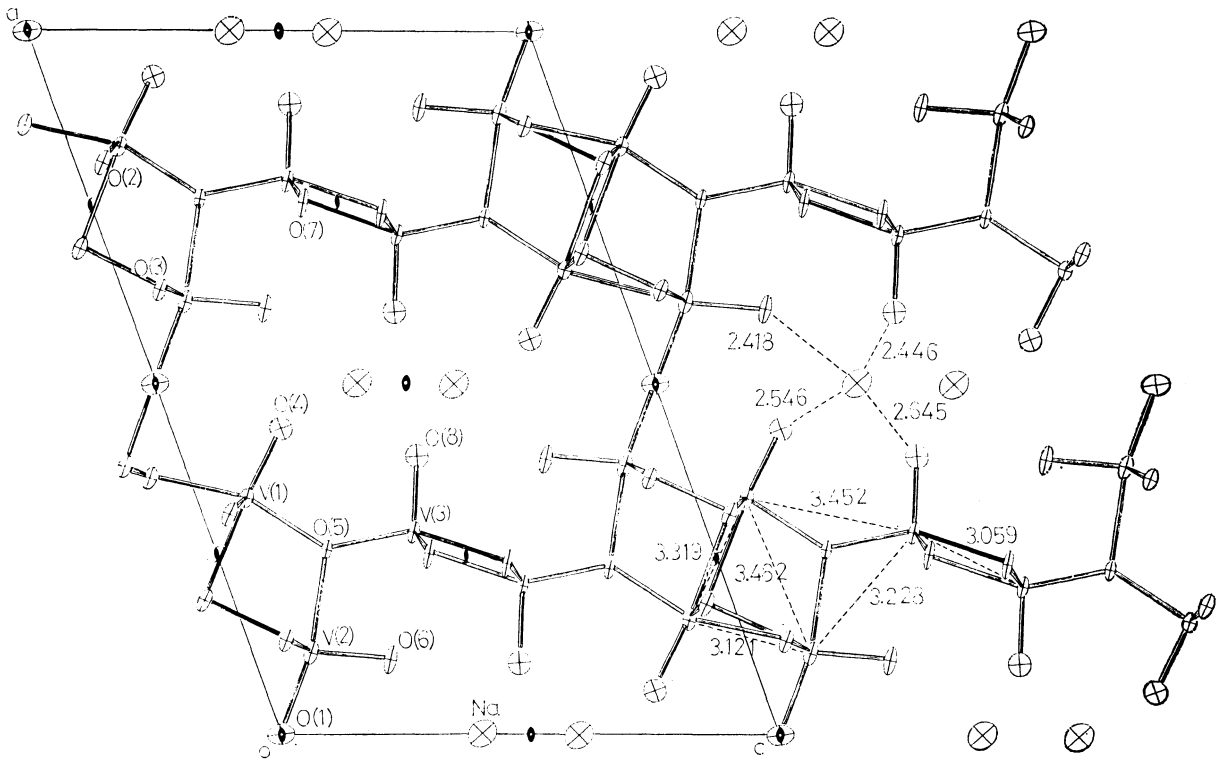

Fig. 1. Projection of the crystal structure.

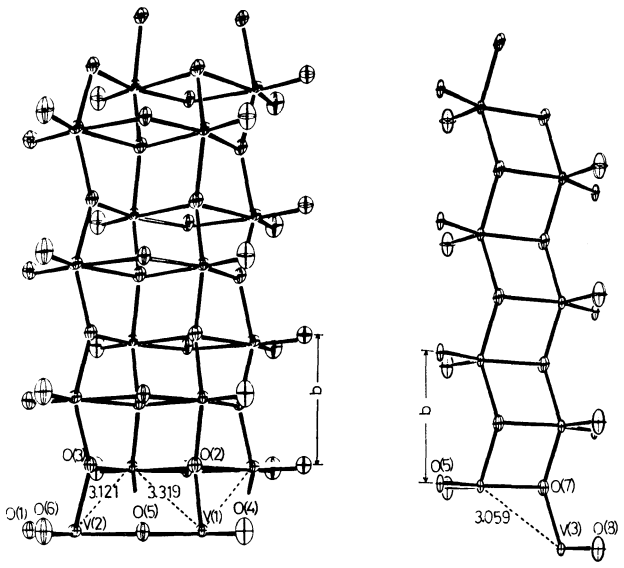

(a) (b)

Fig. 2. Perspective view of the "chain structures" of the vanadium and oxygen atoms.
(a) A complex chain constructed of the 6-coordinated vanadium atoms (V(1) and V(2)). (b) A double chain of the 5-coordinated vanadium atoms (V(3)).

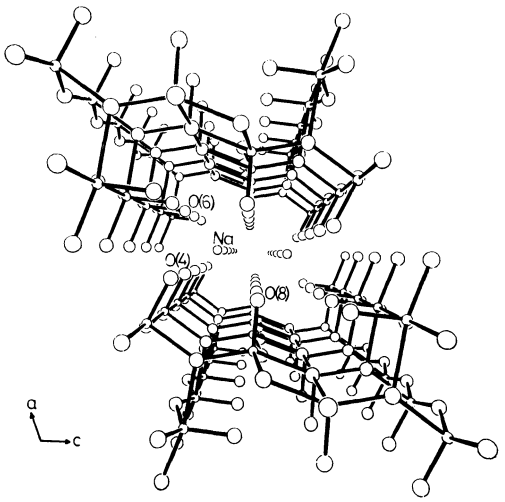

Fig. 3. Perspective view of the tunnel structure.

600 K for several specimens along the needle axis (the b axis) of the crystals using a four-probe method. The crystals were washed with aqueous NH_3. Gold wires 0.025 mm in diameter were bonded to the crystals by silver conducting paint (Shoei 4895). Then the crystals were annealed for about 30 min at about 300 °C. The sample dimensions and probe separations were measured with a microscope. Because of the uncertainty in determining the exact probe separation and sample dimensions, the estimated error in the resistivities is about 50%. The results are shown in Figs. 4 and 5. The room-temperature resistivityis $6.0\pm 3.0\times 10^{-3}\,\Omega$ cm. The logarithmic derivative of the resistance, $-(\mathrm{d}\ln R/\mathrm{d}T)$, *versus* the temperature is also shown in Fig. 4. In a one-dimensional conductor, a metal-insulator (M-I) transition temperature is defined by the peak posotion of $-(\mathrm{d}\ln R/\mathrm{d}T)$ *versus* T.[11,12] The inset of Fig. 4 shows a peak around 130 K.

DTA Experiments. A quasi-one-dimensional conductor exhibits a specific heat anomaly in the temperature range around the M-I transition temperature.[13,14] Judging from the anisotropy of the electric conductivity and the optical reflectivity, the peak of the $\mathrm{d}\ln R/\mathrm{d}T$ *vs.* T curveture around 130 K (Fig. 4) can be considered to be an indication of the occurrence of a M-I transition. The DTA measurements were made to obtain further evidence.

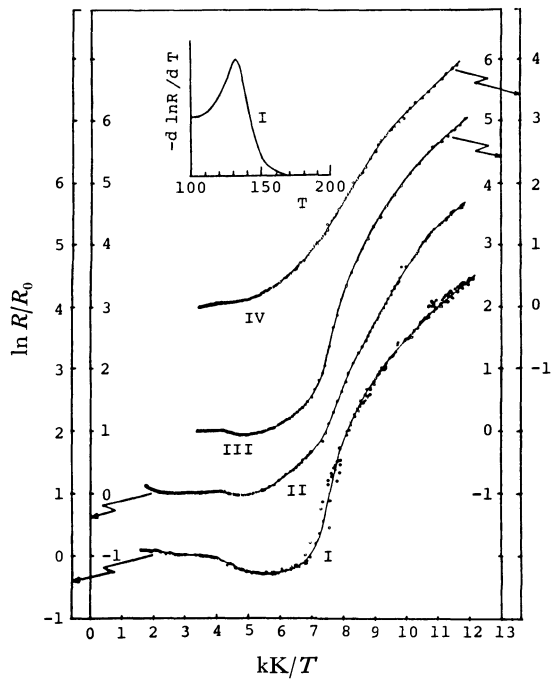

Fig. 4. Logarithm of normalized resistivity *versus* inverse temperature. The inset shows $-(\mathrm{d}\ln R/\mathrm{d}T)$ *versus* T. Curvetures I—IV indicate the resistivities of four different samples.

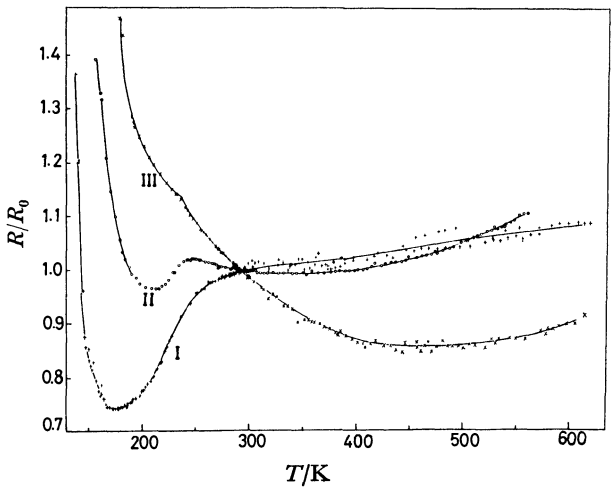

Fig. 5. The temperature dependence of the normalized resistivity. Curvetures I, II, and III show the resistivities of the samples I, II, and IV in Fig. 4, respectively.

The crystals of β-NaVB were ground in a glass mortar and mixed thoroughly with an approximate amount of powdered almina. A copper-Constantan thermocouple was embedded in a quantity of the mixed powder placed in a hole (50 mm × 6 mmϕ) in a cylindrical copper block. The reference thermocouple and the thermocouple used for temperature measurements were in the other two holes, packed with powdered almina. The DTA measurements were made by warming or cooling the copper block. The rate of temperature change was controlled by raising or lowering a liquid-nitrogen vessel with respect to the copper block. Since a small anomaly was observed in the first run, the measurements were repeated eight times to confirm it. On the repeated runs, however,

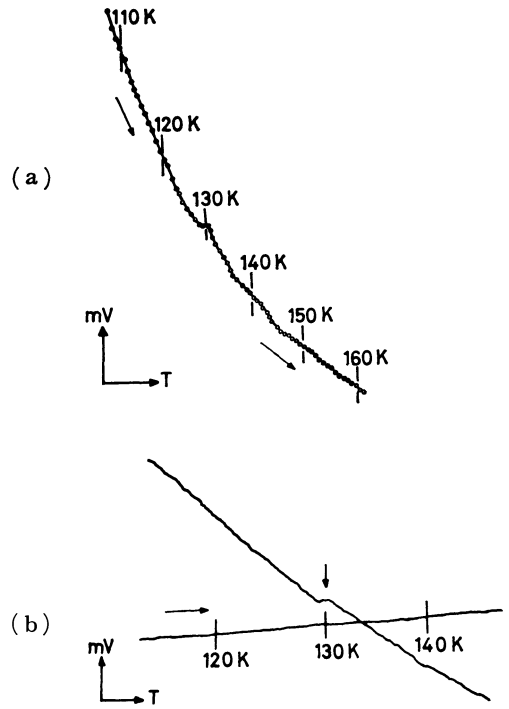

Fig. 6. (a) Averaged thermogram obtained from eight warming curves. (b) An example of the warming curves.

only the warming cycles were examined because of the facility of the temperature control. The voltage readings of the eight thermograms were then added. The dependence on the temperature is shown in Fig. 6a. An anomaly was observed at about 130 K. The measurements were repeated on another sample in order to confirm the reproducibility of the anomaly (Fig. 6b). The heat of transition was roughly estimated to be 10—20 cal/mol by reference to the thermograms of NH_4Cl(T_c=242.8 K, 0.20 kcal/mol) and $NH_4H_2PO_4$ (T_c=148 K, 0.15 kcal/mol).

X-Ray Diffuse Scatterings. X-Ray diffuse scatterings associated with the one-dimensional charge-density waves are among the most direct indications of the metallic state of a system. Besides this, another type of X-ray diffuse scattering can also be expected in β-NaVB. Although crystal-structure analysis shows that the sodium atoms are randomly distributed in two rows in the tunnels, a short-range order among the sodium atoms, which gives rise to X-ray diffuse scatterings, also exists.

Oscillation photographs around the b axis were taken at room temperature using Ni-filtered Cu $K\alpha$ radiation. The exposure times were about 100 h. An example of the photographs is shown in Fig. 7. Weak and broad scatterings are observed between strong layer lines. The existence of the diffuse scatterings was confirmed by comparing the photograph with one taken without mounting a crystal on a glass capillary.

The X-ray diffuse scattering associated with a one-dimensional distortion or a Kohn anomaly generally consists of diffuse, narrow streaks[15] and is inconsistent with the breadth of the observed diffuse scattering. The diffuse scatterings in the middle of the sharp layer lines indicates a tendency of the doubling of the lattice spacing along the b axis. Wadsley has suggested that sodium atoms in a tunnel alternately occupy one of the two possible sites to form a staggered string.[8] If this suggestion were true, the lattice spacing would be doubled along the b axis. Actually, the mode of

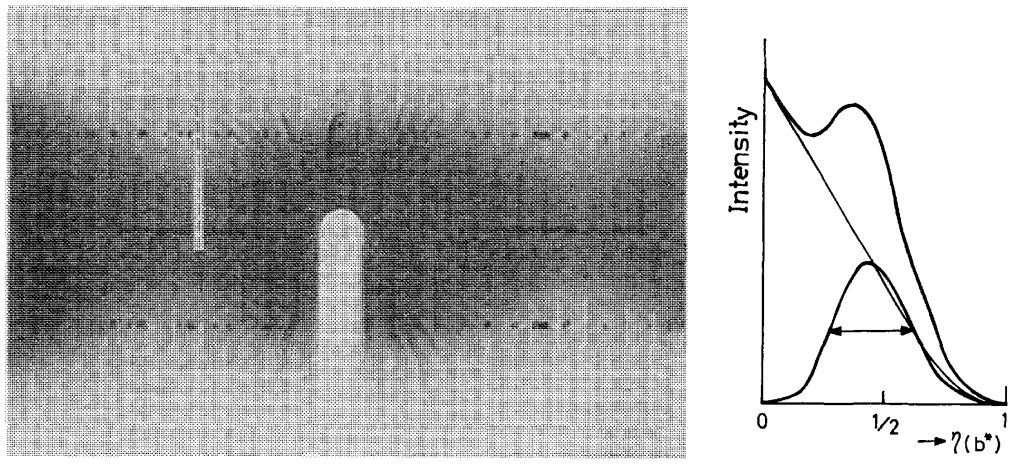

Fig. 7. Oscillation photograph around the **b** axis and the scattering intensity along the dashed line.

the arrangement of sodium atoms is even more complicated because of the nonstoichiometry of the sodium content. The staggered strings may be interrupted. Consequently, the diffuse scatterings may be attributable to existence of "imperfect staggered strings." The constant scattering intensity along the direction perpendicular to ***b*** implies that the correlation between sodium atoms belonging to different tunnels is weak. If the "correlation length ξ" can be estimated by $\xi \approx 2/\Gamma$[16] (Γ is the full width at a half maximum of the diffuse scatterings), it is of the order of 20 Å for the b direction (the width of the "diffuse belt" is about 0.35 b*).

Discussion

The room-temperature conductivity of 200 ± 100 $(\Omega\,\mathrm{cm})^{-1}$ agrees with those values reported by Sienko and Sohn (230 $(\Omega\,\mathrm{cm})^{-1}$)[17] and Wallis, Sol, and Zylbersztejn ($110(\Omega\,\mathrm{cm})^{-1}$);[4] it is also of the same order as that of the well-known one-dimensional metal $K_2Pt(CN)_4Br_{0.3}\cdot 3H_2O$ (≈ 500 $(\Omega\,\mathrm{cm})^{-1}$).[18] In addition, it is compatible with the optical conductivity along the b axis (250 $(\Omega\,\mathrm{cm})^{-1}$) as calculated from $\sigma_{opt}=\omega_p{}^2\tau/4\pi$ using the plasma frequency ($\omega_p=1.44\times10^{15}\,\mathrm{s}^{-1}$) and the electronic relaxation time ($\tau=1.35\times10^{-15}$ s) reported by Kaplan and Zylbersztejn.[6] Needless to say, this agreement does not necessarily support a "simplified one-dimensional metal picture" of this compound. Some crystals show small, but distinct, resistivity minima around 200 K, and the other crystals give an indication of resistivity minima by means of their concave curvatures (Figs. 4 and 5). This is the first observation of the resistivity minimum. However, similar resistivity-*vs.*-temperature behaviour can also be found in papers previousely reported: (1) $\log\sigma$ plotted against $1/T$ of Wallis *et al.*[4] shows a distinct concave curve upwards around 180 K, implying a latent conductivity maximum. (2) Despite the small number of the datum points, a deviation from the smooth curve of resistivity *versus* the inverse temperature around 200 K can be found reported in the paper of Sienko and Sohn.[17]

The existence of the relatively sharp minimum (Fig. 5) shows the non-semiconductive character of the compound. When the resistivity minimum is sharp, the logarithmic derivative of the resistance *versus* temperature gives a well-defined peak at about

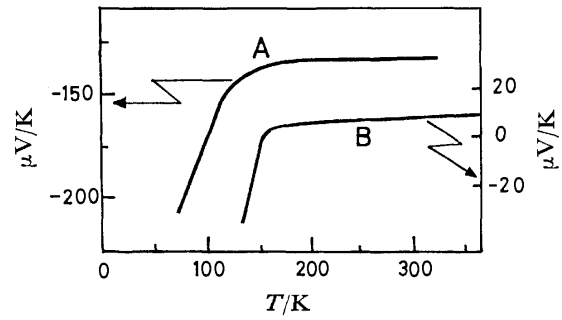

Fig. 8. Seebeck coefficient *versus* temperature of β-NaVB (A) (Ref. 1) and that of one-dimensional conductor, $(TTF)_{12}(SCN)_7$ around its M-I transition temperature ($T_c=169$ K) (B) (Ref. 12).

130 K, which suggests that the phase transition observed by DTA measurements is a M-I transition. The ratio of the low-temperature activation energy to the M-I transition temperature, Δ/T_c. is approximately constant in one-dimenstional systems ($\Delta/T_c=5\pm1$). Wallis *et al*[4] reported that the conductivity shows a simple activated behaviour between 80 K and 125 K, the activation energy being 61 m eV (=708 K). The Δ/T_c ratio is 5.5. Some observations indicating a phase transition can also be seen in the literature: (1) The Seebeck coefficient is almost constant when $T>150$ K and decreases abruptly when $T<110$ K: that is, the temperature dependence changes around $T_c(\approx130\,\mathrm{K})$ (Fig. 8).[1] (2) The susceptibility follows a Curie-Weiss law from 150 K to 450 K, but its temperature dependence becomes more complicated when $T<T_c$.[19] (3) The anisotropy of the conductivity reaches a maximum ($\sigma_\parallel/\sigma_\perp\approx400$) at 125 K ($\approx T_c$).

Thus, the occurrence of the M-I transition appears to be confirmed. On the other hand, on the basis of an examination of the temperature dependence and the anisotropy of electric conductivity, Wallis *et al.* have shown that a variable-range hopping model is applicable at low temperatures ($T<80$ K) and have proposed an interrupted strand model.[4] ESR study by Friederich *et al.* has suggested that the sodium ions are clustered rather than being distributed randomly among

possible sites in the tunnel structure, and that a crystal is separated into regions where the electron concentration is fixed at the value corresponding to $x=1/3$.[19] This picture provides a basis for the interrupted strand model of the electronic-transport mechanism. As has been described above, the observation of diffuse X-ray scattering gives more direct evidence for the "cluster formation" of sodium atoms.

Thus, β-NaVB can be regarded as neither a simple metal nor a simple semiconductor; rather, it has the following two aspects: (1) a one-dimensional metallic character originating from the delocalization states arranged in a linear chain along the b axis,[5] and (2) a semiconductive nature due to the localization of the electron.

On the basis of this information, the temperature variation in Seebeck coefficient will now be interpreted. The room-temperature Seebeck coefficient of $M_xV_2O_5$ (M=Na, Cu, Ag; $0.2<x<0.6$) has been explained by Goodenough in terms of a small polaron formula.[2] Since a Seebeck coefficient, α, is generally small in a metallic state, the large room-temperature value of 135 μV/K (Fig. 8)[1] appears to be inconsistent with the observation of matallic behaviour around room temperature. However, if α includes the sum of α_A (the contribution from the "metallic part"), and α_B (the contribution from the "semiconductive part"), the large room-temperature value can be attributed to α_B. When a one-dimensional metal undergoes a M-I transition, the magnitude of the Seebeck coefficient (α_A) increases abruptly (Fig. 8).[12,20] Thus, the temperature variation of α can be explained.

Figure 9 shows a typical example of the resistivity behaviour of a one-dimensional metal around the M-I transition temperature (A) and that of a variable-range hopping mechanism in a disordered semiconducting system (B).[4,21] The sample dependence of the resistivity (Fig. 5) can be interpreted by the superposition of A and B, if the contribution of A (R_A) and B(R_B) to the resistivity vary from sample to sample ($R=R_A+R_B$). Below the M-I transition temperature, R_A increases exponentially with a decrease in the temperature. Therefore, the magnitude of the resistivity can be mainly determined by the variable-range hopping process ($R\approx R_B$). In fact, Wallis *et al.* have pointed out that the activation energy decreases smoothly below 80 K. On the other hand, at high temperatures R is approximately equal to R_A and the "metallic conductivity" may be observed.

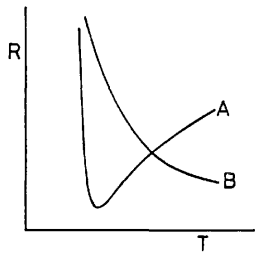

Fig. 9. Schematic illustration of the resistivity *versus* temkerature curve of a one-dimensional metal around the M-I transition temperature (A) and that by one-dimensional variable range hopping conduction (B).

It is well-known that small amounts of disorder and defects in a crystal have a great influence on the electrical conductivity and frequently smear out the M-I transition.[12,22] Kapuskin *et al.* have reported that the lattice parameters of $M_xV_2O_5$ (M=Li, Na, K) are changed slightly by the evolution of oxygen on heating to 730—780 K.[23] Although no more than 0.7 atoms of oxygen are evolved from one elementary cell of bronze, a drastic change in electronic properties is produced. As has been mentioned before, the crystals of β-NaVB were prepared at about 700 °C and then cooled at a rate of 6 °C/h. Since the reaction temperature is higher than 730—780 K, it may be possible that a slight modification is made in the crystalline state, which then gives rise to a sample dependence of the electrical resistivity.

In conclusion, β-NaVB appears to be a non-stoichiometric compound which can behave partly as a one-dimensional metal and partly as an anisotropic semiconductor. The chain-like structure of vanadium and oxygen atoms and a tendency towards the formation of disordered strings of sodium atoms accomondated in the tunnels provide a structural background for this picture of the compound.

Appendix

Refinement of the Crystal Structure. The intensity data were collected with a Rigaku automated four-circle diffractometer using Mo $K\alpha$ radiation. There are 1180 independent reflections ($|F_o|>3\sigma(|F_o|)$) up to $2\theta\leqq 70°$. The systematic abscences indicate the space group to be C2/m, Cm, or C2. The $N(z)$ test and the statistical intensity distribution of $|E|(hkl)$ favoured the centrosymmetrical group; the space group was, therefore, assumed to be C2/m.[10] The atomic parameters and the occupancy probability of the sodium site were refined by a full-matrix least-squares method. The final R-factor is 0.038. The occupancy probability becomes 43% ($Na_xV_2O_5$; $x=0.287$) for the crystal subjected to this structure refinement. The positional and thermal parameters are given in Table 1. The structure

Table 1. Atomic coordinates ($\times 10^5$)
Their standard deviations are in parentheses.

	x	y	z
V(1)	33757(7)	0	10079(10)
V(2)	11624(8)	0	11885(11)
V(3)	28791(7)	0	40997(10)
Na[a]	99(54)	0	40367(84)
O(1)	0	0	0
O(2)	81425(33)	0	5535(49)
O(3)	63373(32)	0	7802(47)
O(4)	43625(35)	0	21898(54)
O(5)	26323(31)	0	22299(45)
O(6)	10674(37)	0	27294(51)
O(7)	75701(36)	0	42520(48)
O(8)	39762(36)	0	47111(54)

a) The occupation probabiliy is 43%.

TABLE 2 INTERATOMIC DISTANCES
Bond lengths and angles around vanadium atoms.

Symmetry code					
None	x, y, z	i	$1-x$, y, $-z$		
ii	$-1/2+x$, $1/2+y$, z	iii	$1-x$, y, $1-z$		
iv	$1/2-x$, $1/2+y$, $1-z$	v	$-x$, y, $1-z$		
V(1)···O(4)	1.588(5) Å		V(1)···O(5)	1.945(5)	
V(1)···O(2)$_{i}$	2.344(4)		V(1)···O(3)$_{i}$	1.996(5)	
V(1)···O(2)$_{ii}$	1.868(1)				
V(2)···O(6)	1.609(6)		V(2)···O(5)	2.157(4)	
V(2)···O(1)	1.792(1)		V(2)···O(3)$_{ii}$	1.892(2)	
V(2)···O(2)$_{i}$	2.346(6)				
V(3)···O(8)	1.596(5)		V(3)···O(5)	1.794(5)	
V(3)···O(6)	2.671(5)		V(3)···O(7)$_{ii}$	1.887(2)	
V(3)···O(7)$_{iii}$	2.005(6)				
O(4)-V(1)-O(5)	97.99(25)°		O(4)-V(1)-O(3)$_{i}$	103.32(23)	
O(4)-V(1)-O(2)$_{ii}$	103.97(17)		O(5)-V(1)-O(2)$_{i}$	75.90(19)	
O(5)-V(1)-O(2)$_{ii}$	92.83(17)		O(2)$_{ii}$-V(1)-O(2)$_{i}$	76.61(11)	
O(2)$_{ii}$-V(1)-O(3)$_{i}$	82.03(16)		O(3)$_{i}$-V(1)-O(2)$_{i}$	82.79(20)	
O(5)-V(2)-O(6)	87.23(24)		O(5)-V(2)-O(2)$_{i}$	72.18(19)	
O(5)-V(2)-O(3)$_{ii}$	84.40(13)		O(6)-V(2)-O(1)	104.51(22)	
O(6)-V(2)-O(3)$_{ii}$	106.03(21)		O(1)-V(2)-O(3)$_{ii}$	92.20(6)	
O(1)-V(2)-O(2)$_{i}$	96.08(6)		O(2)$_{i}$-V(2)-O(3)$_{ii}$	71.69(15)	
O(8)-V(3)-O(5)	103.27(24)		O(8)-V(3)-O(7)$_{iii}$	107.28(25)	
O(8)-V(3)-O(7)$_{ii}$	76.43(18)		O(5)-V(3)-O(7)$_{ii}$	96.62(16)	
O(5)-V(3)-O(7)$_{iii}$	149.45(20)		O(7)$_{ii}$-V(3)-O(7)$_{iii}$	76.43(18)	

viewed down to the b axis is shown in Fig. 1. The bond lengths and angles around vanadium atoms are given in Table 2. The distance of V–V and Na–O are given in Fig. 1.

References

1) J. H. Perlstein and M. J. Sienko, *J. Phys. Chem.*, **48**, 174 (1968).
2) J. B. Goodenough, *J. Solid State Chem.*, **1**, 349 (1970).
3) N. F. Mott, "Metal-Insulator Transitions," Taylor & Francis, London (1974).
4) R. H. Wallis, N. Sol, and A. Zylbersztejn, *Solid State Commun.*, **23**, 539 (1977).
5) G. Sperlich, W. D. Lazé, and G. Bang, *Solid State Commun.*, **16**, 489 (1975).
6) D. Kaplan and A. Zylbersztejn, *J. de Phys.*, **37**, L123 (1976).
7) W. J. Gunning, A. J. Heeger, R. H. Wallis, N. Sol, and A. Zylbersztejn, *Solid State Commun.*, **26**, 155 (1978).
8) A. D. Wadsley, *Acta Crystallogr.*, **8**, 695 (1955).
9) R. P. Ozerov, G. A. Gol'der, and G. S. Zhdanov, *Soviet Phys. Cryst.*, **2**, 211 (1957).
10) The space group A2/m is adopted in Wadsley's paper (Ref. 8).
11) S. Etemad, *Phys. Rev. B*, **13**, 2254 (1976).
12) R. B. Somoano, A. Gupta, V. Hadek, M. Novotny, M. Jones, T. Datta, R. Deck, and A. M. Hermann, *Phys. Rev. B*, **15**, 595 (1977).
13) K. Franulovič and D. Djurek, *Phys. Lett. A*, **51**, 91 (1975).
14) R. A. Craven, M. B. Salamon, G. DePasquali, R. M. Hermann, G. Stuky, and A. Schultz, *Phys. Rev. Lett.*, **32**, 769 (1974); D. Djurek, K. Franulović, M. Prester, S. Tomić, L. Giral, and J. M. Fable, *Phys. Rev. Lett.*, **38**, 715 (1977).
15) R. Comés, "One-Dimensional Conductors," ed by H. J. Keller, Plenum Press, New York and London (1977).
16) D. B. McWhan, P. D. Dernier, C. Vettier, A. S. Cooper, and J. P. Remeika, *Phys. Rev. B*, **17**, 4043 (1978); H. Terauchi, *Phys. Rev. B*, **17**, 2446 (1978).
17) M. J. Sienko and J. B. Sohn, *J. Chem. Phys.*, **44**, 1369 (1966).
18) J. S. Miller and A. J. Epstein, *Progr. Inorg. Chem.*, **20**, 1 (1976).
19) A. Friederich, D. Kaplan, and N. Sol, *Solid State Commun.*, **25**, 633 (1978).
20) J. J. André, A. Bieber, and F. Gautier, *Ann. Phys.*, t.**I**, 145 (1976).
21) A. Bloch, R. B. Weisman, and C. M. Varma, *Phys. Rev. Lett.*, **28**, 753 (1972).
22) R. A. Craven, Y. Tomkiewicz, E. M. Englar, and A. R. Taranko, *Solid State Commun.*, **23**, 429 (1977), S. Etemad, E. M. Englar, T. D. Schultz, T. Penny, and B. A. Scott, *Phys. Rev., B*, **17**, 513 (1978).
23) V. K. Kapustkin, V. L. Volkov, and A. A. Fotiev, *J. Solid State Chem.*, **19**, 359 (1976).

Solubilities and Rates of Dissolution of Diaspore in NaOH Aqueous Solutions

Byong-Tae CHANG,* Li-Hye PAK, and Yu-Suk LI
Department of Chemistry, Korea University, Kodaira, Tokyo 187

(Received October 13, 1978)

The solubility of diaspore(α-$Al_2O_3 \cdot H_2O$ or α-AlOOH) has been measured in NaOH aqueous solutions from 523.15 K to 598.15 K, and at concentrations of Na_2O up to 150.7 g/l. In order to evaluate the equilibrium constant, $K_2^\circ = (a_{AlO_2^-} \cdot a_{H_2O})/a_{OH^-}$, for the dissolution equilibrium of diaspore $AlOOH(s) + OH^-(l) = AlO_2(l) + H_2O(l)$, two methods have been applied to the solubility data. In the first method, analogous to the method previously applied to the dissolution equilibria of gibbsite, bayerite and beohmite, the values of K_2 at relatively low concentrations of NaOH were extrapolated to zero NaOH concentrations. The temperature dependence of K_2° was expressed as $\log K_2^\circ = -(2500/T) + 4.45$. The second method was based on the extended Debye-Hückel theory for the variation in the activity coefficients of AlO_2^-, OH^-, and H^+ ions with ionic strength at any temperature, that is, the value of the solubility product, $K_1^\circ = a_{H^+} \cdot a_{AlO_2^-}$, was obtained at a given temperature by extrapolating values of K_1, equal to $(m_{H^+} m_{AlO_2^-})$, to zero ionic strength. According to the second method, K_2° was expressed as a function of the temperature: $\log K_2^\circ = -(1600/T) + 2.52$ when $A = 2.0$ or $\log K_2^\circ = -(1550/T) + 2.48$ when $A = 1.5$, where A is a parameter. From kinetic analysis of the dissolution rate of diaspore in NaOH solution, the rate constants per unit surface area of diaspore were found to be 0.31, 0.45, and 0.68 $m^{-2}\,h^{-1}$ at 548.15, 573.15, and 598.15 K, respectively.

The dissolution of alumina hydrates in aqueous NaOH solutions is well known, and serves as a key step in the extractive metallurgy of aluminium (the Bayer process). The solubilities of alumina hydrates in NaOH solutions have been measured by Russell, Edward and Taylor.[1] The solubilities of gibbsite, bayerite and boehmite in NaOH solutions from 313.15 K to 473.15 K were reported, and equilibrium constants for the reaction in which alumina hydrates react with OH^- ion to form AlO_2^- ion were presented. The solubility of gibbsite was precisely determined in order to calculate the free energy of formation and to clarify the structures of the aluminate ions in solution at high pH.[2-5] Bernshtein and Matsenok reported the solubilities of boehmite[6] and diaspore[7] at high temperatures between 532.15 and 573.15 K. The data on the solubilities of diaspore, however, appear to be insufficient for discussion of the thermodynamic properties of diaspore in NaOH solutions.

The purpose of this work is to determine the solubilities of diaspore in NaOH solutions and to clarify the thermodynamic and kinetic properties of the dissolution process.

Experimental

Diaspore samples were prepared by the hydrothermal treatment of boehmite in 0.5 M NaOH solution, to which 10 wt % of natural diaspore was added as seed crystals (623 K, 170 atm for two weeks).[8,9] In order to increase the purity of the diaspore samples, the hydrothermal treatment was repeated several times, using the synthesized diaspore as seed crystals. The results of chemical analysis of the samples are listed in Table 1. X-Ray diffraction analysis showed the presence of only diaspore. Furthermore, DTA analysis indicated an endothermic peak from 623 K to 873 K, corresponding to the transformation of diaspore into α-alumina. The above results confirmed the purity of the diaspore to be higher than 99%.

Measurements of the solubility of diaspore were as follows: a sample (0.40 g) and NaOH solution (5 ml) were laid in a Morey-type reactor which was made of Hastelloy with Ag packing. Heat was supplied and the temperature was kept constant in an electric furnace for the attainment of equilibrium. Quenching to room temperature, treatment with hot hydrochloric acid removed the aluminium hydroxide precipitated. Experimentally it was confirmed that the amounts of diaspore dissolved in the hot HCl solution were negligible. The concentrations of alumina dissolved in the NaOH solution, $m_{AlO_2^-}$, were calculated from the differences in the weights of the diaspore before and after dissolution. The concentrations of the OH^- ion at equilibrium, m_{OH^-}, were calculated from the differences between the initial concentration of NaOH, $(m_{OH^-})_0$, and that of $m_{AlO_2^-}$, *i.e.*, $m_{OH^-} = (m_{OH^-})_0 - m_{AlO_2^-}$.

Table 1. CHEMICAL COMPOSITIONS OF DIASPORE SAMPLES (wt %)

Sample	Al_2O_3	SiO_2	Fe_2O_3	TiO_2	Ignition loss
Natural	76.86	4.04	0.43	3.75	15.16
No. 1	83.73	0.00	0.36	0.57	15.49
No. 2	85.22	0.00	0.04	0.10	14.57
Calcd	85.00	—	—	—	15.00

Results and Discussion

Solubility of Diaspore. In Table 2 are shown the results of solubility measurements for diaspore (No. 1) in NaOH solution up to 4.83 M from 523.15 K to 598.15 K. The dissolution process for diaspore in NaOH solution may be expressed as follows;

$$Al_2O_3 \cdot H_2O(s) + 2OH^-(1) = 2AlO_2^-(1) + 2H_2O(1) \quad (1)$$

or

$$AlOOH(s) + OH^-(1) = AlO_2^-(1) + H_2O(1). \quad (2)$$

The equivalent ratio of the AlO_2^- ion to the OH^- ion, α, may be used as a measure of the solubility of diaspore, *i.e.*, as the solubility increases, α approaches unity. As shown in Fig. 1, the values of α shifted to unity not only with increase in the dissolution temperature but also with the initial concentrations of NaOH solution. Bernshtein and Matsenok[7] also observed

TABLE 2. SOLUBILITY AND EQUILIBRIUM CONSTANT OF DIASPORE IN NaOH SOLUTIONS

Run	T (K)	Initial concentration of Na_2O (g/l)	Time (h)	Equilibrium concentration $m_{AlO_2^-}$ (equiv./l)	Equilibrium concentration m_{OH^-} (equiv./l)	H_2O activity (mole fraction)	Equilibrium constant K_2
1	523.15	6.8	116	0.08	0.14	0.996	0.57
2	523.15	13.6	116	0.15	0.30	0.99	0.50
3	523.15	22.3	95	0.22	0.51	0.985	0.43
4	523.15	31.6	97	0.33	0.70	0.98	0.56
5	523.15	63.6	94	0.51	1.55	0.94	0.31
6	523.15	91.5	100	0.77	2.18	0.89	0.31
7	553.15	6.2	72	0.10	0.10	0.996	1.00
8	553.15	13.6	72	0.23	0.21	0.99	1.08
9	553.15	22.3	71	0.34	0.38	0.985	0.88
10	553.15	31.6	71	0.48	0.54	0.98	0.87
11	553.15	63.6	72	1.08	0.97	0.94	1.05
12	553.15	119.0	70	2.29	1.55	0.84	1.24
13	573.15	4.9	82	0.09	0.07	0.997	1.28
14	573.15	9.9	74	0.17	0.15	0.994	1.13
15	573.15	22.3	74	0.39	0.32	0.985	1.20
16	573.15	31.6	48	0.57	0.45	0.98	1.24
17	573.15	45.6	70	0.83	0.64	0.96	1.25
18	573.15	63.6	69	1.16	0.88	0.94	1.24
19	573.15	91.1	7.	1.81	1.13	0.89	1.43
20	573.15	150.7	70	3.73	1.13	0.79	2.61
21	598.15	6.2	56	0.13	0.07	0.996	1.85
22	598.15	13.6	65	0.21	0.11	0.994	1.90
23	598.15	22.3	47	0.46	0.25	0.985	1.81
24	598.15	32.5	48	0.71	0.34	0.98	2.05
25	598.15	63.6	48	1.41	0.63	0.94	2.10
26	598.15	119.0	45	2.80	1.05	0.84	2.24
27	598.15	150.7	45	4.34	0.52	0.79	6.59

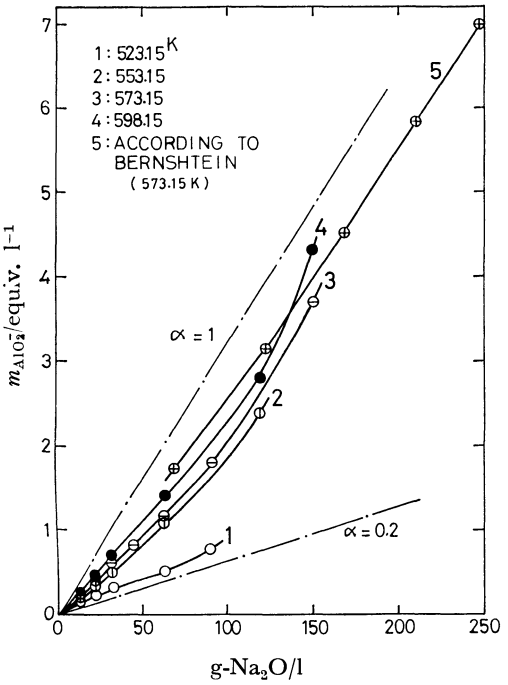

Fig. 1. Solubilities of diaspore in NaOH solutions from 523.15 K to 598.15 K.

similar results in the solubility of diaspore. The values of α for diaspore in this work, however, are lower.

In Fig. 2, the values of α for diaspore are compared with those of α-alumina for approx. equal concentrations of NaOH.[10] At 626 K the two curves intersected which agrees with the transformation temperature of diaspore into α-alumina under 100 atm in the phase diagram of Al_2O_3–H_2O system.[8,9] It is readily seen from Fig. 2 that the temperature dependancy of the solubility of diaspore was much larger

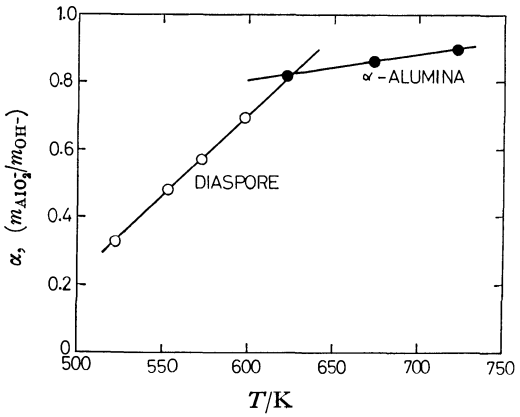

Fig. 2. Comparison of the solubilities of diaspore with those of α-alumina in about 1 M NaOH solution.

than that of α-alumina.

Equilibrium Constants of Dissolution. In order to discuss the dissolution process of diaspore, three equilibrium constants were used as follows:

$$AlOOH(s) = AlO_2^-(1) + H^+(1) \quad (3)$$

$$K_1^\circ = a_{AlO_2^-} \cdot a_{H^+} \quad (4)$$

$$AlOOH(s) + OH^-(1) = AlO_2^-(1) + H_2O(1) \quad (5)$$

$$K_2^\circ = a_{AlO_2^-} \cdot a_{H_2O}/a_{OH^-} \quad (6)$$

$$H_2O(1) = H^+(1) + OH^-(1) \quad (7)$$

$$K_w = a_{H^+} \cdot a_{OH^-}/a_{H_2O} \quad (8)$$

where

$$K_1^\circ = K_2^\circ \cdot K_w. \quad (9)$$

Russell *et al.*[1] derived equilibrium constants, K_2°, at various temperatures by extrapolating $K_2 = m_{AlO_2^-} \cdot m_{H_2O}/m_{OH^-}$ to zero NaOH concentration, assuming that the activity coefficients of the OH^- and AlO_2^- ions are equal and using values of the activity of water in NaOH solutions at 298.15 K. The values of K_2° for diaspore obtained by Russell's method are given in Table 2 and Fig. 3 where the values of K_2° have been neglected at very low NaOH concentration because of large deviations. From the linear relationship between $\log K_2^\circ$ and $1/T$, K_2° was found to be a function of the temperature by the following equation:

$$\log K_2^\circ = -2500/T + 4.45. \quad (10)$$

In Table 3 the equilibrium constants and thermodynamic quantities for the dissolution equilibrium (5) obtained from K_2°, Eq. 10 and the thermodynamic relationships are given. The solubility product of $HAlO_2$, K_1°, was found to be 1.13×10^{-13} at 573.15 K, which was approx. six times greater than at 298.15 K (2×10^{-13}).[1]

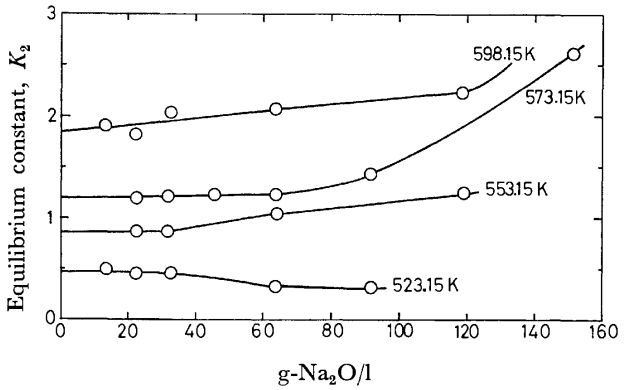

Fig. 3. Equilibrium constants (K_2) obtained by the Russel's method for the dissolution of diaspore in NaOH solutions.

Several assumptions are made in the detremination of equilibrium constants by Russell's method. Firstly, the activity coefficients of AlO_2^- and OH^- ions are assumed to be equal, neglecting the difference in ion size. Secondly, the values of a_{H_2O} at 298.15 K were used at high temperatures without any correction (up to 598.15 K). Thirdly, it is not appropriate to mix units in an equilibrium constants expression by multiplying the activity of water on the mole fraction scale together with the activities of AlO_2^- and OH^- ions on the normality scale.

As described above, generally the value of α at a given temperature becomes larger with increase in the concentration of NaOH solution. The addition of salts such as NaCl, Na_2SO_4, and $NaNO_3$ to the NaOH solution increased the solubility of the alumina hydrates.[4] In the case of diaspore, it was experimentally confirmed that the solubility in a mixed solution containing 1 M NaOH and 1 M NaCl was one and a half times larger than in 1 M NaOH solution at 573.15 K. This indicates that the increase in NaOH concentration raises the solubility of diaspore not only through an increase in the OH^- ion concentration but also through an increase in the ionic strength of the solution. Marshall *et al.* discussed the effect of ionic strength on the solubilities of $CaSO_4$ and its hydrates, and $Ca(OH)_2$ by applying the extended Debye-Hückel theory to high temperature aqueous solution sup to the critical temperature of water.[12,13]

According to Marshall's method, the solubility products are given as follows:

$$K_1^\circ = m_{H^+} \cdot m_{AlO_2^-} \cdot \gamma_{H^+} \cdot \gamma_{AlO_2^-} \quad (11)$$

$$= K_1 \cdot \gamma_\pm^2 \quad (12)$$

where

$$K_1 = m_{H^+} m_{AlO_2^-}. \quad (13)$$

According to the extended Debye-Hückel theory,

$$\log \gamma_\pm = -S_T I^{1/2}/(1 + baI^{1/2})$$
$$= -S_T I^{1/2}/(1 + AI^{1/2}) \quad (14)$$

where S_T is the limiting Debye-Hückel slope, b is a function of temperature and dielectric constant, a is an "ion size parameter," and $A = ba$. From Eqs. 12 and 14,

$$\log K_1^\circ = \log K_1 + 2S_T I^{1/2}/(1 + AI^{1/2}). \quad (15)$$

The ionic strengths, I, are equal to the initial concentrations of NaOH solution expressed as molality, *i.e.*,

Table 3. Equilibrium constants obtained by Russel's method and thermodynamic quantities for the dissolution equilibrium

T (K)	Equilibrium constants			ΔG (kJ)	ΔH (kJ)	ΔS (J/deg)
	K_1°	K_2	K_w[a]			
523.15	4.01×10^{-12}	0.45	8.91×10^{-12}	3.4	47.8	85
553.15	8.70×10^{-12}	0.87	1.00×10^{-11}	0.63	47.8	85
573.15	1.13×10^{-11}	1.24	9.12×10^{-12}	−1.0	47.8	85
598.15	1.29×10^{-11}	1.82	7.08×10^{-12}	−3.0	47.8	85

a) From Ref. 11.

$$I = (m_{AlO_2^-} + m_{OH^-} + m_{Na^+})/2 \quad (16)$$

$$= (m_{NaOH})_0. \quad (17)$$

Figures 4 and 5 presnet the experimental data for the solubilities of diaspore plotted as $\log K_1$ against the Debye-Hückel function, $I^{1/2}/(1+AI^{1/2})$. The values of $A=1.5$ and 2.0 used correspond to $a=3.2$ and4.3 Å

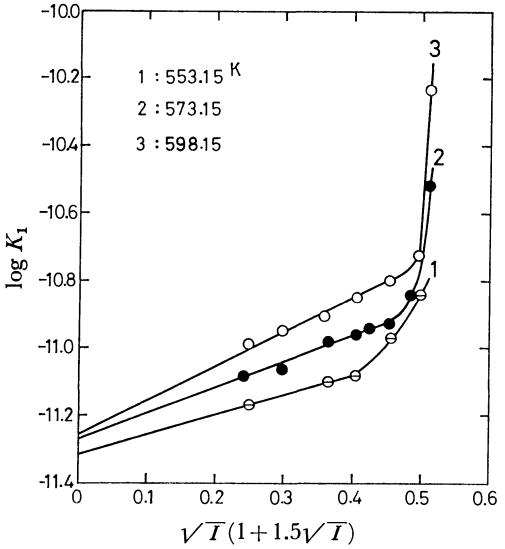

Fig. 4. Logarithm of solubility products (K_1) of diaspore in NaOH solutions *vs.* $I^{1/2}/(1+1.5I^{1/2})$.

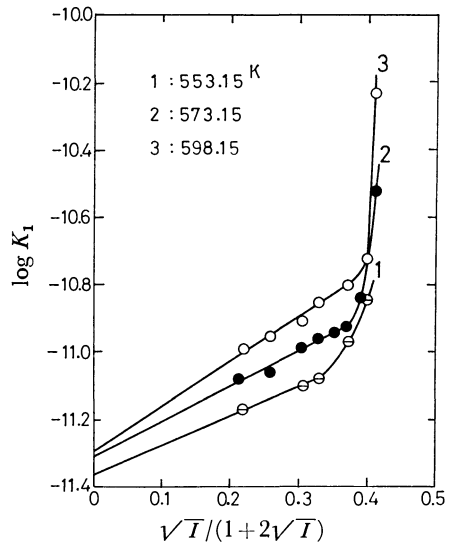

Fig. 5. Logarithm of solubility products(K_1) of diaspore in NaOH solutions *vs.* $I^{1/2}/(1+2I^{1/2})$.

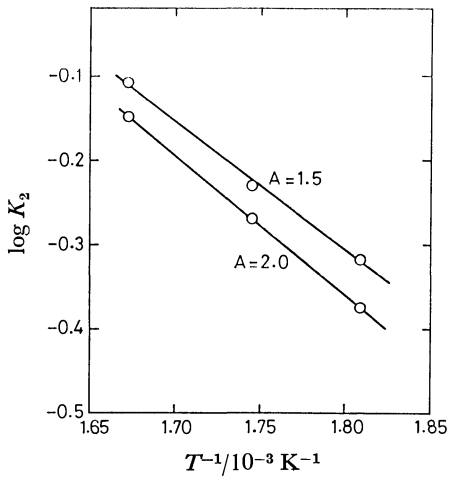

Fig. 6. Temperature dependencies of equilibrium constant K_2 obtained by the Marshall's method.

at 573.15 K, respectively. In the range of relatively low ionic strengths $\log K_1$ changed linearly with the Debye-Hückel function at three temperatures except 523.15 K. The slopes correspond to $2S_T$ in Eq. 15 with the extrapolated values at zero ionic strength corresponding to $\log K_1^\circ$. Figure 6 shows an almost linear relationship between $\log K_2^\circ$ and $1/T$, *i.e.*,

$$\log K_2^\circ = -1550/T + 2.48 \quad (A=1.5) \quad (18)$$

$$\log K_2^\circ = -1600/T + 2.52 \quad (A=2.0). \quad (19)$$

In Table 4 the equilibrium constants and the thermodynamic quantities are listed for Reaction 5 which have been calculated using Eqs. 18 and 19, and thermodynamic relationships. The magnitudes of K_2° were smaller than those obtained by Russell's method. Although the values of S_T were about half the calculated values according to the Debye-Hückel theory, the values of K_2° obtained by Marshall's method may be more reasonable due to the improved extrapolation. As shown in Figs. 4 and 5, $\log K_1^\circ$ deviated from linearity largely at high ionic strength, which may be a direct consequence of ion-solvent interactions[14] and/or the formation of a new solid phase(s) such as $Na_2O \cdot Al_2O_3 \cdot 2.5H_2O$, $3Na_2O \cdot Al_2O_3 \cdot 6H_2O$, *etc.*[15]

Rate of Dissolution of Diaspore. In Fig. 7, the amounts of dissolved diaspore (No. 2) have been plotted as $m_{AlO_2^-}$ against reaction time, t, at three temperatures (548.15, 573.15, and 598.15 K) with a constant initial NaOH concentration of 0.970 M. The times required for the dissolution equilibrium to be

TABLE 4. EQUILIBRIUM CONSTANTS OBTAINED BY MARSHALL'S METHOD AND THERMODYNAMIC QUANTITIES FOR THE DISSOLUTION EQUILIBRIUM

A	T (K)	Equilibrium constants K_1°	K_2	K_w	ΔG (kJ)	ΔH (kJ)	ΔS (J/deg)	Limiting slope S_T
1.5	553.15	4.8×10^{-12}	0.48	1.00×10^{-11}	3.3	29.6	48	0.34
	573.15	5.4×10^{-12}	0.59	9.12×10^{-12}	2.5	29.6	47	0.39
	598.15	5.5×10^{-12}	0.78	7.08×10^{-12}	1.2	29.6	47	0.50
2.0	553.15	4.2×10^{-12}	0.42	1.00×10^{-11}	3.9	30.6	48	0.44
	573.15	4.9×10^{-12}	0.54	9.12×10^{-12}	2.9	30.6	48	0.52
	598.15	5.0×10^{-12}	0.71	7.08×10^{-12}	1.7	30.6	48	0.67

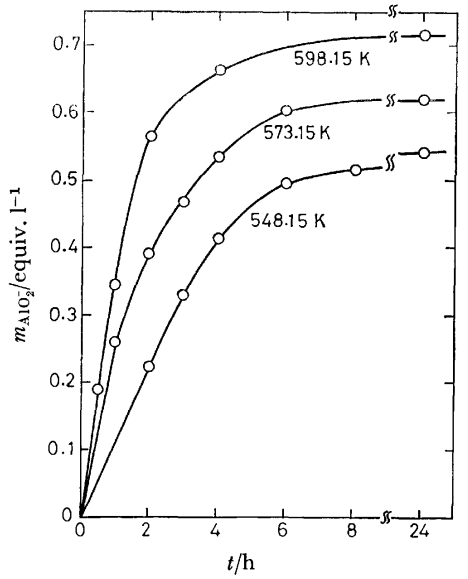

Fig. 7. Dissolution curves of diaspore in 0.970 M NaOH solution at three temperatures.

attained were 40 h(548.15 K), and 24 h(573.15 and 598.15 K). The diaspore sample of No. 2 had a special surface area of 3.40 m^2/g(BET).

Assuming that the chemical reaction of AlOOH with OH^- ions on the surface of the diaspore is the rate-determining step, the rate of dissolution may be expressed as follows:

$$d(m_{AlO_2^-}/m_{OH^-})/dt = kS[(m_{AlO_2^-}/m_{OH^-})_e - (m_{AlO_2^-}/m_{OH^-})] \quad (20)$$

where k is the rate constant per unit of surface area of the sample, S is the total surface area of undissolved diaspore at time t and $(m_{AlO_2^-}/m_{OH^-})$ is the concentration ratio of AlO_2^- to OH^- ions at equilibrium.

In terms of a new variable, x, Eq. 20 becomes

$$dx/dt = kS(x_e - x) \quad (21)$$

where

$$x = m_{AlO_2^-}/m_{OH^-}. \quad (22)$$

From the experimental data, x_e equals 0.59 at 548.15 K, 0.64 at 573.15 K, and 0.74 at 598.15 K, respectively.

The value of S is also a function of x. Introducing the mean size of the diaspore particles, r, S, and the weight of the undissolved diaspore, W, may be expressed as follows:

$$S(r) = a_1 r^2 \quad (23)$$

$$W(r) = a_2 r^3 \quad (24)$$

$$S(r)/S(r_0) = (r/r_0) = [W(r)/W(r_0)]^{2/3} \quad (25)$$

where a_1 and a_2 are proportionality constants and r_0 is the initial mean size. From the mass balance for the diaspore sample,

$$W(r_0) - W(r) = (m_{AlO_2^-} \cdot G \cdot V)/1000. \quad (26)$$

In this equation, G is the gram equivalent of diaspore equal to 60 and V is the volume of the solution. Substituting V=5 ml and G=60,

$$W(r_0) - W(r) = 0.030 m_{AlO_2^-}. \quad (27)$$

Furthermore, since $W(r_0)$=0.40 g and (m_{OH^-})=0.970 M, S may be expressed as a function of x as follows:

$$S(x)/S_0 = [(1+0.27x)/(1+x)]^{2/3} \quad (28)$$

where S_0 is the initial total surface area and equal to 1.36 m^2 when $W(r_0)$=0.40 g. Substituting Eq. 28 into Eq. 20:

$$dx/dt = kS_0[(1+0.27x)/(1+x)]^{2/3}(x_e - x). \quad (29)$$

This differencial equation may be solved as follows:

$$[f(1) - f(y)]/(BS_0) = kt \quad (30)$$

where

$$y = [(1+0.27x)/(1+x)]^{1/3} \quad (31)$$

$$f(y) = n^2\left[\ln(y-m) - \frac{1}{2}\ln(y^2+my+m^2) + 3^{1/2}\tan^{-1}\left(\frac{2y+m}{\sqrt{3}}\right)\right] - m^2\left[\ln(y-n) - \frac{1}{2}\ln(y^2+ny+n^2) + 3^{1/2}\tan^{-1}\left(\frac{2y+n}{\sqrt{3}}\right)\right] \quad (32)$$

$$B = 1.38m^2n^2(m^3-n^2)(1+x_e) \quad (33)$$

$$m = [(1+0.27x_e)/(1+x_e)]^{1/3} \quad (34)$$

$$n = (0.27)^{1/3} = 0.65. \quad (35)$$

Figure 8 shows the linear relationship between t and $[f(1)-f(y)]/(BS_0)$. From the slopes of the straight lines, the values of k were obtained as follows:

$$k = 0.31 \text{ m}^{-2}\cdot\text{h}^{-1} \quad (548.15 \text{ K}) \quad (36)$$

$$= 0.45 \quad (573.15 \text{ K}) \quad (37)$$

$$= 0.68. \quad (598.15 \text{ K}). \quad (38)$$

From the Arrhenius plot between $\log k$ and $(1/T)$, the activation energy for the dissolution of diaspore in NaOH solution was found to be 44 kJ.

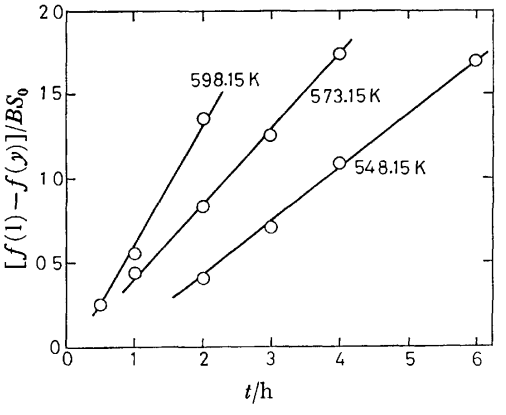

Fig. 8. $f(1)-f(y)/(BS_0)$ *vs.* dissolution time.

References

1) A. S. Russell, J. D. Edwards, and C. S. Taylor, *Trans. AIME J. Metals*, **7**, 1123 (1955).
2) K. Goto, *Nippon Kagaku Zasshi*, **81**, 349 (1960).
3) C. R. Frink and M. Peech, *Soil Sci. Soc. Am., Proc.*, **26**, 346 (1962).
4) A. N. Lypunov, A. G. Khodakova, and Z. G. Galkina, *Tsuvet. Met.*, **37**, 48 (1964).
5) J. A. Kittrick, *Soil Sci. Soc. Am., Proc.*, **30**, 595 (1966).
6) V. A. Bernshtein and E. A. Matsenok, *Zh. Prak.*

Khim., **34**, 982 (1961).
7) V. A. Bernshtein and E. A. Matsenok, *Zh. Prak. Khim.*, **38**, 1935 (1965).
8) A. Neuhaus and H. Heide, *Ber. Dtsch. Keram. Ges.*, **42**, 167 (1965).
9) H. Yanagida and G. Yamaguchi, *J. Ceram. Assoc. Jpn.*, **74**, 94 (1966).
10) G. Yamaguchi, H. Yanagida, and S. Soejima, *Bull. Chem. Soc. Jpn.*, **35**, 1789 (1962).
11) J. R. Fisher and H. L. Barnes, *J. Phys. Chem.*, **76**, 90 (1972).
12) W. L. Marshall, R. Slusher, and E. V. Jones, *J. Chem. Eng. Data*, **9**, 187 (1964); W. L. Marshall and E. V. Jones, *J. Phys. Chem.*, **70**, 4028 (1966).
13) L. B. Yeatts and W. L. Marshall, *J. Phys. Chem.*, **71**, 2641 (1967).
14) J. O'M. Bockris and A. K. N. Reddy, "Modern Electrochemistry," Plenum Press, New York (1970), Vol. 1, p. 238.
15) S. I. Kuznechov, V. A. Tserevyankin, and P. Sh. Shklyan, *Zh. Prak. Khim.*, **35**, 2588 (1962).

Polymer Effects under Pressure. III. Hydrolysis of Normal Alkyl Acetate Catalyzed by Dodecyl Hydrogensulfate Micelle

Yoshihiro TANIGUCHI,* Osamu INOUE, and Keizo SUZUKI

Department of Chemistry, Faculty of Science and Engineering, Ritsumeikan University, Kita-ku, Kyoto, 603

(Received November 6, 1978)

Measurements of the rates of hydrolysis of methyl, ethyl, propyl, and butyl acetates have been made to 2 kbar in water catalyzed by dodecyl hydrogensulfate (DSA) micelle at 40 °C. The rate of hydrolysis decreases with compression up to approximately 1 kbar and then increases above 1 kbar; methyl acetate differs in these respects. The inversion phenomenon under pressure has been explained by the incorporation of both the H_3O^+ ion and ester molecules into the micellar phase. The observed value of the over all activation volume at 1 atm ΔV^* is -5.3 ± 1 cm³/mol for methyl, 0.40 ± 1 cm³/mol for ethyl, 9.7 ± 1 cm³/mol for propyl, and 20 ± 1 cm³/mol for butyl acetate, respectively. From the activation volumes of HCl and DSA micellar catalysts, the volume change accompanying the incorporation of the esters into the micellar phase $\Delta\Delta V_{micelle}$, has been estimated to be 4.0 ± 1 cm³/mol for methyl, 9.8 ± 1 cm³/mol for ethyl, 18.7 ± 1 cm³/mol for propyl, and 27.9 ± 1 cm³/mol for butyl acetate, respectively. The values above have been explained in terms of the contribution to the hydrophobic interaction between the ester molecule and the micelle.

Recently, there have been a large number of publications dealing with the enzyme and enzyme-model reactions as polymer and micellar effects;[1-3] the micellar catalyzed reaction being one of the polymer effects. The incorporation of substrates into the micellar phase is brought about by secondary forces such as the electrostatic and hydrophobic interactions between substrates and micelles. The rate of hydrolysis of esters is recognized to be markedly accelerated above the critical micelle concentration (CMC) and is expected to be retarded under pressure since the volume change accompanying each bond formation is positive. In a previous study,[4] the rate of hydrolysis of alkyl acetates catalyzed by sulfonated polystyrene (PSS) accompanying the hydrophobic incorporation of esters into the polymer domain was shown to be retarded by compression up to about 2 kbar.

It is well documented that hydrophobic interactions participate in micelle formation[5] and a maximum appears in the CMC *vs.* pressure plots at about 1 kbar.[6-13] In the present study, we measured the rate of the hydrolysis of methyl ethyl, propyl, and butyl acetates by dodecyl hydrogensulfate micelle as an acid catalyst up to 2 kbar. The reaction mechanism under pressure is discussed from the activation volume ΔV^* for the micellar catalyzed reaction.

Experimental

Materials. Sodium dodecyl sulfate (SDS) was prepared by the reaction of chlorosulfuric acid and 1-dodecanol, which was fractionally distilled three times and analyzed by gas chromatography. The reaction mixture was neutralized with sodium hydroxide. The crude SDS was extracted three times with petroleum ether in a Soxhlet apparatus for 50 h, and finally recrystallized from methanol. The CMC value of 8.3×10^{-3} mol/kg agrees with those of Hamann[6] and Kaneshina *et al.*[10] A DSA solution was prepared from the SDS solution using an ion exchange resin (Amberlite IR-120). The CMC value was 1.8×10^{-3} mol/kg at atmospheric pressure and 40 °C. An ester was distilled prior to use.

Apparatus and Procedures. The high pressure apparatus for measuring the hydrolysis of the ester has been described in detail elsewhere.[4] Under these experimetal conditions, the rate of hydrolysis of DSA was negligibly smaller than that of the alkyl acetates from the blank test for 3 h, which was compared with the data of Kurz.[14] Analysis of the acetic acid formed was conducted by titration using 1/20 M NaOH solution. The rate constant k_a was obtained by dividing the first-order rate constant by the concentration of acid at atmospheric pressure and 40 °C.

Results

At atmospheric pressure, the catalytic effects of the DSA micelle were greater than that of HCl as shown in Fig. 1. The k_a values for the HCl catalyst are almost identical for all esters, however, those for the micellar catalyst increase with increasing carbon number, *i.e.*, the hydrophobicity of the esters. For example the rates are 2.57, 4.31, 6.87, and 10.2×10^{-2} M^{-1} min^{-1} for methyl, ethyl, propyl, and butyl acetate at 40 °C, respectively. The accelerating effect is similar to that previously reported for PSS catalysts.[4]

Under high pressure, as shown in Fig. 2, the rates showed a minima at approximately 1 kbar, the ex-

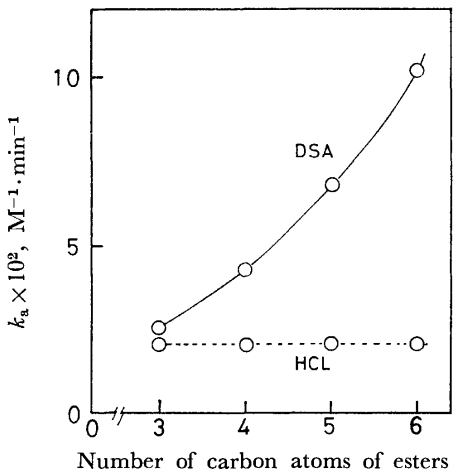

Fig. 1. Plots of k_a *vs.* number of ester carbon atoms for hydrolysis reactions catalyzed by HCl and DSA micelle at 1 atm and 40 °C. Each ester, HCl, and DSA catalysts concentrations are 2×10^{-2} M, 2×10^{-2} M, and 8.3×10^{-3} M.

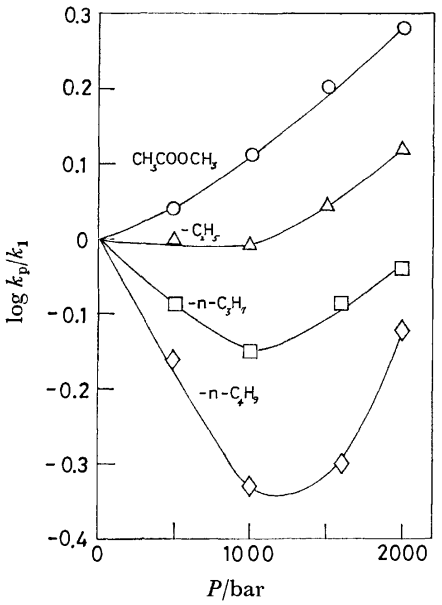

Fig. 2. Plots of $\log k_p/k_1$ *vs.* pressures for hydrolysis reactions catalyzed by DSA micelle at 40 °C. Each ester and DSA catalyst concentrations are 2×10^{-2} M and 8.3×10^{-3} M.

TABLE 1. OBSERVED ACTIVATION VOLUME (ΔV^*) FOR ESTER HYDROLYSIS REACTIONS BY DSA MICELLE AT 40 °C

Catalyst	CH_3COO-R, $\Delta V^*\pm1.0$ cm³/mol			
	-CH_3	-C_2H_5	-n-C_3H_7	-n-C_4H_9
HCl	−9.3[a]	−9.4[a]	−9.0	−7.9[a]
DSA	−5.3	0.40	9.7	20

a) Ref. 4.

ception being methyl acetate, and the pressure effects were larger with longer esters. The inversion phenomena corresponded to the appearance of the maximum of the CMC of DSA at 1 kbar.[12] The observed activation volume ΔV^* is defined by

$$(\partial \ln (k_p/k_1)/\partial P)_T = -\Delta V^*/RT, \quad (1)$$

where R is the gas constant and T the absolute temperature. From the initial slope of the plot of log (k_p/k_1) *vs.* pressure, the ΔV^* values determined graphically have been summarized in Table 1, and compared with previous data for HCl,[4] in addition to the data of propyl acetate catalyzed by HCl.

Discussion

The acid-catalyzed reaction of carboxylic esters in water is generally accepted to occur by an A-2 mechanism,[15,16]

$$H_3O^+ + RCOOR' \overset{K}{\rightleftharpoons} \overset{+}{R}COOHR' + H_2O \quad (2)$$

$$\overset{+}{R}COOHR' + H_2O \xrightarrow{k} R'OH + \overset{+}{R}COOH_2 \quad (3)$$

$$\overset{+}{R}COOH_2 + H_2O \xrightarrow{\text{fast}} RCOOH + H_3O^+ \quad (4)$$

at dilute ester concentration. The rate is given by the equation:

$$(\text{rate})_{HCl} = K\cdot k\cdot C_{ester}\cdot C_{H_3O^+} \quad (5)$$

where C_{ester} and $C_{H_3O^+}$ are the ester and H_3O^+ concentrations. In the micelle catalyst, $C_{H_3O^+}$ is not uniform throught out the solution but is higher near the micellar anion and C_{ester} is also concentrated in the micellar region through hydrophobic interaction. Assuming that $K\cdot k$ in Eq. 5 is approximately independent of the electric field, the rate of acid hydrolysis in the micelle is given by

$$(\text{rate})_{micelle} = K\cdot k\langle C_{ester}\cdot C_{H_3O^+}\rangle, \quad (6)$$

where $\langle C_{ester}\cdot C_{H_3O^+}\rangle$ are the concentrations of the ester and H_3O^+ incorporated into the micellar phase.

A strong acid such as DSA is completely ionized and the counterions are distributed closely to the micellar anion by electrostatic interaction. The effect of added salts on the CMC of SDS surfactants at high pressure was reported by Kaneshina *et al.*,[10] where it was suggested that the ratio of the number of counterions to surfactant in micelles decreases initially with an increase in pressure and then slightly increases with pressure *via* a minimum at 1.5 kbar. This suggests that compression at low pressure causes dissociation of the counterions from the micelle and that compression at higher pressure causes association of the ions to the micelle. If this tendency is the same as for the DSA micelle, the incorporation of the H_3O^+ ion into the micellar phase would show a minimum at approximately 1 to 1.5 kbar independent of the carbon number of the ester.

The driving force of the incorporation of the ester molecules into the micellar phase is expected to be a hydrophobic from Fig. 1. That the rate catalyzed by the DSA micelle increases with increasing carbon number in the ester, indicates a great degree of incorporation of the longer alkyl chain esters into the micellar phase. The methyl acetate, however, would be poorly incorporated into the micelle since the rate catalyzed by DSA is approximately the same as that of the HCl catalyst. Therefore, the rate of methyl acetate catalyzed by DSA micelle under pressure may be expected to increase linearly independently of the behaviour of the micelle under pressure in a similar manner of HCl. The behaviour of the mixed micelle of DSA and ester molecules would be similar to that of the DSA micelle under pressure. From a study of the pressure effect on the CMC of SDS and dodecyltrimethylammonium bromide (DTAB) in water–organic solvent mixtures,[17] the maximum in the CMC–pressure plots gradually shifts to higher values as the alcohol content of the solvent increases, and the effect of 1-butanol is larger than that of methanol. This agrees with the minimum pressure on the rate of hydrolysis for esters having longer alkyl chains under pressure which increase (Fig. 2). Therefore, the inversion phenomena in the rate of hydrolysis for esters having long alkyl chain under pressure has been attributed to the joint effects of the incorporation of the H_3O^+ ion and ester molecules into the micellar phase under pressure in Eq. 6.

Table 2 shows the micellar effects on ΔV^*, $\Delta\Delta V_{micelle}$

Table 2. Micellar effect on ΔV^* for ester hydrolysis compared with PSS polymer effect at 40 °C

Catalyst	CH_3COO-R, $\Delta\Delta V_{micelle}$ ±1.0 cm³/mol			
	-CH_3	-C_2H_5	-n-C_3H_7	-n-C_4H_9
DSA	4.0	9.8	18.7	27.9
PSS(100)[a]	3.4	8.6		10.0
PSS(60)[a]	6.6	12.5		15.5

a) Ref. 4.

compared with the PSS polymer effect. The increase of $\Delta\Delta V_{micelle}$ with increase in the carbon number of the esters needs consideration. The results correspond to the order of the incorporation of the esters into the micelle, and may be explained by the volume increase accompanying rupture of the hydrophobic hydration around the hydrocarbon part of the esters. It has been reported that the volume change for the formation of hydrophobic interaction is 1, 5, and 8 cm³/mol for methyl, ethyl, and propyl groups, respectively.[18] The value of 1—2 cm³/mol per methyl group accompanying the breaking down of hydrophobic hydration is supported by Noguchi,[19] Kaneshina *et al.*,[10] Corkill *et al.*,[20] and Friedman *et al.*[21] For butyl acetate the expected value accompanying the hydrophobic incorporation of ester molecules into the micelle is approximately half the $\Delta\Delta V_{micelle}$ suggesting additional contributions to $\Delta\Delta V_{micelle}$ accompanying a strong hydrophobic atmosphere *e.g.*, the dehydration of H_2O molecules from the carbonyl oxygen atom of the esters for hydrophobic incorporation, which accompanies a positive volume change of 5 to 7 cm³/mol.[22–25] Also, the exclusion of water molecules by strong hydrophobic atmosphere may change the A-2 mechanism into an A-1 mechanism in the *t*-butyl acetate system. Assuming such a development, the ΔV_{HCl} in Eq. 1 becomes small and positive or zero.[26] The $\Delta\Delta V_{micelle}$ for the butyl acetate system is 20 cm³/mol, which is a reasonable value. Further studies are necessary to confirm the A-1 mechanism in the micelle.

References

1) K. J. Laidler and P. S. Bunting, "The Chemical Kinetics of Enzyme Action," 2nd ed, Oxford University Press, London (1973).

2) J. H. Fendler and E. J. Fendler, "Catalysis in Micellar and Macromolecular Systems," Academic Press, New York, N. Y. (1975).

3) "Reaction Kinetics in Micelles," ed by E. H. Cordes, Plenum Press, New York, N. Y. (1973), p. 25.

4) Y. Taniguchi, N. Sugiyama, and K. Suzuki, *J. Phys. Chem.*, **82**, 1231 (1978).

5) C. Tanford, "The Hydrophobic Effect: Formation of Micelles and Biological Membranes," Wiley, New York, N.Y. (1973).

6) S. D. Hamann, *J. Phys. Chem.*, **66**, 1359 (1962).

7) R. F. Tuddenham and A. E. Alexander, *J. Phys. Chem.*, **66**, 1839 (1962).

8) J. Osugi, M. Sato, and N. Ifuku, *Rev. Phys. Chem. Jpn.*, **35**, 32 (1965).

9) J. Osugi, M. Sato, and N. Ifuku, *Rev. Phys. Chem. Jpn.*, **38**, 58 (1968).

10) S. Kaneshina, M. Tanaka, T. Tomida, and R. Matuura *J. Colloid Interface Sci.*, **48**, 450 (1974).

11) M. Ueno, M. Nakahara, and J. Osugi, *Rev. Phys. Chem. Jpn.*, **47**, 25 (1977).

12) K. Suzuki, Y. Taniguchi, and M. Tsuchiya, 6th International Conference on High Pressure, Boulder, July 1977.

13) Recently, from a study of the pressure effect on CMC using naphthalene as a probe, it was found that the CMC of SDS does not invert up to about 5 kbar. See, S. Rodriguez and H. Offen, *J. Phys. Chem.*, **81**, 47 (1977).

14) The rate constants of H^+ catalyzed hydrolysis for sodium alkyl sulfate is 82×10^{-5} to 198×10^{-5} mol^{-1} s^{-1} at 90 °C. See, J. L. Kurz, *J. Phys. Chem.*, **66**, 2239 (1962).

15) C. K. Ingold, "Structure and Mechanism in Organic Chemistry," 2nd ed, Cornell University Press, Ithaca N.Y. (1967), p 1098.

16) K. J. Laidler, "Chemical Kinetics," 2nd ed, McGraw-Hill, London (1965) p. 88.

17) S. Kaneshina, M. Tanaka, and R. Matuura, *Mem. Fac. Sci. Kyushu Univ., Ser. C*, **9**, 71 (1974).

18) K. Suzuki, Y. Taniguchi, and T. Watanabe, *J. Phys. Chem.*, **77**, 1918 (1973).

19) H. Noguchi, *Prog. Polym. Sci.*, **8**, 191 (1975).

20) J. M. Corkill, J. F. Goodmann, and T. Walker, *Trans. Faraday Soc.*, **63**, 768 (1967).

21) M. E. Friedman and H. A. Scheraga, *J. Phys. Chem.*, **69**, 3795 (1965).

22) E. Fishman and H. G. Drickamer, *J. Chem. Phys.*, **24**, 548 (1956).

23) K. Suzuki and M. Tsuchiya, *Bull. Chem. Soc. Jpn.*, **48**, 1701 (1975).

24) Y. Taniguchi and K. Suzuki, *J. Phys. Chem.*, **78**, 759 (1974).

25) K. Suzuki, M. Tsuchiya, and M. Kadono, *Bull. Chem. Soc. Jpn.*, **43**, 3083 (1970).

26) A. R. Osborn and E. Whalley, *Can. J. Chem.*, **39**, 1094 (1961).

Disintegration of Sulfonated Poly(1,4-piperazinediylterephthaloyl) Microcapsules by Poly(diallyldimethylammonium chloride)

Shiro Suzuki and Tamotsu Kondo*,†

Department of Domestic Science, Ferris Women's College, Naka-ku, Yokohama 231

†*Faculty of Pharmaceutical Sciences, Science University of Tokyo, Shinjuku-ku, Tokyo 162*

(Received November 8, 1978)

Partially sulfonated poly(1,4-piperazinediylterephthaloyl) microcapsules were found to undergo disintegration by the action of poly(diallyldimethylammonium) ions if the polycation concentration exceeded a certain value. The polycation concentration at which disintegration started was dependent on the degree of sulfonation of the microcapsules and pH of the medium. Exact electrical equivalence of the polyions involved was shown to be a necessary condition for disintegration of the microcapsules to take place. Disintegration of the microcapsules resulted in a formation of coacervate-like liquid drops. This formation of coacervate-like liquid was accelerated by mechanical and thermal agitation. Crosslinking among the polymers constituting the microcapsules prevented disintegration from occurring.

In a previous paper[1] the disintegration phenomenon of poly(N^{α},N^{ε}-L-lysinediylterephthaloyl) microcapsules by poly(diallyldimethylammonium chloride) was reported. The cationic polyelectrolyte caused disintegration of the microcapsules if its concentration exceeded a certain value which was dependent on the pH of the medium while it acted on the microcapsules to bring about their aggregation at lower concentrations. In any case where disintegration was observed, exact electrical equivalence of the polyions involved was found to exist. The physical process of disintegration was indicated to be a formation of coacervate-like liquid.

As this way of the use of a polycation should be useful to probe the stability and exchangeability of the components of a coacervate film it will be worth while to extend our work to see if the mechanism established for the above system also works in other systems. In view of this, the present paper deals with disintegration of partially sulfonated poly(1,4-piperazinediylphthaloyl) microcapsules by poly(diallyldimethylammonium chloride) in terms of the degree of sulfonation of the polymer and the pH and ionic strength of the medium. The effect of crosslinking of the polymers constituting the microcapsules on disintegration will also be discussed.

Experimental

Preparation of Microcapsules. Sulfonated poly(1,4-piperazinediylterephthaloyl) microcapsules (SPP microcapsules) were prepared in a manner similar to that described in an earlier paper.[2] This way, SPP microcapsules with different degrees of sulfonation were prepared using mixtures of piperazine(Pip) and 4,4′-diaminostilbene-2,2′-disulfonic acid(DASSA) in varying ratios as water-soluble monomers in the interfacial polycondensation reaction between diamine and diacid dichloride, and named SPP-2, -3, and -5 microcapsules, respectively, according to the mixing ratio given in Table 1.

To 7.5 cm³ of aqueous 1% polyethylene glycol(degree of polymerization 4000) solution in a 1 liter round bottom flask surrounded by ice was added an equal volume of 0.4 M solution of a mixture of Pip and DASSA in aqueous 0.45 M sodium carbonate solution containing 1% polyethylene glycol.

To this solution was added 75 cm³ of the mixed solvent (chloroform–cyclohexane 1 : 3, v/v, containing 10% sorbitan trioleate as an emulsifier). The mixture was then mechanically emulsified with a constant speed stirrer for 5 min to yield a water-in-oil emulsion. The alkali served to neutralize hydrogen chloride formed during the polycondensation reaction. Without stopping the stirring, 75 cm³ of terephthaloyl dichloride solution were quickly added to the emulsion, and the stirring was continued for further 3 min. The terephthaloyl dichloride solution was prepared just before use by adding 0.6 g of pure terephthaloyl dichloride to 75 cm³ of the mixed solvent. SPP microcapsules thus obtained were separated from the organic phase by centrifugation at 1000 rpm for 3 min and washed with the mixed solvent containing no emulsifier on the centrifuge at least three times to remove the emulsifier. Then, the washed SPP microcapsules were transferred to aqueous phase with the aid of poly(oxyethylene) sorbitan monolaurate, washed repeatedly with deionized water on the centrifuge, and dialyzed in a Visking tube against distilled water for a week.

Table 1. Molar mixing ratios of Pip to DASSA in diamine mixtures used for preparation of SPP microcapsules and sulfur contents in SPP microcapsules

Microcapsule	Molar mixing ratio Pip : DASSA	Sulfur content %
SPP-2	2 : 1	3.82
SPP-3	3 : 1	3.53
SPP-5	5 : 1	2.89

Microscopic Observation of Microcapsule Disintegration. To the dialyzed suspension of each of SPP-2, -3, and -5 microcapsules in test tubes was added an equal volume of a series of various concentrations of aqueous poly(diallyldimethylammonium chloride)(PDADMA) solution. The pH and ionic strength of the medium were adjusted by the addition of HCl or NaOH and NaCl, respectively. The mixtures were allowed to stand for 1 h with occasional shaking in a thermostated bath kept at 30 °C. At the end of this period, a small portion of each of the mixtures was withdrawn by a capillary tube and placed on a slide glass to observe the state of the SPP microcapsules under an optical microscope. In some cases, the microcapsules were photographed.

Preparation of Dried Samples of SPP Microcapsule Membranes for Adsorption Experiments. Each of SPP-2, -3, and -5 microcapsules in the organic phase was washed repeatedly with the mixed solvent containing no emulsifier, thoroughly dried *in vacuo*, and ground down into fine powder in a porcelain mortar. The powdered samples were stored in a desic-

cator until the time of use.

Measurements of Adsorption of PDADMA to SPP Microcapsule Membranes. To 0.05 g of the powdered samples of SPP microcapsule membranes was added 50 cm³ of various concentrations of aqueous PDADMA solution at different pH(7.0, 4.0, and 2.0) and ionic strengths (0.1 and 0.2). The pH and ionic strength of the medium were adjusted by the addition of HCl or NaOH and NaCl, respectively. The mixtures were permitted to stand for 1 h with continuous stirring in a thermostat maintained at 30 °C to ensure complete dispersion of the samples. At the end of this period, the mixtures were centrifuged at 2000 rpm for 5 min to settle the floating particles. Then, 10 cm³ each of the supernatant solutions was withdrawn by a pipet and titrated with a standardized solution of potassium poly(vinylsulfonate) using toluidine blue as an indicator.[3] The end point of titration could easily be detected visually by the metachromatic color change from blue to purple of the indicator.

Measurements of Electrophoretic Mobility of SPP Microcapsules. To a dialyzed suspension of each of SPP-2, -3, and -5 microcapsules in test tubes was added an equal volume of a series of various concentrations of PDADMA solution. The mixtures were allowed to stand for 1 h with occasional shaking in a thermostated water bath kept at 30 °C. The pH and ionic strength of the medium were adjusted by the addition of the acid or alkali and the salt, respectively, as before.

At the end of this period, nondisintegrated microcapsules were separated from the mixtures by centrifugation at 2000 rpm for 3 min. A small portion of the separated SPP microcapsules as the top layer in the centrifuge tube was withdrawn by a capillary tube and put into a 10^{-3} M NaCl solution. The resulted suspension was used for electrophoresis measurement.

Electrophoretic mobility measurements of the SPP microcapsules were carried out at 30 °C using a microelectrophoresis apparatus(Rank Brothers Co., Ltd., England). For each measurement, at least 20 microcapsules were timed in each direction to eliminate the polarization effect of the electrodes. The mobility of the microcapsules thus obtained was converted into the zeta potential by the Smoluchowski equation.

A portion of disintegrated SPP microcapsules settled in the bottom of the centrifuge tube was also withdrawn by a capillary tube and put into a 10^{-3} M NaCl solution. The mobility of disintegrated SPP microcapsules was converted into the zeta potential in the same way as for nondisintegrated SPP microcapsules.

Preparation of Coacervate-like Liquid Drops from SPP Microcapsules and PDADMA and Measurements of Their Electrophoretic Mobility. On the basis of the microscopic observations of disintegration of SPP microcapsules described later, coacervate-like liquid drops were prepared from SPP-2 and -5 microcapsules and PDADMA under two extreme conditions, *i.e.*, the most favorable and unfavorable conditions for disintegration. In the case of SPP-2 microcapsules, equal volumes of microcapsule suspension and 1.73×10^{-1} N PDADMA solution at pH 7.0 and ionic strength 0.1 were mixed in a 100 cm³ Erlenmeyer flask immersed in a thermostated water bath kept at 30 °C and the mixture was allowed to stand for 1 h. The mixture was then transferred to a 200 cm³ beaker in a water bath at 40 °C, stirred for 30 min, and centrifuged at 2000 rpm for 5 min to sediment coacervate-like liquid.

A small portion of the bottom layer in the centrifuge tube was withdrawn by a microspatula and put into 100 cm³ of 10^{-3}M NaCl solution. The electrophoretic mobility of the drops was measured in the same way as before. A similar procedure was employed to prepare coacervate-like liquid drops from SPP-5 microcapsules and 1.73×10^{-3} M solution of PDADMA. In this case, the pH and ionic strength of the medium were 2.0 and 0.2, respectively.

Treatment of SPP Microcapsules with Glutaraldehyde. The terminal amino groups of the constituent polymers of SPP-2 microcapsules were crosslinked with glutaraldehyde in the following way. Dialyzed suspension of SPP-2 microcapsules and 0.1 M NaCl solution were mixed in a 30 cm³ Erlenmeyer flask. Then, the pH of the resultant suspension was adjusted to about 10 by dropwise addition of 0.1 M NaOH solution to ensure complete deprotonation of the terminal amino groups. Twenty five grams of 25% aqueous glutaraldehyde solution was added to the suspension in the flask and the mixture was kept at 30 °C for 1 h during which the flask was gently shaken. After this treatment, the mixture was centrifuged and the separated SPP-2 microcapsules were redispersed in a medium of pH 7.0 and ionic strength 0.1 containing 1.73×10^{-1} N PDADMA to observe if the polycations would cause disintegration of the aldehyde-treated microcapsules.

Results

Microscopic Observations. In Fig. 1 are shown photomicrographs of intact SPP microcapsules. They were all spherical in shape and well-dispersed in the medium.

Disintegration of SPP microcapsules by PDADMA was found to depend strongly on the polycation concentration, moderately on the pH of the medium, and slightly on the ionic strength of the medium. In Table 2 is shown the dependency of the disintegration phenomenon on the three variables.

At any pH and ionic strength of the medium, disintegration of SPP microcapsules was observed only when the polycation concentration exceeded a certain value though the polycations caused aggregation of the microcapsules at lower concentrations. It was also observed that large microcapsules are readily ruptured by the action of the polycations as compared with small ones.

On the other hand, disintegration was apparently affected by the degree of sulfonation of SPP microcapsules since the pH dependence of the minimum PDADMA concentration required for the microcapsules to undergo disintegration varied with the degree of sulfonation as shown in Table 2. That is to say, disintegration of SPP-5 microcapsules with the lowest degree of sulfonation was prevented at low pH while SPP-2 microcapsules of the highest degree of sulfonation were ruptured independently of the pH of the medium above a certain polycation concentration.

Although the influence of the ionic strength of the medium on disintegration of SPP microcapsules was generally insignificant, it was appreciable in the case of SPP microcapsules of low degree of sulfonation at low pH.

Figure 2 gives the process of disintegration of SPP-2 microcapsules under the most favorable condition for disintegration in the present work, *i.e.*, at pH 7.0 and ionic strength 0.1 when the PDADMA concentration is increased.

At first, a low concentration of PDADMA caused

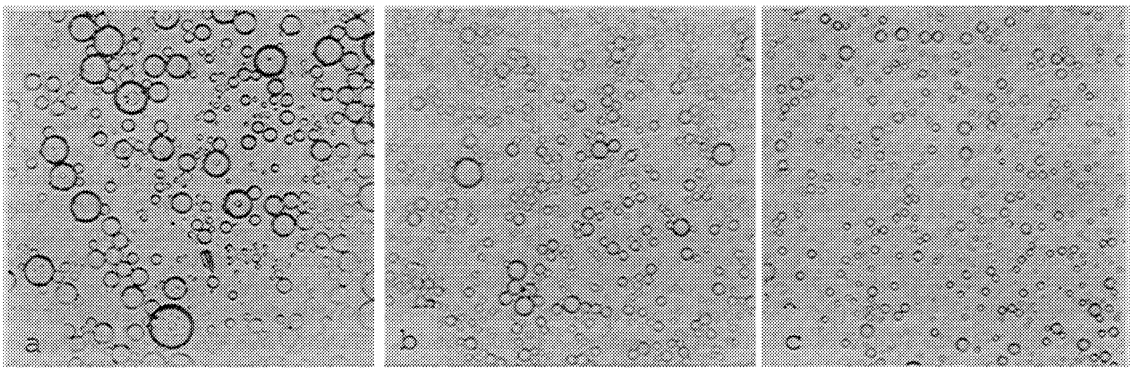

Fig. 1. Photomicrographs of intact SPP-2 (a), -3 (b), and -5 (c) microcapsules (×150).

Table 2. Disintegration of SPP microcapsules by PDADMA

Micro-capsule	pH	Ionic strength	PDADMA concn (N)				
			0.23×10^{-3}	0.33×10^{-3}	1.65×10^{-2}	1.73×10^{-1}	1.77
SPP-2	7.0	0.1	−	−	−	+	++
		0.2	−	−	−	+	++
	4.0	0.1	−	−	−	+	++
		0.2	−	−	−	+	++
	2.0	0.1	−	−	−	+	++
		0.2	−	−	−	+	++
SPP-3	7.0	0.1	−	−	−	+	++
		0.2	−	−	−	+	++
	4.0	0.1	−	−	−	+	++
		0.2	−	−	−	+	++
	2.0	0.1	−	−	−	+	++
		0.2	−	−	−	±	++
SPP-5	7.0	0.1	−	−	−	+	++
		0.2	−	−	−	+	++
	4.0	0.1	−	−	−	+	+
		0.2	−	−	−	±	+
	2.0	0.1	−	−	−	−	+
		0.2	−	−	−	−	+

−: Aggregation alone; ±: very slight disintegration; +: slight disintegration; ++: moderate disintegration.

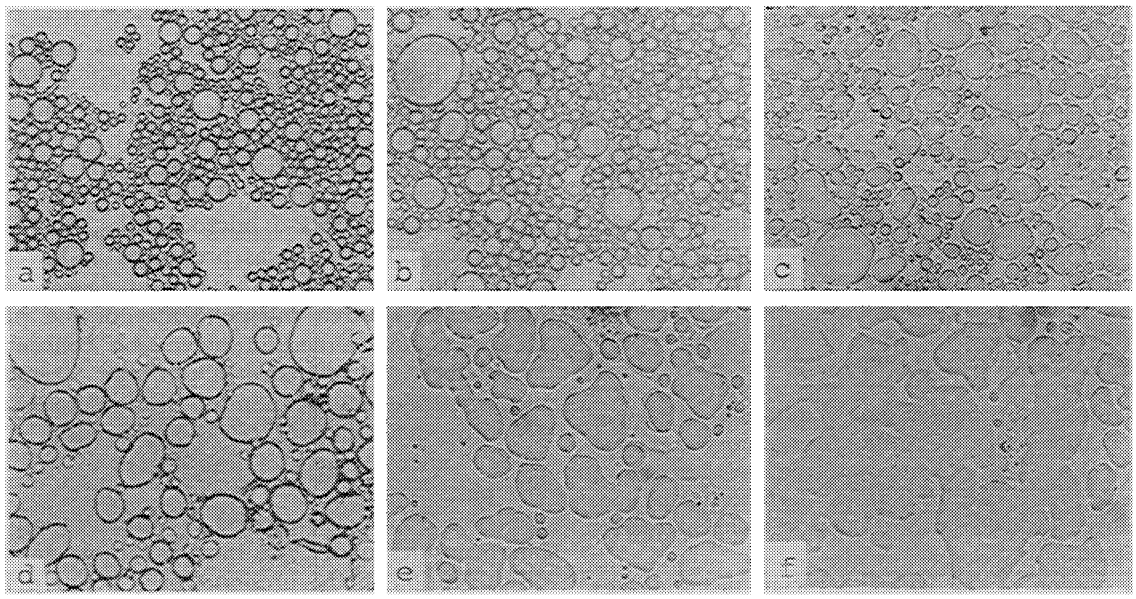

Fig. 2. A series of photomicrographs showing the process of disintegration of SPP-2 microcapsules by PDADMA at pH 7.0 and ionic strength 0.1. PDADMA concentration increases in the alphabetical order of the photos.

aggregation of the microcapsules(a); fusion among the aggregated microcapsules began here and there as the polycation concentration increased, large capsules having been liable to be the centers of fusion(b); the number of the centers from which fusion spread increased rapidly with further increase in the polycation concentration(c); the fusion developed further and large coacervate-like drops were formed(d); coalescence among the large drops proceeded(e); and finally, the microcapsule membranes were almost completely broken to the extent that their original form could not be seen.

Adsorption of PDADMA to SPP Microcapsule Membrane. In Fig. 3 is shown the effect of the degree of sulfonation on the adsorption of PDADMA upon SPP microcapsule membranes at pH 7.0 and ionic strength 0.1. The abscissa represents the logarithm of the initial PDADMA concentration.

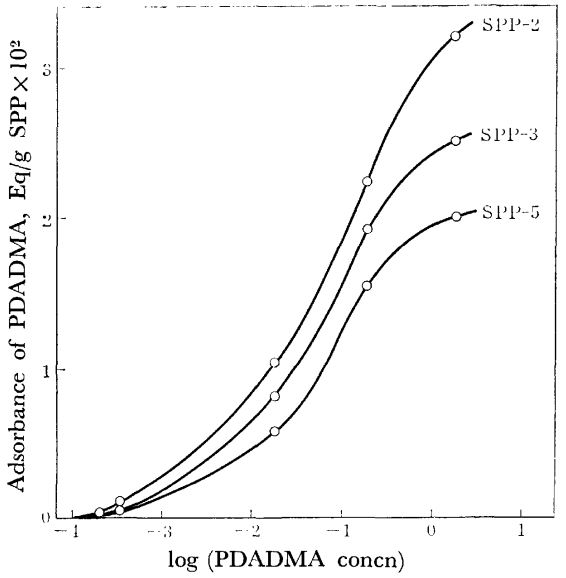

Fig. 3. Adsorption isotherms of PDADMA on SPP microcapsule membranes in a medium of pH 7.0 and ionic strength of 0.1 at 30 °C.

In any case, the PDADMA adsorption increased steeply first and then showed a tendency to saturate as the polycation concentration increased beyond 1.73×10^{-1} N. The adsorption was strongly dependent on the degree of sulfonation. Namely, it increased with increasing degree of sulfonation at all polycation concentrations. Variations in the pH and ionic strength of the medium did not alter this trend though not given here.

The effects of the pH and ionic strength of the medium on the polycation adsorption are illustrated in Fig. 4 for SPP-3 microcapsules.

As the pH was increased the adsorption rose remarkably. An increase in the ionic strength brought about a decrease in the adsorption. The adsorption decrease became less pronounced when the pH was lowered. Similar results were obtained with SPP-2 and -5 microcapsules.

Electrophoretic Behavior of SPP Microcapsules in the Presence of PDADMA. Figure 5 shows the zeta potential of nondisintegrated SPP-3 microcapsules as a function of the polycation concentration and the pH and ionic strength of the medium. The values of these variables are those employed in the preparation of the samples for electrophoresis experiment.

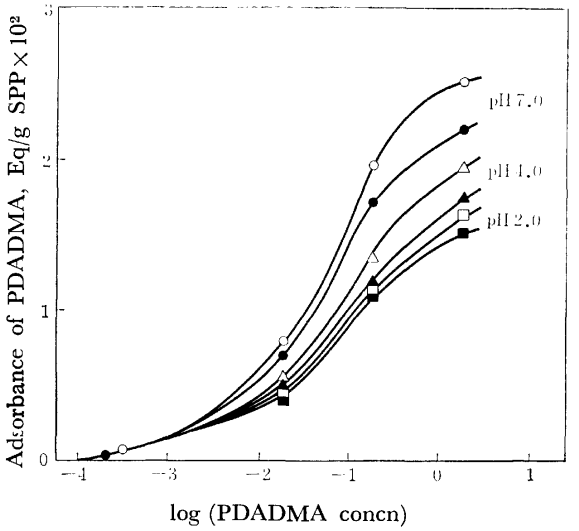

Fig. 4. Adsorption isotherms of PDADMA on SPP-3 microcapsule membranes at 30 °C. Ionic strength: 0.1 (open symbols) and 0.2 (closed symbols).

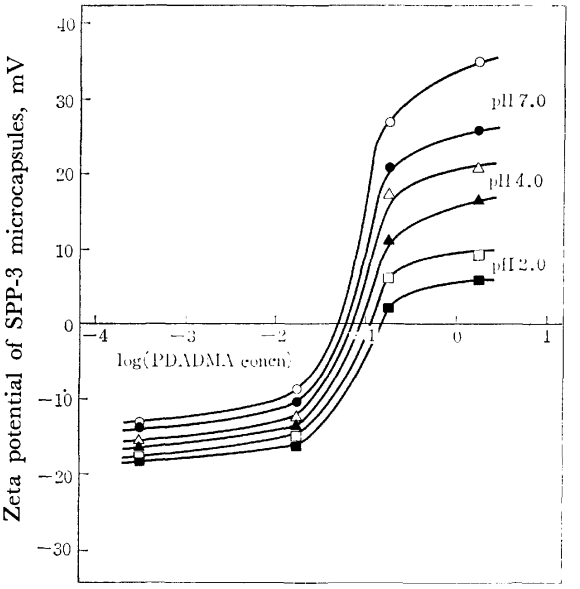

Fig. 5. Zeta potential of SPP-3 microcapsules at 30 °C as a function of PDADMA concentration, pH, and ionic strength. Ionic strength: 0.1 (open symbols) and 0.2 (closed symbols).

In all cases, the zeta potential changed its sign when the polycation concentration attained a value between 1.65×10^{-2} and 1.73×10^{-1} N. The polycation concentration at which the zeta potential reversed its sign shifted downward as the hydrogen ion concentration and ionic strength of the medium were reduced. A decrease in the degree of sulfonation gave rise to an increase in the polycation concentration required to cause reversal of the sign of the zeta potential.

The zeta potential of disintegrated SPP-3 microcap-

sules is shown in Fig. 6 as a function of the polycation concentration and the pH and ionic strength of the medium used for the preparation of the samples for electrophoresis.

Reversal of the sign of the zeta potential was observed as the polycation concentration increased beyond 1.65×10^{-2} N as in the case of nondisintegrated SPP microcapsules. The positive zeta potential after the sign reversal was at most as high as 7 mV and insensitive to changes in the pH and ionic strength of the medium.

Electrophoretic Behavior of Coacervate-like Liquid Drops Prepared from SPP Microcapsules and PDADMA. In Fig. 7 is given a photomicrograph of coacervate-like liquid drops prepared from SPP-2 microcapsules and PDADMA.

The zeta potentials of coacervate-like liquid drops prepared from SPP-2 and -5 microcapsules and PDADMA were almost zero or slightly positive, being indicative of a very low, if any, electric charge of the drops and they were almost independent of the degree of sulfonation and pH and ionic strength of the medium at which the drops were prepared.

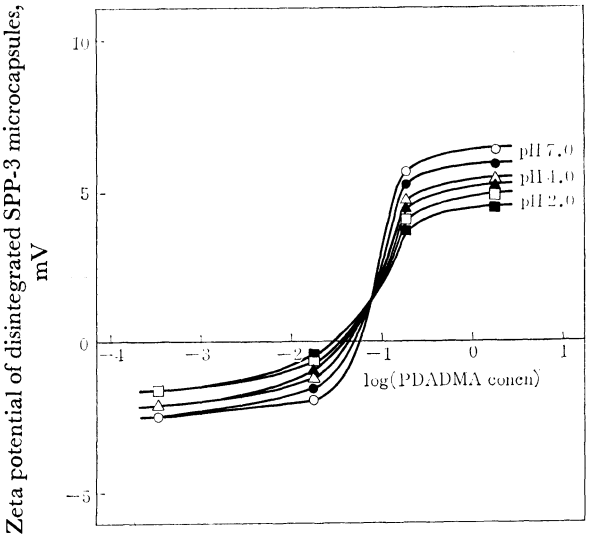

Fig. 6. Zeta potential of disintegrated SPP-3 microcapsules at 30 °C as a function of PDADMA concentration, pH, and ionic strength. Ionic strength: 0.1 (open symbols) and 0.2 (closed symbols).

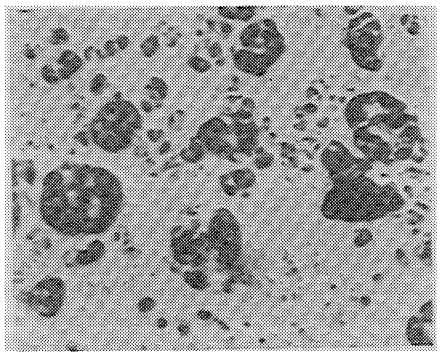

Fig. 7. Photomicrograph of coacervate-like liquid drops prepared from SPP-2 microcapsules and PDADMA.

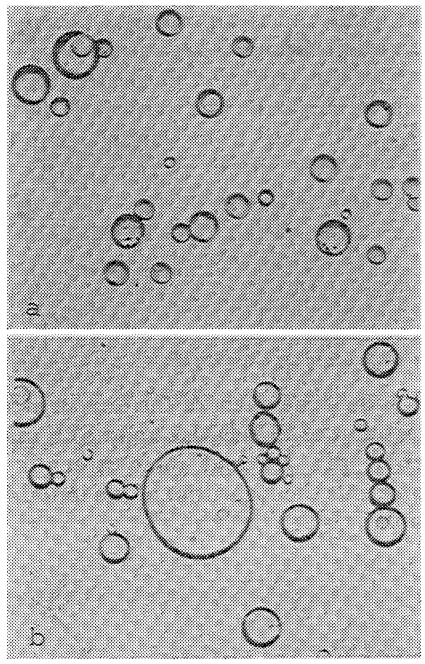

Fig. 8. Photomicrographs of glutaraldehyde-treated SPP-2 microcapsules taken in the absence (a) and presence (b) of PDADMA (×150).

Effect of Glutaraldehyde Treatment on Disintegration of SPP Microcapsules. As described already, SPP-2 microcapsules were appreciably ruptured in 1 h at pH 7.0 and ionic strength 0.1 when the polycation concentration was 1.73×10^{-1} N. On the contrary, glutaraldehyde-treated SPP-2 microcapsules were hardly disintegrated by the action of PDADMA under the same condition. Photomicrographs of glutaraldehyde-treated SPP-2 microcapsules taken in the absence(a) and presence(b) of PDADMA are shown in Fig. 8.

Discussion

As is apparent from the polycondensation reaction utilized in the preparation, SPP microcapsules have a number of sulfonato groups on their constituent polymer molecules as the ionizable group. Disintegration of the microcapsules is clearly caused by the electrostatic interaction between the negatively charged microcapsules and the oppositely charged polycations in the aqueous medium. Namely, it is a prerequisite for disintegration of the microcapsules that PDADMA ions are adsorbed on the sulfonato groups of the microcapsules. However, there seems to be a minimum number of sulfonato groups on the microcapsules for their disintegration to occur because SPP-5 microcapsules are not disintegrated at the PDADMA concentration of 1.73×10^{-1} N when the pH is low though this concentration produces disintegration of the microcapsules with higher degrees of sulfonation at the same pH(Table 2). It is reasonable that the pH effect on disintegration is less significant for SPP microcapsules than for PPL†† microcapsules which have carboxyl groups as the ionizable group since $-SO_3H$ group has

†† Abbreviation for poly(N^{α},N^{ε}-L-lysinediylterephthaloyl).

Table 3. Numbers of quarternary ammonium groups of PDADMA ions adsorbed on SPP microcapsules

Micro-capsule	pH	Ionic strength	PDADMA concn (N)				
			0.23×10^{-3}	0.33×10^{-3}	1.65×10^{-2}	1.73×10^{-1}	1.77
SPP-2	7.0	0.1	5×10^{18}	1.3×10^{19}	6.02×10^{21}	1.32×10^{22}	1.89×10^{22}
		0.2	5×10^{18}	1.3×10^{19}	5.41×10^{21}	1.20×10^{22}	1.74×10^{22}
	4.0	0.1	3×10^{18}	9×10^{18}	3.91×10^{21}	1.08×10^{22}	1.50×10^{22}
		0.2		9×10^{18}	3.61×10^{21}	9.93×10^{21}	1.38×10^{22}
	2.0	0.1		6×10^{18}	3.61×10^{21}	9.03×10^{21}	1.26×10^{22}
		0.2		6×10^{18}	3.31×10^{21}	8.72×10^{21}	1.17×10^{22}
SPP-3	7.0	0.1	2×10^{18}	6×10^{18}	4.81×10^{21}	1.17×10^{22}	1.57×10^{22}
		0.2	2×10^{18}	6×10^{18}	4.21×10^{21}	1.02×10^{22}	1.32×10^{22}
	4.0	0.1		5×10^{18}	3.31×10^{21}	8.12×10^{21}	1.17×10^{22}
		0.2		5×10^{18}	2.70×10^{21}	6.92×10^{21}	1.05×10^{22}
	2.0	0.1		3×10^{18}	2.70×10^{21}	7.22×10^{21}	9.93×10^{21}
		0.2		3×10^{18}	2.40×10^{21}	6.65×10^{21}	9.03×10^{21}
SPP-5	7.0	0.1		5×10^{18}	3.31×10^{21}	9.33×10^{21}	1.20×10^{22}
		0.2		5×10^{18}	2.70×10^{21}	7.22×10^{21}	9.33×10^{21}
	4.0	0.1		3×10^{18}	2.40×10^{21}	5.71×10^{21}	8.72×10^{21}
		0.2		3×10^{18}	1.86×10^{21}	5.41×10^{21}	6.32×10^{21}
	2.0	0.1			2.10×10^{21}	4.81×10^{21}	7.52×10^{21}
		0.2			1.86×10^{21}	4.21×10^{21}	6.02×10^{21}

a lower pK value than –COOH group.

The disintegration phenomenon, polycation adsorption, and zeta potential of SPP microcapsules are closely interrelated. When the PDADMA concentration exceeds a value of 1.65×10^{-2} N the polycation adsorption to the microcapsules begins to increase abruptly (Figs. 3 and 4), disintegration of the microcapsules starts, and the zeta potential of the microcapsules reverses its sign (Fig. 5). In order to give this interrelationship a quantitative basis on which it rests, the numbers of sulfonato groups per unit weight of SPP-2, -3, and -5 microcapsules were first calculated from the sulfur contents. They were 7.08, 6.64, and 5.40×10^{21}, respectively. Secondly, calculations were made of the numbers of quarternary ammonium groups of the PDADMA ions adsorbed on unit weight of the microcapsules based on the adsorption data. The results are given in Table 3.

Interestingly enough, the number of sulfonato groups on the constituent polymers of the microcapsules and that of quarternary ammonium groups on the adsorbed polycations are nearly equal to each other in the polycation concentration region where the disintegration phenomenon is observed. This means that there exists an exact or nearly exact electrical equivalence between the polyanions and the polycations involved in disintegration. In fact, as mentioned before, coacervate-like liquid drops prepared from the microcapsules and the polycations under the conditions favorable to disintegration to occur bear no or little electrical charge, indicating that the electrical equivalence holds in these cases.

Inspection of Fig. 6 seems to give a clue to elucidate the mechanism of disintegration of the microcapsules. Disintegrated SPP microcapsules still have positive zeta potentials though not so high in the polycation concentration region in which coacervate-like liquid drops carry no or little electrical charge. This can be interpreted as showing that interminglement of the polyanions and the polycations is not sufficient and the latter component is still more abundant than the former in the surface layer of the disintegrated microcapsules, thus giving them positive zeta potentials though both components exist on the whole in approximately equivalent amounts in the capsules. Application of thermal and mechanical agitations to the disintegrated capsules should bring about a complete interminglement of the polyion components and this really happens in the preparation of coacervate-like liquid drops. If there are crosslinks among the constituent polymers of the microcapsules random mixing of the polyanions of the microcapsules and the polycations must be prevented and therefore no disintegration is observed.

Interaction between a strongly acidic polyanion and strongly basic polycation in aqueous solution usually yields a colloidal precipitate rather than a gelatinous coacervate.[4,5] The reason why coacervate-like liquid drops were formed in the present work instead of colloidal precipitates as a result of the interaction between SPP polymers and PDADMA polycations both of which are strong polyelectrolytes would presumably be due to a very low charge density of the former as compared with the latter.

It is obvious from the way in which the foregoing argument has been developed that PDADMA ions adsorb on the surface of SPP microcapsules to interact electrostatically with sulfonato groups on the constituent polymers of the microcapsules, causing disintegration of the microcapsules which leads to a complex coacervation under favorable conditions. The electrical equivalence holds in the coacervation and the effects of the degree of sulfonation and the pH and ionic strength of the medium on the disintegration phenomenon can be explained in terms of the effects of these variables

on the electrostatic interaction between the polyions involved. The effect of the molecular sizes of the components is left to be studied in future because there is no way of obtaining samples of the polyanions and the polycations of definite molecular dimensions at present.

This work was supported in part by a Grant-in-Aid for Scientific Research (76-154132) from the Ministry of Education.

References

1) S. Suzuki and T. Kondo, *J. Colloid Interface Sci.*, **67**, 441 (1978).
2) M. Koishi, N. Fukuhara, and T. Kondo, *Can. J. Chem.*, **47**, 3447 (1969).
3) H. Terayama, *J. Polym. Sci.*, **8**, 243 (1952).
4) R. M. Fuoss and H. Sadek, *Science*, **110**, 552(1949).
5) A. S. Michaelis and R. G. Miekka, *J. Phys. Chem.* **65**, 1765 (1961).

Deuteration Kinetics of Tyrosine by Means of Fluorescence Measurement

Mamoru NAKANISHI and Masamichi TSUBOI

Faculty of Pharmaceutical Sciences, The University of Tokyo, Hongo, Bunkyo-ku, Tokyo 113

(Received December 2, 1978)

When tyrosine was rapidly transferred from water into deuterium oxide medium by means of a stopped-flow device, a time-dependent change in the fluorescence intensity at 305 nm (excited at 275 nm) has been observed. The rate constant (k_e) was found to be 116 s^{-1} at pH 5.8 and 14 °C. This k_e value has been attributed to the rate constant of the $O^1H \rightarrow O^2H$ reaction of the phenolic OH group, on the basis of similar fluorescence examinations on phenol, anisole, glycyl-L-tyrosine, and N^{α}-acetyl-*N*-methyl-L-tyrosinamide as well as on the basis of a stopped-flow ultraviolet absorption study of tyrosine. The stopped-flow fluorometry has been applied to a study of tyrosine residues in yeast 3-phosphoglycerate kinase.

Deuteration kinetics can, in general, be a sensitive means of detecting differences in the intramolecular environment of a given functional group in a biological macromolecular system. We have recently shown that an ultraviolet absorption measurement in combination with a stopped-flow device provides a useful method for tracing a rapid deuteration process of tryptophan or tyrosine residues in a protein in an aqueous solution.[1,2] It is known, however, that a fluorescence measurement often provides a greater sensitivity and selectivity than an ultraviolet absorption measurement for an examination of the same chromophore. We, therefore, started a development of "stopped-flow fluorometry," with a possibility in mind that this may be a more useful method for deuteration kinetics.

In general, the isotope effect on fluorescence intensity is not a simple problem.[3,4] There can be a number of possible mechanisms for the occurrence of such an effect, and the intensity does not always reflect the extent of deuteration of the chromophore (or the fluorophore) in question. Indeed, the fluorescence increase of tryptophan on bringing it from ^1H_2O into ^2H_2O medium is attributable to the deuteration of the α-ammonium ($-NH_3^+$) group, but not to that of the imino group of the indole ring.[5,6] For tyrosine, however, the fluorescence increase on bringing it from ^1H_2O into ^2H_2O medium seems to be caused simply by the $O^1H \rightarrow O^2H$ change at its phenolic hydroxyl group. This is shown in this paper, with an example which suggests a possible application to a protein study.

Experimental

Phenol, anisole, L-tyrosine, and glycyl-L-tyrosine were obtained from commercial sources, and were used without further purification. Acetyl-L-tyrosine-*N*-methylamide (N^{α}-acetyl-*N*-methyl-L-tyrosinamide) was prepared by the Protein Research Foundation, Osaka, Japan, and was placed at our disposal by the courtesy of Dr. Y. Koyama, Kansei Gakuin University. Its purity was confirmed by an examination of its proton magnetic resonance. The sample of 3-phosphoglycerate kinase of yeast was purchased from Boeringer, Mannheim. The solvents ^1H_2O and ^2H_2O were used after being distilled. Emission spectra were observed by the use of a Hitachi MPF-4 fluorometer.

The time dependence of the fluorescence intensity or of the ultraviolet absorbance was observed by the use of a Union Giken stopped-flow spectrophotometer RA-401. This is equipped with a rapid-mixing device of dead time 500 μs, and with an ultraviolet monochromator of focal length 25 cm. For stopped-flow fluorometry, a 200 W deuterium discharge lamp was placed at the entrance of the monochromator, and at its exit a cell with optical path length of 2 mm was placed. The solution, after rapid mixing, is led into this cell, and when the flow is stopped the time dependent fluorescence change (if any) should start. The fluorescence is excited by monochromatic light, and is observed through a Hoya UV 30 filter, which allows the emitted light of wavelength longer than 300 nm to come into the detector. For a stopped-flow ultraviolet absorption study, the same deuterium discharge lamp and the same cell were used with the same monochromator as above. Only the location of the photomultiplier was changed. The fluorescence intensity *versus* time curve or the absorbance *versus* time curve was obtained by the use of a Union Giken data processor RA-450, a monitorscope, and an XY recorder.

Results and Discussion

Fluorescence of Tyrosine and Its Change on Deuteration. The observed emission spectra are reproduced in Fig. 1. The fluorescence peaks are found at 296 nm for phenol and at 295 nm for anisole. On transfering from ^1H_2O to $^2H_2O+^1H_2O$, the peak intensity increases by 22% for phenol, but only 2% for anisole. L-Tyrosine, glycyl-L-tyrosine, and N^{α}-acetyl-*N*-methyl-L-tyrosinamide show their fluorescence maxima at 303 nm. On changing the solvent from ^1H_2O to $^2H_2O+^1H_2O$, the intensity increases of 18, 13, and 16% are found, respectively, for these three compounds. Of the total 13% fluorescence increase for L-tyrosine, 9% takes place rapidly within 1 ms, while the remaining 4% increase takes place more slowly, in a period of about 20 ms (see Fig. 2(c)). A re-plot of such a fluorescence intensity on a logarithmic scale against time indicates that the process is apparently a single first order process. The rate constant is found to be 116 s^{-1} at pH 5.8 and 14 °C. This is exactly equal to the rate constant value obtained by a stopped-flow ultraviolet absorption measurement at 285 nm as described in our previous paper[2] (see also the curve given at the bottom of Fig. 2, (c)). This rate constant was assigned to that of the deuteration reaction $O^1H \rightarrow O^2H$ of the phenolic hydroxyl group of tyrosine.[2]

A similar fluorescence increase takes place with nearly equal rate for phenol (Fig. 2, (a)), but not at all for anisole (Fig. 2, (b)). In contrast with glycyl-L-tryptophan, which shows no time-dependent fluorescence increase when it is transferred from ^1H_2O into ^2H_2O medium,[6] glycyl-L-tyrosine shows an increase with nearly an equal rate constant to that for tyrosine (Fig. 2, (d)). All of these facts support the idea that

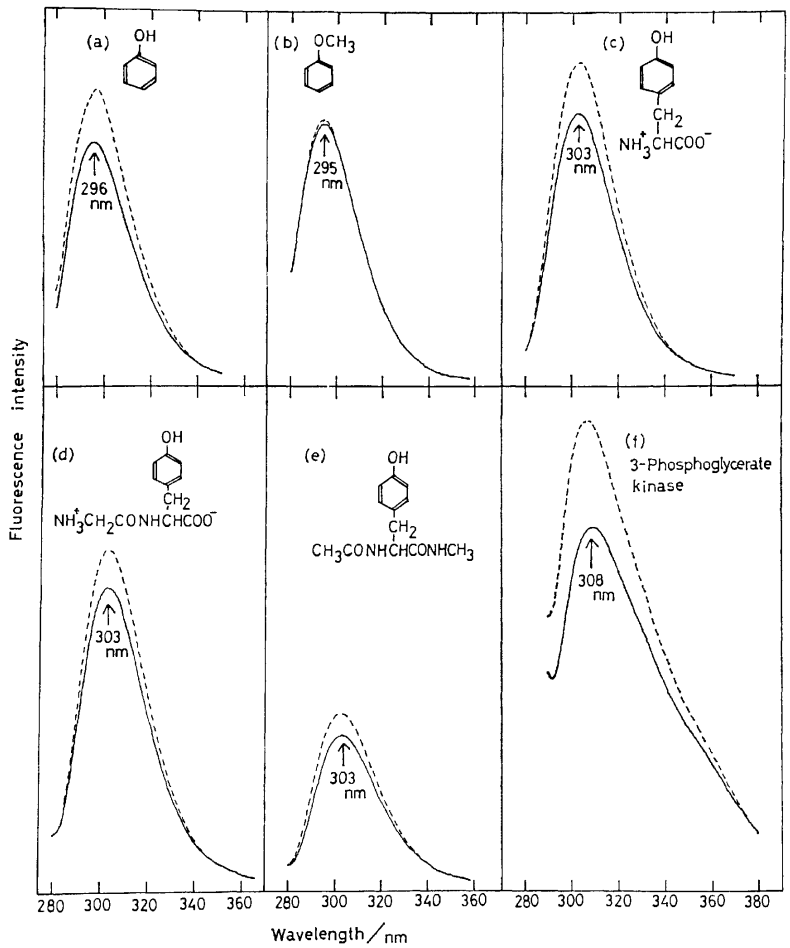

Fig. 1. Emission spectra in ^1H_2O (full line) and in $^2H_2O+^1H_2O$ (broken line), at pH 5.8 and at 14 °C.
(a) Phenol, excited at 270 nm. (b) Anisole, excited at 270 nm. (c) L-Tyrosine (0.15 mM), excited at 275 nm. (d) Glycyl-L-tyrosine, excited at 275 nm. (e) N^{α}-Acetyl-N-methyl-L-tyrosinamide, excited at 275 nm. (f) Yeast 3-phosphoglycerate kinase (0.01%), excited at 280 nm.

the time-dependent fluorescence increase in question is caused by the $O^1H \rightarrow O^2H$ process of the phenolic hydroxyl group.

The amount and the rate of fluorescence increase for N^{α}-acetyl-N-methyl-L-tyrosinamide is also nearly equal (Fig. 2(e)) to those of L-tyrosine or to phenol. Such a rate constant value is to be used as a standard (k_e) value in estimating the attenuation factor $\gamma_j = k_j/k_e$ of a given tyrosine group (j) in a protein molecule whose rate constant value is k_j.

Application to a Protein Study. 3-Phosphoglycerate kinase (EC 2.7.2.3) from yeast contains two tryptophan and eight tyrosine residues per molecule.[7] Nojima *et al.*[8] has found that, in its emission spectrum, a fluorescence maximum is present at 308 nm if excited at 280 nm, while at 329 nm if excited at 295 nm. The former (308 nm) is considered to be caused by the tyrosine residues, and the latter (329 nm) by the tryptophan residues. The emission spectrum of this protein excited at 280 nm is shown in Fig. 1, (f). As may be seen here the fluorescence intensity increases by 28% on bringing it from ^1H_2O to $^2H_2O+^1H_2O$. The same amount (27.5%) of total fluorescence increase was observed when an ^1H_2O solution of this protein is rapidly mixed with the same volume of ^2H_2O by means of the stopped-flow fluorometry technique. Of this total 27.5% increase, 22% takes place within the dead time of the stopped-flow equipment, and the remaining 5% increase takes place very slowly (see Fig. 3). The rate of this slow process was found to be 3.9 s^{-1} at pH 5.9 and at 29 °C. At this pH and at this temperature, k_e of tyrosine is estimated to be 350 s^{-1}, and therefore the attenuation factor $\gamma_i = 3.9/350 = 1/90$. It may be interpreted that the tyrosine residue (or residues) now in question is rather rigidly fixed inside of the protein molecule, and that the chance of its being exposed to the solvent is only 1/90.

In a protein molecule an energy transfer takes place often from tyrosine to tryptophan, and even when a tyrosine residue is excited the fluorescence comes often from the tryptophan residue instead of the tyrosine residue itself.[9] If a protein containing both tyrosine and tryptophan residues gives a tyrosine fluorescence, such a tyrosine residue is considered to be firmly fixed at a particular orientation in the protein molecule, so that no energy transfer takes place between the tyrosine residue now in question and any of the tryptophan residues in the same molecule. Because 3-

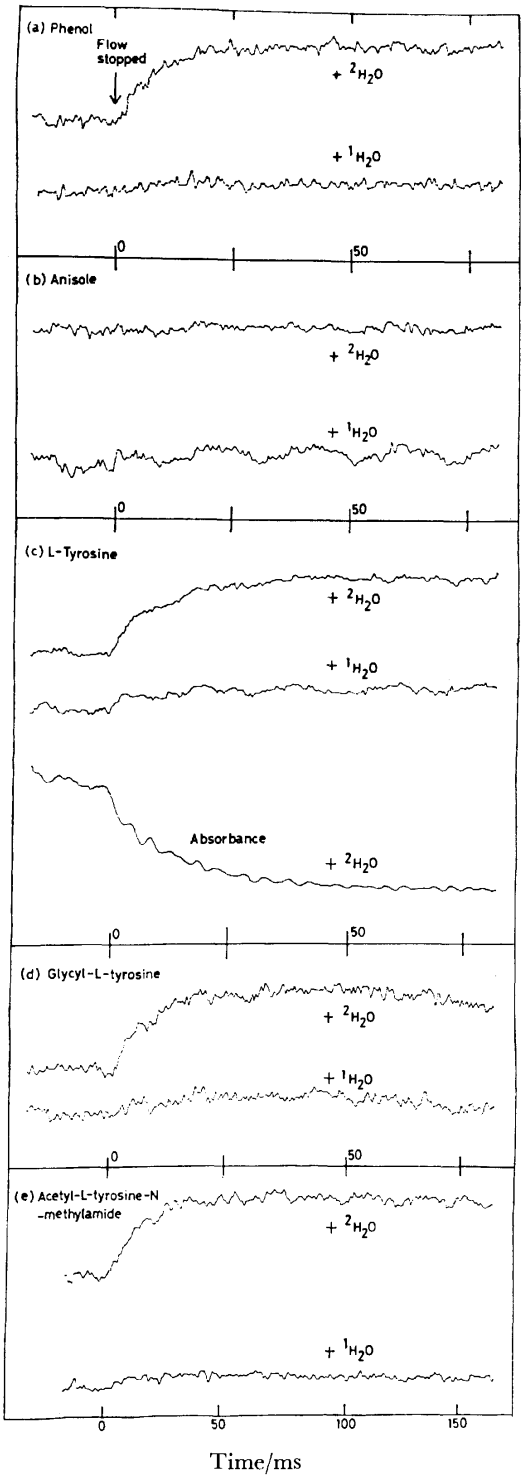

Fig. 2. The time dependence of the fluorescence intensity observed when an ^1H_2O solution of each compound indicated is rapidly mixed with the same volume of ^2H_2O, so that the solvent of the final solution is 1 : 1 $^1H_2O+^2H_2O$. For each compound, a curve recorded in a control experiment in which the same ^1H_2O solution was mixed with ^1H_2O instead of ^2H_2O is also shown.

(a) Phenol (pH 5.3, at 15 °C), excited at 255 nm. (b) Anisole, (pH 5.5, at 15 °C), excited at 255 nm. (c) L-Tyrosine (final concentration 1.2 mM, pH 5.8, at 12.5 °C), excited at 275 nm. The curve at the bottom is the time dependence of the ultraviolet absorbance recorded at 285 nm when an L-tyrosine in ^1H_2O solution was mixed with the same volume of ^2H_2O, so that the final concentration was 1.2 mM, pH 5.8, at 12.5 °C. (d) Glycyl-L-tyrosine, pH 5.5, at 17 °C, excited at 275 nm. (e) N^{α}-Acetyl-N-methyl-L-tyrosinamide pH 5.5, at 17 °C, excited at 275 nm.

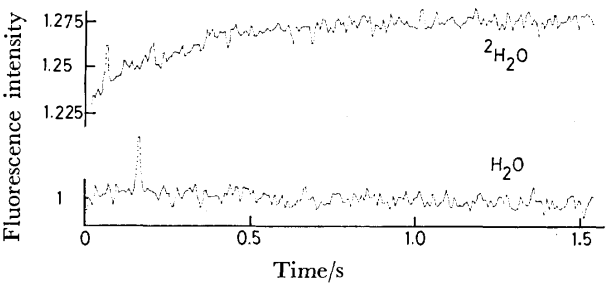

Fig. 3. Change in time of fluorescence intensity at 308 nm (excited at 280 nm) is observed for yeast 3-phosphoglycerate kinase in ^1H_2O upon mixture with ^2H_2O (1 : 1 in volume; final concentration of the protein is 0.05%, pH 5.9) at 29 °C.

phosphoglycerate kinase has both the tyrosine and tryptophan residues, the tyrosine fluorescence (at 309 nm) we have observed is attributed to such a tyrosine residue (or tyrosine residues) rigidly fixed in a special orientation. The fact that the hydrogen-deuterium exchange reaction between this tyrosine residue and the solvent ^2H_2O is 90 times as slow as the tyrosine exposed to the solvent is therefore understandable.

References

1) M. Nakanishi, H. Nakamura, A. Y. Hirakawa, M. Tsuboi, T. Nagamura, and Y. Saijo, *J. Am. Chem. Soc.*, **100**, 272 (1978).
2) M. Nakanishi and M. Tsuboi, *J. Am. Chem. Soc.*, **100**, 1273 (1978).
3) L. Stryer, *J. Am. Chem. Soc.*, **88**, 5708 (1966).
4) J. Eisinger and G. Navon, *J. Chem. Phys.*, **50**, 2069 (1969).
5) S. S. Lehrer, *J. Am. Chem. Soc.*, **92**, 3459 (1970).
6) M. Nakanishi and M. Tsuboi, *Chem. Phys. Lett.*, **57**, 262 (1978).
7) W. K. G. Krietsh and T. Bucher, *Eur. J. Biochem.*, **17**, 568 (1970).
8) H. Nojima, A. Ikai, and H. Noda, *Biochim. Biophys. Acta*, **427**, 20 (1976).
9) R. L. Perlman, A. van Zyl, and H. Edelhoch, *J. Am. Chem. Soc.*, **90**, 2168 (1968).

On the Normal Modes of Vibration in the Uracil Residue — The Use of ^{15}N-Isotope Effects

Yoshifumi NISHIMURA, Hideyuki HARUYAMA, Kimiko NOMURA, Akiko Y. HIRAKAWA, and Masamichi TSUBOI*

Faculty of Pharmaceutical Sciences, The University of Tokyo, Hongo, Bunkyo-ku, Tokyo 113

(Received December 2,1978)

β-Uridine-5′-phosphoric acid-$^{15}N_2$ has been prepared from ^{15}N-RNA of baker's yeast which was grown in $(^{15}NH_4)_2SO_4$ as the sole nitrogen source. Its Raman spectrum has been observed both in ^1H_2O and ^2H_2O solutions. On the basis of the observed ^{15}N isotope effects on the Raman spectra and on the basis of other data previously obtained, normal modes of vibration have been discussed for six Raman bands of the uracil residue that are considered to be in resonance with its electronic transition at 260 nm. The result has led to a conclusion that $C^5=C^6$ is longer and C^4-C^5 is shorter in the excited electronic state $\tilde{A}$ (260 nm) than those in the ground electronic state $\tilde{X}$.

Resonance Raman spectroscopy may sometimes be useful as a tool for exploring the excited state geometry of a molecule.[1,2] Let us suppose that our present aim is to ellucidate the geometrical structure of the electronic excited state of the uracil residue corresponding to its 260 nm absorption band. For this aim we first need to examine which Raman lines of the uracil residue are in resonance with the 260 nm electronic transition ($\tilde{A}$-$\tilde{X}$),[3] and secondly we need to find the normal modes of vibration that are to be assigned to these particular Raman lines. We can then predict that, on going from the ground ($\tilde{X}$) to the excited ($\tilde{A}$) state, a distortion of the molecular conformation takes place along such a normal coordinate or along a linear combination of such normal coordinates. This prediction is based upon a theory which is valid only in a certain approximation.[1,2] In combination with other data, however, this approach often leads to a useful piece of information on the excited state geometry.

In our present study we have used a set of ^{15}N isotope shifts in the vibrational frequencies of the uracil residue, as a data for fixing normal modes, in addition to the usual data obtained by an examination of deuterated products. In our normal coordinate treatment, it has been found that a fixing of the force constant values corresponding to interactions of two bond-stretching motions in the six-membered ring is critical. In this respect, a recent work on the force field in benzene[5] was found to be helpful. On the basis of these data, the normal modes of vibration of the six Raman bands, which were previously found[3,4] to be in resonance with the electronic transition at 260 nm, have now been determined with a considerable reliability.

Experimental

Preparation of ^{15}N RNA. Baker's yeast was grown in a medium in which $(^{15}NH_4)_2SO_4$ is the sole nitrogen source. This part of our experiment was made in collabotation with Dr. Masatsune Kainosho in the Central Research Laboratory, Ajinomoto Company, Ltd. 400 g of wet cells of such yeast were placed in 1 litre of 0.0125 M phosphate buffer (pH 6.8) with 2% sodium dodecyl sulfate and 4.5% ethanol. The suspension was incubated at 95 °C for 5 min, rapidly cooled with dry ice plus methyl cellosolve, and then centrifuged at 4000 rpm for 5 min. From the supernatant, crude RNA was precipitated by adding 2 litre ethanol. The precipitate was washed with 70% ethanol and then with 80% ethanol overnight. The precipitate was dissolved again in 500 ml of 5 mM phosphate buffer, and centrifuged at 4000 rpm for 5 min. RNA was precipitated from the supernatant with 1 M NaCl plus ethanol. This was dissolved in 500 ml of 2.5 mM phosphate buffer and dialyzed against 1 mM phosphate buffer. By an ethanol precipitation, 3.3 g purified ^{15}N RNA was obtained.

Preparation of β-Uridine-5′-phosphoric acid-$^{15}N_2$ (5′-UMP-$^{15}N_2$). ^{15}N-RNA was dissolved in phosphate buffer (pH 5.2) and incubated with nuclease P_1 (kindly provided by Dr. A. Kuninaka, The Research Laboratory of Yamasa Shoyu Co., Ltd., Chyoshi Japan) at 37 °C overnight. After the pH of the digested solution was adjusted to 7.2, the solution was subjected to a Dowex 1X2 column chromatography, where the formic acid form of 200—400 mesh was placed in a 20×1000 mm tube. For elusion, HCOOH gradient (from 0 to 3 M) was used, and 5′CMP, 5′AMP, 5′GMP, and finally 5′UMP came out. 5′UMP-$^{15}N_2$ was recrystallized with ethanol and water. This gave only one spot in a thin-layer chromatography. Its isotopic purity was judged from the isotopic purities determined of 5′AMP-$^{15}N_5$ and 5′-CMP-$^{15}N_3$, prepared from the same batch of ^{15}N-RNA with that for 5′-UMP-$^{15}N_2$. The isotopic purity of each of these two nucleotides was examined by mass-spectrometry of ammonia produced by a micro-Kjeldahl procedure from the nucleotide sample. The ^{15}N content was found to be 89% of the total nitrogen both for 5′-AMP and for 5′-CMP. Because the biosynthesis process is similar for cytosine residue to that for uracil residue, the ^{15}N content of our 5′UMP is considered to be also 89% of its total nitrogen.

Raman Spectroscopic Measurement. Raman spectra of 5′-UMP-$^{14}N_2$ and 5′-UMP-$^{15}N_2$ were examined in neutral ^1H_2O and ^2H_2O solutions. The measurements were made by the use of a JEOL (Japan Electron Optics Laboratory Co.) JRS-Ul spectrophotometer with 514.5 nm line of a Coherent Radiation model 52 GA argon ion laser. The ^{15}N isotope shift was examined for each Raman line by repeating a short-range scan for 5′-UMP-$^{14}N_2$ and for 5′-UMP-$^{15}N_2$ alternately many times by keeping the conditions of the instrument as steady as possible.

Results and Discussions

^{15}N Isotope Effects on the Raman Spectra. In Figs. 1 and 2 are given the observed Raman spectra, observed Raman frequencies (in cm^{-1}), and the amounts of ^{15}N-shifts determined for 5′-UMP, both in ^1H_2O and in ^2H_2O (pH 7.2). In

TABLE 1. THE SET OF FORCE CONSTANTS FOR THE URACIL RESIDUE (md·A^{-1} for K, md·A for H, md·A^{-1} for stretch/stretch interaction constants and md for bend/stretch interaction constants)

1. K(N-C) 6.380; 2. K(C-C) 6.202; 3. K(C=C) 8.900; 4. K(N-R) 5.000;
5. K(C_2=O_8) 11.000; 6. K(N-H) 5.397; 7. K(C_4=O_{10}) 10.800; 8. K(C-H) 5.204;
9. H($C_6N_1C_2$) 1.163; 10. H($C_2N_3C_4$) 1.168; 11. H($N_1C_2N_3$) 1.587;
12. H($N_3C_4C_5$) 1.654; 13. H($C_4C_5C_6$) 0.522; 14. H($C_5C_6N_1$) 0.528;
15. H(RN_1C_2) 1.060; 16. H(RN_1C_6) 1.056; 17. H(OC_2N_3) 1.019;
18. H(OC_2N_1) 1.019; 19. H(OC_4C_5) 1.071; 20. H(OC_4N_3) 1.028;
21. H(HN_3C_4) 0.459; 22. H(HN_3C_2) 0.459; 23. H(HC_5C_6) 0.344;
24. H(HC_5C_4) 0.371; 25. H(HC_6N_1) 0.352; 26. H(HC_6C_5) 0.342;

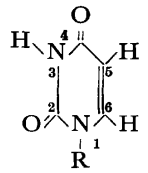

27. f(ν_{ring}, ν_{ring})$_{ortho}$ 0.807; 28. f(ν_{ring}, ν_{ring})$_{meta}$ −0.522; 29. f(ν_{ring}, ν_{ring})$_{para}$ 0.161;
30. f($\nu_{C=O}$, ν_{ring}) 1.207; 31. f($\nu_{C_4=O}$, $\nu_{C=C}$) −0.187; 32. f(δ_{ring}, ν_{ring}) 0.401; 33. f($\delta_{C=O}$, ν_{ring}) 0.279;
34. f(δ_{N-H}, ν_{ring}) 0.072; 35. f(δ_{C-H}, ν_{ring}) 0.197; 36. f($\delta_{C=O}$, $\nu_{C=O}$) 0.980; 37. f(ν_{N-R}, ν_{ring}) 0.471.

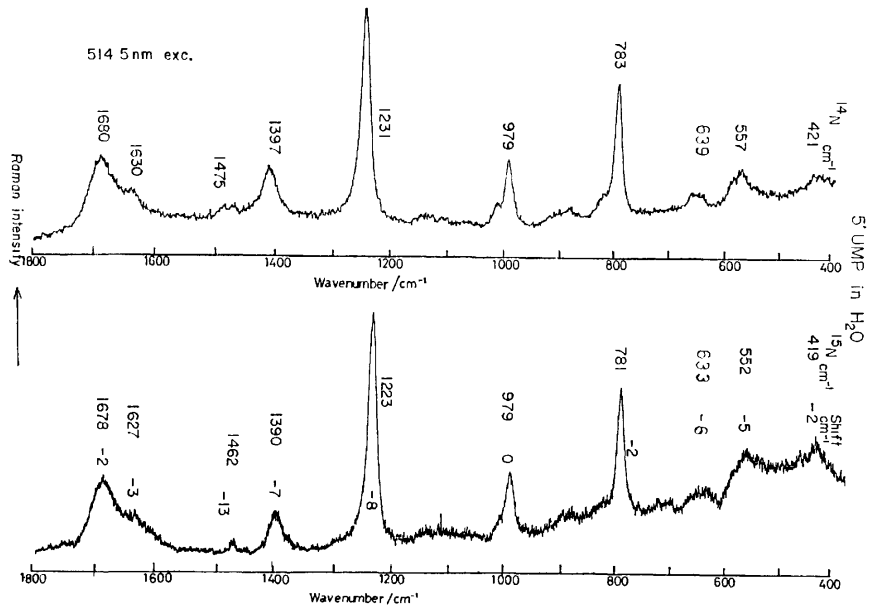

Fig. 1. Raman spectra of β-uridine-5′-phosphoric acid (5′-UMP-$^{14}N_2$ and 5′-UMP-$^{15}N_2$) in ^1H_2O, pH 7.2 at room temperature, concentation 10%. Excited by 514.5 nm line of an Ar^+ laser.

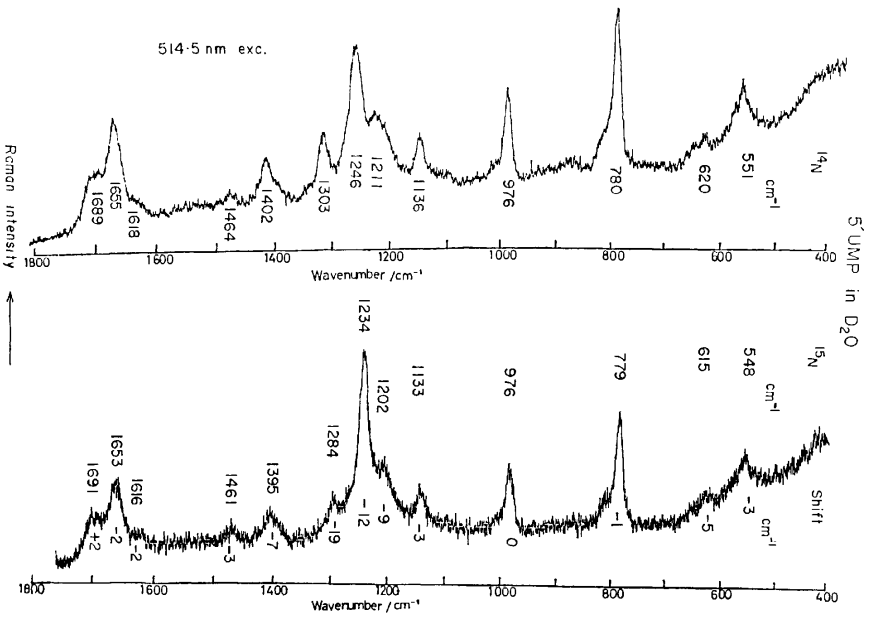

Fig. 2. Raman spectra of β-uridine-5′-phosphoric acid (5′-UMP-$^{14}N_2$ and 5′-UMP-$^{15}N_2$) in ^2H_2O, pH 7.2 at room temperature, concentration 10%. Excited by 514.5 nm line of an Ar^+ laser.

^2H_2O, the NH group at position 3 is deuterated (ND) (for numbering of the positions, see Table 1). As may be seen in Figs. 1 and 2, most of the Raman lines assignable to the uracil residue show appreciable ^{15}N-shifts, while the line at 979 cm^{-1} assignable to the phosphate group[6] shows no shift at all. The observed amounts of ^{15}N-shifts form a useful set of data for determining the force constants and normal modes of vibration of the uracil residue. These are discussed later in this paper. Here, a comment is added as for an interesting isotope effect on the Raman scattering intensity. As may be seen in Fig. 2, the relative intensity of the 1246 cm^{-1} line of 5′-UMP-d_3 is appreciably raised on ^{15}N substitution. This Raman line (let us call its mode "V") is one of the characteristic lines of pyrimidine bases. This is isolated and strong when it is located at about 1235 cm^{-1} or lower frequency (*e.g.*, in uracil residue, and uracil residue-d_1, $^{15}N_2$). On the other hand, it is weaker and has a few satellite lines when it is located at a frequency higher than 1240 cm^{-1} (*e.g.*, in deprotonated uracil residue, deuterated uracil residue, and cytosine residue). This is the strongest Raman line in the uracil residue and shows the greatest intensity enhancement on bringing the exciting wavelength from 514.5 nm to 351.1 nm. The ^{15}N-isotope effect on the intensity of this line may be ascribed to a change in the vibrational mode "V" in the electronic excited state $\tilde{A}$ (260 nm) rather than that in the electronic ground state $\tilde{X}$. It may be explained, in other words, by taking a Duschinsky effect into account.

Thus, it is not improbable that, in the first excited state $\tilde{A}$ (260 nm) of the uracil residue, the $C^5=C^6$ bond order is very low so that its intrinsic stretching frequency is as low as 1234 cm^{-1}. If so, "mode II" (mainly $C^5=C^6$ stretching) and "mode V" have nearly equal frequencies to each other in the upper $\tilde{A}$ state; while, in the ground electronic state, "mode II" (mainly $C^5=C^6$ stretching, at about 1600 cm^{-1}) and "mode V" (1234 cm^{-1}) are orthogonal to each other. In such a situation, the Franck-Condon overlap integrals that cause the Raman scattering of the "V-vibration" may have an appreciable value. If the "V-frequency" is exactly 1234 cm^{-1} (as that for 5′-UMP-$^{15}N_2$, d_3), then the vibrational coupling in $\tilde{A}$ would be very strong and the "V-Raman line" would be strong. If, on the other hand, the "V-frequency" is slightly higher than 1234 cm^{-1} (as that for 5′-UMP-$^{14}N_2$, d_3) the vibrational coupling in $\tilde{A}$ would be weaker and the "V-Raman line" would be weaker.

The Raman Lines That are in Resonance with the 260 nm Electronic Transition. Raman spectra of β-uridine-5′-phosphoric acid (5′-UMP) in neutral aqueous solution were examined with excitation at 647.1, 514.5, 488.0, 457.9, 363.8, and 351.1 nm (Fig. 3). By the use of the 979 cm^{-1} Raman line (PO_3^{2-} symmetric stretching) as an internal intensity standard, the Raman intensity *versus* excitation frequency relation (excitation profile) has been examined for each of the Raman lines of the uracil residue. From a comparison of such an observed excitation profile with theoretical ones, it was shown[4] (i) that the Raman lines at 1231, 1394, and 1475 cm^{-1} are primarily associated with the absorption band at 260 nm, (ii) that, to the 1680, 1630, and 783 cm^{-1} Raman lines, there are appreciable amounts of contribution from the 260 nm absorption band, but contribution from the 210 nm band or from other bands of shorter wavelengths should also be taken into account, and (iii) that the contribution of the 260 nm transition to the 560 cm^{-1} Raman line is rather small.

A rigorous resonance Raman effect of 5′-UMP was examined with 257 nm excitation[3] (see Fig. 3(e)). It became

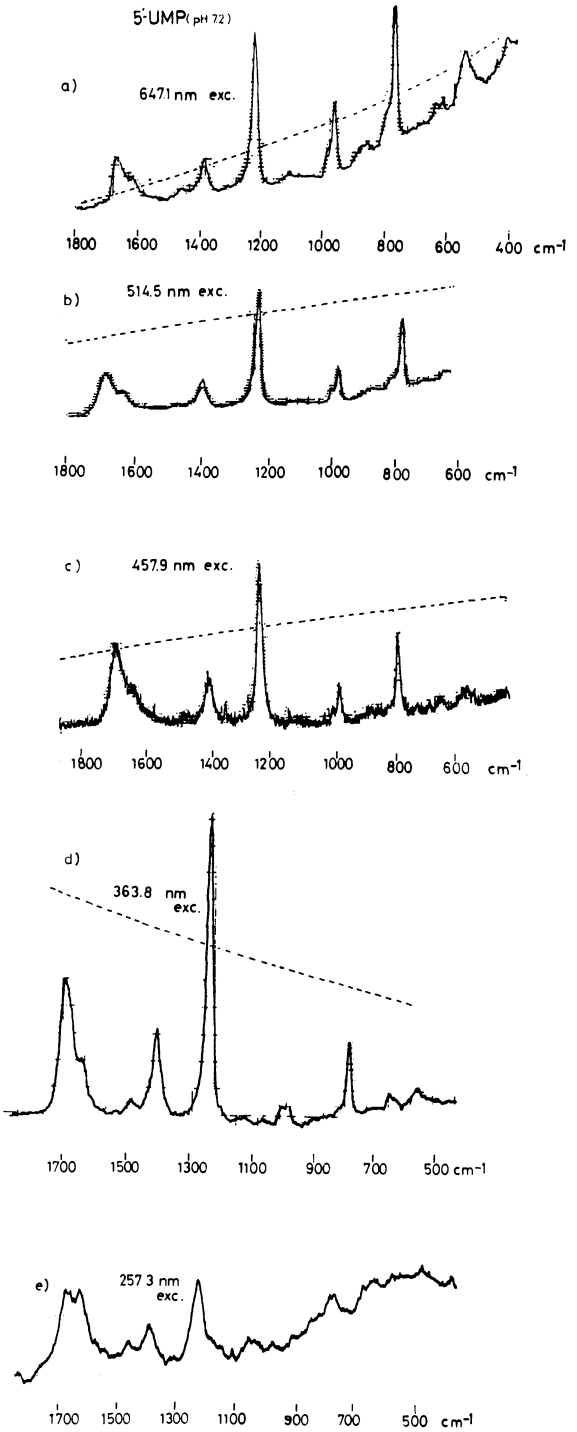

Fig. 3. Raman spectra of 5′-UMP in neutral aqueous solution. Excited by (a) 647.1 nm (Kr), (b) 514.5 nm (Ar), (c) 457.9 nm (Ar), (d) 363.8 nm (Ar), and (e) 257.3 nm (Ar ion laser plus a frequency doubler) lines. Broken lines indicate the spectral sensitivity of the monochromator and detector system.

evident that the six Raman lines at 1680, 1630, 1475, 1395, 1231, and 787 cm^{-1} of the uracil residue are caused by the electronic excited state at 260 nm. Let us call these six Raman lines UrI, UrII, UrIII, UrIV, UrV, and UrVI, respectively.

Characterization of the On-resonance Raman Lines. Pre-resonance and resonance Raman spectra were observed[4] of various related compounds which are considered to be

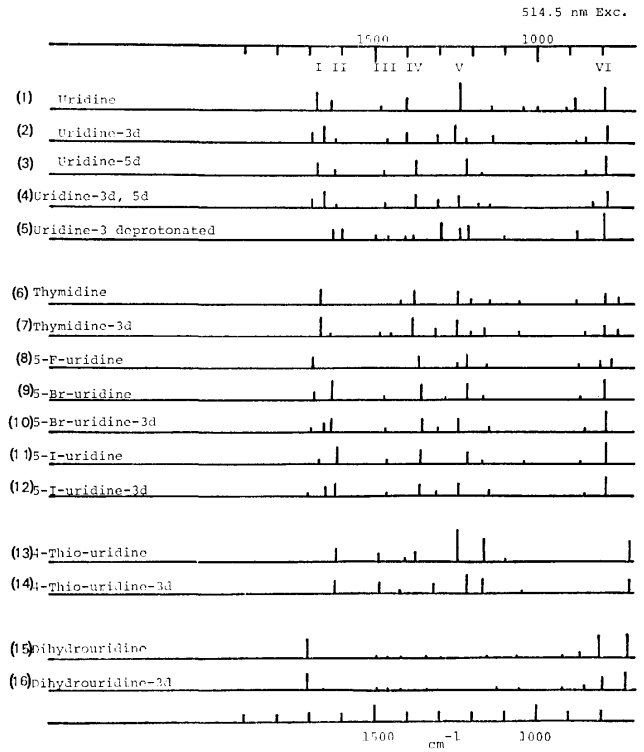

Fig. 4. Raman lines observed for uridine and its derivatives. ^1H is replaced by ^2H at the position indicated.

relevant to the interpretation of the Raman spectrum of the uracil residue. Observed Raman lines of uridine and some uridine derivatives are shown in Fig. 4. On the basis of these data, a detailed discussion were given on the Raman lines of the uracil residue in our previous article.[4] Some of the results and conclusions are briefly summerized below:

a) All of the six Raman lines, UrI to UrVI, are in the skeletal-stretching frequency region. All of these Raman lines, except UrIII, are strong in off-resonance condition. In addition, neither position-3 deuteration nor position-5 deuteration causes a wavenumber shift greater than 100 cm^{-1} for any of these Raman lines. Therefore, all of these are assignable primarily to in-plane skeletal bond-stretching vibrations of the neutral uracil residue.

b) The 787 cm^{-1} line is assignable to a vibration in which all eight skeletal stretching motions take place in-phase (ring breathing).[7,8] It is understandable that, while the relative intensity of this line is very strong in an off-resonance Raman spectrum (see Fig. 3(a)), it is very weak in a rigorous resonance Raman spectrum (Fig. 3(e)) excited in the longest wavelength (260 nm) absorption band ($\tilde{A} \leftarrow \tilde{X}$). The distortion of the uracil residue does not take place along such a ring breathing coordinate on going from $\tilde{X}$ to $\tilde{A}$ states.

(c) In the 1600 to 1700 cm^{-1} region there are three skeletal stretching vibrations expected, because of the three double bonds, $C^2=O$, $C^4=O$, and $C^5=C^6$. Actually there are observed three Raman lines (and three infrared bands) for the position-3 deuterated uracil residues (see Fig. 4; (2), (4), (10), and (12)). In each of the Raman spectra of undeuterated uracil residues (Fig. 4; (1), (3), (9), and (11)), however, one of these three is missing. The missing vibration here must be at 1710 cm^{-1}, because the undeuterated uracil residue gives a strong infrared absorption band at 1710 cm^{-1}.[8] This is assignable to the $C^2=O$ stretching vibration.[9] Thus, the UrI and UrII are probably assignable to a coupled pair of the $C^4=O$ stretching and the $C^5=C^6$ stretching vibrations.

(d) An additional support to the assignments of the UrI and UrII Raman lines is obtained from an examination of the Raman spectrum of 4-thiouridine. This is a derivative of uridine in which the position-4 carbonyl is replaced by thiocarbonyl, so that it has residue. In a resonance condition,

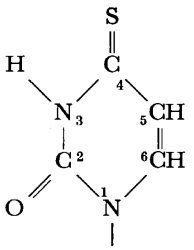

this shows six strong Raman lines at 1619, 1482, 1372, 1243, 1160, and 709 cm^{-1}. In the 1600—1700 cm^{-1} region only one Raman line (assignable to UrII) is observed as is expected. The $C^2=O$ stretching line is missing as it is for the uracil residue, and $C^4=O$ is absent here. Instead, there are two strong Raman lines observed at 1167 and 709 cm^{-1}, which are assignable to the two vibrations caused by a strong coupling of the $C^4=S$ stretching and the ring breathing motions. The three lines at 1482, 1372, and 1243 cm^{-1} are considered to correspond to the UrIII, UrIV, and UrV lines of the uracil residue, respectively.

(e) The Raman lines corresponding to the UrIII and UrIV are found at about 1470 and 1400 cm^{-1}, respectively, for all of the uridine derivatives examined (see Fig. 4) except for dihydrouridine. UrV Raman line is also found for all of the uridine derivatives with high intensities. Deuteration at position-3 causes a slight higher frequency shift of this line and at the same time an appearance of a few satellite lines (see Fig. 4; (2), (4), (7), (10), and (12)). A similar effect is caused also by the position-3 deprotonation (Fig. 4, (5)). Position-5 deuteration, on the other hand, causes a slight lower frequency shift of UrV line (Fig. 4, (3)). This is caused also by the position-5 substitution with bromine or iodine (Fig. 4, (9) and (11)).

(f) Dihydrouridine shows a completely different Raman spectrum (Fig. 4, (15) and (16)) from those of the uridine derivatives with $C^5=C^6$ double bond. Here, no strong Raman lines are found in the 900 to 1500 cm^{-1} region. It is clear that the $C^5=C^6$ double bond, which makes the whole six-membered ring nearly conjugated, is essential for giving rise to the UrI—UrV Raman lines (the $C^5=C^6$ double bond is also essential for the 260 nm absorption band).

Normal Modes of Vibration for the On-resonance Raman Lines. A normal coordinate treatment was made for in-plane vibrations of 1-methyl uracil. Here, every hydrogen atom (except that of the methyl group) was taken as a dynamical unit, while the methyl group was assumed as one dynamical unit. The bond lengths and bond angles in the uracil residue were assumed to be equal to those given by a crystallographic study of 1-cyclohexyluracil (Dr. T. Katsura, personal communication). The calculation was carried out using a HITAC 8800/8700 in the Computer Center at the University of Tokyo, and the programs, BGLZ, and LSMA, written by Shimanouchi and his collaborators.[10] In the calculation, a general valence force field was assumed, where all the bond-stretch bond-stretch interaction terms were taken into consideration. The force constants were determined by a trial and error method so that the calculated frequencies were in the best agreement with the observed frequencies. The adjustment of the force constant values was guided by the Jacobian matrix which was

calculated for each trial set of force constants. The adjustment was made by taking the following items into account:

(a) The calculated ^{15}N-shifts should be in the best agreement with the observed shifts (see Table 2).

(b) The observed effects of the position-3 deuteration and position-5 deuteration on the vibrational frequencies should be well reproduced by the calculation. This was achieved by a proper adjustment of the bending force constant values, so as to bring the N^3H in-plane bending vibration to about 1416 cm^{-1},[11] and the C^5H in-plane bending vibration to about 1100 cm^{-1}.

(c) Not only the Raman frequencies of the uracil residue observed in the aqueous solutions of uridine and its derivatives, but also Raman[12,13] and infrared[11] frequencies observed for powder 1-methyluracil are to be taken as a set of data.

(d) Not only the bond-stretch bond-stretch cross terms for adjacent two bonds (let us call "ortho"), but also those for two bonds "next door but one" from each other (meta) and for two bonds two doors away from each other (para) should have appreciable values. Such force constant values were not found to be negligible in a conjugated double-bond system such as benzene.[5]

The final set of force constant values are given in Table 1, and the calculated vibrational frequencies for the undeuterated and deuterated (at position-3) uracil residues are given in Table 2. The agreement between the observed frequencies (also given in Table 2) and the calculated ones are satisfactory. The agreement between the observed and calculated ^{15}N-isotope shifts are also good except for the 1397 (UrIV) line of the undeuterated uracil residue and for the 1689 (C^2=O), 1464 (UrIII), and 1402 cm^{-1} (UrIV) lines of the deuterated uracil residue . In the actually observed ^{15}N shifts, there must be some factors involved, such as anharmonicity, Fermi resonance, and vibrational couplings with the solvent molecules, which were not taken into consideration in our present calculation. It may also be pointed out here that the amount of the ^{15}N-shift of each vibration is extremely sensitive to the amount of the contribution of the N–H in-plane deformation motion to the vibration now in question. This is, however, not always be properly estimated in our present calculation on the basis of a simple harmonic potential function.

In Fig. 5, are depicted the normal modes of vibration calculated on the basis of the set of force constants given in Table 1. This forms one of the main conclusions of our present study. The modes of the UrI—UrVI vibrations now in question may be characterized as follows:

UrI(1680 cm^{-1}). C^4=O stretching and C^5=C^6 stretching vibrations take place in-phase.

UrII (1630 cm^{-1}). C^4=O stretching and C^5=C^6 stretching vibrations take place with 180° phase difference.

UrIII (1475 cm^{-1}). A skeletal stretching vibration which has a similarity to one of the e_{2g} stretching vibrations of benzene at 1584 cm^{-1}.

UrIV (1397 cm^{-1}). A skeletal stretcing vibration which has a similarity to one of the e_{1u} stretching vibrations of benzene at 1485 cm^{-1}.

UrV (1231 cm^{-1}). A skeletal stretching vibration which has a similarity to the b_{2u} vibration of benzene at 1309 cm^{-1} (Kekulé vibration).

TABLE 2. OBSEVED AND CALCULATED FREQUENCIES OF THE URACIL RESIDUE

Frequency, cm^{-1}		^{15}N-shift, cm^{-1}		PED[b]		Frequency, cm^{-1}		^{15}N-shift, cm^{-1}		PED[b]	
Obsd[a]	Calcd	Obsd	Calcd			Obsd[a]	Calcd	Obsd	Calcd		
Undeuterated						Deuterated (position-3)					
3131*	3132	—	−9	ν N-H (99)		3087*	3100	—	0	ν C-H (99)	
3079*	3100	—	0	ν C-H (98)		3087*	3091	—	0	ν C-H (99)	
3079*	3091	—	0	ν C-H (99)		2260*	2311	—	−12	ν N-D (96)	
1720*	1707	—	−8	ν C_2=O (64)		1689	1698	+2	−5	ν C_2=O (71)	
1680	1673	−2	−4	ν C_4=O, C=C (70)	UrI	1655	1666	−2	−4	ν C_4=O, C=C (75)	UrI
1630	1625	−3	−3	ν C=C, C_4=O (76)	UrII	1618	1622	−2	−2	ν C_4=O, C=C (78)	UrII
1475	1476	−13	−14	ν ring (72)	UrIII	1464	1465	−3	−13	ν ring (81)	UrIII
1423*	1415	—	−9	δ NH (55)		1402	1395	−7	−15	ν ring (51)	UrIV
1397	1397	−7	−15	ν ring (52)	UrIV	1303	1306	−19	−20	ν ring (47)	
1231	1245	−8	−9	ν ring (100)	UrV	1246	1242	−12	−15	ν ring (100)	UrV
1201*	1240	—	−17	δ C-H (56)		1211	1206	−9	−17	ν N-R (22), ν ring (34)	
1156*	1182	—	−18	ν ring (64), ν N-R (32)		1136	1115	−3	−1	δ C-H (83)	
1084*	1115	—	−3	δ C-H (84)		1043*	1102	—	−9	δ N-D (21), ν N-R (15)	
1008*	1001	—	−10	ν ring (47)		914*	886	—	−3	δ N-D (44)	
806*	811	—	−9	δ ring (38)		812*	793	—	−3	δ ring (42)	
783	780	−2	−1	ν ring (52)	UrVI	780	778	−1	−3	ν ring (60)	UrVI
639	622	−6	−4	δ C=O (57)		620	610	−5	−5	δ C=O (56)	
557	546	−5	−3	δ ring (61)		551	543	−3	−4	δ ring (61)	
482	485	—	−3	δ ring (48)		478*	485	—	−3	δ ring (48)	
421	385	−2	−3	δ C=O (65)		395*	384	—	−1	δ ring C=O (64)	
268*	336	—	−1	δ N-R (60)		266*	336	—	0	δ N-R (60)	

a) Raman or infrared frequencies observed[11–13] for powder 1-methyluracil are shown by *. b) Potential energy distribution is given in parenthesis. ν, stretching; δ, bending.

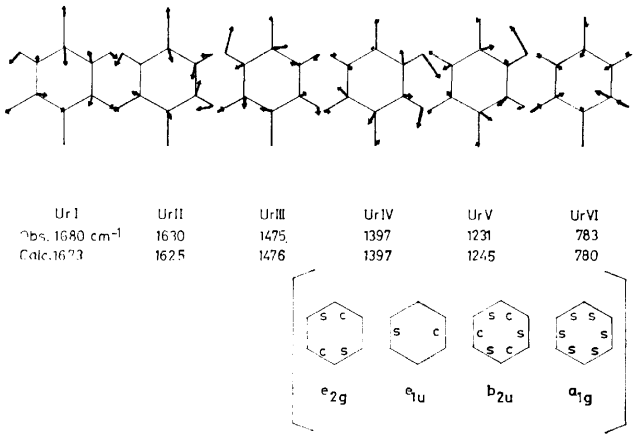

Fig. 5. Normal modes of vibration of the uracil residue, calculated using the set of force constants given in Table 1. Some of the normal modes of the skeletal stretching vibrations of benzene are shown in parentheses for reference. s: stretch, c: contract.

UrVI (783 cm^{-1}). All of the eight bonds, C=C, C–C, C–N, and C=O, stretch and contract in-phase (ring breathing vibration).

Excited State Geometry for the 260 nm Band. Among the six on-resonance Raman lines of the uracil residue, three at 1475 (UrIII), 1397 (UrIV), and 1231 cm^{-1} (UrV) are considered to be most intimately associated to the excited electronic state $\tilde{A}$ corresponding to the 260 nm absorption band. Among the vibrational modes for these three Raman lines, a motion in which the C^4–C^5 stretching and C^5=C^6 stretching take place with 180° phase difference is commonly predominant (see Fig. 5). Therefore, it is probable that, on going from the electronic ground state $\tilde{X}$ to the excited state $\tilde{A}$, a distortion of the molecualr conformation takes place along this coordinate; as shown in Fig. 6, the C^5=C^6 bond is probably longer in $\tilde{A}$ than in $\tilde{X}$, while C^4–C^5 is shorter in $\tilde{A}$ than in $\tilde{X}$. This is another main conclusion of our present study.

The conclusion just reached by our Raman spectroscopic investigation is in an agreement with an expectation from

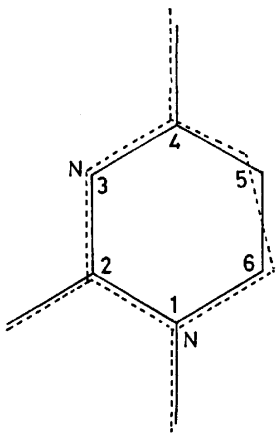

Fig. 6. A schematic drawing to show a possible change in the molecular conformation of the uracil residue on going from the electronic ground state $\tilde{X}$ (shown by full line) to the electronic excited state $\tilde{A}$ (shown by broken line).

theoretical studies on the electronic structure of the uracil residue. Thus, Nagata *et al.*[14] made a semiempirical Pariser-Parr-Pople calculation for the π-electron system of this base residue. This calculation shows that, on going from the highest occupied to the lowest vacant π-orbital, C^5=C^6 bond should change dramatically from *bonding* to *antibonding*, and C^4–C^5 bond should change from *antibonding* to *bonding*, while all other bonds should change only very slightly from *bonding* to *antibonding*. This means that, on going from $\tilde{X}$ to $\tilde{A}$, the bond order of the C^5=C^6 should appreciably decrease, that of the C^4–C^5 should appreciably increase, and those of other bonds should only slightly decrease (see also reference[4]).

Hug and Tinoco[15] made an all-valence electron MO-CI calculation for uracil. It was shown that a marked localization of the monopoles of transitions $\tilde{A}\leftarrow\tilde{X}$ and $\tilde{B}\leftarrow\tilde{X}$ along the acrolein-like fragment O=C^4–C^5=C^6 is expected to take place. For the $\tilde{A}\leftarrow\tilde{X}$ transition, the above view based upon the result of the calculation of Nagata *et al.*[14] is supported by this more elaborate treatment.

We wish to express our thanks to Dr. C. Nagata, National Cancer Center Research Institute, Tokyo, for his kindness in showing an unpublished part of the results of his caluculation and allowing us to use them, and to Dr. S. Nishimura, National Cancer Center Research Institute for his kind instruction in our preparation of ^{15}N-RNA.

References

1) A. Y. Hirakawa and M. Tsuboi, *Science*, **188**, 359 (1975).
2) M. Tsuboi and A. Y. Hirakawa, *J. Raman Spectrosc.*, **5**, 75 (1976).
3) Y. Nishimura, A. Y. Hirakawa, and M. Tsuboi, *Chem. Lett.* **1977**, 907.
4) Y. Nishimura, A. Y. Hirakawa, and M. Tsuboi, "Advances in Infrared and Raman Spectroscopy," ed by R. J. H. Clark and R. E. Hester, Heyden, London (1978), Vol. 5, Chap. 4.
5) A. Y. Hirakawa and Y. Yamamoto, Symposium on the Molecular Structure of the Chemical Society of Japan, Hiroshima, 1978, 1B13.
6) M. Tsuboi, *J. Am. Chem. Soc.*, **79**, 1351 (1957).
7) M. Tsuboi, "XXIIIrd International Congress of Pure and Applied Chemistry," Butterworth, London (1971), Vol. 7, p. 145.
8) M. Tsuboi, S. Takahashi, and I. Harada, "Physicochemical Properties of Nucleic Acids," ed by J. Duchesne, Academic Press, London, New York (1973), Vol. 2 p. 91.
9) M. Tsuboi, Y. Kyogoku, and T. Shimanouchi, *Biochim. Biophys. Acta*, **55**, 1 (1962).
10) T. Shimanouchi, Computer Programs for Normal Coordinate Treatment of Polyatomic Molecules, Department of Chemistry, University of Tokyo.
11) H. T. Miles , T. P. Lewis, E. D. Becker, and J. Frazier, *J. Biol. Chem.*, **248**, 1115 (1973).
12) H. Susi, *Spectrochim. Acta, Part A*, **30**, 1843 (1974).
13) R. C. Lord and G. J. Thomas, Jr., *Biochim. Biophys. Acta*, **23A**, 2551 (1967).
14) C. Nagata, A. Imamura, and H. Fujita, "Advances in Biophysics," ed by M. Kotani, University of Tokyo Press, Tokyo (1973), Vol. 4, p. 1.
15) W. Hug and I. Tinoco, *J. Am. Chem. Soc.*, **95**, 2803 (1973).

Transannular Interaction in the Excited Triplet States of [2.2]Paracyclophane and Related Compounds

Shun-ichi Ishikawa, Junko Nakamura,† Suehiro Iwata,† Minoru Sumitani,‡ Saburo Nagakura,* Yoshiteru Sakata,†† and Soichi Misumi††

The Institute for Solid State Physics, The University of Tokyo, Roppongi, Minato, Tokyo 106

†*The Institute of Physical and Chemical Research, Wako, Saitama 351*

††*The Institute of Scientific and Industrial Research, Osaka University, Suita, Osaka 565*

(Received December 18, 1978)

The triplet-triplet absorption spectra of [2.2]paracyclophane and related cyclophanes (naphthalenophane, pyrenophane, and anthracenophane) were measured. Cyclophanes in which two component subunits fully overlap, show new bands together with monomer-like bands. The electronic structures of triplet states of these cyclophanes were studied theoretically by the "molecules in molecule" method, special attention being paid to the correlations of the electronic structures of cyclophanes with those of corresponding monomers and also to the dependences of the charge transfer interaction upon the overlapping between the component subunits and upon the molecular size.

[2.2]Paracyclophane and other cyclophanes have the conjugated aromatic rings faced to each other and are of particular importance because of the transannular interaction. [2.2]Paracyclophane is regarded as a model of a benzene dimer; especially in the excited state it is a model of a benzene excimer. Thus the electronic structure of this molecule has been studied by several authors.[1)]

Previously, we investigated the singlet states of [2.2]paracyclophane from both experimental and theoretical points of view.[2)] The near and vacuum ultraviolet absorption spectra were well analyzed by considering the configuration interaction (CI) among the ground, locally excited, and charge transfer configurations.

Hausser *et al.* showed in their ODMR (optical detection of magnetic resonance) and ESR studies that in the lowest triplet state, T_1, of cyclophanes which contain two same aromatic molecules two unpaired electrons are rather localized in either ring.[3)] In other words, the charge transfer character is not significant in the lowest triplet state.

In this paper, we have studied the triplet-triplet ($T_n \leftarrow T_1$) absorption spectra of several cyclophanes in order to elucidate the character of the lowest triplet state and higher triplet states, T_n, and also the dependences of the charge transfer interaction upon the ring overlapping and upon the molecular size.

Experimental

Cyclophanes studied here are shown in Fig. 1: [2.2]paracyclophane (PC), *anti*-[2.2](1,4)naphthalenophane (*anti*-NP), *syn*-[2.2](1,4)naphthalenophane (*syn*-NP), [2.2](2,7)-pyrenophane (PyP), *anti*-[2.2](1,4)anthracenophane (*anti*-AP), [2.2](1,4)(9,10)anthracenophane ((1,4)(9,10)-AP), and *syn*-[2.2](1,4)anthracenophane (*syn*-AP). [2.2]Paracyclophane (the Aldrich Chemical Company) was purified by column chromatography and vacuum sublimation. The preparation and purification of other cyclophanes were described previously.[4)]

The $T_n \leftarrow T_1$ absorption spectra of PC, *anti*-NP, *syn*-NP, and PyP were observed at 77 K in 2-methyltetrahydrofuran by an improved "parallel beam method"[5)] in which the exciting light and the monitoring light was set to pass a sample through the same optical path by the use of two sectors synchronized by stepping motors. By setting up the double beam system, the S/N ratio was much improved. Consequently, we could measure the transient spectra with the absorbance less than 0.01. The polarized $T_n \leftarrow T_1$ spectrum of PC was measured by the photoselection method,[6)] two polarizer films being used.

The sensitization method was used for excitation to the triplet states of anthracenophanes since the quantum yields were low for the direct excitation. Biacetyl was added into the sample solution as a triplet sensitizer. Biacetyl was excited with a dye laser pumped with a nitrogen laser at room temperature. Through the energy transfer from triplet biacetyl, anthracenophanes were populated in their T_1 states, and their $T_n \leftarrow T_1$ absorption spectra were measured. The details of the excitation and detection systems used for the measurement were described previously.[7)]

Theoretical

The "molecules in molecule" method was used for the calculation of the energy levels of triplet states of PC in a similar way as for the calculation of singlet states.[2a)]

The energies of the locally excited (LE) configurations for PC were taken to be equal to the observed values of benzene:[8)]

$$E(^3B_{1u}^+) = 3.9\,\text{eV},\ E(^3E_{1u}^\pm) = 4.7\,\text{eV},\ E(^3B_{2u}^-) = 5.6\,\text{eV},$$
$$E(^3E_{2g}^+) = 6.8\,\text{eV},\ E(^3E_{2g}^-) = 9.3\,\text{eV}.$$

The energies of the CT configurations were calculated by the usual method.[9)] The energy, $E_{CT}(i \rightarrow j)$, for the configuration in which one electron transfers from the i-th occupied orbital of one benzene ring to the j-th vacant orbital of the other is given by the following equation:

$$E_{CT}(i \rightarrow j) = I_i - A_j - C_{ij}^{I,II}. \quad (1)$$

Here I_i and A_j are the ionization potential for the i-th orbital and the electron affinity for the j-th orbital, respectively. The Coulombic interaction term, $C_{ij}^{I,II}$, was evaluated with the aid of the Nishimoto-Mataga approximation.[10)]

In actual calculation, I_i and A_j were evaluated by the following equations for the cyclophanes except

‡ Present address: The Institute for Molecular Science, Myodaiji, Okazaki, Aichi 444.

for PC.

$$I_i = I + E_i^+ \quad (2)$$

$$A_j = A - E_j^- \quad (3)$$

Here I and A are the first ionization potential and the electron affinity of an appropriate neutral molecule (naphthalene for naphthalenophane), respectively. E_i^+ and E_j^- are the excitation energies of the corresponding cation and anion determined experimentally,[11] respectively. Since the assignment of spectra has some ambiguity for the benzene cation and anion, Eqs. 2 and 3 are not applicable to PC. Therefore we evaluated I_i and A_j by the following equations:

$$I_i = I + (\varepsilon_{HO} - \varepsilon_i), \quad (4)$$

$$A_j = A - (\varepsilon_j - \varepsilon_{LV}). \quad (5)$$

Here ε_{HO}, ε_{LV}, ε_i, and ε_j are the orbital energies for the highest occupied, lowest vacant, i-th, and j-th orbitals, respectively. They were calculated with the Pariser-Parr-Pople method.[12]

The molecules of *syn*-series, namely, PC, *syn*-NP, PyP, and *syn*-AP belong to the D_{2h} symmetry, and other cyclophanes to the C_{2h} symmetry. The coordinate systems are shown in Fig. 1. In all cyclophanes that belong to D_{2h}, the symmetry of T_1 is $^3B_{2g}$ and the allowed transitions are $^3B_{1u} \leftarrow {}^3B_{2g}$ (x-polarization), $^3A_u \leftarrow {}^3B_{2g}$ (y-polarization), and $^3B_{3u} \leftarrow {}^3B_{2g}$ (z-polarization). In the case of C_{2h}, T_1 is ^3B_g, and the allowed transitions are $^3A_u \leftarrow {}^3B_g$(x,y-polarization) and $^3B_u \leftarrow {}^3B_g$ (z-polarization).

The semi-empirical SCF MO-CI calculation was also made, using MO's calculated by the Pariser-Parr-Pople method.

Results and Discussion

[2.2]*Paracyclophane (PC).* Figure 2 shows the $T_n \leftarrow T_1$ absorption spectrum and its polarization of PC. We found a very weak band at 550 nm and a broad strong band around 330—400 nm. The polarization experiment using the 313 nm light for excitation shows that the strong band consists of two transitions with the polarizations perpendicular to each other. Therefore, three distinct $T_n \leftarrow T_1$ absorption bands were observed for PC. On the other hand, benzene has only two weak $T_n \leftarrow T_1$ transition bands at 430 nm ($^3E_{2g}^+ \leftarrow {}^3B_{1u}^+$)[8b] and at 280 nm ($^3E_{2g}^- \leftarrow {}^3B_{1u}^+$).[8c] The difference in the $T_n \leftarrow T_1$ absorption spectrum between benzene and PC is clearly due to the transannular interaction in the excited triplet states of PC.

In order to analyze the $T_n \leftarrow T_1$ absorption spectra, we performed the semi-empirical SCF MO-CI calculation and the "molecules in molecule" calculation. Figure 3 shows the calculated ("molecules in molecule" method) and observed energy levels of the triplet

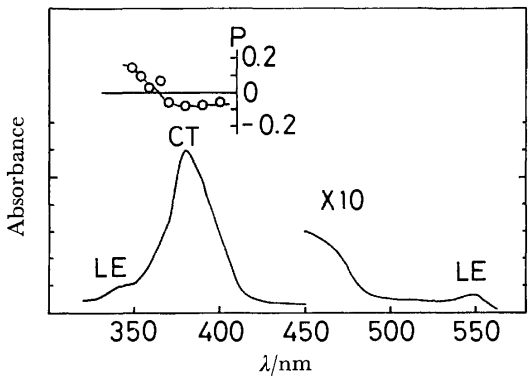

Fig. 2. The $T_n \leftarrow T_1$ absorption spectrum of PC and the polarization, P.

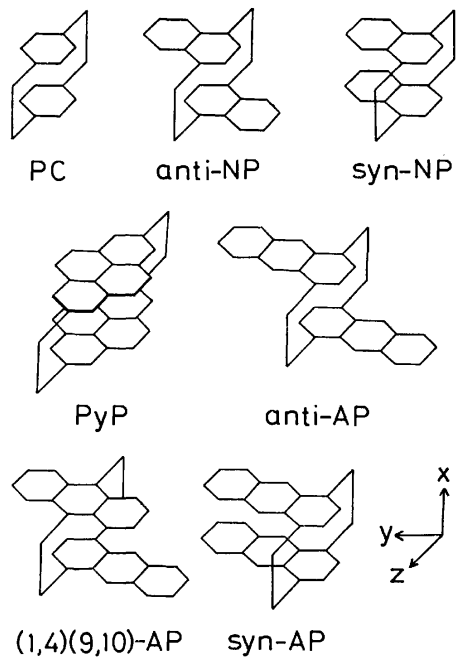

Fig. 1. The molecular structures of PC, *anti*-NP, *syn*-NP, PyP, *anti*-AP, (1,4)(9,10)-AP, and *syn*-AP.

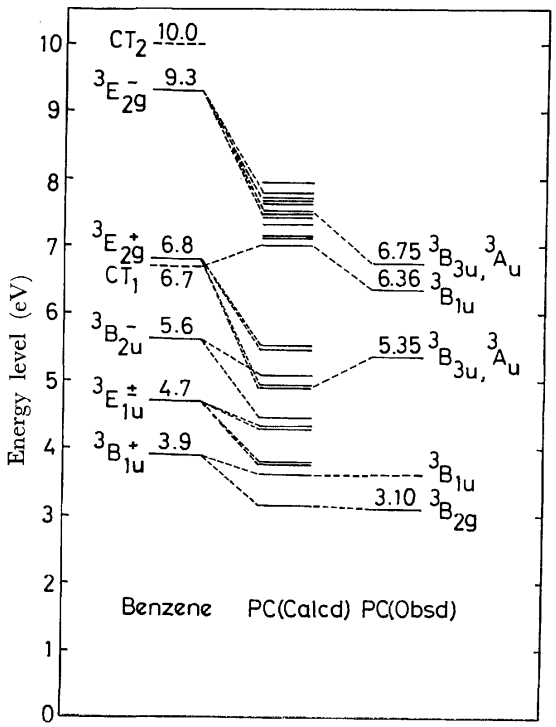

Fig. 3. Observed and calculated energy levels of the triplet states of PC and observed levels of benzene.

states of PC, together with the observed levels of benzene. The zeroth-order LE levels of $^3B_{1u}^-$, $^3E_{1u}^+$, and $^3B_{1u}^+$ of benzene strongly interact with the CT_1 level, and those of $^3E_{2g}^+$ and $^3E_{2g}^-$ with CT_2.

We can see from Fig. 3 that the lowest triplet state of benzene ($^3B_{1u}^+$) is split into two states, $^3B_{2g}$ and $^3B_{1u}$ in PC. The $^3B_{2g}$ state is slightly lower than the $^3B_{1u}$ state and is of the neutral exciton nature. The weight of $^3B_{1u}^+$ of benzene in the T_1 state of PC is more than 80%. Hausser *et al.* recently showed that the zero-field splitting parameter, *D*, of PC is reduced only by 15% with respect to the corresponding monomer, *p*-xylene.[3b] This is consistent with the present result. The present result is also consistent with the result calculated by Hillier *et al.*[1c]

Contrary to the T_1 state, there are no previous studies on higher triplet states. From theoretical consideration we can see that the transitions from the $^3B_{2g}$ state to the $^3B_{3u}$ and ^3A_u states (polarized parallel to the ring), and to the $^3B_{1u}$ state (polarized perpendicularly to the ring) are allowed. These states are shown in Fig. 3. The $^3B_{1u}$ state located at about 7 eV in the column of PC (calcd) is mainly of the CT character. As is clearly seen in this figure, the theoretical study predicts that three bands appear in the observed wavelength region. This prediction agrees well with the experimental result. The semi-empirical SCF MO-CI calculation shows that the intensity ratio of the $T_n \leftarrow T_1$ absorption spectrum is 1 : 0.38 : 0.03 for the $^3B_{1u} \leftarrow {}^3B_{2g}$, ($2^3B_{3u} \leftarrow {}^3B_{2g} + 2^3A_u \leftarrow {}^3B_{2g}$), and ($1^3B_{3u} \leftarrow {}^3B_{2g} + 1^3A_u \leftarrow {}^3B_{2g}$) transitions. With the aid of this intensity ratio together with the calculated and observed transition energies, the three $T_n \leftarrow T_1$ absorption bands are assigned as follows. The most intense band at 380 nm is the CT band ($^3B_{1u} \leftarrow {}^3B_{2g}$) characteristic of the transannular interaction. The band around 340 nm which is polarized perpendicularly to the above CT band, is assigned to the LE band ($2^3B_{3u} \leftarrow {}^3B_{2g} + 2^3A_u \leftarrow {}^3B_{2g}$) and the parentage of this transition is the $^3E_{2g}^- \leftarrow {}^3B_{1u}^+$ transition of benzene. The weak band at 550 nm is ascribed to the LE band ($1^3B_{3u} \leftarrow {}^3B_{2g} + 1^3A_u \leftarrow {}^3B_{2g}$) which comes from the forbidden transition ($^3E_{2g}^+ \leftarrow {}^3B_{1u}^+$) of benzene.

The polarization of the absorption of PC at 313 nm (the excitation wavelength for the measurement of the $T_n \leftarrow T_1$ absorption spectrum of PC) is not clear, since the absorption band in this region consisting of two forbidden transitions, $^1B_{1g} \leftarrow {}^1A_g$ and $^1B_{2g} \leftarrow {}^1A_g$,[2a,13] is only vibrationally allowed. By the polarized absorption spectra of PC crystal measured on the ac plane, the absorbance at 313 nm of the c// spectrum is about twice larger than that of the a// spectrum.[2a] The c axis is parallel to the long axis of the molecule. On the basis of this, the present experiment of the $T_n \leftarrow T_1$ absorption is explained as follows. The degree of polarization, P, is expected to be 1/2 when the $T_n \leftarrow T_1$ transition is polarized parallel to the $S_n \leftarrow S_0$ transition used for excitation, and −1/3 when it is polarized perpendicularly. The band around 380 nm shows the negative value of P. This is consistent with our assignment that the band is the CT band the polarization of which is perpendicular to the benzene plane. In the $T_n \leftarrow T_1$ absorption band around 340 nm, P becomes positive. This indicates that the transition parallel to the $S_n \leftarrow S_0$ excitation is involved in this region.

It is interesting that the CT band was more distinctly observed in the $T_n \leftarrow T_1$ absorption spectrum than in the usual $S_n \leftarrow S_0$ absorption spectrum. This may be because of the weak $T_n \leftarrow T_1$ transition of the component molecule, benzene; that is, the transition localized in one ring is rather weak in the case of PC, and therefore the transition over two rings (CT transition) is observed clearly without the hindrance of LE bands.

anti- *and* syn-*NP*. Figure 4 shows the $T_n \leftarrow T_1$ absorption spectra of *anti*- and *syn*-NP together with that of naphthalene. In the case of naphthalene, the very strong $T_n \leftarrow T_1$ absorption is observed in the visible and ultraviolet regions. The most intense band at 417 nm is known to be polarized parallel to the long axis of the molecule and is assigned to the $^3B_{3g}^- \leftarrow {}^3B_{1u}^+$ transition.[14] The band in the shorter wavelength side is regarded as a vibrational structure. In the $T_n \leftarrow T_1$ absorption spectrum of *anti*-NP, a distinct peak at 447.5 nm was observed but the vibrational structure was not clear. We could not find other bands in the longer wavelength region up to 900 nm. In the spectrum of *syn*-NP, a peak was observed at 465 nm. This is similar to the band of *anti*-NP. In addition, a new broad band was observed around 612.5 nm.

In order to interpret these spectra, the LE and CT levels were also analyzed with the "molecules in molecule" method. The lowest triplet states of *anti*- and *syn*-NP's have mainly a character of T_1 ($^3B_{1u}^+$) of naphthalene. Froines and Hagerman showed that the phosphorescence bands of *anti*- and *syn*-NP shifted

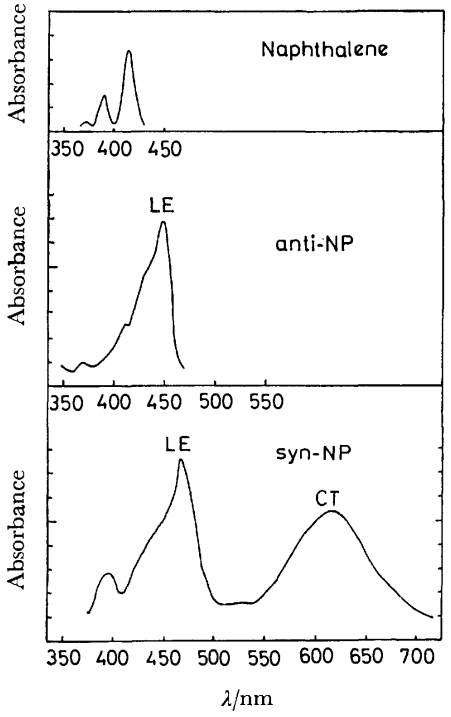

Fig. 4. The $T_n \leftarrow T_1$ absorption spectra of naphthalene, *anti*-NP, and *syn*-NP.

by 1700 cm^{-1} and 2700 cm^{-1}, respectively, to the longer wavelength side from the monomer, 1,4-dimethylnaphthalene, and that the vibrational structures in the phosphorescence spectra of *anti-* and *syn*-NP were rather similar to the monomer's.[15] According to Hausser *et al.* the *D* value of *anti*-NP is reduced by $\approx 10\%$ with respect to 1,4-dimethylnaphthalene.[3a] Therefore, it is concluded that the CT character of T_1 state of NP is small.

Because of the similarity of the spectral shapes, both the $T_n \leftarrow T_1$ absorption bands of *anti*-NP at 447.5 nm and of *syn*-NP at 465 nm are attributed to the LE transitions polarized parallel to the long axes of the molecules. Their parentage is the $^3B_{3g}^- \leftarrow {}^3B_{1u}^+$ transition of naphthalene. On the other hand, we attributed the new band of *syn*-NP around 612.5 nm to the CT band ($^3B_{1u} \leftarrow {}^3B_{2g}$) polarized perpendicularly to the ring plane. The calculated energy levels of the zeroth-order CT states clearly shows that the CT band appears in the longer wavelength side of the LE band at 465 nm. The next problem is why the $T_n \leftarrow T_1$ CT band can be observed in *syn*-NP but not in *anti*-NP. The spacial overlapping of two rings is larger for *syn*-NP than for *anti*-NP. Because of this difference in the overlapping, it is expected that the interaction between the zeroth-order CT level and the zeroth-order lowest triplet LE level is larger for *syn*-NP than for *anti*-NP. This means that absorption intensity of the CT band is larger for *syn*-NP than for *anti*-NP.

Very recently, Subudhi and Lim observed the $T_n \leftarrow T_1$ absorptions of the intramolecular excimers from fluid solutions of di(1-naphthyl)alkanes.[16] The transient absorption spectrum of 1,2-di(1-naphthyl)-ethane observed 150 μs after excitation has a broad band around 470 nm , and the band is continuing up to 600 nm. The band around 470 nm may correspond to our "LE band" observed with *anti-* and *syn*-NP's. Since the LE bands are conceivably rather insensitive to the geometry of the molecule, they are observed at similar positions for *anti-* and *syn*-NP's and also for di(1-naphthyl)alkanes.

Pyrenophane (PyP). The $T_n \leftarrow T_1$ absorption spectra of PyP and pyrene are shown in Fig. 5. In pyrene, the $T_n \leftarrow T_1$ spectrum has a sharp band at 413 nm polarized parallel to the long axis ($^3A_g^- \leftarrow {}^3B_{1u}^+$) and another band at 518 nm polarized parallel to the short axis ($^3B_{3g}^- \leftarrow {}^3B_{1u}^+$).[17] On the other hand, the $T_n \leftarrow T_1$ absorption spectrum of PyP has three bands: a sharp band at 380 nm, a weak band at 480 nm, and a strong band at 625 nm. From the consideration of the spectral shape, the sharp band of PyP can be clearly assigned to the LE band ($^3B_{3u} \leftarrow {}^3B_{2g}$) corresponding to the 413 nm band of pyrene ($^3A_g^- \leftarrow {}^3B_{1u}^+$).

The energy separation between the two absorption peaks of pyrene is about 5000 cm^{-1}, and the separation between the sharp band and the weak band of PyP is 5400 cm^{-1}. Because of this similarity the weak band at 480 nm was assigned to the LE band ($^3A_u \leftarrow {}^3B_{2g}$) corresponding to the 518 nm band of pyrene ($^3B_{3g}^- \leftarrow {}^3B_{1u}^+$). The strong band in the red region can be assigned to the CT transition ($^3B_{1u} \leftarrow {}^3B_{2g}$). It is interesting that the CT band was clearly observed

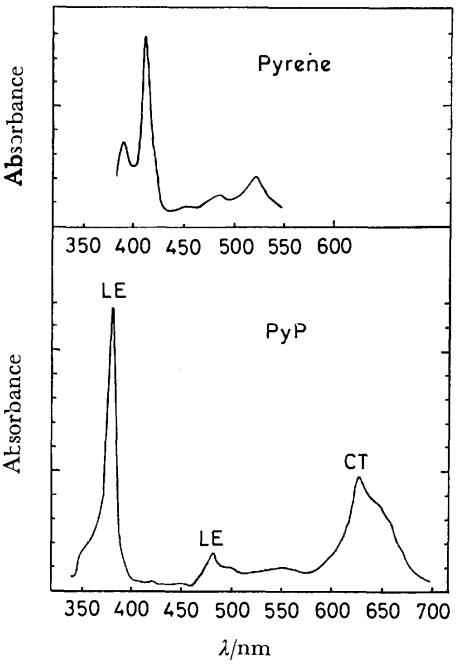

Fig. 5. The $T_n \leftarrow T_1$ absorption spectra of pyrene and PyP.

for PyP as well as for *syn*-NP. This may be due to the whole overlapping of two component subunits.

anti-, *(1,4)(9,10)-, and* syn-*AP.* We measured the $T_n \leftarrow T_1$ absorption spectra of *anti-*, (1,4)(9,10)-, and *syn*-AP by the sensitization method as mentioned in experimental section. The transient spectra observed by the method are confirmed to be the $T_n \leftarrow T_1$ spectra of AP's, since the spectra are quenched by oxygen and the observed rise times of the spectra are

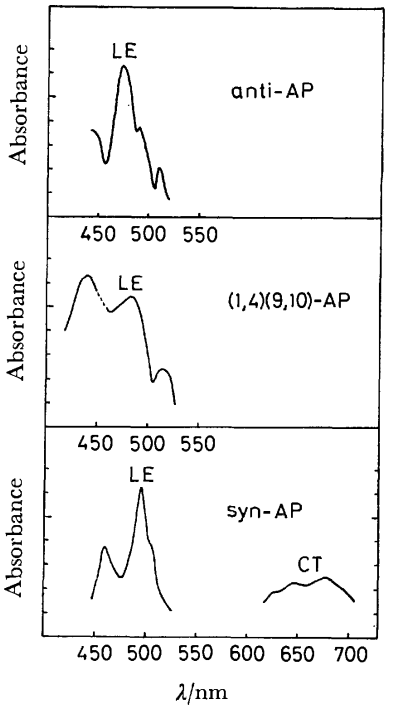

Fig. 6. The $T_n \leftarrow T_1$ absorption spectra of *anti-*, (1,4)-(9,10)-, and *syn*-AP.

well explained in terms of the fact that the related energy transfer process is diffusion controlled. The $T_n \leftarrow T_1$ absorption spectra of *anti*-, (1,4)(9,10)-, and *syn*-AP are shown in Fig. 6. $T_n \leftarrow T_1$ absorption spectra could not be observed for *anti*- and *syn*-AP in the shorter wavelength region than 450 nm, because of the ground state absorption and of scattering of the exciting light.

Anthracene shows the strong $T_n \leftarrow T_1$ absorption band at 425 nm with the polarization parallel to the long axis of the molecule ($^3B_{3g}^- \leftarrow {}^3B_{1u}^+$).[14] Contrary to the cases of NP and PyP, the $T_n \leftarrow T_1$ absorption spectra of AP cannot be interpreted from a simple analogy with the monomer. In *syn*-AP, we found a new band in the red region.

Although it is difficult to assign clearly the bands observed with the three AP's, the strong bands around 500 nm may be due to the LE transition of anthracene, in view of their positions and intensities.

From the calculation of the zeroth-order CT energy level, the CT band is expected to appear for *syn*-AP in the longer wavelength region than the LE band around 500 nm in consistence with the experimental result. The reason why the CT band is observed for *syn*-NP but not for *anti*-NP can be applied to the cases of AP's.

Trend in syn-*Series.* In order to elucidate the dependence of the CT interaction upon the molecular size, the spectra of *syn*-series should be compared. Figure 7 shows the correlation of triplet energy levels of *syn*-series and corresponding monomers. The lower zeroth-order CT levels presented in the columns of monomers interact with the $T_1(^3B_{1u})$ states, and the higher CT with the higher LE ($^3E_{2g}$, $^3B_{3g}$, and ^3A_g). The energy separation between T_1 and CT_1 levels are almost the same in naphthalene, pyrene, and anthracene. In fact, in all of *syn*-NP, PyP, and *syn*-AP spectra the new CT bands are found around 600 nm.

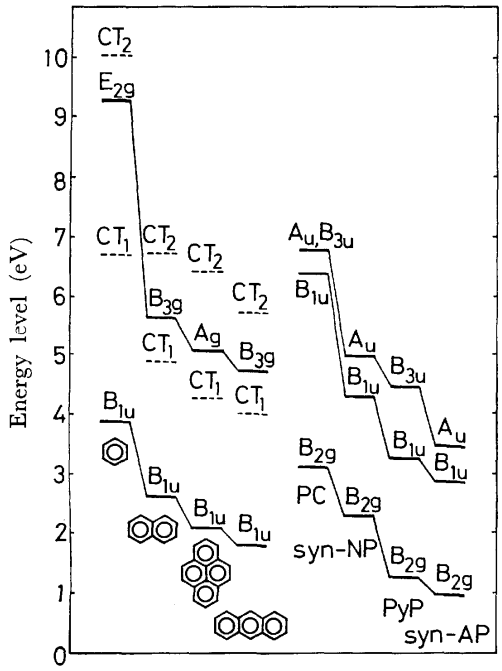

Fig. 7. Energy levels of triplet states of benzene, naphthalene, pyrene, anthracene, PC, *syn*-NP, PyP, and *syn*-AP. The zeroth-order CT levels are also presented in the columns of monomers.

Conclusion

(1) The T_1 states of PC and related compounds are the neutral exciton states.
(2) Higher triplet levels of cyclophanes are well analyzed in terms of the interaction among the zeroth-order LE and CT levels.
(3) CT bands are observed for the *syn*-series : PC, *syn*-NP, PyP, and *syn*-AP in which overlapping between the aromatic rings is large.

The authors should like to express their sincere thanks to Dr. Toshihiko Hoshi, Aoyama Gakuin University, for his kind advice in preparing the polarizer film.

References

1) a) D. J. Cram, N. L. Allinger, and H. Steinberg, *J. Am. Chem. Soc.*, **76**, 6132 (1954); b) M. T. Vala, Jr., I. H. Hillier, S. A. Rice, and J. Jortner, *J. Chem. Phys.*, **44**, 23 (1966); c) I. H. Hillier, L. Glass, and S. A. Rice, *J. Chem. Phys.*, **45**, 3015 (1966); d) C. B. Duke, N. O. Lipari, W. R. Salaneck, and L. B. Schein, *J. Chem. Phys.*, **63**, 1758 (1975).

2) a) S. Iwata, K. Fuke, M. Sasaki, S. Nagakura, T. Otsubo, and S. Misumi, *J. Mol. Spectrosc.*, **46**, 1 (1973); b) K. Fuke and S. Nagakura, *Bull. Chem. Soc. Jpn.*, **48**, 46 (1975); c) K. Fuke, S. Nagakura, and T. Kobayashi, *Chem. Phys. Lett.*, **31**, 205 (1975).

3) a) D. Schweitzer, J. P. Colpa, J. Behnke, K. H. Hausser, M. Haenel, and H. A. Staab, *Chem. Phys.*, **11**, 373 (1975); b) J. P. Colpa, K. H. Hausser, and D. Schweitzer, *Chem. Phys.*, **29**, 187 (1978).

4) a) H. H. Wasserman and P. M. Keehn, *J. Am. Chem. Soc.*, **91**, 2374 (1969); b) A. Iwama, T. Toyoda, T. Otsubo, and S. Misumi, *Tetrahedron Lett.*, **1973**, 1725; c) T. Umemoto, S. Satani, Y. Sakata, and S. Misumi, *Tetrahedron Lett.*, **1975**, 3159.

5) S. Matsumoto, S. Nagakura, S. Iwata, and J. Nakamura *Mol. Phys.*, **26**, 1465 (1973).

6) M. A. El-Sayed and T. Pavlopoulos, *J. Chem. Phys.*, **39**, 834 (1963).

7) M. Sumitani, S. Nagakura, and K. Yoshihara, *Bull. Chem. Soc. Jpn.*, **49**, 2995 (1976).

8) a) S. Iwata and K. F. Freed, *J. Chem. Phys.*, **61**, 1500 (1974); b) R. Astier and Y. H. Meyer, *Chem. Phys. Lett.*, **3**, 399 (1969); c) T. S. Godfrey and G. Porter, *Trans. Faraday Soc.*, **62**, 7 (1966).

9) S. Iwata, J. Tanaka, and S. Nagakura, *J. Am. Chem. Soc.*, **88**, 894 (1966); **89**, 2813 (1967).

10) K. Nishimoto and N. Mataga, *Z. Phys. Chem. (Frankfurt am Main)*, **12**, 335 (1957).

11) T. Shida and S. Iwata, *J. Am. Chem. Soc.*, **95**, 3473 (1973).

12) a) R. Pariser and R. G. Parr, *J. Chem. Phys.*, **21**, 466, 767 (1953); b) J. A. Pople, *Proc. Phys. Soc. London*, **A 68**, 81 (1955).

13) A. Ron and O. Schnepp, *J. Chem. Phys.*, **37**, 2540 (1962).

14) Y. H. Meyer, R. Astier, and J. M. Leclercq, *J. Chem. Phys.*, **56**, 801 (1972).

15) J. R. Froines and P. J. Hagerman, *Chem. Phys. Lett.*, **4**, 135 (1969).

16) P. C. Subudhi and E. C. Lim, *Chem. Phys. Lett.*, **56**, 59 (1978).

17) J. Langelaar, J. Wegdam-van Beek, H. Ten Brink, and J. D. W. van Voorst, *Chem. Phys. Lett.*, **7**, 368 (1970).

Studies of Inorganic Ion Exchangers. III.[1] Ion Exchange Properties of $Ti(HPO_4)_2 \cdot 0—1/2H_2O$ to Alkali Metal and Ammonium Ions

Etsuro KOBAYASHI

National Chemical Laboratory for Industry, Hon-machi, Shibuya-ku, Tokyo 151

(Received April 28, 1978)

In order to develop an inorganic ion exchanger for industrial use, the ion exchange behaviour of $Ti(HPO_4)_2 \cdot 0—1/2H_2O$ with alkali metal and ammonium ions has been investigated. The ion exchange capacities of $Ti(HPO_4)_2 \cdot 1/2H_2O$ (hemihydrate) have been determined by forward and backward titration. The saturation ion exchange capacities (Q^A) of the hemihydrate to Li, Na, K, Cs, and NH_4 (M) ions by the forward titration method were 1.9, 3.2, 4.1, 2.5, and 3.7 meq/g at pH 4.5, respectively. The ion exchange capacities (Q°) of the hemihydrate from 0.1 M MCl were 0.31, 1.84, 2.31, 0.21, and 1.01 meq/g to each of the ions. The selectivity quotients (K_H^M) estimated from the Q^A and Q° were 0.028, 3.77, 15.7 0.008, and 0.255 to each of the ions, and the selectivities of the hemihydrate increased in the order $Cs^+ < Li^+ < NH_4^+ < Na^+ < K^+$. The empirical formula of the 50% ion exchange products derived from the hemihydrate may be represented by $TiMH(PO_4)_2 \cdot 0—1/2H_2O$, (where, M=Na, K, and NH_4). The ion exchange of Li and Cs ions did not take place completely however to give a 50% ion exchanger, and the hemihydrate was then converted into a non-stoichiometric compound.

Certain metal oxides, hydroxides, acid salts, heteropolyacids, insoluble hexacyanoferrate (II), and zeolite have been known as inorganic ion exchangers.[2] Zirconium phosphate, as an acid salt of a multivalent metal is useful as an ion exchanger in analytical chemistry.[3] In order to develop an ion exchanger for industrial use, the ion exchange behavior of various phosphates has been investigated.[4,5] Titanium phosphate as an ion exchanger appears promising because of the stability and low price of the raw material. The titanium(IV) bis(hydrogenphosphate) hemihydrate ($Ti(HPO_4)_2 \cdot 1/2H_2O$) has been synthesized by refluxing amorphous titanium(IV) phosphate (ATP) with concentrated phosphoric acid.[6] The X-ray diffraction pattern of the hemihydrate was entirely different from that of the titanium(IV) bis(hydrogenphosphate) monohydrate ($Ti(HPO_4)_2 \cdot H_2O$), known already.[7] It has been reported[6] that the hemihydrate has an ion exchangeability with ions of relatively large ionic radius, such as potassium and cesium. Further, $Ti(HPO_4)_2 \cdot 0—1/2H_2O$ has also been prepared by refluxing a phosphoric acid and a sulfuric acid solution of $TiOSO_4$, which is the intermediate in the industrial process of titanium(IV) dioxide.[1] In the present work, the ion exchange properties of the hemihydrate toward Li, Na, K, Cs, and NH_4 ions have been investigated. Alberti *et al.*[7] examined the ion exchange properties of $Ti(HPO_4)_2 \cdot H_2O$ with Li, Na, and K ions, and Takaguchi and Tomita[8,9] reported the ion exchange behaviour of the monohydrate with Li and Na ions by forward and backward titration. However, no data of the ion exchange reactions of the hemihydrate exist except for the Na, K, and Cs ions as determined previously by the forward titration.[6] Ion exchange characteristics, such as selectivity quotient, degree of absorption and distribution coefficient for the hemihydrate do not exist. The ion exchange behaviour of the hemihydrate towards Li, Na, K, Cs, and NH_4 ions has been observed by forward and backward titration, and the saturation and equilibrium capacities determined. Ion exchange characteristics have been introduced from the relationship between the capacities. The ion exchange characteristics of the monohydrate have also been estimated and contrasted with the hemihydrate. Moreover, the apparently 50%, 100%, and the 50% →H ion exchange products have been examined by X-ray diffraction and chemical analysis.

Experimental

Preparation of Ion Exchanger. Titanium(IV) bis(hydrogenphosphate) were prepared by the methods described previously,[1,6] the conditions for the monohydrate and hemihydrate and the analytical results being summarized in Table 1.

Analysis. Product components, such as P_2O_5, TiO_2, and H_2O were determined by methods previously reported.[6] The M_2O (M=Li, Na, K, Cs) content was derived from the following equation.

$$100\% - (P_2O_5\% + TiO\% + H_2O\%) = M_2O\%$$

The NH_3 content was determined by Kjeldahl's method. The X-ray diffraction patterns were obtained under the conditions reported previously.[6]

pH *Titration Curves.* *Forward Reaction*: The product (Nos. 1 and 2) (0.100 g)portion was placed in a 20 ml stoppered test tube, and the solutions in the proper ratio of 0.1 M MCl to 0.1 M MOH added (10 ml). The contents in the test tube were shaken periodically and the pH of the supernatant liquid measured after 48 h. The forward titration curve was drawn from the relation between the pH and the ion exchange capacity estimated from the mixed ratio of 0.1 M MCl to 0.1 M MOH.

Backward Reaction: 0.5 M MOH solution (40 ml) was gradually added to the product (0.01 mol)(Nos. 1, 2, and 3); the neutralized product was separated from the mother liquor after 48 h, washed with water, and vacuum-dried over phosphorus pentoxide for 24 h. A portion (0.100 g) of the apparently 100% ion exchange product thus obtained was placed in a (10 ml) stoppered test tube, and the solution 10 ml, mixed in the proper ratio of 0.1 M MCl to 0.1 M HCl added. The contents in the test tube were shaken periodically and the pH of the supernatant liquid measured after 48 h. The backward pH titration curve was then drawn from the relation between the pH and the ion exchange capacity.

Dissolution of Ion Exchanger. A portion of the above supernatant liquid (5.00 ml) was taken, and the phosphorus dissolved determined colorimetrically as phosphomolybdenum blue.

Saturation Capacity at pH 4.5 *(Q°, meq/g).* Titanium(IV) bis(hydrogenphosphate) as an ion exchanger is stable

TABLE 1. SYNTHESIS AND ANALYSIS OF TITANIUM(IV) BIS(HYDROGENPHOSPHATE)

No.	Reaction conditions: Raw material ATP[a] (g)	Raw material $TiOSO_4$[b] (ml)	Mother liquor H_3PO_4 (mol/l)	Mother liquor H_2SO_4 (mol/l)	Volume (ml)	Temp (°C)	Time (h)	Method[c]
1		30.0	8.03	3.40	900	150	50	PPT
2	25.0		13.0	1.80	880	160	50	REF
3		20.0	8.60	2.82	600	163	50	REF
4		30.0	10.9	3.06	900	165	50	REF

No.	Reaction products: TiO_2 (%)	P_2O_5 (%)	H_2O (%)	$TiO_2 : P_2O_5 : H_2O$ (mole ratio)	Estimated formura
1	31.2	54.6	14.2	1.01 : 1.00 : 2.05	$Ti(HPO_4)_2 \cdot H_2O$
2	32.0	56.4	10.1	1.01 : 1.00 : 1.43	$Ti(HPO_4)_2 \cdot 1/2H_2O$
3	32.4	57.5	8.85	1.01 : 1.00 : 1.22	$Ti(HPO_4)_2 \cdot 0—1/2H_2O$
4	32.4	60.7	7.6	0.95 : 1.00 : 0.99	$Ti(HPO_4)_2 \cdot$

a) Amorphous titanium phosphate containing TiO_2 42.7%, P_2O_5 33.8%, H_2O 23.3%. b) Solution containing TiO_2 250 and H_2SO_4 1044 g/l. c) PPT : Precipitation method, REF : Refluxing method.

in an acidic aqueous solution up to a pH of 4.5. Therefore, the ion exchange capacity at pH 4.5 on the forward titration curve was determined as the saturation ion exchange capacity.

The Equilibrium Capacity at pH *4.5 (Q^A, meq/g).* The ion exchanger (0.500 g) was mixed with 0.1 M MCl (25 ml) solution in a 50 ml stoppered Erlenmeyer flask and the contents in the flask periodically shaken. After equilibration, a portion of the supernatant liquid(10.00 ml) was titrated potentiometrically with 0.1 M NaOH using a recording auto titrator (Hiranuma Sangyo Co.). The relation between the pH and the volume of 0.1 M NaOH was drawn as the titration curve. In the titration curve, the ion exchange capacity, corresponding to a volume of 0.1 M NaOH consumed at pH 4.5, was determined as the equilibrium ion exchange capacity.

Selectivity Quotient (K_H^M). This was derived as follows.

$$K_H^M = \frac{(M^+)i}{(H^+)i} \cdot \frac{(H^+)s}{(M^+)s} = \frac{Q^A}{Q^\circ - Q^A} \cdot \frac{Q^A}{C - Q^A},$$

where C is the initial amount (2.5 meq) of 0.1 M MCl used for the determination of the equilibrium ion exchange capacity.

Absorption Quantity (A). This was obtained as follows.

$$Q^A/C \cdot 100 = A(\%).$$

Distribution Coefficient (K_D, ml/g). This was obtained from the expression,

$$\{A/(100-A)\} \cdot S/I = K_D,$$

where S is the volume (25 ml) of 0.1 M MCl used for the determination of the equilibrium ion exchange capacity, and I, the weight (0.500 g) of ion exchanger used.

Results and Discussion

The Ion Exchange Behavior of Titanium(IV) Bis(hydrogenphosphate) Dissolution. The ion exchange titration curves of the hemihydrate to alkali metal (Li, Na, K, Cs) and ammonium ions and solubility curves are shown in Figs. 1, 3, 4, 5, and 6.

Lithium Ion: As shown by the forward titration curve in Fig. 1, the ion exchange capacities of the hemihydrate with Li^+ were 1.9 and 3.9 meq/g at pH 4.5 and 7.0, respectively, and these increased linearly

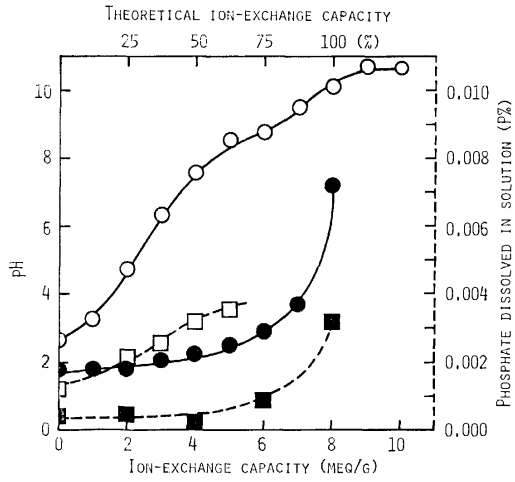

Fig. 1. Li ion-exchange titration curve of and dissolution curve of $Ti(HPO_4)_2 \cdot 1/2H_2O$.
○: Forward titration, ●: backward titration, □: P released to the external solution on the forward titration, ■: P released to the external solution on the backward titration.

in the pH range 2.6—7. The P dissolved in the aqueous solution from the ion exchanger was 0.001—0.005% at pH 1—5. The forward and backward titration curves showed a hysteresis loop, and it is thought that the apparently 100% Li product used for the backward titration did not sufficiently absorb the Li^+. In the backward titration, the dissolved P was smaller than in the forward titration.

The ion exchange titration curve and the solubility curve of the monohydrate with Li^+ have been reported.[7,8] In contrast to the hemihydrate, the results of re-examination with regard to the monohydrate are shown in Fig. 2. The ion exchange behavior in the forward titration agrees with the previous reports.[7,8] The capacities of the monohydrate were 1.9 and 7.0 meq/g at pH 4.5 and 7.0, respectively. In the range of ion exchange capacities 1—6 meq/g, the pH of the

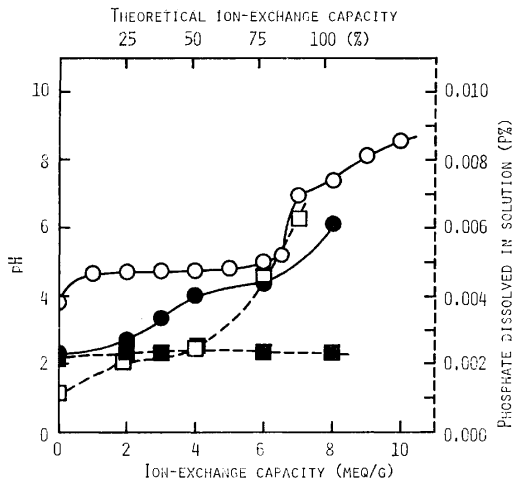

Fig. 2. Li ion-exchange titration curve and dissolution curve of $Ti(HPO_4)_2 \cdot H_2O$.
○: Forward titration, ●: backward titration, □: P released to the external solution on the forward titration, ■: P released to the external solution on the backward titration.

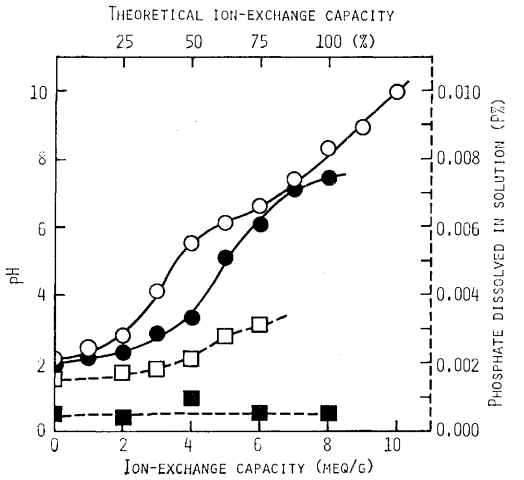

Fig. 3. Na ion-exchange titration curve and dissolution curve of $Ti(HPO_4)_2 \cdot 1/2H_2O$.
○: Forward titration, ●: backward titration, □: P released to the external solution on the forward titration, ■: P released to the external solution on the backward titration.

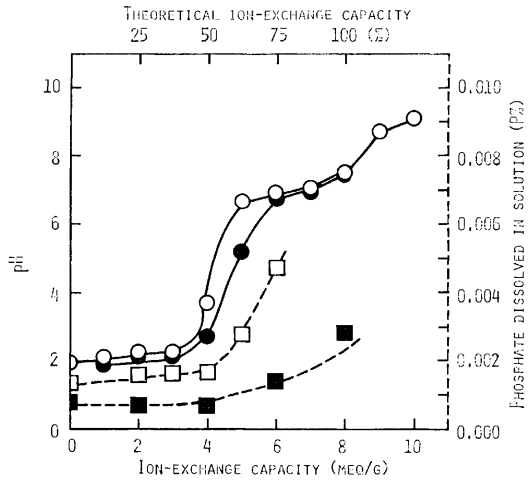

Fig. 4. K ion-exchange titration curve and dissolution curve of $Ti(HPO_4)_2 \cdot 1/2H_2O$.
○: Forward titration, ●: backward titration, □: P released to the external solution on the forward titration, ■: P released to the external solution on the backward titration.

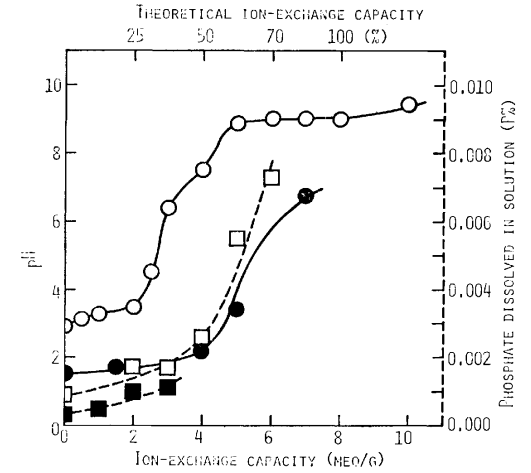

Fig. 5. Cs ion-exchange titration curve and dissolution curve of $Ti(HPO_4)_2 \cdot 1/2H_2O$.
○: Forward titration, ●: backward titration, □: P released to the external solution on the forward titration, ■: P released to the external solution on the backward titration.

solution was 4.5—5.0, and then the change of pH slacked up entirely. The P dissolved in the solution at pH 3.8—7.0 was from 0.001—0.006% and the backward titration curve did not agree with the forward titration curve, the P dissolved in the backward titration being about 0.0025%. As reported above, the pH of the solution equilibrated with the hemihydrate for the forward titration increased with an increase in the ion exchange capacity. The pH in the case of the monohydrate did not change as much in the range of ion exchange capacities 0—6 meq/g. The ion exchange capacities of the hemihydrate and monohydrate at pH 5 were 3.5 and 6.0 meq/g, respectively. It is unreasonable that the ion exchange capacity of the hemihydrate, which provides the large spacings recognized by the X-ray diffraction pattern, should be less than that of the monohydrate which provides the small spacings. The explanation may be that an inorganic ion exchanger can absorb the metal ion, excluding part of the water molecules from the hydrated ion at the cavities and then the ion exchange reaction takes place. When the monohydrate is used as the ion exchanger for Li^+, this explanation is reasonable. Approximately 84% of H^+ in the monohydrate exchanged with Li^+. It is well documented that the size of the alkali metal ions is in the order of $Li^+ < Na^+ < K^+ < Cs^+$, though the degree of hydration is the order of $Cs^+ < K^+ < Na^+ < Li^+$, and the Li^+ is hydrated particularly in neutral and alkaline solutions. It is the hemihydrate which provides the cavities through which large ion particles can pass and when it is used

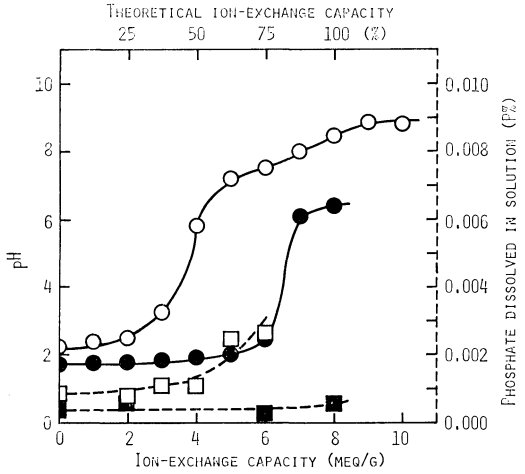

Fig. 6. NH_4 ion-exchange titration curve and dissolution curve of $Ti(HPO_4)_2 \cdot 1/2H_2O$.
○: Forward titration, ●: backward titration, □: P released to the external solution on the forward titration, ■: P released to the external solution on the backward titration.

as the ion exchanger for Li^+, the fully hydrated Li^+ is adsorbed. Consequently the H^+ in the exchanger largely remains further ion exchange is restricted.

Sodium Ion: The forward titration curve in Fig. 3, indicates the ion exchange capacities of the hemihydrate with Na^+ as 3.2 and 6.6 meq/g at pH 4.5 and 7.0, respectively. The P dissolved in the solution was 0.0015—0.003% in the pH range 2.0—6.5. The behavior of the backward titration curve did not agree with that of the forward titration curve. Therefore, it is assumed that the apparently 100% Na product used as the starting material for the backward titration is in reality an 85% ion exchange product. The P dissolved in the backward titration solution was about 0.0005%, the same as with Li^+ and the ion exchange capacities of the hemihydrate with Na^+ were less than those of the monohydrate (5.8, 7.6 meq/g from Fig. 4 in a previous report[6]) at pH 4.5 and 7.0. This may be explained in terms of the adsorption of hydrated ions as mentioned above.

Potassium Ion: In the forward titration curve in Fig. 4 the ion exchange capacities of the hemihydrate to K^+ were 4.1 and 6.7 meq/g at pH 4.5 and 7.0, respectively. The P dissolved in the solution was about 0.0015% in a pH range 2.0—3.7, and then was increased rapidly at higher pH. A 50% K product corresponding to a composition of $TiKH(PO_4)_2 \cdot 1/2H_2O$ was formed from the aqueous solution at pH 4.5, and was stable in weakly acidic solution. The backward titration curve was similar to that of the forward titration curve. The P dissolved in the solution of backward titration was about 0.0007% below pH 4.5.

Cesium Ion: In the forward titration curve in Fig. 5, the ion exchange capacities of the hemihydrate with Cs^+ were 2.5 and 3.3 meq/g at pH 4.5 and 7.0, respectively. The P dissolved in the solution was 0.001—0.002% in the pH range 2.7—3.5, and the dissolubility of the ion exchanger markedly increased above pH 3.5. The backward titration curve was at a considerable distance from the forward titration curve, the explanation being that an apparently 87% Cs product adsorbs Cs^+ to 35% of the theoretical ion exchange capacity of $Ti(HPO_4)_2 \cdot 1/2H_2O$. Also damage is caused to the exchanger by the alkaline aqueous solution.

Ammonium Ion: In the forward titration curve in Fig. 6, the ion exchange capacities of the hemihydrate to NH_4^+ were 3.7 and 4.8 meq/g at pH 4.5 and 7.0, respectively. The P dissolved in the solution was about 0.001%. An apparently 100% NH_4 product was in reality about 50% ion exchanger. Consequently, the backward titration curve, drawn using this product, was at a considerable distance from the forward titration curve. As seen in the X-ray diffraction pattern of Fig. 9, the apparently 100% NH_4 product changed to an amorphous product by the ammoniacal solution. The hemihydrate however provides wide spacings which can adsorb ions of large ionic radii, such as NH_4^+. Therefore, it may be anticipated that the hemihydrate with prove useful for the exclusion of NH_4^+ in a solution below pH 4.5.

The ion exchange properties of the monohydrate with NH_4^+ have not been investigated, since, the behaviors of ion exchange are examined, and shown in Fig. 7. The radius of the NH_4^+ is larger than that of the Li^+ and Na^+. Therefore, the monohydrate, which provides narrow spacings, does not show ion exchangeability with NH_4^+. Part of the ion exchanger dissolved in the ammoniacal solution, and a considerable change in the structure was observed.

Ion Exchange Characters. The titration curves drawn for the estimation of the equilibrium ion exchange capacity are shown in Fig. 8. The various ion exchange characters of titanium(IV) bis(hydrogenphosphate) to the alkali metals and ammonium ions are summarized in Table 2.

The equilibrium ion exchange capacities (Q^A) of

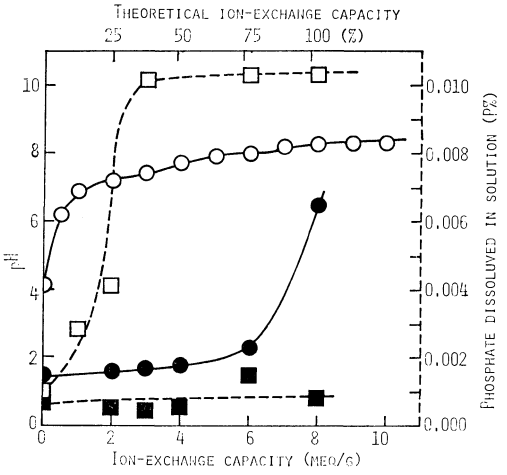

Fig. 7. NH_4 ion-exchange titration curve and dissolution curve of $Ti(HPO_4)_2 \cdot H_2O$.
○: Forward titration, ●: backward titration, □: P released to the external solution on the forward titration, ■: P released to the external solution on the backward titration.

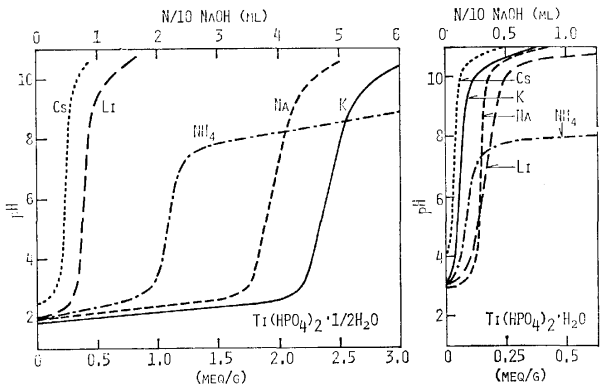

Fig. 8. Titration curves for equilibrium solution of titanium hydrogen phosphate with alkali metal and ammonium chlorides.

the monohydrate with Li^+, Na^+, K^+, Cs^+, and NH_4^+ were 0.025—0.12 meq/g, *i.e.*, the monohydrate hardly adsorbed the above ions in acidic solution at equilibrium. The Q^A of the hemihydrate to NH_4^+, Na^+, and K^+, except for Li^+ and Cs^+, were 1.0, 1.8, and 2.3 meq/g, respectively.

Generally, titanium(IV) bis(hydrogenphosphate) is stable in acid solution below pH 4.5. The saturation ion exchange capacity ($Q°$) of the monohydrate with Na^+ was 5.8 meq/g at pH 4.5. With other ions however, the $Q°$ of the monohydrate was less than 0.6 meq/g. The $Q°$ of the hemihydrate with Li^+, Na^+, K^+, Cs^+, and NH_4^+ was between 1.9—4.1 meq/g.

The selectivity quotients (K_H^M) of the hemihydrate, estimated from the values of Q^A and $Q°$, were 3.77 for Na^+ and 15.7 for K^+. It is thought that the values of K_H^M are significant for the separation of sodium and potassium ions.

The adsorption quantities (A) of the monohydrate for the alkali metal and ammonium ions were less than 5%. However, the A of the hemihydrate increased in the order of $Cs^+<Li^+<NH_4^+<Na^+<K^+$, and exhibited a remarkably high value of 92.4% for K^+.

The distribution coefficients (K_D) of the hemihydrate with Na^+ and K^+ showed remarkably large values. The K_D of K^+ was about 4 times that of K_D for Na^+. Therefore, $Ti(HPO_4)_2 \cdot 0—1/2H_2O$ may be considered as an ion exchanger for the recovery of potassium in sea water and brine.

X-Ray Diffraction Patterns. *Li^+ Exchangers*: A diffraction line of 11.6 Å, which characterized the hemihydrate, disappeared in the pattern of a 50% Li product. Where some lines appeared split in the pattern of the hemihydrate, this disappeared from the pattern of the 50% Li product; *i.e.*, half the diffraction lines decreased. In a previous report,[1] $Ti(HPO_4)_2 \cdot 0—1/2H_2O$ was thought to consist of at least two species and not just one crystallite. The X-ray diffraction pattern of a 50%→H product returned to that of the initial H form. The X-ray diffraction data of an apparently 100% Li product was approximately the same as the 50% Li product, a fact subsequently proved by analysis.

Na^+ Exchanger: The diffraction lines of the hemihydrate at 11.6 and 9.21 Å diasppeared in the 50% Na product. A single diffraction line at 10.2 Å appeared in the 50% Na product. Several lines appeared (in pairs) in the X-ray diffraction pattern of the hemihydrate, but disappeared from the 50% Na product. Therefore, it is assumed that the 50% Na product is a single crystallite. In the 50% Na→H product, the diffraction line at 11.2 Å appeared, and the number of diffraction lines that decreased was greater than in the case of the hemihydrate. The X-ray diffraction data of an apparently 100% Na product was very similar to that of the 50% Na product. The 85% ion exchanger was attacked by the alkaline solution and the intensities of the X-ray diffraction

Table 2. Ion exchange properities of titanium hydrogen phosphate to alkai metal and ammonium ions

Exchanger	Ion	Equilibrium capacity (Q^A, meq/g)	Saturation capacity at pH 4.5 ($Q°$, meq/g)	Selectivity quotient (K_H^M)	Mole fraction ($Q^A/Q°$)	Absortion quantity (A, %)	Distribution coefficient (K_D, ml/g)
$Ti(HPO_4)_2 \cdot H_2O$	Li	0.12	0.6	0.0126	0.20	2.4	1.23
	Na	0.11	5.8	0.0009	0.02	4.4	2.30
	K	0.05	0.6	0.0019	0.01	2.0	1.02
	Cs	0.025	0.4	0.0006	0.07	1.0	0.51
	NH_4	0.035	0.1	0.077	0.35	1.4	0.71
$Ti(HPO_4)_2 \cdot 1/2H_2O$	Li	0.31	1.9	0.028	0.163	12.4	7.08
	Na	1.84	3.2	3.77	0.575	73.6	139.4
	K	2.31	4.1	15.7	0.564	92.4	607.9
	Cs	0.21	2.5	0.008	0.084	8.4	4.59
	NH_4	1.01	3.7	0.255	0.27	40.4	33.9

Equilibrium capacity: Ion exchange capacity at pH 4.5 in Fig 8.
Saturation capacity: Ion exchange capacity at pH 4.5 in Figs. 1, 7, and 4—6.[6]
Selectivity quotient: $K_H^M = \frac{(M^+)I}{(H^+)I} \cdot \frac{(H^+)S}{(M^+)S} = \frac{Q^A}{Q°-Q^A} \cdot \frac{Q^A}{C-Q^A}$.
Absorption quantity: $Q^A/C \times 100 = A$. Distribution coefficient: $K_D = A/I \cdot S/(100-A)$.
C: Initial quantity of MCl (2.5 meq). S: MCl solution (25 ml). I: Ion exchanger (0.5 g).

TABLE 3. X-RAY DIFFRACTION DATA OF TITANIUM HYDROGEN PHOSPHATE AND ION EXCHANGE PRODUCTS

$Ti(HPO_4)_2 \cdot 1/2H_2O$	Exchangers of Li ion			Exchangers of Na ion			Exchangers of K ion			Exchangers of Cs ion			Exchangers of NH_4 ion		
(No. 2) (Å)	50% (Å)	50%→H (Å)	100% (Å)	50% (Å)	50%→H (Å)	100% (Å)	50% (Å)	50%→H (Å)	100% (Å)	50% (Å)	50%→H (Å)	87% (Å)	50% (Å)	50%→H (Å)	100% (Å)
11.6M		11.6M			11.2W	11.6M			12.3 S				11.3 S	11.3 S	11.3W
				10.16 S		10.8W	11.0 S	10.8 S							
9.21M	9.50M	9.21W	9.82M								9.21W			9.21W	
		6.10W			5.98W										
5.60W		5.57W		5.34 S		5.37M	5.47 S	5.50W	5.47W				5.47 S	5.79W	5.53W
5.21 S	5.24 S	5.21 S	5.24 S								5.21M			5.21M	
					4.69W					4.72W					
4.48M	4.41W	4.48M	4.44W	4.57W		4.57W					4.50W			4.41W	
4.31W		4.31W					4.37W	4.35W		4.27W			4.35M		
4.00W	3.97W	3.98W	3.97W	3.97W									4.00 S	4.00M	4.00W
3.90W		3.90W			3.80 S	3.81W	3.93W	3.95W	3.93W	3.93W	3.90W				
3.65M				3.62 S	3.74 S	3.62 S									
	3.53 S		3.56 S	3.54 S			3.59W	3.59W		3.56W	3.56W		3.57W	3.56M	
3.44 S	3.41 S	3.42 S	3.42 S				3.50M	3.46M			3.44M		3.49M	3.42M	
									3.18W				3.19W		
3.16 S	3.14 S	3.16 S	3.16 S	3.15 S	3.16 S	3.16 S	3.16 S	3.15 S	3.14M	3.15M	3.16 S	3.16W	3.14M	3.15M	
3.01W	3.00W	3.00W	3.02W	3.01W	3.02W		3.04W	3.04W		2.96W	3.01W	2.97W	3.04W	2.99W	
							2.79W	2.77W	2.85W	2.86W			2.85W		
							2.71W						2.78W	2.57W	
2.58W	2.53W	2.57W	2.55W	2.54M	2.56W	2.55W	2.52W	2.52W	2.52W	2.55W	2.58W	2.56W	2.52W	2.53W	
2.41W	2.45W	2.41W	2.45W				2.38W						2.40W		

50%: Product of forward titration. 50%→H: Product of backward titration. 100%: Product of forward titration.
Abbreviations: S=strong, M=medium, W=weak.

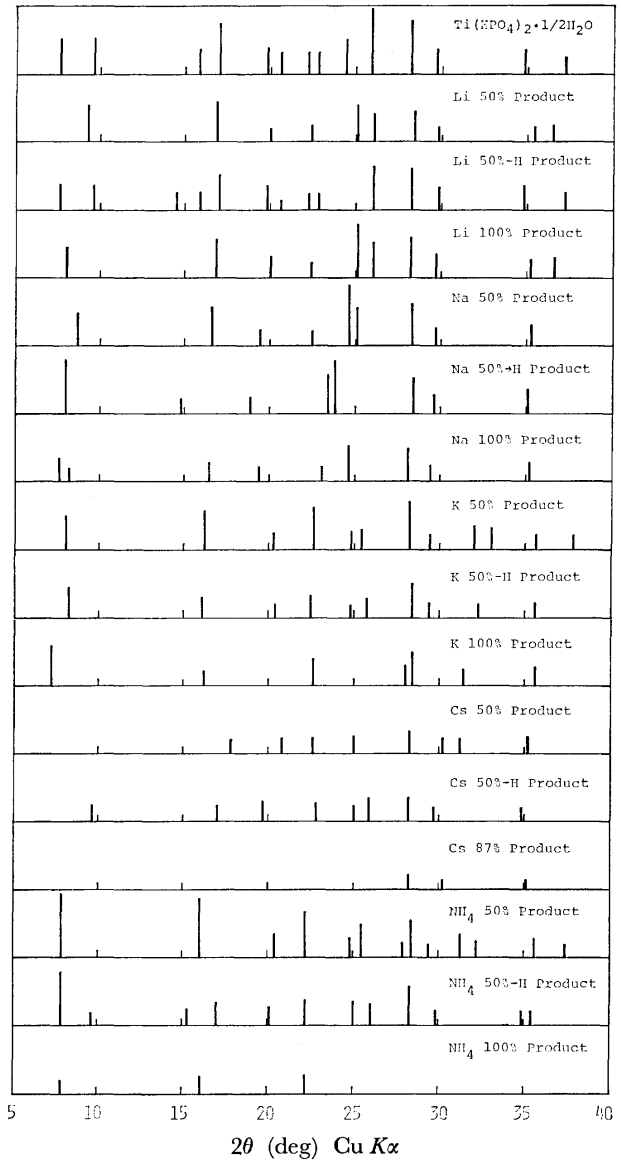

Fig. 9. X-Ray diffraction patterns of titanium hydrogen phosphate and its ion exchange products.

pattern decreased.

K^+ Exchanger: The X-ray diffraction lines at 11.6 and 9.21 Å, which characterized the hemihydrate, disappeared in the X-ray diffraction pattern of the 50% K product. The number of diffraction lines was reduced by a half in contrast with that in the case of the hemihydrate. The diffraction intensities however were increased considirably. As seen in Fig. 4, the 50% K product was in a state of equilibrium with the aqueous solution at pH 4.5. Thus, it is assumed that the composition of this product agrees with that of $TiKH(PO_4)_2 \cdot 0—1/2H_2O$. The X-ray diffraction pattern of a 50% K→H product did not change so much with that of the 50% K product. In an apparently 100% K product, the diffraction line at 12.3 Å reappeared and the intensity of all the diffraction lines increased. As seen in Fig. 4, the apparently 100% K product was in a state of equilibrium with the aqueous solution at pH 7.5. Therefore, it is assumed that the composition of the product agrees with that of $TiK_2(PO_4)_2 \cdot 0—1/2H_2O$.

Cs^+ Exchanger: The 50% Cs product was attacked by the CsOH aqueous solution, and the intensity of the X-ray diffraction pattern decreased. With an apparently 87% Cs product, the ion exchange reaction was not completed, being converted into an amorphous substance.

NH_4^+ Exchanger: In the 50% NH_4 product, the diffraction line at 11.3 Å appeared, and the intensity of all diffraction lines was relatively high. It is assumed from the forward titration curve in Fig. 6 that the product $TiNH_4H(PO_4)_2 \cdot 0—1/2H_2O$, is formed. The diffraction lines at 9.21, 5.21, and 3.42 Å, which characterize the hemihydrate, reappeared in the diffraction pattern of the 50% NH_4→H product. There is the possibility that the product was reconverted to the hemihydrate. The apparently 100% NH_4 product was attacked by the ammoniacal solution, and converted into an amorphous substance.

Composition of the Apparently 50% Ion Exchangers. From the view point of stability, $Ti(HPO_4)_2 \cdot 0—1/2H_2O$ possibly underwent ion exchange to become $TiMH(PO_4)_2 \cdot 0—1/2H_2O$. The conditions for preparation of the 50% products and their analytical results are summarized in Table 4.

From these results, the compositions of the 50% products were estimated as follows; $TiLi_{0.6}H_{1.4}(PO_4)_2 \cdot 1/2H_2O$, $TiNaH(PO_4)_2 \cdot 0.17H_2O$, $TiKH(PO_4)_2 \cdot 0.31H_2O$, $TiNH_4H(PO_4)_2 \cdot 1/2H_2O$, and $Ti_{0.8}Cs_{0.6}H_{2.3}(PO_4)_2 \cdot 0.11H_2O$. As described above, the products of $TiMH(PO_4)_2 \cdot 0—1/2H_2O$ readily obtained by the ion exchange of $Ti(HPO_4)_2 \cdot 0—1/2H_2O$ with Na, K, and NH_4 ions respectively. Ion exchange of the hemihydrate with Li or Cs ions, however, brought about conversion of $Ti(HPO_4)_2 \cdot 0—1/2H_2O$ to a non-stoichio-

Table 4. Preparation of apparently 50% ion exchange products and analysis

Salt	Reaction conditions: $Ti(HPO_4)_2$ (g)	0.1M-MOH[a] (ml)	Temp (°C)	Time (h)	Reaction products: Yield (g)	TiO_2 (%)	P_2O_5 (%)	H_2O (%)	M_2O[b] (%)	$TiO_2 : P_2O_5 : H_2O : M_2O$ (mole ratio)
Li salt	2.40	100	20	48	1.98	30.7	53.1	9.1	7.1	1.03 : 1.00 : 1.45 : 0.63
Na salt	4.80	200	20	48	4.76	30.1	53.4	4.4	12.1	1.00 : 1.00 : 0.65 : 0.52
K salt	4.80	200	20	48	4.73	28.9	49.6	5.1	16.4	1.05 : 1.00 : 0.81 : 0.50
Cs salt	2.40	87	20	48	1.37	20.1	46.0	6.3	27.6	0.78 : 1.00 : 1.25 : 0.30
NH_4 salt	4.86	200	20	48	4.63	31.1	55.1	7.3	6.5[c]	1.00 : 1.00 : 1.04 : 0.99[d]

a) MOH: LiOH, NaOH, KOH, CsOH. b) M_2O: Li_2O, Na_2O, K_2O, Cs_2O. c) % as NH_3. d) Mole ratio as NH_3.

metric compound.

References

1) a) Presented at the 37th National Meeting of the Chemical Society of Japan, Yokohama, April 1978; b) Part II of this series: E. Kobayashi, *Bull. Chem. Soc. Jpn.*, **51**, 2306 (1978).
2) C. B. Amphlett, "Inorganic Ion Exchangers," Elsevier Publishing Company, Amsterdam (1964), p. 15.
3) M. Abe, *Bunseki Kagaku*, **23**, 1254, 1561 (1974).
4) E. Kobayashi and T. Goto, *Kogyo Kagaku Zasshi*, **73**, 692 (1970); *Tokyo Kogyo Shikensho Hokoku*, **66**, 313 (1971).
5) E. Kobayashi, *Kogyo Kagaku Zasshi*, **73**, 1797 (1970); *Tokyo Kogyo Shikensho Hokoku*, **66**, 326 (1971).
6) E. Kobayashi, *Bull. Chem. Soc. Jpn.*, **48**, 3114 (1975); *Tokyo Kogyo Shikensho Hokoku*, **72**, 177 (1977).
7) G. Alberti, P. Cardini-Galli, U. Costantino, and E. Torracca, *J. Inorg. Nucl. Chem.*, **29**, 571 (1967).
8) K. Takaguchi and I. Tomita, *J. Chromatogr.*, **118**, 263 (1976).
9) K. Takaguchi and I. Tomita, The 34th National Meeting of the Chemical Society of Japan, April 1976, Abstr. No. II, 337.

Studies of Inorganic Ion Exchangers. IV.[1] Ion Exchange Equilibrium between Titanium(IV) Bis(hydrogenphosphate) and NaCl–KCl Aqueous Solution

Etsuro KOBAYASHI

National Chemical Laboratory for Industry, Hon-machi, Shibuya-ku, Tokyo 151

(Received July 27, 1978)

In order to develop an inorganic ion exchanger, ion exchange equilibriums between titanium(IV) bis(hydrogenphosphate) and NaCl–KCl aqueous solution have been investigated together with the possibility of separation of Na and K ions. A suitable quantity of $Ti(HPO_4)_2 \cdot H_2O$ (monohydrate), or $Ti(HPO_4)_2$ (anhydrate) was added to a fixed volume of the mixed solution of 0.1 M NaCl with 0.1 M KCl at various ratios. The Na and K ions in the equilibrium solution were determined, and the mole fractions of the ions distributed in the liquid and solid phases estimated. When 0.1 or 0.5 g of the monohydrate were added to 10 ml of each initial solution, the sum of the ion exchange capacities for Na and K ions was approx. 0.1—0.3 meq/g. When 0.1 g of the anhydrate were added to 10 ml of each of the initial solutions, the pH of the final solutions showed values in the range of 1.6—1.9. With the mole fractions of KCl/(NaCl+KCl) above 0.5 in the initial solution, only 2.5—3.5 meq/g of the K ion adsorbed. With an excess (0.5 g exchanger to 10 ml soln) of the anhydrate, all K ions and a part of Na ions were removed together from the solution with the mole fractions of KCl/(NaCl+KCl) being in a range of 0—0.8. The K ion could be effectively separated, when a suitable amount of the anhydrate was added to a solution containing approx. an equimole of NaCl and KCl; however, the elution of K ion with HCl could not be eased by this static method.

Titanium phosphate has been of recent interest as an inorganic ion exchanger similar to zirconium phosphate.[2] In order to develop an ion exchanger for industrial use, titanium(IV) bis(hydrogenphosphate) hemihydrate ($Ti(HPO_4)_2 \cdot 1/2H_2O$) has been synthesized by refluxing amorphous titanium(IV) phosphate with concentrated phosphoric acid.[3] The X-ray diffraction pattern of the hemihydrate differs from that of the titanium(IV) bis(hydrogenphosphate) monohydrate ($Ti(HPO_4)_2 \cdot H_2O$), known already.[4] It has been observed that the hemihydrate has an ion exchangeability toward ions of large size, such as the potassium ion. Further more, $Ti(HPO_4)_2 \cdot 0—1/2H_2O$ was prepared[5] by refluxing concentrated phosphoric acid with a sulfuric acid solution of $TiOSO_4$, the intermediate in the production process of titanium(IV) oxide. In a previous work,[1] the ion exchange properties of the hemihydrate towards alkali metals and ammonium ions have been reported where it was found that the equilibrium ion exchange capacities (Q^A) of the hemihydrate towards Na and K ions were larger than those of the monohydrate, and that the selectivity quotient (K_H^M) and distribution coefficient (K_D) increased in the order $Cs^+ < Li^+ < NH_4^+ < Na^+ < K^+$. This result will aid in the separation of the Na and K ions. In the present work, the ion exchange equilibria between titanium(IV) bis(hydrogenphosphate) and NaCl–KCl aqueous solutions have been examined under various conditions. It has been confirmed that the K ion can be selectively separated from an aqueous solution containing approx. equivalent moles of Na and K ions. In this paper, the experimental data derived will be presented.

Experimental

Preparation of Ion Exchangers. Titanium(IV) bis(hydrogenphosphate) were prepared by the refluxing methods described in previous reports.[3,5] The composition of the monohydrate and hemihydrate, were found as follows: TiO_2, 31.1%; P_2O_5, 54.6%; H_2O, 14.4%; giving an empirical formula of $Ti(HPO_4)_2 \cdot H_2O$. For the hemihydrate: TiO_2, 33.1%; P_2O_5, 58.8%; H_2O, 7.7%; giving the formula as the anhydrous salt, $Ti(HPO_4)_2$.

Ion Exchange Equilibrium and Analysis of Na and K Ions. The ion exchanger (0.100 g) was placed in a 20 ml stoppered test tube, and the initial solution (10 ml), varying in volume ratio of 0.1 M NaCl and 0.1 M KCl added. The contents were shaken periodically and the pH of the supernatant liquid measured after 48 h. A portion of the supernatant liquid (5.00 ml) was taken, and diluted with distilled water to 1000 ml and the Na and K ions determined using a flame photometer at 589 and 768 nm, respectively.

Separation of K Ion from NaCl–KCl Aqueous Solution. The solution mixed in the proper ratio of 0.1 M NaCl and 0.1 M KCl (100 ml) was placed in a 300 ml stoppered Erlenmeyer flask, and to this $Ti(HPO_4)_2$ (2.00 g) was added. The contents of the flask were periodically shaken and the pH of the supernatant liquid and the concentration of Na and K ions determined after 48 h. The ion exchanger was separated from the mother liquor using a centrifugal separator. The adsorbed Na and K ions in the solid phase were eluted with 0.1, 0.5, 1, and 5 M HCl (100 ml) respectively. The K ion in the effluent was determined by flame photometry.

Results and Discussion

Ion Exchange Equilibrium between Titanium(IV) Bis(hydrogenphosphate) and NaCl–KCl Aqueous Solution. When the powder of titanium(IV) bis(hydrogenphosphate) was added to the initial solution varying ratio in volume of 0.1 M NaCl with 0.1 M KCl, the mole fractions of Na and K ions, estimated from the analytical data, are shown in Figs. 1—4.

In No. 1 (Fig. 1), the monohydrate (0.1 g) as ion exchanger was added to the initial solution (10 ml). Consequently, the mole fraction ratios of the Na and K ions in the final solutions were approx. the same as those of the mole fraction of 0.1 M NaCl and 0.1 M KCl in the initial solution at all times and this is indicated by the straight line dividing the L–Na^+ and L–K^+ areas, as seen in Fig. 1. The sum of the mole fractions of the Na and K ions in the solid phase was

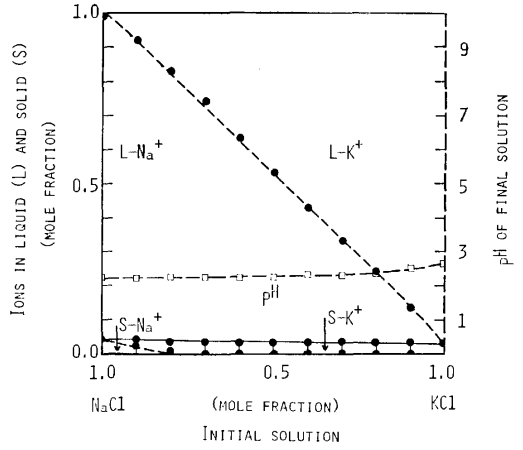

Fig. 1. Distribution of ions in liquid and solid phases on the equilibrium between 0.1 g of $Ti(HPO_4)_2 \cdot H_2O$ and 10 ml of M/10 MCl.

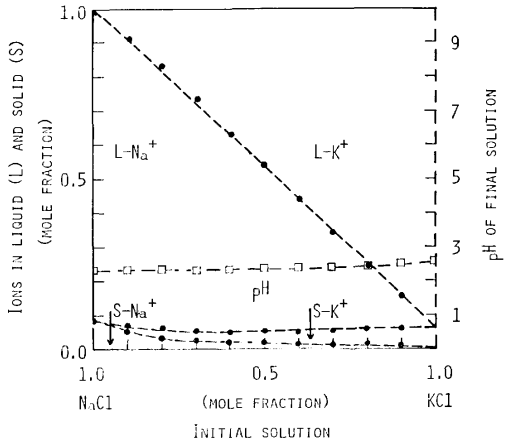

Fig. 2. Distribution of ions in liquid and solid phases on the equilibrium between 0.5 g of $Ti(HPO_4)_2 \cdot H_2O$ and 10 ml of M/10 MCl.

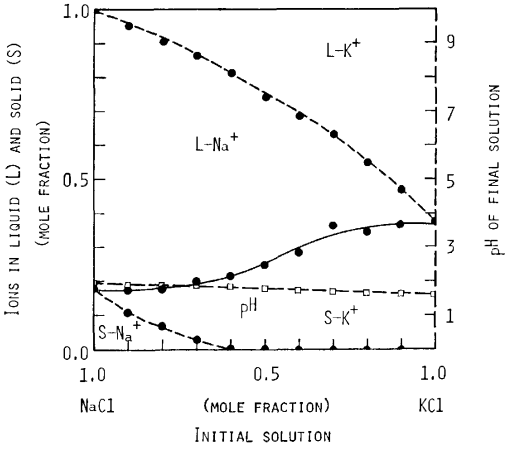

Fig. 3. Distribution of ions in liquid and solid phases on the equilubrium between 0.1 g of $Ti(HPO_4)_2$ and 10 ml of M/10 MCl.

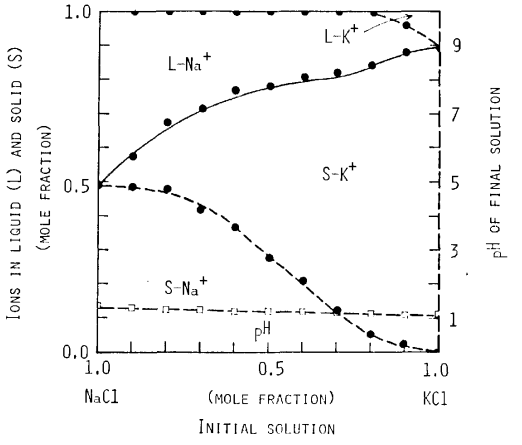

Fig. 4. Distribution of ions in liquid and solid phases on the equilibrium between 0.5 g of $Ti(HPO_4)_2$ and 10 ml of M/10 MCl.

0.03—0.04, a value equivalent to the mole fraction of the H^+ in the final solution, corresponding to an ion exchange capacity of 0.3—0.4 meq/g, *i.e.* the ion exchange capacity of the monohydrate was considerably smaller in weakly acid solution (pH 2.2—2.7). In the mole ratio range 1.0—0.8 (NaCl to NaCl+KCl), the Na ion was absorbed together with the K ion in the solid phase. In the mole ratio 0.8—0.0 (NaCl to NaCl+KCl), only the K ion was adsorbed. However, the ion exchange capacity was small as mentioned above.

In No. 2 (Fig. 2), the monohydrate (0.5 g) was added to the initial solution (10 ml). In this case, the sum of the mole fractions of Na and K ions adsorbed in the solid phase was 0.05—0.08. The ion exchange capacity however was 0.10—0.16 meq/g, and decreased more than No. 1. Both Na and K ions were adsorbed in the solid phase regardless of the mole ratio of NaCl with KCl in the initial solution, *i.e.* neither ion could be separated.

In No. 3 (Fig. 3), the anhydrate (0.1 g) as ion exchanger was added to the initial solution (10 ml). The pH of the final solution showed values in the range 1.6—1.9, and this value decreased gradually with increasing mole fraction of potassium chloride in the final solution. The sum of the mole fractions of Na and K ions adsorbed in the solid phase was 0.18—0.38 corresponding to an ion exchange capacity of 1.8—3.8 meq/g, *i.e.* the ion exchange capacity of the anhydrate was 3.6—4.7 times higher than that of the monohydrate. With a mole ratio of NaCl to NaCl+KCl in the initial solution in the range 0.0—0.5, the ion exchange capacities were 2.5—3.8 meq/g and only the K ion was adsorbed. The above results show that the Na and K ions remained considerably in the final solution, although the anhydrate exhibited selective adsorptive behaviour towards the K ion. Consequently, five times the anhydrate in No.4 (Fig. 4) was used compared to No.3. The sum of the mole fractions of Na and K ions in the solid phase was 0.49—0.89, 2.5 times greater than the sum in No. 3. but the ion exchange capacities derived from the mole fractions were 0.98—1.78 meq/g. When the mole ratio of NaCl to NaCl+KCl was 1.0—0.2, all K ions contained in the solution were adsorbed completely. However, at all points of the mole ratio of NaCl to NaCl+KCl, both the Na and K ions were adsorbed into the solid phase,

Table 1. The distribution of ions in the solid and liquid phases

Ion exchanger $Ti(HPO_4)_2$ No.	(g)	Initial solution M/10 NaCl (ml)	M/10 NaOH (ml)	M/10 KCl (ml)	M/10 KOH (ml)	Final Solid Na^+	Solid K^+	Liquid Na^+ (mole fraction)	Liquid K^+	pH
	0.1	6.0	4.0	—	—	0.34	0.00	0.66	0.00	5.50
	0.1	5.4	3.6	0.6	0.4	0.25	0.10	0.64	0.01	5.50
	0.1	4.8	3.2	1.2	0.8	0.17	0.18	0.62	0.03	5.60
	0.1	4.2	2.8	1.8	1.2	0.11	0.25	0.58	0.06	5.86
	0.1	3.6	2.4	2.4	1.6	0.07	0.30	0.52	0.11	5.72
5	0.1	3.0	2.0	3.0	2.0	0.05	0.32	0.46	0.19	5.86
	0.1	2.4	1.6	3.6	2.4	0.03	0.34	0.38	0.25	5.28
	0.1	1.8	1.2	4.2	2.8	0.01	0.39	0.25	0.35	5.25
	0.1	1.2	0.8	4.8	3.2	0.00	0.40	0.19	0.41	5.22
	0.1	0.6	0.4	5.4	3.6	0.00	0.41	0.09	0.50	5.14
	0.1	—	—	6.0	4.0	0.00	0.42	0.00	0.58	4.00
	0.1	2.0	8.0	—	—	0.64	0.00	0.36	0.00	7.60
	0.1	1.8	7.2	0.2	0.8	0.56	0.08	0.35	0.01	7.64
	0.1	1.6	6.4	0.4	1.6	0.47	0.17	0.33	0.03	7.82
	0.1	1.4	5.6	0.6	2.4	0.38	0.26	0.29	0.07	7.82
	0.1	1.2	4.8	0.8	3.2	0.33	0.31	0.25	0.11	8.02
6	0.1	1.0	4.0	1.0	4.0	0.31	0.35	0.19	0.15	8.10
	0.1	0.8	3.2	1.2	4.8	0.27	0.39	0.13	0.21	8.08
	0.1	0.6	2.4	1.4	5.6	0.23	0.43	0.03	0.31	7.70
	0.1	0.4	1.6	1.6	6.4	0.18	0.46	0.03	0.33	7.66
	0.1	0.2	0.8	1.8	7.2	0.12	0.50	0.02	0.36	7.60
	0.1	—	—	2.0	8.0	0.00	0.58	0.00	0.42	7.36

i.e. it was impossible to separate them. This is the manner in which an excess of ion exchanger is employed toward both ions in the initial solution. Thus, it may be expected from experiments Nos. 3 and 4 that the selective adsorption of the anhydrate towards the K ion is achieved.

Effects of pH *on Ion Exchange Equilibrium.* Generally, the ion exchange capacity of an acid salt as an ion exchanger increased with a rise in pH of the aqueous solution. In a previous work,[1] the equilibrium ion exchange capacities of titanium(IV) bis(hydrogenphosphate) with the alkali metal and ammonium chlorides, and the saturation ion exchange capacities have been estimated. As a direct consequence of this the values of the latter at pH 4.5 were larger than those of the former measured in the acid liberated from the ion exchange. In the present study, the ion exchange equilibrium between $Ti(HPO_4)_2$ and a weak acid-neutral aqueous solution containing the Na and K ions has been examined, the results of which are given in Table 1.

In No. 5 (Table 1), the mole ratio of the sodium and potassium chlorides with the sodium and potassium hydroxides in the initial solution was adjusted to 6 : 4 and consequently the pH values of the initial solutions were about 12.7. On adding the anhydrate to the alkaline aqueous solutions, an ion exchange reaction took place and consequently the pH of the solution dropped to betweeen 4.0 and 5.5. The ion exchange capacities of the anhydrate toward the Na and K ions were 3.4 and 4.2 meq/g at pH 5.5 and 4.0, respectively. The ion exchange capacity toward the K ion did not greatly increase in comparison with that estimated in the acid aqueous solutions of No. 3 (3.8 meq/g).

In No. 6 (Table 1), the mole ratio of the chloride and hydroxide was adjusted to 2 : 8 in the initial solution. The pH values of the initial solutions were about 13.0. When anhydrate was added to the alkaline aqueous solutions, the pH of the solution changed, lying in the range 7.4—8.1. The ion exchange capacities of the anhydrate toward Na and K ions were 6.4 and 5.8 meq/g, respectively. In the presence of both Na and K ions the sum of the ion exchange capacities for both ions was about 6 meq/g in all cases. In that case neither ion could be separated despite the ratio of the Na and K ions in the initial solution.

The ion exchange isotherms for the Na and K ions in Nos. 3, 5, and 6 are shown in Fig. 5.

As reported earlier in No.3, the solutions were acidified by the ion exchange reaction. K ions were adsorbed on the ion exchanger when fractions of K ion in the final solution were in the range of 0.33—1.00 as shown by the isotherm. The ion exchange capacities increased as the pH of the final solution increased. However, it is clear from the isotherms in Nos. 5 and 6 that the separation of Na and K ions using the anhydrate may be progressively more difficult with the increase in pH of the final solution.

Separation of Na^+ with K^+ and Elution of K^+ from Ion Exchanger. From the above results the separation of K ion from a NaCl–KCl solution, such as sea water which contains a small quantity of KCl to NaCl, is

TABLE 2. THE SEPARATION OF Na WITH K IONS FROM THE NaCl-KCl MIXED SOLUTION AND THE ELUTION OF POTASSIUM ION

Ion exchanger $Ti(HPO_4)_2$ (g)	Initial solution			Final					Ions released from solid	
				Solid		Liquid			Elute	
	M/10 NaCl (ml)	M/10 KCl (ml)	$\frac{K}{Na+K}$ (wt %)	Na^+	K^+	Na^+ (mole fraction)	K^+	pH		K^+ (%)
2.00	40	60	66	0.00	0.42	0.40	0.18	1.44	0.1 M HCl	4.2
2.00	50	50	56	0.02	0.40	0.48	0.10	1.43	0.1 M HCl	4.1
2.00	50	50	56	0.03	0.41	0.47	0.09	1.43	0.5 M HCl	6.0
2.00	50	50	56	0.02	0.40	0.48	0.10	1.44	1.0 M HCl	10.5
2.00	50	50	56	0.03	0.40	0.47	0.10	1.43	5.0 M HCl	35.5
2.00	60	40	49	0.05	0.35	0.55	0.05	1.43	0.1 M HCl	4.1

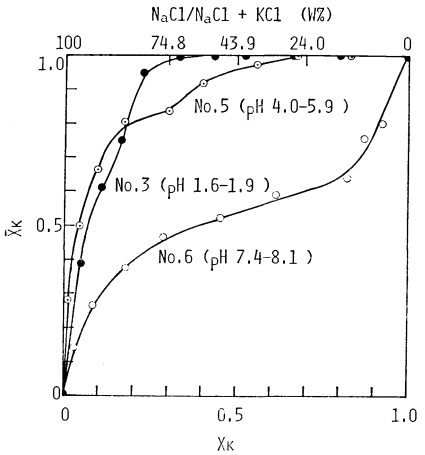

Fig. 5. Ion exchange isotherms between potassium and sodium ions on $Ti(HPO_4)_2$.
X_k: the mole fraction of K^+ in the solution.
$\bar{X}_k$: the mole fraction of K^+ in the exchanger.

difficult. However, K ions can be separated in high yield from an aqueous solution containing approx. an equivalent mole of NaCl and KCl, using an appropriate amount of ion exchanger. The separation of both ions using $Ti(HPO_4)_2$ and the elution of K ion are summarized in Table 2.

These experiments confirm that the K ion can be adsorbed in the solid pahse and that most of the Na ions remain in the liquid phase. With hydrochloric acid as the eluate in the static method, the adsorbed K ions were not released completely from the ion exchanger since the selectivity quotient (K_H^M) of $Ti(HPO_4)_2 \cdot 0—1/2H_2O$ toward K ion is larger than that of the hemihydrate toward other ions as reported in a previous paper.[1] When $Ti(HPO_4)_2$ was used as the ion exchanger for the separation of K ion, the release of K ion was not smooth. The granulation of $Ti(HPO_4)_2$ and the recovery of K ion by the column method need further study.

References

1) a) Presented at the 38th National Meeting of the Chemical Society of Japan, Nagoya, October 1978; b) Part III of this series: E. Kobayashi, *Bull. Chem. Soc. Jpn.*, **52**, 1351 (1979).
2) S. Allulli, C. Ferragina, A. La Cinestra, M. A. Massucci, and N. Tomassini, *J. Inorg. Nucl. Chem.*, **39**, 1043 (1977).
3) E. Kobayashi, *Bull. Chem. Soc. Jpn.*, **48**, 3114 (1975); *Tokyo Kogyo Shikensho Hokoku*, **72**, 177 (1977).
4) G. Alberti, P. Cardini-Galli, U. Costantino, and E. Torracca, *J. Inorg. Nucl. Chem.*, **29**, 571 (1967).
5) E. Kobayashi, *Bull. Chem. Soc. Jpn.*, **51**, 2306 (1978).

Preparation, Optical Resolution, Racemization, and Ligand Isotopic Exchange of Tris(1,3-diphenyl-1,3-propanedionato)-germanium(IV) Perchlorate in Acetonitrile

Fumio B. UENO, Akira NAGASAWA, and Kazuo SAITO*

Chemistry Department, Faculty of Science, Tohoku University, Aoba, Aramaki, Sendai 980

(Received July 17, 1978)

Tris(1,3-diphenyl-1,3-propanedionato)germanium(IV) $[Ge(bzbz)_3]^+$ was prepared as crystalline perchlorate, and resolved by the crystallization of its salt with hydrogen (*R,R*)-*O,O*-dibenzoyltartrate. The patterns of UV and circular dichroism spectra are very similar to those of $[Si(bzbz)_3]ClO_4$. The racemization of the *Δ*-$[Ge(bzbz)_3]ClO_4$ was studied kinetically in acetonitrile at 40—60 °C to find the rate law: Rate$=k_{rac}$[complex], where $k_{rac}=9.86\times10^{-5}$ s^{-1} at 50 °C. The activation parameters ($\Delta H^*=99\pm2$ kJ mol^{-1} and $\Delta S^*=-17\pm2$ J K^{-1} mol^{-1}) are very similar to those of tris(acetylacetonato)germanium(IV) complex. Compared with the rate of ligand isotopic exchange, the racemization should proceed *via* intramolecular mechanism. The steric effect coming from the substituents on the chelate ring should play an important role in determining the racemization rate.

We had studied the kinetics of racemization and ligand isotopic exchange of tris(acetylacetonato)germanium(IV) $[Ge(acac)_3]^+$.[1,2] With aims of understanding the detailed processes of the intramolecular racemization of tris(*β*-diketonato)germanium(IV) complex, our study has been extended to tris(1,3-diphenyl-1,3-propanedionato)germanium(IV) $[Ge(bzbz)_3]^+$. The pK_a value (K_a; acid dissociation constant) of 1,3-diphenyl-1,3-propanedione (Hbzbz) is greater by ten times than that of acetylacetone, and different electronic and steric effects are expected. This paper deals with the synthesis, the resolution and the kinetics of racemization in acetonitrile of this new complex.

Experimental

Materials. Preparation of $[Ge(bzbz)_3]ClO_4$ and $[Ge(bzbz)_3]Cl$: $[Ge(acac)_3]ClO_4$ was synthesized by the reported procedure.[1] An acetonitrile solution (80 cm^3) of $[Ge(acac)_3]ClO_4$ (2.8 g, 6.0×10^{-3} mol) and Hbzbz (14.8 g, 6.6×10^{-2} mol) was refluxed with stirring at *ca.* 110 °C for *ca.* 120 h, and poured into diethyl ether (500 cm^3). The yellow precipitates were filtered off and recrystallized from acetonitrile by adding diethyl ether. Pale-yellow needles melted at 289 °C with decomposition, and are soluble in acetonitrile, chloroform, acetone, nitromethane and glacial acetic acid. Found: C, 64.10; H, 4.21; Ge (as GeO_2 in ash), 8.85%. Calcd for $C_{45}H_{33}O_{10}ClGe$: C, 64.19; H, 3.95; Ge, 8.62%. The UV absorption spectra in acetonitrile are shown in Fig. 1. The IR absorption pattern in KBr disc is very similar to that of $[Si(bzbz)_3]ClO_4$. ^{1}H-NMR spectra in CD_3CN show phenyl peaks at 8.1—8.2(*ortho*), 7.65(*meta*), 7.5(*para*) ppm and a methine peak at 7.75 ppm *vs.* tetramethylsilane (TMS).

$[Ge(bzbz)_3]Cl$ was prepared by treating $[Ge(bzbz)_3]ClO_4$ with the anion exchange resin Amberlyst A-26 (Cl^--type) in acetonitrile, and crystallized by adding diethyl ether.

Optical Resolution: $[Ge(bzbz)_3]Cl$ (320 mg, 8.5×10^{-4} mol) was dissolved in 56 cm^3 of acetonitrile-acetone (5 : 2), and treated with sodium hydrogen (*R,R*)-*O,O*-dibenzoyltartrate (340 mg, 8.5×10^{-4} mol) in 24 cm^3 of aqueous acetone (5 : 1). Two hundred cm^3 of water was dripped to the solution at a rate of 3 cm^3 per minute with stirring at room temperature to give oily precipitates, which were recrystallized from acetonitrile by adding diethyl ether. A solution of this diastereoisomer (0.8 g, 7.2×10^{-4} mol) and magnesium perchlorate (1.0 g, 4.5×10^{-3} mol) in 60 cm^3 of glacial acetic acid was poured into diethyl ether to give partially resolved, optically active $[Ge(bzbz)_3]ClO_4$, which was collected by filtration. The product was fractionally crystallized from chloroform solution by adding diethyl ether. (yield *ca.* 10%) Circular dichroism spectrum of the partially resolved complex is shown in Fig. 1. (The optical resolution seems to be *ca.* 6% in this case.)

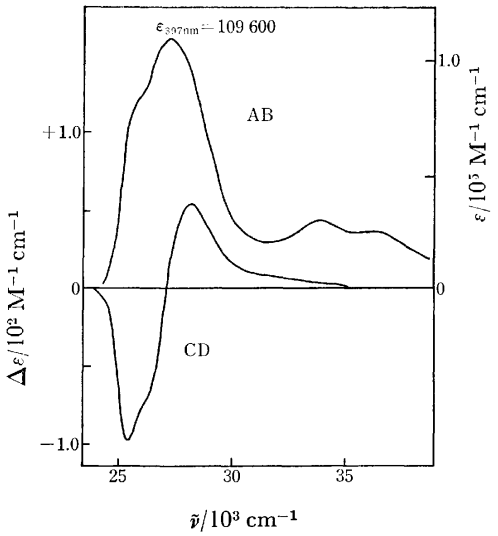

Fig. 1. Ultraviolet absorption (AB) and circular dichroism (CD) spectra of $(-)_{589}$-$[Ge(bzbz)_3]ClO_4$ in acetonitrile.

Other Reagents: Acetonitrile, trichloroacetic acid, pyridine, and tetraethylammonium perchlorate were purified by the ordinary methods. The labelled Hbzbz(Hbzbz[^{14}C]) was prepared by the Claisen condensation between ethyl benzoate[^{14}C] and acetophenone, and purified by recrystallization from ethanol (specific radioactivity; 19.1 mCi/g).

Kinetic Procedure. Racemization: Acetonitrile solution containing the optically active $[Ge(bzbz)_3]ClO_4$, and other reagents whenever necessary, was kept in a thermostatted cell at 40 to 60 °C (±0.1 °C), and the progress of racemization was followed by observing the CD strength at a proper wavelength in the range from 390 to 414 nm. The UV spectra of the reaction mixtures were also recorded before and after the kinetic runs. The water content in the complex solution was determined by Karl Fischer titration.

Isotopic Exchange: The complex and Hbzbz[^{14}C] were dissolved in acetonitrile. Aliquots were sealed in pyrex-glass tubes and placed in a thermostat (60 and 90 °C). The ampoules were chilled one by one at proper time intervals, and the contents were poured into cold diethyl ether. Precipitated $[Ge(bzbz)_3]ClO_4$ was filtered off, dried *in vacuo*, and dissolved in acetonitrile. The solution was divided into two portions. One portion was mixed with *p*-bis(5-phenyl-2-oxazolyl)benzene(POPOP) solution in toluene and the β-activity was counted with a liquid scintillation counter. Another portion was diluted with acetonitrile and the extinction was measured at 377 nm to find the concentration of the complex. The rate of isotopic exchange was calculated on the basis of the change of specific activities of the complex by McKay's formula.[5]

Apparatus. Hitachi 323 Spectrophotometer and JASCO model J-40 Spectropolarimeter were used for recording the UV absorption and CD spectra respectively. The β-activity of ^{14}C was recorded with a Nuclear Chicago Unilux II-A Liquid Scintillation Counter.

Results

The Kinetics of Racemization in Acetonitrile. The logarithm of CD strength decreased linearly with the reaction time. The extinction of UV spectra remained unchanged during several half-lives, and the decrease in CD strength should be due to intrinsic racemization of the complex. The rate was proportional to the complex concentration (5×10^{-6} to 5×10^{-3}M) (Fig. 2), and expressed by the rate law

$$\text{Rate} = k_{obsd}[\text{complex}] = 2k_{rac}[\text{complex}]. \quad (1)$$

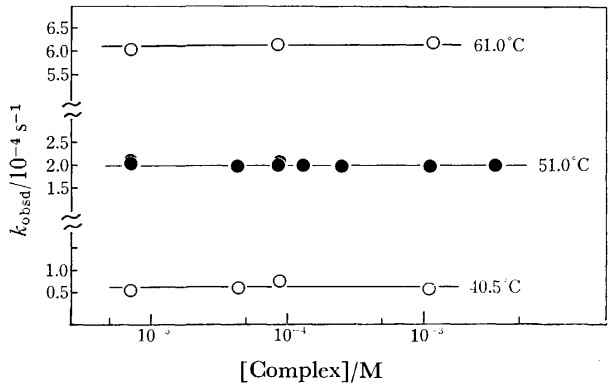

Fig. 2. Influence of the complex concentration upon k_{obsd} in acetonitrile.

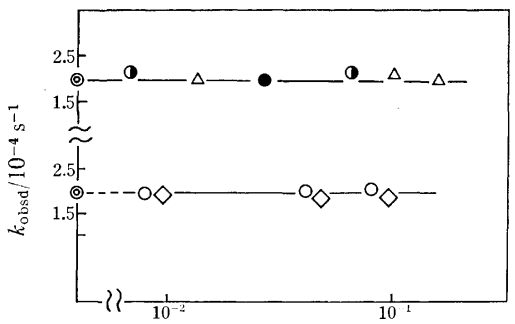

Fig. 3. Influence of water, acid, pyridine, free ligand, and tetraethylammonium perchlorate concentration upon the racemization rate in acetonitrile at 51 °C. △: Water, ◇: trichloroacetic acid, ○: pyridine, ●: dibenzoylmethane, ◑: tetraethylammonium perchlorate, and ◎: without any reagent.

Water (10^{-3} to 10^{-1}M) gave no influence on the racemization rate. (Fig. 3.) Neither did free Hbzbz, trichloroacetic acid, and pyridine in the concentration ranges given in Fig. 3. The rate is insensitive to the ionic strength ($<6.5\times10^{-2}$ mol dm^{-3} by tetraethylammonium perchlorate.) The rate constants and activation parameters are shown in Table 1.

Ligand Isotopic Exchange. Experimental conditions were as follow: $[Ge(bzbz)_3ClO_4]=3.95\times10^{-3}$ M, $[Hbzbz\text{-}^{14}C]=4.97\times10^{-2}$ M, $[H_2O]=3.17\times10^{-2}$ M. No exchange was observed at 60 °C within 1500 min. However, at 90 °C, the ligand exchange was observed and the following rate law was obtained.

$$\text{Rate} = k_{obsd}[\text{complex}],\ k_{obsd} = 2.18\times10^{-8}\ \text{s}^{-1} \quad (2)$$

Discussion

Bond Rupture Mechanism. The results are summarized in Table 1 together with those of the related complexes. The $[Ge(bzbz)_3]^+$ racemizes faster but exchanges the ligand slower than $[Ge(acac)_3]^+$ does. Absence of solvolysis, hydrolysis and ligand isotopic exchange at 40 to 60 °C under the given conditions indicates that the racemization proceeds *via* an intramolecular mechanism. Absence of influence of the concentrations of the complex and the free ligand on the rate also supports this mechanism. The rate

Table 1. Rate constants and activation parameters for the racemization and the ligand isotopic exchange in acetonitrile

Complex[a]	pK_a of ligand[b]	k_1(50 °C) / 10^{-5} s^{-1}	ΔH^* / kJ mol^{-1}	ΔS^* / J K^{-1} mol^{-1}	k_2 / s^{-1}	k_{ex}(90 °C) / s^{-1}
$[Ge(acac)_3]^+$	11.8	2.88	102±2	−18±6	2.7×10^{-4}	6.48×10^{-6} [c]
$[Ge(bzbz)_3]^+$	13.4	9.86	99±2	−17±2	0[d]	2.18×10^{-8}
$[Si(acac)_3]^+$	11.8	3.87	108±1	+2	1.5×10^{-1}	Not observed within 10 h at 50 or 60 °C
$[Si(bzbz)_3]^+$	13.4 (9.70)[e]	5.46	105±4	−4	0[d]	
$[Si(meacac)_3]^+$	(11.8)[e]	180	117±4	+59	3.0×10^{-2}	

Racemization rate: $R=(k_1+k_2[\text{base}])[\text{complex}]$, Ligand isotopic exchange rate: $R=k_{ex}[\text{complex}]$

a) Counter anion is ClO_4^- in all cases. b) In CH_3OH, from Ref. 4. c) Calculated from activation parameters in Ref. 2, and $[H_2O]=3\times10^{-2}$ M. d) Pyridine has no catalitic action in this case. e) In 50% aqueous dioxan, Ref. 6.

was not influenced by water, trichloroacetic acid, pyridine and tetraethylammonium perchlorate. These facts might appear to be consistent with the twist mechanism without bond break throughout the racemization. However, we tend to think that the present racemization proceeds *via* bond break mechanism, by comparing the activation parameters with those of related compounds. Racemization of $[Ge(acac)_3]^+$ was claimed to involve a solvent assisted break of Ge–O bond, on the basis of solvent effect (*i.e.* linear correlation between the racemization rate and the nucleophilicity of the solvents[1]). The ΔH^* and ΔS^* values of the present racemization are very similar to those for the $[Ge(acac)_3]^+$ complex.

Jones and Fay studied the geometrical isomerization of dihalobis(β-diketonato)germanium(IV) in an equimolar mixture of diphenylmethane and 1,3-dimethoxybenzene by the nmr line broadening technique and proposed an intramolecular mechanism involving the break of one Ge–O bond. The activation enthalpy and entropy are respectively 103±6 kJ mol^{-1}, −5±13 J mol^{-1} K^{-1} for $[GeCl_2(dpm)_2]$ (dpm; enolate anion of 2,2,6,6-tetramethyl-3,5-heptanedione). These values are also very similar to ours, and provide support to the postulation that the racemization involves one Ge–O bond break as rate determining step.

$[Ge(bzbz)_3]^+$ with a more basic ligand racemizes faster than $[Ge(acac)_3]^+$. If the racemization rate were governed by the ease of bond break alone, the rate should depend directly on the pK_a of the free ligand. Hence, some other factors must be encountered. The proposed mechanism is visualized in Fig. 4. We studied the racemization kinetics of some tris (β-diketonato)silicon(IV) complexes[3], and found that the $[Si(meacac)_3]^+$(meacac; enolate anion of

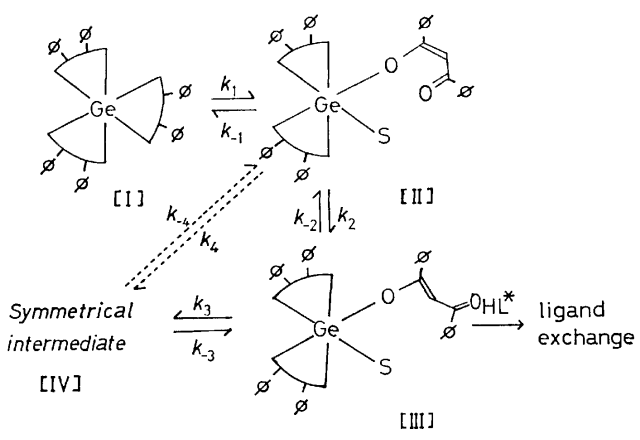

Fig. 4. Racemization mechanism of $[Ge(bzbz)_3]^+$ in acetonitrile.
S; Solvent molecule (acetonitrile). The present kinetics was studied only in acetonitrile because of the solubility, and the role of solvent molecules was not examined. From the analogy to the racemization mechanism of $[Ge(acac)_3]^+$, however, the vacant coordination site formed by the break of one Ge–O bond is likely to be occupied by an acetonitrile molecule (donor number 14.1).[8] HL*; labelled Hbzbz.

3-methyl-2,4-pentanedione)racemizes faster in acetonitrile than $[Si(acac)_3]^+$ does, despite of the larger pK_a of Hmeacac than Hacac. This observation was interpreted by Eq. 3 by considering a mechanism similar to Fig. 4.

$$k_{rac} = k_1 \frac{k_2}{k_{-1}+k_2} \frac{k_3}{k_{-2}+k_3}, \quad (3)$$

where k_1, k_{-1}, k_2, k_{-2}, and k_3 are the rates of Si–O bond break, ring closure, isomerizations of the unidentate ligand (from *cis* to *trans* and *vice versa*) and twist around Si(IV) respectively. The branching ratio $k_2k_3/(k_{-1}+k_2)(k_{-2}+k_3)$ for the meacac complex was considered to be greater than that for the acac complex on the basis of large steric interaction among the methyl groups in the state coresponding to II. A similar interpretation would be applicable to the present racemization, if the branching ratio were greater for the bzbz complex than for the acac complex. This assumption does not seem inadequate because molecular model studies disclose that more repulsive interaction is expected in II around the methine proton for the bzbz complex than for acac complex. However, there remains a possibility that the symmetrical transition state (IV) might be formed directly from II, so that the branching ratio is modified to $k_4/(k_4+k_{-1})$. Nevertheless a steric factor coming from the terminal group must be responsible for the faster racemization of $[Ge(bzbz)_3]^+$ than $[Ge(acac)_3]^+$.

On the other hand, the ligand isotopic exchange of $[Ge(bzbz)_3]^+$ is slower by *ca.* 300 times than of $[Ge(acac)_3]^+$ at 90 °C. On the basis of the ΔS^* value and the deuterium isotopic effect,[2] the isotopic exchange was claimed to be mostly governed by the ease of proton transfer from Hacac* to acac$^-$ in an intermediate of the form $[Ge(O,O\text{-acac})_2(O\text{-acac})(O\text{-acac*}\ H)]^+$. If this mechanism commonly operates in the ligand isotopic exchange of $[Ge(bzbz)_3]^+$, increase in bulkiness of the terminal groups in the ligand will decrease the ease of proton transfer to result in slower isotopic exchange.

The authors wish to thank the Ministry of Education for the Great-in-Aid.

References

1) A. Nagasawa and K. Saito, *Bull. Chem. Soc. Jpn.*, **47**, 131 (1974).
2) A. Nagasawa and K. Saito, *Bull. Chem. Soc. Jpn.*, **51**, 2015 (1978).
3) T. Inoue and K. Saito, *Bull. Chem. Soc. Jpn.*, **46**, 2417 (1973).
4) D. C. Luehrs, R. T. Iwamoto, and J. Kleinberg, *Inorg. Chem.*, **4**, 1738 (1965).
5) H. A. C. McKay, *Nature*, **142**, 997 (1938).
6) "Stability Constants," The Chemical Society, London (1964), 482.
7) R. W. Jones, Jr., Ph. D. dissertation, Cornell University, Ithaca, N. Y. (1971).
8) V. Gutmann, "Coordination Chemistry in Non-Aqueous Solutions," Springer, Berlin (1968), 19.

Precise Coulometric Titration of the Potassium Hydrogen Phthalate (NBS-SRM 84d). The Use of the Faraday Constant as an International Standard†

Takayoshi YOSHIMORI* and Tatsuhiko TANAKA

Faculty of Engineering, Science University of Tokyo, Kagurazaka, Shinjuku-ku, Tokyo 162

(Received July 28, 1978)

The purity of the potassium hydrogen phthalate (NBS SRM 84d) was determined by precise coulometric titration. The purity obtained was 99.995±0.002% (standard deviation: 0.003%), and was in excellent agreement with the purities of the same SRM determined already in three laboratories in U.S.A. These results support the recommendation on the use of the Faraday constant as an international standard for titrimetric analysis.

In 1974, the Commission V.5 of the Analytical Chemistry Division of IUPAC recommended the use of the Faraday constant as an international standard for chemical analysis.[1] This recommendation has been partly supported by Yoshimori.[2] He discussed on the relationship between the results of chemical analysis and the basic SI units, and pointed out that the Faraday constant should be used as the international standard for titrimetric analysis. The results of gravimetric analysis are obtainable as the mass fraction by using the masses of a sample and of a precipitate, and usually the atomic weights or the molar masses of the elements concerned should be used. Therefore, the results of gravimetric analysis can directly be referred to the system of SI units (including the values of international atomic weights). There is no opportunity to use the Faraday constant as the standard for gravimetry.

On the other hand, a standard solution in a titrimetric analysis plays only the role which relates the elementary entities in a weighed portion of a standard reference material (SRM) to those of the material to be determined in a sample. Actually, an SRM of 100% purity is not obtainable, and it is nearly impossible to weigh an SRM without any contamination.[2] Therefore, the concentration of a standard solution and the results obtained by using the solution always include, as a factor, the purity of the SRM which was utilized for the standardization.

The SRMs for titrimetric analysis are now produced and certified individually in many countries. Therefore, the results of titrimetric analysis are internationally not unified yet. Thus, the Faraday constant becomes an excellent standard when it is used as the standard for titrimetric analysis.[2] Since 1973, the Faraday constant has been defined as the electricity of one mole of electrons (or protons).[3] Therefore, the purities (as mass fraction) of the SRMs for titrimetric analysis determined by a precise coulometric titration are obtainable from both the values of molar masses and the physical measurements (weight of sample and electricity consumed), and provide the fundamentals of the system of the SI units. Thus, the results of the titrimetric analysis obtained by using the standard solutions which were standardized with such SRMs, may also be referred to the system of the SI units.

† Presented at the 26th International Congress of Pure and Applied Chemistry, Tokyo, Japan, September 1977.

In order to use the Faraday constant as an international standard for titrimetric analysis, the experimental proof is not enough to get the international concensus, though the opinion has theoretically excellent fundamentals. One of the methods to support the use of the constant is to determine the purity of the same and important SRM for titrimetric analysis in collaboration with many laboratories in various countries by the precise coulometry. This paper presents one of such results, namely, the purity of the potassium hydrogen phthalate given by the National Bureau of Standards (SRM 84d) which was already assayed in three laboratories in U.S.A. by the precise coulometric titration.

Experimental

The instruments for the constant-current coulometric generation of hydroxide ion were similar to those shown previously.[4,5] From the certified values of the measuring devices, it is expected that the standard deviation in the measurement of the generating current was not greater than 0.005%. A 50 Hz electronic oscillator based on the frequency of a quartz crystal and a cycle counter were used to measure the time interval of the electrolysis. All weights were corrected against absolute weights. The other apparatus and reagents were the same as those of the previous paper.[5]

The sample was gently crushed in an agate mortar to about 100 mesh, dried at 120 °C for 2 h and cooled in a desiccator containing magnesium perchlorate before weighing. The procedure for the coulometric titration was the same as that of the previous paper.[5] The following values

TABLE 1. RESULTS OF ASSAY OF NBS 84d POTASSIUM HYDROGEN PHTHALATE

Taken (mg)	Found (mg)	Purity (%)
453.385	453.351	99.993
444.449	444.406	99.990
479.025	479.005	99.996
516.018	516.013	99.999
483.945	483.936	99.998
438.308	438.284	99.995
526.112	526.086	99.995
538.650	538.615	99.994
		Mean=99.995±0.002%[a]
		s_R[b]=0.003%

a) The 95% confidence interval for the mean value.
b) Standard deviation calculated from the range.

Table 2. Summary of the results of assays of NBS 84d potassium hydrogen phthalate

Author	Purity	No. of detns.	Standard deviation (%)	Purity recalculated[a] (%)	Drying condition	Ref.
Bates and Wichers	99.987[b]	3	0.002	—	100 °C	(6)
Taylor and Smith	99.977	5	0.003	99.992	120 °C 2—3 h	(7)
Eckfeldt and Shaffer	99.999	10	0.003	100.002	120 °C 2 h	(8)
Knoeck and Diehl	99.991[c]	6	0.005	99.991	110 °C 24 h	(9)
This work		8	0.003	99.995	120 °C 2 h	

a) Purity recalculated on the basis of the values of the Faraday constant and the molar mass in this work. b) Titrimetric analysis. c) Coulometric titration with the external generation of titrant.

were used for calculating the results; Faraday constant: 96484.6 C mol^{-1}, molar mass of potassium hydrogen phthalate: 204.223 g mol^{-1}, density of the reagent: 1.64 g cm^{-3}.

Results and Discussion

The results obtained by this investigation on the NBS SRM-84d are given in Table 1. The SRM was first assayed in NBS in 1957[6] by titrimetry based on the purity of the single crystal of benzoic acid, then by the precise coulometric titration in 1959.[7] Eckfeldt and Shaffer[8] and more recently Knoeck and Diehl[9] also analyzed the same sample by the precise coulometry. These laboratories are in U.S.A. and based on the same system of prototypes and standards. Their results are summarized in Table 2 in comparison with the results given in Table 1. The purities shown previously were recalculated by using the latest values of the Faraday constant and the molar masses in 1977 (shown above). The recalculated results are in excellent agreement with the purity obtained by this investigation, though they were based on the different prototypes of weight and electricity between Japan and U.S.A. Therefore, the results in Table 2 can be the fundamental data which support the recommendation on the use of the Faraday constant as an international standard for titrimetric analysis.

The authors express their sincere thanks to Dr. John K. Taylor (U.S. National Bureau of Standards) who supplied them the SRM.

References

1) IUPAC Information Bulletin, Appendices on Provisional Nomenclature, Symbols, Units, and Standards—No. 35, "Status of the Faraday Constant as an Analytical Standard," (1974), IUPAC Oxford; *Pure Appl. Chem.*, **45**, 125 (1976).
2) T. Yoshimori, *Bunseki*, **1975**, 551; *Talanta*, **22**, 827 (1975); *Z. Chem. (Leipzig)*, **18**, 211, 251 (1978).
3) IUPAC, "Manual of Symbols and Terminology for Physicochemical Quantities and Units, 1973 ed."
4) T. Yoshimori and I. Hikawa, *Bunseki Kagaku*, **16**, 927 (1967).
5) T. Yoshimori and T. Tanaka, *Anal. Chim. Acta*, **66**, 85 (1973).
6) R. G. Bates and E. Wichers, *J. Res. Natl. Bur. Stand.*, **59**, 9 (1957).
7) J. K. Taylor and S. W. Smith, *J. Res. Natl. Bur. Stand.*, **63A**, 153 (1959).
8) E. L. Eckfeldt and E. W. Shaffer, Jr., *Anal. Chem.*, **37**, 1534 (1965).
9) J. Knoeck and H. Diehl, *Talanta*, **16**, 567 (1969).

Phase Relation in the System PbO–$PbGeO_3$

Kazushi HIROTA* and Toshimori SEKINE

National Institute for Researches in Inorganic Materials, Sakura-mura, Ibaraki 300-31

(Received August 9, 1978)

Phase relations in the system PbO–$PbGeO_3$ were determined using both the quenching and DTA techniques. Two new lead germanate phases Pb_5GeO_7 and $Pb_{11}Ge_3O_{17}$ were found to be stable. It was found that the Pb_5GeO_7 melts incongruently at 738 °C to PbO plus liquid, whereas the $Pb_{11}Ge_3O_{17}$ decomposes into Pb_5GeO_7 plus Pb_3GeO_5 at 728 °C. The compounds Pb_3GeO_5, $Pb_5Ge_3O_{11}$, and $PbGeO_3$ were identified as congruently melting compounds, in accordance with previous investigations. Some other compounds, such as Pb_6GeO_8, Pb_4GeO_6, and $Pb_3Ge_2O_7$, which have been reported previously could not be confirmed as stable phases.

The PbO–GeO_2 binary system has been studied by Speranskaya,[1] Phillips and Scroger,[2] and Gouju *et al.*[3] There is an almost total disagreement regarding intermediate phases. Speranskaya reports Pb_6GeO_8, Pb_3GeO_5, $Pb_5Ge_3O_{11}$, $PbGeO_3$, and $PbGe_3O_7$ as stable compounds, while Phillips and Scroger list Pb_4GeO_6, $Pb_3Ge_2O_7$, $PbGeO_3$, $PbGe_2O_5$, and $PbGe_4O_9$. Only the compound $PbGeO_3$ is common to the two diagrams. Gouju *et al.* report Pb_3GeO_5, $Pb_3Ge_2O_7$, $PbGeO_3$, and $PbGe_4O_9$ in their phase diagram.

Sugii, *et al.*[4] grew crystals of $PbGeO_3$, and $Pb_5Ge_3O_{11}$ successfully by means of the Czochralski method, but were unable to confirm the existence of $Pb_3Ge_2O_7$. Zwicker *et al.*[5,6] also grew crystals of $Pb_5Ge_3O_{11}$ by the Czochralski method. The prototype structures of $Pb_5Ge_3O_{11}$ and Pb_3GeO_5 were described by Newnham *et al.*[7] and Neurgaonkar *et al.*[8] respectively. These studies on single crystals of $Pb_5Ge_3O_{11}$ and Pb_3GeO_5 agree with Speranskaya's data, but disagree with those of Phillips *et al.* and Gouju *et al.* Contrary to Speranskaya's phase diagram, Pentegova *et al.*[9] have concluded that the $Pb_3Ge_2O_7$ is a stable phase.

The aim of the present study is to examine the discrepancies among these phase diagrams and to establish the phase relations of intermediate compounds in the system PbO–$PbGeO_3$.

Experimental

General Procedure. Two different experimental methods were used in the present investigation: quenching and differential thermal analysis (DTA). In the quenching method, samples were heated at given temperatures until an equilibrium was attained among stable phases. The samples were then quenched rapidly to room temperature and the phases present were determined by electron probe microanalysis, X-ray diffraction, and microscopic examination.

Melting and crystallization temperatures were obtained by means of DTA. Melting temperature of each compound obtained was also ascertained by the quenching method.

Starting Materials. Commercial GeO_2 of purity 99.99% and a purified PbO were used as starting materials. The PbO was prepared from basic lead carbonate. A raw basic lead carbonate was brought into a lead nitrate solution by treating with an equivalent nitric acid. The solution was added with aqueous ammonia to form a small amount of lead hydroxide precipitate. After standing in a water bath for about 10 h, the solution was filtered. The solution was then heated again in a water bath, and an equivalent sulfuric acid was added to it. The precipitate with its mother liquid was heated in a water bath for a day and the volume of the precipitate was allowed to decrease. The precipitate was filtered, washed, and mixed with an excess of ammonium carbonate to bring the precipitate into lead carbonate. The mixture was heated overnight in a water bath, filtered, and washed. The washed precipitate was treated with nitric acid to bring the carbonate into a solution of lead nitrate. The solution was kept again in a water bath for a day and filtered. After that, lead nitrate crystals were allowed to deposit from the filtrate. The lead nitrate was heated at 420 °C in air, and PbO was obtained as product. Only about 10 ppm of Al and Ni were detected in the PbO by means of spectroscopic analysis.

Furnace and Temperature Control. A vertical-tube quench furnace with three heating zones was used for the equilibration runs. About 10 cm length of even heating zone reduced the total variation of temperature of the sample to less than ±0.5 °C. The actual temperature in the furnace was measured with a Pt–PtRh (13%) thermocouple which was calibrated against the melting point of gold. Frequent calibration was necessary because a decrease in emf of the thermocouple was found after a series of runs.

Checking of Equilibration and Quenching Procedures. The approach to equilibrium was studied by X-ray diffraction and microscopy. The quenched samples in the equilibration runs were examined as a function of time. Starting from a mixture of PbO and GeO_2, a complex mixture of more than 3 phases of intermediate compounds was obtained for short runs. Two phases or a single phase was found at equilibrium. The equilibrium was approached closely, for example, after several hundred hours of reaction poriod at about 650 °C. Starting from glasses, metastable crystalline phases were found after short runs.

Liquids of high PbO concentrations could not be quenched to glasses. The presence of a liquid phase, therefore, was evidenced by meniscus formation from the powdered compound in question.

Differential Thermal Analysis. About 2 g of PbO and GeO_2 were mixed and enclosed by welding in a platinum capsule, 6 mm in diameter and 35 mm long. The platinum capsule was mounted in a silver block and heated. The use of the silver block, which resulted in a long zone of even heating, reduced the total variation of temperature within the lead germanate sample to less than 2 °C.

Electron Probe Microanalysis. A mixture of PbO and GeO_2, mixed thoroughly in an agate mortar, was enclosed in a platinum tube by welding and kept at 800 °C for several hours in a vertical tube furnace, and allowed to fall into chilled water. Three kinds of glasses thus obtained and the two pure oxides were used as standards of known compositions to determine the correction factor. The oxide binary has been known to have the following linear relationship for C/K *vs.* C:

$$C/K = \alpha + (1-\alpha)C,$$

Table 1. Analytical results by electron probe microanalysis

Starting materials		Temp	Duration		Products						
					Phase 1			Phase 2			
Phase	Composition mol %PbO	°C	h		GeO_2/wt %	PbO/wt %	Pb/Ge	GeO_2/wt %	PbO/wt %	Pb/Ge	Phases
PbO+GeO_2	85.7	730	130		8.6	92.$_6$	5.0$_5$	0	100	—	Pb_5GeO_7+PbO
PbO+GeG_2	86.0	660	290		8.9	92.$_7$	4.8$_8$	0	100	—	Pb_5GeO_7+PbO
PbO+GeO_2	83.4	717	250		8.8	91.$_7$	4.8$_9$	—	—	—	Pb_5GeO_7
Glass	82.0	636	288		8.8	92.$_2$	4.9$_1$	11.$_0$	89.$_6$	3.8$_2$	Pb_5GeO_7+$Pb_{11}Ge_3O_{17}$
PbO+GeO_2	81.0	660	290		8.9	92.$_1$	4.8$_5$	11.$_3$	89.$_7$	3.7$_2$	Pb_5GeO_7+$Pb_{11}Ge_3O_{17}$
Glass	80.0	726	200		9.0	90.$_2$	4.7$_0$	11.$_6$	87.$_9$	3.5$_0$	Pb_5GeO_7+$Pb_{11}Ge_3O_{17}$
				av	8.8	91.$_9$	4.8$_8$				
				(calcd	8.57	91.4	5.00)				(Pb_5GeO_7)
PbO+GeO_2	90.0	602	1840		0	100	—	11.$_5$	89.$_6$	3.6$_5$	PbO+$Pb_{11}Ge_3O_{17}$
Glass	77.7	603	520		13.$_9$	84.$_3$	2.8$_4$	11.$_8$	86.$_3$	3.4$_2$	Pb_3GeO_5+$Pb_{11}Ge_3O_{17}$
Glass	76.0	706	530		13.$_8$	85.$_1$	2.8$_9$	11.$_5$	86.$_8$	3.5$_4$	Pb_3GeO_5+$Pb_{11}Ge_3O_{17}$
								av 11.$_4$	88.$_5$	3.6$_2$	
								(calcd 11.33	88.67	3.67)	($Pb_{11}Ge_3O_{17}$)
PbO+GeO_2	75.0	730	100		13.$_6$	84.$_2$	2.9$_0$	—	—	—	Pb_3GeO_5
PbO+GeO_2	70.0	701	350		13.$_7$	85.$_5$	2.9$_2$	21.$_2$	77.$_4$	1.7$_1$	Pb_3GeO_5+$Pb_5Ge_3O_{11}$
Glass	67.0	603	520		13.$_7$	84.$_8$	2.9$_0$	21.$_6$	79.$_4$	1.7$_2$	Pb_3GeO_5+$Pb_5Ge_3O_{11}$
				av	13.$_7$	84.$_7$	2.8$_9$				
				(calcd	13.51	86.49	3.00)				(Pb_3GeO_5)
PbO+GeO_2	62.5	730	130		—	—	—	22.$_3$	77.$_2$	1.6$_2$	$Pb_5Ge_3O_{11}$
Glass	55.0	706	530		31.$_7$	67.$_8$	1.0$_0$	22.$_1$	76.$_2$	1.6$_2$	$PbGeO_3$+$Pb_5Ge_3O_{11}$
				(calcd	31.91	68.09	1.00	av 21.$_8$	77.$_6$	1.6$_7$	($PbGeO_3$)
								(calcd 21.95	78.05	1.67)	($Pb_5Ge_3O_{11}$)

where C is the concentration of oxide in weight, K is the background-corrected intensity of characteristic radiation relative to that of the element in the pure oxide, and α is the constant introduced by Bence and Albee.[10] Under the present experimental conditions, *i.e.*, 20 kV accelerating potential and 40° take-off angle, the correction factor α was determined as follows: $\alpha^{Pb}_{GeO_2}=1.50$ and $\alpha^{Ge}_{PbO}=1.54$. Relative deviations of the analysis were determined by replicate analysis and are within ±2% for PbO and GeO_2 respectively.

Results and Discussion

Identification of Phases. The phases present in quenched samples were identified by X-ray diffraction and electron probe microanalysis. Selected results are summarized in Table 1.

Four phases with intermediate compositions were detected between PbO and $PbGeO_3$. These compositions of intermediate phases can be represented approximately by the following formulae: Pb_5GeO_7, $Pb_{11}Ge_3O_{17}$, Pb_3GeO_5, and $Pb_5Ge_3O_{11}$. The latter two, Pb_3GeO_5 and $Pb_5Ge_3O_{11}$ have been reported by Speranskaya. But the former two phases, Pb_5GeO_7 and $Pb_{11}Ge_3O_{17}$, have not been reported yet.

Equilibrium relations are illustrated in Fig. 1. The Pb_5GeO_7 was determined to be stable only between 738 °C and 632±7 °C. The composition of this phase was determined to be 4.9±0.2 in atomic ratio of Pb/Ge. The crystal structure determined by Kato indicates that the site ratio of Pb to Ge in the crystal lattice is equal to 5.[11] These results are consistent with each other within the experimental errors.

The phase $Pb_{11}Ge_3O_{17}$ seems the same compound as "Pb_4GeO_6" reported by Phillips and Scroger. X-Ray diffraction data on Pb_4GeO_6 shown by them could be indexed assuming that the sample was mainly $Pb_{11}Ge_3O_{17}$ mixed with a small amount of Pb_5GeO_7.

The analytical results of this phase ranged from 79.3 to 77.4 mol % PbO; this variation is considered to be within analytical errors. This phase is not regarded as a solid solution but as a compound with a constant composition. Preliminary study of the crystal structure of this compound indicates that there are 14 metal sites in a subunit cell, after Kato.[14] The average atomic ratio Pb/Ge=3.62 and the number of metal sites for this compound indicate the formula of $Pb_{11}Ge_3O_{17}$ (Pb/Ge=3.67) to be the compound with the simplest integral ratio.

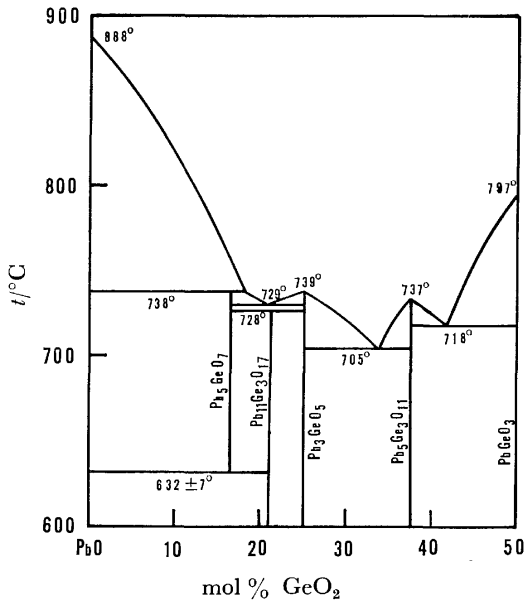

Fig. 1. Phase relations in the system PbO–$PbGeO_3$.

TABLE 2. X-RAY DIFFRACTION DATA OF POWDER SAMPLES

Pb_5GeO_7		$Pb_{11}Ge_3O_{17}$	
d spacing Å	Relative intensity	d spacing Å	Relative insensity
6.70	2	7.35	11
5.78	6	3.534	3
4.082	6	3.286	6
3.715	16	3.268	4
3.341	15	3.188	13
3.290	13	3.159	67
3.064	100	3.122	10
2.950	19	3.054	100
2.885	57	2.951	29
2.848	28	2.763	64
2.776	13	2.668	22
2.756	26	2.576	16
2.327	13	2.499	12
2.260	6	2.333	3
2.216	9	1.983	4
2.041	10	1.928	10
1.907	17	1.879	14
1.877	5	1.851	13
1.842	5	1.838	12
1.811	13	1.796	4
1.800	4	1.591	10
1.752	2	1.580	10
1.742	7		
1.698	24		
1.645	10		
1.562	10		
1.556	11		

Not Substantiated Compounds. No evidence for the existence of the compounds Pb_6GeO_8 and Pb_2GeO_4 was obtained in this work. Speranskaya has reported Pb_6GeO_8 as stable. It is difficult to determine the chemical composition by means of DTA only, when a compound melts incongruently. The phase Pb_5GeO_7, found in the present investigation, melts incongruently at 738±2 °C, while the Pb_6GeO_8 also has been reported to melt incongruently at 740 °C. It is noteworthy that the temperatures of incongruent melting of the two are in good agreement with each other within experimental errors. The methods adopted to determine the chemical composition of the phase Pb_6GeO_8 were not given.

The phase Pb_2GeO_4 has been reported by Merker *et al.*[12] An X-ray diffraction pattern has been given. But Hasegawa *et al.*[13] have pointed out that this diffraction pattern can be completely indexed by as-

suming that the phase is a mixture of $Pb_5Ge_3O_{11}$ and Pb_3GeO_5.

The stability of a $Pb_3Ge_2O_{11}$ compound could not be substantiated at the temperature range in our experiment. The result is in accordance with Zwicker *et al.* and Sugii *et al.* The congruently melting phase in question is not $Pb_3Ge_2O_7$ but $Pb_5Ge_3O_{11}$. Hasegawa *et al.* have reported that $Pb_3Ge_2O_7$ crystallized from a glass at lower temperatures and transformed to $Pb_5Ge_3O_{11}$ at 489 °C. In the present investigation the presence of a phase with composition $Pb_3Ge_2O_7$ could not be verified at 600 °C, the lowest temperature in our experiment; the product after 1600 h of reaction period was a mixture of $Pb_5Ge_3O_{11}$ and $PbGeO_3$.

It may seem surprising that the three published phase diagrams in the system $PbO-GeO_2$ disagree with one another, and that the existence of compounds such as $Pb_5Ge_3O_{11}$ or Pb_3GeO_5 has been questioned several times. One of the reasons for this is probably due to the presence of metastable phases. Slow cooling of melts tried by Pentegova *et al.*, is not necessarily adequate to investigate the phase relations in the system $PbO-GeO_2$. For example, Zwicker *et al.* have shown that, in the system $PbO-GeO_2$, slow cooling can substantially bring about super-cooling of the melt, and rapid crystallization may form metastable crystalline phases.

In order to assure the equilibrium state in this system, therefore, it is essential to keep the sample at constant temperature and composition for a sufficiently long time, this was tried in the present investigation.

References

1) E. I. Speranskaya, *Izv. Acad. Nauk SSSR Otd. Khim. Nauk*, **1959**, 162.
2) B. Phillips and M. G. Scroger, *J. Am. Ceram. Soc.*, **48**, 398 (1965).
3) D. Gouju, J. Fournier, and R. Kohlmuller, *C. R. Acad. Sci., Ser. C*, **266**, 1065 (1968).
4) K. Sugii, H. Iwasaki, and S. Miyazawa, *J. Cryst. Growth*, **10**, 127 (1971); *Mater. Res. Bull.*, **6**, 503 (1971).
5) W. K. Zwicker, H. P. Dougherty, M. Delfino, and J. Ladell, *Ferroelectrics*, **11**, 347 (1976).
6) W. K. Zwicker, M. Delfino, J. P. Dougherty, A. Sicignano, J. Ladell, and J. A. Nicolosi, *J. Electronic Materials*, **6**, 125 (1977).
7) R. E. Newnham, R. W. Wolfe, and C. N. W. Darlington, *J. Solid State Chem.*, **6**, 378 (1973).
8) R. R. Neurgaonkar, R. W. Wolfe, and R. E. Newnham, *J. Appl. Crystallogr.*, **7**, 307 (1974).
9) N. V. Pentegova, V. D. Sal'nikov, and Yu. Ya. Tomashpol'skii, *Kristallografiya*, **19**, 820 (1974), (*Sov. Phys. Crystallogr.*, **19**, 507 (1974)).
10) A. E. Bence and A. L. Albee, *J. Goul.*, **76**, 382 (1968).
11) K. Kato, to be published.
12) Von L. Merker and H. Wondratschek, *Glastechn. Ber.*, **29**, 471 (1957).
13) H. Hasegawa, M. Shimada, and M. Koizumi, *J. Mater. Sci.*, **8**, 1725 (1975).
14) K. Kato, private communication.

Preparations and Characterization of Cycloruthenated Complexes Derived from 1-Phenylpyrazole, 2-Phenylpyridine, and Benzo[*h*]quinoline

Katsuma HIRAKI,* Yayoi OBAYASHI,† and Yoko OKI

Department of Industrial Chemistry, Faculty of Engineering, Nagasaki University, Bunkyo-machi, Nagasaki, 852

(Received September, 1, 1978)

A pale yellow solution, prepared from $RuCl_3 \cdot 3H_2O$ and carbon monoxide in 2-methoxyethanol, reacted with 1-phenylpyrazole (Hphpz), 2-phenylpyridine (Hphpy), and benzo[*h*]quinoline (Hbzqn) to give new chloro-bridging dinuclear cycloruthenated complexes, $[\{RuCl(C\sim N)(CO)_2\}_2]$ (C∼N=cycloruthenated moiety). These complexes reacted with Tl(acac) (acac=acetylacetonato ligand), γ-picoline (pic), and triphenylphosphine resulting in the break-down of the chloro-bridging bond of the complexes, and afforded new mononuclear cycloruthenated complexes, $[Ru(acac)(C\sim N)(CO)_2]$, $[RuCl(C\sim N)(CO)_2(pic)]$, and $[RuCl(C\sim N)(CO)_n(PPh_3)_{3-n}]$ (n=2 for phpz, and n=1 for phpy and bzqn), respectively. The complexes prepared in this study were characterized by IR, ^{1}H-NMR, and mass spectroscopies.

Recently, cyclometallation reactions have become of interest in view of the stabilization of transition metal–carbon σ bonds[1–3] and of availabilities for the syntheses of heterocycles.[3] Several investigations have been reported concerning cycloruthenation reactions of azobenzene,[2,4–7] polyhaloazobenzene,[2,6] benzo[*h*]quinoline,[8] Schiff bases derived from benzaldehyde,[9] triphenylphosphite,[2,7,10] triphenylphosphine[2,7] and 1,3-di-*p*-tolylimidazolidin-2-ylidene group.[11] These cycloruthenation reactions in most cases were carried out using activated ruthenium species, such as $[\{RuCl_2(CO)_3\}_2]$,[4,9] or alkyl-,[6,7] hydrido-,[10] or zerovalent[5,8,9] ruthenium complexes.

This paper deals with direct and convenient cycloruthenation reactions of 1-phenylpyrazole (Hphpz), 2-phenylpyridine (Hphpy), and benzo[*h*]quinoline (Hbzqn) yielding new chloro-bridging dinuclear cycloruthenated complexes, and with some mononuclear complexes prepared by the bridge-splitting reactions of the dinuclear complexes with thallium acetylacetonate [Tl(acac)], γ-picoline (pic), and triphenylphosphine (PPh_3).

Cyclometallated complexes of Hphpz and Hphpy have been obtained with palladium and rhodium,[1–3] whereas those of Hbzqn have been reported for several transition metals.[1,2]

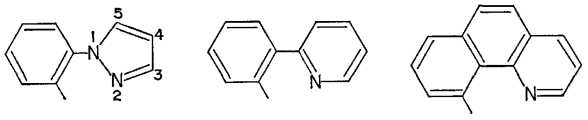

phpz phpy bzqn

Experimental

Materials. Commercial grade ruthenium(III) chloride trihydrate ($RuCl_3 \cdot 3H_2O$), benzo[*h*]quinoline, and γ-picoline were used without further purification. 1-Phenylpyrazole,[12] 2-phenylpyridine,[13] and Tl(acac)[14] were prepared according to the methods described in the literature. Solvents were dried by usual procedures and distilled.

General Procedures. IR spectra were obtained using a Hitachi 285 grating spectrometer. ^{1}H- and ^{31}P-NMR spectra were run on JEOL model-JNM-MH-100 and -FX-100 spectrometers, respectively. Molecular weights were determined using a JEOL model MS-01SG double-focussing mass spectrometer, referring to parent ion peaks. Melting points were determined on a Yanagimoto MP-S3 microstage apparatus and are uncorrected. All preparative operations were performed in an atmosphere of dry dinitrogen.

Cycloruthenation Reactions of Hphpz, Hphpy, and Hbzqn. Carbon monoxide was bubbled into a 2-methoxyethanol solution (30 ml) of $RuCl_3 \cdot 3H_2O$ (1 g) under refluxing for 6 h to give a yellow solution. An excess amount of Hphpz (2.6 g) was added to the yellow solution, and the mixture was refluxed for 3.5 h. A yellow precipitate was separated and washed with diethyl ether and benzene to afford di-μ-chloro-tetracarbonylbis{2-(1′-pyrazolyl)phenyl-1-*C*,2′-*N*}-diruthenium(II) (**1**) in 60% yield. 2-Phenylpyridine and benzo[*h*]quinoline reacted similarly with the yellow solution to yield $[\{RuCl(phpy)(CO)_2\}_2]$ (**2**) and $[\{RuCl(bzqn)(CO)_2\}_2]$ (**3**), respectively.

*Reactions of **1**, **2**, and **3** with Tl(acac).* Thallium acetylacetonate (0.6 mmol) and **1** (0.3 mmol) in 40 ml of dichloromethane were stirred under refluxing for 7 h and then at ambient temperature for 98 h. After the reaction mixture was filtered and concentrated, hexane was added to the resulting solution. A pale reddish gray solid precipitated and was washed with hexane to give mononuclear acetylacetonatodicarbonyl{2-(1′-pyrazolyl)phenyl(1-*C*,2′-*N*)}ruthenium(II) (**4**) in 45.9% yield.

Complexes **2** and **3** also reacted similarly with Tl(acac) to afford $[Ru(acac)(phpy)(CO)_2]$ (**5**) and $[Ru(acac)(bzqn)(CO)_2]$ (**6**), respectively.

*Reactions of **1**, **2**, and **3** with Triphenylphosphine.* A dichloromethane suspension containing **1** (0.4 mmol) and triphenylphosphine (2.0 mmol) was stirred at room temperature for 22 h. The resulting solution was concentrated, and diethyl ether was added. On standing overnight at 5—6 °C, the mixture yielded a white crystal, which was separated and washed with diethyl ether to give mononuclear dicarbonylchloro{2-(1′-pyrazolyl)phenyl(1-*C*,2′-*N*)}triphenylphosphineruthenium(II)-diethyl ether(2/1) (**7**) in 87.4% yield.

Complexes **2** and **3** also reacted analogously with triphenylphosphine to yield $[RuCl(phpy)(CO)(PPh_3)_2]$ (**8**) and $[RuCl(bzqn)(CO)(PPh_3)_2]$ (**9**), respectively.

*Reactions of **1**, **2**, and **3** with γ-Picoline.* A dichloromethane suspension (40 ml) involving **1** (0.4 mmol) and γ-picoline (2.4 mmol) was stirred at room temperature for 3.5 h. After the concentration of the resultant solution, followed by addition of hexane, an off-white powder precipitated. Recrystallization of the off-white powder from dichloromethane gave a mother liquor and a white granule,

† Present address: Sagamidai-jutaku 3-101, Iwase 531, Matsudo 271,

The evaporation to dryness of the mother liquor, followed by recrystallization from dichloromethane-hexane, afforded a pale gray solid, dicarbonylchloro(γ-picoline){2-(1′-pyrazolyl)phenyl-1-*C*,2′-*N*}ruthenium(II) (**10a**) in 46.9% yield. Three times recrystallizations of the white granule from dichloromethane yielded **10b** (2.9% yield), which was ascribed to an isomer of **10a** by elemental analysis, IR, and ^{1}H-NMR data.

Complex **2** reacted similarly with 4-picoline and gave [RuCl(phpy)(CO)$_2$(pic)] (**11a**) and a slight amount of a mixture consisting of **11a** and a by-product. Attempts to separate the mixture into the components were unsuccessful.

A dichloromethane suspension (25 ml) containing **3** (0.27 mmol) and γ-picoline (0.73 mmol) was refluxed for 4 h and stirred at ambient temperature for 14 h. After the concentration of the resulting solution, addition of hexane yielded a dark yellow microcrystal and a mother liquor. A silica-gel chromatography of a dichloromethane solution of the microcrystal afforded a yellow solid [RuCl(bzqn)(CO)$_2$(pic)] (**12a**). An orange-yellow powder, formed gradually from the mother liquor on cooling, produced an orange yellow solid [{RuCl(bzqn)(CO)(pic)}$_2$] (**12b**) with recrystallization from dichloromethane-hexane.

Results and Discussion

Cycloruthenation Reactions of Hphpz, Hphpy, and Hbzqn. Chatt *et al.*[15] reported that the 2-methoxyethanol solution of $RuCl_3 \cdot 3H_2O$ was refluxed under bubbling carbon monoxide to yield the yellow solution, in which a main ruthenium species was represented by [RuCl$_m$(CO)$_n$].[16] This solution reacted easily with tertiary phosphine or arsine resulting in the formation of complexes, [RuCl$_2$(CO)$_2$L$_2$] (L=a neutral donor ligand).[15] In the present study, the yellow solution reacted also with Hphpz, Hphpy, and Hbzqn under reflux to give the cycloruthenated dinuclear complexes, [{RuCl(C∼N)(CO)$_2$}$_2$] (C∼N=cycloruthenated moiety), **1**, **2**, and **3**, respectively (*vide infra* as for configurations). On the other hand, the preparation of a more carbonylated ruthenium complex, [{RuCl$_2$(CO)$_3$}$_2$], needs higher pressure of carbon monoxide than 10 atm.[17] In consideration of these facts, it seems certain that the main ruthenium species in the yellow solution bears two carbonyl groups, and has a divalent state, not the initial trivalent one, judging from the π-back bonding character of the carbonyl groups. Accordingly, the main ruthenium species is represented by [RuCl$_2$(CO)$_2$S$_2$], where S means a solvent molecule or a chloro ligand. The cycloruthenation reactions are shown by the following equation:

$$[RuCl_2(CO)_2S_2] + 2H(C\sim N) \longrightarrow 1/2[\{RuCl(C\sim N)(CO)_2\}_2] + H_2(C\sim N)\cdot Cl + 2S.$$

These reactions proceed fairly smoothly, and seem to provide a convenient route for the syntheses of the cycloruthenated complexes of the aryl-substituted heterocycles. Driving forces for these reactions are possibly associated both with a basicity of the heterocycles and with a structural factor of the aryl-substituted heterocycles susceptible to the cyclometallation.[1-3,8] Tables 1—3 summarize yields, elemental analyses, and some properties of **1**, **2**, and **3** and their derivatives.

Complexes **1**, **2**, and **3** are stable and insoluble in common organic solvents. Each of these complexes contains terminal carbonyls as shown by IR spectra (Table 2), and has one chlorine atom and four other coordination sites per ruthenium atom, as indicated clearly by the elemental analyses (Table 1). It has been well known that most of divalent ruthenium complexes have a six-coordinated structure,[4,8,9,15,17] and that chlorine atoms serve as bridging ligands to form a dinuclear structure in chlororuthenium(II) complexes.[4,17] On the basis of these considerations, of the high insolubilities, and of reactivities towards a few reagents as stated later, each of **1**, **2**, and **3** was assigned to the dinuclear structure having the chlorine bridges, similarly to [{RuCl(azb)(CO)$_2$}$_2$], (Hazb=azobenzene).[4]

Acetylacetonato and Triphenylphosphine Complexes. The dinuclear complexes **1**, **2**, and **3** reacted with Tl(acac) to afford the mononuclear acetylacetonatoruthenium(II) complexes **4**, **5**, and **6**, respectively.

Table 1. Yields and properties of the ruthenium complexes

Complex		Yield (%)	Mp[a] (°C)	Color	C (%)		H (%)		N (%)	
					Calcd	Found	Calcd	Found	Calcd	Found
{RuCl(phpz)(CO)$_2$}$_2$	**1**	60.0	243	Off white	39.36	39.79	2.10	2.09	8.35	8.24
{RuCl(phpy)(CO)$_2$}$_2$	**2**	61.5	262—263	Pale yellow	45.35	45.60	2.31	2.59	4.02	3.99
{RuCl(bzqn)(CO)$_2$}$_2$	**3**	64.8	278—280	Yellow	48.59	49.26	2.17	2.47	3.78	3.78
Ru(acac)(phpz)(CO)$_2$	**4**	45.9	176—178	Pale reddish gray	48.12	47.68	3.53	3.31	7.01	7.06
Ru(acac)(bzpn)(CO)$_2$	**5**	68.6	140—164	Pale brown	52.68	52.53	3.68	3.82	3.41	3.40
Ru(acac)(bzqn)(CO)$_2$	**6**	72.6	213—219	Pale yellowish brown	55.30	56.18	3.48	3.58	3.22	3.34
RuCl(phpz)(CO)$_2$(PPh$_3$)[b]	**7**	87.4	190	White	58.64	58.17	4.29	4.12	4.41	4.43
RuCl(phpy)(CO)(PPh$_3$)$_2$	**8**	47.9	277—231	Yellow	68.39	68.51	4.51	4.49	1.66	1.57
RuCl(bzqn)(CO)(PPh$_3$)$_2$	**9**	57.7	270	Yellow	68.90	69.27	4.42	4.42	1.62	1.61
RuCl(phpz)(CO)$_2$(pic)	**10a**	46.9	187—190	Pale gray	47.61	48.23	3.29	3.24	9.80	9.89
	10b	2.9	164—167	White	47.61	47.53	3.29	3.22	9.80	9.65
RuCl(phpy)(CO)$_2$(pic)	**11a**	40.0	183—188	Dark yellow	51.88	51.58	3.44	3.37	6.37	6.31
RuCl(bzqn)(CO)$_2$(pic)	**12a**	25.2	204—210	Yellow	54.37	54.20	3.26	3.24	6.04	6.00
{RuCl(bzqn)(CO)(pic)}$_2$	**12b**	10.0	270	Orange yellow	55.11	55.14	3.47	3.82	6.48	6.59

a) With decomposition. b) Containing a half mole of diethyl ether as solvent of crystallization.

TABLE 2. CHARACTERISTIC IR BANDS AND MOLECULAR WEIGHTS OF THE COMPLEXES

Complex	ν(C=O) (cm^{-1})[a]	M. W.[c]
1	2038, 1987, 1962, 1941(sh) 1928(w)[b]	—
2	2020, 1975, 1946, 1928(w) 1908(sh)[b]	—
3	2015, 1978, 1960, 1930(w)[b]	—
4	2040, 1978	400(400)
5	2040, 1974	411(411)
6	2030, 1970	—
7	2040, 1985	—
8	1910[b]	—
9	1920[b]	—
10a	2050, 1987	—
10b	2020, 1940[b]	—
11a	2050, 1987	—
12a	2045, 1984	—
12b	1923, 1950(sh), 1975(w), 2040(w)	—

a) In chloroform solution, unless noted elsewhere. b) In KBr disc. c) Calculated value corresponding to ^{102}Ru is given in parentheses.

Triphenylphosphine also cleaved the chloro-bridging bonds of the dinuclear complexes, giving mononuclear complexes **7**, **8**, and **9**. These complexes are stable in a solid state and soluble in dichloromethane and chloroform. The acetylacetonato complexes decompose slowly in the solution, whereas the triphenylphosphine complexes are stable in the solution, too.

^{1}H-NMR spectrum of **4** (Table 3 and Fig. 1) shows two doublets at δ 7.41 (1H, 5′-H, J=2.5 Hz) and 8.09 (1H, 3′-H, J=2.5 Hz), one triplet at δ 6.49 (1H, 4′-H) and two multiplets at δ 7.6—7.75 (1H) and 6.9—7.4 (3H), in addition to signals characteristic of the acac group. The multiplets differ completely from that of Hphpz, and are due to an *o*-phenylene group of the phpz moiety. As for mass spectrum of **4**, peaks of *m/e* corresponding to ^{102}Ru appeared at 400, 372, 344, 301, 273 and 245, which were ascribable to a parent peak [Ru(acac)(phpz)$(CO)_2$]$^+$, and fragment

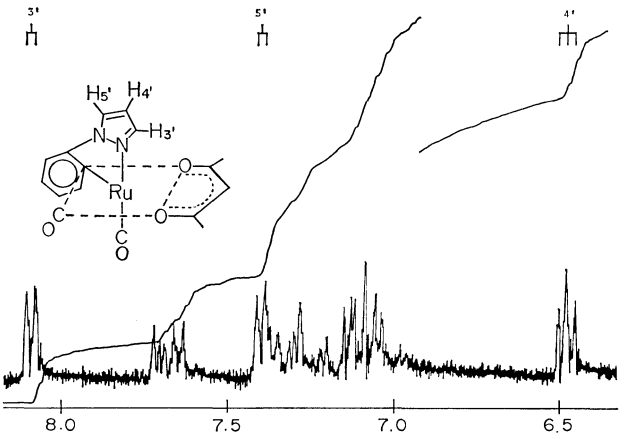

Fig. 1. ^{1}H-NMR spectrum of **4** in CD_2Cl_2 solution (δ-value from TMS).

peaks [Ru(acac)(phpz)(CO)]$^+$, [Ru(acac)(phpz)]$^+$, [Ru(phpz)$(CO)_2$]$^+$, [Ru(phpz)(CO)]$^+$, and [Ru(phpz)]$^+$, respectively. These evidences elucidated unambiguously the cycloruthenated structure of the phpz moiety in **4**. Mass spectrum of **5** gave also a very similar pattern to that of **4**, to which the phpy moiety corresponded in place of the phpz one. This fact and the aromatic proton resonances[18] in ^{1}H-NMR spectrum of **5** indicate analogously the cycloruthenated structure of the phpy moiety in **5**. Complex **6** was similarly ascribed to the cycloruthenated structure on the basis of the ^{1}H-NMR spectrum.[19]

It is noted that **8** and **9** bear two triphenylphosphine ligands and one carbonyl group, while **7** has one triphenylphosphine ligand and two carbonyl groups, similarly to [RuCl(azb)$(CO)_2(PPh_3)$].[4] It is certain that both the phpy and bzqn moieties have a more conjugated skeleton than the phpz and azb moieties. The difference of the skeletal conjugation is probably responsible for that of the substitution of the carbonyl group with triphenylphosphine in these complexes. A proton-decoupled ^{31}P-NMR spectrum of **9** in dichloromethane showed a sharp singlet at 105.20 ppm to upper field from trimethyl phosphite (external standard). This fact proves undoubtedly that two triphenyl-

TABLE 3. ^{1}H-NMR DATA OF THE RUTHENIUM COMPLEXES[a]

Complex	Pyrazolyl group				acac or pic			
	3′-H	4′-H	5′-H	$J_{4,3 \text{ or } 5}$	$C_\gamma H$[b] or H_α[c]	H_β	$J_{\alpha\beta}$	CH_3
	δ, ppm	δ, ppm	δ, ppm	Hz	δ, ppm	δ, ppm	Hz	δ, ppm
4[d]	8.09(d)	6.49(t)	7.41(d)	2.5	b) 5·26(s)[e]	—	—	1.69(s), 2.09(s)
5[f]	—	—	—	—	b) 5.26(s)[e]	—	—	1.68(s), 2.12(s)
6[f]	—	—	—	—	b) 5.47(s)	—	—	1.62(s), 2.23(s)
7[g,h]	8.31(d)	6.47(t)	7.23(d)	2.5	—	—	—	—
10a[d]	8.29(d)	6.55(t)	8.09(d)	2.5	c) 8.37(d)	6.97(d)	6.5	2.24(s)
10b[f]	8.18(d)	6.51(t)	7.2 (d)[i]	2.5	c) 8.97(d)	7.4 (d)[i]	6.0	2.48(s)
11a	—	—	—	—	c) 8.32(d)	6.93(d)	6.5	2.20(s)
12a[g]	—	—	—	—	c) 8.33(d)	6.76(d)	6.3	2.11(s)

a) In CD_2Cl_2, unless noted elsewhere. Abbreviations used: s=singlet, d=doublet, t=triplet, q=quartet. b) Acac group. c) Pic group. d) See the text about the *o*-phenylene protons. e) Confirmed by a measurement in $CDCl_3$ solution. f) See the notes 18, 19, and 21 about the aromatic protons of **5**, **6**, and **10b**, respectively. g) In $CDCl_3$. h) Containing CH_2[δ 3.58(q, J=7.0 Hz, 2H)] and CH_3[δ 1.25(t, 3H)] resonances of diethyl ether. i) Overlapping with the *o*-phenylene protons.

phosphine ligands in **9** are located at *trans* positions to each other, but not at *cis* positions, because the two triphenylphosphine ligands at the latter positions would be magnetically unequivalent and result in two ^{31}P resonances. The *trans* configuration of the ligands is presumably due to a steric interaction among the two triphenylphosphine ligands and the chelating bzqn moiety.

Accordingly, two isomers A and B are possible for **9**, as demonstrated in Fig. 2. IR spectrum of this complex exhibits a comparatively low frequency of ν(CO) band. Low stretching frequencies of carbonyl group have been observed for $[RuCl_2(CO)(pyridine)_3]$[20] and $[Ru(azb)(pz_3BH)(CO)]$ (pz=1-pyrazolyl),[4] possessing the carbonyl group *trans* to a nitrogen donor ligand. In consideration of these facts, **9** was ascribed to configuration A, in which the nitrogen donor site was situated at a *trans* position to the carbonyl group. Complex **8** was also associated with the configuration A, from the similarity of the composition and the ν(CO) frequency.

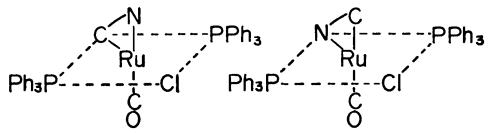

Fig. 2. Possible configurations of the bis(triphenylphosphine) complexes. C∼N=the cycloruthenated moiety.

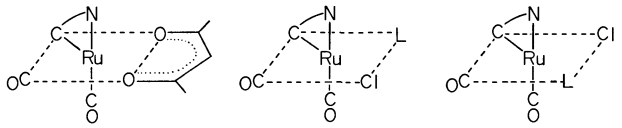

Fig. 3. Possible configurations of the dicarbonyl complexes. L=triphenylphosphine or γ-picoline.

Complexes **4**, **5**, **6**, and **7** show two strong ν(CO) bands near 1978 and 2040 cm^{-1}, revealing a *cis* coordination of the two carbonyl groups. One of the two carbonyl groups is presumably situated at a *trans* position to the nitrogen donor site, analogously to the cases of **8** and **9**, since the coordinations of these ligands are likely to be unaffected by the splitting reactions of the chlorobridging bonds of **1**, **2**, and **3** with Tl(acac) or triphenylphosphine. These discussions lead to proposals that **4**, **5**, and **6** are assignable to configuration C, and that **7** is to configuration D or E (Fig. 3).

γ-Picoline Complexes. γ-Picoline also reacted with **1**, **2**, and **3** to yield corresponding derivatives **10**, **11**, and **12**, respectively. Each of **10** and **12** was separated into a major product **a** and a minor one **b** by means of the repeated recrystallizations. These complexes are stable in a solid state and soluble in dichloromethane and chloroform.

Mononuclear complexes **10a**, **11a**, and **12a** showed very similar ν(CO) bands to those of **4**, **5**, **6**, and **7**, suggesting a similarity among the configurations of these complexes. ^{1}H-NMR spectrum of **10a** contains two multiplets at δ 7.0—7.4 (3H) and 7.7—7.9 (1H) assignable to the *o*-phenylene protons, in addition to γ-picoline and pyrazolyl proton resonances (Table 3), indicating the cycloruthenated structure of the phpz moiety in **10a**. Moreover, ^{1}H-NMR spectrum of **10b**[21] showed lower field γ-picoline proton resonances than that of **10a** did. It is expected that all the protons of γ-picoline *trans* to a carbonyl group are deshielded more strongly owing to a π-back bonding character of the carbonyl group than those of γ-picoline *trans* to the aryl carbon. On the basis of these discussions, **10b** was assigned to configuration D, whereas **10a**, **11a**, and **12a** to configuration E.

Complex **12b** exhibited a medium ν(CO) band at 1923 cm^{-1}, accompanied by very weak bands at 1950, 1975, and 2040 cm^{-1}. Elemental analysis of **12b** reveals that this complex is not an isomer of the main product **12a**, but has one chlorine atom and four other coordination sites per ruthenium atom, similarly to **3**. These data are consistent with a dimeric structure of **12b**, retained even during the reaction of **3** with γ-picoline, although γ-picoline has been regarded as a typical bridge-splitting reagent. Complex **12b** was probably formed by a substitution of two carbonyl groups in **3** with two γ-picoline ligands, in place of the chlorine-bridge splitting reaction. However, further characterization of **12b** was impossible, since its yield was low and irreproducible.

Dinuclear Complexes. All the mononuclear complexes derived from the dinuclear ones **1**, **2**, and **3** had one or two carbonyl ligands, but not more than three. In addition, all the mononuclear dicarbonyl complexes exhibited two strong ν(CO) bands. These facts indicate that each ruthenium atom in the dinuclear complexes is coordinated with two carbonyl groups in a *cis* form, but not in a *trans* form. Accordingly, one of the two carbonyl groups is necessarily located at a *cis* position to the two bridging chlorine atoms. On the basis of these discussions and the conclusion that the nitrogen donor site of the cycloruthenated moiety was situated at the *trans* position to one of the carbonyl groups, as stated above, four isomers are

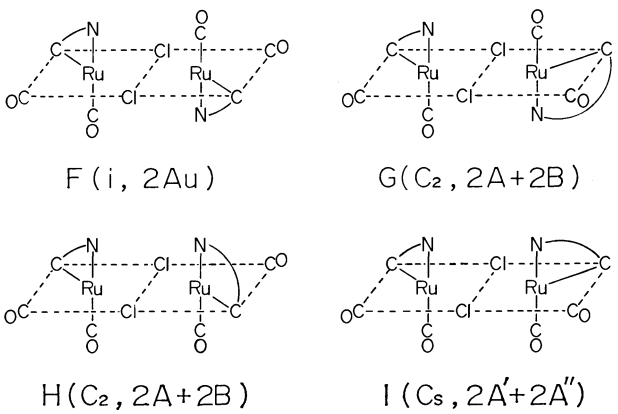

Fig. 4. Possible configurations of the dinuclear complexes. The symmetry and the infrared active mode for the ν(CO) vibrations are given in parenthesis. The cycloruthenated moiety is represented by C∼N.

possible for each of **1**, **2**, and **3**, as depicted in Fig. 4. In Fig. 4, symmetry and an infrared active mode for the carbonyl stretching vibrations are given for each somer.

IR spectrum of **1**, **2**, or **3** shows three strong ν(CO) bands and a few weak ones. In consideration of the steric interaction between the two cycloruthenated moieties, it appears that each of these dinuclear complexes consists of two isomers, F and G. This proposal is reasonable, since all the mononuclear complexes investigated in the present study can be derived by a substitution of the bridging chlorine atoms, and by an additional substitution of one carbonyl group only in the cases of **8** and **9**, from F or G without any rearrangement of the other ligands.

We wish to express our gratitude to Mrs. Hisako Mazume and Miss Yumi Kojima of Nagasaki University for their technical assistances and also to Mr. Toru Hinomoto of Japan Electron Optics Laboratory for the ^{31}P-NMR measurement.

References

1) M. Nonoyama, *Kagaku No Ryoiki*, **28**, 674 (1974) and literatures cited therein.
2) J. Dehand and M. Pfeffer, *Coord. Chem. Rev.*, **18**, 327 (1976) and literatures cited therein.
3) M. I. Bruce, *Angew. Chem. Int. Ed. Engl.*, **16**, 73 (1977) and literatures cited therein.
4) a) M. I. Bruce, M. Z. Iqbal, and F. G. A. Stone, *J. Chem. Soc., Chem. Commun.*, **1970**, 1325; b) M. I. Bruce, M. Z. Iqbal, and F. G. A. Stone, *J. Chem. Soc., A*, **1971**, 2820.
5) J. D. Gilbert, D. Rose, and G. Wilkinson, *J. Chem. Soc., A*, **1970**, 2766.
6) M. I. Bruce, R. C. F. Gardner, and F. G. A. Stone, *J. Chem. Soc., Dalton Trans.*, **1976**, 81.
7) M. I. Bruce, R. C. F. Gardner, and F. G. A. Stone, *J. Organomet. Chem.*, **40**, C 39 (1972).
8) M. I. Bruce, B. L. Goodall, and F. G. A. Stone, *J. Organomet. Chem.*, **60**, 343 (1973).
9) R. L. Bennet, M. I. Bruce, B. L. Goodall, M. Z. Iqbal, and F. G. A. Stone, *J. Chem. Soc., Dalton Trans.*, **1972**, 1787.
10) J. J. Levison and S. D. Robinson, *J. Chem. Soc., A*, **1970**, 639.
11) P. B. Hitchcock, M. F. Lappert, and P. L. Pye, *J. Chem. Soc., Chem. Commun.*, **1977**, 196.
12) I. L. Finar and K. E. Godfrey, *J. Chem. Soc.*, **1954**, 2293.
13) J. C. W. Evans and C. F. H. Allen, *Org. Synth.*, Coll. Vol. II, 517 (1966).
14) W. H. Nelson, W. J. Randall, and D. F. Martin, *Inorg. Synth.*, IX, 53 (1971).
15) J. Chatt, B. L. Shaw, and A. E. Field, *J. Chem. Soc.*, **1964**, 3466.
16) W. P. Griffith, "The Chemistry of the Rarer Platinum Metals," Interscience Publishers, London (1967), p. 185.
17) M. I. Bruce and F. G. A. Stone, *J. Chem. Soc., A*, **1967**, 1238.
18) The aromatic proton resonances were observed at δ 8.10 (1H, doublet, J=6.0 Hz), 7.1—7.3 (3H, multiplet), and 7.5—8.0 (4H, multiplet).
19) Three multiplets were observed for the bzqn moiety of **6**; δ 7.5—7.9 (4H), 7.9—8.3 (2H), and 8.4—8.7 (2H).
20) S. D. Robinson and G. Wilkinson, *J. Chem. Soc., A*, **1966**, 300.
21) *o*-Phenylene proton resonances were observed at δ 7.1—7.3 (2H, multiplet, overlapping with 5′-H), 7.3—7.5 (1H, multiplet, overlapping with H_β of 4-picoline), and 7.6—7.9 (1H, multiplet).

The Absolute Configuration and Circular Dichroism of $(+)_{240}^{CD}$-[(2*S*,7*S*)-2,7-Dimethyl-3,6-diazaoctane-1,8-diamine]platinum(II) Chloride Dihydrate

Yasuji NAKAYAMA, Shun'ichiro OOI,* and Hisao KUROYA

Department of Chemistry, Faculty of Science, Osaka City University, Sumiyoshi-ku, Osaka 558

(Received September 11, 1978)

The title compound was synthesized and characterized by means of absorption, circular dichroism, and its NMR spectra as well as X-ray structure analysis. The crystals are monoclinic, with a $P2_1$ space group, a=9.175(3), b=12.423(5), c=7.434(3) Å, β=108.1(4)°, and Z=2. The structure was determined from the diffractometer data and refined by a least-squares method to R=0.041 for 1732 observed reflections. The Pt atom has an essentially planar coordination with 4 N atoms. The disposition of the four donor atoms is not rectangular, but trapezoidal; it is, moreover, slightly tetrahedral. The quadridentate ligand forms three 5-membered chelate rings with the Pt atom. The two terminal rings are of a δ asymmetric envelope conformation, while the middle ring has a λ symmetric skew conformation. Both of the secondary N atoms possess a R configuration. The complex ion has a pseudo-two-fold axis by which the two terminal rings are related to each other. The circular dichroism spectrum reflects mainly the conformations of the 5-membered chelate rings. The features of the absorption and circular dichroism spectra are discussed on the basis of the geometry of the PtN_4 chromophore.

This work has been undertaken as a part of the investigation into the interrelation between structure and circular dichroism (CD) in the Pt(II) complexes. For the title complex there are three possible isomers, as is shown in Fig. 1, where *RR*, *RS*, and *SS* denote the configurations of the asymmetric nitrogens in each isomer. The information from the PMR spectrum is that the synthesized compound is not a mixture of these isomers, but contains either the *RR*- or the *SS*-isomer. The CD spectrum suggests that the compound consists of the *RR*-isomer, but this is not decisive. Therefore, a single-crystal structure analysis has been performed on the title complex.

Experimental

Preparation of the Compound. The (2*S*,7*S*)-2,7-dimethyl-3,6-diazaoctane-1,8-diamine (=3*S*,8*S*-dimetrien, NH_2CH_2-C*H(CH_3)NH(CH_2)$_2$NHC*H(CH_3)CH_2NH_2) hydrochloride was prepared according to the method described in the literature.[1]

$K_2[PtCl_4]$(3.8 g) and 3*S*,8*S*-dimetrien·4HCl (2.0 g) were dissolved in 50 cm³ of water. The solution was heated at 80 °C, and then a KOH solution (1.4 g in 10 cm³ of water) was added, drop by drop. The precipitate was washed with water and found by analysis to be [Pt(dimetrien)]-[$PtCl_4$].

Found: C, 13.59; H, 3.13; N, 8.01%. Calcd for [Pt-($C_8H_{22}N_4$)][$PtCl_4$]: C, 13.60; H, 3.12; N, 7.93%.

The Magnus-type salt (2.0 g) was dissolved in 2 dm³ of an aqueous $HClO_4$ solution (pH≈3). The resulting solution was passed through an anion-exchange column (Dowex 1X-8) in the chloride form, and the effluent was rotary-evaporated. The single crystals of [Pt(3*S*,8*S*-dimetrien)]Cl_2·$2H_2O$ were subsequently obtained by recrystallization from water–acetone.

Found: C, 20.23; H, 5.57; N, 12.07%. Calcd for [Pt-($C_8H_{22}N_4$)]Cl_2·$2H_2O$: C, 20.16; H, 5.46; N, 11.76%.

Spectral Measurements. The PMR spectrum was recorded at 60 MHz on a JEOL-C-60HL Spectrometer, using DSS as the internal reference. The FT ^{13}C NMR spectrum was obtained at 15.04 MHz with broad-band proton decoupling. Dioxane was used as the internal reference. The values of the chemical shifts in the text have been converted to the TMS scale. The absorption spectrum was measured using a Hitachi EPS-3T Spectrophotometer, while the CD spectrum was recorded on a JASCO J-20 Automatic Recording Spectrometer. In order to protect the asymmetric nitrogens from inversion, samples were dissolved in a 0.01 M DCl solution in the NMR measurements, whereas a 0.03 M HCl solution was used in the absorption and CD measurements.

X-Ray Data Measurement. Crystal Data: C_8Cl_2-$H_{26}N_4O_2Pt$, *F.W.*=476.1, Monoclinic, a=9.175(3), b=12.423(5), c=7.434(3) Å, β=108.1(4)°, U=805.4(5) Å³, D_m=1.93, D_c=1.96 g/cm³, Z=2, μ(Mo $K\alpha$)=94.8 cm^{-1}. The Laue symmetry and approximate unit-cell dimensions were determined from Weissenberg and precission photographs. The unit-cell dimensions were refined by a least-squares analysis of 28 θ values measured on a Philips PW1100 diffractometer.

Data Collection: A unique data set in the $2\theta \leq 55°$ range was collected by a conventional ω-2θ scan method using graphite-monochromated Mo $K\alpha$ radiation. The crystal size was 0.16×0.17×0.19 mm. The scan speed and scan width in ω were 0.017° s^{-1} and (1.0+0.2 tan θ)° respectively. The background was counted for 20 s at each end of the scan range. No significant variations were found in the intensities of three standard reflections menitored every 3 h. A total of 1732 intensities with $I_t - 2\sqrt{I_t} > I_b$ were collected and used for the structure analysis (I_t, intensity at the peak of reflection; I_b, mean background count obtained from preliminary background measurements for 5 s at each side of the peak). Intensity data were corrected for the Lp factors.[2] A spherical absorption correction (r=0.085 mm) was applied.

Structure Determination and Refinement. The crystal structure was solved by the heavy atom method. The positional and thermal parameters were refined by a block-diagonal least-squares method. The minimized function was $\sum w(F_o - |F_c|)^2$. The weighting scheme, w=1.0 for $F_o \leq 96.0$ and $w=(96.0/F_o)^2$ for $F_o > 96.0$, was found to be optimum in order to make $w\Delta F_o^2$ relatively constant over the ranges of F_o. The final R value was 0.041. In the final cycle of refinement all the parameter shifts were less than 0.2σ. The positional and thermal parameters are listed in Table 1.

The atomic scattering factors for all atoms were taken from Ref. 3, with corrections for anomalous scattering for Pt^0 and Cl^-. The absolute crystal structure was determined on the basis of the configuration (*S*) of asymmetric carbons.

TABLE 1. POSITIONAL AND THERMAL PARAMETERS, WITH e.s.d. VALUES IN PARENTHESES

	x	y	z	B/Å^2		x	y	z	B/Å^2
Pt	0.25071(4)	0.0	0.13658(4)	a)	C(3)	0.327(2)	0.196(1)	0.339(2)	3.2(2)
Cl(1)	0.5369(5)	−0.5526(4)	0.2806(5)	a)	C(4)	0.156(2)	0.177(1)	0.316(2)	3.5(3)
Cl(2)	−0.0842(5)	−0.2292(4)	0.2125(6)	a)	C(5)	−0.060(2)	0.066(1)	0.086(2)	3.2(2)
N(1)	0.441(1)	−0.087(1)	0.138(2)	3.0(2)	C(6)	−0.070(1)	−0.007(2)	−0.087(2)	3.1(2)
N(2)	0.400(1)	0.088(1)	0.334(1)	2.6(2)	C(7)	0.677(2)	0.131(2)	0.466(2)	4.2(3)
N(3)	0.096(1)	0.116(1)	0.132(1)	2.5(2)	C(8)	−0.187(2)	0.152(2)	0.038(3)	4.2(3)
N(4)	0.068(1)	−0.077(1)	−0.047(2)	3.0(2)	$O_w(1)$	0.575(1)	−0.305(1)	0.183(2)	4.4(2)
C(1)	0.581(2)	−0.037(1)	0.286(2)	3.3(2)	$O_w(2)$	−0.100(2)	0.397(2)	0.407(3)	7.5(4)
C(2)	0.551(2)	0.086(1)	0.302(2)	3.5(3)					

a) Anisotropic temperature factors ($\times 10^4$) of the exp $[-(B_{11}h^2+B_{22}k^2+B_{33}l^2+B_{12}hk+B_{13}hl+B_{23}kl)]$ form for the parameters:

	B_{11}	B_{22}	B_{33}	B_{12}	B_{13}	B_{23}
Pt	75.9(4)	36.9(2)	90.5(7)	14(1)	70(1)	16(1)
Cl(1)	173(6)	67(3)	154(7)	−20(7)	151(10)	−33(7)
Cl(2)	160(6)	70(3)	204(8)	−63(7)	186(11)	−74(8)

The observed and calculated structure factors are available at the Chemical Society of Japan (Document No. 7916). All the computations were carried out using programs in the UNICS.[4]

Results and Discussion

As is illustrated in Fig. 1, the complex ion may exist in three isomers. In the *RR*-isomer two terminal rings assume a δ conformation, while the middle ring is of a λ conformation, both methyl groups being equatorial with respect to the chelate ring. The *SS*-isomer has a δ middle ring and two λ terminal rings with axial methyl groups. In the *RS*-isomer the middle ring has an envelope conformation, but one of the terminal rings is of a λ conformation and the other is of a δ one. Of the two methyl groups, one is axial, whereas the other is equatorial. Although the *RR*-isomer with equatorial methyl groups seems to be the most probable of the three, the *RS*- and *SS*-isomers should not be left out of account, since, in the planar complex, the methyl group is not always constrained in the equatorial disposition.[5] The *RR*- and *SS*-isomers have a two-fold axis, but the *RS*-isomer has no symmetry.

The PMR spectrum showed one prominent methyl doublet at 1.19 ppm, while four carbon signals appeared at 12.73, 54.94, 56.76, and 61.24 ppm in the ^{13}C NMR spectrum. These observations indicate that the prepared compound is not a mixture of the isomers, but is, rather composed of either the *RR*- or the *SS*-isomer. Since the CD spectrum did not offer data decisive for distinguishing between these isomers, an X-ray structure analysis was performed.

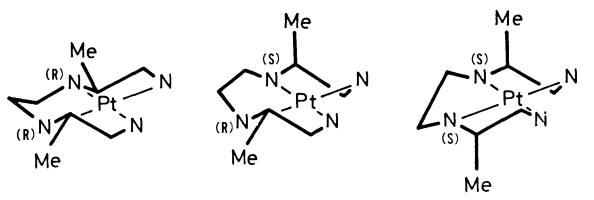

RR *RS* *SS*

Fig. 1. Possible isomers for $(+)^{CD}_{240}$-[Pt(3*S*,8*S*-dimetrien)]$^{2+}$.

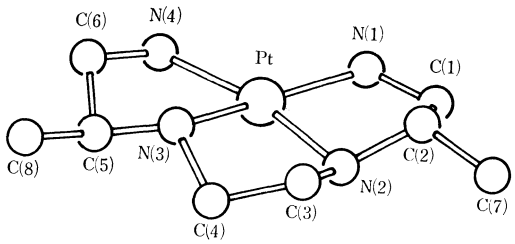

Fig. 2. Structure of $(+)^{CD}_{240}$-[Pt(3*S*,8*S*-dimetrien)]$^{2+}$.

Figure 2 shows a perspective drawing of the complex ion. This structure corresponds to the *RR*-isomer. The ion has an approximate two-fold axis which runs through the Pt atom and bisects the N(1)–Pt–N(4) bond angle. The molecular parameters (Table 2) related by this axis are in good agreement, within the limit of experimental error. In each of the three 5-membered rings, the middle ring is of a symmetric λ skew conformation, while the two terminal rings have an asymmetric δ envelope conformation.

The projection of the complex ion is shown in Fig. 3. The disposition of the 4 N atoms is not square or rectangular, but trapezoidal. Moreover, these atoms are disposed in a slightly tetrahedral configuration around the Pt atom, as may be seen in Fig. 3, where the deviations of atoms from the coordination plane defined by N(1)–N(4) are given in parentheses. Such a trapezoidal disposition of four ligators is usual in the metal chelates of triethylenetetramine (=trien) and its substituted derivatives.[6,7] Although the N(1)–Pt–N(4) angle is considerably larger than 90°, it is comparable to the corresponding angle (104°) in [Pd(trien)] $(PF_6)_2 \cdot KPF_6$.[8] An examination of the scaled model of the complex ion indicates that the slightly tetrahedral disposition of the 4 N atoms results from the conformation of the 3*S*,8*S*-dimetrien ligand, in which both C(*S*)–CH_3 groups are constrained equa-

Table 2. Bond lengths and angles

Bond lengths (l)	l/Å		l/Å
Pt-N(1)	2.05(1)	Pt-N(4)	2.04(1)
Pt-N(2)	1.99(1)	Pt-N(3)	2.02(1)
N(1)-C(1)	1.54(2)	N(4)-C(6)	1.49(3)
N(2)-C(2)	1.48(2)	N(3)-C(5)	1.50(2)
N(2)-C(3)	1.50(2)	N(3)-C(4)	1.50(2)
C(1)-C(2)	1.57(2)	C(5)-C(6)	1.56(3)
C(2)-C(7)	1.50(3)	C(5)-C(8)	1.54(3)
C(3)-C(4)	1.54(2)		
Bond angles (ϕ)			
	ϕ/°		ϕ/°
N(1)-Pt-N(2)	84.1(5)	N(3)-Pt-N(4)	84.2(5)
N(2)-Pt-N(3)	86.3(5)	N(1)-Pt-N(4)	106.2(5)
Pt-N(1)-C(1)	108(1)	Pt-N(4)-C(6)	109(1)
Pt-N(2)-C(2)	110(1)	Pt-N(3)-C(5)	109(1)
Pt-N(2)-C(3)	107(1)	Pt-N(3)-C(4)	107(1)
C(2)-N(2)-C(3)	118(1)	C(5)-N(3)-C(4)	118(1)
N(1)-C(1)-C(2)	109(1)	N(4)-C(6)-C(5)	110(2)
N(2)-C(2)-C(1)	103(1)	N(3)-C(5)-C(6)	104(1)
N(2)-C(2)-C(7)	113(1)	N(3)-C(5)-C(8)	111(1)
C(1)-C(2)-C(7)	108(1)	C(6)-C(5)-C(8)	112(1)
N(2)-C(3)-C(4)	108(1)	N(3)-C(4)-C(3)	104(1)

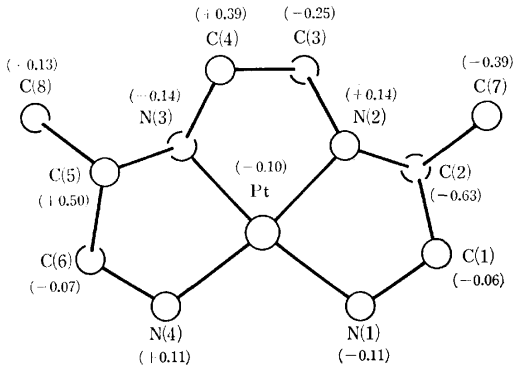

Fig. 3. Projection of $(+)_{240}^{CD}$-[Pt(3*S*,8*S*-dimetrien)]$^{2+}$ on the coordination plane defined by four nitrogen atoms. The deviations (Å) of atoms from the plane are given in parentheses.

torially. Such a disposition seems to be characteristic of the *RR*-isomer. This view is supported by the similar configuration of the 4 N atoms in $(-)_{589}$-*trans*-[Co$(NO_2)_2$(3*S*,8*S*-dimetrien)]ClO_4,[6] in which the dimetrien ligand has the same conformation as the present complex ion.

The Pt–N(secondary) distance seems to be shorter than the Pt–N(primary) distance. Such a tendency was also found in the Pd–N(secondary) and Pd–N(primary) bond lengths in the Pd(II) chelate of trien cited above for comparison. The C(2)–N(2)–C(3) and C(4)–N(3)–C(5) bond angles are significantly larger than the tetrahedral angle. This may be caused by the planar coordination of the quadridentate ligand. The other bond lengths and angles are normal.

Figure 4 shows the crystal structure viewed along the b axis. All amino H atoms participate in the

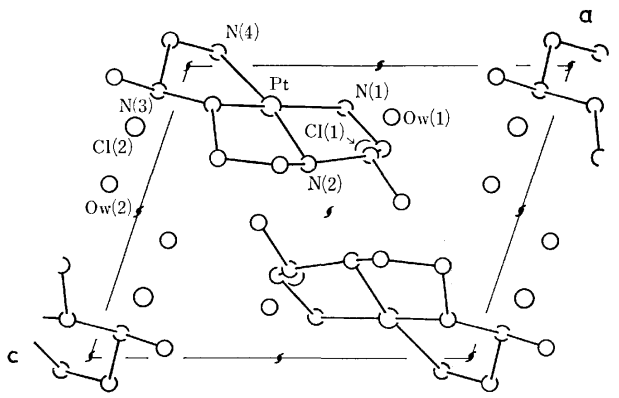

Fig. 4. Crystal structure viewed down the b axis.

Table 3. Possible hydrogen bonds

A	B	A···B (l/Å)	H···B (l/Å)	N-H···B (ϕ/°)
N(1)-H[a]	Cl(1^{III})	3.21(1)	2.19	170
N(1)-H	O_w(1^{I})	2.95(2)	2.18	131
N(2)-H	Cl(1^{III})	3.25(1)	2.25	164
N(3)-H	Cl(2^{IV})	3.18(1)	2.16	168
N(4)-H	Cl(2^{I})	3.30(1)	2.41	145
N(4)-H	O_w(2^{V})	2.81(3)	1.79	168
Cl(1)	O_w(1^{I})	3.20(2)		
Cl(1)	O_w(2^{VII})	3.23(2)		
Cl(2)	O_w(1^{VI})	3.21(2)		
Cl(2)	O_w(2^{VIII})	3.22(2)		

Roman-numeral superscripts refer to atoms in the following equivalent positions:
I x, y, z; II $1+x, (1/2)+y, z$; III $1+x, (1/2)+y, 1+z$; IV $x, (1/2)+y, z$; V $x, -(1/2)+y, z$; VI $-1+x, y, z$; VII $1+x, -1+y, z$; VIII $x, -(1/2)+y, 1+z$

a) The positions of the H atoms in the NH_2 groups were calculated on the assumption that the N-H distance is 1.03 Å.

N–H···Cl^- or N–H···O(H_2O) hydrogen bonding, the data of which are presented in Table 3.

The absorption and CD spectra are presented in Fig. 5. The electronic spectrum shows three bands, at 35000, 41000, and 44200 cm^{-1}. The peak positions are very similar to those in [Pt$(NH_3)_2$ (*RR*-chxn or *R*-pn)]Cl_2 and in [Pt(*RR*-chxn or *R*-pn)$_2$]Cl_2;[9] hence these peaks can be assigned to the $^1A_1 \rightarrow {}^3A_2$ and ^3E, $^1A_1 \rightarrow {}^1A_2$, and $^1A_1 \rightarrow {}^1E$ transitions (D_4 symmetry), respectively (*RR*-chxn = (1*R*,2*R*)-1,2-cyclohexanediamine; *R*-pn = (*R*)-1,2-propanediamine). However, the absorption is generally more intense than those in the chxn and pn complexes. Similarly, the absorption intensity in [Pd(trien)]$^{2+}$ was found to be about three times as intense as that in [Pd(*R*-pn)$_2$]$^{2+}$.[8] The disposition of the 4 N donor atoms is rectangular in [Pt(*R*-pn)$_2$]$^{2+}$;[5] this may also be the case in [Pd(*R*-pn)$_2$]$^{2+}$ and in the Pt(II) chelates of chxn, whereas the disposition is trapezoidal in the 3*S*,8*S*-dimetrien and trien complexes. The PtN_4 and PdN_4 chromophores in the last two complexes lack a center of symmetry, which may be responsible for the enhancement of the absorp-

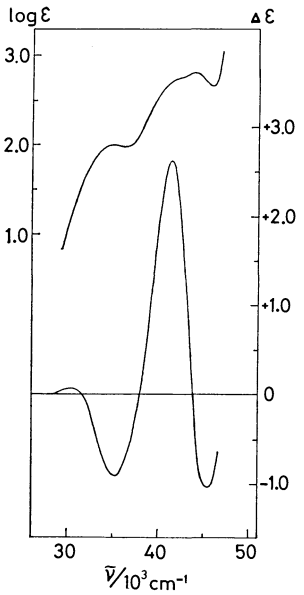

Fig. 5. Absorption (top) and CD (bottom) spectra of $(+)^{CD}_{240}$-[Pt(3*S*,8*S*-dimetrien)]$Cl_2 \cdot 2H_2O$

tion intensity. The enhancement is largest in the $^1A_1 \rightarrow {}^1A_2$ ($d_{xy} \rightarrow d_{x^2-y^2}$) transition. This is compatible with the interpretation of the intensity enhancement, because the electronic transition within the coordination plane should be the most sensitive to the disposition of donor atoms in the plane.

The d→d optical activity of the present complex could be regarded as composed of the contributions from the vicinal effects of the dissymmetric 5-membered rings and that of the asymmetric secondary nitrogen. The second effect may be small in magnitude, since the local effective symmetry around the secondary nitrogen can be taken as C_s. Then, the *RR*-isomer can be anticipated to show a CD pattern similar to that of $[Pt(NH_3)_2(SS\text{-chxn})]^{2+}$,[9] with one δ ring. Indeed, the CD signs of the ^3E and ^1E bands in the present complex are the same as those in the *SS*-chxn complex, but there is a remarkable difference between the CD spectra of these complexes; the $^1A_2$ CD band which appears at 41000 cm^{-1} in the former complex (Fig. 5) is not found in the latter complex. Similarly, the $^1A_2$ band is not observed in the CD spectra of $[Pt(NH_3)_2(S\text{-pn})]^{2+}$ and $[Pt(SS\text{-chxn or } S\text{-pn})_2]^{2+}$.[9] As has been described above, the increase in the electric-dipole transition moment is largest for the $^1A_2$ transition; this is responsible for the emergence of the intense $^1A_2$ CD band in the former. The CD sign of this band is compatible with that of the $^1A_2$ band in *trans*-$[CoCl_2(3S,8S\text{-dimetrien})]^+$.[10] The intensities of the other CD bands are also larger than those in $[Pt(NH_3)_2(SS\text{-chxn})]^{2+}$; this increase is mainly attributable to the increase in the transition moments.

This research was supported by a Grant-in-Aid for Scientific Research from the Ministry of Education.

References

1) M. Saburi and S. Yoshikawa, *Bull. Chem. Soc. Jpn.*, **45**, 1143 (1972).
2) J. Hornstra and B. Stubbe, PW1100 Data Processing Programs, Philips Research Laboratories, Eindhoven, Holland.
3) "International Tables for X-Ray Crystallography," Kynoch Press, Birmingham (1962), Vol. 3, pp. 202, 215.
4) "The Universal Crystallographic Computation Program System," Crystallographic Society of Japan (1969).
5) C. Maeda, K. Matsumoto, S. Ooi, and H. Kuroya, unpublished work; the X-ray structure analysis on $[Pt(R\text{-pn})_2]Cl_2 \cdot 2H_2O$ has revealed that one of the chelate rings is in a λ conformation with the equatorial methyl group, while the other has a δ conformation with the axial one.
6) M. Ito, F. Marumo, and Y. Saito, *Acta Crystallogr., Sect. B*, **28**, 463 (1972).
7) G. Marongiu, E. C. Lingafelter, and P. Paoletti, *Inorg. Chem.*, **8**, 2763 (1969).
8) F. Hori, K. Matsumoto, S. Ooi, and H. Kuroya, *Bull. Chem. Soc. Jpn.*, **50**, 138 (1977).
9) H. Ito, J. Fujita, and K. Saito, *Bull. Chem. Soc. Jpn.*, **40**, 2584 (1967); although the CD data of the Pt(II) complexes of *RR*-chxn and *R*-pn are presented therein, the CD curves of the *S* analogues are assumed to be inversions of the corresponding *R* analogues.
10) M. Goto, A. Okubo, T. Sawai, and S. Yoshikawa, *Inorg. Chem.*, **9**, 1488 (1970).

Kinetic Studies of the Electron Transfer Reaction in Iron(II) and Iron(III) Systems. VIII. The Effect of Hexamethylphosphoric Triamide on the Electron Transfer Reaction in Aqueous Solution

Goro WADA,* Sayuri NAKAGO, and Yuriko ABE

Department of Chemistry, Nara Women's University, Nara 630

(Received September 14, 1978)

The kinetics and mechanism of the electron transfer reaction between Fe(II) and Fe(III) in mixed solvents of water and hexamethylphosphoric triamide (HMPA) were studied. The apparent rate constant k varies depending upon [HMPA] and [H^+]; k exhibits a minimum value at [HMPA]=1.5 M at constant [H^+] and increases linearly with respect to [H^+]$^{-1}$ at constant [HMPA]. Judging from the basicity constant of HMPA, the complex formation constant of Fe(hmpa)$^{3+}$, and the absorption spectra of aqueous solutions containing Fe(II), Fe(III), HMPA, and $HClO_4$, the existing species in the reaction systems are mostly Fe^{2+}_{aq}, Fe^{3+}_{aq}, $Fe(OH)^{2+}$, Fe(hmpa)$^{3+}$, and Fe(hmpa)$(OH)^{2+}$ at low concentrations of HMPA. Therefore, the probable reaction paths are Fe^{2+}–Fe^{3+}, (k_0); Fe^{2+}–$Fe(OH)^{2+}$, (k_H); Fe^{2+}–Fe(hmpa)$^{3+}$, (k_L); and Fe^{2+}–Fe(hmpa)$(OH)^{2+}$, (k_{HL}) at the concentration range of [HMPA]=0—1 M and [$HClO_4$]=0.03—0.2 M. The occurrence of a minimum value of k *vs.* [HMPA] is reasonably understood by taking the complex formation between Fe(III) and HMPA into account in reaction rate equation. If the hydrolysis constants of both $Fe(OH)^{2+}$ and Fe(hmpa)$(OH)^{2+}$ are considered to be nearly of the same order, the value of k_H are approximately ten times larger than that of k_{HL}. At higher concentrations of HMPA, the higher Fe(III)-complexes with HMPA might take part in the electron transfer reaction.

The electron transfer reaction between iron(II) and iron(III) in aqueous media, Fe(II)+*Fe(III)→Fe(III)+*Fe(II), has been studied since the radioactive tracer method by use of ^{59}Fe was first established by Silvermann and Dodson,[1] and it is now well-known that, in case that no catalytic ligand exists, the reaction in aqueous media proceeds predominantly through a hydrogen atom transfer mechanism along the extended chains of the hydrogen bonds between a certain number of water molecules connecting the two reacting species.[2,3] Therefore, in aqueous solvents mixed with aprotic organic substances, such as acetone,[4] nitromethane,[5] and dimethyl sulfoxide,[6] the rate of the electron transfer reaction *via* the hydrogen atom transfer mechanism is made smaller than that in pure water, because of the partial breakdown of the hydrogen bondings by such aprotic molecules.

In this investigation, hexamethylphosphoric triamide (abbreviated HMPA) is adopted as another aprotic substance, since HMPA has come into notice on account of a recent finding that the life time of solvated electrons in this medium is surprisingly long, as compared with those of hydrated electrons or other usual solvated ones.[7] In this connection, it looks to be very interesting to study how the effect of HMPA appears on the electron transfer reaction mechanism of iron(II) and iron(III) system.

Experimental

Materials. The commercially obtained HMPA of guaranteed reagent grade was refined as follows: after it was refluxed over barium oxide at 85—90 °C under a reduced pressure of nitrogen of 5 mmHg for 2 h and the first portion of the distillate was taken out, the rest of the liquid was distilled with iron(II) chloride at 80 °C under reduced pressure of nitrogen, and then the middle portion of the distillate was collected and immediately used for the experiments. Since HMPA had a slight tendency to form a kind of peroxide with time which would perturb our present experiments, iron(II) chloride was adopted for reducing it under nitrogen atmosphere.

The purification of other materials such as $Fe(ClO_4)_2$, $Fe(ClO_4)_3$, $NaClO_4$, and water and the preparation of iron(III) tracer labeled by radioisotope ^{59}Fe were already described elsewhere.[8,9] $NaClO_4$ was used for maintaining the ionic strength of the reaction media at μ=0.2 M.

Procedure of Measurements. For the purpose of determining the basicity constant of HMPA in water, the spectrophotometric indicator method was adopted, using thymol blue as an indicator and a Hitachi-Perkin-Elmer UV-VIS spectrophotometer Model 139 for the observation. The detailed procedure is shown in the literature.[10]

For the determination of formation constant of Fe(hmpa)$^{3+}$, Job's continuous variation method was applied using the same spectrophotometer.[11]

The method to determine the rate constants of the electron transfer reaction was also the same as that described in the literature,[8,9] except that the concentration of iron(III) in the reaction solution was initially kept much lower than those in the cases in other media, because a small amount of iron(II) was inevitably oxidized to iron(III) by the peroxide in HMPA which happened to be formed even during the careful experimental procedure.

Results and Discussion

Basicity Constant of HMPA. Prior to the kinetic observations, the basicity constant of HMPA in water was needed to be known in order to make clear in what form HMPA exists in acidic media. The basicity constant of HMPA is defined as K_a=[HMPA] [H^+]/[HMPA·H^+]. Hence, the optical absorbance of a solution containing thymol blue and $HClO_4$ at a certain wavelength, A, is expressed as follows:[10]

$$A = \frac{\varepsilon_a[H^+]+\varepsilon_b K_{HIn}}{[H^+]+K_{HIn}}[HIn]_0 \quad (1)$$

where ε_a and ε_b stand for the molar absorptivities of thymol blue (HIn) in acid and base forms respectively, $[HIn]_0$ the total concentration of thymol blue, and K_{HIn} the dissociation constant of thymol blue as K_{HIn}=[H^+] [In^-]/[HIn]. When HMPA is added at the total

concentration $[HMPA]_0$ to the initial solution of thymol blue and $HClO_4$, the hydrogen ion concentration and the absorbance would alter as much as $\Delta[H^+]$ and ΔA respectively, in a relation expressed by the following equation.

$$\Delta A = \frac{(\varepsilon_a-\varepsilon_b)K_{HIn}\Delta[H^+]}{([H^+]+\Delta[H^+]+K_{HIn})([H^+]+K_{HIn})}[HIn]_0 \quad (2)$$

Since $\Delta[H^+]$ is equal to $[HMPA.H^+]$, K_a can be calculated by using $\Delta[H^+]$ which is obtained from Eq. 2.[10]

$$K_a = \frac{([HMPA]_0-\Delta[H^+])([HClO_4]_0-\Delta[H^+])}{\Delta[H^+]} \quad (3)$$

Thus, the value of K_a was given $K_a=0.71\pm0.16$ M as the mean value of thirty-one observations at $[HMPA]_0=0.23$—1.15 M, $[HClO_4]_0=0.01$—0.02 M and 25 °C at wavelengths 420, 440, 520, and 540 nm, where HMPA exhibits no absorption.[12] This value corresponds to $pK_a=0.15$, indicating that HMPA is a very weak base although it is a little more basic than *N,N*-dimethylformamide, $pK_a(DMF)=-0.19$[13] and dimethyl sulfoxide, $pK_a(DMSO)=-0.67$.[10] According to the Gutmann's donor numbers, D_{SbCl_5}, the sequence of the basic nature as Lewis bases agrees with the present results, HMPA>DMF>DMSO.[14]

Formation Constant of Fe(hmpa)$^{3+}$. In aqueous solution of iron(III) perchlorate, optical absorbance increases at the shorter wavelengths than 450 nm with decreasing concentration of perchloric acid from 1.0 M to 0.01 M due to the partial hydrolysis of $Fe^{3+}{}_{aq}$ with the hydrolysis constant $K_H=[Fe(OH)^{2+}][H^+]/[Fe^{3+}]=2.2\times10^{-3}$ M at 25 °C.[15] In order to determine the formation constant of $Fe(hmpa)^{3+}$ defined as $K_L=[Fe(hmpa)^{3+}]/[Fe^{3+}][HMPA]$, it is desirable that the acid concentration is chosen to be high enough to be able to avoid the partial hydrolysis of Fe^{3+}, although too high acid concentration would give rise to the protonation of HMPA due to $K_a=0.71$ M, as described above.

Thus, the formation constant K_L was determined under a carefully considered condition of $[HClO_4]_0=1.0$ M by Job's continuous variation method.[11] In Fig. 1, are drawn two Job's curves of $[Fe^{3+}]_0+[HMPA]_0=0.1$ and 0.08 M at 350 nm, where Y is defined by the following relation, in which ε_0 and ε_1 are the molar absorptivities of Fe^{3+} and $Fe(hmpa)^{3+}$ respectively.

$$Y = \varepsilon_0[Fe^{3+}] + \varepsilon_1[Fe(hmpa)^{3+}] - \varepsilon_0[Fe^{3+}]_0$$
$$= (\varepsilon_1-\varepsilon_0)[Fe(hmpa)^{3+}] \quad (4)$$

The curves exhibit maxima both at $x=[Fe^{3+}]_0/([Fe^{3+}]_0+[HMPA]_0)=0.5$ indicating that the predominant species is a 1 : 1 complex between Fe^{3+} and HMPA at these concentration ranges, and give $K_L=1.46\pm0.22$ M^{-1} as a result.[11]

At higher concentrations of HMPA than 0.1 M, higher complexes such as $Fe(hmpa)_n{}^{3+}$ ($n\geqq2$) might be formed.

Effect of Concentration of HMPA on Rates of the Electron Transfer Reaction. The process of the electron transfer reaction between iron(II) and iron(III) obeys the following McKay's relationship, as has been commonly recognized in any exchange reactions;

$$\ln\left(1-\frac{x}{x_\infty}\right) = -([Fe(II)] + [Fe(III)])kt \quad (5)$$

in which x and x_∞ represent the specific radioactivity of Fe(II) species at reaction time t and at equilibrium, respectively. Therefore, the apparent second-order rate constant, k, is expressed by use of half-time period of the reaction, $t_{1/2}$, which is obtained from the linear plot of $\ln(x_\infty-x)$ *vs.* t.

$$k = \frac{0.693}{([Fe(II)]+[Fe(III)])t_{1/2}} \quad (6)$$

When $[H^+]$ is maintained constant, k is affected by addition of HMPA; at a low concentration range of HMPA, k is lowered by HMPA and after passing the minimum point at about $[HMPA]_0=1.5$ M, k increases with increasing $[HMPA]_0$. The variation of k with $[HMPA]_0$ are shown in Fig. 2. Similar

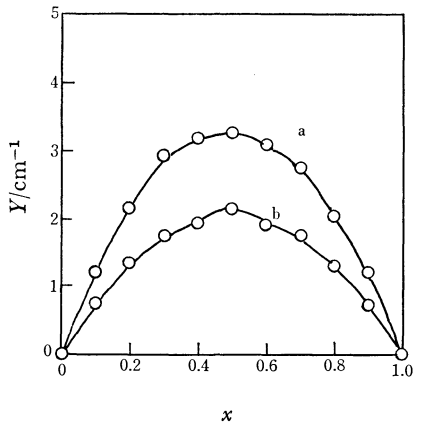

Fig. 1. Job's plot of continuous variation at 350 nm.
$Y=(\varepsilon_1-\varepsilon_0)[Fe(hmpa)^{3+}]$ and $x=[Fe^{3+}]_0/([Fe^{3+}]_0+[HMPA]_0)$.
a: $[Fe^{3+}]_0+[HMPA]_0=0.1$ M, b: $[Fe^{3+}]_0+[HMPA]_0=0.08$ M.

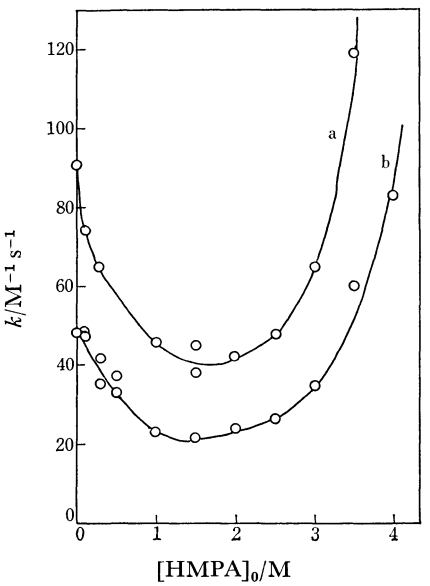

Fig. 2. Variation of k with $[HMPA]_0$ at $\mu=0.2$ M and 25 °C.
a: $[HClO_4]_0=0.05$ M, b: $[HClO_4]_0=0.1$ M.

phenomena have been recognized in water–DMSO systems, with the minimum value of k appearing at the mole fraction of DMSO 0.2—0.3 ([DMSO] =6.5—8.0 M) when $[HClO_4]=5\times10^{-2}$ M,[8] and in water–DMF systems, with the minimum value of k appearing at $[H_2O]=2$ M (namely [DMF]=12.5 M) when $[HClO_4]=1\times10^{-2}$ M.[16]

Dependence of Rate Constants upon Acid Concentration. The apparent rate constant k is also dependent upon $[H^+]$ at constant [HMPA], becoming smaller as $[H^+]$ becomes larger. When k is plotted against the reciprocal $[H^+]$, straight lines are obtained at respectively constant concentration of HMPA, as is reproduced in Fig. 3, at the concentration range of $[HMPA]_0=0$—3 M and $[H^+]=0.03$—0.2 M. Therefore, k is apparently expressed by the following equation at constant [HMPA];

$$k = k_A + \frac{k_B}{[H^+]} \tag{7}$$

where k_A and k_B are the intercept and the slope of an

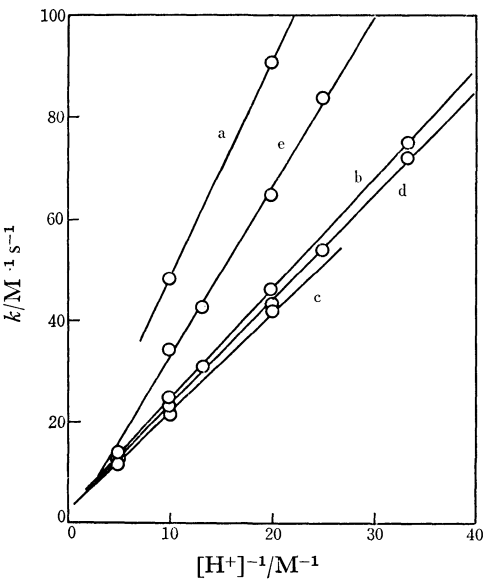

Fig. 3. Linear relationships of k with $[H^+]^{-1}$ at μ= 0.2 M and 25 °C.
a:$[HMPA]_0=0$ M, b: $[HMPA]_0=1.0$ M, c: $[HMPA]_0$ =1.5 M, d: $[HMPA]_0=2.0$ M, e: $[HMPA]_0=3.0$ M.

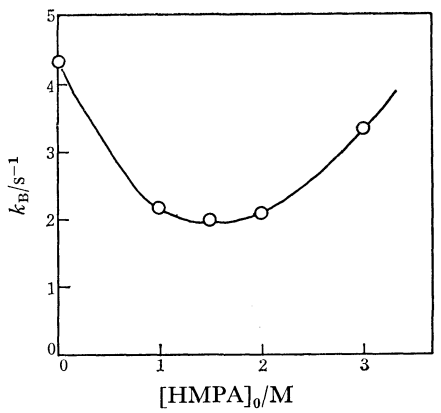

Fig. 4. Variation of k_B with $[HMPA]_0$ at μ=0.2 M and 25 °C.

empirically observed straight line respectively in Fig. 3; k_A's are very small at every $[HMPA]_0$, while k_B varies with $[HMPA]_0$ and exhibits a minimum again at $[HMPA]_0=1.5$ M, as is shown in Fig. 4.

Mechanism. According to the absorption spectra of aqueous solutions containing Fe^{3+}, HMPA, and $HClO_4$ at various concentrations at a wavelength range of 270—500 nm, the following results are observed : in the ultraviolet region, the absorbance increases with increasing [HMPA] and decreasing $[HClO_4]$, whereas in the visible region, it increases with increasing both [HMPA] and $[HClO_4]$, and approximate isosbestic phenomena occur in the vicinity of 340—350 nm among spectra of different $[HClO_4]$ at individually constant [HMPA]. These observed facts are caused by the hydrolysis of iron(III) species and the complex formation between iron(III) and HMPA. Consequently, it can be deduced that in the mixed solvents of water and HMPA, predominant part of iron(III) exists in the forms such as Fe^{3+}, $Fe(OH)^{2+}$, $Fe(hmpa)^{3+}$, and $Fe(OH)(hmpa)^{2+}$, and the rest part is in the forms of some higher complexes of HMPA. Since the pK_a value of HMPA is comparatively small, the occurrence of the protonated species of $Fe(hmpa)^{3+}$ is not probable. In regard to iron(II) species, both the hydrolysis and the complex formation with HMPA would be weak.

Thence, the important reaction paths of the electron transfer would be expressed by the following equations, having the activated complexes composed of $[Fe^{2+}, Fe^{3+}]$, $[Fe^{2+}, OH^-, Fe^{3+}]$, $[Fe^{2+}, HMPA, Fe^{3+}]$, and $[Fe^{2+}, OH^-, HMPA, Fe^{3+}]$ respectively. The asterisked Fe in the equations stands for the labeled species by tracer radioisotope:

$$Fe^{2+} + {}^*Fe^{3+} \rightarrow Fe^{3+} + {}^*Fe^{2+} \quad (k_0) \tag{8}$$

$$Fe^{2+} + {}^*Fe(OH)^{2+} \rightarrow Fe(OH)^{2+} + {}^*Fe^{2+} \quad (k_H) \tag{9}$$

$$Fe^{2+} + {}^*Fe(hmpa)^{3+} \rightarrow Fe(hmpa)^{3+} + {}^*Fe^{2+} \quad (k_L) \tag{10}$$

$$Fe^{2+} + {}^*Fe(OH)(hmpa)^{2+} \rightarrow Fe(OH)(hmpa)^{2+} + {}^*Fe^{2+} \quad (k_{HL}) \tag{11}$$

When the respective rate constants of Reactions 8—11 are denoted by k_0, k_H, k_L, and k_{HL}, the formation constant of $Fe(hmpa)^{3+}$ by K_L, and the hydrolysis constants of $Fe(OH)^{2+}$ and $Fe(OH)(hmpa)^{2+}$ by K_H and K_{HL} respectively, the apparent rate constant k is given by the following equation.

$$k = \frac{k_0 + k_H K_H [H^+]^{-1} + k_L K_L [HMPA] + k_{HL} K_L K_{HL} [HMPA][H^+]^{-1}}{1 + K_H [H^+]^{-1} + K_L [HMPA] + K_L K_{HL} [HMPA][H^+]^{-1}} \tag{12}$$

Since HMPA is slightly basic in aqueous solutions, the concentration of free HMPA, [HMPA], appearing in Eq. 12, has to be strictly expressed by the following equation.

$$[HMPA] = \frac{[HMPA]_0}{1 + K_a^{-1}[H^+] + K_L [Fe^{3+}] + K_L K_{HL} [Fe^{3+}][H^+]^{-1}} \tag{13}$$

By using the values $K_a=0.71$ and $K_L=1.46$ and supposing that K_{HL} would be approximately as small as 10^{-3} of the same order as K_H, the value of the denomi-

nator of Eq. 13 can be regarded as unity at low but not extremely low acid concentrations, and therefore, $[HMPA]_0$ may be plausibly used in place of [HMPA] in Eq. 12.

On the other hand, among the three terms in the denominator of Eq. 12, only $K_L[HMPA]$ is no longer negligible as compared with unity, according to the numerical consideration. Therefore, Eq. 12 can be simplified as follows:

$$k(1+K_L[HMPA]) = (k_0+k_LK_L[HMPA]) + (k_HK_H+k_{HL}K_LK_{HL}[HMPA])[H^+]^{-1} \quad (14)$$

Comparing Eq. 14 with Eq. 7, more accurate straight lines will be obtained when $k(1+K_L[HMPA])$, instead of the mere k, is plotted against $[H^+]^{-1}$, as are shown in Fig. 5, with the intercept k_A' and the slope k_B' of respective straight lines.

$$k_A' = k_0 + k_LK_L[HMPA] \quad (15)$$

$$k_B' = k_HK_H + k_{HL}K_LK_{HL}[HMPA] \quad (16)$$

The values of k_A' as obtained from the extrapolation of the straight lines are small and inaccurate to determine the value, while k_B' is accurately determined and found to increase with the increasing [HMPA], although it is not linear against the expectation from Eq. 16. The variation of k_B' with the function of [HMPA] is shown in Fig. 6, where any minimum phenomenon is no longer observed, which has been observed in the case of plotting k_B *vs.* [HMPA] in Fig. 4.

In both cases of mixed solvents of water–*N*-methylacetamide (NMA) and water–*N*,*N*-dimethylacetamide (DMA),[17] the linear relationship corresponding to Eq. 14 with the same physical meanings of k_A' and k_B' as the present case, was found to hold, and another

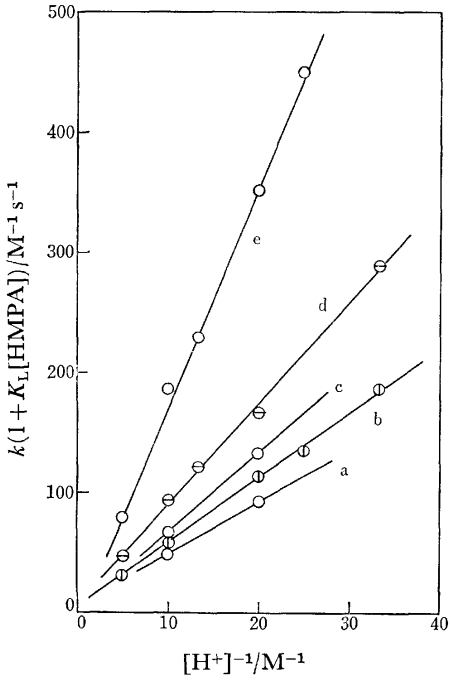

Fig. 5. Linear relationships of $k(1+K_L[HMPA])$ with $[H^+]^{-1}$ at $\mu=0.2$ M and 25 °C.
a, b, c, d, and e: Respectively the same as in Fig. 3.

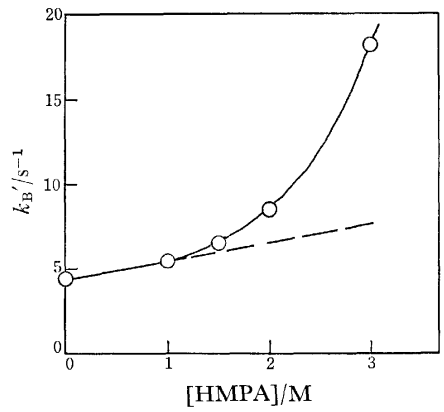

Fig. 6. Variation of k_B' with [HMPA] at $\mu=0.2$ M and 25 °C.

linear relationship of k_B' with [NMA] or [DMA] as represented by Eq. 16 was also noticed, giving reasonable values of k_HK_H and $k_{HL}K_LK_{HL}$.

Both of the observed facts that k exhibits a minimum value as a function of $[HMPA]_0$ as in Fig. 2 and that k_B also shows a minimum at the same $[HMPA]_0$ as in Fig. 4 may result from a same cause and reflect on the failure of k_B' from the linearity with respect to [HMPA] as in Fig. 6.

The abrupt increment of k_B' failing from the linearity in Fig. 6 may indicate a probability that the higher complexes of $Fe(hmpa)_n^{3+}$ ($n\geqq 2$) participate in the total reaction at higher HMPA concentration. From the limiting slope of the curve at $[HMPA]\rightarrow 0$, the value of $k_{HL}K_LK_{HL}$ may be given to be 1.2 $M^{-1}s^{-1}$, which may lead to a further estimation of $k_{HL}=3.7\times10^2$ M^{-1} s^{-1}. Since $k_H=2.7\times10^3 M^{-1}s^{-1}$ at 25 °C,[15] the reaction path (11) is supposed to be about ten times slower than the reaction path (9). The existence of HMPA molecule in coordinate sphere of the iron(III) complex may interfere with the hydrogen atom transfer mechanism of the electron transfer, probably due to both the larger geometrical dimension of an HMPA molecule, and the poorer possibility of hydrogen bonding of an HMPA molecule which is surrounded with as many as six methyl groups towards the outside of the complex, than that of a water molecule.

References

1) J. Silvermann and R. W. Dodson, *J. Phys. Chem.*, **56**, 846 (1952).
2) W. L. Reynolds and R. W. Lumry, *J. Chem. Phys.*, **23**, 2460 (1955).
3) R. A. Horne, *J. Inorg. Nucl. Chem.*, **25**, 1139 (1963).
4) R. A. Horne, "Exchange Reactions," IAEA, Vienna (1965), p. 67.
5) A. G. Maddock, *Trans. Faraday Soc.*, **55**, 1268 (1959).
6) G. Wada and M. Aoki, *Bull. Chem. Soc. Jpn.*, **44**, 3056 (1971).
7) T. Cuvigny, J. Normant, and H. Normant, *C. R. Acad. Sci.*, **258**, 3503 (1964); J. M. Brooks and R. R. Dewalt, *J. Phys. Chem.*, **72**, 2655 (1968).
8) J. Menashi, W. L. Reynolds, and G. Van Auken, *Inorg. Chem.*, **4**, 299 (1965).
9) G. Wada, N. Yoshizawa, and Y. Sakamoto, *Bull. Chem. Soc. Jpn.*, **44**, 1018 (1971).

10) G. Wada, *Bull. Chem. Soc. Jpn.*, **42**, 890 (1969).
11) G. Wada, *Bull. Chem. Soc. Jpn.*, **41**, 882 (1968).
12) Experimental work of spectrophotometry in this section was performed by Miss Mikiko Tabira.
13) G. Wada and T. Takenaka, *Bull. Chem. Soc. Jpn.*, **44**, 2877 (1971).
14) V. Gutmann, "Coordination Chemistry in Non-Aqueous Solutions," Springer Verlag, Wien (1968), p. 19.
15) G. Wada and A. Endo, *Bull. Chem. Soc. Jpn.*, **45**, 1073 (1972).
16) G. Wada, Y. Sahira, K. Ohsaki, and F. Shinoda, *Bull. Chem. Soc. Jpn.*, **47**, 851 (1974).
17) G. Wada and R. Yoshihara, *Kogyo Kagaku Zasshi*, **73**, 2309 (1970).

Synthetic Inorganic Ion-exchange Materials. XX. Ion-exchange Properties of Crystalline Antimonic(V) Acid with Alkaline Earth Metal Ions

Mitsuo ABE

Department of Chemistry, Faculty of Science, Tokyo Institute of Technology, Ookayama, Meguro-ku, Tokyo 152

(Received October 17, 1978)

A stoichiometrical ion-exchange was observed for all the systems of Mg^{2+}, Ca^{2+}, Sr^{2+}, and Ba^{2+} with H^+ in the crystalline antimonic(V) acid as a cation exchanger. The selectivity sequence, $Mg^{2+}<Ba^{2+}<Sr^{2+}<Ca^{2+}$, has been found for the ion-exchange reactions in 0.1 M nitrate salt solutions of different alkaline earth metals. Breakthrough and further elution studies were carried out in order to test the reversibility of the ion-exchange reactions. X-Ray analysis indicates that a solid solution forms for the ion-exchange system of the alkaline earth metal ions in the crystalline antimonic(V) acid.

Antimonic acid, $Sb_2O_5 \cdot 4H_2O$, has been of interest during last two decades because of its high ion-exchange capacity.[1] Various antimonic acid materials have been obtained with different chemical compositions and ion-exchange properties, depending on the method of preparation as well as on aging.[2] The species can be classified into three groups-crystalline, amorphous, and glassy. Among three different antimonic acids, crystalline antimonic(V) acid, C-SbA, shows an unusual selectivity for alkali metal ions as compared with the strong acid-type cation-exchange resins. The increasing selectivity shows: $Li^+<K^+<Cs^+<Rb^+<Na^+$ for microquantities of alkali metal ions in a nitric acid solution.[3,4] Similar unusual selectivity has been observed for polyantimonic acid[5] and hydrated antimony pentoxide.[6] These materials can be applied to the effective separation of sodium ion from certain elements.[3,4,6,7]

An unusual selectivity has been found in the ion-exchange system for microquantities of alkaline earth metal ions in a nitric acid solution.[8] An increasing order of selectivity is: $Mg^{2+}<Ba^{2+}<Ca^{2+}<Sr^{2+}$. A large difference in the distribution coefficients has been observed for the pairs of Mg^{2+}-Ba^{2+}, Ba^{2+}-Sr^{2+}, and Cs^+-Sr^{2+}. Effective separations can be achieved for these pairs.[8] Slightly different selectivities have been found for polyantimonic acid (PAA): $Mg^{2+}<Ca^{2+}<Sr^{2+}<Ba^{2+}$.[9]

In general, the selectivities of the inorganic ion-exchangers vary not only with the solution media, but also with exchange loading as a function of the concentration of the elements.

In this paper, the ion-exchange properties of C-SbA with macroquantities of alkaline earth metal ions will be reported.

Experimental

Reagents. The antimony pentachloride (Yotsuhata Chemical Co., Ltd.) was used without further purification. The other reagents used were all of an analytical grade.

Preparation of C-SbA as an Ion-exchange Material. C-SbA was prepared as has been described previously:[2] the precipitate obtained by the hydrolysis of antimony pentachloride was kept in the mother solution at 40 °C for over 20 days, and then washed with cold demineralized water with the aid of a centrifuge (about 10000 rpm) until it was free from chloride ions. After drying, the product was ground and sieved (100—200 mesh size). The collected sample was rewashed with demineralized water in order to obtain a clear supernatant solution following batch equilibrium experiments and to improve the elution-flow rate.

The Stoichiometry of Ion-exchange. Equilibrations were carried out by the batch technique as follows: a 0.25 g portion of the C-SbA was immersed in 25 ml of a 0.1 M nitrate salt solution of different alkaline earth metals at 30±0.1 °C with intermittent shaking. The amounts of metal ions adsorbed were determined from the changes in the concentrations of the alkaline earth metal ions and hydrogen ions relative to the initial concentration of the solution after equilibration. The emf titration method was employed for determining the hydrogen-ion concentration by means of a standard sodium hydroxide solution.

Breakthrough Curves. A column, 2.3 long and 0.4 cm i.d., containing 0.40 g of C-SbA in hydrogen ion-form, was employed, with a flow rate of 0.3 ml/min. The concentrations of hydrogen ions liberated by the ion-exchange reaction were titrated with a standard sodium hydroxide solution, using methyl red as an indicator.

Elution Curves of Alkaline Earth Metal Ions. A nitric acid solution at different concentrations was passed through the C-SbA column saturated with alkaline earth metal ions with a flow rate of about 0.3 ml/min.

Composition of the Ion-exchanged C-SbA with Different Alkaline Earth Metal Ions. The ion-exchanged C-SbA of a weighed amount (0.1 g) was dissolved by heating in a mixed solution of 25 ml of a 12 M HCl solution and 10 ml of a 0.5 M KI solution. After cooling, a 10 ml portion of a 10% tartaric acid solution was added in order to avoid the hydrolysis of Sb(III) and a 50 mg portion of L-ascorbic acid was added to reduce of the I_3^- formed as a result of the reaction of oxidation-reduction from Sb(V) to Sb(III). The concentrations of the alkaline earth metals and of antimony in the solutions were determined by using a Varian-Techtron 1100 atomic-absorption spectrometer. The water content of the ion-exchanged C-SbA was calculated by subtracting the weights of the corresponding metal oxides from the initial weight.

X-Ray Power-diffraction Analysis. The X-ray data for the ion-exchanged C-SbA were determined by using a JEOL X-ray diffraction meter Model, JDX-7E with, Ni-filtered Cu $K\alpha$ radiation.

Results and Discussion

The results of the TGA, DTA, and X-ray studies of C-SbA in the hydrogen-ion form showed a good

TABLE 1. STOICHIOMETRY OF THE ION-EXCHANGE REACTION OF ALKALINE EARTH METAL IONS ON C-SbA

Ion-exchange system	Amounts meq/g			
	Mg^{2+}/H^+	Ca^{2+}/H^+	Sr^{2+}/H^+	Ba^{2+}/H^+
Adsorbed metal ions	0.61±0.02	3.37±0.02	3.15±0.02	2.55±0.02
Liberated hydrogen ions	0.60±0.05	3.40±0.05	3.10±0.02	2.50±0.05

agreement with our earlier works.[2,10]

Batch Equilibration. The equilibrium for macroquantities of alkaline earth metal ions was attained within 3 months from our preliminary studies. For microquantities of Ca^{2+} and Sr^{2+}, previous work indicated that the exchange equilibrium would be attained in about 6 months. These phenomena may be explained by the presence of limited numbers of sites favorable to Ca^{2+} and Sr^{2+} making for a very tight network structure of the C-SbA. Thus no difference in the adsorbed amounts was observed within the limits of experimental error, although a further uptake of very small amounts occurred for a few consecutive months.

The relation between the liberated hydrogen ions and the adsorbed alkaline earth metal ions indicates a stoichiometry of the ion-exchange reaction for the systems studied (Table 1). The affinity sequence for macroquantities was found to be in this increasing order:

$$Mg^{2+} < Ba^{2+} < Sr^{2+} < Ca^{2+}$$

which was slightly different from the sequence for microquantities presented above. This may suggest that the selectivity sequence varys with the loading of the alkaline earth metal ions in C-SbA, as has been found for the ion-exchange systems of alkali metal ions–hydrogen ions on the C-SbA.[10] A definite selectivity sequence has been reported for both micro- and macroquantities of the same system on PAA by Baetsle and Huys.[5] However, no equilibrium time required has been reported in the literature. The rate of the adsorption of Ca^{2+} and Sr^{2+} was extremely slow, and the same sequence observed on PAA was found at the initial stage of the adsorption within a few weeks.

Breakthrough Curves. The breakthrough curves showed that hydrogen ions are liberated quantitatively for the equivalent uptake of alkaline earth metal ions by the ion-exchange reaction. The elution of the hydrogen ions by the ion-exchange proceeded rapidly at first, but they were still being liberated even after the passage of a relatively large volume of a 0.05 M nitrate salt solution of different alkaline earth metals, except in the case of the 0.05 M $Ba(NO_3)_2$ solution (Fig. 1). The breakthrough curve obtained for Ba^{2+}/H^+ exchange was steeper than those obtained for other systems. This can be explained by the fast rate of the adsorption for Ba^{2+} and the slow rate for the other alkaline earth metal ions, as was to be expected from a previous report.[8] The breakthrough capacities were determined by the analysis of alkaline earth metal and antimony after decomposing the exchanged C-SbA, because the determination from the liberated

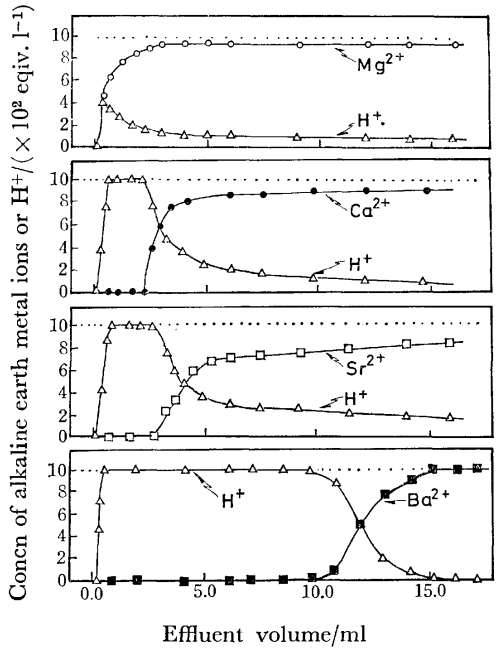

Fig. 1. Breakthrough curves for 0.05 M alkaline earth metal nitrate on C-SbA.
Column: 2.3×0.4 cm i.d., flow rate: 0.3 ml/min, —○—: Mg^{2+}, —●—: Ca^{2+}, —□—: Sr^{2+}, —■—: Ba^{2+}, —△—: H^+.

hydrogen ions may lead to large experimental error because of long tailing.

Elution of the Alkaline Earth Metal Ions Adsorbed on the C-SbA. Individual elution peaks with a sharp front and a tailing rear were observed for the elution of Mg^{2+}, Ca^{2+}, and Sr^{2+} (Figs. 2 and 3). Incomplete regenerations were achieved for the systems of Ca^{2+}/H^+ and Sr^{2+}/H^+, even if a 10 M nitric acid was used as an eluant. These phenomena may be due to the slow rate of desorption and the highly adsorptive ability on the C-SbA for Ca^{2+} and Sr^{2+}.

The adsorbed Ba^{2+} were eluted easily with a relatively small volume of a 1 M HNO_3 as an eluant. The results of the breakthrough and the elution are summarized in Table 2. The breakthrough capacities are found to be in the following increased order: $Mg^{2+}<Ca^{2+}<Ba^{2+}<Sr^{2+}$. The lower value of the breakthrough capacity than the uptake by batch equilibration for Ca^{2+} may be due to the slow rate of adsorption. A complete regeneration was achieved for the Ba^{2+}-exchanged C-SbA. Elutions of 79%, 31% and 43% for the adsorbed metal ions were achieved for Mg^{2+}, Ca^{2+} and Sr^{2+} respectively under the above experimental conditions.

The water contents of the C-SbA exchanged by

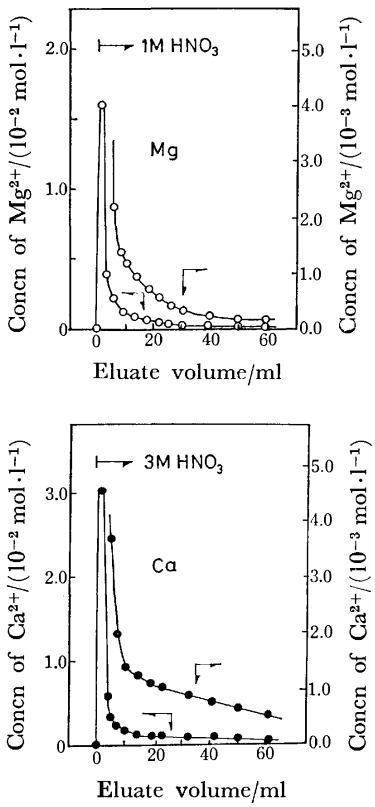

Fig. 2. Elution curves of Mg^{2+} and Ca^{2+} from the ion-exchanged C-SbA.
Column: 2.3×0.4 cm i.d., flow rate: 0.3 ml/min.

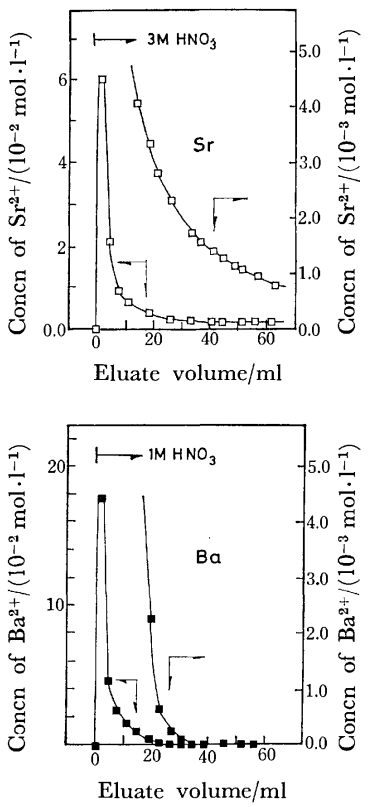

Fig. 3. Elution curves of Sr^{2+} and Ba^{2+} from the ion-exchanged C-SbA.
Column: 2.3×0.4 cm i.d., flow rate: 0.3 ml/min.

Table 2. Preparation and composition of the ion-exchanged C-SbA with different alkaline earth metal ions

Batch No.	Ion-exchange reaction	Influent[c]		M^{2+} Adsorbed (meq/g)[a]	Mole ratio in the exchanger	
		Breakthrough with	Elution with		MO/Sb_2O_5	H_2O/Sb_2O_5
1	$H^+ \rightarrow Mg^{2+}$	40 ml of 0.05 M $Mg(NO_3)_2$		0.53[b]	0.105	2.01
2	$Mg^{2+} \rightarrow H^+$	40 ml of 0.05 M $Mg(NO_3)_2$	70 ml of 1 M HNO_3	0.095	0.019	2.83
3	$H^+ \rightarrow Ca^{2+}$	800 ml of 0.05 M $Ca(NO_3)_2$		2.61[b]	0.516	1.47
4	$Ca^{2+} \rightarrow H^+$	800 ml of 0.05 M $Ca(NO_3)_2$	1500 ml of 3 M HNO_3 and 300 ml of 10 M HNO_3	1.81	0.358	1.85
5	$H^+ \rightarrow Sr^{2+}$	1000 ml of 0.05 M $Sr(NO_3)_2$		3.31[b]	0.654	0.726
6	$Sr^{2+} \rightarrow H^+$	1000 ml of 0.05 M $Sr(NO_3)_2$	1500 ml of 3 M HNO_3 and 300 ml of 10 M HNO_3	1.90	0.375	1.04
7	$H^+ \rightarrow Ba^{2+}$	30 ml of 0.05 M $Ba(NO_3)_2$		3.00[b]	0.594	3.35
8	$Ba^{2+} \rightarrow H^+$	30 ml of 0.05 M HNO_3	60 ml of 1 M HNO_3	0.0	0.0	4.47

a) meq/g of $Sb_2O_5 \cdot 4H_2O$. b) Breakthrough capacity. c) M: $mol \cdot l^{-1}$.

TABLE 3. X-RAY DIFFRACTION DATA OF THE C-SbA EXCHANGED BY DIFFERENT ALKALINE EARTH METAL IONS

Batch No. Exchanged	H+		1 Mg2+		3 Ca2+		5 Sr2+		7 Ba2+	
hkl	*d*(Å)	I/I_0	*d*(Å)	I/I_0	*d*(Å)	I/I_0	*d*(Å)	I/I_0	*d*(Å)	I/I_0
111	5.993	100	6.00_2	100	5.914	85	5.973	59	6.010	50
311	3.131	76	3.134	79	3.091	70	3.120	40	3.139	42
222	2.998	78	3.001	74	2.961	100	2.986	100	3.005	100
400	2.596	15	2.599	17	2.564	18	2.587	19	2.602_5	22
331	2.382	10	2.386	11	2.352	6	2.373	5		
422	2.119	4	2.124_5	1						
511	1.998_5	22	2.001_4	18	1.973_8	19	1.991	11	2.004	11
440	1.835_3	35	1.837_0	34	1.813_1	45	1.828_4	38	1.840_5	34
531	1.755	23	1.756_8	20	1.733_6	18	1.749_1	10	1.759_0	13
533	1.582_9	11	1.585_1	6	1.564_1	9	1.577_4	6	1.587_3	7
622	1.565_2	28	1.566_9	27	1.546_1	31	1.559_2	27	1.569_1	30
444	1.499_4	6	1.500_7	6	1.480_5	8	1.493_3	5	1.502_4	7
711	1.453_9	18	1.455_6	12	1.436_3	10	1.447_9	6	1.457_6	10
731	1.351_3	11	1.353_7	9	1.336_4	12	1.347_4	8	1.355_9	8
$\bar{a}$(Å)	10.38_2		10.39_6		10.25_7		10.34_6		10.40_9	

$\bar{a}$: Mean lattice constant.

different alkaline earth metal ions decrease with an increase in the amounts of the metal ions adsorbed and also with an increase in the crystal ionic radii of the metals, except in the case of Ba^{2+}. This indicates that the net transfer of some water molecules from the solid phase to the solution phase occurs with the ion-exchange of the alkaline earth metal ions on the C-SbA in hydrogen-ion form.

X-Ray Analysis. The X-ray diffraction data of the ion-exchanged C-SbA with different alkaline earth metal ions are summarized in Table 3.

There are changes in the lattice constant of up to a few percent with the cations adsorbed, but no change in the space group, Fd3m. Similar behavior is established for C-SbA and various zeolites on the ion-exchange systems of the alkali metal ions.[10,11] This may be due to the fact that C-SbA does not undergo remarkably any dimensional change with the ion-exchange because of its three-dimensional framework structure, like that of zeolite. In contrast, clay mineral and crystalline zirconium phosphate, possessing two dimensional structure, may undergo swelling or shrinking and may also be converted to two immiscible phases during the ion-exchange of some metal ions.[11,12] All of the X-ray diffraction patterns determined belong to Fd3m, and no immiscible phase was found over the entire range of systems studied. A remarkable decrease in the diffraction intensities of the (111) and (311) planes was observed with an increase in the crystal ionic radii of the adsorbed metal ions, while the (222) plane increased.

The calculated values of the lattice constant of the ion-exchanged C-SbA are plotted against the effective ionic radii of the metal ions in Fig. 4, the data of the C-SbA exchanged with alkali metal ions being included for comparison. The effective ionic radii can be found from the Shannon and Prewitt Table by assuming that the metal ion has six-coordinated

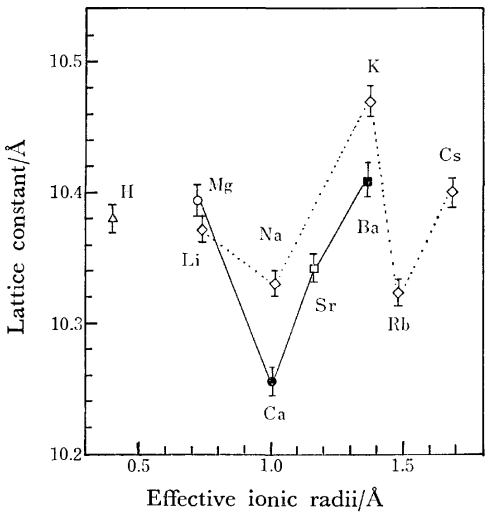

Fig. 4. Changes in the lattice constant of the C-SbA ion-exchanged with alkaline earth metal ions.
△: H-form, ○: (1), ●: (3), □: (5), ■: (7), A numeral in parenthesis indicates batch number.

radii.[13] A strong dependence on the effective ionic radii was noticed for the changes in the lattice constant, although it may be very difficult to explain its relationship quantitatively because of the metal ions adsorbed in different amounts in the C-SbA. When the exchanging cation, Na^+ or Ca^{2+}, has an ionic radii of about 1.0 Å, the lattice constant decreases markedly, as compared with that of the C-SbA in the hydrogen-ion form. Increased lattice constants are observed for the adsorption of a metal ion with effective ionic radii of about 1.3 Å (in the case of K^+ and Ba^{2+}).

Our work indicates that C-SbA has interstitial-(free) water with the chemically bonded water combined as Sb–OH.[14] The shrinking of the crystal lattice makes it progressively easier to exclude some

Table 4. X-Ray diffraction data of the ion-exchanged C-SbA samples after regeneration with nitric acid solutions as eluants

Batch No.	2		4		6		8	
Exchanged	$Mg^{2+}\rightarrow H^+$		$Ca^{2+}\rightarrow H^+$		$Sr^{2+}\rightarrow H^+$		$Ba^{2+}\rightarrow H^+$	
hkl	*d*(Å)	I/I_0	*d*(Å)	I/I_0	*d*(Å)	I/I_0	*d*(Å)	I/I_0
111	6.001	100	5.953	100	5.981	85	5.993	100
311	3.134	67	3.104	82	3.121	61	3.130	58
222	2.999	77	2.973	95	2.987	100	2.995	70
400	2.598	15	2.574	16	2.588	23	2.594_5	14
331	2.384	10	2.362	8	2.374	7	2.381	10
422	2.122	4					2.118	2
511	1.996	14	1.981_5	20	1.991_4	18	1.997_2	17
440	1.836_3	20	1.819_9	44	1.828_7	38	1.834_3	28
531	1.755_8	22	1.740_6	20	1.749_3	17	1.753_9	21
533	1.583_8	6	1.570_4	12	1.577_4	4	1.582_4	9
622	1.566_4	20	1.552_0	33	1.560_1	33	1.564_0	24
444	1.499_2	4	1.486_2	6	1.493_5	8	1.498_3	6
711	1.454_8	13	1.441_4	9	1.449_3	10	1.452_7	12
731	1.352_9	9	1.340_5	12	1.347_5	9	1.351_2	13
$\bar{a}$(Å)	10.38_8		10.29_6		10.34_9		10.37_8	

$\bar{a}$: Mean lattice constant.

of the water molecules of the solid phase by the ion-exchanging metal ions. In contrast, the swelling may cause some of the water molecules to be retained with the exchanging metal ions. If the dimension of the crystal lattice remain constant during the ion-exchange, the net transfer of some of the water molecules from the solid phase to the solution phase are probably caused by the adsorption of the metal ion with large effective ionic radii. The differences in the water content in the C-SbA exchanged with Ba^{2+} and with Ca^{2+} can be explained by the swelling and the shrinking.

The X-ray diffraction data of the C-SbA regenerated by different nitric acid solutions are summarized in Table 4. The X-ray data for the regenerated sample (Batch No.8) show that the conversion from the Ba^{2+}-exchanged C-SbA to the C-SbA in the hydrogen-ion form is indeed reversible within the limit of experimental error. In the other system, the X-ray patterns show intermediate profiles between the fully exchanged C-SbA and the C-SbA in hydrogen-ion form in the diffraction intensities and in values of the lattice constant.

The apparent irreversibility for the ion-exchange systems of Ca^{2+}/H^+ and Sr^{2+}/H^+ may be due to the extremely slow rate of adsorption and desorption in addition to the extremely high adsorptive ability of C-SbA for Ca^{2+} and Sr^{2+}.

Only a single phase is noticed over the entire range of C-SbA ion-exchanged with different alkaline earth metal ions. This indicates that a solid solution forms for the ion-exchange system of the metal ions in the C-SbA.

References

1) M. Abe and T. Ito, *Nippon Kagaku Zasshi*, **87**, 1174 (1966).
2) M. Abe and T. Ito, *Bull. Chem. Soc. Jpn.*, **41**, 333 (1968).
3) M. Abe and T. Ito, *Bull. Chem. Soc. Jpn.*, **40**, 1013 (1967).
4) M. Abe, *Bull. Chem. Soc. Jpn.*, **42**, 2638 (1969).
5) L. H. Baetsle and D. Huys, *J. Inorg. Nucl. Chem.*, **30**, 639 (1968).
6) F. Girardi, R. Pietra, and E. Sabbioni, *J. Radioanal. Chem.*, **5**, 141 (1970).
7) M. Abe, *Sep. Sci. Technol.*, **13**, 347 (1978).
8) M. Abe and K. Uno, *Sep. Sci. Technol.*, **14**, 355 (1979).
9) J. Lefebvre and H. Maria, *C. R. Acad. Sci. Paris*, **256**, 3121 (1964).
10) M. Abe, *J. Inorg. Nucl. Chem.*, **41**, 85 (1979).
11) J. A. Marinsky, "Ion Exchange" Marcel Dekker, New York (1969) Vol. 2, p. 123.
12) A. Clearfield, R. H. Blessing, and J. A. Stynes, *J. Inorg. Nucl. Chem.*, **30**, 2249 (1968).
13) R. D. Shannon and C. T. Prewitt, *Acta Crystallogr., Sect. B*, **25**, 925 (1969).
14) M. Abe and T. Ito, *Bull. Chem. Soc. Jpn.*, **41**, 2366 (1968).

Synthesis, Absorption and CD Spectra of [Co(amino alcohol)$(N)_2(O)_2$]-type Complexes

Kenichi Okazaki and Muraji Shibata*

Department of Chemistry, Faculty of Science, Kanazawa University, Kanazawa 920

(Received October 19, 1978)

Complexes of the [Co(amOH)$(N)_2(O)_2$]-type, where amOH represents 2-aminoethanol or (*S*)-2-amino-1-propanol and $(N)_2(O)_2$ represents $(gly)_2$, $(\beta\text{-ala})_2$, (ox)(en) or (ox)$(NH_3)_2$, have been prepared and characterized on the basis of absorption and PMR spectra. Splitting of the T_{2g} band has been observed in the solution spectra of certain isomers of the [Co$(gly)_2$(eta)], [Co$(gly)_2$(*S*-pra)], or [Co$(\beta\text{-ala})_2$(eta)] complex. Using the crystal spectral data of the isomers of [Co$(gly)_2$(eta)], the σ- and π-antibonding parameters for the ligating alcoholate O atom have been estimated and it has been found that each parameter shows a higher value than the corresponding parameters for the other ligating N and O atoms. The CD spectrum, in the T_{2g} region, of *fac*-[Co$(gly)_2$(eta)] has shown an intense peak at *ca.* 25000 cm^{-1}, and the vicinal effect curve of each isomer of the [Co$(gly)_2$(*S*-pra)] complex has shown an intense peak at the same frequency.

The mixed ligand complex of cobalt(III) containing 2-aminoethanol (Heta) and ethylenediamine, $[Co(en)_2(Heta)]^{3+}$, was first prepared by Buckingham *et al.*[1] Later, Ogino *et al.*[2] prepared optically active complexes such as $[Co(en)_2(S\text{-Hpra})]^{3+}$ (*S*-Hpra denotes (*S*)-2-amino-1-propanol), $[Co(en)_2(Heta)]^{3+}$ and $[Co(NH_3)_4(S\text{-Hpra})]^{3+}$ and reported that dissociation of the hydroxyl protons resulted in changes in the absorption and circular dichroism (CD) spectra; in the spectra of the deprotonated $[Co(eta)(en)_2]^{2+}$ and $[Co(S\text{-pra})(en)_2]^{2+}$ complexes, a shoulder and maximum are observed in the second absorption (T_{2g}) region. In the CD spectra of $[Co(S\text{-pra})(en)_2]^{2+}$ and $[Co(S\text{-pra})(NH_3)_4]^{2+}$ complexes, the vicinal effect curve shows of medium intensity peaks not only in the first absorption (T_{1g}) region but also at the shoulder of the split T_{2g} band. These observations are of interest since, in general, splitting of the T_{2g} band and an intense CD peak in the T_{2g} region are both rare. Nishide *et al.*[3] prepared [Co(amOH)$(N)_4$]-type complexes using a variety of amino alcohols (amOH) and studied the vicinal effect due to the chelated amino alcohols. There is however no study of other complexes which differ from the above in chromophore.

The present work was undertaken to prepare mixed ligand complexes of [Co(amOH)$(N)_2(O)_2$]-type, in which amOH denotes 2-aminoethanol or optically active (*S*)-2-amino-1-propanol and the $(N)_2(O)_2$ moiety denotes two glycinate ions, two β-alaninate ions, ethylenediamine and oxalate ion, or two ammonia and oxalate ions. The complexes obtained exhibited remarked different absorption and CD spectra, and splitting of the second absorption band was observed. In order to clarify the splitting of the T_{1g} and T_{2g} bands, polarized crystal spectra were measured, and from the spectral data, the σ- and π-antibonding parameters of the N and O donor atoms of the 2-aminoethanolate ion evaluated using the Angular Overlap Model.[4]

Experimental

Preparation. *a) (2-Aminoethanol)bis(glycinato)cobalt(III) Perchlorate, [Co(gly)$_2$(Heta)]ClO_4:* To a slurry of K[Co$(CO_3)(gly)_2]\cdot H_2O$ (9.7 g, 0.03 mol)[5] in water (25 cm^3) was added sufficient 3 M $HClO_4$ (M=mol dm^{-3}) to acid-hydrolyze the carbonato complex species. After removal of the precipitated $KClO_4$ by filtration, 2-aminoethanol (1.8 g, 0.03 mol) was added to the filtrate. The solution was stirred at 50 °C for 40 min, during which the pH of the solution was maintained at *ca.* 8.5 by the addition of an aqueous KOH solution. The resulting solution was adjusted to pH *ca.* 2, and the precipitated material filtered off. The filtrate was charged on a column containing 100—200 mesh Dowex 50W-X8 resin (Na^+ form, 5×20 cm). The red violet band held on the top of the column was eluted with 0.3 M NaCl solution and the band separated into four bands, the second and third bands being the desired species. Both eluates were concentrated to a small volume below 35 °C under reduced pressure and the concentrate poured into a column of the same resin (5×45 cm). By elution with water, the concentrate from the second band gave a violet band which was the parent species and a dark blue band which was the desired species (labeled A-1). The concentrate from the third band gave three bands, dark violet, red violet and red bands, of the desired species labeled A-2, A-3, and A-4 respectively. Acidification of the eluates with $HClO_4$ to pH *ca.* 3 brought about a change in colour, A-1, A-2, and A-3 to red violet and A-4 to rose. After concentration of the acidified solutions to small volumes, the A-1 and A-4 concentrates were kept in a refrigerator overnight, A-2 being kept in a refrigerator after the addition of a mixture of ethanol and ether (1 : 1). With respect to A-3, red violet crystals deposited during concentration. The yields of A-1, A-2, A-3, and A-4 were approximately 0.1, 0.2, 2.3, and 0.4 g, respectively.

b) (2-Aminoethanol)(ethylenediamine)(oxalato)cobalt(III) Perchlorate, [Co(ox)(en)(Heta)]ClO_4: To a green solution of tricarbonatocobaltate(III) ($Co(NO_3)_2\cdot 6H_2O$, 0.1 mol)[6] was added the solid material (17 g), prepared previously from ethylenediamine and oxalic acid. The mixture was stirred at 40 °C for 1.5 h, the resulting solution carefully acidified with $HClO_4$ under ice-cold conditions and filtered to remove any material precipitated. To this filtrate was added 2-aminoethanol (6 g, 0.1 mol), and the mixture stirred at 60 °C for 1 h, during which time the pH of the mixture was maintained at *ca.* 8.5 by the addition of an aqueous solution of KOH. The resulting solution was acidified to pH *ca.* 6 and concentrated. After the insoluble material had been filtered off, the filtrate was poured into a column of 100—200 mesh Dowex 50W-X8 resin (Na^+ form, 7×20 cm). Elution with water produced two bands, one dark violet and the other red (B-1 and B-2). Both eluates were adjusted to pH *ca.* 3 and concentrated. The crystals formed were recrystallized several times from aque-

ous solution (pH 2 adjusted with $HClO_4$).

c) (2-Aminoethanol)diamine(oxalato)cobalt(III) Perchlorate and Bis(2-aminoethanol)ammine(oxalato)cobalt(III) Bromide, [Co(ox)-$(NH_3)_2$(Heta)]ClO_4 and [Co(ox)(NH_3)(Heta)$_2$]Br: In the same manner as in a), $K[Co(CO_3)(ox)(NH_3)_2]\cdot H_2O$ (12 g, 0.04 mol)[7] was acid-hydrolyzed with 3 M $HClO_4$ and 2-aminoethanol (2.4 g, 0.04 mol) and ammonium oxalate (0.7 g) added to the solution. After the mixture had been stirred for 40 min at 60 °C, the pH being maintained at 8.5, the solution was acidified to pH *ca.* 6 and concentrated. The material precipitated was filtered off and the filtrate charged on a column of the same resin (Na^+ form, 7×20 cm). Elution with water produced three bands consisting of an anionic species, non-charged dark violet species and a red species. The final eluate (C-1) was further acidified to pH *ca.* 3 with aqueous $HClO_4$, concentrated and kept in a refrigerator overnight. The dark-violet eluate was made pH 2, whereupon the color turned violet. This solution was charged on a column of the same cation exchanger (4.5× 12 cm). Elution with a 0.3 M $NaClO_4$ solution, produced two violet bands (C-2 and C-3). The eluates were adjusted to pH *ca.* 2 and concentrated under reduced pressure, whereby pure violet crystals were obtained with respect to C-3. Crystals of C-2 were obtained as follows; to the concentrate was added a mixture of ethanol and ether (1 : 3), whereby a tarry material separated out. This material was dissolved in a small amount of water and an ethanol–HBr (47%) mixture (4 : 1) and ether added to the solution. The violet crystals (C-2) thus obtained were recrystallized from water by adding the same mixture of ethanol–HBr as above.

d) Bis(β-alaninato)(2-aminoethanol)cobalt(III) Perchlorate and Iodide, [Co(β-ala)$_2$(Heta)]X (X=ClO_4 or I): To a solution of tricarbonatocobaltate(III) ($Co(NO_3)_2\cdot 6H_2O$, 0.05 mol scale)[6] was added β-alanine (10.7 g, 0.12 mol), and the mixture stirred at 50 °C for 3 h. To the resulting solution 2-aminoethanol (3.5 g, 0.05 mol) neutralized previously with aqueous $HClO_4$ and activated charcoal (4 g) were added, and the solution stirred at 50 °C for 30 min. After the activated charcoal had been removed, the solution was neutralized and concentrated. The concentrate was poured into a column of the same resin as above (Na^+ form, 7× 20 cm), and eluted with water. A violet band and some overlapped bands descended after some bands of the anionic species had been eluted. For the sake of convenience, the violet band eluate has been named E-1, and the overlapped ones combined and named E-2. Each fraction was brought to pH 2 and charged on a column containing the same resin as above (5×22 cm). Elution with a 0.3 M $NaClO_4$ solution at pH 2, enabled each band held at the top of the column to be separated into four bands colored red or violet, numbered Nos. 1—4 according to the order of elution. The eluates No. 1 and No. 2 of the E-1 and No. 2 of the E-2, were subsequently concentrated. After the addition of a mixture of ethanol and ether (2 : 1), the concentrates were kept in a refrigerator overnight and the deposited crystals were recrystallized from water. With respect to eluate No. 4 of E-1, the addition of an ethanol–ether mixture (1 : 3) to the concentrate induced immediate crystallization. The crystals thus obtained sparingly recrystallized from aqueous solution due to the ready isomerized to an other species identical to No. 1 of E-1. The No. 1 eluate of E-2 was concentrated until red crystals were found and the crystals recrystallized from aqueous $HClO_4$. The addition of ethanol–ether mixture (1 : 5) to No. 3 of E-2, resulted in a red tarry material separating from the aqueous phase, this being dissolved in a minimum amount of water. To this solution a small amount of NaI and followed by an ethanol–ether mixture were added. On standing in the refrigerator overnight, red crystals deposited. No recrystallization was conducted due to the poor yield of product. The eluates of No. 3 of E-1 and No. 4 of E-2 were too small in quantity for crystals to be obtained.

e) (S)-2-Amino-1-propanolbis(glycinato)cobalt(III) Perchlorate, [Co(gly)$_2$(S-Hpra)]ClO_4: Four fractions were obtained in the same way as in a), except that (*S*)-2-amino-1-propanol (1.5 g, 0.02 mol) was used instead of 2-aminoethanol and that a longer time was necessary for reaction (1 h). The fractions were conveniently named A-1—A-4. The following description concerns the separation of the diastereoisomers for each geometrical isomer: Eluate A-1, adjusted to pH 2 with aqueous $HClO_4$ was charged on a column of the same cation exchanger (3×35 cm). The red violet band held at the top of the column was eluted first with a 0.2 M aqueous solution of sodium $(+)_{589}$-bis(tartrato)diantimonate(III), the pH being controlled to 3.5 with aqueous $HClO_4$, until the band clearly separated into two, and secondly eluted with a 0.3 M aqueous solution of $NaClO_4$. A-2 gave two bands in chromatographic elution conducted in a similar manner to that in A-1, using a 0.3 M $NaClO_4$ solution as the cluent. The effluents were concentrated and ethanol added. The products of the diastereoisomeric pairs were recrystallized from water by the addition of ethanol. The diastereoisomers for A-3 were isolated in the following manner; the eluate containing non-charged species was concentrated and charged on a column of the same resin (5×45 cm). Elution was conducted with water by means of a fraction collector. Frontal fractions, where the intensity ratios of the $\Delta\varepsilon$ values at 530 nm and the ε values at 550 nm were smaller than −0.033 and the rear fractions where the intensity ratios of the $\Delta\varepsilon$ values at 581 nm and the ε values at 550 nm were larger than 0.015 were collected and labeled A-3(−) and A-3(+), respectively. The collected eluates were adjusted to pH *ca.* 3 and evaporated. The violet crystals of A-3(−) separated out during concentration and the crystals of A-3(+) were obtained by adding an ethanol–ether mixture (1 : 1). Recrystallization was repeated until the $\Delta\varepsilon$ of the main CD peak attained a constant value. One of the diastereoisomers of A-4 was obtained as red crystals from the concentrate adjusted to pH *ca.* 3; the crystals were recrystallized repeatedly until the $\Delta\varepsilon$ value remained constant. The solution containing the other diastereoisomer was charged on a column containing the same resin (3×35 cm) and the band held at the top of the column eluted with a 0.3 M $NaClO_4$ solution. The rear fractions exhibiting a (−) CD sign were collected together and concentrated. A mixture of ethanol and ether (1 : 1) was added and the solution kept in a refrigerator until crystals separated. The crystals thus obtained were recrystallized until the $\Delta\varepsilon$ value remained constant.

The elemental analyses are summarized in Table 1.

Resolution. The A-1 and A-3 Isomers of [Co(gly)$_2$-(Heta)]$^+$: In an aqueous, warm solution (*ca.* 40 °C) of the perchlorate (0.76 g, 0.002 mol) was dissolved $(-)_{589}Na[Co(ox)_2(en)]$ (0.34 g, 0.001 mol),[8] whereupon the less soluble diastereoisomeric salt crystallized. The crystals were dissolved in water (100 cm^3) containing some $NaHCO_3$ in order to assist dissolution. The resulting alkaline solution was adjusted to pH 2 with aqueous $HClO_4$ and concentrated until crystallization, after which recrystallization was repeated.

The A-4 Isomer of [Co(gly)$_2$(Heta)]$^+$: The chloride which is more soluble than the perchlorate was prepared in the following manner; the red effluent (A-4) described in a) was acidified with an aqueous HCl solution and concentrated and methanol added to precipitate the chloride. The chlo-

Table 1. Elemental analyses of the prepared complexes

Label	Complex	C%	H%	N%
A-1	$[Co(gly)_2(Heta)]ClO_4 \cdot 0.5\ H_2O$	19.10 (19.13)	4.41 (4.29)	10.82 (11.16)
A-2	$[Co(gly)_2(Heta)]ClO_4 \cdot 0.5\ H_2O$	19.16 (19.13)	4.44 (4.29)	10.91 (11.16)
A-3	$[Co(gly)_2(Heta)]ClO_4$	19.90 (19.60)	4.13 (4.12)	11.45 (11.43)
A-4	$[Co(gly)_2(Heta)]ClO_4 \cdot H_2O$	18.71 (18.69)	4.47 (4.45)	10.92 (10.90)
B-1	$[Co(ox)(en)(Heta)]ClO_4$	19.57 (19.60)	4.14 (4.12)	11.44 (11.43)
B-2	$[Co(ox)(en)(Heta)]ClO_4 \cdot 0.5\ H_2O$	18.95 (19.13)	4.22 (4.29)	11.14 (11.16)
C-1	$[Co(ox)(NH_3)_2(Heta)]ClO_4 \cdot H_2O$	13.39 (13.36)	4.19 (4.21)	11.63 (11.69)
C-2	$[Co(ox)(NH_3)(Heta)_2]Br \cdot H_2O$	19.24 (19.21)	4.80 (5.11)	11.55 (11.20)
C-3	$[Co(ox)(NH_3)_2(Heta)]ClO_4 \cdot H_2O$	13.60 (13.36)	4.10 (4.21)	11.65 (11.69)
No. 1 (E-1)	$[Co(\beta\text{-ala})_2(Heta)]ClO_4$	24.27 (24.29)	4.85 (4.84)	10.52 (10.62)
No. 2 (E-1)	$[Co(\beta\text{-ala})_2(Heta)]ClO_4 \cdot H_2O$	23.30 (23.23)	5.38 (5.12)	10.00 (10.16)
No. 1 (E-2)	$[Co(\beta\text{-ala})_3] \cdot (HClO_4)_2 \cdot 0.5\ H_2O$	20.50 (20.28)	4.08 (3.97)	7.93 (7.88)
No. 2 (E-2)	$[Co(\beta\text{-ala})_2(Heta)]ClO_4 \cdot 0.5\ H_2O$	23.79 (23.75)	4.87 (4.98)	10.03 (10.38)
A-1(+)	$[Co(gly)_2(S\text{-Hpra})]ClO_4 \cdot 0.5\ H_2O$	21.88 (21.58)	4.46 (4.40)	10.76 (10.79)
A-1(−)	$[Co(gly)_2(S\text{-Hpra})]ClO_4 \cdot 0.5\ H_2O$	22.00 (21.58)	4.42 (4.40)	10.61 (10.79)
A-2(+)	$[Co(gly)_2(S\text{-Hpra})]ClO_4 \cdot H_2O$	21.08 (21.09)	4.87 (4.55)	10.58 (10.54)
A-2(−)	$[Co(gly)_2(S\text{-Hpra})]ClO_4 \cdot 1.5\ H_2O$	20.61 (20.63)	4.70 (4.70)	10.37 (10.31)
A-3(+)	$[Co(gly)_2(S\text{-Hpra})]ClO_4 \cdot 1.5\ H_2O$	20.68 (20.63)	4.68 (4.70)	10.44 (10.31)
A-3(−)	$[Co(gly)_2(S\text{-Hpra})]ClO_4 \cdot 0.5\ H_2O$	21.60 (21.58)	4.44 (4.40)	10.85 (10.79)
A-4(+)	$[Co(gly)_2(S\text{-Hpra})]ClO_4 \cdot 1.5\ H_2O$	20.81 (20.63)	4.86 (4.70)	10.28 (10.31)
A-4(−)	$[Co(gly)_2(S\text{-Hpra})]ClO_4 \cdot H_2O$	21.07 (21.09)	4.91 (4.55)	10.49 (10.54)
A-1	$[Co(gly)_2(Heta)][Co(ox)_2(en)] \cdot 2.5\ H_2O$	23.84 (23.70)	4.51 (4.64)	11.55 (11.51)
A-3	$[Co(gly)_2(Heta)][Co(ox)_2(en)] \cdot 0.5\ H_2O$	25.26 (25.19)	4.00 (4.23)	12.26 (12.24)
A-4	$[Co(gly)_2(Heta)][Co(ox)_2(en)] \cdot 3.5\ H_2O$	22.93 (23.01)	4.65 (4.83)	11.15 (11.18)

( ): Calcd.

ride (2 g, 0.0065 mol) was dissolved in warm water (*ca.* 15 cm^3, *ca.* 40 °C), and $(-)_{589}Na[Co(ox)_2(en)]$ (1 g, 0.003 mol)[8] added. The addition of ethanol gave red, needle-like crystals. Which was followed by recrystallization from warm water (*ca.* 40 °C).

The elemental analyses are summarized in Table 1.

Measurements. The absorption spectra were measured with a Hitachi 323 recording spectrophotometer, the absorption spectra of single crystals being measured by a micro-spectrophotometer constructed in this laboratory.[9] The CD spectra were recorded with a JASCO Model ORD/UV-5 spectrometer with CD attachments. Proton magnetic resonance (PMR) spectra were conducted with JEOL Model JNM-PS-100 spectrometer (100 MHz) at *ca.* 24 °C. The values of the chemical shifts were measured in relation to sodium 2,2,3,3-tetradeuterio-3-(trimethylsilyl)propionate (TMSP) as the internal reference. The acid dissociation constants of the complexes were determined by pH titration at 25 °C and the ionic strength 0.1 adjusted by $NaClO_4$.

The absorption and CD spectra were measured in acid (pH 2) or alkaline solutions (pH 8). For the PMR spectra, all of the protons of $-NH_2$ of the isomeric complexes of $[Co(gly)_2(Heta)]^+$ were deuterized in alkaline D_2O solution and the chlorides of the isomers used for the samples in acid solutions (DCl). The PMR spectra of the C-2 and C-3 were measured in D_2O–D_2SO_4 (30%) solutions.

Results and Discussion

Characterization of Complexes. The possible geometrical isomers of a $[Co(Heta)(N)_2(O)_2]$-type complex are illustrated in Fig. 1, where *trans(O)*, *cis·cis*, and *trans(N)* isomers are *mer* isomers with respect to the three N donor atoms. Assuming the $(N)_2(O)_2$ moiety consists of two glycinate or two β-alaninate ions, *i.e.* $(N)_2(O)_2=(gly)_2$ or $(\beta\text{-ala})_2$, then the four isomers are possible. When the moiety consists of (ox)(en), two isomers, *cis·cis* and *fac*, are possible; $(ox)(NH_3)_2$ as the moiety gives, *cis·cis*, *trans(N)* and *fac* isomers.

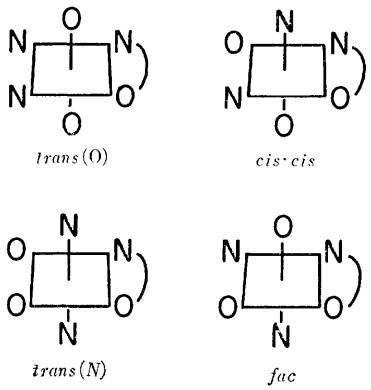

Fig. 1. Possible geometrical isomers of $[Co(Heta)(N)_2(O)_2]$. N–O denotes Heta.

From the absorption spectra of whole complexes, some of which are shown in Figs. 2 and 3, a *fac* isomer is readily distinguishable from the corresponding *mer* isomer, but the *mer* isomers cannot be distinguished from each other despite the fact that there are remarkable differences in the spectra for deprotonated isomers.

Yoneda *et al.*[10] explained theoretically the "through-cobalt effect" which had been found experimentally,[11] and on this basis assigned the signals of a number of complexes in the PMR spectra. The "through-cobalt effect" has been applied to the PMR data of the *mer*-$[Co(gly)_2(eta)]$ isomers and to the C-2 and C-3 isomers for characterization.

The PMR spectra, in alkaline solutions, of the $[Co(gly)_2(eta)]$ isomers are shown in Fig. 4, in which the signals of the methylene groups of the glycinate ions may be distinguished from the multiplets due to the methylene groups of the chelated eta, since the glycinate protons undoubtedly exhibit either a singlet or a doublet. No significant difference in chemical

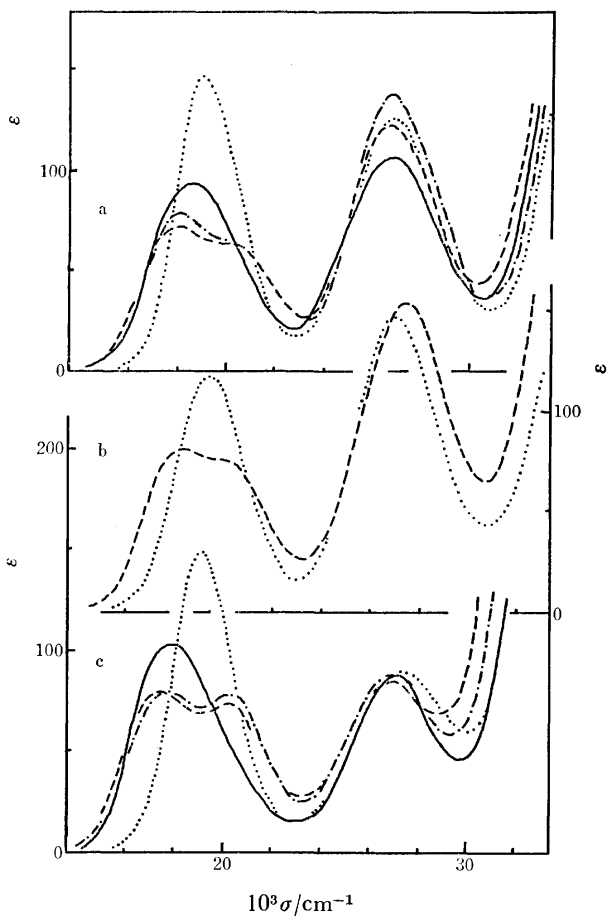

Fig. 2. Absorption spectra of protonated complexes, a) $[Co(gly)_2(Heta)]^+$, b) $[Co(ox)(en)(Heta)]^+$, and c) $[Co(\beta\text{-ala})_2(Heta)]^+$; —— *trans(O)*, –– *cis·cis*, —·— *trans(N)*, and ····· *fac*.
The ε values of *cis·cis*-, *fac*-$[Co(\beta\text{-ala})_2(Heta)]^+$ are taken arbitrarily.

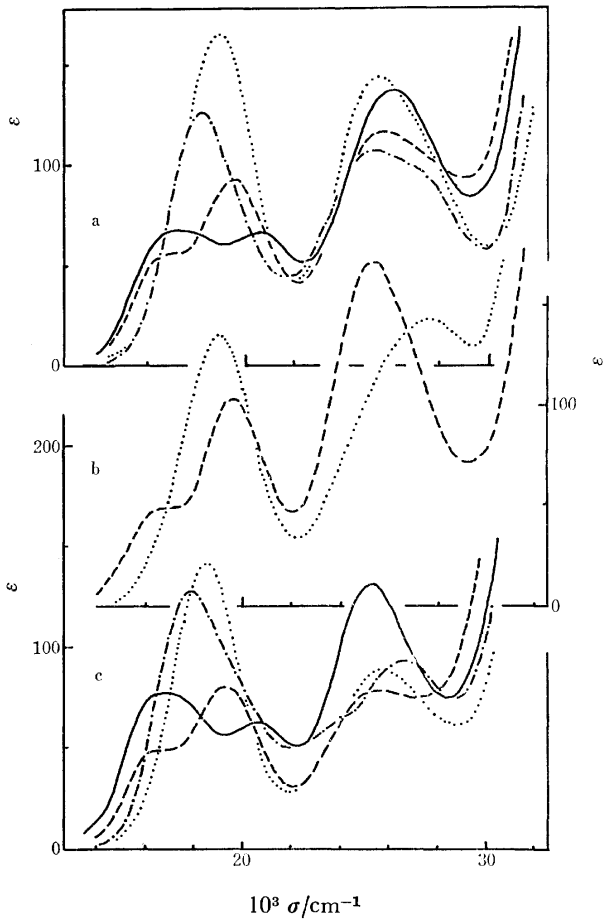

Fig. 3. Absorption spectra of deprotonated complexes, a) $[Co(gly)_2(eta)]$, b) $[Co(ox)(eta)(en)]$, and c) $[Co(\beta\text{-ala})_2(eta)]$; —— *trans(O)*, –– *cis·cis*, —·— *trans(N)*, and ····· *fac*.
The ε values of *cis·cis*-, *fac*-$[Co(\beta\text{-ala})_2(eta)]$ are taken arbitrarily.

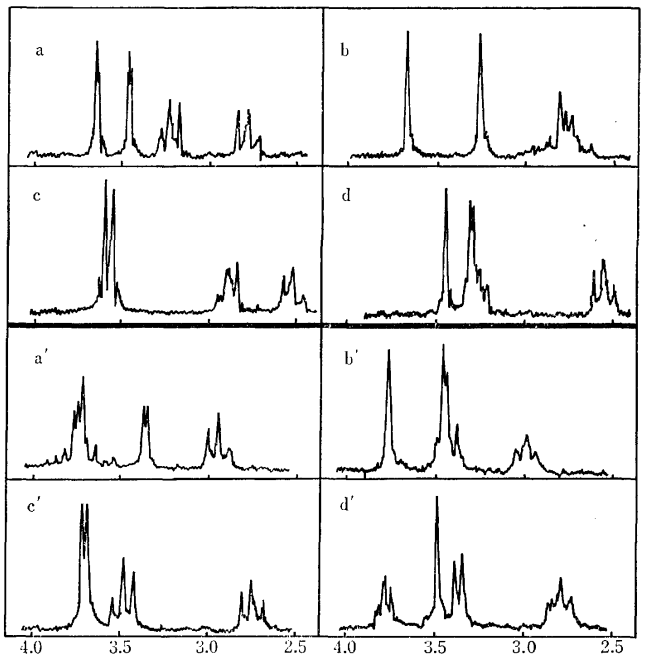

ppm, *vs.* TMSP

Fig. 4. PMR spectra of; a—d) $[Co(gly)_2(eta)]$ (deprotonated form), a'—d') $[Co(gly)_2(Heta)]^+$ (protonated form), a, a') *trans(O)* (A-1), b, b') *cis·cis* (A-2), c, c') *trans(N)* (A-3), d, d') *fac* (A-4).

shift between the two glycinate groups of the *trans(N)* isomer is expected because of the symmetric situations of the two N atoms in the glycinate ions. Thus the spectrum of A-3, which possesses two singlets around 3.6 ppm, has been assumed to be the *trans(N)* isomer. Concerning the signals eminating from the chelated 2-aminoethanol, the multiplet of the CH_2 protons adjacent to the oxygen is thought to appear at lower field than that of the CH_2 protons adjacent to the nitrogen because of the stronger electron-withdrawing effect due to oxygen. The spectrum of the A-1 isomer shows two multiplets at approximately 3.2 and 2.8 ppm, whereas the spectrum of A-2 shows a multiplet around 2.8 ppm, the integrated intensity of which corresponds to the four hydrogens of the 2-aminoethanol, *i.e.*, the protons adjacent to the oxygen induce the signals at approximately 3.2 ppm in the A-1 isomer and at approximately 2.8 ppm in the A-2 isomer. Thus the A-1 isomer may be identified as the *trans(O)*, and the A-2 as the *cis·cis*. The results[12] of X-ray analysis of a crystal of the A-2 isomer supports this.

The PMR spectra of the protonated $[Co(gly)_2(Heta)]^+$ isomers are also shown in Fig. 4. The resonance signals of the protonated and deprotonated forms of the $[Co(gly)_2(Heta)]^+$ isomers may be assigned in the same manner as above, the results of which are summarized in Table 2.

With respect to the C-2 and C-3 isomers, the PMR spectra measured in D_2O–D_2SO_4 (30%) solution are shown in Fig. 5. There are five signals in the C-3 spectrum; the signal at 5.94 ppm is due to the NH_2 protons of the chelated 2-aminoethanol (Deta), where the hydroxyl group is deuterated, and the signals due to the two NH_3 groups are at 4.40 and 3.72 ppm. The other two signals due to the methylene groups of the Deta are at *ca.* 3.6 and 2.9 ppm as multiplets. Since the spectrum indicates the existence of two non-equivalent NH_3 groups, the C-3 isomer is regarded as the *cis·cis* form. Furthermore, from the "through-cobalt effect" the NH_3 proton signal at low field is due to the NH_3 trans to the N atom of the chelated Deta. From elemental analysis and PMR data it is thought that the C-2 isomer is $[Co(ox)(NH_3)(Heta)_2]^+$, in which one of the Heta molecules acts as a bidentate ligand and another as a unidentate ligand. The PMR spectrum of the C-2 isomer is more intricate than C-3; there are two broad signals at 5.9 and 4.4 ppm and multiplets around 3.7 and 2.8 ppm, the integrated ratio

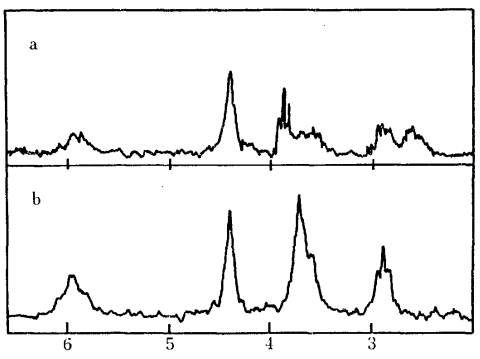

ppm, *vs.* TMSP

Fig. 5. PMR spectra of; a) *cis·cis*-$[Co(ox)(NH_3)(Heta)_2]^+$ (C-2) and b) *cis·cis*-$[Co(ox)(NH_3)_2(Heta)]^+$ (C-3).

Table 2. Assignment of PMR signals[a] of the $[Co(gly)_2(Heta)]^+$ and $[Co(gly)_2(eta)]$ complexes

Complex	Glycine		2-Aminoethanol	
	CH_2	CH_2	O-CH_2	N-CH_2
trans(O)-$[Co(gly)_2(Deta)]^+$	3.75 (o)	3.36 (d)	3.75 (m)	2.95 (m)
trans(O)-$[Co(gly)_2(eta)]$	3.64 (d)	3.45 (d)	3.21 (m)	2.80 (m)
cis·cis-$[Co(gly)_2(Deta)]^+$	3.77 (s)	3.46 (s)	3.43 (m)	2.99 (m)
cis·cis-$[Co(gly)_2(eta)]$	3.68 (s)	3.26 (s)	2.78 (m)	2.78 (m)
trans(N)-$[Co(gly)_2(Deta)]^+$	3.72 (s)	3.69 (s)	3.48 (m)	2.76 (m)
trans(N)-$[Co(gly)_2(eta)]$	3.58 (s)	3.54 (s)	2.88 (m)	2.53 (m)
fac-$[Co(gly)_2(Deta)]^+$	3.36 (d)	3.48 (s)	3.78 (m)	2.78 (m)
fac-$[Co(gly)_2(eta)]$	3.45 (s)	3.31 (o)	3.26 (m)	2.56 (m)

a) Values in ppm from TMSP. (s): Singlet. (d): Doublet. (m): Multiplet. (o): Overlap.

Table 3. Results of the assignment and absorption spectral data

Label	Complex	I band		II band	
		$\tilde{\nu}/10^3$ cm^{-1}	ε	$\tilde{\nu}/10^3$ cm^{-1}	ε
A-1	*trans*(*O*)-[Co(gly)$_2$(Heta)]$^+$	18.6	92.5	26.8	106
	trans(*O*)-[Co(gly)$_2$(eta)]	17.2	66.9	26.0	137
		20.4	65.9		
A-2	*cis*·*cis*-[Co(gly)$_2$(Heta)]$^+$	18.0	72.2	26.8	123
		sh. 19.8	63.0		
	cis·*cis*-[Co(gly)$_2$(eta)]	sh. 17.0	54.6	25.6	117
		19.6	92.9		
A-3	*trans*(*N*)-[Co(gly)$_2$(Heta)]$^+$	18.2	78.0	26.8	138
		sh. 20.2	69.4		
	trans(*N*)-[Co(gly)$_2$(eta)]	18.2	124	25.2	108
A-4	*fac*-[Co(gly)$_2$(Heta)]$^+$	19.2	147	26.8	125
	fac-[Co(gly)$_2$(eta)]	18.8	166	25.4	144
B-1	*cis*·*cis*-[Co(ox)(en)(Heta)]$^+$	18.4	79.5	27.4	156
		sh. 19.8	75.2		
	cis·*cis*-[Co(ox)(en)(eta)]	16.6	48.7	25.2	171
		19.4	103		
B-2	*fac*-[Co(ox)(en)(Heta)]$^+$	19.3	117	26.8	147
	fac-[Co(ox)(en)(eta)]	19.0	134	27.6	143
C-1	*fac*-[Co(ox)(NH$_3$)$_2$(Heta)]$^+$	19.2	94.2	27.0	134
	fac-[Co(ox)(NH$_3$)$_2$(eta)]	19.0	115	27.2	137
C-2	*cis*·*cis*-[Co(ox)(NH$_3$)(Heta)$_2$]$^+$	17.6	82.5	27.0	163
	cis·*cis*-[Co(ox)(NH$_3$)(Heta)(eta)]	sh. 16.6	45.1	24.6	148
		19.0	81.0		
C-3	*cis*·*cis*-[Co(ox)(NH$_3$)$_2$(Heta)]$^+$	18.0	77.7	27.4	155
	cis·*cis*-[Co(ox)(NH$_3$)$_2$(eta)]	sh. 16.6	45.7	25.0	158
		19.2	89.0		
No. 1 (E-1)	*trans*(*O*)-[Co(*β*-ala)$_2$(Heta)]$^+$	18.0	104	27.2	88
	trans(*O*)-[Co(*β*-ala)$_2$(eta)]	16.8	77.2	25.2	133
		20.6	63.4		
No. 2 (E-1)	*trans*(*N*)-[Co(*β*-ala)$_2$(Heta)]$^+$	17.7	79.4	26.8	87.7
		20.4	77.9		
	trans(*N*)-[Co(*β*-ala)$_2$(eta)]	17.8	128	sh. 24.0	64.9
				26.4	94.2
No. 4 (E-1)	*cis*·*cis*-[Co(*β*-ala)$_2$(Heta)]$^+$ [a]	17.4	—	27.0	—
		20.2	—		
	cis·*cis*-[Co(*β*-ala)$_2$(eta)][a]	sh. 16.8	—	25.6	—
		19.2	—		
No. 3 (E-2)	*fac*-[Co(*β*-ala)$_2$(Heta)]$^+$ [a]	19.0	—	27.3	—
	fac-[Co(*β*-ala)$_2$(eta)][a]	18.4	—	25.6	—
A-1	*trans*(*O*)-*Δ*-[Co(gly)$_2$(*S*-Hpra)]$^+$	18.6	89.8	27.1	108
	trans(*O*)-*Δ*-[Co(gly)$_2$(*S*-pra)]	17.2	62.7	26.2	130
		20.6	67.8		
	trans(*O*)-*Λ*-[Co(gly)$_2$(*S*-Hpra)]$^+$	18.7	98.5	26.8	119
	trans(*O*)-*Λ*-[Co(gly)$_2$(*S*-pra)]	17.2	72.7	25.6	159
		20.5	74.2		
A-2	*cis*·*cis*-*Δ*-[Co(gly)$_2$(*S*-Hpra)]$^+$	17.8	71.4	26.7	122
		sh. 20.0	62.9		
	cis·*cis*-*Δ*-[Co(gly)$_2$(*S*-pra)]	sh. 17.0	48.5	25.6	104
		19.6	87.4		
	cis·*cis*-*Λ*-[Co(gly)$_2$(*S*-Hpra)]$^+$	18.0	74.0	26.6	133
		sh. 20.0	62.2		
	cis·*cis*-*Λ*-[Co(gly)$_2$(*S*-pra)]	16.5	65.5	25.4	128
		19.4	105		
A-3	*trans*(*N*)-*Λ*-[Co(gly)$_2$(*S*-Hpra)]$^+$	18.1	70.4	26.7	131
		sh. 20.0	62.0		

TABLE 3. (Continued)

Label	Complex	I band		II band	
		$\tilde{\nu}/10^3$ cm^{-1}	ε	$\tilde{\nu}/10^3$ cm^{-1}	ε
	trans(*N*)-*Λ*-[Co(gly)$_2$(*S*-pra)]	18.1	123	26.0	96.3
	trans(*N*)-*Λ*-[Co(gly)$_2$(*S*-Hpra)]$^+$	18.2	84.4	26.8	146
		sh. 20.0	69.6		
	trans(*N*)-*Λ*-[Co(gly)$_2$(*S*-pra)]	18.2	141	24.8	127
A-4	*fac*-*Λ*-[Co(gly)$_2$(*S*-Hpra)]$^+$	19.2	149	26.8	118
	fac-*Λ*-[Co(gly)$_2$(*S*-pra)]	18.9	183	25.7	132
	fac-*Λ*-[Co(gly)$_2$(*S*-Hpra)]$^+$	19.3	153	26.8	133
	fac-*Λ*-[Co(gly)$_2$(*S*-pra)]	18.9	180	25.2	170

a) The ε values were not obtained because of a lack of elemental analyses.

of the four signals being estimated as 2 : 5 : 4 : 4 (from lower to higher field). The multiplets are due to the methylene groups of the two Deta, while one of the broad signals at 5.9 ppm is assignable to the NH_2 protons of the chelated Deta from a comparison with the spectrum of the C-3 isomer. With respect to the broad signal at 4.4 ppm, it is considered from the integrated ratio that the two types of signal due to the NH_3 and the NH_2 of the unidentately bound amino alcohol overlap. Comparing the signals due to NH_3 and NH_2 in the C-2 isomer spectrum (4.4 and 5.9 ppm) with those in the C-3, *cis*·*cis* configuration with NH_3 in the trans position of the N of the chelated Deta is assumed to this isomer. The remaining isomer for the [Co(ox)$(NH_3)_2$(Heta)]$^+$ complex should be *trans*(*N*), but no band corresponding to such a species has been observed in the chromatographic separation.

The absorption spectra in alkaline solutions for the *cis*·*cis* isomers (A-2, B-1, C-2, and C-3) are similar. The No. 4 isomer of E-1 which exhibits a similar spectrum to those of the *cis*·*cis* isomers has been assigned *cis*·*cis*. On the basis of the similarity of spectra, the No. 1 isomer of E-1 and the No. 2 isomer of E-2 have been assigned *trans*(*O*) and the No. 2 isomer of E-1 *trans*(*N*).

The crystals of the No. 1 isomer of E-2 have been identified as *fac*-[Co(*β*-ala)$_3$]·$(HClO_4)_2$·0.5H_2O from elemental analysis, the absorption spectrum,[13] and the acid-base titration (see below). The complex species in acidified aqueous solution was adsorbed on the cation exchanger and the crystals contained perchloric acid of crystallization, both of which are of interest.

The No. 1 isomer of E-1 and the No. 2 isomer of E-2 have been identified as the same isomer since both species exhibit identical absorption spectra in acidic and basic solution and possess the same pK_a values as seen from Table 4.

Ogino *et al.*[2] assigned the absolute configurations of the [Co(en)$_2$(Heta)]$^{3+}$ and [Co(en)$_2$(*S*-Hpra)]$^{3+}$ complexes by a comparison of the CD spectra with those of the [Co(gly)(en)$_2$]$^{2+}$ and [Co(L-ala)(en)$_2$]$^{2+}$ complexes. Each CD spectrum of the *mer* and *fac* isomers of the present [Co(gly)$_2$(amOH)]$^+$ (amOH=Heta, *S*-Hpra) complexes exhibits a major CD peak in the T_{1g} region, similarly to those of the *mer* and *fac* isomers of [Co(am)$_3$] (am=gly, L-ala)[14,15] complexes, respectively. Thus, the sbaolute configuration of an isomer of [Co(gly)$_2$(amOH)]$^+$, which exhibits (+) CD sign at *ca.* 19000 cm^{-1}, is assignable to *Λ*, and hence, the other isomer to *Δ*. The structures thus assigned are summarized in Table 3.

pK_a *Values.* Nishide *et al.*[3] have reported that the pK_a values of the [Co$(NH_3)_4$(amOH)]$^{3+}$, [Co$(en)_2$-(amOH)]$^{3+}$ and [Co(*R*-chxn)$_2$(amOH)]$^{3+}$ complexes are *ca.* 3.6, 3.2, and 3.2, respectively. From the pK_a values of the present complexes summarized in Table 4, it is seen that the *cis*·*cis* and *trans*(*N*) isomers exhibit lowerer pK_a values (*ca.* 4.2) compare to the *trans*(*O*) and *fac* isomers (*ca.* 5.2). This indicates that the pK_a value of amOH, where the O atom is situated trans to the other O atom, shows *ca.* 4.2, while the value of amOH, where the O atom is situated trans to the N atom, shows *ca.* 5.2. This difference may be due to reduced electron density on the former hydroxyl O atom.

The No. 1 isomer of E-2, which has been assigned as [Co(*β*-ala)$_3$] from the absorption spectrum,[13] behaves as a strong and dibasic acid in titration, this being additional evidence that the chemical formula is [Co(*β*-ala)$_3$]·$(HClO_4)_2$.

Absorption Spectra. A spectra of [Co(gly)$_2$(*S*-Hpra)]$^+$ isomers show great similarity to the spectrum of the corresponding [Co(gly)$_2$(Heta)]$^+$ isomer. The numerical data for all the absorption spectra for the protonated and deprotonated isomers are summarized in Table 3. The spectrum of the *fac*-[Co(gly)$_2$(Heta)]$^+$

TABLE 4. pK_a VALUES

Complex	pK_a
cis·*cis*-[Co(gly)$_2$(Heta)]$^+$	4.1
trans(*N*)-[Co(gly)$_2$(Heta)]$^+$	4.2
cis·*cis*-[Co(ox)(en)(Heta)]$^+$	4.4
cis·*cis*-[Co(ox)$(NH_3)_2$(Heta)]$^+$	4.3
cis·*cis*-[Co(ox)(NH_3)(Heta)$_2$]$^+$	4.4
trans(*N*)-[Co(*β*-ala)$_2$(Heta)]$^+$	4.4
trans(*O*)-[Co(gly)$_2$(Heta)]$^+$	5.1
fac-[Co(gly)$_2$(Heta)]$^+$	5.3
fac-[Co(ox)(en)(Heta)]$^+$	5.2
fac-[Co(ox)$(NH_3)_2$(Heta)]$^+$	5.2
trans(*O*)-[Co(*β*-ala)$_2$(Heta)]$^+$ [a]	5.9

a) No. 1 (E-1) and No. 2 (E-2) complexes.

complex is similar to that of *fac*-[Co(gly)$_3$],[16] suggesting that amino alcohol in the protonated form and the glycinate ion are situated in close positions in the spectrochemical series.[17] For the *mer* isomers of [Co(*β*-ala)$_2$(Hpta)]$^+$, having two six-membered chelate rings, the spectra of the *cis·cis* and *trans*(*N*) isomers exhibit a remarkable degree of splitting in the T_{1g} region, while no splitting has been observed in the spectrum of the *trans*(*O*) isomer. Among the *cis·cis* and *trans*(*N*) isomers of the [Co(gly)$_2$(Heta)]$^+$, [Co(gly)$_2$(*S*-Hpra)]$^+$ and [Co(ox)(Heta)(N)$_2$]$^+$-type complexes, the spectra are similar and show a little splitting; however, no splittings have been observed in the spectra of the *trans*(*O*) isomers in the T_{1g} region.

Each of the deprotonated complexes exhibits quite a different spectrum from the corresponding protonated complex. The *trans*(*O*), *cis·cis*, *trans*(*N*) and *fac* isomers exhibit remarkedly different spectra. The T_{1g} band for each *trans*(*O*) isomer is clearly split into two and the separation between the maxima is in the range 3200—3800 cm^{-1}; the T_{2g} band for each *trans*(*O*) isomer shows a sharp band. For the *cis·cis* isomers, the T_{1g} bands are not split as clearly as the *trans*(*O*) isomers, but each has a noticeable shoulder at lower wave-number, the T_{2g} band exhibiting a broad maximum generally splitting. The exceptions are the *cis·cis* isomers of B-1, C-2, and C-3, which contain no N–O chelate rings beyond eta, which show only sharp bands in the T_{2g} region. For the *trans*(*N*) isomers, recognizable splittings in the T_{2g} region and sharp bands in the T_{1g} region have been observed in contrast to the *trans*(*O*) isomers. The remaining isomers of *fac* give sharp and red-shifted bands in both the T_{1g} and T_{2g} regions. The complexes are, however, shifted to the blue end.

As seen in Fig. 3, there is a remarkable difference between the shapes of the T_{2g} bands for the *trans*(*N*) isomers of the [Co(gly)$_2$(eta)] and [Co(*β*-ala)$_2$(eta)] complexes, both of which have an identical chromophore *trans*(*N*)-[Co(eta)(N)$_2$(O)$_2$]. The same differences in the T_{2g} bands have been observed between the *cis·cis*-[Co(ox)(eta)(N)$_2$] isomer and each *cis·cis* isomer of the [Co(gly)$_2$(eta)] and [Co(*β*-ala)$_2$(eta)] complexes as well as between the *fac* isomers of the [Co(ox)(eta)(N)$_2$] complex and the [Co(gly)$_2$(eta)] and [Co(*β*-ala)$_2$(eta)] complexes. These differences may be related to the manner of chelation of the ligands forming the (N)$_2$(O)$_2$ moiety.

Three possible transitions for the T_{1g} band have been revealed in the polarized crystal spectra of the *trans*(*O*) and *cis·cis* isomers of the [Co(gly)$_2$(eta)] complex, and the polarized crystal spectra of the *cis·cis* and *trans*(*N*) isomers provides clearer splitting of the T_{2g} band (Fig. 6). The *trans*(*O*) isomer shows a large splitting of the T_{1g} band and this together with the X-ray analysis of the *cis·cis* isomer[12] allows assignment of the three bands. The paths of the polarized light are schematically shown in Fig. 7. In the ∥ polarized spectra, a maximum at 15900 cm^{-1} for the *trans*(*O*) isomer and two maxima at 20200 and 16400 cm^{-1} for the *cis·cis* isomer have been assigned to the transitions from the d_{zx} orbital for the *trans*(*O*) and from the d_{yz} and d_{zx} orbitals for the *cis·cis* isomer,

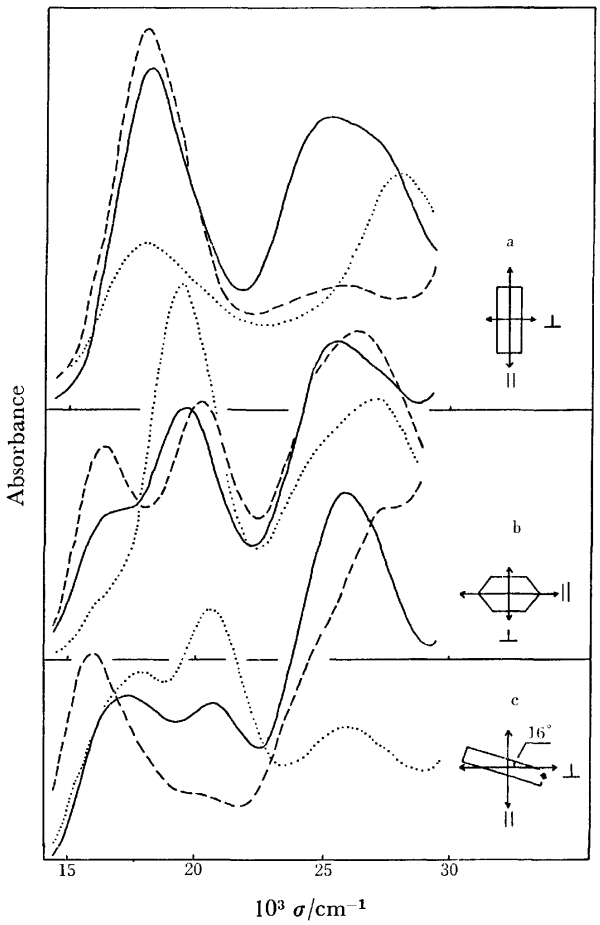

Fig. 6. Absorption spectra of [Co(gly)$_2$(eta)]; a) *trans*(*N*), b) *cis·cis*, and c) *trans*(*O*) (—— solution, —— ∥, ····· ⊥).

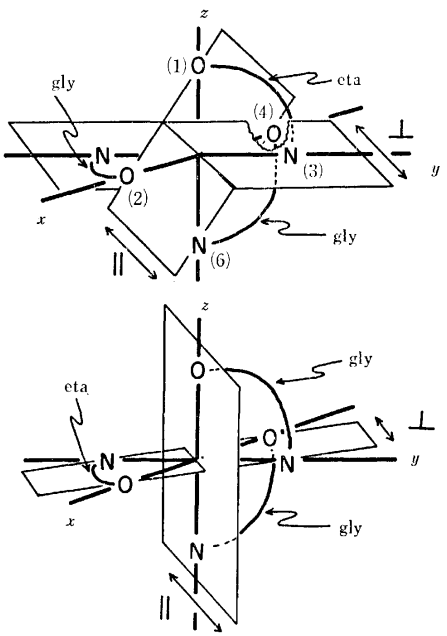

Fig. 7. The arrangements of the donor atoms and the paths of the polarized lights; *trans*(*O*)-[Co(gly)$_2$(eta)] (upper) and *cis·cis*-[Co(gly)$_2$(eta)] (lower).

respectively (Fig. 7). In the spectra with ⊥ polarization two maxima at 20600 and 17800 cm^{-1} for the *trans(O)* and a maximum at 19500 cm^{-1} for the *cis·cis* isomer have been assigned to the transitions from d_{yz} and d_{xy} for the former and from d_{xy} for the latter isomer, respectively. Using the Angular Overlap Model[4] (Appendix), the antibonding parameters, e_σ and e_π, may be obtained from the above data assuming that the $e_\sigma(N)$ parameters of the amino alcoholate and glycinate ions are equal. Assuming $C=4B$ and $B=450$ cm^{-1} (C and B denote the Racah parameters), the most reasonable values are shown in Table 5. Both the e_σ and the e_π values for the alcoholate O atom are large which are comparable with those for the OH^- ligand. The e_σ and e_π values for the OH^- ligand have been reported as 8500 and 2100 cm^{-1}, respectively, for the *trans*-$[Cr(OH)_2(NH_3)_4]^+$ isomer.[18]

CD Spectra. The CD spectra of the protonated and deprotonated forms of the resolved three isomers of the $[Co(gly)_2(Heta)]^+$ complex are shown in Fig. 8, and the configurational and vicinal effect curves, calculated from the CD spectra of the protonated and deprotonated isomers of the $[Co(gly)_2(S\text{-Hpra})]^+$ complex are shown in Fig. 9. The configurational curves show striking resemblances to the CD spectra, in both acidic and basic solutions of the corresponding isomers of the $[Co(gly)_2(Heta)]^+$ complex indicating the additivity of the configurational and vicinal effects in both the $[Co(gly)_2(S\text{-Hpra})]^+$ and $[Co(gly)_2(S\text{-pra})]$

Table 5. The σ- and π-antibonding parameters for the N and O donor atoms of the glycinate and 2-aminoethanolate ions

gly	eta	Value (cm^{-1})
$e_\sigma(N)$	$e_\sigma(N)$	7700
$e_\sigma(O)$		5800
	$e_\sigma(O')$	8100
$e_\pi(O)$		325
	$e_{\pi 1}(O')$[a]	2300
	$e_{\pi 2}(O')$[a]	700

a) Appendix.

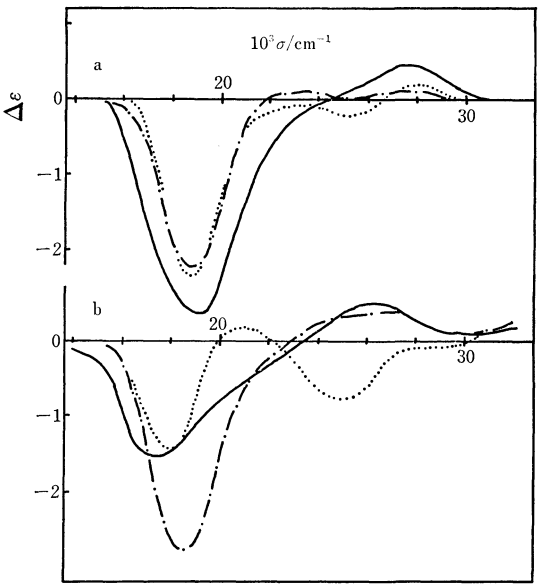

Fig. 8. CD spectra of $[Co(gly)_2(Heta)]^+$ (upper) and $[Co(gly)_2(eta)]$ (lower); —— *trans(O)*, —·— *trans(N)*, and ····· *fac*.

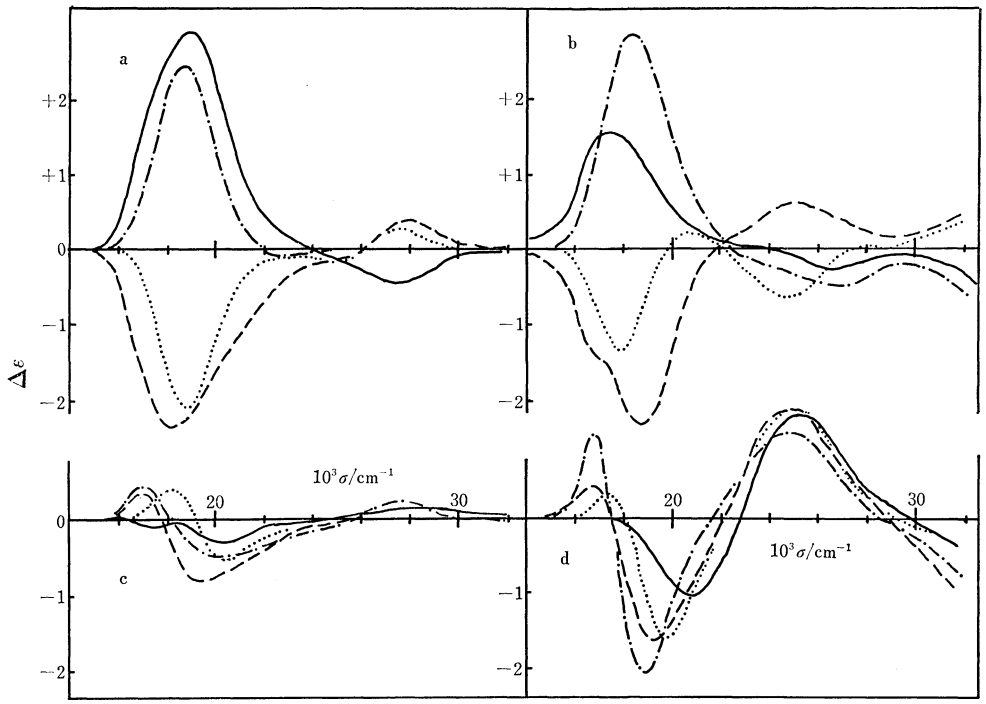

Fig. 9. Configurational and vicinal effect curves of $[Co(gly)_2(S\text{-Hpra})]^+$ (a,c) and $[Co(gly)_2(S\text{-pra})]$ (b, d); upper, configurational effect curves; lower, vicinal effect curves (—— *trans(O)*, —— *cis·cis*, —·— *trans(N)*, and ····· *fac*).

Table 6. CD spectral data

Label	Complex	I band		II band	
		$\tilde{\nu}/10^3$ cm^{-1}	$\Delta\varepsilon$	$\tilde{\nu}/10^3$ cm^{-1}	$\Delta\varepsilon$
A-1	*trans*(*O*)-*Λ*-[Co(gly)$_2$(Heta)]$^+$	19.2	−2.81	27.8	+0.45
	trans(*O*)-*Λ*-[Co(gly)$_2$(eta)]	17.4	−1.51	26.2	+0.48
A-3	*trans*(*N*)-*Λ*-[Co(gly)$_2$(Heta)]$^+$	18.8	−2.21		
	trans(*N*)-*Λ*-[Co(gly)$_2$(eta)]	18.4	−2.76	27.0	+0.40
A-4	*fac*-*Λ*-[Co(gly)$_2$(Heta)]$^+$	18.8	−2.31	25.2	−0.19
				28.0	+0.19
	fac-*Λ*-[Co(gly)$_2$(eta)]	18.0	−1.44	25.0	−0.75
		20.8	+0.16		
A-1	*trans*(*O*)-*Δ*-[Co(gly)$_2$(*S*-Hpra)]$^+$	19.2	−2.99	27.6	+0.56
	trans(*O*)-*Δ*-[Co(gly)$_2$(*S*-pra)]	18.0	−1.55	25.6	+1.57
		sh. 19.8	−1.41		
	trans(*O*)-*Λ*-[Co(gly)$_2$(*S*-Hpra)]$^+$	18.9	+2.77	27.4	−0.33
	trans(*O*)-*Λ*-[Co(gly)$_2$(*S*-pra)]	17.4	+1.49	25.2	+1.21
		21.0	−0.74		
A-2	*cis*·*cis*-*Δ*-[Co(gly)$_2$(*S*-Hpra)]$^+$	18.8	−2.96	28.2	+0.50
	cis·*cis*-*Δ*-[Co(gly)$_2$(*S*-pra)]	18.9	−3.85	24.8	+2.02
	cis·*cis*-*Λ*-[Co(gly)$_2$(*S*-Hpra)]$^+$	17.6	+2.29	27.8	−0.22
	cis·*cis*-*Λ*-[Co(gly)$_2$(*S*-pra)]	17.0	+1.86	24.4	+0.85
		21.2	−0.29		
A-3	*trans*(*N*)-*Δ*-[Co(gly)$_2$(*S*-Hpra)]$^+$	19.1	−2.69	27.6	+0.23
	trans(*N*)-*Δ*-[Co(gly)$_2$(*S*-pra)]	18.7	−4.71	25.4	+1.45
	trans(*N*)-*Λ*-[Co(gly)$_2$(*S*-Hpra)]$^+$	18.6	+2.24	27.4	+0.22
		22.6	−0.32		
	trans(*N*)-*Λ*-[Co(gly)$_2$(*S*-pra)]	17.2	+2.50	24.4	+0.83
		sh. 19.8	+0.44		
A-4	*fac*-*Δ*-[Co(gly)$_2$(*S*-Hpra)]$^+$	19.4	−1.97	27.8	+0.39
	fac-*Δ*-[Co(gly)$_2$(*S*-pra)]	19.2	−1.73	25.6	+0.79
	fac-*Λ*-[Co(gly)$_2$(*S*-Hpra)]$^+$	18.6	+2.38		
	fac-*Λ*-[Co(gly)$_2$(*S*-pra)]	17.8	+1.54	25.0	+2.07
		20.0	−1.58		

complexes. The T_{2g} transitions are magnetic-dipole-forbidden, but nevertheless the configurational effect curve for the *fac*-[Co(gly)$_2$(eta)] isomer exhibits a sharp peak at *ca.* 25000 cm^{-1}.

With respect to the [Co(N)$_5$(O)]-type complexes, Nishide *et al.*[3] reported that all vicinal effect curves for the deprotonated [Co(*S*-pra)(en)$_2$]$^{2+}$ and [Co(*S*-pra)(NH$_3$)$_4$]$^{2+}$ complexes showed a weak positive and an intense negative CD peak in the T_{1g} region and a moderately intense positive CD peak in the T_{2g} region (*ca.* 25000 cm^{-1}). In the [Co(N)$_3$(O)$_3$]-type complexes, all the vicinal effect curves of the deprotonated isomers exhibit a strong negative CD band on the high-frequency-side in the T_{1g} region and a strong positive CD band at *ca.* 25000 cm^{-1} in the T_{2g} region. It is interesting that the strong positive CD peaks in the T_{2g} region for both the [Co(N)$_5$(O)]- and [Co(N)$_3$(O)$_3$]-type have been observed at the same frequency of 25000 cm^{-1}. Among the *mer* isomers the half-width of each T_{1g} band decreases in the order: *trans*(*O*), *cis*·*cis* and *trans*(*N*). In this order each major peak in the vicinal effect shifts to the lower-energy-side, while the minor (+) peak at a lower-energy gradually enhances in intensity.

The authors wish to express sincere thanks to Dr. T. Nishide and Prof. K. Saito, Tohoku University, for the aid in the preparation of the (*S*)-2-amino-1-propanol ligand, and also to Dr. H. Miyamae and Prof. Y. Saito, Tokyo University, for the X-ray analysis of the *cis*·*cis*-[Co(gly)$_2$(eta)] complex.

Appendix

Energy Matrices. For the *trans*(*O*) isomer, the arrangement of gly$^-$ and eta$^-$ is defined as in Fig. 7; all the ligating atoms are placed on the x, y, and z axes, and the lone pairs of the alcoholate ion interact with only the d_{xz} and d_{yz} orbitals. The π orbitals of the chelating carboxylate ions at (2) and (4) in Fig. 7 interact with only d_{xz} and d_{xy}, respectively. Based on these assumptions, the antibonding parameters have been defined as follows:

σ_N=a σ-antibonding parameter for the N donor atom of gly$^-$ or eta$^-$=e_σ(N)

σ=a σ-antibonding parameter for the O donor atom of gly$^-$=e_σ(O)

σ'=a σ-antibonding parameter for the O donor atom of eta$^-$=e_σ(O′)

π=a π-antibonding parameter for the O donor atom of gly$^-$=e_π(O)

π'=a π-antibonding parameter for the O donor atom of eta$^-$ related with the d_{xz} orbital=$e_{\pi 1}$(O′)

π''=a π-antibonding parameter for the O donor atom of

eta⁻ related with the d_{yz} orbital=$e_{\pi_2}(O')$.
The antibonding energies with non-vanishing values are;

$$\langle z^2|\mathbf{A}|z^2\rangle = \frac{3}{2}\sigma_N + \frac{1}{2}\sigma + \sigma'$$
$$\langle yz|\mathbf{A}|yz\rangle = \pi''$$
$$\langle zx|\mathbf{A}|zx\rangle = \pi + \pi'$$
$$\langle xy|\mathbf{A}|xy\rangle = \pi$$
$$\langle x^2-y^2|\mathbf{A}|x^2-y^2\rangle = \frac{3}{2}\sigma_N + \frac{3}{2}\sigma$$
$$\langle x^2-y^2|\mathbf{A}|z^2\rangle = \frac{\sqrt{3}}{2}[\sigma_N-\sigma].$$

Using the above relations, the energy matrix for the *trans(O)* isomer may be obtained.

On the assumption that the N and O donor atoms for the *cis·cis* isomer are arranged as in Fig. 7, the energy matrix can be obtained similarly to that for the *trans(O)* isomer.

Evaluation of Parameters. The three transitions assigned are for the *trans(O)* isomer,

$$E(d_{y^2-z^2} \longleftarrow d_{yz}) = 20600\ cm^{-1}$$
$$E(d_{z^2-x^2} \longleftarrow d_{zx}) = 15900\ cm^{-1}$$
$$E(d_{x^2-y^2} \longleftarrow d_{xy}) = 17800\ cm^{-1},$$

and for the *cis·cis* isomer,

$$E(d_{y^2-z^2} \longleftarrow d_{yz}) = 20200\ cm^{-1}$$
$$E(d_{z^2-x^2} \longleftarrow d_{zx}) = 16400\ cm^{-1}$$
$$E(d_{x^2-y^2} \longleftarrow d_{xy}) = 19500\ cm^{-1}.$$

Assuming the energy differences originating from the off-diagonal elements are negligibly small; the above relations may be rewritten in terms of the diagonal elements of T_{1g} transitions

$$\frac{3}{4}(3\sigma_N+\sigma') - \pi'' - C = 20600 \quad (1)$$
$$\frac{3}{4}(\sigma_N+2\sigma+\sigma') - \pi - \pi' - C = 15900 \quad (2)$$
$$\frac{3}{4}(\sigma_N+\sigma) - \pi - C = 17800 \quad (3)$$
$$\frac{3}{4}(3\sigma_N+\sigma) - C = 20200 \quad (4)$$
$$\frac{3}{4}(\sigma_N+2\sigma+\sigma') - \pi - \pi' - C = 16400 \quad (5)$$
$$\frac{3}{4}(2\sigma_N+\sigma+\sigma') - \pi - \pi'' - C = 19500 \quad (6)$$

The left-hand-sides of the equations are related as follows;
(1)+(3)=(4)+(6)
(2)=(5),
and t .us the six equations may be reduced to four. Assuming $C=4B$, the value of B may be estimated for the [Co(gly)$_2$(eta)] complex (450 cm^{-1}), since the values of B for the *fac*-[Co(gly)$_3$] and *fac*-[Co(eta)$_3$] isomers are equal to 470 and 430 cm^{-1}, respectively. Furthermore, the value of σ_N has been estimated as 7700 cm^{-1}, which is identical with the value of σ_N for the [Co(en)$_3$] complex.

Using these values of B and σ_N, the four independent equations, which have been arbitrarily chosen from the six equations, may be solved and eight groups of $\sigma,\sigma'-4\pi''/3$, π, and $\pi'-\pi''$ values obtained. The average values of each $\sigma,\sigma'-4\pi''/3$, π, and $\pi'-\pi''$ are 5800, 7200, 325, and 1600 cm^{-1}, respectively.

From the above relations, the energies of the diagonal elements of the T_{2g} transitions are expressed by the use of the parameters. By comparing the absorption spectra with the calculated energies of the T_{2g} transitions, the most reasonable value of π'' is 700 cm^{-1}. Consequently, the parameters of σ_N, σ, σ', π, π', and π'' have been evaluated as 7700, 5800, 8100, 325, 2300 and 700 cm^{-1}, respectively.

References

1) D. A. Buckingham, C. E. Davis, and A. M. Sargeson, *J. Am. Chem. Soc.*, **92**, 6159 (1970).
2) K. Ogino, T. Uchida, T. Nishide, J. Fujita, and K. Saito, *Chem. Lett.*, **1973**, 679.
3) T. Nishide, K. Ogino, J. Fujita, and K. Saito, *Bull. Chem. Soc. Jpn.*, **47**, 3057 (1974).
4) C. E. Schäffer, *Structure and Bonding*, **5**, 68 (1968); C. E. Schäffer, *Pure Appl. Chem.*, **24**, 361 (1970).
5) M. Shibata, H. Nishikawa, and Y. Nishida, *Inorg. Chem.*, **7**, 9 (1968).
6) M. Shibata, *Proc. Jpn. Acad.*, **50**, 779 (1974).
7) M. Shibata, *Nippon Kagaku Zasshi*, **87**, 771 (1966).
8) B. E. Douglas, R. A. Haines, and J. G. Brushmiller, *Inorg. Chem.*, **2**, 1194 (1963).
9) S. Nagasaki and M. Shibata, *Bull. Chem. Soc. Jpn.*, **49**, 2329 (1976).
10) H. Yoneda, U. Sakaguchi, and Y. Nakayama, *Bull. Chem. Soc. Jpn.*, **48**, 209 (1975).
11) M. Watabe, K. Onuki, and S. Yoshikawa, *Bull. Chem. Soc. Jpn.*, **48**, 687 (1975).
12) H. Miyamae and Y. Saito, *Acta Crystallogr., Sect. B*, **34**, 937 (1978).
13) M. B. Ćelap, S. R. Niketić, C. J. Janjć, and V. N. Nikolić, *Inorg. Chem.*, **6**, 2063 (1967).
14) B. E. Douglas and S. Yamada, *Inorg. Chem.*, **4**, 1561 (1965).
15) R. G. Denning and T. S. Piper, *Inorg. Chem.*, **5**, 1056 (1966).
16) M. Mori, M. Shibata, E. Kyuno, and M. Kanaya, *Bull. Chem. Soc. Jpn.*, **34**, 1837 (1961).
17) R. Tsuchida, *Bull. Chem. Soc. Jpn.*, **13**, 388 (1938).
18) C. E. Schäffer, *Structure and Bonding*, **14**, 69 (1973).

A Mössbauer Study of the Photolysis of Bis- and Tris-oxalato Iron(III) Complexes in a Solid, Solutions, and Frozen Solutions

Haruo SATO and Takeshi TOMINAGA*

Department of Chemistry, Faculty of Science, The University of Tokyo, Hongo, Tokyo 113

(Received October 31, 1978)

The photolytic reactions of bis- and tris-oxalato iron(III) complexes in a solid, solutions, and frozen solutions were studied by means of ^{57}Fe Mössbauer spectroscopy. An iron(II) species was observed as a metastable intermediate product in the photolysis of tris(oxalato)ferrate(III) in a solid and solutions. A mechanism with a sequence of iron(II) intermediates was tentatively proposed for the photolysis and subsequent reactions in this compound. The Mössbauer technique was also used to examine whether or not tris(oxalato)ferrate(III) was diluted uniformly with diamagnetic substances in the mixed crystals and frozen solutions.

It has been demonstrated in our earlier work that Mössbauer spectroscopy is a useful tool for detecting the changes in oxidation states and structures induced by radiolysis, photolysis, and pyrolysis in solid iron compounds.[1-6] Recently, we have investigated the photolysis of potassium tris(oxalato)ferrate(III) in a solid and solutions[7] and proposed the possible application of Mössbauer spectroscopy in the photochemistry of metal complexes in the liquid and frozen states.

The object of this article is to present a more complete report of our work concerning the photolysis of potassium tris(oxalato)ferrate(III) in a solid and solutions, together with our recent results on the photolysis of potassium diaquabis(oxalato)ferrate(III) in solutions. In addition, the Mössbauer technique has also been applied to the investigation of whether or not potassium tris(oxalato)ferrate(III) is diluted uniformly with diamagnetic substances in mixed crystals and in frozen solutions.

Experimental

Materials. *Potassium Tris(oxalato)ferrate(III) Trihydrate* $K_3[Fe(C_2O_4)_3]\cdot 3H_2O$: An aqueous solution of a (1 : 3) mixture (by mole ratio) of iron(III) chloride and potassium oxalate was heated for 2 h at 80 °C; after the solution had been cooled, the precipitate was collected and recrystallized three times from water. Found: C, 14.6; H, 1.2%. Calcd for $K_3[Fe(C_2O_4)_3]\cdot 3H_2O$: C, 14.7; H, 1.2%.

^{57}Fe-enriched Potassium Tris(oxalato)ferrate(III) Trihydrate $K_3[^{57}Fe(C_2O_4)_3]\cdot 3H_2O$: A 0.2 M potassium hydrogenoxalate solution was added to an excess of freshly precipitated $^{57}Fe_2O_3\cdot nH_2O$, after which the mixture was heated for 1 h at 70 °C (1 M=1 mol dm^{-3}). The resulting solution was filtered, and the filtrate was concentrated in a vacuum.[8] Found: C, 14.7; H, 1.0%. Calcd for $K_3[^{57}Fe(C_2O_4)_3]\cdot 3H_2O$: C, 14.6; H, 1.2%.

^{57}Fe-doped Potassium Tris(oxalato)cobaltate(III) Trihydrate $K_3[(^{57}Fe,Co)(C_2O_4)_3]\cdot 3H_2O$: An aqueous solution containing a (1 : 33) mixture (by weight) of ^{57}Fe-enriched potassium tris(oxalato)ferrate(III) trihydrate and potassium tris(oxalato)cobaltate(III) trihydrate was quenched quickly in liquid nitrogen, and then the frozen solution was condensed in a vacuum at −21 °C by pumping it through a liquid nitrogen trap.

^{57}Fe-enriched Potassium Diaquabis(oxalato)ferrate(III) ($K[^{57}Fe(C_2O_4)_2(H_2O)_2]$) Solutions: A (1 : 3) mixture (by mole ratio) of potassium oxalate and oxalic acid in an aqueous solution was added to an excess of freshly precipitated $^{57}Fe_2O_3\cdot nH_2O$; the solution was then filtered after having been heated for 1 h at 70 °C.

Potassium Diaquabis(oxalato)ferrate(II) $K_2[Fe(C_2O_4)_2(H_2O)_2]$: This compound was prepared according to the procedures described by Temperly *et al.*[9]

Potassium μ-Oxalato-bis[bis(oxalato)ferrate(II)] $K_6[Fe_2(C_2O_4)_5]$: This was prepared by heating potassium tris(oxalato)ferrate(III) for 15 min at 260 °C according to the method described by Bancroft *et al.*[10]

Photoirradiation. Samples were exposed either to a 500-W superhigh-pressure mercury lamp (spectral range: 300—600 nm) or to a 30-W low-pressure mercury lamp (253.7 nm). The solid samples were irradiated as crystals spread over a glass plate or adhesive tape, as film coated on an acrylic plate,[11] or as a disk in KCl.

A quartz cell with a 5-mm optical path was used for the irradiation of the solutions. Frozen solutions were irradiated as dipped directly in liquid nitrogen or as contained in acrylic or Teflon holders designed for Mössbauer measurements.

Freezing of Solutions. Both irradiated and unirradiated solutions were frozen quickly by one of the following procedures, A—D, prior to Mössbauer measurements:

A) The holder containing the solution was placed on Dry Ice.

B) The holder containing the solution was immersed in liquid nitrogen.

C) Droplets of the solution were added directly to liquid nitrogen.

D) A spatula precooled at 77 K was dipped into the solution so that a small amount was condensed on it, and then it was quickly put into liquid nitrogen. By repeating this procedure, small droplets of the frozen solution were collected in the liquid nitrogen.

By Procedures B—D, we may achieve freezing rates of 5—8 K/s, 10—40 K/s, and 100—250 K/s respectively.

Measurements of Mössbauer Spectra, Infrared Spectra, and Powder X-Ray Patterns. The Mössbauer spectra at 77 K and 293 K were measured by using a Hitachi AA-40 or a Shimadzu MEG-2 Mössbauer spectrometer against ^{57}Co in copper or rhodium foil. Acrylic or Teflon holders (32 mm in diameter) were used for the measurements of the solutions.

The curve-fitting of the spectra thus obtained was performed with a HITAC 8800/8700 computer, assuming that they were composed of absorption peaks in a Lorentzian line shape.

The infrared spectra were recorded on a Hitachi EPI-G2 spectrophotometer (400—4000 cm^{-1} region). The powder X-ray patterns of the (1 : 33) mixture of potassium tris(oxalato)ferrate(III) trihydrate with potassium tris(oxalato)cobaltate(III) trihydrate, and ^{57}Fe-doped potassium tris(oxalato)cobaltate(III) trihydrate were taken by using a Rigaku Denki Geigerflex and Fe $K\alpha$-radiation.

Results and Discussion

Photolysis of Potassium Tris(oxalato)ferrate(III) in the Solid Phase. The Mössbauer spectrum at 77 K of the unirradiated solid potassium tris(oxalato)-ferrate(III) (Product I) in Fig. 1a is composed of a single broad absorption indicative of an electronic spin relaxation effect.[12] After irradiation at 253.7 nm for 5 h at room temperature, the Mössbauer spectrum (Fig. 1b) represents two sets of quadrupole doublets for an iron(II) species (Product II) and an iron(III) species (Product III) in addition to the broad single absorption of the unreacted parent compound. After the prolonged standing of the photolyzed sample in air, however, the intensities of the iron(III) doublet peaks (Product III) had increased, while those of the iron(II) doublet (Product II) had decreased and the iron(II) doublet (Product II) had disappeared eventually (Fig. 1c).

When smaller amounts of ^{57}Fe-enriched potassium tris(oxalato)ferrate(III) were irradiated in a solid, in a disk, or on film, two iron(II) species (Products IV and V) other than Product II were obtained as photolysis products, depending on the irradiation conditions (period, temperature, and atmosphere) (Fig. 2).

Table 1 summarizes the Mössbauer parameters of the photolysis products from potassium tris(oxalato)-ferrate(III), together with the identities of those products tentatively deduced on the basis of the results reported previously for the pyrolysis and radiolysis of the same system.[9,10,13,14]

Among such products, Products V and VI[15] are fairly unstable intermediates which have not been observed in the earlier work. The Mössbauer parameters and infrared spectra (Fig. 3) reveal that both products, V and VI, cannot be identical with any of the known products, I to IV, nor with any tetrahedral species. Furthermore, from the conceivable structures for Products V and VI, we may rule out the following ones:

1) $[Fe(C_2O_4)_3]^{4-}$ and $[Fe(C_2O_4)_2(C_2O_4H)(H_2O)]^{3-}$ can be excluded for stoichiometric reasons.

2) $[Fe(H_2O)_6]^{2-}$ and $[Fe(C_2O_4)(H_2O)_4]$ are unlikely because Product VI is stable in solutions containing excess potassium oxalate.

3) Structures with bridging oxalates may also be eliminated because the infrared spectrum of Product

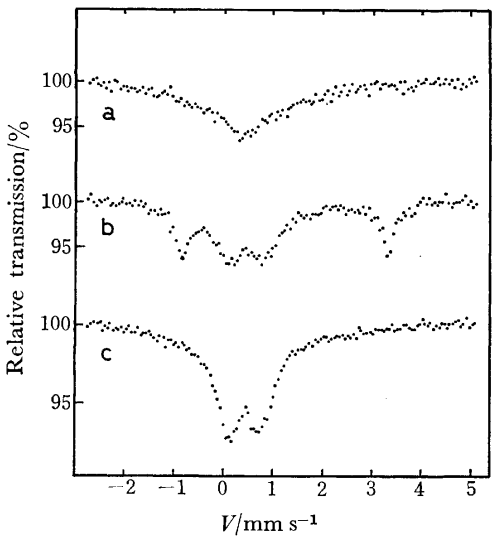

Fig. 1. Mössbauer spectra at 77 K of solid $K_3[Fe(C_2O_4)_3]\cdot 3H_2O$, [$V$: velocity]. a) Unirradiated solid sample, b) solid sample irradiated for 5 h with 253.7 nm light, c) irradiated solid sample after standing for 20 d.

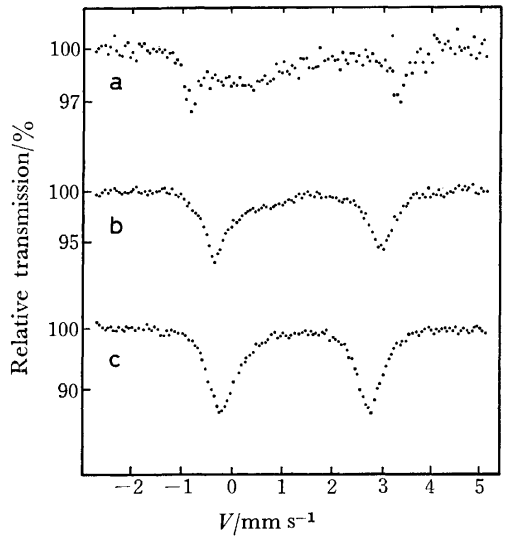

Fig. 2. Mössbauer spectra at 77 K of solid $K_3[^{57}Fe(C_2O_4)_3]\cdot 3H_2O$ (in small amounts) photoirradiated (a) in KCl disk for 3 min at 60 °C in air with 300—600 nm light (Product II), (b) in KCl disk for 2 h at 0 °C in CO_2 with 253.7 nm light (Product IV), and (c) in powder for 1 min at 40 °C in air with 300—600 nm light (Product V).

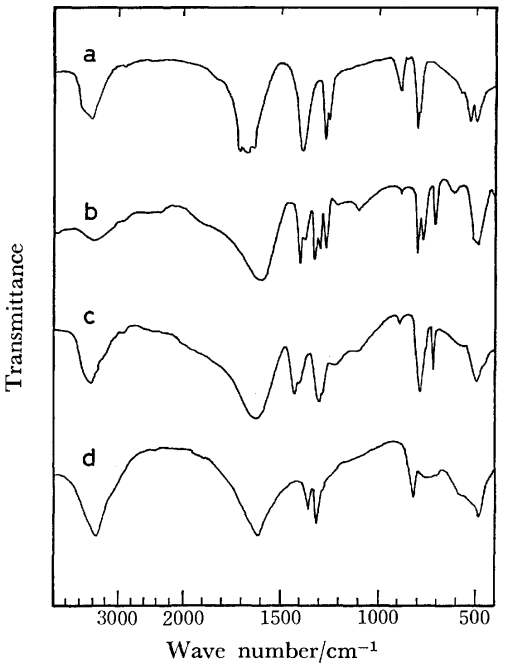

Fig. 3. Infrared spectra of (a) $K_3[Fe(C_2O_4)_3]\cdot 3H_2O$, (b) Product II ($K_6[Fe_2(C_2O_4)_5]$), (c) Product V, and (d) $FeC_2O_4\cdot 2H_2O$.

Table 1. Mössbauer parameters of the photolysis products from potassium tris(oxalato)ferrate(III)

Product	77 K		293 K		Tentative assignment
	δ[a]	ΔE_Q	δ[a]	ΔE_Q	
	mm/s		mm/s		
Product I	0.44±0.02	—	0.33±0.02	—	Parent compound
Product II	1.26±0.02	4.09±0.08	1.16±0.02	3.89±0.08	$[Fe_2^{II}(C_2O_4)_5]^{6-}$
Product III	0.49±0.02	0.70±0.03	0.36±0.03	0.68±0.04	$[Fe^{III}(C_2O_4)_2(H_2O)_2]^-$
Product IV	1.34±0.02	3.27±0.04	1.22±0.02	2.53±0.04	$[Fe^{II}(C_2O_4)_2(H_2O)_2]^{2-}$
Product V	1.28±0.02	2.94±0.03	—	—	Metastable iron(II) species
Product VI	1.29±0.01	2.91±0.01	—	—	Metastable iron(II) species
Freeze drying (Product V)	1.29±0.02	2.94±0.02	—	—	Metastable iron(II) species

a) With respect to the centroid of the spectrum of iron foil at 293 K. Experimental errors are indicated of maximum deviations.

V shows no absorption band in the 1300—1400 cm^{-1} region (characteristic of the iron complexes with oxalate bridging, such as $FeC_2O_4 \cdot 2H_2O$ and $K_6[Fe_2(C_2O_4)_5]$).

Although further investigation will be necessary for determining the identities of Products V and VI, we may assume tentatively that a geometrical isomer of Product IV ($K_2[Fe(C_2O_4)_2(H_2O)_2]$) remains as one of the possible structures for Product V (and VI).

As has been mentioned above, the formation and subsequent conversion of Products II, III, IV, and V were governed mainly by the photoirradiation conditions. A brief irradiation at a lower temperature generally favors the initial formation of Product V. After prolonged standing, Product V is converted into Products IV and II, which are eventually converted into Product III by oxidation in air. Product II also appears on the heating of Product IV at 120 °C. Thus, the overall mechanism for the formation of such products can be generally accounted for by assuming the following sequence of photolytic and subsequent reactions:

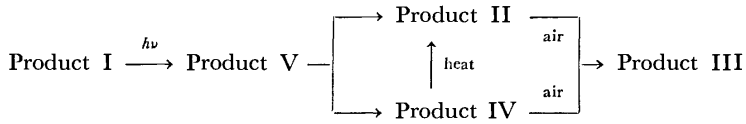

or, in terms of tentative assignments;

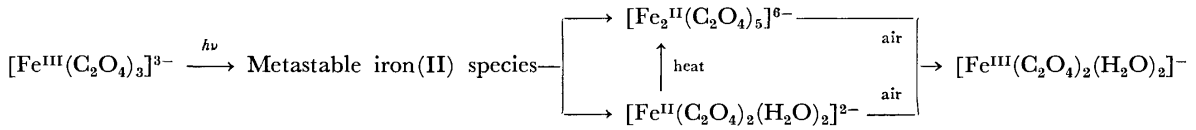

Dilution of Potassium Tris(oxalato)ferrate(III) in Mixed Crystals and Frozen Solutions. As is shown in Fig. 4a, the Mössbauer spectrum of solid potassium tris(oxalato)ferrate(III) trihydrate consists of a remarkably broadened absorption peak, indicating an electronic spin relaxation effect.[12] If this compound is diluted uniformly with a diamagnetic substance (*e.g.*, potassium tris(oxalato)cobaltate(III) trihydrate or water), however, a resolved hyperfine structure is observed in the Mössbauer spectrum due to the developing relaxation effect. In fact, the Mössbauer spectrum of ^{57}Fe-doped potassium tris(oxalato)ferrate(III) trihydrate, $K_3[(^{57}Fe,Co)(C_2O_4)_3] \cdot 3H_2O$ (Fig. 4b), indicates a resolved magnetic hyperfine structure and suggests that potassium tris(oxalato)ferrate(III) trihydrate is diluted uniformly in solid potassium tris(oxalato)cobaltate(III) trihydrate. By comparing the powder X-ray pattern of the ^{57}Fe-doped potassium tris(oxalato)cobaltate(III) with that of a (1 : 33) mixture of potassium tris(oxalato)ferrate(III) trihydrate and potassium tris(oxalato)cobaltate(III) trihydrate, it may be presumed that the ^{57}Fe-doped potassium tris(oxalato)cobaltate(III) trihydrate is constituted of mixed crystals.

In frozen solutions containing uniformly dispersed iron(III) species, Mössbauer spectra have been reported to show similar hyperfine structures resulting from long spin-relaxation times.[16,17] Although we have, in this work, measured the Mössbauer spectra of frozen solutions (quenched by Procedure B) at various concentrations (0.002—1 M) of potassium tris(oxalato)ferrate(III), no significant difference was observed in their spectra over the concentration range studied. For example, the Mössbauer spectrum of the 0.005 M potassium tris(oxalato)ferrate(III) solution (Fig. 4c) quenched by Procedure B resembles that of the same compound in the solid state (Fig. 4a) and suggests that microcrystals of the solute were separated on freezing the solutions. However, the Mössbauer spectrum of the 0.005 M potassium tris(oxalato)ferrate(III) solution containing an excess of potassium hydrogenoxalate, frozen quickly by Procedure D

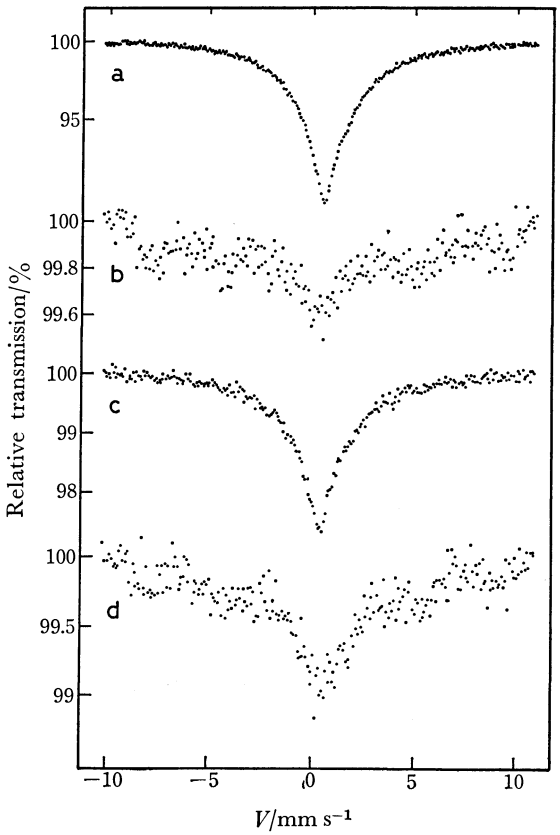

Fig. 4. Mössbauer spectra at 77 K of (a) solid $K_3[Fe(C_2O_4)_3]\cdot 3H_2O$, (b) solid $K_3[(^{57}Fe,Co)(C_2O_4)_3]\cdot 3H_2O$, (c) a 0.005 M $K_3[^{57}Fe(C_2O_4)_3]$ solution quenched by procedure B, and (d) a 0.005 M $K_3[^{57}Fe(C_2O_4)_3]$ solution containing an excess of KHC_2O_4, quenched quickly by procedure D.

(Fig. 4d), shows the hyperfine structure characteristic of the relaxation effect. Accordingly, it is obvious that the solute is diluted more uniformly in this frozen solution. Thus, the Mössbauer technique can be used to examine whether or not solutes are uniformly diluted in quenched solutions.

Photolysis of Potassium Tris(oxalato)ferrate(III) in Aqueous Solutions and Frozen Aqueous Solutions. In Fig. 5 are illustrated the Mössbauer spectra of neutral

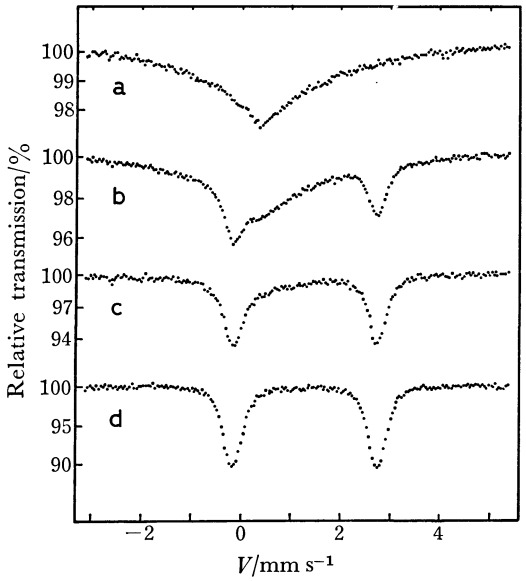

Fig. 5. Mössbauer spectra at 77 K of neutral aqueous solutions of $K_3[^{57}Fe(C_2O_4)_3]$ quenched by procedure B after photoirradiation for various periods. (a) Unirradiated, (b) 3-s irradiated, (c) 10-s irradiated, and (d) 120-s irradiated.

aqueous solutions of potassium tris(oxalato)ferrate(III) quenched by Procedure B after photoirradiation for 3, 10, and 120 s with a superhigh-pressure mercury lamp. The iron(III) single peak of the parent complex (Product I) tended to disappear, yet the iron(II) doublet (Product VI) became predominant with the increase in the irradiation period. Table 2 summarizes the Mössbauer parameters of the products obtained by the photoirradiation of the solutions, together with the percentage photoreduction for various irradiation periods.

The Mössbauer spectrum of the photoirradiated frozen solutions of potassium tris(oxalato)ferrate(III) also indicates the formation of Product VI (Fig. 6a). On 5-min standing at room temperature after 2-min exposure to the superhigh-pressure mercury lamp, iron(II) oxalate has already started precipitating in an aqueous solution of potassium tris(oxalato)-

Table 2. Mössbauer parameters at 77 K of the photolysis products of 0.02 M $K_3[^{57}Fe(C_2O_4)_3]$ aqueous solutions and the percentage photoreduction for various irradiation periods

Product		Period of photoirradiation/s			
		0	3	10	120
Iron(III) species (parent)	δ[a]/(mm/s)	0.44(1)[b]	0.43(1)	0.43(4)	—
	ΔE_Q/(mm/s)	—	—	—	—
	Γ/(mm/s)	2.48(5)	2.41(5)	2.03(15)	—
	ε/%	2.5(1)	2.7(1)	1.2(1)	—
Iron(II) species (Product VI)	δ[a]/(mm/s)	—	1.29(1)	1.29(1)	1.29(1)
	ΔE_Q/(mm/s)	—	2.91(1)	2.91(1)	2.91(1)
	Γ/(mm/s)	—	0.43(2)	0.43(1)	0.44(1)
	ε/%	—	2.4(1)	6.2(1)	10.5(2)
Percentage of photoreduction/%		0	17	59	100

a) With respect to the centroid of the spectrum of iron foil at 293 K. b) Figures in parentheses indicate standard deviations in units of the last significant digit. Γ: Line-width; ε: resonance-effect magnitude.

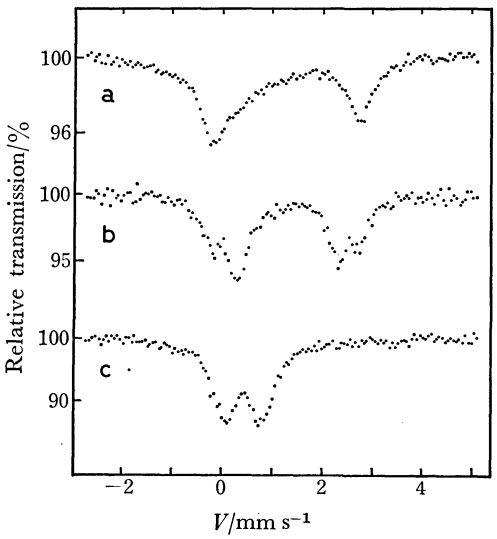

Fig. 6. Mössbauer spectra at 77 K of (a) a photoirradiated frozen aqueous solution of $K_3[^{57}Fe(C_2O_4)_3]$, (b) an aqueous solution of $K_3[^{57}Fe(C_2O_4)_3]$ quenched on 5-min standing at room temperature after photoirradiation, and (c) an aqueous solution of $K_3[^{57}Fe(C_2O_4)_3]$ quenched on prolonged standing at room temperature after photoirradiation.

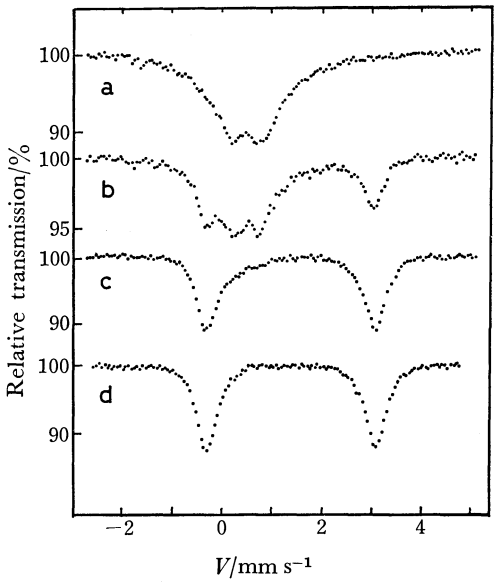

Fig. 7. Mössbauer spectra at 77 K of 0.05 M sulfuric acid solutions of $K_3[^{57}Fe(C_2O_4)_3]$ quenched by procedure A after photoirradiation for (b) 3 s, (c) 10 s, and (d) 60 s. (a): Unirradiated solution.

ferrate(III); Fig. 6b shows the spectrum of this solution quenched quickly. Although Product VI is at first converted into iron(II) oxalate, iron(II) oxalate is in turn oxidized after prolonged standing in air and is dissolved again. The Mössbauer spectrum of the iron(III) species resulting from the oxidation of iron(II) oxalate (Fig. 6c) reveals the formation of potassium diaquabis(oxalato)ferrate(III) and potassium tris(oxalato)ferrate(III).

The Mössbauer parameters and infrared spectra suggest that the product obtained from freeze-drying (at −21 °C) of Product VI may be identical with Product V.

Hence, the photolysis and subsequent reactions of potassium tris(oxalato)ferrate(III) in aqueous solutions presumably proceed as in the following sequence:

$$[Fe(C_2O_4)_3]^{3-} \xrightarrow{h\nu} \underset{\text{species (Product VI)}}{\text{Metastable iron(II)}} \longrightarrow \underset{\text{(precipitate)}}{FeC_2O_4\cdot 2H_2O} \xrightarrow{\text{air}} [Fe^{III}(C_2O_4)_2(H_2O)_2]^- \text{ or } [Fe^{III}(C_2O_4)_3]^{3-}$$

$$\downarrow \text{freeze-drying}$$

Product V

Photolysis of Potassium Tris(oxalato)ferrate(III) in Sulfuric Acid Solutions. Based on spectrophotometric measurements, Parker has reported that both monooxalato- and bisoxalato- iron(III) complexes are present in sulfuric acid solutions of potassium tris(oxalato)ferrate(III).[18]

The Mössbauer spectrum obtained in this work of a frozen 0.05 M sulfuric acid solution of potassium tris(oxalato)ferrate(III) reveals a broad singlet absorption of tris(oxalato)ferrate(III) ion in addition to the mono- and bis-oxalato complexes (Fig. 7a). The relative quantities of mono-, bis-, and tris-oxalato complexes in frozen solutions were found to depend on the freezing rate. Figures 7b—d illustrates the Mössbauer spectra of sulfuric acid solutions of potassium tris(oxalato)ferrate(III) frozen by Procedure A after having been irradiated with the superhigh-pressure mercury lamp for 3, 10, and 60 s. It is obvious that the parent complex was reduced to an iron(II) species (Product VII). The Mössbauer parameters of Product VII (δ=1.4 mm/s, ΔE_Q=3.2—3.4 mm/s) appear to change slightly with the change in the freezing rate. The percentage photoreduction to the iron(II) species was estimated as being about 30, 70, and 100% for 3-, 10-, and 60-s irradiations respectively. The percentage reduction determined spectrophotochemically by means of the *o*-phenanthroline method[19] was in good agreement with the Mössbauer data.

Since Product VII is unstable, iron(II) oxalate has already appeared in the solution after 120-s photoirradiation. When a frozen-sulfuric-acid solution of potassium tris(oxalato)ferrate(III) has been exposed to light, the Mössbauer spectrum also indicates the formation of Product VII.

Photolysis of Potassium Diaquabis(oxalato)ferrate(III) in Aqueous Solutions. Figure 8 demonstrates the Mössbauer spectra of aqueous solutions of potassium diaquabis(oxalato)ferrate(III) frozen by Procedure B after photoirradiation; the percentage photoreduction of the parent complex to iron(II) species increases with the increase in the photoirradiation period. Table

Table 3. Mössbauer parameters at 77 K of the photolysis products of 0.02 M $K[^{57}Fe(C_2O_4)_2(H_2O)_2]$ aqueous solutions for various irradiation periods

Product		Period of photoirradiation/s			
		0	3	10	60
Iron(III) species (parent)	δ[a]/(mm/s)	0.49	0.49	[b]	—
	ΔE_Q/(mm/s)	0.64	0.58	[b]	—
	Γ/(mm/s)	0.54	0.53	[b]	—
	ε/%	7.0	5.6	[b]	—
Iron(II) species (photolysis product)	δ[a]/(mm/s)	—	1.34	1.31	1.29
	ΔE_Q/(mm/s)	—	3.21	2.88	2.83
	Γ/(mm/s)	—	0.48	0.57	0.39
	ε/%	—	3.3	5.5	11.0

a) With respect to the centroid of the spectrum of iron foil at 293 K. b) Reasonable values were not available.

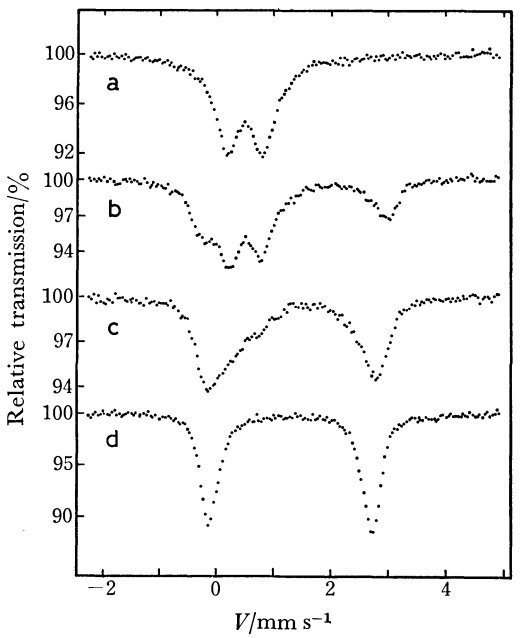

Fig. 8. Mössbauer spectra at 77 K of aqueous solutions of $K[^{57}Fe(C_2O_4)_2(H_2O)_2]$ quenched by procedure B after photoirradiation for (b) 3 s, (c) 10 s, and (d) 60 s. (a): Unirradiated solution.

3 summarizes the Mössbauer parameters obtained from curve-fitting by assuming a quadrupole doublet of the Lorentzian line-shape for the iron(II) species. While the isomer shift and quadrupole splitting of the iron(II) species are decreased with the increase in the irradiation period, the line-width shows anomalous behavior. Although the Mössbauer line-width is, in general, expected to increase with the concentration of iron species,[20] the line-width of the iron(II) species in Fig. 8 does not simply increase with the concentration in terms of the irradiation period; the widths are 0.48, 0.57, and 0.39 mm/s for 3-, 10-, and 60-s irradiations respectively. Such an anomaly can be explained tentatively by assuming that at least two iron(II) species with slightly different parameters are formed in photolysis; one of them is predominant after 3-s irradiation, while the other becomes predominant after 60-s irradiation. Both species can exist after 10-s irradiation. Unfortunately, the Mössbauer spectrum obtained after 10-s irradiation (Fig. 8c) cannot be resolved well by computer curve-fitting because of the broad overlapping absorption of tris(oxalato)ferrate(III), possibly formed by the combination of the parent complex with free oxalate ions.[21]

Further study will be necessary for a complete understanding of the mechanism of the photolysis of diaquabis(oxalato)ferrate(III) in aqueous solutions.

References

1) N. Saito, H. Sano, T. Tominaga, and F. Ambe, *Bull. Chem. Soc. Jpn.*, **38**, 681 (1965).
2) N. Saito, T. Tominaga, and T. Morimoto, *J. Inorg. Nucl. Chem.*, **32**, 2811 (1970).
3) T. Tominaga, M. Takeda, T. Morimoto, and N. Saito, *Bull. Chem. Soc. Jpn.*, **43**, 1093 (1970).
4) N. Saito, M. Takeda, and T. Tominaga, *Radiochem. Radioanal. Lett.*, **6**, 169 (1971).
5) H. Sato and T. Tominaga, *Bull. Chem. Soc. Jpn.*, **49**, 697 (1976).
6) H. Sato and T. Tominaga, *Radiochem. Radioanal. Lett.*, **26**, 185 (1976).
7) H. Sato and T. Tominaga, *Radiochem. Radioanal. Lett.*, **30**, 165 (1977).
8) A. Rosenheim, *Z. Anorg. Chem.*, **11**, 216 (1896).
9) A. A. Temperley and D. W. Pumplin, *J. Inorg. Nucl. Chem.*, **31**, 2711 (1969).
10) G. M. Bancroft, K. G. Dharmawardena, and A. G. Maddock, *J. Chem. Soc., A.*, **1969**, 2914.
11) H. E. Spencer and M. W. Schmidt, *J. Phys. Chem.*, **75**, 2986 (1971).
12) D. Barb, L. Diamandescu, and D. Tarabasan, *J. Phys. Colloq.*, **37**, C6-113 (1976).
13) K. G. Dharmawardena and G. M. Bancroft, *J. Chem. Soc., A.*, **1968**, 2655.
14) G. M. Bancroft, K. G. Dharmawardena, and A. G. Maddock, *Inorg. Chem.*, **9**, 223 (1970).
15) Presumably, the Product VI formed in the photolysis of tris(oxalato)ferrate(III) in solutions has a structure identical with that of Product V.
16) A. J. Nozik and M. Kaplan, *J. Chem. Phys.*, **49**, 4141 (1968).
17) J. W. G. Wignall, *J. Chem. Phys.*, **44**, 2462 (1966).
18) C. A. Parkar, *Trans. Faraday Soc.*, **50**, 1213 (1954).
19) C. G. Hatchard and C. A. Parkar, *Proc. R. Soc., London, Ser. A*, **235**, 518 (1956).
20) H. Sano and R. H. Herber, *J. Inorg. Nucl. Chem.*, **30**, 409 (1968).
21) Tris(oxalato)ferrate(III) appeared in the Mössbauer spectrum of a solution quenched by Freezing Procedure B after a mixture of solutions of potassium diaquabis(oxalato)-ferrate(III) and potassium oxalate had been left standing for 10 s.

Preparation and Stereochemistry of Optical Isomers of the Tris-(3,3′-dimethyl-2,2′-bipyridyl *N,N′*-dioxide)chromium(III) Complex

Hideaki KANNO, Kazuo KASHIWABARA, and Junnosuke FUJITA*

Department of Chemistry, Faculty of Science, Nagoya University, Chikusa, Nagoya 464

(Received October 30, 1978)

A new ligand, (*R*)- and (*S*)-3,3′-dimethyl-2,2′-bipyridyl *N,N′*-dioxide(mbdo) forms three diastereomers(I, II, and III) of $[Cr(mbdo)_3]^{3+}$ by the reaction with $[Cr(H_2O)_6]^{3+}$ in water. (I) was assigned to a pair of enantiomers, $\Delta(RRR)$ and $\Lambda(SSS)$, and (II) and (III) to either a diastereomeric pair of $\Delta(RRS)$ and $\Lambda(SSR)$ or $\Delta(SSR)$ and $\Lambda(RRS)$. While the racemic (I) was resolved by SP-Sephadex column chromatography, (II) and (III) isomerized in water to each other (II$\rightleftarrows$III) by exposure to ultraviolet light, were resolved by the reaction of $[Cr(H_2O)_4$(*R* or *S*)-mbdo$]^{3+}$ with a stoichiometric amount of (*S* or *R*)-mbdo. The circular dichroism spectra of these optically active isomers were measured in aqueous solutions and compared with those of complexes of the $[CrO_6]$-type of known absolute configuration. The optically active free $(+)_{589}$- and $(-)_{589}$-mbdo were isolated by decomposing $\Lambda(SSS)$- and $\Delta(RRR)$-$[Cr(mbdo)_3]^{3+}$, respectively, with $edta^{4-}$. The active mbdo is optically stable even in boiling water.

2,2′-Bipyridyl *N,N′*-dioxide(bpdo) forms a skew seven-membered chelate ring upon coordination to a metal ion. Since the skew chelate ring is chiral (δ or λ), a tris-type complex of bpdo has four theoretically possible diastereomers, each of which has a pair of enantiomers (Δ and Λ).[1] By analogy with the stereoisomerism in $[Co(en)_3]^{3+}$(en=ethylenediamine),[2] these diastereomers can be designated as $lel_3(\Delta(\lambda\lambda\lambda), \Lambda(\delta\delta\delta))$, $lel_2ob(\Delta(\lambda\lambda\delta), \Lambda(\delta\delta\lambda))$, $lelob_2$ $(\Delta(\lambda\delta\delta), \Lambda(\delta\lambda\lambda))$, and $ob_3(\Delta(\delta\delta\delta), \Lambda(\lambda\lambda\lambda))$. However, we have reported that $[Cr(bpdo)_3]^{3+}$ forms only one pair of enantiomers which racemize spontaneously in water at room temperature.[3] This indicates that the bpdo chelate ring is flexible, changing its conformation ($\delta\rightleftarrows\lambda$) very easily. If the rotation around the bond between the 2 and 2′ carbons of bpdo is prohibited by replacing the 3 and 3′ hydrogens with some bulky substituents, such a conformational change is forbidden and the complex ion is expected to exist in some optically stable isomers. This paper deals with the preparation and stereochemistry of the tris-chromium(III) complex with a new chelate ligand, (*R*)- and (*S*)-3,3′-dimethyl-2,2′-bipyridyl *N,N′*-dioxide(mbdo)(Fig. 1).

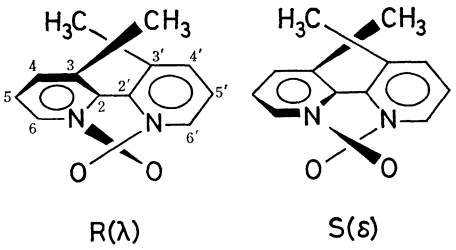

Fig. 1. A pair of enantiomers of mbdo.

Experimental

Preparation of Ligand. 3,3′-Dimethyl-2,2′-bipyridyl *N,N′*-dioxide(mbdo) was prepared from 3,3′-dimethyl-2,2′-bipyridyl[4] according to a method similar to that for 2,2′-bipyridyl *N,N′*-dioxide(bpdo).[5] An acetic acid solution(75 cm^3) of 3,3′-dimethyl-2,2′-bipyridyl(18 g, 0.1 mol) was mixed with 30% aqueous hydrogen peroxide(60 cm^3). The solution was refluxed for 4 h, then mixed with another 50 cm^3 of 30% aqueous hydrogen peroxide and refluxed for 3 h. The resulting pale yellow solution was evaporated under reduced pressure to give an oily residue. A small amount of ethanol was added to the residue and the mixture was evaporated. This procedure was repeated several times to remove water contained in the product. White precipitate was obtained upon addition of a small amount of acetone and then ether to the oily residue. The precipitate was filtered, washed with acetone and then ethanol, and air-dried. Recrystallization from a small amount of hot ethanol gave white cubic crystals. Yield: 12.3 g (60%), mp 212—214 °C (sublimation); IR(KBr disk) 1255 and 1242(ν_{N-O}) and 802 cm^{-1}(δ_{N-O}); ^{1}H-NMR(D_2O) δ=2.17 ppm(s, CH_3). The mbdo ligand exists in a pair of enantiomers. The optically active ligand was obtained by decomposing an optically active $[Cr(mbdo)_3]^{3+}$ complex (*vide post*).

Preparation of $[Cr(mbdo)_3]^{3+}$. A 10^{-2} mol/dm^3 hydrochloric acid solution (40 cm^3) containing $Cr(NO_3)_3\cdot 9H_2O$ (1.2 g, 3 mmol) and racemic mbdo(2.4 g, 11 mmol) was heated at 80 °C for 5 h. After cooling, sodium perchlorate (2 g, 16 mmol) was added to the solution to give green precipitate, which was filtered, washed with water and then ethanol, and recrystallized from warm water. Yield: 1.1 g (73%). This complex perchlorate consists of three pairs of diastereomers of $[Cr(mbdo)_3]^{3+}$.

Separation of Optical Isomers of $[Cr(mbdo)_3]^{3+}$. The $[Cr(mbdo)_3]^{3+}$ complex obtained above was dissolved in water, and the solution was poured on a column(ϕ2.7×130 cm) of SP-Sephadex C-25 resin in the Na^+ form. By eluting the adsorbed band with a 0.2 mol/dm^3 sodium $(+)_{589}$-tartratoantimonate(III) solution, the column gave three separate bands, Ia,Ib, and Ic in the order of elution (Fig. 2a). All the fractions of Ia and of Ib gave positive and negative, respectively, rotations at sodium D line, the CD patterns of Ia and Ib fractions being enantiomeric to each other. Thus, the Ia and Ib bands were assigned to a pair of enantiomers (diastereomer I(Ia, Ib)). The fractions of Ic band were collected and rechromatographed. The adsorbed complex on an SP-Sephadex column(ϕ2.7×130 cm) was eluted with a 0.15 mol/dm^3 Na_2SO_4 solution. Two separate bands (II and III) were obtained (Fig. 2b). The diastereomers in these bands isomerize to each other on exposure to light (II$\rightleftarrows$III), so that the chromatography should be carried out in the dark. The isomers Ia and Ib in solution are stable in the light. The diastereomers II and III were found to be partially resolved by column chromatography. The fractions of Ia, Ib, II, and III bands were collected separately, diluted several times with water, and poured on small columns of SP-Sephadex resin. The adsorbed isomers were eluted with a 2 mol/dm^3 NaCl solution, and the eluates

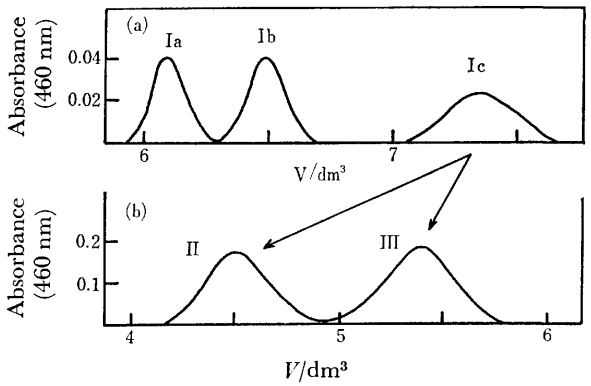

Fig. 2. (a) Elution curve of $[Cr(mbdo)_3]^{3+}$. Eluent: 0.2 mol/dm³ sodium $(+)_{589}$-tartratoantimonate(III). (b) Elution curve of Ic. Eluent: 0.15 mol/dm³ sodium sulfate.

were mixed with $NaClO_4$ to give green crystals, which were filtered, washed with a small amount of cold water, and air-dried. The formation ratio, I(Ia+Ib):II:III was 4 : 1 : 1.

Preparation of $Cr(mbdo)Cl_3 \cdot 5H_2O$. A 10^{-2} mol/dm³ hydrochloric acid solution(50 cm³) containing $Cr(NO_3)_3 \cdot 9H_2O$(0.8 g, 2.0 mmol) and racemic mbdo(0.5 g, 2.3 mmol) was heated at 70 °C for 3 h. After cooling, the resulting solution was poured on a column (ϕ 2.5×80 cm) of SP-Sephadex C-25 resin. The adsorbed product was eluted with a 0.5 mol/dm³ NaCl solution to give three separate bands. The last blue-green band was a mixture of the mono-mbdo complex and $[Cr(H_2O)_6]^{3+}$, which were separated by similar SP-Sephadex column chromatography using a 0.2 mol/dm³ Na_2SO_4 solution as an eluent. The green fraction of the mono-mbdo complex was again poured on a small column(ϕ 2.7×5 cm) of SP-Sephadex after dilution with water. The column was washed well with 10^{-2} mol/dm³ hydrochloric acid in order to replace Na^+ ions on the resin with H^+, and the adsorbed complex was eluted with 3 mol/dm³ hydrochloric acid. The eluate was evaporated to dryness in a vacuum desiccator over P_2O_5 and NaOH to give violet crystals. They were washed with ethanol and air-dried. Yield: 60%. This complex has the composition of $Cr(mbdo)Cl_3 \cdot 5H_2O$, and turns from violet to green in water, indicating that some chloride ions coordinate to the chromium(III) ion in the solid state. On heating an aqueous solution of the complex at 60 °C for a few hours, the absorption spectrum coincides with that of the green fraction ($(Cr(H_2O)_4(mbdo)]^{3+}$) separated by chromatography.

Resolution of mbdo. Optically active mbdo was obtained from the $(+)_{589}$-Ia or $(-)_{589}$-Ib isomer. To an aqueous solution (20 cm³) of the Ia or Ib isomer(50 mg, 0.05 mmol) was added $Na_2H_2edta \cdot 2H_2O$ (100 mg, 0.27 mmol) and the solution was heated at 70 °C for 10 h. During the course of heating, the color of the solution gradually turned from green to red violet. The resulting solution was diluted with 500 cm³ of water, adjusted to pH 9—10 with NaOH. The solution was passed through first a column of Dowex 1X8 anion exchange resin in the Cl^- form (ϕ 2.7×20 cm) to remove $[Cr(OH)(edta)]^{2-}$ produced and other anions, and then through a column of Dowex 50W cation exchange resin in the H^+ form (ϕ 2.7×10 cm) to remove cations such as Na^+ and the unreacted mbdo-chromium(III) complex. The solution was then evaporated to dryness under reduced pressure to give optically active mbdo. The $(+)_{589}$-Ia isomer gave $(+)_{589}$-mbdo ($[\alpha]_{589}^{23} = +10.6°$). The active mbdo is optically stable in solution.

Preparation of Optically Active $[Cr(H_2O)_4((+)_{589}$- *or* $(-)_{589}$-*mbdo)]^{3+}$. This complex was prepared from $[Cr(H_2O)_6]^{3+}$ and optically active mbdo by the method described for the racemic $[Cr(H_2O)_4(mbdo)]^{3+}$ complex. Its isolation was not achieved because of the small amount obtained. The quantitative circular dichroism(CD) spectrum of this complex was determined with the aid of the ε values of the racemate.

Preparation of Optical Isomers of $[Cr((+)_{589}$-*mbdo)*$_2((-)_{589}$-*mbdo)]*$^{3+}$. To an aqueous solution of $[Cr(H_2O)_4((-)_{589}$-mbdo)]$^{3+}$ was added twice the equivalent amount of $(+)_{589}$-mbdo. The solution was heated at 50 °C for 7 h and poured on an SP-Sephadex column (ϕ 2.0×50 cm). The adsorbed product was eluted with a 0.5 mol/dm³ NaCl solution in order to separate the tris-complex from the starting material. The fractions of the second band were collected and rechromatographed. By elution with a 0.2 mol/dm³ Na_2SO_4 solution, two bands(IIa and IIIa) were obtained, corresponding to enantiomers of diastereomers II and III, respectively, described for the racemic complex. Both isomers show positive rotation at 589 nm and epimerize to each other in the light (IIa$\rightleftarrows$IIIa) as observed for the racemic II and III. Diastereomer I was not formed, indicating that no disproportionation took place.

Analytical data of all the new compounds are given in Table 1.

Measurements. Absorption and CD spectra were recorded on a Hitachi 323 spectrophotometer and a JASCO J-40 spectropolarimeter, respectively. Optical rotations were determined with a JASCO DIP-40 digital polarimeter.

Results and Discussion

A new ligand mbdo can exist in a pair of enantiomers, since free rotation around the common axis connecting the two rings is prohibited by the presence of the methyl and NO groups. The ligand molecule has no functional group to form diastereomers with resolving agents, but the optical resolution was achieved by forming optically active $[Cr(mbdo)_3]^{3+}$, the ligands

Table 1. Analytical data

		C/%		H/%		N/%	
		Found	Calcd	Found	Calcd	Found	Calcd
	mbdo[a]	66.64	66.64	5.26	5.60	12.84	12.95
Ia:	$[Cr(mbdo)_3](ClO_4)_3 \cdot 5H_2O$	39.67	39.69	4.06	4.27	7.72	7.72
II:	$[Cr(mbdo)_3](ClO_4)_3 \cdot 2H_2O$	41.68	41.77	3.99	3.90	8.26	8.16
III:	$[Cr(mbdo)_3](ClO_4)_3 \cdot 3H_2O$	40.85	41.05	3.92	4.03	7.90	7.98
	$CrCl_3(mbdo) \cdot 5H_2O$	30.83	31.01	4.41	4.78	6.05	6.03

a) mbdo = $C_{12}H_{12}N_2O_2$.

in which have the same chirality (*vide infra*). The resolved mbdo is optically stable even in boiling water. The enantiomers are denoted by *R* and *S*,[6] as shown in Fig. 1. The *R*-(or *S*-) ligand forms a λ(or δ) skew chelate ring stereoselectively upon coordination. In this paper, the chilarity of the ligand is represented by the symbols δ and λ.

The $[Cr(mbdo)_3]^{3+}$ complex has eight theoretically possible optical isomers; $lel_3(\Delta(\lambda\lambda\lambda),\ \Lambda(\delta\delta\delta))$, $lel_2ob(\Delta(\lambda\lambda\delta),\ \Lambda(\delta\delta\lambda))$, $lelob_2(\Delta(\lambda\delta\delta),\ \Lambda(\delta\lambda\lambda))$, and ob_3 $(\Delta(\delta\delta\delta),\ \Lambda(\lambda\lambda\lambda))$. In the *lel* structure, the line joining the two nitrogen atoms of the mbdo ligand is nearly parallel to the C_3 axis of the complex ion, while in the *ob* structure, it is extremely oblique to the same axis so that the line and the axis are almost perpendicular to each other.

Of the four possible diastereomers, three (I, II, and III) were obtained by the reaction of $[Cr(H_2O)_6]^{3+}$ with racemic mbdo. No indication was found for the presence of more than three diastereomers by column chromatography. The isomers show absorption spectra differing from each other in the region of the first absorption band (Fig. 3). Diastereomer I is completely resolved into enantiomers Ia and Ib by SP-Sephadex column chromatography. The enantiomers are optically stable in solution. On the other hand, diastereomers II and III isomerize to each other in solution by exposure to ultraviolet light. Since the chirality of the ligand is retained in the complexes and no disproportionation takes place, the isomerization between II and III can be attributed to inversion in the arrangement of ligands around the metal ion ($\Delta \rightleftarrows \Lambda$, epimerization). Such epimerization will arise in the following two systems; (1) $lel_3 \rightleftarrows ob_3[\Delta(\lambda\lambda\lambda)(\text{or } \Lambda(\delta\delta\delta)) \rightleftarrows \Lambda(\lambda\lambda\lambda)(\text{or } \Delta(\delta\delta\delta))]$ and (2) $lel_2ob \rightleftarrows lelob_2$ $[\Delta(\lambda\lambda\delta)(\text{or } \Lambda(\delta\delta\lambda)) \rightleftarrows \Lambda(\lambda\lambda\delta)(\text{or } \Delta(\delta\delta\lambda))]$. Reaction (1) does not seem to take place, since molecular models show that the ob_3 isomer forms an extremely crowded structure, while reaction (2) appears to arise without difficulty from the studies of molecular models. Thus, diastereomer I which is stable in solution can be assigned to the lel_3 isomer, and diastereomers II and III to two isomers of the lel_2ob and $lelob_2$. The assignments are supported by the following experimental results. Diastereomer I assigned to the least crowded lel_3 structure is obtained in the largest amount (*vide ante*). The reaction of $[Cr(H_2O)_6]^{3+}$ with optically active mbdo obtained from the Ia (or Ib) enantiomer gives only the Ia (or Ib) enantiomer. Thus, the ligand recovered from Ia (or Ib) is proved to be optically pure, and diastereomer I should be the lel_3 isomer. On the other hand, the tris-complex prepared from $[Cr(H_2O)_4((-)_{589}\text{-mbdo})]^{3+}$ and $(+)_{589}$-mbdo consists of two optically active IIa and IIIa isomers, no diastereomer I being formed (see Experimental). Isomers IIa and IIIa thus formed should be enantiomers of diastereomers II and III, respectively, corresponding to either group of $\Delta(\delta\lambda\lambda)$ and $\Lambda(\delta\lambda\lambda)$ or $\Delta(\delta\delta\lambda)$ and $\Lambda(\delta\delta\lambda)$. The isomers isomerize (epimerize) to each other in solution by exposure to ultraviolet light, distributing in almost equal amounts at equilibrium. Thus, the equilibration study gives no information on the assignment of the structures of diastereomers II and III. In the column chromatography, diastereomer I(lel_3) eluates most quickly. If the elution order of the diastereomers is proportional to the number of the *lel* ligand, diastereomers II and III are assigned to the lel_2ob and $lelob_2$ isomers, respectively.

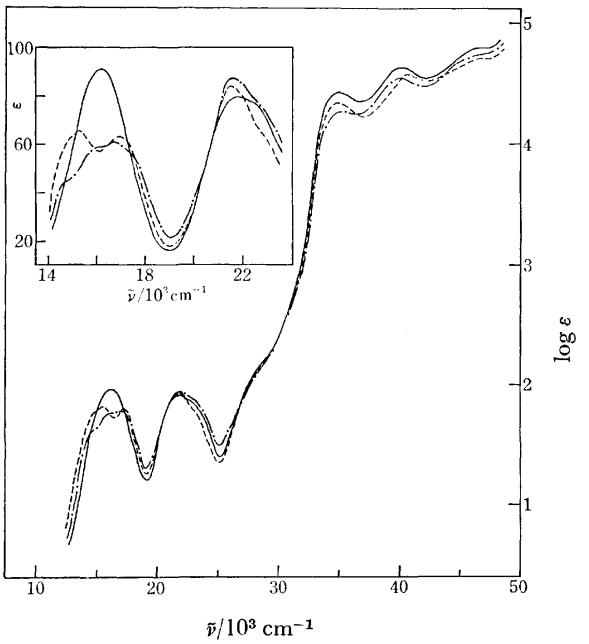

Fig. 3. Absorption spectra of three diastereomers of $[Cr(mbdo)_3]^{3+}$, Ia(——), II(----), and III(—·—).

Figure 3 shows the absorption spectra of diastereomers Ia, II, and III. Their spectral patterns in the region of the first absorption band differ remarkably, while those in the other region are similar to each other. The first absorption band of Ia is sharp and symmetrical, but those of II and III split into three components. All the diastereomers belong to the $[CrO_6]$-type in which the ligating oxygen atoms are the same kind. However, the actual symmetry of the lel_3 isomer will be D_3, and those of both lel_2ob and $lelob_2$ isomers will lower to C_2. In the fields of D_3 and C_2 symmetries, the first absorption band ($^4T_{2g}$) will split into two ($^4A_1$, ^4E) and three (2^4A, ^4B) components, respectively. Although diastereomer Ia shows no splitting in the first absorption band, the fact that diastereomers II and III exhibit the presence of three components in these bands supports the previous assignment for structures of these diastereomers. The absorption spectrum of diastereomer Ia is very similar to that of $[Cr(bpdo)_3]^{3+}$ over the whole region.[3] This indicates that the latter complex in which the ligands can easily change the conformation exists in the lel_3 form in solution. The spectral data are given in Table 2.

Figure 4 shows the CD spectra of $(+)_{589}$-$[Cr((+)_{589}\text{-mbdo})_3]^{3+}$ (Ia), $(+)_{589}$-$[Cr((+)_{589}\text{-mbdo})_2((-)_{589}\text{-mbdo})]^{3+}$(IIa), and $(+)_{589}$-$[Cr((+)_{589}\text{-mbdo})_2((-)_{589}\text{-mbdo})]^{3+}$(IIIa). The Ia isomer gives strong CD in the regions of the first and the ligand absorption bands. On the other hand, isomers IIa and IIIa show very similar spectra to each other over the whole

Table 2. Absorption and CD spectral data

	Absorption $\tilde{\nu}/10^3\ cm^{-1}$ (log ε)	CD $\tilde{\nu}/10^3\ cm^{-1}$ ($\Delta\varepsilon$)
$(+)_{589}$-mbdo	38.61 (4.32)	32.47 (+0.19)
	45.87 (4.57)	36.36 (−2.05)
		38.61 (+5.26)
		42.8 (−0.4)sh
		45.05 (−1.40)
		46.73 (+1.80)
Ia	16.23 (1.96)	16.00 (−2.86)
	21.81 (1.90)	21.21 (+0.46)
	22.5 (1.9)sh	28.65 (+0.45)
	35.09 (4.42)	31.30 (−0.61)
	39.92 (4.46)	36.0 (+63)sh
	46.08 (4.79)	38.10 (+142)
		41.15 (−93.9)
		46.95 (−79.9)
IIa	14.9 (1.8)sh	14.71 (−1.26)
	15.27 (1.82)	15.20 (−1.17)
	16.98 (1.80)	17.24 (+1.21)
	21.51 (1.93)	21.05 (−0.40)
	22.9 (1.8)sh	28.49 (+0.08)
	35.09 (4.33)	34.90 (+13.2)
	40.40 (4.59)	38.54 (+24.4)
	46.30 (4.72)	41.49 (−8.55)
		46.08 (−20.7)
IIIa	14.8 (1.6)sh	14.58 (−0.57)
	15.97 (1.76)	15.22 (−0.63)
	16.92 (1.78)	17.36 (+0.71)
	21.69 (1.94)	21.19 (−0.30)
	23.2 (1.8)sh	28.41 (+0.06)
	35.21 (4.28)	35.46 (+9.47)
	40.00 (4.55)	38.46 (+16.3)
	46.3 (4.8)sh	42.02 (−8.20)
		46.51 (−12.6)
IV	16.89 (1.36)	15.77 (−0.14)
	23.64 (1.55)	16.95 (+0.08)
	34.48 (3.90)	21.23 (−0.01)
	41.49 (4.19)	23.36 (+0.02)
	45.87 (4.38)	27.50 (+0.01)
		34.13 (−0.81)
		38.50 (−9.73)
		41.93 (+11.5)
		46.73 (−12.6)

Ia: $(+)_{589}$-$[Cr((+)_{589}$-mbdo$)_3]^{3+}$
IIa: $(+)_{589}$-$[Cr((+)_{589}$-mbdo$)_2((-)_{589}$-mbdo$)]^{3+}$
IIIa: $(+)_{589}$-$[Cr((+)_{589}$-mbdo$)_2((-)_{589}$-mbdo$)]^{3+}$
IV: $[Cr(H_2O)_4((+)_{589}$-mbdo$]^{3+}$
sh: shoulder.

region, although the strength of the former is somewhat larger. Both isomers consist of the same ligands, two $(+)_{589}$-mbdo and one $(-)_{589}$-mbdo. However, these isomers are antipodal to each other in the arrangement of the ligands around the metal ion. If one is Δ-configuration, the other is Λ-configuration. The similarity in the CD spectra suggests that the circular dichroism in these isomers is mainly caused by the contribution due to the vicinal effect of the chiral mbdo ligand (δ,λ) rather than to the configurational

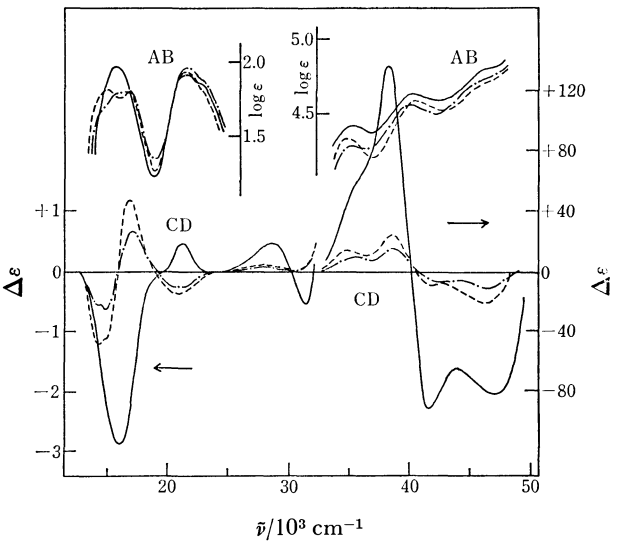

Fig. 4. Absorption(AB) and CD spectra of $(+)_{589}$-$[Cr((+)_{589}$-mbdo$)_3]^{3+}$ (Ia)(——), $(+)_{589}$-$[Cr((+)_{589}$-mbdo$)_2((-)_{589}$-mbdo$]^{3+}$ (IIa)(----), and $(+)_{589}$-$[Cr((+)_{589}$-mbdo$)_2((-)_{589}$-mbdo$)]^{3+}$ (IIIa)(—·—).

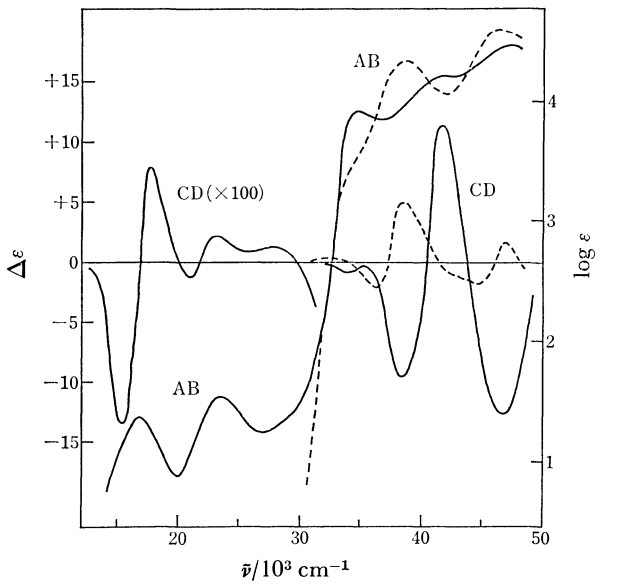

Fig. 5. Absorption(AB) and CD spectra of $[Cr(H_2O)_4$-$((+)_{589}$-mbdo$)]^{3+}$(——) and $(+)_{589}$-mbdo(----).

effect (Δ, Λ). Since these isomers contain two $(+)_{589}$-mbdo and one $(-)_{589}$-mbdo, the vicinal effect would come from one $(+)_{589}$-mbdo, if such effects of chiral ligands function additively. The $[Cr(H_2O)_4((+)_{589}$-mbdo$)]^{3+}$ complex of the $[CrO_6]$-type is a good example for knowing the vicinal effect of $(+)_{589}$-mbdo. However, as Fig. 5 shows, the CD spectrum of this complex is similar in pattern but much weaker in intensity than that of isomers IIa and IIIa, in the region of the first absorption band. In the ultraviolet region, its spectrum differs remarkably from that of the isomers. This indicates that the configurational and vicinal effects do not contribute additively to the CD spectra of these complexes. The additivity rule has been reported to hold for a number of five-membered chelate complexes.[7] The chiral conformation of the mbdo chelate ring does not cause inversion.

However, the chelate ring is large and would be flexible in a certain range. The most stable conformation of the ring may differ more or less from each other in each complex to minimize steric interactions among ligands. The different conformations would bring about different vicinal effects in CD spectra. The reason why the additive rule fails in the mbdo complexes can be attributed to such flexible conformation of the chelate ring. The free $(+)_{589}$-mbdo ligand which should be in a different conformation from those in the complexes exhibits a quite different CD spectrum in the ultraviolet region from that of the complexes. The absolute configurations of isomers IIa and IIIa can not be assigned from the CD spectra.

Isomer Ia, $(+)_{589}$-$[Cr((+)_{589}\text{-mbdo})_3]^{3+}$ shows a strong negative CD band in the region of the first absorption band. The $(+)_{589}$-$[Cr(bpdo)_3]^{3+}$ isomer which gives a similar CD pattern in this region was assigned to the *Λ*-configuration[3] from comparison of the CD patterns of a series of complexes, $[Cr(bpdo)_n(en)_{3-n}]^{3+}$. Figure 6 shows a comparison of the CD spectrum of Ia isomer with that of *Λ*-$[Cr(ox)_3]^{3-}$ (ox= oxalate ion)[8,9] and *Λ*-$[Cr(mal)_3]^{3-}$ (mal=malonate ion).[8,9] The spectral changes for these five-, six-, and seven-membered chelate complexes, are similar to those observed for a series of complexes, $[Co(NH_2(CH_2)_nNH_2)_3]^{3+}$ (n=2, 3, and 4).[10] In the ultraviolet region, the Ia (or Ib) isomer exhibits a characteristic CD pattern with strong intensity; a positive (or negative) and a negative (or positive) CD band from the smaller wavenumber side. The other complexes of mbdo show no such strong CD in this region. The CD bands in this region may be assigned to the $\pi\rightarrow\pi^*$ transitions of the ligand. Since the Ia isomer consists of ligands with the same chirality, $(+)_{589}$-mbdo, such strong CD might be caused by the exciton interaction among the ligands as observed for $[M(phen)_3]^{n+}$ (phen=1,10-phenanthroline).[11] Although the exciton CD for the system consisting of ligands with a twist conformation is unknown, the CD pattern of the Ia isomer resembles that of *Λ*-$[Cr(phen)_3]^{3+}$,[11,12] and the isomer can be assigned to the *Λ*-configuration. The assignment agrees with that based on the CD sign in the region of the first absorption band. If the isomer has the *Λ*-configuration, the $(+)_{589}$-mbdo ligand should be in the *δ*-skew conformation to form the lel_3 structure. Hence the $(+)_{589}$-mbdo can be assigned to the *S*-configuration.

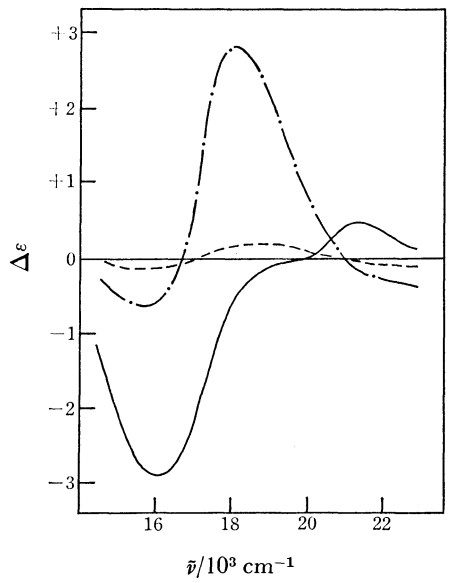

Fig. 6. CD spectra of $[CrO_6]$ complexes in the region of the first absorption band, $(+)_{589}$-$[Cr((+)_{589}\text{-mbdo})_3]^{3+}$ (Ia)(——), *Λ*-$[Cr(mal)_3]^{3-}$ (----), and *Λ*-$[Cr(ox)_3]^{3-}$ (—·—).

This work was carried out with Scientific Research Grant-in-Aid No. 243013 from the Ministry of Education and the Kurata Research Grant.

References

1) A. Vinciguerra, P. G. Simpson, Y. Kakiuti, and J. V. Quagliano, *Inorg. Chem.*, **2**, 286 (1963).
2) E. J. Corey and J. C. Bailar, Jr., *J. Am. Chem. Soc.*, **81**, 2620 (1959).
3) H. Kanno, K. Kashiwabara, and J. Fujita, *Bull. Chem. Soc. Jpn.*, **52**, 761 (1979).
4) F. H. Case, *J. Am. Chem. Soc.*, **68**, 2574 (1946).
5) I. Murase, *Nippon Kagaku Zasshi*, **77**, 682 (1956).
6) R. S. Cahn, C. K. Ingold, and V. Prelog, *Angew. Chem., Int. Ed. Engl.*, **5**, 385 (1966).
7) B. E. Douglas, *Inorg. Chem.*, **4**, 1813 (1965); K. Ogino, K. Murano, and J. Fujita, *Inorg. Nucl. Chem. Lett.*, **4**, 351 (1968).
8) A. J. McCaffery, S. F. Mason, and R. E. Ballard, *J. Chem. Soc.*, **1965**, 2883.
9) K. R. Butler and M. R. Snow, *J. Chem. Soc., Dalton Trans.*, **1976**, 251.
10) M. Kojima, H. Yamada, H. Ogino, and J. Fujita, *Bull. Chem. Soc. Jpn.*, **50**, 2325 (1977).
11) S. F. Mason and B. J. Peart, *J. Chem. Soc., Dalton Trans.*, **1973**, 949.
12) J. Fergason, C. J. Hawkins, N. A. P. Kane-Maquire, and H. Lip, *Inorg. Chem.*, **8**, 771 (196).

Preparation and Circular Dichroism of Dichloro-(*S*)-2-(butylphenylphosphinomethyl)pyrrolidine-palladium(II)([$PdCl_2L$]) and Its Related Complexes, and the Absolute Configuration of [$PdCl_2L$] Determined by X-Ray Analysis

Isamu KINOSHITA, Kazuo KASHIWABARA, Junnosuke FUJITA,* Takashi YAMANE,**
Hitoshi UKAI,** and Tamaichi ASHIDA**

*Department of Chemistry, Faculty of Science, and **Department of Applied Chemistry, Faculty of Engineering, Nagoya University, Chikusa, Nagoya 464*

(Received November 29, 1978)

(*S*)-2-(Butylphenylphosphinomethyl)pyrrolidine(L) was prepared from (*S*)-proline *via* four main reaction steps. A pair of diastereomers of the $PdCl_2L$ complex, the isomerism of which comes from chiral configuration of the phosphorus atom, crystallized in different forms (needle and block), which were separated by hand picking. The molecular structure and absolute configuration of one(block) of the dichloro complexes was determined by X-ray analysis. Crystallographic data are: $P2_12_12_1$, $Z=4$, $a=13.576(4)$, $b=16.351(3)$, $c=8.041(2)$ Å, and $R=7.8\%$ for 1659 reflections. The Pd atom has a distorted square planar coordination of four donor atoms. The Pd–Cl bond distance *trans* to Pd–P, 2.367 Å, is longer than that *trans* to Pd–N, 2.296 Å. The absolute configuration of the coordinated phosphorus atom was determined to be *R* by assuming *S* configuration for the asymmetric carbon atom of the aminophosphine. The corresponding diastereomers of the dibromo complex were also prepared from each diastereomer of the chloro complex. The circular dichroism spectra of these diastereomers were compared with one another and with those of other related complexes, and the vicinal effects due to the chiral phosphorus atoms in these complexes were examined.

There has been much interest in asymmetric syntheses catalized by transition metal complexes, especially by rhodium(I) complexes containing chiral phosphines. These studies have extensively developed preparations[1-5] and optical resolutions[6] for a variety of chiral phosphines. Recently, some of optically active natural products have been used for precursors of chiral phosphines.[7-9] However, tedious procedures are often required for preparing optically active phosphines with a chiral phosphorus atom. The importance of a chiral center at a phosphorus atom has been pointed out for high efficiency of asymmetric hydrogenation.[10]

This paper reports the preparation of (*S*)-2-(butylphenylphosphinomethyl)pyrrolidine, which has three chiral centers at the carbon, nitrogen, and phosphorus atoms, and the isolation of a pair of diastereomers of its dichloro palladium(II) complex caused by a pair of the chiral phosphorus atoms. The chiral carbon atom has *S* configuration and the nitrogen one should yield the same *S* configuration stereoselectively upon coordination as seen in bis(*S*-prolinato)palladium(II).[11] The paper also describes the molecular structure and absolute configuration of one of the diastereomers determined by X-ray analysis.

So far little work has been reported concerning circular dichroism(CD) spectra of metal complexes containing chiral phosphines. The accumulation of CD data of chiral phosphine complexes will be necessary for investigating the stereochemistry of phosphine complexes catalyzing asymmetric syntheses. In this paper the CD spectra of diastereomers of the dichloro complex are compared with those of the related complexes and the vicinal effects due to the coordinated chiral phosphorus atoms are examined. A part of this study has been reported briefly.[12]

Experimental

All the preparations and handlings of the aminophosphines were carried out under an atmosphere of nitrogen or *in vacuo*. The palladium(II) complexes containing the aminophosphines can be handled in air. Absorption, CD, ^{1}H-NMR, and IR spectra were recorded on a HITACHI 323 spectrometer, a JASCO J-20 or J-40 spectropolarimeter, a JEOL PMX-60 spectrometer, and a HITACHI EPI-L 2 spectrometer, respectively.

Preparations. The following compounds were prepared according to the methods previously reported; (*S*)-2-(diphenylphosphinomethyl)pyrrolidine[8] and (*S*)-2-(aminomethyl)-pyrrolidine.[13]

(S)-2-(Phenylphosphinomethyl)pyrrolidine. To liquid ammonia (150 cm^3) in a 500 cm^3 round-bottom, three neck flask with a mechanical stirrer, a dropping funnel, and nitrogen inlet was added sodium metal(3.3 g) and then phenylphosphine(15 g) dropwise with vigorous stirring over 40 min at −78 °C (Dry Ice–methanol). After stirring for further 20 min, (*S*)-2-(bromomethyl)pyrrolidine hydrobromide[14] (17 g) was added in small portions and then the solution was stirred for 2 h at −78 °C. The liquid ammonia was evaporated off at room temperature and oxygen-free tetrahydrofuran(THF) was added on the residue. The undissolved material (sodium bromide) was filtered off and the filtrate was evaporated to remove THF. The oily residue was distilled under reduced pressure to yield colorless liquid. Yield: 7.4 g, bp 140.5—141 °C/933 Pa.

(S)-2-(Butylphenylphosphinomethyl)pyrrolidine. To a mixture of liquid ammonia (150 cm^3) and sodium metal (0.52 g) was added dropwise (*S*)-2-(phenylphosphinomethyl)-pyrrolidine(4.38 g) with vigorous stirring over 20 min at −78 °C. The solution changed from blue green to green. After stirring for 1 h, butylchloride (6 cm^3) was added dropwise to the solution. The color of the solution changed to deep red instantly and the stirring was continued until the color became light yellow. The liquid ammonia was evaporated off at room temperature and oxygen-free THF was added on the residue to extract the object. The undissolved material (sodium chloride) was filtered off and the filtrate was evaporated to give oily residue. It was distilled in vacuo to yield colorless liquid. Yield: 3.6 g, bp 135—136 °C/13.3 Pa.

*{(S)-2-(Butylphenylphosphinomethyl)pyrrolidine}dichloropalladium(II) (**1a** and **1b**).* To an acetonitrile solution (50 cm³) of $PdCl_2(CH_3CN)_2$[15] (198 mg) was added (*S*)-2-(butylphenylphosphinomethyl)pyrrolidine(190 mg). After stirring for 3 h at 50 °C, appropriate amounts of diethyl ether and then hexane were added to the resultant solution to yield yellow precipitate, which was filtered(250 mg). The product was dissolved in a small amount of chloroform and the solution was poured into a column (ϕ 1.2×10 cm) of acidic activated alumina. The adsorbed yellow band was eluted with a mixture of chloroform and ethanol(20 : 1). The yellow eluate was concentrated to a small volume(10 cm³) and mixed with ethanol(50 cm³). The ethanol solution was slowly concentrated at room temperature in air to yield two different crystal forms (total yield 77%), needle (**1a**) and block(**1b**), which were separated by hand picking. The crystals of each form were separately recrystallized from a mixture of chloroform and ethanol. Yield: *ca.* 15% for each isomer. Found for **1a**: C, 42.41; H, 5.66; N, 3.21%. Found for **1b**: C, 42.43; H, 5.68; N, 3.26%. Calcd for $PdCl_2(C_{15}H_{24}NP)$: C, 42.22; H, 5.68; N, 3.28%.

*{(S)-2-(Butylphenylphosphinomethyl)pyrrolidine}dibromopalladium(II) (**2a** and **2b**).* To the complex **1a** or **1b** (60 mg) in a mixture(30 cm³) of chloroform and ethanol (1 : 1) was added an ethanol solution (10 cm³) saturated with sodium bromide. After stirring for 3 h at room temperature, the solution was evaporated to dryness under reduced pressure and dichloromethane was added to the residue to extract the dibromo complex. To the extract was added diethyl ether to yield yellow precipitate, **2a** or **2b** from **1a** or **1b**, respectively. Yield: 50 mg. Found for **2a**: C, 34.65; H, 4.70; N, 2.32%. Found for **2b**: C, 34.77; H, 4.69; N, 2.50%. Calcd for $PdBr_2(C_{15}H_{24}NP)$: C, 34.94; H, 4.70; N, 2.32%.

*{(S)-2-(Diphenylphosphinomethyl)pyrrolidine}dichloropalladium(II) (**3**).* To a suspension of $PdCl_2(CH_3CN)_2$(328 mg) in chloroform(30 cm³) was added a chloroform solution (10 cm³) of (*S*)-2-(diphenylphosphinomethyl)pyrrolidine (341 mg). After stirring overnight, the solution was poured into a column (ϕ 1.5×10 cm) of acidic activated alumina and the adsorbed band was eluted with a mixture of chloroform and ethanol(5 : 1). Diethyl ether was added to the eluate to yield yellow crystals (**3**). Yield: *ca.* 30%. Found: C, 45.38; H, 4.50; N, 3.03%. Calcd for $PdCl_2(C_{17}H_{20}NP)$: C, 45.71; H, 4.52; N, 3.14%.

*{(S)-2-(Aminomethyl)pyrrolidine}dichloropalladium(II) (**4**).* To a chloroform solution(150 cm³) of $PdCl_2(CH_3CN)_2$ (1.1 g) was added a chloroform solution(70 cm³) of (*S*)-2-(aminomethyl)pyrrolidine (0.43 g) and the solution was stirred for 3 h at room temperature to give a precipitate gradually. The precipitate was filtered and dissolved in hot water containing a few drops of concd hydrochloric acid. The solution was concentrated and then potassium chloride was added to the concentrate to yield yellow crystals (**4**). Yield: 0.7 g. Found: C, 21.64; H, 4.37; N, 10.10%. Calcd for $PdCl_2(C_5H_{12}N_2)$: C, 21.39; H, 4.49; N, 10.09%.

*(2-N,N-Dimethylaminoethyldiphenylphosphine)dichloropalladium(II) (**5**).* This complex was prepared according to the method of Meek *et al.*[16]

*Structure Determination of **1b**.* The crystal data of **1b** are as follows: orthorhombic, $P2_12_12_1$, a=13.576(4), b=16.351(3), c=8.041(2)Å, D_m=1.60, D_x=1.588 g cm⁻³, Z=4, and μ(Mo $K\alpha$)=14.1 cm⁻¹. The intensity data were collected on a Hilger & Watts automatic diffractometer using Zr-filtered Mo $K\alpha$ radiation. The crystal used for the data collections had the dimensions of 0.45×0.40×0.25 mm. Independent 1840 reflections with $2\theta \leq 50°$ were measured by the θ-2θ step scan technique, of which non-zero reflections were 1659. The intensity data were corrected for Lorentz and polarization effects. Absorption correction was also carried out by the Furnas's method.[17]

The structure was solved by the heavy atom method. The refinement was carried out by the block-diagonal least-squares method.[18] In the refinement, the weights $w=1/(\sigma^2(F)+a|F_o|+b|F_o|^2)$ for $|F_o|>0$, and $w=c$ for $|F_o|=0$ were assigned ,where $\sigma(F)$ is the standard deviation

TABLE 1. THE ATOMIC PARAMETERS AND THEIR ESTIMATED STANDARD DEVIATIONS (×10⁴) OF **1b**

Thermal parameters are in the form: $\exp(-\beta_{11}h^2-\beta_{22}k^2-B_{33}l^2-\beta_{12}hk-\beta_{13}hl-\beta_{23}kl)$.

	x	y	z	β_{11}	β_{22}	β_{33}	β_{12}	β_{13}	β_{23}
Pd	1983(1)	880(1)	690(1)	45(1)	31(1)	171(1)	1(1)	5(2)	−10(1)
Cl(1)	483(2)	1186(2)	−472(5)	59(2)	48(1)	288(9)	21(3)	−60(8)	−51(6)
Cl(2)	1551(3)	−498(2)	1207(5)	77(2)	35(1)	279(9)	−23(3)	−9(7)	31(5)
P	2575(3)	2101(2)	72(5)	53(2)	30(1)	236(7)	8(3)	51(6)	−20(5)
N	3349(7)	673(5)	1803(14)	64(6)	35(4)	203(20)	−5(8)	31(20)	14(15)
C(1)	3948(10)	1426(8)	2064(22)	67(9)	50(6)	308(38)	−27(13)	−31(33)	−52(27)
C(2)	4998(11)	1097(9)	2347(22)	50(7)	78(8)	326(39)	14(14)	−101(30)	−42(32)
C(3)	5058(11)	335(9)	1310(21)	72(9)	71(7)	313(43)	−2(16)	16(33)	157(30)
C(4)	3972(9)	91(7)	882(18)	53(7)	47(6)	219(27)	30(10)	−46(28)	−1(23)
C(5)	3874(9)	1975(7)	515(23)	54(8)	40(5)	408(43)	5(10)	107(35)	−21(29)
C(6)	2140(9)	2961(6)	1289(15)	77(9)	27(4)	188(24)	16(10)	−37(26)	7(16)
C(7)	1226(8)	2913(7)	2055(16)	41(6)	45(5)	194(25)	7(10)	27(23)	−50(20)
C(8)	886(9)	3599(9)	2987(23)	70(9)	56(6)	288(35)	−3(13)	−101(32)	−48(27)
C(9)	1394(10)	4320(8)	3074(19)	92(10)	58(7)	207(27)	20(14)	19(31)	−63(24)
C(10)	2316(10)	4351(6)	2266(19)	105(11)	40(6)	250(30)	5(13)	−81(33)	−20(21)
C(11)	2676(9)	3683(6)	1363(17)	77(9)	28(4)	254(31)	−11(10)	1(27)	−41(20)
C(12)	2418(10)	2414(7)	−2116(18)	41(13)	47(6)	226(30)	46(16)	151(36)	8(24)
C(13)	2920(20)	3207(11)	−2622(32)	309(31)	81(10)	583(77)	−31(35)	581(91)	177(46)
C(14)	3721(28)	2894(16)	−3672(87)	126(30)	24(10)	1177(99)	−29(29)	292(99)	34(90)
C(14′)	3427(29)	3456(23)	−3761(75)	135(33)	85(21)	983(98)	29(45)	566(99)	245(99)
C(15)	4237(16)	3325(18)	−4692(35)	153(22)	173(22)	448(73)	−13(35)	102(71)	83(66)

Table 2. The positional($\times 10^3$) and thermal(Å^2) parameters of the hydrogen atoms of **1b**
The standard deviations are given in parentheses.

	Bonded to	*x*	*y*	*z*	*B*
H (1)	N	307 (10)	41 (8)	284 (23)	8 (4)
H (2)	C (1)	378 (8)	167 (6)	281 (15)	3 (3)
H (3)	C (2)	503 (11)	106 (7)	346 (17)	6 (4)
H (4)	C (2)	569 (8)	145 (8)	240 (19)	6 (4)
H (5)	C (3)	515 (11)	6 (7)	211 (26)	8 (5)
H (6)	C (3)	532 (10)	60 (9)	13 (22)	7 (5)
H (7)	C (4)	373 (7)	12 (5)	−11 (13)	1 (2)
H (8)	C (4)	373 (8)	−32 (7)	113 (15)	4 (3)
H (9)	C (5)	414 (9)	258 (8)	87 (16)	6 (4)
H (10)	C (5)	426 (8)	178 (7)	−20 (17)	4 (3)
H (11)	C (7)	82 (10)	225 (9)	186 (23)	8 (4)
H (12)	C (8)	33 (8)	333 (8)	390 (16)	5 (4)
H (13)	C (9)	114 (11)	494 (8)	366 (19)	7 (4)
H (14)	C (10)	265 (11)	500 (8)	222 (23)	8 (4)
H (15)	C (11)	344 (9)	361 (7)	69 (17)	5 (3)
H (16)	C (12)	145 (10)	269 (7)	−234 (16)	7 (4)
H (17)	C (12)	267 (10)	222 (8)	−259 (20)	8 (4)

based on counting statistics. A disorder occurs at the butyl group. Both the C^{β} and C^{γ} atoms of the butyl group were located at two sites with occupancies of 0.5 each from the D-map. Finally the C^{β} atom converged into the resultant position, though its temperature factors are significantly larger than those of the other atoms. The H atoms were found on the D-map. However, those bonded to the C^{β}, C^{γ}, C^{δ} atoms of the butyl group were not found, and not included in the further refinement. The final *R* value is 9.9% ($a=-0.1777$, $b=0.0082$, and $c=0.2184$), while it is 7.8% for non-zero reflections.

The atomic scattering factors for the Pd^{2+}, Cl^-, P, N, C, and H were taken from International Tables for X-Ray Crystallography, Vol. IV.[19] Calculations were carried out on the FACOM 230-75 computers at Nagoya University. The final atomic parameters are listed in Tables 1 and 2.[20]

Results and Discussion

Preparation and Properties. Mislow[21] and Horner[22] prepared a number of chiral phosphines and phosphine oxides containing asymmetric phosphorus atoms. However, their methods are somewhat tedious. In the present study, a pair of diastereomers of (*S*)-2-(butylphenylphosphinomethyl)pyrrolidine was easily obtained by the following scheme:

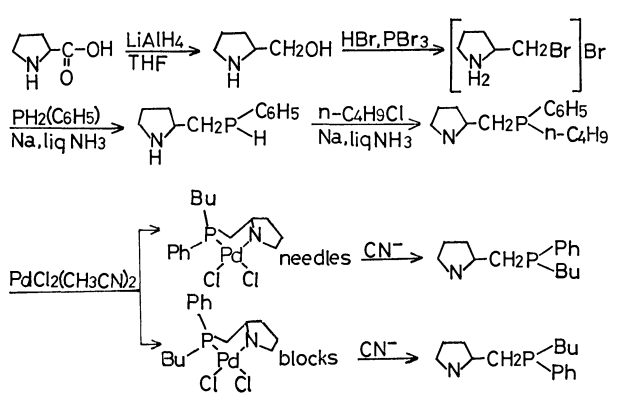

The aminophosphine was prepared from (*S*)-proline by a method similar to those for 2-aminoethylphenylphosphine derivatives reported by Issleib.[23] The dichloro palladium(II) complex of the aminophosphine yields only two diastereomers arising from a pair of chiral phosphorus atoms. The nitrogen atom will have *S* configuration stereoselectively upon coordination as confirmed by X-ray analysis on [Pd(*S*-prol)$_2$].[11] The diastereomers (**1a** and **1b**) crystallize in different forms, needle and block, by slow evaporation of an ethanol solution, and can be separated by hand picking. They are stable in air and do not isomerize in boiling ethanol. The free chiral phosphines are easily liberated from the diastereomers by treating with sodium cyanide in water. The corresponding chiral dibromo complexes (**2a** and **2b**) were derived from each diastereomer of the dichloro complex.

Table 3. NMR spectral data of palladium complexes in $CDCl_3$
(δ/ppm from TMS)

Complex	$-CH_3$	$-CH_2-$	N–H	$-C_6H_5$
1a	0.83	1—4.2	7.0	7.5—8.3
1a[a]	0.93	1—4.0	6.6	7.5—8.3
1b	0.97	1—4.2	6.1	7.4—8.3
1b[a]	0.88	1—4.0	6.2	7.5—8.5
2a	0.85	1—3.9	6.5	7.5—8.3
2b	0.91	1—4.1	5.7	7.5—8.3
3	—	1—4.0	6.9	7.3—8.3

a) solvent: DMSO-d_6.

Table 3 shows the data of ^{1}H-NMR spectra of the aminophosphine complexes prepared. The peaks in the region 5.7—7.0 ppm can be assigned to the N–H protons, since these peaks disappear on deuteration. The N–H protons of **1b** and **2b** resonate at a considerably higher magnetic field than do those of **1a** and **2a** respectively. The chiral phosphorus atoms of **1a**, and **1b** have *S* and *R* configurations, respectively (*vide post*). In the *R* configuration(**1b**), the N–H proton and the phenyl group face each other on the same side of the complex plane. Therefore, the up-field shifts of the N–H protons of **1b** and **2b** indicate that the phenyl group causes the shielding effect to the N–H proton. In a previous paper,[12] such a phenyl group was considered to give the deshielding effect to the N–H proton, hence the absolute configuration of **1b** was assigned reversely. The chemical shifts of these N–H protons seem to be sensitive to environment such as the kinds of ligating halide ions and solvents (Table 3). The complex **3**, which has the phenyl group in the same arrangement as **1b** shows the N–H resonance at nearly the same field, 6.9 ppm as that of **1a**.

In the far IR spectra, all the dichloro-aminophosphine complexes show absorption bands around 280 and 330 cm^{-1}. These bands can be assigned to the ν(Pd–Cl), since the corresponding dibromo complexes show no band in this region. The dichloro-diamine complex (**4**) exhibits two strong bands at 301 and 337 cm^{-1} which may be correspond to the ν(Pd–Cl) of 306 and

327 cm^{-1} observed for *cis*-$[PdCl_2(NH_3)_2]$.[24] The IR spectra of the present complexes are too complicated to be assigned.

Molecular Structure of ***1b*** The stereoscopic view of **1b** (block crystal) drawn by ORTEP II[25] is shown in Fig. 1. The absolute configuration of the phosphorus atom in **1b** becomes *R*, when the asymmetric carbon atom of the pyrrolidine ring is assumed to be *S* configuration. Therefore the phosphorus atom of **1a** (needle crystal) has *S* configuration. The bond lengths and angles concerning non-hydrogen atoms are shown in Fig. 2. The e.s.d.'s are; 0.02—0.03 Å for bond lengths except for Pd–X(0.005—0.014 Å) and C(14)–X(0.05 Å), and 0.7—1.6° for bond angles except for X–Pd–X(0.2—0.4°) and C(13)–C(14)–C(15) (5°). The equations of the best planes and the related data are given in Table 4.

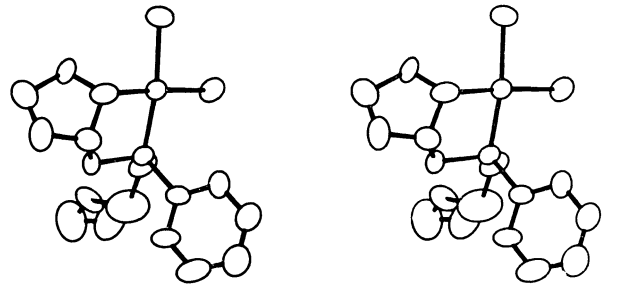

Fig. 1. The stereoscopic view of **1b**.

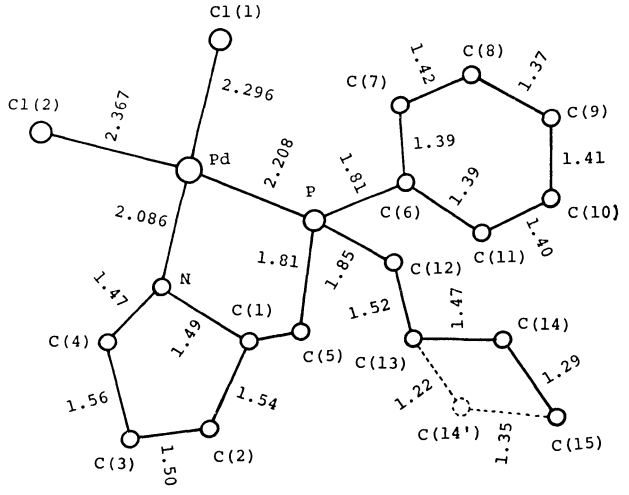

Fig. 2.(a) The bond lengths(Å) of **1b**.

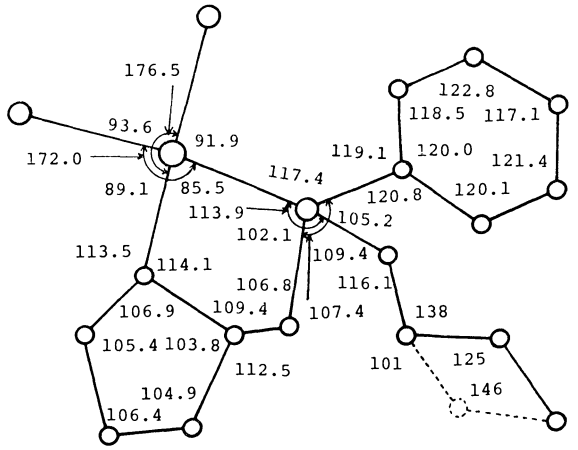

Fig. 2(b). The bond angles (°) of **1b**.

The Pd(II) ion forms a distorted square plane with four donor atoms. The dihedral angle between the plane of Pd, Cl(1), and Cl(2), and that of Pd, P, and N is 174.0°. The P atom deviates by 0.27 Å from the best plane formed with Pd, Cl(1), Cl(2), and N. However, the planarity is rather better than that in $[PdCl_2\{N,N$-dimethyl-α-methyl-*o*-(butylphenylphosphino)benzylamine$\}]$ (BENZYL),[26] in which the N

TABLE 4. THE BEST PLANES OF **1b**

(a) Equations of the best planes

$X=ax,\ Y=by,\ Z=cz$

Plane I: Pd, Cl(1), Cl(2), P, N
$0.3384X-0.3067Y-0.8896Z+0.0011=0$

Plane II: Pd, Cl(1), Cl(2), N
$-0.3693X+0.2483Y+0.8955Z+0.1180=0$

Plane III: Pd, P, N
$0.3515X-0.3562Y-0.8658Z+0.0475=0$

Plane IV: Pd, Cl(1), Cl(2)
$-0.3523X+0.2565Y+0.9001Z+0.0790=0$

Plane V: N, C(2), C(3), C(4)
$-0.0139X+0.5767Y-0.8169Z+0.5990=0$

Plane VI: P, C(6), C(7), C(8), C(9), C(10), C(11)
$-0.4532X+0.3437Y-0.8225Z+0.4784=0$

(b) Dihedral angles (°) between the planes

	I	II	III	IV	V
II	176.2				
III	176.8	173.5			
IV	177.0	178.9	174.0		
V	123.0	125.7	119.8	125.6	
VI	118.2	118.9	115.5	119.5	151.2

(c) Displacements ($\times 10^2$ Å) of atoms from the planes

The atoms with asterisks are not included in the best plane calculations.

I		II		III	
Pd	−2	Pd	2	Pd	0
Cl(1)	−3	Cl(1)	−1	P	0
Cl(2)	10	Cl(2)	0	N	0
P	7	N	−1	Cl(1)*	−8
N	−9	P*	27	Cl(2)*	24
C(1)*	−36	C(1)*	−19	C(1)*	−32
C(2)*	8	C(2)*	26	C(2)*	17
C(3)*	123	C(3)*	134	C(3)*	136
C(4)*	115	C(4)*	120	C(4)*	128
C(5)*	40	C(5)*	63	C(5)*	37
C(6)*	−143	C(6)*	−118	C(6)*	−156
C(12)*	140	C(12)*	162	C(12)*	126
IV		V		VI	
Pd	0	N	−1	P	3
Cl(1)	0	C(2)	1	C(6)	−3
Cl(2)	0	C(3)	−3	C(7)	1
P*	22	C(4)	3	C(8)	−1
N*	−6	C(1)*	52	C(9)	2
		C(5)*	204	C(10)	0
		Pd*	94	C(11)	−2

atom deviates by 0.423 Å from the best plane of Pd, Cl(1), Cl(2), and P. The Pd–Cl(2) (*trans* to Pd–P) length of 2.367 Å is longer than the Pd–Cl(1) (*trans* to Pd–N) length of 2.296 Å. The same trend in the Pd–Cl lengths is seen in BENZYL (2.386 and 2.285 Å). The elongation of Pd–Cl(2) bond may be attributed to the stronger *trans* effect of P than that of N. The Pd–P length of 2.208 Å is significantly short as compared with those of 2.241 Å in BENZYL and of 2.286 Å in [PdCl{(*S*)-isopropyl-*t*-butylphenylphosphine}{(*R*)-*N*,*N*-dimethyl-α-(2-naphthyl) ethylamine-3*C*,*N*}] (NAPHTHYL).[6] The Pd–N length of 2.086 Å is also shorter than those in BENZYL (2.134 Å) and NAPHTHYL (2.167 Å).

The five-membered chelate ring is fairly puckered to form a δ conformation. The torsion angles concerning the ring are: Pd–N–C(1)–C(5), −40.9°; N–C(1)–C(5)–P, 49.7°; C(1)–C(5)–P–Pd, −35.7°; C(5)–P–Pd–N, 11.9°; P–Pd–N–C(1), 13.7°. The deviations of C(1) and C(5) from the plane of Pd, P, and N are 0.32 Å (to the direction to C(6) (phenyl group)) and 0.37 Å(to the direction to C(12) (butyl group)), respectively. The N–Pd–P angle is 85.5°, while that of the six-membered chelate ring in BENZYL is 94.0°. On the contrary, the Cl–Pd–Cl angle (93.6°) is larger than that in BENZYL (88.12°).

The coordinated N atom of the pyrrolidine ring has *S* configuration. The torsion angles of the pyrrolidine ring are; χ_1=32.2, χ_2=−16.8, χ_3=−4.7, and χ_4=25.1°. The C^{α} (=C(1)) atom is puckered out by 0.52 Å in the pyrrolidine ring, while C^{δ} puckering is observed for [Pd(*S*-prol)$_2$].[11]

The disorder occurs at the location of C(14). Therefore the abnormal bond lengths and angles concerning this atom are observed. However, the distance between C(13) and C(15), 2.49 Å is rather normal.

Absorption and CD Spectra. The absorption and CD spectra of the dichloro (**1a** and **1b**) and the dibromo (**2a** and **2b**) complexes are shown in Figs. 3 and 4, respectively. The numerical data are given in Table 5 together with those of the other related complexes. The absorption spectra of a pair of diastereomers quite resemble each other, while the CD spectra are nearly enantiomeric to each other. The diastereoisomerism arises from a pair of enantiomeric configurations of the phosphorus atom, the other chiral centers at the carbon and nitrogen atoms being all *S* configurations. If it is assumed that the vicinal effects due to these three chiral atoms contribute additively to the CD, the vicinal effects of the chiral phosphorus atoms (*S* configuration) in the dichloro and dibromo complexes can be estimated by the following equations, respectively; [Δε(**1a**)−Δε(**1b**)]/2 and [Δε(**2a**)−Δε(**2b**)]/2. (Fig. 5) The calculated curves are very similar in the pattern between the dichloro and dibromo complexes, although the curve of the latter complex shifts to the smaller wavenumber side according to the spectrochemical series. From these curves, it is concluded that the coordinated (*S*)-phosphorus atom shows a positive main CD band in the region of the absorption band of the smallest wavenumbers. On the other hand, the curve of the combined vicinal effect due to both chiral atoms of the carbon and nitrogen can be derived by the equation, [Δε(**1a**)+Δε(**1b**)]/2. The derived curve is shown in Fig. 6 together with the absorption and CD spectra of the related complexes. The curve closely resemble the CD spectrum of **3** in the region of the smallest wavenumber absorption band. The complex **3** has two chiral centers at the carbon and nitrogen atoms with the same *S* chirality as **1a** and **1b**. The curve of the same vicinal effect calculated from **2a** and **2b** also show a pattern similar to that of the dichloro complex. These results indicate that the vicinal effects of the three different chiral atoms are additive in the CD spectra

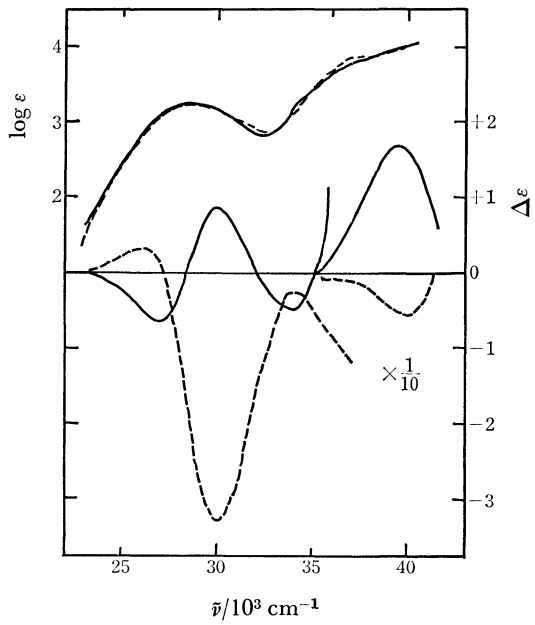

Fig. 3. Absorption and CD spectra of [(*S*)-2-(butylphenylphosphinomethyl)pyrrolidine]dichloropalladium-(II), **1a**(——) and **1b**(----).

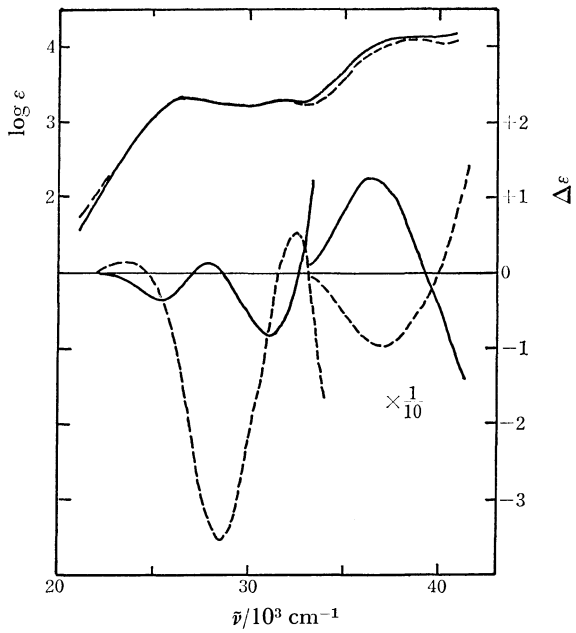

Fig. 4. Absorption and CD spectra of [(*S*)-2-(butylphenylphosphinomethyl)pyrrolidine]dibromopalladium-(II), **2a**(——) and **2b**(----).

TABLE 5. ABSORPTION AND CD SPECTRAL DATA

Complex	Absorption maxima $\tilde{\nu}/10^3$ cm^{-1} (ε/mol^{-1} dm^3 cm^{-1})	CD extrema $\tilde{\nu}/10^3$ cm^{-1} ($\Delta\varepsilon$/mol^{-1} dm^3 cm^{-1})
1a	28.75 (1800)	26.75 (−0.67)
	36.5 (5560 sh[a])	30.0 (+0.86)
		34.0 (−0.49)
		39.6 (+17.0)
1b	28.75 (1790)	26.00 (+0.33)
	37.0 (7270 sh)	30.0 (−3.29)
		40.0 (−5.6)
2a	27.00 (2220)	25.40 (−0.36)
	31.5 (1940)	27.9 (+0.11)
	38.5 (13300)	31.0 (−0.84)
		36.5 (+12.5)
2b	26.75 (2150)	23.50 (+0.16)
	31.4 (1900)	28.6 (−3.52)
	38.5 (12100)	32.7 (+0.54)
		37.0 (−9.57)
3	28.25 (2080)	25.25 (+0.13)
	37.5 (12900)	29.7 (−2.41)
		36.5 (+3.43)
4	26.75 (406)	25.75 (+0.50)
	37.0 (996 sh)	29.0 (−0.28)
		38.3 (+0.41)
5	28.17 (2050)	
	37.2 (13400)	

a) sh: shoulder.

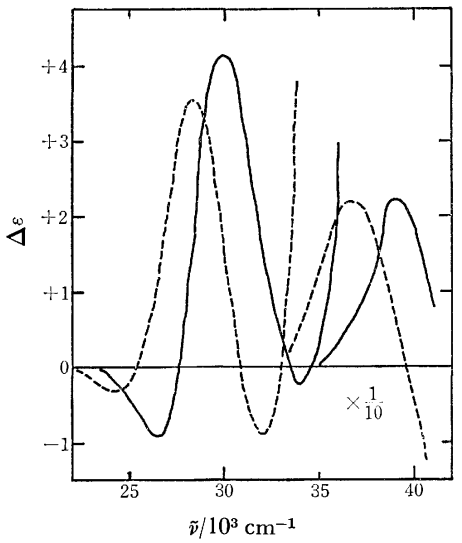

Fig. 5. CD curves calculated from (1/2)[$\Delta\varepsilon$(**1a**)−$\Delta\varepsilon$(**1b**)](——) and (1/2)[$\Delta\varepsilon$(**2a**)−$\Delta\varepsilon$(**2b**)](----).

of the present complexes. The diamine complex (**4**) which has the same chiral atoms as **3** also gives a CD pattern similar to that of **3** in the same region, although the CD intensity of the negative band is very weak.

Meek *et al.*[16] reported that the complex **5** gives absorption bands due to the d-d transitions at *ca.* 21000 cm^{-1}. However, all of the aminophosphine complexes prepared here shows neither absorptions nor

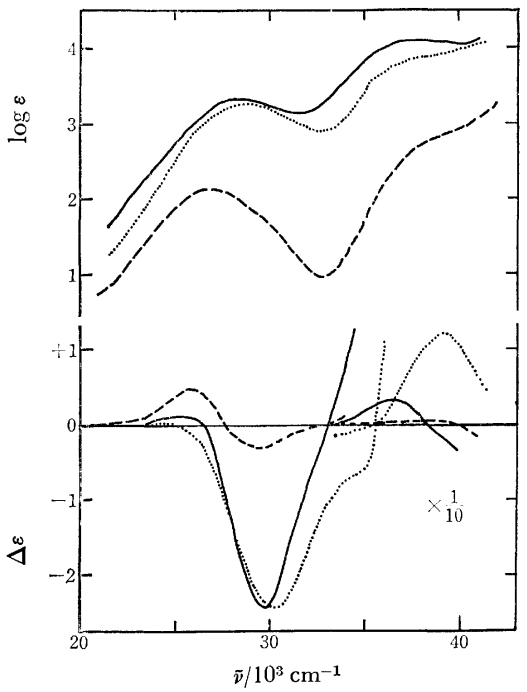

Fig. 6. Absoprtion and CD spectra of [(*S*)-2-(diphenylphosphinomethyl)pyrrolidine]dichloropalladium(II), **3** (——) and [(*S*)-2-(aminomethyl)pyrrolidine]dichloropalladium(II), **4** (----), and CD curve calculated from (1/2)[$\Delta\varepsilon$(**1a**)+$\Delta\varepsilon$(**1b**)] (……).

CD in this region. Therefore, the fairly strong bands at 28000 cm^{-1} of the aminophosphine complexes may be assigned to those associated with the d-d transitions. This assignment will be supported by the fact that the dichloro(diamine)Pd(II) complexes[27] including **4** exhibit similar absorption bands at nearly the same wavenumbers. The nitrogen and phosphorus atoms are known to stand at nearly the same position in the spectrochemical series.[28]

The authors express their thanks to Professor J. Tanaka of Nagoya University, who kindly allowed them to use the diffractometer in his laboratory. The authors also wish to thank the Ministry of Education for Scientific Research Grant-in-Aid No. 243013.

References

1) B. D. Vineyard, W. S. Knowles, M. J. Sabacky, G. L. Bachman, and D. J. Weinkauff, *J. Am. Chem. Soc.*, **99**, 5946 (1977).

2) M. D. Fryzuk and B. Bosnich, *J. Am. Chem. Soc.*, **99**, 6262(1977).

3) T. Hayashi, T. Mise, S. Mitachi, K. Yamamoto, and M. Kumada, *Tetrahedron Lett.*, **1976**, 1133.

4) K. Yamamoto, A. Tomita, and J. Tsuji, *Chem. Lett.*, **1978**, 3.

5) H. B. Kagan, *Pure Appl. Chem.*, **43**, 401 (1975).

6) K. Tani, L. D. Brown, J. Ahmed, J. A. Ibers, M. Yokota, A. Nakamura, and S. Otsuka, *J. Am. Chem. Soc.*, **99**, 7876 (1977).

7) H. B. Kagan and T. P. Dang, *J. Am. Chem. Soc.*, **94**, 6429 (1972).

8) I. Ogata, F. Mizukami, Y. Ikeda, and M. Tanaka, Japan Patent, Kokai, **76**, 43754 (1976); *Chem. Abstr.*, **85**,

124144z(1976).
9) K. Achiwa, *J. Am. Chem. Soc.*, **98**, 8265(1976).
10) W. S. Knowles, M. J. Sabacky, and B. D. Vineyard, *J. Chem. Soc., Chem. Commun.*, **1972**, 10.
11) T. Ito, F. Marumo, and Y. Saito, *Acta Crystallogr., Sect. B*, **27**, 1062 (1971).
12) I. Kinoshita, K. Kashiwabara, and J. Fujita, *Chem. Lett.*, **1977**, 831.
13) S. Schnell and P. Karrer, *Helv. Chim. Acta*, **38**, 2036 (1955).
14) S. Seanles, Jr., G. E. Roelofs, M. Tamres, and R. N. McDonald, *J. Org. Chem.*, **30**, 3445 (1965).
15) R. A. Walton, *Spectrochim. Acta, Part A*, **21**, 1795 (1965).
16) D. W. Meek, P. E. Nicpon, and V. I. Meek, *J. Am. Chem. Soc.*, **92**, 5351 (1970).
17) T. C. Furnas, "Single Crystal Orienter Instruction Manual," General Electric Co., Milwaukee (1956).
18) All the programs used are in the "UNICS-Osaka" system, The Computation Center, Osaka University (1973).
19) "International Tables for X-Ray Crystallography," Kynoch Press, Birmingham (1974), Vol. IV, pp. 72—84.
20) The observed and calculated structure factors are available at the Office of the Editor of the Bulletin of the Chemical Society of Japan as Document No. 7919.
21) O. Kospium, R. A. Lewis, J. Chickos, and K. Mislow, *J. Am. Chem. Soc.*, **90**, 4842(1968); K. Naumann, G. Aon, and K. Mislow, *ibid.*, **91**, 7012 (1969).
22) L. Horner, *Pure Appl. Chem.*, **9**, 225(1964).
23) K. Issleib and H. Oehme, *Chem. Ber.*, **100**, 2685(1967).
24) C. H. Perry, D. P. Athus, E. F. Young, J. R. Durig, and B. R. Mitchell, *Spectrochim. Acta, Part A*, **23**, 1137 (1967).
25) C. K. Johnson, "ORTEP-II," Report ORNL-3794, Oak Ridge National Laboratory, Tennessee (1971).
26) A. Takenaka, Y. Sasada, K. Yamamoto, and J. Tsuji, *Bull. Chem. Soc. Jpn.*, **50**, 3177 (1977).
27) H. Ito, J. Fujita, and K. Saito, *Bull. Chem. Soc. Jpn.*, **42**, 2863 (1969).
28) K. Kashiwabara, I. Kinoshita, and J. Fujita, *Chem. Lett.*, **1978**, 673.

Temperature Dependence of the Optical Resolution and Solubility Isotherm of Bis(ethylenediamine)oxalatocobalt(III) (1*R*,3*S*,4*S*,7*R*)-3-Bromocamphor-9-sulfonate

Akira FUYUHIRO,* Kazuaki YAMANARI, and Yoichi SHIMURA

Department of Chemistry, Faculty of Science, Osaka University, Toyonaka, Osaka 560

(Received December 27, 1978)

The determination of solubility isotherm of a ternary system, *Λ*-[Co(ox)(en)$_2$](*d*-$C_{10}H_{14}OBrSO_3$)–*Λ*-[Co(ox)(en)$_2$](*d*-$C_{10}H_{14}OBrSO_3$)–H_2O, between 5 and 25 °C, revealed that the resolving agent (1*R*,3*S*,4*S*,7*R*)-3-bromocamphor-9-sulfonate ion is applicable to the optical resolution of the $[Co(ox)(en)_2]^+$ ion below 19 °C from the viewpoint of solubility in water, in spite of the formation of a pseudo racemic compound, *Λ*-[Co(ox)(en)$_2$]·*Λ*-[Co(ox)(en)$_2$](*d*-$C_{10}H_{14}OBrSO_3)_2\cdot 2H_2O$.

Some useful informations on optical resolutions have been given from the studies of solubility isotherms for a multi-component system containing a pair of diastereomeric salts of metal complexes[1,2] or organic substances.[3] The previous investigations showed that the formation of a pseudo racemate[1] or solid solutions[3] causes an unsuccessful or difficult optical resolution; for example, the resolving agent, (1*R*, 3*S*,4*S*,7*R*)-3-bromocamphor-9-sulfonate(1−) ion (abbreviated to *d*-bcs$^-$), is not applicable to the optical resolution of $[Co(ox)(en)_2]^+$ ion at 25 °C because of the formation of the pseudo racemate, *Λ*-[Co(ox)(en)$_2$]·*Λ*-[Co(ox)(en)$_2$](*d*-bcs)$_2\cdot 2H_2O$.[1] Successive study to determine the isotherms of the *d*-bcs salts at other temperatures revealed that the optical resolution becomes possible below 19 °C in spite of the formation of the pseudo racemate. Thus the solubility isotherm of the ternary system, *Λ*-[Co(ox)(en)$_2$](*d*-bcs)–*Λ*-[Co(ox)(en)$_2$](*d*-bcs)–H_2O, at 5 °C and the temperature dependence of two invariant points in a region of 5—25 °C are presented here; a short letter of the results was presented elsewhere.[4]

Experimental

Materials. *[Co(ox)(en)$_2$](d-bcs)*: The *Λ*- and *Δ*-diastereomers, and the pseudo racemate were prepared by the method previously reported[1]; ε(497 nm)=120 for each complex, and $\Delta\varepsilon$(523 nm)=+2.71, −2.71, and 0 for the *Λ*- and *Δ*-diastereomers, and the pseudo racemate, respectively. Found: C, 32.47; H, 5.48; N, 9.41%. Calcd for *Λ*-[Co(ox)(en)$_2$](*d*-bcs)·H_2O: C, 32.29; H, 5.42; N, 9.41%. Found: C, 31.93; H, 5.56; N, 9.35%. Calcd for *Λ*-[Co(ox)(en)$_2$](*d*-bcs)·1.5H_2O: C, 31.80; H, 5.50; N, 9.27%. Found: C, 32.30; H, 5.42; N, 9.40%. Calcd for *rac*-[Co(ox)(en)$_2$](*d*-bcs)·H_2O: C, 32.29; H, 5.42; N, 9.41%. The analytical values of the *Λ*-diastereomer corresponded to those of neither tetrahydrate nor 2.5-hydrate[1] but 1.5-hydrate.

Measurements. The solubilities of complexes in water were determined in molality in the same way as previously reported.[2] The solid phases were identified from the elemental analyses, the absorption and CD spectra, and so on. Optical densities were measured with a JASCO UVIDEC-1 spectrophotometer and CD with a JASCO MOE-1 spectropolarimeter.

Results and Discussion

The solubility data obtained are given in Table 1, and Figs. 1 and 2, where any saturated solution is expressed as a point defined by summing up the position vectors of the solubilities of the one or two component salt(s) contained.[2]

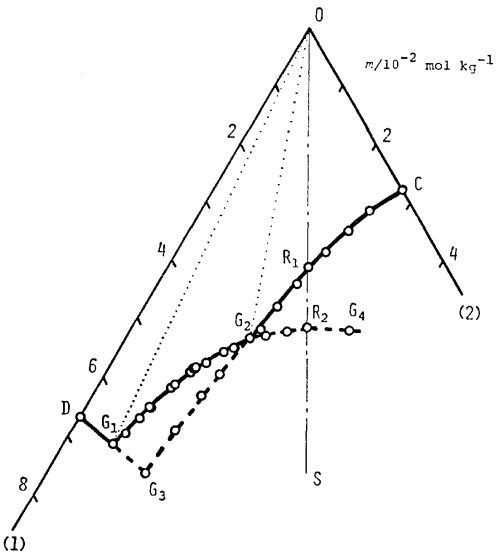

Fig. 1. Solubility isotherm of the ternary system, *Λ*-[Co(ox)(en)$_2$](*d*-bcs)–*Λ*-[Co(ox)(en)$_2$](*d*-bcs)–H_2O, at 5 °C. Solubility is presented in molality *m* of anhydrous salt; *Λ*-[Co(ox)(en)$_2$](*d*-bcs) (1) and *Λ*-[Co(ox)(en)$_2$](*d*-bcs) (2).

Solubility Isotherm of Λ-*[Co(ox)(en)$_2$](d-bcs)*-Δ-*[Co(ox)(en)$_2$](d-bcs)–H_2O at 5 °C.* Figure 1 shows the solubility isotherm of the ternary system, *Λ*-[Co(ox)(en)$_2$](*d*-bcs)–*Λ*-[Co(ox)(en)$_2$](*d*-bcs)–H_2O, at 5 °C. The pseudo racemate, *Λ*-[Co(ox)(en)$_2$]·*Λ*-[Co(ox)(en)$_2$](*d*-bcs)$_2\cdot 2H_2O$, exists in the region G_1G_2 at 5 °C as in the case of 25 °C.[1] At 25 °C the invariant points, G_1 and G_2, appear on the left and the right hand sides of the "racemic line" OS, respectively (see Fig. 2). On the contrary, at 5 °C, both points appear on the left hand side of the "racemic line". Therefore, the isotherms at 5 °C represents the first case that the optical resolution becomes possible in spite of existence of the pseudo racemic compound.

If an aqueous solution of *rac*-[Co(ox)(en)$_2$](*d*-bcs) is concentrated at the constant temperature 5 °C, in other words, if the solution whose composition is on the line OR_1 in Fig. 1 is concentrated, the less soluble diastereomer *Λ*-[Co(ox)(en)$_2$](*d*-bcs)·4H_2O will appear in the solid phase at the point R_1, and then

TABLE 1. EQUILIBRIUM OF THE SYSTEM, Λ-[Co(ox)(en)$_2$](d-bcs)-Λ-[Co(ox)(en)$_2$](d-bcs)-H_2O, AT 5 AND 25 °C, AND THE TEMPERATURE DEPENDENCE OF THE TWO INVARIANT POINTS, G_1 AND G_2

In liquid phase, solubility is presented in molality m of anhydrous salt. Abbreviations are as follows: Λ-[Co(ox)(en)$_2$](d-bcs)·H_2O=Λ, Δ-[Co(ox)(en)$_2$](d-bcs)·$4H_2O$=Δ, and Λ-[Co(ox)(en)$_2$]·Δ-[Co(ox)(en)$_2$](d-bcs)$_2$·$2H_2O$=*rac*; *, metastable state.

T/°C	a)	Liquid phase[b] $m/10^{-2}$ mol kg^{-1} Λ	Liquid phase[b] $m/10^{-2}$ mol kg^{-1} Δ	Solid phase
5	C		2.78 (±0.06)	Δ
	C ↕ G_2	0.66	2.46	
		1.14	2.33	
		1.66	2.18	
		2.04	2.05	
		2.03	2.04	Δ
		2.35	2.04	
		2.84	1.93	
		2.83	1.94	
		3.27	1.89	
	G_2	3.51 (±0.10)	1.79 (±0.08)	Δ + *rac*
	G_4*	1.97*	3.22*	*rac**
	R_2*	2.57*	2.57*	*rac**
	R_2* ↕ G_2	2.89*	2.29*	*rac**
		3.25*	2.02*	
	G_2 ↕ G_1	3.82	1.64	
		3.83	1.66	
		4.00	1.53	
		4.36	1.36	
		4.53	1.23	
		4.55	1.26	
		4.56	1.24	*rac*
		4.66	1.21	
		5.00	1.10	
		5.10	1.06	
		5.53	0.96	
		5.56	0.91	
		5.80	0.86	
		6·11	0.82	
	G_1	6.41 (±0.13)	0.73 (±0.08)	Λ + *rac*
	D	6.65 (±0.03)		Λ
	G_2 ↕ G_3*	4.26*	1.68*	
		4.69*	1.59*	Δ*
		5.38*	1.51*	
	G_3*	6.19* (±0.08)	1.45* (±0.02)	Λ* + Δ*
25	C		5.15 (±0.02)	Δ
	C ↕ G_2	0.72	4.89	
		1.41	4.68	
		1.83	4.55	Δ
		2.18	4.36	
		2.51	4.27	
		2.85	4.19	
	G_2	3.13 (±0.11)	4.13 (±0.06)	Δ + *rac*
	R_4	3.65 (±0.02)	3.65 (±0.02)	*rac*
	R_4 ↕ G_1	3.83	3.50	
		4.67	2.83	
		4.97	2.57	
		5.81	2.10	
		5.99	2.02	
		6.42	1.81	*rac*
		7.27	1.48	
		7.41	1.52	
		7.49	1.48	
		7.54	1.43	
		8.56	1.09	
		8.84	1.11	
	G_1	8.96 (±0.10)	1.06 (±0.08)	Λ + *rac*
	D	9.32 (±0.03)		Λ
10	G_1	6.93	0.78	Λ + *rac*
15	G_1	7.55	0.90	Λ + *rac*
17.5	G_1	7.87	0.93	Λ + *rac*
20	G_1	8.17	0.99	Λ + *rac*
10	G_2	3.39	2.26	Δ + *rac*
15	G_2	3.34	2.75	Δ + *rac*
17.5	G_2	3.31	3.00	Δ + *rac*
20	G_2	3.25	3.39	Δ + *rac*

a) Positions of the points in Figs. 1 and 2. In these expressions, $G_1 \leftrightarrow G_2$, for example, does not contain the points G_1 and G_2. b) The values in parentheses are estimated errors and were calculated from twice the standard deviations of the experimental measurements, which were repeated 3—11 times.

the point of the saturated solution will move along the curve R_1G_2. After the liquid phase composition reaches the point G_2, the less soluble diastereomer will gradually disappear with precipitating the pseudo racemate, Λ-[Co(ox)(en)$_2$]·Δ-[Co(ox)(en)$_2$](d-bcs)$_2$·$2H_2O$, while the liquid phase composition will remain unaltered. Finally, only the solid pseudo racemate will remain. When the solid less soluble diastereomer is removed from the system just before reaching G_2 on the curve R_1G_2, the yield of the diastereomer will be 49% of Δ-[Co(ox)(en)$_2$]$^+$ (25% of the racemic one). Further evaporation will change the composition of the liquid phase from G_2 to G_1 and the second solid, *rac*-[Co(ox)(en)$_2$](d-bcs)·H_2O, will precipitate till the solution composition reaches the point G_1. By separating and re-dissolving this pseudo racemate, successive optical resolution will become possible.

If the initial solution composition is in the region OR_1C in Fig. 1, the isothermal concentration of this solution will also cause the first precipitation of Δ-[Co(ox)(en)$_2$](d-bcs)·$4H_2O$. When the solution composition reaches the point G_2, the second solid,

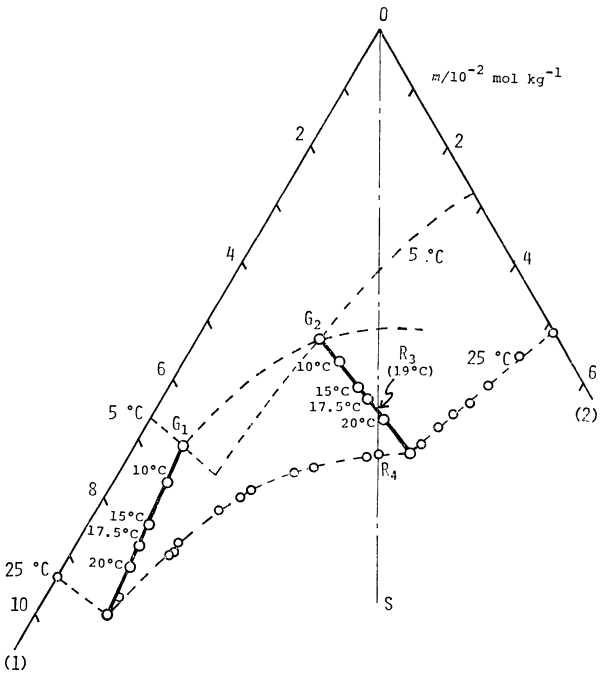

Fig. 2. Temperature dependence of the two invariant points, G_1 and G_2, of the ternary system, *Λ*-[Co(ox)-(en)$_2$](*d*-bcs)–*Λ*-[Co(ox)(en)$_2$](*d*-bcs)–H_2O, at 5—25 °C. Solubility is presented in molality *m* of anhydrous salt; *Λ*-[Co(ox)(en)$_2$](*d*-bcs) (1) and *Λ*-[Co(ox)-(en)$_2$](*d*-bcs) (2).

Λ-[Co(ox)(en)$_2$]·*Λ*-[Co(ox)(en)$_2$](*d*-bcs)$_2$·2H_2O, will begin to precipitate, but the first solid will not completely disappear and both solids will remain to the last. If the initial solution composition is in the region OG_2R_1, the first and the second solids will deposit similarly, and then the solution composition will begin to move along the curve G_2G_1 as soon as all the first solid dissolve in the liquid phase. When the solution composition reaches G_1, the third solid, *Λ*-[Co(ox)(en)$_2$](*d*-bcs)·H_2O, will appear in the system. At last, only the second and the third solids will remain.

Therefore the point G_2 is a kind of "pseudo invariant point", and corresponds to the final liquid phase composition of the right hand region in Fig. 1. Only when the liquid phase composition is in the region OG_1G_2 or on the line OG_2, the pseudo racemic compound, *Λ*-[Co(ox)(en)$_2$]·*Λ*-[Co(ox)(en)$_2$](*d*-bcs)$_2$·2H_2O, deposits as the first precipitation in this system at 5 °C. Thus the pseudo recemate shows the incongruent solubility in water at 5 °C and can be recrystallized at this temperature without decomposition only from an aqueous solution containing an appropriate amount of *Λ*-[Co(ox)(en)$_2$](*d*-bcs) salt.

Certain metastable states which were maintained at least for several hours were observed at 5 °C. On the curve $G_2R_2G_4$ in Fig. 1, the solution is in metastable equilibrium with the solid phase, *Λ*-[Co(ox)(en)$_2$]·*Λ*-[Co(ox)(en)$_2$](*d*-bcs)$_2$·2H_2O, and the point R_2 represents the metastable solubility of the pseudo racemate. The point G_3 corresponds to the metastable invariant point, where both solids, *Λ*-[Co(ox)-(en)$_2$](*d*-bcs)·H_2O and *Λ*-[Co(ox)(en)$_2$](*d*-bcs)·4H_2O, coexist. If the solution composition moves along the curve $R_1G_2G_3$ in an optical resolution, the yield of the *Λ*-diastereomer will increase.

Solubilities of Λ-[*Co(ox)(en)*$_2$](d-*bcs*)–Δ-[*Co(ox)(en)*$_2$]-(d-*bcs*)–H_2O *between 5 and 25 °C.* Figure 2 represents the temperature dependence (5—25 °C) of the two invariant points, G_1 and G_2. The curve of the temperature dependence of G_2 intersects the "racemic line" OS at 19 °C (point R_3). Therefore, the optical resolution using this ternary system becomes possible at temperatures lower than 19 °C. Futhermore, it was found that the solubility data reported previously for *rac*-[Co(ox)(en)$_2$](*d*-bcs)·H_2O at 5, 10, and 15 °C[1] are of metastable states and its value at 5 °C corresponds to the point R_2 in Fig. 1.

The solubility isotherm of the present system at 25 °C has somewhat changed from that previously reported,[1] in which some errors are included with regard to the solubilities of *Λ*-[Co(ox)(en)$_2$](*d*-bcs)·4H_2O, though the principal feature has not altered. Since the phase change in crystals of the *Λ*-diastereomer from the 1.5- or 2.5-hydrate to the tetrahydrate required about half a day with considerable deviations, it seems that the true tetrahydrate was not realized in some determinations of the previous experiment.[1] The corrected data are also given in Table 1.

References

1) Y. Shimura and K. Tsutsui, *Bull. Chem. Soc. Jpn.*, **50**, 145 (1977).
2) A. Fuyuhiro, K. Yamanari, and Y. Shimura, *Bull. Chem. Soc. Jpn.*, **52**, 90 (1979).
3) M. Leclercq and J. Jacques, *Bull. Soc. Chim. Fr.*, **1975**, 2052.
4) A. Fuyuhiro, K. Yamanari, and Y. Shimura, *Chem. Lett.*, **1978**, 1393.

Prefered Orientation and π-Bonding of the Hydroxyl Group in 1,2-Benzocycloalken-3-ols

Nobuo Mori,* Shin-ichi Kasuya, Hitoshi Miyazaki, and Toshiyuki Takezawa
Department of Chemistry, Science University of Tokyo, Shinjuku-ku, Tokyo 162
(Received July 22, 1978)

The various values of ν_{OH} of 1,2-benzocycloalken-3-ols observed in dilute CCl_4 solutions have been explained in terms of the inclination angle of the C–O bond to the plane of the benzene ring (θ) and the conformational isomerism of the OH group with respect to the C–O bond. The ν_{OH} shift caused by OH···π bonding is angle-dependent, *i.e.*, 9 cm^{-1} if θ=50—90°, or 17 cm^{-1} if θ=38—45°.

Intramolecular OH···π bondings have been extensively investigated by IR spectroscopy and have accepted successful application to the conformational and structural elucidation of various systems containing both hydroxyl group and π-source.[1] Oki, Iwamura, *et al.* found the geometry dependence of the π-bonded ν_{OH} or π-bond shift ($\Delta\nu_{OH}$) in biphenyl-2-ols,[2] alkenols,[3] and 2-phenylalkanols.[4] Such dependence has not however been reported in 1-phenylalkanols. The axial and equatorial OH groups of 1,2-benzocyclohexen-3-ols however show π-bonded ν_{OH}'s of 3618 and 3600 cm^{-1} respectively.[4,5]

In the present work, the angular dependence of $\Delta\nu_{OH}$ in a series of 1,2-benzocycloalken-3-ols having different inclination angles between the C–O bond and the plane of the benzene ring (θ's) have been studied. The range of θ has been from 10 to 82°. Table 1 gives the compounds examined and the relevant θ's for the axial and equatorial† C–O bonds (θ_a and θ_e), as measured using Dreiding models. In this work, the cyclopentene, cyclohexene, and cycloheptene rings have been assumed to take the envelope,[6–8] half-chair,[9] and chair conformations,[10–12] respectively. The cyclopentadiene rings of **5**'s have been assumed to be coplanar with the benzene rings.

Table 1. Inclination angles of the C–O bond, θ_a and θ_e (°)

Compound	θ_a	θ_e
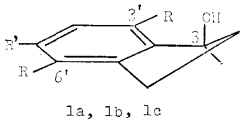 1a, 1b, 1c	75	45
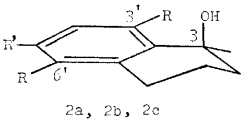 2a, 2b, 2c	82	38
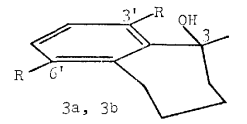 3a, 3b	50	10
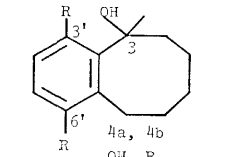 4a, 4b	—	—
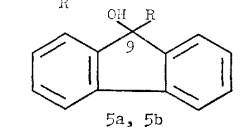 5a, 5b	60	60

Compound number	R	R′
1a—**5a**	H	H
1b—**5b**	CH_3	H
1c and **2c**	H	NO_2

Results and Discussion

Table 2 gives the ν_{OH} data observed in CCl_4, in which each alcohol exhibits at least one maximum at 3600, 3607, 3616, 3620, or 3626 cm^{-1}. The last ν_{OH} is characteristic of monomeric secondary alcohols[13] and the remaining ν_{OH}'s will be assigned later.

In each compound, the prefered orientation of the C–O bond is determined by at least one of the following factors: (1) the interaction between the equatorial hydroxyl group and the *peri*-substituent (*peri*-interaction), (2) 1,3-diaxial and/or other steric interactions, and (3) OH···π bonding. A previous IR study of **2a** and **2b**[5] indicated that an axial orientation, free from factor (1), is prefered. In the IR and NMR studies of substituted 1-tetralols and analogs by Hanaya, *et al.*[14] factor (1) was found to predominate over (2) with a few exceptions. The same will not always apply to the **1**'s and **3**'s, however, since the substituent arrangements in space are different. In the **1**'s where the equatorial hydroxyl and the *peri*-substituent are less eclipsed than in the **2**'s, the *peri*-interaction will be less. In the **3**'s, with the substituents in a more eclipsed position, the *peri*- and also the 1,3-diaxial interactions will be greater. Nevertheless, the prefered orientation will be decided by examining the *peri*-substituent effects on the relative absorption intensities.

The strongest OH bands of **1a** and **1b** appear at 3601 and 3607 cm^{-1} respectively. The shift to higher frequency in **1b** is due to the steric effects of the *peri*-methyl substituent which are expected to cause changes in the population of the OH conformers around the C–O bond and/or conversion of the prefered orientation of the C–O bond. If the former is true and if the most favoured OH conformer of **1a** is that of Type II (see Table 4), this conformer would convert to Type

† In the text, "axial" and "equatorial" mean "quasi-axial" and "quasi-equatorial," respectively.

Table 2. ν_{OH} data for the benzocycloalken-3-ols in dilute CCl_4 solutions (cm^{-1})

Compound	Substituent	Equatorial, bonded ν_{OH}, ε	Axial, bonded ν_{OH}, ε	Free ν_{OH}, ε
1a	—	3601,[b] 52	3616,[b] sh	3627, br[a]
1b	3′,6′-Dimethyl		3607, 60, 20[c]	
			3615, sh	
1c	5′-Nitro	3600, 50	3616, sh	3626, 52
2a[5]	—	3603,[d] 32	3618,[d] 50	
2b[5]	3′,6′-Dimethyl		3610, sh	
			3621, 65	
2c	5′-Nitro	3600, sh	3617, 55	3626, sh
3a	—		3619, 65, 20[c]	3630, br[a]
3b	3′,6′-Dimethyl		3621, 79, 17[c]	
4a	—		3615, 77, 20[c]	
4b	3′,6′-Dimethyl		3620, 80, 18[c]	
5a	—	3601, 110, 14,[c] and 3620, br[a]		
5b	9-Methyl	3599,[e] 140, 11[c]		

a) br: unusually broadened part (ν_{OH} is uncertain). b) Reported: 3594, 3610sh (W. R. Jackson and C. H. McMullen, *J. Chem. Soc.*, **1965**, 1170); 3605, 3620 (J. M. Brewster and J. G. Buta, *J. Am. Chem. Soc.*, **88**, 2233 (1966)). c) Apparent half band width. d) Reported:[4] 3601, 3618. e) Reported: 3602 (A. Allerhand and P. von R. Schleyer, *J. Am. Chem. Soc.*, **85**, 866 (1963)).

Table 3. Chemical shifts (δ) and coupling constants (J) for H(1) of the benzocycloalken-3-ols[a]

Compound	In CCl_4	In $CDCl_3$
1a	4.98, t(J: 5.8, 5.8 Hz)	4.3, t(J: 6, 6 Hz)[15]
2a	4.48, m[c]	3.9, m[15]
3a[b]	4.77, m[d]	4.9, m[15]
4a	4.88, dd(J: 4.5, 11.5 Hz)	—
1b	5.08, dd(J: 2.5, 5.6 Hz)	5.15, dd(J: 2.5, 6.2 Hz)
2b	4.63, t(J: 3.0, 3.0 Hz)	—
3b[b]	5.27, dd(J: 2.5, 6.0 Hz)	5.35, dd(J: 2.5, 6.5 Hz)
4b	5.25, dd(J: 4.5, 9.5 Hz)	—

a) δ of H(1) is concentration-dependent. b) Saturated solution. c) The unresolved multiplet has a width of 12 Hz at the half height and a double intensity at the center relative to the side signals. d) The unresolved multiplet has a width of 12 Hz at the half height.

I by *peri*-methyl substitution, relieving the resulting interaction between the OH hydrogen and *peri*-methyl. This conversion, however, can not explain the observed ν_{OH} shift to higher frequency, since the ν_{OH} of Type I should be lower than that of Type II.[13] Conversion of Type I to II is unlikely. It appears reasonable to assume that **1a** prefers the equatorial C–O orientation (ν_{OH}: 3601 cm^{-1}), not taking into account the question of the prefered OH conformer. The orientation is converted to the axial form (ν_{OH}: 3607 cm^{-1}) by the introduction of the *peri*-methyl group, which relieves the resulting interaction between the equatorial hydroxyl and *peri*-methyl. Both **2a** and **2b** prefer an axial orientation.[4,5] In the case of **3a** and **3b**, the single 3620 cm^{-1} band is practically unchanged by the introduction of the *peri*-methyl group and thus the axial orientation seems to be exclusively prefered.

A comparison of the relative intensities of the axial and equatorial OH bands indicates that the axial orientation is increasingly prefered in the sequence from **1a** to **3a** or with a decrease in θ_e and exclusively prefered in **1b** to **3b**. This result is consistent with the ^1H NMR results (Table 3). Indeed, the J-coupling data for the H(1) of **1a** to **3a** in $CDCl_3$, which are similar to those in CCl_4, suggest the preference for axial orientation in **2a** and **3a** but not in **1a**.[15] The $J_{1,2}$ values for **1b** to **3b** are of a magnitude expected from the Karplus relationship and are very similar to those observed for analogs with equatorial H(1).[8,11,12,16] It appears that the prefered axial orientation is caused predominantly by the *peri*-interaction which becomes greater with decreasing θ_e and increasing size of the *peri*-substituent ($H<CH_3$).

The π-bondings of the axial and the equatorial OH species assigned above may be expected from the considerably low values of ν_{OH}. In fact, the nitro substituent in **1c** and **2c** increases the relative intensity of the free OH band, indicating at least one of the OH species to be π-bonded. Iwamura and Hanaya[4] assigned the 3618 and 3600 cm^{-1} bands of 1,2-benzocyclohexen-3-ols to the axial and equatorial π-bonded OH species, respectively, by taking account of the usual conformational and π-bonding effects on ν_{OH} and expected the π-bond shifts to be 9 and 18 cm^{-1}. On a similar base, the ν_{OH} values in Table 2 may be assigned to Types I, II, and III of the OH conformers,

TABLE 4. TYPES OF OH CONFORMERS AND ASSIGNMENTS OF THE MAXIMUM ν_{OH} BANDS

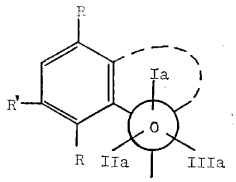

Axial C–O orientation

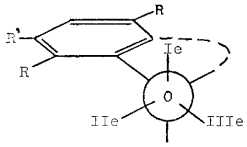

Equatorial C–O orientation

Type of OH conformer	Free ν_{OH} assumed[18]	Compounds **1a—1c**			Compounds **2a—2c**			Compounds **3a, 3b**		
		ν_{OH} observed	$\Delta\nu_{OH}$	$\theta°$	ν_{OH} observed	$\Delta\nu_{OH}$	$\theta°$	ν_{OH} observed	$\Delta\nu_{OH}$	$\theta°$
Ia	3618	3607	11	75	—		82	—		50
IIa	3627	3616sh	11		3618	9		3620	7	
IIIa	3627	3626	1		3626sh	1		—		
Ie	3618	3600	18	45	3602	16	38	—		10
IIe	3627	—			—			—		
IIIe	3627	3626			3626sh	1		—		

as given in Table 4. In each type of conformer, the O–H is assumed to be staggered between the opposing bonds. OH···π bonding occurs in Types I and II in which the OH hydrogen is directed towards the π-cloud. In **1a** to **3a**, Type Ia, in which the O–H is pointing inside the cycloalkene ring, may be sterically unfavorable, since repulsion operates between the OH hydrogen and one or two axial hydrogens on the cycloalkene ring which are in close proximity.[17] In Type IIe also, the OH hydrogen is close to the *peri*-hydrogen. Thus, Types IIa and Ie, in which no overcrowding of the OH hydrogen may be expected, are probably prefered and may largely contribute to the axial and equatorial OH absorptions at 3618 and 3600 cm,$^{-1}$ respectively. The shifts from the free ν_{OH} values ($\Delta\nu_{OH}$)[18] are 7—11 and 16—18 cm^{-1}, respectively, which are ascribable to OH···π bonding.

In **1b** to **3b**, Type IIa may contain an additional interaction between the OH hydrogen and *peri*-methyl. With a decrease of θ_a or in moving from **3b** to **1b**, this interaction will increase and Type IIa becomes less possible, whereas the crowding in Type Ia will be relieved. Thus, the prefered conformer will be IIa in **3b** and **2b** (ν_{OH}: 3620 cm^{-1}; $\Delta\nu_{OH}$: 7 cm^{-1}), but it will be Ia in **1b** (ν_{OH}: 3607 cm^{-1}; $\Delta\nu_{OH}$: 11 cm^{-1}). The weak absorptions at 3610 and 3615 cm^{-1} which **2b** and **1b** exhibit may be assigned to Ia and IIa, respectively, as the less prefered conformers. Benzyl alcohols with θ=90°[19] show π-bonded ν_{OH} (3617 cm^{-1})[13,20] which may be assigned to Type II, so that $\Delta\nu_{OH}$ is 10 cm^{-1}. These results indicate the angular dependence of the π-bond shift: $\Delta\nu_{OH}$ is *ca.* 9 cm^{-1} if θ=50—90°, or *ca.* 17 cm^{-1} if θ=38—45°. **5a** and **5b** (θ=60°) exhibit intense bands at 3600 cm^{-1} which may be assigned to Type I, so that $\Delta\nu_{OH}$ is 18 cm^{-1}. This shift is larger than expected from the above relationship, probably because the OH may be π-bonded with the two benzene rings. The weak 3620 cm^{-1} band of **5a** is probably due to an OH species π-bonded with one benzene ring, so that $\Delta\nu_{OH}$ is 8 cm^{-1}, as expected. The IR and NMR data of **4a** and **4b** are similar to those of **3a** and **3b**. It thus appears that the cyclooctene ring[21] is not as flexible as expected from molecular models.[22] The above relationship between θ and $\Delta\nu_{OH}$ predicts that the C–O bond is axial ($\Delta\nu_{OH}$: 7 or 12 cm^{-1}).

Experimental

Samples. Most of the compounds examined are known substances. 5-Nitroindan-1-ol (**1c**) was prepared from the corresponding ketone by $NaBH_4$ reduction and purified by recrystallization; mp 82.1—82.9 °C; Found: C, 60.43; H, 5.07; N, 7.75%. Calcd for $C_9H_9NO_3$: C, 60.33; H, 5.06; N, 7.82%.

Measurements. IR spectra were recorded on a JASCO DS-403G grating spectrometer. The solvent was CCl_4 distilled over P_2O_5 before use and the concentration selected was *ca.* 0.003 mol/l or less, so as to avoid intermolecular association (cell length: 50 mm). The spectral slit width was 1.5 cm^{-1} at 3600 cm^{-1}.

^{1}H NMR spectra were measured using a JEOL JNM4H-100 spectrometer operating at 100 MHz for *ca.* 10 w/v% solutions in CCl_4 or $CDCl_3$ with TMS as an internal reference. All measurements were carried out at ambient temperature (20—25 °C).

References

1) For a comprehensive review and data of ν_{OH}, see M. Tichý, "Advances in Organic Chemistry," ed by R. A. Raphael, E. C. Taylor, and H. Wynberg, Interscience, New York, N. Y. (1965), Vol. 5, p. 115.

2) M. Oki and H. Iwamura, *J. Am. Chem. Soc.*, **89**, 576 (1967).

3) M. Oki, H. Iwamura, T. Onoda, and M. Iwamura, *Tetrahedron*, **24**, 1905 (1968).

4) H. Iwamura and K. Hanaya, *Bull. Chem. Soc. Jpn.*, **43**, 3901 (1970).

5) N. Mori, M. Yoshifuji, Y. Asabe, and Y. Tsuzuki, *Bull. Chem. Soc. Jpn.*, **44**, 1137 (1971).

6) G. W. Rathjens, *J. Chem. Phys.*, **36**, 2401 (1962); S. S. Butcher and C. C. Costain, *J. Mol. Spectroscopy*, **15**, 40 (1965); J. Laane and R. C. Lord, *J. Chem. Phys.*, **47**, 4941 (1967).

7) M. Hiscock and G. B. Porter, *J. Chem. Soc., B*, **1971**,

1631; W. R. Jackson, C. H. McMullen, R. Spratt, and P. Bladon, *J. Organomet. Chem.*, **4**, 392 (1965); W. E. Rosen, L. Dorfman, and M. P. Linfield, *J. Org. Chem.*, **29**, 1723 (1964).

8) H. R. Buys and E. Havinga, *Tetrahedron*, **24**, 4967 (1968).

9) E. L. Eliel, N. L. Allinger, and G. A. Morrison, "Conformational Analysis," Interscience, New York, N. Y. (1965), p. 109; N. L. Allinger, J. A. Hirsh, M. A. Miller, and I. J. Tyminski, *J. Am. Chem. Soc.*, **90**, 5773 (1968); J. F. Chiang and S. H. Bauer, *ibid.*, **91**, 1898 (1969).

10) S. Kabuss, H. Friebolin, and H. G. Schmidt, *Tetrahedron Lett.*, **1965**, 469; S. Kabuss, H. G. Schmidt, H. Friebolin, and W. Faisst, *Org. Magn. Reson.*, **1**, 451 (1969) and **2**, 19 (1970); N. Neto, C. diLauro, and S. Califano, *Spectrochim. Acta, Part A*, **26**, 1489 (1970).

11) G. L. Buchanan and J. M. McCrae, *Tetrahedron*, **23**, 279 (1967).

12) M. St-Jacques and C. Vaziri, *Org. Magn. Reson.*, **4**, 77 (1972).

13) M. Oki and H. Iwamura, *Bull. Chem. Soc. Jpn.*, **32**, 950, 955 (1959).

14) K. Hanaya, S. Onodera, S. Awano, and H. Kudo, *Bull. Chem. Soc. Jpn.*, **47**, 509 (1974); K. Hanaya, S. Onodera, and H. Kudo, *ibid.*, **47**, 2607 (1974).

15) D. R. Brown and A. B. Turner, *J. Chem. Soc., Perkin Trans.* **2**, **1975**, 1307.

16) S. Mitsui, A. Kasahara, and K. Hanaya, *Bull. Chem. Soc. Jpn.*, **41**, 2526 (1968).

17) Such interaction was assumed to explain the slightly higher value of ν_{OH} for the axial OH group of cyclohexanols; H. S. Aaron and C. P. Rader, *J. Am. Chem. Soc.*, **85**, 3046 (1963); H. S. Aaron, C. P. Ferguson, and C. P. Rader, *ibid.*, **89**, 1431 (1967).

18) In the text, $\Delta\nu_{OH}$ is defined as the difference in ν_{OH} between π-bonded and free OH species both situated in similar steric environments.[3,4] The free ν_{OH}'s for Types I and II are assumed to be 3618 and 3627 cm^{-1}, respectively.

19) J. C. Evans, *Spectrochim. Acta*, **17**, 129 (1961).

20) P. J. Krueger and B. F. Hawkins, *Can. J. Chem.*, **51**, 3250 (1973).

21) Although no reliable experimental estimation has been made for the conformation, strain energy minimization calculations[22,23] predict a nondescript flexible form as the lowest energy conformation.

22) N. L. Allinger and J. T. Sprague, *J. Am. Chem. Soc.*, **94**, 5734 (1972).

23) G. Favini, G. Buemi, and M. Raimondi, *J. Mol. Struct.*, **2**, 137 (1968).

The Regioselective *C*-Hydroxyalkylation of 1,3-Diphenyl-1,3-propanedione with Halo Alcohols, Involving Intramolecular Alcoholysis: the Synthesis of Oxoalkyl Esters†

Hideo Tsutsumi, Kimio Inoue, and Yoshiharu Ishido*

Department of Chemistry, Faculty of Science, Tokyo Institute of Technology, O-okayama, Meguro-ku, Tokyo 152

(Received July 17, 1978)

The reaction of 1,3-diphenyl-1,3-propanedione (**1**) with 2-chloroethanol (**2**) or 3-chloro-1-propanol (**3**) was performed in the presence of potassium carbonate and sodium iodide as an improved procedure for regioselective *C*-hydroxyalkylation, involving intramolecular alcoholysis; the effects of the solvents, the temperature, and the amounts of potassium carbonate and sodium iodide were also investigated. The reaction with **2** afforded 3-benzoylpropyl benzoate (**4**) (*ca.* 70% yield), together with 2-benzoylmethyl-2-phenyl-1,3-dioxolane (**5**) (*ca.* 15% yield). The reaction with **3**, on the other hand, gave 4-benzoylbutyl benzoate (92—94% yield); the corresponding 1,3-dioxane derivative was detected only in a trace. Moreover, the reaction of **1** with 2-hydroxyethyl tosylate was similarly performed, but the yields of both **4** and **5** were unexpectedly low.

The *C*-hydroxyalkylation of 1,3-dicarbonyl compounds was first demonstrated by the reaction of 2,4-pentanedionatosodium with ethylene oxide in ethanol at 0 °C; this gave 3-(2-hydroxyethyl)-2,4-pentanedione (20% yield).[1] On the other hand, the synthesis of methyl ketones has been accomplished by the *C*-alkylation of 2,4-pentanedione with benzyl halides in ethanol in the presence of potassium carbonate, involving simultaneous ethanolysis.[2] Based on these facts, a novel synthetic route to 4-oxoalkanols has been established ; *i.e.*, the reaction of 2,4-pentanedione with 1,2-epoxyoctane in the presence of potassium carbonate and sodium iodide in ethanol under reflux gave a 28% yield of 5-hydroxy-2-undecanone.[3] There have recently been reported the syntheses of some eleven-membered cyclic ketolactones by the *C*-alkylation of 2-substituted dimedones with 4-chloro-2-butenyl acetate in the presence of potassium *t*-butoxide and potassium iodide, followed by the hydrolysis of the esters and intramolecular alcoholysis.[4] On the other hand, we recently demonstrated that the sodium iodide-catalyzed reactions of ethylene carbonate with some active methylene compounds, which are assumed to proceed *via* 2-iodoethanol, afforded the corresponding 4-oxoalkyl esters as predominant products.[5] In view of the mechanism of these reactions, therefore, we set out to develop an improved procedure for a more-highly regioselective and effective *C*-hydroxyaltion of 1,3-dicarbonyl compounds involving intramolecular alcoholysis by the use of 1,3-diphenyl-1,3-propanedione (**1**) and 2-chloroethanol (**2**) or 3-chloro-1-propanol (**3**); we wish now to report our results.

Results and Discussion

Although ethanol has usually been used as a solvent in the alkylation of 1,3-dicarbonyl compounds, we examined a series of solvents for the reaction; a mixture of **1** (10 mmol), **2** (45 mmol), potassium carbonate (10 mmol), and sodium iodide (13 mmol) in a solvent

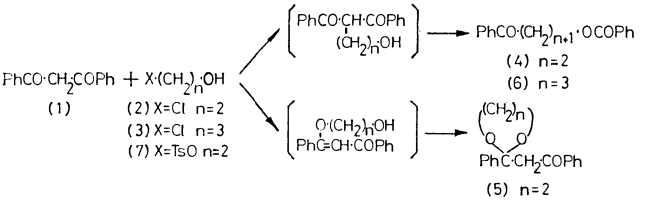

Scheme 1.

Table 1. Examination of solvent effect on the reaction of 1,3-diphenyl-1,3-propanedione (**1**) with 2-chloroethanol (**2**)[a]

Entry	Solvent	Temp (°C)	Yield of product		Recovery of
			4 (%)	**5** (%)	**1** (%)
1	Hexane	80—90	6	—	74
2	Benzene	75—85	trace	—	86
3	Chloroform	80—90	6	—	73
4	Diethyl ether	80—90	—	—	89
5	1,4-Dioxane	80—90	8	2	82
6	Ethyl acetate	85—95	41	trace	53
7	Acetonitrile	70—85	40	trace	44
8	1,2-Dimethoxyethane	85—95	59	trace	26
9	Acetone	80—90	50	trace	38
10	*N*,*N*-Dimethylformamide	80—90	39	7	44
11	Dimethyl sulfoxide	80—90	28	14	22
12	Hexamethylphosphoric triamide	80—90	29	47	20
13[b]	*ditto*	80—90	8	48	34

a) All the reactions were performed by the use of **1** (10 mmol), **2** (45 mmol), K_2CO_3 (10 mmol), and NaI (13 mmol) in a solvent (50 ml). b) This reaction was performed without NaI.

was stirred for 2 days in an autoclave under the conditions given in Table 1. As expected, the products obtained were the same as those formed in the reaction of ethylene carbonate;[5] we obtained small amounts of acetophenone and 2-chloroethyl benzoate in addi-

† This paper was partly presented at 26th International Congress of Pure and Applied Chemistry, Tokyo, Japan, September 4—10, 1977; the Abstract p. 999.

tion to the main products of the corresponding 4-oxoalkyl ester and ethylene acetal derivative, namely, 3-benzoylpropyl benzoate (**4**) and 2-benzoylmethyl-2-phenyl-1,3-dioxolane (**5**). When hexane, benzene, chloroform, diethyl ether, and 1,4-dioxane were used, scarcely none of the benzoate, **4**, was obtained, and the starting material, **1**, was recovered in the yields shown in the table. In contrast with these, ethyl acetate, acetonitrile, 1,2-dimethoxyethane, and acetone were effective for the coupling reaction, giving **4** in 41, 40, 59, and 50% yields respectively, together with traces of **5**. On the increasing polarity of solvents in turn from *N*,*N*-dimethylformamide up to dimethyl sulfoxide and hexamethylphosphoric triamide, however, we obtained **4** (39, 28, and 29% yields respectively) and **5** (7, 14, and 47% yields respectively), in addition to the recoveries of **1** seen in the table. The last entry clearly demonstrated the importance of the addition of sodium iodide to the reaction system, resulting in the formation of **4** in only an 8% yield.

In order to check if an elevated temperature brings about any improvement in the reaction, we performed some of the reactions in acetone, 1,2-dimethoxyethane, acetonitrile, and ethyl acetate at 150 °C. However, no improved results were obtained, giving **4** (49, 28, 21, and 27% yields respectively) and **5** (trace, trace, 9% yield, and trace respectively)(see Table 2). Judging from the yield of **4** and the easy of handling the solvents, it was concluded that it is more advantageous to perform the reaction at around 90 °C in acetone.

Subsequently, the molar proportions of **2** and potassium carbonate in the reaction were examined; the conditions used and the results thus obtained are summarized in Table 3. The results led us to the conclusion that the reaction gives the desired compound, **4**, in 60—71% yields, provided the proportions of **2** and potassium carbonate were 3.75 : 1—1.5 : 1.

The utilization of an excess amount of **2** (75 mmol) in relation to potassium carbonate (2 mmol), however, gave no product at all. This may arise from the predominant reaction of **2** with potassium carbonate, by which the surface of potassium carbonate was covered with the resultant potassium chloride; this may make the potassium carbonate ineffective in the objective reaction. As may be seen from the third entry, the elongation of the reaction time was not fruitful; a 4 day-elongation improved the yield by only 11%. For reference, the reaction in ethyl acetate was checked by the use of 1.5 : 1 **2**–potassium carbonate as is shown in the last entry; this gave **4** (33% yield) in parallel with the results shown in Table 2.

Consequently, the reaction system for a highly regioselective *C*-hydroxyalkylation has been furhter investigated in terms of the reaction involving **3** in

Table 2. The reaction of **1** with **2** in some solvents at an elevated temperature[a]

Entry	Solvent	Yield of product **4** (%)	Yield of product **5** (%)	Recovery of **1** (%)
1	Acetone	49	trace	41
2	1,2-Dimethoxyethane	28	trace	51
3	Acetonitrile	21	9	69
4	Ethyl acetate	27	trace	69

a) All the reactions were performed by the use of **1** (2 mmol), **2** (15 mmol), K_2CO_3 (2 mmol), and NaI (2.7 mmol) in a solvent (20 ml) in an autoclave at 150 °C for 1 day.

Table 3. Examination on effect of the amounts of **2** and K_2CO_3 in the reaction in acetone[a]

Entry	**2** (mmol)	K_2CO_3 (mmol)	Yield of product **4** (%)	Yield of product **5** (%)	Recovery of **1** (%)
1	75	2	—	—	99
2	15	2	18	6	74
3[b]	15	2	29	7	64
4	15	6	69	11	18
5	7.5	2	74	14	12
6	6	2	69	16	14
7	4.5	2	67	14	18
8	3	2	65	13	21
9	6	4	71	17	11
10	3	4	41	10	42
11[c]	6	4	33	3	55

a) All the reactions were performed by the use of **1** (2 mmol) and NaI (2.7 mmol) in acetone (20 ml) at 90 °C for 2 days. b) This reaction was performed for 6 days. c) This reaction was performed in ethyl acetate for the sake of comparison.

Table 4. Reactions of 1,3-diphenyl-1,3-propanedione (**1**) and 3-chloro-1-propanol (**3**) in the presence of potassium carbonate and sodium iodide[a]

Entry	Solvent	**3** (mmol)	Temp (°C)	Period (day[b])	Yield of product **6** (%)	Yield of recovered **1** (%)
1	Acetone	2.3	reflux	2	59	40
2	Acetone	4.6	reflux	2	68	26
3	Acetone	12	reflux	2	71	19
4	Acetone	12	reflux	4	94	trace
5	Acetone	12	90	2	92	—
6	Acetone	12	150	15 h	79	20
7	1,2-Dimethoxyethane	12	reflux	2	80	—

a) All the reactions were performed by the use of **1** (2 mmol), K_2CO_3 (2 mmol), and NaI (2.7 mmol) in a solvent (20 ml). b) Unless otherwise noted.

Table 5. Reactions of 1,3-diphenyl-1,3-propanedione (**1**) with 2-hydroxyethyl tosylate (**7**) in the presence of potassium carbonate and sodium iodide in acetone[a)]

Entry	**7** (mmol)	K_2CO_3 (mmol)	Temp (°C)	Yield of product **4** (%)	Yield of product **5** (%)	Recovery of **1** (%)
1	2.1	4	reflux	10	3	71
2	4.2	4	reflux	21	4	63
3[b)]	2.1	4	reflux	2	20	65
4	2.1	4	90	41	6	41
5	4.2	4	90	35	11	42
6	2.1	8	90	14	5	68

a) All the reaction were performed by the use of **1** (2 mmol) and NaI (2.7 mmol) in acetone (20 ml) for 2 days. b) This reaction was performed without NaI.

place of **2** under the conditions summarized in Table 4. In this case, the reaction was almost regiospecifically induced on the methylene carbon of **1** to give a 92% yield of 4-benzoylbutyl benzoate (**6**) as is shown in the fifth entry. In addition, it should be noticed that this reaction could also be performed in acetone under reflux, giving **6** in a 94% yield together with a trace amount of a by-product which was barely confirmed as 2-benzoylmethyl-2-phenyl-1,3-dioxane by PMR spectroscopy. The sixth entry shows that an elevated temperature is also inadequate for this reaction. Moreover, the reaction in 1,2-dimethoxyethane (Entry 7) also gave **6** in an 80% yield. The mechanism of these reactions is conceivably similar to that proposed in the sodium iodide-catalyzed reaction of ethylene carbonate with **1**[5)] as follows: the chloro-substituent of **2** or **3** may first be replaced by the iodide ion to give the corresponding iodoalkanols, which are then subjected to the coupling reaction with **1** in the presence of potassium carbonate to give the corresponding intermediary 3,3- or 4,4-dibenzoyl-1-alkanol. Subsequently, the resulting dibenzoylalkanols may undergo intramolecular alcoholysis to give **4** or **6** as is depicted in Scheme 1.

Finally, we performed the reaction of 2-hydroxyethyl tosylate (**7**), in place of **2**, with **1** in order to compare it with the above reactions, since **7** seems to behave similarly to **2**, judging from the nucleofugacity of the tosyloxy function. The conditions and the results thus obtained are summarized in Table 5. We observed a similar trend in the yields of **4**, although they were inferior to those obtained in the reactions of **2** with **1**.

Experimental

The PMR spectra were recorded on a Varian T-60 instrument in deuteriochloroform with tetramethylsilane (TMS) as the internal standard. The IR spectra were recorded on a Hitachi 285 spectrophotometer. The column chromatographic separations were performed by the use of Wakogel C-300 (Wako Pure Chemicals, Japan), and TLC, by the use of Merck silica gel 60 F_{254} precoated plates (thickness, 0.25 mm); spots were detected with a UV lamp (S. L. Light, Tokyo Machinery Co., Ltd. 253.7 and 365 nm).

Materials. We purchased commercially 2-chloroethanol (**2**) and 3-chloro-1-propanol (**3**) (Aldrich Chemical Co., Inc.). 1,3-Diphenyl-1,3-propanedione (**1**) was prepared from 1,3-diphenyl-2-propene-1-one according to the method of Allen *et al.*;[6)] mp 77—78 °C (from MeOH) (lit,[6)] 77—78 °C). 2-Hydroxyethyl tosylate (**7**) was prepared according to the method of Rompuy *et al.*;[7)] the PMR spectrum of the product was identical with that of an authetic specimen.

*Examination of the Solvent Effect on the Reaction of **1** with **2**.* A mixture of **1** (2.24 g, 10 mmol), **2** (3 ml, 45 mmol), potassium carbonate (1.40 g, 10 mmol), and sodium iodide (2.0 g, 13 mmol) in a solvent (50 ml) was stirred in an autoclave at 90 °C for 2 days. The resulting mixture was evaporated *in vacuo*, and the residue was triturated with chloroform (50 ml). The supernatant was filtered and evaporated. When DMSO, DMF, or HMPT was used as the solvent, the resulting mixture was made weakly acidific by the use of 1 M (=1 mol dm^{-3}) hydrochloric acid and then extracted with chloroform (20 ml×3). The extracts were combined and evaporated, after drying over anhydrous magnesium sulfate. The syrups thus obtained were subjected to chromatographic separation on a column of silica gel by the use of 1 : 1 v/v benzene-cyclohexane to give 1,3-diphenyl-1,3-propanedione (**1**), 3-benzoylpropyl benzoate (**4**), and 2-benzoylmethyl-2-phenyl-1,3-dioxolane (**5**) in turn. The PMR spectra of these products were superimposable with those of the corresponding authentic specimen.[5)] The results thus obtained are summarized in Table 1.

The Reaction at 150 °C. The products were similarly chromatographed on a column of the silica gel after stirring a mixture of **1** (448 mg, 2 mmol), **2** (1 ml, 15 mmol), K_2CO_3 (280 mg, 2 mmol), and NaI (400 mg, 2.7 mmol) in a solvent at 150 °C for 1 day. The results thus obtained are summarized in Table 2.

*Examination of Appropriate Amounts of **2** and K_2CO_3 in the Reaction.* In acetone, a mixture of the agents as described above with various proportions of **2** and K_2CO_3 was treated in the same way as above; the results thus obtained are summarized in Table 3.

*The Reactions of **1** with **3** in the Presence of K_2CO_3 and NaI.* A mixture of **1** (448 mg, 2 mmol), **3** (2.3—12 mmol), K_2CO_3 (280 mg, 2 mmol), and NaI (400 mg, 2.7 mmol) in a solvent (20 ml) was stirred under reflux, at 90 °C or at 150 °C for 15 h, 2 days, or 4 days in an autoclave. The purification of the products thus obtained was performed in the same way as described above to give **1** and 4-benzoylbutyl benzoate (**6**); IR (NaCl): 1720, 1680, 1270, and 1110 cm^{-1}; PMR ($CDCl_3$-TMS) : δ1.7—2.1 (4H, m, C-CH_2CH_2-C), 3.03* (2H, PhCO-CH_2-), 4.36* (2H, O-CH_2-), and 7.2—8.2 (10 H, m, aromatic). The *J*-values with an asterisk could not be determined by the first-order analysis because of virtual coupling. Found: C, 76.48; H, 6.39%. Calcd for $C_{18}H_{18}O_3$: C, 76.57; H, 6.43%. The results thus obtained are summarized in Table 4.

The Reaction of ***1*** *with* ***7*** *in the Presence of* K_2CO_3 *and NaI.* A mixture of **1** (448 mg, 2 mmol), **7** (2.1 or 4.2 mmol), K_2CO_3 (4 or 8 mmol), and NaI (400 mg, 2.7 mmol) in acetone (20 ml) was treated under reflux or at 90 °C in an autoclave with stirring for 2 days; the solvent was then evaporated after the addition of some water to dissolve the insoluble crystals. The resulting aqueous residue was weakly acidified with 1 M hydrochloric acid, followed by extraction with chloroform (10 ml×3). After the organic layer had been dried over anhydrous sodium sulfate, the filtrate was evaporated; the residue was subjected to chromatographic separation on a column of silica gel. The results thus obtained are summarized in Table 5.

The authors wish to thank the members of the Laboratory of Organic Analysis, Tokyo Institute of Technology, for the elemental analyses, and the Ministry of Education, Japanese Government, for their Scientific Research Grant-in-Aid (No. 947038).

References

1) H. Gault, M. Selm, and N. J. Corre, *C. R. Acad. Sci., Ser. C*, **254**, 2594 (1962); *Chem. Abstr.*, **57**, 2037b (1963).
2) S. Boatman, T. H. Harris, and C. R. Hauser, *J. Org. Chem.*, **30**, 3321 (1965).
3) T.-L. Ho and C. W. Wang, *Experientia*, **29**, 1195 (1973).
4) J. R. Mahajan, *Synthesis*, **1976**, 110; J. R. Mahajan and H. C. Araujo, *Can. J. Chem.*, **55**, 3261 (1977).
5) Y. Ishido, H. Tsutsumi, and S. Inaba, *J. Chem. Soc., Perkin Trans. 1*, **1977**, 521.
6) C. F. H. Allen, R. D. Abel, and J. B. Normington, *Org. Synth.*, Coll. Vol. I, 205 (1944).
7) L. V. Rompuy, N. Schamp, N. D. Kimpe, and R. V. Parijs, *J. Chem. Soc., Perkin Trans. 1*, **1973**, 2503.

Phosphinyl- and Phosphinothioylamino Acids and Peptides. IV. Further Examples of Use of the Diphenylphosphinothioyl Group for the Protection of Amino Acids

Shigeru IKEDA, Fumio TONEGAWA, Etsuro SHIKANO, Kozo SHINOZAKI, and Masaaki UEKI*

Department of Chemistry, Science University of Tokyo, Kagurazaka, Shinjuku-ku, Tokyo 162

(Received July 31, 1978)

The preparation and purification of diphenylphosphinothioyl(Ppt)-amino acids were studied. The side-chain functional groups of tyrosine and cysteine were found to react also with diphenylphosphinothioyl chloride to form *O*-Ppt and *S*-Ppt derivatives. Acidic reagents for the removal of *N*-Ppt group were examined by using *N,O*-bis-Ppt-tyrosine ethyl ester (III) as the most difficult model, HCl in HCO_2H–CH_2Cl_2 being found to be most preferable. The *O*- and *S*-Ppt bonds were stable during the course of acidic treatments, but could be removed by alkaline hydrolysis. An application of Ppt-amino acids to the solid phase peptide synthesis is given.

Selection of the α-amino protecting group is important in working out peptide synthesis because an *N*-terminal elongation strategy is generally favored. Urethane groups such as benzyloxycarbonyl(Z)[1] and *t*-butoxycarbonyl(Boc)[2] have been used since they are superior in selectivity for the removal and prevention of racemization. However, complete prevention of side-reactions by carbonium ions formed during the course of deprotection seems difficult. We have investigated a new series of amino protecting groups not producing such an active species by cleavage.

The phosphazo method[3] is well-known as regards its utilization of the reactivity of trivalent phosphorus-nitrogen compounds with carboxylic acids. The acid lability of P–N bonds decreases in the oxidated state of phosphorus. In fact, the bis(benzyloxy)phosphinylidyne $(C_6H_5CH_2O)_2P(O)$– group has been used as an amino protecting group in the syntheses of amino sugars[4] and peptides.[5] The group can be removed, as in the case of the Z group, by catalytic hydrogenation or hydrogen bromide in acetic acid. In the latter case of deprotection, it is not clear which bond, C–O (a) or P–N (b), is cleaved initially. Recently

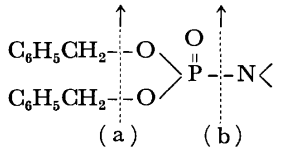

we have used monofunctional phosphinyl, RR'P(O)–, and phosphinothioyl, RR'P(S)–, groups as amino protecting groups and found that they can be removed not only by HBr in acetic acid but also by HCl reagents usually used for the removal of the Boc groups.[6,7] Among various kinds of phosphinyl and phosphinothioyl groups examined the diphenylphosphinothioyl (Ppt) group was thought to be the most useful since diphenylphosphinothioyl chloride can be easily prepared both in laboratories and on an industrial scale starting from benzene and thiophosphoryl chloride by the Friedel-Crafts reaction.[8] This paper gives further examples of the use of the Ppt group for the protection of amino acids.

$$2C_6H_6(\text{benzene}) + S{=}PCl_3 \xrightarrow{AlCl_3} (C_6H_5)_2P(S)\text{-}Cl \quad (\text{Ppt-Cl})$$

$$\text{Ppt-Cl} + H_2N\text{-}CHR\text{-}CO_2R' \xrightarrow{N(C_2H_5)_3} \text{Ppt-NH-CHR-}CO_2R'$$

$$\text{Ppt-NH-CHR-}CO_2R' \xrightarrow[2)\ H^+]{1)\ OH^-} \text{Ppt-NH-CHR-}CO_2H$$

$$\text{Ppt-Cl} + H_2N\text{-}CHR\text{-}CO_2^- \xrightarrow[2)\ H^+]{1)\ OH^-} \text{Ppt-NH-CHR-}CO_2H$$

Ppt-amino acids were prepared by alkaline hydrolysis of Ppt-amino acid esters obtained from Ppt–Cl and amino acid esters.[6] Difficulties in the alkaline hydrolysis of *N*-diisopropoxyphosphinylidyne- and *N*-diphenoxyphosphinylidyneamino acid esters were reported.[9,10] However, no such steric hindrance was encountered in the case of Ppt derivatives. Importance of the Ppt group exists in the direct synthesis of Ppt-amino acids from amino acid betaines.

Phosphinothioyl chlorides are surprisingly resistant to hydrolysis as compared with phosphinyl chlorides.[11] The rate of hydrolysis was accelerated by the addition of a suitable solvent such as dioxane (Fig. 1). Addition of dioxane up to the same volume of water is admissible.

The synthesis of Ppt-amino acids was studied by Schotten-Baumann type reactions in water or aqueous dioxane. An amino acid was dissolved in a 2 M (1 M=1 mol dm^{-3}) NaOH solution and Ppt–Cl was added in one portion. The mixture was stirred vigorously to initiate a rapid reaction within several minutes. Then, 2 M NaOH solution was added, the pH of the solution being kept in the desired range. An 8.5—9.5 pH range was recommended,[6] but yields from

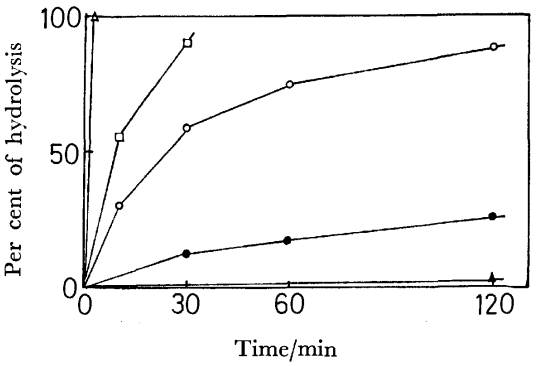

Fig. 1. Rate of hydrolysis of Ppt-Cl in dioxane–water (△: 2/1, □: 1/1, ○: 1/2, ●: 1/5) and in water (▲) at pH 9.5.

reactions in this range were later found to be sometimes poor. This could be attributed to the second reaction of the Ppt-amino acid salt with Ppt–Cl to give the Ppt-amino acid diphenylphosphinothioic anhydride,[12] since better yields were obtained by reactions at higher pH. This was confirmed by isolation of a small amount of dicyclohexylamine salt of Ppt–Gly–Gly–OH, Mp 187—192 °C, Found: C, 63.52; H, 7.46; N, 7.99; P, 5.45%. Calcd for $C_{28}H_{40}N_3O_3PS$: C, 63.53; H, 7.56; N, 7.93; P, 5.85%, from the mother liquor of recrystallization of Ppt–Gly–OH.

Most of the Ppt-amino acids were obtained as free acids which could be easily purified by recrystallization. Complete removal of contaminating diphenylphosphinothioic acid(Ppt–OH) was difficult in the case of oily substances. However, the presence of a small amount of Ppt–OH does not seem to hinder peptide synthesis by the dicyclohexylcarbodiimide (DCC) method since Ppt–OH reacts very rapidly with DCC to produce a stable 1 : 1 adduct.[13] Pure samples of Ppt-amino acids were obtained by utilizing the difference of acid strength of Ppt-amino acids and Ppt–OH. Ppt-amino acids, which are weaker as an acid and more lipophilic than Ppt–OH, can be extracted preferentially by organic solvents from slightly acidic aqueous solution. A considerable amount of dicyclohexylamine(DCHA) salt of Ppt–OH remained without being made free after the usual treatment to regenerate a free Ppt-amino acid from its DCHA salt by shaking with ethyl acetate and 5% aqueous citric acid solution. Ppt-glutamine could be purified by recrystallization from ethyl acetate or by column chromatography on silica gel. When a solution of crude Ppt–Gln–OH in ether saturated with water was passed through a silica gel column, Ppt–Gln–OH was absorbed completely, only Ppt–OH being eluted out. Pure Ppt–Gln–OH was then obtained by eluting with methanol.

In the case of γ-benzyl glutamate and ε-Z-lysine only hydrolysis of Ppt–Cl occurred under the conditions described above. Various conditions were tested; Ppt–Glu(OBzl)–OH can be prepared by using 50% aqueous dioxane as a solvent and triethylamine as a base and isolated in 32% yield as the *t*-butylamine salt.

The reactions of Ppt–Cl with side-chain functional groups were investigated. Alcoholic hydroxyl groups of serine and threonine were not affected by Ppt–Cl since Ppt–Ser–OH and Ppt–Thr–OH were obtained as DCHA salts in 66 and 47% yields, respectively, by the Schotten-Baumann type reactions. Ppt–Ser–OH can be benzylated with benzyl bromide and sodium hydride[14] to give Ppt-*O*-benzyl-serine in 61% yield as the DCHA salt. When tyrosine was treated with 2 molar equiv. of Ppt–Cl under the conditions described above, a mixture of two phosphinothioylated tyrosines was obtained. The mixture was separated by silica gel column chromatography to give *N*-Ppt-tyrosine (I), which was isolated as the DCHA salt, and *N*,*O*-bis-Ppt-tyrosine (II), Mp 117—124 °C, in 6 and 30% yields, respectively. Ethyl tyrosinate also reacted with Ppt–Cl in the presence of triethylamine to give *N*,*O*-bis-Ppt-tyrosine ethyl ester (III) contaminated with *N*-Ppt-tyrosine ethyl ester. When III was hydrolyzed by 1 M NaOH at room temperature for 48 h, both carboxylate ester and phosphinothioate ester bonds were cleaved to afford I in 80% yield. The *O*-Ppt group could also be cleaved slowly by hydrazinolysis.

$$\text{H-Tyr-OH} \xrightarrow[\text{OH}^-]{\text{2 Ppt-Cl}} \underset{\text{(I)}}{\text{Ppt-Tyr-OH}} + \underset{\text{(II)}}{\text{Ppt-Tyr(Ppt)-OH}}$$

$$\text{H-Tyr-OEt} \xrightarrow[\text{N}(C_2H_5)_3]{\text{2 Ppt-Cl}} \underset{\text{(III)}}{\text{Ppt-Tyr-OEt}} + \text{Ppt-Tyr(Ppt)-OEt}$$

The *N*-Ppt group of compound III was found to be unexpectedly slow in cleavage by acidic reagents. Hydrogen bromide in acetic acid could remove the *N*-Ppt group within 5 min, but it took 4 days for complete removal by trifluoroacetic acid–dichloromethane (1/1). Hydrogen chloride in dioxane or acetic acid and triphenylphosphine dihydrochloride solution in dichloromethane[15] were also so impotent that it took more than 2—3 h for complete deprotection. The most preferable reagent for removal of the *N*-Ppt group was HCl in formic acid. When compound III was dissolved in dichloromethane and the same volume of 0.6 M HCl in formic acid was added, complete deprotection took place within 20 min to give *O*-Ppt-tyrosine ethyl ester hydrochloride (IV). These conditions are generally applicable to the removal of *N*-Ppt groups. The *O*-Ppt group was quite stable during the course of acidic treatment since no Pauly positive spot[16] was detected by TLC. The results suggest the possible use of the *O*-Ppt group for the protection of the OH function of tyrosine. This was exemplified in the following synthesis. IV was coupled in the presence of triethylamine with Z–Ser(Bu^t)–OH by DCC to give Z–Ser(Bu^t)–Tyr(Ppt)–OEt(V) in 91% yield. Alternative cleavage of the two *O*-protecting groups was accomplished by alkaline hydrolysis for the *O*-Ppt group and by treatment with trifluoroacetic acid for the *O*-Bu^t group.

$$\text{III} \xrightarrow{0.3\text{M HCl/HCO}_2\text{H-CH}_2\text{Cl}_2(1/1)} \underset{\text{(IV)}}{\text{H-Tyr(Ppt)-OEt}\cdot\text{HCl}}$$

$$\text{Z-Ser(Bu}^t\text{)-OH} + \text{IV} \xrightarrow{\text{DCC}} \underset{\text{(V)}}{\text{Z-Ser(Bu}^t\text{)-Tyr(Ppt)-OEt}}$$

$$\text{V} \begin{cases} \xrightarrow{\text{OH}^-} \text{Z-Ser(Bu}^t\text{)-Tyr-OH} \\ \xrightarrow{F_3CCO_2H} \text{Z-Ser-Tyr(Ppt)-OEt} \end{cases}$$

The SH function of cysteine was more reactive than the amino function with Ppt–Cl. When cysteine methyl ester was treated with equimolar amounts of Ppt–Cl in the presence of triethylamine, *S*-Ppt-cysteine methyl ester hydrochloride (VI) was obtained as the main product. When 2 molar equiv. of the reagent was used, the α-amino group of VI was also phosphinothioylated to give *N*,*S*-bis-Ppt-cysteine methyl ester (VII) in 79% yield. When VI was hydrolyzed by 1 M NaOH in ethanol, selective removal of the methyl ester occurred to give *S*-Ppt-cysteine (VIII) in 61% yield. Stability of the *S*-Ppt group changed

with solvent. When aqueous dioxane was used as a solvent the phosphinothioate ester bond also underwent hydrolysis. However, *N*,*S*-bis-Ppt-cysteine (IX) could be obtained in 12% yield when VIII or cysteine itself was reacted for a short time with Ppt–Cl in aqueous dioxane in the presence of triethylamine. Since the *S*-Ppt group was also stable under the acidic conditions, IX would be useful for the synthesis of cysteine containing peptides.

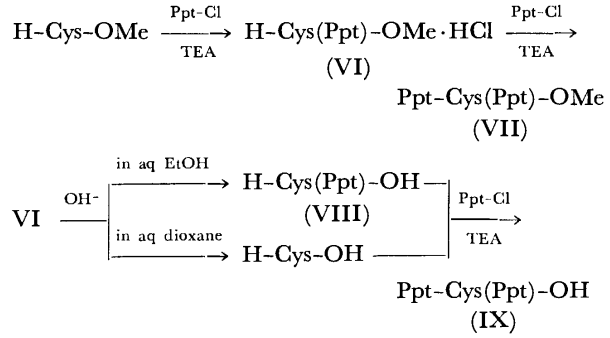

TEA: triethylamine

Arginine reacted very rapidly with Ppt–Cl, but no useful Ppt derivative was obtained probably because of the lactam formation.[17] Since Ppt–Cl is unreactive toward the indole moiety of tryptophan, tryptophan reacted with Ppt–Cl to give Ppt-tryptophan as a sole product. Pure acid was obtained as crystals containing 1 mol of ethanol by recrystallization from ethanol.

The physical properties of Ppt-amino acids prepared in the present experiments are summarized in Table 1.

Coupling of the Ppt-amino acids was successful[6] with use of DCC, mixed anhydride and the oxidation-reduction condensation[18] methods. No steric hindrance was observed in the coupling of the Ppt-amino acids contrary to the case of *N*-trityl-amino acids.[19]

Ppt-amino acids can be used for the solid phase synthesis of peptides.[20] Ppt-glycine was esterified *via* caesium salt[21] to a chloromethylated resin. Deprotection was performed by treatment with 1 M HCl in HCO_2H–CH_2Cl_2(2/1) for 30 min, carried out twice. Couplings were mediated with oxidation-reduction condensation. After incorporation of Ppt–Leu followed by Ppt–Pro, the protected tripeptide

Table 1. Diphenylphosphinothioylamino acids and their salts

Ppt deriv. of	Yield, %[a] (Method)[b]	Mp, (°C)	$[\alpha]_D$[c] (deg.)	TLC R_f[d] A	TLC R_f[d] B	Found (Calcd), % C	H	N	P
Gly	66 (*A*)	118—119		0.53	0.87	57.65 (57.75)	4.53 (4.81)	4.86 (4.81)	10.44 (10.64)
L-Ala	58 (*A*)	120	−13.7	0.55	0.87	58.86 (59.03)	5.31 (5.24)	4.69 (4.57)	10.25 (10.14)
L-Ala·DCHA	e)	177—178	−3.7			67.78 (67.75)	8.06 (8.09)	5.87 (5.75)	6.36 (6.36)
L-Val	62 (*A*)	112—114	−17.5	0.53	0.93	61.12 (61.27)	6.11 (6.00)	4.37 (4.20)	9.33 (9.29)
L-Val·DCHA	e)	149—151	−10.0			67.63 (67.72)	8.33 (8.36)	5.39 (5.44)	5.60 (6.02)
L-Leu	40 (*C*)	60— 70[g]	−17.5	0.52	0.91	59.12 (59.19)[k]	6.41 (6.57)[k]	3.72 (3.83)[k]	8.66 (8.48)[k]
L-Leu·DCHA	e)	137—138	−15.0			67.92 (68.14)	8.78 (8.59)	5.15 (5.29)	6.19 (5.85)
L-Ile·CHA	52 (*E*)	181—183	−7.5	0.54	0.90	64.39 (64.54)	7.89 (7.91)	6.14 (6.27)	6.89 (6.93)
L-Phe·DCHA	75 (*D*)	190—191	+8.7	0.54	0.89	70.72 (70.42)	7.71 (7.71)	5.09 (4.97)	5.30 (5.50)
L-Pro	62 (*A*)	128—130	−15.0	0.52	0.90	61.47 (61.64)	5.45 (5.43)	4.14 (4.22)	9.03 (9.35)
L-Pro·DCHA	e)	194—195	−40.0			67.72 (67.93)	7.87 (8.08)	5.50 (5.46)	5.79 (6.04)
L-Met·DCHA	30 (*D*)	145—146	−1.2	0.52	0.88	63.88 (63.74)	7.84 (7.86)	5.14 (5.12)	5.83 (5.66)
L-Cys(Bzl)·DCHA	30 (*D*)	170—171	+22.5[h]	0.52	0.92	66.96 (67.06)	7.48 (7.46)	4.65 (4.60)	5.00 (5.09)
L-Cys(Ppt)·CHA	12 (*F*)	141—144	+7.5	0.53	0.94	60.36 (60.74)	5.71 (5.82)	4.22 (4.29)	9.18 (9.49)
L-Asp(OBzl)·DCHA	50 (*D*)	156—157	−13.7	0.47	0.96	67.57 (67.75)	7.47 (7.25)	4.51 (4.51)	5.15 (4.99)
L-Glu(OBzl)·TBA	32 (*F*)	94— 98	+10.0	0.53	0.88	63.85 (63.89)	6.93 (6.65)	5.38 (5.32)	5.85 (5.88)
L-Asn	56 (*B*)	163—164 (dec)	−5.0[h]	0.31	0.77	55.19 (55.16)	4.86 (4.93)	7.93 (8.04)	8.79 (8.89)
L-Gln	50 (*B*)	77— 79	+22.5	0.31	0.77	56.04 (56.36)	5.29 (5.24)	7.76 (7.73)	8.38 (8.55)

TABLE 1. (Continued)

Ppt deriv. of	Yield, %[a] (Method)[b]	Mp, (°C)	$[\alpha]_D$[c] (deg.)	TLC R_f[d] A	TLC R_f[d] B	Found (Calcd), % C	H	N	P
L-Gln·DCHA	e)	172—174	+8.7			63.37 (63.05)[i]	7.70 (7.60)[i]	7.74 (7.60)[i]	5.76 (5.60)[i]
L-Ser·DCHA	66 (*D*)	157—158	−5.0	0.29	0.83	64.37 (64.50)	7.80 (7.83)	5.42 (5.57)	6.17 (6.16)
L-Ser(Bzl)·DCHA	39[f]	138—139	+5.0	0.52	0.97	68.74 (68.93)	7.62 (7.59)	4.57 (4.77)	5.25 (5.22)
L-Thr·DCHA	47 (*D*)	147—149	−10.0	0.31	0.84	64.91 (65.08)	8.10 (8.01)	5.39 (5.42)	5.78 (5.99)
L-Tyr·DCHA	6 (*B*)	192—193	−1.2[h]	0.31	0.84	66.18 (66.46)[m]	7.62 (7.54)[m]	4.50 (4.69)[m]	5.12 (5.25)[m]
L-Tyr·(Ppt)	33 (*B*)	117—124	−17.5	0.57	0.93	63.56 (63.68)[n]	4.85 (4.66)[n]	2.01 (2.25)[n]	9.41 (9.95)[n]
L-Tyr(Bzl)·DCHA	43 (*D*)	182—184	+15.0[h]	0.57	0.94	71.89 (71.87)	7.36 (7.33)	4.14 (4.19)	4.62 (4.63)
L-Trp	e)	76— 82	−8.7[j]	0.54	0.92	64.58 (64.39)[o]	5.71 (5.79)[o]	6.05 (6.00)[o]	6.71 (6.64)[o]
L-Trp·DCHA	84 (*E*)	190—191	+7.5			69.74 (69.87)	7.43 (7.31)	6.87 (6.98)	5.33 (5.14)
L-Arg(Tos)	30 (*A*)	199—201	+4.9[j]	0.20	0.84	54.06 (54.26)[p]	5.35 (5.42)[p]	10.29 (10.12)[p]	5.63 (5.60)[p]
L-Arg(NO_2)	61 (*C*)	129—132	+2.5[h]	0.17	0.86	48.23 (48.34)[p]	5.42 (5.22)[q]	15.50 (15.65)[q]	6.86 (6.93)[q]
L-Arg(NO_2)·DCHA	e)	159—161	+5.0[h]			58.08 (58.45)	7.13 (7.30)	13.37 (13.62)	4.94 (5.02)

a) Purified yields. b) Described in Experimental. c) *c* 1 in EtOH unless otherwise stated. d) Solvent systems: A; chloroform: methanol : acetic acid=95 : 5 : 3. B; 1-butanol : acetic acid : water=4 : 1 : 1. e) Pure sample prepared for analytical purpose. f) Yield for the *O*-benzylation. g) Dehydration temperature. h) *c* 1 in MeOH. i) The value we reported previously[23] is corrected. j) *c* 1 in *N*,*N*-dimethylformamide. k) Calcd for $C_{18}H_{22}NO_2PS\cdot H_2O$. l) Calcd for $C_{29}H_{42}N_3O_3PS\cdot 1/2H_2O$. m) Calcd for $C_{33}H_{43}N_2O_3PS\cdot H_2O$. n) Calcd for $C_{33}H_{29}NO_3P_2S_2\cdot 1/2H_2O$. o) Calcd for $C_{23}H_{21}N_2O_2PS\cdot C_2H_5OH$. p) Calcd for $C_{25}H_{29}N_4O_4PS_2\cdot 1/2H_2O$. g) Calcd for $C_{18}H_{22}N_5O_4PS\cdot 1/2H_2O$.

was removed from the resin by transesterification[22] to give Ppt–Pro–Leu–Gly–OMe in 95% yield. No undesirable product, Ppt–Leu–Gly–OMe, was detected by TLC.

Experimental

Diphenylphosphinothioyl chloride (Wako Pure Chemical Ind. Ltd.) was distilled before use.

N-Diphenylphosphinothioylamino acids were prepared by the reaction of diphenylphosphinothioyl chloride and α-amino acids (or α-amino acids bearing a protected side-chain functional group) in aqueous alkaline solution or in aqueous dioxane containing triethylamine. The diphenylphosphinothioylamino acids thus prepared were isolated either as free acids (procedures *A*, *B*, and *C*) or in the form of dicyclohexylamine(DCHA), cyclohexylamine(CHA) or *t*-butylamine(TBA) salt (procedures *D*, *E*, and *F*). They are listed in Table 1.

A. The amino acid (0.85 mol) was dissolved in 400 ml of 2 M NaOH solution. Diphenylphosphinothioyl chloride (214 g, 0.85 mol) was added in one portion and the mixture was stirred vigorously to initiate a rapid reaction within several minutes. 2 M NaOH solution was added at a rate to keep the pH of the solution in the range 9.5—10.0. After the pH change had ended the reaction mixture was diluted with 1 l of water and the remaining chloride was removed by extraction with ethyl acetate. The aqueous layer was acidified to pH 6 with solid citric acid, saturated with NaCl and extracted 3 times with ethyl acetate. Combined ethyl acetate extracts were washed successively with saturated $NaHCO_3$ solution, 5% citric acid solution and saturated NaCl solution, dried over anhydrous Na_2SO_4 and evaporated to give a pasty mass. This was crystallized by trituration with petroleum ether. The crude products were recrystallized from ethyl acetate, ethyl acetate–hexane or benzene–hexane.

B. The amino acid was treated with diphenylphosphinothioyl chloride as described in procedure *A*. The solution was acidified with 5% citric acid solution, ether being added. The resulting precipitate was collected by filtration and washed thoroughly with water and then with ether and dried. In the case of tyrosine, a mixture of *N*,*O*-bis-Ppt-L-tyrosine (II) and *N*-Ppt-L-tyrosine (I) was obtained. The mixture was dissolved in dichloromethane and applied to a silica gel column. II was obtained by elution with the same solvent. Following elution with ether gave I.

C. After synthesis and extraction as described in procedure *A*, dicyclohexylamine was added to the ethyl acetate extracts, the corresponding salt separating out. Sometimes, addition of the same volume of ether was necessary. The product was filtered off and washed with ethyl acetate or ether. The crude salt was shaken vigorously in a separatory funnel with a mixture of ethyl acetate and 5% citric acid solution. After removal of insoluble substance, mainly DCHA salt of diphenylphosphinothioic acid, by filtration, the aqueous layer was separated and extracted twice with ethyl acetate. The combined ethyl acetate extracts were washed with 5% citric acid solution and satu-

rated NaCl solution, dried and evaporated to dryness. Ppt-L-leucine was crystallized as a monohydrate by addition of water and recrystallized from methanol–water.

D. The Ppt-amino acid obtained as in procedure *C* was converted again into the corresponding DCHA salt.

E. After synthesis and extraction as in procedure *A*, cyclohexylamine or dicyclohexylamine was added to the ethyl acetate extracts, the corresponding salt separating out. The product was filtered off, washed with ethyl acetate and recrystallized from methanol or ethanol.

F. The amino acid (0.30 mol) was dissolved in a mixture of 425 ml of water and 425 ml of dioxane by addition of 56 ml (0.4 mol) of triethylamine with vigorous stirring under ice cooling. 90.7 g(0.36 mol) of diphenylphosphinothioyl chloride and 36.4 ml (0.26 mol) of triethylamine in 150 ml of 50% aqueous dioxane were added separately in one portion. Within 5 min a clear solution resulted and was extracted twice with ether. The ether extracts were back extracted with 5% $NaHCO_3$ solution. The combined aqueous solution was acidified to pH 4—5 with 5% citric acid solution and extracted 3 times with ethyl acetate. The ethyl acetate extracts were washed successively with 5% $NaHCO_3$ solution, two portions of 30 ml of 1% $NaHCO_3$ solution, three portions of 150 ml of 5% citric acid solution, two portions of 300 ml of water and saturated NaCl solution. The ethyl acetate layer was dried and concentrated to dryness. The oily residue was dissolved in dichloromethane, applied to a silica gel column (3×40 cm) and eluted with the same solvent (about 1.5 l). After evaporation of the eluate the product was dissolved in ether, the amine shown in Table 1 being added to give the corresponding salt.

Ppt-L-Tyr(Ppt)-OEt (III) and Ppt-L-Tyr-OEt. Ppt-Cl(5.05 g, 20 mmol) was added to a suspension of L-Tyr-OEt·HCl(2.48 g, 10 mmol) in 20 ml of chloroform and 4.2 ml (30 mmol) of triethylamine. After being stirred at room temperature for a day the solution was successively washed with water, 5% citric acid, water, 5% $NaHCO_3$, and water. The chloroform layer was dried and concentrated to dryness. The oily residue was dissolved in benzene, applied to a silica gel column (1.5×30 cm) and eluted with 150 ml of benzene to give III as amorphous white powder; 3.93 g (61%). It was homogeneous chromatographically. $[\alpha]_D$ −10.0° (*c* 1, EtOH); Found: C, 65.81; H, 5.04; N, 2.28%. Calcd for $C_{35}H_{33}NO_3P_2S_2$: C, 65.54; H, 5.14; N, 2.18%. Further elution with CH_2Cl_2 gave Ppt-L-Tyr-OEt; 0.86 g (20%). Mp 93—98 °C; $[\alpha]_D$ −32.5° (*c* 1, EtOH); Found: C, 64.92; H, 5.75; N, 2.90%. Calcd for $C_{23}H_{24}NO_3PS$: C, 64.96; H, 5.64; N, 3.29%.

H-L-Tyr(Ppt)-OEt·HCl (IV). III(0.64 g, 1 mmol) was dissolved in 10 ml of 0.3 M HCl/HCO_2H–CH_2Cl_2(2/1). After being left to stand at room temperature for 30 min the solution was evaporated *in vacuo*, the residue being distributed between water and ether. The layers were separated and the ether layer was extracted with 1 M hydrochloric acid (×5). The combined aqueous extracts were concentrated and dried under reduced pressure over NaOH pellets. The product was triturated with ether to give IV as white crystals; 0.42 g (93%). Mp 137—141 °C; $[\alpha]_D$ +22.5° (*c* 1, EtOH); Found: C, 58.37; H, 5.48; N, 3.07%. Calcd for $C_{23}H_{25}NO_3PSCl\cdot 1/2H_2O$: C, 58.68; H, 5.25; N, 2.97%.

Z-L-Ser(Bu^t)-L-Tyr(Ppt)-OEt (V). IV(0.23 g, 0.5 mmol), Z-L-Ser(Bu^t)-OH(0.15 g, 0.5 mmol) and triethylamine(0.07 ml, 0.5 mmol) were dissolved in 1 ml of chloroform. Dicyclohexylcarbodiimide (0.11 g, 0.5 mmol) was added under stirring at 0 °C. Stirring was continued at 0 °C for 30 min and at room temperature for 12 h. After the usual work-up the product was separated and purified by silica gel preparative layer chromatography to give an oil; 0.33 g (91%). $[\alpha]_D$ +30.0° (*c* 1, EtOH); Found: C, 64.91; H, 6.31; N, 3.86%. Calcd for $C_{38}H_{43}N_2O_7PS$: C, 64.97; H, 6.12; N, 3.99%.

Z-L-Ser-L-Tyr(Ppt)-OEt. V(0.18 g, 0.25 mmol) was treated with anhydrous trifluoroacetic acid(0.25 ml) at 0 °C for 20 min and at room temperature for 2 h. After the removal of trifluoroacetic acid by evaporation *in vacuo* the product was separated and purified by silica gel preparative layer chromatography to give an oil; 0.15 g (91%). $[\alpha]_D$ −5.0° (*c* 1, EtOH); Found: C, 62.71; H, 5.46; N, 4.13%. Calcd for $C_{34}H_{35}N_2O_7PS$: C, 63.17; H, 5.41; N, 4.33%.

Z-L-Ser(Bu^t)-L-Tyr-OH. A solution of 0.14 g (0.2 mmol) of V in 3 ml of ethanol and 0.66 ml of 1 M sodium hydroxide was stirred at room temperature for 3 h. After removal of ethanol *in vacuo* the aqueous solution was extracted with ethyl acetate and acidified to pH 4 with 5% citric acid. The acidified solution was extracted with ethyl acetate. The ethyl acetate extracts were washed with water, dried and concentrated. The oily residue was dissolved in methanol and purified by gel filtration on Sephadex LH-20 (1.7×17 cm) to give a chromatographically homogeneous oil; 0.073 g (80%). $[\alpha]_D$ +40.0° (*c* 1, EtOH); Found: C, 62.04; H, 6.74; N, 6.16%. Calcd for $C_{24}H_{30}N_2O_7\cdot 1/2H_2O$: C, 61.69; H, 6.63; N, 5.99%.

Solid Phase Synthesis of Ppt-L-Pro-L-Leu-Gly-OMe. Chloromethyl resin, prepared by chloromethylating the Bio-Beads S-X1 (Bio-Rad Laboratories), was esterified with Ppt-glycine by means of the caesium salt method(Gly content 0.43 mmol/g). One gram of the ester resin was placed in the reaction vessel of the Beckman model 990 peptide synthesizer. The machine was programmed to perform the following steps automatically: (1) washing three times with CH_2Cl_2, (2) pre-washing with 1 M HCl in HCO_2H–CH_2Cl_2 (2/1), (3) deprotection twice with 1 M HCl in HCO_2-H–CH_2Cl_2 (2/1) for 30 min, (4) washing three times each with CH_2Cl_2, EtOH, and again CH_2Cl_2, (5) neutralization three times with 10% triethylamine in CH_2Cl_2 for 5 min, (6) washing three times with CH_2Cl_2, (7) successive addition of 1.29 mmol each of Ppt-amino acid, tris(*p*-methoxyphenyl)-phosphine and 2,2′-dithiodipyridine in CH_2Cl_2, (8) coupling for 60 min, (9) washing three times with CH_2Cl_2, (10) repetition of steps 7, 8, and 9, (11) washing twice each with *N,N*-dimethylformamide and EtOH. After the completion of coupling the protected peptide was removed from the resin by transesterification with use of 1 M triethylamine in MeOH for 12 h four times. The combined filtrates and washings were evaporated *in vacuo* and the residue was dissolved in ethyl acetate. The solution was washed with water, dried and concentrated to give a pasty mass. This was crystallized slowly by triturating with ether; 0.21 g (95%). Mp 143—144 °C; $[\alpha]_D$ −70.0° (*c* 0.5, EtOH); Found: C, 60.38; H, 6.61; N, 7.89; P, 5.98%. Calcd for $C_{23}H_{34}N_3O_4PS$: C, 60.59; H, 6.59; N, 8.15; P, 6.01%.

References

1) M. Bergmann and L. Zervas, *Chem. Ber.*, **65**, 1192 (1932).
2) L. A. Carpino, *J. Am. Chem. Soc.*, **79**. 98 (1957).
3) S. Goldschmidt and H, Lautenschlager, *Justus Liebigs Ann. Chem.*, **580**, 68(1953); S. Goldschmidt and C. Jutz, *Chem. Ber.*, **86**, 1116 (1953).
4) M. L. Wolfrom, P. J. Conigliaro, and E. J. Soltes, *J. Org. Chem.*, **32**, 653 (1967).
5) L. Zervas and P. Katsoyannis, *J. Am. Chem. Soc.*, **77**, 5351(1955).
6) M. Ueki and S. Ikeda, *Chem. Lett.*, **1976**, 827.

7) M. Ueki and S. Ikeda, Proceedings of the 14th Symposium on Peptide Chemistry (ed by T. Nakajima, Protein Research Foundation, 1977), pp. 1—4.
8) L. Maier, *Helv. Chim. Acta*, **47**, 120(1964).
9) T. Wasner-Jauregg, J. J. O'Nell, and W. H. Summerson, *J. Am. Chem. Soc.*, **73**, 5202 (1951).
10) L. J. Sciarini and J. S. Fruton, *J. Am. Chem. Soc.*, **71**, 2940 (1949).
11) A. A. Neimysheva and I. L. Knunyants, *Zh. Obshch. Khim.*, **36**, 1090 (1966).
12) A. G. Jackson, G. W. Kenner, G. A. Moore, R. Ramage, and W. D. Trop, *Tetrahedron Lett.*, **1976**, 3627.
13) M. Mikołajczyk, P. Kiełbasiński, and Z. Goszczyńska, *J. Org. Chem.*, **42**, 3929(1977).
14) H. Sugano and M. Miyoshi, *J. Org. Chem.*, **41**, 2352 (1976).
15) M. Ueki, S. Ikeda, and F. Tonegawa, Proceedings of the 5th American Peptide Symposium (ed by M. Goodman and J. Meienhofer, John Wiley & Sons, Inc., 1977), pp. 546—548.
16) T. Mann and E. Leone, *Biochem. J.*, **53**, 140 (1953).
17) R. Paul, G. W. Anderson, and F. M. Callahan, *J. Org. Chem.*, **26**, 3347 (1961).
18) T. Mukaiyama, R. Matsueda, and M. Suzuki, *Tetrahedron Lett.*, **1970**, 1901.
19) L. Zervas and D. M. Theodoropoules, *J. Am. Chem. Soc.*, **78**, 1359 (1956).
20) R. B. Merrifield, *J. Am. Chem. Soc.*, **85**, 2149 (1963).
21) B. F. Gisin, *Helv. Chim. Acta*, **56**, 1476 (1973).
22) H. C. Beyerman, H. Hindriks, and E. W. B. de Leer, *J. Chem. Soc., Chem. Commun.*, **1968**, 1668.
23) M. Ueki and S. Ikeda, *Chem. Lett.*, **1977**, 869.

Synthesis of 3-Ethoxycarbonyl-1,2,3,4,5,10-hexahydroindeno[1,2-*d*]azepine

Masaru KIMURA* and Shiro MOROSAWA

Department of Chemistry, Faculty of Science, Okayama University, Tsushima, Okayama 700

(Received August 14, 1978)

3-Ethoxycarbonyl-1,2,3,4,5,10-hexahydroindeno[1,2-*d*]azepine (**10b**) was synthesized from 1-benzylpiperidin-4-one and 1-benzyl-4-[*o*-(hydroxymethyl)phenyl]hexahydroazepin-4-ol. Compound **10b** is of particular interest as an intermediate for the preparation of the hitherto unknown indeno[1,2-*d*]azepine. It was found that 1-ethoxycarbonyl-4-[*o*-(hydroxymethyl)phenyl]hexahydroazepin-4-ol and 1-ethoxycarbonyl-4-[*o*-(hydroxymethyl)-phenyl]piperidin-4-ol (**16b**) give 1-ethoxycarbonylspiro[azepin-4,1′(3*H*′)-isobenzofuran] and 1-ethoxycarbonyl-spiro[3*H*-isobenzofuran-1,4′-piperidine] (**17b**), respectively. Treatment of **16b** with 88% formic acid gave **17b** and 2-ethoxycarbonyl-2,3,4,9-tetrahydro-1*H*-indeno[2,1-*c*]pyridine.

Although several benzazazulenes have been extensively studied in recent years,[1-6] indeno[1,2-*d*]azepine (**1**, 7-azabenz[*a*]azulene) does not seem to have been reported. As the only example of this ring system, 1,2,3,4,5,5a,10,10a-octahydroindeno[1,2-*d*]azepine was reported by Boyakchan *et al.*[6] We wish to report two independent methods A and B for the preparation of the title compound **10a** which might be converted into compound **1** by dehydrogenation.

Method A is characterized by use of **3a**·HCl, the structure of which was determined by X-ray analysis.[7] The structure of the final product **10a** was established as 3-ethoxycarbonyl-1,2,3,4,5,10-hexahydroindeno[1,2-*d*]azepine. The method required 8 steps from **2a**, the overall yield being only 4% on the basis of **2a**. It thus became necessary to develop another facile method for obtaining **10b**.

Recently, Parham *et al.* found that 1-[*o*-(hydroxymethyl)phenyl]cycloheptan-1-ol gives the corresponding 5,6,7,8,9,10-hexahydrobenz[*a*]azulene.[8] We investigated the possibility of preparing **10b** from **14a** according to method B, and attempted application of this method to the preparation of indenopyridine (**18b**, Scheme 2).

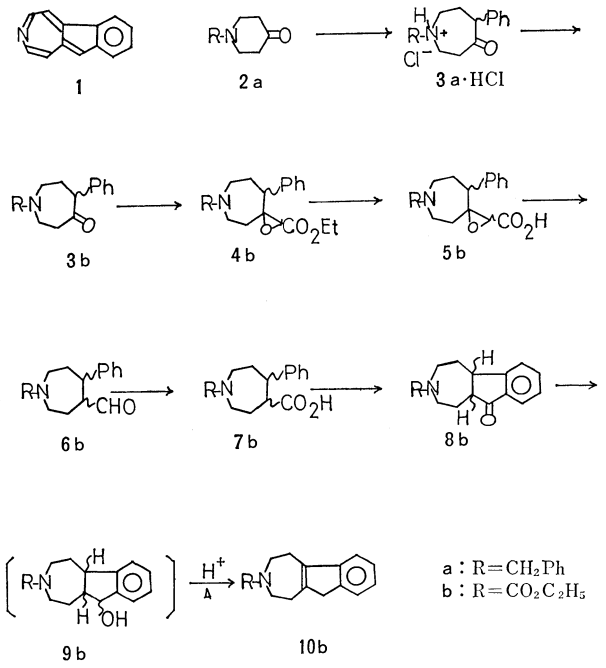

Scheme 1.

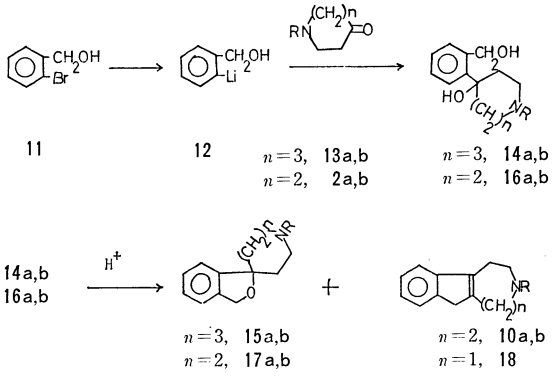

Scheme 2.

Results and Discussion

*Method A. Synthesis of 3-Ethoxycarbonyl-1,2,3,4,5,10-hexahydroindeno[1,2-*d*]azepine (**10b**) from 1-Benzylpiperidin-4-one (**2a**).* 1-Benzyl-5-phenylhexahydroazepin-4-one (**3a**) was obtained by ring expansion of **2a** with ethyl *N*-nitrosobenzylcarbamate in 21% yield. Treatment of **3a**·HCl with ethyl chloroformate gave 1-ethoxycarbonyl-5-phenylhexahydroazepin-4-one (**3b**) quantitatively. Condensation of **3b** with ethyl chloroacetate in the presence of potassium *t*-butoxide by Darzen's method,[10] followed by hydrolysis with KOH in methanol gave the corresponding glycidic acid (**5b**) in 55% yield. When the reaction was stopped in the first step, the corresponding glycidic ester (**4b**) was isolated in 96% yield. Decarboxylation of **5a** at 150—155 °C without a solvent gave 1-ethoxycarbonyl-4-formyl-5-phenylhexahydroazepine (**6b**) in 64% yield. Oxidation of **6a** with silver oxide generated *in situ* gave 1-ethoxycarbonyl-4-phenylhexahydroazepin-5-carboxylic acid (**7b**) in 49% yield. Cyclization of **7b** by the Friedel-Crafts reaction (PCl_5, $SnCl_4$) resulted in the formation of 3-ethoxycarbonyl-1,2,3,4,5,5a,10,10a-octahydroindeno-[1,2-*d*]azepin-10-one (**8b**) in 83% yield. Further transformation of **8b** by hydrogenation ($LiAlH_4$, MeOH), followed by heating with a trace of hydrochloric acid without a solvent at 215 °C gave the indeno-[1,2-*d*]azepine (**10b**, title compound) in 86% yield; the structure of **10b** was deduced by the NMR and IR data and analytical result. The final step from **8b** to **10b** can be explained by acid catalyzed indene formation *via* a transient intermediate **9b** under the above conditions. Indenoazepines, such as **8b** and

10b, are of particular interest as an intermediate in the preparation of the hitherto unknown indeno-[1,2-*d*]azepine (**1**).

Method B. Synthesis of ***10b*** *from 1-Benzyl-4-[o-(hydroxymethyl)phenyl]hexahydroazepin-4-ol (**14a**).* 1-Benzyl- and 1-ethoxycarbonyl-4-[*o*-(hydroxymethyl)-phenyl]hexahydroazepin-4-ol (**14a** and **14b**), and 1-benzyl- and 1-ethoxycarbonyl-4-[*o*-(hydroxymethyl)-phenyl]piperidin-4-ol (**16a** and **16b**) were prepared in a similar way to that employed by Parham and Egberg,[11] as follows. The lithium derivative (**12**) of *o*-bromobenzyl alcohol (**11**) was allowed to react with 1-benzyl- or 1-ethoxycarbonylhexahydroazepin-4-one (**13a** or **13b**), and 1-benzyl- or 1-ethoxycarbonylpiperidin-4-one (**2a** or **2b**) at −40 °C. The usual work-up gave **14a**, **14b**, **16a**, and **16b** in 80, 48, 56, and 31%,[8b] respectively.

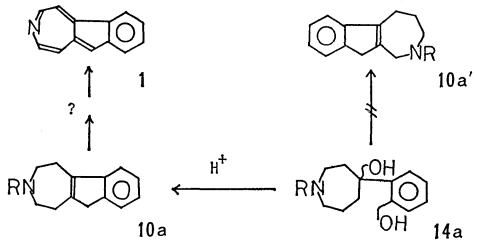

Scheme 3.

The reaction of **14a** in the presence of boron trifluoride etherate in refluxing benzene for 10 h gave indenoazepine (**10a** or **10a'**, Scheme 3) in 10% yield accompanied by 1-benzylspiro[azepine-4,1'(3*H*')-isobenzofuran] (**15a**) in 42% yield. The structure of this indene has two possibilities, since there are two ways to form the indene ring *via* the elimination of water from **14a** as shown in Scheme 3. For the confirmation of the structure, the indene (**10a** or **10a'**) was treated with ethyl chloroformate in refluxing benzene. The expected 1-ethoxycarbonyl-1,2,3,4,5,10-hexahydroindeno[1,2-*d*]azepine (**10b**, title compound) was obtained in 83% yield. **10b** was identified by comparison with the NMR and IR data of the authentic sample obtained by method A. Method B from **14a** requires much shorter steps than method A from **2a**.

On the other hand, the reaction of **14b** and **16b** gave only 1-ethoxycarbonylspiro[azepine-4,1'(3*H*')-isobenzofuran](**15b**) and **17b** in 89 and 49% yields, respectively, under the same conditions as in the case of **14a**. However, the reaction of **16b** in 88% formic acid at 100 °C for 90 min gave 1'-ethoxycarbonylspiro[isobenzofuran-1(3*H*), 4'-piperidine] (**17b**) and the other expected 2-ethoxycarbonyl-2,3,4,9-tetrahydro-1*H*-indeno[2,1-*c*]pyridine (**18b**) in 23 and 30% yields, respectively. **16a** which gave only the corresponding spiro compound (**17a**)[8b] afforded no corresponding indene (**18a**) even in the formic acid at 100 °C.

Experimental

The structures of all the new compounds were confirmed by NMR, IR, and analytical data. All melting points and boiling points are uncorrected. IR (Nujol) spectra were determined on a JASCO IRA-1 grating infrared spectrometer. NMR ($CDCl_3$/TMS, Hitachi-Perkin Elmer R-20) spectra were obtained at 60 MHz. The chemical shifts are represented in terms of δ values. Column chromatography and TLC were performed using Wakogel C-200 and Kieselgel 60F 254, respectively. **2a**, **2b**, **13a**, and **13b** were prepared by the method developed by one of us (S. M).[9]

*HCl Salt of 1-Benzyl-5-phenylhexahydroazepin-4-one (**3a**·HCl).* Ethyl *N*-nitrosobenzyl carbamate (19.8 g, 0.095 mol) was added over a period of 1.5 h to a stirred mixture of freshly distilled 1-benzyl-1-azacyclohexan-4-one (**2a**, 15.5 g, 0.082 mol), finely powdered potassium carbonate (14.5 g) and absolute methanol (8 ml), the reaction temperature being maintained at 25 °C by means of an ice–water bath. The dark red reaction mixture was then allowed to stand at room temperature until the evolution of nitrogen gas ceased (48 h). Ether (50 ml) and water (30 ml) were added to the mixture. After shaking, the two layers were separated. The ethereal solution was washed with saturated aqueous NaCl solution. A white solid appearing in the aqueous layer was collected, washed with a small amount of water and dried in a desiccator (soild KOH). The solid was recrystallized from ethanol to give colorless prisms (**3a**·HCl, 4.5 g, 21%): mp 225 °C (dec); IR 2540, 1710, 760, 740, 700 cm^{-1}; NMR (CCl_4, free **3a**, mp 72 °C) 1.80—3.30 (9H, m), 3.61 (2H, s, $-C\underline{H}_2Ph$), 7.20 (5H, m, aromatic H), 7.28 (5H, m, aromatic H). Found: C, 71.96; H, 6.74; N, 4.62%. Calcd for $C_{19}H_{21}NO$·HCl: C, 72.25; H, 7.02; N, 4.44%.

*1-Ethoxycarbonyl-5-phenylhexahydroazepin-4-one (**3b**).* A mixture of **3a**·HCl (21.76 g, 0.078 mol) and ethyl chloroformate (19.0 g, 0.172 mol) was stirred for 4 h at 140 °C (bath temp). After being cooled to room temperature, excess formate was removed by a rotary evaporator at 50 °C. Benzyl chloride was then distilled at 70—80 °C/20 Torr (9.6 g). Distillation of the residue gave a colorless viscous oil (**3b**, 19.3 g, 95%, bp 171 °C/0.15 Torr): IR (neat) 1700 cm^{-1}(broad); NMR 1.24 (3H, t, J=7Hz), 2.00 (2H, m), 2.70 (2H, m), 2.90—3.65 (2H, m), 3.70—4.40 (3H, m), 4.15 (2H, q, J=7 Hz), 7.28 (5H, m, aromatic H). Found: C, 68.87; H, 7.48; N, 5.16%. Calcd for $C_{15}H_{19}NO_3$: C, 68.94; H, 7.33; N, 5.36%.

*1-Ethoxycarbonyl-5-phenyl-1,2,3,5,6,7-hexahydrospiro[azepine-4(4H),2'-oxirane]-3'-carboxylic Acid (**5b**).* A flask flame-dried at reduced pressure was charged with freshly distilled ethyl chloroacetate (3.07 g, 2.65 mmol) and **3b** (6.98 g, 2.50 mmol). A solution of potassium *t*-butyrate in *t*-butyl alcohol (50 ml, 2.6 mmol) was added from a dropping funnel over a period of *ca.* 30 min to the flask with stirring, the temperature of the reaction mixture being maintained at 10—15 °C on an ice bath. The mixture was stirred for 1—1.5 h at *ca.* 10 °C. Most of the *t*-butyl alcohol was removed by distillation. The oily residue was taken up in ether. The ether solution was washed with water, then with saturated aqueous sodium chloride solution, and was finally dried over anhydrous sodium sulfate. The residue obtained on evaporation of the ether was distilled to give colorless glycidic ester (**4b**, 8.8 g, 96.2%, 195—200 °C/0.2 Torr), ethyl 1-ethoxycarbonyl-5-phenyl-1,2,3,5,6,7-hexahydrospiro[4*H*-azepine-4,2'-oxirane]-3'-carboxylate. IR (neat) 1760 (sh), 1700, 1220, 770, 705 cm^{-1}. No analytical sample could be prepared, since it was partially decomposed during the course of vacuum distillation.

Crude **4b** (8.8 g, 2.5 mmol) was dissolved in a solution of potassium hydroxide (2.65 g, 6.1 mmol) in absolute ethanol (29 ml), and the resulting solution was kept at room temperature under nitrogen atmosphere for 40 min. The mixture was then warmed on a water bath (60 °C) for 7 h, the solvent being evaporated under reduced pressure. The

residue was dissolved in 50 ml of water and extracted with benzene (50 ml). The water layer was acidified with aqueous 10% sulfuric acid, and extracted twice with ether (50 ml portions). After the separation, the ether layer was dried over $MgSO_4$, the solvent being distilled off. A dark-red crude product (**5b**, 6.1 g, 75%) was obtained and crystallized from benzene to give pure **5b** (4.1 g, 56.8%, dec 153 °C): IR 1730, 1630 cm^{-1}; NMR 1.25 (3H, t, J=7 Hz), 1.51—2.28 (4H, m), 2.99—3.95 (5H, m), 4.17 (2H, q, J=7Hz), 7.24(5H, m), 8.45 (1H, bs, COOH). Found: (dried for 3 h at 130 °C): C, 64.20; H, 6.93; N, 4.38%. Calcd for $C_{17}H_{21}NO_5$: C, 63.94; H, 6.63; N, 4.39%.

*1-Ethoxycarbonyl-4-formyl-5-phenylhexahydroazepine (**6b**).* **5b** (2.8 g, 1.0 mmol) was heated on an oil bath (at 150—155 °C) under nitrogen for 4 h. Ether (20 ml) was added. Drying and evaporation of the ether solution gave tan oil. The oil was mixed with 10% sulfuric acid (10 ml) and dioxane (14 ml). The solution was heated under reflux for 14 h. The solution was evaporated under reduced pressure, and the usual work-up gave a reddish residue. The residue was distilled to give **6b** (1.76 g, 64%, 180—183 °C/0 .1 Torr): IR(neat) 1710, 1690 cm^{-1}; NMR 1.24 (3H, t, J=7Hz), 1.59—2.35 (4H, m), 2.59—3.08 (4H, m), 4.14 (2H, q, J=7 Hz), 7.18 (5H, m), 10.29 (1H, s, CHO). Found: C, 69.96; H, 7.86; N, 5.13%. Calcd for $C_{16}H_{21}NO_3$: C, 69.79; H, 7.69; N, 5.09%.

*1-Ethoxycarbonyl-4-phenylhexahydroazepine-5-carboxylic Acid (**7b**).* To a solution of **6b** (2.8 g, 1.1 mmol) and sodium hydroxide (0.79 g, 1.75 mmol) in a mixed solvent (50 ml, ethanol: water=3 : 2) cooled on an ice bath was added a solution of silver nitrate in water (20 ml) in small portions with stirring. The oxidation was complete in *ca.* 5 min after the last addition. The black silver suspension was removed by filtration and washed with several portions of hot water. The cold combined filtrate and washing were acidified with concd hydrochloric acid, a white powder being precipitated out. Recrystallization of this powder from water gave **7b** (2.6 g, 82%, mp 146—147 °C): IR 1720, 1640, 705, 690 cm^{-1}; NMR 1.24 (3H, t, J=7 Hz), 1.60—2.30(4H, b), 2.50—3.10 (2H, b), 3.20—3.90 (4H, b), 4.14 (2H, q, J=7 Hz), 7.18 (5H, s), 10.30 (1H, s, COOH). Found: C, 65.99; H, 6.88; N, 4.54%. Calcd for $C_{16}H_{21}NO_4$: C, 65.96; H, 7.27; N, 4.81%.

*7-Ethoxycarbonyl-4a,5,6,7,8,9,9a,10-octahydro-7-azabenz[a]azulen-10-one (**8b**).* To a suspension of **7b** (1.5 g, 0.55 mmol) in 30 ml of benzene (dried over sodium) was added powdered phosphorus pentachloride (1.14 g, 0.55 mmol) in portions with swirling and cooling on an ice-water bath. After evolution of hydrogen chloride had ceased by the vigorous reaction at 80 °C, all the volatile substances were distilled under reduced pressure at 100 °C. Aluminum chloride (0.5 g, 0.4 mmol) was added to a stirred solution of the residual oily acid chloride in 30 ml of dry benzene at room temperature over a period of 1.5 h. The mixture was then heated at 80 °C for 1.5 h. After being cooled to room temperature, the mixture was poured onto ice and hydrochloric acid, and ether (10 ml) was added for the separation of the layers. The ether layer was concentrated and the product was purified by distillation (**8b**, 1.14 g, 82.6%, bp 180—195 °C/0.1 Torr); IR (neat) 1720, 1680, 770 cm^{-1}; NMR 1.26 (3h, t, J=7Hz), 1.50—3.35 (6H, b), 3.35—3.89 (4H, b), 4.17 (2H, q, J=7 Hz), 7.18—7.91 (4H, m). (the oxime of **8b**, mp 181 °C): Found: C, 66.49; H, 6.99; N, 9.71%. Calcd for $C_{16}H_{20}N_2O_3$: C, 66.65; H, 6.99; N, 9.71%.

*3-Ethoxycarbonyl-1,2,3,4,5,10-hexahydroindeno[1,2-d]azepine (**10b**).* A three-necked flask was charged with 1% aqueous sodium hydroxide (4 ml) and sodium borohydride (0.39 g, 1 mmol) and the system was purged with nitrogen. A solution of the indanone (**8b**, 4.8 g, 1.8 mmol) in methanol (70 ml) was added dropwise over a period of 10—20 min. After addition was complete, the mixture was carefully reheated to reflux for 2 h. The mixture was then cooled on an ice bath, and a sufficient amount of 3 M aqueous hydrochloric acid (50 ml) was carefully added dropwise to decompose excess sodium borohydride. The acidified solution was worked up immediately by extraction with benzene. The benzene extract was washed with saturated aqueous sodium hydrogencarbonate. The benzene solution was dried over anhydrous sodium sulfate, the benzene being removed. The residue was distilled and pressure reduced to give the indene **10b** (4.1 g, 85.4%, bp 215—216 °C/0.23 Torr): IR (neat) 1690, 1600, 760, 720 cm^{-1}; NMR (CCl_4) 1.25(3H, t, J=7Hz, $-CH_3$), 2.50—2.90(4H, b, aliphatic CH_2), 3.25 (2H, s, CH_2 in indene system), 3.45—3.81 (4H, b, aliphatic CH_2N), 4.15 (2H, q, J=7 Hz, CH_2CH_3), 7.02—7.22 (4H, m, aromatic H). Found: C, 74.21; H, 7.51; N, 5.64%. Calcd for $C_{16}H_{19}NO_2$: C, 74.68; H, 7.44; N, 5.44%.

*Reaction of o-Bromobenzyl Alcohol (**11**). Typical Procedure. 1-Benzyl-4-[o-(hydroxymethyl)phenyl]hexahydroazepin-4-ol (**14a**).* Butyllithium (12.2 ml, 3.2 mmol, 2.45 M in hexane) was added to a cold (−40 °C) mixture of **11** (1.3 g, 1.6 mmol) in THF (15 ml) and hexane (10 ml). The mixture was stirred for 5 min at −40 °C and 1-benzylhexahydroazepin-4-one (**13a**, 1.7 g, 0.8 mmol) was added at a rate such that the temperature was maintained at −40 °C for 30 min. The mixture was poured into a large volume of saturated aq NH_4Cl, and extracted with ether. The extract was washed with water, and dried (Na_2SO_4). Removal of the solvent gave a practically pure product. Product **14a** was purified by column chromatography on silica gel eluting with petroleum ether–ethyl acetate (1 : 1): yield 1.83 g (80%); IR (neat) 3360 (OH, hydrogen bonding), and 720 cm^{-1}; NMR (DMSO-d_6) 1.60—2.90 (10 H, two broad peaks, aliphatic CH_2), 3.51 (2H, s, benzylic CH_2N), 4.72 (2H, s, benzylic CH_2O), 4.55—5.32 (2H, bs, alcohol OH), 7.00—7.62 (9H, m, aromatic H). Found: C, 76.83; H, 8.07; N, 4.88%. Calcd for $C_{20}H_{23}NO_2$: C, 77.13; H, 8.09; N, 4.50%.

*1-Ethoxycarbonyl-4-[o-(hydroxymethyl)phenyl]hexahydroazepin-4-ol (**14b**).* The reaction was carried out as described for **14a**. The crude product was purified by preparative TLC (using 50% ethyl acetate in benzene as eluent): **14b**, 47.6%; IR (neat) 3400, 750 cm^{-1}; NMR 1.18 (3H, t, J=7 Hz), 1.50—2.60 (6H, b), 3.00—3.70 (4H, b), 4.06 (2H, q, J=7Hz), 4.30—5.00 (2H, bs, OH), 4.80 (2H, s), 7.10—7.20 (4H, m, aromatic H). Found: C, 65.60; H, 7.82; N, 4.89%. Calcd for $C_{16}H_{23}NO_4$; C, 65.51; H, 7.90; N, 4.78%.

*1-Benzyl-4-[o-(hydroxymethyl)phenyl]piperidin-4-ol (**16a**)* was prepared by the method described in the literature.[8b]

*1-Ethoxycarbonyl-4-[o-(hydroxymethyl)phenyl]piperidin-4-ol (**16b**).* The crude product, obtained in a similar way to that used for **14a**, was crystallized from ethyl acetate to give **16a**: 31.3% yield, mp 113—114 °C; IR 3400, 1670, 750 cm^{-1}; NMR 1.22(3H, t, J=7 Hz), 1.55—3.68 (8H, two broad peaks), 3.95 (2H, s), 4.40 (2H, q), 4.20—5.01 (2H, bs, OH), 7.18—7.28 (4H, m). Found: C, 64.20; H, 7.82; N, 4.91%. Calcd for $C_{15}H_{21}NO_4$: C, 64.49; H, 7.58; N, 5.01%.

*Reaction of **14a**, **14b**, **16a**, and **16b** with Boron Trifluoride Etherate.* 1-Benzylspiro[azepine-4,1′(3*H*′)-isobenzofuran] (**15a**) and 1-benzyl-1,2,3,4,5,10-1*H*-indeno[1,2-*d*]azepine (**10a**). Boron trifluoride etherate (2.0 g, 1.4 mmol) was

added to the benzene (50 ml) solution of **14a** (1.96 g, 0.66 mmol). The reaction mixture was heated to reflux for 2 h. The reaction mixture was poured into a large amount of ice water. The layers were separated and the benzene layer was washed with saturated aqueous sodium hydrogencarbonate followed by water, and dried over $MgSO_4$. The solvent was removed to yield an oil. The oil was chromatographed on silica gel by elution with a mixed solvent (10% ethyl acetate in benzene). From fraction Nos. 17—27, a pale yellow oil (160 mg) was collected . The oil was distilled under reduced pressure to give **10a**: 10% yield, 140—150 °C/0.14 Torr; IR (neat) 1600, 750, 720, 690 cm^{-1}; NMR 2.15—3.10 (8H, two broad peaks), 3.12—3.35 (2H, bs, CH_2 in indene system), 3.76 (2H, s, benzylic CH_2N), 7.00—7.30 (4H, m, aromatic H), 7.32 (5H, m, aromatic H). When **10a** was treated with ethyl chloroformate in refluxing benzene, the less labile oil **10b** was obtained in 83% yield. **10b** was identified by comparison with the sample obtained from **2a** by method A.

*1-Ethoxycarbonylspiro[azepine-4,1'(3H')-isobenzofuran] (**15b**).* The reaction of **14b** was carried out as described for **10a**. The product was purified by preparative TLC (20% ethyl acetate in benzene as eluent). **15b** (R_f=0.38): 89% yield; IR 1690, 1040, 755 cm^{-1}; NMR 1.22(3H, t, J=7 Hz), 1.60—2.50 (6H, b), 2.80—3.90 (4H, b), 4.10 (2H, q, J=7 Hz), 4.98 (2H, s), 6.90—7.30 (4H, m). Found: C, 69.35; H, 7.92; N, 5.03%. Calcd for $C_{16}H_{21}NO_3$: C, 69.79; H, 7.69; N, 5.09%.

*1-Ethoxycarbonylspiro[isobenzofuran-1(3H),4'-piperidine] (**17b**).* The reaction of **16b** was carried out as described for **10a**. The product was purified by preparative TLC (50% chloroform in benzene as eluent). **17b** (R_f=0.4): 43% yield; IR 1700, 1035, 750 cm^{-1}; NMR (CCl_4) 1.24 (3H, t, J=7 Hz), 1.50—1.90 (4H, b), 2.70—4.30 (4H, two broad peaks), 4.10 (2H, q, J=7 Hz), 5.01 (2H, s), 7.00—7.30 (4H, m). Found: C, 69.42; H, 6.63; N, 5.41%. Calcd for $C_{15}H_{17}NO_3$: C, 69.48; H, 6.61; N, 5.40%. The reaction of **16a** was carried out as described for **10a**. When the labile product (**17a**) was treated with ethyl chloroformate in refluxing benzene, **17b** was obtained in 65% yield based on **16a**.

*2-Ethoxycarbonyl-2,3,4,9-tetrahydro-1H-indeno[2,1-c]pyridine (**18b**).* **16b** (0.3 g, 0.11 mmol) was added to 2 ml of 88% formic acid and heated at the reflux temperature for 1.5 h. The reaction mixture was added with stirring to a large amount of ice water and resulting mixture was extracted with benzene. After the usual work-up, the solvent of the extract was removed to give a yellow oil (0.23 g). The crude oil was subjected to preparative TLC on silica gel with 20% ethyl acetate in benzene as eluent. From the first band (R_f=0.55), **18b** was collected: 80 mg, 30% yield; IR (neat) 1695. 1605, 760 cm^{-1}; NMR(CCl_4) 1.26 (3H, t, J=7 Hz), 2.50—3.00 (2H, bt, J=*ca.* 5Hz), 3.24 (2H, bs), 3.40—3.80 (2H, bt, J=*ca.* 5 Hz), 4.24 (2H, q, J=7 Hz), 7.00—7.40 (4H, m). Found: C, 73.92; H, 7.04; N, 5.76%. Calcd for $C_{15}H_{17}NO_2$: C, 74.05; H, 7.04; N, 5.76%. From the second band, **17b** (R_f=0.38) was collected in 23% yield.

When a solution of **16a** in formic acid was refluxed for 1.5 h, only **17a** was obtained. Treatment of **17a** with ethyl chloroformate in refluxing benzene gave **17b** in 90% yield based on **16a**.

References

1) W. Treibs, H. M. Barchet, G. Bach, and W. Kirchhof, *Ann.*, **574**, 54 (1951).

2) G. A. Anderson and J. Tazuma, *J. Am. Chem. Soc.*, **74**, 3455 (1952).

3) T. Nozoe, H. Horino, and T. Toda, *Tetrahedron Lett.*, **1967**, 5349.

4) K. Takase, T. Asao, and N. Hirata, *Bull. Chem. Soc. Jpn.*, **41**, 3027 (1968).

5) K. Yamane and K. Fujimori, *Bull. Chem. Soc. Jpn.*, **49**, 1101 (1976).

6) A. P. Boyakchan, L. L. Oganesyan, and G. T. Tatevosyan, *Khim. Geterotsike. Soedin. (USSR)*, **1974**, 1129.

7) The structure of **3a**·HCl was determined by X-ray analysis. K. Fukuyama, S. Shimizu, S. Kashino, and M. Haisa, *Bull. Chem. Soc. Jpn.*, **47**, 1117 (1974).

8) a) W. E. Parham, L. D. Johnes, and Y. A. Sayed, *J. Org. Chem.*, **41**, 1184 (1976); b) W. E. Parham, D. C. Egberg, Y. A. Sayed, R. W. Thraikill, G. E. Keyser, M. New, W. C. Montgomery, and L. D. Johnes, *ibid.*, **41**, 2628 (1976); c) V. J. Bauer, R. W. Kosley, and W. Raymond (Hoechst A. -G.) D. B. Patent 2458176 (1975) and U. S. Patent 4240080 (1973) cited in *Chem. Abstr.* **83**, 114246d (1975).

9) a) S. Morosawa, *Bull. Chem. Soc. Jpn.*, **31**, 418 (1958); b) S. Morosawa, *ibid.*, **33**, 1113 (1960).

10) M. S. Newman and B. J. Magerlein, *Org. React.*, **5**, 413 (1949).

11) W. E. Parham and D. C. Egberg, *J. Org. Chem.*, **37**, 1545 (1972).

S_N2 Reactions in Dipolar Aprotic Solvents. VIII.[1] Chlorine Isotopic Exchange Reaction of (Arylsulfonyl)chloromethanes, (Arylsulfinyl)chloromethanes, and 2-Chloro-1-arylethanones in Acetonitrile. A Role of the Nucleophile-substrate Interaction in the Finkelstein Reaction

Jun-ichi HAYAMI,*[2] Tohru KOYANAGI, and Aritsune KAJI
Department of Chemistry, Faculty of Science, Kyoto University, Kyoto 606
(Received August 22, 1978)

Chlorine isotopic exchange reactions of substituted chloromethanes [(arylsulfonyl)chloromethanes (**1**), (arylsulfinyl)chloromethanes (**2**), and 2-chloro-1-arylethanones (**4**)] with tetraethylammonium chloride-^{36}Cl were studied in acetonitrile. This study enabled, for the first time, the accurate rate study of the former two classes of compounds (**1** and **2**) of extremely low reactivity. Both the large enthalpies of activation and the positive entropies of activation were the characteristics for these two substrates (**1**-*p*-NO_2 and **2**-*p*-NO_2). High reactivity of 2-chloro-1-phenylethanone was substantiated, and was not associated with the significant secondary kinetic deuterium isotope effect. A nucleophile-substrate association that proceeds the reaction was suggested and the possible role of such an interaction was examined in the light of the intermediary of the nucleophile-substrate complex in the Finkelstein reaction.

The present authors have been investigating the symmetrical Finkelstein reaction between the substituted chloromethanes and radioactive chloride ion in dipolar aprotic solvent.[3] Through the Hammett type analysis of the reaction rates, two factors were pointed out to govern the reactivity of this reaction system: One is the approach of the nucleophile to the substrate, and the other is the electron-donating stabilization of the incipient electro-positive reaction center at the transition state. These findings were accomodated in the framework of the traditional S_N2 reactions.[4]

However, in a recent work, the authors confirmed the presence of an 1 : 1 complex between the substrate and the anionic nucleophile in the Finkelstein reaction mixture. This complex shows many characteristics of the approach of a nucleophile in the S_N2 reactions.[5]

In a separate study, secondary kinetic deuterium isotope effect at the α-hydrogen of the S_N2 reaction center was substantiated for S_N2 substrates of high reactivity.[6] Inverse equilibrium deuterium isotope effects were also found for the substrate-nucleophile association, suggesting that the secondarty isotope effects are explained in terms of the intervention of the complex as the direct precursor of the Finkelstein reaction and in terms of the operation of the electron-donating conjugation at the loose transition state of the unimolecualr scrambling of the complex.[7]

In the present work, chlorine isotopic exchange reactions of (arylsulfonyl)chloromethanes (**1**), (arylsulfinyl)chloromethanes (**2**), and 2-chloro-1-arylethanones (**4**) with tetracthylammonium chloride-^{36}Cl were studied in acetonitrile to get an insight of the rate-controlling factors of the S_N2 reactions.

Results and Discussion

In dry acetonitrile as the solvent, substituted chloromethanes were treated with tetraethylammonium chloride-^{36}Cl as are shown in Scheme 1.

Good second-order kinetics was followed for this isotopic exchange reaction in the every instance. Good

$$X\text{-}C_6H_4\text{-}Y\text{-}CH_2Cl + (C_2H_5)_4N\ ^*Cl \rightleftharpoons X\text{-}C_6H_4\text{-}Y\text{-}CH_2{}^*Cl + (C_2H_5)_4NCl$$

X: a) *p*-NO_2, b) *p*-Cl, c) H, d) *p*-CH_3, e) *p*-CH_3O.
Y: a) SO_2 (**1**), b) SO (**2**), c) CO (**4**).

Scheme 1.

linear free energy relationships held for Hammett σ in each classes of substrates, giving positive ρ values. The accurate rate study for the substrates of diminished reactivity, (arylsulfonyl) and (arylsulfinyl)chloromethanes (**1** and **2**) was achieved for the first time.[8] Results are shown in Table 1.

In Table 2, the second-order rate constants for the substituted chloromethanes with unsubstituted phenyl ring are collected to show the effect of the functional group adjacent to the S_N2 reaction center. Substituent effects on the phenyl moiety are also shown by the Hammett $\rho\sigma$ relationship.

As is shown in Table 2, reactivity spreads in wide range (10^{10}) between the most reactive compound [(phenoxy)chloromethane] and the least reactive one [(phenylsulfonyl)chloromethane]. In 2-chloro-1-arylethanones (**4**), which are about 10^9 times as reactive

Table 1. Observed second-order rate coefficients of symmetrical Finkelstein reactions
$X\text{-}C_6H_4\text{-}Y\text{-}CH_2Cl + (C_2H_5)_4N^{36}Cl$

X	k_{obsd} / $M^{-1}\,min^{-1}$ Y; SO_2[a]	Y; SO[b]	Y; CO[c]
p-NO_2	4.30	5.15	10.4
p-Cl	1.78	1.86	2.71
H	1.24	0.918	1.46
p-CH_3	0.942	0.758	0.962
p-CH_3O	0.801	0.647	0.859
ρ	0.70 (r=0.999)	0.88 (r=0.997)	1.02 (r=0.998)

Throughout this paper, 1 M = 1 mol dm^{-3}, 1 cal_{th} = 4.184 J, °C = K − 273.15. a) At 66.5 °C, $\times 10^6$. b) At 66.5 °C, $\times 10^4$. c) At 0 °C, $\times 10$.

TABLE 2. EFFECT OF THE FUNCTIONAL GROUP ADJACENT TO THE REACTION CENTER. RELATIVE RATES AND ρ VALUES FOR SYMMETRICAL FINKELSTEIN REACTION OF SUBSTITUTED CHLOROMETHANES

(20 °C)

$Ph\text{-}Y\text{-}CH_2Cl + (C_2H_5)_4N^{36}Cl$

Y	$\frac{k_{obsd}}{M^{-1}\,min^{-1}}$	Relative rate	ρ	$\left(\frac{t}{°C}\right)$
O	15.0[a,b]	3.98×10^{10}	−1.56	(−15.9)
CO	1.22	3.24×10^{9}	1.02	(0.0)
S	3.81×10^{-2} [b]	1.01×10^{8}	−0.92	(20.0)
CH=CH	2.54×10^{-2} [b]	6.74×10^{7}	U-shape	(20.0)
NONE	1.23×10^{-2} [b]	3.26×10^{7}	U-shape	(20.0)
C≡C	9.14×10^{-3} [b]	2.42×10^{7}	−0.19	(20.0)
CH_2	3.72×10^{-5} [a,b]	9.87×10^{4}	0.57	(60.0)
SO	1.14×10^{-7} [a]	3.02×10^{2}	0.88	(66.5)
SO_2	3.77×10^{-10} [a]	1.00	0.70	(66.5)

a) Calculated from the data at other temperatures.
b) Ref. 3.

as (arylsulfonyl)chloromethanes (**1**), electron-withdrawing groups on the phenyl ring facilitate the isotope exchange raection. While in all the other reactive substrates studied [especially in (arylthio)chloromethanes (**3**) and (aryloxy)chloromethanes] the effect of the substituent on the phenyl ring is reversed. Therefore, a quite different accelerating factor seems to be operative in the reaction of the halo ketone **4**.

Reaction of 2-Chloro-1-Arylethanone (4). A marked reactivity was shown by 2-chloro-1-arylethanones, which were about 10^7—10^9 times more reactive than (arylsulfinyl)chloromethanes, and (arylsulfonyl)-chloromethanes.

The enhanced reactivity of an α-halo carbonyl compound is often cited[9] and is a matter of controversy considering the presence of the carbonyl group which is an electron-withdrawing group as effective as the sulfinyl and sulfonyl groups.[10]

To get the insight of the reactivity of the 2-chloro-1-arylethanones **4**, substrate–nucleophile interaction was examined first, as the importance of the approach of the nucleophile was implicated by the positive ρ_{obsd}.

On the addition of nucleophile, chloride ion, to the solution of 2-chloro-1-arylethanone in acetonitrile, a significant PMR shift was observed.[5b] As are shown in the left side column of Table 3 for 2-chloro-1-phenylethanone (**4**-H), the representative compound of the class, the enthalpy of formation of the complex ($\Delta H°$) was the most negative among the substrates studied, implicating some interaction other than hydrogen bonding.[11] However, this stabilization (deactivation) is counterbalanced by the extensive decrease in the entropy of formation of the complex ($\Delta S°$) giving rise a fairly small formation constant for the nucleophile-substrate association (Tables 4 and 5).[5b]

A study on the proton spin-lattice relaxation time (T_1) suggested that such a large decrease of the entropy

TABLE 3. ACTIVATION PARAMETERS AND THERMODYNAMIC PARAMETERS IN THE SYMMETRICAL FINKELSTEIN REACTION

Y	$\Delta H°$ [a] kcal·mol^{-1} ($\rho°$)	$\Delta S°$ [a,b] eu	ΔH_1^* kcal·mol^{-1} (ρ_1)	ΔS_1^* [b] eu	ΔH_{obsd}^* kcal·mol^{-1} (ρ_{obsd})	ΔS_{obsd}^* [b] eu
	(a) $Ph\text{-}Y\text{-}CH_2Cl + (C_2H_5)_4N^{36}Cl$					
CO	-4.3_0	$-18._1$	21.0	$6._8$	16.7[c]	$-11._3$[c]
[**4**-H]	(0.52)		(0.50)		(1.02)	
	(b) Substrates with sulfur-containing functional groups $p\text{-}NO_2\text{-}C_6H_4\text{-}Y\text{-}CH_2Cl + (C_2H_5)_4N^{36}Cl$					
SO_2	-1.2_2	$-3._5$	35.1	$12._0$	33.9	$8._5$
[**1**-*p*-NO_2]	(0.54)		(0.16)		(0.70)	
SO	-1.4_0	$-4._2$	30.0	$6._6$	28.6	$2._4$
[**2**-*p*-NO_2]	(0.66)		(0.22)		(0.88)	
S	-1.7_5	$-7._2$	21.3	$-2._8$	19.5	$-10._0$
[**3**-*p*-NO_2]	(0.59)		(−1.51)		(−0.92)	

$\Delta H°$, $\Delta S°$, $\rho°$ are for the association equilibria, ΔH_1^*, ΔS_1^*, ρ_1 are for the rate-determining scrambling in the postulated scheme 2, and ΔH_{obsd}^*, ΔS_{obsd}^*, ρ_{obsd} are for the overall isotope exchange reaction.

a) Throughout this paper, errors for $\Delta H°$ and $\Delta S°$ are estimated to be within 0.5 kcal/mol, and with in 2 eu.

b) At 20 °C. c) $K_{obsd}/M^{-1}\,min^{-1}$: 1.46×10^{-1} (0.0 °C); 4.20×10^{-1} (10.0 °C); 1.22 (20.0 °C). $k_2/M^{-1}\,min^{-1}$: 1.50×10^{-1} (0.0 °C); 4.25×10^{-1} (10.0 °C); 1.23 (20.0 °C). Errors for ΔH_{obsd}^* and ΔS_{obsd}^* are estimated to be within 0.5 kcal/mol, and within 2 eu.

* $k_2 = k_{obsd}\times ab/(a-x)(b-x)$, $x/(a-x)(b-x) = K$

where a=chemical concentration of the substrate [0.1 M for $X\text{-}C_6H_4\text{-}Y\text{-}CH_2Cl$; Y=$SO_2$, SO, and S. 0.05 M for $X\text{-}C_6H_4\text{-}CO\text{-}CH_2Cl$], b=chemical concentration of the nucleophile ($^{36}Cl^-$) [0.1 M for $X\text{-}C_6H_4\text{-}Y\text{-}CH_2Cl$; Y=$SO_2$, SO, and S. 0.05 M for $X\text{-}C_6H_4\text{-}CO\text{-}CH_2Cl$], x=chemical concentration of the association complex, K=formation constant of the association complex.

** k_2 is the second-order rate constant corrected for the decrease in the concentration of both the free nucleophile and the free substrate on the formation of complex. Such correction gave essentially no effect on the Arrhenius parameters.

on complexing was accompanied by the extensive freezing of the intramolecular rotation in the substrate.[11] The examination of the limiting PMR shift and of the thermodynamic parameters of the association equilibria pointed out the possibility that the nucleophilic anion interacts with the carbonyl group, as well as with the α-methylene protons.[11]

Another indication of such an interaction was obtained by the ^{13}C-NMR study. Carbon-13 NMR (CMR) spectra were obtained for 2-chloro-1-phenylethanone-1-^{13}C (C_6H_5–^{13}CO–CH_2Cl), with phenylchloromethane-1-^{13}C (C_6H_5–$^{13}CH_2Cl$) as the reference compound. As are shown in Table 4, α-methylene carbon of phenylchloromethane, carbon at the potential reaction center, showed no significant CMR shift (about 0.1 ppm or less) by the addition of chloride ion.

Table 4. ^{13}C-NMR shift induced by the formation of complex

Ph–Y–CH_2Cl + $(C_2H_5)_4NCl$[a]

Y	δ [b] ppm	δ [c] ppm	δ_c [d] ppm
NONE (Ph–$^{13}CH_2Cl$)	47.2	47.3	(<0.5)
CO (Ph–^{13}CO–CH_2Cl)	192.2	193.3	8.3

a) At 25 °C, in acetonitrile-d_3. b) δ from TMS. 0.1 M standard solution. c) δ from TMS. TEA-Cl (1.0 M) is added to the standard solution. d) $\delta_c=\delta/f$; "f" is the fraction of the complexed substrate. K/M^{-1} (25 °C); 0.132 (Ph–$^{13}CH_2Cl$), 0.157 (Ph–^{13}CO–CH_2Cl).

On the other hand, carbonyl carbon of 2-chloro-1-phenylethanone, located at α-position to the reaction center, gave the low field shift, amounting to 1.1 ppm, on the addition of tetraethylammonium chloride (1.0 M). The amount of the shift is evidently larger than the errors inherent in the present CMR measurements (±0.1 ppm).[12]

When correction is made of the fraction of the complex in the equilibrium, with the due assumption that the equilibration is rapid for the time scale of the NMR spectroscopy, the limiting shift of the complex of 8.3 ppm is obtained for 2-chloro-1-phenylethanone. In PMR spectra, α-methylene proton of this substrate showed limiting complexing shift of −1.52 ppm, indicating the attacking nucleophile resides in the proximity of the methylene protons, at the site of the potential S_N2 displacement.[5b]

These results suggest that, preceding the isotopic exchange reaction, a nucleophilic anion coordinates to both α-methylene protons and the carbonyl group. Hindrance of the internal rotation thus sets in, as reflected on the sharp decrease in ΔS° and the increase in the rotational correlation time (τ_c) of the substrate in the complex.[5b]

Thus, a quite similar structure to that of the transition state of the nucleophilic displacement reaction accompanying "orbital overlap" is suggested for the nucleophile-substrate complex of **4**. In this complex, a coordination of the nucleophile is already accomplished and the "entropy activation", necessary for the S_N2 reaction to take place, is essentially attained.[9a,13]

There seems to be no reason to suppose that such a complex should dissociate to the free components to enter the classical "S_N2" displacement. Possible intermediary of such an association complex was already discussed.[8,9]

As a second approach, the measurement of the secondary α-deuterium isotope effect (α-d effect) using 2-chloro-1-phenylethanone-2-d_2 (**4**-H-d_2) was undertaken to present a clue to the nature of the transition state of the displacement reaction of this chloro ketone. The results are shown in Table 5 along with the results of another reactive substrate, **3**-p-NO_2.

Table 5. α-Deuterium isotope effect of the Finkelstein reaction system in acetonitrile

Substrate	k_2^H/k_2^D	K^H/K^D	k_1^H/k_1^D
Ph–CO–CH_2Cl (0 °C)	0.96_2 [a]	0.94_2 [b]	1.02_1
p-NO_2–C_6H_4–S–CH_2Cl (20 °C)	1.11_9 [c]	0.97_6 [c]	1.14_7 [c]

a) k_2/M^{-1} min^{-1}: 1.50×10^{-1} (for Ph–CO–CH_2Cl), 1.62×10^{-1} (for Ph–CO–CD_2Cl). b) K/M^{-1}: 0.307 (for Ph–CO–CH_2Cl), 0.326 (Ph–CO–CHDCl). c) Ref. 7.

In the symmetrical Finkelstein reaction, the chloro ketone **4**-H gave an inverse α-d effect ($k_2^H/k_2^D=0.96_2$) for the second order rate coefficient.

Such an inverse kinetic isotope effect seems to be too large for a reaction that proceeds through a symmetrical transition state. In a symmetrical S_N2 reaction, Seltzer suggested an operation of a normal isotope effect or an isotope effect of close to unity when the nucleophilicities of the incoming and leaving nucleophile are equal.[14] Interestingly, PMR experiments showed that the α-d effect on the complex formation equilibrium for **4**-H is appreciable and inverse ($K^H/K^D=0.94_2$).

Now an explanation in terms of the operation of an association-scramble mechanism, which was applied to accomodate the kinetic isotope effect of the reactive substrates,[7] is worth trying.

This mechanism postulates an intervention of the nucleophile-substrate association complex as a direct precursor of the rate-determining (unimolecular) scrambling and is depicted in Scheme 2.[5]

As expressed in Scheme 2, α-d effect (k_2^H/k_2^D), kinetic parameters ($\Delta H^\ddagger_{obsd}$, $\Delta S^\ddagger_{obsd}$), and ρ_{obsd} values can be separated into those parameters, both for the complex-forming step and for the unimolecular-scrambling step.

When one postulates the operation of the association-scramble mechanism, α-d effect ascribable to the rate-determining scrambling step of this halo ketone is calculated to be normal and is very close to unity, suggesting a very tight transition state[16] (Table 5).

For the chloro ketone **4**, there is no intramolecular functionality among the substrate itself to stabilize the incipient electropositive center developing in the course of the S_N2 reaction. This is in contrast to the

$$\begin{array}{ccc} X\text{-}C_6H_4\text{-}Y\text{-}CH_2Cl + {}^*Cl^- & & X\text{-}C_6H_4\text{-}Y\text{-}CH_2{}^*Cl + Cl^- \\ K \updownarrow \uparrow\downarrow (rapid) & & (rapid) \uparrow\downarrow K \\ [X\text{-}C_6H_4\text{-}Y\text{-}CH_2Cl\cdot{}^*Cl^-] & \xrightarrow[(slow)]{k_1} & [X\text{-}C_6H_4\text{-}Y\text{-}CH_2{}^*Cl\cdot Cl^-] \end{array}$$

K: Equilibrium constant of the complex formation.
k_1: Rate coefficient of the (unimolecular) scrambling in the complex.

$$K = \frac{[\text{Complex}]}{[\text{Substrate}]\,[\text{Nucleophile}]}$$

$$\text{Rate} = k_1\cdot[\text{Complex}] = K\cdot k_1\,[\text{Substrate}]\,[\text{Nucleophile}]^{15)}$$

$k_2 = K\cdot k_1$
$k_2^H/k_2^D = (K^H/K^D)(k_1^H/k_1^D)$
$\Delta H^*_{obsd} = \Delta H^\circ + \Delta H_1^*$
$\Delta S^*_{obsd} = \Delta S^\circ + \Delta S_1^*$
$\rho_{obsd} = \rho^\circ + \rho_1$
(*Cf.* Table 3, footnote)

Scheme 2. Association-scramble mechanism.

cases of the chloromethyl sulfide **3** and other reactive compounds.

However, it is conceivable that the incoming chloride ion which resides at a position close enough to perturb the carbonyl group keeps interacting in the course of the rate-determining scrambling. This sort of an interaction could energetically be favored by the "orbital overlap" among the π-orbital of the carbonyl group, the incipient p-orbital of the reaction center, and the p-orbital of the nucleophile.[9a)]

Thus a kind of the attraction-dissociation process is feasible. In fact, very small α-d effect can be reasonably interpreted assuming a tight transition state where no significant charge separation around the reaction center is expected.[17)] Positive ρ_1 value in Table 3(a) also are in accord with the above explanation, since the electron-withdrawing group on the phenyl ring facilitates the attraction of the nucleophile.

Effect of the Sulfur-containing Functional Group on the Finkelstein Reactions. As shown in Table 2, marked retardation in reaction was observed for (arylsulfonyl)- and (arylsulfinyl)chloromethanes (**1** and **2**), in contrast to the appreciable rate acceleration in (arylthio)-chloromethanes (**3**). In the present study, the reactivity gap between **2** and **3** was significantly larger than that reported earlier by Bordwell and coworkers.[8)]

For (*p*-nitrophenylsulfonyl)chloromethane (**1**-*p*-NO_2) and for (*p*-nitrophenylsulfinyl)chloromethane (**2**-*p*-NO_2), as the representatives for these classes of the substrates, activation parameters were evaluated. In Table 6, these parameters are given with those for (*p*-nitrophenylthio)chloromethane (**3**-*p*-NO_2) as the reference substrate.

The observed enthalpies of activation (ΔH^*_{obsd}) increase in the order of **3**-*p*-NO_2<**2**-*p*-NO_2<**1**-*p*-NO_2, reflecting the relative reactivities of these substrates. As to the observed entropies of activation (ΔS^*_{obsd}) incontestable positive values were obtained for **1**-*p*-NO_2 and **2**-*p*-NO_2.

This is quite a contrast with the Bordwell's experiment. They found large negative entropies of activation in the reaction of **2** and potassium iodide in acetone. They also claimed only a small difference in the enthalpies of activation between **2** and **3**.[8)]

These findings led Bordwell to accomodate the rate retardation in terms of the steric hindrance (and of the electrostatic repulsion) by sulfinyl (and possibly by sulfonyl) group.[8)] A similar explanation was made of the ring opening of the episulfonium ion, under the nucleophilic attack by chloride ion, substituted with alkylsulfonyl group.[18)]

However, positive entropy of activation obtained in the present study cannot be accomodated in terms of increased steric restriction in the transition state. Thus the cause of the rate retardation other than the steric hindrance must be sought for the least reactive substrates **1** and **2**.

There is a possibility that an isokinetic relationship holds for the symmetrical exchange reaction of **1**, **2**, and **3**, although the apparent linear relationship found can probably be fallacious. If the present observation is not fortuitous in nature, an operation of a common mechanism should be postulated among the three classes of compounds.[19)] This implies a possible intervention of the nucleophile-substrate complex playing a role of the direct precursor of the rate-determining step, as behaviors of the chloromethyl sulfide **3** were better accomodated in the frame work of this mechanism.[7)]

In Table 3(b), there are also shown kinetic and thermodynamic parameters which are obtained by taking into account the intervention of the complex.

Interestingly, an isokinetic relationship about ΔH_1^*-ΔS_1^* suggests a different interaction between chloro ketone **4** and the three classes of the sulfur-containing substrates, while ΔH^*_{obsd}-ΔS^*_{obsd} relationship suggests a single interaction among those four classes of the substrates.

The postulation of the association-scramble mechanism suggests a more comprehensive picture. The effect of a facilitated approach of a nucleophile is separated from k_{obsd} into K, thus the rate retardation observed in **1** and **2** could be an outcome of the lack of the electron-donating capacity of both the sulfinyl and the sulfonyl groups to the reaction center in the

Table 6. Activation parameters for the substrates with sulfur-containing functional groups
$X\text{-}C_6H_4\text{-}Y\text{-}CH_2Cl + (C_2H_5)_4N^{36}Cl$

Y	X	ΔH^*_{obsd} / kcal·mol^{-1}	ΔS^*_{obsd} / eu (20 °C)
SO_2[a)]	*p*-NO_2	33.9±0.6	$8._5$±2.0
SO[b)]	*p*-NO_2	28.6±0.5	$2._4$±2.0
S[c)]	*p*-NO_2	19.5±0.5	$-10._0$±2.0

a) k_{obsd}/M^{-1} min^{-1}: 4.30×10^{-6} (66.5 °C); 1.23×10^{-4} (89.6 °C); 1.42×10^{-3} (110.0 °C). k_2/M^{-1} min^{-1}: 5.15×10^{-6} (66.5 °C); 1.45×10^{-4} (89.6 °C); 1.65×10^{-3} (110.0 °C). b) k_{obsd}/M^{-1} min^{-1}: 5.15×10^{-4} (66.5°C); 8.69×10^{-3} (89.6 °C); 6.95×10^{-2} (110.0 °C). k_2/M^{-1} min^{-1}: 6.09×10^{-4} (66.5 °C); 1.01×10^{-2} (89.6 °C); 7.96×10^{-2} (110.0 °C). c) k_{obsd}/M^{-1} min^{-1}: 7.15×10^{-3} (20.0 °C); 2.27×10^{-2} (30.0 °C); 6.46×10^{-2} (40.0 °C). k_2/M^{-1} min^{-1}: 7.92×10^{-3} (20.0 °C); 2.50×10^{-2} (30.0 °C); 7.03×10^{-2} (40.0 °C). [*Cf.* Ref. 3a.]

(unimolecular) scrambling step of the nucleophilic displacement reaction. There are examples of the difference in the electron-donating capacity of these three sulfur-containing groups.[20]

A conceivable presence of the isokinetic relationship(s) among the nucleophilic displacement reactions studied, suggests a prevailing positive entropy of activation for substrates with extremely high activation enthalpy. However, no indication is obtained from this reasoning about the physical meaning of the positive entropy of activation where a tight transition state can plausibly be ascribed.[21]

At present, the postulation of the intermediary of the nucleophile-substrate complex remains as a proposal. Further studies to support (or disprove) the role of such a complex are necessary to help clarify the situation on the possibility of the intermediary in the Finkelstein reaction system.

Experimental

Preparative gas chromatography was performed on a Varian Model-920 gas chromatograph. The CMR spectra were obtained on a JEOL JNM-FX60 spectrometer. The mass spectra were recorded on a Hitachi M-52 spectrometer. The radioactivity was measured with a Nuclear Chicago Model-6801 liquid scintillation counter.

Materials. Substituted chloromethanes were synthesized according to the standard procedures.[3,8]

2-Chloro-1-phenylethanone-1-^{13}C: (a) Benzoic-*carboxy*-^{13}C Acid:[22] A Grignard solution was prepared from 480 mg (20 mmol) of magnesium turning and 3.1 g (20 mmol) of bromobenzene in absolute ether (20 ml). Phenylmagnesium bromide was carbonated with carbon-^{13}C dioxide liberated from 1 g (5 mmol) of barium carbonate-^{13}C (isotopic enrichment 90%, Prochem). Following hydrolysis with aqueous ammonium chloride, the ethereal solution was extracted repeatedly (5 ml×5) with saturated aqueous sodium hydrogencarbonate solution. Then the alkaline solution was washed with ether, acidified and extracted with a small amount of saturated aqueous sodium hydrogencarbonate solution. The hot aqueous solution was acidified with hydrochloric acid, and cooled to precipitate the product, yield 556 mg (91%). (b) Benzoyl-*carbonyl*-^{13}C Chloride. A mixture of 556 mg (4.6 mmol) of benzoic acid and 4 ml (30 mmol) of purified thionyl chloride was refluxed for 1 h and the excess thionyl chloride was removed under reduced pressure. The residual liquid was used without further purification. (c) 2-Diazo-1-phenylethanone-^{13}C: To a stirred and ice-cooled ethereal solution of diazomethane (65 ml) [from 10.8 g (50 mmol) of *N*-methyl-*N*-nitroso-*p*-toluenesulfonamide] was added dropwise a solution of crude benzoyl chloride in 20 ml of absolute ether. The mixture was stirred for 15 min at 0 °C and for additional 2 h at room temperature. The product was used for the following process without further purification. (d) 2-Chloro-1-phenylethanone-1-^{13}C; Into a stirred dry ethereal solution (20 ml) containing 2-diazo-1-phenylethanone was introduced anhydrous hydrogen chloride for 1 h at 0 °C. Then the solution was concentrated, and the resulting crude material was recrystallized from ethanol, to give a pure product, 506 mg, 72% based on the benzoic acid. Mass; 156 (M^+) (isotopic enrichment 90%).

2-Chloro-1-phenylethanone-2-d_2: To a stirred and ice-cooled solution of 2-diazo-1-phenylethanone (400 mg, 2.7 mmol) in dry ether (20 ml) was bubbled anhydrous deuterium chloride, generated by the reaction between phosphorus pentachloride (24 g, 0.1 mol) and deuterium oxide (2 g, 0.1 mol). The mixture was stirred for 1 h at 0 °C, then concentrated to give the crude material. Recrystallization from ethanol gave a pure product, 407 mg, 82% based on the 2-diazo-1-phenylethanone. Mass; 157 (M^+) (isotopic enrichment 99.7%).

Benzyl-α-^{13}C Chloride: (a) Methyl Benzoate-*carbonyl*-^{13}C; An ethereal solution (10 ml) of 500 mg (4.0 mmol) of benzoic-^{13}CO acid was treated with a cold ethereal solution (65 ml) of diazomethane prepared from 10.8 g (50 mmol) of *N*-methyl-*N*-nitroso-*p*-toluenesulfonamide. The solution was concentrated under reduced pressure, and used for the following step without further purification. (b) Phenylmethanol-1-^{13}C; An ethereal solution (3 ml) of the ester was added dropwise to a stirred ethereal solution (15 ml) of 455 mg (1.2 mmol) of lithium aluminum hydride. The mixture was then refluxed for 2 h, cooled with ice bath, and acidified with dilute hydrochloric acid. The aqueous layer was separated, and extracted with several portions of ether. The ether layer and the extracts were combined and the combined solution was dried over anhydrous magnesium sulfate. Concentration of the solution gave the cited compound as an almost colorless liquid. This product was used without further purification. The yield was essentially quantitative. (c) Benzyl-α-^{13}C chloride; To the crude benzyl alcohol, was added slowly 5 ml (25 mmol) of purified thionyl chloride, and the mixture was refluxed for 1 h. The excess thionyl chloride was distilled off, and the product was purified by preparative gas chromatography. The yield was 370 mg, 71% based on the benzoic acid. Mass; 127 (M^+) (isotopic enrichment, 90%).

Kinetic Measurements. Batch method was employed for kinetic measurements. Procedures were almost similar as previously reported.[3] At the appropriate intervals, the reaction mixture was quenched by cooling and dilution with cold (−78 °C) toluene, while tetraethylammonium chloride was extracted in water. Chlorine-36 radioactivity was measured by liquid scintillation counter. In the measurement of the less reactive substrate, tetraethylammonium chloride-^{36}Cl with high specific activity (10 μCi/mmol) was utilized. In such cases, to avoid the experimental error caused by the contamination of unreacted tetraethylammonium chloride-^{36}Cl to the organic layer, the organic layer was washed repeatedly with water (at least six times) until the radioactivity of the aqueous layer was reduced to that of the natural backgound.

The tracer experiments were carried out at the Radioisotope Research Center of Kyoto University. The authors are grateful to the staffs of this institution. The present work was supported by the Grant-in-Aid for Scientific Research from the Ministry of Education (No. 83151, 84076) and by the grants kindly given from Saneyoshi Shogakukai and from Ito Kagaku Shinkokai. Special thanks are due to the donors of these grants.

References

1) Part of this work was presented before the IInd IUPAC Conference on Physical Organic Chemistry (Noordwijkerhout, 1974), and before the 35th Annual Meeting of the Chemical Society of Japan (Invited Lecture, Fukuoka, 1975, abstract III, p. 1314).

2) Address correspondence to the Department of Chemistry, College of Liberal Arts and Science, Kyoto University.

3) a) J. Hayami, N. Tanaka, S. Kurabayashi, Y. Kotani, and A. Kaji, *Bull. Chem. Soc. Jpn.*, **44**, 3091 (1971); b) J. Hayami, N. Tanaka, and A. Kaji, *ibid.*, **46**, 954 (1973).

4) a) C. K. Ingold, "Structure and Mechanism in Or-

ganic Chemistry," Cornell University Press, Ithaca, 1953; b) A. Streitwieser, Jr., "Solvolytic Displacement Reactions," McGraw-Hill Book Co., Inc., New York, 1962.

5) a) J. Hayami, N. Tanaka, N. Hihara, and A. Kaji, *Tetrahedron Lett.*, **1973**, 385; b) J. Hayami, T. Koyanagi, N. Hihara, and A. Kaji, *Bull. Chem. Soc. Jpn.*, **51**, 891 (1978).

6) N. Tanaka, A. Kaji, and J. Hayami, *Chemistry Lett.*, **1972** 1223.

7) J. Hayami, N. Hihara, N. Tanaka, and A. Kaji, *Bull. Chem. Soc. Jpn.*, **52**, 831 (1979).

8) Bordwell reported a reaction of (phenylsulfinyl)chloromethane with sodium iodide in solvent acetone. However, no absolute kinetic datum was given. F. G. Bordwell and W. T. Brannen, Jr., *J. Am. Chem. Soc.*, **86**, 4645 (1964).

9) a) Ref. 4b. p. 26. b) J. W. Thorpe and J. Warkentin, *Can. J. Chem.*, **51**, 927 (1973); c) R. G. Pearson, S. H. Langer, F. V. Williams, and W. J. McGuire, *J. Am. Chem. Soc.*, **74**, 5130 (1952).

10) F. G. Bordwell and G. D. Cooper, *J. Am. Chem. Soc.*, **74**, 1058 (1952).

11) Ref. 5b and references cited therein.

12) Besides the change in electron density, one should also take into account the electrostatic perturbation by the anion that results in the downfield shift of CMR. This effect should have happened for the case of phenylchloromethane. The absence of complex shift on CMR of this substrate suggests that the chloride ion that makes van der Waals contact with the α-hydrogen locates fairly far from the carbon in question, or that there occurs a fortuitous compensation of up- and downfield shift. The latter possibility seems to be less feasible, as is suggested from the work of Hagen and Roberts. The downfield shift of CMR spectra by the electrostatic perturbation was reported for the carboxylic acids on the ionization of a carboxyl group to a carboxylate anion. The present result suggests that the chloride ion resides in a proximity of the carbonyl group to perturb the CMR shift. *Cf.*, R. Hagen and J. D. Roberts, *J. Am. Chem. Soc.*, **91**, 4504 (1969).

13) R. G. Bergstrom, R. G. M. Londells, G. H. Wahl, Jr., and H. Zollinger, *J. Am. Chem. Soc.*, **98**, 3301 (1976).

14) S. Seltzer, and A. A. Zavitsas, *Can. J. Chem.*, **45**, 2023 (1967).

15) a) Heavy atom isotope effect for both the leaving and the incoming chlorine is ignored. *Cf.*, C. J. Collins and N. S. Bowman, Ed., "Isotope Effects in Chemical Reactions," Van Nostrand-Reinhold, New York, 1970; b) In the isotopic exchange reaction, the (total) chemical concentrations of both the substrate and the nucleophile remain unchanged throughout the reaction. However, formation of the complex causes a decrease in the concentration of the free substrate and the free nucleophile. Thus the corrections must be made for the rate constants, even if the association complex is in merely parasitic equilibrium with the free substrate and the free nucleophile.

For the sake of simplicity and to show the experimental results, rate data in Tables 1 through 2 are not corrected. As is exemplified in the footnote of Table 3, the due correction is often close to 20% for the substrates with a high K. However, as are given in the footnote of Table 3, $\Delta H_1^{\ddagger}$ and $\Delta S_1^{\ddagger}$ (also $\Delta H_{obsd}^{\ddagger}$ and $\Delta S_{obsd}^{\ddagger}$) are affected little by the due correction of the decrease in the concentrations of the reactants and, accordingly, of the rate constants on the complex formation.

16) a) Ref. 7; b) Leffek explained the (overall) kinetic isotope effects in the S_N2 reaction in terms of the loose-tight transition state. *Cf.* K. T. Leffek and A. F. Matheson, *Can. J. Chem.*, **50**, 986 (1972).

17) A. J. Parker, *Chem. Revs.*, **69**, 12 (1969).

18) W. A. Thaler, W. H. Mueller, and P. E. Butler, *J. Am. Chem. Soc.*, **90**, 2069 (1968).

19) J. F. Leffler and E. Grunwald, "Rates and Equilibria of Organic Reactions," John Wiley and Sons, Inc., New York, 1963.

20) J. R. Alexander and H. McCombie, *J. Chem. Soc.*, **1931**, 1913.

21) There is, at least in principle, no guarantee that the bimolecular nucleophilic displacement reaction is a "single interaction reaction". Accordingly, scattered entropy-enthalpy plot can be a sign of the presence of a host of different isokinetic relationships that show different isokinetic temperatures. Thus, with the isokinetic temperature(s) of 300—400 K, available data can predict a positive entropy of activation even for a reasonable activation enthalpy of 25—30 kcal/mol. Isokinetic temperatures calculated from $\Delta H_1^{\ddagger}$-$\Delta S_1^{\ddagger}$ in Table 3 is 926 K, while that from $\Delta H_{obsd}^{\ddagger}$-$\Delta S_{obsd}^{\ddagger}$ is 771 K.

22) A. Murray, III, and D. L. Williams, "Organic Syntheses with Isotopes," Interscience Publishers, Inc., New York (1958), p. 83.

Michael Addition of 4*H*-Cyclopenta[*def*]phenanthrene to 9,9′-Bifluorenylidene and the Related Reactions

Takao KIMURA,*,† Masahiro MINABE, and Kazuo SUZUKI

Department of Industrial Chemistry, Faculty of Engineering, Utsunomiya University, Ishiicho, Utsunomiya 321-31

(Received August 28, 1978)

The compound 9-(4*H*-cyclopenta[*def*]phenanthren-4-yl)-9,9′-bifluorene was synthesized by the Michael addition of 4*H*-cyclopenta[*def*]phenanthrene to 9,9′-bifluorenylidene and also by other reactions. In addition, five kinds of trimers which consisted of 4*H*-cyclopenta[*def*]phenanthrene and fluorene were obtained by the same reactions. The conformation of these trimers is assigned to be the *gauche-gauche* form.

The Michael addition of fluorene (**1**) to 9,9′-bifluorenylidene (**2**) has been reported in detail.[1] In our previous publication,[2] the ring expansions on the active methylene of 4*H*-cyclopenta[*def*]phenanthrene (**3**) were shown to have a property similar to that of **1**. The acidities of methylene protons of hydrocarbons **1** and **3** have been investigated closely, with their analogues, by determination of the dissociation constant in some solvents.[3]

The present paper deals with the Michael additions of **3** and **1** to some fulvalenes in order to compare with additions of **1** to **2**, and also to clarify the conformations of the resulting trimers.

Results and Discussion

The Michael addition of **3** to **2** gave 9-(4*H*-cyclopenta[*def*]phenanthren-4-yl)-9,9′-bifluorene (**4**); the yield of **4** increased (10—35%) with the increase of base concentration (2—10% of sodium ethoxide). This reaction proceeded rapidly under a potassium hydroxide–aqueous pyridine system to give **4** in a reasonable yield. The addition can be explained by the nucleophilic attack of carbanion (A) on the highly-polarized acceptor **2** to form carbanion (B) followed by protonation to give **4** (Scheme 1).

Compound **4** was also prepared by the reaction of 9-lithiofluorene with bromide **5**, and also by dehydrogenation of 9-(8,9-dihydro-4*H*-cyclopenta[*def*]-phenanthren-4-yl)-9,9′-bifluorene (**6**), which was obtained by the addition of hydrocarbon **7**[4] to **2**.

The Michael reactions of fulvalene **8**[5] with **1** and with **3** yielded 4-(9-fluorenyl)-4,4′-bi(4*H*-cyclopenta-[*def*]phenanthrene) (**9**) and 4,4′ : 4′,4″-ter(4*H*-cyclopenta[*def*]phenanthrene) (**10**), respectively. The addition of **1** to unsymmetrical ethylene **11**[5] afforded isomeric **4** and 4,4-di(9-fluorenyl)-4*H*-cyclopenta[*def*]-phenanthrene (**12**) in a ratio of 75 to 25. Furthermore, the reaction of **3** with **11** gave 9,9-di(4*H*-cyclopenta[*def*]phenanthren-4-yl)fluorene (**13**) (73%) and **9** (27%).

The methine protons in the NMR spectrum of hydrocarbon **14** appear as two doublets about 0.3 ppm apart. In addition, the methine signals of alcohol **15** and bromide **5** shift to lower fields than those of alcohol **16** and bromide **17**, respectively. These findings may be explained as due to the difference of

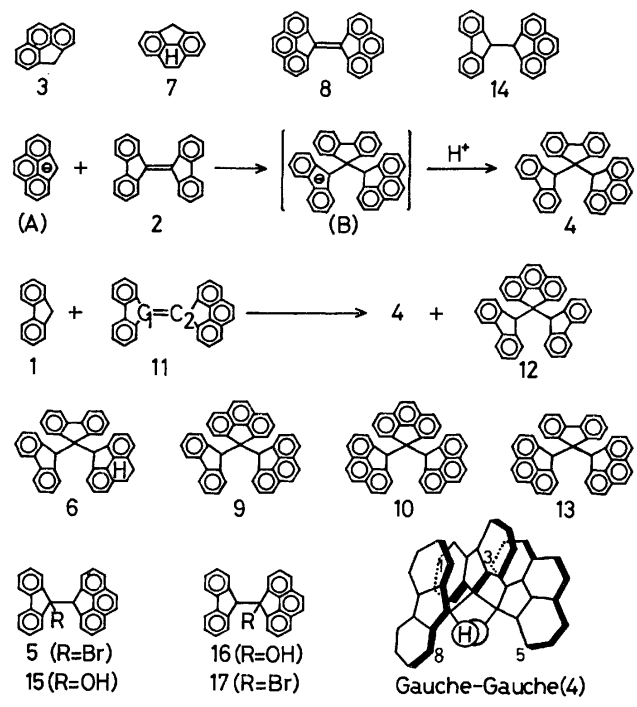

Scheme 1.

the acidities between the methylene protons of fragmental hydrocarbons **1** and **3**.[3] Also, this presumption would be extended reasonably to the reactivity of fulvalene **11**: the electron distribution on the central double bond of **11** lies to the **3** moiety. Therefore, the carbanion preferentially attacks the C_1 atom rather than the C_2 atom on **11**.

The assignment of the methine protons in the NMR spectra of the trimers was confirmed by comparison[6] with the corresponding deuterated compounds, as summarized in Table 1. The methine protons of **6** are observed as a two-proton singlet, which suggests that the electronic property of a methine proton on the **7** moiety of **6** is equivalent to that of a **1** segment. The two methine protons of the unsymmetrical trimers, such as **4** and **9**, are observed as two separate singlets, which may be regarded as the case of **14**. The two methine protons of **4** and **9** are assigned so that the methine on the leaflet of **3** corresponds to the peak in lower field and the methine on the leaflet of **1** to the one in higher field.

The compound **4** would be symmetrical with respect to the central fluorenylidene plane as in the analogues, **10**, **12**, and **13**, whose methine proton NMR

† Present address: Department of Environmental Chemistry, Faculty of Engineering, Utsunomiya University, Utsunomiya 321-31.

TABLE 1. PROTON NMR SPECTRA OF THE MICHAEL ADDUCTS IN PYRIDINE-d_5

Compd	Methine (δ)	Aromatic (δ)
4	5.65 (1H, s), 5.93 (1H, s)	5.68 (2H, d, J=7.2 Hz), 6.46—8.78 (22H, m)
6[a]	5.35 (2H, s)	2.94 (4H, s, $-CH_2-CH_2-$), 4.87 (1H, d, J=7.8 Hz), 5.24 (1H, d, J=7.8 Hz), 6.18—8.70 (20H, m)
9	5.89 (1H, s), 6.18 (1H, s)	5.36 (1H, d, J=6.6 Hz), 5.48 (1H, d, J=6.6 Hz), 6.10—8.83 (22H, m)
10	6.41 (2H, s)	5.45 (2H, d, J=7.2 Hz), 6.52—8.90 (22H, m)
12	5.73 (2H, s)	5.44 (2H, d, J=7.8 Hz), 6.08—8.83 (22H, m)
13	6.14 (2H, s)	5.74 (2H, d, J=7.2 Hz), 6.54—8.86 (22H, m)

a) Measured in DMSO-d_6.

spectra showed a two-proton singlet. An examination of molecular scale models of **4** suggests that the *gauche-gauche* form is more appropriate to the conformation of **4** at the ground state than the *anti-anti* form, due to the steric interaction of the bulky aromatic rings.

The anomalous spread of the aromatic signal zone in the spectrum of **4** is probably attributable to the torsional conformation.[1] The signals at higher fields would be assigned to be the 1-proton of the outside 9-fluorenyl plane and the 3-proton of the 4*H*-cyclopenta[*def*]phenanthren-4-yl plane, because of being located in the shielding zone of the adjacent central aromatic ring,[1,7,8] as simulated in Scheme 1. On the contrary, the peaks at lower fields are due to the 8-proton of the 9-fluorenyl plane and the 5-proton of the 4*H*-cyclopenta[*def*]phenanthren-4-yl plane. The broad aromatic zone on the spectrum of **4** is observed to become narrower with the elevation of temperature. At a high temperature, the central sp^3-sp^3 single bonds may be released from the torsion, which would increase the probability of the *eclipsed-eclipsed* form. Therefore, the shielding effect of the central aromatic ring decreases and results in some reducing of the signal zone. A similar view can be applied to the other analogues: **6**, **9**, **10**, **12**, and **13**.

Experimental

All the melting points are uncorrected. The melting points of deuterated compounds in this series are identical with those of the parent hydrocarbons.

The IR spectra were obtained as KBr disks using a IR-G spectrophotometer (JASCO). The mass spectra were measured with a RMU-6E apparatus (Hitachi). The proton NMR spectra were recorded with a JNM-C-60HL (60 MHz) spectrometer (JEOL) using TMS as an internal reference. The deuterium incorporation was determined from the average value of five peaks on the NMR spectra.

*Michael Reaction of 9,9'-Bifluorenylidene (**2**) with 4H-Cyclopenta[def]phenanthrene (**3**).* To a soln of KOH (0.05 g) in H_2O (1 ml) and pyridine (9 ml), there was added 492 mg (1.5 mmol) of **2** and 285 mg (1.5 mmol) of **3**. The mixture was stirred for 1 h at room temperature under an atmosphere of nitrogen.

The reaction mixture was then poured into HCl (2%, 150 ml) and extracted with benzene (150 ml). The organic layer was dried over Na_2SO_4 and evaporated to dryness, and the residual materials were separated by means of silica-gel column chromatography (2.0×50 cm) in cyclohexane. The first and second eluates gave 34 mg of **3** (mp 114—116 °C) and 72 mg of **2** (mp 185—187 °C), respectively.

The third eluate was evaporated off and the residue was recrystallized from EtOAc to afford 554 mg (71%) of **4**: mp 259—260 °C (dec); MS, *m/e*, 518 (M^+), 353, and 329. Found: C, 94.91; H, 4.94%. Calcd for $C_{41}H_{26}$: C, 94.95; H, 5.05%.

*Michael Reaction between **2** and 8,9-Dihydro-4H-cyclopenta[def]phenanthrene (**7**).* A mixture of **2** (492 mg, 1.5 mmol), **7** (288 mg, 1.5 mmol), and aq K_2CO_3 (1.1 g in 2 ml) in pyridine (8 ml) was heated in a sealed tube at 95—98 °C for 24 h. The reaction mixture was treated in a manner similar to the above to yield 273 mg (35%) of **6**: mp 253—254 °C (dec); MS, *m/e*, 520 (M^+) and 494. Found: C, 94.65; H, 5.46%. Calcd for $C_{41}H_{28}$: C, 94.58; H, 5.42%.

*Michael Addition of **1** to 4,4'-Bi(4H-cyclopenta[def]phenanthren-4-ylidene) (**8**).* A mixture of **1** (249 mg, 1.5 mmol), **8** (564 mg, 1.5 mmol), and aq KOH (0.3 g in 1 ml) in pyridine (9 ml) was refluxed for 8 h under an atmosphere of nitrogen to give 520 mg (64%) of **9**: mp 319—320 °C (dec); MS, *m/e*, 542 (M^+) and 353. Found: C, 95.16; H, 4.67%. Calcd for $C_{43}H_{26}$: C, 95.17; H, 4.83%.

*Addition of **3** to **8**.* To a soln of $NaOPr^n$ prepared from metallic sodium (0.3 g) and *n*-PrOH (13 ml), there were added 564 mg (1.5 mmol) of **8** and 285 mg (1.5 mmol) of **3**. The resulting mixture was refluxed for 8 h under an atmosphere of nitrogen to yield 738 mg (87%) of **10**: mp 327—328 °C (dec); MS, *m/e*, 566 (M^+). Found: C, 95.11; H, 4.30%. Calcd for $C_{45}H_{26}$: C, 95.37; H, 4.63%.

*Michael Reaction of 4-(9-Fluorenylidene)-4H-cyclopenta[def]phenanthrene (**11**) with **1**.* A mixture of **11** (528 mg, 1.5 mmol) and **1** (249 mg, 1.5 mmol) in EtOH (10 ml) containing NaOEt (1.0 g) was heated in a sealed tube at 95—98 °C for 8 h. After cooling, the precipitates were collected and separated by silica-gel column chromatography to afford 381 mg (49%) of the mixture, which consisted of **4** (75% by NMR) and **12** (25%).

*Michael Addition of **3** to **11**.* A mixture of **3** (285 mg) and **11** (528 mg) was allowed to react under the conditions similar to those of **1** and **11** to yield the products (545 mg, 67%), which consisted of **13** (73% by NMR) and **9** (27%).

*9-(4H-Cyclopenta[def]phenanthren-4-yl)-9,9'-bifluorene (**4**).*

a): A soln of 9-lithiofluorene (prepared from 870 mg of **1** according to the procedure described elsewhere[9]) was added dropwise to a soln of bromide **5** (1.00 g, 2.3 mmol) in benzene–xylene (1 : 1, 60 ml) at 0 °C with stirring for 10 min. After being boiled for an additional 2 h, the reaction mixture was treated with aq NH_4Cl (5%, 50 ml), dried over Na_2SO_4, and then evaporated to dryness *in vacuo*. The residue was recrystallized from cyclohexane to afford 550 mg (46%) of **4**, which was identical in all respects with the specimen obtained by the Michael addition of **3** to **2**.

b): A soln of **6** (281 mg, 0.54 mmol) in 10 ml of *p*-cymene was refluxed with Pd–C (5%, 50 mg) for 40 h. The reaction

mixture was filtered and the filtrate was then steam distilled. The residue was chromatographed in cyclohexane on a silica-gel column to give 99 mg (35%) of **4**: mp 259—260 °C (dec).

*4,4-Di(9-fluorenyl)-4*H*-cyclopenta*[def]*phenanthrene* (**12**). A mixture of 9-lithiofluorene and bromide **17** was treated in a manner similar to that used for **4**, giving **12** in a yield of 50%: mp 286—287 °C (dec); MS, *m/e*, 518 (M^+), 353, and 165. Found: C, 94.73; H, 5.06%. Calcd for $C_{41}H_{26}$: C, 94.95; H, 5.05%.

*9,9-Di(4*H*-cyclopenta*[def]*phenanthren-4-yl)fluorene* (**13**). Compound **13** was prepared by the reaction of **3** with **5** according to a procedure similar to the above: yield 42%; mp 308—309 °C (dec); MS, *m/e*, 542 (M^+), 353, and 189. Found: C, 95.08; H, 4.89%. Calcd for $C_{43}H_{26}$: C, 95.17; H, 4.83%.

*9-(4*H*-Cyclopenta*[def]*phenanthren-4-yl)-9-fluorenol* (**15**).[5] A soln of fluorenone (5.4 g, 30 mmol) in xylene (60 ml) was allowed to react with 4-lithio-4*H*-cyclopenta[*def*]phenanthrene[10] (prepared from 5.7 g of **3** with $LiBu^n$ in xylene) at 0 °C. The resulting mixture was refluxed for 1 h to afford 9.85 g (89%) of **15**: mp 188—189 °C (lit,[5] 188—189 °C); IR: 3310 cm^{-1} (–OH); MS, *m/e*, 370 (M^+); NMR (benzene-d_6): δ 1.94 (1H, s, –OH), 5.27 (1H, s, >CH–), and 6.50—7.65 (16H, m, Ar–H).

*4-(9-Fluorenyl)-4*H*-cyclopenta*[def]*phenanthren-4-ol* (**16**). To a soln of 4*H*-cyclopenta[*def*]phenanthren-4-one (3.0 g, 14.7 mmol) in benzene–xylene (1 : 1, 80 ml), there was added dropwise a soln of 9-lithiofluorene (prepared from 2.5 g of **1**) at 0 °C with stirring for 10 min. The mixture was boiled for an additional 2 h to yield 2.77 g (51%) of **16**: mp 202—203 °C; IR, 3275 cm^{-1} (–OH); MS, *m/e*, 370 (M^+); NMR (benzene-d_6): δ 1.98 (1H, s, –OH), 4.96 (1H, s, >CH–), and 6.60—7.50 (16H, m, Ar–H). Found: C, 90.80; H, 4.90%. Calcd for $C_{28}H_{18}O$: C, 90.78; H, 4.90%.

*4-(9-Fluorenylidene)-4*H*-cyclopenta*[def]*phenanthrene* (**11**).[5] A soln of **15** (0.8 g, 2.2 mmol) in AcOH (30 ml) containing concd HCl (0.2 ml) was refluxed for 1 h to give 500 mg (66%) of **11**: mp 197—198 °C (dec) (lit,[5] mp 196 °C, dec); MS, *m/e*, 352 (M^+).

Compound **16** was also converted into **11** in a 68% yield.

*4-(9-Fluorenyl)-4*H*-cyclopenta*[def]*phenanthrene* (**14**). A mixture of **11** (100 mg, 0.28 mmol), Zn powder (1 g), and concd HCl (1 ml) in AcOH (30 ml) was refluxed for 1.5 h to give 97 mg (96%) of **14**: mp 208—209 °C (from EtOAc); MS, *m/e*, 354 (M^+), 189, and 165; NMR (benzene-d_6): δ 5.04 (1H, d, J=4.2 Hz), 5.35 (1H, d), and 6.85—7.79 (16H, m). Found: C, 94.60; H, 5.01%. Calcd for $C_{28}H_{18}$: C, 94.88; H, 5.12%.

*9-Bromo-9-(4*H*-cyclopenta*[def]*phenanthren-4-yl)fluorene* (**5**). Dry HBr was bubbled into a soln of **15** (3.7 g, 10 mmol) in AcOH (135 ml) for 1 h. The reaction mixture was allowed to stand overnight and the precipitate was filtered, dried, and then recrystallized from benzene–cyclohexane (1 : 1) to afford 3.73 g (86%) of **5**: mp 185—187 °C (dec); MS, *m/e*, 434, 432 (M^+), 354, and 352; NMR (benzene-d_6) δ 5.53 (1H, s, >CH–) and 6.46—7.66 (16H, m, Ar–H). Found: C, 77.39; H, 3.74%. Calcd for $C_{28}H_{17}Br$: C, 77.60; H, 3.95%.

*4-Bromo-4-(9-fluorenyl)-4*H*-cyclopenta*[def]*phenanthrene* (**17**). Compound **17** was produced from **16** by a method similar to the above in a 78% yield: mp 171—172 °C (dec); MS, *m/e*, 434, 432 (M^+), 354, and 352; NMR (benzene-d_6): δ 5.24 (1H, s, >CH–) and 6.60—7.60 (16H, m, Ar–H). Found: C, 77.90; H, 3.96%. Calcd for $C_{28}H_{17}Br$: C, 77.60; H, 3.95%.

Syntheses of Deuterated Compounds. Hydrocarbon **3** was deuterated by the method applied in **1**[11] to give 4,4-dideuterio **3** (**3**-4,4-d_2) in a 92% yield. The deuterium incorporation was calculated to be 97% by NMR.

Also, **7**-4,4-d_2 was obtained in a 93% yield (deuterium incorporation, 97%).

Deuterated compounds of **4**, **6**, **9**, **10**, **12**, and **13** were prepared by the Michael reaction using corresponding substrates in a NaOEt–EtOD or NaOD–D_2O–pyridine system. The deuterium contents of these compounds were found to be *ca.* 100% at the methine protons.

References

1) M. Minabe and K. Suzuki, *J. Org. Chem.*, **40**, 1298 (1975).
2) T. Kimura, M. Minabe, and K. Suzuki, *J. Org. Chem.*, **43**, 1247 (1978).
3) J. Hine, "Structural Effects on Equilibria in Organic Chemistry," John Wiley & Sons, New York (1975), p. 172.
4) L. F. Fieser and J. Cason, *J. Am. Chem. Soc.*, **62**, 1293 (1940).
5) G. Wittig and G. Pieper, *Ann.*, **558**, 207, 218 (1947).
6) M. Minabe and K. Suzuki, *Bull. Chem. Soc. Jpn.*, **48**, 2487 (1975).
7) M. Nakamura, N. Nakamura, and M. Ōki, *Bull. Chem. Soc. Jpn.*, **50**, 2986 (1977).
8) T. Ooya, M. Minabe, and K. Suzuki, *Bull. Chem. Soc. Jpn.*, **51**, 1473 (1978).
9) T. Kimura, M. Minabe, M. Tsubota, and K. Suzuki, *Bull. Chem. Soc. Jpn.*, **50**, 258 (1977).
10) A. Streitwieser, Jr., and J. I. Brauman, *J. Am. Chem. Soc.*, **85**, 2633 (1963).
11) D. J. Cram and W. D. Kollmeyer, *J. Am. Chem. Soc.*, **90**, 1791 (1968).

The Total Synthesis of (+)-Totarol and (+)-Podototarin

Takashi MATSUMOTO* and Akira SUETSUGU

Department of Chemistry, Faculty of Science, Hiroshima University, Higashisenda-machi, Hiroshima 730

(Received August 28, 1978)

The Grignard reaction of 7-methoxyphthalide with methylmagnesium iodide, followed by acetylation and dehydration, gave 3-acetoxymethyl-2-isopropenylanisole which, on catalytic hydrogenation, afforded 3-acetoxymethyl-2-isopropylanisole. This was then converted into (2-isopropyl-3-methoxybenzyl)triphenylphosphonium chloride (**8**) *via* 3-hydroxymethyl-2-isopropylanisole and 3-chloromethyl-2-isopropylanisole. The Wittig reaction of (*R*)-(−)-α-cyclocitral with **8** in the presence of butyllithium afforded the corresponding styryl derivative, which was converted into the dihydro compound (**19**) by partial catalytic hydrogenation. The intramolecular cyclization of **19** gave (+)-totaryl methyl ether (**20**) along with its *cis*-isomer. The methyl ether **20** was finally demethylated with boron tribromide to give (+)-totarol (**1**), which was further characterized as its acetate. Since the conversion of (+)-**1** into (+)-podototarin has already been reported, the present work can be regarded as the total synthesis of natural (+)-podototarin.

Totarol, a rare tricyclic diterpene phenol possessing an isopropyl group at the C-14 position, was first isolated as a major constituent of the heartwood of *Podocarpus totara* G. Benn. *ex.* D. Don by Easterfield and McDowell.[1] On the basis of chemical and spectroscopic studies, Short and his coworkers[2] deduced the structure of totarol to be **1**; this was confirmed by the synthesis of the racemate by Barltrop and Rogers.[3] The absolute configuration of totarol was determined by ORD measurements and by direct correlation with dehydroabietic acid by Chow and Erdtman.[4] Podototarin (**2**), a novel bisditerpene, was also isolated from the heartwood of P. *totara* by Brandt and Thomas[5] and Cambie and Mander.[6] The structure of podototarin was determined by the synthesis[7–9] of **2** from natural (+)-totarol. However, no investigation on the total synthesis of optically active totarol has hitherto been reported. It is thus still necessary to synthesize the optically active totarol to complete the total synthesis of natural podototarin. This paper describes the simple syntheses of (+)-totarol (**1**) and, consequently, of (+)-podototarin (**2**).

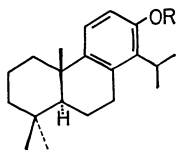

1 R=H
20 R=Me
22 R=Ac

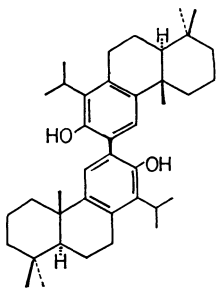

2

Our basic strategy for the synthesis of optically active octahydrophenanthrene backbone (**3**) is shown in Scheme 1. Since there are many precedents for the intramolecular cyclization of phenethylcyclohexene derivatives, the synthetic target is the optically active 3-phenethyl-1-cyclohexene derivative (**4**), which might be constructed by the condensation of optically active cyclohexenylmethyl derivative (**5**) and benzyl derivative (**6**).

In the present study, (*R*)-(−)-α-cyclocitral (**7**)[10,11] and (2-isopropyl-3-methoxybenzyl)triphenylphosphonium chloride (**8**) were chosen as the compounds

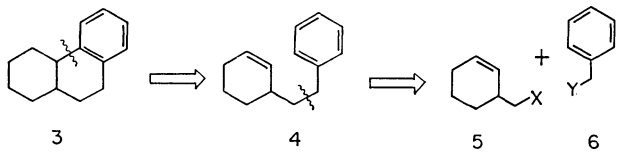

3 4 5 6

Scheme 1.

corresponding to **5** and **6**. Thus, the first synthetic goal was to prepare the phosphonium salt **8**. This was successfully achieved in the following manner. The Grignard reaction of 7-methoxyphthalide (**9**)[12] in tetrahydrofuran with methylmagnesium iodide in ether afforded the corresponding diol (**10**), which was converted into a monoacetate (**11**). The treatment of **11** with *p*-toluenesulfonic acid in hot benzene gave a mixture of the desired 3-acetoxymethyl-2-isopropenylanisole (**12**) and 7-methoxy-1,1-dimethyl-1,3-dihydroisobenzofuran (**13**) in a ratio of *ca.* 2 : 1. Since the separation of **12** and **13** was somewhat difficult, the mixture was directly oxidized with Jones reagent and then purified by column chromatography on silica gel to afford **12** and 4-methoxy-3,3-dimethylphthalide (**14**), which was easily converted into **10** by reduction with lithium aluminium hydride. The catalytic hydrogenation of **12** in ethanol over PtO_2 gave 3-acetoxymethyl-2-isopropylanisole (**15**) which, on reduction with lithium aluminium hydride, afforded 3-hydroxymethyl-2-isopropylanisole (**16**). The alcohol **16** was treated at room temperature with thionyl chloride in ether and the resulting benzyl chloride derivative (**17**), without purification, was converted into the phosphonium salt **8**, by treatment with triphenylphosphine in refluxing benzene. The Wittig reaction of **7** with **8** in benzene in the presence of butyllithium gave 6-(2-isopropyl-3-methoxystyryl)-1,5,5-trimethylcyclohexene (**18**). The NMR spectrum of **18** showed signals at δ 5.63 (dd, J=9 and 15 Hz) and 6.68 ppm (d, J=15 Hz) due to the newly formed olefinic protons. These vicinal coupling constants (J=15 Hz) suggested the presence of a *trans*-disubstituted double bond in **18**. The compound **18** in ethanol was submitted to partial catalytic hydrogenation over Pd–C to afford the corresponding phenethyl derivative (**19**). The intramolecular cyclization of **19** with anhydrous aluminium chloride in dichloro-

methane afforded (+)-totaryl methyl ether (**20**), $[\alpha]_D$ +23.3°(EtOH), as the major product and its *cis*-isomer (**21**), $[\alpha]_D$ −44.3°(EtOH), as the minor one. The *cis*-configuration of the A/B ring junction in **21** was supported by its NMR spectrum, which showed a high field signal, δ 0.41 ppm, due to the $C_{4\beta}$ methyl group and the shielding effect of the aromatic ring. Since the optical rotation of **20** was somewhat lower than that of the natural derivative,[6] it was further purified by crystallization to give the optically pure compound, $[\alpha]_D$ +40.6°(EtOH). The demethylation of **20** with boron tribromide in dichloromethane gave (+)-totarol (**1**), which was characterized as its acetate (**22**).

As has been described above, the partial synthesis of (+)-podototarin from (+)-totarol has already been reported.[7-9] Consequently, the present synthesis of (+)-totarol can be regarded as the total synthesis of (+)-podototarin.

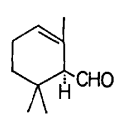

7

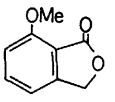

9

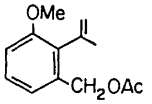

12

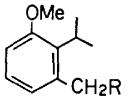

8 R=$\overset{+}{P}Ph_3Cl^-$
15 R=OAc
16 R=OH
17 R=Cl

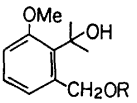

10 R=H
11 R=Ac

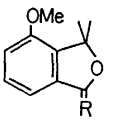

13 R=H2
14 R=O

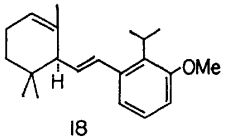

18

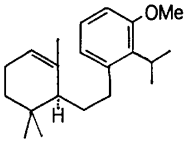

19

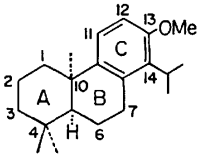

21

Experimental

All melting points are uncorrected. The IR spectra and optical rotations were measured in chloroform, and the NMR spectra in carbon tetrachloride at 60 MHz, with tetramethylsilane as the internal standard, unless otherwise stated. The chemical shifts are presented in terms of δ values; s: singlet, bs: broad singlet, d: doublet, dd: double doublet, m: multiplet. Column chromatography was performed using Merck silica gel (0.063 mm).

*3-Hydroxymethyl-2-(1-hydroxy-1-methylethyl)anisole (**10**).* A solution of 7-methoxyphthalide (**9**)[12] (mp 108—109 °C, 3.347 g) in dry tetrahydrofuran (60 ml) was added dropwise to a stirred solution of methylmagnesium iodide prepared from magnesium (1.239 g) and methyl iodide (3.80 ml) in dry ether (20 ml), with cooling in an ice–water bath. The mixture was stirred at room temperature for 4 h, poured into aqueous ammonium chloride, and extracted with ether. The ether extract was washed successively with aqueous sodium thiosulfate and water, dried over sodium sulfate, and evaporated to give an oil. The crude product was purified by column chromatography on silica gel (100 g) using ether–chloroform (3 : 97) as the eluent to give **10** (2.058 g: 52%), which was recrystallized from hexane–ether: mp 63—64 °C; IR: 3607, 3386 cm^{-1}; NMR: 1.60 (6H, s, $-\overset{|}{C}(CH_3)_2$), 3.78 (3H, s, $-OCH_3$), 4.68 (2H, s, $-CH_2OH$). Found: C, 67.26; H, 8.23%. Calcd for $C_{11}H_{16}O_3$: C, 67.32; H, 8.22%.

*3-Acetoxymethyl-2-(1-hydroxy-1-methylethyl)anisole (**11**).* A solution of **10** (345 mg), acetic anhydride (0.4 ml), and pyridine (0.2 ml) was allowed to stand at room temperature for 15 h and diluted with ether. The ether solution was washed successively with dilute hydrochloric acid, aqueous sodium hydrogencarbonate, and water. After drying over sodium sulfate, the solvent was evaporated to dryness and the residue was chromatographed on silica gel (20 g) using ether–benzene (1 : 9) as the eluent to give a monoacetate (**11**) (352 mg: 84%) which was then recrystallized from petroleum benzin; mp 61—62 °C; IR: 3585, 3511, 1733 cm^{-1}; NMR: 1.63 (6H, s, $-\overset{|}{C}(CH_3)_2$), 2.02 (3H, s, $-OCOCH_3$), 3.00 (1H, bs, –OH), 3.82 (3H, s, $-OCH_3$), 5.48 (2H, s, $-CH_2O-$). Found: C, 65.61; H, 7.58%. Calcd for $C_{13}H_{18}O_4$: C, 65.53; H, 7.61%.

*3-Acetoxymethyl-2-isopropenylanisole (**12**) and 4-Methoxy-3,3-dimethylphthalide (**14**).* A solution of **11** (1.880 g) and *p*-toluenesulfonic acid (200 mg) in dry benzene (20 ml) was heated at 60 °C for 10 min, cooled to room temperature, and then diluted with ether. The solution was washed with aqueous sodium hydrogencarbonate and water, dried over sodium sulfate, and evaporated *in vacuo* to give an oil (1.812 g), whose NMR spectrum suggested the presence of the isopropenyl compound (**12**) and 7-methoxy-1,1-dimethyl-1,3-dihydroisobenzofuran (**13**); NMR: 1.47 (6H, s, $-\overset{|}{C}(CH_3)_2$), 3.83 (3H, s, $-OCH_3$), 4.94 (2H, s, $-OCH_2-$). Since the separation of **12** and **13** was unsuccessful, the above crude oil (1.812 g) was immediately oxidized with Jones reagent (8 N, 3.0 ml) in acetone (8.0 ml) at 16 °C for 1 h. The reaction mixture was diluted with ether, washed with water, and then dried over sodium sulfate. After the solvent had been evaporated, the residue was purified by column chromatography on silica gel (60 g) using benzene as the eluent to give **12** (764 mg: 44%) as an oil. IR: 1731, 1642 cm^{-1}; NMR: 2.00 (6H, s, $=\overset{|}{C}CH_3$ and $-OCOCH_3$), 3.78 (3H, s, $-OCH_3$), 4.79 and 5.23 (each 1H and bs, $-\overset{|}{C}=CH_2$), 5.01 (2H, s, $-CH_2O-$). Found: C, 70.84; H, 7.47%. Calcd for $C_{13}H_{16}O_3$: C, 70.89; H, 7.32%.

Further elution with ether–benzene (1 : 9) gave a phthalide (**14**) (323 mg: 21%) which was recrystallized from hexane: mp 88—89 °C; IR: 1751 cm^{-1}; NMR: 1.65 (6H, s, $-\overset{|}{C}(CH_3)_2$), 3.95 (3H, s, $-OCH_3$). Found: C, 68.90; H, 6.35%. Calcd for $C_{11}H_{12}O_3$: C, 68.73; H, 6.29%.

*Conversion of the Phthalide (**14**) into the Diol (**10**).* A mixture of **14** (1.020 g), lithium aluminium hydride (302 mg), and dry tetrahydrofuran (35 ml) was refluxed for 3 h. The reaction mixture was decomposed with aqueous ammonium chloride, extracted with ether, and the extract was washed with water. After drying over sodium sulfate, the solvent was evaporated *in vacuo* to give the diol (**10**) (968 mg: 93%) as a solid. The IR and NMR spectra were identical with those of the above authentic diol (**10**).

*3-Acetoxymethyl-2-isopropylanisole (**15**).* A mixture of **12** (2.988 g) and PtO_2 (170 mg) in ethanol (10 ml) was subjected to catalytic hydrogenation at room temperature for *ca.* 25 min. After the usual work-up, the crude product was purifi-

ed by column chromatography on silica gel (50 g) using benzene as the eluent to give **15** (2.733 g: 91%), which was recrystallized from methanol: mp 31.5—32 °C; IR: 1731 cm^{-1}; NMR: 1.32 (6H, d, J=7 Hz, $-CH(C\underline{H}_3)_2$), 1.99 (3H, s, $-OCOCH_3$), 3.18 (1H, m, $-C\underline{H}(CH_3)_2$), 3.80 (3H, s, $-OCH_3$), 5.05 (2H, s, $-CH_2O-$). Found: C, 70.48; H, 8.25%. Calcd for $C_{13}H_{18}O_3$: C, 70.24; H, 8.16%.

*3-Hydroxymethyl-2-isopropylanisole (**16**).* A mixture of **15** (2.544 g), lithium aluminium hydride (434 mg), and dry ether (40 ml) was stirred at room temperature for 1.5 h, and then decomposed with aqueous ammonium chloride. The mixture was extracted with ether. The ether extract was washed with water, dried over sodium sulfate, and then evaporated to give an alcohol (**16**) (2.036 g: 99%), which was used directly in the subsequent reaction. For microanalysis an aliquot of the crude product (157 mg) was purified by column chromatography on silica gel (20 g) using ether–benzene (5 : 95) as the eluent to give the pure alcohol (147 mg). IR: 3618, 3415 cm^{-1}; NMR: 1.30 (6H, d, J= 7 Hz, $-CH(C\underline{H}_3)_2$), 1.95 (1H, bs, –OH), 3.29 (1H, m, $-C\underline{H}-(CH_3)_2$), 3.80 (3H, s, $-OCH_3$), 4.51 (2H, s, $-CH_2O-$). Found: C, 73.45; H, 9.02%. Calcd for $C_{11}H_{16}O_2$: C, 73.30; H, 8.95%.

*3-Chloromethyl-2-isopropylanisole (**17**).* A solution of **16** (2.156 g) and thionyl chloride (1.7 ml) in dry ether (5.0 ml) was stirred at room temperature for 2 h, and then evaporated *in vacuo*. The residue was dissolved in dry benzene and the solution was evaporated *in vacuo* to afford **17** (2.278 g: 96%) which, without purification, was used in the next reaction. NMR: 1.36 (6H, d, J=7 Hz, $-CH(C\underline{H}_3)_2$), 3.22 (1H, m, $-C\underline{H}(CH_3)_2$), 3.82 (3H, s, $-OCH_3$), 4.53 (2H, s, $-CH_2-$).

*(2-Isopropyl-3-methoxybenzyl)triphenylphosphonium Chloride (**8**).* A solution of **17** (2.595 g) and triphenylphosphine (3.444 g) in dry benzene (10 ml) was refluxed for 16 h. The precipitates (**8**) (2.627 g, mp 239—241 °C) were filtered and washed with dry benzene. The filtrate was further refluxed for 14 h to give an additional salt (2.299 g, mp 239—242 °C).

*(−)-6-(2-Isopropyl-3-methoxystyryl)-1,5,5-trimethylcyclohexene (**18**).* A solution of butyllithium in hexane (15%; 4.5 ml) was added at room temperature to a stirred suspension of **8** (4.16 g) in dry benzene (25 ml) in a stream of nitrogen. The mixture was stirred at room temperature for 1.5 h and a solution of (*R*)-(−)-α-cyclocitral (**7**)[10,11] (860 mg), $[\alpha]_D$ −710° (EtOH), in dry benzene (5.0 ml) was added. After stirring at room temperature for 4 h, the reaction mixture was poured into a mixture of ice and aqueous ammonium chloride, and extracted with ether. The ether extract was washed with brine, dried over sodium sulfate, and then evaporated. The residue was triturated with hexane and the precipitated triphenylphosphine oxide was removed by filtration. The filtrate was evaporated and the residue was purified by column chromatography on silica gel (100 g) using hexane–benzene (9 : 1) as the eluent to give **18** (733 mg: 44%) as an oil. $[\alpha]_D$ −248°; NMR: 0.92 and 0.96 (each 3H and s, $-\dot{C}(CH_3)_2$), 1.30 (6H, d, J= 7 Hz, $-CH(C\underline{H}_3)_2$), 1.68 (3H, bs, $=\dot{C}CH_3$), 3.38 (1H, m, $-C\underline{H}(CH_3)_2$), 3.80 (3H, s, $-OCH_3$), 5.43 (1H, m, $-CH=\dot{C}-$), 5.63 (1H, dd, J=9 and 15 Hz, $-\dot{C}H-C\underline{H}=CH-$), 6.68 (1H, d, J=15 Hz, $-\dot{C}H-CH=C\underline{H}-$). Found: C, 84.72; H, 10.16%. Calcd for $C_{21}H_{30}O$: C, 84.51; H, 10.13%.

*(−)-2-(2,6,6-Trimethyl-2-cyclohexenyl)-1-(2-isopropyl-3-methoxyphenyl)ethane (**19**).* A suspension of **18** (1.550 g) and 5% Pd–C (700 mg) in ethanol (6.0 ml) was stirred at room temperature in an atmosphere of hydrogen. After one mole equivalent of hydrogen had been absorbed (*ca.* 80 min), the mixture was filtered. The filtrate was evaporated and the residue was purified by column chromatography on silica gel (150 g) using hexane and then hexane–benzene (7 : 3) as the eluents to give the dihydro compound (**19**) (1.253 g: 80%) as an oil. $[\alpha]_D$ −99.7°; NMR: 0.91 and 1.01 (each 3H and s, $-\dot{C}(CH_3)_2$), 1.33 (6H, d, J=7 Hz, $-CH(C\underline{H}_3)_2$), 1.73 (3H, bs, $=\dot{C}CH_3$), 3.18 (1H, m, $-C\underline{H}-(CH_3)_2$), 3.78 (3H, s, $-OCH_3$), 5.29 (1H, m, $-CH=\dot{C}-$). Found: C, 84.24; H, 10.79%. Calcd for $C_{21}H_{32}O$: C, 83.94; H, 10.73%.

*Intramolecular Cyclization of **19**.* Anhydrous aluminium chloride (450 mg) was added at 35 °C to a solution of **19** (1.015 g) in dichloromethane (10 ml). The reaction mixture was stirred at 35 °C for 20 min, poured into ice–water, and then extracted with ether. The ether extract was washed with water, dried over sodium sulfate, and evaporated to dryness. The crude product was chromatographed on silica gel (120 g) using hexane as the eluent to give the *cis*-isomer (**21**) (305 mg: 30%). $[\alpha]_D$ −44.3° (EtOH); NMR ($CDCl_3$): 0.41 (3H, s, $C_{4\beta}-CH_3$), 0.94 (3H, s, $C_{4\alpha}-CH_3$), 1.15 (3H, s, $C_{10}-CH_3$), 1.24 and 1.33 (each 3H, d, and J=7 Hz, $-CH-(C\underline{H}_3)_2$), 3.42 (1H, m, $-C\underline{H}(CH_3)_2$), 3.79 (3H, s, $-OCH_3$), 6.70 and 7.13 (each 1H, d, and J=9 Hz, $C_{11}-H$ and $C_{12}-H$). Found: C, 83.86; H, 10.74%. Calcd for $C_{21}H_{32}O$: C, 83.94; H, 10.73%.

Further elution gave the *trans*-isomer (**20**) (565 mg: 56%), $[\alpha]_D$ +23.3° (EtOH), which was recrystallized from ethanol to give pure totaryl methyl ether. Mp 91—93 °C; $[\alpha]_D$ +40.6° (EtOH) [lit,[6] mp 91—92 °C, $[\alpha]_D$+42° (EtOH)]; NMR ($CDCl_3$): 0.94 (6H, s, $-\dot{C}(CH_3)_2$), 1.20 (3H, s, $C_{10}-CH_3$), 1.31 (6H, d, J=7 Hz, $-CH(C\underline{H}_3)_2$), 3.29 (1H, m, $-C\underline{H}(CH_3)_2$), 3.77 (3H, s, $-OCH_3$), 6.72 and 7.12 (each 1H, d, and J=9 Hz, $C_{11}-H$ and $C_{12}-H$). Found: C, 83.72; H, 10.80%. Calcd for $C_{21}H_{32}O$: C, 83.94; H, 10.73%.

*(+)-Totarol (**1**).* A mixture of **20** (45 mg) and boron tribromide (0.04 ml) in dichloromethane (1.5 ml) was stirred at 0—5 °C for 15 min and then at room temperature for 2 h. The reaction mixture was poured into ice–water and extracted with ether. The ether extract was washed with water, dried over sodium sulfate, and then evaporated to dryness. The crude product was purified by column chromatography on silica gel (10 g) using hexane–benzene (3 : 7) as the eluent to afford totarol (**1**) (38 mg: 88%) which was recrystallized from petroleum ether: mp 132—133 °C; $[\alpha]_D$+41.5° (lit,[13] mp 131—132 °C, $[\alpha]_D$+42°); IR: 3608, 3352 cm^{-1}; NMR ($CDCl_3$): 0.93 and 0.95 (each 3H and s, $-\dot{C}(CH_3)_2$), 1.18 (3H, s, $C_{10}-CH_3$), 1.33 (6H, d, J=7 Hz, $-CH(C\underline{H}_3)_2$), 4.50 (1H, bs, –OH), 6.49 and 7.01 (each 1H, d, and J=9 Hz, $C_{11}-H$ and $C_{12}-H$). Found: C, 83.71; H, 10.63%. Calcd for $C_{20}H_{30}O$: C, 83.86; H, 10.56%.

*(+)-Totaryl Acetate (**22**).* A solution of **1** (60 mg), acetic anhydride (0.2 ml), and pyridine (0.8 ml) was heated at 75—80 °C for 2 h. After the usual work-up, the crude product was purified by column chromatography on silica gel (10 g) using hexane–benzene (1 : 1) as the eluent to give the acetate (**22**) (56 mg: 82%) which was recrystallized from ethanol: mp 122—124 °C (lit,[6] mp 122—124 °C); $[\alpha]_D$+46.0°; IR: 1751 cm^{-1}; NMR: 0.95 (6H, s, $-\dot{C}(CH_3)_2$), 1.20 (3H, s, $C_{10}-CH_3$), 1.21 and 1.24 (each 3H, d, and J= 7 Hz, $-CH(C\underline{H}_3)_2$), 2.21 (3H, s, $-OCOCH_3$), 3.21 (1H, m, $-C\underline{H}(CH_3)_2$), 6.65 and 7.05 (each 1H, d, and J=9 Hz, $C_{11}-H$ and $C_{12}-H$). Found: C, 80.64; H, 9.89%. Calcd for $C_{22}H_{32}O_2$: C, 80.44; H, 9.83%.

References

1) T. H. Easterfield and J. C. McDowell, *Trans. New Zealand Inst.*, **43**, 55 (1911); **48**, 578 (1915).
2) W. F. Short and H. Wang, *J. Chem. Soc.*, **1951**, 2979, and references cited therein.
3) J. A. Barltrop and N. A. J. Rogers, *J. Chem. Soc.*, **1958**, 2566.
4) Y-L. Chow and H. Erdtman, *Acta Chem. Scand.*, **14**, 1852 (1960); **16**, 1305 (1962); *Chem. Abstr.*, **59**, 1689e (1963).
5) C. W. Brandt and B. R. Thomas, *New Zealand J. Sci. Tech.*, **33B**, 950 (1951).
6) R. C. Cambie and L. N. Mander, *Tetrahedron*, **18**, 465 (1962).
7) R. C. Cambie, W. R. J. Simpson, and L. D. Colebrook, *Tetrahedron*, **19**, 209 (1963).
8) C. P. Falshaw, A. W. Johnson, and T. J. King, *J. Chem. Soc.*, **1963**, 2422.
9) A. C. Day, *J. Chem. Soc.*, **1964**, 3001.
10) C. H. Eugster, R. Buchecker, Ch. Tscharner, G. Uhde, and G. Ohloff, *Helv. Chim. Acta*, **52**, 1729 (1969).
11) T. Matsumoto and S. Usui, *Bull. Chem. Soc. Jpn.*, **52**, 212 (1979).
12) M. Uemura, S. Tokuyama, and T. Sak n, *Chem. Lett.*, **1975**, 1195.
13) R. Hodges, *J. Chem. Soc.*, **1961**, 4247.

Improvement of Acetone Yield in the Oxidation of Propylene

Mamoru Ai* and Atsumu Ozaki

Research Laboratory of Resources Utilization, Tokyo Institute of Technology, Nagatsuta, Midori-ku, Yokohama 227

(Received September 1, 1978)

The outstanding property of the SnO_2–MoO_3 catalyst in the oxidation of propylene to acetone was confirmed by tests of various oxide catalysts supported on pumice. The optimum composition was found to be SnO_2-70/MoO_3-30 mol % for the oxidation at from 170 to 260 °C. It was also found that this pumice-supported catalyst is sufficiently selective for the acetone formation even at a high temperature of 260 °C, and that it gives a high yield of acetone while keeping its high selectivity. The selectivity increases up to 90 mol % with an increase in the partial pressure of water vapor and with a decrease in the oxygen partial pressure. On the basis of such information, it can be said that a high yield of acetone can be obtained by the divided introduction of oxygen.

It has been shown that propylene can be oxidized to acetone in the presence of water vapor on molybdenum-containing catalysts,[1–5] whereas the acetone yields attained in the previous works were limited because of low conversion at low temperatures or because of low selectivity at higher temperatures.[2–5] Thus, further study is required to improve the acetone yield.

Experimental

Catalysts. A number of mixed oxide catalysts were prepared by the procedures described in previous papers.[6–8] That is, an aqueous solution or slurry containing the required quantity of metal compounds was mixed with 10—20 mesh pumice in a fixed ratio of one g-atom metal per 500 ml of pumice (in apparent volume), followed by evaporation to dryness with vigorous stirring and calcination in a stream of air at 500 °C for 4—5 h.

Procedures. The catalytic reactions were carried out in a conventional continuous-flow system. The reactor was made of a steel tube coated with aluminum, 50 cm in length and 1.8 cm i.d., which was mounted vertically and immersed in a lead bath. The reactant gas was fed from the top of the reactor, with water or isopropyl alcohol (IPA) being introduced into a preheater section by means of an injection syringe pump.

The amount of catalyst in the propylene oxidation was 20, 30, or 40 g, and the feed rates of the reactants in a standard run were as follows: propylene-20/air-20/water vapor-76 ml (volume at 25 °C)/min. The effluent gas from the reactor was led successively into three chilled water-scrubbers to recover the water-soluble compounds. At the end of a 1-h run, the contents of the scrubbers (about 50 ml) were collected and analyzed by gas chromatography. The inlet and exit gases were intermittently analyzed.

The reaction of IPA was carried out at a fixed concentration of IPA (1.65 mol% in air) and a fixed total flow rate (1.5 l/min), changing the amount of catalyst in the range from 5 to 20 g.

Results and Discussion

Catalyst Screening. Acetone-forming Activities of Various Composite Oxide Catalysts: It seems apparent from the previous studies[8–11] that the propylene oxidation to acetone proceeds through an alcoholic intermediate, requiring two different functions for the catalyst: the hydration of olefin and the oxidative dehydrogenation of the alcoholic intermediate. It can, accordingly, be expected that information regarding the two functions will be helpful in the exploration of an effective catalyst. Since the hydration activity may be expected to run parallel with the activity for the dehydration of IPA, the catalytic activity for the dehydration and dehydrogenation of IPA in the presence of an excess of air would be relevant as measures of the two functions.

Since the first function is generally accepted to be associated with acid catalysts, various binary or ternary mixed oxide catalysts of an acidic property were tested for the ability to form acetone from propylene. The amount of catalyst used was 20 g, and the standard feed rates of the reactants were adopted. The results are summarized in Tables 1 and 2.

Another series of experiments were carried out with each catalyst using a mixture of IPA and air as the reactant. The rates of IPA dehydration, r_p, and dehydrogenation, r_a (mol/h·g-catalyst), were measured at 175 °C. They are also shown in Tables 1 and 2.

The results in Tables 1 and 2 may be summarized as follows.

(i) Acetone is obtained, more or less, with every V_2O_5- or MoO_3-containing catalyst, at least at a low temperature. The acetone yields is likely to increase with an increase in r_p, which can be regarded as a measure of the acidity.[6–8]

(ii) Although it gives a strikingly high value of r_p, WO_3–P_2O_5 does not convert IPA to acetone; thus, it is inactive for the propylene oxidation to actone.

(iii) The SnO_2–MoO_3 catalyst gives a strikingly high yield of acetone. It should be noted that both r_p and r_a are larger on this catalyst than on other catalysts. It is also notable that the high selectivity to acetone is retained at temperatures as high as 220 °C.

(iv) The Sn-60/V-40 is the second best catalyst.

Effect of the SnO_2–MoO_3 Composition on the Yield of Acetone: Five SnO_2–MoO_3 catalysts of different compositions were tested for the yield of acetone as well as for r_p and r_a, where the feed rate of air was twice as large as in the standard condition. The yields of acetone at 175, 190, 210, and 240 °C are plotted in Fig. 1, together with the values of r_p and r_a obtained at 140 °C.

Although the highest yield of acetone is obtained at around 30 atom % Mo at each temperature, it is noticeable that the effect of the temperature increase on the acetone yield is more marked with the catalysts

Table 1. Oxidation of propylene to acetone using various MoO_3-based catalysts[a]

Catalyst (atomic ratio)	Reactions for IPA at 175 °C[b]		Oxidation of propylene					
			Temp (°C)	Conversion (%) of propylene to				
	r_p	r_a		Acetone	(Selectivity)[c]	Acid[d] (×2/3)	$CO+CO_2$ (×1/3)	Total[e]
Mo-P (9-1)	10.6	1.2	330	0.6	(37)	0.25	0.9	1.8
Mo-S (9-1)	12.0	0.5	320	0.83	(35)	0.5	1.0	2.4
Mo-W (8-2)	0.8	1.2	320	0.91	(50)	0.1	0.8	1.8
(2-8)	25.0	8.4	293	3.21	(66)	0.3	1.4	4.9
Mo-U (8-2)	3.4	1.0	369	1.94	(39)	0.8	2.1	4.9
(2-8)	8.8	0.5	300	0.15	(7)	0.3	1.8	2.3
Mo-Ti (5-5)	36.0	5.8	248	2.12	(72)	0.3	0.5	2.9
			290	4.42	(52)	1.3	2.8	8.5
Mo-Ti-P (5-5-1)	32.0	3.2	250	1.8	(69)	0.2	0.6	2.6
			292	2.66	(41)	0.8	3.0	6.4
Mo-Sn (3-7)	217.0	205	182	19.2	(90)	0.8	1.4	21.4
			219	24.5	(87)	1.0	2.5	28.0
Mo-Fe (2-8)	42.0	22.0	235	3.0	(59)	0.9	1.2	5.1
			290	2.25	(22)	2.5	5.5	10.3
Mo-Bi (8-2)	4.6	0.9	330	1.23	(44)	0.5	1.1	2.8
Mo-Bi-P (9-1-2)	15.0	0.1	330	2.20	(46)	1.2	1.4	4.8

a) Feed rates=propylene-20/air-20/water vapor-76 ml/min, amount of catalyst used=20 g. b) IPA concentration =1.65 mol % in air. c) 100×(acetone)/(total). d) Calculated as acetic acid. e) Sum of acetone, acid, CO, and CO_2.

Table 2. Oxidation of propylene to acetone using various V_2O_5- and WO_3-based catalysts[a]

Catalyst (atomic ratio)	Reactions for IPA at 175 °C[b]		Oxidation of propylene					
			Temp (°C)	Conversion (%) of propylene to				
	r_p	r_a		Acetone	(Selectivity)[c]	Acid[d] (×2/3)	$CO+CO_2$ (×1/3)	Total[e]
V-Mo (85-15)	39.0	7.8	214	2.14	(60)	1.1	0.3	3.5
			242	2.40	(38)	1.9	2.0	6.3
V-W (8-2)	47.0	14.0	198	5.20	(53)	2.9	1.8	9.9
			214	4.28	(49)	1.1	3.4	8.8
(2-8)	5.0	2.5						
V-Ti (8-2)	37.0	36.0	209	1.20	(32)	1.7	0.8	3.7
			234	1.04	(15)	1.2	4.8	7.0
(1-9)	2.4	45.0	187	0.27	(20)	0.9	0.2	1.4
			220	0.87	(35)	0.6	1.0	2.4
V-Sn (4-6)	80.0	52.0	176	4.3	(72)	1.2	0.5	6.0
			187	6.36	(69)	1.7	1.2	9.3
			209	10.0	(70)	1.4	2.9	14.3
			234	8.86	(58)	2.4	4.0	15.2
(1-9)	2.0	105.0	220	0.90	(13)	1.8	4.2	6.9
W-P (9-1)	about 400.0	0.0	300	trace	(0)	trace	0.5	0.5

a) Feed rates=propylene-20/air-20/water vapor-76 ml/min, amount of catalyst used=20 g. b) IPA concentration =1.65 mol % in air. c) 100×(acetone)/(total). d) Calculated as acetic acid. e) Sum of acetone, acid, CO, and CO_2.

with a lower Mo content, suggesting that the rate-limiting step may be different depending on the Mo content. In fact, r_p is much larger than r_a on the 40% Mo catalyst, while r_a is much larger than r_p on the 20% Mo catalyst. If r_p and r_a represent the two functions required, the rate-limiting step on the 40% Mo catalyst would be the oxidation of the alcoholic intermediate. The less extensive effect of the temperature would be reasonable, because the equilibrium concentration of the alcoholic intermediate should decrease with an increase in the temperature. On the other hand, the rate-limiting step on the 20% Mo catalyst would be the hydration to form the alcoholic intermediate; this is in agreement with the more marked effect of the temperature. Thus, r_p and r_a can be regarded as parameters for the two functions.

Effect of the Third Components Added to Sn-70/Mo-30: The effect of the third component to improve the ace-

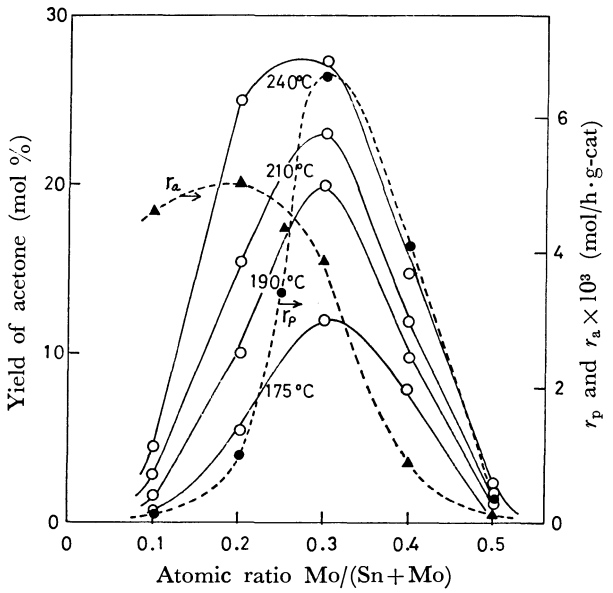

Fig. 1. Effect of SnO_2–MoO_3 composition on the yield of acetone and the values of r_p and r_a.
Oxydation of propylene; catalyst used=20 g, feed rates=propylene-20/air-40/water vapor-76 ml/min (at 25 °C). r_p and r_a; dehydration and dehydrogenation rates of IPA at 140 °C and 1.65 mol % IPA in air.

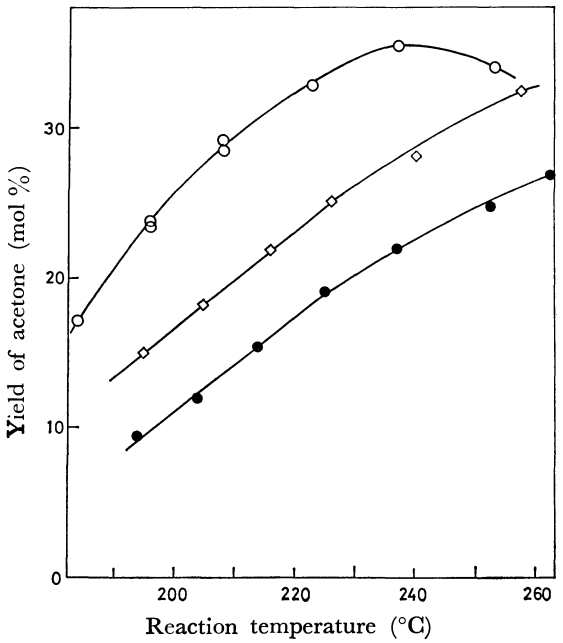

Fig. 2. Effect of reaction temperature on the yield of acetone. Feed rates; propylene-20/oxygen-15/nitrogen-24/water vapor-104 ml/min (at 25 °C), amount of catalyst used; (○)=20 g, (◇)=15 g, (●)=10 g.

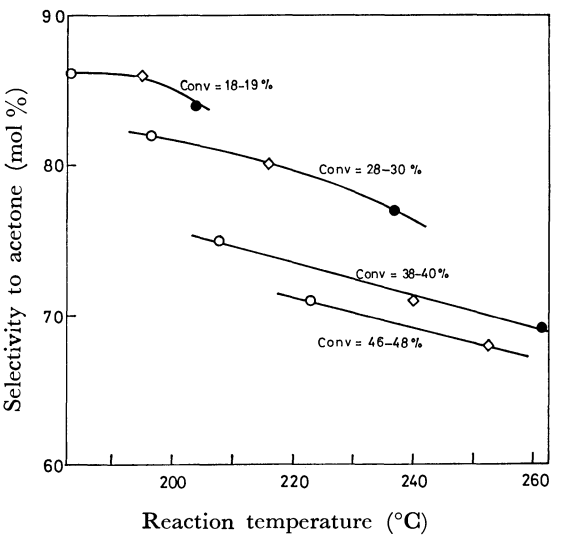

Fig. 3. Effects of reaction temperature and propylene conversion on the selectivity to acetone. Reaction conditions and notations are the same as in Fig. 2.

tone yield was tested with P_2O_5, SO_3, V_2O_5, U_3O_8, TiO_2, Al_2O_3, Fe_2O_3, and SiO_2 by adding 2—10 atom% to Sn-70/Mo-30, whereas none of then showed any improvement.

Effect of the Reaction Conditions on the Yield of Acetone. Since the Sn-70/Mo-30 catalyst proved to be the best, the effect of the reaction conditions were investigated on this catalyst.

Effect of the Reaction Temperature: The effects of the reaction temperature on the selectivity to acetone and on the yield were tested using different amounts of the catalyst. The results are shown in Figs. 2 and 3. At the acetone yield of around 35 mol%, almost all of the oxygen fed in was consumed.

The results may be summarized as follows:

(i) The yield of acetone increases with an increase in the temperature up to about 260 °C provided the oxygen is not completely consumed.

(ii) The selectivity largely depends on the conversion of propylene (Fig. 3), the effect of the temperature being less marked.

Effect of the Feed Rate of Oxygen and Nitrogen: Two series of runs were performed, changing the feed rate of oxygen or nitrogen. The results are shown in Table 3. Except for Run 56, the conversion of oxygen was very close to 100%, so that the total conversion of propylene increased with the flow rate of oxygen.

The results in Table 3 may be summarized as follows:

(i) The selectivity to acetone decreased as the inlet oxygen concentration increases, so that there is an optimum value in the oxygen-flow rate to give the highest yield of acetone for a fixed flow rate of propylene. An acetone yield of 43 mol % was achieved with a selectivity of 78 mol %.

(ii) The selectivity to acetone can be improved by dilution with nitrogen, suggesting a suppression of complete oxidation in the presence of nitrogen.

Effect of the Feed Rate of Water Vapor: The acetone-synthesis runs were carried out at different concentrations of water vapor. The results, shown in Table 4, indicate that the selectivity increases markedly with an increase in the water-vapor pressure. In the absence of water vapor, the catalytic activity was seriously impaired by the deposit of nonvolatile materials, while the catalyst was easily regenerated by air treatment at 500 °C. This suggests that the water vapor serves to prevent catalyst poisoning as well as to suppress complete oxidation.

Table 3. Effects of feed rates of oxygen and nitrogen on the yield of acetone[a]

Run No.	Feed rates of (ml/min)				Conversion (%) of propylene to				
	C_3H_6	H_2O	N_2	O_2	Acetone	(Selectivity)[b]	Acid[c] (×2/3)	$CO+CO_2$ (×1/3)	Total[d]
51	20	76	38	2	15.6	(92)	0.6	0.7	16.9
52	20	76	36	4	26.1	(88)	1.4	1.7	29.2
53	20	76	20	10	36.4	(89)	2.7	1.7	40.8
54	20	76	40	10	37.8	(86)	2.3	3.7	43.8
55	20	76	20	17	43.7	(78)	4.2	7.8	55.7
56	20	76	40	17	40.2	(83)	3.1	5.6	48.9
57	20	76	20	40	34.6	(35)	8.6	55.0	98.2
58	20	76	0	3	21.1	(89)	0.8	1.7	23.6
59	20	76	0	5	29.6	(87)	1.7	2.8	34.1
60	20	76	0	10	33.6	(78)	2.2	7.3	43.1
61	20	76	0	17	40.0	(75)	3.0	10.1	53.1

a) Catalyst=SnO_2-70/MoO_3-30, amount of catalyst used=40 g, temperature=215 °C. b) 100×(acetone)/(total). c) Calculated as acetic acid. d) Sum of acetone, acid, CO, and CO_2.

Table 4. Effect of feed rate of water vapor on the yield of acetone[a]

Run No.	Feed rates of (ml/min)				Conversion (%) of propylene to				
	C_3H_6	H_2O	N_2	O_2	Acetone	(Selectivity)[b]	Acid[c] (×2/3)	$CO+CO_2$ (×1/3)	Total[d]
62	20	0	20	10	12.2	(66)	0.4	5.8	18.4
63	20	20	20	10	22.0	(79)	1.9	4.0	27.9
64	20	76	20	10	36.4	(84)	2.7	4.5	43.6
65	20	150	20	10	47.0	(86)	2.7	5.2	54.9
66	20	152	16	4	27.7	(92)	1.0	1.6	30.3
67	20	152	32	8	44.0	(87)	2.5	4.1	50.6
68	20	152	20	17	46.5	(75)	3.8	11.3	61.6
69	20	152	20	40	53.5	(66)	6.9	20.0	80.4

a) Catalyst=SnO_2-70/MoO_3-30, amount of catalyst used=40 g, temperature=215 °C. b) 100×(acetone)/(total). c) Calculated as acetic acid. d) Sum of acetone, acid, CO, and CO_2.

Table 5. Oxidation of propylene by divided introduction of oxygen[a]

Reactor 1		Reactor 2		Conversion (%) of propylene to				
Temp (°C)	Feed of air (ml/min)	Temp (°C)	Feed of air (ml/min)	Acetone	(Selectivity)[b]	Acid[c] (×2/3)	$CO+CO_2$ (×1/3)	Total[d]
197	20			24.5	(90)	1.2	1.6	27.3
218	20	Without		26.8	(90)	1.1	1.9	29.8
194	40	Reactor 2		23.3	(90)	1.4	1.3	26.0
216	40			33.0	(83)	2.7	4.1	39.8
Without		220	20	23.3	(85)	2.4	1.9	27.6
Reactor 1		220	40	25.7	(85)	2.0	2.8	30.5
193	40	210	0	31.0	(86)	2.5	2.7	36.2
194	20	210	20	35.7	(88)	2.4	2.5	40.6
203	20	210	20	42.5	(88)	2.6	3.2	48.3
220	20	215	20	43.5	(87)	2.6	3.6	49.7
220	40	215	20	48.0	(85)	3.2	4.9	56.1
220	40	218	O_2=10	49.5	(84)	4.0	5.6	59.1

a) Catalyst=SnO_2-70/MoO_3-30, amount of catalyst used=20 g (Reactor 1) and 20 g (Reactor 2), feed rate of propylene=20 ml/min, feed rate of water vapor for each reactor=76 ml/min. b) 100×(acetone)/(total). c) Calculated as acetic acid. d) Sum of acetone, acid, CO, and CO_2.

Improvement of the Acetone Yield. Although a high selectivity to acetone can be obtained by lowering the concentration of oxygen, the yield is limited by the oxygen feed. Thus, the reaction was performed successively in two reactor, with additional air or oxygen supplied to the second reactor. As is shown in Table 5, the yield is markedly improved by such a divided introduction of oxygen, while retaining the high selectivity. In this way, an acetone yield of 48—50 mol % is achieved with a selectivity of about 85 mol %. Although a retardation of acetone formation by product acetone was previously reported[12], the above result shows that the retardation by acetone is not strong.

Conclusion

The selective oxidation of propylene to acetone can be performed on SnO_2–MoO_3/pumice, particularly with a composition of 30% Mo; a high water partial pressure and a low oxygen partial pressure are requisites in improving the acetone yield. The superior performance of the SnO_2–MoO_3 catalyst is understood in terms of two functions: the hydration of propylene and the oxidative dehydrogenation of IPA. When the Mo content is varied, both functions, indicated by r_p and r_a, attain maxima at around 20 to 30% Mo, thus giving rise to an optimum composition of 30% Mo.

References

1) J. Buiten, *J. Catal.*, **10**, 188 (1968).
2) Y. Morooka, S. Tan, and A. Ozaki, *J. Catal.*, **12**, 291 (1968); *Bull. Chem. Soc. Jpn.*, **41**, 2820 (1968).
3) S. Ogasawara, S. Takahashi, A. Fukai, and Y. Nakata, *Kogyo Kagaku Zasshi*, **72**, 2244 (1969).
4) S. Tan, Y. Morooka, and A. Ozaki, *J. Catal.*, **17**, 132 (1970).
5) Y. Morooka, Y. Takita, and A. Ozaki, *J. Catal.*, **23**, 183 (1971).
6) M. Ai, *J. Catal.*, **40**, 318 and 327 (1975).
7) M. Ai, *J. Catal.*, **49**, 305 (1977).
8) M. Ai, *J. Catal.*, **50**, 291 (1977).
9) J. Buiten, *J. Catal.*, **13**, 373 (1969).
10) Y. Morooka, Y. Takita, and A. Ozaki, *J. Catal.*, **27**, 177 (1972).
11) J. Buiten, *J. Catal.*, **27**, 232 (1972).
12) Y. Takita, Y. Moro-oka, and A. Ozaki, *J. Catal.*, **52**, 95 (1978).

The Total Synthesis of (+)-Taxoquinone, (−)-7α-Acetoxyroyleanone, (−)-Dehydroroyleanone, (−)-Horminone, (−)-7-Oxoroyleanone, and (+)-Inuroyleanol

Takashi MATSUMOTO* and Shogo HARADA

Department of Chemistry, Faculty of Science, Hiroshima University, Higashisenda-machi, Hiroshima 730

(Received September 4, 1978)

Methylation of 12-benzoyloxyabieta-8,11,13-trien-11-ol with methyl iodide afforded 11-benzoyloxy-12-methoxyabieta- and 12-benzoyloxy-11-methoxyabieta-8,11,13-triene (**9**). Oxidation of the latter product with chromium trioxide, followed by sodium borohydride reduction and acetylation, gave 7β-acetoxy-12-benzoyloxy-11-methoxyabieta-8,11,13-triene (**17**) and its 7α-acetoxy isomer (**18**) in a ratio of *ca.* 5 : 1. On the other hand, treatment of **9** with lead tetraacetate produced **17** and **18** in a ratio of *ca.* 1 : 2. The 7β-acetate (**17**) was then oxidized with chromium trioxide and the resulting *p*-quinone derivative was hydrolyzed with aqueous sodium hydroxide to give taxoquinone (**1**), which on dehydration gave dehydroroyleanone. Similarly, the 7α-acetate (**18**) was converted into horminone (**4**) *via* the *p*-quinone derivative, which was treated with aqueous sodium hydrogencarbonate to give 7α-acetoxyroyleanone. Oxidation of **4** with manganese dioxide afforded 7-oxoroyleanone. Methylation of **1** with diazomethane, followed by oxidation with a chromium trioxide–pyridine complex, afforded 12-methoxyabieta-8,12-diene-7,11,14-trione, which on reduction with sodium dithionite gave inuroyleanol.

There have been reports on the isolation and structural elucidation of many naturally-occurring highly-oxygenated tricyclic diterpenes possessing an oxygen function at the C-11 position. In previous papers,[1,2] we reported the successful oxidation of the C-11 position in the tricyclic C ring-aromatized diterpenes with benzoyl peroxide. As an extension of that work, our efforts were further directed toward the syntheses of highly-oxygenated tricyclic diterpenes possessing an abietane skeleton. This paper[3] describes the syntheses of (+)-taxoquinone (**1**),[4,5] (−)-7α-acetoxyroyleanone (**2**),[6,7] (−)-dehydroroyleanone (**3**),[5,6,8,9] (−)-horminone (**4**),[5,10] (−)-7-oxoroyleanone (**5**),[5,7] and (+)-inuroyleanol (**6**),[7] all starting from (+)-ferruginol (**7**). Since the total synthesis of optically active ferruginol[11] has recently been accomplished in our laboratory, the present work constitutes the total syntheses of all the above natural diterpenes (**1**—**6**).

The oxidation of ferruginol (**7**) with benzoyl peroxide in chloroform afforded 12-benzoyloxyabieta-8,11,13-trien-11-ol (**8**)[2] which was methylated with methyl iodide and anhydrous potassium carbonate in refluxing ethyl methyl ketone to give the two monomethyl ethers, **9** and **10**, in a ratio of *ca.* 3 : 2. In order to elucidate the structures of these two products, the minor product (**10**) was reduced with lithium aluminium hydride in ether to yield a phenol (**11**) which responded positively to the Gibbs test,[12] suggesting the presence of an aromatic proton para to a phenolic hydroxyl group. Therefore, the structure of **10** was determined as 11-benzoyloxy-12-methoxyabieta-8,11,13-triene.[13] This structure was further confirmed by the following conversion. The oxidation of **10** with chromium trioxide in acetic acid produced the corresponding 7-oxo compound (**12**), which on alkaline hydrolysis gave cryptojaponol (**13**).[2,14] The major product (**9**) was then hydrolyzed with aqueous sodium hydroxide in refluxing methanol to give another phenol (**14**) which, in contrast with **11**, showed a negative Gibbs test,[12] suggesting the presence of a substituent para to a phenolic hydroxyl group. Therefore, the structure of **9** was assigned as 12-benzoyloxy-11-methoxyabieta-8,11,13-triene. The compound **9** was also oxidized with chromium trioxide in acetic acid to give the corresponding 7-oxo compound (**15**) together with the *p*-benzoquinone derivative, which was identical with 12-benzoyloxyabieta-8,12-diene-11,14-dione (**16**)[2] prepared from **8** by oxidation with *m*-chloroperbenzoic acid. The reduction of **15** with sodium borohydride in methanol at 0 °C followed by acetylation of the resulting mixture of epimeric alcohols with acetic anhydride in pyridine at room temperature produced a mixture of 7β-acetoxy-12-benzoyloxy-11-methoxyabieta-8,11,13-triene (**17**) and its 7α-acetoxy isomer (**18**) in a ratio of *ca.* 5 : 1. The stereochemistry of the acetoxyl group was established on the basis of the C-7 proton signals with half-height width of 15 Hz at δ 5.93 ppm in **17** and 5 Hz at δ 5.86 ppm in **18** in their NMR spectra. This reaction procedure leading to the 7-acetoxy compounds (**17** and **18**) is

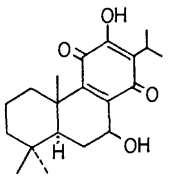

1

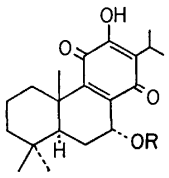

2 R=Ac
4 R=H

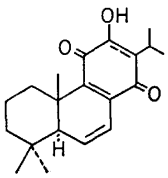

3

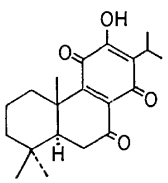

5

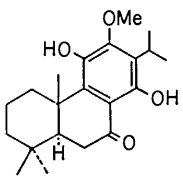

6

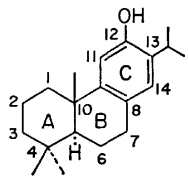

7

suitable for the synthesis of taxoquinone (**1**) possessing a 7β-hydroxyl group. However, for the syntheses of 7α-acetoxyroyleanone (**2**) and horminone (**4**) it is necessary to prepare **18** predominantly. For this purpose, the direct acetoxylation on the C-7 position in **9** was carried out with lead tetraacetate in refluxing acetic acid in a stream of nitrogen. The chromatographic purification of the crude porduct on silica gel afforded a mixture of **17** and **18** in a ratio of *ca.* 1 : 2. The 7β-acetate (**17**) was then oxidized with chromium trioxide in acetic acid at room temperature to yield 7β-acetoxy-12-benzoyloxyabieta-8,12-diene-11,14-dione (**19**) along with the 7-oxo compound (**15**). The hydrolysis of **19** with aqueous sodium hydroxide in refluxing methanol, followed by treatment with dilute hydrochloric acid, afforded taxoquinone (**1**). This was dehydrated[5] with *p*-toluenesulfonic acid in refluxing benzene to give dehydroroyleanone (**3**) and also methylated[5] with diazomethane to give 7β-hydroxy-12-methoxyabieta-8,12-diene-11,14-dione (**20**). Similarly, the 7α-acetate (**18**) was oxidized with chromium trioxide in acetic acid to give 7α-acetoxy-12-benzoyloxyabieta-8,12-diene-11,14-dione (**21**) along with the 7-oxo compound (**15**). The treatment of **21** first with aqueous sodium hydroxide in refluxing methanol, followed with dilute hydrochloric acid, produced horminone (**4**) which on oxidation[5] with manganese dioxide in dioxane afforded 7-oxoroyleanone (**5**). On the other hand, when **21** was hydrolyzed with aqueous sodium hydrogencarbonate in refluxing methanol, 7α-acetoxyroyleanone (**2**) was obtained. The hydroxyquinone (**20**) was then oxidized with a chromium trioxide–pyridine complex to give 12-methoxyabieta-8,12-diene-7,11,14-trione (**22**), which was reduced at 95 °C with sodium dithionite in acetic acid to afford inuroyleanol (**6**).

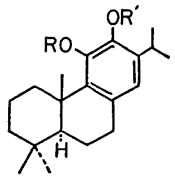

8 R=H, R'=COPh
9 R=Me, R'=COPh
10 R=COPh, R'=Me
11 R=H, R'=Me
14 R=Me, R'=H

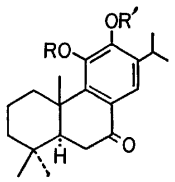

12 R=COPh, R'=Me
13 R=H, R'=Me
15 R=Me, R'=COPh

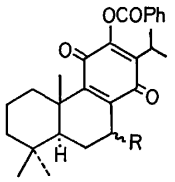

16 R=H
19 R=β-OAc
21 R=α-OAc

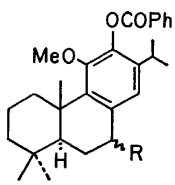

17 R=β-OAc
18 R=α-OAc

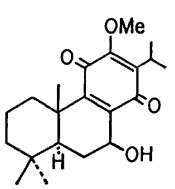

20

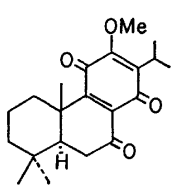

22

Experimental

All melting points are uncorrected. The IR and UV spectra were taken in chloroform and ethanol, respectively. The NMR spectra were obtained in carbon tetrachloride at 60 MHz with tetramethylsilane as an internal standard, unless otherwise stated. The chemical shifts are presented in terms of δ values; s: singlet, d: doublet, bd: broad doublet, dd: double doublet, t: triplet, m: multiplet. The optical rotations were measured in chloroform using a Yanaco OR-50D. Column chromatography was performed using Merck silica gel (0.063 mm).

Methylation of 12-Benzoyloxyabieta-8,11,13-trien-11-ol (8). A mixture of **8**[2] (10.00 g), methyl iodide (16.0 ml), and anhydrous potassium carbonate (40.0 g) in ethyl methyl ketone (50 ml) was refluxed for 8 h. The mixture was cooled to room temperature, poured into water, and extracted with ether. The ether extract was washed with brine, dried over sodium sulfate, and then evaporated *in vacuo*. The residue was chromatographed on silica gel (300 g) using benzene as the eluent to give 12-benzoyloxy-11-methoxyabieta-8,11,13-triene (**9**) (6.25 g: 60%) which was recrystallized from ether–methanol: mp 125—126 °C; $[\alpha]_D$+76.4°; IR: 1735 cm^{-1}; NMR: 0.95 (6H, s, $-\underset{|}{C}(CH_3)_2$), 1.15 and 1.17 (each 3H, d, and J=7 Hz, $-CH(C\underline{H}_3)_2$), 1.30 (3H, s, C_{10}–CH_3), 3.68 (3H, s, $-OCH_3$), 6.67 (1H, s, C_{14}–H), 7.3—8.3 (5H, m, aromatic protons). Found: C, 80.03; H, 8.45%. Calcd for $C_{28}H_{36}O_3$: C, 79.96; H, 8.63%.

Further elution gave 11-benzoyloxy-12-methoxyabieta-8,11,13-triene (**10**) (3.95 g: 38%) which was recrystallized from chloroform–acetone: mp 183.5—184.5 °C; $[\alpha]_D$+76.5°; IR: 1735 cm^{-1}; NMR: 0.91 and 0.96 (each 3H and s, $-\underset{|}{C}-(CH_3)_2$), 1.22 (6H, d, J=7 Hz, $-CH(C\underline{H}_3)_2$), 1.39 (3H, s, C_{10}–CH_3), 3.52 and 3.57 (each *ca.* 1.5 H and s, $-OCH_3$),[15] 6.74 (1H, s, C_{14}–H), 7.3—8.4 (5H, m, aromatic protons). Found: C, 80.24; H, 8.55%. Calcd for $C_{28}H_{36}O_3$: C, 79.96; H, 8.63%.

12-Methoxyabieta-8,11,13-trien-11-ol (11). A mixture of **10** (208 mg) and lithium aluminium hydride (300 mg) in dry ether (15 ml) was refluxed for 2 h. The mixture was poured into ice–dilute hydrochloric acid and extracted with ether. The ether extract was washed with water, dried over sodium sulfate, and then evaporated *in vacuo*. The residue was chromatographed on silica gel (15 g) using benzene as the eluent to give **11** (126 mg: 80%) which responded positively to the Gibbs test.[12] Mp 94—94.5 °C (from methanol); $[\alpha]_D$+67.2°; IR: 3510 cm^{-1}; NMR : 0.94(6H, s, $-\underset{|}{C}(CH_3)_2$), 1.18 (6H, d, J=7 Hz, $-CH(C\underline{H}_3)_2$), 1.28 (3H, s, C_{10}–CH_3), 3.70 (3H, s, $-OCH_3$), 5.79 (1H, s, C_{11}–OH), 6.25 (1H, s, C_{14}–H). Found: C, 79.92; H, 10.21%. Calcd for $C_{21}H_{32}O_2$: C, 79.70; H, 10.19%.

11-Benzoyloxy-12-methoxyabieta-8,11,13-trien-7-one (12). A mixture of **10** (2.00 g) and chromium trioxide (2.00 g) in acetic acid (60 ml) was allowed to stand at room temperature for 24 h. The mixture was poured into ether–aqueous sodium hydrogencarbonate and extracted with ether. The ether extract was washed with brine, dried over sodium sulfate, and then evaporated *in vacuo*. The crude product was chromatographed on silica gel (200 g) using ether–benzene (5 : 95) as the eluent to give **12**[14] (1.24 g: 60%) which was recrystallized from chlroroform–ether : mp 197—198 °C; $[\alpha]_D$+68.9°; IR: 1739, 1676 cm^{-1}; NMR: 0.97 (6H, s, $-\underset{|}{C}(CH_3)_2$), 1.25(3H, s, C_{10}–CH_3), 1.26 and 1.39 (each 3H, d, and J=7 Hz, $-CH(C\underline{H}_3)_2$), 2.56 (2H, bd, J=7 Hz, $-CH_2CO-$), 3.61 and 3.65 (each *ca.* 1.5 H and s, $-OCH_3$),[14] 7.85 (1H, s, C_{14}–H), 7.3—8.3 (5H, m, aromatic protons). Found: C, 77.10; H, 7.85%. Calcd for $C_{28}H_{34}O_4$: C, 77.39; H, 7.89%.

Cryptojaponol (13). A mixture of **12** (600 mg) and 10% aqueous sodium hydroxide (5.0 ml) in methanol (35 ml)

was refluxed for 1 h and then evaporated *in vacuo*. The residue was acidified with dilute hydrochloric acid and extracted with ether. The ether extract was washed successively with water, aqueous sodium hydrogencarbonate, and brine. The dried solution was then evaporated *in vacuo* to afford a solid which was recrystallized from methanol, giving **13** (180 mg), mp 205—207 °C. Found: C, 76.21; H, 9.08%. Calcd for $C_{21}H_{30}O_3$: C, 76.32; H, 9.15%. The mother liquor of crystallization was evaporated *in vacuo* and the residue was chromatographed on silica gel (20 g) using ether–benzene (1 : 99) as the eluent to give an additional **13** (106 mg). The IR and NMR spectra of **13** were identical with those of authentic cryptojaponol.[2]

11-Methoxyabieta-8,11,13-trien-12-ol (14). A mixture of **9** (171 mg) and 10% aqueous sodium hydroxide (1.5 ml) in methanol (10 ml) was refluxed for 1 h. After the same work-up as described for the preparation of **13**, the crude product was chromatographed on silica gel (15 g) using benzene as the eluent to give **14** (124 mg: 80%) which responded negatively to the Gibbs test.[12] Mp 114.5—115 °C (from methanol); $[\alpha]_D$+67.5°; IR: 3545, 3340 cm^{-1}; NMR: 0.95 (6H, s, $-\dot{C}(CH_3)_2$), 1.20 (6H, d, J=7 Hz, $-CH(C\underline{H}_3)_2$), 1.28 (3H, s, $C_{10}-CH_3$), 3.74 (3H, s, $-OCH_3$), 5.18 (1H, s, $C_{12}-OH$), 6.48 (1H, s, $C_{14}-H$). Found: C, 79.98; H, 10.21%. Calcd for $C_{21}H_{32}O_2$: C, 79.70; H, 10.19%.

Oxidation of 9 with Chromium Trioxide. Chromium trioxide (6.0 g) was added to a stirred solution of **9** (5.959 g) in acetic acid (80 ml) over a 1 h period. The mixture was further stirred at room temperature for 5 h and then allowed to stand for 18 h. The mixture was poured into water and extracted with ether. The ether extract was washed successively with water, aqueous sodium hydrogencarbonate, and brine. After drying over sodium sulfate, the solvent was evaporated *in vacuo* and the residue was chromatographed on silica gel (300 g) using benzene as the eluent to give 12-benzoyloxyabieta-8,12-diene-11,14-dione (**16**) (1.630 g: 27%) which was recrystallized from ethanol: mp 196—197 °C. Found: C, 76.97; H, 7.89%. Calcd for $C_{27}H_{32}O_4$: C, 77.11; H, 7.67%. The IR and NMR spectra of **16** were identical with those of authentic royleanone benzoate.[2] Further elution with ether–benzene (1 : 9) afforded 12-benzoyloxy-11-methoxyabieta-8,11,13-trien-7-one (**15**) (2.731 g: 44%) which was recrystallized from methanol: mp 163—163.5 °C; $[\alpha]_D$+38.0°; IR: 1740, 1678, 1600 cm^{-1}; NMR: 0.99 (6H, s, $-\dot{C}(CH_3)_2$), 1.22 and 1.27 (each 3H, d, and J=7 Hz, $-CH(C\underline{H}_3)_2$), 1.40 (3H, s, $C_{10}-CH_3$), 3.70(3H, s, $-OCH_3$), 7.76 (1H, s, $C_{14}-H$), 7.3—8.4 (5H, m, aromatic protons). Found: C, 77.57; H, 7.83%. Calcd for $C_{28}H_{34}O_4$: C, 77.39; H, 7.89%.

7β-Acetoxy-12-benzoyloxy-11-methoxyabieta-8,11,13-triene (17) and Its 7α-Acetoxy Isomer (18). From the Methyl Ether (9): A mixture of **9** (1.00 g) and lead tetraacetate (3.00 g) in acetic acid (30 ml) was refluxed for 40 min with stirring in a stream of nitrogen. The mixture was cooled to room temperature and ethylene glycol (1.0 ml) was added. The mixture was further stirred at room temperature for 30 min, poured into water, and extracted with ether. The ether extract was washed successively with water, aqueous sodium hydrogencarbonate, and brine. After drying over sodium sulfate, the solvent was evaporated *in vacuo*. The residue was chromatographed on silica gel (120 g) using ether–benzene (2 : 98) as the eluent to give a mixture of **17** and **18** (647 mg: 57%) whose NMR spectrum showed the presence of **17** and **18** in a ratio of *ca.* 1 : 2 from the intensities of the C-14 proton signals. The crystallization of the mixture from methanol gave **18** (290 mg): mp 176—177 °C; $[\alpha]_D$+75.2°; IR: 1735 sh, 1725 cm^{-1}; NMR: 0.94 (6H, s, $-\dot{C}(CH_3)_2$), 1.19 and 1.21 (each 3H, d, and J=7 Hz, $-CH(C\underline{H}_3)_2$), 1.28 (3H, s, $C_{10}-CH_3$), 2.04 (3H, s, $-OCOCH_3$), 3.72 (3H, s, $-OCH_3$), 5.86 (1H, m, $W_{1/2}$=5 Hz, $C_{7\beta}-H$), 6.88 (1H, s, $C_{14}-H$), 7.3—8.4 (5H, m, aromatic protons). Found: C, 75.15; H, 7.94%. Calcd for $C_{30}H_{38}O_5$: C, 75.28; H, 8.00%.

The isolation of the pure 7β-acetate (**17**) was difficult; it showed the following NMR spectrum: 0.95 and 1.00 (each 3H and s, $-\dot{C}(CH_3)_2$), 1.18 (6H, bd, J=7 Hz, $-CH(C\underline{H}_3)_2$), 1.37(3H, s, $C_{10}-CH_3$), 2.09 (3H, s, $-OCOCH_3$), 3.70 (3H, s, $-OCH_3$), 5.93 (1H, m, $W_{1/2}$=15 Hz, $C_{7\alpha}-H$), 6.85 (1H, s, $C_{14}-H$), 7.3—8.4 (5H, m, aromatic protons).

From the Ketone (15): Sodium borohydride (600 mg) was added at 0—5 °C to a stirred solution of **15** (1.469 g) in methanol (20 ml). The mixture was further stirred at this temperature for 3 h, acidified with dilute hydrochloric acid, and extracted with ether. The ether extract was washed with brine, dried over sodium sulfate, and then evaporated *in vacuo* to give a mixture of alcohols (1.17 g). IR: 3590, 3350, 1740 cm^{-1}; NMR: 0.95 (6H, s, $-\dot{C}(CH_3)_2$), 1.28 (6H, d, J=7 Hz, $-CH(C\underline{H}_3)_2$), 1.33 (3H, s, $C_{10}-CH_3$), 3.70 (3H, s, $-OCH_3$), 4.3—4.8 (1H, m, C_7-H), 7.25 (1H, s, $C_{14}-H$), 7.3—8.3 (5H, m, aromatic protons).

An aliquot of the above mixture (880 mg) was dissolved in acetic anhydride (15 ml) and pyridine (1.5 ml), allowed to stand at room temperature for 24 h, and then diluted with ether. The ether solution was washed successively with dilute hydrochloric acid and water, dried over sodium sulfate, and evaporated *in vacuo* to give an oil (861 mg) whose NMR spectrum showed the presence of **17** and **18** in a ratio of *ca.* 5 : 1.

Oxidation of the 7α-Acetate (18). Chromium trioxide (900 mg) was added to a stirred solution of **18** (900 mg) in acetic acid (15 ml). The mixture was further stirred at room temperature for 20 h, poured into water, and extracted with ether. The ether extract was washed successively with water, aqueous sodium hydrogencarbonate, and water. After drying over sodium sulfate, the solvent was evaporated *in vacuo*. The residue was recrystallized from methanol to give 7α-acetoxy-12-benzoyloxyabieta-8,12-diene-11,14-dione (**21**)[16] (210 mg: 23%). Mp 261—262 °C; $[\alpha]_D$+42.0°; IR: 1738, 1664, 1655 sh cm^{-1}; MNR ($CDCl_3$): 0.89 (6H, s, $-\dot{C}(CH_3)_2$), 1.23 (6H, d, J=7 Hz, $-CH(C\underline{H}_3)_2$), 1.28 (3H, s, $C_{10}-CH_3$), 2.06 (3H, s, $-OCOCH_3$), 5.99 (1H, m, $W_{1/2}$=5 Hz, $C_{7\beta}-H$), 7.4—8.3 (5H, m, aromatic protons). The mother liquor of crystallization was evaporated *in vacuo* and the residue was chromatographed on silica gel (40 g) using ether–benzene (1 : 99) as the eluent to give **15** (354 mg).

Oxidation of the 7β-Acetate (17). A solution of **17** (900 mg) containing a small amount of **18** was oxidized with chromium trioxide (900 mg) at room temperature for 20 h. After the same work-up as described for the preparation of **21**, the crude product was recrystallized from methanol to afford **21** (40 mg). The mother liquor of crystallization was evaporated *in vacuo* and the residue was chromatographed on silica gel (40 g) using ether–benzene (1 : 99) as the eluent to give a quinone fraction (400 mg) which was recrystallized from methanol to give 7β-acetoxy-12-benzoyloxyabieta-8,12-diene-11,14-dione (**19**)[16] (140 mg). Mp 125—127 °C and 155—160 °C; $[\alpha]_D$+30.0°; IR: 1737, 1663, 1653 sh cm^{-1}; NMR ($CDCl_3$): 0.90 and 0.94 (each 3H and s, $-\dot{C}(CH_3)_2$), 1.20 and 1.26 (each 3H, d, and J= 7 Hz, $-CH(C\underline{H}_3)_2$), 1.39 (3H, s, $C_{10}-CH_3$), 2.08 (3H, s, $-OCOCH_3$), 6.02 (1H, t, J=8.5 Hz, $W_{1/2}$=17 Hz, $C_{7\alpha}-H$),

7.4—8.4 (5H, m, aromatic protons). Further elution gave **15** (68 mg). The mother liquor of the above crystallization was chromatographed on silica gel to afford some additional **15** (201 mg).

Taxoquinone (1). A mixture of **19** (103 mg) and 10% aqueous sodium hydroxide (4.0 ml) in methanol (15 ml) was refluxed for 30 min. After the addition of methanol (5.0 ml) and 10% hydrochloric acid (8.0 ml), the mixture was further refluxed for 5 min, cooled to room temperature, and extracted with ether. The ether extract was washed successively with water, aqueous sodium hydrogencarbonate, and brine, dried over sodium sulfate, and then evaporated *in vacuo*. The residue was chromatographed on silica gel (20 g) using ether–benzene (2 : 98) as the eluent to give taxoquinone (**1**) (49 mg: 68%) which was recrystallized from ether: mp 206—207 °C; $[\alpha]_D$+344° (lit,[4] mp 212—214 °C, $[\alpha]_D$+340°); IR: 3548, 3378, 1671, 1647, 1623, 1597 cm^{-1}; NMR ($CDCl_3$): 0.93 (6H, s, $-\dot{C}(CH_3)_2$), 1.22 (6H, d, J=7 Hz, $-CH(C\underline{H}_3)_2$), 1.35 (3H, s, C_{10}–CH_3), 3.84 (1H, d, J=2 Hz, $C_{7\beta}$–OH), 4.84 (1H, m, $W_{1/2}$=20 Hz, $C_{7\alpha}$–H), 7.33 (1H, s, C_{12}–OH). Found: C, 72.04; H, 8.60%. Calcd for $C_{20}H_{28}O_4$: C, 72.26; H, 8.49%. The synthetic **1** was shown to be identical with natural taxoquinone by mixed melting point determination and IR and NMR spectral comparisons.

Dehydroroyleanone (3). A mixture of **1** (36.1 mg) and *p*-toluenesulfonic acid (40 mg) in dry benzene (10 ml) was refluxed for 30 min. The mixture was cooled to room temperature, stirred with sodium hydrogencarbonate for 30 min, and then filtered. The filtrate was evaporated *in vacuo* and the residue was chromatographed on silica gel (15 g) using ether–benzene (2 : 98) as the eluent to give dehydroroyleanone (**3**) (12.5 mg: 37%) which was recrystallized from petroleum ether: mp 166—167 °C; $[\alpha]_D$−609° (lit,[6] mp 166—168.5 °C, $[\alpha]_D$−620°); IR: 3363, 1665, 1635, 1610 cm^{-1}; UV λ_{max} nm (ε): 247sh (8600), 333 (7100), 459 (610); NMR ($CDCl_3$): 0.98, 1.02, and 1.04 (each 3H and s, $-\dot{C}(CH_3)_2$ and C_{10}–CH_3), 1.22 (6H, d, J=7 Hz, $-CH(C\underline{H}_3)_2$), 2.14 (1H, t, J=3 Hz, C_5–H), 6.45 (1H, dd, J=3 and 10 Hz, C_6–H), 6.81 (1H, dd, J=3 and 10 Hz, C_7–H), 7.32 (1H, s, C_{12}–OH). Found: C, 76.52; H, 8.52%. Calcd for $C_{20}H_{26}O_3$: C, 76.40; H, 8.34%. The IR and NMR spectra of **3** were identical with those of natural dehydroroyleanone.

Further elution gave the recovered **1** (20.0 mg).

7α-Acetoxyroyleanone (2). A mixture of **21** (41.9 mg) in methanol (30 ml) and 5% aqueous sodium hydrogencarbonate (4.0 ml) was refluxed for 45 min and evaporated *in vacuo*. The residue was acidified with dilute hydrochloric acid, refluxed for 5 min, cooled to room temperature, and then extracted with ether. The ether extract was washed successively with aqueous sodium hydrogencarbonate and water, dried over sodium sulfate, and evaporated *in vacuo*. The residue (31.8 mg) was recrystallized from ethanol to give 7α-acetoxyroyleanone (**2**) (11.9 mg: 36%). Mp 212—214 °C; $[\alpha]_D$−7° (lit,[6] mp 212—214.5 °C, $[\alpha]_D$−14°); IR: 3390, 1736, 1671, 1642, 1608 cm^{-1}; UV λ_{max} nm (ε): 272 (12,400), 410 (760); NMR ($CDCl_3$): 0.84 (6H, s, $-\dot{C}(CH_3)_2$), 1.19 and 1.22 (each 3H, d, and J=7 Hz, $-CH(C\underline{H}_3)_2$), 1.24 (3H, s, C_{10}–CH_3), 2.02 (3H, s, $-OCOCH_3$), 5.94 (1H, m, $W_{1/2}$=6 Hz, $C_{7\beta}$–H), 7.13 (1H, s, C_{12}–OH). Found: C, 70.75; H, 8.23%. Calcd for $C_{22}H_{30}O_5$: C, 70.56; H, 8.08%. The synthetic **2** was shown to be identical with natural 7α-acetoxyroyleanone by mixed melting point determination and IR and NMR spectral comparisons.

Horminone (4). A mixture of **21** (105 mg) and 10% aqueous sodium hydroxide (4.0 ml) in methanol (20 ml) was refluxed for 30 min, acidified with 10% hydrochloric acid, and further refluxed for 5 min. After the same work-up as described for the preparation of **1**, the crude product (88.3 mg) was recrystallized from ether–petroleum ether to give horminone (**4**) (39.3 mg: 54%). Mp 176—178 °C; $[\alpha]_D$−120° (lit,[6] mp 172.5—174.5 °C, $[\alpha]_D$−132°); IR: 3570, 3380, 1671, 1647, 1627, 1601 cm^{-1}; NMR ($CDCl_3$): 0.91 and 0.99 (each 3H and s, $-\dot{C}(CH_3)_2$), 1.22 (3H, s, C_{10}–CH_3), 1.22 (6H, d, J=7 Hz, $-CH(C\underline{H}_3)_2$), 4.75 (1H, m, $W_{1/2}$=9 Hz, $C_{7\beta}$–H), 3.05 and 7.27 (each 1H and s, 2-OH). Found: C, 72.11; H, 8.38%. Calcd for $C_{20}H_{28}O_4$: C, 72.26; H, 8.49%. The synthetic **4** was shown to be identical with natural horminone by mixed melting point determination and IR and NMR spectral comparisons.

7-Oxoroyleanone (5). According to the method of Eugster *et al.*,[5] a mixture of **4** (160 mg) and active manganese dioxide (1.80 g) in dioxane (25 ml) was stirred at 75—80 °C for 44 h. The crude product was chromatographed on silica gel (20 g) using ether–benzene (3 : 97) as the eluent to give the recovered **4** (107 mg). Further elution with ether–benzene (1 : 9) afforded 7-oxoroyleanone (**5**) (13.0 mg) which was recrystallized from methanol: mp 202—203 °C dec (lit,[7] mp 204—205 °C); IR: 3400, 1695, 1663, 1645, 1575 cm^{-1}; NMR ($CDCl_3$): 0.93 and 0.96 (each 3H and s, $-\dot{C}(CH_3)_2$), 1.22 (6H, d, J=7 Hz, $-CH(C\underline{H}_3)_2$), 1.36 (3H, s, C_{10}–CH_3), 6.98 (1H, s, C_{12}–OH). The IR and NMR spectra of **5** were identical with those of natural 7-oxoroyleanone.

12-Methoxyabieta-8,12-diene-7,11,14-trione (22). A solution of **1** (110 mg) in ether was methylated at 0—5 °C with diazomethane to give 7β-hydroxy-12-methoxyabieta-8,12-diene-11,14-dione (**20**) (110 mg). The crude ether (**20**) was dissolved in pyridine (2.0 ml) and chromium trioxide (120 mg) was added at 0—5 °C. The mixture was stirred at room temperature for 45 h, poured into dilute hydrochloric acid, and extracted with ether. The ether extract was washed with brine, dried over sodium sulfate, and then evaporated *in vacuo*. The residue was chromatographed on silica gel (20 g) using ether–benzene (3 : 97) as the eluent to give **22** (26 mg) which was recrystallized from petroleum ether: mp 90—92 °C (lit,[7] mp 88—91 °C); IR: 1700, 1663, 1625, 1577 cm^{-1}; NMR ($CDCl_3$): 0.92 and 0.96 (each 3H and s, $-\dot{C}(CH_3)_2$), 1.19 and 1.21 (each 3H, d, and J=7 Hz, $-CH(C\underline{H}_3)_2$), 1.42 (3H, s, C_{10}–CH_3), 3.90 (3H, s, $-OCH_3$).

Inuroyleanol (6). A solution of sodium dithionite (300 mg) in water (1.0 ml) was added at 95—100 °C to a solution of **22** (42.0 mg) in acetic acid (1.5 ml). The mixture was stirred at this temperature for *ca.* 2 min, cooled to room temperature, and extracted with ether. The ether extract was washed successively with water, aqueous sodium hydrogencarbonate, and brine. After drying over sodium sulfate, the solvent was evaporated *in vacuo* and the residue was recrystallized from methanol to give inuroylcanol (**6**) (29.4 mg: 70%). Mp 185—186 °C; $[\alpha]_D$+106° (lit,[7] mp 185—187 °C, $[\alpha]_D$+113.9°); IR: 3520, 1620 cm^{-1}; NMR ($CDCl_3$): 0.96 (6H, s, $-\dot{C}(CH_3)_2$), 1.37 (3H, s, C_{10}–CH_3), 1.39 (6H, d, J=7 Hz, $-CH(C\underline{H}_3)_2$), 3.80 (3H, s, $-OCH_3$), 5.72 (1H, s, C_{11}–OH), 13.30 (1H, s, C_{14}–OH). Found: C, 72.77; H, 8.85%. Calcd for $C_{21}H_{30}O_4$: C, 72.80; H, 8.73%.

The authors are grateful to Arakawa Chemical Co., Ltd. for a generous gift of rosin. Thanks are also due to Professors S. Morris Kupchan, C. H. Eugster, and O. E. Edwards for their kind supply of the natural samples and spectral copies.

References

1) T. Matsumoto, Y. Ohsuga, and K. Fukui, *Chem. Lett.*, **1974**, 297.
2) T. Matsumoto, Y. Ohsuga, S. Harada, and K. Fukui, *Bull. Chem. Soc. Jpn.*, **50**, 266 (1977).
3) This work has been reported in a preliminary form: T. Matsumoto and S. Harada, *Chem. Lett.*, **1976**, 1311.
4) S. M. Kupchan, A. Karim, and C. Marcks, *J. Am. Chem. Soc.*, **90**, 5923 (1968); *J. Org. Chem.*, **34**, 3912 (1969).
5) M. Hensch, P. Rüedi, and C. H. Eugster, *Helv. Chim. Acta*, **58**, 1921 (1975).
6) O. E. Edwards, G. Feniak, and M. Los, *Can. J. Chem.*, **40**, 1540 (1962).
7) S. V. Bhat, B. S. Kalyanaraman, H. Kohl, N. J. de Souza, and H.-W. Fehlhaber, *Tetrahedron*, **31**, 1001 (1975).
8) J. H. Gough and M. D. Sutherland, *Aust. J. Chem.*, **19**, 329 (1966).
9) C. H. Eugster, *Palette*, **1968**, 25; *Chem. Abstr.*, **69**, 54262e (1968).
10) M.-M. Janot and P. Potier, *Ann. Pharm. Fr.*, **22**, 387 (1964).
11) T. Matsumoto and S. Usui, *Bull. Chem. Soc. Jpn.*, **52**, 212 (1979).
12) F. E. King, T. J. King, and L. C. Manning, *J. Chem. Soc.*, **1957**, 563.
13) The methyl ether **10** should be produced by methylation of an intermediate (**8a**).

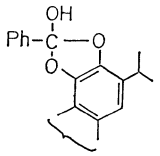

8a

14) T. Kondo, M. Suda, and M. Teshima, *Yakugaku Zasshi*, **82**, 1252 (1962).
15) These signals arose from rotational isomers due to a methoxyl group whose free rotation was restricted by two bulky ortho-substituents, the benzoyloxyl and isopropyl groups.
16) The acetoxyquinone seemed to be too unstable for the chromatographic purification on silica gel.

The Nature of Athabasca Tar Sand (Canada) and Tar Sand Derivatives. A Comparison with Coal-hydrogenolysis Products

Ryoichi Yoshida,[1] Tadashi Yoshida,* Yasuko Ikawa,** Takeshi Okutani, Yasuko Hirama, Yoshinori Nakata, Shinichi Yokoyama, Masataka Makabe,** and Yoshihisa Hasegawa

Government Industrial Development Laboratory, Hokkaido, Sapporo 061-01

***Department of Applied Chemistry, School of Engineering, Hokkaido University, Sapporo 060*

(Received September 21, 1978)

Solvent extracts of Athabasca tar sand were analyzed by the Brown-Ladner method, the Takeya *et al.* method, and the Speight method on the basis of the ^{1}H-NMR data and by ^{13}C-NMR spectroscopy. The structural characteristics of Athabasca tar sand derivatives were also compared with those of coal-hydrogenolysis products. The results show that the structural characteristics of hexane solubles, monomers consisting of one aromatic ring substituted highly with C_6 aliphatic chains, resemble those of the oil fraction produced during the initial stage of the hydrogenolysis of Taiheiyo coal. However, the structural characteristics of the hexane insoluble-benzene solubles, oligomers consisting of 2 aromatic rings substituted highly with C_{4-5} aliphatic chains, are different from those of any coal-hydrogenolysis products. In addition, the close agreement between the f_a value obtained by the Brown-Ladner method and ^{13}C-NMR may indicate that, for solvent extracts of Athabasca tar sand, the assumption in the Brown-Ladner method that the atomic H/C ratio of aliphatic structures is 2 is proper.

From the standpoint of developing alternative resources to petroleum, studies of the chemical structures of coal, tar sand bitumen, and shale oil have been carried out with the view of utilizing these materials as raw material for energy. Studies of the chemical structure of tar sand bitumen have been carried out by the Speight method[2-5] using the data of ultimate analysis, ^{1}H-NMR, and molecular weight. The present authors have previously studied coal-hydrogenolysis products[6-9] using the Brown-Ladner method[10] and the Takeya *et al.* method,[11] which determined the structural parameters for structural units from the data of ultimate analysis and ^{1}H-NMR. Therefore, in the present investigation solvent extracts of Athabasca tar sand were analyzed by the Brown-Ladner method and the Takeya *et al.* method, and the results were compared with the chemical structures of coal-hydrogenolysis products. The aromaticity (f_a) determined by ^{13}C-NMR analysis was compared with the value obtained on the basis of the Brown-Ladner method. The Speight method is also discussed.

Experimental

Solvent Separation. As solvents, hexane and benzene used in the separation of coal-hydrogenolysis products[8,9] were adopted. A portion of about 10—20 g of tar sand was weighed accurately and they extracted with 5 vol of hexane per weight of tar sand. The solution was filtered after it had been stirred for 1 h at room temperature. The residue was again extracted with hexane in the same manner as the first extraction. The yield of hexane solubles (oil) was defined as the sum of the yields of the two hexane extractions. The hexane-insoluble residue was extracted with benzene in the same manner as in the hexane extraction. The yield of the hexane insoluble-benzene solubles (asphaltene) was obtained as the sum of two benzene extractions. Bitumen prepared from tar sand at the Research Council of Alberta was also separated in the same manner as the tar sand.

Analysis of the Hexane Solubles and the Hexane Insoluble-Benzene Solubles. The ultimate analysis,[8,9] ^{1}H-NMR analysis (solvent:$CDCl_3$),[8,9] ^{13}C-NMR analysis(solvent:$CDCl_3$),[12] molecular-weight determination (solvent:$CHCl_3$),[8,9] GPC (solvent:THF),[8] and determination of the hydroxyl-group content by trimethylsilylation[13] were carried out on both fractions in the manners previously reported.[8,9,12,13]

Results and Discussion

The yields of the hexane solubles and the hexane insoluble-benzene solubles are 9.5—10.3% and 2.0—2.2% respectively on the basis of tar sand, and the yield of bitumen is 11.5—12.5%. Consequently, the yields of the hexane solubles and the hexane insoluble-benzene solubles are 82.4—82.6% and 17.4—17.6% respectively on the basis of bitumen. The yield of benzene-insoluble matter, namely sand, is 87.6—88.5% on the basis of tar sand. The ash content of tar sand determined by high-temperature ashing techniques (815 °C) is 87.2%, which is almost equal to the yield of benzene-insoluble matter. These results indicate that the sand obtained here does not contain any organic matter. This fact was confirmed by the TGA of the benzene-insoluble matter. The weight loss of benzene-insoluble matter up to 800 °C is 0.2%.

The data on the ultimate analysis of hexane solubles and the hexane insoluble-benzene solubles are shown in Table 1, along with the data for the coal-hydrogen-

Table 1. Elementary analysis (%)

	C	H	O	N	S
Tar sand					
Hexane solubles	83.9	11.3	0.7	1.1	4.2
Benzene solubles	80.5	9.0	3.4	0.9	7.8
Tar-sand bitumen[a]					
Hexane solubles	84.4	11.4	0.5	1.8	4.2
Benzene solubles	80.4	8.5	2.3	1.0	8.1
Coal-hydrogenolysis products (Taiheiyo coal)					
Hexane solubles	86.4	9.2	3.5	0.7	0.2
Benzene solubles	86.5	6.7	5.0	1.8	0.2

a) This sample was obtained from the Research Council of Alberta.

Table 2. Chemical structure of Athabasca tar-sand bitumen (Brown-Ladner method)

	Hydrogen distribution			Structural parameter							
	H_a	H_α	H_o	f_a[c]	f_a	σ	H_{au}/C_a	H_o/H_α	M_n[d]	M_v[e]	M_v/M_n
Tar sand											
Hexane solubles	0.057	0.166	0.777	0.25	0.24	0.69	1.07	4.9	320	440	1.4
Benzene solubles	0.082	0.202	0.716	0.37	0.39	0.68	0.86	3.5	320	2130	6.7
Tar-sand bitumen[a]											
Hexane solubles	0.049	0.156	0.794	0.26	0.23	0.67	1.07	5.1	330	410	1.2
Benzene solubles	0.101	0.178	0.721	0.44	0.43	0.65	0.79	4.1	360	2250	6.3
Coal-hydrogenolysis products[b]											
Hexane solubles											
$Oil(S_1)$ Taiheiyo coal	0.05—0.13	0.15—0.18	0.69—0.79		0.25—0.40	0.50—0.69	0.90—1.00	3.8—5.2	270—350	220—260	0.7—1.0
$Oil(S_1)$ Oyubari coal	0.15—0.21	0.24—0.29	0.50—0.60		0.42—0.57	0.44—0.50	0.76—0.97	1.7—2.4	260—280	280—300	1.0—1.1
$Oil(S_2)$ Taiheiyo coal	0.15—0.28	0.32—0.34	0.39—0.42		0.57—0.62	0.40—0.45	0.81—0.88	1.2—1.3	190—220	220—260	1.0—1.3
$Oil(S_2)$ Oyubari coal	0.25—0.30	0.31—0.35	0.37—0.40		0.60—0.65	0.38—0.45	0.79—0.84	1.1—1.3	190—230	260—280	1.2—1.5
Benzene solubles											
Taiheiyo coal	0.34—0.39	0.30—0.36	0.30—0.33		0.67—0.71	0.38—0.41	0.77—0.90	0.8—1.0	160	420—470	2.9
Oyubari coal	0.29—0.36	0.30—0.32	0.34—0.40		0.66—0.71	0.39—0.44	0.64—0.75	1.0—1.3	260	490—830	3.2

a) This sample was obtained from the Research Council of Alberta. b) Quoted from the papers of Yoshida *et al.* (1974, 1976):[8,9] Coal → $Oil(S_1)$; Coal → Asphaltene → $Oil(S_2)$

c) Calculated from the data of ^{13}C-NMR. d) Weight of the average structural unit calculated numerically from the value of the structural parameter. e) Molecular weight determined by vapor-pressure osmometry.

Table 3. Comparison of the results obtained by the Speight method with the results obtained by the Brown-Ladner method

	R_a[b]	R'_a[c]	C_{sa}/C_p	σ	C_s/C_{sa}	H_o/H_α	C_p/C_a	H_{au}/C_a	*M.W.*
Hexane solubles	1.2—1.4	*ca.* 1.2—1.4	0.59—0.61	0.67—0.69	5.7—6.2	4.9—5.1	0.89—0.94	1.07	410—440[d]
Oil (Speight, 1970)[a]	1.4		0.58		4.7		0.92		424[e]
Benzene solubles	10.9—15.3	*ca.* 13.4	0.47—0.55	0.63—0.68	4.5—5.1	3.5—4.1	0.56—0.64	0.79—0.86	2130—2250[d]
Asphaltene (Speight, 1970)[a]	57.4		0.52		4.8		0.40		5489[e]
									(2492)[f]

a) Quoted from the paper of Speight (1970).[2] b) Aromatic rings per molecule: $(C_l+2)/2$. c) Aromatic rings per molecule: calculated from H_{au}/C_a and M_v/M_n. d) Solvent: chloroform. e) Solvent: benzene. f) Quoted from the paper of Boyd *et al.* (1962).[16]

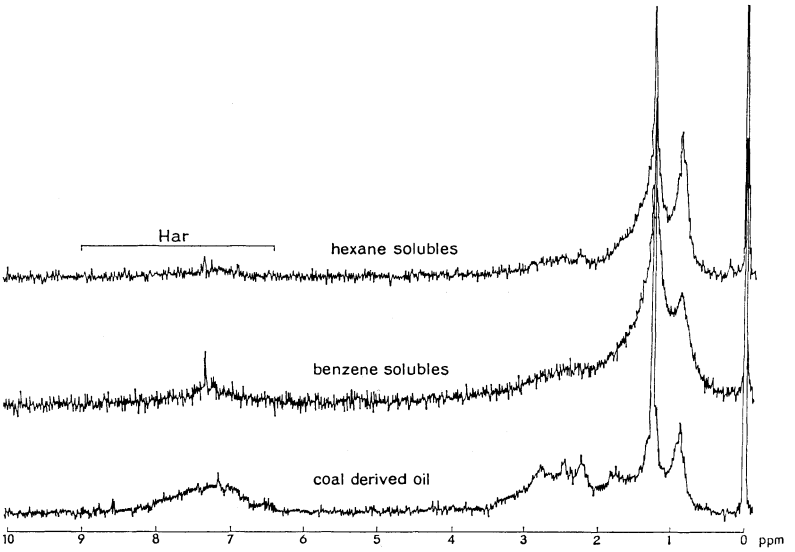

Fig. 1 ^{1}H-NMR spectra of tar sand extracts and coal-hydrogenolysis product.

olysis products. For both fractions of tar sand, the carbon content is lower and the hydrogen content is higher than those of the coal-hydrogenolysis products. The most remarkable differences in ultimate composition between the tar-sand derivatives and the coal-hydrogenloysis products is that the oxygen content of the coal-hydrogenolysis products is higher, while the sulfur content of the tar-sand derivatives is higher. The hydroxyl oxygen content of tar-sand bitumen is 0.3%, lower than that of the coal-hydrogenolysis products(1.1—3.3%).[8] In Figs. 1 and 2 the spectra of the ^{1}H-NMR and ^{13}C-NMR of tar-sand derivatives are compared with those of coal-hydrogenolysis products. In Table 2 the hydrogen distributions determined by means of ^{1}H-NMR, the structural parameters calculated on the basis of the Brown-Ladner method and ^{13}C-NMR, the weights of the average structural units calculated from the values of the

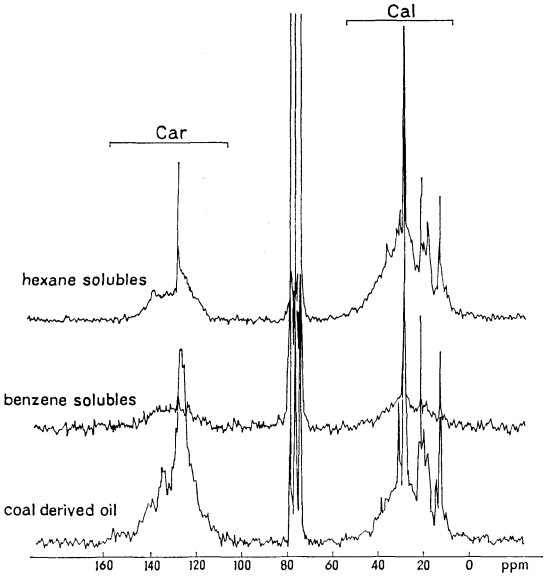

Fig. 2. ^{13}C-NMR spectra of tar sand extracts and coal-hydrogenolysis product.

structural parameters(M_n), and the molecular weights determined by the vapor-pressure osmometry(M_v) of tar-sand derivatives are compared with those of coal-hydrogenolysis products. Regarding the hexane solubles, the aromaticity(f_a) is low, and the f_a values based on the Brown-Ladner method and on ^{13}C-NMR agree closely. The measure of the substitution of the aromatic system(σ) is high, the size of the aromatic rings in the structural unit is 1 ring (H_{au}/C_a : 1.07), and the measure of the aliphatic chain length (H_o/H_α) is about 5, which means that the length of the aliphatic chain is C_6. The molecular weight(M_v) is 410—440, and the degree of polymerization(M_v/M_n) is 1.2—1.4. This shows that hexane solubles consist mostly of monomers. These structural characteristics resemble those of Oil(S_1) from Taiheiyo coal. They are however, different from those of Oil(S_1) from Oyubari coal(C:85.6%), which is of a higher rank than Taiheiyo coal(C : 76.9%), from those of Oil(S_2), and from those of benzene solubles, Asphaltene(R). The following reaction scheme for coal hydrogenolysis has been proposed:[14,15]

$$\text{Coal} \begin{cases} \nearrow \text{Oil}(S_1) \\ \searrow \text{Asphaltene(R)} \longrightarrow \text{Oil}(S_2) \end{cases}$$

Oil(S_1) is the product produced during the initial stage of coal hydrogenolysis. Oil(S_2) is the product produced through the reaction of Coal→Asphaltene(R)→Oil(S_2). Regarding the hexane insoluble-benzene solubles, f_a is higher than for hexane solubles, while the f_a values based on the Brown-Ladner method and on ^{13}C-NMR agree closely. The size of the aromatic rings is larger(about 2 rings, H_{au}/C_a: 0.76—0.86), H_o/H_α is smaller, and M_v and M_v/M_n are much larger than those for the hexane solubles. This is also obvious from the GPC chromatogram in Fig. 3. The structural unit of this fraction resembles Oil(S_1) from Oyubari coal as to f_a and H_{au}/C_a, but compared with Oil(S_2) and Asphaltene(R) f_a is much lower and H_o/H_α is much larger. M_v and M_v/M_n are much larger than those of coal-hydrogenolysis products.

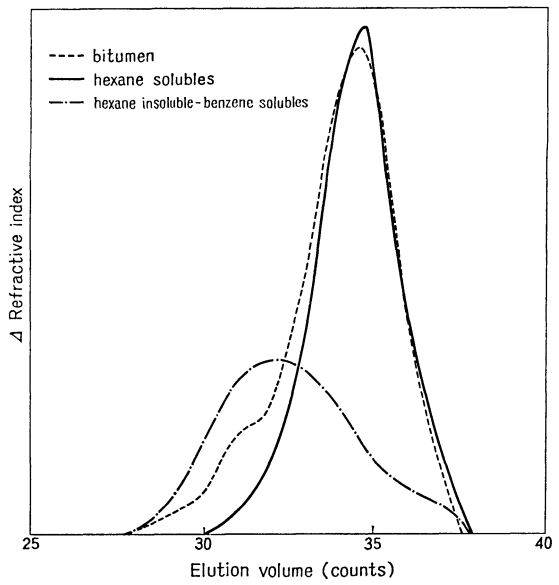

Fig. 3. GPC chromatograms of tar-sand extracts.

This fraction is an oligomer(M_v/M_n: 6.3—6.7) consisting of 2 aromatic rings substituted highly with the C_{4-5} aliphatic chain. In Table 3, a comparison of the results obtained by the Speight method with the results obtained by the Brown-Ladner method is shown. Theoretically, R_a, C_{sa}/C_p, C_s/C_{sa}, and C_p/C_a in the Speight method have the same meaning as R_a'(aromatic rings per molecule, they can be calculated from the values of H_{au}/C_a and M_v/M_n), σ, H_o/H_α, and H_{au}/C_a respectively. Comparing the analytical results obtained by the two methods, R_a and R_a', and C_s/C_{sa} and H_o/H_α, agree precisely, but C_{sa}/C_p and σ, and C_p/C_a and H_{au}/C_a, differ slightly. This may be due to the lack of consideration of heteroatoms in the Speight method. Comparing the present data with Speight's data[2] obtained by the Speight method for the hexane solubles, similar values for molecular weight and R_a are obtained. However, for the hexane insoluble-benzene solubles the molecular weights are remarkably different from each other. There is also a large difference between the values of R_a. The present data on the molecular weight of the hexane insoluble-benzene solubles(2130—2250) agree closely with the data of Boyd *et al.*(2492).[16] The value of R_a in the Speight method varies with the value of the molecular weight according to $R_a=(C_i+1)/2$, where C_i is a function of the molecular weight. In addition, the close agreement between the f_a values obtained by the Brown-Ladner method and by ^{13}C-NMR may indicate that, for Athabasca tar-sand derivatives, the assumption in the Brown-Ladner method of 2 for the atomic H/C ratio of aliphatic structures is correct.

The authors are grateful to Dr. Yosuke Maekawa of the Government Industrial Development Laboratory, Hokkaido, for samples, and would like to thank Prof. D. M. Bodily of the University of Utah for his helpful discussion.

References

1) Visiting fellow at the Coal Research Institute, Hokkaido University.
2) J. G. Speight, *Fuel*, **49**, 76, 134 (1970).
3) I. Fujishima and T. Miyagawa, *Nenryo Kyokai Shi*, **53**, 111 (1974).
4) S. Itoh, M. Yashiro, K. Tomizawa, and H. Tominaga, *Bull. Jpn. Petrol. Inst.*, **19**, 50 (1977).
5) K. Koguchi, *et al.*, The conference on Heavy oil and Gasification (Fuel Soc. Japan), Omuta (1976).
6) R. Yoshida, T. Ishii, and G. Takeya, *Nippon Kagaku Kaishi*, **1972**, 1892.
7) R. Yoshida, Y. Maekawa, and G. Takeya, *Nenryo Kyokai Shi*, **51**, 1225 (1972).
8) R. Yoshida, Y. Maekawa, and G. Takeya, *Nenryo Kyokai Shi*, **53**, 1011 (1974).
9) R. Yoshida, Y. Maekawa, T. Ishii, and G. Takeya, *Fuel*, **55**, 341 (1976).
10) J. K. Brown and W. R. Ladner, *Fuel*, **39**, 87 (1960).
11) G. Takeya, M. Itoh, A. Suzuki, and S. Yokoyama, *Nenryo Kyokai Shi*, **43**, 837 (1964).
12) Y. Maekawa, T. Yoshida, Y. Yoshida, and M. Imanari, *Nenryo Kyokai Shi* **56**, 351 (1977).
13) Y. Hasegawa, S. Yokoyama, S. Ueda, Y. Maekawa, R. Yoshida, and Y. Yoshida, the 13th Sekitan Kagaku Kaigi (1976).
14) T. Ishii, Y. Maekawa, and G. Takeya, *Kagaku Kogaku*, **29**, 988 (1965).
15) R. Yoshida, Y. Maekawa, T. Ishii, and G. Takeya, *Fuel*, **55**, 337 (1976).
16) M. L. Boyd and D. S. Montgomery, *Fuel*, **41**, 355 (1962).

Stereochemical Studies of the Hydrogenation with Asymmetrically Modified Nickel Catalysts; The Hydrogenation of Methyl 2-Alkyl-3-oxobutyrate

Akira TAI,* Hiroshi WATANABE, and Tadao HARADA

Institute for Protein Research, Osaka University, Yamada-kami, Suita, Osaka 565

(Received September 25, 1978)

The hydrogenation of methyl 2-methyl-3-oxobutyrate (I) to methyl 3-hydroxy-2-methylbutyrate (III) was carried out with various types of asymmetrically modified nickel catalysts (MNi). The use of MNi always resulted in the deviation of the ratio, **2S/2R**=((2*S*,3*R*)-III+(2*S*,3*S*)-III)/((2*R*,3*R*)-III+(2*R*,3*S*)-III), from 1/1, in spite of the use of racemic I. A catalyst giving a larger **2S/2R** value always gave a larger **3R/3S** value. These results led to the conclusion that the configurations at the C-2 and C-3 positions of the product were determined in the process of the formation of the complex between the substrate and the modifying reagent (the absorption step), not at the step of the hydrogen addition to the adsorbed substrate (the rate-determining step). The best optical yield and the highest ratio of *erythro*-III/*threo*-III were obtained when (*R*,*R*)-tartaric acid–MNi was used as a catalyst. The amounts of the isomers produced were in the following order: 2*S*,3*R*≫2*R*,3*R*≈2*R*,3*S*>2*S*,3*S*. Stereochemical models are proposed to account for the formation of the 2*S*,3*R*-isomer in a large excess.

The comparative study of the rate and the optical yield of methyl acetoacetate (MAA) over an asymmetrically modified Raney nickel catalyst has revealed that the enantioface-differentiating step of the substrate took place elsewhere than in the step of the hydrogen addition to the adsorbed substrate (the rate-determining step).[1] Although the kinetic study has suggested that the modifying reagent differentiated the enantioface of the substrate by making a complex with the substrate at the adsorption step, the mode of the differentiation has not yet been made clear.

In the hydrogenation of methyl 2-methyl-3-oxobutyrate (I) to *threo*- and *erythro*-methyl 3-hydroxy-2-methylbutyrate (III) over a modified nickel catalyst (MNi), it has been noticed that the function of the modifying reagent is not only to differentiate the enantioface of the substrate, but also to determine the ratio of the diastereomers produced.[2]

The readily interconvertible chiral center at the C-2 position of I may serve as an internal probe for the detection of the substrate-modifying reagent interaction. In this respect, the stereochemical investigation of the hydrogenation of I was expected to give useful information about the mode of the enantio-differentiation.

In this paper, we will present an account of the mode of the enantio-differentiation and evidence which may support the conclusion of our kinetic study with respect to the enantio-differentiating step.

Results and Discussion

The stereochemical relationship between the substrate and the products in the hydrogenation of I is shown in Scheme 1.

The results of the hydrogenations of I as well as of methyl 2-ethyl-3-oxobutyrate (II) and MAA over various sorts of modified nickel catalysts are summarized in Table 1.

The amounts of the four stereoisomers, calculated from the data of Table 1, are listed in Table 2, together with following values: **2R**=(2*R*,3*R*)-III+(2*R*,3*S*)-III, **2S**=(2*S*,3*R*)-III+(2*S*,3*S*)-III, **3R**=(2*R*,3*R*)-III+(2*S*,3*R*)-III, **3S**=(2*R*,3*S*)-III+(2*S*,3*S*)-III, configuration excess at the C-2 position: |**2R**−**2S**|/(**2R**+**2S**), and configuration excess at the C-3 position: |**3R**−**3S**|/(**3R**+**3S**).

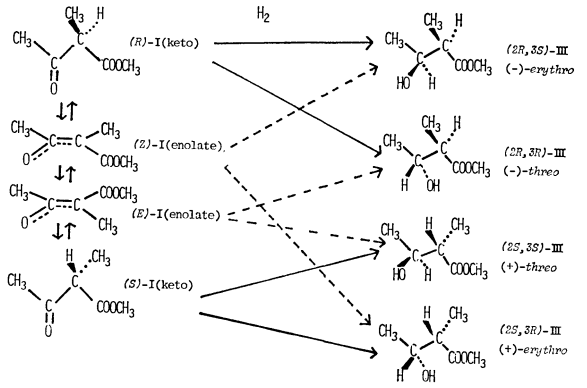

Scheme 1.

The activated nickel powders prepared either by the thermal decomposition of nickel formate (DNi) or by the hydrogenolysis of nickel oxide (HNi), gave better optical yields than did Raney nickel (RNi). As for modifying reagents, the enantio-differentiating abilities were in the order of tartaric acid≫valine≈glutamic acid. These greneal features were the same as those found in the hydrogenation of MAA[3].

Enantio-differentiating Step. The preliminary experiment indicated that an authentic IIIe or IIIt was not epimerized nor racemized under the conditions used for the hydrogenation of I to III.

Therefore, in the course of the reaction, the configuration of the product is determined before the addition of hydrogen to the substrate. Thus, the distribution of stereoisomers in the product directly reflects the equilibrium situation of the substrate, as is shown in Scheme 1.

If the distribution of stereoisomers is different between the modified and unmodified catalysts, the difference indicates the interaction between the substrate and the modifying reagent prior to the step of the hydrogen addition.

As may be seen in Tables 1 and 2, with asymmetrically modified catalysts the values of |**2R**−**2S**|/(**2R**+**2S**) always deviated from zero despite the use of racemic

Table 1. Hydrogenation of the β-keto ester with a modified nickel catalyst

	Catalyst	Modifying reagent	Substrate	Products: Diastereomers ratio (*erythro*/*threo*)	Products: Optical purity(%) *erythro*[d]	Products: Optical purity(%) *threo*[e]
1	MRNi[a]	(*R*,*R*)-Tartaric acid	I	65.1/39.4	24.0	17.3
2	MDNi[b]	(*R*,*R*)-Tartaric acid	I	77.9/22.1	55.8	41.2
3	MHNi[c]	(*R*,*R*)-Tartaric acid	I	78.4/21.6	56.7	64.4
4	MHNi	(2*S*,3*S*)-2-Methyltartaric acid	I	72.0/28.0	46.2[f]	20.5[g]
5	MDNi	(*S*)-Valine	I	62.3/37.7	5.5	0.5
6	MDNi	(*S*)-Glutamic acid	I	67.6/32.4	0.6	0
7	HNi	None	I	62.6/37.4	—	—
8	MHNi	(*R*,*R*)-Tartaric acid	II	70.7/29.3	79.9[h]	71.3[h]
9	NHNi	(*R*,*R*)-Tartaric acid	MAA	—	83.0[i]	

a) RNi: Raney nickel. b) DNi: Activated Ni catalyst prepared by the thermal decomposition of nickel formate. c) HNi: Activated Ni catalyst prepared by the hydrogenolysis of nickel(II) oxide. d) (2*S*,3*R*)-isomer in excess, e) (2*R*,3*R*)-isomer in excess. f) (2*R*,3*S*)-isomer in excess. g) (2*S*,3*S*)-isomer in excess. h) Enantiomer excess was determined by NMR. i) (*R*)-isomer in excess.

Table 2. Isomer distribution of the hydrogenation product of the β-keto ester

	Stereoisomer distribution(%) 2*R*3*R*	2*S*3*R*	2*R*3*S*	2*S*3*S*	**2R** isomers (2*R*3*R*+2*R*3*S*)	**2S** isomers (2*S*3*R*+2*S*3*S*)	**3R** isomers (2*R*3*R*+2*S*3*R*)	**3S** isomers (2*R*3*S*+2*S*3*S*)	$\frlvert{2R-2S}{2R+2S}\times100$	$\frlvert{3R-3S}{3R+3S}\times100$
1	20.5	40.5	24.6	14.4	45.1	54.9	61.0	39.0	8.3	22.0
2	15.6	60.7	17.2	6.5	32.8	67.2	76.3	23.7	34.4	52.6
3	17.8	61.4	17.0	3.8	34.8	65.2	79.2	20.8	30.4	58.4
4	11.2	19.3	52.7	16.8	63.9	36.1	30.5	69.5	27.8	39.0
5	19.0	32.8	29.4	18.8	48.4	51.6	51.8	48.2	3.2	3.6
6	16.2	34.0	33.6	16.2	49.8	50.2	50.2	49.8	0.4	0.4
7	18.7	31.3	31.3	18.7	50.0	50.0	50.0	50.0	0	0
8	25.1	63.6	7.1	4.2	32.2	67.8	88.7	11.3	35.6	77.4
9	91.5		8.5		—	—	91.5	8.5	—	83.0

I, and the ratio of *erthro*-III/*threo*-III was also changed from the value obtained with an unmodified catalyst.

Thus, it is evident that the relative amounts of (*S*)-I (keto) and (*R*)-I(keto), or of (*Z*)-I (enolate) and (*E*)-I (enolate), are changed by the modifying reagent. The present results clearly show the existence of an interaction between the substrate and the modifying reagent before the hydrogenation of the adsorbed substrate took place. In Tables 1 and 2 it can also be seen that the catalyst giving a larger $|\mathbf{2S}-\mathbf{2R}|/(\mathbf{2S}+\mathbf{2R})$ value always gave a larger $|\mathbf{3R}-\mathbf{3S}|/(\mathbf{3R}+\mathbf{3S})$ value. In connection with this relation, the increase in *erythro*-III resulted in an increase in the optical purity of both *erythro*- and *threo*-III. These facts strongly suggest that the configurations at both the C-2 and C-3 positions of III were determined by the same process involving the formation of a substrate-modifying reagent complex. Therefore, the stereochemistry of the product is considered to be fixed at the adsorption step of the substrate.

This conclusion is very compatible with that obtained from our kinetic study.[1]

Mode of Enantio-differentiation. The use of (*R*,*R*)-tartaric acid–MHNi gave the best results with respect to the optical yield and the diastereomer excess. The amounts of stereoisomers produced were in the order of 2*S*,3*R*≫2*R*,3*R*≈2*R*,3*S*>2*S*,3*S*. According to the physicochemical studies, tartaric acid is adsorbed on the catalyst with one of its carboxyl groups; the other carboxyl group and two hydroxyl groups are essentially free from the catalyst surface.[4] The two hydroxyl groups of tartaric acid are expected to play an important role in interacting with the substrate.[5] The excellent enantio-differentiation obtained in the combination of tartaric acid and I as well as MAA can be attributed to the two-point interaction with hydrogen bondings between the modifying reagent and the substrate.

When the substrate takes a keto form, the co-adsorbed species with the best-fitting interaction between I and tartaric acid on the catalyst surface gives the complex shown in Fig. 1, in which the carbonyl group to be hydrogenated faces the catalyst with its *si*-face and the configuration at the C-2 position is *S*, so that the methyl group at the C-2 position is remote from the catalyst. The large deviation of the $|\mathbf{2R}-\mathbf{2S}|/(\mathbf{2R}+\mathbf{2S})$ value from zero indicates that the substrate originally having the 2*R* configuration is converted to the 2*S* configuration in order to make this favorable complex. The addition of hydrogen to this complex gives (2*S*,3*R*)-III.

When the substrate takes an enolate form, the complex of (*Z*)-enolate with (*R*,*R*)-tartaric acid shown in Fig. 2 is the best fitting one. This complex also gives (2*S*,3*R*)-III.

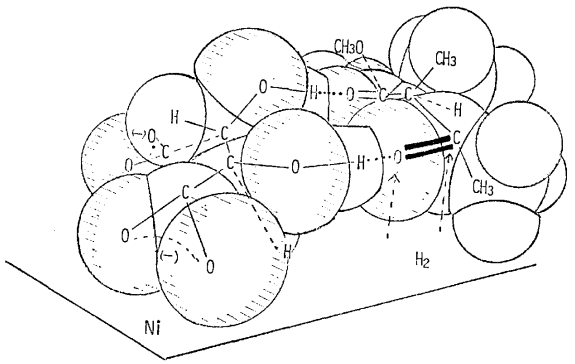

Fig. 1. Schematic representation of the complex between I(keto form) and (*R*,*R*)-tartaric acid on the MNi catalyst. The complex gives (2*S*,3*R*)-III by the attack of hydrogen from the catalyst-side (*si*-face attack)

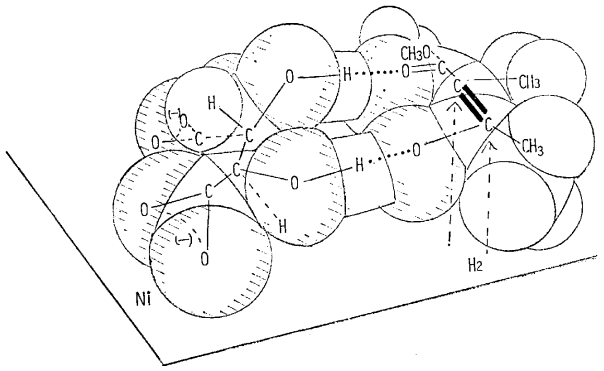

Fig. 2. Schematic representation of the complex between I(enolate) and (*R*,*R*)-tartaric acid on the MNi catalyst. The complex gives (2*S*,3*R*)-III by the attack of hydrogen from the catalyst-side (*si*-face attack).

Thus, the predominant formation of (2*S*,3*R*)-III may be well explained by both of the models. Although it is not clear whether the substrate is hydrogenated in a keto or an enolate form, the mode of the differentiation was found to be well understood without specifying the form of the substrate to be hydrogenated.

The quantitative discussion of the amounts of minor isomers is difficult at present, since the distribution of stereoisomers depends on the relative amount of the unmodified part of the catalyst.[1b] The difference in the results with MRNi and MHNi may be expected to arise in part from the difference in the unmodified part of the catalyst.

The use of (*R*,*R*)-tartaric acid–MNi always gave the 3*R*-isomer in a large excess in the hydrogenation of I as well as those of II and MAA (entries 8 and 9 in Table 2). Thus, it seems that the same mode of interaction between the substrates and the modifying reagent is involved in the enantio-differentiating hydrogenation of β-keto esters with tartaric acid–MNi.

Experimental

The analytical GLC was carried out with a Shimadzu GC-4A-PF gas chromatograph using a 3 m, 5 mm o.d. glass column packed with 15% Ucon 50-HB-2000 on Chromosorb W at the stated temperature. The preparative GLC was carried out with a Shimadzu GC-3HA instrument using a 6 m, 8 mm o.d. stainless column packed with the same packing.

The ^{1}H-NMR spectra were taken with a JEOL-FX-100 spectrometer.

The optical rotations were measured with a Perkin Elmer 241 polarimeter.

Substrate. Methyl 2-methyl-3-oxobutyrate (I) was prepared from methyl acetoacetate and methyl iodide in the presence of sodium methoxide. A slight excess of methyl acetoacetate was used in order to minimize the formation of methyl 2,2-dimethyl-3-oxobutyrate. From 850 g of methyl acetoacetate and 993 g of methyl iodide, 752 g of crude I containing 8% of methyl acetoacetate and 5% of methyl 2,2-dimethyl-3-oxobutyrate was obtained. To 750 g of crude I, 50 g of freshly prepared $Ni(OH)_2$ was added, after which the mixture was stirred for 5 days at room temperature. After removing the insoluble matter by filtration, the filtrate was mixed with 10 g of Raney nickel and allowed to stand overnight at room temperature. After the solid had been removed, the resulting liquid was dried over magnesium sulfate and then distilled under reduced pressure to give 680 g of purified I; bp 88—90 °C/20 mmHg. A GLC (at 90 °C) analysis indicated 95% purity. Also, there were 4% of methyl 2,2-dimethyl-3-oxobutyrate and 1% of methyl acetoacetate.

Methyl 2-ethyl-3-oxobutyrate (III) (bp 75—80 °C/20 mmHg was prepared by the same procedure except for the use of ethyl bromide instead of methyl iodide.

Catalyst. The catalyst from nickel formate (DNi): Well-dried nickel formate prepared from nickel chloride and sodium formate was thermally decomposed at 250—300 °C under a pressure of 20—25 mmHg for 1 h. Reduced nickel oxide (HNi): This was obtained by the reduction of nickel oxide with hydrogen at 350 °C for 1 h. The nickel oxide used for this work was obtained by the dehydration (at 500 °C for 4 h) of nickel hydroxide prepared from nickel nitrate and sodium hydroxide. No active catalyst was obtained from nickel oxide of a commercial grade. Raney nickel (RNi): Raney alloy (Kawaken Fine Chemical Co., Ni 40% Al 60%) was leached with sodium hydroxide in the way previously reported.[1]

Modification of the Catalyst. Each catalyst was soaked in a 1% solution of a modifying reagent adjusted to pH 4.1 with 1 M sodium hydroxide at 85 °C for 1 h. The amount of the modifying solution used was 120 ml per gram of the catalyst.

After the removal of the solution by decantation, the modified catalyst was washed successively with a 60 ml/(g catalyst) portion of water, two 300 ml/(g catalyst) portions of methanol, and a 60 ml/(g catalyst) portion of THF.

Solvent. THF was used as a solvent of the hydrogenation. Commercial THF was dried over NaH overnight and was then distilled under a nitrogen atmosphere.

Hydrogenation of I. In an autoclave (1000 ml capacity), I (100 g) in 300 ml of THF with 1.5 g of acetic acid was hydrogenated over 8 g of a modified catalyst under an initial hydrogen pressure of 110 kg/cm^2 at 120 °C until no more consumption of hydrogen was observed. After the removal of the catalyst, the product was subjected to flash distillation under reduced pressure.

Determination of Stereoisomers in the Hydrogenation Product of I. The flash-distilled hydrogenation product essentially consisted of two components, *erythro*-III (IIIe) and *threo*-III (IIIt), accompanied by less than 5% of an unidentified impurity. The relative amounts of the *erythro* isomer; D_e=

$\frac{\text{IIIe}}{\text{IIIe}+\text{IIIt}}$, and the threo isomer; $D_t=\frac{\text{IIIt}}{\text{IIIe}+\text{IIIt}}$, were determined from the peak area of the analytical GLC (115 °C). The retention times of IIIt and IIIe were 21.6 min and 23.4 min respectively.

The separation of IIIe and IIIt in the reaction product was carried out by the method reported in our previous paper.[6]

The process of separation is illustrated in Scheme 2.

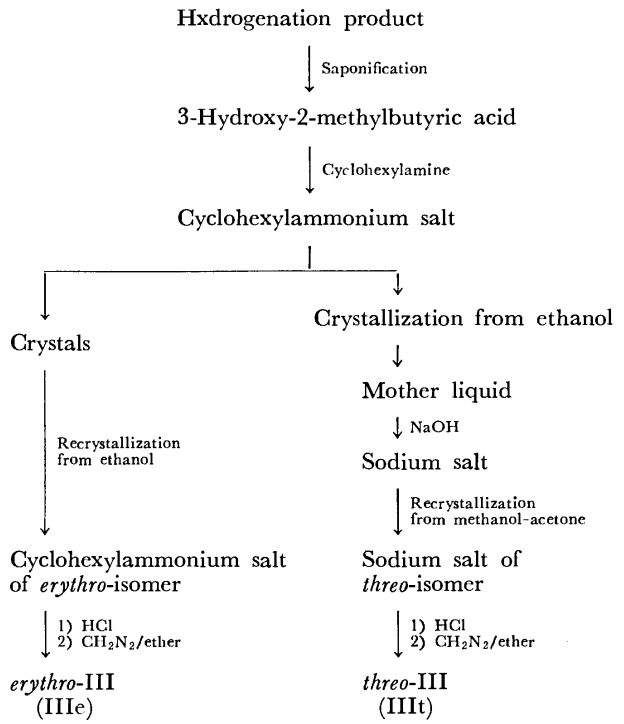

Scheme 2.

The isolated IIIe and IIIt were subjected to the polarimetric determination of their optical purity $(OY)_e=[2S3R-2R3S/(2S3R+2R3S)]\times 100$ and $(OY)_t=[2R3R-2S3S/(2R3R+2S3S)]\times 100$ as a methanol solution (c 5). The values were calculated based on the reported values: $[\alpha]_D^{20}$, (2*S*,3*S*)+36.80° (c 5, methanol) and (2*S*,3*R*), +14.32° (c 5, methanol).[6]

The distribution of each stereoisomer in the reaction product was calculated as follows:

$$2S3R(\%) = D_e \times \left(\frac{100+(OY)_e}{2}\right)$$

$$2R3S(\%) = D_e \times \left(\frac{100-(OY)_e}{2}\right)$$

$$2R3R(\%) = D_t \times \left(\frac{100+(OY)_t}{2}\right)$$

$$2S3S(\%) = D_t \times \left(\frac{100-(OY)_t}{2}\right)$$

The recrystallizations of the authentic sodium *threo*-3-hydroxy-2-methylbutyrate and cyclohexylammonium *erythro*-3-hydroxy-2-methylbutyrate with this separation process under the same conditions resulted in no change in the optical rotations. Thus, the optical purity of diastereomers in the hydrogenation product was proved to be the same as that of the isolated diastereomers.

The Stereochemical Stability of IIIe and IIIt in the Presence of a Catalyst and Hydrogen. An authentic optically active IIIe or IIIt was shaken with MNi under a hydrogen pressure of 100 kg/cm² at 100 °C for one day. The subsequent GLC and polarimetric determination of the recovered IIIe or IIIt indicated that no epimerization and racemization took place on this treatment.

Hydrogenation of II. In an autoclave (100 ml capacity), II (12.5 g) in 25 ml of THF and 1.5 g of acetic acid were hydrogenated over 1 g of the modified catalyst in the way described above.

Determination of Stereoisomers in the Hydrogenation of II. The analytical GLC (140 °C) of the product showed two peaks at the retention times of 7.4 min and 8.8 min.

The two components were isolated by the preparative GLC. The compound with a shorter retention time (7.2 min) in the analytical GLC (140 °C) showed the NMR ($CDCl_3$, TMS) assigned to $\underset{(b)}{CH_3}-\underset{(e)}{\underset{|}{C}}(\underset{(g)}{H})(\underset{(d)}{H})-\underset{(c)}{\underset{|}{C}}(\underset{(a)}{CH_2CH_3})-\underset{(f)}{COOCH_3}$; δ, 0.93 (3H, t, J=7.1 Hz, (a)), 1.23 (3H, d, J=6.3 Hz, (b)), 1.64 (2H, m, (c)), 2.33 (1H, m, (d)), 2.45 (1H, d (broad), (e)), 3.73 (3H, s, (f)), 3.91 (1H, m, (g)).

The compound with a longer retention time (8.8 min) in the analytical GLC (140 °C) showed NMR ($CDCl_3$, TMS) δ, 0.91 (3H, t, J=7.1 Hz (a)), 1.19 (3H, d, J=6.4 Hz, (b)), 1.66 (2H, m, (c)), 2.35 (2H, overlapped two signals, (d) and (e)), 3.72 (3H, s, (f)), 3.90 (1H, broad, (g)).

The compound with a shorter retention time was determined to be *threo*-IV (IVt) by the comparisons of its retention time with that of IIIt[6] or ethyl *threo*-3-hydroxy-2-propylbutyrate[7] and of its NMR spectra with those of ethyl *threo*- and *erythro*-3-hydroxy-2-propylbutyrate.[7]

The ratio in the amounts of *threo*-IV: D_t and *erythro*-IV: D_e was determined by the analytical GLC.

The NMR spectra of IVe and IVt taken in the presence of Eu(hfmc)$_3$ showed two signals of H(f), which correspond to those of the enantiomers. Thus, the enantiomer excess (*e.e.*) of each diastereomer was determined from the relative peak area of the H(f) signals of the solution containing 10 mg of IVe or IVt and 25 mg Eu(hfmc)$_3$ in 500 μl of $CDCl_3$.

The absolute configuration at C-3 of IVe with the low-field H(f) signal and that of IVt with the high-field H(f) signal was assigned to the S-configuration by the use of Horeau's method.[6,8]

When the enantiomer excess of each diastereomer is expressed by *e.e.*(%)=[peak area (high-field)−peak area (low-field)]/peak area (high-field+low-field)×100, the distribution of each stereoisomer is calculated as follows:

$$2R3R(\%) = D_t \times \left(\frac{100+(e.e.)_t}{2}\right)$$

$$2S3S(\%) = D_t \times \left(\frac{100-(e.e.)_t}{2}\right)$$

$$2S3R(\%) = D_e \times \left(\frac{100-(e.e.)_e}{2}\right)$$

$$2R3S(\%) = D_e \times \left(\frac{100+(e.e.)_e}{2}\right)$$

The authors wish to express their gratitude to Professor Yoshiharu Izumi, Osaka University, for his many helpful discussions and suggestions in the course of this work. The work was supported partially by a Grant-in-Aid from the Ministry of Education (No. 203522).

References

1) a) T. Harada, Y. Hiraki, Y. Izumi, J. Muraoka, H. Ozaki, and A. Tai, Proc. 6th Int. Congr. Catal., London (1976), pp. 1024—1033; b) H. Ozaki, A. Tai, S. Kobatake, H. Watanabe, and Y. Izumi, *Bull. Chem. Soc. Jpn.*, **51**, 3559 (1978).

2) A. Tai, M. Imaida, T. Oda, and H. Watanabe, *Chem. Lett.*, **1978**, 61.

3) a) Y. Izumi, *Angew. Chem. Int. Ed. Engl.*, **10**, 871 (1971); b) T. Harada, S. Onaka, A. Tai, and Y. Izumi, *Chem. Lett.*, **1977**, 1131.

4) a) A. Hatta and W. Suetaka, *Bull. Chem. Soc. Jpn.*, **48**, 3441 (1975); b) J. A. Groenewegen and W. M. H. Sachtler, *J. Catal.*, **33**, 176 (1974); c) T. Tanabe, K. Okuda, and Y. Izumi, *Bull. Chem. Soc. Jpn.*, **46**, 514 (1973).

5) a) H. Ozaki, *Bull. Chem. Soc. Jpn.*, **51**, 257 (1978); b) J. A. Groenewegen and W. M. H. Sachtler, *J. Catal.*, **38**, 501 (1975); c) H. Watanabe, T. Harada, A. Tai, and Y. Izumi, 37th National Meeting of the Chemical Society of Japan, April 1978, Abstr. No. 1Q25.

6) A. Tai and M. Imaida, *Bull. Chem. Soc. Jpn.*, **51**, 1114 (1978).

7) K. Masken and N. Polgar, *J. Chem. Soc., Perkin Trans. 1*, **1973**, 109.

8) A. Horeau, *Tetrahedron Lett.*, **1961**, 506.

Kinetics of the Reaction of α-Chloro Aliphatic Acids with Aqueous Ammonia[1)]

Yoshiro OGATA,* Atsushi KAWASAKI, Yasuhiko SAWAKI, and Yuya YAMAUCHI
Department of Applied Chemistry, Faculty of Engineering, Nagoya University, Chikusa-ku, Nagoya 464
(Received November 30, 1978)

The kinetics of the reaction of α-chloro aliphatic acids (CAA's) with aqueous ammonia to form the corresponding α-amino acids and α-hydroxy acids have been studied by measuring the produced chloride ion. The observed rate for CAA's having COOH on a *s*-C (*s*-CAA's) is expressed as: $v=(k_1+k_2[NH_3]_{ex})[CAA]$, while the rate for CAA having COOH on a *t*-C (*t*-CAA): $v=k_1[CAA]$. These results together with previous observations indicate that the mechanism changes with substrate, *i.e.*, pure S_N2 type for chloroacetic acid to pure S_N1 type for α-chloroisobutyric acid. The exclusion of α-lactone mechanism and the effect of carboxylato group are discussed. The reactivity of ammonia toward α-chloro aliphatic acids is as twice as that of hydroxide ion.

The ammonolysis of α-halo aliphatic acids is an important method for preparation of α-amino acids.[2-4)] Generally, α-chloro aliphatic acids (**1**) are treated with a large excess of aqueous ammonia to give α-amino acids (**2**) accompanied by α-hydroxy acids (**3**). (See Eq. 1.)

Cheronis and Spitzmuller[5)] have reported the effect of molar ratio, temperature, and pH on the yields for this ammonolysis, but not the kinetics and mechanism. We have reported the kinetics for the ammonolysis of chloroacetic acid, where the rate law was: $v=k[NH_3][ClCH_2CO_2H]$, suggesting S_N2 mechanism.[6)] But this nucleophilic mechanism may vary with the change of branching at α-position from primary to tertiary.

The present study was undertaken to obtain some information on the kinetics of the reaction of α-chloro aliphatic acids having COOH on *s*-C and *t*-C (abbreviated as *s*-CAA and *t*-CAA, respectively) with aqueous ammonia, and the change of mechanism with structure. The role of carboxylate ion is discussed.

Results and Discussion

Ammonolysis was conducted at 60 °C in aqueous ammonia, and the produced chloride ion was measured to follow the rate of reaction. The reaction gave α-amino acids (**2**) along with α-hydroxy acids (**3**). The products ratios are shown in Table 1.

$$\underset{\text{(1)}}{R^1R^2CCO_2H\ (Cl)} + \text{aq } NH_3 \longrightarrow \underset{\text{(2)}}{R^1R^2CCO_2H\ (NH_2)} + \underset{\text{(3)}}{R^1R^2CCO_2H\ (OH)} \quad (1)$$

General Kinetics of the Ammonolysis. α-Chloro aliphatic acids were treated with over tenfold excess of ammonia. The rate of ammonolysis was first-order in the acid. For the determination of the order with respect to ammonia, the rate constant was measured at constant concentration of α-chloro aliphatic acid and various concentrations of ammonia. The observed rate constants are in Table 2. The plot of the observed rate constants against the initial concentrations of ammonia gave a straight line with an intercept at $[NH_3]_{ex}=0$. Therefore, the rate equation consists of first- and second-order terms, where $[\ ]_{ex}$ means excess concentration to that of CAA.

$$\frac{d}{dt}[Cl^-] = (k_1+k_2[NH_3]_{ex})[CAA] \quad (2)$$

Here, k_1 was evaluated from the intercept of the plot and k_2 from the slope. The results are shown in Table 3. The α-amino acids and α-hydroxy acids produced in the reaction show that the ammonolysis and hydrolysis occur competitively.

Table 1. Product ratio for ammonolysis of α-chloro aliphatic acids (**1**) (See Eq. 1)

	R^1	R^2	$[CAA]_0=0.1$ M $[NH_3]_{ex}=5.1$ M
1a	H	Me	**2a** : **3a** = 83 : 17
1b	H	Et	**2b** : **3b** = 73 : 27
1c	H	*i*-Pr	**2c** : **3c** = 39 : 61
1d	Me	Me	**2d** : **3d** = 14 : 86

s-CAA's. The rate equation for *s*-CAA's (**1a**, **1b**, and **1c**) can be expressed as Eq. 2. (Table 3.) The second-order rate constants decrease in the order; R^2: Me>Et≫*i*-Pr.

The order is due to inductive effect as well as steric effect. Especially, the steric effect is important for the reaction of 2-chloro-3-methylbutyric acid (**1c**). The transition state, crowded with leaving chloride ion, attacking ammonia, and carboxylato and isopropyl groups, reduced the second-order rate constants (k_2).

The accompanying hydrolysis was confirmed by the isolation of α-hydroxy acids. The rate of hydrolysis for α-chloropropionic acid (**1a**) was measured. The rate equation was expressed as

$$v = (0.35+0.76[OH^-])[CH_3CH(Cl)CO_2H]\times 10^{-5} \quad \text{at 60 °C.} \quad (3)$$

Therefore, ammonolysis of secondary α-chloro aliphatic acids is a "border line case" between S_N2 and S_N1.

t-CAA. In contrast to *s*-CAA's, *t*-CAA, α-chloroisobutyric acid (**1d**), has a rate independent of the concentration of nucleophiles.

$$\frac{d}{dt}[Cl^-] = k_1[(CH_3)_2C(Cl)CO_2H] \quad (4)$$

The first-order rate constant is greater than that for analogous secondary substrates. α-Amino acid (**2a**) is the main product of the reaction of α-chloro-

TABLE 2. RATE CONSTANTS FOR THE REACTION OF α-CHLORO ALIPHATIC ACIDS (CAA) WITH AMINO COMPOUNDS IN AN AQUEOUS SOLUTION AT 60±0.1 °C

$[CAA]_0$	$[NH_3]_{ex}$[a]	NaOH	CH_3CHCO_2H | NH_2	$(CH_3CHCO_2H)_2NH$	$k_{obsd}\times10^5$
M	M	M	M	M	s^{-1}
CH_3CHCO_2H | Cl	1.2				1.7
	1.88				2.6
	2.9				3.1
	3.5				4.1
0.10		0.12			0.35
		0.49			0.56
		0.78			0.86
		0.60	0.25		0.63
		1.1	0.50		1.6
		1.6	0.74		2.6
		2.1	1.0		3.3
		0.40		0.10	0.45
		0.55		0.15	0.62
		0.70		0.20	0.71
		1.3		0.40	1.0
		1.6		0.50	1.1
$CH_3CH_2CHCO_2H$ | Cl	1.2				0.86
	1.8				1.4
	2.9				1.5
	4.5				2.3
0.071		0.070			0.38
$(CH_3)_2CHCHCO_2H$ | Cl	1.2				0.42
	2.5				0.44
	3.8				0.50
	5.1				0.52
0.080		0.080			0.36
$(CH_3)_2CCO_2H$ | Cl	1.2				96
	2.5				95
	3.8				96
	5.1				94
0.087		0.090			90

a) Excess ammonia $[NH_3]_{ex}$ means the difference in the concentrations between added ammonia and $[CAA]_0$.

TABLE 3. RATE CONSTANTS FOR THE REACTION OF α-CHLORO ALIPHATIC ACIDS WITH AQUEOUS AMMONIA AT 60±0.1 °C (See Eq. 2)

Substrate	$k_1\times10^5$ (s^{-1})	$k_2\times10^5$ ($M^{-1}\,s^{-1}$)	$k'_1\times10^5$ (s^{-1})[a]
1a	0.68	0.94	0.35
1b	0.48	0.40	0.38
1c	0.38	0.027	0.36
1d	95	—	90

a) k'_1: hydrolysis rate constants for α-chloro carboxylates.

propionic acid (**1a**) with aqueous ammonia, while α-hydroxy acid (**3d**) is the main product from α-chloroisobutyric acid (**1d**) with only a little α-aminoisobutyric acid (**2d**) (Table 1).

The activation parameters were calculated from k_1's at 60 and 30 °C. The energy of activation is 27.9 kcal mol^{-1} and the entropy of activation +9.3 e.u. This consistent with S_N1 mechanism, while the entropy of activation for ammonolysis of chloroacetic acid, where S_N2 mechanism operates, is −16 e.u.[6]

Grunwald and *et al.*[7] suggested α-lactone mechansim for the hydrolysis of α-bromopropionic acid on the basis of the first-order rate equation, the retention of configuration, common ion effect, and a small solvent effect. Hence, solvent effect was studied with our α-chloroisobutyric acid to examine the intermediacy of α-lactone. The results expressed as Grunwald-Winstein equation,[8] $\log(k/k_0)=mY$, are shown in Table 4.

The observed m value for the ammonolysis of α-

TABLE 4. SOLVENT EFFECT ON THE REACTION OF α-CHLOROISOBUTYRIC ACID WITH AMMONIA IN AQUEOUS METHANOL AT 30±0.1°C ($[NH_3]_{ex}$=2.5 M)

Solvent	Y value[8]	$k_1\times10^5$ (s^{-1})
H_2O	3.493	1.4
40 vol % MeOH	2.391	0.64
80 vol % MeOH	0.381	0.19

chloroisobutyric acid (m=0.27) is three times larger than that for the hydrolysis of α-bromopropionic acid (m=0.095); *i.e.*, the former reaction is more susceptible to solvent effect than the latter.[7]

Gripenberg *et al.*[9] proposed that a methyl group increased the unimolecular rate by a factor of 10^4 and a carboxylato group by a factor of about 10^3. Based on these values, we can expect a decrease of the unimolecular rate by a factor of 10 by substitution of carboxylato group for methyl group. Contrary to this expectation, the unimolecular rate constant for the methanolysis of α-bromopropionic acid (5.12×10^{-5} s^{-1} at 64.5 °C)[7] was found to be much larger than that of isopropyl bromide (5.0×10^{-8} s^{-1} at 64.5 °C).[7] This would be ascribed to the neighboring group participation of carboxylate ion in spite of the inductive rate-retarding effect of carboxylate ion. [The comparison of rate constants alone may not be appropriate to judge the participation].

On the other hand, the observed first-order rate constant for the ammonolysis of α-chloroisobutyric acid (1.4×10^{-5} s^{-1} at 30 °C) was much lower than the reported value for the hydrolysis of *t*-butyl chloride (3.3×10^{-2} s^{-1} at 25 °C).[8] Thus, no acceleration by neighboring carboxylate ion was observed; hence the α-lactone mechanism is excluded for the present reaction. Namely, the ammonolysis of α-chloroisobutyric acid proceeds by S_N1 mechanism, *i.e.*, rate-determing dissociation of Cl$^-$ forming zwitter ion $Me_2\overset{+}{C}COO^-$, where carboxylate ion acts as a weaker electron-releasing group than methyl group. The change of mechanism to S_N1 in isobutyric acid may be ascribed to the high stabilization of carbonium ion by the presence of two Me and a solvated COO$^-$.

Subsequent Reaction of α-Chloropropionic Acid with Ammonia. Ammonolysis of α-chloropropionic acid is a consecutive reaction. The kinetics for the reaction of α-chloropropionic acid with α-aminopropionate or α,α′-iminodipropionate ion were studied. The rate constants are listed in Table 5.

Table 5. Rate constants for the reaction of α-chloropropionic acid with α-aminopropionate and α,α′-iminodipropionate ions in aqueous solution at 60±0.1 °C

$v=(k_1+k_2[\text{Amino compound}])$ **[1a]**

Amino compound	$k_1\times10^5$ (s^{-1})	$k_2\times10^5$ (M^{-1} s^{-1})
NH_3	0.68	0.94
$CH_3\underset{\underset{NH_2}{\vert}}{C}HCO_2^-$	0.12	3.1
$(CH_3\underset{\underset{\vert}{}}{C}HCO_2^-)_2NH$	0.33	1.7

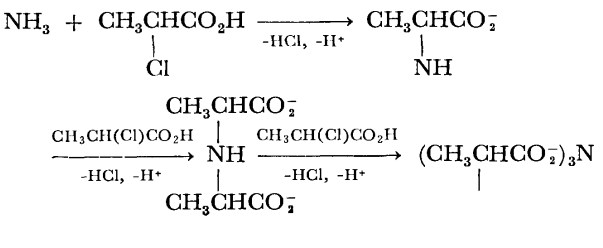

α-Aminopropionate ion having an α-carboxylatoethyl group ($CH_3\underset{\underset{\vert}{}}{C}HCO_2^-$) is about three times as reactive as ammonia in k_2, while α,α′-iminodipropionate ion is no more so stronger nucleophile than ammonia in spite of the presence of two α-carboxylatoethyl groups:

$$CH_3\underset{\underset{NH_2}{\vert}}{C}HCO_2^- \gtrsim (CH_3\underset{\underset{\vert}{}}{C}HCO_2^-)_2NH \gtrsim NH_3$$

We reported that the reactivity toward chloroacetic acid was in the order: $NH_2CH_2CO_2^-\simeq NH(CH_2CO_2^-)_2>NH_3$ in which the steric effect caused a slight decrease in the rate for iminodiacetate ion, compared with the rate for aminoacetate ion.[6] Similarly, a small reactivity of α,α′-iminodipropionate ion is due to the steric effect, because α-carboxylatoethyl group is much bulkier than carboxylatomethyl group.

In aqueous solution, the hydrolysis of α-chloropropionic acid is not negligible. (Eq. 3.) The rate constant for the hydrolysis of chloroacetic acid in an aqueous solution at 60 °C (7.67×10^{-5} s^{-1} M^{-1}) was reported to be *ca.*1/2 of that for the ammonolysis (15.0×10^{-5} s^{-1} M^{-1}).[10] We obtained the rate constants for hydrolysis (0.76×10^{-5} s^{-1} M^{-1}) and for ammonolysis (0.94×10^{-5} s^{-1} M^{-1}) of α-chloropropionic acid in an aqueous solution at 60 °C. Hence, the nucleophilicity of ammonia toward alkyl chloride is *ca.* 1.6 fold higher than that of hydroxide ion. But the relative nucleophilicity of OH$^-$ and NH_3 may depend on the structure of RX and the solvent. Though the Swain-Scott nucleophilicity parameter for ammonia is unavailable, aniline (n=4.49) is twice as reactive as hydroxide ion (n=4.20).[11] Ammonia seems to have the same reactivity as aniline.

Mechanism. The above observations suggest a following scheme for the reaction in an aqueous solution.

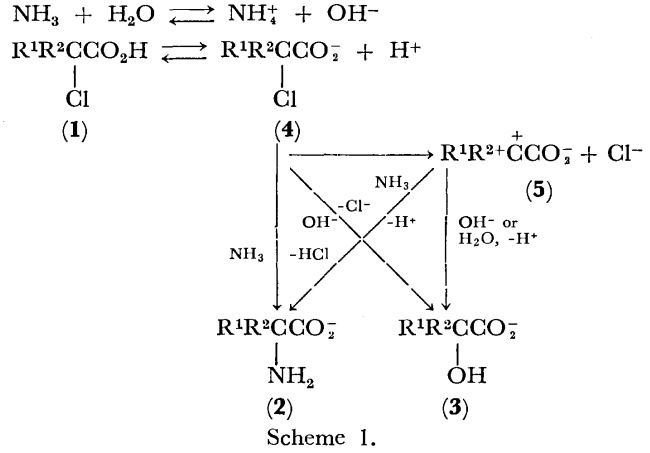

Scheme 1.

The primary reaction is a competition between ammonia and hydroxide ion for α-chloro aliphatic acid. In the ammonolysis of α-chloropropionic acid, a fall of pH by addition of ammonium chloride decreased the formation of lactic acid, which suggests that the hydrolysis proceeds by an attack of hydroxide ion.

The mechanism changes from S_N2 to S_N1, as the alkyl group varies from primary to tertiary. This result agrees with the earlier observation in the sol-

TABLE 6. CHANGE OF MECHAMISM WITH STRUCTURE

R^1	R^2	Mechanism
H	H	S_N2
H	Me	S_N2 + S_N1
H	Et	S_N2 + S_N1
H	*i*-Pr	S_N2 + S_N1
Me	Me	S_N1

volysis of alkyl halides.[12] The hydrolysis occurs competitively, and thus the yields of α-amino acids were lowered. The yields of α-amino acids decreased in the order: **2a>2b>2c>2d**. The results also support this mechanism. The hydrolysis can be suppressed on addition of ammonium chloride as was observed. In these reactions, the carboxylato group acts as a weaker electron-releasing group, but exerts no anchimeric assistance.

Experimental

Melting points were measured by a Yanagimoto micro-melting point apparatus and were corrected. Boiling points were uncorrected. IR spectra were recorded on a Perkin-Elmer 337 grating spectrophotometer, and NMR spectra on a Hitachi R-24B spectrometer.

Materials. Aqueous ammonia, nitric acid, hydrochloric acid, sodium hydroxide, ammonium chloride, α-aminoisobutyric acid, and alanine used were of guaranteed reagent grade. α-Chloropropionic acid was redistilled under vacuum before use: bp 92—93 °C/15 Torr (lit,[13] 82.5—83.5 °C/12 Torr; NMR (CCl_4) δ 1.70 (d, 3H, CH_3), 4.35 (q, 1H, CH).

Preparation of the Other α-Chloro Aliphatic Acids. 2-Chloro-3-methylbutyric, α-chlorobutyric, and α-chloroisobutyric acids were prepared by α-chlorination[14] of the corresponding acids. The corresponding aliphatic acid was reacted with a gaseous mixture of Cl_2–O_2 gas in a molar ratio of 1/2 in the presence of chlorosulfuric acid and chloranil at 120 °C for 6 h. The product was then extracted with ether, the organic layer being distilled to obtain α-chloro aliphatic acid. α-Chlorobutyric acid: bp 101—111 °C/27 Torr (lit,[15] 98 °C/10.5 Torr); NMR(CCl_4) δ 4.2 (t, 1H, CH), 2.5—2.0 (m, 2H, CH_2), 1.1 (t, 3H, CH_3); IR (neat) 1730 cm^{-1} (C=O), 625 (C–Cl). α-Chloroisobutyric acid: bp 97—99 °C/27 Torr; mp 29—30 °C (lit,[16] mp 28—30 °C); NMR (CCl_4) δ 1.75 (s); IR (neat) 1720 cm^{-1} (C=O), 615 (C–Cl). α-Chloroisovaleric acid: bp 108—109 °C/15 Torr (lit,[17] 125—126 °C/32 Torr); NMR (CCl_4) δ 4.05 (d, 1H, CH), 2.5—1.8 (m, 1H, CH), 1.10 (d, 6H, CH_3); IR (neat) 1720 cm^{-1} (C=O), 620 (C–Cl).

Preparation of α-Amino Acid. A mixture of α-chloro aliphatic acids (0.01 mol) and aqueous ammonia (5.2 M, 50 ml) was heated, in the case of α-chloropropionic and α-chlorobutyric acids. A mixture of 2-chloro-3-methylbutyric acid and aqueous ammonia 50 ml (28%) was reacted at room temperature for 3 weeks. The solution was evaporated under vacuum, and α-amino acids were recrystallized from aqueous methanol. The yields of isolated products were based on α-chloro aliphatic acids. Alanine: Yield 55%; NMR (D_2O/DSS) δ 4.2—3.8 (q, 1H, CH), 1.75 (d, 3H, CH); IR (KBr) 3200—3000 cm^{-1}, 2250 (NH_2), 1600 (CO_2^-). α-Aminobutyric acid: Yield 39%; NMR (D_2O/DSS) δ 4.15 (t, 1H, CH), 2.4—2.2 (m, 2H, CH_2), 1.5 (t, 3H, CH_3); IR(KBr) 3200—3000 cm^{-1} (NH_2), 1600 (CO_2^-). Valine: Yield 17%; NMR (D_2O/DSS) δ 3.55 (d, 1H, CH), 2.2—1.9 (m, 1H, CH), 1.0 (dd, 6H, CH_3); IR (KBr) 3200—3000 cm^{-1} (NH_2), 1600 (CO_2^-).

Preparation of α-Hydroxy Aliphatic Acid. An aqueous solution of α-chloro aliphatic acid (0.01 mol) and the equivalent amount of NaOH was refluxed for 24 h. The solution was acidified with HCl and extracted with ether (20 ml). The solution was evaporated to obtain α-hydroxy aliphatic acid. In the case of α-chloropropionic and α-chloroisobutyric acids, the solution was dried without acidification and α-hydroxy aliphatic acid sodium salts were obtained. Sodium lactate: NMR (D_2O/DSS) δ 4.2 (q, 1H, CH), 1.5 (d, 3H, CH_3). α-Hydroxybutyric acid: NMR (CCl_4) δ 7.10 (s, 1H, OH), 4.15 (t, 1H, CH), 2.2—1.9 (m, 2H, CH_2), 1.0 (t, 3H, CH_3); IR (KBr) 3450 cm^{-1} (OH), 1720 (C=O). 2-Hydroxy-3-methylbutyric acid: NMR (CCl_4) δ 7.15 (s, 1H, OH), 4.1 (d, 1H, CH), 2.2—2.0 (m, 1H, CH), 0.9 (dd, 6H, CH_3); IR (KBr) 3420 cm^{-1} (OH), 1720 (C=O). Sodium α-hydroxyisobutyrate: NMR (D_2O/DSS) δ 1.80 (s, CH_3); IR (KBr) 3440 cm^{-1} (OH), 1610 (CO_2^-).

The products were identified similarly by means of NMR in comparison with the authentic samples. The ratio of products of ammonolysis of α-chloropropionic and α-chloroisobutyric acids was estimated by NMR spectra of the reaction mixture after evaporation of the solvent. In the case of α-chlorobutyric and 2-chloro-3-methylbutyric acids, the reaction mixture of α-chloro aliphatic acids and aqueous ammonia was acidified with aqueous HCl and extracted with ether. After evaporation of the solvent the molar ratio of α-amino acids to DMSO was estimated by NMR spectra of the residue of the aqueous layer. Similarly, the ratio's of α-hydroxy aliphatic acids to DMSO were estimated by that of the ether extract. Then, the ratio of products of ammonolysis of α-chlorobutyric and 2-chloro-3-methylbutyric acids was obtained in this way.

Preparation of α,α′-Iminodipropionic Acid. Alanine (25 g, 0.3 mol), 100 ml of aqueous NaOH (24 g, 0.6 mol), and 50 ml of aqueous α-chloropropionic acid (32 g, 0.3 mol) were mixed in a flask equipped with a reflux condenser at room temperature. The solution was refluxed for 24 h. Then, the aqueous solution was acidified with HCl and was washed with ether (50 ml×3) to extract lactic acid. After evaporation of aqueous layer in vacuum to dryness, α,α′-iminodipropionic acid was extracted with ethanol (1.5 l), the ethanol solution being condensed in vacuum and cooled. α,α′-Iminodipropionic acid was slowly crystallized, filtered, washed with cold ethanol, and recrystallized from water-ethanol-ether (1 : 2 : 1). 5.0 g of colorless crystals of α,α′-iminodipropionic acid was obtained: mp 236—238 °C (lit,[18] 238 °C); NMR (D_2O/DSS) δ 3.90 (q, d, 2H, CH), 1.55 (d,d, 6H, CH_3); IR (KBr) 3400 cm^{-1} (NH), 1720 (C=O), 1600 (CO_2^-). Found: C, 43.07; H, 6.45; N, 8.35%. Calcd for $C_6H_{11}NO_4$: C, 44.72; H, 6.88; N, 8.69%.

Kinetics. A solution of α-chloro aliphatic acid (5 ml) was added to an aqueous solution of amino compound (45 ml) in a glass-stoppered flask, which had reached thermal equilibrium in a thermostat. Aliquots (5 ml) were pipetted out at regular intervals of time and cold dilute nitric acid was added to stop the reaction. The chloride ion concentration was determined by the Volhard method.[19]

The rate constants for the reaction of α,α′-iminodipropionate ion and α-chloropropionic acid was rather inaccurate (±10%) because of the lower initial concentration of α,α′-iminodipropionate ion and a small amount of impurity (NaCl), which could not completely be eliminated, but the content of NaCl was determined and subtracted. The initial first-order rate constants (up to 20% conversion) were calculated by the least square method (r>0.98). The

% conversion of the reaction of NH_3 or OH^- was 30—50%. Probable error in rate constants was ±5%.

References

1) Contribution No. 247.

2) (a) W. C. Tobie and G. B. Ayres, *Org. Synth.*, Coll. Vol. I, 23 (1941); (b) C. S. Marvel, *ibid.*, Coll. Vol. III, 495 (1955); (c) C. S. Marvel, *ibid.*, Coll. Vol. III, 523 (1955); (d) H. E. Carter and H. D. West, *ibid.*, Coll. Vol. III, 774 (1955); (e) C. S. Marvel, *ibid.*, Coll. Vol. III, 848 (1955).

3) K. Kraut, *Ber.*, **33**, 2577 (1898).

4) G. R. Robertson, *J. Am. Chem. Soc.*, **49**, 2899 (1927).

5) N. D. Cheronis and H. Spitzmuller, *J. Org. Chem.*, **6**, 349 (1941).

6) Y. Ogata, A. Kawasaki, and T. Goto, *J. Org. Chem.*, **33**, 1107 (1968).

7) E. Grunwald and S. Winstein, *J. Am. Chem. Soc.*, **70**, 841 (1948).

8) (a) E. Grunwald and S. Winstein, *J. Am. Chem. Soc.*, **70**, 846 (1948); (b) J. E. Leffler and E. Grunwald, "Rates and Equilibria of Organic Reactions," Wiley, New York, N. Y. (1963), p. 347.

9) J. Gripenberg, E. D. Hughes, and C. K. Ingold, *Nature*, **164**, 480 (1948).

10) N. I. Darienko and N. V. Sapozhinikova, *Izv. Vyssh. Ucheb. Zaved. Khim., Khim. Tekhnol.*, **3**, 461 (1960); *Chem. Abstr.*, **54**, 21954 (1960).

11) C. G. Swain and C. B. Scott, *J. Am. Chem. Soc.*, **75**, 141 (1953).

12) (a) E. D. Hughes and C. K. Ingold, *J. Chem. Soc.*, **1935**, 244; (b) E. D. Hughes, *ibid.*, **1935**, 255; (c) E. D. Hughes, C. K. Ingold, and U. G. Shapiro, *ibid.*, **1936**, 225; (d) L. C. Bateman, K. A. Cooper, E. D. Hughes, and C. K. Ingold, *ibid.*, **1940**, 925.

13) A. Michael, *Ber.*, **34**, 4049 (1901).

14) Y. Ogata, T. Harada, K. Matsuyama, and T. Ikejiri, *J. Org. Chem.*, **40**, 2960 (1975).

15) R. H. Horn, R. B. Mitter, and S. N. Slater, *J. Chem. Soc.*, **1950**, 2900.

16) M. S. Kharasch and H. C. Brown, *J. Am. Chem. Soc.*, **62**, 925 (1940).

17) M. Renard, *Mem. Soc. Sci. Liege*, **65**, 288 (1948); *Chem. Abstr.*, **42**, 7814 (1948).

18) G. Stadnikoff, *Ber.*, **40**, 1014 (1907).

19) J. R. Coldwell and H. V. Meyer, *Ind. Eng. Chem. Anal. Ed.*, **7**, 38 (1935).

Solvolysis in Carboxamides. V.[1] Solvolytic Elimination of *threo*-1-Methyl-2-phenylpropyl Brosylate in *N,N*-Dimethylacetamide. Kinetic, Product, and Deuterium Tracer Studies

Seiki SAITO,* Kenji DOIHARA, Toshio MORIWAKE, and Kunio OKAMOTO**

Department of Synthetics Chemistry, School of Engineering, Okayama University, Tsushima, Okayama 700

***Department of Hydrocarbon Chemistry, Faculty of Engineering, Kyoto University, Sakyo-ku, Kyoto 606*

(Received October 7, 1978)

Solvolysis of a series of ring substituted *threo*-1-methyl-2-phenylpropyl brosylates has been carried out in *N,N*-dimethylacetamide (DMA) as solvent. Hammett treatment of the rate data indicated that the DMA solvolysis of the unsubstituted brosylate (**1c**) falls into the category of k_s pathway (100%). In order to gain further information of the nature of the k_s pathway, the DMA solvolysis of **1c** or **1c**-2-*d* (labeled at C(2)) has been conducted. The product distribution, effect of water content on it, the composition and deuterium distribution of recovered brosylate, kinetic isotope effect, and the deuterium distribution of product have been investigated. The products consisted of the olefins ((*E*)- and (*Z*)-2-phenyl-2-butenes, and 2- and 3-phenyl-1-butenes), and, in the presence of water in DMA, the carboxylates (*erythro*- and *threo*-1-methyl-2-phenylpropyl acetates) and the small amount of diastereomeric alcohols. The major product was (*Z*)-2-phenyl-2-butene, indicating the occurrence of *anti*-*E*1 process. The deuterium was substantially scrambled in each product. These findings suggest that the reaction proceeds through tight ion-pair and subsequent processes such as *anti*-*E*1, 2,1-phenyl and -hydride shifts, solvent capture, and *threo-erythro* interconversion take place competitively. In view of a substantial extent of intervention of such rearrangement, the involvement of nucleophilic solvent assistance is thought to be less probable in this k_s process.

The β-phenyl participation in solvolytic reactions has been one of interesting subjects in organic reaction mechanism for more than twenty years.[2] Cram has first proposed the phenonium ion as intermediate in the acetolysis of optically active *threo*- and *erythro*-1-methyl-2-phenylpropyl tosylates to account for the remarkable stereospecificity of the reaction.[3] For example, the acetolysis of the *threo*-substrate gave acetate (53% yield) with 94% retention of configuration, accompanied with the olefin formation (35%).[3]

Winstein *et al.*[4] have shown, however, that the rate enhancement expected for the β-phenyl participation is generally quite small. In fact, when titrimetric rate is compared, the rate of the acetolysis of *threo*-1-methyl-2-phenylpropyl tosylate was 0.6 times the rate of *s*-butyl tosylate under the same conditions.[4]

Such an apparent discrepancy between rate data and stereospecificity of product has made it difficult to clarify the role of β-phenyl group in solvolytic reactions and, therefore, was the starting point of the current controversy.[2,5-13]

Schleyer and his collaborators[6] have recently suggested that the solvolysis of β-arylalkyl systems proceeds through discrete aryl-assisted (k_Δ) and/or aryl-unassisted (k_s) pathways. They have developed the method for the dissection of the observed rate constant (k_t) into its Fk_Δ and k_s components by the use of Hammett correlation.[6a]

The application of this approach[6a] to 2-aryl-1-methylpropyl system has been performed by Brown and Kim.[5e] They conducted the acetolysis of a series of ring substituted *threo*-1-methyl-2-phenylpropyl brosylates and found the existence of an excellent rate-product correlation, when $100Fk_\Delta/k_t$ value was compared with the yield of retained acetate. However, since the rate ratio (k_Δ/k_s) of 12 for the unsubstituted derivative (**1c**) was too small to be ascribed to the mechanism involving the simultaneous formation of open and bridged ions,[6] they have proposed a mechanism involving an open tight ion-pair as a common intermediate to which both the aryl-assisted and the aryl-unassisted pathways compete,[5e,f] employing the original formulation of Shiner[14] and Sneen.[15]

In a series of our investigations with respect to the nature of carboxamide solvolysis for typical secondary cycloalkyl systems, 4-*t*-butylcyclohexyl,[16] 7β-methylbicyclo[3.3.1]non-3β-yl,[17] and *exo*-2-norbornyl[1] systems, it has been revealed that the reactions proceed through an initially formed tight ion-pair intermediate [R^+X^-] (classical) which undergoes various subsequent processes such as *E*1 reaction, solvent capture (formation of imidatonium ion), or rearrangements, as is outlined in Scheme 1.

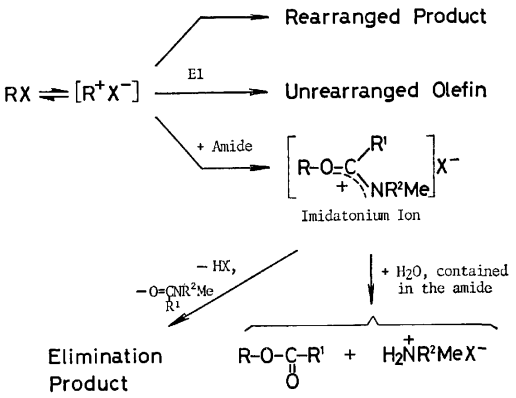

R^1, R^2=H or Me

Scheme 1.

As a principal characteristic of the carboxamide solvolysis, it has been demonstrated that the carboxamides suppress the formation of rearranged products even when the substrate has a structure prone to rearrangement and, in addition, they accelerate *syn*-*E*1 process in the cyclic substrates[1,16,17] to result in an increase in the yield of unrearranged olefin. Based on such trends observed in the previous studies,[1,16,17] it was anticipated that a fraction of the k_Δ pathway

for **1c** might be suppressed in the carboxamide solvolysis as compared with that in the acetolysis.[5e] It appeared also of interest to examine whether the rate-product correlation, observed in the acetolysis,[5e] is observed or not in carboxamide solvolysis of such system.

In this paper, we report on a) the Hammett treatment of rate data for the DMA solvolysis of a series of ring substituted *threo*-1-methyl-2-phenylpropyl brosylates (**1a**—**g**), b) the products of the DMA solvolysis of the unsubstituted derivative **1c** in the presence of various amounts of water, c) the composition and deuterium distribution of the unchanged brosylate recovered from half-life reaction of C(2)-deuterated substrate **1c**-2-*d* in DMA solvent, d) deuterium distribution of the products produced from the DMA solvolysis of **1c**-2-*d*, and e) kinetic isotope effect for **1c**-2-*d* solvolysis in four carboxamide solvents, *i.e.*, *N*-methylformamide (NMF), *N*-methylacetamide (NMA), *N*,*N*-dimethylformamide (DMF), and *N*,*N*-dimethylacetamide (DMA). We also discuss the generality of the mechanism (Scheme 1) and the mechanistic problem[2,5-13] of 2-aryl-1-methylpropyl solvolysis, especially on the nature of the k_s process.

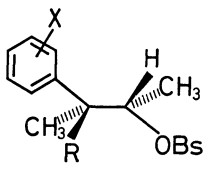

1a R=H, X=*p*-MeO
1b R=H, X=*p*-Me
1c R=H, X=H
1c-2-*d* R=D, X=H
1d R=H, X=*p*-Cl
1e R=H, X=*m*-Cl
1f R=H, X=*m*-CF_3
1g R=H, X=*p*-NO_2

Results

Rate Study and Hammett Correlation for the DMA Solvolysis of ***1a***—***g***. The rates of solvolysis of **1a**—**g** in DMA solvent were determined titrimetrically in the same manner as reported.[1] All the kinetic runs exhibited first-order behavior over two to three half lives. Pyridine, added to neutralize liberated *p*-bromobenzenesulfonic acid, did not alter the rate, presumably indicating that the reaction proceeds through typical *E*1 or S_N1 mechanism. The rate constants and activation parameters are tabulated in Table 1. The Hammett plot for the rates of **1a**—**g** at 75 °C is shown in Fig. 1, together with that for the acetolysis[5e] for the purpose of comparison.

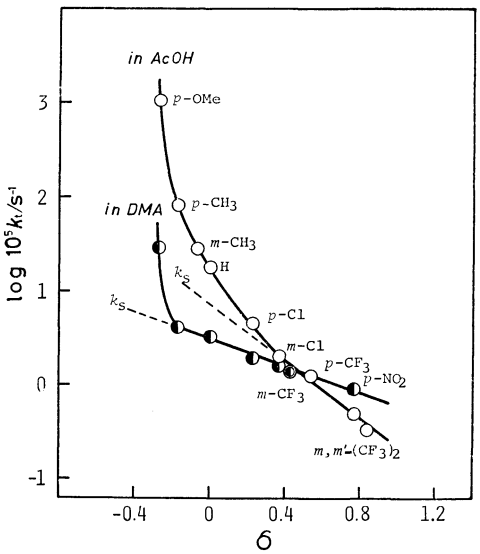

Fig. 1. Plot of $\log k_t$ (*thero*-2-aryl-1-methylpropyl brosylate) for the DMA solvolysis and acetolysis (Ref. 5e) *vs.* σ at 75 °C; ρ-value and correlation coefficient for the DMA line are −0.72 and 0.991, respectively.

A satisfactory linear relation was observed for all the substrates except for *p*-methoxyphenyl derivative **1a**. The k_s line was determined by a least-squares treatment to obtain the ρ-value of −0.72.[18] Unlike the acetolysis,[5e] the k_Δ pathway was suppressed in DMA solvent for *p*-tolyl derivative **1b** as well as the parent phenyl derivative **1c**. Thus the DMA solvolysis of **1c** turned out to be the case of 100% k_s solvolysis. This result is quite notable as compared with previously known solvolyses of unsubstituted phenyl derivatives in the system such as 2-aryl-1-methylpropyl,[5e] 2-aryl-1-methylethyl,[6a-c,19] or *trans*-2-arylcyclopentyl[5f] because these reactions are known to proceed more or less through the k_Δ pathway.

Table 1. Kinetic data for the solvolysis of *threo*-2-aryl-1-methylpropyl brosylates **1a**—**g** in *N*,*N*-dimethylacetamide (DMA)[a]

Substituent	$10^5/s^{-1}$ [b]				$\left(\frac{\Delta H^*}{A}\right)$[c]	$\left(\frac{\Delta S^*}{B}\right)$[d]
	25.0 °C[e]	50.0 °C	75.0 °C	100.0 °C		
p-OCH_3	0.124	0.299[f] 3.21	28.8		22.9	−9.1
p-CH_3	0.00952		4.15	47.1	24.5	−8.5
H	0.00844		3.34	35.9	24.4	−10.8
p-Cl	0.00443		1.90	21.4	24.4	−10.3
m-Cl	0.00341		1.59	18.5	24.7	−9.7
m-CF_3	0.00331		1.44	16.3	24.4	−10.7
p-NO_2	0.00152		0.916[e] 4.41[h]	29.7[g]	25.1	−9.5

a) [ROBs]=0.075 mol/dm³; [C_5H_5N]=0.077 mol/dm³; [H_2O]=0.003 mol/dm³. b) Mean deviation for k_t's is ±2%. c) At 25.0 °C; A=4.184 kJ/mol. d) At 25.0 °C; B=4.184 J/(K mol). e) Extrapolated from data at other temparatures. f) At 33.0 °C. g) At 110.0 °C. h) At 90.0 °C.

Product Distribution and Effect of Water Content for the DMA Solvolysis of **1c**. In the light of the results mentioned above, it is pertinent to investigate the nature of k_s pathway by the use of the DMA solvolysis of **1c**. The product distribution for such reaction was determined by the combined use of gas chromatography and ^1H NMR spectroscopy. As illustrated in Scheme 1, the carboxylates can be formed by rapid hydrolysis of the imidatonium ion. The stereochemistry of solvent capture on initial carbonium ion intermediate could be disclosed by efficient trapping of the imidatonium ion with water. This method has been successfully utilized in the previous works.[1,17] Thus the effect of water content in DMA solvent on the product distribution was examined and the results are summarized in Table 2 and illustrated in Fig. 2.

Similarly to the trends observed for cycloalkyl systems,[1,17] the olefins, (*Z*)-2-phenyl-2-butene (**7**), its (*E*)-isomer (**8**), 2-phenyl-1-butene (**9**), and 3-phenyl-1-butene (**10**), were produced in completley dried DMA. Among them, the (*Z*)-butene **7** was a major product (≈66%). The carboxylates, *erythro*-1-methyl-2-phenylpropyl acetate (**11**) and its *threo*-isomer (**12**), were obtained only in the presence of water and they should stem from the reaction of water and the imidatonium ions, [*erythro*-R-DMA]$^+$OBs$^-$ (**4**) or [*threo*-R-DMA]$^+$OBs$^-$ (**5**), respectively (*vide infra*). These imidatonium ions can be derived from the tight ion-pair intermediate (**2**) by solvent capture (Scheme 3, *vide infra*).

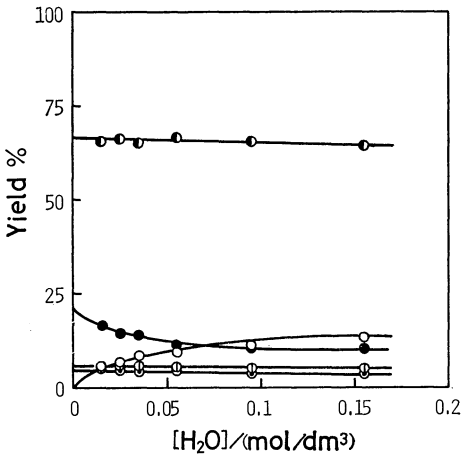

Fig. 2. Effect of water content of DMA on the formation of (*Z*)-olefin **7** (◐), (*E*)-olefin **8** (●), 2-phenyl-1-butene **9** (⊙), 3-phenyl-1-butene **10** (◫), and *erythro*-acetate **11** (○) at 75.0 °C.

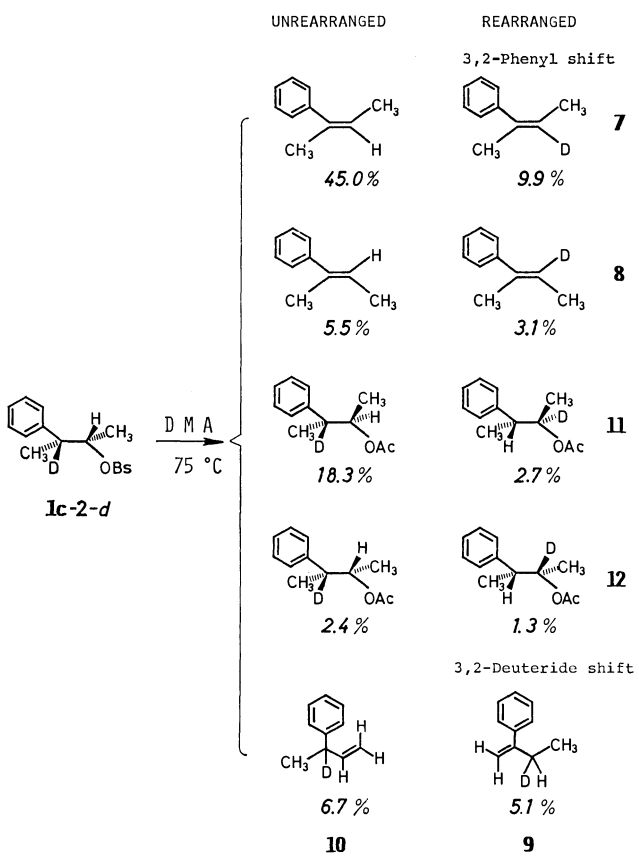

Scheme 2.

Deuterium Distribution in the Products for DMA Solvolysis and for Acetolysis of **1c**-2-d. In the investigation of the product composition, the occurrence of 2,1-hydride shift in the tight ion-pair **2** is disclosed in view of the formation of 2-phenyl-1-butene **9**. However, 2,1-phenyl shift, if any, is impossible to be proved, unless the substrate labeled at C(2). Thus, by the use of **1c**-2-*d*, the extent of phenyl migration can be estimated from the deuterium distributions in the phenylbutenes, **7**, **8**, and **10**, and also in *erythro*- and *threo*-1-methyl-2-phenylpropyl acetates, **11** and **12**.

Table 2. Effects of added H_2O on product distribution for the DMA solvolysis of *threo*-1-methyl-2-phenylpropyl brosylate at 75.0 °C[a]

$\left(\frac{[H_2O]}{mol/dm^3}\right)$	Product yield%						
	Olefin				Acetate		ROH[b]
	7	**8**	**9**	**10**	**11**	**12**	
0.015	65.9	16.5	4.9	5.3	5.8	1.1	0.5
0.025	66.4	14.4	4.5	5.9	6.9	1.3	0.6
0.035	65.1	14.0	4.2	5.8	8.5	1.7	0.7
0.055	66.8	11.5	4.2	5.5	9.3	1.8	0.9
0.095	65.8	10.8	3.8	5.1	11.4	2.2	0.9
0.155	64.5	10.1	3.6	4.9	13.4	2.4	1.1

a) [ROBs]=0.075 mol/dm^3; [C_5H_5N]=0.077 mol/dm^3. b) Diastereomeric 3-phenyl-2-butanols: isomer compositions were comprable with those of the acetates.

Table 3. Isotopic scrambling in the products for DMA solvolysis and acetolysis of *threo*-1-methyl-2-phenylpropyl-2-*d* brosylate **1c**-2-*d* at 75 °C[a]

Product	Yield % (Composition %)[b]		
Solvent:	wet DMA[c]	dry DMA[d]	AcOH
Butene:			
(*Z*)-2-Phenyl-2- (**7**) (3-H : 3-D)	54.9 (82 : 18)	57.5 (73 : 27)	5.8 (55 : 45)
(*E*)-2-Phenyl-2- (**8**) (3-H : 3-D)	8.6 (64 : 36)	26.7 (62 : 38)	19.2 (39 : 61)
3-Phenyl-1- (**10**) (3-D : 2-D)	6.7 (100 : 0)	7.4 (100 : 0)	3.3 (81 : 19)
2-Phenyl-1- (**9**) (3-D,H : 3-H_2)	5.1 (100 : 0)	8.4 (100 : 0)	2.1 (90 : 10[e])
Acetate:			
erythro-1-Me-2-phenylpropyl (2-D : 1-D) (**11**)	21.0 (87 : 13)	trace[f]	2.7 (60 : 40)
threo-1-Me-2-phenylpropyl (2-D : 1-D) (**12**)	3.7 (65 : 35)	0.0	67.0 (51 : 49)

a) [**1c**-2-*d*] = 0.075 mol/dm³; [C_5H_5N] = 0.077 mol/dm³. b) The accuracy for NMR measurement of deuterium content was ≤1%; reproducibility = ±3%. c) [H_2O] = 0.17 mol/dm³. d) [H_2O] < 0.003 mol/dm³. e) See text. f) Deuterium distribution was not determined.

Table 4. Summary of cleavage reaction of recovered brosylate from half-life solvolyses of *threo*-1-methyl-2-phenylpropyl brosylate **1c** and its C(2)-deuterated brosylate **1c**-2-*d* in DMA at 75 °C[a]

ROBs	% Recov.[c]	[$C_5H_5N^+HOBs^-$] (mol/dm³)	3-Phenyl-2-butanol, compn. %[b]			
			threo		*erythro*	
			2-D	3-D	2-D	3-D
1c-2-*d*[d]	—	—	0	100	0	0
1c	98	—	94.1		5.9	
1c	95	0.15	94.9		5.1	
1c-2-*d*	99	—	13.9	80.1	1.3	4.6

a) [ROBs] = 0.075 mol/dm³; [C_5H_5N] = 0.077 mol/dm³; [H_2O] = 0.17 mol/dm³. b) For deuterium distribution analysis: the accuracy ≤1%; reproducibility = ±3%. c) Based on the theoretical amount. d) Control experiment.

The DMA solvolysis of **1c**-2-*d* has been carried out at 75.0 °C, and for the purpose of comparison the acetolysis of **1c**-2-*d* was also conducted at the same temperature. The isotopic distribution was measured by means of ^1H NMR spectroscopy in the Fourier transform mode for all the products, which were separated by the use of column chromatography, preparative gas chromatography, and/or an appropriate chemical transformation. The extent of rearrangement, *i.e.*, 2,1-hydride shift and 2,1-phenyl shift, was calculated from the product composition and the deuterium distribution in the each product. The results are summarized in Table 3 and illustrated in Scheme 2.

Partial Solvolysis and the Analysis of Unchanged Brosylate for the DMA Solvolysis of ***1c*** *and* ***1c***-2-d. Previously, we have demonstrated that 4-*t*-butylcyclohexyl tosylate undergoes rearrangement of the type *cis*⇄*trans* during the solvolysis in phenol–benzene,[20] acetic acid,[21] 60% (v/v) acetone–water,[21] and NMA solvent.[16] From these results, it is anticipated that the rearrangement of **1c** from *threo* to *erythro* configuration may also occur during the DMA solvolysis. Accordingly, the half-life solvolysis of **1c** or **1c**-2-*d* has been carried out in the absence and the presence of added pyridinium brosylate at 75.0 °C and then the unchanged brosylate was isolated. The recovered brosylate was converted into the corresponding alcohol keeping the stereochemical integrity by the use of sodium–naphthalene reagent in tetrahydrofuran at −78 °C. The alcohol was analyzed to determine its isomer composition and/or deuterium distribution by means of gas chromatography and ^1H NMR spectroscopy. As expected, it was disclosed that *threo* brosylate **1c** rearranges to *erythro* brosylate (**13**) during the solvolysis. The results are summarized in Table 4.

Kinetic Isotope Effect. In order to obtain information on the transition-state structure for the DMA solvolysis of **1c**, the isotope effect on the DMA solvolysis rate of **1c** by deuteration of C(2) position was examined at 75.0 °C. Such examination has been also made on the other carboxamide solvolyses in DMA, NMA, and NMF. These results are tabulated in Table 5 together with data pertinent to appropriate systems. The β-effect ($k_H/k_{\beta\text{-}D}$) of 1.93 (DMA solvolysis) appears to be comparable to the values reported for solvolyses of the systems[22–24] with the tertiary β-hydrogen.

Table 5. Summary of isotope effect for solvolysis of secondary alkyl sulfonates bearing tertiary β-hydrogen[a)]

Substrate	Solvent (T/°C)	$k_H/k_{\beta-D}$	Olefin Yield %[b)]	Ref.
threo-1-Methyl-2-phenylpropyl OBs	DMA (75)	1.93	83	this work
	DMF (75)	1.67	—	this work
	NMA (75)	1.63	62	this work
	NMF (75)	1.41	—	this work
cis-2-Phenylcyclopentyl OTs	AcOH (50)	2.07	96	22
threo-2-Cyclohexyl-1-methylpropyl OTs	AcOH (25)	1.87	54[c)]	23
1,2-Dimethylpropyl OTs	AcOH (25)	2.26	70[d)]	24

a) Effect by substituting the tertiary β-hydrogen. b) Data for the unlabeled substrate. c) At 35 °C. d) At 75 °C.

Discussion

Possible Reaction Scheme Drawn on the Basis of the Product Distribution and Effect of Water Content on It for DMA Solvolysis of ***1c***. The yields of the (*Z*)-2-olefin **7** and 1-butenes, **9** and **10**, are virtually unchanged even with the increase in the water content (Fig. 2). In contrast, the yield, though much less, of (*E*)-2-butene **8** decreases with the increase in water content, but becomes actually invariant at the water concentration higher than 0.15 mol/dm³. On the other hand, the yield of the *erythro*-acetate **11** increases complementing the decrease in the yield of (*E*)-2-butene **8**, and it also becomes constant (Fig. 2), although the increase in the acetate **11** yield can not completely compensate the (*E*)-olefin **8** yield.

From these features of the yield variation caused by increase in water content, the following reaction pathway can be depicted as one of the simplest reaction schemes: a) the (*Z*)-olefin **7** and 1-butene **10** are formed from the tight ion-pair **2**, b) the *erythro*-acetate **11** can be produced by the reaction of water with *erythro*-imidatonium ion **4**, partially compensating the decrease in the yield of the (*E*)-2-butene **8**, c) thus the (*E*)-2-butene **8** comes actually from the *erythro*-imidatonium ion **4**, but a part of it can be formed through a rearranged cation (**6**) which is formed after 2,1-hydride shift of the tight ion-pair 2, d) the 1-butene **9** can also be produced from the rearranged cation **6**, and e) the *threo*-acetate **12**, although in very low yield, is derived from the *threo*-imidatonium ion **5**. These pathways are illustrated in Scheme 3, which are essentially the same as those depicted in Scheme 1.

The formation of conjugated terminal olefin **9** suggests the occurrence of 2,1-hydride shift to produce tertiary benzylic cation **6**. Cram and Sahyun[25)] have demonstrated that the acetolysis of a tertiary benzylic system, *i.e.*, 1-methyl-1-phenylpropyl chloride, affords the olefins in 94% yield which consist of (*Z*)-olefin **7**, (*E*)-olefin **8**, and 1-butene **9** in the ratio 9 : 68 : 23. If the same ratio for Saytzeff orientation could be expected on the reaction of benzylic cation **6** in the solvolysis of **1c** in DMA containing 0.155 mol/dm³ of water, the yields of **7** and **8** can be predicted to be 1.4% and 10.6%, respectively, based

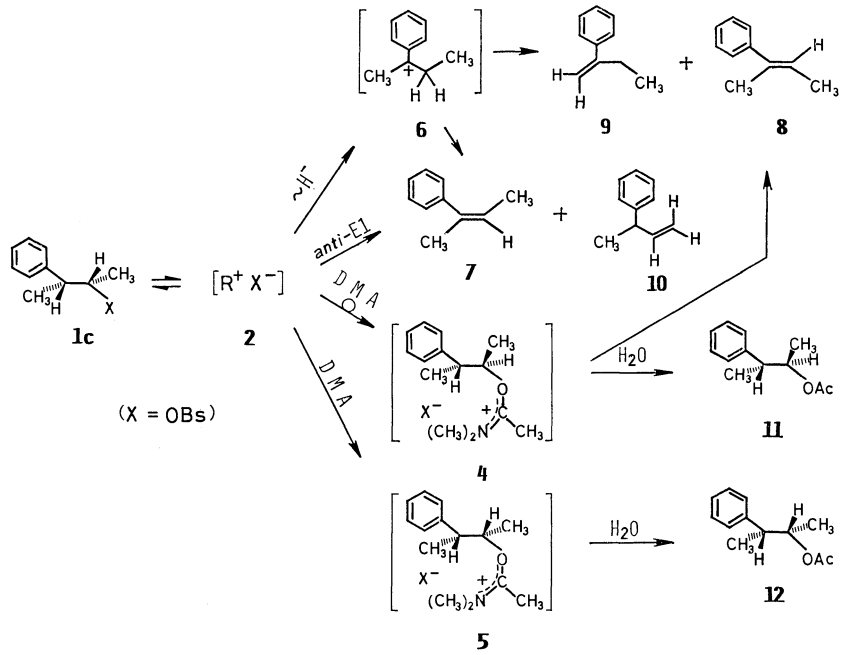

Scheme 3.

on the observed yield (3.6%) of **9** (Table 2; $[H_2O]=0.155$ mol/dm^3). Since the observed yield of (*E*)-olefin **8** (10.1%) is in line with the predicted value (10.6%), most of the (*E*)-olefin **8** should be derived from the benzylic cation **6** (Scheme 3). Obviously, most of (*Z*)-olefin **7** stems from the tight ion-pair **2**, since the yield of **7** is far greater than the expected value (1.4%) from the cation **6**.

Stereochemistry of E1 Reaction. When stereochemistry of the *E*1 reaction was compared with the cyclic systems, in which elimination takes place in *syn*-fashion,[1,16,17] the remarkable contrast was observed. Namely, the formation of (*Z*)-olefin **7** should be ascribed to *anti*-*E*1 reaction from the tight ion-pair **2**; the (*E*)-olefin formation from the imidatonium ion **4** should also be attributed to *anti*-elimination (Scheme 4).

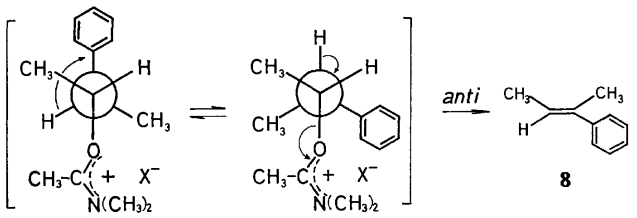

Scheme 4.

In the solvolysis of cyclic substrates,[1,17] which bear no β-hydrogens antiperiplanar to the leaving group, the *syn*-elimination was predominant. However, the tight ion-pair derived from open-chain compound **1c** can rotate easily to afford the conformers capable of both *syn*- and *anti*-eliminations. In the case of solvolysis of 1-methylpropyl-2-*d* tosylate in a dipolar aprotic solvent, *i.e.*, nitrobenzene, Skell and Hall[26] have demonstrated that it gives predominantly *syn*-elimination product. In contrast, the DMA solvolysis of **1c** afforded overwhelmingly *anti*-elimination product **7**. Thus, this feature seems to be characteristic of DMA solvolysis of the open-chain system. Further scrutinies are required to explain such contrasting stereochemical results.

Occurrence of 2,1-Phenyl Shift in the Tight Ion-pair 2. Appearance of the label at C(3) positions of the olefins **7** and **8**, or at C(1) positions of the acetates **11** and **12** (Table 3 or Scheme 2) clearly indicates that 2,1-phenyl shift occurs not only during the acetolysis with k_Δ process, but also actually *in the DMA solvolysis of 100% k_s process.*

It is notable that the isotopic scrambling in the retained acetate **12** is far from complete equilibration (Table 3) for the DMA solvolysis. Consequently, the formation of this product can not be ascribed to intervention of a symmetrical intermediate expected for the phenonium ion pathway. Although Harris *et al.*[6a] have suggested that even the deactivated substrates of a series of ring substituted 2-phenylethyl system undergo a small, almost undetectable amount of aryl participation (Fk_Δ), the present result rules out such a possibility so far as the DMA solvolysis of **1c** is concerned.

Based on the dual mechanism ($k_\Delta+k_s$) of solvolysis of β-arylalkyl system,[6] the inverted acetate should be produced by k_s pathway without any scrambling, unless the starting material has first undergone the k_Δ ionization at first and subsequently internal return to give a scrambled substrate. The DMA solvolysis of **1c** has already turned out to have no k_Δ process but 100% k_s pathway as is shown in Fig. 1 and mentioned above. Therefore, the scrambling of the isotope in the inverted acetate **11** can not be compatible with the previously proposed k_s process without the scrambling.[6]

The extent of rearrangement of the DMA solvolysis and the acetolysis was calculated from the data in Table 3 and Scheme 2, to be 22% and 47%, respectively. Thus, DMA solvent much more suppresses the rearrangement accompanied the solvolytic reaction of the brosylate **1c**-2-*d* than does acetic acid as solvent. For the formation of 2-phenyl-1-butene **9**-3-H_2 (Table 3), 3,1-hydride shift and the subsequent deuteron elimination is conceivable (Scheme 5).

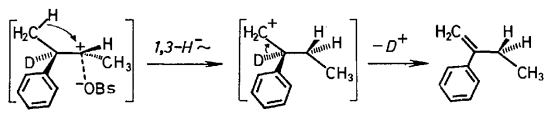

Scheme 5.

Possible Double Inversion Course for the Formation of Retained Acetate 12. As is shown in Table 4, it was revealed that *threo* brosylate **1c** rearranges to *erythro* brosylate (**13**) to a substantial extent (5.9%) during the half-life solvolysis of **1c** in DMA solvent. Furthermore, when the similar analysis has been conducted for the solvolysis in the presence of two-fold excess of pyridinium brosylate, the essentially same result was obtained (Table 4), indicating that the *threo-erythro* interconversion is caused intramolecularly by the rotation of C(1)–C(2) bond at the stage of the tight ion-pair intermediate **2** (Scheme 6). Such crossover by an internal rotation in the tight ion-pair has also been suggested by Cram and Knight[27] and by Collins *et al.*[28]

On the basis of Scheme 6, it is deduced that the formation of the retained acetate **12** in the DMA solvolysis of **1c** should be ascribed, at least partly,

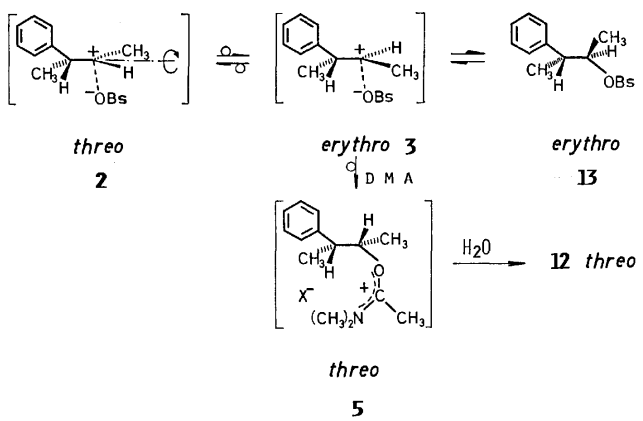

Scheme 6.

to the double inversion course; *erythro*-type ion-pair intermediate (**3**) should intervene between *threo*-type ion pair intermediate **2** and *threo*-type imidatonium ion **5** (Scheme 3).

The Formation of (E)-Olefin 8 from [erythro-*R-DMA*]$^+$-*OBs*$^-$. As mentioned in the foregoing section (Scheme 4), in completely dried DMA, [*erythro*-R-DMA]$^+$OBs$^-$ **4** undergoes *anti*-elimination to give the (*E*)-olefin **8**. The yield of the (*E*)-olefin **8** (8.6% in the wet solvolysis (Table 3)) was increased to 26.7% in the dry solvolysis (Table 3), whereas *erythro*-acetate **11** was reduced from 21% to trace amount under dried conditions. The amounts of the (*E*)-olefin **8** arising from [*erythro*-R-DMA]$^+$OBs$^-$ **4**, therefore, can be calculated to be 18.1%(=26.7—8.6%). If [*erythro*-R-DMA]$^+$OBs$^-$ **4** undergoes *anti*-elimination keeping the same isotopic distribution as that in the *erythro*-acetate **11** (Table 3), the deuterium content at C(3) position of (*E*)-olefin **8** produced can be estimated to be about 20%.[29] However, as is indicated in Table 3, it actually amounts to 38%. This result suggests that [*erythro*-R-DMA]$^+$OBs$^-$ **4** must undergo further 2,1-phenyl shift before it is transformed to (*E*)-olefin **8**. The following scheme can be drawn to account for the situation (Scheme 7), and this scheme appears to be essentially the same as that proposed previously to explain the observed chemical behavior of imidatonium ion derived from *exo*-2-norbornyl cation.[30]

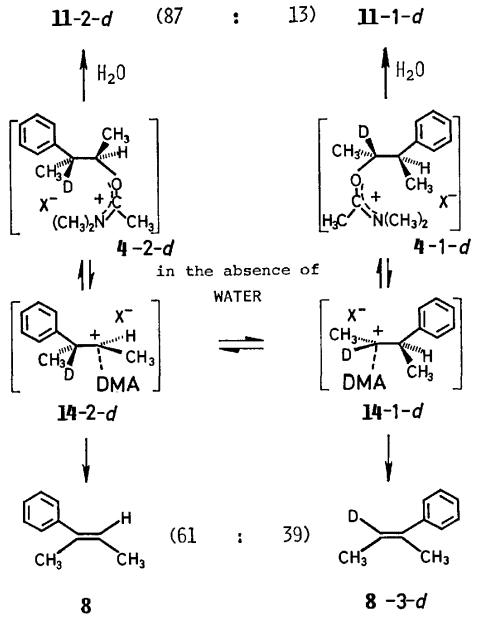

Scheme 7.

Nature of the k_s Pathway. Brown and Kim[5e] have made a detailed comparison of the characteristics of the k_s pathway in secondary β-arylalkyl solvolysis with the corresponding characteristics of primary β-arylalkyl solvolysis in terms of ΔS^*, secondary isotope effect, ρ-value, lyate ion effect, or hydride shift. They have noted on the basis of these features that no evidence for strong nucleophilic solvent participation in the secondary k_s process could be detected and these were considered to lend support to an S_N1 mechanism. The present findings as regards ΔS^* value (Table 1), ρ-value (Fig. 1), the cocurrences of 2,1-hydride as well as 2,1-phenyl shift and of intramolecular *threo-erythro* interconversion of the brosylate **1c** (Table 4), or no effect of added pyridine on the rate (*vide supra*), are in line with the implications pointed out by Brown and Kim.[5e]

An additional mechanistic aspect could be drawn on closer inspection of the data for the kinetic isotope effects (Table 5) and the product distributions (Tables 2 and 3), as in the following. First, the olefins arising from the process involving 2,1-hydride shift are not in large amount (Tables 2 and 3), probably suggesting that the relatively large β-deuterium isotope effect for the DMA solvolysis of **1c** (Table 5) can not be ascribed to hydrogen participation.[23,24] Secondly, although the olefins arising from *anti*-elimination is predominant, its yield is not sufficiently reduced by C(2)-deuteration, clearly indicating that the intervention of *E*2 process can be eliminated from the present reaction: the yield of (*Z*)-olefin **7** is 64.7% for **1c** and is 54.6% for **1c**-2-*d* (Tables 2 and 3). Thus the isotope effect for the DMA solvolysis of **1c** should be predominently associated with a specific transition-state structure of the reaction. Thirdly, when the isotope effects for the solvolysis of **1c**-2-*d* in the four carboxamide solvents (NMF, NMA, DMF, and DMA) are compared with the yields of (*Z*)-olefin **7** in the corresponding reactions (Table 6), the larger isotope effect is accompanied with the increased yield of the (*Z*)-olefin **7**. This may indicate that the magnitude of kinetic isotope effect for the carboxamide solvolysis of **1c** could be correlated to the degree of hyperconjugative stabilization[14,22] of the transition state with antiperiplanar conformation, from which (*Z*)-2-phenyl-2-butene **7** is formed. The larger isotope effect probably means the more stabilization of antiperiplanar transition state which, in turn, results in the more (*Z*)-olefin **7**.

As regards the relatively high β-deuterium isotope effect in the acetolysis of *cis*-2-phenylcyclopentyl tosylate (Table 5), Kim and Brown[22] have recently suggested that it may be the result of the combined effects of hyperconjugative destabilization of the transition state, leading to tight ion-pair intermediate, and of destabilization of the subsequent transition state, leading to tertiary benzylic cation, by the difficulty

Table 6. Comparison between kinetic isotope effect and amount of *anti*-elimination product for the carboxamide solvolyses of **1c**-2-*d* at 75 °C

Amide	$k_H/k_{\beta-D}$[a]	Yield % of (*Z*)-olefin **7**[b]
DMA	1.93±0.01	54.9
DMF	1.67±0.01	43.5
NMA	1.63±0.02	43.0
NMF	1.41±0.01	35.5

a) The k_H values for DMF, NMA, and NMF solvolyses were 4.79, 18.1, and 38.5 (10^{-5} s^{-1}), respectively; for the DMA solvolysis, see Table 1. b) Data for the labeled substrate,

of loosening a C–D bond compared to a C–H bond.

In conclusion, all the results presented above can be explained by the mechanism involving the tight ion-pair intermediate **2** which undergores intramolecular processes, such as *anti-E*1 reaction, phenyl or hydride shift, and *threo-erythro* interconversion, competitively with the solvent capture leading to the imidatonium ion **4**. These rearrangements require that the site of the carbonium center opposite to the leaving group should not be shielded by solvent molecule at the stage of the tight ion-pair intermediate **2**, and this, in turn, suggests that the reaction may proceed without any kinetically significant involvement of nucleophilic solvent assistence.[6h]

Experimental

Melting points determined on a Yamato Model MP-1 apparatus were uncorrected. NMR spectra were recorded in $CDCl_3$ at 60 MHz on a Hitachi R-24 spectrometer or at 100 MHz on a JEOL JNM-MH 100 or JEOL JNM-FX 100 instrument. Infrared spectra were taken on a Hitachi EPI-S2 spectrometer. Both analytical and preparative GLC's were performed on a Hitachi K-53 gas chromatograph equipped with a thermal conductivity detector. The following columns were used: A, 3 m×3 mm 5% Benton 34+5% DIDP on 60—80 mesh Neopak 1A; B, 3 m×3 mm 10% PEG 6000 on 60—80 mesh Chromosorb W (NAW). Silicic acid powder (Wakogel C-200) was employed for column chromatography. For the alumina column, Merck neutral alumina (activity 1) was used.

Materials and Solvents. *N,N*-Dimethylacetamide (DMA) of commercial grade was purified in the same manner as described in the previous paper.[1] $NaBD_4$ (97.0 D-atom %) was supplied from CEA. Ether, diglyme, THF, and pentane used for reaction medium or recrystallization were distilled over sodium–benzophenone ketyl before use. Boron trifluoride etherate was distilled over CaH_2. Pyridine was distilled over BaO. All other solvents and reagents were of reagent grade and liquid materials were distilled before use.

(E)-2-Aryl-2-butenes. These olefins were prepared in the same manner as reported by Brown and Kim.[5e] Treatment of 2-butanone with arylmagnesium bromide (except for *p*-nitrophenyl derivative) gave 2-aryl-2-butanol which was dehydrated to a mixture of (*Z*)- and (*E*)-2-aryl-2-butenes and 2-aryl-1-butene according to the procedure of Garbisch[31] except for *p*-methoxyphenyl derivative for which dehydration was carried out by the use of $POCl_3$–pyridine mixture (0 °C—room temp, 24 h). The olefin mixture was subjected to fractional distillation by the use of a spinning band column and fractions containing gas chromatographically pure (*E*)-2-aryl-2-butene component were collected.

threo-*3-Aryl-2-butanols.* Various *threo*-3-aryl-2-butanols were prepared from corresponding (*E*)-2-aryl-2-butenes by hydroboration-oxidation reaction following the reported method.[5e]

threo-*2-Aryl-1-methylpropyl Brosylates.* These substrates were synthesized from the corresponding alcohols in the usual manner.[32] The melting points of the various brosylates were 100—101 (**1a**), 97—98 (**1b**), 94—95 (**1c**), 91—93 (**1d**), 69.5—71.5 (**1e**), and 50—51 °C (**1f**) (lit, 97.5—98.5 (**1a**),[33] 97—98 (**1b**),[5e] 93—93 (**1c**),[3] 94—95 (**1c**),[5e] 68.5—69.5 (**1d**),[5e,34] 91.5—92.5 (**1e**),[5e,34] and 50—51 °C (**1f**)[5e]).

threo-*3-(p-Nitrophenyl)-2-butanol and Its Brosylate.* *threo*-3-(*p*-Nitrophenyl)-2-butanol was prepared from the parent phenyl derivative similarly to the method reported for the preparation of *cis*-2-(*p*-nitrophenyl)cyclopentanol;[22] *threo*-3-Phenyl-2-butanol (3.1 g, 20.6 mmo) was treated with acetic anhydride (24 cm^3) and pyridine (48 cm^3) at room temp overnight. Workup gave acetate in 95% yield. The acetate was dissolved in a mixture of acetic acid (7 cm^3) and acetic anhydride (10 cm^3) and the resulting solution was cooled to 0 °C. To the solution was added a solution of 90% nitric acid (2 cm^3) in acetic acid (5 cm^3) under stirring at 0 °C and the mixture was stirred for 2 h at 0 °C and overnight at room temp. The mixture was poured on ice–water (100 cm^3) and extracted several times with ether. The ether solutions were washed successively with 10% K_2CO_3 and water, and dried (Na_2SO_4). Evaporation of the ether gave *threo*-1-methyl-2-(*p*-nitrophenyl)propyl acetate in 70% yield (3.3 g). The acetate was dissolved in methanol containing 0.5 mol/dm^3 HCl (43 cm^3) and the resulting solution was heated under reflux for 8 h. After workup, *threo*-3-(*p*-nitrophenyl)-2-butanol was distilled to afford practically pure sample (2.7 g, 98% yield).

The brosylate **1g** was synthesized from this alcohol in the usual manner.[32] **1g**: mp 104—105 °C; NMR (60 MHz) δ=1.25 (d, 3H, CH_3), 1.32 (d, 3H, CH_3), 3.0 (quintet, 1H, C(2)–H), 4.74 (quintet, 1H, C(1)–H), 7.4 (d, 2H, Ar–H), 7.5 (s, 4H, Ar–H), and 8.0 ppm (d, 2H, Ar–H); IR (KBr); 1520 (NO_2), 1350 (SO_2), 1185, and 1170 cm^{-1} (SO_2).

Found: C, 46.50; H, 3.71%. Calcd for $C_{16}H_{16}O_5NSBr$: C, 46.39; H, 3.89%.

threo-*3-Phenyl-2-butan-3-d-2-ol and Its Brosylate* ***1c***-*2*-d. Deuterium at C(2) position was introduced by deuterioboration of (*E*)-2-phenyl-2-butene. Deuterioboration–oxidation was carried out according to the standard procedure.[35] Diborane-d_6 was generated externally from $NaBD_4$ and borontrifluoride etherate in diglyme and was supplied into THF solution of the olefin. After workup, the labeled alcohol was purified by column chromatography (alumina) to give pure alcohol in 90% yield.

Brosylate **1c**-2-*d* was prepared from this alcohol in the usual manner.[32] **1c**-2-*d*: mp 93—94 °C (lit,[5e] 93—94 °C for unlabeled sample). ^1H (100 MHz) and ^{13}C (25 MHz) NMR spectra of **1c**-2-*d* indicated an isotopic purity of 97% and the absence of deuterium scrambling throughout its synthesis.

Product Analysis. A reaction mixture for product study was prepared by the same method as described in the previous paper:[1] [ROBs]=0.075 mol/dm^3; [C_5H_5N]=0.077 mol/dm^3 (in an ampoule). The sealed ampoule was then kept at desired temperature for ten half-lives. The contents of the ampoule were poured on ice-water and extracted with pentane–ether mixture. The pentane–ether solution was washed several times with water, dried ($MgSO_4$), and condensed to 1—2 cm^3 by the use of 30-cm distillation column packed with glass helices. The condensed solution was subjected to GLC on column A. An excellent separation was effected on the column for all the products except for (*Z*)-2-phenyl-2-butene **7** and 3-phenyl-1-butene **10** which were identical in their retention times. The yields of (**7**+**10**), **8**, **9**, **11**, **12**, *erythro*-3-phenyl-2-butanol, and *threo*-3-phenyl-2-butanol were calculated from GLC's peak areas, calibrating based on molar response ratios. The mixture of (**7**+**10**) was isolated by means of preparative GLC and their composition was analyzed from the integral intensities of NMR (100 MHz in the Fourier transform mode) signals of methyl protons for the respective olefins **7** and **10**.

Partial Solvolysis and Isolation of Unchanged Brosylate. The brosylate recovered from half-life solvolysis of **1c** or **1c**-2-*d* in DMA solvent was isolated from the reaction mixture by

repeated recrystallization at −50 °C (ether–pentane). Colorless crystalline brosylate was obtained easily in 98% yield based on the theoretical amount. The brosylate was kept under high vacuum (0.05 mmHg) at room temperature overnight. ^{1}H NMR spectrum (100 MHz) of the sample exhibited no sign of contamination with the solvolysis products.

Cleavage Reaction of the Recovered Brosylate with Sodium–Naphthalene.[36] A mixture of naphthalene (0.49 g, 3.67 mmol), sodium (0.088 g, 3.67 mmol) cut in small pieces, and THF (12.5 cm^3) was stirred at room temp for 2 h to result in a dark-green solution of sodium–naphthalene anion radical, and then, was cooled to −78 °C. To this solution was added the brosylate (0.226 g, 0.61 mmol), recovered from half-life solvolysis of **1c**-2-*d* in DMA solvent, in THF (3 cm^3) by the use of a syringe through a septum. Within a minute, a critical color changeocc urred (from dark green to reddish black). The excess of reagent was quenched by the addition of THF–water (1 : 1, 5 cm^3). Workup followed by column chromatography (silicic acid, 20 g) afforded a diastereomeric mixture of 3-phenyl-2-butanol in 80% yield: column was eluted successively with benzene and CH_2Cl_2, and the mixture was collected from the fractions eluted with CH_2Cl_2. The mixture was subjected to preparative GLC (column B) which provided *threo*- and *erythro*-3-phenyl-2-butanols without mutual contamination. Deuterium distribution in each alcohol was determined by means of ^{1}H NMR spectroscopy as described below.

Isotopic Distribution Analysis. The deuterium distribution analysis of the solvolysis products was carried out by means of ^{1}H NMR spectroscopy (100 MHz) in the Fourier transform mode. A sample for NMR assay was prepared under dry nitrogen in order to avoid contamination with moisture. The combined use of column chromatography and preparative GLC, and, in some cases, an appropriate chemical transformation, provided the compounds that meet the purpose of the determination of isotopic distribution.

Although the separation of the (*Z*)-olefin **7** and nonconjugated terminal olefin **10** could not be effected on GLC, all the NMR signals due to the both olefins **7** and **10** were advantageously well-resolved. The isotopic distribution in **7** and **10** was, therefore, determined from the NMR spectrum of the mixture which was isolated by means of preparative GLC. For the (*Z*)-olefin **7** a decrease in the integral intensity of the olefinic proton signal was measured. The partial labeling at C(3) position was easily verified by the observation that the C(4)-protons (methyl) gave clean doublet and singlet signals when C(1)-protons (methyl) were irradiated.

As for the 3-phenyl-1-butene **10**, integral intensities of the benzylic proton and internal vinylic proton were measured and a relative intensity of the respective signals to that of methyl protons was calculated. The methyl proton signal, consisted of doublet and triplet, and complicated multiplet of the terminal vinylic proton signals indicated that deuterium was situated at both C(2) and C(3) positions of the olefin **10**.

With regard to 2-phenyl-1-butene **9**, relative integral intensity of the methylene protons (C(3)) to that of methyl or olefinic protons was determined. The methyl signal consisted of "doublet of sharp triplets" and clean triplet. The former is considered to be due to the presence of adjoining –CHD– group to which the methyl protons are coupled and the latter undoubtedly indicates that the methyl protons are involved in spin-spin coupling with the adjoining $-CH_2-$ group. The integral intensity ratio for the olefinic proton *cis* to phenyl, that *trans* to phenyl, and the methyl protons was strictly 1 : 1 : 3. These findings clearly demonstrated that partial deuteron loss, though in small amount, actually occurred during the formation of the olefin **9**.

The deuterium content at C(3) position of the (*E*)-olefin **8** was determined similarly to that described above for the (*Z*)-olefin **7**.

The mixture of diastereomeric acetates **11** and **12** was isolated by column chromatography (silicic acid) and was hydrogenolyzed ($LiAlH_4$) into a mixture of *threo*- and *erythro*-3-phenyl-2-butanols from which each isomer was separated by preparative GLC. Deuterium distribution was determined by measuring the relative integral intensity between the C(2)–H and C(3)–H signals. The partial labeling at both positions was easily observed in splitting pattern of the two methyl signals.

The deuterium distribution in each isomer of the diastereomeric 3-phenyl-2-butanol obtained from the cleavage reaction of the recovered brosylate (*vide supra*) was also determined similarly to the method mentioned above.

The operating parameters employed in ^{1}H NMR spectroscopy in the Fourier transform mode were a spectral width of 1000 Hz, a 45° pulse, pulse repetition of 10 s, and an appropriate number of pulses to provide spectra with almost same S/N ratio for each sample. The integral intensity of each observed nuclei was directly computed on a JEOL 980B computer with SYSTEM Q/D PROGRAM FAFT08/11. The spectra of each unlabeled sample were recorded by the use of above-mentioned parameters and were used in order to calibrate the integral intensity obtained for each labeled sample.

Kinetic Measurements. The procedure was described in the previous paper.[1] In determining the kinetic isotope effect, simultaneous rate measurements of two compounds, the parent and C(2)-deuterated compounds **1c** and **1c**-2-*d*, were carried out. Three individual set of such determinations were conducted.

References

1) S. Saito, T. Moriwake, K. Takeuchi, and K. Okamoto, *Bull. Chem. Soc. Jpn.*, **51**, 2634 (1978): Part IV.

2) For a leading review, see C. J. Lancelot, D. J. Cram, and P. v. R. Schleyer, in "Carbonium Ions," ed by G. A. Olah and P. v. R. Schleyer, Wiley-Interscience, New York, N, Y. (1972), Vol. 3, Chap. 27.

3) D. J. Cram, *J. Am. Chem. Soc.*, **71**, 3863 (1949); **74**, 2129 (1952).

4) S. Winstein, B. K. Morse, E. Grunwald, K. C. Schreiber, and J. Corse, *J. Am. Chem. Soc.*, **74**, 1113 (1952).

5) a) H. C. Brown, "The Transition State," Special Publication No.16, The Chemical Society, London, 1962, p. 140 ff.; b) H. C. Brown, K. J. Morgan, and F. J. Chloupek, *J. Am. Chem. Soc.*, **87**, 2137 (1965); c) H. C. Brown, R. Bernheimer, C. J. Kim, and S. E. Scheppele, *ibid.*, **89**, 370 (1967); d) H. C. Brown and C. J. Kim, *ibid.*, **90**, 2082 (1968); e) H. C. Brown and C. J. Kim, *ibid.*, **93**, 5765 (1971); f) C. J. Kim and H. C. Brown, *ibid.*, **94**, 5051 (1972).

6) a) C. J. Lancelot and P. v. R. Schleyer, *J. Am. Chem. Soc.*, **91**, 4291 (1969); b) *ibid.*, **91**, 4296 (1969); c) C. J. Lancelot, J. J. Harper, and P. v. R. Schleyer, *ibid.*, **91**, 4294 (1969); d) P. v. R. Schleyer and C. J. Lancelot, *ibid.*, **91**, 4297 (1969); e) J. M. Harris, F. L. Schadt, P. v. R. Schleyer, and C. J. Lancelot, *ibid.*, **91**, 7508 (1969); f) D. J. Raber, J. M. Harris, and P. v. R. Schleyer, *ibid.*, **93**, 4829 (1971); g) H. C. Brown, C. J. Kim, C. J. Lancelot, and P. v. R. Schleyer, *ibid.*, **92**, 5244 (1970); h) F. L. Schadt III, C. J. Lancelot, and P. v. R. Schleyer, *ibid.*, **100**, 228 (1978).

7) a) D. J. Cram, *J. Am. Chem. Soc.*, **86**, 3767 (1964);

b) D. J. Cram and J. A. Thompson, *ibid.*, **89**, 6766 (1967); **91**, 1778 (1969).
8) B. G. Ramsey and N. K. Das, *J. Am. Chem. Soc.*, **94**, 4233 (1972).
9) J. A. Cramer and J. G. Jewett, *J. Am. Chem. Soc.*, **94**, 1377 (1972).
10) A. Diaz, I. Lazdins, and S. Winstein, *J. Am. Chem. Soc.*, **90**, 6546 (1968).
11) M. D. Bentley and M. J. S. Dewar, *J. Am. Chem. Soc.*, **90**. 1075 (1968).
12) J. E. Nordlander and W. G. Deadman, *J. Am. Chem. Soc.*, **90**. 1590 (1968).
13) a) R. J. Jablonski and E. I. Snyder, *Tetrahedron Lett.*, **1968**, 1103; b) M. G. Jones and J. L. Cokes, *J. Am. Chem. Soc.*, **91**, 4284 (1969).
14) V. J. Shiner, Jr., in "Isotope Effects in Chemical Reactions," ed by C. J. Collins and N. S. Bowman, Van Nostrand-Reinhold, New York, N. Y. (1970), pp 90—159.
15) R. A. Sneen, *Acc. Chem. Res.*, **6**, 46 (1973).
16) S. Saito, T. Yabuki, T. Moriwake, and K. Okamoto, *Bull. Chem. Soc. Jpn.*, **46**, 1795 (1973).
17) S. Saito, T. Yabuki, T. Moriwake, and K. Okamoto, *Bull. Chem. Soc. Jpn.*, **51**, 529 (1978).
18) The ρ-value for various secondary β-arylalkyl systems has been reported to be -0.71— -1.6; see Table II in Ref. 2.
19) S. Winstein, M. Brown, K. C. Schreiber, and A. H. Schlessinger, *J. Am. Chem. Soc.*, **74**, 1140 (1952).
20) K. Okamoto, S. Saito, and H. Shingu, *Bull. Chem. Soc. Jpn.*, **42**, 3298 (1969).
21) K. Okamoto, S. Saito, and H. Shingu, *Bull. Chem. Soc. Jpn.*, **43**, 3008 (1970).
22) C. J. Kim and H. C. Brown, *J. Am. Chem. Soc.*, **94**, 5043 (1972).
23) S. Winstein and J. Takahashi, *Tetrahedron*, **2**, 316 (1958).
24) D. J. Cram and J. Tadanier, *J. Am. Chem. Soc.*, **81**, 2737 (1959).
25) D. J. Cram and N. R. V. Sahyun, *J. Am. Chem. Soc.*, **85**, 1257 (1963).
26) P. S. Skell and W. L. Hall, *J. Am. Chem. Soc.*, **85**, 2851 (1963).
27) D. J. Cram and J. D. Knight, *J. Am. Chem. Soc.*, **74**, 5839 (1952).
28) a) C. J. Collins, B. M. Benjamin, and M. H. Lietzke, *Ann.*, **687**, 150 (1965); b) C. J. Collins, in "Carbonium Ions," ed by G. A. Olah and P. v. R. Schleyer, Wiley-Interscience, New York, N. Y. (1968), Vol. 1, Chap 9.
29) Calculated by $[(8.6\% \times 0.36) + (18.1\% \times 0.13)] \times 10^2/26.7\%$.
30) See Scheme 8 in Ref. 1.
31) E. W. Garbisch, *J. Org. Chem.*, **26**, 4165 (1961).
32) R. S. Tipson, *J. Org. Chem.*, **9**, 235 (1944); see also H. C. Brown and G. Ham, *J. Am. Chem. Soc.*, **78**, 2735 (1956).
33) S. Winstein, E. Clippinger, A. H. Fainberg, R. Heck, and G. C. Robinson, *J. Am. Chem. Soc.*, **78**, 328 (1956).
34) The published data for *p*-Cl and *m*-Cl which appeared in Table V in Ref. 5e should be interchanged with each other.
35) G. Zweifel and H. C. Brown, *Org. React.*, **13**, 1 (1963).
36) W. D. Closson, P. Wriede, and S. Bank, *J. Am. Chem. Soc.*, **88**, 1581 (1966).

New Ring Opening Reactions of Oxiranes with Aryl Carboxylates

Kazutoshi FUNAHASHI

Central Research Institute, Teijin Ltd., Asahigaoka, Hino, Tokyo 191

(Received October 13, 1978)

Oxiranes reacted with aryl esters in the presence of base. The reactions of aryl carboxylates with alkyloxiranes afforded almost exclusively 1-alkyl-2-(aryloxy)ethyl carboxylates, whereas the reactions with aryloxiranes gave a mixture of 1-aryl-2-(aryloxy)ethyl carboxylates and 2-aryl-2-(aryloxy)ethyl carboxylates. Similar results were also obtained in the reaction with *S*-aryl thiocarboxylates and diaryl carbonates. The rate of reaction between phenyl acetate and phenoxymethyloxirane (PMO) in the presence of tributylamine (n-Bu_3N) as a catalyst has been determined in the temperature range 110 to 130 °C and may be expressed by $-d[PMO]/dt=k_2[n\text{-}Bu_3N]\cdot[PMO]$. The apparent activation energy calculated from the Arrhenius plots is 85.8 kJ/mol. The reaction catalyzed by tributylamine is assumed to proceed through zwitter ions, n-$Bu_3\overset{+}{N}CH_2CH(R)O^-$ and n-$Bu_3\overset{+}{N}CH(R)CH_2O^-$, which attack aryl carboxylate.

Oxiranes have drawn much attention recently as starting compounds in chemical syntheses. Reports[1] have been published on the addition reactions of oxiranes, but not on the addition reactions of aryl carboxylates to oxiranes. In this paper it will be reported that an aryl carboxylate adds to an oxirane to give addition products, **1** and **2**, as shown in Scheme 1. The reaction is catalyzed by bases such as pyridine, 1,8-diazabicyclo[5.4.0]undec-7-ene (DBU), tributylamine, and potassium *t*-butoxide. When the substituent R^2 on the oxirane is an electron donating group, *e.g.* methyl or phenoxymethyl, cleavage of the oxirane occurs almost exclusively at the β-position, yielding **1** as the product. When R^2 is an aryl group, a mixture of **1** and **2** is obtained. When aryl carbonates or *S*-aryl thiocarboxylates are employed as aryl esters, similar results are observed.

The reaction rate has been determined in the reaction of phenoxymethyloxirane (abbreviated to PMO hereafter) with phenyl acetate in the presence of tributylamine as the catalyst. A probable reaction mechanism has been proposed.

Results and Discussion

The reaction between an aryl carboxylate and alkyloxirane in the presence of a base produced almost exclusive β-cleavage of the oxirane to form aryl carboxylate adducts **1a—g**, as shown in Scheme 1.

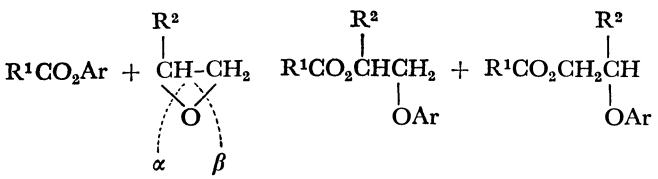

1a—i **2a—i**

a:	R^1=Me	R^2=H	Ar=Ph
b:	Me	Me	Ph
c:	Me	CH_2OPh	Ph
d:	Ph	H	Ph
e:	Ph	H	*p*-$MeOC_6H_4$
f:	Ph	H	*p*-PhC_6H_4
g:	Ph	Me	Ph
h:	Me	Ph	Ph
i:	Ph	Ph	Ph

Scheme 1.

In several reactions, a very small amount of compound resulting from α-cleavage was found in the products. The structure of the products has been confirmed by a comparison of the isolated reaction products with authentic samples prepared by other routes, the results of which are shown in Table 1. For example, the compound isolated from the reaction product of phenyl acetate with methyloxirane has been identified as 1-methyl-2-phenoxyethyl acetate by comparison with an authentic sample of **1b**, synthesized through other routes.[2] In the case of $R^2=CH_2OC_6H_5$ in Scheme 1, the reaction product was similarly compared with an authentic sample of **1c** synthesized separately[5] and found to be pure **1c**.

The reaction between a phenyl carboxylate and phenyloxirane however caused both α- and β-cleavage of the oxirane to form a mixture of the phenyl carboxylate adducts **1** and **2**. For example, the reaction of phenyloxirane with phenyl acetate produced 2-phenoxy-1-phenylethyl acetate **1h** and β-phenoxyphenethyl acetate **2h**, which were identified by comparison with authentic samples derived from 2-phenoxy-1-phenylethanol and 2-phenoxy-2-phenylethanol, each synthesized by Guss's procedure.[3] The ratio of **1** to **2** formed in the reaction has been determined by gas chromatography, the results of which are shown in Table 2.

A similar reaction occurred when diphenyl carbonate was used as an aryl ester.

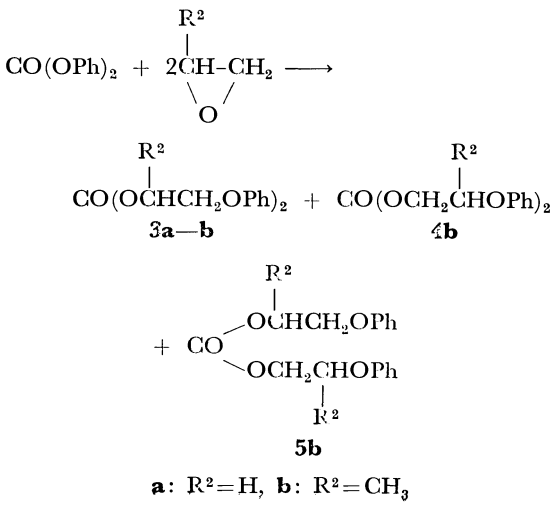

a: R^2=H, **b**: $R^2=CH_3$

Table 1. Reaction of aryl esters with oxiranes[a)]

Initial reagents R¹	R²	Ar	Catalyst	Reaction temp (°C)	time (h)	Product	**1** in the mixture (%)[c)]	Yield[d)] (%)	Mp(Bp/kPa) (°C)	Calcd (Found) (%) C	H
Me	H	Ph	DBU	140	4	**1a**	100	77	131/20 [97.5—98.5/0.27][7)e)]		
Ph	H	Ph	n-Bu_3N	140	7	**1d**	100	84	60	74.63 (74.49	5.82 5.68)
Ph	Me	Ph	Pyridine	150	4	**1g, 2g**	95	82	239—241/4	74.98 (75.14	6.29 6.14)
Ph	H	p-$MeOC_6H_4$	t-BuOK	170	5	**1e**	100	88	71	70.57 (70.72	5.92 5.88)
Ph	H	p-PhC_6H_4	DBU	160	5	**1f**	100	78	95	79.22 (79.35	5.70 5.90)
Me	$PhOCH_2$	Ph	t-BuOK	170	4	**1c**	100	92	185/0.67 [33][5)e)]		
Me	Me	Ph	Pyridine	150	4	**1b, 2b**	97	84	141/3.1		
OPh	H	Ph[b)]	t-BuOK	190	5	**4a**	100	79	91.5—92.5 [92—93][8)e)]		

a) The molar ratio of substrates: aryl esters/oxiranes/catalyst=1/1.2/0.03 except in (b). b) The molar ratio of substrates: diphenyl carbonate/oxirane/catalyst=1/2.4/0.06. c) The ratio was determined by integration of the NMR absorption area. d) Total isolated yield based on the aryl ester used. e) Value described in the literature.

Table 2. Reaction of phenyl ester with phenyloxirane

Phenyl ester[a)]	Catalyst	Reaction temp (°C)	time (h)	Product	Yield[b)] (%)	**1** in the mixture (%)	Bp/kPa (°C)	Calcd (Found) (%) C	H
AcOPh	DBU	140	4	**1h, 2h**	86	75.1	154—157/0.53	75.00 (75.25	6.29 6.37)
AcOPh	Pyridine	180	6	**1h, 2h**	34	59.0			
BzOPh	t-BuOK	200	5	**1i, 2i**	79	79.4	202—205/0.4	79.22 (79.49	5.70 5.58)
BzOPh	DBU	150	6	**1i, 2i**	88	72.9			

a) The molar ratio of substrates: phenyl ester/phenyloxirane/catalyst=1/1/0.015. b) Total isolated yield.

For example, diphenyl carbonate reacted with methyloxirane to give a mixture of **3b**, **4b**, and **5b**, the proportion of **3b** being more than 91% in the product, which was determined by integration of the NMR peak. Product **3b** was identified by comparison with an authentic sample prepared by the reaction of phosgene with 1-phenoxy-2-propanol.

The reaction of *S*-phenyl thiobenzoate with oxirane was conducted in order to determine the reaction mechanism and was found to proceed as follows.

$$PhCOSPh + \overset{\diagdown\!\diagup}{O} \longrightarrow PhCO_2CH_2CH_2SPh$$

6

Product **6** was identified by comparison with an authentic sample prepared by the benzoylation of 2-(phenylthio)ethanol. No other products, for example, *S*-(2-phenoxyethyl) thiobenzoate, were detected. The reaction proved therefore that the aryl ether oxygen of the product came from the aryloxyl group in the aryl carboxylate.

Reaction Rates. The reaction rate was investigated as follows. PMO was chosen as the oxirane and allowed to react with phenyl acetate in nitrobenzene in the presence of tributylamine. The reaction rate was determined by measurement of the unchanged PMO.

Reaction Rate and Catalyst Concentration and Reaction Temperature. The rate of reaction was found to be in linearly related to the PMO concentration as shown in Figs. 1 and 2, *i.e.*,

$$-d[PMO]/dt = k_1[PMO] \quad (1)$$

where k_1 is the first order rate constant and [PMO] is the concentration of PMO.

The reaction rate was also determined at various [PMO]/[Phenyl acetate] ratios and was found to be first order with respect to [PMO] and zero order with respect to [Phenyl acetate] as may be seen in Fig. 1.

The relation between k_1 and catalyst concentration was determined by changing the concentration of n-Bu_3N. A linear relationship passing through the origin was established as shown in Fig. 3.

Eq. 1 may be rewritten:

$$-d[PMO]/dt = k_2[cat][PMO] \quad (2)$$

where k_2 is the second order rate constant and [cat] is the concentration of catalyst. k_2 is equal to $k_1/[cat]$.

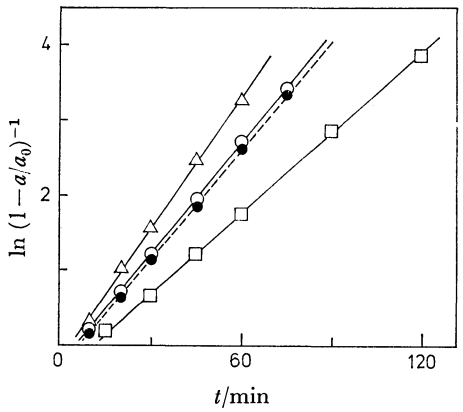

Fig. 1. First-order decrease of [PMO] in the reaction of AcOPh with PMO. The reactions were carried out at various temperatures, △; 130 °C, ○; 120 °C, □; 110 °C, in the reaction system containing AcOPh (1.6 mol), PMO (1.6 mol), *n*-Bu_3N (0.08 mol), and $PhNO_2$ with which the total weight of the system was adjusted to 1 kg. ●; Instead of using 1.6 mol of AcOPh in the system, 3.2 mol was used at 120 °C. a_0; $[PMO]_{initial}$, a; $[PMO]_{decreased}$.

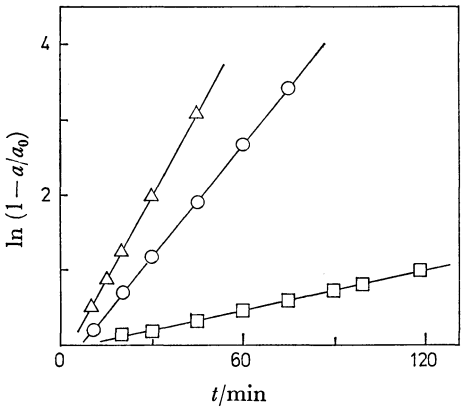

Fig. 2. First-order decrease of [PMO] in the reaction of AcOPh with PMO at 120 °C. The reactions were carried out in the reaction system containing AcOPh (1.6 mol) and PMO (1.6 mol) and various amounts of *n*-Bu_3N, △; 0.12 mol, ○; 0.08 mol, □; 0.016 mol.

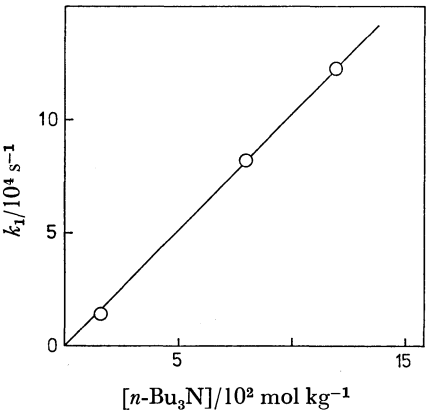

Fig. 3. The relation between the first order rate constant (k_1) and the concentration of *n*-Bu_3N at 120 °C. The reactions were carried out in the reaction system containing AcOPh (1.6 mol), PMO (1.6 mol), and various amounts of *n*-Bu_3N.

TABLE 3. RELATION OF REACTION TEMPERATURES TO k_1 AND k_2 IN THE REACTION SYSTEM CONTAINING AcOPh (1.60 mol), PMO (1.60 mol), *n*-Bu_3N (0.08 mol), AND $PhNO_2$ (TOTAL WEIGHT OF 1 kg)

	110 °C	120 °C	130 °C
10^4k_1 (s^{-1})	6.048	8.222	10.60
10^2k_2 ($l\,mol^{-1}\,s^{-1}$)[a]	0.713	0.979	1.274

a) Converted by the density of the reaction system.

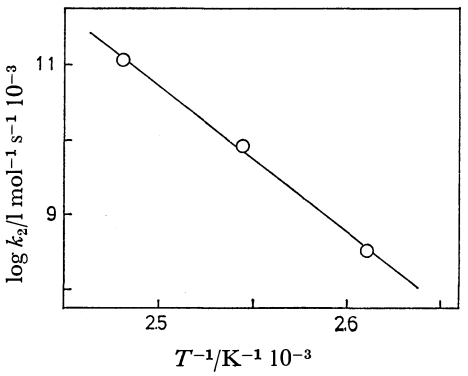

Fig. 4. Arrhenius plots of the second order rate constants.

Values of k_1 and k_2 are given in Table 3.

The Apparent Activation Energy. The Arrhenius plots based on k_2 are shown in Fig. 4 and the apparent activation energy has been estimated as 85.8 kJ/mol in the temperature range 110—130 °C.

The Reaction Mechanism. 1) In the presence of tributylamine and nitrobenzene as catalyst and solvent respectively, the rate of the reaction shown in Scheme 1, may be expressed as follows:

$$-d[PMO]/dt = k_2[n\text{-}Bu_3N][PMO]$$

and is of zero order with respect to the concentration of aryl ester.

2) In the reactions of Scheme 1, with methyloxirane and PMO as oxiranes the reaction products were produced almost exclusively by selective β-cleavage of the oxiranes, *i.e.*, **1b**, and **1c**. This shows that a nucleophile attacks the primary carbon of the oxirane.

3) The formation of **6** in the reaction between *S*-phenyl thiobenzoate and oxirane suggests that the addition of an aryl ester to an oxirane occurs *via* C–O bond cleavage between the carbonyl carbon and the aryloxyl group of an aryl ester.

4) Laird and Parker[4] assumed that the reaction of oxirane with an alcohol in the presence of triethylamine as catalyst formed a intermediate zwitter ion, $Et_3\overset{+}{N}CH_2CH_2O^-$.

On the basis of the above evidence, the reaction of alkyloxirane, catalyzed by a tertiary amine is assumed to proceed as follows. The rate determining step is Eq. 3.

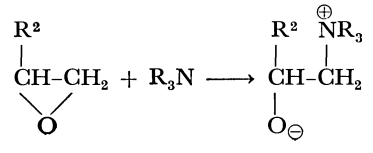

(3)

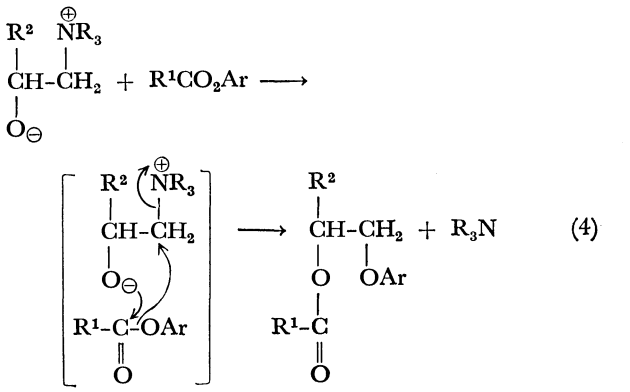

In the reaction of phenyloxirane with a phenyl carboxylate, it appears that the tertiary amine attacks competitively on both the primary and secondary carbons in the oxirane. This is due to inductive and steric effects of the phenyl group in the oxirane, as shown in Eq. 5. Thus, a mixture of **1** and **2** was formed.

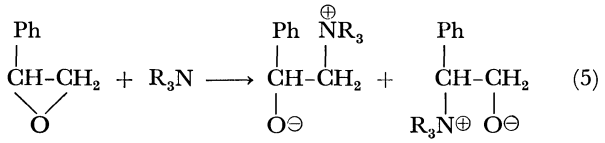

Experimental

All boiling and melting points are uncorrected. The IR and NMR spectra were recorded on a Hitachi EPI-G and JEOL-PS-100/PET-100A spectrometer respectively. Mass spectra (MS) were obtained on a Shimadzu LKB-9000 mass spectrometer at 70 eV.

Reaction between Phenyl Acetate and Methyloxirane. Phenyl acetate (2.72 g, 20 mmol), methyloxirane (1.28 g, 22 mol) and tributylamine (0.11 g, 0.6 mmol) in THF (15 ml) were placed in an autoclave and stirred at 170 °C for 3 h. The reaction mixture was distilled under reduced pressure giving 3.26 g (84%) of **1b**; bp 141 °C/3.1 kPa; IR(neat) 3040(=C–H), 2970(CH_3), 2920(CH_2), and 1740 (C=O) cm^{-1}; MS (70 eV) *m/e* (rel intensity) 194(2), 134(2), 101(46), 77(13), and 43(100); NMR ($CDCl_3$) δ (ppm from TMS) 1.32 (3H, d, J=7.1 Hz, C–C$\underline{H}_3$), 2.01(3H, s, OCOC$\underline{H}_3$), 3.95(2H, d, J=5.2 Hz, C$\underline{H}_2$–OPh), and 5.22(1H, m, CH_3CO_2–C$\underline{H}$). Found: C, 68.21; H, 7.37%. Calcd for $C_{11}H_{14}O_3$: C, 68.02; H, 7.27%.

The product was identified as **1b** by comparison with an authentic sample of **1b** prepared by another route.

Reaction between Phenyl Acetate and Phenyloxirane. Phenyl acetate (6.8 g, 50 mmol), phenyloxirane (6.0 g, 50 mmol) and potassium *t*-butoxide (0.090 g, 0.8 mmol) were heated at 170 °C for 3 h. The reaction mixture was dissolved in ether and the ethereal solution washed with water, and distilled under reduced pressure, giving 11.6 g (91%) of a mixture of **1h** and **2h**; bp 154—157 °C/0.53 kPa; IR (neat) 1747(C=O) cm^{-1}; Found: C, 75,27; H, 6.37%. Calcd for $C_{16}H_{16}O_3$: C, 75.00; H, 6.29%.

The product was found by means of gas chromatography to be a mixture of **1h** and **2h** (1m column of SE-30 on Celite). The products were identified by comparison with authentic samples prepared separately. The proportion of **1h** in the mixture was 68.2% determined by gas chromatography.

Reaction between S-Phenyl Thiobenzoate and Oxirane. *S*-Phenyl thiobenzoate (4.3 g, 20 mmol), oxirane (1.8 g, 41 mmol) and potassium *t*-butoxide (0.06 g, 0.53 mmol) were heated at 180 °C for 6 h to give 3.7 g (71.6%) of **6**: bp 161—162 °C/0.27 kPa; IR (neat) 3050(=C–H), 2920(CH_2), and 1715(C=O) cm^{-1}; NMR ($CDCl_3$) δ 3.24(2H, t, J=6.8 Hz, PhSC$\underline{H}_2$), and 4.45(2H, t, J=6.8 Hz, $CH_3CO_2C\underline{H}_2$). Found: C, 69.49; H, 5.25%. Calcd for $C_{15}H_{14}O_2S$: C, 69.74; H, 5.46%. The product was identified as **6** by comparison with an authentic sample prepared by another route.

Reaction of Diphenyl Carbonate with Methyloxirane. Diphenyl carbonate (3.2 g, 15 mmol), methyloxirane (2.6 g, 45 mmol) and potassium *t*-butoxide (0.09 g, 0.8 mmol) were heated at 170 °C for 4 h to give 3.7 g(75.0%) of a mixture of **3b**, **4b**, and **5b**: bp 182—186 °C/0.27 kPa; IR (neat) 2960(CH_3) and 1735(C=O) cm^{-1}; NMR ($CDCl_3$) δ 1.39 (d, J=6.8 Hz, C$\underline{H}_3$), 3.98(d, J=4.8 Hz, PhOC$\underline{H}_2$), 4.23(d, J=7.9 Hz, $CO_2C\underline{H}_2$), 4.58(m, PhOC$\underline{H}$), and 5.10(m, CO_2-C$\underline{H}$). Found: C, 69.35; H, 6.89%. Calcd for $C_{19}H_{22}O_5$: C, 69.07; H, 6.71%. The proportion of **3b** in the product was more than 82% determined by integration of the NMR absorption area.

Syntheses of Authentic Samples. ***1b***, ***2b***, ***1g***, *and* ***2g***: 1-Phenoxy-2-propanol and 2-phenoxy-1-propanol were prepared by Sexton's procedure[2] and acetylated or benzoylated by Schotten-Baumann's reaction.

1b: Bp 140—142 °C/3.2 kPa. Found: C, 68.09; H, 7.36%.

2b: Bp 134—136 °C/3.3 kPa; NMR ($CDCl_3$) δ 1.30(3H, d, J=6.0 Hz, CHC$\underline{H}_3$), 2.02(3H, s, C$\underline{H}_3$CO), 4.18(2H, m, C$\underline{H}_2$), and 4.58(1H, m, C$\underline{H}$). Found: C 68.16; H, 7.35%. Calcd for $C_{11}H_{14}O_3$: C, 68.02; H, 7.27%.

1g: Bp 135—137 °C/0.2 kPa; NMR ($CDCl_3$) δ 1.47(3H, d, J=6.8 Hz, C$\underline{H}_3$), 4.10(2H, m, C$\underline{H}_2$), and 5.48(1H, m, C$\underline{H}$). Found: C, 74.88; H, 6.27%.

2g: Bp 131—133 °C/0.2 kPa; NMR ($CDCl_3$) δ 1.40(3H, d, J=6.8 Hz, C$\underline{H}_3$), 4.39(2H, m, C$\underline{H}_2$), and 4.72(1H, m, C$\underline{H}$). Found: C, 74.90; H, 6.21%. Calcd for $C_{16}H_{16}O_3$: C, 74.98; H, 6.29%.

1c. **1c** was prepared by Fairbourne's procedure:[5] bp 143—146 °C/0.27 kPa; MS (70 eV) *m/e* 286(M^+); NMR ($CDCl_3$) δ 2.00(3H, s, C$\underline{H}_3$), 4.10(4H, d, J=4.8 Hz, 2 C$\underline{H}_2$), and 5.35(1H, m, C$\underline{H}$).

3b. **3b** was prepared by the reaction of 1-phenoxy-2-propanol with phosgene in pyridine: bp 185—186 °C/0.27 kPa; NMR($CDCl_3$) δ 1.39(6H, d, J=6.8 Hz, 2C$\underline{H}_3$), 3.98(4H, d, J=4.8 Hz, 2C$\underline{H}_2$OPh), and 5.10(2H, m, $2CO_2$-C$\underline{H}$). Found: C, 69.21; H, 6.77%. Calcd for $C_{19}H_{22}O_5$: C, 69.07; H, 6.71%.

1h, ***1i***, ***2h***, *and* ***2i***. 2-Phenoxy-1-phenylethanol and 2-phenoxy-2-phenylethanol were prepared by Guss's procedure[3] and the products acetylated or benzoylated by Schotten-Baumann's reaction.

1h: Bp 148—151 °C/0.4 kPa; MS(12 eV), *m/e* 256(M^+), and 196. Found: C, 75.15; H, 6.17%.

2h: Bp 141—143 °C/0.4 kPa; MS(12 eV), *m/e* 256(M^+), and 183. Found: C, 75.21; H, 6.21%. Calcd for $C_{16}H_{16}O_3$: C, 75.00; H, 6.29%.

1i: Bp 205—208 °C/0.4 kPa; MS(70 eV), *m/e* 318(M^+), and 196. Found: C, 79.29; H, 5.59%.

2i: Bp 200—205 °C/0.4 kPa; MS(70 eV), *m/e* 225($M^+ - C_6H_5O$), and 183. Found: C, 79.34; H, 5.63%. Calcd for $C_{21}H_{18}O_3$: C, 79.22; H, 5.70%.

6. **6** was prepared by benzoylation of 2-(phenylthio)ethanol by Schotten-Baumann's reaction.

6: Bp 162 °C/0.27 kPa. Found: C, 69.83; H, 5.30%. Calcd for $C_{15}H_{14}O_2S$: C, 69.74; H, 5.46%.

Measurement of Reaction Rates. The rate of the reaction between PMO and phenyl acetate in the presence of tributylamine catalyst was determined.

Samples: PMO was prepared from phenol and epichloro-

hydrin by conventional means. The purity was determined according to Stenmark[6] and was greater than 98.1%. Phenyl acetate, and tributylamine were purified by conventional means. Nitrobenzene solvent was a commercially available product which was further purified.

Determination: PMO, phenyl acetate and tributylamine were mixed in the appropriate amounts and nitrobenzene added until the total amount was 2.5 g. The mixture was charged into a sealed glass tube of 0.8 cm inner diameter and 8 cm length. The sealed glass tube was vigorously agitated in a thermostat bath maintained at a specific temperature. After a specified reaction period the sealed tube was taken out of the bath and quenched. Unchanged PMO in the reaction mixture was determined by Stenmark's procedure.[6]

The author wishes to express his thanks to Prof. Takeshi Matsumoto, Faculty of Science, Hokkaido University, for helpful discussions. Thanks are also given to Dr. Takeo Shima for his encouragement and support.

References

1) a) R. J. Gritter, "The Chemistry of the Ether Linkage," ed by S. Patai, Wiley-Interscience, London (1967); b) A. Rosowsky, "Heterocyclic Compounds with Three- and Four-membered Rings," ed by A. Weissberger, Wiley-Interscience, London (1964).
2) A. R. Sexton, and E. C. Britton, *J. Am. Chem. Soc.*, **70**, 3606 (1948).
3) C. O. Guss, *J. Am. Chem. Soc.*, **71**, 3460 (1949).
4) R. M. Laird and R. E. Parker, *J. Chem. Soc., B*, **1969**, 1062.
5) A. Fairbourne, G. P. Gibson, and D. W. Stephens, *J. Chem. Soc.*, **1931**, 445.
6) G. A. Stenmark, *Anal. Chem.*, **29**, 1367 (1957).
7) W. J. Svirbely, W. M. Eareckson III, K. Matsuda, H. B. Pickard, I. S. Solet, and W. B. Tuemmler, *J. Am. Chem. Soc.*, **71**, 508 (1949).
8) J. L. R. Williams, D. D. Reynolds, K. R. Dunham, and J. F. Tinker, *J. Org. Chem.*, **24**, 68 (1959).

Reaction of Coordinated Phosphines. IV. Mechanism of Carbon-Phosphorus Bond Cleavage in Triarylphosphines and Trialkylphosphines by Palladium(II) Acetate

Kiyoshi KIKUKAWA, Makoto TAKAGI, and Tsutomu MATSUDA*

Department of Organic Synthesis, Faculty of Engineering, Kyushu University, Hakozaki, Higashi-ku, Fukuoka 812

(Received October 19, 1978)

Reaction of triphenylphosphine with an equimolar amount of $Pd(OAc)_2$ in acetic acid at room temperature in the presence of styrene gave *trans*-stilbene(94%), H_3PO_4(0.8%), $PhP(O)(OH)_2$(40%), $Ph_2P(O)(OH)$(19%), and $Ph_3P{=}O$(35%). Reactions of tributyl- and trioctylphosphine with $Pd(OAc)_2$ in acetic acid at 90 °C yielded butene(20%) and octene(1-; 22%, 2-; 17%), respectively, as main products. The phenylation of some olefins with triphenylphosphine in acetic acid-*d*, as well as other features of the reaction lead to the conclusion that nucleophilic attack on coordinated phosphorus atom is the most probable pathway for the formation of the phenylation agent (phenylpalladium species) in the reaction system among the others, *ortho*-metallation and oxidative addition.

Tertiary phosphines have been used as versatile and useful ligands in various phases of the chemistry and reactions of transtion-metal complexes, and are considered to bear carbon-phosphorus bond being stable under usual reaction conditions. Only a few has been known about the reaction of tertiary phosphines coordinated to transition metals,[2] except for *ortho*-metallation to arylphosphines and metallation of carbon-hydrogen bond in alkylphosphines which leads to five membered metal cycles.[3] Thus, degradation of the phosphines themselves in the metal complexes has hitherto been ignored or overlooked as a minor side reaction. Recent studies, however, indicated that the degradation of such ligands can take place under suitable conditions with surprising ease.[1,2] These findings suggest that detailed informations of this type of degradation would not only serve for a full understanding of the chemical transformation of transition-metal complexes in general, but also may shed light on a specific problem such as the mechanism of catalyst decay where the transformationof the ligands may result in a significant loss of its activity after repeated reaction cycles.

Previously, we reported that $Pd(OAc)_2(PPh_3)_n$ (n=1 or 2) served as an arylating reagent of various kinds of olefins, and proposed a tentative mechanism involving a facile cleavage of the carbon-phosphorus bond assisted by nucleophilic attack to the phosphorus with acetate ion, mostly based on the effect of *p*-substituents in the aryl groups and the nature of the products.[4] Moreover, a related C–A bond fission in APh_n–PdX_2 system (A=As, Sb, Bi, Se, or Te, n=2 or 3, X=OAc or halogen) evidenced that the behavior of PPh_3–$Pd(OAc)_2$ system was clearly different from those containing Bi, Sb, (or Hg), which proceeded *via* a simple electrophilic attack by bivalent palladium (or metal exchange) without the assistance of acetate ion.[1] Present paper deals with the studies on a stoichiometry of the phosphorus compound and deuterium labeling to substantiate the mechanistic features of the arylation. An analogous carbon-phosphorus bond cleavage of some trialkylphosphines assisted by $Pd(OAc)_2$ is also presented.

Results and Discussion

Reaction of Triphenylphosphine with $Pd(OAc)_2$. A mixture of triphenylphosphine and 1 or 4 equivalents of $Pd(OAc)_2$ in acetic acid was allowed to react at room temperature in the presence of excess styrene. After removal of organic compounds except for phosphorus containing compounds, chromatography of the chloroform extract from aqueous phase afforded triphenylphosphine oxide and the other phosphorus compounds (Reaction 1 and Table 1).

$$PPh_3 + Pd(OAc)_2 + CH_2{=}CHPh \xrightarrow{\text{AcOH, room temp, 48 h}} PhCH{=}CHPh(\mathbf{1}) + PhCH{=}CHOAc(\mathbf{2}) + Ph_3P{=}O(\mathbf{3}) + Ph_2P(O)OH(\mathbf{4}) + PhP(O)(OH)_2(\mathbf{5}) + H_3PO_4(\mathbf{6}) \quad (1)$$

In view of the results that in the absence of $Pd(OAc)_2$ most of triphenylphosphine was recovered unchanged except for oxidation to its oxide, the formation of these compounds are reasonably understood in terms of aerobic oxidation and hydrolysis of probable intermediates acetoxyphenylphosphines, $Ph_n(OAc)_{3-n}P$ (n=3—1), in the treatment. It is to be noted that despite of the recovery of some amount of triphenylphosphine (as its oxide), much of the products was obtained as phenylphosphonic acid, especially in the presence

TABLE 1. REACTION OF TRIPHENYLPHOSPHINE WITH $Pd(OAc)_2$ IN THE PRESENCE OF STYRENE IN ACETIC ACID[a]

Run	Molar ratio	Yield(%) based on PPh_3[b]					Yield(%) based on Pd
	PPh_3 : $Pd(OAc)_2$: Styrene	**1**	**3**	**4**	**5**	**6**	**2**[c]
1	1 : 1 : 4	94	35	19	40	0.8	trace
2	1 : 4 : 16	200	14	8	70	2.0	30

a) At room temp for 2 days. b) Moles of product per moles of PPh_3 utilized. c) The product is contaminated with a small amount of acetophenone and other carbonyl compounds.

of excess $Pd(OAc)_2$. The results in Table 1 indicate that two of the three phenyl groups (and some of the third one) are effectively utilized in the phenylation, and the diphenylphosphine intermediate is more reactive than triphenylphosphine in the present phenyl transfer. The marked depression of the amount of acetoxylated product(**2**) may be explained in terms of decrease of associated palladium(II) species in the presence of the phosphine ligand by considering the recent mechanistic study[5] on olefin-acetoxylation describing that dimeric palladium acetate was the most reactive species. The specific role of $Pd(OAc)_2$ is supported by the observations that none of the phenylated olefins or biphenyl was produced in the reactions of triphenylphosphine with $PdCl_2$ or other transition metal salts, $RhCl_3 \cdot 3H_2O$, $RuCl_3$, $CoCl_2$, $NiCl_2$, and $Ni(OAc)_2 \cdot 4H_2O$, but the systems of $PdCl_2$–NaOAc or $RhCl_3 \cdot 3H_2O$–AgOAc with PPh_3 gave rise to phenylated olefins (54% and a trace amount, respectively, based on PPh_3).

Reaction of Trialkylphosphine with $Pd(OAc)_2$. Although an attempted alkylation of styrene with some trialkylphosphines in place of triphenylphosphine failed under the same conditions described above and even at temperature up to 50 °C, heating of an equimolar mixture of $Pd(OAc)_2$ and tributyl- or trioctylphosphine in acetic acid at 90 °C gave a considerable amount of olefins and a small amount of oxidation product (Reactions 2 and 3) accompanied by precipitation of a considerable amount of palladium black.

$$P(n\text{-Bu})_3 + Pd(OAc)_2 \xrightarrow{\text{AcOH, 90 °C, 3 h}} \text{1-butene(20\%)} + \text{2-butanone(2.5\%)} + \text{2-butenes(traces)} + \text{butane(trace)} \quad (2)$$

$$P(n\text{-}C_8H_{17})_3 + Pd(OAc) \xrightarrow{\text{AcOH, 90 °C, 20 h}} \text{1-octene(22\%)} + \text{2-octene(17\%)} + \text{octane(0.2\%)} + \text{2-octanone(2.2\%)} + \text{octenyl acetates(2.1\%)} \quad (3)$$

Carbon-phosphorus bond cleavage could not be found in the absence of $Pd(OAc)_2$ under the same reaction conditions. Only traces of cyclohexene and cyclohexanone were formed from tricyclohexylphosphine. The formation of the olefins could be explained in terms of alkyl transfer from phosphorus to palladium to form an alkylpalladium species which decomposed to the olefins and palladium hydrides. The low reactivity of the alkylphosphines for the carbon-phosphorus bond cleavage can be understood by considering larger electron donating ability of the alkyl groups as compared to phenyl group and steric effect, especially for tricyclohexylphosphine, if one assumes that nucleophilic attack of acetate ion on the coordinated phosphine is operative in the reaction as proposed previously.[1,4]

Reaction of Triphenylphosphine or Triphenylphosphine-d_{15} with $Pd(OAc)_2$ in Acetic Acid-d. *ortho*-Metallation to coordinated triarylphosphines has been widely observed in transition-metal complexes.[2a,3,6] Furthermore, Nyholm *et al.*[7] reported that in the reaction with osmium carbonyl cluster complex triphenylphosphine was subjected to cleavage of carbon-phosphorus bond to produce a benzyne complex as one of the products. When a solution of $Pd(OAc)_2(PPh_3)_2$ in acetic-d_3 acid-*d* was allowed to stand at room temperature for 11 days, the NMR spectrum showed that 1.2 hydrogens per mole of triphenylphosphine were exchanged. The exchange can be reasonably interpreted by the process which involves the formation of an *ortho*-metallated intermediate as delineated in Reaction 4. This observation led us to inquire the mechanistic relation between the arylation and the *ortho*-metallation.

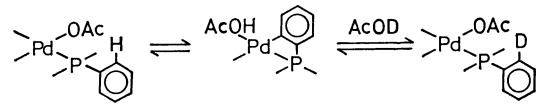

(4)

If the *ortho*-metallation were operative as a crucial step in the formation of a phenylpalladium species, either directly or through a benzyne complex, the arylation with *p*-substituted triphenylphosphine would give rise to the product carrying the substituent(X) at a *meta* position or a mixture of phenylated olefins with *meta* and *para* substituent, as formally shown in Reactions 5, 6, and 7. Similarly *meta*-substituted triphenylphosphine would give rise to a mixture of *ortho*, *meta*, and *para* substituted products.

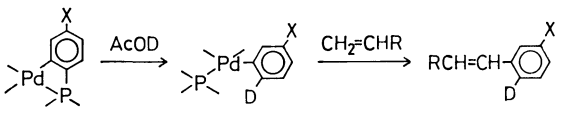

(5)

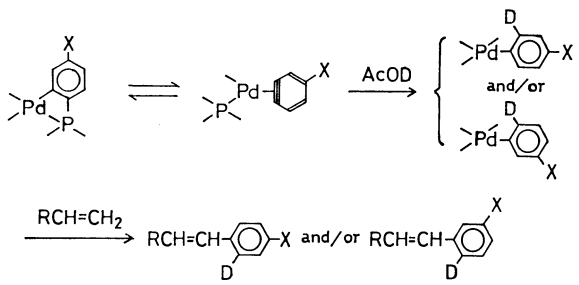

(6)

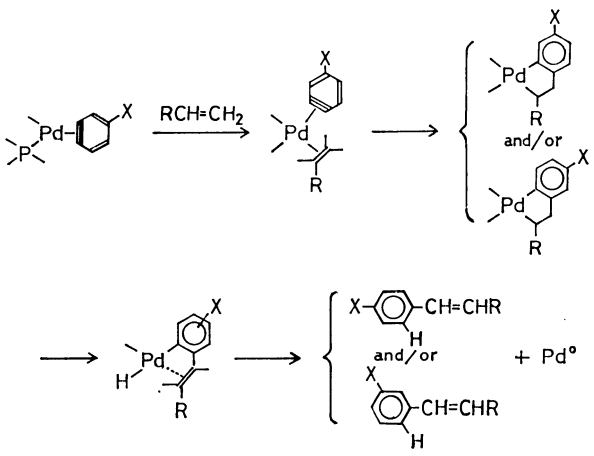

(7)

However, this was not the case for the current arylation, and only *p*-substituted products were obtained in the reactions with several *p*-substituted triphenyl-

Table 2. Phenylation of 1-octene and styrene by PPh_3 or PPh_3-d_{15} with $Pd(OAc)_2$ in acetic acid-d

Run	Phosphine and ratio to $Pd(OAc)_2$		Olefin	Conditions: temp (°C)	Conditions: t (h)	Deuterium content in phenylated olefin[a]
6	PPh_3	2	1-Octene	40	4	$C_6H_{13}CH=CH-Ph-d_{0.15}$
7	PPh_3	2	Styrene	40	4	Stilbene-$d_{0.13}$
8	PPh_3	1	Styrene	r.t.	2	Stilbene-$d_{0.0}$
9	PPh_3-d_{15}	1	Styrene	r.t.	2	Stilbene-$d_{5.08}$

a) Deuterium content was estimated by MS measurement for Runs 6, 7, and 8, and by NMR measurement for Run 9.

phosphines.[4] The regiospecificity of the position where olefin is introduced was further evidenced by the fact that only ethyl *m*-methylcinnamate was formed in the reaction of tri-*m*-tolylphosphine with $Pd(OAc)_2$ in the presence of excess ethyl acrylate. In order to obtain further information relating to the role of the *ortho*-metallation, phenylation of olefins with triphenylphosphine and $Pd(OAc)_2$ in acetic acid-*d* was carried out. The reaction with triphenylphosphine-d_{15} in the same solvent was also conducted to differentiate between the usual route *via* phenylpalladium and the other which might occur through the benzyne intermediate, if it formed (Reactions 6 and 7). As shown in Table 2, when one equivalent of triphenylphosphine or triphenylphosphine-d_{15} was utilized, the phenyl group in the starting phosphines transferred as such without being subjected to any H–D exchange. On the other hand, the presence of another mole of triphenylphosphine gave rise to incorporation of deuterium in the products, though it is to a small extent. It is to be mentioned here that the ratio of triphenylphosphine to $Pd(OAc)_2$ affects the rate of the phenylation as shown in Fig. 1. The reverse relationship between the rate of phenylation and the extent of the H–D exchange strongly suggests that the exchange became recognized only because of the decrease of the phenylation rate and that the *ortho*-metallation (Reaction 4) does not contribute to the formation of the phenylpalladium species for phenylation of olefins.

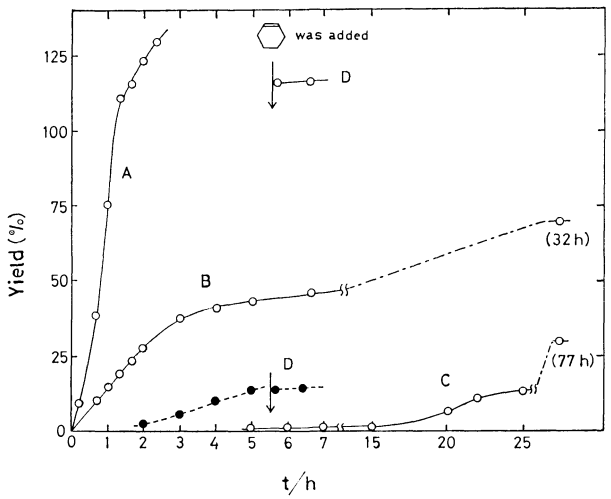

Fig. 1 Time course of phenylation of cyclohexene in acetonitrile. $[Pd(OAc)_2]=0.1$ M, $[PPh_3]=0.05$ M (A), 0.1 M (B), 0.2 M (C), 0.05 M (D), $\left[\bigcirc\right]=$ 0.2 M. Temp: 25.0 °C (A and D), 30.0 °C (B and C). Yields are based on PPh_3.
—○—: Phenylcyclohexenes, —●—: Ph–Ph.

Mechanism of the Arylation. Previously we proposed the tentative mechanism for the facile carbon-phosphorus bond cleavage, which involved an initiatory nucleophilic attack on the coordinated phosphorus atom by acetate ion leading to phenyl transfer to palladium.[4]

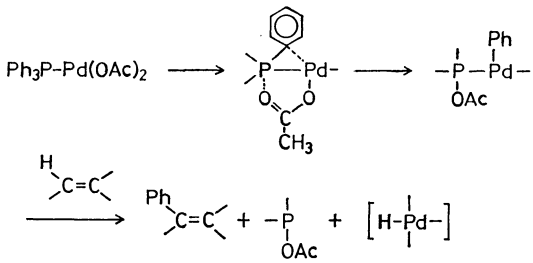

(8)

Recently, Fahey and Mahan[8] have described reversible oxidative addition of triphenylphosphine to zero-valent nickel and palladium complexes (Reaction 9).

$$C_6F_5\text{-}PPh_2 + Pd(0) \longrightarrow C_6F_5\text{-}Pd(II)\text{-}PPh_2 \quad (9)$$

This fact introduces an alternative pathway to be considered for the formation of the phenylpalladium species in the present phenylation, since the reaction proceeds with accompanied formation of zero-valent palladium. If the oxidative addition route is operative in the present system the phenylation should be expected to proceed more favorably under nitrogen atmosphere than under aerobic conditions. The effect of the atmosphere examined in the reaction of $Pd(OAc)_2(PPh_3)_2$ with 1-octene (Table 3) shows that under nitrogen the yield of phenylated olefins decreased remarkably, whereas the addition of an oxidizing agent, $Cu(OAc)_2\cdot 2H_2O$, increases the yield even under nitrogen. Since the phenylation in the system of phenylmercury(II) acetate–$Pd(OAc)_2$ is known to be little affected by the atmosphere,[9] the results can be considered to indicate that the atmosphere influences the step of the formation of the phenylpalladium species, and divalent palladium is principally responsible for the present carbon-phosphorus bond cleavage.

Another feature of the current phenylation is the marked effect of the ratio of triphenylphosphine to $Pd(OAc)_2$ on the reaction rate (Fig. 1). The increase in triphenylphosphine/Pd ratio depressed both the rate and yield of the phenylation. Particularly, the use of double moles of triphenylphosphine to $Pd(OAc)_2$ introduced a long induction period (curve C), and the presence of excess triphenylphosphine substantially

Table 3. The effect of atmosphere on the phenylation of 1-octene by $Pd(OAc)_2(PPh_3)_2$ in acetic acid

Run	Atmosphere	Additive	Conditions t (h), (temp, °C)		Phenylated olefins (%)[a]	Acetoxylated olefins (%)[b]
3	air	—	9	(50)	97	3
4	nitrogen	—	70	(50)	35	5
5	nitrogen	$Cu(OAc)_2 \cdot 2H_2O$	22	(50)	113	2

a) 1- and 2-Phenyl-1-octenes and -2-octenes. Yields are based on the Pd complex. b) A mixture of isomeric octenyl acetates and octan-2-one. Yields are the sum of those of the acetates and the ketones.

inhibited the reaction.[4] It would be unreasonable to consider that the rate of the oxidative addition (Reaction 9) reduces in such a manner as shown in Fig. 1 even in the presence of one or two equivalents of triphenylphosphine. It is most probable that coordination of two phosphine molecules to $Pd(OAc)_2$ somehow prevents the phenyl migration from phosphorus to palladium (Reaction 8). Under aerobic conditions the phosphine is extruded from the coordination sphere by oxidation to the phosphine oxide, thus leaving a vacant site in the palladium complex which serves for the phenyl migration to take place. Under nitrogen atmosphere, such process obviously is not available, and cupric acetate is needed as oxidant or more probably as carrier of the "excess" triphenylphosphine. The reasoning for the formation of the phenylpalladium species directly from $Pd(OAc)_2$ and triphenylphosphine was further evidenced by the following experiment. The reactions A and D in Fig. 1 were carried out under the same conditions except for the mode of addition of cyclohexene. In the reaction A, the olefin was applied to a solution of $Pd(OAc)_2$ just before the addition of triphenylphosphine. When a mixture of triphenylphosphine and $Pd(OAc)_2$ in acetonitrile was allowed to react for 5.5 h, a small amount of biphenyl was detected before the addition of cyclohexene (Reaction D). On addition of the olefin to the mixture, the formation of phenylcyclohexenes took place very rapidly and was completed within 5 min. Nevertheless, the yield (120 %) was comparable to those under the condition A. The results strongly supports the conclusion that the phenylpalladium species are formed to a considerable extent even in the absence of olefins and the presence of zero-valent palladium species is unnecessary for the production of phenylating agent in the present reaction system.

All of the observations are consistent with the following reaction scheme which involves an nucleophilic attack by acetate on the coordinated phosphorus atom. The similar mechanism could be applied for the migration of the second and the third phenyl groups from phosphorus to palladium, though no direct evidence is available at present.

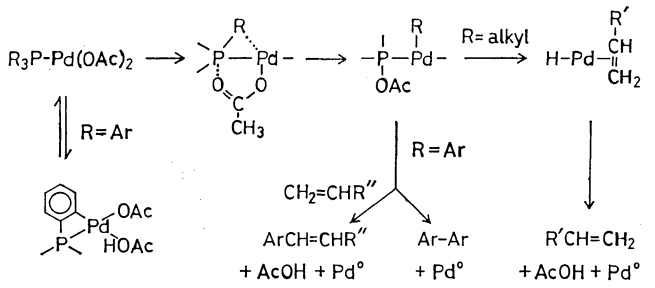

Scheme.

Experimental

Materials. Palladium acetate and bis(triphenylphosphine)palladium(II) acetate were prepared by the method of Wilkinson *et al.*[10] Triphenylphosphine and tributylphosphine were of commercial origin and were used without further purification. Triphenylphosphine-d_{15} was prepared from pentadeuterophenyl magnesium bromide and phosphorus trichloride.[11] Trioctylphosphine was prepared by the similar method described above; bp 183—187 °C/1 mmHg (lit,[12] 173—178 °C/0.3 mmHg). Olefins and solvents were of commercial origin and were used after distillation. Acetic acid was refluxed with potassium permanganate before distillation.

Reaction of Trialkylphosphine with $Pd(OAc)_2$. The solution of trialkylphosphine(5 mmol) and $Pd(OAc)_2$(5 mmol) in acetic acid (20 ml) was heated at 90 °C under stirring for 3 to 20 h. Evolution of gas (24 ml at 15 °C) was observed for tributyl phosphine. The gas was consisted of 1-butene(98%), 2-butene(1%) and butane(1%) according to the analysis with GLC (20% dibenzyl ether on Celite 545). Palladium black deposited was removed by filtration and organic products in the reaction mixture were extracted with ether, neutralized with aq sodium hydrogencarbonate, washed three times with aq sodium chloride and dried. The products were identified by comparison with those of authentic samples and with decane as an internal standard on GLC. The peak assigned to ketones disappeared by the treatment of the ethereal solution with 2,4-dinitrophenylhydrazine.

Reaction of Triphenylphosphine with $Pd(OAc)_2$ in the Presence of Styrene. In a 100 ml flask were placed 1.31 g(5 mmol) of triphenylphosphine, 1.12 g(5 mmol) of $Pd(OAc)_2$, 2.08 g (20 mmol) of styrene and 10 ml of acetic acid. The mixture was stirred at room temperature for 48 h. Excess styrene and acetic acid were evaporated under vacuum at room temperature, and then styrene derivatives were steam-distilled from the residue. The distillate was extracted with ether. Stilbene, acetoxylated styrene and acetophenone in the extract was separated by column chromatography on silica gel (Wakogel, C-100). The residue was extracted with chloroform, and the chloroform layer gave triphenylphosphine oxide and diphenylphosphinic acid after chromatography on silica gel. $Ph_2P(O)OH$, mp 188—192 °C(lit,[13] 194—195 °C). Phenylphosphonic acid was obtained from the aq layer, mp 145—150 °C(without purification, lit,[14]

158—161 °C). A small portion of aq layer was used for the analysis of phosphoric acid.[15] All the phosphorus compounds obtained in the present reaction were identified by comparison of the IR with those of authentic samples except for phosphoric acid. The assignment of the phenylated and acetoxylated products was described previously.[4,16]

*Reaction of Tri-*m*-tolylphosphine with Pd(OAc)$_2$ in the Presence of Ethyl Acrylate.* To a mixture of Pd(OAc)$_2$(5 mmol) and ethyl acrylate(20 mmol) in acetonitrile(30 ml) was added tri-*m*-tolylphosphine at room temperature and stirred for 12 h. Palladium metal deposited was removed by filtration and a distillation of the filtrate gave 0.60 g of ethyl *m*-methylcinnamate(bp 120 °C/5 mmHg). The structure of the product was identified by comparison of IR, NMR, and the retention time on GLC (Reoplex 400, 1.5 m, 140 °C) with an authentic sample. The IR and GLC analysis excluded the formation of ethyl *p*-methylcinnamate.

*Phenylation in Acetic Acid-*d. Reaction procedure in acetic acid-*d* was similar to that in acetic acid except for the protection from the moisture by a calcium chloride tube. *trans*-1-Phenyl-1-octene was separated by preparative GLC as described previously[4] and was analyzed by MS: *m/e*, 188(M^+), relative intensities of isotope peaks; M+1=35.7 (%), M+2=7.15(%) (values from lit[17] for $C_{14}H_{20}$, M+1=15.45, M+2=1.11). Stilbene was isolated in the same way as described above. The relative intensities were as follows. Run 7: *m/e*, 180(M^+); M+1=30.92, M+2=5.01. Run 8: M+1=15.27. Run 9: M+1=15.0 (values from lit,[17] for $C_{14}H_{12}$, M+1=15.32, M+2=1.09). Stilbene from the run 9 was hydrogenated over Pd/$BaCO_3$ to 1,2-diphenylethane. PMR of the product showed two singlets placed at δ 2.86(methylene protons) and 7.12(aromatic protons). The ratio of the peak area of the aromatic to aliphatic protons was 1.23(an average from five measurements) which showed the presence of 5.08 of deuterium in a molecule. The deuterium calcd from MS was 4.83.

Determination of Time Course of Phenylation. Runs A and B: To a solution of Pd(OAc)$_2$(0.5 mmol) in acetonitrile containing an internal standard (diethyleneglycol dibutyl ether), cyclohexene (1.0 mmol) triphenylphosphine (0.25 or 0.5 mmol) were added and stirred in a thermostated cell. Samples were withdrawn at appropriate time intervals by a microsyringe and directly analyzed on GLC equipped with flame ionization detector. Rection procedure for Runs C and D was similar to the above except for the way of addition of cyclohexene and triphenylphosphine. Thus, in Run C, bis(triphenylphosphine)palladium acetate was used and in Run D, triphenylphosphine was allowed to react with Pd(OAc)$_2$ for 5.5 h before the addition of cyclohexene.

References

1) Part III in this series, T. Kawamura, K. Kikukawa, M. Takagi, and T. Matsuda, *Bull. Chem. Soc. Jpn.*, **50**, 2021 (1977).

2) a) R. Mason and D. W. Meek, *Angew. Chem. Int. Ed. Engl.*, **17**, 183 (1978). b) D. R. Coulson, *J. Chem. Soc., Chem. Commun.*, **1968**, 1530. c) A. Nakamura and S. Otsuka, *Tetrahedron Lett.*, **1974**, 463. d) M. L. H. Green, M. J. Smith, H. Felkin, and G. Swierczewski, *J. Chem. Soc., Chem. Commun.*, **1971**, 158. e) R. Asano, I. Moritani, Y. Fujiwara, and S. Teranishi, *Bull. Chem. Soc. Jpn.*, **46**, 2910 (1973).

3) a) A. J. Cheney, B. E. Mann, B. L. Shaw, and R. M. Slade, *J. Chem. Soc., A*, **1971**, 3833. b) G. W. Parshall, W. H. Knoth, and R. A. Schunn, *J Am. Chem. Soc.*, **91**, 4990 (1969). c) S. Hietkamp, D. J. Stufkens, and K. Vrieze, *J. Organometal. Chem.*, **134**, 95 (1977); **139**, 189 (1977). d) A. A. Kiffen, C. Masters, and L. Raynand, *J. Chem. Soc., Dalton Trans.*, **1975**, 853.

4) T. Yamane, K. Kikukawa, M. Takagi, and T. Matsuda *Tetrahedron*, **29**, 955 (1973).

5) S. Winstein, J. McCaskie, H. B. Lee, and P. M. Henry, *J. Am. Chem. Soc.*, **98**, 6913 (1976).

6) G. W. Parshall, *Acc. Chem. Res.*, **3**, 139 (1970).

7) a) G. W. Bradford, R. S. Nyholm, G. J. Gainsford, J. M. Guss, P. R. Ireland, and R. Mason, *J. Chem. Soc., Chem. Commun.*, **1972**, 87; b) C. W. Bradford and R. S. Nyholm, *J. Chem. Soc., Dalton Trans.*, **1973**, 529.

8) D. R. Fahey, and J. E. Mahan, *J. Am. Chem. Soc.*, **98**, 4499 (1976).

9) Unpublished data; T. Kawamura, K. Kikukawa, M. Takagi, and T. Matsuda.

10) T. A. Stephenson, S. M. Morehouse, A. R. Powell, J. P. Heffer, and G. Wilkinson, *J. Chem. Soc.*, **1965**, 3632.

11) M. A. Bennett and D. L. Milner, *J. Am. Chem. Soc.*, **91**, 6983 (1969).

12) M. M. Rauhut, H. A. Currier, A. M. Semsel, and V. P. Wystrach, *J. Org. Chem.*, **26**, 5138 (1961).

13) G. M. Kosolapoff and R. F. Struck, *J. Chem. Soc.*, **1959**, 3950.

14) H. Z. Lecher, T. H. Chao, K. C. Whitehouse, and R. A. Greenwood, *J. Am. Chem. Soc.*, **76**, 1045 (1954).

15) Y. Murakami and M. Takagi, *J. Am. Chem. Soc.*, **91**, 5130 (1969).

16) T. Matsuda, T. Mitsuyasu, and Y. Nakamura, *Kogyo Kagaku Zasshi*, **72**, 1751 (1969).

17) R. M. Silverstein, G. C. Bassler, and T. C. Morrill, "Spectrometric Identification of Organic Compounds," 3rd ed, John Wiley & Sons, Inc. N. Y. (1974), p. 41.

A Simple MO Treatment on the Nucleophilic Substitution Reactions of Six-membered Aza-aromatic Compounds

Minoru HIROTA,* Hideyuki MASUDA, Yoshiki HAMADA,** and Isao TAKEUCHI**

Department of Applied Chemistry, Faculty of Engineering, Yokohama National University, Minami-ku, Yokohama 232

***Department of Pharmacy, Meijo University, Tempaku-ku, Nagoya 468*

(Received October 30, 1978)

Nucleophilic substitution reactions of monoaza- and diaza-naphthalenes and -phenanthrenes were discussed on the basis of an HMO calculation taking the nature of the reagent into consideration. Results were compared with the orientation of some nucleophilic substitution reactions, *i.e.* Chichibabin amination, phenylation by phenyllithium, and methylation by methylsulfinylmethanide ion. The nature of the reagent was explicitly taken into account as the difference in the coulomb integrals and the reagent-dependent orientation of these reactions were explained theoretically.

In recent decades, molecular orbital theory has been applied to many organic reactions and, in most instances, succeeded in interpreting the reactions. In the field of heteroaromatic chemistry, many applications of MO theory were also reported.[1] In an earlier stage the reactivity indices were calculated and shown to reproduce the orientations of substitution reactions.[2-5] However, several heteroaromatic compounds exhibit different orientations depending on the nature of nucleophiles (or electrophiles), which prevents the use of common reactivity indices throughout all kinds of nucleophilic (or electrophilic) reactions. For example, quinoline, a typical of the six-membered aza-aromatics, reacts with amide anion in liquid ammonia to produce 2-aminoquinoline,[6] while it is methylated to produce 4-methylquinoline by methylsulfinylmethanide ion (dimsyl anion) in DMSO.[7] Both reactions are caused by the attack of nucleophile, being usually classified as nucleophilic substitution reactions. The results are embarrassing when the reactions were predicted in terms of reactivity indices. On the other hand, the reactivity indices themselves are also inconsistent, predicting the different sites of reaction depending upon the kinds of the indices. Brown[8] has classified the reactivity indices from the theoretical consideration on the transition states of the reactions and has given a general guideline to select the proper index as follows: When the reagent or the substrate is reactive, orientation of the reaction is determined by localization energy (L_r) or superdelocalizability (S_r), while the orientation is determined by electron density (q_r) or polarizability (π_{rr}) in the case contrary. The classification is rationalized afterwords by several authors by considering the orbital energies of the reagents (and also of the substrates). Klopman[9] has developed a generalized poly-electronic perturbation theory (GE theory) in which the energies of the unoccupied MO's of electrophile (acceptor) and of the occupied MO's of nucleophile (donor) were both taken into accounts and succeeded in explaining the different orientation of the nucleophilic substitution reactions of pyridinium salts. Simonetta[10] has proposed a π-electronic model for the transition state of aromatic substitution reaction in which the AO's of the tetra-valent carbon and the leaving and the substituting groups were treated analogous to the case of hyperconjugation in order to separate the π-orbitals from the σ-orbitals. The reactivity is discussed on the basis of the π-part of MO's alone. Chalvet and Daudel[11-13] have developed a theory for the treatment of the transition state of aromatic substitution, in which, again, π-MO's of the interacting system were solely considered to predict the orientation of the reaction as a function of the HOMO-energies of the attacking nucleophile.

In practice, substituted benzenes are resistant to nucleophilic aromatic substitutions and react only at the ipso position of the nucleophilically activated halogen or alkoxyl substituent. On the contrary, nucleophilic substitution reaction is quite common with so-called π-electron-deficient aza-aromatic compounds,[6,7,14-22] and the orientations of the reactions are dependent on the nature of the attacking nucleophiles. The present authors have reported the nucleophilic substitutions of several monoaza- and diaza-naphthalenes, -phenanthrenes, and -anthracenes,[23-25] and found remarkable differences in orientations depending upon the nature of the nucleophiles. In this paper, the different orientation observed in some nucleophilic reactions will be discussed according to the above mentioned theory developed by Chalvet and Daudel.

Theoretical

In order to predict the orientations of the substitution reactions on the heteroaromatic compounds, the relative MO energies of the transition states leading to variously oriented substituted products were estimated by a method similar to the unified treatment of transition state proposed by Chalvet *et al.* In this theory, a transition state is treated as a heteroaromatic π-system (substrate) with extension of delocalization by reagent, and the MO Φ of the transition state is formed in terms of the linear combination of the reagent atomic orbital (or group orbital) γ and the substrate molecular orbitals ϕ^σ and ϕ^π.

$$\Phi = \lambda\gamma + \sum C_i\phi_i^\sigma + \sum C_j\phi_j^\pi$$
$$= \lambda\gamma + \sum C_m\chi_m^\sigma + \sum C_n\chi_n^\pi$$

As the reagent (X) attacks the periphery of the π-electron cloud of the substrate aromatic molecule, the overlap between the ϕ^σ and γ will be small and can be neglected. Thus,

$$\langle\gamma|\phi^\sigma\rangle = \langle\gamma|\chi_r^\sigma\rangle = 0$$

and

$$\langle\gamma|\boldsymbol{h}|\phi^{\sigma}\rangle = \langle\gamma|\boldsymbol{h}|\chi_{r}^{\sigma}\rangle = 0$$

where r refers to the site of the nucleophilic (or electrophilic) attack in the substrate molecule. This means that the relative energies of the transition state can be estimated by considering solely the following π-MO's.

$$\Phi^{\pi} = \lambda\gamma + \sum C_{n}\chi_{n}^{\pi}$$

The calculation of the Φ^{π}'s can be carried out within the framework of the Hückel MO approximation if the following integrals are properly evaluated.

$$\alpha_{x} = \langle\gamma|\boldsymbol{h}|\gamma\rangle$$

$$\beta_{rx} = \langle\gamma|\boldsymbol{h}|\chi_{r}^{\pi}\rangle$$

These integrals can be evaluated by the following way. The perturbation energy caused by the interaction with the reagent has been shown to increase monotonously as the increase of β_{rx} without significant crossings of the energies within the range of $\beta_{rx}=0$—2.0.[12] Thus the resonance integrals β_{rx} are simply evaluated to be 0.5 after Chalvet *et al.*

The coulomb integrals α_{x} are evaluated with reference to the Mulliken's electronegativities[26,27] of the attacking nucleophiles. Discussions in this paper are confined to the following three reactions; (i) phenylation with phenyllithium, (ii) methylation by dimsyl anion, and (iii) Chichibabin amination. The phenylation with phenyllithium is assumed to be induced by the initial attack of phenyl carbanion. The anion has been proved to be a sigma anion carrying the unshared electron pair in an sp^2 non-bonding AO. The anion is stabilized by the aromatic sextet of electrons as is in the parent hydrocarbon. Methylation of the six-membered aza-aromatic compounds by dimsyl anion is rather complex in the mechanistic point of view, involving an initial addition of the nucleophile and subsequent elimination in some cases. However, the orientation of the reaction is determined by the initial attack of dimsyl anion towards the heteroaromatic nucleus. The transition state energies of this initial process can be properly evaluated by the method mentioned above. The dimsyl anion is a carbanion in conjugation with sulfinyl group, and its anionic center is supposed to be planar. Thus, the unshared electron pair of this anion should occupy a p-AO. Chichibabin amination reactions are carried out in liquid ammonia, and the effective nucleophile is amide anion. The anion is generally supposed to take an angular conformation. However, the hybridization state of its nitrogen atom is not known in details, since the exact geometry of the anion has not been determined. Anyhow the nitrogen atom has a non-bonding AO of which s-character is ranging from 0 to 50%. In other words, the AO has an intermediate character between pure p and sp-hybridized.

Ionization potentials I, electron affinities A, and Mulliken's electronegativities χ_{M} for these AO's are given, together with the estimated α_{x} values, in Table 1. Ionization potentials, electron affinities, and other properties have been correlated with coulomb integrals by many authors.[26,28–31] Nevertheless, coulomb and other integrals for HMO calculations have been assigned in a qualitative manner with reference to these properties

Table 1. The electronegativities and the coulomb integrals of carbon and nitrogen atoms of various valence states

Atom	AO	I/eV	A/eV	χ_{M}	h_{x}
C(sp^2)	2p(π)	11.16	0.03	5.60	−0.5
	tr(σ)	15.62	1.95	8.79	+2.0
N[a]	2p	13.94	0.84	7.39	
N(sp^2)	2p	14.12	1.78	7.95	+1.5
N(sp)	2p	14.11	2.14	8.13	

a) Unhybridized N atom.

in most instances, and such integrals are also employed to formulate the Hückel determinant of the substrate heteroaromatic molecules in this investigation. Thus, the α_{x}'s are also evaluated by taking the following factors into account. Firstly, as the β_{rx} is *a priori* assigned to be 0.5 which corresponds to a rather weak interaction, the effect of electronegativity should be a little exaggerated in the α_{x} integrals to compensate the smaller β_{rx}. Secondly, the coulomb integrals for anionic centers should be shallower than those for the neutral atoms of similar electronic states. Thirdly, the electronegativities of the anionic centers of the reagents increase in the order; dimsyl anion<amide anion<phenyl anion, even though there exists some ambiguity in the χ_{M} value of the nitrogen atom in amide anion. Thence, h_{C}(dimsyl)<h_{N}(amide)<h_{C}-(phenyl). In conclusion, the integrals given in Table 1 were employed in the calculations. These values are carefully adjusted so as to be consistent with other integrals in the substrate heteroaromatic molecules.

Results and Discussion

By performing the MO calculations described in the theoretical part, total π-energies of the models for the transition states were obtained. The total π-energy E_{π}(r) is dependent on the site (r) of reaction in a molecule concerned, and the one with the lowest π-energy corresponds to the transition state for the most feasible reaction path, which should be realized in practice. The relative π-energies for the various reaction sites in the heteroaromatic molecules 1 to 13 are shown graphically in Fig. 1(a)—(n) as a function of the coulomb integral ($\alpha_{x}=\alpha+h_{x}\beta$) of the attacking nucleophiles. In these figures, the "transition state" with the lowest π-energy at $h_{x}=-3$ is chosen as the reference(s) and the energy difference E_{π}(r)−E_{π}(s) in β unit are plotted as a function of h_{x}. Then, the relative "transition state" energy for the site chosen as the reference is given by the straight line E_{π}(s)=0 (which superposed on the abscissa). When the energy curves for other "transition states" do not intersect the abscissa, the relative energies of them are always higher than E_{π}(s), and the heteroaromatic molecule is expected to react at the same site (s) irrespective of the nature of the attacking nucleophiles. When the energy curve(s) of other "transition states" crosses the abscissa, the lowest energy one is replaced as the change in h_{x}. Therefore, the site of the nucleophilic attack is predicted to be altered as the change in the

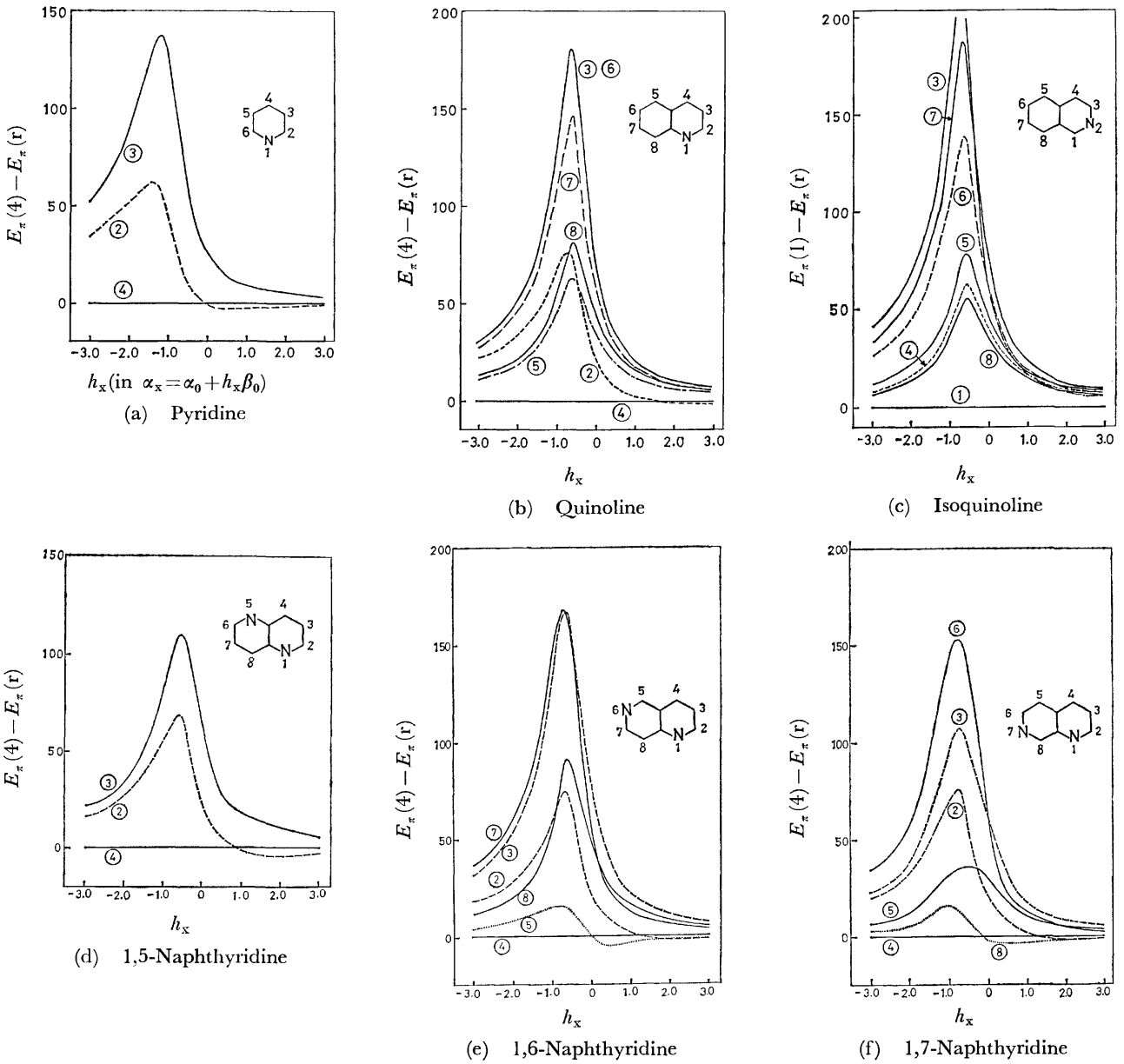

Fig. 1. Relative π-energies for the transition states of various reaction sites (in β units$\times 10^3$).

nucleophilicity of the reagent.

Of all the heterocycles investigated, isoquinoline (**3**), 5-azaphenanthrene (**10**), 4,6-diazaphenanthrene (**12**), acridine (**13**), and 1,10-diazaanthracene (**14**) belong to the former cases. Nucleophilic substitution reactions of these nitrogen heterocycles have been extensively investigated by several authors. Since the first report on pyridine and related substances by Chichibabin and Zeide,[6] the amination by alkali amide in liquid ammonia has been applied to a variety of the six-membered aza-aromatic compounds and called Chichibabin reaction. This modification of amination on a series of naphthyridines have been studied in details by Paudler and Kress,[17] and further extended to the benzo analogs of naphthyridines by the present authors.[23-25] The reaction on 1,5-naphthyridine had been reported to give the 2-amino derivative initially,[17] but the 4-amino derivative was identified as the product of the amination recently.[18,23]

Phenylation by phenyllithium in ether or hydrocarbon medium is also a well-known reaction, and the substitution occurs predominantly on the carbon atom ortho to the ring nitrogen atom in almost all cases reported.[14-16,32] The present authors[25] have investigated on the orientation of the phenylation of 1,*x*-naphthyridines and shown that the main product is the 2-phenyl derivative in the reactions of all isomeric heterocycles. Methylation of these aza-aromatic compounds were first reported by Russel and Weiner.[7] They carried out the reaction on pyridine and several of its benzo analogs and, though pyridine is unreactive to dimsyl anion, showed that the ortho or para-substituted derivatives were produced *via* addition-elimination mechanism. The methylation was applied to diazanaphthalenes and diazaphenanthrenes by the present authors.[24,25] The products of these reactions were summarized in Table 2 together with the orientations predicted from Fig. 1 by assuming the coulomb

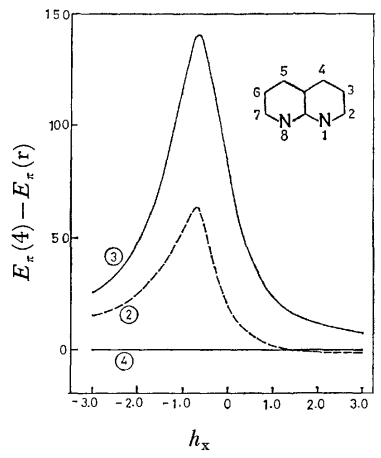

(g) 1,8-Naphthyridine

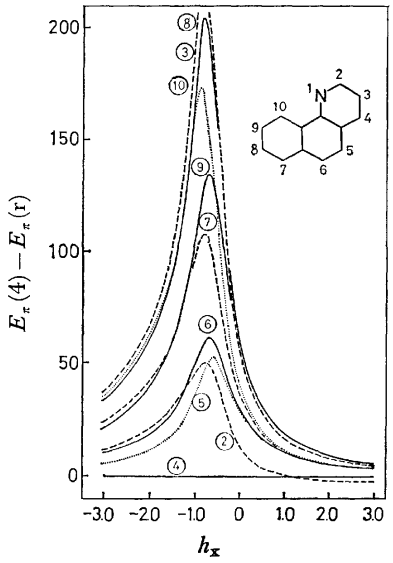

(h) 1-Azaphenanthrene

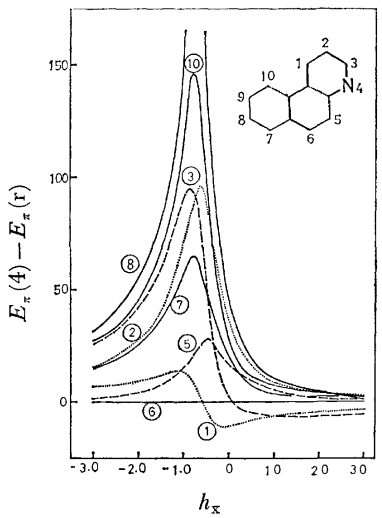

(i) 4-Azaphenanthrene

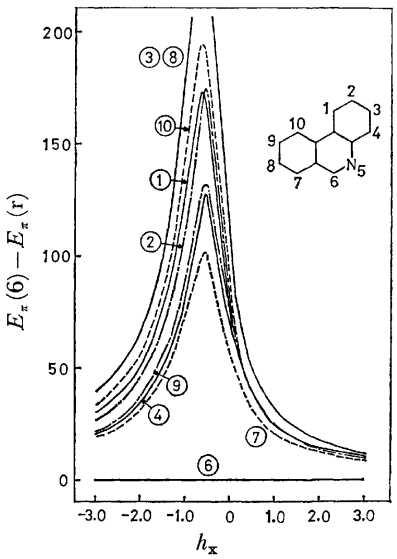

(j) 5-Azaphenanthrene

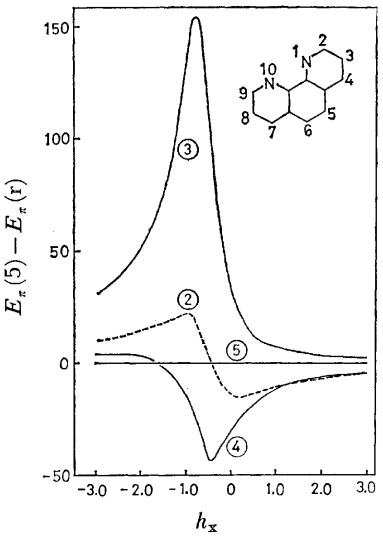

(k) 1,10-Diazaphenanthrene

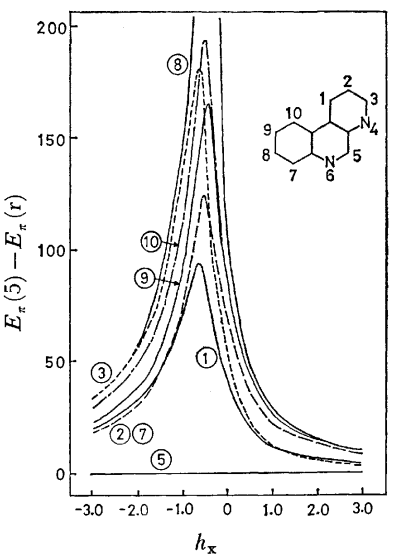

(l) 4,6-Diazaphenanthrene

Fig. 1

integrals of the reagents as given in Table 1.

The orientations of the compounds **3**, **10**, **12**, **13**, and **14** are invariable throughout all three kinds of nucleophilic reaction, and the prediction from Fig. 1 is shown to be consistent with the experimental results. With other heterocycles, the orientation alters with the change in reagents in accord with the crossing of the π-energy curve in Fig. 1. 1,5-Naphthyridine (**4**), for example, produce 2-phenyl-, 2- or 4-amino-, and 4,8-dimethyl-naphthyridines by the above mentioned reactions, and the difference in orientation is properly explained by the crossing of the transition state π-energy curve for the 2 (and 6)-position with abscissa which corresponds to that for the 4(and 8)-position. Thus, the reagent of which h_x is larger than 1 (crossing point) is predicted to attack toward 2 (and 6)-position. The compounds **1**, **2**, **5**, **6**, **7**, **8**, **9**, and **11** also have some similar crossings with abscissa in their "transition state" π-energy curve and expected to behave differently toward the attack of various nucleophiles in orientation. The difference in orientation is verified with all the compounds investigated experimentally (**2**, **5**, **6**, **7**, **8**, and **9**). Phenylation and amination have not yet been carried out on 1,10-diazaphenanthrene (**11**), lacking the evidence for the different orientation, and pyridine (**1**) is unreactive toward dimsyl anion even if it is expected to react at the 4-position.[33] After all the comparison with the experimental consequence illustrates that the method is quite trustworthy and widely applicable to the qualitative prediction of the orientation.

The results are compared with the orientations predicted from reactivity indices. Among various reactivity indices, electron density q_r, as well as superdelocalizability $S_r^{(-)}$ and frontier electron density $f_r^{(-)}$ for nucleophilic reactions, is suitable for this discussion, being given in Table 3. With the heterocycles of which reaction site toward nucleophile is

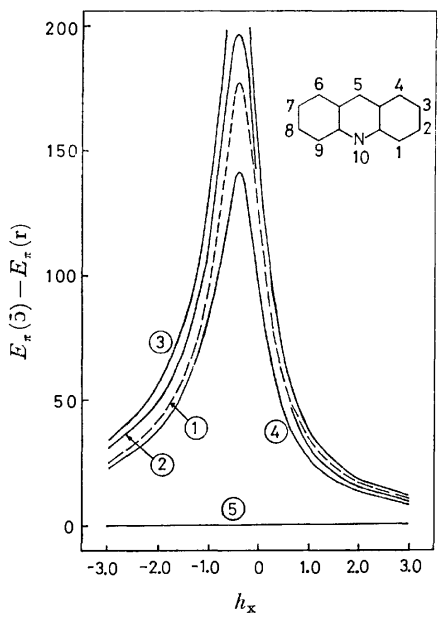

(m) Acridine

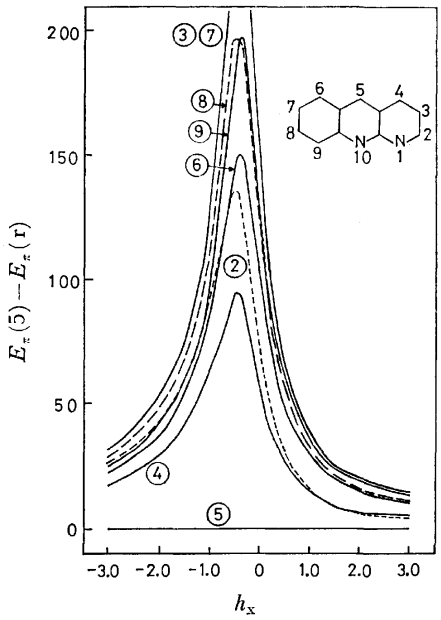

(n) 1,10-Diazaanthracene

Fig. 1.

TABLE 2. PRODUCTS OF SOME NUCLEOPHILIC SUBSTITUTION REACTIONS AS COMPARED WITH THOSE PREDICTED

Compound		Phenylation ($h_x=2.0$)	Amination ($h_x=1.5$)	Methylation ($h_x=-0.5$)
Pyridine (**1**)	th.	2>4	2>4	4>2
	exp.	(2)	(2)	unreact.
Quinoline (**2**)	th.	2>4	2>4	4>5
	exp.	(2)	(2)	(4)
Isoquinoline (**3**)	th.	1>3	1>8	1>8
	exp.	(1)	(1)	(1)
1,5-Naphthyridine (**4**)	th.	2>4	2>4	4>2
	exp.	(2)	(2), (4)[a]	(4, 8)[b]
1,6-Naphthyridine (**5**)	th.	2>5	2>5	4>5
	exp.	(2)	(2)	(4)
1,7-Naphthyridine (**6**)	th.	8≈2	8>2	4>8
	exp.	(2)	(8)	(4, 8)[b]
1,8-Naphthyridine (**7**)	th.	2>4	2>4	4>2
	exp.	(2)	(2)	(4, 5)[b]
1-Azaphenanthrene (**8**)	th.	2>4	2>4	4>2≈5
	exp.		(2)	(4) + (5) + (6) + (4, 6)[b]
4-Azaphenanthrene (**9**)	th.	3>1	3>1	6>1≈5
	exp.		(3)	(5) + (6)
5-Azaphenanthrene (**10**)	th.	6>7	6>7	6>7
				(6)
1,10-Diazaphenanthrene (**11**)	th.	2>4	2>4	4>5
	exp.			(4) + (4, 7)[b]
4,6-Diazaphenanthrene (**12**)	th.	5>3	5>3	5>1
	exp.		(5)	(5)
Acridine (**13**)	th.	5>4	5>4	5>4
	exp.		(5)	(5)
1,10-Diazaanthracene (**14**)	th.	5>2	5>2	5>4
	exp.		(5) + (2, 5)[b]	(5)

a) Different product was reported by several authors.[17,18,23] b) Disubstituted derivative.

TABLE 3. REACTIVITY INDICES FOR THE NUCLEOPHILIC REACTIONS OF AZA-AROMATIC COMPOUNDS

Compound	r	q_r	$S_r^{(-)}$	$f_r^{(-)}$	Compound	r	q_r	$S_r^{(-)}$	$f_r^{(-)}$
Pyridine (**1**)	2, 6	**0.943**	**0.983**	0.271	4-Azaphenanthrene (**9**)	1	0.942	**1.152**	0.265
	3, 5	0.992	0.853	0.107		2	0.999	0.906	0.154
	4	0.951	0.978	**0.627**		3	**0.926**	1.083	0.094
Quinoline (**2**)	2	**0.917**	1.146	0.258		5	1.008	0.998	0.275
	3	1.001	0.881	0.102		6	0.978	1.090	**0.314**
	4	0.932	**1.257**	**0.457**		7	0.995	1.000	0.148
	5	0.989	1.058	0.296		8	0.999	0.864	0.001
	6	0.999	0.884	0.099		9	0.996	0.916	0.157
	7	0.984	0.938	0.145		10	0.999	0.943	0.035
	8	1.007	1.002	0.263	5-Azaphenanthrene (**10**)	1	0.996	0.962	0.099
Isoquinoline (**3**)	1	**0.918**	**1.259**	**0.480**		2	0.999	0.909	0.139
	3	0.968	0.944	0.046		3	0.993	0.884	0.016
	4	0.991	1.039	0.338		4	1.004	0.991	0.191
	5	1.000	1.005	0.296		6	**0.891**	**1.390**	**0.484**
	6	0.984	0.937	0.177		7	0.979	1.072	0.225
	7	0.997	0.884	0.095		8	0.999	0.864	0.001
	8	0.986	1.058	0.352		9	0.980	0.987	0.212
1,5-Naphthyridine (**4**)	2, 6	**0.915**	1.178	0.203		10	1.001	0.943	0.068
	3, 7	0.985	0.953	0.116	1,10-Diazaphenanthrene (**11**)	2, 9	**0.927**	**1.115**	0.249
	4, 8	0.939	**1.293**	**0.360**		3, 8	0.993	0.900	0.001
1,6-Naphthyridine (**5**)	2	**0.901**	1.228	0.285		4, 7	0.940	1.194	0.262
	3	1.000	0.887	0.079		5, 6	0.994	1.035	**0.296**
	4	0.919	1.338	**0.446**	4,6-Diazaphenanthrene (**12**)	1	0.942	1.178	0.176
	5	0.907	**1.339**	0.398		2	0.979	1.014	0.181
	7	0.951	1.003	0.070		3	0.923	1.099	0.054
	8	1.002	1.045	0.264		5	**0.898**	**1.434**	**0.419**
1,7-Naphthyridine (**6**)	2	**0.912**	1.173	0.208		7	1.000	1.022	0.147
	3	0.985	0.953	0.133		8	0.992	0.888	0.005
	4	0.933	1.291	**0.394**		9	0.995	0.938	0.124
	5	0.980	1.115	0.286		10	0.995	0.968	0.051
	6	0.966	0.950	0.323	Acridine (**13**)	1, 9	1.015	1.068	0.137
	8	0.925	**1.296**	0.369		2, 8	0.974	1.075	0.126
1,8-Naphthyridine (**7**)	2, 7	**0.903**	1.235	0.251		3, 7	1.004	0.924	0.065
	3, 6	1.002	0.884	0.078		4, 6	0.981	1.222	0.191
	4, 5	0.992	**1.342**	**0.392**		5	**0.896**	**1.926**	**0.502**
1-Azaphenanthrene (**8**)	2	**0.928**	1.112	0.293	1,10-Diazaanthracene (**14**)	2	0.887	1.477	0.207
	3	0.998	0.874	0.026		3	1.007	0.920	0.053
	4	0.941	**1.188**	**0.396**		4	0.910	1.606	0.270
	5	0.997	1.020	0.303		5	**0.880**	**2.138**	**0.489**
	6	0.997	1.013	0.246		6	0.977	1.273	0.170
	7	0.999	0.981	0.112		7	1.004	0.929	0.053
	8	0.994	0.883	0.008		8	0.970	1.128	0.121
	9	1.000	0.897	0.147		9	1.017	1.070	0.107
	10	0.992	0.963	0.016					

indifferent with varying h_x values (**3**, **10**, **12**, **13**, and **14**), their reactivity indices also foresee the same site for nucleophilic reactions. The predicted sites (indicated by bold letters in Table 3) are always consistent with those from the transition state π-energy curves in Fig. 1.

The reactivity indices for other compounds investigated are apparently inconsistent among them, predicting different sites of nucleophilic reaction for a compound. All of these compounds have crossings with abscissa in the transition state π-energy curves in Fig. 1, and the reagent dependent orientation has been rationalized. As expected by the frontier electron theory, frontier electron density is the most suitable index to predict the site of the attack by dimsyl anion of which HOMO energy is high ($h_x=-0.5$) and close to that of the LUMO of the heteroaromatic compounds reacting as substrates (Fig. 2). The orientations of the methylation agrees with those predicted from $f_r^{(-)}$'s in most instances. Hence, the methylation is frontier-controlled. Only one exception is the case of 1,10-diazaphenanthrene. The 5,6-bonds of azaphenanthrenes usually have higher double bond character than the other bonds in the same molecule, and the bond alter-

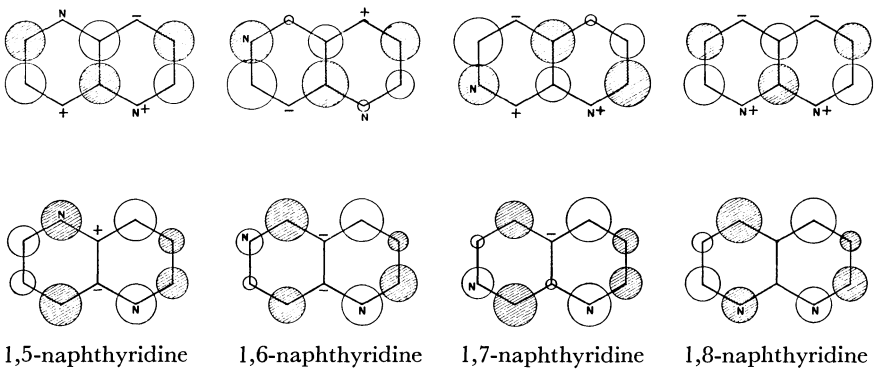

1,5-naphthyridine 1,6-naphthyridine 1,7-naphthyridine 1,8-naphthyridine

Fig. 2. The LUMO's and the next LUMO's of naphthyridines. In this figure, magnitudes of the AO coefficients (c_{ir}'s) are proportional to the radii of circles, and the hatched circles correspond to the coefficients with negative signs. Only the signs of c_{ir}'s are given when they are too small to be illustrated by circles.

nation is significant in the ring annelated by two benzene nuclei. Since both the reactivity indices (Table 3) and the transition state π-energy curves (Fig. 1) are calculated by assuming identical β-values to all C–C and C–N bonds in the rings, the results become less trustworthy by the increase in bond alternation. A variable β-calculation will improve them considerably.

On the other hand, the orientations of the amination and the phenylation are predicted by the electron densities. In these reactions, the HOMO's of the nucleophiles are estimated to be considerably lower than the LUMO's of substrates, being charge-controlled.[34]

Similar quantities for the delocalized π-model of the transition states were also obtained by the perturbational calculations on the PPP-SCF wave functions of these heterocycles.[35] However, the results agree with the experiments only fairly, and no further improvement is expected by the calculations on the basis of more sophisticated MO.

These calculations were carried out using the HITAC 8250 computer of Yokohama National University and the HITAC 8700 computer of the University of Tokyo Computer Center.

The authors thank to Mr. K. Hisada and Mr. N. Hyodo for their assistance in calculations. This research was supported in part by grants from the Asahi Glass Foundation for the Contribution to Industrial Technology to which the authors are grateful. It was also supported in part by the Grant-in-Aid for Special Project Research from the Ministry of Education, Science and Culture.

References

1) J. Ridd, "Physical Methods in Heterocyclic Chemistry," ed by A. R. Katritzky, Academic Press, New York (1963), Vol. 1, p. 109. See also M. Hida, "Kagaku Sosetsu, No. 1," (1973), pp. 120—150.
2) H. C. Longuet-Higgins and C. A. Coulson, *Trans. Faraday Soc.*, **43**, 87 (1947).
3) H. C. Longuet-Higgins and C. A. Coulson, *J. Chem. Soc.*, **1949**, 971.
4) R. D. Brown and R. D. Harcourt, *J. Chem. Soc.*, **1959**, 3451.
5) M. J. S. Dewar and P. M. Maitlis, *J. Chem. Soc.*, **1957**, 944, 2521.
6) A. E. Chichibabin, *Bull. Soc. Chim. Fr.*, [5], **3**, 762 (1936) and reports of the same author cited therein.
7) G. A. Russel and S. A. Weiner, *J. Org. Chem.*, **31**, 248 (1966).
8) R. D. Brown, "Molecular Orbitals in Chemistry, Physics and Biology," ed by Pre-Olov Löwdin and B. Pullman, Academic Press, New York (1964), p. 485.
9) G. Klopman, *J. Am. Chem. Soc.*, **90**, 223 (1968).
10) S. Carra, M. Raimondi, and M. Simonetta, *Tetrahedron*, **22**, 2673 (1966); *ibid.*, **24**, 3402 (1968).
11) O. Chalvet, R. Daudel, T. F. W. McKillop, and G. H. Schmid, *Tetrahedron*, **26**, 339 (1970).
12) O. Chalvet, R. Daudel, and T. F. W. McKillop, *Tetrahedron*, **26**, 349 (1970).
13) O. Chalvet, R. Daudel, G. H. Scmid, and J. Rigaudy, *Tetrahedron*, **26**, 365 (1970).
14) J. C. W. Evans and C. F. H. Allen, *Org. Synth.*, **2**, 517 (1938).
15) K. Ziegler and K. Zeiser, *Chem. Ber.*, **63**, 1849 (1930).
16) K. Ziegler and K. Zeiser, *Ann.*, **485**, 174, 185 (1931).
17) W. W. Paudler and T. J. Kress, *J. Org. Chem.*, **33**, 1384 (1968).
18) E. V. Brown and A. C. Plasz, *J. Heterocycl. Chem.*, **7**, 593 (1970).
19) F. W. Bergstrom, *J. Org. Chem.*, **2**, 411 (1937); **3**, 424 (1938).
20) Y. Kobayashi and I. Kumadaki, *Chem. Pharm. Bull.*, **21**, 2066 (1973).
21) E. P. Hart, *J. Chem. Soc.*, **1954**, 1879.
22) These reactions were reviewed recently by the present authors [Y. Hamada and I. Takeuchi, *Yukigosei Kagaku*, **32**, 602 (1974)].
23) Y. Hamada, I. Takeuchi, and M. Hirota, *Chem. Pharm. Bull.*, **19**, 1751 (1971).
24) Y. Hamada, T. Sato, and I. Takeuchi, *Yakugaku Zasshi*, **95**, 1492 (1975).
25) Y. Hamada, I. Takeuchi, and M. Hirota, *Chem. Pharm. Bull.*, **22**, 485 (1974).
26) R. S. Mulliken, *J. Chem. Phys.*, **2**, 782 (1934).
27) J. Hinze, M. A. Whitehead, and H. H. Jaffé, *J. Am. Chem. Soc.*, **85**, 148 (1963).
28) A. Streitwieser, Jr., "Molecul r Orbital Theory for Organic Chemists," John Wiley & Sons, Inc., New York (1961), pp. 117—135.
29) R. S. Mulliken, *J. Chem. Phys.*, **3**, 573 (1935).

30) G. W. Wheland and D. E. Mann, *J. Chem. Phys.*, **17**, 264 (1949).
31) A. Kuboyama, "Bunshi-Kidoron," ed by T. Nakajima, Kyoritsu Shuppan, Ltd., Tokyo (1966), pp. 207—222.
32) H. Gilman and R. D. Nelson, *J. Am. Chem. Soc.*, **70**, 3316 (1948).
33) Recently 4-methylpyridine was obtained in a poor yield by the methylation carried out under a very low temperature. Y. Hamada, unpublished data.
34) G. Klopman, "Chemical Reactivity and Reaction Paths," G. Klopman, John Wiley & Sons, Inc., New York (1974), pp. 55—82.
35) M. Hirota and H. Masuda, unpublished data.

Double Diels-Alder Reactions of Coumalic Acid with 1,3-Dienes

Takeshi IMAGAWA, Tsunefumi NAKAGAWA, Mituyosi KAWANISI, and Keiiti SISIDO

Department of Industrial Chemistry, Faculty of Engineering, Kyoto University, Sakyo-ku, Kyoto 606

(Received November 9, 1978)

Thermal reaction of coumalic acid with 1,3-butadienes gave after diazomethane treatment dimethyl tricyclo[3.2.1.$0^{2,7}$]oct-3-ene-2,4-dicarboxylate *via* double Diels-Alder reaction. This represents the simplest synthesis of such a tricyclic system. The reaction with cyclopentadiene was also studied.

Diels-Alder reaction of 2-pyrone and esters of some 2-pyronecarboxylic acids are well documented.[1] With acetylenes as dienophile the reaction provided the benzene derivatives by loss of carbon dioxide from the intermediary adduct. With olefinic dienophiles, a decarboxylative double diene synthesis occurred to afford a bicyclo[2.2.2]oct-2-ene system, and with electron-rich dienophiles the so-called Diels-Alder reaction with inverse electron-demand[2] was effected with high regiospecificity.

In view of these facts, the reaction in the combination of coumalic acid (**1**) and 1,3-butadienes (**2**) seems most probably to follow the path A (Scheme 1).

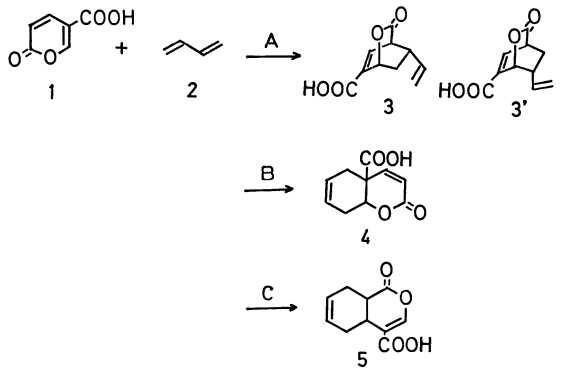

1 2 3 3' 4 5

Scheme 1.

Meanwhile, taking the properties of 1,3-butadienes as a good diene part in Diels-Alder reaction as well as the lesser electron-withdrawing nature of the carboxylic acid **1** than that of the ester in consideration, we are intrigued by the possibility of the reaction path B[3] or C, the product **5** in the latter reaction path being a potential intermediate for the synthesis of natural products.[4]

Evidences to be presented gave the precedence to the reaction path A and the structural investigation and the fate of the adduct **3** will be described in detail in this report.[5]

Results and Discussion

The reaction of **1** with excess of butadiene (**2a**) in anhydrous methanolic solution at 100 °C for 6 h in a pressure bottle gave after treatment with ethereal diazomethane colorless needles **6a**, mp 101—102 °C, in 70% yield. This product was analyzed for C_8H_8-$(COOMe)_2$ by elemental analysis and mass spectrometry. The presence of a saturated ester function and an α,β-unsaturated ester moiety was apparent from the intense IR absorptions at 1735, 1710, and 1620 cm^{-1}. In UV spectrum a maximum at 243 nm (log ε 4.08) was interpreted to show the presence of a

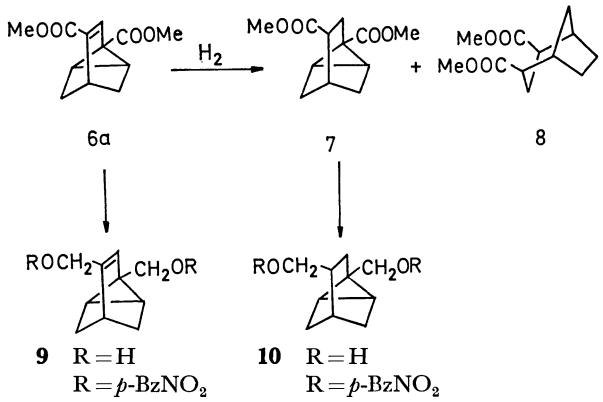

9 R=H, R=*p*-$BzNO_2$ **10** R=H, R=*p*-$BzNO_2$

Scheme 2.

β-cyclopropylacrylic ester chromophore[6] where the arrangement of the cyclopropane ring attains the maximum conjugation with the double bond, *i.e.*, the "bisected" conformation. Catalytic hydrogenation over Raney-Ni resulted in the uptake of one equivalent of hydrogen to yield the saturated ester **7**, but the hydrogenation over Pd–C gave a mixture of **7** and another product **8** resulting from the uptake of two equivalents; this fact clearly suggests the coexistence of a cyclopropane ring and a double bond. The structure of **8** was later deduced from the consideration of the reaction path and the symmetry confirmed by seven signals in its ^{13}C-NMR spectrum.

Lithium aluminum hydride reduction of **6a** and **7**, followed by treatment with *p*-nitrobenzoyl chloride gave the di-*p*-nitrobenzoates **9** and **10**, respectively. Although the NMR spectrum of **9** showed two singlets in the region of acyloxymethyl protons, **10** showed a singlet and a doublet of 6.6 Hz spacing. These facts indicate that **6a** has a carboxyl group on a tertiary carbon atom and an α,β-unsaturated ester group having no hydrogen at the α-position.

The fact that thermal treatment of **6a** over Pd–C at 300 °C gave an aromatic isomer, dimethyl 4-ethylisophthalate (**11**), especially combined with the fact that similar treatment of the 1,3-pentadiene adduct **6d** gave dimethyl 4-propylisophthalate (**12**), implicates the retention of a 1,3-dicarboxylate moiety and a butadiene moiety in **6a** without rearrangement or

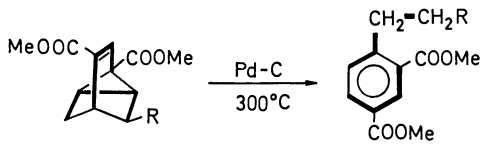

6a R=H **11** R=H
6d R=Me **12** R=Me

Scheme 3.

cleavage as shown by bold lines in Scheme 3. These results, taken together, require the partial structure i in **6a**.

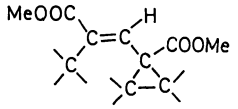

i

Formula 1.

Further structural evidences were obtained from its NMR spectrum which showed five well-separated multiplets for eight ring-protons as well as the two singlets due to the ester methyl protons, indicating the inherent symmetry of the molecule (Fig. 1); its ^{13}C-NMR spectrum confirmed this symmetry. The large coupling constant between H_a and H_b (12.3 Hz) may be ascribed to the geminal coupling of the methylene protons. In view of the observed spin-spin couplings between H_a (2H) and H_b (2H), and H_c (2H) and H_d (1H) (4.8 Hz), these five protons must constitute the partial structure ii, in which the coupling J_{ad} is nearly

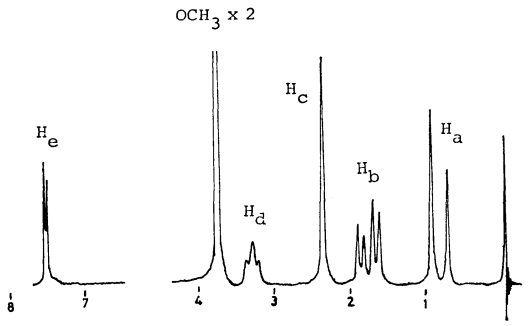

Fig. 1. ^{1}H-NMR spectrum of **6a** (60 MHz).

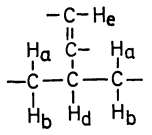

ii

Formula 2.

0 Hz. The triplet signals of H_d are further spin-splitted by the long-range coupling (1.7 Hz) with the olefinic proton H_e; this fact allows us to link the partial structures i and ii. Taking the total number of carbons and hydrogens into account, the other two protons (H_c) causing the 2H singlet may be divided into a cyclopropane ring as shown in the structure iii from consideration of the molecular symmetry. The bonding of C_α and C_β leads to a structure iii.

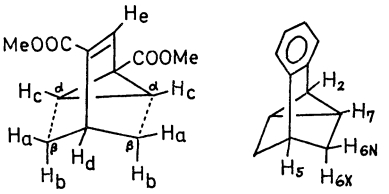

iii **13**

Formula 3.

At this stage, it was helpful to consider the NMR spectral features of the reported tricyclo[3.2.1.0^{2,7}]oct-3-ene system,[7] particularly of benzo[3,4]tricyclo[3.2.1.0^{2,7}]oct-3-ene (**13**).[7a] The cyclopropyl protons of **13** form a doublet due to the coupling with the other cyclopropyl proton H_2, but that of **6a** a singlet. The other coupling feature of the methylene protons is very similar in both compounds. It is well established[7] that, since the dihedral angles of *endo*-H_6–C_6–C_5–H_5 and *endo*-H_6–C_6–C_7–H_7 are close to 80°, little, if any, splitting is expected for these protons.

The reaction of **1** and butadiene **2a** under the same conditions described above gave, without diazomethane treatment, a half-ester **6b**. The structure of **6b** follows from the NMR spectrum which showed a similar pattern of the ring protons to that of **6a** except one ester methyl group. Its IR spectrum displayed strong carbonyl absorptions at 1740 and 1680 cm^{-1}: these bands are characteristic for a saturated ester and an α,β-unsaturated carboxylic acid. Therefore, to the half-ester **6b** is assigned the structure shown. Treatment of **6b** with diazomethane gave **6a** quantitatively.

These findings lead to the conclusion that **6b** is best explained as a result of two sequential Diels-Alder reactions. That is, the thermal [4+2]cycloaddition

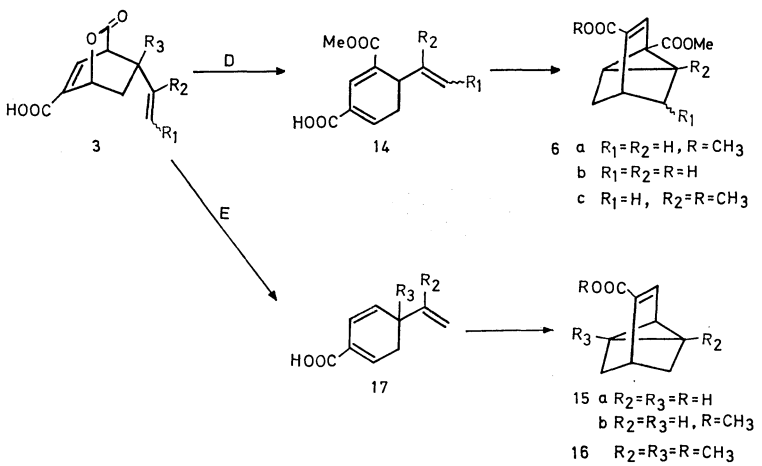

Scheme 4.

reaction between the diene moiety of **1** and the ene part of **2** as the dienophile with inverse electron-demand would generate the bicyclic lactone **3**, which could then undergo methanolysis-dehydration to produce the half-ester of vinylcyclohexadienedicarboxylic acid **14**. The succeeding intramolecular Diels-Alder reaction also takes place with inverse electron-demand, giving the product **6b**. This [4+2]cycloaddition step leading to the cyclopropane ring formation has rather ample analogy.[8] Since the reaction step D in Scheme 4 without added acid-catalyst is unprecedent, the intermediate **3** was trapped to disclose the reaction mechanism. The reaction at lower temperature (80 °C) and in aprotic solvent (benzene) gave the lactone **3**. Thus obtained **3** reacted in anhydrous methanol only very sluggishly at 100 °C and gave at 150 °C **6b** and **15a** in a ratio of 1 : 3. The reaction temperature and course are different from those of the reaction of **1** and **2a**. This difference may be ascribed to the absence or presence of acid catalysis of **1** itself.[9]

The reaction of **1** with isoprene at 100 °C for 20 h gave after diazomethane treatment **6c** in 23% yield. The location of the methyl substitution is clearly demonstrated by consideration of the coupling pattern in the NMR spectrum. In this case, the coupling constant between the cyclopropyl proton H_7 and *endo*-methylene proton H_{6N} was observed as 2.3 Hz.

The reaction of **1** with 1,3-pentadiene at 100 °C for 20 h gave **6d** in 20% yield after diazomethane treatment.

In sharp contrast to the aforementioned case, the reaction of **1** with 2,3-dimethylbutadiene at 100 °C for 30 h gave chiefly a crystalline decarboxylated adduct **15b**. The structure of **15b** follows from its spectral characteristics. Treatment with diazomethane gave an oily ester **16**, which was identical with the tricyclic adduct obtained by the reaction of methyl coumalate with 2,3-dimethylbutadiene.[3]

This fact implies that with the change of the substituent(s) on the butadiene component, the construction of the ene-diene moiety necessary for the posterior Diels-Alder reaction of the primary cycloadduct was achieved by an alternative route E, *i.e.*, a simple decarboxylative step into **17**. Although the concurrent route E is supposed to be the reason for the low yield of **6c** and **6d**, inspection of the fore-run of distillation was fruitless since so many components were included.

We believe that the reaction presented herewith represents the simplest synthesis of the tricyclo[3.2.1.$0^{2,7}$]oct-3-ene system yet reported.[10]

The reaction of **1** with cyclopentadiene in boiling methanol for 3 h gave **18** in 48% yield. Elemental analysis showed it to be an undecarboxylated 1 : 1 adduct and its NMR spectrum revealed a marked similarity to that of the product **19** obtained by the reaction of methyl coumalate with cyclopentadiene. The identity of the skeletal structures of **18** and **19** was established by the fact that both gave the same 1,3-dipolar cycloadduct of the methyl ester **20** by the treatment with excess of ethereal diazomethane. Half hydrogenated product **21** of the adduct **18** showed in its NMR spectrum three well separated, mutually coupled pairs of doublet of doublets in the lower field

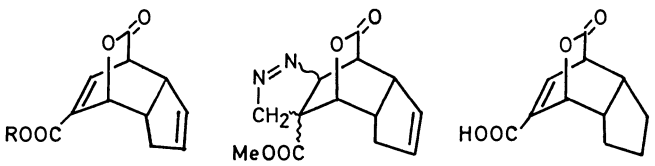

18 R=H
19 R=CH_3

20 **21**

Formula 4.

region (δ 3.97, 5.73, and 7.57): this reinforces the assignment of the signals in the spectrum of **18**.

It should be emphasized that even cyclopentadiene can behave mainly as a dienophile in this type of reaction.

Experimental

All the melting points were determined on a Yanagimoto hot-stage apparatus and are uncorrected. IR spectra were recorded on a Shimadzu IR 27-G spectrometer, and UV spectra on a Hitachi EPS-2 spectrophotometer. Mass spectra (MS) were obtained with a Hitachi RMS-4 spectrometer (70 eV). NMR spectra were measured on a JEOL C-60HL spectrometer using TMS as an internal standard. We are grateful to Dr. S. Kojima for the courtesy that made possible the use of this instrument. ^{13}C-NMR spectra were obtained with a Varian CFT-20 spectrometer at 20 MHz in $CDCl_3$ solution using TMS as an internal standard. Microanalyses were performed by Mrs. K. Fujimoto using a Yanagimoto C.H.N. Corder MT-1. GLC was performed with a Shimadzu GC-4AIT with a 3 mm×3 m column packed with 10% High Vacuum Silicone Grease on Chromosorb W (80—100 mesh).

*Reaction of **1** with Butadiene.* (a) A suspension of **1**[9] (7.0 g) and excess of butadiene (20 ml) in methanol (35 ml) was heated in a pressure bottle at 100—110 °C for 5 h. After removal of the solvent, treatment with ethereal diazomethane, concentration, and distillation gave with a small amount of fore-run, a fraction of bp 172 °C/15 Torr, which crystallized immediately (mp 97—98 °C). Recrystallization from diisopropyl ether or methanol gave **6a** (2.2 g; 70%) as colorless needles: mp 101—102 °C; IR and UV (EtOH): see text; MS, *m/e*(rel intensity) 222(M^+, 44), 207 (16), 191(25), 190(20), 163(100), 131(44), 119(20), 103 (37), 91(26), 77(22), 59(45); NMR (CCl_4): δ 0.84 (2H, d, 12.3 Hz, H_{6N} and H_{8N}), 1.74(2H, dd, 4.9 and 12.3 Hz, H_{6X} and H_{8X}), 2.28(2H, bs, H_1 and H_7), 3.27 (1H, bt, 4.9 and 1.8 Hz, H_5), 7.36(1H, d, 1.8 Hz, H_3), and 3.70 and 3.73(3H each, s, COOMe); ^{13}C-NMR: δ 28.3(t, C_6 and C_8), 29.4(d, C_1 and C_7), 29.7(s, C_2), 31.1(d, C_5), 51.4 and 52.0 (q, OMe), 131.1(s, C_4), 132.4(d, C_3), 164.9 (C=C-C=O), 171.5(s, C=O). Found: C, 65.05; H, 6.38%. Calcd for $C_{12}H_{14}O_4$: C, 64.85; H, 6.35%.

(b) A similar reaction using 2.00 g of **1** afforded without diazomethane treatment 0.89 g (30%) of **6b**, on standing for many days after removal of the solvent: mp 178—178.5 °C (MeOH); IR(Nujol): see text; NMR ($CDCl_3$): δ 0.88 (2H, d, 12.3 Hz, H_{6N} and H_{8N}), 1.82(2H, dd, 12.3 and 4.8 Hz, H_{6X} and H_{8X}), 2.43(2H, bs, H_1 and H_7), 3.32(1H, bt, 4.8 Hz, H_5), 7.70(1H, d, 1.8 Hz, H_3), 3.76 (3H, s, COOMe). Found: C, 63.18; H, 5.65%. Calcd for $C_{11}H_{12}O_4$: C, 63.45; H, 5.81%.

(c) A suspension of **1** (500 mg) and excess of butadiene (1 ml) in benzene (20 ml) with a trace amount of hydroquinone was heated in a pressure bottle at 150 °C for 20 h.

After removal of the solvent, distillation gave a fraction of bp 160—180 °C/25 Torr (381 mg; 71%), which crystallized soon (mp 107—110 °C). Recrystallization from ether gave an analytically pure **15a**: mp 117—118 °C; IR(Nujol): 1660, 1600 cm^{-1}; NMR ($CDCl_3$), δ 0.75(2H, d, 12.0 Hz, H_{6N} and H_{8N}), 1.5—2.0(3H, cm, H_1, H_2, and H_7), 3.23(1H, bt, H_5), 7.24(1H, dd, 5.4 and 2.0 Hz, H_3). Found: C, 71.97; H, 6.65%. Calcd for $C_9H_{10}O_2$: C, 71.98; H, 6.71%.

(d) A similar mixture from 310 mg of **1** was heated at 80 °C for 6 days. After removal of the solvent, preparative TLC separation gave 109 mg of **3a** as thermally very labile oil; NMR($CDCl_3$): δ 1.53 (1H, ddd, 14, 4, and 2 Hz, H_{5N}), 2.52(1H, ddd, 14, 10, and 4 Hz, H_{5X}), 2.90(1H, m, H_4), 3.80(1H, dd, 6.4 and 2.8 Hz, H_3), 5.0—6.0(4H, complex m, H_6 and vinyl H), 7.48(1H, dd, 6.4 and 2.4 Hz, H_2).

The adduct **3a** (72 mg) in anhydrous methanol was heated at 100 °C for 6 h to result in only small conversion. Heating further at 150 °C for 4 h gave a mixture of **6b** and **15a** in a ratio of 1 : 3 (by NMR analysis).

*Catalytic Hydrogenation of **6a**.* A solution of **6a** (111 mg) in methanol (30 ml) was hydrogenated over Raney-Ni, resulting in one equivalent H_2 uptake. Filtration and solvent removal gave oily **7** (110 mg) which showed only one peak on GLC analysis. Analytical sample of **7** had bp 142—143.5 °C/5 Torr: $n_D^{24.8}$ 1.4924; IR(neat): 1750, 1720, 1625 cm^{-1}; MS: *m/e* 224(M^+, 20), 193(35), 192(100), 164 (76), 137(28), 132(49), 105(77), 79(23), 77(22), 59(26): NMR($CDCl_3$): δ 1.4—2.7(10H, m), 3.67 and 3.72(3H each, s, $COOCH_3$); ^{13}C-NMR: δ 19.3(t), 23.1(s), 27.0(t), 27.7(d), 27.6(d), 32.4(t), 32.7(d), 41.8(d), 51.6(q), 51.7(q), 174.7(s), 175.1(s). Found: C, 64.39; H, 7.17%. Calcd for $C_{12}H_{16}O_4$: C, 64.27; H, 7.19%.

A solution of **6a** (444 mg) in ethanol (30 ml) was hydrogenated over 5% Pd–C (400 mg), resulting in 74 ml (1.65 eq) of H_2 uptake. Removal of the catalyst and the solvent gave an oily mixture, which was shown by GLC analysis to consist of two components **7** and **8** in the ratio of 5.9 : 1. After preparative GLC separation, the major component was identified to be **7** by spectral comparison. The minor component **8** had bp 140—145 °C(bath)/5 Torr; NMR ($CDCl_3$): δ 1.4—2.7 (12H, m), 3.78(6H, s, $COOCH_3$); ^{13}C-NMR: δ 21.9(t), 28.8(t×2), 32.5(t), 36.4(d×2), 44.8 (d×2), 51.6(q×2), 175.3(s×2); MS: *m/e* 226 (M^+, 5), 195(23), 194(59), 167(30), 166(100), 162(20), 160(20), 135(31), 134(31), 107(61), 80(31), 79(55), 67(23). Found: C, 63.98; H, 8.06%. Calcd for $C_{12}H_{18}O_4$: C, 63.70; H, 8.02%.

*Di-p-nitrobenzoate **9**.* A solution of **6a** (222 mg) in ether (30 ml) was added dropwise to $LiAlH_4$ (100 mg) suspended in dry ether (30 ml). The mixture was stirred for 2 h and excess of hydride was decomposed by addition of ethyl acetate and then satd. Rochelle salt solution (50 ml). The ethereal solution was dried (Na_2SO_4) and evaporated to give diol (227 mg). The diol without purification was dissolved in pyridine–CH_2Cl_2, and *p*-nitrobenzoyl chloride (371 mg) was added. After standing overnight at room temperature the mixture was poured onto ice water, and extracted with CH_2Cl_2. The organic solution was washed successively with dil HCl, satd. $NaHCO_3$, and water. The solution was dried and evaporated, and digestion of the residue with ethanol and several recrystallizations gave **9**: mp 91—92 °C; IR(Nujol): 1720, 1528, and 1350 cm^{-1}; NMR ($CDCl_3$): δ 0.95 (2H, d, 14 Hz, H_{6N} and H_{8N}), 1.66(2H, bs, H_1 and H_7), 1.7(2H, m, H_{6X} and H_{8X}), 2.76(1H, bt, H_5), 6.17(1H, bs, H_3), 4.47(2H, s, $-OCH_2$), 4.88(2H, s, $-OCH_2$), 8.28(8H, s, Ar-H). Found: C, 61.88; H, 4.23; N, 5.75%. Calcd for $C_{24}H_{20}N_2O_8$: C, 62.06; H, 4.34; N, 6.03%.

*Di-p-nitrobenzoate **10**.* Similarly to the above, the dihydro ester **7** (254 mg) was reduced by $LiAlH_4$ (110 mg). After usual work-up, the resulting diol without purification was treated with 400 mg of *p*-nitrobenzoyl chloride, giving **10**, mp 143—144 °C (EtOH); IR(Nujol): 1722(with shoulder), 1528, 1355 cm^{-1}; NMR($CDCl_3$): δ 1.4—2.3(10H, m), 5.88 (2H, s, $-O-CH_2$), 5.76(2H, d, 6.6 Hz, $-OCH_2$), 8.25(8H, s, Ar-H). Found: C, 61.56; H, 4.78; N, 5.75%. Calcd for $C_{24}H_{22}N_2O_8$: C, 61.80; H, 4.75; N, 6.01%.

*Isomerization of **6a** with Pd–C.* A suspension of 10% Pd–C (500 mg) in **6a** (1.0 g) was heated in a test tube at 300—310 °C for 2 h. Ethereal extract of the reaction mixture was evaporated to give crude oil (802 mg), which showed a single peak on GLC analysis. Distillation gave diemthyl 4-ethylisophthalate[12] (**11**) (591 mg): bp 142—146 °C/5 Torr; $n_D^{26.0}$ 1.5202; IR(neat): 1738(with shoulder), 1614 cm^{-1}; NMR(CCl_4): δ 1.24(3H, t, 7.5 Hz, $CH_2\underline{CH}_3$), 3.04 (2H, q, 7.5 Hz, $\underline{CH}_2CH_3$), 7.27(1H, d, 8.6 Hz, H_5), 8.01 (1H, dd, 8.6 and 2.0 Hz, H_6), 8.44(1H, d, 2.0 Hz, H_2), 3.93(6H, s, $COOCH_3$). (Found: C, 64.94; H, 6.38%).

For comparison, when **6a** (500 mg) was heated without addition of Pd-C at 300—310 °C for 3 h, **6a** (200 mg) was recovered after distillation: mp 98—110 °C.

*Reaction of **1** with Isoprene.* A suspension of **1** (2.0 g) and isoprene (6 ml) in methanol (50 ml) was heated at 100—110 °C for 24 h in a pressure bottle. Removal of the solvent, treatment with ethereal diazomethane and subsequent evaporation gave an oily mixture. Fractional distillation with a Vigreux column gave a fore-run (bp 120—160 °C/15 Torr: 1.01 g) and **6c** (761 mg: 23%); bp 160—165 °C/15 Torr. The fore-run showed on GLC analysis at least six peaks and the structures were not further investigated. Analytically pure **6c** had bp 132—136 °C/5 Torr; IR(neat): 1740 (with shoulder), 1620 cm^{-1}; NMR(CCl_4): δ 0.85(2H, d, 12.3 Hz, H_{6N} and H_{8N}), 1.43 (3H, s, C_1-CH_3), 1.65 (1H, dd, 12.3 and 5.0 Hz, H_{8X}), 1.82(1H, ddd, 12.3, 5.0, and 2.3 Hz, H_{6X}), 2.26(1H, bd, 2 Hz, H_7), 3.22(1H, bt, H_5), 7.32(1H, d, 1.7 Hz, H_3), 3.67 and 3.73(3H each, s, $COOCH_3$). Found: C, 65.91; H, 7.06%. Calcd for $C_{13}H_{16}O_4$: C, 66.08; H, 6.83%.

*Reaction of **1** with 1,3-Pentadiene.* A suspension of **1** (2.0 g) and 1,3-pentadiene (*cis/trans* mixture: 4 ml) in methanol (50 ml) was heated at 110 °C for 9 h. After diazomethane treatment and solvent removal, the residue was fractionally distilled at 4 Torr with a 10 cm Vigreux column, giving four fractions; A: 85—95 °C (470 mg); B: 95—118 °C (837 mg); C: 128—140 °C (725 mg); D: 140—155 °C (249 mg). From the fractions B, C, and D, crystalline **6d** (286 mg) was obtained: mp 98.5—99.5 °C. Column chromatography (Al_2O_3: PhH) of the mother liquid (B,C,D) gave further crop of crystals (415 mg: total 21%); IR(Nujol): 1740 (with shoulder), 1620 cm^{-1}; MS: *m/e* 326(M^+, 77), 221(29), 205(44), 204(60), 177(100), 163(33), 145(61), 117(40), 105(36), 91(31), 59(37); NMR(CCl_4): δ 0.61(3H, d, 7.2 Hz, *endo*-CH_3-C_6), 0.90(1H, d, 12.2 Hz, H_{8N}), 1.87 (1H, ddd, 12.2, 2.0, and 4.8 Hz, H_{8X}), 2.1(1H, ddd lower half was obscured by overlapping, 7.3, 3.7, and 2 Hz, H_{6X}), 2.18 and 2.28 (1H each, AB q with further splitting, 5.4 and 2 Hz, H_1 and H_7), 3.16(1H, bt, H_5), 7.67(1H, d, 2.0 Hz, H_3), 3.76(6H, s, 2×$COOCH_3$). Found: C, 65.96; H, 6.75%. Calcd for $C_{13}H_{16}O_4$: C, 66.08; H, 6.83%.

*Pd–C Treatment of **6d**.* A sample of **6d** (200 mg) was heated with Pd–C at 300—310 °C as described before. Work-up and distillation gave a single substance **12**: bp 150 °C (bath)/5 Torr; IR(neat): 1735 (with shoulder), 1610 cm^{-1}; MS: *m/e* 236 (M^+, 37), 205(100), 189(57); NMR(CCl_4):

δ 1.02(3H, t, 7.0 Hz, CH_3), 1.57(2H, m, $CH_2\underline{CH_2}CH_3$), 2.99 (2H, t, 8.2 Hz, $\underline{CH_2}CH_2CH_3$), 7.31(1H, d, 8.2 Hz, H_6), 8.07 (1H, dd, 8.2 and 1.8 Hz, H_5), 8.53(1H, d, 1.8 Hz, H_2), 3.92(6H, s, $2\times COOCH_3$). Found: C, 66.12; H, 6.91%. Calcd for $C_{13}H_{16}O_4$: C, 66.08; H, 6.83%.

Reaction of ***1*** *with 2,3-Dimethylbutadiene.* A suspension of **1** (2.0 g) and 2,3-dimethylbutadiene (2 ml) in methanol (50 ml) was heated at 100—110 °C for 30 h. Removal of the solvent and distillation gave an oily mixture (2.156 g): bp 150—180 °C/20 Torr. Upon standing **15b** crystallized (378 mg): mp 191—192 °C(CH_2Cl_2); IR(Nujol): 3400—2400, 1670, 1608 cm^{-1}; MS: *m/e* 178(M^+, 82), 163(29), 133(100), 119(26), 117(27), 105(70), 93(33), 91(71), 79(34); NMR ($CDCl_3$): δ 0.82(2H, d, H_{6N} and H_{8N}), 1.63(2H, dd, 12.3 and 3.4 Hz, H_{6X} and H_{8X}), 3.11(1H, bt, H_5), 7.40(1H, dd, 7 and 2 Hz, H_3), 1.28(6H, s, CH_3-C_1 and CH_3-C_7), 1.3 (1H, d, H_2). Found: C, 74.30; H, 7.99%. Calcd for $C_{11}H_{14}O_2$: C, 74.13; H, 7.92%.

The acid **15b** was esterified with CH_2N_2 giving in a quantitative yield the ester **16** which was identical in all respects with an authentic sample.[3]

Reaction of ***1*** *with Cyclopentadiene.* A solution of **1** (2.0 g) and freshly prepared cyclopentadiene (2.5 g) in methanol (80 ml) was heated under reflux for 3 h. Removal of the solvent and dicyclopentadiene gave a crystalline residue. Recrystallization from ethanol gave **17** (1.397 g: 47.5%): mp 198—199 °C(dec); IR($CHCl_3$): 3400—2400, 1738, 1688, 1630 cm^{-1}; NMR($CDCl_3+CF_3COOH$): δ 1.90(1H, d with further splittings, 17.2 Hz, H_{1N}), 2.57(1H, dd, with further splittings, 17.2 and 9.2 Hz, H_{1X}), 3.2(1H, m, H_{7a}), 3.4(1H, m, H_{3a}), 3.93(1H, dd, 6.3 and 2.9 Hz, H_4), 5.38 and 5.58(1H each, AB q with further splittings, 6.8 Hz, H_3 and H_2), 5.67 (1H, dd, H_7), 7.32(1H, dd, 6.3 and 2.3 Hz, H_5). Found: C, 63.82; H, 4.87%. Calcd for $C_{11}H_{10}O_4$: C, 64.07; H, 4.89%.

Partial Hydrogenation of ***18****.* A solution of **18** (1.0 g) in ethanol (100 ml) was hydrogenated over 5% Pd–C (0.5 g) until about one equivalent (120 ml) of H_2-uptake resulted. Immediate removal of the catalyst and the solvent, followed by several recrystallizations from ethanol gave **21** (525 mg): mp 160—161 °C (dec with frothing); IR(Nujol): 1716, 1760(shoulder), 1628 cm^{-1}; NMR ($CDCl_3+CF_3COOH$): δ 0.8—2.2(6H, m, $3\times CH_2$), 2.4—3.2(2H, m, $2\times CH$), 3.97(1H, dd, 6.9 and 3.0 Hz, H_4), 5.73(1H, dd, 4.2 and 2.6 Hz, H_7), 7.57(1H, dd, 6.9 and 2.6 Hz, H_5). Found: C, 63.40; H, 5.69%. Calcd for $C_{11}H_{12}O_4$: C, 63.45; H, 5.81%.

1,3-Dipolar Cycloaddition of Diazomethane. A solution of **19** (650 mg) in CH_2Cl_2 was treated with excess of CH_2N_2. After standing for 4 h, AcOH was added until the faint yellow color of CH_2N_2 was disappeared. Solvent removal followed by recrystallization (MeOH) gave **20** (694 mg): mp[12] 146—147 °C(dec with frothing); IR ($CHCl_3$): 1765, 1746 cm^{-1}; MS: *m/e* 234(M^+, small), 190(20), 175(61), 169(50), 131(100), 129(27), 116(27), 115(30), 91(45), 66(41), 44(93); NMR($CDCl_3$): δ 2.3—2.8(2H, m, CH_2), 2.7—3.5 (4H, m, CH), 4.82 and 4.92(1H each, AB q, NCH_2), 5.6—5.8(2H, m, olefinic H), 3.85(3H, s, $COOCH_3$). Found: C, 59.29; H, 5.32; N, 10.77%. Calcd for $C_{13}H_{14}N_2O_4$: C, 59.53; H, 5.38; N, 10.68%.

A solution of **18** (500 mg) in methanol was treated with CH_2N_2 as described above. The obtained crystals had mp[12] 146—147 °C. The spectral characteristics were consistent with those of the product described above.

References

1) (a) H. Behringer and P. Heckmaier, *Chem. Ber.*, **102**, 2835 (1969); (b) J. A. Reed, C. L. Schilling, Jr., R. F. Tarvin, T. A. Rettig, and J. K. Stille, *J. Org. Chem.*, **34**, 2188 (1969); (c) A. K. Bahl and W. Kemp, *J. Chem. Soc., C*, **1971**, 2268; (d) H. E. Zimmerman, G. L. Grunewald, R. M. Paufler, and M. A. Sherwin, *J. Am. Chem. Soc.*, **91**, 2330 (1969) and the references cited therein.

2) R. Huisgen, R. Grashey, and J. Sauer, "The Chemistry of Alkene," ed by S. Patai, Interscience, New York (1961), p. 922: D. L. Fields, T. Regan, and J. C. Dignan, *J. Org. Chem.*, **33**, 390 (1968).

3) This reaction path has been found: T. Imagawa, N. Sueda, and M. Kawanisi, *J. Chem. Soc., Chem. Commun.*, **1972**, 388 and *Tetrahedron*, **30**, 2227 (1974).

4) G. Büchi, J. A. Carlson, J. E. Powell, Jr., and L-F. Tietze, *J. Am. Chem. Soc.*, **95**, 540 (1973); G. Büchi and J. A. Carlson, *ibid.*, **91**, 6470 (1969): C. R. Hutchinson, K. C. Mattes, M. Nakane, J. J. Partridge, and M. R. Uskovic, *Helv. Chim. Acta*, **61**, 1221 (1978).

5) Preliminary communication: T. Imagawa, M. Kawanisi, and K. Sisido, *Chem. Commun.*, **1971**, 1292.

6) M. J. Jorgenson and T. Leung, *J. Am. Chem. Soc.*, **90**, 3769 (1968).

7) (a) R. C. Hahn and L. J. Rothman, *J. Am. Chem. Soc.*, **91**, 2409 (1969); (b) H. Tanida, K. Tori, and K. Kitahonoki, *ibid.*, **89**, 3212 (1967); (c) N. A. LeBel and J. E. Huber, *ibid.*, **83**, 3193 (1963).

8) (a) C. F. Huebner, E. Donoghue, L. Dorfman, F. A. Stuber, N. Danieli, and E. Wenkert, *Tetrahedron Lett.*, **1966**, 1185; (b) W. v. E. Doering and W. R. Roth, *Tetrahedron*, **19**, 715 (1963); (c) E. N. Marvell and J. Seubert, *Tetrahedron Lett.*, **1969**, 1333; (d) P. Heimbach, K-J. Ploner, and F. Thömel, *Angew. Chem.*, **83**, 285 (1971); (e) R. M. Harrison, J. D. Hobson, and M. M. Al Holly, *J. Chem. Soc., C*, **1971**, 3084; (f) P. Gilgen, J. Zsindely, and H. Schmidt, *Helv. Chim. Acta*, **56**, 681 (1973).

9) Coumalic acid was washed several times with water and recrystallized twice from methanol: see R. H. Wiley and N. R. Smith, *Org. Synth.*, Coll. Vol. IV, 201 (1963) and Ref. 1(d).

10) R. C. Hahn and L. J. Rothman, *J. Am. Chem. Soc.*, **91**, 2409 (1966); C. A. Grob and J. H. Hostynek, *Helv. Chim. Acta*, **46**, 1176 (1963); W. v. E. Doering, E. T. Fossel, and R. L. Kaye, *Tetrahedron*, **21**, 25 (1965); R. R. Sauers, J. A. Beisler, and H. Feilich, *J. Org. Chem.*, **32**, 569 (1967); T. J. Katz and S. Cerefice, *J. Am. Chem. Soc.*, **91**, 2405 (1969); Ref. 8(a).

11) M. J. Strauss, L. J. Andrews, and R. M. Kiefer, *J. Am. Chem. Soc.*, **90**, 3473 (1968).

12) The sample was loaded at 120 °C onto the hot-stage, since the mp of the sample seemed to be variable to the heating speed.

Studies on Chrysanthemate Derivatives. VI.[1] A Stereoselective Synthesis of *trans*-3-(2,2-Dichlorovinyl)-2,2-dimethyl-1-cyclopropanecarboxylic Acid and Related Compounds

Yasuo NAKADA,* Rokuro ENDO, Shigeki MURAMATSU, Junya IDE, and Yasuo YURA[2]
Central Research Laboratories, Sankyo Co., Ltd. 1-2-58 Hiromachi, Shinagawa-ku, Tokyo 140

(Received October 7, 1978)

A new method is described for the stereoselective synthesis of *trans*-3-(2,2-dichlorovinyl)-2,2-dimethyl-1-cyclopropanecarboxylic acid (**2t**) *via* ethyl 3,3-dimethyl-4,6,6,6-tetrachlorohexanoate (**3a**) as a key intermediate. The key intermediate (**3a**) was obtained by addition of carbon tetrachloride to ethyl 3,3-dimethyl-4-pentenoate, prepared by condensation of 3-methyl-2-buten-1-ol and triethyl orthoacetate followed by Claisen rearrangement. Treatment of **3a** with sodium *t*-pentyloxide in benzene gave ethyl *trans*-2,2-dimethyl-3-(2,2,2-trichloroethyl)-1-cyclopropanecarboxylate (**6t**) in good yield. Dehydrochlorination and hydrolysis of **6t** using potassium hydroxide in ethanol afforded **2t** in high yield.

Natural pyrethrins and related synthetic pyrethroids, which consist mainly of furylmethyl and cyclopentenyl derivatives as alcohol moieties and chrysanthemic acid as acid moiety, are unstable in air and light.[3] This property restricts their use, particularly against agricultural pests, in spite of their outstanding potency against many insect species and low mammalian toxicity. 3-Phenoxybenzyl alcohol was discovered by the Sumitomo group to be useful as an alcohol moiety of pyrethroids and the benzyl chrysanthemate (phenothrin) had been known to be relatively resistant to photo-irradiation.[4] Its stability, however, has been assessed to be still insufficient for agricultural use. Recently, Elliott and his coworkers have found a new pyrethroid, 3-phenoxybenzyl 3-(2,2-dichlorovinyl)-2,2-dimethyl-1-cyclopropanecarboxylate (**1**; permethrin) which showed adequate stability in light and air, prominent insecticidal activity, and low mammalian toxicity.[5] This breakthrough focused attention on the potential of synthetic pyrethroids in agricultural pest control. Further detailed investigation on permethrin (**1**) has clarified that the *trans*-isomer of **1** was much less toxic to mammals than the *cis*-isomer.[6]

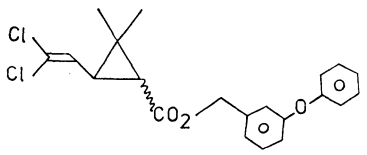

Permethrin (**1**)

The acid moiety of permethrin (**1**), 3-(2,2-dichlorovinyl)-2,2-dimethyl-1-cyclopropanecarboxylic acid (**2**; dichlorovinylchrysanthemic acid), was originally synthesized by Farkas *et al.*[7] by cyclopropanation of 1,1-dichloro-4-methyl-1,3-pentadiene with ethyl diazoacetate. Alternatively, the acid (**2**) was prepared by ozonolysis of the parent chrysanthemate followed by condensation of the resulting 2,2-dimethyl-3-formyl-1-cyclopropanecarboxylate with dichloromethylenetriphenylphosphorane.[8]

These methods, however, provide less satisfactory results from an industrial point of view concerning yield, stereoselectivity of the cyclopropanecarboxylate formation, and cost. Under these considerations, the stereoselective synthesis of **2** deserves high priority.[9] In this report, we describe a new stereoselective synthesis of the *trans*-isomer (**2t**)[10] *via* ethyl 3,3-dimethyl-4,6,6,6-tetrachlorohexanoate (**3a**) as a key intermediate.[11]

3-Methyl-2-buten-1-ol (**4**) was prepared by allylic rearrangement of 2-methyl-3-buten-2-ol in the presence of acetic acid and acetic anhydride followed by hydrolysis with aqueous sodium hydroxide in good yield. Condensation of **4** and triethyl orthoacetate followed by Claisen rearrangement under catalysis of propionic acid gave ethyl 3,3-dimethyl-4-pentenoate (**5**) in 54% yield according to the procedure of Johnson *et al.*[12]

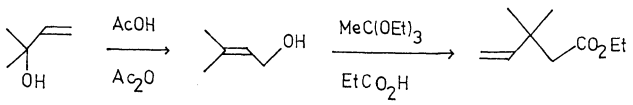

4 **5**

Addition reaction of haloalkanes such as carbon tetrahalides and haloforms to olefins using transition metal halides as catalysts was applied to elongation of the vinyl chain in **5** by trichloromethyl group.[13] In addition of carbon tetrachloride to **5**, the combination of iron(III) chloride and benzoin gave the ester **3a** in satisfactory yield. Addition of bromotrichloromethane to **5** occurred at lower temperature under the same catalyst to give ethyl 4-bromo-3,3-dimethyl-6,6,6-trichlorohexanoate (**3b**) in moderate yield.

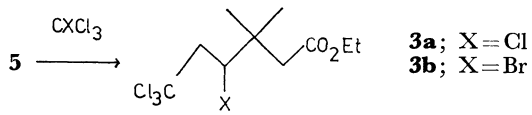

3a; X=Cl
3b; X=Br

The mass spectrum of the adduct (**3a**) showed molecular peaks at *m/e* (relative intensity): 314 (1), 312 (4), 310(9), and 308 (7) suggesting a 1 : 1 adduct between **5** and carbon tetrachloride. The NMR spectrum of **3a** showed two doublets at 2.28 (1H; J=15.1 Hz) and 2.53 ppm (1H; J=15.1 Hz) assignable to nonequivalent methylene protons adjacent to the carboxyl group, and three doubleting doublets at 3.08 (1H; J=6.3 and 16.2 Hz), 3.22 (1H; J=2.8 and 16.2 Hz), and 4.40 ppm (1H; J=2.8 and 6.3 Hz) assignable to nonequivalent two methylene protons and the chloromethine proton, respectively.

Cyclization of **3a** was conducted with the use of a variety of bases (Table 1). The distribution of reaction products substantially depends on the employed bases: sodium *t*-pentyloxide in *t*-pentyl alcohol

Table 1. Cyclization of ethyl 3,3-dimethyl-4,6,6,6-tetrachlorohexanoate (**3a**) with various bases

Run No	Base (2 mmol)	Solvent	Time (h)[a]	Yield (%) 6 *cis*	6 *trans*	7 *cis*	7 *trans*	8
1	EtONa[b]	EtOH	16	>1	1	>1	2	14
2	t-$C_5H_{11}ONa$	t-$C_5H_{11}OH$	2	24	41	2	5	—
3	NaH[c]	DMF	4	5	10	>1	>1	>1
4	$NaNH_2$[d]	DMF	4	1	8	>1	>1	48
5	DBU	THF	16	—	—	—	—	75

a) Reaction temperature: room temperature. b) The starting material (**3a**) was recovered in 67% yield. c) A complex mixture which was not separated was obtained in about 60% yield. d) An unidentified product was obtained in about 20% yield.

gave the cyclized products in good yield, *i.e.*, ethyl 2,2-dimethyl-3-(2,2,2-trichloroethyl)-1-cyclopropanecarboxylate (**6**) as a main product and ethyl dichlorovinylchrysanthemate (**7**), the product of further elimination, as a minor one, whereas the reaction with sodium ethoxide, sodium amide, and 1,8-diazabicyclo[5.4.0]-undec-7-ene (DBU) in the solvents listed in Table 1 only resulted in the formation of the dehydrochlorinated compound, ethyl 3,3-dimethyl-4,6,6-trichloro-5-hexenoate (**8**).

3a ⟶

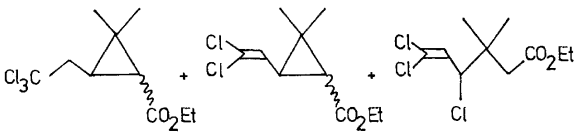

6 **7** **8**

Furthermore scrutiny of cyclization of **3a** and **3b** was made with various solvents using sodium t-pentyloxide as a base (Table 2). In cyclization of the chloride (**3a**), the use of benzene, a less polar aprotic solvent, furnished stereoselectively *trans*-cyclization products (**6t** and **7t**), whereas the use of polar solvents such as dioxane, ether, and tetrahydrofuran (THF) increased the amount of *cis*-cyclization products (**6c** and **7c**). In particular the use of THF as a solvent gave predominantly the products of further elimination (**7c** and **7t**) and the total ratio of *cis*/*trans* (**6c**+**7c**/**6t**+**7t**) was nearly 1 : 1. Eventually combination of inverse addition of the base and controlled reaction temperature provided the maximal ratio of *trans*- and *cis*-isomer (Run 2). However, the cyclization of the bromide (**3b**), even in a less polar aprotic solvent such as benzene, proved to be less stereoselective, resulting in a ratio of 3 : 5 (**6c** and **6t**). The results suggest that the *cis*/*trans* ratio of the product (**6**) depends to a great extent on both the polarity of the solvents and the leaving groups (Cl or Br). Presumably in a less polar aprotic solvent the cyclization of the chloride (**3a**) may proceed by bimolecular 1,3-elimination reaction (E2), prefering *anti*-parallel elimination to *syn*-elimination. On the other hand, in a polar solvent it may proceed by unimolecular 1,3-elimination reaction (E1), leading to a mixture of *cis*- and *trans*-isomers. There would be three conformers (**A**, **B**, and **C**) in the chloride **3a**, among which, however, the conformer **C** would be unfavorable because of nonbonded dipole-dipole interaction between the carbonyl

Table 2. Cyclization of ethyl 3,3-dimethyl-4-halo-6,6,6-trichlorohexanoate (**3a**) and (**3b**) with sodium t-pentyloxide in various solvents

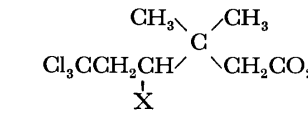

3a: X=Cl, **3b**: X=Br

Run No	X	Solvent[a]	t-$C_5H_{11}ONa$ (mmol)	Yield (%) 6 *cis*	6 *trans*	7 *cis*	7 *trans*
1	Cl	benzene	2	6	69	7	11
2	Cl	benzene[b]	1.5	3	67	5	13
3	Cl	dioxane	2	17	48	14	17
4	Cl	ether	2	24	49	11	12
5	Cl	THF	2	24	15	26	29
6	Cl	THF	5	1	1	47	44
7	Br	benzene	5	29	50	1	1

a) Reaction conditions: room temperature for 2 h. b) Inverse addition of the base and reaction at 15—20 °C for 5 h.

group and the chlorine atom. Of the conformers **A** and **B**, the conformer **A** undergoes cyclization smoothly by bimolecular *anti*-parallel 1,3-elimination of hydrogen chloride in a less polar aprotic solvent to lead to the *trans*-isomer, while the conformer **B** does not cyclize in a such manner because of its having no hydrogen *anti*-parallel to the chlorine atom. The *cis*-isomer would be formed by *syn*-1,3-elimination of the conformer **A** and/or unimolecular 1,3-elimination, which is likely in polar aprotic solvents. Under the same conditions as the case of the chloride (**3a**), the bromide (**3b**) tended to increase the *cis*-isomer. Since the reactivity of the bromine atom as a leaving group is much higher than that of the chlorine atom, the unimolecular reaction may significantly compete with the bimolecular *anti*-parallel 1,3-elimination even in a less polar aprotic solvent such as benzene.

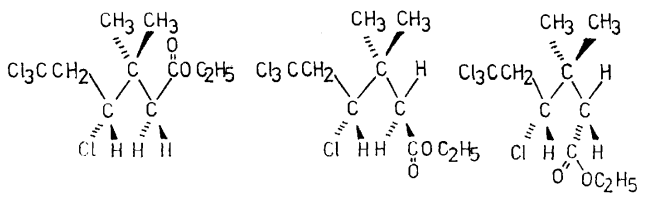

A **B** **C**

Table 3. Dehydrochlorination of ethyl *trans*-2,2-dimethyl-3-(2,2,2-trichloroethyl)-1-cyclopropanecarboxylate (**6t**)[a]

Run No	Reagent (mmol)	Solvent (ml)	Reaction conditions	Product	Yield (%)
1	KOH (25)	EtOH (30)	55 °C, 20 h	**2t**	92
2	DBU (10)	—	90 °C, 15 min	**7t**	96
3	$ZnCl_2$ (0.5)	—	120 °C, 2 h	**7t**	38

a) Compound **6t** (5 mmol) was used.

The *cis*- and *trans*-isomers of **6** were successfully separated by high pressure liquid chromatography (see Experimental part). In the NMR spectrum (100 MHz), the methine proton adjacent to the carboxyl group on the cyclopropane ring of the *cis*-isomer showed a doublet at 1.66 ppm with a coupling constant of J=8.4 Hz, and the corresponding proton of the *trans*-isomer was observed at 1.36 ppm with a coupling constant of J=5.4 Hz. The fact that the methine proton of the *trans*-isomer appeared at higher field than the *cis*-isomer may be due to the shielding effect of the trichloroethyl group in the same side. Furthermore these assignments are consistent with the values of the coupling constants in *cis*- and *trans*-protons on cyclopropane rings.[14]

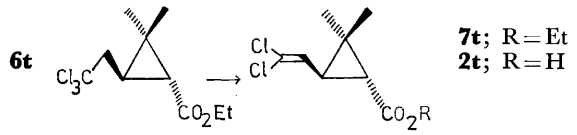

Dehydrochlorination of *trans*-isomer of the ester (**6t**) was examined with several dehydrohalogenation reagents (Table 3). Treatment of **6t** with potassium hydroxide in ethanol and DBU gave the *trans*-acid (**2t**) and the ester (**7t**) respectively in excellent yield. The elimination from **6t** was also effected by zinc chloride to afford **7t** in moderate yield. Under the reaction conditions employed above, no isomerization from *trans*-isomers to *cis*-isomers was observed.

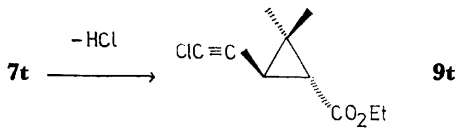

Treatment of **7t** with potassium *t*-butoxide in THF gave ethyl *trans*-3-(2-chloroethynyl)-2,2-dimethyl-1-cyclopropanecarboxylate (**9t**) in good yield.

Experimental

IR spectra were measured on a JASCO IR-A2 Spectrometer. NMR spectra were obtained in a Varian High Resolution NMR Spectrometer A-60 or HA-100 using tetramethylsilane as an internal standard. Chemical shifts are expressed in ppm. Mass spectra were recorded on a Japan Electron Optics Lab. Spectrometer JMS-01SG. All melting and boiling points are uncorrected.

*3-Methyl-2-buten-1-ol (**4**).* To a solution of acetic acid (500 ml), acetic anhydride (200 ml), and *p*-toluenesulfonic acid (20 g) was added dropwise a solution of 2-methyl-3-buten-2-ol (88 g) in acetic acid (100 ml) at 20 °C. After stirring for 15 min at room temperature, the mixture was poured into ice-water, neutralized with 10% aqueous potassium hydroxide, and extracted with ether. The extracts were washed successively with 5% aqueous potassium hydroxide and aqueous sodium chloride and dried over anhydrous sodium sulfate. Distillation gave 79 g of 3-methyl-2-butenyl acetate, bp 69—75 °C/53 mmHg (lit,[15] bp 40—44 °C/15 mmHg). The acetate was hydrolyzed by sodium hydroxide in aqueous methanol to give **4** in 70% yield, bp 65—68 °C/38 mmHg (lit,[15] bp 45—52 °C/15 mmHg).

*Ethyl 3,3-Dimethyl-4-pentenoate (**5**).* The pentenoate **5** was prepared according to the procedure of Johnson *et al.*[12] A solution of the alcohol **4** (8.6 g), triethyl orthoacetate (81 g), and propionic acid (0.45 g) was stirred at 130—140 °C for 4 h under removing of the resulting ethanol. After cooling, the reaction mixture was washed with saturated aqueous solution of sodium hydrogencarbonate and then with that of sodium chloride, and dried over anhydrous magnesium sulfate. The organic fraction was carefully distilled to give 5.3 g of **5**;[16] bp 81—83 °C/47 mmHg (lit,[16a] bp 35—45 °C/0.10 mmHg), IR, ν_{max}^{film} cm^{-1}: 1740, 1645, 1230, and 915, NMR ($CDCl_3$): 1.15 (s, 6H, $2CH_3$), 1.24 (t, 3H; J=7.1 Hz, $OCH_2\underline{CH_3}$), 2.31 (s, 2H, $\underline{CH_2}CO_2$), 4.16 (q, 2H; J=7.1 Hz, $O\underline{CH_2}CH_3$), 5.01 (dd, 1H; J=1.5 and 10.4 Hz, CH=C$\underline{H}$H), 5.03 (dd, 1H; J=1.5 and 18.3 Hz, CH=CH$\underline{H}$), and 6.02 (dd, 1H; J=10.4 and 18.3 Hz, $\underline{CH}$=CHH).

*Addition of Tetrahalomethane to **5**.* A mixture of **5** (0.1 mol), carbon tetrachloride (0.3 mol), isopropyl alcohol (0.2 mol), iron(III) chloride (0.01 mol), benzoin (0.01 mol), and diethylamine hydrochloride (0.015 mol) was heated under nitrogen at 70—80 °C for 8 h. After cooling, the mixture was diluted with 1% hydrochloric acid and extracted with chloroform. The extracts were dried over anhydrous magnesium sulfate and evaporated *in vacuo* to give a residue, which was distilled to afford the 1 : 1 adduct, ethyl 3,3-dimethyl-4,6,6,6-tetrachlorohexanoate (**3a**) in 82% yield, bp 112—117 °C/0.6 mmHg, IR, ν_{max}^{film} cm^{-1}: 1730 and 1200, NMR (CCl_4): 1.10 (s, 3H, CH_3), 1.18 (s, 3H, CH_3), 1.23 (t, 3H; J=7.0 Hz, $OCH_2\underline{CH_3}$), 2.28 (d, 1H; J=15.1 Hz, C$\underline{H}$HHCO$_2$), 2.53 (d, 1H; J=15.1 Hz, CH$\underline{H}$HCO$_2$), 3.08 (dd, 1H; J=6.3 and 16.2 Hz, ClCHC$\underline{H}$H), 3.22 (dd, 1H; J=2.8 and 16.2 Hz, ClCHC$\underline{H}$H), 4.11 (q, 2H; J=7.0 Hz, $O\underline{CH_2}CH_3$), 4.40 (dd, 1H; J=2.8 and 6.3 Hz, ClC$\underline{H}$CHH), MS, *m/e* (relative intensity) for $C_{10}H_{16}O_2{}^{35}Cl_4$: 314 (1), 312 (4), 310 (9), and 308 (M^+, 7). With the same catalyst as the case of the addition of carbon tetrachloride, bromotrichloromethane and **5** were heated at 35—45 °C for 5 h to give ethyl 4-bromo-6,6,6-trichlorohexanoate (**3b**) in 33% yield, IR, ν_{max}^{film} cm^{-1}: 1730, 1150, and 650, NMR ($CDCl_3$): 1.17 (s, 3H, CH_3), 1.26 (s, 3H, CH_3), 1.27 (t, 3H; J=7.2 Hz, $OCH_2\underline{CH_3}$), 2.37 (d, 1H; J=15.1 Hz, C$\underline{H}$HCO$_2$), 2.65 (d, 1H; J=15.1 Hz, CH$\underline{H}$CO$_2$), 3.31 (d, 1H; J=5.0 Hz, BrCHC$\underline{H}$H), 3.32 (d, 1H; J=3.5 Hz, BrCHCH$\underline{H}$), 4.15 (q, 2H; J=7.2 Hz, $O\underline{CH_2}CH_3$), and 4.55 (dd, 1H; J=3.5 and 5.0 Hz, BrC$\underline{H}$CHH). Found: C, 33.90; H, 4.52; Br, 22.60; Cl, 30.11. Calcd for $C_{10}H_{16}O_2BrCl_3$: C, 33.88; H, 4.54; Br, 22.54; Cl, 30.00%.

*Cyclization of **3a** and **3b**.* A solution of **3a** or **3b** (1 mmol) in any one of solvents (1 ml) as listed in Tables 1 and 2 was added dropwise to a solution or suspension of various bases (2—5 mmol) in the same solvent (2—5 ml) at room temperature, with the exception of run 2 in Table 2. In run 2 a solution of sodium *t*-pentyloxide (1.5 mmol) in benzene was added to a solution of **3a** at 10—15 °C. After stirring under the reaction conditions as shown in Tables 1 and 2, the mixture was diluted with ice-water and extracted

with ethyl acetate. The extracts were washed with saturated water solution of sodium chloride and dried over anhydrous magnesium sulfate. Evaporation of the solvent *in vacuo* gave a residue, from which yields were determined by analytical GLC (PEG 20 M, 125 °C). *Cis*- and *trans*-isomers of ethyl 2,2-dimethyl-3-(2,2,2-trichloroethyl)-1-cyclopropanecarboxylate (**6**) were separated by high pressure liquid chromatography on a μ-porasil column (Waters Associates Inc.,) using hexane as the eluent; **6t**, IR, ν_{max}^{film} cm^{-1}: 1729 and 1179, NMR ($CDCl_3$) at 100 MHz: 1.21 (s, 3H, CH_3), 1.25 (s, 3H, CH_3), 1.26 (t, 3H; J=7.2 Hz, OCH_2CH_3), 1.36 (d, 1H; J=5.4 Hz, $CHCHCO_2$), 1.73 (broad q, 1H; J=5.8 Hz, $CHHCHCH$), 2.72 (dd, 1H; J=6.0 and 15.0 Hz, $CHHCH$), 2.77 (dd, 1H, J=6.3 and 15.0 Hz, $CHHCH$), 4.08 (q, 2H; J=7.2 Hz, OCH_2CH_3), MS, *m/e* (relative intensity) for $C_{10}H_{15}O_2{}^{35}Cl_3$: 278 (1), 276 (5.3), 274 (17.1), and 272 (M^+, 12.8) and **6c**, IR, ν_{max}^{film} cm^{-1}: 1725 and 1180, NMR ($CDCl_3$) at 100 MHz: 1.22 (s, 6H, $2CH_3$), 1.23 (t, 3H; J=7.0 Hz, OCH_2CH_3), 1.48 (dt, 1H; J=5.5 and 8.4 Hz, $CHHCHCH$), 1.66 (d, 1H; J=8.4 Hz, $CHCHCO_2$), 3.01 (dd, 1H; J=5.5 and 15.2 Hz, $CHHCH$), 3.13 (dd, 1H; J=5.5 and 15.2 Hz, $CHHCH$), and 4.11 (q, 2H; J=7.0 Hz, OCH_2CH_3), MS, *m/e* (relative intensity): 278 (1), 276 (3.5), 274 (11.0), and 272 (M^+, 9.7). The mixture of *cis*- and *trans*-ethyl dichlorovinylchrysanthemate (**7**) was separated by column chromatography (silica gel-silver nitrate, hexane/ethyl acetate=100/3); **7t**[7], IR, ν_{max}^{film} cm^{-1}: 1730, 1620, and 1180, NMR (CCl_4): 1.20 (s, 3H, CH_3), 1.27 (t, 3H; J=7.2 Hz, OCH_2CH_3), 1.29 (s, 3H, CH_3), 1.53 (d, 1H; J=5.2 Hz, $CHCHCO_2$), 2.19 (dd, 1H; J=5.2 and 8.3 Hz, $=CHCHCH$), 4.12 (q, 2H; J=7.2 Hz, OCH_2CH_3), and 5.63 (d, 1H; J=8.3 Hz, $=CHCH$) and **7c**[7], IR, ν_{max}^{film} cm^{-1}: 1725, 1620, and 1190, NMR ($CDCl_3$): 1.26 (s, 6H, $2CH_3$), 1.27 (t, 3H; J=7.1 Hz, OCH_2CH_3), 1.83 (dd, 1H; J=1.0 and 8.0 Hz, $=CHCHCHCO_2$), 2.02 (t, 1H; J=8.0 Hz, $=CHCHCH$), 4.11 (q, 2H; J=7.1 Hz, OCH_2CH_3), and 6.28 (dd, 1H; J=1.0 and 8.0 Hz, $=CHCHCH$). Ethyl 3,3-dimethyl-4,6,6-trichloro-5-hexenoate (**8**) was purified by column chromatography on silica gel (hexane/benzene=1/1), IR, ν_{max}^{film} cm^{-1}: 1730, 1612, and 1150, NMR ($CDCl_3$): 1.15 (s, 6H, $2CH_3$), 1.28 (t, 3H; J=7.1 Hz, OCH_2CH_3), 2.35 (d, 1H; J=14.5 Hz, $CHHCO_2$), 2.51 (d, 1H; J=14.5 Hz, $CHHCO_2$), 4.21 (q, 2H; J=7.1 Hz, OCH_2CH_3), 4.98 (d, 1H; J=10.5 Hz, $=CHCHCl$), and 6.13 (d, 1H; J=10.5 Hz, $=CHCHCl$), MS, *m/e* (relative intensity) for $C_{10}H_{15}O_2{}^{35}Cl_3$: 278 (1), 276 (7.0), 274 (20.3), and 272 (M^+, 20.4).

Dehydrochlorination of ***6t***. Compound **6t** (5 mmol) was heated with a variety of reagents such as zinc chloride (0.5 mmol), DBU (10 mmol), and potassium hydroxide (25 mmol) under reaction conditions described in Table 3. After the usual work-up, the crude products were chromatographed on silica gel, using benzene and benzene–ethyl acetate (3/1) as eluents for **7t** and **2t**, respectively. Following spectral data were obtained for **2t**, mp 96—97 °C (lit,[7] mp 95—96.5 °C), IR, ν_{max}^{Nujol} cm^{-1}: 2700, 1680, and 1620, NMR (CCl_4): 1.23 (s, 3H, CH_3), 1.35 (s, 3H, CH_3), 1.57 (d, 1H; J=5.6 Hz, $CHCHCO_2$), 2.25 (dd, 1H; J=5.6 and 8.5 Hz, $=CHCH-CHCO_2$), 5.61 (d, 1H; J=8.5 Hz, $=CHCH$), and 11.97 (broad s, 1H, CO_2H).

Ethyl trans*-3-(2-Chloroethynyl)-2,2-dimethyl-1-cyclopropanecarboxylate* ***(9t)***. A solution of **7t** (0.21 g) in THF (2 ml) was added dropwise to a slurry of potassium *t*-butoxide (0.22 g) in THF (5 ml) at room temperature. After stirring for 6 hr, the reaction mixture was poured into ice-water and extracted with ether. The extracts were washed with saturated aqueous sodium chloride and dried over anhydrous sodium sulfate. Evaporation of the solvent *in vacuo* gave a residue, which was chromatographed on silica gel (hexane/benzene=1/1) to afford 0.11 g of **9t**, IR, ν_{max}^{film} cm^{-1}: 2220, 1730, and 1175, NMR (CCl_4): 1.20 (s, 3H, CH_3), 1.27 (t, 3H; J=7.1 Hz, OCH_2CH_3), 1.29 (s, 3H, CH_3), 1.59 (d, 1H; J=5.6 Hz, $CHCHCO_2$), 1.85 (d, 1H; J=5.6 Hz, $CHCHCO_2$), and 4.12 (q, 2H; J=7.1 Hz, OCH_2CH_3), MS, *m/e* (relative intensity) for $C_{10}H_{13}O_2{}^{35}Cl$: 202 (1) and 200 (M^+, 2.7).

The authors wish to express their thanks to Dr. K. Murayama for his encouragement and advice and to Dr. N. Soma for his valuable discussion.

References

1) Part V; Y. Nakada, S. Muramatsu, M. Asai, H. Tsuji, and Y. Yura, *Agric. Biol. Chem.*, **42**, 1767 (1978).
2) Present address: 16-47 Sakuradai, Midori-ku, Yokohama-shi, Kanagawa 227, Japan.
3) Y. Chen and J. E. Casida, *J. Agric. Food Chem.*, **17**, 208 (1969).
4) K. Fujimoto, N. Itaya, Y. Okuno, T. Kadota, and T. Yamaguchi, *Agric. Biol. Chem.*, **37**, 2681 (1973).
5) M. Elliott, A. W. Farnham, N. F. Janes, P. H. Needham, D. A. Pulman, and J. H. Stevenson, *Nature*, **246**, 169 (1973).
6) H. Yoshioka and J. Miyamoto, *Kagaku To Seibutsu*, **14**, 549 (1976).
7) J. Farkas, P. Kourim, and F. Sorm, *Collect. Czech. Chem. Commun.*, **24**, 2230 (1959).
8) M. Elliott, A. W. Farnham, N. F. Janes, P. H. Needham, and D. A. Pulman, *Nature*, **244**, 456 (1973).
9) For recent syntheses of the acid **2** and its ethyl ester (**7**) see: a) N. Itaya, T. Matsuo, N. Ohno, T. Mizutani, F. Fujita, and H. Yoshioka, "Synthetic Pyrethroids In ACS Symposium Series 42," ed by M. Elliott, American Chemical Society, Washington, D. C. (1977), p. 45; b) K. Kondo, K. Matsui, and A. Negishi, *ibid.*, p. 128; c) N. Punja, Japan Patent, Kokai, 51-141842 (1976); d) F. Mori, Y. Ohmura, T. Nishida, and K. Itoi, *ibid.*, 51-141843 (1976).
10) We applied for a patent in 1974: Y. Yura, Y. Nakada, and R. Endo, Japan Patent, Kokai, 51-59839 (1976).
11) Kondo *et al.* presented at the 31st National Meeting of Chemical Society of Japan a synthesis of the ethyl ester (**7**) of the acid **2** by a method similar to ours at the nearly same time as we completed our synthesis: K. Matsui, Y. Takahatake, and K. Kondo, Abstracts of Papers, the 31st National Meeting of Chemical Society of Japan, Sendai, October, 1974, Vol. 1, p. 58.
12) W. S. Johnson, L. Werthemann, W. R. Bartlett, T. J. Brocksom, T. Li, D. J. Faulkner, and M. R. Petersen, *J. Am. Chem. Soc.*, **92**, 741 (1970).
13) a) M. Asscher and D. Vofsi, *J. Chem. Soc.*, **1963**, 1887; b) M. Asscher and D. Vofsi, *ibid.*, **1963**, 3921.
14) a) A. F. Bramwell, L. Crombie, P. Hemesley, G. Pattenden, M. Elliott, and N. F. Janes, *Tetrahedron*, **25**, 1727 (1969); b) H. M. Hutton and T. Schaefer, *Can. J. Chem.*, **40**, 875 (1962).
15) T. G. Halsall and A. R. Hands, *J. Chem. Soc.*, **1961**, 3251.
16) a) J. H. Babler and A. J. Tortorello, *J. Org. Chem.*, **41**, 885 (1976); b) K. Kondo, K. Matsui, and Y. Takahatake, *Tetrahedron Lett.*, **1976**, 4359.

Layered Compounds. LIX.[1] Facile Syntheses and Spectral Properties of [3.3]Cyclophanes and Related Cyclophanes

Tetsuo Otsubo, Masashi Kitasawa, and Soichi Misumi*

The Institute of Scientific and Industrial Research, Osaka University, Suita, Osaka 565

(Received December 18, 1978)

A simple synthetic method of [3.3]cyclophanes *via* dithia[4.4]cyclophanes is presented. The spectra of a variety of cyclophanes were examined and compared to those of [2.2]analogues. It was concluded from the absorption spectra that the transannular π-π interactions of the cyclophanes were strongly dependent on both ring-to-ring distance and overlapping mode. From the emission spectra, it was described that cyclophanes of parallel sandwich type formed easily normal excimers, whereas [2.2]metacyclophane and [2.2]- and [3.3]metaparacyclophanes formed strained excimers showing marked red shifts of fluorescence bands.

Cram and his coworkers reported the first synthesis of [3.3]paracyclophane **1** in the study of a series of [*m.n*]paracyclophanes and pointed out its unique properties, *e.g.*, the formation of a rather stronger tetracyanoethylene complex than [2.2]paracyclophane **31** in spite of longer ring-to-ring distance.[2] In this regard, an investigation was undertaken for comparing the strength of intramolecular charge-transfer interaction in a series of donor-acceptor [*n.n*]paracyclophanes, of which the [3.3]system was expected to provide the most stable intramolecular complex.[3]

It has been well known that [3.3]paracyclophane **1** might be the most suitable system for the transannular electronic interaction because **1** has a parallel sandwich structure of the two benzene rings with considerably short ring-to-ring distance and without severe ring strain.[4] However, further extensive study of **1** has been limited owing to tedius route in the initial synthesis. Although a few synthetic methods of **1** were developed by means of ring expansion of [2.2]paracyclophane,[5] 1,8-cycloaddition,[6] and condensation of malonic ester,[7] a general method has been expected for applying to a variety of [3.3]cyclophanes such as multibridged and multilayered types and donor-acceptor type.

The synthesis of [2.2]cyclophanes by sulfur elimination from dithia[3.3]cyclophanes has proved to be very useful as a general method of [2.2]cyclophanes.[8] This successful approach results from a facile extrusion of sulfur atom bonded to two benzyl groups forming relatively stable radicals in desulfurization, in contrast to stubborn sulfur atom bonded to alkyl groups. When bonded to phenethyl or longer phenylalkyl groups, elimination of sulfur atom was difficult due to predominant decomposition. Recently we found that when either of two interposing groups was benzyl group, a similar extrusion of sulfur smoothly proceeded, and a series of [*n*]cyclophanes was prepared by desulfurization of such type of dithiacyclophanes.[9] Furthermore, this method made it possible to extend to the syntheses of higher homologues of [*n.n*]paracyclophanes. Here we present a general method for syntheses of [3.3]- and [4.4]paracyclophanes **1** and **2** and the application to a variety of [3.3]- and related cyclophanes **3**—**7**.[10] Their absorption and emission spectra are discussed together with those of [2.2]-analogues from view points of transannular electronic interaction and excimer formation.

Results and Discussion

Syntheses: All the starting materials required in

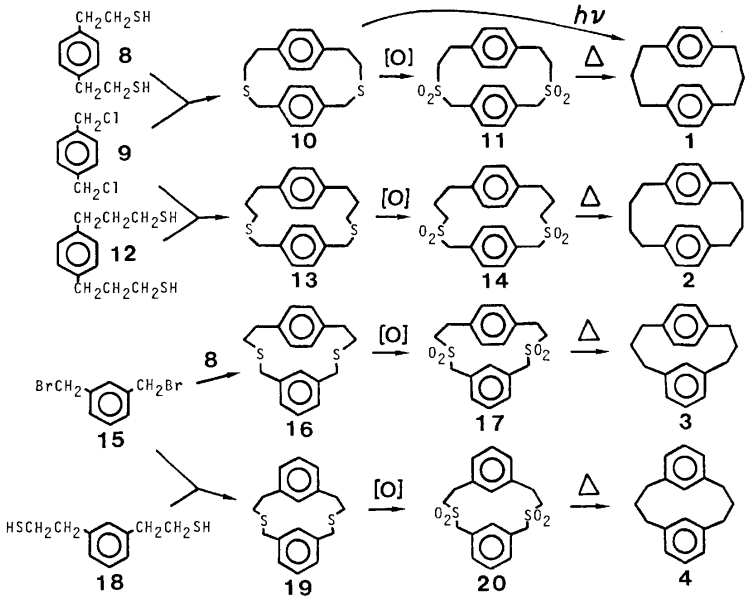

Scheme 1.

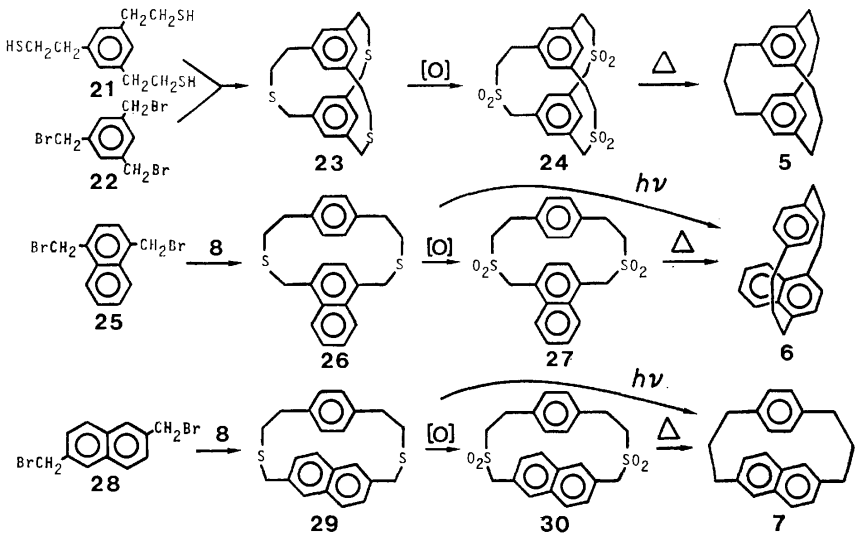

Scheme 2.

the general synthesis of cyclic thia compounds were prepared according to the literatures or conventional methods, except commercially available **9** and **15**.[11] Cyclic thia compounds **10**, **13**, **16**, **19**, **23**, **26**, and **29** were obtained in high yields (60—90%) by the corresponding coupling reactions of these precursors under high dilution conditions. [3.3]Paracyclophane **1** was produced by irradiation of 2,13-dithia[4.4]-paracyclophane **10** in triethyl phosphite with a high pressure mercury lamp for one week in 24% yield or with a low pressure mercury lamp for 15 h in 20% yield. As an alternative route, **10** was oxidized with hydrogen peroxide (95% yield) or *m*-chloroperbenzoic acid (81% yield) to disulfone **11**, and the subsequent pyrolysis of **11** gave **1** in 75% yield (flash pyrolysis) or in 33% yield (flow system pyrolysis).[12] [4.4]-Paracyclophane **2**[13] was similarly prepared by oxidation (97% yield) of 2,15-dithia[5.5]paracyclophane **13**, followed by pyrolysis (76% yield) of disulfone **14**. In this case, the direct photodesulfurization of **13** to **2** was unsuccessful. The pyrolytic method is widely applicable to the syntheses of all the other [3.3]-cyclophanes, *i.e.*, [3.3]metaparacyclophane **3** (40% yield), [3.3]metacyclophane **4**[7] (52%), [3.3.3](1,3,5)-cyclophane **5**[14] (16%), [3.3]paracyclo(1,4)naphthalenophane **6** (37%), and [3.3]paracyclo(2,6)naphthalenophane **7** (13%). The photochemical method was also applied with success for the synthesis of **6** (5.6%) and **7** (12%), but not for **3**, **4**, and **5**. All the new compounds were characterized by NMR and mass spectra and elemental analyses.

Electronic Absorption Spectra: Cram *et al.* reported that the electronic spectra of [*m.n*]paracyclophanes showed bathochromic shift and broadening of absorption bands due to an increasing transannular π-electronic interaction between the two benzenes as the number of *n* and *m* decreased.[2] As seen in the spectra of [2.2]- and [3.3]paracyclophanes (Fig. 1), these anoma-

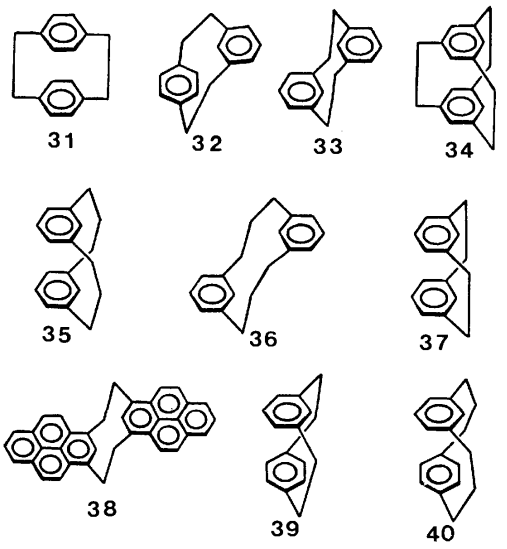

Scheme 3.

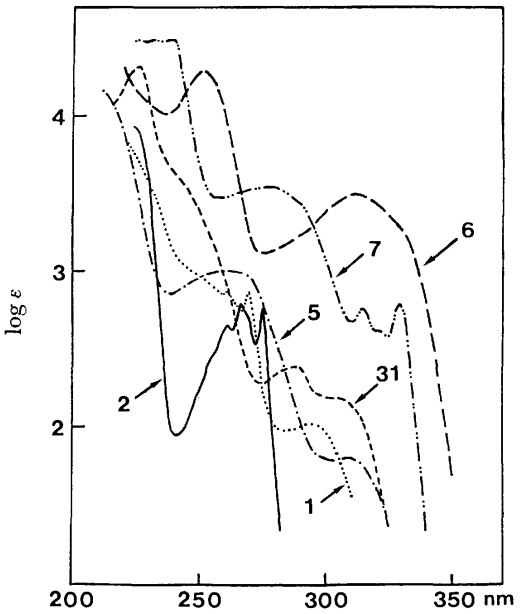

Fig. 1. Electronic spectra of cyclophanes **1**, **2**, **5**, **6**, **7**, and **31** in tetrahydrofuran.

lous phenomena become marked when the two benzene rings were more closely fixed within van der Waals contact.[4,15] It should be noted that the interaction depends not only on ring-to-ring distance but also on overlapping mode. Thus, the two benzenes of [2.2]paracyclophane **31** are well superposed on each other,[15] whereas those of [3.3]paracyclophane **1** are stacked with a little parallel displacement, so that the pπ-pπ overlap somewhat diminishes.[4] The overlapping in [3.3.3](1,3,5)cyclophane **5** is very similar as in **31**, though the ring-to-ring distance is the almost same as that of **1**. If the ring-to-ring distance is main factor for the spectral anomalousness of cyclophanes, **5** should show a spectrum similar to that of **1**. In practice, however, it showed considerable red shift of the longest wavelength band compared to that of **1**, and its maxima (λ_{max} 261 and 310 nm) are, interestingly, quite similar to those (λ_{max} 258 and 312 nm) of the lower homologue, *i.e.*, [2.2.2]-(1,3,5)cyclophane **34**.[16] This result clearly indicates the significance of the overlapping mode rather than the ring-to-ring distance. The spectra of the two paracyclonaphthalenophanes **6** and **7** also reflect the difference in the overlapping mode. According to molecular model examination, the benzene ring of [3.3]paracyclo(2,6)naphthalenophane **7** is stacked above the center of the faced naphthalene ring, but pπ-pπ overlapping may be less effective than that of [3.3]paracyclo(1,4)naphthalenophane **6**. In fact, the longest wavelength band (L_b transition) of **7** shows only a small red shift by *ca.* 5 nm as compared to that of 2,6-dimethylnaphthalene and retains a fine structure, while that of **6** shows a striking red shift by *ca.* 25—30 nm as compared to that of 1,4-dimethylnaphthalene.

[2.2]Metaparacyclophane **32** and [2.2]metacyclophane **33** exhibit weak transannular interaction due to partial overlapping of two benzene rings in the spectra (Fig. 2). [3.3]Metaparacyclophane **3** no longer

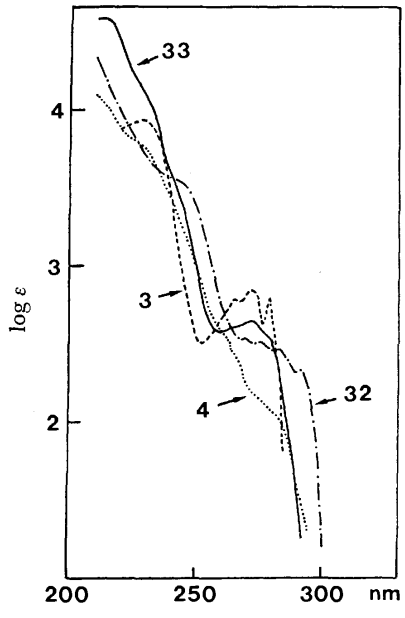

Fig. 2. Electronic spectra of cyclophanes **3** and **4** in tetrahydrofuran and **32** and **33** in cyclohexane.

demonstrates such an effect because the two benzene rings are far apart beyond van der Waals contact. However, [3.3]metacyclophane **4** is not the case, in spite of longer distance between the two benzene rings. Its absorption bands are more broad than that of the lower homologue **33**. This can be explained by a conformational flipping between syn and anti forms, which occurs much easily than the corresponding [2.2] system **33**. Thus, **33** exists only as the anti form,[17] which is hardly interconvertible to syn form, whereas **4** favors the syn form **35** over the anti form **36**, according to molecular model examination. In other words, the increased overlapping of the two benzene rings in the syn form seems to be responsible for the marked interaction in [3.3]system.

Emission Spectra: The emission spectra of paracyclophanes have been studied as a model for examining the structure of benzene excimer, *i.e.*, dimolecular associate in excited state.[18] For example, Vala *et al.* observed the excimer emissions of [2.2]- and [4.4]-paracyclophanes **31** and **2**, indicating that an excimer was formed when two benzene rings were stacked in parallel.[19] Study on the emission spectrum of [3.3]-paracyclophane, in which two benzenes are stacked with little strain, is expected to give further information about the excimer structure. Excimer fluorescences are readily distinguishable from the normal monomer fluorescences, because the former is characterized by large Stokes shifts, broadening, and weak intensity of emission bands.

Table 1 summarizes the emission data of the present cyclophanes measured at 77 K and room temperature (RT). [2.2]- And [3.3]paracyclophanes **31** and **1** and [3.3.3]cyclophane **5** exhibit excimer emissions at both temperatures, although their maxima appear at somewhat longer wavelength due to benzene ring warping than that (*ca.* 330 nm) of ordinary benzene excimer.[20] [4.4]Paracyclophane **4** shows an excimer emission at RT, but a monomer emission at 77 K. These results obviously indicate that the structures of **31** and **1** are favorable for strong π-π interaction even at the ground state, whereas **2** requires a conformational change to bring the two benzene rings close to a certain distance equal to or less than van der Waals contact for the excimer formation.[21]

Shizuka *et al.* reported that **33**, which is consisted of anti form alone in the ground state, exhibited an excimer fluorescence together with a normal fluorescence at RT but no excimer fluorescence at 77 K, and the excimer fluorescence was resulted from its syn form[22] A similar conversion of anti form to syn form in the excited state was observed with [2.2]-(1,3)pyrenophane **38**.[23] The fact that **33** exhibits excimer emission only at RT implies considerable activation energy for syn-anti conversion. In addition, significant red shift of the emission band (392 nm) reflects the severe strain in the syn form. On the other hand, [3.3]metacyclophane, which favors syn form in the ground state in contrast to anti form for **33**, emits an excimer fluorescence characteristic of less strained system even at 77 K.

[2.2]- and [3.3]metaparacyclophanes **32** and **3** exhibit both monomer and excimer emissions at RT and

Table 1. Emission spectra of [2.2]- and [3.3]cyclophanes in EPA

Compound	Temp	Fluorescence	Phosphorescence (nm)
[2.2]Paracyclophane **31**	77 K	354 (excimer)[a]	470[a]
	RT	350 (excimer)[a]	
[3.3]Paracyclophane **1**	77 K	361 (excimer)[a]	463[a]
	RT	358 (excimer)[a]	
[3.3.3](1,3,5)Cyclophane **5**	77 K	374 (excimer)[a]	446[a]
	RT	371 (excimer)[a]	
[4.4]Paracyclophane **2**	77 K	281 (monomer)[b]	379[b]
	RT	335 (excimer)[a]	
[2.2]Metacyclophane **32**	77 K	296 (monomer)[b]	372[b]
	RT	392 (excimer)[a]	
[3.3]Metacyclophane **4**	77 K	284 (monomer),[a] 349 (excimer)[a]	440[a]
	RT	348 (excimer)[a]	
[2.2]Metaparacyclophane **32**	77 K	310 (monomer)[b]	474[a]
	RT	314 (monomer),[a] 393 (excimer)[a]	
[3.3]Metaparacyclophane **3**	77 K	286 (monomer)[b]	398[b]
	RT	292 (monomer),[a] 393 (excimer)[a]	
[3.3]Paracyclo(1,4)naphthalenophane **6**	77 K	370 (excimer)[a]	554[b]
	RT	372 (excimer)[a]	
[3.3]Paracyclo(2,6)naphthalenophane **7**	77 K	346 (monomer)[b]	504[b]
	RT	346 (monomer)[b]	

a) Broad. b) Fine structure.

only monomer emission at 77 K. The maxima of their excimer bands lie at a wavelength comparable to that of **33**. The emission spectra suggest their structures to be of sandwich type with severe strain such as **39** and **40**, in which the two benzene rings are stacked with remarkably different mode compared to the syn form of **33**.

The orientation dependence of excimer formation was found in the case of paracyclonaphthalenophanes **6** and **7**. The 1,4-isomer **6** exhibits an excimer emission at RT and 77 K, whereas the 2,6-isomer **7** a monomer emission at both temperatures. Evidently, $p\pi$-$p\pi$ interaction is also an important factor for excimer formation.

Experimental

Melting points are uncorrected. All solvents are of reagent grade. NMR measurements were made with a Hitachi Perkin-Elmer R-20 spectrometer (60 MHz) or a JEOL JNM-FX100 in deuteriochloroform using tetramethylsilane as an internal standard. Mass spectra were determined on a Hitachi RMU-7 spectrometer at 70 eV using direct insertion technique. UV spectra were recorded on a Hitachi EPS-3T spectrophotometer. Emission spectra were taken on a Hitachi MPF-2A spectrophotometer attached with a HTV R-446F photomultiplier in EPA (ethyl ether–isopentane–ethanol of 5 : 5 : 2 volume ratio). A solution of about 1×10^{-3} M was prepared and degassed by freeze-pump-thaw method. Emission spectra were uncorrected.

1,4-Bis(2-mercaptoethyl)benzene ***8***. A mixture of 1,4-bis(2-bromoethyl)benzene[24] (19.70 g, 0.068 mol) and thiourea (12.32 g, 0.162 mol) in 200 ml of 95% ethanol was refluxed with stirring for 2.5 h. After evaporation of the solvent, the residue was refluxed with potassium hydroxide (80 g) in 400 ml of water for 7 h under nitrogen. The mixture was cooled in an ice bath and acidified with 1 : 1 of concd sulfuric acid–water. The resulting oil was extracted with benzene. The extract was washed with water, dried over anhyd magnesium sulfate, and evaporated to give a colorless oil, 12.83 g (96%), bp 125—127 °C/1 Torr.

NMR ($CDCl_3$, 60 MHz) δ=1.39(m, 2H, SH), 2.4—3.0 (m, 8H, CH_2), 7.14 ppm(s, 4H, ArH). Found: C, 60.29; H, 6.82; S, 32.14%. Calcd for $C_{10}H_{14}S_2$: C, 60.55; H, 7.11; S, 32.33%.

1,4-Bis(3-mercaptopropyl)benzene ***12***. Dithiol **12** was obtained in 97% yield from 1,4-bis(3-bromopropyl)benzene[25] in a similar manner as described in dithiol **8**; colorless oil, bp 165—167 °C/2 Torr.

NMR ($CDCl_3$, 60 MHz) δ=1.34(t, 2H, J=8 Hz, SH), 1.89(quint, 4H, J=7 Hz, CH_2), 2.48(t, 4H, J=7 Hz, CH_2S), 2.71(t, 4H, J=7 Hz, $ArCH_2$), and 7.09 ppm(s, 4H, ArH). Found: C, 63.81; H, 7.95; S, 28.13%. Calcd for $C_{12}H_{18}S_2$: C, 63.66; H, 8.01; S, 28.32%.

1,4-Bis(2-mercaptoethyl)benzene ***18***. Dithiol **18** was led from 1,3-bis(ethoxycarbonylmethyl)benzene[26] as described below.

A solution of 1,3-bis(ethoxycarbonylmethyl)benzene(1.65 g, 6.6 mmol) in 15 ml of dry tetrahydrofuran was slowly added into a suspension of lithium aluminium hydride (0.53g, 13.9 mmol) in 25 ml of dry THF over a period of 30 min at room temperature. After 30 min of reflux, a small amount of ethyl acetate, water, and dil hydrochloric acid were added successively. The mixture was saturated with sodium chloride and extracted with ethyl ether. The extract was washed with satd. aq NaCl solution and dried over magnesium sulfate. Evaporation gave a colorless oil of 1,3-bis(2-hydroxyethyl)benzene, 1.05 g (96%).

NMR ($CDCl_3$, 100 MHz) δ=2.75(t, 4H, J=6.7 Hz, $ArCH_2$), 3.27(bs, 2H, OH), 3.71(t, 4H, J=6.7 Hz, CH_2O), and 6.9—7.3 ppm(m, 4H, ArH).

The above 1,3-bis(2-hydroxyethyl)benzene (1.48 g, 8.9 mmol) was mixed with 100 ml of 48% hydrobromic acid and 6 ml of concd sulfuric acid. The mixture was refluxed for 1.5 h, cooled to room temperature, and extracted with benzene. The extract was washed with water and dried over anhyd magnesium sulfate. Evaporation gave a colorless oil of 1,3-bis(2-bromoethyl)benzene, 3.2 g (84%), bp 141 °C/2 Torr.

NMR ($CDCl_3$, 100 MHz) δ=3.12(A_2B_2m, 4H, $ArCH_2$), 3.53(A_2B_2m, 4H, CH_2Br), and 7.0—7.3 ppm(m, 4H, ArH).

The above dibromide was converted to 1,3-bis(2-mercaptoethyl)benzene **18** in 81% yield as described in the para analogue **8**; colorless oil, bp 115 °C/10 Torr.

NMR ($CDCl_3$, 60 MHz) δ=1.37(m, 2H, SH), 2.5—3.1 (m, 8H, CH_2), and 7.0—7.3 ppm(m, 4H, ArH). Found: C, 60.28; H, 6.81; S, 32.12%. Calcd for $C_{10}H_{14}S_2$: C, 60.55; H, 7.11; S, 32.33%.

General Method of Coupling Reaction. A solution of the corresponding thiol (0.01 mol) and halide (0.01 mol) in 100 ml of benzene was added dropwise into a refluxed ethanol solution (1 l) containing potassium hydroxide (1.78 g) in a nitrogen atmosphere. The addition was complete in 12 h. The mixture was refluxed an additional 12 h and then concentrated. The residue was taken up in benzene and chromatographed over silica gel with benzene–hexane (1 : 1) to give a crystalline solid of the desired cyclic dithia compound from the main fraction of eluates.

2,13-Dithia[4.4]paracyclophane ***10***. Yield 62%, colorless plates from benzene, mp 183—185 °C.

NMR ($CDCl_3$, 60 MHz) δ=2.75(A_2B_2m, 8H, CH_2), 3.39(s, 4H, CH_2), and 6.80 ppm(s, 8H, ArH). MS *m/e* 300(M^+). Found: C, 71.75; H, 6.57; S, 21.11%. Calcd for $C_{18}H_{20}S_2$: C, 71.95; H, 6.71; S, 21.34%.

2,15-Dithia[5.5]paracyclophane ***13***. Yield 91%, colorless scales from benzene–hexane, mp 153—153.5 °C.

NMR ($CDCl_3$, 60 MHz) δ=1.85(m, 8H, CH_2), 2.60 (m, 4H, $ArCH_2$), 3.55(s, 4H, $ArCH_2S$), 6.87(s, 4H, ArH), and 7.03 ppm (s, 4H, ArH). MS *m/e* 328(M^+). Found: C, 72.94; H, 7.36; S, 19.30%. Calcd for $C_{20}H_{24}S_2$: C, 73.12; H, 7.36; S, 19.52%.

3,12-Dithia[4.4]metaparacyclophane ***16***. Yield 76%, colorless needles from benzene–hexane, mp 81—82 °C.

NMR ($CDCl_3$, 60 MHz) δ=2.83(bs, 8H, CH_2), 3.46(s, 4H, $ArCH_2S$), 6.40(bs, 1H, meta ArH), 6.88(s, 4H, para ArH), and 6.98 ppm(bs, 3H, meta ArH). MS *m/e* 300(M^+). Found: C, 71.78; H, 6.53; S, 21.61%. Calcd for $C_{18}H_{20}S_2$: C, 71.95; H, 6.71; S, 21.34%.

2,13-Dithia[4.4]metacyclophane ***19***. Yield 79%, colorless prisms from benzene–hexane, mp 109—109.5 °C.

NMR ($CDCl_3$, 60 MHz) δ=2.74(A_2B_2m, 8H, CH_2), 3.65(s, 4H, $ArCH_2S$), 6.67(bs, 1H, ArH), 7.0—7.2(m, 3H, ArH), and 7.39 ppm(bs, 4H, ArH). MS *m/e* 300(M^+). Found: C, 72.06; H, 6.52; S, 29.49%. Calcd for $C_{18}H_{20}S_2$: C, 71.95; H, 6.71; S, 21.34%.

2,13,22-Trithia[4.4.4](1,3,5)cyclophane ***23***. Yield 65%, colorless plates from benzene–hexane, mp 251—252 °C.

NMR ($CDCl_3$, 100 MHz) δ=2.71(A_2B_2m, 12H, CH_2), 3.31(s, 6H, $ArCH_2S$), 6.56(s, 3H, ArH), and 6.62 ppm (s, 3H, ArH). MS *m/e* 372 (M^+). Found: C, 67.87; H, 6.65; S, 25.57%. Calcd for $C_{21}H_{24}S_3$: C, 67.69; H, 6.49; S, 25.82%.

2,13-Dithia[4.4]paracyclo(1,4)naphthalenophane ***26***. Yield 63%, colorless columns from benzene–hexane, mp 187—188 °C.

NMR ($CDCl_3$, 60 MHz) δ=2.3—3.1(A_2B_2m, 8H, CH_2), 3.86(s, 4H, $ArCH_2S$), 6.45(s, 4H, ArH), 6.72(s, 2H, ArH), 7.53(A_2B_2dd, 2H, J=7 and 3 Hz, ArH), and 8.02 ppm (A_2B_2dd, 2H, J=7 and 3 Hz, ArH). MS *m/e* 350(M^+). Found: C, 75.65; H, 6.17; S, 18.04%. Calcd for $C_{22}H_{22}S_2$: C, 75.38; H, 6.33; S, 18.29%.

2,13-Dithia[4.4]paracyclo(2,6)naphthalenophane ***29***. Yield 89%, colorless plates from benzene–hexane, mp 198—200 °C.

NMR ($CDCl_3$, 60 MHz) δ=2.2—2.8(m, 8H, CH_2), 3.77 (s, 4H, $ArCH_2S$), 6.41(s, 4H, ArH), 7.26(ABd, 2H, J=8 Hz, ArH), 7.36(bs, 2H, ArH), and 7.53 ppm(ABd, 2H, J=8 Hz, ArH). Found: C, 75.52; H, 6.19; S, 18.51%. Calcd for $C_{22}H_{22}S_2$: C, 75.38; H, 6.33; S, 18.29%.

General Synthetic Method of Disulfone. A) With Hydrogen Peroxide: Cyclic disulfide (4 mmol) was mixed with 8 ml of acetic acid and 2.4 ml of 35% hydrogen peroxide, and heated at 100 °C with stirring for 6 h. The mixture was cooled in an ice bath, and the resulting white crystalline solid of disulfone was filtered, washed, and dried.

B) With m-Chloroperbenzoic Acid: A mixture of cyclic disulfide (1 mmol) and *m*-chloroperbenzoic acid (1.1 g, 6 mmol as 85% active) in 20 ml of dichloromethane was stirred at room temperature for 2 d. After some milliliters of dichloromethane was added to dissolve the resulting precipitate, the solution was washed successively with 3M NaOH solution and water, dried, and concentrated to give a white powder of disulfone. Disulfones thus obtained were essentially pure and used in the following pyrolysis without further purification.

2,13-Dithia[4.4]paracyclophane 2,2,13,13-tetraoxide **11**, yield 95%(method A) and 81%(method B), dec 330—340 °C. 2,15-Dithia[5.5]paracyclophane 2,2,15,15-tetraoxide **14**, yield 97%(by A), dec 310—320 °C. 3,12-Dithia[4.4]-metaparacyclophane 3,3,12,12-tetraoxide **17**, yield 90% (by A) and 67%(by B), mp 283—285 °C. 3,12-Dithia-[4.4]metacyclophane 3,3,12,12-tetraoxide **20**, yield 72% (by B), dec 320—325 °C with melting. 2,13,22-Trithia-[4.4.4](1,3,5)cyclophane 2,2,13,13,22,22-hexaoxide **24**, yield 83%(by A), dec 350 °C. 2,13-Dithia[4.4]paracyclo(1,4)-naphthalenophane 2,2,13,13-tetraoxide **27**, yield 82% (by B), dec 240 °C. 2,13-Dithia[4.4]paracyclo(2,6)naphthalenophane 2,2,13,13-tetraoxide **30**, yield 96%(by A), dec 320—330 °C.

General Synthetic Method of [3.3]-, [4.4]-, and [3.3.3]Cyclophanes. A)Flash Pyrolysis: Sulfone (100—500 mg) was packed in a Pyrex tube sealed at one end. The open end was connected to a rotary pump and the system was maintained under 0.1—0.5 Torr. The tube was placed in a furnace (15 cm in length, preheated to 650 °C) in such a way as the middle of the tube could be heated. The sample part was slidden smoothly inside the furnace. As soon as pyrolysis started, an oily product condensed at the opposite cool end. Column chromatography of the product on silica gel with hexane led to the isolation of the desired cyclophane as white crystals.

B) Flow System Pyrolysis: Sulfone (100 mg) was placed in a pyrolytic flow system modelled after that of Boekelheide *et al.*[27] The first furnace was set at 300 °C and the second at 600 °C. The whole system was maintained under 0.1 Torr. The pyrolysis was complete in a few hours. The resulting cyclophane was trapped in the cold finger and purified by column chromatography.

C) Photodesulfurization: Cyclic dithia compound (100 mg) was dissolved in 10 ml of benzene and 5 ml of triethyl phosphite in a quartz tube. The solution was irradiated with a high pressure mercury lamp in a nitrogen atmosphere (one week for [3.3]paracyclophane and 3 h for [3.3]paracyclonaphthalenophane). After removal of the solvent, the residue was chromatographed on silica gel to give white crystals of the desired product.

[3.3]Paracyclophane ***1***. Yield 75% (method A), 33% (method B), and 24%(method C), colorless plates from methanol, mp 103—104 °C (lit[2]), mp 104.3—105.3 °C).

NMR ($CDCl_3$, 60 MHz) δ=2.03(m, 4H, CH_2), 2.72 (t, 8H, CH_2), and 6.66 ppm(s, 8H, ArH). MS *m/e* 236 (M^+).

[4.4]Paracyclophane ***2***. Yield 76%(by A), colorless

plates from ethanol, mp 147.5—149 °C (lit,[13] mp 146.2—147.3 °C).

NMR ($CDCl_3$, 60 MHz) δ=1.6(m, 4H, CH_2), 2.3(m, 4H, $ArCH_2$), and 6.68 ppm(s, 8H, ArH). MS *m/e* 264 (M^+).

[3.3]Metaparacyclophane **3**. Yield 40% (by A), 20% (by B), colorless plates from hexane, mp 90—91 °C.

NMR ($CDCl_3$, 60 MHz) δ=1.9—2.9(m, 8H, CH_2), 2.71(t, 4H, J=6 Hz, CH_2), 5.55(bs, 1H, meta ArH), 6.63 (s, 4H, para ArH), and 6.6—7.2 ppm (m, 3H, meta ArH). MS *m/e* 236(M^+). Found: C, 91.25; H, 8.30%. Calcd for $C_{18}H_{20}$: C, 91.47; H, 8.53%.

[3.3]Metacyclophane **4**. Yield 52% (by A), 2.7% (by B), colorless plates from ethanol, mp 81—82 °C (lit,[7] 79—80 °C).

NMR ($CDCl_3$, 100 MHz) δ=1.92—2.15(m, 4H, CH_2), 2.74(t, 8H, J=5.8 Hz, $ArCH_2$), 6.54—6.84 (A_2B_2m, 6H, outer ArH), and 6.84 ppm(bs, 2H, inner ArH). MS *m/e* 236(M^+).

[3.3.3](1,3,5)Cyclophane **5**. Yiled 16% (by A), colorless plates from pentane, mp 134—135.5 °C (lit,[14] mp 140 °C).

NMR ($CDCl_3$, 100 MHz) δ=2.18(m, 6H, CH_2), 2.75 (t, 12H, J=5.8 Hz, $ArCH_2$), and 6.52 ppm(s, 6H, ArH). MS *m/e* 276 (M^+).

[3.3]Paracyclo(1,4)naphthalenophane **6**. Yield 13% (by A), 12% (by C), colorless fine crystals from pentane, mp 106—107 °C.

NMR ($CDCl_3$, 60 MHz) δ=2.0—3.0(m, 10H, CH_2), 3.4—3.8(m, 2H, CH_2), 5.95(bs, 2H, ArH), 6.70(s, 2H, ArH), 6.76(bs, 2H, ArH), 7.43(A_2B_2dd, 2H, J=7 and 3 Hz, ArH), and 7.94 ppm(A_2B_2dd, 2H, J=7 and 3 Hz, ArH). MS *m/e* 286(M^+). Found: C, 91.82; H, 7.32%. Calcd for $C_{22}H_{22}$: C, 92.26; H, 7.74%.

[3.3]Paracyclo(2,6)naphthalenophane **7**. Yield 37% (by A), 5.6% (by C), colorless plates from benzene-hexane, mp 160—161 °C.

NMR ($CDCl_3$, 60 MHz) δ=1.8—3.0(m, 12H, CH_2), 6.04(s, 4H, ArH), 7.01(bs, 2H, ArH), and 7.13 ppm(bs, 2H, ArH). MS *m/e* 286(M^+).

Found: C, 92.31; H, 7.51%. Calcd for $C_{22}H_{22}$: C, 92.26; H, 7.74%.

The present work was supported by Grant-in-Aid for Scientific Research from the Ministry of Education, to which authors' thanks are due.

References

1) Part LVIII: T. Kawashima, T. Otsubo, Y. Sakata, and S. Misumi, *Tetrahedron Lett.*, **1978**, 5115.

2) D. J. Cram, N. L. Allinger, and H. Steinberg, *J. Am. Chem. Soc.*, **76**, 6132 (1954); D. J. Cram and R. H. Bauer, *ibid.*, **81**, 5971 (1959); M. Sheehan and D. J. Cram, *ibid.*, **91**, 3544, 3553 (1969).

3) It was recently confirmed that a few donor-acceptor [3.3]cyclophanes showed the strongest intramolecular charge-transfer interaction ; T. Shinmyozu, T. Inazu, and T. Yoshino, *Chem. Lett.*, **1977**, 1347; H. Horita, T. Otsubo, and S. Misumi, *ibid.*, **1978**, 807.

4) P. K. Gantzel and K. N. Trueblood, *Acta Crystallogr.*, **18**, 958 (1965).

5) D. J. Cram and R. C. Helgeson, *J. Am. Chem. Soc.*, **88**, 3515 (1966); E. Hedaya and L. M. Kyle, *ibid.*, **88**, 3667 (1966).

6) T. Tsuji, Y. Hienuki, and S. Nishida, *Chem. Lett.*, **1977**, 1015; T. Tsuji, T. Shibata, Y. Hienuki, and S. Nishida, *J. Am. Chem. Soc.*, **100**, 1806 (1978).

7) T. Shinmyozu, T. Inazu, and T. Yoshino, *Chem. Lett.*, **1976**, 1405; T. Shinmyozu, K. Kumagae, T. Inazu, and T. Yoshino, *ibid.*, **1977**, 43.

8) For review, see a) V. Boekelheide, "Topics in Non-benzenoid Aromatic Chemistry," Hirokawa Publ. Co., Tokyo (1973), Vol 1, p. 47; b) F. Vögtle and P. Neumann, *Synthesis*, **1973**, 85; c) S. Misumi and T. Otsubo, *Acc. Chem. Res.*, **11**, 251 (1978).

9) T. Otsubo and S. Misumi, *Synth. Commun.*, **8**, 285 (1978).

10) For a preliminary report, see T. Otsubo, M. Kitasawa, and S. Misumi, *Chem. Lett.*, **1977**, 977.

11) For **21**: A. Ricci, R. Danieli, and S. Rossini, *J. Chem. Soc., Perkin Trans. 1*, **1976**, 1691; **22**: W. P. Cochrane, P. L. Pauson, and T. S. Stevens, *J. Chem. Soc., C*, **1968**, 630; **25** and **28**: W. Ried and H. Bodem, *Chem. Ber.*, **91**, 1981 (1958); **8**, **12**, and **18**: the present experimental part.

12) The pyrolytic synthetic method of [3.3]cyclophanes was independently reported by other groups at the nearly same time; M. W. Haenel, A. Flatow, V. Taglieber, and H. A. Staab, *Tetrahedron Lett.*, **1977**, 1733; D. T. Longone, S. H. Küsefoglu, and J. A. Gladysz, *J. Org. Chem.*, **42**, 2787 (1977); L. Rossa and F. Vögtle, *J. Chem. Res.*, (S), **1977**, 264.

13) D. J. Cram and N. L. Allinger, *J. Am. Chem. Soc.*, **76**, 726 (1954).

14) A. J. Hubert, *J. Chem. Soc., C*, **1967**, 6.

15) H. Hope, J. Bernstein, and K. W. Trueblood, *Acta Crystallogr., Sect. B*, **28**, 1733 (1972).

16) V. Boekelheide and R. A. Hollins, *J. Am. Chem. Soc.*, **95**, 3201 (1973).

17) C. J. Brown, *J. Chem. Soc.*, **1953**, 3278.

18) For review, see Th. Förster, *Angew. Chem. Int. Ed. Engl.*, **8**, 333 (1969).

19) M. T. Vala, J. Haebig, and S. A. Rice, *J. Chem. Phys.*, **43**, 886 (1965).

20) F. Hirayama, *J. Chem. Phys.*, **42**, 3163 (1965); F. Hirayama and S. Lipsky, *ibid.*, **51**, 1939 (1969).

21) The ring-to-ring distance of [4.4]paracyclophane was estimated to be 3.73 Å; D. J. Cram, N. L. Allinger, and H. Steinberg, *J. Am. Chem. Soc.*, **76**, 6132 (1954).

22) H. Shizuka, T. Ogiwara, and T. Morita, *Bull. Chem. Soc. Jpn.*, **48**, 3385 (1975).

23) T. Hayashi, N. Mataga, T. Umemoto, Y. Sakata, and S. Misumi, *J. Phys. Chem.*, **81**, 424 (1977).

24) K. -B. Augustinson and H. Hasselguist, *Acta Chem. Scand.*, **17**, 953 (1963).

25) T. Matsuoka, T. Negi, T. Otsubo, Y. Sakata, and S. Misumi, *Bull. Chem. Soc. Jpn.*, **45**, 1825 (1972).

26) A. F. Titley, *J. Chem. Soc.*, **1928**, 2571.

27) S. A. Sherrod, R. L. da Costa, R. A. Barnes, and V. Boekelheide, *J. Am. Chem. Soc.*, **96**, 1565 (1974).

NOTES

BULLETIN OF THE CHEMICAL SOCIETY OF JAPAN, VOL. 52 (5), 1521—1522 (1979)

Photochemical Reduction of Di-*t*-butyl Thioketone

Atsuyoshi OHNO,* Misao UOHAMA, Kaoru NAKAMURA, and Shinzaburo OKA
Institute for Chemical Research, Kyoto University, Uji, Kyoto 611

(Received December 4, 1978)

Synopsis. Photochemical reduction of the title compound has been studied and the result is compared with that from the reaction with thiobenzophenone, an aromatic thioketone.

In a previous communication, we reported the result from the photoreaction of di-*t*-butyl thioketone (**1**) in the n,π^* triplet state (T_1, E_T=43—45 kcal/mol) with various olefins.[1] The thioketone **1** reacted with electron-rich olefins affording open-chain photo-adducts instead of cycloadducts. This is a marked contrast between **1** and other thioketones such as thiobenzophenone and adamantanethione.[2]

It is known that thiobenzophenone in the n,π^* triplet state abstracts a hydrogen from various hydrogen-donors yielding the corresponding thiol or disulfide.[2,3] Hydrogen-abstraction by aliphatic thioketones are scarcely studied,[2,4] and we now wish to report some interesting observation in the photohydrogen-abstraction of **1** from various hydrogen-donors.

Results and Discussion

The photo-irradiation was continued until the color of **1**(λ_{max}=540 nm) disappeared. The reaction is summarized in Table 1. Since hydrogen-donors presently employed for the reaction have no absorption above 300 nm, there is no doubt that the reaction takes place through the excitation of **1** into the n,π^* singlet state (S_1) with the lights of 550 and 580 nm.[5] Namely, it has been confirmed that the reaction of tetraphenylethylene with thiobenzophenone under the irradiation for 60 days with the light of 589 nm from sodium lamps (8×60 W)[6] yields 9,10-diphenylphenanthrene. The photoreaction of 9,10-dihydroanthracene with thiobenzophenone has already been reported.[7] Although we did not study the reaction quantitatively, existence of self-quenching, that is, the retardation of reaction by the increase of the concentration of **1**, suggests that the T_1 state of **1** is responsible to the reaction.[2,8]

Table 1 reveals a remarkable reactivity of excited (S_1 or T_1) **1** toward the hydrogen-abstraction; generally, the reactivity of 2-propanol is larger than, or at least comparable to, that of toluene toward hydrogen-abstraction,[9,10] whereas toluene and even tetraphenylethylene are much better hydrogen-donors than aliphatic alcohols and ethers in the present photo-reduction. The large reactivity of aromatic compound can be corelated with their ionization potentials[11] and seems to imply the formation of a charge-transfer-type complex between **1** (in S_1 or T_1) and a hydrogen-donor. Similar process has been suggested for the photo-reductions of benzophenone,[12] α,α,α-trifluoroacetophenone,[13] and thiobenzophenone.[7] The intermediacy of the charge-transfer-type complex is also witnessed by facile reaction with amines.[3a,14] That is, the photo-excited **1** does not abstract a hydrogen from ethanol, whereas it does in the presence of aniline, an electron-donor.

TABLE 1. PHOTOREDUCTION OF DI-*t*-BUTYL THIOKETONE

Hydrogen-donor	Reaction time, day	Yield of Bu^t_2CHSH, %
$PhBH_3$	28	72
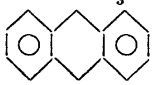 /in C_6H_6 (400 mg) (10 ml)	21	85[a]
$Ph_2C{=}CPh_2$/in C_6H_6 or $CHCl_3$ (800 mg) (10 ml)	14	70[b]
$PhCH_2OH$	6	82[c]
EtOH	≈60	0[d]
i-PrOH	≈60	0[d]
Et_3N	2	80
i-$BuNH_2$	7	27[e]
$PhNH_2$/in EtOH (5 ml) (10 ml)	28	24[f]
Et_2O	≈60	0[d]
	≈60	0[d]

a) Anthracene was isolated in 90% yield. b) 9,10-Diphenylphenanthrene was isolated in 70% yield. c) Benzaldehyde was detected on VPC. d) No reaction took place. **1** was recovered quantitatively. e) **1** was recovered in 49% yield. f) **1** was recovered in 61% yield.

It is noteworthy that the excitation of **1** into the π,π^* state results in completely different reactivity from **1** in the n,π^* state.[15] It is also interesting to compare the reactivity of **1** with that of thiobenzophenone, an aromatic thioketone, by the following two sets of reactions.[3a,12,16]

$$\left\{\begin{array}{l} Ph_2C{=}S + EtOH \xrightarrow{h\nu} Ph_2\dot{C}SH + Me\dot{C}HOH \\ \qquad\qquad \longrightarrow Ph_2CHSH \xrightarrow{h\nu} Ph_2CHSSCHPh_2 \\ Bu^t_2C{=}S + EtOH \xrightarrow{h\nu} \text{no reaction} \end{array}\right.$$

$$\left\{\begin{array}{l} Ph_2C{=}S + PhCH_3 \overset{h\nu}{\rightleftharpoons} Ph_2CSH + PhCH_2\cdot \\ \qquad\qquad\qquad\qquad \longrightarrow \text{no reaction} \\ Bu^t_2C{=}S + PhCH_3 \xrightarrow{h\nu} Bu^t_2CSH + PhCH_2\cdot \\ \qquad\qquad\qquad \xrightarrow{PhCH_3} Bu^t_2CHSH + PhCH_2CH_2Ph \end{array}\right.$$

The results clearly suggest that, in their biradical-type excited states, thiobenophenone has more radical-character on sulfur than on thiocarbonyl-carbon, and the reverse is true for **1**. That is, the electronic configuration of thiocarbonyl group is much affected by the substituent. This is also true for their ground-state chemistry.[17]

Experimental

Materials. Di-*t*-butyl thioketone (**1**) and thiobenzophenone were prepared as previously mentioned.[6,18] Solvents were dried and distilled prior to the use.

Procedure. As a standard procedure, 300 mg of **1** in 10 ml of a hydrogen-donor solvent was sealed in a Pyrex tube (10 mmϕ) under an atmosphere of nitrogen. The mixture was irradiated with a 500 W high-pressure mercury lamp at a temperature of running water. After the reaction, the solvent was evaporated under a reduced pressure and the residual oil was subjected to column chromatography on silica gel with an eluent of hexane–benzene (4 : 1 v/v) mixture. The product isolated was identified to be 2,2,4,4-tetramethyl-3-pentanethiol by comparing the spectral data with those of the authentic sample.

References

1) A. Ohno, M. Uohama, K. Nakamura, and S. Oka, *Tetrahedron Lett.*, **1977**, 1905.

2) P. de Mayo, *Acc. Chem. Res.*, **9**, 52 (1976).

3) a) A. Ohno and N. Kito, *Int. J. Sulfur Chem., Part A*, **1**, 26 (1971); b) N. Kito and A. Ohno, *Bull. Chem. Soc. Jpn.*, **46**, 2487 (1973).

4) a) D. S. L. Blackwell and P. de Mayo, *J. Chem. Soc., Chem. Commun.*, **1973**, 30; b) J. R. Bolton, K. S. Chem, A. H. Lawrence, and P. de Mayo, *J. Am. Chem. Soc.*, **97**, 1832 (1975).

5) The reaction also proceeds in a tube of ordinal glass which cuts the light below 400 nm.

6) A. Ohno, Y. Ohnishi, and G. Tsuchihashi, *J. Am. Chem. Soc.*, **91**, 5038 (1969).

7) Y. Ohnishi and A. Ohno, *Bull. Chem. Soc. Jpn.*, **46**, 3868 (1973).

8) C. C. Liao and P. de Mayo, *Chem. Commun.*, **1971**, 1525.

9) C. Walling and M. J. Gibian, *J. Am. Chem. Soc.*, **94**, 4040(1972).

10) A. Beckett and G. Porter, *Trans. Faraday Soc.*, **59**, 2038 (1963).

11) J. L. Franklin, J. G. Dillard, H. M. Rosenstock, J. T. Hesson, K. Draxl, and F. H. Field, "Ionization Potentials, Appearance Potentials and Heat of Formation of Gaseous Positive Ions," U.S. Department of Commerce, National Bureau of Standards, 1969.

12) J. B. Guttenplan and S. G. Cohen, *J. Am. Chem. Soc.*, **94**, 4040 (1972).

13) P. J. Wagner and R. A. Leavitt, *J. Am. Chem. Soc.*, **95**, 3669 (1973).

14) *Cf.* S. G. Cohen and G. Parsons, *J. Am. Chem. Soc.*, **92**, 7603 (1970).

15) R. Rajee and V. Ramamurthy, *Tetrahedron Lett.*, **1978**, 3463.

16) N. Kito and A. Ohno, *Chem. Commun.*, **1971**, 1338.

17) A. Ohno, K. Nakamura, M. Uohama, S. Oka, T. Yamabe, and S. Nagata, *Bull. Chem. Soc. Jpn.*, **48**, 3718 (1975).

18) A. Ohno, K. Nakamura, Y. Nakazima, and S. Oka, *Bull. Chem. Soc. Jpn.*, **48**, 2403 (1975).

BULLETIN OF THE CHEMICAL SOCIETY OF JAPAN, VOL. 52 (5), 1523—1524 (1979)

Optical and Magnetic Properties of Solid Cation Radical Salts Derived from Some Aromatic Hydrocarbons

Yôichi IIDA

Department of Chemistry, Faculty of Science, Hokkaido University, Sapporo 060

(Received September 21, 1978)

Synopsis. The optical and magnetic properties of solid cation radical salts derived from 9,10-dimethylanthracene and 9,10-dichloroanthracene were explained in terms of one-dimensional Hubbard model composed of equivalent sites of the cation radicals, while those of perylene cation radical salt, in terms of Hubbard model of cation radical dimer.

There have been made extensive investigations concerning the optical and magnetic properties of a number of crystalline ion radical salts.[1-10] On one hand, a deviation from the Curie or Curie-Weiss law has often been found in the temperature dependence of their magnetic susceptibilities, and this deviation has been explained in terms of an existence of spin exchange interaction between ion radicals.[1-3] On the other hand, the electronic spectrum of such solid ion radical salt is found to be different from the monomer spectrum of the corresponding ion radical molecule, but shows a charge-transfer transition between ion radicals in the low-energy region.[3-5]

In most solid ion radical salts, the planar ion radical molecules are known to form, in themselves, a segregated stacking into one-dimensional columns.[5] In this respect, the intermolecular charge-transfer interaction between ion radical molecules is important for the solid-state properties of ion radical salts. In order to understand this situation in more detail, we have applied half-filled Hubbard model to the segregated stack of ion radical molecules and investigated the optical and magnetic properties characteristic of solid ion radical salts.[6-10] Earlier, Sato *et al.* examined the optical absorptions and the magnetic susceptibilities of crystalline cation radical salts of 9,10-dimethylanthracene (DMA), 9,10-dichloroanthracene (DCA) and perylene (P) with antimony pentachloride and perchlorate anions.[3] In the present paper, we shall explain their experimental results in terms of our Hubbard model and understand the electronic states of those crystalline cation radical salts.

A compound of DMA–$SbCl_5$ was obtained as chemically stable cation radical salt. Its solid-state spectrum showed a band peak at 14400 cm^{-1} and a shoulder around 11600 cm^{-1}.[3] The high-energy peak at 14400 cm^{-1} corresponds to the monomer absorption of the 9,10-dimethylanthracene cation radical at 14800 cm^{-1}. The shoulder in the lower-energy region is characteristic of the solid salt and was assigned to the charge-transfer transition between the 9,10-dimethylanthracene cation radicals.[3] On the other hand, the temperature dependence of the paramagnetic susceptibility of DMA–$SbCl_5$ showed a broad maximum at approximately 80 K. The observed magnetic properties could be well explained in terms of antiferromagnetic linear Ising model with exchange coupling constant $J=56$ cm^{-1}.[3] In order to understand those optical and magnetic properties, we consider a system of non-alternant one-dimensional stack of 9,10-dimethylanthracene cation radicals in terms of Hubbard Hamiltonian, which can be written by

$$\mathscr{H} = \sum_{i,j,\sigma} T_{ij} C_{i\sigma}^{+} C_{j\sigma} + I \sum_{i} n_{i\downarrow} n_{i\uparrow}, \tag{1}$$

where $n_{i\sigma}=C_{i\sigma}^{+}C_{i\sigma}$, and $C_{i\sigma}^{+}$ and $C_{i\sigma}$ are the creation and annihilation operators of an electron with σ-spin at the i-th site, respectively, and where $T_{ij}(<0)$ is the transfer matrix element between the i-th and j-th sites. The Coulomb repulsion potential, I, appears only when two electrons with up and down spins are at the same site. For non-alternant one-dimensional column of the 9,10-dimethylanthracene cation radicals, we consider the half-occupied molecular orbital of the unpaired electron as one site of cation radical molecule, and take into account only the transfer matrix element between the nearest neighbor sites. Hereafter, it is simply denoted by $T(<0)$. The shape of the intermolecular charge-transfer absorption spectrum of this system, $\sigma(\omega)$, is then given by[6]

$$\sigma(\omega) \propto \frac{e^2}{4} \frac{I^2}{\omega^2 \sqrt{\omega^2 - I^2}} \sqrt{4T^2 - \omega^2 + I^2}. \tag{2}$$

Here, a δ-function was assumed for each elementary transition in which the spin and the wave vector of an electron are conserved. The charge-transfer absorption of Eq. 2 has a sharp divergent peak at $\omega=I$ and has a band width of $\sqrt{I^2+4T^2}-I$ in the region $\omega>I$. On the other hand, for the magnetic properties of the same system, the Hubbard model leads to, in a region of small $|T|$ limit, a non-alternant one-dimensional antiferromagnet with an exchange interaction $J \approx 2T^2/I$.[8,9] Therefore, if we combine the experimental data on the peak energy of the observed charge-transfer absorption and the exchange interaction parameter, we can uniquely determine the magnitudes of I and T of Eq. 1. For the cation radical salt of DMA–$SbCl_5$, the observed peak energy of the charge-transfer absorption, 11600 cm^{-1}, thus corresponds to $I=11600$ cm^{-1}. As for the antiferromagnetic exchange interaction, rigorously speaking, the J value of Heisenberg model should correspond to $2T^2/I$, but only the J value estimated with linear Ising model is available at the present time. Therefore, we approximately use the estimated $J=56$ cm^{-1} value as $J \approx 2T^2/I$. By putting the $I=11600$ cm^{-1} value into this relation, we obtain $T \approx -570$ cm^{-1} for the one-dimensional system of the DMA–$SbCl_5$ salt.

The optical and magnetic properties of DCA–

$SbCl_5$ salt can be understood in quite a similar way. Sato *et al.* observed a weak charge-transfer absorption at 11200 cm^{-1}.[3] The observed temperature dependence of the magnetic susceptibility was again analyzed in terms of antiferromagnetic linear Ising model with exchange coupling constant $J=56$ cm^{-1}. Then, the application of non-alternant one-dimensional Hubbard model gives $I=11200$ cm^{-1} and $T\approx-560$ cm^{-1} for the cation radical salt of DCA–$SbCl_5$.

Next, we consider the electronic state of P–ClO_4 salt. Its magnetic susceptibility was weakly paramagnetic and the intrinsic paramagnetism decreased with decrease of temperature. The observed magnetic susceptibility *versus* temperature curve fitted closely to the curve calculated from the singlet-triplet model, where the excited triplet state lies 1370 cm^{-1} above the ground singlet state.[3] Therefore, the perylene cation radicals appear to form dimers in the solid state. In contrast to the DMA–$SbCl_5$ and DCA–$SbCl_5$ salts, the electronic spectrum of the solid P–ClO_4 salt showed a strong low-energy absorption at 7700 cm^{-1}, which was attributable to the charge-transfer absorption of the dimer of the perylene cation radicals.[3] We consider the above optical and magnetic properties of the P–ClO_4 salt in terms of the dimer model of Hubbard Hamiltonian, which can be written by

$$\mathscr{H} = \sum_{\sigma} T(C_{1\sigma}^{+}C_{2\sigma}+C_{2\sigma}^{+}C_{1\sigma}) + I(n_{1\downarrow}n_{1\uparrow}+n_{2\downarrow}n_{2\uparrow}), \quad (3)$$

where the notations are common to those in Eq. 1. The suffixes, 1 and 2, denote two sites of perylene cation radicals in a dimer, and $T(<0)$ is the transfer matrix element between the cation radicals in the dimer. If we again take the half-occupied molecular orbital of the cation radical for each site, there are six bases of the wave functions for the dimer. After solving the eigenvalue problem, we have three singlet states and one triplet state. A detail of the wave functions and the energy levels are described in a previous paper.[8] The energy of the charge-transfer absorption, $h\nu_{CT}$, and the singlet-triplet energy separation, δ, are given by

$$h\nu_{CT} = \{(I/2)^2+(2T)^2\}^{1/2} + I/2, \quad (4)$$

$$\delta = \{(I/2)^2+(2T)^2\}^{1/2} - I/2. \quad (5)$$

This dimer model was then applied to the above optical and magnetic properties of the P–ClO_4 salt. By putting the observed values of $h\nu_{CT}=7700$ cm^{-1} and $\delta=1370$ cm^{-1} into Eqs. 4 and 5, we obtain $I=h\nu_{CT}-\delta=6330$ cm^{-1} and $T=-1630$ cm^{-1}, respectively.

The transfer matrix elements thus estimated are considered as a measure of the intermolecular interaction between cation radicals in the solid state. In this respect, the intermolecular interaction in the dimer of the perylene cation radicals of the P–ClO_4 salt should be strongest, while the intermolecular interactions between the 9,10-dimethylanthracene cation radicals in the DMA–$SbCl_5$ salt and between the 9,10-dichloroanthracene cation radicals in the DCA–$SbCl_5$ salt will be of the same order but will be much weaker than that of the P–ClO_4 system. Sato *et al.* noted that the intensity of the charge-transfer band observed in solid spectrum was correlated to the magnitude of exchange coupling constant.[3] In fact, solid P–ClO_4 shows the large values both in exchange coupling constant and intensity of the charge-transfer band, while DMA–$SbCl_5$ and DCA–$SbCl_5$ have weak charge-transfer absorptions and small exchange coupling constants. Although their suggestion was qualitative, we can verify quantitatively their idea on the basis of our Hubbard model. According to our theoretical work,[10] in the region of small $|T|$ limit, the intensity of the intermolecular charge-transfer absorption in non-alternant one-dimensional system of ion radicals is given by CT^2/I, where C is a constant including electric charge, unit cell length and number of sites of the system. On the other hand, the absorption intensity in the dimer model is expressed by $C'T^2/I$,[8] where the constant C' is somewhat different from C. Regardless of this minor difference, the intensity of charge-transfer absorption is predominantly governed by the magnitude of T^2/I. If we take into consideration the T and I values estimated above, the charge-transfer absorption intensity of the P–ClO_4 salt will be ten times or more stronger than those of the DMA–$SbCl_5$ and DCA–$SbCl_5$ salts. Moreover, we have found that, since the antiferromagnetic exchange coupling constant is given by $J\approx 2T^2/I$, the charge-transfer absorption intensity is approximately proportional to the magnitude of J.[10] In this respect, Sato's suggestion that the observed charge-transfer absorption intensity in solid spectrum may be greatly dependent on the magnitude of J receives strong evidence from our Hubbard model.

References

1) R. G. Kepler, *J. Chem. Phys.*, **39**, 3528 (1963).
2) Z. G. Soos and R. C. Hughes, *J. Chem. Phys.*, **46**, 253 (1967).
3) Y. Sato, M. Kinoshita, M. Sano, and H. Akamatu, *Bull. Chem. Soc. Jpn.*, **42**, 3051 (1969).
4) Y. Iida, *Bull. Chem. Soc. Jpn.*, **42**, 71, 637 (1969).
5) J. Tanaka, M. Tanaka, T. Kawai, T. Takabe, and O. Maki, *Bull. Chem. Soc. Jpn.*, **49**, 2358 (1976), and the references cited therein.
6) Y. Iida, *Bull. Chem. Soc. Jpn.*, **50**, 1445 (1977).
7) Y. Iida, *Bull. Chem. Soc. Jpn.*, **50**, 2481 (1977); **51**, 631 (1978).
8) Y. Iida, *Bull. Chem. Soc. Jpn.*, **51**, 2523 (1978).
9) Y. Iida, *Bull. Chem. Soc. Jpn.*, **51**, 3637 (1978).
10) Y. Iida, Paper presented at The Symposium on Molecular Structure, Hiroshima, Japan, 2B22 (1978).

BULLETIN OF THE CHEMICAL SOCIETY OF JAPAN, VOL. 52 (5), 1525—1526 (1979)

An INDO-MO Study of Peroxyacetyl Nitrate Formation

Katsutoshi OHKUBO* and Hiroyuki SATO

Department of Synthetic Chemistry, Faculty of Engineering, Kumamoto University, Kumamoto 860

(Received September 29, 1978)

Synopsis. The process of peroxyacetyl nitrate (PAN) formation has been disscussed on the basis of INDO calculations. The acetylperoxy radical (APR) has been found to be more reactive towards nitrogen monoxide than towards nitrogen dioxide. The bond strength of the O–O linkage in $CH_3C(=O)OONO$, however, is weaker than that of PAN or H_2O_2.

Peroxyacetyl nitrate (PAN) is a major class of eye irritant (lachrymators) in photochemical smog,[1–9] exhibiting toxicity in the inactivation of enzymes such as hemoglobin, papain, reduced ribonuclease and glutathione, and coenzyme A by the oxidation of the susceptible mercapto groups.[8,10,11] PAN has hitherto been considered to be formed in two distinct ways:

$$CH_3C{=}O \xrightarrow{O_2} CH_3C(=O)O_2 \xrightarrow{NO_2} CH_3C(=O)O_2NO_2 \quad \text{(Stephens's mechanism[2,6,8])} \quad (1)$$

$$[CH_3C(=O)O_2NO] \xrightarrow{-NO_2} [CH_3C(=O)O] \xrightarrow{NO_3} CH_3C(=O)O_2NO_2 \quad \text{(Hanst's mechanism[4])} \quad (2)$$

where the acetyl radical is produced by the photochemical decomposition of ketones or the oxidation of olefins and aldehydes in smog.[7] Louw *et al.*[6] and Cox *et al.*[12] recently supported Stephens's mechanism, but suggested the presence of a competitive reaction between $CH_3C(=O)O_2$ (APR) and NO.[12] Although there are some IR spectroscopic studies of PAN,[1,3,13] PAN has hitherto been the object of only limited investigation in terms of the molecular orbital treatment. The present MO study deals with the process of PAN formation.

Method of Calculation

Conformational optimizations were performed on $CH_3C{=}O$ $CH_3C(=O)O_2$, $CH_3C(=O)O_2NO$, and $CH_3C(=O)O_2NO_2$ by means of the INDO method[14] which is reliable for bond angles but less so for bond lengths.[14,15] The optimization, by means of a repeated SCF-procedure for the minimization of the total energy of a molecule, was conducted by changing the geometric parameters in turn until the optimum conformations of identical bond length and angle (within ±0.01 Å and 1°) were reached, the parameters of which are shown in Fig. 1.

Results and Discussion

The σ-type acetyl radical undergoes a rapid reaction with O_2 in air to form the acetylperoxy radical (APR) *via* the overlapping between the singly-occupied (SO), sp^2-like hybridized carbon orbital (spin density=0.62) on $CH_3C{=}O$ and the SO π_g-orbital of O_2 with a binding energy of 180.6 kcal/mol. APR

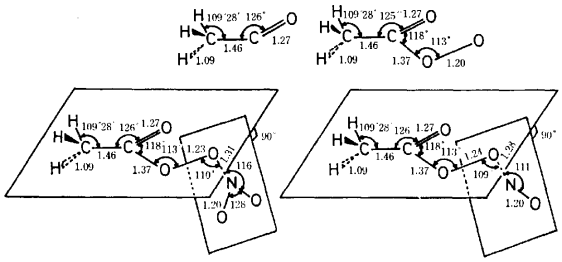

Fig. 1. Optimized geometric parameters for $CH_3C{=}O$, $CH_3C(=O)O_2$ $CH_3C(=O)O_2NO_2$, and $CH_3C(=O)O_2$-NO. (The HC-C(=O)-OO fragment is on the same plane.)

$$CH_3C{=}O \xrightarrow{O_2} CH_3\text{-}C(=O)\text{-}O\text{-}O^{\bullet} \text{ or } CH_3\text{-}C(=O)\text{-}O^{\bullet}\text{-}O \quad (3)$$

(I) (II)

corresponds to I which is energetically more stable than II by 1.03 kcal/mol (rotational barrier around the C–O bond=4.86 kcal/mol). The SO orbital (located at −0.504 a.u.) on the terminal oxygen (spin density=0.819) in APR, which expands perpendicularly to the C(=O)–O–O plane, is capable of coupling with the nitrogen SO orbital (at −0.489 a.u.) on the NO_2 (spin density=0.383) or with that (at −0.454 a.u.) on the NO (spin density=0.468). The minimized energetic process of the above coupling reaction was followed by the optimization of the geometric parameters of $CH_3C(=O)O_2$–NO or $CH_3C(=O)O_2$–NO_2 along the O–N bond. As can be seen from Table 1, the APR–NO_2 reaction is more energetically favored than the APR–NO_2 reaction. The most stable $CH_3C(=O)O_2NO$ and $CH_3C(=O)$-O_2NO_2 are obtained at an O–N distance of 1.28 and 1.31 Å respectively. The nuclear-electron attraction (E_I) makes the APR–NO_2 reaction more favorable than the APR–NO reaction, but the increase in the internuclear and interelectron repulsions (E_N and E_{II} respectively) in the reaction is more remarkable in the APR–NO_2 reaction. That the APR–NO reaction predominates the APR–NO_2 reaction agrees with the priority of $CH_3C(=O)O_2NO$ formation in the following competitive reactions:

$$\text{APR} \left\{ \begin{array}{ll} \xrightarrow[k]{NO} & CH_3C(=O)O_2NO \quad (4a) \\ \xrightarrow[k']{NO_2} & CH_3C(=O)O_2NO_2 \quad (4b) \end{array} \right. \qquad (k/k' \simeq 1.7^{12})$$

The relatively small amount of NO as compared with that of NO_2 in air ([NO]/[NO_2]=0.1(daytime)—1.0(night) in towns[12]), however, does not make Reaction 4a predominate over Reaction 4b in photochemical smog. The calculated binding energy of

Table 1. Changes in the geometric parameters and total energies (ΔE) along the reaction between APR and NO_2 and between APR and NO

R_{NO}/Å	∞	2.20	1.75	1.50	1.31	1.28
r_{OO}/Å	1.20 (1.20)	1.20 (1.21)	1.22 (1.22)	1.23 (1.23)	1.23 (1.24)	(1.24)
r_{NO}/Å	1.20 (1.16)	1.20 (1.16)	1.20 (1.16)	1.20 (1.16)	1.20 (1.16)	(1.20)
ϕ/deg.		100 (90)	102 (98)	105 (107)	110 (113)	(109)
ω/deg.[a]		0.0 (180)	0.0 (180)	0.0 (180)	0.0 (180)	(180)
θ/deg.	138.5	142 (92)	136 (100)	134 (109)	128 (115)	(111)
ΔE/a.u.[b]	0.0 (0.0)	0.135 (0.122)	−0.058 (−0.069)	−0.213 (−0.230)	−0.292 (−0.319)	(−0.324)

Values in parentheses are those for the APP-NO system. a) $\omega=0°$ in the following conformations. b) $\Delta E=E_{total}$(APR-NO_2 or APR-NO)$-E_{total}$(APR)$-E_{total}$(NO_2 or NO).

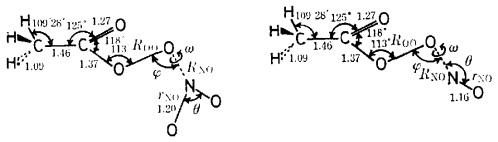

(HC-C(=O)-OO fragment is in the same plane).

the weakest O–O bond in $CH_3C(=O)OONO$ (249 kcal/mol) is less than that of the same bond in H_2O_2 (281 kcal/mol). Consequently, $CH_3C(=O)O_2NO$ undergoes thermal decomposition through the following reaction.

$$CH_3C(=O)O_2NO \xrightarrow{\Delta} CH_3C(=O)O + NO_2 \quad (5)$$

PAN formed by Reaction 4b has many rotational isomers (Fig. 2). The rotational barrier around the $O–NO_2$ bond was found to be 10.2 kcal/mol, around the O–O bond 1.66 kcal/mol, and around the C–O bond 11.9 kcal/mol. The bond strength of the O–O linkage (binding energy=273 kcal/mol) in PAN

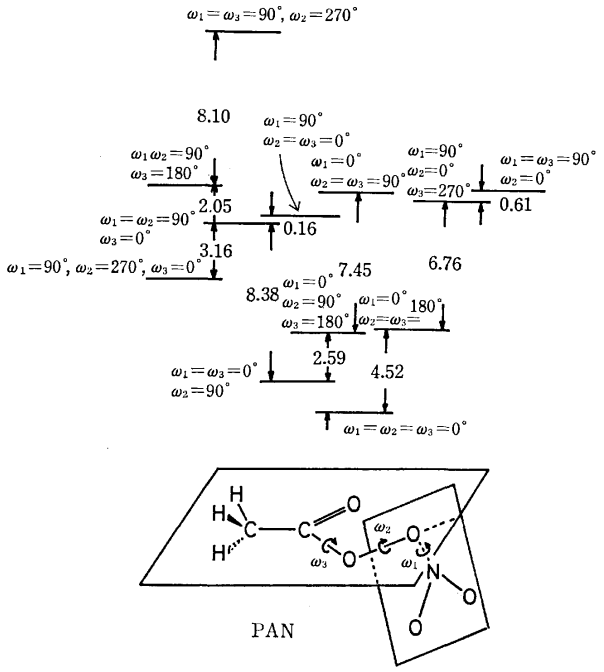

Fig. 2. Relative stability of the rotamers of PAN (energy difference: kcal/mol. $\omega_1=\omega_2=\omega_3=0$ and dihedral angle of the two planes=90° in the above energetically most stable conformation of PAN).

is of the same magnitude as that of H_2O_2, so that PAN is also thermally decomposed in the following way:[7]

$$PAN \xrightarrow{\Delta} [CH_3C(=O)O\text{-}\text{-}ONO_2] \longrightarrow$$

$$[CH_3\text{-}\text{-}C(=O)O] + ONO_2 \longrightarrow CH_3ONO_2 + CO_2 \quad (6)$$

where the binding energy of the C–C bond in CH_3-C(=O)O has been calculated as 249 kcal/mol. The photo-irradiation of PAN in the daytime, however, may bring about [n→π^*] type electron excitation on the carbonyl group (calculated excitation energy =227 kcal/mol). Such an electron excitation on the carbonyl group results in a weakening of the neighboring acyl bond in addition to that of the C=O bond *per se*; the excitation decreased the overlap population of the acyl bond by more than 10% with respect to the same bond in the ground state. Thus, the decomposition of PAN in the daytime may be expressed as follows:[7]

$$PAN \xrightarrow{h\nu} CH_3C{=}O + O_2NO_2 \xrightarrow{H_2O}$$

$$CH_3ONO_2 + CH_4 + CH_3OH + HCO_2H + NO_2 + O_2. \quad (7)$$

The radicals formed through the photochemical decomposition of PAN possibly abstract hydrogen from the SH group of the enzymes, thereby inactivating the enzymes *via* the formation of disulfides which are unobtainable from the *S*-acetyl group oxidation by PAN (or by H_2O_2).[11]

References

1) S. W. Nicksic, J. Harkins, and P. K. Mueller, *Atmos. Environ.*, **1**, 11 (1967).
2) E. R. Stephens, "Advances in Environmental Science," Wiley, New York (1969).
3) I. Fild and D. J. Lovell, *J. Opt. Soc. Am.*, **60**, 1315 (1970).
4) P. L. Hanst, *J. Air Pollution Control Assoc.*, **21**, 269 (1971).
5) P. H. Wendschuh, C. T. Pate, and J. N. Pitts, Jr., *Tetrahedron Lett.*, **1972**, 2931.
6) R. Louw, J. V. Ham, and H. Nieboer, *J. Air Pollution Control Assoc.*, **23**, 716 (1973).
7) F. K. V. Leh and P. K. C. Lak, "Environment and Pollution," C. C. Thomas Publisher, I11. (1974), pp. 15, 56.
8) J. W. Moore and E. A. Moore, "Environmental Chemistry," Academic Press, New York (1976), p. 222.
9) W. A. Glasson and J. M. Heuss, *Environ. Sci. Technol.*, **11**, 395 (1977).
10) J. B. Mudd, *Arch. Biochem. Biophys.*, **102**, 59 (1963).
11) J. B. Mudd and T. TMcManus, *Arch. Biochem. Biophys.*, **132**, 237 (1969).
12) R. A. Cox and M. J. Roffery, *Environ. Sci. Tech.*, **11**, 900 (1977).
13) E. L. Varetti and G. C. Pimentel, *Spectrochim. Acta, Part A*, **30**, 1069 (1974).
14) J. A. Pople and D. L. Beveridge, "Approximate Molecular Orbital Theory," McGraw-Hill, New York (1970), p. 80.
15) M. D. Newton, W. A. Lathan, W. J. Hehre, and J. A. Pople, *J. Chem. Phys.*, **52**, 4064 (1970).

BULLETIN OF THE CHEMICAL SOCIETY OF JAPAN, VOL. 52 (5), 1527—1528 (1979)

Lifetime Measurement of HO_2 Radical

Soji Tsuchiya* and Tomiji Nakamura

Department of Pure and Applied Sciences, College of General Education, The University of Tokyo, Komaba, Meguro-ku, Tokyo 153

(Received October 25, 1978)

Synopsis. The formation and dissipation kinetics of HO_2 radical was investigated by means of UV absorption measurement in a gas mixture, H_2+*ca.* 1% O_2+a trace of Hg vapor which was irradiated by a 253.7 nm light pulse. The rate constant of the reaction $2HO_2 \rightarrow H_2O_2+O_2$ was determined to be $(2.8\pm0.3)\times10^{12}$ cm^3 mol^{-1} s^{-1}.

The reported values of the reaction rate constants of HO_2 which is relevant to photochemical pollution are not in very good agreement with each other.[1] This may be attributed partly to lack of a reliable recombination rate constant of HO_2, since in most reactions the rate constants are determined relative to that of the recombination reaction. However, because of the difficulty in observing accurately the absolute concentration of HO_2, the recombination rate constants determined in different reaction systems show a relatively large scatter.[2-4]

In this note, the direct lifetime measurement as well as the determination of its absolute concentration are described. The method of HO_2 formation is based on the association reaction of H and O_2, the former of which is produced by the Hg photo-sensitized decomposition of H_2. The method is essentially similar to the one employed by Hunziker and Wendt who observed the near IR absorption spectrum of HO_2.[5]

The experimental apparatus is schematically shown in Fig. 1. The H_2 gas containing *ca.* 1% O_2 with a trace of Hg vapor is passed through a quartz cell, whose diameter and length are 3 and 30 cm, respectively, its flow rate being controlled to be several tens cm^3 s^{-1} at 1 atm and at room temperature. The cell was surrounded by six low pressure Hg lamps which were turned on periodically with a pulse width of *ca.* 20 ms and with a repetition frequency of several Hz. A d.c. source for the lamps was controlled by power transistors whose base current was supplied from a pulse generator. Thus, the Hg resonant light pulse with a rise time of 30 μs and variable pulse width was obtained. The UV light beam from a D_2 discharge lamp was passed through the cell, and fed into a monochromator. In order to measure a very weak absorption, the signal from the monochromator was digitized and accumulated to obtain the averaged signal of repeated light pulses. This made it possible to observe a change of transmittance as small as 5×10^{-5}. When a signal change Δ is obtained with the original light intensity of I_0, the optical density of the absorption is defined by

$$D \equiv \ln [I_0/(I_0-\Delta)] = \Delta/I_0 = \beta l[HO_2], \quad (1)$$

where β is the absorption coefficient of HO_2 and l is an optical pathlength.

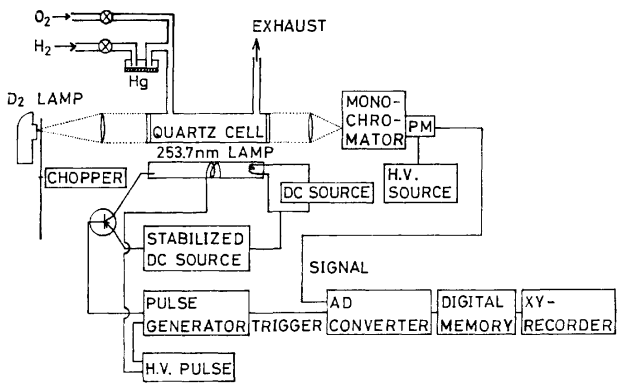

Fig. 1. Block diagram of the apparatus.

A transmittance change following the irradiation of the 253.7 nm light and its recovery after termination of the irradiation were found in the wavelength range of 200—250 nm as shown in Fig. 2. The absorption, which has a maximum intensity around 205 nm, is assigned to that of HO_2 since the absorption disappears with reduction of the O_2 content even if its fraction in H_2 is less than 10^{-2}. HO_2 must be formed by the reaction mechanism:

$$Hg + h\nu\ (253.7\ nm) \longrightarrow Hg^*, \quad (R1)$$

$$Hg^* + H_2 \longrightarrow Hg + 2H, \quad (R2)$$

$$H + O_2 + H_2 \longrightarrow HO_2 + H_2. \quad (R3)$$

A large Hg* quenching cross section of H_2 leads to the instantaneous formation of H atoms by irradiation of the Hg resonant light pulse. In Fig. 2, the transmission of the 205 nm light begins to decrease at the onset of the 253.7 nm light pulse approaching gradually a stationary value. After termination of the light pulse, the transmission recovers to some extent, and for com-

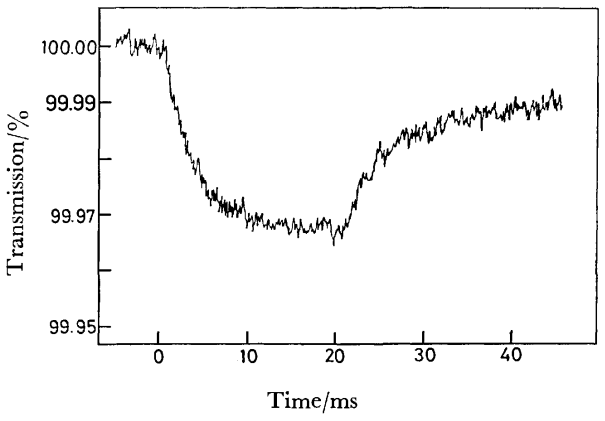

Fig. 2. An example of the observed transmittance change at 205 nm. The flow rates of H_2 and O_2 are 500 and 5 cm^3 min^{-1}, respectively, and the 253.7 nm light pulse width is 20 ms with its repetition frequency of 4 Hz. Number of data accumulated is 256.

plete recovery a fairly long time, during which the cell is refilled with fresh gas, is necessary.

Referring to the table of the reaction rate constants of HO_2,[1] the most probable reactions for the dissipation of HO_2 must be as follows:

$$HO_2 + HO_2 \longrightarrow H_2O_2 + O_2, \quad (R4)$$

$$HO_2 + H \longrightarrow H_2 + O_2. \quad (R5)$$

Reaction R5 is excluded because $[HO_2]$ is at most on the order of 10^{-11} mol cm^{-3} in comparison with *ca.* 10^{-7} mol cm^{-3} of the O_2 concentration. Thus, H atoms react with O_2 rather than with HO_2. Hence, the following kinetic relation is derived;

$$d[HO_2]/dt = \alpha I - 2k_5[HO_2]^2, \quad (2)$$

where I represents the 253.7 nm radiation intensity per unit volume and time and α is a constant to describe the conversion of the absorbed light quantum to moles of HO_2. After termination of the light pulse, Eq. 2 is integrated to give the relation

$$(1/[HO_2]_t) - (1/[HO_2]_{t=\tau}) = 2k_5(t-\tau), \quad (3)$$

where τ is the duration of the light pulse. This equation is modified by substituting Eq. 1 as

$$(1/D_t) - (1/D_{t=\tau}) = 2(k_5/\beta l)(t-\tau). \quad (4)$$

Thus, the absorption coefficient must be known in order to determine the relevant reaction rate.

Inspecting the data of Fig. 2, it is found that a stationary concentration of HO_2 is not realized strictly during the irradiation of 253.7 nm light, and that the UV light does not recover its original intensity long after the termination of the light pulse. These facts may be attributed to the formation of H_2O_2 which absorbs the UV light with an absorption coefficient smaller than that of HO_2. Hence, Eq. 1 should be corrected to

$$D = \beta l[HO_2] + \beta' l[H_2O_2], \quad (5)$$

where β' is the absorption coefficient of H_2O_2. On the beginning of the irradiation, the increase of absorption intensity can be assumed to be solely due to the formation of HO_2, *i.e.*,

$$(dD/dt)_{t=0} = \beta l(d[HO_2]/dt)_{t=0} = \beta l\alpha I. \quad (6)$$

Since the absorption at the final stage should originate from H_2O_2, that is the end product, the stoichiometric relation

$$D_{t=\infty} = \beta' l[H_2O_2]_{t=\infty} = \beta' l\alpha I\tau/2_2 \quad (7)$$

is satisfied. Substituting Eq. 7 into Eq. 6, the absorption coefficient β may be determined by the use of the equation

$$2D_{t=\infty}/(dD/dt)_{t=0}\tau = \beta'/\beta, \quad (8)$$

where β' is known accurately.[6] The absorption coefficient thus determined is $(1.80\pm0.14)\times10^6$ cm^2 mol^{-1} at 205 nm in good agreement with the value reported.[4]

If we deal with the behavior of HO_2 after termination of the light pulse, the following stoichiometric relation is obtained:

$$[HO_2]_t + 2[H_2O_2]_t = 2[H_2O_2]_{t=\infty}, \quad (9)$$

where $t \geq \tau$. Then, $[HO_2]_t$ may be determined by the equation

$$[HO_2]_t = [D(t) - D(t=\infty)]/l(\beta - 0.5\beta'). \quad (10)$$

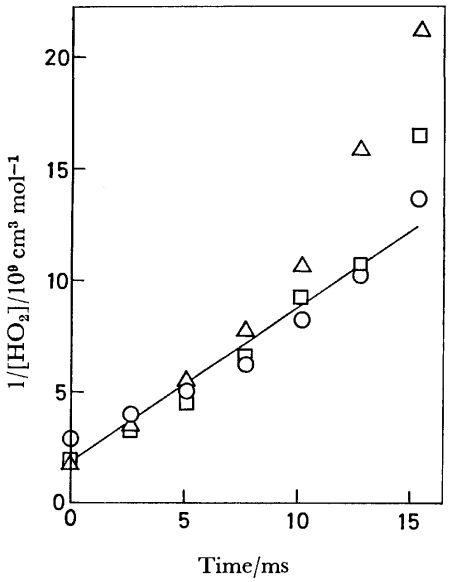

Fig. 3. Plots of $[HO_2]^{-1}$ *vs.* time after the termination of the light pulse. △: 1% O_2 in H_2, ○: 2%O_2, □: 0.5% O_2.

Table 1. Rate constant of $2HO_2 \rightarrow H_2O_2 + O_2$

Investigator	$k_5/10^{12}$ cm^3 mol^{-1} s^{-1}
Foner & Hudson[2]	*ca.* 1.8
Hochanadel *et al.*[4]	5.7±0.5
Paukert & Jonston[3]	2.2±0.3
This work	2.8±0.3

The reciprocals of the obtained values of $[HO_2]_t$ are plotted in Fig. 3 as a function of time lapse after termination of the light pulse, $(t-\tau)$. According to Eq. 3 the initial slope gives the relevant rate constant. A good linearity is found for the initial decay of $[HO_2]$ supporting the second order reaction of the HO_2 dissipation. However, in a later stage, the bimolecular process becomes a minor one since atomic hydrogen or impurity molecules may react with HO_2, so that the plots of $[HO_2]^{-1}$ *vs.* $(t-\tau)$ deviate significantly from the linear line, although the quantity of HO_2 which reacts in non-bimolecular processes is fairly small, probably less than 10% of the original $[HO_2]$. The rate constant obtained is given in Table 1 together with the literature values.

This work was supported partly by a Grant-in-Aid for Scientific Research from the Ministry of Education (No. 111202).

References

1) A. C. Lloyd, *Int. J. Chem. Kinet.*, **6**, 169 (1974).
2) S. N. Foner and R. L. Hudson, *J. Chem. Phys.*, **21**, 1608 (1953).
3) T. T. Paukert and H. S. Johnston, *J. Chem. Phys.*, **56**, 2824 (1972).
4) C. J. Hochanadel, J. A. Ghormley, and P. J. Ogren, *J. Chem. Phys.*, **56**, 4426 (1972).
5) H. E. Hunziker and H. R. Wendt, *J. Chem. Phys.*, **60**, 4622 (1974).
6) R. B. Holt, C. K. McLane, and O. Oldenberg, *J. Chem. Phys.*, **16**, 255, 638 (1948).

BULLETIN OF THE CHEMICAL SOCIETY OF JAPAN, VOL. 52 (5), 1529—1530 (1979)

Matrix Representation of an Olefinic Reference Structure for Monocyclic Conjugated Compounds

Jun-ichi AIHARA

Department of Chemistry, Faculty of Science, Hokkaido University, Sapporo 060

(Received November 13, 1978)

Synopsis. A reference polynomial which represents an olefinic reference structure of a monocyclic conjugated system can be expressed in the form of a Hermitian matrix. Some interesting features of the reference structure have been deduced from it.

The author has developed a graph theory of aromaticity,[1,2] in which the resonance energy due to aromaticity is given as the difference between the total π-electron energy of a conjugated compound and that of its olefinic reference structure. The reference energy of a conjugated hydrocarbon, *i.e.*, the total π-electron energy of its reference structure, has been defined by the following reference polynomial:[1]

$$R(X) = X^N + \sum_{r=1}^{[N/2]} (-1)^r p(r) X^{N-2r}, \quad (1)$$

where N is the number of sp^2-carbon atoms in a conjugated system, $[N/2]$ is the maximum integer not exceeding $N/2$, and $p(r)$ is the number of ways of choosing r disjoint π bonds from the conjugated system.[3] The reference energy is given as twice the sum of the larger $[N/2]$ roots of the equation

$$R(X) = 0. \quad (2)$$

A matrix representation of such a reference polynomial is possible for any monocyclic conjugated system, and is discussed below.

Consider a monocyclic conjugated hydrocarbon with N sp^2-carbon atoms, M of which constitute a closed π ring. The other carbon atoms, if any, belong to the substituent(s). Let an adjacency matrix[4] for this conjugated system be denoted by A and the elements by a_{ij}. The matrix element a_{ij} is therein equal to unity if there is a π bond between the atoms i-j. All the other matrix elements are zero. The eigenvalues of this matrix represent the orbital energies of a conjugated system.

The elements of the matrix A are then changed as follows. If matrix element a_{ij} corresponds to one of the M π bonds forming a π ring, it is weighted with a factor $\exp(i\eta_{ij}\theta)$, where the numerical value of θ is $\pi/(2M)$, and

$$\eta_{ij} = \begin{cases} +1 & \text{if atoms i}\rightarrow\text{j are arranged clockwise in a } \pi \text{ ring of a conjugated system, and} \\ -1 & \text{if not.} \end{cases}$$

The remaining matrix elements are left unchanged. The resulting matrix is denoted by B and the elements by b_{ij}. Matrix B is thus a weighted adjacency matrix.

Next, consider a secular determinant defined by

$$Q(X) = (-1)^N \det|B - EX|, \quad (4)$$

where E is a unit $N \times N$ matrix. On expansion, $Q(X)$ leads to a polynomial in X, the coefficients all being expressible in terms of the closed cyclic products of the type $b_{ij}b_{jk}\cdots b_{pq}b_{qi}$.[5] Such products of more than two matrix elements represent a cyclic array of π bonds, *i.e.*, a π ring, in a conjugated system. These products, however, vanish in the present case since

$$b_{ij}b_{jk}\cdots b_{pq}b_{qi} + b_{ji}b_{kj}\cdots b_{qp}b_{iq} = 2\cos\left(\frac{\pi}{2}\right) = 0. \quad (5)$$

The non-zero cyclic product is represented by

$$b_{ij}b_{ji} = \exp(0) = 1 \quad (6)$$

for each π bond. Then, apply an extended version of Sachs' graph-theoretical theorem[5] to the secular determinant $Q(X)$ with Eqs. 5 and 6 in mind, and the determinant will necessarily be expanded into the same polynomial as the reference polynomial for the same conjugated system, namely,

$$R(X) \equiv Q(X). \quad (7)$$

It has thus been proved that a reference polynomial for a monocyclic conjugated system can be expressed in the form of Eq. 4. Since matrix B is a Hermitian matrix, the eigenvalues of the matrix, *i.e.*, the roots of the equation $Q(X)=0$, are all real.

For example, matrix B for styrene in Fig. 1 is

$$B = \begin{pmatrix} 0 & 1 & 0 & 0 & 0 & 0 & 0 & 0 \\ 1 & 0 & 1 & 0 & 0 & 0 & 0 & 0 \\ 0 & 1 & 0 & z & 0 & 0 & 0 & z^* \\ 0 & 0 & z^* & 0 & z & 0 & 0 & 0 \\ 0 & 0 & 0 & z^* & 0 & z & 0 & 0 \\ 0 & 0 & 0 & 0 & z^* & 0 & z & 0 \\ 0 & 0 & 0 & 0 & 0 & z^* & 0 & z \\ 0 & 0 & z & 0 & 0 & 0 & z^* & 0 \end{pmatrix}, \quad (8)$$

where

$$z = \exp\left(\frac{\pi}{12}\,\mathrm{i}\right). \quad (9)$$

This matrix leads to the same polynomial as $R(X)$ for this compound, *i.e.*,

$$Q(X) = R(X) = X^8 - 8X^6 + 19X^4 - 14X^2 + 2. \quad (10)$$

From the present definition of matrix B, the following

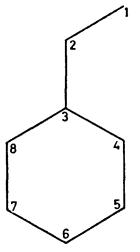

Fig. 1. A conjugated system of styrene.

equalities have been clarified for monocyclic conjugated hydrocarbons:

$$\mathrm{Tr}\, B = \mathrm{Tr}\, A = 0, \tag{11}$$

$$\mathrm{Tr}\, B^2 = \mathrm{Tr}\, A^2 = 2H, \tag{12}$$

where H is the number of π bonds in an entire conjugated system. Note that the trace of a matrix is the sum of the eigenvalues. Equation 11 indicates that the sum of the orbital energies vanishes both for a conjugated system and its reference structure. Equation 12 indicates that the sum of the orbital energies squared for a conjugated system is equal to that for its reference structure. According to extensive numerical analysis, these equalities appear to hold true for polycyclic conjugated hydrocarbons without exception. Since the sum of the orbital energies squared is preserved in the reference structure, it can be deduced that some of the occupied orbitals in a conjugated system must be energetically higher than the corresponding orbitals in its reference structure[6] even if the conjugated system is aromatic with positive resonance energy.

A reference polynomial for a monocyclic heterocyclic conjugated system can also be derived from the secular determinant simply by weighting the matrix elements with the same factors $\exp(i\eta_{ij}\theta)$ as in the case of monocyclic conjugated hydrocarbons. It is interesting to note that, if $\theta=\pi/M$, matrix B represents a Möbius conjugated system, *i.e.*, a singly twisted conjugated system.[7]

References

1) J. Aihara, *J. Am. Chem. Soc.*, **98**, 2750 (1976); **99**, 2048 (1977); **100**, 3339 (1978); *J. Org. Chem.*, **41**, 2488 (1976); *Bull. Chem. Soc. Jpn.*, **50**, 3057 (1977); **51**, 1541 (1978).

2) Gutman *et al.* independently arrived at the same theory of aromaticity: I. Gutman, M. Milun, and N. Trinajstić, *J. Am. Chem. Soc.*, **99**, 1692 (1977).

3) H. Hosoya, *Bull. Chem. Soc. Jpn.*, **44**, 2332 (1971); *Theor. Chim. Acta*, **25**, 215 (1972).

4) F. Harary, "Graph Theory," Addison-Wesley, Reading, Mass. (1969), Chap. 13.

5) J. Aihara, *J. Am. Chem. Soc.*, **98**, 6840 (1976).

6) J. Aihara, *Bull. Chem. Soc. Jpn.*, **50**, 2010 (1977); **51**, 1788 (1978).

7) E. Heilbronner, *Tetrahedron Lett.*, **1964**, 1923.

BULLETIN OF THE CHEMICAL SOCIETY OF JAPAN, VOL. 52 (5), 1531—1532 (1979)

Determination of Self-diffusion Coefficient of Nickel in Nickel Sulfide

Kazuo KOTANI,** Kenichiro OTA,* Takemi AIZAWA,*** and Kazuo FUEKI

Department of Industrial Chemistry, Faculty of Engineering, The University of Tokyo, Hongo, Bunkyo-ku, Tokyo 113

(Received December 2, 1978)

Synopsis. The self-diffusion coefficient of nickel in nonstoichiometric nickel sulfide, $Ni_{1-\delta}S$, was measured as a function of δ, using ^{63}Ni in the temperature range of 550—750 °C. At $\delta=0.028$, the self-diffusion coefficient, D^*_{Ni}, was expressed by the following equation:

$$D^*_{Ni} = 3.3 \times 10^{-7} \exp\left(-\frac{73.2\pm9.2/\text{kJ mol}^{-1}}{RT}\right) \text{m}^2\,\text{s}^{-1}.$$

At 550 °C and 650 °C, D^*_{Ni} increased with an increase in δ from 0 to 0.04 and tended to reach the saturation point above $\delta=0.04$.

Generally, the self-diffusion in inorganic crystals takes place *via* point defects, so it is necessary to know the relation between the self-diffusion coefficient and the defect concentration in order to elucidate the diffusion mechanism. There have, however, been only a few studies which have determined the self-diffusion coefficient as a function of the defect concentration. $Ni_{1-\delta}S$ has a wide nonstoichiometric region, δ.[1-3] The purpose of the present study is to determine the self-diffusion coefficient of nickel in $Ni_{1-\delta}S$ as a function of δ at 550—750 °C.

Experimental

Specimen. The nickel sulfide was prepared by sulfidizing electrolytic nickel powder (99.99% purity) with sulfur purified by distillation *in vacuo*.

They were reacted in a Vycor reaction tube, first at 400 °C for a week and then at 900 °C for 4 days to complete the sulfidization. A single crystal of nickel sulfide, 5 mm in diameter and 50 mm long, was grown by the Bridgeman method. The crystal orientation was determined by the Laue method. Disks, 2 mm in thickness, were cut perpendicular to the c-axis from the single crystal by means of a crystal cutter and polished with polishing paper.

Controlling of δ. A sulfide specimen and sulfur were sealed in an evacuated Vycor tube and placed in an electric furnace which had two different temperature zones. The specimen was set in the high-temperature zone (700 °C), while the sulfur was placed in the low-temperature zone. The specimen was then annealed for 4 days in sulfur vapor, whose vapor pressure was controlled by the lowest temperature of the tube. The δ was determined using the relation between the sulfur pressure and δ,[2] and doubly checked by means of the lattice constant using Laffitte's results.[3]

Diffusion Annealing. About 10 μCi of ^{63}Ni was applied to one end of the disk specimen, after which the specimen was placed in a Vycor tube, evacuated, and sealed. Then the tube was placed in an electric furnace kept at a desired temperature for diffusion annealing. In order to avoid any change in composition resulting from the decomposition of sulfide, the volume of the reaction tube was minimized to about 3 cm^3.

Measurement of the Self-diffusion Coefficient. After the diffusion-annealing the specimen was taken out and sectioned by successive grinding by means of a grinding machine which has been described elsewhere.[5] The thickness of each layer was 5—10 μm, as determined from the weight decrease in the specimen after grinding.

The radioactivity of ^{63}Ni on the polishing paper was counted by the liquid-scintillator-method, since β-rays from ^{63}Ni are too weak for the radioactivity to be measured by the use of a Geiger-Muller counter, especially at low radioactivity. Polishing paper smeared with sulfide powder was immersed in the liquid scintillator, and photons activated by β-rays were measured by means of a photomultiplier.

Results and Discussion

Figure 1 shows the Arrhenius plot for the self-diffusion coefficient, D^*_{Ni}, in $Ni_{1-\delta}S$ at $\delta=0.028$. The D^*_{Ni} value obtained by Klotsman at $\delta=0.03$ is also shown in the same figure for the sake of comparison. There is a good agreement between the two results. The present result at $\delta=0.028$ can be expressed by the following equation:

$$D^*_{Ni} = 3.3 \times 10^{-7} \exp\left(-\frac{73.2\pm9.2/\text{kJ mol}^{-1}}{RT}\right) \text{m}^2\,\text{s}^{-1}$$

Since δ is constant, the activation energy, 73.2 kJ mol^{-1}, indicates the enthalpy of activation for the migration of nickel in $Ni_{1-\delta}S$.

Figure 2 shows the relation between D^*_{Ni} and δ at 550 °C and 650 °C. D^*_{Ni} increases with an increase in δ from 0 to 0.04 at both temperatures. However,

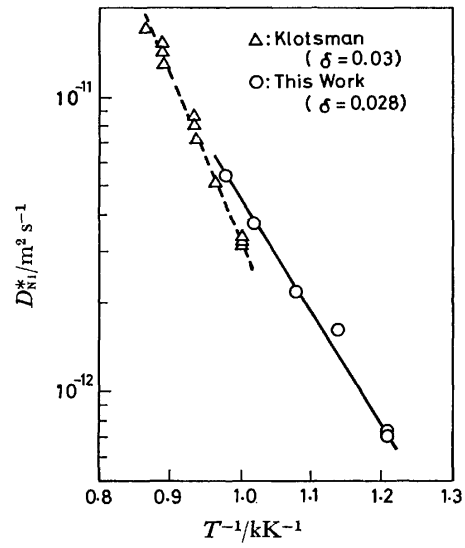

Fig. 1. Arrhenius plot of D^*_{Ni} in $Ni_{1-\delta}S$.

**Present address: National Institute for Researches in Inorganic Materials, Sakura-mura, Ibaragi.

***Present address: Onoda Cement Co., Ltd., Fujiwara-cho, Mie.

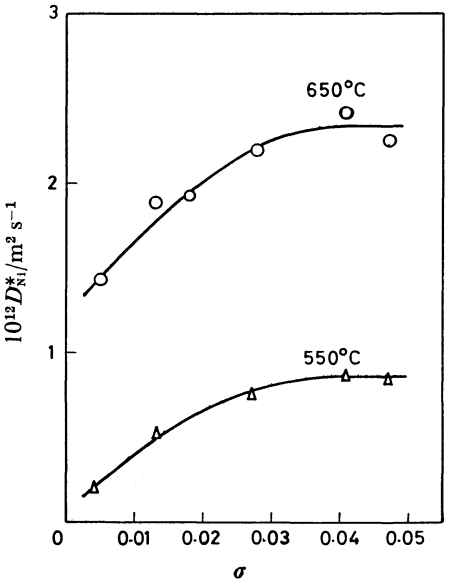

Fig. 2. Relation between D^*_{Ni} and δ in $Ni_{1-\delta}S$.

D^*_{Ni} is not linearly related to δ and tends to reach the saturation point above $\delta=0.04$. A simple defect model would thus appear to be inappropriate for $Ni_{1-\delta}S$.

The same tendencies for the D^*_{Fe} in $Fe_{1-\delta}S$, which has the same Ni–As type of crystal structure,[6] and also for D^*_{Fe} in $Fe_{1-\delta}O$[7] have been reported. The dependence of the D^*_{Fe} in $Fe_{1-\delta}O$ on δ was explained by the formation of clusters of iron vacancies.[7] If the defect clusters are formed in $Ni_{1-\delta}S$, the concentration of free vacancies that are responsible for the diffusion process would not be expected to be linearly related to the deviation from stoichiometry. To ascertain the defect structure of $Ni_{1-\delta}S$, detailed studies, for example, neutron and X-ray diffraction studies, are necessary.

The authors wish to thank Dr. Koichi Kitazawa for his helpful discussions.

References

1) T. Rosenqvist, *J. Iron Steel Inst.*, **176**, 37 (1954).
2) H. Rau, *J. Phys. Chem. Solids*, **36**, 1199 (1975).
3) M. Laffitte and J. Benard, *C. R. Acad. Sci., Ser. C*, **242**, 518 (1956).
4) S. M. Klotsman, A. N. Timofeyev, and I. Sh. Trakhtenberg, *Fiz. Met. Metalloved.*, **16**, 743 (1963).
5) H. Letaw, J. L. M. Slifkin, and W. M. Portnoy, *Rev. Sci. Instrum.*, **25**, 865 (1954).
6) R. H. Condit, R. R. Hobbins, and C. E. Birchenall, *Oxid. Met.*, **8**, 409 (1974).
7) W. K. Chen and N. L. Peterson, Proc. U. S.-Japan Joint Seminar on Defects and Diffusion in Solids, Tokyo, Oct., 1976, p. 177.

BULLETIN OF THE CHEMICAL SOCIETY OF JAPAN, VOL. 52 (5), 1533—1534 (1979)

1,3,5-Triarylpyrazoles as Phosphorescing Impurities in 1,3,5-Triaryl-2-prazolines

Hiroyoshi YAMAMOTO, Yumiko SANO, Yasuhiko SHIROTA,* Hajime SEKI,** and Hiroshi MIKAWA

Department of Applied Chemistry, Faculty of Engineering, Osaka University, Yamadakami, Suita, Osaka 565

***IBM Research Laboratory, San Jose, California 95193*

(Received December 5, 1978)

Synopsis. The origin of the phosphorescence observed for 1,3,5-triphenyl-2-pyrazoline and its substituted derivatives was investigated. Unlike the previously accepted conclusion, our conclusion is that the phosphorescence originates from the corresponding pyrazoles formed from the pyrazolines by the action of light.

Numerous studies have been made of the electronic absorption and emission spectra of 1,3,5-triphenyl-2-pyrazoline (TPP) and its derivatives. These compounds exhibit three absorption bands, *i.e.*, two intense bands in the wavelength regions at around 230—260 nm and 350—420 nm, and a less intense one appearing frequently in the form of an inflection at the 300—330 nm region.[1,2] On excitation in the longest wavelength absorption band, an intense fluorescence with a quantum yield of close to unity appears in nonpolar solvents, no phosphorescence being observed.[3,4] It has been reported, however, that a weak, long-lived green phosphorescence is observed with TPP and some of its derivatives on excitation in the shorter wavelength absorption band by the light of 313 nm, and the phosphorescence has been ascribed as due to the 5-aryl group that constitutes an independent set of singlet and triplet levels from the conjugated π-electron system Ar–N–N=C–Ar in the pyrazoline ring which is responsible for the characteristic spectral features of TPP and its derivatives.[2] This conclusion has been cited also in a recent publication by an independent researcher.[5]

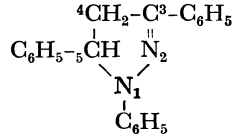

TPP

As a part of our studies on the physical and chemical properties of TPP and its derivatives,[6] we have reinvestigated the origin of the phosphorescence emission observed for TPP and its derivatives. Three compounds, *i.e.*, TPP, 1,5-diphenyl-3-(*p*-methoxyphenyl)-2-pyrazoline (MTPP), and 1,5-diphenyl-3-(*p*-dimethylaminophenyl)-2-pyrazoline (DMATPP), were examined in the present study. The use of the amino-substituted TPP has made the assignment of the phosphorescence emission easy and successful. As shown in Fig. 1, TPP and MTPP purified by repeated recrystallizations exhibit a very weak phosphorescence in the wavelength region of 400 to 500 nm on excitation by the light of 300 to 320 nm, whereas only intense fluorescence appears in the wavelength region of 400 to 500 nm on excitation in the long-wavelength absorption band of these compounds. The phosphorescence was so weak that it was detected under conditions of the maximum sensitivity of the instrument with a wide slit width. On the other hand, DMATPP purified by repeated recrystallizations shows a much more intense phosphorescence in the wavelength region of 440 to 550 nm on excitation by the light of 300 to 340 nm (Fig. 2d), whereas on excitation in the long-wavelength absorption band, only intense fluorescence of DMATPP appears in the wavelength region of 400 to 500 nm (Fig. 2a). It was also found that, in the total emission spectrum (Fig. 2c), the appearance of the phosphorescence is accompanied by the appearance of a new fluorescence at around 350 to over 400 nm. The excitation spectra for the phosphorescence and the new fluorescence were found to be the same with each other, but different from that for the DMATPP fluorescence at the 400 to 500 nm region which corresponds to the absorption spectrum of DMATPP.

These results indicate that the phosphorescence and the new fluorescence (in the case of DMATPP) observed on excitation by the light of 300 to 340 nm do not result from the singlet and triplet levels of the 5-phenyl group in the pyrazoline ring as has been stated in the literature. Emitting impurities conceivable to be incorporated into the pyrazoline compounds during the synthetic process were examined, but their emission spectra did not agree with those shown in Figs. 1 and 2. It was found that the intensity of the phosphorescence and the new fluorescence observed for DMATPP increases when a sample solution was left to stand as it is for long days or after spectral measurements were repeated, and that these emissions are extremely weak with respect to a virgin sample prepared in the dark throughout the processes of purification, drying, and preparation of a solution (Fig. 2b). These

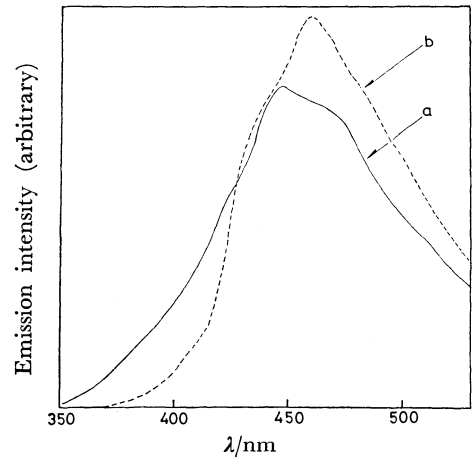

Fig. 1. Corrected phosphorescence spectra observed for TPP (a) and MTPP (b) on excitation by the light of 320 nm in MTHF at 77 K.

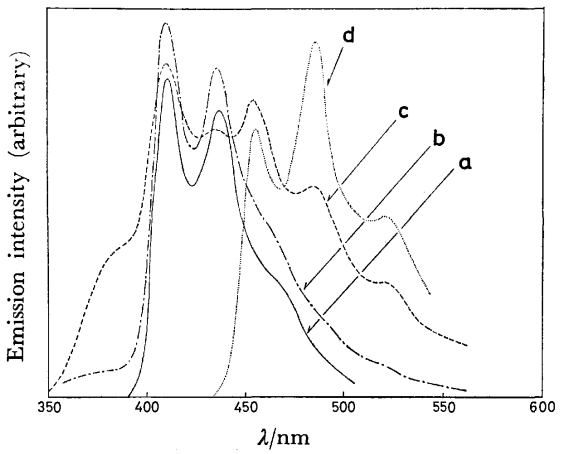

Fig. 2. Corrected emission spectra observed for DMATPP in MTHF at 77 K.
a, b, and c: Total emission spectra; d: delayed emission spectrum.
a: Fluorescence spectrum inherent to DMATPP observed on excitation by the light of 370 nm. b: Emission spectrum observed for a virgin smaple prepared in the dark on excitation by the light of 320 nm. c: Emission spectrum observed on excitation by the light of 320 nm. d: Phosphorescence spectrum observed on excitation by the light of 320 nm.

results indicate that the impurity which is responsible for these emissions is derived from the pyrazoline compound probably by the action of light such as sunlight, light from fluorescent room lamps, and the light employed for spectral measurements. Confirmation for this conjecture was obtained from the result that the intensity of the new emissions for DMA-TPP increases gradually on illuminating a sample solution by the light of 366 nm using a 500 W high pressure mercury lamp, while the intensity of the DMATPP fluorescence decreases with an isoemissive point at 396 nm.[7]

The phosphorescence and the new fluorescence observed for DMATPP on excitation in the ostensible shorter wavelength absorption band were identified as the ones originating from the excitation of 1,5-diphenyl-3-(*p*-dimethylaminophenyl)pyrazole (DMATPPzole) based on the identity of the shape and position of the emission bands, the excitation spectra, and the lifetimes of the emissions with those of the authentic DMATPPzole (τ_f=7.2 ns at room temp, τ_p=0.97 s at 77 K, in a degassed solution of 2-methyltetrahydrofuran). Likewise, the phosphorescences observed for TPP and MTPP were found to be identical with those of the corresponding pyrazoles, although the resolution of the vibrational structure of the phosphorescence bands shown in Fig. 1 is lower as compared with the phosphorescence bands of the authentic 1,3,5-triphenylpyrazole (TPPzole) and 1,5-diphenyl-3-(*p*-methoxyphenyl)pyrazole (MTPPzole). The major reason why the emission due to the impurity pyrazole is much more intense for DMATPP as compared with TPP and MTPP is that DMATPPzole absorbs the light of 300 to 340 nm much more strongly than TPPzole and MTPPzole (λ_{max}(log ε) in MTHF at room temp: 257 nm(4.46) for TPPzole; 261 nm (4.51) for MTPPzole: 290 nm(4.54) for DMATPPzole).

Although the photochemical conversion of TPP and its derivatives into the corresponding pyrazoles has been known,[8] the present sudy of the measurement of the emission spectra has revealed that these compounds are very sensitive to light. The phenomena observed in the emission spectra seem to be general with many other derivatives of TPP which undergo photodehydrogenation. TPP and its derivatives have found applications for practical use, *e.g.*, as fluorescent whitening agents,[9] and as material for electrophotography.[10] The chemical properties described above should be taken into account in evaluating the function of these materials.

Experimental

Materials. TPP (mp 141—2 °C), MTPP (mp 140.5—141.5 °C) were prepared according to the known procedure,[11] purified by repeated recrystallizations from EtOH and dried *in vacuo*. DMATPP (mp 199.5—201 °C) was synthesized in a similar manner by the reaction of phenylhydrazine with 1-(*p*-dimethylaminophenyl)-3-phenyl-2-propenone which was obtained by the reaction of *p*-dimethylaminoacetophenone with benzaldehyde, purified by repeated recrystallizations from EtOH and dried *in vacuo*. TPPzole (mp 138—138.5 °C), MTPPzole (mp 141—142 °C), and DMATPPzole (149—149.5 °C) were prepared from the corresponding pyrazolines by the dehydrogenation reaction with chloranil in refluxing xylene, followed by column chromatography over neutral alumina, recrystallized several times from EtOH, and dried *in vacuo*.

Spectral Measurement. The electronic absorption spectra were recorded with a Hitachi 124 spectrophotometer. The emission and excitation spectra were recorded with a Hitachi MPF-3 spectrofluorometer fitted with a R446 photomultiplier. The concentration of the solution was *ca.* 2×10^{-5} mol/l. The fluorescence lifetime was measured by means of a pulsed N_2 laser with a pulse width of *ca.* 2 ns and repetition of *ca.* 3 Hz.

References

1) R. N. Nurmukhametov and V. B. Tishchenko, *Opt. Spectrosc.*, **23**, 43 (1967).
2) R. N. Nurmukhametov, N. A. Lodygin, and G. I. Grishina, *Opt. Spectrosc.*, **25**, 118 (1968).
3) I. H. Leaver and D. E. Rivett, *Mol. Photochem.*, **6**, 113 (1974).
4) H. Strahle, W. Seitz, and H. Guster, *Ber. Bunsenges. Phys. Chem.*, **80**, 288 (1967).
5) I. H. Leaver, *Mol. Photochem.*, **5**, 411 (1973).
6) a) Y. Sano, K. Kato, M. Yokoyama, Y. Shirota, and H. Mikawa, *Mol. Cryst. Liq. Cryst.*, **36**, 137 (1976); b) F. Iinuma, H. Mikawa, and Y. Shirota, *Polym. Bull.*, in press (1979).
7) The photodehydrogenation of the pyrazolines occurred in solution under evacuation at 2×10^{-2} Torr.
8) L. Schrader, *Tetrahedron Lett.*, **1971**, 2977.
9) A. Wagner, C. W. Schellhammer, and S. Peterson, *Angew. Chem. Int. Ed. Engl.*, **5**, 699 (1966).
10) P. J. Melz, R. B. Champ, L. S. Chang, C. Chiou, G. S. Keller, L. C. Liclican, R. R. Neiman, M. D. Shattuck, and W. J. Weiche, *Photogr. Sci. Eng.*, **21**, 73 (1977).
11) R. H. Wiley, C. H. Jarboe, F. N. Hayes, E. Hansbury, J. T. Nielsen, P. X. Callahan, and M. C. Sellars, *J. Org. Chem.*, **23**, 732 (1958).

BULLETIN OF THE CHEMICAL SOCIETY OF JAPAN, VOL. 52 (5), 1535—1536 (1979)

Rate and Mechanism of the Complex Formation of Thallium(III) with 4-(2-Pyridylazo)resorcinol (PAR) in Aqueous Solution†

Ryuichi FUNADA,†† Taira IMAMURA, and Masatoshi FUJIMOTO*
Department of Chemistry, Faculty of Science, Hokkaido University, Sapporo 060
(Received July 26, 1978)

Synopsis. The kinetics of complex formation of Tl(III) with PAR (LH_3^+) was studied in aqueous solution at 25 °C, $[H^+]=0.1$—1.0 mol dm^{-3}, and ionic strength $I=2.0$ mol dm^{-3} ($NaClO_4$). The formation rate constants k_1 and k_2 assigned to the reactions of Tl^{3+} and $TlOH^{2+}$ with LH_3^+ were determined to be 4.1×10^4 and 1.8×10^5 mol^{-1} dm^3 s^{-1}, respectively. The rate data were discussed in comparison with those for Tl(III)-Semi-Xylenol Orange system.

Thallium(III) has been reported to form colored complexes with some *o*-hydroxy azo multidentate ligands as PAR and its analogs even in acidic media.[1,2] However, no kinetic studies have been reported so far except for our early work on the complex formation of Tl(III) with Semi-Xylenol Orange, SXO, which gives the rate constant 3×10^5 mol^{-1} dm^3 s^{-1} for the reaction of $TlOH^{2+}$ and a neutral species of SXO, H_4SXO^0.[3,4] In the present paper we report the kinetic data for the complex formation of Tl(III) with PAR, in order to compare the rate constants with those for the reaction of Tl(III) with SXO.

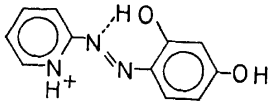

PAR (LH_3^+)

In the proton concentrations 0.1—1.0 mol dm^{-3} the formation of 1 : 1 Tl(III)–PAR complex was confirmed by means of the method of continuous variation at 520 nm, the absorption maximum of the complex.[5] For the kinetic measurements the total concentration of Tl(III) was kept at least in tenfold excess over the PAR concentration. The change in the absorbance at 560 nm, a shoulder of the absorption spectrum of 1 : 1 complex, was followed by stopped-flow technique. This wavelength was adopted for the measurements in order to avoid the influence of the absorbance of the free ligand. Under the experimental conditions the value of the pseudo-first-order rate constants, k_{obsd}, did not depend on the total concentrations of PAR.

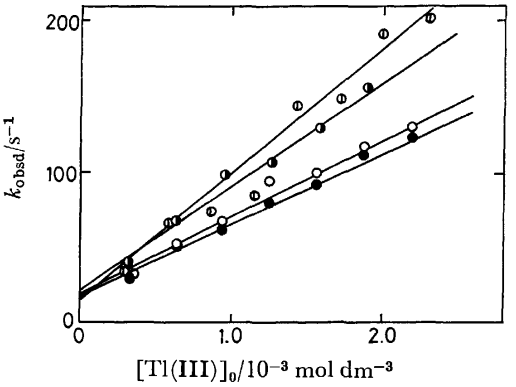

Fig. 1. Dependence of rate constants, k_{obsd}, on total concentrations of Tl(III) at various proton concentrations. $[H^+]=0.2$ (◑), 0.3 (◑), 0.5 (○), and 0.6 mol dm^{-3} (●). $[PAR]_0=2.49\times10^{-5}$ mol dm^{-3}. $I=2.0$ mol dm^{-3} ($NaClO_4$-$HClO_4$) and 25 °C.

Figure 1 shows the dependence of the pseudo-first-order rate constants, k_{obsd}, on the total concentration of Tl(III), $[Tl(III)]_0$, at various proton concentrations. The slopes and the intercepts of the straight lines give the overall rate constants, k_f and k_d, for the formation and dissociation of 1 : 1 complexes, respectively.

The acid-dissociation constants of PAR, $K_c=[LH_2]\times[H^+]/[LH_3^+]=10^{-3.1}$ mol dm^{-3},[1] suggests that the protonated species of PAR, LH_3^+, should be the main species responsible for the complex formation in the acidic region as $[H^+]=0.1$—1.0 mol dm^{-3}.

According to the following scheme with due considerations on the contribution of a base-catalyzed path and the equilibria for very fast protolytic reactions

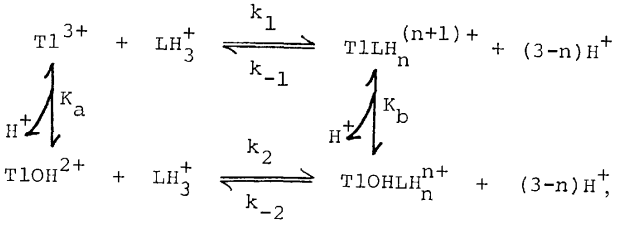

the formation rate constant k_f can be expressed as follows,

$$k_f = \frac{k_1[H^+] + k_2K_a}{[H^+] + K_a}$$

or

$$k_f([H^+]+K_a) = k_1[H^+] + k_2K_a.$$

The plot of $k_f([H^+]+K_a)$ against $[H^+]$ gives a straight line as shown in Fig. 2.[6] From the slope and the intercept the rate constants were determined to be $k_1=4.1\times10^4$ and $k_2=1.8\times10^5$ mol^{-1} dm^3 s^{-1}, respectively.

The value of k_2 was in the same order of magnitude as the formation rate constant for the reaction of $TlOH^{2+}$ and H_4SXO^0. For the completion of the complex formation between Tl(III) and multidentate ligand SXO, the cleavage of the hydrogen-bond

† Presented at the 1978 Winter Meeting in Hokkaido of the Chemical Socity of Japan and the Japan Society for Analytical Chemistry, Sapporo, February 2, 1978.

†† Present address: Hitachi, Ltd., Hitachi 317.

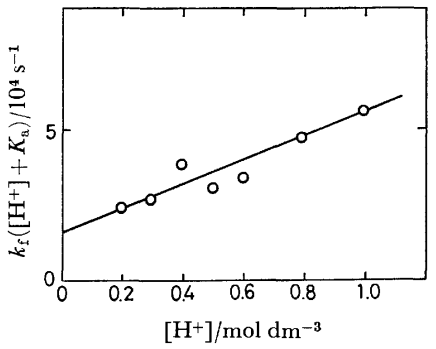

Fig. 2. Plots of $k_f([H^+]+K_a)$ *versus* $[H^+]$ at 25 °C and $I=2.0$ mol dm^{-3} ($NaClO_4$-$HClO_4$). $K_a=10^{-1.14}$ mol dm^{-3}.[10]

between the *o*-hydroxyl group and the nitrogen of iminodiacetate group should necessarily be involved. As regards the first step of the complex formation of PAR with Tl(III) two reaction paths are possible, namely, the first attack of metal ion on the protonated pyridyl nitrogen or the first attack of metal ion on the intramolecular hydrogen-bond between the *o*-hydroxyl group and the azo nitrogen. However, the attack at the protonated unipositive pyridyl group of PAR is very unlikely as reported in the case of the Co(II)–PAR[7] and the Ni(II)–PAR system.[8] Furthermore, it is surprising that the rate constant for the complex formation of Tl(III) with PAR is in the same order of magnitude as that of Tl(III)–SXO despite the differences in the structure, charge type, and the donor atoms between these two ligands. This fact suggests the control of the reaction rate by the step of dissociation of the coordinated water molecule from aqua Tl(III) ion. It is likely that the first attack of Tl(III) ion occurs on the hydrogen-bond between the *o*-hydroxyl group and azo nitrogen of PAR to form the complex.[9]

Experimental

Measurements. All measurements were carried out at 25.0±0.2 °C and ionic strength 2.0 ($NaClO_4$–$HClO_4$). The kinetic measurements were carried out with a stopped-flow spectrometer Yanagimoto SPS-1. The absorption spectra were measured with a Hitachi recording spectrophotometer EPS-3T.

Materials. All reagents are of analytical grade, unless otherwise specified. Water was deionized and distilled. A stock solution of Tl(III) perchlorate was prepared by anodic oxidation of Tl(I) perchlorate in 2 mol dm^{-3} perchloric acid.[10] The concentration of Tl(III) was determined titrimetrically with EDTA using XO as an indicator.[11] The stock solution was stored in the dark. The monohydrate of monosodium salt of PAR was synthesized and purified by repeating recrystallization from ethanol.[2] The purity was confirmed by elemental analysis.[7]

References

1) M. Hniličková and L. Sommer, *Talanta*, **16**, 83 (1969).
2) S. Shibata, "2-Pyridylazo Compounds in Analytical Chemistry," in "Chelates in Analytical Chemistry," ed by H. A. Flaschka and A. J. Barnard, Jr., Marcel Dekker, Inc., New York, N. Y. (1972), Vol. 4, p. 1.
3) Y. Kawai, T. Takahashi, K. Hayashi, T. Imamura, H. Nakayama, and M. Fujimoto, *Bull. Chem. Soc. Jpn.*, **45**, 1417 (1972).
4) Sutin estimated the characteristic rate constant for the replacement of a coordinated water molecule from hydrated Tl(III) ion to be larger than 3×10^9 s^{-1}. The value was calculated from the data for the reaction of iron(III) and chloride ion. See N. Sutin, *Ann. Rev. Phys. Chem.*, **17**, 119 (1966).
5) Tl(III) ion was reported to form a 1 : 1 complex with PAR in aqueous solution at pH lower than 2. At higher pH a 1 : 2 complex was also formed.[1]
6) The dependency of the value of k_d on the proton concentration is not clear owing to the large experimental error (±30%) for the intercepts in Fig. 1. The average value of k_d was calculated to be 10±5 s^{-1} at various proton concentrations.
7) K. Mochizuki, T. Imamura, T. Ito, and M. Fujimoto, *Bull. Chem. Soc. Jpn.*, **51**, 1743 (1978).
8) M. Fujimoto, presented at the 21st Annual Meeting on Coordination Chemistry, Nagoya, October 17, 1971, Abstracts, p. 87.
9) The results of the equilibrium measurements suggest the possibility of the formation of a bidentate PAR complex of Tl(III). Further studies using another method, *e.g.*, NMR, would be necessary to confirm whether the ligand PAR is coordinated to Tl(III) as a bidentate ligand or as a terdentate ligand under the experimental conditions.
10) G. Biedermann, *Arkiv. Kem.*, **5**, 441 (1953).
11) J. Kinnunen and B. Wennerstrand, *Chemist-Analyst*, **46**, 92 (1957).

BULLETIN OF THE CHEMICAL SOCIETY OF JAPAN, VOL. 52 (5), 1537—1538 (1979)

Kinetics of the Substitution of Acetonitrile in (Acetonitrile)chlorobis(triphenylphosphine)rhodium(I) by Triphenylphosphine

Yoshimi OHTANI, Akihiko YAMAGISHI, and Masatoshi FUJIMOTO*

Department of Chemistry, Faculty of Science, Hokkaido University, Sapporo 060

(Received September 7, 1978)

Synopsis. The substitution of coordinated acetonitrile in (acetonitrile)chlorobis(triphenylphosphine)rhodium(I) by triphenylphosphine was studied in benzene by the stopped-flow method under anaerobic conditions. The reaction was found to proceed through both an associative and a dissociative path to yield chlorotris(triphenylphosphine)rhodium(I).

The catalytic activity of Wilkinson's complex, $RhClL_3$ ($L=PPh_3$), in homogeneous hydrogenations strongly depends on the nature of the solvent. The highest activities are usually observed in weakly coordinating solvents.[1] Hydrogenation is practically inhibited in a strongly coordinating solvent such as acetonitrile.[2,3] Since kinetic data on coordination of the solvent molecule to the rhodium catalyst are limited,[4,5] we have carried out a kinetic study on the coordination of an acetonitrile molecule to the Wilkinson's complex:

$$RhClL_3 + CH_3CN \underset{}{\overset{K}{\rightleftharpoons}} RhCl(NCCH_3)L_2 + L. \quad (1)$$

Since the direct measurement of the reaction between $RhClL_3$ and CH_3CN was difficult because of the small equilibrium constant K and partial dimerization of $RhClL_3$, $2RhClL_3 \rightleftharpoons (RhClL_2)_2 + 2L$, we measured the reverse reaction observed upon addition of PPh_3 to $RhCl(NCCH_3)L_2$ in benzene.

Equilibria. When a solution of PPh_3 is added to a solution of $RhCl(NCCH_3)L_2$, the absorption spectrum of the latter changes to that of $RhClL_3$. The equilibrium constant for Reaction 1 is expressed as follows:

$$K = \frac{[RhCl(NCCH_3)L_2][L]}{[RhClL_3][CH_3CN]} \simeq \frac{(A_\infty - A)[L]_{add}}{(A - A_0)[CH_3CN]}, \quad (2)$$

where A, A_0, A_∞, and $[L]_{add}$ denote the absorbance at equilibrium, the initial absorbance, the limiting absorbance at high $[PPh_3]$, and the concentration of PPh_3 added, respectively. Figure 1 shows a typical change in absorbance at 500 nm at $[CH_3CN]=1.9$ mol dm^{-3}. The solid line is reproduced by assuming $K=1.0\times10^{-3}$, $A_0=0.077$, and $A_\infty=0.330$ in Eq. 2, the result showing good agreement with experimental values.

At $[CH_3CN]=1.0$ and 3.8 mol dm^{-3}, the value of K was calculated to be 1.3×10^{-3} and 0.9×10^{-3}, respectively, giving the average equilibrium constant $K_{av}=1.1\times10^{-3}$.

Kinetics. The rate of substitution of CH_3CN in $RhCl(NCCH_3)L_2$ by PPh_3 was measured at 500 nm using a single exponential change observed upon addition of a solution of PPh_3 to a solution of $RhCl(NCCH_3)L_2$. Observed rate constants, k_{obsd}, were proportional to $[PPh_3]$ at constant $[CH_3CN]$ (Fig. 2). The dependence of k_{obsd} on $[CH_3CN]$ at constant

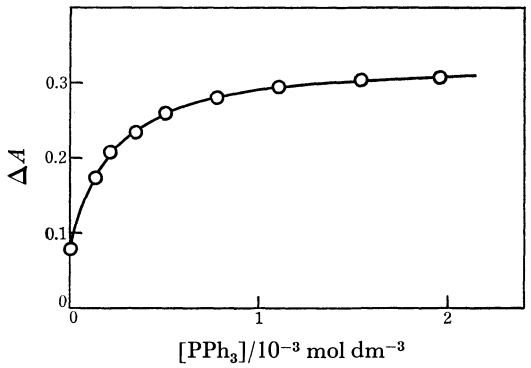

Fig. 1. Change in absorbance of the solution of $RhCl(NCCH_3)(PPh_3)_2$ by the addition of PPh_3 at 500 nm. Solid line is reproduced by assuming Eq. 2 with $K=1.0\times10^{-3}$, $A_0=0.077$, and $A=0.330$. $[RhCl(NCCH_3)(PPh_3)_2]_0=5.4\times10^{-4}$ mol dm^{-3}.

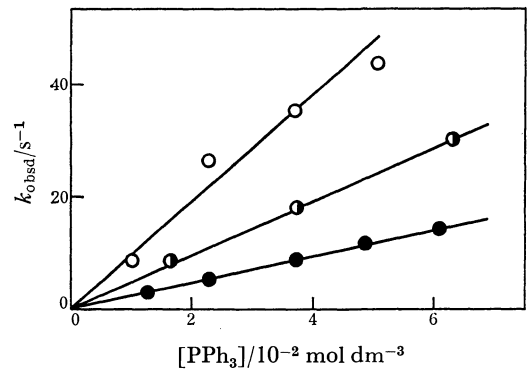

Fig. 2. The dependence of k_{obsd} on the concentration of PPh_3; $[RhCl(NCCH_3)(PPh_3)_2]_0=3.9\times10^{-4}$ mol dm^{-3} and $[CH_3CN]=0.50$ (○), 1.0 (◑), and 2.9 (●) mol dm^{-3}.

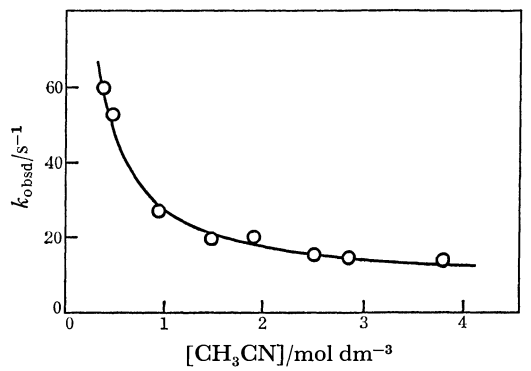

Fig. 3. The dependence of k_{obsd} on the concentration of CH_3CN. $[RhCl(NCCH_3)(PPh_3)_2]_0=4.0\times10^{-4}$ and $[PPh_3]=3.7\times10^{-2}$ mol dm^{-3}.

[PPh_3] is shown in Fig. 3. From Figs. 2 and 3 the observed rate constant is given by

$$k_{obsd} = \left\{k + k' \frac{1}{[CH_3CN]}\right\}[L]. \quad (3)$$

The following reaction mechanism is postulated for the interpretation of the above relationship:

$$\begin{array}{ccc} RhClL_3 + CH_3CN & \underset{k_{-1}}{\overset{k_1}{\rightleftharpoons}} & RhCl(NCCH_3)L_3 \\ k_3 \downarrow\uparrow k_{-3} & & k_4 \downarrow\uparrow k_{-4} \\ RhClL_2 + CH_3CN & \underset{k_{-2}}{\overset{k_2}{\rightleftharpoons}} & RhCl(NCCH_3)L_2. \\ +L & & +L \end{array} \quad (4)$$

By applying the steady-state approximation to the intermediate species, $RhClL_2$ and $RhCl(NCCH_3)L_3$, we obtain

$$k_{obsd} = \frac{k_1k_4[CH_3CN] + k_{-1}k_{-4}[L]}{k_{-1} + k_4} + \frac{k_2k_3[CH_3CN] + k_{-2}k_{-3}[L]}{k_2[CH_3CN] + k_{-3}[L]}. \quad (5)$$

The rate terms for the reaction between $RhClL_3$ and CH_3CN, $k_1k_4[CH_3CN]$ and $k_2k_3[CH_3CN]$, can be neglected, since Equilibrium 1 lies far to the left-hand side under the reaction conditions. If $k_{-3}[L]$ is small as compared with $k_2[CH_3CN]$, *viz.*, the step $RhCl(NCCH_3)L_2 \rightleftharpoons RhClL_2 + CH_3CN$ is pre-equilibrated, Eq. 5 is modified as

$$k_{obsd} = \left\{\frac{k_{-1}k_{-4}}{k_{-1} + k_4} + \frac{k_{-3}}{K_2} \cdot \frac{1}{[CH_3CN]}\right\}[L]. \quad (6)$$

The equation was found to fit the kinetic data for the values, $k_{-1}k_{-4}/(k_{-1}+k_4) = 2.4 \times 10^2$ mol^{-1} dm^3 s^{-1} and $k_{-3}/k_2 = 3.5 \times 10^2$ s^{-1}. The value of k_3 is calculated to be 0.39 s^{-1} from the overall equilibrium constant $K = K_2k_3/k_{-3} = 1.1 \times 10^{-3}$. The value of k_3 agrees with the value 0.4 s^{-1} obtained from the experiment on the substitution of a coordinated PPh_3 in $RhClL_3$ by C_2H_4,[6] even when an experimental error (about 20%) is taken into consideration. The results indicate that both the associative and dissociative paths exist.

Schrock and Osborn suggested that an acetonitrile should compete with an olefin for coordination site on the central metal.[5] Thus, it is expected that an olefin cannot coordinate to $RhCl(NCCH_3)L_2$ without prior dissociation of CH_3CN (Eq. 7) as observed in the case of $RhClL_3$ (Eq. 8).[6] Actually, ethylene cannot coordinate to $RhCl(NCCH_3)L_2$ without dissociation of CH_3CN.[7]

$$RhCl(NCCH_3)L_2 + Ol \overset{K'}{\rightleftharpoons} RhCl(ol)L_2 + CH_3CN \quad (7)$$

$$RhClL_3 + Ol \overset{K''}{\rightleftharpoons} RhCl(ol)L_2 + L, \quad (8)$$

where Ol denotes olefin. In the case of cyclohexene, K'' is too small to be determined by the spectrophotometric method; styrene has an even smaller K'' (2.4×10^{-4})[8] than K for acetonitrile. Thus, Reaction 7 in the solution containing a considerable amount of acetonitrile lies far to the left-hand side under the conditions of hydrogenation. The coordination of CH_3CN suppresses the formation of olefin complexes, $RhCl(ol)L_2$ and $RhClH_2(ol)L_2$, the rate of hydrogenation of the olefins being lowered in acetonitrile.

Experimental

$RhCl(C_2H_4)(PPh_3)_2$ was prepared according to Osborn *et al.*[2] A solution of $RhCl(NCCH_3)(PPh_3)_2$ was prepared by dissolving $RhCl(C_2H_4)(PPh_3)_2$ in benzene containing an appropriate amount of CH_3CN, the coordinated C_2H_4 being easily replaced by CH_3CN.[9] Benzene and acetonitrile were distilled. Distilled acetonitrile contained 0.06 mol dm^{-3} of water, which affected neither the spectrum nor the reaction rate. All the measurements were carried out at 20±0.2 °C in oxygen-free benzene. Equilibrium measurements were carried out *in vacuo* with a Hitachi EPS-3T spectrophotometer. The rate of substitution of the coordinated CH_3CN in $RhCl(NCCH_3)(PPh_3)_2$ by PPh_3 was measured with a Union Giken RA-1300 stopped-flow apparatus under nitrogen atmosphere.

References

1) B. R. James, "Homogeneous Hydrogenation," Wiley, New York (1973), pp. 204—248.
2) J. A. Osborn, F. H. Jardine, J. F. Young, and G. Wilkinson, *J. Chem. Soc., A*, **1966**, 1711.
3) J. P. Candlin and J. A. Oldham, *Discuss. Faraday Soc.*, **46**, 60 (1968).
4) J. R. Shapley, R. R. Schrock, and J. A. Osborn, *J. Am. Chem. Soc.*, **91**, 2816 (1969).
5) R. R. Schrock and J. A. Osborn, *J. Am. Chem. Soc.*, **98**, 2134 (1976).
6) Y. Ohtani, M. Fujimoto, and A. Yamagishi, *Bull. Chem. Soc. Jpn.*, **50**, 1453 (1977).
7) Y. Ohtani, A. Yamagishi, and M. Fujimoto, *Bull. Chem. Soc. Jpn.*, in press.
8) Y. Ohtani, A. Yamagishi, and M. Fujimoto, *Bull. Chem. Soc. Jpn.*, **52**, 69 (1979).
9) Y. Ohtani, A. Yamagishi, and M. Fujimoto, *Bull. Chem. Soc. Jpn.*, **51**, 2562 (1978).

BULLETIN OF THE CHEMICAL SOCIETY OF JAPAN, VOL. 52 (5), 1539—1540 (1979)

Studies on Unusual Amino Acids and Their Peptides. X. The Convenient Synthesis of *t*-Leucine and the Optical Resolution of the *N*-Benzyloxycarbonyl Derivative[1)]

Toshifumi MIYAZAWA, Katsumi TAKASHIMA, Yoshikazu MITSUDA,** Takashi YAMADA, Shigeru KUWATA, and Hiroshi WATANABE*

Laboratory of Chemistry, Faculty of Science, Kōnan University, Okamoto, Higashinada-ku, Kobe 658

(Received March 28, 1978)

Synopsis. *t*-Leucine has been conveniently prepared on a large scale from the phenylhydrazone of trimethylpyruvic acid, which was readily obtained as a precipitate from the oxidation of pinacolone. The *N*-benzyloxycarbonyl derivative of DL-*t*-leucine has been resolved with quinine and quinidine in ethanol.

In the course of investigation,[2)] it has been necessary to prepare optically active *t*-leucine on a large scale. For this purpose the route shown in Scheme was chosen.

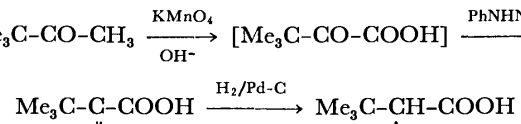

Scheme.

Pinacolone has been oxidized with aqueous alkaline permanganate to trimethylpyruvic acid.[3)] This keto acid has been converted, without isolation, into the insoluble phenylhydrazone (I) and separated by filtration. Hydrogenation of I in the presence of palladium on carbon gave *t*-leucine (II) in good yield.

N-Z-DL-*t*-Leucine (III) has been resolved with quinine and quinidine in ethanol, and the optical purities of the resolved isomers confirmed by gas chromatographic analysis[4)] after conversion to the *N*-pivaloyl-*t*-leucyl-L-valine methyl ester.

Experimental

All melting points are uncorrected. Optical rotations have been measured by Yanagimoto OR-10 and JASCO DIP-4 polarimeters.

Phenylhydrazone of Trimethylpyruvic Acid (I). Pinacolone (50 g) was oxidized with alkaline potassium permanganate (160 g) by Knoop's method.[3)] To the filtrate of the reaction mixture (*ca.* 5.5 l), after neutralization with HCl, was added phenylhydrazine (65 g) dissolved in acetic acid (250 ml) and the mixture allowed to stand at room temperature overnight. The resulting precipitates were separated by filtration, dried, and recrystallized from 70% ethanol, affording pale yellow needles (84 g, 76%) of mp 157—158 °C (lit,[5)] mp 157—158 °C).

Hydrogenation of the Phenylhydrazone (I). The phenylhydrazone (I) (100 g) was dissolved in a mixture of ethanol and water (510 ml EtOH+75 ml H_2O), and hydrogenated with 5% Pd–C (20 g) at 70 °C under an initial pressure of 50—140 kg/cm². The resulting solution was removed from the catalyst and evaporated to dryness under reduced pressure. The residue was dried sufficiently and washed repeatedly with dry benzene. The crude DL-*t*-leucine (II) (53.7 g; mp 248—251 °C (sublime)) was recrystallized from aqueous acetone; yield, 41.6 g (70%); mp 250—251 °C (sublime) (lit,[6,7)] mp 250 °C (sublime)).

Optical Resolution of N-*Z*-DL-t-*Leucine(III).* Thirty-eight mmol of III[8)] and quinine (or quinidine) were dissolved in hot ethanol (90 ml), and the precipitated white crystals recrystallized from ethanol four times. The purified salt was suspended in ethyl acetate, and shaken with 2 M HCl to remove the base, and subjected to the usual work-up. The optically active *t*-leucine was obtained by hydrogenation of the corresponding *N*-Z-derivative.

N-Z-D-*t*-Leucine quinine salt: mp 166—167 °C, $[\alpha]_D^{20}$ −106.5° (*c* 1.0, MeOH). Found: C, 69.46; H, 7.47; N, 7.12%. Calcd for $C_{34}H_{43}N_3O_6$: C, 69.24; H, 7.35; N, 7.13%.

N-Z-D-*t*-Leucine: syrup, $[\alpha]_D^{20}$ +5.9° (*c* 1.0, MeOH).

N-Z-D-*t*-Leucine dicyclohexylamine (DCHA) salt: mp 165.5—166 °C (from EtOH–Et_2O), $[\alpha]_D^{20}$ +8.5° (*c* 1.0, MeOH). Found: C, 69.90; H, 9.56; N, 6.04%. Calcd for $C_{26}H_{42}N_2O_4$: C, 69.92; H, 9.48; N, 6.27%.

D-*t*-Leucine: mp 250—252 °C (sublime), $[\alpha]_D^{21}$ +10.5° (*c* 1.0, H_2O), $[\alpha]_D^{20}$ −29.1° (*c* 1.0, AcOH) (lit,[9)] $[\alpha]_D^{20}$ +10.01° (*c* 5.19, H_2O) (*cf.* Refs. 3 and 10)). Found: C, 54.74; H, 9.87; N, 10.35%.

N-Z-L-*t*-Leucine quinidine salt: mp 134—136 °C (*ca.* 98 °C sinter), $[\alpha]_D^{20}$ +127.7° (*c* 1.0, MeOH).

N-Z-L-*t*-Leucine: syrup, $[\alpha]_D^{20}$ −6.0° (*c* 1.0, MeOH).

N-Z-L-*t*-Leucine DCHA salt: mp 166—166.5 °C (from EtOH–Et_2O), $[\alpha]_D^{20}$ −8.7° (*c* 1.0, MeOH) (lit,[11)] mp 165—168 °C, $[\alpha]_D$ −8.4° (*c* 0.59, MeOH)). Found: C, 69.79; H, 9.35; N, 5.98%.

L-*t*-Leucine: mp 250—252 °C (sublime), $[\alpha]_D^{21}$ −10.9° (*c* 1.0, H_2O), $[\alpha]_D^{26}$ +30.0° (*c* 1.0, AcOH) (lit, mp 250 °C (sublime),[12)] $[\alpha]_D^{28.5}$ −10.15° (*c* 4.63, H_2O)[9)] (*cf.* Refs. 3, 10, and 13), $[\alpha]_D^{25}$ +36.0° (*c* 2, AcOH)[3)]). Found: C, 54.77; H, 9.91; N, 10.35%.

The present work was supported by a Grant-in-Aid for Scientific Research from the Ministry of Education.

References

1) A part of this work was presented at the 36th National Meeting of the Chemical Society of Japan, Higashi-Osaka, April 1977, Abstr. No. 3U09.

2) T. Yamada, K. Takashima, T. Miyazawa, S. Kuwata, and H. Watanabe, *Bull. Chem. Soc. Jpn.*, **51**, 883 (1978).

3) J. P. Greenstein and M. Winitz, "Chemistry of the Amino Acids," John Wiley & Sons, Inc., New York (1961), Vol. 3, p. 2580.

** Morishita Pharmaceutical Co., Ltd., 29, 4-Chome, Doshomachi, Higashi-ku, Osaka 541.

4) E. Frauendorfer, W. Steglich, and F. Weygand, *Chem. Ber.*, **106**, 1019 (1973).
5) "Dictionary of Organic Compounds," 4th ed, Eyre & Spottiswoode, London (1965), Vol. 5, p. 3187.
6) F. Knoop and G. Landmann, *Hoppe-Seyler's Z. Physiol. Chem.*, **89**, 157 (1914).
7) D. Bonner, E. L. Tatum, and G. W. Beadle, *Arch. Biochem. Biophys.*, **3**, 88 (1944).
8) N. Izumiya, S.-C. J. Fu, S. M. Birnbaum, and J. P. Greenstein, *J. Biol. Chem.*, **205**, 221 (1953).
9) E. Abderhalden, W. Faust, and E. Haase, *Hoppe-Seyler's Z. Physiol. Chem.*, **228**, 187 (1934).
10) H. Pracejus and S. Winter, *Chem. Ber.*, **97**, 3173 (1964).
11) J. Pospíšek and K. Bláha, *Collect. Czech. Chem. Commun.*, **42**, 1069 (1977).
12) W. Steglich, E. Frauendorfer, and F. Weygand, *Chem. Ber.*, **104**, 687 (1971).
13) T. Tanabe, S. Yajima, and M. Imaida, *Bull. Chem. Soc. Jpn.*, **41**, 2178 (1968).

BULLETIN OF THE CHEMICAL SOCIETY OF JAPAN, VOL. 52 (5), 1541—1542 (1979)

Preparation and Reaction of *N*-Imidoyliminotriphenylphosphoranes

Hiroshi YOSHIDA,* Tsuyoshi OGATA, and Saburo INOKAWA

Department of Synthetic Chemistry, Faculty of Engineering, Shizuoka University, Johoku, Hamamatsu 432

(Received May 2, 1978)

Synopsis. *N*-Imidoyliminotriphenylphosphoranes **2** have been prepared by the reaction of triphenylphosphine with *N*-chloroamidines followed by treatment with base. **2** can react readily with hydrochloric acid or methyl iodide to give the corresponding salts. Treatment of **2** with carbon disulfide gave *N*-(thioacyl)iminotriphenylphosphoranes together with isothiocyanates.

In a previous paper[1] the reaction of imidoyltriphenylphosphonium methylides **1** with carbon disulfide was reported. The products were a result of the attack on either the ylide carbon atom or the imidoyl nitrogen atom.

Iminophosphoranes show similar chemical properties to those of phosphonium methylides.[2] In this paper the reaction of *N*-imidoyliminotriphenylphosphoranes **2** with carbon disulfide and halides will be reported.

Iminophosphoranes **2** have been prepared by the reaction of *N*-(1-chloro-2,2-diphenylvinyl)iminophosphorane, prepared from chlorodiphenylacetonitrile and triphenylphosphine, with aromatic amines[3] or the reaction of *N*-chlorobenzamidines with triphenylphosphine followed by treatment with base.[4] In the reports however, no information of the nature of the compounds **2** was reported. Based on the second route, several iminophosphoranes **2** have been synthesized to give moderate yields, the results of which are given in Table 1. The hydrochloric acid salts of **2** (R^1=aryl, R^2=$CHPh_2$), prepared by the reaction of **2** with hydrochloric acid, have been found to be **3**(R^1=aryl, R^2=$CHPh_2$)[3] [protonation on imidoyl nitrogen] not **4** [protonation on the nitrogen atom of iminophosphorane].

The structure of **3** has been elucidated by NMR analysis of the N–C=NH proton,[3] which shows a down field shift due to the electron withdrawing group R^1.[3] The NH protons in **3** (R^1=*p*-$Me_2NC_6H_4$, R^2=$CHPh_2$) and **3** (R^1=*p*-$NO_2C_6H_4$, R^2=$CHPh_2$) appear at δ 11.4 and 12.8 in $CDCl_3$, respectively.

Elucidation of the structure of the hydrochloric acid salts of **2a—i** posed difficulties. The salt of **2h**, however, was confirmed as **3h** and not **4h** on the basis of the NMR studies. The NMe protons of **2h** appear at δ 3.23 as a doublet due to coupling with phosphorous ($^5J_{PNCNCH}$=2 Hz). The NMe protons of the hydrochloride of **2h** in $CDCl_3$ appear at δ 3.36 as a doublet (J=5 Hz). The addition of D_2O to the solution disappeared the splitting indicating that the splitting is due to HNCH interaction not PNCNCH.

The reaction of **2** with methyl iodide was conducted at room temperature to give **5** (R=Me). The structures of the products were elucidated on the basis of the NMR results (Table 3). The NMe protons of

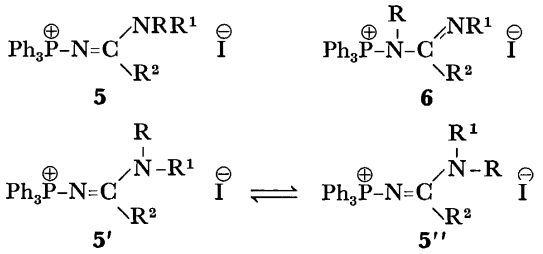

5 show no coupling with phosphorus, indicating that methylation of the nitrogen atom in the imidoyl group occurs, since $^3J_{PNCH}$=10—12 Hz[5] has been reported for compounds of the type $Ph_3\overset{\oplus}{P}NCH_3$.

The NMR spectra of **5** derived from **2h** with ethyl iodide and **2i** with methyl iodide showed two groups of peaks of the same intensity (Table 3), indicating the presence of two isomers **5′** and **5″**,[6] especially in the case of sterically hindered compounds **5e, f, h, i**.

The reaction of *N*-alkyl or aryl iminotriphenylphosphoranes with carbon disulfide has been shown to give phosphine sulfide and isothiocyanates.[2] In contrast, it was found here that iminophosphorane **2**

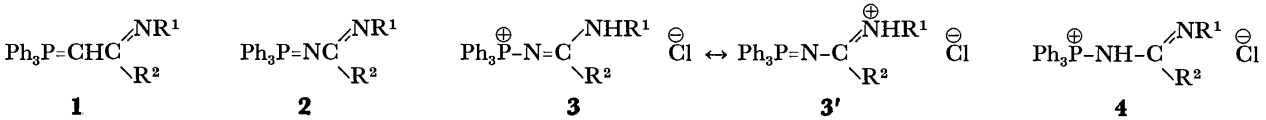

Table 1. Preparation and physical properties of **2**

	R^1	R^2	Yield (%)	Mp (°C)	NMR (δ in $CDCl_3$)	IR (KBr) cm^{-1} $\nu_{C=N}$	IR (KBr) cm^{-1} $\nu_{P=N}$	M^+	Found (Calcd) (%) C	Found (Calcd) (%) H	Found (Calcd) (%) N	Reaction with CS_2 Temp (°C)	Time (d)	Products (%)
2a	*p*-MeC_6H_4	Ph	37	161—163	2.17(s, Me), 6.7—7.7(m, arom)	1530	1340	470	81.32(81.68)	5.92(5.78)	5.81(5.95)	25	3	**6a**(96), R^1NCS(85)
2b	Ph	*p*-MeC_6H_4	48	199—202	2.20(s, Me), 6.3—8.1(m, arom)	1530	1340	470	81.52(81.68)	5.64(5.78)	6.01(5.95)	25	3	**6b**(92), R^1NCS(81)
2c	*m*-MeC_6H_4	Ph	39	177—180	2.13(s, Me), 6.2—8.2(m, arom)	1530	1340	470	81.74(81.68)	5.81(5.78)	5.77(5.95)	25	3	**6a**(90), R^1NCS(79)
2d	Ph	*m*-MeC_6H_4	44	173—174	2.18(s, Me), 6.3—8.1(m, arom)	1530	1340	470	81.43(81.68)	5.71(5.78)	5.84(5.95)	25	3	**6c**(87), R^1NCS(88)
2e	*o*-MeC_6H_4	Ph	23	172—174	2.18(s, Me), 7.1—8.1(m, arom)	1520	1330	470	81.63(81.68)	6.04(5.78)	5.83(5.95)	70	2	**6a**(89), R^1NCS(64)
2f	Ph	*o*-MeC_6H_4	38	169—172	2.15(s, Me), 6.1—8.1(m, arom)	1500	1300	470	81.55(81.68)	5.54(5.78)	6.19(5.95)	70	3	**6d**(72), R^1NCS(57)
2g	Ph	Ph	49	157—159	6.6—8.3(m, arom)	1520	1340	456	81.33(81.56)	5.37(5.52)	5.94(6.14)	25	3	**6a**(94), R^1NCS(83)
2h	Me	Ph	30	172—175	3.23(d, J=2, Me), 6.9—8.0(m, arom)	1630	1390	394	78.98(79.19)	6.03(5.88)	6.91(7.10)	25	1	**6a**(93), R^1NCS(95)
2i	Et	Ph	25	160—161	1.84(t, J=7, Me), 4.16(q, CH_2) 6.5—7.7(m, arom)	1630	1390		79.73(79.39)	6.03(6.17)	6.41(6.86)			

Table 2. The HCl salts of **2**

	Mp (°C)	NMR (δ in $CDCl_3$)	IR(KBr) cm^{-1}
3a	262—264	2.27(s, Me), 6.8—8.4(m, arom), 12.57(broad s, NH)	1530
3b	232—334	2.22(s, Me), 6.7—8.4(m, arom), 12.73(broad d, J=6, NH)	1530
3c	192—195	2.31(s, Me), 6.8—7.9(m, arom), 12.92(broad s, NH)	1530
3d	205—210	1.96(s, Me), 6.8—8.1(m, arom), 12.28(broad d, J=5, NH)	1530
3e	251—253	2.36(s, Me), 6.5—8.0(m, arom), 12.66(broad d, J=7, NH)	1580, 1500
3f	167—169	1.92(s, Me), 6.6—8.2(m, arom), 12.53(broad d, J=6, NH)	1530
3g	240—242	6.6—8.2(m, arom), 12.61(broad s, NH)	1530
3h	257—262	3.36(d, J=5, NMe), 6.8—8.0(m, arom), 10.28(broad s, NH)	1640, 1590
3i	146—148	1.47(t, J=7, Me), 3.87(q, CH_2), 6.8—8.0(m, arom), 10.32(broad s, NH)	1640, 1600

Table 3. Alkylation of **2** with alkyl iodide in chloroform

5	Mp (°C)	RI	NMR (δ in $CDCl_3$)
5a	Resinous	MeI	2.15(s, Me), 4.04(s, NMe), 6.6—7.9(m, arom)
5b	142—144	MeI	2.10(s, Me), 3.98(s, NMe), 6.4—7.9(m, arom)
5c	Resinous	MeI	2.21(s, Me), 4.00(s, NMe), 7.0—7.9(m, arom)
5d	Resinous	MeI	1.84(s, Me), 4.03(s, NMe), 6.4—8.0(m, arom)
5e	203—206	MeI	1.39 and 1.46(s, 44 : 56, Me), 3.39 and 4.02 (s, 56 : 44, NMe), 6.7—8.0(m, arom)
5f	255—256	MeI	1.65 and 1.88(s, 56 : 44, Me), 3.27 and 4.07 (s, 44 : 56, NMe), 6.5—7.8(m, arom)
5g	Resinous	MeI	3.92 (s, NMe), 6.5—8.0(m, arom)
5h	230—232	MeI	3.09 and 3.75(s, NMe), 6.8—7.8(m, arom)
	214—216[a)] + 230—232	EtI	1.18 and 1.59(t, J=7, 59 : 41, Me), 3.07 and 3.74(s, 41 : 59, NMe), 3.44 and 3.80(q, J=7, 59 : 41, CH_2), 6.8—8.0(m, arom)
5i	216—218[a)] + 230—232	MeI	1.18 and 1.59(t, J=7, 63 : 37, Me), 3.07 and 3.74(s, 37 : 63, NMe), 3.44 and 3.80(q, J=7, 63 : 37, CH_2), 6.8—8.0(m, arom)

a) A mixture of two crystalline compounds.

readily reacted with carbon disulfide to give *N*-(thioacyl)iminophosphorane **6** and isothiocyanate:

$$Ph_3P{=}NC(=NR^1)R^2 \; (\mathbf{2}) + CS_2 \longrightarrow Ph_3P{=}NC(=S)R^2 \; (\mathbf{6}) + R^1NCS$$

Iminophosphoranes **6** have been considered as intermediates in the reaction of thiobenzoyl azide (phenyl thiatriazole) with triphenylphosphine,[7] giving benzonitrile and phosphine sulfide. In the thermolysis of the phosphonium salts **7** (R=Me, *t*-Bu), the isolation of **6** have not been successful.[3,7] The structure of **6** has been confirmed on the basis of NMR, IR, and MS.[8]

$$Ph_3\overset{\oplus}{P}{-}N{=}C(CHPh_2)SR \; \overset{\ominus}{Cl} \quad \mathbf{7}$$

Experimental

Preparation of **2**. As a typical experiment the preparation of **2a** will be given. *N*-Phenyl-*N'*-chlorobenzamidine was prepared according to the literature[9] and used without purification. To a stirred solution of *N*-phenyl-*N'*-chlorobenzamidine(0.01 mol) in dry benzene(30 ml) was added a solution of triphenylphosphine(0.01 mol) in dry ether(20 ml), the temperature being kept below 10 °C. After 2 h the oily precipitate was separated and dissolved in EtOH (20 ml). To the solution was added in one step a solution of KOH (0.03 mol) in EtOH(10 ml) and the solution stirred vigorously. After 3 min the mixture was quenched with water (60 ml) and extracted with $CHCl_3$(50 ml). The extract was dried over Na_2CO_3 and concentrated *in vacuo* to give a crystalline material. Crystallization from $CHCl_3$–petroleum ether gave **2a** in 37% yield, the results of which are shown in Table 1.

Preparation of the Hydrochloric Acid Salts of **2**. To a solution of **2a**(5 mmol) in $CHCl_3$(20 ml) was added concd HCl(1 ml) in one portion. The mixture was stirred and the organic layer separated. Concentration of the solution *in vacuo* gave white crystalline substance **3a** quantitatively (Table 2).

Alkylation of **2** *with Alkyl Iodide*. To a solution of **2a** (5 mmol) in $CHCl_3$(20 ml) was added MeI(0.5 ml) in one portion. The mixture was left at room temperature for 24 h. Concentration of the solution *in vacuo* gave a white resin **5a**(R=Me)quantitatively.

The Reaction of **2** *with Carbon Disulfide*. A solution of **2a** (10 mmol) and CS_2(100 mmol) in $CHCl_3$(30 ml) was left to stand for 3 days at room temperature. The mixture was dried *in vacuo* and extracted with petroleum ether. On crystallization from AcOEt the extracts gave **6a** in 96% yield. The mother liqour was found to be *p*-tolyl isothiocyanate by comparison of the IR spectrum with that of authentic sample. The yield was determined by VPC (Silicone Grease 20% on celite) using mesitylene as an internal standard.

6a(R^2=Ph): mp 158—160 °C. NMR($CDCl_3$) δ=6.6—8.2(m, arom). M^+ 397. IR(KBr) 1340 cm^{-1}(P=N). Found: C, 75.23; H, 4.98; N, 3.61%. Calcd for $C_{25}H_{20}NSP$: C, 75.55; H, 5.07; N, 3.53%.

6b(R^2=*p*-MeC_6H_4): mp 159—160 °C. NMR($CDCl_3$) δ =2.31(s, Me), 6.9—8.1(m, arom). M^+ 411. IR(KBr) 1350 cm^{-1}(P=N). Found: C, 75.96; H, 5.43; N, 3.21%. Calcd for $C_{26}H_{22}NSP$: C, 75.89; H, 5.39; N, 3.40%.

6c(R^2=*m*-MeC_6H_4): mp 144—145 °C. NMR($CDCl_3$) δ= 2.38(s, Me), 6.9—8.2(m, arom). M^+ 411. IR(KBr) 1350 cm^{-1}(P=N). Found: C, 75.64; H, 5.14; N, 3.26%. Calcd for $C_{26}H_{22}NSP$: C, 75.89; H, 5.39; 3.40%.

6d(R^2=*o*-MeC_6H_4): mp 143—145 °C. NMR($CDCl_3$) δ= 2.54(s, Me), 6.9—8.1(m, arom). M^+ 411. IR(KBr) 1350 cm^{-1}(P=N). Found: C, 75.81; H, 5.26; N, 3.49%. Calcd for $C_{26}H_{22}NSP$: C, 75.89; H, 5.39; N, 3.40%.

References

1) H. Yoshida, T. Ogata, and S. Inokawa, *Bull. Chem. Soc. Jpn.*, **50**, 3315(1977).

2) a) A. W. Johnson, "Ylid Chemistry," Academic Press, New York and London(1966); b) H. J. Bestmann and K. Zimmermann, "Organic Phosphorous Compounds," ed by G. M. Kosolapoff and L. Mair, Wiley-Interscience, New York (1972), Vol 3.

3) R. D. Partos and K. W. Ratts, *J. Am. Chem. Soc.*, **88**, 4996 (1966).

4) G. I. Derkach and A. W. Kirsanov, *J. Gen. Chem. USSR*, **32**, 2221 (1962).

5) N. F. Chamberlain, "The Practice of NMR Spectroscopy," Plenum Press, New York and London (1974), p 332.

6) a) L. M. Jackman, "Dynamic Nuclear Magnetic Resonance Spectroscopy," ed by L. M. Jackman and F. A. Cotton, Academic Press, New York (1975), p. 203; b) G. Häfelinger, "The Chemistry of Amidines and Imidates," ed by S. Patai, John Wiley & Sons, London (1975).

7) L. Horner and A. Gross, *Justus Liebigs Ann. Chem.*, **591**, 117 (1955).

8) The reaction of **6** will be shown in detail in a forthcoming paper.

9) T. Fuchigami, E. Ichikawa, and K. Odo, *Bull. Chem. Soc. Jpn.*, **46**, 1765 (1973).

BULLETIN OF THE CHEMICAL SOCIETY OF JAPAN, VOL. 52 (5), 1543—1544 (1979)

The Formation of 3,4,5-Tris(substituted phenyl)-4,5-dihydro-1,2-oxazole *N*-Oxides in the Oxidations of (Substituted phenyl)nitromethanide Anions with Silver Nitrate or Peroxodisulfate

Kimitoshi FUKUNAGA,* Kenji HAMANAKA, and Makoto KIMURA

Faculty of Engineering, Yamaguchi University, Tokiwadai, Ube, Yamaguchi 755

(Received May 11, 1978)

Synopsis. The reaction of an alkali metal salt of (substituted phenyl)nitromethane (**1**) with silver nitrate or peroxodisulfates in dimethyl sulfoxide (DMSO) gives 3,4,5-tris(substituted phenyl)-4,5-dihydro-1,2-oxazole *N*-oxides (**2**) in a good yield.

The oxidations of an alkali metal salt of primary nitroalkane with peroxodisulfates[1-3] or silver ions[1,3,4] have been known to be a general method for the formation of vicinal dinitro compounds. Particularly, the oxidation of the alkali metal salt of α-arylnitroalkane with silver nitrate in aqueous dimethyl sulfoxide (DMSO) or acetonitrile has been recognized as one of the most convenient methods for the formation of vicinal dinitro compounds.[4] Little information is, however, available about the formation of 4,5-dihydro-1,2-oxazole *N*-oxides in the oxidation of an alkali metal salt of nitroalkane under similar reaction conditions to those described above. Shechter and Kaplan[1] have reported that the reaction of nitroethane with peroxodisulfate in alkaline medium gives 3,4,5-trimethyl-1,2-oxazole in a 25% yield. Nenitzescu[5] has reported that anodic oxidation of an aqueous solution of sodium salt of phenylnitromethane (**1a**) gives 3,4,5-triphenyl-1,2-oxazole (**4a**). The mechanism of these reactions has not been discussed but it should involve the intermediate 4,5-dihydro-1,2-oxazole *N*-oxide ring formation. Recent studies by Pagano and Shechter have shown that the sodium salt of **1a** reacts with ammonium peroxodisulfate in aqueous sodium hydroxide to give 3,4,5-triphenyl-4,5-dihydro-1,2-oxazole *N*-oxide (**2a**) in a 1.3% isolated yield together with other products.[3] We describe here the reactions of alkali metal salts of (substituted phenyl)nitromethanes (**1a**—**e**) with peroxodisulfates or silver nitrate[6] in DMSO to give 3,4,5-tris(substituted phenyl)-4,5-dihydro-1,2-oxazole *N*-oxides (**2a**—**e**) without concomitant formation of the corresponding vicinal dinitro compounds (**3a**—**e**).

Alkali metal salts of **1a**—**e** were allowed to react with an equimolar amount of silver nitrate in DMSO according to methods A and B, and the corresponding **2a**—**e** were obtained in good yields, as shown in Scheme 1. The structures of **2a**—**e** were confirmed by the analytical and spectral data reported in Ref. 6.

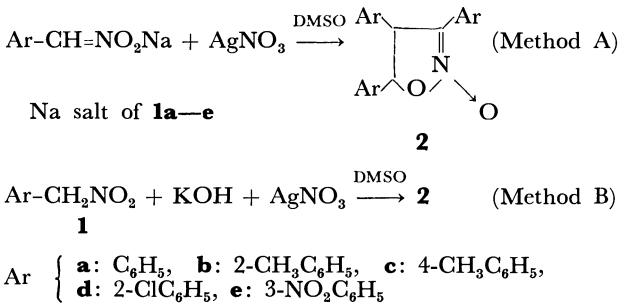

Scheme 1.

The reaction of the sodium salt of **1a** with silver nitrate in *N*,*N*-dimethylformamide (DMF) or acetonitrile, however, gave yellow (*E*)-α-nitrostilbene (**5a**) as the main product. When a mixture of the sodium salt of **1a** and peroxodisulfate was stirred in DMSO at room temperature for 1 h, only **2a** was obtained. The reaction also took place in other solvents such as DMF and acetonitrile, but it was slower and the yield of **2a** was lower than that in DMSO. Typical results are summarized in Tables 1 and 2. The reason for the ineffectiveness of silver nitrate or peroxodisulfate

TABLE 1. REACTION OF (SUBSTITUTED PHENYL)NITROMETHANIDE ANION WITH SILVER NITRATE[a]

Run	Substrate (mmol)	$AgNO_3$ (mmol)	Solvent (ml)	Reaction time (h)	Products and yields[b] (%)
1	**1a** (50)	60	DMSO (150)	2	**2a** (57.1[c], 49.5[d])
2	**1b** (44)	45	DMSO (120)	4	**2b** (41.9[c], 44.0[d])
3	**1c** (44)	45	DMSO (120)	4	**2c** (46.3[c], 41.9[d])
4	**1d** (44)	45	DMSO (120)	4	**2d** (47.2[c], 43.8[d])
5	**1e** (25)	28	DMSO (120)	4	**2e** (40.4[d])
6[c]	**1a** (25)	26	DMF (30)	2	**2a** (3.8), **5a** (16.5), benzaldehyde[e] (8.2), **1a**[f] (trace)
7[c]	**1a** (25)	26	CH_3CN (50)	2	**2a** (7.6), **5a** (17.8), benzaldehyde[e] (8.9), **1a**[f] (trace)
8	**1a** (20)	23	DMSO (90) $+H_2O$ (25)	2	**2a** (50.5[c])

a) All the reactions were conducted at room temperature. b) Yields were based upon **1**, and referred to isolated ones. c) By Method A. d) By Method B. e) Benzaldehyde was identified and analyzed as its 2,4-dinitrophenylhydrazone. f) A trace amount of **1a** was determined by means of gas chromatography using Tenax GC column at 240 °C.

Table 2. Reactions of sodium salt of phenylnitromethane (**1a**) with peroxodisulfates[a]

Run	Peroxodisulfate (mmol)	Solvent (ml)	Reaction time (h)	Product and yield[b] (%)
1	$K_2S_2O_8$ (15)	DMSO (30)	12	**2a** (62.4)
2	$K_2S_2O_8$ (15)	DMF (30)	12	**2a** (22.8)
3	$K_2S_2O_8$ (15)	CH_3CN (50)	12	**2a** (19.0)
4	$(NH_4)_2S_2O_8$ (15)	DMSO (25)	12	**2a** (63.5)
5	$K_2S_2O_8$ (25)	DMSO (25)	1	**2a** (64.7)

a) All the reactions were carried out using 3.98 g (25 mmol) of sodium salt of **1a** and 1.05 g (12.5 mmol) of sodium hydrogencarbonate at room temperature. The amounts of peroxodisulfates and solvents are given in parentheses. b) Yields were based upon **1a**, and referred to isolated ones.

in DMF or acetonitrile seems to be the low solubility of the sodium salt of **1a** in these cases. Two possible mechanisms for this reaction may be considered. The first mechanism is an ionic pathway postulated originally by Pagano and Shechter[3] for the reaction of the sodium salt of **1a** with ammonium peroxodisulfate. The second possible mechanism involves both $S_{RN}1$ and $E_{RC}1$ reactions, as shown in Scheme 2. This Scheme is based on the observation that the reaction of α-bromophenylnitromethane with the sodium salt of **1a** in DMSO gives also **2a**.[6,8] The exclusive formation of **2** can be well explained by S_{RN} and E_{RC} processes, but there is no experimental evidence for excluding an ionic pathway.

$$\mathrm{Ar\text{-}CH{=}NO_2^-} \xrightarrow{+AgNO_3} \mathrm{Ar\text{-}\dot{C}HNO_2} + NO_3^- + Ag \quad (Ia)$$

$$\mathrm{Ar\text{-}CH{=}NO_2^-} \xrightarrow{+1/2S_2O_8^{2-}} \mathrm{Ar\text{-}\dot{C}HNO_2} + 1/2HSO_4^- + 1/2SO_4^{2-} \quad (Ib)$$

$$\mathrm{Ar\text{-}\dot{C}HNO_2} + \mathrm{Ar\text{-}CH{=}NO_2^-} \longrightarrow \mathrm{[Ar\text{-}CH(NO_2)\text{-}CH(NO_2)\text{-}Ar]^{\cdot -}} \quad (II)$$

3

$$\mathbf{[3]}^{\cdot -} \longrightarrow \mathrm{Ar\text{-}\dot{C}H\text{-}CH(NO_2)\text{-}Ar} + NO_2^- \quad (III)$$

$$\mathrm{Ar\text{-}\dot{C}H\text{-}CH(NO_2)\text{-}Ar} + \mathrm{Ar\text{-}\dot{C}HNO_2} \longrightarrow \mathrm{Ar\text{-}CH(NO_2)\text{-}CH(Ar)\text{-}CH(NO_2)\text{-}Ar} \quad (IV)$$

6

$$\mathbf{6} \longrightarrow \mathbf{2} + NO_2^- \quad (V)$$

Ar=phenyl and substituted phenyl group

Scheme 2.

The only alternative route to **2a** is the reaction of **5a** with **1a**,[7] but the present reaction seems to provide a more convenient one-step method for preparation of **2**, because readily available **1** is the only starting material.

Experimental

Materials. Silver nitrate, potassium peroxodisulfate, ammonium peroxodisulfate, and sodium hydrogencarbonate were commercial reagent-grade. Commercial DMSO, DMF, and acetonitrile were distilled prior to use. (Substituted phenyl)nitromethanes (**1a—d**) were prepared from the corresponding arylacetonitriles[9] according to the method of Black and Bakers.[10] 3-Nitrophenylnitromethane (**1e**) was prepared by nitration of **1a** with fuming nitric acid.[11] The sodium salts of **1a—e** were prepared by addition of methanol solution of **1a—e** to an equivalent amount of sodium methoxide in methanol.

General Procedure for Reaction of 1 with Silver Nitrate. General Procedure by Method A. A sodium salt of **1** (0.05 mol) was added in portions to a stirred solution of silver nitrate (0.06 mol) in DMSO (150 ml) at room temperature. The mixture was stirred at the same temperature for 2 h, and then the silver deposited was removed by filtration, and washed with small amounts of DMSO. The filtrate and washings were poured into cold water to give a pale yellow precipitate, which was collected by filtration, washed with water, and dried. Crystallization from acetic acid or ethanol gave **2** as colorless needles.

General Procedure by Method B. A mixture of **1** (0.05 mol), water (20 ml), and potassium hydroxide (0.05 mol) was added rapidly to a solution of silver nitrate (0.06 mol) in DMSO (150 ml) with stirring. The mixture was stirred at room temperature for 2 h and work-up was carried out as described under Method A.

General Procedure for Reaction of the Sodium Salt of 1a with Peroxodisulfates. To a stirred mixture of potassium peroxodisulfate (0.015 mol) and sodium hydrogencarbonate (0.0125 mol) in DMSO (30 ml), the sodium salt of **1a** (0.025 mol) was added in portions and the mixture was stirred at room temperature for 12 h. The solution was then poured into cold water to give slightly yellow precipitates, which were collected, washed with water, and dried. Crystallization from acetic acid gave **2a**.

References

1) H. Schechter and R. B. Kaplan, *J. Am. Chem. Soc.*, **75**, 3980 (1953).
2) A. Dornow and K. J. Fust, *Chem. Ber.*, **90**, 1774 (1957).
3) A. H. Pagano and H. Shechter, *J. Org. Chem.*, **35**, 295 (1970).
4) R. B. Kaplan and H. Shecter, *J. Am. Chem. Soc.*, **83**, 3535 (1961).
5) C. D. Nenitzesuch, *Chem. Ber.*, **62**, 2669 (1929).
6) A part of this work was published in a communication form: K. Fukunaga, *Synthesis*, **1978**, 58.
7) E. P. Kohler and G. R. Barrett, *J. Am. Chem. Soc.*, **46**, 1733 (1924).
8) It has been found that α-halonitroalkanes, on treatment with nucleophiles, undergo substitution in which the halogen rather than the nitro group is displaced and that these reactions all show the characteristics of radical anion-free radical chain processes (*cf.* N. Kornblum, *Angew. Chem. Int. Ed. Engl.*, **14**, 734 (1975)).
9) K. Fukunaga, S. Ide, M. Mori, and M. Kimura, *Nippon Kagaku Kaishi*, **1977**, 1379; "Shin Zikken Kagaku Koza," ed by The Chemical Society of Japan, Maruzen, Tokyo (1978), Vol. 14, p. 1434.
10) A. P. Black and F. H. Bakers, *Org. Synth.*, Coll. Vol. II, 512 (1943).
11) L. F. Fieser and M. Gates, *J. Am. Chem. Soc.*, **68**, 2249 (1949).

BULLETIN OF THE CHEMICAL SOCIETY OF JAPAN, VOL. 52 (5), 1545—1546 (1979)

The Glow-discharge Reactions of Amines

Hideki ASADA, Masakatsu NOMURA, and Shōichi KIKKAWA*

Department of Applied Chemistry, Faculty of Engineering, Osaka University, Yamadakami, Suita 565

(Received July 10, 1978)

Synopsis. The glow-discharge reactions of propylamine, dipropylamine, and *N*,*N*-dimethyl-2-methyl-1-propenylamine were studied. The results show that the primary amines yield RN=CHR′ and $RNHCH_2CN$, and that the secondary amines produce R(R′)NCH(R″)CN. *N*,*N*-Dimethyl-2-methyl-1-propenylamine produces a series of imine and nitrile.

We have already reported that the glow-discharge reactions of butylamine, pyrrolidine, and pyrrole[1] gave characteristic products. In this note, propylamine, dipropylamine, and *N*,*N*-dimethyl-2-methyl-1-propenylamine, whose double bond may be supposed to stabilize the active species produced by a C–N fission, were chosen as the starting materials in order to clarify the glow-discharge reactions of amine derivatives. Their glow-discharge reactions were discussed principally on the basis of detailed product analyses.

Propylamine gave such products as could be deduced from the reaction of butylamine, while dipropylamine gave the same kind of products that could be deduced from the products of pyrrolidine, considered as a typical secondary amine, so it has become apparent that primary and secondary amines gave characteristic products in the discharge field.

N,*N*-Dimethyl-2-methyl-1-propenylamine was prepared by the dehydration of dimethylamine with isobutylaldehyde. From the product analyses, the double bond of enamine may be supposed to stabilize the N-radical produced by the cleavage of the weakest C–N bond in the discharge field, accordingly, several characteristic products were produced. These results will be reported in this note.

Experimental

The propylamine and dipropylamine were obtained from Wako Pure Chemical Industries, Ltd., and were used without further purification. *N*,*N*-Dimethyl-2-methyl-1-propenylamine, which was composed of a fraction with a bp of 87—88 °C/760 mmHg, was prepared according to the ordinary method.[2] The apparatus was a fast-flow system which has been previously described,[3] it was operated in a similar way. The rate of the reactants was adjusted by being controlled the heating of their reservoir. The reaction products were collected in the liquid nitrogen trap.

The principal liquid products were isolated from an appropriate fraction using preparative gas chromatography (Shimadzu GC-2C, Silicone DC 550, 4.5 m, H_2), and were identified by the analyses of their NMR spectra, IR spectra, and mass spectra obtained using GC-MS, and by comparing their retention times with those of the authentic samples in the gas chromatogram. The quantitative analyses of the liquid products were undertaken by comparing the area of the chromatogram using a Shimadzu GC-4BPTF apparatus (4.4 m×3 mm column packed with 10% and 20% SE-30 on Chromosorb W and Uniport B respectively; oven temp: 30—270 °C; program rate: 10 °C/min; H_2 was used as the carrier gas).

Results and Discussion

N-Propylidenepropylamine, *N*-ethylidenepropylamine, and (propylamino)acetonitrile were produced by the glow-discharge reaction of propylamine. *N*-Propylidenepropylamine and *N*-ethylidenepropylamine are assumed to be formed by the attack of the propyl and ethyl radicals upon the N-atom of propylamine, followed by dehydrogenation. (Propylamino)acetonitrile is supposed to be produced by the reaction of $\dot{C}H_2CN$ with propylamine. It is obvious that these compounds correspond to the reaction products of butylamine.

The results of both reactions under similar conditions are cited in Table 1 in an attempt to deduce a general rule with regard to the behavior of primary aliphatic amines under the influence of the glow discharge. The glow-discharge reactions of $CH_3(CH_3)CHCH_2NH_2$ and $CH_3CH_2(CH_3)CHNH_2$ also gave the products deduced from the above results.

Table 1. General products of primary amines

	(%)[a]		(%)[a]
n-$PrNH_2$	25.9	*n*-$BuNH_2$	38.8
n-PrN=CHR	(35.1)	*n*-BuN=CHR	(22.3)
R=CH_3	30.5	R=CH_3	21.0
R=CH_2CH_3	4.6	R=CH_2CH_3	tr
		R=$CH_2CH_2CH_3$	1.3
n-$PrNHCH_2CN$	34.3	*n*-$BuNHCH_2CN$	27.7

a) Ratio in the liquid products.

Concerning the cleavage of the secondary amines obtained in the mass spectra, β-fission is very important; also, in the discharge field, the $CH_3CH_2CH_2NH\dot{C}H_2$ formed according to the β-fission of dipropylamine is considered to rearrange to $CH_3CH_2\dot{C}HCN$ accompanying dehydrogenation. The α-fission of dipropylamine formed $CH_3\dot{C}HCN$, and the double β-fission of dipropylamine yielded $\dot{C}H_2CN$. The reactions of these radicals with dipropylamine were supposed to lead to 2-aminonitriles. As the process caused by β-fission is supposed to be a main one, it seems probable that the amount of 2-(dipropylamino)propionitrile is less than that of 2-(dipropylamino)butyronitrile.

The discharge reaction of pyrrolidine also gave a series of 2-(1-pyrrolidinyl)nitrile as the main products; therefore, the formation of such products seems to be a general feature in the glow-discharge reactions of secondary aliphatic amines (see Table 2).

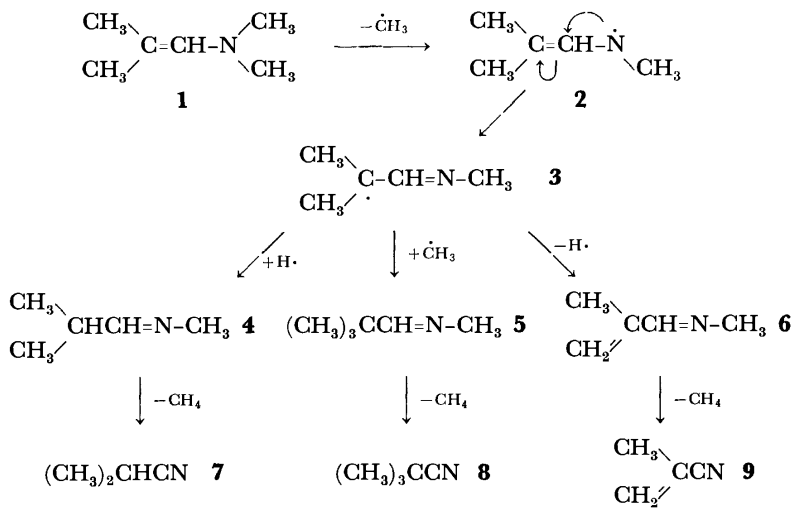

Scheme 1.

Table 2. General products of secondary amines

	(%) [a]		(%) [a]
$(n\text{-Pr})_2NH$	25.4	NH	19.9
$(n\text{-Pr})_2NCH(R)CN$	(40.8)	NCH(R)CN	(47.8)
R=H	17.7	R=H	20.4
$R=CH_3$	4.7	$R=CH_3$	16.0
$R=CH_2CH_3$	18.4	$R=CH_2CH_3$	11.4

a) Ratio in the liquid products.

Thus, the glow-discharge reactions of primary amines gave RN=CHR′ and $RNHCH_2CN$, while that of secondary amines gave R(R′)NCH(R″)CN.

Table 3 shows the results of the glow-discharge reaction of *N,N*-dimethyl-2-methyl-1-propenylamine. This table indicates the formation of many kinds of nitrile and imine under the present experimental conditions. The process leading to these products could be reasonably deduced in the following way (see Scheme 1). According to the evaluation of the bond energy of *N,N*-dimethyl-2-methyl-1-propenylamine on the basis of the data of Egger and Cocks,[4] the (a) bond in $C=C-N^{(a)}-C$ is believed to be the weakest in the molecule. The largest fragment in the mass spectrum of *N,N*-dimethyl-2-methyl-1-propenylamine is also M—Me. The N-radical produced by a cleavage of the N–Me bond in the discharge field attacked the neighboring sp^2-carbon, forming an imine, and produced a relatively stable tertiary radical at the β-position. Supposing the existence of this radical in the middle of the way, we can explain the formation of **4**, **5**, and **6**. The doubly-occurring cleavage of the N–Me bonds in the starting enamine, followed by the elimination of hydrogen, leads to **7**, **8**, and **9**. The formation of other identified products, such as propionitrile, acrylonitrile, and hydrogen cyanide, are attributed to the further decomposition of **7**, **8**, and **9**.

Another feature of the discharge reaction of *N,N*-dimethyl-2-methyl-1-propenylamine is the formation of *N,N*-dimethyl-1-cyano-2-methyl-1-propylamine, produced by HCN addition to the enamine, which occurred during the warming up of the reaction mixture in the trap to room temperature.

Table 3. Experimental conditions and yields of the liquid products for the glow-discharge reaction of *N,N*-dimethyl-2-methyl-1-propenylamine

Reaction condition	Run No. 1	2	3
Anodic current of discharge (mA)	50	65	80
Reactant fed in (g)	3.13	2.54	4.06
Liquid products (g)	3.00	2.07	3.00
% in liquid products			
C_4	0.9	2.0	2.8
$CH_2=CHCN$	3.1	4.7	6.1
CH_3CH_2CN	1.5	2.8	1.1
$CH_2=C(CH_3)CN$	1.2	2.5	4.1
$(CH_3)_2CHCN$	0.4	0.8	1.5
$(CH_3)_3CCN$	0.6	1.7	1.7
$CH_2=C(CH_3)CH=NCH_3$	4.9	5.8	5.6
$(CH_3)_2CHCH=NCH_3$	2.3	1.5	0.9
$(CH_3)_3CCH=NCH_3$	3.1	3.5	1.0
$(CH_3)_2NCH_2CN$	0.5	0.2	1.0
$(CH_3)_2CHCH(CN)N(CH_3)_2$	0.9	1.5	5.0
Others (50 peaks)	5.9	11.2	25.5
$[(CH_3)_2C=CHN(CH_3)_2]$	74.7	61.8	43.7

References

1) S. Kikkawa, M. Nomura, and N. Hosokawa, *Bull. Chem. Soc. Jpn.*, **50**, 2700 (1977).
2) K. C. Brannock, A. Bell, R. D. Burpitt, and C. A. Kelly, *J. Org. Chem.*, **29**, 801 (1964).
3) S. Kikkawa, M. Nomura, and Y. Morita, *J. Synth. Org. Chem. Jpn.*, **34**, 36 (1976).
4) K. W. Egger and A. T. Cocks, *Helv. Chim. Acta*, **56**, 1516 (1973).

BULLETIN OF THE CHEMICAL SOCIETY OF JAPAN, VOL. 52 (5), 1547—1548 (1979)

The Crystal and Molecular Structure of an Isomer of Dibromoperylenes[1)]

Tokiko UCHIDA,* Kozo KOZAWA, Yukinori NAGAO, and Takahisa MISONOO

Department of Industrial Chemistry, Faculty of Science and Technology, Science University of Tokyo, Yamazaki, Noda, Chiba 278

(Received August 10, 1978)

Synopsis. Of two isomers of dibromoperylene, the one possessing the higher melting point has been determined to be 3,9-dibromoperylene from the X-ray diffractometer data. The crystals are monoclinic, with a space group of $P2_1/a$, $a=15.238$, $b=11.826$, $c=3.928$ Å, $\beta=95.53°$, $D_m=1.90$, $D_x=1.94$ g cm^{-3}, and $Z=2$. The structure was solved by the heavy-atom method. The final R value was 0.090 for 931 reflections.

As early as 1925, Zinke *et al.*[2)] obtained two kinds of dibromoperylene, **1** and **2**, by adding bromine to perylene. They presumed the one with the lower melting point, **2**, to be 3,10-dibromoperylene, since it was oxidized in sulfuric acid to produce 3,10-perylenequinone. However, the other dibromoperylene, **1**, has remained ambiguous as to the positions of its substituted bromine atoms. From the view point of our systematically synthetic study of perylene derivatives, the above-mentioned ambiguity is not permissible. Therefore, we have now determined the crystal and molecular structure of **1** from the three-dimensional X-ray data.

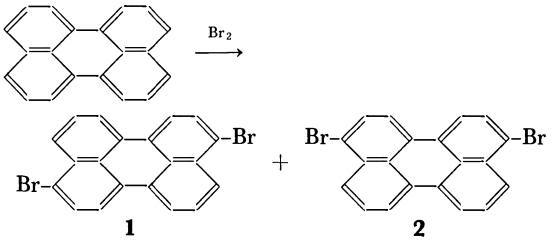

Experimental

Materials. Perylene (2.5 g) was dissolved in benzene (375 ml) at 80 °C; the solution was then cooled and the temperature kept at 35 °C with stirring. After adding bromine (7.5 g) to it in a drop-by-drop manner for about 10 min, the mixture was cooled and 3.9 g of solid products were separated. Then, the reaction products were fractionated into two parts, **1** and **2**, with aniline–nitrobenzene (1/1 v/v), the fractionation being done on the basis of the difference in their solubility.

The **1** portion was purified by repeated recrystallizations from aniline–nitrobenzene (1/1 v/v). Yield, 0.51 g; mp 289—293 °C. Found: C, 58.96; H, 2.28%. Calcd for $C_{20}H_{10}Br_2$: C, 58.57; H, 2.46%. **2** was obtained similarly by recrystallization from aniline–toluene (5/3 v/v). Yield, 0.71 g; mp 218—223 °C.[3)] Found: C, 58.16; H, 2.34%. Calcd for $C_{20}H_{10}Br_2$: C, 58.57; H, 2.46%.[4)]

Procedures. A c-elongated needle crystal of **1**, $0.05\times0.1\times0.5$ mm, was grown in a benzene solution. The reflection intensities and cell parameters were determined with a Rigaku four-circle diffractometer at the University of Tokyo with LiF-monochromatized Mo $K\alpha$ radiation ($\lambda=0.7107$ Å). The data were collected by the 2θ-ω scan method up to $2\theta\leqq55°$. Lorentz and polarization corrections were applied, but no absorption correction was made. The profiles of the reflection peaks showed that the crystal was rather poor in quality. Of the 1845 independent measured reflections, 931 (with $|F_o|>3\sigma(F)$) were used in the analysis.

Crystal Data. $C_{20}H_{10}Br_2$, $M_r=410.11$, monoclinic, space group $P2_1/a$, $a=15.238(3)$, $b=11.826(3)$, $c=3.928(3)$ Å, $\beta=95.53(2)°$, $U=704.5$ Å^3, $D_m=1.90$ (flotation), $D_x=1.94$ g cm^{-3}, $Z=2$, $\mu=59.8$ cm^{-1} (Mo $K\alpha$).

Structure Determination and Discussion

The structure was solved by the heavy-atom method and refined by the block-diagonal least-squares procedure. The discrepancy index, R, was finally reduced to 0.090 with the anisotropic thermal parameters for non-hydrogen atoms, a constant isotropic thermal parameter (4.0 Å^2) for hydrogen atoms, and an anomalous dispersion correction for the bromine atom. The atomic scattering factors were adopted from the International Tables for X-Ray Crystallography, Vol. IV.[5)] All the computations were performed at the Computer Centre of the University of Tokyo, using the UNICS program system.[6)]

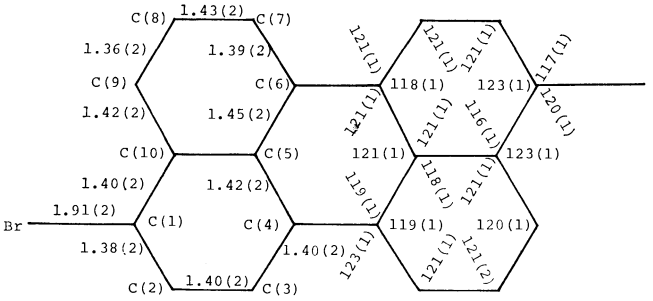

Fig. 1. Bond distances (Å) and angles(°). Estimated standard deviations are shown in parentheses.

The structure analysis indicates that the molecule has a center of symmetry and is 3,9-dibromoperylene. Table 1 gives the positional and thermal parameters,[7)] while the bond distances and angles are shown in Fig. 1. Though the relatively high value of the estimated standard deviations (esd's) prevents any precise discussion of the results, the structure of the perylene skeleton is not affected by the substituted bromine atoms.[8,9)] These large esd's might due to the poor crystallinity, as has been mentioned above.

The molecule makes the following least-squares plane:

$$0.3524X - 0.1280Y + 0.9270Z = 0$$

where X, Y, and Z are coordinates (in Å) referred to the a, b, and c* crystal axes respectively. The largest atomic deviation from this plane is 0.02 Å for C(7).

The dibromoperylene molecules stack to form a

TABLE 1. THE FINAL ATOMIC PARAMETERS ($\times 10^4$), WITH THEIR ESTIMATED STANDARD DEVIATIONS
The anisotropic thermal parameters are of the form: $\exp[-(B_{11}h^2+B_{22}k^2+B_{33}l^2+B_{12}hk+B_{13}hl+B_{23}kl)]$

	x	y	z	B_{11}	B_{22}	B_{33}	B_{12}	B_{13}	B_{23}
Br	−1350 (1)	4166 (1)	3826 (4)	58 (1)	62 (1)	697 (11)	43 (2)	52 (5)	−27 (6)
C(1)	−1087 (11)	2631 (11)	2813 (34)	50 (7)	41 (9)	378 (80)	19 (13)	−3 (38)	71 (45)
C(2)	−1711 (9)	1834 (13)	3469 (33)	29 (6)	79 (12)	343 (78)	40 (14)	−3 (34)	−3 (50)
C(3)	−1567 (9)	697 (12)	2731 (37)	29 (6)	67 (11)	502 (87)	11 (13)	74 (35)	71 (54)
C(4)	−799 (8)	348 (11)	1357 (33)	26 (6)	48 (9)	457 (85)	23 (12)	72 (34)	21 (46)
C(5)	−163 (8)	1176 (11)	734 (30)	19 (5)	53 (9)	346 (74)	22 (11)	−74 (30)	−35 (42)
C(6)	655 (8)	848 (12)	−628 (30)	22 (5)	73 (10)	308 (70)	3 (13)	−3 (31)	−46 (50)
C(7)	1271 (10)	1685 (14)	1161 (42)	35 (7)	83 (13)	630 (110)	22 (15)	94 (44)	119 (61)
C(8)	1103 (10)	2849 (14)	−454 (40)	31 (7)	76 (12)	601 (104)	14 (14)	66 (42)	15 (57)
C(9)	346 (9)	318 (13)	810 (39)	28 (6)	78 (12)	559 (100)	−9 (14)	−115 (40)	134 (58)
C(10)	−301 (8)	2358 (11)	1446 (33)	24 (6)	46 (9)	463 (83)	12 (11)	3 (34)	37 (46)
H(2)	−2211 (144)	1813 (164)	4842 (579)						
H(3)	−2020 (139)	238 (182)	3359 (530)						
H(7)	1609 (135)	1463 (177)	−2943 (529)						
H(8)	1695 (143)	3353 (173)	−996 (544)						
H(9)	332 (149)	4134 (151)	2245 (547)						

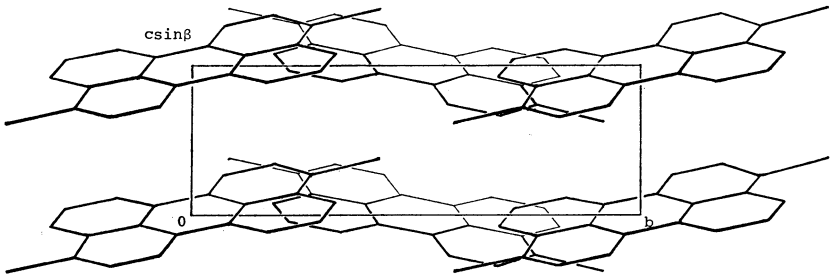

Fig. 2. The structure viewed along the a axis.

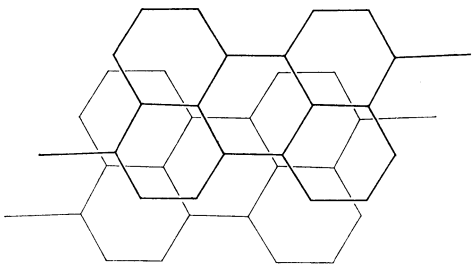

Fig. 3. Molecular overlap projected to the best plane.

column parallel to the c axis, as is shown in Fig. 2. Figure 3 gives the overlapping scheme of two adjacent molecules in a column projected on the molecular plane. The ovelapping manner of the perylene skeleton is very similar to that in the α-form crystal of perylene.[9] All the intermolecular Br···H distances exceed 3.0 Å. Since the sum of the van der Waals radii of Br and H is 3.12 Å, there might well not be any special interaction between intercolumnar atoms.

The authors wish to thank Dr. Maki Sato of the University of Tokyo for his help in the data collection.

References

1) Presented at the 37th National Meeting of the Chemical Society of Japan, Yokohama, April, 1978.
2) A. Zinke, F. Linner, and O. Wolfbauer, *Chem. Ber.*, **58**, 323 (1925).
3) Lit (Ref. 2) mp: **1**, 289.5—291.0 °C; **2**, about 190 °C.
4) The mass spectra of **1** and **2** showed identical patterns of ion peaks over the entire region examined, and gave the parent ion peaks at *m/e* 408, 410, and 412 corresponding to two bromine atoms. The IR spectra of both **1** and **2** also exhibited almost identical absorption patterns.
5) "International Tables for X-Ray Crystallography," Vol. IV, Kynoch Press, Birmingham (1974), pp. 72, 73, 80, and 149.
6) "Universal Crystallographic Computation Program System," ed by T. Sakurai, Crystallographic Society of Japan, Tokyo (1967).
7) The structure-factor table is kept in the office of the Chemical Society of Japan (Document No. 7919).
8) J. Tanaka, *Bull. Chem. Soc. Jpn.*, **36**, 1237 (1963).
9) A. Camerman and J. Trotter, *Proc. R. Soc. London, Ser. A*, **279**, 129 (1964).

BULLETIN OF THE CHEMICAL SOCIETY OF JAPAN, VOL. 52 (5), 1549—1550 (1979)

New Azulene Derivatives Obtained by the Sulfur Dehydrogenation of Guaiene: 3,6,9-Trimethylazuleno[4,5-*b*]thiophene and 2-Methylthioguaiazulene[1)]

Kazuko KOHARA,* Hojun TACHIBANA, Yukio MASUYAMA, and Yasushi OTANI
Konan Chemical Industry, Co. Ltd., 5-21, Nakagawa-cho, Takatsuki, Osaka 569

(Received October 2, 1978)

Synopsis. Two new azulene derivatives, 2-methylthioguaiazulene and 3,6,9-trimethylazuleno[4,5-*b*]thiophene, have been obtained and characterized, along with known 3,5,8-trimethylazuleno[6,5-*b*]thiophene and 2,2′-biguaiazulenyl, by the sulfur dehydrogenation of guaiene.

Guaiazulene[2)] is a well-known azulene derivative and is readily accessible as a major product of the sulfur dehydrogenation of guaiene. In our factory, guaiazulene was produced in large quantities as a precursor for sodium salt of guaiazulene-3-sulfonic acid. During the production of the guaiazulene, several products retaining an azulene skeleton were obtained as minor ingredients. This paper will deal with the isolation and structural elucidation of these minor products.

Experimental

All the melting points are uncorrected. The infrared spectra were determined with a Hitachi Model EPI-G2 spectrometer. The proton nuclear magnetic resonance spectra were recorded as a solution in chloroform-*d*, with internal tetramethylsilane, on a Varian T-60, a Varian A-60D, or a Varian XL-100-15 spectrometer. The mass spectra were measured at 70 eV. The guaiene was prepared by the dehydration of guaiol with formic acid.[3)]

The dehydrogenation of guaiene was performed with sulfur at 200—260 °C for 2—3 h. After the separation of guaiazulene by extraction with sulfuric acid, followed by distillation, the mother liquor of the recrystallization of guaiazulene from methanol was extracted again with 55% sulfuric acid. The extract was diluted with water, and the products were taken into benzene and washed with an aqueous solution of sodium carbonate. The solvent was removed by distillation, and the residue was subjected to fractional vacuum distillation. Seven fractions; i) bp 155 °C/3.5 Torr, ii) bp 155—160 °C/3.5 Torr, iii) bp 160—170 °C/3.5 Torr, iv) bp 170—185 °C/3.5 Torr, v) bp 185—190 °C/3.5 Torr, vi) bp 190—195 °C/3.5 Torr, vii) bp 195—203 °C/3.5 Torr, were thus obtained. Fractions i, ii, and iii contain mainly guaiazulene. From the latter fractions, four kinds of crystalline products were obtained through repeated column chromatography on alumina and/or silica gel as follows:

Product ***A***: Fraction iii was dissolved in hexane and they allowed to stand in a refrigerator. The crystals thus separated were recrystallized from hexane and benzene (10 : 1) to give purple crystals; mp 116—117 °C (≈1%).[4)] Found: C, 79.34; H, 6.14%. Calcd for $C_{15}H_{14}S$: C, 79.60; H, 6.23%.

Product ***B***: After the separation of a small quantity of Product **A** from Fraction vii, the residue was extracted with 40% sulfuric acid. The usual work-up of the extract afforded blue crystals with a mp of 73—74 °C (recrystallized from hexane) in a 0.3% yield.[4)] $\lambda_{max}^{c\text{-hexane}}$ nm (log ε) 235 (4.24), 259 (4.46), 300 (sh, 4.18), 321 (4.37), 335 (4.34), 365 (3.52), 383 (3.58), 403 (3.12), 622 (2.72), 650 (sh, 2.67), 683 (2.59), 725 (sh, 2.28). Found: C, 79.54; H, 6.21%. Calcd for $C_{15}H_{14}S$: C, 79.60; H, 6.23%.

Product ***C***: Products **A** and **B** were removed from Fraction v in the usual manner, and the residue was dissolved in hexane and allowed to stand in a refrigerator. The crystals thus separated were purified by repeated column chromatography on silica gel containing 3% of water eluted with hexane. Product **C** was thus obtained as blue crystals with a mp of 58.5—59 °C in a 0.1% yield.[4)] $\lambda_{max}^{c\text{-hexane}}$ nm (log ε) 254 (4.28), 307 (4.70), 316 (4.74), 348 (3.45), 365 (3.66), 383 (3.89), 403 (4.03), 570 (2.60), 605 (2.58), 670 (sh, 2.18). Found: C, 78.63; H, 8.24; S, 12.74%. Calcd for $C_{16}H_{20}S$: C, 78.63; H, 8.25; S, 13.12%.

Product ***D***: This product was separated from Fraction vii through repeated column chromatography on alumina with hexane. Pure Product **D** was obtained as blue crystals with a mp of 176 °C (recrystallized from hexane) in a ≈0.05% yield.[4)]

Results and Discussion

Product **A** was easily identified as 3,5,8-trimethylazuleno[6,5-*b*]thiophene (**1**) on the basis of a comparison of its melting point and ^{1}H-NMR spectrum with those of the authentic sample reported by Hayashi *et al.*[5)]

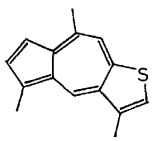

1

The structure of Product **B** was unambiguously established by an examination of its ^{1}H-NMR spectrum, which exhibited two sets of AB-quartets at δ 6.94 and 7.68 (J=11 Hz) and 7.29 and 7.57 (J=4.5 Hz), indicating the presence of vicinal hydrogens on both seven- and five-membered rings. Along with the resonance of two methyl groups at δ 2.88 (6H, s), a signal at δ 2.42 (3H, d, J=1.5 Hz) and a broad singlet at δ 7.07 (1H, bs) indicate that the condensed thiophene ring is substituted with the methyl group at the β-position.[6)] In trifluoroacetic acid, Product **B** exists as its conjugate acid (**2′**), showing three methyl groups at δ 2.92 (3H, d, J=1.0 Hz, 3-CH_3), 3.04 (3H, q, J=1.5 Hz, 9-CH_3), and 3.22 (3H, s, 6-CH_3), a two-proton multiplet at δ 4.15 (7,7′-H), a one-proton multiplet at δ 7.85 (8-H), a one-proton broad singlet at δ 8.65 (2-H), and an AB-quartet at δ 8.58 and 9.11 (J=10.5 Hz, 5-, 4-H). These NMR data are fully consistent with the formulation of Product **B** as 3,6,9-trimethylazuleno[4,5-*b*]thiophene (**2**). To the best of

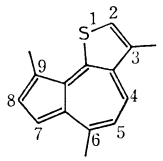

2

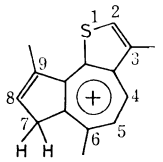

2′

our knowledge, Compound **2** is the second example of an azulene derivative in which a thiophene ring is annulated to the seven-membered ring of an azulene skeleton.

The fact that Product **C** retained a guaiazulene structure was confirmed by the absorption in the ^{1}H-NMR spectrum at δ 1.33 (6H, d, J=7 Hz, $-CH(\mathbf{CH_3})_2$), 3.07 (1H, septet, J=7 Hz, $-\mathbf{CH}(CH_3)_2$), 2.76 (3H, s, 4-CH_3), and 2.63 (3H, s, 1-CH_3). Furthermore, seven-membered ring protons appeared as a doublet at 7.97 (1H, d, J=2.0 Hz, 8-H) and AB-quartet, with further small doublet splittings in the lower-field half of the signals at 6.98 (1H, d, J=10.0 Hz, 5-H), 7.26 (1H, dd, J=10.0, 2.0 Hz, 6-H). In addition, a one-proton singlet attributable to 3-H appeared at δ 6.99. Since the methyl protons characteristic of the methylthio group were observed at δ 2.49 as a singlet,[7] it may be concluded that Product **C** is to be identified as 2-methylthioguaiazulene (**3**). Further support for the structure of **3** was obtained from the sodium periodate oxidation of **3**. The sulfoxide (**4**) was easily obtained in a pure form by chromatography on alumina eluted with benzene as a blue oil. The 4-CH_3 hydrogen resonance in the NMR spectrum of **4** appeared as a

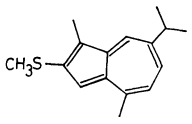

3

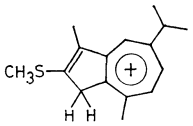

3′

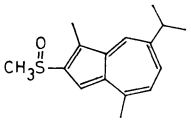

4

singlet at δ 2.68 which is comparable to that of **3**. As expected, 1-CH_3, S-CH_3, and 3-H resonated at δ 2.89 (6H, bs) and 7.72 (1H, s) respectively, points lower than those for the corresponding signals of **3**. The spectrum of **3** taken in trifluoroacetic acid can also be interpreted as supporting the assignment as a conjugate acid (**3′**) of **3**.

Product **D** was identified as 2,2′-biguaiazulenyl since its physical and spectral data are identical with those of the reported values for 2,2′-biguaiazulenyl.[8]

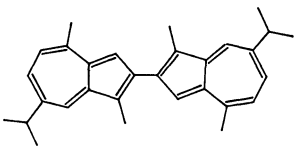

5

References

1) A preliminary report of this work was presented at the 7th International Congress of Essential Oils, Kyoto, Japan, October 1977.

2) T. Kariyone, S. Naito, and J. Chatani, *Pharm. Bull. (Japan)*, **2**, 339 (1954); I. Ognjanoff, D. Ivanoff, V. Herout, M. Horak, J. Pliva, and F. Sorm, *Chem. Ind. (London)*, **1957**, 820; V. Herout, M. Romanuk, and F. Sorm, *Collect. Czech. Chem. Commun.*, **21**, 1359 (1956).

3) M. V. Kadival, M. S. Nair, and S. C. Bhattacharyya, *Tetrahedron*, **23**, 1241 (1967).

4) Isolated yield based on the guaiene used.

5) S. Hayashi, S. Kurokawa, M. Okano, and T. Matsuura, *Tetrahedron Lett.*, **35**, 3443 (1967).

6) S. Sternhell, *Rev. Pure Appl. Chem.*, **14**, 15 (1964).

7) The corresponding *S*-methyl protons of 3-methylthioguaiazulene resonated at δ 2.43 ppm: L. L. Replogle, R. M. Arluck, and J. R. Maynard, *J. Org. Chem.*, **30**, 2715 (1965).

8) R. Hagen, E. Heilbronner, and P. A. Straub, *Helv. Chim. Acta*, **51**, 45 (1968).

BULLETIN OF THE CHEMICAL SOCIETY OF JAPAN, VOL. 52 (5), 1551—1552 (1979)

The Reaction of Methylferrocene with Manganese(III) Acetate

Taeko IZUMI, Yoshibumi SATOU, Yoshio YOSHIDA, and Akira KASAHARA*

Department of Applied Chemistry, Faculty of Engineering, Yamagata University, Yonezawa 992

(Received October 24, 1978)

Synopsis. The oxidation of methylferrocene with manganese(III) acetate in acetic acid yielded three products which arose from the ferrocenylmethylation of methylferrocene. The reaction of methylferrocene with manganese(III) acetate in presence of styrene was also examined.

Previously, Heiba *et al.*[1] have reported the oxidation of aromatic hydrocarbons by manganese(III) acetate in acetic acid; they suggested that a free radical mechanism involving the selective generation and oxidation of organic free radicals is present. For example, the reaction of toluene with manganese(III) acetate led to the formation of a mixture of benzyl acetate, methylbenzyl acetate, and tolylacetic acid. The present investigation deals with the manganese(III) acetate oxidation of methylferrocene (**1**).

Results and Discussion

In a solution of acetic acid containing manganese(III) acetate and anhydrous potassium acetate, **1** was heated at 120 °C until the dark brown color of Mn(III) ion disappeared. Ferrocenyl(2-methylferrocenyl)methane (**2**), ferrocenyl(3-methylferrocenyl)methane (**3**), and ferrocenyl(1′-methylferrocenyl)methane (**4**) were obtained as the products.

In general, the thermolysis of manganese(III) acetate leads almost exclusively to the formation of $\cdot CH_2COOH$ radicals.[1,2] On the other hand, ferrocene does not appear to be particularly susceptible to attack by free radicals.[3] Consequently, in the reaction of **1** with manganese(III) acetate, the attack by the $\cdot CH_2COOH$ radical most likely occurs at the methyl group of **1**; this mechanism is shown in Scheme 1. Kochi *et al.*[4] suggested that the $\cdot CH_2COOH$ radical is oxidized relatively slowly to the correposnding carbonium ion, in contrast to the benzylic radical. In the oxidation of **1** with manganese(III) acetate, the formation of **2**, **3**, and **4** indicates therefore that the $\cdot CH_2COOH$ radical reacts more rapidly with **1** than the radical is oxidized by Mn(III) and the ferrocenylmethyl radical (**5**) is oxidized somewhat more rapidly to the corresponding carbonium ion (**6**) than the $\cdot CH_2COOH$ radical is oxidized by Mn(III). Furthermore, the absence of the formation of ferrocenylmethyl acetate (**7**), which is an expected side product in this reaction, indicated that the **6** carbonium ion reacts more rapidly with **1** than with acetic acid.

Heiba and Dessau[5] described a reaction of olefins with aromatic ketones such as acetophenone in the presence of manganese(III) acetate, leading to the formation of cyclized ketones together with noncyclized products. We have now found that the reaction of **1** with manganese(III) acetate in the presence of

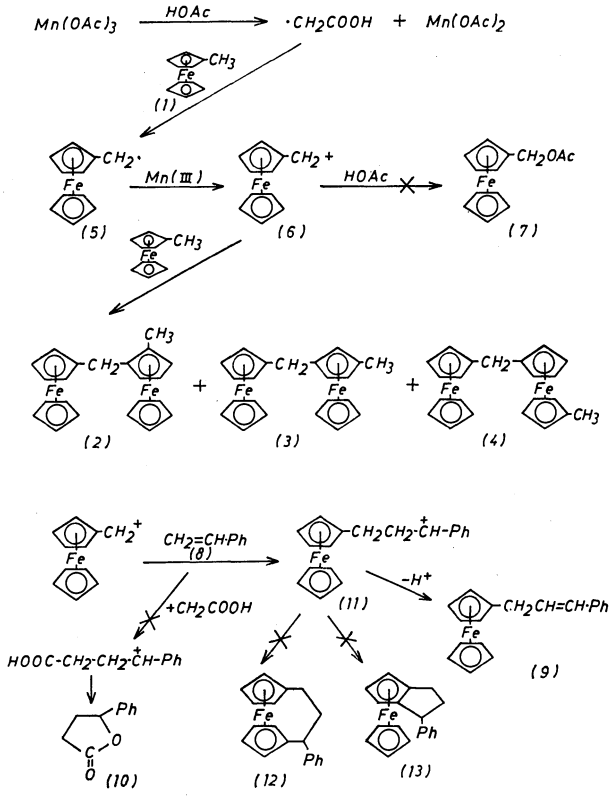

styrene (**8**) led to the formation of a noncyclized product (**9**), together with **2**, **3**, and **4**. The formation of **9** and the absence of γ-lactone (**10**), which is an expected product in the reaction, indicate that the **6** carbonium ion adds to the olefin more quickly than the $\cdot CH_2COOH$ radical adds to the olefin and that the H^+ abstraction from an intermediate (**11**) is faster than the intramolecular cyclization of **11** to **12** or **13**.

Experimental

Materials. All the melting points are uncorrected. The IR and mass spectra were measured using a Hitachi 215 spectrophotometer and a Model RMU-6M mass spectrometer at 70 eV. The NMR spectra were obtained on a Hitachi Model R-22 (90 MHz), using TMS as an internal standard.

The preparation of the following compounds has already been reported: methylferrocene (**1**)[6] and manganese(III) acetate dihydrate.[1]

*The Reaction of Methylferrocene (**1**) with Manganese(III) Acetate.* A mixture of **1** (3.0 g, 15 mmol) and anhydrous potassium acetate (7.4 g) in 75 ml of acetic acid was heated at 120 °C under nitrogen with manganese(III) acetate dihydrate (4.0 g, 15 mmol) until the brown color of Mn(III) ion disappeared (14 h). The reaction mixture was diluted with water and extracted several times with ether. The ether extracts were then dried over anhydrous magnesium sulfate

and evaporated. The residue was chromatographed on silica gel with hexane as the eluent.

The first elution with hexane gave 1.82 g of the starting material (**1**).

The second elution with hexane–benzene (1 : 1) gave 0.38 g (6.4%[7]) of **2**, mp 95—97 °C (ethanol). Found: C, 66.21; H, 5.43%. Calcd for $C_{22}H_{22}Fe_2$: C, 66.37; H, 5.56%; mol wt, 398. IR: 3090, 2980, 2920, 1100, 1000, and 910 cm^{-1}. NMR ($CDCl_3$): δ 1.90 (3H, s, CH_3), 3.33 (2H, s, CH_2), 3.97, 4.01, and 4.05 ppm (17H, m, Cy protons). MS: *m/e* 398 (M^+ for $C_{22}H_{22}Fe_2$). The physical constants and IR and NMR spectra were identical with those of ferrocenyl(2-methylferrocenyl)methane (**2**), which was prepared by the reduction with $LiAlH_4$–$AlCl_3$ of ferrocenyl 2-methylferrocenyl ketone (mp 102—103 °C).

The third elution with benzene–hexane (1 : 1) gave 0.47 g (7.8%) of **3**, mp 83—85 °C (ethanol). Found: C, 66.22; H, 5.45%. Calcd for $C_{22}H_{22}Fe_2$: C, 66.37; H, 5.56%, mol wt, 398. IR: 3090, 2980, 2920, 1100, 1000, 920, and 910 cm^{-1}. NMR ($CDCl_3$): δ 1.87 (3H, s, CH_3), 3.28 (2H, s, CH_2), 3.96, 4.03, and 4.07 ppm (17H, m, Cy protons). MS: *m/e* 398 (M^+ for $C_{22}H_{22}Fe_2$). The **3** compound is identical in all respects with ferrocenyl(3-methylferrocenyl)-methane, which was prepared by the reduction of ferrocenyl 3-methylferrocenyl ketone (mp 90—92 °C) with $LiAlH_4$–$AlCl_3$.

The following elution with benzene–hexane (1 : 1) gave 0.43 g (7.0%) of **4**, mp 85—97 °C (ethanol). Found: C, 66.31; H, 5.48%. Calcd for $C_{22}H_{22}Fe_2$: C, 66.37; H, 5.56%; mol wt, 398. IR: 3090, 2980, 2920, 1100, 1000, and 910 cm^{-1}. NMR ($CDCl_3$): δ 1.91 (3H, s, CH_3), 3.36 (2H, s, CH_2), 3.97, 4.02, and 4.07 ppm (17H, m, Cy protons). MS: *m/e* 398 (M^+ for $C_{22}H_{22}Fe_2$). The **4** compound is identical in all respects with ferrocenyl(1′-methylferrocenyl)-methane, which was prepared by the reduction of ferrocenyl 1′-methoxycarbonylferrocenyl ketone (mp 180—182 °C)[8] with $LiAlH_4$–$AlCl_3$.

*The Reaction of Methylferrocene (**1**) with Manganese(III) Acetate in the Presence of Styrene.* A mixture of **1** (3.0 g, 15 mmol), styrene (1.54 g, 15 mmol), and anhydrous potassium acetate was heated at 120 °C under nitrogen with manganese(III) acetate dihydrate (4.0 g, 15 mmol) until the brown color of Mn(III) ion disappeared (10 h). The isolation of the products in the same manner as was used for the oxidation of **1** with manganese(III) acetate gave **2** (mp 95—97 °C, 0.35 g, 6.0%), **3** (mp 83—85 °C, 0.41 g, 7.0%), **4** (mp 85—87 °C, 0.38 g, 6.3%), and **9** (mp 68—70 °C, 0.52 g, 11.5%).

The **9** compound is identical in all respects with 3-ferrocenyl-1-phenyl-1-propene, which was prepared by the reduction of cinnamoylferrocene (mp 139—140 °C)[9] with $LiAlH_4$–$AlCl_3$. Found: C, 75.38; H, 5.83%. Calcd for $C_{19}H_{18}Fe$: C, 75.51; H, 6.00%; mol wt, 3.02. IR: 3090, 2980, 2920, 1100, 1000, 905, and 960 cm^{-1} (trans –CH=CH–). NMR ($CDCl_3$): δ 3.21 (2H, t, CH_2), 4.10 (5H, s, Cy protons), 4.16 (4H, br-s, Cy protons), 6.40 (1H, m, J=15 Hz, –CH=C–Ph), and 7.20—7.40 ppm (6H, m, –C=CH–Ph+Ph protons). MS: *m/e* 302 (M^+ for $C_{19}H_{18}Fe$).

References

1) E. I. Heiba, R. M. Dessau, and W. J. Koehl, Jr., *J. Am. Chem. Soc.*, **91**, 138 (1969).

2) R. E. Van Der Ploeg, R. W. DeKorte, and E. C. Kooyman, *J. Catal.* **10**, 52 (1968).

3) M. Rosenblum, "Chemistry of the Iron Group Metallocenes," John Wiley & Sons, New York (1965), p. 208.

4) J. K. Kochi, J. D. Bacha, and T. W. Bethea, III, *J. Am. Chem. Soc.*, **89**, 6538 (1967).

5) E. I. Heiba and R. M. Dessau, *J. Am. Chem. Soc.*, **94**, 2888 (1972).

6) R. A. Benkeser and J. R. Bach, *J. Am. Chem. Soc.*, **86**, 890 (1964).

7) The calculation of the yield is based on the stoichiometry of 2 mol of manganic acetate/mol of **2**, **3**, **4**, and **9** produced. This stoichiometry is required by the mechanism presented in this paper.

8) T. H. Barr, H. L. Lentzner, and W. E. Watts, *Tetrahedron*, **25**, 6001 (1969).

9) K. Schlogl and A. Molar, *Monatsh. Chem.*, **93**, 861 (1962).

BULLETIN OF THE CHEMICAL SOCIETY OF JAPAN, VOL. 52 (5), 1553—1554 (1979)

A Novel Approach to *cis*-Jasmone and Dihydrojasmone from 2-(2-Benzothiazolylthio)-2-(3-oxobutyl)oct-5-en(or -an)oic Acid by Electrolytic Procedure

Sigeru Torii,* Hideo Tanaka, Yuichi Kobayasi, Junzo Nokami,** and Mikio Kawata**

Department of Industrial Chemistry, School of Engineering, Okayama University, Okayama 700

***Okayama University of Science, Ridai, Okayama 700*

(Received November 21, 1978)

Synopsis. *cis*-Jasmone (**7a**) and dihydrojasmone (**7b**) have been synthesized by facile five-step processes starting from methyl acetoacetate involving electrolysis procedure. Methyl 2-(2-benzothiazolylthio)oct-5-en(or -an)oate, prepared from methyl 2-acetyloct-5-en(or -an)oate (**1**) by the reaction with the *N*-(2-benzothiazolylthio)morpholine, were allowed to react with methyl vinyl ketone, leading to the Michael adducts **4**. After hydrolysis of **4**, the corresponding acids **5** were electrolyzed to afford the desired 1,4-diketone **6** in 45—48% overall yields (based on **1**), whose base-catalyzed cyclization gave **7** smoothly.

As part of our program to investigate the electrochemical functionalization of carboxylates, we examined the conversion of the carboxylates bearing 2-benzothiazolylthio group in the α-position into the corresponding oxo compounds by electrolysis. Our efforts to utilize 2-(2-benzothiazolylthio)-2-(3-oxobutyl)oct-5-en(or -an)oic acid (**4**) in such a reaction led successfully to the expected 1,4-diketone **6**,[1] important precursors of *cis*-jasmone (**7a**) and dihydrojasmone (**7b**).

Methyl 2-(2-benzothiazolylthio)oct-5-en(or -an)oate (**2**) was smoothly prepared by treatment of methyl 2-acetyloct-5-en(or -an)oate (**1**) with *N*-(2-benzothiazolylthio)morpholine (**3**)[2] in methanol under refluxing for *ca.* 16 h.[3] The reaction of **2** with methyl vinyl ketone was carried out successfully in refluxing acetone using excess amounts of potassium carbonate for 12 h in the presence of a trace of 2,5-di-*t*-butylhydroquinone as a polymerisation inhibitor. This afforded **4a** in 87% yield and **4b** in 79% yield. Hydrolysis of Michael adducts **4** in aqueous methanol in the presence of potassium carbonate at 45—55 °C for 14 h afforded the corresponding acids **5** in 92—96% yields.

The electrolysis of **5a** using carbon rod electrodes in acetic acid–*t*-butyl alcohol–triethylamine (6/3/0.2, v/v) at a current of 20 mA/cm² (applied voltage 18—25 V) at 45—55 °C for 2.5 h gave **6a** in 61% yield. Similarly, the electrolysis of **5a** could be carried out using platinum electrodes in methanol–triethylamine (10/0.2, v/v) at a current of 30 mA/cm² (applied voltage 18—22 V) at 45—50 °C for 2.5 h, giving **6a** in 54% yield. On the other hand, the acid **5b** favored the electrolysis in the two-phase system, consisting of water and hexane (extracting solvent) layers as described in the preceeding paper.[4] Thus, an aqueous solution of **5b** and sodium hydroxide was electrolyzed using an undivided cell fitted with two platinum electrodes under a current of 30 mA/cm² (applied voltage 7—9 V) at 46—50 °C for 4 h, giving the desired **6b** in 64% after evaporation of the organic layer.

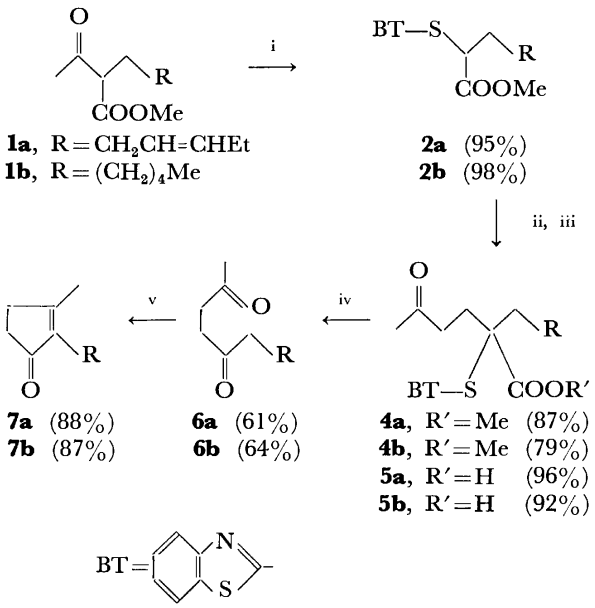

The carbonyl group of **6** seems to be formed by electrolytic decarboxylation of **5** followed by hydroxylation (methoxylation, acetoxylation), leading to intermediate (A), and subsequent elimination of 2-benzothiazolylthio group.[5]

The base-catalyzed cyclization of the 1,4-diketones **6** afforded *cis*-jasmone (**7a**) and dihydrojasmone (**7b**), respectively.[1]

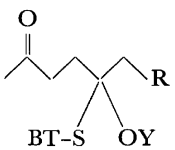

(A)

Y=H, Me, or Ac

Experimental

All boiling points were uncorrected, the boiling points indicated being air-bath temperatures. IR spectra were determined with a JASCO Model IRA-1 spectrophotometer

with a grating. ^{1}H NMR spectra were obtained with Hitachi R-24 and/or JEOL MH-100 spectrometers. Elemental analyses were carried out in this laboratory.

*Methyl (Z)-2-Acetyl-5-octenoate (**1a**).* A suspension of methyl acetoacetate (540 mg, 4.65 mmol), (*Z*)-3-hexenyl bromide (836 mg, 5.13 mmol), K_2CO_3 (2.57 g, 18.6 mmol), and KI (1.07 g, 6.45 mmol) in acetone (20 ml) was heated to reflux for 6 h. Insoluble materials were filtered off and the filtrate was concentrated. The residue was chromatographed (SiO_2, benzene/AcOEt, 30/1) to give **1a** (840 mg, 91%): bp 94—98 °C/9 Torr; IR (neat) 1745 (ester C=O), 1717 (C=O), 1649 cm^{-1}; ^{1}H NMR (CCl_4) δ 0.98 (t, 3, J=7 Hz, CH_3), 1.55—2.34 (m, 9), 3.34 (t, 1, J=7 Hz, CH), 3.70 (s, 3, CH_3O), 4.89—5.66 (m, 2, HC=CH). Found: C, 66.56; H, 9.14%. Calcd for $C_{11}H_{18}O_3$: C, 66.44; H, 9.15%.

*Methyl (Z)-2-(2-Benzothiazolylthio)-5-octenoate (**2a**).* A solution of **1a** (619 mg, 3.12 mmol) and *N*-(2-benzothiazolylthio)morpholine[2] (**3**, 886 mg, 3.51 mmol) in MeOH (7 ml) was heated to reflux for 15 h. After evaporation of the solvent, the residue was chromatographed (SiO_2, benzene/hexane/AcOEt, 20/10/1) to give **2a** (955 mg, 95%): bp 120—124 °C/0.01 Torr; IR (neat) 3056 (HC=C), 1734 cm^{-1} (C=O); ^{1}H NMR (CCl_4) δ 0.93 (t, 3, J=7 Hz, CH_3), 1.72—2.30 (m, 6, CH_2), 3.70 (s, 3, CH_3O), 4.68 (t, 1, J=7 Hz, CH), 5.22—5.57 (m, 2, HC=CH), 7.02—7.92 (m, 4, HC=C). Found: C, 59.61; H, 6.11%. Calcd for $C_{16}H_{19}NO_2S_2$: C, 59.78; H, 5.96%.

Similarly, *methyl 2-(2-benzothiazolylthio)octanoate (**2b**)* was obtained in 98% yield, bp 120—123 °C/0.004 Torr (lit,[3] bp 123—126 °C/0.005 Torr).

*Methyl (Z)-2-(2-Benzothiazolylthio)-2-(3-oxobutyl)-5-octenoate (**4a**).* A mixture of **2a** (515 mg, 1.60 mmol), methyl vinyl ketone (562 mg, 8.01 mmol), K_2CO_3 (443 mg, 3.21 mmol), and 2,5-di-*t*-butylhydroquinone (7 mg) in acetone (7 ml) was heated to reflux for 12 h. The insoluble materials were filtered off and the filtrate was concentrated. The residue was chromatographed (SiO_2, benzene/AcOEt, 15/1) to give **4a** (547 mg, 87%): bp 150—154 °C/0.005 Torr; IR (neat) 3061 (HC=C), 1729 (ester C=O), 1717 cm^{-1} (C=O); ^{1}H NMR (CCl_4) δ 0.92 (t, 3, J=7 Hz, CH_3), 1.68—2.85 (m, 13), 3.69 (s, 3, CH_3O), 5.12—5.50 (m, 2, HC=CH), 7.10—8.00 (m, 4, HC=C). Found: C, 61.43; H, 6.69%. Calcd for $C_{20}H_{25}NO_3S_2$: C, 61.35; H, 6.44%.

Similarly, *methyl 2-(2-benzothiazolylthio)-2-(3-oxobutyl)-octanoate (**4b**)* was obtained in 79% yield, bp 152—155 °C/0.01 Torr; IR (neat) 3058 (HC=C), 1731 (ester C=O), 1716 cm^{-1} (C=O); ^{1}H NMR (CCl_4) δ 0.62—1.04 (m, 3, CH_3), 1.04—2.81 (m, 17), 3.71 (s, 3, CH_3O), 7.08—8.02 (m, 4, HC=C). Found: C, 60.95; H, 7.04%. Calcd for $C_{20}H_{27}NO_3S_2$: C, 61.04; H, 6.92%.

*(Z)-2-(2-Benzothiazolylthio)-2-(3-oxobutyl)-5-octenoic Acid (**5a**).* A solution of **4a** (950 mg, 2.43 mmol) and K_2CO_3 (1.01 g, 7.31 mmol) in MeOH (20 ml) containing water (5 ml) was stirred at 45—55 °C for 14 h. The solution was concentrated to *ca.* 5 ml of total volume, diluted with brine, acidified with aqueous 10% HCl, and extracted with AcOEt. The extracts were washed with brine, dried (Na_2SO_4) and concentrated. The residue was chromatographed (SiO_2, benzene/AcOEt/MeOH, 30/3/1) to give **5a** (882 mg, 96%): IR (neat) 3650—2200 (COOH), 1713 cm^{-1} (C=O); ^{1}H NMR ($CDCl_3$) δ 0.86 (t, 3, J=7 Hz, CH_3), 1.69—2.95 (m, 15), 5.14—5.54 (m, 2, HC=CH), 7.20—8.08 (m, 4, HC=C), 10.41 (s, 1, COOH). Found: C, 60.40; H, 6.13%. Calcd for $C_{19}H_{23}NO_3S_2$: C, 60.45; H, 6.14%.

Similarly, hydrolysis of **4b** afforded **5b** in 92% yield, IR (Nujol) 2996 (COOH), 1713 cm^{-1} (C=O); ^{1}H NMR ($CDCl_3$) δ 0.86 (t, 3, J=6 Hz, CH_3), 1.02—2.96 (m, 17), 7.22—8.07 (m, 4, HC=C), 12.10 (s, 1, COOH). Found: C, 60.34; H, 6.64%. Calcd for $C_{19}H_{25}NO_3S_2$: C, 60.13; H, 6.64%.

*Electrolytic Decarboxylation of **5**. Method A*: A solution of **5a** (51 mg, 0.14 mmol) in AcOH (6 ml), *t*-BuOH (3 ml), and Et_3N (0.2 ml) was electrolyzed under a constant current of 20 mA/cm^2 (applied voltage 18—25 V) at 42 °C using two carbon electrodes (1.5×2 cm^2) for 2.5 h. Evaporation of the solvents followed by column chromatography (SiO_2, benzene/AcOEt, 10/1) gave **6a** (15 mg, 61%), whose IR and NMR spectra were identical with those of reported one.[1]

Method B: The electrolysis of **5a** (48 mg, 0.13 mmol) in MeOH (10 ml) and Et_3N (0.2 ml) at 30 mA/cm^2, 18—22 V, at 45—55 °C using platinum electrodes (1.5×2 cm^2) for 2.5 h gave **6a** (12.5 mg, 54%). Similarly, the electrolysis of **5b** gave **6b** in 54% yield.

Method C: The electrolysis of **5b** (101 mg, 0.27 mmol) in aqueous 0.025 M NaOH (20 ml) covered with hexane (10 ml) using platinum electrodes (1.5×2 cm^2) at 30 mA/cm^2, 7—9 V, at 46—50 °C for 4 h gave **6b** (31 mg, 64%) after evaporation of the organic layer (upper layer). Extractive workup of the aqueous alkaline solution gave **5b** (7 mg, 5%).

*cis-Jasmone (**7a**) and Dihydrojasmone (**7b**).* According to the reported procedure,[1a] a solution of **6a** (15 mg, 0.08 mmol) in aqueous 2% KOH was heated to reflux for 3 h. Extractive workup of the solution gave **7a** (12 mg, 89%). Similarly, **7b** was obtained in 87% yield. Their spectral data were identical with those of reported ones.[1]

References

1) (a) S. Torii, H. Tanaka, and Y. Tomotaki, *Bull. Chem. Soc. Jpn.*, **50**, 537 (1977); (b) S. Torii and H. Tanaka, *Koryo*, **114**, 41, (1976); (c) T.-L. Ho, *Synth. Commun.*, **4**, 256 (1974); (d) R. A. Ellison, *Synthesis*, **1973**, 397, and references cited therein.

2) *N*-(2-Benzothiazolylthio)morpholine (**3**) has been electrosynthesized: S. Torii, H. Tanaka, and M. Ukida, *J. Org. Chem.*, **43**, 3223 (1978).

3) S. Torii, H. Tanaka, and H. Okumoto, *Bull. Chem. Soc. Jpn.*, **52**, 267 (1979).

4) S. Torii, T. Okamoto, and T. Oida, *J. Org. Chem.*, **43**, 2294 (1978).

5) Bis(2-benzothiazolyl) disulfide was isolated in 20—45% yields. The details of the reaction mechanism will be discussed elsewhere.

The Crystal and Molecular Structure of Perylene-2,5-Dibromo-3,6-dichloro-*p*-benzoquinone Complex

Kozo Kozawa* and Tokiko Uchida

Department of Industrial Chemistry, Faculty of Science and Technology, Science University of Tokyo, Noda, Chiba 278

(Received June 14, 1978)

Crystals of the 1 : 1 molecular complex of perylene–2,5-dibromo-3,6-dichloro-*p*-benzoquinone are triclinic, with $a=8.669$, $b=9.697$, $c=7.321$ Å, $\alpha=103.20$, $\beta=110.92$, $\gamma=64.60°$, space group $P\bar{1}$, $Z=1$. The structure has been determined from diffractometer data by the heavy atom method and refined using the full-matrix least-squares method to R 0.069 for 2241 independent reflections. Stacks, with alternating donor and acceptor molecules, extend along the **c** direction. The acceptor molecule assumes two orientations, with a population ratio 1 : 1. A small degree of correlative change in the C–C bond lengths has been found in the perylene molecule on complex formation. The geometry of the quinonoid skeleton of the acceptor is similar to those of the anils and their complexes.

Perylene is a characteristic electron donor among polycyclic aromatic hydrocarbons. The perylene-iodine possesses the lowest electrical resistivity among hydrocarbon-iodine complexes.[1] And the perylene-antimony pentachloride is highly conductive in complexes which include antimony pentachloride as an electron acceptor.[2] Recently, perylene and 7,7,8,8-tetracyanoquinodimethane (TCNQ) were found to form a new type of complex, composed of three perylene molecules and one TCNQ moiety.[3,4] It is very rare in TCNQ complexes that more than two molecules of donor adduct to an acceptor molecule.

Tetrahalobenzoquinones are very useful electron acceptors, forming mainly π-π type donor-acceptor complexes. Their high electron affinity often gives complexes of ionic ground states.[5]

In this paper, the crystal structure of the 1 : 1 complex of perylene and 2,5-dibromo-3,6-dichloro-*p*-benzoquinone (BCQ) will be reported.

Experimental

Dark blue prismatic crystals of perylene-BCQ complex have been grown in a toluene solution. The crystal ($2.0\times0.5\times0.2$ mm^3) was mounted with the c axis parallel to the ϕ axis of a Rigaku four-circle automated diffractometer. The cell parameters and intensity data were obtained with LiF-monochromatized Mo $K\alpha$ radiation ($\lambda=0.7107$ Å). The intensities of the 2916 unique reflections were collected by the 2θ-ω scan technique with a scan speed of 1° min^{-1} in 2θ in the range $2\theta\leq60°$, 2241 reflections ($F_o\geq3\sigma(F)$) were used in the calculations. The scan range for each reflection was $(1+0.45\tan\theta)°$, and the background measurements were made 15 s at the extremeties of the scan range. Four reflections were monitored every 50 measurements and the fluctuations in the intensities of the monitored reflections were within ±2 %. Lorentz and polarization corrections were made, but no absorption correction was applied.

Crystal Data. $C_{20}H_{12}\cdot C_6Br_2Cl_2O_2$, *F.W.* =587.1; Triclinic, $a=8.669(3)$, $b=9.697(3)$, $c=7.321(3)$ Å, $\alpha=103.20(2)$, $\beta=110.92(2)$, $\gamma=64.60(1)°$, $V=517.2$ Å^3; $D_m=1.87$, $D_x=1.885$ g cm^{-3}, $Z=1$, μ(Mo $K\alpha$)=43.9 cm^{-1}, $F(000)=288$. Space group $P\bar{1}$.

The density was measured by the flotation method in an aqueous solution of K_2HgI_4. Structure determination was conducted assuming the space group $P\bar{1}$, and the possibility of P1 was excluded at the refinement step.

Structure Determination

The structure was solved by the heavy atom method. Several block-diagonal, least-squares calculation cycles for non-hydrogen atoms gave convergence at a residual index $R=0.176$. At this stage, the electron densities about the Br and Cl atoms, both in the Fourier and difference Fourier maps, suggested the existence of orientational disorder in the BCQ molecule. Subsequent full-matrix, least-squares refinements were performed with two sets of Br and Cl atoms positionally overlapping, based on the assumption that the two kinds of overlapping halogen atoms had equal probability of occupancy (0.5 : 0.5). The anomalous dispersion corrections for the Br and Cl atoms, reduced the value of R to 0.074. The positional parameters of the six hydrogen atoms attached to perylene, were estimated, assuming a C–H bond distance of 1.08 Å. The next refinement including the hydrogen atoms with an isotropic temperature factor of 4.5 Å^2 converged at $R=0.069$. In the final cycle, the average parameter shift/e.s.d. for non-hydrogen atoms was 0.26.

The final difference map showed maxima about 1.3 e Å^{-3} and only around the halogen atoms. This may be due to systematic error arising from the Br and Cl atoms being located at almost the same positions.

The quantity minimized in the refinement was $\sum w(|F_o|-k|F_c|)^2$, $w=1.0$. The numerical calculations were carried out on a HITAC 8800/8700 computer at the Computer Centre of the University of Tokyo with UNICS program[6] and XRAY system.[7] The atomic scattering factors and anomalous dispersion factors were taken from "International Tables for X-Ray Crystallography" (1974).[8] The final atomic parameters are shown in Tables 1 and 2 and the F_o-F_c data is kept as Document No. 7918 at the Bulletin.

Results and Discussion

Figure 1 shows the molecular packing in the crystal and the numbering of the atoms. Each molecule occupies a center of symmetry. As is common to π-π complexes, the donor and the acceptor molecules alternately stack in a plane-to-plane manner along the c axis, forming columns. The molecular overlapping

Table 1. The final atomic parameters ($\times 10^4$) for non-hydrogen atoms

The anisotropic thermal parameters are of the form:
$\exp[-(B_{11}h^2+B_{22}k^2+B_{33}l^2+2B_{12}hk+2B_{13}hl+2B_{23}kl)]$.

Atom	x	y	z	B_{11}	B_{22}	B_{33}	B_{12}	B_{13}	B_{23}
Br(1)*	2945(10)	1339(8)	3028(10)	104(6)	95(6)	148(9)	−43(5)	49(4)	−39(4)
Cl(1)*	3866(19)	−2295(19)	2248(22)	442(36)	548(37)	541(46)	199(27)	90(31)	295(32)
Br(2)*	3899(3)	−2310(2)	2304(3)	91(3)	88(2)	169(4)	−6(2)	15(3)	31(2)
Cl(2)*	2686(24)	1590(18)	3249(23)	81(11)	51(8)	126(15)	−17(7)	68(8)	−49(7)
O	−889(7)	3034(6)	600(9)	156(11)	72(7)	274(16)	−27(7)	48(10)	7(8)
C(1)	1320(9)	556(8)	1395(10)	104(11)	83(9)	151(15)	−39(8)	32(10)	1(9)
C(2)	1728(8)	−950(8)	1050(10)	96(11)	89(9)	127(13)	−19(8)	24(9)	20(8)
C(3)	−493(9)	1657(8)	317(10)	106(11)	78(9)	157(14)	−27(8)	31(10)	10(9)
C(4)	−2744(11)	4179(8)	4339(13)	152(15)	67(9)	235(20)	−4(9)	33(14)	17(10)
C(5)	−3830(10)	3544(9)	2992(13)	135(14)	89(10)	232(20)	3(9)	36(13)	34(11)
C(6)	−3335(10)	1950(8)	2690(11)	125(13)	95(9)	167(16)	−28(9)	32(11)	14(10)
C(7)	−1699(8)	976(7)	3825(10)	93(10)	81(8)	140(13)	−24(7)	43(10)	11(8)
C(8)	−1156(9)	−700(7)	3526(10)	105(11)	78(8)	137(14)	−33(8)	42(10)	−3(8)
C(9)	−2215(10)	−1412(8)	2162(11)	128(13)	93(9)	196(17)	−48(9)	32(12)	−2(10)
C(10)	−1681(11)	−3007(9)	1889(12)	183(16)	116(11)	209(19)	−81(11)	27(14)	−11(12)
C(11)	−70(11)	−3919(8)	3036(13)	197(17)	68(9)	242(21)	−53(10)	68(15)	−20(11)
C(12)	1055(10)	−3250(8)	4441(11)	148(13)	65(8)	194(17)	−30(8)	48(12)	4(9)
C(13)	546(9)	−1634(7)	4732(10)	101(10)	78(8)	133(13)	−27(7)	35(9)	7(8)

*Br(1) and Cl(1) are located at the same positions of Cl(2) and Br(2) respectively.

Table 2. The final positional parameters of hydrogen ($\times 10^3$)

Isotropic thermal parameter B=4.5 Å^2.

Atom	x	y	z
H(4)	−284(14)	532(12)	450(15)
H(5)	−506(14)	427(12)	192(15)
H(6)	−424(14)	144(12)	169(15)
H(9)	−335(13)	−80(12)	91(15)
H(10)	−243(14)	−352(12)	92(15)
H(11)	23(14)	−501(12)	286(15)

manner of BCQ onto perylene, shown in Fig. 2, is the same as that in the perylene-fluoranil complex.[9] The perylene and the BCQ molecules are planar within standard deviations except for the halogen atoms. The shifts of Br(1) (0.074 Å) and Cl(2) (0.151 Å) from the least-squares BCQ plane are nine and eight times as large as the e.s.d.'s, but the existence of disorder qualifies the significance of these values. The equations of the

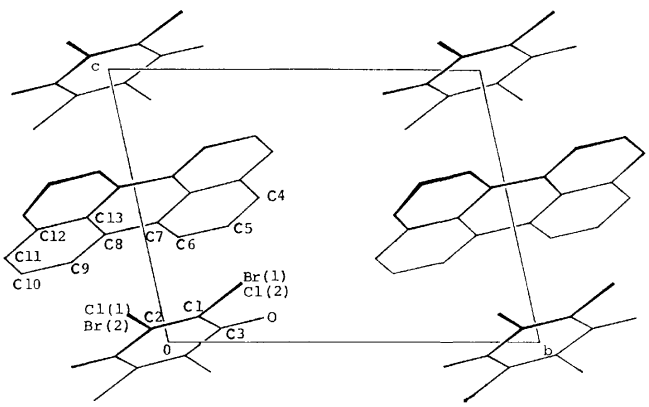

Fig. 1. Projection of the molecular arrangement onto the (100) plane.

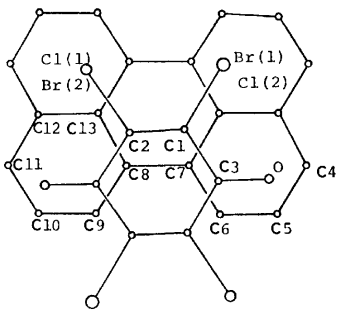

Fig. 2. Two overlapping molecules, viewed along normal to least-squares plane of a perylene molecule.

least-squares planes of the perylene and the BCQ molecules (calculated without hydrogen and halogen atoms) are

$0.7345X + 0.0132Y - 0.6784Z = -3.270$ and

$0.6752X + 0.0292Y - 0.7370Z = 0.0$ respectively,

where X, Y, and Z are orthogonal coordinates (in Å) given by the following equation.

$$\begin{pmatrix} X \\ Y \\ Z \end{pmatrix} = \begin{pmatrix} a & b\cos\gamma & c\cos\beta \\ 0 & b\sin\gamma & -c\sin\beta\cos\alpha^* \\ 0 & 0 & c\sin\beta\sin\alpha^* \end{pmatrix} \begin{pmatrix} x \\ y \\ z \end{pmatrix}$$

The mean separation between the two planes (in the region of overlap) is 3.35 Å and the angle between the plane normals is 4.9°. The values are larger than those of the perylene-fluoranil complex (3.23 Å, 1.8°),[9] which may be explained in terms of the difference between the van der Waals radii of the halogen atoms. The minimum interatomic distances between the overlapping molecules are 3.334 Å for O′–C(10), 3.350 Å for C(3′)–C(9), 3.371 Å for C(3′)–C(8), 3.376 Å for C(3)–C(6), 3.378 Å for C(3)–C(7), and 3.395 Å for O–C(5).

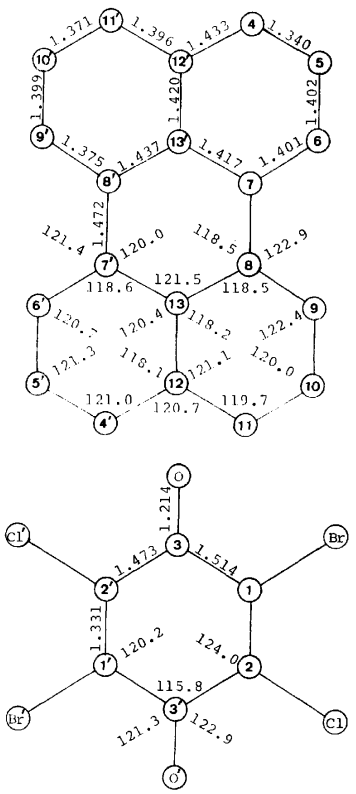

Fig. 3. Bond lengths (Å) and bond angles (°).
(a) Perylene; mean e.s.d.'s are 0.011 Å and 0.7° respectively.
(b) BCQ (quinonoid skeleton); mean e.s.d.'s are 0.010 Å and 0.7° respectively.

The bond distances and angles of the constituent molecules are shown in Fig. 3, in which the thermal vibrational motion has not been corrected for. The largest difference in the chemically equivalent bonds in the perylene skeleton is 0.037 Å between C(4)–C(12′) and C(11)–C(12) (2.2σ). Thus, in the perylene skeleton, all C–C lengths do not differ from the chemically equivalent bonds within experimental error. The geometry of the perylene molecule is similar to that of perylene itself (α-form)[10] or the complexes.[9,11–14]

Table 3 shows the bond lengths of the perylene skeleton together with six references.[9–14] The seven perylene skeletons show the following trends: (1) the longest bond length, C(7)–C(8), is close to a single bond as expected, and the lengths of C(4)–C(5) and C(10)–C(11) are the shortest within the same skeleton, (2) shortening of the C(7)–C(8) bond is accompanied by elongations of the C(8)–C(13), C(7)–C(13′), C(8)–C(9), and C(6)–C(7) bonds, (3) the chemically equivalent bond lengths slightly deviate from each other when the acceptors on both sides of the perylene are symmetrically situated about the molecular axis through C(12) and C(12′). The deviations become relatively large when the acceptors are not symmetrically situated about the axis.

Figure 3b shows the geometry of the quinonoid skeleton in BCQ. Although it is similar to that of other anils and their complexes,[9,15–30] the positional and thermal parameters of the halogen atoms are little reliable and the lengths of C–X bonds are not standard because of disorder. The bond lengths of C(1)–Br(1), C(2)–Br(2), C(2)–Cl(1), and C(1)–Cl(2) are 1.814, 1.820, 1.786, and 1.870 Å respectively. A similar effect, caused by disorder, was reported for benzo[*c*]phenanthrene and 2,3-dichloro-5,6-dicyanobenzoquinone.[31]

The authors would like to thank Mr. Teruyuki Kodama of the University of Tokyo for his help in the data collection and also to Mr. M. Kaneko and Mr. N. Edeh for their co-operation in this work as undergraduate students.

References

1) J. Kommandeur and F. R. Hall, *J. Chem. Phys.*, **34**, 129 (1961); T. Uchida and H. Akamatu, *Bull. Chem. Soc. Jpn.*, **34**, 1015 (1961); M. Schwarz, H. W. Davies, and B. J. Dobriansky, *J. Chem. Phys.*, **40**, 3257 (1964); W. H. Bentley and H. G. Drickamer, *ibid*, **42**, 1573 (1965); I. Shirotani, H. Inokuchi, and S. Minomura, *Bull. Chem. Soc. Jpn.*, **39**, 386 (1966).

Table 3. Bond lengths of the perylene skeleton

	Perylene-BCQ	Perylene-TCNE[a]	Perylene-TCNQ[b]	Perylene[c]	Perylene-fluoranil[d]	Perylene-PMDA[e]	Perylene-Ni Thiete[f]
C(4)–C(5)	1.340	1.362	1.364	1.373	1.364	1.366	1.37
C(10)–C(11)	1.371	1.347	1.353	1.366	1.358	1.364	1.34
C(5)–C(6)	1.402	1.430	1.394	1.421	1.401	1.383	1.41
C(9)–C(10)	1.399	1.435	1.403	1.416	1.419	1.407	1.45
C(6)–C(7)	1.401	1.395	1.387	1.391	1.379	1.381	1.35
C(8)–C(9)	1.375	1.429	1.392	1.404	1.380	1.393	1.37
C(4)–C(12′)	1.433	1.391	1.408	1.397	1.415	1.445	1.41
C(11)–C(12)	1.396	1.408	1.425	1.402	1.406	1.366	1.39
C(7)–C(13′)	1.417	1.441	1.432	1.434	1.427	1.407	1.43
C(8)–C(13)	1.437	1.440	1.419	1.417	1.431	1.423	1.42
C(12)–C(13)	1.420	1.413	1.428	1.424	1.434	1.443	1.44
C(7)–C(8)	1.472	1.456	1.464	1.471	1.473	1.493	1.50
σ	0.011	0.01	0.005	0.005	0.005	0.01	0.02

a) Perylene-tetracyanoethylene; Ref. 13. b) Perylene-7,7,8,8-tetracyanoquinodimethane; Ref. 14. c) Ref. 10. d) Ref. 9. e) Perylene-pyromelliticdianhydride; Ref. 11. f) Perylene-bis[*cis*-1,2-bis-(perfluoromethyl)ethylene-1,2-dithiolato]nickel; Ref. 12.

2) G. E. Blomglen and J. Kommandeur, *J. Chem. Phys.*, **35**, 1636 (1961); F. Gutmann and L. E. Lyons, "Organic Semiconductors," John Wiley and Sons, Inc., New York (1966).
3) K. D. Truong and A. D. Bandrauk, *Chem. Phys. Lett.*, **44**, 232 (1976); A. W. Hanson, *Acta Crystallogr., Sect. B*, **34**, 2339 (1978).
4) K. Ishii, Abstr. No. 1O45, 37th National Meeting of the Chemical Society of Japan, Yokohama, April 1978.
5) B. G. Anex and E. B. Hill Jr., *J. Am. Chem. Soc.*, **88**, 3648 (1966); Y. Matsunaga, *Nippon Kagaku Zasshi*, **89**, 905 (1968); Y. Sato, M. Kinoshita, M. Sano, and H. Akamatu, *Bull. Chem. Soc. Jpn.*, **43**, 2370 (1970); T. Nogami, K. Yoshihara, and S. Nagakura, *ibid.*, **44**, 295 (1971).
6) UNICS. "Universal Crystallographic Computation Program System," Crystallographic Society of Japan (1967).
7) J. M. Stewart, G. J. Kruger, H. L. Ammon, C. Dickinson, and S. R. Hall, Technical Report TR-192 (June, 1972) The X-Ray System of Crystallographic Programs for Any Computer, Computer Science Center, University of Maryland.
8) "International Tables for X-Ray Crystallography," Birmingham, Kynoch Press (1974), Vol. IV.
9) A. W. Hanson, *Acta Crystallogr.*, **16**, 1147 (1963).
10) A. Camerman and J. Trotter, *Proc. R. Soc. London, Ser. A*, **279**, 129 (1963).
11) J. C. A. Boeyens and F. H. Herbstein, *J. Phys. Chem.*, **69**, 2160 (1965).
12) R. D. Schmitt, R. M. Wing, and A. H. Maki, *J. Am. Chem. Soc.*, **91**, 4394 (1969).
13) I. Ikemoto, K. Yakushi, and H. Kuroda, *Acta Crystallogr., Sect. B*, **26**, 800 (1970).
14) I. J. Tickle and C. K. Prout, *J. Chem. Soc., Perkin Trans. 2*, **1973**, 720.
15) I. Ueda, *J. Phys. Soc. Jpn.*, **16**, 1185 (1961).
16) S. S. C. Chu, G. A. Jeffrey, and T. Sakurai, *Acta Crystallogr.*, **15**, 661 (1962).
17) N. D. Jones and R. E. Marsh, *Acta Crystallogr.*, **15**, 809 (1962).
18) B. Kamenar, C. K. Prout, and J. D. Wright, *J. Chem. Soc.*, **1965**, 4851.
19) C. K. Prout and A. G. Wheeler, *J. Chem. Soc., Ser. A*, **1967**, 469.
20) J. L. De Boer and A. Vos, *Acta Crystallogr., Sect. B*, **24**, 720 (1968).
21) K. Yakushi, I. Ikemoto, and H. Kuroda, *Acta Crystallogr., Sect. B*, **27**, 1710 (1971).
22) K. J. van Weperen and G. J. Visser, *Acta Crystallogr., Sect. B*, **28**, 338 (1972).
23) I. J. Tickle and C. K. Prout, *J. Chem. Soc., Perkin Trans. 2*, **1973**, 731.
24) K. Yakushi, I. Ikemoto, and H. Kuroda, *Acta Crystallogr., Sect. B*, **29**, 2640 (1973).
25) K. Prout and I. J. Tickle, *J. Chem. Soc., Perkin Trans. 2*, **1973**, 1212.
26) I. J. Tickle and C. K. Prout, *J. Chem. Soc., Perkin Trans. 2*, **1973**, 724.
27) M. Konno, H. Kobayashi, F. Marumo, and Y. Saito, *Bull. Chem. Soc. Jpn.*, **46**, 1987 (1973).
28) H. Kobayashi, T. Danno, and I. Shirotani, *Bull. Chem. Soc. Jpn.*, **47**, 2333 (1974).
29) A. Meresse, C. Courseille, and N. B. Chanh, *Acta Crystallogr., Sect. B*, **30**, 524 (1974).
30) P. J. Munnoch and J. D. Wright, *J. Chem. Soc., Perkin Trans. 2*, **1975**, 1071.
31) J. Bernstein, H. Regev, and F. H. Herbstein, *Acta Crystallogr., Sect. B*, **33**, 1716 (1977).

Effect of Etching on Intrinsic and Dye-sensitized Photocurrents in Zinc Oxide Electrodes

Michio MATSUMURA, Yoichi NOMURA, and Hiroshi TSUBOMURA*

Department of Chemistry, Faculty of Engineering Science, Osaka University, Toyonaka, Osaka 560

(Received August 7, 1978)

The photoelectrochemical behavior of sintered zinc oxide electrodes was studied. The intrinsic photocurrent, generated by ultraviolet illumination of the zinc oxide electrode, significantly diminished by grinding the electrode surface with an abrasive, and was restored by etching in 2 M(M= mol dm^{-3})HCl for *ca.* 120 s. The dye-sensitized photocurrent caused by rose bengal was also lowered by grinding, but the effect was not as large as in the case of the intrinsic photocurrent, and the photocurrent was restored in a much shorter time of etching. The dye-sensitized photocurrent for an insufficiently etched electrode was enhanced by addition of a reducing agent, *e.g.*, hydroquinone or allylthiourea. However, no enhancement was observed for a well etched electrode. The results, together with the luminescence and reflection spectra of zinc oxide, were discussed by means of models for the semiconductor electronic bands.

Many studies have been carried out on electrochemical solar cells each comprising a semiconductor electrode such as ZnO, TiO_2, or CdS, an electrolyte solution, and a metal counter electrode.[1-6] In these cells, the photocurrent generally arises by the band gap excitation of the semiconductor. The photocurrent is referred to as intrinsic photocurrent, i_{int}, of the semiconductor electrode.

The dye-sensitized photocurrents in the semiconductor electrodes, i_{dye}, have also been studied.[7-11] The dye-sensitized photocurrents are caused by the dye adsorbed on the electrode, but not by those dissolved in the solution.[11-13] Stationary photocurrents can be obtained only when reducing agents are added to the solution.[12,14] Relatively high photocurrents have been obtained by use of rose bengal as a sensitizer and a porous zinc oxide electrode.[15,16] In this paper, further results on some fundamental aspects of the dye-sensitization effects are reported.

Experimental

Zinc oxide sintered disks were prepared by heating compressed zinc oxide powder at 1300 °C in the air for 1 h. The dye adsorptivity on the disk varies a great deal with the source of zinc oxide powder. This seems to be due to impurities such as $ZnCO_3$ present in a small amount. In the present experiment, the powder (Kanto Chemical Co.) was used without further purification. The sinter made from this material has low adsorptivity, giving a reproducible photocurrent. The density of the sinter is almost equal to that of a single crystal. The scanning electron micrograph shows a very compact array of crystalline grains and no visible pore (Fig. 1). The sinter has low electric resistivity $\approx 10\ \Omega$ cm. The shape of the electrode is the same as that described previously.[15] All the other chemicals were of reagent grade and used without further purification.

The photocurrents were measured under potentiostatic conditions with a Hokutodenko HA-101 potentiostat and a saturated calomel electrode (SCE). A 500 W xenon lamp (Ushio Electric, Inc.) was used as the light source. The light was monochromatized by use of a Japan-Jarrell Ash 0.25 m Ebert type monochromator. The light intensity was measured with an Eppley bismuth-silver thermopile. The dye-sensitized photocurrents were studied in aqueous solutions of rose bengal and 0.2 M (mol dm^{-3}) potassium nitrate, the pH of the solution being 6.1. For the measurements of intrinsic photocurrents,

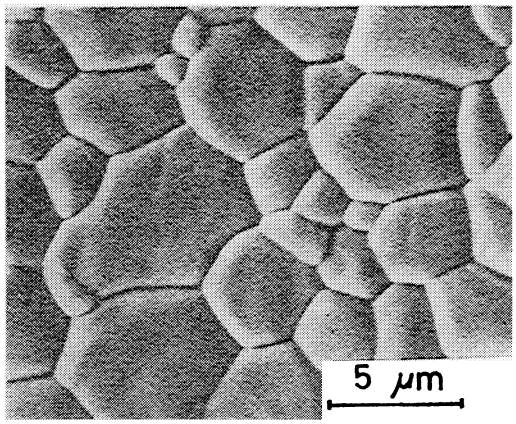

Fig. 1. The scanning electron micrograph of the zinc oxide sinter.

the pH of the solution was adjusted to 7.8 with a borate buffer. Dissolved oxygen was removed by bubbling the solution with high purity nitrogen. In many cases, the zinc oxide sinter was ground with a silicon carbide abrasive (No. 2000), etched in 2 M hydrochloric acid, washed with water and dried.

The luminescence intensity of zinc oxide sinter excited by the same light source as above was measured by use of an RCA 1P28 photomultiplier equipped with Toshiba B46 and 052 glass filters. The luminescence spectra were measured with an Aminco-Bowman spectrofluorimeter. The absorption spectra and the diffuse reflectance spectra were measured with a Shimadzu MPS-50L spectrophotometer. The ZnO sinter was colored slightly after dipping in the dye solution. The amount of the dye adsorbed on the electrode was estimated from the diffuse reflectance spectra of the ZnO sinter taken out of the dye solution, the residual solution on the sinter being soaked with a filter paper.

The differential capacitance at the semiconductor-electrolyte interface was measured with a Yokogawa Hewlett-Packard 4265B universal bridge at a frequency of 1 kHz.

Results

The dye-sensitized photocurrent under steady illumination decayed exponentially during the first several seconds (curve 1, Fig. 2). The initial value of the dye-sensitized photocurrent, i°_{dye}, was determined by extrapolating the curve to zero time of the illumination. When the dye solution contained a reducing agent such

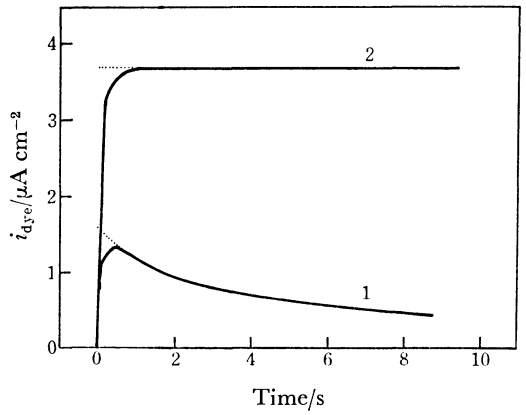

Fig. 2. Change of photocurrent *vs.* time for un-etched electrodes in a solution of 2×10^{-5} M Rose Bengal at potential of 0.4 V (*vs.* SCE). Curve 1, without hydroquinone. Curve 2, with 1.6×10^{-3} M hydroquinone.

as hydroquinone, allylthiourea, or potassium iodide, the decay was suppressed. In some cases the initial value of the photocurrent was enhanced as shown by curve 2 for the case of hydroquinone as a reducing agent. The decay of i_{dye} was suppressed by addition of hydroquinone or allylthiourea at a concentration as low as 5×10^{-5} M, while the increase of i°_{dye} was small at such a low concentration and reached saturation at *ca.* 1×10^{-3} M. In the case of iodide ion, the decay of i_{dye} was not prevented at concentrations below 5×10^{-2} M, and the increase of i°_{dye} could not be observed even at 1.0 M. The difference seems to arise from the weaker electron donor strength of the iodide ion than hydroquinone or allylthiourea. On the other hand, the intrinsic photocurrent did not decay even when the electrolyte solution contained no reducing agent, nor was it affected by the reducing agent.

The photocurrent-potential curves of both i_{int} and i°_{dye} for electrodes etched for various periods of time are shown in Fig. 3. The photocurrents are proportional to the illumination intensity, the shapes of the photocurrent-potential curves not being changed by decrease in the illumination intensity to 1/7. The apparent quantum efficiency of i_{int}, defined as the number of electrons flowing per the number of incident photons on the electrode, is *ca.* 80% for the electrode etched for more than 120 s and polarized at a higher electrode potential than 0.3 V (*vs.* SCE). The onset potentials of the photocurrents did not change with etching. The flat band potentials of ZnO electrodes in the solutions used for the measurements of i_{int} and i_{dye} as determined by the Mott-Schottky plots of the differential capacitance are *ca.* −0.48 and −0.32 V (*vs.* SCE), respectively, agreeing nearly with the onset potentials of photocurrents. The donor densities were determined to be in the range 4.9×10^{22}—7.1×10^{22} m^{-3} by assuming the roughness factor of 2 for the electrode surface.

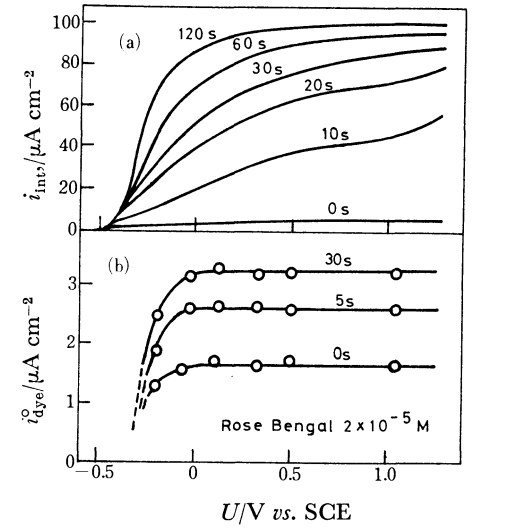

Fig. 3. Current-potential curves of (a) intrinsic photocurrents (excited at λ 360 nm) and (b) the initial values of dye-sensitized photocurrents (λ 562 nm) of ZnO electrode etched for various periods of time.

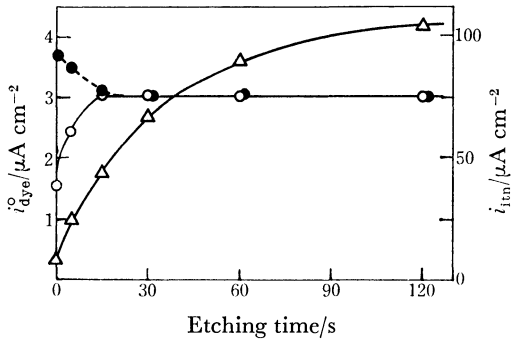

Fig. 4. The photocurrent (at 0.4 V *vs.* SCE) *vs.* etching time in the electrode ground with an abrasive.
○: Initial values of dye-sensitized photocurrent (λ 562 nm) in the presence of 2×10^{-5} M Rose Bengal, ●: the dye-sensitized photocurrent obtained by addition of 1.6×10^{-3} M hydroquinone into the solution; △: the intrinsic photocurrent (λ 360 nm).

The photocurrents observed at the electrode potential of 0.4 V (*vs.* SCE) are plotted against the etching time in Fig. 4. The i°_{dye} value becomes constant at an etching time much shorter than that for the i_{int}. The enhancement of i°_{dye} by hydroquinone occurs only at an etching times less than 15 s. The addition of hydroquinone up to the concentration of 10^{-2} M did not affect the adsorptivity of dye. The amount of the dye adsorbed on the electrode changed slightly by etching, being approximately proportional to the i_{dye} observed in the presence of hydroquinone. This might be due to the change of the surface area caused by etching.

The ZnO sinter emits luminescence when exposed to ultraviolet light. The emission band lies in the range 400—750 nm with a maximum near 530 nm (Fig. 5). The luminescence intensity was quenched drastically by grinding the sinter, but was gradually restored with etching. By etching for 150 s, the luminescence intensity returned to the value before grinding. Figure 6 shows the luminescence intensity at various electrode potentials. The luminescence intensity falls near the onset potential of the photocurrents, decreasing nearly to zero at potentials where the i_{int} value is saturated.

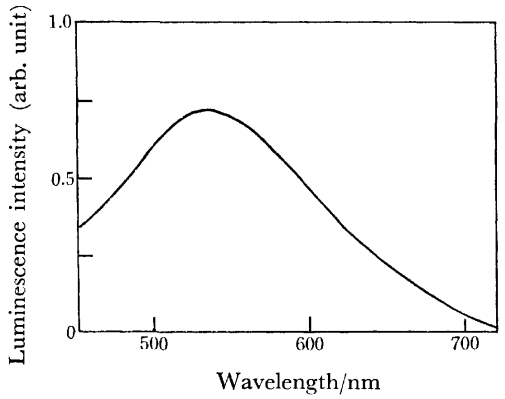

Fig. 5. The luminescence spectrum of ZnO sinter excited at 360 nm.

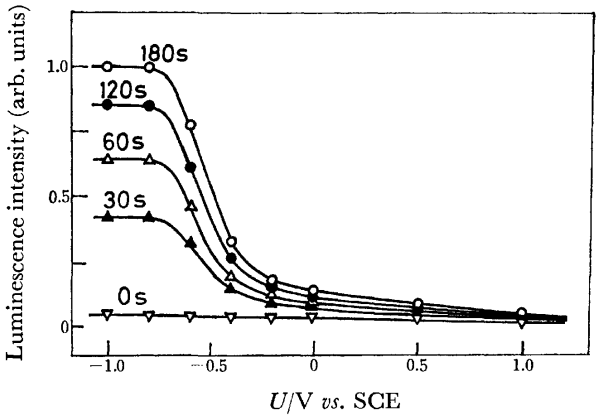

Fig. 6. The luminescence intensity of zinc oxide electrode etched for various periods of time *vs.* electrode potential. The luminescence was excited at 360 nm.

By measuring the weight loss of the ZnO sinter etched in 2 M HCl, the average thickness of the ZnO sinter dissolved by the solution was determined to be 4.3 μm min^{-1}.

Discussion

Our results have revealed that there are fundamental differences between the behavior of the intrinsic photocurrent (i_{int}) and that of the dye-sensitized photocurrent (i_{dye}):

1. The i_{int} is weakened to a greater extent than i_{dye} by grinding the electrode.
2. The increase in i_{dye} with etching reaches saturation when etching time is *ca.* 15 s. The i_{int} value increaes much more slowly by etching, reaching saturation at *ca.* 120 s.
3. The i_{int} value for an insufficiently etched electrode rises gradually as the electrode becomes anodically polarized up to quite high voltages, whereas i_{dye} rises sharply and is saturated at 0.0 V (Fig. 3).
4. By addition of reducing agents to the solution, the decay of i_{dye} is suppressed. Sometimes i°_{dye} increases, whereas i_{int} is hardly affected.

Based on these results, we shall discuss the mechanism of these photocurrents.

Intrinsic Photocurrent. The mechanism of the generation of i_{int} is shown in Fig. 7a. When an n-type semiconductor immersed in an electrolyte is polarized anodically, a potential gradient develops in the space charge layer. By the band gap excitation, the electrons in the valence band are excited to the conduction band. The electron-hole pairs thus generated in the space charge layer are separated efficiently by the electric field.

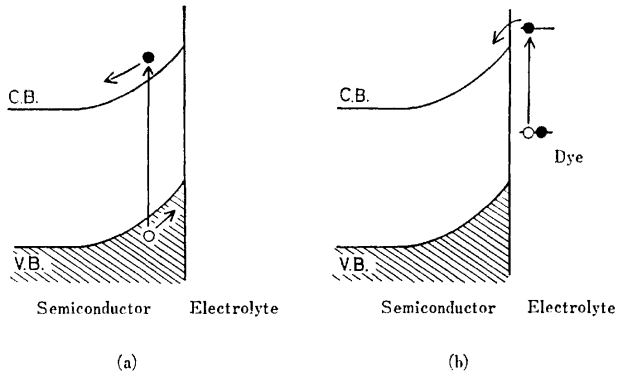

Fig. 7. The energy level diagrams of the semiconductor illustrating the mechanisms of the intrinsic photocurrent (a) and dye-sensitized photocurrent (b).

The i_{int} value of a well etched electrode reaches saturation at the electrode potential of *ca.* 0.3 V (Fig. 3). The quantum efficiency of the saturated i_{int} is regarded to be almost 100% if the reflection of the incident light at the surface is taken into account.

The depth of the space charge layer, L, is approximately given by[17]

$$L = \sqrt{2(U - U_{fb})\varepsilon\varepsilon_0/N_d e} \quad (1)$$

where U is the electrode potential in the bulk, U_{fb} the flat band potential, ε the dielectric constant, ε_0 the permittivity of vacuum, and e the elementary electric charge. The value of L is calculated to be 110 nm at the electrode potential of 0.3 V, at which i_{int} of a well-etched electrode reaches saturation, by substituting $U_{fb} = -0.48$ V, $\varepsilon = 8.5$, $N_d = 6 \times 10^{22}$ m^{-3} (the mean value of the observed donor density) into Eq. 1. On the other hand, the penetration depth of the incident light (λ 360 nm) in ZnO, l, defined as the distance at which the light intensity becomes 5%, is calculated to be *ca.* 100 nm from the absorption constant of *ca.* 3×10^7 m^{-1},[18] in good agreement with the above derived L value. The result suggests that the recombination is negligible in the space charge layer of a well-etched electrode.

On the other hand, the i_{int} value for an insufficiently etched electrode did not reach saturation even when the electrode potential was raised to 5 V (*vs.* SCE). This cannot be explained by the relation between the penetration depth of the light and the depth of the space charge layer, but by taking into account the recombination center of electron-hole pair in the space charge layer generated by the grinding. At a higher anodic polarization, the electric field strength near the surface of the electrode increases and the electrons and holes are separated more rapidly, leading to a higher photocurrent.

This mechanism is supported by the measurements of luminescence from ZnO. The luminescence drops sharply at around −0.5 V (*vs.* SCE) to the more positive region where i_{int} begins to rise (Figs. 3 and 6). This is reasonable since the luminescence is caused by a recombination of the electron-hole pairs. The figures also indicate that non-radiative recombination centers are generated by grinding the electrode, since both the luminescence and i_{int} are weak when the etching time is short, increasing in a similar way with longer etching.

Dye-sensitized Photocurrent. It is generally admitted that the dye sensitized photocurrent (i_{dye}) is caused by an electron injection from the excited dye into the conduction band, the electrons being driven inward by the electric field in the space charge layer (Fig. 7b). In the case of i_{dye}, free holes do not exist in the valence band, and, therefore, the recombination process does not take place even though defects are present in the space charge layer. This can explain i_{dye} being less affected than i_{int} by grinding of the electrode.

The effect of grinding on i°_{dye} can be explained by assuming the formation of electron traps near the surface which capture electrons injected from the dye and send them back to the dye. The fact that the photocurrent at sufficiently high anodic polarization became constant by etching for 15 s indicates that the density of the traps is high in the region very close to the surface (Fig. 4).

Sintered ZnO, normally slight yellow, turns deep yellow on grinding. The increase in absorbance of the sinter from 380 to 650 nm thus produced can be measured by diffuse reflectance spectroscopy. This can be removed by etching for *ca.* 15 s, which is comparable to that necessary to make i°_{dye} reach saturation. The increased absorbance seems to be due to the surface defects, which trap the injected electrons.

The Effect of Reducing Agents on i_{dye}. There are two features of the effect of reducing agents on i_{dye},[12] the increase of i°_{dye} and the prevention of decay of i_{dye}.

Hydroquinone increases i°_{dye} for an electrode etched for less than 15 s, but not for a sufficiently etched electrode (Fig. 4). This can be explained by assuming the presence of surface traps (Fig. 8). Without a reducing agent, a part of the injected electrons are capturated by the surface traps, returning to the dyes which have injected these electrons. Such a backward movement of electrons is prevented by a rapid electron supply from the reducing agent, increasing i°_{dye}.

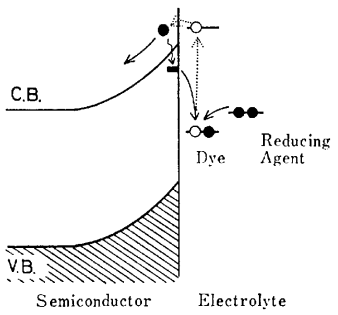

Fig. 8. The energy level diagrams explaining the influence of the surface defect and the reducing agent on the dye-sensitized photocurrent.

Some authors pointed out that the effect of reducing agents on i_{dye} is attributable to either an electron transfer from the reducing agent to the dye in excited state or an exciplex formation between the dye and the reducing agent. In the present case, however, the results are explained in terms of the electron transfer from the reducing agents to the photo-oxidized dye. There seems to be no general "super sensitization" effect of the reducing agents.

From the present study, the dye-sensitized photocurrent has been proved to be less sensitive to the defects in the electrode than the intrinsic photocurrent, especially when the solution contains reducing agents. This is one of the advantages of the dye-sensitized photocurrent as regards utilization of imperfect solid specimens for electrochemical photocells.

The present work was partially supported by a Grant-in-Aid for Scientific Research from the Ministry of Education (No. 911504).

References

1) A. B. Ellis, S. W. Kaiser, and M. S. Wrighton, *J. Am. Chem. Soc.*, **98**, 6855 (1977).
2) B. Miller and A. Heller, *Nature*, **262**, 680 (1976).
3) A. Fujishima, K. Kohayakawa, and K. Honda, *Bull. Chem. Soc. Jpn.*, **48**, 1041 (1975).
4) H. Minoura, M. Tsuiki, and T. Oki, *Ber. Bunsenges. Phys. Chem.*, **81**, 588 (1977).
5) H. Yoneyama, H. Sakamoto, and H. Tamura, *Electrochim, Acta*, **20**, 341 (1975).
6) Y. Nakato, K. Abe, and H. Tsubomura, *Ber. Bunsenges. Phys. Chem.*, **80**, 1002 (1976).
7) H. Gerischer and F. Willig, "Topics in Current Chemistry," Springer, New York (1976), Vol. 61, p. 31.
8) T. Watanabe, A. Fujishima, and K. Honda, *Ber. Bunsenges. Phys. Chem.*, **79**, 1213 (1975).
9) H. Tributsch and H. Gerischer, *Ber. Bunsenges. Phys. Chem.*, **73**, 251 (1969).
10) U. Bode, K. Hauffe, Y. Ishikawa, and H. Pusch, *Z, Phys. Chem. N. F.*, **85**, 144 (1973).
11) R. Memming, *Photochem. Photobiol.*, **16**, 325 (1972).
12) M. Matsumura, Y. Nomura, and H. Tsubomura, *Bull. Chem. Soc. Jpn.*, **50**, 2533 (1977).
13) M. Matsumura, Y. Nomura, and H. Tsubomura, *Bull. Chem. Soc. Jpn.*, **49**, 1409 (1976).
14) M. Matsumura, K. Yamamoto, and H. Tsubomura, *Nippon Kagaku Kaishi*, **1976**, 399.
15) H. Tsubomura, M. Matsumura, Y. Nomura, and T. Amamiya, *Nature*, **261**, 402 (1976).
16) H. Tsubomura, M. Matsumura, K. Nakatani, K. Yamamoto, and K. Maeda, *Solar Energy*, **21**, 93 (1978).
17) H. Gerischer, *J. Electroanal. Chem. Interfac. Electrochem.*, **58**, 236 (1975).
18) G. Heiland, E. Mollwo, and F. Stöckmann, "Solid State Physics," Academic Press, New York (1959), Vol. 8, p. 191.

Association and Photolysis of 1-Benzyl-4-methoxycarbonylpyridinyls

Yusaku IKEGAMI,* Shozo KUBOTA, and Hidetoshi WATANABE[1)]

Chemical Research Institute of Non-aqueous Solutions, Tohoku University, Katahira-2-chome, Sendai 980

(Received August 31, 1978)

1-Benzyl- and 1-(4-methylbenzyl)-4-methoxycarbonylpyridinyl radicals have been prepared by reducing the corresponding pyridinium iodides with sodium amalgam. Hyperfine structures of the ESR spectra were analyzed. The radicals were decomposed photochemically with visible light in the region 380—440 nm in order to generate the intermediate benzyl radicals which were identified spectroscopically at 77 K. Association of each radical at low temperature forms a diamagnetic radical dimer, which is transformed by irradiating the solution with 440—470 nm light into the triplet dimer with zero-field parameters, $D=ca.$ 0.017 cm^{-1} and $E\approx 0$. Another radical, 1-(4-nitrobenzyl)-4-methoxycarbonylpyridinyl, is unstable at room temperature.

Pyridinyl radicals play an important role in studies on radical structure, radical reactions and radical association since the radicals are stable, neutral, and aromatic.[2)] One peculiar property of pyridinyls is the association to form both the diamagnetic singlet (A_S) and paramagnetic triplet (A_T) dimers at low temperature. Another triplet species (B_T) is generated from A_S by irradiating the radical solution with visible light.[3,4)] 1-Benzyl-4-methoxycarbonylpyridinyl (**1**) was prepared in order to investigate the effect of *N*-substituent on stability and association.[5)] In the course of the study, an unexpected sensitivity of the radical to light was observed. The photosensitivity as well as the association were examined for the radical and its derivatives.

Results and Discussion

Preparation. Generation of radicals **1**—**3** for preliminary study was performed by electrolytic reduction of the corresponding pyridinium iodides in degassed acetonitrile or *N*,*N*-dimethylformamide using tetrapropylammonium perchlorate as the supporting electrolyte. Each radical was generated in a stable form, exhibiting the expected ESR spectrum.

Treatment of 1-benzyl-4-methoxycarbonylpyridinium iodide with 3% sodium amalgam in degassed acetonitrile under ice-cooling in the dark afforded a green solution. Removal of the solvent gave blue crystals composed of **1** and NaI. The radical is slightly soluble

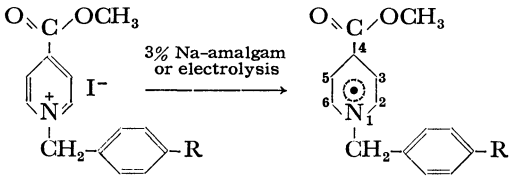

1: R=H
2: R=CH_3
3: R=NO_2

in hydrocarbons, soluble in ethereal and aprotic polar solvents, and not distillable in a vacuum. In solution it is stable for a long period at room temperature in the dark, but decomposes gradually in the light and rapidly in contact with alcohols, water, or air. Yield of the radical in preparation, based on spectroscopic titration, was over 85%. The 4-methylbenzyl derivative **2** prepared in a similar manner to the above showed

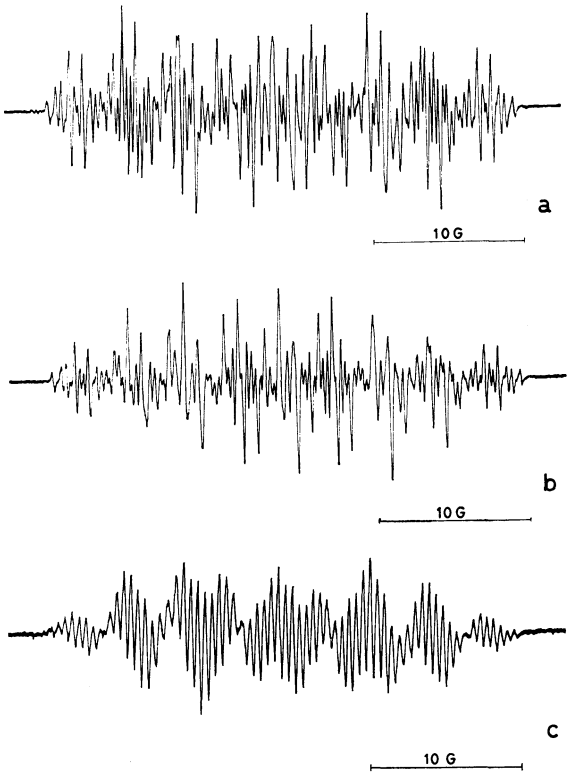

Fig. 1. ESR spectra of 1-benzyl- (a), 1-(4-methylbenzyl)- (b), and 1-(4-nitrobenzyl)-4-methoxycarbonylpyridinyls (c) in acetonitrile at room temperature. The 4-nitrobenzyl derivative was generated electrolytically.

similar properties. On the other hand, the 4-nitrobenzyl derivative **3** was not so stable as **1** and **2**. The deep blue color of **3** turned gradually yellow even in the dark. Approximate half-life for the decomposition, estimated by the ESR signal intensity, was *ca.* 15 min in acetonitrile at 20 °C. Because of the instability, spectroscopic examination of **3** was not carried out.

ESR spectra of radicals **1**—**3** in acetonitrile at room temperature are shown in Fig. 1. The hyperfine structure of each spectrum is interpreted as arising from the radical structure with six splitting constants. The constants observed in two solvents are summarized in Table 1, the assignments being given tentatively according to the type of splitting and by comparing them with the assignments to the constants of 1-methyl-4-methoxycarbonylpyridinyl.[6)] The coplanarity of the carbonyl

TABLE 1. HYPERFINE SPLITTING CONSTANTS FOR RADICALS **1**—**3** AT ROOM TEMPERATURE

Assignment	Splitting constant, *G*				
	1 (R=H)		**2** (R=CH_3)		**3** (R=NO_2)
	In CH_3CN	In MTHF	In CH_3CN	In MTHF	In CH_3CN
CH_3	0.88	0.84	0.91	0.80	0.92
3,5-H	0.56	0.42	0.58	0.40	0.54
2-H	3.73	3.95	3.70	3.98	3.95
6-H	3.83	4.05	3.80	4.08	4.07
N	6.30	6.26	6.24	6.28	6.28
$-CH_2-$	3.56	3.56	3.59	3.60	3.51

group with pyridinyl ring is clearly seen in the nonequivalence of the constants at positions 2 and 6.

The radical concentration of the solution of **1** or **2** for spectroscopic studies was determined spectroscopically by the following electron-transfer reaction.

1 (or **2**) + 1,1′-Dimethyl-4,4′-bipyridinium (MB^{2+})
$\longrightarrow$ $\mathbf{1}^{+}$ (or $\mathbf{2}^{+}$) + MB^{+}

The reaction of a dilute solution of the radical (concn$<5\times10^{-3}$ M) with an excess of solid 1,1′-dimethyl-4,4′-bipyridinium (MB^{2+}) dichloride in acetonitrile in the dark proceeded rapidly to form the corresponding radical cation (MB^{+}) (Paraquat radical cation). The absorption intensity of the resulting cation at 605 nm ($\varepsilon=10060$)[7] was used to calculate the radical concentration.

TABLE 2. ABSORPTION MAXIMA OF RADICALS **1** AND **2** IN ACETONITRILE (23 °C)

Radical	λ_{max} (ε)			
1	246(25300)	302(14900)	393(6830)	630(91)
2	241(22380)	303(14970)	393(6840)	630(104)

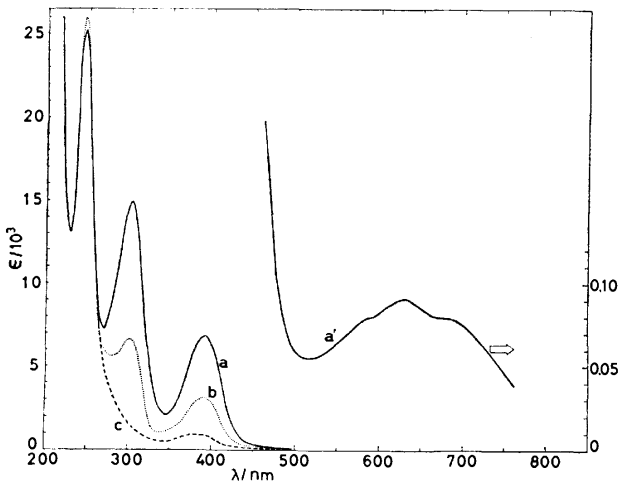

Fig. 2. Absorption spectrum of **1** in acetonitrile and the spectral change on light irradiation at room temperature: (a) 3.9×10^{-3} M and (a′) 2.6×10^{-2} M before irradiation; (b) after 100 s irradiation of (a) with visible light; (c) after 5 min irradiation. A 100 W tungsten lamp equipped with a Toshiba filter UV-39 was used for the irradiation.

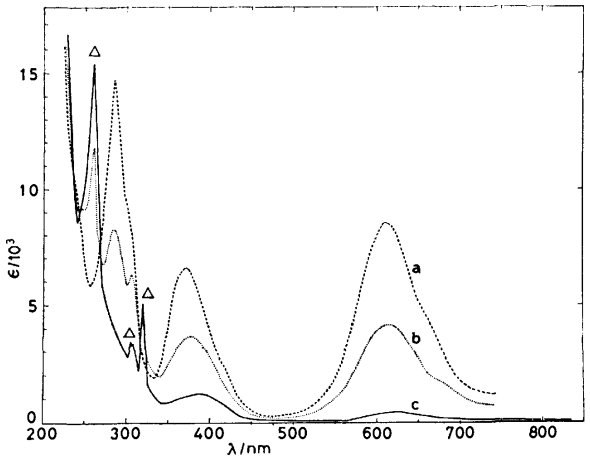

Fig. 3. Absorption spectrum of **1** in MTHF and the spectral change on light irradiation at 77 K: (a) 8.8×10^{-3} M before irradiation; (b) after 1 min irradiation; (c) after 6 min irradiation with a 100 W tungsten lamp. △: Indicates the bands due to the products.

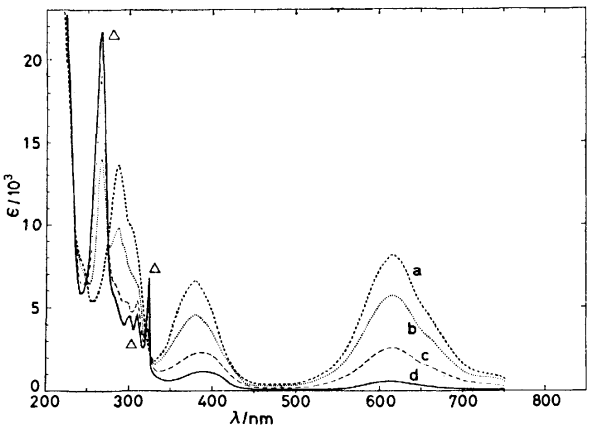

Fig. 4. Absorption spectrum of **2** in MTHF and the spectral change on light irradiation at 77 K: (a) 6.8×10^{-4} M before irradiation; (b) after 1.5 min irradiation; (c) after 6 min irradiation; (d) after 32 min irradiation. A 500 W xenon lamp equipped with a Toshiba filter UV-39 was used for the irradiation.

Spectra and Photolysis. Radical **1** shows absorption maxima given in Table 2 with features similar to 1-alkyl homologs.[8–10] Irradiation of the solution with visible light caused the disappearance of the three longer bands as a result of photolysis; the dispersed weak light in the spectrometer caused no photolysis. The effect of irradiation on the spectrum is shown in Fig. 2; the same phenomenon is observed in MTHF at room temperature. The photolysis occurred also in MTHF glass at 77 K, leading to the spectral change shown in Fig. 3, in which the disappearance of strong bands at 286, 372, and 616 nm on irradiation is accompanied by the appearance of new bands at 260, 306, and 319 nm. The new bands coincide in their wavelengths with those of the benzyl radical generated in 2-methylpentane at 77 K.[11] Irradiation of radical **2** also led to its substantial loss. The absorption bands at 267, 300, 311, and 323 nm

(Fig. 4) correspond to those of the 4-methylbenzyl radical.[11] Thus, the photolysis is interpreted to be the following C–N bond cleavage.

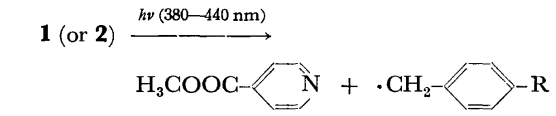

The photolysis occurred with 380—440 nm wavelengths. Strong irradiation of the solution with light of wavelength shorter than 350 nm from a 500 W mercury lamp led to further photoreaction showing a complex spectral change with time. Photolytic change was also observed in the ESR spectrum of a dilute solution at 77 K, an example of which is shown in Fig. 5 for radical **2**. The hyperfine structure appearing on irradiation is ascribed to the 4-methylbenzyl radical. Irradiation of **1** in a similar way resulted in appearance of hyperfine structure in the ESR spectrum differing from that in Fig. 5.

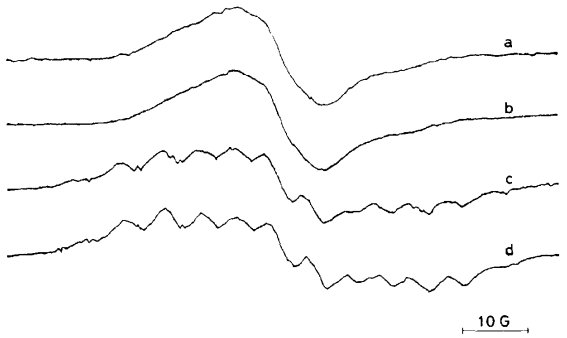

Fig. 5. The ESR spectral change observed by irradiating the dilute solution of **2** in MTHF at 77 K: (a) 1.2×10^{-4} M before irradiation; (b) after 10 min irradiation of (a) with a 500 W xenon lamp using a Toshiba filter VY-50; (c) after 1 min irradiation of (b) using a Toshiba filter VY-42; (d) after further 9 min irradiation of (c).

Since 1-alkylpyridinyls are not sensitive to visible light, the photolysis should be interpreted in terms of a photochemical interaction between the arene ring and the pyridinyl ring. One possible explanation is that excitation of the pyridinyl radical leads to the formation of an intramolecular exciplex *via* electron transfer to the aryl ring, followed by dissociation to an unstable free radical and a stable molecule, methyl isonicotinate.[12] If this is the case, the instability of the 4-nitrobenzyl derivative (**3**) can be explained by a thermal mechanism analogous to the photochemical one, as Mochida *et al.*[13] recently substantiated a general formulation, originally put forth by Kosower,[14] that electron-transfer processes resulting from charge-transfer interaction can share common photochemical and thermal pathways.

Radical Association and Associated Triplet State. The absorption spectrum of **1** at low temperature (Fig. 3a) has an intense band at 616 nm, while the absorption in this region at room temperature (Fig. 2a′) is very weak. The strong absorption is due to the radical dimer denoted by π-mer.[15] Since the solution contains a considerable amount of sodium iodide, the strong intensity might be partially due to the complex formation of the radical with sodium iodide. Complex formation can account for the hypsochromic shifts of the bands at 300 and 391 nm to 286 and 372 nm, respectively, on lowering the temperature in MTHF.[16] The spectrum of **2** can be interpreted similarly (Fig. 4a).

The radical association is also observed as conspicuous decrease in the ESR signal intensity with fall in temperature. The decrease in intensity for the solution of **1** at −150 °C is less than 2% of that at room temperature. (Fig. 6). This can be ascribed to the formation of the diamagnetic radical dimer at low temperature.

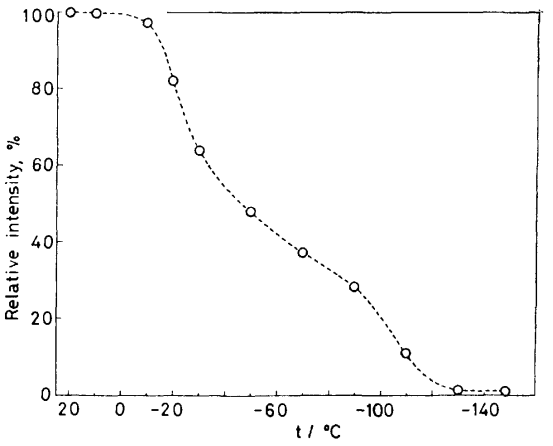

Fig. 6. Decrease of the ESR signal intensity with lowering temperature for the radical **1** in MTHF at the concentration, 4.0×10^{-2} M.

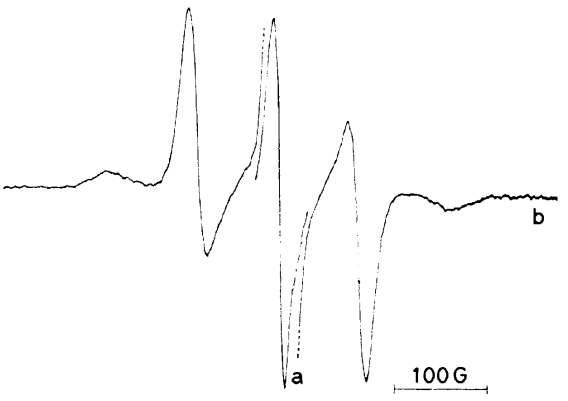

Fig. 7. ESR spectrum of **1** in MTHF at 77 K. 2.5×10^{-2} M. (a) Before irradiation; (b) after 20 min irradiation with a 500 W xenon lamp using a Toshiba filter VY-46. (a) was recorded with 1/2.5 gain amplitude of that for (b).

It has been demonstrated for 1-alkyl-4-methoxycarbonylpyridinyls that the diamagnetic dimer (A_S) is convertible into the triplet dimer (B_T) by light irradiation.[3,4] The same phenomenon is observed for the radicals. Radicals **1** in MTHF at 77 K shows a very weak signal corresponding to the central line in Fig. 7. Irradiation of the solution with light of wavelength longer than 440 nm added a new triplet signal to the ESR spectrum, with no significant change in the central

line. Appearance of the $\Delta M=2$ transition in the ESR spectrum at around 1650 G confirms the triplet. The zero-field parameters estimated roughly are $D=0.0174$ cm^{-1} and $E\approx0$, with $2D=372$ G. The D value is consistent with a spin-spin dipolar interaction for an average separation of 5.3 Å, using the relation $D=-(3/2)g^2\beta^2r^{-3}$.[17] A similar triplet spectrum was obtained for radical **2**, the zero-field parameters, $D=0.0166$ cm^{-1} and $E\approx0$ with $2D=356$ G, corresponding to the spin-spin interaction for an average separation of 5.4 Å. These D values for the association of **1** and **2** are close to those of 1-methyl- and 1-ethyl-4-methoxycarbonylpyridinyls. This indicates that the *N*-substituent has no significant influence upon the structure of the triplet dimer formed by an access of pyridinyl rings.

No spectral change was observed by irradiation with light of wavelength longer 470 nm. The singlet-triplet transformation occurred with visible light in the region 440—470 nm, which differs from both the light specific to the photolysis and the light corresponding to the long-wavelength charge-transfer absorption of π-mer at *ca.* 620 nm. Since no strong absorption was observed in the 440—470 nm region (Figs. 3 and 4), excitation expected in this region, corresponding to the band at 437 nm observed before irradiation for pure 1-methyl-4-methoxycarbonylpyridinyl in MTHF at 77 K,[4] might cause the dynamic reorientation of the radicals in a dimer to the positions capable of triplet transition.

Experimental

Solvents. Acetonitrile (guaranteed reagent, Kanto Chemical Co.) was passed through an alumina (Woelm, neutral) column and distilled. After being degassed by at least five freezing-pumping cycles, the solvent was treated with 1-methyl-4-methoxycarbonylpyridinyl radical, prepared by the reaction of the pyridinium iodide with sodium amalgam, to remove radical-reactive impurities. The solvent was distilled again in a vacuum system at low temperature and left to stand over previously degassed molecular sieves (4A) in a storage vessel. 2-Methyltetrahydrofuran (MTHF) (Eastman Organic) was refluxed over sodium for 3 days and then distilled. The solvent was degassed and then distilled onto sodium and anthracene in a storage vessel. Solvents were transferred, when needed, by distillation into the apparatus using a vacuum system.

Salts. 1-Benzyl-4-methoxycarbonylpyridinium iodide was prepared by the method of Craig *et al.* through the chloride.[18] Mp 163—164 °C. 1-(4-Methylbenzyl)-4-methoxycarbonylpyridinium iodide was prepared as follows. A solution of 4-methylbenzyl chloride (0.04 mol) in acetone (50 ml) was refluxed with an excess of sodium iodide (0.05 mol) under nitrogen for 2 h. The sodium chloride produced was filtered off. Methyl isonicotinate was added to the solution, the temperature being maintained at 50 °C for 2 h, the solution allowed to cool overnight, then left at 0 °C for 40 h. The yellow crystals were filtered off and recrystallized from ethanol and then from methanol. Mp 151—152 °C. Found: C, 49.12; H, 4.34; N, 3.97%. Calcd for $C_{15}H_{16}NO_2I$: C, 48.80; H, 4.37, N, 3.79%. 1-(4-Nitrobenzyl)-4-methoxycarbonylpyridinium iodide was prepared by the method of Kosower *et al.*[19] as orange red crystals, mp 152 °C. 1,1′-Dimethyl-4,4′-bipyridinium dichloride (Wako Chemical Co.) was recrystallized from ethanol, and then dried thoroughly.

Radicals. Pyridinyl radicals were prepared using the apparatus shown in Fig. 8. A pyridinium iodide (0.001 mol), 3 % sodium amalgam, and a magnetic stirrer were put into A and the apparatus was evacuated with an oil diffusion pump to 2×10^{-6} Torr. After the addition of solvent acetonitrile into A by distillation, the mixture was stirred under ice-cooling (1—2 h) until a clear green color was obtained. The solution was filtered in order to remove insoluble substance and the filtrate was put into three tubes (B, C, and D), which were subjected to determination of radical concentration and spectral measurements.

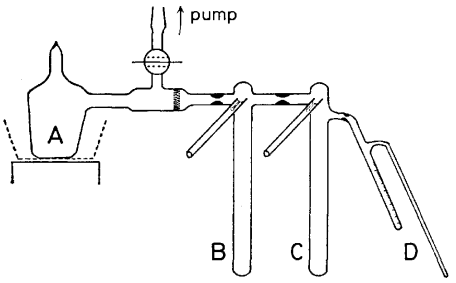

Fig. 8. Apparatus for radical preparation.

Spectral Measurements. A Cary 14 spectrophotometer was used to record absorption spectra. A specially constructed glass Dewar vessel[20] was used to measure the spectra at 77 K. ESR spectra were measured with a Varian E-4 ESR spectrometer. Electrolytic generation of radicals was carried out in the cavity of the spectrometer using acetonitrile or *N,N*-dimethylformamide as the solvent and tetrapropylammonium perchlorate as the supporting electrolyte. A JEOL spectrum computer, JEC-5, was used for spectral simulation.

The investigation was supported by the Asahi Glass Technological Foundation. We thank Prof. Shuichi Seto for his advice and Mr. Takashi Muramatsu for the preparation of pyridinium salts.

References

1) Present address: Central Laboratory of Sankyo Co., Ltd., Tokyo 140.
2) For the review, see E. M. Kosower, "Pyridinyl Radicals in Biology," in "Free Radicals in Biology," ed by W. A. Pryor, Academic Press, New York (1976), Vol. 2, Chap. 1, pp. 1—53.
3) Y. Ikegami, H. Watanabe, and S. Seto, *J. Am. Chem. Soc.*, **94**, 3274 (1972).
4) Y. Ikegami and S. Seto, *J. Am. Chem. Soc.*, **96**, 7811 (1974).
5) Briefly communicated in Y. Ikegami and H. Watanabe, *Chem. Lett.*, **1976**, 1007.
6) S. Kubota and Y. Ikegami, *J. Phys. Chem.*, **82**, 2739 (1978).
7) E. M. Kosower and J. L. Cotter, *J. Am. Chem. Soc.*, **86**, 5524 (1964).
8) E. M. Kosower and E. J. Poziomek, *J. Am. Chem. Soc.*, **86**, 5515 (1964).
9) M. Itoh and S. Nagakura, *Bull. Chem. Soc. Jpn.*, **39**, 369 (1966).
10) E. M. Kosower, H. P. Waits, A. Teuerstein, and L. C. Butler, *J. Org. Chem.*, **43**, 800 (1978).
11) P. M. Johnson and A. C. Albrecht, *J. Chem. Phys.*, **48**, 851 (1968).
12) E. M. Kosower and A. Teuerstein, *J. Am. Chem. Soc.*, **100**, 1182 (1978).

13) K. Mochida, J. K. Kochi, K. S. Chen, and J. K. Wan, *J. Am. Chem. Soc.*, **100**, 2927 (1978).
14) E. M. Kosower, "Reactions through Charge-transfer Complexes," in "Progress in Physical Organic Chemistry," ed by S. G. Cohen, A. Streitwieser, Jr., and R. W. Taft, Interscience Publisher, New York (1965), Vol. 3, pp. 81—163.
15) E. M. Kosower and J. Hajdu, *J. Am. Chem. Soc.*, **93**, 2534 (1971).
16) Coexistence of a pyridinyl radical and sodium iodide brings about the spectral change at low temperature as a result of the complex formation; see also the note in Ref. 4.
17) N. Hirota, *J. Am. Chem. Soc.*, **89**, 32 (1967).
18) J. C. Craig, J. L. Garnett, and D. M. Temple, *J. Chem. Soc.*, **1964**, 4057.
19) E. M. Kosower, D. Hofman, and K. Wallenfels, *J. Am. Chem. Soc.*, **84**, 2755 (1962).
20) Z. Matsumura and Y. Ikegami, *Bull. Chem. Res. Inst. Nonaqueous Solutions, Tohoku Univ.*, **22**, 193 (1972).

Hydrogen Atom Abstraction of *p*-Chloranil Triplet in 1,4-Dioxane in the Presence and Absence of Tetrachlorohydroquinone

Harumichi KOBASHI,* Yasunaka TOMIOKA, and Toshifumi MORITA

Department of Chemistry, Gunma University, Kiryu, Gunma 376

(Received September 7, 1978)

Mechanisms of hydrogen atom abstraction by triplet *p*-chloranil [CA(T)] from 1,4-dioxane (DOH) and tetrachlorohydroquinone (CAH_2) were studied in detail by means of nanosecond laser flash photolysis. A broad band around 740 nm in the transient absorption spectrum of CA in DOH was assigned to the charge-transfer band of the triplet EDA complex between CA and DOH. Efficiencies for the hydrogen atom abstraction from DOH and CAH_2 were determined to be 0.13 and 0.58, respectively. The former value indicates that the hydrogen atom abstraction from DOH is less effective than a physical process in deactivation of the triplet complex. From the latter value together with the measured value of the quenching rate constant (1.7×10^9 dm^3 mol^{-1} s^{-1}) of the triplet by CAH_2, it is inferred that the hydrogen atom abstraction of CA(T) from CAH_2 takes place competing with an efficient radiationless deactivation *via* the triplet exciplex between CA(T) and CAH_2 as a common intermediate.

In a previous work a report was given on the interaction of *p*-chloranil triplet with several vinyl monomers and solvents.[1] It was found that the hydrogen atom abstraction by CA(T) depends remarkably on the charge-transfer (CT) interaction between CA(T) and the hydrogen donors, and that CAH_2 added quenches CA(T) efficiently in company with simultaneous formation of *p*-chloranil semiquinone radical (CAH·) through the CA(T)$+CAH_2\rightarrow$2CAH· reaction. We have carried out an extended study on the mechanism, especially on the possible existence of exciplex as an intermediate for the hydrogen atom transfer. In general, the intersystem crossing (ISC) can be enhanced as in EDA system,[2] when a remarkable CT interaction occurs. Deactivation of CA(T) may thus be considered to proceed through the triplet exciplex as a common intermediate for the hydrogen atom transfer from CAH_2 competing with physical quenching leading to the ground state. In order to confirm this the determination of efficiency of CAH· formation due to hydrogen atom transfer might be valuable. This work deals with the nanosecond laser flash photolysis of CA in DOH and the addition effect of CAH_2 on the efficiency of CAH· formation.

Experimental

The nanosecond flash photolysis at 347 nm by a ruby laser was carried out at room temperature with use of the apparatus described previously.[1] Photomultipliers HTV-1P28 and HTV-R106 were used for analysis in the wavelength ranges of $\leq$650 nm and 650—1000 nm, respectively, according to the low noise operation technique developed by Hunt and Thomas.[3] The intensity of the laser pulse was measured with a photodiode (HP 4220), the output being recorded digitally on a hand-made peak-hold meter[4] calibrated with a thermopile (TRG, Model 107) and a pulse generator (Anritsu, MG 411B). When the laser intensity was too high the decay of the triplet chloranil showed a considerably nonexponential feature at the initial stage owing to the triplet-triplet annihilation. In order to reduce this effect the energy of the excitation pulse was attenuated to less than 25 mJ/pulse by glass plates.

p-Chloranil (CA), tetrachlorohydroquinone (CAH_2), and benzophenone were the same as used previously.[1] 1,4-Dioxane (DOH, the letter H is used separately from others in order to emphasize a hydrogen atom which is abstracted) and benzene (Dotite spectrograde) were used without purification. The benzophenone solution in benzene was used as a reference for the determination of the extinction coefficient of CA(T). The concentrations of CA and CAH_2 were 2.5×10^{-3} mol dm^{-3} and $\leq2.5\times10^{-3}$ mol dm^{-3}, respectively. The sample solutions subjected to photolysis were degassed by freeze-pump-thaw cycles. Fresh solutions were used separately for time resolved spectral measurements, determination of efficiencies of CAH· formation, and measurement of extinction coefficient of CA(T), respectively.

Results and Discussion

CA–DOH System. Figure 1a shows the ground state absorption spectrum of CA in DOH. The absorption with a maximum at *ca.* 335 nm can be assigned to the CT band of the EDA complex between CA and DOH according to the linear relationship[2] between the CT band energies and ionization potentials of donors. The intensity of the CT absorption band at 347 nm is considerably higher than that of the absorption of CA in non-interacting solvent such as 1,2-dichloroethane (DCE) (Fig. 1b). The laser light for excitation is thus absorbed pracically only by the EDA complex between CA and DOH.

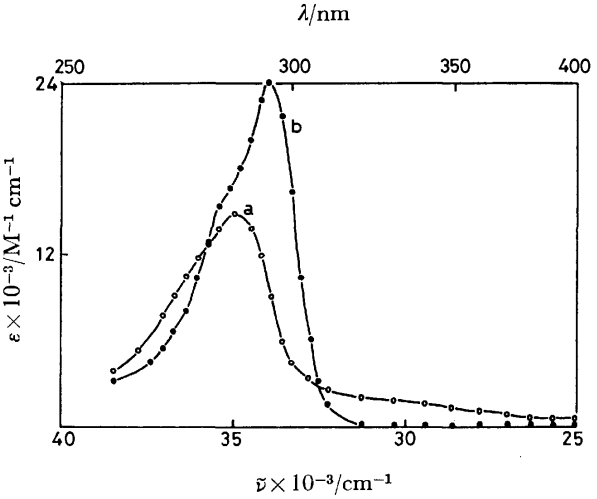

Fig. 1. Electronic absorption spectra of *p*-chloranil in 1,4-dioxane (a) and 1,2-dichloroethane (b).

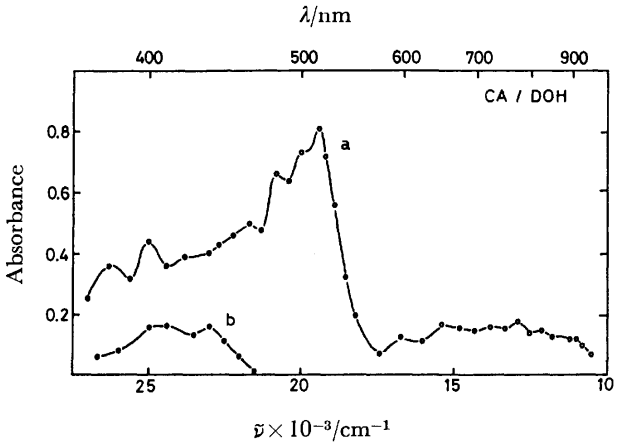

Fig. 2. Transient spectra from laser photolysis of degassed solution of CA (2.5×10^{-3} mol dm^{-3}) in DOH taken at different time after the end of excitation pulse: (a) $t=0$ and (b) $t=8$ μs.

The transient absorption spectra obtained by laser photolysis are shown in Fig. 2. The spectrum immediately after excitation (Fig. 2a) consists of a strong band with a maximum at 515 nm and a weak, broad band in the region 600—900 nm. The spectrum in the wavelength region less than 400 nm has only a qualitative significance since the ground state absorption of CA considerably overlaps in this region and the transient absorption is distorted by the recovery of CA after the photolysis. Concerning the identification of the spectrum (Fig. 2a), the following observations are noted. (1) The strong absorption band around 515 nm is very similar in wavelength position and shape to that of CA(T) in other solvent systems.[1] The decay time of this band which obeys pseudo-first order kinetics in the time range from just after pulsing to 10 μs is obtained to be 3.4 μs. (2) The absorption in the long wavelength region has a maximum at *ca.* 740 nm, its decay profile being almost the same as that of the 515 nm band. (3) By addition of CAH_2 to the solution, the two bands were quenched efficiently, decaying with an identical time constant. (4) The transient absorption spectrum obtained on photolysis of an aerated solution of CA resembles very closely that shown in Fig. 2a. It decays rapidly keeping its whole spectral feature, no new bands appearing after complete decay.

We identified the spectrum immediately after excitation (Fig. 2a) as the one attributable to the triplet EDA complex between CA and DOH, although the band due to CA(T) free from the CT interaction with the solvent would be superposed a little. Thus, the band located around 515 nm can be assigned to the local triplet-triplet absorption in CA moiety. On the other hand, the band in the longer wavelength region may be assigned to the CT transition from DOH to CA(T) for the following reasons. Ionization potentials, 9.13 eV,[5] of 1,4-dioxane is comparable with 9.245 eV[5] of benzene. Both of the CT bands of CA complexes with 1,4-dioxane and benzene in the ground state are located closely together in energy *i.e.*, 3.7 and 3.6 eV,[6] respectively. Since benzene forms a triplet complex with CA having the CT absorption band beyond 550 nm,[7] it is expected that the triplet complex of CA–DOH also has the corresponding absorption in a similar wavelength region. By the same consideration as given by Kawai *et al.*,[7] the CT band of the complex between CA(T) and DOH can be roughly estimated by

$$E_{CT}^{T} = E_{CT}^{G} - E_{T}$$

where E_{CT}^{T} and E_{CT}^{G} are the CT transition energies of the complex in the triplet and the ground state, respectively, and E_T is the energy of CA(T) above the ground state. When we take 3.7 eV for E_{CT}^{G} and 2.1 eV[8] for E_T, E_{CT}^{T} is calculated to be 1.6 eV (=770 nm), in agreement with the experimental value, 1.68 eV (=740 nm). The assignment for the long wavelength band seems to be reasonable.

After the disappearance of the 515 and 740 nm bands, the relatively weak absorption with maximum at 435 nm still remains. Figure 2b shows the absorption at 8 μs after the end of the excitation pulse, the band shape resembling that of CAH· in CA–DCE system.[1] The absorption also resembles that of CAH· produced through the $CA(T)+CAH_2\rightarrow 2CAH\cdot$ reaction. The decay of this long-lived transient was approximately of the second order. We thus identify, the transient spectrum as that of CAH·. Wong *et al.*[9] identified the corresponding transient in the same system as CAH· which decays by the disproportionation with a second order rate as observed by means of electron spin resonance spectroscopy. It is obvious that the CAH· has been produced through the interaction of CA(T) with the solvent, since no absorption around 435 nm could be detected by the addition of a quenching species for CA(T) as in styrene[1] or air.

If the intersystem crossing of CA from S_1 to T_1 proceeds with unit efficiency ($\Phi_{ISC}=1$) as is the case for duroquinone,[10] the extinction coefficient of CA(T), $\varepsilon_{CA(T)}$, interacting with DOH can be determined by comparison with that of benzophenone triplet.[1] The value of $\varepsilon_{CA(T)}$ at 515 nm was found to be $(5.8\pm0.1)\times10^3$ dm^3 mol^{-1} cm^{-1}. The extinction coefficient of CAH· in DOH, $\varepsilon_{CAH\cdot}$, is known to be 7.7×10^3 dm^3 mol^{-1} cm^{-1} at 435 nm.[9] Using these values, we can estimate the yield (Φ_r^0) of CAH· produced from CA(T) in DOH by

$$\Phi_r^0 = \frac{D_{CAH\cdot}(435)/\varepsilon_{CAH\cdot}(435)}{D_0(515)/\varepsilon_{CA(T)}(515)}$$

where $D_0(515)$ is the absorbance at 515 nm just after the cessation of the pulse and $D_{CAH\cdot}(435)$ is the residual absorbance at 435 nm at the time when CA(T) disappeared completely. A small amount of CAH· absorption decayed before this was neglected because the cecay of CAH· is considerably slower than that of CA(T). Φ_r^0 was estimated to be 0.13 ± 0.03 by five runs. The error indicated is the maximum deviation from the mean. Since CAH· is considered to be produced through the reaction sequence, $CA(S_0)\cdots DOH \xrightarrow{h\nu} CA(S_1)\cdots DOH \xrightarrow{ISC} CA(T)\cdots DOH \rightarrow CAH\cdot + DO\cdot$, the efficiency ($\phi_r^0$) of CAH· formation from CA(T) interacting directly with solvent DOH is related to Φ_r^0 by $\Phi_r^0=\Phi_{ISC}\phi_r^0$ where $\Phi_{ISC}=1$. We then have $\phi_r^0=0.13$. This indicates that the hydrogen atom abstraction from the solvent contributes to deactivation of CA(T) to a smaller

extent than the physical quenching process. The first order rate constants of CAH· formation (k_r^0) and another deactivation process (k_d^0) of CA(T) are evaluated to be 3.8×10^4 s^{-1} by use of $k_r^0=\phi_r^0/\tau_T^0$ and 2.6×10^5 s^{-1} by use of $k_d^0=(1-\phi_r)/\tau_T^0$, respectively, where τ_T^0 is the lifetime of CA(T). Thus, the deactivation processes of CA(T) interacting with DOH [CA(T)···DOH] are expressed as follows:

$$\mathrm{CA(T)\cdots DOH} \longrightarrow \mathrm{CAH\cdot + DO\cdot}, \quad k_r^0 = 3.8\times10^4\ \mathrm{s^{-1}} \qquad (1)$$

$$\mathrm{CA(T)\cdots DOH} \longrightarrow \mathrm{CA\cdots DOH}, \quad k_d^0 = 2.6\times10^5\ \mathrm{s^{-1}} \qquad (2)$$

CA–CAH$_2$–DOH System. The ground state absorption spectrum in CA–CAH$_2$–DOH system, which is not illustrated here, was exactly the same as that constracted by the superposition of individual spectrum of CA and CAH$_2$ in DOH up to the maximum concentration of CAH$_2$. No spectral evidence of complexation was obtained between CA and CAH$_2$ in the ground state at room temperature.

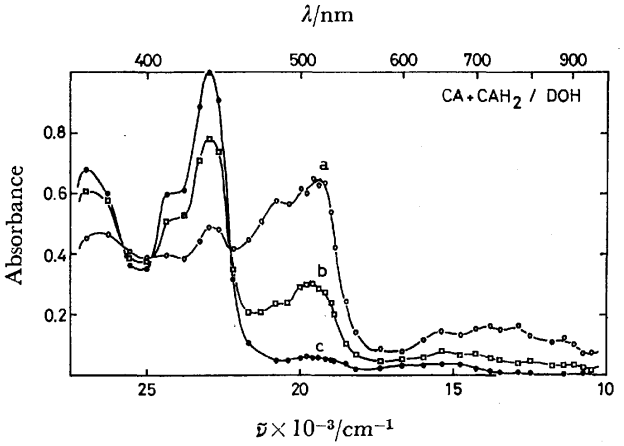

Fig. 3. Transient spectra observed in CA (2.5×10^{-3} mol dm^{-3})–CAH$_2$ (2.5×10^{-3} mol dm^{-3})–DOH system: (a) $t=0$, (b) $t=200$, and (c) $t=600$ ns after pulsing.

Figure 3 shows the transient spectra in CA–CAH$_2$–DOH system at an equal concentration of CA and CAH$_2$, 2.5×10^{-3} mol dm^{-3}. The spectrum obtained immediately after pulsing is very similar to that shown in Fig. 2a except for a small increase around the 435 nm band. With the lapse of time the triplet absorption beyond 500 nm decays rapidly and the 435 nm band grows remarkably. It is apparent that the band around 435 nm is attributed to the characteristic band of CAH· produced by the CA(T)···DOH+CAH$_2$→2CAH· reaction. This is also confirmed by the simultaneous increase of another characteristic band of CAH· at *ca.* 370 nm. There are isosbestic points at 22.3×10^3, 24.8×10^3, and 25.8×10^3 cm^{-1}. This indicates that the growing-up of CAH· absorption around 435 nm is not disturbed by any transient species formed by processes other than the CA(T)···DOH+CAH$_2$→2CAH· reaction. The CAH· absorption decays exactly according to the second order kinetics after reaching the maximum. The decay rate constant (k_t) obtained is 4.5×10^8 dm^3 mol^{-1} s^{-1}, in good agreement with the reported value, 4.1×10^8 dm^3 mol^{-1} s^{-1}. [9]

The small peak at 435 nm (Fig. 3a) may be assumed to be due to absorption of CAH· produced within the time of excitation pulse width. This is understandable on the basis of the following observations. The 435 and 515 nm-band intensities immediately after pulsing show dependence upon the concentrations of CAH$_2$ added; increase of CAH$_2$ concentration makes the 515 nm band decrease and the 435 nm band increase. This shows that the small peak at 435 nm immediately after pulsing is due to CAH· produced within the pulse width. This is also supported by the kinetic analysis at 435 nm. After subtraction of the 435 nm absorbance presumed to be due to CAH· produced within laser excitation and the absorbance due to CA(T) contributing to 435 nm from the observed absorbance, the remaining absorbance which corresponds to that of CAH· produced gradually by the reaction between CA(T)···DOH and CAH$_2$ gives a rise time approximately equal to the decay time of the triplet monitored at 515 nm. The kinetic behavior of 435 nm absorption can thus be analyzed. Production of CAH· from the excited singlet state of CA would be rare if occurring at all. The finite difference between the 435 nm absorbances (Figs. 2a and 3a) does not indicate the existence of the triplet exciplex between CA(T) and CAH$_2$.

In general, the quenching processes of CA(T) interacting with DOH by CAH$_2$ can be represented by

$$\mathrm{CA(T)\cdots DOH + CAH_2} \longrightarrow \mathrm{2CAH\cdot + DOH}, \quad k_r \qquad (3)$$

$$\mathrm{CA(T)\cdots DOH + CAH_2} \longrightarrow \mathrm{CA\cdots DOH + CAH_2}. \quad k_d \qquad (4)$$

Reaction 3 represents the hydrogen atom abstraction from CAH$_2$ and Reaction 4 the physical quenching. The relation between the yield (Φ_r) of CAH· generated after the cessation of pulsing and the efficiency (ϕ_r) of CAH· formation through the interaction between the triplet and CAH$_2$, is expressed by

$$\Phi_r = \frac{\phi_r^0(k_r^0+k_d^0)+2\phi_r k_q[\mathrm{CAH_2}]}{(k_r^0+k_d^0)+k_q[\mathrm{CAH_2}]} = \{(\phi_r^0/\tau_T^0)+2\phi_r k_q[\mathrm{CAH_2}]\}\tau_T, \qquad (5)$$

where, τ_T and τ_T^0 are lifetimes of CA(T) in the presence and absence of CAH$_2$, respectively, ϕ_r^0 is the efficiency of CAH· formation by the interaction with solvent (DOH in this case), $k_q(=k_r+k_d)$ is the quenching rate constant of CA(T)···DOH by CAH$_2$, and [CAH$_2$] is the molar concentration of CAH$_2$. The value of k_q was determined to be 1.7×10^9 dm^3 mol^{-1} s^{-1} from the plot corresponding to the $1/\tau_T=1/\tau_T^0+k_q[\mathrm{CAH_2}]$ equation. Since k_q is so high as to be close to the value for diffusion control, when CAH$_2$ of adequate concentration is present, Eq. 5 can be simplified to

$$\Phi_r = 2\phi_r(1-\tau_T/\tau_T^0) \qquad (6)$$

for the case of $\phi_r^0/\tau_T^0 \ll 2\phi_r k_q[\mathrm{CAH_2}]$, or

$$\Phi_r = 2\phi_r \qquad (7)$$

for the case of $\tau_T \ll \tau_T^0$. When CAH$_2$ is absent, Eq. 5 becomes $\Phi_r=\phi_r^0$ in accordance with Φ_r^0. On the other

hand, Φ_r is obtained experimentally from absorbance changes:

$$\Phi_r = \frac{\{D_{max}(435) - \Delta D_0(435)\}/\varepsilon_{CAH\cdot}(435)}{D_0(515)/\varepsilon_{CA(T)}(515)} \quad (8)$$

where $D_0(515)$ is the absorbance at 515 nm immediately after pulsing, $D_{max}(435)$ the maximum absorbance at 435 nm, and $\Delta D_0(435)$ the absorbance at 435 nm of CAH· formed within laser excitation. $\varepsilon_{CA(T)}(515)$ and $\varepsilon_{CAH\cdot}(435)$ are as noted before. Hence, $\phi_r(=k_r/(k_r+k_q)=k_r/k_q)$ can be calculated by combining Eq. 5 with Eq. 8. The average value of ϕ_r was found to be 0.58 ± 0.05[11] from 15 different observations for three different concentrations of CAH_2, 2.5×10^{-3}, 2.0×10^{-3}, and 1.5×10^{-3} mol cm^{-3}. The error indicated is the standard deviation. The results are summarized in Table 1.

Table 1. Rate parameters and the extinction coefficient obtained by laser flash spectroscopy in CA–DOH and CA–CAH_2–DOH systems

CA(T)···DOH	CA(T)···DOH+CAH_2
$\phi_r^0=0.13$	$\phi_r=0.58$
$\tau_T^0=3.4$ μs	$k_q=1.7\times10^9$ dm^3 mol^{-1} s^{-1}
$k_r^0=0.4\times10^5$ s^{-1}	$k_r=1.0\times10^9$ dm^3 mol^{-1} s^{-1}
$k_d^0=2.5\times10^5$ s^{-1}	$k_d=0.7\times10^9$ dm^3 mol^{-1} s^{-1}
$\varepsilon_{CA(T)}(515)=5.8\times10^3$ cm^3 mol^{-1} cm^{-1}	$k_t=4.5\times10^8$ dm^3 mol^{-1} s^{-1}

In the absence of CAH_2, CA(T)···DOH decays by the hydrogen atom abstraction from DOH but mainly by the physical process of deactivation. This is similar to the previous result in DCE or acrylonitrile.[1] It is evident from k_r and k_d values that Reaction 4 is present competing with Reaction 3 in the efficient quenching (see k_q value) of CA(T)···DOH by CAH_2 and the two processes take place with almost the same probability, indicating that ISC of CA(T) is enhanced by the interaction with CAH_2. This is often observed in the excited singlet[12] and the triplet state[13] in electron transfer or charge-transfer quenching. Recently, Steiner and Winter elucidated the mechanism of the physical quenching of thionine triplet competing with radical formation by halogenated anilines.[14] Their result is explained in terms of a heavy atom effect on ISC (occurring after nearly complete electron transfer) in a triplet exciplex. In the present hydrogen atom abstraction, the existence of such an enhanced ISC also seems to favor an exciplex as an intermediate. Results suggesting the existence of exciplex are as follows. (1) A study[15] on the solvent effect of CAH· formation yield strongly suggests the CT nature of the intermediate in question; the efficiency of the hydrogen atom abstraction increases with solvent polarity. (2) In fluid media no CT band is found in the CA and CAH_2 system nor in the duroquinone and durohydroquinone system.[16] However, DOH solution of the former system shows pink coloration in the frozen state at liquid nitrogen temperature. Even *p*-benzoquinones substituted by very bulky groups such as chlorine or methyl form the quinhydrone type complexes[17] with hydroquinone in the solid state.[18] The above finding seems to be attributed to the same type of complex under restricted conditions. In the triplet state the electron affinity of CA becomes greater than in the ground state. Thus, even in fluid media, CA(T) might form a quinhydrone type complex with CAH_2 by the aid of the CT force surpassing the steric hindrance caused by bulky chlorine atoms. We may assume that the triplet exciplex between CA(T) and CAH_2 exists as a precursor for the hydrogen atom abstraction. This is essentially the same as suggested by Amouyal and Bensasson for duroquinone triplet reduction by durohydroquinone.[10]

From an unified point of view, deactivation processes of CA(T)···DOH in the absence and presence of CAH_2 are as follows:

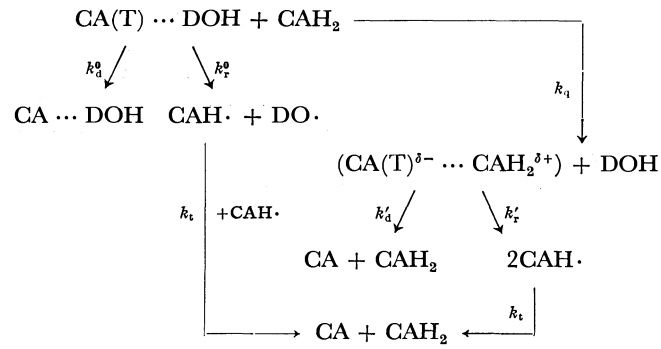

where the ground state CA is the same as CA···DOH in the DOH solvent, $(CA(T)^{\delta-}\cdots CAH_2^{\delta+})$ represents the triplet exciplex with some charge-transfer interaction between CA(T) and CAH_2, k_d' and k_r' are the first order rate constants for the ISC and the semiquinone radical formation in the exciplex, respectively, and other rate constants having their usual meanings. If we define the quenching probability per collision as γ, k_q is replaced by γk_D where k_D is the diffusion controlled rate constant calculated by $8RT/(3000\,\eta)$. The value of γ is obtained as 0.34 in DOH at 24 °C. In other solvents γ values were found to be of the same order of magnitude.[19] The quenching reaction can be considered as a diffusion controlled reaction. The parameters given in Table 1 are related to the rate parameters in this scheme:

$$k_q = \gamma k_D$$
$$k_r = \gamma k_D \cdot k_r'/(k_r'+k_d')$$
$$k_d = \gamma k_D \cdot k_d'/(k_r'+k_d')$$
$$\phi_r = k_r'/(k_r'+k_d')$$

The values of k_r' and k_d' would be so large that no exciplex absorption could be observed.

Although no absorption spectrum due to exciplex could be detected, the existence of the triplet exciplex from which the hydrogen atom abstraction takes place competing with the intersystem crossing to the ground state may be postulated in order to understand the mechanism of the hydrogen atom abstraction by CA(T) from CAH_2.

References

1) H. Kobashi, H. Gyoda, and T. Morita, *Bull. Chem. Soc. Jpn.*, **50**, 1731 (1977).

2) For example, J. B. Birks, "Photophysics of Aromatic Molecules," Wiley-Interscience, London (1970), Chap. 9; S. P. McGlynn, T. Azumi, and M. Kinosita, "Molecular Spectroscopy of the Triplet State," Prentice-Hall Inc., Englewood Cliff, New-Jersy (1969), Chap. 8.

3) T. W. Hunt and J. K. Thomas, *Radiat. Res.*, **32**, 149 (1967).

4) We are grateful to Dr. H. Masuhara (The Osaka University) for supplying us with an electric circuit diagram of the peak-hold meter.

5) K. Watanabe, T. Nakayama, and J. Mottl, *J. Quant. Spectrosc. Radiat. Transfer*, **2**, 369 (1962).

6) G. Briegleb, "Electron-Donator-Acceptor-Komplexe," Springer-Verlag, Berlin (1962), p. 30.

7) K. Kawai, Y. Shirota, H. Tsubomura, and H. Mikawa, *Bull. Chem. Soc. Jpn.*, **45**, 77 (1972).

8) Since determination of the O–O band of CA phosphorescence is difficult the value of E_T used previously in Ref. 7 was used. If we take the value, 2.7 eV, estimated from CA phosphorescence in EPA (M. Kasha, *Chem. Rev.*, **47**, 401 (1947)), E_{CT}^{T} becomes 1.0 eV which may be considered as the lower limit.

9) S. K. Wong, L. Fabes, W. J. Green, and J. K. S. Wan, *J. Chem. Soc., Faraday Trans. 1*, **68**, 2211 (1972).

10) E. Amouyal and R. Bensasson, *J. Chem. Soc., Faraday Trans. 1*, **72**, 1274 (1976).

11) The value of ϕ_r, 0.54, given in a previous paper[15] is the one for 2.0×10^{-3} mol dm^{-3} solution of CAH_2.

12) a) K. Shulten, H. Staerk, A. Weller, H.-J. Werner, and B. Nickel, *Z. Phys. Chem. (Frankfurt am Main)*, **101**, 371 (1976); b) A. R. Watkins, *J. Phys. Chem.*, **77**, 1207 (1973); **78**, 1885 (1974); *Chem. Phys. Lett.*, **43**, 299 (1976).

13) U. Steiner, G. Winter, and H. E. A. Kramer, *J. Phys. Chem.*, **81**, 1104 (1977).

14) U. Steiner and G. Winter, *Chem. Phys. Lett.*, **55**, 364 (1978).

15) H. Kobashi, T. Nagumo, and T. Morita, *Chem. Phys. Lett.*, **57**, 369 (1978).

16) L. Michaelis and S. Granick, *J. Am. Chem. Soc.*, **66**, 1023 (1944).

17) H. Tsubomura, *Bull. Chem. Soc. Jpn.*, **26**, 304 (1953); A. Kuboyama and S. Nagakura, *J. Am. Chem. Soc.*, **77**, 2644 (1955).

18) M. A. Slifkin and R. H. Walmsley, *Spectrochim. Acta, Part A*, **26**, 1237 (1970).

19) Unpublished data.

Anodic Oxidation of *N,N*-Dimethyl-*m*-toluidine at a Platinum Electrode in an Acetonitrile Solution

Kazuo YASUKOUCHI, Isao TANIGUCHI,* Hiroko YAMAGUCHI, and Tatsuya TANOUE

Department of Industrial Chemistry, Faculty of Engineering, Kumamoto University, 2-39-1, Kurokami, Kumamoto 860

(Received September 9, 1978)

The electrochemical behavior of *N,N*-dimethyl-*m*-toluidine (DMMT) in an acetonitrile solution at a Pt electrode was investigated. By controlled-potential oxidation at 0.65 V (*vs.* Ag/0.01 mol dm^{-3} $AgClO_4$), the dihydro compound (**I-a**), which had been considered to be an intermediate in the reaction forming benzidine, was probably obtained. **I-a** was gradually converted to *N,N,N',N'*-tetramethyl-2,2'-dimethylbenzidine (TMMB) in the solution within several hours. **I-a** was easily converted to TMMB by the cathodic re-reduction at −0.9 V or by adding either pyridine or water; this reaction pathway is useful for the synthesis of TMMB. Preliminary mechanistic information on the anodic oxidation of DMMT is also given by cyclic and ring-disk electrode voltammetry, current-reversal chronopotentiometry, and controlled-potential coulometry. The proposed reactions are: A$-$e$\rightarrow$A$^+$, A$^+$+A$\xrightarrow{k}$A-A$^+$, and A-A$^+-$e$\rightarrow DH_2^{2+}$, where A and A$^+$ are, respectively, DMMT and its cation radical, DH_2^{2+} is the dihydro compound (**I-a**), and k is the rate constant of the coupling reaction (*ca.* 5×10^3 dm^3 mol^{-1} s^{-1}). TMMB is formed by: DH_2^{2+}+2e(or 2Py)$\rightarrow$D+H_2(or 2PyH$^+$), where D is TMMB and Py is pyridine.

N,N-dialkyl-substituted aromatic amines show very similar behavior to each other on the anodic oxidation in a nonaqueous solution. In the case of *N,N*-dimethylaniline (DMA),[1] the primary electrode reaction is a one-electron transfer to form a cation radical which then couples to form *N,N,N',N'*-tetramethylbenzidine (TMB) with simultaneous loss of protons. TMB thus formed is more readily oxidized than the starting amine and is converted to the diquinoid structure (TMB^{2+}). Thus, a general reaction scheme is

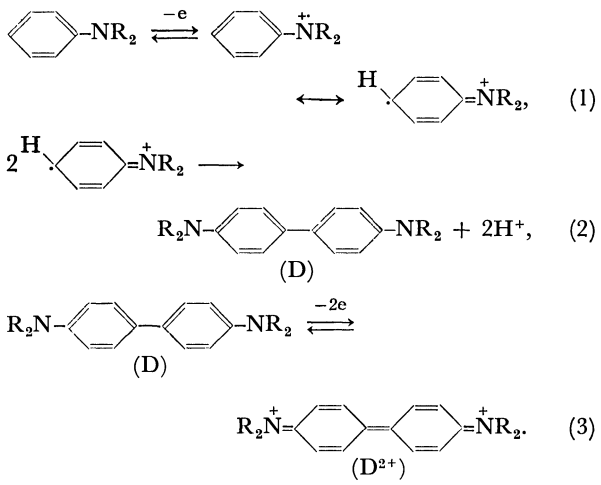

In the coupling reaction (Eq. 2), the dihydro compound (DH_2^{2+}) is considered to be an intermediate,[2]

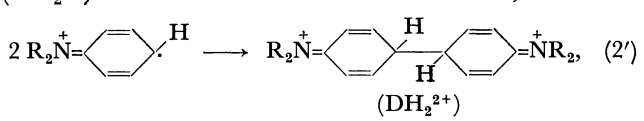

and D is formed by loss of protons from DH_2^{2+}.

The same reactions as Eqs. 1—3 were proposed for DMA also in $AlCl_3$–NaCl melts.[3] However, an intermediate such as DH_2^{2+} is usually unstable and has not yet been isolated. Furthermore, some coupling reactions other than Eq. 2 are possible, but the mechanism has usually not been clarified.

The aims of this paper are to describe the interesting fact that a DH_2^{2+}-like compound was formed by the anodic oxidation of *N,N*-dimethyl-*m*-toluidine (DMMT), to give preliminary information on the mechanism of this electrode reaction, and also to describe the fact that *N,N,N',N'*-tetramethyl-2,2'-dimethylbenzidine (TMMB) was easily synthesized by the re-reduction of the oxidation product of DMMT or by adding a base to the product.

DMMT was adopted for the present study because (i) the ring-substituted methyl group makes the cation radical stable, and thus the coupling reaction may be easily examined, (ii) the low basicity of DMMT[4] compared to its isomers may decrease the complication of the oxidation pathway due to protonation of the parent molecule, and (iii) no study has been reported on the anodic oxidation of DMMT in a nonaqueous solution.

Experimental

DMMT (analytical GR grade) was used as received. Sodium perchlorate (analytical EP grade) was recrystallized twice from ethanol, dried overnight under a reduced pressure (3 mmHg, 1 mmHg≈133.3 Pa), and stored over silica gel. Acetonitrile (MeCN) was purified by distillation from P_2O_5, from K_2CO_3, and then three times by slow fractional distillation. The water content of the MeCN (0.18 wt %) was determined by the Karl-Fischer titration.

Cyclic voltammograms were measured at a Pt disk electrode (1.96×10^{-3} cm^2) sealed in a soft glass using a set of Yanaco P8 polarographs. The working electrode was polished with an oilstone before each measurement. The counter electrode was an Hg pool (*ca.* 3 cm^2). A Ag/0.01 mol dm^{-3} $AgClO_4$ couple in MeCN, which was connected to the test solution with a 1 mol dm^{-3} $NaClO_4$ agar bridge, was used as a reference electrode. All potentials appearing in this paper are referred to this electrode (whose potential was 0.19 V *vs.* SCE).

Macro-scale electrolyses were carried out using a Nikko Keisoku NPGS 301 potentiostat. A two-compartment cell with a fine glass frit was used. The anode electrolyte was usually 200 ml in volume. The working and the counter electrodes were planar Pt. During electrolysis, cyclic voltammograms of the solution were measured at suitable times to check the changes of the composition of the solution. Low concentrations of DMMT (<10 mmol dm^{-3}) were used

because a benzidine-type product was generally formed predominantly at a low concentration of a starting amine.[5] After exhaustive oxidation at 0.65 V (*vs.* Ag/Ag^+), the product I was obtained as follows: After evaporation of the solvent and then addition of 100 ml of aqueous 0.2 mol dm^{-3} $HClO_4$ to remove the supporting electrolyte, I was extracted with benzene and was obtained by evaporation of the benzene. When the supporting electrolyte was removed by water with no perchloric acid, the same product as II described below was obtained. Since the product I was gradually converted to product II in the test solution within several hours and its stability depended sensitively upon the concentration of water contained in the solution, repeated trials for obtaining I were made to get reproducible data. The product II, which was produced by re-reduction at −0.9 V of the solution obtained by exhaustive oxidation at 0.65 V, was obtained by the same method as that used for the product I except for the use of water to remove the supporting electrolyte. To check the purity of the products, they were chromatographed on both an alumina (Wako B-10F) and a silica gel (Wako B-10) with benzene, and the chromatograms obtained were developed with iodine. For both products, three spots due to products I and II, and DMMT which remained unreacted, were detected. Thus, I obtained here contained II (typically about 10—20 %) and a small amount (less than 5 %) of DMMT, while II obtained here contained only a small amount of DMMT and a trace amount of I. For both products I and II without further purification, IR (in KBr wafer using a Hitachi 125 G spectrophotometer), NMR (in $CDCl_3$ using a Hitachi R-24 at 60 MHz), and mass (at 75 eV using a JOEL JMS D-100) spectra were measured. A UV spectrum of the test solution was measured by a Hitachi 200-10 spectrophotometer.

Other electrochemical measurements for rotating ring-disk electrode (RRDE) voltammetry and current-reversal chronopotentiometry (CRC) were carried out by using commercially available apparatuses constructed by Nikko Keisoku. All experiments were carried out at 25±0.3 °C.

Results and Discussion

The cyclic voltammogram of DMMT exhibited one anodic wave (Ia) having a peak potential (E_p) of 0.45 V (Fig. 1a), and no other appreciable wave was observed near this peak. To obtain the oxidation product, controlled-potential electrolysis at 0.65 V was carried out. During electrolysis the height of the wave Ia decreased and a new irreversible reduction wave (IIc) appeared at $E_p = -0.83$ V (Fig. 1b). Since no wave was observed at the potential near 0.45 V, TMMB was not produced because TMMB, if formed, must be oxidized at a somewhat less anodic potential than that for the wave of DMMT. The vicinity of the anode was colored pink, which might be due to the formation of the cation radical of DMMT, and the bulk solution became green. By coulometry for a 5 mmol dm^{-3} DMMT solution, 0.97 electrons/molecule of DMMT were consumed and the product I was obtained.

Controlled-potential re-reduction at −0.9 V was carried out consecutively after exhaustive oxidation at 0.65 V. 0.9 electrons/molecule of DMMT were consumed to make the reduction wave IIc on the voltammogram of the solution disappear; the solution turned dark brown and this color no longer changed to green by the anodic re-oxidation. The cyclic voltammogram of the solution obtained by the re-reduction showed one reversible wave (IIIa/IIIc) at a somewhat less anodic ($E_p = 0.42$ V for IIIa) potential than that for DMMT (Fig. 1c). This suggests that TMMB is produced by the re-reduction of the product I. In confirmation of this consideration product II was isolated after exhaustive re-reduction of I. Both products I and II thus obtained were analyzed to determine their structures, and the characteristics of the analytical data are summarized in

Table 1. Analytical data on the products (I and II) and DMMT

Compound	I	II	DMMT
IR[a] (KBr) (cm^{-1})	1687 (νC=N), 1120 (ClO_4^-), 1607, 1491 (Ring νC=C), 2800—3000 (Me νC–H)	1610, 1498 (Ring νC=C), 1350, (1228) (Ar. *t*-amine νC–N), 815, 808, 832 (1,2,4-trisubstituted benzene δC–H), 2800—3000 (Me νC–H)	1607, 1500 (Ring νC=C), 1350, (1230) (Ar. *t*-amine νC–N), 767, 692 (1,3-disubstituted benzene δC–H), 2800—3000 (Me νC–H)
UV_{max} (MeCN) (nm) (log ε)	255 (<3), 300 (<2.6)	265 (4.36), 300 (3.8—3.9 shoulder)	255 (4.19), 300 (3.34)
NMR[b] ($CDCl_3$) δ (ppm)	2.08 (3H, s, Me), 3.08 (6H, s, Me_2N), 6.8—7.3 (3-4H, m, Ar–H)	2.04 (3H, s, Me), 2.92 (6H, s, Me_2N), 6.5—7.3 (3H, m, Ar–H)	2.30 (3H, s, Me), 2.83 (6H, s, Me_2N), 6.5—7.3 (4H, m, Ar–H)
MS[c] (75 eV) *m/e* (rel intensity)	269.5 (17.9), 268.5 (51.6), 267.5 (14.7), 254.5 (9.5), 253.5 (12.1), 209 (10.5), 135 (67.4), 134 (100), 121 (25.3), 120 (32.6), 119 (29.5), 118 (23.2), 91 (34.7)	269 (21.2), 268.5 (100), 267.5 (24.1), 253 (16.6), 252 (11.2), 209 (10.7), 157 (20.2), 133 (31.6)	135 (66.3), 134 (100), 121 (10.0), 120 (13.7), 119 (12.1), 118 (8.4), 91 (19.5), 77 (9.5), 69 (13.2), 65 (10.5)
Elemental analysis Found (%) (Calcd)	C: 50.413 (46.055)[d] H: 5.631 (5.543) N: 6.100 (5.970) Others: 37.856 (42.431)	80.207 (80.471)[e] 8.696 (8.941) 9.673 (10.439) 1.424 (—)	—

a) Absorption bands are listed in the order of their strength except for those in the parentheses. ν= stretching, δ=bending, t=tertiary, Ar=aromatic, and Me=methyl. b) TMS was used as the internal standard. s=singlet and m=multiplet. c) Only main peaks are listed. d) Calcd for **I-a**. e) Calcd for TMMB.

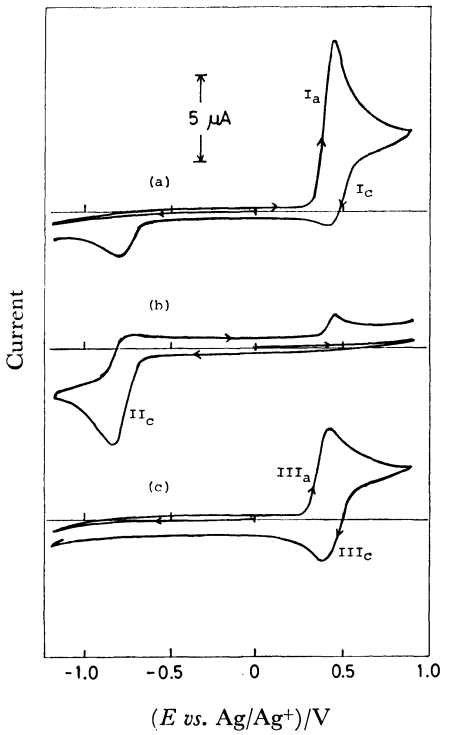

Fig. 1. Cyclic voltammograms of 5 mM DMMT in MeCN–0.4 M $NaClO_4$. Scan rate: 0.5 V s^{-1}. The direction of the potential scan is shown by arrows on the voltammograms.
a) Before controlled-potential electrolysis, b) after exhaustive oxidation at 0.65 V, and c) after exhaustive re-reduction at −0.9 V.

Table 1.

Re-reduction Product II. Comparing the analytical data on II with those on DMMT, we easily find that II is TMMB, as was suggested by the cyclic voltammetric behavior. The reasons for the conclusion that II is identical with TMMB are as follows. a) The IR data on II show that (i) C–N stretching absorption of the tertiary aromatic amine at 1350 cm^{-1} remains and (ii) absorption due to C–H bending of the 1,3-substituted aromatic ring at 692 and 767 cm^{-1} observed for DMMT changes to those of the 1,2,4-substituted one at 808, 815, and 832 cm^{-1}. b) The NMR data on II indicate that (i) since the peak of methyl protons on the ring shifts to a higher field (δ=2.04 for II and δ=2.30 for DMMT), a shift which probably results from the ring-current effect, the methyl group is not coplanar to the ring and thus a 2,2′-dimethylbiphenyl-type structure is suggested, and (ii) the number of aromatic protons reduces to three-fourths of that of DMMT. c) In the mass spectrum, the parent ion peak of TMMB is observed (Found: *m/e* 268.5, Calcd for TMMB: M, 268.4) and the fragmentation is also reasonably explained. d) The UV spectrum of II is similar to that of 2,2′-dimethylbenzidine[6] (the red-shift of λ_{max} for II is explained in terms of the replacement of H atoms on nitrogen with methyl groups). e) The electrochemical data are also consistent with the conclusion of the formation of TMMB, and the reaction for the wave IIIa/IIIc is

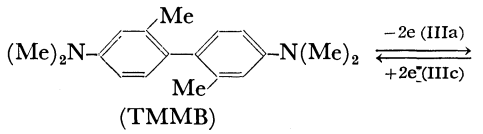

(TMMB)

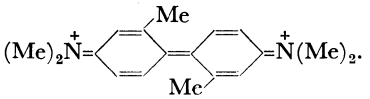

(TMMB^{2+}) (4)

Furthermore, anodic oxidation of II gave a blue solution having absorption maxima at 378 and 680 nm, a result which is similar to that reported for the oxidation of 3,3′-dimethylbenzidine.[7] Thus, TMMB was formed either by the re-reduction or by adding a base after exhaustive oxidation of DMMT in MeCN. This simple method is useful for the synthesis of TMMB in the yield of 80—90%.

Oxidation Product I. Some remarkable differences in the analytical data on I from those on DMMT and TMMB are observed. However, since TMMB is easily produced by the reduction of I or by adding pyridine (or a base) to I, the structure of I must be similar to that of II. The strong absorption at 1120 cm^{-1} in the IR spectrum shows that I forms a salt with a perchlorate anion; the NMR data also support this conclusion because the electron density near *N,N*-dimethyl protons of I (δ=3.08) is lower than those of DMMT (δ=2.83) and TMMB (δ=2.92). The methyl-proton peak of I shifts to a higher field (δ=2.08) than that of DMMT (δ=2.30), as is observed for TMMB (δ=2.04), a fact which indicates that the structure of I is similar to that of TMMB. These results and the fact that no strong UV absorption of I was observed suggest the following two possible structures:

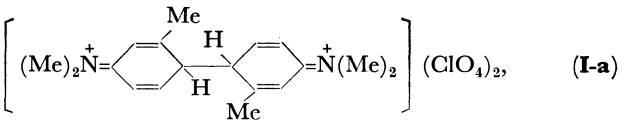

(I-a)

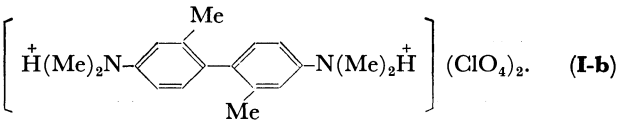

(I-b)

Thus, to determine the structure of I, we tried to distinguish between **I-a** and **I-b** by measuring the number of aromatic protons by integration of the NMR spectrum, but no reproducible result was obtained (the number of protons was 3—4). No appreciable absorption was observed for an N–H proton. However, the structure **I-b** is rejected because (i) in the IR spectrum of I, the C=C ring stretching absorption at 1491 and 1607 cm^{-1} is reduced and the C=N stretching absorption at 1687 cm^{-1} appears, and (ii) in the mass spectrum of I, the peaks at *m/e*=134 and 135 have larger intensity than that of the parent ion peak, a fact which shows that I has an unstable structure which can be split easily into two halves. On the other hand, the largest-intensity peak of **I-b** may be the parent ion peak, as is observed for TMMB. Thus, product I is determined to be the dihydro compound (**I-a**).

I-a was easily converted, as is expected from its

structure, to TMMB by cathodic reduction or by adding pyridine (or a base):

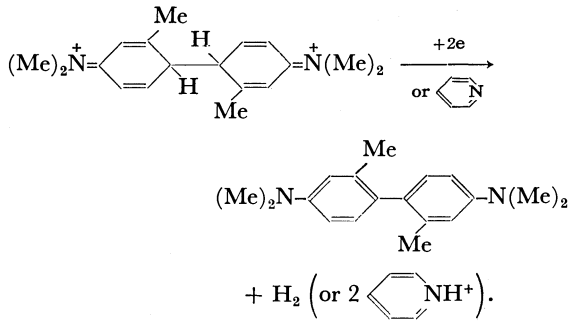

(5)

Oxidation Mechanism. To obtain mechanistic information on the formation of the dihydro compound (**I-a**), some preliminary experiments were carried out. By cyclic voltammetry, the ratio of the anodic peak current of the wave Ia to the square root of the scan rate, $i_{pa}/v^{1/2}$, decreased with increasing scan rate, and the ratio of the cathodic reversal current (i_{pc}) to i_{pa}, i_{pc}/i_{pa}, decreased with an increase in the concentration of DMMT (Table 2). These results are explained in terms of the reactions in which a second-order chemical reaction is involved between two charge-transfer reactions (so-called an ECE mechanism). Usually two possible types of coupling reactions are considered. One is dimerization of intermediates and the other is the coupling of an intermediate with a parent molecule. These two mechanisms are distinguishable by both RRDE voltammetry[8,9] and CRC.[10] Thus, RRDE voltammetry was first applied to obtain precise information. On the basis of Bard's method, the kinetic collection efficiency, $N_k(=-i_r/i_d$ where i_r and i_d are the ring and the disk currents, respectively), was measured as a function of the disk current, CONI ($=i_d/i_{d,l}$ where $i_{d,l}$ is a limiting disk current for the oxidation of DMMT). The N_k values decreased with increasing 1-CONI (Fig. 2). This trend shows[8] that the intermediate generated by the first charge-transfer reacts with the parent molecule and is further oxidized to form the dimer:

$$A - e \rightleftarrows A^+, \quad (6)$$

$$A^+ + A \xrightarrow{k} A\text{-}A^+, \quad (7)$$

$$A\text{-}A^+ - e \rightleftarrows DH_2^{2+}, \quad (8)$$

where A and A^+ are DMMT and its cation radical and DH_2^{2+} is the dihydro compound (**I-a**).

Table 2. Cyclic voltammetric data for oxidation of DMMT in MeCN– 0.4 M $NaClO_4$ (1 M=1 mol dm^{-3})

Concn of DMMT (C) / mM	Scan rate (v) / V s^{-1}	i_{pa} / μA	$i_{pa}/v^{1/2}C$ / μA $V^{-1/2}$ $s^{1/2}$ mM^{-1}	i_{pc}/i_{pa}
1.0	0.05	0.82	3.67	—
	0.1	1.18	3.73	—
	0.25	1.70	3.40	—
	0.5	2.32	3.28	0.48
	1.0	2.78	2.78	0.53
2.0	0.05	1.58	3.53	—
	0.1	2.16	3.42	—
	0.25	3.12	3.12	—
	0.5	3.96	2.80	0.42
	1.0	4.88	2.44	0.55
4.0	0.25	6.40	3.20	—
	0.5	7.80	2.76	0.39
	1.0	10.1	2.53	0.52
7.0	0.25	11.4	3.26	—
	0.5	13.5	2.73	0.39
	1.0	15.4	2.20	0.52
10.0	0.25	13.9	2.78	—
	0.5	18.6	2.63	0.39
	1.0	23.9	2.39	0.45

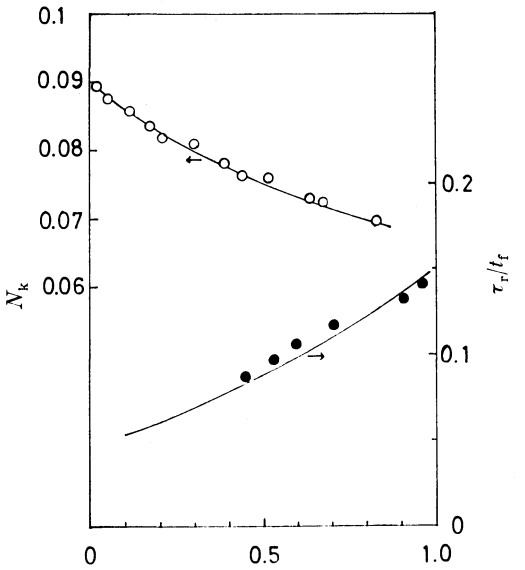

Fig. 2. Collection efficiency (N_k) *vs.* 1-CONI and τ_r/t_f *vs.* t_f/τ_r for oxidation of 1 mM DMMT in MeCN–0.1 M $NaClO_4$. Points are experimental data. For RRDE voltammetry the ring electrode was maintained at 0 V and the rotation rate of the electrode was 105 rad s^{-1}. For CRC the ratio of reverse to forward currents was 1/2 and $t_f=1.0$ s. Solid lines are simulated results corresponding to the rate constant of 5×10^3 M^{-1} s^{-1} (for RRDE) and 7×10^3 M^{-1} s^{-1} (for CRC) for Eqs. 6—8.

To give further support for this mechanism, CRC using the method developed by Evans[10] was also applied. The plots of τ_r/t_f *vs.* t_f/τ_f, where τ_f and τ_r are the forward and the reverse transition times, respectively, and t_f is the forward electrolysis time, showed an upward trend in τ_r/t_f values with increasing t_f/τ_f (Fig. 2); this trend also indicates[10] the above reaction pathway (Eqs. 6—8). By using a digital simulation method the rate constant for the coupling reaction (Eq. 7) was estimated to be approximately 5×10^3 dm^3 mol^{-1} s^{-1} (Fig. 2). To obtain an accurate value of k and more precise mechanistic information, the details of the kinetics of the reaction are being investigated by CRC and RRDE voltammetry and will be reported later.

This work was partially supported by the Asahi Glass Foundation for the Contribution to Industrial Technology. Mass spectra associated with this work were measured at the Japan Atomic Energy Research Institute at Tokai. The authors would like to thank Mr. Ichiro Tsuji for his help in the experiment.

References

1) R. N. Adams, "Electrochemistry at Solid Electrodes," Mercel Dekker, Inc., New York (1969), p. 351, and references cited therein.

2) S. D. Ross, M. Finkelstein, and E. J. Rudd, "Anodic Oxidation," Academic Press, Inc., New York (1975), pp. 203—207.

3) H. L. Jones and R. A. Osteryoung, *J. Electroanal. Chem. Interfacial Electrochem.*, **49**, 281 (1974).

4) R. A. Benkeser and H. R. Krysiak, *J. Am. Chem. Soc.*, **75**, 2421 (1953); N. F. Hall and M. R. Sprinkle, *ibid.*, **54**, 3469 (1932).

5) R. Hand and R. F. Nelson, *J. Electrochem. Soc.*, **117**, 1353 (1970).

6) R. B. Carlin and R. C. Odioso, *J. Am. Chem. Soc.*, **76**, 2345 (1954).

7) J. W. Strojek and T. Kuwana, *J. Am. Chem. Soc.*, **90**, 1353 (1968); H. N. Blount and T. Kuwana, *ibid.*, **92**, 5773 (1970).

8) U. J. Puglisi and A. J. Bard, *J. Electrochem. Soc.*, **119**, 829, 833 (1972).

9) T. H. Teharani, L. A. Tinker, and A. J. Bard, *J. Electroanal. Chem. Interfacial Electrochem.*, **90**, 117 (1978), and references therein.

10) S. C. Rifkin and D. H. Evans, *J. Electrochem. Soc.*, **121**, 769 (1974).

Clustering Reactions of the Protonated Nitrogen N_2H^+ with Hydrogen Molecule in the Gas Phase

Kenzo HIRAOKA

Faculty of Engineering, Yamanashi University, Takeda, Kofu 400

(Received September 28, 1978)

Clustering reactions of the protonated nitrogen N_2H^+ with hydrogen molecule, $N_2H^+(H_2)_{n-1}+H_2=N_2H^+(H_2)_n$ $(n-1, n)$, were studied in a pulsed electron beam mass spectrometer with a high-pressure ion source. The values of enthalpy change $-\Delta H_{n-1,n}$(kcal/mol) and the entropy change $-\Delta S_{n-1,n}$(e.u.) obtained from the van't Hoff plots of equilibrium constants were (0, 1) 7.2, 22.6, (1, 2) 1.5, 14.0. No cluster ions larger than $N_2H^+(H_2)_2$ were observed even at −187 °C. The relatively low values of enthalpy change for the clustering reactions (0, 1) and (1, 2) suggest that the positive charge in N_2H^+ is delocalized, the N_2H^+ ion very weakly interacting with additional hydrogen molecules electrophilicly. The calculated entropy change also suggests that hydrogen molecules in $N_2H^+(H_2)_n$ are weakly bound to the core ion N_2H^+, having considerable freedom of motion in the cluster ion. The thermochemical study proves that the cluster ion $N_2H^+(H_2)_2$ does not have the structure of the protonated hydrazine $N_2H_5^+$.

Studies of ion-solvent molecule interactions in solution date back to the beginning of physical chemistry. However, it is only 10 years since a systematic study of ion-solvent molecule interactions in the gas phase was begun. Studies of ion-solvent clustering reactions in the gas phase provide direct indication of the preferred coordination of ions by solvent molecules and the energy relations between solvated species in the gas phase containing different numbers of coordinated solvent molecules.

A merit of studies in the gas phase by means of mass spectrometry is that the stoichiometry of detectable species can be deduced exactly. The mass spectrometric method also permits measurements of gas phase ion equilibria and their temperature dependence. These data in turn lead to enthalpies, entropies and free energies for ionic reactions. These thermochemical data often give information on the structure of ionic species.

A mass spectrometric study of the ions present in the air at near atmospheric pressures (≈100 Torr) led to the incidental observation[1,2] of the proton hydrates $H^+(H_2O)_n$ formed by ion-molecule reactions involving a trace of water vapor. The observation of clusters such as $NH_4^+(NH_3)_m(H_2O)_n$ and $H^+(CH_3OH)_n$ in ammonia, methanol and other gases led to the systematic study of ion-solvent molecule interactions and ion equilibria in the gas phase.[3] Because of hydrogen bonding, bond energies are very large in the water. Since the charge is very efficiently dispersed by hydrogen bonding, the relative stability difference between the favorable and the unfavorable structures is small.

Recently, Hiraoka and Kebarle investigated two clustering reactions, $H_3^+(H_2)_{n-1}+H_2=H_3^+(H_2)_n$ and $CH_5^+(CH_4)_{n-1}+CH_4=CH_5^+(CH_4)_n$.[4,5] From the thermochemical data obtained, they predicted the structure of H_3^+, CH_5^+ and of cluster ions $H_3^+(H_2)_n$ and $CH_5^+(CH_4)_n$. In both systems, the positive charge is not so well dispersed in the cluster ions as in the case of water system, because hydrogen and methane have no hydrogen bonding ability. Since the charge is not efficiently dispersed in the cluster ions, the relative stability differences between the favorable and the unfavorable structures are larger, thus making it easier to predict the structure of cluster ions.

In this investigation, the clustering reactions of the protonated nitrogen N_2H^+ with hydrogen molecule were studied. Since the protonated molecule and the solvent molecule are different, new information was expected.

Experimental

The ion-molecule reaction ion source and the mass spectrometer were described;[6] only a brief description of the procedures is given herewith.

The H_2 gas(Linde UHP) was purified by passing through a liquid nitrogen cooled trap containing molecular sieve 5 Å at atmospheric pressure. Downstream of this trap, the H_2 gas passed through a variable needle valve in order to reduce the pressure to 1—6 Torr, flowing in and out of the ion source. The H_2 gas thus prepared contains no impurities except a trace amount of nitrogen.[7]

Ionization is produced by a short pulse of 2 keV electrons which enters the sourse through a small slit (12 μm×2 mm, razor blade edges) of the field free ion source. The electron beam is pulsed "on" for 10 μs and "off" for 5 ms. Each pulse contains some 10^6 electrons. The primary ions H_2^+ and H^+ are rapidly converted by ion-molecule reactions into H_3^+. This species reacts further giving H_5^+, H_7^+, *etc.* The reaction occurs due to proton transfer from H_3^+ and H_5^+ to impurity N_2 leading to N_2H^+ and its hydrogen clusters. The vast majority of ions are ultimately destroyed by diffusion towards the wall. Some ions diffuse to the vicinity of an ion exit slit (12 μm×3 mm, razor blade edges) and escape into an evacuated region where they are accelerated, magnetically mass analyzed and detected with counting equipments attached to a multichannel analyser. Collection of some 10^4 pulses at a given m/e gave a satisfactory temporal profile of the ion with a channel dwell time of 20—30 μs.

The equilibrium constants for the clustering reactions $(n-1, n)$ were calculated by

$$K_{n-1,n} = I_n/I_{n-1} \times P_s$$

where I_n/I_{n-1} is the stationary intensity ratios of the corresponding cluster ions and P_s is the solvent (hydrogen) pressure.

Results and Discussion

General. The solvation of ions by neutral molecules is an exothermic process. Since the solvated

ions may fall apart or be collisionally dissociated to reform the original reactants, it is possible that thermodynamic equilibrium can be achieved under conditions where the complex can undergo sufficient collisions to remove the heat of reaction. By the rule of thumb the achievement of equilibrium can be determined by the rate of the slow reaction, which has a rate constant $k \approx 10^{-29}$ cm^6 molecule^{-2} s^{-1}. With this value one can calculate the half-life for the clustering reaction at 3 Torr of H_2 as 2×10^{-6} s or less. The subsequent steps in the clustering sequence require considerably shorter time since their rate constants are considerably higher. Thus, thermodynamic information about the clustering reactions can be obtained from equilibrium constants. At equilibrium we have

$$-RT \ln K = \Delta G = \Delta H - T\Delta S \qquad (1)$$

The enthalpy of reaction can be obtained from the slope of a van't Hoff plot. We can evaluate ΔS if ΔG and ΔH are known.

Results. Figure 1 shows the temperature and pressure ranges for the (0, 1) equilibrium. The equilibrium constant is independent of the hydrogen pressure. Figure 2 gives the van't Hoff plots of the

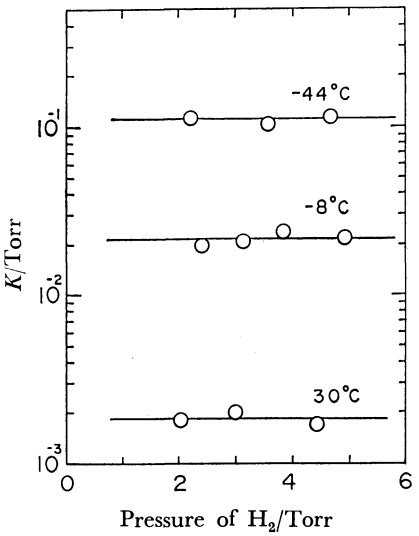

Fig. 1. Equilibrium constant $K_{0,1}$ for the reaction $N_2H^+ + H_2 = N_2H^+(H_2)$ at 3 temperatures plotted *vs.* hydrogen pressure. Standard state for K as given in these plots is 1 Torr.

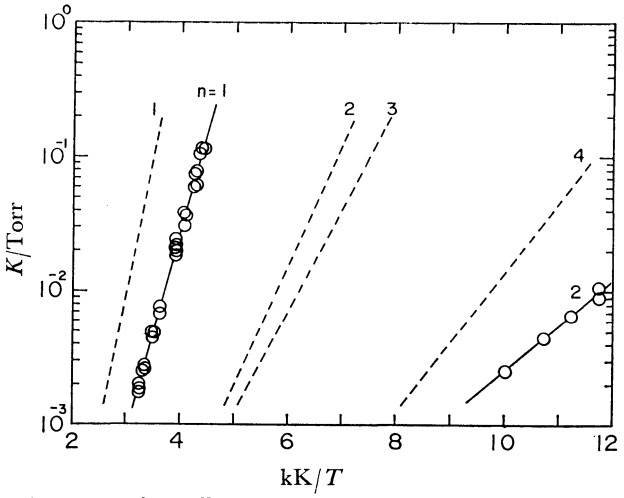

Fig. 2. van't Hoff plots for the reactions $N_2H^+(H_2)_{n-1} + H_2 = N_2H^+(H_2)_n (n-1, n)$. (----) plots for the reactions $H_3^+(H_2)_{n-1} + H_2 = H_3^+(H_2)_n$ $(n-1, n)$, Ref. 4.

clustering reactions of N_2H^+ with hydrogen molecule. For the sake of comparison the results of the clustering reactions of H_3^+ with hydrogen molecule[4] are given in Fig. 2. The thermochemical values obtained are given in Table 1 together with the results of H_2 solvation reaction of HCO^+.[8] The solvent molecule is hydrogen for all the reactions.

Free Energy and Enthalpy Change. Decrease in $\Delta H_{n,n-1}$ ($\Delta H_{n,n-1} = -\Delta H_{n-1,n}$) with n is observed as is always the case for ion clusters. The decrease is expected because of gradual charge dispersal with the addition of new clustering molecules. The irregularity of the van't Hoff plots for the clustering reactions of H_3^+ with H_2 shown in Fig. 2 was discussed.[4] In the hydrogen experiment, cluster ions $H_3^+(H_2)_n$ for $n=1$ to 4 were observed as major ions between room temperature and -170 °C. However, in the present experiment, the ion $N_2H^+(H_2)_2$ $(n=2)$ was the largest cluster observed at low temperatures, no higher clusters $(n>2)$ being observed even at -187 °C; N_2H^+ has much lower hydrogen molecule affinity than H_3^+. The vertical distance between two adjacent van't Hoff plots taken at a constant $1/T$ corresponds to $(\Delta G_{n+1,n} - \Delta G_{n,n-1})(1/2 \cdot 3RT)$, being proportional to the free energy difference at a certain temperature T. A big gap between two van't Hoff plots thus indicates a big drop of stability

Table 1. Thermochemical data obtained from measurement of equilibria
$BH^+(H_2)_{n-1} + H_2 = BH^+(H_2)_n$ $(n-1, n)$

Reaction	$-\Delta H_{n-1,n}$ [a]	$-\Delta S_{n-1,n}$ [b]	$-\Delta G_{n-1,n}$ [a]
(1) $N_2H^+ + H_2 = N_2H^+(H_2)$	7.2±0.2	22.6±1.0	0.4±0.4
(2) $N_2H^+(H_2) + H_2 = N_2H^+(H_2)_2$	1.5±0.3	14.0±2.0	−3.3±0.5
(3) $H_3^+ + H_2 = H_3^+(H_2)$	9.6	24.6	2.3
(4) $H_3^+(H_2) + H_2 = H_3^+(H_2)_2$	4.1	19.8	−1.8
(5) $H_3^+(H_2)_2 + H_2 = H_3^+(H_2)_3$	3.8	20.2	−2.3
(6) $H_3^+(H_2)_3 + H_2 = H_3^+(H_2)_4$	2.4	19.3	−3.4
(7) $HCO^+ + H_2 = (H_2)HCO^+$	3.9	20.5	−2.3

a) ΔH and ΔG values in kcal/mol. Standard state 1 atm. ΔG values are for 298 K. b) ΔS values in entropy units (cal/deg). Standard state 1 atm. ΔS values are for temperatures in the temperature range in which each reaction was studied.

toward dissociation of one molecule. We see from Fig. 2 that there is a very big gap between plots $n=1$ and 2 (Reactions 1 and 2, Table 1), indicating that (a) the first incoming H_2 molecule interacts with reasonable strength with N_2H^+, but the second molecule experiences very weak interactions with $N_2H^+(H_2)$, and (b) the stability of $N_2H^+(H_2)_2$ is remarkably lower than that of $H_3^+(H_2)_2$.

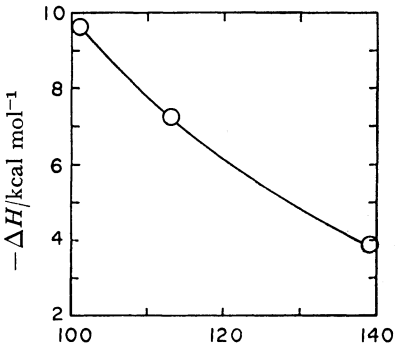

Fig. 3. Relationsflip between $-\Delta H_{0,1}$ for the reaction $BH^+ + H_2 = BH^+(H_2)$ and proton affinity for molecule B as H_2, N_2 and CO. See text.

The values of enthalpy change $\Delta H_{1,0}$ (Table 1) give the order $\Delta H(H_3^+\cdots H_2) > \Delta H(N_2H^+\cdots H_2) > \Delta H(HCO^+\cdots H_2)$, *i.e.*, the order of the hydrogen molecule affinity for each protonated species is $H_3^+ > N_2H^+ > HCO^+$. The order is opposite that of proton affinities of H_2, N_2, and CO, which are 101.0, 113.7, and 139.1 kcal/mol, respectively.[9] The relationship between proton affinities and $-\Delta H_{0,1}$ is shown in Fig. 3. For all Reactions 1, 3, and 7, the solvent molecule is hydrogen which interacts nucleophilicly with each protonated molecule. If the positive charge is more delocalized in the protonated species, the interaction of the solvent molecule with the ion should be weaker, and *vice versa*. The larger proton affinity indicates that the positive charge is more dispersed in the protonated species, and the following clustering step should be less favorable (Fig. 3). This is also the case for polar molecules which have a strong tendency to hydrogen bonding. Water has been known as the best solvent for proton. However, the proton affinity of water is the lowest among all other oxygen containing hydrocarbons.[10]

The Structure of $N_2H^+(H_2)$ and $N_2H^+(H_2)_2$. The characteristic enthalpy changes for Reactions 3—6 led to the prediction of the structure of $H_3^+(H_2)_n$.[4] For the present clustering Reactions 1 and 2, the big drop of $-\Delta H_{n-1,n}$ seems somewhat unusual. A theoretical calculation predicts that N_2H^+ has a linear equilibrium geometry.[11] However, no theoretical work has been carried out on the structure of $N_2H^+(H_2)_n$ for $n=1$. Tentatively two possible structures are suggested (Fig. 4), a solvent hydrogen molecule interacting with the terminal hydrogen atom in structure(a), and with the central nitrogen atom in structure(b). From the large electronegativity of a nitrogen atom and the relatively low proton affinity of a nitrogen molecule, an appreciable amount of positive charge is considered to be on the hydrogen atom in N_2H^+. Because of the smaller size of the hydrogen atom, the nucleophilic interaction between a solvent hydrogen molecule and the terminal hydrogen atom may be stronger than that between a solvent hydrogen molecule and the central nitrogen atom. We would like to suggest that the cluster ion(a) would be the most stable isomer of the cluster ion $N_2H^+(H_2)$. In (a), the proton is sandwiched between N_2 and H_2 molecules. In such a structure, the potential energy curve for the proton may have double potential minima.[12] Since the proton affinity of nitrogen is larger than that of hydrogen, the proton in $N_2H^+(H_2)$ should be closer to the nitrogen molecule (Fig. 4(a)).

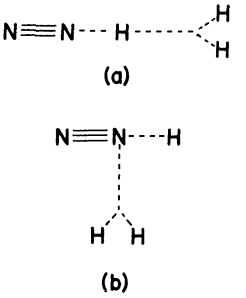

Fig. 4. Possible structures of cluster $N_2H^+(H_2)$,

When the cluster ion $N_2H^+(H_2)$ has structure(a), the second incoming hydrogen molecule would interact either with the central hydrogen atom or the nitrogen atom adjacent to the central hydrogen atom. In either case, the nucleophilic interaction would be much weaker than that for the first clustering step, since the positive charge is already dispersed in $N_2H^+(H_2)$. This might explain the big drop of the enthalpy changes for Reactions 1 and 2.

$N_2H^+(H_2)_2$ has the same chemical formula as the protonated hydrazine, $N_2H_5^+$. From a comparison of heat of formation of $N_2H^+(H_2)_2$ and $N_2H_5^+$, it can easily be shown that the cluster ion $N_2H^+(H_2)_2$ does not have the structure of protonated hydrazine. The heat of formation of $N_2H^+(H_2)_2$ can be obtained from the proton affinity of N_2 and the enthalpy changes of Reactions 1 and 2 as 244.6 kcal/mol. So far no proton affinity of hydrazine has been measured. The proton affinity of hydrazine is considered to be equal or larger than that of ammonia (202 kcal/mol) because of the inductive effect of $-NH_2$ group. Thus the heat of formation of the protonated hydrazine should be $\leqq$187.8 kcal/mol. The difference between these two values is large enough to conclude that $N_2H^+(H_2)_2$ and $N_2H_5^+$ are structural isomers. Although the reaction of the formation of protonated hydrazine, $N_2H^+(H_2) + H_2 = N_2H_5^+$, is highly exothermic ($\approx$60 kcal/mol), it must have a large free energy barrier, *i.e.*, an activation energy barrier as well as an entropy barrier, since the reaction sould undergo the rearrangement of atoms.

Entropy Change. The entropy of a molecule in the gas phase is given by

$$S = S_t + S_r + S_v + S_e \qquad (2)$$

where S_t, S_r, S_v, and S_e are translational, rotational, vibrational and electronic entropy, respectively. The

contribution of the electronic entropy S_e is usually negligible at normal temperatures. The translational entropy is evaluated by

$$S_t = \frac{3}{2}R\ln M + \frac{5}{2}R\ln T - R\ln P - 2.315 \quad (3)$$

where R, M, T, and P are gas constant, molecular weight in atomic unit, temperature, and gas pressure in atmospheric pressure unit, respectively. The rotational entropy for a linear molecule and that for a non-linear molecule are respectively given by the equations

$$S_r = R\ln I + R\ln T - R\ln\sigma + 177.671 \quad (4)$$

$$S_r = \frac{R}{2}\ln I_A I_B I_C + \frac{3}{2}R\ln T - R\ln\sigma + 267.644 \quad (5)$$

where I and σ are the moment of inertia and the symmetry number of the molecule, respectively. The vibrational entropy is given by

$$S_v = R\sum_i\left[-\ln(1-\exp(-h\nu_i/kT)) + \frac{h\nu_i/kT}{\exp(-h\nu_i/kT)-1}\right] \quad (6)$$

where ν_i is the frequency of the i-th fundamental vibration.

The translational entropy change which is by far the most important term is readily evaluated for Reaction 1 by means of the Sackur-Tetrode equation

$$\Delta S_t = \frac{3}{2}R\ln\frac{M_3}{M_1\cdot M_2} - \frac{5}{2}R\ln T + R\ln P + 2.315 \quad (7)$$

where M_1, M_2, and M_3 are the molecular weights of N_2H^+, H_2, and $N_2H^+(H_2)$, respectively. Substituting 265 K for T, we obtain $\Delta S_t = -27.3$ e.u. The temperature 265 K corresponds to the average in the temperature range of the van't Hoff plot from which $\Delta H_{0,1}$ and also $\Delta S_{0,1}$ were obtained (Fig. 2).

In order to evaluate the rotational entropy change, we should know the structure of N_2H^+ and $N_2H^+(H_2)$. The linear structure of N_2H^+[11] theoretically predicted leads to the moment of inertia of $N\equiv N\cdots H^+$ of 1.74×10^{-39} g·cm². The following assumptions will be made for the possible structures of $N_2H^+(H_2)$ shown in Fig. 4. Since the $N_2H^+\cdots H_2$ ion consists of weakly bonded N_2H^+ and H_2, the vibrational modes in H_2 and N_2H^+ would be essentially preserved in $N_2H^+\cdots H_2$. The distance between H atom and H_2 in structure(a), and N atom and H_2 in structure(b) is 1.9 Å. This value is adopted on the basis of the theoretical calculation done by Yamabe, Hirao and Kitaura.[13] They predicted the bond distance $H_3^+\cdots H_2$ of 1.857 Å. Since the bond energy of $H_3^+\cdots H_2$ (9.6 kcal/mol) is of the same order as that of $N_2H^+\cdots H_2$ (7.2 kcal/mol), the predicted value would not be in large error. Actually, the calculated rotational entropy changes are rather insensitive to a small change in the molecular structure. Substitution of these values in Eqs. 4 and 5 leads to $\Delta S_r = 1.3$ e.u. for the cluster ion(a) and $\Delta S_r = 4.2$ e.u. for the cluster ion(b). The total entropy change $\Delta S_{0,1}$ experimentally determined is -22.6 e.u., indicating that $\Delta S_v \approx 3$ e.u. for the formation of the cluster ion(a) and $\Delta S_v \approx 1$ e.u. for that of the cluster ion(b). The new vibrational modes in $N_2H^+(H_2)$ can be represented by a rocking motion with ω_1 in which alternately one end of H_2 and then the other swings toward N_2H^+, a nearly free internal rotation with ω_2 of H_2 around the bond $N_2H^+\cdots H_2$, a bond stretching vibration ω_3, and two normal bending vibrations ω_4 and ω_5. Salmon and Poshusta[14] have estimated $\omega_1\approx\omega_2\approx 200$ cm^{-1} and $\omega_4\approx\omega_5\approx 50$ cm^{-1} for $H_3^+\cdots H_2$. Frequencies of 50 and 200 cm^{-1} lead to vibrational entropy changes of -1.8 and -2.44 e.u. at 265 K, respectively. If the values are used for vibrations in $N_2H^+\cdots H_2$, the four vibrations lead to $\Delta S_v = -8.5$ e.u. Evidently the actual vibrations in $N_2H^+\cdots H_2$ should be considerably milder than the predicted vibrations in $H_3^+\cdots H_2$. Certain vibrations with the frequency of 30 cm^{-1} ($\Delta S_v \approx 1.6$ e.u) or less and the near free internal rotation of H_2 ($\Delta S_v \approx 2$ e.u.) should be taken into consideration in order to explain the estimated ΔS_v.

A number of assumptions would be required for the evaluation of the entropy change for Reaction 2. The translational entropy change $\Delta S_{1,2}$ calculated by Eq. 7 is -21.9 e.u. at 90 K. The temperature 90 K corresponds to the average in the temperature range of the van't Hoff plot for Reaction 2. The total entropy change $\Delta S_{1,2}$ experimentally determined is -14.0 e.u., indicating that $\Delta S_r + \Delta S_v = 7.9$ e.u. We obtain $\Delta S_r \approx 1$ e.u. by assuming several structures of $N_2H^+(H_2)_2$ in which an additional hydrogen molecule interacts with clusters(a) and (b) with the bond length of 2 Å. This value leads to the value of 7 e.u. for ΔS_v. The large positive value of the predicted vibrational entropy change strongly suggests that bonds in $N_2H^+(H_2)_2$ are very loose, additional hydrogen molecules having a large freedom of motion in the cluster ion.

The author is greatly indebted to Professor P. Kebarle for valuable discussions and for the use of the high pressure mass spectrometer.

References

1) P. Kebarle and E. W. Godbole, *J. Chem. Phys.*, **39**, 1131 (1963).

2) Proton hydrates had been spectrometrically observed earlier in flames; P. F. Knewstubb and T. M. Sugden, *Proc. R. Soc. London, Ser. A*, **255**, 520 (1960), field emission; H. D. Beckey, *Z. Naturforsch. A*, **15**, 822 (1960), and gas discharges; P. F. Knewstubb and A. W. Tickner, *J. Chem. Phys.*, **38**, 464 (1963).

3) P. Kebarle, "Ions and Ion Pairs in Organic Reactions," ed by M. Szwarc, Wiley, New York, N. Y. (1972); P. Kebarle, "Ion-Molecule Reactions," ed by J. L. Franklin, Plenum Press, New York, N. Y. (1972); P. Kebarle, *Ann. Rev. Phys. Chem.*, **28**, 445 (1977).

4) K. Hiraoka and P. Kebarle, *J. Chem. Phys.*, **62**, 2267 (1975).

5) K. Hiraoka and P. Kebarle, *J. Am. Chem. Soc.*, **97**, 4179 (1975).

6) A. J. Cunningham, J. D. Payzant, and P. Kebarle, *J. Am. Chem. Soc.*, **94**, 7627 (1972).

7) K. Hiraoka and P. Kebarle, *J. Chem. Phys.*, **63**, 746 (1975).

8) K. Hiraoka and P. Kebarle, *J. Chem. Phys.*, **63**, 1688 (1975).

9) D. K. Bohme, "Interactions between Ions and Molecules," ed by P. Ausloos, Plenum Press, New York, N. Y. (1975).
10) R. Yamdagni and P. Kebarle, *J. Am. Chem. Soc.*, **98**, 1320 (1976).
11) N. L. Summers and J. Tyrrell, *Theor. Chim. Acta*, **47**, 223 (1978).
12) This prediction is based on theoretical calculations done by W. P. Kraemer and G. H. F. Diercksen, *Chem. Phys. Lett.*, **5**, 463 (1970).
13) S. Yamabe, K. Hirao, and K. Kitaura, *Chem. Phys. Lett.*, **56**, 546 (1978).
14) W. I. Salmon and R. D. Poshusta, *J. Chem. Phys.*, **59**, 4867 (1973).

An Empirical Relation between the Quenching Cross-sections of Metastable Argon and the Molecular Diameter of the Quenchers

Kazuhiro MATSUBARA, Yoshitsugu OONO,* Shoichi KAI,** and Yukio NISHIMURA

Research Institute of Industrial Science, Kyushu University, Fukuoka 812

***Department of Electronics, Kyushu University, Fukuoka 812*

(Received October 4, 1978)

For polyatomic quenchers there is a fairly accurate linear relation between $\sigma_Q^{1/2}$ and r, where σ_Q is the quenching cross-section of rare gas metastables (especially $Ar(^3P_2)$) and r, the effective radius of the quencher.

The quenching process for metastable rare gas atoms by neutral molecules is one of the simplest and most elementary chemical reactions. So far many workers have studied the quenching cross-sections, σ_Q (esp. for metastable argon), and also discussed the quenching mechanism.[1-5] However, as will be summarized in the next section, there seems to have been no definite conclusion as to the quenching mechanism. All the theoretical approaches are also unsuccessful.[6] Therefore, what we should do first is to study the existing experimental data systematically and to search for empirical laws. As will be mentioned in the next section, some attempts of this kind have already been done, but the empirical laws they have proposed are not sufficiently quantitative.

The purpose of the present paper is to give a much more quantitative empirical law than has ever been reported: a linear relation between $\sigma_Q^{1/2}$ (esp. for metastable argon) and the effective diameter of the quencher. Empirical laws of this type for several gaseous processes have already been given in a previous paper.[7] Our study shows that diatomic quenchers and polyatomic quenchers are rather clearly different. All the quenching cross-sections cited in this paper are those obtained from $k/\bar{v}$, where k is the rate constant and $\bar{v}$, the mean velocity of the colliding particles.

TABLE 1. THE QUENCHERS CONSIDERED IN THIS REPORT

Mono- and diatomic quenchers
1: Krypton, 2: Xenon, 3: Hydrogen, 4: Deuterium, 5: Nitrogen, 6: Carbon monoxide, 7: Nitrogen monoxide, 8: Oxygen, 9: Hydrogen chloride, 10: Hydrogen bromide, 11: Hydrogen iodide, 12: Chlorine, 13: Bromine, 14: Iodine monochloride,

Polyatomic quenchers
15: Water, 16: Ammonia, 17: Methane, 18: Dinitrogen oxide, 19: Carbon dioxide, 20: Methanol, 21: Acetylene, 22: Ethylene, 23: Ethane, 24: Acetaldehyde, 25: Hydrogen sulfide, 26: Nitrosyl chloride, 27: Chloromethane, 28: Carbonyl sulfide, 29: Sulfur dioxide, 30: Propane, 31: Propionaldehyde, 32: Isobutane, 33: Butane, 34: Benzene, 35: Carbon disulfide, 36: Dichloromethane, 37: 1-Butanol, 38: Phenol, 39: Bromomethane, 40: Pentane, 41: Toluene, 42: Benzaldehyde, 43: Chlorobenzene, 44: Chloroform, 45: *o*-Xylene, 46: *m*-Xylene, 47: *p*-Xylene, 48: 1-Hexanol, 49: *p*-Chlorotoluene, 50: 1-Naphthol, 51: 2-Naphthol, 52: Phosphorus trichloride, 53: *o*-Dichlorobenzene, 54: Carbon tetrachloride, 55: Iodomethane,

Fluorine-containing quenchers
56: Fluorine, 57: Nitrosyl fluoride, 58: Fluorine oxide, 59: Fluoromethane, 60: Nitrogen trifluoride, 61: Fluoroform, 62: Carbon tetrafluoride, 63: Trifluoromethoxy fluoride, 64: Dinitrogen tetrafluoride, 65: Thionyl fluoride, 66: Sulfur hexafluoride, 67: *p*-Fluorotoluene

Summary of the Present View on the Quenching Mechanism

Bourène and Calvé suggested that the ionization potential, I, is relevant to σ_Q from the fact that there is a rough inverse relation between σ_Q and I. As will be discussed later, this suggestion does not hold. Moreover, there is an experiment[8] showing that the ionization process does not contribute to the quenching process of $Ar(^3P_2)$. Bourène and Calvé[3] also suggested that the dispersion force is relevant and obtained a rough linear relation between σ_Q and the polarizability, α_Q, of the quencher. We reexamined this plot and obtained an approximate relation, $\sigma_Q \propto \alpha_Q^{2/3}$ (Fig. 1). However, if α_Q governs σ_Q, a dimensional analysis asserts that $\sigma_Q \propto \alpha_Q^{1/3}$. Hence, their second suggestion is also doubtful. Later we will see that the empirical relation just mentioned is one derivable from other empirical relations which appear more fundamental.

Setser *et al.*[1,2,8] have been studying the quenching

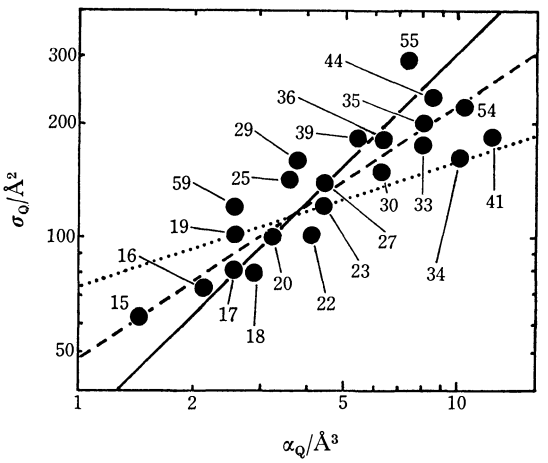

Fig. 1. The relation between σ_Q for $Ar(^3P_2)$ and the polarizability α_Q of quenchers. The slope of the lines are: ——1,– – –2/3,·····1/3. Thus the line with the slope 1/3 (which is suggested by a dimensional analysis or quantum mechanical considerations) does not fit the data, which are taken from Ref. 3. The line with the slope 2/3 best fits the data. The data for α_Q are taken from Ref. 11. All the numbers correspond to those in Table 1.

process extensively; they have also considered quenching mechanisms. Their conclusions thus far are summarized in Ref. 6. They plotted log σ_Q *vs.* log C_6, where C_6 is the van der Waals coefficient, and obtained a linear relation with a unit slope. Their experiments showed that the nature of the product channel is irrelevant to σ_Q. Therefore, they suggested that σ_Q is determined by the long-range forces in the entrance channel. Hereafter we will interpret the long-range interaction as the interaction which does not include the direct repulsive interaction due to the molecular core, *i.e.*, the overlap of electron clouds. As is the case of σ_Q *vs.* α_Q, however, the slope of the log σ_Q *vs.* log C_6 plot apparently contradicts the mechanism suggested (a dimensional analysis shows $\sigma_Q \propto C_6^{1/3}$). King and Setser[6] suggested that this contradiction is either because the long-range forces are not properly represented by C_6, or because the probability of quenching increases in a systematic way, making the slope larger than 1/3. Thus, they seem to assert that the relevant mechanism is due to long-range interactions (esp. dipole-dipole interaction). However, apart from the *ad hoc* nature of their explanation of the value of the slope, the long-range-force mechanism contradicts the facts that σ_Q for $Ar(^3P_2)$ and that for $Ar(^1P_1)$ have the same order of magnitude and that permanent dipoles are irrelevant to σ_Q, as will be shown below (Fig. 6).

Thus, we may conclude that there is no conclusive view on the quenching mechanism of metastable rare gas atoms.

Phenomenological Survey of the Quenching Process

As was discussed in the introductory part of this paper, the $\sigma_Q \propto \alpha_Q^x$ ($x \approx 2/3$) and $\sigma_Q \propto C_6^y$ ($y \approx 1$) relations afford universal phenomenological relations independent of the detailed nature of the quenchers. However, these relations are not sufficiently quantitative.

It has been shown[7] that the effective hard-core radius of the molecule, r, appearing in the statistical mechanics of liquids can be successfully used as the representative length of the molecules in gaseous reactions. Therefore, it is natural to try to find the relation between r and σ_Q. It is known that r is a good measure of the radius of the repulsive core of molecules, *i.e.*, a good measure of the effective radius of the electron cloud of molecules. A dimensional analysis suggests a linear relation between $\sigma_Q^{1/2}$ and r. As a convenient measure of r, we adopted $r_w = (3V_w/4\pi N)^{1/3}$, where V_w is the van der Waals volume of the quencher, which is calculated by using the tables of Bondi,[9] and N, the Avogadro constant. A linear relation holds between r and r_w, as has been shown in Ref. 10. First, we will consider $Ar(^3P_2)$.

Figure 2 shows the linear relation for polyatomic molecules involving only atoms belonging to the first and second periods of the periodic table. The linear relation is much more accurate than any previously reported. Note that the plot is not a log-log one, in contrast to the relations previously obtained. This linear relation, however, does not hold accurately for quenchers containing sulfur, bromine, *etc.* Still, we can

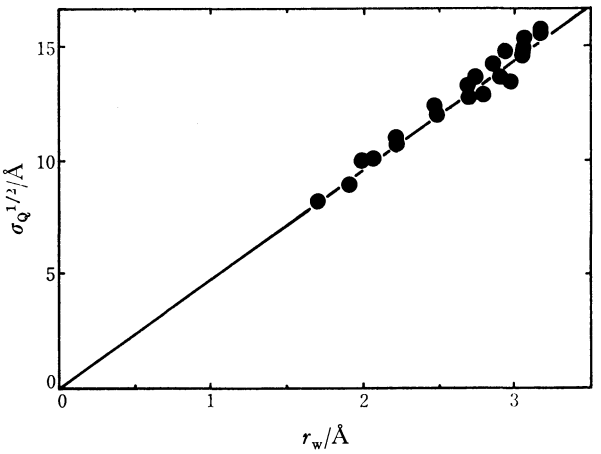

Fig. 2. The linear relation between r_w (see the text) and $\sigma_Q^{1/2}$ for polyatomic quenchers consisting of atoms belonging to the first and second periods of the periodic table. The data are taken from Ref. 4.

get a universal linear law similar to it. For this purpose we systematically modify the van der Waals volumes allotted to the larger atoms as follows: for the atoms belonging to the $(n+2)$-th ($n>0$) period of the periodic table, the modified van der Waals volume, V_w', is related to that of Bondi[9] as $V_w' = (1.7)^n V_w$. This modification seems to reflect the extension of the outermost shell of atoms, but we cannot give a clear physical meaning for it. At any rate, by this modification of the van der Waals volume allotted to the larger atoms, we get the linear relation shown in Fig. 3 for all polyatomic quenchers except those containing fluorin atoms. The accuracy of the linear relation is excellent. The effect of the modification of the van der Waals volumes is shown in Fig. 4. As may clearly be seen from Fig. 5, the diatomic quenchers and the polyatomic quenchers

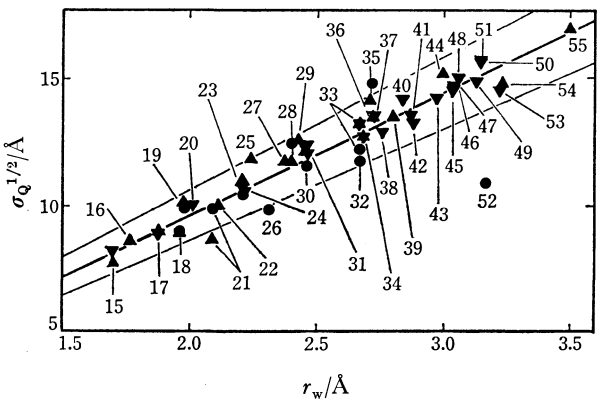

Fig. 3. The linear relation between r_w and $\sigma_Q^{1/2}$. r_w is calculated from the modified van der Waals volumes in the text. The line denotes $\sigma_Q^{1/2} = 4.80\, r_w$. The thin lines show $\sigma_Q^{1/2} = (4.80 \pm 0.48)\, r_w$. Thus our empirical relation is very accurate than those so far obtained. All the numbers in the figure correspond to those in Table 1. The data are taken from Refs. 1, 2 (●), Ref. 3 (▲), and Ref. 4 (▼). The quenchers containing fluorine atoms deviate from the linear law wildly. This suggests that the quenching mechanism for these compounds are different from other quenchers.

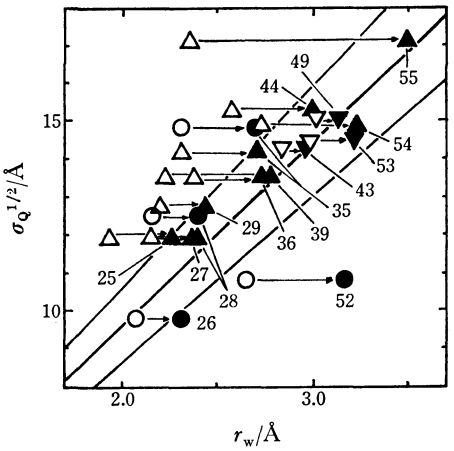

Fig. 4. The effect of the modification of the van der Waals volumes. Open symbols show the $\sigma_Q^{1/2}$ *vs.* r_w relation before the modification of the van der Waals volumes and solid symbols show that after the modification. All the numbers correspond to those in Table 1. Triangles and circles correspond to those in Fig. 3.

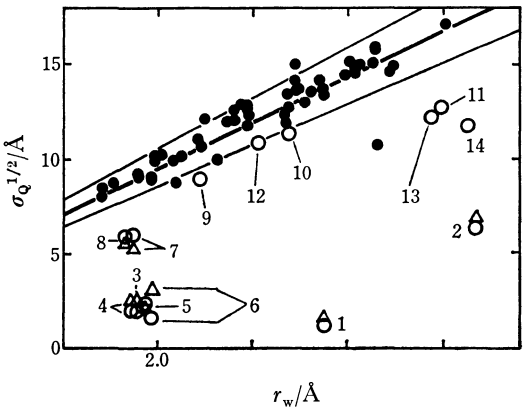

Fig. 5. The $\sigma_Q^{1/2}$ *vs.* r_w relation for mono- and diatomic quenchers. The σ_Q of these quenchers are systematically smaller than those of polyatomic quenchers (denoted by solid symbols). All the numbers correspond to those in Table 1.

Table 2. Irrelevance of the polarizability α_Q (Å^3) to whether or not $\sigma_Q^{1/2} \propto r_w$ holds

Although King and Setser[6] suggested that the quenchers with smaller α_Q values are different from other quenchers, their suggestion does not hold. In the table, the numbers in parentheses show the α_Q values in Å^3.

Mono- and diatomic quenchers		Polyatomic quenchers	
O_2	(1.57)		
N_2	(1.74)	H_2O	(1.45)
NO	(1.70)		
CO	(1.94)	NH_3	(2.16)
Kr	(2.48)	CO_2	(2.59)
HCl	(2.58)	CH_4	(2.56)
HBr	(3.49)	H_2S	(3.61)
		SO_2	(3.78)
		CH_3OH	(3.25)

are different. This difference could not be found, though, as long as we had only the rough empirical laws mentioned above.

The difference cannot be ascribed to that of the number of (valence) electrons nor to that of the ionization potential (see also the next section). Furthermore, although the magnitude of the polarizability may seem relevant, as has been suggested by Setser *et al.*, α_Q has no direct effect on whether $\sigma_Q^{1/2} \propto r$ holds or not (Table 2). Therefore, in so far as we base our conclusions on the existing data, the most natural conclusion is that the number of nuclei in the quencher is relevant to the quenching process (mechanism). This further suggests that the number of vibrational degrees of freedom of the quencher is relevant.

Irrelevance of Other Quantities

The irrelevance of other quantities, such as the permanent dipole moment, the ionization potential, *etc.*, to the quenching mechanism can be seen as follows. Possible relevant quantities, other than r, may include the reduced mass, μ, of colliding particles; the de Broglie wave length, λ; the permanent dipole moment, D; the ionization potential, I; the initial relative velocity, $v(=(3kT/\mu)^{1/2})$, and the initial kinetic energy, $E(=3kT/2)$. A dimensional analysis implies the following functional relation:

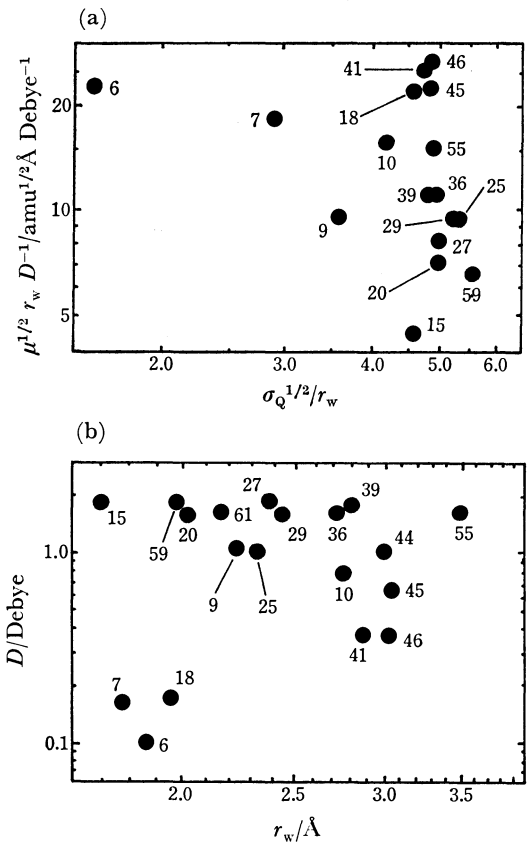

Fig. 6. Irrelevance of dipole moment D of quenchers. (a) Shows that there is no direct relation between D and σ_Q. (b) Shows, furthermore, that D is irrelevant to r_w. Therefore there is no indirect relation between D and σ_Q either.

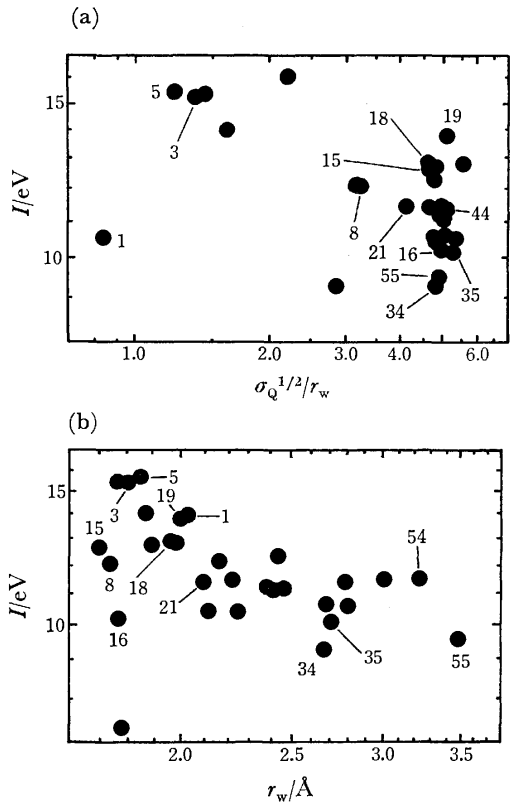

Fig. 7. Irrelevance of the ionization potential I of quenchers. (a) Shows that there is no direct relation between I and σ_Q. Although (b) shows a vague correlation between r_w and I (this is the reason why Bourène and Calvé suggested the relevance of I), but (a) and (b) show that I is substantially irrelevant to σ_Q. All the numbers correspond to those in Table 1. The data for I are taken from Ref. 2.

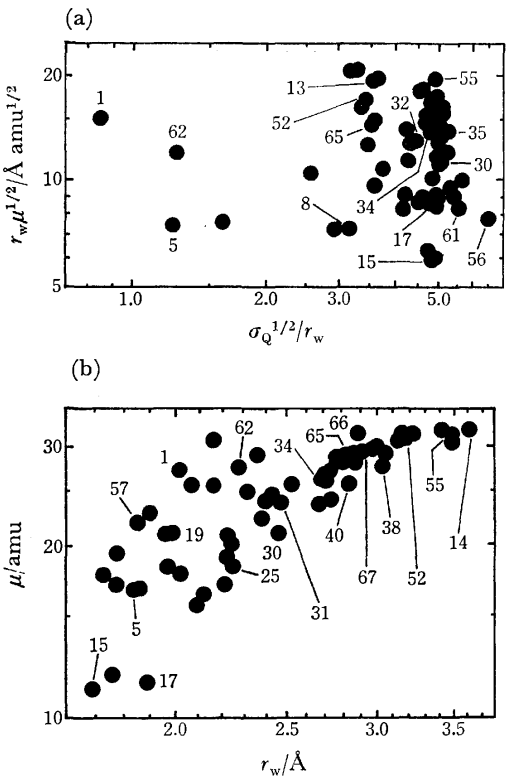

Fig. 8. Irrelevance of the reduced mass μ or the de Broglie wavelength of quenchers. (a) Shows that there is no direct relation between μ and σ_Q. Of course, as is shown in (b), there is a positive correlation between μ and r_w, but the comparison of the scattered distribution of points in (b) and fairly compact distribution of points in (a) implies that reduced mass (and de Broglie wave length) are irrelevant to σ_Q. All the numbers correspond to those in Table 1.

$$\sigma_Q^{1/2} = rf(\lambda/r,\ I,\ D^{1/2}/\mu^{1/2}r,\ \cdots)$$

where constant dimensional quantities are suppressed. All the existing data are obtained from experiments performed under almost the same E (or T). Figures 6—8 show that all the quantities other than r have no direct relevance to σ_Q. The irrelevance of the permanent dipole moment is evidence that the interaction due to the so-called long-range forces has no direct effect on σ_Q, as we suggested at the beginning of this paper.

Discussion

It may seem quite curious that the number of nuclei in the quencher is relevant. There is a possibility that the relevance is explained by the relation between the stochasticity of the motion of a nonlinear oscillator and its number of degrees of freedom. The stochasticity of the internal motion of the quencher enhances its quenching ability. Diatomic quenchers never exhibit stochastic internal motion, so that the quenching cross-section is smaller than would be expected from the empirical law for polyatomic molecules. This explanation is mere speculation, but it is fascinating because there is a growing interest in the chaos appearing in dynamical systems with even a small number of degrees of freedom.

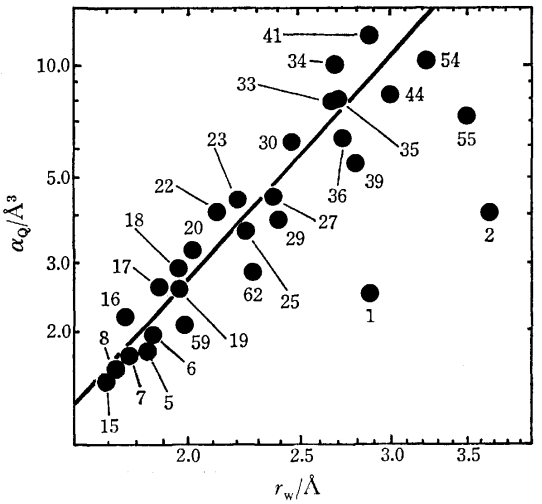

Fig. 9. The relation between modified r_w and the polarizability α_Q. The slope of the line is 3, *i.e.*, $\alpha_Q \propto r_w^3$. α_Q are taken from Ref. 11. All the numbers correspond to those in Table 1.

A close examination of σ_Q suggests that there is some effect of the shape of the quencher. For the series of quenchers with the same van der Waals volume, we have the order of: butane>isobutane and *p*-xylene>

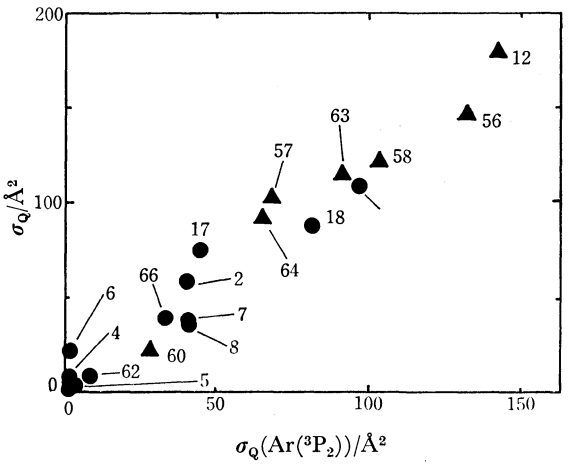

Fig. 10. The relation between the quenching cross sections of $Ar(^3P_2)$ and $Ar(^3P_0)$[1] (●) or Kr $(^3P_2)$[2] (▲). All the numbers correspond to those in Table 1.

m-xylene>*o*-xylene. Thus, the deviation from the spherical shape increases σ_Q slightly. These deviations are, however, very small, and the main feature is that σ_Q is governed by the effective radius of the quencher.

The empirical relation, $\sigma_Q \propto \alpha_Q^{2/3}$, mentioned earlier is derived from $\sigma_Q^{1/2} \propto r_w$ and the empirical relation $\alpha_Q \propto r_w^3$ shown in Fig. 9.

Figure 10 suggests that the quenching mechanisms for $Ar(^3P_2)$ and $Ar(^3P_0)$ or $Kr(^3P_2)$ are the same. However, since only a few results are known for $Kr(^3P_2)$ for polyatomic quenchers, we cannot make a $\sigma_Q^{1/2}$ *vs.* r_w plot. It seems that the same conclusion can be drawn for $Xe(^3P_2)$, but there are not sufficient data in this case, either. For $He(2^1S)$, as was shown in a previous paper,[7] no universal relation between σ_Q and r was found.

One of the authors (Y. O.) is grateful to Dr. M. Tsuji for informing him of Ref. 1—3. He would also like to thank Professor K. Hirakawa and Professor T. Oyama for their stimulating discussions and encouragement.

References

1) L. G. Piper, J. E. Velazco, and D. W. Setser, *J. Chem. Phys.*, **59**, 3323 (1973).
2) J. E. Velazco, J. H. Kolts, and D. W. Setser, *J. Chem. Phys.*, **65**, 3468 (1976).
3) M. Bourène and J. Le Calvé, *J. Chem. Phys.*, **58**, 1452 (1973).
4) H. J. De Jong, *Chem. Phys. Lett.*, **25**, 129 (1974).
5) A. L. Schmeltekopf and F. C. Fehsenfeld, *J. Chem. Phys.*, **53**, 3173 (1970).
6) D. L. King and D. W. Setser, *Ann. Rev. Phys. Chem.*, **27**, 407 (1976).
7) Y. Oono and Y. Nishimura, *Bull. Chem. Soc. Jpn.*, **50**, 1379 (1977).
8) L. A. Gundel, D. W. Setser, M. A. A. Clyne, J. A. Coxon, and W. Nip, *J. Chem. Phys.*, **64**, 4390 (1976).
9) A. Bondi, *J. Phys. Chem.*, **68**, 441 (1964).
10) Y. Oono, *Bull. Chem. Soc. Jpn.*, **48**, 2270 (1975).
11) E. W. Rothe and R. B. Bernstein, *J. Chem. Phys.*, **31**, 1619 (1959).

The Electronic Spectra and Nonaqueous Oxidation and Reduction Potentials of Azoxybenzenes, and Their Mutual Correlation

Tanekazu KUBOTA,* Hiroshi MIYAZAKI, Masumi YAMAKAWA, Kiyoshi EZUMI, and Yoshiko YAMAMOTO

Shionogi Research Laboratory, Shionogi and Co., Ltd., Fukushima-ku, Osaka 553

(Received October 20, 1978)

The near-ultraviolet absorption spectra of various *p,p'*- and *m,m'*-disubstituted azoxybenzenes were recorded in aprotic and protic solvents. The PPP-SCFMO-CI calculation was used in analyzing the spectra and the solvent effect on them. The π-π^* bands of azoxybenzene could be well interpreted on the basis of the electronic structure of benzaldehyde *N*-phenyl oxime (a nitrone). In addition, the half-wave potentials of reduction ($E_{1/2}^{red}$) and oxidation ($E_{1/2}^{oxd}$) were also measured in nonaqueous solvents. These electrochemical data and the above spectral data satisfied a good linear relation: $(E_{1/2}^{oxd}-E_{1/2}^{red})=k_1\cdot E_{ho\to lu}^{UV}+k_2$, this equation having been previously proposed by us. In the Appendix, we have discussed the physical meaning of the constant term, k_2, from the quantitative standpoint, using a series of alternant hydrocarbons as a typical example. Finally, a good linear relation between the $E_{1/2}^{red}$ or $E_{1/2}^{oxd}$ values and the substituent constants was demonstrated and discussed in azoxybenzenes.

So far the electronic spectra and the electronic states of multifarious aromatic amine oxides have been extensively studied experimentally and theoretically in singlet, doublet, and triplet states.[1] Various kinds of experimental techniques have also been used in the studies.[1] However, as far as we know, there have been only a few discussions of the electronic state of azoxybenzenes (AOB's),[2-6] which are classified as one of the aromatic amine oxides. In this report, the electronic spectra and the half-wave potentials of the oxidation ($E_{1/2}^{oxd}$) and reduction ($E_{1/2}^{red}$) of various substituted AOB's have been systematically examined from the viewpoint of experimental and theoretical treatments. For the $E_{1/2}^{oxd}$ and $E_{1/2}^{red}$ values, the interrelation of the half-wave potentials and the electronic spectra is also discussed.[7]

Experimental

Spectral and Polarographic Measurements. The absorption

TABLE 1. SUBSTITUTED AZOXYBENZENES INVESTIGATED, WITH THEIR SYNTHETIC AND PURIFICATION METHODS, MELTING POINTS, AND DIPOLE MOMENTS

Substituent[e]	Mp[b] °C	Dipole moment (D.U.)[c]	Synthesic method[a]	Refining method[d]
H(=AOB)	37(34.5—35.5)[10]	1.93(1.72, 1.57)[14]		R
4,4'-$[N(CH_3)_2]_2$	249—250(252)[11]		B	R
4,4'-$(OCH_3)_2$	119.5—120.5(116.5—118.5)[10]			R
4,4'-$(OC_2H_5)_2$	138—139			R
4,4'-$(CH_3)_2$	71.0—71.5(66—68)[10]		A	R
4,4'-Cl_2	157.5—157.8(154—156)[10]	1.76	A	T
4,4'-$(COOC_2H_5)_2$	115.5—116.0		C	R
4,4'-$(CN)_2$	227.5		C	AC
4,4'-$(NO_2)_2$	194.5—195(190—192)[12]		C	TR
m,m'-$(OCH_3)_2$	53.0—53.5	2.66	A	R
m,m'-$(CH_3)_2$	35.0—35.5(33—35)[10]		A	R
m,m'-Cl_2	98.5—99.0(95.5—97)[10]		A	R
m,m'-$(COOC_2H_5)_2$	80.5—81.0		C	R
m,m'-$(CN)_2$	134.5—135.5		C	R
3,3'-$(NO_2)_2$	149(143)[3]	4.74		T

a) The compounds designated by A, B, and C were synthesized according to Refs. 10, 11, and 12 in the text respectively. The others were commercially available. b) The melting points are uncorrected. The values in parentheses were taken from the literature in the text. c) Measured at 25 °C in dioxane.[13] The values in parentheses were taken from Refs. 14a (1.57: 27 °C, benzene) and 14b (1.72: 22 °C, benzene). d) R: Recrystallized from ethanol except for *m,m'*-$(CN)_2$ and 4,4'-$[N(CH_3)_2]_2$, where benzene and chloroform were suitable as the solvents respectively. T: Purified by preparative thin-layer chromatography. For 4,4'-Cl_2 it was developed with heptane and then recrystallized from ethanol. For 3,3'-$(NO_2)_2$, benzene was used for both the development and the recrystallization. AC: Alumina column chromatography was used for 4,4'-$(CN)_2$. Elution was made first with benzene and then with a benzene(1)–ether(1) mixture, the latter portion being recrystallized from ethanol. TR: Although purification was tried repeatedly by thin-layer chromatography (TLC) and by recrystallization for this compound, its purity was not sufficient judging from the TLC and the elemental analyses. Its purity, however, may be about 95%. e) See text and Ref. 50.

spectra were recorded in the usual manner with a Beckman DK-2A Far-UV spectrometer at room temperature. The organic solvents used were CCl_4, CH_2Cl_2, CH_3CN, heptane, ethanol, and methanol, all of which were spectrograde in purity. They were desiccated sufficiently with a suitable drying agent, such as $CaCl_2$, Na, or Mg ribbon, and then carefully rectified.[1b,d] The electrochemical data were obtained using the polarographic technique, whose details have been described in a previous paper.[7a] The DC and AC polarograms were measured with a Yanagimoto polarograph, Model P8-AP (three-electrode system), a saturated calomel electrode (SCE) being used as the reference electrode. The capillary used for the dropping mercury electrode to yield the $E_{1/2}^{red}$ was: $m=0.855$ mg/s and $t=5.17$ s at $h=70$ cm in distilled water at an open circuit. Alternatively, the $E_{1/2}^{oxd}$ values were obtained with a rotating platinum electrode, the type and the manipulation of which are exactly the same as in our previous report.[7a] All the experiments were carried out at 25 ± 0.1 °C in *N*,*N*-dimethylformamide (DMF) or CH_3CN containing 0.1 mol dm^{-3} terapropylammonium perchlorate (TNPAP). The method used in the purification of DMF, CH_3CN, and TNPAP was also the same as in our references.[7a,8,9]

Samples. The substances employed here are listed in Table 1 along with their synthetic and purification methods and the melting points. The compounds whose preparation method and physical constants have not yet been reported were synthesized and purified by applying the methods of similar substances known already (see Table 1). The structure and purity of the samples were checked by means of TLC, IR, UV, dipole moment, and elemental analyses. A good agreement was obtained between the calculated and experimental values of elemental analyses except for the 4,4′-dinitroazoxybenzene, the purity of which is less than the others. The structure of the AOB's synthesized here is well known to be the *trans*-in plane-form, just like [I].

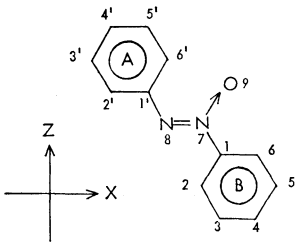

[I]

For the *m*,*m*′-derivatives, however, we could not determine any accurate configuration[50] except for the dinitro derivative, whose NO_2 groups are judged to be in the 3 and 3′ positions from a comparison of the observed (see Table 1) and calculated dipole moments. The latter value is 5.31D, as the vector sum of 1.93D (AOB, whose moment is assumed to be in the direction of the N→O σ moment) and the NO_2 group moment (3.98D)[15] at the 3 and 3′ positions. If two NO_2 groups are in the 5 and 5′ positions, the calculated value is 8.62D.

Results and Discussion

Electronic Spectra of Azoxybenzene Derivatives. As a typical example, the spectrum of AOB is shown in Fig. 1 and compared with that of benzaldehyde *N*-phenyl oxime (BANO: a kind of nitrone),[16] since these are isoelectronic in π-electron systems. It can easily be understood from the figure that the spectra of AOB and BANO are quite similar to each other, especially

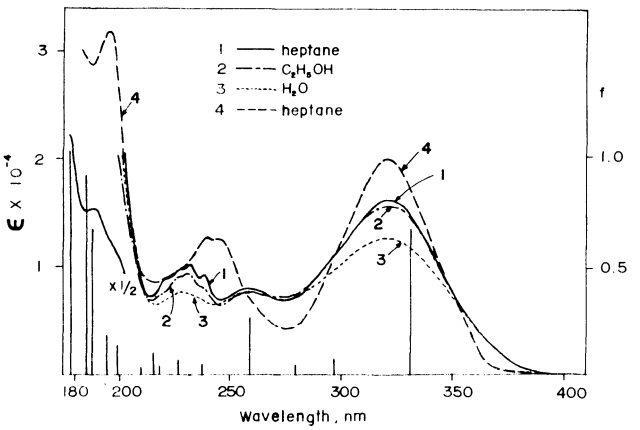

Fig. 1. Electronic spectra of azoxybenzene in aprotic (curve 1) and protic (curves 2 and 3) solvents and of benzaldehyde *N*-phenyl oxime (curve 4) in heptane.

for the characteristic strong π-π^* band appearing in the longest wavelength region, although the bands in the 275—217 nm region is more clearly separated for AOB. This spectral behaviour is very reasonable, as the molecules are the *trans*-in plane-form for both the benzene rings,[17] and suggests that the electronic spectra and the electronic structures of AOB's can be interpreted on the basis of those of BANO previously reported (*vide infra*).[3,16] In the spectra of various substituted AOB's, the spectral pattern of the compounds with electron-donating or electron-accepting substituents at the *p*,*p*′-positions is quite similar to that of AOB, as may be seen in Fig. 2 for 4,4′-bis(dimethylamino)-AOB.

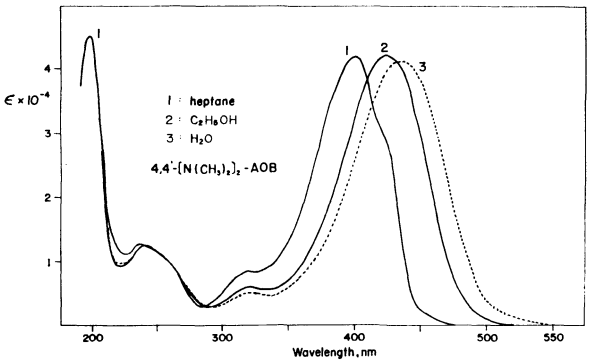

Fig. 2. Electronic spectra of 4,4′-bis(dimethylamino)-azoxybenzene in aprotic (curve 1) and protic (curves 2 and 3) solvents.

For the case of *m*,*m*′-substituents, the weak electron-donating groups like CH_3 and Cl lead also to spectra analogous to that of AOB. On the other hand, if the groups showing quite a large substituent effect are introduced in the *m*,*m*′-positions of AOB, the spectral patterns become very different from that of AOB, as may be understood from Fig. 3. The spectral data are collected in Table 2. Alternatively, the main difference in the spectral behaviour of AOB and BANO is that the well-known blue-shift phenomena found in protic solvents on aromatic amine *N*-oxides including nitrones and nitrile *N*-oxides[18] could not be generally observed

TABLE 2. SPECTRAL AND POLAROGRAPHIC DATA AND SUBSTITUENT CONSTANTS ON VARIOUS SUBSTITUTED AZOXYBENZENES

Compound[j]	First π-π^* band[a]			First wave[b]				First wave[b,e]			Substituent constant[g]	
	λ_{max} (nm)	ε_{max}	$\Delta\tilde{\nu}$[c] (cm^{-1})	$E_{1/2}^{red}$ (volt)[d]	$E_{1/2}^{red}$ (volt)[e]	I_{DC}[d] ($\mu A/mol\ m^{-3}$)	I_{AC}[d] ($\mu\mho/mol\ m^{-3}$)	$E_{1/2}^{oxd}$ (volt)	I_{DC} ($\mu A/mol\ m^{-3}$)	I_{AC} ($\mu\mho/mol\ m^{-3}$)	σ	σ^+
AOB	321.5	16050	−50	−1.396	−1.413	2.28	541	2.028	20.7	175	0	0
4,4′-$(CH_3)_2$	330.3	19620	+120	−1.490	−1.505	2.19	575	1.835	18.7	216	−0.170	−0.311
4,4′-Cl_2	333.2	21370	−150	−1.226	−1.260	2.36	589	2.055	14.5	190	0.227	0.114
4,4′-$(OCH_3)_2$	350[h]	23780	+700	−1.596	−1.586	2.04	508	1.463	17.7	298	−0.268	−0.778
4,4′-$(OC_2H_5)_2$	349.5	26910	+690	−1.586	−1.605	2.06	489	1.446	16.8	281	−0.250	—
4,4′-$[N(CH_3)_2]_2$	400.3	40640[f]	+1390	−1.766	−1.748	2.00	439	0.757	11.3	532	−0.600	−1.78
4,4′-$(CN)_2$	334.8	18350[f]	−320	−0.844	−0.900	2.19	541	2.382	16.5	164	1.00[i]	0.659
4,4′-$(COOC_2H_5)_2$	335.5	22180	−160	−0.969	−1.025	2.09	514	2.272	16.1	76	0.678[i]	0.482
4,4′-$(NO_2)_2$	—	—	—	−0.615	−0.705	2.55	307	2.467	20.9	183	1.270[i]	0.790
m,m′-$(CH_3)_2$	324.6	16120	−80	−1.425	−1.435	2.31	551	1.962	16.8	146	−0.069	−0.066
m,m′-Cl_2	322.8	15410	−170	−1.133	−1.183	2.24	565	2.198	22.8	186	0.373	0.399
m,m′-$(OCH_3)_2$	320.0	14090	+40	−1.364	−1.382	1.93	523	1.760	11.1	126	0.115	0.047
m,m′-$(CN)_2$	320.4	16560	−70	−1.001	−1.060	2.22	518	2.350	26.6	172	0.56	0.562
m,m′-$(COOC_2H_5)_2$	321.7	15920	+70	−1.191	−1.234	1.79	435	2.280	22.1	125	0.398	0.366
3,3′-$(NO_2)_2$	316.4	15380	−30	−0.930	−0.947	2.24	438	2.423	29.2	189	0.710	—

a) Data in heptane. b) Data *vs.* S.C.E. c) $\Delta\tilde{\nu}=\tilde{\nu}$ (heptane) − (ethanol). d) Obtained with a dropping mercury electrode in DMF. e) Obtained with a rotating platinum electrode ($\phi=1$ mm, 600 rpm) in CH_3CN. f) Values in CH_3CN. g) Taken from Refs. 7a, 8, 45, and 46 given in the text. h) The symmetry of this absorption curve is bad. The 350 nm is the weighted mean wavelength (center of gravity) of the curve, but the peak is 345.4 nm. i) This is a σ^- value (Jaffé's σ^*) cited from Ref. 47. j) See text and Ref. 50.

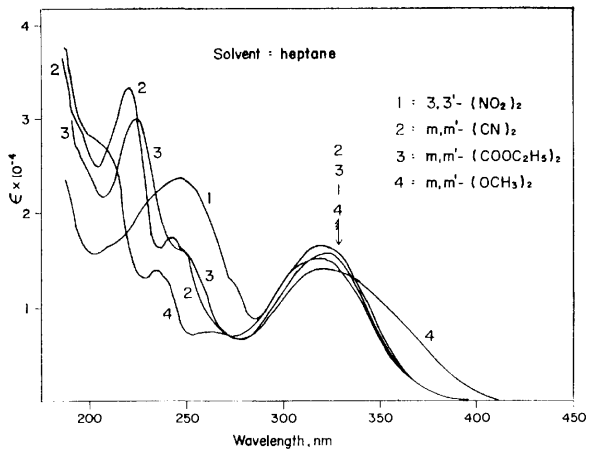

Fig. 3. Electronic spectra of azoxybenzenes substituted at *m,m′*-positions with the groups showing quite a large substituent effect.

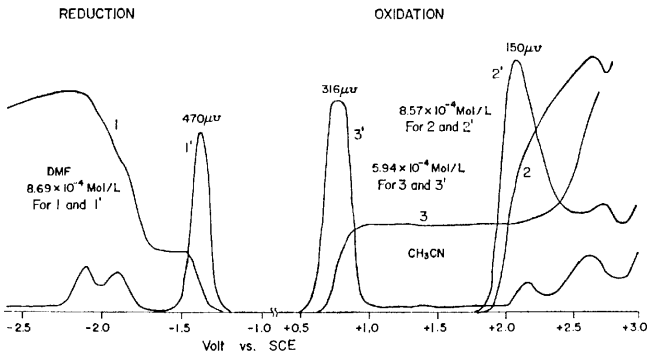

Fig. 4. DC(1) and AC(1′) reduction polarograms in DMF and DC(2) and AC(2′) oxidation voltammograms in CH_3CN of azoxybenzene respectively. Curves 3 and 3′ are DC and AC voltammograms of 4,4′-bis-(dimethylamino)azoxybenzene respectively. The absolute value of current is taken at the ordinate for the conveniences's sake.

for AOB and its derivatives. The red shift, rather than the blue shift, of the strong π-π^* band in the longest-wavelength region was observed in protic solvents in the case of substituted AOB's. This red shift is especially large for the AOB's with 4,4′-$[N(CH_3)_2]_2$ (2003 cm^{-1}), 4,4′-$(OC_2H_5)_2$ (976 cm^{-1}), and 4,4′-$(OCH_3)_2$ (949 cm^{-1}): the values in parentheses are the red shift from heptane to aqueous ethanol (C_2H_5OH: H_2O=3: 2). The spectral change with protic solvents is illustrated in Fig. 2 for the AOB substituted with 4,4′-$[N(CH_3)_2]_2$. The mechanism of the effect of protic solvents on the π-π^* band seems to be more or less different between –N=N→O and –C=N→O groups, the former having two active sites for intermolecular hydrogen-bonding interaction.

Nonaqueous Polarograms and Half-wave Potentials of Reduction and Oxidation. In Fig. 4 are illustrated the reduction polarogram in DMF and the oxidation voltammogram in CH_3CN on AOB as an example. The first reduction wave in Fig. 4 is due to the formation of the corresponding anion radical in the reversible process. This was inferred from the high value (541 $\mu\mho/mol\ m^{-3}$) of the AC wave, and directly verified by recording the ESR spectrum at the potential of the first limiting current. The same circumstances as the above

can be applied to the substituted AOB's, the first wave of which is quite a bit similar to that of AOB in showing a high AC wave. Almost the same reduction DC and AC waves which were obtained with a dropping Hg electrode were also yielded with a rotating Pt electrode. These first waves may be attributed to the anion radical formation. The data are listed in Table 2. On the other hand, the first oxidation wave of AOB, depicted in Fig. 4, seems not only to be overlapped with the next waves, but also the reversibility is less[19] than in the case of the reduction wave. The AC waveheight (175 μC/mol m^{-3}) is considerably smaller than that (*vide supra*) of the reduction wave. Of the AOB derivatives, 4,4'-bis(dimethylamino)-AOB showed a typical oxidation wave. The ESR measurement at the oxidation wave of the compound has ravealed a well-resolved spectrum due to the cation redical. Although the reversibility of the first oxidation wave of all the other AOB's is less than that of 4,4'-bis(dimethylamino)-AOB mentioned above, the $E_{1/2}^{oxd}$ values were determined by the wave analysis as reasonably as possible. All the data are included in Table 2.

Molecular Orbital (MO) Calculation and the Character of the Electronic Spectra. Some qualitative discussions of the excited states of AOB's have previously been reported,[2-6] but there have been no systematic considerations of their electronic states. In order to interpret the electronic spectra and their correlation with the $E_{1/2}^{red}$ and $E_{1/2}^{oxd}$ values, we have carried out the so-called PPP-SCFMO-CI calculations of the AOB's. As has been discussed in the "Electronic Spectra" section, the spectrum of AOB is quite similar to that of BANO (a nitrone). Since the electronic structures of nitrones including BANO were previously studied in detail,[16] the electronic states of AOB's may reasonably be understood by replacing the carbon atom in the bridge part of nitrones with a nitrogen atom, whose valence-state ionization potential (I_P: 14.51) and electron affinity (E_A: 1.20) are taken for the π electron in sp^2 hybridization.[20] The substituents employed in the calculations are the CH_3, Cl, OCH_3, and $N(CH_3)_2$ groups, the I_P, E_A, and core resonance energy (β_{XY}^{core}) of which are the same as those reported in a foregoing paper.[1d] The benzene ring in AOB was assumed to be a regular hexagon with the distance of 1.384 Å, cited from the X-ray analysis data of substituted AOB's.[17a]

The β_{XY}^{core} values in the bridge part, *i.e.*, β_{C-N}^{core} and $\beta_{N=N}^{core}$, were evaluated as follows. The β_{CN}^{core} was estimated by applying the Nishimoto and Forster equation,[21] $\beta_{CN}^{core}=-0.53P_{CN}-2.24$, where the bond order, P_{CN}, was calculated from the $R_{CN}=1.451-0.18P_{CN}$ relation and where the observed CN distance, $R_{CN}=1.496$ Å.[17a] The obtained value is $\beta_{CN}^{core}=-2.108$ eV. Alternatively, the value of $\beta_{N=N}^{core}$ tentavively estimated by employing the various equations connecting the $\beta_{\mu\nu}^{core}$, $S_{\mu\nu}$, valence state I_P, *etc.* led to the conclusion

Table 3. Calculated values of transition energies, oscillator strengths, and main singly excited configurations of azoxybenzene and benzaldehyde *N*-phenyl oxime, with their experimental data

Compound	$\tilde{\nu}_{calcd}$ (10^3 cm^{-1})	f_{calcd}	$\tilde{\nu}_{obsd}$[a] (10^3 cm^{-1})	ε_{max}[a]	Main configuration (%)[b]
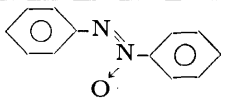	30.28	0.679	31.10	16050	92.6(8/9)
	33.63	0.064			77.8(7/9), 12.9(8/12)
	35.89	0.044			76.2(6/9), 13.8(5/10)
	38.65	0.261	38.94	7945	93.9(5/9)
	42.09	0.038			56.1(8/12), 15.2(7/13), 13.9(7/9)
	44.09	0.050			78.0(4/9)
	45.90	0.027	43.09	10180	76.6(8/11)
	46.43	0.081			39.5(8/10), 19.9(6/11), 17.0(6/9)
	47.57	0.012			55.8(8/10), 29.3 (5/10)
	50.06	0.134	50.61	27520	35.1(8/13), 30.8(7/12), 10.9(8/11)
	51.20	0.175			57.2(6/10), 24.8(5/11)
	53.54	0.670	53.25	35340	27.7(7/13), 26.0(7/11), 19.8(7/12)
	54.44	0.905			29.8(7/12), 28.7(8/13)
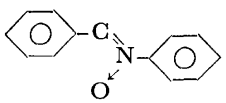	29.76	0.666	31.14	18600	97.5(8/9)
	34.66	0.007			61.7(7/9), 26.6(8/12)
	37.36	0.040			61.8(5/9), 13.9(6/10)
	38.94	0.398			85.8(6/9)
	41.42	0.004	41.25	11500	73.0(8/11), 17.0(8/12)
	42.13	0.000	42.05	11800	84.2(8/10)
	42.47	0.266	44.58	8540	46.4(8/12), 25.3(7/9), 12.9(8/11)
	43.60	0.011			80.8(4/9)
	48.09	0.018			41.7(6/10), 21.3(8/13), 16.7(5/9)
	48.89	0.253	51.33	32300	46.7(8/13), 12.9(7/12), 11.2(5/11)
	51.16	0.321			64.5(5/10), 23.1(6/11)
	53.10	0.803			62.6(7/12), 12.7(8/13)

a) All the experimental data are in heptane. See Ref. 16 for the spectral data of benzaldehyde *N*-phenyl oxime (BANO). b) For example, (8/9) means a singly excited configuration from ϕ_8 to ϕ_9.

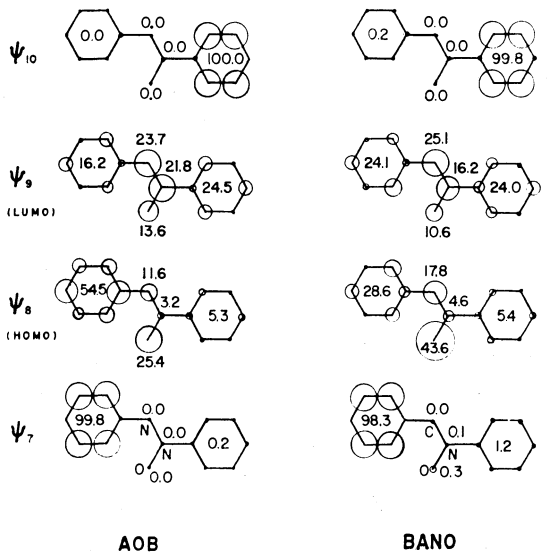

Fig. 5. Comparison of the orbital charge distributions, which are pertinent to the longer wavelength absorption bands, between azoxybenzene and benzaldehyde *N*-phenyl oxime.

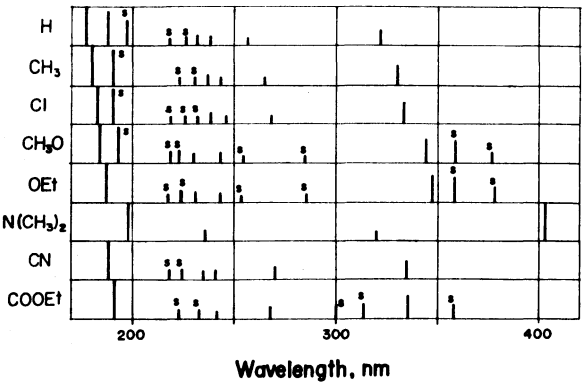

Fig. 6. Effect of substituents at *p,p'*-positions on the electronic spectra of azoxybenzene. The "s" in the figure means the shoulder band.

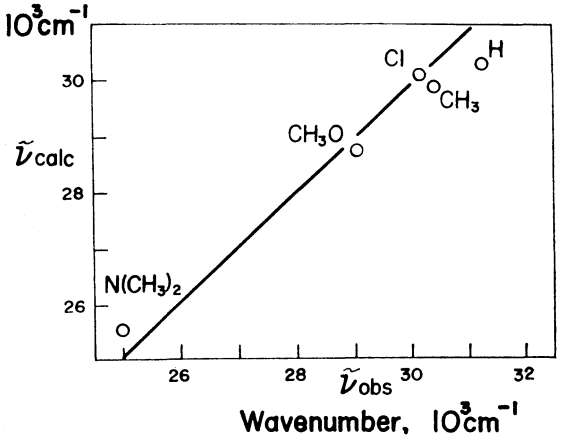

Fig. 7. Mutual correlation of calculated and observed values for the first strong π-π^* band of *p,p'*-disubstituted azoxybenzenes.

that the $\beta_{N=N}^{core}$ is in the range 2.00—3.00 eV. With this result in mind, the $\beta_{N=N}^{core}$=2.75 eV was the most suitable for reproducing the observed UV spectra and dipole moments of AOB's.[22] The N atoms in the –N=N(O)– bridge group are assumed to be in sp^2 hybridization, so that the angles of ∠CNN and ∠CNO are 120° in the *trans*-form, as is shown in [I]. Here, one-electron transitions alone were taken into account in the UV spectral calculation. The excited-state energies of AOB are illustrated in Fig. 1 as stick diagram, while all the calculated and experimental spectral data on it are collected in Table 3, where the corresponding data of BANO are included for the sake of comparison. The orbital electron densities pertinent to the UV spectra are also shown in Fig. 5 for AOB and BANO. It is clear from Table 3 that the strong band of AOB (≈321.5 nm) and that (≈321.1 nm) of BANO appearing in the longest-wavelength region are mainly contributed by the HOMO→LUMO transition. This conclusion is the same as that reported hitherto by other workers;[2-6] their discussions were, however, in the framework of HOMO, without any CI treatment. The tentative assignment of the other bands of AOB and BANO is indicated in Table 3. Quite a good similarity is observed between the two calculations, which may suggest that the two bands recorded at 256.8 and ≈232.1 nm on AOB are coagulated into one band (263—224 nm) for BANO. The orbital-charge distribution (25.4%) on the *N*-oxide group oxygen atom in the HOMO of AOB is much less than that (43.6%) of BANO, so the charge-transfer (CT) character[24] from the above oxygen atom to the π-residual system is also smaller for AOB than in BANO for the case of the HOMO→LUMO transition (the strong band at ≈322 nm). For AOB, this transition is, rather, considered to be an intramolecular CT from the A ring to the bridge N=N(O) group and to the B ring (see Fig. 5 and [I]).[26]

Let us now focus our attention on the substituent effect on the spectrum of AOB. As may be seen in Table 2 and Fig. 6, the first strong π-π^* band is quite sensitive to the 4,4'-substituents with an electron-donor nature, and shows a red shift which is particularly large for the $N(CH_3)_2$ group. This result was confirmed by the present MO calculation, as Fig. 7 shows. The calculation indicates that the first strong π-π^* band observed on the 4,4'-substituted AOB's is also contributed mainly by the HOMO→LUMO transition. On the other hand, the shift of the first strong π-π^* band is small for the case of *m,m'*-substitution of AOB. The results, listed in Table 2, may be explained qualitatively as follows. The MO coefficients of AOB at the *m,m'*-positions are quite small (see Fig. 5) for the HOMO and LUMO, which contribute greatly to the above π-π^* band. Therefore, the small perturbation of these orbitals can be expected from the introduction of *m,m'*-substituents, leading to the small spectral shift. The red shift of the spectra of AOB's due to the solvent change from heptane to protic solvents was described in the foregoing section. The general rule pertaining to the blue-shift phenomena[27] caused by the solvent effect on the electronic spectra of aromatic tertiary amine *N*-oxides seems not to hold for AOB's.[28] That the first strong π-π^* band of AOB is somewhat different in CT

nature from that of BANO has already been discussed. This tendency increases with, for example, an increasing electron-donor nature of the substituents introduced at 4,4′-positions. For 4,4′-$(OCH_3)_2$ or 4,4′-$[N(CH_3)_2]_2$, the electron densities on the *N*-oxide-group oxygen atom are quite small at HOMO (14.36 and 6.33% for the former and the latter respectively), so there is almost no CT from the oxygen atom to the π-residual system in the case of the HOMO→LUMO transition. On the other hand, the electron densities at the N(8) atom (see [I]) always increased upon the HOMO→LUMO transition. These circumstances would be favorable to the red shift of the π-π^* band in protic solvents; that is, such intermolecular interactions as hydrogen bonding with protic solvents would become more or less stronger in the excited π-π^* state than in the ground state.

The Correlation of the Electronic Spectra and Half-wave Potentials. The fact that the first strong π-π^* band of substituted AOB's at the 4,4′-positions is mainly contributed by the HOMO→LUMO transition has been shown in the previous chapter. The linear relation written as Eq. 1 can thus be expected for the AOB's:

$$(E^{oxd}_{1/2} - E^{red}_{1/2}) = k_1 \cdot {}^1E^{UV}_{ho\to lu} + k_2 \qquad (1)$$

Here, ${}^1E^{UV}_{ho\to lu}$ is the singlet electronic transition energy, in which the HOMO→LUMO transition is the main configuration.[30] Of course, if the configuration of triplet excited states (${}^3E^{UV}_{ho\to lu}$) is localized mainly in the HOMO→LUMO transition, Eq. 2 can also be expected:

$$(E^{oxd}_{1/2} - E^{red}_{1/2}) = k_1 \cdot {}^3E^{UV}_{ho\to lu} + k_3 \qquad (2)$$

This relation was recently observed by Loutfy and Loutfy.[31] Figure 8 gives the correlation of Eq. 1, each of the experimental data being taken from Table 2. A good linear relation is found there for 4,4′-substituents, as is to be expected from the MO calculation.[32] The observed k_1 value is 1.27, which is near the theoretical value, 1. Alternatively, the k_2 value of −1.44 was obtained. In the case of the *m*,*m*′-substituents, the shift of the UV spectra is insensitive even to the groups of a stronger electron-donor or -acceptor, as may be seen in Fig. 3 so that the correlation of Eq. 1 was not obtained. The character of the absorption bands for these substances seems to be somewhat different from those of 4,4′-substituents. For the physical meaning of the k_2 and k_3 terms in Eq. 1 or 2, see the Appendix.

Substituent Effect on the $E^{oxd}_{1/2}$ and $E^{red}_{1/2}$ values. In a previous paper we have already pointed out that, in the electrode oxidation process, the σ^+ substituent constant is the better parameter to explain the substituent effect on the $E^{oxd}_{1/2}$ values.[7a] On the other hand, the usual σ or σ^- scales afford a better description of the substituent effect on the $E^{red}_{1/2}$ values.[8,33] In the series of AOB's these same relationships have also been observed. The plotting of the $E^{oxd}_{1/2}$ values against the $2\sigma^+$ gave a nice linear relation, as is indicated in Fig. 9.[34] In the case of the $E^{red}_{1/2}$ values, the good linearity shown in Fig. 10 was also found for 2σ and partly $2\sigma^-$ parameters; σ^- values were adopted for 4,4′-$(NO_2)_2$, 4,4′-$(CN)_2$, and 4,4′-$(COOC_2H_5)_2$, because the electron-accepting ability in the transition state is large for these. The above fact indicates that the treatment of a linear free-energy approximation can safely be applied to the half-wave potentials of AOB's in nonaqueous media, and that

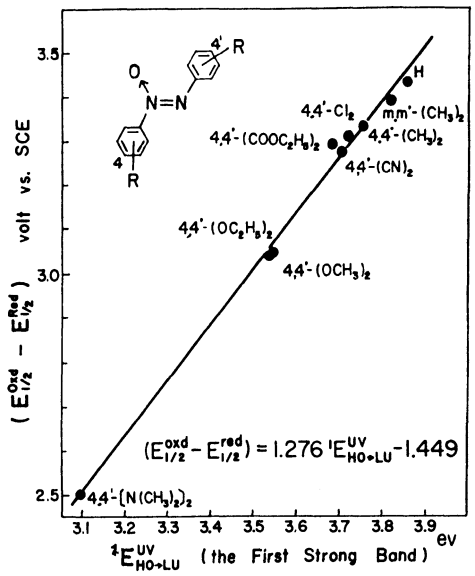

Fig. 8. The relationship between $(E^{oxd}_{1/2} - E^{red}_{1/2})$ values and the first strong π-π^* band energies for 4,4′-disubstituted azoxybenzenes.

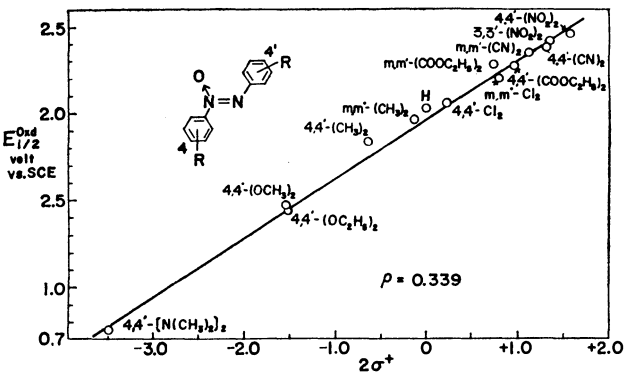

Fig. 9. Linear relationship between the σ^+ values (see Table 2) and the first $E^{oxd}_{1/2}$ values for substituted azoxybenzenes.

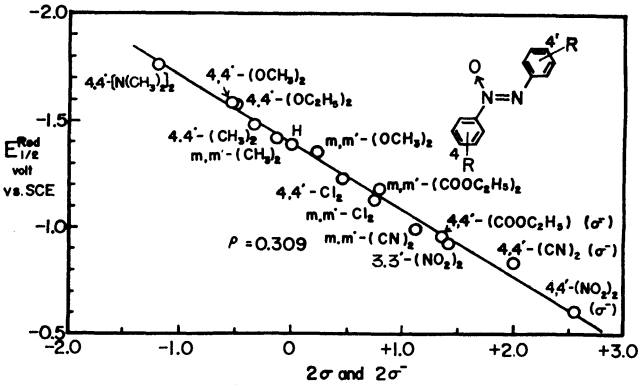

Fig. 10. Linear relationship between the σ and σ^- values (see Table 2) and the first $E^{red}_{1/2}$ values for substituted azoxybenzenes.

the above-mentioned linear relations make it easy to predict the $E_{1/2}^{red}$ and $E_{1/2}^{oxd}$ of substituted AOB's.

Appendix

In our previous papers[7] we did not discuss quantitatively the physical meaning of the constant terms, k_2 and k_3, in Eqs. 1 and 2 respectively. Here an interpretation of the k_2 and k_3 terms will be given. Let us now consider a reversible system of anion-radical formation, such as $R+e \rightleftarrows R^{\pm}$, so that the k_1 value of Eqs. 1 and 2 becomes 1 when the electron volt (eV) is adopted as the energy unit.[36] Applying the Born-Haber-type[35] thermochemical cycle given in Scheme 1 for anion-radical formation in solution, the $E_{1/2}^{red}(R^{\pm}/R)$ can be written by Eq. 3 in eV units, where the energy zero level is placed *in vacuo*:[31,37]

$$E_{1/2}^{red}(R^{\pm}/R) = \Delta G^{\circ} - \varepsilon_{lu} - \Delta E_{solv}^{\pm} \quad (3)$$

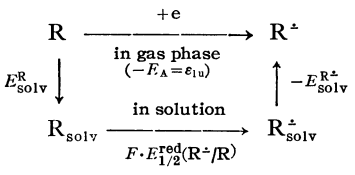

Scheme 1.

$\Delta E_{solv}^{\pm}$ is the solvation energy difference of the anion radical and neutral species; $\Delta E_{solv}^{\pm} = E_{solv}^{R\pm} - E_{solv}^{R}$. The contribution from the $E_{solv}^{R\pm}$ term is predominant. The absorolute potential of the reference electrode is expressed as ΔG°, which is -4.70 eV in the case of the (Ag/Ag^{+}) electrode in acetonitrile (0.01 mol dm^{-3} $AgClO_4$, 0.1 mol dm^{-3} $Et_4N^{+}ClO_4^{-}$).[37] Similarly the $E_{1/2}^{oxd}(R^{+}/R)$ is given by:

$$E_{1/2}^{oxd}(R^{+}/R) = \Delta G^{\circ} - \varepsilon_{ho} + \Delta E_{solv}^{+} \quad (4)$$

The ΔE_{solv}^{R+} equals $(E_{solv}^{+} - E_{solv}^{R})$. Taking account of the difference between Eqs. 3 and 4, Eq. 5 is obtained under the same experimental conditions, *i.e.*, the ΔG° term is cancelled out:[38]

$$(E_{1/2}^{oxd} - E_{1/2}^{red}) = \varepsilon_{lu} - \varepsilon_{ho} + \Delta E_{solv}^{+} + \Delta E_{solv}^{\pm} \quad (5)$$

Note that the $(E_{1/2}^{oxd} + E_{1/2}^{red})/2 \approx E^{\circ}(R^{\pm}/R^{+})$ may become $(-\varepsilon_{ho} - \varepsilon_{lu})/2 + \Delta G^{\circ} = (I_P + E_A)/2 + \Delta G^{\circ}$ when we use Eqs. 3 and 4 and $\Delta E_{solv}^{\pm} = \Delta E_{solv}^{+}$. This relation was employed by Senda and Takahashi to determine the standard electrode potential in nonaqueous solvents.[37b,49] We will now combine Eq.5 with this relation: $^1E_{ho\to lu}^{UV} = \varepsilon_{lu} - \varepsilon_{ho} - J_{ho\cdot lu} + 2K_{ho\cdot lu} + {}^1E_{CI}$, where the small contribution from the CI energy ($^1E_{CI}$) is postulated.[7] Thus, the k_2 value in Eq. 1 is given by Eq. 6 in eV units for a completely reversible system:

$$k_2 = J_{ho\cdot lu} - 2K_{ho\cdot lu} - {}^1E_{CI} + \Delta E_{solv}^{\pm} + \Delta E_{solv}^{+}$$
$$\approx J_{ho\cdot lu} - 2K_{ho\cdot lu} - {}^1E_{CI} + 2\Delta E_{solv}^{\pm} \quad (6)$$

Similarly, the k_3 value in Eq. 2 is given by

$$k_3 = J_{ho\cdot lu} - {}^3E_{CI} + \Delta E_{solv}^{\pm} + \Delta E_{solv}^{+}$$
$$\approx J_{ho\cdot lu} - {}^3E_{CI} + 2\Delta E_{solv}^{\pm} \quad (7)$$

Recently Loutfy and Loutfy discussed the meaning of the k_2 and k_3 values.[31] However, they completely neglected the term of $(\Delta E_{solv}^{\pm} + \Delta E_{solv}^{+})$. In addition, their MO's participating in the UV transition, which they interpreted as the "molecular orbital in solution" of neutral species, should rather be ascribed to those of the anion and cation radicals ($^2\Gamma$ state) generated by electrolysis. Also, they used the $E_{1/2}^{red}$ and $E_{1/2}^{oxd}$ values obtained in different solvents (CH_3CN and DMF) for plotting Eqs. 1 and 2 in the case of AH hydrocarbons, so the $(\Delta G_{CH_3CN}^{\circ} - \Delta G_{DMF}^{\circ})$ term should appear in Eq. 5. They did not take care in this point. Their discussions, therefore, are erroneous.

In the case of the AH hydrocarbons there are some experimental data by which to estimate the k_2 and k_3 values. In addition, the fact that the k_1 value of Eq. 1 is experimentally almost 1 has already been reported.[7] The $\Delta E_{solv}^{\pm}$ and ΔE_{solv}^{+} values can be estimated from Eqs. 3 and 4 respectively by adopting the experimentally determined I_P, E_A, $E_{1/2}^{red}$, and $E_{1/2}^{oxd}$ values.[37] In turn, the value of $(J_{ho\cdot lu} - 2K_{ho\cdot lu} - {}^1E_{CI})$ can be experimentally derived from the evaluation of the $(I_P - E_A - {}^1E_{ho\to lu}^{UV})$ value. The ^1L_a bands of AH's correspond to the $^1E_{ho\to lu}^{UV}$ value.[7] Here note that, in the foregoing papers,[7] we discussed how the value of the $(J_{ho\cdot lu} - 2K_{ho\cdot lu} - {}^1E_{CI})$ term becomes nearly constant from the standpoint of the PPP-SCFMO-CI calculation in a series of similar com-

Table 4. The k_2 and k_3 values theoretically estimated on the alternate hydrocarbons, with some physical constants (see text) necessary for deriving the k_2 and k_3 values

Compound	$-E_{1/2}^{red}$ (V)[a]	$E_{1/2}^{oxd}$ (V)[a]	I_P (eV)[b]	E_A (eV)[c]	^1L_a (eV)[d]	k_2^{theo} (eV)[g,i]	^3L_a (eV)	k_3^{theo} (eV)[h,i]
Anthracene	2.37	0.99	7.66 7.47	0.552	3.310	0.05	1.838[e]	1.522
Pyrene	2.49	1.12	7.72 7.41	0.579	3.718	−0.108	2.083[e]	1.527
Chrysene	2.73	1.29	8.01 7.60	0.419	3.886	0.134	2.455[e]	1.565
Phenanthrene	2.88	1.45	8.06 7.86	0.288	4.238	0.082	2.689[f]	1.631
Benz[*a*]anthracene	2.40	1.16	7.74 7.47	0.696	3.491	0.069	2.050[f]	1.510
Triphenylene	2.87	1.50	8.19 7.89	0.284	4.365	0.005	2.907[f]	1.463
						0.039 ±0.083		1.551 ±0.057

a) Taken from Ref. 37a. b) Taken from Refs. 37a, 37b, and 40. c) Taken from Refs. 37b and 41. d) Taken from Refs. 7b and 42. e) Taken from Ref. 43. f) Taken from Ref. 44. g) The constant term in Eq. 1 in the test. h) The constant term in Eq. 2 in the text. i) The k_2 or k_3 value listed for each compound was obtained by averaging the values derived from the two different I_p's.

pounds such as AH's or aromatic *N*-oxides.[48] The same treatment as the above leads to the evaluation of the ($J_{ho\cdot lu} - {}^3E_{CI}$) term, which is obtained from the calculation of ($I_P - E_A - {}^3E^{UV}_{ho\to lu}$). Here, ${}^3E^{UV}_{ho\to lu}$ is for the ${}^3L_a$ bands. We can now obtain the k_2 and k_3 values in Eqs. 6 and 7 respectively from the experimental values alone. The results thus obtained are listed in Table 4, from which it may be understood that the k_2 value is $\approx$0.04 eV and quite small, while the k_3 value is $\approx$1.55 eV. The $E^{red}_{1/2}$ and $E^{oxd}_{1/2}$ values in Table 4 are those reported under the same conditions as were used for the determination of $\Delta G^\circ = -4.70$ eV,[37] so these are the best values for the evaluation of k_2 and k_3. The plotting of Eqs. 1 and 2 was as follows: $(E^{oxd}_{1/2} - E^{red}_{1/2}) = 1.011\ {}^1L_a - 0.001$ with $n=6$, $s=0.094$, $r=0.980$, and $(E^{oxd}_{1/2} - E^{red}_{1/2}) = 1.018\ {}^3L_a + 1.496$ with $n=6$, $s=0.067$, $r=0.990$.[39] Note that our previously reported result[7b,c] was $(E^{oxd}_{1/2} - E^{red}_{1/2}) = 0.941\ {}^1L_a + 0.092$. The values of the constant term given above seem to be in good agreement with the ones estimated theoretically in the order of magnitude and in the approximation adopted. For AOB's we did not attempt to evaluate the k_2 term in Eq. 1 because of the lack of experimental data and because of the smaller reversibility of the $E^{red}_{1/2}$ and, especially, $E^{oxd}_{1/2}$ values.

References

1) a) J. Bastide, J. P. Maier, and T. Kubota, *J. Electron Spectrosc.*, **9**, 307 (1976); b) M. Yamakawa, T. Kubota, K. Ezumi, and Y. Mizuno, *Spectrochim. Acta*, **30**, 2103 (1974); c) K. Ezumi, T. Kubota, and T. Shida, *Chem. Lett.*, **1977**, 181; d) M. Yamakawa, K. Ezumi, Y. Mizuno, and T. Kubota, *Bull. Chem. Soc. Jpn.*, **47**, 2982 (1974); e) Y. Kawamura, K. Nishikida, and T. Kubota, *Bull. Chem. Soc. Jpn.*, **46**, 737 (1973), and other articles listed in the above papers.

2) a) W. Maier and A. Saupe, *Z. Phys. Chem., N. F.*, **6**, 327 (1956); b) W. Maier, A. Saupe, and A. Englert, *Z. Phys. Chem., N. F.*, **10**, 273 (1957); c) W. Maier and G. Englert, *Z. Elektrochem.*, **62**, 1020 (1958); d) A. Saupe, *Z. Naturforsch., Teil A*, **18**, 336 (1963).

3) P. H. Gore and O. H. Wheeler, *J. Am. Chem. Soc.*, **78**, 2160 (1956).

4) a) D. L. Webb and H. H. Jaffé, *J. Am. Chem. Soc.*, **86**, 2419 (1964); b) H. H. Jaffé and M. Orchin, "Theory and Application of Ultraviolet Spectroscopy," John Wiley and Sons, (1962).

5) C. Tosi, *Spectrochim. Acta*, **22**, 1701 (1966).

6) The discussions in Refs. 2—5 are based on the naive MO approximation.

7) a) H. Miyazaki, T. Kubota, and M. Yamakawa, *Bull. Chem. Soc. Jpn.*, **45**, 780 (1972); b) T. Kubota, H. Miyazaki, K. Ezumi, and M. Yamakawa, *Bull. Chem. Soc. Jpn.*, **47**, 491 (1974); c) T. Kubota and H. Miyazaki, *Bunseki Kiki*, **11**, 639 (1973).

8) T. Kubota, K. Nishikida, H. Miyazaki, K. Iwatani, and Y. Ōishi, *J. Am. Chem. Soc.*, **90**, 5080 (1968).

9) K. Nishikida, T. Kubota, H. Miyazaki, and S. Sakata *J. Magn. Reson.*, **7**, 260 (1972).

10) A. McKillop, R. A. Raphael, and E. C. Taylor, *J. Org. Chem.*, **35**, 1670 (1970).

11) J. F. Corbett, *Chem. Commun.*, **1968**, 1257.

12) W. H. Linnell and M. Khalifa, *J. Chem. Soc.*, **1959**, 1315.

13) T. Kubota and H. Watanabe, *Bull. Chem. Soc. Jpn.*, **36**, 1093 (1963).

14) a) K. E. Calderbauk and R. J. W. LeFévre, *J. Chem, Soc.*, **1948**, 1949; b) R. A. Gehrchevs and E. Müller, *Ann.*, **500**, 296 (1933).

15) T. Shimozawa, "Interpretation of Dielectric Behavior (Experimental Method of Dipole Moment and Its Interpretation)," Kyōritsu Press, Tokyo (1967), p. 55 (in Japanese).

16) The electronic spectra and their interpretation of various nitrones have already been reported in detail. a) T. Kubota, M. Yamakawa, and Y. Mori, *Bull. Chem. Soc. Jpn.*, **36**, 1552 (1963); b) T. Kubota and M. Yamakawa, *Bull. Chem. Soc. Jpn.*, **36**, 1564 (1963); c) M. Yamakawa, T. Kubota, and H. Akazawa, *Theor. Chim. Acta*, **15**, 244 (1969); d) J. Bastide, J. P. Maier, and T. Kubota, *J. Electron Spectrosc. Relat. Phenom.*, **9**, 307 (1976); e) K. N. Houk, P. Caramella, L. L. Munchausen, Y-M. Chang, A. Battaglia, J. Sims, and D. C. Kaufman, *J. Electron. Spectrosc. Relat. Phenom.*, **10**, 441 (1977).

17) See the following papers on the molecular structure of azoxybenzenes; a) W. R. Krigbaum, Y. Chatani, and P. G. Barber, *Acta Crystallogr., Sect. B*, **26**, 97 (1970); b) W. R. Krigbaum and P. G. Barber, *Acta Crystallogr., Sect. B*, **27**, 1884 (1971).

18) N. Mataga and T. Kubota, "Molecular Interactions and Electronic Spectra," Marcel Dekker, New York (1970), Chap. 8.

19) Just before the use of the Pt-electrode the plane platinum head was polished with very fine emery paper; therefore, the reproducibility of the AC wave was good. See also Ref. 7a.

20) a) G. Pilcher and H. A. Skinner, *J. Inorg. Nucl. Chem.* **24**, 937 (1962); b) J. Hinze and H. H. Jaffé, *J. Am. Chem. Soc.*, **84**, 540 (1962).

21) K. Nishimoto and L. S. Forster, *Theo. Chim. Acta*, **4**, 155 (1966).

22) The parameters other than those written in the text are the same as in our previous reports.[1d,16c,23]

23) T. Kubota, M. Yamakawa, and Y. Mizuno, *Bull. Chem. Soc. Jpn.*, **45**, 3282 (1972).

24) This type of intramolecular CT is generally found in the case of aromatic amine oxides such as heterocyclic amine N-oxides, nitrones, and nitrile *N*-oxides.[1b,16,18,25]

25) T. Kubota, *Bull. Chem. Soc. Jpn.*, **35**, 946 (1962).

26) Quite recently a conclusion similar to this was reported on the basis of an INDO/S calculation of AOB; N. J. Bunce, J-P. Schoch, and M. C. Zerner, *J. Am. Chem. Soc.*, **99**, 7986 (1977).

27) T. Kubota and H. Miyazaki, *Chem. Pharm. Bull.*, **9**, 948 (1961).

28) AOB itself shows a blue shift of 50 cm^{-1} alone from heptane to ethanol. Also, our experiments have revealed that the hydrogen-bonding interaction ability of AOB with phenol is $K=2$—5 $dm^3\ mol^{-1}$ in CCl_4 at 25 °C and that the shift of the phenol OH-stretching band is 174 cm^{-1} in CCl_4. Note that the shift of the methanol OH-stretching band brought about by the intermolecular hydrogen bonding with benzaldehyde *N*-methyl oxime (nitrone) is 238 cm^{-1} in CCl_4.[29] These findings indicate AOB to be much weaker a proton-acceptor in the ground state than in a nitrone such as BANO.[29]

29) a) T. Kubota, M. Yamakawa, M. Takasuka, K. Iwatani, H. Akazawa, and I. Tanaka, *J. Phys. Chem.*, **71**, 3597 (1967); b) T. Kubota, *J. Am. Chem. Soc.*, **88**, 211 (1966), and other papers cited in Ref. 29.

30) The derivation and the examination of Eq. 1 have already been reported elsewhere by us.[7] See also the Appendix for the physical meaning of the constant term (k_2) of Eq. 1.

31) Rafik O. Loutfy and Raouf O. Loutfy, *Can. J. Chem.*, **54**, 1454 (1976).

32) Although the MO calculation for the AOB substituted with 4,4'-$(CN)_2$ and 4,4'-$(COOC_2H_5)_2$ was not attempted, the first strong π-π^* band seems to be mainly contributed by the HOMO→LUMO transition, judging from our previous calculation of 4-nitropyridine *N*-oxide, *etc.*[1b]

33) T. Kubota and H. Miyazaki, *Bull. Chem. Soc. Jpn.*, **39**, 2057 (1966).

34) If the plotting is made for usual σ values, the linearity in Fig. 8 becomes quite bad, particularly for the strong electrondonating substituents.

35) L. Pauling, "The Nature of the Chemical Bond," 3rd ed, Cornell University Press, Ithaca, New York (1960), p. 510.

36) This is because the Faraday constant becomes 1 eV/1 V, so that in Eqs. 3, 4, and 5 in the text $F \cdot E_{1/2}$ is simply expressed by $E_{1/2}$.

37) a) B. Case, N. S. Hush, R. Parsons, and M. E. Peover, *J. Electroanal. Chem.*, **10**, 360 (1965); b) M. Senda and R. Takahashi, *Rev. Polarog. (Kyoto)*, **20**, 56 (1974); c) M. E. Peover, "Electroanalytic Chemistry," ed by A. J. Bard, Marcel Dekker, New York, N. Y. (1967), Vol. 2, Chap. 1; d) Rafik O. Loutfy and Raouf O. Loutfy, *J. Phys. Chem.*, **77**, 336 (1973).

38) In these equations the solvation energy of the ion radicals indicates the so-called "real solvation energy," which includes the energy term $F \cdot \chi$. Here χ is the surface potential caused by transferring the ion redical from the gas phase to the solvent phase, both the phases being electrically neutral. The χ value for CH_3CN may be expected to be small.[37a,c]

39) Here, n, s, and r indicate the number of samples adopted for the least-squares calculation, the standard deviation, and the correlation coefficient respectively.

40) R. Boschi, E. Clar, and W. Schmidt, *J. Chem. Phys.*, **60**, 4406 (1974).

41) a) W. E. Wentworth, E. Chen, and J. E. Lovelock, *J. Phys. Chem.*, **70**, 445 (1966); b) W. E. Wentworth, L. W. Kao, and R. S. Becker, *J. Phys. Chem.*, **79**, 1161 (1975).

42) E. Clar, "Polycyclic Hydrocarbons," Academic Press, London (1964), Vols. 1 and 2.

43) S. P. McGlynn, T. Azumi, and M. Kinoshita, "Molecular Spectroscopy of the Triplet State," Prentice-Hall, Englewood Cliffs, New Jersey (1969).

44) P. S. Engel and B. M. Monroe, *Adv. Photochem.*, **8**, 245 (1971).

45) H. C. Brown and Y. Okamoto, *J. Am. Chem. Soc.*, **80**, 4979 (1958).

46) T. Kubota and H. Miyazaki, *Bull. Chem. Soc. Jpn.*, **39**, 2057 (1966).

47) a) H. H. Jaffé, *Chem. Revs.*, **53**, 191 (1953); b) M. Yoshioka, K. Hamamoto, and T. Kubota, *Bull. Chem. Soc. Jpn.*, **35**, 1723 (1962); c) C. Hansch, A. Leo, S. H. Unger, K-H. Kim, D. Nikaitani, and E. J. Lien, *J. Med. Chem.*, **16**, 1207 (1973); d) C. Hansch, S. D. Rockwell, P. Y. C. Jow, A. Leo, and E. E. Steller, *J. Med. Chem.*, **20**, 304 (1977).

48) In the present series, almost constant negative values of $\Delta E^{\pm}_{solv}$ and $\Delta E^{\pm}_{solv}$ were also obtained from Eqs. 3 and 4.

49) T. Kakutani, Y. Morihiro, M. Senda, R. Takahashi, and K. Matsumoto, *Bull. Chem. Soc. Jpn.*, **51**, 2847 (1978).

50) For this reason, the notation of *m,m'* is adopted in this report for the compounds whose accurate configurations in the *m,m'*-positions could not be determined.

Thermodynamic Study on the Adsorption of Dioctadecyl Ether at Hexane/Water Interface

Norihiro MATUBAYASI,† Masatake DOHZONO, Makoto ARATONO, Kinsi MOTOMURA, and Ryohei MATUURA*

Department of Chemistry, Faculty of Science, Kyushu University, Hakozaki, Fukuoka 812

(Received October 27, 1978)

The adsorption of dioctadecyl ether was studied at hexane/water interface, as functions of temperature, pressure, and mole fraction of dioctadecyl ether in hexane. The phase transition between expanded and condensed films was observed with decreasing temperature and increasing pressure and concentration. The thermodynamic quantities associated with the adsorption such as entropy, volume, and energy change were evaluated and comparison was made with the adsorbed films of 1-octadecanol at the same interface in which phase transition takes place. It is found that the dioctadecyl ether shows small negative discontinuous changes of the thermodynamic quantities with the transition from the expanded to the condensed films.

It is of great importance from the viewpoint of surface chemistry to clarify the structure and properties of adsorbed films at interface. In recent papers, we have shown that it can be achieved by applying the thermodynamic treatment developed previously.[1,2] Further we have revealed that the adsorbed film of 1-octadecanol at hexane/water interface shows a phase transition from an expanded to a condensed one and this phase transition is characterized by large negative discontinuous changes of the thermodynamic quantities associated with the adsorption.[3]

As an extension of this study, measurements are made for the adsorbed film of dioctadecyl ether at the same interface, in which the phase trandition takes place.

Experimental

Dioctadecyl ether was purified by repeated recrystallization. The purity was checked by the gas-liquid chromatography. Only one peak was obtained. Hexane used in this study was dehydrated and the impurity was removed by passing through an activated alumina column. Water distilled thrice from alkaline permanganate solution was used. The purity of hexane and water was always checked by the value of the interfacial tension between them.

The interfacial tension was measured by the pendant drop method. Detailed description of the apparatus and the method was given previously.[2,4]

Results

According to the phase rule the state of the system under consideration is completely specified by three independent variables and the structure and properties of interface are speculated by the thermodynamic quantities.[1,2] Then, the interfacial tension γ is measured as functions of temperature T and pressure p at the constant mole fraction of dioctadecyl ether in hexane x_1^0. Plots of γ against T under atmospheric pressure are shown in Fig. 1. At low concentrations the interfacial tension decreases linearly with increasing temperature. At higher concentrations, on the other hand, it increases. At intermadiate concentrations, the γ *vs.* T curve appeares to have a break point. This behavior is

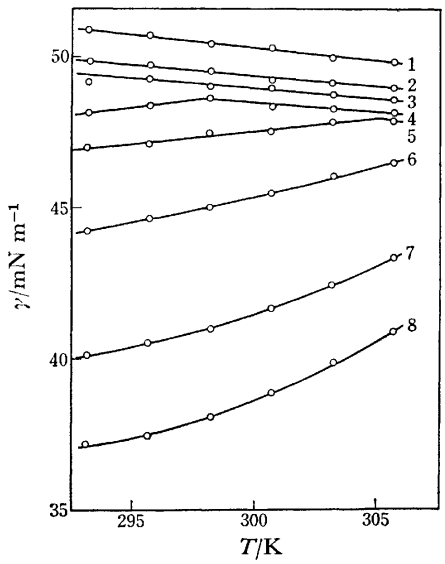

Fig. 1. Interfacial tension *vs.* temperature curves at various concentrations under 0.1 MPa.
1) $x_1^0=0$; 2) 7.88×10^{-5}; 3) 2.66×10^{-4}; 4) 3.11×10^{-4}; 5) 3.35×10^{-4}; 6) 4.00×10^{-4}; 7) 5.46×10^{-4}; 8) 7.19×10^{-4}.

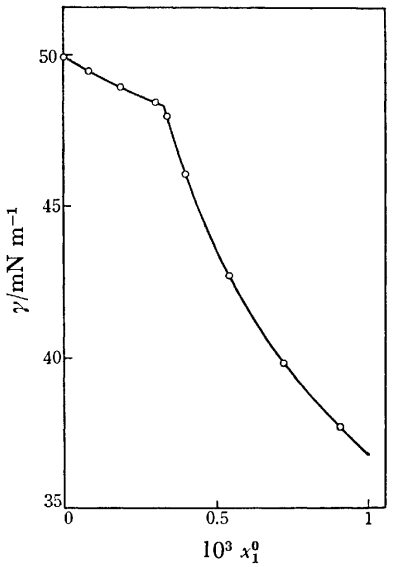

Fig. 2. Interfacial tension *vs.* mole fraction of dioctadecyl ether in hexane curve at 303.15 K under 0.1 MPa.

† Present address: Fuculty of Fisheries, Nagasaki University, Bunkyo-cho, Nagasaki 852.

similar to that of the adsorption of 1-octadecanol at hexane/water interface.[3] However, the break point is limited within a very narrow concentration range, *i.e.* between 2.7×10^{-4} and 3.6×10^{-4} of x_1^0 in this work. In Fig. 2 the interfacial tension *vs.* composition curve at 303.15 K is drawn which is prepared from Fig. 1. It has a sharp break point. In the study of the adsorption of 1-octadecanol, we observed that the first order phase transition is reflected on the γ *vs.* x_1^0 curves as a break point.[3] It is, therefore, conceivable that in the adsorbed film of dioctadecyl ether a similar phase transition takes place. Further, it is observed that at concentrations corresponding to the expanded state γ reaches rapidly its equilibrium value and at concentrations corresponding to the condensed state γ decreases gradually to an equilibrium value.

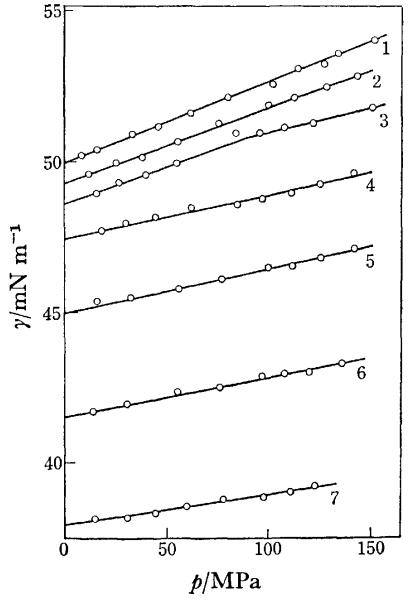

Fig. 3. Interfacial tension *vs.* pressure curves at various concentrations at 303.15 K.
1) $x_1^0=0$; 2) 1.02×10^{-4}; 3) 1.77×10^{-4}; 4) 3.54×10^{-4}; 5) 4.25×10^{-4}; 6) 6.04×10^{-4}; 7) 8.66×10^{-4}.

In Fig. 3 the interfacial tension is plotted against the pressure at various concentrations. The slope of γ *vs.* p curve is linear and positive except the curve at $x_1^0=1.77\times10^{-4}$ which has the break point at about 90 MPa. This figure is considerably different from that of 1-octadecanol.

Discussion

Taking into account that the mutual solubility of hexane and water is in fact negligible and dioctadecyl ether is soluble only in hexane, the thermodynamic quantities associated with the adsorption are estimated by applying the treatment developed previously.[1] The measurements being made on the solution of solute mole fraction below 1.0×10^{-3}, the solution is assumed to be ideal. Thus the interfacial density of surface active solute Γ_1^{H} is calculated by

$$\Gamma_1^{\mathrm{H}} = -(x_1^0/RT)(\partial\gamma/\partial x_1^0)_{T,p} \qquad (1)$$

and other thermodynamic quantities are given as the derivatives of γ with T and p, that is

$$\Delta s = -(\partial\gamma/\partial T)_{p,x_1^0} \qquad (2)$$

$$\Delta v = (\partial\gamma/\partial p)_{T,x_1^0} \qquad (3)$$

and

$$\Delta u = \gamma - T(\partial\gamma/\partial T)_{p,x_1^0} - p(\partial\gamma/\partial p)_{T,x_1^0}, \qquad (4)$$

where Δs, Δv, and Δu are the entropy, volume, and energy changes associated with the adsorption, respectively.

First Γ_1^{H} was calculated by Eq. 1 at various temperatures and pressures. Its value increases with concentration and pressure and decreases with temperature. An abrupt change is seen on the Γ_1^{H} *vs.* x_1^0 curve at the break point at which the expanded and condensed films coexist in equilibrium. Its values of the expanded and condensed states are 0.410 and 4.43 μmol m^{-2}, respectively. This significant behavior of dioctadecyl ether in the interface is revealed more clearly by drawing the interfacial pressure π *vs.* area per molecule A curve on the assumption that the adsorbed film is monomolecular. The π *vs.* A curve at 303.15 K and at 80 MPa is shown in Fig. 4 in which the curve of 1-octadecanol is

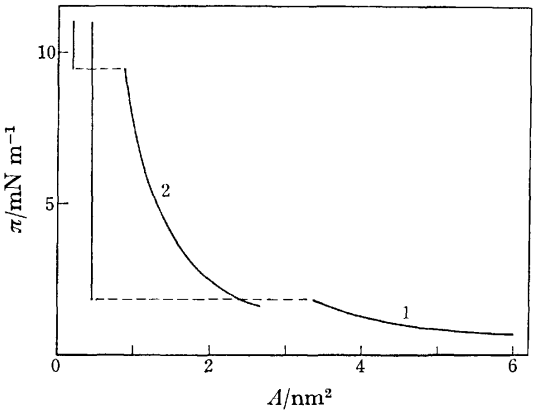

Fig. 4. Interfacial pressure *vs.* area curves at 303.15 K under 80 MPa. 1) Dioctadecyl ether; 2) 1-octadecanol.

also drawn. Although they seem somewhat different in shape, they are essentially identical with each other. In the condensed state the value of A of dioctadecyl ether is almost twice that of 1-octadecanol. Then it can be expected that the molecule adsorbes at the interface in such a way that its polar part is directed to the water phase and its two hydrocarbon chains are perpendicular to the interface. This restricted conformation might be related to the fact that the time dependence of interfacial tension is pronounced for the concentrated solutions.

It is now interesting to compare the entropy change of the adsorption on dioctadecyl ether and that of 1-octadecanol. The value of Δs evaluated by Eq. 2 is shown grafically as a function of x_1^0 at 303.15 K under atmospheric pressure in Fig. 5. The corresponding one of 1-octadecanol is also shown in this figure. It is seen apparently that dioctadecyl ether has a larger value than 1-octadecanol in the expanded state although

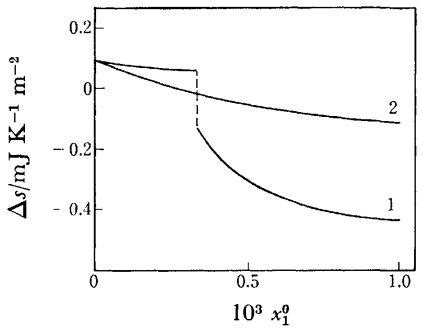

Fig. 5. Entropy change *vs.* concentration curves at 303.15 K under 0.1 MPa. 1) Dioctadecyl ether; 2) 1-octadecanol.

dioctadecyl ether has a more restricted conformation. We notice here that in such a comparison the difference between their interfacial densities is ignored. In Fig. 7A, Δs is plotted against Γ_1^H. As expected, the value of Δs of dioctadecyl ether is smaller than that of 1-octadecanol when compared at the same value of Γ_1^H. Thus we may say that the dioctadecyl ether molecule makes more negative contribution to Δs than 1-octadecanol molecule. It is also found that the entropy change associated with the phase transition, $\Delta s^c - \Delta s^e$, in which the superscripts c and e represent the condensed and expanded states, respectively, has a significantly small negative value compared with that of 1-octadecanol, *i.e.*, -1.4 mJ K^{-1} m^{-2} at 303.15 K and at 80 MPa. This small negative value might be ascribed in part to a loosely packed structure of the condensed film.

It is worthwhile to note that the fact that the break point on the γ *vs.* T curve is observed in a limited range of the concentration is related closely to a small difference between Δs^c and Δs^e. The variation of the equilibrium interfacial tension γ^{eq} between the expanded and condensed phases with temperature is given by[3]

$$(\partial\gamma^{eq}/\partial T)_p = -(\Delta s^c/\Gamma_1^{H,c} - \Delta s^e/\Gamma_1^{H,e})/(1/\Gamma_1^{H,c} - 1/\Gamma_1^{H,e}). \quad (6)$$

The left side of Eq. 6 is given by the slope of the locus of break points in Fig. 1; its value estimated roughly is *ca.* -0.12 mN m^{-1} K^{-1}. On the other hand, the numerical value of the right side, calculated from the experimental results of Figs. 3 and 5, is -0.087 mJ K^{-1} m^{-2} (mN m^{-1} K^{-1}). Taking account of some uncertainty in accuracy, the agreement of these numerical values is not unsatisfactory.

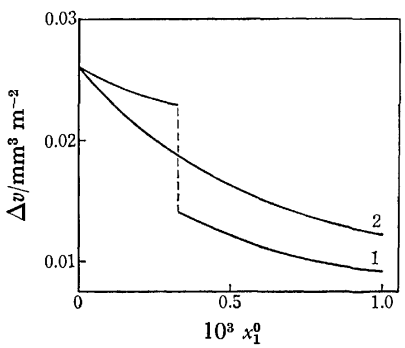

Fig. 6. Volume change *vs.* concentration curves at 303.15 K under 0.1 MPa. 1) Dioctadecyl ether; 2) 1-octadecanol.

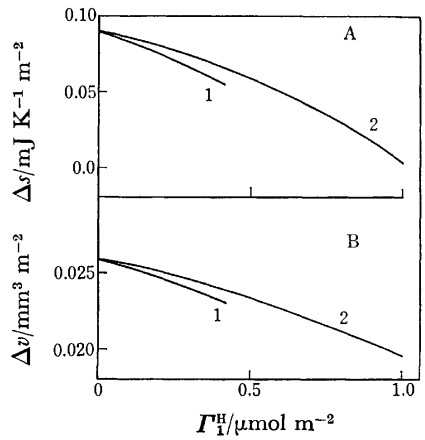

Fig. 7. A) Variation of entropy change with interfacial density at 303.15 K under 0.1 MPa.
B) Variation of volume change with interfacial density at 303.15 K under 0.1 MPa. 1) Dioctadecyl ether; 2) 1-octadecanol.

Lutton *et al.*[5] measured the interfacial tension as a function of temperature for the systems of monoglyceride and diglyceride solutions in cotton seed oil and water. Although the data are not complete, it is found that the difference in the slope of γ *vs.* T curve at the break point obtained for diglyceride is fairly smaller than that obtained for monoglyceride. Their data seem to support our observation that the phase transition of dioctadecyl ether is characterized by the small difference in Δs.

By use of Eq. 3 the value of Δv was evaluated from Fig. 3. The comparison of Δv *vs.* x_1^0 curves between dioctadecyl ether and 1-octadecanol is also made in Fig. 6. This figure is quite similar in appearance to Fig. 5. Further, a figure analogous to Fig. 7A is obtained when Δv is plotted against Γ_1^H (Fig. 7B). This fact indicates that the change in entropy associated with the adsorption is interrelated to the changes in volume. It is also explicable by the corresponding equation to Eq. 6 that the break point in the γ *vs.* p curve is observed only in a limited range of concentration as seen in Fig. 3.

Let us now calculate the energy of interface formation Δu by applying Eq. 4 to the above data. In Fig. 8, the

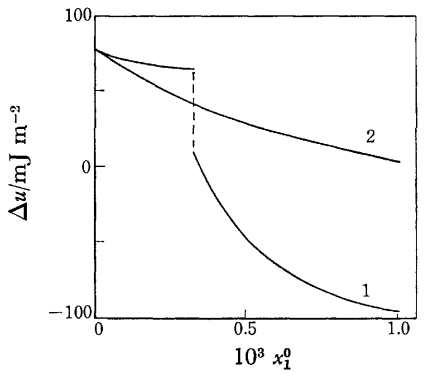

Fig. 8. Energy change *vs.* concentration curves at 303.15 K under 0.1 MPa. 1) Dioctadecyl ether; 2) 1-octadecanol.

value of Δu is plotted against x_1^0 at 303.15 K under atmospheric pressure. It varies with x_1^0 in a similar manner as Δs and Δv do. In the condensed state, however, its decrease with increase in x_1^0 is found to be relatively steep. This might reflect a gradual change of the structure of dioctadecyl ether film at the hexane/water interface with the concentration.

References

1) K. Motomura, *J. Colloid Interface Sci.*, **64**, 348 (1978).
2) K. Motomura, N. Matubayasi, M. Aratono, and R. Matuura, *J. Colloid Interface Sci.*, **64**, 356 (1978).
3) N. Matubayasi, K. Motomura, M. Aratono, and R. Matuura, *Bull. Chem. Soc. Jpn.*, **51**, 2800 (1978).
4) N. Matubayasi, K. Motomura, S. Kaneshina, M. Nakamura, and R. Matuura, *Bull. Chem. Soc. Jpn.*, **50**, 523 (1977).
5) E. S. Lutton, C. E. Stauffer, J. B. Martin, and A. J. Fehl, *J. Colloid Interface Sci.*, **30**, 283 (1969).

Excited-state Electronic Interaction of *m*-Aminoacetophenone with Aliphatic Alcohols

Yoshifumi TANIMOTO,* Kenji INOUE, Yoshihiko FURUKAWA, Yoko SEGAWA, and Michiya ITOH

Faculty of Pharmaceutical Sciences, Kanazawa University, Takara-machi, Kanazawa 920

(Received November 1, 1978)

The electronic interaction of both ground-state and excited-state *m*-aminoacetophenone (MAAP) with several aliphatic alcohols in nonpolar viscous solvent was investigated by steady-state and nanosecond fluorescence spectroscopies. Concentration dependence of several alcohols in liquid paraffin-hexane (LPH) mixed solvent upon fluorescence and absorption spectra suggests a complex formation of MAAP with aliphatic alcohols in the ground state. In the typical LPH solution of MAAP containing high concentration of alcohol, the complex fluorescence exhibits two-component decay and a longer wavelength fluorescence than the complex fluorescence exhibits a rise and decay. The results demonstrate that the complex in the excited state further associates with alcohol to make an exciplex including an alcohol molecule.

The fluorescence properties of many aromatic molecules strongly depend on the solvent system; fluorescence maximum, fluorescence quantum yield, and lifetime remarkably change from nonpolar to polar solvent. In most cases, these changes have been explained in terms of "the solvent effect," which usually involves dispersion force of solvent, and dipole-dipole and dipole-induced dipole interactions between solute and solvent.[1] However, the possibility of a new type of the electronic interaction was reported by Lumry and his coworkers;[2] they suggested the importance of the excited-state solute-solvent complex (exciplex) formation in the polar solvent. Actually, they investigated the fluorescence of indole and indole derivatives in the mixed systems of nonpolar-polar solvents (mainly in pentane–alcohol systems), and showed that an excited-state solute-solvent complex is responsible to a large red shift and loss of vibrational structure in the fluorescence spectra of indole and indole derivatives in the polar solvents. However, since the possibility of the ground state solute-solvent complex was not strictly excluded and since they did not show any dynamical experimental evidence, their explanation does not seem to be generally accepted. On the other hand, Ware and his coworkers[3] investigated the problem of the origin and nature of the temperature-dependent spectral shift characteristic of aminophthalimides in alcoholic solvents by the aid of nanosecond time-resolved emission techniques. They showed that at least two relaxation times characterize the phenomenon. One relaxation time was observed to be subnanosecond in character and may be associated with the exciplex that presumably is present in the system. The other relaxation time was presumably associated with the nonspecific dipolar reorientation. Recently, the interaction of 2-anilinonaphthalene with ethyl alcohol and glycerol in the excited state was studied by DeToma and Brand.[4] They showed a direct kinetic evidence that 2-anilinonaphthalene undergoes a specific reversible association with ethyl alcohol and glycerol in the excited state.

In the previous paper,[5,6] we have clarified that *m*-aminoacetophenone (MAAP) makes a complex with *t*-pentyl alcohol in the ground state and that the complex further associates with alcohol in the excited state (*i.e.*, the complex in the excited state makes an exciplex with alcohol). However, *t*-pentyl alcohol may be not so popular as ethyl alcohol in spectroscopic studies, and the results look some special case. Therefore, we have extended the study to other alkanols. This paper describes the excited-state complex formation (exciplex formation) of MAAP with several alcohols, and the results clearly suggest the general importance in studying the fluorescence properties of polar aromatic molecules in the alcoholic solvents.

Experimental and Kinetic Analysis

MAAP (Nakarai EP Grade) was recrystallized twice from ethyl alcohol, followed by vacuum sublimation. *t*-Butyl alcohol, butyl alcohol (both Nakarai EP Grade) were dried with molecular sieve and thereafter distilled. Isopropyl alcohol (Merck Uvasol) and ethyl alcohol (Nakarai Spectro Grade) were used as supplied. Liquid paraffin and hexane (both Nakarai Spectro Grade) were also used as supplied. The mixture of them (9: 1 volume ratio) was used as a viscous nonpolar solvent. Solutions for lifetime measurements were degassed with the freeze-thaw technique.

Absorption and fluorescence spectra were measured on Hitachi 323 and MPF-4 spectrophotometers at room temperature unless denoted. Fluorescence lifetimes were measured with a similar method described in a previous paper.[5] Observed lifetimes were analyzed by a nonlinear least-squares method including the exciting pulse shape.[7]

For the fluorescence quantum yield measurements,[8] the spectral response of the observed system was corrected by using the fluorescence of quinine sulfate in 0.5 M sulfuric acid as a standard. Fluorescence spectra of both ethyl alcohol solutions of MAAP and quinine sulfate standard solution were measured successively, and after correcting absorbances and refractive indices, the quantum yield of ethyl alcohol solution of MAAP was determined. Here, the quantum yield of quinine sulfate solution was assumed to be 0.55, and solutions were excited by the 360 nm light. The yields of other solutions were then determined by using the ethyl alcohol solutions of MAAP as a second standard and by correcting similarly.

The experimental results are shown to be consistent with the kinetic scheme given below.[9]

$$\mathrm{MAAP} + \mathrm{A} \underset{}{\overset{K}{\rightleftharpoons}} \mathrm{C} \qquad (1)$$

$$\mathrm{C} \xrightarrow{h\nu} \mathrm{C}^* + \mathrm{A} \underset{k_4}{\overset{k_3}{\rightleftharpoons}} \mathrm{E}^* \qquad (2)$$

$$\mathrm{C}^* \xrightarrow{k_1} \mathrm{C} + h\nu' \qquad \mathrm{C}^* \xrightarrow{k_2} \mathrm{C} \qquad \mathrm{E}^* \xrightarrow{k_5} \mathrm{C} + \mathrm{A} + h\nu'' \qquad \mathrm{E}^* \xrightarrow{k_6} \mathrm{C} + \mathrm{A}$$

where A, C, C*, and E* are alcohol, the complex, the complex in the excited state, and excited-state complex (exciplex) generated from C* and A, respectively; K is equilibrium constant of the complex formation in the ground state, and k's are rate constants of respective processes.

Under photostationary state, the process 2 gives the following equations;

$$[C]/F_C = c'\{k_3(k_5+k_6)[A]/(k_4+k_5+k_6)+k_1+k_2\} \quad (3)$$

$$F_E/F_C = c''k_3k_5[A]/\{k_1(k_4+k_5+k_6)\} \quad (4)$$

$$\phi = \{(k_4+k_5+k_6)k_1+k_3k_5[A]\}/\{(k_1+k_2+k_3[A]) \times (k_4+k_5+k_6)-k_3k_4[A]\} \quad (5)$$

In Eqs. 3, 4, and 5, F_C and F_E are the fluorescence intensities of C* and E*, respectively; [A] and [C] are the concentrations of the alcohol and the complex, respectively, ϕ is the fluorescence quantum yield of total emission, and c' and c'' are proportional constants.

For the pulse excitation, following equations are also obtained.

$$[C^*] = c_1 \exp(-\lambda_1 t) + c_2 \exp(-\lambda_2 t) \quad (6)$$

$$[E^*] = c_3\{\exp(-\lambda_1 t)-\exp(-\lambda_2 t)\} \quad (7)$$

where

$$\lambda_{1,2} = 1/2[k_1+k_2+k_3[A]+k_4+k_5+k_6 \mp \{(k_4+k_5+k_6 -k_1-k_2-k_3[A])^2+4k_3k_4[A]\}^{1/2}]$$

$$c_1 = [(\lambda_2-X)/(\lambda_2-\lambda_1)][C^*]_0$$

$$c_2 = [(X-\lambda_1)/(\lambda_2-\lambda_1)][C^*]_0$$

$$c_3 = k_3[A][C^*]_0/(\lambda_2-\lambda_1)$$

$$X = k_1 + k_2 + k_3[A]$$

and

$$\lambda_1 + \lambda_2 = k_1 + k_2 + k_3[A] + k_4 + k_5 + k_6 \quad (8)$$

Results and Discussion

Absorption and Fluorescence Spectra of MAAP. Figure 1 shows the absorption and fluorescence spectra of MAAP in several solvents. In hexane, absorption maximum appears at 325 nm and no fluorescence band is practically observed. In 2-methyltetrahydrofuran (MTHF), the absorption maximum of MAAP shifts to the longer wavelength (λ_{max} 340 nm), while a strong fluorescence band appears at ≈420 nm. The absorption maxima of this compound in tetrahydrofuran, MTHF, and several alcohols appear in similar wavelength region each other, while the fluorescence in alcohols remarkably shifts to 490—510 nm. The Stokes shifts in alcoholic solvents are about 9000—10000 cm^{-1}, though about 5600 cm^{-1} in MTHF. The unusually large Stokes shift seems to suggest some specific interaction between MAAP and alcohols. Since general feature of the absorption and fluorescence spectra was common in all systems reported here (*i.e.*, MAAP–*t*-butyl alcohol, MAAP–butyl alcohol, MAAP–isopropyl alcohol, and MAAP–ethyl alcohol), the results on the MAAP–*t*-butyl alcohol in liquid paraffin–hexane mixed system (abbreviated to LPH hereafter) were mainly described in this paper. Figure 2 shows the concentration dependence of *t*-butyl alcohol (TBA) in the LPH solution of MAAP upon fluorescence spectra. Although MAAP is practically non-fluorescent in LPH, the fluorescence with a short lifetime appears at ≈430 nm by adding a small amount of TBA, and the band increases in intensity with increasing the concentration of TBA (<0.2 M) (1 M=1 mol dm^{-3}). Furthermore, including a small red shift, a new band with a long lifetime appears at ≈490 nm, and increases in intensity with further increasing the concentration of the alcohol (>0.2 M).

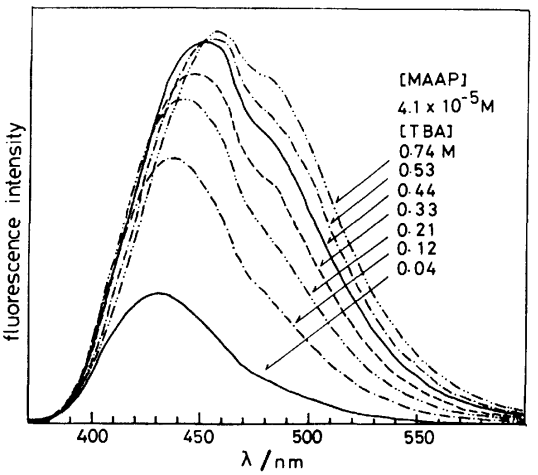

Fig. 2. Fluorescence spectra of MAAP in LPH containing several concentrations of TBA. The excitation wavelength is 360 nm.

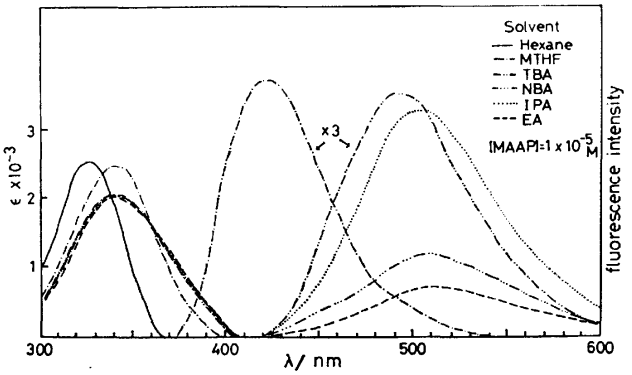

Fig. 1. Absorption and fluorescence spectra of MAAP in various solvents; MTHF, 2-methyltetrahydrofuran; TBA, *t*-butyl alcohol; BA, butyl alcohol: EA, ethyl alcohol. The excitation wavelength is 360 nm.

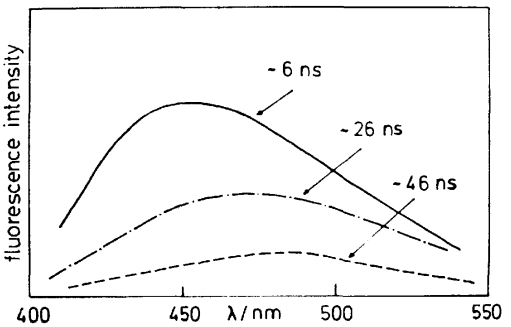

Fig. 3. Time-resolved fluorescence spectra of MAAP (1.4 $\times 10^{-5}$ M) in LPH containing TBA (1×10^{-1} M). Times indicated are after a peak of an exciting laser pulse.

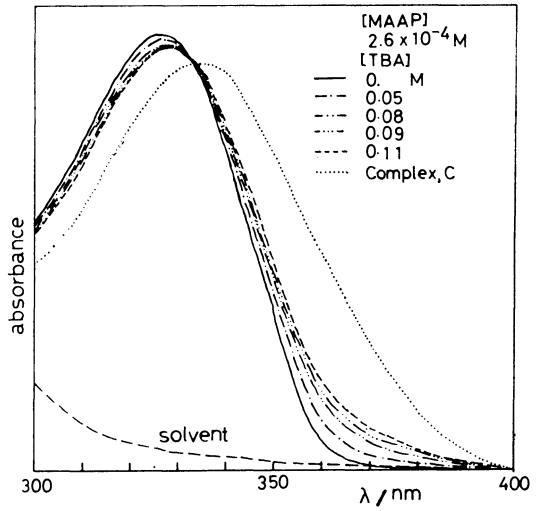

Fig. 4. Absorption spectra of MAAP in LPH, containing several concentrations of TBA. Absorption spectrum of the complex, C, was depicted from K and concentrations of MAAP and TBA.

Time-resolved fluorescence spectra in Fig. 3 exhibit these two kinds of fluorescence bands. Since it can be expected that MAAP and TBA make a hydrogen-bonding complex in the ground state, the shorter wavelength band, which is predominant in the low concentration of TBA, is most probably due to the hydrogen-bonding complex. Figure 4 shows the effect of TBA concentration upon the absorption spectra of MAAP in LPH. A new band appears at ≈360 nm and gradually increases in intensity with increasing the concentration of TBA (an isosbestic point at 334 nm). Therefore, assuming the complex formation in the ground state, the spectra were analyzed in terms of an ordinary 1 : 1 complex formation, shown in Eq. 1.[6] Figure 5 shows the Scott plots of absorption intensity of the new band (I_C) *vs.* [TBA]. The plots exhibit linear relationship, as is clear from Fig. 5, affording an equilibrium constant of 4.6 M^{-1}. Fluorescence intensity of the shorter wavelength band (F_C) was also analyzed in the same manner by assuming that the intensity is proportional to the absorption intensity of the new band. Figure 6 shows the plots of $[TBA]/F_C$ *vs.* [TBA], which afford the equilibrium constant of 3.4 M^{-1}. Both results agree each other within experimental errors.

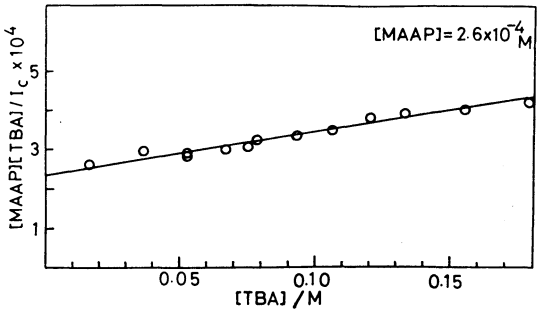

Fig. 5. Plots of $[MAAP][TBA]/I_C$ *vs.* [TBA]. Absorption intensities (I_C) were monitored at 370 nm.

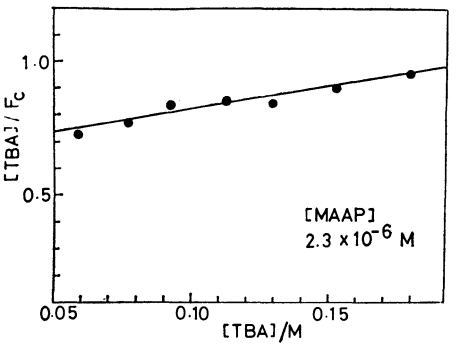

Fig. 6. Plots of $[TBA]/F_C$ *vs.* [TBA]. Fluorescence intensities (F_C) were monitored at 430 nm. In the range of TBA concentration (0.05—0.2 M), spectral shift of the fluorescence was small.

Now, let us examine the longer wavelength fluorescence which appears at rather concentrated solution of TBA. The excitation spectrum monitored at 530 nm (*i.e.*, at the longer wavelength band) is identical with that at 430 nm (*i.e.*, at the shorter wavelength band). Fluorescence intensity of the longer wavelength band increases with increasing the concentration of TBA, as mentioned above. Figures 7 and 8 show the plots of

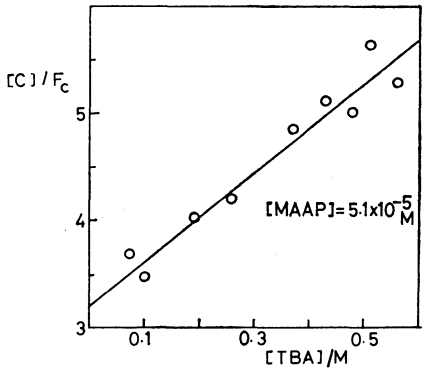

Fig. 7. Plots of $[C]/F_C$ *vs.* [TBA]. Fluorescence intensities (F_C) were monitored at 430 nm. Concentrations of C in the plots were evaluated from K, [MAAP] and [TBA].

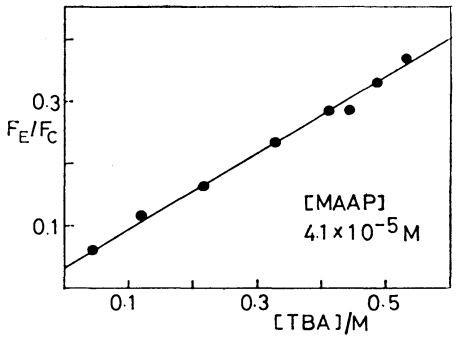

Fig. 8. Plots of F_E/F_C *vs.* [TBA]. Fluorescence intensities, (F_C and F_E) were monitored at 430 nm and at 530 nm, respectively.

[C]/F_C *vs.* [TBA], and F_E/F_C *vs.* [TBA], respectively. They show the linear relationships expected from Eqs. 3 and 4, respectively, though fluorescence intensities, F_C and F_E, may include the spectral shift owing to the change of solvent polarity. With these findings and time evolution of the fluorescence intensities which will be mentioned later, the longer wavelength fluorescence is tentatively ascribed to the exciplex (E*) formed between the complex in the excited state (C*) and TBA.

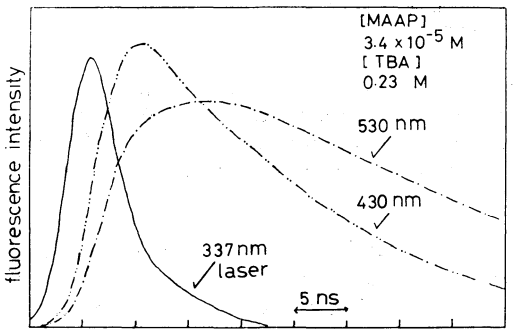

Fig. 9. Time evolution of the fluorescence intensities of MAAP in LPH.

The Time Evolution of Fluorescence and the Estimation of Kinetic Parameters. From Eq. 1, one can expect a simple two-component decay for [C*] and a growth and decay for [E*]. Figure 9 shows the typical time evolutions of the fluorescence of [C*] and [E*], in the MAAP–TBA–LPH system. The shorter wavelength band (C*) exhibits typical two-component decay, and the longer one (E*) shows a growth and decay as expected. The λ_1 and λ_2 obtained from both fluorescence bands coincide with each other within experimental errors. Therefore, these findings provide an evidence that the longer wavelength fluorescence (F_E) is ascribed to the exciplex, E*, generated from C* and TBA.

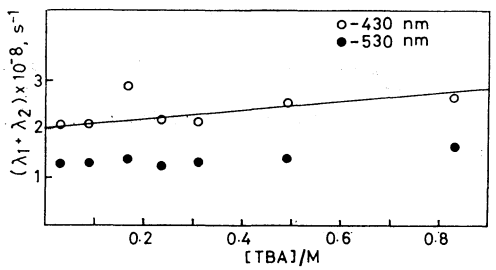

Fig. 10. Plots of $\lambda_1+\lambda_2$ *vs.* [TBA]. Fluorescence intensities were monitored both at 430 nm and at 530 nm. The fluorescence intensities at 530 nm was analyzed as a superposition of the fluorescence of both C* and E*, since both spectra partly overlapped each other in this region. Concentration of MAAP is 3.4×10^{-5} M.

Equation 8 gives k_3 from the plots of $\lambda_1+\lambda_2$ *vs.* [TBA]. As [TBA]$\longrightarrow$0,

$$\lambda_1 \longrightarrow k_1 + k_2$$

$$\lambda_2 \longrightarrow k_4 + k_5 + k_6$$

Thus k_3, k_1+k_2, and $k_4+k_5+k_6$ can be obtained (see Fig. 10). The results were shown in Table 1. Then combining Eq. 4 and the above values obtained, k_4 and k_5+k_6 can be calculated separately (see Fig. 7). If one may calculate the fluorescence quantum yields of more than two TBA concentrations of the solution, one may solve Eq. 5 to estimate k_1 and k_5. From this analysis, the radiative and nonradiative rate constants of respective states, C* and E*, were estimated to be of nearly the same order of magnitude. Furthermore, if only the exciplex formation is an activation process, the energy barrier may be obtained from the plots of F_E/F_C *vs.* $1/T$ (T: temperature, K), assuming that only k_3 in Eq. 4 is temperature dependent.[10] Figure 11 shows this relationship and the activation energy was obtained to be 7 kcal mol^{-1}.

Table 1. KINETICAL PARAMETERS OF THE MAAP–ALCOHOL SYSTEMS IN LPH AT ROOM TEMPERATURE

Alcohol	TBA	BA	IPA	EA
ε[a]	12.5	17.5	19.9	24.5
ϕ[b]	0.56	0.08	0.19	0.05
K, M^{-1} [c]	4.6	5.7	5.6	12.2
$k_3\times10^{-9}$, M^{-1} s^{-1}	0.09	0.31	0.19	0.68
$(k_1+k_2)\times10^{-8}$, s^{-1}	0.58	0.49	0.52	0.69
$(k_4+k_5+k_6)\times10^{-9}$, s^{-1}	0.17	0.15	0.14	0.35

a) Dielectric constant of alcohol. b) Total fluorescence quantum yield (see text). c) Equilibrium constant of the complex formation at room temperature.
TBA, *t*-butyl alcohol; BA, butyl alcohol; IPA, isopropyl alcohol; EA, ethyl alcohol.

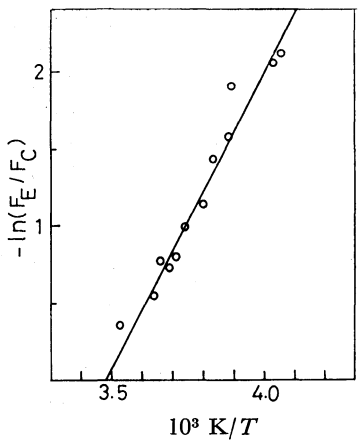

Fig. 11. Plots of $-\ln(F_E/F_C)$ *vs.* $1/T$. Fluorescence intensities, F_C and F_E, were monitored at 430 nm and at 530 nm, respectively. Concentrations of MAAP and TBA are 3.4×10^{-5} M and 0.82 M, respectively.

Fluorescence behavior of the MAAP–butyl alcohol, MAAP–isopropyl alcohol, and MAAP–ethyl alcohol in LPH is essentially parallel to that of MAAP–TBA mentioned above, and observed data in these systems were analyzed in the same procedure as mentioned above. Unfortunately, the activation energy of these systems could not be obtained, because of lack of the solubility of the alcohols at low temperature. The results obtained were listed in Table 1. From the Table,

equilibrium constants of the complex formation seem to increase with increasing strength of the dielectric constant of the alcohols. The rate constants of the exciplex formation, k_3, also seem to increase with the dielectric constant of the alcohols.

Generally, unusually large spectral change observed in the high concentration of TBA (>0.2 M) (see Fig. 2) might be explained in terms of following mechanisms; 1) the internal rotation of MAAP leading to the intramolecular CT interaction in MAAP, 2) the general solvent effect, 3) the reorientation of alcohols around MAAP, and 4) the exciplex formation with the solvent molecules. As for the mechanism 1, the process may be expected to occur very fast in the order of some picoseconds, which is inconsistent with our observation. The mechanism 2 means that the long-range intermolecular interaction between solute and solvent molecules such as dispersion force, dipole-dipole interaction, *etc.*[1] In this mechanism, the effect of alcohol upon the fluorescence band shape may be considered to be small, and wavelength-independent decay in a certain fluorescence spectrum may be expected. However, these are in contradiction to the observation reported here, since Figs. 2, 3, and also 9 show the drastic change of fluorescence band with increasing the TBA concentration, and the time-resolved fluorescence spectra including two different fluorescent species. Then, the mechanism 3 may be ruled out as follows. If MAAP molecule may be surrounded by TBA molecules by adding small amount of TBA in the LPH solution, it is unlikely that there are the two different fluorescent states stable in the excited state of MAAP surrounded by unspecified alcohol molecules. The rate for the reorientation of surrounding molecules may be of the order of picosecond. However, if the alcohol molecule may diffuse to make an interaction with MAAP in LPH, the rate may be of the order of some nanosecond. The diffusion rate constant in LPH is approximately estimated to be of the order of 10^8 M^{-1} s^{-1} from the viscosity of LPH ($\approx$100 cp). With this mechanism, observations shown in Figs. 2, 3, and 9 may be qualitatively explained. Figure 8 shows a linear relationship of F_E/F_C *vs.* [TBA], and may strongly suggest the stochiometric complex formation in the excited state. The mechanism 4 may suggest the specific intermolecular interaction between the complex and another alcohol molecule (*i.e.*, stochiometric excited-state complex formation). As already shown, all the observations have been quantitatively explained with this mechanism. The mechanism 4 seems to be most reasonable in the interpretation of the results observed in this paper.

Preliminary results on the fluorescence of *m*-dimethylaminoacetophenone[11,12] (DMAAP) show essentially the similar fluorescence property to that of MAAP. Although the weak fluorescence band appears at $\approx$405 nm in LPH, a new fluorescence band appears at $\approx$430 nm by adding a small amount of TBA, and increases in intensity with increasing the TBA concentration (<0.15 M). Furthermore, with further increasing the TBA concentration, another new fluorescence band appears at $\approx$490 nm (>0.15 M). The LPH solution of DMAAP containing high concentration of TBA exhibits the two-component decay of the shorter wavelength (at 440 nm), and the rise and decay of the longer wavelength fluorescence (at 530 nm). The similar kinetic analysis suggests that DMAAP makes the 1:1 complex with TBA in the ground state (K=4—10 M^{-1}), and the complex in the excited state (C*) further associate with the alcohol molecule ($k_3=0.08\times10^9$ M^{-1} s^{-1}, $k_1+k_2=0.4\times10^8$ s^{-1}, and $k_4+k_5+k_6=0.1\times10^9$ s^{-1}). Here, if the complex formation in the ground state might be tentatively attributable to a kind of the hydrogen-bonding with alcohol, the interaction between carbonyl of MAAP and hydroxylic hydrogen of alcohol seems to be most reasonable to the complex formation in the ground state. Furthermore, it is likely that the exciplex may be stabilized by the weak electronic interaction such as charge-transfer between C* and alcohol molecule, as already discussed in indole fluorescence by Lumry and his coworkers.[2] However, this is not obvious at this stage.

The authors wish to thank Dr. Kiyokazu Fuke for his help in the analysis of fluorescence lifetimes by a nonlinear least-squares fit, and for valuable discussions.

References

1) N. Mataga and T. Kubota, "Molecular Interactions and Electronic Spectra," Dekker, New York (1970), p. 371.

2) M. S. Walker, T. W. Bednar, and R. Lumry, *J. Chem. Phys.*, **45**, 3455 (1966); M. S. Walker, T. W. Bednar, and R. Lumry, *J. Chem. Phys.*, **47**, 1020 (1967); M. S. Walker, T. W. Bednar, and R. Lumry, "Molecular Luminescence," ed by E. C. Lim, Benjamin, New York (1969), p. 135; M. S. Walker, T. W. Bednar, R. Lumry, and F. Humphries, *Photochem. Photobiol.*, **14**, 147 (1971).

3) W. R. Ware, S. K. Lee, C. J. Brant, and P. P. Chow, *J. Chem. Phys.*, **54**, 4729 (1971).

4) R. P. DeToma and L. Brand, *Chem. Phys. Lett.*, **47**, 231 (1977).

5) Y. Tanimoto and M. Itoh, *Chem. Phys. Lett.*, **57**, 179 (1978).

6) In Ref. 5, the 1:2 complex formation of the ground-state MAAP with *t*-pentyl alcohol was presented. The discrepancy between the previous and present results may be explained by the following two possibilities. The difference might be attributable to the nature of *t*-pentyl alcohol somewhat different from others, since the dielectric constant of *t*-pentyl alcohol (ε: 5.8) is much smaller than that of alcohols used in the present work. Otherwise, the spectral changes observed in the previous system may exhibit the 1:2 complex formation in appearence, since the equilibrium constant of the 1:1 complex of MAAP with *t*-pentyl alcohol may be very small.

7) P. R. Berington, "Data Reduction and Error Analysis for the Physical Sciences," McGraw-Hill, New York (1969).

8) J. N. Demas and G. A. Crosby, *J. Phys. Chem.* **75**, 991 (1971).

9) W. R. Ware, D. Watt, and J. C. Holmes, *J. Am. Chem. Soc.*, **96**, 7853 (1974).

10) M. Itoh, T. Mimura, H. Usui, and T. Okamoto, *J. Am. Chem. Soc.*, **95**, 4388 (1973), and references therein.

11) H. Rupe, A. Braun, and K. von Zembrzuski, *Ber.*, **34**, 3522 (1901).

12) R. Nakagaki, S. Nagakura, T. Kobayashi, and S. Iwata, *Bull. Chem. Soc. Jpn.*, **51**, 2867 (1978).

Anharmonic Potential Functions of Simple Molecules. III. Computation of Vibration-Rotation Energies of XYZ and X_2Y_2 Type Linear Molecules through Direct Numerical Diagonalization: Application to the N_2O Molecule

Isao SUZUKI

Institute of Information Sciences, University of Tsukuba, Sakuramura, Niihari-gun, Ibaraki 300-31

(Received December 9, 1978)

A formalism has been developed for the calulation of vibration-rotation energy levels of linear XYZ and X_2Y_2 type molecules through direct numerical diagonalization of vibration hamiltonian matrix. The procedure of evaluating vibration as well as vibration-rotation energies can be described mostly in matrix algebra and thus easily converted to computer languages. The N_2O molecule was chosen as an example of numerical treatment. Several approaches have been checked in evaluating B_v and D_v and they are discussed from the view point of accuracy and efficiency in computations. It is found that the variational approach of computing B_v^r, contribution of rotational hamiltonian to B_v, is very efficient and accurate. Some peculiar features of the molecular potential of the X_2Y_2 type molecule are discussed in connection with their adaptation on the direct numerical diagonalization method.

There has been an increasing number of studies on the direct numerical diagonalization method of vibrational hamiltonian matrix in terms of a large number of harmonic oscillator basis wave functions.[1-7] The major advantages of reducing the vibrational hamiltonian numerically to fit the observed spectroscopic quantities are threefold. (1) Accidental degeneracies, which require special and somewhat cumbersome treatments in conventional perturbation method, are automatically taken care of. (2) Higher order terms in vibrational potential as well as in expansions of moment of inertial tensor are incorporated without changing the general scheme of computations. (3) Orthonormal vibrational wave functions are readily available through diagonalization as linear combinations of basis harmonic oscillator wave functions. These wave functions may be used to compute any average molecular properties in a given vibrational state.

It is also possible, at least in principle, to apply this method to individual vibration-rotation energy levels. The Coriolis coupling terms in the hamiltonian, however, interact the ro-vibrational states with $\Delta l=\pm 1$ in linear polyatomic molecules, and the factorization is no longer possible for the vibration-rotation states with $J\neq 0$. Therefore, an entire vibration-rotation hamiltonian matrix (unfactorized) must be solved at a time, which forces to use a huge number of basis wave functions (usually products of harmonic oscillator wave function and symmetric rotor type wave function). Since the vibration-rotation coupling constants are as important as the vibrational wavenumbers themselves in the determination of molecular force field, several less rigorous methods have been proposed to calculate vibration-rotation levels. Recent studies of Whiffen *et al.*[6,7] on the OCS molecule have made a significant contribution to this field.

This is our third report on the above subject and the method previously reported (hereafter referred to as I and II) has been extended to include the XYZ and X_2Y_2 type linear molecules. It is shown that the rotational and Coriolis parts of the vibration-rotation hamiltonian are reduced to almost identical forms for these two types of molecule. Several methods have been tested for the evaluation of vibration rotation levels and in each case these levels are converted to the corresponding rotational constant (B_v) and the centrifugal distortion constant (D_v). The results are compared from the view point of accuracy and efficiency in computations.

Extensive numerical calculations have been made on the N_2O molecule and the results are given in the present paper. This molecule is of particular interest, for we plan to apply the resultant vibrational wave functions to the intensity problem for N_2O. In some cases we also used the OCS molecule so that the direct comparison is possible for the results of Whiffen *et al.*[6,7]

The X_2Y_2 type molecule requires some extra handling since it has two degenerate modes and individual l_4 and l_5 are no longer "good" quantum numbers. The proper treatment in direct diagonalization procedure has also been discussed.

Hamiltonian

The general form of the vibration-rotation hamiltonian of a polyatomic molecule given by Goldsmith, Amat, and Nielsen[8] is reduced to a much simpler form for a linear molecule.[9,10] It is conveniently expressed as the sum of the vibrational, rotational, and Coriolis hamiltonians:

$$\mathbf{H} = \mathbf{H}_{vib} + \mathbf{H}_{rot} + \mathbf{H}_{Cor}, \quad (1)$$

$$\mathbf{H}_{vib} = V_h(q_s^2, j_s^2) + V_{anh}(q_s) + \mathbf{H}'_{vib}, \quad (2)$$

$$\mathbf{H}'_{vib} = B(j_x^2 + j_y^2) = (B/2)(j_+j_- + j_-j_+), \quad (3)$$

$$\mathbf{H}_{rot} = B(J_x^2 + J_y^2) = (B/2)(J_+J_- + J_-J_+), \quad (4)$$

$$\mathbf{H}_{Cor} = -2B(j_xJ_x + j_yJ_y) = -B(j_+J_- + j_-J_+). \quad (5)$$

The definitions for symbols appearing in Eqs. 1—5 are summarized in Table 1. All the operators are dimensionless, hamiltonains and other constants are given in cm^{-1} as in I and II. The reduced moment of inertia, I', can be expressed in the following form.[9,10]

$$I' = I_e[1 + \gamma_1 q_1 + \gamma_s q_s]^2. \quad (6)$$

For the molecules of current interest, the expansion coefficients, γ's, are given as

Table 1. Listings of symbols to describe vibration-rotation hamiltonians

q_s	Dimensionless normal coordinate
j_s	Dimensionless vibrational momentum conjugated to q_s $[j_s=p_s/\hbar=\hbar^{-1}(\partial T/\partial \dot{q}_s)]$
V_h	Harmonic part of vibrational potential
V_{anh}	Anharmonic part of vibrational potential
j_x, j_y	x,y-Components of vibrational angular momenta $(j_x=p_x/\hbar, j_y=p_y/\hbar)$
j_+, j_-	Ladder operators for vibrational angular momenta $(j_\pm=j_x\pm ij_y)$
J_x, J_y	Dimensionless total angular momenta $(J_x=P_x/\hbar, J_y=P_y/\hbar)$
J_+, J_-	Ladder operators for total angular momenta $(J_\pm=J_x\pm iJ_y)$
I_e	Equilibrium moment of inertia
B_e	Equilibrium rotational constant $\hbar=/(4\pi cI_e)$
I'	Instantaneous moment of inertia with correction of Coriolis effect
B	Instantaneous rotational constant defined as $\hbar/(4\pi cI')$

a) The molecular axis coincides with the z-axis.

XY_2: $\gamma_1 = (2B_e/\omega_1)^{1/2}$ $s=3$ $\gamma_3=0$

XYZ: $\gamma_1 = (2B_e/\omega_1)^{1/2}|\zeta_{23}{}^x|$ $s=3$ $\gamma_3=(2B_e/\omega_3)^{1/2}|\zeta_{21}{}^x|$

X_2Y_2: $\gamma_1 = (2B_e/\omega_1)^{1/2}|\zeta_{42}{}^x|$ $s=2$ $\gamma_2=(2B_e/\omega_2)^{1/2}|\zeta_{41}{}^x|$

This is the results from the fact that only $a_1{}^{xx}=a_1{}^{yy}$ and $a_s{}^{xx}=a_s{}^{yy}$ are nonvanishing among the derivatives of moment of inertia with respect to normal coordinate: *i.e.* $a_{s\sigma}^{\alpha\beta}=(\partial I^{\alpha\beta}/\partial Q_{s\sigma})$. See, for example, Eq. 17 of Ref. 10. The phases of normal coordinates q_1 and q_s are taken so that the coefficients $a_1{}^{xx}$ and $a_s{}^{xx}$, and thus γ_1 and γ_s, are positive. Taking the reciprocal of I' and expanding it in terms of the related normal coordinates, B is given as

$$B = B_e\sum_{k=0}(-1)^k(k+1)(\gamma_1q_1+\gamma_sq_s)^k$$
$$= B_e[1+\sum_{k=1}(-1)^k(k+1)(\gamma_1q_1+\gamma_sq_s)^k]. \quad (7)$$

Equation 7 reflects the vibrational effects on rotational constants through the changes in moment of inertia. Coupling between the vibrational and rotational angular momenta also affects vibration-rotation energies. Vibrational angular momentum operators $j_\pm$ are given as the sum of

$$j_\pm = \sum_{i=1}^{m} j_\pm^{(s_i,d_i)}, \quad (8)$$

where m is a number of nonvanishing Coriolis coupling constants, s_i and d_i denote nondegenerate and degenerate dimensionless normal coordinates associated with the Coriolis coupling constant. Each term in summation is given as

$$j_\pm^{(s,d)} = \pm i\cdot\zeta_{ds}{}^x[(\omega_d/\omega_s)q_sp_\pm-(\omega_s/\omega_d)j_sq_\pm], \quad (9)$$

where $q_\pm=q_{dx}\pm iq_{dy}$ and $p_\pm=j_{dx}\pm ij_{dy}$ and the suffix i for the coordinate is dropped in Eq. 9. For the present case, the relevant indeces are:

XY_2: $m=1$ $(s_1=3, d_1=2)$,

XYZ: $m=2$ $(s_1=1, d_1=2)$ and $(s_2=3, d_2=2)$,

X_2Y_2: $m=3$ $(s_1=1, d_1=4)$, $(s_2=2, d_2=4)$, and $(s_3=3, d_3=5)$

Substitutions of $j_\pm$ into Eqs. 3 and 5 yield the final forms of hamiltonians in terms of dimensionless normal coordinates and their conjugate momenta.

Energy Levels

Vibrational Energy and Its Matrix Representation. Pure vibrational energies are determined from harmonic and anharmonic potential as well as from squared angular vibrational momenta designated as $\mathbf{H}'_{vib}$ in Eq. 3. The number of nonvanishing force constants are

Table 2. Non-vanishing force constants in general quartic force field

	Quadratic[a]	Cubic	Quartic	Total
XY_2	3	3	6	12
XYZ	4	6	9	19
X_2Y_2	6	11	23	40

a) This column corresponds to the sum of harmonic frequencies and independent Coriolis coupling constant(s) in normal coordinate space. Because of the Coriolis sum rule, only one Coriolis coupling constant is independent in XYZ and X_2Y_2 type molecules. (None in XY_2 type)

tabulated in Table 2 for the three types of linear molecules. As in II, the force constants in curvilinear internal coordinates are transformed into normal coordinate space. It is also convenient to set up the vibrational hamiltonian matrix as the sum of its component matrices for individual force constants.

$$\boldsymbol{H}_v = \sum_{i=1}^{f+1} k^{(i)}\boldsymbol{Z}^{(i)}, \quad (10)$$

where f is a total number of force constants, $k^{(i)}$ could be either ω_s, $k_{ss's''}$ or $k_{ss's''s'''}$. The matrix element $Z_{nn'}^{(i)}$ is defined as

$$Z_{nn'}^{(i)} = \langle n|U^{(i)}(q)|n'\rangle \quad (11)$$

If $k^{(a)}=k_{111}$, for example, $U^{(a)}=q_1{}^3$, and if $k^{(b)}=k_{1122}$, then $U^{(b)}=q_1{}^2q_2{}^2$, $|n\rangle$ represents harmonic oscillator wave function. To be more precise it is either $|n\rangle=|n_1, n_2, l_2, n_3\rangle$ or $|n_1, n_2, n_3, n_4, l_4, n_5, l_5\rangle$. It is convenient to include the term arising from $\mathbf{H}'_{vib}$ in $\boldsymbol{Z}^{(i)}$ and treat as if it were the $(f+1)$th force constant, *i.e.* $k^{(f+1)}=B_e$ and $Z_{nn'}^{(f+1)}=(1/2)\langle n|j_+j_-+j_-j_+|n'\rangle$+higher terms. By selecting a proper set of basis functions, $\boldsymbol{H}_v$ is divided into a desired number of symmetry manifolds (σ, π, δ, $\cdots$), each of which may be treated seperately. Then the eigenvalue problem is solved which yields a diagonal eigen value matrix $\boldsymbol{W}_v$ and the eigen vector matrix $\boldsymbol{A}_v$, the n-th column corresponds to the eigenvector of the n-th eigenvalue.

$$\boldsymbol{H}_v\boldsymbol{A}_v = \boldsymbol{A}_v\boldsymbol{W}_v \quad (12)$$

As described in I and II, only a limited number of lower eigenvalues, which is of immediate interest to us, is usually obtained by a modified Givens-Housholder method for symmetric matrices.[11] Therefore, $\boldsymbol{A}_v$ is not necessarily a square matrix but may be considered as a rectangular matrix. A set of orthonormal vibrational wave functions is readily obtained as a linear combination of the harmonic oscillator wave functions:

$$|v\rangle = \sum_n a_{vn}|n\rangle, \tag{13}$$

where a_{vn} is a corresponding element of $\boldsymbol{A}_v$.

Vibration-rotation Energy. The contributions from $\mathbf{H}_{rot}$ as well as from $\mathbf{H}_{Cor}$ must be considered to obtain the rotational energies of a given vibrational state. The basis function is usually in the form of $|n,J\rangle=|n\rangle\cdot|J\rangle$, the latter being a symmetric rotor type wave function. Since the matrix elements are diagonal with respect to J, the vibration-rotation hamiltonian matrix may be set for any required value of J. Since the operators $J_x^2+J_y^2$ can be replaced by $[J(J+1)-l^2]$ for practical purposes, the effect of $\mathbf{H}_{rot}$ is most conveniently treated as the $(f+2)$th component of $\boldsymbol{Z}$:

$$\boldsymbol{H}_r(J) = k^{(f+2)}\boldsymbol{Z}^{(f+2)}, \tag{14}$$

$$k^{(f+2)} = B_e[J(J+1)-l^2], \tag{15}$$

$$Z_{nn'}^{(f+2)} = \sum_{k=0}(-1)^k(k+1)[\sum_{m=0}^{k} {}_kC_m\gamma_1^{k-m}\gamma_s^m \times\langle n|q_1^{k-m}q_s^m|n'\rangle| \tag{16}$$

The γ's are given in Eq. 6 and ${}_kC_m=k!/[m!(k-m)!]$. The contribution from $\mathbf{H}_{rot}$ may be obtained either by diagonalizing directly $\boldsymbol{H}_{vr}(J)$

$$\boldsymbol{H}_{vr}(J) = \boldsymbol{H}_v + \boldsymbol{H}_r(J) = \sum_{i=1}^{f+2} k^{(i)}\boldsymbol{Z}^{(i)},$$

$$\boldsymbol{H}_{vr}(J)\boldsymbol{A}_{vr}(J) = \boldsymbol{A}_{vr}(J)\boldsymbol{W}_{vr}(J) \tag{17}$$

or by using a variation method: $\boldsymbol{Z}^{(f+2)}$ is transformed by $\boldsymbol{A}_v$ in Eq. 12 and the diagonal elements are taken to represent the rotational contribution.

$$\boldsymbol{W}_{vr}(J) \cong \boldsymbol{W}_v + k^{(f+2)}[\tilde{\boldsymbol{A}}_v\boldsymbol{Z}^{(f+2)}\boldsymbol{A}_v]_{diagonal} \tag{18}$$

In either case we define $\boldsymbol{W}_v^r(J)$ as the contribution from $\mathbf{H}_{rot}$ to the energy specified by J and v.

$$\boldsymbol{W}_v^r(J) = \boldsymbol{W}_{vr}(J) - \boldsymbol{W}_v = \boldsymbol{W}_{vr}(J) - \boldsymbol{W}_{vr}(0) \tag{19}$$

The Coriolis hamiltonian, $\mathbf{H}_{Cor}$, consists essentially of the products of the total and vibrational angular momentum operators and thus has no diagonal matrix elements with respect to vibrational quantum numbers. The total hamiltonian matrix with an arbitary nonzero J is schematically shown in Fig. 1, where each small square represents the submatrix of the size up to 200 by 200 and a superscript l specifies symmetry manifold. Let this total hamiltonian matrix be $\boldsymbol{H}(J)=\boldsymbol{H}_{vrc}(J)$, then the ultimate purpose of our calculation is to obtain $\boldsymbol{W}(J)$ in Eq. 20,

$$\boldsymbol{H}(J)\boldsymbol{A}(J) = \boldsymbol{A}(J)\boldsymbol{W}(J) \tag{20}$$

We may also define $\boldsymbol{W}_v^c(J)$ as the contribution from $\mathbf{H}_{Cor}$,

$$\boldsymbol{W}_v^c(J) = \boldsymbol{W}(J) - \boldsymbol{W}_{vr}(J) = \boldsymbol{W}_{vrc}(J) - \boldsymbol{W}_{vr}(J) \tag{21}$$

However, the total hamiltonian matrix for the states with $|l|\leq 3$ is well over one thousand. This total hamiltonian matrix may be divided into two blocks (so called c- and d-states) by taking symmetric and antisymmetric combinations of the basis functions with respect to $\pm l$, which seperates the l-type doublets (see Fig. 2). Still the size of the matrices is beyond the present practical limit and introduction of a certain approximation is inevitable. The second-order perturbation theory was used in II to calculate the Coriolis effects, however, this method requires summation over the third vibrational states and takes considerable computing time. A double diagonalization method is employed in the present case, which is almost equivalent to the perturbation method, but is much simpler to handle in computer since each step is described by matrix algebra. First, we start with $\boldsymbol{A}_{vr}^l(J)$ in Eq. 17, which is rectangular in most cases, a superscript being added again to specify the symmetry manifold. The original $\boldsymbol{H}_c^{ll'}$ matrices are successively transformed by using the related $\boldsymbol{A}_{vr}^l$ and $\boldsymbol{A}_{vr}^{l'}$, where $l'=l\pm 1$. Finally an assembly of the transformed matrices is diagonalized again to yield (approximate) solutions, $\boldsymbol{W}(J)$. The total process is schematically shown in Fig. 3.

The rotational levels in the n-th vibrational state are given for linear molecules as

$$E_v(J) = \nu_0(v) + B_v[J(J+1)-l^2] - D_v[J(J+1)-l^2]^2 + \cdots \tag{22}$$

where B_v and D_v are the rotational and centrifugal

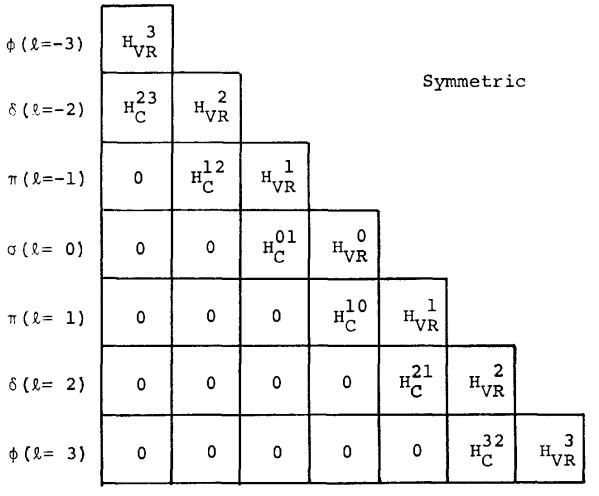

Fig. 1. A full vibration-rotation hamiltonian matrix with $|l|\leq 3$. Each square represents the matrix of size up to 200 by 200. The Coriolis hamiltoniam matrix $\boldsymbol{H}_C$ is off-diagonal with respect to l. For rotationless state ($J=0$), $\boldsymbol{H}_C$ vanishes and each $\boldsymbol{H}_{VR}$ matrix can be treated separately.

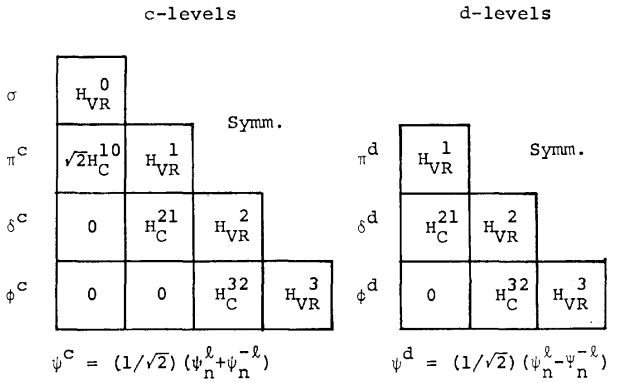

Fig. 2. The seperation of c- and d-states which causes l-type doubling. It is easily seen from the figure that π-states are most strongly affected.

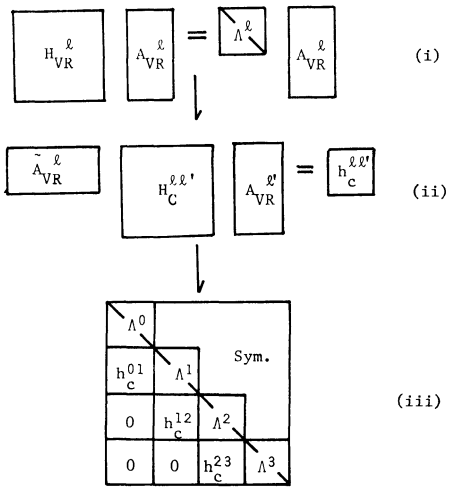

Fig. 3. Schematic representation of double diagonalization procedure. (i) The first diagonalization of $\boldsymbol{H}^{l}_{\mathrm{VR}}$ (The matrix size is usually 200 by 200, and $l=0, 1, 2, \cdots$) The lowest fortv eigenvalues are obtained: $\boldsymbol{\Lambda}^{l}$ is a diagonal matrix of 40 by 40 and $\boldsymbol{A}^{l}_{\mathrm{VR}}$ is an eigen vector matrix of 40 by 200. (ii) Transformation of $\boldsymbol{H}^{ll'}_{\mathrm{C}}$ matrix (iii) Reassembled matrix which is subjected to the second diagonalization to yield (approximate) solutions to $W(J)$ in Eq. 20.

distortion constants, respectively. They are usually determined from the observed transitions experimentally. Theoretical values of B_{v} and D_{v} are obtained by solving Eq. 12 first, then Eq. 20 for two different nonzero J's, say 5 and 10. The contributions from $\mathbf{H}_{\mathrm{rot}}$ and $\mathbf{H}_{\mathrm{Cor}}$ to B_{v} and D_{v} may be written as

$$B_{\mathrm{v}} = B_{\mathrm{e}} + B_{\mathrm{v}}^{\mathrm{r}} + B_{\mathrm{v}}^{\mathrm{c}} \tag{23}$$

and

$$D_{\mathrm{v}} = D_{\mathrm{e}} + D_{\mathrm{v}}^{\mathrm{r}} + D_{\mathrm{v}}^{\mathrm{c}} \tag{24}$$

Each term in Eqs. 23 and 24 gives a good measure for the effect of $\mathbf{H}_{\mathrm{rot}}$ or $\mathbf{H}_{\mathrm{Cor}}$ and can easily be obtained from $W_{\mathrm{v}}^{\mathrm{r}}(J)$ and $W_{\mathrm{v}}^{\mathrm{c}}(J)$. The calculated values of $B_{\mathrm{v}}^{\mathrm{r}}$ and $B_{\mathrm{v}}^{\mathrm{c}}$ are used to compare the results of different approaches and approximations.

The variational method given in Eq. 18 for evaluation of $B_{\mathrm{v}}^{\mathrm{r}}$ and the analytical method of Foord, Smith, and Whiffen (hereafter referred to as FSW method[6]) have also been tested. The latter uses the analytical expressions derived from the second-order perturbation theory, however, the vibrational quantum numbers in the expression are replaced by the "averaged" quantum numbers obtained from the perturbed wave functions. Their formula can easily be extended to cover X_2Y_2 type molecules and it is in the following form,

$$B_{\mathrm{v}}^{e} = \sum_{i=1}^{m} (\zeta_{\mathrm{ds}}^{x})^2 \left[2f(\omega_{\mathrm{s}}, \omega_{\mathrm{d}}) \left(\hat{n}_{\mathrm{s}} + \frac{1}{2} \right) + f(\omega_{\mathrm{d}}, \omega_{\mathrm{s}})(\hat{n}_{\mathrm{d}} + 1) \right], \tag{25}$$

where $f(x,y)=(3x^2+y^2)/[x(x^2-y^2)]$, $\hat{n}_{\mathrm{s}}$ and $\hat{n}_{\mathrm{d}}$ are averaged contributions of n_{s} and n_{d} to a particular vibrational level. Their values are readily obtained from the corresponding $a_{\mathrm{v}n}$'s. Although this treatment ignores certain off-diagonal effects, it is nonetheless an attractive approximation if it works reasonably well, since this approach requires only $\boldsymbol{A}_{\mathrm{v}}$ in Eq. 12 and the second diagonalization process may be skipped altogether.

Computational Procedures

Most of numerical computations have been carried out by a Hitac 8800/8700 system in Computer Centre in the University of Tokyo. As described in II the harmonic oscillator basis functions are specified either by a set of four integers corresponding to n_1, n_2, n_3, and l_2 for XYZ or by a set of seven integers corresponding to n_1 through n_5, l_4 and l_5 for X_2Y_2. A desired number of basis functions is systematically generated with the condition $\sum_{\mathrm{s}} n_{\mathrm{s}} \leq n_{\max}$ ($l_{\mathrm{t}}=n_{\mathrm{t}}, n_{\mathrm{t}}-2, \cdots 1$ or 0). For the case of N_2O, l_2 uniquely specifies the symmetry species, while the following simple rule applies for X_2Y_2.

(1) $n_3 + n_5$ (even, odd) (g, u)

(2) $l = l_4 + l_5$ (0, 1, 2, 3, $\cdots$) ($\sigma, \pi, \delta, \phi, \cdots$)

The generation of matrix elements was described in II in detail and it is not repeated here. As indicated in Eq. 8, the vibrational angular momentum operators $j_{\pm}$ have more than one term in the present case. The evaluation of $Z_{nn'}^{(f+1)}$ involves the product of operator $j_{+}^{(s_i,d_i)} \cdot j_{-}^{(s_j,d_j)}$ with $i \neq j$. Therefore, the treatment of $\mathbf{H}'_{\mathrm{vib}}$ has been modified to incorporate the cases mentioned above. A modified version of the Givens-Housholder method for real symmetric matrices, which allows to compute a limited number of either lowest or highest eigenvalues has been used as in II. Usually 200 basis functions are used for each symmetry species and the lowest 40 eigenvalues and eigenvectors are obtained; This saves considerable computing time and memories as compared with the case where a full set of eigenvalues and eigenvectors is forced to acquire.

Results and Discussion

The general quartic force field previously determined for the nitrous oxide molecule[12] has been used in the present calculation. These force constants are transformed into dimensionless normal coordinate space and their values are listed in Table 3. Within the framework of the second-order perturbation scheme three quartic force constants, k_{1113}, k_{1333}, and k_{1223} do not contribute to the vibrational energy and thus their values were not listed in the original paper,[12] however, they are all included in the present calculation. The bond lengths initially used were the same as those

Table 3. Force constants of N_2O in dimensionless normal coordinates (cm^{-1})

ω_1	1300.44	k_{1111}	2.96
ω_2	596.49	k_{1113}	−8.59
ω_3	2281.57	k_{1122}	−10.15
		k_{1133}	20.10
k_{111}	−59.72	k_{1223}	2.76
k_{113}	80.76	k_{1333}	1.66
k_{122}	54.40	k_{2222}	2.13
k_{133}	−226.60	k_{2233}	−30.40
k_{223}	51.06	k_{3333}	7.14
k_{333}	−64.82		

previously given.[12] Later the more recent values of $r_e(NN)=1.1282$ and $r_e(NO)=1.1843$ Å are used, which yield $B_e=0.4211312$ cm^{-1}. [13]

The requirement of $a_1^{xx}>0$ and $a_3^{xx}>0$ determines the phases of q_1 and q_3 uniquely. The transformation coefficients from mass-adjusted Cartesian to dimensionless normal coordinates (Nielsen's $l_{is\sigma}$[14]) are as follows.

$l_{is\sigma}$	z_1 (N)	z_2 (N)	z_3 (O)
q_1	−0.6184	−0.1952	0.7612
q_3	−0.5471	0.8023	−0.2387
	x_1 (y_1)	x_2 (y_2)	x_3 (y_3)
$q_{2x}(q_{2y})$	−0.4228	0.8247	−0.3760

TABLE 4. CALCULATED VIBRATIONAL LEVELS OF N_2O AND THEIR CONVERGENCE TEST.

The major components of eigenvector coefficients a_{vn}'s are also given.

v	$\nu(200)$[a]	$\Delta\nu(150)$[b]	Major components of a_{vn}[c]
(1) σ-state ($l_2=0$)			
1	0.00	0	0.996(000)[d]
2	1167.51	1	0.944(020) 0.316*(100)
3	1284.08	2	0.925(100) 0.320(020)
4	2223.41	5	0.967(001)
5	2316.40	2	0.828(040) 0.533*(120)
6	2460.88	4	0.706(120) 0.520(040) 0.430*(200)
7	2559.20	10	0.807(200) 0.437(120) 0.263(300)
8	3362.60	8	0.935(021) 0.253*(101)
9	3446.60	8	0.695(060) 0.636*(140) 0.262(220)
10	3479.67	34	0.850(101) 0.313(021)
15	4489.16	38	0.829(041) 0.472*(121)
20	4899.29	155	0.590(320) 0.499*(160) 0.409*(080) 0.223*(400)
(2) π-state ($l_2=1$)			
1	588.67	0	0.998(010)
2	1746.84	0	0.901(030) 0.420*(110)
3	1878.23	2	0.890(110) 0.422(030)
4	2795.99	7	0.971(011)
5	2886.33	2	0.769(050) 0.592*(130)
6	3043.30	6	0.569(130) 0.566(050) 0.551*(210)
7	3158.18	14	0.738(210) 0.546(130) 0.237(050) 0.211(310)
8	3929.43	12	0.897(031) 0.355*(111)
9	4006.93	11	0.652(150) 0.634*(070) 0.324*(230)
10	4054.22	49	0.826(111) 0.359(031) 0.276(211)
15	5048.57	48	0.767(051) 0.542*(131)
20	5470.11	215	0.547(330) 0.432*(171) 0.430*(090) 0.327*(410)

a) $\nu(n)$ in cm^{-1}: obtained by solving $n\times n$ eigenvalue problem. b) $\Delta\nu(m)$ in 10^{-2} cm^{-1}: $\Delta\nu(m)=\nu(m)-\nu(200)$. c) Asterisks indicate negative coefficients. d) The basis functions are given as a set of three integers $(n_1n_2n_3)$, l_2 is omitted since it is constant in a given symmetry block.

The molecular axis coinsides with z-axis, the phases of q_{2x} and q_{2y} are chosen so that they go smoothly to the case of the XY_2 type molecules where ζ_{23}^x is taken to be +1.0.

Convergence Test. As described in I and II, the accuracy of the present treatment depends on the number of the basis functions used. Ten lowest wavenumbers of the σ- and π-species with 200 basis functions are listed in Table 4 along with the 15 and 20th wavenumbers for comparison. In this case n_{max} is about 13 which is smaller than the corresponding value of 19 for XY_2, because of lower symmetry. Calculation has also been made with 150 basis functions and the differences in wavenumbers are entered in the second column of Table 4. Also listed are some coefficients a_{vn}'s which contribute significantly to the vibrational levels in Table 4. Similar treatment has been done for the calculated values of B_v^r and the results are given in Table 5. The terms up to $k=4$ in Eq. 7 are retained in $\mathbf{H}_{rot}$. The accuracy of the computed B_v^c depends on the second factor, namely the number of eigenvalues and eigen-

TABLE 5. CALCULATED ROTATIONAL CONSTANTS OF N_2O AND THEIR CONVERGENCE TEST

All Units are given in 10^{-6} cm^{-1}.

v	B_v-B_0	B_v^r	ΔB_v^r	B_v^c	ΔB_v^c (I)	ΔB_v^c (II)	ΔB_v^c (III)
(1) σ-state ($l_2=0$)							
1	0	−2030	0	−127	0	0	2
2	928	−378	0	−851	0	0	26
3	−1872	−3881	1	−148	0	0	22
4	−3363	−5930	2	410	0	2	−46
5	1787	1144	1	−1513	1	3	85
6	−1010	−2237	3	−929	−1	2	13
7	−3692	−5648	8	−201	0	1	−40
8	−2458	−4310	5	−305	−1	13	63
9	2708	2715	0	−2163	0	25	166
10	−5185	−7799	24	457	1	0	−125
15	−1555	−2793	27	−918	−6	749	81
20	−2161	−2943	101	−1375	−11	108	−212
(2) π-state ($l_2=1$)							
1	511	−1110	0	−536	0	0	18
2	1370	427	1	−1213	−1	0	61
3	−1335	−2869	2	−622	0	0	2
4	−2933	−5079	3	−10	−1	5	23
5	2241	1948	0	−1863	0	11	133
6	−650	−1501	5	−1305	0	10	58
7	−3114	−4517	12	−754	−1	6	−19
8	−2036	−3523	8	−669	−5	287	38
9	3232	3572	1	−2495	−1	307	208
10	−4750	−6898	29	−9	4	125	−115
15	−739	−2020	29	−876	10	*	443
20	−1047	−2312	137	−892	−47	*	*

$B_v=B_v(40/200)$, $B_v^r=B_v^r(40/200)$, and $B_v^c=B_v^c(40/200)$. (m/n) means that the value is calculated from an n by n eigenvalue problem, and the lowest m eigenvalues are obtained.

$\Delta B_v^r=B_v^r(40/150)-B_v^r$, $\Delta B_v^c(I)=B_v^c(40/150)-B_v^c$, $\Delta B_v^c(II)=B_v^c(30/200)-B_v^c$, and $\Delta B_v^c(III)=B_v^c(FSW)-B_v^c$, where $B_v^c(FSW)$ is estimated from Eq. 25.

vectors actually obtained. By varying this number with the fixed basis functions, another convergence test is performed for B_v^c. Only a leading term is retained in $\mathbf{H}_{Cor}$ so that direct comparison is possible for the FSW method in dealing $\mathbf{H}_{Cor}$. The last column in Table 5 shows the differences of B_v^c's computed by the two different methods.

The convergence test for wavenumbers and rotational constants has a markedly similar trend to that of CO_2. This result is in accordance with the earlier conclusion (II) that γ_s is a good measure for the convergence. The value $\gamma_1(N_2O)=0.025$ is very close to that of $\gamma_1(CO_2)=0.024$. The value of γ_3, which is zero for XY_2, is still very small (0.0036). It is gratifying to know that for most low-lying vibrational levels, the present method of the 200 basis functions with the 40 eigenvalues yields the wavenumbers and rotational constants free from the truncation effect of matrix sizes. It must be pointed out here, however, that the 10th lowest wavenumber of N_2O in the π-species, for example, is around 4000 cm^{-1} which is much lower than the corresponding value of 7000 cm^{-1} for the π_g-species of CO_2. A test run for the OCS molecule, of which γ_1 value is 0.021, has been attempted. This molecule shows much quicker convergence than N_2O.

As mentioned earlier, the quartic force constants k_{1333}, k_{1223}, and k_{1113}, do not contribute to the vibrational energies within the second-order perturbation theory. To see the actual effects of these force constants, the calculation is proceeded to drop these force constants one at a time. The results are summarized in Table 6, where only differences in 10^{-2} cm^{-1} are given. Table 6 shows in a way a limitation of the second order perturbation theory. The effect of k_{1113} is the largest, but this may be due to its relatively large value.

If we compare the present results with those calculated earlier by perturbation theory, discrepancies as large as 20 cm^{-1} are found for some levels involved in Fermi resonance. This has also been observed for the CO_2 molecule. More strictly, the quintic force constants, k_{11122}, k_{12222}, and k_{12233} must be considered to make the present calculation directly comparable with that of perturbation theory, since these quintic force constants were implicitly included as the parts of the third-order parameters in Fermi resonance.[12] This has not been tested, although the values of these force constants have become available recently.[15] The agreements of wavenumbers and rotational constants are much better for the levels which are relatively free from the effect of Fermi resonance. For example, discrepancies are within 0.6 cm^{-1} for the 001 and 002 levels located at 2223.7 and 4417.3 cm^{-1}, respectively.

Variational Method in Computing B_v^r. Off-diagonal matrix elements of transformed $\boldsymbol{Z}$ matrix were ignored in Eq. 18. This may be justified since the off-diagonal elements contribute mostly to higher order rotational terms: $[J(J+1)-l^2]^n$, where n is greater than one. The equation may be rewritten so as to give the explicit expression for B_v^r,

$$B_v^r = B_e[\tilde{\boldsymbol{A}}_v \boldsymbol{Z}^{(J+2)} \boldsymbol{A}_v]_{diagonal} \qquad (26)$$

The B_v^r values computed from Eq. 26 are found to agree almost exactly with those obtained by solving Eq. 17 successively with three J's (0, 5, 10) and then fitting the energies to Eq. 22. Discrepancies are less than 10^{-8} cm^{-1}. The agreements are less perfect ($\simeq 5\times10^{-6}$ cm^{-1}) if we drop the centrifugal term in Eq. 22 and fit the remaining two parameters from the results of $J=0$ and $J=5$, as has been done in II. In a way this is a numerical verification that Eq. 26 holds rigorously since B_v^r is a coefficient of $[J(J+1)-l^2]$, which is the leading term in the rotational energy expansion. It also implies that the consideration of centrifugal distortions is required to obtain an accurate value of rotational constant.

FSW Method in Evaluating B_v^c. Although the Coriolis coupling is considered as the second-order effect, the B_v^c values are far from negligible. On the average the $|B_v^c|$ value is smaller than the $|B_v^c|$ value, however, in some vibrational levels this tendency is reversed. The treatment of $\mathbf{H}_{Cor}$ may be the most cumbersome and time-consuming in the direct diagonalization procedure and this makes the FSW method mentioned earlier quite attractive. In the last column of Table 5 entered the calculated differences of B_v^c. The discrepancies are in the order of 10 to 15%. This was rather expected since Eq. 25 was derived by dropping some off-diagonal terms: Eq. 25 is independent of the sign of

Table 6. Effects of "Off-Diagonal" force constants to vibrational frequencies[a]

σ-species	k_{1333} (1.66)	k_{1223} (2.76)	k_{1113} (−8.59)	π-species	k_{1333} (1.66)	k_{1223} (2.76)	k_{1113} (−8.59)
1	0	0	0	1	1	1	−2
2	−2	−9	9	2	−4	−33	21
3	11	21	−135	3	18	58	−165
4	−9	−3	−133	4	−3	−1	−126
5	−10	−86	50	5	−16	−160	−85
6	18	85	−163	6	19	95	−191
7	28	60	502	7	45	161	−624
8	−6	−4	119	8	−9	−16	−116
9	−25	−273	149	9	−34	−420	224
10	13	35	788	10	57	86	−779
15	−22	43	−94	15	−34	94	−69
20	54	301	835	20	−25	306	−880

a) Only the differences are listed in 10^{-2} cm^{-1}: $\Delta\nu=\nu$(without k listed in column head) $-\nu(200)$.

ζ's, while sign dependent terms are expected as off-diagonal contribution.[7] However, the overall errors due to this are relatively small for the total computed value of B_v. In addition, this method is not affected by the second truncation problem discussed earlier. It is more robust and may give better approximation for higher vibrational levels.

If only wavenumbers and rotational constants are to be computed, the logical approach is to solve pure vibrational hamiltonian, Eq. 12, and then to apply Eqs. 25 and 26 to obtain B_v^r and B_v^c, respectively. This is particularly useful in the refinement process in which a number of cycles of calculations should be carried out. The more exact method may be applied in the final stage of refinement.

Centrifugal Distortion and l-Type Doubling Constants. If the centrifugal distortion constants are also to be computed, the procedure given in Eq. 12 through Eq. 21 cannot be avoided. To obtain an accurate D_J value the third-order term $H_J[J(J+1)-l^2]^3$ should be added to Eq. 22 and the four parameters must be fit from four sets of calculations ($J=0$ and three nonzero J's). This has already been done by Whiffen for the OCS molecule.[7] The present calculation shows that the D_v^r values are almost constant and in the range of 35—40 (10^{-8} cm^{-1}). The variations of the D_v values seem to arise mostly from D_v^c, the contribution of $\mathbf{H}_{Cor}$ to D_v.

Table 7. Observed and calculated l-type doubling constants (q_v) for the π-species of N_2O in the unit of 10^{-6} cm^{-1}

Level	Obsd	Ref	Calcd
1	792	a	834
2			1556
3	909	a	988
4	777	a	819
5			2252
6			1724
7	1075	a	1190
8	1459	b	1518
9			2918
10	883	b	928

a) Ref. 16. b) Ref. 17.

The l-type doubling constants are obtained by a procedure analogous to that given in II (see also Fig. 2). The comparison of experimental and calculated constants are listed in Table 7. Just in the cases of CO_2 and CS_2, the calculated values slightly exceed the observed values, but overall profile is well represented by the calculation.

The X_2Y_2 Type Molecule. Acetylene may be an only X_2Y_2 type molecule on which the general quartic force field has been studied in some detail.[18-20] Numerical computations were carried out by using a modified GVFF[19] to test an extended portion of the direct diagonalization procedure. However, the details of numerical computations are not given here. Acetylene has two CH stretching fundamentals over 3000 cm^{-1}, it seems necessary to use more than 200 basis functions because of slower convergence. Rotational expansion is also slow in convergence with $\gamma_2=0.033$. Peculiar features of the X_2Y_2 molecular potential and their treatment in the direct diagonalization method are briefly described here. This type of molecule has non-vanishing force constants k_{345} (k_{1345} and k_{2345} as well) and k'_{4455} which appear in V_{anh} as[21]

$$k_{345}q_3r_4r_5\cos(\chi_4-\chi_5) \text{ and } k'_{4455}r_4^2r_5^2\cos(2\chi_4-2\chi_5).$$

They have off-diagonal matrix elements with respect to individual l_s, although the final matrix elements are always diagonal with respect to $l=l_4+l_5$. These force constants cause the well-known vibrational l-type doubling or resonance. In the σ_g- and σ_u-species, it is possible to reduce the size of hamiltonian matrices by taking linear combinations such as $|1^1 1^{-1}\rangle \pm |1^{-1}1^1\rangle$. However, the merit of taking similar combinations diminishes in the states with $l \neq 0$. In the present calculation no attempts have been made to separate + and − states. They are mixed in the σ_g- or σ_u-species, but their symmetries are obvious from the corresponding signs of a_{vn}'s.

The angular parts as well as the radial parts of degenerate normal coordinates have to be considered in evaluating the matrix elements associated with the above force constants, the subroutine OPERR is modified to allow this type of operations.

Concluding Remarks. A general algorithm for the direct diagonalization method of vibrational hamiltonian matrix has been extended to the XYZ and X_2Y_2 type linear molecules. The use of matrix algebra makes it easily adaptable to the computer programs. Some improvements have been made on the treatment of vibration-rotation energies. As pointed out in II, the present method yields an improved set of orthonormal vibrational wave functions, which may be used to evaluate an expectation value of any physical property P for a given vibrational level, where P is a function of normal coordinates.

$$\bar{P}_v = \langle v|P(q)|v\rangle = \sum_{n,m} a_{vn}a_{vm}\langle n|P(q)|m\rangle \qquad (27)$$

Formula for the transition moment has been given in II and extensive studies have been done on the dipole moment functions of the CO_2 and N_2O molecules and the vibrational wave functions obtained here are very useful, the details will be given elsewhere.[22]

A part of this work was done while the author was visiting the University of Minnesota. The author expresses his gratitude to Prof. John Overend for his hospitality and fruitful discussions, particularly on the phases of normal coordinates and vibrational wave functions.

References

1) I. Suzuki, *Bull. Chem. Soc. Jpn.*, **44**, 3277 (1971).
2) A. Foord and D. H. Whiffen, *Mol. Phys.*, **26**, 959 (1973).
3) L. A. Gribov and G. V. Khovrin, *Opt. Spectrosk.*, **36**, 475 (1974); *Opt. Spectrosc.*, **36**, 274 (1974).
4) I. Suzuki, *Bull. Chem. Soc. Jpn.*, **48**, 3565 (1975).
5) R. J. Whitehead and N. C. Handy, *J. Mol. Spectrosc.*, **55**, 356 (1975).

6) A. Foord, J. G. Smith, and D. H. Whiffen, *Mol. Phys.*, **29**, 1685 (1975).
7) D. H. Whiffen, *Mol. Phys.*, **31**, 989 (1976).
8) M. Goldsmith, G. Amat, and H. H. Nielsen, *J. Chem. Phys.*, **24**, 1178 (1956); **27**, 838 (1957).
9) G. Amat and L. Henry, *Cahiers Phys.*, **12**, 273 (1958).
10) T. Oka, *J. Chem. Phys.*, **47**, 5410 (1967).
11) J. Ortega, "Givens-Housholder Method for Symmetric Matrices" in "Mathematical Method for Digital Computers," ed by A. Ralston and H. S. Wilf, John Wiley (1967), Vol. 2, pp. 94—115.
12) I. Suzuki, *J. Mol. Spectrosc.*, **32**, 54 (1969).
13) C. Amiot, *J. Mol. Spectrosc.*, **59**, 380 (1976).
14) H. H. Nielsen, *Rev. Mod. Phys.*, **23**, 90 (1951).
15) A. Chedin, C. Amiot, and Z. Cihla, *J. Mol. Spectrosc.*, **63**, 348 (1976).
16) C. Amiot and G. Guelachrili, *J. Mol. Spectrosc.*, **59**, 171 (1976).
17) J. Pliva, *J. Mol. Spectrosc.*, **25**, 62 (1968).
18) I. Suzuki and J. Overend, *Spectrochim. Acta, Part A*, **25**, 977 (1969).
19) I. Suzuki, presented at Symposium of Molecular Structure and Spectroscopy, Fukuoka, Oct. 1969.
20) G. Strey and I. M. Mills, *J. Mol. Spectrosc.*, **59**, 103 (1976).
21) L. Henry and G. Amat, *J. Mol. Spectrosc.*, **5**, 319 (1960).
22) I. Suzuki, *J. Mol. Spectrosc.*, in press.

HeI and HeII Photoelectron Study of N_2O_4

Katsunori NOMOTO, Yohji ACHIBA, and Katsumi KIMURA*

Physical Chemistry Laboratory, Institute of Applied Electricity, Hokkaido University, Sapporo 060

(Received December 11, 1978)

A 304 Å HeII photoelectron spectrum of N_2O_4 in the gaseous phase has been deduced in the region up to 29 eV from a HeII spectrum of NO_2–N_2O_4 mixture obtained with a nozzle beam technique, indicating three new maxima in the region between 20 and 29 eV. A 584 Å HeI spectrum of N_2O_4 was also obtained here. From a comparison of the HeI and HeII spectra of N_2O_4 below 20 eV, it was confirmed that two ionization bands exist at 16.5 and 18.2 eV which appear as shoulders in the HeII spectrum. At least fourteen ionization bands have been identified from the HeII spectrum in the region studied. The thirteen bands below 24 eV have been assigned on the basis of a recent Green's function study of von Niessen *et al.*

It is well known that there exists a monomer-dimer equilibrium between NO_2 and N_2O_4 ($N_2O_4 \rightleftharpoons 2NO_2$) in the gaseous phase. Its thermodynamic properties have been studied extensively by Hisatsune.[1] Anomalous geometric features such as an unusually long N–N distance (1.78 Å) and planar structure for N_2O_4 have been found from a gas-phase electron diffraction study by Hedberg *et al.*[2] Furthermore a relatively high barrier to internal rotation (2.9 kcal mol^{-1}) and a relatively small heat of dissociation (12.7 kcal mol^{-1}) have been reported for N_2O_4 by Snyder and Hisatsune.[3] Because of such anomalous features, N_2O_4 has been received much attention in molecular structure and electronic structure from both experimental and theoretical points of views.

Vacuum UV photoelectron (PE) spectroscopy provides ionization energy data useful for studying valence electron orbitals.[4] HeI and HeII PE spectra of the NO_2 monomer have well been studied by Edqvist *et al.*[5] and Brundle *et al.*[6] For its bonded dimer (N_2O_4), however, there is some difficulty in obtaining PE spectra for N_2O_4 with a conventional PE spectrometer, because of its rapid dissociation in the ionization chamber in which the sample pressure is normally the order of 10^{-3} Torr. In order to overcome this difficulty, special gas inlet systems have recently been used to measure HeI PE spectra for mixtures of NO_2 and N_2O_4 by Ames and Turner,[7] Yamazaki and Kimura,[8] Frost *et al.*,[9] and Gan *et al.*[10] Ames and Turner[7] have used a nozzle inlet system in which rapid expansion of gas takes place by a large pressure difference through a pinhole with a nozzle pressure of about 1 atm. In a previous work in our laboratory, Yamazaki and Kimura[8] have used a long-path cooling inlet system in which the gas sample is cooled to −60 °C. Frost *et al.*[9] have used two kinds of gas samples one of which is a vapor from a frozen N_2O_4 sample condensed in the inlet system and the other is a continuous rapid flow of a cold NO_2 gas (−30—−50 °C). In those works of Ames and Turner[7] and Frost *et al.*,[9] the effused gas in the ionization chamber has been pumped out by an additional pumping system to increase the mole fraction of N_2O_4 up to 60—70%. Gan *et al.*[10] have also used a nozzle inlet system with a pressure near 1 atm.

In each of those PE studies,[7–10] the HeI spectrum of N_2O_4 has been deduced from that of the NO_2–N_2O_4 mixture by subtracting the NO_2 component in an appropriate manner. Spectral assignments already reported on the HeI spectra however differ largely from one another, although they are based on *ab initio* MO calculations. A number of theoretical studies on molecular orbitals of N_2O_4 have been published, employing *ab initio* methods[11–14] and many kinds of semiempirical methods.[15] Very recently, von Niessen *et al.*[16] have carried out *ab initio* many-body Green's function calculations on the photoionization of N_2O_4.

In order to obtain a further information about the photoionization of N_2O_4, in the present work we considered it important to compare HeI and HeII PE spectra with each other in spectral shape and intensity, as well as to find new PE bands in the region above 21 eV.

Experimental

PE measurement by HeI (584 Å) and HeII (304 Å) resonance radiations were carried out with our PE spectrometer with some improvements in the gas inlet system and a data accumulation system. The spectrometer is essentially the same as used previously,[17,18] containing a hemispherical electrostatic analyzer of 10 cm in diameter. The resolution is about 25—30 meV as measured for Ar using 584 Å radiation. The improvements of the gas inlet system and the data accumulation system are the following.

The gas inlet system used here is shown schematically in Fig. 1. Gas sample was introduced into the ionization chamber through a pinhole of a glass tube connected to a 2-litre gas reservoir in which the sample was contained at about 600

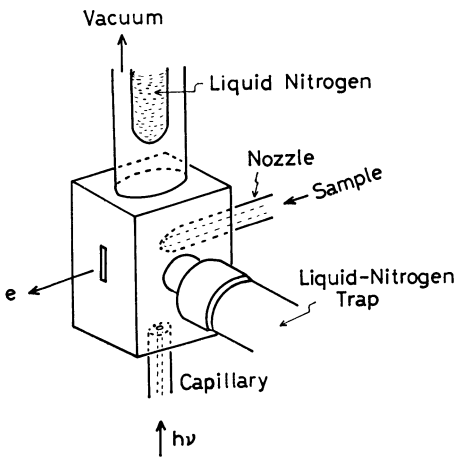

Fig. 1. Schematic drawing of the ionization chamber, the gas inlet system and the cold traps.

Torr. The nozzle pinhole was formed by discharge with a Tesla coil and then appropriately expanded by slowly dissolving in an aqueous HF solution so as to keep the pressure of the ionization chamber in the order of 1×10^{-3} Torr. (The diameter of the pinhole is approximately 50—60 μm.) In order to prevent accumulation of a static charge, the glass nozzle was covered with a brass cap coated by Aquaduck. The effused gas in the ionization chamber was pumped out with two additional diffusion pumps (2″ and 6″) as well as a liquid nitrogen trap, since N_2O_4 rapidly decomposes upon wall collision.

The data accumulating and processing system used consists of a multichannel analyzer (16 bit, 4 K memory) and a computer (YHP 2105-A). The PE spectrum was repeatedly measured, stored in the multichannel analyzer. After improved in signal-to-noise ratio by numerous numbers of repetitions, the data were transferred from the multichannel analyzer to the computer for data analysis. HeI and HeII spectra of pure NO_2 monomer were also measured in order to subtract them from those of the mixture. The procedure of extracting the dimer component is the following. (1) The spectra of both the monomer and the mixture were corrected in intensity for electron collecting efficiency on the basis of the intensity data of N_2, O_2 and CO_2 reported by Gardner and Samson.[19] (2) All the HeI and HeII spectra were smoothed by a moving average method[20] with which five successive points were averaged making each point. The number of points to be averaged was selected as it does not affect spectral resolution seriously. (3) Finally, HeI and HeII spectra of N_2O_4 were obtained from those of NO_2–N_2O_4 mixture by substracting the NO_2 component. Before each substraction, a slight correction for PE kinetic energy was also carried out for the NO_2 spectrum, since the abscissa of the spectrum depends slightly on the sample pressure.[21] (The spectra of NO_2–N_2O_4 mixture and pure NO_2 were observed under different pressure conditions.)

A relatively intense DC-discharge lamp which has recently been designed and constructed in our laboratory[22] was used for measurements of HeII spectra. With this HeII lamp, the PE count rate obtained as a test for the first ionization peak of N_2 was 400 cps under discharge conditions of 500 V, 100 mA and 0.7 Torr He pressure. Under such conditions, count rates of about 70 and 50 cps were obtained at highest peaks for the pure NO_2 and NO_2–N_2O_4 mixed samples.

Results

The HeI PE spectra obtained here for pure NO_2 and a mixture of NO_2 and N_2O_4 are shown in Fig. 2 (a and b, respectively) already corrected for analyzer transmission. The spectrum of pure NO_2 in Fig. 2a was obtained with an ordinary gas inlet system, while the spectrum of NO_2–N_2O_4 mixture in Fig. 2b was obtained with the pinhole nozzle. The spectrum of N_2O_4 in Fig. 2c

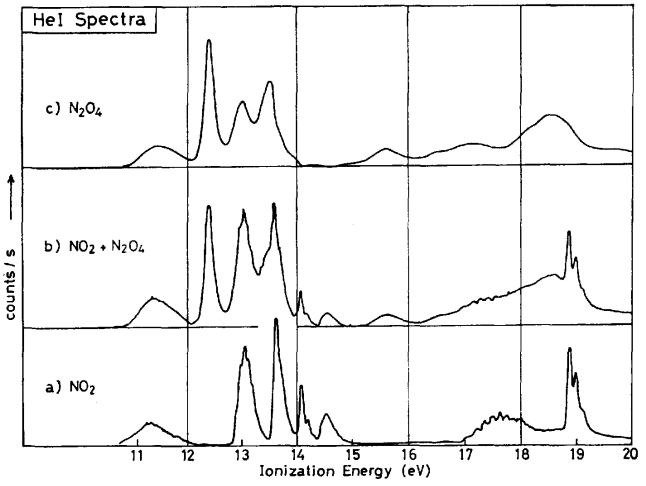

Fig. 2. HeI PE spectra corrected for analyzer transmission. (a) Spectrum of pure NO_2, obtained with a normal inlet system. (b) Spectrum of NO_2–N_2O_4 mixture, obtained with a nozzle inlet system at a total pressure of 600 Torr. (c) Spectrum of N_2O_4, deduced by subtraction of Spectrum a from Spectrum b. Spectra a and b are those already smoothed by a moving averaged method.

Table 1. Vertical ionization energies (eV) obtained here for N_2O_4 and those reported by other workers

This work HeI, HeII (Tentative assignment)[a]	Ames, Turner[b] HeI	Frost *et al.*[d] HeI	Gan *et al.*[e] HeI
$11.4_5\pm0.1$ ($6a_g$)	11.6 ($6a_g$)	11.4 ±0.1 ($6a_g$)	11.4 ($6a_g$)
12.39±0.03 ($4b_{2g}$)	12.4[c] ($1a_u$)	12.35±0.03 ($1a_u$)	12.4 ($4b_{2g}$)
$13.0_5\pm0.1$ ($1a_u$)	12.4[c] ($1b_{1g}$)	13.0 ±0.1 ($1b_{1g}$)	13.0 ($1a_u$)
$13.5_5\pm0.1$ ($1b_{1g}$), ($4b_{3u}$)	13.0[c] ($4b_{2g}$)	13.5 ±0.1 ($4b_{2g}$)	13.4 ($1b_{1g}$)
	13.5[c] ($4b_{3u}$)	15.6 ±0.1 ($4b_{3u}$)	13.5 ($4b_{3u}$)
15.6 ±0.1 ($5b_{1u}$)	15.5 ($5b_{1u}$)	17.1 ±0.2 ($5b_{1u}$)	15.6 ($5b_{1u}$)
16.5 ±0.3 ($1b_{3g}$)	16.9 ($3b_{2g}$)	18.0 ±0.3 ($1b_{3g}$)	17.1 ($1b_{3g}$)
17.2 ±0.3 ($3b_{2g}$)	18.6[c] ($1b_{3g}$)	18.6 ±0.3 ($3b_{2g}$)	18.1 ($3b_{2g}$)
18.2 ±0.3 ($3b_{3u}$)	($3b_{3u}$)		18.6 ($3b_{3u}$)
18.6 ±0.3 ($1b_{2u}$)			19.0 ($1b_{2u}$)
(19.5) ($5a_g$)			19.7 ($5a_g$)
20.7 ($4b_{1u}$)			
22.5 ($4a_g$)			
25.9			

a) Based on the Green's function study of von Niessen *et al.* (Ref. 16). Throughout this paper, the z axis is put on the N–N bond and the y axis is perpendicular to the molecular plane. b) Ref. 7. c) Read from the positions of band maxima. d) Ref. 9. e) Ref. 10.

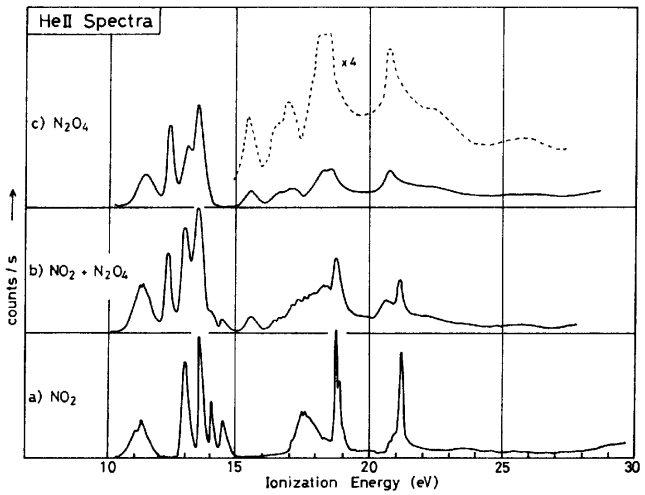

Fig. 3. HeII PE spectra corrected for analyzer transmission. (a) Spectrum of pure NO_2, obtained with a normal inlet system. (b) Spectrum of NO_2–N_2O_4 mixture, obtained with a nozzle inlet system at a total pressure of 450 Torr. (c) Spectrum of N_2O_4, deduced by subtraction of Spectrum a from Spectrum b. Spectra a and b are those already smoothed by a moving averaged method.

was obtained by subtracting a from b. Essentially no NO_2 peaks remain in the subtracted spectrum shown in Fig. 2c.

Similarly, HeII PE spectra obtained here for the monomer and dimer of NO_2 and their mixture are shown in Fig. 3 (a, c, and b, respectively). In the HeII spectrum of N_2O_4 in Fig. 3c, there appear three new maxima at 20.7, 22.5, and 25.9 eV. Results on ionization energies obtained here for N_2O_4 are summarized in Table 1, together with literature data for comparison. Relative intensities of the first five PE bands obtained from the HeI and HeII spectra of N_2O_4 are summarized in Table 2.

TABLE 2. EXPERIMENTAL RELATIVE INTENSITIES (BAND AREAS) IN THE TRANSMISSION-CORRECTED HeI AND HeII SPECTRA OF N_2O_4

Band maximum (eV)	Relative band area	
	HeI	HeII
11.4_5	0.71	1.13
12.39	1.00	1.00
13.0_5	0.8	2.4
13.5_5	1.2	
15.6	0.36	0.49

Discussion

The mole fraction of N_2O_4 in the reservoir behind the nozzle was 65% in the HeI PE measurements, while it was 58% in the HeII measurements. However, the mole fraction in the ionization chamber is not the same as that in the reservoir. The HeI spectrum of the mixture (Fig. 2b) indicates that the N_2O_4 mole fraction in our HeI measurements is very close to that in the work of Gan *et al.*,[10] and considerably higher than those in the works of Ames and Turner[7] and Frost *et al.*[9] The peak height ratio of the 12.39 eV band to the 13.0_5 eV band is about 1 : 1 in our intensity-corrected HeI spectrum, while it is 0.8 : 1 in the spectrum of Ames and Turner[7] and 0.6 : 1 in the spectrum of Frost *et al.*[9]

The reported HeI spectra of N_2O_4 more or less differ in band shape from one another, and there are some discrepancies in the number of PE bands.[7,9,10] It should be mentioned that the HeI spectrum of N_2O_4 shown in Fig. 2c is most close in spectral shape to that reported by Gan *et al.*[10] For HeII spectra of N_2O_4, no reports have been published so far. From the present HeII spectrum of N_2O_4, two interesting facts may be pointed out, one of which is the fact that three broad maxima appear in the region beyond 20 eV, and the other is that the HeI and HeII spectra below 20 eV considerably differ from each other in spectral shape and relative intensity.

Region below 14 eV. The HeI and HeII spectra below 14 eV, showing four maxima, largely differ in the relative intensity from each other. In the previous HeI studies[7–10] there have been large discrepancies in spectral interpretation in this region. Ames and Turner[7] have assigned the 12.39 eV band as a serious overlap of two ionization bands. Frost *et al.*[9] have considered that each of the maxima corresponds to a single ionization. Gan *et al.*[10] have interpreted that two ionization bands exist very closely at 13.4 and 13.5 eV to form apparently one maximum.

If Koopmans' theorem[23] is assumed, the first five ionic states are given in the order of $(6a_g)^{-1}<(1a_u)^{-1}<(1b_{1g})^{-1}<(4b_{2g})^{-1}<(4b_{3u})^{-1}$ with increasing ionization energy on the basis of *ab initio* MO calculations.[11–13] Such Koopmans' theorem assignment has been used in the previous PE studies except that of Gan *et al.*[10] who have proposed the following order on the basis of relative band intensities as well as orbital interactions between two NO_2 moieties: $(6a_g)^{-1}<(4b_{2g})^{-1}<(1a_u)^{-1}<(1b_{1g})^{-1}<(4b_{3u})^{-1}$. This PE assignment of Gan *et al.*[10] that differs from the Koopmans' theorem assignment has been supported by the recent Green's function study of von Niessen *et al.*[16]

In Fig. 4 the HeII spectrum obtained from the present work is compared with a theoretical ionization spectrum obtained by von Niessen *et al.*[16] If the Green's function calculation of von Niessen *et al.*[16] is correct, the three maxima in the 12—14 eV region should correspond to four rather than three ionized states. Considering the fact that the 13.5 eV band is highest in intensity in the HeII spectrum, there may be a large possibility that this band is due to two ionizations. Such interpretation of the 13.5_5 eV band supports the spectral assignment of Gan *et al.*[10] At the present stage, however, it is difficult to interpret unambiguously the HeI and HeII spectra in the 12—14 eV region in terms of the Green's function results. The relative intensity data given in Table 2 will give a clue to solve this question in future theoretical studies.

Region from 14 to 20 eV. In this region, the HeI and HeII spectra considerably resemble each other in spectral shape except that a bump is observed at 18.2 eV

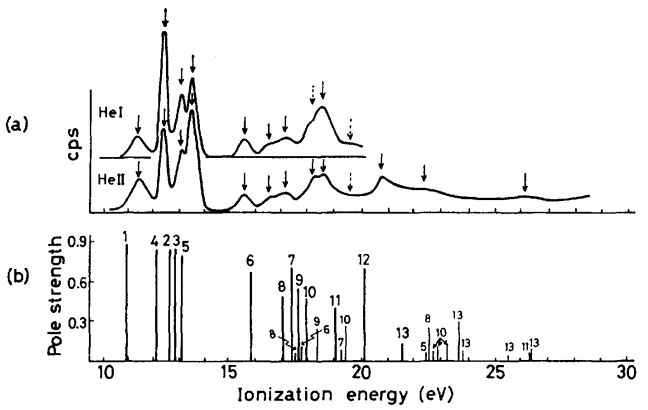

Fig. 4. Comparison of (a) the PE spectra and (b) the theoretical spectrum of von Niessen *et al.* (Ref. 16) in which lines with pole strengths larger than 0.05 are shown and the numbers indicate the following ionized states: $1=(6a_g)^{-1}$, $2=(1a_u)^{-1}$, $3=(1b_{1g})^{-1}$, $4=(4b_{2g})^{-1}$, $5=(4b_{3u})^{-1}$, $6=(5b_{1u})^{-1}$, $7=(3b_{2g})^{-1}$, $8=(1b_{3g})^{-1}$, $9=(2b_{3u})^{-1}$, $10=(1b_{2u})^{-1}$, $11=(5a_g)^{-1}$, $12=(4b_{1u})^{-1}$, $13=(4a_g)^{-1}$.

in the latter. As can be seen from Fig. 3c, two band maxima are clearly observed at 15.6 and 17.2 in the HeII spectrum.

The 15.6 eV band has previously been assigned to the $(5b_{1u})^{-1}$ ionization by Ames and Turner[7] and Gan *et al.*[10] This assignment has also been supported by the Green's function calculation of von Niessen *et al.*[16]

The shoulder appearing at 16.5 eV in the HeI spectrum has been neglected in the previous PE studies in which, for instance, Gan *et al.*[10] have assigned it to a HeI β (537 Å) band of the 18.6 eV peak. However, this 16.5 eV shoulder has been confirmed to appear also in the HeII spectrum, so that there should be at least one ionization band around here. Gan *et al.*[10] have mentioned that there are two ionization bands at 19.0 and 19.7 eV in the HeI spectrum. In the present work, however, we have not been able to identify any shoulder at 19.0 eV from the HeII as well as the HeI spectra. A slight shoulder may be seen at about 19.5 eV in the HeI spectrum, although there is no such shoulder in the HeII spectrum. From the HeI and HeII spectra, it may be considered that there is at least one ionization band in the 19—20 eV region. From their HeI spectra Gan *et al.*[10] have taken a total of six ionization energies, 15.6, 17.1, 18.1, 18.6, 19.0, 19.7 eV in the 14—20 eV region. In the present work, however, we have selected a different set of six ionization energies (15.6, 16.5, 17.2, 18.2, 18.6, 19.5 eV) in this region.

As shown in the theoretical spectrum of von Niessen *et al.*[16] in Fig. 4b, there are several main ionization lines in the 14—20 eV together with many satellite lines due to strong correlation effects. In this region, the main lines (6—11) are located in the order of the Koopmans' theorem assignment except that two lines 7 and 8 are reversed. Taking these theoretical results into account, we may point out a possibility that the six maxima or shoulders in the 14—20 eV correspond to theoretical lines 6, 8, 7, 9, 10, and 11 in this order, besides the satellite lines.

Region above 20 eV. The HeII spectrum obtained here shows three additional maxima at 20.7, 22.5, and 25.9 eV. There are no available spectra for comparison in this region. From the *ab initio* MO calculations,[11–13,16] it has been known that the first thirteen valence MO's are located between −12 and −30 eV in orbital energy and the remaining four valence MO's of oxygen 2s-type are between −40 and −50 eV. If Koopmans' theorem is assumed, thirteen PE bands would be observed below about 30 eV. However, according to the Green's function study of von Niessen *et al.*,[16] thirteen main ionizations occur below about 22 eV and the last two main lines (12 and 13) appear with a separation of about 1.5 eV in the region 20—22 eV, as shown in Fig. 4b. Therefore, it may be possible to correspond the two main theoretical lines (12 and 13) to the two PE maxima observed at 20.7 and 22.5 eV with a separation of 1.8 eV. The remaining broad maximum appearing at 25.9 eV may be due to a contour of many satellite lines.

Finally it may also be pointed out that the minima of the HeII spectrum above 17 eV are considerably lifted upwards from the base line, this suggesting the existence of many satellite ionizations indicated by von Niessen *et al.*[16] According to von Niessen *et al.*,[16] there are many satellite lines with considerably strong intensities even in the higher-energy region up to 50 eV. In the present work we were unable to deduce any HeII spectrum above 29 eV for N_2O_4 owing to a serious overlap of the HeI spectrum. A further experimental study on such higher-energy region is quite interesting in testing a validity of the Green's function calculations.

References

1) I. C. Hisatsune, *J. Phys. Chem.*, **65**, 2249 (1961).
2) a) D. W. Smith and K. Hedberg, *J. Chem. Phys.*, **25**, 1282 (1956); b) B. W. McCelland, G. Gundersen, and K. Hedberg, *J. Chem. Phys.*, **56**, 4541 (1972).
3) R. G. Snyder and I. C. Hisatsune, *J. Mol. Spectrosc.*, **1**, 139 (1957).
4) D. W. Turner, C. Baker, A. D. Baker, and C. R. Brundle, "Molecular Photoelectron Spectroscopy," Wiley, New York (1969).
5) O. Edqvist, E. Lindholm, L. E. Selin, L. Åsbrink, C. E. Kuyatt, S. R. Mielczarek, J. A. Simpson, and I. Fischer-Hjalmers, *Phys. Scr.*, **1**, 172 (1970).
6) C. R. Brundle, D. Neumann, W. C. Price, D. Evans, A. W. Potts, and D. G. Streets, *J. Chem. Phys.*, **53**, 705 (1970),
7) D. L. Ames and D. W. Turner, *Proc. R. Soc. London. Ser. A*, **348**, 175 (1976).
8) T. Yamazaki and K. Kimura, *Chem. Phys. Lett.*, **43**, 502 (1976).
9) D. C. Frost, C. A. McDowell, and N. P. C. Westwood, *J. Electron Spectrosc.*, **10**, 293 (1977).
10) T. H. Gan, J. B. Peel, and G. D. Willett, *J. Chem. Soc., Faraday Trans. 2*, **73**, 1459 (1977).
11) R. Ahlrichs and F. Keil, *J. Am. Chem. Soc.*, **96**, 7615 (1974).
12) J. M. Howell and J. R. Van Wazer, *J. Am. Chem. Soc.* **96**, 7902 (1974).
13) L. C. Snyder and H. Basch, "Molecular Wave Functions and Properties," Wiley, New York (1972).
14) R. L. Griffiths, R. G. A. R. McClagan, and L. F.

Phillips, *Chem. Phys.*, **3**, 451 (1974).
15) S. Kishner, M. A. Whitehead, and M. S. Gopinathan, *J. Am. Chem. Soc.*, **100**, 1365 (1978). Papers cited therein.
16) W. von Niessen, W. Domcke, L. S. Cederbaum, and J. Schirmer, *J. Chem. Soc., Faraday Trans. 2*, **74**, 1550 (1978).
17) K. Kimura, S. Katsumata, T. Yamazaki, and H. Wakabayashi, *J. Electron Spectrosc.*, **6**, 41 (1975).
18) S. Katsumata and K. Kimura, *J. Electron Spectrosc.*, **6**, 309 (1975).
19) J. L. Gardner and J. A. R. Samson, *J. Electron Spectrosc.*, **8**, 469 (1976).
20) A. Savitzky and M. J. E. Golay, *Anal. Chem.*, **36**, 1627 (1964).
21) K. Kimura, T. Yamazaki, and K. Osafune, *J. Electron Spectrosc.*, **6**, 391 (1975).
22) S. Katsumata, K. Nomoto, K. Ohmori, Y. Kirihata, T. Yamazaki, Y. Achiba, and K. Kimura, to be published.
23) T. Koopmans, *Physica*, **1**, 104 (1933).

On the Phase Transitions in Hydrazinium(2+) Sulfate

Takeo OKAMOTO,† Nobuo NAKAMURA, and Hideaki CHIHARA*
Department of Chemistry, Faculty of Science, Osaka University, Toyonaka, Osaka 560
(Received January 10, 1979)

The existence of a "diffuse" phase transition below room temperature has been confirmed in $N_2H_6SO_4$ crystal by powder X-ray and DTA experiments. The transition temperature is very sensitive to the grain size. This size effect was discussed on the basis of the thermodynamic nucleation theory taking into account the interfacial energy between the high and the low temperature phases. The diffuse nature of the transition was interpreted by a theory proposed by Tobolsky *et al.* The spin-lattice relaxation times of ^1H were redetermined and the nature of the cationic motion in each phase was discussed.

Hydrazinium(2+) sulfate ($N_2H_6SO_4$) crystallizes in two modifications at room temperature, one orthorhombic and the other monoclinic.[1] The orthorhombic form has been studied extensively by the X-ray and neutron diffraction methods.[2-4] Its crystal structure is described by the space group D_2^4-$P2_12_12_1$ with four formula units in the unit cell; the crystal is ionic and contains distorted $N_2H_6^{2+}$ and SO_4^{2-} ions. The N–H bond distances in one of the two NH_3-groups, NH_3(I), in an $N_2H_6^{2+}$ ion distribute between 0.965 and 0.981 Å and those in the other NH_3-group (NH_3(II)) between 1.048 and 1.061 Å, the latter seems to form stronger hydrogen bonds with SO_4^{2-} groups than the former. The proton spin-lattice relaxation time T_1 was measured by Harrell and Howell in 1972 and there was found a first order phase transition at 481 K.[5] More recently Harrell and Peterson measured the spin-lattice relaxation time in the rotating frame, $T_{1\rho}$, in $N_2H_6SO_4$ as well as the line shapes of the deuteron resonance in $N_2D_6SO_4$.[6] They ascribed each of the two minima obserbed in both $T_{1\rho}$ and T_1 in the room temperature phase to the reorientation of the NH_3-groups about the N–N axis and to the 180°-flips of $N_2H_6^{2+}$ cation as a whole. They explained the steep decrease in $T_{1\rho}$ above the transition point in terms of translational diffusion of $N_2H_6^{2+}$.

Raman spectra were studied with regard to the distortion of the ionic species and the existence of the high temperature phase change at about 200 °C was also reported in Ref. 7. While these NMR and Raman studies failed to "see" any phase transition below room temperature, there is a report on the existence of a phase transition at −50 °C.[8] This phase transition was recognized by Power *et al.* in the process of their neutron diffraction experiment[4] and later examined in detail by Caville by Raman measurements.[9,10] Caville pointed out that the lowest temperature phase could exist in a metastable state even at room temperature.

We were interested in the nature of the lower phase transition and undertook a differential thermal analysis (DTA) and X-ray measurements on powdered specimens of $N_2H_6SO_4$ as well as remeasurements of proton spin-lattice relaxation time T_1. This paper reports the results of these experiments; an interesting grain-size dependence of the transition temperature will be described. A possible interpretation for the mechanism of the phase transition will be presented.

† Present address: The Institute for Solid State Physics, University of Tokyo, Roppongi, Tokyo 106.

Experimental

Polycrystalline specimens were obtained by recrystallization from an aqueous solution of $N_2H_6SO_4$ (Reagent Grade), followed by desiccation over 4 days. The crystals were ground to fine powders for X-ray, NMR, and DTA measurements. The grain-size effect on the lower phase transition was examined on the specimens which were divided into four parts by use of three sieves of different mesh dimensions. X-Ray powder patterns were obtained with a diffractometer (Rigaku Denki Kogyo Co.) at room temperature (≈18 °C). Proton magnetic relaxation times were determined by the saturation-90°method with a homemade pulsed spectrometer at 10 MHz. The exponential recovery of the magnetization was confirmed over the entire temperature range of the experiments. The details of the NMR measurements have been published elsewhere.[11] DTA experiments were carried out by use of a homemade DTA apparatus with about 1 g of specimen for each experiment. Chromel-*p*-constantan thermocouples (Driver and Harris Co., Ltd.) were used as the thermal sensors. Errors in the temperature measurements were within ±1 °C.

Results and Discussion

X-Ray Powder Diffraction. Figure 1 shows the X-ray powder patterns obtained at room temperature. Sample I in this figure is a specimen grown from an aqueous solution; the diffraction peaks of this sample were indexed consistently by use of the reported cell dimensions, $a=8.232$, $b=9.145$, and $c=5.535$ Å[4] together with the intensity data.[3] Samples II and III were obtained by cooling Sample I down to 189 and 77 K, respectively, kept at each temperature for a few minutes, and warmed up to the room temperature. One may see that Sample III gives a different powder pattern from that of Sample I, suggesting that the original orthorhombic crystals (hereafter referred to as Phase II) have transformed almost completely into the lowest temperature phase by cooling down to 77 K. Sample II, on the other hand, gives a powder pattern which is a superposition of those of Samples I and III. Therefore, one may understand that the phase transition occurred only in part by cooling down to 189 K. Annealing Sample III at 381 K for 2 h gave the pattern of Sample IV in which the majority of the crystal is transformed back to Phase II but some part still remains as a metastable phase even after the annealing.

Differential Thermal Analysis. A unique behavior of this material as mentioned above was also evidenced by a DTA experiment as shown in Fig. 2. When the

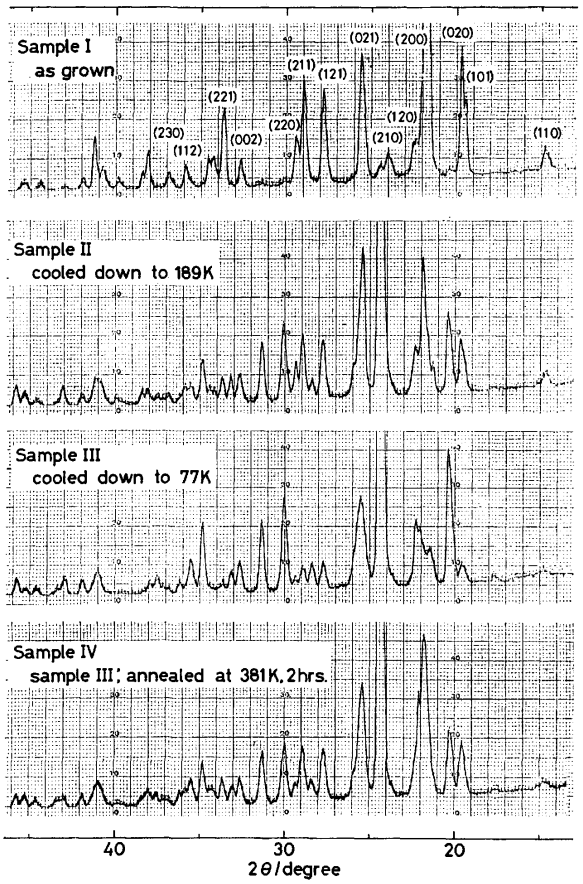

Fig. 1. X-Ray powder diffraction patterns of $N_2H_6SO_4$ at room temperature.

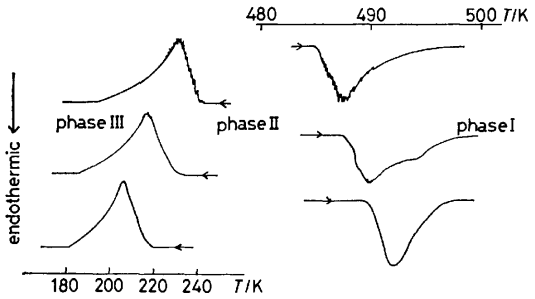

Fig. 2. DTA curves of $N_2H_6SO_4$ obtained by recrystallization (upper curves); after experienced the II→III transition once (middle) and twice (lower).

polycrystalline sample obtained by recrystallization (Phase II) was heated it transformed into Phase I, the highest temperature phase, at 485 K, but the DTA peak associated with this transition had some fine structure. Upon cooling, Phase I transformed into Phase II at 474 K, showing obvious thermal hysteresis as had been observed in Ref. 5. By further cooling a thermal anomaly with fine structure was observed between 242 and 200 K, indicating the transition from Phase II to III. Phase III did not give significant endothermic effect up to 488 K where there is a heat absorption corresponding to the transition from Phase II to I.[12] This fact suggests that Phase III can exist as a metastable state at least up to room temperature as evidenced in the X-ray study and can be transformed very gradually to Phase II at higher temperatures in such a way as to show no discernible DTA peaks.

The occurrence of this gradual transition was confirmed by the following experiments: First, after Phase III is heated up to 420 K a small peak was observed on cooling at 234 K, corresponding to the partial transition from Phase II to Phase III. Secondly, when Phase III had been annealed at about 380 K for 12 h it gave an anomaly on cooling at about 230 K as shown in Fig. 2 corresponding to the transition from Phase II to III; thus we concluded that Phase III had been transformed into Phase II during the annealing period.

The feature of the transition from Phase II to III will be summarized as follows: 1) This transition occurs over a very wide temperature range, namely 40 K, 2) the temperature at which the anomaly begins becomes displaced to a successively lower temperature after repeated thermal cycling, and 3) the fine structure in the DTA peak disappears gradually by repeating the thermal cycle. The shift of the transition point as well as disappearance of the fine structure of the DTA peak was also observed at the higher transition from Phase II to I, though only after the material had experienced the lower transition.

Grain-size Effect on the II—III Transition Point. Among the three characteristics of the II—III transition mentioned above, 2) and 3) may directly be interpreted in terms of a "size effect." The shattering of the crystal upon cooling down through the lower transition has been recognized by Caville.[9] Let us assume that the specimen with a smaller grain size undergoes the transition from Phase II to III at a lower temperature and that each grain shatters to finer ones as it passes its transition point. It follows then that the apparent transition point should be shifted to a lower temperature after each successive thermal cycle. If there is an

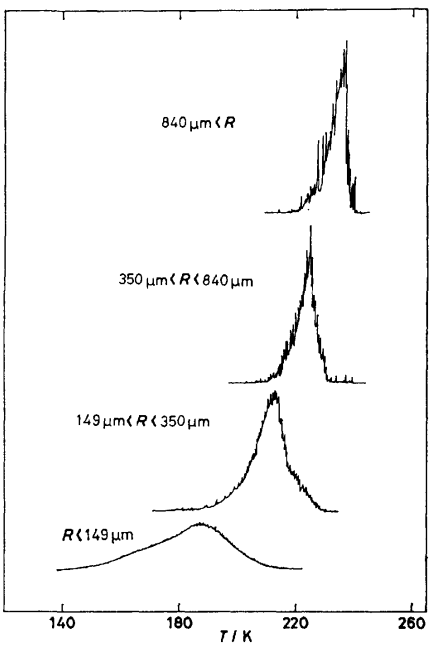

Fig. 3. DTA peaks of II→III transition in specimens with different grain sizes.

ultimate grain size obtained by such thermal cyclings, the specimen would have a homogeneous distribution in grain size and show a single, not composite, DTA peak with no fine structure.

In order to confirm the suggested size effect on the transition point we carried out the DTA on specimens with reasonably defined grain sizes. The results are shown in Fig. 3, which clearly demonstrate that the transition point becomes higher for larger grains. Also the structure of the peak is more prominent for larger grains whereas the transition region spreads broader for smaller grains. By plotting the temperature T_c at which the transition begins to occur against the reciprocal of the average grain size R a linear relation

$$T_0 - T_c = c/R \tag{1}$$

was obtained as given in Fig. 4, with c=2.36 mm K and T_0=237.5 K (the bulk transition point).

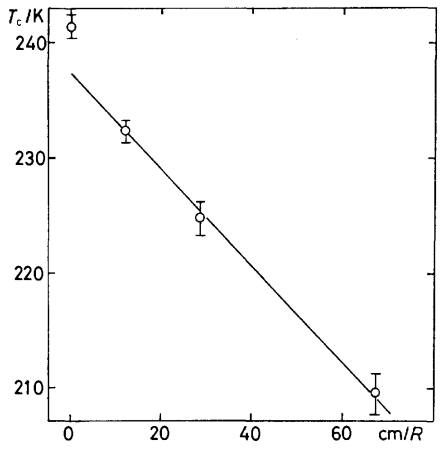

Fig. 4. The II→III transition temperature plotted against the reciprocal of the grain size.

Equation 1 has the form that has been derived for the first order phase transition from thermodynamic cosiderations which take into account the interfacial energy $\gamma_{\alpha\beta}$ between the high temperature parent modification (α-form) and the low temperature β-form.[13] There the coefficient depends totally on the "model" of the α-β interface: In the case of the liquid-to-solid phase change c is shown related to γ_{sl}, the interfacial energy between the solid and the liquid through

$$c = 2T_0\gamma_{sl}/L\rho_s \tag{2}$$

by assuming that a spherical nucleus of solid is in equilibrium with the surrounding bulk liquid phase,[14] where L is the latent heat of fusion and ρ_s the density of the solid. On the other hand the relation for the reverse (melting) transition

$$c = (2T_0/L\rho_s)\{\gamma_{sl} + (1-\rho_s/\rho_l)\gamma_l\} \tag{3}$$

was derived on the assumption that a crystallite can melt below the bulk melting point by the formation of a liquid skin which covers the entire crystal surface so as to make full use of the surface energy of the particle.[15] In this case T_0 is the "skin melting temperature." In Eq. 3 γ_l denotes the surface tension of the liquid and ρ_l the density of the liquid.

Validity of Eqs. 2 and 3 as well as of some other theoretical models was recently examined in relation to experiments on the melting transition of small lead particles. For the melting of lead particles Eqs. 2 and 3 predicted c=360 and 270 nm K, respectively, latter being found close to the experimental results.[13]

The value of c in our present study of II→III solid-solid transition of $N_2H_6SO_4$ is surprisingly large in comparison with that for the melting transition of lead (by a factor of 10^4). Although a value of c can not be estimated theoretically for $N_2H_6SO_4$ because of the lack of the knowledge of the interfacial energies, it seems that not only the interfacial energy but also some other factors will contribute to the large supercooling phenomenon. These factors are, *e.g.*, the large molecular misfit across the boundary of the two phases,[16] and the facility with which the nucleus of the new phase is formed in the mother crystal.[17]

In the case of the phase transition from Phase II to I the DTA peak is displaced to the higher temperature side as the grains become finer. This tendency is opposite to that in the II→III transition. If one is to apply Eq. 3 for the II→I transition, the surface tension of Phase I, γ_I, must be larger than $\gamma_{I,II}/(\rho_{II}/\rho_I - 1)$. Since ρ_{II} could be larger than ρ_I no more than 10%, this would mean that $\gamma_I > 10\gamma_{I,II}$ which is very questionable. Therefore, there will be other reason or reasons for the shift of the transition point in the II→I transition.

Diffuseness of the II—III Transition. As is pointed out in a previous section the phase transition between Phases II and III occurs gradually over a wide range. The possible origin of such a sluggish or diffuse phase transition was examined by Tobolsky *et al*:[18] They developed an *a posteriori* theory for the diffuse phase transition which is by nature the transition of the first order but actually occurs over a wide temperature range. They postulated the existence of a boundary phase K between two different phases A and B which are stable at high and low temperatures, respectively.

By solving for eigenvalues of an Ising matrix of molecular partition functions f_A, f_B, and f_K they obtained an expression for the number n_A or the number fraction x_A of molecules in the phase A as

$$x_A = \frac{n_A}{n_0} = \frac{1-y+(\varepsilon y)^{1/2}+[(1-y)^2+4(\varepsilon y)^{1/2}]^{1/2}}{(1-y)^2+4(\varepsilon y)^{1/2}+(1+y)[(1-y)^2+4(\varepsilon y)^{1/2}]^{1/2}} \tag{4}$$

where

$$y = \exp(-\Delta G_t/RT) \tag{5}$$

and

$$\varepsilon = \exp(-2\Delta G_K/RT). \tag{6}$$

Here ΔG_t and ΔG_k are changes of the molar Gibbs functions associated with A-to-B and A-to-K transitions, respectively, the latter being taken as infinite for an infinitely sharp transition. The expressions of x_B and x_K has also been given in Ref. 18. The anomalous part $\Delta C_p(T)$ of the heat capacity at a temperature T is written as

$$\Delta C_p(T) = -\{(\Delta H_t)^2/RT^2\}y(dx_A/dy) \tag{7}$$

where ΔH_t is the molar enthalpy change in the transition.

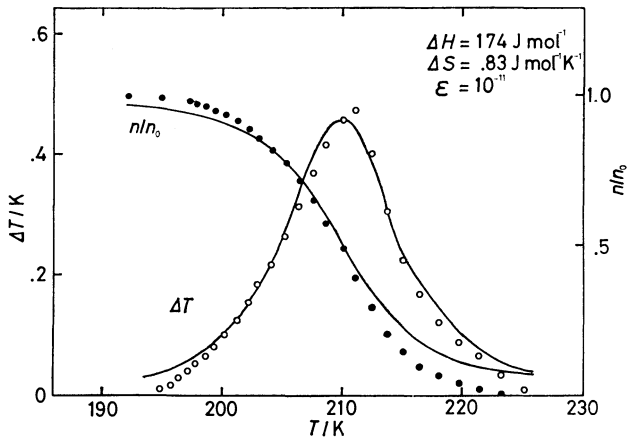

Fig. 5. The DTA curve (open circles) and the fraction of molecules in Phase III (filled circles) in II→III transition of the specimen with 149 μm $<R<$ 350 μm.

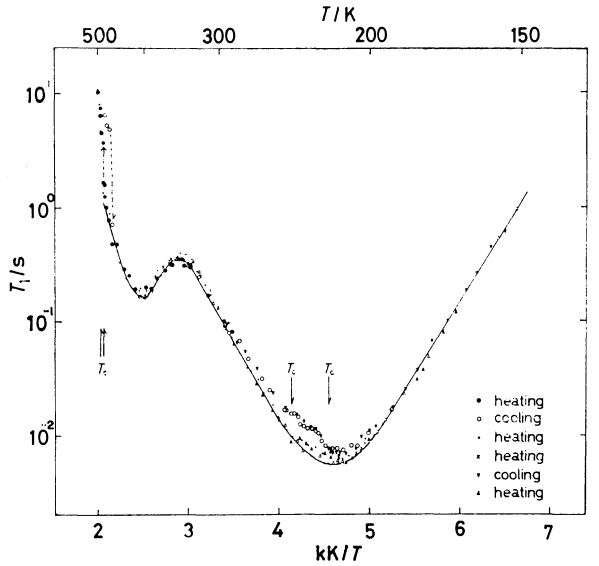

Fig. 6. T_1 of ^1H in polycrystalline $N_2H_6SO_4$ at 10 MHz. The two pairs of arrows indicate the transition regions. The solid curve is calculated with Eqs. 8 and 9. For the illustration of the symbols see in text.

Tobolsky *et al.* applied the theory to the heat capacity anomaly in several materials in detail and found that the heat capacity curve can be described using only one numerical parameter, ε or ΔG_k. In the present case of $N_2H_6SO_4$ no heat capacity data are available. But the shape of the anomaly in the DTA curve reasonably represents what one would expect for the anomalous part of the heat capacity curve. Thus, as an example, the DTA curve in the cooling direction for the specimen of the size 149 μm $<R<$ 350 μm in Fig. 3 was then fitted to Eqs. 4 and 7, the result being shown in Fig. 5. In this figure the fraction of the low temperature phase n/n_0 at each temperature was obtained by integrating the DTA thermogram (the height of which stands for ΔT, the temperature difference between the reference material and the sample under investigation).

Such a fitting gave the thermodynamic functions for the transition the values, $\Delta H_t=174$ J mol^{-1}, $\Delta S_t=0.83$ J mol^{-1} K^{-1}, and $\varepsilon=10^{-11}$, corresponding to $2\Delta G_k\approx 44$ kJ mol^{-1}. ΔG_k, the Gibbs energy of formation of a boundary phase K from Phase II, is not too large to neglect the formation of the phase K in the transition from Phase II to III. The disappearance of the reverse phase transition in the heating run as mentioned in the preceding section can also be accounted for if $\varepsilon>10^{-7}$ is assumed for the formation of phase K from Phase III. In such a case the theoretical curve becomes so flat that one can hardly "observe" any evidence of the phase transition.

The postulate of the boundary phase K has no direct bearing with the particle size effect but it certainly will be one form of manifestation of the significance of the interface energy. Unfortunately it is not possible to relate the value of ΔG_k derived here to any realistic structural model of the transition.

Spin-lattice Relaxation Time. Since the general nature of the phase transitions in $N_2H_6SO_4$ has been understood in the X-ray and the DTA experiments, we proceed to the results of measurements of the spin-lattice relaxation time T_1 on a polycrystalline sample in order to shed some light on the type of motion that $N_2H_6^{2+}$ cations undergo in each phase.

The results are shown in Fig. 6. On heating the specimen obtained by recrystallization from room temperature upwards the T_1 behavior was very similar to that reported by Harrell and Howell[5] as shown by filled circles in Fig. 6. However, on initial cooling of Phase II, the values of T_1 longer than those given in Ref. 5 were obtained (open circles); we also observed a significantly irregular behavior of T_1 in the transition region between about 210 and 250 K as will be described in the following. On heating, Phase III gave T_1 value shorter than those in Phase II, the former being shown by dots and open triangles.

Our values of T_1 for Phase III agree with the Harrell and Howell's results, indicating that what they were looking at was Phase III without being aware of the occurrence of the II—III transition when they cooled their specimen. As one sees in Fig. 6 the difference in T_1 between Phases II and III becomes smaller with increase in temperature and converges to zero somewhere around 300 K. This fact suggests that the transition from Phase III to II proceeds continuously during the T_1 measurements.

The T_1 data were interpreted according to the BPP type of formulation for the dipole-dipole interaction between protons in the form[19]

$$T_1^{-1} = K\{\tau_c/(1+\omega_0^2\tau_c^2) + 4\tau_c/(1+4\omega_0^2\tau_c^2)\} \quad (8)$$

where ω_0 is the Larmor frequency of the nuclear spin, τ_c the correlation time of a specified motion, and K a factor representing reduction of the strength of dipolar interaction due to that motion. If the two crystallographically nonequivalent NH_3-groups rotate about their figure axes (C_3-rotation) with different correlation times (τ_{ci}), the relaxation rate can be written as

$$T_1^{-1} = 1/2\sum_i K_i\{\tau_{ci}/(1+\omega_0^2\tau_{ci}^2)+4\tau_{ci}/(1+4\omega_0^2\tau_{ci}^2)\}, \quad i=1,2. \quad (9)$$

By fitting Eq. 9 to the experimental T_1^{-1} curve in Phase III as shown in Fig. 6 by solid line the activation

Table 1. The activation parameters for the motion of $N_2H_6^{2+}$ cations

Phase	Mode of Motion	$K/10^8$ s^{-1}	E_a/kJ mol^{-1}	$\tau_0/10^{-15}$ s
I	Translational diffusion[a]	—	184	—
II	C_3-rotation of NH_3-group	—	24.9	—
	180°-flip of $N_2H_6^{2+}$	2.5	54.0	1.0
	180°-flip of $N_2H_6^{2+}$[a]	1.9	40.5	166
III	C_3-rotation of NH_3(I)	104	24.9	7.9
	C_3-rotation of NH_3(II)	66	27.8	3.9
	C_3-rotation of NH_3[b]	—	26.2	6.0

a) Ref. 6. b) Ref. 6. A single correlation time was assumed for the motion of two kinds of NH_3-groups.

energies and τ_{0i}'s were obtained for the C_3-rotation as listed in Table 1. Here the Arrhenius activation process was assumed for the motion:

$$\tau_{ci} = \tau_{0i} \exp(E_{ai}/RT). \quad (10)$$

Of the two sets of values for activation parameters for Phase III, the one with the smaller E_a and the larger K may be assigned to NH_3(I) and the other set to NH_3(II). This is because NH_3(II) forms stronger hydrogen bonding with the surrounding SO_4^{2-} groups than NH_3(I) does.

Only the average activation energy was calculated for the C_3-rotation in Phase II from the slope of ln T_1 *vs.* $1/T$ between 250 and 295 K by assuming $\omega_0\tau_c \ll 1$ (see in Table 1). The activation parameters for the 180°-flip of $N_2H_6^{2+}$ were obtained by fitting Eq. 8 to the observed T_1^{-1} by assuming that the correlation time of this motion is so large in comparison with τ_c of C_3-rotation that the two modes of motion can be treated independently. The analysis gave E_a and τ_0 in Table 1 and the solid line in Fig. 6.

The activation energy and τ_0 for the 180°-flip of $N_2H_6^{2+}$ in the present work are significantly different from those in Ref. 6 which have been deduced from the $T_{1\rho}$ data. Such a discrepancy may have come from the ambiguity in fitting the theoretical T_1 curve to the experimental one in a rather narrow temperature range.

It is interesting to note, however, that the free energy of formation of a boundary phase K between Phases II and III is comparable to the activation energy for the 180°-flip of $N_2H_6^{2+}$, suggesting some rearrangement of $N_2H_6^{2+}$ cations takes place in the phase change process.

We are grateful to Mr. Takechika Iida for his assistance in the DTA measurements. Acknowledgment is made to the Mitsubishi Foundation for financial support of this research.

References

1) P. Groth, "Chemische Krystallographie," Verlag von Wilhelm Engelmann, Leipzig (1908), II. Teil, p. 385.
2) I. Nitta, K. Sakurai, and Y. Tomiie, *Acta Crystallogr.*, **4**, 289 (1951).
3) P. G. Jonsson and W. C. Hamilton, *Acta Crystallogr., Sect. B*, **26**, 536 (1970).
4) L. F. Power, K. E. Turner, and J. A. King, *Acta Crystallogr., Sect. B*, **31**, 2470 (1975).
5) J. W. Harrell, Jr. and F. L. Howell, *J. Magn. Reson.*, **8**, 311 (1972).
6) J. W. Harrell, Jr. and E. M. Peterson, *J. Chem. Phys.*, **63**, 3609 (1975).
7) M. Guay, J. Weber, and R. Savoie, *Can. J. Spectrosc.*, **19**, 127 (1974).
8) P. Pepinsky, K. Vedam, Y. Okaya, and S. Hoshino, *Phys. Rev.*, **111**, 1467 (1958).
9) C. Caville, *Can. J. Spectrosc.*, **20**, 123 (1975).
10) C. Caville, *Solid State Commun.*, **21**, 475 (1977).
11) T. Tsuneyoshi, N. Nakamura, and H. Chihara, *J. Magn. Reson.*, **27**, 191 (1977).
12) In our course of the DTA experiments a small and very broad endothermic anomaly has occasionally been observed above 330 K, indicating the probable occurrence of the transition from Phase III to Phase II, but we could not ascertain the neccessary conditions for the reproducibility of such an anomaly.
13) S. J. Peppiatt and J. R. Sambles, *Proc. R. Soc. London, Ser. A*, **345**, 387 (1975) and the references therein.
14) E. Rie, *Z. Phys. Chem.*, **104**, 354 (1923).
15) A. E. Curzon, Thesis, 1960, University of London, cited in Ref. 13.
16) D. Turnbull, "Solid State Physics," ed by F. Seitz and D. Turnbull, Academic Press, New York (1956), Vol. 3, p. 225.
17) M. J. Buerger, "Phase Transformations in Solids," ed by R. Smoluchowski, J. E. Mayer, and W. A. Weyl, John Wiley and Sons, New York (1951), p. 183.
18) A. V. Tobolsky, J. J. Kozak, and N. H. Canter, *Phys. Rev.*, **138**, A651 (1965).
19) A. Abragam, "The Principles of Nuclear Magnetism," Oxford, London (1961), Chap. 8.

Wheland Polynomial. I. Graph-theoretical Analysis of the Contribution of the Excited Resonance Structures to the Ground State of Acyclic Polyenes

Noriko OHKAMI and Haruo HOSOYA*

Department of Chemistry, Ochanomizu University, Bunkyo-ku, Tokyo 112

(Received January 30, 1979)

The Wheland polynomials, the set of the numbers, $w(G,j)$, of the j-th excited resonance structures, for a number of acyclic polyenes were calculated. The relations of $w(G,j)$ with the non-adjacent numbers, $p(G,k)$, topological index, Z_G, and the total π-electronic energy, E_π, were analyzed in detail for linear polyenes. For branched polyenes similar results were obtained, and it was found and proved that E_π is linearly related with the number of Dewar (singly excited)structures. Method for the numbering of atoms to generate the canonical resonance structures was discussed.

Recently a number of interesting relations between the Hückel molecular orbital (MO) and resonance or valence bond (VB) theories have been found and/or reinterpreted by the application of the graph theory (GT) and combinatorial theory to the electronic structures of conjugated molecules.[1-7] The essence of these lines of studies does not lie in the accurate prediction of certain properties of molecules by the use of many sophisticated parameters and approximations but in the physical interpretation of the empirical relations and also in the analysis of the mathematical structures of the theories which have been proposed.

Enumeration of the resonance structures of conjugated hydrocarbons is one of the revived problems, yielding abundant crops.[1,3,8-13] Although it has long been pointed out that as the size of the conjugated molecule increases the weight of the contribution of the Kekulé structures in the ground state rapidly decreases, the total π-electronic energy E_π of conjugated hydrocarbons is shown to be closely related to the number of the Kekulé structures, K.[2,3,7] From quite a different point of view one of the present authors has proposed the non-adjacent numbers $p(G,k)$ and topological index for characterizing the topological structure of a graph,[14] and found the relations of the $p(G,k)$ numbers with K and D, the number of the (singly excited) Dewar structures.[5] Further, the topological index Z_G, namely, the sum of the $p(G,k)$ numbers, for a tree graph is known to be closely related to the E_π value of the corresponding hydrocarbon molecule.[15] Then there must be also some useful relations between E_π and the numbers of higher excited resonance structures.

However, very few studies have been done on the analysis of the excited resonance structures. An effective method (hereinafter called as Wheland polynomial) for enumerating the set of numbers of the canonical resonance structures was proposed by Wheland[8] in 1935 but has been overlooked ever since.[16] The aims of the present paper are to generate the Wheland polynomials for a number of tree graphs, *i.e.*, the carbon atom skeletons of acyclic conjugated hydrocarbons, to find out the relations among these quantities of different origins, *i.e.*, of VB, MO, and GT, and to analyze these relations.

Definitions and Calculations[8]

Consider $N(=2n)$ circularly arranged and numbered points representing the carbon-atom skeleton of either an annulene or a linear polyene, and draw n non-crossing bonds. We get $C_n=(2n)!/\{n!(n+1)!\}$[17] patterns as exemplified in Fig. 1a for the case with $N=6$. When each pattern is projected back onto the σ-bond skeleton of the structural formula of the conjugated molecule concerned, a resonance structure is obtained. The degree of excitation of each resonance structure is defined as the number of "ineffective" or long bonds. The $(2n)!/\{n!(n+1)!\}$ resonance structures thus obtained form a set of the canonical structures.

The Wheland polynomial $W_G(x)$ is defined as

$$W_G(x) = \sum_{k=0}^{m} w(G,k)x^k \qquad (1)$$

where $w(G,k)$ is the number of the k-th excited structures for a given set of the canonical structures of graph G. Given any graph with N numbered points, a set of the canonical structures are automatically obtained by the above procedure (see Fig. 1b). All the $w(G,k)$ numbers in this paper were obtained by computers.[18] Note that the set of $w(G,k)$ numbers, or the Wheland polynomial $W_G(x)$ depends on the numbering of points, or atoms, as shown in Fig. 1c. Among a set of various $W_G(x)$ expressions for a given graph, let the highest priority be given to the one which would be the first entry when aligned in the "dictionary order." Such $W_G(x)$ may have the property that, if a proper value δ is chosen such that $0<\delta\ll 1$, the value of $W_G(\delta)$ is the largest among the set of the possible numberings. In Appendix some discussion on the numbering will be given.

Results and Discussion

In order to clarify the relation between the Wheland polynomial and the π-electronic energy of conjugated hydrocarbons, first the results of the linear polyenes will be analyzed in detail, and the effect of the branching will be discussed later.

Linear Polyene. Let us denote a linear polyene with n double bonds, or $2n(=N)$ sp^2 carbon atoms, by $\bar{n}$.[19] The Wheland polynomials for smaller members

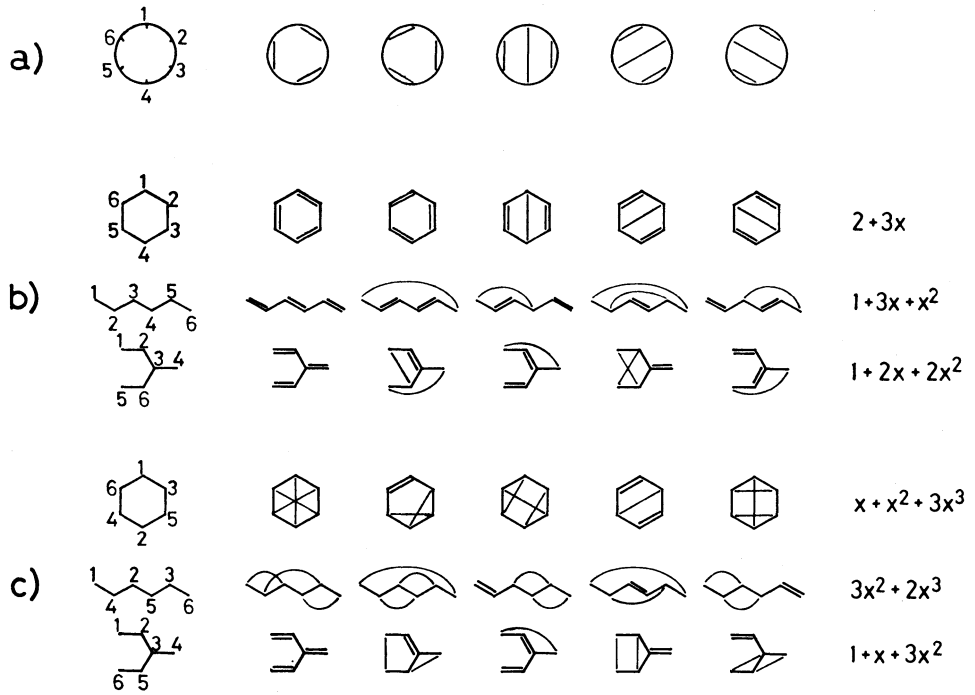

Fig. 1. Generation of the canonical set of the resonance structures and Wheland polynomial.
a) The standard patterns.
b) The Wheland polynomials of the highest priority obtained by the proper numbering.
c) The Wheland polynomials obtained by the improper numbering.

Table 1. Coefficients of the Wheland polynomial for linear polyenes[a)]

n[b)]	$w(\bar{n}, j)$									$\sum w(\bar{n}, j)$[c)]
	$j=0$	1	2	3	4	5	6	7	8	
0	1									1
1	1									1
2	1	1								2
3	1	3	1							5
4	1	6	6	1						14
5	1	10	20	10	1					42
6	1	15	50	50	15	1				132
7	1	21	105	175	105	21	1			429
8	1	28	196	490	490	196	28	1		1430
9	1	36	336	1176	1764	1176	336	36	1	4862

a) $W_G(x)=\sum_{j=0} w(G, j)x^j$. b) Number of double bonds. c) Catalan number.

Table 2. Non-adjacent numbers and topological index for linear polyenes[a)]

n[b)]	$p(\bar{n}, k)$										$Z_{\bar{n}}=p(\bar{n}, k)$[c)]
	$k=0$	1	2	3	4	5	6	7	8	9	
0	1										1
1	1	1									2
2	1	3	1								5
3	1	5	6	1							13
4	1	7	15	10	1						34
5	1	9	28	35	15	1					89
6	1	11	45	84	70	21	1				233
7	1	13	66	165	210	126	28	1			610
8	1	15	91	286	495	462	210	36	1		1597
9	1	17	120	455	1001	1287	924	330	45	1	4181

a) $P_G(x)=\sum_{k=0} p(G, k)\, x^k$. b) Number of double bonds. c) $Z_{\bar{n}}$ is the $2n$-th Fibonacci number, F_{2n}. $F_n=F_{n-1}+F_{n-2}$ with $F_0=F_1=1$.

of the series are given in Table 1, from which the general expressions are derived,

$$W_{\bar{n}}(x) = \sum_{j=0}^{n-1} w(\bar{n}, j)x^j \qquad (n>0) \tag{1'}$$

$$w(\bar{n}, j) = \frac{n!(n-1)!}{j!(j+1)!(n-j)!(n-j-1)!} = \frac{1}{n}\binom{n}{j}\binom{n}{j+1}. \tag{2}$$

By definition $W_{\bar{0}}(x)=1$.

The following relations have been known.[8]

$$W_{\bar{n}}(x) = W_{\overline{n-1}}(x) + x\sum_{j=1}^{n-1} W_{\bar{j}}(x)W_{\overline{n-j-1}}(x), \tag{3}$$

$$W_{\bar{n}}(1) = \sum_{j=0}^{n-1} w(\bar{n}, j) = \frac{(2n)!}{n!(n+1)!}, \tag{4}$$

or

$$\frac{1}{n}\sum_{j=0}^{n-1}\binom{n}{j}\binom{n}{j+1} = \frac{(2n)!}{n!(n+1)!}. \tag{4'}$$

The non-adjacent number $p(G,k)$, *i.e.*, the number of ways for choosing k disjoint lines, for linear polyene $\bar{n}$ is given by[14]

$$p(\bar{n}, k) = \binom{2n-k}{k}, \tag{5}$$

or

$$p(\bar{n}, n-k) = \binom{n+k}{n-k}. \tag{6}$$

The topological index Z_G is defined as the sum of the $p(G,k)$'s for graph G,[14]

$$Z_G = \sum_{k=0}^{m} p(G, k). \tag{7}$$

For a linear polyene

$$Z_{\bar{n}} = \sum_{k=0}^{n} p(\bar{n}, k) = \sum_{k=0}^{n} p(\bar{n}, n-k). \tag{8}$$

These values are given in Table 2.

In order to get the relation between $w(G,k)$ and $p(G,k)$, try to take the summation of $w(G,k)$ with weight as

$$S = \frac{k!(k+1)!}{(2k)!}\sum_{j=0}^{k}\binom{n-j}{k-j}w(\bar{n}, j) = \frac{(k+1)!(n-1)!}{(2k)!(n-k)!}\sum_{j=0}^{k}\binom{n}{j+1}\binom{k}{k-j}. \tag{9}$$

By using the Vandermonde convolution formula[20]

$$\binom{n+p}{m} = \sum_{k=0}^{m}\binom{n}{m-k}\binom{p}{k}, \tag{10}$$

one gets

$$\sum_{j=0}^{k}\binom{n}{j+1}\binom{k}{k-j} = \binom{n+k}{k+1}, \tag{11}$$

which gives

$$S = \binom{n+k}{n-k}.$$

That is, Eqs. 6 and 9 are found to be equal,

$$p(\bar{n}, n-k) = \frac{k!(k+1)!}{(2k)!}\sum_{j=0}^{k}\binom{n-j}{k-j}w(\bar{n}, j). \tag{12}$$

This is the relation between the coefficients of the Wheland polynomial and the non-adjacent numbers for a linear polyene. Similarly we get

$$w(\bar{n}, j) = \sum_{k=0}^{k}(-1)^{j-k}\frac{(2k)!}{k!(k+1)!}\binom{n-k}{j-k}p(\bar{n}, n-k). \tag{13}$$

Specifically, the following relations for a linear polyene are to be noted:

$$w(\bar{n}, 0) = K \quad \text{(number of "Kekulé structures")} = p(\bar{n}, n) \tag{14}$$

$$w(\bar{n}, 1) = D \quad \text{(number of "Dewar structures")} = p(\bar{n}, n-1) - np(\bar{n}, n) \tag{15}$$

$$w(\bar{n}, 2) = D_2 \quad \text{(number of "double Dewar structures")} = 2p(\bar{n}, n-2) - (n-1)p(\bar{n}, n-1) + \frac{n(n-1)}{2}p(\bar{n}, n). \tag{16}$$

By substituting Eq. 12 into Eq. 8, followed by the substitution $k=j+i$, one gets the relation between the topological index and the coefficients of the Wheland polynomial for a linear polyene as

$$Z_{\bar{n}} = \sum_{k=0}^{n}\sum_{j=0}^{k}\frac{k!(k+1)!}{(2k)!}\binom{n-j}{k-j}w(\bar{n}, j) = \sum_{j=0}^{n} C(n, j)\,w(\bar{n}, j) \tag{17}$$

$$C(n, j) = \sum_{i=0}^{n-j}\frac{(j+i)!(j+i+1)!}{(2j+2i)!}\binom{n-j}{i}. \tag{18}$$

For an acyclic hydrocarbon, whose carbon atom skeleton is expressed as a tree graph, the total π-electronic energy E_π calculated by the Hückel molecular orbital method is known to be related to Z_G as[15]

$$E_\pi = A \ln Z_G \qquad (G \in \text{tree}), \tag{19}$$

which, by the substitution of Eq. 17, yields

Table 3. Weight of the coefficients of the Wheland polynomial in the π-electronic energy for linear polyenes

n	$C(n,j)$								
	$j=0$	1	2	3	4	5	6	7	8
0	1.0000								
1	2.0000	1.0000							
2	3.5000	1.5000	0.5000						
3	5.7000	2.2000	0.7000	0.2000					
4	8.8714	3.1714	0.9714	0.2714	0.0714				
5	13.3810	4.5095	1.3381	0.3667	0.0952	0.0238			
6	19.7219	6.3409	1.8314	0.4933	0.1266	0.0314	0.0076		
7	28.5554	8.8335	2.4926	0.6612	0.1679	0.0413	0.0099	0.0023	
8	40.7648	12.2094	3.3759	0.8833	0.2221	0.0542	0.0129	0.0030	0.0007

$$E_\pi = A \ln \sum_{j=0}^{n} C(n,j) w(\bar{n},j). \quad (20)$$

From this equation one can obtain the contribution or weight of each coefficient $w(\bar{n},j)$ of the Wheland polynomial to the total π-electronic energy.

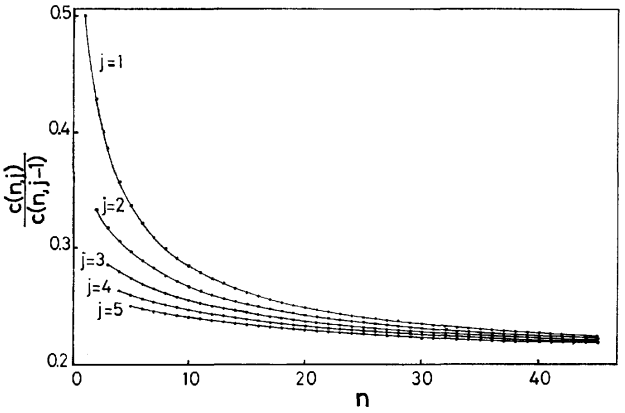

Fig. 2. Convergence of the ratio $C(n, j)/C(n, j-1)$ for larger polyenes. See also Table 3.

The values of $C(n,j)$ for smaller n and j's are given in Table 3, which shows a rapid decrease of $C(n,j)$ with the increase of j. Further, as seen in Fig. 2 the ratio of $C(n,j)$ to $C(n,j-1)$ converges to a certain value for larger n, or

$$C(n,j) \rightarrow C(n,0)\alpha^j, \quad (21)$$

with the value of α a little above 0.2.

By the substitution of Eq. 21 into Eq. 20, it turns out that E_π can approximately be expressed in terms of the Wheland polynomial,

$$E_\pi = A \ln \{C(n,0) W_{\bar{n}}(\alpha)\}, \quad (22)$$

or simply as

$$E_\pi = a \ln W_G(\alpha) + b \quad (\alpha=0.2). \quad (23)$$

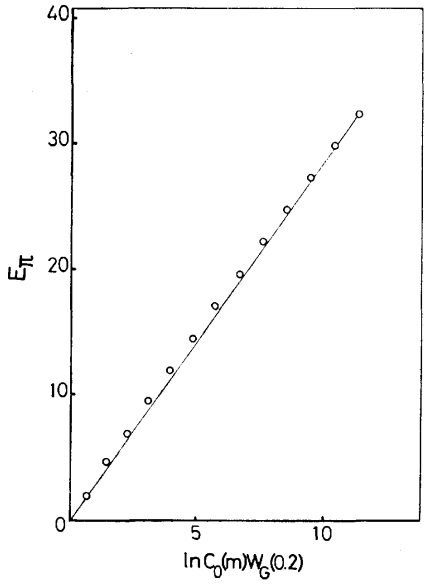

Fig. 3. Linearity between E_π and $\ln\{C_0(m) W_G(0.2)\}$. The straight line is drawn so as to pass the origin.

Although Eq. 22 has been derived for larger n, numerical calculation shows that this relation is also fairly valid even for smaller linear polyenes (Fig. 3). Later it will be shown that Eq. 23 can also be applied to branched polyenes.

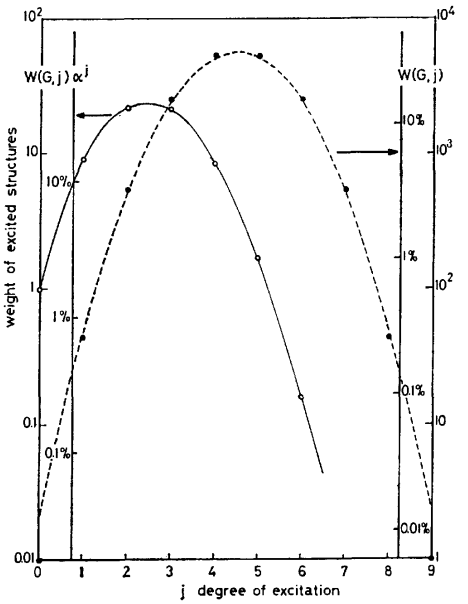

Fig. 4. Dependence of $w(G, j)$ and $w(G, j)\alpha^j$ on the degree of excitation for polyene $C_{20}H_{22}$.
—•—: $w(G, j)$.
——: Gaussian curve, $5600 \exp\{-0.392(j-4.5)^2\}$, to fit the $w(G, j)$ values.
—o—: $w(G, j)\alpha^j$.

Among the whole spectrum of the resonance structures scanned with the order of excitation, one can analyze what is the largest contribution to the energy of the ground state. The values of $w(G,j)$ and $w(G,j)\alpha^j$ with $\alpha=0.2$ for linear polyne $\overline{10}$ are plotted in Fig. 4, where two remarkable features are seen. Although a rigorous proof can not be obtained yet, the smoothed curve of $w(\bar{n},j)\alpha^j$ against j is symmetric with respect to $j=n/2$ and very close to that of the Gaussian curve, $\exp(-x^2)$ (see the broken line). Next the peak of the smoothed curve of $w(\bar{n},j)\alpha^j$ is found at about $j=0.3n$. This can be proved as follows.

For larger n the value of j at which the curve $w(\bar{n},j)\alpha^j$ is an extremum is the root of the following equation

$$\frac{1}{n}\binom{n}{j}\binom{n}{j+1}\alpha^j = \frac{1}{n}\binom{n}{j-1}\binom{n}{j}\alpha^{j-1},$$

and is found to be approximately as

$$j = \sqrt{\alpha}\, n/(\sqrt{\alpha}+1),$$

or

$$j/n = \sqrt{\alpha}/(\sqrt{\alpha}+1) = 0.309, \quad (24)$$

if α takes 0.2.

As has been pointed out earlier,[21] this result confirms that the contributions of the Kekulé structures and even of the lower excited structures get vanishingly small with the increase of the size of the molecule. However, it might still be possible that the numbers of the lower

Table 4. Topological characteristics of hexatriene and octatetraene isomers

Isomer[a]	b)	$w(G,j)$					$p(G,k)$					Z_G	E_π[c]
		$j=0$	1	2	3	4	$k=0$	1	2	3	4		
3-1	I_3	1	3	1			1	5	6	1		13	6.9879
3-2	A_3	1	2	2			1	5	5	1		12	6.8990
4-1	I_4	1	6	6	1		1	7	15	10	1	34	9.5175
4-2	B_4, C_4	1	5	5	3		1	7	14	9	1	32	9.4459
4-3	A_4	1	4	8	0	1	1	7	14	8	1	31	9.4093
4-4	D_4	1	3	9	1		1	7	13	7	1	29	9.3317

a) See Chart 1 for the structure and numbering of carbon atoms. b) X_m refers to the polyene of the series X with m double bonds. See Chart 3. c) Total Hückel π-electronic energy in β units.

Table 5. Topological characteristscs of decapentaene isomers

Isomer[a]	b)	$w(G,j)$					$p(G,k)$						Z_G	E_π[c]
		$j=0$	1	2	3	4	$k=0$	1	2	3	4	5		
5-1	I_5	1	10	20	10	1	1	9	28	35	15	1	89	12.0534
5-2	B_5	1	9	15	14	3	1	9	27	32	14	1	84	11.9852
5-3	C_5	1	8	18	11	4	1	9	27	32	13	1	83	11.9669
5-4	A_5	1	7	21	8	5	1	9	27	31	12	1	81	11.9375
5-5	—	1	8	14	18	1	1	9	26	30	13	1	80	11.9248
5-6	—	1	6	22	8	5	1	9	27	31	11	1	80	11.9180
5-7	E_5,F_5	1	6	20	12	3	1	9	26	29	11	1	77	11.8747
5-8	—	1	6	17	11	6	1	9	26	28	11	1	76	11.8636
5-9	D_5	1	5	22	12	2	1	9	26	28	10	1	75	11.8428
5-10	—	1	5	20	8	7	1	9	26	27	10	1	74	11.8314
5-11	—	1	4	19	13	4	1	9	25	25	9	1	70	11.7636

a) See Chart 2 for the structure and numbering of carbon atoms. b) X_m refers to the polyene of the series X with m double bonds. See Chart 3. c) Total Hückel π-electronic energy in β units.

excited structures are good indicators for E_π. This will be the case if the shape of the curve $w(G,j)\alpha^j$ does not appreciably change from isomer to isomer or does change somewhat systematically so that some cancellation occurs.

Branched Polyenes. Analysis on the relation between the Wheland polynomial and the electronic energy can be extended to branched polyenes in two different aspects, *i.e.*, difference among isomers and general properties within a series of branched hydrocarbons. Questions are: 1) does relation 23 hold for a group of isomers, and 2) does Eq. 12 or 13 hold for a series of branched polyenes?

The Wheland polynomials for smaller branched polyenes are given in Tables 4 and 5, where the $p(G,k)$ numbers, topological index, and the total π-electronic Hückel energy E_π are also given. Here the isomers are numbered according to the values of E_π. It is to be noted that with only one exception (between compounds 5-4 and 5-5) for each group of isomers with $n\leq 5$ this is just the order of decreasing the number of the first excited or Dewar structures, $w(G,1)=D$. For the group of isomers with the same D, the larger the number of the second excited or double Dewar structures, $w(G,2)=D_2$, the larger the E_π value.

To be more quantitative, the E_π values of the decapentaene isomers are plotted against the $\ln\{W_G(0.2)\}$ values in Fig. 5a (see also Table 5). The linearity is a little worse than the remarkably good plot of $E_\pi - \ln Z_G$ (Fig. 5c), but unexpectedly good in spite of the several assumptions and approximations we have made. Similar linearity, though a little more scattered than the smaller polyenes, was obtained for the twenty four isomers of dodecahexaenes. It was found, further, that the contributions of only the first and second excited structures, $\alpha D+\alpha^2 D_2$, can predict the order of E_π value as well as the $\ln\{W_G(\alpha)\}$ value with $\alpha=0.2$ (see Fig. 5b). Namely, for a group of isomers of acyclic polyenes, the E_π values are linearly related with the numbers of the

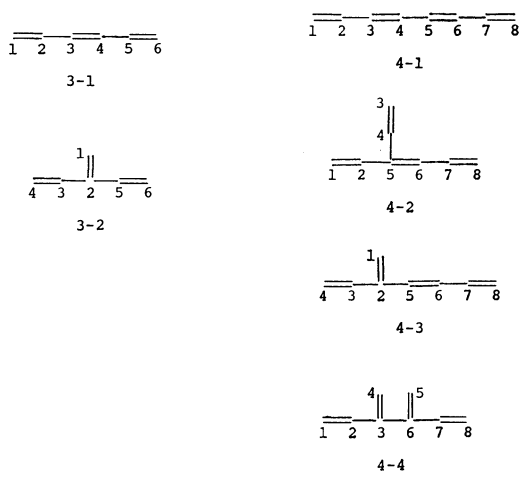

Chart 1.

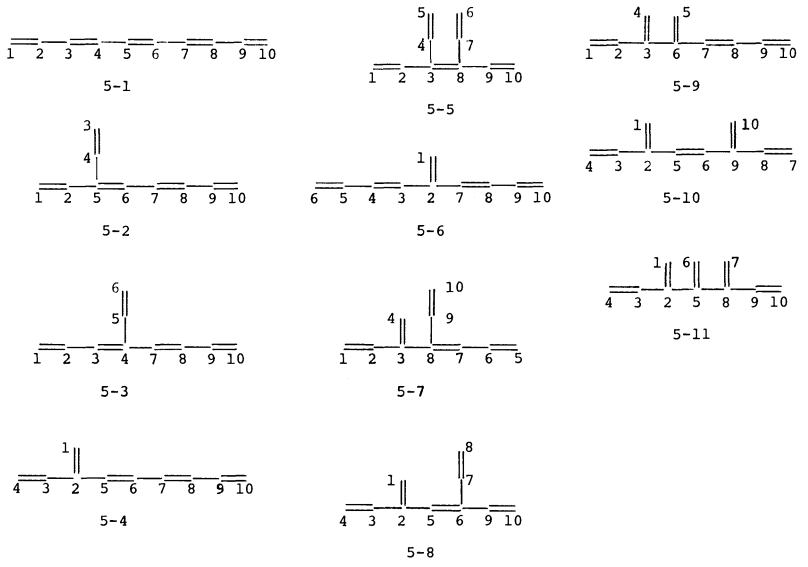

Chart 2.

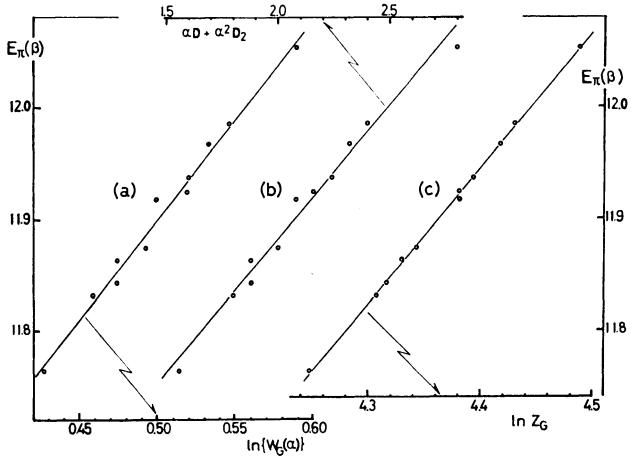

Fig. 5. Dependence of the E_π value of the decapentaene isomers on the various topological quantities. See also Table 5.
(a) Eq. 23, (b) Eq. 25, (c) Eq. 19.

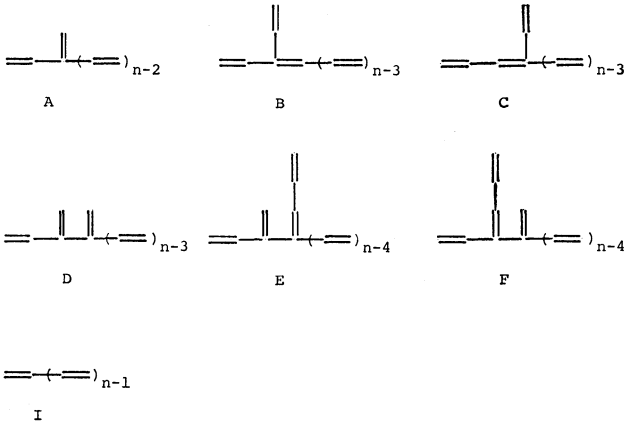

Chart 3.

first and second excited structures as

$$E_\pi \approx D + 0.2D_2. \tag{25}$$

This is also an unexpectedly good correlation, if one knows that the numbers of the Dewar structures for decapentaene and dodecahexaene isomers are, respectively, around 20 and 10% of the total number of the resonance structures.

In order to clarify the secret of this fortuitous result, the distributions of the $w(G,j)$ coefficients of the Wheland polynomial for the following six typical series of branched polyenes were studied (see Chart 3 and Table 6).

In Fig. 6 are plotted the $w(G,j)$ and $w(G,j)\alpha^j$ values against j for linear polyene 14 and one of its isomers. Although both the two curves of the isomer shift a little toward larger j values, the overall shapes are simulated fairly well by Gaussian functions. Both the $w(G,j)$ and $p(G,n-j)$ values for an isomer with n double bonds in each series studied are expressed by

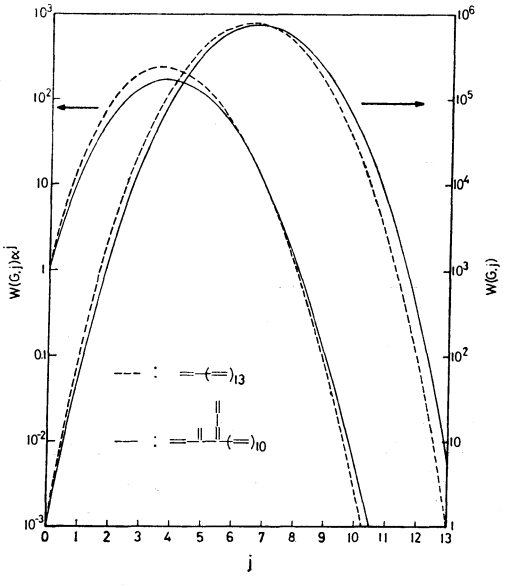

Fig. 6. Similar behaviors of $w(G,j)$ and $w(G,j)\alpha^j$ against j for $C_{28}H_{30}$ and one of its isomer.

Table 6. General expressions for the coefficients of Wheland polynomial and the non-adjacent numbers for various series of branched acyclic graphs

Series	j	$w(G,j)$	$p(G,n-j)$	$\Delta p(G,n-j)$
I	1	$\frac{1}{2}n(n-1)$	$\frac{1}{2}n(n+1)$	0
	2	$\frac{1}{12}n(n-1)^2(n-2)$	$\frac{1}{24}(n-1)n(n+1)(n+2)$	0
	3	$\frac{1}{144}n(n-1)^2(n-2)^2(n-3)$	$\frac{1}{720}(n-2)(n-1)n(n+1)(n+2)(n+3)$	0
A	1	$\frac{1}{2}(n^2-3n+4)$	$\frac{1}{2}(n^2-n+4)$	0
	2	$\frac{1}{12}(n-2)(n^3-6n^2+29n-36)$	$\frac{1}{24}(n-1)(n^3-n^2+22n-24)$	$\frac{1}{2}(n-2)$
	3	$\frac{1}{144}(n-2)(n-3)(n-4)(n^3-6n^2+59n-78)$	$\frac{1}{720}n(n-1)(n-2)(n^3+53n-66)$	$\frac{1}{10}(n-1)(n-2)(n-3)$
B	1	$\frac{1}{2}(n+1)(n-2)$	$\frac{1}{2}(n-1)(n+2)$	0
	2	$\frac{1}{12}(n^4-4n^3-7n^2+58n-60)$	$\frac{1}{24}(n^4+2n^3-13n^2+58n-72)$	$\frac{1}{2}(n-2)$
	3	$\frac{1}{144}(n-2)(n-3)\times(n^4-4n^3-25n^2+220n-264)$	$\frac{1}{720}(n-2)(n-1)\times(n^4+6n^3-19n^2+216n-360)$	$\frac{1}{10}(n-1)(n-2)(n-3)$
C	1	$\frac{1}{2}(n^2-3n+6)$	$\frac{1}{2}(n^2-n+6)$	0
	2	$\frac{1}{12}(n^4-8n^3+53n^2-202n+276)$	$\frac{1}{24}(n^4-2n^3+35n^2-130n+168)$	$(n-3)$
	3	$\frac{1}{144}(n-3)(n^5-12n^4+133n^3-1026n^2+3808n-4848)$	$\frac{1}{720}(n-2)(n^5-n^4+83n^3-479n^2+1476n-1800)$	$\frac{1}{5}(n-1)(n-3)^2$
D	1	$\frac{1}{2}(n^2-5n+10)$	$\frac{1}{2}(n^2-3n+10)$	0
	2	$\frac{1}{12}(n-2)(n^3-10n^2+63n-102)$	$\frac{1}{24}(n^4-6n^3+59n^2-174n+192)$	$\frac{1}{4}(n^2-5n+8)$
	3	$\frac{1}{144}(n-2)(n-3)(n^4-16n^3+173n^2-734n+1008)$	$\frac{1}{720}(n-2)(n^5-7n^4+131n^3-593n^2+1548n-1800)$	$\frac{1}{40}(n-2)(n-3)(n^2-5n+16)$
E	1	$\frac{1}{2}(n^2-5n+12)$	$\frac{1}{2}(n^2-3n+12)$	0
	2	$\frac{1}{12}(n^4-12n^3+89n^2-294n+360)$	$\frac{1}{24}(n^4-6n^3+71n^2-282n+456)$	$\frac{1}{2}(n^2-7n+14)$
	3	$\frac{1}{144}(n-4)(n-3)(n^4-14n^3+161n^2-688n+1404)$	$\frac{1}{720}(n^6-9n^5+175n^4-1395n^3+6664n^2-18396n+21600)$	$\frac{1}{20}(n^4-14n^3+89n^2-280n+348)$
F	1	$\frac{1}{2}(n^2-7n+22)$	$\frac{1}{2}(n^2-5n+22)$	0
	2	$\frac{1}{12}(n^4-16n^3+161n^2-662n+900)$	$\frac{1}{24}(n^4-10n^3+131n^2-578n+936)$	$\frac{1}{2}(n^2-7n+14)$
	3	$\frac{1}{144}(n-3)(n^5-24n^4+397n^3-3150n^2+11320n-14736)$	$\frac{1}{720}(n^6-15n^5+325n^4-2865n^3+13714n^2-34920n+36720)$	$\frac{1}{20}(n^4-14n^3+89n^2-280n+348)$

polynomials of n with order $2j$. The results for smaller j values are given in Table 6. All these results confirm that the values of $w(G,j)$ and $w(G,j)\alpha^j$ for the isomers behave quite similarly with those for the linear polyene.

Try to expand the function below

$$\left(1+\frac{w_1\alpha}{n}\right)^n = 1 + w_1\alpha + \binom{n}{2}\left(\frac{w_1\alpha}{n}\right)^2 + \binom{n}{3}\left(\frac{w_1\alpha}{n}\right)^3 + \cdots$$

$$= 1 + w_1\alpha + \frac{n-1}{2n}\cdot w_1^2\alpha^2 + \frac{(n-1)(n-2)}{6n^2}\cdot w_1^3\alpha^3 + \cdots$$

$$= \sum_{j=0} A_j\alpha^j, \tag{26}$$

where w_1 is $w(\bar{n},1)$, or the number of the Dewar structures

of linear polyene $\bar{n}$. Note that the coefficient A_i to α^j is proportional to $w_1{}^j$ or to the $2j$-th power of n. Compare this expansion with the Wheland polynomial for $\bar{n}$ as

$$W_{\bar{n}}(\alpha) = \sum_{j=0} w(\bar{n}, j)\alpha^j, \tag{27}$$

whose coefficient $w(\bar{n},j)$ is also proportional to the $2j$-th power of n (see Eq. 2). Owing to the small value of α, $W_{\bar{n}}(\alpha)$ can be approximated, though not accurately but reasonably well, as expression 26, namely,

$$W_{\bar{n}}(\alpha) \sim \left(1+\frac{w_1\alpha}{n}\right)^n. \tag{28}$$

As inferred from the behavior of $w(\mathrm{G},j)$ observed above, we may also assume

$$W_{\mathrm{G}}(\alpha) \approx \left(1+\frac{w_1'\alpha}{n}\right)^n \tag{29}$$

for an isomer G with $w_1'=w(\mathrm{G},1)$. Then from Eq. 23 one gets

$$\begin{aligned}\Delta E_\pi &= E_\pi(\bar{n}) - E_\pi(\mathrm{G}) \\ &\approx \ln\{W_{\bar{n}}(\alpha)/W_{\mathrm{G}}(\alpha)\} \\ &\approx n \ln\left\{\left(1+\frac{w_1\alpha}{n}\right)\Big/\left(1+\frac{w_1'\alpha}{n}\right)\right\}.\end{aligned} \tag{30}$$

Since w_1 is equal to $n(n-1)/2$ (from Eq. 2), the value $w_1\alpha/n$ is smaller than unity for small n. Then ΔE_π can be approximated as

$$\Delta E_\pi \approx \alpha(w_1-w_1'). \tag{31}$$

This is a partial proof of relation 25. For larger n, however, the expression 31 would no longer be a good expansion of ΔE_π. In this case one has to expand $W_{\mathrm{G}}(\alpha)$ by the inclusion of higher $w(\mathrm{G},j)$ terms. This means that the larger the molecule the larger the weight of higher excited structures. However, for a group of moderate size of acyclic polyenes, the number of the Dewar structures is thus shown to be a good measure of the π-electronic energy.

Next the relation between $w(\mathrm{G},j)$ and $p(\mathrm{G},n-k)$ was studied. For $j,k\leq 1$ the results are the same as the case of linear polyenes. Namely, for polyene G with n double bonds,

$$K = w(\mathrm{G}, 0) = p(\mathrm{G}, n) \tag{14'}$$

and

$$D = w(\mathrm{G}, 1) = p(\mathrm{G}, n-1) - n\,p(\mathrm{G}, n). \tag{15'}$$

However, for larger values of j and k small correction should be introduced into relations 12 and 13.

Relation 14' is guaranteed by definition. Relation 15' has already been presented without proof by one of the present authors.[3,22] Since an acyclic polyene is an alternant hydrocarbon, namely, the corresponding graph is bipartite, the carbon atoms are grouped into starred and unstarred so that all the bonds are formed between atoms of different groups. As will be exemplified in Appendix, all the ineffective bonds in an excited canonical structure are also formed between atoms of different groups.

Suppose the C–C single bond skeleton of polyene G with n double bonds and choose $n-1$ disjoint bonds on which double bonds are to be drawn. There are $p(\mathrm{C},n-1)$ different ways. Since each double bond is so chosen as to span a couple of starred and unstarred atoms, there are left a couple of starred and unstarred atoms. Irrespective of the situation that they may or may not be adjacent, join them to form the n-th π bond. The resultant $p(\mathrm{G},n-1)$ graphs are the candidates for the set of the first excited canonical structures, or Dewar structures. It is obvious that no other candidate is possible. If the n-th π bond is formed between two adjacent atoms, the resultant graph is nothing else but the unexcited Kekulé structure to be deleted from the counting of $w(\mathrm{G},1)$ or D, and there are n such possible ways for each Kekulé structure. This completes the proof of Eq. 15'. Note that this relation is valid even for a graph with more than one Kekulé structures.

Let the difference between the right and left hand sides of Eq. 12 be defined as

$$\Delta p(\mathrm{G}, n-k) = p(\mathrm{G}, n-k) - \frac{k!(k+1)!}{(2k)!}\sum_{j=0}^{k}\binom{n-j}{k-j}w(\mathrm{G}, j) \tag{32}$$

which was shown to be always positive for $k\geq 2$ of all the series studied. In Table 6 are given the general expressions of the $\Delta p(\mathrm{G},n-2)$ and $\Delta p(\mathrm{G},n-3)$ for each series. It is seen from the expression of $p(\mathrm{G},n-k)$ and $\Delta p(\mathrm{G},n-k)$ that the relative correction is at most in the order of n^{-2} and negligible for larger polyenes. This is also the case with the higher values of k. Thus the number of the higher excited structures can be approximated by Eq. 13 for branched polyenes in terms of the set of the $p(\mathrm{G},k)$ numbers, which can systematically be obtained by the use of several recursion formulas.[14,23]

It is worth mentioning here that the quantities independently obtained from VB and GT are thus found to be closely related with each other through the quantity of MO. Work in these lines is in progress for the mathematical properties of the number of the resonance structures of polycyclic hydrocarbons.

Appendix

A Note on the Numbering of Atoms for Acyclic Polyenes. At present we are not yet in a position to state the unambiguous method for numbering the atoms to generate the Wheland polynominal of the highest priority for an arbitrary acyclic polyene. However, our experience on a number of examples has led to several empirical rules for the numbering of a polyene with a few branches.

Consider first the mapping procedure for generating the

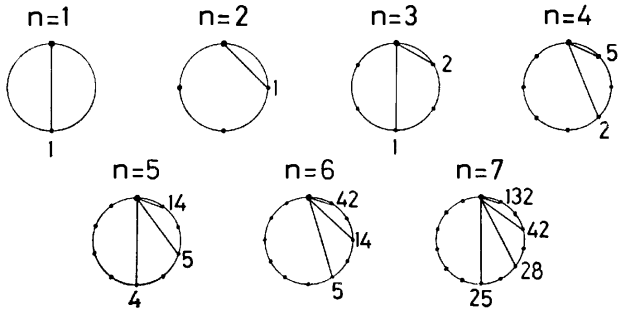

Fig. 7. Distribution of the numbers of the effective and ineffective bonds spanning from a pivot point among a set of C_n standard patterns. No bond is found between a pair of atoms of the same parity, and the distribution is symmetrical.

Wheland polynomial exemplified in Fig. 1. Draw $C_n=(2n)!/\{n!(n+1)!\}$ standard patterns for the set of circularly arranged and numbered $2n(=N)$ points. In each pattern n non-crossing lines are drawn. Choose a point as the pivot from the $2n$ points. Then for each member of the $2n-1$ points count the number of patterns in which it is connected with the pivot point. The results for smaller n's are shown in Fig. 7. Observe that no line is drawn between a pair of points of the same parity. Namely, an alternant hydrocarbon has no bond between a pair of starred atoms and also between a pair of unstarred atoms. The number of the effective bonds are the largest, and the number of the ineffective bonds rapidly decreases with the increase of the length. The sum of these numbers is C_n.

Recall that the set of the canonical resonance structures are obtained by mapping the given arbitrary numbered graph G (or the π-electron skeleton) onto each of the C_n standard patterns. The degree of excitation j for a resonance structure is the number of the ineffective bonds and $w(G, j)$ is the number of j-th excited structures for G. Then the total number of the effective bonds J in the set of the C_n resonance structures is given by

$$J = n \cdot C_n - \sum_{j=1} j \cdot w(G, j).$$

Note that the summation in the second term is equal to $W_G'(1)=(dW_G(x)/dx)_{x=1}$, where $W_G(x)$ is the Wheland polynomial $W_G(x)=\sum_{j=0} w(G, j)\cdot x^j$. The highest priority is given to such a $W_G(x)$ expression that has the top-heaviest set of the coefficients, which we are going to search. It is not sufficient but necessary for that expression to have the largest J value, or the smallest $W_G'(1)$ value.

For convenience's sake let us define the term "number difference", $d_{ij}=\min(|i-j|, 2n-|i-j|)$, for a pair of atoms i and j forming a bond. All the bonds are then classified into the following three types according to their d_{ij} value as,

α-type with $d_{ij}=1$

β-type with $d_{ij}=2, 4, 6, \cdots$

γ-type with $d_{ij}=3, 5, 7, \cdots$

Unless confusion may occur α, β, and γ stand also for the numbers of the bonds of the corresponding types. Then all the above observations and discussions lead to the following recipes for the numbering of atoms so as to give the largest J value, or the smallest $W_G'(1)$ value.

(1) Every bond should be composed of a pair of atoms of different parity, or $\beta=0$.

(2) The number of γ-type bonds should be minimized. There are several possible ways for satisfying the conditions (1) and (2). In these cases recipe (3) would be applied.

(3) The sum $D=\sum_{i<j} d_{ij}$ of the "number difference" for all the bonds should be minimized. Further, to the case where several numberings are still possible in which recipes (1)—(3) are obeyed we may apply.

(4) The sizes of the polyene fragments obtained by excising the γ-(and also β-) type bonds should be as uniform as possible.

However, (3) and (4) should not necessarily be obeyed, and their relative priority seems to change from case to case.

Linear Polyene. Application of recipes (1) and (2) to a linear polyene assures that the following numbering gives the Wheland polynomial of the highest priority,

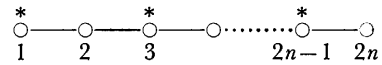

The cyclic change of numbering as

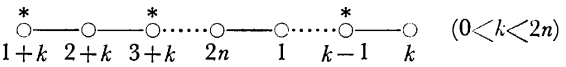

$(0<k<2n)$

gives the same result.

Polyene with One Branch. Three carbon chains, P_1, P_2, and P_3, emanate, from the carbon atom as the junction of the polyene with one branch, where P_1 is an odd chain, P_2 a shorter even chain, and P_3 longer even chain. Application of recipes (1) and (2) gives the numbering as shown in Chart 4a. For graph 4-3 in Chart 1 the following two numberings give the same result,

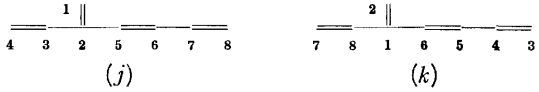

since they are related to each other by the formula

$$j + k = l \text{ or } l + 2n,$$

where j and k are the numberings given to the same atoms, respectively, by the numbering systems (j) and (k), and l is an arbitrary integer (here $l=3$).

Polyene with Two Branches. Consider first those polyenes with two branches, which are separated by one bond. There

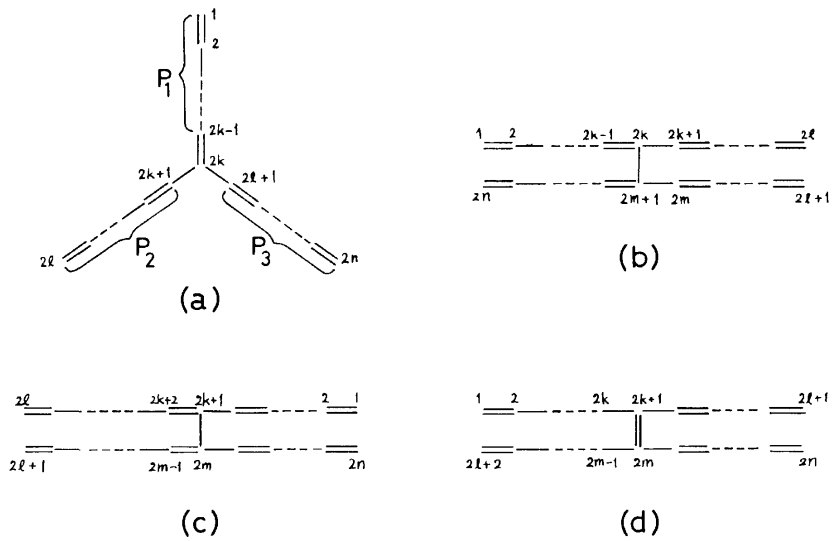

Chart 4.

Table 7. An example showing the factors for determining the coefficients of the Wheland polynomial

Numbering[a]	$W_G(x)$	$W_G'(1)$	β[b]	γ[c]	Fragment[d]
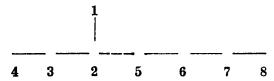	$1+4x+8x^2+x^4$	24	0	1	4+4
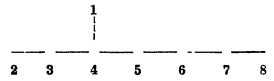	$1+4x+7x^2+2x^3$	24	0	1	1+7
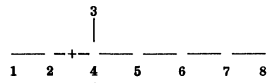	$1+3x+7x^2+3x^3$	26	1	0	2+6
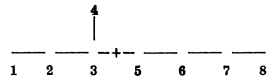	$1+2x+10x^2+x^4$	26	1	0	4+4

a) ——: α-type bond, −+−: β-type bond, ——: γ-type bond. b) Number of the β-type bond. c) Number of the γ-type bond. d) Indicates the sizes of the polyene chains obtained by excising the β- and γ-bonds.

are two cases depending that the central bond is single or double. For the former case the two numberings in Charts 4b and c are the candidates for the highest priority. Then compare the number differences at the central bridge bond, and the numbering giving the smaller value is chosen as the best.

In the case of the polyene with a central bridge double bond, the numbering with the highest priority can be chosen as the one having the smallest number difference at the bridge from the possible numberings of the types as in Chart 4d.

Table 7 shows how the Wheland polynomial depends on the recipes for the numbering given above.

References

1) W. C. Herndon, *Tetrahedron*, **29**, 3 (1973).
2) G. G. Hall, *Int. J. Math. Educ. Sci. Technol.*, **4**, 233 (1973).
3) H. Hosoya, *Kagaku No Ryoiki*, **29**, 719 (1975).
4) J. Aihara, *Kagaku No Ryoiki*, **30**, 269, 379, 812 (1976).
5) H. Hosoya and K. Hosoi, *J. Chem. Phys.*, **64**, 1065 (1976).
6) A. Graovac, I. Gutman, and N. Trinajstić, *Lecture Notes in Chem.*, No. 4, Springer-Verlag, Berlin (1977).
7) R. Swinborne-Sheldrake, W. C. Herndon, and I. Gutman, *Tetrahedron Lett.*, **1975**, 755.
8) G. W. Wheland, *J. Chem. Phys.*, **3**, 356 (1935).
9) M. Gordon and W. H. T. Davison, *J. Chem. Phys.*, **20**, 428 (1952).
10) D. Cvetković, I. Gutman, and N. Trinajstić, *Chem. Phys. Lett.*, **16**, 614 (1972).
11) H. Hosoya and T. Yamaguchi, *Tetrahedron Lett.*, **1975**, 4659.
12) D. Cvetković and I. Gutman, *Croat. Chem. Acta*, **46**, 15 (1974).
13) M. Randić, *J. Chem. Soc. Faraday Trans. 2*, **72**, 232 (1976).
14) H. Hosoya, *Bull. Chem. Soc. Jpn.*, **44**, 2332 (1971).
15) H. Hosoya, K. Hosoi, and I. Gutman, *Theor. Chim. Acta*, **38**, 37 (1975).
16) This algorithm is indeed time-consuming for larger graph even with a computer, since the time required for the enumeration inceases with the factorial of the number of points in the graph.
17) The series C_n of the numbers 1, 2, 5, 14, 42, ···, thus derived, are known as the Catalan numbers.
18) By the use of a HITAC 8700/8800 computer of the University of Tokyo, it took 10 s for the graph with 20 points below which the machine time is negligible. However, as the machine time increases exponentially in this region, an estimated time for a graph with 30 points would be 1.5 h.
19) Note that this notation differs from what was used by one of the present authors elsewhere.[14] In this paper all the molecules have even number of carbon atoms.
20) J. Riordan, "Combinatorial Identities," John Wiley and Sons, Inc., New York (1968).
21) R. Daudel and A. Pullman, *J. Phys.*, **7**, 105 (1946).
22) I. Gutman and H. Hosoya, *Theor. Chim. Acta*, **48**, 279 (1978).
23) H. Hosoya, *Fibonacci Quart.*, **11**, 255 (1973).

X-Ray Molecular Structure of 1-Cyano-7,8-benzo-11-oxatricyclo-[4.2.2.1^{2,5}]undeca-3,7,9-triene†

Kojiro KAN, Yasushi KAI, Noritake YASUOKA, and Nobutami KASAI*

Department of Applied Chemistry, Faculty of Engineering, Osaka University, Yamadakami, Suita, Osaka 565

(Received February 9, 1979)

$C_{15}H_{11}ON$, *M.W.* 221.17, monoclinic, space group $P2_1/c$, $a=9.451(1)$, $b=8.267(1)$, $c=14.336(2)$ Å, $\beta=94.37(1)°$, $D_m=1.31$, $D_c=1.32$ g cm^{-3}, $Z=4$, $R=0.088$ for 1300 non-zero reflections. The molecule has an *endo*-configuration, and the furan ring has an envelope form.

Photoreaction between 1-naphthonitrile and furan gave a single cycloaddition product, although *endo*- and *exo*-isomers were expected to be formed.[1]

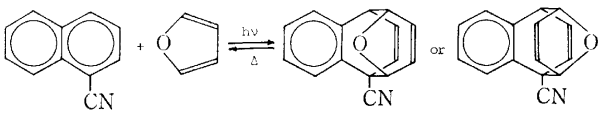

exo-form *endo*-form

In order to determine the stereochemistry of the cycloadduct, an X-ray analysis of the product has been carried out.

Experimental

For the data collection, a crystal with suitable size was mounted on a G.E. single crystal orienter equipped on a Rigaku SG-2 goniometer. Stationary crystal-stationary counter method was applied. During the data collection the intensity of the standard reflections decreased; as it did so uniformly with time, a linear correction factor was applied. 1397 unique data collected up to $2\theta=110°$ were then corrected for Lp effect but not for absorption [μ(Cu $K\alpha$)=6.70 cm^{-1}]. The structure was solved by the symbolic addition method.[2] Signs of 181 $|E|$'s ($|E|>1.4$) were determined, and all the non-hydrogen atoms

Table 1. Fractional atomic coordinates ($\times 10^4$ for C, N, and O atoms and $\times 10^3$ for H atoms) and thermal parameters with e.s.d.'s in parentheses

Anisotropic thermal parameters ($\times 10^4$) expressed in the form: $\exp\{-(\beta_{11}h^2+\beta_{22}k^2+\beta_{33}l^2+\beta_{12}hk+\beta_{13}hl+\beta_{23}kl)\}$.

Atom	x	y	z	β_{11} or B	β_{22}	β_{33}	β_{12}	β_{13}	β_{23}
O	2756(4)	9468(4)	4979(2)	190(6)	102(6)	46(2)	−66(10)	28(6)	−25(6)
N	1952(6)	4576(6)	6412(3)	270(10)	178(10)	48(3)	−51(16)	45(9)	31(9)
C(1)	3253(6)	6508(6)	3440(3)	143(8)	113(9)	37(3)	−60(14)	13(7)	7(8)
C(2)	3225(7)	5868(7)	2544(4)	191(10)	161(10)	35(3)	−9(17)	23(8)	−5(9)
C(3)	2536(6)	4412(7)	2346(4)	181(9)	144(10)	40(3)	12(16)	−1(8)	−29(9)
C(4)	1894(7)	3606(6)	3022(4)	194(10)	101(9)	51(3)	−13(15)	−32(9)	−46(9)
C(5)	1921(6)	4210(6)	3939(3)	154(8)	104(8)	40(3)	−9(14)	6(8)	−3(8)
C(6)	2596(5)	5675(6)	4138(3)	132(7)	92(8)	30(3)	−15(13)	4(7)	−4(7)
C(11)	2764(6)	6482(6)	5104(3)	137(7)	104(8)	31(3)	−32(13)	5(7)	−4(8)
C(12)	4312(6)	6903(6)	5284(4)	154(8)	109(9)	42(3)	−28(14)	2(8)	−11(8)
C(13)	4945(6)	7701(7)	4616(4)	154(8)	118(9)	53(3)	−69(15)	8(8)	−28(9)
C(14)	4001(6)	8099(7)	3728(4)	175(9)	131(9)	40(3)	−2(15)	4(8)	−2(9)
C(21)	2894(7)	9450(6)	3973(4)	195(10)	96(9)	48(3)	−50(15)	29(9)	15(9)
C(22)	1409(6)	9044(6)	3615(4)	170(9)	102(9)	54(3)	−6(15)	11(8)	−2(9)
C(23)	750(6)	8258(6)	4268(4)	156(8)	113(9)	53(3)	22(14)	27(18)	−2(9)
C(24)	1822(6)	8137(6)	5116(3)	173(9)	104(8)	35(3)	−34(14)	12(8)	−16(8)
C(31)	2307(7)	5383(7)	5840(4)	212(10)	120(9)	36(3)	−3(16)	6(9)	−16(8)
H(2)	364(5)	635(6)	207(3)	1.6(11)					
H(3)	240(6)	393(7)	167(4)	4.0(15)					
H(4)	146(5)	269(6)	289(3)	1.6(11)					
H(5)	130(6)	370(7)	442(4)	3.6(14)					
H(12)	502(6)	642(7)	587(4)	3.5(14)					
H(13)	625(5)	792(7)	463(4)	2.7(13)					
H(14)	463(7)	865(9)	316(5)	6.1(19)					
H(21)	306(6)	66(7)	375(4)	3.5(14)					
H(22)	83(6)	926(7)	297(4)	3.9(15)					
H(23)	−38(6)	783(8)	424(4)	4.7(16)					
H(24)	141(5)	838(6)	574(3)	2.2(12)					

† Read at the 28th National Meeting of the Chemical Society of Japan, Tokyo, April 1973.

were located in the *E*-map. All the H atoms were located by difference syntheses. The refinements was carried out by block-diagonal least-squares (*HBLS V*)[3] with anisotropic temperature factors for non-hydrogen atoms. The final *R* values were 0.088 for 1300 non-zero and 0.094 for all reflections. Atomic scattering factors for C, N, and O were taken from Hanson and coworkers,[4] and H from Stewart and coworkers.[5] The final atomic parameters are listed in Table 1.††

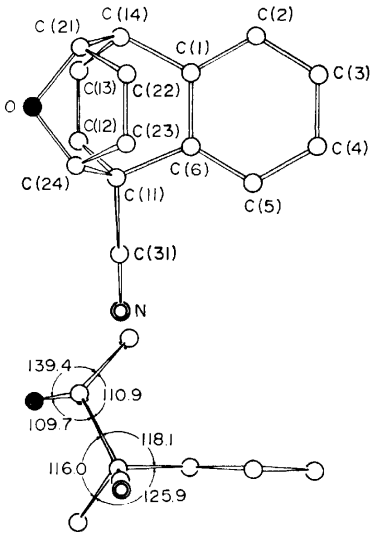

Fig. 1. Molecular structure with the numbering scheme of atoms.

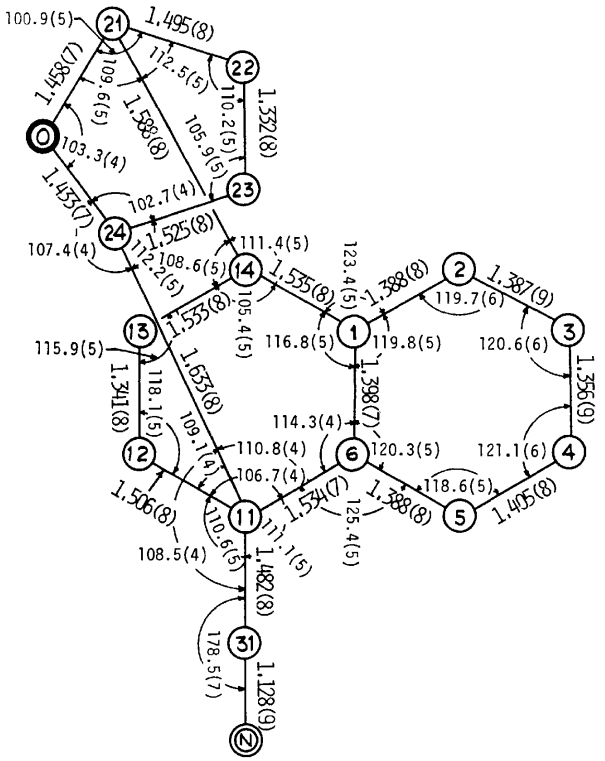

Fig. 2. Bond lengths and bond angles with e.s.d's in parentheses.

†† A Table of observed and calculated structure factors are kept as Document No. 7922 at the Chemical Society of Japan.

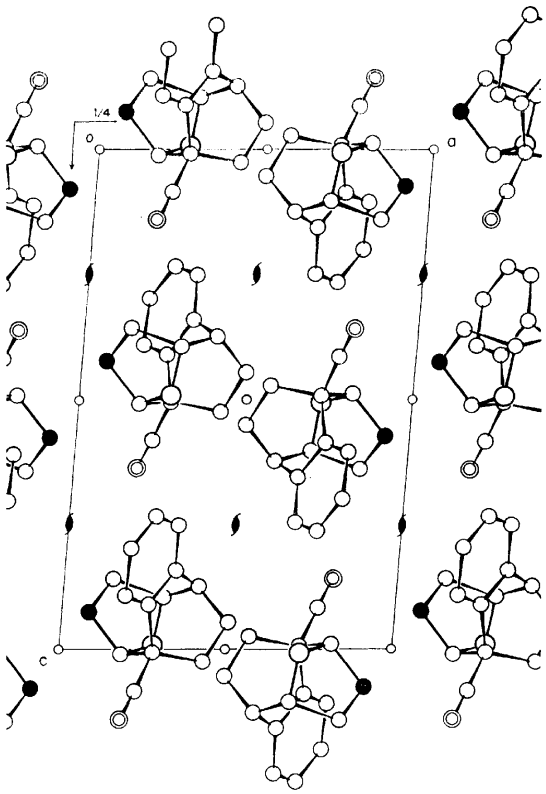

Fig. 3. Crystal structure projected along the b axis.

Results and Discussion

The molecular structure is shown in Fig. 1, which indicates that the cycloadduct has the *endo*-configuration. Bond lengths and bond angles are given in Fig. 2. The C(11)–C(24) and C(14)–C(21) bonds [1.633(8) and 1.588(8) Å, respectively] involved by the photocycloaddition are comparable with those observed in photodimers of anthracene [1.62(2) Å],[6] 2-methoxynaphthalene [1.610(5) Å][7] and 9-anthracenecarbaldehyde[1.61(1) Å],[8] which are longer than the usual $C(sp^2)$–$C(sp^3)$ bond length. The furan ring has an envelope form, the O atom is located by 0.58 Å out of the plane containing C(21) through C(24) atoms. The dihedral angle between the planes defined by O, C(21), and C(24) and C(21), C(22), C(23), and C(24) is 139.4°. The dihedral angle between C(1), C(6), C(11), and C(14) and C(11), C(12), C(13), and C(14) planes is 125.9° (Fig. 1).

The crystal structure is shown in Fig. 3. No close intermolecular atomic contact less than usual van der Waals distance can be observed.

The authors wish to express their deep thanks to Professor H. Sakurai and coworkers for crystals.

References

1) C.-J. Pac, T. Sugioka, and H. Sakurai, *Chem. Lett.*, **1972**, 39.
2) J. Karle and I. L. Karle, *Acta Crystallogr.*, **21**, 849 (1966).
3) T. Ashida, "The Universal Crystallographic Computing System-Osaka," The Computation Center, Osaka Univ.

(1973), p. 55.
4) P. Hanson, F. Herman, J. D. Lea, and S. Skillman, *Acta Crystallogr.*, **17**, 1040 (1764).
5) R. F. Stewart, E. R. Davidson, and W. T. Simpson, *J. Chem. Phys.*, **42**, 3175 (1965).
6) M. Ehrenberg, *Acta Crystallogr.*, **20**, 177 (1966).
7) B. K. Selinger and M. Sterns, *J. Chem. Soc., D*, 978 (1969).
8) M. Ehrenberg, *Acta Crystallogr.*, **24**, 1123 (1968).

Properties and Structure of Alkali Aluminophosphate Glass

Akira KISHIOKA

Department of Chemistry, Faculty of Science and Technology, Sophia University, Kioicho, Chiyoda-ku, Tokyo 102

(Received July 14, 1978)

Several series of alkali (sodium and potassium) aluminophosphate glasses were prepared with compositions of 32—63 mol % of P_2O_5 and the properties of these glasses were determined. In the glasses with a higher P_2O_5 content ($P_2O_5 \gtrsim 42.5$ mol % in the Na_2O–Al_2O_3–P_2O_5 glass and $P_2O_5 \gtrsim 45$ mol % in the K_2O–Al_2O_3–P_2O_5 glass), the density, refractive index, and chemical resistivity increased with increasing amounts of Al_2O_3. In the glasses with a lower P_2O_5 content ($P_2O_5 \lesssim 37.5$ mol % in the Na_2O glass and $P_2O_5 \approx 40$ mol % in the K_2O glass), however, almost no increase of the density was found by an increase of Al_2O_3; the increases in the refractive index and chemical resistivity were also smaller than those in the glasses with a higher P_2O_5 content. The infrared absorption spectra of the glasses varied also with the P_2O_5 content. These changes in the properties are due to a marked structural difference between the glasses with a higher P_2O_5 content and those with a lower P_2O_5 content, and are also associated closely with the structural role of Al^{3+} ions in the glass.

The structure and the role of Al^{3+} ions in aluminophosphate glasses are attracting the attention of many investigators because Al_2O_3 can be incorporated in fairly large quantities into phosphate glass and stabilizes the glass structure. Kreidl and Weyl[1] considered that the ($AlPO_4$) group was formed by AlO_4 and PO_4 tetrahedra in the glass structure. On the other hand, Sakka[2,3] has reported that there are two kinds of Al^{3+} ions with different coordination numbers in phosphate glass. The present authors[4] have investigated the formation of the glasses in the three-component diagram in alkali (sodium and potassium) aluminophosphate systems and found one Al_2O_3 peak in about 65 mol % of P_2O_5 and another peak in about 35 mol % of P_2O_5. We also reported the structural difference between the glasses with a higher P_2O_5 content and those with a lower P_2O_5 content. Reports concerning the fundamental properties such as density, refractive index, viscosity, *etc.* of aluminophosphate glass, however, are relatively few compared with those of aluminosilicate glass. Therefore, it may be interesting to investigate the changes of the properties of the glass with regard to the difference in glass structure.

In this investigation, the density, refractive index, and infrared absorption spectra and also the molar volume, volume per mole of oxygen, and molar refraction were determined for several series of the Na_2O–Al_2O_3–P_2O_5 and K_2O–Al_2O_3–P_2O_5 glasses with the same contents of P_2O_5, which ranged from 32 to 63 mol %. For Na_2O–Al_2O_3–P_2O_5 glass the chemical resistivity and solubility in water or hydrochloric acid were examined. From these results, the changes in the properties were discussed in connection with the glass structure.

Experimental

Preparation of Series of Glasses with the Same P_2O_5 Contents. The glass specimens containing 32.5—45 mol % of P_2O_5, as reported in the previous paper,[5] were used as the lower P_2O_5 alkali aluminophosphate glasses in this investigation. Furthermore, about fifty glass specimens containing more than 45 mol % of P_2O_5 were prepared in the glass-forming regions of the Na_2O–Al_2O_3–P_2O_5 and K_2O–Al_2O_3–P_2O_5 systems.[4] The materials used were reagent grade chemicals of sodium dihydrogenphosphate, potassium dihydrogenphosphate, aluminum oxide, and orthophosphoric acid (85 %). A batch (40-g) obtained by mixing appropriate amounts of the above chemicals was placed in Al_2O_3 crucible and heated in an electric furnace. After dehydration, the temperature of the batch was raised to 1350 °C and kept at this temperature for 1 h. The melt was poured out and quenched by pressing it with a copper plate cooled with water. All the quenched melts were obtained as transparent colorless glasses. The composition of these glasses were determined by chemical analyses and several series of glasses with the same P_2O_5 contents were selected and used in this experiment.

Determination of Al_2O_3. Glass powder containing about 0.1 g of Al_2O_3 was fused with 5—9 g of sodium carbonate and dissolved in 200 cm^3 of 1 mol/dm^3 hydrochloric acid. The Al^{3+} ion in the obtained solution was determined gravimetrically as $AlPO_4$.[6]

Determination of P_2O_5. Glass powder containing about 0.1 g of P_2O_5 was fused with about 3 g of sodium carbonate and dissolved in 100 cm^3 of 1 mol/dm^3 hydrochloric acid. The PO_4^{3-} ion in the solution was determined gravimetrically as $Mg_2P_2O_7$.[7]

Determination of H_2O. The H_2O content of the glass was determined gravimetrically by the method of Naruse *et al.*,[8] namely from the weight loss incurred by heating a mixture of the pulverized glass and preignited zinc oxide at 700 °C for 2 h.

Density and Volume of Glass. The density of the glass was determined pycnometrically using 1-butanol at 25 °C.

The molar volume and the volume per mole of oxygen of the glass were calculated by the following equations:[9]

$$V = \frac{W_f}{\rho} \tag{1}$$

and

$$V_0 = \frac{V}{N_0} \tag{2}$$

where V is the molar volume of the glass, V_0 is the volume per mole of oxygen, W_f is the gram formular weight of the glass based on the composition determined by chemical analyses, ρ is the density of the glass, and N_0 is the number of gram molecular weight of oxygen (32 g units) in the glass.

Refractive Index and Molar Refraction of Glass. The refractive index was estimated by the Becke oil immersion method.

The molar refraction of the glass was calculated by the following equation:[9]

$$R = \frac{n^2-1}{n^2+2}V \qquad (3)$$

where R is the molar refraction of the glass, n is the refractive index, and V is the molar volume.

Chemical Resistivity and Solubility of Glass. Glass grains (0.25—1 mm) of about 1 g were placed in a 100-cm^3 Erlenmeyer flask and 50 cm^3 of either water or hydrochloric acid were added into the flask. After shaking at a speed of 80 strokes per minute in the thermostat, the weight loss and the Al_2O_3/P_2O_5 (molar ratio) in the residual glass were determined. The experimental conditions: concentration of hydrochloric acid, temperature of the thermostat, and shaking time were selected so as to be suitable for the sample glass or the series of samples.

Infrared Spectra. The infrared absorption spectra ranging from 1500 to 600 cm^{-1} of the glasses were recorded by means of a Hitachi EPI-2G spectrophotometer, using the KBr pellet technique.

Results and Discussion

Composition of Glass. The analyses of the glasses with more than 45 mol % of P_2O_5 are given in Tables 1 and 2. The Na_2O or K_2O content was calculated by subtracting the Al_2O_3 and P_2O_5 contents from the weight of the sample. The H_2O content was in the range from 0.11 to 0.42 wt % in eight kinds of the glasses of two series of the Na_2O–Al_2O_3–P_2O_5 glass with 59—61 mol % of P_2O_5 and K_2O–Al_2O_3–P_2O_5 glass with 61—62 mol % of P_2O_5, and the H_2O content tended to decrease with an increase in the amount of Al_2O_3. Since the H_2O content was less than 0.42 wt % in the above glasses, even though they were prepared by adding a large amount of orthophosphoric acid, it is considered that the properties of the glass are not seriously effected by water.

Table 1. Composition of Na_2O–Al_2O_3–P_2O_5 glass

	P_2O_5/mol %[a]	Composition		
		Na_2O/mol %	Al_2O_3/mol %	P_2O_5/mol %
(1)	49	45.74	5.00	49.26
		39.99	9.81	49.20
(2)	55	39.68	5.03	55.29
		33.38	11.40	55.22
(3)	59—61	34.08	4.92	61.00
		29.24	10.78	59.98
		25.81	14.77	59.42
		20.86	18.70	60.43
(4)	63	20.53	16.59	62.88
		17.69	19.02	63.30
		13.38	23.31	63.32

a) P_2O_5 content in the glass.

Table 2. Composition of K_2O–Al_2O_3–P_2O_5 glass

	P_2O_5/mol %[a]	Composition		
		K_2O/mol %	Al_2O_3/mol %	P_2O_5/mol %
(1)	49	40.67	9.95	49.38
		36.19	14.61	49.20
(2)	55—56	38.89	4.98	56.13
		33.17	11.35	55.48
(3)	61—62	32.40	5.14	62.46
		27.68	10.20	62.12
		25.10	13.83	61.08
		21.41	17.34	61.25

a) P_2O_5 content in the glass.

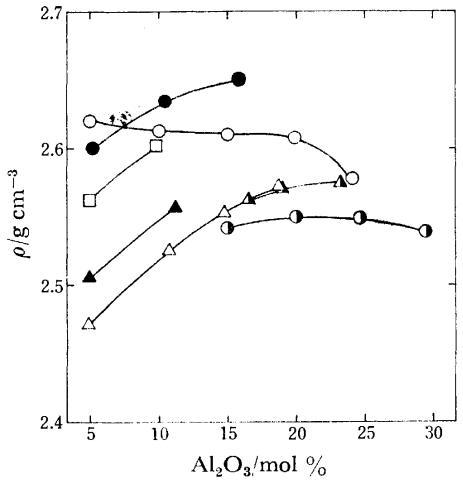

Fig. 1. Density (ρ) of Na_2O–Al_2O_3–P_2O_5 glass.
▲: 63 mol % P_2O_5, △: 59—61 mol % P_2O_5, ▲: 55 mol % P_2O_5, □: 49 mol % P_2O_5, ●: 42.5 mol % P_2O_5, ○: 37.5 mol % P_2O_5, ◑: 32.5 mol % P_2O_5.

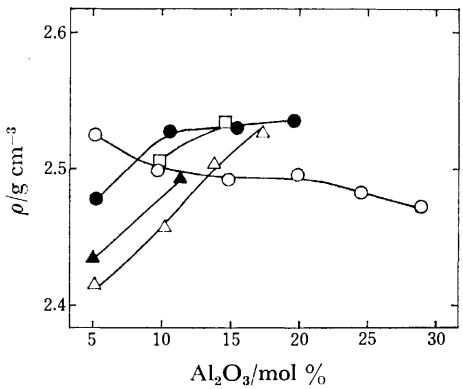

Fig. 2. Density (ρ) of K_2O–Al_2O_3–P_2O_5 glass.
△: 61—62 mol % P_2O_5, ▲: 55—56 mol % P_2O_5, □: 49 mol % P_2O_5, ●: 45 mol % P_2O_5, ○: 40 mol % P_2O_5.

Density and Volume. The densities of these glasses are given in Figs. 1 and 2. In Fig. 1 the densities in the Na_2O–Al_2O_3–P_2O_5 glasses with the same P_2O_5 contents are plotted *vs.* the Al_2O_3 content; also in Fig. 2 those in the K_2O–Al_2O_3–P_2O_5 glasses are similarly plotted. The density of the Na_2O glass was larger than that of the K_2O glass in the same composition.

As shown in Figs. 1 and 2, a marked difference in the changes of the densities can be recognized between the glasses with a higher P_2O_5 content and those with a lower P_2O_5 content. The densities increased with an increase in the Al_2O_3 content in the glasses in the Na_2O–Al_2O_3–P_2O_5 system with 42.5 mol % of P_2O_5 or more and those in the K_2O–Al_2O_3–P_2O_5 system with 45 mol % of P_2O_5 or more. On the contrary, no increase of the densities was found in the glasses of 32.5, 37.5 (Na_2O system), and 40 mol % of P_2O_5 (K_2O system). Furthermore, the densities of the glasses

with a lower Al_2O_3 content in both systems decreased with an increase in the P_2O_5 content. In the glasses with 32.5, 37.5, and 40 mol % of P_2O_5, the P–O–P chain is changed to the P–O–Al chain by an increase in the Al_2O_3 content.[5] The density should tend to decrease rather than to increase because the Na_2O or K_2O content decreases with increasing amounts of Al_2O_3 and also because the P–O–Al chain formed is not very long in such a glass. On the other hand, the increase in the densities in the glasses with a higher P_2O_5 content may be interpreted from the assumption that most of the Al^{3+} ions do not form the chain and network consisting of P–O–Al linkages. The Al^{3+} ions outside the P–O–P chain should easily strengthen the glass structure because the ionic field strength $(Z_i/(r_i+r_0)^2$; where Z_i: charge of cation, r_i: radius of cation, r_0: radius of oxygen ion)[10] of the Al^{3+} ion is much larger than that of the Na^+ or K^+ ion. In addition, the decrease in the densities with an increase in the P_2O_5 content in the glasses with a lower Al_2O_3 content may be interpreted from the following facts: an increase of PO_4 groups having one nonbridging O^{2-} ion in each and decrease of Na^+ or K^+ ions tend to open the structure compared with that of the glass with a lower P_2O_5 content.

The molar volumes and the volumes per mole of oxygen in the Na_2O–Al_2O_3–P_2O_5 glass are given in Figs. 3(a) and 3(b) and those in the K_2O–Al_2O_3–P_2O_5 glass are given in Figs. 4(a) and 4(b). The molar volumes increased with an increase in the P_2O_5 content, while the volumes per mole of oxygen decreased. This indicates that the O^{2-} ions are packed more closely together as the Al_2O_3 and P_2O_5 contents increased. In

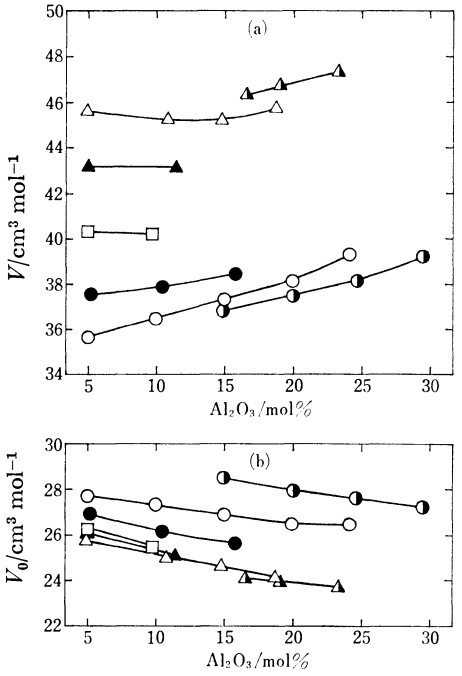

Fig. 3. (a) Molar volume (V) and (b) volume per mole of oxygen (V_0) of Na_2O–Al_2O_3–P_2O_5 glass.
▲: 63 mol % P_2O_5, △: 59—61 mol % P_2O_5, ▲: 55 mol % P_2O_5, □: 49 mol % P_2O_5, ●: 42.5 mol % P_2O_5, ○: 37.5 mol % P_2O_5, ◑: 32.5 mol % P_2O_5.

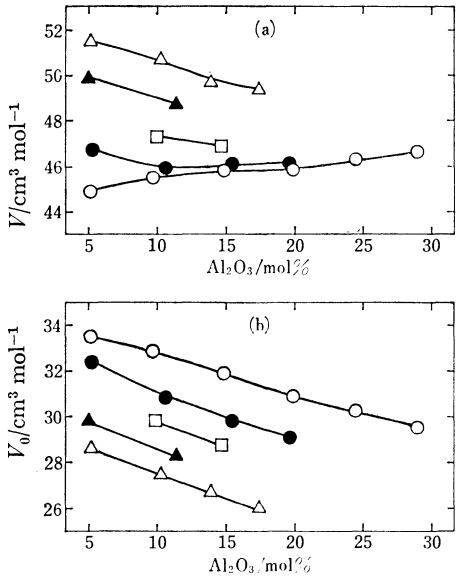

Fig. 4. (a) Molar volume (V) and (b) volume per mole of oxygen (V_0) of K_2O–Al_2O_3–P_2O_5 glass.
△: 61—62 mol % P_2O_5, ▲: 55—56 mol % P_2O_5, □: 49 mol % P_2O_5, ●: 45 mol % P_2O_5, ○: 40 mol % P_2O_5.

the glasses with a lower P_2O_5 content in both systems the molar volumes exhibited the tendency to increase slightly with an increase in the Al_2O_3 content.

Refractive Index and Molar Refraction. The refractive indices of the Na_2O–Al_2O_3–P_2O_5 glass were in the range of 1.482—1.513 and those of the K_2O–Al_2O_3–P_2O_5 glass were 1.474—1.501. The values increased with increasing amounts of Al_2O_3 and P_2O_5, as shown in Figs. 5 and 6. The extent of the increase in the refractive indices with increasing amounts of Al_2O_3 in the glasses with a higher P_2O_5 content was much larger than that in the glasses with a lower P_2O_5

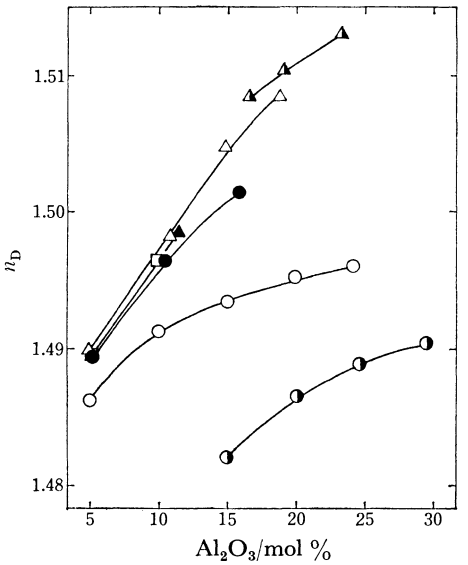

Fig. 5. Refractive index (n_D) of Na_2O–Al_2O_3–P_2O_5 glass.
▲: 63 mol % P_2O_5, △: 59—61 mol % P_2O_5, ▲: 55 mol % P_2O_5, □: 49 mol % P_2O_5, ●: 42.5 mol % P_2O_5, ○: 37.5 mol % P_2O_5, ◑: 32.5 mol % P_2O_5.

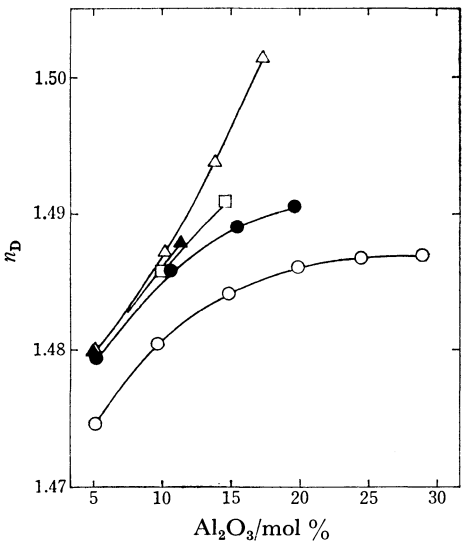

Fig. 6. Refractive index (n_D) of K_2O–Al_2O_3–P_2O_5 glass. △: 61—62 mol % P_2O_5, ▲: 55—56 mol % P_2O_5, □: 49 mol % P_2O_5, ●: 45 mol % P_2O_5, ○: 40 mol % P_2O_5.

content. In the glasses with a lower Al_2O_3 content in both systems, however, the increase in the refractive indices with an increase in the P_2O_5 content was extremely small in the compositions with more than 42.5 mol % of P_2O_5 (Fig. 5) and 45 mol % of P_2O_5 (Fig. 6).

On the other hand, as shown in Figs. 7 and 8, the changes in the molar refractions *vs.* the Al_2O_3 content were almost the same as those in the molar volumes of the glasses in both systems (Figs. 3(a) and 4(a)).

From the measurements of the chemical shift of the Al $K\alpha$ line by X-ray emission spectroscopy, Sakka has reported that most of the Al^{3+} ions in the glasses with a higher P_2O_5 content (P/O≈0.33) are 6-fold coordinated, while those with a lower P_2O_5 content (P/O≲0.25) are 4-fold coordinated.[2,3] In the present investigation, the P/O ratios of the glasses with more than 42 mol % of P_2O_5 are in the range of 0.28—0.35 and those of the

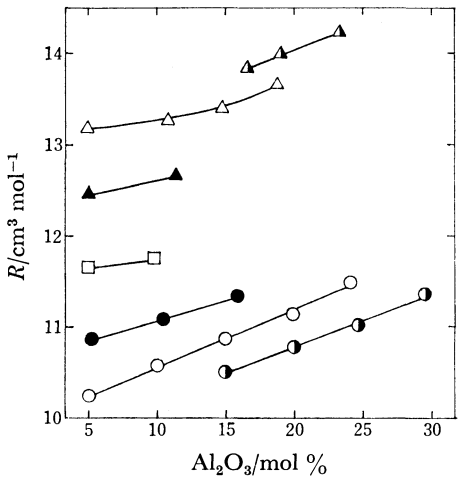

Fig. 7. Molar refraction (R) of Na_2O–Al_2O_3–P_2O_5 glass. ▲: 63 mol % P_2O_5, △: 59—61 mol % P_2O_5, ▲: 55 mol % P_2O_5, □: 49 mol % P_2O_5, ●: 42.5 mol % P_2O_5, ○: 37.5 mol % P_2O_5, ◑: 32.5 mol % P_2O_5.

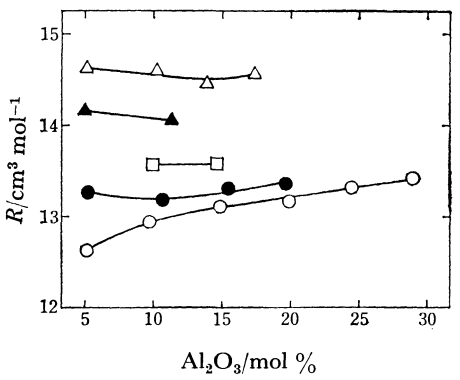

Fig. 8. Molar refraction (R) of K_2O–Al_2O_3–P_2O_5 glass. △: 61—62 mol % P_2O_5, ▲: 55—56 mol % P_2O_5, □: 49 mol % P_2O_5, ●: 45 mol % P_2O_5, ○: 40 mol % P_2O_5.

glasses with less than 42 mol % of P_2O_5 are 0.22—0.30. Therefore, the above results concerning the densities as well as the refractive indices can also be related with the difference in the coordination number of the Al^{3+} ion. From the changes in the densities and refractive indices with increasing amounts of Al_2O_3 shown in Figs. 1, 2, 5, and 6, it may be considered that the marked structural changes in the glasses with P_2O_5 content take place between 37.5 and 42.5 mol % of P_2O_5 in the Na_2O–Al_2O_3–P_2O_5 system and also between 40 and 45 mol % of P_2O_5 in the K_2O–Al_2O_3–P_2O_5 system. Therefore, in both systems the P_2O_5 content of 41—42 mol % may be taken as the boundary composition where the structural change occurs. This is associated closely with the above-mentioned change in the coordination number of Al^{3+} ion between the glasses with a higher P_2O_5 content and those with a lower P_2O_5 content.

Chemical Resistivity and Solubility of Glass. The chemical resistivities in hydrochloric acid in two series of the Na_2O–Al_2O_3–P_2O_5 glasses with 37.5 mol % and 59—61 mol % of P_2O_5 are given in Fig. 9. Although

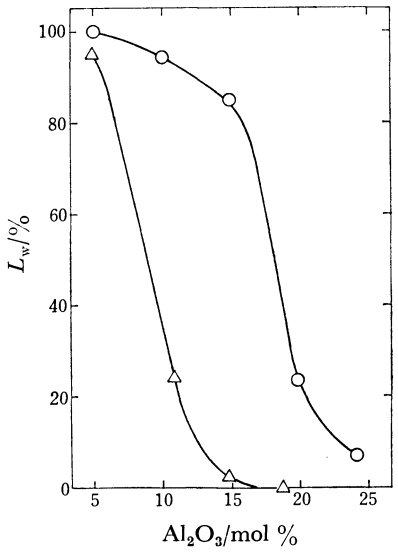

Fig. 9. Chemical resistivity of Na_2O–Al_2O_3–P_2O_5 glass in hydrochloric acid (L_w: weight loss).
○: 37.5 mol % P_2O_5, 1 mol/dm^3 HCl, 25 °C, 1 h, △: 59—61 mol % P_2O_5, concd HCl, 50 °C, 1 h.

the glasses of both series are strengthened chemically with an increase in the Al_2O_3 content, the resistivity of the glass with 59—61 mol % of P_2O_5 is very much larger than that of the glass with 37.5 mol % of P_2O_5. This indicates that the strengthening of the structure by the incorporation of Al_2O_3 is very effective in the glasses with a higher P_2O_5 content. This seems to be due to the tightening of the structure by the Al^{3+} ions outside the P–O–P network or chain in these glasses.

Table 3. Solubility of $52.5Na_2O \cdot 10Al_2O_3 \cdot 37.5P_2O_5$ glass in H_2O (25 °C)

t_s[b]/h	L_w[c]/%	Al_2O_3/P_2O_5[d]
0	—	0.27
1	14.51	0.28
3	38.99	0.29
5	59.30	0.29

b) t_s is the shaking time. c) L_w is the weight loss.
d) Molar ratio in the glass.

Table 4. Solubility of $42.5Na_2O \cdot 20Al_2O_3 \cdot 37.5P_2O_5$ glass in 0.5 mol/dm³ HCl (25 °C)

t_s[b]/h	L_w[c]/%	Al_2O_3/P_2O_5[d]
0	—	0.54
1	8.64	0.53
3	21.75	0.52
5	37.82	0.52
7	48.12	0.53

b) t_s is the shaking time. c) L_w is the weight loss.
d) Molar ratio in the glass.

Table 3 shows the solubility of the $52.5Na_2O \cdot 10Al_2O_3 \cdot 37.5P_2O_5$ glass in water and Table 4 shows that of the $42.5Na_2O \cdot 20Al_2O_3 \cdot 37.5P_2O_5$ glass in 0.5 mol/dm³ hydrochloric acid. The increase in the weight loss of each glass is approximately proportional to the shaking time. The molar ratio Al_2O_3/P_2O_5 in the residual glass is substantially the same value as that in the original glass. These facts indicate that a network consisting of PO_4 tetrahedra does not exist but short P–O–P or short P–O–Al chains exist in the glasses with a lower P_2O_5 content, and thus the structure of such a glass may be taken as "aggregates of molecules." This is an important result for the structure of the glasses with a lower P_2O_5 content.

Infrared Spectra. The infrared absorption spectra of the Na_2O–Al_2O_3–P_2O_5 and K_2O–Al_2O_3–P_2O_5 glasses are given in Figs. 10 and 11, respectively. Between the glasses with a higher P_2O_5 content ((1), (2), and (3) in Figs. 10 and 11) and those with a lower P_2O_5 content ((4), (5), and (6) in Fig. 10; (4) and (5) in Fig. 11), the following marked differences are found in the absorption bands: the absorptions in 1300 cm^{-1} (P=O stretching[8,11,12,13]) move to lower frequencies with decreasing P_2O_5 content and those in 900 cm^{-1} (P–O–P stretching[8,11,12,13]) to higher frequencies with increasing Al_2O_3 content, and also the absorptions in 1000 cm^{-1} (PO_4^{2-} group[8,11,12,13]) increase in intensity with increasing Al_2O_3 content in the glasses with a lower P_2O_5 content. These results show the structural changes

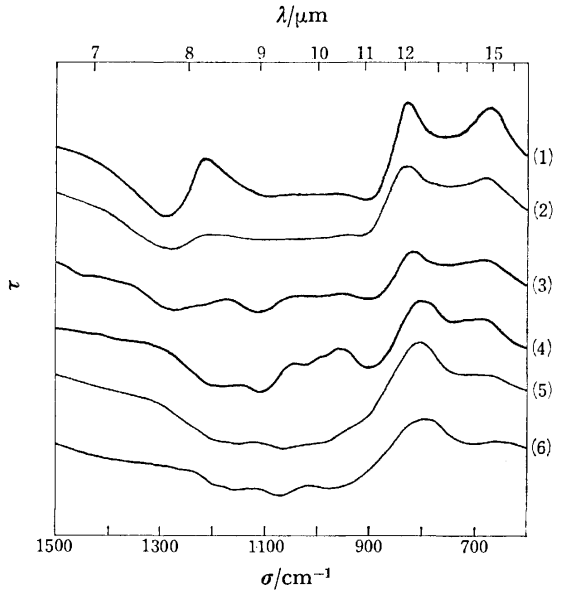

Fig. 10. Infrared spectra of Na_2O–Al_2O_3–P_2O_5 glass (τ: transmittance, σ: wave number).
(1) $29.24Na_2O \cdot 10.78Al_2O_3 \cdot 59.98P_2O_5$,
(2) $20.86Na_2O \cdot 18.70Al_2O_3 \cdot 60.43P_2O_5$,
(3) $39.99Na_2O \cdot 9.81Al_2O_3 \cdot 49.20P_2O_5$,
(4) $52.5Na_2O \cdot 10Al_2O_3 \cdot 37.5P_2O_5$,
(5) $42.5Na_2O \cdot 20Al_2O_3 \cdot 37.5P_2O_5$,
(6) $47.5Na_2O \cdot 20Al_2O_3 \cdot 32.5P_2O_5$.

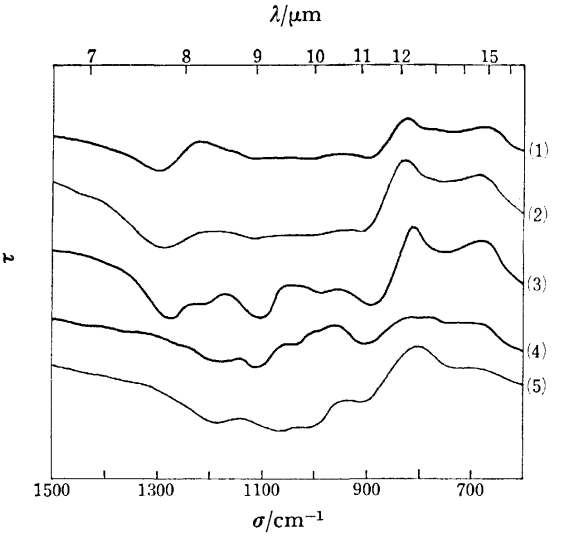

Fig. 11. Infrared spectra of K_2O–Al_2O_3–P_2O_5 glass (τ: transmittance, σ: wave number).
(2) $27.68K_2O \cdot 10.20Al_2O_3 \cdot 62.12P_2O_5$,
(2) $21.41K_2O \cdot 17.34Al_2O_3 \cdot 61.25P_2O_5$,
(3) $40.67K_2O \cdot 9.95Al_2O_3 \cdot 49.38P_2O_5$,
(4) $50K_2O \cdot 10Al_2O_3 \cdot 40P_2O_5$,
(5) $40K_2O \cdot 20Al_2O_3 \cdot 40P_2O_5$.

of the glasses corresponding to the variation of P_2O_5 and Al_2O_3 contents. Especially in the glasses with a lower P_2O_5 content the infrared spectra indicate the change of the short P–O–P chain to the short P–O–Al chain with increasing amounts of Al_2O_3.

From the changes in the properties described above and the coordination number of the Al^{3+} ion in phos-

phate glass,[2,3] the structure of alkali aluminophosphate glass may be considered to be as follows: the glasses with a higher P_2O_5 content consist of a network or long chain of PO_4 tetrahedra, Al^{3+}, and alkali metal ions, while those with a lower P_2O_5 content are formed from random aggregates of short P–O–P chains, Al^{3+}, and alkali metal ions (low Al_2O_3 glass) or random aggregates of short P–O–Al chains of PO_4 and AlO_4 tetrahedra and alkali metal ions (high Al_2O_3 glass).

The author wishes to thank Associate Professor Makio Kinoshita of Sophia University for his interest and encouragement.

References

1) N. J. Kreidl and W. A. Weyl, *J. Am. Ceram. Soc.*, **24**, 372 (1941).
2) S. Sakka, *Bull. Inst. Chem. Res., Kyoto Univ.*, **49**, 349 (1971).
3) S. Sakka, *Yogyo Kyokai Shi*, **85**, 299 (1977).
4) A. Kishioka, M. Hayashi, and M. Kinoshita, *Bull. Chem. Soc. Jpn.*, **49**, 3032 (1976).
5) A. Kishioka, *Bull. Chem. Soc. Jpn.*, **50**, 2088 (1977).
6) E. P. Treadwell and W. T. Hall, "Analytical Chemistry," 9th English ed, (1951), Vol. 2, pp. 150—151.
7) A. Kishioka and M. Kinoshita, *Nippon Kagaku Kaishi*, **1976**, 608.
8) A. Naruse, Y. Abe, and H. Inoue, *Yogyo Kyokai Shi*, **76**, 36 (1968).
9) Bh. V. J. Rao, *Phys. Chem. Glasses*, **4**, 22 (1963).
10) T. Kokubo and M. Tashiro, *Bull. Inst. Chem. Res., Kyoto Univ.*, **52**, 633 (1974).
11) D. E. C. Corbridge and E. J. Lowe, *J. Chem. Soc.*, **1954**, 493.
12) D. E. C. Corbridge and E. J. Lowe, *J. Chem. Soc.*, **1954**, 4555.
13) "Topics in Phosphorus Chemistry," ed by M. Grayson and E. J. Griffith, Interscience Publishers, New York (1969), Vol. 6, pp. 307, 320—321.

Complexation Equilibria of Vanadium(V) with 8-Quinolinolate in Aqueous Solutions

Akio YUCHI, Shinkichi YAMADA, and Motoharu TANAKA*

Laboratory of Analytical Chemistry, Faculty of Science, Nagoya University, Chikusa-ku, Nagoya 464

(Received January 25, 1979)

The complexation equilibria of vanadium(V) with 8-quinolinolate ion(ox^-) were investigated spectrophotometrically. Depending upon the acidity of the solution various 1:1 and 1:2 complexes are formed: VO_3ox^{2-}, VO_3Hox^-, VO_2ox, and $VO_2ox_2^-$. The formation and protonation constants of these complexes are discussed in terms of their structures.

Vanadium(V) reacts with 8-quinolinol(Hox) to give a black precipitate in weakly acidic solution. This complex has been identified to be $V_2O_3ox_4$ or $VO(OH)ox_2$ from the vanadium content.[1-5] This complex, reacting with alcohols (ROH), gives rise to a red complex, of which the structure has been established as $VO(OR)ox_2$ by X-ray study.[6] Furthermore, a yellow precipitate has also been isolated from nearly neutral solution, for which the composition $NaVO_2ox_2$ has been given according to the elemental analysis.[1,4,7] It seems interesting to make it clear why the protonation of $NaVO_2ox_2$ causes such a pronounced color change.

The solvent extraction of vanadium(V) with 8-quinolinol has also revealed the metal to ligand ratio of 1:2, from which the composition of $VO(OH)ox_2$ has been given to the black extracted species.[8,9] This extraction system has been utilized to determine the hydrolysis constants of dioxovanadium(V).[9,10] In these studies no complexed species being assumed in the aqueous phase, it is sometimes indispensable to take into account the formation of lower complexes especially in the extraction of multivalent metals.[11,12] Vanadium(V) itself tends to be hydrolyzed and is correspondingly expected to form various 1:1 and 1:2 complexes with 8-quinolinolate of various degree of hydrolysis. The complexation reactions of Mo(VI) and W(VI) with 8-quinolinolate were studied under limited conditions.[13] However, the stepwise complex formation of multivalent ions has been little studied.

In order to understand the complexation reaction and the extraction behavior of vanadium(V) with 8-quinolinol, we first study the complexation reaction of vanadium(V) with 8-quinolinolate under conditions where no black precipitate appears in the aqueous solution.

Experimental

Reagent. *Dioxovanadium(V) Perchlorate*: Ammonium metavanadate, recrystallized from isothermally distilled ammonia, was dissolved in sodium hydroxide solution. Then the solution was heated with nitrogen gas bubbling to expell ammonia. After cooling, perchloric acid was added to obtain dioxovanadium(V) perchlorate solution, which was standardized titrimetrically against a standard potassium permanganate solution.

8-Quinolinol: Reagent grade 8-quinolinol was recrystallized twice from aqueous acetone.

The method of preparation of sodium perchlorate and sodium hydroxide has been described previously.[11]

Measurement. All the experiments were carried out in a room thermostated at 25±0.5 °C. All the measurements were performed in a thermoelectric circulating bath thermostated at 25±0.1 °C. The ionic strength was maintained at 1.00 mol dm^{-3} with sodium perchlorate. Spectrophotometric measurements were performed on a UNION High Sens Spectrophotometer SM-401 with a thermostated cell compartment. Hydrogen ion concentration was determined by a Radiometer pH meter (PHM 22 type) with a Radiometer glass electrode (G 202 C type) and a calomel electrode filled with a saturated sodium chloride as an internal solution. A 1.00×10^{-2} mol dm^{-3} perchloric acid solution of ionic strength 1 mol dm^{-3} was used as a standard of hydrogen ion concentration: $-\log[H^+]=2.00$. The change of a liquid-junction potential was taken into account.[14]

In order to avoid the polymerization of vanadium(V),[15] it is indispensable to control the total concentration of vanadium(V), to observe the order of mixing various solutions, and to stir the solution vigorously. All the experiments have been carried out under conditions where no polymerized species occurs. The formation of polymers was always monitored by the near ultraviolet and visible spectra.

Results

Protonation Equilibria of 8-Quinolinolate Ion. The protonation equilibria of 8-quinolinolate are expressed by Eqs. 1 and 2:

$$ox^- + H^+ \overset{K_{Hox}}{\rightleftharpoons} Hox \quad (1)$$

$$Hox + H^+ \overset{K_{H_2ox}}{\rightleftharpoons} H_2ox^+ \quad (2)$$

The absorbance at 350 nm of the solution containing 3.91×10^{-4} mol dm^{-3} 8-quinolinol was plotted against $-\log[H^+]$. According to the plot we have two equilibria, which are separated enough to treat them as two independent steps. The plot was compared with a set of normalized curves; $X=\log x$, $Y=a/(1+x)$. The values of the protonation constants and the molar extinction coefficients obtained are as follows:

$$\log K_{H_2ox} = 5.36 \pm 0.02;\ \varepsilon_{H_2ox} = 1560;$$
$$\log K_{Hox} = 9.43 \pm 0.02;\ \varepsilon_{Hox} = 260;$$
$$\varepsilon_{ox} = 2710$$

at 25±0.1 °C and at an ionic strength of 1.0($NaClO_4$).

Protonation Equilibrium of Hydrogen Orthovanadate Ion. The protonation of hydrogen orthovanadate ion is expressed by Eq. 3:[16]

$$HVO_4^{2-} + H^+ \overset{K_{VO_3}}{\rightleftharpoons} VO_3^- \quad (3)$$

The ultraviolet spectra of the solutions containing about

5×10^{-4} mol dm^{-3} vanadium(V) were measured at various hydrogen ion concentrations. A distinct isosbestic point is observed at 290 nm over the range of $-\log[H^+]=7.6$—10. The deviation of the isosbestic point at $-\log[H^+]$ value lower than 7.6 was thought to be due to the formation of polymers. The absorbance change at 265 nm was plotted against $-\log[H^+]$ over the range of $-\log[H^+]=7.6$—10. The plot was compared with a normalized curve; $X=\log x$, $Y=a/(1+x)$ and we obtained $\log K_{VO_2}=8.07\pm0.06$. The value obtained by Schwarzenbach and Geier ($\log K_{VO_2}=8.04$ at 20 °C and 1 mol dm^{-3} KCl)[17] agrees with ours.

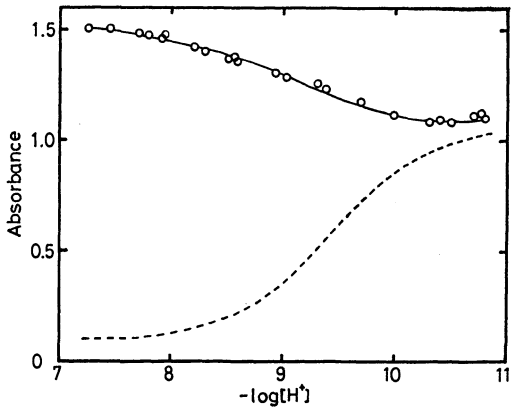

Fig. 1. Absorbance change at 350 nm as a function of $-\log[H^+]$. $C_V=1.39\times10^{-3}$ mol dm^{-3}, $C_{Hox}=3.93\times10^{-4}$ mol dm^{-3}. The solid line: the calculated curve with the constants obtained; the dotted line: data in the absence of vanadium(V).

Complexation Equilibria. The absorbance at 350 nm of the solution containing 1.39×10^{-3} mol dm^{-3} vanadium(V) and 3.93×10^{-4} mol dm^{-3} 8-quinolinol was plotted against $-\log[H^+]$ (Fig. 1). The absorbance change under the same conditions without vanadium(V) is also shown by the dotted line. Thus the difference between these two lines can be ascribed to the complex formation.

In the presence of an excess amount of vanadium(V), the formation of only 1 : 1 complex is anticipated and the equilibrium is generally expressed by Eq. 4:

$$HVO_4^{2-} + mH^+ + ox^- \overset{\beta_{1m1}}{\rightleftharpoons} VO_4H_{m+1}ox^{(3-m)-} \quad (4)$$

where m is the number of protons involved in the complexation reaction and β_{1m1} is the overall formation constant of the species formed. We have Eqs. 5 and 6:

$$\frac{A-A'}{\varepsilon_{1m1}C_{Hox}-A} = \beta_{1m1}\frac{[HVO_4^{2-}][H^+]^m}{\alpha_{ox}} \quad (5)$$

$$[HVO_4^{2-}] = \frac{1}{\alpha_{HVO_4}}\left(C_V - \frac{A-A'}{\varepsilon_{1m1}C_{Hox}-A'}\times C_{Hox}\right) \quad (6)$$

where A and A' are observed absorbances in the presence and in the absence of vanadium(V), respectively, C_{HOX} and C_V are the total concentration of 8-quinolinol and vanadium(V), respectively, and α_{OX} and α_{HVO_4} are the side reaction coefficients taking into account the protonation reaction of 8-quinolinolate ion and hydrogenorthovanadate ion, respectively. At 350 nm the molar extinction coefficients of the uncomplexed vanadium(V) species are negligibly small as compared with those of the complexes and the ligand. ($\log((A-A')/(\varepsilon_{1m1}C_{Hox}-A))-\log[HVO_4^{2-}]+\log\alpha_{ox}$) being plotted against $-\log[H^+]$, a straight line with a slope of m and an intercept of $\log\beta_{1m1}$ will be obtained, provided only one complex is involved in reaction given by Eq. 4.

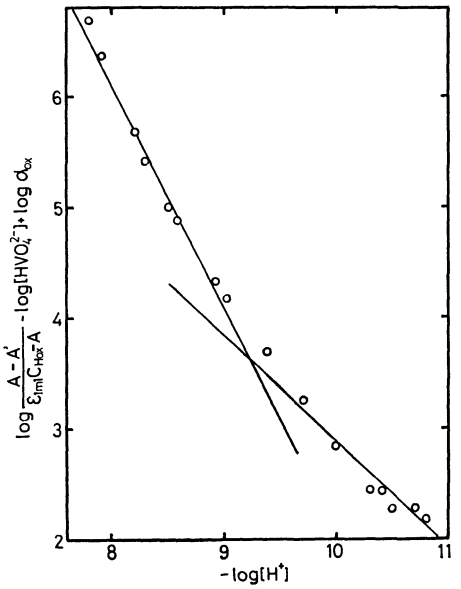

Fig. 2. Determination of the formation constants of vanadium(V)-8-quinolinolate complexes. Plot of $\log((A-A')/(\varepsilon_{1m1}C_{Hox}-A))-\log[HVO_4^{2-}]+\log\alpha_{ox}$ *vs.* $-\log[H^+]$.

The slope of the plot is close to 2 at lower value of $-\log[H^+]$, while at higher value of $-\log[H^+]$ it tends to be unity (Fig. 2). This points to the formation of two types of 1 : 1 complex, namely VO_3Hox^- and VO_3ox^{2-}. The complex is now described not to have more than 1 proton by the repeated elimination of two protons with one oxo group as one water (see Discussion). The overall formation constants and the molar extinction coefficients obtained by the graphical plot were refined with an electronic computer to have the following values:

$$\log\beta_{121} = 22.1\pm0.1;\ \varepsilon_{121} = \varepsilon_{VO_2Hox} = 3830\pm50;$$
$$\log\beta_{111} = 12.8\pm0.1;\ \varepsilon_{111} = \varepsilon_{VO_2ox} = 3650\pm100.$$

The data for the solution containing 1.48×10^{-4} mol dm^{-3} vanadium(V) and 7.82×10^{-5} mol dm^{-3} 8-quinolinol are also well interpreted with the above constants. This confirms the absence of polymerization under the present experimental conditions: the above results are regarded as reliable.

Equilibria in more acidic media were studied by decreasing the total concentrations of vanadium(V) and 8-quinolinol to 5.92×10^{-5} and 3.13×10^{-5} mol dm^{-3}, respectively, the polymerization of vanadium(V) being avoided. The absorbance of the solution at 400 nm was measured at various hydrogen ion concentration and plotted against $-\log[H^+]$ (Fig. 3). Under these conditions protonation equilibria of vanadium(V), Eqs. 7 and 8, must also be considered:[18]

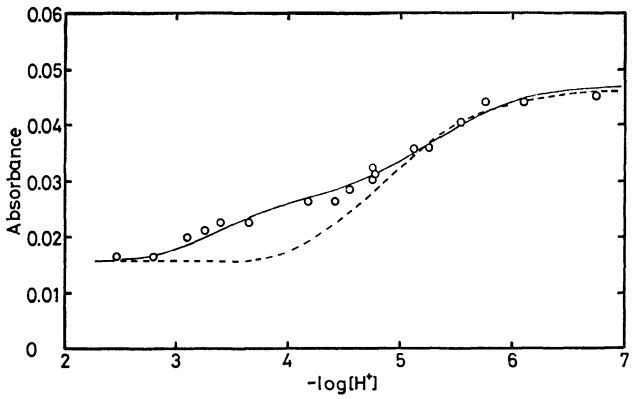

Fig. 3. Absorbance change at 400 nm as a function of $-\log[H^+]$. $C_V=5.92\times10^{-5}$ mol dm^{-3}, $C_{Hox}=3.13\times10^{-5}$ mol dm^{-3}. The solid line: the calculated curve with the constants obtained; the dotted line; the calculated curve without taking into account the formation of VO_2ox.

$$VO_3^- + H^+ \overset{K_{HVO_3}}{\rightleftarrows} HVO_3 \quad (7)$$

$$HVO_3 + H^+ \overset{K_{VO_2}}{\rightleftarrows} VO_2^+ \quad (8)$$

The assumption of VO_3Hox^- as a sole species leads to the deviation at lower value of $-\log[H^+]$ as shown by the dotted line in Fig. 3. This deviation points to the formation of a further protonated species, for example VO_2ox. The combination of the formation constants and the molar extinction coefficients of the above two protonated species, VO_3Hox^- and VO_2ox, leads to the best fit curve indicated by the full line in Fig. 3 with the following:

$$\log\beta_{131} = 27.5\pm0.1;\ \varepsilon_{131} = \varepsilon_{VO,ox} = 1100\pm50.$$

The absorbance at 350 nm of the solution containing 7.00×10^{-5} mol dm^{-3} vanadium(V) and 3.91×10^{-4} mol dm^{-3} 8-quinolinol was plotted against $-\log[H^+]$ (Fig. 4). In the presence of excess amounts of 8-quinolinol the formation of 1:2 complex is also anticipated:

$$HVO_4^{2-} + mH^+ + 2ox^- \overset{\beta_{1m2}}{\rightleftarrows} VO_4H_{m+1}ox_2^{(4-m)-} \quad (9)$$

It was revealed that in addition to 1:1 complexes only $VO_2ox_2^-$ with $m=3$ forms. The combination of the overall formation constant and the molar extinction coefficient giving a minimum error square sum is as follows:

$$\log\beta_{132} = 36.0\pm0.1;\ \varepsilon_{132} = \varepsilon_{VO,ox_2} = 7660\pm100.$$

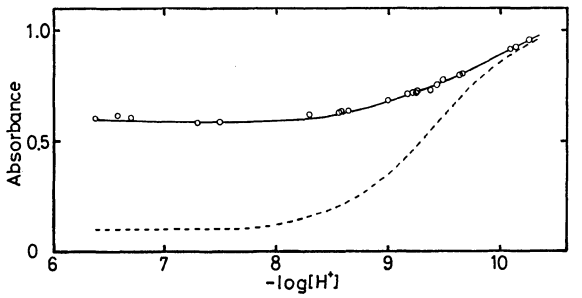

Fig. 4. Absorbance change at 350 nm as a function of $-\log[H^+]$. $C_V=7.00\times10^{-5}$ mol dm^{-3}, $C_{Hox}=2.91\times10^{-4}$ mol dm^{-3}. The solid line: the calculated curve with the constants obtained; the dotted line: data in the absence of vanadium(V).

Discussion

Species identified in this study are represented in Scheme 1 together with pK_a and logarithmic formation constants.[18,19]

In Scheme 1 the changes from left to right correspond to hydrolytic reactions and the changes from upper to lower complexation reactions. It can be seen that the complexation ability decreases with increasing degree of hydrolysis of vanadium(V): the formation constant of VO_3ox^{2-} is $10^{5.6}$ times as low as that of VO_3Hox^-. The same trend has been observed in the complexation of tungsten(VI) with 8-quinolinolate,[13] where the formation constant of WO_4Hox^{2-} is $10^{5.6}$ times as low as that of WO_3ox^-, as evident from the following scheme:

$$\begin{array}{ccccc} H_2WO_4 & \overset{3.5}{\rightleftarrows} & HWO_4^- & \overset{2.3}{\rightleftarrows} & WO_4^{2-} \\ \Big\updownarrow 14.2 & & \Big\updownarrow 8.6 & & \\ WO_3ox^- & \overset{9.1}{\rightleftarrows} & WO_4Hox^{2-} & & \end{array}$$

This difference is mainly attributable to the effect of charge and the number of oxo groups.

The formation constants of the dioxovanadium complexes with various ligands are summarized in Table 1, in which $\sum pK_a$, the summation of the loga-

Table 1. Formation constants of dioxovanadium complexes with various ligands at 25 °C

Number	Ligand	Ionic strength mol dm^{-3}	$\log\beta$	$\sum pK_a$	Reference
1	$edda^{2-}$	1.0($NaClO_4$)	14.5	20.5	14
2	nta^{3-}	1.0($NaClO_4$)	13.8	14.5	14
3	$mida^{2-}$	1.0($NaClO_4$)	10.2	13.4	14
4	pda^{2-}	1.0($NaClO_4$)	8.7	7.3	20
5	$edta^{4-}$	3.0($NaClO_4$)	15.5	20.3	21
6	nta^{3-}	3.0($NaClO_4$)	13.8	15.1	21
7	$2ox^-$	1.0($NaClO_4$)	21.0	29.6	this work

$edda^{2-}$, nta^{3-}, $mida^{2-}$, pda^{2-} and $edta^{4-}$ denote ethylenediamine-*N*,*N*′-diacetate, nitrilotriacetate, *N*-methyliminodiacetate, 2,6-pyridinedicarboxylate and ethylenediamine-*N*,*N*,*N*′,*N*′-tetraacetate, respectively.

$$\begin{array}{ccccccccc} VO_2^+ & \overset{3.2}{\rightleftarrows} & HVO_3 & \overset{3.8}{\rightleftarrows} & VO_3^- & \overset{8.1}{\rightleftarrows} & HVO_4^{2-} & \overset{13}{\rightleftarrows} & VO_4^{3-} \\ \Big\updownarrow 12.4 & & \Big\updownarrow 10.3 & & \Big\updownarrow 4.7 & & & & \\ VO_2ox & \overset{5.3}{\rightleftarrows} & VO_3Hox^- & \overset{9.3}{\rightleftarrows} & VO_3ox^{2-} & & & & \\ \Big\updownarrow 8.6 & & & & & & & & \\ \text{black ppt.} & \rightleftarrows & VO_2ox_2^- & & & & & & \end{array}$$

Scheme 1.

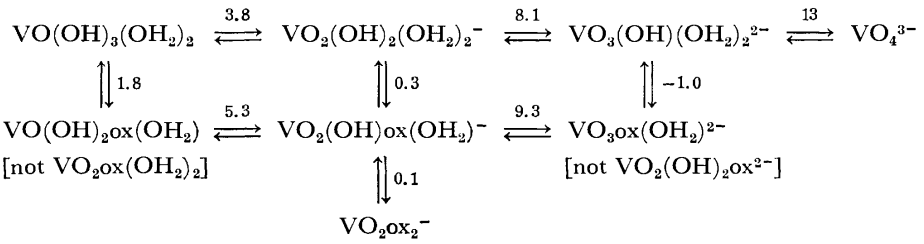

Scheme 2.

rithmic stepwise protonation constants for the donor atoms which actually coordinate to the central metal, is also listed. When the overall formation constant is plotted against $\sum pK_a$, a fairly good linear relationship is observed (Fig. 5).[22]

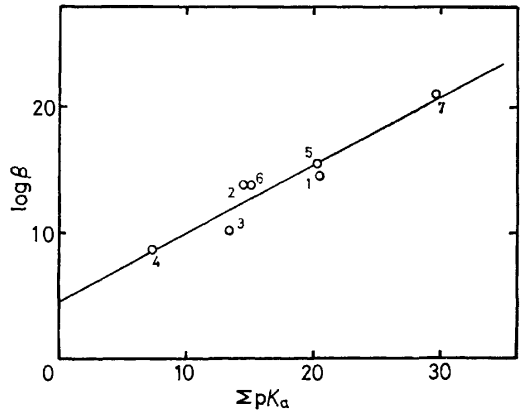

Fig. 5. Correlation of the overall formation constant of vanadium(V) complex with $\sum pK_a$ of the ligand. For the number Table 1 should be referred to.

In order to compare pK_a values Scheme 1 is rewritten as Scheme 2 with probable structures[23] and logarithmic constants. In Scheme 2 the species are arranged to have a same charge in a row. So the change from upper to lower is the substitution reaction of hydroxo group by 8-quinolinolate. VO_2ox and VO_3ox^{2-} have more than one possible structures.

The pK_a of a neutral acid of the formula H_aXO_{a+1}, which have one oxo group, lies in the range of 2—3 and increases by 4—5 for each successive proton dissociation with increase of oxo groups.[25,26] Vanadic acid belongs to this category and can be described as $VO(OH)_3(OH_2)_2$, which gives rise to $VO_2(OH)_2(OH_2)_2^-$ and $VO_3(OH)(OH_2)_2^{2-}$ upon proton dissociation. The formulation $VO(OH)_4(OH_2)^-$ for metavanadate ion[10] seems unlikely.

When pK_a values of complexes are compared with those of the corresponding vanadic acid, nearly the same difference is observed: 3.8 as compared to 5.3 for the first proton dissociation (difference of 1.5) and 8.1 as compared to 9.3 for the second proton dissociation (difference of 1.2). These differences may be ascribed to the difference in electron donating ability between hydroxide and 8-quinolinolate. Thus we may conclude that the change in the number of oxo groups during the hydrolysis of the complex is the same as in the proton dissociation of vanadic acid and that the skeleton of vanadium(V) species is retained during the complexation. Thus VO_2ox is $VO(OH)_2ox(OH_2)$ and not $VO_2ox(OH_2)_2$, and VO_3ox^{2-} is $VO_3ox(OH_2)^{2-}$ and not $VO_2(OH)_2ox^{2-}$.

Furthermore, this Scheme suggests that the constant of the substitution reaction of one hydroxide by 8-quinolinolate is largely affected by the number of coordinated oxo groups: 1.8 for $VO(OH)_2ox$, 0.3 for $VO_2(OH)ox^-$, and -1.0 for VO_3ox^{2-}. On the other hand, the coordinated 8-quinolinolate does not affect much the subsequent coordination of the same ligand: 0.3 for $VO_2(OH)ox^-$ as compared to 0.1 for $VO_2ox_2^-$ in Scheme 2.

The pK_a values are also available for *N*-methyliminodiacetato and 2,6-pyridinedicarboxylato complexes:[14,20]

$$VO_2(mida)(OH_2)^- \rightleftharpoons VO_2(mida)(OH)^{2-} + H^+ \qquad pK_a = 6.13 \pm 0.05$$

$$VO_2(pda)(OH_2)^- \rightleftharpoons VO_2(pda)(OH)^{2-} + H^+ \qquad pK_a = 5.87 \pm 0.02$$

However these reactions involving no increase of oxo groups, they can not be discussed on the same ground as in the present case.

Among the species which have been identified, VO_3ox^{2-}, VO_3Hox^-, and $VO_2ox_2^-$ have the absorption maximum at 363 nm. On the survey of ultraviolet and visible spectra of various metal 8-quinolinolate complexes, it is noticed that the absorption maximum depends upon the oxidation number of metal ions, *e.g.* 410—460 nm for Mox_2, 380—420 nm for Mox_3, 380 nm for Mox_4, and 360—370 nm for MO_2ox_2 (hexavalent).[27] Vanadium(V) complexes mentioned above are well lined up in this series, whereas the black complex has absorption maximum at 550 nm. On the other hand complexes with the dimeric $Mo_2O_3^{4+}$ unit have a fairly strong absorption maximum near 510 nm and monomeric species containing the same ligand do not.[28] This absorption maximum is attributable to the oxo bridged structure of molybdenum and the absorption maximum at 550 nm for the black vanadium(V) complexes also seems to be ascribed to the oxo bridged dimeric structure. The dimeric structure of black vanadium(V) 8-quinolinolate has recently been established by the solvent extraction in our laboratory. Details on this point will be shortly published elsewhere.

References

1) R. Montequi and M. Gallego, *Anales. Soc. Espan. Fis. Quim.*, **32**, 134 (1934).
2) S. Ishimaru, *J. Chem. Soc. Jpn.*, **56**, 72 (1935).
3) M. Borrel and R. Paris, *Anal. Chim. Acta*, **4**, 267 (1950).

4) H. J. Bielig and E. Bayer, *Ann. Chem.*, **584**, 96 (1953).
5) A. J. Blair and D. A. Pantony, *Anal. Chim. Acta*, **13**, 1 (1955); A. J. Blair, D. A. Pantony, and G. J. Minkoff, *J. Inorg. Nucl. Chem.*, **5**, 316 (1958).
6) W. R. Scheidt, *Inorg. Chem.*, **12**, 1758 (1973).
7) H. Nakamura, Y. Shimura, and R. Tsuchida, *Bull. Chem. Soc. Jpn.*, **34**, 1143 (1961).
8) N. Kurmaiah, D. Satyanarayana, and V. P. R. Rao, *Talanta*, **14**, 495 (1967).
9) M. Tanaka and I. Kojima, *J. Inorg. Nucl. Chem.*, **29**, 1769 (1967).
10) S. Yamada, S. Funahashi, and M. Tanaka, *J. Inorg. Nucl. Chem.*, **37**, 835 (1975).
11) J. Rydberg, *Acta Chem. Scand.*, **4**, 1503 (1950).
12) D. Dyrssen, *Sv. Kem. Tidskr.*, **65**, 43 (1953).
13) P. F. Knowles and H. Diebler, *Trans. Faraday Soc.*, **64**, 977 (1968); H. Diebler and R. E. Timms, *J. Chem. Soc. A*, **1971**, 273.
14) S. Yamada, J. Nagase, S. Funahashi, and M. Tanaka, *J. Inorg. Nucl. Chem.*, **38**, 617 (1976).
15) F. J. C. Rossotti and H. Rossotti, *Acta Chem. Scand.*, **10**, 957 (1956).
16) The formulation of species involved in Eq. 3 does not strictly correspond to the actual structure in solution (see Discussion).
17) G. Schwarzenbach and G. Geier, *Helv. Chim. Acta*, **46**, 906 (1963).
18) D. Dyrssen and T. Sekine, *J. Inorg. Nucl. Chem.*, **26**, 981 (1964).
19) L. Newman, W. J. La Fleur, F. J. Brousaides, and A. M. Ross, *J. Am. Chem. Soc.*, **80**, 4491 (1958).
20) S. Funahashi, K. Haraguchi, and M. Tanaka, *Inorg. Chem.* **16**, 1349 (1977).
21) J. Lagrange, P. Lagrange, and K. Zare, *Bull. Soc. Chim. Fr. I*, **1978**, 7.
22) This type of linear free energy relationship generally holds in the complexation of multivalent metal ions; *e.g.* Ti(IV), Zr(IV), Hf(IV), and Mo(VI) and W(VI). A. Yuchi, unpublished results.
23) Some vanadium(V) complexes are characterized structurally by X-ray studies,[6,24] which indicated the octahedral configuration with a comparably long weak bond *trans* to oxo ligand and when more than one oxo ligands are involved they are *cis* to each other.
24) W. R. Scheidt, C. Tsai, and J. L. Hoard, *J. Am. Chem. Soc.* **93**, 3867 (1971); W. R. Scheidt, D. M. Collins, and J. L. Hoard, *ibid*, **93**, 3873 (1971); W. R. Scheidt, R. Countryman, and J. L. Hoard, *ibid*, **93**, 3878 (1971).
25) L. Pauling, "General Chemistry," W. H. Freeman and Co., San Francisco (1947).
26) J. E. Ricci, *J. Am. Chem. Soc.*, **70**, 109 (1948).
27) I. U. P. A. C., "Tables of Spectrophotometric Absorption Data of Compounds Used for the Colorimetric Determination of Elements," Butterworths, London (1963).
28) E. I. Stiefel, "Progress in Inorganic Chemistry," John Wiley and Sons, Inc. (1977), Vol. 22.

Circular Dichroism and Stereochemistry of Tetranuclear Cobalt(III) Complexes of Hexol Type. I. Dodecaammine-hexa-μ-hydroxo-tetracobalt(III) Ion, $[Co\{(OH)_2Co(NH_3)_4\}_3]^{6+}$

Tomikatsu KUDO* and Yoichi SHIMURA

Department of Chemistry, Faculty of Science, Osaka University, Toyonaka, Osaka 560

(Received February 9, 1979)

From the circular dichroism spectra of optically active dodecaammine-hexa-μ-hydroxo-tetracobalt(III) ion, $(+)_{589}$-$[Co\{(OH)_2Co(NH_3)_4\}_3]^{6+}$, measured in the visible and ultraviolet region in several solvents such as 0.01M-HCl and 0.17M-Na_2SeO_3, the d-d transitions of the complex are assigned in consideration of the ion-pairing effect. The absolute configuration of $(+)_{589}$ isomer is assigned as Δ based upon a negative sign of the E_a component for the CoO_6 chromophore. The circular dichroism change by the ion-pairing is attributed to the vicinal effect of chiral oxygen centers stereospecifically produced by the ion-pair formation, and the importance of the oxygen chirality is discussed on the basis of the time-course of circular dichroism change in the solutions.

Dodecaammine-hexa-μ-hydroxo-tetracobalt(III) complex salt was firstly prepared by Jörgensen,[1] and was resolved into optical isomers as the first purely inorganic complex by Werner,[2] who named the complex "hexol" after the bridging ligands. The structure of the polynuclear cation has been established by an X-ray crystal structure analysis of the racemic chloride salt,[3] and there have been done several investigations concerning the optical activity of the resolved isomers and related hexa-μ-hydroxo-tetracobalt(III) type complex ions.[2,4-7] Heretofore there have been two different assignments for the absolute configuration of this type of complexes.[5,7] To solve the problem, a detailed CD investigation of the dodecaammine-hexa-μ-hydroxo-tetracobalt(III) ion, $[Co\{(OH)_2Co(NH_3)_4\}_3]^{6+}$, which is the most basic of this type of complexes, will be reported in the present paper; the absolute configuration will be determined mainly on the basis of the effect of ion-pairing on the CD spectra.

Experimental

Preparation and Optical Resolution. *(1)* $[Co\{(OH)_2Co(NH_3)_4\}_3]Cl_6\cdot 6H_2O$: The sulfate salt $[Co\{(OH)_2Co(NH_3)_4\}_3](SO_4)_3\cdot 4H_2O$ which was prepared by an established method[8] was converted into the chloride salt by treating with $BaCl_2$. Found: H, 6.13; N, 19.29; Cl, 25.05 %. Calcd for $H_{42}O_6N_{12}Cl_6Co_4\cdot 6H_2O$: H, 6.31; N, 19.48; Cl, 24.65%.

(2) $(+)_{589}$-$[Co\{(OH)_2Co(NH_3)_4\}_3](ClO_4)_6\cdot 2.5H_2O\cdot 0.5NaClO_4$: The optical resolution was achieved by a modification of the procedure of Goodwin *et al.*,[4] which was for the corresponding ethylenediamine complex $[Co\{(OH)_2Co(en)_2\}_3]^{6+}$. The racemic chloride hexahydrate (2.00 g, 2.32×10^{-3} mol) was dissolved in 200 cm^3 of cold water, and to this dark brown solution the first quarter of cold solution of $Na_2[Sb_2(d\text{-}C_4H_2O_6)_2]\cdot 2.5H_2O$ (2.18 g, 3.48×10^{-3} mol) in 160 cm^3 of water was added dropwise with stirring. During the reaction the vessel was cooled in an icebath. A voluminous pale-brown precipitate of the less soluble diastereoisomer deposited, which was filtered, washed with cold water, and air-dried. The filtrate was again cooled in an icebath, whereupon the second quarter of $[Sb_2(d\text{-}C_4H_2O_6)_2]^{2-}$ solution was added to it, and the second fraction of the diastereoisomer was obtained. The procedure was repeated 4 times in total. The time for the separation of each fraction did not exceed 20 min.

Each fraction was converted into the perchlorate as follows. A mixture of the less soluble diastereoisomer and solid $NaClO_4$ (*ca.* 2 g) was ground up finely in a mortar, and then to this mixture was added 7 cm^3 of ice-cold water which was in advance acidified to pH 5 with $HClO_4$. This mixture was rubbed with a pestle, the vessel being cooled in an ice bath. The resulting mixture was filtered, washed with an ethanol–water (2: 1) mixture, ethanol and then ether. The brown violet powdery crystals were dried in a vacuum desiccator over $CaCl_2$. The $\Delta\varepsilon_{614}$ values of the fractions were -13.5, -12.9, -6.23, and -1.35 in the order of precipitation. In other experiments the racemic compound was treated to yield 8 fractions or 16 fractions. But the $\Delta\varepsilon_{614}$ value of each the first fraction was same as that described above ($\Delta\varepsilon_{614}=-13.5$). Found: H, 3.78, N, 13.56 %. Calcd for $H_{42}O_{30}N_{12}Cl_6Co_4\cdot 2.5H_2O\cdot 0.5NaClO_4$: H, 3.80; N, 13.50 %.

Measurement. The visible and ultraviolet absorption measurements were made by a Shimadzu UV-200 spectrophotometer. The CD spectra were recorded on a JASCO MOE-1 spectropolarimeter. The time-course of CD change was followed at 614 and 505 nm in H_2O, 0.01M-HCl, 0.17M-Na_2SeO_3, 0.17M-Na_2tart, 0.17M-H_2tart, and NaOH aqueous solutions (pH 8.1 and 10.4) at 22 °C (tart stands for $(+)_{589}$-tartrate(2−) ion). The time-course of absorption change was followed at 625 and 505 nm in each case. The CD measurements in 0.17M-Na_2SeO_3 were made with the solutions prepared freshly every about 10 minutes, and the CD curve was obtained by extrapolating the spectra back to zero time.

Results and Discussion

The absorption and CD spectra are shown in Fig. 1 and the numerical data in Table 1. Since mutarotation of this complex was very fast in water, the CD spectra were measured in 0.01M-HCl solution, in which the complex is considerably stable for the mutarotation. The CD spectra in 0.17M-Na_2SeO_3 were obtained by extrapolating the observed $\Delta\varepsilon$ values back to zero time. The dodecaammine-hexa-μ-hydroxo-tetracobalt(III) ion, $[Co\{(OH)_2Co(NH_3)_4\}_3]^{6+}$, is regarded as composed of a $Co(OH)_6$ and three $Co(OH)_2(NH_3)_4$ chromophores. In the following discussion the former chromophore will be abbreviated to CoO_6 one, and the latter to CoN_4O_2 one. The CoO_6 chromophore has a configurational chirality, Δ or Λ, due to the tris-chelate type structure of the whole complex, while each the CoN_4O_2 chromo-

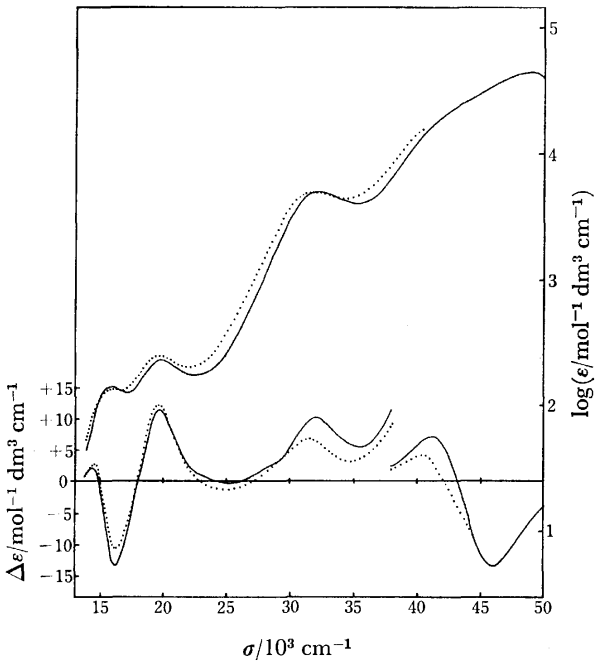

Fig. 1. Absorption and CD curves of $(+)_{589}$-$[Co\{(OH)_2Co(NH_3)_3\}_3]^{6+}$ in 0.01 M-HCl (——) and 0.17 M-Na_2SeO_3 (……).

TABLE 1. THE ABSORPTION AND CD DATA OF $(+)_{589}$-$[Co\{(OH)_2Co(NH_3)_4\}_3]^{6+}$ (Wave numbers are given in $10^3 cm^{-1}$ unit and logε or $\Delta\varepsilon$ values (in parentheses) $mol^{-1}\,dm^3\,cm^{-1}$).

solvent	σ_{max}	(log ε)	σ_{ext}	($\Delta\varepsilon$)
0.01M-HCl			14.47	(+ 2.07)
	15.97	(2.15)	16.28	(−13.5)
	19.86	(2.36)	19.78	(+11.3)
			25.44	(− 0.29)
	32.21	(3.70)	32.00	(+10.0)
			41.20	(+34.4)
	48.90	(4.64)	46.00	(−67.1)
0.17M-Na_2SeO_3			14.61	(+ 2.63)
	16.27	(2.13)	16.30	(−10.8)
	19.76	(2.39)	19.60	(+11.9)
			25.09	(− 1.34)
	31.85	(3.70)	31.55	(+ 6.65)
			40.40	(+19.9)

phore itself has no chirality.

The first and second d-d transition bands of $[Co(H_2O)_6]^{3+}$ are located at 16500 and 24700 cm^{-1}, respectively,[9] and those of *cis*-$[Co(NH_3)_4(H_2O)_2]^{3+}$ at 19900 and 28100 cm^{-1}. Therefore, the absorption bands of $[Co\{(OH)_2Co(NH_3)_4\}_3]^{6+}$ at 15970 and 19860 cm^{-1} in 0.01M-HCl are assigned to the first d-d transition bands of CoO_6 and CoN_4O_2 chromophores, respectively. The second d-d transition bands of both chromophores seem to be masked by an intense band at 32210 cm^{-1}, which is due to the charge transfer transition from the OH bridge group to the central metal, $p_\pi(O)\rightarrow e_g(Co)$. These assignments of the absorption bands are consistent with earlier assignments for those of similar hexa-μ-hydroxo-tetracobalt(III) type ions.[5-7]

Upon going from in 0.01M-HCl to in 0.17M-Na_2SeO_3, the peak of the first d-d absorption band of CoO_6 chromophore shifted to higher energy side, while the peak of CoN_4O_2 chromophores to lower energy side. The charge transfer band shifted to lower energy side. For the CD spectra, the intensity of the longer wavelength extremum of CoO_6 chromophore increased with shifting to higher energy side, but the intensity of the shorter wavelength one of CoO_6 chromophore drastically decreased without shifting. The CD band of CoN_4O_2 chromophore shifted to lower energy side and the intensity increased slightly. Both CD bands at about 32000 and 41000 cm^{-1} shifted to lower energy side and their intensities decreased.

It has been well known that the CD spectra of *Λ*-$[Co(en)_3]^{3+}$ with D_3 symmetry show strong ion-pairing effect in the region of the first d-d absorption band when a kind of oxoanion species such as PO_4^{3-} or SeO_3^{2-} is added; the CD intensity of E_a component of the first d-d transition decreases, and those of A_2 component of the first d-d transition and E_b component of the second d-d transition increase.[10-12] Mason and Norman proposed that hydrogen bonds played an important role in the ion-pair formation between PO_4^{3-} and $[Co(en)_3]^{3+}$,[11] and this view has been supported by an X-ray crystal structure analysis of $[Co(en)_3]_2(HPO_4)_3\cdot 9H_2O$[13] and another CD study of $[Co\{1,1,1\text{-tris}(2\text{-aminoethylaminomethyl})\text{ethane}\}]^{3+}$.[14] In a similar way, hydrogen bonds may occur between SeO_3^{2-} and the OH bridge groups of $[Co\{(OH)_2Co(NH_3)_4\}_3]^{6+}$, because a set of three OH groups is available each on the upper face and below the downward face of the ion of D_3 symmetry. The CD intensities increased at the bands of 14500, 19800, and 25400 cm^{-1}, while decreased at the band of 16300 cm^{-1} (Fig. 1 and Table 1). Therefore, the bands at 14500 and 16300 cm^{-1} can be assigned to A_2 and E_a component of the CoO_6 chromophore respectively.

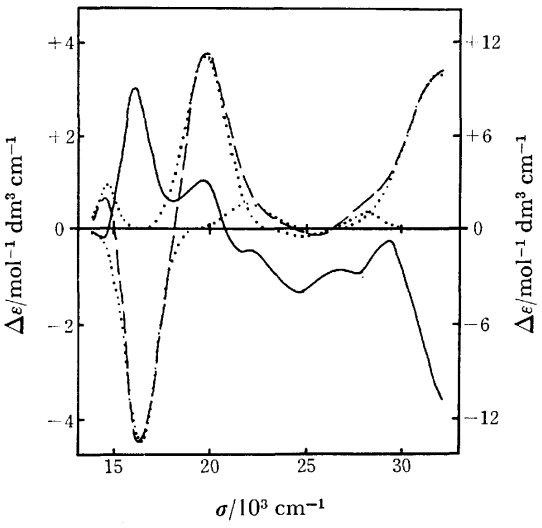

Fig. 2. The ion-pairing effect curve, $\{\Delta\varepsilon_{(in\ 0.17M\text{-}Na_2SeO_3)} - \Delta\varepsilon_{(in\ 0.01M\text{-}HCl)}\}$, (——) (the left ordinate), and CD curve of $(+)_{589}$-$[Co\{(OH)_2Co(NH_3)_4\}_3]^{6+}$ in 0.01 M-HCl (----) and its component curves separated by curve analysis (……) (the right ordinate).

Figure 2 shows the difference CD curve between in 0.01M-HCl and in 0.17M-Na_2SeO_3; this presents the ion-pairing effect of SeO_3^{2-} ion on the CD of $(+)_{589}$-$[Co\{(OH)_2Co(NH_3)_4\}_3]^{6+}$. The curve have six extrema at 14200, 16000, 19600, 21600, 24600, and 27800 cm^{-1} in the d-d transition region. The first and next extrema, at 14200 and 16000 cm^{-1}, correspond to the increment of the positive A_2 component and the decrement of the negative E_a component, respectively, of the first d-d transition of CoO_6 chromophore. The extrema at 19600 and 21600 cm^{-1} correspond to the first d-d transition components of CoN_4O_2 chromophores, and it seems that the last two extrema, at 24600 and 27800 cm^{-1}, correspond to the second d-d transition components of CoO_6 or CoN_4O_2 chromophores. Since the second d-d transition CD bands have been observed at 24300 and 26500 cm^{-1} for Λ-$[Co(ox)_3]^{3-}$[15] and at 26500 and 29400 cm^{-1} for Λ-$[Co(en)_2(H_2O)_2]^{3+}$,[16] it seems that the extremum at 24600 cm^{-1} shows the increment due to the ion-pairing effect on the longer wavelength negative CD component of the second band of CoO_6 chromophore. The extremum at 27800 cm^{-1} corresponds to the longer wavelength CD component of the second band of CoN_4O_2 chromophore or the shorter wavelength CD component of the CoO_6 one. Gaussian curve analysis of the CD spectra measured in 0.01M-HCl showed six CD components at 14680 cm^{-1} ($\Delta\varepsilon=+3.00$), 16340 (-13.54), 19690 ($+11.10$), 21980 ($+1.65$), 24460 (-0.28), and 28120 ($+1.07$) (Fig. 2). These extremum positions are well close to the extrema on the ion-pairing effect curve.

As for the chirality of the hexol type ions, two different assignments of absolute configuration have been offered.[5,7] Both assignments based on the CD sign of E_a component of CoO_6 chromophore, the assignments of the E_a component being reversed. Mason and Wood[5] have assigned the E_a component from the intensity, because the E_a component is invariably stronger than the A_2 component in many trigonal cobalt(III) complexes. The major CD band of CoO_6 chromophore of the hexol type complexes situated at higher energy side than the minor band, and they assigned Λ-configuration to the complex which has a positive sign in the higher energy CD component. On the other hand, Masuda and Douglas[7] have assigned the E_a component on the basis of the CD extremum position, because the E_a component appears usually at lower energy side of the A_2 component for many trigonal cobalt(III) complexes. Thus they assigned the complex which has a positive sign in the lower energy CD band as having the absolute configuration Λ.

From the present study of the ion-pairing effect, it is shown that the intensity of the lower energy CD band of CoO_6 chromophore increases upon ion-pairing, while that of the higher energy CD band decreases. In consequence the higher energy band can be assigned to the E_a component; this suports the assignment of Mason and Wood. As a conclusion the $(+)_{589}$-$[Co\{(OH)_2Co(NH_3)_4\}_3]^{6+}$ which shows a negative sign in the 16280 cm^{-1} CD band is assigned as having Λ-configuration.

Table 2 summarizes the rates of mutarotation, k, of the $(+)_{589}$ isomer determined from the time-course of CD change at 614 and 505 nm for the early reaction stage. The values of $\Delta\varepsilon_{614}$ and $\Delta\varepsilon_{505}$ are also presented, which were obtained by extrapolating the CD values back to zero time by using the rate constants k_{614} and k_{505}. In a NaOH solution of pH 8.1, $(+)_{589}$ isomer lost the optical activity completely within 3 min. In a NaOH solution of pH 10.4 the complex decomposed immediately. During the mutarotation, the absorption intensities at 625 and 505 nm did not change for more than 30 min in H_2O, for more than 120 min in 0.17M-H_2tart, 0.17M-Na_2tart, and 0.17M-Na_2SeO_3, for more than 2 days in 0.01M-HCl, and for more than 5 min in a NaOH solution of pH 8.1; in these periods the absorption spectra did not change in the d-d transition region.

As Table 2 shows, the $\Delta\varepsilon_{614}$ values in 0.01M-HCl and H_2O were -13.5 and -13.7, respectively; they are approximately equal. In 0.17M-Na_2SeO_3, 0.17M-Na_2tart, and 0.17M-H_2tart, they were -10.5, -12.4, and -12.2, respectively. On the other hand, the $\Delta\varepsilon_{505}$ values were almost equal for different solvents. The ion-pair formation affects strongly the $\Delta\varepsilon_{614}$ values, but not the $\Delta\varepsilon_{505}$ values. Thus the ion-pairing affects in a large extent the CoO_6 chromophore and less the CoN_4O_2 chromophores. This means that the hydrogen bonding between oxygen atoms of the counter ion and the OH bridge groups of the complex is more important than that between the counter ion and the ammonia ligands.

It may be worthwhile to consider the chirality of the oxygen atoms of the bridging OH groups, because they bonded directly to the cobalt(III) atoms and it is expected to produce rather strong vicinal effect on the CD bands of the CoO_6 and CoN_4O_2 chromophores. Since each oxygen atom of the six OH bridge groups has probably a pseudo-tetrahedral configuration of the three different attached groups and a lone pair of electrons, it must be asymmetric. For the complexes of Λ-configuration, axial disposition of the OH bond (parallel to

TABLE 2. RATES OF MUTAROTATION FOR THE EARLY STAGE AND THE INITIAL $\Delta\varepsilon$ VALUES AT 614 nm (16280 cm^{-1}) AND 505 nm (19780 cm^{-1}) ($\Delta\varepsilon$ values are given in mol^{-1} dm^3 cm^{-1} unit).

Solvent	$\Delta\varepsilon_{614}$	$\Delta\varepsilon_{505}$	k_{614}/s^{-1}	k_{505}/s^{-1}	k_{mean}/s^{-1}
0.01M-HCl	-13.48	$+11.26$	1.63×10^{-6}	2.40×10^{-6}	2.01×10^{-6}
0.17M-H_2tart	-12.19	$+11.64$	2.67×10^{-5}	1.85×10^{-5}	2.26×10^{-5}
0.17M-Na_2tart	-12.36	$+11.34$	5.10×10^{-4}	4.17×10^{-4}	4.64×10^{-4}
0.17M-Na_2SeO_3	-10.53	$+11.87$	3.52×10^{-4}	3.18×10^{-4}	3.35×10^{-4}
H_2O	-13.67	$+11.11$	1.78×10^{-3}	2.98×10^{-3}	—
NaOH (pH 8.1)			*ca.* 4×10^{-2}	*ca.* 5×10^{-2}	—

the C_3 axis) constraint (*S*) chirality for the asymmetric oxygen atom. Recently, Dixon *et al.*[17] made an X-ray crystal structure analysis of *rac*-$[Co\{(OH)_2Co(en)_2\}_3](SCN)_4(NO_3)_2\cdot 2H_2O$, and the two allowed (tetrahedral) positions were calculated for the hydrogen atoms of the OH bridge groups and the correct choice was made on the basis of difference maps, which revealed that all five but one of the six oxygen atoms take the axial disposition, only one OH group taking equatorial disposition. A molecular model consideration also shows that the axial orientation of the OH bridge groups may be more stable than the equatorial orientation because of some steric repulsion found in the latter case. It can therefore, be pressumed that the six asymmetric oxygen atoms of the *Δ*-$(+)_{589}$-$[Co\{(OH)_2Co(NH_3)_4\}_3]^{6+}$ complex have predominantly (*S*) configurations in the perchlorate crystals.

From absorption measurements during the time-course of CD change, other species expected for the original complex ion were not detected in the experimental time. Therefore the CD intensity decrease for the time-course can be ascribed to the racemization of *Δ*-$(+)_{589}$-$[Co\{(OH)_2Co(NH_3)_4\}_3]^{6+}$. The origin of optical activity decrease of this complex is divided into the racemization of the chirality *Δ* for the CoO_6 chromophore and that of the chirality (*S*) for the asymmetric oxygen atoms. In an acid solution oxonium ions rapidly attack the lone-pair electrons enforcing the inversion of the oxygen chiral center, and the oxygen center may be regarded as being in an equilibrium (*R*)⇌(*S*) (this kind of configurational equilibrium is denoted by *E* in the following); thus the racemization in this case corresponds to the reaction *Δ*(*EEEEEE*)→*Λ*(*EEEEEE*). On the other hand, in the SeO_3^{2-} solution, the oxoanion enforces the OH groups to take the axial positions; then the racemization in this case corresponds predominantly to *Δ*(*SSSEEE*)→*Λ*(*RRREEE*) or *Δ*(*SSSSSS*)→*Λ*(*RRRRRR*), if 1:1 or 1:2 ion-pairing is assumed, respectively. Since the Na_2SeO_3 solution is alkaline (pH=10.4), the *k* value is much greater for the SeO_3^{2-} solution than for the HCl solution. Nevertheless the *k* value in SeO_3^{2-} solution is much less than that in NaOH solution of pH 10.4. Evidently the ion-pairing depressed the racemization. The *k* value in 0.17M-Na_2tart solution (pH=8.1) is about 10^{-1} min^{-1} and that in a NaOH solution of pH 8.1 about 2—3 min^{-1}. It has been well established that the $tart^{2-}$ ion is also capable of forming ion-pairs with several cobalt(III) complexes.[18-20] Therefore, the difference in the *k* values at equal pH is due to the ion-pairing between the OH bridge groups and the doubly charged tartrate anion in the 0.17M-Na_2tart solution. It may be expected that the *k* value is smaller in 0.17M-Na_2tart (pH 8.1) than in 0.17M-Na_2SeO_3 (pH 10.4) in terms of the pH values. However the *k* value in 0.17M-Na_2tart (about 5×10^{-4} s^{-1}) is larger than that in 0.17M-Na_2SeO_3 (about 3×10^{-4} s^{-1}) (Table 2). This is because the ion-pairing effect of Na_2SeO_3 is larger than that of Na_2tart, as can be seen from the comparison of the $\Delta\varepsilon_{614}$ values.

Some plots of $\ln|\Delta\varepsilon|$ *vs.* time (min) for the mutarotation of $(+)_{589}$-$[Co\{(OH)_2Co(NH_3)_4\}_3]^{6+}$ were given in Figs. 3—5. The plots for the early stage gave a straight

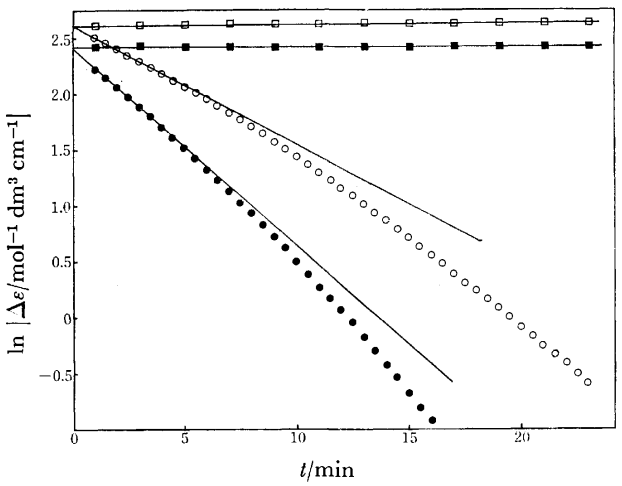

Fig. 3. Plots of $\ln|\Delta\varepsilon|$ *vs.* time for $(+)_{589}$-$[Co\{(OH)_2Co(NH_3)_4\}_3]^{6+}$ in 0.01 M-HCl ($\Delta\varepsilon_{614}$; □, $\Delta\varepsilon_{505}$; ■) and in water ($\Delta\varepsilon_{614}$; ○, $\Delta\varepsilon_{505}$; ●).

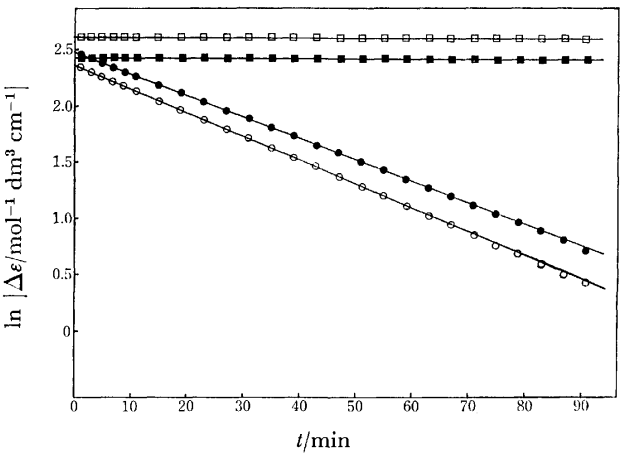

Fig. 4. Plots of $\ln|\Delta\varepsilon|$ *vs.* time for $(+)_{589}$-$[Co\{(OH)_2Co(NH_3)_4\}_3]^{6+}$ in 0.01 M-HCl ($\Delta\varepsilon_{614}$; □, $\Delta\varepsilon_{505}$; ■) and in 0.17 M-Na_2SeO_3 ($\Delta\varepsilon_{614}$; ○, $\Delta\varepsilon_{505}$; ●).

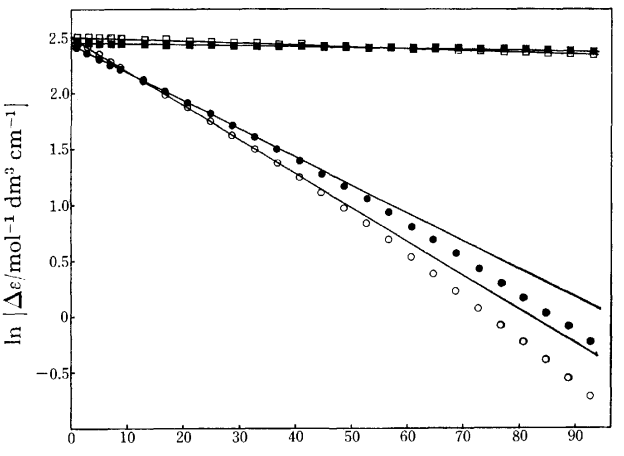

Fig. 5. Plots of $\ln|\Delta\varepsilon|$ *vs.* time for $(+)_{589}$-$[Co\{(OH)_2Co(NH_3)_4\}_3]^{6+}$ in 0.17 M-H_2tart ($\Delta\varepsilon_{614}$; □, $\Delta\varepsilon_{505}$; ■) and in 0.17 M-Na_2tart ($\Delta\varepsilon_{614}$; ○, $\Delta\varepsilon_{505}$; ●).

line; the lines in Figures were calculated by the least square method on the basis of the plots of initial stage. With elapse of time, a steep departure from the line was observed in H_2O (Fig. 3). In 0.17M-Na_2tart and 0.17M-Na_2SeO_3, with elapse of time, a slight departure from the line was observed (Figs. 4 and 5). While in 0.01M-HCl and 0.17M-H_2tart, only a slight departure from the line was observed (Figs. 4 and 5); the mutarotations in the latter two cases represent a true racemization $\Delta(EEEEEE) \rightarrow \Lambda(EEEEEE)$, $\Delta(SSSEEE) \rightarrow \Lambda(RRREEE)$, or $\Delta(SSSSSS) \rightarrow \Lambda(RRRRRR)$. It can be considered that the departure from a line, especially in the case in water, is due to a complicated configurational change due to the coexistence of different kinds of chiralities.

Sarneski and Ulbach[14] pointed out that the major source of CD change in the d-d transition region of Λ-$[Co(en)_3]^{3+}$–PO_4^{3-} ion-pair system may be the vicinal effect of chiral nitrogen centers stereospecifically produced at the primary amine donors by the ion-pair formation of Mason type. Similarly in the present polynuclear complex, the difference CD curve between in 0.01M-HCl and 0.17M-Na_2SeO_3 (Fig. 2) is regarded to have the origin in the vicinal effect of chiral oxygen centers stereospecifically produced by the ion-pair formation, because this curve corresponds to the difference $\Delta(SSSEEE) - \Delta(EEEEEE)$ or $\Delta(SSSSSS) - \Delta(EEEEEE)$. Thus the vicinal effect of the (*S*) oxygen atoms has a positive sign in the E_a component of the CoO_6 chromophore and this is in accord with the fact that the vicinal effect of (*R*) nitrogen center in the Λ-$[Co(en)_3]^{3+}$–PO_4^{3-} ion-pair system has a negative sign in the E_a component of the CoN_6 chromophore.

The authers are grateful to Dr. Takashi Komorita of Osaka University for his help in calculation of CD curve analysis.

References

1) S. M. Jörgensen, *Z. Anorg. Chem.*, **16**, 184 (1898).
2) A. Werner, *Ber.*, **47**, 308 (1914).
3) I. Sötofte and E. Bang, *Acta Chem. Scand.*, **25**, 1164 (1971).
4) H. A. Goodwin, E. C. Gyarfas, and D. P. Mellor, *Aust. J. Chem.*, **11**, 426 (1958).
5) S. F. Mason and J. W. Wood, *Chem. Commun.*, **1967**, 209.
6) R. D. Kern and R. A. D. Wentworth, *Inorg. Chem.*, **6**, 1018 (1967).
7) I. Masuda and B. E. Douglas, *J. Coord. Chem.*, **1**, 189 (1971).
8) G. B. Kauffman and R. P. Pinnell, *Inorg. Synth.*, **6**, 176 (1960).
9) D. A. Johnson and A. G. Sharpe, *J. Chem. Soc., A*, **1966**, 798.
10) R. Larsson, S. F. Mason, and B. J. Norman, *J. Chem. Soc., A*, **1966**, 301.
11) S. F. Mason and B. J. Norman, *J. Chem. Soc., A*, **1966**, 307.
12) H. L. Smith and B. E. Douglas, *Inorg. Chem.*, **5**, 784 (1966).
13) E. N. Duesler and K. N. Raymond, *Inorg. Chem.*, **10**, 1486 (1971).
14) J. E. Sarneski and F. L. Ulbach, *J. Am. Chem. Soc.*, **93**, 884 (1971).
15) A. J. McCaffery, S. F. Mason, and R. E. Ballard, *J. Chem. Soc.*, **1965**, 2883.
16) A. J. McCaffery, S. F. Mason, and B. J. Norman, *J. Chem. Soc.*, **1965**, 5094.
17) D. A. Dixon, R. E. Marsh, and W. P. Schaefer, *Acta Crystallogr., Sect. B*, **34**, 807 (1978).
18) K. Ogino and U. Saito, *Bull. Chem. Soc. Jpn.*, **40**, 826 (1969).
19) M. Fujita and H. Yamatera, *Bull. Chem. Soc. Jpn.*, **49**, 1301 (1976).
20) H. Yoneda and T. Taura, *Chem. Lett.*, **1977**, 63; K. Miyoshi, C. E. Oh, H. Nakazawa, and H. Yoneda, *Bull. Chem. Soc. Jpn.*, **51**, 2946 (1978); T. Taura, H. Tamada, and H. Yoneda, *Inorg. Chem.*, **17**, 3127 (1978).

Phase-transfer Reactions Catalyzed by Phosphoric Triamides Containing Hydrophobic Groups

Masao TOMOI,* Takashi HASEGAWA, Manabu IKEDA, and Hiroshi KAKIUCHI

Department of Applied Chemistry, Faculty of Engineering, Yokohama National University, Yokohama 232

(Received July 4, 1978)

Aqueous organic two-phase reactions (halogen exchange, cyanation, and borohydride reduction) have been catalyzed by phosphoric triamides containing hydrophobic groups. The phosphoric triamides, which have a high cation binding ability, exibited high catalytic activity for the two-phase reactions. The catalytic activity of *N*-alkylteramethylphosphoric triamides (**1**) was higher than that of the corresponding pentamethyl derivatives and the difference has been explained in terms of the contribution of the dimeric species of **1** and/or hydrogen bonding between the NH of **1** and the anionic moieties of inorganic reagents.

Aqueous organic two-phase reactions are catalyzed by quaternary ammonium or phosphonium salts,[1] crown ethers,[2] cryptands,[3] and α-phosphoryl sulfoxides[4] and have found use in organic syntheses.[5] Recently, it was found that *N*-alkylpentamethylphosphoric triamides (**1**)[6] and *N*-alkyltetramethylphosphoric triamides (**2**) catalyzed two-phase reactions, the activity being dependent on the structure of the compounds.

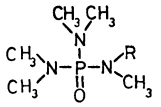

1

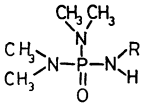

2

In this report, the relationship between the structure and the catalytic activity will be discussed.

Experimental

Reagents. *N*-Alkylpentamethylphosphoric triamides (**1**) have been prepared by the reaction of the sodium salt of pentamethylphosphoric triamide[7] and the corresponding alkyl halides in toluene at 0 °C. *N*-Alkyltetramethylphosphoric triamides (**2**) have been synthesized by the reaction of bis(dimethylamino)chlorophosphine oxide[8] with the corresponding primary amine, in the presence of triethylamine, in refluxing benzene. **1** and **2** were purified by distillation under reduced pressure or recrystallization, and the structure confirmed by NMR, IR, and MS. The yields and physical properties are summarized in Table 1.

TABLE 1. YIELDS AND PHYSICAL PROPERTIES OF PHOSPHORIC TRIAMIDES

Name	Alkyl group (R)	Yield %	Bp/mmHg (mp) °C
Pentamethylphosphoric triamide derivatives			
1a	CH_3[a]	—	68/1
1b	$PhCH_2$	81	117/0.5
1c	$PhCH{=}CH{-}CH_2$	80	155/1
1d	$Ph(CH_2)_3$	44	144/0.5
1e	$1\text{-}C_{10}H_7CH_2$	75	(116—119)[b,c]
1f	$C_{12}H_{25}$	66	142/0.5
1g	$C_{16}H_{33}$	70	165/0.01
Tetramethylphosphoric triamide derivatives			
2a	CH_3	72	103/0.5
2b	$PhCH_2$	78	(84—90)[b,c]
2c	$1\text{-}C_{10}HCH_2$	56	(119—124)[b,c]

a) Commercial product. b) Hygroscopic. c) Uncorrected.

N-Benzylformamide,[9] tridecyl methyl sulfoxife,[10] 18-crown-6,[11] and benzo-18-crown-6[12] were prepared by the methods described in the literature. *N*-Dodecyl-2-pyrrolidone (Mitsubishi Petrochemical) was distilled under reduced pressure prior to use. Other organic reagents were obtained from commercial sources and distilled under reduced pressure prior to use. Inorganic reagents and quaternary ammonium salts were obtained commercially, and used without further purification.

Reaction Procedure. The two-phase reactions were conducted under standard phase-transfer conditions[2,3] and the yields determined by gas chromatography.

Measurements. The cation binding ability of the phosphoric triamides was evaluated by the procedure described by Smid *et al.*[13] and the degree of association measured cryoscopically in benzene.

Results

Halogen Exchange Reaction. Table 2 shows the results of the reaction of octyl bromide with potassium

TABLE 2. REACTION OF $C_8H_{17}Br$[a] WITH KI[b] UNDER PHASE-TRANSFER CONDITIONS[c]

Catalyst[d]	Time h	Yield[e] %
None	24	<5
1a	24	5
1b	6	25
1c	6	77
1d	6	32
1e	6	11
1f	6	38
1g	6	21
2a	24	5
2b	6	73
2c	6	92
$PhCH_2NHCHO$	24	5
$C_{13}H_{27}SOCH_3$	24	26
NDP[f]	24	5
18-Crown-6	6	16
Benzo-18-crown-6	6	68
$PhCH_2N(CH_3)_3{}^+Cl^-$	8	<5
$C_{16}H_{33}N(CH_3)_3{}^+Br^-$	2	100[g]

a) No solvent was used for the substrate. b) Saturated aqueous solution, 5.0 mol equiv. c) Reaction temp, 80 °C; internal standard, tetralin. d) 0.08 mol equiv. e) GLPC analysis. f) *N*-Dodecyl-2-pyrrolidone. g) Emulsified reaction.

iodide under phase-transfer conditions. Both hexamethylphosphoric triamide (**1a**) and pentamethylphosphoric triamide (**2a**) were not effective catalysts for the halogen exchange. *N*-Alkylpentamethylphosphoric triamides (**1b**—**1g**) and *N*-alkyltetramethylphosphoric triamides (**2b**, **2c**) containing higher aliphatic or arylalkyl groups were however found to catalyze the reaction. In particular, the tetramethylphosphoric triamide derivatives showed high catalytic activity.

Formamide, sulfoxide, and 2-pyrrolidone derivatives having hydrophobic groups in the molecules exibited low catalytic activity. Benzo-18-crown-6 was effective as a catalyst, while 18-crown-6 was not. Benzyltrimethylammonium chloride was also not effective. Hexadecyltrimethylammonium bromide (CTAB) showed the highest catalytic activity of all the catalysts used.

Table 3. Reaction of $C_8H_{17}Br$[a] with NaCN[b] under phase-transfer conditions[c]

Catalyst[d]	Time h	Yield[e] %
None	24	11
1a	8	22
1b	10	47
1c	10	70
1d	10	34
1e	10	68
2a	8	24
2b	10	76
2c	10	91
$PhCH_2NHCHO$	10	7
$C_{13}H_{27}SOCH_3$	10	6
NDP[f]	10	4
Benzo-18-crown-6	8	84
$C_{16}H_{33}N(CH_3)_3{}^+Br^-$	6	98[g]

a) No solvent was used for the substrate. b) 33 wt % aqueous solution, 1.5 mol equiv. c) Reaction temp, 80 °C; internal standard, naphthalene. d) 0.05 mol equiv. e) GLPC analysis. f) *N*-Dodecyl-2-pyrrolidone. g) Emulsified reaction.

Cyanation. Table 3 shows the results of the reaction of octyl bromide with sodium cyanide. The cyanation, as well as the halogen exchange reaction, was catalyzed by **1b**—**1e** and **2b**—**2c**, the catalytic activity of the latter being higher than that of the former. Benzo-18-crown-6 and CTAB showed high catalytic activity, but CTAB emulsified the system with increasing conversion of the reaction.

Reduction of Ketone. The results of the reduction of acetophenone and 2-octanone with sodium borohydride are shown in Table 4. The reduction proceeded very slowly in the absence of phosphoric triamide catalysts. This reaction, and the two reactions described above, were catalyzed by the phosphoric triamides, especially **2b** and **2c**.

Interaction between Phosphoric Triamides and Picrate Salts. The cation binding ability of the phosphoric triamides was investigated by the extraction method described by Smid *et al.*[13] and the results of the extraction of potassium picrate by the phosphoric triamides are shown in Table 5. The cation binding ability of **1a** and **2a** was very low. Tetramethylphosphoric triamides containing the benzyl (**2b**) or 1-naphthylmethyl (**2c**) group exibited high cation binding ability, compared with the other phosphoric triamides. Pentamethylphosphoric triamides possessing benzyl (**1b**), cinnamyl (**1c**), or 1-naphthylmethyl (**1e**) groups also proved efficient in the extraction of potassium picrate. The pentamethylphosphoric triamides having a dodecyl (**1f**) or hexadecyl (**1g**) group showed very low cation binding ability.

The cation binding ability of the phosphoric triamides was largely independent of the species of alkali cations,[6] in contrast with the observations on crown ethers.[13]

Association of Phosphoric Triamides. Table 6 shows the degree of association of the phosphoric triamides in benzene which for **2b** and **2c** was 1.2, and for **1b** and **1e** was 1.0. **1b** and **2b** were found to be present as monomeric forms in dioxane.

Table 4. Reduction of ketones[a] with $NaBH_4$[b] under phase-transfer conditions[c]

Ketone $RCOCH_3$	Catalyst[d]	Time h	Yield[e] %
R=Ph[f]	None	8	10
	1b	8	65
	1e	8	69
	2b	6	94
	2c	6	92
$R=C_6H_{13}$[g]	None	24	3
	1b	8	93
	1e	8	87
	2b	3	>95
	2c	3	>95

a) 25.5 mmol. b) 0.76 mol equiv. c) Benzene (4 ml) was used as solvent; 1 wt % aqueous NaOH (1 ml); room temp. d) 0.10 mol equiv. e) GLPC analysis. f) Internal standard, diphenyl. g) Internal standard, ethylbenzene.

Table 5. Extraction of potassium picrate by phosphoric triamides[a]

Phosphoric triamide	Potassium picrate extracted[b] %
1a[c]	1
1b	4
1c	8
1d	1
1e	11
1f	1
1g	1
2a[c]	1
2b	12
2c	12

a) Solvent system, H_2O–CH_2Cl_2 (50:50, v/v); [Picric acid]$=7.0\times10^{-5}$ M: [KOH]$=0.01$ M; [Phosphoric triamide]$=7.0\times10^{-3}$ M. b) Based on total amount of potassium picrate. The picrate concentration was measured by optical spectroscopy, using $\varepsilon=1.8\times10^4$ in CH_2Cl_2. c) [Phosphoric triamide]$=7.0\times10^{-2}$ M.

Table 6. Association of phosphoric triamides in benzene and dioxane

Phosphoric triamide	Concn M	Degree of association in	
		benzene	dioxane
1b	0.055	1.0	
1b	0.013		1.0
1e	0.037	1.0	
2b	0.051	1.2	
2b	0.011		1.0
2c	0.039	1.2	

Discussion

It has been shown that the phosphoric triamides containing hydrophobic groups are effective as phase-transfer catalysts. The catalytic activity of some of the phosphoric triamides was comparable to that of benzo-18-crown-6, and somewhat lower than that of CTAB. The activity was considerably higher than that of formamide, sulfoxide, and pyrrolidone derivatives containing hydrophobic groups. The donor numbers of the corresponding compounds containing methyl, in place of the higher groups are as follows:[14] hexamethylphosphoric triamide, 38.8; *N,N*-dimethylformamide, 26.6; dimethyl sulfoxide, 29.8; *N*-methyl-2-pyrrolidone, 27.3. On the basis of this data, it is suggested that the phosphoric triamides containing hydrophobic groups interact strongly with the cationic moieties of inorganic reagents through pole-dipole interactions.

The mechanism of two-phase reactions catalyzed by ammonium or phosphonium salts was first proposed by Starks,[1] and supported by Herriot and Picker.[15] In the system, the onium salts are thought to extract the anionic reagent into the organic phase. In the reactions catalyzed phosphoric triamides, the compounds which were efficient extractors of potassium picrate from the aqueous to the organic phase (CH_2Cl_2), exibited high catalytic activity for the two-phase reactions (see Tables 2, 3, 4, and 5). These observations may be explained in terms of the mechanism proposed by Starks,[1] *i.e.*, the phosphoric triamides, and the onium salts, transfer the inorganic reagent from the aqueous phase to the organic phase, and thereby catalyze the two-phase reaction.

The catalytic activity of the phosphoric triamides was found to be dependent on the structure of the hydrophobic groups. In this study, the activity of the phosphoric triamides having arylalkyl groups such as benzyl or 1-naphthylmethyl groups was higher than those having alkyl groups such as dodecyl or hexadecyl.

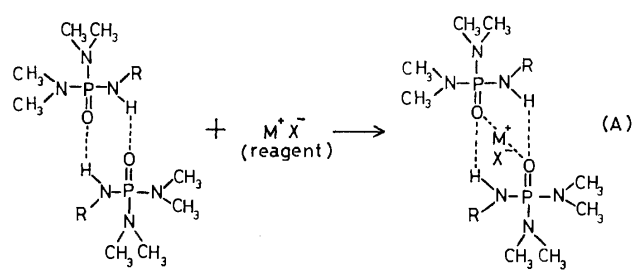

(A)

The catalytic activity of **2** is higher than that of **1**, although the electron-donating power of the dialkylamino group is stronger than that of the monoalkylamino group.[16] This result may be explained as follows; **2** slightly associates in benzene (Table 6) and the hydrogen of NH in **2** is weakly acidic (**2** reacts easily with NaH) suggesting the participation of a dimeric species. This is formed through hydrogen bonding, in the two-phase reaction (Scheme **A**).

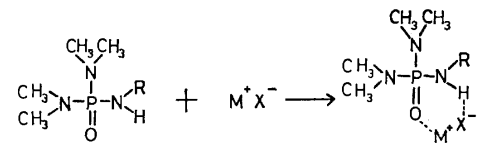

(B)

Moreover, it appears reasonable to assume that the anionic moiety (X^-) of the inorganic reagent (M^+X^-) may interact with the acidic hydrogen of **2** through hydrogen bonding (Scheme **B**). The enhanced interaction of **2** with M^+X^-, as described in schemes **A** and **B**, will result in an increase in the solubility of M^+X^- in the organic phase, and thereby an increase in the catalytic activity of **2**. In the case of **1** which does not contain an acidic hydrogen, the interaction of **1** with X^- is not expected.

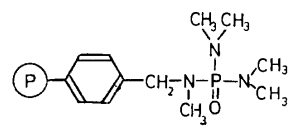

3

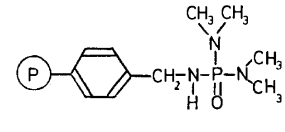

4

Solid-phase catalysts (**3** and **4**), prepared by the reaction of chloromethylated polystyrene resin cross-linked with divinylbenzene and the sodium salts of pentamethylphosphoric triamide or tetramethylphosphoric triamide, were found to be effective for two-phase reactions.[17] In the tri-phase[18] and the two-phase system, the activity of the tetramethyl derivative **4** was higher than that of the pentamethyl derivative **3**. Such a difference between **3** and **4** may be interpreted by assuming a strong interaction of **4** with M^+X^- through hydrogen bonding as shown in scheme **B**, since the cooperative interaction of the phosphoric triamide groups, with M^+X^- as shown in scheme **A**, may be assumed to occur with difficulty in the immobilized system.[19]

References

1) C. M. Starks, *J. Am. Chem. Soc.*, **93**, 195 (1971).
2) D. Landini, F. Montanari, and F. M. Pirisi, *J. Chem. Soc., Chem. Commun.*, **1974**, 879.
3) M. Cinquini, F. Montanari, and P. Tundo, *J. Chem. Soc., Chem. Commun.*, **1975**, 393.
4) M. Mikolajczyk, S. Grzejszczak, A. Zatorski, F. Montanari, and M. Cinquini, *Tetrahedron Lett.*, **1975**, 3757.
5) (a) J. Dockx, *Synthesis*, **1973**, 441; (b) E. V. Dehmlow, *Angew. Chem.*, **86**, 187 (1974); (c) G. W. Gokel and H. D. Durst, *Synthesis*, **1976**, 168; E. V. Dehmlow, *Angew. Chem.*, **89**, 521 (1977).
6) M. Tomoi, T. Takubo, M. Ikeda, and H. Kakiuchi,

Chem. Lett., **1976**, 473.
7) R. L. Arceneau, J. G. Frick, Jr., E. K. Leonard, and J. D. Reid, *J. Org. Chem.*, **24**, 1419 (1959).
8) P. Lester, U. S. Patent 2678335 (1954); *Chem. Abstr.*, **49**, 6300 g (1955).
9) M. Liler, *J. Chem. Soc., B*, **1971**, 334.
10) I. D. Entwinstle and R. A. W. Johnstone, *J. Chem. Soc., Chem. Commun.*, **1965**, 29.
11) G. W. Gokel, D. J. Cram, C. L. Liotta, H. P. Harris, and F. L. Cook, *J. Org. Chem.*, **39** 2445 (1974).
12) C. J. Pedersen, *J. Am. Chem. Soc.*, **89**, 7017 (1967).
13) S. Kopolow, T. E. Hogen Esch, and J. Smid, *Macromolecules*, **6**, 133 (1973).
14) V. Gutmann, *Electrochim. Acta*, **21**, 661 (1976).
15) A. W. Herriott and D. Picker, *J. Am. Chem. Soc.*, **97**, 2345 (1975); A further mechanism for two-phase reactions was proposed by Landini *et al.* *Cf.* D. Landini, A. Maia, and F. Montanari, *ibid.*, **100**, 2796 (1978).
16) *Cf.* for example J. D. Roberts and M. C. Caserio, "Basic Principles of Organic Chemistry," 2nd ed, W. A. Benjamin, Inc., Menlo Park, California (1977), p. 1112.
17) M. Tomoi, M. Ikeda, and H. Kakiuchi, *Tetrahedron Lett.*, **1978**, 3757.
18) *Cf.* S. L. Regen, *J. Am. Chem. Soc.*, **97**, 5965 (1975); *ibid.*, **98**, 6270 (1976).
19) *Cf.* for example D. C. Neckers, *J. Chem. Educ.*, **52**, 695 (1975).

α,β-Unsaturated Carboxylic Acid Derivatives. XVII. The Facile Synthesis of Ethyl α-Azido-α-alkenoates and Reduction to Ethyl α-Amino-α-alkenoates[1]

Chung-gi SHIN,* Yasuchika YONEZAWA, Kazuo UNOKI, and Juji YOSHIMURA**

Laboratory of Organic Chemistry, Faculty of Technology, Kanagawa University, Rokkakubashi, Kanagawa-ku, Yokohama 221

***Laboratory of Chemistry for Natural Products, Faculty of Science, Tokyo Institute of Technology, Nagatsuta, Midori-ku, Yokohama 227*

(Received July 25, 1978)

Several pathways leading to ethyl α-azido-α-alkenoates (**8**) by the β-elimination to ethyl α-azido-β-substituted (hydroxy-, acetoxy-, or mesyloxy)-alkanoates with NaN_3 or Et_3N have been examined. The optimized procedure, in combination with subsequent reduction provides a general synthetic route to α-amino-α-alkenoic acid esters (**9**). The configuration of **8** and **9** have been shown to be of (*Z*)-geometry.

α,β-Unsaturated α-amino acid (α-dehydroamino acid; DHA) or the α-imino form has been postulated as the intermediate in the biological epimerization of the L-α-amino acid into the enantiomer by the process of dehydrogenation-hydrogenation.[2] In addition, DHA is of great importance as a starting material for the incorporation and synthesis of dehydropeptides and peptide antibiotics.[2-5]

In previous papers,[6,7] the facile synthesis of ethyl 2-amino-2-alkenoates (**9**) by reduction of the corresponding 2-azido compounds (**8**) with aluminium-amalgam (Al–Hg) have been reported. Schmidt *et al.* reported the preparation of methyl 2-amino-2-alkenoates by the elimination of methanol from the corresponding α-methoxy α-amino acids[8] or the dehydrochlorination of α-chloro amino acid derivatives.[9]

The synthesis of **8** and the subsequent selective reduction of **8** into **9** will be reported in detail. The

TABLE 1. ETHYL 2-BROMO-3-SUBSTITUTED ALKANOATES (**2**, **3**, AND **4**)

Compound No.	Yield (%)	Bp °C/mmHg[a] (Mp °C)	Formula	Found (Calcd), % C	Found (Calcd), % H	IR spectrum,[b] cm⁻¹ OH	IR spectrum,[b] cm⁻¹ COOEt $COCH_3$ SO_2O	NMR spectrum,[c] δ 2-proton (Hz)	NMR spectrum,[c] δ 3-proton (Hz)	NMR spectrum,[c] δ SCH_3
2a	58	65—70/3	$C_6H_{11}O_3Br$	34.11 (34.12)	5.43 (5.21)	3450,	1750	4.15d(7.6),	4.01—4.22m	
2b	51	67—71/1.5	$C_7H_{13}O_3Br$	37.39 (37.33)	5.66 (5.78)	3440,	1743	4.15d(7.6),	3.85—4.08m	
2c	48	72—75/0.5	$C_8H_{15}O_3Br$	39.98 (40.17)	6.23 (6.28)	3440,	1743	4.14d(7.6),	3.85—4.09m	
2d	50	70—73/0.5	$C_8H_{15}O_3Br$	40.11 (40.17)	6.15 (6.28)	3450,	1740	4.19d(7.9),	3.86dd(4.0)	
2e	45	(72—73)[d]	$C_{11}H_{13}O_3Br$	48.40 (48.35)	4.80 (4.76)	3400,	1720	4.34d(8.0),	5.05dd(5.1)	
3a	83	67—73/1.5	$C_8H_{13}O_4Br$	37.85 (37.94)	5.19 (5.14)		1755	4.29d(7.7),	5.23dq(6.0)	
3b	85	78—80/1	$C_9H_{15}O_4Br$	41.08 (40.70)	5.40 (5.62)		1750	4.32d(7.8),	5.12—5.56m	
3c	86	82—86/1	$C_{10}H_{17}O_4Br$	42.27 (42.70)	6.15 (6.05)		1755	4.32d(7.1),	5.26—5.36m	
3d	84	80—85/1	$C_{10}H_{17}O_4Br$	42.78 (42.70)	6.18 (6.05)		1755	4.28d(9.0),	5.35dd(3.7)	
3e	90	syrup	$C_{13}H_{15}O_4Br$	49.66 (49.52)	4.78 (4.76)		1750	4.48d(10.0),	6.16d(10.0)	
4a	59	110—115/1	$C_7H_{13}O_5SBr$	29.10 (29.06)	4.56 (4.50)		1741, 1365 1180	4.32d(8.0),	4.95—5.22m,	3.06s
4b	51	120—122/1	$C_8H_{15}O_5SBr$	31.74 (31.68)	4.87 (4.95)		1740, 1360 1180	4.41d(8.0),	4.91—5.08m,	3.06s
4c	53	120—125/0.8	$C_9H_{17}O_5SBr$	34.13 (34.07)	5.42 (5.36)		1740, 1360 1175	4.46d(7.0),	4.95—5.12m,	3.04s
4d	46	121—125/0.8	$C_9H_{17}O_5SBr$	34.12 (34.07)	5.56 (5.36)		1745, 1360 1175	4.36d(8.3),	4.96—5.10m,	3.05s
4e	81	(70—71)[e]	$C_{12}H_{15}O_5SBr$	41.00 (41.08)	4.30 (4.29)		1750, 1368 1180	4.50d(10.0),	5.90d(10.0),	2.71s

a) Colorless oil. b) Recorded in KBr. c) Measured in $CDCl_3$. d) Colorless needles from benzene–cyclohexane (1: 4 v/v). e) Colorless needles from hexane.

geometric structure of **8** and **9** has been shown to be of (*Z*)-configuration.

Results and Discussion

The starting material, ethyl 2-bromo-3-hydroxyalkanoate (**2**) were readily prepared by treating ethyl (*E*)-2-alkenoates (**1**) with *N*-bromosuccinimide (NBS) or *N*-bromoacetamide (NBA) and water.[6]

The direct reaction of **2** with 3M NaN_3 in hexamethylphosphoric triamide (HMPA) gave **8** in low yield (Procedure A).

To effect β-elimination after azidation, **2** was converted into ethyl 3-acetoxy-2-bromo (**3**)- and 2-bromo-3-mesyloxyalkanoates (**4**) by conventional means, and subjected to a similar substitution-elimination. The

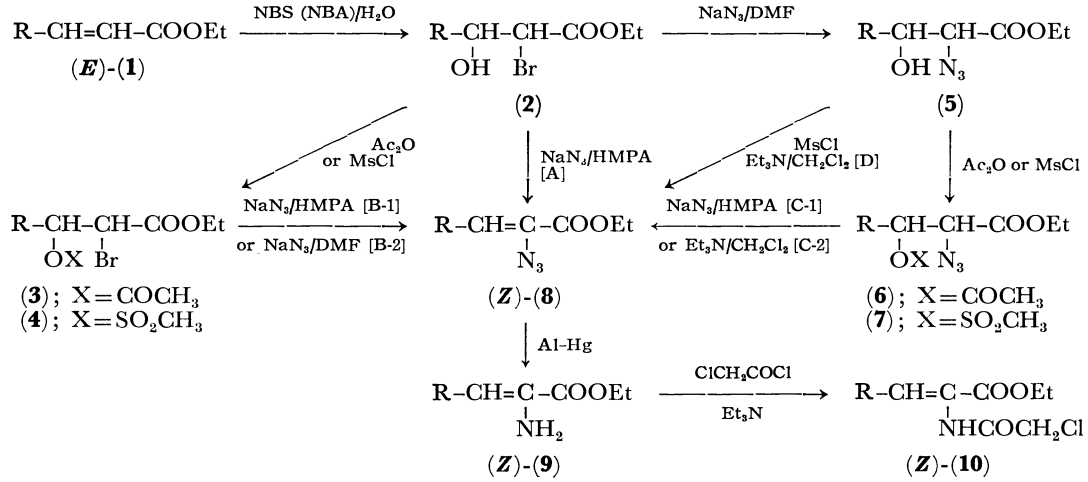

a; R=CH_3, **b**; R=C_2H_5, **c**; R=*n*-C_3H_7, **d**; R=*i*-C_3H_7, **e**; R=C_6H_5

Scheme 1. Alphabet in brackets is the type of procedure.

TABLE 2. ETHYL 2-AZIDO-3-SUBSTITUTED ALKANOATES (**5**, **6**, AND **7**)

Compd No.	Yield (%)	Bp °C/mmHg[a] (Mp °C)	Formula	Found (Calcd), % C	H	N	IR spectrum,[b] cm^{-1} OH	N_3	COOEt $COCH_3$	SO_2O	NMR spectrum,[c] δ 2-proton (Hz)	3-proton (Hz)	SCH_3
5a	75	72—75/1.5	$C_6H_{11}N_3O_3$	41.71 (41.61)	6.45 (6.40)	24.30 (24.27)	3450,	2100,	1750		3.79d(4.0),	4.02—4.32m	
5b	80	75—80/1.7	$C_7H_{13}N_3O_3$	45.12 (44.91)	7.10 (7.00)	22.39 (22.45)	3450,	2100,	1740		3.84d(3.5),	3.85—4.20m	
5c	75	81—83/1	$C_8H_{15}N_3O_3$	47.79 (47.75)	7.70 (7.51)	20.90 (20.88)	3450,	2100,	1740		3.85d(3.4),	3.81—4.18m	
5d	72	80—82/1.5	$C_8H_{15}N_3O_3$	47.61 (47.75)	7.56 (7.51)	20.92 (20.88)	3450,	2100,	1740		3.86d(3.0),	3.70dd(6.9)	
5e	70	syrup	$C_{11}H_{13}N_3O_3$	56.18 (56.16)	5.65 (5.57)	17.76 (17.86)	3450,	2100,	1740		3.98d(4.0),	4.50d(4.0)	
6a	92	73—76/1	$C_8H_{13}N_3O_4$	44.58 (44.64)	6.12 (6.09)	19.61 (19.53)		2100,	1750		3.72d(3.5),	5.36dq(6.6)	
6b	91	75—81/1	$C_9H_{15}N_3O_4$	47.19 (47.15)	6.70 (6.60)	18.43 (18.33)		2100,	1750		3.78d(3.5),	5.26dt(6.9)	
6c	95	80—82/0.2	$C_{10}H_{17}N_3O_4$	49.43 (49.37)	7.10 (7.04)	17.32 (17.28)		2100,	1750		3.74d(3.2),	5.36dt(6.5)	
6d	92	80—82/0.5	$C_{10}H_{17}N_3O_4$	49.56 (49.37)	6.98 (7.04)	17.33 (17.28)		2100,	1750		3.18d(3.0),	5.12dd(7.8)	
6e	89	syrup	$C_{13}H_{15}N_3O_4$	56.58 (—)	5.44 (—)	15.31 (—)		2100,	1755		4.02d(5.0),	6.23d(5.0)	
7a	75	135—140/1.5	$C_7H_{13}O_5SN_3$	33.56 (33.47)	5.19 (5.18)	16.77 (16.73)		2110,	1750,	1370 1190	3.85d(3.8),	5.20dq(6.2),	3.05s
7b	82	135—137/1	$C_8H_{15}O_5SN_3$	36.32 (36.23)	5.78 (5.66)	15.86 (15.85)		2110,	1750,	1370 1185	3.89d(3.2),	5.04dt(6.9),	3.06s
7c	81	138—139/1	$C_9H_{17}O_5SN_3$	38.88 (38.71)	5.87 (6.09)	15.23 (15.05)		2110,	1755,	1370 1190	3.87d(3.2),	5.14dt(6.8),	3.06s
7d	80	140—142/1.5	$C_9H_{17}O_5SN_3$	38.75 (38.71)	6.11 (6.09)	14.98 (15.05)		2110,	1760,	1380 1190	3.87d(3.2),	4.86dd(7.8),	3.08s
7e	76	(68—69)[d]	$C_{12}H_{15}O_5SN_3$	45.79 (46.01)	4.77 (4.79)	13.45 (13.42)		2100,	1745,	1370 1187	4.16d(5.9),	5.94d(5.9),	2.88s

a) Colorless oil. b) Recorded in KBr. c) Measured in $CDCl_3$. d) Colorless needles from hexane.

Table 3. The percentage yields and NMR spectra (δ) of **8**

Compound No.	Procedures and yields (%)						NMR spectrum,[a] δ	
	A	B		C		D	3-proton (Hz)	3-alkyl (Hz)
		1	2	1	2			
8a	45	90	68	90	92	91	6.18qa[a] (7.0)	1.80d (7.0)
8b	40	81	71	81	90	92	6.15t (7.2)	2.24qi[c] (7.2)
8c	35	74	69	74	89	96	6.16t (7.6)	2.21qa[b] (7.6)
8d	37	75	69	75	88	93	5.96d (7.4)	2.80m[d] (6.3)
8e	41	95	43	95	90	85	6.96s —	(7.32—7.52m 7.80—7.92m)[e]

a) Measured in $CDCl_3$. b) Quartet. c) Quintet. d) Multiplet. e) Phenyl protons.

Table 4. The percentage yietds and NMR spectra of **9** and **10**

Compound No.	Yield (%)	NMR spectrum, δ in $CDCl_3$			Compound No.	Yield (%)
		3-proton (Hz)	NH_2	3-alkyl		
9a	75.6	5.65q[a] (7.2)	3.50	1.68q	**10a**	86
9b	85.7	5.56t[b] (7.1)	3.45	2.07t	**10b**	87
9c	80.0	5.59t[b] (7.3)	3.50	2.04t	**10c**	79
9d	84.5	5.46d[c] (9.1)	3.52	2.45m[c]	**10d**	85
9e	70.9	6.50s[d]	4.30	7.20—7.55m[e]	**10e**	65

a) Quartet. b) Triplet. c) Doublet. d) Singlet. e) Multiplet.

reaction of **4** in *N,N*-dimethylformamide (DMF) gave **8** in *ca.* 65% yield together with the direct β-elimination product, the ethyl 2-bromo-2-alkenoates (Procedure B-2). **3** was completed in HMPA in *ca.* 80% yield (Procedure B-1).

In subsequent experiment, **2** was firstly converted into ethyl 2-azido-3-hydroxyalkanoate (**5**), and subsequently into ethyl 3-acetoxy-2-azido (**6**)- and 2-azido-3-mesyloxyalkanoates (**7**) in good yields. The similar elimination reaction of **6** in HMPA in the presence of NaN_3 (Procedure C-1) and **7** in CH_2Cl_2 in the presence of Et_3N (Procedure C-2) proceeded more smoothly to give **8** in *ca.* 85 and 90% yields respectively. The reaction of **5** with mesyl chloride in CH_2Cl_2 in the presence of Et_3N was completed immediately to give **8** quantitatively (Procedure D).

Procedure D is the most satisfactory method for the preparation of **8** from **2** and is generally applicable for the conversion of α-hydroxy azides into the corresponding azido olefin, the results of which will be published elsewhere.

The reduction of **8** with Al–Hg in ether readily gave the expected **9** in *ca.* 80% yield.[7] In order to determine the geometric configuration of **9**, chloroacetylation was performed to give ethyl 2-(chloroacetylamino)-2-alkenoates (**10**). All physical constants and spectral data of **10** were in good agreement with the authentic samples of the (*Z*)-configuration.[10] Therefore, the structures of **8**, **9**, and **10** have been unambiguously assigned the (*Z*)-configuration.

The configuration of the addition products (**2**—**4**), have been the erythro-isomer from the observed $J_{2,3}$ values of over 7.0 Hz. Similarly, from the $J_{2,3}$ values (*ca.* 3.5 Hz), the configuration of **5**, **6**, and **7** has been assigned to the threo-isomer.

Consequently it is considered that the stereospecific *trans* addition to (***E***)-**1**[11] gave the erythro-isomer, which was converted into the threo-isomer by substitution and *trans* β-elimination of the two isomers above proceeded to give (***Z***)-**8**.

Experimental

All boiling and melting points are uncorrected. The IR and NMR spectra were recorded with Hitachi EPI-G3 and JNM-PS-100 Spectrometers with tetramethylsilane as the internal standard respectively.

Preparation of **2**. To a solution of **1** (0.5 mol) in H_2O (300 ml) and tetrahydrofuran (300 ml) was added portionwise NBS or NBA (0.6 mol) below 10 °C. After reaction at the same temperature for 12 h, the resulting solution was allowed to stand for 24 h at room temperature. The solution was extracted four times with ether (200 ml) and the ethereal extracts washed twice with water and dried over anhydrous $MgSO_4$. Evaporation of the ether gave a syrup, which was distilled under reduced pressure to give **2**.

Preparation of **5**. A mixture of **2** (0.1 mol) and NaN_3 (0.25 mol) in DMF (150 ml) was heated with stirring at 60—70 °C for 20 h. The reaction solution was poured into ice-

water (400 ml) and the aqueous solution extracted three times with benzene (100 ml). The combined benzene extracts were washed twice with water and dried over anhydrous $MgSO_4$. Evaporation of the solvent gave **5**.

Preparation of 3 and 6. Two drops of concentrated H_2SO_4 were added to a solution of **2** (0.1 mol) in acetic anhydride (0.15 mol). After stirring at 50—60 °C for 30 min, the reaction mixture was diluted with benzene (60 ml). The benzene solution was washed once with aqueous $NaHCO_3$ and twice with water and dried over anhydrous Na_2SO_4. Concentration of the benzene solution gave a syrupy residue, which was distilled under reduced pressure to give **3**. A similar reaction of **5** gave **6**.

Preparation of 4 and 7. To a solution of **2** (0.05 mol) and mesyl chloride (0.05 mol) in CH_2Cl_2 (50 ml) was added Et_3N (0.05 mol) under nitrogen at 0—3 °C. The chilled solution was allowed to stand at room temperature and the reaction solution continuously stirred at room temperature for 30 min. The reaction solution was washed three times with water and the solution dried over anhydrous Na_2SO_4 and evaporated. The syrup obtained was distilled under reduced pressure to give **4**. A similar reaction of **5** gave **7**.

Preparation of 8. Procedure A. A solution of **2** (0.05 mol) and NaN_3 (0.15 mol) in HMPA (70 ml) was stirred at 30—35 °C for 24 h. The reaction solution was poured into ice-water (300 ml) and the aqueous solution extracted three times with benzene (60 ml). The benzene extracts were washed twice with water, dried over anhydrous $MgSO_4$, and evaporated under reduced pressure. The syrupy residue obtained was purified on a silica gel column using a mixture of hexane and benzene (2: 1 v/v) as eluentent to give **8**.

Procedure B. B-1: A solution of **3** (0.05 mol) and NaN_3 (0.15 mol) in HMPA (70 ml) was stirred at room temperature for 20 h. The reaction solution was poured into ice-water (300 ml) and the aqueous solution similarly worked up to give **8**. *B-2*: Similarly, **4** (0.05 mol) was treated with NaN_3 in DMF (70 ml) at 40—45 °C for 48 h to give **8**.

Procedure C. C-1: Similarly, **6** (0.05 mol) and NaN_3 (0.1 mol) in HMPA (70 ml) was worked up for 12 h to give **8**. *C-2*: To a solution of **7** (0.05 mol) in CH_2Cl_2 (50 ml) was added dropwise Et_3N (0.08 mol) with stirring under nitrogen below 5 °C. After stirring at room temperature for 30 min, the reaction solution was washed once with 3 M HCl and three times with water and dried over anhydrous $MgSO_4$. A similar work-up of the residual syrup gave pure **8**.

Procedure D. To a solution of **5** (0.05 mol) and mesyl chloride (0.06 mol) in CH_2Cl_2 (50 ml) was added dropwise Et_3N (0.15 mol) with stirring under nitrogen below 3 °C. After stirring at room temperature for 40 min, the precipitated salt was filtered off and the filtrate washed once with 3 M HCl and three times with water and dried over anhydrous $MgSO_4$. Finally, a similar purification gave **8**.

Preparation of 9. A solution of **8** (0.05 mol) in ether (30 ml) was added dropwise to a suspension of Al-Hg (made from 4 g of Al) in ether (50 ml) with vigorous stirring at room temperature. After a few minutes, the ether began to reflux, and the refluxing was maintained by the addition of a few drops of water at 20 min intervals. After the addition of the solution was completed, stirring was continued for 3 h. The mixture was extracted several times with an ether-ethyl acetate mixture (1: 3 v/v). The combined extracts were evaporated and distilled under reduced pressure to give **9**.

Preparation of 10. To a solution of **9** (0.02 mol) and Et_3N (0.025 mol) in dry ether (20 ml) was added chloroacetyl chloride (0.025 mol) dropwise with stirring at room temperature. After stirring for 4 h, the salt separating out was filtered. The filtrate was washed once with 3 M HCl, once with aqueous $NaHCO_3$, and twice with water and dried over anhydrous Na_2SO_4. The ether solution was evaporated to give a viscous syrup, which was purified on a silica-gel column using a benzene-acetone mixture (8: 1 v/v) as the eluentent. The fraction obtained was concentrated under reduced pressure to give **10**.

References

1) Part XVI: C. Shin, M. Yamaura, E. Inui, Y. Ishida, and J. Yoshimura, *Bull. Chem. Soc. Jpn.*, **51**, 2618 (1978).
2) B. W. Bycroft, *Nature*, **224**, 595 (1969).
3) M. Bodanszky and D. Perlman, *Nature*, **218**, 291 (1968).
4) E. Gross and J. L. Morell, *J. Am. Chem. Soc.*, **93**, 4634 (1971); E. Gross, H. H. Kiltz, E. Nebelin, *Hoppe-Seyler's Z. Physiol. Chem.*, **354**, 799 (1973).
5) J. M. Liesch and K. L. Rinehart, Jr., *J. Am. Chem. Soc.*, **99**, 1645 (1977).
6) C. Shin, Y. Yonezawa, and J. Yoshimura, *Chem. Lett.*, **1976**, 1063.
7) C. Shin, Y. Yonezawa, and J. Yoshimura, *Chem. Lett.*, **1976**, 1095.
8) H. Poisel, *Chem. Ber.*, **110**, 942 (1977).
9) U. Schmidt and E. Öhler, *Angew. Chem.*, **89**, 344 (1977); *Angew. Chem. Ind. Ed. Engl.*, **16**, 327 (1977).
10) C. Shin, M. Hayakawa, T. Suzuki, A. Ohtsuka, and J. Yoshimura, *Bull. Chem. Soc. Jpn.*, **51**, 550 (1978).
11) L. von Auwers and H. Wissebach, *Ber.*, **56**, 715 (1923).

Disproportionation of Propylene over MoO_3-SiO_2 Catalyst with Various Treatments

Toshiaki SODESAWA,*,** Eisuke OGATA, and Yoshio KAMIYA

Department of Reaction Chemistry, Faculty of Engineering, The University of Tokyo, Hongo, Bunkyo-ku, Tokyo 113

(Received August 25, 1978)

Disproportionation of propylene over MoO_3-SiO_2 (atomic ratio: Mo/Si=1/25) catalyst treated with HCl and aqueous ammonia was studied in the temperature range 350—600 °C under atmospheric pressure. The activity of MoO_3-SiO_2 catalyst extracted with aqueous ammonia remained for a long time, since most of free MoO_3 was removed from the MoO_3-SiO_2 surface. This gave rise to increase in the selectivity for disproportionation of propylene to ethylene and butenes and decrease in the selectivity for hydrogenation, isomerization and polymerization. When MoO_3-SiO_2 not subjected to treatment was pretreated by H_2 gas, it showed higher catalytic activity and lower selectivity for disproportionation than the one treated by N_2 gas.

In previous papers[1-4] we reported that MoO_3-Al_2O_3 shows high catalytic activity for the olefin disproportionation in the temperature range 100—200 °C and that Re_2O_7-Al_2O_3 has high catalytic activity even at ambient temperature. Ogasawara *et al.* reported that the pretreatment by H_2 gas makes active MoO_3-SiO_2 catalyst which has much free MoO_3 on its surface.[5] It is assumed that the free MoO_3 accompanies side reactions such as polymerization and hydrogenation which cause the catalytic degradation.[6] We have carried out disproportionation of propylene using MoO_3-SiO_2 catalyst treated with HCl and aqueous ammonia at relatively high temperatures.

The oxidation states of transition metal affect the catalytic activity of the disproportionation of olefins. It is known that MoO_3-Al_2O_3 catalyst is highly active even in hexa-valent state, and the lower the oxidation state of Mo, the greater the decrease in catalytic activity. It has been reported that the oxidation value of Mo over MoO_3-SiO_2 catalyst is lower than that over MoO_3-Al_2O_3.[7] We wish to consider the difference in oxidation state of Mo between the case of pretreatment of MoO_3-SiO_2 by H_2 and that by N_2.

Experimental

The MoO_3-SiO_2 catalyst was prepared by impregnating a $(NH_4)_6Mo_7O_{24}\cdot 4H_2O$ solution with silica which was evaporated to dryness "Snowtex" (Nissan Kagaku Co., Ltd.), and then by calcining in a flow of air at 550 °C for 5 h. The atomic ratio of Mo to Si was 1: 25, the same as that of Mo to Al, and Re to Al previously reported (A and B catalyst without treatment).[1-4]

The MoO_3-SiO_2 catalysts (C′, C″, C‴) were extracted with aqueous ammonia of various concentrations for 24 h. They were first filtered and washed with water, and then evaporated to dryness prior to calcination in a flow of air at 550 °C for 5 h. The catalysts (D′, D″) treated with HCl solution were evaporated to dryness in a flow of N_2 gas at 100 °C and then calcined at 550 °C for 1 h in a stream of air.

After pretreatment of the A catalyst with N_2 gas and the other catalysts with H_2 gas for 2 h, the reaction was carried out by the conventional fixed bed flow system with a U type reactor in the temperature range 350—600 °C. The reaction products were periodically analyzed by a gas chromatogram connected to the reaction system.

Results and Discussion

Effects of Various Treatments of MoO_3-SiO_2 on the Catalytic Activity. The profiles of the activity change of propylene disproportionation over MoO_3-SiO_2 catalyst with various treatments are shown in Fig. 1. In the initial reaction time, the catalytic activity for the disproportionation was in the order MoO_3-SiO_2 treated with HCl>MoO_3-SiO_2 without treatment>MoO_3-SiO_2 extracted with aqueous ammonia. The activity of catalysts extracted with aqueous ammonia differs greatly from that of catalysts not subjected to such treatment but treated with HCl solution. In the former case, the catalytic activity shows a maximum value at 25 min of the reaction time and then decreases gradually. Even after 20 h, its activity remains high. In the latter case

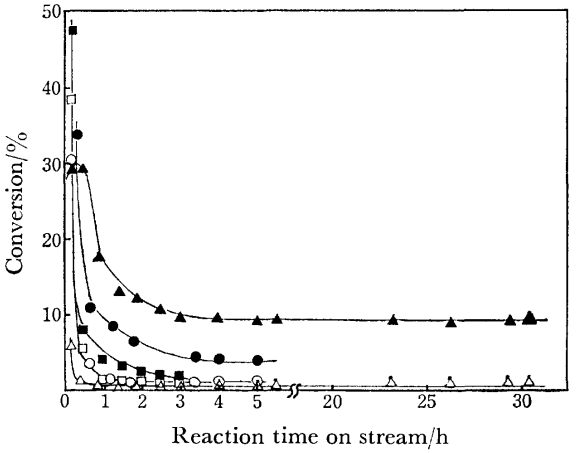

Fig. 1. Effect of various treatments of MoO_3-SiO_2 catalyst on the gas phase disproportionation of propylene at 500 °C and GHSV=60 (h^{-1}).
MoO_3-SiO_2 catalyst without treatment;
●: disproportionation, ○: hydrogenation.
MoO_3-SiO_2 catalyst extracted with 5 % aqueous ammonia;
▲: disproportionation, △: hydrogenation.
MoO_3-SiO_2 catalyst treated with 5 % HCl solution;
■: disproportionation, □: hydrogenation.

** Present address: Department of Industrial Chemistry, Faculty of Engineering, Chiba University, Yayoi-cho, Chiba 260.

the catalytic activity decreases rapidly with the reaction time. The catalytic activity for hydrogenation over MoO_3–SiO_2 extracted with aqueous ammonia was suppressed and the disproportionation to ethylene and butenes was promoted.

Effects of Reaction Temperature. In the temperature range 350—6000 °C, the activity for the disproportionation and hydrogenation of propylene changes within 60 min (Figs. 2—4). At all temperatures examined, the activity of the catalyst extracted with aqueous ammonia for the disproportionation shows a maximum value at 25 min. The new active sites seem to be formed by the reduction of the catalyst with H_2 or aqueous ammonia. At 600 °C, the catalytic activity remains unchanged during the course of reaction. At temperatures below 400 °C, the activity for the disproportionation becomes much lower. This indicates that the suitable reaction temperatures for the disproportionation are above 450 °C.

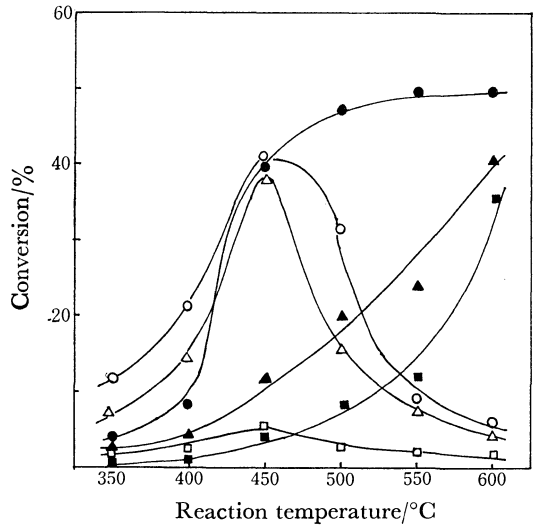

Fig. 2. Effect of temperature on the catalytic activity of MoO_3–SiO_2 without treatment in the gas phase disproportionation at GHSV=60 (h^{-1}).
Disproportionation; ●: 10 min, ▲: 25 min, ■: 60 min.
Hydrogenation; ○: 10 min, △: 25 min, □: 60 min.

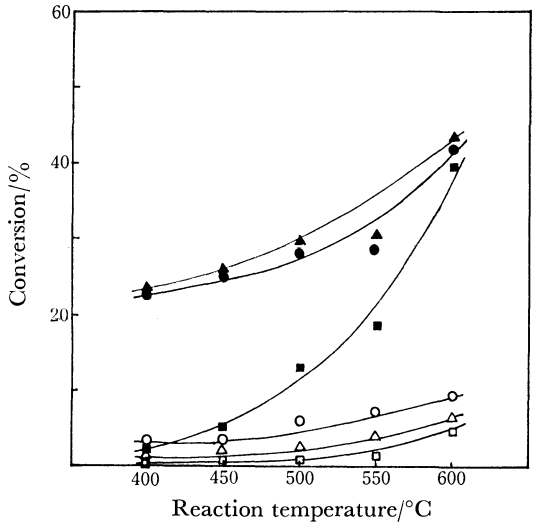

Fig. 3. Effect of temperature on the catalytic activity of MoO_3–SiO_2 extracted with 5 % aqueous ammonia in the gas phase disproportionation at GHSV=60 (h^{-1}).
Disproportionation; ●: 10 min, ▲: 25 min, ■: 60 min.
Hydrogenation; ○: 10 min, △: 25 min, □: 60 min.

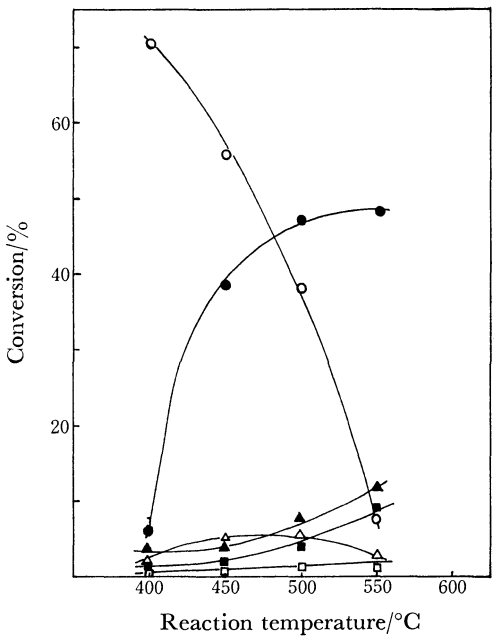

Fig. 4. Effect of temperature on the catalytic activity of MoO_3–SiO_2 treated with 5 % HCl solution in the gas phase disproportionation at GHSV=60 (h^{-1}).
Disproportionation; ●: 10 min, ▲: 25 min, ■: 60 min.
Hydrogenation; ○: 10 min, △: 25 min, □: 60 min.

The mode of activity change for hydrogenation reaction vary with catalyst. In the catalyst not subjected to treatment, the activity for the hydrogenation becomes maximum at 450 °C.

Effects of Concentration of Aqueous Ammonia. The initial activity of the catalyst extracted with various concentrations of aqueous ammonia is shown in Fig. 5.

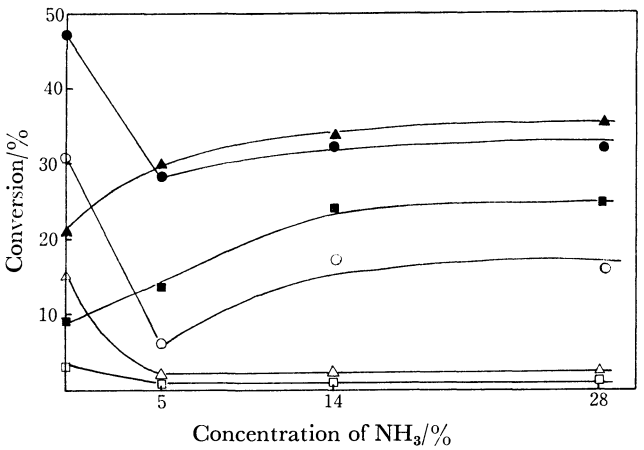

Fig. 5. Effect of concentration of aqueous ammonia on the catalytic activity of MoO_3–SiO_2 in the disproportionation of propylene at 500 °C and GHSV=60 (h^{-1}).
Disproportionation; ●: 10 min, ▲: 25 min, ■: 60 min.
Hydrogenation; ○: 10 min, △: 25 min, □: 60 min.

In each case, the catalytic activity after 10 min was lower than that not subjected to treatment. This seems to be due to the decrease of Mo metal by the extraction with aqueous ammonia. After 25 min the activity of the catalyst extracted with aqueous ammonia had higher value than that of the other catalysts. It seems that the hydrogenation over MoO_3–SiO_2 extracted with aqueous ammonia is suppressed, and the active sites for the disproportionation increase.

The hydrogenation decreased gradually with increase in reaction time. Yermakov *et al.* suggested that the oxidation state of Mo for the disproportionation or polymerization is +4, and that for hydrogenation is +2.[8] It seems that many active sites are formed for the disproportionation, the oxidation state of Mo being +4, but few for hydrogenation, the oxidation state of Mo being +2.

After removal of the free MoO_3 over MoO_3–SiO_2 catalyst by leaching with aqueous ammonia, the activity for the disproportionation remained unchanged as shown in Fig. 5. It is assumed that the increase in the acidity of the catalyst is due not to SiO_2 or MoO_3, but to the new acidic sites formed by the interaction of the two. The free MoO_3 can be extracted with aqueous ammonia. In the case of MoO_3–Al_2O_3 catalyst, 80% of free MoO_3 is removed from the catalyst surface, whereas in the MoO_3–SiO_2, 30% of free MoO_3 is taken off from the surface of MoO_3–SiO_2.[5] Vaghi *et al.* reported that the removal of polymolybdate by leaching with aqueous ammonia restores the activity in the tetrahedral Mo(VI) region, and the decomposition of the molybdosilicate anion occurs at pH 10.[9,10] From our results, it seems that leaching of MoO_3–SiO_2 with aqueous ammonia prefers the removal of free MoO_3 to the decomposition of Mo–O–Si bonds.

Product Distribution. An example of products distribution is given in Table 1. The catalysts extracted with aqueous ammonia (C′, C″, C‴) exhibit higher selectivity to ethylene and butenes as compared with the catalysts, the one without treatment and the other with treatment by HCl (D′, D″). On the other hand, the selectivity for hydrogenation of propylene to propane over MoO_3–SiO_2 extracted with aqueous ammonia is lower than that of the other catalysts. The isomerization of 2-butene to 1-butene produced *via* the disproportionation over the catalysts treated with aqueous ammonia decreases. This shows that the disproportionation over the catalysts subjected to aqueous ammonia extraction is promoted more selectively by suppression of self-hydrogenation or polymerization.[11,12]

The difference in products distribution between the catalyst pretreated by H_2 (A) and that by N_2 (B) shows that the oxidation state of Mo for each case is different. It may be assumed that the oxidation state of Mo in the case of H_2 becomes +4 according to Yermakov *et al.*[8]

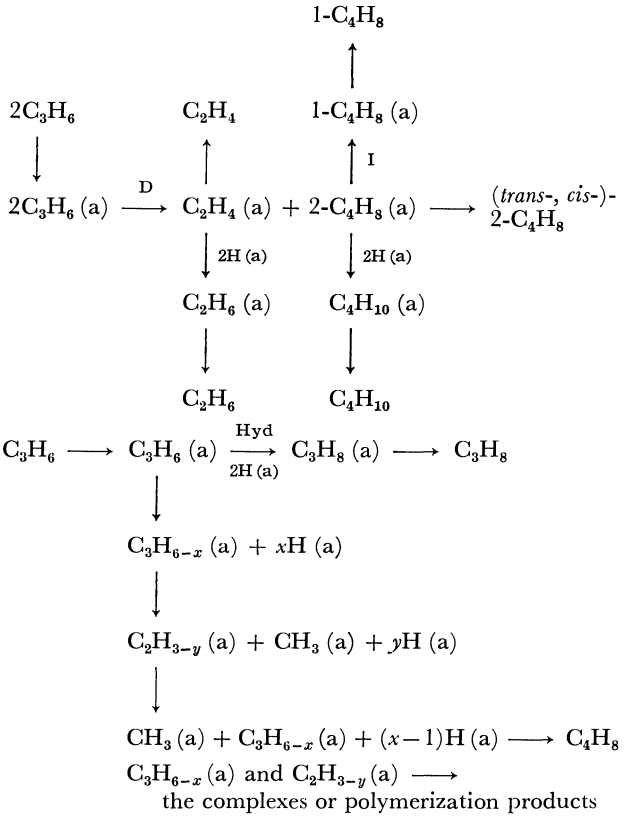

D: Disproportionation, I: isomerization, Hyd: hydrogenation, (a): adsorbed species.

Reaction Scheme.

Table 1. Products distribution in the gas phase disproportionation of propylene over MoO_3–SiO_2 catalyst at 500 °C and GHSV=60 (after 25 min of reaction)

Catalyst	A[a]	B[b]	C′[c]	C″[c]	C‴[c]	D′[d]	D″[d]
Conversion for disproportionation (%)	17.3	6.23	29.0	32.8	35.7	7.63	6.51
(C_2+C_2'+C_4+C_4') selectivity (%)	60.5	80.7	92.2	92.4	90.0	58.5	62.2
(C_4+C_4')/(C_2+C_2') ratio	0.183	0.231	0.757	0.603	0.641	0.172	0.153
C_4'/C_2' ratio	0.380	0.675	0.807	0.660	0.711	0.391	0.373
$C_2/(C_2+C_2')$ (%)	53.0	68.0	7.62	9.93	11.8	60.5	63.3
$C_4/(C_4+C_4')$ (%)	15.5	6.74	1.59	1.42	2.10	10.2	10.6
$1\text{-}C_4'/C_4'$ (%)	46.8	47.2	31.0	39.9	42.5	39.6	47.2
trans-/*cis*- ratio in $2\text{-}C_4'$	1.33	1.31	1.30	1.34	1.35	1.30	1.31
Conversion for hydrogenation (%)	15.2	1.42	0.90	1.55	2.38	5.29	3.80
C_3 selectivity (%)	40.7	18.5	3.31	4.53	6.26	40.9	36.9

a) Pretreated with H_2. b) Pretreated with N_2. c) Extracted with 5% aqueous ammonia (C′), 14% aqueous ammonia (C″), and 28% aqueous ammonia (C‴). d) Treated with 5% HCl (D′) and 14% HCl solution (D″).

Since the ratio of (C_4+C_4') to (C_2+C_2') is lower than C_4'/C_2' and the ratio of C_2 to (C_2+C_2') is larger than that of C_4 to (C_4+C_4'), hydrogenation of ethylene to ethane proceeds more rapidly than that of butenes to butane during the course of disproportionation. The ratio of *trans-* to *cis-* in 2-butenes approximates to equilibrium value at each reaction temperature.

In the catalyst subjected to aqueous ammonia extraction, the molar ratios C_4'/C_2' and $(C_4+C_4')/(C_2+C_2')$ in the temperature range 400—600 °C decrease with increase in the reaction temperature (Fig. 6). At all temperatures, the values increase with reaction time. In the initial reaction periods, the desorption of C_4 and C_4' from the catalyst surface is more difficult than that of C_2 and C_2', the decomposition of C_4 and C_4' proceeding very rapidly at high temperature.

The molar ratios C_4'/C_2' and $(C_4+C_4')/(C_2+C_2')$ for the catalysts treated with aqueous ammonia are greater than those not subjected to such treatment but treated with HCl. It seems that the active sites for disproportionation are formed. In the reaction below 450 °C, the ratio C_4'/C_2' or $(C_4+C_4')/(C_2+C_2')$ after 25 min of the reaction is approximately 1.0, indicating the most selective disproportionation.

The molar ratios of 1-butene in all butenes are shown in Fig. 7. At temperatures below 550 °C, each ratio in the catalyst extracted with aqueous ammonia is the lowest among the catalysts subjected to various treatments. The ratio in the case of the catalyst treated with HCl is lower than that of the catalyst not subjected to treatment. Decrease in the ratio in aqueous ammonia shows that acid sites are necessary for the isomerization over MoO_3–SiO_2 catalyst. On the other hand,

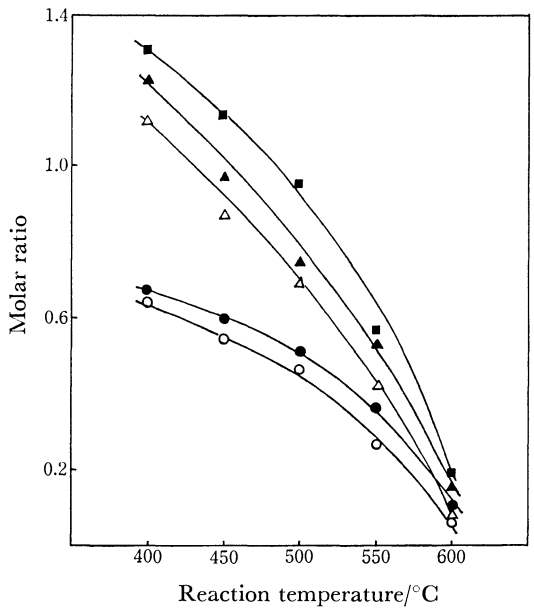

Fig. 6. Effect of temperature on C_4'/C_2' and $(C_4+C_4')/(C_2+C_2')$ molar ratio in the disproportionation of propylene over MoO_3–SiO_2 catalyst extracted with 5 % aqueous ammonia.
Reaction after 10 min; ●: C_4'/C_2', ○: $(C_4+C_4')/(C_2+C_2')$, 25 min; ▲: C_4'/C_2', △: $(C_4+C_4')/(C_2+C_2')$, 300 min; ■: C_4'/C_2'.

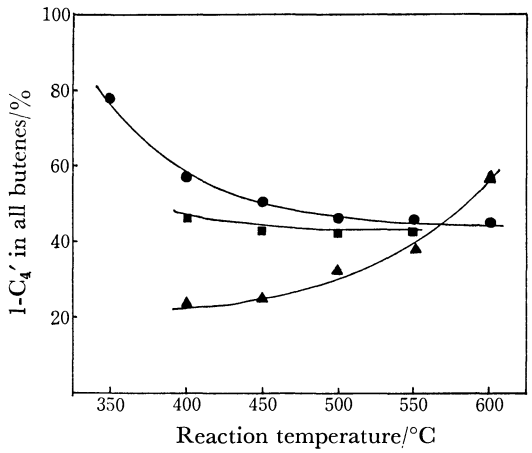

Fig. 7. Effect of temperature on molar ratio of 1-butene in all butenes in the gas phase disproportionation over MoO_3–SiO_2 catalyst at GHSV=60 (h^{-1}) after 25 minutes of reaction time.
●: MoO_3–SiO_2 catalyst. ▲: MoO_3–SiO_2 catalyst extracted with 5 % aqueous ammonia. ■: MoO_3–SiO_2 catalyst treated with 5 % HCl solution.

HCl which neutralizes basic sites is also effective for decreasing the isomerization activity of MoO_3–SiO_2 catalyst. This suggests that both acid and basic sites function effectively in isomerization of 2-butenes to 1-butene over MoO_3–SiO_2 catalyst.

The behavior of MoO_3–SiO_2 catalyst in the shift of the double bond from 2-butenes to 1-butene may be explained as follows.[13] The mechanism of this reaction involves the existence of an electron accepting (oxidative, *i.e.*, acid) center in the vicinity of the π-bond between carbons 2 and 3 and the presence of an electron donating (reducing, *i.e.*, basic) center in the vicinity of the σ-bond between carbons 1 and 2. The shift of the double bond is of a concerted type.

References

1) T. Sodesawa, E. Ogata, and Y. Kamiya, *Nippon Kagaku Kaishi*, **1975**, 1046.
2) E. Ogata, T. Sodesawa, and Y. Kamiya, *Bull. Chem. Soc. Jpn.*, **49**, 1317 (1976).
3) T. Sodesawa, E. Ogata, and Y. Kamiya, *Bull. Jpn. Petrol. Inst.*, **18**, 162 (1976).
4) T. Sodesawa, E. Ogata, and Y. Kamiya, *Bull. Chem. Soc. Jpn.*, **50**, 998 (1977).
5) S. Ogasawara, Y. Nakada, Y. Iwata, and H. Sato, *Kogyo Kagaku Zasshi*, **73**, 509 (1970).
6) S. Furukawa, Y. Kamiya, and N. Ohta, *Kogyo Kagaku Zasshi*, **74**, 2471 (1971).
7) R. Nakamura, Y. Morita, and E. Echigoya, *Nippon Kagaku Kaishi*, **1970**, 420.
8) Yu. I. Yermakov, B. N. Kuznetsov, and Yu. A. Ryndin, *J. Catal.*, **42**, 73 (1976).
9) A. Vaghi, A. Castellan, J. C. J. Bart, and N. Giordano, *J. Catal.*, **42**, 381 (1976).
10) A. Castellan, J. C. J. Bart, A. Vaghi, and N. Giordano, *J. Catal.*, **42**, 162 (1976).
11) M. Taniewski and M. Ofremba, *Tetrahedron Lett.*, **1967**, 1983.
12) J. W. Begley and R. T. Wilson, *J. Catal.*, **9**, 375 (1967).
13) A. Ghorbel, C. Houng-Van, and S. J. Teichner, *J. Catal.*, **33**, 123 (1974).

Syntheses of Several Muramyl Peptides in Relation to Chemical Structures of Less Immunoadjuvant Bacterial Cell Walls

Shoichi KUSUMOTO, Kazuhiro IKENAKA, and Tetsuo SHIBA*

Department of Chemistry, Faculty of Science, Osaka University, Toyonaka, Osaka 560

(Received September 21, 1978)

Various structural analogs of *N*-acetylmuramyl-L-alanyl-D-isoglutamine, which had been shown to be the minimum structure required for the immunoadjuvant activity of bacterial cell walls, were synthesized in order to investigate in more detail the relationship between the activity and chemical structures. Particularly, the compounds of the structures corresponding to the cell walls of special bacteria without immunoadjuvant activity were prepared in this study. Several novel procedures including the preparation of a branched glutamyl peptide were newly exploited to accomplish the syntheses of muramyl peptides with complicated structures. As a result of this synthetic study, new informations were obtained on the structural requirement for the immunoadjucant activity.

Since *N*-acetylmuramyl-L-alanyl-D-isoglutamine (MurNAc–L-Ala–D–Glu(OH)–NH_2)[1] (**1**) had been shown to be the minimum structure required for the immunoadjuvant activity of the bacterial cell walls,[2,3] investigations on the relationship between the structure and the adjuvant activity from the view point of synthetic approaches were much urged. In fact, we reconfirmed the more significance of the structure of MurNAc–L-Ala–D-Glu(OH)–NH_2 (**1**) by comparison with various synthetic analogs.[2]

Thereafter, we extended the study in the above line to the investigation on the structural relation of adjuvant inactive cell walls. According to the recent study of Kotani *et al.*,[4] there have been known quite a few bacteria whose cell walls do not show the immunoadjuvant activity, although usual bacteria possess the significant activities. It should be noted that most of inactive bacteria belong to plant pathogenic ones and are not familiar to mammals. Although MurNAc–L-Ala–D-Glu(OH)–NH_2 (**1**) mentioned above is the common structural unit in many bacterial peptidoglycan, a number of variations are often encountered especially in adjuvant inactive bacteria, for instance, replacement of L-Ala with Gly or L-Ser residue, or linkage of α-carboxyl group of D-Glu residue to the other amino acid.[5] In these respects, we synthesized now *N*-acetyl-

Table 1. Synthetic *N*-acetylmuramyl peptides

MurNAc peptides		Corresponding original bacterium[b]
MurNAc-L-Ala-D-Glu(OH)–NH_2[a]	(**1**)	*Staphylococcus aureus*
MurNAc-L-Ala-D-Glu(–L-Lys-D-Ala-OH[a])–NH_2		*Staphylococcus aureus*
MurNAc– Gly– D -Glu(OH)–NH_2	(**2c**)	*Microbacterium lacticum*[c]
MurNAc-L-Ser-D-Glu(OH)–NH_2	(**3c**)	*Eubacterium limosum*[c]
MurNAc-D-Ala-D-Glu(OH)–NH_2	(**4c**)	
MurNAc-L-Ala-D-Glu(OH)–Gly–OH	(**5c**)	*Micrococcus lysodeikticus*
MurNAc-L-Ala-D-Glu(–L-Lys-D-Ala-OH)–Gly–OH	(**6c**)	*Micrococcus lysodeikticus*
MurNAc–Gly– D -Glu(OH)–Gly–OH	(**7c**)	*Corynebacterium poinsettiae*
MurNAc-L-Ala-D-Glu(OH)–D-Ala–NH_2	(**8c**)	*Arthrobacter* sp. (NCIB 9423)
MurNAc-L-Ala-D-Glu(OH)–Gly–NH_2	(**9c**)	*Arthrobacter atrocyaneus*

a) These are prepared in our previous study. See Ref. 2b in the text. b) The names of the corresponding representative bacteria are given, that have the partial structure mentioned in each line. See Ref. 9. c) In the cell walls of these bacteria, the α-carboxyl group of glutamic acid does not exist actually as a simple amide but further links with a basic amino acid participating in a cross linkage.

muramyl peptides corresponding to the partial structures of inactive cell walls in order to investigate whether changes in rather small moieties are reflected in the inactivities of cell walls.

The *N*-acetylmuramyl peptides (**2c**—**9c**) prepared in this study are summarized in Table 1 together with the names of the representative bacteria in which the corresponding structures are involved. For the synthesis of these compounds, the same strategy was employed as described previously for the muramyl dipeptide (**1**).[2] Thus, peptide portions (**2a**—**9a**) were prepared in principle by conventional methods using Boc[1] and Bzl[1] groups for amino and carboxyl protections, respectively. After removal of the *N*-terminal Boc groups, the resulting peptide benzyl esters were coupled with protected muramic acid, *i.e.*, 1-α-*O*-benzyl-4,6-*O*-benzylidene-*N*-acetylmuramic acid (**10**), by means of the active ester method to give protected muramyl peptides (**2b**—**9b**), whose protecting groups were then removed simultaneously by catalytic hydrogenolysis. This procedure is illustrated for the preparation of **2c** in Fig. 1 for an example. In some syntheses, modifications were required as described below.

The first group of muramyl peptides (**2c**, **3c**, and **4c**) were synthesized in order to elucidate the role of the amino acid adjacent to the muramic acid moiety; the L-Ala residue in **1** was replaced with Gly or L-Ser as models of plant pathogenic and adjuvant-inactive cell walls and with D-Ala as non-natural peptidoglycan analog. Thus, the synthesis of MurNAc–L-Ser–D-Glu(OH)–NH_2 (**3c**) and MurNAc–D-Ala–D-Glu(OH)–NH_2 (**4c**) were performed in a similar manner to that illustrated for MurNAc–Gly–D-Glu(OH)–NH_2 (**2c**) (Fig. 1) except that the mixed anhydride method was used for the coupling of **10** with the peptide moieties.

In the another group of the analogs prepared so far, the α-carboxyl group of D-Glu is linked with an amino acid (**5c**, **6c**, and **7c**) or an amino acid amide (**8c** and **9c**) in place of ammonia in **1**. This type of variations has been mostly found also in adjuvant-inactive cell walls. For instance, the muramyl tri- and pentapeptides, *i.e.*, MurNAc–L-Ala–D-Glu(OH)–Gly–OH (**5c**) and MurNAc–L-Ala–D-Glu(L-Lys–D-Ala–OH)–Gly–OH (**6c**) are involved in the cell wall of *Micrococcus lysodeikticus* which shows exceptionally no adjuvant activity though this bacteria is familiar to human beings.

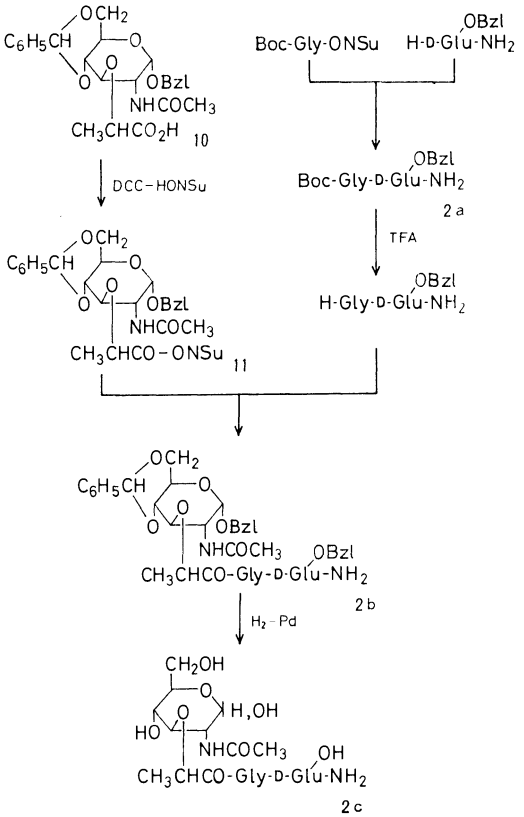

Fig. 1. Synthetic scheme for **2c**.

Though the compound **5c** was obtained according to usual series of reactions, some difficulty was encountered in the synthesis of muramyl pentapeptide (**6c**) particularly for a construction of the branched peptide structure at the D-Glu residue. Therefore, we improved a classical reaction of Boc-D-glutamic anhydride with H–Gly–OBzl to obtain the key intermediate Boc–D-Glu(OH)–Gly–OBzl (**13**) directly by a simple procedure. In this reaction, the isomeric γ-peptide, Boc–D-Glu(Gly–OBzl)–OH (**14**), formed simultaneously must be removed anyhow. LeQuesne and Young[6a] employed fractional extraction for this purpose, but their pro-

Table 2. Physical and analytical data of synthetic *N*-acetylmuramyl peptides

Compd[a]	Yield (%)	$[\alpha]_D$ [b] after 5 min	$[\alpha]_D$ [b] after 24 h	(*c*)	Molecular formula	Found (Calcd) C%	H%	N%
4c	97	+67°	+64°	(0.45)	$C_{19}H_{32}O_{11}N_4 \cdot 1/2H_2O$	45.58 (45.50	6.63 6.63	11.21 11.17)
5c	60	+42° [c]	+39° [d]	(0.48)	$C_{21}H_{34}O_{13}N_4 \cdot 3/4H_2O$	44.62 (44.72	6.30 6.34	10.51 9.93)
6c	90	+19°	+19°	(0.63)	$C_{30}H_{51}O_{15}N_7 \cdot 3/2H_2O$	46.54 (46.38	6.81 7.01	12.64 12.62)
7c	95	+45°	+42°	(0.54)	$C_{20}H_{31}O_{13}N_4 \cdot 3/4H_2O$	43.83 (43.75	5.95 5.97	10.27 10.21)
8c	98	+49°	+48°	(0.52)	$C_{22}H_{37}O_{12}N_4$	46.70 (46.88	6.60 6.62	12.36 12.43)
9c	94	+42°	+38°	(0.50)	$C_{21}H_{35}O_{12}N_5 \cdot H_2O$	44.31 (44.44	6.35 6.57	12.44 12.34)

a) All these compounds were obtained by precipitation from abs ethanol–abs ether followed by lyophilization. See Ref. 18 in the text. b) In H_2O at 25—28 °C. c) At 19 °C. d) At 15 °C.

cedure was too tedious to be applied in a preparative scale.[6b] We improved the procedure as follows. Boc-D-glutamic anhydride was added to a solution of H–Gly–OBzl in THF and the resulting mixture of α- and γ-peptides (**13** and **14**) was dissolved in ethyl acetate. On addition of 1 equivalent of DCHA[1] to this solution, the desired α-peptide (**13**) was obtained as pure DCHA salt in 60% yield, where the γ-peptide (**14**) remained in the mother liquor. The idea came from the method of a selective precipitation of α-esters of *N*-protected glutamic acid,[7] but no one has yet applied it in direct peptide formation. The structure of the α-peptide obtained was checked after deprotection by amino acid analyzer and TLC in comparison with the authentic free dipeptides, *i.e.*, H–D-Glu(OH)–Gly–OH (**15**) and H–D-Glu(Gly–OH)–OH (**16**), which were obtained *via* unequivocal ways (see experimental). Meanwhile, we recognized a fact that the amount of α-peptide (**13**) decreased slightly in the presence of DCHA as compared to that in its absence at the stage of anhydride ring opening. The ratio of α- and γ-peptides was measured for the reaction mixture of Boc–D-glutamic anhydride and H–Gly–OBzl after deprotection by amino acid analyzer. That in the presence of DCHA was actually 2.0: 1.0 and in its absence 2.6: 1.0. These ratios did not change in a range of the reaction temperature between −70 and 20 °C. Furthermore, the same technique in our method was also applicable to the reaction of Z-D-glutamic anhydride with H–Gly–OBzl as described in the experimental section. In this case, the pure γ-peptide, *i.e.*, Z–D-Glu(Gly–OBzl)–OH, could be also isolated from the mother liquor, besides the crystalline α-peptide DCHA salt.

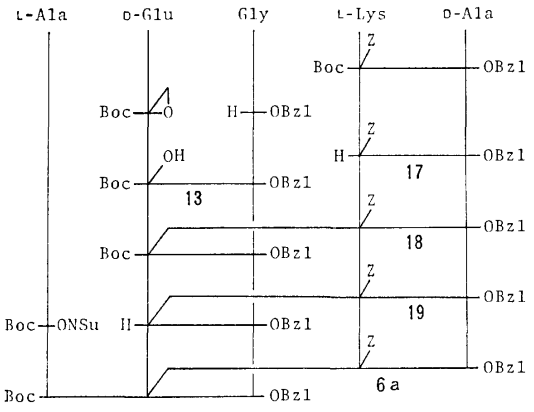

Fig. 2. Synthetic scheme for **6a**.

Concerning with the muramyl pentapeptide (**6c**), Boc–D-Glu(OH)–Gly–OBzl (**13**) was first condensed with H–L-Lys(Z)–D-Ala–OBzl (**17**) to give a branched tetrapeptide, *i.e.*, Boc–D-Glu(L-Lys(Z)–D-Ala–OBzl)–Gly–OBzl (**18**), whose Boc group was then selectively removed by treating with TFA (100 equivalents) at room temperature for 5 min.[8] The resulting H–D-Glu(L-Lys(Z)–D-Ala–OBzl)–Gly–OBzl (**19**) was successively coupled with Boc–L-Ala–OH. After removal of the Boc group, the product was condensed with the protected muramic acid 1-succinimidyl ester (**11**) to give the muramyl pentapeptide derivative (**6b**). Finally, hydrogenolysis of **6b** afforded MurNAc–L-Ala–D-Glu(L-Lys–D-Ala–OH)–Gly–OH (**6c**).

The muramyl tripeptide containing glycine, *i.e.*, MurNAc–Gly–D-Glu(OH)–Gly–OH (**7c**) was also prepared in a similar manner to that described above for **5c**.

Concerning with the syntheses of two muramyl tripeptides containing acid amide groups at their termini, *i.e.*, MurNAc–L-Ala–D-Glu(OH)–D-Ala–NH_2 (**8c**) and MurNAc–L-Ala–D-Glu(OH)–Gly–NH_2 (**9c**), the former (**8c**) could be prepared by conventional method starting from D-alanine amide, whereas a modified procedure should be used for the latter (**9c**) to avoid difficulties in experimental procedures due to high solubility of glycine amide derivatives in water. Thus, a tripeptide ester, *i.e.*, Boc–L-Ala–D-Glu(OBzl)–Gly–OEt (**22**), was first prepared by conventional method and its terminal ethyl ester was converted into amide function after selective removal of γ-benzyl ester group (Fig. 3). Other-

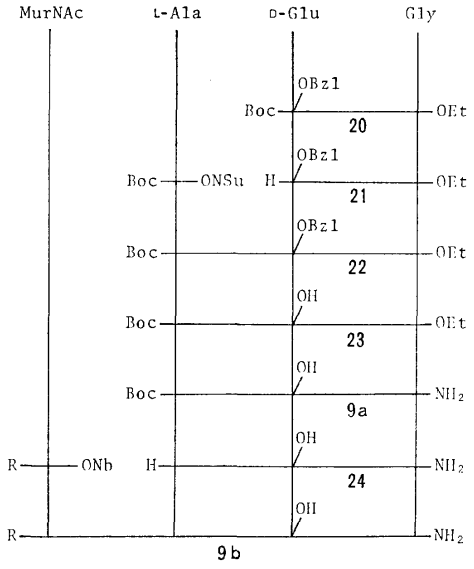

R = 1-α-*O*-benzyl-4,6-*O*-benzylidene

Fig. 3. Synthetic scheme for **9b**.

wise, α,γ-peptide migration would occur in the ammonolysis step. For the coupling of the protected muramic acid (**10**) with the ambient tripeptide, H–L-Ala–D-Glu(OH)–Gly–NH_2 (**24**) (Fig. 3), with less solubility in organic solvent and high solubility in aqueous media, we adopted HONb[1] ester method, particularly since this active ester has been known to afford relatively good yields in condensation in aqueous media.[9] In fact, the desired 1-α-*O*-benzyl-4,6-*O*-benzylidene-MurNAc-L-Ala-D-Glu(OH)-Gly-NH_2 (**9b**) was obtained in a satisfactory yield by this method. The product (**9b**) was then hydrogenolyzed to give the free *N*-acetylmuramyl tripeptide (**9c**). This advantageous method for the coupling of the active ester of muramic acid with a free peptide moiety was further utilized in our another synthesis of MurNAc–L-[U-^{14}C]Ala–D-Glu(OH)–NH_2 successfully.[10]

The immunoadjuvant activities of the muramyl pep-

tides (**2c**—**9c**) prepared above were measured by Kotani *et al.*[11,12] From these results, the relationship between the structure and the adjuvant activity had been already discussed.[11] For the reference, only the conclusion is now summarized as follows. i) The L-Ala residue in MurNAc–L-Ala–D-Glu(OH)–NH_2 (**1**) can be replaced with L-Ser without significant decrease in the activity. On the other hand, less activity is observed in the Gly analog and complete inactivity in the D-Ala analog. ii) Coupling of another amino acid residue at the α-carboxyl terminal of D-glutamic acid in **1** in place of the simple amide caused a remarkable decrease in the activity, while replacement with an amino acid amide kept the high activity. Therefore, the termination with an amide group in the molecule of muramyl peptide seems to be advisable in order to maintain the adjuvant activity in higher level.

Experimental

All melting points are uncorrected. Silica gel 60 (0.063—0.2 mm), Merck, was used for column chromatography and silica gel G, Merck, for thin layer chromatography. THF as solvent was purified by refluxing with $LiAlH_4$ followed by distillation and stored with Na-wire.

Boc–Gly–D-Glu(OBzl)–NH_2 (2a). Boc–Gly–ONSu (2.72 g, 10.0 mmol) was added to a mixture of H–D-Glu(OBzl)–NH_2·HCl (2.36 g, 8.7 mmol) and triethylamine (1.50 ml, 11.0 mmol) in THF (40 ml). After the usual work-up, the product was recrystallized from ethyl acetate–hexane; yield, 3.08 g (90%); mp 112—113 °C; $[\alpha]_D^{29}$ +4.95° (*c* 2.00, ethyl acetate).

Found: C, 57.76; H, 6.90; N, 10.64%. Calcd for $C_{19}H_{27}O_6N_3$: C, 58.00; H, 6.92; N, 10.68%.

1-α-O-Benzyl-4,6-O-benzylidene-MurNAc-Gly-D-Glu(OBzl)–NH_2 (2b). Compound **2a** (2.36 g, 6.0 mmol) was dissolved in TFA (6 ml) and allowed to stand at room temperature for 1 h. On addition of abs ether and hexane, an oily layer separated. The supernatant was removed by decantation, the remaining oil was dissolved in THF, and then the solvent was removed *in vacuo*. The residue solidified by drying over KOH *in vacuo*. It was triturated with abs ether and filtered to give H–Gly–D-Glu(OBzl)–NH_2 TFA salt; yield, 2.08 g (85%).

A solution of 1-α-*O*-benzyl-4,6-*O*-benzylidene-MurNAc-ONSu[2b] (**11**) (0.57 g, 1.0 mmol) in DMF (10 ml) was added to a solution of the TFA salt obtained above (0.41 g, 1.0 mmol) and triethylamine (0.14 ml, 1.0 mmol) in THF (15 ml) with stirring. After the mixture had been kept at room temperature overnight, THF was evaporated *in vacuo* and ethyl acetate was added to the remaining mixture. The resulting gelatinous solid was filtered and recrystallized from dioxane–water; yield, 0.57 g (75%); mp 234 °C (dec); $[\alpha]_D^{28}$ +82° (*c* 0.95, DMF).

Found: C, 61.50; H, 6.24; N, 7.40%. Calcd for $C_{39}H_{46}O_{11}N_4 \cdot H_2O$: C, 61.24; H, 6.33; N, 7.33%.

MurNAc–Gly–D-Glu(OH)–NH_2 (2c). A solution of **2b** (0.30 g, 0.39 mmol) in acetic acid (20 ml) was hydrogenolyzed in the presence of palladium black catalyst. After removal of the catalyst, the filtrate was diluted with water and then evaporated *in vacuo*. The residue was crystallized from methanol; yield, 0.19 g (quantitative); mp 234 °C (dec); $[\alpha]_D^{28}$ +35° (after 5 min), +33° (after 24 h) (*c* 0.46, H_2O).

Found: C, 44.08; H, 6.32; N, 11.55%. Calcd for $C_{18}H_{30}O_{11}N_4 \cdot 1/2H_2O$: C, 44.35; H, 6.41; N, 11.49%.

Boc–L-Ser–D-Glu(OBzl)–NH_2 (3a). A mixture of Boc–L-Ser–OH (1.54 g, 7.5 mmol), H–D-Glu(OBzl)–NH_2·HCl (2.04 g, 7.5 mmol), and *N*-methylmorpholine (0.82 ml, 7.5 mmol) in THF was treated with DCC (1.70 g, 8.2 mmol) and HOBt[1] (1.01 g, 7.5 mmol) under ice-cooling. After the usual work-up, the product was recrystallized form ethyl acetate–hexane; yield, 3.13 g (98%); mp 73—75 °C; $[\alpha]_D^{29}$ +0.70° (*c* 2.98, ethyl acetate).

Found: C, 56.61; H, 7.02; N, 9.90%. Calcd for $C_{20}H_{29}O_7N_3$: C, 56.72; H, 6.90; N, 9.92%.

1-α-O-Benzyl-4,6-O-benzylidene-MurNAc-L-Ser-D-Glu(OBzl)–NH_2 (3b). Compound **3a** (1.27 g, 3.0 mmol) was dissolved in TFA (3 ml) and set aside at room temperature for 35 min. Evaporation of TFA *in vacuo* afforded H–L-Ser–D-Glu(OBzl)–NH_2 TFA salt as a syrup, which was dried over KOH *in vacuo*. Ethyl chloroformate (0.29 ml, 3.0 mmol) was added to a solution of the protected *N*-acetylmuramic acid (**10**) (1.42 g, 3.0 mmol) and triethylamine (0.42 ml, 3.0 mmol) in THF (20 ml) at −19 °C. After being stirred at the same temperature for 15 min, a solution of the above TFA salt and triethylamine (0.42 ml, 3.0 mmol) in THF (15 ml) was added to the mixture, and stirring was continued overnight. Gelatinous solid obtained by addition of water was collected by filtration; yield, 1.95 g (82%). Recrystallization was effected from dioxane–water; mp 197 °C (dec); $[\alpha]_D^{28}$ +81.6° (*c* 1.12, DMF).

Found: C, 60.56; H, 6.19; N, 7.08%. Calcd for $C_{40}H_{48}O_{12}N_4 \cdot H_2O$: C, 60.44; H, 6.34; N, 7.05%.

MurNAc–L-Ser–D-Glu(OH)–NH_2 (3c). Compound **3b** (0.30 g, 0.38 mmol) was dissolved in acetic acid (35 ml) and hydrogenolyzed in the presence of palladium black catalyst. After addition of water, the solvent was evaporated *in vacuo* and the residue was precipitated from abs ethanol–abs ether to afford colorless hygroscopic solid. It was again dissolved in a small amount of water, and subjected to lyophilization;[13] yield, 0.11 g (55%); $[\alpha]_D^{28}$ +39° (after 5 min), $[\alpha]_D^{29}$ +35° (after 24 h) (*c* 0.49, H_2O).

Found: C, 44.29; H, 6.41; N, 10.91%. Calcd for $C_{19}H_{32}O_{12}N_4 \cdot 1/2H_2O$: C, 44.10; H, 6.43; H, 10.83%.

Boc–D-Ala–D-Glu(OBzl)–NH_2 (4a). This compound was prepared from Boc–D-Ala–OH (1.25 g, 6.6 mmol) and H–D-Glu(OBzl)–NH_2·HCl (1.79 g, 6.6 mmol) by means of the DCC–HONSu method in THF and recrystallized from ethyl acetate–hexane; yield, 2.33 g (87%); mp 130.5—131.5 °C; $[\alpha]_D^{29}$ +19.2° (*c* 1.88, ethyl acetate).

Found: C, 59.03; H, 7.20; N, 10.37%. Calcd for $C_{20}H_{29}O_5N_3$: C, 58.95; H, 7.17, N, 10.31%.

1-α-O-Benzyl-4,6-O-benzylidene-MurNAc–D-Ala-D-Glu(OBzl)–NH_2 (4b). Compound **4a** (1.22 g, 3.0 mmol) was treated with TFA (3 ml) and the resulting H–D-Ala–D-Glu(OBzl)–NH_2 was coupled with **10** (1.42 g, 3.0 mmol) by means of the mixed anhydride method as described for **3b**; yield, 1.69 g (73%). Recrystallization was effected from dioxane–water; mp 223 °C (dec); $[\alpha]_D^{28}$ +83.5° (*c* 1.09, DMF).

Found: C, 62.40; H, 6.39; N, 7.05%. Calcd for $C_{40}H_{48}O_{11}N_4 \cdot 1/2H_2O$: C, 62.40; H, 6.42; N, 7.28%.

MurNAc–D-Ala–D-Glu(OH)–NH_2 (4c) and Other MurNAc Peptides (5c—9c). These compounds were prepared by hydrogenolytic deprotection in acetic acid of **4b** and **5b**—**9b** whose syntheses are described below, followed by precipitation from abs ethanol–abs ether in a similar way to that for **3c**. The hygroscopic powders thus obtained were dissolved in water and lyophilized,[13] respectively. The yields, $[\alpha]_D$ values and the results of elemental analyses are summarized in Table 2.

Boc–D-Glu(OBzl)–Gly–OBzl (12). Boc–D-Glu(OBzl)–ONSu (8.69 g, 20.0 mmol) was added to a mixture of H–

Gly–OBzl·HCl (4.03 g, 20.0 mmol) and triethylamine (2.82 ml, 20.0 mmol) in THF (100 ml). After the usual work-up, the product was recrystallized from ethyl acetate–hexane; yield, 8.67 g (89%); mp 71—72 °C; $[\alpha]_D^{20}$ +6.99° (*c* 1.03, ethyl acetate).

Found: C, 64.07; H, 6.75; N, 5.83%. Calcd for $C_{26}H_{32}O_7N_2$: C, 64.45; H, 6.66; N, 5.78%.

*Boc–L-Ala–D-Glu(OBzl)–Gly–OBzl (**5a**).* The TFA salt of H–D-Glu(OBzl)–Gly–OBzl obtained from **12** (4.32 g, 8.9 mmol) was neutralized with triethylamine and then coupled with Boc–L-Ala–OH (1.70 g, 9.0 mmol) by means of DCC in a usual manner. The product was recrystallized from ethyl acetate–hexane; yield, 2.38 g (48%); mp 107 °C; $[\alpha]_D^{19}$ +6.5° (*c* 1.01, DMF).

Found: C, 62.68; H, 6.77; N, 7.63%. Calcd for $C_{29}H_{37}O_8N_3$: C, 62.69; H, 6.71; N, 7.56%.

*1-α-O-Benzyl-4,6-O-benzylidene-MurNAc-L-Ala-D-Glu(OBzl)-Gly-OBzl (**5b**).* Compound **5a** (0.28 g, 0.50 mmol) was treated with TFA as described in the synthesis of **3b**. The syrupy H–L-Ala–D-Glu(OBzl)–Gly–OBzl TFA salt solidified on trituration with abs ether. It was filtered and dried over KOH *in vacuo*. A mixture of **10** (0.24 g, 0.51 mmol), HONSu (0.063 g, 0.55 mmol) and DCC (0.10 g, 0.49 mmol) in THF was stirred under ice-cooling for 4 h. After *N,N'*-dicyclohexylurea had been filtered off, the filtrate was again cooled in an ice bath, and a solution of the TFA salt and triethylamine (0.70 ml, 0.50 mmol) in a small amount of THF was added. The mixture was stirred overnight, and gelatinous solid was collected by filtration and then recrystallized from dioxane–water; yield, 0.28 g (63%); mp 220 °C (dec); $[\alpha]_D^{19}$ +68° (*c* 0.49, DMF).

Found: C, 64.48; H, 6.23; N, 6.26%. Calcd for $C_{49}H_{56}O_{13}N_4$: C, 64.74; H, 6.21; N, 6.16%.

*Boc–D-Glu(OH)–Gly–OBzl (**13**) DCHA Salt.* A mixture of H–Gly–OBzl·HCl (8.87 g, 44.0 mmol) and triethylamine (6.20 ml, 44.0 mmol) in THF (100 ml) was stirred at room temperature for 3 h, and then triethylamine hydrochloride was filtered off. The filtrate was cooled in an ice bath and Boc-D-glutamic anhydride (9.17 g, 40.0 mmol) was added with stirring. After being stirred in an ice bath for 6 h, the solvent was evaporated *in vacuo*. The residue was dissolved in ethyl acetate, washed with 1 M citric acid and water, and dried over Na_2SO_4. After addition of DCHA (8.0 ml, 40 mmol), the mixture was left stand at room temperature to afford crude crystalline material, which was collected by filtration (20.1 g). This was recrystallized from methanol–ethyl acetate–hexane; yield, 12.40 g (53%); mp 164—167 °C. The mother liquor of the recrystallization was condensed *in vacuo*, and the residue was shaken with ethyl acetate and 1 M citric acid. The organic layer was washed with water, dried and again treated with DCHA (2.0 ml, 10 mmol) to give an additional amount of the product; 1.46 g (6%); mp 165.5—167.5 °C.

Found: C, 64.30; H, 8.67; N, 7.04%. Calcd for $C_{31}H_{49}O_7N_3\cdot 1/4H_2O$: C, 64.17; H, 8.60; N, 7.24%.

Compound **13** was hydrogenolyzed in the presence of palladium black and then treated with TFA to give a free dipeptide, which was identified with the authentic specimen of H–D-Glu(OH)–Gly–OH (**15**) described below by means of TLC and amino acid analysis.

*Determination of the Ratio of **13** to **14**.* A solution of H–Gly–OBzl (0.11 g, 0.55 mmol) in THF (3 ml) was prepared as above and stirred at −70, 0, or 20 °C with or without addition of DCHA (0.10 ml, 0.50 mol). Boc-D-glutamic anhydride (0.11 g, 0.50 mmol) was added to the solution and the mixture was stirred overnight. After the solvent was removed *in vacuo*, the residue was dissolved in ethyl acetate and washed with 1 M citric acid and water. Hydrogenolysis with palladium black followed by treatment with TFA at room temperature afforded a mixture of free dipeptide **15** and **16**, whose ratio was determined by means of amino acid analyser. The standard color values for each substance were obtained using the pure authentic samples described below.

DCHA Salts of Z–D-Glu(OH)–Gly–OBzl and Z–D-Glu(Gly–OBzl)–OH. For the synthesis of these compounds, a similar procedure to that described for **13** was employed. A solution of *Z*-D-glutamic anhydride (0.53 g, 2.0 mmol) in THF (10 ml) was added to an ice-cooled solution of H–Gly–OBzl (2.2 mmol) in THF (8 ml). After being stirred overnight, the mixture was worked up as above and dissolved in ethyl acetate. After addition of DCHA (0.40 ml, 2.0 mmol), the mixture was left stand in a refrigerator for 4 days to afford Z–D-Glu(OH)–Gly–OBzl DCHA salt; yield, 0.57 g (48%); R_f on TLC, 0.60 ($CHCl_3$–acetone–acetic acid, 16:4:1). When the mother liquor was seeded with Z–D-Glu(Gly–OBzl)–OH DCHA salt and again left stand in a refrigerator for further 2 days, the γ-peptide DCHA salt was solidified; yield, 0.52 g (43%); R_f on TLC, 0.50.

*H–D-Glu(OH)–Gly–OH (**15**).* *i) TFA Salt as a Standard Sample*: Boc–D-Glu(OBzl)–Gly–OBzl (**12**) (0.70 g, 1.4 mmol) was deprotected by hydrogenolysis followed by action of TFA to afford white precipitate; yield, 0.43 g (94%); mp 139—140 °C (dec); R_f on TLC, 0.41 (1-butanol–acetic acid–water, 4:1:2).

ii) From Z–D-Glu(OH)–Gly–OBzl DCHA Salt: This salt (0.30 g, 0.50 mmol) was washed with aqueous citric acid and hydrogenolyzed in ethyl acetate with palladium black. The product was recrystallized from water–ethanol–ether; yield, 0.070 g (68%); mp 177.5—178.5 °C (dec).

Found: C, 40.74; H, 5.98; N, 13.66%. Calcd for $C_7H_{12}O_5N_2\cdot 1/8H_2O$: C, 40.72; H, 5.98; N, 13.57%.

*H–D-Glu(Gly–OH)–OH (**16**).* *i) TFA Salt as a Standard Sample*: Coupling of Boc–D-Glu(OH)–OBzl derived from its DCHA salt (2.60 g, 5.0 mmol) with H–Gly–OBzl *p*-toluenesulfonate (1.69 g, 5.0 mmol) by means of ethyl chloroformate afforded Boc–D-Glu(Gly–OBzl)–OBzl, which was recrystallized from ethyl acetate–hexane; mp 98—99 °C.

Found: C, 64.42; H, 6.63; N, 5.81%. Calcd for $C_{26}H_{32}O_7N_2$: C, 64.45; H, 6.66; N, 5.78%.

This dipeptide (0.23 g, 0.47 mmol) was deprotected as described in the preparation of **15** to afford **16** TFA salt; yield, 0.14 g (94%); mp 42 °C (dec); R_f on TLC, 0.29 (1-butanol–acetic acid–water, 4:1:2).

ii) From Z–D-Glu(Gly–OBzl)–OH DCHA Salt: A similar procedure to that described above for **15** afforded a product, which was recrystallized from water–ethanol–ether; mp 196—197 °C (dec).

Found: C, 40.55; H, 5.90; N, 13.53%. Calcd for $C_7H_{12}O_5N_2\cdot 1/8H_2O$: C, 40.72; H, 5.98; N, 13.57%.

*H–L-Lys(Z)–D-Ala–OBzl (**17**) HCl Salt.* A 2 M solution of dry HCl in ethyl acetate (60 ml, 120 mmol) was added to a solution of Boc–L-Lys(Z)–D-Ala–OBzl[2b] (8.21 g, 15.2 mmol) in ethyl acetate (70 ml) under ice-cooling. After the mixture had been kept at room temperature overnight, the crystalline product was filtered; yield, 7.00 g (95%); mp 142—144 °C.

Found: C, 59.51; H, 6.70; N, 8.73; Cl, 7.42%. Calcd for $C_{24}H_{32}O_5N_3Cl\cdot 1/4H_2O$: C, 59.74; H, 6.79; N, 8.71; Cl, 7.35%.

*Boc–D-Glu(L-Lys(Z)–D-Ala–OBzl)–Gly–OBzl (**18**).* A solution of **13** DCHA salt (1.20 g, 2.1 mmol) in $CHCl_3$ (30 ml) was shaken twice with 0.3 M citric acid solution, washed with water, dried over $MgSO_4$, and then added to a mixture of **17** HCl salt (1.00 g, 2.1 mmol) and triethylamine (0.29

ml, 2.1 mmol) in $CHCl_3$ (30 ml). To the total mixture was added DCC (0.50 g, 2.4 mmol) with stirring under ice-cooling. Stirring was continued at room temperature for 67 h with further addition of DCC (0.80 g, 3.9 mmol) during the first 48 h. After the usual work-up, the product was purified by silica gel column chromatography ($CHCl_3$–acetone, 1: 1), and then recrystallized successively from methanol–ether and ethanol–water; yield, 0.92 g (54%); mp 175.5—176 °C; $[\alpha]_D^{22}$ +1.9° (*c* 2.16, DMF).

Found: C, 62.92; H, 6.92; N, 8.69%. Calcd for $C_{43}H_{55}O_{11}N_5$: C, 63.14; H, 6.78; N, 8.56%.

Boc-L-Ala-D-Glu(L-Lys(Z)-D-Ala-OBzl)-Gly-OBzl (**6a**). Compound **18** (0.87 g, 1.1 mmol) was dissolved in TFA (8 ml). After 2.5 min at room temperature, abs ether and hexane were added to the mixture. The resulting gelatinous precipitate was crystallized from abs ethanol–ethyl acetate–hexane to give **19** TFA salt; yield, 0.86 g (98%).

To a suspension of **19** TFA salt (0.40 g, 0.48 mmol) obtained above in THF (20 ml) was added 1 M triethylamine in THF (0.48 ml, 0.48 mmol). The mixture was then cooled in an ice bath and Boc-L-Ala-ONSu (0.29 g, 1.0 mmol) was added. After being stirred overnight, the insoluble gelatinous solid was filtered and washed successively with acetone, water, acetone and then ether; yield, 0.29 g (67%); mp 173—174 °C (with softening at 167 °C); $[\alpha]_D^{26}$ +0.50° (*c* 1.99, DMF).

Found: C, 61.58; H, 6.82; N, 9.27%. Calcd for $C_{46}H_{60}O_{12}N_6$: C, 62.14; H, 6.80; N, 9.45%.

1-α-O-Benzyl-4,6-O-benzylidene-MurNAc-L-Ala-D-Glu(L-Lys(Z)-D-Ala-OBzl)-Gly-OBzl (**6b**). Compound **6a** (0.30 g, 0.34 mmol) was dissolved in TFA(2.5 ml). After 2.5 min at room temperature, abs ether was added and the precipitate of the TFA salt was filtered. It was dissolved in DMF (30 ml), treated with 1 M triethylamine in THF (0.32 ml, 0.32 mmol), and then cooled in an ice bath. 1-α-*O*-Benzyl-4,6-*O*-benzylidene-MurNAc-ONSu (**11**) (0.28 g, 0.50 mmol) was added to the cooled solution, and the mixture was stirred overnight. The insoluble solid was filtered and washed with THF; yield, 0.22 g. An additional amount of the product (0.12 g) was recovered by condensation of the mother liquor *in vacuo* followed by removal of THF-soluble materials from the residue. The combined products were reprecipitated from dioxane–water; yield, 0.30 g (75%); mp 220 °C (dec); $[\alpha]_D^{25}$ + 56° (*c* 0.50, DMA).

Found: C, 63.37; H, 6.47; N, 7.70%. Calcd for $C_{66}H_{79}O_{17}N_7 \cdot 1/2H_2O$: C, 63.34; H, 6.44; N, 7.84%.

Boc-Gly-D-Glu(OBzl)-Gly-OBzl (**7a**). After removal of the Boc group in **12** (2.42 g, 5.0 mmol) with TFA (4 ml) in a usual way, the resulting TFA salt was dissolved in THF (30 ml). To the solution were added *N*-methylmorpholine (0.55 ml, 5.0 mmol), Boc-Gly-ONSu (1.50 g, 5.5 mmol) and K_2CO_3 (0.5 g) under ice-cooling. The mixture was worked up as usual and then subjected to silica gel column chromatography. Elution with benzene–ethyl acetate (3: 1) gave pure **7a** as a syrup; yield, 2.1 g (78%). The structure was confirmed by means of NMR spectrum.

H-Gly-D-Glu(OBzl)-Gly-OBzl. *i) HCl Salt*: Compound **7a** (80 mg, 0.15 mmol) was treated with 2 M dry HCl in ethyl acetate (1 ml) in a usual way and the product was recrystallized from methanol–ether; yield, 60 mg (84%); mp 133—134 °C; $[\alpha]_D^{30}$ +13.7° (*c* 1.74, methanol).

Found: C, 57.53; H, 5.88; N, 8.77; Cl, 7.38%. Calcd for $C_{23}H_{28}O_6N_3Cl$: C, 57.80; H, 5.91; N, 8.79; Cl, 7.42%.

ii) TFA Salt: Compound **7a** (80 mg, 0.15 mmol) was treated with TFA (1 ml), and the product was recrystallized from THF–abs ether; yield, 80 mg (97%); mp 84 °C (dec). This substance was identified with the HCl salt mentioned above on TLC.

1-α-O-Benzyl-4,6-O-benzylidene-MurNAc-Gly-D-Glu(OBzl)-Gly-OBzl (**7b**). This compound was prepared in a similar manner to that described for **6b** from H-Gly-D-Glu(OBzl)-Gly-OBzl TFA salt (0.56 g, 1.0 mmol) and **11** (0.68 g, 1.2 mmol), and recrystallized from dioxane–water; yield, 0.70 g (78%); mp 203 °C.

Found: C, 63.94; H, 6.03; N, 6.23%. Calcd for $C_{48}H_{54}O_{13}N_4 \cdot 1/2H_2O$: C, 63.77; H, 6.13; N, 6.20%.

Boc-D-Glu(OBzl)-D-Ala-NH₂. This compound was prepared from Boc-D-Glu(OBzl)-ONSu (3.04 g, 7.0 mmol) and H-D-Ala-NH_2·HCl (0.93 g, 7.5 mmol) and recrystallized from ethyl acetate–hexane; yield, 2.57 g (90%); mp 139.5—140.5 °C.

Found: C, 58.94; H, 7.20; N, 10.19%. Calcd for $C_{20}H_{29}O_6N_3$: C, 58.95; H, 7.17; N, 10.31%.

Boc-L-Ala-D-Glu(OBzl)-D-Ala-NH₂ (**8a**). After removal of the Boc group in Boc-D-Glu(OBzl)-D-Ala-NH_2 (2.42 g, 5.9 mmol) with TFA (6 ml), the resulting TFA salt was treated with triethylamine (0.83 ml, 5.9 mmol) and Boc-L-Ala-ONSu (1.43 g, 5.0 mmol) in THF. The product was recrystallized from $CHCl_3$–hexane; yield, 2.35 g (98%); mp 182.5—183.5 °C (dec); $[\alpha]_D^{28}$ −4.98° (*c* 2.03, DMF).

Found: C, 57.73; H, 7.14; N, 11.61%. Calcd for $C_{23}H_{34}O_7N_4$: C, 57.72; H, 7.16; N, 11.71%.

1-α-O-Benzyl-4,6-O-benzylidene-MurNAc-L-Ala-D-Glu(OBzl)-D-Ala-NH₂ (**8b**). Compound **8a** (0.57 g, 1.2 mmol) was treated with TFA (2 ml) in a usual manner, and the resulting TFA salt was neutralized with triethylamine and coupled with **11** (0.57 g, 1.0 mmol) in a mixture of DMF (8 ml) and THF (30 ml) overnight. Water was added to the mixture to afford gelatinous solid, which was filtered and then washed with 0.2 M citric acid and water. Reprecipitation was carried out from dioxane–water; yield, 0.60 g (72%); mp 275 °C (dec); $[\alpha]_D^{28}$ +83° (*c* 0.10, DMF).

Found: C, 61.77; H, 6.40; N, 8.31%. Calcd for $C_{43}H_{52}O_{12}N_5$: C, 62.28; H, 6.42; N, 8.42%.

Boc-D-Glu(OBzl)-Gly-OEt (**20**). This compound was prepared from H-Gly-OEt·HCl (1.66 g, 11.9 mmol) and Boc-D-Glu(OBzl)-ONSu (5.18 g, 11.9 mmol) in THF and was recrystallized from CH_2Cl_2–hexane; yield, 3.96 g (79%); mp 71—72 °C; $[\alpha]_D^{25}$ +6.20° (*c* 2.34, ethyl acetate).

Found: C, 59.79; H, 7.14; N, 6.59%. Calcd for $C_{21}H_{30}O_7N_2$: C, 59.70; H, 7.16; N, 6.63%.

Boc-L-Ala-D-Glu(OBzl)-Gly-OEt (**22**). Compound **20** (3.00 g, 7.1 mmol) was treated with 1 M dry HCl in ethyl acetate (50 ml), and the product was crystallized from $CHCl_3$–ether to give H-D-Glu(OBzl)-Gly-OEt (**21**) HCl salt (2.15 g, 84%). This salt (2.00 g, 5.6 mmol) was neutralized with triethylamine and coupled with Boc-L-Ala-ONSu (1.63 g, 5.7 mmol) in a usual manner. The product was recrystallized from ethyl acetate–hexane; yield, 2.55 g, (92%); mp 104—105 °C; $[\alpha]_D^{28}$ +7.19° (*c* 2.31, ethyl acetate).

Found: C, 58.37; H, 7.13; N, 8.45%. Calcd for $C_{24}H_{35}O_8N_3$: C, 58.40; H, 7.15; N, 8.51%.

Boc-L-Ala-D-Glu(OH)-Gly-OEt (**23**) *DCHA Salt.* Compound **22** (1.03 g, 2.1 mmol) was hydrogenolyzed in the presence of palladium black in ethanol (30 ml). The product was dissolved in ethyl acetate, and DCHA (0.42 ml, 2.1mmol) and ether were added to the solution to afford **23** DCHA salt as colorless crystals; yield, 1.04 g (83%); mp 138—139 °C; $[\alpha]_D^{26}$ +3.1° (*c* 2.06, methanol).

Found: C, 58.94; H, 9.05; N, 9.42%. Calcd for $C_{29}H_{52}O_8N_4 \cdot 1/2H_2O$: C, 58.66; H, 9.00; N, 9.44%.

Boc-L-Ala-D-Glu(OH)-Gly-NH₂ (**9a**) *DCHA Salt.* DCHA salt of **23** (0.29 g, 0.49 mmol) was dissolved in methanol (15 ml). The solution was saturated with NH_3 and left stand at room temperature in a pressure bottle for 3 days. After

removal of the solvent *in vacuo*, the residue was triturated with ether to afford **9a** DCHA salt; yield, 0.28 g (quantitative). Recrystallization was effected from ethanol–ethyl acetate–ether; mp 183 °C (dec); $[\alpha]_D^{25}$ −10.5° (*c* 1.99, methanol).

Found: C, 57.61; H, 8.78; N, 12.57%. Calcd for $C_{27}H_{49}O_7N_5 \cdot 1/2H_2O$: C, 57.42; H, 8.92; N, 12.40%.

1-α-O-Benzyl-4,6-O-benzylidene-MurNAc-L-Ala-D-Glu(OH)-Gly-NH₂ (9b). A solution of **9a** DCHA salt (0.56 g, 1.0 mmol) in water was passed through a column of Dowex 50 (H^+ form). The column was washed with water, and the combined eluate and washings was condensed *in vacuo*. The residue was twice dissolved in abs ethanol and the solvent was evaporated *in vacuo* to remove water completely. The final residue was dissolved in TFA (2 ml) and allowed to stand at room temperature for 20 min. Addition of abs ether to the solution afforded white precipitate of H–L-Ala–D-Glu(OH)–Gly–NH_2 (**24**) TFA salt (0.35 g, 0.90 mmol). An aqueous solution of this TFA salt was adjusted to pH 8 by addition of aqueous 1 M K_2CO_3 solution and mixed with a solution of 1-α-*O*-benzyl-4,6-*O*-benzylidene-MurNAc-ONb (0.44 g, 0.70 mmol) in THF (10 ml). The reaction mixture was stirred at room temperature for 4.5 h, and then brought to pH 3 by addition of 2 M HCl. Water was added to the mixture to afford gelatinous solid, which was collected by filtration; yield, 0.39 g (76%). Reprecipitation was effected from DMF–ethanol; mp 240 °C (dec); $[\alpha]_D^{25}$ +100° (*c* 0.95, DMF).

Found: C, 57.10; H, 6.28; N, 9.55%. Calcd for $C_{35}H_{45}O_{12}N_5 \cdot 1/2H_2O$: C, 57.05; H, 6.29; N, 9.51%.

References

1) Abbreviations according to IUPAC-IUB comission, *J. Biol. Chem.*, **247**, 977 (1972), are used throughout. Boc: *t*-butoxycarbonyl, Z: benzyloxycarbonyl, Bzl: benzyl, DCC: dicyclohexylcarbodiimide, HONSu: *N*-hydroxysuccinimide, HOBt: 1-hydroxybenzotriazole, HONb: *N*-hydroxy-5-norbornene-2,3-dicarboximide, THF: tetrahydrofuran, DMF: *N,N*-dimethylformamide, DMA: *N,N*-dimethylacetamide, TFA: trifluoroacetic acid, DCHA: dicyclohexylamine.

2) a) S. Kotani, Y. Watanabe, F. Kinoshita, T. Shimono, I. Morisaki, T. Shiba, S. Kusumoto, Y. Tarumi, and K. Ikenaka, *Biken J.*, **18**, 105 (1975); b) S. Kusumoto, Y. Tarumi, K. Ikenaka, and T. Shiba, *Bull. Chem. Soc. Jpn.*, **49**, 533 (1976).

3) a) F. Ellouz, A. Adam, R. Ciorbaru, and E. Lederer, *Biochem. Biophys. Res. Commun.*, **59**, 1317 (1974); b) C. Merser, P. Sinaÿ, and A. Adam, *Biochem. Biophys. Res. Commun.*, **66**, 1316 (1975).

4) S. Kotani, Y. Watanabe, F. Kinoshita, K. Kato, K. H. Schleifer, and H. R. Perkins, *Biken J.*, **20**, 1 (1977).

5) K. H. Schleifer and O. Kandler, *Bacteriol. Rev.*, **36**, 407 (1972).

6) a) W. J. LeQuesne and G. T. Young, *J. Chem. Soc.*, **1952**, 24; b) T. Shiba, N. Yamakita, and T. Kaneko, *J. Inst. Polytech. Osaka City Univ.*, **5**, 144 (1956).

7) E. Krieger and H. Gibian, *Justus Liebigs Ann. Chem.*, **655**, 195 (1962).

8) Considerable cleavage of Z group was observed when **18** was treated with 10—15 equivalents of TFA at room temperature for 30 min.

9) M. Fujino, S. Kobayashi, M. Obayashi, T. Fukuda, S. Shinagawa, and O. Nishimura, *Chem. Pharm. Bull.*, **22**, 1857 (1974).

10) S. Kusumoto, K. Ikenaka, and T. Shiba, *Tetrahedron Lett.*, **1977**, 4055.

11) a) S. Kotani, Y. Watanabe, F. Kinoshita, I. Morisaki, K. Kato, T. Shiba, S. Kusumoto, Y. Tarumi, and K. Ikenaka, *Biken J.*, **20**, 39 (1977); b) S. Kotani, F. Kinoshita, Y. Watanabe, I. Morisaki, T. Shimono, K. Kato, T. Shiba, S. Kusumoto, K. Ikenaka, and Y. Tarumi, *Biken J.*, **20**, 125 (1977).

12) French authors also reported independently the activities and syntheses of four analogs (**2c**, **3c**, **4c**, and **5c**) which were the same to those described in this paper. A. Adam, M. Devys, V. Souvanavong, P. Lefrancier, J. Choay, and E. Lederer, *Biochem. Biophys. Res. Commun.*, **72**, 339 (1976). P. Lefrancier, J. Choay, M. Derrien, and I. Lederman, *Int. J. Peptide Protein Res.*, **9**, 249 (1977).

13) Samples of free *N*-acetylmuramyl peptides precipitated from ethanol–ether contained considerable amount of ethanol, which could not be otherwise removed.

Synthesis of a Protected Hexadecapeptide Corresponding to Positions 1—16 of Human Lysozyme

Shoko YOSHIMURA, Kunitatsu IZUMI, and Yasutsugu SHIMONISHI*

Institute for Protein Research, Osaka University, Yamada-kami, Suita, Osaka 565

(Received September 22, 1978)

For a semi-synthesis of human lysozyme by coupling its natural fragment with synthetic peptides, a protected hexadecapeptide corresponding to positions 1—16 of the enzyme was constructed from three protected peptide fragments (V, IX, and XII) by the conventional method in pure state on the basis of analyses.

Lysozyme, isolated from the urine of patients with monocytic or monomyelocytic leukemia[1] and from human milk,[2] is a basic single-chain protein, 130 amino acid residues in length, cross-linked by four disulfide bridges.[3-5] The three dimensional structure[6] of human lysozyme shows considerable homology with that of hen egg-white lysozyme, in spite of the insertion of a glycine residue between positions 47 and 48 and the substitutions of about 40% of the amino acid residues of the latter. The enzyme can be unfolded by reduction with dithiothreitol, and the rapid refolding of the reduced disordered enzyme can be achieved in a high yield in the presence of oxidized and reduced glutathione,[7] as in the case of hen egg-white lysozyme. Recently,[8] investigation was made on the influence of anhydrous liquid hydrogen fluoride (HF) on human lysozyme. It was found that the original intact lysozyme can be recovered in fair yield from HF-solutions of native lysozyme and its derivative substituted by the 2-chlorobenzyloxycarbonyl group.

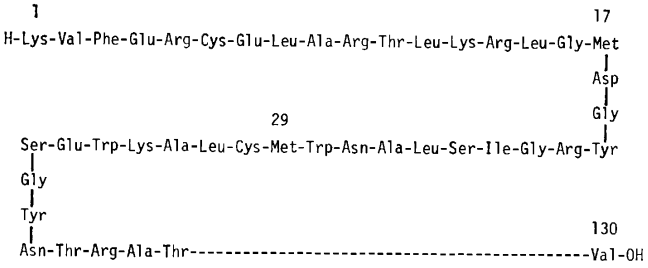

Fig. 1. N-Terminal region of human lysozyme.[3,4]

Human lysozyme contains two residues of methionine located in the N-terminal region of the peptide chain of the enzyme (Fig. 1). Cleavage by cyanogen bromide[9] of the methionyl bonds in the derivative[8] of the enzyme in which all the amino groups are substituted with 2-chlorobenzyloxycarbonyl group, followed by reductive alkylation[10] of the disulfide linkages gives a large fragment lacking the 29 amino acid residues at the N-terminal of the enzyne. The fragment seems to be a suitable material for a semi-synthesis[11,12] of the enzyme, because it has only one free amino group at the amino end. The coupling of the natural fragment with a synthetic peptide leads to the semi-synthesis of the enzyme. This prompted us to synthesize protected peptide fragments containing the N-terminal section of human lysozyme removed from the enzyme by cleavage with cyanogen bromide.

This paper describes the synthesis of a protected hexadecapeptide corresponding to positions 1—16 of human lysozyme. The procedure for synthesis of this peptide is outlined in Figs. 2—5. Figure 2 shows the synthesis of protected hexapeptide V with sqeuence [Lys[1]

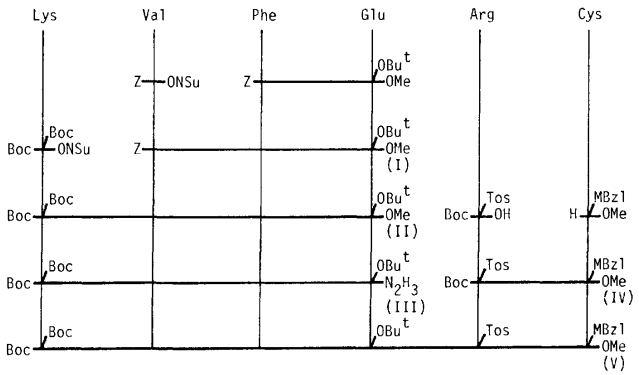

Fig. 2. Scheme for synthesis of sequence 1—6.

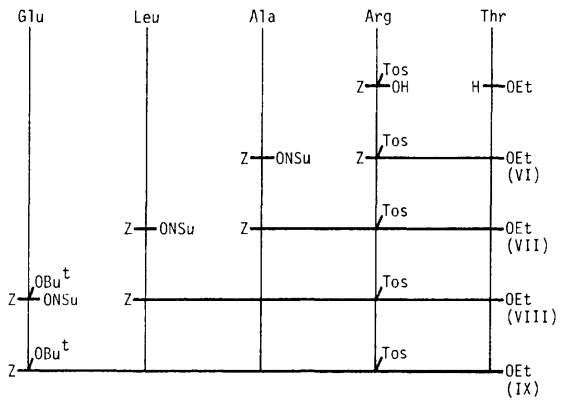

Fig. 3. Scheme for synthesis of sequence 7—11.

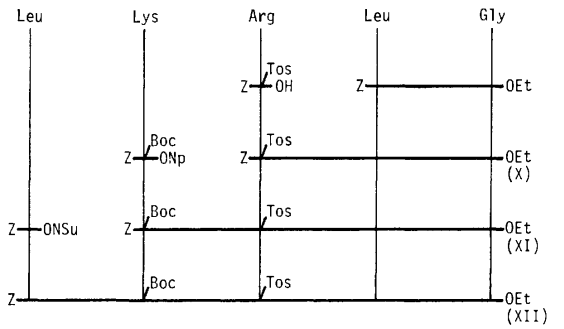

Fig. 4. Scheme for synthesis of sequence 12—16.

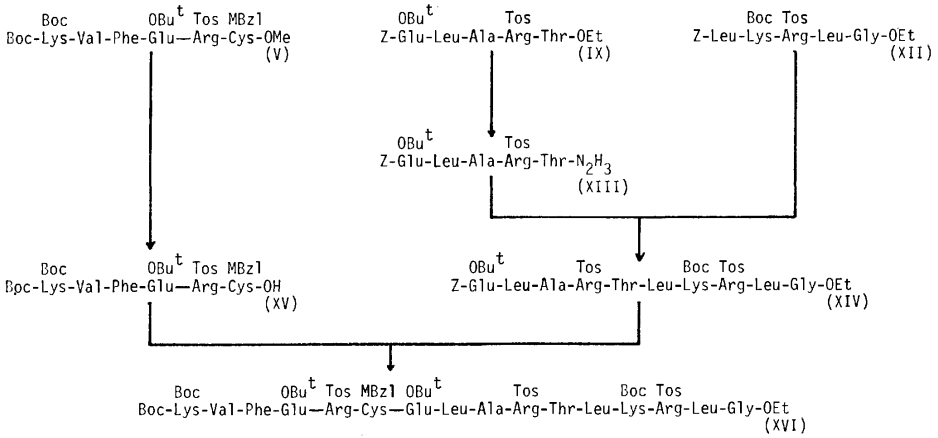

Fig. 5. Scheme for synthesis of the hexadecapeptide corresponding to positions 1—16 of human lysozyme.

to Cys[6].[13] Namely, Z–Phe–Glu(OBu^t)–OMe[14] was subjected to catalytic hydrogenation and the peptide ester obtained was not isolated but allowed to react with Z–Val–ONSu[15] to give Z–Val–Phe–Glu(OBu^t)–OMe (I). The protecting group was removed by catalytic hydrogenation and the resulting tripeptide methyl ester was condensed with Boc–Lys(Boc)–ONSu[12] to yield Boc–Lys(Boc)–Val–Phe–Glu(OBu^t)–OMe (II). The tetrapeptide methyl ester was converted to the corresponding hydrazide (III). Boc–Lys(Boc)–Val–Phe–Glu(OBu^t)–N_3 prepared from compound III was not isolated, but allowed to react directly with H–Arg(Tos)–Cys(MBzl)–OMe prepared by removal of the Boc group from Boc–Arg(Tos)–Cys(MBzl)–OMe (IV) by trifluoracetic acid. In this way Boc–Lys(Boc)–Val–Phe–Glu(OBu^t)–Arg(Tos)–Cys(MBzl)–OMe (V) was obtained.

Figure 3 illustrates the synthesis of protected pentapeptide IX with sequence [Glu[7] to Thr[11]]. First, Z–Arg(Tos)–OH·CHA[16] was condensed with HCl·H–Thr–OEt in the presence of HOBt by DCC.[17] Z–Arg(Tos)–Thr–OEt (VI) thus obtained was hydrogenated catalytically and then coupled with Z–Ala–ONSu[15] to give Z–Ala–Arg(Tos)–Thr–OEt (VII). The protecting group was removed by catalytic hydrogenation and the resulting tripeptide ethyl ester was condensed with Z–Leu–ONSu[15] to give Z–Leu–Ala–Arg(Tos)–Thr–OEt (VIII). The Z group was cleaved by catalytic hydrogenation and the tetrapeptide ethyl ester thus obtained was coupled with Z–Glu(OBu^t)–ONSu[18] to yield Z–Glu(OBu^t)–Leu–Ala–Arg(Tos)–Thr–OEt (IX).

As shown in Fig. 4, protected pentapeptide XII with sequence [Leu[12] to Gly[16]] was constructed by stepwise elongation using Z–Leu–Gly–OEt[19] as starting material. The Z group was removed by catalytic hydrogenation, and the resulting peptide ester was coupled with Z–Arg(Tos)–OH[16] in the presence of HOBt by DCC. The protected tripeptide ester (X) was hydrogenated catalytically, the peptide chain being elongated by stepwise acylation with Z–Lys(Boc)–ONp[20] and Z–Leu–ONSu.[15] The pentapeptide derivative, Z–Leu–Lys(Boc)–Arg(Tos)–Leu–Gly–OEt (XII), was thus obtained.

Construction of the sequence [Lys[1] to Gly[16]] was carried out as illustrated in Fig. 5. Namely, the pentapeptide ethyl ester (IX) was converted to the corresponding hydrazide (XIII) by usual hydrazinolysis. The hydrazide (XIII) was converted to the corresponding azide by the method of Honzl and Rudinger[21] and coupled directly with pentapeptide ethyl ester, which was obtained by removal of the Z group of pentapeptide ethyl ester (XII) by catalytic hydrogenation. The decapeptide derivative (XIV) thus obtained was then hydrogenated over a palladium-catalyst in DMF and the resulting decapeptide ester was coupled with hexapeptide acid (XV) in the presence of HOBt by DCC[17] prepared from the corresponding methyl ester (V) by saponification. However, the resulting material could not be easily purified. Therefore, the decapeptide derivative (XIV) was hydrogenated over a palladium-catalyst in methanol, the catalyst was filtered off and the filtrate was mixed with DMF. Only the methanol in the mixture was evaporated under reduced pressure, and the remaining solution was mixed with hexapeptide acid (XV), and treated under the same conditions as those described above. Thus, a protected hexadecapeptide (XVI) corresponding to positions 1—16 of human lysozyme, Boc–Lys(Boc)–Val–Phe–Glu(OBu^t)–Arg(Tos)–Cys(MBzl)–Glu(OBu^t)–Leu–Ala–Arg(Tos)–Thr–Leu–Lys(Boc)–Arg(Tos)–Leu–Gly–OEt, could be prepared in pure form. Investigations toward a semisynthesis of the enzyme by coupling its natural fragment with synthetic peptides given in this and the following[22] papers are in progress.

Experimental

All melting points were measured by the capillary method and are uncorrected. Thin layer chromatography was performed on silica gel G (Merck) using the following solvent systems (volume ratios); $CHCl_3$: MeOH: AcOH (95: 5: 3), AcOEt: benzene (1: 1), 1-butanol: AcOH: H_2O (4: 1: 1), and $CHCl_3$: MeOH : AcOH : H_2O (10 : 10 : 1 : 10, lower phase). Peptide derivatives were hydrolyzed in 6 M HCl with phenol in sealed tubes at 105 °C for 24 or 48 h, and the hydrolysates were analyzed in a Hitachi KLA-5 analyzer by the method of Moore *et al.*[23] The purity of the peptide derivatives synthesized was confirmed by thin layer chromatography and by the ratio of their constituent amino acids measured in acid hydrolysates by amino acid analysis. Optical

rotations of the peptide derivatives synthesized were measured with a Perkin-Elmer Model 241 polarimeter. The chemicals used in this paper were of reagent grade and were used without further purification. All the amino acids used except glycine were of the L-configuration.

Z-Val-Phe-Glu(OBu^t)-OMe (I). Z-Phe-Glu(OBu^t)-OMe[14] (14.7 g, 29.5 mmol) was dissolved in MeOH (400 ml), and hydrogenated at atmospheric pressure over 5% palladium-charcoal catalyst. The catalyst was filtered off and the filtrate was concentrated to an oil *in vacuo*. The oil was dissolved with Z-Val-ONSu[15] (10.3 g, 29.5 mmol) in $CHCl_3$ (200 ml). The solution was stirred overnight at room temperature and mixed with *N,N*-dimethyl-1,3-propanediamine (3 ml). After 1 h the solution was diluted with $CHCl_3$ and then washed successively with 0.1 M HCl, 5% aqueous $NaHCO_3$ and H_2O. The washed solution was dried over Na_2SO_4, and the dried solution was concentrated to a solid *in vacuo*. The solid was collected with $CHCl_3$ and ether, and then recrystallized from $CHCl_3$ and hexane; wt 15.5 g (85.6%), mp 175—178 °C, $[\alpha]_D^{25}$ −40.6° (*c* 0.6, MeOH).

Found: C, 64.14; H, 7.29; N, 7.06%. Calcd for $C_{32}H_{43}O_8N_3$: C, 64.30; H, 7.25; N, 7.03%.

Boc-Lys(Boc)-Val-Phe-Glu(OBu^t)-OMe (II). Compound I (11.9 g, 19.9 mmol) was dissolved in MeOH (350 ml), and hydrogenated at atmospheric pressure over 5% palladium-charcoal catalyst. The catalyst was filtered off and the filtrate was concentrated to an oil *in vacuo*. The oil was dissolved with Boc-Lys(Boc)-ONSu[12] (8.85 g, 19.9 mmol) in DMF (100 ml) under cooling. The solution was stirred at room temperature for 2 days, and then concentrated to a syrup *in vacuo*. The syrup was dissolved in $CHCl_3$ and washed successively with 0.1 M HCl, 5% aqueous $NaHCO_3$ and H_2O. The washed solution was dried over Na_2SO_4 and then concentrated *in vacuo* to an oil, which was repeatedly crystallized from EtOH and ether; wt 10.3 g (65.3%), mp 168—170 °C, $[\alpha]_D^{25}$ −43.5° (*c* 1.0, MeOH).

Found: C, 60.63; H, 8.30; N, 8.83%. Calcd for $C_{40}H_{65}O_{11}N_5$: C, 60.66; H, 8.27; N, 8.85%.

Boc-Lys(Boc)-Val-Phe-Glu(OBu^t)-N$_2$H$_3$ (III). Compound II (7.93 g, 10.0 mmol) was dissolved in DMF (56 ml) and mixed with 90% hydrazine hydrate (5.6 ml). The mixture was stirred at room temperature overnight, and concentrated *in vacuo* to a gelatinous residue, which was triturated with H_2O; wt 7.87 g (99.2%), mp 188.5—191 °C.

Found: C, 59.04; H, 8.32; N, 12.35%. Calcd for $C_{39}H_{65}O_{10}N_7$: C, 59.14; H, 8.27; N, 12.38%.

Boc-Arg(Tos)-Cys(MBzl)-OMe (IV). Boc-Arg(Tos)-OH[16] (4.14 g, 9.88 mmol) was added to a solution of HCl·H-Cys(MBzl)-OMe (3.50 g, 12.0 mmol) and TEA (1.68 ml) in DMF (50 ml), and cooled to −10 °C—−20 °C. HOBt (1.50 g, 11.1 mmol) and DCC (2.30 g, 11.2 mmol) were added to the cooled mixture. The mixture was stirred at the same temperature for 1 h and at 0 °C for 2 days. The precipitate formed was filtered off and the filtrate was concentrated to an oily residue *in vacuo*. The residue was dissolved in AcOEt and the solution was washed successively with 0.2 M HCl, 5% aqueous $NaHCO_3$ and H_2O. The washed solution was dried over Na_2SO_4 and then concentrated to an oil *in vacuo*. The oil was purified on a column of silica gel using a solvent mixture of AcOEt and benzene (1: 1, v/v). A syrupy material was obtained; wt 5.85 g.

Boc-Lys(Boc)-Val-Phe-Glu(OBu^t)-Arg(Tos)-Cys(MBzl)-OMe (V). Compound III (2.38 g, 3.00 mmol) was dissolved in DMF (17 ml), cooled below −20 °C and mixed with 4.60 M HCl in dioxane (2.50 ml). The solution was mixed with isopentyl nitrite (0.37 g, 3.15 mmol) and stirred at the same temperature for 45 min, the solution was then mixed with a solution in DMF (10 ml) of the material prepared by treatment of compound IV (2.55 g, *ca.* 3.9 mmol) with trifluoracetic acid (10 ml) at 0 °C for 60 min. The solution was made slightly basic by adding TEA below −30 °C, and stirred at 0 °C for a day. The precipitate formed was filtered off and the filtrate was concentrated to half its volume *in vacuo*, and then diluted with $CHCl_3$ under cooling. The diluted solution was washed successively with 0.3 M HCl, 5% aqueous $NaHCO_3$ and H_2O, and dried over Na_2SO_4 and concentrated to an oil *in vacuo*. The oil was solidified in AcOEt and hexane; wt 3.83 g. The crude product was recrystallized from MeOH; wt 2.65 g (66.6%), mp 217—218 °C (dec), $[\alpha]_D^{20}$ −23.0° (*c* 1.0, DMF). Amino acid ratio in the acid hydrolysate: Glu, 1.00 (1); Cys, 0.49 (1); Val, 0.89 (1); Phe 1.00 (1); Lys, 0.91 (1); Arg, 1.06 (1).

Found: C, 57.15; H, 7.28; N, 10.24; S, 4.71%. Calcd for $C_{64}H_{96}O_{16}N_{10}S_2\cdot H_2O$: C, 57.21; H, 7.35; N, 10.43; S, 4.77%.

Z-Arg(Tos)-Thr-OEt (VI). A solution of HCl·H-Thr-OEt (14.7 g, 80.0 mmol) in tetrahydrofuran (100 ml) was added to a suspension of Z-Arg(Tos)-OH·CHA[16] (42.0 g, 75.0 mmol) in tetrahydrofuran (300 ml). The resulting solution was mixed with HOBt (10.8 g, 80.0 mmol), cooled to −10 °C and then mixed with a solution of DCC (16.5 g, 80.0 mmol) in tetrahydrofuran (100 ml). The mixture was stirred at −10 °C for 1 h and then overnight at room temperature. The precipitate thus formed was filtered off and the filtrate was concentrated to a syrup *in vacuo*. The syrup was dissolved in AcOEt and washed successively with 0.5 M HCl, 5% aqueous $NaHCO_3$ and H_2O. It was then dried over Na_2SO_4 and concentrated to an oily residue *in vacuo*. The oily residue was purified on a column of silica gel using a mixture of AcOEt and benzene (1: 1, v/v). The purified material was solidified in $CHCl_3$ and ether; wt 37.0 g (83.5%), mp 64—66 °C, $[\alpha]_D^{24}$ −6.4° (*c* 1.1, MeOH).

Found: C, 54.39; H, 6.42; N, 11.60; S, 5.21%. Calcd for $C_{27}H_{37}O_8N_5S$: C, 54.81; H, 6.30; N, 11.84; S, 5.40%.

Z-Ala-Arg(Tos)-Thr-OEt (VII). Compound VI (30.0 g, 50.0 mmol) was dissolved in MeOH (800 ml) and hydrogenated at atmospheric pressure over 5% palladium-charcoal catalyst. The catalyst was filtered off and the filtrate was concentrated to an oil under reduced pressure. The oil was dissolved with Z-Ala-ONSu[15] (19.2 g, 60.0 mmol) in DMF (50 ml). The mixture was stirred at room temperature for a day, and concentrated to a residue under reduced pressure. The residue was dissolved in AcOEt, and washed successively with 0.5 M HCl, 5% aqueous $NaHCO_3$ and H_2O, and dried over Na_2SO_4. The dried solution was concentrated *in vacuo* to a syrup, which was solidified in a mixture of $CHCl_3$ and ether. The crude product was reprecipitated from a mixture of $CHCl_3$, MeOH, and ether; wt 26.5 g (80.2%), mp 66 °C (sintered), $[\alpha]_D^{24}$ −25.1° (*c* 0.9, MeOH).

Found: C, 54.10; H, 6.52; N, 12.74; S, 5.23%. Calcd for $C_{30}H_{42}O_9N_6S$: C, 54.37; H, 6.39; N, 12.68; S, 4.83%.

Z-Leu-Ala-Arg(Tos)-Thr-OEt (VIII). Compound VII (19.9 g, 30.0 mmol) was dissolved in MeOH (500 ml) and hydrogenated at atmospheric pressure over 5% palladium-charcoal catalyst. The catalyst was filtered off and the filtrate was concentrated to an oil under reduced pressure. The oil was dissolved with Z-Leu-ONSu[15] (13.0 g, 36.0 mmol) in DMF (65 ml). The solution was stirred at room temperature for 24 h, and then concentrated to a residue under reduced pressure. The residue was dissolved in AcOEt and washed successively with 0.7 M HCl, 5% aqueous $NaHCO_3$ and H_2O. The solution was dried over Na_2SO_4, and concentrated to a syrupy residue under reduced pressure. The residue was precipitated repeatedly with $CHCl_3$ and ether; wt 19.3 g

(82.6%), mp 80—85 °C, $[\alpha]_D^{24}$ −32.6° (*c* 1.0, MeOH).

Found: C, 54.44; H, 6.95; N, 12.48; S, 4.01%. Calcd for $C_{36}H_{53}O_{10}N_7S$: C, 54.46; H, 6.98; N, 12.35; S, 4.12%.

Z-Glu(OBu^t)-Leu-Ala-Arg(Tos)-Thr-OEt (IX). Compound VIII (15.5 g, 20.0 mmol) was dissolved in MeOH (350 ml) and hydrogenated at atmospheric pressure over 5% palladium-charcoal catalyst. The catalyst was filtered off and the filtrate was concentrated to a foaming residue *in vacuo*. The residue was dissolved with Z-Glu(OBu^t)-ONSu[18] (10.7 g, 24.0 mmol) in DMF (40 ml). The solution was stirred at room temperature for a day, and then concentrated to a residue *in vacuo*. The residue was dissolved in AcOEt, and washed successively with 0.5 M HCl, 5% aqueous $NaHCO_3$ and H_2O. The washed solution was dried over Na_2SO_4 and then concentrated *in vacuo* to a syrup, which was precipitated from a mixture of AcOEt, EtOH, and ether. The crude product was reprecipitated from the same solvent mixture; wt 13.3 g (69.3%), mp 151—153 °C, $[\alpha]_D^{24}$ −37.6° (*c* 0.9, MeOH). Amino acid ratio in the acid hydrolysate: Thr, 0.89 (1); Glu, 1.02 (1); Ala, 1.00 (1); Leu, 1.00 (1); Arg, 1.07 (1).

Found: C, 55.73; H, 7.18; N, 11.30; S, 3.02%. Calcd for $C_{45}H_{68}O_{13}M_8S\cdot 1/2H_2O$: C, 55.71; H, 7.17; N, 11.55; S, 3.33%.

Z-Arg(Tos)-Leu-Gly-OEt (X). Z-Leu-Gly-OEt[19] (17.5 g, 50.0 mmol) was dissolved in MeOH (500 ml) and hydrogenated at atmospheric pressure over 5% palladium-charcoal catalyst. The catalyst was filtered off and the filtrate was concentrated to a gelatinous solid *in vacuo*. The solid was dissolved with Z-Arg(Tos)-OH obtained from Z-Arg(Tos)-OH·CHA[10] (28.1 g, 50.0 mmol), and HOBt (8.1 g, 60.0 mmol) in tetrahydrofuran (400 ml) at 0 °C. The solution was cooled to −10 °C and mixed with a solution of DCC (12.4 g, 60.0 mmol) in tetrahydrofuran (150 ml). The mixture was stirred at −10 °C for 4 h and overnight at room temperature. The precipitate formed was filtered off and the filtrate was concentrated to a syrup *in vacuo*. The syrup was dissolved in AcOEt, and washed successively with 0.5 M HCl, 5% aqueous $NaHCO_3$ and H_2O. The washed solution was dried over Na_2SO_4, and concentrated to a syrup *in vacuo*. The syrup was purified by chromatography on a column of silica gel using a mixture of AcOEt and benzene (1: 1, v/v). The main fractions were collected and concentrated to a syrupy residue *in vacuo*. The residue was repeatedly precipitated from $CHCl_3$ and ether; wt 25.0 g (75.8%), mp 65—68 °C, $[\alpha]_D^{24}$ −24.8° (*c* 1.0, MeOH).

Found: C, 55.06; H, 6.62; N, 12.35; S, 4.77%. Calcd for $C_{31}H_{44}O_8N_6S\cdot H_2O$: C, 54.87; H, 6.83; N, 12.38; S, 4.84%.

Z-Lys(Boc)-Arg(Tos)-Leu-Gly-OEt (XI). Compound X (19.8 g, 30.0 mmol) was dissolved in MeOH (500 ml) and hydrogenated at atmospheric pressure over 5% palladium-charcoal catalyst. The catalyst was filtered off and the filtrate was concentrated to a syrup *in vacuo*. The syrup was dissolved with Z-Lys(Boc)-ONp[20] (16.5 g, 33.0 mmol) in DMF (100 ml). The solution was stirred at room temperature for a day and concentrated *in vacuo* to a syrupy residue, which was dissolved in AcOEt. The solution was washed successively with 1 M citric acid, 5% aqueous $NaHCO_3$ and H_2O, dried over Na_2SO_4, and concentrated *in vacuo* to a gelatinous solid, which was collected with a mixture of AcOEt, EtOH, and hexane. The crude material was recrystallized from the same mixture; wt 23.5 g (88.4%), mp 147—149 °C, $[\alpha]_D^{24}$ −20.4° (*c*, 1.0, DMF).

Found: C, 55.87; H, 7.24; N, 12.41; S, 3.52%. Calcd for $C_{42}H_{64}O_{11}N_8S\cdot 1/2H_2O$: C, 56.17; H, 7.30; N, 12.48; S, 3.60%.

Z-Leu-Lys(Boc)-Arg(Tos)-Leu-Gly-OEt (XII). Compound XI (17.8 g, 20.0 mmol) was dissolved in MeOH (500 ml) and hydrogenated at atmospheric pressure over 5% palladium-charcoal catalyst. The catalyst was filtered off and the filtrate was concentrated to a syrup *in vacuo*. The syrup was dissolved with Z-Leu-ONSu[15] (8.4 g, 22.0 mmol) in DMF (50 ml). The solution was stirred at room temperature for 36 h and concentrated to a syrup *in vacuo*. The syrup was dissolved in AcOEt, and washed successively with 5% aqueous $NaHCO_3$ and H_2O. The washed solution was dried over Na_2SO_4, and concentrated to a solid *in vacuo*. The solid was dissolved in a mixture of AcOEt and EtOH and precipitated by adding a mixture of ether and hexane. The crude product was reprecipitated from a mixture of EtOH, hexane and ether; wt 16.0 g (80.8%), mp 159—161 °C, $[\alpha]_D^{27}$ −18.8° (*c* 1.0, DMF). Amino acid ratio in the acid hydrolysate: Gly, 1.00 (1); Leu, 1.96 (2); Lys, 1.00 (1); Arg, 0.98 (1).

Found: C, 56.32; H, 7.44; N, 12.32; S, 3.13%. Calcd for $C_{48}H_{75}O_{12}N_9S\cdot H_2O$: C, 56.50; H, 7.61; N, 12.36; S, 3.19%.

Z-Glu(OBu^t)-Leu-Ala-Arg(Tos)-Thr-N_2H_3 (XIII). Compound IX (19.2 g, 20.0 mmol) was dissolved in a mixture of EtOH (200 ml) and DMF (50 ml) by gentle heating. The solution was cooled to 0—5 °C and mixed with 90% hydrazine hydrate (60 ml). The mixture was stirred at room temperature for a day and concentrated to a residue *in vacuo*. The residue was collected with ether, and reprecipitated from EtOH and ether. The crude material was redissolved in a mixture of DMF and EtOH, and reprecipitated by adding a mixture of hexane and ether; wt 16.9 g (89.9%), mp 125—128 °C, $[\alpha]_D^{24}$ −22.0° (*c* 1.0, DMF).

Found: C, 53.80; H, 7.19; N, 14.84; S, 3.32%. Calcd for $C_{43}H_{66}O_{12}N_{10}S\cdot H_2O$: C, 53.51; H, 7.19; N, 14.51; S, 3.38%.

Z-Glu(OBu^t)-Leu-Ala-Arg(Tos)-Thr-Leu-Lys(Boc)-Arg(Tos)-Leu-Gly-OEt (XIV). Compound XII (3.00 g, 2.94 mmol) was dissolved in MeOH (300 ml) and hydrogenated over 5% palladium-charcoal catalyst in a water bath at 35 °C. The catalyst was filtered off and the filtrate was mixed with DMF (5 ml). Only the methanol in the filtrate was evaporated off under reduced pressure and the remaining solution was left to stand in a refrigerator. Meanwhile, compound XIII (3.13 g, 3.24 mmol) was dissolved in DMF (12 ml) by gentle heating, cooled to −20 °C——30 °C, and mixed with 3 M HCl in dioxane (6 ml) and isopentyl nitrite (0.48 ml, 3.7 mmol). The solution was stirred at the same temperature for 45 min and mixed with the solution obtained above and TEA (2.5 ml). The mixture was stirred at 0 °C for 10 days in a refrigerator. The precipitate formed was filtered off and the filtrate was concentrated to a syrup *in vacuo*. The syrup was triturated in cold 0.2 M HCl (250 ml), filtered and washed well with H_2O. The crude material was repeatedly crystallized from MeOH; wt 1.89 g (35.7%), mp 224—226 °C, $[\alpha]_D^{24}$ −20.3° (*c* 0.50, dimethyl sulfoxide). Amino acid ratio in the acid hydrolysate: Glu, 1.05 (1); Leu, 3.01 (3); Ala, 0.95 (1); Arg, 1.94 (2); Thr, 1.02 (1); Lys, 1.03 (1); Gly, 1.00 (1).

Found: C, 54.55; H, 7.48; N, 13.19; S, 3.69%. Calcd for $C_{83}H_{131}O_{22}N_{17}S_2\cdot 2H_2O$: C, 54.80; H, 7.48; N, 13.09; S, 3.52%.

Boc-Lys(Boc)-Val-Phe-Glu(OBu^t)-Arg(Tos)-Cys(MBzl)-OH (XV). Compound V (5.29 g, 3.94 mmol) was dissolved in a mixture of MeOH (100 ml) and DMF (20 ml), mixed with 1 M NaOH (8 ml) in an ice-bath under cooling and stirred at room temperature for 3 h. The solution was made neutral by adding 1 M HCl and concentrated to a syrupy residue under reduced pressure. The residue was triturated in cold 0.2 M HCl (300 ml), filtered and washed well with H_2O. The crude material was repeatedly crystallized from MeOH and ether; wt 4.27 g (81.5%), mp 234—236

°C, $[\alpha]_D^{24}$ −13.6° (*c* 0.51, dimethyl sulfoxide).

Found: C, 56.83; H, 7.29; N, 10.45; S, 4.95%. Calcd for $C_{63}H_{94}O_{16}N_{10}S_2 \cdot H_2O$: C, 56.91; H, 7.28; N, 10.54; S, 4.81%.

Boc–Lys(Boc)–Val–Phe–Glu(OBu^t)–Arg(Tos)–Cys(MBzl)–Glu(OBu^t)–Leu–Ala–Arg(Tos)–Thr–Leu–Lys(Boc)–Arg(Tos)–Leu–Gly–OEt (XVI). Compound XIV (0.89 g, 0.49 mmol) was dissolved in MeOH (200 ml) and hydrogenated over 5% palladium–charcoal catalyst at 35 °C for 3 h in a water-bath. The catalyst was filtered off and the filtrate was mixed with DMF (4 ml). Only the methanol in the filtrate was evaporated *in vacuo*. The remaining solution was mixed with HOBt (0.14 g, 1.0 mmol) and compound XV (0.79 g, 0.59 mmol), cooled below −20 °C and mixed with DCC (0.15 g, 0.7 mmol). The mixture was stirred at −20 °C for 50 min and at room temperature for 2 days. The gelatinous mixture formed during the course of reaction was made clear by adding a small volume of dimethyl sulfoxide. The precipitate formed was filtered off and the filtrate was concentrated to a residue under reduced pressure. The residue was precipitated from MeOH and ether; wt 0.85 g. The crude product was reprecipitated from acetonitrile and MeOH; wt 0.57 g (39.6%), mp 244 °C (dec), $[\alpha]_D^{24}$ −22.0° (*c* 0.49, dimethyl sulfoxide). Amino acid ratio in the acid hydrolysate: Lys, 1.85 (2); Val, 0.88 (1); Phe, 0.95 (1); Glu, 2.23 (2); Arg, 3.00 (3); Cys, not determined; Leu, 3.11 (3); Ala, 1.00 (1); Thr, 1.10 (1); Gly, 0.97 (1).

Found: C, 56.02; H, 7.42; N, 12.80; S, 4.31%. Calcd for $C_{138}H_{217}O_{35}N_{27}S_4$: C, 56.33; H, 7.43; N, 12.85; S, 4.35%.

This work was supported by a Grant-in-Aid (247128, 1977) for Scientific Research from the Ministry of Education, Science and Culture.

References

1) E. Osserman and D. P. Lawlor, *J. Exp. Med.*, **124**, 921 (1966).
2) P. Jollès, *Angew. Chem.*, **81**, 244 (1969).
3) J. Jollès and P. Jollès, *Helv. Chim. Acta*, **52**, 2671 (1969); **54**, 2668 (1971).
4) R. E. Canfield, S. Kammerman, J. H. Sobel, and F. J. Morgan, *Nature New Biology*, **232**, 16 (1971).
5) J. Thomsen, E. H. Lund, K. Kristiansen, K. Brunfeld, and J. Malmquist, *FEBS Lett.*, **22**, 34 (1972).
6) C. C. F. Blake and I. D. A. Swan, *Nature New Biology*, **232**, 12 (1971).
7) D. B. Wetlaufer, E. R. Johnson, and D. M. Clauss, "Lysozyme," ed by E. F. Osserman, R. E. Canfield, and S. Beychok, Academic Press, New York and London (1974), p. 269.
8) M. Okamoto, S. Aimoto, and Y. Shimonishi, "Peptide Chemistry 1977," Proc. 15th Symposium on Peptide Chemistry, ed by T. Shiba, Osaka (1977), p. 205.
9) E. Gross and B. Witkop, *J. Am. Chem. Soc.*, **83**, 1510 (1961).
10) S. Aimoto and Y. Shimonishi, *Bull. Chem. Soc. Jpn.*, **51**, 205 (1978).
11) R. E. Goldberger and C. B. Anfinsen, *Biochemistry*, **1**, 401 (1962).
12) Y. Shimonishi, *Bull. Chem. Soc. Jpn.*, **43**, 3251 (1971).
13) The abbreviations used are those recommended by IUPAC-IUB: *J. Biol. Chem.*, **247**, 977 (1972). Additional abbreviations: MBzl, *p*-methoxybenzyl; CHA, cyclohexylamine; HOBt, 1-hydroxybenzotriazole; DCC, dicyclohexylcarbodiimide: DMF, *N*,*N*-dimethylformamide; TEA, triethylamine.
14) A. Ali and B. Weinstein, *J. Org. Chem.*, **36**, 3022 (1971).
15) G. W. Anderson, J. E. Zimmerman, and F. M. Callahan, *J. Am. Chem. Soc.*, **86**, 1839 (1964).
16) J. Ramachandran and C. H. Li, *J. Org. Chem.*, **27**, 4006 (1962).
17) W. König and R. Geiger, *Chem. Ber.*, **103**, 788 (1970).
18) J. Beacham, G. Dupuis, F. M. Finn, H. T. Storey, C. Yanaihara, N. Yanaihara, and K. Hofmann, *J. Am. Chem. Soc.*, **93**, 5526 (1971).
19) M. Bodanszky and V. du Vigneaud, *J. Am. Chem. Soc.*, **81**, 5688 (1959).
20) R. Schwyzer and W. Rittel, *Helv. Chim. Acta*, **44**, 159 (1961).
21) J. Honzl and J. Rudinger, *Collect. Czech. Chem. Commun.*, **26**, 2333 (1961).
22) S. Yoshimura and Y. Shimonishi, *Bull. Chem. Soc. Jpn.*, **52**, 1677 (1979).
23) S. Moore, D. H. Spackman, and W. Stein, *Anal. Chem.*, **30**, 1185 (1958).

Synthesis of a Protected Tridecapeptide Corresponding to Positions 17—29 of Human Lysozyme

Shoko YOSHIMURA and Yasutsugu SHIMONISHI*

Institute for Protein Research, Osaka University, Yamada-kami, Suita, Osaka 565

(Received September 22, 1978)

For a semi-synthesis of human lysozyme by coupling its natural fragment with synthetic peptides, a protected tridecapeptide corresponding to positions 17—29 of the enzyme was prepared from three protected peptide fragments (II, VI, and XI) by the conventional method in pure form on the basis of analyses.

Human lysozyme[1] contains two residues of methionine at the positions 17 and 29 of the peptide chain of the enzyme.[2,3] Cleavage by cyanogen bromide[4] of the methionyl bonds in the enzyme followed by reductive alkylation[5] of the disulfide linkages give a fragment lacking the 29 amino acid residues at the N-terminus of the enzyme. The natural fragment is considered to be a suitable material for a semi-synthesis,[6,7] as described in the preceding paper.[8] Coupling of the natural fragment with synthetic peptides *via* the formation of peptide linkages will give a covalent semi-synthesis of human lysozyme. For the aim, we have attempted to isolate the natural fragment[5] and synthesize complementary peptide fragments. The peptide fragments refer to the N-terminal region corresponding to positions 1—29 of human lysozyme, which is liberated from the enzyme by treatment with cyanogen bromide. The N-terminal section of the enzyme was divided into two parts and synthesized; a hexadecapeptide[8] corresponding to positions 1—16 and a tridecapeptide corresponding to positions 17—29. This paper reports the synthesis of the latter peptide.

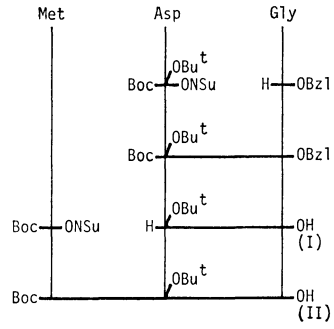

Fig. 1. Synthesis of sequence 17—19.

The peptide was constructed from three peptide fragments, Boc–Met–Asp(OBu^t)–Gly–OH (II),[9] Boc–Tyr–Arg(Tos)–Gly–Ile–Ser–OMe (VI), and Boc–Leu–Ala–Asn–Trp–Met–OMe (XI). The first fragment was synthesized by coupling Boc–Met–ONSu[10] with H–Asp–(OBu^t)–Gly–OH (I) (Fig. 1). The dipeptide (I) was obtained by the catalytic hydrogenation of the syrupy material, Z–Asp(OBu^t)–Gly–OBzl, which was prepared by condensing Z–Asp(OBu^t)–ONSu[11] with H–Gly–OBzl. The synthesis of the second fragment, Boc–Tyr–Arg(Tos)–Gly–Ile–Ser–OMe (VI), was started by coupling Z–Ile–ONp[12] with H–Ser–OMe (Fig. 2). Z–Ile–Ser–OMe (III) thus obtained was catalytically hydrogenated and the resulting dipeptide methyl ester was

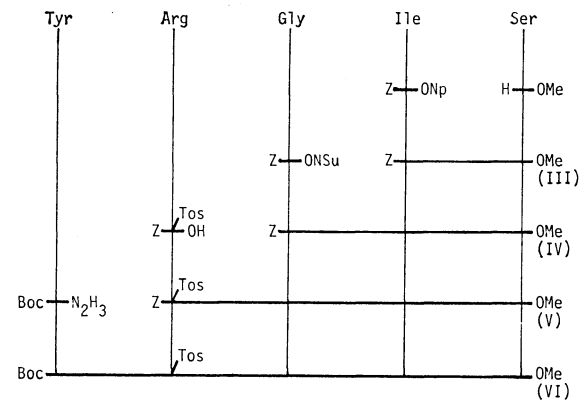

Fig. 2. Synthesis of sequence 20—24.

acylated with Z–Gly–ONSu[10] to give Z–Gly–Ile–Ser–OMe (IV). The tripeptide (IV) was catalytically hydrogenated and condensed with Z–Arg(Tos)–OH[13] by DCC in the presence of HOBt.[14] The resulting tetrapeptide, Z–Arg(Tos)–Gly–Ile–Ser–OMe (V), was catalytically hydrogenated. The tetrapeptide methyl ester was not isolated, but directly coupled with Boc–Tyr–N_3 prepared from the corresponding hydrazide,[15] to give Boc–Tyr–Arg(Tos)–Gly–Ile–Ser–OMe (VI).

For the synthesis of the last fragment, Boc–Leu–Ala–Asn–Trp–Met–OMe (XI), Boc–Asn–ONp[16] was first coupled with H–Trp–OMe. The resulting dipeptide, Boc–Asn–Trp–OMe (VII), was converted to the corresponding hydrazide (VIII) by usual hydrazinolysis. The hydrazide (VIII) was allowed to react with isopentyl nitrite by Rudinger's method,[17] the resulting

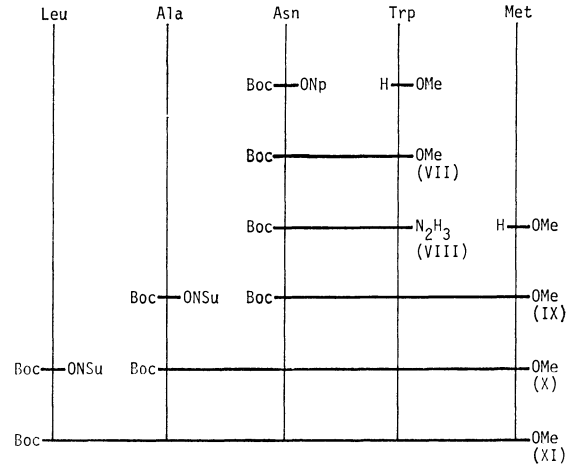

Fig. 3. Synthesis of sequence 25—29.

Table 1. Amino acid analyses of hydrolysates of oligopeptides containing the Asn–Trp linkage

1 2 3 4 5[a]	Acid hydrolysis[b]					Enzymatic hydrolysis				
	1	2	3	4	5	1	2	3	4	5
Boc–Asn–Trp–Gly–OEt			0.78	0.58	1.00					
H–Asn–Trp–Gly–OH			0.81	0.78	1.00			1.01	0.97	1.00
Z–Asn–Trp–Ile –OBzl			0.67	0.45	1.00					
Boc–Asn–Trp–Phe–OEt			0.65	0.50	1.00					
Z–Ala–Asn–Trp–OMe		1.00	0.82	—[c]						
Boc–Leu–Ala–Asn–Trp–OMe	0.97	1.00	0.69	—[c]						
Boc–Ala–Asn–Trp–Met–OMe		1.00	0.64	—[c]	0.59					
Boc–Leu–Ala–Asn–Trp–Met–OMe	0.99	1.00	0.48	—[c]	0.56					
	0.96	1.00	0.59	—[c]	0.59[d]					
H–Leu–Ala–Asn–Trp–Met–OH	0.92	1.00	0.84	—[c]	0.88	1.00	1.00	0.96	1.07	1.05
	0.92	1.00	0.79	—[c]	0.84[d]					

a) Residue number from N-terminus. b) Value obtained after hydrolysis for 24 h. c) Not determined.
d) Value obtained after hydrolysis for 72 h.

Table 2. Analytical data of synthetic peptides containing the Asn–Trp linkage

	Mp (°C)	$[\alpha]_D^{23}$		Analysis (%)		
				C	H	N
Boc–Asn–Trp–Gly–OEt	106—108	−21.9° (*c* 1.0, DMF)	Found	57.18	6.69	13.58
			Calcd	57.24	6.61	13.19
Z–Asn–Trp–Ile–OBzl	207—208	−18.9° (*c* 1.0, DMF)	Found	65.35	6.22	10.53
			Calcd	65.94	6.30	10.68
Boc–Asn–Trp–Phe–OEt	129—131	−31.8° (*c* 1.0, DMF)	Found	62.41	6.72	11.56
			Calcd	62.71	6.62	11.80
Z–Ala–Asn–Trp–OMe	162—165 (dec)	+11.2° (*c* 0.5, DMF)	Found	60.03	5.86	12.89
			Calcd	60.32	5.81	13.03
Boc–Leu–Ala–Asn–Trp–OMe	146 (sintered) 153 (melted and dec)	+0.2° (*c* 1.0, DMF)	Found	57.98	7.36	13.39
			Calcd	58.42	7.19	13.63

azide being condensed *in situ* with H–Met–OMe to give Boc–Asn–Trp–Met–OMe (IX). The tripeptide (IX) was treated with formic acid for removal of the Boc group, and elongated by two single-step reactions using Boc–Ala–ONSu[10] and Boc–Leu–ONSu[10] for acylation, the pentapeptide, Boc–Leu–Ala–Asn–Trp–Met–OMe (XI), thus being obtained (Fig. 3). Amino acid analysis of the acid hydrolysate of pentapeptide (XI) showed that the recovery of aspartic acid is low. The same phenomenon was observed on analyses of the acid hydrolysates of the peptides containing Asn–Trp linkage given in Table 1, which were synthesized separately (Table 2). In contrast, amino acid analyses of enzymatic[18] hydrolysates of the corresponding free peptides gave a theoretical recovery of asparagine. The results are summarized in Table 1.

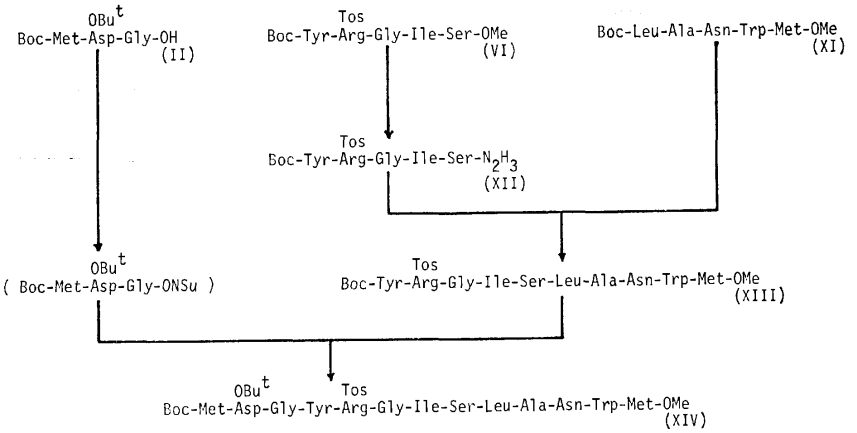

Fig. 4. Synthesis of the tridecapeptide corresponding to positions 17—29 of human lysozyme.

The tridecapeptide, Boc–Met–Asp(OBu^t)–Gly–Tyr–Arg(Tos)–Gly–Ile–Ser–Leu–Ala–Asn–Trp–Met–OMe (XIV), was obtained as shown in Fig. 4. First, the second fragment (VI) was combined with the third fragment (XI). The Boc group of the protected pentapeptide methyl ester (XI) was removed by treatment with formic acid in the presence of mercaptoacetic acid. The resulting pentapeptide with a free amino group was coupled with Boc–Tyr–Arg(Tos)–Gly–Ile–Ser–N_3, prepared from the corresponding hydrazide (XII) by the method of Honzl and Rudinger,[17] to give a decapeptide, Boc–Tyr–Arg(Tos)–Gly–Ile–Ser–Leu–Ala–Asn–Trp–Met–OMe (XIII). The decapeptide (XIII) thus obtained was treated with formic acid for removal of the Boc group and the resulting peptide was coupled with Boc–Met–Asp(OBu^t)–Gly–ONSu obtained from the first fragment (II) as an oily material and used without further purification. Thus, a protected tridecapeptide corresponding to positions 17—29 in the amino acid sequence of human lysozyme, Boc–Met–Asp(OBu^t)–Gly–Tyr–Arg(Tos)–Gly–Ile–Ser–Leu–Ala–Asn–Trp–Met–OMe (XIV), was obtained.

Experimental

The experimental and analytical methods are the same as described in the preceding paper.[8]

H–Asp(OBu^t)–Gly–OH (I). Z–Asp(OBu^t)–ONSu[11] (42.1 g, 0.1 mol) was added to a solution of TosOH·H–Gly–OBzl (33.7 g, 0.1 mol) and TEA (14.0 ml) in DMF (150 ml). The solution was stirred at room temperature for a day and then concentrated to an oily residue under reduced pressure. The residue was dissolved in AcOEt. The solution was washed successively with 0.5 M HCl, 5% aqueous $NaHCO_3$ and H_2O, and then dried over Na_2SO_4 and concentrated to an oil. The oil was dissolved in a mixture of EtOH (600 ml) and H_2O (150 ml), and hydrogenated over 5% palladium–charcoal catalyst under atmospheric pressure. The catalyst was filtered off and the filtrate was concentrated *in vacuo*. The residue was repeatedly flashed with benzene and then crystallized from MeOH and ether; wt 22.5 g (91.5%), mp 158—159 °C, $[\alpha]_D^{24}$ +18.5° (*c* 1.0, AcOH).

Found: C, 48.12; H, 7.45; N, 11.05%. Calcd for $C_{10}H_{18}O_5N_2$: C, 48.77; H, 7.37; N, 11.38%.

Boc–Met–Asp(OBu^t)–Gly–OH·DCHA (II). Boc–Met–ONSu[10] (24.2 g, 69.9 mmol) and TEA (8.4 ml) were added at 0 °C to a suspension of compound I (14.8 g, 60.1 mmol) in a mixture of DMF (200 ml) and H_2O (70 ml). The mixture was stirred at room temperature for 3.5 h to give a clear solution, which was concentrated to an oil under reduced pressure. The oil was redissolved in AcOEt and the solution was washed with 0.5 M HCl and H_2O, dried over Na_2SO_4, and concentrated to an oily residue *in vacuo*. The oil was dissolved in a mixture of ether (1 litre) and AcOEt (200 ml), and then mixed with DCHA (10.8 g). The resulting precipitate was filtered and recrystallized from EtOH, AcOEt, and hexane; wt 27.7 g (69.9%), mp 165—166 °C, $[\alpha]_D^{18}$ −19.4° (*c* 1.0, DMF).

Found: C, 58.08; H, 8.99; N, 8.41; S, 4.88%. Calcd for $C_{32}H_{58}O_8N_4S$: C, 58.33; H, 8.87; N, 8.50; S, 4.87%.

Z–Ile–Ser–OMe (III). Z–Ile–ONp[12] (38.6 g, 0.1 mol) was added to a solution of HCl·H–Ser–OMe (17.0 g, 0.11 mol) and TEA (15.4 ml) in DMF (100 ml). The solution was stirred at room temperature for 3 days, and then concentrated to an oily residue *in vacuo*. The residue was dissolved in AcOEt and H_2O. The AcOEt layer was separated, washed successively with 5% aqueous $NaHCO_3$, 0.7 M HCl and H_2O and dried over Na_2SO_4. The dried solution was concentrated to half its volume, and mixed with hexane and ether. Resulting crystals were separated and recrystallized from AcOEt; wt 31.1 g (85.0%), mp 179—181 °C, $[\alpha]_D^{18}$ +4.3° (*c* 1.0, DMF).

Found: C, 58.76; H, 7.11; N, 7.95%. Calcd for $C_{18}H_{26}O_6N_2$: C, 59.00; H, 7.15; N, 7.65%.

Z–Gly–Ile–Ser–OMe (IV). Compound III (22.0 g, 60.1 mmol) was dissolved in a mixture of MeOH (600 ml) and 4.74 M HCl in dioxane (14 ml), and then hydrogenated under atmospheric pressure over 5% palladium–charcoal catalyst. The catalyst was filtered off and the filtrate was concentrated to a solid residue *in vacuo*. The solid was dissolved in DMF (150 ml), and then mixed with TEA (8.4 ml) and Z–Gly–ONSu[10] (20.2 g, 66.0 mmol). The solution was stirred at room temperature for 2 days, and then concentrated to a syrup under reduced pressure. The syrup was dissolved in AcOEt, and washed successively with 0.7 M HCl, 5% aqueous $NaHCO_3$ and H_2O. The washed solution was dried over Na_2SO_4, and then concentrated to a syrup *in vacuo*. The material was then crystallized from AcOEt and hexane, and recrystallized from AcOEt, ether and hexane; wt 23.0 g (90.6%), mp 137—139 °C, $[\alpha]_D^{18}$ −0.2° (*c* 1.0, DMF).

Found: C, 56.29; H, 6.97; N, 9.81%. Calcd for $C_{20}H_{29}O_7N_3$: C, 56.72; H, 6.90; N, 9.92%.

Z–Arg(Tos)–Gly–Ile–Ser–OMe (V). Compound IV (12.7 g, 30.0 mmol) was dissolved in MeOH (1 litre) and hydrogenated over 5% palladium–charcoal catalyst at atmospheric pressure in a water bath at 30—35 °C. The catalyst was filtered off and the filtrate was concentrated to a solid under reduced pressure. The solid was dissolved with Z–Arg(Tos)–OH, obtained from the corresponding cyclohexylammonium salt[13] (18.4 g, 32.7 mmol), and HOBt (8.1 g, 60.0 mmol) in a mixture of DMF (100 ml) and tetrahydrofuran (200 ml). The solution was cooled to −20 °C in a cold bath, and mixed with a solution of DCC (6.8 g, 33.0 mmol) in tetrahydrofuran (40 ml). The mixture was stirred at −10 °C for an hour and at room temperature overnight, and then concentrated to a solid residue under reduced pressure. The residue was suspended in AcOEt, the insoluble material being filtered off. The filtrate was washed successively with 0.7 M HCl, 5% aqueous $NaHCO_3$ and H_2O. The washed solution was dried over Na_2SO_4, and then concentrated to an oily material *in vacuo*. The material was dissolved in a mixture of EtOH and AcOEt, and crystallized by adding hexane. The crude product was recrystallized from EtOH, AcOEt, and hexane; wt 18.8 g (85.5%), mp 138 °C (sintered) and 152 °C (melted), $[\alpha]_D^{18}$ −1.9° (*c* 1,1, DMF).

Found: C, 53.86; H, 6.52; N, 13.29; S, 4.58%. Calcd for $C_{33}H_{47}O_{10}N_7S$: C, 54.01; H, 6.46; N, 13.36; S, 4.37%.

Boc–Tyr–Arg(Tos)–Gly–Ile–Ser–OMe (VI). Compound V (14.7 g, 20.0 mmol) was dissolved in MeOH (350 ml) and hydrogenated over 5% palladium–charcoal catalyst under atmospheric pressure. The catalyst was filtered off and the filtrate was concentrated to a foaming residue *in vacuo*. Boc–Tyr–N_2H_3[15] (6.5 g, 22.0 mmol) was dissolved in DMF (80 ml). The solution was cooled below −20 °C in a cold bath and mixed with 4.74 M HCl in dioxane (21.6 ml) and then isopentyl nitrite (3.6 ml). The solution was stirred at the same temperature for 45 min and mixed with a solution of the foaming residue in DMF (20 ml) as described above and then with TEA (14.5 ml). The mixture was stirred at 0 °C for 5 days. The precipitate was then filtered off and the filtrate was concentrated to a small volume under reduced

pressure. The remaining solution was diluted with AcOEt, and washed successively with 0.4 M HCl, 5% aqueous $NaHCO_3$ and H_2O. The washed solution was dried over Na_2SO_4 and then concentrated to a foaming residue under reduced pressure, the residue being solidified in a mixture of EtOH, AcOEt, and hexane. The crude material was repeatedly crystallized from a mixture of EtOH, AcOEt, and ether, and then a mixture of CH_3CN, AcOEt, and ether; wt 13.7 g (77.8%), mp 138 °C (sintered) and 142 °C (melted), $[\alpha]_D^{18}$ −4.8° (*c* 1.2, DMF). Amino acid ratio in the acid hydrolysate: Tyr, 0.99 (1); Arg, 0.96 (1); Gly, 1.00 (1); Ile, 0.96 (1); Ser, 0.91 (1).

Found: C, 53.38; H, 6.72; N, 12.52; S, 3.81%. Calcd for $C_{39}H_{58}O_{12}N_8S \cdot H_2O$: C, 53.17; H, 6.86; N, 12.72; S, 3.64%.

Boc-Asn-Trp-OMe (VII). H-Trp-OMe·HCl (22.8 g, 89.4 mmol) was dissolved in DMF (150 ml) and mixed with TEA (12.6 ml). Boc-Asn-ONp[16] (28.2 g, 79.9 mmol) was added to the solution which was stirred at room temperature for a day and then concentrated to a syrup *in vacuo*. The syrup was dissolved in AcOEt and washed successively with 5% aqueous $NaHCO_3$, 0.5 M HCl, and H_2O. The washed solution was dried over Na_2SO_4 with active charcoal, and then concentrated to a solid *in vacuo*. The solid was dissolved in a mixture of EtOH and AcOEt and crystallized by adding hexane. The crude material was recrystallized from the same solvent mixture; wt 30.2 g (86.5%), mp 132—133 °C, $[\alpha]_D^{24}$ +14.3° (*c* 1.0, DMF).

Found: C, 57.75; H, 6.53; N, 13.00%. Calcd for $C_{21}H_{28}O_6N_4 \cdot 1/4H_2O$: C, 57.72; H, 6.57; N, 12.82%.

Boc-Asn-Trp-N_2H_3 (VIII). Compound VII (30.2 g, 69.1 mmol) was dissolved in MeOH (350 ml) and cooled to 0 °C in an ice-bath. Then 90% hydrazine hydrate (100 ml) was added to the chilled solution. The solution was stirred at room temperature for 2 h, and concentrated to an oil *in vacuo*. The oil was triturated with cold water, and washed thoroughly with water. The crude product was crystallized from EtOH, ether, and hexane; wt 26.6 g (88.4%), mp 151—153 °C, $[\alpha]_D^{24}$ −24.6° (*c* 1.0, DMF).

Found: C, 55.09; H, 6.64; N, 18.93%. Calcd for $C_{20}H_{28}O_5N_6 \cdot 1/4H_2O$: C, 54.97; H, 6.58; N, 19.23%.

Boc-Asn-Trp-Met-OMe (IX). Compound VIII (21.6 g, 49.4 mmol) was dissolved in DMF (120 ml) and cooled below −20 °C in a cold bath and mixed with 4.74 M HCl in dioxane (33 ml) and then isopentyl nitrite (7.5 ml). The solution was stirred at −20 °C for 45 min, and then mixed with H-Met-OMe·HCl (12.0 g, 60.0 mmol) and TEA (30.4 ml) below −20 °C and stirred at 0 °C for a day. The precipitate was filtered off and the filtrate was concentrated to a small volume under reduced pressure. The remaining solution was diluted with AcOEt and washed successively with 0.3 M HCl, 5% aqueous $NaHCO_3$ and H_2O. The washed solution was dried over Na_2SO_4 with active charcoal. The dried solution was concentrated under reduced pressure to a solid, which was crystallized from AcOEt, EtOH, and hexane. The crude material was recrystallized from EtOH, hexane, and ether; wt 21.9 g (77.9%), mp 140—144 °C, $[\alpha]_D^{14}$ −39.0° (*c* 1.0, DMF).

Found: C, 54.99; H, 6.70; N, 12.29; S, 5.95%. Calcd for $C_{26}H_{37}O_7N_5S \cdot 1/4H_2O$: C, 54.96; H, 6.65; N, 12.33; S, 5.64%.

Boc-Ala-Asn-Trp-Met-OMe (X). Compound IX (16.9 g, 29.8 mmol) was mixed with 98% formic acid in an ice-bath, and the mixture was kept at room temperature overnight. The clear solution obtained was evaporated *in vacuo* and the residue was mixed with 2.5 M HCl in AcOEt under cooling. The mixture was concentrated to dryness *in vacuo*, and then triturated with ether. The powder was filtered and dried *in vacuo*. The dried powder was dissolved in DMF (60 ml) and mixed with TEA (4.2 ml) and Boc-Ala-ONSu[10] (9.5 g, 33.2 mmol). The mixture was stirred at room temperature for 2 days, and then concentrated to a syrupy residue *in vacuo*. The residue was dissolved in AcOEt and washed successively with 0.4 M HCl, 5% aqueous $NaHCO_3$, and H_2O. The washed solution was dried over Na_2SO_4, and concentrated *in vacuo* to a syrup, which was triturated in a mixture of AcOEt, EtOH, and hexane. The crude product was repeatedly crystallized from CH_3CN and ether; wt 15.8 g (83.2%), mp 134—136 °C, $[\alpha]_D^{24}$ −44.8° (*c* 1.0, DMF).

Found: C, 54.52; H, 6.72; N, 12.96; S, 5.07%. Calcd for $C_{29}H_{42}O_8N_6S \cdot 1/4H_2O$: C, 54.48; H, 6.70; N, 13.15; S, 5.02%.

Boc-Leu-Ala-Asn-Trp-Met-OMe (XI). Compound X (12.7 g, 19.9 mmol) was mixed with 98% formic acid (40 ml) containing mercaptoacetic acid (4 ml) under cooling, and the mixture was left to stand at room temperature overnight. The solvent was evaporated under reduced pressure, and the residue was mixed with 2.5 M HCl in AcOEt (20 ml) under cooling. The mixture was concentrated under reduced pressure to a solid, which was collected with ether. The solid was dissolved in DMF (50 ml) and mixed with TEA (2.8 ml) and Boc-Leu-ONSu[10] (7.2 g, 22.0 mmol). The mixture was stirred at room temperature for 6 days, and then concentrated to a syrup *in vacuo*. The syrup was dissolved in AcOEt containing a small amount of EtOH. The solution was washed successively with 0.3 M HCl, 5% aqueous $NaHCO_3$, and H_2O. The washed solution was dried over Na_2SO_4 and concentrated *in vacuo* to a syrup, which was crystallized from EtOH and hexane. The crude product was recrystallized from CH_3CN and ether; wt 8.0 g (53.3%), mp 173—175 °C. The material thus obtained was further purified by chromatography on silica gel, using a solvent mixture of $CHCl_3$ and MeOH (v/v, 5/1); wt 6.6 g (44.0%), mp 174—176 °C, $[\alpha]_D^{24}$ −41.0° (*c* 1.0, DMF). Amino acid ratio in the acid hydrolysate: Leu, 0.99 (1); Ala, 1.00 (1); Asp, 0.48 (1); Trp, not determined (1); Met, 0.56 (1).

Found: C, 55.87; H, 7.15; N, 12.57; S, 4.38%. Calcd for $C_{35}H_{53}O_9N_7S \cdot 1/4H_2O$: C, 55.87; H, 7.17; N, 13.03; S, 4.26%.

Boc-Tyr-Arg(Tos)-Gly-Ile-Ser-N_2H_3 (XII). Compound VI (25.9 g, 29.4 mmol) was dissolved in EtOH (250 ml) by gentle heating. The solution was cooled to 0 °C in an ice-bath and mixed with 90% hydrazine hydrate (70 ml). The mixture was stirred at room temperature for a day, and then concentrated and flashed repeatedly with benzene. The resulting solid was filtered with a mixture of AcOEt and EtOH. The solid was crystallized from DMF, EtOH, and ether; wt 23.8 g (92.0%), mp 156—158 °C, $[\alpha]_D^{18}$ −7.2° (*c* 1.1, DMF).

Found: C, 51.78; H, 6.95; N, 15.64; S, 3.70%. Calcd for $C_{38}H_{58}O_{11}N_{10}S \cdot H_2O$: C, 51.85; H, 6.87; N, 15.90; S, 3.63%.

Boc-Tyr-Arg(Tos)-Gly-Ile-Ser-Leu-Ala-Asn-Trp-Met-OMe (XIII). Compound XI (4.75 g, 6.31 mmol) was dissolved in 98% formic acid (60 ml) containing mercaptoacetic acid (0.5 ml). The solution was stirred at room temperature for 3.5 h, and then concentrated to a syrupy residue *in vacuo*. The residue was mixed for 1 min with 4 M HCl in dioxane (1.5 ml) under cooling and concentrated *in vacuo* to a syrup, which was triturated in ether. The powder was dried over NaOH *in vacuo*. Compound XII (3.74 g, 4.25 mmol) was dissolved in DMF (20 ml). The solution was cooled below −20 °C in a cold bath and mixed with 4 M HCl in dioxane (7 ml) and isopentyl nitrite (0.78 ml). The solution was stirred at the same temperature for 30 min and then mixed with the powder described above in dimethyl sulfoxide (15 ml), and *N*-methylmorpholine (4.0 ml), and stirred at 0 °C for

7 days. The precipitate formed was filtered off, and the filtrate was concentrated to a small volume under reduced pressure. The residual solution was poured into ice–water, and the precipitate formed was filtered, washed thoroughly with H_2O and dried over P_2O_5 *in vacuo*. The crude material was dissolved in a mixture of MeOH (300 ml) and $CHCl_3$ (200 ml), and insoluble material was filtered off. The filtrate was concentrated *in vacuo* to a residue, which was boiled in a mixture of MeOH (100 ml) and AcOEt (300 ml) and mixed with ether under cooling. The precipitated material was boiled in a mixture of CH_3CN (100 ml) and MeOH (20 ml), and reprecipitated with ether under cooling; wt 3.70 g (57.5%), mp 228—230 °C, $[\alpha]_D^{26}$ −21.2° (*c* 1.0, DMF). Amino acid ratio in the acid hydrolysate: Tyr, 0.95 (1); Arg, 1.08 (1); Gly, 1.01 (1); Ile, 0.93 (1); Ser, 0.83 (1); Leu 0.90 (1); Ala, 1.00 (1); Asp, 0.55 (1); Trp, 0.62 (1); Met, 0.66 (1).

Found: C, 53.84; H, 6.73; N, 13.71; S, 4.40%. Calcd for $C_{68}H_{99}O_{18}N_{15}S_2 \cdot 2H_2O$: C, 53.92; H, 6.85; N, 13.87; S, 4.23%.

Boc–Met–Asp(OBu^t)–Gly–Tyr–Arg(Tos)–Gly–Ile–Ser–Leu–Ala–Asn–Trp–Met–OMe (XIV). Compound II (2.70 g, 4.10 mmol) was suspended in AcOEt (150 ml), and washed with 1 M H_2SO_4 and then H_2O. The washed solution was dried over Na_2SO_4, and then concentrated to an oily material under reduced pressure. The oil was dissolved in a mixture of AcOEt (50 ml) and dioxane (30 ml). The solution was cooled to 0 °C in an ice bath, and mixed with HONSu (0.52 g, 4.5 mmol) and DCC (0.93 g, 4.5 mmol). The mixture was stirred at room temperature for a day. The precipitate formed was filtered off and the filtrate was concentrated to an oily material *in vacuo*.

Compound XIII (3.70 g, 2.44 mmol) was dissolved in 98% formic acid (50 ml). The solution was stirred at room temperature for 3 h and then concentrated to a residue *in vacuo*. The residue was stirred with 2.5 M HCl in AcOEt (5 ml) for 1 min in an ice bath, and then concentrated *in vacuo* to a syrup, which was solidified in ether and dried over NaOH under reduced pressure. The dried material was dissolved in a mixture of dimethyl sulfoxide (10 ml) and DMF (5 ml) with TEA (0.35 ml). The solution was mixed with the oily substance obtained as described above from compound II in DMF (5 ml). The mixture was stirred at room temperature for 4 days and then concentrated to a syrup *in vacuo*. The syrup was triturated in a mixture of AcOEt and ether, and the crude product was crystallized from MeOH. The crystallized material was repeatedly precipitated from a mixture of DMF and ether; wt 3.30 g (72.2%), mp 203 °C, $[\alpha]_D^{24}$ −28.1° (*c* 1.0, DMF). Amino acid ratio in the acid hydrolysate: Met, 1.33 (2); Asp, 1.54 (2); Gly, 1.88 (2); Tyr, 0.99 (1); Arg, 0.98 (1); Ile, 0.99 (1); Ser, 0.85 (1); Leu, 0.99 (1); Ala, 1.00 (1); Trp, not determined.

Found: C, 52.91; H, 6.83; N, 13.31; S, 4.80%. Calcd for $C_{83}H_{123}O_{23}N_{18}S_3 \cdot 2H_2O$: C, 53.19; H, 6.88; N, 13.45; S, 5.13%.

This work was supported by a Grant-in-Aid (247128, 1977) for Scientific Research from the Ministry of Education, Science and Culture.

References

1) E. Osserman and D. P. Lawlor, *J. Exp. Med.*, **124**, 921 (1966).
2) J. Jollès and P. Jollès, *Helv. Chim. Acta*, **52**, 2671 (1969); **54**, 2668 (1971).
3) R. E. Canfield, S. Kammerman, J. H. Sobel, and F. J. Morgan, *Nature New Biology*, **232**, 16 (1971).
4) E. Gross and B. Witkop, *J. Am. Chem. Soc.*, **83**, 1510 (1961).
5) M. Okamoto, S. Aimoto, and Y. Shimonishi, "Peptide Chemistry 1977," Proc. 15th Symposium on Peptide Chemistry, ed by T. Shiba, Osaka (1977), p. 205.
6) R. E. Goldberger and C. B. Anfinsen, *Biochemistry*, **1**, 401 (1962).
7) Y. Shimonishi, *Bull. Chem. Soc. Jpn.*, **43**, 3251 (1971).
8) S. Yoshimura, K. Izumi, and Y. Shimonishi, *Bull. Chem. Soc. Jpn.*, **52**, 1672 (1979).
9) The abbreviations used are those recommended by IUPAC-IUB: *J. Biol. Chem.*, **247**, 977 (1972). Additional abbreviations: DCC, dicyclohexylcarbodiimide; HOBt, 1-hydroxybenzotriazole; DMF, *N*,*N*-dimethylformamide; TEA, triethylamine; DCHA, dicyclohexylamine.
10) G. W. Anderson, J. E. Zimmerman, and F. M. Callahan *J. Am. Chem. Soc.*, **86**, 1839 (1964).
11) K. Hofmann, W. Haas, M. J. Smithers, and G. D. Zanetti, *J. Am. Chem. Soc.*, **87**, 631 (1965).
12) M. Bodanszky and V. du Vigneaud, *J. Am. Chem. Soc.*, **81**, 5688 (1959).
13) J. Ramachandran and C. H. Li, *J. Org. Chem.*, **27**, 4006 (1962).
14) W. König and R. Geiger, *Chem. Ber.*, **103**, 788 (1970).
15) E. Schröder, *Justus Liebigs Ann. Chem.*, **670**, 127 (1963).
16) G. R. Marshall and R. B. Merrifield, *Biochemistry*, **4**, 2394 (1965).
17) J. Honzl and J. Rudinger, *Collect. Czech. Chem. Commun.*, **26**, 2333 (1961).
18) K. Hofmann, F. M. Finn, M. Limetti, J. Montibeller, and G. Zanetti, *J. Am. Chem. Soc.*, **88**, 3633 (1966).

Restricted Rotation Involving the Tetrahedral Carbon. XXV. Barriers to Exchange between *dl* and *meso* Forms of 9-(Arylmethyl)triptycenes[1]

Motomichi KONO, Hiroshi KIHARA, Nobuo NAKAMURA, Fumio SUZUKI, and Michinori ŌKI*

Department of Chemistry, Faculty of Science, The University of Tokyo, Tokyo 113

(Received November 17, 1978)

Barriers to exchange between *dl* and *meso* forms *via* rotation about the C_9–C_{subst} bond of 9-(arylmethyl)-1,4-dimethoxytriptycenes are obtained by the use of the methoxyl signals in the ^1H NMR spectra. It is found that, although the population ratios are affected by the substituent in the 9 position, the enthalpy of activation for the rotation is almost invariant at *ca.* 10 kcal/mol.

9-Substituted triptycenes constitute a unique system in that unusually high barriers are observed for rotation about the C_9–C_{subst} bond.[2] Thus freezing the rotation of even methyl groups on the NMR time scale has been realized[3] and stable rotational isomers isolated at room temperature.[4] Whereas barriers to rotation about the C_9–C_{subst} bond are known in the cases where the substituent is a tertiary alkyl,[5] an isopropyl,[6] or a methyl group,[3] barriers to rotation about the C_9–CH_2 bond have not been known except for one case, 9-(chloromethyl)triptycene, where signals due to ring protons[7] and ring carbons[8] have been used for the analysis.

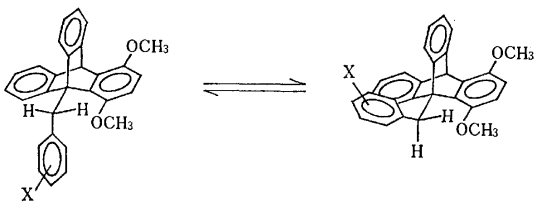

dl-form *meso*-form

(1)

9-Benzyltriptycenes are interesting in that there is an attractive interaction between the 9-benzyl group and the benzo group of the triptycene skeleton:[9] the *dl* forms are unusually favored if there is an electron-attracting substituent in the benzyl group and the benzo group has a group of low ionization potential. The interaction should affect the enthalpy of activation for rotation if other conditions are the same. This paper describes the reinvestigation of the population ratios of the *dl* and the *meso* forms of 9-(arylmethyl)-1,4-dimethoxytriptycenes (**1**) using the FT NMR technique to obtain better data and the study of the barrier to exchange between the *dl* and the *meso* forms by internal rotation using the line shapes of the methoxyl signals in ^1H NMR spectra.

Experimental

Syntheses of Triptycenes. The substituted benzyltriptycenes were prepared by the Diels-Alder reaction between the corresponding 9-benzylanthracenes (**2**) and *p*-benzoquinone followed by enolization and methylation.

9-(m-Nitrobenzyl)anthracene. *m*-Nitrobenzylideneanthrone[10] (3 g) was heated under reflux with 10 ml of ethanol and 3 ml of water and 3 g of sodium borohydride was

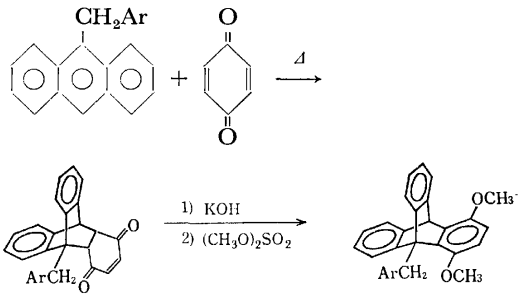

(**1**)

added in small portions. The mixture was heated for 1 h and cooled. The insoluble material was removed by filtration and the mother liquor was concentrated. The residue was taken up in 200 ml of carbon tetrachloride and the solution was heated for 2 h with 20 g of phosphorus pentaoxide. The solution was decanted and evaporated. The residue was chromatographed on silica gel, using benzene as an eluent. The desired product was obtained in 70% yield and used directly for subsequent reactions.

9-(Arylmethyl)-1,4-dimethoxytriptycenes. These compounds were prepared by the following general procedure. The compounds were known unless otherwise stated and their physical properties agreed well with those reported.

A solution of 1.3 g (0.005 mol) of 9-benzylanthracene and 1.1 g (0.01 mol) of *p*-benzoquinone in 20 ml of acetonitrile was refluxed for 24 h and evaporated. The residue was chromatographed on silica gel and eluted with benzene–chloroform (10: 1). An adduct was obtained in over 90% yield. To a solution of the adduct (0.6 g) in 20 ml of dioxane was added 20 ml of 1 M aqueous potassium hydroxide in 10 min and the mixture was treated with 5 ml of dimethyl sulfate in small portions. The potassium hydroxide solution was added in small portions to the mixture until the addition caused no color change. After 10 min stirring, the precipitate was collected and purified by alumina chromatography using hexane–benzene (4: 1) as an eluent. The yield was over 90%.

1,4-Dimethoxy-9-(p-methylbenzyl)triptycene: Mp 223—224 °C. Found: C, 85.94; H, 6.25%. Calcd for $C_{30}H_{26}O_2$: C, 86.09; H, 6.26%. ^1H NMR ($CDCl_3$) δ=2.28 (CH_3), 3.21 (CH_3O), 3.80 (CH_3O), 4.64 (CH_2), 5.95 (bridgehead), 6.47 (AB quartet for dimethoxybenzo H's, J_{AB}=9.0 Hz, $\Delta\nu_{AB}$=6.3 Hz), 6.8—7.5 (aromatic H's).

1,4-Dimethoxy-9-(m-nitrobenzyl)triptycene: Mp 301—305 °C (dec). Found: C, 77.34; H, 4.95; N, 3.10%. Calcd for $C_{29}H_{23}NO_4$: C, 77.48; H, 5.16; N, 3.12%. ^1H NMR ($CDCl_3$–CS_2, integrated for 70 times) δ=3.19 (CH_3O), 3.85 (CH_3O), 4.70 (CH_2), 5.92 (bridgehead), 6.48 (AB quartet for dimethoxybenzo H's, J_{AB}=9.0 Hz, $\Delta\nu_{AB}$=11.0 Hz),

6.8—7.6 (aromatic H's).

^1H NMR Spectra. The spectra were obtained on a JEOL FX60 spectrometer equipped with FT facilities. The solvent was a 3:1 mixture of chloroform and carbon disulfide and sample tubes were of 10 mm diameter. In one case dichloromethane-d_2 was used as a solvent. The temperature was read by a thermocouple directly dipped into the mixed solvent placed in the probe. The error in reading the temperature was ± 0.6 °C. Pulses of 20 μs duration was used with 5 s intervals. The data were accumulated *ca.* 40 times except for the *m*-nitro derivative which required 400 time accumulation.

Total Line Shape Analysis. It was performed with the use of a modified Binsch program,[11] treating the spectra as a pair of uncoupled A⇄B exchanges. Populations were obtained as described in Results and Discussion and the rate constant (k_1) of the *meso*→*d* (or *l*) process was varied in the calculation, the rate constant (k_{-1}) of the reverse process being put outside of the consideration. Since there are two identical processes transforming the *meso* to the *dl* form, $2k_1[meso]=k_{-1}[d \text{ and } l]$ is obtained: namely $K(dl/meso)=2k_1/k_{-1}$. Thus the rate obtained by the computer simulation was divided by 2 to obtain k_1. Chemical shift differences were used as observed. T_2 was calculated from the half band width of the tetramethylsilane signal added as an internal standard.

The signal due to the 4-methoxyl group was always included in the calculation. *p*-Chloro and *m*-nitro compounds gave excellent results by this method. The presence of the *p*-methoxyl group in the *p*-methoxybenzyl compound gave a strong drawback to this method. Thus the line shape analysis was performed only at the higher field. The spectra of the *p*-methylbenzyl and the benzyl compounds were analyzed similarly. The calculated spectra were compared with the observed and the best fit spectra were chosen by visual fitting. The agreement between the observed and the calculated spectra was excellent.

Results and Discussion

Assignment of the Spectra. Fig. 1 shows ^1H NMR spectra of 9-(*p*-chlorobenzyl)-1,4-dimethoxytriptycene at three temperatures. Apparently the methoxyl and the methylene signals broaden on lowering the temperature. The latter splits into a quartet signal and a singlet. Assignments of the spectral peaks of the methylene part is straightforward: a quartet is due to the *dl* form and a singlet the *meso* form (see Newman projections). The former has two singlets which split into two large singlets and a small singlet at the lower temperature. The former two singlets are assigned to the *dl* forms and the latter to the *meso* form from the intensity considerations. The methoxyl groups of the *dl* form in 1- and 4-positions suffer from a large difference in magnetic environment because of the presence of the benzylic phenyl group in the proximity of the 1-position: the signal at the higher field is thus assigned to the 1-methoxyl group. In contrast, the two methoxyl groups of the meso form seem to be in similar magnetic environments.

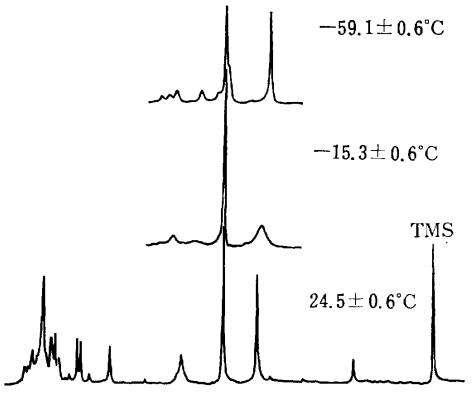

Fig. 1. ^1H NMR spectra of 9-(*p*-chlorobenzyl)-1,4-dimethoxytriptycene at three temperatures.

The aromatic region of the *p*-chloro compound showed temperature dependence in its spectrum but the change was too complicated to analyze.

Other compounds showed similar behavior in the ^1H NMR spectra at various temperatures. The assignments were performed similarly.

Populations of Rotamers. In principle, it should be possible to obtain population ratios at various temperatures by calculation, because the ratios can be used as variants in the total line shape analysis. In practice, however, it will add another uncertainty in the simulation. It was also hoped to reduce the number of parameters in simulations of the line shapes of the methylene part.[12] Thus we decided to obtain the ratios from other sources.

There are two signal pairs to be used for the population analysis. The methylene signals appear as an AB quartet and a singlet. Integration of these signals should produce the population ratio at a given temperature. However, in practice, there are some overlaps in the down-field part of the AB signal with that of the *meso* and in the up-field part of the AB signal with that of the methoxyl signal. The signal due to the methoxyl groups of the *meso* form heavily overlaps with that due to the 4-methoxyl of the *dl* form in the down-field. Thus integration of the methoxyl signals is less hopeful.

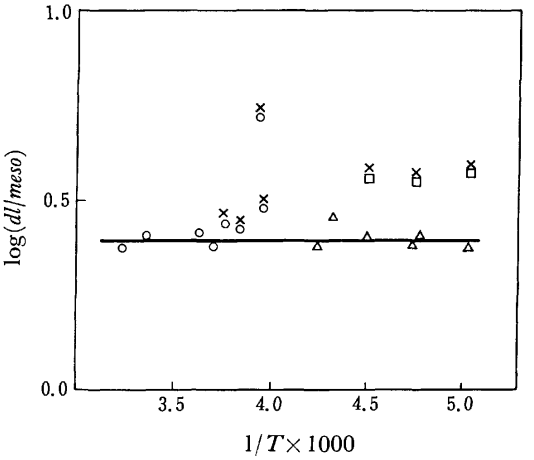

Fig. 2. Population ratios (*dl*/*meso*) of 9-(*p*-methylbenzyl)-1,4-dimethoxytriptycene at various temperatures: □ by integration of the methylene region, △ by integration of the methoxyl region, ○ by the drift in the chemical shift of the methoxyl signal after coalescence. Those with cross marks are rejected in drawing the straight line. See text for the reasons.

Table 1. Equilibrium constants and thermodynamic parameters pertaining to rotamers of 9-arylmethyl-1,4-dimethoxytriptycenes

Aryl	Representative K's (*dl*/*meso*) (Obsd)		$-\Delta H$ (kcal/mol)	ΔS (e.u.)
	−20 °C	−50 °C		
p-$CH_3OC_6H_4$	2.7±0.2	3.0±0.2	0.32±0.02	−1.5±0.5
p-$CH_3C_6H_4$	2.5±0.2	2.5±0.2	0.05±0.01	−1.1±0.2
C_6H_5	2.8±0.2	2.8±0.2	0.57±0.03	+0.3±0.1
p-ClC_6H_4	4.1±0.2	4.5±0.2	0.44±0.06	−1.6±0.1
m-$NO_2C_6H_4$	4.4±0.2	4.9±0.2	0.36±0.12	−0.7±0.1

To avoid these uncertainties, we decided to use the cross-check method of using both the methylene and the methoxyl signals. For the latter, both the integrated intensities and the chemical shift drift at temperatures higher than the coalescence were used. The results are shown in Fig. 2, taking the case of the *p*-methylbenzyl compound as an example. As is seen in the figure, the chemical shift method gives apparently absurd values at temperatures close to the coalescence, which are rejected as the unreliable. Those data obtained by integration of the AB signals were found to give apparently larger values in the cases where the population of the *meso* form was large. Therefore these were also abandoned in the least squares treatment.

The equilibrium constants and thermodynamic parameters thus obtained are tabulated in Table 1. The equilibrium data are in general accordance with those reported,[9] but we take the values reported here to be more reliable because of the better S/N ratios relative to the previously reported. The results confirm that the *dl* form is stabilized relative to the *meso* form and the stabilization is enhanced when the benzyl part carries an electronegative substituent.

Barriers to Exchange between the dl *and the* meso *Forms.* There are 6 rotational processes as depicted in Fig. 3. However, since we are looking at the signals due to the *dl* forms as a package, we can neglect the $d \rightleftharpoons l$ processes. Thus there remain 4 processes of which *meso*→*d* and *meso*→*l* are identical and so are the reverse processes, because *d* and *l* forms are not distinguishable.

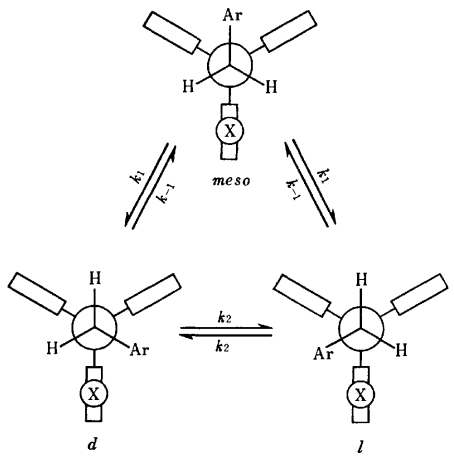

Fig. 3. Processes of mutual exchanges among *meso*, *d*, and *l* forms.

For the *m*-nitro compound, it is possible to take two conformations for the *meso* and the *dl* forms with respect to the nitrophenyl group, although that phenyl group will assume the conformation in which the π-system bisects the H–C–H angle of the α-methylene group.[9] They are NO_2-inside and NO_2-outside conformations. However, these species were not distinguishable by the present technique. We tentatively assume that the average processes are observed, although it is likely that the NO_2-inside conformations are unstable and we are observing processes which involve the NO_2-outside conformations.

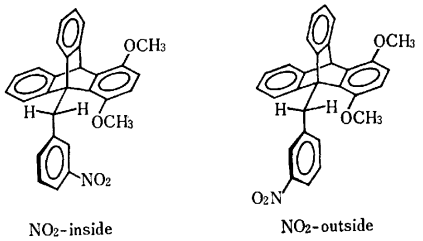

Fig. 4. NO_2-inside and NO_2-outside conformations of a *d* (or *l*) form.

Fig. 5. Computed and observed spectra of 9-(*p*-chlorobenzyl)-1,4-dimethoxytriptycene at various temperatures.

In Fig. 5 the results of computer simulation of the line shapes of the *p*-chloro compound are shown with the rate constants and compared with the observed spectra. These results were put into the Eyring's plot and excellent linear relationships were obtained. From the slopes and the intercepts, the activation parameters were obtained as shown in Table 2.

It is interesting to note that the ground state stabilities seen in the equilibrium constants K(*dl*/*meso*) is

Table 2. Activation parameters for the exchange between the *meso* and the *dl* forms of 9-arylmethyl-1,4-dimethoxytriptycenes in $CDCl_3$–CS_2 (3: 1)

Aryl	$\Delta H^{\neq}$(kcal/mol)		$\Delta S^{\neq}$(e.u.)		$\Delta G^{\neq}$(kcal/mol) (−15 °C)	
	meso→*dl*	*dl*→*meso*	*meso*→*dl*	*dl*→*meso*	*meso*→*dl*	*dl*→*meso*
p-$CH_3OC_6H_4$	8.8±0.3	9.1±0.3	−13.6±0.3	−12.9±1.4	12.3±0.5	12.4±0.5
p-$CH_3C_6H_4$	11.8±0.4	11.8±0.4	−2.6±0.5	−2.8±1.5	12.4±0.3	12.5±0.3
p-$CH_3C_6H_4$[a]	11.3±0.4	12.1±0.4	−4.4±1.4	−1.5±1.8	12.4±0.1	12.4±0.1
C_6H_5	10.0±0.1	10.7±0.2	−7.7±0.6	−5.5±1.0	11.9±0.2	12.1±0.2
p-ClC_6H_4	11.8±0.3	12.1±0.3	−3.4±1.3	−3.7±1.3	12.6±0.2	13.0±0.2
m-$NO_2C_6H_4$	9.6±0.1	10.0±0.1	−12.3±0.4	−12.3±0.4	12.8±0.2	13.2±0.2

a) These values were obtained with a solution in CD_2Cl_2.

not reflected in the $\Delta H^{\neq}$'s. All the compounds examined show almost the same $\Delta H^{\neq}$'s irrespective to the substituent. Since the ground state stability of the compounds with electronegative substituents is ascribable to the charge transfer interaction, it should be reflected in the $\Delta H^{\neq}$'s, if the other factors are the same. Although we must carefully discuss the entropy of activation derived by the total line shape analysis,[13] it is tempting to consider that in the transition state of rotation the *m*-nitro compound suffers from the decrease in entropy probably due to change in solvation which counterbalances the enthalpy factor in the ground state.

References

1) Preceding paper: M. Nakamura and M. Ōki, *Tetrahedron Lett.*, **1979**, 527.
2) M. Ōki, *Angew. Chem. Int. Ed. Engl.*, **15**, 87 (1976).
3) M. Nakamura, M. Ōki, H. Nakanishi, and O. Yamamoto, *Bull. Chem. Soc. Jpn.*, **47**, 2415 (1974).
4) G. Yamamoto, M. Nakamura, and M. Ōki, *Bull. Chem. Soc. Jpn.*, **48**, 2592 (1975).
5) G. Yamamoto and M. Ōki, *Bull. Chem. Soc. Jpn.*, **48**, 3686 (1975).
6) F. Suzuki, M. Ōki, and H. Nakanishi, *Bull. Chem. Soc. Jpn.*, **47**, 3114 (1974).
7) N. M. Sergeyev, K. F. Abdulla, and V. R. Skvarchenko, *J. Chem. Soc., Chem. Commun.*, **1972**, 368.
8) Y. K. Grishin, N. M. Sergeyev, O. A. Subbotin, and Y. A. Ustynyuk, *Mol. Phys.*, **25**, 297 (1973).
9) F. Suzuki and M. Ōki, *Bull. Chem. Soc. Jpn.*, **48**, 596 (1975).
10) V. M. Ingram, *J. Chem. Soc.*, **1950**, 2318.
11) G. Binsch, "Topics in Stereochem.," ed by E. L. Eliel and N. L. Allinger, Interscience, New York (1970), Vol. 3, p. 97.
12) M. Kono and M. Ōki, *Bull. Chem. Soc. Jpn.*, **52**, 1686 (1979).
13) R. R. Shoup, E. D. Becker, and M. L. McNiel, *J. Phys. Chem.*, **76**, 71 (1972).

Restricted Rotation Involving the Tetrahedral Carbon. XXVI. Certainties and Uncertainties Involved in the Rates of Exchange among Three Sites as Obtained by Total Line Shape Analyses of ^{1}H NMR Spectra: The Case of Methylene Signals[1]

Michinori Ōki,* Motomichi Kono, Hiroshi Kihara, and Nobuo Nakamura
Department of Chemistry, Faculty of Science, The University of Tokyo, Tokyo 113
(Received November 17, 1978)

Benzyl methylene signals, which split into an AB quartet and a singlet and show temperature dependence, are obtained at various temperatures and are simulated with the use of two independent rates of rotation. Certain limitations of accuracy are found in this method. The uncertainty becomes less if additional data are provided from other sources, but never becomes negligible. Contribution of the slower process is found difficult to detect especially when the population involved in the process are the less.

The total line shape analysis of the NMR spectra is becoming increasingly popular due to the widespread utilization of high-speed computers and availability of the computing program.[2] The method furnishes the rate constants of 10^{-1}—10^5 s^{-1} easily and the data are favorably compared[3] with those obtained by other methods, when the exchanging sites are two, although there is a warning that the entropy of activation thus obtained may include a considerable error.[4]

As to the exchanging sites of more than two, there are some scattered reports which claim the rates of different processes are separately obtained. A typical example is a combination of internal rotation about the C-N bond and inversion with respect to the nitrogen atom of amines. Bushweller *et al.* succeeded in separating the two processes in a deuterated *N*-ethyl-*N*-methylisopropylamine (**1**) and obtained the rates of the respective process.[5] This method takes advantage of the fact that the rates of the two processes are so much different that the coalescence phenomena are found at two temperatures. The classical example of the carbon skeleton in this type of exchange was reported by Kessler *et al.* on *cis*-1,2-di-*t*-butylcyclohexane (**2**) in which rotation about the C_1–C_2 bond and ring inversion are observed at different temperatures.[6] A recent report by Anet and coworkers[7] on a 1,2-cyclononadiene (**3**) also falls into this category.

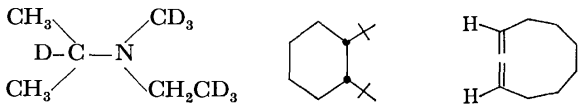

(**1**) (**2**) (**3**)

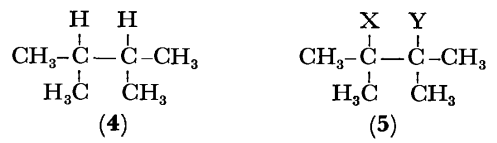

(**4**) (**5**)

Reports from this laboratory made use of the fact that *d* and *l* isomers are not distinguishable by ^{1}H NMR spectroscopy and treated many ethane derivatives, as if there were only two sites exchanging, although there are actually three sites.[8a] The use of ^{13}C NMR in the rate analysis of internal rotation[8b] also falls in this category. This type of treatment seems to be convenient when one barrier is high relative to others. Thus Lunazzi *et al.* treated the ^{13}C NMR spectra of 2,3-dimethylbutane (**4**) in this manner and good agreement between the observed and the calculated spectra was obtained.[9] By *ab initio* calculation barrier to gauche-to-gauche transformation is found to be *ca.* 8 kcal/mol, whereas the line shape analysis (4.3 kcal/mol) and *ab initio* calculation (4.6 kcal/mol) afforded barriers to gauche-to-trans transformation which are in good accordance. Bushweller *et al.* performed also total line shape analysis on 2,3-dimethylbutane derivatives (**5**) by assuming that the gauche-to-gauche barrier is high and the agreement between the observed and the calculated spectra was good.[10] The rotation of gauche-to-gauche seems to contribute little to the whole process.

The above cited cases are not general, of course. In the rotamer exchange, the barriers to rotation of gauche-to-gauche and gauche-to-trans are in general close to each other. Namely two processes of rotation compete in the general case. Then a question arises: to what extent can we rely upon the total line shape analysis in obtaining rate data when more than two independent processes are competing? To answer this question we have analyzed the line shape of benzyl methylene protons of 9-benzyltriptycenes (**6**) which exist as a mixture of *meso*, *d*, and *l* isomers, by taking all the processes

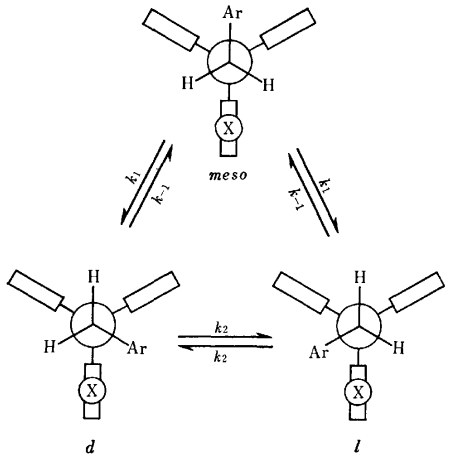

Fig. 1. Exchanging conformers and exchange processes.

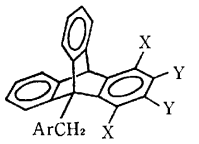

(6)

into consideration. In this case three back-and-forth processes are possible, but, due to the presence of a pair of enantiomers, the number of rate constants converges to three: k_1, k_{-1}, and k_2, as shown in Fig. 1.

In this paper we describe the results of the total line shape analysis and discuss uncertainties associated with the calculation.

Experimental and Data Processing

Materials. The syntheses of 9-arylmethyl-1,4-dimethoxytriptycene and 9-(*p*-chlorobenzyl)-1,2,3,4-tetrachlorotriptycene used in this study have been reported elsewhere.[1,11]

Measurement. The spectral measurement was performed on a JEOL FX 60 spectrometer equipped with FT facilities. The conditions of the measurements were the same as described in a previous paper.[1]

Total Line Shape Analysis. The benzyl methylene signals consisted of an AB quartet and a singlet due to the *dl* and the *meso* forms, respectively. The system was treated as the exchange of AB-BA-C_2 by the modified Binsch program.[12] The chemical shift difference and the coupling constant are used as observed. T_2 was calculated from the line width of TMS added as an internal standard. Population ratios derived in the previous paper were used for the calculation except for 9-(*p*-chlorobenzyl)-1,2,3,4-tetrachlorotriptycene, with which determination of the population ratio was straightforward because clear AB quartet and C_2 signals were observed owing to the absence of the methoxyl signals which prevented the accurate determination in the other compounds. Other pertinent considerations are described in the previous paper.

Results and Discussion

General Consideration. As a starting point, we discuss the limitation of the usefulness of the total line shape analysis. Shown in Fig. 2 are the computed spectra of various relative rates of the two processes using the chemical shift differences and the coupling constant of 9-benzyl-1,4-dimethoxytriptycene. The

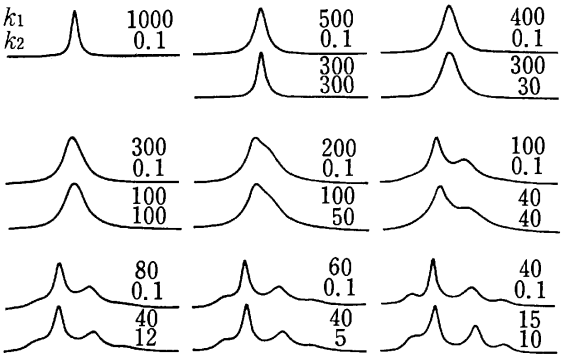

Fig. 2. Computed spectra with the use of various k_1's and k_2's taking other necessary data from those of 9-benzyl-1,4-dimethoxytriptycene.

variables are limited to two because k_1 and k_{-1} are related by the equilibrium constant: $K(dl/meso)=2k_1/k_{-1}$. In our cases the population ratios are available from the integrated intensities and/or the chemical shifts as discussed in the previous paper.[1] We stick to the two independent variables because, although it is possible to obtain k_1 and k_{-1} independently in the computation of the spectra, increasing the number of the variables will increase the uncertainty in the obtained data. The used parameters were as follows: $\Delta\nu_{AB}$ 38.33 Hz, $\Delta\nu_{AC}$ 3.395 Hz, J_{AB} 17.46 Hz, T_2 0.318 s, molar fractions of the *meso* and the *d* (or *l*) forms 0.22 and 0.39, respectively.

In the rows 1, 3, and 5, are shown the line shapes computed with a constant k_2 of 0.1 s^{-1} and various k_1's from 1000 s^{-1} to 40 s^{-1}. The line shapes seem to be determined by the main process at the level of this slow process, because changing the k_2's to 0.01 s^{-1}, while using the k_1's of the same range as above, did not produce any significant change. It may be concluded that a process, the rate constant of which is less than 1/100 of that of a main process has no effect on the line shape of the NMR spectra.

In the rows 2, 4, and 6, are shown the line shapes computed using relatively large k_2 values. As is seen from the simpler spectra, it is clear that a unique combination of two rates cannot be obtained if the spectral shape is simple (compare for example, the shape of $k_1=300$ and $k_2=0.1$ s^{-1} with that of $k_1=100$ and $k_2=100$). Thus we may better exclude one-peaked spectra from the calculation as was pointed out previously.[3] In sharp contrast, the computed spectra with a constant k_2 of 0.1 s^{-1} can differentiate the k_1's of 80, 60, and 40 s^{-1} as shown in the row 5 and the rate of a slow process may be reflected if it becomes 1/10 of that of a fast process as is shown in the bottom row. It seems that, if the spectra are complex, there is a possibility that the rates of the two processes are uniquely determined by this method. Thus we will discuss the line shapes of considerable complexity in the following text to make the discussion more reliable. Another point worthy of note is that, if we neglect a process which does exist, the apparent rate constant of the main process is obtained larger than the real: if k_2 is practically neglected by putting the value of 0.1, the top right curve is simulated by using k_1 of 400 s^{-1}, whereas the curve may actually correspond to k_1 and k_2 of 300 and 30 s^{-1}, respectively (second from top, right curve). Therefore we should take the rate constant as a maximum value even though the main process could explain the line shape completely and the minor process is negligible.

If we assume that the transition state of rotation is a fully eclipsed form, the transition state of the highest energy is the one (**7**) in which the aryl group eclipses

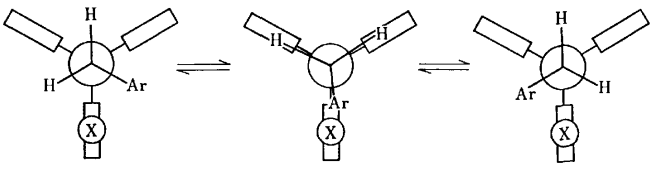

d (or *l*) (**7**) *l* (or *d*)

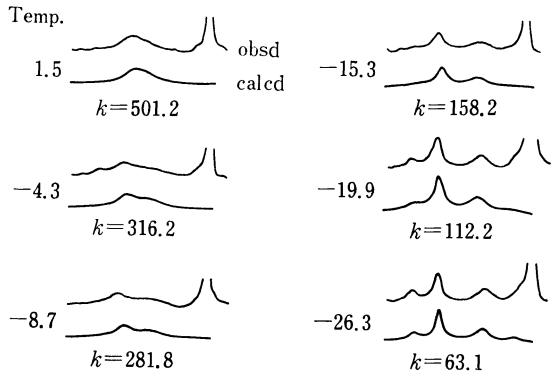

Fig. 3. Observed and calculated spectra of the methylene region of 9-(*p*-chlorobenzyl)-1,4-dimethoxytriptycene at various temperatures. The strong signal at the higher field corresponds to the methoxyl signal and is neglected in the computation.

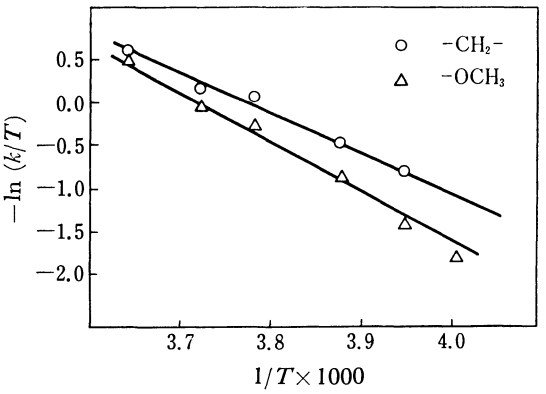

Fig. 4. Comparison of the Eyring's plots using k_1's obtained by the analysis of the methylene part and the methoxyl signals of 9-(*p*-chlorobenzyl)-1,4-dimethoxytriptycene.

the peri substituent. This transition state is realized when the rotation occurs from a *d* form to an *l* form or *vice versa* but never appears in the process of *meso*→*d* (or *l*). Therefore we can reasonably assume that k_1 and k_{-1} are larger than k_2.

Since the line shapes are affected by fast processes to a greater extent than slower processes, we may be able to obtain fairly good agreement between the real and the calculated rates which are obtained by neglecting the $d \rightleftarrows l$ process. Fig. 3 shows the observed spectra at the methylene and methoxyl region of 9-(*p*-chlorobenzyl)-1,4-dimethoxytriptycene at various temperatures and the computed spectra which were obtained by neglecting the $d \rightleftarrows l$ process and the methoxyl signal and were considered the best fit. The used parameters for computation were differences in chemical shifts of $\Delta\nu_{AB}$−40.52 Hz and $\Delta\nu_{AC}$ 2.148 Hz, coupling constant of 17.4 Hz, and T_2's and populations[1] at the respective temperatures. Fig. 4 shows the Eyring's plot using the rate constants thus obtained and compares the result with the straight line corresponding to the *meso*$\rightleftarrows$*d* (or *l*) process as obtained by the total line shape analysis of the methoxyl singnals.[1] Apparently this treatment gives higher rate values and a lower $\Delta H^{\ddagger}$, the difference amounting over 3 times of the standard deviation. Thus the results indicate that we should not overlook the process $d \rightleftarrows l$, although the rate may be small.

Aquisition of Two Independent Rate Constants by Calculation. We tried to evaluate the best k_1 and k_2 of the 9-(chlorobenzyl)-1,4-dimethoxytriptycene by using the computation only. For each spectrum, population ratio at that temperature, coupling constant, differences in chemical shifts, and T_2 are put as constants and k_1 and k_2 as variables. The rate constants are roughly changed by the scale of log *e* for the convenience of computation and an array of line shapes is made. From

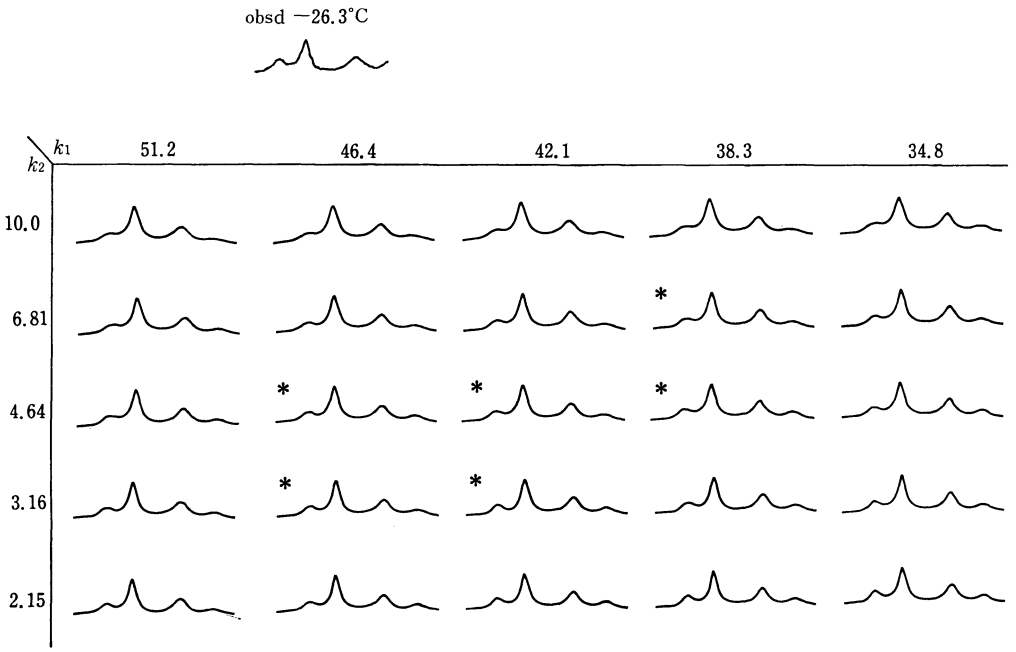

Fig. 5. Computed line shapes with various k_1's and k_2's using the data of *p*-(chlorobenzyl)-1,4-dimethoxytriptycene at −26.3 °C. Those marked with stars are the best fit spectra.

the array a seemingly best fit region is picked up and the portion is expanded with small variations in k_1 and k_2 to make a finer array. An example is shown in Fig. 5, taking the spectrum at −26.3 °C. By visual fitting, we cannot specify a single computed spectrum but can pick up 6 spectra which fit best. Thus it is possible to obtain k_1 and k_2 with certain ranges. Similarly at other temperatures, sets of 2 to 6 best fit spectra are obtained. The results are shown in Table 1.

TABLE 1. RATE CONSTANTS OBTAINED BY THE VISUAL FITTING OF THE COMPUTED SPECTRA WITH THE OBSERVED FOR 9-(*p*-CHLOROBENZYL)-1,4-DIMETHOXYTRIPTYCENE AT VARIOUS TEMPERATURES

Temperature (°C)	Rate constants (s^{-1})	
	k_1	k_2
−15.3	110—90.9	14.7—6.81
−19.9	75.0—48.6	14.7—4.64
−26.3	46.4—38.3	6.81—3.16
−31.1	21.5—19.6	6.81—4.64
−37.3	16.2—13.3	3.16—1.47

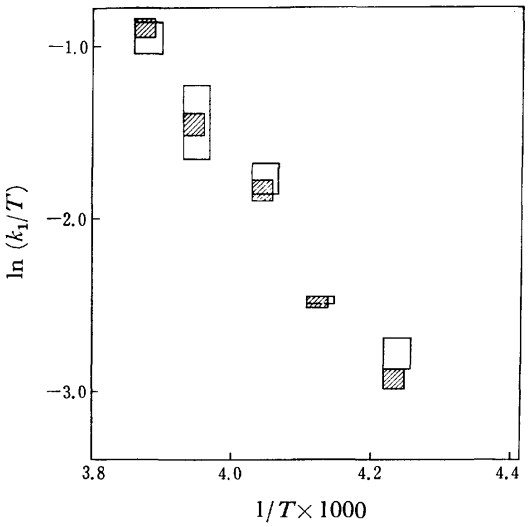

Fig. 6. Eyring's plot showing the ranges of possible errors for the process *meso*→*d*(or *l*) of 9-(*p*-chlorobenzyl)-1,4-dimethoxytriptycene. Open rectangles correspond to those obtained by computation only and hatched rectangles to those derived by the methoxyl signals, the temperature ranges of the latter being changed slightly for the convenience of comparison.

Figure 6 illustrates an Eyring's plot pertaining to the rate constants k_1 with probable error ranges indicated by the widths in the ordinate direction. The widths in the direction of abscissa is written by taking the error of temperature reading, which is ±0.6 °C, into consideration. Similarly Fig. 7 shows an Eyring's plot pertaining to the rate constants k_2. Although it is possible to obtain $\Delta H^{\ddagger}$ and $\Delta S^{\ddagger}$ as 10.2±0.6 kcal/mol and −9.6±2.3 e.u., respectively, for the process *meso*→*d* (or *l*) with a percent error of 5.6, it may contain errors derived by the ambiguity in the k_1's. It is difficult to draw a straight line in the case of k_2's.

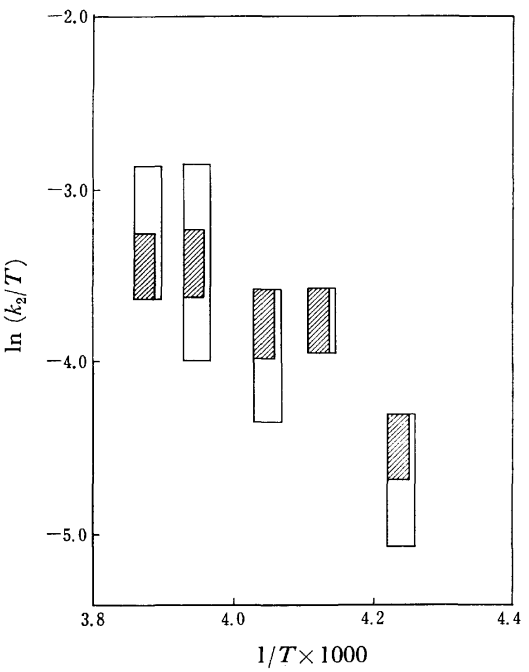

Fig. 7. Eyring's plot showing the ranges of possible errors for the process $d \rightleftharpoons l$ of 9-(*p*-chlorobenzyl)-1,4-dimethoxytriptycene. Open rectangles correspond to those obtained by computation only and hatched rectangles to those derived by using k_1's obtained from the methoxyl signals. For the temperature ranges of the latter, see the caption of Fig. 6.

Barrier to the Minor Process. As pointed out in the previous paper, the rate constants k_1 may be obtained by analyzing the line shapes of the methoxyl signals. One may hope then that if we put these data to obtain the best fit spectra, we should be able to obtain k_2's of better quality. Indeed, the rate constants were obtained as follows at the temperatures where we have the methylene data, using the methoxyl signal shapes (units are s^{-1}): 106 (−15.3 °C), 59.5 (−19.9 °C), 39.8 (−26.3 °C), 19.9 (−31.1 °C), 12.6 (−37.3 °C). These data are also shown in Fig. 6, taking the error limit as ±5%, because we selected the best fit spectra by comparing the computed spectra of *ca.* 5% intervals of rates. The ranges of the k_2's can then be reduced and are shown in Fig. 7. Apparently the linear relation may not be claimed: although we can treat the data by the least squares method to draw a straight line, its percent error amounts to 20.7. Thus it is not practical to obtain the kinetic parameters for the $d \rightleftharpoons l$ process from these data.

It is noteworthy, however, that the calculated spectra suggest that k_2 is close to 1/10—2/10 of k_1. This corresponds to the difference of *ca.* 1 kcal/mol in the barriers to the two processes. Therefore we conclude that the $d \rightleftharpoons l$ process possesses a higher barrier to rotation than the *meso*→*d* (or *l*) process by *ca.* 1 kcal/mol.

The Case of 9-Benzyl-1,2,3,4-tetrachlorotriptycene. This compound is picked up as a model because it poses another problem: does lesser population have any influence on determing a rate constant? Variation of the temperature influenced the spectra of the methylene

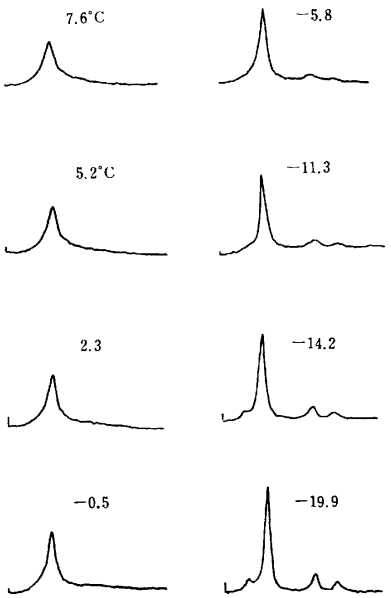

Fig. 8. Temperature dependent spectra of the methylene region of 9-benzyl-1,2,3,4-tetrachlorotriptycene.

Table 2. Populations of the *meso* and the *dl* forms and equilibrium constants of 9-benzyl-1,2,3,4-tetrachlorotriptycene at various temperatures

Temperature (°C)	Populations		K
	meso	*d* (or *l*)	(*dl*/*meso*)
7.6	0.63	0.18	0.58
5.2	0.62	0.19	0.59
2.3	0.62	0.19	0.61
−0.5	0.61	0.19	0.63
−5.8	0.60	0.20	0.66
−11.3	0.59	0.21	0.70
−14.2	0.58	0.21	0.73
−19.9	0.56	0.22	0.78

part as shown in Fig. 8. The population was *ca.* 6 to 4 (*meso*: *dl*). The temperature dependence of the population ratios was determined as shown in Table 2 and the thermodynamic parameters were obtained as follows: ΔH -2.3 ± 0.3 kcal/mol, ΔS -9.8 ± 1.4 e.u. Therefore this compound is a model which possesses less populations of which exchange corresponds to the slow process.

Typical calculated spectra are shown in Fig. 9, where the spectrum at −14.2 °C is taken as an example. Parameters used for the calculation were as follows: $\Delta\nu_{AB}$ −52.29 Hz; $\Delta\nu_{AC}$ 4.095 Hz; J_{AB} 18.6 Hz; populations, *meso* 0.58 and *d* (or *l*) 0.21. T_2's were observed at respective temperatures. As is seen in the figure, it is hardly possible to detect the effect of the slower process, although the rate constant was changed by a factor of almost 50. Thus we may be able to specify the rate constant of the faster process but not the slower one in this case: the line shapes are controlled by the faster process almost exclusively. We may obtain the rates of exchange *meso*⇌*d* (or *l*) independently by looking

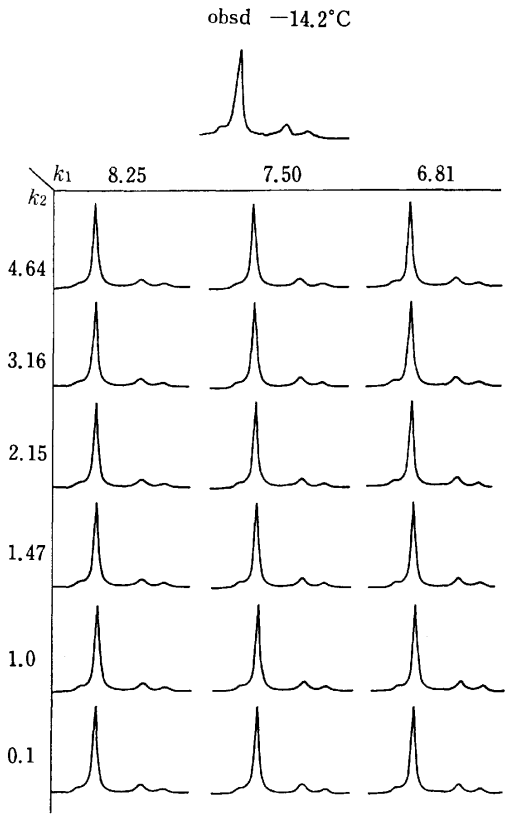

Fig. 9. Computed spectra of 9-benzyl-1,2,3,4-tetrachlorotriptycene at −14.2 °C using various k_1's and k_2's.

at the ^{13}C NMR line shape but the rates thus obtained do not help in obtaining the rates of the slower process.

The rate constants k_1's were obtained as follows (given in s^{-1}): 56.2 (7.6 °C), 46.4 (5.2 °C), 42.1 (2.3 °C), 26.1 (−0.5 °C), 14.7 (−5.8 °C), 12.1 (−11.3 °C), 7.50 (−14.2 °C), 4.64 (−19.9 °C). The Eyring's plot using these values affords ΔH^* 12.5 ± 0.3 kcal/mol and ΔS^* -6.0 ± 1.3 e.u. for the *meso*→*d* (or *l*) process. The activation parameters for the reverse process *d* (or *l*)→*meso* are then ΔH^* 14.0 ± 0.3 kcal/mol and ΔS^* 2.0 ± 0.2 e.u. We may have to expect that these values contain errors as large as 10% in addition to that of the least squares treatment.

Conclusion

We conclude that, in 9-benzyltriptycenes possessing a substituent in one of the peri positions which are close to the substituent, the barrier to rotation is *ca.* 13 kcal/mol. The activation parameters may be obtained by treating the rate constants obtained by the total line shape analysis of the methylene part in ^1H NMR spectra. However, the following should be kept in mind in discussing the data.

1) The process with a large rate constant plays a decisive role in determining the line shape, as was pointed out by Bushweller *et al.*[10] and the rate of the slow process, if obtained, includes a larger error.

2) If the rate constant of a slower process is less than a hundredth of that of a faster process, the former

cannot be detected by the visual fitting of calculated spectra with the obersved. The difference in free energies of activation for the two processes must be smaller than 2—3 kcal/mol to be detected.

3) It is extremely difficult to obtain accurate data for a slow process by comparison of the observed and the calculated spectra. Neglect of the slow process results in overestimation of a fast process, the enthalpy of activation of which is obtained smaller than the true.

4) The populations in the exchange sites have influence on the detectability of a slow process. The exchange between two sites with fewer populations contribute to the line shape too little to affect, if the rate is small.

5) The ambiguity in determining the rates of two exchanging processes is reduced to some extent by utilization of information obtained by other means. However, it was not possible to erase all the ambiguities in the present case.

References

1) Preceding paper: M. Kono and M. Ōki, *Bull. Chem. Soc. Jpn.*, **52**, 1682 (1979).

2) "Dynamic Nuclear Magnetic Resonance Spectroscopy," ed by L. M. Jackman and F. A. Cotton, Academic Press, New York (1975).

3) M. Nakamura, H. Kihara, N. Nakamura, and M. Ōki, *Org. Magn. Reson.*, in press.

4) R. R. Shoup, E. D. Becker, and M. L. McNiel, *J. Phys. Chem.*, **76**, 71 (1972).

5) C. H. Bushweller, C. Y. Wang, J. Reny, and M. E. Lourandos, *J. Am. Chem. Soc.*, **99**, 3938 (1977).

6) H. Kessler, V. Husowski, and M. Hanack, *Tetrahedron Lett.*, 4665 (1968).

7) F. A. L. Anet and I. Yavari, *J. Am. Chem. Soc.*, **99**, 7640 (1977).

8) a) M. Ōki, *Angew. Chem. Int. Ed. Engl.*, **15**, 87 (1976); b) H. Nakanishi and O. Yamamoto, *Bull. Chem. Soc. Jpn.*, **51**, 1777 (1978).

9) L. Lunazzi, D. Macciantelli, F. Bernardi, and K. U. Ingold, *J. Am. Chem. Soc.*, **99**, 4573 (1977).

10) C. Y. Wang and C. H. Bushweller, *J. Am. Chem. Soc.*, **99**, 313 (1977).

11) F. Suzuki and M. Ōki, *Bull. Chem. Soc. Jpn.*, **48**, 596 (1975).

12) G. Binsch, "Topics in Stereochem.," ed by E. L. Eliel and N. L. Allinger, Interscience, New York (1970), Vol. 3, p. 97.

Molecular Dynamics of the Inclusion Complexes of Cyclohexaamylose with Some Aromatic Amino Acids and Dipeptides

Yoshio INOUE,* Yukio KATÔNO, and Riichirô CHÛJÔ

Department of Polymer Chemistry, Tokyo Institute of Technology, O-okayama 2-12-1, Meguro-ku, Tokyo 152

(Received November 29, 1978)

The molecular dynamics of the inclusion complexes of cyclohexaamylose as a model of enzyme have been studied by means of carbon-13 NMR spectroscopy. As substrates we have chosen L-phenylalanine, L-tyrosine, L-tryptophan, glycyl-L-phenylalanine, and L-phenylalanyl-L-lysine. The molecular motion of both the cyclohexaamylose and the substrates in D_2O–DCl solutions have been investigated by dividing the spin-lattice relaxation time into two contributions, the overall molecular reorientation and the anisotropic internal rotation. Upon complex formation, the correlation times for the internal motion of the phenyl ring of phenylalanine residue increase by a factor of up to 8, while those for the overall reorientation increase by a factor of only 2. These results indicate that the complex formation of the substrate with the cyclohexaamylose are induced by the insertion of aromatic side chain into a cavity of cyclohexaamylose even in the aqueous solution. The overall correlation times of the substrates are about three to seven times shorter than those of the host molecule. Thus the forces which bind the host cyclohexaamylose and the substrate are relatively weak. It was observed that the tightness of the inclusion varies with the types of aromatic amino acids and dipeptides.

Cycloamylose (cyclodextrin, CD) is known to form inclusion complexes with various types of small molecules of appropriate size in solution as well as in the crystalline state.[1-3] Cyclohexaamylose (α-CD, cyclohexaglucopyranose) has the shape of a hollow truncated cone with 6 primary and 12 secondary hydroxyl groups crowning opposite ends of its torus. All the glucose units in CD are present in the Cl chair conformation, and the CH groups of carbons 3 and 5 of each unit compose the inside of the hollow torus, even in the aqueous solution.[1,2,4-6] Thus, the hollow space should be relatively hydrophobic.

Cycloamyloses have been used as models for enzymes[7] because their structures are well defined and because they can specifically bind substrates into their hydrophobic cavity. Cycloamyloses are especially good models at present for hydrolytic enzyme, chymotrypsin.[2-7] It is well known that chymotrypsin does not cleave all peptide bonds at a significant rate, and rather it is selective for peptide bonds on the carboxyl side of residues with aromatic side chains, tryptophan, tyrosine, and phenylalanine, and of large bulky hydrophobic residues such as methionine.[8] In these residues aromatic or bulky nonpolar side chains are assumed to be fitted neatly into a nonpolar pocket on chymotrypsin chain.

It is of great interest to investigate the molecular dynamics of inclusion complexes between CD and aromatic amino acids and peptide as models for enzyme-substrate specific binding. Interactions between phenylalanine and α-CD and β-CD (cycloheptaamylose) in aqueous solution have been studied using ^{1}H NMR.[5,6] It has been also studied the thermodynamics of binding of the aromatic guest molecules, including L-phenylalanine (Phe), L-tyrosine (Tyr), and L-tryptophan(Try), to α- and β-CD.[9] These studies have been providing the evidence for the inclusion nature of CD's complex formation with the aromatic side chain of amino acids. Since measurements of carbon-13 spin-lattice relaxation times are particularly useful for the investigation of molecular dynamics of CD inclusion complexes in detail,[10,11] we will study the molecular motion of both guest and host molecules in the inclusion complexes of α-CD with amino acids and dipeptides having aromatic side chain in aqueous solution by means of carbon-13 spin-lattice relaxation. As substrates we will chose Phe, Tyr, Trp, glycyl-L-phenylalanine(Gly–Phe), and N^{α}-(*N*-acetyl-L-phenylalanyl)-L-lysine methyl ester(Phe–Lys) for studying the effect of the types of aromatic ring and of the peptide sequence on the dynamics of the inclusion complex.

Experimental

Materials. α-CD, Phe, Tyr, Try, and Gly–Phe were purchased from Tokyo Kasei Kogyo Co., Ltd. Phe–Lys was supplied by the courtesy of Mr. M. Sakurai of our laboratory. D_2O (isotopic purity: 99.7 atom %D) and 38% (w/w) DCl solution in D_2O were used as solvents and the deuterium field-frequency lock signal in ^{13}C NMR measurement. These deuterated compounds were purchased from Merck Sharp and Dohme Canada Ltd.

Methods. ^{13}C spin-lattice relaxation times (^{13}C-T_1) were measured by the inversion-recoverly method using a 180°-*t*-90° pulse sequence as described by Freeman and Hill,[12] where *t* is time in seconds between the 180° and 90° pulses, on a JEOL JNM PS-100 spectrometer (25 MHz) equipped with a PFT-100 Fourier-transform system and a proton noise decoupler. Data were accumulated in a JEOL JEC-6 computer using 4000 Hz sweep widths in 4096 points (resolution: 2.0 Hz). The 90° pulse recycle times were chosen to be at least five times the longest ^{13}C-T_1 to be measured. The molar concentrations in D_2O–DCl solutions of both α-CD and the substrates for the ^{13}C NMR measurements were kept *ca.* 0.1 M, namely the molar ratio of α-CD to the substrate was 1:1 in the mixture. Samples in D_2O–DCl solutions were thoroughly deoxygenated with nitrogen in order to prevent from the paramagnetic effect of oxygen molecules on T_1 values, because ^{13}C-T_1 of protonated carbon nucleus obtained on such samples may be identical with those from samples degassed by repeated freeze-pump-thaw cycles.[13,14] In all experiments the decrease in amplitude of each resonance with increasing *t* followed an exponential curve characterized by a single T_1, and there was no evidence of heterogeneous relaxation times. The estimated error in T_1 was less than ±10%.

Ultraviolet absorption (UV) spectra were taken on a Beckman-25 spectrometer. For the UV measurements, the

molar concentrations of the aromatic substrates were kept *ca.* 5×10^{-5} M and those of α-CD were varied from zero to 10^{-2} M.

The pH values, read on a TOA pH meter HM-7A, of all samples were adjusted to *ca.* 2 unless otherwise stated. The temperature was kept at 32 ± 2 °C for all experiments.

Results and Discussion

Association Constants. The association constants (K_a) for the complexation of Phe, Tyr, and Trp with α-CD have been estimated by the UV spectral changes induced by the addition of α-CD.[15] The K_a values obtained by assuming the 1:1 complexation[5,6,9] were *ca.* $2\times10^2-6\times10^2$ M for these three α-CD-substrate systems. These values are comparable with those of closely related systems,[2,3,6,9] where the complexes are of the 1:1 inclusion types. Thus, in this paper, the values of ^{13}C-T_1 were analysed by assuming that the complexation of the substrates with α-CD are induced by the insertion of an aromatic side chain of the substrate into a cavity of α-CD.

Carbon-13 NMR Spectra. All peaks in the ^{13}C NMR spectra of both α-CD and the substrates have been assigned based on the assignments previously given by several authors.[16] The ^{13}C NMR spectrum of each α-CD-substrate system consists of only one set of peaks, indicating that only one type of complexation occur and/or the chemical exchange process expressed by Eq. 1 is rapid on the ^{13}C NMR time scale,

$$\alpha\text{-CD} + \text{S} \rightleftarrows [\alpha\text{-CD, S}] \qquad (1)$$

where S and [α-CD, S] are the substrate and α-CD-substrate complex, respectively. The ^{13}C chemical shifts induced in the spectra of α-CD by complexation with the substrates were less than 0.40 ppm of upper-field shifts, which could be attributed to the hydrophobic nature of the interaction between α-CD and the substrate.[11,17]

^{13}C Relaxation Times. In the limit of rapid exchange process of Eq. 1, one measures an average relaxation rate[18]

$$\frac{1}{T_1} = p_f\frac{1}{T_{1f}} + p_c\frac{1}{T_{1c}} \qquad (2)$$

where T_{1f} and T_{1c} are intramolecular spin-lattice relaxation times for a spin at the free and complex states, and p_f and p_c ($=1-p_f$) are the probabilities that α-CD or the substrate is found in the free and complex states, respectively. Eq. 2 is valid only if the relaxation times T_{1f} and T_{1c} are much larger than the life times in the free and complex states. Since the association-dissociation process between α-CD and the aromatic substrates in the aqueous solution is performed in the microsecond to millisecond range[3] and the observed values of ^{13}C-T_1 are in the order of 1—10^{-1} s (see below), the Eq. 2 is applicable to the present study.

For the reaction of Eq. 1, the probability p_c to find a α-CD or a substrate molecule in the complex state can be expressed by

$$p_c = \frac{1}{2}(1+k)\left\{1-\left[1-\frac{4K_a}{K_a+1}\cdot\frac{k}{(1+k)^2}\right]^{1/2}\right\} \qquad (3)$$

where k is the molar ratio of α-CD to substrate S (or converse). In the present case, $K_a\simeq10^2\gg1$ and $k=1$, hence $p_c\simeq1$. Eq. 2 can be, therefore, simplified as,

$$\frac{1}{T_1} \simeq \frac{1}{T_{1c}} \qquad (4)$$

that is, the ^{13}C-T_1 values observed in the present α-CD-substrate mixed system can be considered to be exclusively that of the complex state.

The values of ^{13}C relaxation time measured for the free substrates, free α-CD, and the complexes between them are listed in Table 1. From this table we shall analyse the molecular motions in the inclusion complexes.

For molecules of medium size whose motion is rapid on the ^{13}C NMR time scale, it is likely that the ^{13}C-T_1 value of the carbon atom directly linked at least one proton is governed by ^{13}C-^{1}H dipole-dipole relaxation brought about by a rotational motion.[19] In this case, if the overall molecular reorientation is isotropic, ^{13}C-T_1 is given by

$$\frac{1}{T_1} = \hbar^2\gamma_C^2\gamma_H^2 N r_{CH}^{-6}\tau_{eff} \qquad (5)$$

where τ_{eff} is the effective correlation time for overall molecular reorientation, r_{CH} is the carbon-hydrogen bond length, γ_H and γ_C are the gyromagnetic ratios of ^{1}H and ^{13}C nuclei, and N is the number of directly bonded proton. This τ_{eff} can be related to the isotropic rotational diffusion constant D, and according to the Brownian diffusion model[20-22]

$$\tau_{eff} = \frac{1}{6D} = \frac{8\pi\eta f_r r_0^3}{6kT} = \frac{V_m\eta f_r}{kT} \qquad (6)$$

where k is Boltzmann's constant, T is the absolute temperature, η is the viscosity of the solution in poise, f_r is a microviscosity factor, r_0 is the radius of a spherical solute molecule, and V_m is the molecular volume $V_m=4/3\pi r_0^3$. From Eqs. 5 and 6, a relationship between NT_1 value and the molecular volume is derived as follows

$$\frac{1}{NT_1} = \hbar^2\gamma_C^2\gamma_H^2 r_{CH}^{-6}\eta f_r V_m/kT. \qquad (7)$$

If α-CD is considered to be a spherical molecule of 7.31×10^{-10} m radius,[2,3] and the viscosity of the solution is assumed to be determined mainly by the solvent D_2O ($=1.04\times10^{-2}$ poise at 32 °C[24]), NT_1 values for the ring carbons of α-CD in the free states can be calculated from Eq. 7 using a value of f_r equal to unity[20] and the temperature equal to 305 K. We have 0.122 s for NT_1 value which agrees well with the observed mean value of 0.132 s for ring carbons C_{1-5} within experimental error. For the carbons of the free amino acids and dipeptides NT_1 values were calculated by a similar way. Here, the values of molecular volume of these molecules were calculated by the atomic increments method based on the van der Waals radii of the constituent atoms.[25] Since the molecules investigated here have the freedom of local internal rotation in the side chain and the backbone in addition to the overall motion, it is difficult to find the NT_1 value of the carbon which is determined mainly by the overall reorientation of the molecule. In general, the additional internal

TABLE 1. VALUES OF ^{13}C NT_1[a,b] FOR CYCLOHEXAAMYLOSE (α-CD), SUBSTRATES, AND MOLECULAR INCLUSION COMPLEXES BETWEEN THEM MEASURED IN D_2O–DCl SOLUTIONS AT 32 °C AND pH 2

Compd[c]	^{13}C NT_1(s)±10%						
	1	**2**	**3**	**4**	**5**	**6**	$\langle T_1\rangle_{1-5}$ [α-CD][d]
[α-CD]	0.127	0.136	0.128	0.133	0.135	0.168	0.132
[α-CD, Phe]	0.115	0.119	0.131	0.120	0.119	0.140(0.83)	0.121(0.92)
[α-CD, Tyr]	0.124	0.113	0.110	0.105	0.118	0.164(0.98)	0.114(0.86)
[α-CD, Trp]	0.121	0.124	0.127	0.127	0.119	0.164(0.98)	0.124(0.94)
[α-CD, Gly–Phe]	0.097	0.114	0.115	0.114	0.099	0.124(0.74)	0.108(0.82)
[α-CD, Phy–Lys]	0.083	0.090	0.098	0.081	0.088	0.100(0.60)	0.088(0.67)
	α	β	δ	ε	ζ		
[Phe]	1.34	1.60	1.44	1.44	1.08		
[α-CD, Phe]	1.06(0.79)	1.18(0.74)	0.91(0.63)	0.91(0.63)	0.82(0.76)		
[Tyr]	0.99	1.26	1.16	1.16			
[α-CD, Tyr]	0.67(0.68)	0.86(0.68)	0.87(0.75)	0.87(0.75)			
	α	β	δ_1	ε_3	ζ_2	η	ζ_1
[Trp]	0.81	0.84	0.76	0.73	0.84	0.73	0.73
[α-CD, Trp]	0.61(0.75)	0.76(0.90)	0.40(0.53)	0.36(0.49)	0.41(0.49)	0.41(0.56)	0.37(0.51)
	Phe-α	β	δ	ε	ζ	Gly-α	
[Gly–Phe]	0.99	1.14	1.05	1.02	0.75	1.42	
[α-CD, Gly–Phe]	0.56(0.57)	0.82(0.72)	0.66(0.63)	0.62(0.61)	0.51(0.68)	0.64(0.45)	
[Phe–Lys][e]	Phe-α	β	δ	ε	ζ		
	0.34	0.42	0.53	0.54	0.37		
	Lys-α	β	γ	δ	ε		
	0.39	0.40	0.72	0.92	1.14		
[α-CD, Phe–Lys][e]	Phe-α	β	δ	ε	ζ		
	0.28(0.82)	0.34(0.81)	0.25(0.47)	0.24(0.44)	0.22(0.59)		
	Lys-α	β	γ	δ	ε		
	0.24(0.62)	0.34(0.81)	0.48(0.67)	0.54(0.59)	0.78(0.68)		

a) Here, T_1 is the spin-lattice relaxation time and N is the number of hydrogens attached to the carbon. The measured NT_1 values correspond to the underlined species. b) The values shown in parentheses are the NT_1 ratios of the complexed states to the free states. c) Assignments of carbon atoms are as follows. d) The mean values of T_1 for C_{1-5}. e) Measured at pH 7.0.

α-CD

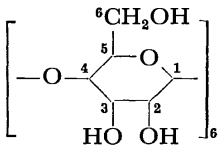

Phe(Tyr)

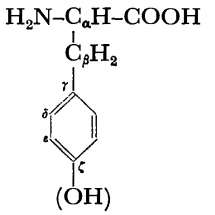

Trp

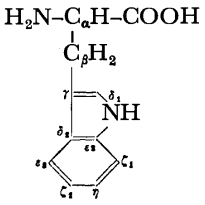

TABLE 2. OBSERVED AND CALCULATED NT_1 VALUES, IN SECONDS, OF SUBSTRATE AMINO ACIDS AND DIPEPTIDES

Compd		Observed NT_1	Calculated NT_1	V_m[a]
Phe	C_ζ	1.08	1.01	148
Tyr	C_α	0.99	0.96	156
Trp	C_α	0.81	0.85	176
	$C_{\varepsilon,\eta,\zeta}$	0.73		
Gly–Phe	C_ζ	0.75	0.76	197
Phe–Lys	C_α(Phe)	0.34		
	C_ζ(Phe)	0.37	0.45	329
	C_α(Lys)	0.39		

a) The molecular volume used for the calculation of NT_1 value, estimated by the atomic increments method.[25]

motion faster than the overall one makes the NT_1 value lengthen.[19] Therefore, we regarded the smallest NT_1 values as the representative of the measure of the overall reorientation. Agreements between the calculated and the observed NT_1 values are well as shown in Table 2, notwithstanding the values of molecular volume used in the calculation of NT_1 are only approximate. Thus we can use Eq. 5 for the analyses of the overall molecular reorientation of both α-CD and the substrates in the free states. Eq. 5 might be applicable, at least qualitatively, to the analyses of molecular motions of both α-CD and substrate molecules in the complex states.

For the group undergoing an additional internal motion, the NT_1 value of a protonated carbon with N directly bonded hydrogens is given by[19,26]

$$\frac{1}{NT_1} = \frac{\hbar^2\gamma_H^2\gamma_C^2}{r_{CH}^6}\tau_{eff}\left[A+B\frac{6\tau_G}{6\tau_G+\tau_{eff}}+C\frac{3\tau_G}{3\tau_G+2\tau_{eff}}\right] \quad (8)$$

where τ_G is the correlation time for internal motion and

$$A = 1/4(3\cos^2\theta-1)^2 \quad (9)$$

$$B = 3\sin^2\theta\cos^2\theta \quad (10)$$

$$C = 3/4\sin^4\theta. \quad (11)$$

Here θ is the angle between the C–H vector and the axis of internal rotation. In the case of rotation of a tetrahedral C–H bond about the C–C bond, $\theta=109°$, this yields $A=1/9$, $B=8/27$, and $C=16/27$. Similarly, in the case of a phenyl ring rotation about C_β–C_γ bond of the Phe residue, C_δ–H and C_ε–H vectors intersect with the rotational axis at $\theta=60°$ and 120°, respectively, and then $A=1/64$, $B=9/16$, and $C=27/64$.

From Eqs. 5 and 8, it is clear that the greater the NT_1 value, the more mobile is the ^{13}C moiety, and that the additional internal rotation faster than the overall one makes the NT_1 value lengthen as mentioned in the preceding paragraph.

As shown in Table 1, for α-CD in the free and the complex states, the NT_1 values for the ring carbons (C_{1-5}) are equal within experimental error in each system, indicating the absence of specific fast internal motion in the pyranose ring.[10] Thus the mean value $\langle T_1\rangle_{1-5}$ could be used to calculate the effective correlation times for overall molecular reorientation of α-CD. The NT_1 values show the existence of rapid internal rotation of the primary alcohol group of α-CD, the phenyl group of Phe and Tyr residues, and all the C_β-methylene groups even in the complex states. Definite increase is observed in NT_1 values in Lys residues when going from the α-carbon to the terminal ε-carbon. These results also show the existence of the internal motion.[27] In the case of Phe residue, the axis of rotation of the phenyl ring about C_β–C_γ bond coincides with the C_ζ–H bond. Therefore, the rotation about C_β–C_γ bond cannot affects the T_1 value of C_ζ, since $\theta=0$ and thus Eq. 8 is reduced to Eq. 5. Then we can estimate the τ_G value for the internal rotation of phenyl ring of Phe residue by using the τ_{eff} value for C_ζ. Since the phenyl ring of Tyr has no C–H bond on the prefered axis of internal rotation, we cannot estimate accurately the τ_G value. The results of calculation of the correlation times are shown in Table 3. Here the correlation time τ_{eff} for the substrate was calculated by adopting the smallest NT_1 value in each substrate as the representative of the overall molecular reorientation having no or a little contribution from the internal motion. Throughout these calculation we have assumed that all C–H bond lengths (r_{CH}) are 1.10×10^{-10} m.

Effect of Complex Formation on the Molecular Motion of α-CD and the Substrates. As can be seen in Tables 1 and 3, all the values of NT_1 (τ_{eff}, τ_G) for both α-CD and the substrates decrease (increase), namely, the motions of these molecules slow down by complexation between them. The reductions of NT_1 are qualitatively explainable as a consequence of the increases in apparent molecular volume by complexation as expected from Eq. 7. The change in molecular dimension induced by complexation is relatively small for α-CD and relatively large for substrates, namely the reduction in NT_1 value of the former is smaller than the latter. For the substrates, it is noticeable that the NT_1 values of aromatic groups show larger changes by complex formation than those of other groups. The effect of the complex formation on the molecular motion could be discussed quantitatively in terms of correlation time. Despite the lack of accurate C–H lengths, the results shown in Table 3 are giving some interesting facts.

Table 3. Rotational correlation time τ_{eff} and τ_G of α-CD, substrates, and molecular inclusion complexes between them[a]

Compd[b]	Correlation time (10^{-11} s)	
	α-CD overall (τ_{eff})[c]	$-CH_2OH$ internal (τ_G)
[α-CD]	37	55
[α-CD, Phe]	41(1.1)	100(1.8)
[α-CD, Tyr]	43(1.2)	36(0.7)
[α-CD, Trp]	40(1.1)	49(0.9)
[α-CD, Gly–Phe]	46(1.2)	130(2.4)
[α-CD, Phe–Lys]	56(1.5)	170(3.1)
	substrate overall (τ_{eff})[d]	phenyl internal (τ_G)[e]
[Phe]	4.6	4.6
[α-CD, Phe]	6.0(1.3)	19 (4.1)
[Tyr]	5.0	4.2[f]
[α-CD, Tyr]	7.2(1.4)	5.6(1.3)[f]
[Trp]	6.7	
[α-CD, Trp]	13 (1.9)	
[Gly–Phe]	6.6	5.6
[α-CD, Gly–Phe]	9.7(1.5)	13 (2.3)
[Phe–Lys]	13	9.0
[α-CD, Phe–Lys]	22 (1.7)	69 (7.7)

a) The values shown in parentheses are the ratios of the correlation times of the complexed to the free states. b) The calculated values correspond to the underlined species. c) Calculated by using the mean values of T_1 for C_{1-5}. d) Calculated by using the smallest NT_1 values shown in Table 1. e) The average T_1 values for $C_{\delta,\varepsilon}$ and for τ_{eff} for C_ζ were used for the calculation of τ_G. f) The values of τ_{eff} were shown, so these values could not compare directly with other τ_G values.

The correlation times for the internal motion of the phenyl ring are clearly showing the mechanism of complex formation. The values of τ_G for the free substrates are comparable or slightly smaller than those of τ_{eff}, indicating the existence of rapid internal rotation of the phenyl ring. Upon complex formation with α-CD, the internal motion of the phenyl ring slows down by a factor of up to *ca.* 8, while the reduction factor of the overall motion is only less than 2. These results support the assumption that the substrates investigated here form the complexes with α-CD by the insertion of an aromatic side chain into a cavity of α-CD even in the aqueous solution. The τ_G values of the phenyl ring in the inclusion complexes show still the existence of apprecia-

bly rapid internal rotation. The results that the NT_1 values of C_δ and C_ϵ in phenyl ring agree with each other and they are always larger than those of C_ζ indicate that α-CD favors the axial inclusion in which the internal rotational axis C_γ–C_ζ of the phenyl ring of the guest is parallel to the axis of the α-CD cavity. According to the space-filling models, the diameter of the cavity of α-CD is about 6.0×10^{-10} m.[3] The molecular diameter, including the van der Waals radii of the proton, of the benzene nucleus is about 6.8×10^{-10} m, thus the axial inclusion is the most natural mode of inclusion.[5]

For the substrates themselves the overall correlation time τ_{eff} increases in the order Phe<Tyr<Gly–Phe≃Trp<Phe–Lys, and this order is also valid after the complex formation. The τ_{eff} value of the three substrates Phe, Tyr, and Trp in the free states are about same and are in the range expected for a molecule of similar size. The Trp, however, shows the prominent increase in τ_{eff} by the formation of complex. The peculiarity of Trp should be a partly due to the difference of the inclusion mode and a partly due to the bulkiness of the indolyl group. In the most probable inclusion mode of the indolyl group, the long axis of the benzene ring $C_{\epsilon3}$–$C_{\zeta1}$ may crosses at about right angles with the axis of the α-CD cavity. This inclusion mode induces larger steric interactions between the indolyl group of Trp and the internal and peripheral group of the α-CD's cavity due to the bulkiness of indolyl group as compared with the axial inclusion of the monocyclic aromatic ring of Phe and Tyr. Thus the bulkiness and type of the aromatic side chain are important factors determining the tight packing of the substrate into the cavity.

Several mechanisms have been proposed for the formation of CD inclusion complex,[2,3,28] but the force driving complex formation and the mechanism of inclusion are still unclear and a matter of speculation.[28] A formation of hydrogen bond between α-CD and substrate may promote complex formation and stabilize resulting complex. It is generally accepted that many benzene derivatives and α-CD form 1 : 1 complexes with benzene ring inserted into the cavity from the secondary hydroxyl side.[3,6,15] According to this model several groups of the substrates investigated here have the hydrogen-bonding capabilities to the α-CD's hydroxyl groups located on the outside of the torus. The existence of hydrogen bond may be confirmable from an analyses of NT_1 values.[29,30] The hydroxyl group of Tyr has no noticeable influence, as compared to the other substrates, on the molecular motions of both α-CD and Tyr in the complexed state, indicating the absence of strong hydrogen bonding interaction between Tyr hydroxyl group and α-CD primary hydroxyl group. The NT_1 value of Gly–C_α in Gly–Phe, in spite of the adjoining carbon to the end group, reveals a significant decrease of motion by complex formation, while that in the free state indicates an evidence of appreciable internal motion. The reduction of Gly–C_α motion may be due to the anchoring effect of the hydrogen bond at the chain end on the molecular motion.[29]

Upon complex formation of Phe–Lys with α-CD, the NT_1 values of alkyl chain carbons of Lys residue show slightly larger reductions as compared with those of C_α and C_β of Phe and Lys residues of Phe–Lys, suggesting an existence of further weak interaction between alkyl chain of Lys residue and α-CD. In this case, two causes can be pointed out as the origin of interaction, *i.e.*, steric hindrance due to access of huge α-CD to Phe residue and $N_\epsilon H$ hydrogen bonding to α-CD. The changes of NT_1 values, however, are too small to clear the causes.

Phe dipeptide, Phe–Lys, in both free and complexed states shows the largest τ_{eff} and τ_G values among the corresponding values of all substrates. The magnitude of Phe–Lys's τ_{eff} is not unreasonable as compared with those of other substrates. However, Phe–Lys shows an unexpected increase in τ_G value of phenyl group by complex formation. Since, in the complex state, the phenyl τ_G value of Gly–Phe is shorter than that of Phe, a largeness of molecular volume or molecular weight of Phe–Lys is not a only reason for this unusual increase in τ_G value. From these results, we can say that the type of the amino acid residue adjoining to aromatic residue in peptide chain is also one of the factors for the tight packing of the substrate into the cavity.

It is noteworthy that, in the complexes, the overall correlation times of the five substrates are about three to seven times shorter than those of the host α-CD molecule. This result indicates the weakness of a dynamic coupling between α-CD and the substrates, namely the extensive independency of a overall motion between them. This result further suggests the shallowness of penetration of the aromatic ring of the substrates into the cavity of α-CD. If the penetration is deep, all motions of aromatic ring other than anisotropic internal rotation about C_β–C_γ bond are greatly restricted within narrow limits due to the steric hindrance. In this case, however, the NT_1 values of C_ζ of Phe residue are too large to explain because the internal rotation about C_β–C_γ bond cannot affects the T_1 values of C_ζ. Thus the penetration of the aromatic ring into the cavity may be an extent to allow the substrate a relatively rapid motion. The shallowness of the insertion is suggested by the absence of hydrogen bond between the hydroxyl group of Tyr and the primary hydroxyl group of α-CD. The results of ^1H NMR study also support the shallow insertion of phenyl ring of Phe into the α-CD cavity.[6] The inclusion of the phenyl ring of D- and L-Phe into the cavity is evident from the upperfield shift of the α-CD's H_3 resonances, but the H_5 resonances are not affected by complexation and furthermore the magnitude of the H_3 upperfield shift induced by complexation is only 0.10 ppm.[6] The three times larger shifts (0.31 ppm) of the H_3 resonances have been observed in the complex between α-CD and *p*-iodoaniline.[6] The strongest coupling between α-CD and the substrate overall motions is seen in [α-CD, Phe–Lys] system, where several intermolecular interaction may participate in the dynamic coupling.

In conclusion, the inclusion complexes between α-CD and the aromatic amino acids and dipeptides investigated here show some characteristics like general peculiarities of enzyme-substrate complex.[8] The host

α-CD has the cavity leading to substrate specifity and the shape matching between the cavity and the substrate is one of the factors determining the strong coupling between them. A nonpolar character of the host cavity and a intermolecular hydrogen bond enhance the binding of substrate and α-CD, but the forces which bind them are relatively weak. The strength of the dynamic coupling also depends on the types of dipeptides.

References

1) F. Cramer, "Einschlussverbindungen," Springer-Verlag, Heiderberg (1954).
2) F. Cramer and H. Hettler, *Naturwissenschaften*, **54**, 625 (1967).
3) F. Cramer, W. Saenger, and H.-Ch. Spatz, *J. Am. Chem. Soc.*, **89**, 14 (1967).
4) C. A. Class, *Can. J. Chem.*, **43**, 2652 (1965).
5) P. V. Demarco and A. L. Thakkar, *Chem. Commun.*, **1970**, 2.
6) D. J. Wood, F. E. Hruska, and W. Saenger, *J. Am. Chem. Soc.*, **99**, 1735 (1977).
7) M. Komiyama and M. L. Bender, *J. Am. Chem. Soc.*, **99**, 8021 (1977); B. Siegel, A. Pinter, and R. Breslow, *ibid.*, **99**, 2309 (1977), and references cited therein.
8) L. Stryer, "Biochemistry," W. H. Freeman and Co., San Francisco (1975).
9) E. A. Lewis and L. D. Hansen, *J. Chem. Soc. Perkin Trans. 2*, **1973**, 2081.
10) J. P. Behr and J. M. Lehn, *J. Am. Chem. Soc.*, **98**, 1743 (1976).
11) K. Uekama, F. Hirayama, and H. Koinuma, *Chem. Lett.*, **1977**, 1393.
12) R. Freeman and H. D. W. Hill, *J. Chem. Phys.*, **53**, 4103 (1970).
13) Y. K. Levine, N. J. M. Birdsall, A. G. Lee, and J. C. Metcalfe, *Biochemistry*, **11**, 1416 (1972).
14) Y. Inoue, A. Nishioka, and R. Chujo, *J. Polym. Sci, Polym. Phys. Ed.*, **11**, 2237 (1973).
15) R. L. VanEtten, J. F. Sebastian, G. A. Clowes, and M. L. Bender, *J. Am. Chem. Soc.*, **89**, 3242 (1967).
16) (a) For α-CD: T. Usui, N. Yamaoka, K. Matsuda, T. Tuzimura, H. Sugiyama, and S. Seto, *J. Chem. Soc. Perkin Trans. 1*, **1973**, 2425; P. Colson, H. J. Jennings, and I. C. P. Smith, *J. Am. Chem. Soc.*, **96**, 8081 (1974); H. Friebolin, N. Frank, G. Keilich, E. Siefert, *Makromol. Chem.*, **177**, 845 (1976). (b) For amino acids and small peptides: W. J. Horsely and H. Sternlicht, *J. Am. Chem. Soc.*, **90**, 3738 (1968); M. Christl and J. D. Roberts, *J. Am. Chem. Soc.*, **94**, 4565 (1972); S. Fermandjian, S. Tran-Dinh, S. Saŭrda, E. Sala, R. Mermet-Bouvien, E. Bricas, and P. Fromageot, *Biochim., Biophys. Acta*, **399**, 313 (1975); O. W. Howarth and D. M. J. Lilley, *Prog. NMR Spectrosc.*, **12**, 1 (1978).
17) W. W. Conover and J. Fried, *Proc. Nat. Acad. Sci. USA*, **71**, 2157 (1974).
18) J. R. Zimmerman and W. E. Brittin, *J. Chem. Phys.*, **61**, 1328 (1957).
19) A. Allerhand, D. Doddrell, and R. Komoroski, *J. Chem. Phys.*, **55**, 189 (1971).
20) J. H. Noggle and R. E. Schirmer, "The Nuclear Overhauser Effect," Academic Press, New York, N. Y. (1971).
21) R. D. Deslauriers, A. C. M. Paiva, K. Schaumburg, and I. C. P. Smith, *Biochemistry*, **14**, 878 (1975).
22) R. D. Deslauriers, Z. Grzonka, K. Schaumburg, T. Shiba, and R. Walter, *J. Am. Chem. Soc.*, **97**, 5093 (1975).
23) A. Hybl, R. E. Rundle, and D. E. Williams, *J. Am. Chem. Soc.*, **87**, 2779 (1965).
24) C. F. Prutton and S. H. Maron, "Fundamental Principles of Physical Chemistry," Macmillan, New York, N. Y. (1951), p 679.
25) J. T. Edward, *J. Chem. Educ.*, **47**, 261 (1970).
26) D. Doddrell, V. Glushko, and A. Allerhand, *J. Chem. Phys.*, **56**, 3683 (1972).
27) H. Saito and I. C. P. Smith, *Arch. Biochem. Biophys*, **158**, 154 (1973).
28) W. Saenger, M. Noltemeyer, P. C. Manor, B. Hingerty, and B. Klar, *Bioorg. Chem.*, **5**, 187 (1976).
29) D. Doddrell, A. Allerhand, *J. Am. Chem. Soc.*, **93**, 1558 (1971).
30) U. Edlund, C. Holloway, and G. C. Levy, *J. Am. Chem. Soc.*, **98**, 5069 (1976).

Structure of Alnustic Acid, a New Secodammarane-type Triterpenic Acid from *Alnus sieboldiana*

Takayuki SUGA,* Tadashi AOKI, Toshifumi HIRATA,
Keiko AOKI (*née* SUKEMIYA), and Yoshinori ASAKAWA
Department of Chemistry, Faculty of Science, Hiroshima University, Higashisenda-machi, Hiroshima 730
(Received December 4, 1979)

A novel C_{31} 3,4-secodammarane-type triterpenoid, alnustic acid, was isolated from the male flowers of *Alnus sieboldiana* Matsum. (Betulaceae). Its structure was elucidated to be (12*R*,20*S*)-12,20-dihydroxy-24-methylene-3,4-secodammar-4(28)-en-3-oic acid by a combination of chemical and spectroscopic methods.

The occurrence of only aromatic ring-containing compounds, such as phenyl propane derivatives, flavonoids, and stilbenes, in the male flowers of *Alnus sieboldiana* Matsum. (Betulaceae) was previously reported from our laboratory.[1-5] Ohmoto *et al.* also described the presence of a flavone glucoside in the pollens of this plant.[6] Our further investigation of the male flowers has newly led to the isolation of a novel C_{31} 3,4-secodammarane-type triterpenic acid, named alnustic acid, differing from the above-described group of compounds. We here wish to report evidence which led to the establishment of its structure.

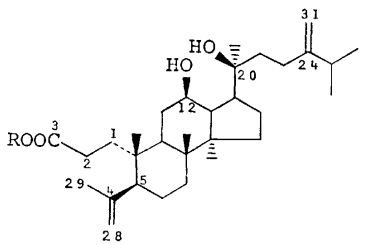

1 R=H
2 R=CH_3

Results and Discussion

The male flowers of *Alnus sieboldiana* Matsum. were collected just before the flowering and immersed in benzene. The benzene extract was subjected to chromatography on a silica gel column and then to preparative thin layer chromatography to give alnustic acid.

Alnustic acid (**1**), $C_{31}H_{52}O_4$, showed the IR absorption bands due to a carboxyl and a hydroxyl group. Methylation of **1** with CH_2N_2 gave a methyl ester (**2**), which upon Jones oxidation yielded a keto alcohol (**3**). Acetylation of **2** with acetic anhydride under mild conditions gave a methyl ester monoacetate (**4**), which was found to possess another unaltered hydroxyl group from the IR spectrum. This inidcates that **1** possesses both a secondary and a tertiary hydroxyl group. The ORD curve pattern, as well as the CD curve, of **3** resembled to those of the previously-described dammaran-12-one derivatives,[7-9] implying the presence of the secondary hydroxyl group located at position 12 in the acid (**1**) and the similarity in surroundings of the newly-formed carbonyl chromophore in the keto alcohol (**3**). The presence of both the carboxyl group located at position 3 and the secondary hydroxyl group occupying the *R* position on C-12 (δ_c 70.6 ppm) was demonstrated by comparing the CMR chemical shifts (Table 1) with those of the corresponding carbon atoms of alnuseric acid (**5**) and the methyl ester (**6**)[10,11] and protopanaxadiol.[12] Simultaneously, the presence of an isopropenyl group on C-5 was shown by the CMR spectra (δ_c 147.3 and 113.6 ppm), as well as by the IR bands, the PMR signals, and the MS fragment. These findings indicate that alnustic acid is a 3,4-secodammarane-type derivative. On the other hand, the mass spectral fragmentation pattern (Scheme 1) indicated the presence of an

TABLE 1. ^{13}C-CHEMICAL SHIFTS OF **1**, **2**, **5**, AND **6** IN $CDCl_3$

Carbon No.	Compds			
	1	**2**	**5**	**6**
1	24.8	24.7	24.7	24.9
2	33.6	30.4	34.0	29.7
3	177.8	174.5	180.2	175.8
4	147.3	147.1	147.4	147.4
5	40.6	40.6	41.0	39.9
6	28.4	28.4	28.4	29.5
7	33.6	33.5	34.3	34.7
8	39.5	39.4	40.1	40.5
9	50.7	50.7	50.4[a]	52.1
10	39.5	39.1	39.1	38.8
11	31.8	31.8	22.1	71.2
12	70.6	70.6	25.5	42.0
13	47.5	47.7	43.2	42.3
14	52.1	52.0	50.4	50.1
15	31.2	31.1	31.1	30.5
16	26.6	26.5	26.8	25.5
17	53.5	53.7	50.9[a]	49.9
18	15.5	15.5	15.4	16.0
19	20.0	20.1	20.1	20.4
20	74.2	73.6	85.3	85.3
21	26.6	26.7	25.1	24.6
22	34.0[a]	33.9[a]	37.3[b]	37.4[a]
23	34.5[a]	34.4[a]	36.1[b]	36.0[a]
24	156.7	156.9	85.8	85.3
25	28.6	29.0	38.0	38.0
26	22.0	22.0	18.8	18.7
27	22.0	22.0	17.6	17.5
28	113.6	113.6	113.4	113.7
29	23.2	23.2	23.2[c]	23.1[b]
30	16.9	16.7	16.3	16.4
31	106.3	106.2	22.9[c]	22.9[b]
OMe		51.6		51.4

a), b), and c): Values in any vertical column may be reversed although those given here are preferred.

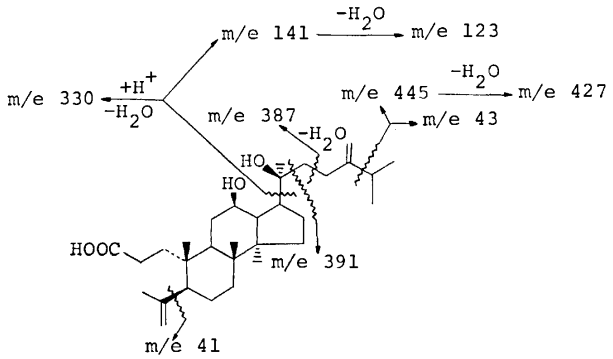

Scheme 1. Mass spectral fragmentation pattern of alnustic acid (**1**).

acyclic side chain. The presence of a terminal methylene and a tertiary hydroxyl group located, respectively, on C-24 and C-20 of the side chain was established by a combination of the IR bands, the PMR signals, the MS peaks (Scheme 1), and the CMR signals (Table 1). In addition, the comparison of these CMR chemical shifts with those of alnuserrudiolone (**7**),[8,9] alnuserrutriol,[9] and protopanaxadiol[12] demonstrated that the chirality at C-20 (δ_c 74.2 ppm) is *S*. This was supported by occurrence of both the free and the intramolecularly hydrogen-bonded hydroxyl bands between the 12-carbonyl and the 20-hydroxyl groups in **3**.[13] We here wish to propose structure **1** for alnustic acid. This proposed structure (**1**) possesses all the features necessary to explain all the spectral data of the acid.

The structure (**1**) was confirmed by its synthesis starting from alnuserrudiolone (**7**)[8,9] following the method established for ring-opening at the 3,4-position in ring A of β-amyrenone.[14] Acetylation of **7** gave a monoacetate, which was then transformed to the corresponding ketoxime, followed by treating with *p*-toluenesulfonyl chloride to yield an abnormal Beckmann rearrangement product (**8**). Hydrolysis of the product (**8**) with alkali under mild conditions gave (12*R*,20*S*)-12,20-dihydroxy-24-methylene-3,4-secodammar-4(28)-en-3-oic acid. Identity of an authentic sample of this acid with naturally occuring alnustic acid was established by direct comparison of a mixed melting point, thin layer chromatogram, and the infrared, mass, and nuclear magnetic resonance spectra.

Thus, the structure of alnustic acid (**1**) has been elucidated to be (12*R*,20*S*)-12,20-dihydroxy-24-methylene-3,4-secodammar-4(28)-en-3-oic acid.

Experimental

The mass spectral analyses were performed on a Hitachi RMS-4 mass spectrometer at 70 eV. The PMR spectra were taken on a Varian T-60 spectrometer using TMS as an internal standard. The CMR spectra were obtained on a JEOL JNM FX-100 spectrometer operating at 15.1 MHz ($\delta_{TMS}=0$).

Extraction and Isolation. The male flowers (95.0 kg) of *Alnus sieboldina* Matsum. naturally grown on a hill in suburbs of Hiroshima city were collected just before the flowering in March. After minced mechanically, the flowers were immersed in benzene at room temp for 2 months. The benzene extract was chromatographed on a silica gel column (Merck; type 60) with a hexane-EtOAc mixture with EtOAc increasing 0 to 100%. The eluate with 50% EtOAc in hexane, after removal of the solvent, was subjected to repeated preparative TLC (silica gel, Merck GF_{254}; EtOAc–$CHCl_3$–hexane (5: 1: 1, v/v); R_f 0.47) to give alnustic acid (577 mg), which was recrystallized from a hexane–EtOAc mixture to yield colorless needles.

*Alnustic Acid (**1**).* Mp 195—196 °C; $[\alpha]_D^{25}$ +27.8° (*c* 0.52, $CHCl_3$); IR (Nujol) ν_{max}3400—2800 and 1710 (COOH), 1640 and 892 cm^{-1} (>C=CH_2); PMR ($CDCl_3$) δ 0.88—1.19 (Me×6), 1.75 (3H, s, >C=C (CH_3)–), 3.60 (1H, br, >C<u>H</u>–OH), 4.71 and 4.87 (4H, br, >C=CH_2×2), 7.36 (1H, s, –COOH); MS, *m/e* (rel intensity), 470 ($(M-H_2O)^+$, 8), 445 (4), 427 (6), 391 (13), 387 (7), 330 (21), 141 (42), 123 (68), 43 (100), and 41 (71).

Found: C, 75.88; H, 10.56%. Calcd for $C_{31}H_{52}O_4$: C, 76.18; H, 10.72%.

*Methylation of **1**.* **1** (363 mg) was methylated with CH_2N_2, followed by purification with preparative TLC [silica gel; benzene–dioxane–acetic acid (90: 25: 4, v/v)], to give a methyl ester (**2**) (389 mg): mp 157—158 °C; $[\alpha]_D^{25}$ +42.7° (*c* 0.59, $CHCl_3$); IR (0.001 M, CCl_4) ν_{max} 3610 (free OH), 3435 (intramolecularly hydrogen-bonded OH), 1730 cm^{-1} (COOMe); PMR ($CDCl_3$) δ 0.98—1.18 (Me×6), 1.73 (3H, s, >C=C(CH_3)–), 3.60 (1H, br, >C<u>H</u>–OH), 3.65 (3H, s, –$COOCH_3$), 4.73 and 4.86 (4H, br, >C=CH_2×2).

Found: C, 76.20; H, 10.92%. Calcd for $C_{32}H_{54}O_4$: C, 76.44: H, 10.83%.

*Acetylation of **2**.* A mixture of **2** (380 mg), dry pyridine (4 ml), and acetic anhydride (8 ml) was allowed to stand overnight at room temp and the product, obtained on treatment of the reaction mixture in the usual method, was subjected to preparative TLC [silica gel; hexane–EtOAc (7: 3, v/v)] to give a methyl ester monoacetate (**4**) (376 mg): IR (Liquid) ν_{max} 3530 (OH), 1738 (C=O), 1642 and 900 cm^{-1} (>C=CH_2); PMR ($CDCl_3$) δ 0.85—1.10 (Me×6), 1.71 (3H, s, >C=C-(CH_3)–), 2.02 (3H, s, –$OCOCH_3$), 3.65 (3H, s, –$COOCH_3$), 4.67 (1H, br, >CH–OAc), 4.77 and 4.84 (4H, br, >C=CH_2×2).

*Oxidation of **2**.* A soln of **2** (58 mg) in dry pyridine (2 ml) was added to the CrO_3–pyridine complex prepared from 100 mg of CrO_3 and 4 ml of pyridine. The reaction mixture was stirred overnight to give a keto alcohol (**3**) (49 mg): IR (0.001 M, CCl_4) ν_{max} 3620 (free OH), 3450 (intramolecularly hydrogen-bonded OH), 1735 (COOMe), 1707 cm^{-1} (C=O); PMR ($CDCl_3$) δ 0.80—1.20 (Me×6), 1.72 (3H, s, >C=C (CH_3)–), 2.92 (2H, d, J=10 Hz, >CH–C<u>H_2</u>–CO–), 3.65 (3H, s, –COOMe), 4.70 and 4.88 (4H, br, >C=CH_2×2); ORD (*c* 0.75, dioxane) $[\Phi]_{600}$ +117°, $[\Phi]_{589}$ +117°, $[\Phi]_{309}$ −780°, $[\Phi]_{303}$ −552°, $[\Phi]_{300}$ −584°, $[\Phi]_{263}$ +1218°; CD (*c* 0.75, dioxane) $[\theta]_{312}$ 0, $[\theta]_{284}$ −244, $[\theta]_{250}$ 0.

*Synthesis of **1**.* *i) Acetylation of **7**:* A mixture of **7** (290 mg), dry pyridine (2 ml), and acetic anhydride (2.5 ml) was left overnight at room temp and, after treatment as usual method, the product obtained was subjected to preparative TLC [silica gel; hexane–EtOAc (7: 3, v/v)] to give a monoacetate (260 mg): IR (Nujol) ν_{max} 3550 (OH), 1730 (COOMe), 1710 (C=O); PMR ($CDCl_3$) δ 2.06 (3H, s, –COOMe).

*ii) Cleavage of Ring A of **7**:* According to the previously-described procedure,[14] a mixture of 12β-acetoxy-alnuserrudiolone oxime (145 mg) and *p*-toluenesulfonyl chloride (100 mg) in dry pyridine (4 ml) was kept for 24 h at room temp. After addition of a few drops of water, the reaction mixture

was further stirred for 30 min at room temp, acidified with 5% hydrochloric acid (15 ml), and extracted with ether to give a solid mass. This mass was subjected to preparative TLC to give (12*R*,20*S*)-12-*O*-acetoxy-3-cyano-20-hydroxy-24-methylene-3,4-secodammar-4(28)-ene (**8**) (16 mg): MS, *m/e* (rel intensity), 511 (M^+, 1), 414 (3), 311 (7), 141 (10), 123 (14), 43 (100), and 41 (72); IR (Nujol) ν_{max} 3550 (OH), 2250 (-C≡N), 1730 (OCOMe), 3077, 1638, and 888 cm^{-1} (>C=CH_2); PMR ($CDCl_3$) δ 2.05 (3H, s, -OCOMe), 4.73 and 4.90 (4H, br, >C=CH_2×2).

iii) Hydrolysis of 8: A soln of **8** (16 mg) in 20% KOH/MeOH (6 ml) was refluxed for 15 h. The reaction mixture, after acidification with 5% hydrochloric acid, was extracted with ether. The ether extract was subjected to preparative TLC [silica gel; EtOAc–benzene (7: 3, v/v)] to give (12*R*, 20*S*)-12,20-dihydroxy-24-methylene-3,4-secodammar-4(28)-en-3-oic acid (**1**) (14 mg): mp 195—196 °C; IR (Nujol) ν_{max} 3400—2800 and 1713 (COOH), 1638 and 890 cm^{-1} (>C=CH_2); PMR ($CDCl_3$) δ 0.88—1.18 (Me×6), 1.73 (3H, s, >C=C(CH_3)–), 3.58 (1H, br, >C<u>H</u>–OH), 4.73 and 4.90 (4H, br, >C=CH_2×2), 5.90 (1H, br, -COOH); MS, *m/e* (rel intensity), 470 ($(M-H_2O)^+$, 5), 445 (4), 427 (4), 391 (6), 387 (4), 330 (6), 141 (20), 123 (26), 43 (100), and 41 (82).

The authors thank JEOL Co., Ltd. for obtaining the ^{13}C-NMR spectra. The present work was partially supported by a Grant-in-Aid for Scientific Research Nos. 234033 and 247027 (1977 and 1978, to T.S.) and No. 354189 (1978, to T.A.) from the Ministry of Education, Science, and Culture and Matsunaga Science Foundation in 1977 (to T.H.).

References

1) Y. Asakawa, *Bull. Chem. Soc. Jpn.*, **43**, 575 (1970).
2) Y. Asakawa, *Bull. Chem. Soc. Jpn.*, **43**, 2223 (1970).
3) Y. Asakawa, F. Genjida, and T. Suga, *Bull. Chem. Soc. Jpn.*, **44**, 297 (1971).
4) Y. Asakawa, *Bull. Chem. Soc. Jpn.*, **44**, 2761 (1972).
5) Y. Asakawa, *Bull. Chem. Soc. Jpn.*, **45**, 1794 (1972).
6) T. Ohmoto, T. Nikaido, T. Nozaki, and M. Ikuse, *Yakugaku Zasshi*, **97**, 176 (1977).
7) O. Tanaka, M. Nagai, and S. Shibata, *Chem. Pharm. Bull.*, **14**, 1150 (1966).
8) T. Suga, T. Hirata, and N. Iwata, *Chem. Lett.*, **1974**, 971.
9) T. Suga, T. Hirata, and T. Aoki, *Bull. Chem. Soc. Jpn.*, to be submitted for publication.
10) T. Hirata, R. Ideo, and T. Suga, *Chem. Lett.*, **1977**, 283.
11) T. Suga and T. Hirata, *Bull. Chem. Soc. Jpn.*, **52**, 1153 (1979).
12) J. Asakawa, R. Kasai, Y. Yamasaki, and O. Tanaka, *Tetrahedron*, **33**, 1935 (1977).
13) Y. Nagai, O. Tanaka, and S. Shibata, *Tetrahedron*, **27**, 881 (1971).
14) G. H. Whitham, *J. Chem. Soc.*, **1960**, 2016.

Syntheses of Cecropia Juvenile Hormones by Selective Side-chain Methylation of (*E,E*)-Farnesol[1)]

Arata YASUDA,*,† Shin TANAKA, Hisashi YAMAMOTO,†† and Hitosi NOZAKI

Department of Industrial Chemistry, Kyoto University, Yoshida, Kyoto 606

(Received December 6, 1978)

The stereoselective route to the title insect hormones (JH-1 & JH-2) depends crucially on the epoxidation of allylic alcohols with *t*-butyl hydroperoxide in the presence of oxobis(2,4-pentanedionato-*O,O'*)vanadium(IV). The oxidation of 2-methyl-1-hepten-3-ol exclusively produces the (2*R**,3*S**) isomer of the diastereomeric epoxy alcohols. This is converted into (*Z*)-6-methyl-5-undecene by the sequence involving oxirane reaction with lithium dibutylcuprate(I) and the removal of both hydroxyl groups of the resulting 1,2-diol. Extension of the series of reactions to the mono- and bisoxirane derived from (*E,E*)-farnesol gives JH-2 and JH-1, respectively.

Since C_{18}-Cecropia juvenile hormone (**1**), now called JH-1, was first synthesized in a nonstereoselective manner, no less than ten syntheses of **1** and the lower homolog, JH-2 (**2**), have appeared.[2)]

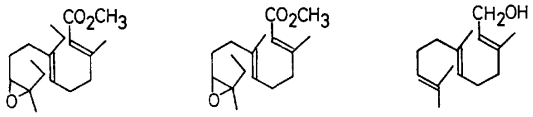

1 **2** **3**

Apparently of great interest are those routes which give only the required stereoisomer with the right configuration about each of the double bond. This paper presents a simple and efficient route starting from the readily available (*E,E*)-farnesol (**3**) and giving the desired products selectively.

The approach is based on a combination of catalyzed, stereoselective epoxidation of allylic alcohols and the transformation of the resulting glycidols into 3-alkylated 1,2-diols.

The principle is first illustrated with a simple example, then its application to syntheses of insect hormones being described.

Stereoselective Preparation of (Z)-6-Methyl-5-undecene (7) and Its Isomer (9). Sharpless *et al.* showed that catalytic epoxidation of cyclic allylic alcohols with *t*-butyl hydroperoxide proceeds with high degrees of stereoselectivity.[3)] The same technique can be successfully extended to a variety of acyclic allylic alcohols.[1)] Of special interest for the syntheses of **1** and **2** is the observation that epoxidation of the allylic alcohol **4** with $VO(acac)_2$-*t*-BuOOH reagent in benzene at room temperature produced (2*R**, 3*S**) epoxy alcohol **5** in 96% selectivity. This was improved (>99%) when the epoxidation was carried out in toluene at 0 °C. In contrast, *m*-chloroperbenzoic acid epoxidation of **4** gave a 62 : 38 mixture of (2*R**,3*S**) and (2*S**,3*S**) epoxy alcohols. The (2*R**,3*S**) structure of **5** was established, after acetylation, by GLPC comparison with the known data.[4,5)] Further study is required before stereochemical and mechanistic details can be understood.[6)] However, from the observation that cyclic allylic alcohols exhibit a strong preference for epoxidation *cis* to the hydroxyl group, we can assume that the preferred conformation of this allylic alcohol at the epoxidation transition state might be the one illustrated, close to that proposed in the case of cyclic allylic alcohols. The epoxy oxygen is then introduced on the same side as the hydroxyl group to give (2*R**,3*S**) epoxy alcohol **5**.[2,4,7)]

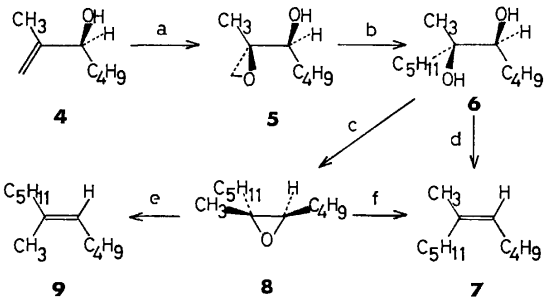

a) $VO(acac)_2$-*t*-BuOOH; b) Bu_2CuLi; c) BuLi, *p*-TsCl; d) $Me_2NCH(OMe)_2$, Ac_2O; e) NaI–AcOH, $SnCl_2$–$POCl_3$–C_5H_5N; f) $LiPPh_2$, MeI.

Treatment of the epoxy alcohol **5** with excess lithium dibutylcuprate(I) in ether at −26 °C for 2 h produced (5*R**,6*S**) diol **6** in 88% overall yield from **4**. As expected from earlier reports,[8)] dibutylcuprate-(I) exclusively attacked the unsubstituted carbon atom of the epoxide ring to furnish 1,2-diol as the sole product. Several methods for stereospecific deoxygenation of diols have been given;[9)] the one reported by Eastwood *et al.*[9c)] ($Me_2NCH(OMe)_2$, Ac_2O) afforded (*Z*)-6-methyl-5-undecene (**7**) in 80% yield. GLPC analysis of the olefin **7** displayed two peaks in the ratio 97 : 3. The major peak, having a shorter retention time, was ascribed to the *Z* isomer[10)] and this was supported by a vinyl methyl signal appearing at δ 1.65.[11)]

On the other hand, the geometrical isomer **9** was obtained from epoxide **8** by the Cornforth procedure[12)] in 80% yield, whose NMR spectrum supports the *E* configuration.[11)] The epoxide **8** was also converted into *Z* olefin **7** by treatment with lithium diphenylphosphide and then with methyl iodide (80% yield).[13)]

Stereospecific Synthesis of dl-*JH-2 (2).* Two methods of nonselective homologation of (*E,E*)-farnesol (**3**)

† Present address: The Institute for Molecular Science, Myodaiji, Okazaki 444.

†† Present address: Department of Chemistry, University of Hawaii at Manoa, Honolulu, Hawaii 96822.

are known to afford a triene having the skeleton of JH-1 (**1**).[14,15] We now report a stereoselective route to hormones **1** and **2** which utilizes the series of reactions mentioned above.

The key intermediate in the synthesis of *dl*-JH-2 (**2**) is the allylic alcohol **13** prepared as follows. The epoxide **11**[16] was efficiently converted into bis-allylic alcohol **12** (90% yield) by reaction with diethyl-

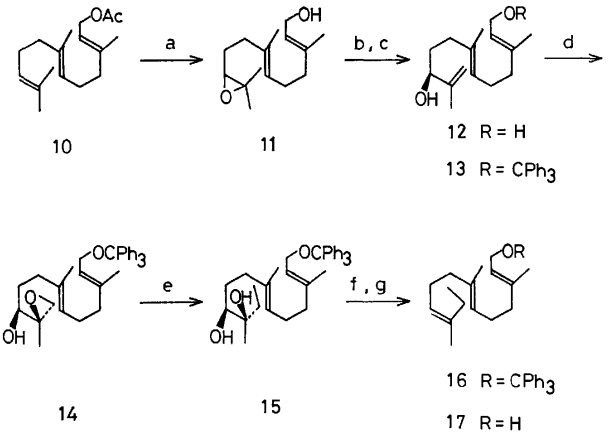

a) NBS, NaOPr-*i*; b) Et_2Al-TMP; c) Ph_3CCl-*p*-TsOH; d) $VO(acac)_2$-*t*-BuOOH; e) Me_2CuLi; f) $(CH_3)_2NCH(OCH_3)_2$, Ac_2O; g) $HClO_4$.

aluminum 2,2,6,6-tetramethylpiperidide,[17] followed by tritylation of the primary hydroxyl group (88% yield). The trityl ether **13** was oxidized to the epoxy alcohol **14**[18] by the $VO(acac)_2$-*t*-BuOOH reagent and the resulting crude **14** was methylated to furnish the diol **15**[18] (81% yield after preparative TLC purification), which was found to be homogeneous upon TLC analysis. Application of the Eastwood procedure[9c] gave the triene trityl ether **16** stereospecifically in 55% yield. Removal of the protecting group by perchloric acid furnished the desired homofarnesol **17** almost quantitatively. The homogeneity of **17** was indicated by TLC analysis, its infrared and NMR spectra being identical with those obtained for homofarnesol.[19] The synthesis of JH-2 (**2**) from **17** has been reported.[19]

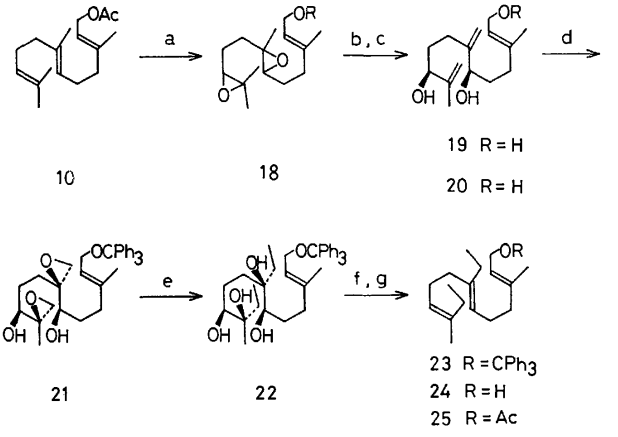

a) MCPBA, K_2CO_3; b) $LiNEt_2$; c) Ph_3CCl-*p*-TsOH; d) $VO(acac)_2$-*t*-BuOOH; e) $(CH_3)_2CuLi$; f) $(CH_3)_2OCH_3)_2$, Ac_2O; g) $HClO_4$.

Synthesis of dl-*JH-1 (1).* (*E,E*)-Farnesol (**3**) was transformed by the van Tamelen-McCormick procedure[15] into the triene trityl ether **20**. The conversion of the intermediate **20** into the bishomofarnesol **24** was accomplished by the sequence of steps described above. The IR and NMR spectra of **24** were entirely analogous to those reported,[15,19] its structure and homogeneity being further confirmed, after acetylation, by TLC and GLPC comparison with an authentic sample of the acetate **25**.[21] The transformation of **24** into JH-1 (**1**) has been reported.[15,19]

Experimental

IR spectra were determined on a Shimadzu IR-27-G spectrometer, mass spectra on a Hitachi RMU-6L mass spectrometer, and NMR spectra on a Varian EM-360 or JEOL-C-60-H spectrometer; chemical shifts are given in δ with tetramethylsilane as an internal standard. Microanalyses were carried out at the Elemental Analyses Center of Kyoto University, and GLPC analyses on a Yanagimoto GCG-550F. All experiments were carried out under an atmosphere of dry nitrogen or argon, preparative thin layer chromatography on silica gel 60 PF_{254} (Merck, Art. 7747) plates, and preparative column chromatography on silica gel 60 (Merck, Art. 7734).

(2R,3S*)-2-Methyl-1,2-epoxyheptan-3-ol (5).* *t*-Butyl hydroperoxide (90%, 600 mg, 6.0 mmol) was added dropwise over a period of 10 min at room temperature to a solution of 2-methyl-1-hepten-3-ol (**4**) (512 mg, 4.0 mmol) and oxobis(2,4-pentanedionato-*O,O'*)vanadium(IV) (32 mg, 0.12 mmol) in benzene (15 ml). After being stirred at ambient temperature for 2 h, the resulting solution was poured into saturated aqueous sodium sulfite. The mixture was vigorously stirred for 20 min and extracted with ether. The ethereal phase was washed with water, dried (anhydrous sodium sulfate), and concentrated *in vacuo* to give the epoxy alcohol **5** as a pale yellow liquid: bp 80 °C (bath temp, 1 Torr); TLC, R_f 0.55 (3:1 hexane–ethyl acetate); IR (neat), 3400 (s), 1470 (m), and 1110 cm^{-1} (m); NMR (CCl_4), 1.28 (3H, s, CH_3–CO), 2.61 (2H, dd, CH_2–O), and 3.32—3.67 (1H, m, CH–OH).

A small aliquot was acetylated by stirring with acetic anhydride in pyridine. GLPC analysis (10% PEG 20 Mesh, 110 °C, 1.0 kg/cm^2) of the resulting acetates showed a peak at 6.5 min (96%), corresponding to the (2*R**,3*S**) epoxy acetate, and a small peak at 5.8 min (4%), corresponding to the (2*S**,3*S**) isomer: bp 80 °C (bath temp, 1 Torr); TLC, R_f 0.53 (1:1 hexane–ether); IR (neat), 1735(s), 1360 (m), 1230—1240(s), and 1110 cm^{-1}(m); NMR (CCl_4), 1.21 (3H, s, CH_3–CO), 1.91 (3H, s, CH_3–CO_2), 2.50 (2H, dd, CH_2–O), and 4.32 (1H, t, CH–O); MS (*m/e*), 186 (7), 156 (14), 144 (23), 127 (100), and 114 (52).

Found: C, 64.4; H, 9.5%. Calcd for $C_{10}H_{18}O_3$: C, 64.5; H, 9.7%.

(5R,6S*)-6-Methylundecane-5,6-diol (6).* Lithium dibutylcuprate(I) was prepared by the addition of 32.0 mmol (16.2 ml of 1.98 M hexane solution) of butyllithium to a vigorously stirred suspension of 3.04 g (16.0 mmol) of copper(I) iodide in 40 ml of ether at −26 °C. After being stirred at this temperature for 20 min, the crude epoxy alcohol **5** dissolved in 20 ml of ether was added at the same temperature. Stirring was continued for 2 h, then the product was isolated by quenching the reaction mixture in ether, filtering through a pad of Celite 545, extracting with ether, drying over sodium sulfate, and concentrating to give an

oil. Preparative TLC (3:1 hexane–ethyl acetate) afforded 663 mg (82% yield from **4**) of the (5*R**,6*S**) diol **6**, which showed a single spot of R_f 0.60 upon TLC analysis (3:1 hexane–ethyl acetate): bp 120 °C (bath temp, 1 Torr); IR (neat), 3450(s), 1470(m), and 1035 cm^{-1}(s); NMR ($CDCl_3$), 3.10—3.36 (1H, m, CH–OH); MS (*m/e*), 182 (18), 157 (36), 115 (36), 63 (100), and 57 (100).

Found: C, 71.2; H, 13.0%. Calcd for $C_{12}H_{26}O_2$: C, 71.2; H, 13.0%.

(Z)-6-Methyl-5-undecene (7). *A. From Diol 6*: A mixture of the (5*R**,6*S**) diol **6** (606 mg, 3.0 mmol) and *N,N*-dimethylformamide dimethyl acetal (3.0 ml) was stirred at room temperature for 17 h. After removal of the volatile material *in vacuo*, the resulting dioxolane derivative was heated in acetic anhydride (3.0 ml) at 130 °C for 17 h. The reaction mixture was allowed to cool to room temperature, poured into water, and the product was extracted with pentane. After being washed with saturated aqueous sodium hydrogencarbonate, saturated brine, and water, the organic phase was dried (Na_2SO_4), and concentrated. Column chromatography using pentane as an eluent gave (*Z*)-6-methyl-5-undecene (**7**) (403 mg, 80% yield) as a clear oil: bp 130 °C (bath temp, 24 Torr); TLC, R_f 0.80 (hexane); IR (neat), 1660—1675(w), 1385(m), and 840 cm^{-1}(w); NMR (CCl_4), 1.65 (3H, s, CH_3–C=), and 5.03 (1H, bt, CH=); MS (*m/e*), 168(12), 114(10), 94(31), 68(72), and 55(100).

Found: C, 85.8; H, 14.6%. Calcd for $C_{12}H_{24}$: C, 85.6; H, 14.4%.

B. From Oxirane 8: According to the procedure of Vedejs and Fuchs,[13] lithium diphenylphosphide in tetrahydrofuran (0.83 M) was prepared from chlorodiphenylphosphine (0.92 ml, 5.0 mmol) and lithium wire (140 mg, 20.0 mmol) in THF (5 ml). A solution of the oxirane **8** (184 mg, 1.0 mmol) in THF (5 ml) was added over a period of 5 min to the solution of lithium diphenylphosphide in THF (3.0 ml, 2.5 mmol) at ambient temperature. The resulting mixture was stirred at the same temperature for 17 h. Methyl iodide (0.27 ml, 4.3 mmol) was then added and the mixture was allowed to stand at room temperature for 1 h. After aqueous workup, the organic phase was dried (Na_2SO_4), and freed of the solvent. The residual liquid was subjected to column chromatography with pentane as an eluent to give pure olefin **7** (132 mg, 80% yield).

(E)-6-Methyl-5,6-epoxyundecane (8). A 1.83 M hexane solution of butyllithium was added dropwise at 0 °C to an ethereal solution (2 ml) of the diol **6** (202 mg, 1.0 mmol) containing a trace of 1,10-phenanthroline until the initially colorless solution turned orange. After 10 min, hexamethylphosphoric triamide (1 ml) and *p*-toluenesulfonyl chloride (229 mg, 1.2 mmol) were successively added and then the whole mixture was stirred at ambient temperature for 6 h. The crude product obtained on extractive workup was purified by preparative TLC (benzene) which furnished 166 mg (90% yield) of the oxirane **8**. GLPC analysis (10% PEG 20 Mesh, 90 °C, 1.0 kg/cm^2) showed the oxirane to be >97% pure: bp 86 °C (bath temp, 2 Torr); TLC, R_f 0.65 (benzene); IR (neat), 1470(s), 1376(m), and 1120 cm^{-1}(w); NMR ($CDCl_3$), 1.18 (3H, s, CH_3–CO), and 2.30—2.67 (1H, bt, CH–O); MS (*m/e*), 184(2), 155(6), 127(10), 114(18), and 58(100).

Found: C, 78.2; H, 13.3%. Calcd for $C_{12}H_{24}O$: C, 78.3; H, 13.0%.

(E)-6-Methyl-5-undecene (9). The oxirane **8** (80 mg, 0.44 mmol) was added to a cooled (−16 °C) solution of sodium iodide (150 mg, 1.0 mmol) and sodium acetate (15 mg, 0.18 mmol) in acetic acid (0.6 ml). After 1 h, the mixture was warmed to room temperature and poured into ether and aqueous sodium hydrogencarbonate. The ethereal solution was washed with a little sodium hydrogensulfite and water, dried (Na_2SO_4), and freed of the solvent. The resulting iodohydrin was added to a cooled (0 °C) solution of tin(II) chloride (230 mg, 1.21 mmol) in pyridine (0.9 ml). Phosphoryl chloride (0.06 ml, 0.40 mmol) in pyridine (0.2 ml) was then added with cooling, and the mixture was allowed to stand at room temperature overnight. After being diluted with hexane, the organic phase was washed with 1 M hydrochloric acid, and water, dried (Na_2SO_4), and concentrated. The crude product was subjected to column chromatography with hexane as an eluent. The olefin **9** (62 mg, 80% yield) was obtained as a colorless oil: bp 130 °C (bath temp, 24 Torr); TLC, R_f 0.80 (hexane); IR (neat), 1665—1675(w) and 840—860 cm^{-1}(sh); NMR (CCl_4), 1.59 (3H, s, CH_3–C=) and 5.05 (1H, bt, CH=); MS (*m/e*), 168 (16), 112(10), 96(30), 59(78), and 55(100).

Found: C, 85.7; H, 14.5%. Calcd for $C_{12}H_{24}$: C, 85.6; H, 14.4%.

(2E,6E)-3,7,12-Trimethyl-2,6,11-dodecatriene-1,10-diol (12). Diethylaluminum 2,2,6,6-tetramethylpiperidide was prepared *in situ* from diethylaluminum chloride (1.7 ml of 1.0 M benzene solution) and 1.68 mmol of lithium 2,2,6,6-tetramethylpiperidide in benzene (5 ml) at 0 °C for 30 min.[17] To this slurry was added dropwise the epoxy alcohol **11**[16] (80 mg, 0.34 mmol) dissolved in 4 ml of benzene at the same temperature. After being stirred for 2 h, 5 ml of 1 M hydrochloric acid was added. Ethereal extracts were dried (Na_2SO_4) and freed of the solvent. The remaining liquid was subjected to preparative TLC (5: 2 ether–hexane) to give pure **12** (71 mg, 90% yield); TLC, R_f 0.41 (2:1 ether–hexane); IR (neat), 3300—3420(s), 1650—1675(m), 1450 (m), 1000(m), and 895 cm^{-1}(m); NMR ($CDCl_3$), 1.59 (3H, s, CH_3–C= on C-3), 1.67 (3H, s, CH_3–C=, C-11), 3.86 (1H, bt, CH–OH), 3.97 (2H, d, CH_2–OH), 4.69 (2H, dd, CH_2=), and 4.82—5.40 (2H, m, CH=).

Microanalysis was performed after trimethylsilylation of both hydroxyl groups:

Found: C, 66.1; H, 11.2%. Calcd for $C_{21}H_{42}O_2Si_2$: C, 65.9; H, 11.1%.

(10R,11S*)-(2E,6E)-3,7,11-Trimethyl-1-trityloxy-2,6-tridecadiene-10,11-diol (15).* The diol **12** (71 mg, 0.31 mmol) was converted into the primary mono(trityl ether) **13** by reaction with trityl chloride (92 mg, 0.33 mmol) in 2 ml of pyridine at 50 °C for 2.5 h. Preparative TLC (1 : 1 hexane–ether) gave purified **13** (130 mg, 88% yield).

t-Butyl hydroperoxide (90%, 32 mg, 0.33 mmol) was added to a mixture of oxobis(2,4-pentanedionate-*O,O'*)-vanadium(IV) (11 mg, 0.04 mmol), the allylic alcohol **13** (130 mg, 0.27 mmol), and benzene (3 ml) as described above, yielding the epoxy alcohol **14** as a pale yellow liquid: TLC, R_f 0.68 (1 : 1 hexane–ether); NMR ($CDCl_3$), 1.23 (3H, s, CH_3–CO), 1.62 (3H, s, CH_3–C= on C-7), 1.95 (3H, s, CH_3–C=, C-3), 2.25—2.70 (2H, m, CH_2–O, C-12), 3.19 (1H, m, CH–O), 3.31—3.70 (2H, bd, CH_2–O, C-1), 5.03—5.52 (2H, m, CH=), and 7.00—7.40 (15 H, m, aromatic).

The crude epoxy alcohol **14** in ether (1 ml) was added at −26 °C to a solution of lithium dimethylcuprate(I) (0.56 mmol) in ether (3 ml) and the whole mixture was stirred at 0 °C for 12 h. According to the procedure described above, the trityl ether **15** (113 mg, 81% yield from **13**) was obtained as a pale yellow liquid after purification by preparative TLC (1 : 1 hexane–ether): TLC, R_f 0.54 (1 : 1 hexane–ether); IR (neat), 3410—3490(s), 1480(m), 1450 (s), 1380(m), and 1050 cm^{-1}(s); NMR ($CDCl_3$), 1.12 (3H, t, CH_3–CH_2), 1.45 (3H, s, CH_3–C= on C-7), 1.62 (3H, s,

CH_3–C= on C-3), 3.15—3.56 (1H, m, CH–OH), 4.94—5.53 (2H, m, CH=), and 7.05—7.45 (15H, m, aromatic).

Microanalysis was performed with the 10,11-*O*-isopropylidene-1-trimethylsilyl ether derivative:

Found: C, 69.1; H, 11.3%. Calcd for $C_{22}H_{42}O_3Si$: C, 69.1; H, 11.1%.

*(2E,6E,10Z)-3,7,11-Trimethyl-2,6,10-tridecatrien-1-ol (**17**).* The diol **15** (113 mg, 0.22 mmol) was transformed into the triene trityl ether **16** (56 mg, 55% yield) as described above for **7**: TLC, R_f 0.54 (3 : 1 petroleum ether–benzene); IR (neat), 1490(w), 1055(s), and 790 cm^{-1}(s); NMR ($CDCl_3$, 100 MHz), 0.95 (3H, t, J=8 Hz, CH_3–CH_2), 1.65 (6H, s, CH_3–C= on C-7 and C-11), 1.88—2.40 (12H, m, methylenes except C-1), 1.96 (3H, s, CH_3–C= on C-3), 3.60 (2H, d, J=7 Hz, CH_2–O), 5.09 (2H, bt, CH= on C-6, 10), 5.44 (1H, bt, CH= on C-2), and 7.16—7.68 (15H, m, aromatic).

The trityl ether **16** thus obtained was treated with 3 ml of 5% perchloric acid in tetrahydrofuran at 0 °C for 1.5 h. After being diluted with ether, the mixture was washed with water, saturated sodium hydrogencarbonate, and saturated brine, dried (Na_2SO_4), and concentrated *in vacuo*. Chromatography on silica gel (1 : 1 hexane–ether) gave the purified homofarnesol **17** (28 mg, 99% yield) which exhibited appropriate physical properties:[19] TLC, R_f 0.41 (2 : 1 ether–hexane); IR (neat), 3250—3380(s), 1665(m), 1450(s), 1380(s), and 1000—1020 cm^{-1} (s); NMR ($CDCl_3$, 100 MHz), 0.95 (3H, t, J=7 Hz, CH_3–CH_2), 1.58 (3H, s, CH_3–C=, C-3), 1.65 (6H, s, CH_3–C=, C-7, 11), 1.85—2.16 (11H, m, methylenes except C-1 and OH), 4.05 (2H, d, J=7 Hz, CH_2–OH), 4.89—5.14 (2H, m, CH=, C-6, 10), and 5.35 (1H, bt, CH=, C-2); MS (*m/e*), 236(2), 218(2), 160(5), 83(71), and 55(100).

*(2E,6E,10Z)-7-Ethyl-3,11-dimethyl-2,6,10-tridecatrien-1-ol (**24**).* According to the same procedure as aforementioned, compound **24** was obtained in 25% overall yield from the diol **20**.[15] The bisoxirane **21**:[18] TLC, R_f 0.68 (ethyl acetate); NMR ($CDCl_3$), 1.23 (3H, s, CH_3–CO), 1.95 (3H, s, CH_3–C=), 2.25—2.80 (4H, m, CH_2–O, C-7, C-12), 3.19 (2H, m, CH–OH), 3.31—3.70 (2H, bd, CH_2–O, C-1), 5.13—5.52 (1H, bt, CH=), and 7.00—7.40 (15H, m, aromatic). The tetrol **22**: TLC, R_f 0.60 (ethyl acetate); NMR ($CDCl_3$), 1.65 (3H, s, CH_3–C=), 2.90—3.35 (2H, m, CH–OH), 3.60 (2H, d, CH_2–O, C-1), 5.46 (1H, bt, CH=), and 7.10—7.55 (15H, m, aromatic). The bishomofarnesol **24** so obtained was spectrometrically identical with the reported data:[14,17] TLC, R_f 0.54 (1 : 1 hexane–ether); IR(neat), 3280—3370(s), 1665(w), 1450(s), 1380(m), and 1000—1020 cm^{-1}(s); NMR ($CDCl_3$, 100 MHz), 0.95 (6H, t, J=7 Hz, CH_3–CH_2), 1.65 (3H, s, CH_3–C= on C-3), 1.90—2.35 (13H, m, methylenes except C-1 and OH), 4.12 (2H, d, J=7 Hz, CH_2–OH), 5.04 (2H, bt, CH=, C-6, 10), and 5.40 (1H, t, J=7 Hz, CH=, C-2); MS (*m/e*), 232(3), 203(3), 175(5), 149(12), 83(50). and 55(100).

The structure and homogeneity of the alcohol **24** were further confirmed, after acetylation, by TLC and GLPC comparison with an authentic sample of acetate **25**. TLC analysis showed a single spot of R_f 0.24 (3 : 1 hexane–ether). The substance was found to be >93% pure by GLPC analysis (10% PEG 20 Mesh, 165 °C, 45 ml/min, 14.1 min retention time).

The work was carried out with Grants-in-Aid 911506, 011010, 110309, 203014, and 303023 from the Ministry of Education.

References

1) A preliminary account of this work has appeared: S. Tanaka, H. Yamamoto, H. Nozaki, K. B. Sharpless, R. C. Michaelson, and J. D. Cutting, *J. Am. Chem. Soc.*, **96**, 5254 (1974).

2) For a review of juvenile hormone syntheses, see a) J. ApSimon, "The Total Syntheses of Natural Products," John Wiley & Sons, Inc., New York, N. Y. (1973), Vol. 2, p. 207; b) K. Mori, *Kagaku To Seibutsu*, **13**, 138 (1975).

3) a) K. B. Sharpless and R. C. Michaelson, *J. Am. Chem. Soc.*, **95**, 6136 (1973); b), F. List and L. Kuhnen, *Erdol Kohle, Erdgas, Petrochem. Brennst.-Chem.*, **20**, 192 (1967).

4) a) G. Berti, "Topics in Stereochemistry," Wiley-Interscience, New York, N. Y. (1973), Vol. 7, p. 93; b) J. L. Pierre, P. Chantemps, and P. Arnaud, *Bull. Soc. Chim. Fr.*, **1968**, 1317.

5) M. L. Sassiver and J. English, *J. Am. Chem. Soc.*, **82**, 4891 (1960).

6) R. C. Michaelson, R. E. Palermo, and K. B. Sharpless, *J. Am. Chem. Soc.*, **99**, 1990 (1977).

7) a) P. Chamberlain, M. L. Roberts, and G. H. Whitham, *J. Chem. Soc., B*, 1374 (1970); b) T. Itoh, K. Kaneda, and S. Teranishi, *J. Chem. Soc., Chem. Commun.*, **1976**, 421.

8) a) C. R. Johnson, R. W. Herr, and M. Wieland, *J. Org. Chem.*, **38**, 4263 (1973); b) B. C. Hartman, T. Livinghouse, and B. Rickborn, *ibid.*, **38**, 4346 (1973).

9) a) E. J. Corey and J. I. Shulman, *Tetrahedron Lett.*, **1968**, 3655 and references cited therein; b) J. N. Hines, M. J. Peagram, G. H. Whitham, and M. Wright, *J. Chem. Soc., Chem. Commun.*, **1968**, 1593; c) F. W. Eastwood, K. J. Harrington, J. S. Josan, and J. L. Pura, *Tetrahedron Lett.*, **1970**, 5223.

10) G. D. Abrams, W. R. Bartlett, V. A. Fung, and W. S. Johnson, *Bioorg. Chem.*, **1**, 243 (1971).

11) R. B. Bates and D. M. Gale, *J. Am. Chem. Soc.*, **82**, 5749 (1960).

12) J. W. Cornforth, R. H. Cornforth, and K. K. Mathew, *J. Chem. Soc.*, **1959**, 112.

13) E. Vedejs and P. L. Fuchs, *J. Am. Chem. Soc.*, **95**, 822 (1973).

14) a) R. J. Anderson, C. A. Henrick, and J. B. Siddall, *J. Am. Chem. Soc.*, **92**, 735 (1970); b) C. A. Henrick, F. Schaub, and J. B. Siddall, *ibid.*, **94**, 5374 (1972); c) R. J. Anderson, C. A. Henrick, J. B. Siddall, and R. Zurflueh, *ibid.*, **94**, 5379 (1972).

15) E. E. van Tamelen and J. P. McCormick, *J. Am. Chem. Soc.*, **92**, 737 (1970).

16) E. E. van Tamelen, M. A. Schwartz, E. Hessler, and A. Storni, *J. Chem. Soc., Chem. Commun.*, **1966**, 409.

17) A. Yasuda, S. Tanaka, K. Oshima, H. Yamamoto, and H. Nozaki, *J. Am. Chem. Soc.*, **96**, 6513 (1974).

18) Both the (10*R**,11*S**) configuration of **14**, and the (6*R**,7*S**,10*R**,11*S**) or (6*R**,7*S**,10*S**,11*R**) configuration of **21** were assumed on the stereochemical outcome of the previous example, as well as on the stereochemistry of the double bonds of the products **17** and **24**, since NMR analyses were not sufficiently effective. The stereochemical analysis of **21** was complicated by the fact that no stereochemical data were available allowing inference on the relative arrangement of the 6 and 10 positions in the MCPBA epoxidation step (**10**→**18**).

19) E. J. Corey and H. Yamamoto, *J. Am. Chem. Soc.*, **92**, 6636 (1970).

20) We thank Dr. K. Kondo and associates for providing the reference sample of the acetate **25**.

A Highly Stereospecific Isomerization of Oxiranes into Allylic Alcohols by Means of Organoaluminum Amides[1]

Arata YASUDA,*,† Hisashi YAMAMOTO,†† and Hitosi NOZAKI

Department of Industrial Chemistry, Kyoto University, Yoshida, Kyoto 606

(Received December 6, 1978)

Organoaluminum reagents of type $R^1R^2NAlR_2$ allow highly stereospecific oxirane ring opening producing allylic alcohols under mild conditions. *trans*-Epoxycyclododecane is converted to (*E*)-2-cyclododecen-1-ol by reaction with diethylaluminum 2,2,6,6-tetramethylpiperidide (DATMP) in quantitative yield, while the *cis*-isomer gives only 8% yield of the same alcohol. Furthermore, this reagent enables us to perform the stereospecific isomerization of trisubstituted oxiranes: *c*-3-butyl-2-methyl-*r*-2-pentyloxirane is transformed into 2-pentyl-1-hepten-3-ol and the diastereomeric oxirane into (*E*)-6-methyl-6-undecen-5-ol, respectively. Such a rigorous stereospecificity is rationalized on the basis of a concerted syn elimination *via* the boat-like six membered ring imtermediary stage, in which the substituents of the oxirane ring should be arranged so as to minimize the severe nonbonded interactions.

A variety of synthetic methods have been developed to bring about the introduction of the allylic alcohol moiety.[2] Among them oxirane-allylic alcohol conversion by means of a strong base offers the advantage of wide spread applicability and experimental simplicity to a unique degree.[3–7] While lithium diethylamide has been widely used for this reaction, the rather vigorous conditions required decrease its practicability.[4–6] A further limitation arises in the reaction with unsymmetrical oxiranes and this reagent is rather nonspecific in the sense that the side chain methyl usually contributes proton to be removed. Accordingly the double bond of the resulting allylic alcohol is located rarely on the main chain. These facts led us to search for a new reagent allowing stereospecific isomerization of oxiranes into allylic alcohols under mild conditions which forms the subject of this paper.

Our attention has been focused on organoaluminum amides, since organoaluminum compounds in general are markedly strong Lewis acids and many of them are known to form stable 1 : 1 complexes with neutral bases such as amines or even ethers. In addition, the aluminum-nitrogen bond is cleaved readily by the attack of proton bearing base such as alcohol to leave aluminum-oxygen bond.[8] It was anticipated that an aluminum amide should be active with respect to both the oxirane ring and the proton to be removed simultaneously.

A series of dialkylaluminum *N,N*-dialkylamides were prepared *in situ* from (1) diethylaluminum chloride and lithium amides[9] obtained from secondary amines and butyllithium,[10] or from (2) diisobutylaluminum hydride and amines.[11] Reactions with *trans*-epoxycyclododecane (**1**)[7] under mild conditions (0 °C, 1 h) are summarized in Table 1. Best results were obtained upon the use of four equiv. of diethylaluminum 2,2,6,6-tetramethylpiperidide (DATMP) in benzene or hexane.[12] Other aluminum amides also gave (*E*)-2-cyclododecen-1-ol (**2**) as a sole product, however the rates of conversion were lower than that observed with DATMP. Thus the reactivity of alminum amides is apparently dependent on the structure of amine component.[13] Either benzene or hexane proved to be effective, as these do not solvate the aluminum species.[14]

TABLE 1. CONVERSION OF **1** TO **2** BY VARIOUS ALUMINUM AMIDES[a]

Aluminum amide[b]	Solvent	Yield (%)[c]
Et_2Al–TMP[d]	benzene	99
Et_2Al–TMP	hexane	99
Et_2Al–TMP	ether	76
Et_2Al–TMP	tetrahydrofuran	5
Et_2Al–N(*i*-Pr)$_2$[d]	benzene	65
Et_2Al–N(Cy)$_2$[d]	benzene	36
Et_2Al–NEt_2[d]	benzene	5
(*i*-Bu)$_2$Al–NPh_2[e]	benzene	48
(*i*-Bu)$_2$Al–NMePh[e]	benzene	69
(*i*-Bu)$_2$Al–N(*i*-Pr)$_2$[e]	benzene	30

a) For detailed reaction conditions, see Experimental part. b) Abbreviations used here are in accordance with those cited in Ref. 10. c) Yields are based on material isolated by preparative TLC. d) Prepared from diethylaluminum chloride and the corresponding lithium amide at 0 °C for 30 min. e) Prepared from diisobutylaluminum hydride and the corresponding amine.

Remarkably, the *cis* isomer **3** ($n=10$) reacted very reluctantly with DATMP under the same conditions (8 % yield of **2**). In addition, attempts to obtain allylic alcohols from medium ring-attached oxiranes **3** ($n=3$, 4, 5, and 6) were unsuccessful. Most of starting oxiranes were recovered unchanged.

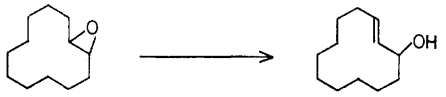

1 2

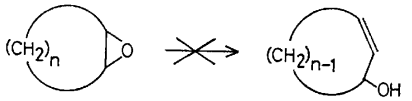

3

A few examples illustrate the efficient conversion of oxiranes to allylic alcohols in the presence of DATMP.

† Present address: The Institute for Molecular Science, Myodaiji, Okazaki 444.

†† Present address: Department of Chemistry, University of Hawaii at Manoa, Honolulu, Hawaii 96822.

The oxirane **4** was smoothly converted to **5** in 92% yield, while in contrast the reaction with lithium amide yielded less than 5 % of **5**. Oxiranes **6**[7] and **8**[15] gave allylic alcohols **7** and **9** in 98 and 96% yield, respectively. Notably, none of cyclized byproducts was produced in these two cases.

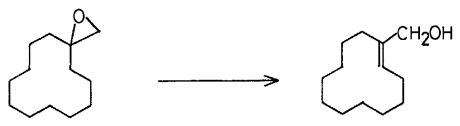

4 5

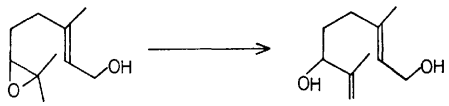

6 7

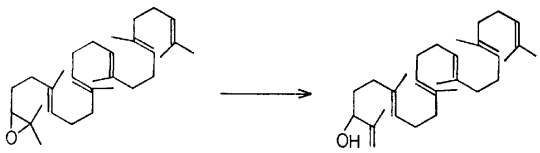

8 9

With the demonstration of the facility and effectiveness of this reagent, attention was directed toward the orientational selectivity in the reaction of unsymmetrical trisubstituted oxiranes. Remarkably, DATMP did react with oxiranes **10** and **12** under sharp discrimination of the configuration of oxiranes. Thus, the reaction of DATMP with oxirane **10** in benzene at 0 °C for 30 min gave the disubstituted allylic alcohol **11** in 96% yield. In marked contrast, the diastereomeric oxirane **12**[16] gave under the same conditions the trisubstituted (*E*)-allylic alcohol **13** predominantly in 83% yield. The structure of the product was unambiguously confirmed by the alternative synthesis of **13** and **14** by means of the β-oxido ylide technique.[17]

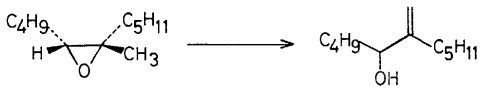

10 11

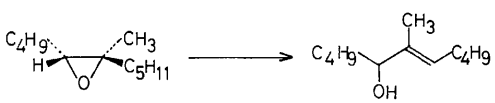

12 13

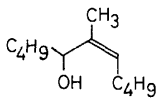

14

Aluminum amides preferentially abstract α-proton of the alkyl group located on the same side as hydrogen of oxirane to give the corresponding allylic alcohols (see Fig. 1). This is attributed to the attack of the aluminum reagent from the less hindered side of the oxirane group ("steric approach control"). This is supported by the

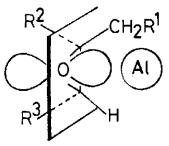

Fig. 1.

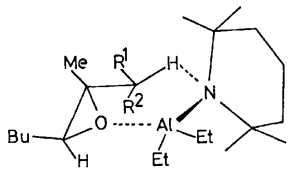

Conformer A (R^1=Bu, R^2=H)
B (R^1=H, R^2=Bu)

Fig. 2.

above finding that only sluggishly *cis*-2,3-disubstituted oxiranes **3** reacted with DATMP. In addition, the resulting allylic double bond prefers the (*E*)-configuration. Such significantly high stereoselectivity observed with DATMP is rationalized by presuming intermediary stage illustrated in Fig. 2 with respect to the reaction of the oxirane **12** with DATMP. Of the possible conformers, the chair ones should suffer from substantial steric interference because of the bulk of the extremely large TMP group. Moreover, of the two boat conformers (A and B), obviously the conformer A has the least steric crowdedness and the subsequent collapse would certainly furnish trisubstituted (*E*)-allylic alcohol **13**. The conformer B has severe crowdedness below the six-membered plane and this explains the minor amount of (*Z*)-allylic alcohol **14**.

Such a remarkable selectivity inherent in DATMP is further demonstrated by the following example. Bisoxirane **15** gives triol **16** upon exposure to lithium diethylamide,[18] while treatment of **15** with DATMP has converted it to the isomeric triol **17**[19,20] in 41% yield.

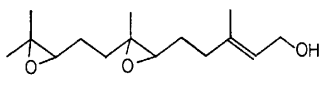

15

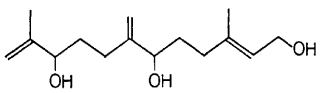

16

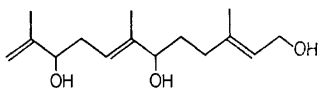

17

The selection rules of the DATMP isomerization of oxiranes into allylic alcohols are therefore:

(1) The sole product is a secondary allylic alcohol.

(2) The required proton is supplied by the alkyl group located on the same side as hydrogen of oxirane C(3).

(3) The resulting double bond prefers the (*E*) configuration.

Experimental

The infrared spectra were determined on a Shimadzu IR-27-G spectrometer; the mass spectra on a Hitachi RMU-6L mass machine; the GLPC analyses on a Yanagimoto GCG-550F; and NMR spectra on a JNM-PMX 60 or Varian EM-360 spectrometer. The chemical shifts are given in δ in ppm with TMS as the internal standard. Splitting patterns are designated as s, singlet; d, doublet; t, triplet; q, quartet; m, multiplet. The microanalyses were carried out by the staffs at the Elemental Analyses Center of Kyoto University. All experiments were carried out under an atmosphere of dry argon. In experiments requiring dry solvents, tetrahydrofuran was distilled from sodium-benzophenone. Ether, benzene, and hexane were dried over sodium metal. During workup, drying of the organic solution was performed over anhydrous sodium sulfate. Thin layer or preparative thick layer plates were made of E. Merck PF-254, and preparative column chromatography on silica gel E. Merck Art. 7734.

Preparation of Dialkylaluminum N,N-*Dialkylamides. From Diethylaluminum Chloride and Lithium Amides*:[9] A benzene solution of diethylaluminum chloride (1 equiv) was added at 0 °C dropwise to a solution of lithium *N,N*-dialkylamide (1 equiv) in benzene. The resulting slurry was stirred at the same temperature for 30 min and used immediately. The following aluminum amides were prepared by this method: diethylaluminum 2,2,6,6-tetramethylpiperidide (DATMP); diethylaluminum diisopropylamide; diethylaluminum diethylamide.

From Diisobutylaluminum Hydride and Amines:[11] Diisobutylaluminum hydride (1 equiv) dissolved in benzene was added drop by drop to a solution of amine (1 equiv) in benzene at 0 °C. The resulting solution was gently heated until theoretical volume of hydrogen gas was evolved. The reaction mixture was allowed to cool to 0 °C and then used immediately. The following aluminum amides were prepared by this method: diisobutylaluminum diphenylamide; diisobutylaluminum *N*-methylanilide; diisobutylaluminum diisopropylamide.

Preparation of Oxiranes. 1-Oxaspiro[2,11]tetradecane (**4**): To a mixture of methylenecyclododecane[21] (540 mg, 3.0 mmol) and dichloromethane (15 ml) *m*-chloroperbenzoic acid (712 mg, 3.3 mmol) was added at 0 °C in small portions. The whole mixture was stirred at the same temperature for 1.5 h. After dilution with ether, the mixture was poured into ice-cold saturated sodium sulfite. The separated organic phase was washed with saturated sodium sulfite and saturated sodium bicarbonate, dried, and concentrated *in vacuo*. The residue was submitted to column chromatography using 10: 1 hexane–ether as an eluent to give 534 mg (91% yield) of pure **4** as a clear oil: bp 90 °C (bath temp, 1 Torr); TLC, R_f 0.28 (5: 1 hexane–ether); IR (neat), 2940 (s), 1470 (s), 1445 (m), and 1150 cm^{-1} (w); NMR (CCl_4), 2.39 (2H, s, CH_2–O); MS (*m/e*), 196 (13), 178 (12), 153 (25), 125 (70), and 111 (100).

Found: C, 79.3; H, 12.3%. Calcd for $C_{13}H_{24}O$: C, 79.5; H, 12.3%.

c-*3-Butyl-2-methyl*-r-*2-pentyloxirane* (**10**). A solution of (*Z*)-6-methyl-5-undecene[16] (250 mg, 1.50 mmol) in dichloromethane (8 ml) was treated with *m*-chloroperbenzoic acid (354 mg, 1.65 mmol) as described above to furnish **10** (250 mg, 90 % yield) as a colorless liquid: bp 64 °C (1 Torr); TLC, R_f 0.65 (1: 1 hexane–ether); IR (neat), 1470 (s), 1370 (s), and 1115 cm^{-1} (m); NMR (CCl_4), 1.19 (3H, s, CH_3–CO), and 2.48 (1H, bt, CH–O); MS (*m/e*), 184 (13), 155 (4), 141 (38), 127 (12), and 71 (100).

Found: C, 78.2; H, 13.4%. Calcd for $C_{12}H_{24}O$: C, 78.2; H, 13.1%.

Reaction of Oxiranes with Aluminum Amides. A General Procedure: To a stirred mixture of aluminum amide (4.0 mmol) and benzene (10 ml) a solution of oxirane (1.0 mmol) in benzene (3 ml) was added at 0 °C drop by drop over a period of 5 min. The whole mixture was stirred at the same temperature until oxirane could not be detected by TLC analysis. The reaction was quenched by the addition of ice-cold 1 M hydrochloric acid and the resulting organic phase was separated. The aqueous layer was extracted with ether. The organic solutions were combined, washed with saturated brine, dried, and concentrated *in vacuo*. The residue was submitted to preparative TLC to give the desired allylic alcohol.

(E)-*2-Cyclododecen-1-ol* (**2**):[6] TLC, R_f 0.22 (2: 1 hexane–ether); IR (neat), 3330—3370 (s), 1465 (s), 1450 (m), and 970 cm^{-1} (s); NMR (CCl_4), 3.73—4.20 (1H, m, CH–OH), and 4.97—5.82 (2H, m, CH=); MS (*m/e*), 182 (16), 164 (13), 139 (32), 125 (46), and 98 (100).

1-Cyclododecenylmethanol (**5**): This is an (*E,Z*)-mixture, bp 110 °C (bath temp, 1 Torr); TLC, R_f 0.40 (1: 1 hexane–ether); IR (neat), 3300—3360 (s), 1665 (w), 1470 (s), 1000—1010 (s), and 800 cm^{-1} (w); NMR (CCl_4), 3.96 and 4.10 (2H, s, CH_2–O), and 5.15—5.71 (1H, m, CH–); MS (*m/e*), 196 (19), 178 (6), 149 (8), 109 (35), and 83 (100).

Found: C, 79.3; H, 12.5%. Calcd for $C_{13}H_{24}O$: C, 79.5; H, 12.3%.

A small aliquot of **5** was acetylated by stirring with acetic anhydride in pyridine. GLPC analysis (10 % Apiezon, 230 °C, 1.3 kg/cm^2) showed a 69: 31 mixture of (*E*) and (*Z*)-allylic acetates.

(E)-*3,7-Dimethyl-2,7-octadiene-1,6-diol* (**7**):[22] The title compound was prepared according to the general procedure, except the use of 5 equiv. of DATMP; TLC, R_f 0.28 (ether); IR (neat), 3340—3400 (s), 1650 (m), 1440 (m), 1000 (s), and 890 cm^{-1} (s); NMR ($CDCl_3$), 1.67 (3H, s, CH_4–C= on C-3), 1.73 (3H, s, CH_3–C= on C-7), 3.87—4.23 (3H, d and t, CH–O and CH_2–O), 4.90 (2H, bd, CH_2=), and 5.43 (1H, bt, CH=); MS (*m/e*), 152 (2), 134 (10), 119 (30), 84 (95), and 67 (100).

(E,E,E,E)-*2,6,10,15,19,23-Hexamethyltricosa-1,6,10,14,18,22-hexaen-3-ol* (**9**): Bp 195 °C (bath temp, 0.5 Torr); TLC, R_f 0.45 (1: 1 hexane–ether); IR (neat), 3400—3480 (m), 1710 (m), 1450 (s), 1380 (s), and 895 cm^{-1} (m); NMR (CCl_4), 3.92 (1H, bt, CH–O), and 4.60—5.33 (7H, m, CH= and CH_2=).

Found: C, 84.6; H, 11.7 %. Calcd for $C_{30}H_{50}O$: C, 84.4; H, 11.8 %.

2-Pentyl-1-hepten-3-ol (**11**): Bp 105 °C (bath temp, 1 Torr); TLC, R_f 0.64 (30: 1 benzene–ethyl acetate, 3 developments); IR (neat), 3310—3400 (s), 1650 (m), 1465 (s), 1015 (s), and 895 cm^{-1} (s); NMR (CCl_4), 3.97 (1H, m, CH–O), 4.80 and 4.96 (2H, s, CH_2=); MS (*m/e*), 184 (2), 155 (3), 127 (15), 113 (25), and 71 (100).

Found: C, 78.1; H, 13.0%. Calcd for $C_{12}H_{24}O$: C, 78.2; H, 13.1%.

(E)-*6-Methyl-6-undecen-5-ol* (**13**). A sample free from **11** was produced by preparative TLC purification (30: 1 benzene–ethyl acetate, 3 developments): bp 105 °C (bath temp, 1 Torr); TLC, R_f 0.55 (30: 1 benzene–ethyl acetate, 3 developments); IR (neat), 3310—3400 (s), 1470 (s), 1010 (s), and 850 cm^{-1} (w); NMR (CCl_4), 1.60 (3H, s, CH_3–C=), 3.90 (1H, bt, CH–O), and 5.33 (1H, t, CH=); MS (*m/e*), 184 (4), 155 (8), 127 (66), 109 (30), and 71 (100).

Found: C, 78.0; H, 13.1%. Calcd for $C_{12}H_{24}O$: C, 78.2; H, 13.1%.

A small aliquot was acetylated with Ac_2O–pyridine. GLPC analysis (10% Apiezon, 210 °C, 1.0 kg/cm^2) showed that the product was $>$96 % pure.

Alternative Synthesis of a Mixture of ***13*** *and* ***14****.*[17] To a slurry of ethyltriphenylphosphonium bromide (2.32 g, 6.0 mmol) in THF (10 ml) was added dropwise butyllithium (4.6 ml of a 1.3 M hexane solution, 6.0 mmol) at 0 °C. After stirring at 0 °C for 30 min, the resulting red ylide solution was cooled to −78 °C and treated with pentanal (516 mg, 6.0 mmol) dissolved in THF (5 ml). Butyllithium (4.6 ml of a 1.3 M hexane solution, 6.0 mmol) was added dropwise at this temperature to effect immediate red coloring. To this solution was added pentanal (516 mg, 6.0 mmol) dissolved in THF (5 ml), and the solution was brought to room temperature and stirred for 2 h. The reaction mixture was poured into ice-cold water, and the product was extracted with ether. The ethereal solution was dried and freed of the solvent to leave a crude oil, which was purified by preparative TLC (4: 1 hexane–ether) to furnish a mixture of **13** and **14** (820 mg, 74% yield). GLPC analysis as described above showed the ratio of **13**: **14** 84: 16.

*(E,E)-3,7,11-Trimethyldodeca-2,7,11-triene-1,6,10-triol (****17****)*: The title compound was prepared from **15** by the reaction of 10 equiv. of DATMP in benzene at 0 °C for 3 h: TLC, R_f 0.25 (ether); IR (neat), 3260—3400 (s), 1650 (m), 1450 (s), 1000 (s), and 900 cm^{-1} (m); NMR ($CDCl_3$), 1.64—1.80 (9H, bs, CH_3–C=), 3.83—4.69 (4H, m, CH_2–O and CH–O), 4.80—5.12 (2H, d, CH_2=), and 5.20—5.77 (2H, m, CH=).

The microanalysis was performed after trimethylsilylation of both hydroxyl groups.

Found: C, 61.5; H, 10.5%. Calcd for $C_{21}H_{50}O_3Si_3$: C, 61.3; H, 10.6%.

The authors wish to thank the Ministry of Eduction, Japan, for Grant-in-Aid (No. 011010, 110309, 203014, and 303023).

References

1) A preliminary account of this work has appeared: A Yasuda, S. Tanaka, K. Oshima, H. Yamamoto, and H. Nozaki, *J. Am. Chem. Soc.*, **96**, 6513 (1974).

2) a) J. Reucroft and P. G. Sammes, *Quart. Rev. (London)*, **25**, 135 (1971); b) R. S. Lenox and J. A. Katzenellenbogen, *J. Am. Chem. Soc.*, **95**, 957 (1973); c) A. Yasuda, H. Yamamoto, and H. Nozaki, *Tetrahedron Lett.*, **1976**, 2621.

3) A. Rosowsky, "Heterocyclic Compounds with Three- and Four-Membered Rings," ed by A. Weissberger, Interscience, New York, N. Y. (1964), pp. 1—523.

4) a) A. C. Cope, H. H. Lee, and H. E. Petree, *J. Am. Chem. Soc.*, **80**, 2849 (1958); b) A. C. Cope, G. A. Berchtold, P. E. Peterson, and S. H. Sharman, *ibid.*, **82**, 6370 (1960); c) A. C. Cope and J. K. Heeren, *ibid.*, **87**, 3125 (1965); d) A. C. Cope, M. Brown, and H. H. Lee, *ibid.*, **80**, 2855 (1958).

5) a) J. K. Crandall, *J. Org. Chem.*, **29**, 2830 (1964); b) J. K. Crandall and L. Chang, *ibid.*, **32**, 435, 532 (1967); c) J. K. Crandall and L. C. Lin, *J. Am. Chem. Soc.*, **89**, 4526, 4527 (1967).

6) a) B. Rickborn and R. P. Thummel, *J. Org. Chem.*, **34**, 3583 (1969); b) R. P. Thummel and B. Rickborn, *J. Am. Chem. Soc.*, **92**, 2064 (1970); c) R. P. Thummel and B. Rickborn, *J. Org. Chem.*, **36**, 1365 (1971); d) C. L. Kissel and B. Rickborn, *ibid.*, **37**, 2060 (1972).

7) a) K. B. Sharpless and R. F. Lauer, *J. Am. Chem. Soc.*, **95**, 2697 (1973); b) B. M. Trost and J. Bogdanowicz, *ibid.*, **95**, 5311 (1973).

8) a) T. Mole and E. A. Jeffery, "Organoaluminium Compounds," Elsevier, Amsterdam (1972); b) K. Gosling, J. D. Smith, and D. H. W. Wharmby, *J. Chem. Soc., A*, 1738 (1969).

9) T. Hirabayashi, H. Imaeda, K. Itoh, S. Sasaki, and Y. Ishii, *J. Organomet. Chem.*, **19**, 299 (1969).

10) R. A. Olofson and C. M. Dougherty, *J. Am. Chem. Soc.*, **95**, 583 (1973).

11) W. P. Neumann, *Justus Liebigs Ann. Chem.*, **629**, 23 (1960).

12) It should be noted that LiTMP itself was an unsatisfactory reagent for this transformation under the same reaction conditions (<5 % of **2** and >70 % of the starting oxirane was recovered).

13) E. C. Ashby, J. P. Sevenair, and F. R. Dobbs, *J. Org. Chem.*, **36**, 197 (1971).

14) For example, a) H. C. Brown and K. Ishikawa, *J. Am. Chem. Soc.*, **83**, 4372 (1961); b) B. Franzus and E. J. Snyder, *ibid.*, **87**, 3423 (1965); see also Ref. 7b.

15) E. E. van Tamelen and T. J. Curphey, *Tetrahedron Lett.*, 121 (1962).

16) S. Tanaka, H. Yamamoto, H. Nozaki, K. B. Sharpless, R. C. Michaelson, and J. D. Cutting, *J. Am. Chem. Soc.*, **96**, 5254 (1974).

17) E. J. Corey and H. Yamamoto, *J. Am. Chem. Soc.*, **92**, 226, 3523 (1970).

18) E. E. van Tamelen and J. P. McCormick, *J. Am. Chem Soc.*, **92**, 737 (1970).

19) The (*E*) configuration of the central double bond was assumed on the basis of the stereochemical outcomes of other examples, since NMR analysis was not effective enough in this case.

20) The low yield of the reaction was attributed to the thermal lability of the resulting triol **17**.

21) J. Casanova and B. Waegell, *Bull. Soc. Chim. Fr.*, 1295 (1971).

22) E. Buchta and F. Andree, *Justus Liebigs Ann. Chem.*, **639**, 9 (1961).

Syntheses of Capreomycin Analogs in Relation to Their Antibacterial Activities[1)]

Shinya NOMOTO and Tetsuo SHIBA*

Department of Chemistry, Faculty of Science, Osaka University, Toyonaka, Osaka 560

(Received December 11, 1978)

Six analogs of an antituberculous antibiotic capreomycin were synthesized in order to clarify the structure-activity relationship, especially with regard to the significance of the β-amino group in α,β-diaminopropionic acid residue as well as the position of linkage of the branch residue, β-lysine, to the cyclic peptide moiety. All the synthetic products were found to have the same conformations in solution as those of the natural antibiotics in terms of NMR spectra. It was found from their antibacterial activities that an amino group located at β-position of the α,β-diaminopropionic acid residue adjacent to ureidodehydroalanine residue remarkably strengthens the biological activity, and that the position of a branch does not significantly influence the antibacterial potency.

Peptide antibiotics such as, capreomycin,[2)] viomycin,[3)] and tuberactinomycin,[4)] show comparable antituberculous activities. From a structural point of view, these antibiotics constitute one group of branched cyclic pentapeptides with analogous amino acid sequence (Figs. 1 and 2). However, capreomycin, whose chemical structure was established,[5)] is structurally unique. The Ser[4] residue[6)] in all tuberactinomycins including viomycin (tuberactinomycin B) is replaced by A_2pr[7)] residue in capreomycins. This antibiotic contains one more amino group in its molecule than in tuberactinomycin. Capreomycin differs from tuberactinomycin in the position of linkage of the branch part, *i.e.*, β-Lys or γ-Hy-β-Lys,[7)] to the cyclic pentapeptide moieties, which is of interest in connection with the structure-activity relationship as well as biosynthesis of capreomycin.

Little is known about structural requirements for the antimicrobial activity of capreomycin so far. Syntheses of several capreomycin analogs have been carried out in the present study in order to clarify how the above-mentioned structural differences between capreomycin and tuberactinomycin are reflected on the antibacterial activity.

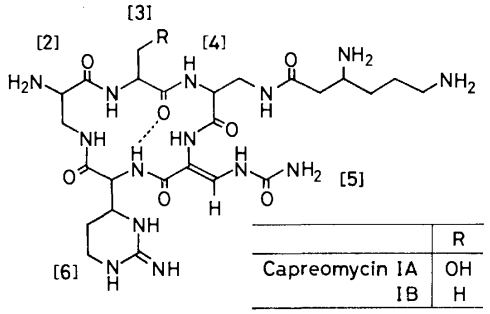

	R
Capreomycin IA	OH
IB	H

Fig. 1. Structures of capreomycins.

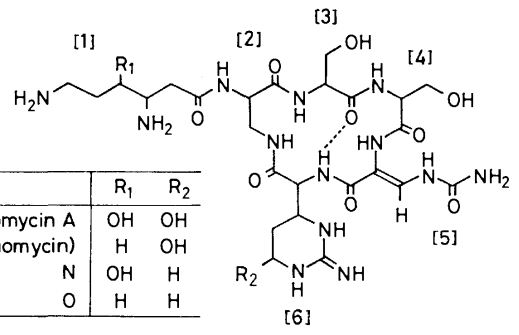

	R_1	R_2
Tuberactinomycin A	OH	OH
B (Viomycin)	H	OH
N	OH	H
O	H	H

Fig. 2. Structures of tuberactinomycins.

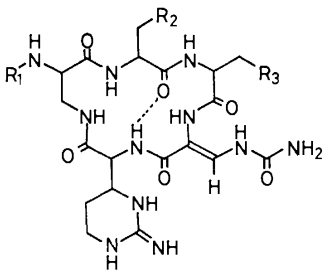

	R_1	R_2	R_3
Capreomycin IIA (2a)	H	OH	NH_2
IIB (2b)	H	H	NH_2
Pseudocapreomycin IB (4)	β-Lys	H	NH_2
Reversecapreomycin IIB (11a)	H	NH_2	H
[Orn[4]]-Capreomycin IIB (11b)	H	H	$CH_2CH_2NH_2$
Di-β-Lys-capreomycin IIB (13)	β-Lys	H	β-Lys-NH

Fig. 3. Structures of capreomycin analogs synthesized.

Capreomycin analogs and related compounds synthesized are summarized in Fig. 3. Capreomycin IIA and IIB lacking β-Lys residue in capreomycin IA and IB molecules, respectively, were obtained from natural sources as minor components of the antibiotics.[8)] Capreomycin IIA and IIB have comparable antibacterial activities to those of IA and IB,[9)] whereas a similar cyclic moiety of tuberactinomycin, *i.e.*, tuberactinamine N shows less activity than tuberactinomycin itself.[10)] It was suggested that the β-amino group of A_2pr[4] residue[6)] in capreomycin II might act to enhance the antibacterial activity. For the sake of confirmation, we compared not only the antimicrobial spectra of tuberactinamine N and capreomycin IIA and IIB synthesized here, under the same conditions, but also those of tuberactinomycin O and so-called pseudocapreomycin IB whose branch part is linked to the second amino acid (A_2pr) residue in a similar way to that of the former. [Orn[4]]-Capreomycin IIB[6)] and reversecapreomycin IIB, in which the positions of Ala[3] and A_2pr[4] residue in capreomycin IIB are exchanged, were also synthesized for the purpose of observing the effects of the length of the side chain in the basic amino acid residue and its sequential position.

In order to prepare a more potent analog of this antibiotic than natural capreomycin or tuberactinomycin, and taking into account the fact that the addition of β-lysine branch to the cyclic peptide moiety virtually increases the biological activity in the case of tuberactinomycin, introduction of β-Lys to the free α-amino group of A_2pr^2 residue[6] in capreomycin IB, *viz.*, the preparation of di-β-Lys-capreomycin IIB, was undertaken.

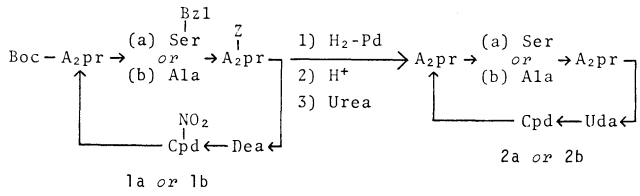

Fig. 4. Synthetic scheme for capreomycin IIA(**2a**) and IIB(**2b**).

Syntheses of Capreomycin IIA and IIB. The protected cyclopentapeptides **1a** and **1b** (Fig. 4), whose syntheses were reported in the total syntheses of capreomycin IA and IB,[5] were deprotected by catalytic reduction followed by acid treatment. The products were immediately treated with excess urea in order to convert the aldehyde group liberated from Dea[7] into Uda[7] residue, affording capreomycin IIA and IIB (**2a** and **2b**).

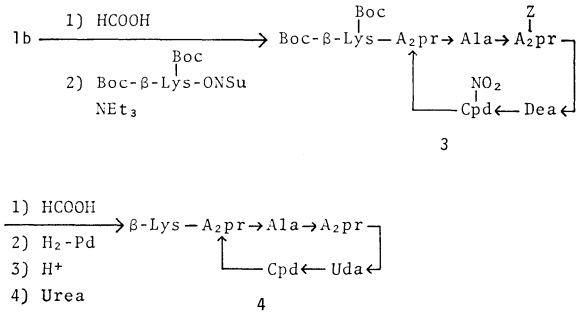

Fig. 5. Synthetic scheme for pseudocapreomycin IB(**4**).

Synthesis of Pseudocapreomycin IB. After cleavage of the Boc[7] group in **1b** (Fig. 5) with 99 % formic acid, Boc-β-Lys(Boc) residue was introduced to the α-amino group of the A_2pr^2 residue by the ONSu[7] active ester method. The product **3** was subsequently converted into pseudocapreomycin IB (**4**) through successive removal of Boc, Z, and nitro groups followed by the transformation of Dea into Uda residue.

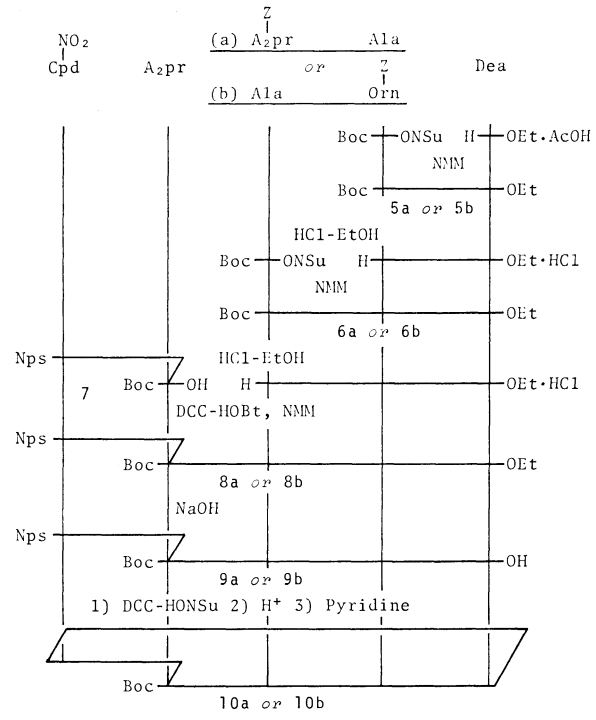

Fig. 6. Synthetic scheme for protected cyclopentapeptides **10a** and **10b**.

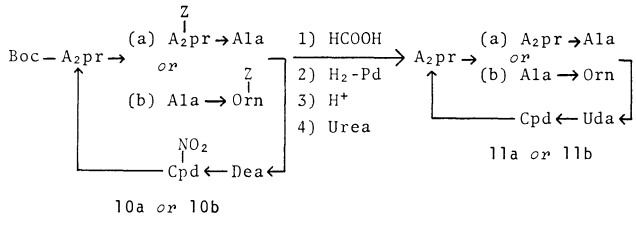

Fig. 7. Synthetic scheme for reversecapreomycin IIB (**11a**) and [Orn[4]]-capreomycin IIB(**11b**).

Syntheses of Reversecapreomycin IIB and [Orn[4]]-Capreomycin IIB. The synthetic schemes for these compounds

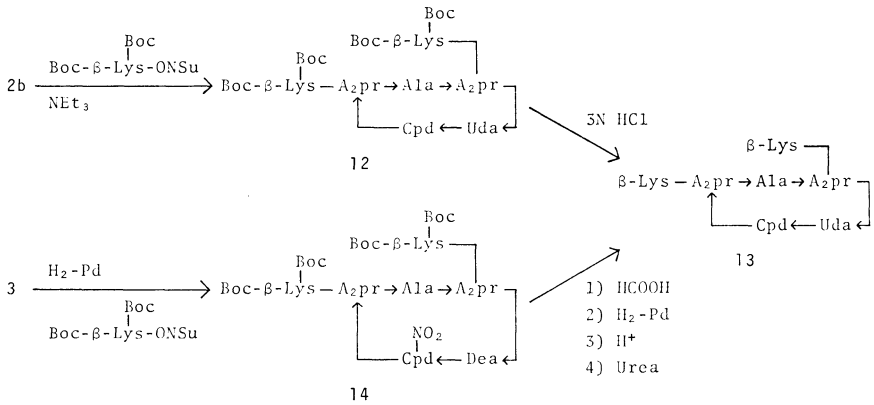

Fig. 8. Synthetic scheme for di-β-Lys-capreomycin IIB (**13**).

are given in Figs. 6 and 7. The C-terminal tripeptides (**6a**) and (**6b**) were prepared by the stepwise elongation method from the C-terminal utilizing ONSu active esters. Cleavage of Boc groups in dipeptides (**5a**) and (**5b**) was carried out in ethanol, otherwise severe decomposition occurred at diethyl acetal group of Dea residue.

The N-terminal dipeptide **7**[12] was condensed with deprotected C-terminal tripeptides (**6a**) and (**6b**) by means of DCC-HOBt[7] to afford linear pentapeptides (**8a**) and (**8b**), which were then cyclized by the ONSu active ester method. Conversion of the protected cyclic pentapeptides (**10a**) and (**10b**) thus obtained into the final products (**11a**) and (**11b**) were carried out as in the preparation of capreomycin IIA (**2a**) or IIB (**2b**).

Synthesis of Di-β-Lys-capreomycin IIB. This analog was prepared in the following two ways. Route A (Fig.

Table 1.[a] Chemical shifts (δ) of capreomycin analogs in D_2O–TFA (4: 1)

Position of amino acid residue		Cpm IA	Cpm IB	Cpm IIA	Cpm IIB
1	α-CH_2	2.63(dd)	2.50(dd)		
		2.85(dd)	2.81(dd)		
	β-CH	3.8 (m)	3.7 (m)		
	γ-CH_2	1.8 (m)	1.8 (m)		
	δ-CH_2	1.8 (m)	1.8 (m)		
	ε-CH_2	3.10(m)	3.08(m)		
2	α-CH	4.3—4.5(m)	4.2—4.5(m)	4.3—4.6(m)	4.3—4.6(m)
	β-CH_2	3.3 (m)	3.3(m)	3.3 (m)	3.3 (m)
		3.8 (m)	3.8(m)	4.1 (m)	4.1 (m)
3	α-CH	4.86(t)	4.67(q)	4.84(t)	4.68(q)
	β-CH_2	3.84(d)		3.95(d)	
	β-CH_3		1.43(d)		1.45(d)
4	α-CH	4.3—4.5(m)	4.2—4.5(m)	4.3—4.5(m)	4.3—4.5(m)
	β-CH_2	3.7—4.3(m)	3.7—4.2(m)	3.7—4.2(m)	3.79(dd)
					3.8—4.2(m)
5	β-CH	8.04(s)	8.03(s)	8.05(s)	8.04(s)
6	α-CH	5.01(d)	4.96(d)	5.01(d)	4.95(d)
	β-CH	4.5 (m)	4.5 (m)	4.5 (m)	4.5 (m)
	γ-CH_2	1.6—2.3(m)	1.6—2.3(m)	1.6—2.3(m)	1.6—2.3(m)
	δ-CH_2	3.3 (m)	3.3 (m)	3.3 (m)	3.3 (m)

Position of amino acid residue		Pseudo Cpm IB	Reverse Cpm IIB	[Orn[4]]-Cpm IIB	Di-β-Lys-Cpm IIB
1	α-CH_2	2.65(dd)			2.7—3.0(m)
		2.83(dd)			
	β-CH	3.7 (m)			3.8 (m)
	γ-CH_2	1.8 (m)			1.8 (m)
	δ-CH_2	1.8 (m)			1.8 (m)
	ε-CH_2	3.08(m)			3.10(m)
2	α-CH	4.68(dd)	4.3—4.6(m)	4.1—4.4(m)	4.68(dd)
	β-CH_2	3.2 (m)	3.3 (m)	3.4 (m)	3.4 (m)
		4.1 (m)	4.1 (m)	4.1 (m)	4.0 (m)
3	α-CH	4.74(q)	5.18(dd)	4.68(q)	4.69(q)
	β-CH_2		3.60(dd)		
			4.0—4.4(m)		
	β-CH_3	1.45(d)		1.47(d)	1.43(d)
4	α-CH	4.3—4.5(m)	4.33(q)	4.1—4.5(m)	4.3—4.6(m)
	β-CH_2	3.6—4.1(m)		2.0 (m)	3.6—4.1(m)
	β-CH_3		1.46(d)		
	γ-CH_2			1.8 (m)	
	δ-CH_2			3.08(t)	
5	β-CH	8.03(s)	8.05(s)	8.06(s)	8.02(s)
6	α-CH	4.97(d)	5.02(s)	4.97(d)	5.97(d)
	β-CH	4.5 (m)	4.5 (m)	4.4 (m)	4.4 (m)
	γ-CH_2	1.6—2.3(m)	1.6—2.3(m)	1.6—2.3(m)	1.6—2.3(m)
	δ-CH_2	3.3 (m)	3.3 (m)	3.3 (m)	3.3 (m)

a) Abbreviation: Cpm, capreomycin.

TABLE 2.[a] CHEMICAL SHIFTS (δ) OF NH PROTONS OF CAPREOMYCIN ANALOGS IN H_2O (pH 2.5)

	Cpm IA	Cpm IB	Cpm IIA	Cpm IIB	Pseudo Cpm IB	Reverse Cpm IIB	[Orn^4]-Cpm IIB	Di-β-Lys-Cpm IIB
1	9.33(d)	9.72(d)	9.60(d)	9.50(d)	9.43(d)	9.61(d)	9.39(d)	9.20(d)
2	9.24(d)	9.24(d)	9.33(d)	9.30(d)	9.29(d)	9.25(d)	9.28(d)	9.19(d)
3	8.82(s)	8.76(s)	9.10(s)	9.10(s)	9.05(s)	8.88(s)	8.82(s)	8.77(s)
4	8.64(d)	8.68(d)	8.73(d)	8.73(d)	8.59(d)	8.78(d)	8.78(d)	8.58(d)
5					8.44(d)			8.41(d)
6[b]	8.22(t)	8.15(t)						8.12(t)
7[b]	8.10(t)	8.15(t)	8.19(t)	8.08(t)	7.95(t)	8.27(t)	8.09(t)	8.00(t)
8	7.61(d)	7.62(d)	7.50(d)	7.49(d)	7.50(d)	7.68(d)	7.72(d)	7.61(d)
9	7.46(s)	7.42(s)	7.44(s)	7.44(s)	7.44(s)	7.41(s)	7.39(s)	7.40(s)
10	7.46(s)	7.42(s)	7.31(s)	7.18(s)	7.23(s)	7.41(s)	7.17(s)	7.40(s)
11	6.48(s)	6.49(s)	6.43(s)	6.34(s)	6.44(s)	6.45(s)	6.49(s)	6.46(s)
12	6.29(s)	6.34(s)	6.29(s)	6.27(s)	6.29(s)	6.23(s)	6.31(s)	6.30(s)

a) Abbreviation: Cpm, capreomycin. b) The chemical shifts of protons 6 and 7 are exchangeable.

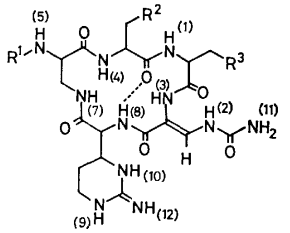

(6)
R^3: β-Lys-NH- in Cpm IA, IB and di-β-Lys-Cpm IIB

8): Boc-β-Lys(Boc) residue was introduced simultaneously to both the α-amino group of A_2pr^2 and β-amino group of A_2pr^4 in capreomycin IIB (**2b**). Subsequently, four Boc groups in the product **12** were removed to afford di-β-Lys-capreomycin IIB (**13**). Route B (Fig. 8): when the protected hexapeptide (**3**, Fig. 5) was hydrogenated in the presence of Boc-β-Lys(Boc)-ONSu, a heptapeptide **14** was directly obtained in a good yield without cleavage of the nitro group as well as *N*,*N*-acyl migration at the A_2pr^4 residue.[5] The hexapeptide **14** was then subjected to deprotection followed by conversion of Dea into Uda residue.

The advantage of route B over route A lies in its applicability to a possible need in which analogs possessing different kinds of amino acid residues at two branch positions are required.

NMR Analysis. The NMR spectral data of capreomycin analogs prepared in this study are summarized in Tables 1 and 2, together with those of natural antibiotics for comparison. Assignment of each signal was performed by means of decoupling technique and a comparison with the spectra of natural antibiotics.[11,12]

The cyclic peptide moieties of tuberactinomycin and capreomycin as well as tuberactinomycin analogs have a stable and rigid conformation with an intramolecular hydrogen bond in commom as shown in Figs. 1 and 2.[11a] This is shown in particular by constant chemical shifts of each α-NH and α-CH signal in all the cyclic moieties. The fact that all capreomycin analogs show similar NMR spectral patterns to those of the natural ones, especially with respect to signals of α-NH and α-CH, indicates the conformational similarity of the analogs to the natural antibiotics.

Antibacterial Activities. The minimum inhibitory concentrations of capreomycin analogs were determined by a serial agar dilution method (Table 3). Both capreomycin IIA and IIB showed apparently greater activities than the corresponding tuberactinamine N,

TABLE 3. MINIMUM INHIBITORY CONCENTRATIONS (mcg/ml) OF CAPREOMYCIN ANALOGS

Test organism	Cpm IA	Cpm IB	Tum O	Tua N	Cpm IIA	Cpm IIB	Pseudo Cpm IB	Reverse Cpm IIB	[Orn^4]-Cpm IIB	Di-β-Lys-Cpm IIB
Staphylococcus epidermidis sp-al-1	100	>100	>100	>100	>100	>100	50	>100	>100	50
Streptococcus pyogenes 1022	>100	>100	>100	>100	50	50	50	100	100	>100
Streptococcus agalactiae 1020	>100	>100	—	—	50	100	>100	>100	100	>100
Corynebacterium diphtheriae P.W.8	3.1	3.1	3.1	50	6.3	6.3	1.6	100	25	1.6
Bacillus subtilis ATCC 6633	25	25	50	>100	50	25	6.3	100	50	3.1
Escherichia coli B	50	100	100	>100	50	100	50	>100	>100	100
Klebsiella pneumoniae ATCC 10031	25	50	25	>100	25	25	25	>100	100	50
Salmonella typhosa H 901	25	50	100	>100	50	50	25	>100	>100	50
Shigella sonnei E 33	50	100	50	>100	100	100	100	>100	>100	100
Proteus vulgaris OX 19	50	50	50	>100	50	100	50	>100	>100	100
Mycobacterium ATCC 607	6.3	6.3	6.3	50	25	12.5	12.5	100	25	3.1

a) Abbreviations: Cpm, capreomycin; Tum tuberactinomycin; Tua, tuberactinamine.

being comparable to Tum O, whereas activities of both reversecapreomycin IIB and [Orn^4]-capreomycin IIB proved to be weaker than that of capreomycin IIB, being comparable to that of tuberactinamine N. On the other hand, pseudocapreomycin IB and di-β-Lys-capreomycin IIB showed even slightly greater activities than those of capreomycin IB or tuberactinomycin O.

Structure-activity Relationship. Both capreomycin IIA and IIB lacking the β-Lys branch showed stronger activities than tuberactinamine N which is also a cyclic peptide having no branch part. It is suggested that the β-amino group of A_2pr^4 residue promotes biological potency, although no such effect could be recognized for the same β-amino group of A_2pr^4 residue in pseudocapreomycin IB as compared with tuberactinomycin O. A possible explanation is as follows: the antibacterial potency of tuberactinomycin or capreomycin I might reach the upper limit in this sort of peptide antibiotics, since no synthetic analog has been found remarkably more active than the natural antibiotics so far.

Weaker activities of both [Orn^4]- and reversecapreomycin IIB apparently indicate the significance of the location of β-amino group of A_2pr^4 residue for its function as an activity-enhancing group.

A comparable activity of pseudocapreomycin IB to natural capreomycin IA or IB may imply that the effectiveness of β-Lys residue does not differ so much at either position of A_2pr residues for the enhancement of antibacterial activity. However, even if two β-Lys residues were attached to both amino groups, no significant increase of the activity was observed as seen in the case of di-β-Lys-capreomycin IIB.

Experimental

All the melting points are uncorrected. NMR spectra were recorded with a Varian XL-100-15 spectrometer using sodium dimethylsilapentanesulfonate as an internal standard. Specific rotations were measured with a Perkin-Elmer 141 Polarimeter. Molecular weights were determined with a Knauer vapor pressure osmometer using DMF as a solvent.

*Capreomycin IIA (**2a**).* A protected cyclopentapeptide **1a**[5] (170 mg, 0.180 mmol) was treated with 99 % formic acid (5 ml) at room temperature for 1 h. After removal of formic acid by evaporation, the product was hydrogenated with palladium black in methanol. The filtrate from catalyst was concentrated *in vacuo*. The residue was dissolved in 1 M hydrochloric acid–acetone (1: 1) (5 ml) and heated under reflux for 10 min. To the cooled solution was added urea (500 mg, 8.33 mmol) and the mixture was stirred at room temperature overnight. After evaporation of the solvent *in vacuo*, ethanol was added to the residue to form a white precipitate, which was reprecipitated from water–methanol–ethanol, yield 99 mg (84.6 %), mp 250 °C (dec), $[\alpha]_D^{23}$ +9.3° (*c* 2.8, H_2O). Found: C, 34.77; H, 5.60; N, 25.13; Cl, 15.35 %. Calcd for $C_{19}H_{35}N_{12}O_7Cl_3 \cdot 1/2H_2O \cdot 1/2CH_3OH$: C, 34.70; H, 5.67; N, 24.90; Cl, 15.76 %.

*Capreomycin IIB (**2b**).* The compound was prepared from a protected cyclopentapeptide **1b**[5] (150 mg, 0.179 mmol) in a similar manner to that for **2a**, yield 93 mg (81.6 %), mp 252 °C (dec), $[\alpha]_D^{23}$ −24.9° (*c* 0.57, H_2O). Found: C, 31.99; H, 6.15; N, 23.82; Cl, 15.24 %. Calcd for $C_{19}H_{35}N_{12}O_6Cl_3 \cdot 4H_2O$: C, 32.32; H, 6.14; N, 23.81; Cl, 15.07 %.

*Cyclo[Boc-β-Lys(Boc)-A_2pr-Ala-A_2pr(Z)-Dea-Cpd(NO_2)] (**3**).* Compound **1b**[5] (300 mg, 0.359 mmol) was treated with 99 % formic acid at room temperature for 2 h. Formic acid was removed *in vacuo* and the residue was dried over sodium hydroxide under reduced pressure. The white powder thus obtained was then coupled with Boc-β-Lys(Boc)-ONSu[10] (191 mg, 0.431 mmol) in DMF (2 ml) in the presence of triethylamine (54 mg, 0.538 mmol) at room temperature for 40 h. To the reaction mixture was added chloroform to form a gelatinous precipitate (335 mg, 87.7 %). The product was reprecipitated from DMF–ether for elemental analysis, mp 240 °C (dec), $[\alpha]_D^{23}$ −43.7° (*c* 0.90, DMF). Found: C, 50.36; H, 6.81; N, 17.13 %. Calcd for $C_{46}H_{73}N_{13}O_{16} \cdot 3/2H_2O$: C, 50.63; H, 7.02; N, 16.69 %.

*Pseudocapreomycin IB (**4**).* Deprotection of **3** (110 mg, 0.132 mmol) and conversion of Dea into Uda residue were carried out as in the preparation of **2a**, yield 62 mg (74 %), mp 245 °C (dec), $[\alpha]_D^{23}$ −30.7° (*c* 0.61, H_2O). Found: C, 37.44; H, 6.09; N, 24.27 %. Calcd for $C_{25}H_{48}N_{14}O_7Cl_4$: C, 37.60; H, 6.06; N, 24.56 %.

*Boc-Orn(Z)-Dea-OEt (**5b**).* Z-Dea-OEt[5b] (12.4 g, 36.6 mmol) was hydrogenated with palladium black catalyst in ethanol (100 ml) in the presence of acetic acid (4.40 g, 73.2 mmol) to give an oil of H-Dea-OEt·AcOH. This was then dissolved in ethyl acetate (30 ml) and added dropwise to an ice-cooled solution of Boc-Orn(Z)-ONSu (17.0 g, 36.6 mmol) in ethyl acetate (30 ml) with stirring. Subsequently, *N*-methylmorpholine (4.44 g, 43.9 mmol) was added dropwise and the mixture was stirred at 0 °C for 2 h and at room temperature for 16 h. The solution was washed with 10 % aqueous citric acid, saturated aqueous sodium hydrogencarbonate and brine. The organic layer was dried over anhydrous magnesium sulfate and concentrated *in vacuo* to afford a white solid (17.1 g, 84.7 %). It was recrystallized from ethyl acetate–hexane, mp 62—63 °C, $[\alpha]_D^{23}$ −5.9° (*c* 2.4, DMF). Found: C, 57.91; H, 7.96; N, 7.27 %. Calcd for $C_{27}H_{43}N_3O_9 \cdot 1/2H_2O$: C, 57.67; H, 7.89; N, 7.47 %.

*Boc-A_2pr(Z)-Ala-Dea-OEt (**6a**),* A protected tripeptide **6a** was obtained from Boc-A_2pr(Z)-ONSu[12] (10.0 g, 22.9 mmol) and Z-Ala-Dea-OEt (**5a**)[12] (9.40 g, 22.9 mmol) in a similar way to that in the preparation of **5b**, yield 11.7 g (85.3 %), mp 94—96 °C, $[\alpha]_D^{23}$ −10.7° (*c* 2.4, DMF). Found: C, 56.69; H, 7.48; N, 9.45%. Calcd for $C_{28}H_{44}N_4O_{10}$: C, 56.36; H, 7.43; N, 9.39 %.

*Boc-Ala-Orn(Z)-Dea-OEt (**6b**).* Compound **5b** (6.00 g, 10.8 mmol) was treated with 28 ml of 5.8 M hydrogen chloride in ethanol at room temperature for 90 min. Benzene (300 ml) was added to the solution, which was then lyophilized. After the same procedure had been repeated twice, the resulting white powder was dried over sodium hydroxide under reduced pressure. To a solution of the deprotected dipeptide thus obtained and Boc-Ala-ONSu (3.10 g, 10.8 mmol) in ethyl acetate (70 ml) was added *N*-methylmorpholine (1.32 g, 13.0 mmol) dropwise at 0 °C with stirring. After being stirred at 0 °C for 2 h and then at room temperature for 16 h, the solution was washed with 10 % aqueous citric acid, saturated aqueous sodium hydrogencarbonate and brine successively, and dried over anhydrous magnesium sulfate. When ethyl acetate was removed *in vacuo*, a white solid (6.06 g, 89.5 %) was obtained. For elemental analysis, the product was recrystallized from ethylacetate–hexane, mp 70—75 °C, $[\alpha]_D^{23}$ −4.3° (*c* 2.3, DMF). Found: C, 57.49; H, 7.68; N, 8.96%. Calcd for $C_{30}H_{48}N_4O_{10}$: C, 57.68; H, 7.74; N, 8.97 %.

*Boc-A_2pr(Nps-Cpd(NO_2))-A_2pr(Z)-Ala-Dea-OEt (**8a**).* Removal of Boc group in **6a** (2.36 g, 3.95 mmol) was carried out as in the preparation of **6b**. The deprotected tripeptide obtained above was dissolved in DMF (15 ml) together with dipeptide **7**[12] (2.00 g, 3.59 mmol), HOBt (680 mg, 5.03 mmol),

N-methylmorpholine (436 mg, 4.31 mmol), and DCC (815 mg, 3.95 mmol) at 0 °C with stirring. Stirring was continued at 0 °C for 2 h and at room temperature for 16 h. The solution was filtered and concentrated *in vacuo*. The resulting oily residue was dissolved in ethyl acetate, washed with 10 % aqueous citric acid, saturated aqueous sodium hydrogencarbonate and brine successively and dried over anhydrous magnesium sulfate. The solution was concentrated *in vacuo* to give a yellow solid (3.30 g, 88.7 %). For elemental analysis, it was reprecipitated from THF–ether, mp 136—140 °C (dec), $[\alpha]_D^{23}$ +32.9° (*c* 2.0, DMF). Found: C, 49.19; H, 6.08; N, 15.78; S, 2.96 %. Calcd for $C_{43}H_{62}N_{12}O_{16}S \cdot H_2O$: C, 49.04; H, 6.13; N, 15.96; S, 3.04 %.

*Boc–A_2pr(Nps–Cpd(NO_2))–Ala–Orn(Z)–Dea–OEt (**8b**).* The compound was obtained from **6b** (3.37, 5.39 mmol) and **7**[12] (3.00 g, 5.39 mmol) as a yellow solid according to the method used for **8a**, yield 4.89 g (85.3 %), mp 155—160 °C (dec), $[\alpha]_D^{23}$ +38.0° (*c* 1.8, DMF). Found: C, 50.70; H, 6.33; N, 15.40; S, 3.03 %. Calcd for $C_{45}H_{66}N_{12}O_{16}S$: C, 50.84; H, 6.26; N, 15.81; S, 3.02 %.

*Boc–A_2pr(Nps–Cpd(NO_2))–A_2pr(Z)–Ala–Dea–OH (**9a**).* To a suspension of **8a** (3.00 g, 2.90 mmol) in ethanol (5 ml) was added 2.2 ml of 2 M aqueous sodium hydroxide. After being stirred at room temperature for 30 min, the solution was diluted with water (50 ml), and acidified with 10 % aqueous citric acid. The precipitated oil was extracted with ethyl acetate. The organic layer was washed with brine and dried over anhydrous magnesium sulfate. When the solvent was removed *in vacuo*, a yellow solid (2.45 g, 83.9 %) was obtained. It was reprecipitated from THF–ether for elemental analysis, mp 134—137 °C (dec), $[\alpha]_D^{23}$ +42.5° (*c* 1.7, DMF). Found: C, 48.64; H, 6.05; N, 15.98; S, 3.07 %. Calcd for $C_{41}H_{58}N_{12}O_{16}S \cdot 1/2H_2O \cdot 1/2C_4H_8O$: C, 49.09; H, 6.04; N, 15.98; S, 3.05 %.

*Boc–A_2pr(Nps–Cpd(NO_2))–Ala–Orn(Z)–Dea–OH (**9b**).* This peptide was obtained as a yellow solid from **8b** (4.44 g, 4.18 mmol) according to the method used in the preparation of **9a**: yield 3.91 g (90.5 %), mp 125—130 °C (dec), $[\alpha]_D^{23}$ +34.0° (*c* 1.9, DMF). Found: C, 49.94; H, 6.27; N, 15.18; S, 2.79 %. Calcd for $C_{43}H_{62}N_{12}O_{16}S \cdot 1/2H_2O \cdot 1/2C_4H_8O$: C, 50.04; H, 6.25; N, 15.56; S, 2.97 %.

*Cyclo[Boc–A_2pr–A_2pr(Z)–Ala–Dea–Cpd(NO_2)] (**10a**).* To a solution of **9a** (2.20 g, 2.19 mmol) and HONSu (276 mg, 2.40 mmol) in THF (10 ml), was added DCC (496 mg, 2.40 mmol) with stirring room temperature. After being stirred for 5 h, the solution was filtered and concentrated *in vacuo*. The residual yellow oil was triturated with hexane to give a yellow powder of the ONSu ester of **9a**, yield 2.51 g. Only an oil was obtained in spite of efforts to crystallize the product.

To a solution of the active ester obtained above in THF (3 ml) was added 1.85 ml of 2.7 M hydrogen chloride in THF dropwise with stirring at 0 °C, stirring being continued for 30 min. Ether was added to the solution to obtain a pale yellow powder (1.94 g).

The deprotected peptide active ester thus prepared was then dissolved in DMF (200 ml) and added slowly to pyridine (2 l) with vigorous stirring for 40 h, stirring being continued for 20 h. The solution was then concentrated *in vacuo*. The desired cyclic pentapeptide **10a** was isolated by silica gel column chromatography using a mixture of chloroform and methanol (19: 1) as an eluting solvent. The product was recrystallized from hot methanol to give fine needles (441 mg, 26.5 % based on **9a**), mp >250 °C, $[\alpha]_D^{23}$ −38.1° (*c* 1.2, DMF). Found: C, 49.42; H, 6.32; N, 18.21 %; molecular weight, 781. Calcd for $C_{35}H_{53}N_{11}O_{13} \cdot H_2O$: C, 49.23; H, 6.49; N, 18.04 %; molecular weight, 854.

*Cyclo[Boc–A_2pr–Ala–Orn(Z)–Dea–Cpd(NO_2)] (**10b**).* The cyclopentapeptide was obtained from **9b** (3.70 g, 3.57 mmol) according to the method used for **10a** as fine needles (561 mg, 20.1 %), mp 250 °C, $[\alpha]_D^{23}$ −44.7° (*c* 1.6, DMF). Found: C, 51.04; H, 6.64; N, 17.66 %; molecular weight, 743. Calcd for $C_{37}H_{57}N_{11}O_{13} \cdot 1/2H_2O$: C, 50.91; H, 6.70; N, 17.65 %; molecular weight, 873.

*Reversecapreomycin IIB (**11a**).* This analog was synthesized from **10a** (150 mg, 0.179 mmol) as in the preparation of capreomycin IIA, yield 101 mg (88.6 %), mp >250 °C, $[\alpha]_D^{23}$ +29.2° (*c* 0.26, H_2O). Found: C, 31.15; H, 5.99; N, 22.80; Cl, 14.55 %. Calcd for $C_{19}H_{35}N_{12}O_6Cl_3 \cdot 5.5H_2O$: C, 31.13; H, 6.33; N, 22.93; Cl, 14.51 %.

*[Orn[4]]-Capreomycin IIB (**11b**).* This analog was obtained from **10b** (150 mg, 0.174 mmol) in a similar way to that for the preparation of capreomycin IIA, yield 107 mg (93.0 %), mp 245—248 °C (dec), $[\alpha]_D^{23}$ −51.5° (*c* 1.5, H_2O). Found: C, 33.02; H, 6.24; N, 22.07; Cl, 14.14 %. Calcd for $C_{21}H_{39}N_{12}O_6Cl_3 \cdot 5.5H_2O$: C, 33.14; H, 6.62; N, 22.09; Cl, 13.98 %.

*Di-β-Lys-capreomycin IIB (**13**). Route A*: To a suspension of capreomycin IIB·3HCl (**2b**) (45 mg, 0.071 mmol) in DMF (2 ml) were added Boc-β-Lys(Boc)–ONSu[10] (79 mg, 0.18 mmol) and triethylamine (18 mg, 0.18 mmol) with stirring at room temperature. After being stirred for 48 h, the solution was concentrated *in vacuo*. To the residual oil was added 3 M hydrochloric acid (5 ml). The mixture was stirred at room temperature for 1 h and then neutralized with 4 M aqueous sodium hydroxide. The solution was applied to a column (2.5×80 cm) of Sephadex G10. The desired product **13** was eluted with water, yield 51 mg (75 %). For elemental analysis the product was reprecipitated from water–methanol–ethanol, mp 245 °C (dec), $[\alpha]_D^{23}$ −50.5° (*c* 1.3, H_2O). Found: C, 35.01; H, 6.89; N, 20.23; Cl, 16.44 %. Calcd for $C_{31}H_{61}N_{16}O_8Cl_5 \cdot 6H_2O \cdot CH_3OH$: C, 34.83; H, 7.03; N, 20.31; Cl, 16.07 %.

Route B: The hexapeptide **3** (150 mg, 0.141 mmol) was hydrogenated with palladium black catalyst in DMF (15 ml) in the presence of Boc–β-Lys(Boc)–ONSu[10] (94 mg, 0.21 mmol) for 40 h. To the filtrate from catalyst was added ethyl acetate (50 ml) to form a gelatinous precipitate of **14**, which was collected by centrifugation, yield 147 mg (83.1 %). It was reprecipitated from DMF–chloroform–ether for elemental analysis, mp >250 °C, $[\alpha]_D^{23}$ −43.1° (*c* 0.42, DMF). Found: C, 50.07; H, 7.52; N, 16.61 %. Calcd for $C_{54}H_{95}N_{15}O_{19} \cdot 2H_2O$: C, 50.10; H, 7.71; N, 16.23 %.

Deprotection and conversion of Dea to Uda residue in compound **14** (66 mg, 0.052 mmol) were carried out by a similar procedure to that in the preparation of **2a**, yield 39 mg (78 %). The product thus obtained was identical with the product in route A in thin-layer chromatography (silica gel; phenol–water–concd aqueons ammonia 30: 10: 1; R_f 0.22).

The authors are indebted to The Research Laboratories, Toyo Jozo Co., Ltd. for measurements of antibacterial activities, and to Dr. Kenji Okawa and his coworkers for use of the vapor pressure osmometer.

References

1) This study was presented at the 36th National Meeting of the Chemical Society of Japan, Yokohama, April 1978, II, p. 1122.

2) a) E. B. Herr, M. E. Haney, G. E. Pittenger, and C. E. Higgins, *Proc. Indiana Acad. Sci.*, **69**, 134 (1960); b) S. Nomoto, T. Teshima, T. Wakamiya, and T. Shiba, *J. Antibiot.*, **30**, 955 (1977).

3) a) A. C. Finlay, G. L. Hobby, F. Hochstein, T. M. Lees, F. F. Lenert, J. A. Means, S. Y. Pan, P. P. Regma, J. B. Rontier, B. A. Sobin, K. B. Tate, J. H. Kane, *Am. Rev.*

Tuberac., **63**, 1 (1951); b) S. Noda, T. Take, A. Nagata, T. Wakamiya, and T. Shiba, *J. Antibiot.*, **25**, 427 (1972).

4) a) A. Nagata, T. Ando, R. Izumi, H. Sakakibara, T. Take, K. Hayano, and J. Abe, *J. Antibiot.*, **21**, 681 (1968); b) H. Yoshioka, T. Aoki, H. Goko, K. Nakatsu, T. Noda, H. Sakakibara, T. Take, A. Nagata, J. Abe, T. Wakamiya, T. Wakamiya, Shiba, and T. Kaneko, *Tetrahedron Lett.*, **1971**, 2043.

5) a) T. Shiba, S. Nomoto, T. Teshima, and T. Wakamiya, *Tetrahedron Lett.*, **1976**, 3907; b) S. Nomoto, T. Teshima, T. Wakamiya, and T. Shiba, *Tetrahedron*, **34**, 921 (1978).

6) Numbering of positions of the amino acid residues in the cyclic peptide moiety is given in Fig. 1. It is in line with numbering for tuberactinomycin (Fig. 2), *cf.* footnote 11) in Ref.[12].

7) Abbreviations according to IUPAC-IUB recommendation, *J. Biol. Chem.*, **247**, 977 (1972), are used. A_2pr: α,β-diaminopropionic acid, Cpd: capreomycidine, Uda: β-ureidodehydroalanine, β-Lys: β-lysine, Dea: β,β-diethoxyalanine, Boc: *t*-butoxycarbonyl, Z: benzyloxycarbonyl, Nps: *o*-nitrophenylsulfenyl, DCC: dicyclohexylcarbodiimide, HONSu: *N*-hydroxysuccinimide, HOBt: 1-hydroxybenzotriazole. All amino acids used in this study except DL-Dea are of L-configurations.

8) E. B. Herr and M. O. Redstone, *N. Y. Acad. Sci.*, **135**, 940 (1966).

9) W. M. Stark, C. E. Higgens, R. N. Wolfe, M. M. Hoehn, and J. M. McGuire, *Antimicrobi. Agents Chemothe.*, **1962**, 596.

10) T. Wakamiya and T. Shiba, *J. Antibiot.*, **28**, 292 (1975).

11) a) T. Wakamiya and T. Shiba, *Bull. Chem. Soc. Jpn.*, **48**, 2502 (1975); b) T. Shiba, S. Nomoto, and T. Wakamiya, *Experientia*, **32**, 1109 (1976).

12) T. Teshima, S. Nomoto, T. Wakamiya, and T. Shiba, *Bull. Chem. Soc. Jpn.*, **50**, 3372 (1977).

Alkylation and Acylation of Active Methylene Compounds Using 1,8-Diazabicyclo[5.4.0]undec-7-ene as a Base[1)]

Noboru Ono,* Tetsuji Yoshimura, Tadashi Saito, Rui Tamura, Rikuhei Tanikaga, and Aritsune Kaji

Department of Chemistry, Faculty of Science, Kyoto University, Sakyo-ku, Kyoto 606

(Received December 13, 1978)

Active methylene compounds are selectively monoalkylated with alkyl halides in benzene using 1,8-diazabicyclo[5.4.0]undec-7-ene (DBU) as a base. Selectivity of monoalkylation decreases when the reaction is carried out in a polar solvent. Ethyl acetoacetate is O-acylated with acyl halides in the presence of DBU in acetonitrile to give the (*E*)-enol esters stereoselectively.

Alkylation and acylation of active methylene compounds are important reactions in organic chemistry and have been studied extensively.[2)] Most reactions have been carried out in hydroxylic or dipolar aprotic solvents, for the anion species of active methylene compounds are not soluble in less polar solvents. Recent development of phase transfer method[3)] or the method of ion pair extraction[4)] has enabled this reaction to be carried out in a nonpolar solvent. The merits of the reaction in a nonpolar solvent are found in the simple work-up better yields and better selectivity.[3-4)] In a previous paper it has been shown that carboxylic acids are esterified with alkyl halides in the presence of 1,8-diazabicyclo[5.4.0]undec-7-ene (DBU) in benzene.[5)] In this paper we wish to report that active methylene compounds are alkylated or acylated with alkyl halides or acyl halides, respectively, in the presence of DBU. The new procedure is noteworthy for affording the selectively monoalkylated products in alkylation of active methylene compounds and the (*E*)-enol esters stereoselectively in acylation of ethyl acetoacetate.

Results and Discussion

Alkylation of active methylene compounds (Ia—f) was carried out as follows. A mixture of Ia—f, DBU, and alkyl halides (RX) in benzene was stirred at room temperature for an appropriate period, after which the DBU-hydrogen halide (DBU·HX) was either filtered off or washed out with water from the reaction mixture. The products were purified by distillation, recrystallization or column chromatography. The products of the reaction of Ia—c were also analyzed by GLPC to

$$\underset{\text{Ia—f}}{CH_2(Y)(Z)} + RX \xrightarrow[\text{benzene}]{\text{DBU}} \underset{\text{IIa—f}}{RCH(Y)(Z)} + \underset{\text{IIIa—f}}{RRC(Y)(Z)} + DBU\cdot HX \quad (1)$$

Ia: Y=CN, Z=$COOC_2H_5$
Ib: Y=CCH_3 (=O), Z=CCH_3 (=O)
Ic: Y=CCH_3 (=O), Z=$COOCH_3$
Id: Y=$COOCH_3$, Z=$SO_2C_6H_4$-CH_3-(*p*)
Ie: Y=CC_6H_5 (=O), Z=SO_2CH_3
If: Y=CCH_3 (=O), Z=$SO_2C_6H_5$

determine the exact ratio of monoalkylation to dialkylation (II/III). Results are summarized in Table 1. The O-alkylated products are also formed in alkylation of Ib or Ic, but the yields of them are poor, so discussion of O-alkylation is omitted in this paper.

The monoalkylated products (IIa—f) are important intermediates in organic synthesis, for example, they are readily coverted to the corresponding nitriles, ketones or esters by dealkoxycarbonylation or desulfonylation, and IIa, IIc, or IId can be the starting materials for the preparation of α,β-unsaturated nitriles,[6)] α,β-unsaturated ketones,[7)] or α,β-unsaturated esters,[8)] respectively.

Alkylation of Ia—f has been done by various method, but the present procedure has some advantages over the conventional methods. First, the reaction proceeds in benzene, making the work-up very simple. Secondly, as seen in Table 1, the new procedure gives the monoalkylated products exclusively. In general, the selective monoalkylation of relative stable carbanions involves difficulties such as concurrent dialkylation.[9)] This problem becomes paticularly serious in alkylation of ethyl cyanoacetate (Ia). Alkylation of Ia with ethyl iodide was carried out under various conditions to search for the best monoalkylation method. Results are summarized in Table 2. As can be seen from Table 2, the method using DBU in benzene gives monoalkylated products more selectively than the other methods and is far more superior to the ion pair extractive method of Bröndstrom[4)] which has been the best monoalkylation method known to date.[10)] The use of a nonpolar solvent such as benzene is important for this selective monoalkylation, since the ratio of mono to dialkylation decreases when the reaction is carried out in a polar solvent. The ratio of monoalkylation increases when alkylation of Ia is carried out in a nonpolar solvent, but such a tendency is not observed in alkylation of the sodium salt of Ia(Table 2). Bröndstrom and Junggern also point out that polarity of the solvent causes no appreciable effect on the ratio of mono to dialkylation in alkylation of the tetrabutylammonium salt of Ia.

The concurrent occurrence of mono and dialkylation can occur if the proton transfer equilibrium between the unreacted anion (I^-) and the monoalkylated product (II) is established at a rate comparable with that of the alkylation process.[11)] The small ratio of dialkylation in the reaction using DBU in benzene can be explained by assuming that this conditions suppress proton transfer relative to alkylation. However, it is difficult to discuss

Table 1. Alkylation of active methylene compounds (Ia—f) with alkyl halides (RX) in benzene in the presence of DBU

Substrate	RX	Time (h)	Composition of products (%)				Isolated yield of II (%)
			I[a]	II[b]	III[c]	IV[d]	
Ia	C_2H_5I	3.0	9	83	8		80
Ia	n-C_3H_7I	3.0	17	76	7		
Ia	i-C_3H_7I	4.0	38	61	1		
Ia	n-C_4H_9Br	15.0	8	88	4		65
Ia	n-C_4H_9I	5.0	6	90	4		77
Ib	C_2H_5I	2.0	11	81	5	3	
Ib	n-C_3H_7I	4.5	8	82	4	6	
Ib	n-C_4H_9Br	6.5	9	80	1	10	
Ic	C_2H_5I	1.0	7	85	3	5	
Ic	n-C_4H_9I	3.0	6	87	0	7	
Id	n-C_4H_9Br	15.0					93
Id	n-$C_8H_{17}Br$	15.0					81
Id	CH_2=CH–CH_2Br	15.0					96
Ie	CH_3I	1.0					80
Ie	C_2H_5I	5.0					76
If	CH_2=CH–CH_2Br	5.0					80
If	n-C_3H_7I	15.0					72

a) Starting materials. b) Monoalkylated products. c) Dialkylated products. d) O-alkylated products.

Table 2. Effects of base and solvent on alkylation of ethyl cyanoacetate with ethyl iodide

Base	Solvent	Composition of products (%)		
		I[a]	II[b]	III[c]
DBU	benzene	9	83	8
DBU	THF	18	72	10
DBU	CH_3CN	17	66	17
DBU	DMF	8	64	28
NaH	THF	26	29	45
NaH	CH_3CN	23	55	22
NaH	DMF	9	58	33
C_2H_5ONa	C_2H_5OH	21	42	37
$(n\text{-}C_4H_9)_4N^+OH^-$	$CHCl_3$	14	72	14[d]

a) Starting materials. b) Monoalkylated products. c) Dialkylated products. d) Data from Ref. 4a.

this matter further at the present stage, for we do not have the precise information about the structures of the reactive species in such solvents.[12]

Recently, it has been reported that DBU is effective as a base for dialkylation of active methylene compounds in *N*,*N*-dimethylformamide (DMF).[13] This and the results in Table 2 tell us that the use of DBU in a polar solvent is preferable when dialkylation or second alkylation in stepwise alkylation of I is the desired reaction. In fact, alkylation of Ia successively with butyl iodide in benzene and with ethyl iodide in DMF gave ethyl 2-cyano-2-ethylhexanoate in a good overall yield (60 %). The second step could also be carried out in benzene, but the reaction proceeded more slowly in benzene than in DMF.

$$\text{Ia} + n\text{-}C_4H_9I \xrightarrow[\text{benzene}]{\text{DBU}} n\text{-}C_4H_9\text{-}\underset{\displaystyle CN}{\overset{\displaystyle COOC_2H_5}{\underset{|}{\overset{|}{CH}}}} \quad (77\%) \qquad (2)$$

$$n\text{-}C_4H_9\text{-}\underset{\displaystyle CN}{\overset{\displaystyle COOC_2H_5}{\underset{|}{\overset{|}{CH}}}} + C_2H_5I \xrightarrow[\text{DMF}]{\text{DBU}} n\text{-}C_4H_9\text{-}\underset{\displaystyle CN}{\overset{\displaystyle COOC_2H_5}{\underset{|}{\overset{|}{C}}}}\text{-}C_2H_5 \quad (78\%) \qquad (3)$$

Acylation of ethyl acetoacetate with acyl chlorides was carried out in the presence of DBU. Various bases such as sodium hydride, triethylamine, or pyridine have so far been used for this reaction. In general, the reaction using sodium hydride gives the C-acylated products and the reaction using triethylamine or pyridine gives the O-acylated products consisted of the mixture of the *E* and *Z* enol esters.[14] The composition of these mixtures depends on the initial concentration of the enolate, for acyl chlorides are much more reactive than most alkylating reagents. The DBU salt of ethyl acetoacetate upon treatment with acyl chlorides gave the *E* enol esters stereoselectively, the selectivity became poor when acylation was carried out in benzene. The results of acylation are summarized in Table 3. Selectivity of the formation of the *E* isomers is poor in acylation induced by triethylamine. These results suggest that the reactive forms of the enolate consist of the mixture of the *E* and *Z* form and the ratio of them depends on the nature of solvent and bases. The ^1H NMR and carbon spectra indicate that the triethylamine salt of β-dicarbonyl compounds in a nonpolar solvent is best described as one in which the chelated enol form of β-dicarbonyl compounds is hydrogen bonded to triethylamine.[15] From the analogy of the triethylamine salt, the DBU salt is also considered as the similar hydrogen bonded complex in a nonpolar solvent. In a polar solvent, these complexes become the solvent separated ions, where the *E* conformation would be preferred since the oxygen atoms bearing negative charge are maximally separated. The DBU salt is more easily solvated than the triethylamine salt, for the DBU salt has a larger and more delocalized cation than the triethylamine salt.

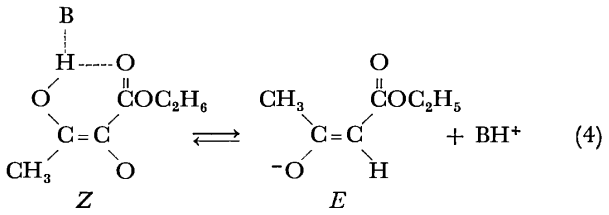

Consequently, acylation of ethyl acetoacetate with acyl chlorides using DBU in acetonitrile gives the *E* enol esters stereoselectively. For synthetic purposes, the *E* enol esters are very important, for the reaction of them with dialkyl cuprates gives the *E* isomers of β-dialkyl-α, β-unsaturated esters in good yields with high stereospecificity, which are important intermediates in the synthesis of natural products.[14]

Table 3. The reaction of ethyl acetoacetate with acyl chloride in the presence of DBU

RCCl ‖ O	Solvent	Yield (%)[a]	Isomer distribution of product	
			E(%)	*Z*(%)
CH_3CCl ‖ O	CH_3CN	53	97	3
C_6H_5CCl ‖ O	CH_3CN	79	97	3
$(CH_3)_3CCCl$ ‖ O	CH_3CN	95	100	0
C_6H_5CCl ‖ O	benzene	55	67	33
C_6H_5CCl ‖ O	CH_3CN[b]	75	84	16

a) Yield of isolated products. b) Triethylamine was used as a base.

In summary, DBU can be used as a base for alkylation of various active methylene compounds and acylation of ethyl acetoacetate, and the reaction proceeds both in a polar and in a nonpolar solvent. The merit of the use of DBU can be found in that the reaction course is easily controlled by polarity of the solvent.

Experimental

Solvents, DBU, and other commercially obtained materials were purified by distillation. The IR spectra were recorded with a Hitachi 215 spectrophotometer. The ^1H NMR spectra were recorded using a JEOL PS-100 spectrometer with TMS as an internal standard. GLPC analyses were performed with a Varian Aerograph 920 using a column containing Silicone-DC-550 (20%). Most of the starting materials and products were prepared by the literature methods. Sulfonyl ester (Id) was prepared by the reaction of methyl chloroacetate with sodium *p*-toluenesulfinate in DMF.[16] Keto sulfone (Ie) was prepared by the reaction of ethyl benzoate with the anion of dimethyl sulfone.[17] Keto sulfone (If) was prepared by the reaction of chloroacetone with sodium benzenesulfinate in DMF.[16]

Alkylation of Ia—c. A solution of alkyl halides (0.01 mol) in benzene (10 ml) was added to a stirred solution containing Ia—c (0.01 mol) and DBU (0.01 mol) in 50 ml of benzene. The reaction mixture was stirred at room temperature for the period indicated in Table 1, then washed with water, and the organic layer was dried over anhydrous magnesium sulfate. After removal of the solvent the residue was analyzed by GLPC. The results are given in Table 1. Some typical procedure to isolate the pure products is given below. Physical and spectral properties of the products are in good agreement with the literature value.

Ethyl 2-Cyanohexanoate (IIa, R=n-C_4H_9) from Butyl Bromide. A solution of butyl bromide (13.7 g, 0.1 mol) in 50 ml of benzene was added to a solution of ethyl cyanoacetate (11.3 g, 0.1 mol) and DBU (15.2 g, 0.1 mol) in 100 ml of benzene and the mixture was stirred at room temperature for 15 h. The reaction mixture was then washed with water, the organic layer was dried over anhydrous magnesium sulfate, and distilled. Ethyl 2-cyanohexanoate; bp 130°C/22 mmHg (lit,[18] 108 °C/8 mmHg), 11.0 g (65% yield). NMR (CCl_4) δ=0.95 (3H, t, J=4.8 Hz), 1.2—1.4 (7H, m), 1.9 (2H, m), 3.5 (1H, t, J=5.6 Hz), 4.25 (2H, q, J=7.2 Hz); IR (neat) 2250 cm^{-1} (CN), 1740 cm^{-1} (C=O).

Ethyl 2-Cyanohexanoate from Butyl Iodide. A mixture of ethyl cyanoacetate (6.7 g, 0.05 mol), DBU (7.6 g, 0.05 mol), and butyl iodide (9.2 g, 0.05 mol) in 150 ml of benzene was stirred at room temperature for 5 h, and was worked up as above to give ethyl 2-cyanohexanoate (6.5 g, 77% yield). The purity of the product was more than 95 %.

Ethyl 2-Cyano-2-ethylhexanoate. A mixture of ethyl 2-cyanohexanoate (3.4 g, 0.02 mol), DBU (3.1 g, 0.02 mol), and ethyl iodide (3.2 g, 0.02 mol) in 50 ml of DMF was stirred at room temperature for 5 h. The reaction mixture was worked up as above. Ethyl 2-cyano-2-ethylhexanoate; bp 141 °C/22 mmHg, 3.1 g (78% yield). NMR (CCl_4) δ=0.9 (6H, t, J=4.8 Hz), 1.25 (3H, t, J=7.2 Hz), 1.3 (4H, m), 1.8 (4H, m), 4.2 (2H, q, J=7.2 Hz); IR (neat) 2250 cm^{-1} (CN), 1740 cm^{-1} (C=O).

Ethyl 2-Cyanobutanoate (IIa, R=C_2H_5). A mixture of ethyl cyanoacetate (10.4 g, 0.1 mol), DBU (15.2 g, 0.1 mol), and ethy iodide (15.6 g, 0.1 mol) in 200 ml of benzene was stirred at room temperature for 3 h. The reaction mixture was then worked up as above to give 2-cyanobutanoate (11 g, 80% yield, bp 109 °C/29 mmHg) which contains ethyl cyanoacetate (about 5%) and dialkylated product (about 5%). They could not be separated by simple distillation.

Alkylation of Id. Methyl 2-(p-Tolylsulfonyl)hexanoate (IId, R=n-C_4H_9). A mixture of Id(11.0 g, 0.05 mol), DBU (7.6 g, 0.05 mol), and butyl bromide (6.9 g, 0.05 mol) in benzene (150 ml) and DMF (5 ml) was stirred at room temperature for 15 h. The reaction mixture was then washed with water and the organic layer was dried over anhydrous magnesium sulfate. After removal of the solvent, the residue was chromatographed on silica gel with benzene as an eluent to give methyl 2-(*p*-tolylsulfonyl) hexanoate (13.6 g, 93% yield). Mp 54—55 °C; NMR ($CDCl_3$) δ=0.9 (3H, t, J=4.8 Hz), 1.28 (4H, m), 1.90 (2H, m), 2.48 (3H, s), 3.60 (3H, s), 3.70 (1H, t, J=5.6 Hz), 7.3 (2H, d, J=8.0 Hz), 7.6 (2H, d, J=8.0 Hz); IR (Nujol) 1740 cm^{-1} (C=O), 1320, 1140 cm^{-1} (SO_2).

Methyl 2-(p-Tolylsulfonyl)decanoate (IId, R=n-C_8H_{17}). A mixture of Id (2.3 g, 0.01 mol), DBU (1.52 g, 0.01 mol), and octyl bromide (1.94 g, 0.01 mol) in benzene (20 ml) and DMF (5 ml) was stirred at room temperature for 15 h. The reaction mixture was worked up as above, and the crude product was chromatographed on silica gel with benzene as an eluent to give methyl 2-(*p*-tolylsulfonyl)decanoate as a colorless oil in 81 % yield (2.7 g). NMR ($CDCl_3$) δ=0.88 (3H, t, J=4.8 Hz), 1.22 (12H, m), 1.82 (2H, m), 2.42 (3H, s), 3.60 (3H, s), 3.70 (1H, s, J=5.6 Hz), 7.30 (2H, d, J=8.0 Hz), 7.60 (2H, d, J=8.0 Hz); IR (neat) 1740 cm^{-1} (C=O), 1320, 1140 cm^{-1} (SO_2).

Methyl 2-(p-Tolylsulfonyl)-4-pentenoate (IId, R=CH_2–CH=CH_2). A mixture of Id (4.56 g, 0.02 mol), DBU (3.04 g, 0.02 mol),

and allyl bromide (2.44 g, 0.02 mol) in benzene (100 ml) and DMF (5 ml) was stirred at room temperature for 5 h. The reaction mixture was worked up as above to give methyl 2-(*p*-tolylsulfonyl)-4-pentenoate (5.1 g, 96% yield) as a colorless oil. NMR ($CDCl_3$) δ=2.40 (3H, s), 2.60 (2H, m), 3.60 (3H, s), 3.80 (3H, s), 5.00 (2H, m), 5.58 (1H, m), 7.25 (2H, d, J=8.0 Hz), 7.60 (2H, d, J=8.0 Hz); IR (neat) 1740 cm^{-1} (C=O), 1600 cm^{-1} (C=C), 1320, 1140 cm^{-1} (SO_2).

Alkylation of Ie. α-Methylsulfonylpropiophenone (IIe, R=CH_3). A mixture of Ie (1.0 g, 0.005 mol), DBU (0.76 g, 0.005 mol), and methyl iodide (0.71 g, 0.005 mol) in benzene (10 ml) and DMF (2 ml) was stirred at room temperature for 1 h. The reaction mixture was then washed with water and the organic layer was dried over anhydrous magnesium sulfate. After removal of the solvent, the residue was recrystallized from ethanol to give colorless needles (0.85 g, 80% yield), mp 55 °C (lit,[16] 56—57 °C). NMR ($CDCl_3$) δ=1.80 (3H, d, J=7.8 Hz), 2.98(3H, s), 4.98 (1H, q, J=7.8 Hz), 7.7—8.2 (5H, m).

α-Methylsulfonylbutyrophenone (IIe, R=C_2H_5). A mixture of Ie (1.0 g, 0.005 mol), DBU (0.76 g, 0.005 mol), and ethyl iodide (0.8 g, 0.005 mol) in benzene (10 ml) and DMF (2 ml) was stirred at room temperature for 5 h. The reaction mixture was worked up as above, and the crude product was recrystallized from ethanol to give the product (0.86 g, 76 % yield) as colorless needles, mp 110 °C (lit,[19] 113 °C). NMR ($CDCl_3$) δ=1.0 (3H, t, J=7.8 Hz), 2.3 (2H, q, J=7.8 Hz), 1.98 (3H, s), 4.80 (1H, t, J=7.8 Hz), 7.5—7.8 (5H, m).

Alkylation of If. 3-Phenylsulfonylhex-5-en-2-one (IIf, R=CH_2–CH=CH_2). A mixture of If (1.93 g, 0.01 mol), DBU (1.52 g, 0.01 mol), and allyl bromide (1.27 g, 0.01 mol) in 50 ml of benzene was stirred at room temperature for 5 h. The reaction mixture was worked up as above, and the crude product was chromatographed on silica gel with benzene as an eluent to give the product (1.8 g, 80% yield) as a colorless oil. NMR (CCl_4) δ=2.30 (3H, s), 2.50 (2H, m), 4.15 (1H, t, J=7.2 Hz), 5.00 (2H, m), 5.51 (1H, m), 7.6 (5H, m); IR (neat) 1725 cm^{-1} (C=O), 1310, 1140 cm^{-1} (SO_2).

3-Phenylsulfonyl-3-hexanone (IIf, R=n-C_3H_7). A mixture of IIf (1.93 g, 0.01 mol), DBU (1.52 g, 0.01 mol), and propyl iodide (1.7 g, 0.01 mol) in 50 ml of benzene was stirred at room temperature for 15 h. The reaction mixture was worked up as above and the crude product was chromatographed on silica gel with benzene as an eluent give the product (1.7g, 72 % yield as a colorless oil. NMR (CCl_4) δ=0.85 (3H, t, J=4.8 Hz), 1.20 (2H, m), 1.78 (2H, m), 2.38 (3H, s), 4.16 (1H, t, J=5.6 Hz), 7.6—7.9 (5H, m); IR (neat) 1725 cm^{-1} (C=O), 1310, 1140 cm^{-1} (SO_2).

General Procedure of Acylation of Ethyl Acetoacetate. A solution of an acyl chloride (0.012 mol) in 10 ml of acetonitrile was added dropwise over 30 minutes to a stirred solution of ethyl acetoacetate (1.3 g, 0.01 mol) and DBU (1.8 g, 0.012 mol) in 10 ml of acetonitrile maintained below 5 °C by an ice bath. The reaction mixture was then stirred at room temperature for 3 h and was worked up by addition of water and ether, separation, and extaction of water layer with ether. The combined ethereal layers were washed with water, dried over anhydrous magnesium sulfate, and distilled to give the O-acylated product (enol ester), and the *E*/*Z* ratio of the product was determined by GLPC. The yield and the *E*/*Z* ratio of the product are given in Table 3. The following enol esters were prepared by this procedure.

Ethyl (E)-3-Benzoyloxy-2-butenoate: Bp 112 °C/0.4 mmHg (lit,[14a] 111 °C/0.4 mmHg); NMR (CCl_4) δ=1.30 (3H, t, J=7.2 Hz), 2.45 (3H, s), 4.20 (2H, q, J=7.2 Hz), 5.82 (1H, s), 7.2—8.2 (5H, m); IR (neat) 1750, 1725 cm^{-1} (C=O).

Ethyl (E)-3-Acetoxy-2-butenoate: Bp 110 °C/19 mmHg (lit,[14c] 78 °C/5 mmHg); NMR (CCl_4) δ=1.25 (3H, t, J=7.2 Hz), 2.10 (3H, s), 2.30 (3H, s), 4.05 (2H, q, J=7.2 Hz), 5.50 (1H, s); IR (neat) 1755, 1730 cm^{-1} (C=O).

Ethyl (E)-3-Pivaloyloxy-2-butenoate: Bp 103 °C/3 mmHg (lit,[20] 100 °C/2.5 mmHg); NMR (CCl_4) δ=1.26 (9H, s), 1.35 (3H, t, J=7.2 Hz), 2.32 (3H, s), 4.12 (2H, q, J=7.2 Hz), 5.55 (1H, s); IR (neat) 1755, 1730 cm^{-1} (C=O).

The authors are grateful to the Sanyo Chemical Co., Ltd. (Kyoto) for the supply of DBU.

References

1) Nucleophilic Substitution Reaction in a Nonpolar Solvent. Part IV. Part III; N. Ono, T. Yamada, T. Saito, K. Tanaka, and A. Kaji, *Bull. Chem. Soc. Jpn.*, **51**, 2401 (1978). For a preliminary communication on portions of this work, see, N. Ono, T. Yoshimura, R. Tanikaga, and A. Kaji, *Chem. Lett.*, **1977**, 871.

2) H. O. House, "Modern Synthetic Reactions," 2nd ed, Benjamin Inc., Menlo Park, Calif. (1972), p. 492 ff.

3) E. V. Dehmlow, *Angew. Chem. Int. Ed. Eng.*, **13**, 170 (1974), **16**, 493 (1977).

4) a) A. Bröndstrom and U. Junggern, *Acta Chem. Scand.*, **23**, 2203 (1969); b) A. Bröndstrom and U. Junggern, *Acta Chem. Scand.*, **23**, 2204 (1969); c) A. Bröndstrom and U. Junggern, *Acta Chem. Scand.*, **23**, 3585 (1969); d) A. Bröndstrom and U. Junggern, *Acta Chem. Scand.*, **25**, 1469 (1971).

5) N. Ono, T. Yamada, T. Saito, K. Tanaka, and A. Kaji, *Bull. Chem. Soc. Jpn.*, **51**, 2401 (1978).

6) N. Ono, H. Eto, R. Tamura, J. Hayami, and A. Kaji, *Chem. Lett.*, **1976**, 757.

7) N. Ono, R. Tamura, J. Hayami, and A. Kaji, *Chem. Lett.*, **1977**, 189.

8) N. Ono, R. Tamura, J. Hayami, and A. Kaji, *Tetrahedron Lett.*, **1978**, 763.

9) For example, alkylation of ethyl isocyanoacetate or tosylmethyl isocyanide affords mainly dialkylation products: U. Schöllkopf, D. Hoppe, and R. Jentsch, *Chem. Ber.*, **108**, 1580 (1975). A. M. van Leusen, G. J. M. Boerm, R. B. Helmholdt, H. Siderius, and J. Strating, *Tetrahedron Lett.*, **1972**, 2367.

10) a) R. B. Miller and B. F. Smith, *Synth. Commun.*, **3**, 413 (1973), where monoalkylation of methyl cyanoacetate was carried out by the extractive alkylation procedure; b) A. M. van Leusen, R. J. Bouma, and O. Possel, *Tetrahedron Lett.*, **1975**, 3487, where monoalkylation of tosylmethyl isocyanide was carried out by the phase transfer procedure.

11) L. M. Jackman and B. C. Lange, *Tetrahedron*, **33**, 2737 (1977).

12) The triethylamine salt of I is proposed to be hydrogen bonded between triethylamine and I in a nonpolar solvent.[15] If the DBU salts of I are also hydrogen bonded in a similar way in benzene, such anions may suppress proton transfer. But we have no data to support this idea at the present stage,

13) H. Oediger and F. Möller, *Justus Liebigs Ann. Chem.*, **1976**, 348.

14) a) C. P. Casey and D. F. Marten, *Tetrahedron Lett.*, **1974**, 925; b) C. Ouannes and Y. Langlois, *Tetrahedron Lett.*, **1975**, 3461; c) M. Suama, Y. Murata, and K. Ichikawa, *Nippon Kagaku Zasshi*, **91**, 162 (1970).

15) M. Raban and G. Yamamoto, *J. Org. Chem.*, **42**, 2549 (1977).

16) G. Beck and D. Günther, *Chem. Ber.*, **106**, 2758 (1973).

17) H. O. House and J. K. Larson, *J. Org. Chem.*, **33**, 61 (1968).

18) E. R. Alexander and A. C. Cope, *J. Am. Chem. Soc.*, **66**, 886 (1944).

19) B. Samuelsson and B. Lamm, *Acta Chem. Scand.*, **25**, 1555 (1971).

20) R. Gelin, S. Gelin, and A. Galliaud, *Bull. Soc. Chim. Fr.*, **1973**, 3416.

Synthesis of *D*:*A*-Friedo-18β-lupane Derivatives[1]

Yasushi YOKOYAMA, Takahiko TSUYUKI, Yoshihiko MORIYAMA, Tatsushi MURAE, Hirokazu TOYOSHIMA, and Takeyoshi TAKAHASHI*

Department of Chemistry, Faculty of Science, The University of Tokyo, Hongo, Bunkyo-ku, Tokyo 113

(Received December 19, 1978)

D: *A*-Friedo-18β-lup-19-ene and *D*: *A*-friedo-18β-lup-19-en-3-one with a new migrated lupane framework were synthesized and the former compound was converted into known methyl trinorshionanoate.

There have been reported a number of migrated triterpene compounds with *D*-, *D*: *C*-, *D*: *B*-, and *D*: *A*-friedo-type frameworks. Among them, a series of migrated oleanane derivatives, taraxerol, multiflorenol, walsurenol, alnusenone (=glutinone), and friedelin (**1**) are well known.[2] In a series of migrated lupane derivatives, however, only guimarenol (**2**) has been isolated from *Ceropegia dichotoma* as a migrated lupane derivative, which has been shown to possess a *D*: *B*-friedolupane framework.[3] Neither isolation nor synthesis of a triterpene with a *D*: *C*- or *D*: *A*-friedolupane framework has yet been reported. We wish to describe a synthesis of *D*: *A*-friedo-18β-lup-19-ene (**3**) and *D*: *A*-friedo-18β-lup-19-en-3-one (**4**) from friedelin (**1**) and also conversion of **3** into known methyl trinorshionanoate (**5**)[4] *via* a trinor ketone (**6**).

Friedelan-19α-ol (**7**),[5] prepared from friedelin (**1**) *via* friedel-18-ene (**8**), was treated with phosphorus pentachloride in toluene at 0 °C to give an olefin mixture. The mixture was separated by column chromatography on silica gel impregnated with silver nitrate into an olefin (**3**; yield 61%) and friedel-18-ene (**8**; yield 4%). The olefin (**3**) has a molecular formula $C_{30}H_{50}$ determined by elemental analysis and mass spectrum, and shows a signal at δ 1.64 characteristic of an isopropylidene group together with signals at δ 0.78—0.90 due to six methyl groups in the ^{1}H NMR spectrum. These observations indicate the occurrence of *E*-ring contraction during the dehydration reaction and, therefore the structure of **3** could be inferred to be *D*: *A*-friedo-18β-lup-19-ene. The structure **3** was further confirmed by the following transformation.

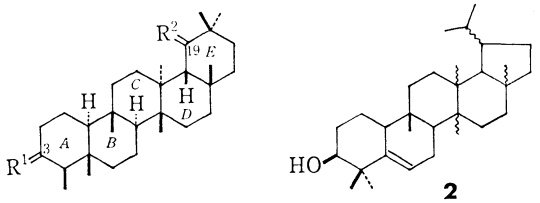

	R^1	R^2
1	O	H_2
7	H_2	β-H, α-OH
11	O	O
13	β-H, α-OH	α-H, β-OH
14	-O(CH$_2$)$_2$O-	O
15	-O(CH$_2$)$_2$O-	β-H, α-OH
16	O	β-H, α-OH

2

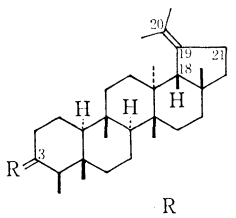

R	
3	H_2
4	O

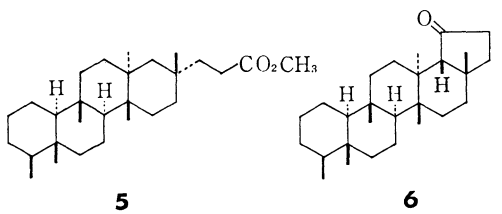

5 **6**

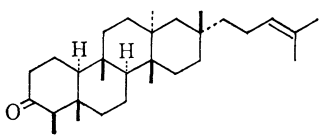

9

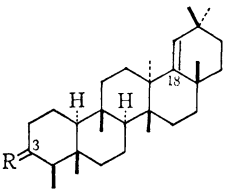

R	
8	H_2
10	O

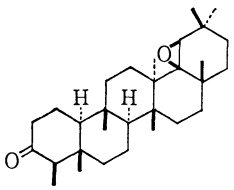

12

Oxidation of the olefin (**3**) with ruthenium tetraoxide[6] in carbon tetrachloride at room temperature gave a ketone (**6**), $C_{27}H_{44}O$. The presence of α-monosubstituted five-membered ketone was demonstrated for **6** by IR ($\nu_{C=O}$ 1725 cm^{-1}) and NMR (δ 2.18, 2H, m and δ 2.20, 1H, s) spectra. CD measurement showed a positive Cotton effect. Godtfredsen *et al.*[7] reported that 3α,11α-diacetoxy-13β-fusidan-17-one showed a positive Cotton effect, while its 13α-isomer a strong negative maximum. Therefore the *D*/*E* ring juncture in **6** could be determined to be *cis*, leading to 18βH configuration.

The trinor ketone (**6**) in methanol was irradiated using a high pressure mercury lamp to afford methyl trinorshionanoate (**5**), which was identical with a specimen obtained from shionone (**9**).[5] The framework of **6** was thus confirmed and the structure of the olefin (**3**) was shown to be *D*: *A*-friedo-18β-lup-19-ene.

Since a C$_{(3)}$-functionalized *D*: *A*-friedolupane derivative is considered to be one of the important key compounds for preparation of migrated lupane derivatives with *D*: *B*- and *D*: *C*-friedo-type frameworks, *D*: *A*-friedo-18β-lup-19-en-3-one (**4**) was prepared as follows.

Friedel-18-en-3-one (**10**)[8] was converted into friedelane-3,19-dione (**11**)[9] *via* 18β,19β-epoxyfriedelan-3-one (**12**)[9] and friedelane-3α,19β-diol (**13**).[10] The diketone

(**11**) was stable to an alkaline treatment. This suggests an 18βH configuration (ring juncture *C/D/E*: *trans*-anti-*cis*) for **11**. The 18αH isomer (*trans*-syn-*trans*) is considered to be much less stable than the 18βH isomer.[5,11]

Treatment of the diketone (**11**) with ethylene glycol in the presence of *p*-toluenesulfonic acid in benzene gave a mono-ethylene acetal (**14**). The absorption band at 1685 cm^{-1} in the IR spectrum of **14** indicated that the carbonyl group at C-19 was left unchanged and that the ethylene acetalization occurred on the carbonyl group at C-3. Reduction of **14** with lithium aluminium hydride in tetrahydrofuran gave 19α-hydroxyfriedelan-3-one 3-ethylene acetal (**15**), which, on treatment with *p*-toluenesulfonic acid in acetone, afforded 19α-hydroxyfriedelan-3-one (**16**; ν_{OH} 3450 and 3620 and $\nu_{C=O}$ 1705 cm^{-1}) in about 76% yield from **11**. The NMR spectrum of **16** showed a multiplet at δ 2.1—2.5 due to three protons α and α′ to the carbonyl group and a doublet at δ 3.79 (J=5.5 Hz)[5] due to a proton on C-19β. The 19α-hydroxy configuration for **15** and **16** received support from the fact that the reduction of friedelan-19-one with lithium aluminium hydride gave friedelan-19α-ol (**7**) as a sole product.[5]

The dehydration reaction of the hydroxy ketone (**16**) with phosphorus pentachloride was examined under various conditions and it was found that the best results were obtained under the following reaction conditions. The hydroxy ketone (**16**; 0.012 mmol) in toluene (5 ml) was treated with phosphorus pentachloride (*ca.* 10 mg) at −10 °C for 20 h to give an olefin (**4**) as a single reaction product in 90% yield. Reaction under reflux conditions resulted in the formation of undesired friedel-18-en-3-one (**10**), and reaction with a larger amount of phosphorus pentachloride gave an unidentified olefin in considerable amounts (see Experimental).

The olefin (**4**), mp 276—278 °C, gave a molecular formula $C_{30}H_{48}O$ (by elemental analysis and mass spectrometry) and showed the presence of a carbonyl group ($\nu_{C=O}$ 1710 cm^{-1}) and an isopropylidene group (δ 1.65, br s, 6H) in the IR and NMR spectra, indicating that the olefin (**4**) corresponds to an *E*-ring contraction product. On Huang-Minlon reduction, the olefin (**4**) gave *D*: *A*-friedo-18β-lup-19-ene (**3**) identical with a specimen obtained from **7** (*vide supra*). Therefore, the structure of the olefin (**4**) was shown to be *D*: *A*-friedo-18β-lup-19-en-3-one.

Experimental

General Procedures. Melting points were measured on a Mel-temp capillary melting point apparatus (Laboratory Devices) and were uncorrected. IR spectra were measured in Nujol mull using a Hitachi EPI-G2 spectrometer. CD measurement was carried out on a JASCO Model J-20 spectrometer. Optical rotations were measured on a JASCO DIP-SL polarimeter. Mass spectra were taken on a Hitachi RMU-6-Tokugata mass spectrometer at 70 eV with a direct inlet system. The relative intensity was expressed in the parenthesis. ^1H NMR spectra were measured using a Hitachi R-20 spectrometer. Chemical shifts were expressed in δ downfield from TMS as an internal standard and coupling constants in Hz. GLC analyses were made using a Shimadzu Gas Chromatograph GC-6A equipped with a hydrogen flame ionization detector (column: Dexsil 300GC, temperature 290 °C). HPLC analyses were carried out on a Waters Liquid Chromatograph ALC/GPS 202/401 at room temperature with an RI detector (column: μ-Porasil 1/8 (inch) × 1 (foot); solvent system: 5% ether–hexane; flow rate: 0.5 ml/min; pressure: *ca.* 250 psi). TLC was carried out on Kieselgel G (E. Merck) coated in 0.25 mm thickness. Wakogel C-200 (Wako) was used for column chromatography.

Dehydration of Friedelan-19α-ol (7). To a solution of friedelan-19α-ol[5] (**7**; 407 mg) in toluene (100 ml) kept at 0 °C, phosphorus pentachloride (*ca.* 660 mg) dissolved in toluene (25 ml) was added and the reaction mixture was stirred for 1.5 h at 0 °C. After addition of 15% sodium carbonate solution (70 ml), the reaction product was treated in usual way and subjected to separation by column chromatography on silica gel (40 g) impregnated with 20% silver nitrate. Elution with petroleum ether (320 ml) gave an isopropylidene derivative (**3**; 236 mg) and further elution with benzene (160 ml) and then with ether (80 ml) gave friedel-18-ene (**8**; 15 mg). The isopropylidene derivative (**3**) was recrystallized from acetone to afford *D*: *A*-friedo-18β-lup-19-ene (**3**; 218 mg), mp 181.5—182.5 °C; NMR ($CDCl_3$) δ 0.78—0.90 (6×CH_3), 1.64 (6H, s; $(CH_3)_2C{=}C\langle$), and the absence of signals due to olefinic proton; MS *m/e* (%) 410 (M^+; 14), 395 (12), 259 (39), and 121 (100); Found: C, 87.86; H, 12.43%. Calcd for $C_{30}H_{50}$: C, 87.73; H, 12.27%.

Oxidation of D: A-*Friedo-18β-lup-19-ene (3).* A ruthenium tetraoxide solution was prepared according to Nakata's procedure[6c] as follows. To ruthenium dioxide (83.6 mg) dissolved in carbon tetrachloride (10 ml), a solution of sodium periodate (361.4 mg) in water (10 ml) was added and the mixture was stirred for 19 h initially at 0 °C then at room temperature.

A solution of *D*: *A*-friedo-18β-lup-19-ene (**3**; 33.4 mg) in carbon tetrachloride (3 ml) was covered with water (2 ml) and stirred. The carbon tetrachloride solution (5 ml) of ruthenium tetraoxide was added dropwise and the stirring was continued for 21 h at room temperature. An excess of the oxidizing reagent was destroyed by addition of 2-propanol (2 ml). The reaction product was treated as usual and purified by column chromatography on silica gel (5 g). The unchanged hydrocarbon (6.2 mg) was eluted with petroleum ether (20 ml) and subsequent elution with petroleum ether–benzene (1: 1, 100 ml) gave a trinor ketone (**6**; 17.0 mg), mp 217—218 °C (crystallized from acetone); IR 1725 cm^{-1}; CD (*c* 0.0014, dioxane, at 26 °C) $[\theta]_{302}$ +7570, $[\theta]_{313}$ +7710, and $[\theta]_{325}$ +4190; NMR ($CDCl_3$) δ 0.77—1.00 (6×CH_3), 2.18 (2H, m; $-CH_2-CO-$), and 2.20 (1H, s; $-\dot{C}H-CO-$); MS *m/e* (%) 384 (M^+; 32), 369 (37), 259 (39), 257 (41), 245 (29), 190 (41), 149 (82), and 109 (100); Found: C, 84.19; H, 11.73%. Calcd for $C_{27}H_{44}O$: C, 84.31; H, 11.53%.

Photoirradiation of Trinor Ketone (6). A solution of trinor ketone (**6**; 27.2 mg) in methanol (35 ml) in a quartz vessel was irradiated using a high pressure mercury lamp (100 W) for 2.5 h under a nitrogen atmosphere at room temperature. Column chromatographic separation on silica gel (6 g) gave methyl trinorshionanoate (**5**; 14.4 mg) together with unidentified hydrocarbons and the unchanged starting material (4 mg). The photo-produced methyl trinorshionanoate (**5**) was identical (mp, IR, NMR, MS, and TLC) with an authentic specimen prepared from shionone (**9**).[5]

Treatment of Friedelane-3,19-dione (11) with Alkali. Friedelane-3,19-dione[9] (**11**; 14.6 mg) in methanol (15 ml) was heated under reflux with sodium methoxide (*ca.* 55 mg) for 2 h. The residue, after removal of the solvent, was extracted with ether. The ethereal extract was worked up as usual and the examination on TLC showed only one spot identical with that of the starting diketone (**11**).

*Ethylene Acetalization of Friedelane-3,19-dione (**11**).* A mixture of friedelane-3,19-dione (**11**; 2.9 g), ethylene glycol (5 ml), *p*-toluenesulfonic acid (*ca.* 100 mg), and benzene (600 ml) was heated under reflux using Dean-Stark apparatus for 2.5 h. The reaction mixture was worked up as usual, and crystallization from dichloromethane–ether gave friedelane-3, 19-dione 3-ethylene acetal (**14**; 2.7 g), mp 271—272 °C) crystallized from chloroform–acetone); IR 1685 cm^{-1}; NMR ($CDCl_3$) δ 0.77 (3H, d, J=7 Hz; *s*-CH_3), 0.89 (9H, s; 3× *t*-CH_3), 1.01, 1.18 (each 3H, s; *t*-CH_3), 1.11 (6H, s; 2×*t*-CH_3), 2.19 (1H, s; 18β-H), and 3.8—4.0 (4H, m; –O–CH_2–CH_2–O–); MS *m/e* (%) 484 (M^+; 5), 469 (4), 317 (7), 139 (35), and 99 (100); Found: C, 79.22; H, 10.62%. Calcd for $C_{32}H_{52}O_3$: C, 79.28; H, 10.81%.

*Reduction of Friedelane-3,19-dione 3-Ethylene Acetal (**14**).* The ethylene acetal (**14**; 2.7 g) dissolved in tetrahydrofuran (500 ml) was treated with lithium aluminium hydride (300 mg) at reflux temperature for 6.5 h and the reaction mixture was worked up as usual to give 19α-hydroxyfriedelan-3-one 3-ethylene acetal (**15**; 2.6 g), mp 287—289 °C (crystallized from chloroform–acetone); IR 3500 cm^{-1}; NMR ($CDCl_3$) δ 0.78 (3H, d, J=7 Hz; *s*-CH_3), 0.88, 1.08 (each 6H, s; 2× *t*-CH_3), 0.90, 1.01, 1.25 (each 3H, s; *t*-CH_3), and 3.7—4.0 (5H, m; 19β-H and –O–CH_2–CH_2–O–); MS *m/e* (%) 486 (M^+; 6), 471 (4), 468 (4), 317 (14), and 99 (100).

*Deacetalization of Hydroxy Ethylene Acetal (**15**).* A solution of the hydroxy ethylene acetal (**15**; 160 mg) in acetone (160 ml) was heated with a catalytic amount of *p*-toluenesulfonic acid. The reaction product was purified by column chromatography on silica gel (20 g) to give 19α-hydroxyfriedelan-3-one (**16**; 139 mg), mp 261—265 °C; IR 3620, 3450, and 1705 cm^{-1}; $[\alpha]_D^{24}$ −9.9° (*c* 0.25, $CHCl_3$); NMR ($CDCl_3$) δ 0.74, 0.90, 1.02 (each 3H, s; *t*-CH_3), 0.88 (3H, d, J=7 Hz; *s*-CH_3), 1.09, 1.26 (each 6H, s; 2×*t*-CH_3), 2.1—2.5 (3H, m; –CH_2–CO–CH–), and 3.79 (1H, d, J=5.5 Hz; 19β-H); MS *m/e* (%) 442 (M^+; 3), 424 (13), 409 (13), 273 (43), 186 (31), and 123 (100); Found: C, 81.29; H, 11.32%. Calcd for $C_{30}H_{50}O_2$: C, 81.39; H, 11.38%.

*Dehydration of 19α-Hydroxyfriedelan-3-one (**16**).* Five portions of 19α-hydroxyfriedelan-3-one (**16**; each *ca.* 2 mg) dissolved in toluene (each 3 ml) were treated with phosphorus pentachloride (each *ca.* 10 mg) at reflux temperature, 60 °C, 40 °C, room temperature, and at −10 °C, respectively, and the reaction product was examined by GLC. A single product was obtained at reflux temperature and was shown to be friedel-18-en-3-one (**10**). A mixture of *D*: *A*-friedo-18β-lup-19-en-3-one (**4**) and an unidentified dehydration product was obtained in a ratio of 3: 4 and 1: 2 in the reactions at 60 °C and 40 °C, respectively. This mixture was inseparable by HPLC, silica gel chromatography, and by recrystallization. Reactions at room temperature and at −10 °C gave the same mixtures as above in a ratio of 3: 1 and 8: 1, respectively.

A solution of **16** (5.6 mg) in toluene (5 ml) was treated with phosphorus pentachloride (*ca.* 63 mg) at −10 °C for 20 h, and the reaction product was examined by GLC. Only the unidentified dehydration product was detected. A solution of **16** (5.4 mg) in toluene (5 ml) was treated with phosphorus pentachloride (*ca.* 10 mg) under the same conditions to yield a reaction product (4.6 mg), which was shown to be the desired isopropylidene derivative (**4**), mp 276—278 °C (crystallized from chloroform–acetone); IR 1710 cm^{-1}; $[\alpha]_D^{24}$ −24° (*c* 0.22, $CHCl_3$); NMR ($CDCl_3$) δ 0.73, 0.83 (each 3H, s; *t*-CH_3), 0.78 (3H, d, J=6 Hz; *s*-CH_3), 0.93 (9H, s; 3×*t*-CH_3), 1.65 (6H, br s; $(CH_3)_2C$=C<), and 2.0—2.5 (6H, m; –CH_2–CO–CH– and 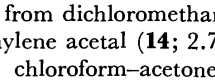 ; MS *m/e* (%) 424 (M^+; 13), 409 (4), 273 (33), and 121 (100); Found: C, 85.02; H, 11.48%. Calcd for $C_{30}H_{48}O$: C, 84.84; H, 11.39%.

Huang-Minlon Reduction of D: A-*Friedo-18β-lup-19-en-3-one(**4**).* A mixture of *D*: *A*-friedo-18β-lup-19-en-3-one (**4**; 23 mg), hydrazine hydrate (100 %, 0.3 ml), potassium hydroxide (200 mg), and diethylene glycol (2 ml) was heated under reflux for 1 h. An excess of hydrazine was distilled off and the distillation was continued until the vapor temperature reached to about 220 °C. Then the reaction mixture was heated under reflux for 4 h. Usual work up gave a residue, which was subjected to separation by column chromatography on silica gel (3 g) impregnated with 20% silver nitrate. Elution with hexane (20 ml) gave a hydrocarbon (11 mg), which was completely identical with *D*: *A*-friedo-18β-lup-19-ene (**3**) prepared from **7**.

References

1) A part of this work was reported in a preliminary form: Y. Yokoyama, T. Hirao, T. Tsuyuki, Y. Moriyama, T. Murae, and T. Takahashi, *Tetrahedron Lett.*, **1977**, 273.

2) *E.g.* T. K. Devon and A. I. Scott, "Handbook of Naturally Occurring Compounds," Academic Press, New York and London (1972), Vol. II (Terpenes), p. 282; "Terpenoids and Steroids," ed by K. H. Overtone, The Chemical Society, London, (1974), Vol. 4, p. 209 and (1975), Vol. 5, p. 137.

3) A. G. González, F. G. Jerez, and M. L. Escalona, *An. Quim.*, **69**, 921 (1973).

4) Y. Tanahashi, Y. Moriyama, T. Takahashi, F. Patil, J.-F. Biellmann, and G. Ourisson, *Bull. Soc. Chim. Fr.*, **1966**, 1670.

5) T. Tsuyuki, T. Hoshino, M. Ito, and T. Takahashi, *Bull. Soc. Chim. Fr.*, **1968**, 2895.

6) a) C. Djerassi and R. R. Engle, *J. Am. Chem. Soc.*, **75**, 3838 (1953); b) G. Snatzke and H. W. Fehlhaber, *Justus Liebigs Ann. Chem.*, **663**, 123 (1963); c) H. Nakata, *Tetrahedron*, **19**, 1959 (1963).

7) W. O. Godtfredsen, W. von Daehne, S. Vangedal, A. Marquet, D. Arigoni, and A. Melera, *Tetrahedron*, **21**, 3505 (1965).

8) V. V. Kane and R. Stevenson, *Tetrahedron*, **15**, 223 (1961).

9) Compounds, **11** and **12**, were formed by dry ozonation of friedelin (**1**): E. Akiyama, M. Tada, T. Tsuyuki, and T. Takahashi, *Bull. Chem. Soc. Jpn.*, **52**, 164 (1979).

10) Ozonation of friedel-18-ene (**8**) to yield 18β,19β-epoxyfriedelane, and subsequent treatment of this epoxide with Li–$EtNH_2$–*t*-BuOH to give friedelan-19β-ol were described in Ref. 5.

11) E. L. Eliel, "Stereochemistry of Carbon Compound," McGraw-Hill, New York (1962), p. 282.

Synthesis and Reactions of Perylenecarboxylic Acid Derivatives. VI. Sulfonation of 3,4-Perylenedicarboximide

Yukinori NAGAO* and Takahisa MISONO

Department of Industrial Chemistry, Faculty of Science and Technology, Science University of Tokyo, Yamazaki, Noda-shi, Chiba 278

(Received July 3, 1978)

The sulfonation of 3,4-perylenedicarboximide (**1**) with sulfuric acid has been studied. The position of the sulfo group in the monosulfonated product (**2**) obtained at 100 °C has been discussed on the basis of the NMR and IR spectra of **2** and the related compounds, and has been confirmed to be the 9-sulfoperylene-3,4-dicarboximide. The localized treatment of **1** by Hückel and Pople MO calculations confirmed substitution at the 9-position. Paper chromatographic analysis indicated that the reaction product was only **2** in the temperature range 60—120 °C, and the reaction rate was determined spectroscopically. The maximum formation of **2** was approximatedly 97% at 100 °C. The rate of reaction was found to be a pseudo first order process and the activation energy found to be 19.5 kcal/mol.

In a previous publication the 3,4-perylenedicarboximide (PDCI) (**1**) was sulfonated at 100 °C, and the *N*-substituted-perylene-3,4-dicarboximide (*N*-R-PDCI) (**5**) prepared from the sulfonic acid (PDCI-SO_3H) (**2**) *via* **3** and the *N*-substituted-sulfoperylene-3,4-dicarboximide (*N*-R-PDCI-SO_3H) (**4**), as presented below.[1]

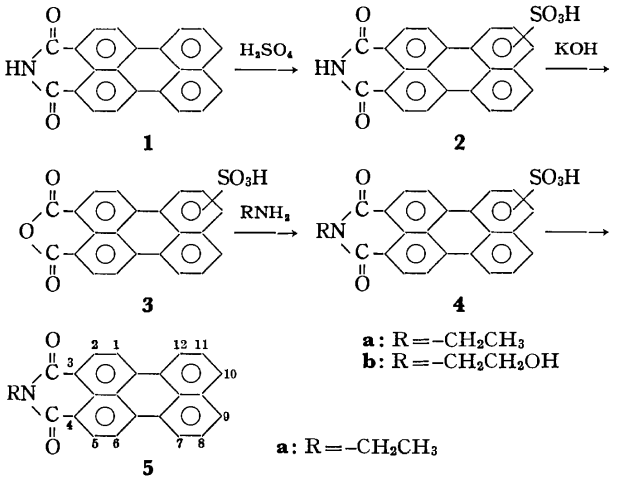

The substituted position of the sulfo group in **2**, however, remains. The position of substitution has been discussed on the basis of the NMR and IR spectra data of **2** and related compounds; **4a**, **4b**, **5a**, **7**, **8a**, perylene, perylenedisulfonic acids, and **8b**. The kinetics of the sulfonation of **1** have also been determined.

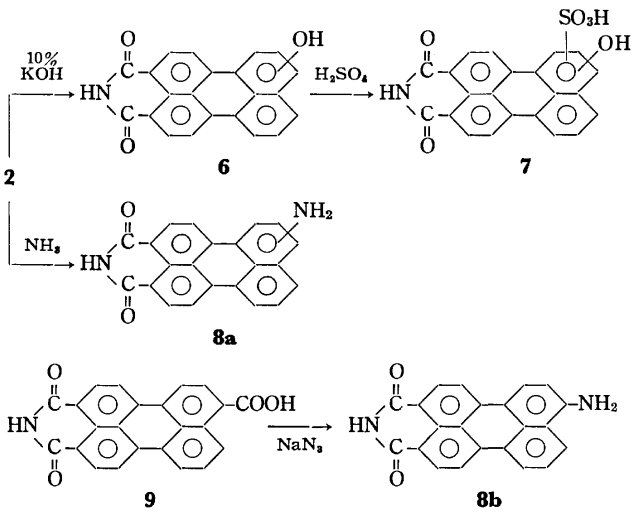

Experimental

Materials. PDCI (**1**), the potassium salt of PDCI-SO_3H (PDCI-SO_3K), the potassium salt of *N*-(2-hydroxyethyl)-PDCI-SO_3H (**4b**), the potassium salt of *N*-ethyl-PDCI-SO_3H (**4a**), and *N*-ethyl-PDCI (**5a**) were prepared and purified by previous methods.[1] The free sulfonic acid was prepared by adding hydrochloric acid to the solution of the potassium salt. PDCI-SO_3H was confirmed to be a free sulfonic acid by titration with potassium hydroxide solution and in the TG analysis the water of hydration was lost at 100 °C. PDCI-SO_3H dried at 100 °C was used as the standard reagent for spectroscopical determination.

Perylene was prepared from 3,4,9,10-perylenetetracarboxylic dianhydride by the method of Goto *et al.*[2] Perylenedisulfonic acid was prepared by the methods of Marschalk.[3]

Measurements and Molecular Orbital Calculations. The NMR spectra were obtained using a JNM-4H-100 spectrometer (Japan Electron Optics Laboratory Co.) at 100 MHz. All spectra were measured in DMSO-d_6 using TMS as an internal standard and samples for measurement at 150 °C were contained in sealed tubes. Mass spectra were obtained using a Hitachi RMU-7M mass spectrometer. Visible spectra were measured using a Hitachi 124 spectrometer for solutions in concd sulfuric acid and IR spectra on a Nippon Bunko IR-E spectrophotometer. The developing solvent used in paper chromatography was a 1-butanol–pyridine–28 % ammonia–water mixture (1 : 1 : 1 : 1). The molecular orbitals were calculated using an IBM 370 computer with a modification of the program of Wiberg.[4]

Sulfonation of Hydroxyperylene-3,4-dicarboximide. Hydroxyperylene-3,4-dicarboximide (6): In an autoclave was added PDCI-SO_3K 0.60 g and 10% KOH 50 ml. The autoclave was heated at 200 °C for 10 h with stirring. The reaction mixture was filtered, the precipitate washed with water, and poured into water. The suspension was acidified with hydrochloric acid and filtered and the precipitate washed with water, and dried, **6** 0.50 g: λ_{max} (H_2SO_4) 620 nm; R_f 0.78 (violet); MS (70 eV), *m/e* 337 (M^+). After sublimation at 400 °C/3—5 mmHg, an analytical sample was given.

Found: C, 77.53; H, 3.05; N, 4.08%. Calcd for $C_{22}H_{11}O_3N$: C, 78.33; H, 3.29; N, 4.15%.

Sulfonation of Hydroxyperylene-3,4-dicarboximide: Into a three

necked flask fitted with a stirrer was added concentrated sulfuric acid 20 ml and **6** 0.10 g. The mixture was warmed at 50 °C for 2 h with stirring, and the cooled mixture poured into ice water 100 ml. The mixture was filtered and the solid dissolved in refluxing ethanol, and filtered to remove the unreacted **6**. The solution was concentrated in an evaporator, and concentrated hydrochloric acid added until the material solidified. The solid was filtered and dried, giving the sulfonic acid **7** 0.08 g: λ_{max} (H_2SO_4) 623 nm; R_f 0.62 (violet).

Aminoperylene-3,4-dicarboximide. Preparation from PDCI-SO_3K: In an autoclave was added PDCI-SO_3K 0.50 g and 28% ammonia 50 ml, followed by ammonia gas until a pressure of 10 kg/cm² was attained. The autoclave was heated at 200 °C for 10 h. The reaction mixture was filtered, and the precipitate washed with hot 1% potassium hydroxide to remove the unreacted PDCI-SO_3K. The precipitate was washed with water and dried, giving the amine **8a** 0.32 g: λ_{max} (H_2SO_4) 609 nm; R_f 0.88 (blue); MS (70 eV), *m/e* 336 (M^+). After sublimation at 400 °C/1 mmHg, an analytical sample was given.

Found: C, 78.23; H, 3.31; N, 7.72%. Calcd for $C_{22}H_{12}N_2O_2$: C, 78.56; H, 3.60; N, 8.33%.

Preparation from 9-Carboxy-3,4-perylenedicarboximide (9): **9** 0.50 g was dissolved in concentrated sulfuric acid 25 ml and to the solution was slowly added sodium azide 0.10 g. The solution was maintained at 50 °C for 4 h and then the reaction mixture was poured into water and filtered. The precipitate was washed with hot 1% potassium hydroxide, water, ethanol, and dried, giving the amine **8b** 0.22 g: λ_{max} (H_2SO_4) 609 nm; R_f 0.88 (blue); MS (70 eV), *m/e* 336 (M^+). The DMSO solution gave an analytical sample by acidification with hydrochloric acid.

Found: C, 71.08; H, 3.23; N, 6.59 %. Calcd for $C_{22}H_{12}N_2O_2$+HCl: C, 70.88; H, 3.51; N, 7.51%.

Sulfonation of PDCI. In order to study the rate of sulfonation, concentrated sulfuric acid 25 ml was added into a three neeked flask, and the temperature of the flask adjusted to the temperature of the rate measured. To the flask was added PDCI 0.50 g and the flask maintained at the same temperature with stirring. An aliquot of the reaction mixture was withdrawn periodically and analyzed by paper chromatography and spectroscopy.

Paper Chromatography: The reaction mixture was poured into water and the precipitated reaction mixture separated by centrifuging. The precipitate was dissolved in 1% potassium hydroxide, placed on the paper and developed by the solvent.

Determination by Spectroscopy: The reaction mixture were diluted with concentrated sulfuric acid, and the absorbance at two wavelength (570 and 585 nm) measured. The mole ratio of PDCI and PDCI-SO_3H to the mixture was calculated from the following relationship:

$$A_{570} = 0.743 \times (\text{PDCI}) + 0.583 \times (\text{PDCI-SO}_3\text{H})$$

$$A_{585} = 0.714 \times (\text{PDCI}) + 0.726 \times (\text{PDCI-SO}_3\text{H})$$

A_{570} and A_{585}; Absorbances of the reaction mixture at 570 and 585 nm. (PDCI) and (PDCI-SO_3H) are the concentrations of PDCI and PDCI-SO_3H (mg/ml), respectively.

Results and Discussion

NMR Spectra of Sulfonic Acids. The sulfonic acid **2** was confirmed to be a mono-sulfonic acid by the potassium analysis of the potassium salt of **2**.[1] The position of the sulfo group in **2** has been evaluated by comparing the NMR spectra of the related compounds, the spectra data being shown in Table 1. Assignment of the proton positions has been assumed on the basis of the perylene spectrum (in CCl_4).[5,6] The differences between the spectra in DMSO-d_6 and CCl_4 were significantly small.

Table 1. NMR spectra of perylene derivatives

Compound	Chemical shift δ/ppm	Position
2[a]	11.5—11.6 (1H, singlet)	N
	8.8—9.1 (1H, doublet)	10
	8.0—8.5 (7H, multiplet)	1, 2, 3, 6, 7, 8, 12
	7.5—7.8 (1H, triplet)	11
4a[a]	8.8—9.1 (1H, doublet)	10
	8.0—8.5 (7H, multiplet)	1, 2, 3, 6, 7, 8, 12
	7.5—7.8 (1H, triplet)	11
4a[b]	9.0—9.2 (1H, doublet)	10
	8.4—8.6 (6H, multiplet)	1, 2, 3, 6, 7, 12
	8.1—8.2 (1H, doublet)	8
	7.5—7.8 (1H, triplet)	11
4b[a]	8.8—9.1 (1H, doublet)	10
	8.0—8.5 (7H, multiplet)	1, 2, 3, 6, 7, 8, 12
	7.5—7.8 (1H, triplet)	11
10[a]	8.3—8.5 (4H, doublet)	X
	7.8—7.9 (4H, doublet)	B
	7.4—7.7 (4H, triplet)	A
11[a]	8.7—8.9 (2H, doublet)	4, 10
	8.3—8.5 (4H, triplet)	1, 6, 7, 12
	7.9—8.1 (2H, doublet)	2, 8
	7.4—7.7 (2H, triplet)	5, 11
5a[b]	8.2—8.6 (6H, multiplet)	1, 2, 5, 6, 7, 12
	7.7—8.0 (2H, doublet)	9, 10
	7.5—7.7 (2H, triplet)	8, 11
7[a]	11.4—11.6 (singlet)	N
	8.0—8.5 (multiplet)	
	7.4—7.9 (triplet)	

a) Measured at 25 °C. b) Measured at 150 °C.

Both **4a** and **4b** exhibited similar peaks to **2** except the peak δ 11.5—11.6 — the addition of D_2O to the solution of **2**, caused the peak at 11.5—11.6 to diminish. The potassium salt showed a similar relation. Thus in the spectrum of **2**, the δ 11.5—11.6 peak has been assigned to the proton of the imide group, and δ 8.8—9.1 and 7.5—7.8 to the single proton in the perylene ring.

The structures of the perylenedisulfonic acids have not been confirmed as 3,9- or 3,10-disulfonic acids, and it is expected that there will be no significant differences in the spectra due to the symmetrical structures. Consequently the structure of the 3,9-derivative (**11**) has been tentatively assigned on the following basis (Table 1): the δ 8.3—8.5 triplet signals appear to overlap the two doublet signals, and the δ 8.7—8.9 signal has been attributed to the 4 and 10 positions, since the steric effect of the sulfo group is larger than that of the others.

The NMR spectrum of **5a**† shows that the imide group does not influence the protons at the 8, 9, 10, and 11 positions.

† In order to examine the influence of the imide group the NMR spectrum of **5a** was taken at 150 °C—**5a** has the greatest solubility among the other *N*-substituted PDCI.

Table 2. Electron densities and the chemical shifts of **5a**

Position	Electron densities		Chemical shifts (ppm)	
	Hückel	Pople	**5a**	Perylene
1, 6	1.007	1.297	8.2—8.6	8.3—8.5
2, 5	0.895	0.596	8.2—8.6	7.4—7.7
7, 12	0.914	0.785	8.2—8.6	8.3—8.5
8, 11	1.001	1.124	7.5—7.7	7.4—7.7
9, 10	0.918	0.826	7.7—8.0	7.8—7.9

The ring proton shift has been found to be approximately proportional to the calculated charge densities on the attached ring-carbon sites.[7] In the polycyclic molecules however, the resonance shifts of a particular ring proton need be corrected for the ring current of the neighbouring rings.[8] There have been several theoretical studies of NMR chemical shifts in polycyclic aromatic hydrocarbons on the basis of the ring current theory.[5,6,9,10] For a complex molecule such as **5a** both the charge densities and ring currents must be considered. The electron densities of **5a** (see later) and the chemical shifts of the protons are shown together with the chemical shifts of perylene in Table 2. The lowest density position showed the largest proton shift to lower field for perylene.

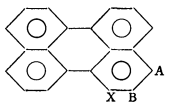

10

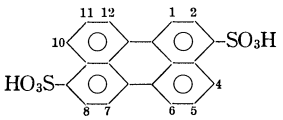

11

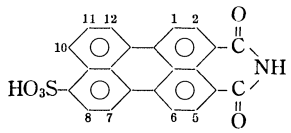

2a

The NMR spectra of **4a** at 150 °C gave sharper peaks than at room temperature. The peaks at δ 9.0—9.2, 8.1—8.2, and 7.5—7.8 almost coincide with the peaks at 8.7—8.9, 7.9—8.1, and 7.4—7.7 of perylenedisulfonic acids. Therefore on the basis of the NMR spectra of the related compounds, **2** has been estimated as the 9-sulfonic acid (**2a**), and the position of the proton assigned as in the Table. Substitution of the sulfo group confirmed that the peak near δ 9.1 was not observed, as shown in the spectrum of **7**.

Preparation of the Amine from the Sulfonic Acid. By the reaction of the sulfonic acid **2** with NH_3, the corresponding amine **8a** has been prepared and compared with the amine **8b**, prepared by the Schmidt reaction from 9-carboxy-3,4-perylenedicarboximide (**9**). These compounds were very difficult to purify due to poor properties of sublimation and solubility in the solvent. Subsequent analysis gave rather low N analysis (%) but the effect of impurities on the spectra as shown in Fig. 1 is negligible since paper chromatography gave only one spot. Both the IR (Fig. 1) and mass spectra of **8a** and **8b** showed the same spectra.

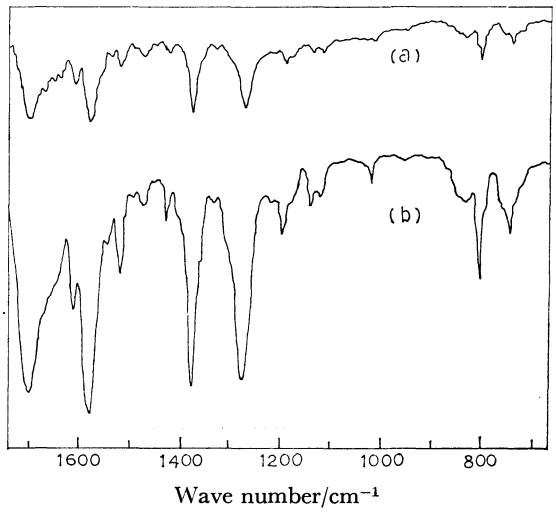

Fig. 1. IR spectra of aminoperylene-3,4-dicarboximide; (a) **8b**, (b) **8a**.

Localized Treatment of the Hückel and Pople Method. The total energies of the calculated models (Fig. 2) for perylene and PDCI by the methods of Hückel[11,14] and Pople[12,13] have been calculated for the localized treatment of electrophilic aromatic substitution.[15,16] The parameters used are shown in Table 3 and the calculated total energies are shown in Table 4. The results show that 9-substitution for PDCI and 3-substitution for perylene have the lowest energy and thus the quantum chemical calculations support the conclusions.

Sulfonation of PDCI. Yields of Sulfonation: From paper chromatography, the reaction products were

Table 3. Parameters for Hückel and Pople calculations

Hückel[a]

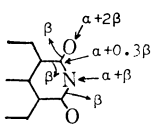

Pople[b] (eV)

	W_{2pi}	(ii,ii)
C^+	−11.16	10.988
N^{2+}	−28.53	16.574
O^+	−17.70	13.827
$\beta_{C=C}$;	−1.7515	
β_{C-N};	−1.4030	
β_{C-O};	−2.220	

$$(ii,jj)$$

$$\frac{e^2}{\{r_{ij}^2+\frac{1}{4}[(ii,ii)+(jj,jj)]^2\}^{1/2}}$$

a) Ref. 15. b) Ref. 13, W_{2pi}; ionization potentials, (ii,ii) and (jj,jj); one-center repulsion integrals, (ii,jj); two-center repulsion integrals, r_{ij}; distances, β; resonance integrals.

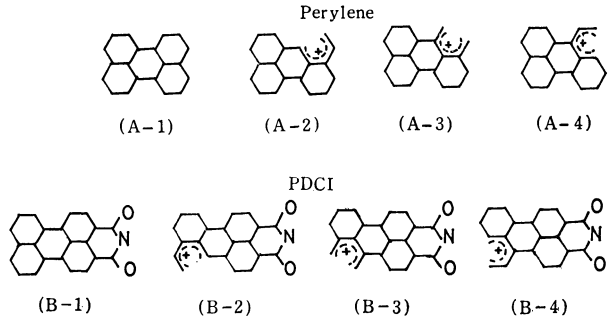

Fig. 2. Calculation models for perylene and PDCI.

TABLE 4. THE TOTAL ENERGIES OF THE MODELS

	Perylene			PDCI	
	Hückel ($-\beta$)	Pople (eV)		Hückel ($-\beta$)	Pople (eV)
(A-1)	−28.245	−259.086	(B-1)	−43.042	−369.942
(A-2)	−26.042	−237.604	(B-2)	−40.562	−345.386
(A-3)	−25.735	−235.935	(B-3)	−40.501	−345.470
(A-4)	−26.106	−237.864	(B-4)	−40.654	−345.776

shown to contain only one product **2** until 120 °C, then the reactions were followed spectroscopically. The maximum yield of sulfonic acid was approximately 97% at 100 °C as shown in Fig. 3.

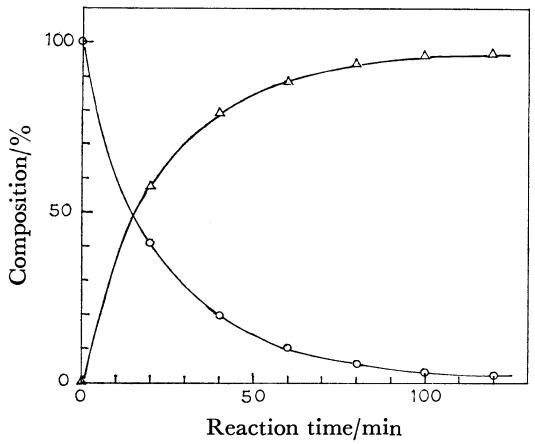

Fig. 3. Sulfonation of PDCI (**1**) at 100 °C.
○; PDCI, △: PDCI-SO_3H.

Pseudo First Order Reaction Constant and Activation Energy:

$$\underset{a-x}{\text{PDCI}} \xrightarrow{k} \underset{x}{\text{PDCI-SO}_3\text{H}}$$

The linear plots of $\ln(a-x)/a$ against reaction time t at 63, 80, 100, and 119 °C were obtained at the initial stages in the reaction, where a and x represent the concentrations of initial PDCI and PDCI-SO_3H, respectively. The rate constants k, estimated from the slopes have been compared in Table 5. The activation energy was obtained as 19.5 kcal mol^{-1}.

TABLE 5. RATE CONSTANTS FOR SULFONATION OF PDCI WITH H_2SO_4

Temp (°C)	Rate constant k (min^{-1})
119	1.26×10^{-1} a)
100	3.11×10^{-2} b)
80	6.74×10^{-3} a)
63	2.02×10^{-3} a)

a) Average of two measurements.
b) Average of four measurements.

References

1) Y. Nagao and T. Misono, *Shikizai Kyokai Shi*, **49**, 29 (1976).
2) N. Goto, T. Kosuka, and Y. Koga, *Kogyo Kagaku Zasshi*, **72**, 890 (1969).
3) C. Marschalk, *Bull. Soc. Chim. Fr.*, **41**, 74 (1927).
4) K. B. Wiberg, "Computer Programming for Chemists," W. A. Benjamin, Inc., New York (1965), p. 225.
5) N. Jonathan, S. Cordon, and B. P. Dailey, *J. Chem. Phys.*, **36**, 2443 (1962).
6) C. W. Haigh and R. B. Mallion, *Mol. Phys.*, **18**, 737, 751 (1970).
7) A. Zweig, J. E. Lehnsen, J. E. Langaster, and M. T. Nagliz, *J. Am. Chem. Soc.*, **85**, 3940 (1963).
8) T. Schaeffer and W. G. Schneider, *Can. J. Chem.*, **41**, 966 (1963).
9) J. D. Memory, G. W. Parker, and J. C. Halsey, *J. Chem. Phys.*, **45**, 3567 (1966); T. R. Cobb and J. D. Memory, *ibid.*, **47**, 2020 (1967); E. R. Long and J. D. Memory, *ibid.*, **61**, 3865 (1974).
10) A. T. Amos and H. G. Ff. Roberts, *Mol. Phys.*, **20**, 1073 (1971).
11) E. Hückel, *Z. Phys.*, **70**, 204 (1931).
12) J. A. Pople, *Trans. Faraday Soc.*, **49**, 1375 (1953).
13) M. J. S. Dewar, *J. Chem. Phys.*, **44**, 759 (1966).
14) A. Streitwiser, "Molecular Orbital Theory For Organic Chemists," John Wiley and Sons, Inc., New York (1961).
15) Y. Yukawa, R. Mikawa, and K. Ito, "Bunshikidoho Keisan Enshu," Hirokawa, Tokyo, (1967), p. 212.
16) M. J. S. Dewar, "The Molecular Orbital Theory of Organic Chemistry," (1969).

Preparation of Model Polymers for Visual Pigment and Spectral Changes

Masato NANASAWA* and Hiroyoshi KAMOGAWA
Faculty of Engineering, Yamanashi University, Takeda, Kofu 400
(Received July 11, 1978)

N-(8′-Apocarotene-8′-ylidene)butylamine (Bu-SB) has been protonated with amino acid derivatives in aqueous solution and the absorption maxima of the protonated products observed at 500 nm. Copolymers (from N^{α}-methacryloyl-L-lysine methyl ester and α-methyl *N*-methacryloyl-L-glutamate) bearing long conjugated double bonds as a side chain have been synthesized for the simulation of rhodopsin. The absorption spectra shifted to longer wavelengths, and the absorbances amounted to 4—8%, based on the maximum peaks.

The literature is extensive concerning the photochromic process in visual pigments and a number of interesting observations and results have been reported.[1] Nevertheless the mechanism remains unclarified. Absorption maxima (λ_{max}) of pigments bonded to opsin by Schiff base (SB) linkages are observed at approximately 500 nm, although the 11-*cis*-retinylidene analogue in solution absorbs in the ultraviolet. The bathochromic shift was thought due to the protonation of the SB linkage,[2] this hypothesis being qualitatively supported by indirect methods and theory.

The absorption spectra of long pendant conjugated chains attached to peptide backbones was reported to shift approximately 120 nm to longer wavelengths by the addition of acceptors with strong electron affinities and small molecular sizes.[3] It is difficult to produce an experimental model identical with rhodopsin in which the absorption peak shifts reversibly to the red region, but the following models have been prepared with the intention of simulating a visual pigment and examining spectral changes: amino acid derivatives have been employed as protonating agents for low molecular SB, since the acid components reported to date were mineral acids[4] and organic acids possessing a strong proton transfer constant such as trichloroacetic acid;[5] other models have been vinyl polymers bearing N^{ε}-(8′-apocarotene-8′-ylidene)-L-lysine methyl esters and α-methyl L-glutamates as side chains. The spectral changes of the amino acid derivatives have been investigated.

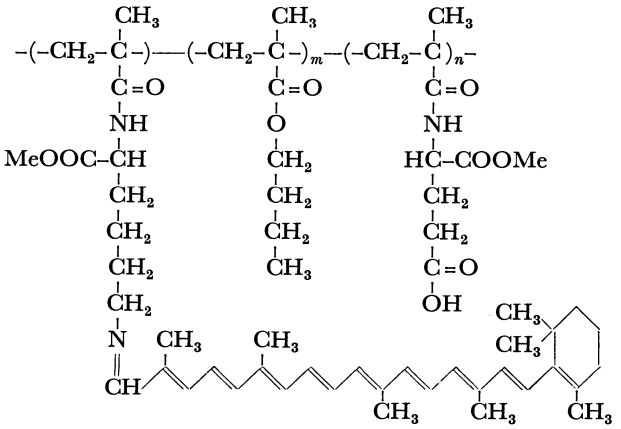

m: 0—4, *n*: 0—2.

The methacryloyl chain has been employed as the polymer backbone in place of peptides, since poly(amino acid)s are insoluble in organic solvents by denaturation during cleavage of the protecting groups and subsequent purification, bringing about low yields

Table 1. Poly(vinyl amino acid)s and SB

	Poly-Ly	Poly-Ly-1	Copoly-1	Copoly-2	Copoly-3
Composition[a]					
Vinyl-Z-Ly(OMe)	1	1	1	1	1
Vinyl-Glu-OBzl(OMe)	0	0	1	1	2
BMA	0	4	0	4	4
Yield %	54.0	73.1	63.8	78.8	68.4
$[\eta]$ dl/g[b]	0.235	0.392	0.182	0.180	0.295
Content mM/g[c]					
$-NH_2$	3.32 (75.9)	1.07 (85.6)	1.85 (87.2)	0.65 (66.6)	0.37 (77.9)
-COOH			1.77 (83.2)	0.70 (72.7)	0.66 (69.8)
Spectra of SB					
λ_{max}	428	430		415	416
$E_{1\%}$	208	127		26.3	8.3
Amount of SB[d] mol%	38.0	44.4		11.0	6.1

a) Composition of monomer for polymerization. b) In DMF at 25 °C. c) Content of ω-group in polymer measured by titration with 0.1 M NaOH or 0.1 M HCl in THF–H_2O, figures in parentheses indicate calculated values in %. d) Calculated values from the absorptivity of Bu-SB (λ_{max} 440 nm, $E_{1\%}$ 826) and amino residue in polymer.

of SB and difficulties in measurement of the shift magnitude in a heterogeneous system. N^{α}-Methacryloyl-N^{ε}-benzyloxycarbonyl-L-lysine methyl ester [Vinyl-Z-Ly(OMe)] has been prepared by the esterification of Z-Ly with thionyl chloride–methanol,[6] followed by amidation with methacryloyl chloride. Attempts to esterify γ-benzyl L-glutamate by conventional means were unsuccessful due to ready hydrolysis and ester exchange. Consequently γ-benzyl α-methyl N-methacryloyl-L-glutamate [Vinyl-Glu-OBzl(OMe)] has been prepared by the amidation of Glu-OBzl in cold alkaline solution with methacryloyl chloride, followed by the esterification with ethereal diazomethane solution. In order to examine the effect of neighboring groups and increase in solubility of the polymers, the vinyl amino acid derivatives have been copolymerized with butyl methacrylate (BMA) in dioxane by conventional free radical polymerization. The protecting groups at the amino acid ω-position have been cleaved with hydrogen bromide.

Table 1 gives the polymers and the SB linkages synthesized. The ω-group contents are seen to be slightly lower than the calculated values due to the preferential polymerization of BMA and the presence of protecting groups. The copolymer of Vinyl-Glu (OMe) and Vinyl-Ly(OMe) which consisted of 1:1 or 2:1 molar ratios did not bond with 8′-apocarotene-8′-al presumably due to salt formation of the amino groups with neighboring carboxyl groups in the polymer molecule. It was reported that only 11-*cis*- and 9-*cis*-retinal combine with opsin to form pigments and that only the 11-*cis* pigment has an absorption spectrum identical with that of rhodopsin.[7] In this study, however, the effect of the isomers of carotenal was not examined and 8′-apocarotene-8′-al, which was readily obtained by the potassium permanganate oxidation of β-carotene[8] and put up resistance to oxidation, was used as a pigment.

The absorption maxima (λ_{max}) of Poly-SB shifted to shorter wavelengths compared with Bu-SB (Table 1). This tendency increased after isolation and drying for Poly-SB (*e.g.* Poly-Ly-1: λ_{max}, 427 nm; $E_{1\%}$, 118), which may indicate that the delocalization of the π-electrons involved in the long pendant conjugated chain is affected by steric hindrance. The absorptivities were lower than the calculated values based on the amino group content in the polymer and the $E_{1\%}$ of Bu-SB, especially that of Copoly-SB being below 10. The measurements were conducted in the concentration range satisfying Lambert's Law, so that the low absorptivities indicate that SB formation is affected by the polymer backbones and the amount of amino group available for SB formation is decreased by salt formation in the polymer.

The spectrum of Bu-SB protonated with hydrochloric acid shifted 95 nm to longer wavelengths as previously reported.[9] For amino acid derivatives with low acidic dissociation constants (pK_a), Bu-SB remained unprotonated in non aqueous solvents but protonated in strong organic acids such as p-toluenesulfonic acid. In aqueous solvents, however, the spectrum of Bu-SB shifted to the red on mixing with amino acid derivatives,

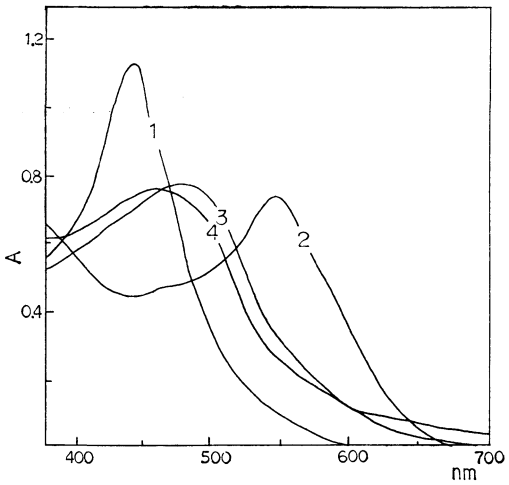

Fig. 1. Absorption spectra of Bu-SB with amino acids. 1; Bu-SB, 2; Bu-SB with HCl, 3; Bu-SB with Z-Glu, 4: Bu-SB with Poly-Glu(OMe). Solvent: 80% DMF.

although new peaks were observed at shorter wavelengths than that with hydrochloric acid (Fig. 1). The cause of this may be the difference in electrostatic energies of the counter ions.[10] The region of the maximum peaks are not clear with α- and γ-carboxy groups of amino acids. The absorptivity of Bu-SB protonated with poly(α-methyl N-methacryloyl-L-glutamate) [Poly-Glu(OMe)] was approximately half the value with low molecular amino acids, probably due to limited protonation by steric hindrance.

The spectra of Poly-Ly-SB protonated with amino acids were similar to those of Bu-SB, but the shifts were smaller. The amino acids as proton donors were in a large excess to the amino residue of Poly-Ly, and consequently neutralization was negligible. The positive charge on the nitrogen of the protonated lysine delocalized throughout the π-electron system is presumably interfered with the torsion of the conjugated chains and a small amount of acid components may be brought in

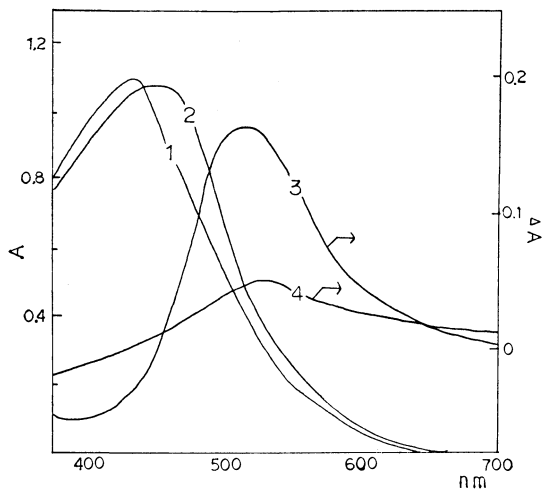

Fig. 2. Absorption spectra of Poly-SB and Copoly-SB 1: Poly-Ly-SB, 2: Poly-Ly-SB with Poly-Glu(OMe), 3: ΔA for Poly-Ly-SB with Z-Glu, 4: ΔA for Copoly-SB. Solvent: 80% DMF.

the proximity of the C=N bond due to steric hindrance of the polymer backbone or the long side chains. The low absorbance of Poly-Ly-SB with acids possessing large molecular sizes are analogous to those of Bu-SB and may be interpreted in terms of the steric hindrance discussed above. The bathochromic shift decreased in the order Z-Glu and Poly-Glu(OMe) (72, 47 nm respectively), indicating that the poorly dissociated carboxylic acid is incompletely bonded to the nitrogen in the hydrophobic region of the polymer matrix, thereby bringing about the poor delocalization of the positive charge throughout the conjugated double bonds.

The spectrum of Copoly-SB, which possesses an environment analogous to rhodopsin slightly shifted towards a longer wavelength by the addition of water. In order to obtain more obvious magnitude of the shift, the difference in absorbance (ΔA) plotted against the wavelength of Copoly-SB and Bu-SB in aqueous solution, the ΔA at the maximum peak being 4% of that for the λ_{max} of Copoly-SB (Fig. 2). This low absorbance appears to be due to there being fewer opportunities for collision between the SB linkage and the carboxylic acids fixed as side chains in the copolymer, since the addition of a lower molecular acid instead of an acid component as the side chain increases the absorbance (9%). The ΔA_{max} of Copoly-SB and with the addition of low molecular acids in aqueous solution was located at a slightly longer wavelength (5—10 nm) compared with Poly-SB and Bu-SB with the addition of amino acids. This suggests that the pendant polar groups such as the carboxylate anions and the salts in the vicinity of the chromophore pull the positive charge into the conjugate chain,[11] thus increasing the contribution to the resonance structure.

It is experimentally impossible to produce a highly selective and restrictive model which forms a SB in the aqueous phase and protonates quantitatively. It has been possible, however, to synthesize a simple polymer model simulating rhodopsin, in which the absorption spectrum shifted towards the longer wavelength *via* intramolecular protonation without the addition of external acid components. The magnitude of the shift, however, was small.

Experimental

The infrared, visible, ^{1}H-NMR and mass spectra were obtained using a Hitachi 215, a Hitachi 200-10, a JEOL-PXM60 and a Hitachi RMU-6MG spectrometer respectively. Elemental analyses were conducted using a Perkin-Elmer 250 instrument. 8′-Apocarotene-8′-al was prepared by the $KMnO_4$-oxidation of β-carotene and purified by aluminum oxide chromatography (Woelem-neutral), followed by partition separation.

Preparation of Vinyl-Z-Ly(OMe): Z-Ly(OMe) was prepared with Z-Ly and methanol–thionyl chloride.[6] To Z-Ly(OMe) HCl (10 g, 30.3 mM) in DMF–THF (2: 5, 70 ml) was added triethylamine (8.9 ml, 60 mM) and the Et_3N–HCl precipitated was filtered off. Methacryloyl chloride (3.5 ml) was added to the filtrate maintained below 5 °C. Stirring was maintained overnight in an ice bath, after which the mixture was filtered and washed with benzene. The filtrate, washed with dil.HCl, 10 % $NaHCO_3$ and water, was dried over anhydrous sodium sulfate and concentrated *in vacuo*. The oily residue was purified by precipitation with a mixture of carbon tetrachloride and hexane. Yield 11.0 g. Found: C, 62.23; H, 7.08; N, 7.13%. Calcd for $C_{19}H_{26}N_2O_5$: C, 62.64; H, 7.14; N, 7.69%. IR (CCl_4): 3400 (NH), 1730 (ester C=O), 1700 (carbamate C=O), 1670 (amide C=O), 945 (C=C) cm^{-1}. ^{1}H-NMR (CCl_4), δ: 1.4—1.7 (m, 6H, lysine CH_2), 1.9 (s, 3H, methacryl CH_3), 3.1 (d, 2H, lysine δ-CH_2), 3.6 (s, 3H, ester CH_3), 4.3 (s, 1H, lysine α-CH), 5.1 (s, 2H, benzyl CH_2), 5.3, 5.6 (s, 2H, CH_2–C), 7.3 (s, 5H, phenyl) ppm. Mass (*m/e*): 364 (M^+, 5 % to CH_2=C–CH_3^+).

Preparation of Vinyl-Glu-OBzl(OMe): A finely powdered Glu–OBzl (7.13 g, 30 mM) was vigorously stirred for one minute with Et_3N (5 ml) in H_2O (50 ml) in an ice bath, followed by the immediate addition of methacryloyl chloride (3 ml) below 5 °C. The mixture was vigorously stirred for 15 min, after which the reaction mixture was extracted with two portions of chloroform (100 ml). The extract, washed with dil.HCl and water was dried over anhydrous sodium sulfate and concentrated *in vacuo*. The Vinyl-Glu-OBzl thus obtained was esterified with an ethereal diazomethane solution and the solution washed with 10 % $NaHCO_3$ and water, dried over anhydrous sodium sulfate and concentrated *in vacuo*. The reaction product was purified by precipitation with a mixture of carbon tetrachloride and hexane. Yield 4.7 g. Found: C, 63.34; H, 6.36; N, 5.23%. Calcd for $C_{17}H_{21}NO_5$: C, 63.95; H, 6.58; N, 4.39%. IR (CCl_4); 3400 (NH), 1740 (ester C=O), 1675 (amide C=O), 920 (C=C) cm^{-1}. ^{1}H-NMR (CCl_4), δ: 1.9 (s, 3H, methacryl CH_3), 2.2—2.4 (m, 4H, glutamate CH_2), 3.8 (s, 3H, ester CH_3), 4.6 (t, 1H, α-CH), 5.1 (s, 2H, benzyl CH_2), 5.3, 5.8 (s, 2H, CH_2=C), 7.4 (s, 5H, phenyl) ppm. Mass (*m/e*): 319 (M^+, 15 % to benzyl ion).

Preparation of Poly-SB: A portion of the monomer (5 g), the composition of which is listed in Table 1, the α,α'-azobisisobutyronitrile (50 mg) and dioxane (10 ml) were placed in a Pyrex glass ampoule which had been previously flushed with nitrogen, sealed, and heated at 75 °C for 48 h. The polymer thus obtained was precipitated by ether, washed with ether, and dried *in vacuo*. The polymer (1 g) was dissolved in trifluoroacetic acid (3 ml). Cleavage of the protecting groups was conducted with a 30 % solution of hydrobromic acid in acetic acid (3 ml) at 50 °C for 1 h. The polymer thus obtained was tranformed into the free state of the ω-position by the following procedure: Poly-Ly HBr in H_2O (10 ml) was basified with Et_3N, precipitated into acetone, and freeze-dried from H_2O; Poly-Glu(OMe) was dissolved in 5% Na_2CO_3 solution and acidified with dil.HCl to pH 2, the polymer thus precipitated was washed with water and dried *in vacuo*; the copolymer dissolved in a mixture of THF and H_2O was neutralized with 0.1 M NaOH to the isoelectric point[12] and stirred at this point for 10 h. The polymer thus precipitated was washed with water and freeze-dried from dioxane. IR (KBr) and ^{1}H-NMR (DMSO-d_6) indicated no absorption peak at 695 cm^{-1} and 7—8 ppm.

Poly-SB was prepared as follows: 0.5 mM of polymer (based on lysine residue) and 1 mM of 8′-apocarotene-8′-al were stirred in DMF (10 ml) with a molecular sieve (3A) under nitrogen and allowed to stand in the dark for several days. The reaction mixture was poured into ether, dissolved in DMF without drying, and the DMF solution extracted with petroleum ether using a Soxhlet liquid extractor to attain a sufficient removal of remaining 8′-apocarotene-8′-al. The spectra were measured in a 1 mm cell approximately 5 min after 10^{-3} M/l of SB (1 ml) and 10^{-3} M/l of amino acid derivatives (10 ml) in DMF were mixed.

References

1) G. H. Brown, "Photochromism," John Willy and Sons, New York (1971), p. 708; B. Honig and T. G. Ebrey, *Ann. Rev. Biophys. Bioeng.*, **3**, 151 (1974).
2) R. Morton and G. Pitt, *Biochem. J.*, **59**, 128 (1955).
3) M. Nanasawa and H. Kamogawa, *Chem. Lett.*, **1977**, 1183.
4) W. Waddell and R. S. Becker, *J. Am. Chem. Soc.*, **93**, 3788 (1971).
5) P. E. Blatz and D. L. Pippert, *J. Am. Chem. Soc.*, **90**, 1296 (1968).
6) T. Shibata, *Bull. Chem. Soc. Jpn.*, **33**, 1721 (1960).
7) R. Hubbard and G. Wald, *J. Gen. Physiol.*, **36**, 269 (1952).
8) R. Karrer and V. Solmssen, *Helv. Chim. Acta*, **21**, 682 (1937).
9) W. H. Waddell, A. M. Schaffer, and R. S. Becker, *J. Am. Chem. Soc.*, **99**, 8456 (1977).
10) P. E. Blatz, *Chem. Commun.*, **1970**, 614.
11) B. Honig, A. D. Greenberg, U. Dinur, and T. G. Ebrey, *Biochemistry*, **15**, 4593 (1976).
12) Calculated from the equation: $H^+=(K_wK_a/K_b)^{1/2}$.

The Ullmann Condensation Reaction of Haloanthraquinone Derivatives with Amines in Aprotic Solvents. IV. Kinetic Studies of the Condensation with Ethylenediamine

Sadao ARAI, Akira TANAKA, Mitsuhiko HIDA,* and Takamichi YAMAGISHI

Department of Industrial Chemistry, Faculty of Technology, Tokyo Metropolitan University, Fukazawa, Setagaya-ku, Tokyo 158

(Received September 8, 1978)

In the Ullmann condensation of bromoanthraquinones (AQBr) with ethylenediamine using copper(I) bromide as a catalyst, the reaction rate decreased with time which has been interpreted in terms of the formation of the ineffective copper(II) species. The kinetic investigation showed the reaction rate to be first order both for the copper(I) species and AQBr. After prolonged reaction the copper(I) species was quantitatively converted to the copper(II) species, the copper(II) species appearing to have little catalytic activity due to strong coordination with ethylenediamine. The reactivities of the haloanthraquinones were dependent on the ease of coordination with Cu(I) and the rate of Cu(II) formation. The mechanism, including the reaction between Cu^{I}(AQBr) and ethylenediamine, has been proposed and discussed.

Aryl halides readily undergo nucleophilic replacement of the halogen atom by moieties such as OR and NH_2, with the aid of a copper catalyst. The reaction mechanism, has however, been the subject of little research and the catalytic action of the copper species remains obscure.

The authors have reported the mechanism of the Ullmann condensation reaction for haloanthraquinones with amines using copper salts as the catalyst in protic and aprotic solvents.[1-4] In aprotic solvents, the effective copper(I) species oxidizes to the ineffective copper(II) species during the course of reaction and the formation of the copper(II) species has been shown to have an important role in the reaction.[2,3] Thus, in the condensation with 2-aminoethanol, the resulting copper(II) species increased the catalytic activity of the copper(I) species. The pseudo-first order rate constant may be expressed as follows:

$$k = k_1[Cu^{I}] + k_2[Cu^{I}][Cu^{II}].^{4)}$$

In this paper the reaction of haloanthraquinones with ethylenediamine, will be reported which is more reactive than 2-aminoethanol, by copper(I) catalyst in aprotic media.

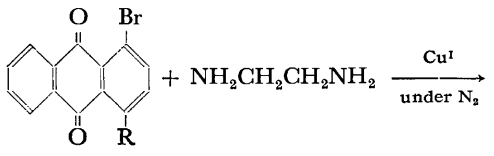

1: R=H
2: R=NH_2

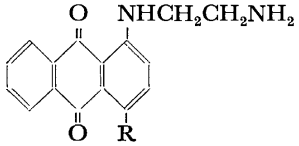

3: R=H
4: R=NH_2

Experimental

General. 1-Bromoanthraquinone (**1**), 1-amino-4-bromoanthraquinone (**2**), and copper(I) bromide were prepared by the methods described in a previous paper.[2] Commercially available ethylenediamine was dried over sodium, distilled, and stored under nitrogen. The solvents used were dried by standard procedures, distilled, and stored under nitrogen. The details of the kinetic measurements have been described in Part I of this series.[2] The anthraquinone and 1-aminoanthraquinone formed in the course of reaction were analyzed by high speed liquid chromatography in a manner similar to that described in a preceding paper[4]: column, Zorbax ODS 25 cm; mobile phase, methanol–water 67: 33; temperature, 40 °C; detector, UV-254 nm. ESR spectra were measured as described in preceding papers.[3,4] IR and UV and visible spectra were recorded with JASCO IRA-1 and Shimadzu UV-200 spectrophotometers respectively. NMR spectra were obtained on a Hitachi R-24 spectrometer for solutions in dimethyl-d_6 sulfoxide with tetramethylsilane as an internal reference. Mass spectra were taken on a JEOL JMS-D 100 mass spectrometer by direct insertion.

Condensation Products. The condensation product, 1-(2-aminoethylamino)anthraquinone (**3**), was very liable, cyclizing thermally to give compound (**5**).[5] The condensation reaction of **1** and **2** with ethylenediamine in 1,2-dimethoxyethane–methyl cellosolve (4: 1) solution were conducted at temperatures below 100 °C in order to avoid possible side reactions, *e.g.*, cyclization of the condensation products.

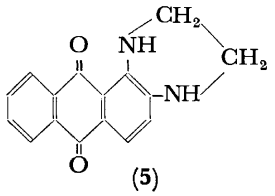

(**5**)

The condensation products were obtained from the reaction mixture in a following manner: The solvents were removed under reduced pressure and the reaction mixture poured into water. After filtration, the products were washed with water and dried and the precipitate chromatographed on a silica gel column with benzene–methanol (4: 1, v/v) as the eluent. No formation of ring closed compounds were observed.

1-(2-Aminoethylamino)anthraquinone (3): λ_{max}(C_2H_5OH) 501 nm (ε 6460); IR (KBr) 1660 cm^{-1} (C=O); NMR δ=2.37 (2H, disappearing on deuteration, NH_2), 2.85 (2H, $-CH_2-$), 3.25 (2H, $-CH_2-$), 6.95—8.35 (7H, quinone ring), 9.80 (1H, NH); MS, *m/e*=266 (M^+).

1-Amino-4-(2-aminoethylamino)anthraquinone (4): λ_{max}(C_2H_5-OH) 501 nm (ε 15700), 571 nm (ε 14100); NMR δ=2.85 (2H, $-CH_2-$), 3.44 (2H, $-CH_2-$), 7.10—8.40 (6H, quinone

ring), 10.91 (1H, disappearing on deuteration, NH); MS, m/e=281 (M^+).

Results and Discussion

The reactivities of the haloanthraquinones in the presence or absence of copper(I) catalyst have been compared in Fig. 1 and indicate the following observations:

(i) The copper(I) catalyst greatly enhanced the reactivities of the haloanthraquinones.

(ii) 1-Bromoanthraquinone (**1**) was more reactive than 1-amino-4-bromoanthraquinone (**2**), both in the absence and presence of catalyst. The relative initial rates have been calculated as follows: **1** (without catalyst): **2** (without catalyst): **1** (with catalyst): **2** (with catalyst)=20: 1: 5900: 5500.

(iii) The catalytic activity decreased as the reaction proceeded, a tendency more marked in reaction **2** than in **1**.

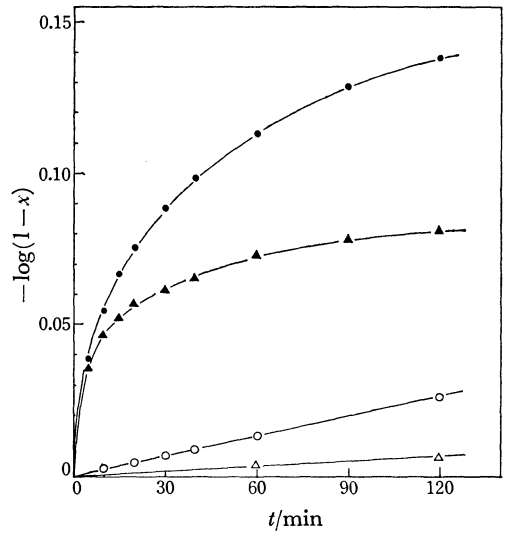

Fig. 1. Pseudo-first order plots of the reaction between bromoanthraquinones and ethylenediamine. $[AQBr]_0 = 5\times10^{-3}$ mol/l, $[EN]_0$=0.5 mol/l, $[CuBr]_0 = 1\times10^{-3}$ mol/l, temp 70 °C, solvent 1,2-dimethoxyethane–methyl cellosolve 4: 1.
●: 1-BrAQ(**1**)–EN–CuBr, ▲: 1-NH_2-4-BrAQ(**2**)–EN–CuBr, ○: 1-BrAQ–EN, △: 1-NH_2-4-BrAQ–EN.

The above results may be explained in terms of the change in catalyst from copper(I) to copper(II). The following kinetic studies of the reaction between the haloanthraquinones and ethylenediamine reasonably support this reasoning.

Kinetics of Catalyst-free Reactions. Figure 1 shows that both the reactions of **1** and **2** in the absence of copper(I) bromide catalyst can be interpreted in terms of pseudo-first order kinetics. Since ethylenediamine (EN) was in a large excess, the second order rate constants were obtained by dividing the pseudo-first order rate constants by the concentration of amine. The second order rate constants of **1** and **2** (k_I and k_{II}) are expressed by Eqs. 1 and 2:

$$k_I\ (l\cdot mol^{-1}\cdot min^{-1}) = (3.2[EN]+7.0)\times10^{-4}, \quad (1)$$

$$k_{II}\ (l\cdot mol^{-1}\cdot min^{-1}) = (7.16\pm1.22)\times10^{-5}. \quad (2)$$

Bunnett *et al.* reported that the nucleophilic substitution reactions of halonitrobenzenes with amines were accelerated, strongly or mildly with an increase in the concentration of amine or by the addition of bases.[6] Under these conditions the second order rate constant largely conform to Eq. 1. This observation has been interpreted by the following scheme:

$$ArX + RNH_2 \underset{k_{-a}}{\overset{k_a}{\rightleftharpoons}} \left[\begin{matrix} & X \\ Ar & \\ & NH_2R \\ & + \end{matrix}\right] \underset{k_c[RNH_2]}{\overset{k_b}{\circlearrowright}} ArNHR. \quad (3)$$

Application of steady state hypothesis to this mechanism gives a second order rate constant (k') expressed by

$$k' = \frac{k_a k_b}{k_{-a}+k_b+k_c[RNH_2]} + \frac{k_a k_c[RNH_2]}{k_{-a}+k_b+k_c[RNH_2]}. \quad (4)$$

Assuming k_{-a} is much larger than $(k_b+k_c[RNH_2])$ in the reaction of **1**, k_I may be expressed as follows:

$$k_I = \frac{k_a k_b}{k_{-a}} + \frac{k_a k_c[RNH_2]}{k_{-a}}. \quad (5)$$

By comparing Eq. 5 with Eq. 1, $k_a k_b/k_{-a}$ and $k_a k_c/k_{-a}$ have been evaluated as 7.0×10^{-4} $l\cdot mol^{-1}\cdot min^{-1}$ and 3.2×10^{-4} $min^{-1}\cdot l^2\cdot mol^{-2}$, respectively. Thus, the ratio of k_c to k_b has been calculated as 0.46 $mol^{-1}\cdot l$ indicating that the reaction of **1** with ethylenediamine is mildly accelerated. Assuming k_{-a} is much less than $(k_b+k_c[RNH_2])$, Eq. 4 simplifies to $k'=k_a$ and the reaction is not base catalyzed. The reaction of **2** may correspond to this instance.

Kinetics of Copper(I) Catalyzed Reactions. The pseudo-first order plots for the reaction using copper(I) bromide as a catalyst were not linear (Fig. 1) presumably indicating that the reaction rate decreased with the formation of the ineffective copper(II) species. The rate equation has been interpreted as first order in concentration of bromoanthraquinones (AQBr) and copper(I) species. Thus,

$$-\frac{d[AQBr]}{dt} = (k_0+k_1[CuBr])[AQBr], \quad (6)$$

where k_0 denotes the pseudo-first order rate constant ($k_1[EN]$ or $k_{II}[EN]$) of the catalyst-free reactions.

ESR measurements suggested that the copper(I) species was oxidized to the copper(II) species exponentially increased during the course of reaction. Then, the concentration of CuBr may be mathematically expressed by Eq. 7:

$$[CuBr] = a\cdot\exp(-\gamma t) + b. \quad (7)$$

The initial concentration of CuBr is given by

$$[CuBr]_0 = a + b, \quad (8)$$

and the concentration of CuBr approaches b after prolonged reaction.

Combining Eq. 6 with Eq. 7 and integrating gives Eq. 9.

$$-\ln(1-x) = \frac{k_1 a}{\gamma}(1-e^{-\gamma t}) + (k_1 b+k_0)t \quad (9)$$

This may be rewritten:

$$-\frac{\ln(1-x)}{t} = A\cdot\frac{(1-e^{-\gamma t})}{t} + B, \quad (10)$$

where x denotes the yield of the condensation product, and $A=k_1a/\gamma$ and $B=k_1b+k_0$. By assuming a value of γ, A and B were determined by means of linear regression analysis. The values of the parameters (A, B, and γ), which gave the maximum correlation coefficient, were taken to be the most suitable parameters. The agreement between calculated and observed data was very good, since the correlation coefficients were greater than 99% in all cases.

The rate constant k_1 can be obtained from Eq. 11,

$$k_1 = \frac{\gamma A+B-k_0}{[\mathrm{CuBr}]_0} \tag{11}$$

and the values of k_1 and γ are summarized in Tables 1

Table 1. Rate constant k_1, γ, and the value of $b/(a+b)$ for the reaction of 1-bromoanthraquinone (**1**) with ethylenediamine (EN)

	mol·l^{-1}	k_1 (l·mol^{-1}·min^{-1})	γ	$\frac{b}{a+b}\times 100$ (%)
EN	0.256	17±0.5	0.16	0.9
	0.502	23±1	0.17	2.0
	0.669	23±0.5	0.17	8.6
	0.998	25±0.5	0.12	3.3
	1.410	31±1	0.15	6.2
CuBr	3.72×10^{-4}	15±1	0.14	0
	7.57	26±2	0.16	3.4
	10.7	23±1	0.17	2.0
	15.2	23±1	0.18	3.1
1	1.07×10^{-3}	26±0.5	0.07	12.8
	2.50	22±1.6	0.11	7.2
	5.02	23±1	0.17	2.0
	7.53	23±1	0.19	1.2
	10.1	20±1	0.20	0

Temp 70 °C, solvent 1,2-dimethoxyethane–methyl cellosolve 4: 1.

Table 2. Rate constant k_1, γ, and the value of $b/(a+b)$ for the reaction of 1-amino-4-bromoanthraquinone (**2**) with ethylenediamine (EN)

	mol·l^{-1}	k_1 (l·mol^{-1}·min^{-1})	γ	$\frac{b}{a+b}\times 100$ (%)
EN	0.260	23±2	0.29	2.1
	0.516	29±3	0.26	2.9
	0.747	33±2	0.25	4.1
	1.00	34±3	0.19	4.8
	1.42	40±2	0.18	8.0
CuBr	4.34×10^{-4}	47±4	0.27	3.1
	7.07	33±2	0.26	2.9
	9.51	29±3	0.26	2.9
	11.76	32±3	0.27	3.2
2	2.59×10^{-3}	29±1	0.15	2.7
	5.01	29±3	0.26	2.9
	7.54	23±3	0.35	1.2
	10.03	21±4	0.35	1.7

Temp 70 °C, solvent 1,2-dimethoxyethane–methyl cellosolve 4: 1.

and 2. Tables 1 and 2 show that the rate constant k_1 is approximately independent of the initial concentration of CuBr. The plot of γA against the initial concentration of CuBr gives a straight line supporting the assumption that the condensation with ethylenediamine is first order with respect to copper(I) bromide. The values of the ratio $b/(a+b)$ are given by Eq. 12:

$$\frac{b}{a+b} = \frac{B-k_0}{\gamma A+B-k_0}. \tag{12}$$

As shown in Tables 1 and 2, the value of $b/(a+b)$ was less than about 4% in most cases indicating that the copper(I) species is almost perfectly oxidized to the copper(II) species after prolonged reaction.[7] Under these condensation conditions debrominated products were also produced suggesting that the copper(II) species was formed by an electron transfer from copper(I) to bromoanthraquinone (AQBr+Cu(I)⟶AQBr$^{\cdot}$ +Cu(II)) in a similar manner to the condensation with 2-aminoethanol and that part of the resulting bromoanthraquinone anion radical may be debrominated.[4]

The catalytic activity of copper(I) species in the reaction with ethylenediamine was insensitive to the resulting copper(II) species. This is presumably because ethylenediamine strongly coordinates to the copper(II) species and thereby prevents cooperation between the copper(I) and copper(II) species. It has been reported that copper(II) forms stable chelate complex with ethylenediamine ($[Cu(EN)]^{2+}$ and $[Cu(EN)_2]^{2+}$).[8]

The catalytic activity of the copper(I) species in the reaction with ethylenediamine was 20 times greater than that with 2-aminoethanol. After a statistical correction of 2 was applied, ethylenediamine was more reactive than 2-aminoethanol by a factor of 10. This has been attributed to the fact that electrons are more delocalized in the copper(I) species with a bidentate amine such as ethylenediamine.

Reaction Mechanism. As indicated in Tables 1 and 2, the rate constant k_1 increased with increasing concentration of amine, the plot of $1/k_1$ against 1/[EN] giving a linear relationship (Fig. 2). On the other hand, the rate constant k_1 decreased with increasing concentration of bromoanthraquinone ([AQBr]), the plot of $1/k_1$ against [AQBr] giving a straight line (Fig. 3).

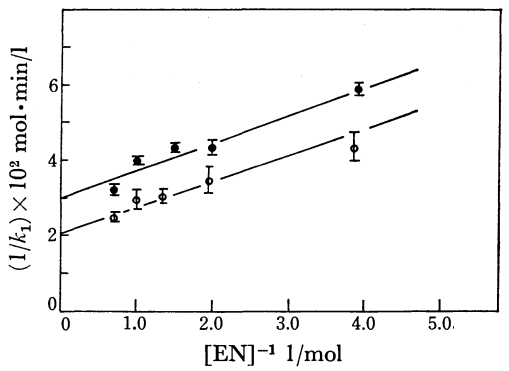

Fig. 2. Plots of $1/k_1$ against 1/[EN]. Temp 70 °C, solvent 1,2-dimethoxyethane–methyl cellosolve 4: 1.
●: 1-BrAQ–EN–CuBr, ○: 1-NH_2-4-BrAQ–EN–CuBr.

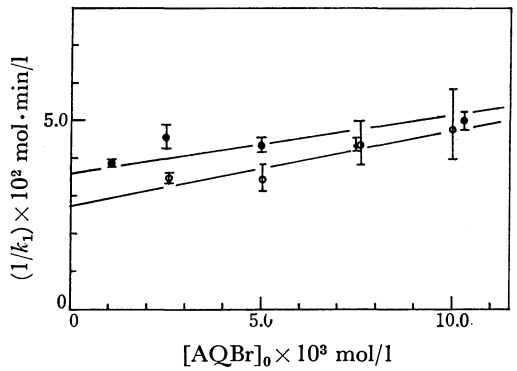

Fig. 3. Plots of $1/k_1$ against [AQBr]. Temp 70 °C, solvent 1,2-dimethoxyethane–methyl cellosolve 4: 1. ●: 1-BrAQ–EN–CuBr ○: 1-NH_2-4-BrAQ–EN–CuBr.

All results can be interpreted by assuming the following reaction scheme (Eq. 13):

$$\begin{aligned} &Cu^I + EN \overset{K_1}{\rightleftharpoons} Cu^I(EN) \\ &Cu^I + AQBr \overset{K_2}{\rightleftharpoons} Cu^I(AQBr) \xrightarrow[k_r]{EN} \text{product.} \end{aligned} \tag{13}$$

On the basis of this (Eq. 13), the rate constant k_1 is expressed by

$$k_1 = \frac{k_r K_2[EN]}{1+K_1[EN]+K_2[AQBr]}. \tag{14}$$

The concentration of AQBr under smal conversion is approximately equal to the initial concentration ($[AQBr]_0$). Thus equation 14 may be rewritten:

$$k_1^{-1} = \frac{k_1}{k_r K_2} + \frac{1+K_2[AQBr]_0}{k_r K_2} \cdot \frac{1}{[EN]}, \tag{15}$$

$$k_1^{-1} = \frac{1+K_1[EN]}{k_r K_2[EN]} + \frac{K_2}{k_r K_2[EN]} \cdot [AQBr]_0. \tag{16}$$

The values k_r, K_1, and K_2 can be evaluated from the slope and the intercept of Figs. 2 and 3, and the concentrations of AQBr and EN, the values of which are shown in Table 3. Since the equilibrium between Cu^I and EN does not include haloanthraquinone, there should not be any difference in the magnitude of K_1 between **1** and **2**. Table 3 shows that K_1 in the reaction of **1** is approximately equal to that in the reaction of **2**, which supports the above mechanism.

The parameter γ corresponds to the decreasing rate of copper(I) species. As shown in Tables 1 and 2, the magnitude changes with the initial concentrations of haloanthraquinone and copper(I) bromide, but it is little affected by the concentration of amine. The kinetics of the formation of the copper(II) species, however, is not yet clearly understood.

Table 3. Rate parameters

Rate parameter	1-BrAQ (**1**)	1-NH_2-4-BrAQ (**2**)
k_r ($mol^{-1}\cdot l\cdot min^{-1}$)	1.24	0.98
K_1 ($l\cdot mol^{-1}$)	8.9	10.0
K_2 ($l\cdot mol^{-1}$)	243	500

Temp 70 °C, solvent 1,2-dimethoxyethane–methyl cellosolve 4: 1, $[AQBr]_0=5\times 10^{-3}$ $mol\cdot l^{-1}$, $[EN]_0=5\times 10^{-1}$ $mol\cdot l^{-1}$.

As previously reported, in the presence of copper(I) catalyst, **1** is more reactive than **2** and this may be reasonably explained as follows: The rate constant k_r of **2** is smaller than that of **1**, while the equilibrium constant between Cu(I) and **2** has a greater value than that between Cu(I) and **1**. Thus, **2** has an initial rate similar to that of **1**. The reaction rate of **2**, however, diminishes more rapidly than that of **1** with time, an observation caused possibly by the concentration of copper(I) species decreasing more rapidly in the reaction of **2** than in the reaction of **1**, since the magnitude of the parameter γ of **2** is greater than that of **1**.

The authors wish to thank Dr. Kinji Anda and Mr. Masao Usui of the Tokyo Metropolitan Industrial Technical Institute for assistance with the mass spectral measurements.

References

1) a) T. D. Tuong and M. Hida, *Bull. Chem. Soc. Jpn.*, **43**, 1763 (1970); b) T. D. Tuong and M. Hida, *ibid.*, **44**, 756 (1971); c) T. D. Tuong and M. Hida, *J. Chem. Soc., Perkin Trans. 2*, **1974**, 676.

2) Part I of this series, S. Arai, T. Yamagishi, S. Ototake. and M. Hida, *Bull. Chem. Soc. Jpn.*, **50**, 547 (1977).

3) Part II, S. Arai, M. Hida, T. Yamagishi, and S. Ototake, *Bull. Chem. Soc. Jpn.*, **50**, 2982 (1977).

4) Part III, S. Arai, M. Hida, and T. Yamagishi, *Bull. Chem. Soc. Jpn.*, **51**, 277 (1978).

5) H. P. Kolliker and P. Caveng, *Chimia*, **20**, 281 (1966), M. S. Simon and D. P. Waller, *Tetrahedron Lett.*, **1967**, 1527.

6) J. F. Bunnett and R. H. Garst, *J. Am. Chem. Soc.*, **87**, 3875 (1965).

7) In the condensation with 2-aminoethanol, the copper(I) species was not perfectly oxidized to the copper(II) species even after prolonged reaction.

8) a) H. B. Jonassen and T. H. Dexter, *J. Am. Chem. Soc.*, **71**, 1553 (1949); b) G. Gordon and P. K. Birdwhistell, *ibid.*, **81**, 3567 (1959).

The Regioselective Amino-exchange Reaction of β-Amino Conjugated Enones

Choji KASHIMA* and Yasuhiro YAMAMOTO

Department of Chemistry, University of Tsukuba, Sakura-mura, Niihari-gun, Ibaraki 300-31

(Received September 21, 1978)

By heating with various amines, the amino-exchange reaction of β-amino conjugated enones was regioselectively accomplished on β-carbon to give the corresponding β-amino conjugated enones. The resulting β-dialkylamino conjugated enones could then be used for the synthesis of β,β-disubstituted conjugated enones by treatment with Grignard reagents.

Previously, it has been reported that *cis*-1-substituted-4-amino-3-penten-2-ones were regioselectively prepared from 2,4-pentanedione through 5-substituted 3-methylisoxazoles by catalytic hydrogenation.[1] Benary described[2] how β-dialkylamino conjugated enones reacted with Grignard reagents to afford β,β-disubstituted conjugated enones. However, *N*-unsubstituted and *N*-monosubstituted β-amino conjugated enones are inert toward Grignard reagents, even under forced conditions. Therefore, the conversion from *N*-unsubstituted β-amino conjugated enones to *N*,*N*-disubstituted analogues seems to be the key step in the regioselective synthesis of β,β-disubstituted conjugated enones.

The reactions of β-amino conjugated enones with hydroxylamine[3] and ureas[4] have already been reported. In both cases, nucleophiles attack first the β-carbon of β-amino conjugated enones as a Michael-type addition, and then eliminate the amine or ammonia to afford the corresponding heterocycles. By analogy, we expected the amino-exchange reaction of β-amino conjugated enones upon the treatment with a primary or secondary amine to afford *N*-monosubstituted or *N*,*N*-disubstituted β-amino conjugated enones. (Scheme 1).

When *cis*-4-amino-3-penten-2-one (**1**) was treated with dimethylamine, *trans*-4-dimethylamino-3-penten-2-one (**2a**) was formed in a quantitative yield. In this reaction, the β-amino conjugated enone has two reaction sites, on the β-carbon and on the carbonyl carbon atoms. In the case of the reaction of *cis*-2-amino-2-hepten-4-one (**3**) with dimethylamine, four reaction products, *trans*-2-dimethylamino-2-hepten-4-one (**4a**), *trans*-4-dimethylamino-3-hepten-2-one, and their *cis* isomers, could be expected. When **3** was treated with dimethylamine under the same conditions, however, only one product was obtained. This product was independently prepared from **3** by direct methylation on nitrogen in the presence of sodium hydride. This result showed that the amino-exchange reaction occurred regioselectively on β-carbon to afford 2-dimethylamino-2-hepten-4-one. For determining the configuration, the NMR spectrum of this product was compared with those of **1**, **2a**, **2d**, **2e**, **2f**, and **2h**, which configurations had already been confirmed by means of the IR, UV, and olefinic proton NMR spectra.[5] The allyl methyl proton signal appeared at δ 2.49 ppm, and the molarinduced shift (Δδ) by Eu(fod)$_3$ was larger than that of the olefinic proton signal. This was similar not to the cases of **1** and **2h**, but to those of **2a**, **2d**, **2e**, and **2f** (*cf.* Table 2). These results indicated that *trans*-2-dimethylamino-2-hepten-4-one (**4a**) was more favorable for the reaction product from **3** and dimethylamine.

Similarly, **1** and **3** were treated with various secondary amines to give the corresponding β-amino conjugated enones, **2** and **4**, with *trans* configurations, as are listed in Table 1. On the contrary, the reaction products from primary amines with **3** and **5** were found to be the corresponding *cis*-β-(*N*-monosubstituted)-amino conjugated enones, **4h**, **4i**, and **6j**, which showed allyl methyl protons and the chelated NH signals at about δ 1.9 and 10.5 ppm in NMR respectively. These results suggested that the configurations of the resulting β-amino conjugated enones were easily changed to the thermodynamically stable form under an amino-exchange reaction or on alkylation reaction. In the cases of piperidine, morpholine, diethylamine, diisopropylamine, aniline, *N*-methylaniline, acetamide, and *N*-methylacetamide, the reaction did not occur, even at high temperatures, because of their bulkiness and/or the lack of nucleophilicity.

As applications of this amino-exchange reaction, the syntheses of several terpens, such as ar-turmerone (**9**)[6] and targetone (**12**),[7] were demonstrated. The synthesis of **11** was carried out from *cis*-2-amino-6-*p*-tolyl-2-

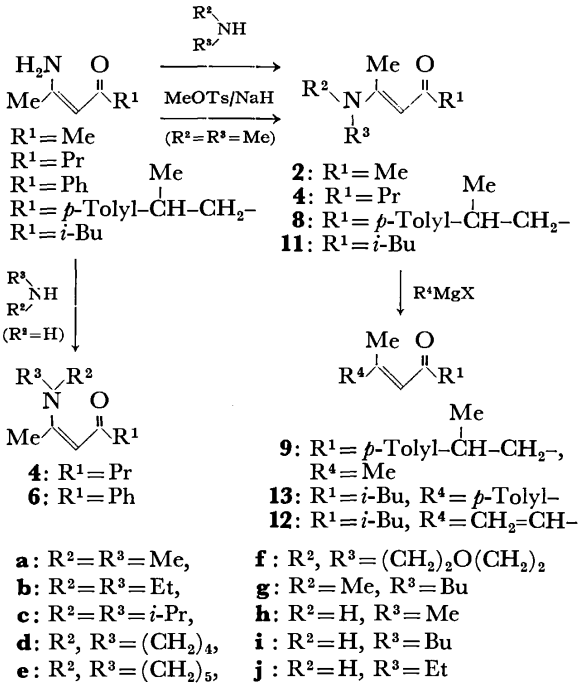

Scheme 1.

TABLE 1. THE YIELDS OF AMINO-EXCHANGE REACTION PRODUCTS

	Product			Temp (°C)	Time (h)	Yield (%)
	R^1	R^2	R^3			
2a	Me	Me	Me	90	12	90
2b	Me	Et	Et	150	24	0
2c	Me	*i*-Pr	*i*-Pr	150	24	0
2d	Me	$-(CH_2)_4-$		90[a]	6	98
2e	Me	$-(CH_2)_5-$		105[a]	24	0
2e	Me	$-(CH_2)_5-$		125	12	13
2f	Me	$-(CH_2)_2O(CH_2)_2-$		130[a]	48	0
2g	Me	Me	Bu	90[a]	48	46
4a	Pr	Me	Me	90	12	92
4b	Pr	Et	Et	150	24	0
4d	Pr	$-(CH_2)_4-$		90[a]	6	100
4e	Pr	$-(CH_2)_5-$		105[a]	24	0
4f	Pr	$-(CH_2)_2O(CH_2)_2-$		130[a]	24	0
4h	Pr	H	Me	120	12	96
4i	Pr	H	Bu	130	12	79
6j	Ph	H	Et	110	24	95
8d	*p*-Tolyl-CH(Me)-CH_2-	$-(CH_2)_4-$		90[a]	12	65
11d	*i*-Bu	$-(CH_2)_4-$		90[a]	12	73

a) The reaction was carried out under refluxing without benzene.

TABLE 2. THE NMR DATA OF β-AMINO CONJUGATED ENONES [R^2R^3N-C(Me)=CH-CO-R^1]

Compd	Conf.	δ^{Me}	δ^{CH}	δ^{R^2}	δ^{R^3}	δ^{R^1}	$\Delta\delta^{Me}$	$\Delta\delta^{CH}$
1	*cis*	1.90	5.01	9.6	6.4	1.99	3.78	6.50
2h	*cis*	1.90	4.98	10.7	2.93	2.00	3.36	5.48
3	*cis*	1.90	4.97	9.7	5.2	0.95, 1.2—1.9, 2.25		
4h	*cis*	1.92	5.00	10.8	2.92	0.92, 1.6, 2.2		
4i	*cis*	1.92	4.95	11.0	0.93, 1.55, 3.25	0.93, 1.55, 2.22		
5	*cis*	2.00	5.70	10.2	5.5	7.2—7.5, 7.7—8.0		
6j	*cis*	2.07	5.66	10.5	1.19, 4.1—4.5	7.2—7.5, 7.7—8.0		
7	*cis*	1.82	4.93	9.6	5.15	1.23, 2.27, 2.5, 3.2, 7.1		
10	*cis*	1.90	5.00	9.7	4.9—5.2	0.93, 2.11		
2a	*trans*	2.41	4.95	2.92		1.96	8.32	5.90
2d	*trans*	2.48	4.95	1.94, 3.14		2.01	8.18	5.74
2e	*trans*	2.42	5.14	1.63, 3.32		1.98	7.81	5.61
2f	*trans*	2.48	5.25	3.52		2.09	8.29	6.34
2g	*trans*	2.35	4.82	2.79	0.88, 1.38, 3.17	1.85		
4a	*trans*	2.49	5.00	2.95		0.92, 1.6, 2.15	5.99[a]	1.31[a]
4d	*trans*	2.51	4.91	1.94, 3.31		0.91, 1.53, 2.25		
8d	*trans*	2.49	4.85	1.9, 3.25		1.23, 2.29, 2.5, 3.25, 7.1		
11d	*trans*	2.45	4.80	2.0, 3.32		1.90, 2.0		

hepten-4-one (**7**) through *trans*-2-(1-pyrrolidinyl)-6-*p*-tolyl-2-hepten-4-one (**8d**). Similarly, **12** was synthesized by the reaction of *cis*-2-amino-6-methyl-2-hepten-4-one (**10**) and pyrrolidine, followed by the reaction with vinylmagnesium bromide. The total yields of **9** and **12** were 22 and 9%, based on the corresponding *N*-unsubstituted β-amino conjugated enones respectively.

In conclusion, the treatment of *N*-unsubstituted β-amino conjugated enones with various amines afforded *N*-substituted β-amino conjugated enones by the regioselective amino-exchange reaction. The resulting β-dialkylamino conjugated enones should be very useful intermediates for the synthesis of β,β-disubstituted conjugated enones in combination with the Grignard reaction.

Experimental

The Preparation of N-*Unsubstituted β-Amino Conjugated Enones.* *cis*-4-Amino-3-penten-2-one (**1**) was prepared from 2,4-pentanedione by treatment with anhydrous ammonia in anhydrous ethanol.[8] By hydrogenation on platinum, *cis*-2-amino-2-hepten-4-one (**3**) was prepared from 3-methyl-5-propylisoxazole, which had itself been obtained by the action of ethyl bromide on 3,5-dimethylisoxazole in the presence of sodium amide in liquid ammonia.[1] The configurations of all the β-amino conjugated enones were confirmed by the chemical shifts of the allyl methyl and the chelated NH proton signals, and the

shifts of the allyl methyl and olefinic proton signals induced by Eu(fod)$_3$, on NMR in chloroform-d_1, as are listed in Table 2.

cis-*2-Amino-6-*p*-tolyl-2-hepten-4-one (7).* According to the alkylation method,[1] 3,5-dimethylisoxazole was treated with 1-bromo-1-*p*-tolyl-ethane to afford 3-methyl-5-[1-methyl-2-(*p*-tolyl)ethyl]isoxazole; yield, 37 %. Bp 110 °C/3 mmHg. IR (liquid film): 2950, 1610, 1530, 1450, 1420, 1120, and 815 cm^{-1}. Found: C, 78.09; H, 7.93; N, 6.13%. Calcd for $C_{14}H_{17}NO$: C, 78.10; H, 7.96; N, 6.51 %. This isoxazole derivative was then hydrogenated to Compound **7**, which was purified by distillation *in vacuo*; yield, 95%. Bp 137 °C/4 mmHg. IR (liquid film): 3350, 3200, 2950, 1615, 1530, 1410, 1020, and 815 cm^{-1}.

cis-*2-Amino-6-methyl-2-hepten-4-one (10).* By the hydrogenation of 3-methyl-5-isobutylisoxazole, **10** was obtained and purified by recrystallization from hexane; yield, 57%. Mp 56—57 °C, bp 102—105 °C/5 mmHg. Found: C, 67.82; H, 10.57; N, 9.82%. Calcd for $C_8H_{15}NO$: C, 68.04; H, 10.71; N, 9.82%.

General Procedure of Amino-exchange Reaction. A solution of β-amino conjugated enone (5 mmol) and primary or secondary amine (6 mmol) in 2 ml of benzene was heated in a sealed tube. The mixture was then cooled to room temperature and concentrated. The crude *N*-substituted β-amino conjugated enone was purified by fractional distillation and/or recrystallization. The product was identified with an authentic sample by means of VPC and the spectral data.

trans-*2-Dimethylamino-2-hepten-4-one (4a).* Compound **4a** was prepared from **3** and dimethylamine. The NMR peaks were shifted by Eu(fod)$_3$ (*cf.* Table 2). Bp 100—110 °C/3 mmHg. Mass (*m/e*): 155 (M), 140 (M−15), 138, 127 (M−28), 112 (M−43), 98, 85, 84, 70, 69, 56, and 44. Found: C, 68.80; H, 11.07; N, 8.82%. Calcd for $C_9H_{17}NO$: C, 69.63; H, 11.03; N, 9.02%.

trans-*2-(1-Pyrrolidinyl)-2-hepten-4-one (4d).* Compound **4d** was prepared from **3** and pyrrolidine. Bp 112—114 °C/5 mmHg. IR (liquid film): 2950, 2910, 1630, 1530, 1340, and 1020 cm^{-1}. Found: C, 72.44; H, 10.40; N, 7.88%. Calcd for $C_{11}H_{19}NO$: C, 72.88; H, 10.57; N, 7.73%.

cis-*2-Methylamino-2-hepten-4-one (4h).* Compound **4h** was prepared from **3** and methylamine. Bp 53—55 °C/5 mmHg. Found: C, 68.33; H, 10.46; N, 9.90%. Calcd for $C_8H_{15}NO$: C, 68.04; H, 10.71; N, 9.92%.

cis-*2-Butylamino-2-hepten-4-one (4i).* Compound **4i** was prepared from **3** and butylamine. Bp 105 °C/3 mmHg. IR (liquid film): 2950, 2915, 1605, 1580, 1300, and 735 cm^{-1}. Found: C, 72.19; H, 11.21; N, 7.65%. Calcd for $C_{11}H_{21}NO$: C, 72.08; H, 11.55; N, 7.64%.

trans-*2-(1-Pyrrolidinyl)-6-*p*-tolyl-2-hepten-4-one (8d).* Compound **8d** was obtained from **7** and pyrrolidine, and subsequently purified by distillation. Bp 130 °C/5 mmHg. IR (liquid film): 2950, 1630, 1340, 1020, 815, and 730 cm^{-1}.

trans-*2-(1-Pyrrolidinyl)-6-methyl-4-hepten-2-one (11d).* Compound **11d** was obtained by the amino-exchange reaction from **10** and pyrrolidine, and subsequently purified by recrystallization from hexane. Mp 67—68.5 °C. Found: C, 73.26; H, 10.57; N, 7.15%. Calcd for $C_{10}H_{21}NO$: C, 73.79; H, 10.84; N, 7.17%.

The Direct Methylation of 3. Sodium hydride in Bayol was washed with dry ether 2 times. To the suspension of sodium hydride in dry ether, **3** (5 mmol) was then added, drop by drop, at 0 °C to precipitate a pasty mass. Then methyl tosylate (12 mmol) in dry ether was added slowly to the mixture. After the reaction mixture had been stirred at room temperature for 5 h, the reaction mixture was washed with aqueous sodium chloride and dried over anhydrous magnesium sulfate. The ether was evaporated off, and the residue was distilled *in vacuo* to afford **4a**, which was identified with amino-exchange reaction product by means of VPC and the spectral data; yield, 34%.

ar-Turmerone (9). The title compound was obtained from **8d** and methylmagnesium iodide, and the product was identified with authentic sample by means of its spectral data;[6] yield, 28 %.

ar-Dihydroturmerone (14). By the treatment of **11d** with *p*-tolylmagnesium bromide, 2-*p*-tolyl-6-methyl-2-hepten-4-one (**13**) was prepared; yield, 24 %. Bp 70—75 °C/2 mmHg. NMR ($CDCl_3$): 0.92 (d, 6H, J=7.0 Hz), 2.0 (m, 1H), 2.3 (m, 2H), 2.34 (s, 3H), 2.47 (s, 3H), 6.35 (broad s, 1H), 7.04 (d, 2H, J=10.0 Hz), and 7.30 ppm (d, 2H, J=10.0 Hz). IR (liquid film): 2950, 1680, 1600, 1195, 1060, and 810 cm^{-1}. Found: C, 82.23; H, 9.20%. Calcd for $C_{15}H_{20}O$: C, 83.28; H, 9.32%. Compound **13** was hydrogenated on platinum in ethanol to afford Compound **14**; yield, 36 %. Bp 111—114 °C/6 mmHg. NMR (CCl_4): 0.90 (d, 6H, J=7.0 Hz), 1.16 (d, 3H, J=7.5 Hz), 2.06 (m, 3H), 2.27 (s, 3H), 2.48 (m, 2H), 3.21 (m, 1H), and 7.0 ppm (s, 4H). Found: C, 82.95; H, 10.25%. Calcd for $C_{15}H_{22}O$: C, 82.51; H, 10.16%.

The title compound was also obtained by the hydrogenation of **9** on platinum in ethanol; the two products were identical in their spectral data.

Targetone (12). The title compound was prepared from **11d** and vinylmagnesium bromide, and subsequently purified by distillation. The product was identified with an authentic sample by means of its spectral data.[8]

References

1) C. Kashima, S. Tobe, N. Sugiyama, and M. Yamamoto, *Bull. Chem. Soc. Jpn.*, **46**, 310 (1973).

2) E. Benary, *Chem. Ber.*, **64**, 2543 (1931); J. Ficinni and Normant, *Bull. Soc. Chim. Fr.*, **1964**, 1294.

3) C. Kashima, Y. Yamamoto, Y. Omote, and Y. Tsuda, *Bull. Chem. Soc. Jpn.*, **50**. 543 (1977).

4) C. Kashima, Y. Yamamoto, Y. Omote, T. Otsuka, and Y. Tsuda, *Heterocycles*, **4**, 1387 (1976).

5) C. Kashima, H. Aoyama, Y. Yamamoto, T. Nishio, and K. Yamada, *J. Chem. Soc., Perkin Trans. 2*, **1975** 665.

6) R. P. Gandhi, O. P. Vig, and S. M. Mukheji, *Tetrahedron*, **7**, 236 (1959); V. K. Honwad and A. S. Rao, *Tetrahedron*, **20**, 2921 (1964); K. S. Ayyor and G. S. K. Rao, *Can. J. Chem.*, **46**, 1467 (1968).

7) E. E. Boehm, V. Thaller, and M. C. Whiting, *J. Chem. Soc.*, **1963**, 2535.

8) A. Combes and C. Combes, *Bull. Soc. Chim. Fr.*, [3] **7**, 778 (1892).

The Hydrogen-transfer Reaction of a Diazo Compound Catalyzed by a Cobalt Complex

Kenji YOSHINO, Yasukazu OHKATSU, and Teiji TSURUTA*

Department of Synthetic Chemistry, Faculty of Engineering, University of Tokyo, Hongo, Bunkyo-ku, Tokyo 113

(Received September 27, 1978)

Acetophenone α-methylbenzylhydrazone was produced by the thermolysis of 1,1′-diphenylazoethane in the presence of a cobalt complex in benzene. In this reaction, the cobalt complex seemed to stabilize the radicals formed from the azo compound by the elimination of α-hydrogen. The stabilized radicals underwent 1,3-rearrangement to form acetophenone α-methylbenzylhydrazone. The driving force of this rearrangement is considered to be the nature of the cobalt atom, which prefers a bond formation with a more electronegative nitrogen atom to a carbon atom.

In our previous study,[1] it was found that scarcely no inner olefin 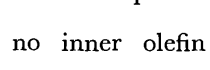 was produced by the thermolysis of 2,2′,3,3′-tetramethyl-2,2′-azodibutyronitrile in benzene, but the substance was produced in quantity in the presence of a cobalt complex such as Co(II)TPP. The mechanism for the formation of the inner olefin was explained by the following scheme:

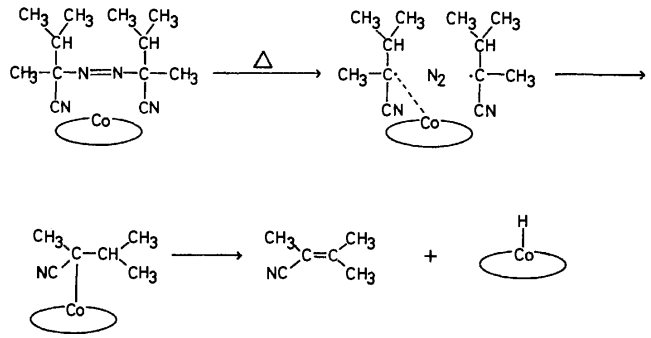

Scheme 1.

where the participation of Co(II)TPP was assumed in a certain hydrogen-transfer reaction.

A typical example of a hydrogen-transfer reaction catalyzed by a metal complex is a reaction in the co-enzyme vitamin B_{12}. Particularly, 1,2-hydrogen transfer processes from glycol to aldehyde catalyzed by diol dehydrase were studied; the co-enzyme B_{12} was established as playing an important role in the hydrogen-transfer reaction.[2]

The present paper reports that acetophenone α-methylbenzylhydrazone is produced from 1,1′-diphenylazoethane by thermolysis in the presence of a cobalt complex as a result of a hydrogen-transfer reaction (1,3-rearrangement). This reaction provides not only evidence for a possible interaction between a transition-metal complex and a free radical, but also a model for the rearrangement reaction of vitamin B_{12}.

Experimental

Syntheses of Azo Compounds. (*S*)-(−)-α-Methylbenzylamine and (*R*)-(+)-α-methylbenzylamine were obtained using the resolution method of Theilacker.[3]

The levorotatory amine: $\alpha_D^{23}=-38.2°$(neat) ($\alpha_D^{22}=-38.3°$).[3]

The dextrorotatory amine: $\alpha_D^{23}=+38.3°$(neat) ($\alpha_D^{22}=+37.16°$).[3]

(*S,S*)-(−)-1,1′-Diphenylazoethane (*SS*-Azo compound) was prepared according to the method of Green *et al.*[4]

$[\alpha]_D^{18}=-284.2°$ (453.8 mg/5 ml CCl_4) ($[\alpha]_D^{25}=-304.9°$ (35.8 mg/2 ml CCl_4)).[4]

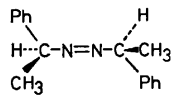 *SS*-Azo compound

(*R,R*)-(+)-1,1′-Diphenylazoethane (*RR*-Azo compound) was prepared by means of the procedure used in the case of the *SS*-Azo compound except for the use of (*R*)-(+)-α-methylbenzylamine in place of (*S*)-(−)-α-methylbenzylamine.

$[\alpha]_D^{18}=+288.8°$(156.8 mg/5 ml CCl_4)

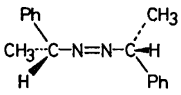 *RR*-Azo compound

meso-1,1′-Diphenylazoethane (*RS*-Azo compound) was prepared starting with racemic α-methylbenzylamine according to the procedure described above; when the reaction products (mixtures of *SS*, *RR*, and the *RS*-Azo compound) were allowed to stand in a refrigerator, crystals of the *RS*-Azo compound were formed. The crystals were recrystallized twice from ethanol; white prism crystals; mp 72.5—73.5 °C (72—73 °C).[4]

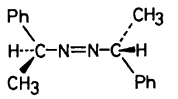 *RS*-Azo compound

Preparation of Metal Complexes. Tetraphenylporphyrin (H_2TPP) was prepared according to the method of Falk.[5] Cobalt(II) tetraphenylporphyrin [Co(II)TPP] was prepared according to the method of Rothemund and Menotti.[6] Ni(II)-TPP, Mn(II)TPP, and Cu(II)TPP were prepared using nickel(II) acetate, manganese(II) acetate, and copper(II) acetate, respectively, in place of cobalt(II) acetate.

(1*R*,2*R*)-*N*,*N*′-Disalicylidene-1,2-cyclohexanediaminatocobalt(II) [Co(II)(sal)$_2$(*R*-CHXDA)] was prepared according to the method of Aoi *et al.*[7] Ni(II)(sal)$_2$(*R*-CHXDA), Mn(II)-(sal)$_2$(*R*-CHXDA), and Cu(II)(sal)$_2$(*R*-CHXDA) were prepared using nickel(II) acetate, manganese(II) acetate, and copper(II) acetate, respectively, in place of cobalt(II) acetate.

Preparation of Acetophenone α-Methylbenzylhydrazone. A mixture of 1-bromo-1-phenylethane (50 g, 0.27 mol), 100 % hydrazine hydrate (103 g, 2.06 mol), triethylamine (50 ml), and benzene (100 ml) was refluxed for 6 h. The contents were then poured into an aqueous solution of sodium hydroxide

and extracted five times with 400 ml of diethyl ether. After drying over Na_2CO_3 and removing the ether, the resulting α-methylbenzylhydrazine was purified by distillation (64.5—66.0 °C/1.6 mmHg); yield, 31.2 g (78 %); IR: 3280 cm^{-1} (N–H); and PMR: 1.24 ppm (methyl), 3.16 ppm (N–H), 3.66 ppm (methine), and 7.25 ppm (phenyl).

A mixture of α-methylbenzylhydrazine (31.2 g, 0.211 mol), acetophenone (25.3 g, 0.211 mol), acetic acid (40 mg), and anhydrous ethanol (50 ml) was purged with nitrogen and then refluxed for 12 h. After the solvent had been removed, a pale yellow viscous liquid was obtained; yield, 50 g (94 %); IR: 3275 cm^{-1} (N–H) and 1597 cm^{-1} (C=N); PMR: 2.02 ppm (a), 1.56 ppm (b), 4.55 ppm (c), 7.25 ppm (d), 7.55 ppm (e), and 4.87 ppm (f); and GC-MS: *m/e* (rel intensity), 238 (parent peak, 0.6), 237 (2.9), 222 (3.8), 133 (2.3), 118 (2.9), 105 (100), 104 (2.4), and 92 (2.3).

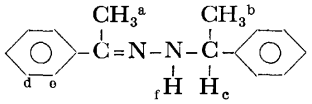

Decomposition of Azo Compound. A benzene solution of an Azo compound with or without a metal complex was charged into an ampoule and degassed twice by a freeze-thaw method to remove the oxygen; the ampoule was then sealed *in vacuo*. After standing at 104 °C in a light-shielded oil bath for 2 days, the contents of the ampoule were subjected to analysis.

Analysis of Decomposition Products. 2,3-Diphenylbutane was isolated from the decomposition products by using column chromatography (silica gel–hexane). It was identified by PMR: 1.01 ppm (methyl), 2.78 ppm (methine), and 7.20 ppm (phenyl); and GC-MS: *m/e* (rel intensity), 210 (parent peak, 1.1), 106 (9.5), 105 (100), 104 (25), 79 (4.4), and 77 (1.9).

It was not easy to isolate acetophenone α-methylbenzylhydrazone from the decomposition products because of the oxygen-sensitive nature of the hydrazone. Therefore, a reaction mixture was freeze-dried for six hours, and the remaining oily residue (C) was subjected to elemental analysis and PMR, GC-MS, and IR analyses. The oily residue (C) was found to be almost pure acetophenone α-methylbenzylhydrazone (purity 98 %, by GLC determination) when the thermolysis was carried out with the *RS*-Azo compound (512.1 mg) and Co(II)TPP (15.6 mg) in benzene (50 ml) at 104 °C. The PMR, GC-MS, and IR spectra of (C) agreed well with those of acetophenone α-methylbenzylhydrazone synthesized separately. Found: C, 80.76; H, 7.57; N, 11.09%. Calcd:** C, 80.57; H, 7.51; N, 11.65%.

Quantitative analyses of the products were carried out by means of GLC techniques using a column packed with Silicone DC-550. The column temperatures were 120 °C for ethylbenzene and styrene, 200 °C for 2,3-diphenylbutane, and 250 °C for acetophenone α-methylbenzylhydrazone. Benzene, the solvent, was used as the internal standard.

Measurement of Decomposition Rates. The decomposition rates of the azo compounds were measured in benzene using a differential pressure gauge at 70 °C. After the calculation of the rates, the vapor pressure of the benzene used as the solvent was corrected. AIBN: 3.7×10^{-5} mol l^{-1} s^{-1}, *SS*-Azo compound: 1.1×10^{-6} mol l^{-1} s^{-1}.

Measurement of ESR. The ESR of a benzene solution of the reaction mixture was measured under nitrogen at room temperature or at −196 °C. A benzene solution of Co(II)TPP and a mixture of Co(II)TPP and acetophenone α-methylbenzylhydrazone synthesized separately were measured in the manner described above.

Measurement of the Specific Rotation of the Hydrogen-transfer Product. The *SS*-Azo compound (3.67×10^{-2} M) was decomposed in the presence of Co(II)TPP (6.3×10^{-5}—1.56×10^{-4} M) in benzene at 104 °C. An optical rotation of the benzene solution containing decomposition products was measured using a 100 mm quartz cell at 20 °C. The optical rotation was reduced to optically active products, especially the hydrogen-transfer product, based on a quantitative analysis of the products by means of GLC.

Results and Discussion

General Aspects of Decomposition. The yield distribution of the thermolysis products from 1,1′-diphenylazoethane (Azo compound) with or without a metal complex are summarized in Table 1. The products from the Azo compound by thermolysis in the presence of a metal complex are identified as ethylbenzene, styrene, 2,3-diphenylbutane, and acetophenone α-methylbenzylhydrazone (called hereafter the hydrogen-transfer product).

The hydrogen-transfer product is resistant to heat (unchanged at 104 °C for 10 days) or light (unchanged for 60 min under UV light), but it is very sensitive to oxygen and turns to acetophenone and 1-phenylethanol when placed in contact with oxygen.[8] Table 1 shows that the hydrogen-transfer product is formed in the presence of a metal complex such as Co(II)TPP or Co(II)(sal)$_2$(*R*-CHXDA) (Scheme 2(b)), and that the yield is increased with an increase in the concentration of the metal complex. The Azo compound was changed into the hydrogen-transfer product almost quantitatively with 1 mol % of Co(II)TPP for the Azo compound. No hydrogen-transfer product is produced in the absence of the metal complex.

The mode of the decomposition of the Azo compound without a metal complex, on the other hand, is shown in Scheme 2(a).[9] The decomposition products are styrene, ethylbenzene, and 2,3-diphenylbutane derived from the 1-phenylethyl radical.

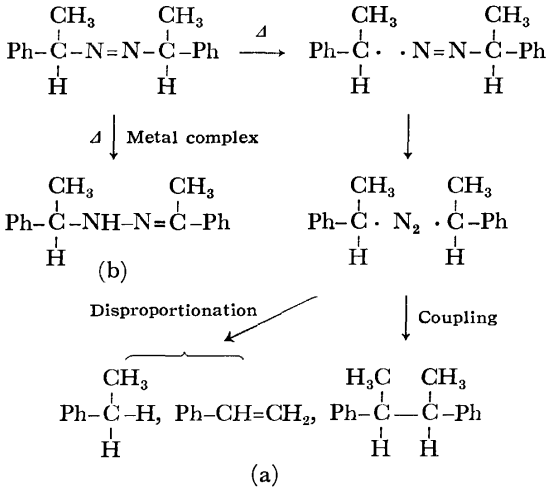

Scheme 2.

** The values calculated in consideration of Co(II)TPP (15.6 mg) and the hydrogen-transfer product (512.1 mg) contained in (C).

Table 1. Yields of products from 1,1′-diphenylazoethane by thermolysis in the presence of a metal complex

Azo compd ($\times 10^2$ M)	Cobalt complex ($\times 10^4$ M)	Co complex./Azo compd (molar ratio) ($\times 10^3$)	Products (%)			
			Ph–CH_2CH_3	Ph–CH=CH_2	Ph–C(CH_3)H–C(CH_3)H–Ph	Ph–C(CH_3)=N–NH–CH(CH_3)–Ph
SS 4.3	0	0	1.1	0.4	79.5	0
SS 4.3	CoTPP 0.38	0.88	0.7	0.6	36.5	59.8
SS 4.3	CoTPP 1.1	2.6	0.4	0.8	14.8	82.0
SS 4.3	CoTPP 3.4	7.9	0.3	1.7	5.9	91.1
SS 7.1	CoTPP 17	24	0.1	1.6	0	98.0
SS 4.7	Co* 11	23	2.0	1.3	50.8	29.5
SS 4.7	Co* 22	47	1.8	1.4	43.8	40.0
SS 6.7	Co* 40	60	2.0	1.8	55.9	41.1
SS 4.7	Co* 44	94	1.8	1.9	40.0	47.4
RR 4.6	Co* 11	24	2.0	1.3	52.2	25.1
RR 4.6	Co* 22	48	1.8	1.4	48.1	33.1
RR 4.6	Co* 44	96	1.8	1.9	46.8	35.1
RS 4.3	0	0	1.6	0.4	95.0	0
RS 3.7	CoTPP 3.0	8.1	0.4	1.6	6.4	89.5
RS 4.3	CoTPP 3.5	8.1	0.2	1.4	4.2	93.3
RS 5.3	CoTPP 6.4	12	0.1	1.8	0	98.0
RS 4.7	Co* 1.1	2.4	1.8	0.6	92.1	4.6
RS 4.8	Co* 2.3	4.7	2.0	0.7	91.2	8.4
RS 5.2	Co* 16	30	2.4	1.3	63.9	26.4
RS 5.6	Co* 23	41	2.4	1.4	68.4	18.5
RS 5.5	Co* 26	47	2.4	1.4	61.9	25.6
RS 4.5	Co* 52	114	2.1	2.4	43.2	45.8

Co*: Co(II)$(sal)_2$(*R*-CHXDA). Reaction Conditions: 104 °C, 2 days, in benzene (50 ml).

Stabilization of the Radical by Metal Complexes. The formation of the hydrogen-transfer product is not observed at room temperature, regardless of the presence of a metal complex in the reaction system. A comparison of the yield of the hydrogen-transfer product from the *SS*-Azo compound with Co(II)TPP in the presence and in the absence of AIBN at 70 °C is shown in Fig. 1. The rates of the decomposition reaction at 70 °C were found to be 3.7×10^{-5} M s^{-1} for AIBN and 1.1×10^{-6} M s^{-1} for the *SS*-Azo compound, AIBN being decomposed 34 times more rapidly than the *SS*-Azo compound. The radical concentration in the reaction system with AIBN should be much higher than that in the system without AIBN. As may be seen in Fig. 1, the rate of the formation of the hydrogen-transfer product is very high in the reaction system containing AIBN (A). This shows that a radical formation is necessary for the formation of the hydrogen-transfer product.

Table 2 shows the influence of the central metal and its ligand on the yield of the hydrogen-transfer product. The yields of the hydrogen-transfer product decreased in this order; Co>Ni>Mn>Cu, and TPP>$(sal)_2$(*R*-

Table 2. Influence of the central metal of the complexes on the yield of the hydrogen-transfer product

SS-Azo compd ($\times 10^2$ M)	Metal complex ($\times 10^3$ M)	Products (%)			
		Ph–CH_2CH_3	Ph–CH=CH_2	Ph–C(CH_3)H–C(CH_3)H–Ph	Ph–C(CH_3)=N–NH–CH(CH_3)–Ph
8.45	CoTPP 8.04	0.2	1.4	8.9	88.0
8.45	NiTPP 8.04	0.5	0.3	34.7	53.6
8.45	MnTPP 8.10	0.9	0.4	60.8	41.3
8.45	CuTPP 8.00	1.2	1.2	91.5	3.2
4.3	Co* 13.2	2.0	1.3	48.8	34.6
4.3	Ni* 10.6	0.8	0.8	92.2	1.3
4.3	Mn* 15.5	0.8	1.0	90.6	1.0
4.3	Cu* 10.4	0.8	0.8	94.3	0.8

Co*, Ni*, Mn*, Cu*: Co(II), Ni(II), Mn(II), Cu(II)$(sal)_2$(*R*-CHXDA).
Reaction conditions: 104 °C, 2 days, in benzene (50 ml).

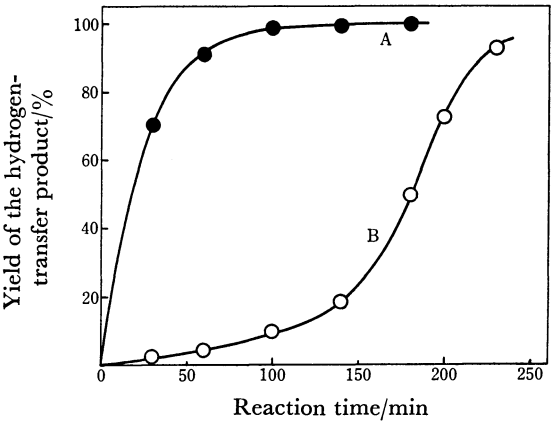

Fig. 1. Effect of AIBN on amount of acetophenone α-methylbenzylhydrazone formed.

	A	B
SS-Azo compd	8.9×10^{-2} M	8.4×10^{-2} M
Co(II)TPP	6.0×10^{-4} M	5.3×10^{-4} M
AIBN	2.1×10^{-2} M	0 M

Reaction Conditions: at 70 °C in benzene.

CHXDA). This order is in good agreement with that of the ability of metal complexes to stabilize 1-cyano-1,2-dimethylpropyl radical ($CH_3\dot{C}(CN)CH(CH_3)_2$), Co(II)-TPP>Ni(II)TPP>Mn(II)TPP>Cu(II)TPP.[1] It may be supposed that the α-hydrogen of the Azo compound is easily abstracted by a radical. By the elimination of the α-hydrogen, Ph–$\dot{C}(CH_3)$–N=N–$CH(CH_3)$–Ph (I) is produced as is shown below:

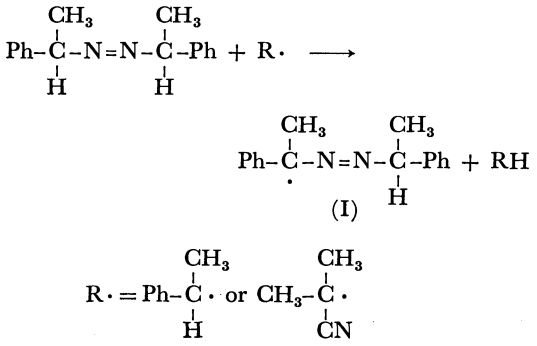

It is considered that the dependence of the yield of the hydrogen-transfer product on kinds of metal complex is attributable to degree of interaction between radical(I) and the metal complex, that is, the stability of the intermediate(II) formed in the reaction system.

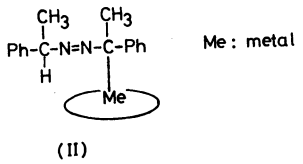

(II)

The ESR spectra of a reaction mixture which contains decomposition products from the *SS*-Azo compound in the presence of Co(II)TPP are shown in Fig. 2. A peak of Co^{II} was observed when the reaction mixture was measured at room temperature (a). At −196 °C, on the other hand, a characteristic octet of Co^{II} was observed, and each peak was split into a triplet, indicating the N–Co^{II} bond (b). Furthermore, a very small peak ($g=2.001_2$) was observed at −196 °C; the intensity of this peak increased upon irradiation with UV light (c). It is considered that the peaks in Figs. 2(a) and 2(b) are attributable to an intermediate(III) which has a cobalt nitrogen bond, while the peak in Fig. 2(c) is attributable to a radical(IV) formed possibly by the cleavage of the cobalt-nitrogen bond of the intermediate(III), as is shown below:

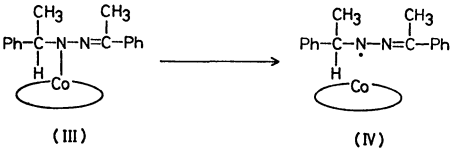

(III) (IV)

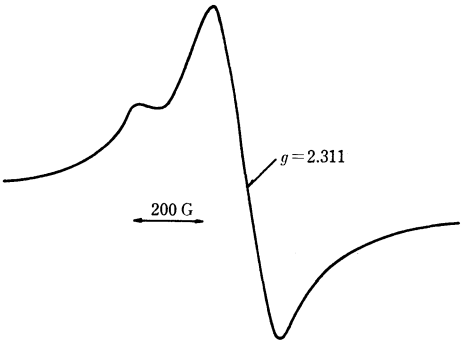

Fig. 2(a). ESR spectrum of reaction mixture of *SS*-Azo compound in the presence of Co(II)TPP at room temperature.

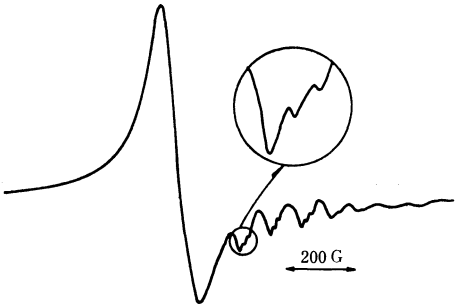

Fig. 2(b). ESR spectrum of reaction mixture of *SS*-Azo compound in the presence of Co(II)TPP at −196 °C.

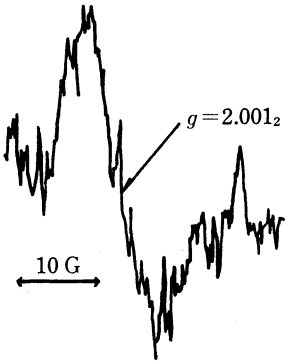

Fig. 2(c). ESR spectrum of reaction mixture of *SS*-Azo compound in the presence of Co(II)TPP at −196 °C.

In this connection, it should be noted that carbon-cobalt bond of alkyl cobalamine or vitamine B_{12} is cleaved by UV light.[10]

No peaks were observed, at room temperature, for either the benzene solution of Co(II)TPP only, or the benzene solution of Co(II)TPP and the hydrogen-transfer product synthesized separately. This means that the peaks in Fig. 2 can not result from an interaction of Co(II)TPP and the hydrogen-transfer product.

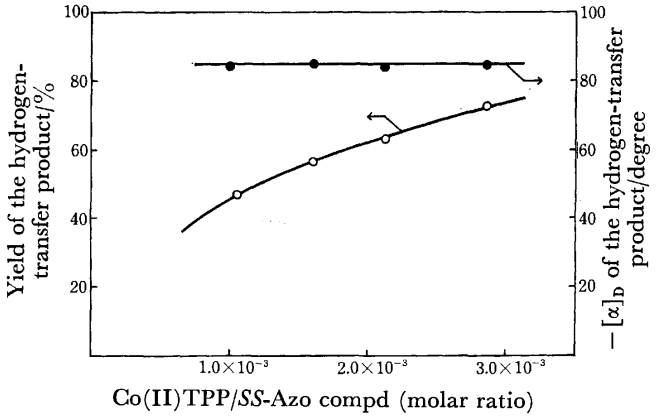

Fig. 3. Yield and specific rotation of the hydrogen-transfer product obtained from *SS*-Azo compound in the presence of Co(II)TPP in benzene at 104 °C for 2 days.

Stereochemistry of Acetophenone α-Methylbenzylhydrazone. The specific rotation of the hydrogen-transfer product, which was obtained from the *SS*-Azo compound by thermolysis in the presence of Co(II)TPP, was almost constant ($[\alpha]_D=-88°$), regardless of its yield (Fig. 3). This means that the configuration of one of the two asymmetric carbons of the original *SS*-Azo compound is probably retained in the hydrogen-transfer product.

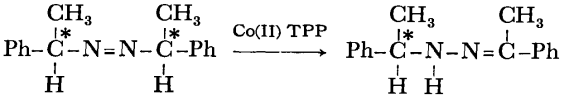

A Possible Mechanism:

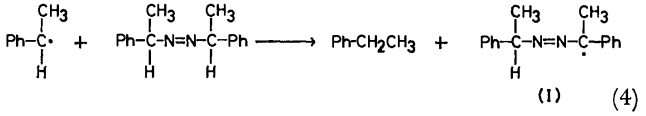

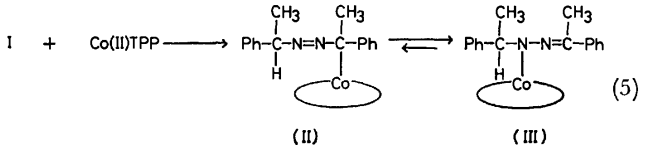

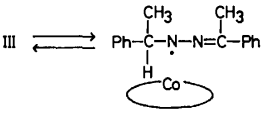

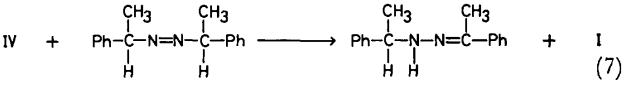

Scheme 3 is a step in which radicals are released by thermolysis. In the beginning, the concentration of the radical is very low; therefore, scarcely no coupling and disproportionation reactions of the diffusion radicals occurs, and the diffusion radical formed abstracts the α-hydrogen of the Azo compound (Scheme 4). The radical(I) thus formed is immediately stabilized by a cobalt complex (Scheme 5) or abstracts the α-hydrogen from another Azo compound to form the radical(I) again. However, the latter mechanism is not probable in the light of the results shown in Fig. 3. The intermediate(II) undergoes a rearrangement reaction to the intermediate(III), in which a nitrogen-cobalt bond is newly formed. The intermediates(II) and (III) are presumably equilibrated with each other (Scheme 5). The existence of the intermediate(III) is suggested by the results of the ESR spectra, shown in Fig. 2. The series of steps from Scheme 4 to Scheme 7 is a chain reaction.

The authors would like to express their thanks to Professor Shohei Inoue for giving useful advice.

References

1) K. Yoshino, Y. Ohkatsu, and T. Tsuruta, *Polym. J.*, **9**, 275 (1977).
2) R. B. Silverman and D. Dolphin, *J. Am. Chem. Soc.*, **98**, 4626 (1976).
3) W. Theilacker and H.-G. Winkler, *Chem. Ber.*, **87**, 690 (1954).
4) F. D. Greene, M. A. Berwick, and J. C. Stowell, *J. Am. Chem. Soc.*, **92**, 867 (1970).
5) J. E. Falk, "Porphyrins and Metalloporphyrins," Elsevier, Amsterdam (1964).
6) P. Rothemund and A. R. Menotti, *J. Am. Chem. Soc.*, **70**, 1808 (1948).
7) H. Aoi, M. Ishimori, S. Yoshikawa, and T. Tsuruta, *J. Organomet. Chem.*, **85**, 241 (1975).
8) K. Yoshino, Y. Ohkatsu, and T. Tsuruta, *Chem. Lett.*, **1978**, 915.
9) S. Seltzer and F. Dunne, *J. Am. Chem. Soc.*, **87**, 2628 (1965).
10) T.H. Finlay, J. E. Valinsky, A. S. Mildram, and R. H. Abeles, *J. Biol. Chem.*, **248**, 1285 (1973).

Temperature Effects on the Stereochemistry of the Solvolysis of *trans*-2,3-Diphenyloxirane†

Masashi INOUE, Yoshio TAGUCHI, Toshio SUGITA, and Katsuhiko ICHIKAWA*

Department of Hydrocarbon Chemistry, Faculty of Engineering, Kyoto University, Yoshida, Kyoto 606

(Received November 8, 1978)

The temperature effects on the stereochemistry of the acid-catalyzed ethanolysis of *trans*-2,3-diphenyloxirane were examined. The stereochemistry of the reaction became more retentive as the reaction temperature was raised. The reaction mechanisms are discussed, and it is concluded that concurrent reactions take place in the ethanolysis, one of them giving an inverted product, and the other, a retained one, and that the former reaction is caused by a nucleophilic attack of ethanol on the carbon of the conjugate acid of the epoxide, while the latter proceeds *via* an intermediate which has a carbonium-ion character.

Nucleophlic ring-opening reactions of epoxide have been widely studied.[1] It is now generally accepted that epoxides react by means of an S_N2 mechanism under basic conditions. The mechanism of the ring opening of epoxides in acidic media is, however, quite a complex matter. The initial protonation to the epoxide oxygen atom is recognized as a fast, reversible step.[2] In the limiting form, two mechanisms are possible for the ring opening and the attack of the nucleophile, *i.e.*, *A*1 and *A*2 mechanisms. As the attacking nucleophile is the solvent in the solvolyses, though, both mechanisms lead to the same rate expression. Thus, alternative criteria have been used. They have been carefully discussed by Chapman and his coworkers.[3] Long *et al.*,[4] following a suggestion by Taft and his coworkers,[5] proposed the use of ΔS^* as a criterion for the mechanism of a hydrolytic reaction. The entropies of activation for the acid-catalyzed hydrolysis of simple epoxides are between -6.1 and -3.9 cal mol^{-1} K^{-1},[6] much lower than those of the reactions of the established *A*1 mechanism and yet greater than those of the established *A*2 mechanism; these values can be explained in terms of a borderline *A*2 mechanism.[1a,7]

A nucleophilic attack by an *A*2 mechanism involves complete inversion of configuration, whereas an *A*1 mechanism involves racemization in the limiting form. It is generally recognized that simple aliphatic epoxides give inverted products in acid-catalyzed ring opening.[1a] The only exception is the reaction of *cis*- and *trans*-2,3-dimethyloxirane with aluminum chloride in nitromethane, which yields more than 85% retained 3-chloro-2-butanol.[8]

In aryl- or carbonyl-substituted epoxides, reactions are known in which epoxides ring-open with retention of configuration at the position attacked. In a few epoxides, ring openings give rise to both stereoisomeric products. Parker and Isaacs concluded that concurrent S_Ni and S_N2 mechanisms take place in reactions of this type.[1a]

Recently Chapman and his coworkers have studied the acid-catalyzed ethanolysis of 2-phenyloxirane both kinetically and stereochemically.[3,9] The reaction yielded a mixture of 89% inverted and 11% retained products at 23 °C. They explained their observation by only a borderline *A*2 mechanism involving the transition states depicted in Scheme 1. Obviously, the two transition states, which have different situations around

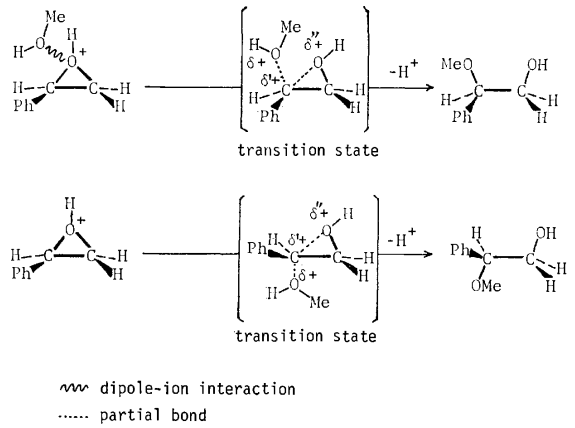

Scheme 1.

the carbon atom attacked by ethanol, are different in energy. Therefore, the reaction parameters, activation enthalpy and activation entropy, are different for the two reactions, one of which yields a retained product, while the other gives an inverted one. As the two reactions have different activation parameters, it is ridiculous to discuss the two reactions in terms of a single pair of ΔH^* and ΔS^*. The stereochemical outcome must also be altered by the variation in the reaction temperatures. They did not, however, explore the temperature effects on stereochemistry.

Although a number of papers, including those of Chapman *et al.*, have discussed the temperature effects on reaction kinetics, *i.e.*, activation parameters, only a few papers have dealt with the effects on stereochemistry. Even so, two contrasting results have appeared in the literature. Fisher and Koch reported the acid-catalyzed hydrolysis of *trans*- and *cis*-2-methyl-3-phenyloxiranes in aqueous dioxane.[10] The reaction afforded 67% inverted and 33% retained glycols from the trans epoxide and 76% inverted and 24% retained ones from the cis isomer, and the stereochemistry of the reaction did not change in the temperature range of 20—45 °C. From these results, one can expect that the reaction has only one transition state, yielding both retained and inverted products.

On the other hand, Macchia *et al.* reported that the acid-catalyzed solvolysis of 1-aryl-1,2-epoxycyclohexane afforded larger amounts of the retained product at higher reaction temperatures.[11] From this observation,

† Taken from Ph D. thesis of M. I.

one can expect that concurrent reactions take place, one of which leads to a inverted product, and the other, to a retained one.

A previous paper has described the co-solvent effects on the stereochemistry of the ethanolysis of *trans*-2,3-diphenyloxirane (**1**). In that paper, we reported that the steric course of the reaction can be controlled from 85% retention–15% inversion (nitromethane: ethanol= 20: 2 by volume) to 10% retention–90% inversion (HMPA: ethanol=10: 12) by the choice of co-solvent.[12] This paper will report the temperature effects on the stereochemistry of the ethanolysis of **1** and will discuss the mechanism of the reaction.

Results and Discussion

In the study of the stereochemistry of the acid-catalyzed ethanolysis of **1** in the temperature range below the boiling point of ethanol, the same experimental conditions as in the previous paper were chosen. The results are summarized in Table 1. The reaction products were *threo*-2-ethoxy-1,2-diphenylethanol (*threo*-**2**, the retained product), the erythro isomer (*erythro*-**2**, the inverted product), 1,1-diethoxy-2,2-diphenylethane (**3**), and benzophenone (**4**, an oxidized product of diphenylacetaldehyde (**5**) in the course of the work-up); the identification and an outline of the sequence of the formation of these products have already been presented in the previous paper. As is shown in Table 1, the proportion of the retained product *threo*-**2** increased as the reaction temperature was raised. Similar temperature effects were observed in the experiments in binary solvent systems.

To examine the stereochemistry of the reaction at temperatures higher than the boiling point of ethanol, experiments were carried out in an autoclave. Unexpectedly, sulfuric acid, which was used as a catalyst in the experiments listed in Table 1 and in those of the previous paper, has no catalytic activity in the temperature range higher than 130 °C; only the starting material, **1**, accompanied by traces of 1,2-diphenylethanol (**6**) and 2,2-diphenylethanol (**7**), 1,2-diphenyl-2-hydroxyethanone (**8**), and/or diphenylethanedione (**9**), was detected on GLC analysis when an ethanolic solution of **1** containing sulfuric acid was allowed to stand at 200 °C for 4 h. This observation may be attributed to the facts that sulfuric acid acts as an oxidizing agent and that the reduced material of sulfuric

Table 1. Temperature effects on the ethanolysis of *trans*-2,3-diphenyloxirane (**1**)[a]

Reaction temp (°C)	Solvent	Product distribution (%)				Retention[b] (%)
		3	**4**	*threo*-**2**	*erythro*-**2**	
30	EtOH	8	tr	18	74	20
50	EtOH	12	tr	23	65	26
70	EtOH	16	tr	26	58	31
50	EtOH–CH_3CN (46: 54, vol)	9	15	36	40	48
70	EtOH–CH_3CN (46: 54, vol)	18	12	37	33	53

a) The experimental conditions were described in a previous paper (Ref. 12).
b) The proportion of *threo*-**2** to the total **2**.

Table 2. Typical results of acid-catalyzed ethanolysis of *trans*-2,3-diphenyloxirane at high temperatures

Temp (°C)	Time (h)	Acid[c] (μl)	Product distribution[a] (%)								Retention (%)
			1	**3**	**4**	*threo*-**2**	*erythro*-**2**	**11**	**10**	Others[b]	
90±2	4	100	37.3	0.4	1.1	18.5	41.7	0.6			29.6
103±1	4	100	29.2	1.3	1.0	22.9	45.1	0.5			33.7
120±3	3.5	100	22.1	3.2	2.3	27.1	43.8	0.6		0.1	38.9
130±2	3	100	17.9	5.0	1.1	30.7	44.7	0.6		tr	40.7
140±1	3	80	18.9	5.5	1.3	30.7	42.6	0.7			41.9
149±1	2	100	19.8	6.1	0.5	30.7	42.9	tr			41.3
165±1	2	100	5.7	16.1	0.8	30.9	39.5	1.1	5.9		43.9
190±4	2	75	22.0	4.3	3.6	30.3	36.2	3.2		0.4	45.6
206±3	2	20	57.6	0.2	4.9	13.9	14.8	5.7		2.6	48.4
220±3	2	50	28.5	3.0	3.2	28.3	29.4	3.9	1.2	2.1	49.1
130±2	3	200	0.4	10.6	0.5	28.0	50.9	0.4	9.2		35.5
130±2	3	150	0.7	15.3	0.4	28.6	48.3	0.4	6.3		37.2
130±2	3	80	25.5	2.7	1.7	28.1	41.0	0.8		0.2	40.7
130±2	3	50	49.3	0.3	1.4	19.7	28.6	0.7			40.8
130±2	3	30	68.9	0.1	0.8	12.2	17.7	0.6			41.3

a) Determined by the relative area ratio on GLC. b) The oxidation-reduction products, **6**, **7**, **8**, and **9**. c) Hydrochloric acid (*ca.* 0.005 mol/l) in ethanol was added to 1 ml of an ethanolic solution containing 10 mg of **1**.

acid has no catalytic activity toward the ethanolysis. Therefore, hydrochloric acid was used as the catalyst for the experiments at higher reaction temperatures. Some typical results are given in Table 2. As is shown in Table 2, larger proportions of the retained product were observed at higher temperatures, and almost equal amounts of retained and inverted products were formed at 200 °C. Although it is interesting whether or not the proportion of the retained product increases monotonously at more higher temperatures, no clear-cut results could be obtained because of the formation of undesired products, *i.e.* rearranged products (**3**, **5**, 1,2-diphenyl-1-ethoxyethylene (**10**), and benzyl phenyl ketone (**11**)) and oxidation-reduction products (**6**, **7**, **8**, and **9**). It must be noted that the yield of **11** increased suddenly at higher than 160 °C; **11** has previously been reported not to be formed in the rearrangement by acid.[13]

Higher acid concentrations gave more inverted product; this forms a striking contrast to the results mentioned in the previous paper, in which we reported that the stereochemical outcome of the sulfuric acid-catalyzed ethanolysis of **1** at ordinary temperatures was not affected by the variation in the acid concentration. Four reasons for this can be considered: **a** the effects of a trace of water contaminating the acid solution; **b** the contamination of the non-acid-catalyzed reaction which yields the retained product; **c** the formation of chlorohydrin, or the subsequent ethanolysis of the chlorohydrin, and **d** the effects of the ion-pairing of the acid. To examine the effects of water, reactions were carried out with small amounts of water added. The results are shown in Fig. 1. As the proportion of the retained product increased with an increase in the amount of water added, the **a** reason can be excluded. The **b** reason can also be easily excluded because no reaction occurred without an acid catalyst. The **c** reason was recently proposed by Whalen *et al.* as the specific effects of chloride ion in the hydrolysis of phenanthrene 9,10-oxide;[14] it cannot be completely excluded in the present case, though no chlorohydrin was detected in the reaction products and the chloride-ion concentrations are a hundred times smaller than those of **1**. The **d** reason was proposed by Wylde and his coworkers;[15] it seems to be the most probable explanation in the present case. As the counter anion exists near the protonated oxygen in the ion pair of protonated epoxide and chloride, the probability of the existence of ethanol in the front side of the epoxide ring decreases as compared with that in free ion, and an inversion reaction is favored by the ion pair. As the dilution of the acid solution causes the ion pair to dissociate into free ions, the reaction becomes more retentive with a lowering in the acid concentration.

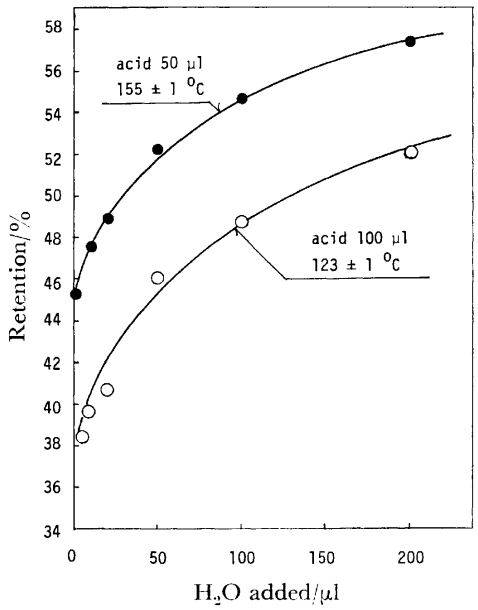

Fig. 1. Effects of water on ethanolysis of *trans*-2,3-diphenyloxirane.

As the stereochemistry of the ethanolysis is affected by the reaction temperatures, two reaction are expected to take place in the ethanolysis. If Parker-Isaacs' conclusion is true, the overall kinetical expression is as follows:

$$k_{obsd} = k'K[H^+] = (k_{ret}+k_{inv})K[H^+]$$

in which k_{ret} is a second-order rate constant for the reaction which gives the retained product, while k_{inv} is that for the inversion reaction. The pre-equilibrium constant between **1** and the oxonium ion is presented as K. Then, the reaction parameters for each of the reactions can be defined as[16]

$$k_{ret} = \gamma \exp\left(\frac{-\Delta G^{\ddagger}_{ret}}{RT}\right) = \exp\left(\frac{T\Delta S^{\ddagger}_{ret}-\Delta H^{\ddagger}_{ret}}{RT}\right)$$

$$k_{inv} = \gamma' \exp\left(\frac{-\Delta G^{\ddagger}_{inv}}{RT}\right) = \exp\left(\frac{T\Delta S^{\ddagger}_{inv}-\Delta H^{\ddagger}_{inv}}{RT}\right).$$

Therefore,

$$\frac{k_{ret}}{k_{inv}} = \frac{\gamma}{\gamma'} \exp\left(\frac{\Delta S^{\ddagger}_{ret}-\Delta S^{\ddagger}_{inv}}{R}\right) \exp\left(-\frac{\Delta H^{\ddagger}_{ret}-\Delta H^{\ddagger}_{inv}}{RT}\right)$$

Assuming that the activation parameters are constant in the temperature range of the experiments, the following equation can be deduced:

$$\ln\left(\frac{k_{ret}}{k_{inv}}\right) = -\frac{\Delta H^{\ddagger}_{ret}-\Delta H^{\ddagger}_{inv}}{RT} + \text{Const.}$$

If two reactions have the same reaction order, which was proved to be the case by the constancy of the stereochemical outcomes with the variation in the reaction times, the ratio of the two rate constants, k_{ret}/k_{inv}, can be substituted for the ratio of the two reaction products, *threo*-**2**/*erythro*-**2**. Therefore, a straight line should be obtained if $\ln$(*threo*-**2**/*erythro*-**2**) is plotted *vs.* $1/T$; the results are shown in Fig. 2. From the results, $\Delta H^{\ddagger}_{ret} > \Delta H^{\ddagger}_{inv}$ and $\Delta S^{\ddagger}_{ret} > \Delta S^{\ddagger}_{inv}$ are obtained. The enthalpic factor favors the formation of the inverted product, whereas the entropic factor favors the retention reaction.

Macchia *et al.* proposed the mechanism shown in Scheme 2 for the acid-catalyzed solvolysis of 1-aryl-1,2-epoxycyclohexanes.[11] However, we cannot agree with their mechanism in view of the following considerations: (1) the entropy of the transition state, **12**, is expected to be equal to, or smaller than, that of **13**, because **12** involves a molecule of ethanol and (2) the enthalpy of

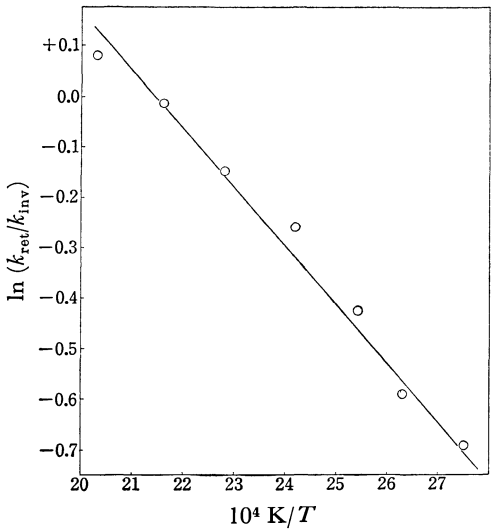

Fig. 2. Plot of $\ln(k_{ret}/k_{inv})$ *vs.* $1/T$ for the ethanolysis of *trans*-2,3-diphenyloxirane.

12 is expected to be smaller than that of **13**, because hydrogen bonding from the ethanol involved in the transition state to the oxygen of the epoxide supplies an additional stabilization energy to **12**. Both suppositions are contrary to the observations.

Bruice *et al.* examined the temperature effects on the product distribution of the hydrolysis of phenanthrene

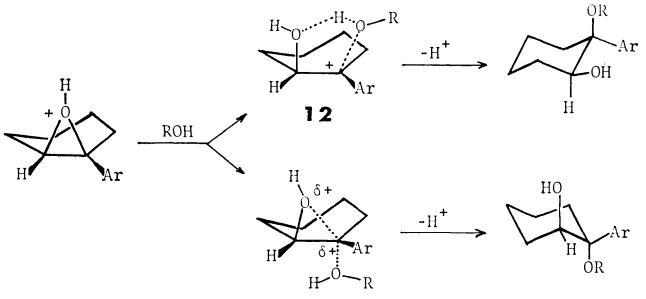

Scheme 2.

9,10-oxide[18] and reported those relative activation parameters: $\Delta H^{\neq}_{ret}-\Delta H^{\neq}_{inv}=2.05$ kcal mol^{-1} and $\Delta S^{\neq}_{ret}-\Delta S^{\neq}_{inv}=5.0$ cal deg^{-1} mol^{-1}. They explained their observations in terms of an S_N1 mechanism. The energy difference, 2.05 kcal mol^{-1}, however, seems to be rather large for the fast reaction step after the rate-determining formation of a carbonium ion.

A possible mechanism for the reaction is shown in Scheme 3, in which (A) is the conjugate acid of the epoxide and (C) is a completely developed carbonium ion. The intermediate (B) is considered to be in a circumstance in which *p*-obital of the carbon is solvated by the intramolecular hydroxyl group. As the broken C–O bond provides more freedom to the system, the reaction which yields the retained product should have a lower activation entropy than the reaction yielding the inverted product.

Finally, we shall discuss briefly the rearrangement of **1**. Blum *et al.* reported that $Rh_2(CO)_4Cl_2$ catalyzed rearrangement of **1** gave 8% of **11**, 25% of **5**, 11% of diphenylmethane, 12% of 1,2-diphenylethylene, and 18% of *cis*-2,3-diphenyloxirane after 2 h at 210 °C, while the same catalyst gave 25% of **5**, 5% of 1,2-diphenylethylene, and 65% of unchanged **1** without **11** after 5 h in boiling benzene.[18] These results, together with the results shown in Table 2, indicate that the predominant factor affecting the rearranged-product distribution is the reaction temperature, and that high reaction temperatures favor the formation of **11**. These observations may be explained by Pearson's HSAB principle.[19] At low temperatures C–O bond breaking is assisted by the more polarizable (softer than hydride) phenyl group, resulting in phenyl migration to give **5**. On the other hand, the fully developed carbonium ion formed at a high temperature is attacked by the more electronegative (harder) hydride ion, since the positive charge of the cation is easily neutralized by the electron density of the hydride ion.

Experimental

The materials and analytical methods have been described in a previous paper.[12]

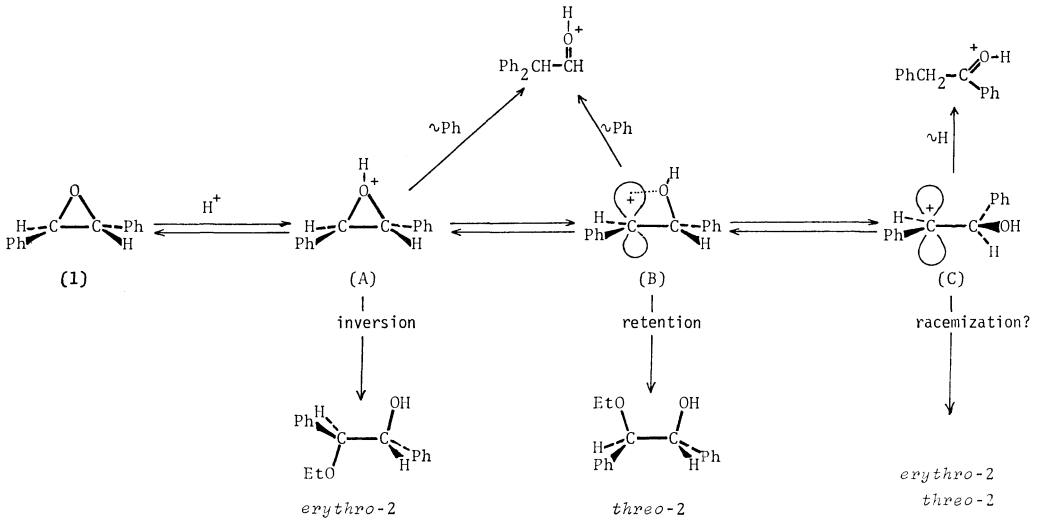

Scheme 3.

Ethanolysis of **1** *in an Autoclave.* To a 1-ml portion of an ethanolic solution containing 10 mg of **1**, a definite volume of hydrochloric acid in ethanol (*ca.* 0.005 mol/l) was added. The reaction mixture was then shaken vigorously, set in an autoclave, and heated to the desired temperature. Ten minutes usually (and thirty minutes at the longest) were required to arrive at the reaction temperature. After an appropriate time interval at that temperature, the mixture was cooled and poured into sampling tube containing a small amount of potassium carbonate. The quenched sample was then kept at room temperature for a day and analyzed by GLC.

Isolation of the Product. To a mixture of 206.4 mg of **1** and 20 ml of ethanol, 0.5 ml of ethanolic hydrochloric acid (*ca.* 0.005 mol/l) was added. The reaction mixture was then shaken vigorously, set in an autoclave, and heated to 240 °C. Thirteen minutes were required to arrive at that temperature; the autoclave was then held at that temperature (237—260 °C) for 3 h. To the cooled reaction mixture, a portion of potassium carbonate was added. The filtered mixture was washed with water, and the aqueous layers were extracted with ether. After the removal of the solvent, the dried product was chromatographed on an $8\phi \times 720$ mmH silica-gel column under a 1-m head of elutant (hexane, hexane–benzene and benzene–diethyl ether successively, with concentration gradients). The products (in the order of elution) and the yields were as follows: **10** (0.4%), recovered **1** (4%), **5** (9%), **4** (8%), **9** (0.5%), **3** (2%), **8** (0.3%), **6** (3%), **2** (50%), and **7** (3%).

The authors wish to thank Professor Kunio Okamoto of this Department for his critical discussion.

References

1) a) R. E. Parker and N. S. Isaacs, *Chem. Rev.*, **59**, 737 (1959); b) A. Rosowsky, "Heterocyclic Compounds with Three- and Four-Membered Rings," Part 1, ed by A. Weissberger, Interscience, New York (1964), p. 1.

2) J. G. Pritchard and F. A. Long, *J. Am. Chem. Soc.*, **78**, 6008 (1956).

3) J. Biggs, N. B. Chapman, A. F. Finch, and V. Wray, *J. Chem. Soc., B*, **1971**, 55.

4) F. A. Long, J. G. Pritchard, and F. E. Stafford, *J. Am. Chem. Soc.*, **79**, 2362 (1957); L. L. Schaleger and F. A. Long, *Adv. Phys. Org. Chem.*, **1**, 1 (1963).

5) R. W. Taft, Jr., *J. Am. Chem. Soc.*, **74**, 5374 (1952); R. W. Taft, Jr., E. L. Purlee, P. Riesz, and C. A. DeFazio, *ibid.*, **77**, 1584 (1955).

6) Long *et al.* themselves concluded from the results that ring epening proceeds by means of an *A*l mechanism.

7) Parker-Isaacs' conclusion was criticized again; J. G. Pritchard and I. A. Siddiqui, *J. Chem. Soc., Perkin Trans. 2*, **1973**, 452.

8) M. Inoue, T. Sugita, Y. Kiso, and K. Ichikawa, *Bull. Chem. Soc. Jpn.*, **49**, 1063 (1976).

9) L. Biggs, N. B. Chapman, and V. Wray, *J. Chem. Soc., B*, **1971**, 63, 66, and 71.

10) F. Fisher and H. Koch, *Chem. Ber.*, **99**, 2000 (1966).

11) C. Battistini, P. Crotti, and F. Macchia, *Tetrahedron Lett.*, **1975**, 2091.

12) M. Inoue, Y. Taguchi, T. Sugita, and K. Ichikawa, *Bull. Chem. Soc. Jpn.*, **51**, 2098 (1978).

13) H. O. House, *J. Am. Chem. Soc.*, **77**, 3070 (1955).

14) D. L. Whalen, A. M. Ross, P. M. Dansette, and D. M. Jerina, *J. Am. Chem. Soc.*, **99**, 5672 (1977).

15) G. Lamaty, R. Maleq, C. Selve, A. Sivade, and J. Wylde, *J. Chem. Soc., Perkin Trans. 2*, **1975**, 1119.

16) The vapor pressure of ethanol at 230 °C is 50 atm. The pressure effects on the reaction kinetics are ignored, since they are rather small in the pressure range of these experiments.

17) P. Y. Bruice, T. C. Bruice, P. M. Dansette, H. G. Selander, H. Yagi, and D. M. Jerina, *J. Am. Chem. Soc.*, **98**, 2966 (1976).

18) D. Milstein, O. Buchman, and J. Blum, *Tetrahedron Lett.*, **1974**, 2257; *J. Org. Chem.*, **42**, 2299 (1977).

19) R. G. Peason, *J. Chem. Educ.*, **45**, 581 (1968).

Modified Preparation of Sodium Guaiazulenide and Reaction of the Reagent with 3-Formylguaiazulene

Shinji KUROKAWA

Department of Chemistry, Faculty of Education, Saga University, Honjo-machi, Saga 840

(Received November 10, 1978)

As a modification for facilitating small-scale reactions, sodium *N*-methylanilinide was prepared from sodium hydride and *N*-methylaniline instead of by the usual method from sodium, *N*-methylaniline, and naphthalene (as assistant). Sodium *N*-methylanilinide, made by this procedure, was successively converted to sodium guaiazulenide, the formation of which was checked by tracing known reactions. The reaction of the reagent with 3-formylguaiazulene was also studied, and found to yield 4-substituted 2-formyl-1,4-dihydroguaiazulene and 6-substituted 2-formyl-3,6-dihydroguaiazulene. In this case, nucleophilic addition of guaiazulenide anion occured not at the carbonyl group but at the 6- and 8-positions of the seven-membered ring of formylguaiazulene, accompanied by formyl group and hydrogen migrations.

In the previous paper we reported that 1-[2-(4-azulenyl)vinyl]azulene and 1-[2-(1-azulenyl)vinyl]-azulene derivatives were formed by thermolysis of 3-formylguaiazulene (**9**).[1] One of the skeletal hydrocarbons, 1-[2-(1-azulenyl)vinyl]azulene, has already been synthesized from azulenylmethylphosphonium salt and formylazulene.[2]

As a means of access to hitherto unknown 1-[2-(4-azulenyl)vinyl]azulene, the reaction of sodium guaiazulenide (**1**) with **9** was studied, since the reaction was thought, if followed by dehydration of the resulting alcohol, to be a possible route to 1-[2-(7-isopropyl-1-methyl-4-azulenyl)vinyl]guaiazulene.[3,4]

Sodium *N*-methylanilinide, used for preparation of **1**,[3] is usually made from sodium wire and *N*-methylaniline, using naphthalene as an assistant.[5] However, the procedure was not satisfactory for our purpose of small-scale experiments, due to the technical problem of how to make such fine wires as would allow a fairly smooth reaction with a millimol-order quantity of *N*-methylaniline. For this reason, the sodium hydride available as fine powder (as oil mull) was used instead of sodium metal, without the aid of the assistant, for the preparation of **1** in this paper.

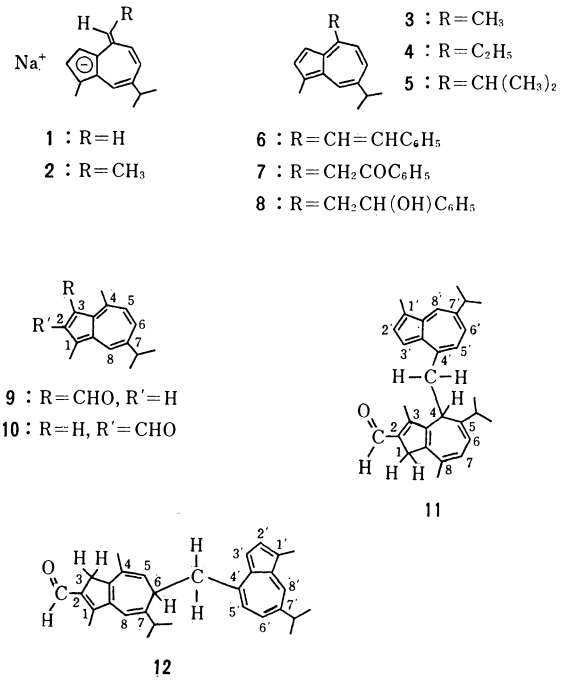

Fig. 1.

Results and Discussion

Sodium hydride and *N*-methylaniline reacted smoothly with evolution of hydrogen when a suspension in THF was heated, to form a pale yellow solution of sodium *N*-methylanilinide, which was subsequently changed into **1** by addition of **3**. The formation of **1** was apparent from the immediate color change of **3** from blue to brown, but was also proved by the reaction of **1** with methyl iodide to afford 4-ethyl-7-isopropyl-1-methylazulene (**4**),[3] though the yield (27.6%) was slightly lower than that (35%) in Ref. 3.

In this reaction, a by-product $C_{17}H_{22}$ (MS) was also found in a 3.4% yield. This compound is thought to be 4,7-diisopropyl-1-methylazulene (**5**) formed from **2**, because an alternative structure, 1,4-diethyl-7-isopropylazulene, is impossible owing to the lack of 1-ethyl-7-isopropyl-4-methylazulene in the reaction products.

For an additional proof of **1**, the reactivity toward formyl groups was examined by reaction of **1** with benzaldehyde.[4] The same products **6**, **7**, and **8** were isolated as in Ref. 4 and identified by UV, IR, NMR, and mass, but the yield of dehydration product **6** was prominent in our case (in THF) in contrast to the mere trace of **6** in Ref. 4 (in benzene).[7]

Reaction of **1** with **9** yielded two products: 1,4-dihydro-5-isopropyl-4-(7-isopropyl-1-methyl-4-azulenyl)-methyl-3,8-dimethyl-2-azulenecarbaldehyde (**11**) and 3,6-dihydro-7-isopropyl-6-(7-isopropyl-1-methyl-4-azulenyl)methyl-1,4-dimethyl-2-azulenecarbaldehyde (**12**), in 25.6 and 19.6% yields, respectively. Contrary to our expectation that addition of **1** would occur at carbonyl group, as in benzaldehyde, the nucleophilic addition of methylene carbanion of **1** took place at 6- and 8-positions of **9**, followed by migrations of the formyl group and hydrogen.

Rearrangement of the formyl group was shown by dehydrogenation of **11** and **12** with chloranil or *o*-chloranil, yielding 2-formylguaiazulene (**10**). The substitution mode of five-membered ring was also indicated by the NMR of **11** and **12**, in which the

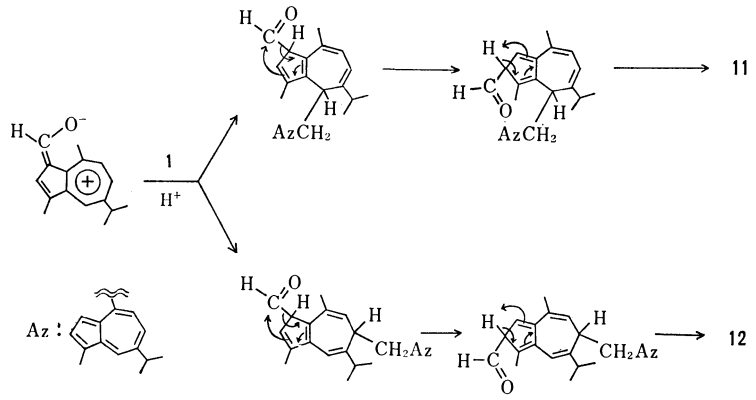

Fig. 2.

coupling constant 2.2 Hz (or 2.3 Hz) of 3-methyl and 1-methylene protons (or 1-methyl and 3-methylene protons) is in good agreement with 1.9 Hz of those of azulenium cations.[8,9]

In the NMR of **11**, moreover, 6-, 7-, and 4-hydrogens appeared as doublet (6.06), double quartet (6.44) (quartet is due to allyl coupling with 8-methyl protons), and double doublet signals (3.96 ppm), respectively, in accordance with the 4-substituted 1,4-dihydroguaiazulene structure. Also, the 6-substituted 3,6-dihydroguaiazulene structure of **12** was supported by the appearance of singlet (6.33), double quartet (5.34), and doublet signals (2.84) for 8- and 5-hydrogens and for the 6-methylene group, though splitting of 6-hydrogen signals were not clear owing to the overlapping with 3-methylene signals. Furthermore, all of these assignments were ascertained by double resonance spectra.

Addition of a nucleophilic strong base at 4- and 6-positions of the azulene nucleus was already observed by NMR spectroscopy.[10] In the present reaction, 4- (or 8-) and 6-positions of **9** would become reactive toward nucleophiles owing to the contribution of the mesomeric form of a tropylium cation type, in which the formyl group plays an important role. This may cause an exclusive addition of the methylene carbanion of **1** to the seven-membered ring and thus would explain the difference between this reaction and that with benzaldehyde. This conclusion is supported by the fact that the seven-membered ring of diethyl 1,3-azulenedicarboxylate and its derivatives is activated enough to react with Grignard reagents.[11]

On the other hand, conjugation of the formyl group with double bonds of dihydroguaiazulene is only attainable in **11** and **12** in a successive reaction course, and this might act as a driving-force of subsequent migrations of the formyl group and hydrogen.

Experimental

NMR spectra were taken in $CDCl_3$ with TMS as internal standard on a JEOL MH-100 spectrometer (100 MHz), or on a JEOL FX-90Q instrument (90 MHz) for spin-decoupling experiments. Mass spectra (MS) were obtained at 70 eV with a JEOL JMS-O1SG spectrometer, or at 24 eV with a JEOL-D300 instrument for GC-MS. UV spectra were recorded in cyclohexane on a Hitachi 624 digital spectrometer with a Hitachi 056 recorder, and IR spectra (liquids as films; solids as CCl_4 solutions) on a Hitachi 260-10 spectrometer. Mps are uncorrected. GLC was carried out on a Shimadzu GC-3AH instrument.

Preparation of Sodium Guaiazulenide (1). Under dry nitrogen 500 mg (10.4 mmol) of sodium hydride (50% dispersion in Bayol 85) was washed with hexane (10 cm^3), then with dry THF (10 $cm^3 \times 2$), and suspended in a solution of 3.62 g (33.8 mmol) of *N*-methylaniline in 20 cm^3 of THF. This suspension was heated to refluxing for 30 min, and the resulting pale yellow solution was refluxed for 30 more min to complete the reaction. To this solution, at room temperature, was added another solution of 1.98 g (10.0 mmol) of **3** in 10 cm^3 of THF over a period of 20 min. The color of **3** changed from blue to brown at each moment of addition, and finally yielded a brown solution of **1** in THF, which was used for successive reactions without further purification.

Reaction of 1 with Methyl Iodide. To a stirred solution of **1** in THF was added dropwise 2.20 g (15.5 mmol) of methyl iodide over a period of 5 min; stirring was continued for an additional 1 h. The reaction mixture, after evaporation of THF (reduced pressure), was taken up into 200 cm^3 of hexane and the insoluble sodium iodide was filtered off. The filtrate was washed with 7% hydrochloric acid (100 $cm^3 \times 3$), then with water, dried on sodium sulfate, and concentrated(reduced pressure) to give a blue oil. Successive hexane–silica gel elution chromatography afforded blue fractions containing **3**, **4**, **5**, and unknown minor components. From GLC analysis of these fractions, the yields of **3** (recovery), **4**, and **5** are calculated to be 47.4, 27.6, and 3.4%, respectively, based on **3**. Purification of each compound was not successful by means of elution chromatography, except that **4** was isolated as a mixture with **3** and **5**, and characterized by its NMR spectrum. **3**: GC-MS, *m/e* (rel intensity), 198 (66), 183 (100), 168 (17), 167 (18), 155 (17), 153 (26), and 128 (12). **4**: GC-MS, 212 (100), 197 (94), 169 (13), 167 (15), 154 (11), and 153 (12); NMR $\delta = 1.26$ (6H, d, $J = 7.0$ Hz, $CH(C\underline{H}_3)_2$), 1.34 (3H, t, $J = 7.5$ Hz, $CH_2C\underline{H}_3$), 2.64 (3H, s, 1-CH_3), 3.04 (2H, q, $J = 7.5$ Hz, $CH_2C\underline{H}_3$), 3.84 (1H, m, $J = 7.0$ Hz, $C\underline{H}(CH_3)_2$), 3.82 (1H, d, $J = 11.0$ Hz, 5-H), 7.23 (1H, dd, $J =$ 11.0 and 2.0 Hz, 6-H), 7.24 (1H, d, $J = 3.8$ Hz, 3-H), 7.58 (1H, d, $J = 3.8$ Hz, 2-H), and 8.16 (1H, d, $J = 2.0$ Hz, 8-H). **5**: GC-MS, 226 (100), 211 (76), 183 (39), 181 (17), 169 (17), and 155 (23).

Reaction of 1 with Benzaldehyde. To a stirred solution of **1** in THF (from 10 mmol of **3**) was added dropwise 2.5 g

(24 mmol) of benzaldehyde over a period of 20 min; stirring was continued for 4 h. The reaction mixture was worked up in the usual manner,[3,4] and **6**, **7**, and **8** were isolated in 64, 12, and 24% relative yields (**6**+**7**+**8**=100%).[7] **6**: NMR δ=1.32 (6H, d, J=7.0 Hz, CH(C$\underline{H}_3$)$_2$), 2.64 (3H, s, 1-CH$_3$), 3.04 (1H, m, J=7.0 Hz, C$\underline{H}$(CH$_3$)$_2$), 7.08—7.60 (9H, m, 3-H, 5-H, 6-H, vinyl-H, and Ph), 7.60 (1H, d, J=4.0 Hz, 2-H), 7.94 (1H, d, J=17.0 Hz, vinyl-H (*trans*)), and 8.14 (1H, d, J=2.0 Hz, 8-H); MS, *m/e* (rel intensity), 286 (100), 285 (38), 284 (27), 271 (97), 243 (45), 241 (31), 239 (22), and 228 (26). **7**: NMR δ=1.32 (6H, d, J=7.0 Hz, CH(C$\underline{H}_3$)$_2$), 2.64 (3H, s, 1-CH$_3$), 3.04 (1H, m, J=7.0 Hz, C$\underline{H}$(CH$_3$)$_2$), 4.76 (2H, s, CH$_2$), 6.99 (1H, d, J=10.0 Hz, 5-H), 7.16—7.72 (6H, m, 2-H, 3-H, 6-H, and B_2C part of A_2B_2C system of Ph), 8.00—8.20 (2H, m, A_2 part of A_2B_2C system of Ph), and 8.08 (1H, d, J=2.0 Hz, 8-H); MS, 302 (95), 105 (100), and 77 (28). **8**: NMR δ=1.38 (6H, d, J=7.0 Hz, CH(C$\underline{H}_3$)$_2$), 2.70 (3H, s, 1-CH$_3$), 3.12 (1H, m, J=7.0 Hz, C$\underline{H}$(CH$_3$)$_2$), 3.56 (2H, d, J=8.0 Hz, CH$_2$), 5.20 (1H, m, C$\underline{H}$(OH)), 7.03 (1H, d, J=10.0 Hz, 5-H), 7.20—7.80 (8H, m, 2-H, 3-H, 6-H, and Ph), and 8.24 (1H, d, J=2.0 Hz, 8-H); MS, 304 (100), 198 (69), 185 (90), 184 (25), 183 (63), 167 (21), 165 (21), 155 (57), 149 (97), 143 (25), 107 (21), 105 (46), 84 (27), 79 (33), 78 (24), 77 (33), 43 (21), and 41 (26).

*Reaction of **1** with 3-Formylguaiazulene (**9**).* A solution of 1.13 g (5.00 mmol) of **9** in 15 cm^3 of THF was added to a solution of **1** in THF (from 10.0 mmol of **3** and 25 cm^3 of THF) drop by drop over a period of 40 min. The reaction mixture was stirred for an additional 4 h, diluted with water (20 cm^3), and extracted with benzene (100 cm^3×3); the extract was washed with 7% hydrochloric acid (100 cm^3×3), then with water, dried, and concentrated (reduced pressure) to give a green oil. The oil was subsequently submitted to silica gel chromatography with hexane–AcOEt (4: 1) as the eluant, and separated into 331 mg (16.7%) of unchanged **3**, 543 mg (25.6 %) of **11**, 417 mg (19.6%) of **12**, 89.6 mg of unknown mixture, and 336 mg (29.7%) of recovery of **9**.

Dimer **11** was obtained as a green oil, which solidified in a refrigerator to give green microprisms, mp 113—115 °C. TLC (hexane–AcOEt) R_f 0.30. UV_{max} 205 nm (log ε 4.50), 246 (4.44), 287 (4.61), 305 (sh 4.17), 341 (sh 4.09), 353 (4.17), 366 (sh 4.14), 543 (sh ε 269), 568 (sh 384), 592 (sh 469), 610 (543), 632 (493), 667 (485), 698 (sh 254), and 739 (192); IR 1650 (C=O), 2720 and 2825 cm^{-1} (formyl CH); NMR[12] δ= 1.10 (6H, q, J=6.8 Hz, 5-CH(C$\underline{H}_3$)$_2$), 1.30 (6H, d, J=6.8 Hz, 7′-CH(C$\underline{H}_3$)$_2$), 1.55 (3H, t, J=2.2 Hz, 3-CH$_3$), 2.26 (3H, broad s, 8-CH$_3$) (broadening is due to couplings with 6-H and 7-H), 2.47 (1H, m, J=6.8 Hz, 5-C$\underline{H}$(CH$_3$)$_2$), 2.62 (3H, s, 1′-CH$_3$), 2.93 (1H, m, J=6.8 Hz, 7′-C$\underline{H}$(CH$_3$)$_2$), 3.04 (2H, dd, J=8.8 and 6.6 Hz, 4-CH$_2$), 3.27 (2H, q, J=2.2 Hz, 1-H$_2$), 3.96 (1H, dd, J=8.8 and 6.6 Hz, 4-H) (double doublets look like a broad triplet due to allyl coupling with 6-H), 6.06 (1H, broad d, J=7.0 Hz, 6-H) (broadening is due to couplings with 4-H and 8-CH$_3$), 6.44 (1H, dq, J=7.0 and 1.3 Hz, 7-H), 6.52 (1H, d, J=10.6 Hz, 5′-H), 7.15 (1H, d, J=4.0 Hz, 3′-H), 7.21 (1H, dd, J=10.6 and 1.8 Hz, 6′-H), 7.59 (1H, d, J=4.0 Hz, 2′-H), 8.08 (1H, d, J=1.8 Hz, 8′-H), and 9.62 (1H, s, 2-CHO); MS, *m/e* (rel intensity), 424 (4), 227 (100), 226 (11), 199 (13), 183 (14), 157 (21), and 142 (14).

Found: C, 87.79; H, 8.35%. Calcd for $C_{31}H_{36}O$: C, 87.69; H, 8.55%.

Dimer **12** was obtainde as a blue oil, which also solidified in a refrigerator to give blue crystals, dec at *ca.* 70 °C. TLC (hexane–AcOEt) R_f 0.26. UV_{max} 202 nm (log ε 4.44), 249 (sh 4.51), 285 (4.62), 289 (sh 4.61), 303 (sh 4.18), 346 (sh 4.10), 352 (4.14), 368 (sh 4.03), 543 (sh ε 298), 565 (sh 402), 591 (sh 489), 609 (557), 632 (500), 666 (482), 699 (sh 238), and 738 (182); IR 1655 (C=O), 2720 and 2825 cm^{-1} (formyl CH); NMR[12] δ=1.02 (6H, d, J=6.8 Hz, 7-CH(C$\underline{H}_3$)$_2$), 1.35 (6H, d, J=7.0 Hz, 7′-CH(C$\underline{H}_3$)$_2$), 1.96 (3H, d, J=1.3 Hz, 4-CH$_3$), 2.40 (1H, m, J=6.8 Hz, 7-C$\underline{H}$(CH$_3$)$_2$), 2.48 (3H, t, J=2.3 Hz, 1-CH$_3$), 2.65 (3H, s, 1′-CH$_3$), 2.84 (2H, d, J=7.9 Hz, 6-CH$_2$), 3.06 (1H, m, J=7.0 Hz, 7-C$\underline{H}$(CH$_3$)$_2$), 3.50 (1H, broad m, J=9.0 and 7.9 Hz, 6-H) (broadening is due to allyl coupling with 8-H), 3.61 (2H, m, J=2.3 Hz, 3-H$_2$), 5.34 (1H, dq, J=9.0 and 1.3 Hz, 5-H), 6.33 (1H, broad s, 8-H) (broadening is due to allyl coupling with 6-H), 6.62 (1H, d, J=10.8 Hz, 5′-H), 7.06 (1H, d, J=3.7 Hz, 3′-H), 7.32 (1H, dd, J= 10.8 and 2.0 Hz, 6′-H), 7.60 (1H, d, J=3.7 Hz, 2′-H), 8.13 (1H, d, J=1.7 Hz, 8′-H), and 10.08 (1H, s, 2-CHO); MS, 424 (7), 227 (100), 157 (15), 149 (19), 142 (11), and 43 (11).

Found: C, 87.80; H, 8.35 %. Calcd for $C_{31}H_{33}O$: C, 87.69; H, 8.55 %.

*2-Formylguaiazulene (**10**). A. From **11**.* A solution of 10 mg (0.024 mmol) of **11** and 15 mg (0.061 mmol) of chloranil in 2 cm^3 of benzene was stirred for 12 h at room temperature. The reaction mixture was diluted with petroleum ether (20 cm^3), shaken with a 4% aqueous solution of potassium hydroxide (25 cm^3), washed with water, dried, and the resultng green precipitates, insoluble in most organic solvents, were filtered off. Evaporation of the solvent and subsequent benzene–silica gel elution chromatography yielded 0.33 mg (6.2%) of **10**, identical with the authentic specimen in TLC, IR, and MS.

*B. From **12**.* The procedure given in *A* afforded 0.71 mg (4.7%) of **10**, identical (TLC and IR) with that from *A*, from 28 mg (0.067 mmol) of **12** and 60 mg (0.24 mmol) of *o*-chloranil.

As a control experiment, **9** was treated with a mixture of chloranil and *o*-chloranil in the same manner as described in *A*. In this case, however, only unchanged **9** was observed and formation of **10** was not detected in TLC of the reaction mixture.

The author wishes to thank Miss Naoko Kitahara of Saga University for her assistance in the experimental work as a part of her graduation thesis of Saga University. Thanks are also due to Dr. Hajime Koga of Hisamitsu Pharmaceutical Co., Ltd., and Dr. Toru Hinomoto of JEOL, Ltd., for their kind measurements of mass spectra and double resonance spectra.

References

1) S. Kurokawa, T. Safo, T. Noguchi, and K. Yano, *Bull. Chem. Soc. Jpn.*, **48**, 1559 (1975).

2) J. O. Currie, Jr., R. A. LaBar, R. D. Breazeal, and A. G. Anderson, Jr., *Justus Liebigs Ann. Chem.*, **1973**, 166.

3) K. Hafner, H. Pelster, and H. Patzelt, *Justus Liebigs Ann. Chem.*, **650**, 80 (1961).

4) M. Scholz, L. Vien, G. Fischer, B. Tschapke, and M. Muhlstädt, *Chem. Ber.*, **100**, 375 (1967).

5) H. E. Schroeder, Ph. D. Thesis, Harvard University, Massachusetts, U. S. A., 1938. *Cf.*, L. F. Fieser and M. Fieser, "Reagents for Organic Synthesis," John Wiley and Sons, New York (1967), Vol. 1, p. 1095; and literature cited therein.

6) Ref. 3 reported a 52% yield of **4** from **1**, and a 68% yield of **1** from **3**. From these data, an overall yield of **4** was calculated to be 35% based on **3**.

7) Ref. 4 reported that the relative yields of **6**, **7**, and **8** were trace, 98, and 2% when a 1: 1 ratio of **1** and benzaldehyde was used in a benzene solution, while the yield of **8**

increased to 28—73% for the reagent ratio of 1: 2.

8) D. Meuche, B. B. Molloy, D. H. Reid, and E. Heilbronner, *Helv. Chim. Acta*, **46**, 2483 (1963).

9) An alternative structure having 1-methyl (or 3-methyl) and 2-methylene groups was also possible if the migration of formyl group could occur by dehydrogenation of **11** and **12**. This possibility was excluded, because the coupling constant expected for that structure was less than 1 Hz according to Ref. 8.

10) R. N. MacDonald, H. E. Petty, N. L. Wolfe, and J. V. Paukstelis, *J. Org. Chem.*, **39**, 1877 (1974).

11) N. Abe, T. Morita, and K. Takase, *Tetrahedron Lett.*, **1973**, 3883: N. Abe and K. Takase, *ibid.*, **1973**, 4739.

12) Assignments were based on spin-decoupling experiments.

A Highly Stereospecific Procedure for the Transformation of Allylic Alcohols into 1,3-Dienes[1)]

Arata YASUDA,*,† Shin TANAKA, Hisashi YAMAMOTO,†† and Hitosi NOZAKI

Department of Industrial Chemistry, Kyoto University Yoshida, Kyoto 606

(Received December 6, 1978)

The title synthesis involves (1) epoxidation of allylic alcohols with *t*-butyl hydroperoxide in the presence of vanadium catalyst followed by trimethylsilylation, (2) specific oxirane ring opening by means of diethylaluminum 2,2,6,6-tetramethylpiperidide and subsequent desilylation producing 3-ene-1,2-diols, and (3) removal of both hydroxyl groups through bromination with a mixture of phosphorus tribromide and copper(I) bromide and the successive zinc debromination. The sequence of reactions has been extended with considerable success to the preparations of *β*-myrcene from nerol, *trans*-*β*-ocimene from geraniol in a specific way, and *α*- and *β*-farnesenes from their biological precursors. A C_{12} sex pheromone of red bollworm moth has been prepared efficiently by this method with cyclododecene as a starting material.

The high regio- and stereospecific isomerization of oxiranes into allylic alcohols has recently been accomplished by means of aluminum amides, especially diethylaluminum 2,2,6,6-tetramethylpiperidide(DATMP).[2)] To explore the applicability of this technique, we have undertaken an investigation of the reactions with a variety of oxirane derivatives.

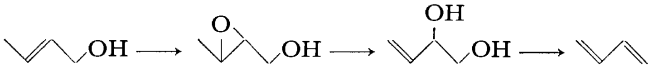

Of particular interest among them should be the conversion of 2,3-epoxy alcohols to 3-ene-1,2-diols. The recent development of effective methods of catalytic epoxidation of allylic alcohols with *t*-butyl hydroperoxide has made 2,3-epoxy alcohol species readily available for synthetic purpose.[3)] Furthermore, it could be envisioned that such ene-diols would provide us with the chance of success in the stereocontrolled synthesis of 1,3-dienes.[4)]

Epoxidation of nerol (**1a**) with the Sharpless reagent ($VO(acac)_2$–*t*-BuOOH) furnished epoxy alcohol **2a** in quantitative yield. Although the direct transformation of **2a** into 3-ene-1,2-diol **4a** by means of DATMP did not proceed smoothly, the problem was easily solved by protection of the hydroxyl group with either trimethylsilyl ether or 1-ethoxyethyl group. Of the two protecting groups, the trimethylsilyl group was more favorable for our purpose for ease of both introduction and removal. Thus, the epoxy alcohol **2a** was converted *in situ* to the epoxy silyl ether **3a** by the successive addition of pyridine, hexamethyldisilazane, and chlorotrimethylsilane at 0 °C. The crude product was immediately subjected to the action of DATMP, followed by desilylation with potassium fluoride in aqueous methanol, to furnish **4a** in 79% overall yield from **1a**. A striking feature is that none of the vinyl silyl ether was detected in the crude reaction mixture before KF treatment. As anticipated from the previous results,[2)] geraniol (**5a**) gave the isomeric diol **8a** as a predominant product. The detailed product distribution in the reaction of **7a** with DATMP and diethylaluminum diisopropylamide

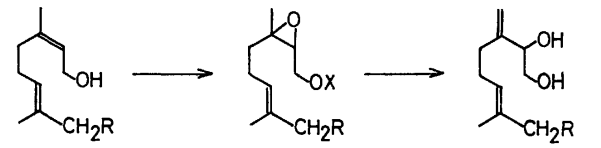

1a R=H **2a** R=H, X=H **4a** R=H
2b R=Me_2C=$CHCH_2$, X=H
1b R=Me_2C=$CHCH_2$ **3a** R=H, X=$SiMe_3$ **4b** R=Me_2C=$CHCH_2$
3b R=Me_2C=$CHCH_2$, X=$SiMe_3$

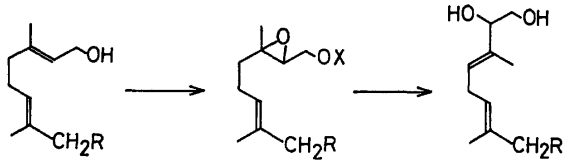

5a R=H **6a** R=H, X=H **8a** R=H
6b V=Me_2C=$CHCH_2$, X=H
5b R=Me_2C=$CHCH_2$ **7a** R=H, X=$SiMe_3$ **8b** R=Me_2C=$CHCH_2$
7b R=Me_2C=$CHCH_2$, X=$SiMe_3$

Table 1. Product distribution in the reaction of **7** with aluminum amides

Aluminum amide[a)]	Isomer distribution[b)] **8a** : **9***) : **4a**	Yield (%)[c)]
DATMP	90 : 5 : 5	65
Et_2Al–$N(i\text{-}Pr)_2$	44 : 48 : 8	64

*) 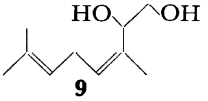

9

a) Aluminum amide reagents were prepared as previously reported.[2)] b) Isomer ratio was determined as follows. After KF treatment, the resulting crude 1,2-diols were converted to the corresponding aldehydes by the reaction with sodium periodate in ethanol. The chemical shifts ($CDCl_3$, TMS) of aldehyde protons appeared at *δ* 9.3 (the aldehyde derived from **8a**); 10.1 (the aldehyde derived from **9**); 9.5 (the aldehyde derived from **4a**). The ratio was determined by their intensities. c) Yields are based on material isolated by preparative TLC.

† Present Address: The Institute for Molecular Science, Myodaiji, Okazaki 444.

†† Present Address: Department of Chemistry, University of Hawaii at Manoa, Honolulu, Hawaii 96822.

are listed in Table 1. In addition to the previous observation, Table 1 shows following points of interest:

(1) This transformation can be believed to involve initial complex formation where aluminum amides approach the oxirane so as to enable a greater orbital overlap. Then the presence of the bulky trimethylsiloxyl group should make the attack of aluminum amides even more selective so that the reagents attack the oxirane group exclusively on the less hindered side (on the same side as hydrogen of oxirane) to produce trisubstituted olefinic diol **8a** or the isomer **9**.

(2) Substitution of diisopropylamide for tetramethylpiperidide moiety results in the complete lack of the (*E*) preference, which supports that the bulk of the extremely large TMP group did play an even more significant role in determining the course of elimination. Thus, in the abstraction stage of hydrogen, the favored direction is to be strictly arranged so as to minimize the severe nonbonded interactions. It should be added that using *t*-butyldimethylsilyl protecting group[5] in place of trimethylsilyl moiety even more improved the selectivity (**4a**: **8a**: **9**=2: 96: 2).

A similar sequence was extended to transform (2*Z*,6*E*)-farnesol (**1b**) to ene-diol **4b** (71% yield) and the isomer **5b** to **8b** (70% yield), respectively.

Now the remaining step toward 1,3-dienes consists in selective transformation of 1,2-diol group into vinyl moiety. Attempted application of the Eastwood method[6] proved to be disappointing. Treatment of the diol **4a** with *N*,*N*-dimethylformamide dimethyl acetal and the subsequent heating of the resulting dioxolane derivative in acetic anhydride at 110 °C afforded myrcene (**10a**)[7] in less than 20% yield.[8] Reaction of the benzaldehyde acetal of the diol with butyllithium was also tested without any success.[9] We therefore developed the following alternative route. The diol **4a** was initially brominated with a mixture of copper(I) bromide (2.5 equiv) and phosphorus tribromide (1.2 equiv) at 0 °C for 1 h and then successively treated with excess zinc dust at room temperature for 2 h to furnish myrcene (**10a**) in 58% yield. Similarly, the following terpenes were prepared efficiently from the corresponding ene-diols: *trans*-β-ocimene (**11a**),[10] from diol **8a**; β-farnesene (**10b**),[11] from **4b**; *trans*-α-farnesene (**11b**),[12] from **8b**. The homogeneity of each product was attested by the NMR analysis. Although the role of excess copper(I) bromide in this process is still obscure, it

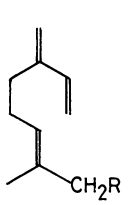

10a R=H
10b R=Me_2C=$CHCH_2$

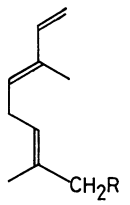

11a R=H
11b R=Me_2C=$CHCH_2$

appears to facilitate both bromination and debromination and is essential for securing good yields. The synthesis of **10b** and **11b** should be monitored by TLC assay, since the longer reaction time causes cyclization induced by zinc bromide at the expense of the desired product.

The present method permitted the facile synthesis of the following 1,3-diene compounds. 1,3-Cyclododecadiene (**15**) was prepared from (*E*)-2-cyclododecen-1-ol (**12**).[13] In addition, (*E*)-9,11-dodecadienyl acetate (**19**), which was known as the major sex pheromone of the red bollworm moth,[14] was prepared smoothly from the diol **14** as a starting material. Thus, **14** was converted to the open chain diol **16** by sodium periodate oxidation followed by sodium tetrahydroborate reduction. The same series of reactions transformed **16** into the triol **17**. The terminal alcohol (C-12) was converted to the

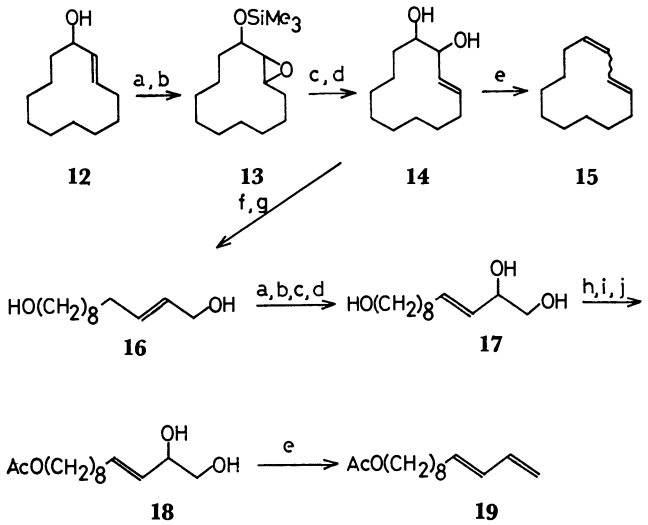

a, $VO(acac)_2$–*t*-BuOOH; b, Me_3SiCl–$(Me_3Si)_2NH$–C_5H_5N; c, DATMP; d, KF; e, PBr_3–Cu_2Br_2–Zn; f, $NaIO_4$; g, $NaBH_4$; h, $Me_2C(OMe)_2$–*p*-TsOH; i, Ac_2O–C_5H_5N; j, $(CH_2OH)_2$–*p*-TsOH.

acetate **18** as follows. Treatment of **17** with 2,2-dimethoxypropane with a catalytic amount of *p*-toluenesulfonic acid followed by acetylation (acetic anhydride-pyridine) afforded acetonide acetate, which was transformed to diol **18** using ethylene glycol and trace *p*-toluenesulfonic acid. The desired diene **19** was obtained by the similar treatment with PBr_3–Cu_2Br_2–Zn.

Finally a further extension of the sequence should be added. Reaction of an epoxy silyl ether **20** with DATMP and then KF gave 2-methylene-1,3-diol **21**. Although this class of compounds are potential intermediates for

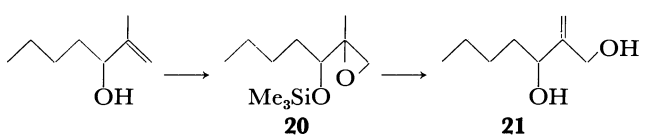

20 **21**

the synthesis of substituted trimethylenemethane and other related compounds, there exist few synthetic routes available.[15]

Experimental

The infrared spectra were determined on a Shimadzu IR-27-G spectrometer; the mass spectra on a Hitachi RMU-6L mass machine; and NMR spectra on a JNM-PMX 60 or

Varian EM-360 spectrometer. The chemical shifts are given in δ in ppm with TMS as the internal standard. Splitting patterns are designated as s, singlet; d, doublet; t, triplet; q, quartet; m, multiplet. The microanalyses were carried out by the staffs at the Elemental Analyses Center of Kyoto University. All experiments were carried out under an atmosphere of dry argon. In experiments requiring dry solvents, tetrahydrofuran was distilled from sodium-benzophenone. Ether and benzene were dried over sodium metal. During workup, drying of the organic solution was performed over anhydrous sodium sulfate. Thin layer or preparative thick layer plates were made of E. Merck PF-254, and preparative column chromatography on silica gel E. Merck Art. 7734.

*Synthesis of Myrcene (**10a**). 2-Methyl-r-2-(4-methyl-3-pentenyl)-c-3-trimethylsiloxymethyloxirane (**3a**).* The epoxy alcohol **2a** was prepared as previously reported.[3a] A solution of *t*-butyl hydroperoxide (300 mg, 3.0 mmol) in benzene (3 ml) was added at 0 °C dropwise to a mixture of nerol (**1a**) (308 mg, 2.0 mmol) and oxobis(2,4-pentanedionato-*O*,*O*')vanadium-(IV) (16 mg, 0.06 mmol) in benzene (10 ml). Stirring was continued at room temperature for 3 h (TLC analysis indicated the absence of starting material). The epoxy alcohol **2a** was converted *in situ* to the epoxy silyl ether **3a** by the successive addition of pyridine (4.0 ml), hexamethyldisilazane (0.8 ml), and chlorotrimethylsilane (0.4 ml) at 0 °C. The reaction was completed in 1 h at room temperature, then saturated sodium sulfite was added and the whole mixture was vigorously stirred at ambient temperature for 20 min. The separated organic phase was washed with saturated copper(II) sulfate and water, dried, and concentrated *in vacuo*. The crude product was immediately subjected to the next reaction.

A sample was purified by column chromatography on silica gel (20: 1 hexane–ether) followed by bulb-to-bulb distillation: bp 92—94 °C (bath temp, 1 Torr); TLC, R_f 0.49 (2: 1 hexane–ether); IR (neat), 1450 (m), 1245 (s), 1122 (s), 1080 (s), and 845 cm^{-1} (s); NMR (CCl_4), 0.11 (9H, s, CH_3–Si), 1.25 (3H, s, CH_3–CO), 1.59 (3H, s, CH_3–C=), 1.65 (3H, s, CH_3–C=), 2.63 (1H, t, J=6 Hz, CH–O), 3.54 (2H, dd, CH_2–O), and 5.00 (1H, bt, CH=); MS (*m/e*), 242 (1), 181 (8), 173 (10), 160 (100), and 145 (44).

Found: C, 64.4; H, 10.7 %. Calcd for $C_{13}H_{26}O_2Si$: C, 64.4; H, 10.8 %.

*7-Methyl-3-methylene-6-octene-1,2-diol (**4a**).* To a benzene solution (20 ml) of diethylaluminum 2,2,6,6-tetramethylpiperide (8.0 mmol) a solution of crude **3a** (*ca.* 2.0 mmol) in benzene (2 ml) was added at 0 °C dropwise and the mixture was stirred at the same temperature for 1 h. The reaction mixture was quenched with dil. hydrochloric acid at 0 °C and the resulting organic phase was separated. The aqueous layer was extracted with ether, and the combined organic solutions were washed with saturated brine, dried, and freed of the solvent. The residue was dissolved in 80 % aqueous methanol (5 ml) and potassium fluoride (1.2 g, 20.0 mmol) was added at 0 °C. After stirring at room temperature for 3 h, the volatile material was removed under reduced pressure. The residue was partitioned between saturated brine and ethyl acetate, and the aqueous phase was extracted several times with ethyl acetate. The combined organic phase was washed with saturated brine, dried, and concentrated *in vacuo*. The remaining liquid was submitted to preparative TLC (1: 1 hexane–ethyl acetate) to give pure **4a** (269 mg, 79% yield from **1a**) as a clear oil: bp 130 °C (bath temp, 1 Torr); TLC, R_f 0.41 (ether); IR (neat), 3350—3440 (s), 1440—1455 (m), 1065—1090 (s), and 905 cm^{-1}(m); NMR ($CDCl_3$), 1.61 (3H, s, CH_3–C=), 1.69 (3H, s, CH_3–C=), 4.00—4.33 (1H, m, CH–O), and 4.83—5.27 (3H, bd, CH= and CH_2–); MS (*m/e*), 170 (1), 152 (4), 127 (9), 109 (18), and 69 (100).

Microanalysis was performed after converting the 1,2-glycol group to isopropylidene acetal group by treating the glycol with 2,2-dimethoxypropane in dichloromethane in the presence of a catalytic amount of *p*-toluenesulfonic acid:

Found: C, 74.4; H, 10.7%. Calcd for $C_{13}H_{22}O_2$: C, 74.2; H, 10.5%.

*Myrcene (**10a**).*[7] To an ethereal solution (10 ml) of diol **4a** (200 mg, 1.2 mmol), copper(I) bromide (860 mg, 3.0 mmol) and phosphorus tribromide (0.09 ml, 0.5 mmol) were successively added at −78 °C, and the whole mixture was stirred at 0 °C for 1 h. Zinc dust (392 mg, 6.0 mmol) was added at 0 °C and stirring was continued at room temperature for 2 h. Dilution of the mixture with pentane, folowed by workup and short-path column chromatography (pentane as an eluent), furnished myrcene (**10a**) (98 mg, 58 % yield) as a colorless oil: TLC, R_f 0.80 (hexane); IR (neat), 1600 (s), 1435—1450 (m), 1365 (m), 990 (s), and 890 cm^{-1} (s); NMR (CCl_4), 1.53 (3H, s, CH_3–C=), 1.62 (3H, s, CH_3–C=), 2.20 (4H, d, CH_2–C=), 4.98 (2H, s, CH_2= on C-3), 4.81—5.46 (3H, m, CH_2= on C-1 and CH= on C-6), and 6.35 (1H, dd, J=18 and 10 Hz, CH= on C-2); MS (*m/e*), 136 (8), 121 (7), 107 (5), 93 (100), and 69 (99).

Synthesis of trans-*β-Ocimene (**11a**). 2-Methyl-r-2-(4-methyl-3-pentenyl)-t-3-trimethylsiloxymethyloxirane (**7a**).* The epoxy alcohol **6a**[3a] was converted to epoxy silyl ether **7a** as described above, and used for the next reaction without purification.

A small aliquot was purified by column chromatography (20: 1 hexane–ether) followed by evaporative distillation: bp 95 °C (bath temp, 1 Torr); TLC, R_f 0.50 (2: 1 hexane–ether); IR (neat), 1450 (m), 1240 (m), 1120 (s), 1065—1080 (s), and 840 cm^{-1} (s); NMR (CCl_4), 0.11 (9H, s, CH_3–Si), 1.19 (3H, s, CH_3–CO), 1.59 (3H, s, CH_3–C=), 1.65 (3H, s, CH_3–C=), 2.63 (1H, t, J=5 Hz, CH–O), 3.54 (2H, dd, CH_2–O), and 5.00 (1H, bt, CH=); MS (*m/e*), 242 (1), 181 (14), 160 (100), 145 (45), and 103 (76).

Found: C, 64.2; H, 10.7%. Calcd for $C_{13}H_{26}O_2Si$: C, 64.4; H, 10.8 %.

*(E)-3,7-Dimethyl-3,6-octadiene-1,2-diol (**8a**).* The title compound was prepared from the crude **7a** by treatment with DATMP (4 equiv) at 0 °C for 1.5 h in benzene and then with potassium fluoride (10 equiv) at room temperature for 3 h (59 % yield based on geraniol **5a**): bp 135 °C (bath temp, 1 Torr); TLC, R_f 0.37 (ether); IR (neat), 3250—3400 (s), 1430—1445 (s), 1035—1070 (s), and 880—890 cm^{-1} (m); NMR ($CDCl_3$), 1.64 (6H, s, CH_3–C=), 1.69 (3H, s, CH_3–C=), 2.52—2.94 (2H, t, J=8 Hz, CH_2–C=), 3.80—4.32 (1H, m, CH–O), 5.12 (1H, bt, CH= on C-6), and 5.46 (1H, bt, CH= on C-4); MS (*m/e*), 170 (6), 152 (11), 139 (36), 109 (60), and 81 (100).

Microanalysis was performed with the isopropylidene acetal derivative:

Found: C, 74.4; H, 10.5%. Calcd for $C_{13}H_{22}O_2$: C, 74.2; H, 10.5%.

trans-*β-Ocimene (**11a**).*[10] The title compound was prepared from sequential treatment of the diol **8a** with copper-(I) bromide, phosphorus tribromide, and zinc as described above. The desired triene **11a** (66 % yield) formed a clear oil: TLC, R_f 0.80 (hexane); IR (neat), 1650 (m), 1610 (s), 1380 (s), 990 (s), and 890 cm^{-1} (s); NMR (CCl_4), 1.65—1.72 (9H, m, CH_3–C=), 2.79 (2H, bt, CH_2–C=), 4.58—5.55 (4H, CH= on C-4 and C-6, CH_2=), and 6.26 (1H, dd, J=18 and 10 Hz, CH= on C-2); MS (*m/e*), 136 (13), 121 (24), 105 (18), 93 (100), and 79 (47).

*Synthesis of β-Farnesene (**10b**). r-2-[(3E)-4,8-Dimethyl-3,7-nonadienyl]-2-methyl-c-3-trimethylsiloxymethyloxirane (**3b**):* Bp 135 °C (bath temp, 1 Torr); TLC, R_f 0.48 (5: 1 hexane–ether); IR (neat), 1450 (m), 1245 (s), 1120 (s), 1080 (s), and 845 cm^{-1} (s); NMR (CCl_4), 0.09 (9H, s, CH_3–Si), 1.23 (3H, s,

CH_3–CO), 2.67 (1H, t, CH–O), 3.54 (2H, d, J=6 Hz, CH_2–O), and 4.82—5.23 (2H, m, CH=); MS (*m/e*), 310 (M^+).

Found: C, 69.7; H, 11.2 %. Calcd for $C_{18}H_{34}O_2Si$: C, 69.6; H, 11.0 %.

*(6E)-7,11-Dimethyl-3-methylene-6,10-dodecadiene-1,2-diol (**4b**).* The title compound (169 mg, 71 % yield) was prepared from **1b** employing a series of reactions as aforementioned: TLC, R_f 0.53 (ether); IR (neat), 3330—3420 (s), 1438—1454 (m), 1065—1090 (s), and 905 cm^{-1} (s); NMR ($CDCl_3$), 1.61 (6H, s, CH_3–C= on C-7 and C-11), 1.69 (3H, s, CH_3–C= on C-11), 3.39—3.91 (2H, m, CH_2–O), 4.00—4.36 (1H, m, CH–O), and 4.70—5.34 (4H, bd, CH_2= and CH=).

Microanalysis was performed with its isopropylidene acetal derivative:

Found: C, 77.9; H, 10.9 %. Calcd for $C_{18}H_{30}O_2$: C, 77.7; H, 10.8 %.

*β-Farnesene (**10b**).*[11] The preparation of the diene **10a** was repeated, except stirring was stopped in 1.5 h to suppress the formation of by-products. β-Farnesene (**10b**) (78 mg) was obtained from the diol **4b** (238 mg) in 38 % yield as a colorless liquid: TLC, R_f 0.80 (hexane); IR (neat), 1600 (s), 1440—1465 (s), 990 (s), 910 (sh), and 895 cm^{-1} (s); NMR (CCl_4), 1.60 (6H, s, CH_3–C=), 1.69 (3H, s, CH_3–C=), 4.82—5.41 (6H, m, CH_2= and CH= on C-6, C-10), and 6.32 (1H, dd, J=18 and 11 Hz, CH= on C-2); MS (*m/e*), 204 (8), 161 (10), 133 (20), 93 (59), and 69 (100).

Synthesis of trans-α-*Farnesene (**11b**).* r-2-[*(3E)-4,8-Dimethyl-3,7-nonadienyl*]-2-methyl-t-3-trimethylsiloxymethyloxirane (**7b**): Bp 135 °C (bath temp, 1 Torr); TLC, R_f 0.53 (5:1 hexane–ether); IR (neat), 1450 (m), 1250 (s), 1120 (s), 1060—1080 (s), and 835 cm^{-1} (s); NMR (CCl_4), 0.09 (9H, s, CH_3–Si), 1.19 (3H, s, CH_3–CO), 2.67 (1H, t, CH–O), 3.54 (2H, d, J=6 Hz, CH_2–O), and 4.82—5.23 (2H, m, CH=); MS (*m/e*), 310 (M^+).

Found: C, 69.6; H, 11.1 %. Calcd for $C_{18}H_{34}O_2Si$: C, 69.6; H, 11.0 %.

*(3E,6E)-3,7,11-Trimethyl-3,6,10-dodecatriene-1,2-diol (**8b**).* The same sequence as aforementioned furnished the diol **8b** (168 mg, 70 % yield) from (*E,E*)-farnesol (**5b**) (222 mg) as a clear oil: TLC, R_f 0.48 (ether); IR (neat), 3340—3420 (s), 1440—1455 (m), 1060—1080 (m), and 890 cm^{-1} (w); NMR ($CDCl_3$), 1.61 (6H, s, CH_3–C= on C-7 and C-11), 1.65 (3H, s, CH_3–C= on C-3), 1.69 (3H, s, CH_3–C= on C-11), 2.72 (2H, t, J=7 Hz, CH_2–C= on C-4), 3.92—4.31 (1H, m, CH–O), 5.12 (2H, bt, CH= on C-6 and C-10), and 5.46 (1H, bt, CH= on C-4).

Microanalysis was performed with its isopropylidene acetal derivative:

Found: C, 77.9; H, 11.1 %. Calcd for $C_{18}H_{30}O_2$: C, 77.7; H, 10.8 %.

trans-α-*Farnesene (**11b**).*[12] The title compound was obtained in 45 % yield from **8b**: TLC, R_f 0.80 (hexane); IR (neat), 1610 (m), 1440—1455 (s), 1380 (s), 990 (s), 910 (sh), and 895 cm^{-1} (s); NMR (CCl_4), 1.50—1.74 (12H, m, CH_3–C=), 2.80 (2H, bt, CH_2–C= on C-4), 4.60—5.66 (5H, m, CH_2= and CH= on C-4, C-6, and C-10), and 6.32 (1H, dd, J=18 and 11 Hz, CH= on C-2); MS (*m/e*), 204 (9), 135 (14), 119 (48), 107 (43), and 93 (100).

*Synthesis of 1,3-Cyclododecadiene (**15**).* trans-*1,2-Epoxy-3-trimethylsiloxycyclododecane (**13**)*: Bp 110—112 °C (bath temp, 1 Torr); TLC, R_f 0.59 (3:1 hexane–ether); IR (neat), 1240 (s), 1105 (m), 950 (w), 865 (m), and 840 cm^{-1} (s); NMR (CCl_4), 0.10 (9H, s, CH_3–Si), 2.42—2.90 (2H, m, CH–O on C-1 and C-2), and 3.83—4.16 (1H, m, CH–O on C-3); MS (*m/e*), 270 (1), 255 (48), 185 (6), 129 (100), and 95 (38).

Found: C, 66.9; H, 11.4 %. Calcd for $C_{15}H_{30}O_2Si$: C, 66.6; H, 11.2 %.

*(E)-3-Cyclododecene-1,2-diol (**14**).* This compound was prepared from **12** in 63 % yield: mp 89—91 °C (benzene–hexane); TLC, R_f 0.68 (ether); IR (Nujol), 3300—3410 (s), 1450 (s), 1030 (s), 980 (s), and 915 cm^{-1} (m); NMR ($CDCl_3$), 3.20—3.98 (2H, m, CH–O), and 5.39—5.83 (2H, m, CH=).

Found: C, 72.7; H, 11.3 %. Calcd for $C_{12}H_{22}O_2$: C, 72.7; H, 11.2 %.

*1,3-Cyclododecadiene (**15**).*[16] The diol **14** was transformed to the title compound in 70 % yield: TLC, R_f 0.80 (hexane); IR (neat), 1470—1485 (s), 1445 (m), 980 (s), and 950 cm^{-1} (m); NMR (CCl_4), 5.00—6.59 (4H, m, CH=); MS (*m/e*), 164 (37), 121 (25), 93 (37), 79 (100), and 67 (100).

*Synthesis of (E)-9,11-Dodecadienyl Acetate (**19**). (E)-2-Dodecene-1,12-diol (**16**).* Sodium periodate (3.08 g, 14.4 mmol) was added at 0 °C to a solution of diol **14** (1.42 g, 7.2 mmol) in 80 % aqueous ethanol (26 ml). After stirring at 0 °C for 1.5 h, the solid was filtered off and the filtrate was concentrated *in vacuo*. The residue was partitioned between saturated brine and ether, then the ethereal solution was washed with saturated brine, dried, and freed of the solvent to yield dialdehyde: TLC, R_f 0.60 (2:1 ether–hexane); IR (neat), 1720—1730 (s), 1690 (s), 1460—1470 (m), and 980 cm^{-1} (m); NMR (CCl_4), 6.00 (1H, dd, J=16 and 8 Hz, CH= on C-2), 6.80 (1H, dt, J=16 and 7 Hz, CH= on C-3), 9.43 (1H, d, J=7 Hz, CH=O on C-1), and 9.70 (1H, t, CH=O on C-12); MS (*m/e*), 196 (3), 98 (48), 83 (76), 70 (74), and 55 (100).

The crude product was treated with sodium tetrahydroborate (274 mg, 7.2 mmol) in methanol (10 ml) at room temperature for 1 h. Acetic acid was then added dropwise to hydrolyze the excess hydride and the volatile material was removed *in vacuo*. The residue was diluted with ethyl acetate and the organic phase was washed with saturated brine, dried, and concentrated *in vacuo*. Purification by column chromatography (1:1 benzene–ethyl acetate) furnished the diol **16** (1.05 g, 73 % yield from **14**) as a semi-solid: TLC, R_f 0.13 (1:2 hexane–ether); IR (neat), 3350—3450 (s), 1480 (m), 1470 (s), 1090 (s), and 970 cm^{-1} (s); NMR ($CDCl_3$), 3.60 (2H, t, CH_2–O on C-12), 4.05 (2H, d, CH_2–O on C-1), and 5.41—5.73 (2H, m, CH=).

Microanalysis was performed after trimethylsilylation of both hydroxyl groups:

Found: C, 63.0; H, 12.0 %. Calcd for $C_{18}H_{40}O_2Si_2$: C, 62.8; H, 11.7 %.

*(E)-9,11-Dodecadienyl Acetate (**19**).*[14] The sequence as described above converted the diol **16** to the triol **17** in 75 % yield: TLC, R_f 0.31 (ethyl acetate); IR (neat), 3300—3450 (s), 1450—1480 (m), 1050—1070 (s), and 970 cm^{-1} (s); NMR ($CDCl_3$), 3.20—4.05 (5H, m, CH_2–O and CH–O), and 5.51—5.73 (2H, m, CH=).

Before the synthesis of diene **19**, the terminal alcohol (C-12) was converted to the acetate as follows. To a mixture of triol **17** (80 mg, 0.37 mmol), 2,2-dimethoxypropane (0.07 ml, 0.55 mmol), and THF (3 ml) was added *p*-toluenesulfonic acid (4 mg, 0.02 mmol) at 0 °C, and the solution was stirred at room temperature for 4 h. A drop of pyridine was added and the mixture was diluted with ether. The organic solution was washed with saturated brine, dried, and freed of the solvent. The residue was treated with acetic anhydride (0.5 ml) in pyridine (0.5 ml) at ambient temperature for 5 h. Aqueous workup in the usual manner, drying, and concentrating *in vacuo* gave acetonide acetate, which was treated with *p*-toluenesulfonic acid (4 mg, 0.02 mmol) in ethylene glycol (2 ml) at room temperature for 4 h to furnish diol **18** (89 % yield based on **17**) after purification by preparative TLC (2:1 ether–hexane): TLC, R_f 0.53 (2:1 ether–hexane); IR (neat), 3400—3450 (s), 1740 (s), 1370 (m), 1235—1255 (s), and 970 cm^{-1} (m); NMR ($CDCl_3$), 1.96 (3H, s, CH_3–CO), 3.59 (2H, t, CH_2–OAc), 3.87—4.38 (3H, m, CH–O and CH_2–O), and

5.18—6.09 (2H, m, CH=).

The diol **18** was converted to the desired diene **19** with the Cu_2Br_2–PBr_3–Zn system in 75 % yield: TLC, R_f 0.38 (5: 1 hexane–ether); IR (neat), 1740 (s), 1260 (s), 1005 (m), 960(w), and 900 cm^{-1} (m); NMR ($CDCl_3$, 100 MHz), 2.02 (3H, s, CH_3–CO), 1.95—2.21 (2H, m, CH_2–C=), 4.06 (2H, t, J=7 Hz, CH_2–O), and 4.85—6.50 (5H, m, CH= and CH_2=, 5.00, 5.15, 5.61, 5.69, 5.75, 5.82, 5.92, 6.03, 6.15, 6.24, 6.30, 6.40, and 6.50); MS (*m/e*), 224 (7), 164 (18), 135 (15), 121 (20), and 67 (100).

*2-Methyl-2-(1-trimethylsiloxypentyl)oxirane (**20**)*: Bp 60 °C (bath temp, 1 Torr); TLC, R_f 0.68 (1: 1 hexane–ether); IR (neat), 1450—1700 (w), 1245 (s), 1090 (s), 940 (m), 865 (sh), and 840 cm^{-1} (s); NMR (CCl_4), 0.53 (9H, s, CH_3–Si), 1.67 (3H, s, CH_3–CO), 2.68—3.16 (2H, dd, CH_2–O), and 3.50—3.90 (1H, bt, CH–O); MS (*m/e*), 216 (2), 201 (25), 160 (43), 131 (34), and 75 (100).

Found: C, 61.3; H, 11.3 %. Calcd for $C_{11}H_{24}O_2Si$: C, 61.1; H, 11.2 %.

*2-Methylene-1,3-heptanediol (**21**)*. Treatment of **20** (216 mg, 1.0 mmol) with DATMP (4.0 mmol) and then with KF furnished the diol **21** (108 mg) in 75 % yield: TLC, R_f 0.33 (ether); IR (neat), 3340—3400 (s), 1655 (w), 1010—1060 (s), and 905 cm^{-1} (m); NMR ($CDCl_3$), 3.84—4.48 (3H, m, CH–O and CH_2–O), and 5.09 (2H, s, CH_2=).

Found: C, 66.5; H, 11.5 %. Calcd for $C_8H_{16}O_2$: C, 66.6; H, 11.2 %.

The authors wish to thank the Ministry of Education, Japan, for a Grant-in-Aid (No. 011010, 110309, 203014, and 303023).

References

1) A preliminary account of this work has appeared: S. Tanaka, A. Yasuda, H. Yamamoto, and H. Nozaki, *J. Am. Chem. Soc.*, **97**, 3252 (1975).

2) A. Yasuda, S. Tanaka, K. Oshima, H. Yamamoto, and H. Nozaki, *J. Am. Chem. Soc.*, **96**, 6513 (1974).

3) (a) K. B. Sharpless and R. C. Michaelson, *J. Am. Chem. Soc.*, **95**, 6136 (1973); (b) S. Tanaka, H. Yamamoto, H. Nozaki, K. B. Sharpless, R. C. Michaelson, and J. D. Cutting, *ibid.*, **96**, 5254 (1974); (c) R. C. Michaelson, R. E. Palermo, and K. B. Sharpless, *ibid.*, **99**, 1990 (1977).

4) The dehydration of allylic alcohol generally gives rise to a complex mixture from which the isolation of the desired product is a rather tedious task; see A. Bhati, *Perfum. Essent. Oil Rec.*, **54**, 376 (1963); B. M. Mitzner, S. Lemberg, and E. T. Theimer, *Can. J. Chem.*, **44**, 1090 (1966).

5) E. J. Corey and A. Venkateswarlu, *J. Am. Chem. Soc.*, **94**, 6190 (1972).

6) F. W. Eastwood, K. J. Harrington, J. S. Josan, and J. L. Pura, *Tetrahedron Lett.*, **1970**, 5223.

7) G. Ohloff, J. Seibl, and E. Kovats, *Justus Liebigs Ann. Chem.*, **675**, 83 (1964).

8) D. Chambencis, G. Mousset, *Bull. Soc. Chim. Fr-Part II*, **1974**, 2969.

9) J. N. Hines, M. J. Peagram, G. H. Whitham, and M. Wright, *J. Chem. Soc., Chem. Commun.*, **1968**, 1593.

10) B. M. Mitzner, E. T. Theimer, L. Steinbach, and J. Wolt, *J. Org. Chem.*, **30**, 646 (1964).

11) K. E. Murray, *Aust. J. Chem.*, **22**, 197 (1969).

12) G. W. K. Cavill, P. J. Williams, and F. B. Whitfield, *Tetrahedron Lett.*, **1967**, 2201.

13) K. B. Sharpless and R. F. Lauer, *J. Am. Chem. Soc.*, **95**, 2697 (1973); see also Ref. 2.

14) (a) B. F. Nesbitt, P. S. Beevor, R. A. Cole, R. Lester, and R. G. Poppi, *Nature (London), New Biol.*, **244**, 208 (1974); (b) B. F. Nesbitt, P. S. Beevor, R. A. Cole, R. Lester, and R. G. Poppi, *Tetrahedron Lett.*, **1973**, 4669; (c) K. Mori, *Tetrahedron*, **30**, 3807 (1974).

15) F. Weiss, *Q. Rev., Chem. Soc.*, **24**, 278 (1970).

16) A. J. Hubert and J. Dale, *J. Chem. Soc.*, **1965**, 6674.

A Stereoselective 1,3-Transposition Reaction of Allylic Alcohols[1)]

Arata YASUDA,*,† Hisashi YAMAMOTO,†† and Hitosi NOZAKI
Department of Industrial Chemistry, Kyoto University, Yoshida, Kyoto 606
(Received December 6, 1978)

Reduction of glycidyl mesylate with dissolving metal produces allylic alcohol in fair to excellent yield. Combined with the highly stereoselective epoxidation of allylic alcohols with *t*-butyl hydroperoxide and oxobis(2,4-pentanedionato-*O*,*O*')vanadium(IV) as a catalyst, the sequence provides a new and efficient means for 1,3-transposition of allylic alcohols, by which geraniol is transformed into linalool, farnesol into nerolidol, and furthermore, (−)-*cis*-carveol into the (+) antipode and vice versa in a stereospecific way.

The recently discovered procedure for making 2,3-epoxy-1-alkanols by catalytic epoxidation of allylic alcohols[2)] has initiated an investigation into the possible utilization of the dissolving metal reduction of glycidyl mesylate (methanesulfonate) obtained therefrom as a possible way of 1,3-transposition of allylic alcohols.

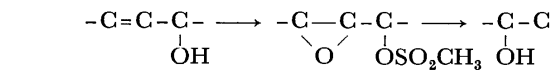

The epoxy alcohol **2** was treated with methanesulfonyl chloride and triethylamine in dichloromethane at −26 °C to give the mesylate **3**. Reduction of **3** with calcium metal in liquid ammonia-tetrahydrofuran furnished linalool (**4**) (88% yield). Some variations in the metal reagent have been studied: sodium, 87% yield; lithium, 50% yield. The use of methylamine, ethylamine, and hexamethylphosphoric triamide in place of liq. ammonia was tested without any success. Reduction with sodium-naphthalene in THF also effected the same transformation yielding linalool. This procedure gave the best result when a THF solution of the mesylate was added to a THF solution of the radical anion.[3,4)] Nerolidol (**8**)[5)] was similarly obtained by reaction of the mesylate **7** with sodium-metal in liq. ammonia-THF.

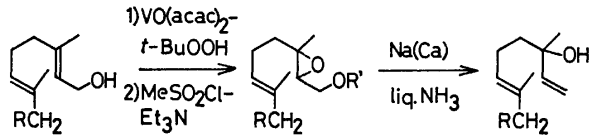

1 R=H **2** R=R'=H **4** R=H
3 R=H, R'=SO_2Me
5 R=Me_2C=$CHCH_2$ **6** R=Me_2C=$CHCH_2$, R'=H **8** R=Me_2C=$CHCH_2$
7 R=Me_2C=$CHCH_2$, R'=SO_2Me

Although the facility and directness of this procedure are appealing, even more important is the advantage that glycidols are prepared from allylic alcohols with high stereospecificity by the Sharpless reagent.[2)] For example, (−)-*cis*-carveol (**9**) was selectively oxidized to the *cis*-epoxy alcohol **10**. Treatment of the mesylate **11** with either Na–NH_3 or Na-naphthalene furnished (+)-*cis*-carveol (**12**) in good yield. The reverse transformation of **12** into **9** was smoothly carried out by employing the same sequence as described above. From the known specific rotation,[6)] each product was found to be no less than 90% optically pure.

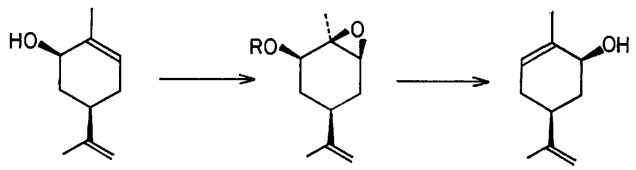

9 **10** R=H, **11** R=Ms **12**

In order to examine the stereochemistry of the reduction of an open-chain glycidyl mesylate, (2*R**,3*S**)-glycidol **14**[2b)] was prepared and subjected to the transformation.

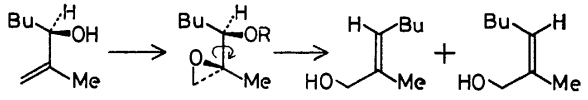

13 **14** R=H, **15** R=Ms **16**

Reduction of the mesylate **15** with dissolving calcium furnished an (*E*), (*Z*) mixture of allylic alcohols **16** in a ratio of ≈4: 1. Obviously, the oxirane ring opening is not in concert with the reductive cleavage of the mesylate moiety, but the indicated rotation around the C–C bond is allowed in the acyclic mesylate **15**.

Experimental

The optical rotations were measured using a Yanaco-OR-50 polarimeter. The infrared spectra were determined on a Shimadzu IR-27-G spectrometer; the mass spectra on a Hitachi RMU-6L mass machine; the glpc analyses on a Yanagimoto GCG-550F; and the NMR spectra on a JNM-PMX 60 or Varian EM-360 spectrometer. The chemical shifts are given in δ in ppm with TMS as the internal standard. Splitting patterns are designated as s, singlet; d, doublet; t, triplet; q, quartet; m, multiplet. The microanalyses were carried out by the staffs at the Elemental Analyses Center of Kyoto University. All experiments were carried out under an atmosphere of dry argon. Tetrahydrofuran was dried by distillation from sodium-benzophenone. During workup, drying of the organic solutions was performed over anhydrous sodium sulfate. Thin layer or preparative thick layer plates were made of E. Merck PF-254, and preparative column chromatography on silica gel E. Merck Art. 7734.

† Present Address: The Institute for Molecular Science, Myodaiji, Okazaki 444.
†† Present Address: Department of Chemistry, University of Hawaii at Manoa, Honolulu, Hawaii 96822.

Transformation of Geraniol (1) into Linalool (4). To a mixture of epoxy alcohol **2** (340 mg, 2.0 mmol) prepared from geraniol (**1**) according to the procedure of Sharpless,[2a] and triethylamine (0.3 ml, 2.2 mmol) dissolved in dichloromethane (3 ml) a solution of mesyl chloride (252 mg, 2.2 mmol) in dichloromethane (3 ml) was added drop by drop at −26 °C. After stirring at this temperature for 1 h, the reaction mixture was quenched in ice-cold water. The organic phase was removed and the aqueous layer was extracted with ether. The combined organic solutions were washed with saturated brine, dried, and concentrated *in vacuo* to leave a crude oil, which was purified by preparative TLC (1:1 hexane–ether) to furnish epoxy mesylate **3** (436 mg, 96 % yield): TLC, R_f 0.50 (1: 1 hexane–ether, 2 developments); IR (neat), 1450 (m), 1340—1360 (s), 1240 (w), 1170 (s), and 940—980 cm^{-1} (s); NMR ($CDCl_3$), 1.34 (3H, s, CH_3–CO), 1.64 (3H, s, CH_3–C=), 1.71 (3H, s, CH_3–C=), 2.89—3.24 (1H, m, CH–O), 3.03 (3H, s, CH_3–S), 4.13 and 4.41 (2H, dd, J=11 and 5 Hz, CH_2–OS), and 5.07 (1H, bt, CH=).

To a mixture of the mesylate **3** (248 mg, 1.0 mmol), THF (1 ml), and redistilled ammonia (10 ml) freshly polished calcium metal was added in small pieces at −35 to −37 °C (cooling bath temperature) with vigorous stirring and as rapidly as the metal dissolved, until the blue color persisted. After another 10 min, ammonium chloride (1.00 g) was added carefully to discharge the blue color. The cooling bath was removed and the mixture was poured into ice-cold water. The product was extracted with ether, dried, and freed of the solvent. The residue was submitted to preparative TLC (1: 1 hexane–ether) to give linalool (**4**) (136 mg, 88 % yield) as a clear oil which was homogeneous by TLC. IR and NMR spectra were superimposable on those of authentic specimen.

Linalool (**4**) was also prepared from **3** using the sodium-naphthalene reagent as follows. A green solution of sodium-naphthalene (3.0 mmol) in THF (10 ml) was prepared in the usual manner.[7] To this a solution of the mesylate **3** (124 mg, 0.5 mmol) in THF (1 ml) was added drop by drop over a period of 10 min at room temperature. Stirring was continued for 10 min and the reaction was terminated by the addition of ammonium chloride (1.00 g). The resulting mixture was partitioned between ether and ice-cold water and the organic layer was washed with saturated brine, dried, and concentrated *in vacuo*. Preparative TLC purification (1: 1 hexane–ether) of the residue gave linalool (**4**) (64 mg, 83 % yield). NMR analysis indicated that the product was almost free from impurities.

Transformation of Farnesol (5) into Nerolidol (8). The epoxy alcohol **6**[8] was converted to the mesylate **7** in 97 % yield as described above: TLC, R_f 0.23 (1: 1 hexane–ether); IR (neat), 1450 (s), 1350 (s), 1250 (m), 1160—1180 (s), and 950—980 cm^{-1} (s); NMR ($CDCl_3$), 1.33 (3H, s, CH_3–CO), 2.85—3.20 (1H, m, CH–O), 2.99 (3H, s, CH_3–S), 4.10—4.35 (2H, dd, CH_2–OS), and 4.82—5.23 (2H, m, CH=).

Freshly cut sodium was added in small pieces to a mixture of the mesylate **7** (316 mg, 1.0 mmol), THF (1 ml), and redistilled ammonia (10 ml) at −37 °C (cooling bath temperature) until the blue color persisted. After stirring for another 10 min, the reaction mixture was worked up according to the above mentioned procedure. After drying and concentrating *in vacuo*, the remaining liquid was submitted to preparative TLC (1: 1 hexane–ether) to furnish nerolidol (**8**)[5] (194 mg, 87 % yield) as a clear oil. This material was identical in all respects with the reported one.[5]

*Transformation of (−)-*cis*-Carveol (9) into the (+) Antipode (12).* According to the previously reported procedure,[9] (−)-*cis*-carveol (**9**) (18.24 g, 80 % yield, $[\alpha]_D^{25}$ −26.4 (c=5.6, C_2H_5OH)) was prepared from (−)-carvone (22.50 g, $[\alpha]_D^{25}$ −58 (neat)) by reduction with lithium aluminum hydride (226 mg) in THF (150 ml) and purified by column chromatography (5: 1 hexane–ether) followed by distillation (106—107 °C/10 Torr). From the known specific rotation,[6] the product was estimated to contain 98 % of (−)-*cis*-carveol (**9**) and 2 % of the *trans* isomer. GLPC analysis (10 % PEG 20 Mesh, 120 °C, 0.2 kg/cm^2) also showed the same isomer ratio.

A solution of *t*-butyl hydroperoxide (600 mg, 6.0 mmol) in benzene (8 ml) was added drop by drop to a mixture of (−)-*cis*-carveol (**9**) (608 mg, 4.0 mmol) and oxobis(2,4-pentanedionato-*O*,*O*′)vanadium(IV) (16 mg, 0.06 mmol) dissolved in benzene (8 ml) at 0 °C. After stirring at 50 °C for 4.5 h, the reaction mixture was cooled to room temperature and poured into saturated sodium sulfite. The product was extracted with ether, washed with water, dried, and freed of the solvent. The residue was submitted to column chromatography (5: 1 hexane–ether) to give epoxy alcohol **10** (420 mg, 64 % yield) as a pale yellow oil:[10] TLC, R_f 0.18 (1: 1 hexane–ether); IR (neat), 3400—3500 (s), 1370 (m), 1065 (m), 890 (s), and 860 cm^{-1} (m); NMR ($CDCl_3$), 1.25 (3H, s, CH_3–CO), 1.60 (3H, s, CH_3–C=), 3.10—3.25 (2H, m, CH–O), and 4.95 (2H, s, CH_2=). GLPC analysis (5 % PEG 20 Mesh, 140 °C, 0.2 kg/cm^2) showed that the product was >94 % chemically pure.

Treatment of **10** with mesyl chloride–triethylamine as described above afforded the epoxy mesylate **11** in 87 % yield: TLC, R_f 0.15 (1: 1 hexane–ether); IR (neat), 1450 (m), 1350 (s), 1170 (s), 960 (s), and 890 cm^{-1} (s); NMR ($CDCl_3$), 1.34 (3H, s, CH_3–CO), 1.60 (3H, s, CH_3–C=), 3.10 (3H, s, CH_3–S), 3.50—4.55 (2H, m, CH–O), and 4.98 (2H, s, CH_2=).

Dissolving sodium reaction with the epoxy mesylate **11** (246 mg, 1.0 mmol) furnished 57 % yield of (+)-*cis*-carveol (**12**)[11] (87 mg) as a clear oil: $[\alpha]_D^{25}$ +35.9 (c=4.3, C_2H_5OH), >92 % optically pure. IR, NMR, and mass spectra were identical with those of the authentic sample.

The sodium-naphthalene reagent also effected the same reductive cleavage to give **12** in 54 % yield.

*Transformation of (+)-*cis*-Carveol (12) into the (−) Antipode (9).* The same sequence described above afforded (−)-*cis*-carveol (**9**) $[\alpha]_D^{25}$ −23.0 (c=5.6, C_2H_5OH) (98 % optically pure) from **12** $[\alpha]_D^{25}$ +35.9 (c=5.6, C_2H_5OH) (95 % optically pure).

Preparation of (E)-2-Methyl-2-hepten-1-ol (16). The epoxy alcohol **14**[2b] was converted to the mesylate **15** in 95 % yield: bp 110 °C (bath temp, 1 Torr); TLC, R_f 0.28 (1: 1 hexane–ether); IR (neat), 1450 (s), 1360 (m), 1230—1240 (w), 1100 (m), and 970 cm^{-1} (s); NMR ($CDCl_3$), 1.21 (3H, s, CH_3–CO), 2.96 (2H, dd, CH_2–O), 3.03 (3H, s, CH_3–S), and 4.32 (1H, t, CH–O). Found: C, 48.8; H, 8.2 %. Calcd for $C_9H_{18}O_4S$: C, 48.6; H, 8.2 %.

The epoxy mesylate **15** (222 mg, 1.0 mmol) was treated with calcium metal in liq NH_3–THF as described above to give the alcohol **16** (74 mg, 58 % yield) as a clear oil: bp 120 °C (bath temp, 25 Torr); TLC, R_f 0.35 (1: 1 hexane–ether); IR (neat), 3300—3360 (s), 1470 (m), 1380 (m), and 1005 cm^{-1} (s); NMR (CCl_4), 1.75 (3H, s, CH_3–C=), 4.12 (2H, s, CH_2–O), and 5.29 (1H, bt, CH=); MS (m/e), 128 (M^+).

Found: C, 74.7; H, 12.7 %. Calcd for $C_8H_{16}O$: C, 74.9; H, 12.6 %.

GLPC analysis (20 % PEG 20 Mesh, 130 °C, 0.4 kg/cm^2) of the product showed two peaks in the ratio of 81: 19. The major peak, having the longer retention time, was ascribed to the (*E*) isomer by comparison with the previously reported results.[12]

The authors wish to thank the Ministry of Education, Japan, for Grant-in-Aid (No. 011010, 110309, 203014,

and 303023).

References

1) A preliminary account of this work has appeared: A. Yasuda, H. Yamamoto, and H. Nozaki, *Tetrahedron Lett.*, **1976**, 2621. *Cf.* After the publication of our preliminary results, Marshall *et al.* employed the similar procedure in the synthesis of confertin: J. A. Marshall and R. H. Ellison, *J. Am. Chem. Soc.*, **98**, 4312 (1976).

2) (a) K. B. Sharpless and R. C. Michaelson, *J. Am. Chem. Soc.*, **95**, 6136 (1973); (b) S. Tanaka, H. Yamamoto, H. Nozaki, K. B. Sharpless, R. C. Michaelson, and J. D. Cutting, *ibid.*, **96**, 5254 (1974).

3) (a) J. C. Carnahan, Jr. and W. D. Closson, *Tetrahedron Lett.*, **1972**, 3447; (b) S. Bank and M. Platz, *ibid.*, **1973**, 2097.

4) Several related methods were reported for preparing linalool from derivatives of geraniol; (a) From citral, G. V. Nair and G. D. Pandit, *Tetrahedron Lett.*, **1966**, 5097; (b) From geranyl iodide, S. K. Pradhan and V. M. Girijavollabhan, *ibid.*, **1968**, 3103.

5) L. Ruzicka, *Helv. Chim. Acta*, **6**, 483, 492 (1923).

6) R. G. Johnson and J. Read, *J. Chem. Soc.*, **1934**, 233.

7) W. D. Closson, P. Wriede, and S. Bank, *J. Am. Chem. Soc.*, **88**, 1581 (1966).

8) S. Tanaka, A. Yasuda, H. Yamamoto, and H. Nozaki, *J. Am. Chem. Soc.*, **97**, 3252 (1975).

9) H. G. Kuivila and O. F. Beumel, Jr., *J. Am. Chem. Soc.*, **83**, 1246 (1961).

10) M. Narayanaswamy, V. M. Sathe, and A. S. Rao, *Chem. Ind. (London)*, **1969**, 921.

11) R. H. Reitsema, *J. Am. Chem. Soc.*, **75**, 1996 (1953).

12) E. J. Corey and H. Yamamoto, *J. Am. Chem. Soc.*, **92**, 226, 3523 (1970), and references cited therein.

A Highly Stereoselective Synthesis of Trisubstituted Ethylenes from α-Trialkylsilyl Ketones[1,2]

Michio OBAYASHI, Kiitiro UTIMOTO,* and Hitosi NOZAKI
Department of Industrial Chemistry, Kyoto University, Yoshida, Kyoto 606
(Received February 19, 1979)

A novel procedure for preparing trisubstituted ethylenes stereoselectively is based on the reaction of α-trialkylsilyl-substituted ketones with alkyllithium reagents and on the following highly discriminative elimination of the silyl and oxido (or hydroxyl) groups from the resulting adducts. The *syn*-elimination of both groups is observed under basic conditions, while the reaction proceeds in *anti*-fashion on acid treatment. Furthermore α-trimethylsilylated ketones are shown to be readily obtained from 2-trimethylsilyl-2,3-dialkyloxiranes. The reaction sequence is applied to the stereoselective synthesis of tetrahomonerol which has been obtained from the codling moth.

Synthesis of trisubstituted ethylenes[3,4] has received considerable attention because of the widespread occurrence of these olefin units in many classes of naturally occurring compounds. Furthermore, recent progress in organic synthesis *via* silicon compounds[5] has disclosed novel methods for the synthesis of 1,2-disubstituted ethylenes with rigorous stereochemistry.[6] This paper describes a facile procedure for the stereoselective synthesis of trisubstituted ethylenes *via* reaction of α-trialkylsilyl ketones with alkyllithium reagents followed by *syn*-elimination under basic conditions or by *anti*-elimination on acid treatment.[7,8]

Reaction of 5-trimethylsilyl-4-decanone (Ia)[1] with MeLi in THF at −78 °C afforded a reaction mixture containing IIa.[9] Treatment of the reaction mixture directly with KO^{t}Bu (Run 1 in Table 1) afforded (*E*)-4-methyl-4-decene (III)[10] in 76% overall yield as shown in Scheme 1. When the reaction mixture was treated with glacial acetic acid saturated with sodium acetate (Run 5), the (*Z*)-isomer IV was obtained with *E*/*Z* ratio of 12/88.[11] On the contrary the elimination with concentrated sulfuric acid (Run 7) gave less the stereoselectivity. Similar results were obtained in the case of 5-triethylsilyl-4-decanone (Ib). These and other data are summarized in Table 1.[12,13]

Further information about the stereoselectivity of this olefin synthesis was obtained from the reaction of 3-trimethylsilyl-2-octanone with *n*-PrLi. Treatment of the reaction mixture with KO^{t}Bu gave IV in 21% yield (*E*/*Z*=4/96) *via* the diastereomer of II.[15]

Clearly β-trialkylsilyl alcoholates II are produced from α-trialkylsilyl ketones and alkyllithium reagents with high stereoselectivity. Although it was unsuccessful to directly determine the diastereomeric composition of the alcoholate II or the respective alcohol, the composition was inferred from the *E*/*Z* ratios of the olefins obtained in the elimination reactions. The high selectivity of this carbonyl addition is explained formally by the Felkin model,[16] in which the separation between the trialkylsilyl group and the incoming alkyllithium is the greatest.

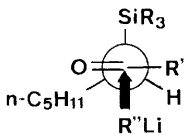

The lithium salt or the potassium salt of the alcohol produces a trisubstituted ethylene by *syn*-elimination of trialkylsilyl and oxido groups. Comparison of Runs 1 and 2, or Runs 3 and 4 as well, indicates that the *syn*-elimination from the lithium salt is slower than that from the potassium salt. On the other hand, acidic treatment of the alcoholates II directly or of the isolated alcohols induces *anti*-elimination of trialkylsilyl and hydroxyl groups as shown in Scheme 2.[6a-c] Poor stereoselectivity is observed when such nucleophiles having weak affinity to silicon as HSO_4^- or H_2O are present (Runs 7 and 8). Meanwhile, nucleophiles with strong affinity to silicon such as AcO^- and F^- give much improved selectivity data (Runs 5, 9—12). Probably in the absence of suitable nucleophiles, C–C bond rotation of the β-silyl carbocation V competes with the *anti*-elimination. The effective nucleophiles obviously favor the concerted *anti*-elimination of the intermediate VI without the loss of stereochemistry. Runs 11 and 12, indicate that the acid strength is an additional factor influencing the *E*/*Z* ratio.

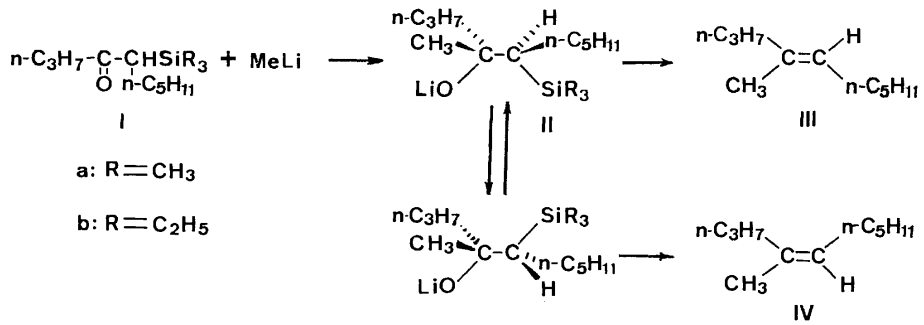

Scheme 1.

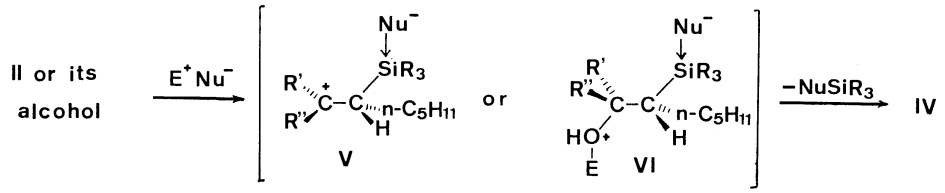

Scheme 2.

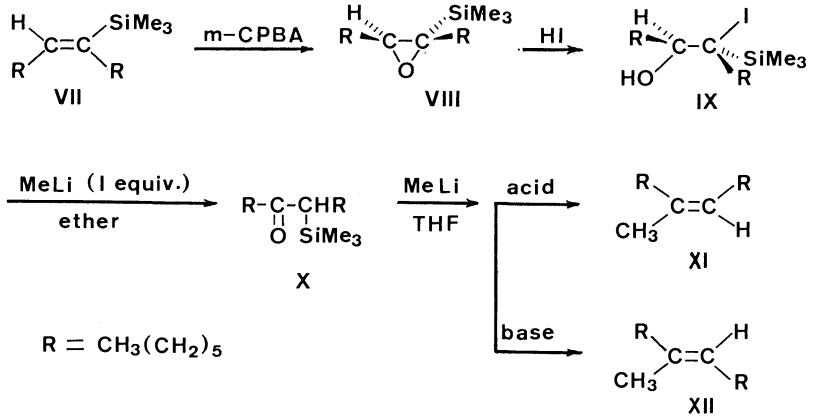

Scheme 3.

Furthermore as shown in Scheme 3, both isomers (XI and XII) of a trisubstituted ethylene have been obtained from the silylated olefin (VII) *via* the trialkylsilyloxirane (VIII) and the iodohydrin (IX). Treatment of IX with 1 equivalent of MeLi in ether afforded α-trimethylsilyl ketone (X). The resulting mixture was further treated with MeLi (3 equiv.) at −78 °C affording (*Z*)-7-methyl-7-tetradecene (XI) after acidic work-up (Scheme 3 and Table 2). Reaction of IX with 4 equivalents of MeLi in ether at −78 °C gave the same result. The stereoselectivity of the olefin formation is rather low as compared with the previous reaction (for example, Run 5 in Table 1). Remarkably, the *E*/*Z* selectivity of olefin formation is much improved by the coexistence of THF in the MeLi-treatment of X.

An application of these stereoselective olefin formations has provided (2*Z*,6*Z*)-7-methyl-3-propyl-2,6-decadien-1-ol (XIX), which is known to be a tetrahomonerol obtained from the codling moth (Scheme 4).[17] Silyloxirane (XIV) prepared from XIII[6k] was converted to XVII by the following two ways. Isomerization of silyloxirane XIV[1b] in the presence of MgI_2 gave α-trimethylsilyl ketone (XVI). Further treatment

Table 1. Transformation of 5-trialkylsilyl-4-decanone (Ia and Ib) to 4-methyl-4-decene (III and IV)

Run No.	I	Addition[a] condition	Elimination condition (temp)	Olefin %[b]	III/IV[c] (*E*/*Z*)
1	a	A	KO^{t}Bu (refl.)	76	91/9
2	a	B	— (refl.)	53	86/14
3	b	B	KO^{t}Bu (refl.)	76	91/9
4	b	B	— (refl.)	30	—[e]
5	a	A	AcONa/AcOH (−20 °C)	69	12/88
6	a	0 °C-r.t./ 0.5 h	AcONa/AcOH (−20 °C)	—[e]	20/80
7	a	A	H_2SO_4 (r.t.)[d]	69	24/76
8	a	B	H_2SO_4 (r.t.)[d]	80	50/50
9	b	B	AcONa/AcOH (−20 °C)	57	10/90
10	b	B	AcONa/AcOH (−20 °C)[d]	46	10/90
11	b	B	KF/AcOH (r.t.)[d]	72	12/88
12	b	B	KF/H_2SO_4 (r.t.)[d]	84	18/82

a) A: Addition of MeLi was carried out at −78 °C and then the mixture was allowed to stand at a room-temperature for 1—1.5 h. B: The addition occurred at −78 °C and then the reaction completed at a room-temperature overnight. b) Yield determined by GLPC using dodecane as an internal standard. c) Determined by GLPC. d) Carried out after hydrolytic work-up of II. e) Not determined.

Table 2. Conversion of iodohydrin (IX) to trisubstituted ethylenes (XI and XII)

MeLi[a] Equiv.	MeLi[a] Temp	MeLi[b] Equiv.	Elimination condition	Olefin %[d]	XI/XII[c] (*Z*/*E*)
1	−20 °C	3[c]	AcONa/AcOH	84	86/14
4	−78 °C	—	AcONa/AcOH	85	84/16
1	−20 °C	3	AcONa/AcOH	74	91/9
4	−78 °C	—	KO^{t}Bu	78	15/85
1	−20 °C	3	KO^{t}Bu	79	9/91

a) The amount of MeLi (ether) admixed initially. b) The amount of MeLi (ether) added (at −78 °C) to the isomerization mixture, which was diluted with THF in advance. c) Without dilution with THF, the reaction was carried out in ether. d) Overall yield from VIII. e) Determined by GLPC.

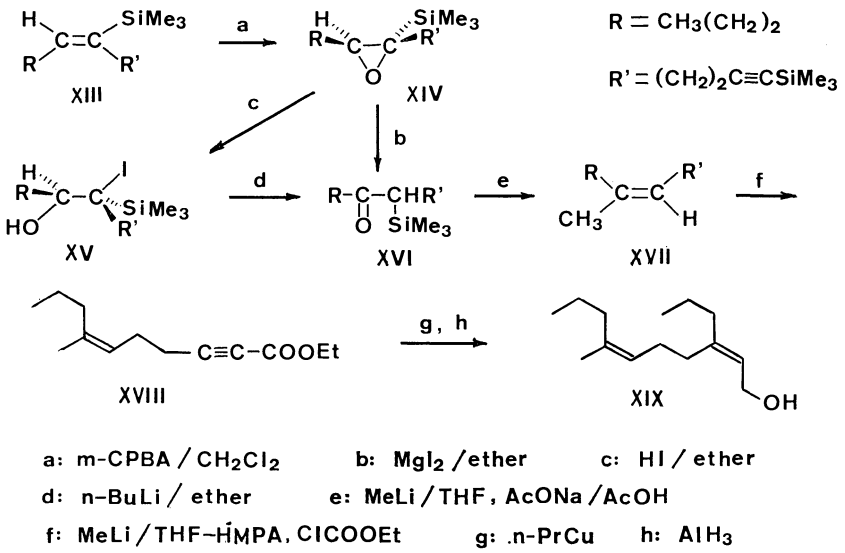

Scheme 4.

of XVI with MeLi, AcONa/AcOH afforded XVII. Secondly, iodohydrin (XV) obtained from XIV was treated with *n*-BuLi (1 equiv.) followed by MeLi giving XVII after acidic work-up. Direct ethoxycarbonylation of XVII to acetylenic ester XVIII was effected by treatment with MeLi/THF–HMPA[18] and then with ClCOOEt. The acetylenic ester was finally transformed into XIX by the reported procedure.[17]

Experimental

GLPC was performed on Shimadzu GC-4BPT with 3 m×3 mm glass column packed with 20 % polyethylene glycol and 20 % HVSG on Chromosorb W-AW (80—100 mesh). Mass spectra were obtained on Hitachi RMU-6L with 70 V chamber voltage. NMR were measured on Varian EM-360, JEOL JNM-PMX 60, and Varian EM-390 with Me_4Si as internal standard and CCl_4 as solvent. IR on Shimadzu IR-27G spectrometer. Elemental microanalyses were performed by Elemental Analyses Center of Kyoto University. All the reactions were carried out under an atmosphere of dry argon.

Reaction of α-Trialkylsilyl Ketones (I) with Alkyllithium Reagents. (E)-4-Methyl-4-decene (III, Run 1): To a solution of 5-trimethylsilyl-4-decanone (Ia, 0.23 g, 1 mmol) in 5 ml of THF was added MeLi (3 mmol, 3.5 ml of 0.87 M ethereal solution) at −78 °C. The mixture was stirred at a room-temperature for 1 h and treated with KO^{t}Bu (1.0 g, 9 mmol) at reflux for 1 h. The resulting mixture was poured into aq NH_4Cl overlaid with hexane, washed (aq NH_4Cl, sat. NaCl), and dried (Na_2SO_4). GLPC analysis indicated that III was formed in 76 % overall yield (E/Z=91/9). Bp 93—96 °C/21 mmHg; IR (neat) 1380 cm^{-1}; MS *m/e* (rel. %), 154 (M^+, 11), 111 (13), 97 (22), 84 (16), 69 (52), 55 (100); NMR (CCl_4) δ=0.60—1.03 (6H, m), 1.03—1.70 (8H, m), 1.55 (3H, br-s), 1.70—2.20 (4H, m), 5.03 (1H, t, J=7 Hz).

Found: C, 85.50; H, 14.45 %. Calcd for $C_{11}H_{22}$: C, 85.63; H, 14.37 %.

(Z)-4-Methyl-4-decene (IV, Run 5): The reaction mixture from Ia (1 mmol) and MeLi (3 mmol) was treated with 10 ml of glacial acetic acid saturated with sodium acetate under stirring at −20 °C for 30 min and at a room-temperature overnight. The resulting mixture was poured into sat. NaCl overlaid with hexane, washed (sat. $NaHCO_3$, sat. NaCl), and dried (Na_2SO_4). GLPC analysis indicated that IV was formed in 69 % overall yield (E/Z=12/88). Bp 90—95 °C/21 mmHg; IR (neat) 1380 cm^{-1}; MS *m/e* (rel. %), 154 (M^+, 15), 111 (15), 97 (23), 84 (19), 69 (57), 55 (100); NMR (CCl_4) δ=0.60—1.03 (6H, m), 1.03—1.70 (8H, m), 1.63 (3H, br-s), 1.70—2.15 (4H, m), 5.01 (1H, t, J=7 Hz).

Found: C, 85.77; H, 14.40 %. Calcd for $C_{11}H_{22}$: C, 85.63; H, 14.37 %.

4-Phenyl-4-decene: To a solution of Ia (0.23 g, 1 mmol) in 5 ml of THF was added PhLi (3 mmol, 3.5 ml of 0.87 M ethereal solution) at −78 °C. The mixture was stirred at a room-temperature for 1 h and poured into aq NH_4Cl overlaid with ether. The ether layer was washed (aq NH_4Cl, sat. NaCl) and dried (Na_2SO_4). The concentrate was dissolved in 5 ml of THF and treated with a few drops of concentrated H_2SO_4 at a room-temperature for 1 h. The reaction mixture was poured into sat. $NaHCO_3$ overlaid with hexane, washed (sat. $NaHCO_3$, sat. NaCl), and dried (Na_2SO_4). Chromatography of the concentrate on silica-gel column (hexane) afforded 0.11 g (52 %) of 4-phenyl-4-decene (E/Z=39/61). The mixture formed an oil; IR (neat) 1601, 1492, 1380, 705 cm^{-1}; NMR (CCl_4) δ=0.65—1.10 (6H, m), 1.10—1.67 (8H, m), 1.67—2.60 (4H, m), 6.90—7.70 (5H, m) and two olefinic signals at 5.35 (br-t, J=7 Hz, C=CH of (4*Z*)-isomer) and 5.58 (br-t, J=7 Hz, C=CH of (4*E*)-isomer). The sum of these olefinic signals was equal to 1H. GLPC gave each isomer in pure form.

(4E)-Isomer: MS *m/e* (rel. %), 216 (M^+, 19), 173 (31), 159 (16), 131 (20), 118 (33), 117 (100), 105 (14), 91 (49), 77 (7), 55 (5), 41 (12), 40 (48), 29 (32).

Found: C, 88.80; H, 11.44 %. Calcd for $C_{16}H_{24}$: C, 88.82; H, 11.18 %.

(4Z)-Isomer: The mass spectrum was very similar to that of (4*E*)-isomer.

Found: C, 88.55; H, 11.24 %. Calcd for $C_{16}H_{24}$: C, 88.82; H, 11.18 %.

Reaction of (7S,8S*)-8-Iodo-8-trimethylsilyl-7-tetradecanol (IX) with MeLi.* Iodohydrin (IX) was prepared according to the reported procedure from (2*S**,3*S**)-2-trimethylsilyl-2,3-dihexyloxirane (VIII).[1c]

(Z)-7-Methyl-7-tetradecene (XI): To a solution of IX (0.41

g, 0.98 mmol) in 5 ml of ether was added MeLi (0.98 mmol, 0.61 ml of 1.63 M ethereal solution) at −20 °C. The mixture was stirred at a room-temperature for 1 h and treated with 5 ml of THF and MeLi (3 mmol, 1.84 ml of 1.63 M ethereal solution) at −78 °C. The resulting mixture was stirred at a room-temperature for 1 h and treated with 5 ml of glacial acetic acid saturated with sodium acetate under stirring at −20 °C for 0.5 h and at a room-temperature overnight. The mixture was poured into sat. NaCl overlaid with hexane, washed (sat. $NaHCO_3$, sat. NaCl), and dried ($MgSO_4$). Chromatography of the concentrate on silica-gel column (hexane) afforded 0.16 g of XI (yield, 74 % based on 1 mmol of VIII, E/Z=9/91). Bp 115—120 °C/4 mmHg; IR (neat) 1368 cm^{-1}; MS *m/e* (rel. %) 210 (M^+, 12), 181 (0.6), 140 (10), 125 (16), 112 (14), 111 (17), 97 (26), 84 (25), 83 (65), 71 (17), 70 (100), 43 (33), 41 (50), 29 (23); NMR (CCl_4) δ=0.88 (6H, t, J=6 Hz), 1.05—1.50 (16H, m), 1.62 (3H, s), 1.70—2.10 (4H, m).

Found: C, 85.22; H, 14.33 %. Calcd for $C_{15}H_{30}$: C, 85.63; H, 14.37 %.

(E)-7-Methyl-7-tetradecene (XII): The reaction mixture from IX (0.39 g, 0.94 mmol) and MeLi (0.94 mmol, 0.58 ml of 1.63 M ethereal solution) was treated with 5 ml of THF and MeLi (3 mmol) at −78 °C. The resulting mixture was stirred at a room-temperature for 1 h and poured into sat. $NaHCO_3$ overlaid with ether. The ether layer was washed (sat. $NaHCO_3$, sat. NaCl) and dried ($MgSO_4$). The concentrate was dissolved in 5 ml of THF and treated with KO^{t}Bu (1.0 g, 8 mmol) at a room-temperature for 1 h. The resulting mixture was poured into aq. NH_4Cl overlaid with hexane, washed (aq NH_4Cl, sat. NaCl) and dried ($MgSO_4$). Chromatography of the concentrate on silica-gel column (hexane) afforded 0.17 g of XI (yield, 79 % based on 1 mmol of VIII, E/Z=91/9). Bp 115—120 °C/4 mmHg; IR (neat) 1368 cm^{-1}; NMR (CCl_4) δ=0.88 (6H, t, J=6 Hz), 1.05—1.50 (16H, m), 1.53 (3H, s), 1.75—2.10 (4H, m). The mass spectrum was very similar to that of (7*Z*)-isomer.

Found: C, 86.27; H, 14.47 %. Calcd for $C_{15}H_{30}$: C, 85.63; H, 14.37 %.

(2Z,6Z)-7-Methyl-3-propyl-2,6-decadien-1-ol (XIX). (2S, 3S*)-2-Trimethylsilyl-2-(4-trimethylsilyl-3-butynyl)-3-propyloxirane (XIV)*: Treatment of (*E*)-1,5-bis(trimethylsilyl)-5-nonen-1-yne (XIII, 1.0 g, 3.9 mmol) with *m*-chloroperbenzoic acid (85 % purity, 1.0 g, 5 mmol) in CH_2Cl_2 at 0 °C overnight gave 1.1 g (quantitative yield) of XIV. IR (neat) 2200, 1245, 837, 758, 696, 640 cm^{-1}; MS *m/e* (rel. %), 282 (M^+, 0.2), 267 (0.2), 253 (2), 239 (3), 225 (8), 171 (9), 169 (5), 147 (15), 133 (5), 91 (5), 83 (4), 75 (13), 74 (9), 73 (100), 59 (8), 43 (5); NMR (CCl_4) δ=0.03 (9H, s), 0.10 (9H, s), 0.75—1.15 (3H, m), 1.15—2.50 (8H, m), 2.61 (1H, br-t, J=6 Hz).

Found: C, 63.82; H, 10.88 %. Calcd for $C_{15}H_{30}OSi$: C, 63.76; H, 10.70 %.

Conversion of XIV to (Z)-1-Trimethylsilyl-6-methyl-5-nonen-1-yne (XVII) Involving the Isomerization of XIV to 5,9-Bis(trimethylsilyl)-8-nonyn-4-one (XVI) in the Presence of MgI_2: To a solution of MgI_2 (10 mmol) in 10 ml of ether was added XIV (0.28 g, 1 mmol dissolved in 10 ml of ether). The resulting mixture was stirred at reflux for 2 h and then treated with 6 ml of 1,4-dioxane at 0 °C overnight. The solution was freed from solids by filtration. The solids were washed with hexane several times and the combined organic layer was washed (sat. $NaHCO_3$, sat. NaCl), dried ($MgSO_4$), and concentrated affording 0.28 g (98 %) of XVI. Oil; IR (neat) 2200, 1686, 1246, 840, 761, 700, 642 cm^{-1}; MS *m/e* (rel. %), 282 (M^+, 1), 267 (2) 253 (3), 239 (2), 225 (2), 209 (5), 172 (10), 171 (61), 147 (11), 143 (12), 130 (32), 115 (5), 75 (22), 74 (9), 73 (100), 59 (7), 45 (16), 43 (7). To a solution of XVI (0.28 g, 0.98 mmol) in 2 ml of THF was added MeLi (3 mmol, 2.9 ml of 1.04 M ethereal solution) at −78 °C. The mixture was stirred at 0 °C for 1 h and treated with 3 ml of glacial acetic acid saturated with sodium acetate under stirring at −20 °C for 30 min and at a room-temperature overnight. The resulting mixture was poured into sat. NaCl overlaid with hexane, washed (sat. $NaHCO_3$, sat. NaCl), and dried (Na_2SO_4). Chromatography of the concentrate on silica-gel column (hexane) afforded XVII (0.11 g, yield, 51 % based on XIV, E/Z=5/95). Bp 104—108 °C/17 mmHg; IR (neat) 2210, 1247, 844, 763, 701, 645 cm^{-1}; MS *m/e* (rel. %), 208 (M^+, 0.6), 193 (3), 179 (4), 165 (2), 149 (5), 144 (12), 119 (6), 105 (5), 97 (37), 96 (15), 83 (7), 81 (16), 75 (3), 74 (7), 73 (65), 69 (10), 59 (22), 55 (100), 43 (12); NMR (CCl_4) δ=0.10 (9H, s), 0.90 (3H, t, J=6 Hz), 1.10—1.65 (2H, m), 1.67 (3H, br-s), 1.80—2.40 (6H, m), 5.14 (1H, br-t, J=6 Hz).

Found: C, 75.05; H, 11.74 %. Calcd for $C_{13}H_{24}Si$: C, 74.92; H, 11.61 %.

Conversion of XIV to XVII via (4S,5S*)-5,9-Bis(trimethylsilyl)-5-iodo-8-nonyn-4-ol (XV)*: To a solution of XIV (0.37 g, 1.3 mmol) in 5 ml of ether was added 0.6 ml of 57 % HI at −20 °C. After 20 min the mixture was poured into sat. $NaHCO_3$ overlaid with ether. The ether layer was washed (10 % $Na_2S_2O_3$, sat. $NaHCO_3$, sat. NaCl), dried ($MgSO_4$), and concentrated, affording 0.50 g (29 %) of XV. To a solution of XV (0.50 g, 1.2 mmol) in 5 ml of ether was added *n*-BuLi (1.2 mmol, 1.5 ml of 0.82 M hexane solution) at −20 °C. The mixture was stirred at room temperature for 0.5 h and treated with 5 ml of THF and MeLi (3.7 mmol, 2.2 ml of 1.63 M ethereal solution) at −78 °C. Work-up gave XVII (0.16 g, yield, 57 % based on XIV, E/Z=5/95).

Transformation of XVII into (2Z,6Z)-7-Methyl-3-propyl-2,6-decadien-1-ol (XIX): To a solution of XVII (0.10 g, 0.48 mmol) in 2 ml of THF and 1 ml of HMPA was added MeLi (0.6 mmol, 0.58 ml of 1.04 M ethereal solution) at −78 °C. The mixture was stirred at −30 °C for 1 h and treated with ClCOOEt (0.06 ml, 0.6 mmol) at −78 °C. The resulting mixture was stirred at a room-temperature for 0.5 h and poured into sat. $NaHCO_3$ overlaid with ether. The ether layer was washed (sat. $NaHCO_3$, sat. NaCl) and dried ($MgSO_4$). Chromatography of the concentrate on silica-gel column (benzene) gave 70 mg (70 %) of ethyl (*Z*)-7-methyl-6-decen-2-ynoate (XVIII, E/Z=4/96). IR (neat) 2265, 1709, 1371, 1360, 1243, 1070, 757 cm^{-1}; MS *m/e* (rel. %), 208 (M^+, 0.5), 193 (1), 180 (16), 151 (7), 149 (5), 135 (8), 134 (7), 121 (7), 112 (15), 111 (7), 97 (26), 84 (16), 69 (11), 56 (8), 55 (100), 43 (8), 41 (13); NMR (CCl_4) δ=0.88 (3H, t, J=6 Hz), 1.25 (3H, t, J=7 Hz), 1.10—1.53 (2H, m), 1.65 (3H, br-s), 1.75—2.15 (2H, m), 2.15—2.40 (4H, m), 4.04 (2H, q, J=7 Hz), 4.80—5.25 (1H, m). The product XVIII was transformed into the tetrahomonerol XIX according to the reported procedure.[16] IR (neat) 3300, 1659, 1366, 1239, 1002, 833, 750 cm^{-1}; MS (as trimethylsilyl ether) *m/e* (rel. %), 282 (M^+, 10), 267 (3), 239 (12), 197 (13), 192 (10), 171 (11), 169 (15), 161 (25), 156 (15), 155 (11), 149 (48), 143 (10), 129 (12), 121 (24), 119 (25), 97 (38), 93 (18), 91 (20), 81 (20), 79 (22), 75 (59), 73 (81), 55 (100), 43 (23), 41 (22); NMR (CCl_4) δ=0.90 (6H, t, J=6 Hz), 1.10—1.77 (4H, m), 1.67 (3H, br-s), 1.77—2.40 (9H, m), 4.02 (2H, br-d, J=7 Hz), 5.10 (1H, m), 5.33 (1H, t, J=7 Hz).

The authors wish to thank the Ministry of Education, Science and Culture, Japan, for the Grant-in-Aid (911506, 011010, 110309, 203014, 303023).

References

1) Preliminary reports dealing with certain aspects of this

work have appeared: (a) K. Utimoto, M. Obayashi, and H Nozaki, *J. Org. Chem.*, **41**, 2940 (1976); (b) M. Obayashi, K. Utimoto, and H. Nozaki, *Tetrahedron Lett.*, **1977**, 1807; (c) M. Obayashi, K. Utimoto. and H. Nozaki, *ibid.*, **1978**, 1383.

2) α-Trialkylsilyl ketone means α-trialkylsilyl-substituted ketone in this paper.

3) For reviews of olefin synthesis see (a) I. Reucroft and P. G. Sammes, *Q. Rev. Chem. Soc.*, **25**, 135 (1971); (b) A. S, Arora and I. K. Ugi, "Methoden der Organischen Chemie (Houben-Weyl)," 4th ed, ed by E. Müller, G. Thieme Verlag, Stuttgart (1972), Vol. V/lb, pp. 728—945.

4) For recent methods for the synthesis of trisubstituted ethylenes see (a) A. Marfat, P. R. McGuirk, and P. Helquist, *Tetrahedron Lett.*, **1978**, 1363; (b) D. E. van Horn and E. Negishi, *J. Am. Chem. Soc.*, **100**, 2252 2254 (1978) and references cited therein.

5) For recent reviews see (a) I. Fleming, *Chem. Ind. (London)*, **1975**, 449; (b) P. F. Hudrlik, "New Application of Organometallic Reagents in Organic Synthesis," J. Organomet. Chem. Library, ed by D. Seyferth, Elsevier, Amsterdam (1976), Vol. 1, p. 127; (c) E. W. Colvin, *Chem. Soc. Rev.*, **7**, 15 (1978).

6) (a) P. F. Hudrlik and D. Peterson, *Tetrahedron Lett.*, **1974**, 1133; (b) P. F. Hudrlik and D. Peterson, *J. Am. Chem. Soc.*, **97**, 1464 (1975); (c) P. F. Hudrlik, D. Peterson, and R. J. Rona, *J. Org. Chem.*, **40**, 2263 (1975); (d) K. Utimoto, M. Kitai, and H. Nozaki, *Tetrahedron Lett.*, **1975**, 2825; (e) P. B. Dervan and M. A. Shippey, *J. Am. Chem. Soc.*, **98**, 1265 (1976); (f) J. J. Eisch and G. A. Damasevitz, *J. Org. Chem.*, **41**, 2214 (1976); (g) K. Uchida, K. Utimoto, and H. Nozaki, *ibid.*, **41**, 2215 (1976); (h) K. Uchida, K. Utimoto, and H. Nozaki, *ibid.*, **41**, 2941 (1976); (i) K. Uchida, K. Utimoto and H. Nozaki, *Tetrahedron*, **33**, 2987 (1977); (j) T. H. Chan, W. Michajlowskij, B. S. Ong, and D. N. Harpp, *J. Organomet. Chem.*, **107**, Cl (1976); (k) M. Obayashi, K. Utimoto, and H. Nozaki, *Tetrahedron Lett.*, **1977**, 1805; (l) W. Michajl owskij and T. H. Chan, *ibid.*, **1976**, 4439.

7) Stereochemistry of olefin-forming reaction from β-trialkylsilyl alcohols was studied in ref. 6a—c and 6e.

8) 1,1-Disubstituted ethylenes were prepared by analogous procedures: (a) P. F. Hudrlik and D. Peterson, *Tetrahedron Lett.*, **1972**, 1785; (b) R. A. Ruden and B. L. Gaffney, *Synth. Commun.*, **5**, 15 (1975).

9) The corresponding alcohol was obtained in 80 % yield by hydrolytic work-up.

10) The structures of III and IV are based on NMR analysis.

11) This mixture did not contain other isomers. We could not detect (*E*)- and (*Z*)-4-methyl-3-decene from the product mixture.

12) In further attempts for preparation of IV treatment of IIb with $HSCH_2COOH$ gave IV in 61 % yield, *E*/*Z*=46/54; with BF_3-OEt_2, 82 %, 37/63.

13) When α-trimethylsilylketone (Ia) was treated with MeMgBr in place of MeLi, IV was obtained in 22 % yield (*E*/*Z*=23/77) after acidic work-up (AcONa/AcOH). Reaction of Ia with PhLi gave 4-phenyl-4-decene in 52 % yield (*E*/*Z*=39/61) after treatment of the reaction mixture with H_2SO_4.[14]

14) Treatment of the reaction mixture with KO^{t}Bu or AcONa/AcOH gave no olefinic products. Sulfuric acid produces a benzyl-type cation which gives 4-phenyl-4-decene by the elimination of Me_3Si group.

15) Propyllithium may abstract proton from methyl ketone in 3-trimethylsilyl-2-octanone. This side reaction may be responsible for the decreased overall yield of IV.

16) M. Cherst, H. Felkin, and N. Prudent, *Tetrahedron Lett.*, **1968**, 2199.

17) (a) S. B. Bowlus and J. A. Katzenellenbogen, *Tetrahedron Lett.*, **1973**, 1277; (b) S. B. Bowlus and J. A. Katzenellenbogen, *J. Org. Chem.*, **38**, 2733 (1973); (c) M. P. Cooke, *Tetrahedron Lett.*, **1973**, 1281.

18) This procedure is, to the best of our knowledge, the first, direct,[19] and irreversible transformation of silylacetylene to the acetylide. The same treatment of *n*-$C_6H_{13}C{\equiv}CSiMe_3$ gave *n*-$C_6H_{13}C{\equiv}CCOOEt$ in 93 % yield.

19) For stepwise transformation of silylacetylene to the acetylide see E. J. Corey, J. A. Katzenellenbogen, N. W. Gilman, S. A. Roman, and B. W. Erickson, *J. Am. Chem. Soc.*, **90**, 5618 (1968).

A Theoretical Treatment of the Difference in the Fragmentation of Urea and Acetamide

Tsutomu TAKAGI* and Masayoshi OIWA

Department of Applied Chemistry, Faculty of Engineering, Kansai University, Suita, Osaka 564

(Received June 21, 1978)

The difference in the hydrogen migration in urea and acetamide under electron impact has been discussed from the standpoint of the all-valence electron semi-empirical SCF-MO theory (CNDO/2). The features of the molecular ion in the ground state and the hydrogen-migration models for both compounds were estimated based on the variations in the total and the partitioned energies. The variation in the total energy with the hydrogen migration in urea was smaller than that in acetamide. Moreover, the bonding interaction between carbon and nitrogen becomes weak; the cleavage of the migrated molecular ion to NH_3 was predicted. On the other hand, the weak bonding interaction between carbon and carbon in acetamide does not change through the migration of hydrogen. It is predicted that the α-cleavage in the C–C bond will occur in preference to the migration of hydrogen. Finally, in acetamide, it was found that the possibility of the migration of hydrogen is lower than that in urea, judging from the variations in the total and the partitioned energies.

It is interesting to ascertain the hydrogen-migration process involved in fragmentation from the standpoint of the molecular orbital (MO) theory. The analyses, by MO theory, of the mass spectral data of the organic compounds have not been completely established because of the complexity of the driving factors governing the cleavage of the molecular ion ($M^{\ddagger}$) on electron-impact collision.

The mass spectra of urea[1] and acetamide[2] have been reported. In the mass spectrum of urea, a peak thought to be the ion formed by the migration of hydrogen has been observed. This shows that the NH_3 ion with *m/e* 17 is richly abundant, accompained by the migration of hydrogen from one nitrogen to another nitrogen. On the other hand, in acetamide the most important fragmentation arises from α-cleavage, resulting in the formation of an ion with a mass of 44. The migration of hydrogen from carbon to nitrogen does not appear as clearly as that of urea. This fragmentation of acetamide has, however, not been fully elucidated, but only speculated from the mass spectral data.

This paper will describe an attempt to analyze the hydrogen migration in urea and the possibility of the migration of hydrogen in acetamide by calculations based on the CNDO/2 method.

Method and Calculations

Interaction Energies. These discussions were supported by unrestricted open-shell SCF calculations with a CNDO/2 approximation. The total molecular energy, E, can be expressed by the sum of one- and two-center terms:[3]

$$E_{\text{total}} = \sum_{A} E_A + \sum_{A<B} E_{AB}$$

where

$$E_A = \sum_{r}^{A} p_{rr} U_{rr} + \frac{1}{2} \sum_{r}^{A} \sum_{s}^{A} \{p_{rr} P_{ss} - (p_{rs}^{\alpha})^2 - (p_{rs}^{\beta})^2\} \gamma_{AA}$$

$$E_{AB} = \sum_{r}^{A} \sum_{s}^{B} 2 p_{rs} \beta_{AB}^{\circ} S_{rs} - \sum_{r}^{A} \sum_{s}^{B} \{(p_{rs}^{\alpha})^2 + (p_{rs}^{\beta})^2\} \gamma_{AB} + (Z_A - P_{AA})(Z_B - P_{BB}) \gamma_{AB}$$

E_{AB} is the contribution to the total energy from all the two-center integrals involving A and B centers; it can be partitioned into covalent binding, core repulsion, and ionic terms. The total E_{AB} is used for discussing the nature of each bond with a hydrogen migration.

Table 1. Molecular geometries[c] for the $M^{\ddagger}$ ions

Urea		Acetamide	
r_1	1.2875[a]	r_1	1.220
r_2	1.375[a]	r_2	1.540
r_3	1.375	r_3	1.3675[b]
∠OCN	121.5°	∠OCN	125.0°

a) The total energy shows minimum at 1.2875 Å and 1.375 Å. b) This value was decided from the minimum total energy as a function of r_3. c) Lengths in Ångström.

Geometry. It is difficult to determine absolutely the reaction coordinate in the hydrogen-migration process under electron impact.[4] Consequently, the parameters for the geometry of the $M^{\ddagger}$ ion employed here were decided as is shown in Table 1. These values of the bond lengths and the bond angles for the starting geometry, with the exception of the r_1, r_2, and r_3, were taken from the standard tables.[5]

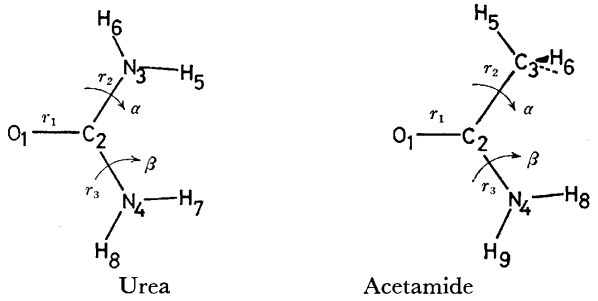

Fig. 1. Representation of the geometries of urea and acetamide.

The basic conformations in the $M^{\ddagger}$ ions of urea and acetamide are shown in Fig. 1. As the lengths of the N–H bonds in urea and acetamide we employed 1.000 Å, and as that of the C–H bonds in acetamide, 1.080 Å.

Migration Model. The total energy contour

TABLE 2. E_{AB} VALUES[a] BETWEEN NITROGEN AND HYDROGEN IN UREA

	$\beta(\alpha=0°)$			
	0°	30°	60°	90°
E_{total}	−1399.511	−1399.300	−1398.843	−1398.600
N_4–H_5	−0.168	−0.202	−0.282	−0.311
	$\beta(\alpha=30°)$			
	30°	60°	90°	
E_{total}	−1399.052	−1398.563	−1398.316	
N_4–H_5	−0.222	−0.305	−0.335	

a) Energies in eV.

TABLE 3. E_{AB} VALUES[a] BETWEEN NITROGEN AND HYDROGEN IN ACETAMIDE

	$\alpha(\beta=0°)$		
	0°	90°	180°
E_{total}	−1295.831	−1278.794	−1295.797
N_4–H_5		0.011	0.057
N_4–H_6	−0.031	−0.079	
	$\beta(\alpha=0°)$		
	30°	60°	90°
E_{total}	−1295.577	−1294.967	−1294.644
N_4–H_6	−0.071	−0.062	−0.121
N_4–H_7	−0.025	−0.117	−0.121

a) Energies in eV.

diagram[6] of the M^+ ion for the origin of the migration shows the deep energy minima at $\alpha=0°$ and $\beta=0°$ in both compounds, adopting the values in Table 1. The variation in the E_{AB} of the N_4H_5 by the rotation by β is shown in Table 2 for urea. The bonding interaction between N_4 and H_5 is strong at $\beta=90°$. These results suggest that the possibility of the migration of hydrogen to N_4 is large in this conformation. However, in this conformation the variation in the total energy with the hydrogen migration in the first stage was large. On the other hand, in acetamide the bonding interaction in the possible conformation of the hydrogen migration was weak, as is shown in Table 3. Consequently, as a model of the hydrogen migration, the planar geometries shown in Fig. 2 were employed, judging from the E_{AB} values and the total energies.

Models of both compounds, in which the migration of hydrogen was assumed to follow the curve path(2),

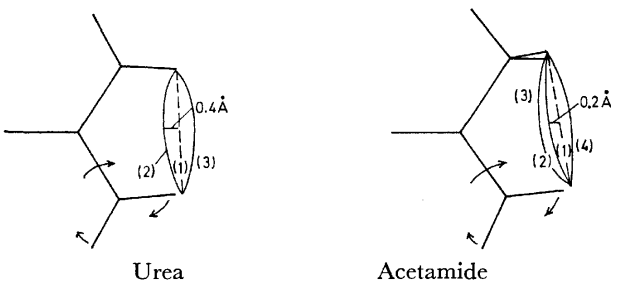

Urea Acetamide

Fig. 2. Migration model and paths.

show that the migrating hydrogen moves to N_4. The deviations from the least-motion path[7] at the transition state are at 0.4 Å in urea and 0.2 Å in acetamide. The variations in the total energies with the hydrogen migration in the models, caused by the least-motion path(1) and the other paths, were large in comparison with that caused by the curve path. The curve-path model was, therefore, chosen for the hydrogen migration in both compounds.

Results and Discussion

Urea. The results calculated by using the curve path are shown in Table 4 and Fig. 3. It is apparent from the shape of the curve that the total energy of the transition state, in which the N_3–H_5 distance is 1.306 Å, was low in the curve path. The potential energy was 4.736 eV. The total energy tends to decrease in the latter half of the migration of hydrogen. It is thought that a comparatively stable state results from the hydrogen migration. In this case, the variation in the total energy between the origin and the terminus of the migration was 2.105 eV.

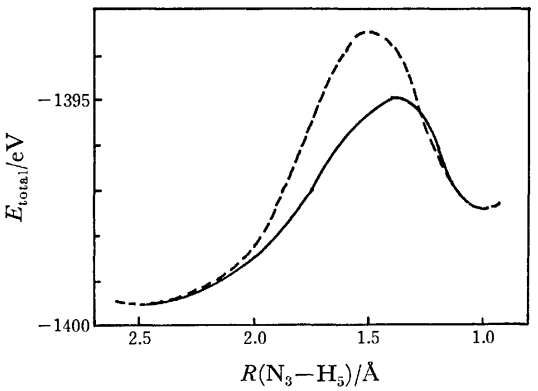

Reaction coordinate for hydrogen migration

Fig. 3. Variation of the total energies in urea.
——: The curve path (1). – – –: The least-motion path (2).

TABLE 4. VARIATIONS IN THE TOTAL ENERGY AND E_{AB}[a]

	Point	1	3	5
E_{total}		−1399.511	−1394.775	−1397.406
$R(N_4$–$H_5)$/Å		2.494	1.359	1.000
E_{AB}	O_1–C_2	−34.266	−33.787	−37.462
	C_2–N_3	−36.436	−37.299	−37.607
	C_2–N_4	−36.436	−30.561	−26.857
	N_3–H_5+N_4–H_5	−20.934	−18.056	−19.843

a) Energies in eV.

The increase in the total energy results from the increases in the E_{AB} value of the C_2–N_4 and the sum of the E_{AB} values of the two bonds (N_3–H_5 and N_4–H_5), as is shown in Table 4.

Although it is thought that the slight increase in the sum of the E_{AB} values of the two bonds hinders the migration of hydrogen, there is a tendency to decrease

near the terminus of the migration.

The tendency of the E_{AB} value of the C_2–N_4 bond to increase with the approach of H_5 to N_4 shows that the interaction between C_2 and N_4 is weakened; this results from the change in the bond length of this bond through the hydrogen migration. On the other hand, the variations in the E_{AB} values of the C_2–N_3 and the O_1–C_2 were small; this shows a slight tendency to decrease, after which these values were large and negative. This phenomenon may be related to the cleavage of the migrated M^+ ion to the fragment ion, *m/e* 17 or *m/e* 42.

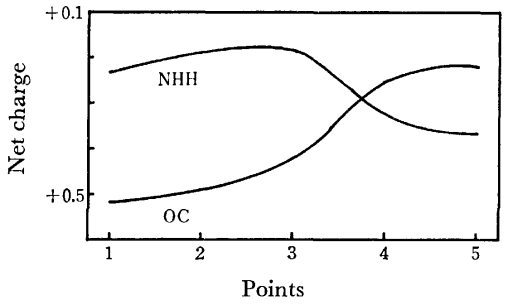

Fig. 4. Variation of the net electric charges.

Next, the variation in the net eleetric charge is shown in Fig. 4. The charge of the CO tends to be positively small with the hydrogen migration, while that of the N_4HH is large and positive. In the OCN_3H, after the migration of hydrogen, the density increases. These results may be reflected in the intense peak height of the NH_3 ion.

Acetamide. The most apparent fragmentation arises from cleavage, resulting in the formation of the ion with a mass of 44. If the migration of hydrogen as well as urea occurs, the hypothetical process for the migration of hydrogen can be expected to be energetically favored.

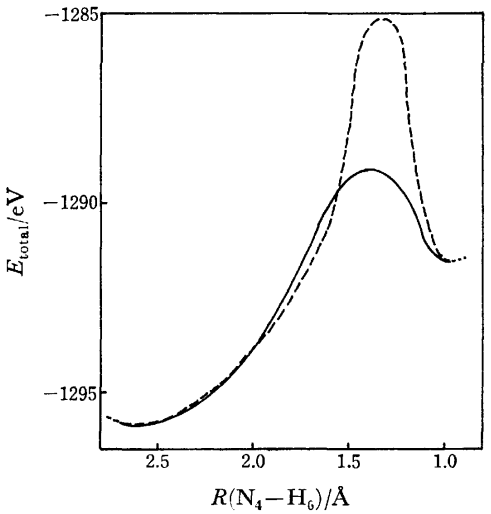

Fig. 5. Variation of the total energies in acetamide.
——: The curve path (1). – – –: The least-motion path (2).

The variation in the total energy in the model was larger than that in urea, as is shown in Fig. 5. This variation in the least-motion path was larger than that in the curve path. The potential energy in this curve-path process was 6.675 eV, which is larger by 2.0 eV than that in urea. Moreover, the variation in the total energy between the point of origin and the terminus of the migration was 4.075 eV, which is large. The variation in the total energy with the hydrogen migration at the conformation at $\alpha=180°$ and $\beta=0°$ was also large, similar to that at $\alpha=0°$ and $\beta=0°$, which was 11.284 eV.

Difference in Urea and Acetamide. The values of the E_{AB} of the N_4–H_6 in $\alpha=0°$ and of the N_4–H_5 in $\alpha=180°$ were −0.031 and 0.057 eV respectively, as is shown in Table 3. The values of the resonance interaction were positive (0.097 and 0.144 eV) in acetamide, while in urea this value of the N_4–H_5 was −0.168 eV. Therefore, the bonding interaction between hydrogen and nitrogen in urea is strong; this may be related to the ease of the migration of hydrogen. It may be predicted that the chance of the migration of hydrogen in urea is fairly strong.

Although the decrease in the E_{AB} values of the two bonds is not smooth, the variation in this energy in urea is smaller than that in acetamide. In acetamide, the increase (from −20.185 to −16.561 eV) shows the hindrance of the migration of hydrogen.

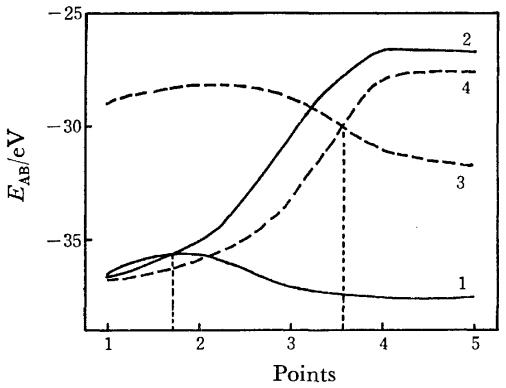

Fig. 6. Variation of the E_{AB} values of the skeletal bonds with the hydrogen migration.
——: Urea, 1: C_2–N_3, 2: C_2–N_4. – – –: Acetamide, 3: C_2–C_3, 4: C_2–N_4.

Fig. 6 shows the variations in the E_{AB} values of the C–C and C–N bonds. The E_{AB} value of the C_2–N_4 decreases smoothly. In acetamide, that of the C_2–C_3 is negatively small in comparision with the other bonds, including that of urea, in the origin of the migration. Moreover, the variation in this value is small, as in the case of the C_2–N_4 bond in urea.

It is found that the bonding interaction between C_2 and N_4 in acetamide is weaker than that of the C_2–C_3 bond after Point 3. However, the interaction in the first stage is strong. These features in acetamide show a great difference from urea. It may be thought that, even if the hydrogen migration occurs, the cleavage of the C_2–C_3 bond will occur preferentially to that of the C_2–N_4.

Conclusion

The estimation of the CNDO scheme provides fairly good information with respect to the fragmentation, including the migration of hydrogen in urea and acetamide. The treatment for the M^+ ion in the ground state shows a different profiles for the hydrogen migrations in the two compounds. As for the variation in the total energy in acetamide, the potential energy is large; therefore, there are large differences in the changes in E_{AB} values of the skeletal bonds. It is, therefore, found that the possibility of the migration of hydrogen is undoubtedly large in urea.

Finally, the quantitative discussion was unsatisfactory; the precise relation between the relative intensity of the rearranged ion and the estimation of the energy by the migration process has not been established. However, the possibility of the migration of hydrogen was qualitatively predicted by this treatment with respect to urea and acetamide, based on the partitioned energy and the migration model.

References

1) M. A. Baldwin, A. M. Kirkien-Konasiewicz, A. G. London, A. Maccoll, and D. Smith, *J. Chem. Soc.*, **1968**, 34.
2) J. A. Gilpin, *Anal. Chem.*, **31**, 935 (1959).
3) a) J. A. Pople and P. K. Nesbet, *J. Chem. Phys.*, **27**, 571 (1955); b) J. A. Pople, D. P. Santry, and G. A. Segal, *J. Chem. Phys.*, **43**, S129 (1965); c) H. Fischer and H. Kollmar, *Theoret. Chim. Acta*, **16**, 163 (1970).
4) a) T. Takagi and M. Oiwa, *Bull. Chem. Soc. Jpn.*, **48**, 2979 (1975); b) T. Takagi and M. Oiwa, *Bull. Chem. Soc. Jpn.*, **51**, 1931 (1978).
5) "Table of Interatomic Distances," Chem. Soc., Spec. Publs, No. 11 (1958); No. 18 (1965).
6) T. Takagi and M. Oiwa, *Bull. Chem. Soc. Jpn.*, submitted for publication.
7) F. O. Rice and E. Teller, *J. Chem. Phys.*, **6**, 489 (1938); **7**, 199 (1938).

A Theoretical Approach to the Possible Hydrogen Migration in Butadiene under Electron Impact

Tsutomu TAKAGI* and Masayoshi OIWA

Department of Applied Chemistry, Faculty of Engineering, Kansai University, Suita, Osaka 564

(Received July 13, 1978)

The hydrogen migration in butadiene under electron impact was studied by means of the calculated potential energy surfaces. The all-valence electron semi-empirical SCF-MO(MINDO/2-Unrestricted Hartree Fock) theory was employed. The possibility of the migration of hydrogen has been discussed. Moreover, the mechanisms (I—IV) including the hydrogen migration for the formation of the C_3H_3 ion have been discussed. The hydrogen-migration models are presented based on the variations in the total and the partitioned energies. It is very probable that the hydrogen on C_1 in the M^+ ion migrates to the other carbon, C_4, *via* Models 1 and 2 in Mechanism IV. It was predicted that the formation of the C_3H_3 ion occurs by means of the fragmentation of the migrated M^+ ion, although the other mechanisms can not always be ignored. Finally, for the hydrogen-migration models, the theoretical predictions were found to be in good agreement with the available experimental results.

The fragmentation in the unsaturated hydrocarbons is more complex than in the case of the saturated hydrocarbons. The hydrogen migration in the molecular ion(M^+) can be expected to be essentially prevalent if the M^+ ion possesses a large amount of excess vibrational energy. In this case, it is thought that the hydrogen migration proceeds *via* the four- or six-ring transition state.[1,2]

The possibility of the migration of hydrogen in butadiene can not always be neglected, judging from the mass number of the produced fragment ions. In butadiene, the C_3H_3, C_2H_3, and C_4H_5 ions are found in the mass spectrum in rich abundance. The precise mechanisms for the formation of these fragment ions, especially the C_3H_3 ion, have, however, not yet been elucidated, but only speculated from the mass spectral data.

By the way, the Woodward-Hoffmann rule is very useful in discussing the migration of hydrogen. However, with respect to the mechanism of the formation of the C_3H_3 ion including the hydrogen migration, the contribution of the hydrogen migration to the cleavage of the C–C bond can not be discussed in terms of the W-H rule. Therefore, it is necessary that the role of the M^+ ion for the hydrogen migration be discussed in terms of energy.

The mechanisms for the C_3H_3 ion with *m/e* 39 are thought to be as follows:

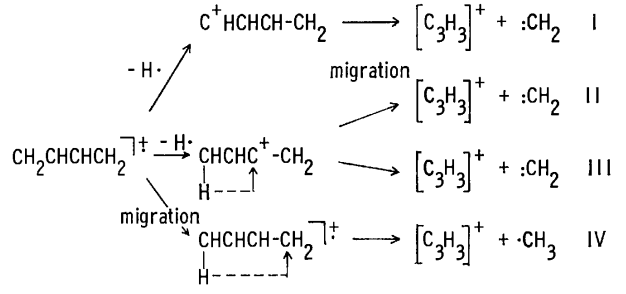

Mechanism I shows the formation of the C_3H_3 ion by the scission of the C–C bonds in the $[M-H]^+$ion. The mechanism with the hydrogen migration to the carbon atom loses a hydrogen atom as is shown in II. In Mechanism III, this process shows the simple fragmentation of the $[M-H]^+$ion. If the existence of the five-ring transition state in Mechanism IV is real, *i.e.*, if it is estimated that the hydrogen-migration process is energetically favorable, Mechanism IV should not be ignored. Mechanism IV shows the process with the migration of hydrogen.

The present paper is concerned with a discussion of the migration of hydrogen and with the treatment by the simple models for the formation of the C_3H_3 ion in order to gain a better understanding of the fragmentation in butadiene from the standpoint of the MO theory.

Method and Conformation

Computations. All the computations were carried out on a FACOM 230-48 computer at Kansai University. The wave functions were calculated by means of the MINDO method, with the original parameterization.[3] The MINDO calculation of the open shell-configuration was carried out using the method reported by Dewar.[3]

The total energy, E, can be partitioned into these chemically useful terms:[4,5]

$$E = \sum_A E_A + \sum_{A<B} E_{AB}$$

E_A is the energy due to the atom A. E_{AB} is the contribution to the total energy from all two-center integrals involving A and B centers, and can be partitioned into covalent binding, core repulsion, and ionic terms.[6]

Geometry. The starting geometry for the hydrogen-migration model requires a minimization of the total energy of the system with respect to all its independent internal coordinates, as has been discussed in a previous paper.[7] Moreover, it is difficult to determine absolutely the reaction coordinate passing through the equilibrium geometry. A full optimization of the

TABLE 1. MOLECULAR GEOMETRIES FOR THE M^+ ION

Parameter		Parameter	
r_1	1.37 Å	α	122°
r_2	1.47 Å	β	125°
r_3	1.06 Å	θ	119°

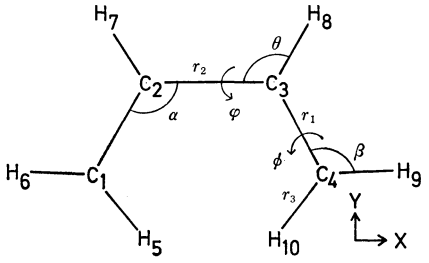

Fig. 1. Definition of the geometrical parameters for the M^+ ion.

geometries at each point in the migration process is thus quite impractical. Consequently, we employed the parameters[8] for the geometry of the M^+ ion as shown in Fig. 1 and Table 1.

The geometries were chosen by assuming the same valence angles for the hydrogen atoms on the CH_2 groups and by neglecting the changes in the C–C bond lengths in the migration process. The twisting of the carbon frame is expressed by φ, the dihedral angle between the $C_1C_2C_3$ and $C_4C_3C_2$ planes; $\varphi=0°$ for *cis*. The CH bond length was changed from 1.06 Å in the starting geometry to 1.09 Å in the terminus of the migration. At the terminus of the hydrogen migration, the angles of β and φ are 109.5° and 90° respectively.

Rotation. The variation in the total energy of the M^+ ion, as a function of the angle, φ, keeping the other internuclear distances and angles constant, is shown in Table 2.

The bond distance between C_4 and H_5 is 2.691 Å in *cis*($\varphi=0°$) and 2.812 Å in $\varphi=30°$, while the bond distance between C_4 and H_7 is 2.720 Å in *trans*($\varphi=180°$). Upon the rotation in φ from 0° to 180°, the chance of the migration of H_7 to C_4 becomes large. The resonance interaction (E^R) between C_4 and H_5 is slightly stronger at 30° than at 0°. Therefore, as a starting conformation, it seems reasonable to adopt that one at $\varphi=30°$ with respect to the migration of H_5 to C_4.

By the way, the net electric charge on C_4 is 0.2048, which is larger and more positive than that as C_3. If the migration of hydrogen is induced by the positive charge, it can be predicted that the migration of hydrogen to the end carbon atom is possible. One findings are, of course, as yet insufficient for us to discuss the possibility of the migration of hydrogen.

Energy Contour. In order to ascertain the migration path, a two-dimensional energy surface was generated by calculating the energy minimum as a function of the α angle, as well as of φ, assuming the other parameters in Table 1. The calculations were carried out with the φ angle increased from 0° to 90°, and at each value of φ, with α varying from 60° to 122°.

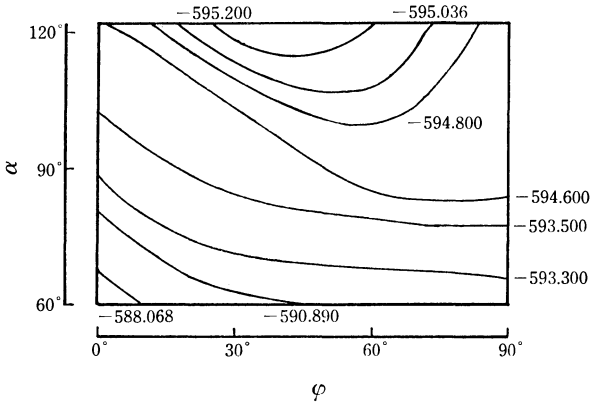

Fig. 2. Energy contours (in eV) of the M^+ ion of the origin of the migration of bent and twisted butadiene, as a function of the angles α and φ. Note that the contours are not separated by equal intervals of energy.

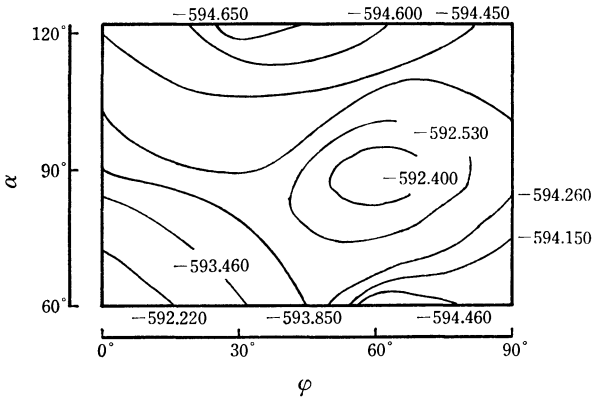

Fig. 3. Energy contours (in eV) of the M^+ ion of the terminus of the migration of bent and twisted butadiene, as a function of the angles α and φ. Note that the contours are not separated by equal intervals of energy.

The total energy-contour diagram for the origin of the migration is given in Fig. 2. The most obvious feature was the deep energy minimum at $\varphi=30°$ and $\alpha=122°$. It can be predicted that this feature results from the electron deficiency; the rotation of the C_2–C_3 bond is comparatively more favorable than a neutral molecule. On the other hand, the total energy-contour diagram calculated for the terminus of the migration is given in Fig. 3. The energy minimum was situated

Table 2. Variations in the total energy and the physical parameters

Angle/φ	0°	30°	60°	90°	120°	150°	180°
E_{total}[a]	−594.560	−595.270	−595.203	−594.702	−595.150	−595.301	−594.716
$R(C_4$–$H_5)$[b]	2.691	2.812	3.118	3.494	3.833	4.063	4.144
$R(C_4$–$H_7)$	3.422	3.379	3.260	3.091	2.911	2.773	2.720
C_3[c]	0.0506	0.0324	0.0422	0.0555	0.0138	−0.0091	0.0355
C_4	0.2048	0.1559	0.1386	0.1576	0.1572	0.2020	0.2372
$E^R(C_4$–$H_5)$[d]	−0.031	−0.033	−0.019	0.009	−0.004	0.001	0.000

a) Energies in eV. b) Distances in Ångströms. c) Net electric charge. d) $E^R=2\sum_r^A\sum_s^B p_{rs}\beta^\circ_{AB}S_{rs}$ in E_{AB}.

Table 3. Variations in the total energy and E_{AB}[a] in Model 1

	Points	1	2	3	4	5
$R(C_4-H_5)$/Å		2.812	2.320	1.849	1.422	1.090
E_{total}		−595.270	−595.476	−594.186	−594.664	−594.966
E_{AB}	C_1-C_2	−19.984	−20.377	−21.365	−21.157	−21.367
	C_2-C_3	−16.164	−17.114	−16.756	−17.255	−17.094
	C_3-C_4	−21.135	−20.304	−19.599	−17.556	−17.207
	$C_1-H_5+C_4-H_5$	−12.507	−12.284	−9.634	−10.772	−12.520

a) Energies in eV.

at $\varphi=30°$ and $\alpha=122°$, while the local minimum energy was −594.662 eV at $\varphi=60°$ and $\alpha=60°$. If this local minimum-energy state is formed by the hydrogen migration, an interesting feature emerges: the formation of the C_3H_3 ion with a three-memberd ring will be accelerated by the fragmentation of the M^+ ion after the hydrogen migration.

Results and Discussion

Migration Models. Mechanism IV was also discussed assuming several models for the hydrogen migration. Model 1, in which the starting and final geometry are $\varphi=30°$ and $\alpha=122°$, is the migration process of H_5 to C_4. The C_4 carbon atom was then changed from sp^2 to sp^3 hybridization by means of the C_3–C_4 bond through the hydrogen migration, as is shown in the following figure. The other parameters were kept constant.

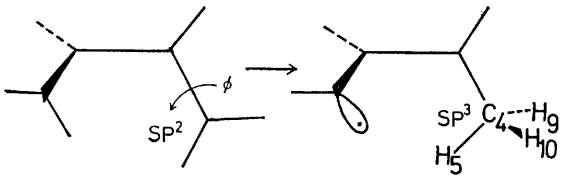

Table 3 shows the variation in the total and the partitioned energies. It is apparent from the variation in the total energy that the transition state lies at Point 3 along the coordinate representing the migration of hydrogen from C_1 to C_4. The potential energy in this process in Model 1 was 1.290 eV, smaller than the minimum energy required for the scission of the C–C bond. The total energy in the first stage shows a tendency to decrease. This results from the decrease in the sum of the two-center energies of the C–C bonds. The increase in the total energy from Point 2 to the transition state results from the increase in the sum of the E_{AB} values of the two bonds (C_1–H_5 and C_4–H_5).

The variation in the bonding interaction of each C–C bond is shown in Fig. 4. The variation in the E_{AB} value of the C_3–C_4 bond increases remarkably with the approach of H_5 to C_4; this shows that the interaction between C_3 and C_4 is weakened by the hydrogen migration, while the variations in the E_{AB} values of the C_1–C_2 and C_2–C_3 bonds are small, which shows a slight decreasing trend. These results may be related to the fragmentation of the migrated M^+ ion to the $[M-CH_3]^+$ ion.

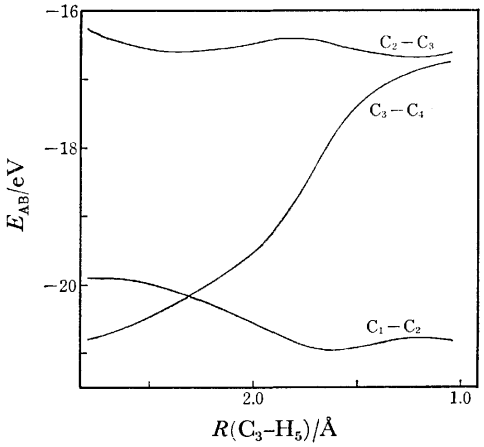

Fig. 4. Variation of E_{AB} of the C–C bonds due to the hydrogen migration in Model 1.

Table 4. Charge distribution of the M^+ ion

	Origin			Terminus	
	0°	30°	180°	0°	30°
C_1	0.2048	0.1699 (0.2465)[a]	0.2372	0.1791	0.1453
C_2	0.0506	0.1210 (0.1535)	0.0356	−0.0966	−0.0541
C_3	0.0506	0.0324 (0.0109)	0.0356	0.3551	0.3220
C_4	0.2048	0.1559 (0.2803)	0.2372	−0.0267	−0.0190

a) The values in parentheses correspond to the net electric charge on the p_z orbital.

The sum of the E_{AB} values of the C_1–H_5 and C_4–H_5 bonds decreases in the latter half of the reaction. This implies that the bonding interaction between C_4 and H_5 becomes strong through the migration process.

The net electric charge of the C_4 atom is large and positive, as is summarized in Table 4. The net electric charge on the p_z orbital on C_4 at $\varphi=30°$ is very positively large. It seems, therefore, that the possibility of the migration of hydrogen to C_4 is certainly large. There is also an electron flow of the $C_1C_2C_3$ moiety, changing from +0.3233 to +0.4132 by the migration of hydrogen. Consequently, it is apparent that the charge on the migrated M^+ ion remains on the CH_3 moiety, suggesting the formation of the $[M-CH_3]^+$ ion with *m/e* 39. These features are shown in the following process:

TABLE 5. VARIATIONS IN THE TOTAL ENERGY AND E_{AB}[a] IN MODEL 2

	Points	1	2	3	4	5
$R(C_4-H_5)$/Å		2.691	1.948	1.716	1.322	1.090
E_{total}		−594.560	−594.824	−594.151	−594.382	−594.662
E_{AB}	C_1-C_2	−20.359	−19.619	−19.354	−19.154	−18.519
	C_2-C_3	−17.059	−16.971	−16.580	−15.479	−14.109
	C_3-C_4	−20.359	−20.928	−19.905	−16.143	−14.423
	$C_1-H_5+C_4-H_5$	−12.484	−11.426	−11.738	−11.660	−12.396

a) Energies in eV.

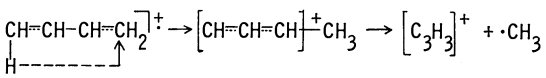

In the simple model employed here, these results indicate that the migration of H_5 to C_4 is very probable. Moreover, the hydrogen migration gives fairly good information with respect to the formation of the C_3H_3 ion.

In Model 2, the calculations were carried out with the $C_1C_2C_3$ chain bent at C_2 with the α values varying from 122° to 60° in 15.5° increments; then, at each value of α, the calculations were made by increasing φ from 0° to 60° in 15° increments. For the other parameters we adopted the same values as in Model 1.

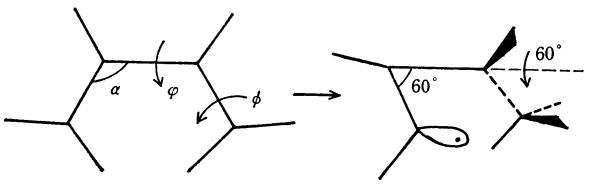

Table 5 shows the variations in the total and the partitioned energies in Model 2. The energy profile is depicted by the curve, as in Model 1. The total energy at the terminus of the migration is −594.662 eV, nearly equal to that in Model 2. The most remarkable difference from Model 2 is that the bonding interaction between C_1 and C_3 becomes strong. These results indicate that the hydrogen-migration process in Model 2 is energetically favorable, as in Model 1.

Next, the starting geometry at $\varphi=90°$ and $\alpha=122°$, in which H_5 migrates to C_4, is shown as Model 3. The migration path of H_5 was chosen as the least-motion path[9] from C_1 to C_4. This release of H_5 from C_1 requires more energy than in Models 1 and 2; the potential

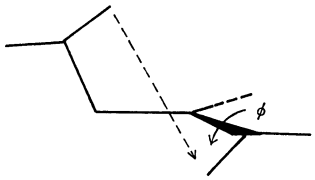

energy in this process was 1.367 eV. This is related to the increase in the sum of the E_{AB} values of the C_1-H_5 and C_4-H_5 bonds; this remarkable increase shows that the migration of H_5 is prevented in this process. The bonding interaction between C_2 and C_3 was almost unchanged with the hydrogen migration. The value of the C_2-C_3 bond is larger than that of the C_3-C_4 bond; it may be thought, therefore, that the scission of the C_2-C_3 bond occurs in preference to that of the C_3-C_4 bond. As a result, judging from this variation, it may be predicted that the C_2H_3 ion is formed.

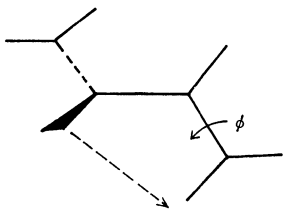

In Model 4, the variation in the total energy between the origin and terminus of the migration was 0.276 eV; the potential energy was, then, 1.448 eV. It is possible to form the resonance structure by the migration of H_7 as follows:

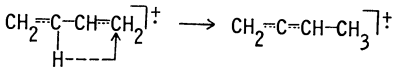

TABLE 6. VARIATIONS IN THE TOTAL ENERGY AND E_{AB}[a] IN MODELS 3 AND 4

	Points	1	2	3	4	5
				Model 3		
E_{total}		−594.702	−594.527	−593.335	−593.751	−594.435
E_{AB}	C_2-C_3	−16.852	−14.973	−14.812	−16.074	−16.233
	C_3-C_4	−20.536	−21.849	−20.733	−17.049	−17.392
	$C_1-H_5+C_4-H_5$	−12.621	−11.539	−5.804	−10.106	−12.476
				Model 4		
E_{total}		−595.301	−595.561	−593.853	−594.323	−595.025
E_{AB}	C_2-C_3	−17.273	−15.259	−15.080	−16.683	−16.993
	C_3-C_4	−21.016	−21.046	−20.021	−17.374	−17.174
	$C_1-H_7+C_4-H_7$	−12.657	−12.136	−9.734	−10.693	−12.434

a) Energies in eV.

The bonding interaction energy between C_2 and C_3 was larger than that between C_3 and C_4. This is the same as in Model 3. On the other hand, the variation in the sum of the E_{AB} values of the C_2–H_7 and C_4–H_7 bonds in Model 4 was similar to that in Model 1. Therefore, the possibility of the migration of H_7 to C_4 is larger than in Model 3.

Table 7. The total energies and the net electric charges in the $[M-H]^+$ ions

	$[M-H_5]^+$	$[M-H_6]^+$	$[M-H_8]^+$
		Trans	
E_{total}/eV	−578.031	−578.196	−578.219
C_3			0.3138
C_4			0.0118
		Cis	
E_{total}/eV	−578.034	−575.796	−578.191

$[M-H]^+$ Ion. In order to discuss Mechanism II, the calculations for the $[M-H]^+$ ion were carried out using the same parameters as in Model 1. The stable structure of the $[M-H]^+$ ion was in a state which lost H_7 and H_8 in *trans*; this phenomenon is estimated to be more energetically favorable than in *cis*. Table 7 shows the total energies of the several structures for the $[M-H]^+$ ion and the net electric charges on the carbon atoms. The net electric charge of the C_3 which had lost H_8 was +0.3138, which is large and positive. If the driving force is this positive charge, as much as in the M^+ ion, in the $[M-H]^+$ ion it can be predicted that the possibility of the migration of hydrogen to C_3 is large. Therefore, as a model, the migration process of H_5 to C_3 was discussed.

The total energy in the $[M-H]^+$ ion upon the rotation of the C_2–C_3 bond was the energy minimum at 90°. Therefore, this starting geometry for the migration of H_5 from C_1 to C_3 at 90° was chosen:

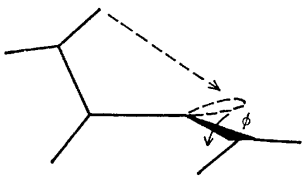

The variation in the total energy in this process is shown in Table 8. The position of the H_5 atom at Point 3 was decided on the basis of the energy-minimum state; the position of H_5, in which the $C_1H_5C_3$ angle is 90°, was chosen.

The potential energy in this process was 3.251 eV, larger than those in the models of the M^+ ion. Moreover, the bonding interaction between C_2 and C_3 was weakened, contrary to the case of the C_2–C_3 bond in the M^+ ion. Therefore, it can be predicted that this bond is easy to cleave in the $[M-H]^+$ ion. The bonding interaction of this bond at 180° was also weakened from −17.257 to −15.210 eV by the loss of the hydrogen atom; in other $[M-H]^+$ ions this trend also appeared. Consequently, it seems that it is more difficult for the

Table 8. Variations in the total energy and E_{AB}[a] in the $[M-H]^+$ ion

Points	1	2	3	4	5
$R(C_3$–$H_5)$/Å	2.783	2.301	1.716	1.313	1.060
E_{total}	−578.563	−578.069	−575.312	−577.413	−578.028
E_{AB} C_2–C_3	−16.286	−16.222	−16.316	−14.079	−14.788
E_{AB} C_3–C_4	−23.761	−23.689	−22.937	−22.831	−22.910

a) Energies in eV.

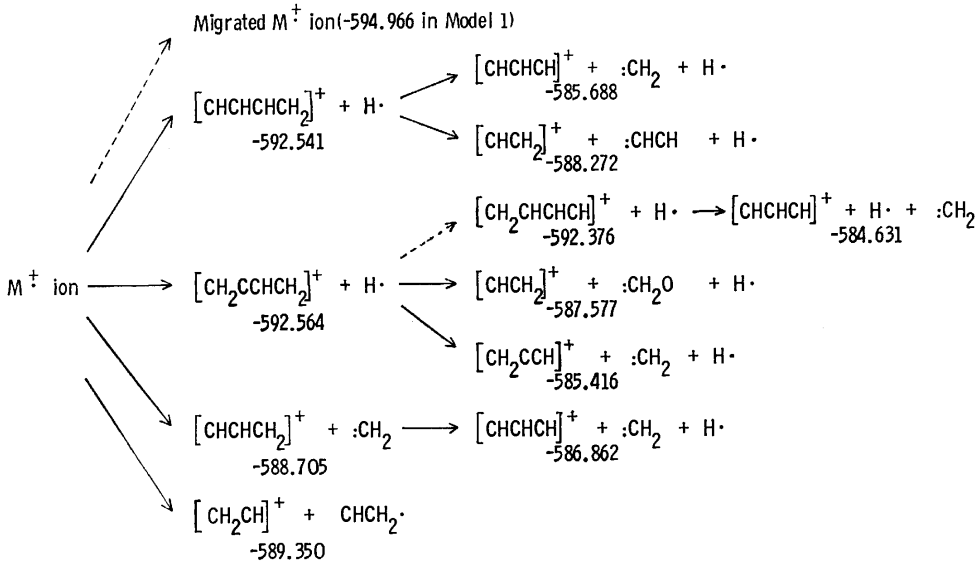

Fig. 5. Fragmentation pattern of butadiene. The dotted arrow shows the hydrogen-migration process. The total energies of the fragments are the sum of the fragments.

migration of H_5 to occur in the $[M-H]^+$ ion than in the M^+ ion.

Fragmentation Pattern. Considering the variation in the total energies in the fragmentation process, the energy relations are shown in Fig. 5. It is apparent from the total energies that the variation for the hydrogen migration is smaller than that for the simple fragmentation. The variation for the C_3H_3 ion which is produced from the $[M-H]^+$ ion is larger than that for the C_2H_3 ion. The fragmentation of the M^+ ion to the C_3H_4 ion is energetically less favorable than the direct cleavage to the C_2H_3 ion; it may, then, be asserted that the formation of the C_3H_4 ion by the direct release of the CH_2 radical is energetically less favorable. This tendency causes the $[M-H]^+$ ion to appear. Moreover, by the fragmentation of the migrated $[M-H]^+$ ion, the scission of the C_2–C_3 bond occurs in preference to that of the C_3–C_4 bond.

Conclusion

Calculations have been presented in support of a discussion of the possibility of the hydrogen migration in butadiene, taking account of the variations in the total and the partitioned energies with respect to the migration of hydrogen in the M^+ ion.

This treatment is not absolutely essential, but it is a very convenient starting point.

The following features were postulated: (1) The net electric charges on the C_1 and C_4 atoms were large and positive in the M^+ ion. The positive charge on the carbon atom was one of the driving factors in the migration of hydrogen. (2) It is very probable that the hydrogen atom migrates *via* Models 1 and 2 in Mechanism IV, judging from the variation in the total energy. (3) The migration of hydrogen from C_1 to C_4 migrates in the M^+ ion, and then the C_3H_3 ion is produced by the hydrogen migration. (4) It was found that the positive charge remains in the $C_1C_2C_3$ moiety after the hydrogen migration. (5) It can be predicted that the formation of the C_3H_3 ion results from the fragmentation of the M^+ ion. (6) The fragmentation of the $[M-H]^+$ ion leads to the formation of the C_2H_3 ion. Finally, this treatment for the migration of hydrogen gives fairly good information as the mass spectrum of butadiene.

References

1) F. W. McLafferty, *Appl. Spectrosc.*, **11**, 148 (1957).
2) F. W. McLafferty, *Anal. Chem.*, **31**, 82, 2072 (1959).
3) M. J. S. Dewar and E. Haselbach, *J. Am. Chem. Soc.*, **92**, 590, 3854 (1970).
4) a) H. Fischer and H. Kollmar, *Theoret. Chim. Acta*, **16**, 163 (1970); b) M. J. S. Dewar and D. H. Lo, *J. Am. Chem. Soc.*, **93**, 7201 (1971).
5) M. S. Gordon, *J. Am. Chem. Soc.*, **91**, 3122 (1969).
6) J. A. Pople and G. A. Segal, *J. Chem. Phys.*, **44**, 3289 (1966).
7) T. Takagi and M. Oiwa, *Bull. Chem. Soc. Jpn.*, **51**, 1931 (1978).
8) a) V. Schomaker and L. Pauling, *J. Am. Chem. Soc.*, **61**, 1769 (1958); b) "Table of Interatomic Distances," Chem. Soc., Spec. Publs., No. 11 (1958); No. 18 (1965).
9) F. O. Rice and E. Teller, *J. Chem. Phys.*, **6**, 489 (1938).

A Study of the Reduction Mechanism of *p*-Dimethylaminobenzaldehyde to 1,2-Bis(*p*-dimethylaminophenyl)-1,2-ethanediol by Rotating Disk Electrode Voltammetry

Isao TANIGUCHI,* Kazuo YASUKOUCHI, Akiko YOSHIYAMA,† and Taro SEKINE†

Department of Industrial Chemistry, Faculty of Engineering, Kumamoto University, 2-39-1, Kurokami, Kumamoto 860

†*Department of Electronic Chemistry, Graduate School at Nagatsuta, Tokyo Institute of Technology, 4259, Nagatsuta, Midori-ku, Yokohama 227*

(Received August 22, 1978)

Rotating disk electrode voltammetry was applied to study the reduction mechanism of *p*-dimethylaminobenzaldehyde (**1**) in water–ethanol alkaline solutions by using a mercury-plated platinum rotating disk electrode. In the logarithmic analysis of the wave, the plots of log $[i^{2/3}/(i_d-i)]$ *vs.* E showed good linearity, and the shifts of the half-wave potential with an increase in the rotation speed of the electrode (ω) and in the initial concentration of **1** (C) were $\partial E_{1/2}/\partial \log \omega = -22 \pm 2$ mV and $\partial E_{1/2}/\partial \log C = 19 \pm 2$ mV, respectively. On the other hand, no appreciable change in $E_{1/2}$ was observed with varying alkalinities of the solutions. These results and the large shift of $E_{1/2}$ with an increase in the concentration of water ($\partial E_{1/2}/\partial \log[H_2O] = ca.$ 50 mV) are explained in terms of the following reactions:

$$R + e \rightleftarrows R^{\cdot} \text{ (solvated by water)}, \quad (1)$$

$$2R^{\cdot} \xrightarrow{k} D^{2-} \text{ (r.d.s.)}, \quad (2)$$

$$D^{2-} + 2H_2O \longrightarrow DH_2 + 2OH^-, \quad (3)$$

where R and $R^{\cdot}$ are the molecule and the radical of **1**, respectively, D^{2-} is the dimer of $R^{\cdot}$ and DH_2 is the hydrodimer (**2**) of R. The rate of the dimerization reaction (k in Eq. 2) was estimated to be 2.5×10^4 M^{-1} s^{-1} from the shift of $E_{1/2}$ with log ω for the 50% water–ethanol solution containing 1 M NaOH, and this rate constant decreased with decreasing water concentration.

Rotating disk electrode voltammetry (RDEV) is one of the most useful techniques for studying an electrode reaction. It is more advantageous than polarography using a dropping-mercury electrode because (i) the rotation speed of the electrode can be varied over a wide range, whereas the variation of the drop-time is limited, and (ii) even in a high concentration of a reactant the current-potential curve at an RDE can be obtained and the reaction mechanism may be examined under conditions similar to those for a macro-scale electrolytic synthesis. Furthermore, recently Saveant *et al.* have reported[1,2] the theoretical relationship between current and potential at a rotating disk electrode (RDE) and have given some diagnostic criteria for determining the correct mechanism among various types of hydrodimerization reactions coupled to an electron transfer.

On the other hand, Allen reported[3] that *p*-dimethylaminobenzaldehyde (**1**) was reduced to 1,2-bis(*p*-dimethylaminophenyl)-1,2-ethanediol (**2**) (the mixture of *dl* and *meso* types) in a water–alcohol solution of KOH with a mercury electrode at −1.9 V (*vs.* NCE) in 97% yield. However, no report has been published for the reduction mechanism. Thus, to clarify the reaction pathway, RDEV was applied for the reduction of **1** to **2** in alkaline solutions at a mercury-plated rotating disk electrode (MPRDE).

Experimental

The voltammograms were measured using a set of apparatuses for RDEV (Nikko Keisoku RRD-1, SC-2, NPS-2, and NPGS-1) and an X-Y recorder (Riken D-72BP). The electrolytic cell (NKC-1) and the platinum rotating disk electrode (PRDE) were also constructed by Nikko Keisoku. The MPRDE ($r = 0.302$ cm) was prepared for each set of runs as follows: The PRDE was first polarized cathodically at 5 mA and at the rotation speed of the electrode of 104.7 rad s^{-1} for 10 min in a copper sulfate solution used commonly for a copper coulometer, and then the copper-plated platinum electrode was dipped into a saturated $Hg(NO_3)_2$ solution for 30 s. The MPRDE thus prepared was set into the apparatus immediately after being washed with distilled water.

The test solution was a 1 M NaOH solution containing 50 % v/v ethanol, unless stated otherwise, and the solution was deaerated by bubbling with purified nitrogen. The measurements were carried out at 25±0.5 °C under continuous flow of nitrogen over the solution surface. The rate of potential sweep used was 16.7 mV s^{-1}. The reference electrode was a saturated calomel electrode (SCE); the potentials given in this paper are referred to this electrode without any correction the liquid junction potential. The value of the half-wave potential adopted is the average of values obtained by several experiments. The uncertainty is within ±3 mV. The kinematic viscosity (ν) of the solution (0.0331 cm^2 s^{-1} for a 1 M NaOH solution containing 50% v/v ethanol) was measured by using a viscometer (Shibata SF 7741). The diffusion coefficient (D) of **1** (3.09×10^{-6} cm^2 s^{-1}) was determined by using the Levich equation, and this value was also assumed to be valid for the diffusion coefficient of the anion radical of **1**.

The macro-scale electrolyses were carried out in 100 ml of 1 M NaOH water–ethanol solutions containing 1 g (67 mM) of **1** by controlling the cathode potential at −1.8 V *vs.* SCE. An H-type electrolytic cell, which is the same as that described elsewhere,[4] was used. The cathode was a mercury pool (20 cm^2) and the anode was a platinum plate (4 cm^2). During electrolysis, one electron/molecule of **1** was consumed. After reduction, the products were separated into *dl* and *meso* types of **2** by Allen's method,[3] and were weighed to determine the *dl*/*meso* ratio. After electrolysis, *meso*-**2** was always obtained from 50 % water–ethanol solution, by adding water when necessary. The total yield of the products was *ca.* 70%.

The diastereomers were identified by means of both their NMR spectra[5] (100 MHz at room temperature) and melting points.[3] The characteristics obtained are:
dl; mp 113 °C, NMR (DMSO-d_6) δ=5.0 (2H, s, hydroxylic),
meso; mp 178 °C, NMR (DMSO-d_6) δ=4.76 (2H, s, hydroxylic).

All reagents used were analytical GR grade without further purification. Throughout this paper 1 M=1 mol dm^{-3}.

Results

The voltammograms for the reduction of **1** at the MPRDE were measured in water–ethanol alkaline solutions by changing the rotation speed of the electrode (ω), the initial concentration of **1** (C), and the alkalinity of the solution. The results are shown in Figs. 1—4. In the logarithmic analysis of the wave (Fig. 1), the relationship between log $[i^{2/3}/(i_d-i)]$ and the cathode potential (E) shows good linearity, with the slope of the line being 57±3 mV (the plots of log $[i/(i_d-i)]$ *vs.* E are also shown for comparison in Fig. 1). The half-wave potential ($E_{1/2}$) shifted to more negative potentials with increasing ω ($\partial E_{1/2}/\partial \log \omega = -22\pm2$ mV, see Fig. 2) and to more positive potentials with increasing C ($\partial E_{1/2}/\partial \log C = 19\pm2$ mV, see Fig. 3). On the other hand, no appreciable change in $E_{1/2}$ was observed with alkalinity of the solution (Fig. 4), when we take into account the liquid junction potential (from the Henderson equation, the liquid junction potentials between the test solution and the saturated KCl solution are: 8.5 mV (1 M NaOH), 0.44 mV (0.1 M NaOH+0.9 M $NaClO_4$), and 0.01 mV (0.01 M NaOH+0.99 M $NaClO_4$)).

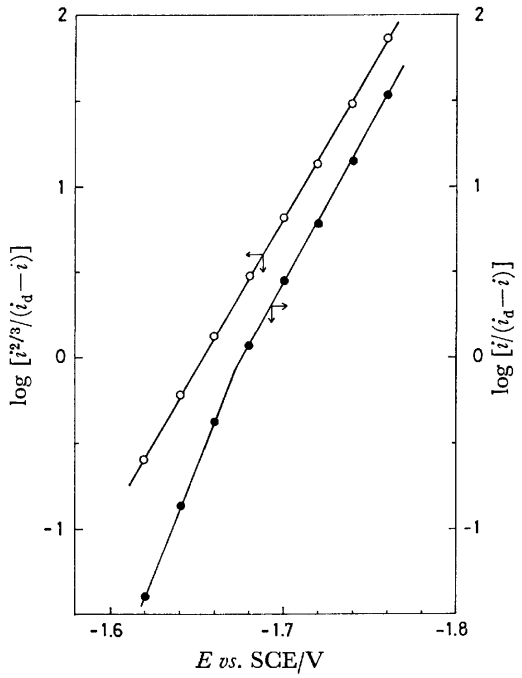

Fig. 1. Logarithmic analysis of the wave for 9.7 mM of **1** at ω=261.8 rad s^{-1}.

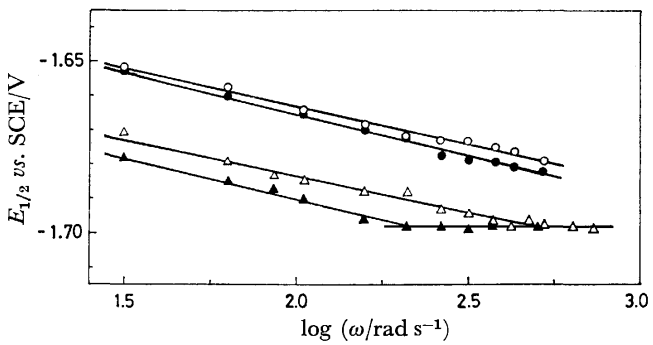

Fig. 2. Variations of half-wave potential as a function of the rotation speed of the electrode at various concentrations of **1**; ○: 15.7 mM, ●: 9.71 mM, △: 1.19 mM, ▲: 0.406 mM.

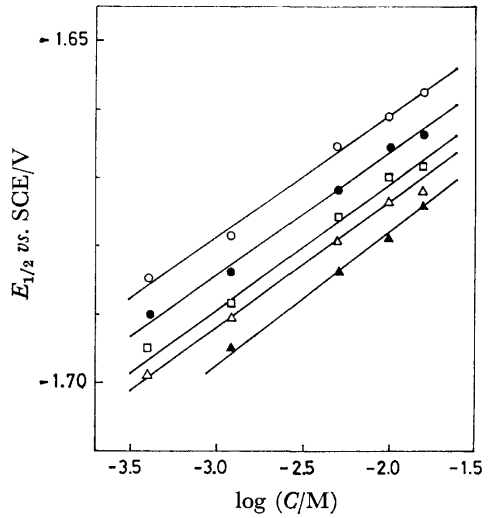

Fig. 3. Variations of half-wave potential as a function of the concentration of **1** at various rotation speeds of the electrode; ○: 62.8 rad s^{-1}, ●: 104.7 rad s^{-1}, □: 157.1 rad s^{-1}, △: 209.4 rad s^{-1}, ▲: 314.2 rad s^{-1}.

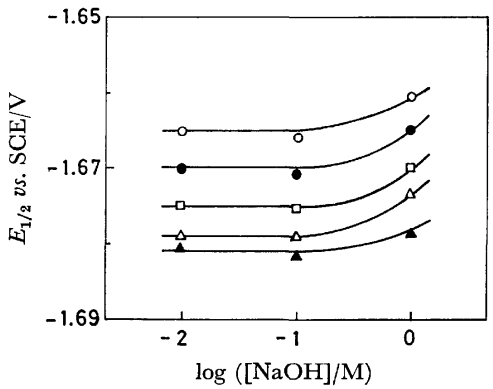

Fig. 4. Variations of half-wave potential as a function of NaOH concentration at various rotation speeds of the electrode; ○: 62.8 rad s^{-1}, ●: 104.7 rad s^{-1}, □: 157.1 rad s^{-1}, △: 209.4 rad s^{-1}, ▲: 314.2 rad s^{-1}. [**1**]=10 mM. The ionic strength and sodium ion concentration were maintained constant (1 M) by adding $NaClO_4$ crystals.

Discussion

Reduction Mechanism. The results shown in Fig. 1 indicate that the reduction of **1** is successfully explained

in terms of Eq. 13 in the appendix of the present paper, for $n=1$. This mechanism is also consistent with the facts that (i) the n-value (electrons consumed/molecule of **1**) obtained by coulometry was one, (ii) **2** was produced by controlled-potential electrolysis, and (iii) the dependences of $E_{1/2}$ on both ω and C were in good agreement with those estimated by Eq. 14 in the appendix. Thus, when we take into account the diagnostic criteria (see Tables 3 and 4 in Ref. 2), **1** was reduced by

$$R + e \rightleftarrows R^{\cdot}, \quad (1)$$

$$2R^{\cdot} \longrightarrow D^{2-} \text{ (r.d.s.)}, \quad (2)$$

$$D^{2-} + 2H_2O \longrightarrow DH_2 + 2OH^-, \quad (3)$$

where R and $R^{\cdot}$ are the molecule and the anion radical of **1**, respectively, D is the dimer of R, and thus DH_2 is the hydrodimer (**2**). It should be noted that, as is shown by Eq. 2, the dimerization reaction occurred between two anion radicals of **1**.

For dimerization reactions, (i) the coupling between two anion radicals (DIM I mechanism) has been excluded because of the coulombic repulsive force between the radicals, and the coupling between an anion radical and a neutral radical produced by a protonation to the anion radical (DIM II mechanism) has generally been considered to be the predominant reaction in aqueous alkaline solutions, and (ii) in a non-aqueous medium without proton-donating reagents, an ion-pair formation of an anion radical with the cation of a supporting electrolyte (DIM III mechanism) has been reported to be important for the coupling reaction. Both these considerations were examined. For the DIM II mechanism, $E_{1/2}$ must vary in 19.7 mV/pH (in fact, for the reduction of benzaldehyde, $E_{1/2}$ shifts in this manner[6]), but in the present experiment, since no appreciable change in $E_{1/2}$ was observed with alkalinity of the solution (see Fig. 4), the DIM II mechanism must be rejected. When the anion radical forms an ion-pair with the cation of a supporting electrolyte, $E_{1/2}$ is affected by the concentration and the kind of the cation. Thus the variation of $E_{1/2}$ was tested by changing the supporting electrolyte. No appreciable difference in $E_{1/2}$ was observed when either 0.1 M tetraethylammonium hydroxide or 0.1 M sodium hydroxide was used as a supporting electrolyte.

According to recent developments in the study of ion-pair formations,[7,8] not only does an anion radical form a contact ion-pair ($R^{\cdot}/M^+$, where M^+ is the cation of a supporting electrolyte), but an anion radical interacts with water molecules; thus solvation ($R^{\cdot}/H_2O$) and/or a separated ion-pair ($R^{\cdot}/H_2O/M^+$) formation are to be considered when water concentration is greater than 1 M. In both cases the electric repulsion between anion radicals diminishes. Recently, Lamy *et al.*[9] have concluded from the results obtained by linear sweep voltammetry that for the electrohydrodimerization of activated olefines, the coupling of two anion radicals solvated by water molecule was the most probable reaction in a low acidity media.

The effect of water concentration of $E_{1/2}$ was then examined. The $E_{1/2}$ shifted to a more negative potential with a decrease in the concentration of water (Fig. 5).

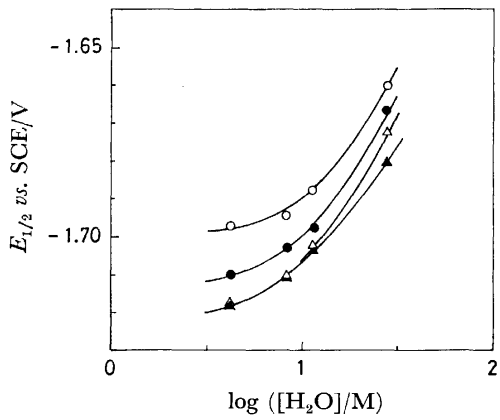

Fig. 5. Variations of half-wave potential as a function of water concentration in 1 M NaOH water–ethanol solutions containing 10 mM of **1** at various rotation speeds of the electrode; ○: 62.8 rad s^{-1}, ●: 104.7 rad s^{-1}, △: 209.4 rad s^{-1}, ▲: 314.2 rad s^{-1}.

Though the shift of $E_{1/2}$ may include the variation of the liquid junction potential which results from the change of the composition of the test solution, the large shift of $E_{1/2}$ (*ca.* 50 mV/log [H_2O]) suggests strongly that an increase of the number of anion radicals solvated by water facilitates the rate of coupling between the anion radicals because of a decrease in the coulombic repulsive force between two anion radicals.

To examine whether or not the reactions (Eqs. 1—3) are applicable in the solution containing a low concentration (7.5%) of water, the voltammograms for the reduction of **1** were also measured by changing the experimental parameters. In the 7.5% water–ethanol solution, results similar to those obtained in the 50% water–ethanol solution were obtained. That is, the plots of log $[i^{2/3}/(i_d-i)]$ *vs.* E showed a straight line having a slope of 53 mV, and the dependences of $E_{1/2}$ on both ω and C, $\partial E_{1/2}/\partial \log \omega$ and $\partial E_{1/2}/\partial \log C$, were −25 and 20 mV, respectively. Thus, we concluded that no serious change in the mechanism occurred in the water concentration range tested.

The dl/meso *Ratio of the Products.* To give further experimental support for the formation of the solvated anion radical, the variation of isomer ratio (*dl*/*meso*) of **2** was examined. On steric grounds, when the water concentration is high enough to solvate all anion radicals, the most favorable conformation in the transition state of the dimerization reaction is I, whereas when a part of the radicals are solvated, structure II is more attractive than I because of the aid of inter-radical hydrogen bonding.

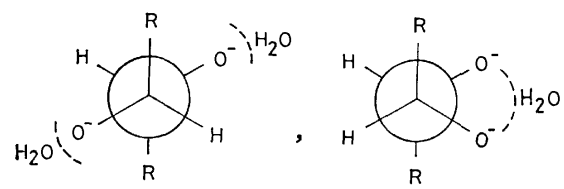

where R=$-C_6H_4N(CH_3)_2$.

TABLE 1. ISOMER RATIOS IN REDUCTION PRODUCTS OF **1**

Run	Solvent[a]	Amount of **1** g	(mM)	Charge passed mF	Yield of product (**2**) *meso* g	*dl* g	Ratio of *dl*/*meso*	Total yield of product %
1	50% H_2O + 50% EtOH	1.0045	(67.0)	6.57	0.38	0.32	0.84	70
2		1.0090	(67.3)	6.57	0.38	0.31	0.82	68
3		1.0011	(66.7)	6.57	0.38	0.30	0.79	68
							Av 0.82	
4	5% H_2O + 95% EtOH	1.0236	(69.4)	6.94	0.23	0.45	2.0	66
5		1.0116	(67.3)	8.66	0.28	0.44	1.6	71
6		1.0044	(67.0)	6.58	0.24	0.47	2.0	71
							Av 1.9	

a) The volume of all solutions was 100 ml.

Thus, the *dl*/*meso* ratio of the products must increase with a decrease in the concentration of water. According to the macroscale electrolysis data obtained (Table 1), the *dl*/*meso* ratio changed from 0.8 in the 50% water–ethanol solution to 1.9 in the 5% water–ethanol solution. In the latter case, the current decreased to less than one-tenth of the current in the former case at the same cathode potential, −1.8 V *vs.* SCE; this is because the rate of dimerization decreased with decreasing water concentration, as will be described later. The result of the *dl*/*meso* ratio is consistent with the above consideration about the formation of the solvated anion radical.

For some aromatic aldehydes, the DIM II mechanism which was rejected in the present experiment for **1** has been proposed in aqueous basic solutions. This unusual behavior for **1** is probably because the electron density on the oxygen atom of the carbonyl group is high, due to the extremely strong electron-donating effect of the *N*,*N*-dimethylamino group, and thus the hydrogen bonding with a water molecule is facilitated. To clarify the structure of the anion radical and the mechanism of the solvation, further experiments are required.

TABLE 2. RATE CONSTANT CALCULATED FROM Eq. 4

Concentration of Water[a] vol %	**1** mM	log ω_0	ω_0 rad s^{-1}	k[b] $M^{-1}\,s^{-1}$
50	1.19	2.70	501.2	2.21×10^4
50	0.406	2.34	218.8	2.38
				Av 2.5×10^4
15	9.31	2.38	239.9	1.4×10^3
7.5	10.0	2.25	177.8	9.6×10^3

a) Water–ethanol solution containing 1 M NaOH.
b) For the calculation, the diffusion coefficient (D) of **1** and the kinematic viscosity of the solution obtained for each solution were used.

Rate of the Dimerization. The rate constant of the dimerization (k) can be estimated from the variation of $E_{1/2}$ with log ω.[2] The value of ω at the intersection of the oblique linear part of the $E_{1/2}$—log ω plots with the horizontal part, ω_0, gives

$$(1/3)kC(\delta^2/D) = 1, \tag{4}$$

where $\delta = 1.61\,D^{1/3}\nu^{1/6}\omega_0^{-1/2}$.

As can be seen in Fig. 2, an intersection in the $E_{1/2}$—log ω plots is observed for the concentrations of **1** lower than 1.2 mM in 50% water–ethanol solutions containing 1 M NaOH. Thus the apparent rate constant for the dimerization is calculated to be 2.5×10^4 $M^{-1}\,s^{-1}$ by using Eq. 4 (Table 2), where the value of k obtained is the total value of the rate constants for the two reactions of $R^{\cdot}$ to both *dl* and *meso* types of **2**. When the water concentration decreased, the intersection in $E_{1/2}$—log ω plots was observed even in the solution containing 10 mM of **1** (Fig. 5); this is because the rate of dimerization decreased. For 7.5 and 15% water–ethanol solutions, the values of k thus obtained are listed in Table 2. The decrease in the k value at low concentrations of water indicates that an increase in the coulombic repulsive force between the anion radicals lowered the rate of the dimerization.

The authors wish to express their thanks to Associate Professor Tsutomu Nonaka of Tokyo Institute of Technology for his useful advice.

Appendix

Let us consider the following reactions:

$$A + ne \rightleftarrows B \text{ (reversible)}$$

$$2B \xrightarrow{k} B_2 \text{ (irreversible fast dimerization)}$$

At the steady state, the boundary value problem of the above reactions at an RDE can be formulated as follows, under the usual experimental conditions:

$$D_A\frac{d^2A}{dx^2} - V_x\frac{dA}{dx} = 0, \tag{1}$$

$$D_B\frac{d^2B}{dx^2} - V_x\frac{dB}{dx} - kB^2 = 0, \tag{2}$$

where $V_x = -0.51\,\omega^{3/2}\nu^{-1/2}x^2$, with the boundary conditions of

$$x = 0\text{: } A = A_0,\ B = B_0, \text{ and } D\frac{dA}{dx} = -D\frac{dB}{dx} = \frac{i}{nF}$$

$$(D_A = D_B = D \text{ is assumed}), \tag{3}$$

$$x \to \infty\text{: } A = A^*, \text{ and } B = 0, \tag{4}$$

where A^* is the bulk concentration of A, and A_0 and B_0 are, respectively, the concentrations of A and B at the surface of the RDE. The symbols used without definition have their ordinary meanings.[10]

The solution of Eq. 1 is

$$A = A_0 + (A^*-A_0)\frac{\int_0^x \exp\left(\int_0^x \frac{V_x}{D}dx\right)dx}{\int_0^\infty \exp\left(\int_0^\infty \frac{V_x}{D}dx\right)dx}, \quad (5)$$

and the concentration gradient of A at the electrode surface is

$$\left(\frac{dA}{dx}\right)_{x=0} = \frac{A^*-A_0}{\int_0^\infty \exp\left(\int_0^\infty \frac{V_x}{D}dx\right)dx}, \quad (6)$$

and thus the current density (i) is represented by

$$i = nFD\left(\frac{dA}{dx}\right)_{x=0} = nFD(A^*-A_0)/\delta \quad (7)$$

where $\delta = 1.61\ D^{1/3}\ \nu^{1/6}\ \omega^{-1/2}$.

By using the limiting current, i_d ($A_0=0$ in Eq. 7), we obtain

$$A_0 = \left(\frac{i_d-i}{nFD}\right)\delta. \quad (8)$$

On the other hand, Eq. 2 can not be solved analytically, but we may use the simplified model.[11] Here, let us neglect the second term in Eq. 2; thus we obtain

$$D\frac{d^2B}{dx^2} - kB^2 = 0. \quad (9)$$

After satisfying the boundary conditions, we obtain the solution of Eq. 9:

$$B = \frac{6D/k}{(\sqrt{6D/(kB_0)}+x)^2}, \quad (10)$$

Thus, the current is

$$i = -nFD\left(\frac{dB}{dx}\right)_{x=0} = (nFD)^{3/2}B_0^{3/2}/\varepsilon \quad (11)$$

where $\varepsilon = (3/2)^{1/3}\ (nF)^{1/3}\ D^{2/3}\ k^{-1/3}$,
and we obtain

$$B_0 = \left(\frac{i^{2/3}}{nFD}\right)\varepsilon. \quad (12)$$

Under the condition of the Nernst equation holding for the electron transfer reaction ($A+n\ e \rightleftarrows B$), we obtain

$$\begin{aligned} E &= E_0 - \frac{RT}{nF}\ln\frac{B_0}{A_0} \\ &= E_0 - \frac{RT}{nF}\ln\frac{i^{2/3}}{(i_d-i)}\frac{\varepsilon}{\delta} \\ &= E_0 - \frac{RT}{nF}\ln\frac{\varepsilon}{\delta} - \frac{RT}{nF}\ln\frac{i^{2/3}}{(i_d-i)}. \end{aligned} \quad (13)$$

By substituting $i=(1/2)i_d$ and $i_d = nFDA^*/\delta$ into Eq. 13, we get the half-wave potential:

$$\begin{aligned} E_{1/2} &= E_0 - \frac{RT}{nF}\ln\frac{2^{1/3}\varepsilon}{i_d^{1/3}\delta} \\ &= E_0 - \frac{RT}{nF}\ln\frac{3^{1/3}D^{1/3}k^{-1/3}A^{*-1/3}}{\delta^{2/3}} \\ &= E_0 - \frac{RT}{3nF}\ln\frac{3D}{kA^*\delta^2} \end{aligned} \quad (14\text{-}1)$$

or

$$= E_0 - \frac{RT}{3nF}\ln\frac{3D^{1/3}}{1.61^2\nu^{1/3}} + \frac{RT}{3nF}\ln\frac{kA^*}{\omega}. \quad (14\text{-}2)$$

Equations 13 and 14 obtained here are the same as those derived by other workers,[2,12] and were used in the present work.

References

1) C. P. Andrieux, L. Nadjo, and J. M. Saveant, *J. Electroanal. Chem. Interfacial Electrochem.*, **42**, 223 (1973).
2) L. Nadjo and J. M. Saveant, *J. Electroanal. Chem. Interfacial Electrochem.*, **44**, 327 (1973).
3) M. J. Allen, *J. Org. Chem.*, **15**, 435 (1950).
4) I. Taniguchi and T. Sekine, *Denki Kagaku*, **43**, 201 (1975); I. Taniguchi, A. Yoshiyama, and T. Sekine, *ibid.*, **45**, 442 (1977).
5) J. A. Stocker and D. H. Kern, *J. Org. Chem.*, **33**, 1271 (1968).
6) L. Nadjo and J. M. Saveant, *J. Electroanal. Chem. Interfacial Electrochem.*, **33**, 419 (1971).
7) M. Lipsztajn, T. M. Krygowski, and Z. Galus, *J. Electroanal. Chem. Interfacial Electrochem.*, **49**, 17 (1974).
8) L. A. Avaca and A. Bewick, *J. Electroanal. Chem. Interfacial Electrochem.*, **41**, 405 (1973).
9) E. Lamy, L. Nadjo, and J. M. Saveant, *J. Electroanal. Chem. Interfacial Electrochem.*, **50**, 141 (1974).
10) V. G. Levich, "Physicochemical Hydrodynamics," Prentice-Hall Inc., Englewood Cliffs, New Jersey (1962), Chap. 2.
11) L. K. J. Tong, K. Liang, and W. R. Ruby, *J. Electroanal. Chem. Interfacial Electrochem.*, **13**, 245 (1967).
12) R. Bonnaterre and G. Cauquis, *J. Electroanal. Chem. Interfacial Electrochem.*, **33**, 199 (1971).

Electron Spin Resonance Study of the Pyramidal Geometry around the Tervalent Carbon Atom of the Bicyclo[2.1.1]hexan-5-yl Radical[1)]

Takashi KAWAMURA,* Shigeru HAYASHIDA, and Teijiro YONEZAWA
Department of Hydrocarbon Chemistry, Faculty of Engineering, Kyoto University, Sakyo-ku, Kyoto 606
(Received September 11, 1978)

The bicyclo[2.1.1]hexan-5-yl and the 5-deuteriobicyclo[2.1.1]hexan-5-yl radicals have been examined using ESR. A comparison of the spectra confirmed that geometry around C_5 is pyramidal and showed highly stereoselective long-range spin-transfer from C_5 to the endo proton on C_6; $a(H_{6endo})=28.22$ and $a(H_{6exo})=0.49$ G. A potential curve for the out-of-plane bending motion of the C_5–H_5 bond, selected from the trial curves gave a reasonable simulation of the temperature dependence and isotope effects on $a(H_5)$ and $a(H_{6endo})$. The curve has two minima with a relatively low barrier to inversion; the geometry of the C_5–H_5 bond bent in the exo direciton has been estimated as approximately 0.9 kcal/mol more stable than that with the C_5–H_5 bond located in the endo direction.

Stereospecific intramolecular interactions in bicyclo[2.1.1]hexanes have been of theoretical and experimental interest for several years and large long-range nuclear spin couplings between the two endo protons on methano bridges of bicyclo[2.1.1]hexanes have been observed.[2)] A strong interaction has been revealed by the nonempirical molecular orbital calculation of bicyclo[2.1.1]hexane between the two endo C–H bonds on the methano bridges.[3)] Furthermore the *endo*-bicyclo[2.1.1]hexan-5-yl tosylate has been found to undergo faster solvolysis, by a factor of 10^8 than the exo isomer.[4)] All these results indicate a strong stereospecific intramolecular interaction operating between the two endo C–H bonds on the methano bridges.

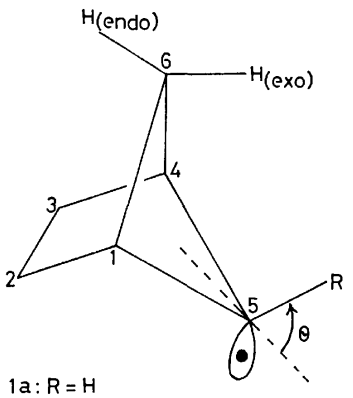

1a: R = H
1b: R = D

The potential curves for the umbrella-mode vibrations around tervalent carbon atoms of several alkyl radicals have been correlated with the temperature dependence and the isotope shifts of hyperfine splitting constants (hfsc) of α carbon nuclei and/or α protons.[5)] In the bicyclo[2.1.1]hexan-5-yl radical (**1a**), the temperature dependences of $a(H_5)$ and $a(H_{6endo})$ and their shifts upon replacement of H_5 with a deuterium atom are closely correlated with the out-of-plane bending motion of the C_5–H_5 bond.[1b)] The potential curve for this motion will be estimated by simulating the temperature dependence and isotope effects with the aid of geometrical dependence of spin distribution calculated from INDO-UHF method.[6)]

Results and Discussion

ESR Spectra and Stable Geometry of ***1****.* The radical **1a** and the 5-deuteriobicyclo[2.1.1]hexan-5-yl radical, **1b**, have been generated in an ESR cavity by the photolysis of bis(bicyclo[2.1.1]hexane-5-carbonyl) peroxide and bis(5-deuteriobicyclo[2.1.1]hexane-5-carbonyl) peroxide in cyclopropane solvent, respectively. Typical ESR spectra for these radicals and the computer simulations have been published elsewhere.[1)] The spectrum of **1a** at −115 °C has been analyzed as three sets of doublets (28.22, 9.14, and 0.49 G), split further into three sets of 1 : 2 : 1 triplets (0.80, 0.49, and 0.25 G) with a g factor of 2.0027_6. At the same temperature the spectrum of **1b** consisted of two sets of doublets (28.80 and 0.50 G), three sets of 1 : 2 : 1 triplets (0.82, 0.36, and 0.11 G), and a 1 : 1 : 1 triplet of 1.34 G. The principal difference between the spectrum of **1a** and that of its deuterated analogue, **1b**, is the replacement of the large doublet of 9.14 G by the 1 : 1 : 1 triplet of 1.34 G. This result reconfirms the assignment[1a)] of $|a(H_5)|=9.14$ G for **1a** and previous estimations of the stable geometry of **1a**;[1a)] **1a** has a pyramidal radical center with C_5–H_5 bent in the exo direction (*i.e.*, $\theta>0$).

The remaining two sets of doublets of 28.22 and 0.49 G for **1a** should belong to H_{6endo} and H_{6exo}. The C_6–H_{6endo} bond is arranged in a double W-plan[7)] with respect to the odd electron orbital in the stable geometry of **1**, suggesting that $a(H_{6endo})$ is larger than $a(H_{6exo})$. This is consistent with the INDO-UHF calculations.[1a)] Thus the largest doublet of 28.22 G has been assigned to H_{6endo} and the smallest doublet of 0.49 G to H_{6exo}. It should be pointed out that the long-range spin-transfer from the tervalent carbon atom to the two hydrogen atoms on C_6 is highly stereoselective. The remaining three sets of triplets of 0.80, 0.49, and 0.25 G of **1a** are expected to arise from H_1, H_{2syn} and H_{2anti} and their equivalents, but the assignments remain uncertain. Table 1 summarizes the observed hfsc's of **1a** and **1b** together with the assignments.

Temperature Dependence and Isotope Shift of hfsc's. The replacement of H_5 with a deuterium atom shifted not only the splitting pattern attributed to H_5 but also the hfsc's of other protons; a typical example is the increase of the hfsc of H_{6endo} from 28.22 to 28.80 G

Table 1. Observed hfsc's of **1a** and **1b** at −115 °C

Radical	hfsc's (G)[a]					
1a	28.22 d	9.14 d	0.49 d	0.80 t	0.49 t	0.25 t
1b	28.80 d	1.34 t[b]	0.50 d	0.82 t	0.36 t	0.11 t
assignt.	H_{6endo}	H_5	H_{6exo}	(H_1	H_{2anti}	H_{2syn})[c]

a) d: doublet; t: triplet. b) Triplet due to a deuterium nucleus c) The hfsc's of the protons in the parentheses have not been assigned.

upon the deuteration.[1b] The ratio of the observed splitting of [$a(D_5)$ of **1b**]/[$a(H_5)$ of **1a**] at −115 °C is 0.147[1b] which is smaller than that of the magnetic moments of the nuclei (0.1535).

The temperature dependence of the hfsc's of **1a** are illustrated in Figs. 1 and 2. The hfsc's of H_5 and H_{6endo} depend on the temperature (T) as $d|a(H_5)|/dT=7.9$ mG deg^{-1} and $d|a(H_{6endo})|/dT=-33$ mG deg^{-1}, respectively.

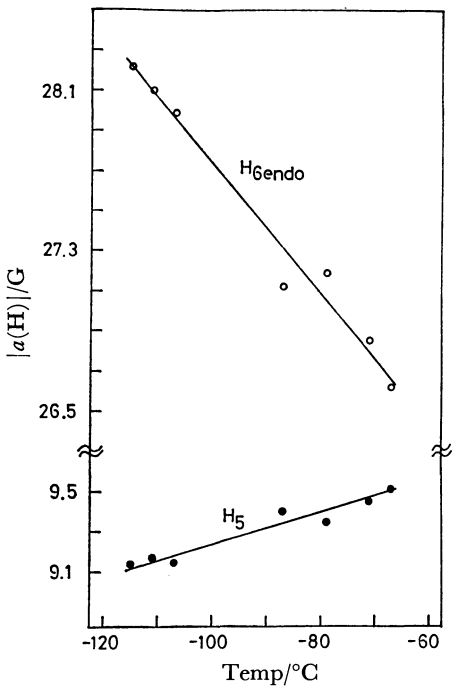

Fig. 1. Temperature dependence of $a(H_5)$ and $a(H_{6endo})$.

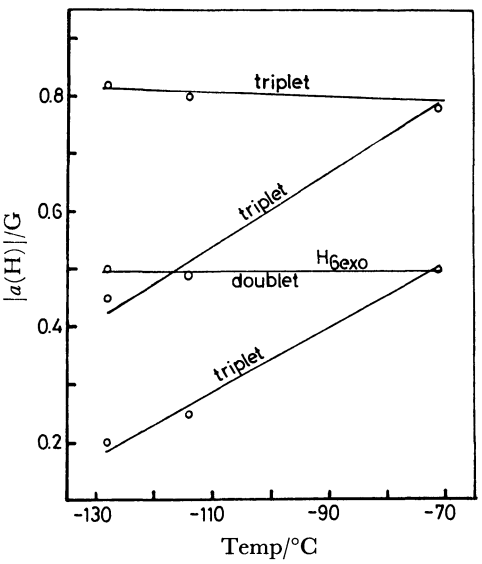

Fig. 2. Temperature dependence of the small hfsc's of **1a**.

The replacement of an α hydrogen atom with a deuterium atom has a similar effect as the lowering of the temperature for the out-of-plane bending mode vibration of the C_α–H_α (or C_α–D_α) bond; both effects decrease the average amplitude of the vibration. Therefore, the small ratio of $a(D_5)$ of **1b** to $a(H_5)$ of **1a** and the positive temperature dependence of $|a(H_5)|$ may be assumed to originate largely from the shift of the average amplitude of the out-of-plane bending vibration of the C_5–H_5 (or C_5–D_5) bond.

The temperature effect on $a(H_{6endo})$ of **1a** may result from the temperature dependence of the out-of-plane bending vibration of the C_5–H_5 bond or of some mode(s) of vibration(s) resulting in a shift of the time-averaged arrangement between the odd electron orbital on C_5 and the C_6–H_{6endo} bond. The observed increase of $a(H_{6endo})$ upon replacement of the H_5 with a deuterium atom was 28.80−28.22=0.58 G, which is similar to the observed increase of the hfsc upon lowering the temperature 15—20 °C. This indicates that the temperature and isotope effects result from the out-of-plane bending mode (and/or the in-plane bending and the stretching modes) vibration of the C_5–H_5 bond. Otherwise, the observed isotope effect on $a(H_{6endo})$ is unreasonably large, since the replacement of H_5 with a deuterium atom has only a small effect on the reduced masses of the other modes of vibrations.

The small triplets of 0.49 and 0.25 G of **1a** (at −115 °C) exhibit a relatively large temperature dependence (Fig. 2). The corresponding splitting of the deuterated analogue, **1b**, at −115 °C are 0.36 and 0.11 G, respectively, which are similar to those of **1a** at a 15 to 20 °C lower temperature. These results indicate that the temperature dependences and deuterium isotope shifts of the hfsc's of **1** may originate largely from the out-of-plane bending vibration of the C_5–H_5 bond.

Procedure for Estimation of the Potential Curve for the Out-of-plane Bending Motion of the C_5–H_5 Bond. The potential curve for the out-of-plane bending vibration of the C_5–H_5 bond may be estimated by reproducing the four experimental values (the temperature dependences and the isotope shifts of the hfsc's of H_5 and H_{6endo}) with trial potential functions.

For this procedure the geometrical dependences of the hfsc's of **1** are required. Calculations using the UHF-INDO method have been shown to give reliable geometrical dependences of the spin distribution. The valence s orbital spin densities on the hydrogen atoms of **1** were calculated at 7.5° intervals of θ, where θ is

defined as the angle between the C_5–H_5 bond and the $C_1C_5C_4$ plane. The remaining geometry of **1** is assumed to be the same as the parent hydrocarbon reported by Chiang.[8] The INDO spin densities, ρ, on H_5 and H_{6endo} have been fitted to fourth-order polynomials in θ in order to evaluate ρ at any value of θ desired, and multiplied by C, which converts the spin density into the hfsc:

$$a(\theta) = C(\rho_0+\rho_1\theta+\rho_2\theta^2+\rho_3\theta^3+\rho_4\theta^4). \quad (1)$$

Figure 3 illustrates the calculated geometrical dependence of the hfsc's of H_5 and H_{6endo}. The conversion factor C was set tentatively to 1100 G in Fig. 3.

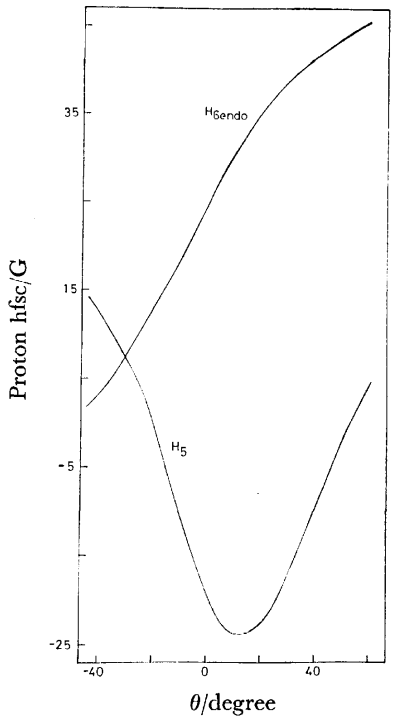

Fig. 3. Geometrical dependence of $a(H_5)$ and $a(H_{6endo})$.

The vibrations of the C_5–H_5 bond have been treated as motions of H_5 bonded to an infinite mass. The hamiltonian for the out-of-plane motion is expressed by the following equation:

$$\mathcal{H} = -\frac{\hbar^2}{2\cdot I}\frac{\partial^2}{\partial\theta^2} + V(\theta) \quad (2)$$

where I is the moment of inertia and $V(\theta)$ an arbitrary potential function which is expressed by an eighth-order polynomial in θ. The eigenfunctions, ψ_i, are calculated as linear combinations of the lowest twenty eigenfunctions of an appropriate harmonic oscillator that minimizes the difference between the square of the expectation value of the hamiltonian and the expectation value of the square of the hamiltonian in the lowest state,

$$|\langle\psi_0|\mathcal{H}|\psi_0\rangle^2-\langle\psi_0|\mathcal{H}^2|\psi_0\rangle|.$$

The expectation values, $a_i=\langle\psi_i|a(\theta)|\psi_i\rangle$, for each vibrational level i were then calculated using the wave functions obtained for the particular potential. The hfsc of a proton at a given temperature, $a(T)$, is expressed as an average of the expectation values weighted by Boltzmann populations:

$$a(T) = [\sum_i a_i\cdot\exp(-\varepsilon_i/kT)]/[\sum_i \exp(-\varepsilon_i/kT)]. \quad (3)$$

For convenience in the comparison between the experimental and calculated values, the isotope shift of the hfsc of H_5, $\Delta|a(H_5)|$, is defined as shown below from the hfsc's of **1a** and **1b** observed at -115 °C:

$$\Delta|a(H_5)| = [|a(D_5)| \text{ of } \mathbf{1b}]/0.1535-[|a(H_5)| \text{ of } \mathbf{1a}], \quad (4)$$

where 0.1535 is the ratio of the magnetic moments of the deuterium nucleus and proton. The isotope shift of the hfsc of H_{6endo} is simply given as the difference between the observed hfsc's of the H_{6endo} of **1a** and **1b** at -115 °C. The temperature coefficient, $d|a(T)|/dT=[|a(T_2)|-|a(T_1)|]/(T_2-T_1)$, and the isotope shift, $\Delta|a(H)|$, are divided by $|a(-115\ °C)|$ in order to get rid of the somewhat arbitrary multiplication factor, C, in Eq. 1:

$$\begin{aligned} d|A(H)|/dT &= [d|a(T)|/dT]/|a(-115\,°C)|, \\ \Delta|A(H)| &= \Delta|a(H)|/|a(-115\,°C)|. \end{aligned} \quad (5)$$

The experimental values are $d|A(H_5)|/dT=+0.86\times10^{-3}$ deg^{-1}, $\Delta|A(H_5)|=-4.5\times10^{-2}$, $d|A(H_{6endo})|/dT=-1.2\times10^{-3}$ deg^{-1}, and $\Delta|A(H_{6endo})|=+2.1\times10^{-2}$. From this point $d|A(H)|/dT$ and $\Delta|A(H)|$ are defined as the temperature dependence and isotope shift of the hfsc of a particular proton.

Effect of Vibrations of In-plane Bending and of Stretching Modes of the C_5–H_5 Bond. The wave numbers of the vibrations of the in-plane (or in-cone) bending mode and the stretching mode of the C_5–H_5 bond are expected to be around 1000 and 3000 cm^{-1}, respectively.[9] The energy gaps between these vibrational levels are too large for effective thermal excitation; these vibration modes can not effectively contribute to the temperature dependence of the hfsc's of H_5 and H_{6endo}. However, the replacement of H_5 with a deuterium atom changes the average amplitude of these modes of vibration, possibly resulting in isotope shifts of the hfsc's of H_5 and H_{6endo}.

The isotope shifts of the hfsc's of H_5 and H_{6endo} due to these two modes of vibration have been examined. The motions of the in-plane bending and the stretching vibrations taken into account are shown below:

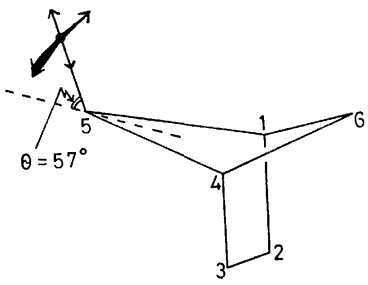

The angle $\theta=57°$ is the estimated potential minimum for the out-of-plane bending of the C_5–H_5 bond (*vide infra*). The stretching and in-plane bending vibrations have been assumed harmonic with wave numbers in the range 2800—3100 and 800—1500 cm^{-1}, respectively. The geometrical dependence of the spin densities on H_5 and H_{6endo} for these modes of motions may be calculat-

ed using the UHF-INDO method and expressed in quadratic forms (*cf.* Eq. 1). The isotope shifts of the hfsc's of H_5 and H_{6endo} due to in-plane bending vibration of C_5–H_5 are then obtained[10] as $\Delta|A(H_5)|=(0.22—0.75)\times10^{-2}$ (−5——17% of the observed) and $\Delta|A(H_{6endo})|=(0.05—0.17)\times10^{-2}$ (2—8% of the observed). The calculated values of the isotope shifts resulting from the stretching vibration of the C_5–H_5 bond are $\Delta|A(H_5)|=(1.8—1.9)\times10^{-2}$ (−40——42% of the observed) and $\Delta|A(H_{6endo})|\approx-0.02\times10^{-2}$ (−1% of the observed). These modes of vibration have negligible effects on the isotope shift of the hfsc of H_{6endo}. These vibrations, however, have quite a large contribution to the isotope shift of the hfsc of H_5, and the estimated contribution of both vibrations are opposite to the experimental observation and also opposite to the contribution of the out-of-plane bending motion (*vide infra*).

The foregoing analyses show that the temperature dependence of the hfsc's of H_5 and H_{6endo} and the deuterium isotope shift of the hfsc of H_{6endo} arise largely from the out-of-plane bending vibration of the C_5–H_5 bond. The isotope shift of the hfsc of H_5 is, however, a result of the counteracting contributions from the out-of-plane bending motion and the stretching and in-plane bending vibrations. Therefore, the isotope shift of the hfsc of H_5 is not such a good indicator as the other three experimental values in the estimation of the potential curve for the out-of-plane bending motion of the C_5–H_5 bond. Calculations, taking only into account the out-of-plane bending vibration, may overestimate the isotope shift of the hfsc of H_5.

Estimation of the Potential Curve. The dependence of the hfsc of H_5 on the pyramidal deformation of C_5 in Fig. 3 reveals that the hfsc of H_5 should be negative, otherwise the radical center must have an unreasonably pyramidal geometry. Thus the hfsc of H_5 has been assumed negative. Based on this assumption the observed positive temperature dependence of the absolute value of the hfsc of H_5 indicates that the potential curve for the out-of-plane vibration of C_5–H_5 bond is anharmonic.[5a,5e] Several typical trial anharmonic potential functions, selected from more than thirty trials, are illustrated in Fig. 4. Table 2 summarizes the calculated temperature dependences and isotope shifts of the hfsc's of H_5 and H_{6endo}.

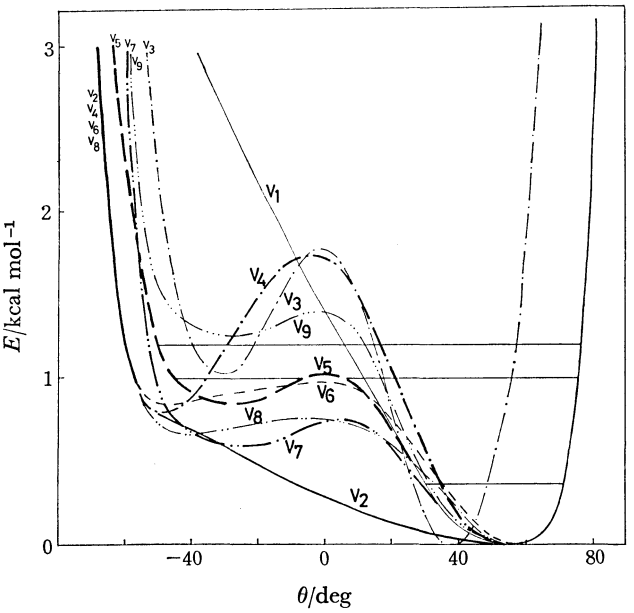

Fig. 4. Trial potential curves. Horizontal solid lines are vibrational levels calculated with curve V_5 for **1a**.

Simple single-minimum anharmonic potential curves (V_1, V_2) gave calculated values which were too small for the temperature dependence of the hfsc of H_{6endo}. The reason for this is that the expectation values of $a(H_{6endo})$ for the second and higher vibrational levels of **1a** are not sufficiently shifted from the lowest vibrational level to reproduce the observed large temperature dependence of $a(H_{6endo})$. In order to reproduce the experimentally observed large negative temperature dependence of the hfsc of H_{6endo}, the lowest vibrational level needs to be restricted in the positive range of θ, whereas in the second and higher excited vibrational levels, the extent of the vibration of C_5–H_5 bond needs to be extended to a very large negative value of θ. Such requirements can be satisfied by unsymmetrical double-minimum potential curves. ΔE (kcal/mol) is defined as the difference between the two minima and $\Delta\varepsilon$ (kcal/mol) as the barrier to inversion measured from the higher minimum. Double-minimum potential curves with relatively high barrier to inversion (V_3, V_4)

Table 2. Calculated temperature dependences and isotope shifts of hfsc's of H_5 and H_{6endo}

Curve	$d\|A(H_{6endo})\|/dT$ [a]	$d\|A(H_5)\|/dT$ [a]	$\Delta A(H_{6endo})$ [a]	$\Delta A(H_5)$ [a]	ΔE [b]	$\Delta\varepsilon$ [b]
V_1	15	229	40	341	c)	c)
V_2	68	−154	76	94	c)	c)
V_3	62	−127	54	22	0.95	0.75
V_4	26	235	46	458	0.79	0.96
V_5	76	76	142	246	0.89	0.18
V_6	104	88	92	494	0.87	0.15
V_7	92	−1.5	361	−43	0.60	0.20
V_8	104	d)	92	413	0.66	0.10
V_9	29	208	48	341	1.30	0.17
obsd	-1.2×10^{-3}	0.86×10^{-3}	2.1×10^{-2}	-4.5×10^{-2}	—	—

a) Calculated values are given as a per cent of the experimental values. b) In kcal/mol.
c) Single-minimum. d) Not monotonous and very small.

predict a too small temperature dependence and a too small isotope shift of the hfsc of H_{6endo}.

The potential curves with a ΔE of around 0.9 kcal/mol and a relatively low barrier to inversion (V_5, V_6) give reasonable temperature dependences of the hfsc's of H_5 and H_{6endo} and an acceptable isotope shift for H_{6endo}. The isotope shifts of the hfsc of H_5 calculated with V_5 and V_6 are acceptable since the contributions of the in-plane and stretching vibrations to the isotope effects on $a(H_5)$ (*vide supra*) have been ignored. Potential curves with small values of ΔE gave an unacceptable small temperature dependence of $a(H_5)$ (V_7, V_8) and a curve with a large value of ΔE gave a too large temperature dependence of $a(H_5)$ (V_9).

Thus the potential curve for the out-of-plane vibration of C_5–H_5 bond is suggested as a double-minimum potential with a small barrier to inversion with an energy difference of around 0.9 kcal/mol between the two energy minima. The geometry with the C_5–H_5 bond tilting in the exo direction is about 0.9 kcal/mol more stable than that with the C_5–H_5 bond located on the endo side. The barrier to inversion, $\Delta\varepsilon$, is very small and there is no vibrational steady state in which the C_5–H_5 bond is localized in the endo side of the $C_1C_5C_4$ plane ($\theta<0$); even the zero-point vibrational level in the left well ($\theta<0$) is located above the barrier top and effectively mixed with the vibrational state(s) in the right well ($\theta>0$).

Estimation of the Potential Curve. The dependence of $a(H_{6endo})$ on the out-of-plane deformation angle, θ, is large and monotonic. This feature was helpful in estimating the potential curve of the out-of-plane vibration of C_5–H_5 bond. However, in the case of most alkyl radicals, the parameters available for estimation of the potential curve would be only the temperature dependence of the hfsc of α proton(s). In such cases, it would be impossible to estimate the potential curve only from the temperature dependence of the hfsc of the α proton(s). For example in the case of the present radical, the results in Table 2 show that at least three potential curves would give acceptable temperature dependence of the hfsc of H_5: a single-minimum curve lying between V_1 and V_2, a double-minimum curve with a relatively high barrier to inversion lying between V_3 and V_4, and a double-minimum potential with a low barrier to inversion similar to V_5 or V_6.

Experimental

ESR Measurements. The ESR spectra of **1a** and **1b** were obtained during photolysis of bis(bicyclo[2.1.1]hexane-5-carbonyl) peroxide and bis(5-deuteriobicyclo[2.1.1]hexane-5-carbonyl) peroxide, respectively. The solvent was deoxygenated liquid cyclopropane. Measurements were conducted on a JEOL PE-2X spectrometer modified with a JEOL ES-SCXA gunn diode X-band microwave unit equipped with a cylindrical mode cavity with slits for UV irradiation. The field sweep was monitored during each ESR measurement with ^1H NMR using a water sample, which was set just outside the ESR cavity. A tunable NMR radio frequency was supplied from a JEOL ES-FC3 oscillator and counted on a Takeda-Riken TR-5501 frequency counter. The magnetic field difference between the ESR and NMR sample position was calibrated daily with perylene cation in concentrated sulfuric acid. ($g=2.002583$).[11] Photolysis was performed with a Philips SP-500 super-high-pressure mercury lamp focused with two quartz lenses and filtered through a distilled water cell of 45 mm path length. Accumulations and simulations were performed using a JEOL JEC-6 minicomputer.

The g factor and hfsc's were corrected against the microwave frequency drift,[12] which may result from the heating of the cavity by radiation and/or the change of chemical constituents in the sample through photochemical reactions.

The ESR samples were cooled with a cold nitrogen gas flow controlled by a JEOL JES-VT-3A temperature controller. The heating of samples by radiation was calibrated by measuring the temperature of liquid cyclopropane in a sample tube during irradiation and the temperature of the cooling nitrogen gas.

For the measurements of the isotope shifts of the hfsc's, the spectrum of **1b** was measured immediately after observation of the spectrum of **1a** without any change in the setting of the temperature of the nitrogen gas flow cooling the sample.

Bicyclo[2.1.1]hexane-5-carbonyl Chloride. A mixture of bicyclo[2.1.1]hexane-5-carboxylic acid[13] (3.0 g, 24 mmol) and thionyl chloride (8.7 g, 73 mmol) in chloroform (14 ml) was refluxed for 4 h. The chloroform was removed by distillation under atmospheric pressure. Distillation of the residue gave a forerun of the excess thionyl chloride (52—54 °C/400 Torr) followed by bicyclo[2.1.1]hexane-5-carbonyl chloride (2.8 g 19 mmol) (bp 68—74 °C/21 Torr); yield 80 %.

Bis(bicyclo[2.1.1]hexane-5-carbonyl) Peroxide. To a suspension of sodium peroxide (290 mg, 3.7 mmol) in dry ether (12 ml) cooled in an ice bath was added a solution of bicyclo-[2.1.1]hexane-5-carbonyl chloride (1.0 g, 6.9 mmol) in dry ether (8 ml) and two drops of water. The mixture was stirred overnight in an ice bath and then at room temperature for several hours followed by the dropwise addition of cold water (20 ml) to dissolve the excess sodium peroxide and the generated sodium chloride. The ethereal layer was washed with a saturated sodium hydrogencarbonate aqueous solution and then with a sodium chloride aqueous solution and finally dried over anhydrous magnesium sulfate. The ether was evaporated to dryness by a flow of nitrogen gas; yield 50 %. The white crystalline peroxide was stored as a pentane solution (or suspension).

5-Deuteriobicyclo[2.1.1]hexane-5-carboxylic Acid. A solution of norbornane diazo ketone[13] (3.5 g, 0.026 mol) in a mixed solvent of 1,4-dioxane (70 ml) and D_2O (50 ml) was irradiated under nitrogen with a 200 W medium-pressure mercury lamp. The course of the reaction was monitored by the disappearance of the diazo band at 4.80 μm in the infrared absorption, and required about 1.5 h. Approximately 100 ml of the mixed solvent was removed by distillation through a 30-cm Vigreux column under reduced pressure (bp 43—44 °C/100 Torr). The residue was made alkaline with 1 M sodium hydroxide and extracted with three 50 ml portions of ether to remove the neutral materials. The aqueous solution was acidified with hydrochloric acid and extracted with four 50 ml portions of ether, and dried over anhydrous magnesium sulfate. The ether solvent was removed and distillation of the residue gave 0.88 g of 5-deuteriobicyclo[2.1.1]hexane-5-carboxylic acid, bp 106—109 °C at 7 Torr; yield 27 %.

Bis(5-deuteriobicyclo[2.1.1]hexane-5-carbonyl) Peroxide. The 5-deuteriobicyclo[2.1.1]hexane-5-carboxylic acid was converted to the acid chloride with thionyl chloride and treated with sodium peroxide to obtain the peroxide.

The authors would like to thank Dr. S. Kato (Institute of Molecular Science) for the computer program to solve the anharmonic oscillation. This work was partly

supported by a grant from the Ministry of Education. INDO-UHF calculations are performed with FACOM M190 computer at Data Processing Center of Kyoto University.

Note Added in Proof

The potential curve for the out-of-plane bending motion of the C_5–H_5 bond of **1** was calculated with *ab initio* UHF method. Basis functions were the STO-3G set[14] except those for the tervalent carbon atom, for which Dunning's 4s/2p basis set[15] was adopted. The calculated curve resembles the curve V_3 in Fig. 4. The extrema of the calculated curve are (θ deg, E kcal/mol): (−22, 1.2), (7, 2.1), and (42, 0.0). This result is consistent with the present conclusion.

We thank Dr. H. Nakatsuji and Mr. K. Ohta (Kyoto) for discussions and Gauss-70 program. *Ab initio* calculations were performed on HITAC M-180 computer at Institute of Molecular Science.

References

1) Preliminary accounts have been published: a) M. Matsunaga and T. Kawamura, *J. Am. Chem. Soc.*, **97**, 3519 (1975); b) T. Kawamura, S. Hayashida, and T. Yonezawa, *Chem. Lett.*, **1977**, 267.

2) K. B. Wiberg, B. R. Lowry, and B. J. Nist, *J. Am. Chem. Soc.*, **84**, 1594 (1962).

3) J. M. Lehn and G. Wipff, *Theor. Chim. Acta*, **28**, 2769 (1973).

4) K. B. Wiberg, R. A. Fenoglio, V. Z. Williams, Jr., and R. W. Ubersax, *J. Am. Chem. Soc.*, **92**, 568 (1970).

5 a) S. Y. Chang, E. R. Davidson, and G. Vincow, *J. Chem. Phys.*, **52**, 5596 (1970); b) P. J. Krusic and P. Meakin, *J. Am. Chem. Soc.*, **98**, 228 (1976); c) J. B. Lisle, L. F. Williams, and D. E. Wood, *ibid.*, **98**, 227 (1976); d) J. K. Kochi, P. Bakuzis, and P. J. Krusic, *ibid.*, **95**, 1516 (1973); e) T. Kawamura, Y. Sugiyama, M. Matsunaga, and T. Yonezawa, *ibid.*, **97**, 1627 (1975); f) B. T. Sutcliffe and C. Gaze, *Mol. Phys.*, **35**, 525 (1978).

6) J. A. Pople, D. L. Beveridge, and P. A. Dobosh, *J. Am. Chem. Soc.*, **90**, 4201 (1968).

7) a) F. W. King, *Chem. Rev.*, **76**, 157 (1976); b) T. Kawamura, M. Matsunaga, and T. Yonezawa, *J. Am. Chem. Soc.*, **100**, 92 (1978).

8) J. F. Chiang, *J. Am. Chem. Soc.*, **93**, 5044 (1971).

9) *Cf.* D. L. Beveridge and K. Miller, *Mol. Phys.*, **14**, 401 (1968).

10) For the procedure of calculation, see Eq. 18 of Ref. 5a.

11) B. G. Segal, M. Kaplan, and G. K. Fraenkel, *J. Chem. Phys.*, **43**, 4191 (1965).

12) T. Kawamura, M. Tsumura, Y. Yokomichi, and T. Yonezawa, *J. Am. Chem. Soc.*, **99**, 8251 (1977).

13) K. B. Wiberg, B. R. Lowry, and T. H. Colby, *J. Am. Chem. Soc.*, **83**, 3998 (1961).

14) W. J. Hehre, R. F. Stewart, and J. A. Pople, *J. Chem. Phys.*, **51**, 2657 (1969).

15) T. H. Dunning, *J. Chem. Phys.*, **53**, 2823 (1970).

The Correlation of Basicity and Equilibrium Constants Evaluated from Lanthanoid-induced Shifts in the Eu(fod)$_3$-*p*-Substituted Aniline Systems

Masatoshi HIRAYAMA* and Masashiro OWADA

Department of Chemistry, Ibaraki University, 2-1-1 Bunkyo, Mito 310

(Received September 18, 1978)

An approximate linear correlation has been found between the basicity of substrate (pK_a) and the logarithm of the equilibrium constant K_1 for 1:1 adducts evaluated from the least squares analysis of lanthanoid-induced shifts (LIS) for the systems containing Eu(fod)$_3$ and a series of *p*-substituted anilines in $CDCl_3$. In contrast, both the observed *S*-values and intrinsic shifts have shown no simple correlation to pK_a's of substrates.

The equilibrium constants (K) and chemical stoichiometry for several systems containing shifts reagents (LSR) and substrates (S) in solution have quantitatively been investigated by several workers in terms of the least-squares analysis of lanthanoid-induced shifts (LIS).[1-9] The orders of magnitude of K have, though roughly, been estimated for several functional groups as a coordination site. The validity of these estimates of K values has been checked solely by the degree of fits of the LIS data to the equilibrium system and by the magnitude of the free energy change, ΔG. Indeed, it has generally been confirmed that such a fit to each envelope of proton data in a substrate molecule is satisfactory (measured in terms of the standard deviation, σ). However the variation in K-values with the position in a molecule is relatively large. It has not been investigated which of some possible origins of errors is directly related to this variation in K.

From the characteristics of LSR as a Lewis acid it is reasonable to expect that the K-values should be correlated to the basicity of the substrate, the degree of steric hindrance on complexation, and the nature of the solvent, *e.g.*, the dielectric constant. It has recently been found in our laboratory that there is a qualitative correspondence between K and the degree of steric hindrance on complexing to LSR for the Eu(fod)$_3$–alkylaniline system in CCl_4.[6]

This paper will report on the relation of K to the basicity of the substrate for a selected series of *p*-substituted anilines with similar steric effects and various pK_a's with Eu(fod)$_3$ in $CDCl_3$.

Experimental

Eu(fod)$_3$ dried over P_2O_5 in a vaccum desiccator was used immediately after sublimation. $CDCl_3$ as the solvent and liquid amine samples were dried over molecular sieves in the dark, the solid samples being recrystallized. The sample solutions were prepared by the so-called "S_0-incremental dilution method,"[11] with a constant concentration of substrate (S_0), 0.2 M. The maximum ratio, $[L_0]/[S_0]$ (ρ), was 2.4 to 3.4, where $[L_0]$ is the total concentration of Eu(fod)$_3$, the number of data points, 23 to 28. NMR spectra were recorded on a Hitachi R-20A at 60 MHz at 34 °C in the frequency-swept mode, using TMS as an internal standard. The program used for the fitting analysis was LISA[5] developed by Shapiro *et al.* and partially modified in this laboratory. All computations were made on HITAC 8800/8700 computers at The University of Tokyo.

Results and Discussion

The systems consisting of aniline and Ln(fod)$_3$ in $CDCl_3$ at room temperature fullfil "the condition of fast substrate exchange" for the measurement of NMR shifts,[6,11,12] as well as those studied in most literatures. It has been found for most substrates with Ln(fod)$_3$ that the highest complex present in solution is LS_2 for very small values of ρ.[1,3-9] Consequently, the equilibria to be considered are 1) $L+S \rightleftharpoons LS \cdots K_1$, 2) $LS+S \rightleftharpoons LS_2 \cdots K_2$, and 3) $L+2S \rightleftharpoons LS_2 \cdots K_3$. Eq. 3 may be neglected because its formation constant is expected to be much smaller than for the others. The formation of L_2 dimer ($L+L \rightleftharpoons L_2 \cdots K_L$ (4)) has been considered in the literature through vapor phase osmometric measurements.[13] The introduction of this effect to the fitting analysis of LIS gave poorer fits for several substrates in solution.[4,5] This suggests that K_L has a very small value, even if the dimerization reaction were considered. Thus, in the present analysis for each substrate, the attempts were made for fitting the LIS data to the four equilibrium systems; (a) only (1), (b) (1)+(4), (c) (1)+(2), and (d) (1)+(2)+(4). For the two step equilibrium (c), the appropriate ranges of K_1 and K_2 were first estimated on the basis of the K-values[6] already obtained for analogous substrates. The respective Q-values ($Q = \sum_i^N (\delta_{exp,i} - \delta_{calcd,i})^2$, where the δ-values represent the LIS's and N the number of data points) for *o*- and *m*-proton data, Q_o and Q_m, were calculated by the introduction of a set of K_1 and K_2 values common to the two data series. The Q_{av}-value was evaluated as the

Table 1. Substrates and pK_a[a]-values

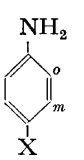

	Compound	pK_a[a]
1	X=CH_3	4.90
2	F	4.48
3	C_6H_5	4.22
4	Cl	3.83
5	Br	3.73
6	I	3.65
7	CN	1.75
8	NO_2	0.93
9	OCH_3	5.16
10	$COOCH(CH_3)_2$	2.49
11	$COCH_3$	2.20

a) Taken from Ref. 10.

TABLE 2. EQUILIBRIUM CONSTANTS AND INTRINSIC SHIFTS[a]

Compound		δ_1[b]	δ_2[b]	K_1	K_2	$Q_{av,min}(\sigma)$[c]
1	*o*-H	−10.00±0.21	−7.07±0.05	212± 30.5	13±12.7	1.03×10^{-2} (0.021)
	m-H	−2.38±0.16	−1.54±0.08			
2	*o*-H	−13.89±0.21	−8.91±0.11	228±100.0	55±14.5	8.00×10^{-3} (0.018)
	m-H	−2.89±0.03	−1.91±0.03			
3	*o*-H	−10.73±0.19	−7.03±0.09	153±29.9	26±14.1	9.20×10^{-3} (0.019)
	m-H	−2.56±0.08	−1.22±0.06			
4	*o*-H	−10.60±1.27	−6.59±0.36	69± 7.4	20±27.6	4.50×10^{-2} (0.046)
	m-H	−2.17±0.23	−1.52±0.10			
5	*o*-H	−9.91±0.13	−5.67±0.82	91±33.9	15±6.4	3.27×10^{-1} (0.128)
	m-H	−2.07±0.03	−1.27±0.21			
6	*o*-H	−13.60±0.35	−5.51±0.04	84±4.0	193±61.6	7.50×10^{-2} (0.061)
	m-H	−2.84±0.66	−1.25±0.00$_7$			
7[e]	*o*-H	−11.30±0.14	−3.93±0.14	14.8±1.14	2.6±0.14	2.42×10^{-2} (0.032)
	m-H	−6.93±0.88	−2.65±0.10			
	o-H	−11.90±0.16		11.2±0.76	0.7±0.07[d]	2.83×10^{-2} (0.035)
	m-H	−7.37±0.12				
8	*o*-H	−11.47±2.39		3.0±0.57	23.0±5.7[d]	2.60×10^{-3} (0.011)
	m-H	− 8.98±1.85				

a) The values of K_1, K_2, δ_1 and δ_2 are those corresponding to $Q_{av,min}$. The standard deviations given in parentheses were evaluated on the basis of each pair of parameters corresponding to $Q_{o,min}$ and $Q_{m,min}$. b) Measured in ppm. Negative signs designate shifts to lower field. c) See text for $Q_{av,min}$. σ is the standard deviation for the fitting analysis, $\sqrt{Q_{av,min}/N}$, where N is the number of date points. d) K_L-values. e) Two sets of parameters obtained by the fitting analyses to both the equilibrium systems are listed. See text.

average which was weighted for the respective δ_1-values corresponding to Q_o and Q_m, where δ_1 is the intrinsic shift for the 1 : 1 complex (LS). The minimum value of Q_{av}, $Q_{av,min}$, was found from the Q_{av}-map in the range of K_1 and K_2 selected above. In the equilibrium system (d), after the introduction of the appropriate value ($0.01 \leqq K_L \leqq 50$) into K_L, the above procedure was conducted. For the one step mechanisms, (a) and (b), the Q_{av}-map for K_1 and K_L was prepared, where K_L was assumed to be zero for (a).

For compounds **1** to **6**, the best results were obtained from the analysis using (c), satisfactorily small values being observed for $Q_{av,min}$. Thus, the set of K_1 and K_2 values which gives the $Q_{av,min}$ value, is a reasonable one, and the values are shown in Table 2 together with the $Q_{av,min}$ values. Simultaneously, the $Q_{o,min}$ and $Q_{m,min}$ for the *o*- and *m*-proton data were independently determined from the Q_o and Q_m maps, respectively. The values of Q_{min} were satisfactorily small except for the *o*-proton data of **5**. The standard deviations for each of the values of K_1 and K_2 decided above were evaluated from the respective K_1 and K_2 values corresponding to $Q_{o,min}$ and $Q_{m,min}$ (Table 2). Representative examples of the analysis and Q-map's are shown in Figs. 1 and 2 for the two step equilibrium, respectively. The values of K vary widely from the *o*- to the *m*-system, especially for the K_2-values as presumed. It is, however, difficult to determine the error responsible for this variation and some explanations will be given later.

The optimum values for the intrinsic shifts, δ_1 and δ_2, were obtained from the set of K_1 and K_2 values which gave $Q_{av,min}$, and each standard deviation was calculated on the basis of the δ_1 and δ_2 values corresponding to $Q_{o,min}$ and $Q_{m,min}$, as the case of K. As may be seen

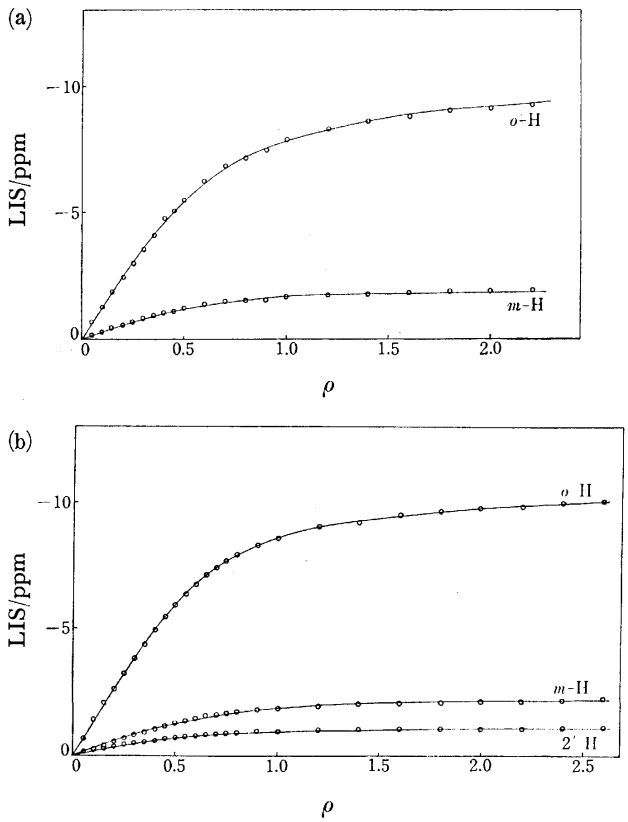

Fig. 1. Results of theoretical fits of the observed Eu(fod)$_3$-induced shifts to the two step mechanism for (a) *p*-chloroaniline and (b) 4-aminobiphenyl.
○: The observed data.

from Table 2, the values of the intrinsic shift do not vary so widely as the K-values, since they are not so

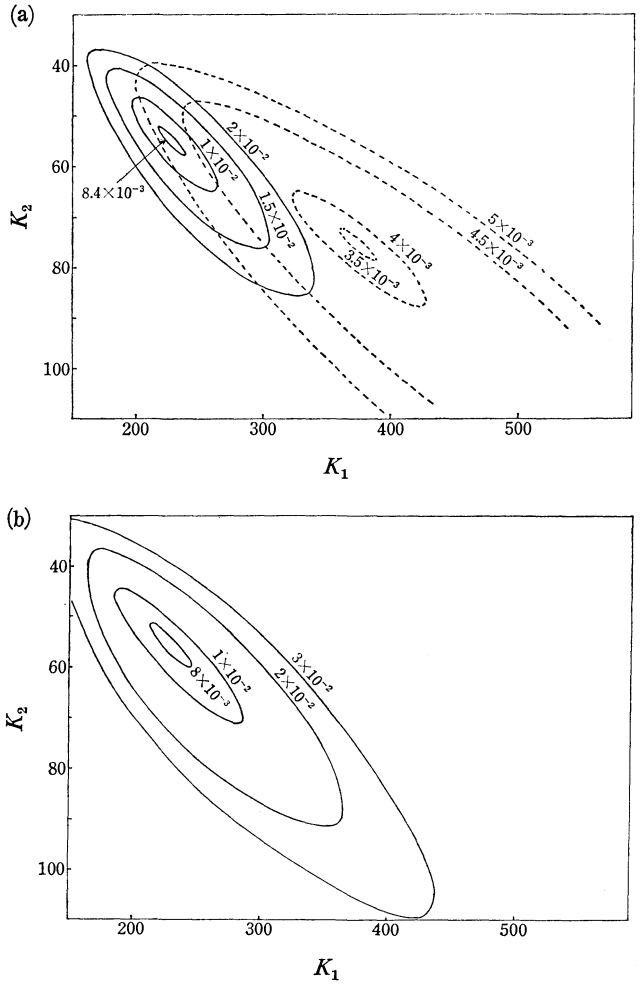

Fig. 2. Contour plots of Q calculated by fitting the LIS's to the equilibrium system, L+S⇄LS and LS+S⇄LS$_2$, for the *p*-fluoroaniline–Eu(fod)$_3$ system in $CDCl_3$ at 34 °C. a) The results calculated independently for *o*- and *m*-proton data. Solid and broken lines denote Q_o and Q_m, respectively. b) The average of Q_o and Q_m, Q_{av}.

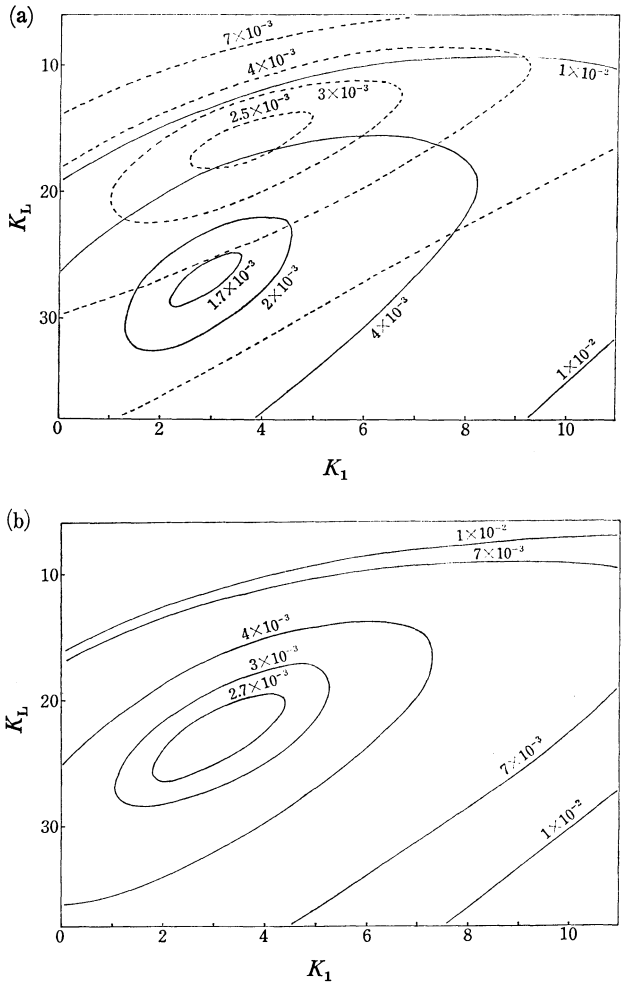

Fig. 3. Contour plots of Q calculated by fitting the LIS's to the equilibrium system, L+S⇄LS and L+L⇄L$_2$, for the *p*-nitroaniline–Eu(fod)$_3$ system in $CDCl_3$ at 34 °C. a) Solid and broken lines denote Q_o and Q_m, respectively. b) Q_{av}.

sensitive to small variations in Q near Q_{min} as the K-value.

For **8**, while the data did not fit well (c), the considerably small value of $Q_{av,min}$ was observed solely by the application of (b) to the analysis of data; the Q-map's are shown in Fig. 3. Attempts to fit the data for **7** to both (b) and (c) resulted in similar small magnitudes of $Q_{av,min}$, and further small variation in values of K, δ_1 and δ_2. It is difficult to select the equilibrium system for the determination of K_1, and however, (b) appears preferable to (c), from the view point of the linearity of log K_1 *vs.* pK_a (Fig. 4). The considerably small or zero values of K_2 obtained for compounds **7** and **8**, appear consistent with the fact that these pK_a values are smaller than for **1** to **6**. Furthermore, it is very plausible from the view point of the competing effect of coordination that only the data for the compound **8** having the smallest pK_a value can be well explained in terms of the addition of the effect of self-association of Eu(fod)$_3$ in solution. In Fig. 4, log K_1 is plotted *vs.* pK_a, where the approximately linear relationship is valid from the nature of the Lewis acid of Eu(fod)$_3$. This is supported by the larger shifts observed for methoxy protons than those expected from the adduct formed by coordination through the N-lone pair. For **10** and **11**, the fits of data to (a) were relatively good for the envelope of *m*-proton shifts ($Q\approx0.01$), but very poor for the *o*-proton shifts. These two substrates did not lead to a clear minimum of Q from the fitting analysis to any other equilibrium systems. This may be due also to the expected effect of coordination of the X-group to the Eu(fod)$_3$. For this type of bifunctional substrate, an additional coordination state, Eu···X-ϕ-NH_2 needs to be taken into account in the equilibrium system.[14] However, the number of parameters determined by least squares analysis becomes considerably greater. Even if more parameters could be evaluated, the results would have no physical significance.

The possible sources of scatter in data in Fig. 4 may be attributed to the following facts; (1) the steric accessibility of the substrate to Eu(fod)$_3$ may be affected by X, (2) the substrate molecule in the present system may be under somewhat different condition from that under which the pK_a-value was measured in Ref. 10, (3) the effect of the coordination effect of X to Eu(fod)$_3$

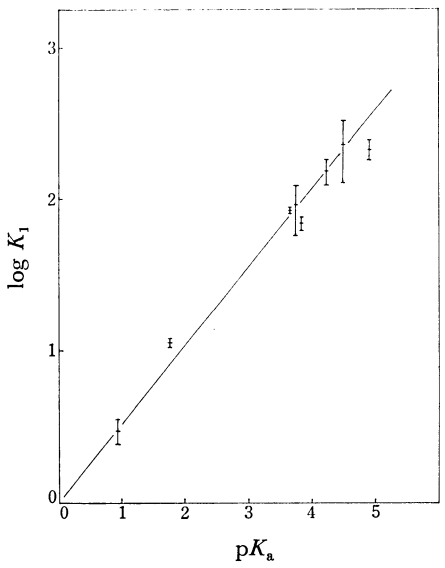

Fig. 4. The logarithms of the equilibrium constants for 1 : 1 adducts (K_1) formed between Eu(fod)$_3$ and *p*-substituted anilines in $CDCl_3$ at 34 °C, *vs.* pK_a-values. The range of each data point corresponds to its standard deviation.

on the observed shifts is not taken into account for all the groups, and (4) a small error may be inherent in the measurement of the concentration of substrate or shift reagent.

The weighting average of K_1, 667, obtained for aniline (pK_a=4.46) with Eu(fod)$_3$ in $CDCl_3$ is very large in the tendency of variation of K_1 in Fig. 4. It may be thought that aniline is not subject to the steric hindrance anticipated for *p*-substituted anilines.[16] However, such a large magnitude of K_1 may not be ascribed solely to this effect. From Table 2, no correlation may be seen between the K_2 and pK_a values for **1** to **6**. This seems acceptable from the possible expectation that the relative acidity and geometry of 1 : 1 adducts (LS) and the steric effect of LS on the accessibility of the second amine molecule may vary with X. On the other hand, the *S*-values and intrinsic shifts estimated in the present investigation also showed no correlation to the pK_a values, in contrast to the linear correlation of *S*-values to pK_a's for the same substrate with Eu(dpm)$_3$ obtained by Ernst *et al.*[11] There may be several explanations to account for such different results with the Eu-chelete, containing the observation of the larger *S*-values with Eu(dpm)$_3$ than with Eu(fod)$_3$.[17] It appears that the difference in contact shift contribution to LIS may dominate among the various explanations.

The authors would like to express their grateful appreciation to Professor B. L. Shapiro for the LISA program.

References

1) B. L. Shapiro and M. D. Johnston, Jr., *J. Am. Chem. Soc.*, **94**, 8185 (1972).
2) J. K. M. Sanders, S. W. Hanson, and D. H. Williams, *J. Am. Chem. Soc.*, **94**, 5325 (1972).
3) J. W. ApSimon, H. Beierbeck, and A. Fruchier, *J. Am. Chem. Soc.*, **95**, 939 (1973).
4) J. Reuben, *J. Am. Chem. Soc.*, **95**, 3534 (1973).
5) M. D. Johnston, Jr., B. L. Shapiro, M. J. Shapiro, T. W. Proulx, A. D. Godwin, and H. S. Pearce, *J. Am. Chem. Soc.*, **97**, 542 (1975).
6) M. Hirayama and N. Ishida, *Bull. Chem. Soc. Jpn.*, **50**, 779 (1977).
7) F. Inagaki, S. Takahashi, M. Tasumi, and T. Miyazawa, *Bull. Chem. Soc. Jpn.*, **48**, 853 (1975).
8) F. Inagaki, M. Tasumi, and T. Miyazawa, *Bull. Chem. Soc. Jpn.*, **48**, 1427 (1975).
9) H. N. Cheng and H. S. Gutowsky, *J. Phys. Chem.*, **82**, 914 (1978).
10) D. D. Perrin, "Dissociation Constants of Organic Bases in Aqueous Solutions," Butterworth, London, 1965.
11) L. Ernst and A. Mannschreck, *Tetrahedron Lett.*, **1971**, 3023.
12) M. Hirayama, M. Sato, M. Saito, and M. Takeuchi, *Bull. Chem. Soc. Jpn.*, **48**, 2690 (1975).
13) C. S. Springer, Jr., *et al.*, "NMR Shift Reagents," ed by R. E. Sievers, Academic Press, New York, N. Y. (1973); R. Porter, T. J. Marks, and D. F. Schriver, *J. Am. Chem. Soc.*, **98**, 3548 (1973); J. F. Desreaux, L. E. Fox, and C. N. Reilley, *Anal. Chem.*, **44**, 2217 (1972).
14) Such discussion has been carried out for 1 : 1 adducts[2] and the shifts explained in terms of the superposition of the corresponding monofunctional substrate.[15] This treatment, however, may not be explicitly applied to the present system.
15) H. Hart and G. M. Love, *Tetrahedron Lett.*, **1971**, 625.
16) It has been reported that such aniline derivatives coordinate to Eu(fod)$_3$ with the angle between the N–C and N–Eu bonds ranging from 120° to 140°.[12] It may be presumed on the basis of this assertion that the *p*-substituent causes the aniline molecule to be less accessible to Eu(fod)$_3$.
17) B. L. Shapiro, M. D. Johnston, Jr., A. D. Godwin, T. W. Proulx, and M. J. Shapiro, *Tetrahedron Lett.*, **1972**, 3233.

Studies of the Dissolved State of Sodium Tetradecyl Sulfate in Ethanol-Water Mixtures by Measurements of the Activity

Masakatsu KOSHINUMA*

Department of Chemistry, Faculty of Science, Tokyo Metropolitan University, Setagaya, Tokyo 158

(Received September 25, 1978)

The details of electromotive-force measurement by means of a concentration cell consisting of sodium tetradecyl sulfate (NaTS) in ethanol–water mixtures and of anionic and cationic ion-exchange membranes as septams were described. The membranes used proved to be permeable exclusively to the surfactant (TS^-) and Na^+ ions respectively. The activities of the TS^- and Na^+ ions were measured separately, and then the mean activity was computed as a function of the ethanol content in the solvent. Below the CMC, the activities for TS^- and Na^+ ions and the mean activity increased with an increase in the NaTS concentration, but decreased with an increase in the ethanol concentration. Above the CMC, the activity of the TS^- ion decreased, whereas that of the Na^+ ion increased; the mean activity also slightly increased with an increase in the NaTS concentration. The values of CMC obtained were 1.5×10^{-3}, 1.7×10^{-3}, and 2.2×10^{-3} mol/dm^3 for 5, 10, and 15 vol % ethanol concentrations respectively. The mechanism of mixed micelle formation was also expressed by a charged phase-separation model in an ethanol–water mixture much as in the case of a simple aqueous solution. The degrees of counterion attachment were found to be 0.73, 0.68, and 0.62 for 5, 10, and 15 vol % ethanol respectively. The intermicellar concentrations of TS^-, (C_{TS}), and Na^+ ions, (C_{Na}), were calculated. With an increase in the NaTS concentration, C_{Na} monotonously increased, but C_{Na} decreased. At a given NaTS concentration, C_{Na} increased with an increase in the ethanol concentration, while C_{Na} was approximately constant.

It is well known that the addition of a nonelectrolyte to a surfactant solution greatly affects the nature of the solution. Many studies regarding the influence of nonelectrolytes on the CMC values have been performed with anionic[1–4] and cationic[1,5,6] surfactants. On the addition of alcohols, the decrease in the CMC was explained by the diluted surface-charge density and the enhanced hydrophobic interaction on a micelle.[7,8] The increase in the CMC was correlated by the hydrophobic nature of the additives and their micellar breaking-up power.[1] Though there have been investigations of the effects of the addition of nonelectrolytes, there have been relatively few studies of the adsorption from the solution,[9] the state of the solution[10] and the micellar state;[11] this has been due in part to the difficulty of activity measurement. In a previous report, the various properties of an aqueous sodium tetradecyl sulfate (NaTS) solution were investigated by measuring its activity.[12] In the present paper, the dissolved state of NaTS in an ethanol–water mixture was studied by measuring the electromotive force (EMF) of the concentration cell. Ethanol was used as a nonelectrolyte additive since it mixes with water in all proportions; also, it is a good solvent for the surfactant. From the activity measurements, the mechanism of micelle formation, the degree of counterion attachment to the micelle, and the intermicellar concentration will be discussed.

Experimental

Materials. The sodium tetradecyl sulfate used was synthesized and purified as in the previous paper.[12] Special-grade ethanol was dehydrated by calcium oxide and distilled before use. Deionized water was used for the EMF measurement.

Procedure. The construction of the concentration cell and the method of measurement were the same as in the previous paper.[12] For the EMF measurements, a solution of 4.0×10^{-3} mol/dm^3 NaTS was used as a reference for each composition of the ethanol–water mixture. The surface tension was measured by the Wilhelmy plate method.[13]

Results and Discussion

Calculation of Activities. The values of the EMF of the TS^- ion, E_{TS}, and of the Na^+ ion, E_{Na}, were obtained from the concentration cells. According to Nernst's equation, E_{TS} and E_{Na} in an ethanol–water mixture are given by

$$E_{TS} = (\lambda_{TS}-\lambda_{Na})(2.303RT/F)\log(a_{TS}/a_{OTS}) \quad (1)$$

$$E_{Na} = (\lambda'_{TS}-\lambda'_{Na})(2.303RT/F)\log(a_{Na}/a_{ONa}) \quad (2)$$

where λ_{TS}, and λ_{Na} are the transport numbers of the TS^- and Na^+ ions for an anionic exchange membrane, and λ'_{TS}, and λ'_{Na}, those for a cationic membrane; F, the Faraday constant; R, the gas constant, and T, the absolute temperature. The values of a_{TS} and a_{Na} are the activities of the TS^- and Na^+ ions in a given solution, and a_{OTS} and a_{ONa}, the corresponding values in a reference solution. If the following Eqs. 3 and 4, may be assumed:

$$\lambda_{TS} = 1, \quad \lambda_{Na} = 0, \quad (3)$$

$$\lambda'_{TS} = 0, \quad \lambda'_{Na} = 1. \quad (4)$$

Eqs. 5 and 6 are obtained:

$$E_{TS} = (2.303RT/F)\log(a_{TS}/a_{OTS}) \quad (5)$$

$$E_{Na} = -(2.303RT/F)\log(a_{Na}/a_{ONa}). \quad (6)$$

If the values of a_{OTS} and a_{ONa} are known, the activities of the given solutions can be computed from Eqs. 5 and 6 by the substitution of the E_{TS} and E_{Na} measured. Plotting the following extrapolation function,[14] a_{OTS} and a_{ONa} can be obtained:

$$E'_{TS} = (2.303RT/F)\log C - E_{TS}$$
$$= (2.303RT/F)(-\log f_{TS}+\log a_{OTS}) \quad (7)$$

$$E'_{Na} = (2.303RT/F)\log C + E_{Na}$$
$$= (2.303RT/F)(-\log f_{Na}+\log a_{ONa}). \quad (8)$$

* Present address: Laboratory of Chemistry, Faculty of Education, Chiba University, Chiba 260.

Here, C denotes the concentration of NaTS, and f_{TS} and f_{Na}, the activity coefficients of the TS^- and Na^+ ions at the C concentration respectively. If E'_{TS} and E'_{Na} are plotted against $C^{1/2}$ and the curves are extrapolated C to 0, a_{OTS} and a_{ONa} can be calculated by Eq. 9 from the extrapolated values of E'_{OTS} and E'_{ONa};

$$\left.\begin{aligned}\log a_{OTS} &= (F/2.303RT)E'_{OTS}\\ \log a_{ONa} &= (F/2.303RT)E'_{ONa}\end{aligned}\right\} \quad (9)$$

because f_{TS} and f_{Na} are unity at $C=0$ in Eqs. 7 and 8. The mean activity and also each activity are calculated by introducing Eq. 9 into Eqs. 5 and 6.

The assumption of Eqs. 3 and 4 of NaTS in an ethanol–water mixture must be confirmed by experiments; however, verification is difficult. The influences were examined, as the addition of ethanol might affect the nature of the ion-exchangers by swelling, dissociation of ion-exchange fixed groups, and transport of the solvent through them; (osmosis effect), depending on the ethanol concentration. It has been reported that swelling, which is closely related to the effective mean pore size of a membrane, its decrease interfering with the ion transport because of the steric disturbance, is little affected by the addition of a low concentration of a lower alcohol, and even in a 20% concentration is nearly equal to that in water.[15] Therefore, the other influences were investigated from the point of view of whether or not Eqs. 10 and 11 for the anionic and cationic exchange membranes hold, using NaCl, the activities of which have been established.

$$\lambda_{Cl} = 1, \quad \lambda_{Na} = 0 \quad (10)$$

$$\lambda'_{Cl} = 0, \quad \lambda'_{Na} = 1 \quad (11)$$

The EMF values of the Cl^- ion, E_{Cl}, and of the Na^+ ion, E_{Na}, resulting from the concentration cell with the reference solution containing the 4.0×10^{-3} mol/kg mixed solvent, were measured for NaCl in an ethanol–water mixture containing 20 wt % ethanol at 25 °C in a manner similar to that used for NaTS. The results obtained are shown in Fig. 1. The value of E_{Cl} increased, and that of E_{Na} decreased, linearly with an increase in the logarithmic concentration of NaCl in a way analogous

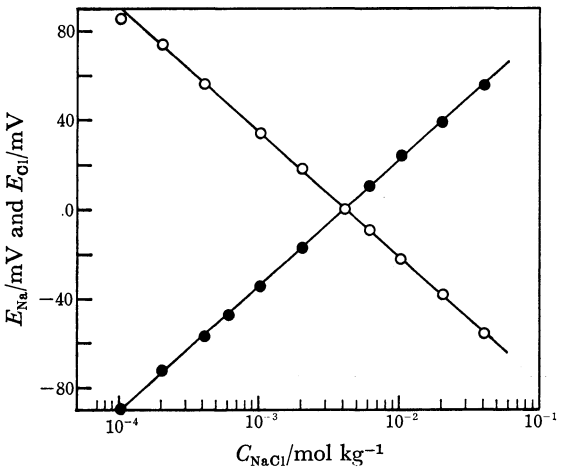

Fig. 1. Electromotive force of Na^+ and Cl^- ions against NaCl concentration.
○; Na^+ ion, ●; Cl^- ion.

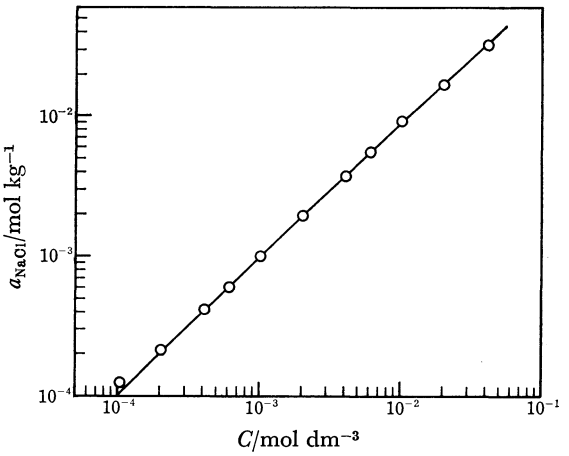

Fig. 2. Mean activity of NaCl in the 20 wt % ethanol–water mixture against NaCl concentration.
○; Experimental value, ——; calculated value by the Eqs. 12 and 13.

to that in water. The activities were calculated from these results. The equations corresponding to those from 1 to 9 were also set up in the case of NaCl. The extrapolated E'_{OCl} and E'_{ONa} values were obtained as −144.3 and −144.5 mV respectively; then, a_{OCl} and a_{ONa} were calculated to be 3.64×10^{-3} and 3.61×10^{-3} mol/kg mixed solvent respectively. The activities of the Cl^- and Na^+ ions and the mean activity were calculated separately. The mean activities of NaCl in the ethanol–water mixture are shown by the circles in Fig. 2. A rule for the activity coefficients of NaCl in ethanol–water mixtures has been states as[16,17]

$$(f_{\pm NaCl})_{org} = (f_{\pm NaCl})_{water}[(f_{\pm HCl})_{org}/(f_{\pm HCl})_{water}]. \quad (12)$$

Here, $(f_{\pm NaCl})_{water}$ and $(f_{\pm HCl})_{water}$ are the activity coefficients of NaCl and HCl respectively, in water and $(f_{\pm NaCl})_{org}$ and $(f_{\pm HCl})_{org}$ are the activity coefficients of NaCl and HCl respectively in ethanol–water mixtures. In Eq. 12, $(f_{\pm NaCl})_{water}$ and $(f_{\pm HCl})_{water}$ were calculated using the Debye-Hückel equation, with the mean ionic radii of 4.0 Å for NaCl and of 4.3 Å for HCl. On the other hand, $(f_{\pm HCl})_{org}$ has been given by this empirical equation:[18]

$$\log (f_{\pm HCl})_{org} = -[0.6428C^{1/2}/(1+1.529C^{1/2})] + 0.1293 - \log(1+0.04104m) \quad (13)$$

where C and m denote the concentrations of NaCl in a mol/dm^3-mixture and in a mol/kg-mixture respectively. The computed mean activities of NaCl in an ethanol–water mixture containing 20 wt % ethanol are shown as a solid line in Fig. 2. The experimental mean activities were in good agreement with the values calculated by means of Eqs. 12 and 13; therefore, Eqs. 10 and 11 were verified. Even in an ethanol–water mixture containing below 20 wt % ethanol, no significant changes occur in the characteristics of anionic and cationic exchange membranes; that is they swell well, their ion-exchange fixed groups fully dissociate, and no solvent transport takes place, as in water. Eqs. 3 and 4 for NaTS can also be established as in water.[12]

The values of E_{TS} and E_{Na} measured for NaTS in ethanol–water mixtures containing 5, 10, and 15 vol %

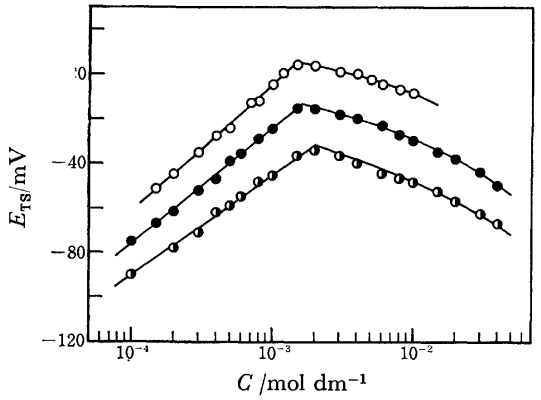

Fig. 3. Electromotive force of TS^- ion against NaTS concentration. Ethanol concentrations for 5 vol %; ○, 10 vol %; ●, and 15 vol %; ◑.
The curves for 10 and 15 vol % ethanol were transferred downward by 20 and 40 mV respectively.

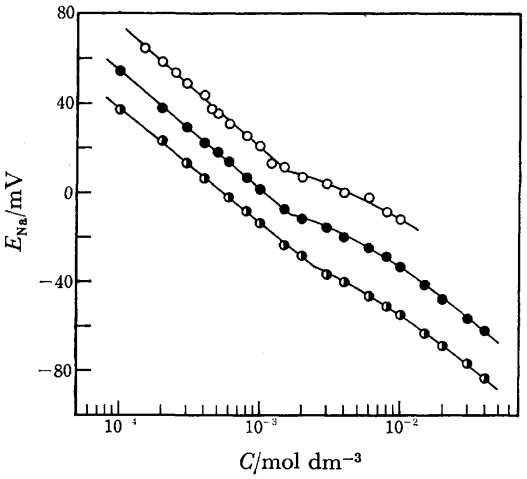

Fig. 4. Electromotive force of Na^+ ion against NaTS concentration. Ethanol concentrations for 5 vol %; ○, 10 vol %; ●, and 15 vol %; ◑.
The curves for 10 and 15 vol % ethanol were transferred downward by 20 and 40 mV respectively.

ethanol are shown in Figs. 3 and 4. With an increase in the logarithmic concentration of NaTS, E_{TS} increased linearly to the CMC and then decreased, while E_{Na} decreased linearly to the CMC and through a plateau region decreased in all ethanol concentrations. In order to calculate the activities of the TS^- and Na^+ ions, the plots by the extrapolation functions, 7 and 8, are shown in Fig. 5 for 5 and 15 vol % ethanol concentrations. The extrapolated values of E'_{OTS} and E'_{ONa}, and also the activities of a_{OTS} and a_{ONa} as computed by Eq. 9,

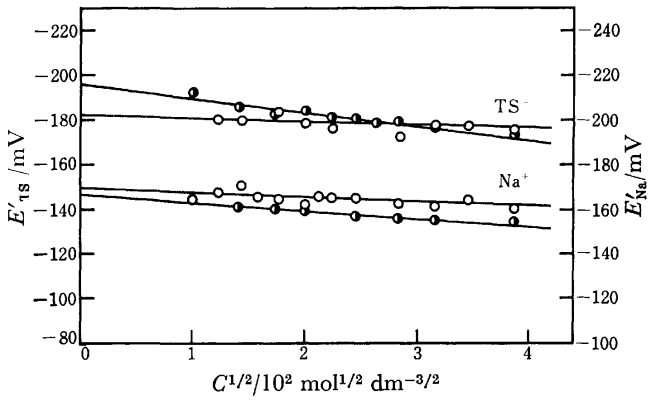

Fig. 5. Extrapolation of E'_{TS} and E'_{Na} against NaTS concentration.
○; 5 vol % etflanol concentration,
◑; 15 vol % etflanol concentration.

are shown in Table 1. The activities of the TS^- and Na^+ ions, as calculated from Eqs. 5 and 6, are shown in Figs. 6 and 7. With an increase in the NaTS concentration, the activities of the TS^- and Na^+ ions increased, but above a breaking point concentration that of the TS^- ion decreased. The increase in the ethanol concentration caused a decrease in the activities of the TS^- and Na^+ ions. The breaking points agreed with the CMC's determined from the surface-tension measurements, which are shown in Fig. 8 for different ethanol concentrations. The CMC values were 1.5×10^{-3} for 5 vol%, 1.7×10^{-3} for 10 vol%, and 2.2×10^{-3} mol/dm^3 or 15 vol% ethanol. The mean activities, as calculated from the definition, are shown in Fig. 9. Above the

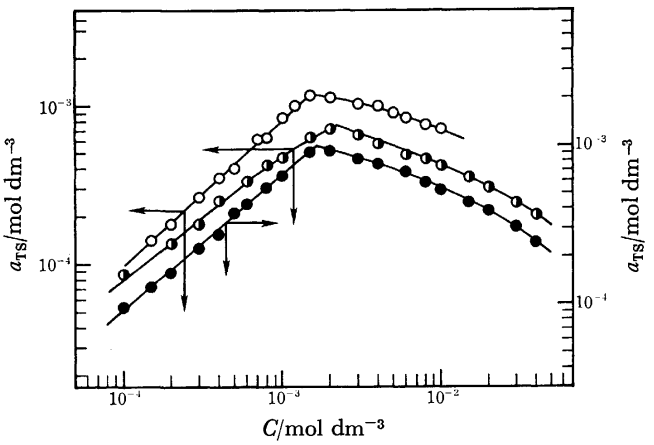

Fig. 6. Activity of TS^- ion against NaTS concentration. Ethanol concentrations for 5 vol %; ○, 10 vol %; ●, and 15 vol %; ◑.

TABLE 1. CALCULATED VALUES OF E_0' AND a_0 AT VARIOUS ETHANOL CONCENTRATIONS

C_E/vol %	E'_{OTS}/mV	E'_{ONa}/mV	a_{OTS}/mol dm^{-3}	a_{ONa}/mol dm^{-3}
0[a)]	−183.0	−155.0	9.59×10^{-4}	2.78×10^{-3}
5	−182.1	−169.0	9.93×10^{-4}	1.63×10^{-3}
10	−189.0	−169.3	7.64×10^{-4}	1.61×10^{-3}
15	−196.3	−166.3	5.79×10^{-4}	1.81×10^{-3}

a) The data for 0 vol % ethanol are quoted from a previous report,[12] where the 10.0×10^{-3} mol/dm^3 NaTS solution was chosen as the reference solution.

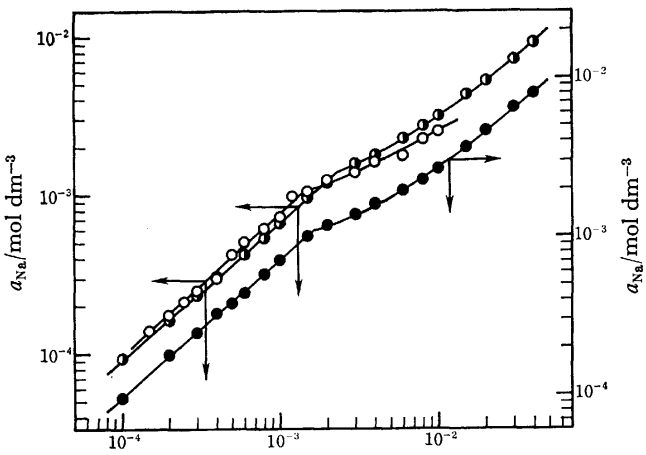

Fig. 7. Activity of Na^+ ion against NaTS concentration. Ethanol concentrations for 5 vol %; ○, 10 vol %; ●, and 15 vol %; ◑.

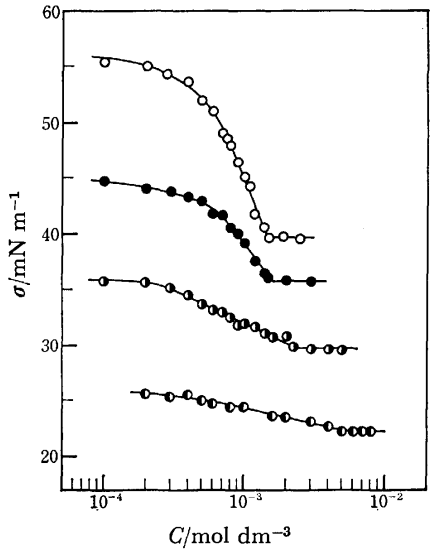

Fig. 8. Surface tension of NaTS in ethanol–water mixtures against NaTS concentration.
Ethanol concentrations for 5 vol %; ○, 10 vol %; ●, 15 vol %; ◑, and 20 vol %; ◐.
The curves for 10, 15, and 20 vol % ethanol were transferred downward by 5, 10, and 15 mN/m respectively.

CMC, the mean activities were not constant, but increased slightly with an increase in the NaTS concentrations, as in the aqueous solution without ethanol;

Table 2. Constant values of α and β below and above the CMC at various ethanol concentrations

C_E/vol %	$C \leqq$ CMC		$C >$ CMC	
	α	β	α	β
0	0.070	0.283	0.996	2.702
5	0.102	0.421	0.924	2.932
10	0.157	0.648	0.904	2.725
15	0.212	0.890	0.868	2.673

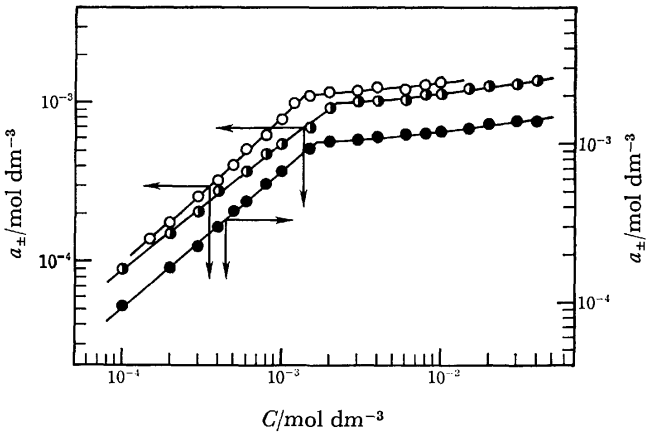

Fig. 9. Mean activity of NaTS against NaTS concentration. Ethanol concentrations for 5 vol %; ○, 10 vol %; ●, and 15 vol %; ◑.

also, the tangents increased with an increase in the ethanol concentration. The mean activity coefficients of NaTS are given for different ethanol concentrations, both below the CMC down to 1.0×10^{-4} mol/dm^3 and above it up to 40.0×10^{-3} mol/dm^3, by

$$\log f_{\pm} = -(\alpha \log C + \beta), \tag{14}$$

where α and β are constants, the values of which are shown in Table 2.

Micelle Formation and Counterion Attachment. It has been reported that the micelle formation of NaTS in water can be explained by the charged phase-separation model[12] according to

$$p\mathrm{TS}^- + q\mathrm{Na}^+ \rightleftarrows \mathrm{TS}_p\mathrm{Na}_q^{-(p-q)}$$

where a micelle consists of pTS$^-$ ions and qNa$^+$ ions; therefore,

$$p \log a_{TS} + q \log a_{Na} = \text{constant}. \tag{15}$$

Since, in the ethanol–water mixture, the mixed micelles are considered to be formed by the penetration of ethanol, penetration is taken account of in the discussion of the micelle-formation mechanism. If the charged phase-separation model holds in the mixed micelles, the formation of a mixed micelle, which consists of pTS$^-$ ions, qNa$^+$ ions, and n ethanol molecules, can be expressed as follows:

$$p\mathrm{TS}^- + q\mathrm{Na}^+ + n\mathrm{EtOH} \rightleftarrows \mathrm{TS}_p\mathrm{Na}_q\mathrm{EtOH}_n^{-(p-q)}$$

and also: $(a_{TS})^p(a_{Na})^q(a_E)$=constant where EtOH denotes ethanol. Then, the following equation is given:

$$p \log a_{TS} + q \log a_{Na} + n \log a_E = \text{constant}. \tag{16}$$

In the present study, the activity of ethanol is considered to be constant in Eq. 16 because the experiments were performed with the concentration of ethanol kept constant when that of NaTS was varied. Moreover, the decrease in the ethanol activity due to the formation of the mixed micelle can be neglected because the concentration of ethanol was much larger than that of NaTS. The value of n can be regarded as constant, since the concentrations of NaTS were varied within a narrow range of NaTS concentrations above the CMC. Therefore, Eq. 16 can be simplified to

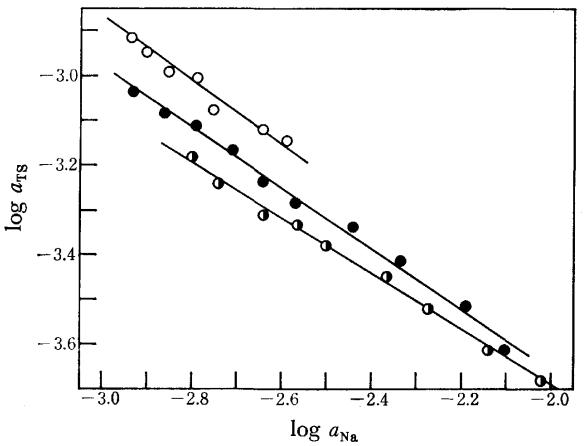

Fig. 10. Relation between log a_{TS} and log a_{Na} above the CMC. Ethanol concentrations for 5 vol %; ○, 10 vol %; ●, and 15 vol %; ◑.

$$p \log a_{TS} + q \log a_{Na} = \text{constant}, \quad (17)$$

which can then be reduced to the same form as Eq. 15. According to Eq. 17, the degree of counterion attachment can be estimated from the slope of the curves if a linear relation is obtained when log a_{TS} is plotted against log a_{Na}. We attempted to examine whether or not Eq. 17 holds. The relations between log a_{TS} and log a_{Na} are shown in Fig. 10, where the plots give good linear relationships for each ethanol concentration. Thus, the mixed-micelle formation in the ethanol–water mixtures can also be explained by the charged phase-separation model. Moreover, the value of n proves to be constant in each concentration range. The degree of counterion attachment, $r=-q/p$, was obtained as 0.73 for 5 vol %, 0.68 for 10 vol %, and 0.62 for 15 vol % ethanol. Figure 11 shows the degrees of counterion attachment and the CMC values obtained. The CMC values decrease, pass through a minimum near the 5 vol % ethanol concentration, and then increase, while the degree of counterion attachment gradually decreases with an increase in the ethanol concentration.

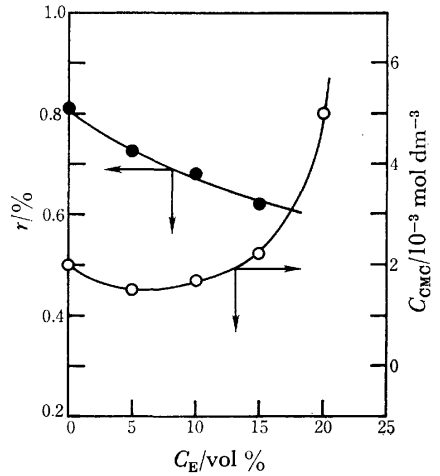

Fig. 11. Degree of counterion attachment and CMC value against ethanol concentration.
●; Degree of counterion attachment,
○; CMC value.

The decrease in the CMC value in the low ethanol-concentration range can be explained by the penetration of ethanol into the NaTS micelle forming the mixed micelle; this causes the decrease in the electrostatic energy on the micelle surface by the dilution of the charge density and the increase in the entropy of mixing.[7,8] The increase in the CMC value in the high ethanol-concentration range results from the increasing affinity of the hydrocarbon chain for ethanol; consequently, the ethanol-rich mixture is a good solvent for NaTS. The degree of counterion attachment gradually decreases; therefore, the charge density on the micelle surface decreases, the result mainly of the penetration of ethanol into the micelle and the decrease in the micelle size.[19]

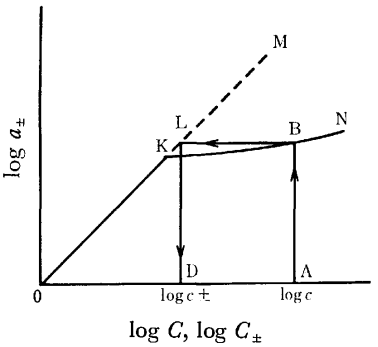

Fig. 12. Schematic representation of calculation of intermicellar concentration.
The broken line determined by the Eq. 14.

Calculation of Intermicellar Concentration. The principles of the calculation of the intermicellar concentration are shown schematically in Fig. 12, where the OKBN line represents the mean activity curve observed and where the K point is the CMC. If a relation between the mean activities and the concentrations of NaTS below the CMC is held similarly above the CMC, the broken line, KLM, which is obtained by the extension of the OK line to above the CMC indicates the relation between the mean activity and the intermicellar concentration. It can be considered that the micelles have no effects upon the relation between the mean activity above the CMC and the intermicellar concentration; that is the activity cofficient for the mean intermicellar concentration behaves the same as just below the CMC when the micelle concentration is very dilute. The mean concentration is defined by the same relation as that of below the CMC;

$$a_{\pm} = f_{\pm} \cdot C_{\pm} \quad (18)$$

where $f_{\pm}$ and $C_{\pm}$ denote the intermicellar activity coefficient and the intermicellar concentration respectively. The value of $f_{\pm}$ is assumed to be expressed by Eq. 14. On the other hand, the mean intermicellar concentration is given by

$$C_{\pm} = (C_{Na} \cdot C_{TS})^{1/2}. \quad (19)$$

Here, C_{TS} and C_{Na} express the intermicellar concentrations of the TS^- and Na^+ ions, since they are not necessarily equal to each other. Then, the intermicellar mean concentration corresponding to the total concen-

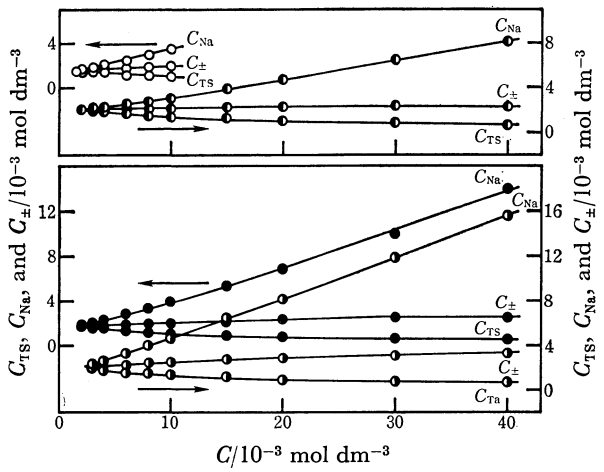

Fig. 13. Intermicellar concentrations of Na^+ and TS^- ions and intermicellar mean concentration.
C_{Na}, C_{TS}, and $C_{\pm}$ represent intermicellar concentrations of Na^+, TS^- ions and intermicellar mean concentration respectively. Ethanol concentrations for 0 vol %; ◐, 5 vol %; ○, 10 vol %; ●, and 15 vol %; ◑.

tration, C, of NaTS is obtained by the process of ABLD on the diagram shown in Fig. 12, while the intermicellar concentration of the TS^- and Na^+ ions for the solution with a total concentration of C are related to each other[20] thus:

$$C_{Na} = (C - C_{TS})(1-r) + C_{TS} \quad (20)$$

where r denotes the degree of counterion attachment. From Eqs. 18, 19, and 20, the intermicellar concentrations are given thus:

$$C_{TS} = -(1-r)(C/2r) + (1/2r)[(1-r)^2C^2 + 4rC_{\pm}^2]^{1/2},$$
$$C_{Na} = -(1-r)(C/2) - (1/2)[(1-r)^2C^2 + 4rC_{\pm}^2]^{1/2}. \quad (21)$$

The results calculated are shown in Fig. 13 for the four ethanol-water mixtures; in the calculation for the 0 vol% ethanol medium, the experimental data are quoted from the previous paper.[12] The intermicellar concentration of C_{Na} increased monotonously, while that of C_{TS} decreased and then asymptotically approached a constant value, with an increase in the NaTS concentration. It was noticed further that C_{TS} was approximately constant, independent of the ethanol concentration, while C_{Na} increased with an increase in the ethanol concentration. The intermicellar mean concentration also increased with increases in both the NaTS and ethanol concentrations. This increase indicates the effect of a good solvent for NaTS, as has been mentioned previously. Also, the difference in inclinations between the C_{TS} and C_{Na} curves in Fig. 13 is roughly proportional to $(1-r)$, which is the degree of dissociation of the Na^+ ion from the micelles.

It should be noted that such relations[21] as

$$C_{Na} = (C - C_{CMC})(1-r) + C_{CMC}$$

and

$$a_{Na} = f_{Na}(C - C_{CMC})(1-r) + C_{CMC}$$

are not correct because C_{CMC} varies with an increase in C, as is shown in Fig. 13. The problem, however, remains of to what extent the presence of micelles influences the activity of intermicellar ions.

The author wishes to express his hearty thanks to Professor Tsunetaka Sasaki of Tokai University for his encouragement and guidance throught the experiments.

References

1) M. F. Emerson and A. Holtzer, *J. Phys. Chem.*, **71**, 3320 (1967).
2) M. J. Schick, *J. Phys. Chem.*, **68**, 3585 (1964).
3) K. Shirahama and R. Matuura, *Bull. Chem. Soc. Jpn.*, **38**, 373 (1965).
4) H. Uehara, M. Manabe, and R. Matuura, *Mem. Fac. Sci. Kyushu Univ., C*, **8**, 55 (1972).
5) S. H. Herzfeld, M. L. Corrin, and W. D. Harkins, *J, Phys. Colloid Chem.*, **54**, 271 (1950).
6) P. Mukerjee and A. Ray, *J. Phys. Chem.*, **67**, 190 (1963).
7) K. Shinoda, *Bull. Chem. Soc. Jpn.*, **26**, 101 (1953).
8) K. Shirahama and T. Kashiwabara, *J. Colloid Interface Sci.*, **36**, 65 (1971).
9) K. Shirahama, K. Nakao, H. Endo, and R. Matuura, *Bull. Chem. Soc. Jpn.*, **39**, 1017 (1966).
10) G. D. Parfitt and A. L. Smith, *Trans. Faraday Soc.*, **61**, 2736 (1965).
11) S. Miyagishi, *Bull. Chem. Soc. Jpn.*, **47**, 2972 (1974).
12) M. Koshinuma and T. Sasaki, *Bull. Chem. Soc. Jpn.*, **48**, 2755 (1975).
13) M. Koshinuma, A. Nakamura, T. Seimiya, and T. Sasaki, *Bull. Chem. Soc. Jpn.*, **45**, 344 (1972).
14) R. A. Robinson and R. H. Stokes, "Electrolyte Solutions," Butterworth Pub., London (1959), p. 190.
15) T. Yamabe and M. Senō, "Ion Kokan Jushimaku," Gihōdō Pub., Tokyo (1964), p. 80.
16) H. S. Harned, *J. Phys. Chem.*, **66**, 589 (1962).
17) R. D. Lainier, *J. Phys. Chem.*, **69**, 2697 (1965).
18) H. S. Harned and C. Calmon, *J. Am. Chem. Soc.*, **61**, 1491 (1939).
19) H. Suzuki and T. Sasaki, Synopsis of Annual Meeting of 26th Colloid and Interface Chemistry Section in Chem. Soc. Japan, Held at Fukui (1973), p. 60.
20) T. Sasaki, M. Hattori, J. Sasaki, and K. Nukina, *Bull. Chem. Soc. Jpn.*, **48**, 1397 (1975).
21) C. Botre, V. L. Crescenz, and A. Mele, *J. Phys. Chem.*, **63**, 650 (1959).

The Similarity between the π,π^* Absorption Spectra of 1-Indenone and 1,2-Naphthoquinone

Akira KUBOYAMA* and Hitoshi MATSUMOTO†

National Chemical Laboratory for Industry, Shibuya-ku, Tokyo 151

†*School of Pharmacy, Tokushima University of Arts and Science, Yamashiro-cho, Tokushima 770*

(Received October 6, 1978)

The π,π^* absorption spectrum and its solvent effect of 2-methyl-1-indenone have been found to be similar to those of 1,2-naphthoquinone. This fact is discussed on the basis of the results calculated using the P-P-P method. The similarity of the calculated π-electronic structures in the low-energy π,π^* singlet states between 1-indenone and 1,2-naphthoquinone is not so good as that between fluorenone and 9,10-phenanthrenequinone.

Recently, we have found a similarity between the π,π^* absorption spectra of fluorenone and 9,10-phenanthrenequinone.[1] This similarity is thought to be due to a similarity between the π-electronic systems of the two compounds, on the assumption that the carbonyl group of fluorenone and the α-dicarbonyl group of phenanthrenequinone are equivalent. According to this idea, the above similarity has been reasonably explained on the basis of the results calculated using the P-P-P method. Such a similarity may be expected to exist between 1-indenone and 1,2-naphthoquinone. Heretofore, scarcely nothing has been known about the π,π^* absorption spectra of 1-indenone and its alkyl derivatives.[2] In this work, we have obtained the π,π^* absorption spectra of relatively stable 2-methyl-1-indenone in solutions and have studied the similarity between the π,π^* absorption spectra of 2-methyl-1-indenone and 1,2-naphthoquinone.[3,4]

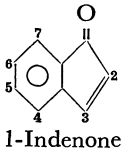

1-Indenone

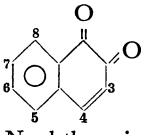

1,2-Naphthoquinone

Experimental

Measurements. The absorption spectra of 2-methyl-1-indenone and 1,2-naphthoquinone were measured with a Hitachi 200-20 and a Cary 14 spectrophotometer respectively. Hexane, heptane, benzene, and methanol were used as the solvents.

Materials. According to an earlier article,[5] 2-methyl-1-indenone was synthesized from *trans*-α-methylcinnamic acid by UV inside irradiation (Hg 253.7 nm line) in the ethanol solution,[6,7] and then by a ring-closure reaction in sulfuric acid. The product thus obtained was purified by vacuum distillation and then by recrystallization from a diluted aqueous solution of ethanol (mp 46.5—47.0 °C). It began to decompose four days after its preparation. The 1,2-naphthoquinone was the same as that used in a previous work.[4] The solvents used were of a commercially available spectrograde.

Results. The absorption spectra obtained and the numerical data about them are shown in Fig. 1 and Table 1 respectively.

Calculations

Method. In the calculations using the P-P-P method for 1-indenone, the values of the core and electronic repulsion integrals were the same as those used for 1,2-naphthoquinone in the previous work.[4] As for the effect of alkyl-group substitution, the core Coulomb integral of the substituted carbon atoms was taken as −9.00 eV, considering only the inductive effect, as in the previous work. In the calculations, all the singly-excited configurations were included. The molecular dimensions[8] of 1-indenone assumed are shown in Fig. 2.

Results. The calculated results are shown in Tables 2 and 3 and in Fig. 3. In Table 2, the first column

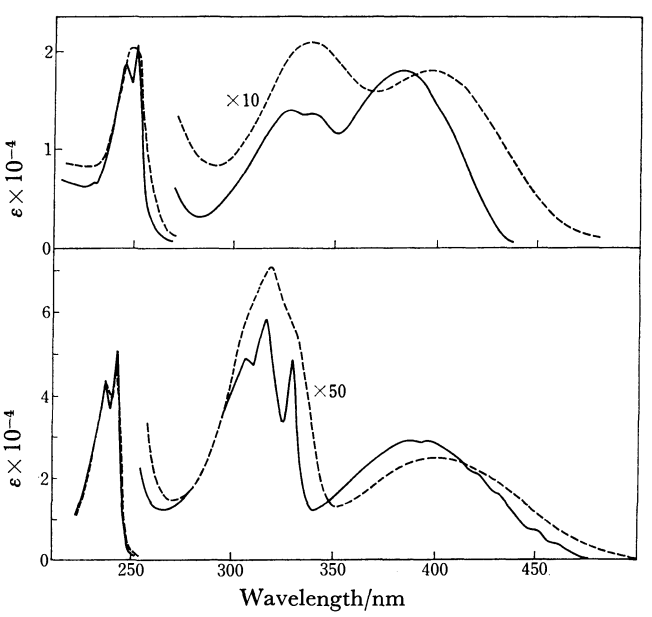

Fig. 1. Absorption spectra of 2-methyl-1-indenone and 1,2-naphthoquinone in solutions.
Lower curves: 2-methyl-1-indenone (——: hexane, – – –: methanol). Upper curves: 1,2-naphthoquinone (——: heptane, – – –: methanol). ε denotes molar absorption coefficient/10^{-3} mol cm^{-2}. In the heptane solution of 1,2-naphthoquinine, the scale of the ordinate is arbitrary.

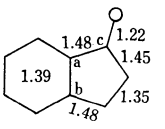

Fig. 2. Molecular dimension of 1-indenone (A).
a: 108.5°, b: 108.5°, c: 127.5°.

Table 1. Wavelengths (λ) and molar absorption coefficients (ε) of the absorption maxima and the oscillator strengths (f) of the absorption bands

Solvent	λ / nm	ε / 10^{-3} mol cm^{-2}	f	Band
(1) 2-Methyl-1-indenone				
Hexane	396	565	0.013	I
	387.5	574		
	329.5	975	0.020	II
	316	1100		
	306	1000		
	242	50300	0.56	III
	236	43800		
Benzene	397	558		I
	331	929		II
	319	1265		
Methanol	401.5	492	0.012	I
	318.5	1385	0.027	II
	242	47400	0.56	III
	237	42700		
(2) 1,2-Naphthoquinone				
Heptane	382			I
	337.5			II
	326			
	251			III
	245			
Methanol	396	1710	0.034	I
	337	1990	0.050	II
	249	19200	0.36	III

Table 2. Calculated results

No.	1-Indenone E / eV	1-Indenone f	1,2-Naphthoquinone[4] E / eV	1,2-Naphthoquinone[4] f	Band
1	4.16	0.043	4.32	0.077	I
2	4.39	0.023	4.49	0.091	II
3	5.45	0.655	5.29	0.587	III

Table 3. Calculated results for the configurational mixings[a]

(1) 1-Indenone				
State	(5→6)	(4→6)	(5→7)	(4→7)
No. 1	0.872	0.013	0.029	0.044
No. 2	0.003	0.603	0.150	0.085
No. 3	0.083	0.337	0.143	0.239
(2) 1,2-Naphthoquinone				
State	(6→7)	(5→7)	(6→8)	(5→8)
No. 1	0.481	0.175	0.169	0.030
No. 2	0.464	0.277	0.133	0.000
No. 3	0.015	0.488	0.247	0.108

a) ($i\rightarrow j$) denotes the electron configuration due to the one-electron promotion of i-MO→j-MO. Each configuration of 1-indenone in the table corresponds to that of 1,2-naphthoquinone directly below it.

denotes the numbering of the states in the order of increasing excitation energies (calculated).

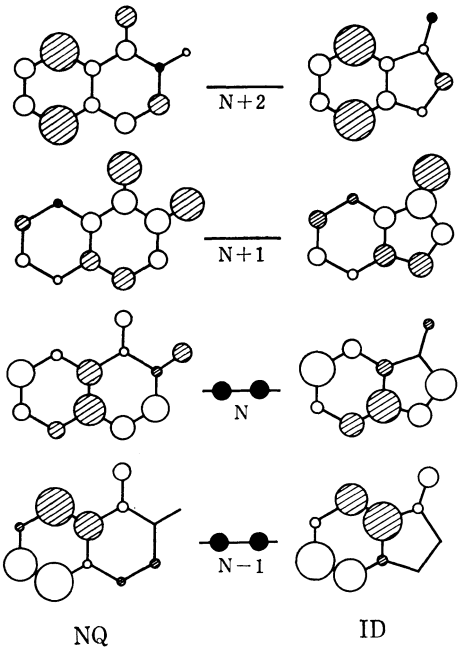

Fig. 3. π-Molecular orbitals of 1-indenone and 1,2-naphthoquinone. The N and N+1 MO energy levels denote the highest occupied and lowest vacant levels respectively. The figures on both sides denote the π-electron distributions and the signs of coefficients of the 2pπ AO's in the corresponding MO's.

Discussion

As may be seen in Fig. 2, both 2-methyl-1-indenone and 1,2-naphthoquinone have two weak π,π^* bands at the longer wavelengths and a strong π,π^* band at the shorter wavelengths. These π,π^* bands are denoted as Bands I—III, as is shown in Table 1. Bands I—III of 2-methyl-1-indenone[9] are located close to the corresponding bands of 1,2-naphthoquinone. In the hexane solution of 2-methyl-1-indenone, Band II has a far sharper structure than Band I. On the other hand, in the heptane solution of 1,2-naphthoquinone, while Band II has a structure, Band I has no structure at all. In the solvent effects of Bands I—III, the following two similarities are found between the two compounds. First, Band I in the methanol solutions, where the hydrogen bond may be formed between the solute and solvent molecules, lies at longer wavelengths than that in the cyclohexane solutions, while Bands II and III lie at almost the same position in both solutions. Second, the intensity ratio of Band I to Band II in the methanol solutions is similar than that in the cyclohexane solutions. The π,π^* absorption spectrum and its solvent effect of 1-indenone are thought to be similar to those of 2-methyl-1-indenone. Therefore, the above discussion may also equally hold good between the π,π^* absorption spectra of 1-indenone and 1,2-naphthoquinone.

On the other hand, in Table 2, the calculated results for the low-energy π,π^* singlet states of 1-indenone and 1,2-naphthoquinone are similar and Bands I—III are favorably assigned on the basis of them. The assignment of Band I of 1,2-naphthoquinone in Table 2 was sup-

ported by the consistency between the experimental and calculated results for the energy shift of Band I through alkyl-group substitutions in the previous work.[4] As may be seen in Fig. 3, the corresponding highest occupied and lowest vacant π-MO's of the two compounds are similar if we assume that the carbonyl group of 1-indenone and the α-dicarbonyl group of 1,2-naphthoquinone are equivalent, as in the case of the pair of fluorenone and 9,10-phenanthrenequinone. However, the similarity between the π-MO's of 1-indenone and 1,2-naphthoquinone is less than that between the above pair. This may be due to the poor molecular symmetry of 1-indenone and 1,2-naphthoquinone. In a previous work,[1] a close similarity of the configurational mixings in the low-energy π,π^* singlet states was found between fluorenone and 9,10-phenanthrenequinone. On the other hand, in Table 3, although the configurational mixings in 1-indenone and 1,2-naphthoquinone are similar in the No. 3 state, those in the Nos. 1 and 2 states are not so similar. Therefore, the similarity between the π,π^* absorption spectra of 1-indenone and 1,2-naphthoquinone can not be so clearly explained as that between fluorenone and 9,10-phenanthrenequinone. The above-mentioned dissimilarity between the configurational mixings in the two compounds is puzzling in view of the similarity between their π-MO's.

As for the change in the calculated excitation energy of the No. 1 state of 1-indenone through an alkyl-group substitution, it is found that the energy decrease ($\Delta E=-0.094$ eV) for the 2-position is the largest and that there is an energy increase ($\Delta E=0.014$ eV) for the 5-position. The 2- and 5-positions in 1-indenone are the positions α and para to the carbonyl group respectively. In 1,2-naphthoquinone, similar calculated results have been obtained in a previous work.[4] Therefore, these findings may support the assignment of Band I of 1-indenone to the transition, the No. 1 state←ground state, in Table 2. After all, it may be concluded that the similarity between the calculated π-electronic structures in the low-energy π,π^* singlet states of 1-indenone and 1,2-naphthoquinone is not so good as that between fluorenone and 9,10-phenanthrenequinone.

Recently, data about the π,π^* absorption spectrum of *p*-tropoquinone 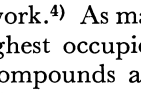 have been obtained by Ito *et al.*[11] which are similar to those of *p*-benzoquinone.[12] This similarity can be clearly explained, on the basis of the calculated results, much as that between fluorenone and 9,10-phenanthrenequinone.

The authors are grateful to Drs. Hideaki Tanaka and Koichi Honda of this laboratory for their helpful advice about the photochemical *trans*→*cis* isomerization of α-methylcinnamic acid in the preparation of 2-methyl-1-indenone.

References

1) A. Kuboyama, *Chem. Phys. Lett.*, **41**, 544 (1976); *Tokyo Kogyo Shikensho Hokoku*, **73**, 348 (1978).
2) E. D. Bergmann, A. Heller, and H. Weiler-Feilchenfeld, *Bull. Soc. Chim. Fr.*, **1959**, 635.
3) S. Nagakura and A. Kuboyama, *J. Am. Chem. Soc.*, **76**, 1003 (1954); *Nippon Kagaku Zasshi*, **74**, 97 (1953).
4) A. Kuboyama and H. Arano, *Bull. Chem. Soc. Jpn.*, **49**, 1401 (1976); *Tokyo Kogyo Shikensho Hokoku*, **72**, 170 (1977).
5) R. Stoermer and G. Voht, *Justus Liebigs Ann. Chem.*, **409**, 55 (1915).
6) H. Tanaka and K. Honda, private communication.
7) Y. Urushibara and M. Hirota, *Nippon Kagaku Zasshi*, **82**, 354 (1961).
8) H. R. Luss and D. L. Smith, *Acta Crystallogr., Sect. B*, **28**, 884 (1872).
9) In 2-methyl-1-indenone, the n,π^* band may be hidden under Band I, as in the case of fluorenone.[10] In Fig. 1, the fine structures on Band I in the cyclohexane solution may be partly due to this n,π^* band.
10) A. Kuboyama, *Bull. Chem. Soc. Jpn.*, **37**, 1540 (1964).
11) S. Ito, Y. Shoji, H. Takeshita, M. Hirama, and K. Takahashi, *Tetrahedron Lett.*, **1975**, 1075.
12) W. Flaig, J.-C. Salfeld, and E. Baume, *Justus Liebigs Ann. Chem.*, **618**, 117 (1958); A. Kuboyama, S. Matsuzaki, M. Takagi, and H. Arano, *Bull. Chem. Soc. Jpn.*, **47**, 1604 (1974); *Tokyo Kogyo Shikensho Hokoku*, **71**, 180 (1976).

Solvent Extraction Equilibria of Acids. VII. The Co-extraction of Water with Strong Mineral Acids by Trioctylphosphine Oxide

Masaru Niitsu,* Nobuhiko Iritani, and Tatsuya Sekine†

Faculty of Pharmaceutical Sciences, Josai University, Sakado, Saitama 350-02

†*Department of Chemistry, Science University of Tokyo, Kagurazaka, Shinjuku-ku, Tokyo 162*

(Received October 27, 1978)

The extraction of water from a 1 mol dm^{-3} sodium perchlorate solution with trioctylphosphine oxide (TOPO) in four organic solvents and the co-extraction of water with hydrochloric, hydrobromic, hydroiodic, perchloric, nitric, and thiocyanic acids from 1 mol dm^{-3} of the acid solution by TOPO in hexane have been studied at 25 °C. The extraction constants of water in the absence of any of the acids, $K'_{H_2O}=[TOPO\cdot H_2O]_{org}[TOPO]_{org}^{-1}$, were determined to be $10^{0.40}$, $10^{0.00}$, $10^{-0.12}$, and $10^{-0.36}$ in benzene, hexane, carbon tetrachloride, and chloroform respectively. A discrepancy from the 1 : 1 molar ratio of TOPO and water in the extract was observed in the higher-TOPO-concentration region in the hexane system. The co-extraction of water with the acids disolvated by TOPO was greater in the order of $HCl \simeq HBr > HI > HClO_4$, and it was much poorer with the monosolvated acids, nitric and thiocyanic acid. The equilibria for these co-extractions of water with the acids are complicated.

The co-extraction of water with various acids by oxygen-containing solvents has been studied with ethers, ketones, alcohols, and tributyl phosphate.[1,2] The extraction of acids and the co-extraction of water with the acids into various organic diluents containing trioctylphosphine oxide (TOPO) have also been studied, and the equilibria have been considered from several standpoints.[3-8]

After a series on the extraction equilibria of several acids with TOPO,[9-14] the present authors have studied the co-extraction of water with some of these acids. The present paper will describe the experimental results and will discuss the equilibria of these co-extractions.

Experimental

All of the experiments were carried out in a thermostatted room at 25 °C in a manner essentially similar to that described previously.[9-14] A portion of a 1 mol dm^{-3} aqueous electrolyte solution and the same volume of an organic solution were placed in a stoppered glass tube, and the contents were vigorously agitated and centrifuged. The concentration of water in the organic phase was determined by the Karl Fischer method.

Statistical

In the present paper, HX and E denote an acid and TOPO, and the subscript "org" denotes chemical species in the organic phase.

In the absence of any acid, the extraction equilibrium of water with TOPO may be written by the following equations, on the basis of the results to be presented later:

$$E(org) + H_2O \rightleftarrows E\cdot H_2O(org) \quad (1)$$

$$K'_{H_2O} = [E\cdot H_2O]_{org}[E]_{org}^{-1} \quad (2)$$

The concentration of water in the organic phase is written as

$$[H_2O]_{org,total} = [H_2O]_{org,blank} + [H_2O]_{org,E} \quad (3)$$

where $[H_2O]_{org,blank}$ and $[H_2O]_{org,E}$ are the concentrations of free water in the diluent and of bound water with TOPO respectively.

In the presence of an acid, the concentration of water in the organic phase may be written as

$$[H_2O]_{org,total} = [H_2O]_{org,blank} + [H_2O]_{org,E} + [H_2O]_{org,HX} \quad (4)$$

where $[H_2O]_{org,HX}$ is the concentration of the water co-extracted with the acid. Since the extraction of the acids in the absence of TOPO is negligible, the concentration of the extractant may be written as

$$[E]_{org,total} - a[H^+]_{org} = [E]_{org} + [E\cdot H_2O]_{org} \quad (5)$$

where $[H^+]_{org}$ is the concentration of the acid in the organic phase and where a is the mole of TOPO combined with one mole of the acid. As has been described previously,[9,10,13] the value for this a is two for hydrochloric, hydrobromic, hydroiodic, and perchloric acid, while it is one for nitric and thiocyanic acid.

The concentration of the acid-free TOPO, that is, TOPO combined with no acid, can be calculated by means of Eq. 5, and the amount of water combined with the acid-free TOPO, $[H_2O]_{org,E}$, can be calculated from the calibration curves, $\log [H_2O]_{org,E}$ *vs.* $\log [E]_{org,total}$. Finally, the concentration of the water co-extracted with the acid can be calculated by introducing this calculated value of $[H_2O]_{org,E}$ and the experimentally obtained value of $[H_2O]_{org,blank}$ into Eq. 4.

Results

The concentrations of water in the organic solvents containing no TOPO and being equilibrated with an aqueous 1 mol dm^{-3} sodium perchlorate solution are listed in Table 1. The amounts of water in the organic phases containing TOPO and being equilibrated with this aqueous solution (thus, no extraction of any acid

Table 1. The values of the extraction constant in Eq. 2 and those of the water concentration dissolved by the diluent at equilibrium

	$\log [H_2O]_{org,blank}$	$\log K'_{H_2O}$
Benzene	−1.45	0.40
Hexane	−2.39	0.00
Carbon tetrachloride	−2.02	−0.12
Chloroform	−1.14	−0.36

Org. phase: diluent containing TOPO. Aq. phase: 1 mol dm^{-3} sodium perchlorate solution.

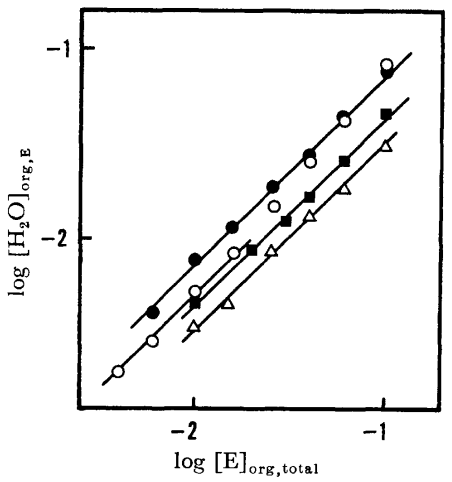

Fig. 1. Variation of water content of the organic phase with total TOPO concentration in benzene (●), hexane (○), carbon tetrachloride (■), or chloroform (△), after correction for the dissolved water by the diluent. The straight lines are slope of +1. The aqueous phase was 1 mol dm^{-3} sodium perchlorate solution.

was expected) were also determined; the $[H_2O]_{org,E}$ values were calculated by means of Eq. 3. Figure 1 shows these calculated values as a function of the total TOPO concentration in the organic phase. The values of $K'_{H,O}$ were calculated from these data by using Eq. 2; they are listed in Table 1. (For the calculation of the value in the hexane system, only those data which fitted with the straight line of a slope one were employed).

The co-extraction of water with mineral acids by TOPO was studied only when the diluent was hexane. The concentration of the co-extracted water with the acid by TOPO was calculated by means of Eq. 4.

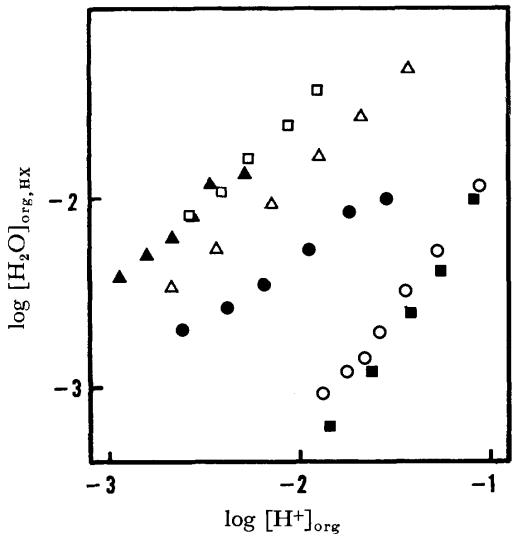

Fig. 2. Co-extracted water with hydrochloric (▲), hydrobromic (□), hydroiodic (△), perchloric (●), nitric (○), or thiocyanic (■) acid-TOPO complex in the hexane phase containing various amount of TOPO, where the aqueous phase for thiocyanic acid system was 0.9 mol dm^{-3} hydrochloric acid and 0.1 mol dm^{-3} sodium thiocyanate, and that for others was 1 mol dm^{-3} only the acid.

Figure 2 shows the values as a function of the concentration of the extracted acid in the organic phase. In these experiments, the aqueous phase was a solution of the acid at 1 mol dm^{-3} except in the thiocyanic acid system; in this case, the aqueous phase contained 0.9 mol dm^{-3} of hydrochloric acid and 0.1 mol dm^{-3} of sodium thiocyanate, and the calculation was made by assuming that the extraction of the hydrochloric acid was negligible compared to that of the thiocyanic acid (*cf.* Refs. 10 and 13).

It is anticipated that the error in the water co-extracted with hydrochloric acid is greater than that co-extracted with the other acids, because its extraction with TOPO was poor, and so much smaller amounts of co-extracted water had to be determined.

Another series of experiments on the co-extraction of water were also made by keeping the TOPO concentration at 0.04 mol dm^{-3}, while changing the hydrogen-ion concentration in the 1 mol dm^{-3} (H,Na)ClO_4 or 1 mol dm^{-3} (H,Na)NO_3 ionic media. The log $[H_2O]_{org,HX}$ *vs.* log $[H^+]_{org}$ plots obtained from these data were found to overlap approximately with those shown in Fig. 2.

Discussion

The above results may be summarized as follows.

i) TOPO in benzene, carbon tetrachloride, and chloroform, and that in hexane at its low concentrations (below 0.02 mol dm^{-3}), extract water from a 1 mol dm^{-3} sodium perchlorate solution as a 1:1 species, TOPO·H_2O. The mole fractions of the TOPO·H_2O species relative to the total TOPO are 0.72, 0.50, 0.43, and 0.30 in benzene, hexane, carbon tetrachloride, and chloroform respectively. Thus, the TOPO is not completely hydrated. In hexane, a discrepancy from the 1:1 mole ratio in the extract was observed when the TOPO concentration was higher.

ii) The amount of water co-extracted into hexane with the three hydrohalogenic acids was proportional to the amount of acid extracted. One mole of hydrochloric and hydrobromic acid in hexane which is combined with two moles of TOPO[10,13] co-extracted approximately three moles of water, but one mole of hydroiodic acid which is also combined with two moles of TOPO[13] co-extracted only approximately 1.3 moles of water.

iii) One mole of perchloric acid which is combined with two moles of TOPO in hexane[9] co-extracts less than one mole of water, and the amounts of water co-extracted per mole of the acid decrease with an increase in the acid concentration.

iv) The co-extractions of water with nitric and with thiocyanic acid, each of which is combined with one mole of TOPO in hexane,[9,13] are approximately the same as each other, and much less than with the other acids; only about one-tenth mole of water is co-extracted with one mole of each of the acids, but the mole ratio of water and acid slightly increases with an increase in the acid concentration.

The extraction of water in the absence of acid in the present work is similar to that in the previous reports;[3-5] moreover, the present results when the solvent is hexane

are similar to those when the solvent was cyclohexane or isooctane in the previous reports.

Attempts were made to find species other than $TOPO \cdot H_2O$ in the hexane system in the higher TOPO concentrations by statistical treatments of the data, but they were not successful. Thus, the present authors can not conclude whether the discrepancy from unity of the slope of the plot in Fig. 1 is due to the formation of higher aggregates such as $(TOPO)_b(H_2O)_c$ (where b/c is lower than unity) or is due to changes in the chemical activities of the solutes. The same kind of discrepancy found in the previous work was explained in terms of the formation of a species, $(TOPO)_3(H_2O)_4$.[15]

It is noticeable that, although a 1:1 species of TOPO and water is formed in the organic phase, still a certain fraction of TOPO, sometimes more than a half of the total TOPO, is in the unhydrous state. Although the salt in the aqueous phase may affect the extraction of water, this can not be explained by the decrease in the water activity because the water activity in a 1 mol dm^{-3} sodium perchlorate solution is about 0.96; thus, the change is not serious.[16]

As may be seen from Fig. 2, the co-extraction of water was proportional to the extraction of the acid when it was a hydrogen halogenide. However, the slope of the $\log [H_2O]_{org,HX}$ *vs.* $\log [H^+]_{org}$ plot was somewhat lower than unity when the acid was perchloric acid and higher than unity when the acid was nitric or thiocyanic acid (in the latter cases, the slopes were about 1.5). It is difficult to give an explanation of these values of the slope of the $\log [H_2O]_{org,HX}$ *vs.* $\log [H^+]_{org}$ plot or of the observation that the molar ratio of the extracted acid and the co-extracted water is quite different when the acid is different. Furthermore, these results can not explain why certain monoprotonic acids are extracted with two molecules of TOPO in the organic phase.

As was previously reported,[9,10,13] only perchloric and the three hydrohalogenic acids among the monoprotonic inorganic acids we have studied were disolvated with TOPO in hexane. One of the explanations for this disolvation to one proton may be that the proton in the extract is in the oxonium-ion form; two of the hydrogens are combined with the phosphoryl oxygen of TOPO, and the last hydrogen is combined with the anion. However, this does not explain the finding that the average composition of the extract was $(TOPO)_2(HClO_4)(H_2O)_d$, where d is a number decreased by an increase in the acid concentration in the organic phase and always lower than unity. Moreover, for the three extracted hydrohalogenic acid species, whose average compositions were $(TOPO)_2(HX)(H_2O)_e$, where e was about 1.3 for hydroiodic acid and about 3 for the other two acids, we should consider that a certain proportion of co-extracted water was in a form other than the oxonium-ion form.

Diamond and his coworkers studied the co-extraction of water with hydrochloric, hydrobromic, perchloric, perrhenic, and tetrachloroauric acid by TOPO in various solvents and reported a tendency similar to that shown by the present results.[3-6] Since less than one mole of water was co-extracted with one mole of the perchloric, perrhenic, and tetrachloroauric acid which were disolvated with TOPO, they concluded that the proton combined with the TOPO molecules was not a oxonium-ion, but was unhydrous, and that the anion which was assumed to combine with the proton as an ion pair was responsible for the co-extraction of water.

However, when the water is assumed to be co-extracted only by an "ion-paired" anion, the very poor co-extraction of water with nitric and thiocyanic acid can not be explained; a nitrate ion should interact with water molecules more strongly than a perchlorate ion.

It is noticeable that the two monoprotonic acids which co-extracted water only poorly were monosolvated by TOPO in the organic phase, while the other monoprotonic acids, which co-extracted greater amounts of water than nitric and thiocyanic acid, were disolvated. It is also marked that these monosolvated acids were weaker acids than the disolvated ones. These facts seem to lead us to other kinds of explanations. For example, none of the anions of the monosolvated acids are in the form of an ion pair in the organic phase; they all interact with the proton more strongly, and thus are less available for the water molecules than the ion-paired anion, and/or each of the two phosphoryl oxygens of TOPO in the disolvated acid species interact with the proton less strongly than that in the monosolvated acid species, thus becoming more available for hydration. However, since spectroscopic measurements have not been made, no final conclusion can be reached on the basis of only the results in the present study.

References

1) Y. Marcus and A. S. Kertes, "Ion Exchange and Solvent Extraction of Metal Complexes," Wiley-Interscience, New York (1969).

2) T. Sekine and Y. Hasegawa, "Solvent Extraction Chemistry," Marcel Dekker, New York (1977).

3) T. J. Conocchioli, M. I. Tocher, and R. M. Diamond, *J. Phys. Chem.*, **69**, 1106 (1965).

4) J. J. Bucher, M. Zirin, R. C. Laugen, and R. M. Diamond, *J. Inorg. Nucl. Chem.*, **33**, 3869 (1971).

5) J. J. Bucher and R. M. Diamond, *J. Inorg. Nucl. Chem.*, **34**, 3531 (1972).

6) J. A. Labinger, B. A. Sudbury, and R. M. Diamond, *J. Inorg. Nucl. Chem.*, **37**, 221 (1975).

7) M. Senegacnik, C. Klofutar, S. Paljk, and L. Smrekar, *J. Inorg. Nucl. Chem.*, **32**, 1659 (1970).

8) A. I. Mikhailichenko, *Radiokhimiya*, **12**, 594 (1970).

9) M. Niitsu and T. Sekine, *J. Inorg. Nucl. Chem.*, **37**, 1054 (1975).

10) M. Niitsu and T. Sekine, *J. Inorg. Nucl. Chem.*, **38**, 1053 (1976).

11) M. Niitsu and T. Sekine, *J. Inorg. Nucl. Chem.*, **38**, 1057 (1976).

12) T. Sekine, Y. Zeniya, and M. Niitsu, *Bull. Chem. Soc. Jpn.*, **49**, 2629 (1976).

13) M. Niitsu and T. Sekine, *Bull. Chem. Soc. Jpn.*, **50**, 1015 (1977).

14) M. Niitsu and T. Sekine, *Bull. Chem. Soc. Jpn.*, **51**, 705 (1978).

15) M. A. Lodhi, P. R. Danesi, and G. Scibona, *J. Inorg. Nucl. Chem.*, **33**, 1889 (1971).

16) Y. Hasegawa, *Bull. Chem. Soc. Jpn.*, **42**, 1429 (1969).

Molecular Weight Distribution and Kinetics of Low-temperature Propene Polymerization with Soluble Vanadium-based Ziegler Catalysts

Yoshiharu Doi,* Morio Takada, and Tominaga Keii

Department of Chemical Engineering, Tokyo Institute of Technology, Ookayama, Meguro-ku, Tokyo 152

(Received November 8, 1978)

A kinetic study has been carried out on the low-temperature polymerization of propene with the soluble catalyst system, VCl_4 and alkylaluminium ($AlEt_2Cl$, $AlEt_2Br$, or $AlEt_3$). The rate coefficients of the elementary reactions were evaluated at −78 °C. The molecular weight distribution function was derived on the basis of the polymerization mechanism. The theoretical distribution curves and experimental distribution curves obtained by use of a gel permeation chromatography agree, supporting the mechanism proposed for the coordination polymerization.

The molecular weight distribution (MWD) of polymers depends on the kinetic scheme of polymerization. Flory[1] and Bamford *et al.*[2] derived some distribution functions related to kinetic parameters for vinyl polymerization. Since the advent of gel permeation chromatography,[3] detailed kinetic investigations on the basis of the MWD data of polymers produced have been carried out for various models of polymerization, such as the radical polymerization of styrene with benzoyl peroxide as initiator[4] and the radiation-induced polymerization of styrene[5] and α-methylstyrene.[6] Agreement between the theoretical and experimental MWD curves can be regarded as evidence for the proposed kinetic scheme. However, this type of investigation does not seem to have been applied to the coordination polymerizaton of α-olefin with Ziegler-type catalysts.

In the present study, carrying out the polymerization of propene with the soluble catalyst mixture of VCl_4 with alkylaluminium [$AlEt_2Cl$, $AlEt_2Br$, or $AlEt_3$ ($Et=C_2H_5$)] at −78 °C, we compare the experimental MWD curves with a theoretical one derived from a proposed kinetic scheme. The catalyst system, VCl_4/$AlEt_2Cl$[8] or VCl_4/$AlEt_2Br$,[7] at −78 °C gives the syndiotactic form of polypropylene, whereas VCl_4/$AlEt_3$[10] gives the stereoirregular (atactic) form of polypropylene.

The kinetic scheme for polymerization is discussed, values being then determined for the rate coefficients of elementary reactions along the scheme.

Kinetic Scheme

The mechanism of syndiotactic polymerization of propene with the soluble catalyst system VCl_4/$AlEt_2Cl$ has been extensively investigated by Natta and coworkers.[8–11] Their kinetic data[9,10] on the polymerization and spectroscopic data[11] of the catalyst system suggest the following mechanistic features concerning the polymerization of propene. The catalytically active vanadium formed by the reaction of VCl_4 with $AlEt_2Cl$ is only a small fraction (less than 1%) of the total amount of vanadium[9] and a trivalent state.[11] The polymerization of propene takes place *via* two successive reactions, propene monomer coordination to the active vanadium and the subsequent insertion of the coordinated monomer into the growing chain attached to the metal.[10] The molecular weight of the growing chain is restricted either by the propene monomer coordinated or by the attack of alkylaluminium.[9,10] The chain transfer with monomer may be caused by a hydrogen transfer from the growing chain to the coordinated monomer with the subsequent formation of a new growing chain and a dead polymer. In the chain transfer with alkylaluminium, the growing chain attached to the vanadium may be replaced by the alkyl group on aluminium. In both cases the number of polymerization centers remains unchanged. For the purpose of calculation, the above reactions are written as follows.

Coordination to monomer

$$R_n + M \overset{K_m}{\rightleftharpoons} C_n \tag{1}$$

Propagation

$$C_n \xrightarrow{k_p} R_{n+1} \tag{2}$$

Chain transfer with monomer

$$C_n \xrightarrow{k_{tm}} R_1 + Y_n \tag{3}$$

Chain transfer with alkylaluminium

$$R_n + A \xrightarrow{k_{tal}} R_1 + Z_n \tag{4}$$

Here C_n and R_n represent the growing chain with n units attached to the active vanadium metal with and without the monomer coordinated, respectively. M, A, Y_n, and Z_n represent the propene monomer, alkylaluminium, polymer with n units and polymer molecule with n units attached to inactive aluminium metal, respectively.

The overall rates of propagation, R_p, and chain transfer, R_t, are given by

$$R_p = k_p\sum_1^\infty[C_n] = k_pK_m\sum_1^\infty[R_n][M]$$

$$= k_p\left(\frac{K_m[M]}{1+K_m[M]}\right)\sum_1^\infty([C_n]+[R_n]) \tag{5}$$

$$R_t = (k_{tm}K_m[M]+k_{tal}[A])\sum_1^\infty[R_n] \tag{6}$$

The number average degree of polymerization of the isolated polymers, $\bar{P}_n$, at a given time, t, is given by

$$\bar{P}_n = \frac{\int_0^t R_p dt}{\sum_1^\infty([C_n]+[R_n])+\int_0^t R_t dt} \tag{7}$$

If we assume the steady-state conditions under which R_p and R_t remain constant during the course of polymerization, the reciprocal of $\overline{P}_n$ can be expressed as

$$\frac{1}{\overline{P}_n} = \left(\frac{1+K_m[M]}{k_p K_m[M]}\right)\cdot\frac{1}{t} + \frac{R_t}{R_p} \quad (8)$$

Under the conditions that $t \gg 0$, Eq. 8 can be approximated as

$$\frac{1}{\overline{P}_n} \simeq \frac{R_t}{R_p} = \frac{k_{tm}}{k_p} + \frac{k_{tal}}{k_p K_m}\cdot\frac{[A]}{[M]} \quad (9)$$

We now derive the MWD function in this polymerization. The formation of the growing chain with n units is given by

$$\frac{d[R_n+C_n]}{dt} = k_p K_m[M]([R_{n-1}]-[R_n]) - (k_{tm}K_m[M]+K_{tal}[A])[R_n] \quad (10)$$

When the polymerization is stationary, *i.e.*, $[C_n]$ and $[R_n]$ remain constant during the course of polymerization, the right-hand side of Eq. 10 is zero. Thus we have

$$[R_n] = \beta[R_{n-1}] = \beta^{n-1}[R_1] \quad (11)$$

with

$$\beta = \frac{k_p K_m[M]}{k_p K_m[M]+k_{tm}K_m[M]+k_{tal}[A]} \quad (12)$$

The rate of formation of the polymer with n units is given by

$$\frac{d[Y_n+Z_n]}{dt} = (k_{tm}K_m[M]+k_{tal}[A])[R_n] \quad (13)$$

For a low conversion of monomer the concentration of polymer, $[Y_n+Z_n]$, may be expressed as a function of t.

$$[Y_n+Z_n] = (k_{tm}K_m[M]+k_{tal}[A])\beta^{n-1}[R_1]t \quad (14)$$

Thus, we have the mole fraction of polymer with n units, $X(n)$

$$X(n) = (1-\beta)\beta^{n-1} \quad (15)$$

which is the same as the MWD function derived by Flory.[1)]

Experimental

Reagents. Propene (Mistubishi Petrochemical Co. 99.7 % purity, the impurity being propane) was dried by passing through columns of NaOH and P_2O_5. Heptane (reagent grade) was dried by refluxing over sodium metal under nitrogen atmosphere after distillation. Alkylaluminiums (Japan Aluminium Alkyl Co.) and VCl_4 (Wako Pure Chemicals) were used without further purification.

Polymerization Procedure. A three-neeked glass flask with a magnetic stirrer was used as a reactor. Propene was condensed into heptane in the reactor kept at −78 °C with methanol–Dry Ice. The amount of heptane used was adjusted to be 100 ml as the total volume of solution. Prescribed amounts of alkylaluminium and VCl_4 were charged one after the other. Polymerization was timed from the addition of the VCl_4 component, and quenched at a given time by introducing 100 ml of an ethanol solution of hydrochloric acid cooled at −78 °C. The polymers obtained were washed several times with 200—300 ml ethanol and dried *in vacuo* at room temperature.

Gel-permeation Chromatography Analysis. Molecular weight distributions of polymers were measured by gel permeation chromatography (GPC) (Waters Associates, Model 200) with the use of five polystyrene gel columns (10^7, 10^6, 10^5, 10^4, and 10^3 Å pore sizes) and *o*-dichlorobenzene as a solvent at 135 °C. The solvent flow rate was maintained at 1.0 ml/min. A molecular weight calibration curve was obtained on the basis of the universal calibration,[12,13)] with 10 standard samples of monodisperse polystyrene of molecular weights 2100—2610000. From the GPC data, the number-average and weight-average molecular weights ($\overline{M}_n$, $\overline{M}_w$) were obtained by standard procedures by using the data at 1/2 count (2.5 ml elution volume).

Results and Discussion

The polymerization results obtained at −78 °C under various conditions are summarized in Tables 1, 2, and 3 for the $VCl_4/AlEt_2Cl$, $VCl_4/AlEt_2Br$, and $VCl_4/AlEt_3$ catalysts, respectively. Polymerization was carried out in the range of a low conversion of propene monomer up to several percents. The concentration of monomer may be regarded as constant during the course of polymerization. Kinetic analysis for the polymerization was made from the data given in the Tables.

Polymerization Rate. The time dependence of the yields of polymers produced in the course of polymerizations with different catalyst systems is shown in Fig. 1. The yield-time curves are almost linear with no induction periods. This shows that the formation of the polymerization centers is complete just after the start of polymerization and the number of the centers remains constant during the course of polymerization.

The polymer yields at a given polymerization time were of first-order, as anticipated, with respect to the amount of vanadium tetrachloride at a constant concentration of alkylaluminium. On the other hand, it was found that the relationship between polymerization rate and propene monomer concentration is not of simple first-order kinetics. The polymerization rate, R_p, increased to a constant value with increase in monomer

Table 1. Polymerization results obtained at −78 °C under different experimental conditions with $VCl_4/AlEt_2Cl$ catalyst system

Sample	$AlEt_2Cl$ (mol/l)	C_3H_6 (mol/l)	Polymerization period (h)	Polymer yield (g)	$\overline{M}_n$ ($\times 10^4$)	Q ($\overline{M}_w/\overline{M}_n$)
A-1	0.05	8.4	0.5	0.05	2.39	1.4
A-2	0.05	8.4	0.75	0.14	2.32	1.5
A-3	0.05	8.4	1.0	0.19	2.99	1.5
A-4	0.05	8.4	2.0	0.49	3.06	1.5
A-5	0.05	8.4	3.0	0.72	3.19	1.5
A-6	0.05	8.4	4.0	1.01	3.73	1.6
A-7	0.05	8.4	5.0	1.39	3.58	1.7
A-8	0.05	8.4	7.0	2.00	4.07	1.7
A-9	0.03	8.4	3.0	0.52	3.28	1.5
A-10	0.10	8.4	3.0	0.99	2.93	1.6
A-11	0.15	8.4	3.0	0.96	3.06	1.7
A-12	0.20	8.4	3.0	0.97	2.68	1.8
A-13	0.25	8.4	3.0	0.94	2.87	1.6
A-14	0.05	1.2	3.0	0.23	1.92	1.9
A-15	0.05	2.4	3.0	0.46	2.27	1.7
A-16	0.05	4.8	3.0	0.66	2.97	1.7
A-17	0.05	11.7	3.0	0.66	—	—

VCl_4 concentration of 0.01 mol/l, polymerization solution of 0.1 l.

Table 2. Polymerization results obtained at −78 °C with $VCl_4/AlEt_2Br$ catalyst system

Sample	$AlEt_2Br$ (mol/l)	C_3H_6 (mol/l)	Polymerization period (h)	Polymer yield (g)	$\bar{M}_n$ ($\times 10^3$)	Q ($\bar{M}_w/\bar{M}_n$)
B-1	0.050	8.4	2.0	0.06	3.34	2.3
B-2	0.050	8.4	3.0	0.08	5.17	3.0
B-3	0.050	8.4	5.0	0.10	6.58	2.7
B-4	0.050	8.4	6.5	0.16	5.50	2.6
B-5	0.015	8.4	3.0	0.05	—	—
B-6	0.025	8.4	3.0	0.09	4.24	2.5
B-7	0.075	8.4	3.0	0.04	4.61	1.7
B-8	0.100	8.4	3.0	0.04	4.40	1.6
B-9	0.200	8.4	3.0	0.03	3.34	1.6
B-10	0.025	4.8	3.0	0.06	3.02	2.0
B-11	0.025	12.3	3.0	0.14	4.93	2.3

VCl_4 concentration of 0.01 mol/l, polymerization solution of 0.1 l.

Table 3. Polymerization results obtained at −78 °C with $VCl_4/AlEt_3$ catalyst system

Sample	$AlEt_3$ (mol/l)	C_3H_6 (mol/l)	Polymerization period (h)	Polymer yield (g)	$\bar{M}_n$ ($\times 10^5$)	Q ($\bar{M}_w/\bar{M}_n$)
C-1	0.025	8.4	0.5	0.30	2.57	1.6
C-2	0.025	8.4	1.0	0.49	3.43	1.8
C-3	0.025	8.4	1.5	0.92	5.45	2.0
C-4	0.025	8.4	2.5	1.25	7.55	2.0
C-5	0.025	8.4	3.0	1.43	7.75	2.0
C-6	0.005	8.4	3.0	1.08	6.81	2.1
C-7	0.015	8.4	3.0	0.83	5.97	2.4
C-8	0.100	8.4	3.0	0.57	4.86	2.6
C-9	0.150	8.4	3.0	0.40	3.46	2.6
C-10	0.200	8.4	3.0	0.47	3.82	2.2
C-11	0.025	1.2	2.5	0.22	2.74	2.1
C-12	0.025	4.8	2.5	0.82	5.74	2.0
C-13	0.025	11.9	2.5	1.42	10.7	1.8

VCl_4 concentration of 0.001 mol/l, polymerization solution of 0.1 l.

concentration, [M].[14] $1/R_p$ is plotted against 1/[M] for the respective catalyst system in Fig. 2. The linearity of the plots indicate that Eq .5 is applicable to the polymerization of propene with soluble vanadium-based catalysts. The values of the coordination equilibrium constant of monomer, K_m, were determined from the slopes and the intercepts of the straight lines. The results are given in Table 4.

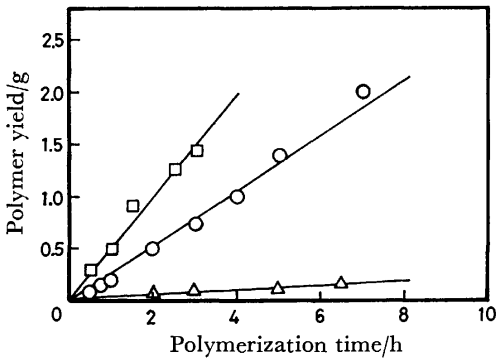

Fig. 1. Polymer yield-time curves of the polymerizations with different catalyst systems.
(○); $VCl_4/AlEt_2Cl$ system (samples A-1—A-8), (△); $VCl_4/AlEt_2Br$ system (samples B-1—B-4), (□); $VCl_4/AlEt_3$ system (samples C-1—C-5).
For experimental conditions see Tables 1—3.

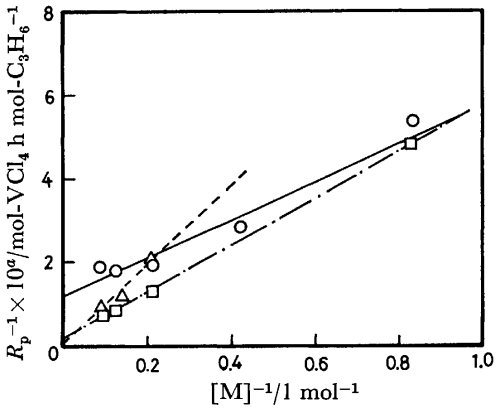

Fig. 2. Plots of the reciprocal of polymerization rate, R_p^{-1}, against the reciprocal of propene monomer concentration, $[M]^{-1}$.
(○); $VCl_4/AlEt_2Cl$ system ($a=1$ for $R_p^{-1}\times 10^a$), (△); $VCl_4/AlEt_2Br$ system ($a=0$ for $R_p^{-1}\times 10^a$), (□); $VCl_4/AlEt_3$ system ($a=2$ for $R_p^{-1}\times 10^a$).
−78 °C, $[AlEt_2Cl]=[AlEt_2Br]=0.05$ mol/l or $[AlEt_3]=0.025$ mol/l.

The effect of alkylaluminium concentration on the polymerization rate is complicated (Fig. 3). The polymerization rate rises to a maximum value followed by a gradual fall with increase in the concentration of alkylaluminium, *i.e.*, in the Al/V ratio. The polymerization rate is correlated with the following function of the concentration of alkylaluminium [A].

$$R_p \propto \frac{K_A[A]}{(1+K_A[A])^2} \tag{16}$$

Table 4. Rate coefficients of elementary reactions in the polymerization of propene with $VCl_4/AlEt_2X$ (X=Cl, Br, Et) catalyst systems at −78 °C

	$AlEt_2Cl$	$AlEt_2Br$	$AlEt_3$
K_m(l·mol^{-1})	0.26±0.03	0.02±0.01	0.04±0.01
K_A(l·mol^{-1})	6.8±0.3	31±3	46±2
k_p(h^{-1})	(4.3±1.0)×10^3	(2.5±1.2)×10^2	(5.3±0.6)×10^4
k_{tm}(h^{-1})	5.4±0.1	1.7±0.1	2.3±0.3
k_{tal}(l·mol^{-1}·h^{-1})	18±6.5	3.5±2.0	9.0±1.5

The value of the constant, K_A, decreases in the order: $AlEt_3$>$AlEt_2Br$>$AlEt_2Cl$ (Table 4). The order appears to correspond to the reducing powers of the alkylaluminium for VCl_4. Though we can not present a conclusive explanation for Eq. 16, alkylaluminium seems to take part in the deactivation of polymerization centers as well as in the formation of the centers through the alkylation and complexation of VCl_4. This is supported by the obervation of Lehr[15] that higher Al/V ratios result in some reduction of vanadium to its divalent state at −78 °C in the $VCl_4/Al(i\text{-}Bu)_3$ catalyst system. The influence of the alkylaluminium concentration on the polymerization rate is thus understandable as a result of the change in the number of polymerization centers, $\sum_1^\infty([C_n]+[R_n])$.

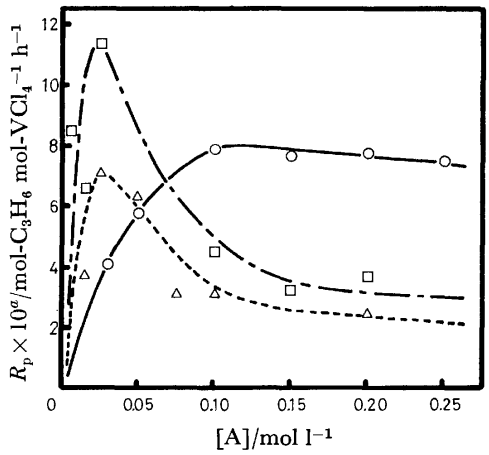

Fig. 3. Influence of alkylaluminium concentration, [A], on polymerization rate, R_p.
(○); $VCl_4/AlEt_2Cl$ system (a=0 for $R_p\times10^a$), (△); $VCl_4/AlEt_2Br$ system (a=−1 for $R_p\times10^a$), (□); $VCl_4/AlEt_3$ system (a=1 for $R_p\times10^a$).
−78 °C, [M]=8.4 mol/l.

Average Molecular Weight. The number-average molecular weghts, $\overline{M}_n$, of polymers produced increase with the polymerization time, attaining constant values in a few hours for all the catalyst systems (Tables 1—3). The plots of $1/\overline{M}_n$ *vs.* $1/t$ are shown for different catalyst systems in Fig. 4. The linearity of plots indicates that the experimental results are satisfactorily correlated by Eq. 8, which is a linear form of Eq. 7. Using the values of K_m given in the preceding section, we can estimate the values of the propagation rate coefficient of monomer, k_p, from the slopes of the straight lines. The values of k_p for different catalyst systems are summarized in Table 4.

The values of $\overline{M}_n$ of the polymers produced at 3 h increase with increase in the concentration of propene monomer, [M]. The dependence of the value of $\overline{M}_n$ on [M] is given by Eq. 9. The relation between the value of $\overline{M}_n$ of the polymers produced and the concentration of alkylaluminiums, [A], also follows Eq. 9 (Figs. 5—7). The values of intercepts of both straight lines in the respective figure agree closely with each other. This suggests that the chain terminating steps other than the transfer with monomer and alkylaluminium is not significant in the polymerization. The values of the rate coefficients of the chain transfers, k_{tm} and

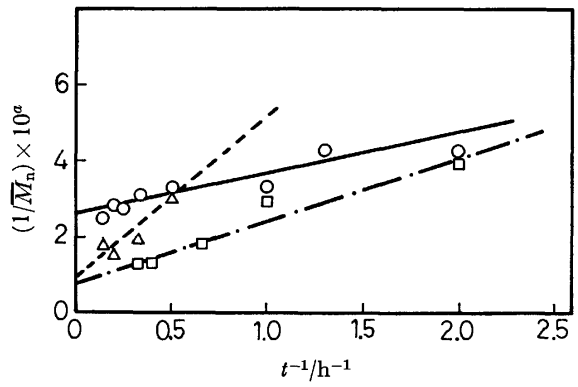

Fig. 4. Plots of $1/\overline{M}_n$ *vs.* $1/t$.
(○); $VCl_4/AlEt_2Cl$ system (a=5 for $1/M_n\times10^a$, samples A-1—A-8), (△); $VCl_4/AlEt_3Br$ system (a=4 for $1/M_n\times10^a$, samples B-1—B-4), (□); $VCl_4/AlEt_3$ system (a=6 for $1/M_n\times10^a$, samples C-1—C-5).
For experimental conditions see Table 1—3.

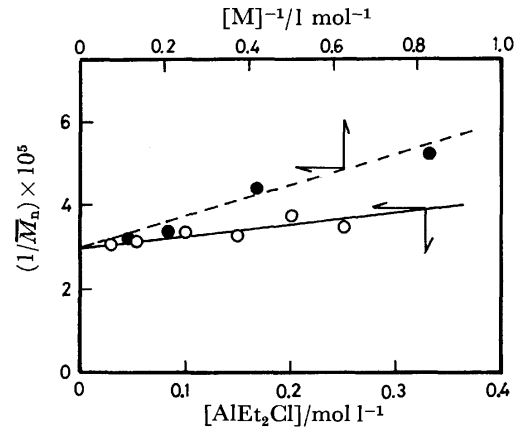

Fig. 5. Plots of $1/\overline{M}_n$ *vs.* $1/[M]$ and *vs.* [A] for $VCl_4/AlEt_2Cl$ system.
(●); Samples A-14—A-16 and A-5, (○); Samples A-9—A-13 and A-5.
For experimental conditions see Table 1.

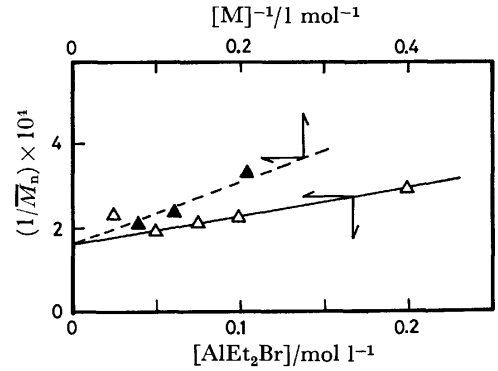

Fig. 6. Plots of $1/\overline{M}_n$ *vs.* $1/[M]$ and *vs.* [A] for $VCl_4/AlEt_2Br$ system.
(▲); Samples B-10, B-11 and B-2, (△); Samples B-6—B-9 and B-2.
For experimental conditions see Table 2.

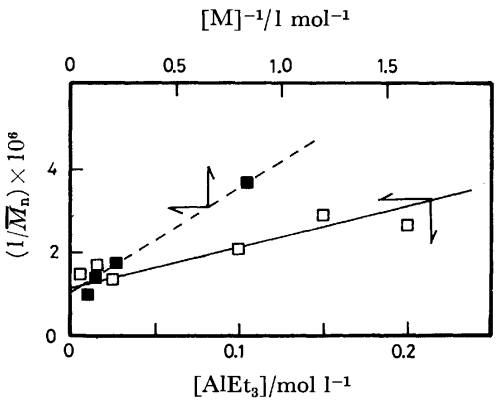

Fig. 7. Plots of $1/\overline{M}_n$ *vs.* 1/[M] and *vs.* [A] for VCl_4/$AlEt_3$ system.
(■); Samples C-11—C-13 and C-4.
(□); Samples C-5—C-10.
For experimental conditions see Table 3.

k_{tal}, may be obtained from the intercepts and slopes of the straight lines. The values of k_{tm} and k_{tal} are given in Table 4 with the experimental deviation for each catalyst system.

The rate coefficients of the elementary reactions are remarkably affected by the type of alkylaluminium used. The mole fraction of syndiotactic dyads of the polypropylene produced decreases as follows.[7]

$$AlEt_2Cl\ (86) > AlEt_2Br\ (65) > AlEt_3\ (50) \qquad (17)$$

The remarkable influence of the type of alkylaluminium on the elementary reaction rates and stereospecificity may be interpreted in terms of the bimetallic structure of the polymerization center, first proposed by Zambelli *et al.*,[11] in which the alkylaluminium complexed with alkylvanadium chloride regulates the catalytic capability.

Molecular Weight Distributions. Comparison has been made between the theoretical and experimental MWD curves of the polypropylene samples. Three

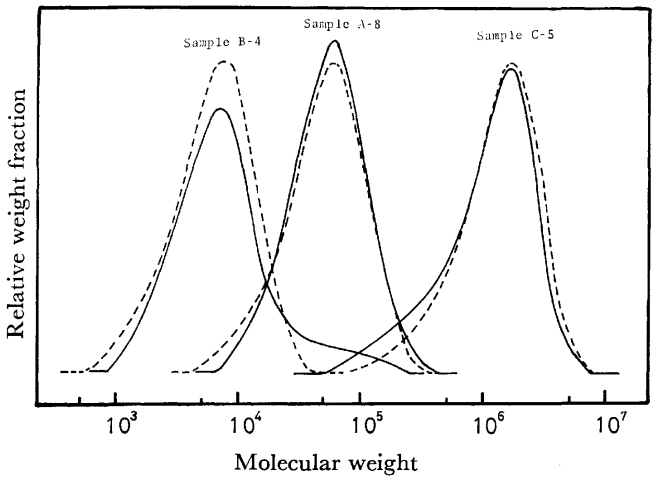

Fig. 8. Experimental and theoretical molecular weight distribution curves of polypropylenes prepared at −78 °C with different soluble vanadium-based catalysts.
(——): Experimental curves, (– – –) theoretical curves.

nomalized GPC curves of samples A-8, B-4 and C-5 are shown in Fig. 8 by solid lines. The polypropylene samples were prepared by the polymerization with different catalyst systems. The weight fraction of polymer is plotted against common logarithms of molecular weight. For the sake of comparison the theoretical MWD curves of the three samples were calculated from a plot of $42 \cdot n^2 \cdot [X(n)]$ *vs.* $\log (42 \cdot n)$, with $[X(n)]$ by means of Eq. 15 and the values of β (0.99865 for sample A-8, 0.98915 for sample B-4 and 0.99995 for sample C-5) were determined using the kinetic parameters (Table 4), taking the conditions for the preparation into consideration. The results are shown in Fig. 8 by dotted lines. The modes of curves and the values of maxima are in close agreement between theory and experiment, except sample B-4 prepared with $VCl_4/AlEt_2Br$ system. The shoulder at the higher molecular weights observed in the GPC curve of sample B-4 may be due to the coexistence of $AlEt_2Cl$ formed by the halogen interchange between VCl_4 and $AlEt_2Br$.

It may be concluded that the molecular weight distributions of polymers produced with soluble vanadium-based catalysts are expressed by the distribution function of Eq. 15 derived from the kinetic scheme proposed.

References

1) P. J. Flory, "Principles of Polymer Chemistry," Cornel Univ. Press, Ithaca, N. Y. (1953).
2) C. H. Bamford, W. G. Bard, A. D. Jenkins, and P. F. Onyon, "The Kinetics of Vinyl Polymerization by Radical Mechanisms," Butterworths, London, (1958).
3) J. C. Moore, *J. Polym. Sci. A-2*, **2**, 835 (1964).
4) J. A. May, Jr., and W. B. Smith, *J. Phys. Chem.*, **72**, 216 (1968).
5) S. Machi, J. Silverman, and D. Metz, *J. Phys. Chem.*, **76**, 930 (1972).
6) A. S. Chawla, and R. Y. Hung, *J. Polym. Sci., Polym. Chem. Ed.*, **13**, 1271 (1975).
7) Y. Doi, M. Takada, and T. Keii, *Makromol. Chem.*, **180**, 57 (1979).
8) G. Natta, I. Pasquon, and A. Zambelli, *J. Am. Chem. Soc.*, **84**, 1488 (1962).
9) G. Natta, A. Zambelli, G. Lanzi, I. Pasquon, E. R. Mognaschi, A. L. Segre, and P. Centola, *Makromol. Chem.*, **81**, 161 (1965).
10) A. Zambelli, G. Natta, I. Pasquon, and R. Signorini, *J. Polym. Sci., Part C*, **16**, 2485 (1967).
11) A. Zambelli, I. Pasquon, R. Signorini, and G. Natta, *Makromol. Chem.*, **112**, 160 (1968).
12) Z. Grubisic, P. Rempp, and H. Bonoit, *J. Polym. Sci., Part B*, **5**, 753 (1967).
13) T. Ogawa, S. Tanaka, and S. Hoshino, *Kobunshi Kagaku*, **29**, 6 (1972).
14) Further purification of monomer by bubbling in the heptane solution of $AlEt_3$ was made to remove the trace of O_2 prior to use in the VCl_4–$AlEt_2Cl$ catalyst system. However, no effect of purification was observed on the polymerization rates. It is concluded that the unusual dependence of monomer concentration on the polymerization rate can not be interpreted in terms of the inhibiting effect of O_2 trace in the monomer.
15) M. H. Leher, *Macromolecules*, **1**, 178 (1968).

Temperature Effects on CD Spectra of β-Cyclodextrin Complexes with 2-Substituted Naphthalenes

Kazuaki HARATA

Research Institute for Polymers and Textiles, Sawatari 4, Kanagawa-ku, Yokohama 221

(Received November 13, 1978)

CD spectra of β-cyclodextrin complexes with 2-naphthol, 2-naphthyloxyacetic acid, potassium 2-naphthoate, and potassium 2-naphthylacetate were measured at various concentrations of β-cyclodextrin and at temperatures ranging from 10 to 70 °C. The temperature-dependent CD spectra of the 2-naphthyloxyacetic acid complex clearly show the 1 : 1 complex formation, but the other three complexes give CD intensity changes which are inexplicable in terms of the 1 : 1 stoichiometry. The molecular ellipticity and thermodynamic parameters were determined by the least-squares method. Enthalpy and entropy are in the ranges from −22.2 to −26.8 kJ·mol^{-1} and from −24 to −38 J·K^{-1}·mol^{-1}, respectively. They are strongly correlated to the volume of the substituent of the guest molecule, although the free energy is found in a quite narrow region (from −14.3 to −15.4 kJ·mol^{-1}). The correlation is explained on the basis of the β-cyclodextrin–guest interaction and the solvation around the guest molecule.

Cyclodextrins, which are α-1,4-linked cyclic oligosaccharides, form a number of inclusion complexes with a variety of guest molecules owing to the large cylindrical cavity in the center of the molecule.[1,2] Since cyclodextrins are asymmetric molecules, optical activity is induced when an optically inactive guest is included in the cavity.[3–7] For the cyclodextrin complexes with aromatic guests, the origin of induced optical activity was reasonably explained in terms of the Kirkwood-Tinoco coupled oscillator model.[5–7] Although CD spectra of many cyclodextrin complexes have already been reported, the molecular ellipticity of the complex has not been precisely determined. Since the induced CD is caused by cyclodextrin–guest interactions, CD spectra are expected to give information on the structure of the complex in solution. In the previous paper,[8] we reported the temperature dependence of CD spectra of α-cyclodextrin complexes with *m*- and *p*-nitrophenols. We present here the temperature effects on CD spectra of β-cyclodextrin complexes with 2-substituted naphthalenes and will discuss the structure and binding force of the complexes on the basis of the thermodynamic parameters determined by the least-squares method.

Experimental

Materials. β-Cyclodextrin (G. R., Tokyo Kasei Co.) was twice recrystallized from water and dried *in vacuo* over phosphorous pentaoxide. 2-Naphthol and 2-naphthyloxyacetic acid (G. R., Tokyo Kasei Co.) were recrystallized from ethanol. Potassium 2-naphthoate and potassium 2-naphthylacetate were prepared from 2-naphthoic acid and 2-naphthylacetic acid, which were treated by KOH-saturated ethanol, and were recrystallized from water.

CD Measurements. Solutions were prepared with deionized and distilled water. The CD spectra were recorded on a JASCO J-40A circular dichrograph with a J-DPZ data-processor. The recording of each spectrum was repeated four times, and the averaged spectra were obtained on the data-processor. The temperature was regulated by using a Tokyo Rico TC-100 thermo-controller with an accuracy of ±0.5 °C inside the cell.

Results

The CD spectra measured at 30 °C are shown in Fig. 1. The concentrations of β-cyclodextrin, 2-naphthol, 2-naphthyloxyacetic acid, potassium 2-naphthoate, and potassium 2-naphthylacetate are 5.0×10^{-3}, 1.89×10^{-4}, 2.12×10^{-4}, 1.90×10^{-4}, and 2.02×10^{-4} M, respectively. Each complex shows negative CD bands in the wavelength region longer than 250 nm. The CD bands found in the 250—300 nm region give a peak intensity higher than the intensity of the 300—350 nm bands. A large positive-signed CD band was found in the wavelength region from 200 to 250 nm. The temperature dependence of the CD intensity was measured by increasing the temperature from 10 to 70 °C. After the measurement at 70 °C, the temperature was again lowered to 10 °C. Then, the CD intensity returned to the initial value.

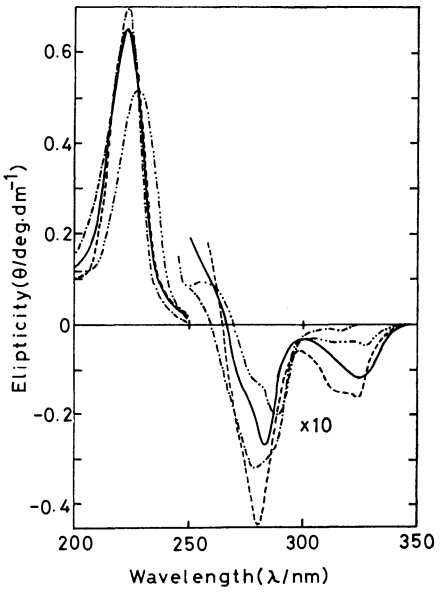

Fig. 1. CD spectra of β-cyclodextrin complexes with 2-naphthol (——), 2-naphthyloxyacetic acid (– – –), potassium 2-naphthylacetate (–·–·), and potassium 2-naphthoate (–··–) at 30 °C. The concentrations of β-cyclodextrin, 2-naphthol, 2-naphthyloxyacetic acid, potassium 2-naphthylacetate, and potassium 2-naphthoate are 5.0×10^{-3}, 1.89×10^{-4}, 2.12×10^{-4}, 2.02×10^{-4}, and 1.90×10^{-4} M, respectively.

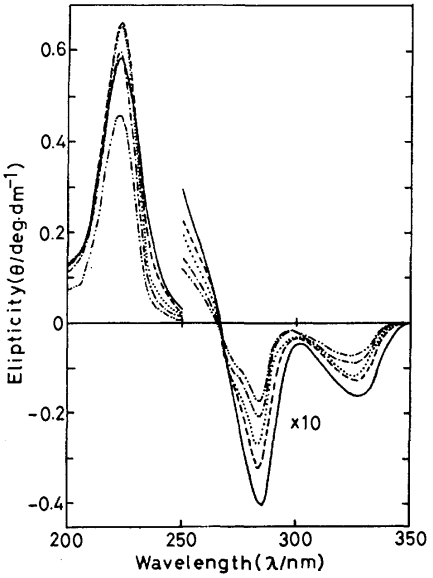

Fig. 2. CD spectra of β-cyclodextrin–2-naphthol complex measured at 10 °C (——), 20 °C (——), 30 °C (·····), 50 °C (-·-·), and 70 °C (-···-). The concentrations of β-cyclodextrin and 2-naphthol are 5.0×10^{-3} and 1.89×10^{-4} M, respectively.

β-Cyclodextrin–2-Naphthol Complex. The CD spectra measured at 10, 20, 30, 50, and 70 °C are shown in Fig. 2. With the increase of temperature, the negative CD bands lower their intensity. The intensity change in these bands is more rapid at lower temperature conditions. When the temperature is raised from 10 to 30 °C, the CD intensity of the 285 nm band decreases by 0.14 deg·dm^{-1}, which corresponds to 33% of the intensity measured at 10 °C. On the other hand, the intensity change is only 0.035 deg·dm^{-1} between the temperatures of 50 and 70 °C. The 285 nm band is slightly sharpened by increasing the temperature, and a shoulder appears at 274 nm. A similar sharpening is observed in the positive CD band centered at 222 nm. The intensity change in the 222 nm band is different from that of the negative-signed bands measured in the longer wavelength region. The CD intensity enhances when the temperature is raised up to 20 °C; after that, however, the intensity lowers with increasing temperature. Figure 4a gives the more detailed intensity change measured at 222 nm. In this case, the concentration of 2-naphthol is adjusted to 1.83×10^{-4} M, and the intensity was measured at β-cyclodextrin concentrations of 1.0×10^{-3}, 2.0×10^{-3}, and 9.0×10^{-3} M. At each β-cyclodextrin concentration, the highest CD intensity was not observed at 10 °C. The temperature which gives the maximum CD intensity becomes lower with the decrease of the β-cyclodextrin concentration. At 9.0×10^{-3} M β-cyclodextrin concentration, the CD intensity increases with the temperature up to 40 °C, and after that decreases gradually. The intensity maxima were also observed at 20 and 15 °C at the β-cyclodextrin concentrations of 2.0×10^{-3} and 1.0×10^{-3} M, respectively. The molecular ellipticity of the complex and thermodynamic parameters were determined by the least-squares method (see Appendix) on the basis of the assumption of the 1 : 1 stoichiometry. The intensity data measured at temperatures lower than 40 °C (9.0×10^{-3} M), 30 °C (2.0×10^{-3} M), and 25 °C (1.0×10^{-3} M) were not included in the calculation, since these values systematically deviated from the expected ones and can not be explained on the basis of the 1 : 1 stoichiometry. The calculated intensity is shown by the solid line in Fig. 4a. The 1 : 1 stoichiometry predicts the monotonous decrease of the CD intensity with the increase of the temperature. The molecular ellipticity of the complex is $5.7(1)\times10^{4}$ deg·cm^{2}·dmol^{-1}, and the dissociation constant at 25 °C is $2.0(2)\times10^{-3}$ mol. The free energy at 25 °C, enthalpy, and entropy for the complex formation are −15.4(3), −26.8(9) kJ·mol^{-1}, and −38(3) J·K^{-1}·mol^{-1}, respectively.

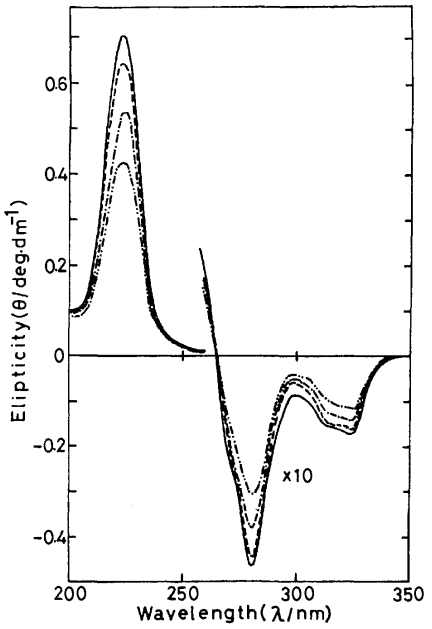

Fig. 3. CD spectra of β-cyclodextrin–2-naphthyloxyacetic acid complex measured at 10 °C (——), 30 °C (——), 50 °C (-·-·), and 70 °C (-···-). The concentrations of β-cyclodextrin and 2-naphthyloxyacetic acid are 5.0 $\times10^{-3}$ and 2.13×10^{-4} M, respectively.

β-Cyclodextrin–2-Naphthyloxyacetic Acid Complex. The CD spectra of the 2-naphthyloxyacetic acid complex measured at 10, 30, 50, and 70 °C are shown in Fig. 3. Unlike the 2-naphthol complex, the intensity change is slow in the temperature range from 10 to 30 °C. Two weak CD bands are centered at 313 and 326 nm, while the larger negative band found at 280 nm has a weak shoulder at 273 nm. The intensity of these CD bands becomes lower with the increase of the temperature, and the intensity change is more rapid at higher temperature. The intensity of the 280 nm peak reduces to *ca.* 65% of the intensity measured at 10 °C when the temperature is raised to 70 °C. The intensity of the positive CD band, which is centered at 224 nm, also decreases with increasing temperature. The intensity at 70 °C is about 60% of that measured at 10 °C. Figure 4b shows plots of the intensity change measured at 224 nm against the temperature. The concentration of

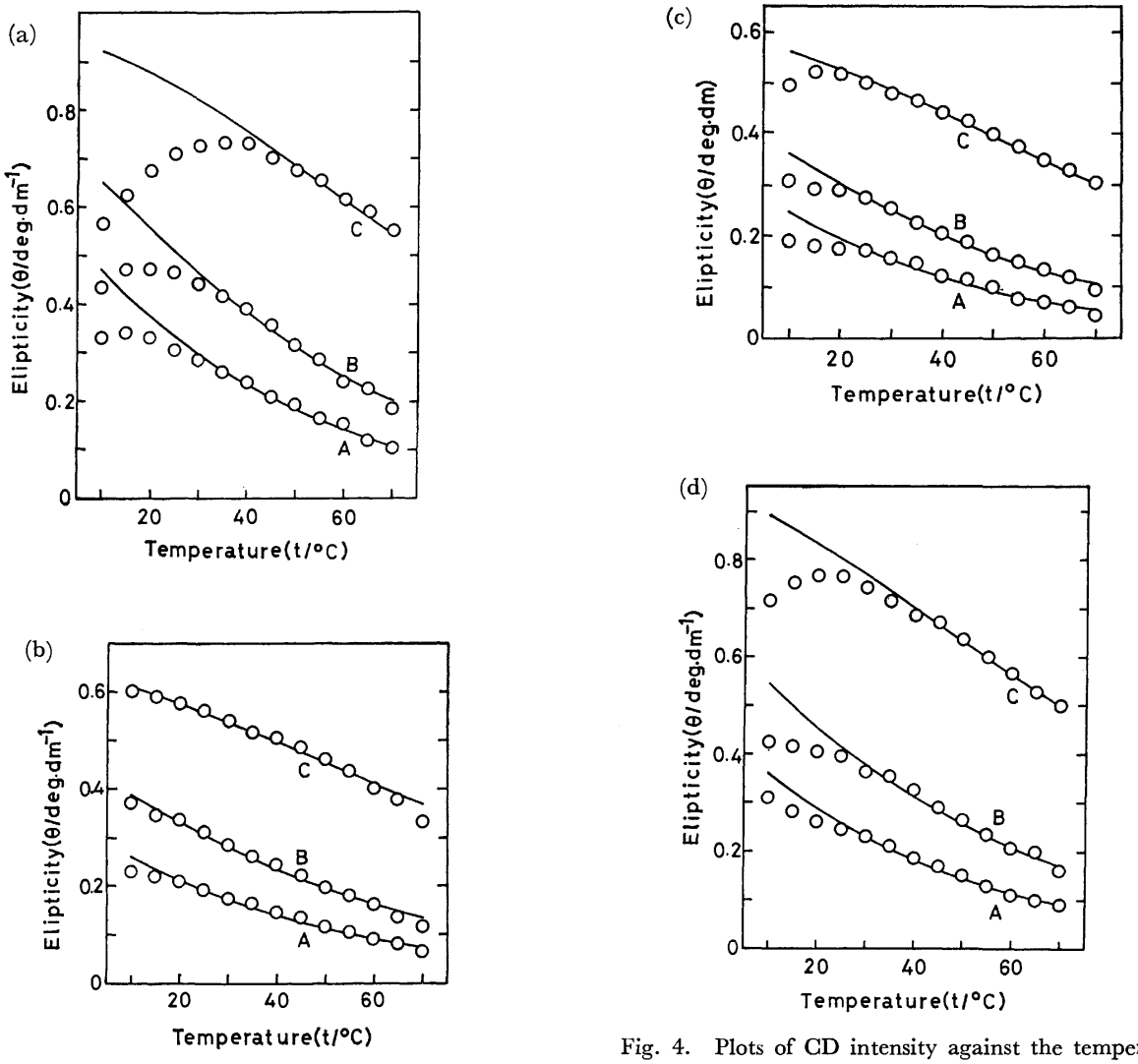

Fig. 4. Plots of CD intensity against the temperature; the intensity is measured at 222 nm for the 2-naphthol complex (a), 224 nm for the 2-naphthyloxyacetic acid complex (b), 230 nm for the potassium 2-naphthoate complex (c), and 224 nm for the potassium 2-naphthylacetate complex (d) with the concentrations of 1.83×10^{-4}, 1.73×10^{-4}, 1.71×10^{-4}, and 1.96×10^{-4} M, respectively. The concentration of β-cyclodextrin is 1.0×10^{-3} (A), 2.0×10^{-3} (B), and 9.0×10^{-3} M (C). Solid lines are calculated intensity by using molecular ellipticity and thermodynamic parameters which are determined by the least-squares method on the basis of a 1:1 complex.

2-naphthyloxyacetic acid is 1.73×10^{-4} M, and the measurement was carried out at the β-cyclodextrin concentrations of 1.0×10^{-3}, 2.0×10^{-3}, and 9.0×10^{-3} M. The least-squares calculation was done by using all the intensity data measured. The CD intensity decreases monotonously with the temperature increase, and the calculated values (shown by solid lines) fitted well with the observed ones. In this case, the molecular ellipticity is $4.20(4)\times10^{4}$ deg·cm²·dmol⁻¹, and the dissociation constant at 25 °C is $2.7(1)\times10^{-3}$ mol. The free energy at 25 °C, enthalpy, and entropy are −14.6(1), −22.5(5) kJ·mol⁻¹, and −24(2) J·K⁻¹·mol⁻¹, respectively.

β-Cyclodextrin–Potassium 2-Naphthoate Complex. This complex shows two weak peaks at 328 and 312 nm in the longer wavelength region, while in the 250—300 nm region there is found a negative CD peak at 289 nm and a shoulder at 281 nm. The positive CD band is observed at 230 nm. The intensity change measured at 230 nm is shown in Fig. 4c. The concentration of the guest is 1.71×10^{-4} M. At the β-cyclodextrin concentration of 9.0×10^{-4} M, an enhancement of the CD intensity is observed when the temperature is raised from 10 to 15 °C, but after that, the intensity decreases with the increase of the temperature. At the β-cyclodextrin concentrations of 2.0×10^{-3} and 1.0×10^{-3} M, an intensity decrease was observed during the temperature increase up to 70 °C. In the least-squares calculation, the intensity data measured at temperatures less than 20 °C were not included because of the reasons mentioned above. The molecular ellipticity of the complex is $3.88(7)\times10^{4}$ deg·cm²·dmol⁻¹, and the dissociation constant at 25 °C was determined to be $2.7(2)\times10^{-3}$ mol. The free energy at 25 °C, enthalpy, and entropy are −14.6(2), −25.5(8) kJ·mol⁻¹, and −37(2) J·K⁻¹·mol⁻¹, respectively.

β-Cyclodextrin–Potassium 2-Naphthylacetate Complex.

TABLE 1. MOLECULAR ELLIPTICITY AND THERMODYNAMIC PARAMETERS OF β-CYCLODEXTRIN COMPLEXES WITH 2-SUBSTITUTED NAPHTHALENES

	λ_{max}	$[\theta]$	K_d(298 K)	ΔG(298 K)	ΔH	ΔS
	nm	10^4 deg·cm²·dmol^{-1}	10^{-3}·mol	kJ·mol^{-1}	kJ·mol^{-1}	J·K^{-1}·mol^{-1}
2-Naphthol	222	5.7(1)	2.0(2)	−15.4(3)	−26.8(9)	−38(3)
2-Naphthyloxyacetic acid	224	4.20(4)	2.7(1)	−14.6(1)	−22.2(5)	−24(2)
Potassium 2-naphthoate	230	3.88(7)	2.7(2)	−14.6(2)	−25.5(8)	−37(2)
Potassium 2-naphthylacetate	224	5.5(1)	3.1(2)	−14.3(2)	−23.0(6)	−29(2)

In the longer wavelength region, a very weak CD band is centered at 318 nm. The larger negative peak is observed at 279 nm, while a shoulder is observed at 288 nm. In the shorter wavelength region, a positive CD band is found at 224 nm. The temperature dependence of the 224 nm band was measured at the guest concentration of 1.96×10^{-4} M, as shown in Fig. 4d. At the β-cyclodextrin concentration of 9.0×10^{-3} M, the CD intensity increased with the temperature up to 20 °C, then decreases with increasing temperature. Only an intensity decrease was observed at the β-cyclodextrin concentrations of 2.0×10^{-3} and 1.0×10^{-3} M. The least-squares calculation was done by using the intensity data measured at the temperatures higher than 30 °C for the β-cyclodextrin concentration of 9.0×10^{-3} M and 20 °C for the concentrations of 2.0×10^{-3} and 1.0×10^{-3} M. The molecular ellipticity of the complex is $5.5(1)\times10^4$ deg·cm²·dmol^{-1}, and the dissociation constant at 25 °C is $3.1(2)\times10^{-3}$ mol. The free energy at 25 °C, enthalpy, and entropy are −14.3(2), −23.0(6) kJ·mol^{-1}, and −29(2) J·K^{-1}·mol^{-1}, respectively.

Discussion

Structure and Stoichiometry of the Complex. β-Cyclodextrin complexes with four 2-substituted naphthalenes give similar CD spectra: two negative CD bands in the 250—350 nm region and a positive CD band in the 200—250 nm region. The origin of induced CD by cyclodextrins is reasonably interpreted in terms of the Kirkwood-Tinoco coupled oscillator model.[5-7] The rotational strength with an electric transition-dipole-moment of μ_{oa} is given by

$$R_{oa} \approx (A_{oa}+B_{oa}\cos 2\theta)\mu_{oa}^2 \qquad (1)$$

where A_{oa} and B_{oa} are constants dependent only on the wavelength, and θ is the angle made by the dipole moment and the molecular axis of β-cyclodextrin. Since A_{oa} and B_{oa} are positive values and A_{oa} is about one-third of B_{oa}, the sign of the induced CD is determined only by the relative orientation of the dipole moment in the β-cyclodextrin cavity. The dipole moment parallel to the molecular axis of β-cyclodextrin gives a positive CD and the perpendicularly polarized dipole moment produces a negative CD. The CD bands observed in the 200—250 and 250—300 nm regions indicate that the guest molecule is included with the naphthyl group parallel to the molecular axis of β-cyclodextrin. The CD band found in the 300—350 nm region may be ruled out since the Kirkwood-Tinoco model should be applied to the transition with a strong electric dipole moment.

In the complexes with 2-naphthol, the temperature dependent CD intensity change can not be fully explained on the basis of a 1:1 complex model. The 1:1 stoichiometry predicts the monotonous decrease of the CD intensity with the increase of the temperature. But, an intensive enhancement of the CD intensity is observed in the lower temperature region. The discrepancy in these results may be interpreted in terms of the structural change of the complex with the temperature increase and/or the formation of the complexes with higher stoichiometry than a 1:1 molar ratio. But the structural change seems to be less likely in this case if we consider only a 1:1 complex. The guest molecule must rotate around the axis perpendicular to the naphthyl plane to reduce the CD intensity of the 222 nm band. But such a rotation also decreases the intensity of the 285 nm band, although the observed intensity change clearly shows the opposite tendency. The displacement of the naphthyl group either to the primary hydroxyl side or to the secondary hydroxyl side also decreases the intensity of both 222 and 285 nm bands. Moreover, according to the inspection of molecular models, the naphthyl group is expected to be tightly packed in the β-cyclodextrin cavity. The tight packing may impose a strong restriction upon the translational and rotational freedom of the naphthyl group because of the repulsive interaction between hydrogen atoms of β-cyclodextrin and the naphthyl group.

The formation of a complex with higher stoichiometry than a 1:1 molar ratio is more plausible. The temperature which gives the intensity maxima of positive CD bands becomes lower with the increase of β-cyclodextrin concentration. The discrepancy found between observed and calculated intensities is more remarkable at higher β-cyclodextrin concentrations. These facts suggest that the association at lower temperature produces a complex in which two or more β-cyclodextrin molecules are bound to one guest molecule. It seems unlikely that β-cyclodextrin binds two or more guest molecules since the concentration of the guest is lower than one-fifth of the β-cyclodextrin concentration. In the crystalline complexes,[9-11] two β-cyclodextrin molecules are linked by many hydrogen bonds between secondary hydroxyl groups to form a dimer structure with a head-to-head arrangement. Therefore, the β-cyclodextrin dimer with the same structure may be formed in aqueous solutions.[11] The rotational strengths of a 2:1 complex were estimated by assuming that the transition-dipole-moment is located at the center of the dimer; the structure of β-cyclodextrin and the parameters used in the calculation were those used in the earlier work.[5] For the transition-dipole-moments parallel and perpendicular to the β-cyclodex-

trin axis, the rotational strengths are $1.25\times10^{-4}\,\mu_{\parallel}^2$ (at 222 nm) and $-0.26\times10^{-4}\,\mu_{\perp}^2$ (at 285 nm), respectively. On the other hand, the corresponding rotational strengths in the 1:1 complex are $1.53\times10^{-4}\,\mu_{\parallel}^2$ and $-0.15\times10^{-4}\,\mu_{\perp}^2$. Therefore, the formation of the 2:1 complex may decrease the intensity of positive CD and enhance the negative CD, giving an explanation for the observed intensity change.

In the 2-naphthyloxyacetic acid complex, the calculated CD intensity based on the thermodynamic parameters determined by the least-squares method is in good agreement with the observed intensity (Fig. 4d). This indicates that the association of two or more β-cyclodextrin molecules does not occur in this case. The guest molecule has a relatively large substituent, so that the substituent group may hinder the formation of complexes with higher stoichiometry.

Thermodynamic Parameters and Binding Force in the Complex. Free energies at 298 K are in the range from −14.3 to −15.4 kJ·mol^{-1}, a remarkably narrow region in spite of the different guest molecules. Enthalpy and entropy are in the range from −22.2 to −26.8 kJ·mol^{-1} and −24 to −38 J·K^{-1}·mol^{-1}, respectively. A plot of ΔH against ΔS is given in Fig. 5. ΔH is linearly correlated to ΔS. A similar correlation has been also observed in the α-cyclodextrin complexes.[12] Changes in ΔH are almost compensated by changes in ΔS. Therefore, the free energy is restricted in a quite narrow region. Such compensation phenomena are widely observed in water solutions.[13]

The thermodynamic parameters indicate that ΔH and ΔS are strongly correlated to the molecular volume of the guest. Figure 6 shows plots of ΔH and ΔS against the van der Waals volume of the substituent in the guest molecule. The volumes were estimated according to Bondi.[14] ΔH and ΔS decrease in magnitude with an increase of the substituent volume. Changes in ΔH and ΔS can be explained on the basis of the β-cyclodextrin–guest interaction and solute–solvent interaction. Owing to the cylindrical cavity of β-cyclodextrin, a guest molecule with a smaller substituent may fit better into the cavity. A bulky substituent seems to inhibit the close packing of the guest molecule, and to impose an unfavorable conformational change on β-cyclodextrin. The tight inclusion of the guest molecule also imposes restrictions on the conformational flexibility of β-cyclodextrin as well as on translational and rotational freedom of the guest molecule.[15] Therefore, a guest molecule with a small substituent may give large values of enthalpy and entropy of complex formation compared with the guest molecule having a bulky substituent.

In the uncomplexed state, the guest molecule is surrounded by solvent molecules, while some water molecules are included in the β-cyclodextrin cavity.[16] These water molecules may be removed by the complex formation and become bulk water. The enthalpy change for the process is expressed as

$$\Delta H^{s} = H^{s}(\beta\text{-cyclodextrin–guest}) + H^{s}(n\mathrm{H_2O}) - H^{s}(\beta\text{-cyclodextrin–}n\mathrm{H_2O}) - H^{s}(\text{guest}) \quad (2)$$

$$= \Delta H_{c}^{s} + \Delta H_{e}^{s} + \Delta H_{v}^{s}. \quad (3)$$

H_{c}^{s} is the energy required to create a cavity to accomodate the solute molecule in solution, and is calculated according to Pierotti.[17] H_{e}^{s} and H_{v}^{s} are the electrostatic interaction energy and the van der Waals interaction energy, respectively, between solute and solvent molecules. The detailed descriptions of H_{e}^{s} and H_{v}^{s} are given in the earlier paper.[18] In the crystalline state, the uncomplexed β-cyclodextrin contains 2.5 water molecules in the center of the cavity.[16] Therefore, $n=2.5$ was assumed in this calculation. The calculated enthalpy, which is in the range from −21.9 to −24.3 kJ·mol^{-1} (Table 2), suggests that the bulky substituent group decreases the enthalpy of complex formation.

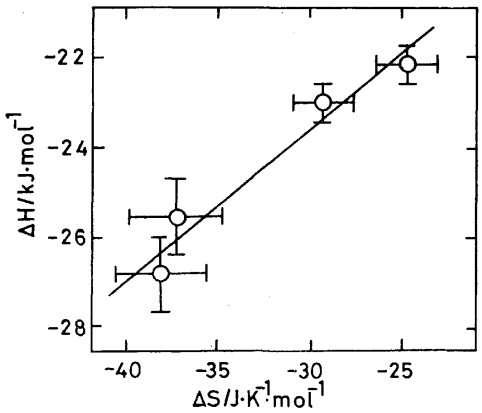

Fig. 5. Plot of ΔH against ΔS. Vertical and horizontal bars indicate error limits.

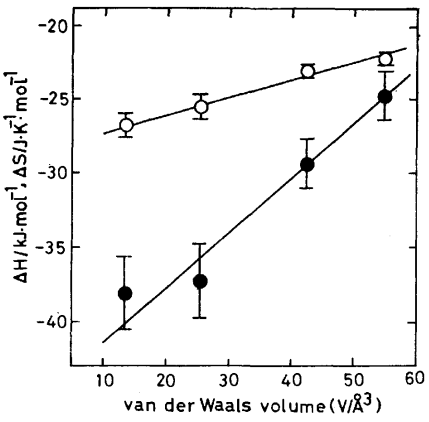

Fig. 6. Plots of ΔH (○) and ΔS (●) against van der Waals volumes of substituent in naphthalene derivatives. Vertical bars indicate error limits.

Table 2. Calculated solvation effects on ΔH for the complex formation of β-cyclodextrin with 2-substituted naphthalenes

	$V^{a)}$ / Å^3	ΔH / kJ·mol^{-1}
2-Naphthol	13.4	−24.3
2-Naphthoate ion	25.6	−21.9
2-Naphthylacetate ion	42.5	−24.1
2-Naphthyloxyacetic acid	55.1	−22.1

a) The van der Waals volume of the substituent.

The calculated results also indicate that the naphthyl group is highly hydrophobic, so that it may be more favorable for the group to be located in the hydrophobic cavity of β-cyclodextrin than in the aqueous environment.

Appendix

When β-cyclodextrin forms a 1:1 complex with a guest in an aqueous solution,

$$\beta\text{-cyclodextrin} + \text{guest} \rightleftarrows \beta\text{-cyclodextrin–guest}, \quad \text{(A1)}$$

the dissociation constant at the temperature of T_i K is given by

$$K_{di} = (a-x_{ij})(b_j-x_{ij})/x_{ij} \quad \text{(A2)}$$

where a, b_j, and x_{ij} are the concentrations of the guest, β-cyclodextrin, and the complex, respectively. The observed CD intensity is expressed by using the molecular ellipticity of θ_m: as

$$\theta_{ij} = \theta_m x_{ij}. \quad \text{(A3)}$$

Then, by substituting Eq. A3 to Eq. A2,

$$K_{di} = \frac{ab_j\theta_m}{\theta_{ij}} - a - b_j + \frac{\theta_{ij}}{\theta_m} \quad \text{(A4)}$$

If we assume that the enthalpy (ΔH) and entropy (ΔS) for the complex formation are independent of temperature under the experimental conditions, the free energy for the complex formation is given by

$$\Delta G_i = \Delta H - T_i\Delta S \quad \text{(A5)}$$

$$= RT_i \ln K_{di}. \quad \text{(A6)}$$

By substituting Eq. A4 to Eq. A6, we obtain

$$\ln\left(\frac{ab_j\theta_m}{\theta_{ij}} - a - b_j + \frac{\theta_{ij}}{\theta_m}\right) - \frac{\Delta H}{RT_i} + \frac{\Delta S}{R} = 0 \quad \text{(A7)}$$

θ_m, ΔH, and ΔS can be determined by the least-squares technique if we know the rough values of θ_m°, ΔH°, and ΔS°:

$$\theta_m = \theta_m^\circ + \Delta\theta_m \quad \text{(A8)}$$

$$\Delta H = \Delta H^\circ + \Delta(\Delta H) \quad \text{(A9)}$$

$$\Delta S = \Delta S^\circ + \Delta(\Delta S). \quad \text{(A10)}$$

Then, by expanding $\ln K_{di}$, we obtain

$$\ln K_{di} = \ln K_{di}^\circ + \Delta\theta_m\left(\frac{ab_j}{\theta_{ij}} - \frac{\theta_{ij}}{\theta_m^{\circ 2}}\right)\Big/K_{di}^\circ \quad \text{(A11)}$$

where

$$K_{di}^\circ = \frac{ab_j\theta_m^\circ}{\theta_{ij}} - a - b_j + \frac{\theta_{ij}}{\theta_m^\circ} \quad \text{(A12)}$$

Therefore, the quantity to be minimized is given by

$$M = \sum_{ij}\left[\left(\frac{ab_j}{\theta_{ij}} - \frac{\theta_{ij}}{\theta_m^{\circ 2}}\right)\Delta\theta_m/K_{di}^\circ - \frac{\Delta(\Delta H)}{RT_i} + \frac{\Delta(\Delta S)}{R} + \Delta_{ij}\right]^2 \quad \text{(A13)}$$

with

$$\Delta_{ij} = \ln K_{di}^\circ - \frac{\Delta H^\circ}{RT_i} + \frac{\Delta S^\circ}{R} \quad \text{(A14)}$$

If θ_{ij} is measured at more than two β-cyclodextrin concentrations, θ_m°, ΔH°, and ΔS° are determined by Eqs. 4, 5, and 6. But if the measurement is carried out without changing the concentration, θ_m° may be estimated on the basis of the observed θ_{ij}. By solving the simultaneous equation of

$$\partial M/\partial\Delta\theta_m = 0, \quad \partial M/\partial\Delta(\Delta H) = 0,$$

and

$$\partial M/\partial\Delta(\Delta S) = 0 \quad \text{(A15)}$$

$\Delta\theta_m$, $\Delta(\Delta H)$, and $\Delta(\Delta S)$ are obtained. This procedure should be repeated until the magnitudes of $\Delta\theta_m$, $\Delta(\Delta H)$, and $\Delta(\Delta S)$ are sufficiently smaller than the corresponding standard deviation, which is given by

$$\sigma_p = [m_{pp}^{-1}(\sum_{ij}\Delta_{ij}^2)/(N-3)]^{1/2} \quad \text{(A16)}$$

where m_{pp}^{-1}, Δ_{ij}, and N are the p-th diagonal element of the inverse matrix, the residual for θ_{ij}, and the number of data, respectively. Usually, the convergence is achieved within ten cycles.

References

1) J. A. Thoma and L. Stewart, "Starch: Chemistry and Technology," ed by R. L. Whistler and E. F. Pashall, Academic Press, New York (1965), Vol. I, pp. 209—249.
2) F. R. Senti and S. R. Erlander, "Non-stoichiometric Compounds," ed by R. L. Mandelcorn, Academic Press, New York (1964), pp. 568—605.
3) K. Takeo and T. Kuge, *Staerke*, **24**, 281 (1972).
4) M. Otagiri, K. Ikeda, K. Uekama, O. Ito, and M. Hatano, *Chem. Lett.*, **1974**, 679.
5) K. Harata and H. Uedaira, *Bull. Chem. Soc. Jpn.*, **48** 375 (1975).
6) K. Harata and H. Uedaira, *Sen'i Kobunshi Zairyo Kenkyusho Kenkyu Hokoku*, **112**, 1 (1976).
7) R. Bergeron and P. McPhie, *Bioorg. Chem.*, **6**, 465 (1977).
8) K. Harata, *Bull. Chem. Soc. Jpn.*, **51**, 2727 (1978).
9) J. A. Hamilton, M. N. Sabesan, I. K. Steinrauf, and A. Gedds, *Biochem. Biophys. Res. Commun.*, **73**, 659 (1976).
10) M. M. Harding, J. M. MacLennan, and R. M. Paton, *Nature*, **274**, 621 (1978).
11) J. J. Stezowski, K. H. Jogun, E. Eckle, and K. Bartels, *Nature*, **274**, 627 (1978).
12) E. A. Lewis and L. D. Hansen, *J. Chem. Soc., Perkin Trans. 2*, **1973**, 2081.
13) R. Lumry and S. Rajender, *Biopolymers*, **9**, 1125 (1970).
14) A. Bondi, *J. Phys. Chem.*, **68**, 441 (1964).
15) J. P. Behr and J. M. Lehn, *J. Am. Chem. Soc.*, **98**, 1743 (1976).
16) R. A. Pierotti, *J. Phys. Chem.*, **69**, 281 (1965).
17) K. Linder and W. Sanger, *Angew. Chem.*, **90**, 738 (1978).
18) K. Harata, H. Uedaira, and J. Tanaka, *Bull. Chem. Soc. Jpn.*, **51**, 1627 (1978).

Acidic Property and Oxidation Activity of MoO_3-V_2O_5-P_2O_5 Ternary Oxides

Mamoru Ai

Research Laboratory of Resources Utilization, Tokyo Institute of Technology, 4259 Nagatsuta, Midori-ku, Yokohama 227

(Received December 13, 1978)

The relationship between the acid-base properties and the oxidation activity of a series of ternary oxide catalysts, MoO_3-V_2O_5-P_2O_5, with different V/Mo composition and a constant phosphorus content, P/(Mo+V)=0.1, was investigated. The acidity was determined by means of the NH_3 adsorption and by studying the catalytic activity for acid-catalyzed reactions, such as dehydration of isopropyl alcohol and isomerization of 1-butene, in the presence of an excess of air. A new acidic site is generated by the combination of two binary oxides, *i.e.*, MoO_3-P_2O_5 and V_2O_5-P_2O_5, and a broad maximum in the acidity occurs at V/(Mo+V)=0.4—0.9. The basic property is so small that no satisfactory data can be obtained from the adsorption of acidic molecules such as CO_2, SO_2, and acetic acid. The catalysts, regardless of composition, are inactive for reactions which are accelerated by basic sites, such as oxidative dehydrogenation of isopropyl alcohol to acetone, oxidative decomposition of formic acid to CO_2, and oxidation of methanol to CO_2. The oxidation activities for butadiene and methanol can be tied to the acidity of the catalysts.

A variety of multi-component oxides containing more than three kinds of metal oxides have been proposed as being effective as practical catalysts. Why can a good performance be obtained only by the combination of several oxides? What is the role of each component in the catalytic action of a multi-component oxide? Moreover, what are the functions universally required for an oxidation catalyst?

We have studied selective oxidations on the basis of the idea that an acid-base-type interaction between the catalyst surface and the organic substance to be oxidized plays the determining role in mild oxidations, and as a result, the combination of metal oxides contributes to an enhancement or modification of the acid-base properties.[1]

MoO_3, V_2O_5, and P_2O_5 are all typical acidic oxides. Therefore, composite oxides consisting of these oxides, naturally, are characterized by their acidic property. Actually, they have been proposed as catalysts suited only for "acid-formation" reactions, such as syntheses of maleic anhydride, phthalic anhydride, acrylic acid, and methacrylic acid.[2-4]

As for the three binary systems made up by two of the three oxides, *i.e.*, MoO_3-V_2O_5, MoO_3-P_2O_5, and V_2O_5-P_2O_5, the relationship between the acid-base properties and the catalytic behavior in mild oxidations has been studied earlier.[5-7]

In this work, we were interested in seeing how the replacement of molybdenum in the MoO_3-P_2O_5 (P/Mo=0.1) catalyst by vanadium induces a change in the catalytic behavior and, then, in confirming whether or not the change in the catalytic activity can be interpreted by the change of the acid-base properties.

Experimental

The catalysts used in this study were a series of ternary oxides, MoO_3-V_2O_5-P_2O_5, with nine different V/Mo compositions and a constant phosphorus content, P/(Mo+V)=0.1 (atomic ratio). The method of the preparation was the same as that employed in the previous studies.[5-7] That is, the required quantities of $(NH_4)_6Mo_7O_{24}\cdot 4H_2O$, NH_4VO_3, and 85 wt % H_3PO_4 were dissolved in hot water by using oxalic acid, if necessary, and to this was added 10—20 mesh pumice. Then, the mixture was evaporated with stirring. The catalyst were calcined in a stream of oxygen at 500 °C for 4—5 h.

The techniques of acidity measurement and the reaction procedures were the same as those employed earlier.[8]

Results

Surface Properties. In Table 1 are shown the specific surface areas. They are of the order of 1 m^2/g over the entire range of composition and the effect of composition is found to be small.

Table 1. Surface areas of the MoO_3-V_2O_5-P_2O_5 catalysts

Composition[a] V/(Mo+V)	Surface area (m^2/g)	Composition[a] V/(Mo+V)	Surface area (m^2/g)
0	1.2	0.60	1.0
0.05	1.1	0.80	0.9
0.10	1.2	0.90	0.9
0.20	1.0	1.0	1.5
0.40	1.1		

a) P/(Mo+V)=0.10: atomic ratio.

The acidity (number of acidic sites) was measured directly by the irreversible adsorption of NH_3 at 200 °C using the static method.[8] The results are shown in Fig. 1.

It seems difficult to determine in this way the acidity with satisfactory accuracy. Therefore, another attempt was made to determine the acidity indirectly, that is, the catalytic activity for certain acid-catalyzed reactions was investigated. The dehydration of isopropyl alcohol (IPA) to propylene and the isomerization of 1-butene to 2-butenes, in the presence of an excess of air, were chosen as the model reactions, as in the previous studies.[4-8]

The reactions were carried out at the IPA and 1-butene concentrations of 1.33 and 1.0 mol% in air, respectively, and the total flow rate of 1.0 l/min, by changing the amounts of the catalysts in the range of 1

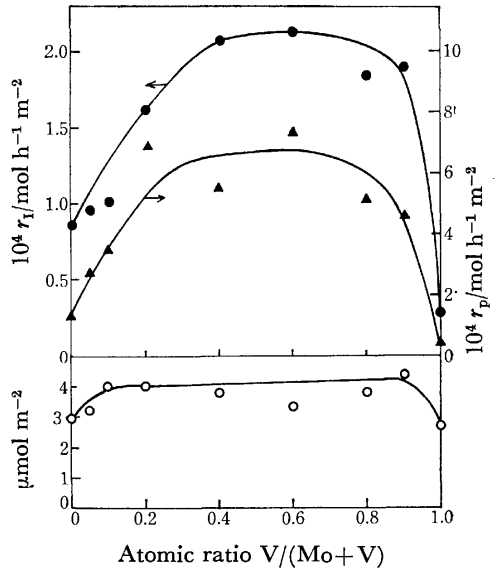

Fig. 1. Acidity of MoO_3–V_2O_5–P_2O_5 as a function of the V/(Mo+V) ratio. P/(Mo+V)=0.1.
○: Irreversible adsorption of NH_3 at 200 °C, ▲: dehydration activity for IPA at 145 °C, r_p, ●: isomerization activity for 1-butene at 172 °C, r_I.

to 20 g. The MoO_3–V_2O_5–P_2O_5 catalysts exhibit a very high activity for the two reactions and, therefore, the reactions can occur, to a considerable extent, at a fairly low temperature. Propylene is the sole product in the reaction of IPA. The initial rate of IPA dehydration at 145 °C, r_p, and the rate of butene isomerization at 172 °C, r_I (mol/h·m² of catalyst), are plotted together with the amounts of adsorbed NH_3 in Fig. 1.

As for the basicity, we tried to measure it by the adsorption of SO_2 as well as CO_2, using the static method, and by the adsorption of acetic acid using the pulse method.[8] However, the amounts were so small that the effect of catalyst composition could not be obtained.

Decomposition of Formic Acid. It has been reported that the catalytic activity for decomposition of formic acid to CO and that for the oxidative decomposition to CO_2 can be tied to the acidic and basic properties, respectively, of the metal oxide catalysts.[9] Because of the simplicity of the reaction system, the catalytic activity for these reactions was tested.

The reaction was carried out at the concentration of 1.8 mol% HCOOH in air and the total flow rate of 1.0 l/min. The catalysts weighed 2 to 20 g. Details of the reaction procedures were described earlier.[9] The products were CO and H_2O, and the amount of CO_2 was negligibly small regardless of the catalyst composition. The initial rate of CO formation at 259 °C, r_{CO} (mol/h·m² of catalyst), are plotted in Fig. 2.

Oxidation of Butadiene. Since the MoO_3–V_2O_5–P_2O_5 catalysts are fairly acidic and rarely basic, satisfactory results can be expected merely for the activity in the oxidation of basic reactants and for the selectivity in the "base to acid" type reactions.[1] Therefore, the oxidation of butadiene was chosen as a model reaction.

The reaction was carried out in an excess of air (C_4H_6=1.0 mol%) at 360—450 °C and at a constant

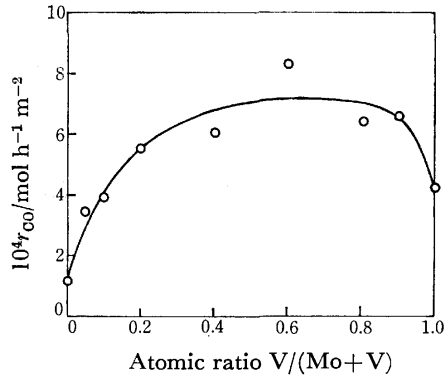

Fig. 2. Catalytic activity for the decomposition of formic acid to CO at different V/Mo compositions. r_{CO}: Rate of CO formation at 259 °C and 1.8 mol % HCOOH in air.

total flow rate (1.0 l/min). The amounts of the catalysts were varied in the range of 1 to 20 g to achieve a proper conversion. The rate of butadiene consumption at 365 °C, r_B (mol/h·m² of catalyst), was adopted as a measure of the activity, for convenience in the experimental procedures. The results are shown in Fig. 3.

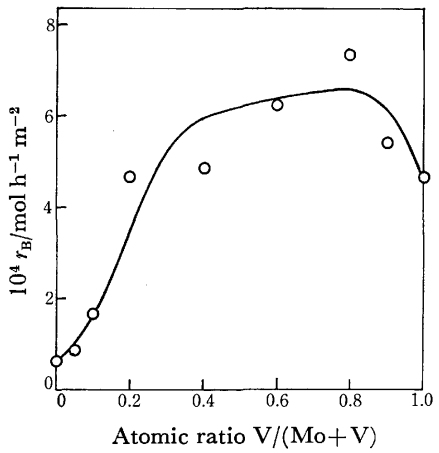

Fig. 3. Oxidation activity for butadiene as a function of the V/(Mo+V) ratio. r_B: Consumption of butadiene at 365 °C and 1.0 mol % C_4H_6 in air.

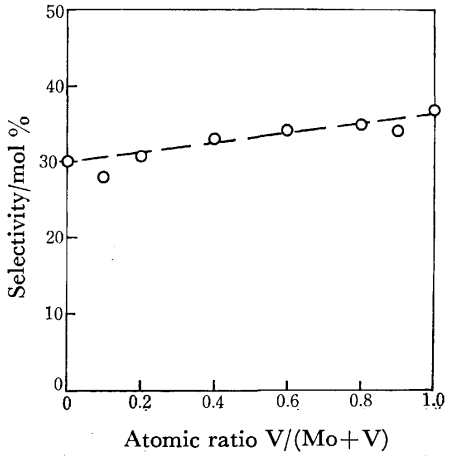

Fig. 4. Selectivity of butadiene to maleic anhydride at a total conversion of 40—50 %. T=360—450 °C, C_4H_6=1.0 mol % in air.

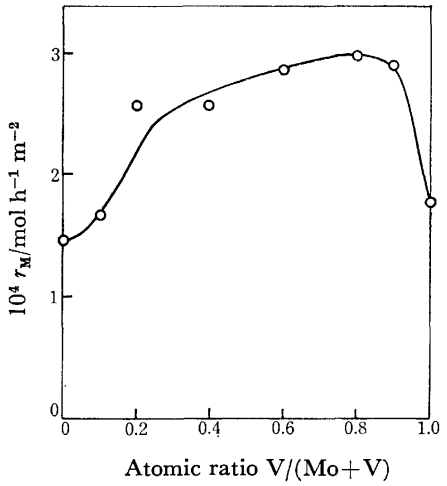

Fig. 5. Oxidation activity for methanol as a function of the V/(Mo+V) ratio. r_M: Rate of formaldehyde formation at 250 °C and 2.6 mol % CH_3OH in air.

The main products were maleic anhydride, CO, and CO_2. The selectivity of butadiene to maleic anhydride at a fixed conversion, 40—50%, was measured with each catalyst; it is shown in Fig. 4.

Oxidation of Methanol. The oxidation of methanol was tested, because the catalytic activity for this reaction was found to be correlated with the acid-base properties of the catalysts.[10]

The reaction was carried out at 2.6 mol% CH_3OH in air. Formaldehyde was almost the sole product and the amounts of CO_2 and CO were very small, even when the conversion was about 50%. The rate of formaldehyde formation at 250 °C, r_M (mol/h·m^2 of catalyst), is shown in Fig. 5.

Discussion

The activities for the two acid-catalyzed reactions vary in the same fashion with the variation of V/Mo composition. However, the shape of the NH_3-curve in Fig. 1 is not the same as that of the activity-curves. With regard to these results, one may be led to consider that the catalytic activities reflect the true acidity better than the amounts of NH_3, because the surface areas of the catalysts are so small that it is difficult to measure, with satisfactory accuracy, the amounts of adsorbed NH_3. In the following, it is sure that a new acidic site is generated by the combination of the MoO_3–P_2O_5 (P/Mo=0.1) and the V_2O_5–P_2O_5 (P/V=0.1) or by the replacement of molybdenum in the MoO_3–P_2O_5 by vanadium. The acidity attains a broad maximum at V/(Mo+V)=0.4—0.9. This feature of the acid-generation is different from that observed in the case of MoO_3–V_2O_5 binary system, where a sharp maximum in acidity occurs at V/(Mo+V)=0.85—0.90[5].

The possession of a very high activity for the two acid-catalyzed reactions proves that the MoO_3–V_2O_5–P_2O_5 catalysts are eminent in acidic property, as can easily be expected from the natures of MoO_3–P_2O_5 and V_2O_5–P_2O_5. On the other hand, the absence of the catalytic activity for the reactions which are promoted by basic sites, for example, the oxidative dehydrogenation of IPA to acetone,[1] the oxidative decomposition of formic acid to CO_2,[9] and the oxidation of methanol to CO_2,[10] indicates that the catalysts regardless of the V/Mo composition are very poor in basic property. The basic property of MoO_3 and V_2O_5 may be extinguished completely by P_2O_5.[7]

The presence of a parallelism between the activity for decomposition of formic acid to CO (Fig. 2) and the acidity (the activities for IPA dehydration and butene isomerization) supports the earlier view that catalytic activity for the CO formation is tied to the acidic property of the catalyst.[9]

The catalytic activity for the oxidation of butadiene (Fig. 3) also varies in the same fashion as do the activities shown in Fig. 1, except for the V/(Mo+V)=1 catalyst. This finding suggests that the oxidation of butadiene is decided mainly by the activation of butadiene by the acidic sites, as has been pointed out earlier.[1]

The selectivity to maleic anhydride is relatively high over the entire range of composition. This can easily be understood from the fact that the catalysts, regardless of composition, are fairly acidic and rarely basic, because one of requirements for an effective catalyst suited for "acid-formation" reactions is the possession of a sufficient acidic property.[1]

The catalysts, regardless of the composition, exhibit a very good selectivity in the oxidation of methanol to formaldehyde, which is consistent with the earlier proposal that formaldehyde is the sole product as long as the catalyst is acidic enough.[10] The presence of a parallelism between the catalytic activity for the formaldehyde formation (Fig. 5) and the acidities shown in Fig. 1 also supports the view that the activity for formaldehyde formation is decided mainly by the activation of methanol on acidic sites.[10]

It is concluded that the MoO_3–V_2O_5–P_2O_5 catalysts are eminent in acidic property but poor in basic property, regardless of the V/Mo composition, that a new acidic site is generated by the combination of the MoO_3–P_2O_5 and the V_2O_5–P_2O_5, and that the acidity attains a broad maximum at V/(Mo+V)=0.4—0.9. The catalytic behavior in the oxidation of butadiene and methanol can be explained relatively well in terms of the acid-base properties of the catalysts.

References

1) M. Ai, *Yuki Gosei Kagaku Kyokai Shi*, **35**, 202 (1977).
2) R. J. Sampson and D. Shooter, "Oxidation and Combustion Reviews," ed by C. F. H. Tipper, Elsevier, Amsterdam (1965), Vol. 1, p. 282.
3) D. J. Hucknall, "Selctive Oxidation of Hydrocarbons," Academic Press, New York (1974), pp. 47—51.
4) T. Ohara, *Yuki Gosei Kagaku Kyokai Shi*, **29**, 52 (1971); *Shokubai*, **19**, 157 (1977).
5) M. Ai and S. Suzuki, *Nippon Kagaku Kaishi*, **1973**, 260.
6) M. Ai and S. Suzuki, *J. Catal.*, **30**, 362 (1973).
7) M. Ai and S. Suzuki, *Bull. Chem. Soc. Jpn.*, **47**, 3074 (1974).
8) M. Ai, *Bull. Chem. Soc. Jpn.*, **49**, 1328 (1976); *J. Catal.*, **40**, 318 (1975); **49**, 305 (1977).
9) M. Ai, *J. Catal.*, **50**, 291 (1977).
10) M. Ai, *J. Catal.*, **54**, 462 (1978).

Solvent Effects and Hyrogen-bonding Interactions on Absorption and Fluorescence Spectra of 1-Methyl-2-pyridone

Akira FUJIMOTO and Kozo INUZUKA*

Department of Applied Science, Faculty of Technology, Tokyo Denki University, Kanda, Chiyoda-ku Tokyo 101

(Received December 21, 1978)

The electrostatic solvent effects and hydrogen-bonding interactions on IR and UV absorption and fluorescence spectra of 1-methyl-2-pyridone has been investigated. It was found that the UV absorption and fluorescence bands of 1-methyl-2-pyridone shifted towards the shorter-wavelength region with increasing solvent polarity and that these bands exhibited a blue shift on hydrogen bond formation with alcohols and chloroform. The excited-state dipole moment of 1-methyl-2-pyridone, and the equilibrium constants in the ground and excited states and enthalpy change in the ground state for hydrogen-bond formation between 1-methyl-2-pyridone and ethanol have been determined from the spectroscopic studies.

Kimura *et al.*[1] have suggested from fluorescence data, that the lowest excited singlet state of 1-methyl-2-pyridone (abbreviated to MPD) is π-π^* in character in alcoholic solution. It was not reported that the fluorescence band characterized by the π-π^* transition shifted towards the shorter-wavelength region with increasing solvent polarity and that the band exhibited a blue shift on hydrogen bond formation with alcohols.

As part of this study[2] on the electronic spectra of heterocyclic compounds, the solvent effects and hydrogen-bonding interactions on UV absorption and fluorescence spectra of MPD in isooctane (2,2,4-trimethylpentane) have been investigated. The presence of an intermolecular hydrogen bond between MPD and ethanol has been confirmed by IR analysis.

Experimental

MPD was purified by vacuum distillation to give a sample of boiling point 103.0—103.5 °C/930 Pa. The solvents used were commercially available and further purified by distillation. IR spectra were measured using a Hitachi Model 260-30 infrared spectrophotometer; measurements were conducted at ambient temperature, a cell of 0.5 mm path length being used. Measurements of UV absorption and fluorescence were conducted with the spectrophotometers reported previously.[2a] The temperature of the UV absorption cells (10 mm) was regulated by a Komatsu-Yamato Model CTR-120 electronic cooling circulator within the temperature range 8 to 50 °C.

Results and Discussion

The C=O absorption bands of MPD observed in the several solvents at room temperature are given in Table 1. As may be seen the C=O band shifted to the lower-frequency region with increasing polarity of the solvents; notably the frequency shift of the corresponding band is appreciably larger in alcohols and chloroform than in other solvents. As Fig. 1 illustrates remarkable changes are produced in the IR spectra of MPD by the addition of ethanol to the carbon tetrachloride solution: the C=O streching band of MPD was observed at 1667 cm^{-1} in CCl_4, while the corresponding band shifted to the lower-frequency region with increasing ethanol concentration (1660 cm^{-1}, ethanol concentration=2.14 mol dm^{-3}). A similar frequency-shift was observed on the addition of chloroform to a carbon

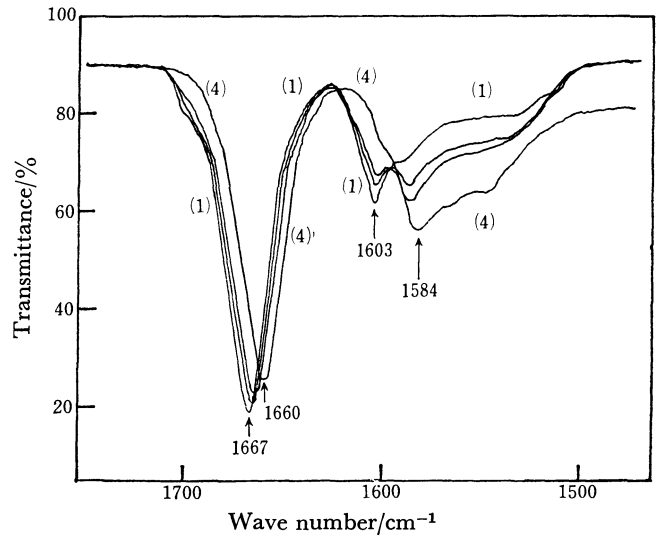

Fig. 1. IR spectra of the MPD–ethanol–carbon tetrachloride system. Concentration of MPD: 8.26×10^{-3} mol dm^{-3}. Concentrations of ethanol (mol dm^{-3}): (1) 0, (2) 8.8×10^{-2}, (3) 1.76×10^{-1}, (4) 2.14.

tetrachloride solution of MPD. Such frequency-shifts in alcohol and chloroform may be attributed to intermolecular hydrogen bonding between the C=O group of MPD and alcohol, and between the C=O group of MPD and chloroform. The hydrogen bond between MPD and ethanol is represented by the following equilibrium:

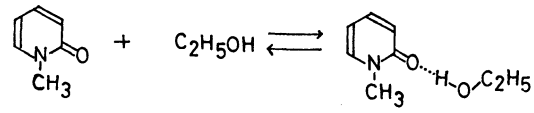

(1)

Here MPD acts as a proton acceptor and ethanol as a proton donor. In Fig. 1, the absorption band at 1603 cm^{-1}, corresponding to the ring streching vibration of MPD[3] disappeared, while a new band maximum was observed at 1584 cm^{-1}, attributed to the redistribution of the ring electrons as a result of hydrogen-bond formation with the OH group of ethanol.

The solvent effects on the electronic spectra of organic compounds have been studied by many workers: Lippert,[4] Mataga *et al.*,[5] and McRae[6] proposed the following equation (Eq. 2) for the evaluation of the

difference in the dipole moments of the excited and ground states, *i.e.* $\Delta\mu = \mu_e - \mu_g$.

$$hc\Delta\sigma = \text{const} + 2F(D, n)(\Delta\mu)^2/a^3, \quad (2)$$

where

$$\Delta\sigma = \sigma_a^m - \sigma_f^m$$

and

$$F(D, n) = \left(\frac{D-1}{2D+1} - \frac{n^2-1}{2n^2+1}\right).$$

In Eq. 2 σ_a^m and σ_f^m represent the wave number of the peak of the UV absorption band and the fluorescence band maximum, respectively. D and n represent the dielectric constant and refractive index of the solvent and a represents Onsager's reaction radius of the solute molecule.

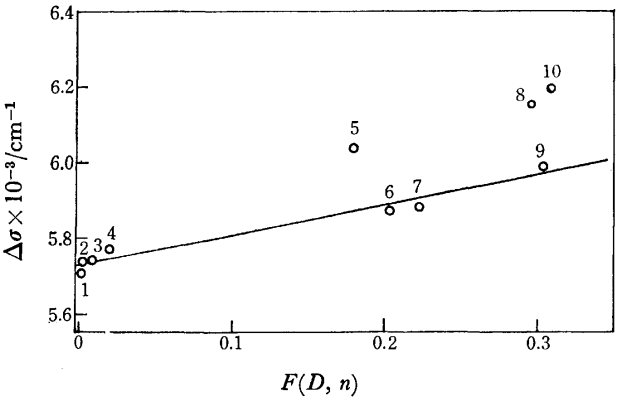

Fig. 2. The plot of $\Delta\sigma$ *vs.* $F(D, n)$.

Table 1. Wave numbers of the C=O band maxima (ν), UV absorption maxima (σ_a^m), and fluorescence band maxima (σ_f^m) of MPD measured in solvents of different polarity at room temperature

No.	Solvent	$F(D,n)$	ν / cm^{-1}	σ_a^m / cm^{-1}	σ_f^m / cm^{-1}
1	Isooctane	0.000	1677	32410	26700
2	Benzene	0.002	1667	32440	26700
3	Carbon tetrachloride	0.010	1667	32440	26700
4	Dioxane	0.020	1666	32420	26700
5	Chloroform	0.185	1660	32840	26800
6	Ethyl acetate	0.202	—[a]	32570	26700
7	Dichloromethane	0.218	1665	32680	26800
8	Ethanol	0.298	1660	32950	26800
9	Acetonitrile	0.304	1664	32790	26800
10	Methanol	0.308	1659	33000	26800

a) The C=O band of MPD was hidden by the intense absorption band of the C=O group of ethyl acetate.

The observed values of σ_a^m and σ_f^m are given in Table 1, together with the values of $F(D,n)$.[4,5] It may be seen that the UV absorption and fluorescence band maxima tend to shift towards the shorter-wavelength region with increasing solvent polarity and the blue shift of the UV absorption band maximum is much larger than that of the fluorescent counterpart. A similar phenomenon has been observed for the UV absorption and fluorescence spectra of pyridine *N*-oxide in several solvents.[7] In analogy with pyridine *N*-oxide the above experimental facts indicate that the π-electron transfer from the oxygen atom to the pyridine ring is much larger in the excited state than in the ground state. Accordingly, the dipole moment appears to be larger in the ground state than in the excited state, $\mu_g > \mu_e$. In Fig. 2 the $\Delta\sigma$ has been plotted against $F(D,n)$ and as can be seen there is a linear relationship between $\Delta\sigma$ and $F(D,n)$ except for alcohols and chloroform. The linear relationship between $\Delta\sigma$ and $F(D,n)$ corresponds to Eq. 2 and may be approximately represented as follows:

$$\Delta\sigma = 5730 + 770F(D, n). \quad (3)$$

From this equation, the $\Delta\mu$ value for MPD has been evaluated as -1.1 D, assuming 2.5 Å for a. μ_e has been estimated to be 2.94 D, using the values $\Delta\mu$ and μ_g (4.04 D) determined by Krackov *et al.*[8] In Fig. 2 the solvents such as alcohol and chloroform cause a large deviation and this has been attributed to hydrogen-bonding as described in the experimental section.

The equilibrium constant in the ground state (K_g),

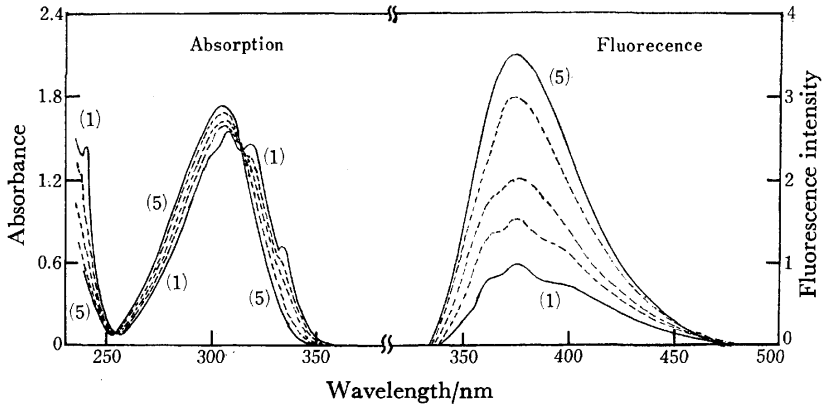

Fig. 3. UV absorption and fluorescence spectra of the MPD–ethanol–isooctane system at ambient temperature. Concentration of MPD: 4.2×10^{-4} mol dm^{-3}. Concentrations of ethanol (mol dm^{-3}): (1) 0, (2) 7.0×10^{-2}, (3) 1.5×10^{-1}, (4) 5.0×10^{-1}, (5) 2.0. Excitation wavelength: 300 nm.

enthalpy change ($-\Delta H$), and entropy change ($-\Delta S$) due to hydrogen-bond formation have been obtained by UV spectroscopy.[9] As shown in Fig. 3, considerable changes are produced in the UV spectra of MPD by the addition of ethanol to the isooctane solution. In order to eliminate the interference of the ordinary solvent effect, a three-component system was employed.[9] Consequently, it may be assumed that the spectral changes are due to the formation of a hydrogen-bonded complex between MPD and ethanol. It has been found that the UV absorption spectra, characterized by the π-π^* transition[1] exhibits a large blue-shift and an increase in total absorption intensity with increasing ethanol concentration. The values, 5.91 mol^{-1} dm^3 for K_g, 18 kJ mol^{-1} for $-\Delta H$, and 45.6 J K^{-1} mol^{-1} for $-\Delta S$ which were interpolated at 25.0 °C, were obtained from the UV spectra of the MPD-ethanol-isooctane system.

The fluorescence spectra of the MPD-ethanol-isooctane system are presented in Fig. 3. A blue shift of the fluorescence band maximum is evident and the intensity of the fluorescence band increases with increasing concentration of ethanol. The degree of spectral shift of the band maximum caused by hydrogen bonding is smaller in the fluorescence spectrum than in the absorption one. Experimentally it has been established that the addition of ethanol to the isooctane solution of MPD does not change either the fluorescence or absorption spectra when the concentration of ethanol is more than 2.0 mol dm^{-3}. From the fluorescence and absorption band spectra and the concentration of ethanol being 2.0 mol dm^{-3}, the fluorescence and absorption band maxima wave numbers were found to be 26800 and 32950 cm^{-1}, respectively. These values agree with the values of σ_f^m and σ_a^m in ethanol, respectively (Table 1).

The equilibrium constant of the hydrogen-bond formation in the excited state (K_e) may be related to K_g using the UV absorption and fluorescence spectral data in Eq. 4:[10]

$$\log K_e = \log K_g - 0.625\,\delta\sigma/T, \qquad (4)$$

where

$$\delta\sigma = (\delta\sigma_a + \delta\sigma_f)/2.$$

$\delta\sigma_a$ (540 cm^{-1}) is the difference between the UV absorption band maxima of MPD in isooctane and ethanol, and $\delta\sigma_f$ (100 cm^{-1}) corresponds to the difference between the fluorescence band maxima in the above two solvents and T is the absolute temperature. The value of K_e at 25.0 °C has been estimated to be 1.3 mol^{-1} dm^3 from Eq. 4. The equilibrium constant in the excited state may also be obtained *via* Eq. 5.[11]

$$[1-(f_0/f_m)(d_m/d_0)]/[D] = -K_e + \alpha K_e(f_0/f_m)(d_m/d_0) \qquad (5)$$

$$\alpha = \Phi_a/\Phi_c,$$

where f_m and f_0 correspond to the fluorescence intensities with and without the addition of donor, and d_m and d_0, the absorbances at a definite wavelength with and without the addition of donor, respectively. Φ_c and Φ_a correspond to the quantum yields of fluorescence of the acceptor and hydrogen-bonded complex, respectively, and [D] is the concentration of donor. The analysis of the fluorescence intensities is shown in Fig. 4 where it may be seen that K_e is approximately 1.8 mol^{-1} dm^3. This value is in reasonable agreement with the K_e value obtained by Eq. 4. Both K_e values are smaller than the K_g value indicating that the hydrogen-bonding is weaker in the excited state than in the ground state.

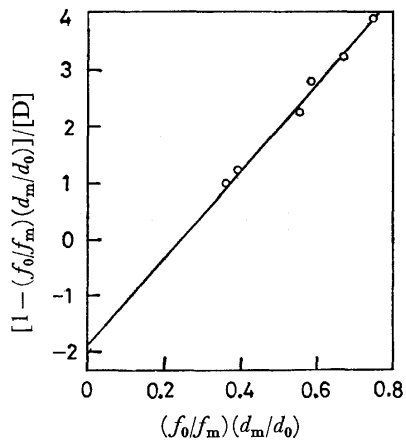

Fig. 4. The plot of $[1-(f_0/f_m)(d_m/d_0)]/[D]$ *vs.* $(f_0/f_m)(d_m/d_0)$. From the observed change of fluorescence intensity at 375 nm, the equilibrium constant of hydrogen bond formation in the excited state (K_e) was obtained.

This work was supported by grants from the Tokyo Denki University Research Fund.

References

1) K. Kimura and R. Nagai, *Bull. Chem. Soc. Jpn.*, **49**, 3343 (1976).
2) a) A. Fujimoto, A. Sakurai, H. Midorikawa, and E. Iwase, *Nippon Kagaku Kaishi*, **1974**, 1; b) A. Fujimoto and K. Inuzuka, *Bull. Chem. Soc. Jpn.*, **51**, 2781 (1978); c) K. Inuzuka and A. Fujimoto, *ibid.*, **51**, 2786 (1978); d) A. Fujimoto and H. Hirose, *ibid.*, **51**, 3377 (1978). e) K. Inuzuka and A. Fujimoto, *ibid.*, **52**, 939 (1979).
3) A. R. Katritzky and R. A. Jones, *J. Chem. Soc.*, **1960**, 2947.
4) Lippert, *Z. Electrochem.*, **61**, 962 (1957).
5) N. Mataga, Y. Kaifu, and M. Koizumi, *Bull. Chem. Soc. Jpn.*, **29**, 465 (1956); N. Mataga, *ibid.*, **36**, 654 (1963).
6) E. G. MaRae, *J. Phys. Chem.*, **61**, 562 (1957).
7) T. Kubota and M. Yamakawa, *Bull. Chem. Soc. Jpn.*, **35**, 555 (1962).
8) M. H. Krackov, C. M. Lee, and H. G. Mautner, *J. Am. Chem. Soc.*, **87**, 892 (1964).
9) H. Baba and S. Suzuki, *J. Chem. Phys.*, **35**, 1118 (1961).
10) A. Weller, *Z. Elektrochem.*, **61**, 1956 (1957).
11) N. Mataga and S. Tsuno, *Bull. Chem. Soc. Jpn.*, **30**, 368 (1957).

Spectroscopic and Equilibrium Dialysis Studies of the Poly(acrylic acid)-Cu(II) Complex in the pH Range 3.5—7[1)]

Kiwamu YAMAOKA* and Tsutomu MASUJIMA

Faculty of Science, Hiroshima University, Higashisenda-machi, Hiroshima 730

(Received December 25, 1978)

The complex formation between poly(acrylic acid), poly(Acr), and Cu^{2+} ion was studied in 150 mM NaCl solutions at 25 °C and at the mixing ratios of Acr residues-to-Cu^{2+}, *R*, of 32, 16 and 8, in the pH range of 3.5—7 by the spectroscopic and equilibrium dialysis methods. The dialysis results showed that more than 90% of the Cu^{2+} ions remain bound to the polymer at pH's higher than 4.5, but the bound Cu(II) begins to dissociate at lower pH values. The data also revealed that the true absorption spectra of poly(Acr)–Cu(II) complexes varied with pH and *R* in a complicated manner. The analysis of the bound Cu(II) spectra disclosed the presence of three different kinds of Cu(II)–Acr complexes over the entire pH range. It is the relative amounts of these three complexes that vary with pH and *R*. With a newly devised plot of the dialysis data, the stability constant for each Cu(II)–Acr complex was determined. In the poly(Acr)–Cu(II) macrocomplex, each Cu(II) was estimated to bind to two or four carboxylato ligands.

In a previous investigation in which the complex formation of poly(α-L-glutamic acid), poly(Glu), with Cu^{2+} was studied in the pH range between 7 and 3, poly(acrylic acid), poly(Acr), was chosen as the polymeric model of poly(Glu).[2)] The absorption spectra of poly(Glu)- and poly(Acr)–Cu(II) systems were both found to vary with pH in an unexpectedly complicated manner, but their pH dependence differed from each other. The finding was qualitatively attributed to the difference in the conformational change between poly(Glu) and poly(Acr) to which Cu(II) is bound, and also to the fact that the peptide nitrogen, a likely ligand to Cu(II), is lacking in the poly(Acr) residue. The finding also indicated that Cu(II)-residue complexes of various types are present in each polyanion–Cu(II) system. It is thus quite significant to study the structural details of poly(Glu)- and poly(Acr)–Cu(II) complexes by analyzing their absorption spectra quantitatively.

Spectroscopic and structural studies of the poly(Acr)–Cu(II) system in solutions are numerous;[2–10)] however, some conflicting views have been given on the nature of the binding of Cu(II) to poly(Acr). For example, the pH variation of the absorption intensity was attributed either to the conformational change of the macromolecular complex[3)] or to the change in the amount of bound Cu(II).[8)] Two binding schemes between Cu^{2+} and the side-chain carboxylato groups of poly(Acr) have been presented: Cu(II) binds to two adjacent[3,7)] or distant[8)] carboxylato groups. In addition, the number of the ligands participating in the complex formation has been suggested to be either two carboxylato groups[3,7–10)] or more than two,[4)] or both depending on the conditions.[6)] The same points of controversy have also been noted in the reports on the poly(methacrylic acid)–Cu(II) complex.[4,5,11–16)]

In order to clarify those unresolved questions, the visible-UV absorption spectra of poly(Acr)–Cu(II) solutions were measured in the pH range 7—3.5. The concentration and the molar absorption coefficient of the *bound* Cu(II), ε^b, were directly determined by the equilibrium dialysis method. The ε^b values vary in a complicated way, but systematically depend on both pH and the mixing ratio of Acr residues-to-Cu^{2+} ion. The ε^b *vs.* pH curves could be explained reasonably well as the interplay of three limiting spectra which characterize three types of Cu(II)–Acr complexes in poly(Acr). The binding schemes between Cu^{2+} and poly(Acr), the dissociation constants of poly(Acr), and the stability constants of poly(Acr)–Cu(II) complexes were also determined by means of graphical plots. The schemes of two and four side-chain carboxylato groups bound by a Cu(II) are sufficient to explain the binding data. By comparing those new data with the spectra of such low molecular weight models as the glutaric acid- and malonic acid–Cu(II) complexes, the nature of the poly(Acr)–Cu(II) complex will be discussed.

Experimental

Materials. Poly(sodium acrylate), abbreviated simply as poly(Acr), was purchased from Nakarai Chemical Co., Kyoto, and purified from an aqueous solution by means of dialysis against redistilled water for 24 h. The sample solution was freeze-dried and then vacuum-dried at 56 °C for 7 h. The degree of polymerization was determined to be *ca.* 7700 from the intrinsic viscosity in 1 M (=mol dm^{-3}) NaCl.[17)] Reagent grade copper(II) chloride dihydrate was crystallized from redistilled water before use. All other chemicals were of reagent grade and used without further purification.

Preparation of Sample Solutions. Each of the NaCl, $CuCl_2$, and HCl solutions was added to a stock polymer solution in this order. In every poly(Acr)–Cu(II) solution, the concentration of the polymer and the total of the concentrations of HCl and NaCl were always kept constant at 8 mM and 150 mM, respectively. The mixing ratio, *R*, defined as the mean residue weight concentration of Acr residues to the total concentration of Cu^{2+} in the sample solution, was adjusted by changing the initial Cu^{2+} concentration. The pH of the sample solution was adjusted by the addition of 0.125 M HCl.

Equilibrium Dialysis. The procedures and device for equilibrium dialysis were described elsewhere.[18)] The volumes of the two chambers of the dialysis cell were designed to be *ca.* 14 and 3.5 ml. The poly(Acr)–Cu(II) solution (13 ml) and the 150 mM NaCl solution (3.3 ml) were filled in the larger and smaller chambers, respectively, in order to minimize the changes in both *R* and pH of the poly(Acr)–Cu(II) solution during dialysis. The assembled dialysis cells were rotated continuously for 45 h at 15 rpm and at 25 °C. A period of 24 h was sufficient for a Cu^{2+} solution to reach a complete equilibrium. The adsorption of Cu^{2+} on the dialysis membrane was negligible. When the dialysis was completed, the absorp-

tion spectra and pH of the sample solution in the larger cell chamber were measured in sequence. The colorimetric determination of unbound Cu^{2+} ions in the smaller chamber was carried out as described below.

Colorimetric Determination of Cu^{2+} Ions. 2,2'-Biquinoline (Merck Co., Ltd.) was used as a chelating agent to determine the Cu^{2+} concentration. The procedure for this colorimetry is given in Merck Cat. No. 2955. A molar absorption coefficient of 5780 at 546 nm was used for the chelated Cu(II). The calibration curve obeyed Beer's law up to 15 μM of Cu^{2+}. With the concentration of the unbound Cu^{2+}, $[Cu]_f$, thus determined from the dialysate, the concentration of the bound Cu(II) in the dialyzed poly(Acr)–Cu(II) solution, $[Cu]_b$, was calculated as:

$$[Cu]_b = [Cu]_0 - [Cu]_f\frac{(V_1+V_2)}{V_1}, \quad (1)$$

where $[Cu]_0$ is the initial concentration of Cu^{2+} in the poly(Acr)–Cu(II) solution; V_1 and V_2 are the initial volumes of the poly(Acr)–Cu(II) and 150 mM NaCl solutions, respectively. The volume change in the poly(Acr)–Cu(II) solution before and after dialysis was *ca.* 1.5 % at most, even in the high pH and R range where the Donnan effect could possibly be appreciable. Thus, the Donnan effect should be negligible under the present experimental conditions. The binding fraction of Cu(II), f_b, is obtained as follows:

$$f_b = \frac{[Cu]_b}{[Cu]_b+[Cu]_f}. \quad (2)$$

Measurements of Absorption Spectra and pH. The absorption spectra and pH of sample solutions were measured as described elsewhere.[2] The pH calibration was made against the standard pH solutions (pH 6.88 and 4.00). All experiments were carried out at 25±1 °C.

Results

Absorption Spectra of Poly(Acr)–Cu(II) Solutions. The absorption spectra of poly(Acr)–Cu(II) solutions at various pH and R are shown in Fig. 1. The spectra are characterized by three new bands: a peak at 250—260 nm ($\varepsilon \leq 5000$), a weak shoulder near 370 nm ($\varepsilon \leq 40$), and a peak at 680—710 nm ($40 \leq \varepsilon \leq 120$). These bands are denoted as the UV-, near UV-, and visible bands from the short wavelength end. The spectrum of the $CuCl_2$ solution in 150 mM NaCl (pH 3.45—5.74) shows a shoulder near 250 nm ($\varepsilon \approx 230$) and a weak peak near 800 nm ($\varepsilon \approx 13$) (Fig. 1(a)). The spectrum of the poly(Acr) solution in 150 mM NaCl also shows only an ascending curve below 250 nm (Figs. 1(a)—(c)). The new three bands clearly reflect the formation of the poly(Acr)–Cu(II) complex. However, no isosbestic point was observed in either band in the pH range 4—7.

The spectra of poly(Acr)–Cu(II) solutions vary in a complicated manner depending on pH and R. In Fig. 2, the apparent molar absorption coefficients, ε_i, at 250 and 710 nm are plotted against pH. The wavelengths are close to the peaks of the UV- and visible bands, respectively. The ε values at the two wavelengths vary differently in the pH range 6.5—4.3. As the pH is lowered from 6, the visible band intensity increases and reaches a maximum at a pH of 4.4—4.3, while the UV-band intensity remains almost unchanged. At the pH lower than 4.3, however, all of the ε *vs.* pH curves descend monotonically.

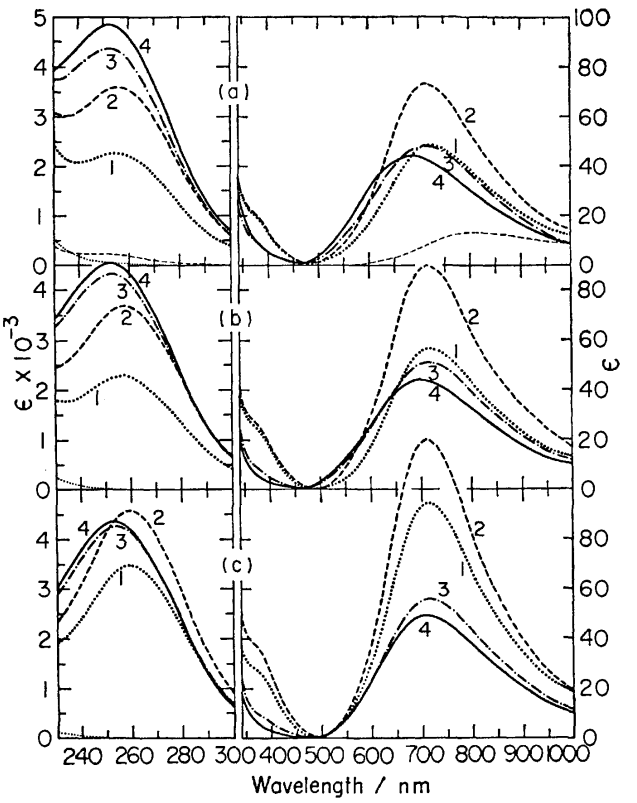

Fig. 1. The UV and visible absorption spectra of Cu^{2+} in the presence of poly(Acr) in 150 mM NaCl at various pH. (a): R=32; pH=3.85 (1), 4.11 (2), 5.50 (3), and 6.60 (4). (b): R=16; pH=3.90 (1), 4.17 (2), 5.87 (3), and 6.51 (4). (c): R=8; pH=3.94 (1), 4.21 (2), 6.09 (3), and 6.42 (4). The numeral in the parentheses corresponds to the numbered spectrum. The molar absorption coefficient, ε, is expressed in terms of the total concentration of Cu^{2+} present in solution. The dotted curves (without number) in the UV region are the spectra of poly(Acr) expressed in terms of $\varepsilon \cdot R$. The spectra of $CuCl_2$ solutions are constant in the pH range 3.54—5.74. An example is given in (a) (—— without number).

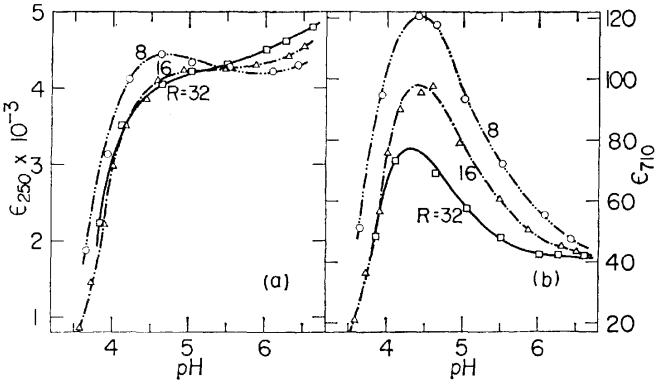

Fig. 2. The variation of the molar absorption coefficients of Cu^{2+}, ε, with pH in the presence of poly(Acr) at various R and at selected wavelengths of (a) 250 nm and (b) 710 nm.

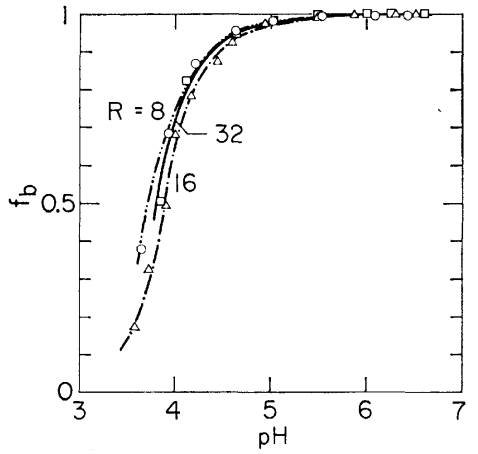

Fig. 3. The variation of the binding fraction of Cu(II), f_b, with pH at various R.

The Binding Fraction of Cu^{2+} and Its Variation with pH. In order to express the pH dependence of the absorption intensity in terms of the amount of the *bound* Cu(II), the binding fraction, f_b, was estimated from the dialysis data with the aid of Eq. 2. The results are shown in Fig. 3. Almost all the Cu^{2+} ions added in the poly(Acr) are bound to the polymer at pH values higher than 5.5, and more than 90% of the total Cu^{2+} indeed remain bound in the pH range 5.5—4.5. The bound Cu(II) begins to dissociate from the polymer site with the further decrease in pH. Only at a pH lower than 4.5 do the f_b *vs.* pH curves behave similarly to the ε *vs.* pH curves (*cf.* Fig. 2). These dialysis results show that the variation in ε at a pH higher than 4.5 is not due to the change of the amount of the bound Cu(II), but to the change in the ε of the bound Cu(II) itself.

The pH *Dependence of the Molar Absorption Coefficient and the Peak Position of the Bound Cu(II).* Since the bound and unbound Cu^{2+} concentrations are now available, the molar absorption coefficient of the *bound* Cu(II), ε^b, can be determined by using f_b in the following equation:

$$\varepsilon_\lambda^b = \frac{1}{f_b}(\varepsilon_\lambda - \varepsilon_\lambda^f) - \frac{[Cu]_0}{[Cu]_b} R \cdot \varepsilon_\lambda^p + \varepsilon_\lambda^f, \qquad (3)$$

where ε_λ, ε_λ^p, and ε_λ^f are the molar absorption coefficients at wavelength λ of the poly(Acr)–Cu(II), poly(Acr), and unbound Cu^{2+} in 150 mM NaCl solutions, respectively. The ε^b values are evaluated at four wavelengths: 250 and 710 nm (near the peaks of UV- and visible bands), 370 nm (the shoulder of near UV-band), and 880 nm (a hump of the visible band). The results are shown in Figs. 4(a)—(d), together with the peak wavelengths of the UV- and visible bands, denoted as λ_{max}, in Figs. 4(e) and (f). It should be noted that these ε^b *vs.* pH curves demonstrate the real changes in the optical property of the *bound* Cu(II) in poly(Acr)–Cu(II).

The ε_{250}^b *vs.* pH curves are peculiar in that they show a U-type change (Fig. 4(a)). On the other hand, the ε_{710}^b and ε_{880}^b curves are sigmoidal (Figs. 4(b) and (d)). In both sets of these curves, however, the ε^b converges to the limiting ε^b values on the high and low pH sides, as indicated by broken lines I and III. The limiting

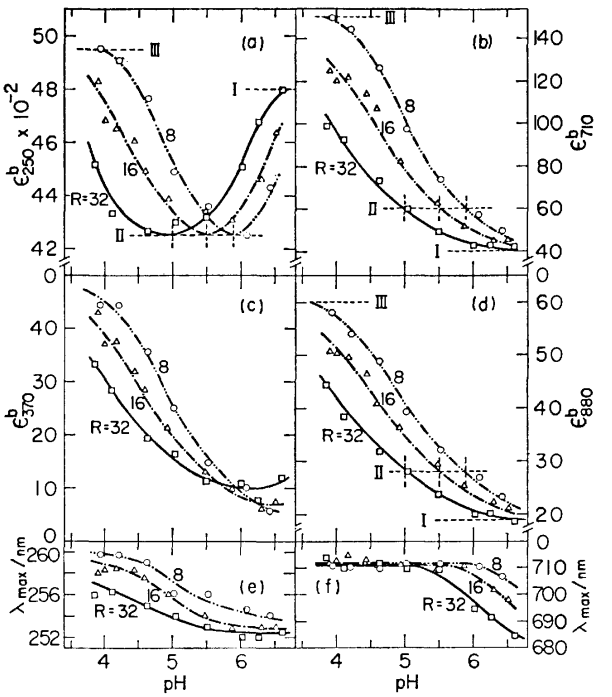

Fig. 4. The pH variation of the absorption coefficients of bound Cu(II), ε^b, at selected wavelengths of (a) 250 nm, (b) 710 nm, (c) 370 nm, and (d) 880 nm, and the variation of the peak positions of (e) the UV- and (f) visible-bands, λ_{max}. The ε^b and λ_{max} were estimated by applying Eq. 3 to each absorption spectrum of poly(Acr)–Cu(II) solution. The broken lines in (a), (b), and (d) show the characteristic values of ε^b at three pH regions of I, II, and III.

ε_{250}^b values are 4800 (pH$\geq$6.8 and R=32) and 4950 (pH$\leq$3.6 and R=8) in Fig. 4(a), while the limiting ε_{710}^b and ε_{880}^b values are 40 and 19 (pH$\geq$6.8 and R=32), and 150 and 60 (pH$\leq$3.6 and R=8) in Figs. 4(b) and (d), respectively. The minimum points in the ε_{250}^b *vs.* pH curves yield a constant value of 4250 regardless of R (pH=5.0 and R=32, pH=5.5 and R=16, and pH=5.9 and R=8), as indicated by broken line II in Fig. 4(a). Interestingly, the ε_{710}^b and ε_{880}^b values are also constant regardless of R at these respective pH values, becoming 60 and 28 respectively, as indicated by broken line II in Figs. 4(b) and (d).

Concurrently with the changes in ε^b, the peak positions, λ_{max}, in the spectra of bound Cu(II) vary with pH in two steps, as shown in Figs. 4(e) and (f). The λ_{max} of the UV-band is almost constant (252.5 nm (R=32), 253 nm (R=16), and 254 nm (R=8)) in the

Table 1. The molar absorption coefficients, ε_λ^b in $cm^{-1}\cdot mol^{-1}\cdot dm^3$, and the peak positions, λ_{max} in nm, in the spectra of Cu(II) bound to poly(Acr) in three pH regions I, II, and III

pH	ε_{250}^b	λ_{max}	ε_{710}^b	ε_{880}^b	λ_{max}
I	4800	252.5—253.5	40	19	685
II	4250	254.0—254.5	60	28	710—713
III	4950	260	150	60	710—713

pH range between 6.8 and 5.9—5.5, where the ε^b_{250} values are lowest, and then begins to shift to *ca.* 260 nm with the further lowering of pH. On the other hand, the λ_{max} of the visible band varies from 685 nm (R=32 at pH=6.8) to near 711 nm and remains constant in the lower pH range (pH≤5.0). These data are summarized in Table 1. The two-step change of the respective absorption peaks of the visible and UV-bands for the bound Cu(II) suggests the presence of two or three kinds of the Cu(II)–Acr complexes in poly(Acr)–Cu(II).

Assignment of ε^b-Values to the Three Complexes. The complicated variations of the ε^b_λ of bound Cu(II) with pH in Fig. 4 can be best explained as an interplay of three limiting ε^b_λ-values over the entire pH range under consideration of the data given in the preceding section. These limiting ε^b_λ-values may then be either characteristic of three different chemical species of the Cu(II)–Acr complexes or representative of three different states of a single or a mixture of Cu(II)–Acr complex(es) formed in poly(Acr)–Cu(II).

On the assumption that three limiting values of ε^b_λ in Table 1 specify three structurally different Cu(II)–Acr complexes, which are denoted as complexes I, II, and III, the fraction of each complex i (i=I, II, III) to the total of the bound Cu(II), f_I, f_{II}, and f_{III}, may be calculated at a given pH and at a selected wavelength of λ as follows:

$$\varepsilon^b_\lambda = \sum_{i=I}^{III} f_i(\varepsilon^b_\lambda)_i \text{ and } \sum_{i=I}^{III} f_i = 1, \quad (4)$$

where $(\varepsilon^b_\lambda)_i$ is the ε^b_λ-value characteristic of complex i. With the values of $(\varepsilon^b_\lambda)_i$ at 250 and 710 nm in Table 1, Eq. 4 can be written explicitly as follows:

$$\begin{aligned} \varepsilon^b_{250} &= 4800f_I + 4250f_{II} + 4950f_{III}, \\ \varepsilon^b_{710} &= 40f_I + 60f_{II} + 150f_{III}, \text{ and } f_I + f_{II} + f_{III} = 1. \end{aligned} \quad (5)$$

By solving these simultaneous equations for f_I, f_{II}, and f_{III} with the observed ε^b_{250} and ε^b_{710} at given pH and R values, the pH dependence of the f_i's may be obtained.

Figure 5 shows the variation of the fraction of complex i, f_i, with pH at three different R. At R=32 (Fig. 5(a)), complex I is dominant at high pH(≥6.1) and then its fraction decreases on lowering the pH. Simultaneously, the fraction of complex II, f_{II}, increases to unity at pH=5 and then decreases in the lower pH range where complex III now becomes dominant. With decrease in R (Figs. 5(b) and (c)), the f_i *vs.* pH curves shift to the high pH region as compared with the curves for R=32. These shifts may result from the lowering of the degree of dissociation, α^*, of the side-chain carboxylato groups by the binding of Cu(II) even at the same pH. In order to test this hypothesis, the pH should be converted into the α^*, which is defined as

$$\alpha^* = 1 - \frac{[HCl]_{add} + 2[Cu]_b}{[Acr]_0}, \quad (6)$$

where $[Acr]_0$ is the initial residue concentration of poly(Acr), and $[HCl]_{add}$ is the concentration of HCl added to the solution.

The dependence of f_i on α^* is shown in Fig. 5(d). The f_i *vs.* α^* curves at three R do not coincide with one another in this plot. Thus the horizontal displacement of the f_i toward higher pH is not due solely to the

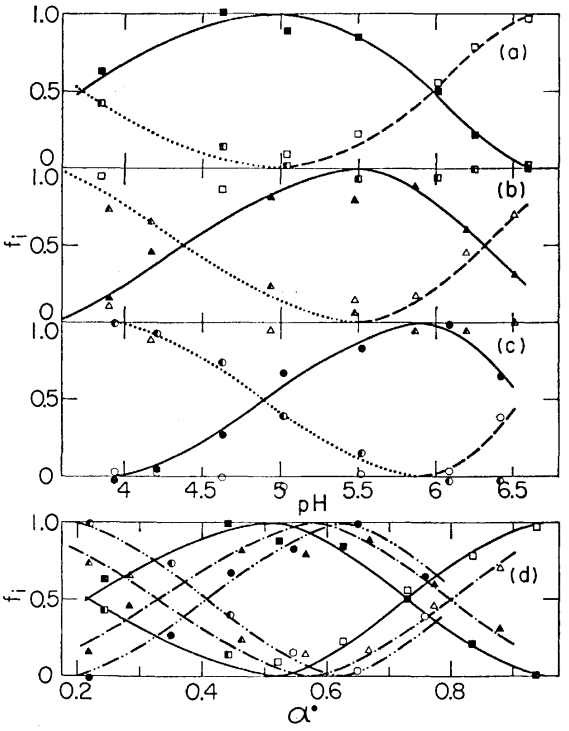

Fig. 5. The pH dependence of the fraction of the Cu(II)–Acr complex i (i=I, II, and III) to the total bound Cu(II), f_i, at various R; (a) R=32, (b) 16, and (c) 8; Complex I (—— and open symbols), complex II (—— and filled symbols), and complex III (····· and half-filled symbols), together with the variation of the f_i with the degree of dissociation of poly(Acr), α^*, at various R (32 —, 16 –·, 8 –··) in (d).

neutralization of the carboxylato group by Cu(II) but due also to the change in the ε^b of the bound Cu(II) with R. In any case, complex II is most dominant when about half of the carboxyl groups of poly(Acr) are ionized, while complexes I and III become a major entity in the fully ionized and un-ionized conformations of poly(Acr)–Cu(II), respectively. Accordingly, the pH region may also be divided into three subregions, *i.e.*, pH regions I, II, and III.

Component Spectra of the Bound Cu(II) in Poly(Acr)–Cu(II). Since the overall spectrum of the bound Cu(II) in the poly(Acr)–Cu(II) could be obtained in terms of ε^b_λ (Eq. 3), it is now possible to divide it into three component spectra characteristic of complexes I, II, and III by using the results shown in Fig. 5. For the poly(Acr)–Cu(II) at a given R (=32, 16 or 8), the pH-independent component spectra can be calculated from Eq. 4 first by solving simultaneous equations for $(\varepsilon^b_\lambda)_I$, $(\varepsilon^b_\lambda)_{II}$, and $(\varepsilon^b_\lambda)_{III}$ at a wavelength of λ with both ε^b_λ- and f_i-values at any three pH, and then by repeating the same calculations at other wavelengths in the 940—230 nm regions. Several of those spectra were derived by employing the data at different sets of three pH values and averaged. The mean spectra were designated as component spectra I, II, and III for complexes I, II, and III at a given R. The results are shown for the visible and UV-bands in Fig. 6. It should be noted that each of the component spectra is

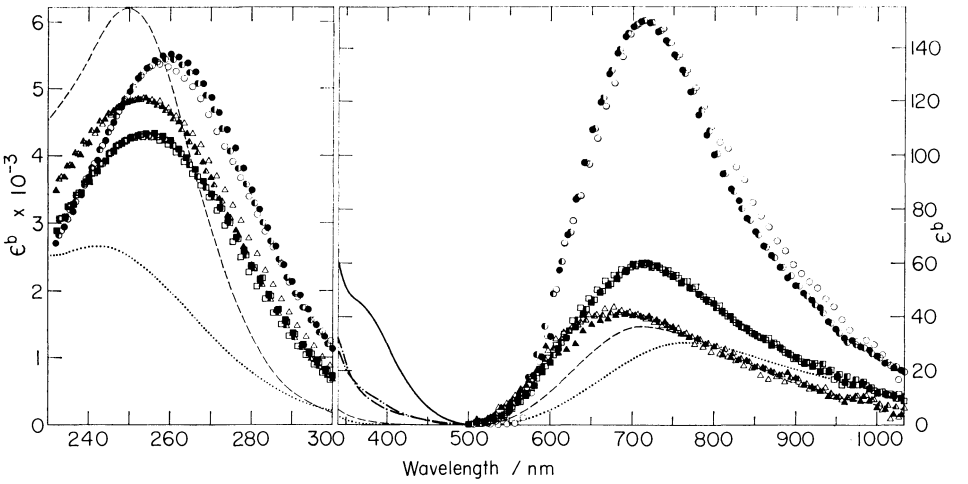

Fig. 6. The spectra of complexes I, II, and III in poly(Acr)–Cu(II). Complex I: R=32 (△), 16 (▲), and 8 (▲). Complex II: R=32 (□), 16 (◧), and 8 (■). Complex III: R=32 (○), 16 (◐), and 8 (●). For the procedure of the determination of these spectra, see text. This procedure could not be applied to the near UV-band because of the low absorption intensity. Instead, some typical spectra, which are closest to f_i=1, are shown (Complex I –·–·, Complex II –···–, and Complex III ——). The spectra of Cu(II)–glutarate (·····) and –malonate (–––––) complexes (R=[carboxyl group]/$[Cu^{2+}]_0$=80) are also shown for comparison.

nearly independent of the R and pH values. It is component spectrum III, which represents the dominant complex in the low pH region, that is most intense in the visible wavelength and gives rise to a considerable shoulder in the near UV-band. Although component spectra II and III both show the peak of the visible band at the same wavelength of 710 nm, they differ from each other in that II is weaker but broader than III.

The spectra of the bound Cu(II) in the glutaric acid- and malonic acid–Cu(II) complexes are also shown in Fig. 6 for comparison. Glutaric acid was chosen as the model for the nearest neighbor ligands of poly(Acr), because it has the same number of carbon atoms between two carboxylato groups. Malonic acid is known to form a four-coordinated complex with Cu(II) at the high carboxylate-to-Cu(II) ratio.[19] The spectra of the glutaric acid–Cu(II) complex with the R values up to 60 never resemble any of those component spectra I, II, and III as regards the peak position and intensity. However, the spectra of malonic acid–Cu(II) complexes at high R are quite similar to component spectrum II of the Cu(II)–Acr complex in the poly(Acr)–Cu(II) as regards the general spectral features in the visible band. This similarity is suggestive of the structure of complex II.

Formation of Cu(II)–Acr Complexes in Poly(Acr)–Cu(II). The structure of the Cu(II)–Acr complex may be reflected in the stoichiometry of the complex formation between the Acr residue and Cu^{2+}. On the basis that the equilibrium constant depends inversely on the first power of $[Acr]_0$, Wall and Gill[3] have concluded that a pair of the intramolecular adjacent carboxylato groups is chelated with a Cu(II). On the other hand, Tamaoki *et al.*[8] considered that two carboxyl ligands separated from each other on a single polyanion are associated with a Cu(II), because the Cu(II) showed almost the same binding strength for polycarboxylates of varying tacticities. In order to clarify the binding process between Cu^{2+} and poly(Acr) from the equilibrium dialysis data, some graphical methods were devised.

The following equilibrium schemes are considered for the binding between Cu^{2+} and carboxylato ligands of poly(Acr).

$$\text{Scheme A: } \mathrm{COOH} \overset{K_1}{\rightleftharpoons} \mathrm{COO^-} + \mathrm{H^+},$$

$$(\mathrm{COO^-})_2 + \mathrm{Cu^{2+}} \overset{K_2}{\rightleftharpoons} (\mathrm{COO})_2\mathrm{Cu}. \quad (7)$$

$$\text{Scheme B: } \mathrm{COOH} \overset{K_1}{\rightleftharpoons} \mathrm{COO^-} + \mathrm{H^+},$$

$$2(\mathrm{COO^-}) + \mathrm{Cu^{2+}} \overset{K_3}{\rightleftharpoons} \mathrm{COOCuOOC}. \quad (8)$$

In these schemes, the K_1, K_2, and K_3 are the dissociation constant of poly(Acr) and the stability constants of two different Cu(II)-residue complexes and are given as

$$K_1 = \frac{[\mathrm{COO^-}][\mathrm{H^+}]}{[\mathrm{COOH}]}, \quad (9)$$

$$K_2 = \frac{[(\mathrm{COO})_2\mathrm{Cu}]}{[(\mathrm{COO^-})_2][\mathrm{Cu^{2+}}]}, \quad (10)$$

and

$$K_3 = \frac{[\mathrm{COOCuOOC}]}{[\mathrm{COO^-}]^2[\mathrm{Cu^{2+}}]}. \quad (11)$$

In Scheme A, a Cu^{2+} ion binds to two adjacent carboxylato groups, whereas in Scheme B it binds to any two carboxylato groups. All the values of K_1, K_2, and K_3 are only apparent, since they are expressed in terms of concentrations and include the contribution of the electrostatic potential field of the polyanion. The total concentration of the ligands of poly(Acr) is given as

$$P_0 \equiv [\mathrm{Acr}]_0 = [\mathrm{COO^-}] + [\mathrm{COOH}] + 2[(\mathrm{COO})_2\mathrm{Cu}]. \quad (12)$$

The concentration of the pairs of nearest-neighbor carboxylato groups in poly(Acr), $[(COO^-)_2]$, may be given as:

$$[(COO^-)_2] = q[COO^-]. \quad (13)$$

Equations 9, 10, 12, and 13 are combined for Scheme A:

$$\frac{q(P_0-2\beta)}{\sigma} = \frac{[H^+]}{K_1K_2} + \frac{1}{K_2}, \quad (14)$$

or

$$\log\left(\frac{q(P_0-2\beta)K_2}{\sigma} - 1\right) = -pH + pK_1. \quad (15)$$

Equations 9, 11, and 12 are combined for Scheme B:

$$\frac{P_0-2\beta}{\sqrt{\sigma}} = \frac{[H^+]}{K_1\sqrt{K_3}} + \frac{1}{\sqrt{K_3}}, \quad (16)$$

or

$$\log\left(\frac{(P_0-2\beta)\sqrt{K_3}}{\sqrt{\sigma}} - 1\right) = -pH + pK_1, \quad (17)$$

where β is the concentration of bound Cu(II) or Cu(II)–Acr complex, and σ is the ratio of the concentration of the bound Cu(II) to that of unbound Cu^{2+}. The quantities P_0, β, σ, and $[H^+]$ are all obtained experimentally. When the left-hand side of Eq. 14 or 16 is plotted against $[H^+]$, a straight line would result, provided that the complex formation occurs according to Scheme A or B. The intercept and tangent of this line give the K_2 or K_3 together with K_1. The results are shown in Fig. 7, where the value of q is assumed to be 0.5.[3] Alternatively, Eqs. 15 and 17 may be utilized, in the cases where the intercepts are too small to estimate K_1, K_2, and K_3 unambiguously. With a number of assumed K_2 and K_3 values, the left-hand side of Eq. 15 or 17 is plotted against pH, until a straight line with a slope of -1 is obtained. Then the assumed

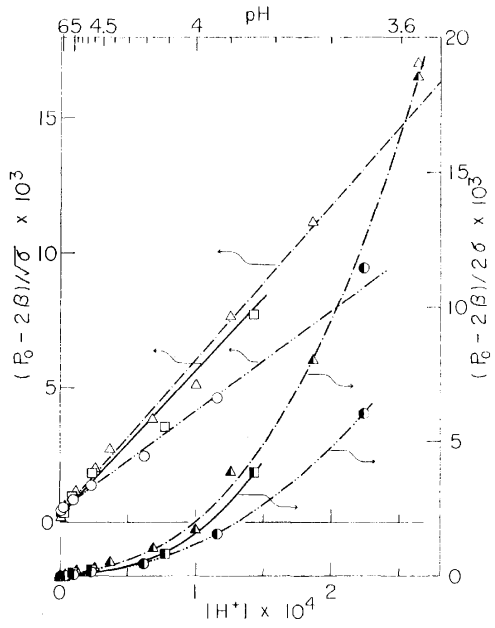

Fig. 7. The binding plots at three R for Scheme A (the right ordinate) and for Scheme B (the left ordinate). R=32 (◧ and □), 16 (◭ and △), and 8 (◐ and ○). See text for other details.

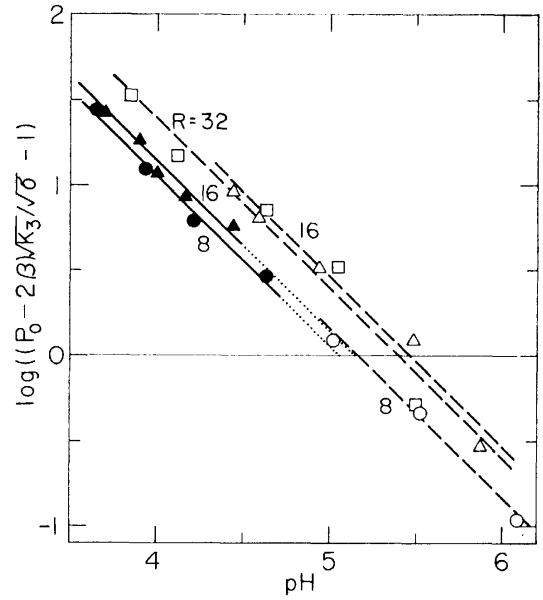

Fig. 8. The logarithmic binding plot at various R for Scheme B in pH regions II (open symbols) and III (filled symbols). The straight lines are best fitted by the f_i-weighted least-squares method. See text for other details.

K_2 or K_3 is the desired value and, in this case, the pK_1 is equal to the pH at which the straight line crosses the abscissa. The results are shown in Fig. 8.

If Scheme A describes the complex formation between Cu^{2+} and Acr ligands in all three pH regions I, II, and III, the above plot (Eq. 14) should give rise to a straight line over an entire range of $[H^+]$. This is not the case, as is demonstrated in Fig. 7. Scheme A may tentatively be concluded not to describe adequately the complex formation in the lower pH regions II and III, at least, under the assumption that the concentration of the adjacent two carboxylato groups is proportional to the concentration of the side-chain carboxylato groups remaining on poly(Acr),[3] *i.e.*, q is constant in Eq. 13. However, the validity of this assumption is believed open to further investigations. On the other hand, Scheme B is adequate to describe the complex formation in pH regions II and III, because the points of the R=32, 16, and 8 complexes fall approximately on straight lines which yield positive intercepts as required by Eq. 16. From those graphic methods, however, no clear conclusion can be given on whether or not Scheme A is the correct one in pH region I. This is mainly because the unbound Cu^{2+} ion is almost undetectable in the high pH ($\geq$6) region, regardless of R, and also because the intervals between experimental points become narrow exceedingly as the pH becomes larger than about 5. These factors introduce large errors in the plots in Fig. 7.

From the logarithmic plots shown in Fig. 8, the values of K_1 and K_3 were estimated in pH regions II and III and are summarized in Table 2. It is interesting to note that the apparent dissociation constants, pK_1, of poly(Acr)–Cu(II) vary from pH region II to pH region III, as the R=8 and 16 plots indicate in Fig. 8. The

Table 2. The pK_1, log K_3, and log $(K_2 \cdot K_4)$ of Cu(II)–Acr complexes in poly(Acr)–Cu(II) at various R in pH regions II and III

	pH	II (Scheme B)		III (Scheme B)		II (Scheme C)	
		pK_1 / mol·dm^{-3}	log K_3 / (mol·dm^{-3})$^{-2}$	pK_1 / mol·dm^{-3}	log K_3 / (mol·dm^{-3})$^{-2}$	pK_1 / mol·dm^{-3}	log$(K_2 \cdot K_4)$ / (mol·dm^{-3})$^{-2}$
R	32	5.4	7.3	—	—	5.4	8.0
	16	5.5	7.2	5.1	6.8	5.5	7.9
	8	5.2	6.8	5.1	6.9	5.2	7.8

pK_1 values are in good agreement with those previously obtained for poly(Acr)–Cu(II) by the potentiometric titration method (4.91 in 0.2 M $NaNO_3$[5] and 5—6 in 0.25 M $NaNO_3$[6]). The stability constants, log K_3, are quite large as compared with those for Cu(II)–dicarboxylic acid complexes, suggesting a strong binding of Cu(II) to two carboxylato ligands of poly(Acr).

A slightly more complicated class of the binding reaction schemes involves four Acr residues per Cu(II). On the assumption that the four ligands are paired and each pair consists of two adjacent carboxylato groups of poly(Acr), the binding scheme may be written as

$$\text{Scheme C: } \mathrm{COOH} \overset{K_1}{\rightleftharpoons} \mathrm{COO^-} + \mathrm{H^+},$$

$$(\mathrm{COO^-})_2 + \mathrm{Cu^{2+}} \overset{K_2}{\rightleftharpoons} (\mathrm{COO})_2\mathrm{Cu},$$

$$(\mathrm{COO})_2\mathrm{Cu} + (\mathrm{COO^-})_2 \overset{K_4}{\rightleftharpoons} [(\mathrm{COO})_2\mathrm{Cu}(\mathrm{COO})_2]^{2-} \quad (18)$$

The overall stability constant $K_2 \cdot K_4$ is then given as

$$K_2 \cdot K_4 = \frac{[\mathrm{Cu(COO)_4^{2-}}]}{[(\mathrm{COO^-})_2]^2[\mathrm{Cu^{2+}}]}. \quad (19)$$

By combining K_1 and $K_2 \cdot K_4$, the following expression results:

$$\frac{2q((P_0/2)-2\beta)}{\sqrt{\sigma}} = \frac{[\mathrm{H^+}]}{K_1\sqrt{K_2 \cdot K_4}} + \frac{1}{\sqrt{K_2 \cdot K_4}}. \quad (20)$$

This expression is close to Eq. 16. The plots at three R values also give straight lines in pH region II similar to those in Fig. 8, when a value of 0.5 is again assumed for q throughout pH regions II and III (*cf.* Table 2). It should be noted then that the coordination of any two residues by a Cu(II), *i.e.*, Scheme B, can not be discriminated from the coordination of any two pairs of four residues by a Cu(II), *i.e.*, Scheme C, provided that each pair consists of two nearest neighbor carboxylato groups.

Discussion

The Absorption Spectra of Poly(Acr)–Cu(II) Macrocomplex. The UV-, near UV-, and visible bands have been reported for poly(Acr)- and poly(methacrylic acid)–Cu(II) systems.[2-4,8,10,12,15,16] The UV- and visible bands are commonly observed in the Cu(II)-complexes with low molecular weight carboxylic acids of various types.[20,21] The UV-band at 250 nm may be assigned to an allowed charge-transfer band between the carboxyl ligands of poly(Acr) and Cu(II) on the basis of its peak position and high intensity.[2,20] The skewed visible band at 700 nm should be the d-d transition on the basis of its peak position and low absorption intensity.[10,15,20] The skewed shape suggests the composite nature of this band, which should involve two or more d-d transitions.[20,22] The existence of such multiple transitions was noted in the 860—890 nm region for the poly(methacrylic acid)–Cu(II) complex.[15]

Leyte *et al.*[15] have observed the near UV-band at 380 nm in the poly(methacrylic acid)–Cu(II) system and suggested a binuclear Cu(II) complex of the acetate type by comparing their results with the studies of the Cu(II) complexes with acetate,[23] unsaturated acid,[24] and α,ω-dicarboxylic acid.[25,26] However, the appearance of the near UV-band can not be considered as conclusive evidence of the binuclear Cu(II) complex.[21] On the contrary, Graddon[27] has assigned this band to the d_{xy}, $d_{yz} \rightarrow d_{x^2-y^2}$ transition of the planar, coordinated cupric ion from the results of the Cu(II)-acetylacetonate complex which has no dimeric structure. Hence, it is still unresolved whether or not the 370 nm band reflects the presence of the binuclear Cu(II) complex in poly(Acr)–Cu(II). This band appears even at a high ratio of the side-chain carboxyl groups to bound Cu(II) and is remarkable only in the low pH region III. Therefore, the Cu(II)–Acr complexes, which give rise to component spectra II and III (Fig. 6), could possibly be related structurally to the Cu(II)-acetylacetonate complex.

Structures of Cu(II)–Acr Complexes in Poly(Acr)–Cu(II) and Their Dependence on pH. The presence of three kinds of Cu(II)–Acr complexes in poly(Acr)–Cu(II) has been unraveled in the present work. However, it is not verified at present whether or not complexes, I, II, and III have unique structures. It is possible that each kind of complex i (i=I, II, III) is a mixture of several chemical species whose structures differ from each other slightly but do not affect the optical spectra appreciably. Figure 9 shows some of the likely chemical species for Cu(II)–Acr complexes. The structures of the species are by no means a complete list nor a conclusion introduced by this work, but should be considered as a working hypothesis. As regards the number of the ligands bound by a Cu(II), two carboxylato groups of poly(Acr) are normally considered because of the electric charge neutrality.[3,8,10] As the remaining ligands to Cu(II), the solvent water, hydroxide ion, counter-ion (Cl^-), and the additional carbonyl and carboxyl groups of poly(Acr) are all possible participants in the coordination with Cu(II), on the analogy of the Cu(II)–complexes with the small-molecular-weight ligands.[19-21] The Cl^- ion may be discounted because the spectra of poly(Acr)–Cu(II)

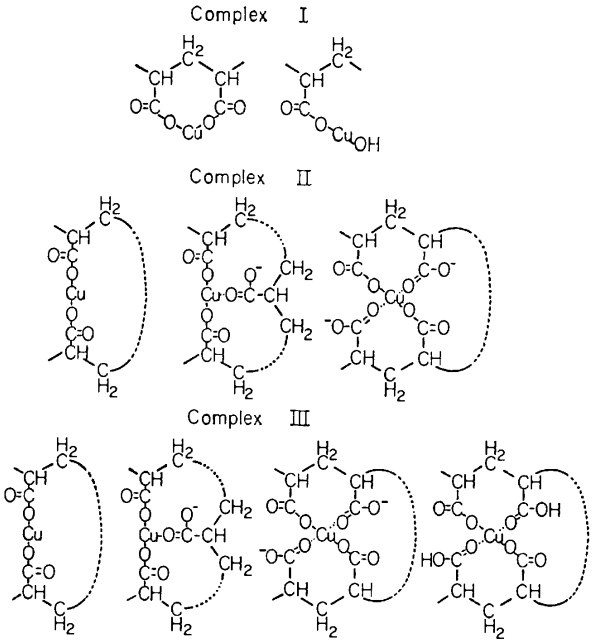

Fig. 9. Some possible structures of Cu(II)–Acr complexes in poly(Acr)–Cu(II). Neither hydration of water nor geometric isomer was explicitly considered. Complexes were assumed to be formed between Cu(II) and the side-chain carboxyl groups of a single poly(Acr) strand.

in 150 and 7.5 mM[2] NaCl solutions show no essential differences.

Although the present data fail to confirm that the complex formation reaction involves the $[Acr]^{-1}$-term in the high pH region (Scheme A), complex I is likely to be a bidentated-type complex, as already reported.[3,7] Poly(Acr) is in a rather extended conformation in this pH region because of the charge repulsion, so that the Cu(II) may bind to a pair of nearest-neighbor carboxylato groups. Nevertheless, the binding of Cu^{2+} to a carboxylato groups and an OH^- ion could not be omitted. The complex formation reaction depends on the $[Acr]^{-2}$-term (Scheme B) in the intermediate and low pH regions II and III where complexes II and III are dominant, respectively. This finding substantiates the notion that a bound Cu(II) is associated with the two carboxylato groups which are separated from, and independent of, each other on a single polymer strand (or possibly on different strands). The Cu(II) may also be coordinated by four carboxylato groups, as indicated by Scheme C. The profile of the component spectrum for complex II is very close to the spectrum of the Cu(II)–malonate complex which is also coordinated by four carboxylato groups (Fig. 6).[19]

It is impossible at present to discriminate whether or not the chemical species for complexes II and III are formed between carboxylato groups of intra- or inter-chains. The poly(Acr)–Cu(II) complex may take on a compact or aggregated conformation, as the ionization of the side-chains is suppressed by the added protons. This view is supported by the remarkable decrease in the viscosity of poly(Acr) solutions in the presence of Cu^{2+} or H^+.[8,10] However, the bound Cu(II) can also bridge two polymer-strands by forming a planar, four-coordinated complex with two each out of four carboxylato groups (Scheme C). The overall conformation of the poly(Acr)–Cu(II) macro-ion should be studied by the light-scattering or sedimentation method to draw a definite conclusion on the role of the bound Cu(II) in the low pH regions.

The stability constants, in terms of $\log K_3$, of the Cu(II)–Acr complexes (*cf.* Table 2) are three to four orders of magnitude greater than the $\log K$ of Cu(II)–glutarate [3.16 (no salt),[28] 3.88 (no salt), and 3.64 (in 0.2 M $NaNO_3$)[5]] and are comparable with those of Cu(II)–malonate and –oxalate complexes (*ca.* 8 and 5.54[5]). Gregor *et al.*[5] considered that the enormous electrostatic attraction of poly(Acr) toward Cu^{2+} contributes to the formation of a Cu(II)–Acr complex in poly(Acr) as stable as the Cu(II)–alkanoate complexes composed of five- and six-membered rings. However, it is also possible that the electrostatic repulsion is effectively suppressed in the presence of 150 mM NaCl and the conformation of poly(Acr) becomes either in the compact-coil or in the multi-stranded aggregates. The peculiar feature of the ligand field of the carboxyl groups of poly(Acr) toward the Cu^{2+} ion and the flexible backbone structure thereof may be the important cause to produce stable and large-ring Cu(II)–Acr complexes in poly(Acr).

Conclusion

The complicated pH dependence of the absorbance and peak position of the UV and visible absorption spectra of poly(Acr)–Cu(II) solutions was verified to be due partly to the dissociation of bound Cu(II) from the polymer sites in the low pH range ($\leq$4.3), but mostly to the genuine variation of the spectra of the bound Cu(II) with pH. This variation with pH was interpreted as being due to the interplay of three component spectra characteristic of Cu(II)–Acr complexes I, II, and III. The fractions of complexes I, II, and III vary with pH, becoming most dominant in the high, intermediate, and low pH regions, respectively. The analysis of the binding reactions showed that the chemical species constituting those complexes involve both chelation and coordination of two to four side-chain carboxylato groups of poly(Acr). The present study strongly suggests the possibility that the bound Cu(II) also bridges two or more poly(Acr) strands to form multi-strand aggregates.

References

1) Macromolecule–Metal Ion Complexes. V. For the preceding paper, see Ref. 2.
2) K. Yamaoka and T. Masujima, *Bull. Chem. Soc. Jpn.*, **52**, 1286 (1979).
3) F. T. Wall and S. J. Gill, *J. Phys. Chem.*, **58**, 1128 (1954).
4) A. M. Kotliar and H. Morawetz, *J. Am. Chem. Soc.*, **77**, 3692 (1955).
5) H. P. Gregor, L. B. Luttinger, and E. M. Loebl, *J. Phys. Chem.*, **59**, 34, 366, 559 (1955).
6) J. V. McLaren, J. D. Watts, and A. Gilbert, *J. Polym. Sci., Part C*, **16**, 1903 (1967).
7) P. Monjol, *Bull. Soc. Chim. Fr.*, **1972**, 1319.

8) K. Tamaoki, K. Imai, J. Nishino, and Y. Sakaguchi, *Kobunshi Kagaku*, **30**, 608 (1973).
9) J. A. Marinsky, N. Imai, and M. C. Lim, *Isr. J. Chem.*, **11**, 601 (1973).
10) H. Nishikawa and E. Tsuchida, *Bull. Chem. Soc. Jpn.*, **49**, 1545 (1976).
11) M. Mandel and J. C. Leyte, *J. Polym. Sci.*, **56**, S23 (1962).
12) M. Mandel and J. C. Leyte, *J. Polym. Sci., Part A*, **2**, 2883, 3771 (1964).
13) R. L. Gustafson and J. A. Lirio, *J. Phys. Chem.*, **69**, 2849 (1965).
14) J. J. O'Neill, E. M. Loebl, A. Y. Kandanian, and H. Morawetz, *J. Polym. Sci., Part A*, **3**, 4201 (1965).
15) J. C. Leyte, L. H. Zuiderweg, and M. van Reisen, *J. Phys. Chem.*, **72**, 1127 (1968).
16) J. A. Marinsky and W. M. Anspach, *J. Phys. Chem.*, **79**, 439 (1975).
17) S. Inoue, K. Yamaoka, and M. Miura, *J. Sci. Hiroshima Univ., Ser. A*, **39**, 27 (1975).
18) K. Yamaoka and M. Masujima, *Biopolymers*, **17**, 2485 (1978).
19) D. P. Graddon, *J. Inorg. Nucl. Chem.*, **7**, 73 (1958).
20) D. P. Graddon, *J. Inorg. Nucl. Chem.*, **17**, 222 (1961).
21) M. Kato, H. B. Jonassen, and J. C. Fanning, *Chem. Rev.* **64**, 99 (1964).
22) R. Hirasawa and H. Kon, *J. Chem. Phys.*, **56**, 4467 (1972).
23) R. Tsuchida and S. Yamada, *Nature*, **176**, 1171 (1955).
24) B. J. Edmondson and A. B. P. Lever, *Inorg. Chem.*, **4**, 1608 (1965).
25) L. Dubicki, C. M. Harris, E. Kokot, and R. L. Martin, *Inorg. Chem.*, **5**, 93 (1966).
26) B. N. Figgis and D. J. Martin, *Inorg. Chem.*, **5**, 100 (1966).
27) D. P. Graddon, *J. Inorg. Nucl. Chem.*, **14**, 161 (1960).
28) J. M. Peacock and J. C. James, *J. Chem. Soc.*, **1951**, 2233.

Molecular Dynamics of Polystyrene Model Molecules; Reorientational Correlation Times of Phenyl Groups of 2,4-Diphenylpentane

Shinbu KODA,† Hiroyasu NOMURA,* and Yutaka MIYAHARA

Department of Chemical Engineering, Faculty of Engineering, Nagoya University, Chikusa-ku, Nagoya 464
†*Department of Synthetic Chemistry, Faculty of Engineering, Nagoya University, Chikusa-ku, Nagoya 464*

(Received December 27, 1978)

The reorientational correlation times of phenyl groups in 2,4-diphenylpentane in solution were measured as a function of the temperature by means of Raman line-shape analysis. The reorientational correlation times of both isomers increase as the temperature increases, that is, the reorientational motion of phenyl groups in molecules gradually become active. In the low-temperature region, the reorientational correlation times of the meso 2,4-diphenylpentane are longer than those of the racemic one. This fact that the molecular motion of phenyl groups of the racemic isomer rotates more easily than that of the meso one is in agreement with the results obtained from ultrasonic study by Monnerie *et al.* On the other hand, in the higher-temperature region, the reorientational correlation times of the meso isomer are shorter than those of the racemic one. In addition, the potential barriers for the reorientational motion of phenyl groups are found to be (3.3±0.3) kcal/mol for the meso isomer and (2.0± 0.3) kcal/mol for the racemic isomer.

Ultrasonic absorption studies of vinyl polymers in solution, especially of polystyrene, have shown that local segmental motions of the backbone and motions of the side chains themselves were observed for the ultrasonic relaxation phenomena in the megahertz region.

Recently, in order to clarify the nature of the elementary motion of polymer chains in solution, Monnerie *et al.*[1] have reported very interesting results on the ultrasonic relaxation of 2,4-diphenylpentane in solution. The 2,4-diphenylpentane is the simplest polystyrene model molecule; two configurational isomers are present of the racemic and meso types. Monnerie *et al.* have indicated that the single relaxation observed for both racemic and meso types of 2,4-diphenylpentane in solution is due to the equilibrium reaction of the rotational isomers between g^-t and tt, and between tt and g^-g^-, conformations for the meso and racemic isomers respectively. Though they have suggested that the observed ultrasonic relaxation can be explained by taking into account the rotational motions of phenyl groups, the ultrasonic studies did not give any detailed information.

In our previous papers,[2,3] we reported that the reorientational correlation times of phenyl groups in polystyrene chains in solution could be determined by means of laser Raman spectroscopy. The same quantities can also, in principle, be determined by means of NMR relaxation experiments, infrared-band-shape analysis, and depolarized Rayleigh scattering. Compared with these methods, however, Raman studies can give information of interest more directly.

In the present paper, we will report on the temperature dependence of the reorientational correlation times of phenyl groups in *racemic*- and *meso*-2,4-diphenylpentane in solutions and will discuss the molecular motions of the phenyl groups in these molecules in solution.

Experimental

The apparatus used consisted of an argon-ion laser (800 mW at 488 nm) manufactured by the Coherent Radiation Co., Ltd. and a JRS-U1 Laser Raman Spectrometer of the Japan Electron Laboratory Co., Ltd. The Raman spectrum was observed at 90° with respect to linearly polarized incident light. In the analysis of the Raman line shape of the $\nu_2(a_{1g})$ mode of the phenyl group, all the experiments were carried out with a fixed slit width (40 μm).

The measuring temperatures were in the range from −90 °C to 40 °C. A variable-temperature Raman cell of the Harney-Miller type was used. The details of the experimental procedures were described previously.[4]

The meso and racemic 2,4-diphenylpentane, abbreviated *m*-DPP and *r*-DPP respectively, were kindly provided by Prof. Monnerie; these samples were the same as those used for ultrasonic studies. The detailed properties of the samples used have been given in detail in the literature.[5,6,7] By means of NMR and IR studies, the samples used have been confirmed for the following points; for *m*-DPP, the twofold degenerated g^-t (or tg^+) state is predominant, and the other conformations of *r*-DPP are 75% in the tt state and 25% in the g^-g^- state at room temperature.

The chloroform used as a solvent was commercial product, a spectral-grade regent. The concentrations of *m*-DPP and *r*-DPP were both 20.0 wt %.

Results and Data Analysis

Before we determined the reorientational correlation times of phenyl groups of *m*- and *r*-DPP in solution, we confirmed that the Raman spectra of DPP did not change in the pure liquid state nor in chloroform solutions over the whole temperature range. This fact clearly indicate that the conformational changes of *m*- and *r*-DPP in solution do not occur in these experiments.

The reorientational correlation times (τ(or)) of the phenyl group of DPP were determined by means of the Raman-line-shape analysis of stretching mode. For example, the Raman-line-shapes of $I_\parallel(\omega)$ and $I_\perp(\omega)$ of the $\nu_2(a_{1g})$ band are shown in Fig. 1, where $I_\parallel(\omega)$ and $I_\perp(\omega)$ represent the paralleled and polarized Raman intensities respectively with respect to the linearly polarized incident light.

As the ν_2 band of DPP shown in Fig. 1 overlapped the other bands, it was extracted by resolving these Raman lines into their components with Lorentzian functions, using the non-linear least-mean squares method of

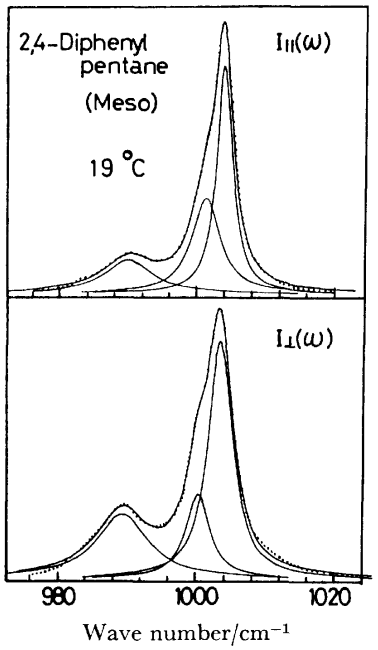

Fig. 1. Raman line shape of ν_2 band meso 2,4-diphenylpentane at 19 °C. Dotted line; observed, solid line; composed and decomposed with Lorentzian functions.

Fletcher-Powell.[8] After the correction for the line-boading effects of the instrumental slit width,[9] the true half-widths were determined for each one, $I_{\parallel}(\omega)$ and $I_{\perp}(\omega)$. As we found the depolarization ratio, $\rho_s(=I_{\perp}(\omega)/I_{\parallel}(\omega))$, to be about 0.02 for each isomer in throughout the temperature range, the intrinsic vibrational line shape, $I_{isot}(\omega)$, and the measured line shape, $I_{\parallel}(\omega)$, can be considered to be the same without the introduction of any significant errors.

The temperature dependences of the half-width of the isotropic and anisotropic parts of the Raman scattering, $\omega_{1/2}$(isot) and $\omega_{1/2}$(anis), are shown in Fig. 2. As was seen in Fig. 1, the Raman line shapes of $I_{\parallel}(\omega)$ and $I_{\perp}(\omega)$ can be represented by the Lorentzian curve within the limits of experimental error, also, we can estimate

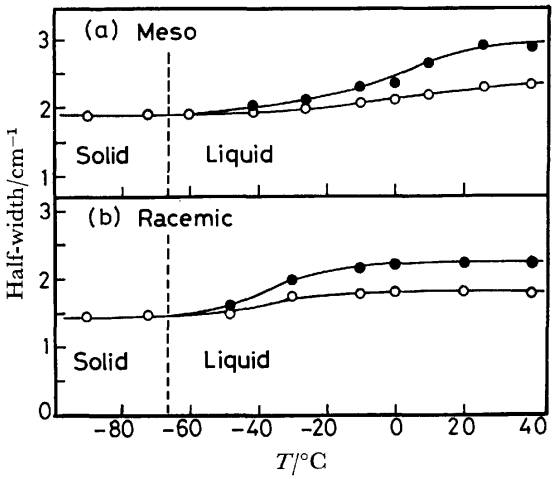

Fig. 2. Temperature dependence of $\omega_{1/2}$(isot) (○) and $\omega_{1/2}$(anis) (●) for each isomer. a); Meso isomer, b); racemic isomer.

the reorientational correlation times, τ(or), by means of the following relations;

$$\omega(\text{or}) = \omega_{1/2}(\text{anis}) - \omega_{1/2}(\text{isot}), \quad (1)$$

$$\tau(\text{or}) = (\pi c\omega(\text{or}))^{-1}, \quad (2)$$

where c is the velocity of light.

The molecular symmetries of *r*- and *m*-DPP are C_1 and C_2 respectively. As has clearly been mentioned by Nafie and Peticolas,[10] in the DPP molecule the reorientational correlation time obtained from the $\nu_2(a_{1g})$ band of the ring-stretching vibration of phenyl groups should be related to a set of motions about the axes which diagonalize the moment-of-inertia tensor and also diagonalize the rotational diffusion tensor. However, the reorientation about the axis of the phenyl group, $C–C_{ring}$, will be faster than those about the other axes, taking into account the moment-of-inertia of each axis in the *m*- and *r*-DPP molecules. Accordingly, we may consider that the reorientational correlation time obtained from the $\nu_2(a_{1g})$ mode of the phenyl group is mainly concerned with the motion about the $C–C_{ring}$ axis.

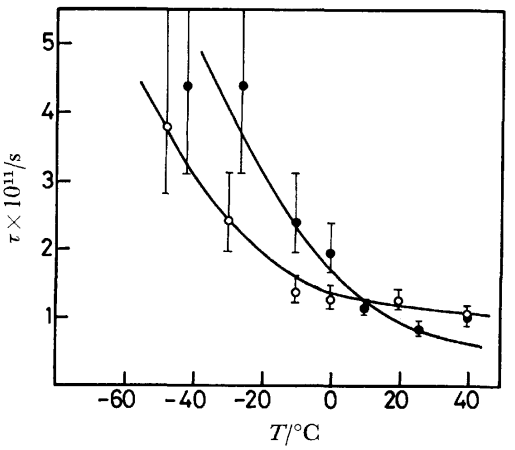

Fig. 3. Temperature dependence of the reorientational correlation time. ○; Racemic isomer, ●; meso isomer.

The temperature dependence of τ(or) for each isomer of DPP in solution shown in Fig. 3. In the low-temperature region, the reorientational correlation times, τ(or), of both isomers decrease sharply with an increase in the temperature and the values of τ(or) of the racemic-type DPP are longer than those of the meso-type DPP at the same temperature. On the contrary, with an increase in the temperature, the temperature dependences of their τ(or) become smaller and the τ(or) values of meso-type DPP are longer than those of the racemic-type one.

Discussion

At the lowest temperature measured (−90 °C), of course, the solution was in a solid state (the melting point of chloroform is −63.5 °C), therefore, all the molecular reorientational motions were frozen out, that is, $\omega_{1/2}(\text{anis}) \simeq \omega_{1/2}(\text{isot})$.

Even in the liquid state, below temperatures of

about −30 to −40 °C, the differences between $\omega_{1/2}$(isot) and $\omega_{1/2}$(anis) can hardly be distinguished, taking the experimental accuracy into account. This fact clearly indicated that the reorientational motion of phenyl groups in *m*- and *r*-DPP is frozen out and/or is extremely slow. In both isomers, as the temperature inceases, the differences between $\omega_{1/2}$(isot) and $\omega_{1/2}$(anis) increase. The reorientational motion of phenyl groups in a molecule gradually becomes active.

In the low-temperature region, the reorientational correlation times, τ(or), of *m*-DPP are longer than those of *r*-DPP; that is, the molecular motion of phenyl groups of the latter in the tt state rotates more easily than that of the former in the tg^- state. This fact is in agreement with the results obtained by ultrasonic study.

However, at higher temperature, it seems that the reorientational motion of the phenyl groups of *m*-DPP becomes faster than that of racemic ones. As has been mentioned above, the conformational changes in each isomer could not be observed at any temperature. This suggests that there are some changes in the intermolecular relations in solution and open the way to further investigation of this subject.

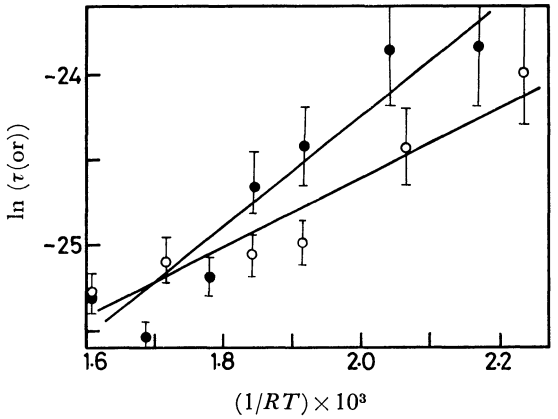

Fig. 4. Natural logarithmic reorientational correlation time *versus* $1/RT$. ○; Racemic isomer, ●; meso isomer.

The potential barrier for the reorientational motin of phenyl groups can be estimated from the following equation;[11]

$$\tau(\text{or}) \propto \exp(U_r/RT) \quad (3)$$

where R is the gas-constant, T is the absolute temperature, and U_r is the potential barrier. Figure 4 shows the relationship between ln (τ(or)) and $1/RT$. As may be shown in Fig. 4, the difference between the meso and racemic isomers can be observed. The values obtained are (3.3±0.3) kcal/mol and (2.0±0.3) kcal/mol for the meso and racemic isomers respectively.

Usually, in solution the rotational relaxation time can be expressed by the Debye-Einstein relation;

$$\tau(\text{or}) = 4\pi a^3\eta/(3RT) \quad (4)$$

where η is the viscosity coefficient of the solvent in a dilute solution. For chloroform, the activation energy obtained from the viscosity data[12] is 1.65 kcal/mol. This value is comparable to that obtained from the plot of ln(τ(or)) *vs.* $1/RT$ for *r*-DPP. The value of U_r for *m*-DPP is larger than that for the racemic one. The intramolecular interaction of phenyl groups in *m*-DPP may contribute to this difference in the rotational potential barrier. This fact shows that the rotational molecular motion of phenyl groups in *m*-DPP is hindered more than that of *r*-DPP.

TABLE 1. REORIENTATIONAL CORRELATION TIME

Sample	τ(or)/s
Toluene	0.60×10^{-11}
1,2-Diphenylethane	0.96
2,4-Diphenylpentane	2.4
Polystyrene M_w = 600	4.6
2200	6.4

(20 wt % in $CHCl_3$).

In Table 1, the τ(or) of DPP at room temperature is compared with those of several other molecules.[2,3] As the two phenyl groups in DPP are located at the 2 and 4 positions in normal pentane, the interaction between phenyl groups in DPP is much stronger than that of the 1,2-diphenylethane, where the two phenyl groups are located at the terminal carbon atoms. Therefore, the τ(or) of DPP is much longer than those of 1,2-diphenylethane and toluene, in which the phenyl group rotates freely. Moreover, the τ(or) values of polystyrene are longer than that of DPP and increase with the molecular weights, because of the short-range interaction between phenyl groups in the polymer chain.

In conclusion, the molecular motion of phenyl groups in DPP is very slow, and the rotation is almost completely hindered at low temperatures, where the single relaxation has been observed by ultrasonics. Accordingly, the single relaxation observed by ultrasonics should be considered to be due to the chain-conformational change in the molecule, as has mentioned by Monnerie *et al.* This is because the reorientational relaxation time of phenyl groups is of an order of 10^{-11} s, therefore, this motion should not be coupled with the rotational motion of the alkyl chain itself.

In addition, we can not consider that the elementary motion of polymer chains in solution is a conformational change, tt and tg^+ and/or tg^- and g^-g^-, observed in 2,4-diphenylpentane. Usually in polystyrene solutions, the ultrasonic relaxations have been observed in the regions of MHz and several hundred MHz at room temperature.[13] Extrapolating the data obtained by Monnerie *et al.* to room temperature, the relaxation should be observed at 204 MHz in the $tg^-(tg^+)\rightarrow tt$ process and at 575 MHz in $tt\rightarrow g^-g^-$. Besides, the relaxation amplitude, A, in those frequency regions is of an order of $1—2\times10^{-17}$ neper/s^2 cm^{-1}; this value can hardly be detected at higher frequencies by means of present-day experimental techniques. Therefore, the unit of elementary motion of polymer chains in solution must be longer than the 2,4-diphenylpentane molecule.

The authors wish to thank Professor Lucien Monnerie for supplying the meso and racemic 2,4-diphenylpentane.

References

1) B. Froelich, C. Noel, B. Jasse and L. Monnerie, *Chem. Phys. Lett.*, **15**, 159 (1976).
2) H. Nomura and Y. Miyahara, *Polym. J.*, **8**, 30 (1976).
3) S. Koda, H. Nomura, and Y. Miyahara, *Macromolecules*, **11**, 604 (1978).
4) H. Nomura and Y. Miyahara, *Bull. Chem. Soc. Jpn.*, **48**, 2779 (1975).
5) B. Jasse, A. Lety, and L. Monnerie, *J. Mol. Struct.*, **18**, 413 (1973).
6) B. Jasse and L. Monnerie, *J. Phys. D*; *Appl. Phys.*, **8**, 863 (1975).
7) B. Jasse, A. Lety, and L. Monnerie, *Spectrchim. Acta, Part A*, **31**, 391 (1975).
8) H. Nomura, S. Koda, and Y. Miyahara, *Appl. Spectrsc.*, in press.
9) H. Nomura, S. Koda, and Y. Miyahara, to be published.
10) L. A. Nafie and W. L. Peticolas, *J. Chem. Phys.*, **57**, 3145 (1972).
11) A. V. Rakov, *Opt. Spektrosk.*, **7**, 128 (1959).
12) "Kagaku Binran" ed by the Chemical Society of Japan, Maruzen (1941).
13) H. Nomura, S. Kato, and Y. Miyahara, *Mem. Fac. Eng., Nagoya Univ.*, **27**, 72 (1975).

Metal Complexes with Amino Acid Amides. IV. Relationship between the CD Spectra of Palladium, Nickel, and Copper Complexes with *cis*-Bis(amino carboxamidato)metal(II) Type

Takashi KOMORITA* and Yoichi SHIMURA

Department of Chemistry, Faculty of Science, Osaka University, Toyonaka, Osaka 560

(Received November 6, 1978)

Square planar complexes of [ML] type, where M=Pd^{2+}, Ni^{2+}, and Cu^{2+} for L=*N,N'*-bis(L-alanyl)-1,3-propanediaminate anion and M=Ni^{2+} and Cu^{2+} for L=*N,N'*-bis(L-alanyl)-1,2-ethanediaminate anion, were synthesized. Their absorption and CD spectra were measured in aqueous, ethanol, and DMF solutions. The results are discussed in comparison with those of *cis*- and *trans*-bis(amino carboxamidato)complexes. Definite correspondence is found between the component d-d bands of *N,N'*-bis(L-alanyl)-1,3-propanediaminatopalladium(II) and those of its nickel analog, in line with a similar correspondence for the corresponding *trans*-bis(L-amino carboxamidato) complexes. Assignment of the component d-d bands has been reexamined for the copper complexes of bis(amino carboxamidato) type by comparing their CD data with those for the palladium and nickel analogs.

Solvent effects on CD spectra have been studied for a large number of square planar bis(amino carboxamidato) complexes.[1-4] A definite correspondence has been found between the ligand field bands of trans palladium(II) complexes and those of nickel(II) analogs.[3,4] However, no similar examination has been carried out on the cis type or copper(II) complexes, due to the labile nature of the copper(II) and nickel(II) complexes.

This paper presents spectral relationship found for the nickel(II), palladium(II), and copper(II) complexes of *cis*-bis(L-amino carboxamidato) type. The work was achieved by use of tetradentate ligands, *N,N'*-bis(L-alanyl)-1,3-propanediamine and -1,2-ethanediamine, which make the complexes take the *cis* geometry.

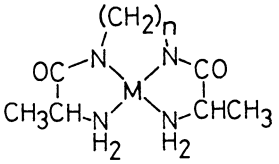

Experimental

Materials. The ligands, *N,N'*-bis(L-alanyl)diamines were synthesized according to Scheme 1.

N,N'-Bis(N-benzyloxycarbonyl-L-alanyl)-1,2-ethanediamine (1): *N*-Benzyloxycarbonyl-L-alanine (31.6 g, 0.14 mol) was dissolved in 700 cm^3 of absolute tetrahydrofuran (THF). The resulting solution was cooled to the temperature range −10—−5 °C, and 14.4 g (0.14 mol) of triethylamine was added to it under stirring. The temperature was kept in the range, stirring being continued. A solution of 19.4 g (0.14 mol) of isobutyl chloroformate in 60 cm^3 of absolute THF was added dropwise to the reaction mixture. After the addition had been completed, the mixture was stirred for 20 min, and a solution of 3.3 g (0.055 mol) of 1,2-ethanediamine in 250 cm^3 of absolute THF was added dropwise. The mixture which turned curdy was gradually warmed to room temperature under stirring for several hours and then allowed to stand overnight.

The white precipitate, which contained triethylammonium chloride as well as the desired compound, was separated by a glass filter, washed with water three times and recrystallized from ethanol: the compound crystallizes in needles if it is of adequate purity. The samples for elemental analyses were dried *in vacuo* over $CaCl_2$. Another crop of the product was obtained from the mother liquor. Total yield, 19.1 g (74 %); mp 188.5—190.5 °C (uncorr.).

Found: C, 61.15; H, 6.45; N, 11.82 %. Calcd for $C_{24}H_{30}N_4O_6$: C, 61.26; H, 6.43; N, 11.91 %.

This compound is readily soluble in ethanol, ethyl acetate, chloroform, and THF only when hot.

N,N'-Bis(L-alanyl)-1,2-ethanediamine Dihydrobromide Hemihydrate, L,L-balaenH_2·2HBr·0.5H_2O (2): A 1:2 mixture (100 g) of hydrogen bromide–acetic acid was added to 23.0 g of **1** previously damped with 50 cm^3 of gracial acetic acid. On stirring the whole mixture for 80 min, the starting material **1** was dissolved and the desired product deposited as a resinous mass. An additional amount of the product was precipitated as a powder by adding 300 cm^3 of ether. Recrystallization of the crude product from ethanol–ether yielded colorless microcrystals. These were washed with a 1:2 mixture of ethanol–ether and dried *in vacuo* over P_2O_5 at about 75 °C overnight. Yield, 15.4 g (86 %); $[\alpha]_{589}^{16}$ =+4.1° (*c*=0.114; water); mp *ca.* 135 °C (dec).

Found: C, 25.81; H, 5.67; N, 15.03 %. Calcd for $C_{16}H_{42}N_8O_5Br_4$: C, 25.75; H, 5.67; N, 15.02 %.

N,N'-Bis(N-benzyloxycarbonyl-L-alanyl)-1,3-propanediamine (3). A solid product was obtained by a procedure similar to that for the 1,2-ethanediamine analog **1**, except for the use of 1,3-propanediamine in place of 1,2-ethanediamine. It was separated by a glass filter and washed with THF, water, aqueous 5 % $NaHCO_3$ solution, and water, successively. Recrystallization from THF yielded fibrous crystals which were dried *in vacuo* over $CaCl_2$. An addtional amount of the compound was obtained from the mother liquor. Total yield was 8.00 g (88 %) starting with 11.2 g (50 mmol) of *N*-benzyloxycarbonyl-L-alanine and 1.4 g (19 mmol) of 1,3-propanediamine: mp 192.5—193.5 °C (uncorr).

Found: C, 61.86; H, 6.74; N, 11.44 %. Calcd for $C_{25}H_{32}N_4O_6$: C, 61.97; H, 6.66; N, 11.56 %.

This compound is easily soluble only in hot THF, chloroform, and ethanol.

N,N'-Bis(L-alanyl)-1,3-propanediamine Dihydrobromide, L,L-balatnH_2·2HBr (4): This compound can be derived from **3** by a similar procedure to that for the 1,2-ethanediamine analog **2**, but does not seem to be so easily crystallizable as **2**: Thus, the resinous mass of the crude product **4** was obtained from an appropriate amount of **3** each time before the preparation of metal complexes.

Cu(L,L-balaen)·2H_2O: A solution containing 1.5 g (4.1

mmol) of **2** in 25 cm³ of water was poured into a column (1.3 cm × 10 cm) packed with Amberlite IRA-410 of OH^- form and the column was eluted with water. To the eluate was added $Cu(OH)_2$ freshly prepared from 1.03 g (4.1 mmol) of $CuSO_4 \cdot 5H_2O$, and the mixture was stirred until it turned red. The solution was evaporated to dryness below 35 °C *in vacuo*. To the residual reddish violet powder was added 20 cm³ of water, and a small amount of insoluble substances was filtered off. From the filtrate diluted with 80 cm³ of ethanol, a small amount of less soluble bluish precipitate and a large amount of brick-red needles (or plates), the desired complex, were deposited successively by careful addition of ether. After the supernatant suspension of the bluish precipitate had been decanted, the brick-red crystals were washed with ether by decantation and dried in air. Additional crops of these crystal, were obtained by fractional treatment of the supernatant solution with ether. Total yield, 0.78 g (72 %).

Found: C, 31.97; H, 6.73; N, 18.63 %. Calcd for $C_8H_{20}N_4O_4Cu$: C, 32.05; H, 6.72; N, 18.69 %.

*Cu(*L,L*-balatn)·3H₂O*: An aqueous solution (40 cm³) containing **4** derived from 4.84 g (10 mmol) of **3** was neutralized with an aqueous KOH solution and mixed with $Cu(OH)_2$ prepared from 2.25 g (9 mmol) of $CuSO_4 \cdot 5H_2O$. To the resulting violet solution was added such an amount of aqueous KOH solution as necessary to raise the pH to 8.5, where the color of the solution turned pink. The solution was evaporated to dryness on a rotary evaporator below 35 °C. The desired complex was extracted with ethanol from the residue and recrystallized as shiny reddish violet plates, the trihydrate, by addition of ether. The crystals were dried in air: yield, 1.80 g (64 %).

Found: C, 32.23; H, 7.20; N, 16.94 %. Calcd for $C_9H_{24}N_4O_5Cu$: C, 32.57; H, 7.29; N, 16.88 %.

*Cu(*L,L*-balatn)·2H₂O*: The crystals of the trihydrate, described above, released a part of the water of crystallization to give an orange solid upon exposure to dry atmosphere. The sample for elemental analyses was prepared by drying the trihydrate over $CaCl_2$ overnight.

Found: C, 34.06; H, 6.99; N, 17.75 %. Calcd for $C_9H_{22}N_4O_4Cu$: C, 34.44; H, 7.07; N, 17.85 %.

*Ni(*L,L*-balaen)·2H₂O*: A solution of 2.00 g (5.5 mmol) of **2** in 10 cm³ of water was neutralized with a solution containing 0.62 g (11.1 mmol) of KOH in 10 cm³ of water. To the resulting solution was added a solution of 1.50 g (5.2 mmol) of $Ni(NO_3)_2 \cdot 6H_2O$ in 10 cm³ of water. The blue solution was neutralized with a KOH solution (0.62 g in 10 cm³ of water). A green precipitate appeared immediately, disappearing almost within 40 min under stirring. Desalting was performed from the resulting dark yellow solution by a few cycles of successive procedures: evaporation to dryness and extraction of the desired complex into ethanol. Brown yellow needles were separated from the ethanol extract by adding a small amount of water and a large amount of ether and dried in air: yield, 0.71 g (47 %).

Found: C, 32.26; H, 6.75; N, 18.70 %. Calcd for $C_8H_{20}N_4O_4Ni$: C, 32.57; H, 6.83; N, 18.99 %.

*Ni(*L,L*-balatn)·2H₂O*: An ethanol solution containing the complex was prepared by a similar procedure described for the balaen analog, by use of 2.62 g (9 mmol) of $Ni(NO_3)_2 \cdot 6H_2O$ and 4.84 g (10 mmol) of **3**, the volume being reduced *in vacuo* to a few cubic centimeters. Orange-yellow microcrystals of the desired complex were separated from the concentrated solution by adding several drops of water. These were collected on a glass filter, washed with a mixture of water–ethanol–ether (roughly 1 : 4 : 3) and dried in air: yield, 1.97 g (71 %).

Found: C, 34.73; H, 7.24; N, 18.10 %. Calcd for $C_9H_{22}N_4O_4Ni$: C, 34.98; H, 7.18; N, 18.13 %.

*Pd(*L,L*-balatn)·2.5H₂O*: The crude compound **4** derived from 2.42 g (5 mmol) of **3** was dissolved in 25 cm³ of water and neutralized with 10 cm³ of a 1 M NaOH solution. To the resulting solution was added a solution containing 1.18 g (4 mmol) of Na_2PdCl_4 in 10 cm³ of water. A brownish precipitate was immediately formed. The solution suspending the precipitate was subjected to a similar neutralization procedure, by use of 1 M NaOH.[4] During the course of procedure followed by stirring for 2.5 h, most of the precipitate was dissolved. The residue was then filtered off. Mixed salts and yellow sirup were obtained by evaporating the yellow solution *in vacuo*. Most of the salts were removed by a similar procedure to that described for Ni(L,L-balaen)·$2H_2O$, except for the use of methanol in place of ethanol. The resulting methanol extract was evaporated to dryness. The residue was dissolved in a small amount of water, poured into a column (1.3 cm × 23 cm) packed with Amberlite IRA-410 of OH^- form and eluted with water. The eluate was concentrated *in vacuo* below 35 °C to give pale yellow needles which were washed with a small amount of cold water and dried over $CaCl_2$: yield, 0.42 g (29 %).

Found: C, 29.46; H, 6.37; N, 15.19 %. Calcd for $C_{18}H_{46}N_8O_9Pd_2$: C, 29.56; H, 6.34; N, 15.32 %.

Measurements. The absorption and CD measurements were made with a Shimadzu UV-200 spectrophotometer and a JASCO MOE-1 spectropolarimeter, respectively, at room temperature. The solvents employed were the same as those reported.[2]

Gaussian Analyses. Gaussian analyses for selected absorption and CD curves were performed by use of a slightly modified version of program LGNS:[5,6] best fit between the observed and calculated curves was obtained by use of 35—49 spectral points per curve; each point was weighted with the square of ε in the least-squares treatment in absorption-curve analyses, but not in CD analyses. The number of components of ligand field ansorption and CD bands was fixed to three and four for the nickel and palladium complexes, respectively. All the calculations were performed at Computation Center, Osaka University.

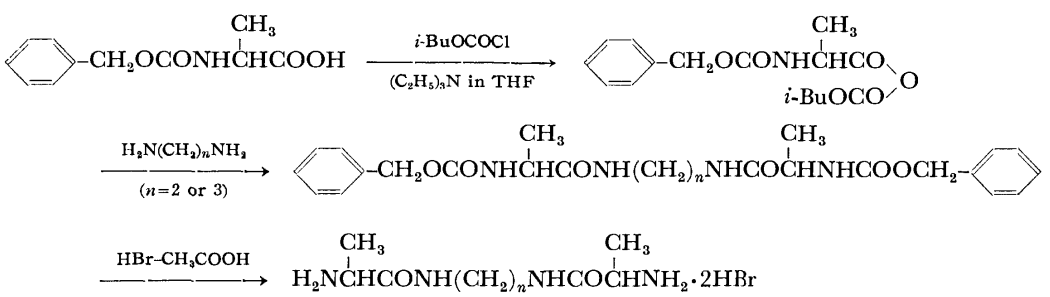

Scheme 1.

Results and Discussion

Absorption and CD data of the complexes are shown in Tables 1 and 2 and Figs. 1—5. The absorption and CD spectra of [Cu(L,L-balaen)] in aqueous solution have been recorded by Parris and Hodges, without isolation of the complex.[7] Our data do not differ much from theirs.

Gaussian Analyses. Gaussian analyses were performed for the CD spectra of the palladium and nickel complexes and for the absorption spectra of [Ni(L,L-balatn)] in three kinds of solvents. The results are given in Table 3.

For the analysis of CD curves of the palladium complex, the position of the first component, a spin-forbidden band,[1] was assumed to be equal to the corresponding output value[8] of *cis*-bis(L-valinamidato)-palladium(II). This does not seem to affect the overall results seriously, since the component is small enough. Overlapping of the intense charge transfer bands might affect the results seriously if inappropriate data in the overlapping region were chosen as inputs.

All the standard deviations of $\Delta\varepsilon$ values (Table 3) are within experimental error. On the other hand, those of ε values are, seemingly, of considerable magnitude, but the deviations in the region of relatively large ε values should be much smaller due to the weight scheme adopted.

The results of absorption- and CD-curve analyses for [Ni(L,L-balatn)] coincide with each other as regards the positions. This shows the validity of the assumption of three components in the ligand field band region of this or similar nickel complexes.

Absorption Spectra. The complex, [Ni(L,L-balatn)], exhibits an absorption maximum with a little higher intensity at a slightly lower wave number than the *trans*-bis(amino carboxamidato)nickel(II) complexes,[1,4] in each of the solvents (Table 1 and Fig. 1). This behavior is in line with that found between the absorption spectra of *cis*- and *trans*-bis(amino carboxamidato)-palladium(II) complexes.[1,4] Consequently, the absorp-

TABLE 1. ABSORPTION DATA OF THE COMPLEXES

Complex	Solvent[a]	Maxima[b]
Pd(L,L-balatn)·2.5H_2O	(W)	*ca.* 27sh 34.8br(2.64)
	(Et)	*ca.* 27sh *ca.* 32sh 34.9(2.68)
	(DMF)	*ca.* 29sh 35.3(2.81)
Ni(L,L-balatn)·2H_2O	(W)	22.8(1.85)
	(Et)	*ca.* 21sh 22.9(1.88)
	(DMF)	*ca.* 20.5sh 23.1(1.88)
Ni(L,L-balaen)·2H_2O	(W)	*ca.* 22sh 24.5(2.36)
	(Et)	*ca.* 21.5sh 24.6(2.41)
	(DMF)	*ca.* 21.5sh 24.7(2.46)
Cu(L,L-balatn)·3H_2O	(W)	19.8(1.81)
	(Et)	20.6(1.85) *ca.* 22.5sh
	(DMF)	21.0br(1.83)
Cu(L,L-balaen)·2H_2O	(W)	19.6(2.24)
	(Et)	20.2(2.24) *ca.* 23sh
	(DMF)	20.4(2.35) *ca.* 23sh

a) W: water, Et: ethanol. b) Wave numbers given in 10^3 cm^{-1} unit; intensities, log ε, in parentheses. sh: shoulder, br: broad peak.

TABLE 2. CD DATA OF THE COMPLEXES

Complex	Solvent[a]	Extrema[b]
Pd(L,L-balatn)·2.5H_2O	(W)	29.7(+0.07) 36.4(−0.80)
	(Et)	*ca.* 32sh(−) 36.7(−0.72)
	(DMF)	*ca.* 31.5br(+0.16) 36.8(−0.29)
Ni(L,L-balatn)·2H_2O	(W)	23.7(−0.62)
	(Et)	*ca.* 21sh(−) 24.0(−0.54)
	(DMF)	21.0(+0.15) 24.3(−0.42)
Ni(L,L-balaen)·2H_2O	(W)	21.9(−0.70) *ca.* 24.5sh(−)
	(Et)	21.6(−0.51) 24.9(−0.47)
	(DMF)	20.0(−0.02) 22.4(+0.13) 25.5(−0.19)
Cu(L,L-balatn)·3H_2O	(W)	19.7(−0.48)
	(Et)	19.9(−0.50) 23.9(+0.008)
	(DMF)	20.1(−0.30) 23.3(+0.05)
Cu(L,L-balaen)·2H_2O	(W)	20.0(−0.80)
	(Et)	20.1(−0.80)
	(DMF)	16.3(+0.004) 19.9(−0.37) 24.9br(+0.008)

a), b) See footnotes of Table 1.

TABLE 3. RESULTS OF GAUSSIAN ANALYSES[a]

Solvent[b]	[Ni(L,L-balatn)] Absorption components			[Ni(L,L-balatn)] CD components			[Pd(L,L-balatn)][e] CD components			[Ni(L,L-balaen)] CD components		
	σ_{max}	ε_{max}	Band-width[c]	σ_{ext}	$\Delta\varepsilon_{ext}$	Band-width	σ_{ext}	$\Delta\varepsilon_{ext}$	Band-width	σ_{ext}	$\Delta\varepsilon_{ext}$	Band-width
(W)							27.00[f]	+0.011	3.25			
	21.38	13.5	3.48	21.44	−0.066	3.31	31.24	+0.130	4.44	21.52	−0.462	2.36
	21.99	22.9	3.86	21.98	+0.111	3.93	32.79	−0.239	3.10	22.54	−0.068	3.63
	23.58	46.2	4.38	23.60	−0.658	3.94	36.50	−0.792	5.17	24.53	−0.485	4.85
	SD[d]=1.4			SD=0.009			SD=0.003			SD=0.007		
(Et)							26.83[f]	+0.047	3.31			
	20.80	8.5	3.57	20.90	−0.175	2.45	31.35	−0.053	4.25	21.39	−0.439	2.43
	21.98	29.1	4.10	21.89	+0.336	2.73	34.42	+0.153	3.14	22.93	+0.112	3.31
	23.59	50.5	4.45	23.65	−0.622	3.99	36.46	−0.770	4.43	24.59	−0.511	4.67
	SD=1.8			SD=0.004			SD=0.007			SD=0.006		
(DMF)							26.80[f]	−0.011	3.43			
	20.54	27.8	3.32	20.59	+0.147	3.06	29.49	+0.140	4.57	20.81	−0.072	2.33
	22.10	16.0	3.82	22.20	+0.291	2.29	33.51	+0.155	3.96	22.47	+0.228	3.17
	23.68	59.3	4.02	23.60	−0.481	4.27	36.63	−0.313	4.10	25.08	−0.215	4.44
	SD=2.2			SD=0.005			SD=0.002			SD=0.003		

a) σ's and band widths are given in 10^3 cm^{-1} unit. b) See footnote a) of Table 1. c) Half-value width. d) Standard deviation of the calculated values of ε or $\Delta\varepsilon$ from the corresponding observed values. e) For the input data used, see Fig. 5. f) Fixed values; see text.

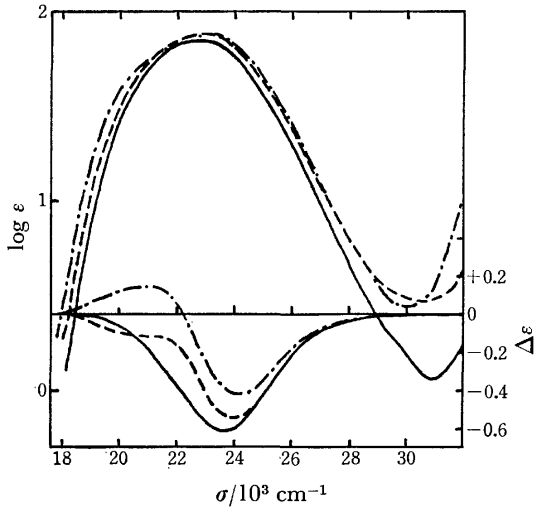

Fig. 1. Absorption and CD spectra of [Ni(L,L-balatn)] in water (——), in ethanol (----), and in DMF(-·--·).

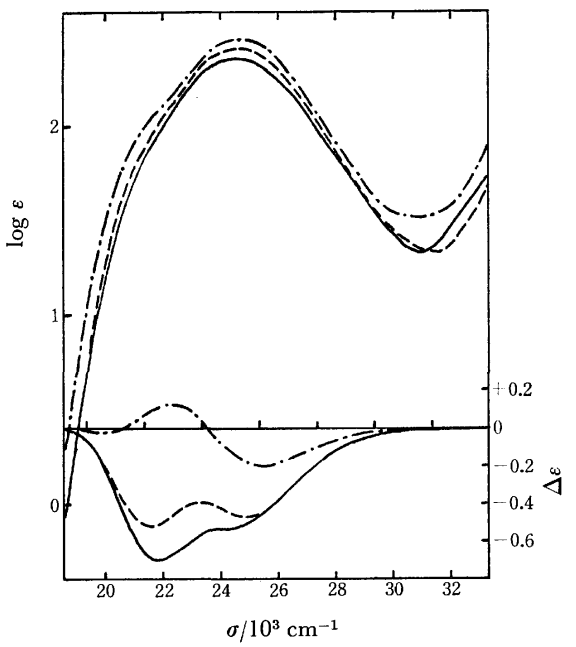

Fig. 2. Absorption and CD spectra of [Ni(L,L-balaen)] in water (——), in ethanol (----), and in DMF (-·--·).

tion spectra of [Ni(L,L-balatn)] are considered to correspond to those of a *cis*-bis(amino carboxamidato)-nickel(II) complex, which has not been isolated so far.

The absorption spectra of [Ni(L,L-balaen)] (Table 1 and Fig. 2) suggest an abnormally strong ligand field in this complex. The absorption maximum shifts toward blue by 1000—1500 cm^{-1} as compared with those of the *trans*-bis(amino carboxamidato)nickel(II) complexes, in each solvent. Such a blue shift is found also for each component band of the balaen complex (Table 3). This suggests that the ligand fits a nickel(II) ion so closely as to cause a constrictive effect found in different kinds of macrocyclic complexes.[9]

In contrast with the complexes of nickel(II) ion, both ligands, balatn and balaen, give ligand field strengths of the same order of magnitude as the copper(II) ions. The absorption peak of [Cu(L,L-balaen)] lies near that of the balatn analog in each solvent (Table 1 and Figs. 3 and 4). This is in line with the fact that metal–nitrogen bonds are longer for copper(II) than for nickel(II) by roughly 8 pm[10] in square-planar complexes of similar type.

The absorption spectra of [Pd(L,L-balatn)] (Table 1 and Fig. 5) essentially coincide with those of the *cis*-bis(amino carboxamidato)palladium(II) complexes in

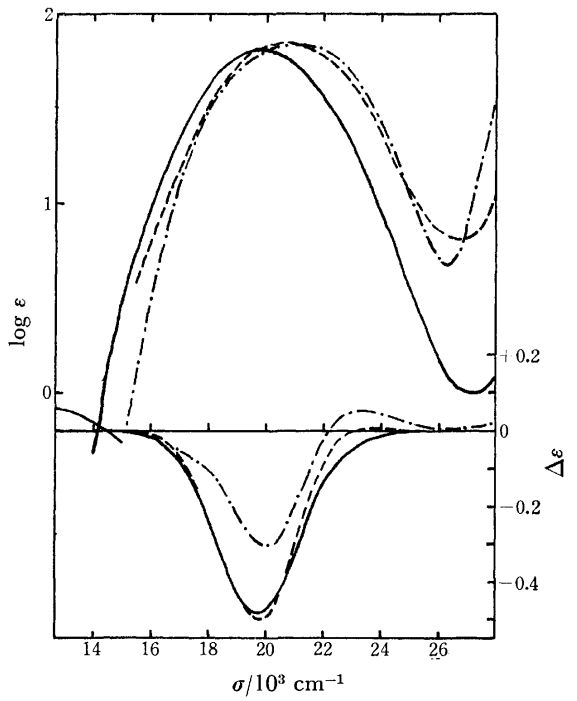

Fig. 3. Absorption and CD spectra of [Cu(L,L-balatn)] in water (——), in ethanol (----), and in DMF (-·-·).

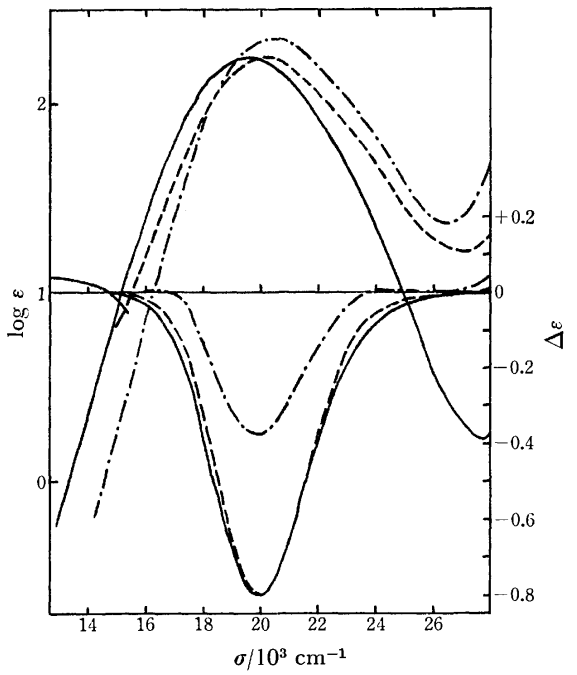

Fig. 4. Absorption and CD spectra of [Cu(L,L-balaen)] in water (——), in ethanol (----), and in DMF (-·-·).

respective solvents. However, attempts to prepare the monomeric balaen complex, [Pd(L,L-balaen)], under similar conditions to those adopted for the balatn analog, have so far been unsuccessful. The results are understandable if palladium(II) ion were of favorable size for balatn to form a stable mononuclear complex but not for balaen. However, this is not the case, since available data of X-ray analyses[11] show that metal–nitrogen distances are nearly equal to each other

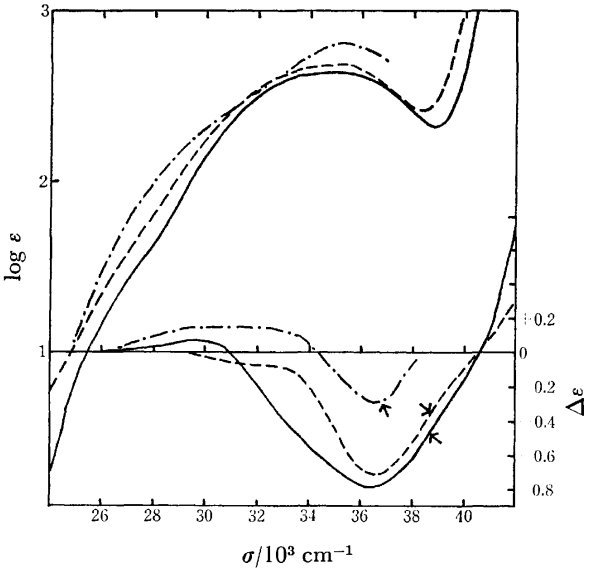

Fig. 5. Absorption and CD spectra of [Pd(L,L-balatn)] in water (——), in ethanol (----), and in DMF (-·-·). Arrows signify the terminal points of input data used in the Gaussian analyses.

between some square-planar complexes of palladium(II) and of copper(II).

CD Correspondence between Palladium and Nickel Complexes. The CD spectra of [Pd(L,L-balatn)] apparently resemble those of the nickel analog (Figs. 1 and 5). Thus Gaussian analyses (Table 3) are expected to disclose the relationship between the spectra of both complexes in more detail. Since the three component bands of the nickel complex have comparable absorption intensities, they should correspond to the second, third, and fourth components (Table 3) of the palladium complex. For the corresponding components of *cis*-bis(amino carboxamidato)palladium(II) complexes, three of the four spin-allowed d-d transitions, ν_3', ν_2', and ν_4', respectively, have already been assigned.[4,12] As regards the three components, the CD sign patterns for the nickel complex coincide with those for the palladium complex in ethanol and in DMF solutions.[13] It might be concluded that the first, second, and third components of [Ni(L,L-balatn)] should correspond to the second, third, and fourth of the palladium analog, respectively. Thus a definite correspondence was found between the ligand field bands of nickel(II) and of palladium(II) complexes with *cis*-bis(amino carboxamidato) type, as already found for the trans analogs.

The CD-sign patterns of [Ni(L,L-balaen)] differ from those of the balatn analog in aqueous and DMF solution (Table 3 and Figs. 1 and 2), but differ from that of *cis*-bis(L-valinamidato)palladium(II) only in aqueous solution. Gaussian analyses for the last complex showed (−,+,−) pattern in water, ethanol and DMF. A question still remains about the (−,−,−) pattern of the balaen complex in aqueous solution.

Band Assignment for the Copper Complexes. There are at least three components at roughly 17000, 19000, and 21000—22000 cm^{-1} in the ligand field band region of bis(amino carboxamidato)copper(II) complexes and the three components have been tentatively assigned to

the electronic transitions, ν_2, ν_3, and ν_4, respectively.[4] However, there are many copper complexes that exhibit a small positive extremum on the longer wavenumber end of CD spectrum.[2,4] In most cases it seems inadequate to regard the extremum as a residue of compensation among those three components. This is also the case for [Cu(L,L-balaen)] in DMF (Fig. 4).

Let us reexamine the four components inferred to exist in the ligand field band region of the copper complexes. The balatn and the balaen complexes (Figs. 3 and 4) display similar CD patterns to the bis(L-amino carboxamidato) complexes with alaninamidato, leucinamidato, and valinamidato ligands, although the latter complexes may be trans or predominantly so in the solutions. It seems reasonable to assume that the d-level orderings are essentially the same for the *trans* and *cis* complexes of bis(amino carboxamidato) type.

The order $\nu_2<\nu_3<\nu_4$ has been inferred for the trans complexes.[4] The corresponding order $\nu_2'<\nu_3'<\nu_4'$ should hold for the *cis*-type complexes with balatn and balaen.

The second and third CD components, which closely overlap each other to give a negative extremum in most of the complexes including [Cu(L,L-balatn)] and [Cu(L,L-balaen)], are much larger than the others, having net negative sign.[2] For most of the similar nickel or palladium complexes, the two components due to ν_3 and ν_4 (or ν_3' and ν_4') exhibit large and net negative CD, irrespective of the geometrical structures.

Thus it is preferable to assign the four components of the copper complexes to the transitions ν_2', ν_3', ν_4', and ν_1' (or ν_2, ν_3, ν_4, and ν_1), respectively, in the order of increasing wavenumbers.

The assignment is supported by the following observations: (1) The component due to ν_2 corresponds to a positive CD band in most of the bis(L-amino carboxamidato)-type complexes irrespective of the central metal ions and geometrical structures, (2) the component due to ν_1, which can be found only in the copper complexes, exhibits a small positive CD extremum or none in most cases (Table 2 and Figs. 3 and 4).[2] This is in line with the theory that the transition ν_1 is magnetically forbidden in first-order approximation.[14] Remarkable exceptions to (2) are the ν_1 components of the L-prolinamidato, L-phenylalaninamidato, and (*S*)-2-amino-4-methyl-*N*-methylpentanamidato complexes; the ν_1 component seems to correspond to a large negative CD extremum in these complexes.

References

1) T. Komorita, J. Hidaka, and Y. Shimura, *Bull. Chem. Soc. Jpn.*, **41**, 854 (1968).
2) T. Komorita, J. Hidaka, and Y. Shimura, *Bull. Chem. Soc. Jpn.*, **42**, 168 (1969).
3) T. Komorita, J. Hidaka, and Y. Shimura, *Bull. Chem. Soc. Jpn.*, **42**, 1782 (1969).
4) T. Komorita, J. Hidaka, and Y. Shimura, *Bull. Chem. Soc. Jpn.*, **44**, 3353 (1971).
5) D. B. Siano and D. E. Metzler, *J. Chem. Phys.*, **51**, 1856 (1969).
6) A list of the program written by D. B. Siano, J. A. Thomson, C. H. Harris, and D. E. Metzler was kindly supplied by the authors.
7) M. Parris and A. E. Hodges, *J. Am. Chem. Soc.*, **90**, 1909 (1968).
8) T. Komorita, unpublished work.
9) L. Y. Martin, L. J. DeHayes, L. J. Zompa, and D. H. Busch, *J. Am. Chem. Soc.*, **96**, 4046 (1974).
10) This value was estimated by use of data of the X-ray analyses: E. N. Baker, D. Hall, and T. N. Waters, *J. Chem. Soc., C*, **1966**, 680; J. M. Stewart and E. C. Lingafelter, *Acta Crystallogr.*, **12**, 842 (1959); M. Mathew and N. R. Kunchur, *Acta Crystallogr., Sect. B*, **26**, 2054 (1970); B. L. Holian and R. E. Marsh, *ibid.*, **26**, 1049 (1970); L. M. Shkol'nikova, E. M. Yutal, E. A. Shugam, and V. A. Voblikova, *Zh. Strukt. Khim.*, **11**, 886 (1970); D. Hall and T. N. Waters, *J. Chem. Soc.*, **1960**, 2644; E. C. Lingafelter and P. C. Jain, *Acta Crystallogr.*, **22**, 922 (1967); L. L. Merritt, C. Guare, and A. E. Lessor, *ibid.*, **9**, 253 (1956); M. A. Jarski and E. C. Lingafelter, *ibid.*, **17**, 1109 (1964).
11) C. E. Pfluger, R. L. Harlow, and S. H. Simonsen, *Acta Crystallogr., Sect. B*, **26**, 1631 (1970); M. A. Jarski and E. C. Lingafelter, *Acta Crystallogr.*, **17**, 1109 (1964); E. Frasson, C. Panattoni, and L. Sacconi, *ibid.*, 477; D. Hall, R. H. Summer, and T. N. Waters, *J. Chem. Soc., A*, **1969**, 420; C. Panattoni, E. Frasson, and R. Zannetti, *Gazz. Chim. Ital.*, **89**, 2132 (1959); E. Frasson, R. Bardi, and S. Bezzi, *Acta Crystallogr.*, **12**, 201 (1959).
12) ν_1, ν_2, ν_3, and ν_4 denote transitions from (z^2), (xy), (xz), and (yz) to (x^2-y^2), and ν_1', ν_2', ν_3', and ν_4' those from (z^2), (x^2-y^2), (xz), and (yz) to (xy), respectively, where (k) indicates a molecular orbital composed mainly of d_k-orbital. The x axis is fixed to be nearly colinear with metal–N(amido) linkage in *trans*-bis(amino carboxamidato) complex, but to bisect N–metal–N angle within each chelate ring in *cis* complex. The y axis is fixed also within coordination square in both *trans* and *cis* complexes.
13) The output data of CD analysis for [Ni(L,L-balatn)] in aqueous solution may be relatively unreliable regarding the first two components since these heavily overlap each other.
14) This means that the matrix element of electronic angular momentum, $\langle d_{x^2-y^2}|l_i|d_{z^2}\rangle$, is equal to zero irrespective of chromophore symmetries, where i=x, y, or z.

Palladium(II) Complexes Derived from the Reactions of Bis-(3-hydroxy-2-methyl-4-pyronato)palladium(II) with Several Nitrogen Bases

Hideyoshi MORITA,* Shigeru SHIMOMURA, and Shinichi KAWAGUCHI†

Faculty of Pharmaceutical Sciences, Tokushima University, Shomachi, Tokushima 770

†*Department of Chemistry, Faculty of Science, Osaka City University, Sumiyoshi-ku, Osaka 558*

(Received November 8, 1978)

The preparation and properties of the palladium(II) amine complexes containing 3-hydroxy-2-methyl-4-pyronate ions as the counter anions, $[Pd(N)_4]L_2$ and $[Pd(NN)_2]L_2 \cdot nH_2O$, are reported, where N=propylamine or benzylamine, NN=ethylenediamine, trimethylenediamine or *N,N*-dimethylethylenediamine, HL=3-hydroxy-2-methyl-4-pyrone, and n=2—4. The unidentate-amine complex, $[Pd(N)_4]L_2$, reacts with NaI to afford $[PdI_2(N)_2]$, whereas the bidentate-amine complex, $[Pd(NN)_2]L_2 \cdot nH_2O$, reacts with NaI to give $[Pd(NN)_2]I_2$. The mixed-ligand complexes, [PdL(bpy)]X and [PdL(phen)]X (where bpy=2,2′-bipyridine, phen=1,10-phenanthroline, X=ClO_4 or $B(C_6H_5)_4$), are also reported. On the basis of the PMR spectra, the IR spectra, and the electric conductivities, the structures of the isolated complexes are discussed.

3-Hydroxy-2-methyl-4-pyrone (HL) has some resemblance to the β-diketones, all being monobasic acids and usually functioning as O,O′-chelating agents.[1,2] The bis-chelates of these ligands with bivalent metal ions, such as Co(II), Ni(II), and Zn(II), react with nitrogen bases to form five- or six-coordinate adducts.[3,4] On the other hand, the corresponding Pd(II) complexes, $[Pd(\beta\text{-dik})_2]$, react with an excess of amine to afford $[Pd(\beta\text{-dik})(amine)_2](\beta\text{-dik})$ or $[Pd(amine)_4](\beta\text{-dik})_2$, depending upon whether the amine is secondary or primary respectively.[5] As was reported in a preliminary communication,[6] the Pd(II) complex of 3-hydroxy-2-methyl-4-pyrone, PdL_2, also reacts with ethylenediamine to result in $[Pd(en)_2]L_2 \cdot 2H_2O$. As an extension of this study, the present paper will report on the syntheses and properties of several Pd(II) amine complexes containing the 3-hydroxy-2-methyl-4-pyronate anion as a counter ion. The complexes obtained by the reactions of the above Pd(II) amine complexes with sodium iodide or lithium bromide will also be described.

Experimental

*Preparation of Complexes. Bis(3-hydroxy-2-methyl-4-pyronato)palladium(II), $[PdL_2]$ (**1**).* Palladium(II) chloride (10 mmol) was dissolved in a hot aqueous solution (100 ml) of NaCl (15 g), after which the mixture was cooled to 0—5 °C in an ice-bath. Into this solution we then vigorously stirred, a cold aqueous solution (0—5 °C, 50 ml) containing HL (20 mmol) and NaOH (20 mmol). A brown precipitate was formed immediately. After the solution had been stirred for 1 h at room temperature, a crude precipitate was filtered; this was then dissolved in chloroform (400 ml) at 40—50 °C. After the filtration of the insoluble materials, the solvent was evaporated at 35 °C. The brown residue was washed with ethanol and ether and then dried *in vacuo*. Yield: 86 %.

*Tetrakis(propylamine)palladium(II) 3-Hydroxy-2-methyl-4-pyronate, $[Pd(pa)_4]L_2$ (**2a**)*: Complex **1** (1.5 mmol) was dissolved in 10 ml of benzene containing propylamine (8 mmol) at room temperature. After the removal of the insoluble materials by filtration, the solvent was evaporated at *ca.* 25 °C. A white residue was collected on a glass filter, washed with cold acetone, and dried *in vacuo*. Yield: 40 %. By using benzylamine instead of propylamine, a white precipitate of $[Pd(ba)_4]L_2$ (**2b**) was also obtained in a 50 % yield.

*Bis(ethylenediamine)palladium(II) 3-Hydroxy-2-methyl-4-pyronate Dihydrate, $[Pd(en)_2]L_2 \cdot 2H_2O$ (**3a**)*: To a stirred suspension of Compound **1** (1.5 mmol) in chloroform (10 ml) we added a chloroform solution (10 ml) of ethylenediamine (10 mmol), after which the mixture was stirred for 30 min. A pale yellow precipitate was filtered and washed with cold ethanol and ether. The precipiate was then dissolved in warm ethanol (15 ml). After the removal of the insoluble materials by filtration, ether (100 ml) was added to the pale yellow filtrate. The white precipitate thus obtained was filtered, washed with cold ethanol and ether, and then dried *in vacuo*. Yield: 64 %.

*Bis(trimethylenediamine)palladium(II) 3-Hydroxy-2-methyl-4-pyronate–Water(1/2.5), $[Pd(tn)_2]L_2 \cdot 2.5H_2O$ (**3b**)*: To a stirred suspension of Compound **1** (1.5 mmol) in benzene (6 ml) we added a benzene solution (20 ml) of trimethylenediamine (40 mmol), after which the mixture was stirred for *ca.* 2 h. The crude pale yellow precipitate thus obtained was filtered and washed with ether. The precipitate was then dissolved in ethanol (15 ml). After the removal of the insoluble materials by filtration, ether (150 ml) was added to the pale yellow filtrate to obtain a white precipitate, which was then filtered washed with ether, and dried *in vacuo*. Yield: 67 %.

*Bis(N,N-dimethylethylenediamine)palladium(II) 3-Hydroxy-2-methyl-4-pyronate Tetrahydrate, $[Pd(N,N\text{-}Me_2en)_2]L_2 \cdot 4H_2O$ (**3c**)*: To a stirred suspension of Compound **1** (1.5 mmol) in benzene (6 ml) we added a benzene–ethanol (5:2 by volume) solution (14 ml) containing *N,N*-dimethylethylenediamine (10 mmol), after which the mixture was stirred for *ca.* 1 h. After the removal of the insoluble materials by filtration, the solvent was evaporated at *ca.* 27 °C. The white residue was collected on a glass filter, washed with ether, and dried *in vacuo*. Yield: 74 %.

*(2,2′-Bipyridine)(3-hydroxy-2-methyl-4-pyronato)palladium(II) 3-Hydroxy-2-methyl-4-pyronate, [PdL(bpy)]L (**4a**)*: To a stirred suspension of Compound **1** (3 mmol) in chloroform (15 ml) we added a chloroform solution (2 ml) of 2,2′-bipyridine (3 mmol), after which the mixture was stirred for *ca.* 1 h. The yellow precipitate thus obtained was filtered, washed with chloroform and ether, and then dried *in vacuo*. Yield: 76 %. This compound is fairly hygroscopic, and a color change from yellow to reddish yellow occurs in the presence of moisture. By using 1,10-phenanthroline instead of 2,2′-bipyridine, a yellow precipitate of [PdL(phen)]L (**4b**) was also obtained in a 43 % yield. This compound is also hygroscopic, and a change in color to reddish yellow also takes place in the presence of moisture.

Although we could not isolate Compounds **4a** and **4b** in a satisfactory purity, as the analytical data in Table 1 indicate, we obtained stable complex salts, **4c**—**4f**, by replacing the counter ion, L, with a perchlorate or tetraphenylborate anion.

(2,2'-Bipyridine)(3-hydroxy-2-methyl-4-pyronato)palladium(II) Perchlorate, [PdL(bpy)]ClO$_4$ (4c): To an aqueous ethanol (1: 1 by volume) solution (40 ml) of 2,2'-bipyridine (1.5 mmol) we added Compound **1** (1.5 mmol); then we stirred the mixture for *ca.* 1 h at room temperature. After the removal of the insoluble materials by filtration, an aqueous solution (10 ml) of $NaClO_4$–H_2O (1.5 mmol) was added to the yellow filtrate. The yellow precipitate thus obtained was filtered, washed with water, ethanol, and ether successively, and then dried *in vacuo*. Yield: 73 %. By using $NaB(C_6H_5)_4$ in place of $NaClO_4 \cdot H_2O$, a yellow precipitate of $[PdL(bpy)]B(C_6H_5)_4$ (**4d**) was also obtained in a 71 % yield.

The corresponding 1,10-phenanthroline complexes, [PdL(phen)]ClO$_4$ (**4e**) and $[PdL(phen)]B(C_6H_5)_4$ (**4f**), were obtained as yellow precipitates by the same methods as were used for Compounds **4c** and **4d** respectively, using 1,10-phenanthroline instead of 2,2'-bipyridine. The yields were 80 and 76 % respectively.

Reactions of [Pd(N)$_4$]L$_2$ (2) and [Pd(NN)$_2$]L$_2 \cdot n$H$_2$O (3) with Sodium Iodide. To an ethanol solution (5 ml) containing Compound **2a** (0.5 mmol) we added an ethanol solution (3 ml) of NaI (1.0 mmol), after which the mixture was stirred for *ca.* 45 min. The red brown precipitate thus obtained, $[PdI_2(pa)_2]$, was filtered, washed with ethanol and then ether, and dried *in vacuo*. Yield: 60 %. (Found: C, 14.95; H, 3.84; N, 5.60 %. Calcd for $[PdI_2(pa)_2] = C_6H_{18}N_2I_2Pd$: C, 15.06; H, 3.79; N, 5.86 %.) Other compounds, $[PdI_2(ba)_2]$, $[Pd(en)_2]I_2$, $[Pd(tn)_2]I_2$, and $[Pd(N,N\text{-}Me_2en)_2]I_2$, were also obtained similarly from the reactions of Compounds **2b**, **3a**, **3b**, and **3c** with NaI, in the mole ratio of one to two in each case. (Found for $[PdI_2(ba)_2]$: C, 29.08; H, 3.13; N, 4.90 %. Calcd for $C_{14}H_{18}N_2I_2Pd$: C, 29.27; H, 3.16; N, 4.88 %. Found for $[Pd(en)_2]I_2$: C, 10.41; H, 3.45; N, 11.72 %. Calcd for $C_4H_{16}N_4I_2Pd$: C, 10.00; H, 3.36; N, 11.66 %. Found for $[Pd(tn)_2]I_2$: C, 14.19; H, 4.08; N, 10.84 %. Calcd for $C_6H_{20}N_4I_2Pd$: C, 14.17; H, 3.96; N, 11.02 %. Found for $[Pd(N,N\text{-}Me_2en)_2]I_2$: C, 17.92; H, 4.52; N, 10.39 %. Calcd for $C_8H_{24}N_4I_2Pd$: C, 17.91; H, 4.51; N, 10.44 %.)

Reaction of [PdL(bpy or phen)]L with Lithium Bromide and Sodium Iodide. An ethanol solution (10 ml) of LiBr–H_2O (15 mmol) was stirred into a yellow aqueous ethanol solution (1: 3 by volume) of [PdL(bpy)]L (1.5 mmol) *in situ*. After the stirring had continued for *ca.* 40 min, the yellowish brown precipitate thus obtained was filtered, washed with ethanol and ether, and then *in vacuo*. Yield: 70 %. (Found: C, 28.42; H, 1.89; N, 6.43 %. Calcd for $[PdBr_2(bpy)] = C_{10}H_8N_2Br_2Pd$: C, 28.44; H, 1.91; N, 6.63 %.) By using phen instead of bpy, a yellowish brown precipitate of $[PdBr_2(phen)]$ was obtained in an 82 % yield (Found: C, 33.29; H, 1.98; N, 6.03 %. Calcd for $[PdBr_2(phen)] = C_{12}H_8N_2Br_2Pd$: C, 32.29; H, 1.81; N, 6.28 %.). The corresponding iodo complexes, $[PdI_2(bpy)]$ and $[PdI_2(phen)]$, were also obtained similarly as red brown precipitates from the reactions of [PdL(bpy or phen)]L with twice as many moles of NaI (Found: C, 23.92; H, 1.75; N, 5.32 %. Calcd for $[PdI_2(bpy)] = C_{10}H_8N_2I_2Pd$: C, 23.26; H, 1.56; N, 5.42 %. and Found: C, 27.49; H, 1.56; N, 5.18 %. Calcd for $[PdI_2(phen)] = C_{12}H_8N_2I_2Pd$: C, 26.67; H, 1.49; N, 5.18 %.).

Measurements. The IR spectra in the 200—4000 cm^{-1} region were recorded on a JASCO DS-701G infrared spectrophotometer in Nujol mulls between CsI plates. The PMR spectra were obtained with a JEOL JNM-PS-100 spectrometer. The water contents in the hydrated complexes were determined from the thermogravimetric curves, which had themselves been obtained with a Shimadzu TGA-30 thermobalance at a heating rate of 5 °C/min in an atmosphere of nitrogen flowing at 50 ml/min. The electric conductivities of the solutions were measured with a Toa Electronics CM-2A conductivity meter. The molecular weight was determined with a Hitachi Perkin-Elmer 115-type vapor-pressure osmometer, employing benzil as the reference substance.

Results and Discussion

Bis(3-hydroxy-2-methyl-4-pyronato)palladium(II), $[PdL_2]$ (**1**), reacts with an excess amount of an aliphatic amine to give a complex of the $[Pd(N)_4]L_2$ type (**2**) (where N is propylamine (pa) (**2a**) or benzylamine (ba) (**2b**)) or the $[Pd(NN)_2]L_2 \cdot n$H$_2$O type (**3**) (where NN is ethylenediamine (en) (**3a**), trimethylenediamine (tn) (**3b**), or *N,N*-dimethylethylenediamine(*N,N*-Me$_2$en) (**3c**)). These Pd(II) amine complexes contain the 3-hydroxy-2-methyl-4-pyronate ion as counter anions. When Compounds **2a** and **2b**, which have monodentate amines, were reacted with twice as many moles of NaI, two of the coordinated amines were replaced by two iodide anions to afford neutral complexes, $[PdI_2(pa)_2]$ and $[PdI_2(ba)_2]$ respectively. On the other hand, when Compounds **3a**, **3b**, and **3c**, which have bidentate amines, were treated with twice as many moles of NaI, the 3-hydroxy-2-methyl-4-pyronate ions were replaced by iodide anions to give $[Pd(en)_2]I_2$, $[Pd(tn)_2]I_2$, and $[Pd(N,N\text{-}Me_2en)_2]I_2$ respectively.

The parent complex, Complex **1**, reacts with an equimolar amount of a heterocyclic nitrogen base such as bpy and phen to give rise to [PdL(bpy or phen)]L, (**4a**, **4b**). Even when twice as many or more moles of bpy or phen were used, a complex of the $[Pd(NN)_2]L_2$ type was not afforded, but **4a** or **4b** resulted. Although Compounds **4a** and **4b** could not be isolated in a satisfactory purity, their PMR spectra in the intact solutions indicate unequivocally that two kinds of L exist, one in the coordination sphere and the other in the outer sphere (Table 2). By replacing the counter ion, L, with perchlorate and tetraphenylborate anions, stable complex salts, **4c**—**4f**, were obtained. When the ethanol solutions of **4a** and **4b** *in situ* were treated with an excess amount of LiBr$\cdot$H$_2$O or twice as many moles of NaI, the coordinated 3-hydroxy-2-methyl-4-pyronate ligand was replaced by two bromide or iodide ions to give $[PdX_2(bpy \text{ or } phen)]$, where X is Br or I. The analytical and IR data of the newly isolated compounds are listed in Tables 1 and 3 respectively.

[PdL$_2$] (1). Compound **1** exhibits strong IR bands at 1600, 1564, and 1545 cm^{-1}; the former band can be assinged to the C=O, and the latter two, to the C=C stretching vibrations, by reference to the data of the other metal complexes of 3-hydroxy-2-methyl-4-pyrone.[1] The band observed at 419 cm^{-1} can tentatively be assigned to the Pd–O stretching vibration by reference to the data of the bis(acetylacetonato)palladium(II).[7]

In the PMR spectrum of Compound **1** in $CDCl_3$, the signal of the 5-position proton is composed of two doublets, the area ratio of which is 1: 1, as is listed in

TABLE 1. COLOR AND ANALYTICAL DATA OF THE PALLADIUM(II) COMPLEXES

Complex		Color	Found (Calcd), %			
			C	H	N	H_2O
1	$[PdL_2]$	brown	40.26 (40.42)	2.90 (2.83)		
2a	$[Pd(pa)_4]L_2$	white	48.44 (48.61)	7.92 (7.82)	9.33 (9.45)	
2b	$[Pd(ba)_4]L_2$	white	61.41 (61.18)	6.15 (5.91)	6.99 (7.14)	
3a	$[Pd(en)_2]L_2 \cdot 2H_2O$	white	37.52 (37.47)	5.99 (5.90)	10.83 (10.92)	6.78 (7.03)
3b	$[Pd(tn)_2]L_2 \cdot 2.5H_2O$	white	39.01 (39.32)	6.67 (6.42)	10.61 (10.19)	7.43 (8.19)
3c	$[Pd(N,N\text{-}Me_2en)_2]L_2 \cdot 4H_2O$	white	39.80 (39.71)	7.16 (7.00)	9.15 (9.26)	11.69 (11.91)
4a	[PdL(bpy)]L	yellow	47.33 (51.53)	3.23 (3.54)	4.87 (5.46)	
4b	[PdL(phen)]L	yellow	51.11 (53.70)	3.31 (3.37)	4.87 (5.22)	
4c	$[PdL(bpy)]ClO_4$	yellow	38.91 (39.45)	2.68 (2.69)	5.67 (5.75)	
4d	$[PdL(bpy)]B(C_6H_5)_4$	yellow	67.90 (67.96)	4.68 (4.71)	3.83 (3.96)	
4e	$[PdL(phen)]ClO_4$	yellow	42.03 (42.29)	2.49 (2.56)	5.53 (5.48)	
4f	$[PdL(phen)]B(C_6H_5)_4$	yellow	69.30 (69.01)	4.47 (4.55)	3.85 (3.83)	

TABLE 2. PMR SPECTRA OF THE PALLADIUM(II) COMPLEXES AT ROOM TEMPERATURE

Compound	Solvent	L			Bases
		CH_3	H^5	H^6	
1	$CDCl_3$[a]	2.42 (6H, s)	6.29 (1H, d) 6.52 (1H, d)	7.66 (2H, d)	
2a	$CDCl_3$[a]	2.17 (6H, s)	6.11 (2H, d)	7.44 (2H, d)	0.79 (12H, t, $-C\underline{H}_3$), 1.48 (8H, unresolved sex, $-CH_2-C\underline{H}_2-CH_3$), 2.62 (8H, broad, $-C\underline{H}_2-NH_2$), 5.80—6.40 (8H, $-N\underline{H}_2$)[c]
	D_2O[b]	2.75 (6H, s)	6.78 (2H, d)	8.23 (2H, d)	1.36 (12H, t, $-C\underline{H}_3$), 2.09 (8H, sex, $-CH_2-C\underline{H}_2-CH_3$), 3.04 (8H, t, $-C\underline{H}_2-NH_2$)
2b	$CDCl_3$[a]	1.20 (6H, s)	5.74 (2H, d)	d)	3.78 (8H, broad, $-C\underline{H}_2-NH_2$), 6.70—7.80 (m, $\underline{H}^6$, $-CH_2-N\underline{H}_2$ and $-CH_2-$)
3a	D_2O[b]	2.73 (6H, s)	6.75 (2H, d)	8.20 (2H, d)	3.10 (8H, s, $-C\underline{H}_2-NH_2$)
3b	D_2O[b]	2.75 (6H, s)	6.78 (2H, d)	8.24 (2H, d)	2.14 (4H, quin, $-CH_2-C\underline{H}_2-CH_2-$), 3.08 (8H, t, $-C\underline{H}_2-NH_2$)
3c	D_2O[b]	2.69 (6H, s)	6.72 (2H, d)	8.20 (2H, d)	3.05 (s, $-N-(C\underline{H}_3)_2$, 3.04—3.20 (m, $-C\underline{H}_2-N-(CH_3)_2$),[e] 3.20—3.28 (4H, m, $-C\underline{H}_2-NH_2$)
4a	D_2O[b]	2.52 (3H, s) 2.80 (3H, s)	6.76 (1H, d) 6.87 (1H, d)	f)	7.70—8.70 (m, $\underline{H}^6$ and bpy)
4b	D_2O[b]	2.22 (3H, s) 2.70 (3H, s)	6.31 (1H, d) 6.75 (1H, d)	g)	7.20—8.80 (m, $\underline{H}^6$ and phen)
4c	$(CD_3)_2SO$[a]	2.20 (3H, s)	6.53 (1H, d)	f)	7.50—8.40 (9H, m, $\underline{H}^6$ and bpy)

a) TMS was used as an internal reference. b) TMS was used as an external reference. c) The signal overlaps with 5-position proton of the pyronate anion, the composite area corresponding to 10H. d) The signal overlaps with the amine and phenyl protons of ba. e) The signal overlaps with the methyl protons of the *N,N*-Me_2en, the composite area corresponding to 16H. f) The signal overlaps with the bpy resonances. g) The signal overlaps with the phen resonances.

TABLE 3. CHARACTERISTIC IR BANDS (cm^{-1}) OF THE PALLADIUM(II) COMPLEXES

Compound	ν (C=O)	ν (C=C)			ν (M–O)	ν (M–N)	δ (N–M–N)	Others			
1	1600	1564	1545		419						
2a	1612	1573	1514								
2b	1612	1573	1516								
3a	1607	1595	1552			520	288				
3b	1604	1559	1499			512	257				
3c	1603	1567—1558		1510		510	269				
4c	1594	1564	1543		411			768	722	1110—1075	622
4d	1604	1565	1550		411			764	720		
4e	1596	1564	1550		410			1632	1520	1090—1074	622
4f	1598	1566	1548		410			1633	1520		

Table 2. The spectral pattern suggests the coexistence of two different magnetic environments for the 5-position protons. The complex may exist as a mixture of *cis* and *trans* isomers, as is shown below:

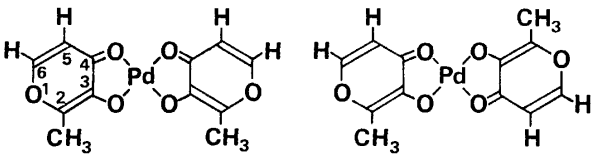

cis *trans*

Whether the two carbonyl groups occupy mutually *cis* or *trans* positions seems to exert a different influence on the proton in question. The nearly equal intensities of the two signals at 6.29 and 6.52 ppm indicate that the *cis* and the *trans* isomers exist in equal amounts in chloroform, although the signal assignments to the two isomers are not possible. The methyl protons and the 6-position protons resonate as a singlet and a doublet respectively. Their insensitivity to the geometrical structure might arise from the fact that they are farther from the donor atoms than the 5-position protons.

Table 4. Molar conductivities of the palladium(II) complexes[a)]

Complex	Solvent	Λ_M
2a	H_2O	119
	EtOH	16.4
2b	EtOH	17.3
3a	H_2O	165
3b	H_2O	163
3c	H_2O	165
4c	DMSO	28.9
4e	DMSO	17.3
$[Pd(pa)_2I_2]$	DMSO	0
$[Pd(ba)_2I_2]$	DMSO	0
$[Pd(en)_2]I_2$	DMSO	95.2
$[Pd(tn)_2]I_2$	DMSO	135
$[Pd(N,N\text{-}Me_2cn)_2]I_2$	DMSO	133
$[Pd(bpy)I_2]$	DMSO	4.2
$[Pd(phen)I_2]$	DMSO	8.7

a) Molar conductivity of the 10^{-3} M solution at 25 °C ($ohm^{-1}\cdot cm^2\cdot mol^{-1}$).

$[Pd(N)_4]L_2$ (2). As may be seen in Table 3, these complexes exhibit the ν(C=O) and ν(C=C) bands at 1612 cm^{-1}, and at 1573 and 1515 cm^{-1}, respectively. The ν(C=O) frequency is slightly higher than that for **1**, but it is not diagnostic for the presence of L in the outer sphere. On the other hand, no band is observed in the Pd–O stretching region (400—500 cm^{-1}), suggesting that the 3-hydroxy-2-methyl-4-pyronate anion is not coordinated to the Pd(II) ion. The molar conductivity data (Table 4) indicate that Compound **2a** is a 1:2 electrolyte in water, while Compounds **2a** and **2b** do not dissociate completely in ethanol.[8)] The molecular-weight data of these complexes (Table 5) also show that they are partially dissociated in ethanol. During the measurements of the conductivity and the molecular

Table 5. Molecular-weight data for the $[Pd(N)_4]L_2$ complexes[a)]

Compound	Solvent	Temp °C	Concentration ($\times 10^{-3}$ M)	Calcd	Found
2a	EtOH	40	1.33	593	342
	EtOH	40	3.32		401
	EtOH	40	4.65		435
	$CHCl_3$	30	1.70		606[b)]
2b	EtOH	40	2.51	758	367
	$CHCl_3$	30	2.53		256[c)]

a) The molecular-weight values listed were determined *ca.* 30 min after dissolution. b) This value changed with the time, reaching 538 and 399 *ca.* 1 and 25 h after dissolution respectively. c) This value changed with the time, reaching 240 *ca.* 25 h after dissolution.

weight in ethanol, the color of the solution gradually changed from faintly yellow to yellow orange. These results seem to be caused by ionization and the following ligand substitution:

$$[Pd(N)_4]L_2 \rightleftarrows [PdL(N)_2]L + 2N \quad (1)$$

The molecular weight of **2a**, determined *ca.* 30 min after dissolution in chloroform, nearly coincides with the calculated value, reflecting poor ionization in this solvent, but the value diminishes with time, suggesting the gradual progress of the ligand substitution of **2a** according to Eq. 1.

In the PMR spectrum of **2a** in D_2O, the signals of the methyl, 5-position, and 6-position protons of 3-hydroxy-2-methyl-4-pyronate anion were observed at 2.75 s, 6.78 d ($J_{5,6}$=5.2 Hz), and 8.23 d ppm respectively. These values coincide with those for the protons of L in $[Pd(NN)_2]L_2\cdot nH_2O$ (**3**), which are 1:2 electrolytes in D_2O, suggesting again that **2a** dissociates completely in D_2O.

On the other hand, Table 5 shows that **2a** exists as the ion aggregate for at least 30 min after dissolution in chloroform; thereafter the substitution and decomposition occur gradually with time. Compound **2b** changes more rapidly in chloroform than does **2a**. The PMR data for **2a** and **2b** in chloroform (Table 2) were taken immediately after dissolution. The protons of L in **2b** resonate at a much higher field than these in **2a**. The benzylamine molecules in the coordination sphere may exert an anisotropic magnetic effect on L in the outer sphere.

Recently, Okeya *et al.*[9)] found that hydrogen exchange occurs between $CDCl_3$ and amine protons in palladium(II) amine complexes containing a β-diketonate anion in the outer sphere, $[PdL_4](\beta\text{-dik})_2$ and $[Pd(\beta\text{-dik})L'_2](\beta\text{-dik})$, where L=primary amine, L'=secondary amine, and β-dikH=acetylacetone or trifluoroacetylacetone. In the present PMR studies of **2a** and **2b** in $CDCl_3$, the hydrogen-exchange reactions between $CDCl_3$ and propylamine and benzylamine are also observed, the signal due to the amine proton diminishing and the peak due to $CHCl_3$ growing concurrently with time (Fig. 1). The pK_a value of HL (8.61)[10)] is near that of acetylacetone (8.82),[10)] and the pyronate anion, L, in

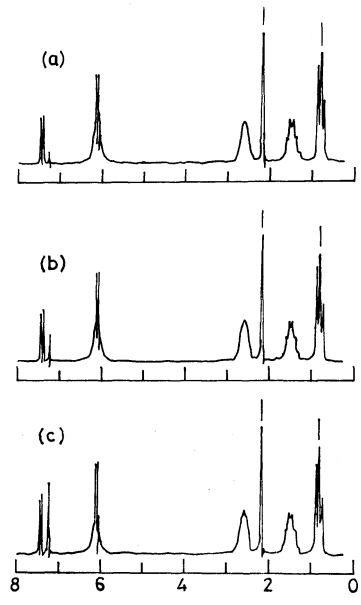

Fig. 1. The PMR spectra of $[Pd(pa)_4]L_2$ [**2a**] in $CDCl_3$ 5 min (a), 30 min (b) and 100 min (c) after dissolution, respectively.

the outer sphere may accept a hydrogen ion from the amine in the coordination sphere:

$$[Pd(RNH_2)_4]^{2+}(L^-)_2 \rightleftarrows [Pd(RNH)(RNH_2)_3]^+L^-(HL) \quad (2)$$

$$[Pd(RNH)(RNH_2)_3]^+L^-(HL) + CDCl_3 \longrightarrow [Pd(RNHD)(RNH_2)_3]^{2+}(L^-)_2 + CHCl_3 \quad (3)$$

$[Pd(NN)_2]L_2 \cdot nH_2O$ (3). The water contents of **3a**, **3b**, and **3c** were determined from the thermogravimetric curves of these complexes. The TG curves show that the liberation of the water occurs at around 45—110 °C in either case. In the IR spectra of the dehydrated complexes, the intensity of the fairly strong and broad bands which appeared at 3170 (**3a**), at 3460 and 3340 (**3b**), and at 3325 and 3180 (**3c**) cm^{-1}, diminished, although none of these bands except the 3460 and 3340 cm^{-1} bands disappeared completely. These results suggest that the bands observed in the 3170—3460 cm^{-1} region are mainly due to the O–H stretching vibration, although the NH_2 stretching bands also appear in this region. These complexes exhibit no band in the Pd–O stretching region, but they do show the Pd–N stretching and N–Pd–N bending bands, suggesting that L is contained in the outer sphere, as in the cases of **2a** and **2b**. The tentative assignment of the ν(Pd–N) and δ(N–Pd–N) bands is based on the data for $[Pd(en)_2]X_2$ (where X=Cl, Br, or I).[11] The molar conductivity data of these complexes also indicate that all three complexes are 1:2 electrolytes in water.

In the PMR spectra of these complexes in D_2O, the signals due to the methyl, 5-position, and 6-position protons of the 3-hydroxy-2-methyl-4-pyronate anion were observed at about 2.72 s, 6.75 d, and 8.22 d ppm respectively, as is shown in Table 2. Although *cis* and *trans* isomers are possible for Compound **3c**, the methyl and methylene $-C\underline{H}_2-NH_2$ protons of *N,N*-dimethylethylenediamine appear as a kind of singlet and a kind of multiplet at 3.05 and 3.26 ppm respectively, while the methylene $-C\underline{H}_2-N-(CH_3)_2$ protons overlap with the methyl protons of *N,N*-Me_2en. This spectral behavior seems to suggest that **3c** exists in D_2O solely as the *trans* or *cis* isomer or that, alternatively, the two isomers exhibit identical chemical shifts by chance.

The counter anion, L, in $[Pd(NN)_2]L_2 \cdot nH_2O$ (**3**) can readily be replaced by treating it with double the molar amount of sodium iodide in ethanol to precipitate the $[Pd(NN)_2]I_2$ complex in a 75—85% yield. This behavior is contrasted with that of the unidentate-amine complex, Complex **2**, which readily reacts with sodium iodide in ethanol to precipitate $[PdI_2(N)_2]$. The bidentate-amine in **3** is bonded to Pd(II) much more strongly than is the unidentate-amine in **2** and resists being displaced by the iodide ion.

$[PdL(bpy\ or\ phen)]X$ ($X=ClO_4$ or $B(C_6H_5)_4$) (4). The infrared data of these complexes suggest that: (a) The perchlorate ion is not coordinated to the palladium ion, since the bands at 1070—1110 *vs.* and 622 cm^{-1} assigned to the perchlorate ion are not split in Compounds **4c** and **4e**. (b) The bpy ligand is coordinated to the palladium ion, since the characteristic band (751 cm^{-1}) of the free bpy is shifted and split to 765 and 720 cm^{-1} in **4c** and **4d**.[12] (c) The phen ligand is coordinated to the palladium ion, since the characteristic bands (1505 and 1605 cm^{-1}) of the free phen are shifted to 1520 and 1632 cm^{-1} respectively in **4e** and **4f**.[13] (d) The 3-hydroxy-2-methyl-4-pyronate anion is coordinated to the palladium ion, since the band (410 cm^{-1}) assignable to the Pd–O stretching vibration is observed for all the complexes, **4c**, **4d**, **4e**, and **4f**. The molar conductivity data of **4c** and **4e** indicate that these complexes are 1:1 electrolytes in dimethyl sulfoxide,[8] supporting the idea that the perchlorate ion is not coordinated to the palladium ion. Compounds **4d** and **4f** are not soluble in common solvents and prevent any conductivity measurement. In the PMR spectrum of **4c** in $(CD_3)_2SO$, the signals of the methyl protons and the 5-position proton of the pyronate ligand were observed at 2.20 s and 6.53 d ppm ($J_{5,6}=5.2$ Hz) respectively, but no signal of the 6-position proton is discernible because of overlapping with the bpy resonances. The appearance of one kind of doublet due to the 5-position proton is in accordance with the lack of geometrical isomers for this complex, contrary to the coexistence of the *cis*- and *trans*-$[PdL_2]$ isomers in the $CDCl_3$ solution. Unfortunately, **4e**, like **4d** and **4f**, is not soluble enough in common solvents to give PMR spectra.

The authors would like to thank Miss Yoshimi Murooka and Miss Keiko Fujita for their experimental assistance. The present work was partially supported by a Grant-in-Aid for Scientific Research from the Ministry of Education.

References

1) H. Morita, Y. Hayashi, S. Shimomura, and S. Kawaguchi, *Chem. Lett.*, **1975**, 339; H. Morita, S. Shimomura, and S. Kawaguchi *Bull. Chem. Soc., Jpn.*, **49**, 2461 (1976).

2) J. P. Fackler, Jr., *Prog. Inorg. Chem.*, **7**, 361 (1966).
3) H. Morita, S. Shimomura, and S. Kawaguchi, *Bull. Chem. Soc., Jpn.*, **51**, 3213 (1978).
4) D. P. Graddon, *Coord. Chem. Rev.*, **4**, 1 (1969).
5) S. Okeya, Y. Onuki, Y. Nakamura, and S. Kawaguchi, *Chem. Lett.*, **1977**, 1305.
6) H. Morita, H. Sakurai, S. Shimomura, and S. Kawaguchi, *Transition Metal Chem.*, **2**, 210 (1977).
7) K. Nakamoto, "Infrared Spectra of Inorganic and Coordination Compounds," 2nd ed, Wiley-Interscience, New York (1970), pp. 247—256.
8) W. J. Geary, *Coord. Chem. Rev.*, **7**, 81 (1971).
9) S. Okeya, Y. Nakamura, and S. Kawaguchi, *J. Chem. Soc., Chem. Commun.*, **1977**, 914.
10) L. G. Sillen and A. E. Martell, "Stability Constants of Metal-Ion Complexes," Supplement No. 1, The Chemical Society, London (1971), pp. 365 and 404. The pK_a values were obtained in an aqueous solution at 25 °C and μ= 0.1($NaClO_4$).
11) G. W. Watt and D. S. Klett, *Inorg. Chem.*, **5**, 1278 (1966).
12) S. P. Shinha, *Spectrochim. Acta*, **20**, 879 (1964).
13) A. A. Schilt and R. C. Taylor, *J. Inorg. Nucl. Chem.*, **9**, 211 (1959).

The Separation of Tin from Water and Sea-water by Flotation and the Determination of Tin by Atomic Absorption Spectrophotometry Following Stannane Generation

Susumu NAKASHIMA

Institute for Agricultural and Biological Sciences, Okayama University, Kurashiki-shi, Okayama 710

(Received November 30, 1978)

A method is described for the separation and determination of sub-microgram levels of tin in water. A sub-microgram amount of tin(II, IV) in a 1000-ml sample of water is coprecipitated with iron(III) hydroxide at pH 4.0 ± 0.2. The precipitate is floated with the aid of sodium dodecyl sulfate and small air bubbles, and then separated and dissolved in 2 ml of 6 M hydrochloric acid and diluted to 10 ml with water. Finally, the tin content is determined by the generation of stannane, using sodium borohydride as a reductant, followed by atomic absorption spectrophotometry with a long absorption cell (60×1.2 cm i.d.). This separation technique has also been successfully applied to the determination of sub-microgram amounts of tin in natural sea-water. The time required for the pre-concentration of tin from a 1000-ml volume of solution is about 15 min per sample after 15 min of stirring.

It is important to establish a rapid, sensitive, and accurate method to determine tin in natural waters from the viewpoints of environmental chemistry, geochemistry, marine biology, and limnology. Tin has so far received little attention as an environmental pollutant in natural waters. Furthermore, almost nothing is known about the tin content in natural waters. Tin probably exists at concentrations below 1 $\mu g\ l^{-1}$ in natural water samples. At such low concentrations, a precise, direct determination is impractical, even by the atomic absorption spectrophotometry of stannane, which has a high sensitivity.[1-3] In addition, nickel(II) causes serious negative interference in the determination of tin by the above hydride-generation method. Hence, it is necessary to pre-concentrate tin from water and separate it from nickel(II) prior to determination.

Coprecipitation with iron(III) hydroxide[4-6] or zirconium hydroxide[7,8] is used as a pre-concentration technique for the determination of tin in aqueous systems. These bulky amorphous precipitates, however, are difficult to filter, and centrifugation is cumbersome for larger volumes.

Mizuike and Hiraide[9] reported a flotation technique carried out with the aid of a hot ethanolic paraffin solution and small nitrogen bubbles for the separation of the tin(IV) coprecipitated with iron(III) hydroxide. This separation technique was successfully applied to the spectrophotometric determination of tin at the ppb level in high-purity zinc metal.

In a previous paper,[10] a flotation technique[9,11,12] in which the precipitate of iron(III) hydroxide is floated with the aid of sodium oleate and small air bubbles was used for the pre-concentration of arsenic in natural non-saline waters.

This communication will describe the application of this separation technique, with suitable modifications, to the pre-concentration of sub-microgram amounts of tin(II, IV) in water. The precipitate is readily separated from the mother liquor and then dissolved in dilute hydrochloric acid for the atomic absorption spectrophotometry by the generation of stannane, using sodium borohydride as a reductant. The various parameters that affect the flotation and determination of tin were investigated. This method is simple and rapid, and it is applicable to the extraction of tin at low ppb levels from large volumes of water and sea-water.

Experimental

Apparatus. A Nippon Jarrell-Ash, Model AA-1 Mark II, atomic absorption spectrophotometer equipped with a Jarrell-Ash tin hollow-cathode lamp and a custom-made silica absorption cell (60×1.2 cm i.d.) was used, along with a Beckman burner supplied with nitrogen and hydrogen.

The apparatus used for the stannane generation was a modified Nippon Jarrell-Ash, Model ASD-1A, hydride-measurement unit coupled to a custom-made hydride-generating cell. The schematic diagram of the analytical system is similar to that described previously.[10]

All the pH measurements were carried out with a Hitachi-Horiba, Model M-5, pH meter, together with a combined glass electrode.

The flotation and separation apparatus was similar to that described by Mizuike and his coworkers.[11,12] The flotation cell was a glass cylinder, 40×6.5 cm i.d., which was fitted with a sintered-glass filter (No. 4) to generate small bubbles. A side arm was added near the bottom of the cell in order to drain out the mother liquor rapidly after the flotation, as is shown in Fig. 1.

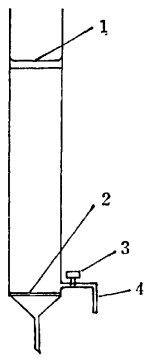

Fig. 1. Flotation cell for pre-concentration of tin.
1: Foam layer containing iron(III) hydroxide and tin, 2: sintered-glass disk (porosity 4), 3: cock, 4: drain pipe.

Reagents. All the reagents were of an analytical-reagent grade except for sodium dodecyl sulfate and sodium oleate. The aqueous reagents were prepared in de-ionized, distilled water. The tin standard solutions were freshly prepared by diluting stock solutions before use.

Tin(IV) Stock Solution (1 mg ml^{-1}): Some (500 mg) high-purity tin metal was dissolved in 40 ml of concentrated sulfuric acid by heating. After cooling, the solution was made up to 500 ml with 2 M hydrochloric acid.

Tin(II) Stock Solution (1 mg ml^{-1}): Some (950 mg) stannous chloride dihydrate was freshly dissolved in 50 ml of concentrated hydrochloric acid, and then the solution was made up to 500 ml in 2 M hydrochloric acid.

Iron(III) Solution (5 mg ml^{-1}): Some (43.17 g) ammonium iron sulfate was dissolved in water, after which the solution was diluted to 1000 ml in 1 M hydrochloric acid.

Sodium Dodecyl Sulfate Solution (1 mg ml^{-1}): Sodium dodecyl sulfate (powder, extra-pure reagent, Wako Pure Chemical Industries, Ltd.) was dissolved in 99.5 v/v % ethanol.

Sodium Oleate Solution (1 mg ml^{-1}): Sodium oleate (powder, extra-pure reagent, Wako Pure Chemical Industries, Ltd.) was dissolved in 99.5 v/v % ethanol with stirring.

Sodium Borohydride Solution (5 w/v %): This solution was used in a 0.1 M sodium hydroxide solution.

Procedure for the Flotation Step. One thousand ml of acidified water is placed in a 1000-ml beaker, and 2 ml of an iron(III) solution is added. The pH of the solution is adjusted to 4.0±0.2 with an aqueous ammonia solution, while being stirred magnetically, in order to precipitate iron(III) hydroxide, and the mixture is stirred for 15 min. After adding 2 ml of a sodium dodecyl sulfate solution to the beaker, the contents of the beaker are transferred to a flotation cell and the residue in the beaker is washed into the cell by using three small portions of water. Air is passed through at a flow rate of 50 ml min^{-1} from the lower end of the cell for about 2 min in order to obtain a complete mixing and flotation of the precipitate. Most of the mother liquor is drained from the side arm by opening the cock of the drain pipe. After closing the cock, the residual mother liquor is sucked off through the sintered-glass disk, and the precipitate is washed with 30 ml of water. Two ml of 6 M hydrochloric acid is added to the cell to dissolve the precipitate, the filtrate is collected by suction in a 10-ml calibrated flask, the sintered-glass disk is washed with water, the washings are added to the flask, and the mixture is diluted to 10 ml with water.

Procedure for the Determination of Tin. One ml of a freshly prepared 5 w/v % sodium borohydride solution is transferred into a stannane-generating cell and the cell is attached to the apparatus. A plastic syringe containing 1 ml of the sample solution is inserted into the side-arm seal of the cell. The four-way stopcock of the apparatus is turned to the sweep position in order to introduce nitrogen into the system, and the sample is injected into the cell. The stannane thus generated is swept into the long absorption cell with nitrogen and then atomized in the nitrogen-hydrogen flame, and the absorption signal is recorded on a recorder. The stopcock is returned to the by-pass position. The cell is carefully rinsed with distilled water.

A calibration curve is constructed using 1.2 M hydrochloric acid solutions containing 1.0 mg ml^{-1} of iron(III) and 0—0.10 μg ml^{-1} of tin(IV); this curve is linear within the above range of tin. The detection limit of tin was found to be 0.5 ng ml^{-1}. No appreciable difference in sensitivity was observed between tin(II) and tin(IV). The coefficients of variations were 1.5 and 1.4 % in 10 replicate runs of 0.04 and 0.08 μg ml^{-1} of tin(IV) respectively.

The atomic absorption apparatus was operated under the following conditions: wavelength, 286.3 nm; lamp current, 8 mA; gas-flow rates: nitrogen, 1.5; hydrogen, 1.5, and auxiliary nitrogen, 6 liter min^{-1}; slit (spectral band width), 1 nm.

Results and Discussion

The Optimum Conditions for the Determination of Tin. The effect of the sodium-borohydride concentration on the evolution of stannane was investigated. As is shown in Fig. 2, it was found that more than 3 w/v % of the reductant concentration (1 ml volume) can quantitatively reduce up to 0.10 μg of tin to stannane. In this work, 1 ml of 5 w/v % of the solution was used.

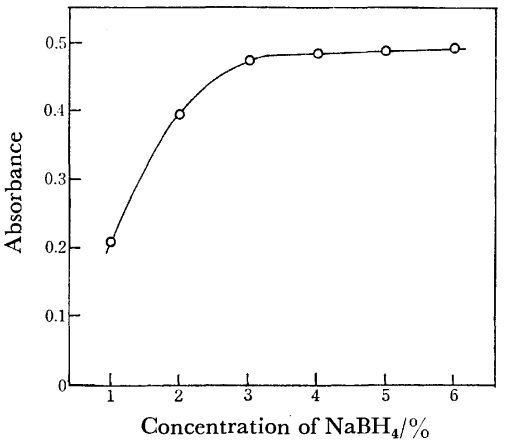

Fig. 2. Effect of sodium borohydride concentration on the evolution of stannane.
Solution containing 0.10 μg of Sn(IV), sample volume: 1 ml.

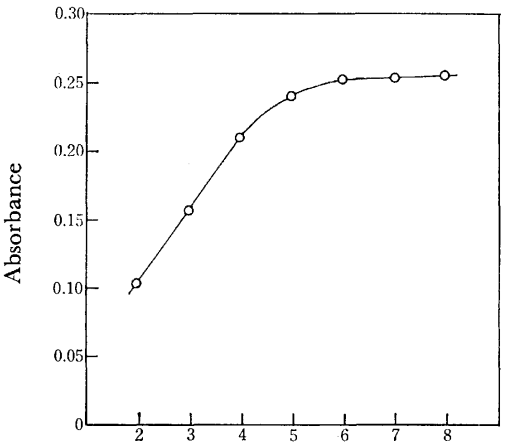

Fig. 3. Effect of nitrogen flow-rate on the evolution of stannane.
Solution containing 0.05 μg of Sn(IV), sample volume: 1 ml.

The optimum conditions for the sensitivity of tin were dependent on the flow rate of auxiliary nitrogen, as is shown in Fig. 3. The tin absorbance increased with an increase in the flow rate of auxiliary nitrogen up to 6 l min^{-1} when the flow rates of both nitrogen and hydrogen were 1.5 l min^{-1}. The optimum sensitivity was obtained with a flow rate of auxiliary nitrogen

between 6 and 8 l min^{-1}; a flow rate of auxiliary nitrogen of 6.0 l min^{-1} was, therefore, adopted throughout.

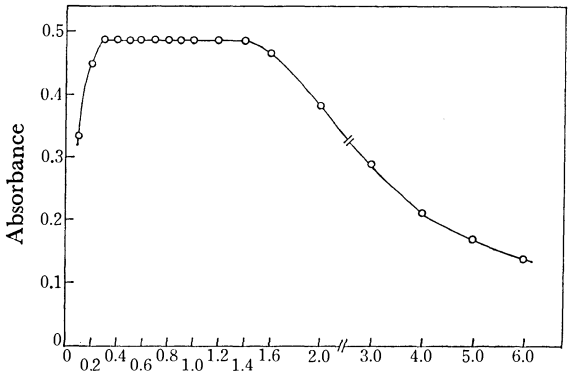

Fig. 4. Effect of hydrochloric acid concentration on the evolution of stannane.
Solution containing 0.10 μg of Sn(IV), sample volume: 1 ml.

Figure 4 shows the effect of the hydrochloric-acid concentration on the generation of stannane. The optimal concentration of hydrochloric acid is between 0.3—1.4 M and is critical because of the pronounced decrease in sensitivity with an increase in the acid concentration. Therefore, it is necessary to adjust the acid concentration of the sample solution carefully for reliable results. The use of a tin(II) solution gave similar results. Thus, the final acidity of hydrochloric acid was maintained at 1.2 M in further work.

The effect of iron(III) added as a collector on the generation of stannane was also studied. A slighter larger suppression (about 6%) of the tin absorbance was observed in the presence of 0.25—2.5 mg ml^{-1} of iron(III) in comparison with that in the absence of iron(III). Therefore, a calibration curve for tin was constructed using tin(IV) solutions containing 1.0 mg ml^{-1} of iron(III).

The Optimum Conditions for the Flotation of Tin.

Effect of pH: The effect of the pH of a 1000-ml solution containing 0.8 μg of tin(II, IV), 10 mg of iron(III) and 2.0 mg of surfactant on the coprecipitation of tin was studied. Hydrochloric acid and an aqueous ammonia solution was used to adjust the pH to values within the range of 3.4—10.0. The results are shown in Fig. 5. Quantitative recoveries of both the divalent and the tetravalent states of tin were obtained over this range, as well as in the case of arsenic(III, V).[10] The most stable layer of surface foam supporting the precipitate of iron(III) hydroxide when sodium dodecyl sulfate was

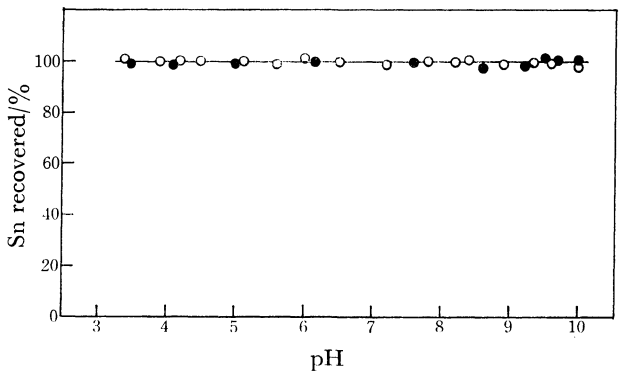

Fig. 5. Coprecipitation of tin with iron(III) hydroxide as a function of pH.
Solution containing 0.8 μg of Sn and 10 mg of Fe(III), sample volume: 1000 ml, ●: Sn(II), ○: Sn(IV).

used was found within the pH range of 3.4—7.0; the pH of 4.0±0.2 was, therefore, used throughout the work. At a pH above 7, a stable surface-foam layer was obtained by using sodium oleate as a surfactant.

Amounts of Iron(III) and Surfactant: The recovery of tin as a function of the amount of iron(III) added to the solution is given in Table 1. Quantitative recoveries of tin were obtained above 5.0 mg of iron(III). In this work, therefore, 10 mg of iron(III) was added to 1000 ml of a solution. The amount of sodium dodecyl sulfate required for the complete flotation of the precipitate was also studied. Quantitative recoveries of tin were obtained between 0.5—8.0 mg of sodium dodecyl sulfate, and so 2.0 mg of it in a 1000 ml solution was added in further work.

Stirring Time: The relation between the stirring time and the recovery of tin was investigated. The results are shown in Table 2. Coprecipitation was quantitative over the range of 5—40 min; stirring for 15 min was found best.

Table 2. Relation between stirring time and recovery of tin[a)]

Stirring time (min)	5	10	15	20	25	30	40
Sn recovered (%)	95	99	100	98	99	102	100

a) Solution containing 0.8 μg of Sn(IV) and 10 mg of Fe(III); pH, 4.0±0.2; sample volume, 1000 ml.

Effect of Foreign Ions: By following the proposed procedure, the effects of various ions on the separation and determination of tin(IV) were investigated. Table 3 compares the permissible amounts of foreign ions for the determination of tin(IV) with and without coprecipitation. As can be seen, when coprecipitation at

Table 1. Relation between amount of iron(III) added and recovery of tin[a)]

Fe(III) added (mg)	2.5	5.0	7.5	10.0	15.0	20.0	25.0
Sn recovered (%)	91	99	100	99	99	100	101

a) Solution containing 0.8 μg of Sn(IV) and 2 mg of sodium dodecyl sulfate; pH, 4.0±0.2; sample volume, 1000 ml.

Table 3. Comparison of permissible amounts of foreign ions for determination of tin with and without coprecipitation

Ion	Limit, [Ion]/[Sn]		Ion	Limit, [Ion]/[Sn]	
	Direct[a]	With copptn[b]		Direct[a]	With copptn[b]
Mo^{6+}	600	1000	Sb^{3+}	100	100
Hg^{2+}	400	1000	Cu^{2+}	60	800
Te^{4+}	400	400	As^{3+}	50	50
Se^{6+}	200	1000	As^{5+}	50	50
Bi^{3+}	100	100	Se^{4+}	40	40
Co^{2+}	100	1000	Ni^{2+}	2	800

The following are tolerable: Na^+, K^+, Ca^{2+}, Mg^{2+}, Cl^-, SO_4^{2-}, NO_3^-, SiO_3^{2-} (excess, $\times 10000$), Sr^{2+}, Ba^{2+}, Cd^{2+}, Zn^{2+}, Mn^{2+}, Al^{3+}, Cr^{3+}, Cr^{6+}, Pb^{2+}, V^{5+}, PO_4^{3-} (excess, $\times 1000$). a) Solution containing 0.10 μg of Sn(IV); sample volume, 1 ml. b) Solution containing 1.0 μg of Sn(IV) and 10 mg of Fe(III); sample volume, 1000 ml.

pH 4.0±0.2 is used, most foreign ions normally present in natural waters hardly interfere at all with the determination of tin(IV), and suppressive effects by diverse ions, especially, those by nickel(II), copper(II), cobalt(II), selenium(VI) and mercury(II), were found to be largely eliminated in comparison with those which occur when tin is directly determined without coprecipitation. The values of the permissible amounts (Ion/Sn in weight) of these ions in the proposed method increased from 2, 60, 100, 200, and 400 to 800, 800, 1000, 1000, and 1000 for nickel(II), copper(II), cobalt(II), selenium(VI), and mercury(II) respectively, compared with the values permissible in the direct determination. However, hydride-forming elements, such as selenium(IV), antimony(III), arsenic(III, V) and bismuth(III), are coprecipitated with iron(III) hydroxide in the same way as tin and had a relatively great effect on the generation of stannane.

Recovery of Tin: The solutions (1000 ml) at pH 4.0±0.2 containing 10 mg of iron(III), 2.0 mg of sodium dodecyl sulfate, and 0.2, 0.4, 0.6, 0.8, 1.0, 2.0, 4.0, 6.0, 8.0, 10.0, 15.0, and 20.0 μg of tin(IV) were analyzed by the procedure described above. The recoveries of the tin that had been added were greater than 95% in all instances. No blank value was detected throughout the whole analytical process. The proposed conditions, therefore, appear to be optimal for 1000-ml volumes of a solution containing up to 20 μg of tin(IV).

The relative standard deviations of ten-times-repeated analyses of the solutions containing 0.4 and 0.8 μg of tin(IV) per 1000 ml were 2.4 and 2.3% respectively.

Applications to Natural Sea-water: In order to investigate the applicability of this method to sea-water, the recoveries of known amounts of tin(IV) added to natural sea-water samples taken up at two different locations were examined by the above procedure. The analyses were carried out 1000-ml aliquots of clear, uncontaminated sea-water, filtered through 0.45 μm Millipore filters after the addition of hydrochloric acid immediately after sampling. Table 4 presents the recovery data of the tin. These results indicate that the analytical process had a satisfactory recovery of tin from sea-water at pH 4.0±0.2. The average tin concentrations for both sea-water samples were low, 0.07 and 0.14 μg l^{-1}.

Table 4. Recovery of tin added to natural sea-water samples[a]

Tin added (μg)	Tin[b] found (μg)	Tin recovered (μg)	Mean recovery (%)	Tin in sample (μg l^{-1})	
None	0.139±0.004			0.14	c)
0.200	0.338±0.008	0.199	100		
None	0.068±0.003			0.07	d)
0.400	0.459±0.009	0.391	98		

a) Volume of sample, 1000 ml. b) The mean value of four measurements. c) This sample was taken at Shibukawa, Okayama Prefecture. d) This sample was taken at Ajino, Okayama Prefecture.

Hamaguchi *et al.*[5,6] reported an average of 0.81 μg l^{-1} in the range of 0.30—1.22 μg l^{-1} of the tin concentrations in four sea-water samples collected from the Pacific Ocean. Moreover, Kodama and Tsubota[13] reported that the tin concentrations in six water samples from the North Pacific ranged from 0.63 to 1.93 μg l^{-1}, showing an average of 1.15 μg l^{-1}. The reason for the discrepancy between the values reported in this work and those in the literature is not clear. A possible explanation may be that the former sea-water samples were collected near the seashore, and the latter ones, in the ocean.

Conclusions

The flotation of sub-microgram amounts of tin(II, IV) coprecipitated with iron(III) hydroxide is useful as a pre-concentration technique for the extraction of tin(II, IV) from a large volume of water, and subsequent atomic-absorption measurement in a long absorption cell of the stannane from the tin(II, IV) is an accurate method for the determination of tin. In addition, the satisfactory isolation of tin from such interfering ions as nickel(II) and copper(II) present in water is the advantage of the proposed method.

The author wishes to thank Professor Atsushi Mizuike and Dr. Masataka Hiraide of Nagoya University for their helpful advice on the flotation technique, and Assistant Professor Fuji Morii of Okayama University for her useful discussions.

References

1) K. C. Thompson and D. R. Thomerson, *Analyst (London)*, **99**, 595 (1974).
2) P. N. Vijan and C. Y. Chan, *Anal. Chem.*, **48**, 1788 (1976).
3) H. D. Fleming and R. G. Ide, *Anal. Chim. Acta*, **83**, 67 (1976).
4) K. Shimizu and N. Ogata, *Bunseki Kagaku*, **12**, 526 (1963).

5) H. Hamaguchi, K. Kawaguchi, N. Onuma, and R. Kuroda, *Anal. Chim. Acta*, **30**, 335 (1964).
6) H. Hamaguchi, R. Kuroda, N. Onuma, K. Kawaguchi, T. Mitsubayashi, and H. Hosohara, *Geochim. Cosmochim. Acta*, **28**, 1039 (1964).
7) W. Yoshimura, *Bunseki Kagaku*, **24**, 714 (1975).
8) E. Amakawa, K. Onishi, N. Taguchi, and H. Seki, *Bunseki Kagaku*, **27**, 81 (1978).
9) A. Mizuike and M. Hiraide, *Anal. Chim. Acta*, **69**, 231 (1974).
10) S. Nakashima, *Analyst(London)*, **103**, 1031 (1978).
11) M. Hiraide, Y. Yoshida, and A. Mizuike, *Anal. Chim. Acta*, **81**, 185 (1976).
12) M. Hiraide and A. Mizuike, *Bunseki Kagaku*, **26**, 47 (1977).
13) Y. Kodama and H. Tsubota, *Bunseki Kagaku*, **20**, 1554 (1971).

NOTES

BULLETIN OF THE CHEMICAL SOCIETY OF JAPAN, VOL. 52 (6), 1849—1850 (1979)

C_2^- Ion as Impurity from Halogen Ion Source and a Possibility of Its Application to Reaction Kinetics Studies

Nobuyuki KASHIHIRA*,† and Egon VIETZKE

Institut für Chemie der Kernforschungsanlage Jülich GmbH, Institut 1: Nuklearchemie, 5170 Jülich, FRG

(Received August 16, 1978)

Synopsis. Negative ions from a hot LaB_6 surface were studied with a quadrupole mass filter. C_2^- ion was formed *via* a charge exchange process. About 10^{-11} A of mass-selected C_2^- ion current was obtained above 40 eV of ion energies. A possibility of employing this to study a reaction kinetics is discussed.

We constructed an ion source for the negative atomic halogen ions based on surface ionization[1,2] and successfully applied it to a study on the ion-molecule reactions of $Br^- + CH_4$,[3] $Br^- + CH_3F$.[4] The ion source delivered *ca.* 10^{-8} A of the atomic halogen ion current above 20 eV of the ion energy with caesium halide as the source material and LaB_6 as ionizing material. The ion beam was checked in terms of energy spread and purity. The intrinsic energy spread at the zero energy was found to be 0.55 eV[2] from measurement of dependence of the energy spread on ion energy with an electrostatic energy analyzer of parallel plate type. The purity of the beam was studied by mass analysis with a RF quadrupole mass filter. The result indicated that the ion beam is quite pure, no measurable amounts of impurity ions being observed.

In the present paper we report on the ionic impurities in the ion beam observed with more sensitive electrometer under optimal conditions for the minority ions but not necessarily for the main ion, and discuss their possible use as an ion beam. In the case of caesium bromide as the source material such negative ions as F^- ($m/e=19$), C_2^- ($m/e=24$), CN^- ($m/e=26$), O_2^- ($m/e=32$), and Cl^- ($m/e=35$ and 37) were observed as the minority ions besides Br^- ion, although their ion intensities were less than 100 ppm of Br^- ion under normal operating conditions and *ca.* 10^{-11} A for C_2^- ion with a kinetic energy of 40 eV and less for others under optimal conditions. As the Br^- ion,[1,2] the halogen ions Cl^- and F^- are formed by a negative surface ionization on the hot LaB_6 surface which has a small work function of 2.6 eV,[5] due to the large electron affinities of their neutral species, Br, Cl, and F being 3.54 eV, 3.76 eV and 3.58 eV, respectively.[6] Since the neutral species of these minority halogens exist as an impurity in CsBr, the contribution of the corresponding ions can be in the same order of magnitude as an impurity content.

Of the minority ions, the particularly interesting one is C_2^- ion which is the second abundant ionic species next to Br^- ion in the mass spectrum. Contrary to the halogens, the neutral species for C_2^- and CN^- ions may not be impurities of the source material but are formed only at the hot graphite surface as seen in an emission study with a graphite electrode. Furthermore, C_2 has the electron affinity of 3.54 eV[6] which is large enough to be surface ionized on the hot LaB_6 surface. However, the experimental result shows that no such ion was formed when no CsBr was supplied. Thus, it is concluded that C_2^- ion is not produced by the surface ionization. As an alternative process for the formation of this ion we assign the accidental near resonance charge exchange between Br^- and C_2, since the electron affinity of C_2 matches that of Br. The cross section for this process is supposed to be large, possibly in the order of 10×10^{-16} cm^2.[7] However, the correct mechanism for C_2^- ion formation remains open to question.

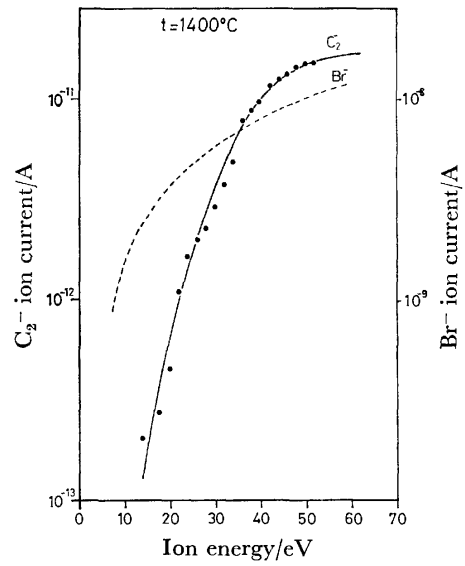

Fig. 1. Energy dependence of C_2^- ion current with CsBr at 1400 °C.

Although the ion source was originally designed and operated only for the sake of the major ion, we tested the possibility of employing it as the beam source for the minority ions. The C_2^- ion current was measured under the optimum operating conditions in order to get a maximum current. The variation of the ion intensity as a function of the ion energy is shown in Fig. 1. The ion intensity of C_2^- ion is *ca.* 10^{-11} A above 40 eV, declining sharply for lower ion energies. The behavior is similar to that of the major ion indicating a space charge effect. However, the intensities for these ions can not be directly compared since they were measured

* Present address: Training Institute for Environmental Pollution Control, 526 Tokorozawa, Tokorozawa 359.

under optimal conditions for each ion.

The energy spread of the C_2^- ion beam was also measured, an intrinsic energy spread of *ca.* 0.55 eV being obtained as the major ion by extrapolating an energy spread-ion energy curve to zero energy.

In applying this ion source to the reaction kinetics for the minority ions, however, a mass discrimination of the desired ion from others, especially the major ion, is necessary prior to the deceleration and focussing of ion beam onto a scattering cell. This can be easily achieved with a small permanent magnet or a RF quadrupole mass filter, since only a moderate mass resolution is required. Furthermore, a very small number of ionic products can be detected by mass analysis in combination with a pulse counting technique.

Since C_2^- ion is very stable and an important precursor in flame reactions reacting with such molecules as H_2, H_2O and hydrocarbons, it would be interesting to study such ion-molecule reactions by means of the present source.

Experimental

The apparatus consists of an ion emitter, a magnet, an acceleration-deceleration multistage lens and a RF quadrupole mass filter. The ion source chamber and the chamber which accomodates a mass filter are separately pumped with oil diffusion pumps. The operating pressures of both chambers are maintained below 10^{-6} Torr (1 Torr=133.322 Pa). The ion source, unless otherwise specified, is constructed of stainless steel. The main part of the ion source is the ion emitter made of a rear-fed layer of LaB_6 as the ionizing material (Fig. 2).

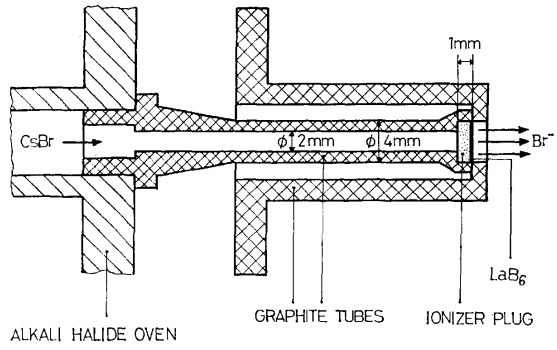

Fig. 2. Cross sectional view of the alkali halide type ion emitter.

Graphite (type EK 87, Ringsdorff, Bonn) was used as a structural material. However, since graphite does not bind firmly with LaB_6, LaB_6 powder was suspended in a small amount of methanol and then pressed onto the porous graphite plug; after evaporation of the solvent in a vacuum, it was heated to its operating temperature, affording a mechanically stable sedimentary layer of LaB_6. The concentric graphite tubes are in contact with each other at their front ends and heated by an alternating current of *ca.* 100 A to 1300 °C in the region of the ionizing area. The desired halogen is supplied as caesium halide from the oven heated by means of a molybdenum wire to 500 °C or higher. The vapor passes the inner graphite tube and diffuses through the porous graphite plug and the sedimentary layer of LaB_6, at which the alkali halide molecules are eventually surface ionized. The negative ions thus formed are extracted and simultaneously accelerated in order to avoid a space charge effect. After being focused by a couple of lenses and then decelerated to the desired ion energy equal to the voltage applied to the ion emitter, the ions are subjected to mass analysis with a RF quadrupole mass filter (Extranuclear Laboratries, Model 324-9) and collected on a cylindrical Faraday cup, the current from which is measured with a Keithley 414S Picoammeter. At the operating temperature 1300 °C, the LaB_6 surface also emits electrons, in a number at least three orders of magnitude greater than that of major negative ions. The electrons are removed from the ions by means of a magnetic field perpendicular to the beam axis. The ions proceed practically unaffected by the field due to their far larger masses. When necessary, energy analysis is carried out after deceleration by means of an electrostatic energy analyser.

The authors thank Professor G. Stöcklin for his encouragement and advice. One of them (N.K.) thanks him particularly for the opportunity to carry out the experiments at K.F.A.

References

1) N. Kashihira and E. Vietzke, *Report Jül-1032-NC*, Jülich (1973).

2) N. Kashihira, E. Vietzke, and G. Zellermann, *Rev. Sci. Instr.*, **48**, 171 (1977).

3) N. Kashihira, E. Vietzke, and G. Zellermann, *Chem. Phys. Lett.*, **39**, 316 (1976).

4) N. Kashihira, E. Vietzke, and G. Zellermann, "Proceeding of the 9th International Symposium on Hot Atom Chemistry," Blacksburg, USA, September 18—23, (1977).

5) J. M. Lafferty, *J. Appl. Phys.*, **22**, 299 (1951).

6) V. I. Vedenyv, L. V. Gurvich, V. N. Kondratyev, V. A. Medveden, and Ye. L. Frankevich, "Bond Energies, Ionization Potentials and Electron Affinities (English Edition)," St. Martins Press, New York, N. Y. (1966).

7) R. F. Stebbings, "Molecular Beam," ed by J. Ross, Interscience Publishers, New York, N.Y. (1966), p. 242.

BULLETIN OF THE CHEMICAL SOCIETY OF JAPAN, VOL. 52 (6), 1851—1852 (1979)

The Crystal Structure of the 1: 2 Tetrapropylammonium Guanidinium Bromide Complex

Tooru TAGA,* Makoto OHASHI, Kenji OSAKI, Koichiro MIYAJIMA, and Hiromitsu YOSHIDA

Faculty of Pharmaceutical Sciences, Kyoto University Yoshidashimoadachi-cho, Sakyo-ku, Kyoto 606

(Received November 27, 1978)

Synopsis. The crystal of the title complex is monoclinic, $P2_1/a$ with these unit cell dimensions: $a=16.16$, $b=19.18$, $c=15.46$ Å, and $\beta=98°$. The crystal structure has layers of hydrogen-bond networks formed by the guanidinium and bromide ions. Two different conformers of the tetrapropylammonium ions are packed between the networks.

This work is one of a series of X-ray studies on the crystal structures of tetraalkylammonium guanidinium halide complexes.[1-3] Two kinds of the crystals of tetrapropylammonium guanidinium bromide complexes, 1 : 2 and 2 : 1 $(Pr)_4NBr$–GuBr, were obtained from the aqueous solutions of the mixed tetrapropylammonium bromide and guanidinium bromide salts.[1] The crystal structure of the 1 : 2 complex described in this note received attention in relation to that of the 2 : 1 complex reported previously.[2]

Experimental

The crystals obtained by the evaporation method were very unstable in the air. Thus, the X-ray experiments were performed by sealing the crystals in a capillary tube. The crystals are monoclinic, space group $P2_1/a$, as indicated by the systematic absences of $h0l$ for h odd and $0k0$ for k odd. The cell dimensions are $a=16.65(9)$, $b=19.18(5)$, $c=15.46(14)$ Å, and $\beta=98(2)°$. The observed crystal density is 1.415 g/cm^3, while the calculated density is 1.485 g/cm^3 if eight chemical unit, $[N(C_3H_5)_4][C(NH_2)_3]_2Br_3$, are assumed in the unit cell. The higher order reflections were not observed in the Weissenberg films taken by rotating the crystals about the b- and c-axes, using Ni-filtered Cu $K\alpha$ radiation. Intensity data of 1498 reflections were collected by the use of a SYNTEX AD-1 densitometer.

The structure was solved by the heavy-atom method. The six bromide ions were determined by the direct method using the program MULTAN. The structure was refined by successive cycles of the block-diagonal and full-matrix least-squares methods with the anisotropic thermal parameters of the bromide ions. The refinement was terminated at the stage where an R-value was reduced to 0.15, since the temperature factor of this crystal is large ($\bar{B}=4.9$). All computations were performed on a FACOM M-190 in the Data Processing Center of Kyoto University, using the program system KPAX which included the UNICS program.

Results and Discussion

Table 1 lists the positional parameters and their estimated standard deviations, and Figs. 1 and 2 show the crystal structures projected along the a- and b-axes, respectively.

The structure is composed of the two-dimensional hydrogen-bond network formed by the guanidinium ions and the bromide ions. The tetrapropylammonium groups are packed between these hydrogen-bond networks. This layer-like structure resembles that observed previously in the crystal of tetrabutylammonium guanidinium bromide monohydrate complex.[3] However, an interesting aspect of this crystal structure is found in its unique hydrogen-bond networks. Each guanidinium ion is bonded to three bromide ions by the six NH···Br hydrogen-bonds, and forms a rigid triangular $GuBr_3$ group; the average N···Br distance is 3.45 Å. The $GuBr_3$ groups are linked together in a

TABLE 1. POSITIONAL PARAMETERS AND THEIR ESTIMATED STANDARD DEVIATIONS

The values have been multiplied by 10^4.

Atom	x	y	z	Atom	x	y	z
Br(1)	3797(5)	1728(4)	4054(5)	N(P1)	3625(28)	3065(22)	6308(31)
Br(2)	13(6)	−20(5)	2409(6)	C(11)	3311(60)	3371(47)	7142(62)
Br(3)	3842(5)	1755(4)	8725(5)	C(12)	2764(57)	3804(48)	7048(64)
Br(4)	2400(4)	5047(4)	4808(6)	C(13)	2418(45)	4055(37)	7930(51)
Br(5)	2704(5)	303(6)	222(6)	C(21)	3918(31)	3601(25)	5791(37)
Br(6)	31(5)	4719(5)	2504(6)	C(22)	4325(49)	3554(39)	5080(54)
				C(23)	4760(44)	4089(36)	4746(49)
C(G1)	505(46)	4261(38)	5526(53)	C(31)	4228(44)	2518(36)	6557(52)
N(11)	958(31)	4740(25)	5989(34)	C(32)	5075(54)	2689(44)	7212(61)
N(12)	642(25)	4049(20)	4814(29)	C(33)	5721(53)	2272(44)	7484(60)
N(13)	−238(27)	4210(21)	5770(30)	C(41)	3062(50)	2742(42)	5740(57)
				C(42)	2414(70)	2145(56)	6087(76)
C(G2)	513(36)	4345(29)	333(43)	C(43)	1671(38)	2043(32)	5254(44)
N(21)	1079(31)	4642(27)	880(35)				
N(22)	541(35)	4274(30)	−452(40)	N(P2)	3509(23)	3079(20)	1265(27)
N(23)	−99(26)	3988(22)	575(31)	C(51)	2932(42)	3508(35)	1904(48)
				C(52)	2511(59)	3077(50)	2469(64)
C(G3)	2137(58)	759(47)	2230(62)	C(53)	2333(44)	3549(37)	3139(49)
N(31)	2860(30)	885(24)	2225(33)	C(61)	3804(44)	3678(36)	784(50)
N(32)	1506(32)	667(26)	1570(37)	C(62)	4349(64)	3349(50)	105(68)
N(33)	1849(32)	882(25)	3092(37)	C(63)	4624(49)	4028(40)	−196(53)
				C(71)	4184(31)	2630(26)	1836(38)
C(G4)	2201(49)	655(40)	7314(55)	C(72)	4737(40)	2966(33)	2355(45)
N(41)	2936(34)	601(29)	7359(38)	C(73)	5453(35)	2460(29)	2751(43)
N(42)	1629(36)	297(30)	6718(40)	C(81)	2825(44)	2643(37)	659(51)
N(43)	1878(35)	772(28)	8041(40)	C(82)	2105(33)	2979(28)	105(38)
				C(83)	1477(65)	2323(55)	−219(75)

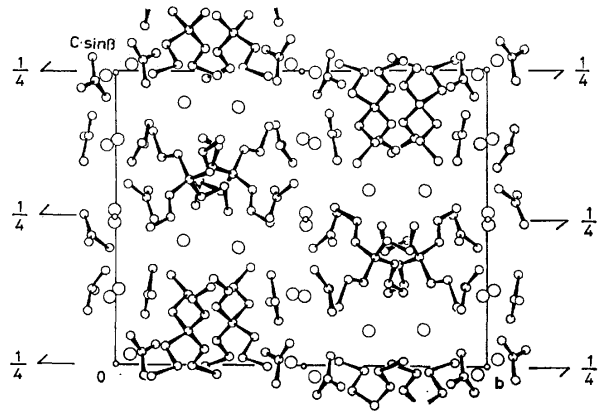

Fig. 1. The [100] projection of the structure of 1 : 2 tetrapropylammonium guanidinium bromide complex. The large circle indicates a bromide ion.

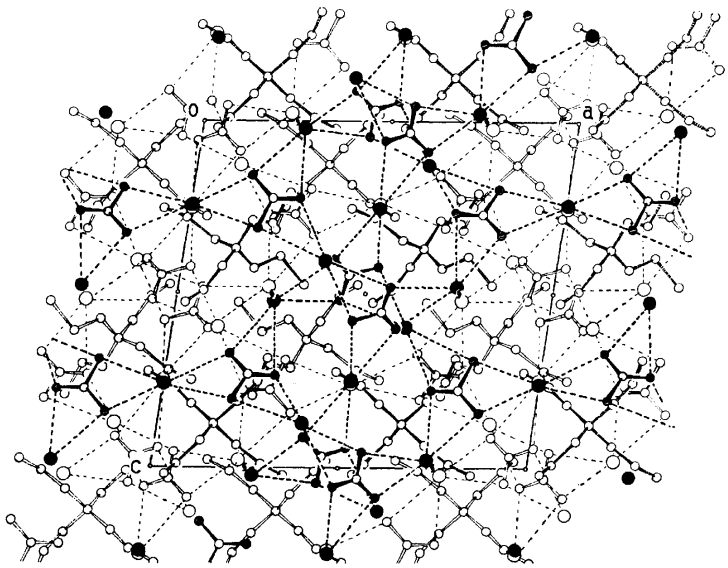

Fig. 2. The [010] projection of the structure of 1 : 2 tetrapropylammonium guanidinium bromide complex. The broken line indicates a NH···Br hydrogen-bond.

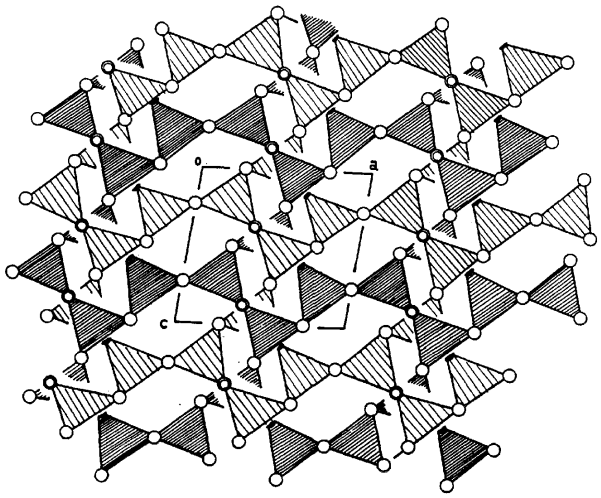

Fig. 3. A schematical drawing of the hydrogen-bond networks composed of the $GuBr_3$ groups.
The two networks weaved into each other are viewed down the b-axis.

manner such that the bromide ion forms four hydrogen-bonds with the nitrogen atoms of the two adjacent guanidinium ions, and they form four-membered rings and eight-membered rings in an infinite two-dimensional network. As is shown schematically in Fig. 3, the two networks related by the $\bar{1}$ symmetry are, furthermore, interwoven with each other; the four-membered rings and the eight-membered rings in the different networks are entangled together. The closest approach of these networks is found between the antiparallel guanidinium planes at the entanglement point of the two rings.

When the crystal structure described above is compared with that of the 2 : 1 complex,[2] one of the common structural features is that two different conformers of tetrapropylammonium groups exist in both structures. The two conformers have approximately $\bar{4}$ mm and $\bar{4}$ symmetries, as reported previously.[2] This common fact will provide the evidence that these two conformations for tetrapropylammonium are energetically very close. The second point of the common features is that the guanidinium ion forms a $GuBr_3$ group with three bromide ions. A similar $GuCl_3$ group has been observed in the crystal structure of guanidinium chloride salt.[4] These facts may indicate that the $GuBr_3$ formation is favorable in a crystalline state. A definite difference between the three structures is how these stable $GuBr_3$ groups link in the structure. In the 2 : 1 complex, each $GuBr_3$ group is apart from the others and act as a divalent anion.[2] On the other hand, in the 1 : 2 complex, the $GuBr_3$ groups are linked together at the bromide ion, and they form a two-dimensional network as mentioned above. In the case of guanidinium chloride salt, three $GuCl_3$ groups are linked together at a chloride ion, and they form a complicate three-dimensional network as a whole.[4] The apparent charge of the $GuBr_3$ group in the 1 : 2 complex is smaller than in the 2 : 1 complex, since each bromide ion contributes half a unit of charge onto the $GuBr_3$ group in the network. Hence, the ionic character of the crystal of the 1 : 2 complex is considered to be smaller than that of the 2 : 1 complex.

References

1) K. Miyajima, H. Yoshida, and M. Nakagaki, *Bull. Chem. Soc. Jpn.*, **50**, 2854 (1977).
2) T. Taga, M. Ohashi, K. Miyajima, H. Yoshida, and K. Osaki, *Chemistry Lett.*, **1977**, 917.
3) T. Taga, M. Ohashi, K. Miyajima, H. Yoshida, and K. Osaki, *Chemistry Lett.*, **1977**, 921.
4) D. J. Hass, D. R. Harris, and H. H. Mills, *Acta Crystallogr.*, **19**, 676 (1965).

BULLETIN OF THE CHEMICAL SOCIETY OF JAPAN, VOL. 52 (6), 1853—1854 (1979)

ESR Studies of a New Stable π-Conjugated Bisaryloxyl Biradical

Kazuo MUKAI,* Tsukasa HARA, and Kazuhiko ISHIZU

Department of Chemistry, Faculty of Science, Ehime University, Matsuyama 790

(Received December 9, 1978)

Synopsis. The new stable π-conjugated bisaryloxyl biradical, 4,4′-(*m*-phenylene)bis(2,6-di-*t*-butylphenoxyl), was prepared, and the ***g***- and ***D***-tensor values of the biradical were determined from an analysis of an asymmetric ESR spectrum of a frozen solution containing the biradical. A resolved hyperfine structure was observed in the ESR spectrum of a liquid solution of the biradical, giving the hyperfine splitting values theoretically expected for the triplet state of the biradical.

2,6-Di-*t*-butyl-4-phenylphenoxyl (aryloxyl (I)) (see Fig. 1) is a fairly stable phenoxyl radical, first prepared by Müller *et al.*, which can be separated as a solid with 90% radical concentration.[1] 4,4′,4″-(1,3,5-Benzenetriyl)tris(2,6-di-*t*-butylphenoxyl) (trisaryloxyl) is also known as a stable phenoxyl triradical prepared by Kothe *et al.*[2] The existence of a quartet state in the trisaryloxyl radical has been confirmed by ESR measurements in rigid media at 77 K.[3] These radicals can be prepared from their phenol and triphenol precursors by their PbO_2 oxidation in toluene under vacuum or nitrogen gas, respectively

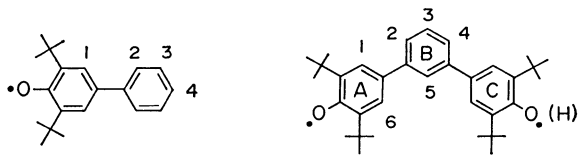

(I) (II) and (II-AB)

Fig. 1. Molecular structures of aryloxyl radical (I), bisaryloxyl biradical (II), and monoradical precursor (II-AB) of the biradical (II), and the atomic numbering system.

We have prepared the bisphenol precursor (IV) which is related to the above phenol and triphenol precursors, and have succeeded in synthesizing the corresponding π-conjugated bisaryloxyl biradical (II), 4,4′-(*m*-phenylene)bis(2,6-di-*t*-butylphenoxyl), (see Fig. 1). Zero-field splitting parameters and hyperfine splitting constants of the biradical (II) have been determined from its frozen and fluid solution ESR spectra, respectively.

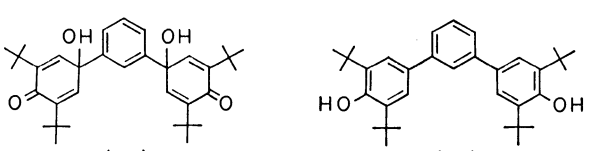

(III) (IV)

Experimental

m-*Bis(4-oxo-1-hydroxy-3,5-di*-t-*butyl-2,5-cyclohexadienyl)benzene (quinol (III))*. Quinol (III) was synthesized by a Grignard reaction of 2,6-di-*t*-butyl-*p*-benzoquinone with *m*-dibromobenzene and Mg in tetrahydrofuran (THF) under an atmosphere of nitrogen, following a method similar to that used with 4-hydroxy-2,6-di-*t*-butyl-4-phenyl-2,5-cyclohexadien-1-one.[4] The viscous reaction mixture obtained was added to an aqueous ammonia, then they were taken up in diethyl ether, washed with water, and dried over anhydrous sodium sulfate. After removal of the diethyl ether, a pasty solid remained. By adding petroleum ether (bp 50—70 °C) to the pasty residue, some white solids were precipitated. The solids were filtered off, washed with petroleum ether, and recrystallized from methyl alcohol. Mp 248—251 °C. (Found: C, 78.42; H, 9.16%. Calcd for $C_{34}H_{46}O_4$: C, 78.72; H, 8.94%). UV spectrum (λ_{max}=231 nm, log ε=4.50 in THF). NMR spectrum (δ=1.24 ppm (36 H, s, *t*Bu), 2.35 (2H, s, OH), 6.53 (4H, s, *m*-ring), 7.33 (3H, s, phenylene ring), 7.52 (1H, s, phenylene ring); δ in $CDCl_3$ with TMS as internal standard).

m-*Bis(3,5-di*-t-*butyl-4-hydroxyphenyl)benzene (bisphenol (IV))*. Bisphenol (IV) was synthesized by reduction of quinol (III) with Zn powder and concd HCl in methyl alcohol, following the same process as that of Rieker *et al.*[4] The white solids obtained were recrystallized twice from methyl alcohol. Mp 223—225 °C. (Found: C, 82.95; H, 9.73%. Calcd for $C_{34}H_{46}O_2$: C, 83.90; H, 9.53%). UV spectrum (λ_{max}=268 nm, log ε=4.57 in THF). NMR spectrum (δ=1.53 ppm (36H, s, *t*Bu), 5.24 (2H, s, OH), 7.42 (4H, s, *m*-ring), 7.42 (3H, s, phenylene ring), 7.65 (1H, s, phenylene ring); δ in $CDCl_3$ with TMS as internal standard).

All the ESR measurements were carried out using a JES-ME-3X spectrometer equipped with a Takeda-Riken microwave frequency counter. The ESR splittings were determined using $(KSO_3)_2NO$ as a standard. The *g*-values were measured relative to the value of Li-TCNQ powder, calibrated with $(KSO_3)_2NO$ (g=2.0054).[5]

Results and Discussion

When the bisphenol precursor of the bisaryloxyl biradical (II) was oxidized with PbO_2 in toluene under vacuum, the color of the bisphenol solution immediately became purple. The ESR spectrum of this solution (see Fig. 2(a)) showed a sextet-doublet hyperfine pattern (g_{iso}=2.00419±0.00003), and we assigned the spectrum to the primary aryloxyl monoradical (II-AB) formed from the parent phenol by abstraction of a phenolic hydrogen atom. The large sextet splitting (a^H=1.72±0.04 G) in the primary radical will be due to five magnetically equivalent ring protons (H_1, H_2, H_4, H_5, H_6) and the doublet splitting (a^H=0.71±0.04 G) is explained by a ring proton (H_3). These hyperfine splittings and g_{iso}-value are in good agreement with those ($a^H_{1,2,4}$=1.74±0.04, a^H_3=0.74±0.04 G and g_{iso}=2.00415±0.00003) for the aryloxyl radical (I) in toluene. By further oxidation, the purple color changed to yellow-brown, and the sextet-doublet spectrum of the monoradical was altered to a twelve-line spectrum of the bisaryloxyl biradical (II) with an equivalent splitting distance of 0.86 G and with g_{iso}=2.00414±

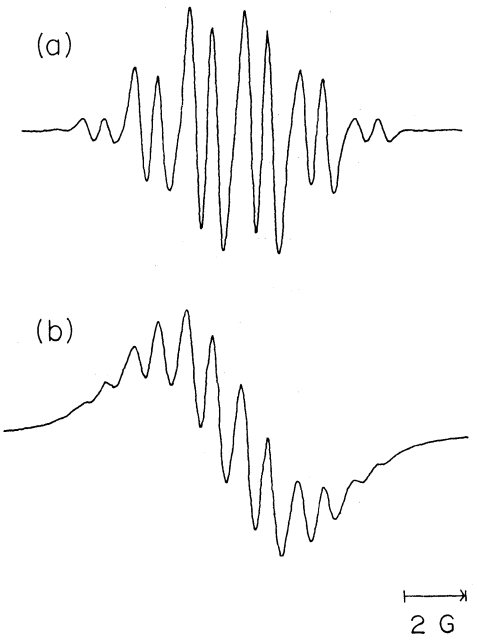

Fig. 2. (a) ESR spectrum of the monoradical precursor (II-AB) of the bisaryloxyl biradical (II) in toluene at 20 °C. (b) ESR spectrum of the bisaryloxyl biradical (II) in toluene at 20 °C.

0.00003, as shown in Fig. 2(b). The radical was stable for many weeks in toluene under vacuum at room temperature. The spectrum can be reconstructed with two sets of three and five equivalent protons ($a^{H}=1.72$ (3H), $a^{H}=0.86$ G (5H)).

Rather few triplet molecules show resolved proton hyperfine structure, because of the spin-spin dipolar broadening. The ESR spectrum of the bisaryloxyl biradical (II) shows twelve lines from the hyperfine interaction of the electrons with the eight ring protons, as described above. Kopf *et al.*[6] have proposed a simple theory to explain the hyperfine splitting of weakly π-conjugated verdazyl biradicals; their results indicate that the splitting constants of nuclei contained in rings connecting the two monoradical halves are the average of splittings from protons in corresponding positions in the monoradical, while the splitting constants for nuclei in other parts of the molecules were one-half of the monoradicals splittings. The bisaryloxyl biradical (II) is considered to be a strongly π-conjugated biradical consisting of two aryloxyl groups (AB- and BC-types) with two unpaired electrons in a molecular orbital, in which ring B is common to both monoradical-AB and -BC. Therefore, in the biradical (II), the theoretically expected values for the hyperfine splittings of the eight ring protons from those of the monoradical precursor (III-AB) are $a^{H}_{2,4,5}=1.72$ G (3H), $a^{H}_{1,6}=0.86$ G (4H), and $a^{H}_{3}=0.71$ G (1H); the observed hyperfine splittings ($a^{H}_{2,3,5}=1.72$ G (3H) and $a^{H}_{1,3,6}=0.86$ G (5H)) for the biradical (II) agree exceedingly well with the ones calculated from the monoradical precursor; this strongly supports the above explanation.

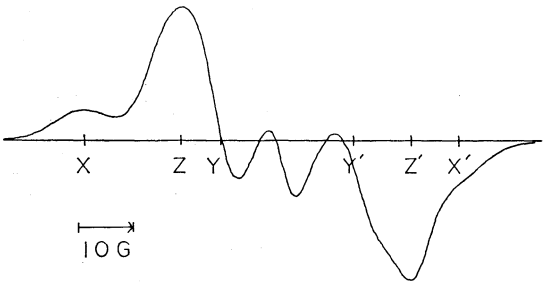

Fig. 3. ESR spectrum of the bisaryloxyl biradical (II) in toluene at 77 K.

When a solution containing the bisaryloxyl biradical (II) is frozen into glass at 77 K, one can observe dipolar splittings, as is shown in Fig. 3. A central weak line at $g=2$ is attributable to the monoradical impurity. Assuming non-axial symmetry, the zero-field splitting parameters D and E were tentatively estimated from the positions of the three pairs of turning points ZZ', YY', and XX' in Fig. 3, as performed for the bisgalvinoxyl biradicals in Refs. 7 and 8. The values are $D=34.0\pm1.0$ G and $E=3.0\pm1.0$ G. Because of the symmetry of the biradical molecule, we can expect that the principal axes of the $\boldsymbol{D}$- and $\boldsymbol{g}$-tensors are coaxial. Consequently, the frequency centers of these three pairs of absorption lines, ZZ', YY', and XX', give $g_{zz}=2.0024\pm0.0004$, $g_{yy}=2.0035\pm0.0004$, and $g_{xx}=2.0051\pm0.0004$, respectively. The average $g_{av}=1/3(g_{xx}+g_{yy}+g_{zz})=2.0037\pm0.0004$ is in agreement with the isotropic $g_{iso}=2.00414\pm0.00003$ value measured at room temperature, indicating that the $\boldsymbol{g}$-tensor values obtained by the above analysis are consistent.

References

1) E. Müller, A. Schick, and K. Scheffler, *Chem. Ber.*, **92**, 474 (1959).

2) G. Kothe, C. Nowak, K. H. Denkel, E. Ohmes, and H. Zimmermann, *Angew. Chem.*, **82**, 521 (1970). *Angew. Chem. Int. Ed. Engl.*, **9**, 520 (1970).

3) C. Nowak, G. Kothe, and H. Zimmermann, *Ber. Bunsenges. Phys. Chem.*, **78**, 265 (1974).

4) A. Rieker and K. Scheffler, *Justus Liebigs Ann. Chem.*, **689**, 78 (1965).

5) J. J. Windle and A. K. Wiersma, *J. Chem. Phys.*, **39**, 1139 (1963).

6) P. Kopf, K. Morokuma, and R. Kreilick, *J. Chem. Phys.*, **54**, 105 (1971).

7) K. Mukai and T. Tamaki, *Bull. Chem. Soc. Jpn.*, **50**, 1239 (1977).

8) K. Mukai and J. Sakamoto, *J. Chem. Phys.*, **68**, 1432 (1978).

BULLETIN OF THE CHEMICAL SOCIETY OF JAPAN, VOL. 52 (6), 1855—1856 (1979)

Secondary Deuterium Isotope Effects in the Intramolecularly-competing Methoxymercuration of Ethylene-1,1-d_2 and *cis*-2-Butene-2-d_1

Sumio SHINODA, Masashi ISEMURA,† and Yasukazu SAITO*

Institute of Industrial Science, The University of Tokyo, 22-1, Roppongi 7-Chome, Minato-ku, Tokyo 106

(Received December 19, 1978)

Synopsis. Secondary deuterium isotope effects in the intramolecularly-competing methoxymercuration of ethylene-1,1-d_2 and *cis*-2-butene-2-d_1, determined from the rate ratio (k(β-deuteriomercurial)/k(α-deuteriomercurial)=1.12, 1.06), indicate that the transition state for the methoxymercuration of ethylene and *cis*-2-butene does not have a symmetrical structure such as a mercurinium ion, but is accompanied by considerable C–O bond formation.

The oxymercuration of olefins followed by reductive demercuration with sodium borohydride is a synthetically important method for the synthesis of alcohols and ethers.[1] The remarkable feature of the oxymercuration is that the reaction has almost all the usual features of an electrophilic addition but structural rearrangement, substitution, and conjugate addition do not accompany the reaction.[2] The process is strictly a 1,2-addition in the Markownikov sense and occurs in a stereospecific anti fashion for unstrained simple olefins.[3]

Although extensive studies have been accumulated,[4] there is still dissension regarding the mechanism of this reaction, as was comprehensively reviewed by Ambidge *et al.* recently.[5] One convincing line of approach has involved an application of a linear free-energy relationship,[6] but the interpretation of the rate data seems rather diverse, and depends on the category of olefins selected. In order to remove the ambiguity in the mechanistic problem, it is important to determine accurately the mechanism for the most simple olefin, ethylene.

From this viewpoint, we utilized here the secondary deuterium isotope effect to elucidate the transition-state structure for the methoxymercuration of ethylene together with *cis*-2-butene. Isotopic substitution is unique in that it generates no variation of electronic potential-energy surfaces for molecules.[7] When ethylene-1,1-d_2 (**1**) or *cis*-2-butene-2-d_1 (**2**) is oxymercurated, two isomeric adducts are obtained, *i.e.*, α- and β-deuterio-oxymercurials where the designation of α and β is made from the mercurated carbon. Because the formation of these isomers is competitive, the ratio of the product isomers is equivalent to the corresponding rate constants, k_β/k_α.

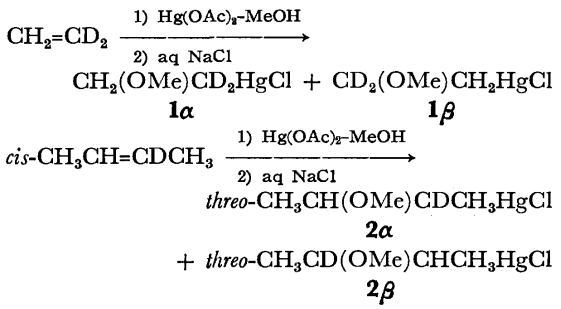

Scheme 1.

Secondary deuterium isotope effects on reaction rates have been generally recognized as evidence of hybridization change at the position of isotopic substitution between reactant and transition state.[7,8] Accordingly, we can directly deduce the symmetry concerning the hybridization of α- and β-carbons in the transition state by examining the value of k_β/k_α.

Results and Discussion

Methoxymercuration of **1** and **2** was effected at 25 °C by standard procedures (Scheme 1).[9] In the absence of mineral acid, oxymercuration of olefins with mercury(II) acetate gives kinetically controlled products,[10] and there was no possibility of discrepancies of temperature or other conditions in the formation of the two isomers. The ratio of the product isomers was determined by using PMR spectroscopy carefully for the quantitative analysis.

The PMR spectrum of the methoxymercurials formed from **1** is shown in Fig. 1. Obviously two peaks with unequal intensity appear at δ 2.16 and 3.60; deuterium decoupling did not alter the peak ratio. It is evident from Fig. 1 that **1β** (δ 2.16) was formed in preference to **1α** (δ 3.60). The isomer ratio for the methoxymercuration of **2** was determined with methyl peaks. The results are tabulated in Table 1.

Table 1. Rate ratio for the intramolecularly-competing methoxymercuration of deuterio-olefins

Olefin	k_β/k_α
$CH_2=CD_2$	1.21
cis-$CH_3CH=CDCH_3$	1.06

For unsymmetrically deuterium-substituted symmetrical olefins such as **1** or **2**, the olefinic carbons are equivalent on the electronic potential-energy surface. If the transition state for the methoxymercuration of ethylene or *cis*-2-butene is symmetrical, retaining the equivalence of the two carbons, the secondary deuterium isotope effect would be identical for the two isomers. The observed substantial deviation of k_β/k_α from unity, therefore, indicates that the symmetrical transition state such as **3** or **4** is unfavorable for ethylene and *cis*-2-butene, despite the symmetry in substituents.

An intervention of oxy-addendum in the transition state has been claimed by several authors on the basis of the substituent effect on the rate of oxymercuration[2,11] On the assumption of the inverse α-deuterium

† Present address: Sumitomo Chemical Company Limited, 7-9, Nihonbashi 2-Chome, Chuo-ku, Tokyo 103.

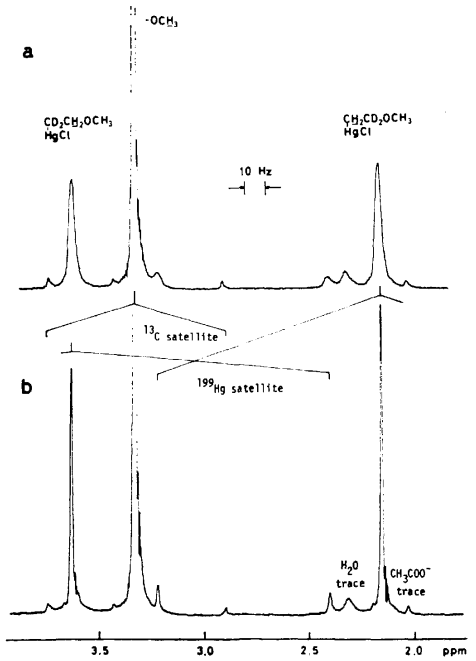

Fig. 1. PMR spectrum of the methoxymercurials of ethylene-1,1-d_2 at 25 °C and 100 MHz in $CDCl_3$ solution; (a) without deuterium irradiation; (b) with deuterium irradiation at 15.349345 MHz which corresponds to the center of the α- and β-deuterium resonance.

isotope effect ($k_H/k_D<1$), which has been usually observed when there is a change from sp^2 to sp^3 in the carbon bond hybridization,[7,8] the observed magnitude of the rate ratio for the intramolecularly-competing process, k_β/k_α, directly shows that the C–O bond is considerably formed in the transition state. Hence, the transition-state structure for the methoxymercuration of ethylene and *cis*-2-butene would be represented as **5**. The position of mercury along the C–C bond axis may be of interest, but seems to be a complicated problem since the molecular orbital calculation[12] suggests that rather small energy is required to shift the mercury along that axis (as compared with halonium ions), and that the ease of the displacement depends appreciably on the kind of the ligand bonded to mercury(II). The "mercurinium ion" intermediate, formulated frequently as **3** in analogy to olefin-Ag(I) π-complex or bromonium ion,[12] may be involved in the reaction path, possibly in the pre-rate-determining step equilibria,[13] but its formation is not a rate-determining step.[14]

It is noteworthy that **5** is similar to the transition-state structure proposed by Kreevoy and coworkers for the deoxymercuration reaction.[15] In view of the reversible nature of the oxymercuration of olefins and the deoxymercuration of the formed adducts, it is reasonable that their transition-state structures resemble each other, although the content of C–Hg and C–O bond formation may be variable with the kind of olefin substituents or mercury ligands.

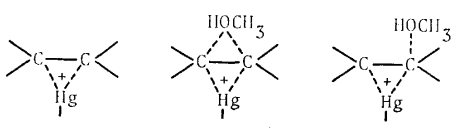

3 **4** **5**

Experimental

Preparations of **1** and **2** were described elsewhere.[16,17] All the reagents and solvents were commercially available. PMR spectra were recorded on a JEOL PS-100 spectrometer. Deuterium decoupling was carried out with a JEOL OA-1 synthesizer.

In determining the isomer ratios, both radio-frequency power and sweep rate were selected to avoid saturation of signal intensity. Spectra were obtained in both the frequency-increasing and -decreasing conditions ten times on a 4- or 10-fold expanded scale of the standard sweep width, so as to secure the precision of area measurement. Reported values were the avarage of three independent runs with an error of 3% (standard deviation) for the total measurement.

Methoxymercuration was performed by introducing **1** or **2** *via* a vacuum line into the solution consisting of methanol (5 cm^3) and mercury(II) acetate (2 mmol) at 25 °C, which was stirred by a magnetic stirring bar until all the mercury(II) ions were consumed to yield a homogeneous solution. Mercurials were isolated in the form of chloride by the method described by Ichikawa *et al.*[9]

References

1) H. C. Brown and P. J. Geoghegan, Jr., *J. Org. Chem.*, **35**, 1844 (1970).
2) R. C. Fahey, *Top. Stereochem.*, **3**, 237 (1968).
3) T. Ibusuki and Y. Saito, *J. Organomet. Chem.*, **56**, 103 (1973).
4) W. Kitching, *Organomet. Chem. Rev.*, **3**, 61 (1968); T. G. Traylor, *Acc. Chem. Res.*, **2**, 152 (1969).
5) I. C. Ambidge, S. K. Dwight, C. M. Rynard, and T. T. Tidwell, *Can. J. Chem.*, **55**, 3086 (1977).
6) J. E. Leffler and E. Grunwald, "Rates and Equilibria of Organic Reactions," John Wiley and Sons, New York, N. Y. (1963).
7) "Isotope Effects in Chemical Reactions," ed by C. J. Collins and N. S. Bowman, Van Nostrand Reinhold Co., New York, N. Y. (1970).
8) S. Seltzer, *J. Am. Chem. Soc.*, **83**, 1861 (1961); A. Streitwieser, Jr., R. H. Jagow, R. C. Fahey, and S. Suzuki, *ibid.*, **80**, 2326 (1958).
9) K. Ichikawa, H. Ouchi, and S. Araki, *J. Am. Chem. Soc.*, **82**, 3880 (1960).
10) S. Bentham, P. Chamberlain, and G. H. Whitham, *Chem. Commun.*, **1970**, 1528.
11) R. D. Bach and R. F. Richter, *Tetrahedron Lett.*, **1973**, 4099; *J. Org. Chem.*, **38**, 3442 (1973).
12) R. D. Bach and H. F. Henneike, *J. Am. Chem. Soc.*, **92**, 5589 (1970).
13) D. J. Pasto and J. A. Gontarz, *J. Am. Chem. Soc.*, **92**, 7480 (1970); **93**, 6902 (1971).
14) W. Kitching, "Organometallic Reactions," ed by E. I. Becker and M. Tsutsui, Wiley-Interscience, New York, N. Y. (1972), Vol. 3, pp. 319—398.
15) M. M. Kreevoy and B. M. Eisen, *J. Org. Chem.*, **28**, 2104 (1963).
16) M. Kosaki, M. Isemura, Y. Kitaura, S. Shinoda, and Y. Saito, *J. Mol. Catal.*, **2**, 351 (1977).
17) S. Shinoda and Y. Saito, *Bull. Chem. Soc. Jpn.*, **47**, 2948 (1974).

BULLETIN OF THE CHEMICAL SOCIETY OF JAPAN, VOL. 52 (6), 1857—1858 (1979)

Crystal and Molecular Structure of Bis(1-diphenylphosphinothioyl-3-methylthioureato)nickel(II)

Toschitake IWAMOTO,* Fujio EBINA, Hiroshi NAKAZAWA, and Chiaki NAKATSUKA

Department of Chemistry, College of General Education, The University of Tokyo, Komaba, Meguro, Tokyo 153

(Received November 24, 1978)

Synopsis. The title compound [Ni{$(C_6H_5)_2$PSNCSNHCH$_3$}$_2$] was found to crystallize in the monoclinic space group C2/c with a=23.29(1), b=9.457(2), c=16.40(1) Å, β=121.33(8)°, Z=4. The six-membered chelate ring built of five kinds of atoms, Ni, 2S, P, N, and C, was demonstrated.

Ojima *et al.*[1,2] proposed that some diphenylphosphinothioylthioureatometal(II) complexes have a chelate structure consisting of five kinds of atoms, M(II), 2S, P, N, and C. In order to confirm the existence of such a chelate ring, the title compound was subjected to X-ray structural analysis.

Experimental

Among the complexes reported,[1,2] a complex previously described as bis(3-diphenylphosphinothioyl-1,1-dimethylthioureato)nickel(II) was chosen because of its good appearance as fine crystals. A 0.2×0.4×0.6 mm single crystal grown up from a dichloromethane–ethanol solution was used for the X-ray diffraction experiments. In the course of structure refinement, the crystal was confirmed to be that of the title compound, bis(1-diphenylphosphinothioyl-3-methylthioureato)nickel(II). After preliminary Weissenberg photographs were taken, precise determination of lattice parameters and collection of intensity data were carried out on a Rigaku automated four-circle diffractometer using Cu $K\alpha$ radiation, the procedure being similar to that reported.[3] Of 4142 observed reflections with $2\theta \leq 120°$, 1671 with $|F_o| \geq 3\sigma(|F_o|)$ were used for the structure refinement. The absorption corrections[4] were applied together with Lp ones. The density was measured by the flotation method using potassium tetraiodomercurate solution. Crystal data: $NiC_{28}H_{28}N_4P_2S_4$, $F.W.$=669.44. Monoclinic, space group C2/c, a=23.29(1), b=9.457(2), c=16.40(1) Å, β=121.33(8)°, Z=4. D_m=1.45, D_x=1.44 g cm^{-3}. Systematic absences: hkl, $h+k=2n+1$; $h0l$, $l=2n+1$. μ(Cu $K\alpha$)=45.36 cm^{-1}.

The structure was solved by the heavy-atom method. All the calculations were carried out on a HITAC 8800/8700 computer at the Computatinon Center of this University. The programs used were those in UNICS[5] and their local versions. The atomic scattering factors were taken from those of Cromer and Waber.[6] From the three-dimensional Patterson synthesis, the Ni atoms were located at the inversion centers in the c glide planes. In successive Fourier syntheses, the positions of all the remaining non-hydrogen atoms could be found out except that of the second methyl-C atom should have been found for the dimethyl compound around the N(2) atom of the side chain. Since the measured density was smaller by 0.02 g cm^{-3} than that calculated for the dimethyl compound, the refinement was progressed assuming this crystal to be that of the title compound. Several cycles of block-diagonal least-squares calculations were carried out to the final R=0.093, the real and imaginary parts of the anomalous dispersion

Table 1. Positional and thermal parameters for [Ni{$(C_6H_5)_2$PSNCSNHCH$_3$}$_2$][a]

Atom	x	y	z	U_{11}	U_{22}	U_{33}	U_{12}	U_{13}	U_{23}
Ni	5000	5000	5000	11(1)	23(1)	19(1)	−2(1)	6(1)	−2(1)
S(1)	4786(1)	4419(2)	3560(1)	17(1)	40(1)	21(1)	−3(1)	8(1)	−5(1)
S(2)	3948(1)	5125(2)	4664(1)	13(1)	28(1)	29(1)	−3(1)	10(1)	−6(1)
P	3555(1)	3349(2)	3889(1)	13(1)	25(1)	23(1)	−3(1)	8(1)	−2(1)
N(1)	3529(3)	3260(7)	2890(4)	26(4)	41(4)	27(3)	−9(3)	14(3)	−4(2)
N(2)	3908(4)	3545(8)	1869(4)	30(4)	61(4)	19(3)	−14(3)	12(3)	−10(3)
C(1)	4000(4)	3668(8)	2747(4)	32(5)	28(4)	22(3)	0(4)	12(3)	−3(3)
C(2)	3272(5)	2920(12)	1092(5)	53(6)	91(7)	23(4)	−39(6)	12(4)	−18(4)
C(11)	2966(4)	3230(7)	3587(4)	7(4)	35(4)	22(3)	−5(3)	4(3)	0(3)
C(12)	2494(4)	3796(10)	4179(5)	27(5)	55(5)	40(4)	−8(4)	19(4)	−11(4)
C(13)	1839(4)	3637(11)	3966(6)	12(4)	73(6)	57(5)	−14(5)	23(4)	−7(4)
C(14)	1390(4)	2842(10)	3196(6)	26(5)	59(6)	43(5)	−4(4)	13(4)	−1(4)
C(15)	1590(4)	2261(11)	2599(6)	14(4)	63(6)	53(5)	−18(4)	9(4)	−13(4)
C(16)	2231(4)	2480(10)	2783(6)	28(5)	52(5)	42(4)	−12(4)	18(4)	−18(4)
C(21)	3955(4)	1788(8)	4574(5)	17(4)	27(4)	46(4)	1(3)	27(4)	4(3)
C(22)	3721(5)	475(10)	4132(6)	46(6)	37(5)	59(6)	−6(5)	32(5)	−12(4)
C(23)	4006(6)	−759(10)	4645(7)	92(9)	33(5)	71(7)	9(5)	45(6)	8(4)
C(24)	4536(5)	−690(10)	5606(8)	40(6)	40(5)	102(8)	15(5)	52(6)	21(5)
C(25)	4757(5)	580(10)	6030(7)	24(5)	57(6)	66(6)	10(5)	24(4)	24(4)
C(26)	4480(4)	1851(9)	5533(5)	19(4)	43(4)	44(4)	9(4)	15(4)	12(3)

a) The positional and thermal parameters have been multiplied by 10^4 and 10^3, respectively, the numbers in parentheses being esd's in the last signigicant digits. The form of thermal parameters is $\exp[-2\pi^2(U_{11}h^2a^{*2}+U_{22}k^2b^{*2}+U_{33}l^2c^{*2}+2U_{12}hka^*b^*+2U_{13}hla^*c^*\cos\beta^*+2U_{23}klb^*c^*)]$.

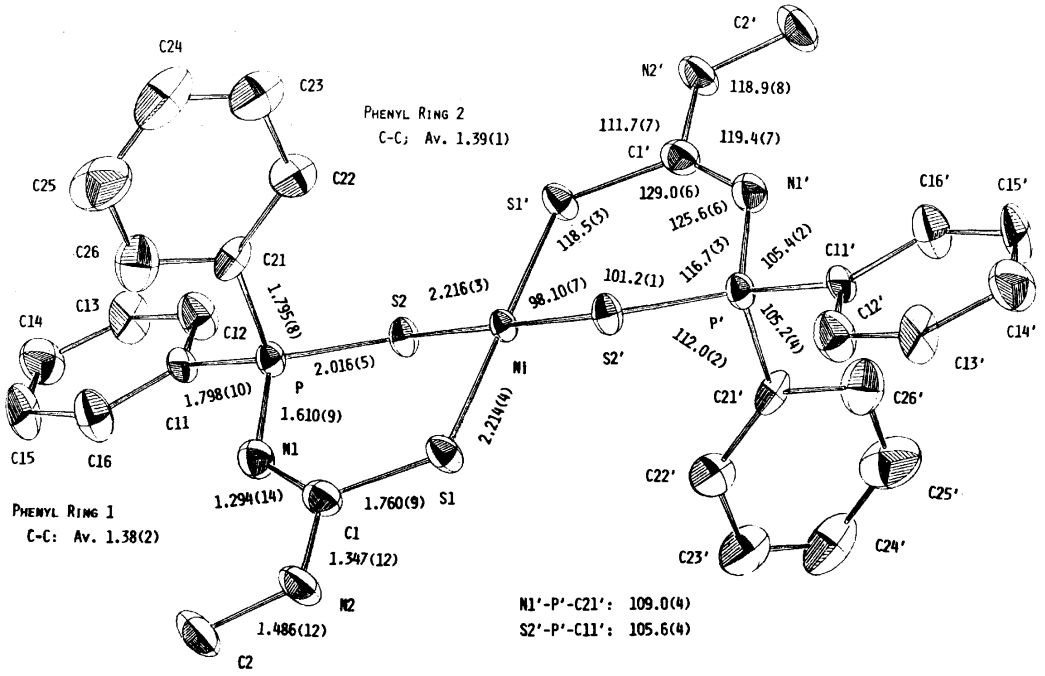

Fig. 1. An ORTEP view of $[Ni\{(C_6H_5)_2PSNCSNHCH_3\}_2]$ molecule using 50% probablity ellipsoids. The bond distances and angles are given in Å and degree, respectively, and the numbers in parentheses are esd's in the last significant digits.

correction being also made.[7] The shift of each atomic parameter was within one-third of the estimated standard deviation at the last two cycles. The final difference Fourier map showed no significant peak attributable to the "second" methyl-C atom. This shows that the analyzed crystal is composed of the title compound. The refinement with the Cc space group, another possible one for the observed systematic absences, afforded no improvement.

Description of the Structure

The final atomic parameters are given in Table 1. The molecular structure of the complex is shown in Fig. 1 with the values of important bond distances and angles. The Ni atom is bonded to S(1) and S(2) atoms of the ligands in a square-planar trans configuration. The six-membered chelate ring is built of Ni, S(1), C(1), N(1), P, and S(2) atoms as proposed by Ojima *et al.*[1,2] The chelate ring, the phenyl ring 1, and the methylamino side chain are roughly parallel to the ac plane, and the phenyl ring 2 protrudes from the P atom of the chelate ring into a direction approximately parallel to the b axis. The NiS_4 coordination sphere resembles that in bisdithioacetylacetonatonickel(II)[8] and other conjugated bis(thioketo-thiolato)nickel(II) complexes. The chelate ring has the following features of bond distances. The average Ni–S bond length 2.215 Å is longer than those in the conjugated thioketo-thiolato type complexes. The C(1)–S(1) bond is comparable in length to that in bismaleonitrildithiolatonickelate(II).[9] The P–S(2) and P–N(1) bonds appear to be partially double. The N(1)–C(1) bond is too short for a C=N bond. Although these features could support a partial conjugation of π-orbitals in the chelate ring, the unfavorable deviations of the relevant atoms from the calculated best plane are: P 0.59, N(1) 0.19, Ni 0.08, C(1) −0.11, S(1) −0.16, and S(2) −0.47 Å.

References

1) I. Ojima, T. Iwamoto, T. Onishi, N. Inamoto, and K. Tamaru, *Chem. Commun.*, **1969**, 1501.
2) I. Ojima, T. Onishi, T. Iwamoto, N. Inamoto, and K. Tamaru, *Bull. Chem. Soc. Jpn.*, **44**, 2150 (1971).
3) T. Iwamoto and M. Kiyoki, *Bull. Chem. Soc. Jpn.*, **48**, 2414 (1975).
4) "International Tables for X-Ray Crystallography," Kynoch Press, Birmingham Vol. II, p. 291. The crystal elongated along b axis could not be cut down into smaller pieces.
5) Universal Crystallographic Computation Program System (UNICS), ed by T. Sakurai, Crystallographic Society of Japan, Tokyo (1967).
6) "International Tables for X-Ray Crystallography," Kynoch Press, Birmingham (1974), Vol. IV.
7) The table of the structure factors is kept as Document No. 7920 at the Chemical Society of Japan.
8) R. Beckett and B. F. Hoskins, *J. Chem. Soc., Dalton Trans.*, **1974**, 622.
9) R. Eisneberg and J. A. Ibers, *Inorg. Chem.*, **4**, 605 (1965).

BULLETIN OF THE CHEMICAL SOCIETY OF JAPAN, VOL. 52 (6), 1859—1860 (1979)

Studies of the Separation Mechanism in Ion-exchange Chromatography. I. Inversion of the Elution Order of cis and trans Isomers of Metal Complexes

Hayami YONEDA* and Shigeo YAMAZAKI

Department of Chemistry, Faculty of Science, Hiroshima University, Hiroshima 730

(Received December 4, 1978)

Synopsis. The inversion of the elution order in ion-exchange chromatography was found for cis and trans isomers of $[Co(X)_2(en)_2]^+$ ($X=N_3^-$, NO_2^-, and NCS^-) by the addition of dioxane to NH_4Cl or $(NH_4)_2SO_4$ aqueous solution as eluent, and the separation mechanism was discussed.

Since King and Walters[1] reported the chromatographic separation of the cis and trans isomers of $[Co(NO_2)_2(NH_3)_4]^+$ by ion-exchange technique, it has been accepted as a general rule that the trans isomer is eluted earlier than the cis isomer.[2,3] This is quite understandable when we consider that the cis isomer has a dipole moment and is adsorbed more strongly than the trans isomer having no dipole moment. This explanation is based on the assumption that separation is carried out mainly by adsorption, although chromatography consists of two processes, adsorption and elution. Here it must be pointed out that the dielectric constant is fairly smaller in the stationary phase (resin phase) than in the moving phase (aqueous solution), so that ion association in the stationary phase should be more effective than in the moving phase, that is, adsorption should be more decisive than elution. Thus, it is natural to consider that the elution order is determined by the strength of adsorption. Therefore, if we set up conditions under which ion association in the moving phase is more effective than that in the stationary phase, the elution order of the cis and trans isomers is expected to be reversed.

Based on this consideration, we tried to chromatograph the cis and trans pairs of three cobalt(III) complexes through the column packed with SP-Sephadex C-25 using dioxane–water mixed solution of an electrolyte as an eluent. As such Sephadex contains many hydrophilic functional groups, the dielectric constant in the stationary phase should be fairly large and it can be easily overtaken by the dielectric constant in the moving phase (aqeuous solution) with the addition of some amount of dioxane to the eluent, which should result in the inversion of the elution order. This expectation was fulfilled in the present study.

Experimental

Samples. All the complexes were prepared according to the literature, and identified by UV absorption spectra and elemental analyses. Complexes used were the cis and trans pairs of $[Co(NO_2)_2(en)_2]ClO_4$, $[Co(NCS)_2(en)_2]Cl\cdot H_2O$, and $[Co(N_3)_2(en)_2]ClO_4$.

Sample solutions were prepared by dissolving 10 mg of the complex in a few ml of an eluent.

Eluent. The eluents were aqueous solutions of 0.4 mol dm^{-3} NH_4Cl, 0.4 mol dm^{-3} NH_4NCS and 0.05 mol dm^{-3} $(NH_4)_2SO_4$ containing various amounts of dioxane. Dioxane was distilled before use.

Apparatus. All the works were carried out on a laboratory-built chromatographic unit at room temperature. The column size was 25 cm long and 6.5 mm in diameter. SP-Sephadex C-25 (Pharmacia, Sweden) was used as a packing material. The flow rates were ranged from 0.8 ml/min for zero dioxane to 0.25 ml/min for 60% dioxane content. The detector was operated at the first absorption band of each complex. The adjusted retention volume was measured from the elution curve. $(NH_4)_3[Cr(NCS)_6]$ was used as a marker.[4] The sample solution 20 μl being typical was injected by a syringe into the column.

Results and Discussion

Fig. 1(a) shows the trend of the retention volumes of the cis and trans pairs of three cobalt(III) complexes with increasing dioxane content of 0.4 mol dm^{-3} NH_4Cl solution. As expected, in the low dioxane content region, the retention volume of the cis isomer having a dipole moment is larger in all three cases than that of the trans isomer having no dipole moment. This suggests that the electrostatic interaction between the complex cation and the functional group (SO_3^-) of Sephadex ion-exchanger plays a decisive role in chromatographic separation. The situation is reversed in the high dioxane content region where the retention volume of the cis isomer becomes smaller than that of the trans isomer. This means that the electrostatic interaction between the complex cation and the counter anion in the moving phase plays a dominant role in chromatographic separation.

The most important factors which govern the electrostatic interaction are the charge density of the counter ion (ionic charge times concentration) and the dielectric constant of the medium. In the case of SP-Sephadex C-25, the exchange capacity and the bed volume of the gel at ionic strength 0.4 are known to be 2.3 m equivalent/g(dry gel) and 6 ml/g(dry gel) respectively. Since the real volume of the swelling gel is estimated to be 2/3 of the bed volume, the concentration of the SO_3^- group in the swelling gel is calculated to be 0.57 mol dm^{-3} which is larger than 0.4 mol dm^{-3}, the Cl^- concentration of the eluent. In addition, the water caught in the Sephadex matrix is presumed to be less structured than the water in the moving phase. Since the electrostatic interaction is dependent upon the product of the charge density of the counter ion and the inverse of the dielectric constant, it should be larger in the stationary phase than in the moving phase in the absence or at the low content of dioxane.

Although the addition of dioxane decreases the magni-

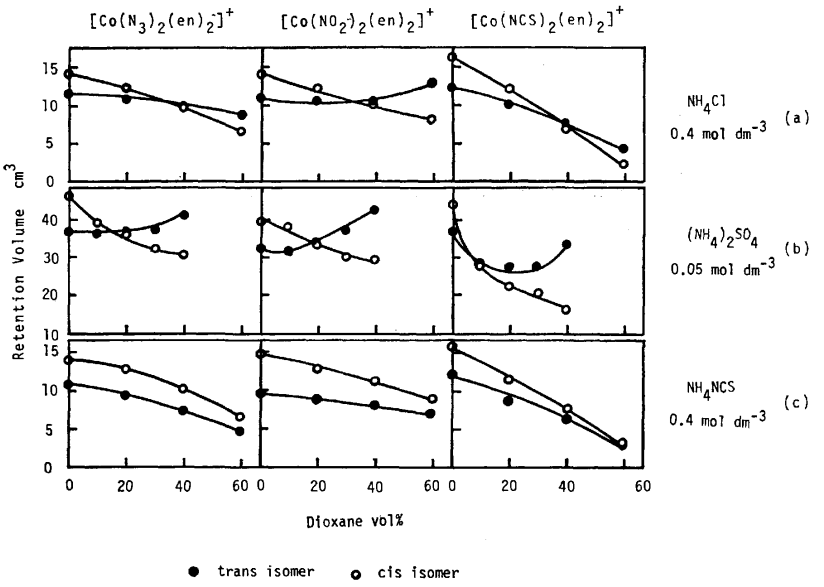

Fig. 1. Retention volume of trans(●) and cis(○) pairs of $[Co(X)_2(en)_2]^+$ ($X=N_3^-$, NO_2^-, and NCS^-) *vs.* dioxane content in 0.4 mol dm^{-3} NH_4Cl, 0.05 mol dm^{-3} $(NH_4)SO_4$ and 0.4 mol dm^{-3} NH_4NCS solution as eluent.

tude of the dielectric constant both in the stationary and moving phases, the rate of decrease should be larger in the moving phase. Since Sephadex contains many hydrophilic groups, it can hold much water strongly. Thus, the Sephadex matrix contains more water than the moving phase when the dioxane–water mixed solution is kept in equilibrium with Sephadex.[5] Therefore, the increase of dioxane content in the eluent results in a more gradual decrease of the dielectric constant in the stationary phase than in the moving phase. Thus, the magnitude of the dielectric constant in both phases becomes closer with the increasing content of dioxane, and at a certain content of dioxane the inversion of the magnitude of the dielectric constant takes place. The inversion of the elution order can be thus understood. In the case of 0.4 mol dm^{-3} NH_4Cl, the inversion of the elution order takes place at about 35—40% (v/v) dioxane content above which the cis isomer is eluted earlier than the trans isomer. The inversion should take place at much lower dioxane content for the bivalent anion SO_4^{2-} than for the univalent anion Cl^-. Thus, for 0.05 mol dm^{-3} $(NH_4)_2SO_4$ solution, the inversion takes place at about 10—20% dioxane content as shown in Fig. 1(b).

However, it must be noted that for $(NH_4)_2SO_4$ solution, the retention volume of the trans isomer does not decrease but rather increase with increasing content of dioxane. This means that the effective concentration of SO_4^{2-} to catch the complex cation decreases with increasing content of dioxane. The addition of dioxane decreases the dielectric constant of the moving phase which results in strengthening the association of SO_4^{2-} not only with the complex cation but also with NH_4^+. Since the cis isomer has a dipole moment and a great tendency toward association with SO_4^{2-}, it is not so much influenced by the presence of NH_4^+. However, for the trans isomer having no dipole moment, the existence of a large amount of NH_4^+ results in the decrease of the effective concentration of SO_4^{2-} in the eluent of high dioxane content, so that the retention volume increases.

If this interpretation is valid, the retention volume should decrease regularly with increasing content of dioxane, when an eluent contains a salt which has little tendency toward ion association even in the solution of high dioxane content. Ammonium thiocyanate solution as eluent is considered to be the case as shown in Fig. 1(c). Here, NCS^- solvates dioxane strongly and is presumed to be dissociated from NH_4^+ even in the high dioxane content. Such strong solvation of NCS^- anion causes the decrease in its association with the complex (cis and trans) too, so that the association-promoting tendency due to the decrease of the dielectric constant is almost cancelled. Thus the inversion of the elution does not take place.

Reference

1) E. L. King, and R. R. Walter, *J. Am. Chem. Soc.*, **74**, 4471 (1952).
2) M. Mori, M. Shibata, and M. Nanasawa, *Bull. Chem. Soc. Jpn.*, **29**, 947 (1956); M. Mori, M. Shibata, and K. Hori, *ibid.*, **34**, 1809 (1961).
3) Y. Yoshikawa, M. Kojima, M. Fujita, M. Iida, and H. Yamatera, *Chem. Lett.*, **1974**, 163.
4) S. Yamazaki and H. Yoneda, *J. Chromatogr.*, in press.
5) N. Yoza, *Kagaku No Ryoiki*, **25**, 1041 (1971).

BULLETIN OF THE CHEMICAL SOCIETY OF JAPAN, VOL. 52 (6), 1861—1862 (1979)

EPR Studies of the Cobalt(II)-(N_2S_2)-Schiff Base Complex with Lewis Bases and CO

Matsujiro SAKURADA,* Yoshihiro SASAKI, Masakazu MATSUI, and Tunenobu SHIGEMATSU
Institute for Chemical Research, Kyoto University, Uji, Kyoto 611

(Received December 6, 1978)

Synopsis. The EPR and optical spectra of *N,N'*-bis-3-thioxo-1-methylbutylidene) ethylenediaminatocobalt(II) in the presence of Lewis bases and CO were measured. The cobalt(II) complex formed five-coordinate adducts with Lewis bases and CO, which had a rhombic symmetry with a $(d_{x^2-y^2}, d_{xz}, d_{yz})^6(d_{z^2})^1$ ground configuration.

Basolo *et al.* have reported that several cobalt(II)–Schiff base complexes (N_2O_2 type) from monomeric oxygen adducts reversibly in the presence of nitrogen donors at a low temperature.[1,2] Recently, Corrigan *et al.* has demonstrated that *N,N'*-bis(2-mercaptobenzylidene)ethylenediaminatocobalt(II) (N_2S_2 type) reacts with molecular oxygen in the presence of pyridine at low temperatures.[3] We have found ourselves that *N,N'*-bis(3-thioxo-1-methyl-butylidene) ethylenediaminatocobalt(II) (N_2S_2 type) is capable of forming monomeric oxygen adducts in the presence of Lewis bases.[4] Here we will report the axial ligation of the cobalt(II) complex with Lewis bases and CO, as studied by the EPR method.

Experimental

N,N'-Bis(3-thioxo-1-methylbutylidene) ethylenediaminatocobalt(II), Co(tacacen), was prepared according to the literature.[5] (Found: C, 45.90; H, 6.06; N, 8.73%. Calcd for $C_{12}H_{18}N_2S_2Co$: C, 46.00; H, 5.79; N, 8.94%). Pyridine, piperidine, and *N*-methylimidazole obtained commercially were purified by distillation, but triphenylphosphine, tributyl phosphine, tributyl phosphite, and trimethyl phosphite were used without further purification. All the EPR samples except the CO sample were prepared by dissolving Co(tacacen) in a toluene solution containing a proper quantity of the Lewis base. Prior to measurements, the samples were degassed thoroughly. The CO sample was prepared by exposing a degassed Co(tacacen) toluene solution to CO gas (500 Torr) at room temperature for three days. The EPR spectra were measured with a JEOL-ME-3X EPR spectrometer at X-band frequencies and calibrated with Mn^{2+} in MgO and DPPH. The optical spectra were measured in dichloromethane with a Hitachi 323 automatic recording spectrophotometer.

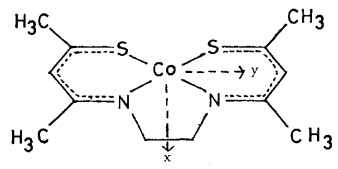

N,N'-bis(3-thioxo-1-methylbutylidene)ethylenediaminatocobalt(II), Co(tacacen).

Results and Discussion

The EPR spectra for Co(tacacen) with pyridine, CO, and triphenylphosphine are shown in Fig. 1. The EPR parameters are tabulated in Table 1. The nitrogen-14 ($I=1$) superhyperfine structure, split into a triplet component, appears in the EPR spectrum for the pyridine system; this indicates that only one pyridine molecule coordinates to Co(tacacen). The phosphorus-31 ($I=1/2$) superhyperfine splitting similarly demonstrates that one triphenylphosphine molecule coordinates to Co(tacacen). Though we measured the EPR spectra of Co(tacacen) toluene solutions containing higher concentrations of these Lewis bases, no evidence for six-coordinate complexes, $Co(tacacen)(LB)_2$, was obtained. The CO adduct was obtained by exposing a Co(tacacen) toluene solution to CO gas, but it did not form in the presence of the Lewis bases.

When the $\boldsymbol{g}$- and $\boldsymbol{A}$-tensors have the same principal axes, the first-order relationships between an electronic structure for the $(d_{z^2})^1$ ground state and the EPR parameters are given according to the following equations:[6]

$$\begin{aligned} g_{xx} &= 2.002 - 6\lambda/\Delta E_{yz} \\ g_{yy} &= 2.002 - 6\lambda/\Delta E_{xz} \\ g_{zz} &= 2.002 \\ A_{xx} &= P[-K-2/7+(g_{xx}-2.002) \\ &\quad +(1/14)(g_{yy}-2.002)] \\ A_{yy} &= P[-K-2/7+(g_{yy}-2.002) \\ &\quad +(1/14)(g_{xx}-2.002)] \\ A_{zz} &= P[-K+4/7+(1/14)\{(g_{xx}-2.002) \\ &\quad +(g_{yy}-2.002)\}] \end{aligned} \qquad (1)$$

TABLE 1. EPR PARAMETERS FOR Co(tacacen)(LB) COMPLEXES

LB	g_1	g_2	g_3	$-A_1$	$-A_2$	A_3	A_3^N	A_1^P	A_3^P	ΔE_{xz}	ΔE_{yz}	$P(cm^{-1})$	K
N-Methylimidazole	2.421	2.219	1.993	3.6	37.8	65.0	16.3			10.2	5.1	0.0169	0.169
Pyridine	2.444	2.207	1.993	−16.2	21.6	77.2	15.3			10.2	5.1	0.0173	0.077
Piperidine	2.432	2.189	2.004	−9.1	26.3	67.1	7.5			10.2	5.1	0.0157	0.099
Carbon monoxide	2.290	2.070	2.029	25.6	58.7	62.0						0.0162	0.165
Triphenylphosphine	2.320	2.161	2.014	8.8	28.9	67.7		149	175	10.4	5.2	0.0136	0.108
Tributylphosphine	2.348	2.175	2.012	8.9	32.6	61.3		140	162	10.4	5.2	0.0148	0.133
Trimethyl phosphite	2.364	2.185	2.012	7.8	33.6	65.1		124	211	10.4	5.2	0.0155	0.140
Tributyl phosphite	2.376	2.189	1.998	12.7	40.4	59.6		126	199	10.4	5.2	0.0160	0.181

A: 10^{-4} cm^{-1}. ΔE: 10^3 cm^{-1} (in dichloromethane solvent).

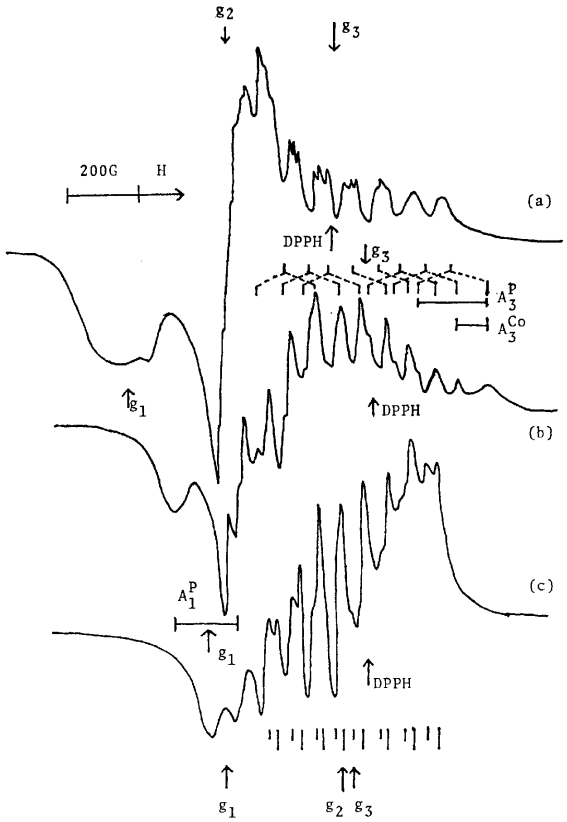

Fig. 1. EPR spectra of Co(tacacen) in the presence of Lewis bases at 77 K. (a) 10 % Pyridine; (b) 10^{-1} M triphenylphosphine; (c) CO gas (500 Torr).

where λ is the effective spin-orbit coupling constant, and where ΔE_{xz} and ΔE_{yz} are the energy separations for the $d_{z^2} \rightarrow d_{xz}$ and $d_{z^2} \rightarrow d_{yz}$ states respectively. $P = gg_n\beta\beta_n\langle r^{-3}\rangle_{3d}$ and PK is the Fermi contact term. The second-order contribution has little significance where $\Delta E \gg \lambda$. The g_3 values in the five-coordinate Co(tacacen) (LB) complexes we studied are nearly 2.002. This implies that the five-coordinate complexes have the $(d_{x^2-y^2}, d_{xz}, d_{yz})^6(d_{z^2})^1$ ground configuration.

The optical spectra for Co(tacacen) with N-donors and P-donors were measured in order to estimate the energy separations. The absorption bands were observed at 10200 cm^{-1} ($\varepsilon \simeq 80$) and 5,100 cm^{-1} ($\varepsilon \simeq 40$) for the N-donors, and at 10400 cm^{-1} ($\varepsilon \simeq 40$) and 5,200 cm^{-1} ($\varepsilon \simeq 10$) for the P-donors. Wayland *et al.* reported that the effective spin-orbit coupling constants for five-coordinate complexes of *N,N'*-disalicylideneethylenediaminato cobalt(II), Co(salen), with Lewis bases, which have the $(d_{z^2})^1$ ground state, are 20—30% less than the free-ion value.[7] In Co(tacacen)(pyridine), when it is assumed that $\Delta E_{xz} = 10200$ cm^{-1}, that $\Delta E_{yz} = 5100$ cm^{-1}, and that the spin-orbit coupling constant is less than the free-ion value by the same degree as in Co(salen)(pyridine), g_{xx}, g_{yy}, and g_{zz} for $(d_{z^2})^1$ ground state are equal to 2.425, 2.214, and 2.002 respectively. These values are in good agreement with the g values observed. No such consistency is found for the other ground states. Therefore, it is concluded that the five-coordinate complexes in this study have

Table 2. Cobalt-59 spin densities for Co(tacacen)(LB) complexes

LB	$-A_c$	A_d	ρ_{3d}	ρ_{4s}	ρ_{Co}	%4s
N-Methyl-imidazole	30.7	104.0	0.717	0.024	0.740	3.24
Pyridine	13.2	98.3	0.678	0.036	0.714	5.04
Piperidine	15.6	89.6	0.617	0.029	0.647	4.48
Carbon monoxide	26.8	89.0	0.639	0.022	0.661	3.33
Triphenyl-phosphine	14.7	77.8	0.536	0.025	0.561	4.46
Tributyl-phosphine	19.6	84.6	0.583	0.024	0.607	3.95
Trimethyl phosphite	21.7	88.5	0.610	0.024	0.634	3.79
Tributyl phosphite	28.9	91.4	0.630	0.020	0.650	3.08

A: 10^{-4} cm^{-1}. $A_c = -PK$. $A_d = (4/7)P$.
$\%4s = (\rho_{4s}/\rho_{Co}) \times 100$.

the $(d_{x^2-y^2}, d_{xz}, d_{yz})^6$ $(d_{z^2})^1$ ground configuration.

The cobalt-59 spin densities can be evaluated from the EPR parameters. The Fermi term has two main factors: (1) the polarization of filled 1s, 2s, and 3s orbitals, which causes a negative spin on the cobalt nucleus because of the unpaired electron in the 3d orbital, and (2) the admixture of the $3d_{z^2}$ orbital into the 4s orbital, which causes a positive spin. Thus, $A_{contact}$ is written as follows:

$$A_{contact} = -PK = \rho_{4s}[A(\text{Co4s})] + \rho_{3d}[A(\text{Co3d})] \quad (2)$$

where $A(\text{Co4s}) = 0.1232$ cm^{-1} and $A(\text{Co3d}) = 0.00840$ cm^{-1}.[8] ρ_{3d} and ρ_{4s} are the spin densities of the cobalt $3d_{z^2}$ and 4s orbitals respectively. The cobalt $3d_{z^2}$ spin density is estimated by comparing the observed dipolar coupling constant with the theoretical value ($A_d = (4/7)P_0 = 0.0145$ cm^{-1}) according to this equation: $\rho_{3d} = (A_d)_{obsd}/(A_d)_{obsd}$. The results for the cobalt-spin density are given in Table 2. The total cobalt-spin densities increase in the order of: N-donors>CO>P-donors. This suggests that the N-donors have a smaller mixing between the cobalt $3d_{z^2}$ and the ligand σ-donor orbitals than do CO and the P-donors. This order also agrees with the tendency of the electronegativity of the ligand-donor atoms.

References

1) B. M. Hoffman, D. I. Diemente, and F. Basolo, *J. Am. Chem. Soc.*, **92**, 61 (1970).
2) M. J. Carter, D. P. Rillema, and F. Basolo, *J. Am. Chem. Soc.*, **96**, 392 (1974).
3) M. F. Corrigan, K. S. Murry, and B. O. West, *J. Chem. Soc., Dalton Trans.*, **1977**, 1478.
4) M. Sakurada, Y. Sasaki, M. Matsui, and T. Shigematsu, *Bull. Inst. Chem. Res., Kyoto Univ.*, **55**, 466 (1977).
5) P. R. Blum, R. M. C. Wei, and S. C. Cummings, *Inorg. Chem.*, **13**, 450 (1974).
6) A. H. Maki, N. Edelstein, A. Davison, and R. H. Holm, *J. Am. Chem. Soc.*, **86**, 4850 (1964).
7) B. B. Wayland, M. E. Abd-Elmageed, and L. F. Mehne, *Inorg. Chem.*, **14**, 1456 (1975).
8) M. C. R. Symons and J. G. Wilkinson, *J. Chem. Soc., A*, **1971**, 2069.

BULLETIN OF THE CHEMICAL SOCIETY OF JAPAN, VOL. 52 (6), 1863—1864 (1979)

Diffusion Coefficients of Thallium(I) and Cadmium(II) Ions in Aqueous Nitrate Solutions Determined Chronoamperometrically with a Thin-walled Hanging Mercury Drop Electrode

Haruko IKEUCHI, Kyoichi IWAI, Mamoru KANEKO, Muneo MAYA, and Gen P. SATÔ*

Department of Chemistry, Faculty of Science and Technology, Sophia University, Kioicho, Chiyoda-ku, Tokyo 102

(Received January 12, 1979)

Synopsis. The diffusion coefficients (D) of Tl^+ in 0.1 and 0.5 mol dm^{-3} KNO_3 and of Cd^{2+} in 1.0 mol dm^{-3} KNO_3 in the temperature range 5 °C—35 °C are given with additional data including activation energies. $kT/D\eta$, where η is the viscosity of the nitrate solution, depends primarily on the diffusing species.

A stationary mercury drop electrode hanging from a thin-walled capillary (HMDE) was found to be one of the most suitable means for reliable electrochemical determination of diffusion coefficients.[1,2] This report gives the diffusion coefficients measured by the HMDE method for thallium(I) and cadmium(II) ions in aqueous nitrate solutions at several temperatures.

When the diffusion current I_d at a spherical electrode is plotted against $t^{-1/2}$, where t is the time of electrolysis, a straight line should be obtained.[3] From the slope and intercept of the plot, with the known size of the electrode, the diffusion coefficient (D) and the product nc are determined independently from a single chronoamperogram, n being the charge number of the electrode reaction and c the bulk concentration of the electroactive species. A comparison of the observed value, $(nc)_{obsd}$, with the known value, $(nc)_{calcd}$, provides a useful means of assessing the extent to which the obtained D is reliable.

The linearity of the I_d *vs.* $t^{-1/2}$ plot is a qualitative criterion of experimental validity, but it is not sufficient. An example is given to demonstrate the importance of the "nc test" in a reliable diffusion coefficient measurement. All the plots for $[Fe(CN)_6]^{3-}$ in 1.0 mol dm^{-3} KCl were quite linear even when the $(nc)_{obsd}$ values were incorrect. The D values calculated from such linear plots were unreasonably high, scattered, and varied with the cyanoferrate concentration. Thus, besides the reproducible surface of known area with high hydrogen overvoltage, an essential advantage of the use of an appropriately designed HMDE is its ability to approximate spherical diffusion satisfactorily.

Experimental

In earlier experiments a balanced-type HMDE[1] was used. Later a micrometer-type HMDE assembly MCI AS01 (Mitsubishi Chemical Industries, Ltd.) was adopted, its capillary end being drawn to give a tip of *ca.* 0.2 mm in outer diameter, from which a mercury drop of 0.8 mm—1.0 mm diam. was produced. The size of the drop was read by the rotation of the micrometer, which had been calibrated by weighing the mercury delivered. For such an HMDE the total error due to the shielding and the non-sphericity is estimated to be 1% or less.[2] Constancy and uniformity of the solution temperature were essential to maintain stagnancy. It was controlled within $\pm$(0.002—0.05) °C, the fluctuation being larger at lower and higher temperatures.

The potentiostat with a current follower was essentially the same as that used previously[1] except that the high-speed pen recorder was replaced by a digital memory device (Biomation, Transient Recorder, Model 802), and the current signals stored therein were printed out. This arrangement eliminated the positive deviation at $t<1.5$ s caused by the delay in response of the pen recorder.[1] Another type of positive error in current magnitude was observed at much shorter times, $t<20$ ms, attributable to the saturation of the current follower during the initial period of electrolysis. The difficulty was readily circumvented by appropriate adjustment in the gain

Table 1. Diffusion coefficients of thallium(I) ions in aqueous potassium nitrate solutions

Supporting electrolyte[a]	T/K	Number of runs	$10^{10}D$/m^2 s^{-1}	Δ^*E_A/kJ mol^{-1}	$\lambda\exp\left(\frac{\Delta^*S}{2R}\right)$/nm	$kT/D\eta$/nm
0.1 M KNO_3	288	6	15.3±0.2	15.8±1.7	0.26±0.09	2.3
	293	6	17.5±0.2			2.3
	298	29	19.4±0.1			2.4
	303	6	21.6±0.2			2.4
	308	4	23.5±0.5			2.5
0.5 M KNO_3	278.20	6	11.5±0.4	16.6±1.3	0.30±0.08	2.3
	283.22	6	12.8±0.1			2.4
	288.24	6	14.5±0.2			2.5
	293.48	6	16.9±0.2			2.5
	298.52	6	18.7±0.3			2.5
	302.89	3	20.3±0.4			2.6
1.0 M KNO_3	298.19	11	17.3±0.2	—	—	2.7

The uncertainty is 95% confidence limit. a) M=mol dm^{-3}.

Table 2. Diffusion coefficients of cadmium(II) ions in aqueous nitrate solutions

Supporting electrolyte[a)]	T/K	Number of runs	$10^{10}D$/m^2 s^{-1}	Δ^*E_A/kJ mol^{-1}	$\lambda\exp\left(\frac{\Delta^*S}{2R}\right)$/nm	$kT/D\eta$/nm
0.1 M KNO_3	298.35	4	7.40±0.03	—	—	6.3
1.0 M KNO_3	278.12	8	4.18±0.03			6.4
	283.17	12	4.89±0.03			6.6
	288.25	13	5.67±0.06			6.5
	295.17	10	6.76±0.08	18.5±0.9	0.27±0.05	6.3
	298.15	3	7.31±0.10			6.4
	303.01	6	8.26±0.08			6.3
	308.34	7	9.07±0.05			6.5
1.0 M $NaNO_3$	298.01	12	6.71±0.05	—	—	6.4

The uncertainty is 95% confidence limit. a) M=mol dm^{-3}.

of the follower. The whole system is capable of recording diffusion currents from a few milliseconds. The time range 100 ms—10 s was used in the present set of experiments.

Preparation of the reagents and solutions and the procedure of chronoamperometry have been described in detail.[1)] The chronoamperograms were first examined for linearity against $t^{-1/2}$. The deviating points that reflected the convective disturbance of diffusion layer at longer times[1)] were omitted, and the values of $(nc)_{obsd}$ were calculated for each set of measurements. If the mean value of $(nc)_{obsd}$ agreed with $(nc)_{calcd}$ within the limits of experimental error for 95% confidence, the value of D that best reproduced the observed chronoamperogram was obtained by the least-squares method by using the value of $(nc)_{calcd}$.

Results and Discussion

The diffusion coefficients for thallium(I) and cadmium (II) ions in nitrate solutions (Tables 1 and 2, respectively) were critically selected from the data obtained in the authors' laboratory since 1970. The values for 0.1 mol dm^{-3} KNO_3 at 25 °C supersede the corresponding ones presented earlier.[1)]

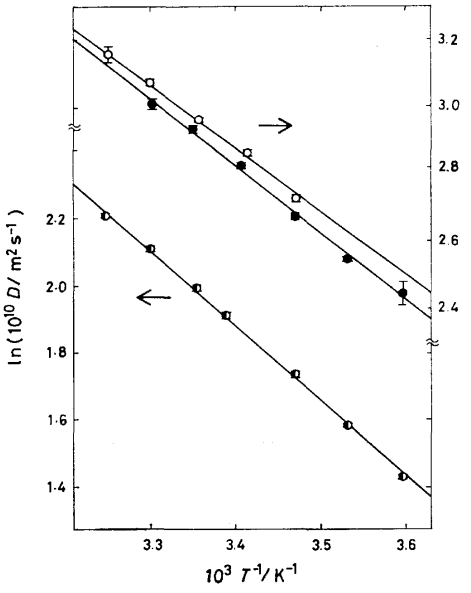

Fig. 1. Arrhenius plots of D.
○: Tl^+ in 0.1 mol dm^{-3} KNO_3, ●: Tl^+ in 0.5 mol dm^{-3} KNO_3, ◐: Cd^{2+} in 1.0 mol dm^{-3} KNO_3. The error bars correspond to the uncertainty at 95% confidence.

The Arrhenius plots of the three systems gave curves slightly convex upward (Fig. 1). The average experimental activation energies of diffusion, Δ^*E_A, are calculated by linearly approximating the curved plots. It is noted that these figures are comparable to 16.7 kJ mol^{-1} of the diffusion of water molecules in 0.1 mol dm^{-3} KNO_3.[4)]

According to Eyring's absolute rate theory, the intercept of the Arrhenius plot is related to $\lambda\exp(\Delta^*S/2R)$, where Δ^*S is the entropy of activation of diffusion, λ is the distance between two successive equilibrium positions of the diffusing particle in the solution, and R the gas constant.[5)] The values for this quantity falling around 0.3 nm suggest that Δ^*S cannot differ appreciably from zero. A similar value, 0.34 nm, is calculated from the data[4)] for the diffusion of water in 0.1 mol dm^{-3} KNO_3.

The viscosity, η, of the supporting electrolyte solutions was estimated by inter- and extrapolation of the tabulated data,[6)] and $kT/D\eta$ are calculated. The result seems to depend primarily on the diffusing species, being fairly insensitive to the temperature and concentration of the supporting electrolyte, as might be expected from the Einstein-Stokes relation or Eyring's theory.[5)]

The authors thank Sr. Jean Michalec for correcting the manuscript. One of the authors (H.I.) gratefully acknowledges financial support granted by the Saneyoshi Scholarship Foundation.

References

1) H. Ikeuchi, Y. Fujita, K. Iwai, and G. P. Satô, *Bull. Chem. Soc. Jpn.*, **49**, 1883 (1976).
2) H. Ikeuchi, T. Yazaki, and G. P. Satô, *Bunseki Kiki*, **14**, 207 (1976).
3) For example, I. M. Kolthoff and J. J. Lingane, "Polarography," 2nd ed, Interscience Publishers, New York (1952), Chap. 2.
4) K. Tanaka, *J. Chem. Soc., Faraday Trans. 1*, **71**, 1127 (1975).
5) S. Glasstone, K. J. Laidler, and H. Eyring, "The Theory of Rate Processes," McGraw-Hill Book Co., New York (1941), Chap. IX.
6) "Kagaku Binran," 2nd ed, ed by the Chemical Society of Japan, Maruzen, Tokyo (1975), p. 579.

BULLETIN OF THE CHEMICAL SOCIETY OF JAPAN, VOL. 52 (6), 1865—1866 (1979)

2-Alkylation Reactions of Thiophene and 1-Methylpyrrole with Trialkylboranes

Toshiki SOTOYAMA, Shoji HARA, and Akira SUZUKI*

Department of Applied Chemistry, Faculy of Engineering, Hokkaido University, Sapporo 060

(Received December 9, 1978)

Synopsis. The reactions of iodine with ate-complexes prepared from trialkylboranes and 2-thienyllithium or 1-methyl-2-pyrrolyllithium were found to give the corresponding 2-alkylthiophenes or 1-methyl-2-alkylpyrroles, respectively, in good yields.

Useful methods for obtaining functionalized organic compounds can be found by employing a heterocycle with one hetero atom either as a precursor, reagent, or vehicle for the formation. The most general synthesis of pyrroles and thiophenes involves, as observed in the Knorr reaction, condensation of a carbonyl compound with the corresponding hetero atom containing compound.[1] On the other hand, probably the most available procedure for the synthesis of 2-alkylated derivatives of such heterocycles involves the reaction of the corresponding 2-lithio derivatives with alkyl halides.[2] However, the synthesis is satisfactory only for primary alkyl halides which readily undergo nucleophilic substitution reactions. In the case of *s*-alkyl halide, it may involve a competitive elimination reaction.[3] We wish to report that the reaction of 2-lithiothiophene or 2-lithio-1-methylpyrrole with trialkylboranes, followed by treatment with iodine gives the corresponding 2-alkylated derivatives in good yields (Eq. 1).[4]

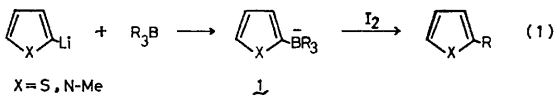

(1)

Addition of an equimolar amount of butyllithium in ether to thiophene in ether containing tetramethylethylenediamine (TMEDA) at room temperature resulted in quantitative metalation to give 2-lithiothiophene, which was then treated at room temperature with a solution of triisobutylborane in THF. The reaction of the resulting solution of the ate-complex (**1**) thus obtained with iodine, followed by the usual alkaline hydrogen peroxide oxidation to remove the residual organoborane, provided 2-isobutylthiophene in a 95% yield. The results of reactions with representative trialkylboranes are summarized in Table 1.

In the present reaction, secondary alkyl and aryl groups appear to be introduced as readily as primary alkyl groups. It seems that the reaction proceeds through the same type of reaction path as considered in the reaction of 1-alkynyltriorganoborates with iodine,[5] *i.e. via* three stages: (1) coordination of trialkylboranes with the carbanion derived from the heterocyclic compound, (2) iodine cation attack of the 5-position in the hetero ring with migration of an alkyl group from boron to 2-position, and (3) intermediate (**2**) gives the product by the elimination of dialkyliodoborane (Eqs. 2, 3, and 4).

TABLE 1. 2-ALKYLATION OF THIOPHENE AND 1-METHYLPYRROLE WITH TRIALKYLBORANES[a]

Hetero-cycle	Organoborane R_3B R=	Product	Yield %[b]
Thiophene	Propyl	2-Propylthiophene	62
	Butyl	2-Butylthiophene	91
	Isobutyl	2-Isobutylthiophene	95
	s-Butyl	2-*s*-Butylthiophene	100
	Octyl	2-Octylthiophene	66
	Cyclopentyl	2-Cyclopentylthiophene	100
	Phenyl[c]	2-Phenylthiophene	42[d]
1-Methyl-pyrrole[e]	Propyl	1-Methyl-2-propylpyrrole	92
	Butyl	1-Methyl-2-butylpyrrole	98
	Isobutyl	1-Methyl-2-isobutylpyrrole	80
	s-Butyl	1-Methyl-2-*s*-butylpyrrole	95
	Hexyl	1-Methyl-2-hexylpyrrole	70
	Cyclopentyl	1-Methyl-2-cyclopentylpyrrole	73

a) Thiophene or 1-methylpyrrole: trialkylborane= 1.2: 1 b) Based on organoborane used. Analyzed by VPC. c) Prepared from PhMgBr and BF_3 etherate. d) Refluxed for 4 h. e) Metalation of 1-methylpyrrole: To a stirred solution of 1-methylpyrrole and TMEDA in dry ether was added butyllithium, followed by heating at reflux temperature for 2 h.

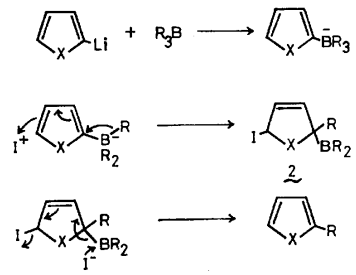

(2)

(3)

(4)

Experimental

Materials. All the chemicals and solvents were purified by distillation. Trialkylboranes were prepared by the usual procedure.[6]

The IR and NMR spectra were taken on a Hitachi-Perkin-Elmer Model 125 spectrophotometer and Hitachi R-22 spectrometer at 90 MHz using tetramethylsialne as an internal standard, respectively.

General Procedure. A representative procedure for the preparation of 2-butylthiophene is as follows. A dry 50 ml-flask equipped with a magnetic stirring bar, a septum inlet, and a reflux condenser was flushed with nitrogen. The flask

was charged under nitrogen gas with thiophene (0.378 g, 4.5 mmol), TMEDA (0.627 g, 5.4 mmol) and anhydrous ether (5 ml). Butyllithium (4.5 mmol, 3 ml of 1.5 M solution in ether) was then added at room temperature and the mixture was stirred for 1 h. After metalation was complete, tributylborane (3 mmol, 2 ml of 1.5 M solution in THF) was added at room temperature, followed by reflux for 2 h. The solution was cooled to −78 °C and iodine (1.143 g, 4.5 mmol) in 10 ml of dry ether was added. The reaction mixture was stirred for 30 min and allowed to warm to room temperature. After being stirred for 2 h, the mixture was treated with 5 ml of 3 M aqueous sodium hydroxide and 5 ml of 30% hydrogen peroxide at room temperature for 2 h. Saturation of the aqueous solution with potassium carbonate yielded an organic phase. The product was extracted with ether and analyzed by VPC. Analysis indicated the presence of 2.73 mmol (91%) of 2-butylthiophene. An analytically pure material was obtained by preparative VPC. (10% Carbowax 20 M on Uniport B, 3 m) with Varian autoprep Model-2800.

Identification of the Products. *2-Propylthiophene*: n_D^{20} 1.5060. Found: C, 66.48; H, 7.86%. Calcd for $C_7H_{10}S$: C, 66.61; H, 7.99%. Mass; *m/e*=126 (M^+). IR(neat); 3050, 1460, 850, 820, 690 cm^{-1}. NMR (CCl_4); τ, 9.00 (3H, t, J=6.0 Hz), 8.40 (2H, m), 7.18 (2H, t, J=7.0 Hz), 2.90—3.40 (3H, m).

2-Butylthiophene: n_D^{20} 1.5064. Found: C, 68.47; H, 8.51%. Calcd for $C_8H_{12}S$: C, 68.51; H, 8.62%. Mass; *m/e*=140 (M^+). IR (neat); 3050, 1460, 850, 820, 690 cm^{-1}. NMR (CCl_4); τ, 9.10 (3H, t, J=7.0 Hz), 8.45 (4H, m), 7.20 (2H, t, J=7.0 Hz), 2.92—3.36 (3H, m).

2-Isobutylthiophene: n_D^{20} 1.4980. Found: C, 68.63; H, 8.59%. Calcd for $C_8H_{12}S$: C, 68.51; H, 8.62%. Mass; *m/e*=140 (M^+). IR (neat); 3050, 1460, 1385, 1370, 1170, 700 cm^{-1}. NMR (CCl_4); τ, 9.05 (6H, d, J=6.0 Hz,) 8.08 (1H, m), 7.30 (2H, d, J=7.0 Hz), 2.92—3.35 (3H, m).

2-s-Butylthiophene: n_D^{20} 1.5006. Found: C, 68.63; H, 8.58%. Calcd for $C_8H_{12}S$: C, 68.51; H, 8.62%. Mass; *m/e*=140 (M^+). IR(neat); 3050, 1450, 1380, 860, 820, 690 cm^{-1}. NMR (CCl_4); τ, 9.15 (3H, t, J=6.0 Hz), 8.76 (3H, d, J=7.0 Hz), 8.43 (2H, m), 7.20 (1H, m), 2.92—3.35 (3H, m).

2-Octylthiophene: n_D^{20} 1.4922. Found: C, 73.21; H, 10.35%. Calcd for $C_{12}H_{20}S$: C, 73.40; H, 10.27%. Mass; *m/e*=196 (M^+). IR (neat); 3050, 1450, 850, 820, 690 cm^{-1}. NMR (CCl_4); τ, 9.10 (3H, t, J=6.0 Hz), 8.10—8.80 (12H, m), 7.17 (2H, t, J=7.0 Hz), 2.90—3.35 (3H, m).

2-Cyclopentylthiophene: n_D^{20} 1.5365. Found: C, 70.88; H, 7.98%. Calcd for $C_9H_{12}S$: C, 71.00; H, 7.94%. Mass; *m/e*=152 (M^+). IR (neat); 3050, 1440, 859, 820, 690 cm^{-1}. NMR (CCl_4); τ, 7.72—8.55 (8H, m), 6.75 (1H, m), 2.90—3.33 (3H, m).

2-Phenylthiophene: Mp 34—35 °C. Found: C, 74.82; H, 5.11%. Calcd for $C_{10}H_8S$: C, 74.96; H, 5.03%. Mass; *m/e*=160 (M^+). IR (Nujol); 3050, 1940, 1780, 1590, 1440, 860, 825, 760, 690 cm^{-1}. NMR (CCl_4); τ, 2.18—3.18 (8H, m).

1-Methyl-2-propylpyrrole: n_D^{20} 1.504. Found: C, 77.85; H, 10.59%. Calcd for $C_8H_{13}N$: C, 77.99; H, 10.64%. Mass; *m/e*=123 (M^+). IR (neat); 3100, 1500, 1310, 1100, 710 cm^{-1}. NMR (CCl_4); τ, 9.00 (3H, t, J=7.0 Hz), 8.37 (2H, m), 7.52 (2H, t, J=7.0 Hz), 6.48 (3H, s), 4.06—4.35 (2H, m), 3.17 (1H, t, J=2 Hz).

1-Methyl-2-butylpyrrole: n_D^{20} 1.486. Found: C, 78.89; H, 10.96%. Calcd for $C_9H_{15}N$: C, 78.77; H, 11.02%. Mass; *m/e*=137 (M^+). IR (neat); 3100, 1500, 1310, 1100, 710 cm^{-1}. NMR (CCl_4); τ, 9.04 (3H, t, J=6.0 Hz), 8.35 (4H, m), 7.50 (2H, t, J=7.0 Hz), 6.48 (3H, s), 4.06—4.35 (2H, m), 3.17 (1H, t, J=2 Hz).

1-Methyl-2-isobutylpyrrole: n_D^{20} 1.515. Found: C, 78.83; H, 11.11%. Calcd for $C_9H_{15}N$: C, 78.77; H, 11.02%. Mass; *m/e*=137 (M^+). IR (neat); 3100, 1490, 1380, 1360, 1090, 700 cm^{-1}. NMR (CCl_4); τ, 9.05 (6H, d, J=6.4 Hz), 8.16 (1H, m), 7.64 (2H, d, J=7.0 Hz), 4.50 (3H, s), 4.06—4.35 (2H, m), 3.17 (1H, t, J=2 Hz).

1-Methyl-2-s-butylpyrrole: n_D^{20} 1.454. Found: C, 78.65; H, 11.13%. Calcd for $C_9H_{15}N$: C, 78.77; H, 11.02%. Mass; *m/e*=137 (M^+). IR (neat); 3100, 1490, 1310, 1100, 700 cm^{-1}. NMR (CCl_4); τ, 9.11 (3H, t, J=7.3 Hz), 8.80 (3H, d, J=6.4 Hz), 8.44 (2H, m), 7.36 (1H, m), 6.42 (3H, s), 4.06—4.35 (2H, m), 3.17 (1H, t, J=2 Hz).

1-Methyl-2-hexylpyrrole: n_D^{20} 1.482. Found: C, 79.85; H, 11.63%. Calcd for $C_{11}H_{19}N$: C, 79.94, H, 11.59%. Mass; *m/e*=165 (M^+). IR (neat); 3100, 1490, 1310, 1090, 700 cm^{-1}. NMR (CCl_4); τ, 9.10 (3H, t, J=5.0 Hz), 8.20—8.82 (8H, m), 7.49 (2H, t, J=8 Hz), 6.46 (3H, s), 4.06—4.35 (2H, m), 3.17 (1H, t, J=2 Hz).

1-Methyl-2-cyclopentylpyrrole: n_D^{20} 1.518. Found: C, 80.55; H, 10.06%. Calcd for $C_{10}H_{15}N$: C, 80.48, H, 10.13%. Mass; *m/e*=149 (M^+). IR (neat); 3100, 1490, 1100, 715 cm^{-1}. NMR (CCl_4); τ, 7.82—8.59 (8H, m), 7.04 (1H, m), 6.46 (3H, s), 4.06—4.35 (2H, m), 3.17 (1H, t, J=2 Hz).

References

1) For example, see R. M. Acheson, "An Introduction to the Chemistry of Heterocyclic Compounds," John Wiley and Sons, New York (1976).

2) V. Ramanathan and R. Levine, *J. Org. Chem.*, **27**, 1216 (1962).

3) B. J. Wakefield, "The Chemistry of Organolithium Compounds," Pergamon Press, Oxford, (1976), p. 144.

4) Alkylation of furan is also possible; this is to be published in connection with the synthesis of 1,4-dicarbonyl compounds using organoboranes. I. Akimoto and A. Suzuki, *Synthesis*, in press (1978).

5) A. Suzuki, N. Miyaura, S. Abiko, M. Itoh, H. C. Brown, J. A. Sinclair, and M. M. Midland, *J. Am. Chem. Soc.*, **95**, 3080 (1973).

6) H. C. Brown, "Organic Synthesis *via* Boranes," John Wiley and Sons, New York, (1975).

BULLETIN OF THE CHEMICAL SOCIETY OF JAPAN, VOL. 52 (6), 1867—1868 (1979)

Steric Effect in 3,7-Disubstituted Tropolone. Chemical and Physical Properties of 3-Phenyl- and 3-Isopropyl-7-(2,4,6-cycloheptatrienyl)tropolones[1]

Takahiro TEZUKA*,† and Tetsuo NOZOE††

Department of Chemistry, Faculty of Science, Tohoku University, Sendai 980

(Received August 28, 1978)

Synopsis. The preparation and chemical and spectroscopic properties of 3-phenyl-7-(2,4,6-cycloheptatrienyl)-tropolone (**1**) and 3-isopropyl-7-(2,4,6-cycloheptatrienyl)-tropolone (**2**) are described. The somewhat unusual properties of **1** and **2** have been discussed in terms of the steric effect of the two substituent groups at positions 3 and 7 in the tropolone ring.

X-Ray crystallographic studies have revealed the distortion of the heptagon in tri and tetra-substituted tropolones.[2] In this connection, this report will show that the 3,7-disubstituted tropolones (**1** and **2**) possess chemical and physical properties which differ from the parent tropolone.

3-Phenyl- and 3-isopropyl-7-(2,4,6-cycloheptatrienyl)-tropolones (**1** and **2**) have been prepared in good yield from 3-phenyl- and 3-isopropyltropolones, respectively, by reaction with di(2,4,6-cycloheptatrienyl) ether. The structures of **1** and **2** have been assigned on the basis of the spectral and chemical data (see Experimental). Compounds **1** and **2** afforded azo derivatives **4a** (71%), **4b** (63%), and **5** (68%) by the action of the corresponding aryldiazonium chlorides. Compound **1** gave, on reaction with diazomethane, two kinds of methyl ethers **6** (61%) and **7** (24%), both of which reverted to **1** by acid hydrolysis. The isomeric structures of **6** and **7** have been tentatively assigned on the basis that a less hindered methyl ether would be formed in higher yield.[3] The methoxyl group of the ethers (**6** and **7**) was replaced by an amino group in the reaction of ammonia in methanol, giving amino derivatives **8** and **9**, the isomeric structures of which are again tentative. The properties of **1** and **2** described are consistent with those of the parent tropolone.[3]

The properties of **1** and **2**, however, differ from tropolone in the following respects: (i) the compounds do not show a ferric chloride coloration characteristic of tropolones in benzene and ethanol, but show a pale green coloration in 1-butanol. It is well documented that the ferric chloride coloration of tropolones in benzene and ethanol is due to the formation of the tropolone-iron (III) 3:1 or 2:1 complex.[3,4] (ii) The hydroxyl absorption bands of **1** and **2** do not appear in the ordinary region (3200—3500 cm^{-1}),[5] appearing at 3050 cm^{-1} in low intensity (CCl_4). The absorption bands of the conjugated carbonyl appear at 1600 and 1550 cm^{-1} for **1**, and 1590 and 1540 cm^{-1} for **2**. The band positions are as expected,[5] but the intensities are extremely small compared with those of tropolone. (iii) Compounds **1** and **2** are inert to nitration with nitric acid in acidic medium, with which tropolone readily reacts to give nitrotropolone.[3] Similar chemical and spectroscopic properties were found for 3,7-di(2,4,6-cycloheptatrienyl)tropolone (**3**)[6] prepared from 3-(2,4,6-cycloheptatrienyl)tropolone and di(2,4,6-cycloheptatrienyl) ether.

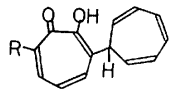

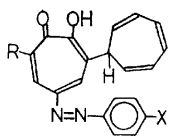

1: R=Phenyl
2: R=Isopropyl
3: R=2,4,6-Cycloheptatrienyl

4a: R=Ph; X=Me
4b: R=Ph; X=Br
5: R=*i*-C_3H_7; X=Me

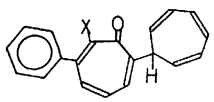

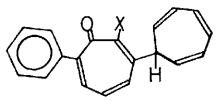

6: X=OMe
8: X=NH_2

7: X=OMe
9: X=NH_2

The distortion of the heptagon and bond fixation in crowded tropolones such as 3,5,7-tribromohinokitiol and 3,7-dibromohinokitiol have been reported by Itô *et al.*[2] The somewhat unusual properties of **1**, **2**, and **3** found in this study may be related to the steric effect of the bulky substituent groups at the 3 and 7 positions of the tropolone ring. The boat conformation of 2,4,6-cycloheptatriene is well documented and the steric hindrance caused by the 2,4,6-cycloheptatrienyl group may be comparable with that by the isopropyl group.[7]

Experimental

Preparation of 3-Phenyl-7-(2,4,6-cycloheptatrienyl)tropolone (1) and 3,7-Di(2,4,6-cycloheptatrienyl)tropolone (3). A mixture of 3-phenyltropolone (5 g, 0.025 mol) and di(2,4,6-cycloheptatrienyl) ether (3 g, 0.015 mol) in dry ethanol (5 ml) was refluxed for 20 min. The precipitate formed was collected by filtration and crystalized (6.8 g; 94%). Recrystallization from benzene gave **1** as yellow needles, mp 141—142 °C: λ_{max}^{MeOH} (log ε) 242 (4.36), 268 (4.33), 348 (3.84), 385 (3.86), and 410 (3.70) nm; δ (CCl_4) 3.63 (1H, t, J=4.8 Hz), 5.18 (2H, dd, J=4.8 and 8.2 Hz), 6.13 (2H, m), 6.37 (2H, broad t), and around 8 (8H). Found: C, 83.17; H, 5.38%. Calcd for $C_{20}H_{16}O_2$: C, 83.31; H, 5.59%.

Similarly, heating a mixture of 3-(2,4,6-cycloheptatrienyl)-tropolone (250 mg, 1.2 mmol) and di(2,4,6-cycloheptatrienyl)-

† Present address: Department of Chemistry, The University of Tsukuba, Sakura-mura, Ibaraki 300-31.

†† Present address: Tokyo Research Laboratory, Kao Soap Ltd., Bunka, Sumida-ku, Tokyo 131.

ether (117 mg, 0.59 mmol) in dry ether (2.5 ml) under reflux for 3 h gave crystals (365 mg, 100%). Recrystallization from ethanol gave **3** as yellow needles, mp 137 °C, identical with an authentic sample.[6]

Preparation of 3-Isopropyl-7-(2,4,6-cycloheptatrienyl)tropolone (2). A mixture of 3-isopropyltropolone (12.6 g, 0.0768 mol) and di(2,4,6-cycloheptatrienyl) ether (8.6 g, 0.0434 mol) was heated on a water bath for 20 min. The reaction mixture was extracted with benzene and the extract treated with aqueous copper(II) sulfate. The precipitate formed was collected by filtration, giving copper salts of **2** (20 g, 91%) as green needles (mp 229 °C). Dry hydrogen sulfide gas was passed through a suspension of the copper salts of **2** (200 mg, 0.035 mmol) in chloroform (4 ml) for 30 min. and the mixture allowed to stand for 1 h. The copper(II) sulfide precipitate was filtered, and the filtrate was treated with active charcoal, washed with water and dried over sodium sulfate. Evaporation of the solvent gave crystals of **2** (91 mg, 51%). Recrystallization from a mixed solvent of ethanol and benzene gave **2** as colorless needles, mp 77—78 °C: λ_{max}^{MeOH} (log ε) 255 (4.18), 321 (3.70), 363 (3.68), 374 (3.72), and 396 (3.58) nm; δ (CCl_4) 1.24 (6H, d, J=4.0 Hz), 3.30 (1H, m), 3.42 (1H, t, J=4.2 Hz), 5.28 (2H, dd, J=4.2 and 8.8 Hz), 6.20 (2H, m), 6.54 (2H, m), and 7.25 (3H, m). Found: C, 80.52; H, 7.32%. Calcd for $C_{17}H_{18}O_2$: C, 80.28; H, 7.13%.

3-Phenyl-5-(p-tolylazo)-7-(2,4,6-cycloheptatrienyl)tropolone (4a). To a pyridine solution (1 ml) of **1** (100 mg, 0.35 mmol) was added with stirring at 0 °C an aqueous solution of *p*-toluenediazonium chloride, prepared from *p*-toluidine (41 mg, 0.38 mmol), 6 M hydrochloric acid (0.3 ml), sodium nitrite (35 mg, 0.51 mmol), and water (0.1 ml). The stirring was continued for 1—1.5 h at 0 °C. After the addition of a small amount of water, the reaction mixture was extracted with chloroform and the extract washed with water and dried over sodium sulfate. Evaporation of the solvent gave **4a** (100 mg, 71%) as crystals. Recrystallization from benzene afforded **4a** as orange needles, mp 201.5—202.5 °C. Found: C, 79.60; H, 5.36%. Calcd for $C_{27}H_{22}O_2N_2$: C, 79.78; H, 5.46%.

3-Isopropyl-5-(p-tolylazo)-7-(2,4,6-cycloheptatrienyl)tropolone (5). To a pyridine solution (1 ml) of **2** (100 mg, 0.39 mmol) was added with stirring at 0 °C an aqueous solution of *p*-toluenediazonium chloride, prepared from *p*-toluidine (46 mg, 0.43 mmol), 6 M hydrochloric acid (0.4 ml), sodium nitrite (40 mg, 0.58 mmol), and water (0.2 ml). The stirring was continued for 1.5 h at 0 °C. Work-up of the reaction mixture as described above gave **5** (100 mg, 68%) as crystals. Recrystallization from benzene afforded **5** as orange needles, mp 164—165 °C. Found: C, 77.65; H, 6.76; N, 7.49%. Calcd for $C_{24}H_{24}O_2N_2$: C, 77.39; H, 6.50; N, 7.52%.

3-Phenyl-5-(p-bromophenylazo)-7-(2,4,6-cycloheptatrienyl)tropolone (4b). To a pyridine solution (0.1 ml) of the sodium salts of **1** (100 mg, 0.32 mmol) was added with stirring at 0 °C an aqueous solution of *p*-bromobenzenediazonium chloride prepared from *p*-bromoaniline (62 mg, 0.36 mmol), 6 M hydrochloric acid (0.2 ml), sodium nitrite (30 mg, 0.43 mmol), and water (0.3 ml). The mixture was continuously stirred for 1 h at 0 °C. Work-up of the reaction mixture gave crystals of **4b** (95 mg, 63%). Recrystallization from benzene gave **4b** as orange needles, mp 197—198 °C. Found: C, 65.96; H, 4.20; N, 6.21%. Calcd for $C_{26}H_{19}O_2N_2Br$: C, 66.24; H, 4.03; N, 5.94%.

Formation of Methyl Ethers (6 and 7) from 1. To an ethereal solution of **1** (1 g, 3.5 mmol) was added an ethereal solution of diazomethane (8 ml) prepared from *N*-nitrosomethylurea and potassium hydroxide.[8] After the addition of methanol (one drop), the mixture was allowed to stand at room temperature for 30 min. The precipitate formed was collected by filtration giving crystals of **6** (640 mg, 61%). Recrystallization from ethanol gave **6** as yellow needles, mp 133—134 °C. Found: C, 83.22; H, 6.03%. Calcd for $C_{21}H_{18}O_2$: C, 82.42; H, 6.00%. Concentration of the filtrate gave crystals of **7** (250 mg, 24%). Recrystallization from ethanol gave **7** as yellow needles, mp 112—113 °C. Found: C, 83.23; H, 5.86%. Calcd for $C_{21}H_{18}O_2$: C, 83.42; H, 6.00%.

Hydrolysis of 6 and 7. A mixture of **6** (1 mg) or **7** (1.5 mg) and 3 M sulfuric acid (one drop) in ethanol (0.1 ml) was refluxed for 10 min. The reaction mixture was extracted with benzene and the extract washed with water and dried. Evaporation of the solvent gave a crystalline compound which had an R_f value identical with that of **1**.

Formation of Amino Derivatives 8 and 9. A mixture of the methyl ethers (**8** and **9**) (110 mg) prepared from **1** with diazomethane (*vide supra*) was dissolved in methanolic ammonia (25 volume %, 20 ml) and the mixture allowed to stand at room temperature for 48 h. Evaporation of the methanol and excess ammonia gave an oil which solidified on the addition of a small amount of ethanol to give crystals (65 mg). Recrystallization from a mixture of ethanol and benzene gave yellow prisms (**8**), mp 126—127 °C. Found: N, 4.54%. Calcd for $C_{20}H_{17}ON$: N, 4.88%. The filtrate gave, after alumina chromatographic purification, crystals of **9** (10 mg), mp 65 °C. Found: N, 4.50%. Calcd for $C_{20}H_{17}ON$: N, 4.88%.

Nitration of 1, 2, and 3. To an acetic acid solution (2 ml) of **1** (200 mg, 0.69 mmol) was added with stirring an acetic acid solution (0.5 ml) of 92% nitric acid (140 mg, 2.4 mmol) and the mixture continuously stirred for 3 h. The precipitate formed by the addition of water was collected by filtration giving crystals (200 mg). Recrystallization from benzene gave yellow needles, mp 142 °C, identical with **1**.

Under similar conditions the nitration of **2** and **3** was attempted which again leads to the quantitative recovery of the starting materials.

References

1) Taken from a part of Tezuka's Doctor Thesis, Tohoku University (1962); a part of this work was presented at the Local Meeting of the Chemical Society of Japan, Akita, October 1961.

2) S. Itô, Y. Fukazawa, and Y. Iitake, *Tetrahedron Lett.*, **1972**, 741, 745.

3) T. Nozoe, K. Takase, H. Matsumura, T. Asao, K. Kikuchi, and S. Ito, "Dai Yuki Kagaku," Asakura Pub. Co., Tokyo (1960), Vol. 13.

4) Y. Oka and S. Matsuo, *Sci. Rept. Res. Inst. Tohoku Univ.*, **A8**, 532 (1956); *Bunseki Kagaku*, **7**, 215 (1958).

5) Y. Ikegami, "Kagaku No Ryoiki," Extra Vol. 38, Nankodo (1959).

6) T. Nozoe, T. Tezuka, and T. Mukai, *Bull. Chem. Soc. Jpn.*, **36**, 1470 (1963).

7) T. Tezuka, *Bull. Chem. Soc. Jpn.*, **37**, 1113 (1964); F. A. L. Anet, *J. Am. Chem. Soc.*, **86**, 458 (1964); M. Traetterberg, *ibid.*, **86**, 4265 (1964).

8) F. Arndet, *Org. Synth.*, Coll. Vol., II, 165, 461 (1943).

BULLETIN OF THE CHEMICAL SOCIETY OF JAPAN, VOL. 52 (6), 1869—1870 (1979)

The Carbonylation of α-Haloacetophenones and Benzyl Halides by Disodium Tetracarbonylferrate

Yoshihisa WATANABE,* Kenichi TANIGUCHI, Masataka SUGA, Take-aki MITSUDO, and Yoshinobu TAKEGAMI

Department of Hydrocarbon Chemistry, Kyoto University, Sakyo-ku, Kyoto 606

(Received August 31, 1978)

Synopsis. α-Haloacetophenones and benzyl chlorides can be converted into derivatives of β-keto acid and phenylacetic acid respectively by two succesive reactions, with $Na_2Fe(CO)_4$ and then with nitrobenzenes or iodine-ethanol as the oxidizing reagents.

Tetracarbonylferrate, such as potassium tetracarbonylhydridoferrate and disodium tetracarbonylferrate, are excellent reagents for the carbonylation of alkyl halides.[1] These reactions involve acylcarbonylferrates as the key intermediates, from which the corresponding carbonylated products, such as aldehydes, ketones, and acid derivatives are derived.[2] The reaction of the ferrates with α-haloacetophenones and benzyl chloride, however, has been shown to give only alkyl complexes, β-oxoalkyl- (**1**)[3] and benzyltetracarbonylferrate (**2**).[1b] An attempt to prepare the cor-

$[Ph-\overset{\overset{O}{\|}}{C}-CH_2-Fe(CO)_4]^-$ **1** $\qquad [Ph-CH_2-Fe(CO)_4]^-$ **2**

responding acyl complexes from **1** and **2** in the manner described in the literature[1b] has been unsuccessful. **1** and **2** give acetophenone and toluene respectively upon protonation. **1** shows specific behavior in the reaction with acyl halides. The treatment of **1** with acyl halides and then with acetic acid gives enol esters.[3] Acyl- and carbamoyltetracarbonylferrates are excellent reagents for the reductive acylation and carbamoylation of nitro compounds into amides and ureas respectively.[2d,4]

$$[RCOFe(CO)_4]^- + ArNO_2 \longrightarrow RCONHAr$$

The present study will deal with the transformation of **1** and **2** into β-keto acid derivatives and phenylacetic acid derivatives respectively by the treatment of **1** and **2** with nitrobenzenes and iodine-ethanol as oxidizing reagents.

Results and Discussion

Derivatives of tetracarbonylferrates are powerful reducing reagents for the reduction of nitro compounds, giving amines, amides, and ureas. The alkyl complexes, **1** and **2**, also have a great reactivity for nitrobenzene, nitrotoluene, and *p*-chloronitrobenzene. The nitro compounds react smoothly with **1** and **2** at room temperature, with the evolution of gas. The reaction is completed in less than 30 min. The major products are β-keto amides (**3**) and phenylacetamides (**4**) from **1** and **2** respectively. The treatment of **2a** with iodine-ethanol gives ethyl phenylacetate. The results are summarized in Table 1.

Table 1. The carbonylation of α-haloacetophenones and benzyl chlorides with disodium tetracarbonylferrate

Run	Halide	Oxidizing agent	Product (Yield % per halide)
1	α-Chloroacetophenone	Nitrobenzene	**3a** (44) and *N*-Phenacylaniline (trace)
2	α-Chloroacetophenone	*p*-Nitrotoluene	**3b** (22)
3	α-Chloroacetophenone	*p*-Chloronitrobenzene	**3c** (11)
4	α-Bromo-*p*-phenylacetophenone	Nitrobenzene	**3d** (50) and 4-Acetylbiphenyl (50)
5	Benzyl chloride	Nitrobenzene	**4a** (35)
6	*p*-Chlorobenzyl chloride	Nitrobenzene	**4b** (24)
7	*o*-Chlorobenzyl chloride	Nitrobenzene	**4c** (16)
8	Benzyl chloride	Iodine-ethanol	Ethyl phenylacetate (38)

These results indicate that α-haloacetophenones and benzyl halides can be transformed into carbonylated derivatives by a two-step procedure, a reaction with the ferrate and then with an oxidizing agent. *N*-Phenacylaniline, an expected products from **1a**, was obtained, but in only a poor yield. Although the reaction mechanism is not clear, the alkyl groups of **1** and **2** appear to be transformed into the corresponding acyl types through the reaction. With the reaction of iodine, an oxidative addition of iodine to the alkyl ferrate(0) seems to be the first step; the coordination of iodine may cause an alkyl migration to one of the coordinated carbon mon-

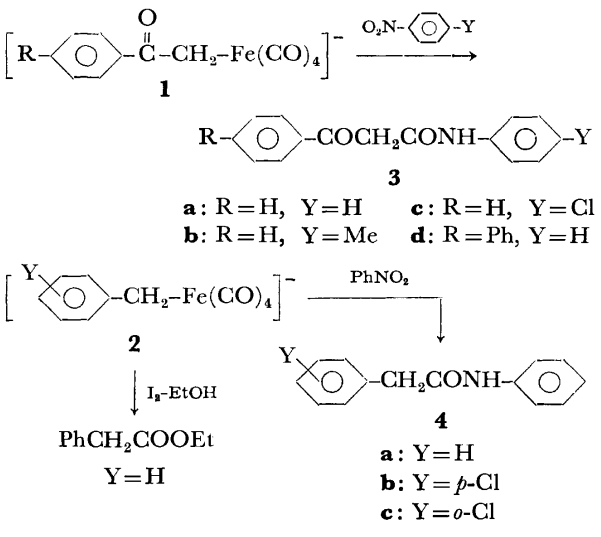

oxides to give an acyl iron(II) complex such as [RCOFe-$(CO)_3I_2$], from which an acyl iodide may be formed. The cleavage of acylcarbonylmetal complexes with iodine and bromine has already been reported in manganese and cobalt series.[5] The reaction of nitrobenzenes also seems to involve an oxidizing step to iron(II) complexes, which may be favorable for the formation of acyl complexes.[6] Thus, the reduction of nitrobenzenes with the ferrate, **1** and **2**, is completed by *N*-acylation.

Experimental

Materials. The tetrahydrofuran was distilled over $LiAlH_4$ prior to use. The disodium tetracarbonylferrate was prepared according to the method described an earlier article.[1b] The benzyl chloride, *o*- and *p*-chlorobenzyl chloride, α-chloroacetophenone, α-bromo-*p*-phenylacetophenone, and nitrobenzenes were all commercial products. The nitrobenzenes were dried over a molecular sieve (3A) and distilled before use.

General Reaction Procedure. To the ferrate (11 mmol) in tetrahydrofuran (40 ml), were added an α-haloacetophenone or benzyl chloride (11 mmol) solution in tetrahydrofuran (10 ml); the reaction mixture was then stirred under an argon atmosphere at room temperature for 30 min. To this solution, an oxidizing agent, such as a nitrobenzene (11 mmol) solution in tetrahydrofuran (10 ml) or an iodine-saturated solution in ethanol (30 ml), was added drop by drop, and then the mixture was stirred for about 1 h until the evolution of gas ceased.

Analyses. The ethyl phenylacetate was analyzed by GLC using a column (3 mmϕ, 3 m) packed with Apiezone Grease L (10%) on Neopak 1A. The other products were isolated by chromatography and analyzed by means of IR, PMR, and elemental analysis. The IR spectra were recorded on a 215 Hitachi spectrometer. The ^1H NMR spectra were taken on a JEOL-PM-60 spectrometer. All the chemical shifts are given in δ values relative to a Me_4Si standard. All the melting points were taken on a Yanagimoto apparatus and are uncorrected. All the products (**3** and **4**) are known compounds and were identified by means of their IR and PMR spectra. The elemental analyses of the products gave satisfactory results.

*Benzoylacetanilide (**3a**).* The filtered and concentrated reaction mixture was chromatographed on a 2×30 cm florisil column. The elution of the chromatogram with benzene gave brown crystals: Found: C, 79.53; H, 5.90; N, 6.35; O, 8.22%. Calcd for $C_{14}H_{13}NO$: C, 79.62; H, 6.16; N, 6.64; O, 7.58%. This compound appeared to be *N*-phenacylaniline, but its yield was not big enough for further analysis. Further elution of the chromatogram with ether gave colored crystals (**3a**; yield, 44%), which was later recrystallized from ethanol/petroleum ether. The IR and PMR spectra of the crystals were identical with those of an authentic benzoylacetanilide (Aldrich). Mp, 107.5—108.5 °C.

N-*(p-Tolyl)benzoylacetamide (**3b**).* Chromatography on a 2×30 cm florisil column, using methanol as an eluant, gave crystals (**3b**; yield, 22%), which were later recrystallized from ethanol. Mp, 142.0—143.0 °C. IR (KBr): ν(NH) 3300(m), ν(COAr) 1690(s), ν(CONH) 1640(s) cm^{-1}. PMR (d^6 DMSO): δ 2.3 (s, 3H), 4.1 (s, 2H), 7.0—8.2 (m, 9H), 10.1 (s, 1H) ppm.

N-*(p-Chlorophenyl)benzoylacetamide (**3c**).* Chromatography on a 2×30 cm silica gel column, using ether as an eluant, gave crystals (**3c**; yield, 11%). Mp, 163.0—164.0 °C. IR (KBr): ν(NH) 3300(w), ν(CO) 1690(s) and 1660(s) cm^{-1}. PMR (d^6 DMSO): δ 4.2 (s, 2H), 7.2—8.1 (m, 9H) ppm.

*(p-Phenylbenzoyl)acetanilide (**3d**).* Chromatography on a 2×30 cm silica gel using dichloromethane gave yellow crystals (4-acetylbiphenyl; yield, 50%), identified by means of the IR and PMR spectra using an authentic sample. The further elution of the chromatogram with ethanol gave crystals (**3d**; yield, 50%), later recrystallized from chloroform. Mp, 181.0—184.0 °C. IR(KBr): ν(NH) 3300(m), ν(CO) 1690(s) and 1660(s) cm^{-1}. PMR (d^6 DMSO): δ 4.2 (s, 2H), 6.7—8.3 (m, 14H), 10.2 (s, 1H) ppm.

*Phenylacetanilide (**4a**).* The filtered and concentrated reaction mixture was extracted with ethanol to give crystals (**4a**; yield, 35%). Mp, 116.5—117.5 °C. IR (KBr): ν(NH), 3300(m), ν(CO) 1655(s) cm^{-1}. PMR ($CDCl_3$): δ 3.7 (s, 2H), 6.8—7.9 (m, 10H) ppm.

*(p-Chlorophenyl)acetanilide (**4b**).* Chromatography on a 2×30 cm silica gel column, using ether and ethanol as eluants, gave crystals (**4b**; yield, 24%). Mp, 169.5—171.5 °C. IR (KBr): ν(NH) 3300(m), ν(CO) 1660(s) cm^{-1}. PMR ($CDCl_3$): δ 3.7 (s, 2H), 6.8—7.7 (m, 9H), 10.1 (s, 1H) ppm.

*(o-Chlorophenyl)acetanilide (**4c**).* Chromatography on a 2×30 cm silica gel column, using dichloromethane and ether as eluants, gave crystals (**4c**; yield, 16%), which were then recrystallized from ethanol. Mp, 138.0—141.0 °C. IR (KBr): ν(NH) 3300(m), ν(CO) 1660(s) cm^{-1}. PMR ($CDCl_3$): δ 3.9 (s, 2H), 6.8—7.8 (m, 9H), 10.1 (s, 1H) ppm.

References

1) See, for example, a) Y. Takegami, Y. Watanabe, H. Masada, and I. Kanaya, *Bull. Chem. Soc. Jpn.*, **40**, 1456 (1967); b) M. P. Cooke, Jr., *J. Am. Chem. Soc.*, **92**, 6080 (1970); W. O. Siegel and J. P. Collman, *ibid.*, **94**, 2516 (1972).

2) a) Y. Watanabe, T. Mitsudo, M. Tanaka, K. Yamamoto, T. Okajima, and Y. Takegami, *Bull. Chem. Soc. Jpn.*, **44**, 2569 (1971); b) J. P. Collman, S. R. Winter, and D. R. Clark, *J. Am. Chem. Soc.*, **94**, 1788 (1972); c) J. P. Collman, S. R. Winter, and R. G. Komoto, *ibid.*, **95**, 249 (1973); d) M. Yamashita, Y. Watanabe, T. Mitsudo, and Y. Takegami, *Tetrahedron Lett.*, **1976**, 1585.

3) T. Mitsudo, Y. Watanabe, T. Sasaki, H. Nakanishi M. Yamashita, and Y. Takegami, *Tetrahedron Lett.*, **1975**, 3163.

4) M. Yamashita, K. Mizushima, Y. Watanabe, T. Mitsudo, and Y. Takegami, *J. Chem. Soc., Chem. Commun.*, **1976**, 670.

5) T. H. Coffield, J. Kozikowski, and R. D. Closson, *J. Org. Chem.*, **22**, 598 (1957); R. H. Heck, *J. Am. Chem. Soc.*, **86**, 5138 (1964).

6) J. C. Case and M. C. Whitting, *J. Chem. Soc.*, **1960**, 4632; Y. Watanabe, T. Mitsudo, M. Yamashita, and Y. Takegami, *Bull. Chem. Soc. Jpn.*, **48**, 1478 (1975).

BULLETIN OF THE CHEMICAL SOCIETY OF JAPAN, VOL. 52 (6), 1871—1872 (1979)

Preparation of 1,3-Bis(4-aminobutyl)-1,3-dimethyl-1,3-diphenyldisiloxane and Siloxane-containing Polyamides

Toshio TAKIGUCHI,* Kazuo AMAGAI, and Hisashi KAWABATA

Department of Synthetic Chemistry, Faculty of Technology, Gunma University, Kiryu, Gunma 376

(Received October 4, 1978)

Synopsis. 1,3-Bis(4-aminobutyl)-1,3-dimethyl-1,3-diphenyldisiloxane has been readily obtained by the reduction of 1,3-bis(3-cyanopropyl)-1,3-dimethyl-1,3-diphenyldisiloxane, the hydrolysate of chloro(3-cyanopropyl)methylphenylsilane. The diamine reacted with abietic acid forming an equimolar crystalline adduct which gave a siloxane-containing polyamide by the conventional salt fusion technique.

Several preparations of compounds with the general formula $[NH_2–R–Si(R')(R'')]_2O$, (carbofunctional α,ω-diamino substituted disiloxanes) have been reported.

In the preparation of siloxane-containing α,ω-difunctional oligomeric compounds, 1,3-bis(4-aminobutyl) tetraorganodisiloxanes have been obtained in good yield by the reduction of the corresponding dinitriles by lithium aluminum hydride, followed by alkaline hydrolysis. The tetraorganodisiloxane segments were wholly retained during the procedure.

The preparation of α,ω-diamino compounds has been conducted according to the following scheme:

$$R'R''HSiCl \xrightarrow{CH_2=CHCH_2CN,\ H_2PtCl_6} ClSi(R')(R'')CH_2CH_2CH_2CN \xrightarrow{H_2O} [CNCH_2CH_2CH_2(R')(R'')Si]_2O \xrightarrow{LiAlH_4} [NH_2CH_2CH_2CH_2CH_2(R')(R'')Si]_2O$$

All products were well defined spectroscopically and the NMR and IR data were consistent with the assigned structures.

The obtained diamines further underwent polycondensation with organic dibasic acids to give modified polyamides containing disiloxane linkages in the chain backbone.

Experimental

Starting Materials. Dichloromethylsilane (bp 41 °C) and chlorodimethylsilane(bp 36 °C) in purified grades were received from Shin-etsu Chem. Ind. Co.; chloromethylphenylsilane(bp 66—67 °C/15 mmHg) was synthesized from Grignard reagents. 1,3-Dimethyl-1,3-diphenyldisiloxane (bp 90 °C/0.25 mmHg; n_D^{24} 1.5250) was prepared by the acid hydrolysis[2] of chloromethylphenylsilane (yield 86%). Commercial grade allyl cyanide (bp 119 °C) was purified by distillation immediately prior to use.

3-Cyanopropylchloromethylphenylsilane. A mixture of allyl cyanide (20 g, 0.30 mol), chloromethylphenylsilane (61 g, 0.39 mol), and hexachloroplatinic(IV) acid solution[3] (300 μl), was sealed in a stainless bomb maintained at 120 °C for 24 h. Fractionation of the resultant products gave 59 g (88%) pure 3-cyanopropylchloromethylphenylsilane (**1**), bp 95—96 °C/0.08 mmHg.

IR (neat): 2225 (ν_{CN}), 1425 (Si–C_6H_5), 1255 (Si–CH_3), 490 (Si–Cl).

NMR (CCl_4): δ=0.65 (3H, s, –CH_3), 1.12 (2H, m, Si–CH_2–), 1.72 (2H, m, C–CH_2–C), 2.23 (2H, t, –CH_2–CN), 7.40 (5H, m, –C_6H_5).

1,3-Bis(3-cyanopropyl)-1,3-dimethyl-1,3-diphenyldisiloxane. Hydrolysis of **1** under refluxing for 1 h, accompanied by conventional treatment gave quantitatively the dimeric product, 1,3-bis(3-cyanopropyl)-1,3-dimethyl-1,3-diphenyldisiloxane (**2**). (bp 193—195 °C/0.05 mmHg, n_D^{20} 1.5298).

IR (neat): 2225 (ν_{CN}), 1425 (Si–C_6H_5), 1255 (Si–CH_3), 1055 (Si–O–Si).

NMR (CCl_4): δ=0.33 (6H, s, –CH_3), 0.85 (4H, m, Si–CH_2–), 1.53 (4H, m, C–CH_2–C), 2.10 (4H, t, –CH_2–CN), 7.30 (10H, m, –C_6H_5).

1,3-Bis(4-aminobutyl)tetraorganodisiloxanes. A typical preparation will be given for 1,3-bis(4-aminobutyl)-1,3-dimethyl-1,3-diphenyldisiloxane (**3**):

To a suspension consisting of lithium aluminum hydride (4.3 g, 0.114 mol) and anhydrous ether (230 ml) cooled below 0 °C, a solution of **2** (18.7 g, 0.0476 mol) in anhydrous ether (30 ml) was added dropwise under vigorous stirring for 20 min. The resultant mixture was further stirred for an additional 40 min and water (5 ml). 20% aqueous sodium hydroxide solution (3.5 ml) and water (16 ml) were added in succession. The contents were stirred with continuous cooling to ensure completion of the reaction.

After removal of the inorganic salts formed by filtration, the ethereal layer was dried over anhydrous sodium sulfate and successively fractionated to give 14.9 g (78%) of **3** (bp 182—184 °C/0.1 mmHg; n_D^{20} 1.5312). **1**, **2**, and **3** are new compounds not found in the literature.

The preparation of the intermediate, **2** from the hydrosilylation of 1,3-dimethyl-1,3-diphenyldisiloxane and allyl cyanide in the presence of platinum catalyst was unsuccessful, yielding only a small amount of 3-cyanopropyl-1,3-dimethyl-1,3-diphenyldisiloxane as an addition product.

The use of chlorodimethylsilane in place of chloromethylphenylsilane in the platinum-catalyzed hydrosilylation of allyl cyanide followed by a similar procedure as above, unfailingly yielded the tetramethyl analog, 1,3-bis(4-aminobutyl)tetramethyldisiloxane (**4**), (bp 119—122 °C/0.04 mmHg; n_D^{20} 1.4360).

Compd 3:

Found: C, 65.78; H, 8.93; N, 6.99; Si, 13.92%. Calcd for $C_{22}H_{36}N_2OSi_2$: C, 65.95; H, 9.06; N, 6.99; Si, 14.02%.

IR (neat): 3350 (ν_{NH}), 1590 (δ_{NH}), 1425 (Si–C_6H_5), 1250 (Si–CH_3), 1055 (Si–O–Si).

NMR (CCl_4): δ=0.28 (6H, s, –CH_3), 0.83 (4H, br, Si–CH_2–), 1.38 (8H, br, C–CH_2–C), 2.60 (4H, br, –CH_2–N), 3.00 (4H, br, –NH_2), 7.30 (10H, m, –C_6H_5).

Compd 4:

Found: C, 52.22; H, 11.72; N, 9.86; Si, 20.28%. Calcd for $C_{12}H_{32}N_2OSi_2$: C, 52.12; H, 11.66; N, 10.13; Si, 20.31%.

IR (neat): 3340, 3270 (ν_{NH}), 1590 (δ_{NH}), 1250 (Si–CH_3), 1055 (Si–O–Si).

NMR (CCl_4): δ=0.03 (12H, s, –CH_3), 0.48 (4H, m, Si–CH_2–), 1.05 (4H, br, –NH_2), 1.37 (8H, m, C–CH_2–C), 2.62 (4H, t, –CH_2–N).

Polymerization. Compound **3** behaved in a similar manner as the polymethylenediamines towards organic dibasic acids,

an example of which will be given as follows:

To a stirred solution of adipic acid (11.0 g, 75.4 mmol) in ethanol (85 ml), a solution of **3** (30.8 g, 77 mmol) in ethanol (60 ml) was added. On standing overnight the solution deposited a fine colorless crystalline mass from which was obtained by recrystallization from ethanol–benzene (1: 1) 31.7 g (77%) of the pure adipic acid salt of **3**, melting at 174—175 °C.

Found: C, 61.61; H, 8.29; N, 5.20; Si, 10.22%. Calcd for $C_{23}H_{46}N_2O_5Si_2$: C, 61.54; H, 8.42; N, 5.13; Si, 10.26%.

IR (neat): 1630, 1540 (NH_3^+), 1580, 1390 (COO^-), 1420 (Si–C_6H_5), 1250 (Si–CH_3), 1055 (Si–O–Si).

X-Ray powder pattern (Cu $K\alpha$/Ni)

d, kX: 7.628 6.919 6.707 6.326 4.848 4.770 4.671 4.462 4.291 4.230 4.058 3.802 3.708 3.520 3.440 3.376 3.187 2.950 2.622 2.557

I/I_0 0.63 0.17 0.69 0.54 0.29 0.58 0.42 1.00 0.73 0.44 0.80 0.38 0.19 0.24 0.20 0.20 0.15 0.13 0.11 0.17.

Melt-polymerization of the salt was conducted according to the method of S. B. Speck,[4] and the final beating was conducted at 270 °C under a pressure less than 0.5 mmHg.

The polymer obtained was a pale yellow, transparent, tough solid softening over the range of temperature 100—150 °C to give a sticky highly viscous liquid with high spinnability and insolubility in ordinary organic solvents except for *m*-cresol. The intrinsic viscosity of the polyamide measured at 25 °C in *m*-cresol was [0.46].

IR (neat): 3300 (ν_{NH}), 1640 ($\nu_{C=O}$), 1540 (δ_{NH}), 1425 (Si–C_6H_5), 1255 (Si–CH_3), 1055 (Si–O–Si).

Terephthalic acid and sebacic acid were also found to give similar solids with different softening points when analogously treated.

The authors would like to thank Shin-etsu Chem. Ind. Co. for the supply of the organochlorosilanes.

References

1) a) [R=*m*-C_6H_4; R′,R″=Me] J. C. Bonnet and E. Marechal, *Bull. Soc. Chim. Fr.*, **1972**, 3561; b) (R=*m*,*p*-C_6H_4; R′,R″=Ph) L. W. Breed and J. C. Wiley. Jr., *J. Organomet. Chem.*, **102**, 29 (1975); c) [R=$(CH_2)_2$; R′,R″=Me] L. H. Sommer, N. S. Marans, G. M. Goldberg, J. Rockett, and R. P. Pioch, *J. Am. Chem. Soc.*, **73**, 882 (1951); d) [R=$(CH_2)_3$; R′,R″=Me] J. C. Saam and J. L. Speier, *J. Org. Chem.*, **24**, 119 (1959); T. A. Sladkova and L. Kh. Freidlin, *Izv. Akad. Nauk SSSR, Ser. Khim.*, **1965**, 1061; *Chem. Abstr.*, **63**, 8395a (1965); e) [R=$(CH_2)_8$; R,R″=Et] T. A. Sladkova and L. Kh. Freidlin, *Izv. Akad. Nauk SSSR, Ser. Khim.*, **1965**, 1061; *Chem. Abstr.*, **63**, 8395a (1965); f) [R=$(CH_2)_4$; R′,R″=Me; R′=Me, R′=Et; R′,R″=Et] A. D. Petrov, L. Kh. Freidlin, G. I. Kudryavtsev, T. A. Sladkova, V. M. Vdovin, and T. I. Shein, *Doklady Akad. Nauk SSSR*, **129**, 1064 (1959); *Chem. Abstr.*, **54**, 13718 (1960); g) [R=CH_2: R′,R″=Me] J. E. Noll, R. F. Daubert, and J. L. Speier, *J. Am. Chem. Soc.*, **73**, 3871 (1951).

2) M. C. Harvey, W. H. Nebergall, and J. S. Peake, *J. Am. Chem. Soc.*, **79**, 1437 (1957).

3) H_2PtCl_6·$6H_2O$ (1 g) was dissolved in *i*-PrOH (20 ml).

4) S. B. Speck, *J. Org. Chem.*, **18**, 1689 (1953).

BULLETIN OF THE CHEMICAL SOCIETY OF JAPAN, VOL. 52 (6), 1873—1874 (1979)

Friedel-Crafts Reaction of Anisole with 2-*t*-Butyloxirane

Masashi INOUE, Masatsune HARADA,† Nobuyuki UMAKI, and Katsuhiko ICHIKAWA*

Department of Hydrocarbon Chemistry, Faculty of Engineering, Kyoto University, Yoshida, Kyoto 606

(Received November 2, 1978)

Synopsis. The title reaction in excess anisole gave a mixture composed of 3-(methoxyphenyl)-2,3-dimethyl-1-butanols (**2**) (a mixture of ortho and para isomers), 2-(*p*-methoxyphenyl)-2-methybutane (**3**), and oligomer of 2-*t*-butyloxirane, while the same reaction in nitromethane gave a product composed of **2** (only the para isomer) and hexylanisoles, but not **3**. The reaction sequences to give the products are discussed in terms of step-by-step and concerted alkylation mechanisms.

A recent paper has described that epoxides react competitively with the aromatic substance under Friedel-Crafts conditions *via* two different paths:[1] Path a; a nucleophilic attack of aromatics on epoxide to yield 2-aryl-1-alkanols,[2] and Path b; a rearrangement of the epoxide to a carbonyl compound, followed by condensation with aromatics. It was also found that the alkylation of anisole with epoxides in a nitromethane solvent takes place preferentially through Path b. In the course of our study of Friedel-Crafts reactions with epoxides, we found a curious behavior of 2-*t*-butyloxirane (**1**) under Friedel-Crafts conditions.

When **1** was allowed to react with an excess of anisole in the presence of aluminum chloride, 3-(methoxyphenyl)-2,3-dimethyl-1-butanols (**2**) (21% yield;[3] ortho isomer 50% and para isomer 50%) and 2-(methoxyphenyl)-2-methylbutane (**3**) (14% yield; only para isomer) were found, together with the oligomer (**4**).

The retention volumes on GLC suggested that **4** was a mixture of dimer (8 wt% on the basis of the weight of the **1** used) and trimer (8 wt%) of **1**. When the reaction was carried out in nitromethane, a 14% yield of **2** (only para isomer) and a 30% yield of a mixture of isomer of hexylanisole were obtained, but no formation of **3** was observed.

As the ring-opening and the rearrangement of simple epoxide are widely accepted as proceeding without the formation of a fully developed carbonium ion,[4] the formation of **2**, which appears to be derived from a neopentyl rearrangement, is interesting. Although the base-catalyzed ring-opening and polymerization of **1** have been well established,[5] no report concerning a reaction under acidic conditions has appeared to our knowledge. Therefore, several kinds of acid-catalyzed ring-openings of **1** were carried out in order to examine the possibility of such a rearrangement.

As is shown in Table 1, the products are those which are formed by the direct attack on the epoxide carbon of **1**; no product could be detected which is to be expected from the neopentyl rearrangement, followed by nucleophilic attack. The results of the alkylation reported here are the first example of this kind of rearrangement in a simple aliphatic epoxide.[6]

† Present address: Research Center, Osaka Gas Co., Ltd., Konohana, Osaka 554.

TABLE 1. ACID-CATALYZED RING-OPENING OF *t*-BUTYLOXIRANE (**1**)

Reaction condition	Product (isolated yield)
35% HCl, dioxane, 10 °C, 3 h.	1-Chloro-3,3-dimethyl-2-butanol (**10**) (90%)
$AlCl_3$, 1,2-dichloroethane, ice bath, 2.5 h.	**10** (8.4%)
Acetic acid, 70 °C, 48 h, then 10% NaOH.	3,3-Dimethyl-1,2-butanediol (**11**) (92%)
Formic acid, ice bath, 24 h.	*t*-Butylethylene diformate (18%), 2-hydroxy-3,3-dimethyl formate (19%), 1-(hydroxymethyl)-2,2-dimethylpropyl formate (8%), and **11** (8%)
Ethanol, a drop of H_2SO_4, room temp, 8 days.	1-Ethoxy-3,3-dimethyl-2-butanol (89%)

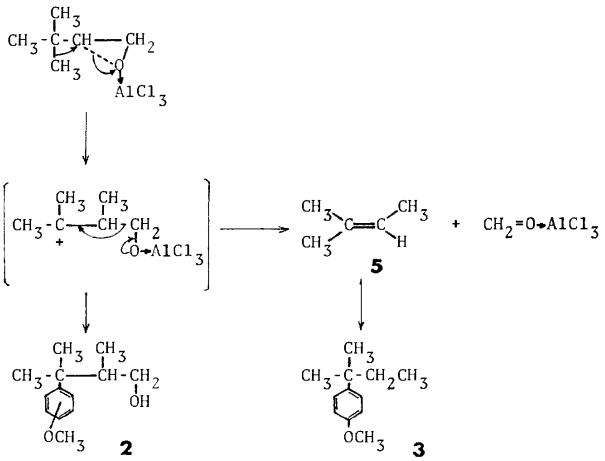

Scheme 1. Proposed reaction sequences for the reaction of **1** in excess anisole.

Product **3** is also an abnormal product. It is well known that undesired reactions always take place as the side reactions of Friedel-Crafts reaction.[7] The reaction sequences which have thus far been proposed to explain the side reactions, however, cannot explain the formation of **3**. The most probable reaction sequence is as follows: **1** undergoes ring-opening, rearrangement of methyl group, and β-cleavage to yield 2-methyl-2-butene (**5**), which then reacts with anisole to give **3** (Scheme 1). A similar cleavage was reported in the BF_3-catalyzed rearrangement of pinene oxide (**6**).[8] In the Lewis acid-catalyzed rearrangement of epoxide, the migrating groups are usually the substituents attached directly to

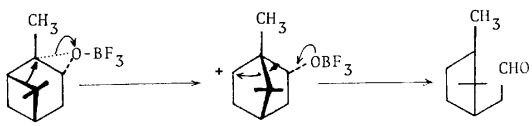

the epoxide ring. In contrast, the alkyl groups which are in the β-position to the epoxide ring shift in the reactions of **1** and **6**. As the backside of the epoxide C–O bond is shielded by the bulky *t*-butyl group in **1** or the methyl group on the bridge carbon in **6**, alkyl groups attached to the epoxide rings are prevented from approaching the carbonium-ion center.

As the reaction of anisole with 2,3-dimethyl-2-butene affords a product consisting of more than 95% para isomer (as shown by a separate control experiment), the high proportion of the ortho isomer in **2** formed in the reaction of excess anisole seems to be unusual. Kretchmer and McCloskey[9] found that ethyl allylmalonate and 5-hexen-2-one (**7**) react preferentially with anisole at the ortho position and explained the mechanism by a cyclic process, in which both anisole and the alkylating agent coordinate to an aluminum atom. A similar mechanism might be applied to the ortho alkylation of anisole with **1**. But in the reaction of **1**, the exchange of the solvent from excess anisole to nitromethane reduced the proportion of ortho alkylation from 50% to 0%, whereas the alkylation of anisole with **7** was reported to yield 65% and 55% ortho product in excess anisole and in 1-nitropropane respectively. The solvent effects of the reaction reported here seem to be too large to be explained by the ortho-alkylation mechanism.

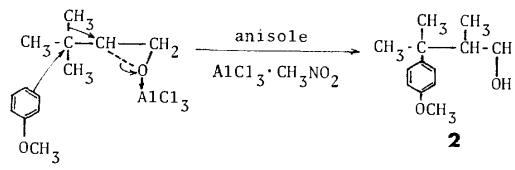

Scheme 2.

Nakajima *et al.* reported an asymmetric induction in the reaction of benzene with optically active 1,2-epoxybutane to yield 3-phenyl-1-butanol.[10] From their results, one can consider that the hydride shift from the β to the α position occurs in concert with the alkylation step of benzene. In the reaction of **1** in nitromethane, the alkylation step seems similarly to occur in concert with the methyl migration and ring-opning of epoxide, as is shown in Scheme 2. An S_N2-like transition state favors an attack on the para position of anisole because of steric hinderance. Scheme 2 can also explain the fact that the reaction in nitromethane does not give **3**, because this reaction mechanism does not involve a fully developed carbonium ion. In the case of the anisole solvent, the reacting species have a more carbonium-ion character (Scheme 1) and the proportion of the ortho isomer increases.

Experimental

Into a mixture of aluminum chloride (2.7 g) and anisole (25 ml) held in an ice bath, a solution of **1** (1.00 g) in anisole (10 ml) was added dropwise under vigorous stirring over a period of 30 min; stirring was then continued for an additional 2 h at the ice-bath temperature. After the usual work-up, the products were separated by column chromatography on silica gel, using benzene as the elutant. The distillation of the least polar fraction by means of a ball-oven apparatus yielded 230 mg (13%) of **3**, which was identical with a sample prepared by the alkylation of anisole with **5**; NMR ($CDCl_3$): 0.6[7] (3H, t), 1.2[5] (6H, s), 1.6[0] (4H, q), 3.7[8] (3H, s), and 6.7—7.3 (4H, phenyl). MS *m/e* (rel intensity) 180 (M^+, 13), 149 (100), 121 (17), and 90 (10). IR; 830 cm [1]. Found: C, 81.09; H, 9.94%. From the middle fraction was obtained 170 mg of **4**; NMR ($CDCl_3$): 0.9[2] (3H, s) and 3.1—4.0 (unresolved multiplets, 1H). IR: 3600, 3450, 1480, 1365, 1120, 1095, and 1060 cm^{-1}.

The distillation of the most polar fraction by means of the ball-oven apparatus yielded 350 mg (17%) of two isomers of **2**. Para isomer of **2**: NMR ($CDCl_3$): 0.9[2] (3H, d, J=6.4 Hz), 1.7[2] (6H, s), 1.8 (2H, m, methine and OH), 3.3[5] (1H, d, d, J=7.6 and 10.6 Hz), 3.7[8] (1H, d, d, J=4.8 and 10.6 Hz), 3.7[8] (3H, s, OCH_3), and 6.7—7.3 (4H, AA'BB' coupling, phenyl). IR: 3350, 1610, 1580, 1518, 1300, 1260, 1190, 1030, and 830 cm^{-1}.

References

1) M. Inoue, T. Sugita, and K. Ichikawa, *Bull. Chem. Soc. Jpn.*, **51**, 174 (1978).
2) T. Nakajima, S. Suga, T. Sugita, and K. Ichikawa, *Tetrahedron*, **25**, 1807 (1969).
3) The yields (after isolation) are the average values of the three experiments.
4) R. E. Parker and N. S. Isaacs, *Chem. Rev.*, **59**, 737 (1959); J. Biggs, N. S. Chapman, A. F. Finch, and V. Wray, *J. Chem. Soc., B*, **1971**, 55; G. Berti, B. Macchia, F. Macchia, and L. Monti, *J. Chem. Soc., C*, **1971**, 3371; Y. Pocker and B. P. Ronald, *J. Am. Chem. Soc.*, **100**, 3122 (1978), and references cited therein.
5) J. K. Crandall and L-H. C. Lin, *J. Am. Chem. Soc.*, **89**, 4527 (1967); C. C. Price, M. K. Akkapeddi, B. T. DeBona, and B. C. Furie, *ibid.*, **94**, 3964 (1972); C. C. Price and D. D. Carmelite, *ibid.*, **88**, 4093 (1966).
6) The backbone rearrangement of steroid epoxide is of a type analogous to a neopentyl rearrangement; J. W. Blunt, M. P. Hartshown, and D. N. Kirk, *Tetrahedron*, **25**, 149 (1969).
7) M. Inoue, N. Umaki, T. Sugita, and K. Ichikawa, *Nippon Kagaku Kaishi*, **1978**, 775, and references cited therein.
8) J. B. Lewis and G. W. Hendrick, *J. Org. Chem.*, **30**, 4271 (1965).
9) R. A. Kretchmer and M. B. McCloskey, *J. Org. Chem.*, **37**, 1989 (1972).
10) T. Nakajima, Y. Nakamoto, and S. Suga, *Bull. Chem. Soc. Jpn.*, **48**, 960 (1975).
11) The starting material, **1**, was prepared by two different methods: the *m*-chloroperbenzoic acid oxidation of commercially available 3,3-dimethyl-1-butene, and the cyclization of 2-bromo-3,3-dimethyl-1-butanol.[12]
12) S. J. Hurst and J. M. Bruce, *J. Chem. Soc.*, **1963**, 1321.

BULLETIN OF THE CHEMICAL SOCIETY OF JAPAN, VOL. 52 (6), 1875—1876 (1979)

Oxidation-reduction Equilibrium between Anion Radicals. Electron-accepting Property of 2,3-Dichloro-5,6-dicyano-*p*-benzoquinone

Yôichi IIDA

Department of Chemistry, Faculty of Science, Hokkaido University, Sapporo 060

(Received December 18, 1978)

Synopsis. The electron affinity and the oxidation-reduction potential of 2,3-dichloro-5,6-dicyano-*p*-benzoquinone were estimated by means of the equilibrium constant of the preferred electron transfer reaction between anion radicals in acetonitrile solution.

It is known that 7,7,8,8-tetracyanoquinodimethane (TCNQ) and cyano-substituted *p*-benzoquinone molecules are strong electron acceptors, forming stable anion radical salts with some diamagnetic counter cations.[1-6]

A method was worked out for determining the electron affinity values of electron acceptor molecules by means of preferred electron transfer reaction between anion radicals in solution.[1] By measuring the equilibrium constant of such a reaction, we can estimate the difference of the electron-accepting strengths between two acceptor molecules. The method was applied to the following electron-transfer (oxidation-reduction) reaction in acetonitrile solution:

$$\mathrm{TCNQ}^{\cdot} + p\text{-}\mathrm{X_2QCy_2} \rightleftarrows \mathrm{TCNQ} + p\text{-}\mathrm{X_2QCy_2}^{\cdot}, \quad (1)$$

where p-H_2QCy_2 (X=H) and p-Cl_2QCy_2 (X=Cl) stand for 2,3-dicyano-*p*-benzoquinone and 2,3-dichloro-5,6-dicyano-*p*-benzoquinone, respectively. The equilibrium constant K of this reaction is given by

$$K = \frac{[\mathrm{TCNQ}][p\text{-}\mathrm{X_2QCy_2}^{\cdot}]}{[\mathrm{TCNQ}^{\cdot}][p\text{-}\mathrm{X_2QCy_2}]}. \quad (2)$$

Chemical equilibrium was easily observable in the reaction between $TCNQ^{\cdot}$ and p-H_2QCy_2, when p-H_2QCy_2 was added to an acetonitrile solution of the sodium salt of TCNQ anion radical. The effect of cations was neglected, the activity coefficients of the solutes being assumed to be unity since their concentrations were of the order 10^{-5} mol/l. The concentrations of $[TCNQ^{\cdot}]$ and $[p$-$H_2QCy_2^{\cdot}]$ in the equilibrium state were easily estimated spectrophotometrically, the K value in acetonitrile being determined as $K=30$ at 20 ± 1 °C.

In the reaction between $TCNQ^{\cdot}$ and p-Cl_2QCy_2, however, the chemical equilibrium was not easily observed when p-Cl_2QCy_2 was added to an acetonitrile solution of TCNQ anion radical. An unpaired electron of TCNQ anion radical is transferred almost completely to p-Cl_2QCy_2, the equilibrium constant K being so great that we can hardly determine the $[TCNQ^{\cdot}]$ concentration in the equilibrium state by the usual spectrophotometric method. We could determine only the lower limit of K as $K\geq2\times10^3$ in acetonitrile solution at 20 ± 1 °C. This hampered the quantitative estimation of the electron affinity and the oxidation-reduction potential of p-Cl_2QCy_2. Yamagishi overcame the above difficulty and succeeded in determining the K value for the reaction between $TCNQ^{\cdot}$ and p-Cl_2QCy_2.[4] By adding p-Cl_2QCy_2 to an acetonitrile solution containing the TCNQ anion radical in the presence of large excess of TCNQ and p-$Cl_2QCy_2^{\cdot}$, the equilibrium concentration of $[TCNQ^{\cdot}]$ can be estimated spectrophotometrically. The equilibrium constant of Eq. 2 for the case of X=Cl was then determined to be $K=(4.7\pm1.0)\times10^5$ at 15 °C in acetonitrile solution.[4]

First, we estimate the oxidation-reduction potential of p-Cl_2QCy_2 by the use of the K value obtained and the equation

$$E_0(\mathrm{TCNQ},\ \mathrm{TCNQ}^{\cdot}) - \frac{RT}{F}\ln\frac{[\mathrm{TCNQ}^{\cdot}]}{[\mathrm{TCNQ}]} = E_0(p\text{-}\mathrm{Cl_2QCy_2},\ p\text{-}\mathrm{Cl_2QCy_2}^{\cdot}) - \frac{RT}{F}\ln\frac{[p\text{-}\mathrm{Cl_2QCy_2}^{\cdot}]}{[p\text{-}\mathrm{Cl_2QCy_2}]}, \quad (3)$$

where R, T, and F are the gas constant, the observed temperature and the Faraday constant, respectively, E_0 (TCNQ, $TCNQ^{\cdot}$) and E_0 (p-Cl_2QCy_2, p-$Cl_2QCy_2^{\cdot}$) representing the standard oxidation-reduction potentials in the formation of the anion radicals of $TCNQ+e \rightleftharpoons TCNQ^{\cdot}$ and p-$Cl_2QCy_2+e \rightleftharpoons p$-$Cl_2QCy_2^{\cdot}$, respectively. These reactions are assumed to be reversible electrode reactions in acetonitrile solution. When the value of $K=(4.7\pm1.0)\times10^5$ determined spectrophotometrically is put into Eq. 3, we have

$$E_0(p\text{-}\mathrm{Cl_2QCy_2},\ p\text{-}\mathrm{Cl_2QCy_2}^{\cdot}) = E_0(\mathrm{TCNQ},\ \mathrm{TCNQ}^{\cdot}) + 0.32\ \mathrm{V}. \quad (4)$$

The oxidation-reduction potential in the formation of p-H_2QCy_2 anion radical was obtained as E_0 (p-H_2QCy_2, p-$H_2QCy_2^{\cdot}$)$=E_0$ (TCNQ, $TCNQ^{\cdot}$)$+0.09$ V in acetonitrile solution. Thus, the value of E_0 (p-Cl_2QCy_2, p-$Cl_2QCy_2^{\cdot}$) is larger than E_0 (p-H_2QCy_2, p-$H_2QCy_2^{\cdot}$) by 0.23 V. The increase in the E_0 (p-Cl_2QCy_2, p-$Cl_2QCy_2^{\cdot}$) value is caused by the introduction of two chlorine substituents into 2,3-dicyano-*p*-benzoquinone. In view of the magnitudes of these oxidation-reduction potentials, the electron-accepting strengths of acceptor molecules lie in the range TCNQ$<p$-$H_2QCy_2<p$-Cl_2QCy_2.

Next, we examine the electron affinities of these acceptors. The observed equilibrium constant of Eq. 2 is related to electron affinity by

$$-RT\ln K = E_A(\mathrm{TCNQ}) - E_A(p\text{-}\mathrm{X_2QCy_2}) + \Delta\Delta G^{\circ}_{\mathrm{solv}}(\mathrm{TCNQ},\ \mathrm{TCNQ}^{\cdot}) - \Delta\Delta G^{\circ}_{\mathrm{solv}}(p\text{-}\mathrm{X_2QCy_2},\ p\text{-}\mathrm{X_2QCy_2}^{\cdot}), \quad (5)$$

where $E_A(M)$ is the electron affinity of neutral acceptor molecule M, and $\Delta\Delta G^{\circ}_{\mathrm{solv}}$ (M, $M^{\cdot}$) the difference in the free energy of solvation between the molecule and its anion radical. As long as the molecular sizes and

shapes of the acceptors are similar, we can reasonably assume $\Delta\Delta G^{\circ}_{solv}$ (TCNQ, TCNQ$^{\cdot-}$)$\approx\Delta\Delta G^{\circ}_{solv}$ (p-X_2QCy_2, p-$X_2QCy_2^{\cdot-}$), and we have

$$-RT\ln K = E_A(\text{TCNQ}) - E_A(p\text{-}X_2QCy_2). \quad (6)$$

Thus, the absolute values of E_A (p-X_2QCy_2), (X=H or Cl), will be determined from this relation if the value is once given for E_A (TCNQ). So far, Briegleb's value of E_A (TCNQ)=1.7 eV has been taken as a reference,[2,5] but the value appears to be underestimated. Farragher and Page measured the E_A (TCNQ) value by magnetron method and proposed E_A (TCNQ)=2.88 eV as a standard.[6] Their value is considered to be more reliable. If we take E_A (TCNQ)=2.88 eV, we can estimate the values of E_A (p-H_2QCy_2) and E_A (p-Cl_2QCy_2) by Eq. 6 to be 2.97 eV and 3.20 eV, respectively. The electron-accepting strength of p-Cl_2QCy_2 is very strong but somewhat weaker than that of hexacyanobutadiene; Farragher and Page reported the electron affinity of the latter compound to be 3.30 eV.[6]

It is of interest to compare the E_A (p-X_2QCy_2)$-E_A$ (TCNQ), (X=H or Cl), values obtained from Eq. 6 with those estimated from the charge-transfer absorption spectra. The acceptors of TCNQ, p-H_2QCy_2, and p-Cl_2QCy_2 form charge-transfer complexes with various electron donors in solution. For a common donor, D, the energy difference of the charge-transfer bands, $h\nu_{CT}$ (D, TCNQ)$-h\nu_{CT}$ (D, p-X_2QCy_2), (X=H or Cl), can be approximately written as

$$h\nu_{CT}(\text{D, TCNQ}) - h\nu_{CT}(\text{D, } p\text{-}X_2QCy_2) = E_A(p\text{-}X_2QCy_2) - E_A(\text{TCNQ}). \quad (7)$$

The charge-transfer complexes with various donor molecules of polycyclic aromatic hydrocarbons were examined in 1,2-dichloroethane. By observing the charge-transfer absorptions, together with Eq. 7, E_A (p-X_2QCy_2)$-E_A$ (TCNQ), (X=H or Cl), was evaluated for each common donor. For five donors, the average value of E_A (p-H_2QCy_2)$-E_A$ (TCNQ) was 0.05 ± 0.05 eV, while that of E_A (p-Cl_2QCy_2)$-E_A$ (TCNQ) was 0.29 ± 0.05 eV. On the other hand, from Eq. 6, the experimental results of oxidation-reduction equilibrium give E_A (p-H_2QCy_2)$-E_A$ (TCNQ)=0.09 eV and E_A (p-$Cl_2QCy)_2-E_A$ (TCNQ)=0.32 eV. The values agree, within experimental error, with those estimated from the charge-transfer absorptions, respectively. This, in return, supports the assumption $\Delta\Delta G^{\circ}_{solv}$ (TCNQ, TCNQ$^{\cdot-}$)$\approx$ $\Delta\Delta G^{\circ}_{solv}$ (p-X_2QCy_2, p-$X_2QCy_2^{\cdot-}$), (X=H or Cl), in deriving Eq. 6.

In conclusion, the present technique of oxidation-reduction equilibrium between anion radicals is useful for determining the electron affinity values of electron acceptor molecules as well as the oxidation-reduction potentials in the formation of anion radicals of these acceptors.

The author wishes to thank Dr. Akihiko Yamagishi for his helpful discussions.

References

1) Y. Iida and H. Akamatu, *Bull. Chem. Soc. Jpn.*, **40**, 231 (1967).
2) Y. Iida, *Bull. Chem. Soc. Jpn.*, **44**, 1430 (1971).
3) Y. Iida, *Bull. Chem. Soc. Jpn.*, **49**, 3691 (1976).
4) A. Yamagishi, *Chem. Lett.*, **1975**, 899.
5) G. Briegleb, *Angew. Chem.*, **76**, 326 (1964).
6) A. L. Farragher and F. M. Page, *Trans. Faraday Soc.*, **63**, 2369 (1967).

BULLETIN OF THE CHEMICAL SOCIETY OF JAPAN, VOL. 52 (6), 1877—1878 (1979)

Synthesis of Disubstituted Benzoquinones by the Photochemical Reaction of Acetylenes with $Fe(CO)_5$

Kazuhiro MARUYAMA,* Toru SHIO, and Yoshinori YAMAMOTO
Department of Chemistry, Faculty of Science, Kyoto University, Kyoto 606

(Received November 17, 1978)

Synopsis. Internal acetylenes substituted with alkyl groups and terminal acetylenes substituted with alkyl, aryl, and functionallized alkyl groups are converted to disubstituted quinones by the photochemical reaction with $Fe(CO)_5$ followed by treatment with Ce(IV).

In the course of our investigations on quinonoid compounds,[1] we required a new synthetic methodology for disubstituted benzoquinone derivatives. Indirect methods,[2] whereby two substituents are introduced stepwise into benzoquinone, suffer from several difficulties, such as low yields and frequent need for long reaction steps. Direct conversion can be achieved by the photochemical reaction of acetylenes with $Fe(CO)_5$.[3] It appeared that this procedure would provide an attractive route to disubstituted benzoquinones because of a simple operation and a satisfactory yield. However, a curious thing was that any systematic investigations had not been performed and the ratio of products (2,5- and 2,6-isomers) had not been established. Consequently, we decided to explore the reaction of various types of acetylenes with $Fe(CO)_5$ in hopes of developing a practical procedure and establishing the scope and limitations.

Results and Discussion

A benzene solution of an acetylene and $Fe(CO)_5$ was irradiated by a high pressure Hg lamp under N_2, and the reaction was followed by GLPC. After most of the starting acetylene was consumed, treatment of the reaction mixture with ceric ammonium nitrate produced the desired quinones. The results are summarized in Table 1. The structure of 2,5-(**2**) and 2,6-isomers (**3**) was determined by the ^1H NMR spectra of their acetyl derivatives. Reductive acetylation of **2** and **3** produced **4** and **5**, respectively, in a good yield. Since the two acetyl groups of **4** possess an identical chemical shift and those of **5** two different chemical shifts, two isomers could be easily discriminated.

TABLE 1. REACTION OF VARIOUS ACETYLENES WITH $Fe(CO)_5$[a]

Acetylene **1** R		Products, % (isold) **2**	**3**	Conversion %
$-(CH_2)_5CH_3$	(**1a**)	28	22	94
$-(CH_2)_3Cl$	(**1b**)	11	9	96
$-(CH_2)_8CO_2CH_3$	(**1c**)	22	16	93
$-C_6H_5$	(**1d**)	22	9	96
$-C_6H_4CH_3$	(**1e**)	18	9	96
$-C_6H_4Cl$	(**1f**)	17	10	85

a) Conversion indicates the amounts of acetylene consumed after 2 h irradiation.

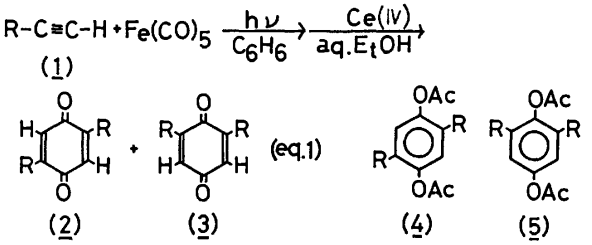

As is apparent from Table 1, the terminal acetylenes can be converted to the corresponding quinones and the functional groups can be introduced into the side chain. Normally, 2,5-isomer (**2**) is obtained predominantly, presumably owing to the steric reason. However, diphenylacetylene does not give the desired quinone, though dimethylacetylene can be converted to duroquinone.[3] Since the reaction of phenylacetylene, *p*-methylphenylacetylene, and *p*-chlorophenylacetylene proceeds in a similar fashion and the product distributions are nearly identical, it seems that the electronic circumstances around the triple bond do not influence the reaction cource. Other acetylenes such as 2-propyn-1-ol, 3-bromo-1-propyne, 3-methoxy-1-propyne, and 1-butyne-3-one, where the functional groups are involved in the alpha-position, did not produce the desired quinones.

We next examined the reaction of acyclic alkadiynes with $Fe(CO)_5$ in hopes of obtaining cyclophanes bearing quinonoid structure.[4] Unfortunately, however, similar treatment of 1,9-decadiyne with $Fe(CO)_5$ did not produce the desirable methylene bridged benzoquinone but afforded the normal intermolecular cyclization products. Other diynes such as 1,7-octadiyne and 1,11-dodecadiyne gave the similar results. Consequently, the intramolecular cyclization is an unfavorable reaction at least in the above three diynes.

Finally the reaction of trimethylethynylsilane was examined to explore a possibility of obtaining quinone metalloids bearing a silyl group. Such a metalloid may be converted further to a number of functionallized quinone derivatives, since the transformation of C–Si bond to various C–Hetero bonds and C–C bond is well established.[5] Unexpectedly, the reaction took an entirely different course. Cyclopentadienone derivative was isolated from among tarry materials. Although the structure was assigned as the cyclopentadienone–Fe complex (**6** or **7**), the discrimination between both isomers

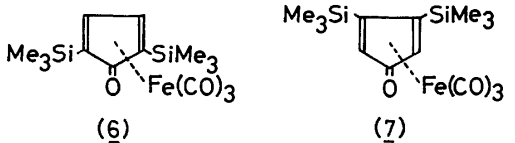

Table 2. The relationship between the substituents of acetylenes and the reaction products[a)]

R–C≡C–R′ R	R′	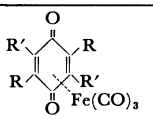	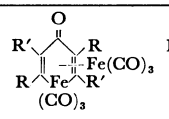	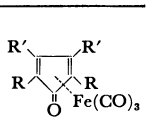
$-(CH_2)_mX$	H[b)]	Yes	No	No
$-C_6H_4-Y$	H[b)]	Yes	No	No
$-C_6H_5$	C_6H_5[6)]	No	Yes	Yes
$-SiMe_3$	H[b)]	No	No	Yes
cyclo-C_3H_4–	H[7)]	Yes	No	No
Me–	Me[3)]	Yes	No	No

a) Yes indicates that the product is obtained, and No means the reverse.
b) Our own works.

was not possible. The reaction of trimethylpropynylsilane or trimethyl-1-hexynylsilane was quite sluggish, and these acetylenes were recovered even after irradiation for 24 h.

In conclusion, the course of the reaction highly depends upon the structure of acetylenes. The results of our own experiments and others are summarized in Table 2. The requirement for obtaining quinone derivatives is that i) internal acetylenes are substituted not with aryl groups but with alkyl groups, and that terminal acetylenes are substituted with ii) alkyl groups, iii) aryl groups, and with iv) functionallized alkyl groups where the functional groups are separated from the quinone moiety at least by two methylene units.

Experimental

General Procedure for the Reaction of Acetylenes with $Fe(CO)_5$. Oxygen-free dry benzene solution of an acetylene (0.025 mol) and $Fe(CO)_5$ (4.9 g, 0.025 mol) was irradiated by a high pressure Hg lamp under N_2 at 20 °C. GLPC examination revealed that generally the acetylene was almost consumed after 2 h. Then, the solvent was removed under reduced pressure, giving black oil. To an acetone solution of this oil was added an ethanol–water (72: 25) solution of $(NH_4)_2Ce(NO_3)_6$ (13.7 g, 0.025 mol) with stirring and the resulting mixture was stirred overnight at room temperature. The organic materials were extracted with benzene and dried over anhyd. Na_2SO_4. The products were filtered through the column of silica, and benzene eluted the desired quinones in substantially pure form. These quinones (a mixture of 2,5- and 2,6-isomers) were further filtered through the column of silica to separate the isomers, and to obtain analytically pure materials. **2a** (yellow needles); mp 83—83.5 °C; NMR (CCl_4) 0.89 (t, 6H), 1.70—1.10 (m, 16H), 2.40 (t, 4H), 6.50 (s, 2H); IR (KBr) 1652, 1615 cm^{-1}; Mass *m/e* 276; Found; C, 78.38; H, 10.24%. Calcd for $C_{18}H_{28}O_2$: C, 78.21; H, 10.21%. **3a** (brown oil); NMR (CCl_4) 0.90 (t, 6H), 1.80—1.10 (m, 16H), 2.45 (t, 4H), 6.52 (s, 2H); IR (neat) 1659, 1615 cm^{-1}; Mass *m/e* 276; Elemental analysis was not performed since the pattern of mass spectra was identical with **2a**. **2b** (yellow crystal): mp 66—69 °C; NMR ($CDCl_3$) 2.08 (m, 4H), 2.62 (t, 4H), 3.56 (t, 4H), 6.57 (s, 2H); IR (KBr) 1649 cm^{-1}; MS *m/e* 260.040. Calcd for $C_{12}H_{14}O_2Cl_2$; 260.037079. **3b** (brown oil); NMR ($CDCl_3$) 1.99 (m, 4H), 2.61 (t, 4H), 3.55 (t, 4H), 6.50 (s, 2H); IR (neat) 1655, 1616 cm^{-1}. **2c** (pale yellow needles); mp 94—94.5 °C; NMR ($CDCl_3$) 1.60—1.20 (m, 28H), 2.40 (t, 4H), 3.67 (s, 6H), 7.16 (s, 2H); IR (KBr) 1733, 1651 cm^{-1}; Found; C, 69.52; H, 9.01%. Calcd for $C_{26}H_{40}O_6$; C, 69.61; H, 8.99%. **3c** (yellow oil); NMR ($CDCl_3$) 1.60—1.20 (m, 28H), 2.30 (t, 4H), 3.68 (s, 6H), 6.50 (s, 2H); IR (neat) 1740, 1665 cm^{-1}; Found; C, 69.52; H, 9.01%. Calcd for $C_{26}H_{40}O_6$; C, 69.61; H, 8.99%. **2d** (orange-yellow plates); mp 214—215 °C (lit,[8)] 214 °C); NMR ($CDCl_3$) 6.84 (s, 2H), 7.36 (m, 10H); IR (KBr) 1646 cm^{-1}. **3d** (reddish needles); mp 137—138 °C (lit,[9)] 135 °C); NMR ($CDCl_3$) 6.82 (s, 2H), 7.36 (m, 10H); IR (KBr) 1652 cm^{-1}. **2e** (orange-yellow plates); mp 222—223 °C (lit,[10)] 220 °C); NMR ($CDCl_3$) 2.42 (s, 6H), 6.88 (s, 2H), 7.50—7.10 (m, 8H); IR (KBr) 1657 cm^{-1}. **3e** (orange-red needles); mp 150—155 °C (lit,[9)] 161 °C); NMR ($CDCl_3$) 2.40 (s, 6H), 6.84 (s, 2H), 7.30—7.00 (m, 8H); IR (KBr) 1668 cm^{-1}. **2f** (orange needles); mp 223—224 °C; NMR ($CDCl_3$) 6.94 (s, 2H), 7.50—7.20 (m 8H); IR (KBr) 1652 cm^{-1}; Found; C, 65.59; H, 2.89; Cl, 21.43%. Calcd for $C_{18}H_{10}O_2Cl_2$; C, 65.67; H, 3.07; Cl, 21.54%. **3f** (orange crystal); mp 112—116 °C; NMR ($CDCl_3$) 6.82 (s, 2H), 7.50—7.20 (m, 8H); IR (KBr) 1660 cm^{-1}; Found; C, 65.59; H, 2.89; Cl, 21.43%. Calcd for $C_{18}H_{10}O_2\ Cl_2$; C, 65.67; H, 3.07; Cl, 21.54%.

The reductive acetylation was carried out by the reported procedure.[11)] The reaction proceeded quite smoothly, and the reaction product was directly analyzed by ^1H NMR spectra without further purification. **4a**; NMR (CCl_4) 0.88 (t, 6H), 1.70—1.10 (m, 16H), 2.19 (s, 6H), 2.43 (t, 4H), 6.77 (s, 2H). **5a**; NMR (CCl_4) 0.90 (t, 6H), 1.70—1.10 (m, 16H), 2.19 (s, 3H), 2.24 (s, 3H), 2.40 (t, 4H), 6.75 (s, 2H). **4d**; NMR ($CDCl_3$) 2.07 (s, 6H), 7.16 (s, 2H), 7.50—7.30 (m, 10H). **5d**; NMR ($CDCl_3$) 2.05 (s, 3H), 2.10 (s, 3H), 7.00 (s, 2H), 7.50—7.30 (m, 10H). **4e**; NMR ($CDCl_3$) 2.08 (s, 6H), 2.36 (s, 6H), 7.12 (s, 2H), 7.40—7.20 (m, 7H). **5e**; NMR ($CDCl_3$) 2.06 (s, 3H), 2.11 (s, 3H), 2.35 (s, 6H), 7.05 (s, 2H), 7.40—7.20 (m, 8H). Other isomers (**2b** and **3b**, **2c** and **3c**, **2f** and **3f**) were determined by their carbonyl stretching frequencies.

The reaction of ethynylsilane with $Fe(CO)_5$ was performed similarly. After irradiation for 4 h, evaporation of the solvent followed by filtration through the column of florisil gave the complex (**6** or **7**); pale yellow needles (mp 135—138 °C); yield 2%; NMR ($CDCl_3$) 0.32 (s, 18H), 5.52 (s, 2H); IR KBr) 2055, 1993, 1960, 1606 cm^{-1}; UV ($CHCl_3$) λ_{max} 302 nm, log ε=3.5; Mass *m/e* 364; Found; C, 45.39; H, 5.54%. Calcd for $C_{13}H_{20}O_4Si_2Fe$; C, 46.15; H, 5.53%.

References

1) K. Maruyama, *Kagaku No Ryoiki*, in press (1978); *Reactive Intermediate*, in press.
2) H. J. Teuber, *Chem. Ber.*, **98**, 2465 (1965); "The Chemistry of the Quinonoid Compound," ed by S. Patai, Wiley, New York (1974).
3) H. W. Sternberg, R. Markby, and I. Wender, *J. Am. Chem. Soc.*, **80**, 1009 (1958).
4) S. Misumi, *Kagaku No Ryoiki*, **32**, 651 (1978).
5) P. F. Hudrlik, "New Applications of Organometallics in Organic Synthesis," ed by D. Seyferth, Elsevier, New York (1976), p. 127.
6) G. N. Shrauzer, *J. Am. Chem. Soc.*, **81**, 5307 (1959).
7) R. Victor, R. B-Shoshan, and S. Sarel, *Tetrahedron Lett.*, **1973**, 4211; R. Victor, V. Usieli, and S. Sarel, *J. Organomet. Chem.*, **129**, 387 (1977).
8) D. E. Kvalnes, *J. Am. Chem. Soc.*, **56**, 2478 (1934).
9) E. C. S. Jones and J. Kenner, *J. Chem. Soc.*, **1931**, 1851.
10) R. Pummerer and E. Prell, *Chem. Ber.*, **55**, 3111 (1922).
11) J. F. McOmie and J. M. Blatchly, "Organic Reactions," Wiley, New York (1972), Vol. 19, p. 199.

BULLETIN OF THE CHEMICAL SOCIETY OF JAPAN, VOL. 52 (6) 1879—1880 (1979)

A Convenient Method of Preparing *p*-Toluenesulfonates of Ethyl Esters of Amino Acids Using Ethyl *p*-Toluenesulfonate

Kazuo UEDA

Department of Chemistry, Faculty of Liberal Arts, Nagasaki University, Bunkyo-machi, Nagasaki 852

(Received November 4, 1978)

Synopsis. The treatment of amino acids with ethyl *p*-toluenesulfonate affords the *p*-toluenesulfonates of the ethyl esters in good yields. Tryptophan ethyl-ester *p*-toluenesulfonate was also prepared in an 81% yield.

In the peptide synthesis, the *p*-toluenesulfonates of ethyl esters of amino acids are of importance as starting materials.[1]

The *p*-toluenesulfonates of the ethyl esters of amino acids have previously been prepared by the use of *p*-toluenesulfonic acid as a catalyst; the synthesis involved the azeotropic distillation of a mixture of amino acid, *p*-toluenesulfonic acid, ethanol, and carbon tetrachloride.[2]

We have now found that amino acids are easily converted to the *p*-toluenesulfonates of the ethyl esters in good yields by treatment with ethyl *p*-toluenesulfonate. The results thus obtained are summarized in Table 1. The method was very convenient and required neither special apparatus nor complicated manipulation: the ethanolic suspension of amino acid was refluxed while being stirred for 24—30 h in the presence of ethyl *p*-toluenesulfonate. We have not observed any *N*-ethylation or *N*-tosylation of the amino acids under these conditions. Tryptophan ethyl-ester *p*-toluenesulfonate has not been synthesized previously, probably because of its instability to *p*-toluenesulfonic acid. However, we succeeded in synthesizing this compound in an 81% yield by the use of our method.

It has previously been reported that the reaction of 3β-steroidal tosylates with tetrabutylammonium acetate in acetone gives 3α-acetates in good yields and appears to be a nucleophilic bimolecular S_N2 displacement by acetate.[3] Taking into account the fact that the tosylate is a very good leaving group,[3-5] the esterification may be explained as is shown in the following reaction scheme.

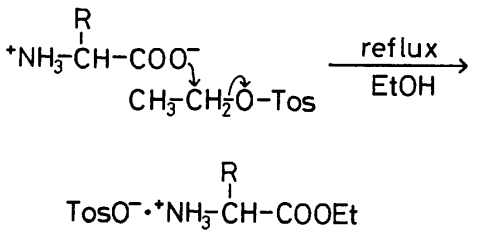

Experimental

All the melting points were uncorrected. The TLC was carried out on a silica-gel 60 F_{254} pre-coated plate (Merck and Co.) with the following solvent systems: $R_{f,1}$ $CHCl_3$–MeOH (5: 1, v/v); $R_{f,2}$ *n*-BuOH–AcOH–pyridine–H_2O (15: 3: 10: 12, v/v). The optical rotations were measured on an Atago polarimeter Polax. The IR spectra were recorded on a Hitachi EPI-2 spectrometer. Ethyl *p*-toluenesulfonate was purified by distillation under reduced pressure, a fraction with a bp of 121 °C/2 mmHg being used. All the amino acids used in this experiment, except glycine and 4-aminobutyric acid (4-Abu), had an L-configuration.

General Esterification Procedure. A suspension of the amino acid (10 mmol) and ethyl *p*-toluenesulfonate (11 mmol) in absolute ethanol (40 ml) was refluxed while being stirred for 24—30 h, during which dissolution occurred. After the evaporation of the solvent, the residual material was treated with ether. The precipitate filtered off was recrystallized from hot ethanol–ether.

L-*Tryptophan Ethyl-ester* p-*Toluenesulfonate.* This was prepared from Trp (2.04 g, 10 mmol) and ethyl *p*-toluenesulfonate (2.20 g, 11 mmol) as has been described above. Yield 3.28 g (81%); mp 139—140 °C; $[\alpha]_D^{30}$ +15.4° (*c* 4, EtOH); IR (Nujol) 3370 (indole NH) and 1730 cm^{-1} (C=O); $R_{f,1}$ 0.49, $R_{f,2}$ 0.81. Found: C, 59.38; H, 6.09; N, 6.67%. Calcd for $C_{20}H_{24}O_5N_2S$: C, 59.39; H, 5.98; N, 6.92%.

TABLE 1. *p*-TOLUENESULFONATES OF ETHYL ESTERS OF AMINO ACIDS

Amino acid	Yield[a] (%)	Mp (°C)		$[\alpha]_D^t$ (°)	
		Obsd	Lit[2]	Obsd (*c*, solvent, *t* °C)	Lit[2] (*c* 2, DMF, 20 °C)
Gly	100[b]	oil	oil		
4-Abu	86	82—84	83		
Val	87	147—149	143—144	+12.5 (4 DMF 20)	+10.2
Leu	92	153—154	158	+6.0 (4 DMF 18)	+ 7.8
Phe	89	153.5—154	153	+14.9 (2 DMF 17)	+15.5
Tyr	93	190—190.5	193	+12.3 (4 DMF 21)	+12.6
Met	86	128—129	127	+6.9 (4 DMF 22)	+ 6.5
Trp	81	139—140		+15.4 (4 EtOH 30)	
Pro	100[b]	oil	oil		

a) Yields were of recrystallized products. b) Yield was estimated by TLC.

References

1) M. Bodanszky, Y. S. Klausner, and M. A. Ondetti, "Peptide Synthesis," 2nd ed, John Wiley and Sons, New York (1976), p. 51.
2) T. Kato, S. Makisumi, M. Ohno, and N. Izumiya, *Nippon Kagaku Zasshi*, **83**, 1151 (1962).
3) R. Baker, J. Hudec, and K. L. Rabone, *J. Chem. Soc., C*, **1969**, 1605.
4) S. Winstein, E. C. Friedrich, R. Baker, and Yang-i Lin, *Tetrahedron, Suppl.*, **8**, 621 (1966).
5) A. Streitwieser, Jr., *Chem. Rev.*, **56**, 571 (1956).

^{14}N Nuclear Quadrupole Relaxation in Sulfuric Diamide and Methanesulfonamide

Hisao NEGITA,* Tsuneo KUBO, Michio MAEKAWA, Akinobu UEDA, and Tsutomu OKUDA

Department of Chemistry, Faculty of Science, Hiroshima University, Hiroshima 730

(Received July 20, 1978)

The ^{14}N nuclear quadrupole resonances (NQR) in sulfuric diamide (sulfamide), $H_2NSO_2NH_2$, and methanesulfonamide, $CH_3SO_2NH_2$, were studied by the pulse method. The resonance frequency and the spin-lattice relaxation time (T_1) were measured in the temperature range from liquid nitrogen temperature to room temperature. In the case of sulfuric diamide, T_1 decreases monotonously as the temperature rises, and is dominated by the thermal torsional motion below 140 K. On the other hand, T_1 is attributed to the reorientation of the amino group in the temperature range from 200 to 240 K, whereas it is due to the reorientation of the molecule above 240 K; the activation energies in these orientations are 43.5 and 61.5 kJ·mol^{-1} respectively. In the case of methanesulfonamide, the minimum of T_1 is found near 130 K. This is caused by the rotation of the methyl group. The activation energy for this motion is calculated to be 9.6 kJ·mol^{-1}. The dominant relaxation mechanism is attributed to the reorientation of the amino group from 200 to 240 K and to the reorientation of the molecule above 240 K. The activation energies for these motions are 19.2 and 40.6 kJ·mol^{-1} respectively.

Structural studies on sulfuric diamide (sulfamide), $H_2NSO_2NH_2$, and methanesulfonamide, $CH_3SO_2NH_2$, have been performed by various spectroscopic means. The ^{14}N nuclear quadrupole resonance (NQR) study on the former compound was recently reported by our group.[1] We hope to obtain further information on the dynamical properties of the two materials from ^{14}N nuclear quadrupole relaxation. We have measured the spin-lattice relaxation time (T_1) by the pulse method and will discuss the molecular motions in these compounds.

Experimental

^{14}N NQR measurements were carried out using a pulse spectrometer, consisting of a Matec gating modulator Model 5100, a R. F. gated amplifier Model 515, and a tuned receiver Model 615, which was designed by Petersen.[2,3] The resonance frequency and the spin-lattice relaxation time were measured in the temperature range from liquid nitrogen temperature to room temperature by the repeating 90° pulse method.[4] The pulse width was about 25—50 μs. The free induction decay signal was averaged in a Nicolet Instrument Model 527 signal averager. The temperature was controlled by the method of Abe[5] or Petersen.[2,3] The temperature was measured by the use of a copper-constantan thermocouple and stabilized within ±0.1 K. The frequency was checked by means of a frequency counter, TR-5104, from the Takeda Riken Co.

The sulfuric diamide was obtained by the reaction of sulfuryl chloride with liquid ammonia and was purified by recrystallization from acetone.[6] On the other hand, the methanesulfonamide was prepared by the reaction of methanesulfonyl chloride with liquid ammonia and was purified by recrystallization from 1:2 ethanol–benzene.[7] In the present measurements, we used about a 20-g portion of each sample melted in a glass ampoule.

Results and Discussion

Generally a pair of ^{14}N NQR frequencies, ν_- and ν_+, are observed for a species of nitrogen atom:

$$\nu_\pm = \frac{|e^2Qq|}{4h}(3\pm\eta), \qquad (1)$$

where $|e^2Qq/h|$ and η are the quadrupole coupling constant and the asymmetry parameter, respectively. In methanesulfonamide, a pair of resonance lines were found: $\nu_-=2442.1$ kHz and $\nu_+=3400.2$ kHz (at liquid nitrogen temperature). The quadrupole coupling constant and asymmetry parameter derived from these frequencies are as follows: $|e^2Qq/h|=3894.9$ kHz and $\eta=49.20\%$. These values are to be compared with those for sulfuric diamide: $|e^2Qq/h|=3905.3$ kHz and $\eta=50.82\%$.[1]

The temperature dependence of the resonance frequencies, ν_- and ν_+ lines, in sulfuric diamide and methanesulfonamide is shown in Fig. 1. The temperature dependence in sulfuric diamide is smaller than that in methanesulfonamide. This fact may be explained by the intermolecular interaction, probably by the difference in the number of the hydrogen bonds between sulfuric diamide and methanesulfonamide. That is, the vibration of the nitrogen atom in sulfuric diamide is more suppressed than in methanesulfonamide.

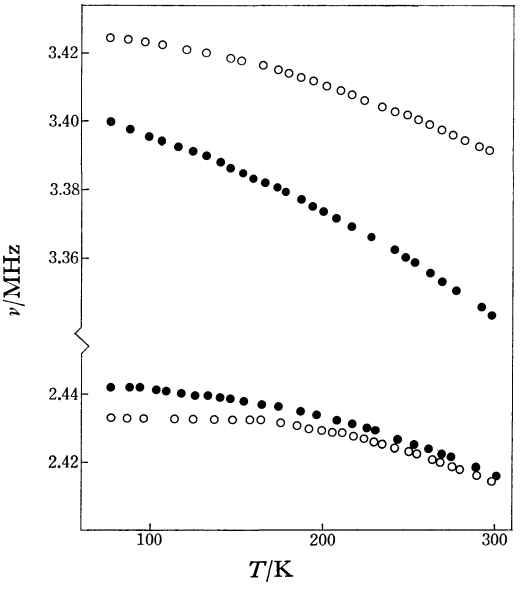

Fig. 1. The temperature dependence of the resonance lines in sulfuric diamide (○) and methanesulfonamide (●).

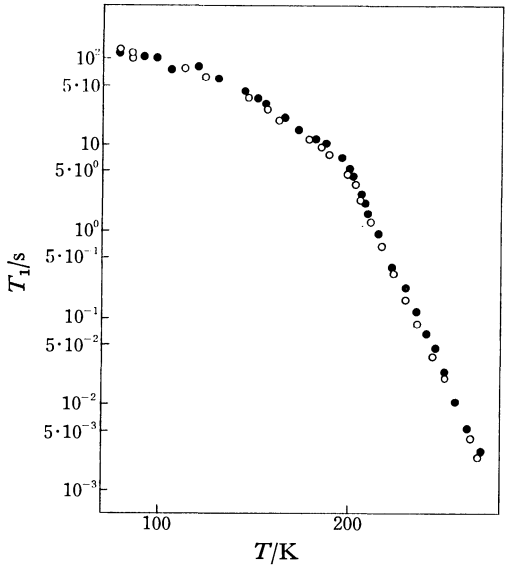

Fig. 2. The temperature dependence of the spin-lattice relaxation times in sulfuric diamide. ○: ν_- line; ●: ν_+ line.

The temperature dependence of the spin-lattice relaxation times (T_1) for ν_- and ν_+ lines in sulfuric diamide is shown in Fig. 2. Both curves are coincident within the experimental error. This fact suggests that the molecular motions equally contribute to T_1 for ν_- and ν_+ lines.

Below 140 K, the spin-lattice relaxation time is determined by torsional lattice vibration and is dominated by indirect two-phonon processes so that $1/T_1 \propto T^2$.

Above 200 K, the spin-lattice relaxation time drops exponentially as the temperature rises. This process can probably be attributed to the reorientation of the amino group around the S–N bond or to the reorientation of the molecule. In this case, the relaxation time is given by the following equation:[8]

$$1/T_1 = C\tau/(1+\omega_i^2\tau^2) \quad (i=+, -, \Delta), \tag{2}$$

where C is a constant related to the intrinsic nature of the molecular motion, τ is the correlation time, and ω_i is the resonance angular frequency. In the low temperature region of the T_1 minimum, $\omega_i\tau \gg 1$, and assuming the Arrhenius' relation for the correlation time, the following equation holds:

$$\tau = \tau_0 \exp(E_a/RT), \tag{3}$$

where τ_0 is the inverse frequency factor and E_a is the activation energy of the motion. Accordingly, we get

$$1/T_1 = f(\omega_i)\cdot\exp(-E_a/RT). \tag{4}$$

Equation 4 can be rewritten as follows:

$$\ln(1/T_1) = -E_a/RT + f'(\omega_i) \tag{5}$$

where $f'(\omega_i)$ is a function of ω_i, whose temperature dependence is negligible. In Fig. 3, the $\ln(1/T_1)$ value is plotted as a function of $1/T$. A break point is found near $10^3/T=4.2$/K (about 240 K) as is shown in Fig. 3. This suggests that T_1 above 240 K and T_1 below 240 K are dominated by different molecular motions. That is, the dominant relaxation mechanism below 240 K is considered to be caused by the reorientation of the amino group around the S–N bond, whereas that above 240 K is brought about by the reorientation

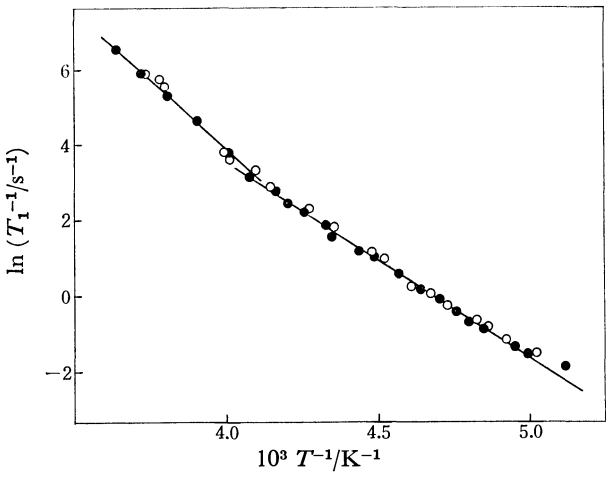

Fig. 3. $\ln(1/T_1)$ *vs.* $10^3/T$ in sulfuric diamide. ○: ν_- line; ●: ν_+ line.

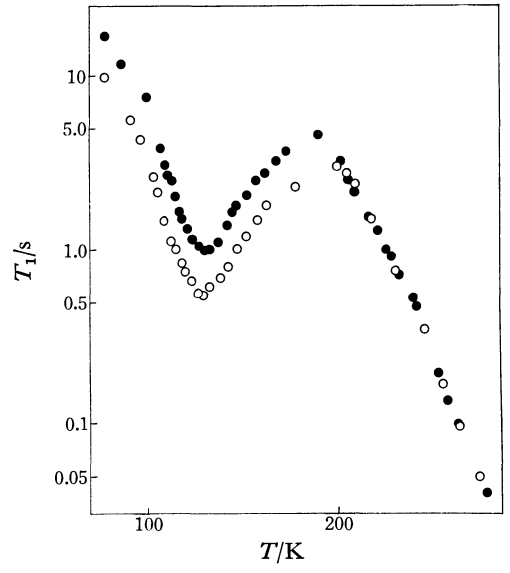

Fig. 4. The temperature dependence of the spin-lattice relaxation times in methanesulfonamide. ○: ν_- line; ●: ν_+ line.

of the molecule. In fitting Eq. 5 to the experimental T_1 values, the activation energies for these motions are determined: 43.5±4.3 kJ·mol^{-1} for the former motion and 61.5±6.2 kJ·mol^{-1} for the latter.

The temperature dependence of the spin-lattice relaxation times for ν_- and ν_+ lines in methanesulfonamide is shown in Fig. 4. In the temperature region from liquid nitrogen temperature to 200 K, T_1 for the ν_+ line, *i.e.*, $T_1(\nu_+)$, are longer than those for the ν_- line, *i.e.*, $T_1(\nu_-)$. However, above 200 K both relaxation times are coincident within the experimental error. This fact suggests that the molecular motion contributes differently to $T_1(\nu_-)$ and $T_1(\nu_+)$ below 200 K, but equally above 200 K.

In the temperature range from liquid nitrogen temperature to 170 K, a T_1 minimum is found near 130 K, as is shown in Fig. 4. This is caused by the introduction of the methyl group, and accordingly by the rotation of the group. The activation energy for this motion is calculated to be 9.6±0.9 kJ·mol^{-1} by

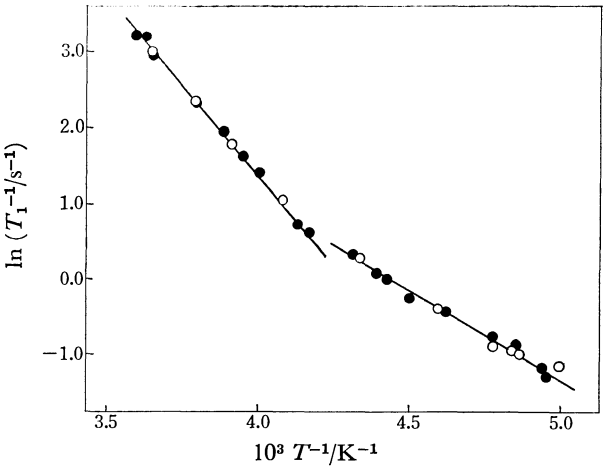

Fig. 5. $\ln(1/T_1)$ *vs.* $10^3/T$ in methanesulfonamide. ○: ν_- line; ●: ν_+ line.

the BPP theory.[9] This value is to be compared with 9.2 kJ·mol^{-1} for the rotation of the methyl group in acetonitrile.[10]

Above 200 K, T_1 drops exponentially as the temperature rises; this is shown in Fig. 4. As is shown in Fig. 5, in the $\ln(1/T_1)$ plot against $1/T$, a break point is found near $10^3/T$=4.2/K (about 240 K). This fact is explained in the same manner as for sulfuric diamide. That is, T_1 is dominated by the reorientation of the amino group around the S–N bond below 240 K and by the reorientation of the molecule above 240 K. In fitting Eq. 5 to the experimental T_1 values, the E_a values are determined: 19.2±1.9 kJ·mol^{-1} for the former motion and 40.6±4.1 kJ·mol^{-1} for the latter. These values are smaller than those in sulfuric diamide. This suggests that the intermolecular interaction in methanesulfonamide is weaker than that in sulfuric diamide, that is, the number of the hydrogen bonds per molecule in the former compound is smaller than that in the latter.

Takagi *et al.*[11] calculated the energy of the hydrogen bonds in sulfuric diamide to be 19.7 kJ·bond^{-1}, assuming that there are only two N–H···O hydrogen bonds per molecule, although there are other weak N–H···N hydrogen bonds.[12] Assuming that the activation energy (E_a) for the reorientation of the amino group comes mostly from breaking the hydrogen bonds, N–H···O, it is estimated to be 39.3 kJ·mol^{-1}, which is in good agreement with our experimental value, 43.5 kJ·mol^{-1}. In the case of methanesulfonamide, the E_a value for the reorientation of the amino group is 19.2 kJ·mol^{-1}, which is nearly equal to 19.7 kJ·bond^{-1}. Accordingly, it is concluded that there is one hydrogen bond, N–H···O, per molecule, although there may exist other weak hydrogen bonds, for example N–H···N.

References

1) H. Negita, T. Kubo, and K. Shibata, *Bull. Chem. Soc. Jpn.*, **48**, 675 (1975).
2) G. L. Petersen, Ph. D. thesis, Brown University, 1975.
3) G. L. Petersen and P. J. Bray, *J. Chem. Phys.*, **64**, 522 (1976).
4) S. Alexander and A. Tzalmona, *Phys. Rev. A*, **138**, 845 (1965).
5) Y. Abe, *J. Phys. Soc. Jpn.*, **18**, 1804 (1963).
6) Ed. F. Degering and G. C. Gross, *Ind. Eng. Chem.*, **35**, 751 (1943).
7) L. Field and F. A. Grunwald, *J. Am. Chem. Soc.*, **75**, 934 (1953).
8) Y. Abe, Y. Ohneda, H. Niki, and S. Kojima, *J. Phys. Soc. Jpn.*, **40**, 530 (1976).
9) Y. Abe, Y. Ohneda, M. Hirota, and S. Kojima, *J. Phys. Soc. Jpn.*, **37**, 1061 (1974).
10) A. Tzalmona, *Phys. Lett. A*, **34**, 289 (1971).
11) S. Takagi, R. Shintani, H. Chihara, and S. Seki, *Bull. Chem. Soc. Jpn.*, **32**, 137 (1959).
12) K. N. Trueblood and S. W. Mayer, *Acta Crystallogr.*, **9**, 628 (1956).

Ultrasonic Absorption in Dodecane Solution of Aerosol OT

Teruyo YAMASHITA, Hiroshige YANO,* and Tatsuya YASUNAGA**

Daiichi College of Pharmaceutical Science, Minami-ku, Fukuoka 815

***Department of Chemistry, Faculty of Science, Hiroshima University, Hiroshima 730*

(Received August 2, 1978)

The ultrasonic absorptions of Aerosol OT in dodecane solution were measured in the frequency range 5—95 MHz at various temperatures. An excess absorption caused by single relaxation was observed above the second critical micelle concentration. This is attributed to the conformational change in structure of two kinds of Aerosol OT micelles, since the maximum excess absorption per wave length depends on the concentration and temperature. The thermodynamic and kinetic parameters were determined in relation to the reaction.

The kinetics of micelle formation in surfactant solutions have been extensively studied in aqueous solutions by means of various relaxation methods.[1-10] However, few studies have been performed on the kinetics of reverse micelles in nonpolar solvents.

Aerosol OT (sodium 1,2-bis(2-ethylhexyloxycarbonyl)ethanesulfonate) forms reverse micelles in dodecane and its solution properties have been extensively investigated by static methods.[11-13] The purpose of the present investigation is to clarify the kinetic behavior of dodecane solutions of Aerosol OT by means of ultrasonic absorption.

Experimental

Dodecane was dried on P_2O_5 and distilled under reduced pressure (8 mmHg). Aerosol OT (guaranteed reagent grade) was dried at 105 °C under reduced pressure (8 mmHg) until the weight became constant. The concentration of the sample solution was given in terms of weight.

Ultrasonic absorptions were measured at the odd harmonics of 0.5, 5, and 20 MHz X-cut quartz transducers by means of pulse technique. The frequencies of the measurement were in the range 5—95 MHz. The major mechanical features of the apparatus were reported by Tatsumoto.[14] The sound velocity was measured by the sing-around method operating at 2.0 MHz, the density being determined with a pycnometer. All the measurements were carried out at concentrations 33.4—80 wt % and at temperatures 20—40 °C.

Results and Discussion

The concentration dependence of the ultrasonic absorption spectra of dodecane solution of Aerosol OT is shown in Fig. 1 and the temperature dependence of the absorption spectra in Fig. 2. All the spectra can be represented by

$$\alpha/f^2 = A/[1+(f/f_r)^2] + B, \quad (1)$$

where α is the absorption coefficient, f the frequency, f_r the relaxation frequency, A the amplitude of the excess absorption, and B the residual absorption. The ultrasonic parameters A, B, and f_r were so determined as to give the best fit of the experimental data to Eq. 1. The results are given in Table 1. Figure 3 shows the concentration dependence of the sound velocity at 20 °C. We see anomaly at concentrations of *ca.* 5 and 35%. The former is equal to the first critical micelle concentration(CMC) of Aerosol OT in dodecane reported by Mattoon and Mathews.[15] The latter can thus be assigned to the second CMC. Considering that the excess absorption appears near the second

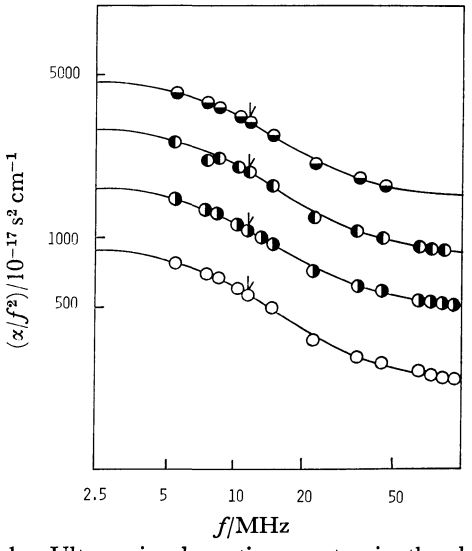

Fig. 1. Ultrasonic absorption spectra in the dodecane solutions of Aerosol OT at 20 °C. ◒ 74.5%, ◐ 67.4%, ◑ 59.1%, ○ 45.4%

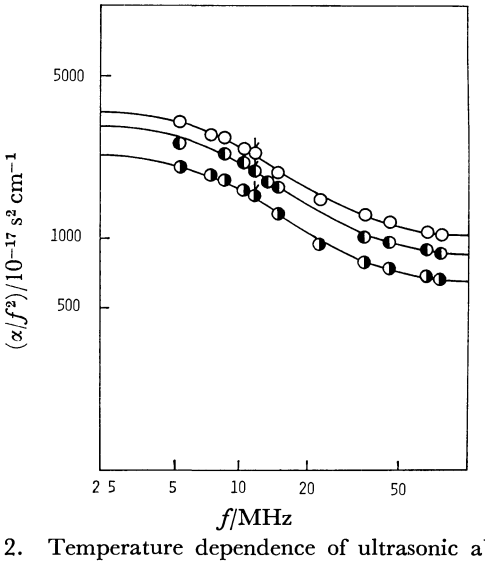

Fig. 2. Temperature dependence of ultrasonic absorption spectra in the 70% dodecane solution of Aerosol OT. ○ 20 °C, ◐ 30 °C, ◑ 40 °C

CMC, the cause of the excess absorption is presumed to be associated with the second CMC of Aerosol OT. Peri[11] reported that two types of micelles exist in hydrocarbon solutions of Aerosol OT, their size changing slightly with concentration and temperature. Taking this into account together with our results in which the relaxation frequencies show no concentra-

Table 1. Ultrasonic and thermodynamic parameters of dodecane solutions of Aerosol OT at 20 °C

wt %	A (10^{-15} s^2 cm^{-1})	B	f_r (MHz)	ρ (g cm^{-3})	β (10^{-4} °C^{-1})	c (10^5 s^{-1} cm)
33.4	4.26	1.58	11.5	0.8443	7.98	1.2888
40.0	6.68	1.96	11.5	0.8663	7.82	1.2865
45.4	6.68	2.45	11.5	0.8864	7.76	1.2877
50.0	8.63	3.11	11.5	0.9022	7.54	1.2891
55.0	9.78	3.91	11.5	0.9219	7.41	1.2900
59.1	11.5	5.12	11.5	0.9397	7.23	1.2926
64.7	14.9	7.25	11.5	0.9603	6.97	1.2959
67.4	21.3	8.61	11.5	0.9720	6.67	1.3007
70.0	26.5	10.1	11.5	0.9812	5.95	1.3046
74.5	33.4	14.9	11.5	1.0035	5.22	1.3142
78.6	57.6	18.4	11.5	1.0226	4.59	1.3238
80.0	72.5	19.6	11.5	1.0267	3.80	1.3247

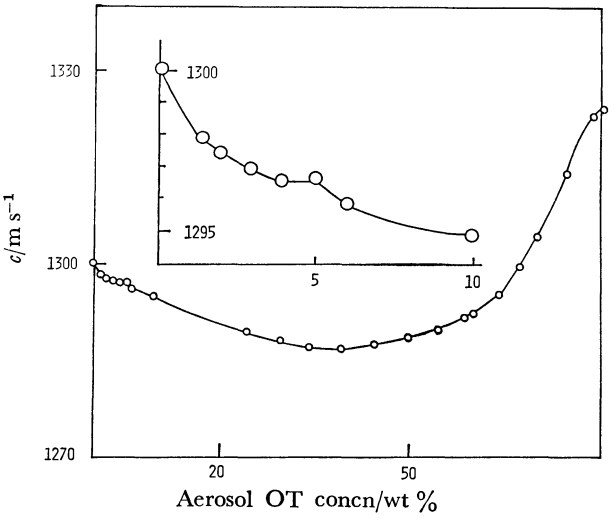

Fig. 3. Concentration dependence of the sound velocity in the dodecane solutions of Aerosol OT at 20 °C.

tion dependence (Table 1), we postulate a two state model for the relaxation mechanism:

$$A \underset{k_b}{\overset{k_f}{\rightleftharpoons}} B, \tag{2}$$

where A and B are the two types of micelles. On the assumption that the relaxation strength is much smaller than unity and the total specific heat capacity is equal to the instantaneous specific heat capacity, the relaxation frequency and the maximum excess absorption per wave length μ_{max} are expressed by the following equations.[16]

$$2\pi f_r = k_f + k_b, \tag{3}$$

$$\mu_{max} = \psi\rho\pi c^2 V(\Delta V/V - \Delta H\beta/C_p)^2/2RT, \tag{4}$$

and

$$\psi = K(1-x_{1st\ CMC})/(1+K)^2, \tag{5}$$

where k_f and k_b are respectively the forward and backward rate constants, ρ is the density, c the sound velocity, V the molar volume, β the thermal expansion coefficient, C_p the specific heat at a constant pressure, and ΔV and ΔH are the standard volume change and the enthalpy change of the reaction, respectively. The equilibrium constant, K, is defined to be $K=x_b/x_a=$

Table 2. Thermodynamic parameters associated with the conformational change in dodecane solution of Aerosol OT

	T (°C)	K	ΔV (cm^3 mol^{-1})	ΔH (kcal mol^{-1})	ΔS (cal mol^{-1} K^{-1})
a)	20	0.089	24	9.8	29
	40	0.24	24	9.8	29
b)	20	0.089			
	25	0.11			
	30	0.15	23	9.2	27
	35	0.18			
	40	0.24			

a) Determined from the concentration dependence of μ_{max} in the concentration range 33.4—80%. b) Determined from the temperature dependence in 70% solution.

Table 3. Rate constants for the conformational change of the micelle

T (°C)	k_f (10^6 s^{-1})	k_b (10^7 s^{-1})
20	5.9	6.6
25	7.7	6.4
30	9.4	6.3
35	11	6.1
40	14	5.8

$k_f/k_b=\exp\{-(\Delta H-T\Delta S)/RT\}$, where x_a and x_b are the mole fraction of species A and B, respectively, and ΔS is the entropy change. With C_p values determined by the interpolation of the values given by Finke *et al.*[17] and Rihani and Doraiswamy,[18] the thermodynamic parameters, K, ΔV, ΔH, and ΔS were so determined as to give the best fit of the experimental values of μ_{max} to Eq. 4. The values obtained are given in Table 2; the yields are shown by solid lines in Figs. 4 and 5. The parameters were also determined from the temperature dependence of μ_{max} at a constant concentration (Table 2). The thermodynamic parameters determined by these two procedures are very close to each other, indicating that the interpretation of the excess absorption mechanism by the two state

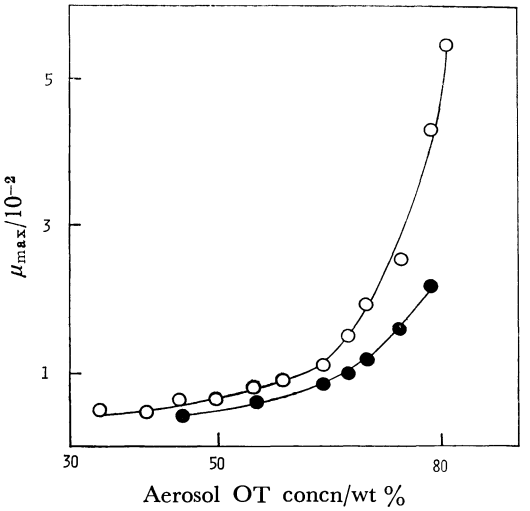

Fig. 4. Concentration dependence of the maximum excess absorption per wavelength at 20 °C (○) and 40 °C (●). The solid lines represent the theoretical curves calculated by Eq. 4 using the parameters in Table 2.

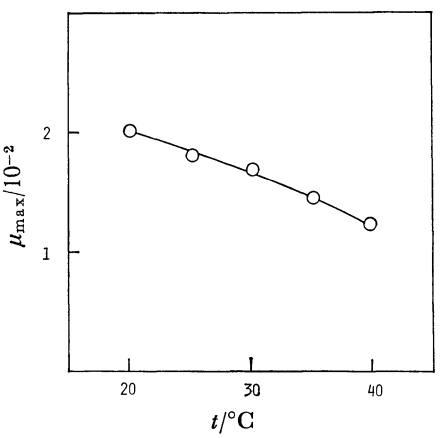

Fig. 5. Temperature dependence of the maximum excess absorption per wavelength in the 70% dodecane solution of Aerosol OT. The solid line was calculated from Eq. 4.

model is reasonable.

The forward and backward rate constants represent the rate of transition from the micelle formed above the first CMC to that above the second CMC and the rate of reverse transition, respectively. The rate constants were calculated from the relaxation frequency and the equilibrium constant at various temperatures (Table 3). The forward rate constant changes with temperature while the backward rate constant remains constant. This indicates that the free energy of activation of state B is almost constant and that of state A decreases with the temperature; micelles formed above the first CMC are destabilized with rise in temperature as compared with other micelles.

References

1) K. Takeda, *J. Sci. Hiroshima Univ., Ser. A*, **40**, 87 (1976).
2) J. Lang, C. Tondre, R. Zana, R. Bauer, H. Hoffman, and W. Ulbricht, *J. Phys. Chem.*, **79**, 276 (1975).
3) J. Rassing, P. J. Sams, and E. Wyn-Jones, *J. Chem. Soc., Faraday Trans. 2*, **70**, 1247 (1974).
4) E. Graber, J. Lang, and R. Zana, *Kolloid Z. Z. Polym.*, **238**, 479 (1970).
5) G. C. Kresheck, E. Hamori, G. Davenport, and E. M. Scheraga, *J. Am. Chem. Soc.*, **88**, 246 (1966).
6) K. Takeda and T. Yasunaga, *J. Colloid Interface Sci.*, **45**, 406 (1973).
7) J. Lang and E. M. Eyring, *J. Polym. Sci. A-2*, **10**, 89 (1972).
8) K. Takeda, *J. Sci. Hiroshima Univ., Ser. A*, **40**, 69 (1976).
9) K. Takeda, N. Tatsumoto, and T. Yasunaga, *J. Colloid Interface Sci.*, **47**, 128 (1974).
10) T. Nakagawa and H. Jizomoto, *Kolloid Z. Z. Polym.*, **250**, 594 (1972).
11) J. B. Peri, *J. Colloid Interface Sci.*, **29**, 6 (1969).
12) M. B. Mathews and E. Hirschhorm, *J. Colloid Interface Sci.*, **8**, 86 (1953).
13) M. Ueno and H. Kishimoto, *Bull. Chem. Soc. Jpn.*, **50**, 1631 (1977).
14) N. Tatsumoto, *J. Chem. Phys.*, **47**, 4561 (1967).
15) R. W. Mattoon and M. B. Mathews, *J. Chem. Phys.*, **17**, 496 (1949).
16) K. R. Hertzfeld and T. A. Litovitz, "Absorption and Dispersion of Ultrasonic Wave," Academic Press, New York (1959).
17) H. L. Finke, M. E. Gross, G. Waddington, and H. M. Huffman, *J. Am. Chem. Soc.*, **76**, 333 (1954).
18) D. N. Rihani and L. K. Doraiswamy, *Ind. Eng. Chem. Fundamentals*, **4**, 17 (1965).

Intramolecular Charge-transfer Absorption Spectra of Tetracyanotetrathiafulvalene

Shigeo YONEDA, Tokuzo KAWASE, and Zen-ichi YOSHIDA*

Department of Synthetic Chemistry, Kyoto University, Yoshida, Kyoto 606

(Received August 28, 1978)

The electronic spectrum and structure of tetracyanotetrathiafulvalene have been investigated by the ASMO-SCF-CI method, in which the 3d orbitals of sulfur atoms are taken into account. The calculated results showed that the absorption band at the longest wavelength can be interpreted in terms of intramolecular charge-transfer.

In preceding papers,[1,2] we reported the syntheses of several electronegative substituted tetrathiafulvalenes such as tetracyanotetrathiafulvalene (**1**).

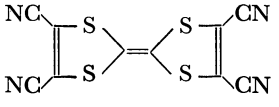

1

The compound **1** is composed of two parts, that is, the electron-donating part (the central electron-rich olefin moiety) and the electron-accepting part (the dicyanoethylene moiety). It seems reasonable to expect the appearance of an intramolecular charge-transfer[3] band in the electronic spectrum of **1**. In the present work, experimental and theoretical investigations of the electronic spectrum of **1** were carried out, and the absorption band at the longest wavelength (502 nm in benzene) was shown to be due to an intramolecular charge-transfer transition.

In addition, the electronic structure of **1** in the ground state will be discussed and compared with that of the parent tetrathiafulvalene (TTF).

Experimental

The compound, **1**, was prepared from 4,5-dicyano-1,3-dithiole-2-thione in the presence of triphenyl phosphite; mp 264—265 °C (dec).[2] The ultraviolet and visible absorption spectra of **1** were recorded on a Hitachi EPS-3T spectrophotometer in benzene, dichloromethane, acetonitrile, and methanol. The observed spectra were analyzed by assuming Gaussian curves for the absorption bands. Three absorption bands thus obtained and their molecular extiction coefficients are presented in Table 1.

Calculation

The calculations were carried out by the use of the semiempirical ASMO-SCF-CI method involving all valence electrons.[4] The sulfur atom has not only 3s and 3p, but also 3d orbitals in the valence shell. As regards unsubstituted TTF, it was pointed out that the inclusion of sulfur 3d orbitals is necessary to explain the relative bond lengths of the two carbon-carbon double bonds obtained from the X-ray analysis of TTF.[5] Accordingly, in this calculation the 3d orbitals of the sulfur atom were taken into account.

The overlap integrals were calculated using Slater-type atomic orbitals, where the orbital exponents are taken from Clementi and Raimondi.[6] The one-center exchange integrals were estimated from the Slater-Condon parameters evaluated by Hinze and Jaffé.[7] The Slater exponents (ζ_r), valence-state ionization potentials (I_r) of atomic orbitals, one-center Coulomb integrals (rr|rr), and one-center exchange integrals (rr'|rr') used in the present calculations are listed in Table 2.

The structural model for **1** is shown in Fig. 1. The molecule is assumed to have D_{2h} symmetry; the interatomic distances are taken from the X-ray data of TTF[5] and the book by Pople and Beveridge.[8]

The MO energies for each of the six occupied and vacant levels, and their approximate descriptions are shown in Table 3, although the LCAO coefficients of the MO's are not given.

In calculating the electronic transition energies, the 36 lowest singly-excited configurations were considered. The calculated singlet transition energies

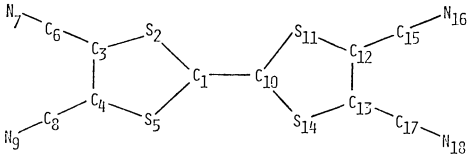

$\angle S_5C_1S_2 = 114.5°$ C_1-C_{10} = 1.349 Å
$\angle C_1S_2C_3 = 94.4°$ C_1-S_2 = 1.757 Å
$\angle S_2C_3C_4 = 118.3°$ S_2-C_3 = 1.731 Å
$\angle C_6C_3C_4 = 120.0°$ C_3-C_4 = 1.314 Å
C_3-C_6 = 1.450 Å
C_6-N_7 = 1.160 Å

Fig. 1. Geometries and bond lengths of tetracyanotetrathiafulvalene.

TABLE 1. ELECTRONIC SPECTRA OF TETRACYANOTETRATHIAFULVALENE

Solvent	A-band		B-band		C-band	
	λ_{max} (nm)	($\log \varepsilon_{max}$)	λ_{max} (nm)	($\log \varepsilon_{max}$)	λ_{max} (nm)	($\log \varepsilon_{max}$)
Benzene	502	(3.30)	328	(4.18)		
Dichloromethane	500	(3.36)	326	(4.20)	262	(4.41)
Acetonitrile	492	(3.30)	323	(4.16)	261	(4.33)
Methanol	480	(3.30)	320	(4.04)	261	(4.20)

TABLE 2. SLATER EXPONENTS (ζ_r) AND VALENCE STATE IONIZATION POTENTIALS (I_r)[a] OF ATOMIC ORBITALS AND ELECTRON REPULSION INTEGRALS[a]

		ζ_r	I_r	(rr|rr)[b]	(rr'|rr')[c]
C	2s	1.6083	−20.01	12.10	(2s2p|2s2p) =2.30
	2p	1.5679	−11.27	10.93	(2p2p'|2p2p')=0.54
N	2s	1.9237	−26.92	12.87	(2s2p|2s2p) =2.99
	2p	1.9170	−14.42	11.88	(2p2p'|2p2p')=0.77
S	3s	2.1223	−20.08	8.54	(3s3p|3s3p) =1.02
	3p	1.8273	−13.32	9.82	(3p3p'|3p3p')=0.55
	3d	0.8400	−3.67	5.90	

a) Energy in eV. b) $(rr|rr)=I_r-E_r$. c) Ref. 7.

TABLE 3. ENERGIES AND APPROXIMATE DESCRIPTION OF THE MOLECULAR ORBITALS OF TETRACYANOTETRATHIAFULVALENE

MO No.	Energy eV	Symbol	Description	D_{2h} Symmetry label
12	−3.13	σ		B_{3u}
11	−3.14	π	Delocalized over bridge carbons and sulfur atoms	B_{1g}
10	−3.19	σ		A_g
9	−3.42	σ		A_g
8	−3.53	π	Node at bridge carbons (delocalized over DCNE)[a]	B_{1g}
7	−3.54	π	Node at bridge carbons (delocalized over DCNE)[a]	B_{2u}
6	−10.47	π	Delocalized over TTE[b]	A_g
5	−12.65	π	Delocalized over whole molecule (TTF)	B_{3u}
4	−13.78	π	Node at bridge carbons (delocalized over DTE)[c]	B_{1g}
3	−13.84	π	Node at bridge carbons (delocalized over DTE)[c]	B_{2u}
2	−13.88	σ		B_{2u}
1	−13.98	σ		B_{2u}

a) DCNE: Dicyanoethylene moiety. b) TTE: Tetrathioethylene moiety. c) DTE: Dithioethylene moiety.

and oscillator strengths are presented in Table 4. For comparison, the results calculated both including and neglecting 3d orbitals of sulfur atoms are listed in Table 4.

The electron densities and overlap populations of **1** are also shown, together with those of parent TTF, in Fig. 2.

Discussion

In the calculations of transition energies of organic compounds with a bivalent sulfur atom, the contribution of sulfur 3d orbitals is usually not evaluated and often neglected. However, as seen in Table 4, the transition energies calculated with 3d orbitals were in better agreement with the observed ones than those calculated without 3d orbitals. This evidently suggests that the 3d orbitals of the sulfur atom are essential for the explanation of the electronic structure of the system **1**.

Intramolecular Charge-transfer Absorption Band. According to the calculated results, since the wave

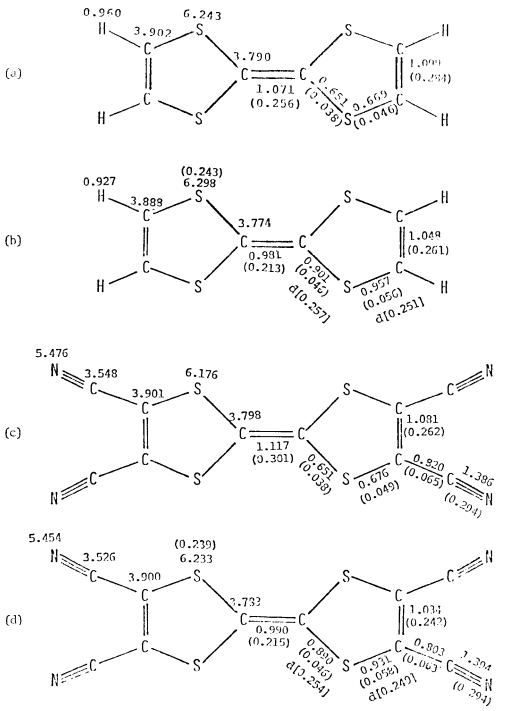

Fig. 2. Electron densities and overlap populations of tetrathiafulvalene (TTF) and tetracyanotetrathiafulvalene. (a): The results of TTF in the case of neglecting d orbitals, (b) the results of TTF in the case of including d orbitals, (c) the results of tetracyanotetrathiafulvalene in the case of neglecting d orbitals, (d) the results of tetracyanotetrathiafulvalene in the case of including d orbitals. The numbers in the parentheses, ( ) and [ ], indicate π- and d-overlap populations, respectively.

function for the excitation at 2.48 eV was composed of V_{6-7} (95%), V_{5-8} (4%), and V_{4-11} (1%), where V_{m-n} represents the singly excited configuration from the m-th level to the n-th (Table 3), the absorption band at 2.48 eV can be assigned to the excitation from the 6th orbital (HOMO) to the 7th (LUMO):

$$\begin{aligned}\Phi_6 = &-0.332(\chi_1+\chi_{10})_{2pz} + 0.383(\chi_2+\chi_5+\chi_{11}+\chi_{14})_{3pz}\\ &+0.007(\chi_2+\chi_5-\chi_{11}-\chi_{14})_{3dxz}\\ &+0.113(\chi_2-\chi_5+\chi_{11}-\chi_{14})_{3dyz}\\ &-0.177(\chi_3+\chi_4+\chi_{12}+\chi_{13})_{2pz}\\ &-0.002(\chi_6+\chi_8+\chi_{15}+\chi_{18})_{2pz}\\ &+0.087(\chi_7+\chi_9+\chi_{16}+\chi_{18})_{2pz} \qquad (1)\\ \Phi_7 = &-0.147(\chi_2+\chi_5+\chi_{11}+\chi_{14})_{3pz}\\ &+0.172(\chi_2-\chi_5+\chi_{11}+\chi_{14})_{3dxz}\\ &-0.091(\chi_2+\chi_5+\chi_{11}+\chi_{14})_{3dyz}\\ &+0.360(\chi_3-\chi_4+\chi_{12}-\chi_{13})_{2pz}\\ &+0.148(\chi_6-\chi_8+\chi_{15}-\chi_{17})_{2pz}\\ &-0.216(\chi_7-\chi_9+\chi_{16}-\chi_{18})_{2pz}, \qquad (2)\end{aligned}$$

where the m of χ_m corresponds to the number of atoms in Fig. 1.

As can be seen from Eqs. 1 and 2, the large contribution of the tetrathioethylene part ($S_2C{=}CS_2$) to the highest occupied π-MO and that of the dicyanoethylene part (NC–C=C–CN) to the lowest vacant

Table 4. Calculated transition energies[a] and oscillator strengths

ΔE_{obsd}	ASMO-SCF-CI (with d)		ASMO-SCF-CI (without d)		Assignment[b]
	ΔE_{calcd}	f	ΔE_{calcd}	f	
2.48 (3.30)[c]	3.22	0.357	4.07	0.527	$\pi_{TTE}\rightarrow\pi^*_{DCNE}$
3.54 (4.18)[c]	3.36	0.656	5.80	0.506	$\pi_{TTF}\rightarrow\pi^*_{TTE}$
4.77	5.41	0.519	8.12	0.347	$\pi_{TTF}\rightarrow\pi^*_{DCNE}$
	5.75	0.130			$\pi_{DTE}\rightarrow\pi^*_{DCNE}$
	6.21	0.585			$\pi_{DTE}\rightarrow\pi^*_{TTE}$

a) Energy in eV. b) TTE: Tetrathioethylene component. DCNE: Dicyanoethylene component. TTF: Tetrathiafulvalene component. DTE: Dithioethylene component. c) The numbers in parentheses indicate $\log \varepsilon_{max}$, obtained from measurements.

π^*-MO are clearly represented. Thus, this $\pi_{TTE}\rightarrow\pi^*_{DCNE}$ transition is reasonably understood as the transition from the electron-rich moiety ($S_2C{=}CS_2$) to the electron-deficient moiety (NC–C=C–CN). Consequently, the absorption band at the longest wave length is well interpreted in terms of intramolecular charge-transfer.

A similar result was obtained in the calculations of **1** by the CNDO/2-CI method. If 3d orbitals of the sulfur atom are considered, the longest wave length absorption band can also be reasonably assigned to the $\pi_{TTE}\rightarrow\pi^*_{DCNE}$ transition.

This interpretation is also supported by the results that the absorption band at the longest wave length exhibits blue shifts upon changing the polarity of solvents from benzene (502 nm) to methanol (480 nm); these results are listed in Table 1.

The strong absorption band at 3.54 eV can be assigned to the excitation from the tetrathiafulvalene moiety to the tetrathioethylene moiety, since the molecular orbitals of the ground and excited states for this transition correspond to π_{TTF} and π^*_{TTE}, respectively (Table 4). Similarly, the absorption band at 4.77 eV is assigned to the excitation from the tetrathiafulvalene moiety to the dicyanoethylene moiety.

In the case of the TTF's substituted with electron-donating groups (such as methyl, hydroxyl and amino groups), the transition from the highest occupied MO to the lowest vacant MO could not be assigned to the $\pi\rightarrow\pi^*$ one; this is obviously a different result from that of the calculation for **1**. Therefore, it is reasonably concluded that the phenomenon of the intramolecular charge-transfer is characteristic of electronegatively substituted tetrathiafulvalenes.

Electron Population Analysis. As seen in Fig. 2(b), the total electron densities on the carbons, C_1 and C_3, in TTF are smaller than 4.0, but those of the 2pz orbitals are 1.058 and 1.027, respectively, indicating that TTF can be considered to be an electron-rich olefin so far as π-electron system is concerned. The formal charge of the sulfur atom in TTF, in spite of a rather large positive charge (+0.17) in the $3p_\pi$ net charge, is negative (−0.30) as a result of the back donation of the σ electrons. This back donation of electrons is mainly caused by the 3d orbitals of the sulfur atom, to which indeed considerable charge densities (about 0.24) are attributed.

With regard to the overlap populations of TTF, in comparing the values calculated by including 3d orbitals with those found by neglecting 3d orbitals, the values for C_1–C_3 and C_3–C_4 bonds are smaller. Those for C_1–S_2 and S_2–C_3 bonds reveal the most significant difference, in amount 0.25—0.29, between the case of including 3d orbitals and the case of neglecting them. This prominent difference of overlap populations can be explained by the concept of the partial overlap populations between 3d orbitals of sulfur and 2pz orbitals of carbon atoms, whcih distributes to the C–S bonds in the amount of 0.25. Such participations of 3d orbitals should strengthen the C–S bonds up to those comparable to the double bond. These results indicate that the 3d orbitals of sulfur atoms are quite important in tetrathiafulvalene systems.

Similar aspects in the electronic structure of **1** were obtained by comparing the results calculated by including and neglecting 3d orbitals with each other.

It may be expected that the charge density of the central ethylene carbon atom would be decreased by the substitution of an electron-withdrawing group (CN). However, the calculated result shows that the charge density of the central carbon atom increases and that of the sulfur atom decreases, which indicates a transfer of electrons from the sulfur atoms of the central tetrathioethylene part to the dicyanoethylene part. This suggests that **1** is composed of two separable components, namely, a dicyanoethylene part and a tetrathioethylene part, which is coincident with the result obtained from the study of the electronic absorption spectra of **1**.

References

1) Z. Yoshida, T. Kawase, and S. Yoneda, *Tetrahedron Lett.*, **1975**, 331.
2) S. Yoneda, T. Kawase, M. Inaba, and Z. Yoshida, *J. Org. Chem.*, **43**, 595 (1978).
3) S. Nagakura, *Pure Appl. Chem.*, **7**, 79 (1963); *Mol. Phys.*, **3**, 105 (1960).
4) T. Yonezawa, H. Konishi, and H. Kato, *Bull. Chem. Soc. Jpn.*, **42**, 933 (1969).
5) W. F. Cooper, N. C. Kenny, J. W. Edmons, A. Nagel, F. Wudl, and P. Coppens, *Chem. Commun.*, **1971**, 889.
6) E. Clementi and D. L. Raimondi, *J. Chem. Phys.*, **38**, 2686 (1963).
7) J. Hinze and H. H. Jaffé, *J. Chem. Phys.*, **38**, 1834 (1963).
8) J. A. Pople and D. L. Beveridge, "Approximate Molecular Orbital Theory," McGraw-Hill Book Company (1970), p. 111.

The Determination of the Chemical Diffusion Coefficients for AgBr and α-AgI by Means of an Improved d.c. Polarization Cell

Junichiro MIZUSAKI,* Kazuo FUEKI,* and Takashi MUKAIBO

Department of Industrial Chemistry, Faculty of Engineering, The University of Tokyo, Hongo, Bunkyo-ku, Tokyo 113

(Received September 7, 1978)

In order to determine the chemical diffusion coefficients for AgBr and α-AgI, a new experimental technique was developed. A Pt probe was inserted into the middle of the AgX (X=Br or I) pellet in an improved d.c. polarization cell of the Ag/AgX/carbon type, and the applied potential difference between the Ag and carbon electrodes was changed abruptly. The accompanying change in $E(L/2)$, the EMF between the Ag electrode and the Pt probe, was followed, and the chemical diffusion coefficient, $\tilde{D}$, was determined by the analysis of the change in $E(L/2)$ with the time. In the temperature range from 325 to 400 °C, $\tilde{D}$ for AgBr with excess silver was found to be

$$\tilde{D} = 7.10 \times 10^{2} \exp\left(-\frac{1.96\times10^{4}\ \text{cal mol}^{-1}}{RT}\right) \text{cm}^2\ \text{s}^{-1}. \quad \text{(i)}$$

In the temperature range of 330 to 500 °C, $\tilde{D}$ for α-AgI was

$$\tilde{D} = 4.95 \times 10^{-1} \exp\left(-\frac{7.71\times10^{3}\ \text{cal mol}^{-1}}{RT}\right) \text{cm}^2\ \text{s}^{-1}. \quad \text{(ii)}$$

Using these chemical diffusion coefficients and the electronic conductivity data, the nonstoichiometry, and apparent mobility of electronic carriers of AgBr and α-AgI were determined.

Generally, the chemical diffusion coefficient for a solid compound is obtained from the measurement of the responding weight change or electrical conductivity change, both of which changes are caused by the sudden change in the chemical potential of its components. Gravimetric measurements are useful when the solid compound has a large nonstoichiometry, while the measurement of the electrical conductivity is effective when the conductivity of the sample is quite sensitive to the chemical potential of its components.

However, in the case of the silver halides, the nonstoichiometry is too small to be detected by the gravimetric method, and the electrical conductivity, which is essentially ionic, is constant, irrespective of the chemical potential of silver. Therefore, the chemical diffusion coefficients for silver halides cannot be determined by means of conventional techniques, and new techniques must be developed.

Weiss has carried out some pioneering work on the determination of the chemical diffusion coefficient for AgBr.[1,2] He employed a Hebb-Wagner d.c. polarization cell of the type:

(I) Ag/AgBr/carbon, inert atmosphere

and tried to determine the chemical diffusion coefficient by two methods. In the first method, a constant potential was applied to the cell until a stationary state was reached. Then, the potential was removed abruptly and the EMF decay was followed. From the decay constant, the chemical diffusion coefficient was then determined. In the second method, the current decay was followed after the step-like change in the potential difference applied between the electrodes. However, a large discrepancy was found between the results of these two measurements.

Recently, the present authors have investigated the cell of the (I) type. They have found that the electrical potential of the electrode attached to the surface of AgX pellet is quite sensitive to the activity of the halogen, X, in the atmosphere in contact with the AgX surface and does not show the activity of the X in the AgX.[3] Also, the ionic current due to the electrolysis of AgX was found not to be blocked completely in the cell of the (I) type, because the carbon electrode is exposed to an inert atmosphere and the halogen partial pressure around the electrode is considerably lower than that at the AgX/carbon interface.[4] These findings suggest problems with Weiss' experiments. In Weiss' first method, the carbon electrode was exposed to an inert atmosphere, so the EMF decay might have reflected the decomposition of AgBr at the AgBr/carbon interface. In his second method, an appreciable ionic current due to the decomposition of AgBr might have flowed in the cell.

The purpose of the present study is to present a new polarization technique, one which is free from the problems encountered in Weiss' experiments, and to report the results of measurements, made using a new technique, of the chemical diffusion coefficients for AgBr and α-AgI.

Theoretical

Distribution Profiles of Nonstoichiometry in a d.c. Polarization Cell. A schematic drawing of the d.c. polarization cell employed in the present study is shown in Fig. 1. It is constructed of an AgX pellet with the length, L, sandwiched between an Ag electrode and a so-called 'ion-blocking' electrode.[4] When an inactive electrode is inserted into AgX as a probe at a certain distance, x, from the Ag/AgX interface, and when a potential difference, $E(L)$, is then applied between the Ag electrode and the ion-blocking electrode, an electrical potential difference, $E(x)$, is observed between the Ag electrode and the probe. Denoting the electrochemical potential of electrons in AgX by η_e, we can express $E(x)$ by

$$E(x)F = -\{\eta_e(x) - \eta_e(0)\} \quad (1)$$

where $\eta_e(x)$ denotes η_e at the x position, $\eta_e(0)$ represents η_e at the Ag/AgX interface, and F denotes the Faraday constant. Expressing the chemical potential of silver in AgX by μ_{Ag}, and the electrochemical potential of silver ions in AgX by η_{Ag^+}, we obtain

$$\eta_e(x) = \mu_{Ag}(x) - \eta_{Ag^+}(x). \quad (2)$$

From Eqs. 1 and 2,

$$E(x)F = -\{\mu_{Ag}(x) - \mu_{Ag}(0)\} + \{\eta_{Ag^+}(x) - \eta_{Ag^+}(0)\}$$
$$= E'(x)F + E''(x)F, \quad (3)$$

where

$$E'(x)F = -\{\mu_{Ag}(x) - \mu_{Ag}(0)\}, \quad (4)$$

and

$$E''(x)F = \eta_{Ag^+}(x) - \eta_{Ag^+}(0). \quad (5)$$

When the ionic current in the cell is completely blocked, η_{Ag^+} in the cell is constant throughout the AgX pellet. Thus,

$$E'' = 0. \quad (5)'$$

From Eqs. 3, 4, and 5′,

$$E(x)F = -\{\mu_{Ag}(x) - \mu_{Ag}(0)\}. \quad (6)$$

When the chemical potential of silver in AgBr is close to that of metallic silver, AgBr is known to show the n-type electronic conduction. In this case, the electronic conductivity, σ_e,[4] is expressed by

$$\sigma_e = \sigma_e^\circ \exp\{(\mu_{Ag} - \mu_{Ag}^\circ)/RT\}, \quad (7)$$

where μ_{Ag}° and σ_e° are the μ_{Ag} and σ_e of AgBr in equilibrium with metallic silver, and where R is the gas constant, and T, the temperature. The n-type electronic conduction is caused by the conduction electrons released from the excess silver atoms. When we represent the nonstoichiometry of AgBr by δ, the metal–excess silver bromide is expressed by the chemical formula $Ag_{1+\delta}Br$ and the concentration of the conduction electrons and the conductivity, σ_e, of AgBr are both proportional to δ. Therefore,

$$\delta = \delta^\circ \exp\{(\mu_{Ag} - \mu_{Ag}^\circ)/RT\}, \quad (8)$$

where δ° is δ in AgBr in equilibrium with metallic silver. From Eqs. 6 and 8,

$$\delta(x) = \delta^\circ \exp\left\{-\frac{E(x)F}{RT}\right\}, \quad (9)$$

where $\delta(x)$ is δ at a ceretain distance, x, from the Ag/AgX interface. As α-AgI shows the p-type electronic conduction due to electron holes, the electronic conductivity, σ_h, can be expressed as[4]

$$\sigma_h = \sigma_h^\circ \exp\{(\mu_{Ag}^\circ - \mu_{Ag})/RT\}, \quad (10)$$

where σ_h° is the σ_h of AgI in equilibrium with metallic silver. The p-type conduction indicates that α-AgI is a metal-dificient compound with the chemical formula of $Ag_{1-\delta}I$. The hole concentration and electronic conductivity of α-AgI are proportional to δ. Thus,

$$\delta = \delta^\circ \exp\{(\mu_{Ag}^\circ - \mu_{Ag})/RT\}. \quad (11)$$

From Eqs. 6 and 11,

$$\delta = \delta^\circ \exp\left\{\frac{E(x)F}{RT}\right\}. \quad (12)$$

In a previous paper[3] the present authors have shown that, under ion-blocking conditions, $E(x)$ in the n-type region of AgBr shows a steady-state distribution

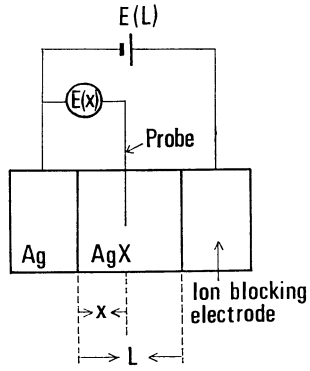

Fig. 1. Schematic diagram of experimental method.

$$\frac{x}{L} = \frac{1 - \exp\left\{-\frac{E(x)F}{RT}\right\}}{1 - \exp\left\{-\frac{E(L)F}{RT}\right\}}. \quad (13)$$

Similarly, for AgI with the p-type conduction,

$$\frac{x}{L} = \frac{\exp\left\{\frac{E(x)F}{RT}\right\} - 1}{\exp\left\{\frac{E(L)F}{RT}\right\} - 1}. \quad (14)$$

The combination of Eqs. 9 and 13 yields

$$\frac{x}{L} = \frac{\delta(x) - \delta^\circ}{\delta(L) - \delta^\circ}. \quad (15)$$

The combination of Eqs. 12 and 14 also results in the same equation. Equation 15 shows that when a steady state is reached under the ion-blocking conditions, the nonstoichiometry of AgBr and α-AgI is linearly distributed in the d.c. polarization cell.

Determination of the Chemical Diffusion Coefficient for AgBr and α-AgI. When a constant potential difference, $E_1(L)$, is applied between the electrodes of the cell in Fig. 1 for a time sufficient to attain the steady-state, and is then changed to $E_2(L)$ abruptly, the distribution of δ in AgX gradually changes with the time from one steady state to another steady state. This process is controlled by the chemical diffusion in AgX. If the molar amount of X in a unit volume of AgX is expressed by C, the amount of silver excess or silver deficit in a unit volume will be given by $C\delta$. Therefore, the diffusion equation is

$$\frac{\partial(C\delta)}{\partial t} = \tilde{D}\frac{\partial^2(C\delta)}{\partial x^2}, \quad (16)$$

where $\tilde{D}$ denotes the chemical diffusion coefficient, and t, the time. Because C is constant, Eq. 16 can be rewritten as

$$\frac{\partial\delta}{\partial t} = \tilde{D}\frac{\partial^2\delta}{\partial x^2}. \quad (17)$$

In the case of AgBr, the boundary conditions are

$$\frac{\delta(x, 0) - \delta^\circ}{\delta(L, 0) - \delta^\circ} = \frac{x}{L} \quad \text{for } t = 0 \quad (18)$$

$$\delta(L) = \delta^\circ \exp\left\{-\frac{E_1(L)F}{RT}\right\} \quad \text{for } t < 0 \quad (19)$$

$$\delta(L, t \geq 0) = \delta^\circ \exp\left\{-\frac{E_2(L)F}{RT}\right\} \quad \text{for } t \geq 0 \quad (20)$$

$$\delta(0,\ t) = \delta^{\circ} \qquad \text{for } x=0. \qquad (21)$$

Solving Eq. 17 under the condition of Eqs. 18—21, we obtain

$$\frac{\delta(L/2,t)-\delta(L/2,0)}{\delta(L/2,\infty)-\delta(L/2,0)} = \frac{4}{\pi}\sum_{n=1}^{\infty}\frac{(-1)^n}{2n-1}\exp\left\{-\frac{\tilde{D}\pi^2(2n-1)^2t}{L^2}\right\}, \qquad (22)$$

where n is the integer. The same solution as Eq. 22 is obtained in the case of α-AgI. When t becomes large, the $n>2$ terms in the series of Eq. 22 become negligibly small. It follows that

$$\frac{\delta(L/2,\infty)-\delta(L/2,t)}{\delta(L/2,\infty)-\delta(L/2,0)} = \frac{4}{\pi}\exp\left(-\frac{\tilde{D}\pi^2t}{L^2}\right). \qquad (23)$$

The change in $\delta(L/2)$ with the time can be calculated from $E(L/2)$ by using Eqs. 9 and 13. From the slopes of the plots of $\log[\{\delta(L/2,\infty)-\delta(L/2,t)\}/\{\delta(L/2,\infty)-\delta(L/2,0)\}]$ *versus* t, we can determine the chemical diffusion coefficient, $\tilde{D}$.

Chemical Diffusion Coefficient and Electronic Conductivity. According to Wagner's theory of metal oxidation,[5] the diffusion through the oxide layer is generally interpreted as consisting of migration processes of ions and electrons, and, in the case of diffusion-controlled oxidation, the chemical diffusion coefficient, $\tilde{D}$, is given by

$$\tilde{D} = \frac{V_m}{Z_1F^2}\frac{(\sigma_1+\sigma_2)\sigma_3}{\sigma_1+\sigma_2+\sigma_3}\frac{\partial\mu_M}{\partial\delta}, \qquad (24)$$

where σ_1, σ_2, and σ_3 are the conductivities of cations, anions, and electrons respectively, and where Z_1 is the number of the charge of the cations, μ_M is the chemical potential of metal, and V_M is the molar volume.

The same diffusion situation as in the metal oxidation is set up in the present experiment, except for the initial several seconds, where the transient current flows to charge or discharge the cell. For AgBr with the n-type conduction, the diffusion of Ag^+ ions and electrons contributes most to the chemical diffusion. Therefore,

$$\tilde{D} = \frac{\sigma_{Ag^+}\sigma_e V_m}{(\sigma_{Ag^+}+\sigma_e)F^2}\frac{\partial\mu_{Ag}}{\partial\delta}. \qquad (25)$$

Since σ_{Ag^+} is much larger than σ_e, Eq. 25 becomes

$$\tilde{D} = \frac{\sigma_e V_m}{F^2}RT\frac{1}{\delta}. \qquad (26)$$

Here Eq. 8 is used. Equation 26 indicates that the nonstoichiometry can be determined by chemical diffusion measurements and electronic conductivity measurements.

Similarly, the diffusion of Ag^+ ions and positive holes occurs during the chemical-relaxation process in α-AgI.

From Eq. 24,

$$\tilde{D} = \frac{\sigma_{Ag^+}\sigma_h V_m}{(\sigma_{Ag^+}+\sigma_h)F^2}\frac{\partial\mu_{Ag}}{\partial\delta}. \qquad (27)$$

Since $\sigma_{Ag^+} \gg \sigma_h$, using Eq. 10 we obtain

$$\tilde{D} = \frac{\sigma_h V_m}{F^2}RT\frac{1}{\delta}. \qquad (28)$$

Experimental

Cells and Samples. Figure 2 shows the cell structure and the block-diagram of the circuit used for the measurement. The samples were prepared in the way described elsewhere.[3] The cell construction was essentially the same as that of the improved d.c. polarization cell,[4] except that in the present work the platinum probe was placed in the middle of the AgX pellet. A hole, 0.8 mm in diameter, was drilled along the axis of the silver electrode to the middle of the AgX pellet. In this hole, a platinum wire 0.2 mm in diameter, protected by an alumina tube (0.8 mm in outer diameter and 0.4 mm in inner diameter), was buried as a probe so that only the tip of the wire was in contact with the AgX pellet.

Measurement Procedure. The cell was set in an electrical furnace, the temperature of which was controlled within ±1 °C. Then a constant potential difference, $E_1(L)$, was created between the silver and carbon electrodes by means of a potentiostat. The potential difference, $E(L/2)$, between the silver electrode and the platinum probe was recorded by means of high-input-impedance voltage follower and a recorder. After $E(L/2)$ had reached a steady value, $E_1(L)$ was changed abruptly to $E_2(L)$ by means of a function generator and the time change of $E(L/2)$ was recorded. In several runs, the time change in the current passing through the cell was also recorded. The chemical diffusion coefficient was determined by the analysis of the recorded curve of $E(L/2)$ *versus* the time.

The measurement for AgBr was performed in the temperature range from 325 to 400 °C, with $E(L)$ values of from 10 to 200 mV. Under these conditions, AgBr showed the n-type electronic conduction. The measurements for α-AgI were performed in the temperature range from 330 to 500 °C, with $E(L)$ values of from 300 to 550 mV.

Results and Discussions

Several examples of the time change of $E(L/2)$ for AgBr (L=6.0 mm) are shown in Figs. 3(a) and 3(b).

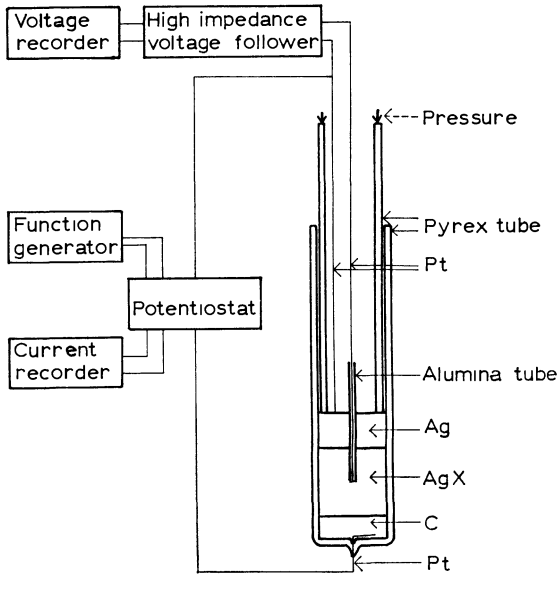

Fig. 2. Construction of cell and block-diagram of circuit.

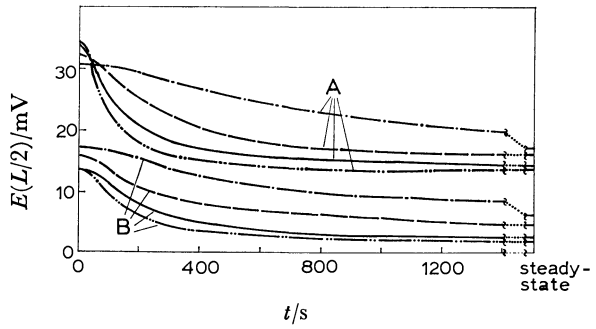

Fig. 3(a). Time change of $E(L/2)$ for AgBr, $L=6.0$ mm.
—·—·—; 325 °C, — — —; 350 °C, ——; 375 °C,
—··—··—; 400 °C.
Curves A; Results for the step of $E(L)$ from 200 mV to 40 mV. Curves B; Results for the step of $E(L)$ from 40 mV to 10 mV.

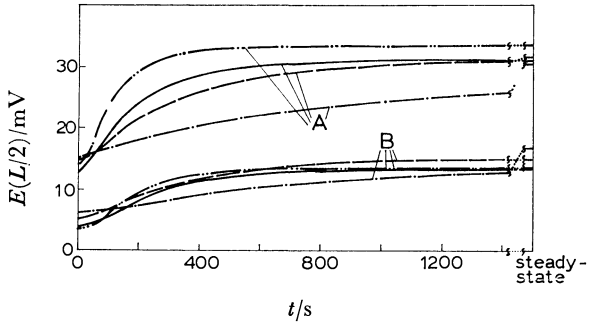

Fig. 3(b). Time change of $E(L/2)$ for AgBr, $L=6.0$ mm.
—·—·—; 325 °C, — — —; 350 °C, ——; 375 °C,
—··—··—; 400 °C.
Curves A; Results for the step of $E(L)$ from 40 mV to 200 mV. Curves B; Results for the step of $E(L)$ from 10 mV to 40 mV.

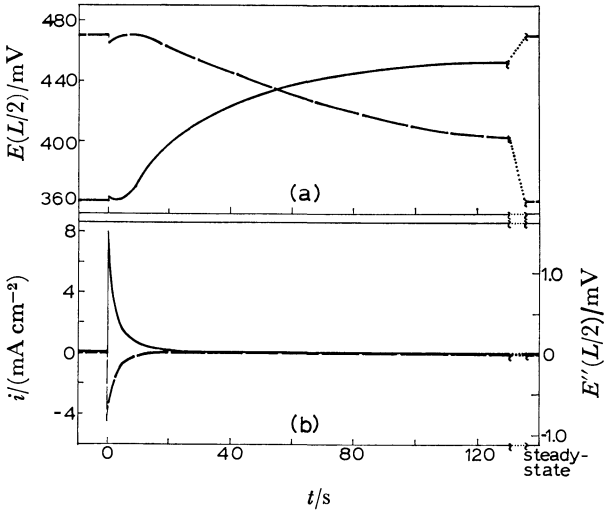

Figs. 4(a), 4(b). Time change of $E(L/2)$, i, and $E''(L/2)$ for α-AgI at 330 °C, $L=7.0$ mm.
——; Step of $E(L)$ from 400 mV to 500 mV.
— — —; Step of $E(L)$ from 500 mV to 400 mV.

The time changes of $E(L/2)$ and the current for AgI ($L=7.0$ mm) at 330 °C are shown in Figs. 4(a) and 4(b).

Table 1. Comparison of calculated and observed values of $E(L/2)$ in a steady state (AgBr)

Temp °C	$E(L)$ mV	$E(L/2)$ mV Calcd	$E(L/2)$ mV Obsd $L=4.7$ mm	$E(L/2)$ mV Obsd $L=6.0$ mm
325	10	4.8	7.2	6.4
	40	16.2	17.4	16.0
	200	34.6	33.5	31.0
400	10	4.8	6.5	3.3
	40	16.6	17.8	14.0
	200	38.4	40.7	34.3

Table 2. Comparison of calculated and observed values of $E(L/2)$ in a steady state (α-AgI)

Temp °C	$E(L)$ mV	$E(L/2)$ mV Calcd	$E(L/2)$ mV Obsd $L=7.0$ mm	$E(L/2)$ mV Obsd $L=10.0$ mm
330	375	339	345	—
	400	364	364	375
	430	394	—	405
	500	464	470	—
	530	494	—	504
500	300	254	256	—
	400	354	363	345
	500	454	452	450

In Tables 1 and 2, the observed steady-state values are compared with those calculated by using Eqs. 13 and 14. Both agree within the limits of experimental error; this error can be attributed to the inaccuracy in the positioning of the platinum probe, because the platinum wire itself has a diameter of 0.2 mm and a slight plastic deformation of pellets prior to the experiments may also result in a small displacement of the probe.

As is shown in Fig. 4(b), the cell exhibits a transient current for several seconds after the sudden change of $E(L)$. It appears to be an ionic one which flows to charge or discharge the improved d.c. polarization cell.[4] The ionic current, i_{ion}, can be expressed by

$$i_{ion}=\frac{\sigma_{Ag^+}}{F}\frac{\partial\eta_{Ag^+}}{\partial x}=\sigma_{Ag^+}\frac{E''(x)}{x}=\sigma_{Ag^+}\frac{E''(L/2)}{L/2}. \quad (29)$$

Using the values of σ_{Ag^+} given by Biermann and Jost,[6] we can calculate the $E''(L/2)$ values, which are shown by the subscale in Fig. 4(b). Obviously $E''(L/2)$ decays to 0 ± 1 mV within 2 s after the sudden change in $E(L)$. When $E''(L/2)$ actually vanishes,

$$E(L/2)F=-\{\mu_{Ag}(L/2)-\mu_{Ag}(0)\}. \quad (30)$$

In the case of AgBr, Eq. 30 is found to hold within 0.5 s after the sudden change in $E(L)$.

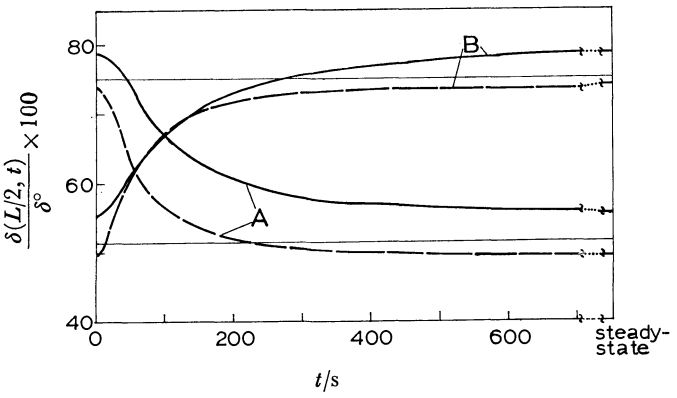

Fig. 5. Plots of $\delta(L/2,t)/\delta^\circ$ *versus* t for AgBr at 400 °C.
——; L=6.0 mm. — — —; L=4.7 mm.
Curves A; Step of $E(L)$ from 40 mV to 200 mV.
Curves B; Step of $E(L)$ from 200 mV to 40 mV.

Figure 5 shows some typical examples of the plot of $\delta(L/2)$ *versus* t. The plots of $\log[\{\delta(L/2,\infty)-\delta(L/2,t)\}/\{\delta(L/2,\infty)-\delta(L/2,0)\}]$ *versus* t are shown in Fig. 6. Clearly, the plots in Fig. 6 fall on a straight line. Thus, the chemical diffusion coefficient, $\tilde{D}$, is calculated from the slope of the plots. Figure 7 shows the $\tilde{D}$ values obtained in the present work. The $\tilde{D}$ values show a good linearity in the figure. $\tilde{D}$ for AgBr can be expressed by this equation

$$\tilde{D} = 7.10\times 10^{2}\exp\left(-\frac{1.96\times 10^{4}\ \text{cal mol}^{-1}}{RT}\right)\text{cm}^2\,\text{s}^{-1}, \quad (31)$$

and $\tilde{D}$ for α-AgI can be given by

$$\tilde{D} = 4.95\times 10^{-1}\exp\left(-\frac{7.71\times 10^{3}\ \text{cal mol}^{-1}}{RT}\right)\text{cm}^2\,\text{s}^{-1}. \quad (32)$$

Using Eq. 26, the nonstoichiometry of AgBr in equilibrium with metallic silver can be calculated from the σ_e° obtained by Ilschner.[7] The plot A in Fig. 8 shows δ° of AgBr. From the intercept of the plot at the ordinate and the slope of the plot, the molar entropy, $\Delta\overline{S}$, and the molar enthalpy, $\Delta\overline{H}$, of the dissolution of silver can be calculated. The results are $\Delta\overline{S}$= 2.87eu and $\Delta\overline{H}$= −21.4 kcal mol^{-1} respectively. Since the dissolution of silver into AgBr consists of the transfer of atoms between two solid phases, the entropy change is close to zero.

In a previous paper,[4] the present authors have determined σ_h*, the hole conductivity of α-AgI in equilibrium with 1 atm of iodine gas. We can calculate δ*, the nonstoichiometry of α-AgI in equilibrium with 1 atm of iodine gas, by using Eq. 28 and σ_h*. The calculated results are shown as the B plot in Fig. 8. The entropy and enthalpy of the dissolution of iodine into α-AgI in equilibrium with 1 atm of iodine gas are $\Delta\overline{S}$= −21.8 eu and $\Delta\overline{H}$=1.51 kcal mol^{-1} respectively. As iodine atoms are transferred from the gas phase to the solid phase, $\Delta\overline{S}$ takes a large negative value.

The apparent mobility of electrons in AgBr, m_e, and that of holes in α-AgI, m_h, are calculated by means of the following equations:

$$\sigma_e^\circ = \left(\frac{N\delta^\circ}{V_m}\right)m_e e, \quad (33)$$

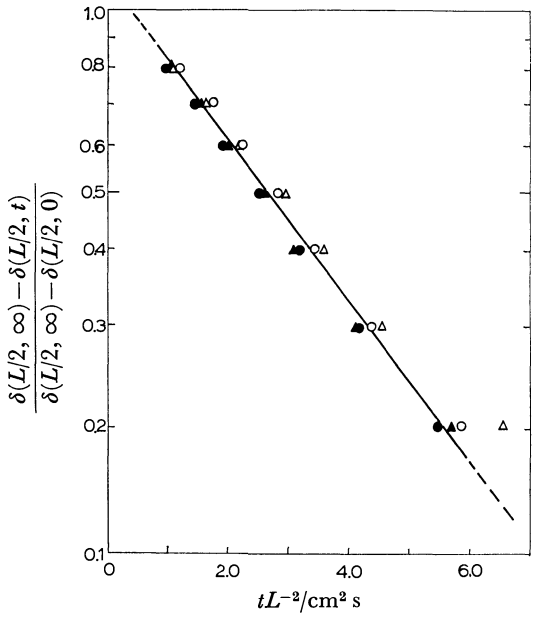

Fig. 6. Plots of $\{\delta(L/2,\infty)-\delta(L/2,t)\}/\{\delta(L/2,\infty)-\delta(L/2,0)\}$ *vs.* tL^{-2} for AgBr at 400 °C.
○; L=6.0 mm, step of $E(L)$ from 200 mV to 40 mV.
△; L=6.0 mm, step of $E(L)$ from 40 mV to 200 mV.
●; L=4.7 mm, step of $E(L)$ from 200 mV to 40 mV.
▲; L=4.7 mm, step of $E(L)$ from 40 mV to 200 mV.

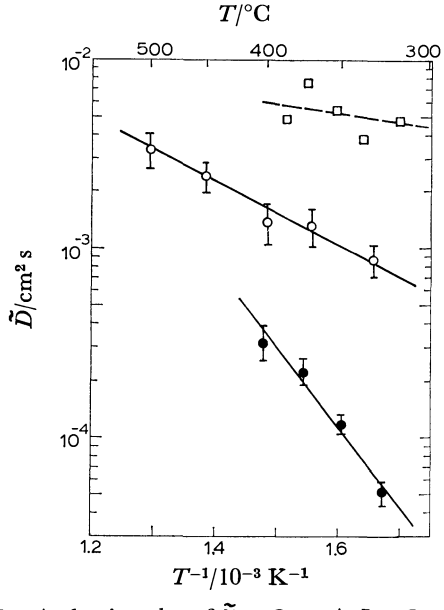

Fig. 7. Arrhenius plot of $\tilde{D}$. ○; α-AgI. ●; AgBr by this work. □; AgBr by Weiss.[1]

$$\sigma_h^* = \left(\frac{N\delta^*}{V_m}\right)m_h e, \quad (34)$$

where N denotes Avogadro's constant and where e denotes the charge of an electron. At 400 °C, m_e= 5.5×10^{-3} cm^2 V^{-1} s^{-1} for AgBr and m_h=2.5×10^{-2} cm^2 V^{-1} s^{-1} for α-AgI.

In Fig. 7, the $\tilde{D}$ values obtained by Weiss in his first work[1] are also plotted. His results showed larger $\tilde{D}$ values than those obtained in the present work, and the Arrehnius plot was not linear. When the applied potential difference is removed in Weiss'

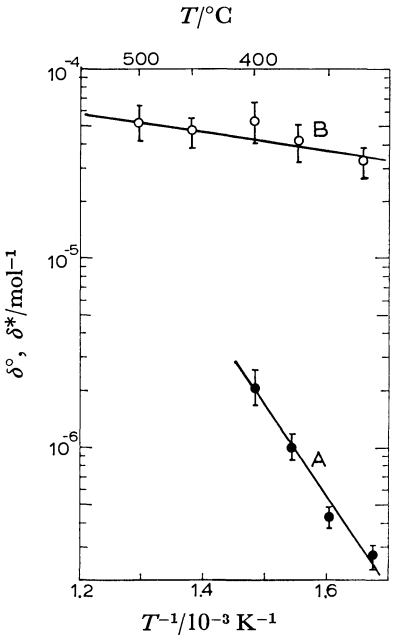

Fig. 8. Plots of δ° and δ^* *vs.* T^{-1}. A; δ° of AgBr. B; δ^* of α-AgI.

cell, the activity of the silver at the AgBr/carbon interface rises as a result of the diffusion of silver atoms toward the interface from the interior of AgBr, and also as a result of bromine gas be being released and silver atoms leaving at the interface due to the decomposition. This decomposition causes a faster decay of EMF, whcih results in the apparent $\tilde{D}$ values being larger than the real values. Because the decomposition rate is often controlled by the flow rate of the inert gas around the carbon electrode, the reproducibility may not be good. Figure 7 suggests the high probability that the measurements in Weiss' first work were disturbted by the decomposition of AgBr.

The $\tilde{D}$ values in Weiss' second work[2] were ten times or more larger than those in his first work. We can see in Fig. 4(b) that the decay in the current occurs much faster than the chemical relaxation of the sample. This fact can explain why Weiss' second work resulted in such extraordinarily large $\tilde{D}$ values.

Weiss' first method can be useful when the chemical relaxation due to the chemical diffusion in the sample occurs faster than the relaxation by other effects, while the second method can be applied to a sample in which the transient ionic current is small enough. However, it seems AgBr was not a sample suitable for either of these measuring methods.

Summary

1) A new technique for the detemination of the chemical diffusion coefficients in ionic crystals was devised and applied to AgBr and α-AgI. The chemical diffusion coefficient for AgBr was found to be much smaller than that reported by a previous investigator. 2) Using the chemical diffusion coefficient and electronic conductivity of AgX, the nonstoichiometry, electron and hole mobilities, and entropy and enthalpy of the dissolution of elements into AgX were calculated.

References

1) K. Weiss, *Z. Phys. Chem., NF*, **59**, 242 (1968).
2) K. Weiss, *Electrochim. Acta*, **16**, 201 (1971).
3) J. Mizusaki, K. Fueki, and T. Mukaibo, *Bull. Chem. Soc. Jpn.*, **48**, 428 (1975).
4) J. Mizusaki, K. Fueki, and T. Mukaibo, *Bull. Chem. Soc. Jpn.*, **51**, 694 (1978).
5) C. Wagner, *Z. Phys. Chem.*, **B 11**, 139 (1930); **B 32**, 447 (1936).
6) W. Biermann and W. Jost, *Z. Phys. Chem., NF*, **25**, 139 (1960).
7) B. Ilschner, *J. Chem. Phys.*, **28**, 1109 (1958).

Crystal and Molecular Structure of *trans*-1,4-Dibenzoyl-2,5-dimethylpiperazine†

Kojun Okamoto,* Kiyotane Sekido, Jun Itoh,** Teruo Noguchi,** and Sakutaro Hirokawa

Department of Chemistry, The National Defense Academy, Hashirimizu, Yokosuka 239
***Koa Oil Co., Ltd., Ōtemachi, Tokyo 100*

(Received September 18, 1978)

The crystal structure of *trans*-1,4-dibenzoyl-2,5-dimethyl-piperazine has been determined by the X-ray method. The space group is $P2_1/c$, with $a=7.483$, $b=6.577$, $c=19.939$ Å, $\beta=116.71°$ and $Z=2$. The structure was solved by the direct method and refined by the least-squares method to the final R factor of 0.094 for 2559 independent reflections. A nitrogen atom and three carbon atoms bonded to the nitrogen atom are approximately in a plane. The molecule is centrosymmetric, the piperazine ring having a *chair*-form. The methyl groups are in the axial position. The oxygen atom is approximately in a plane formed by N, C(carbonyl), and C(benzene). The dihedral angle between this plane and the benzene ring is approximetely 70°.

1,4-Dibenzoyl-2,5-dimethylpiperazine (DDP) has two isomers, the *trans*-form (mp 225 °C) and the *cis*-form (mp 146 °C). The crystal structure of the *cis*-form was reported by Sakurai *et al.*[1] We have studied the *trans*-form in order to discuss the molecular geometry in both forms. The results are given below.

Experimental

Colorless prisms elongated along the b axis were obtained by slow evaporation from an ethanol solution of *trans*-DDP. The crystal is built upon a monoclinic unit cell.

Crystal Data. Oscillation and Weissenberg photographs were taken with Cu $K\alpha$ radiation. The systematically absent reflections indicated that the space group is $P2_1/c$. The cell dimensions were refined by least-squares calculations on the basis of higher-order reflections measured on a diffractometer. The density of the crystal was measured by the flotation method. Since there are two formula units per cell, the molecule has a center of symmetry. The crystal data are summarized in Table 1.

Intensity Data. A prismatic crystal was ground to a cylinder 0.4 mm in diameter and 0.4 mm in length. This was mounted on a four-circle diffractometer (Rigaku AFC-III) with Nb-filtered Mo $K\alpha$ radiation from a graphite monochromator, and the intensity data were collected for 2559 independent reflections with $|F_o| \geqq 3\sigma(F_o)$ with $2\theta \leqq 60.0°$, using the ω-2θ scan technique with a scanning speed of 4° min^{-1} in 2θ. No corrections were made for absorption or extinction.

Table 1. Crystal data

Experimental error given in parentheses refers to the last figure.

Molecular formula	$C_{20}H_{22}N_2O_2$
Formula weight	322.4
Mp	225 °C
Crystal system	Monoclinic
a	7.483 (1) Å
b	6.577 (1)
c	19.939 (4)
β	116.71 (2)°
Space group	$P2_1/c$
V	876.5 (7) Å^3
Z	2
D_m	1.229 g cm^{-1}
D_x	1.221
μ(Mo $K\alpha$)	0.856 cm^{-1}

Structure Determination

The structure was analyzed by the direct method using MULTAN.[2] Phases were determined for the 346 reflections with $|E|>1.50$, eight E maps being calculated. The phases set with the lowest residual (33.1) and the highest figure of merit (1.10) produced a significant E map, which revealed the positions of all the non-hydrogen atoms. The atomic coordinates and temperature factors were refined by the block-diagonal matrix least-squares method until R was reduced to 0.190. Locations of the hydrogen atoms were obtained by assuming a tetrahedral angle for each carbon atom and a bond length of 1.09 Å for each C–H bond. Further refinements were made on a CDC-6600 computer at Century Research Center Co., Tokyo, using anisotropic thermal parameters for the non-hydrogen atoms and isotropic B for the hydrogen atoms. Convergence was attained with $R=0.094$ after six cycles of the procedure. The atomic scattering factors were taken from International Tables for X-Ray Crystallography[3]. The final parameters with their standard deviations are given in Tables 2 and 3***.

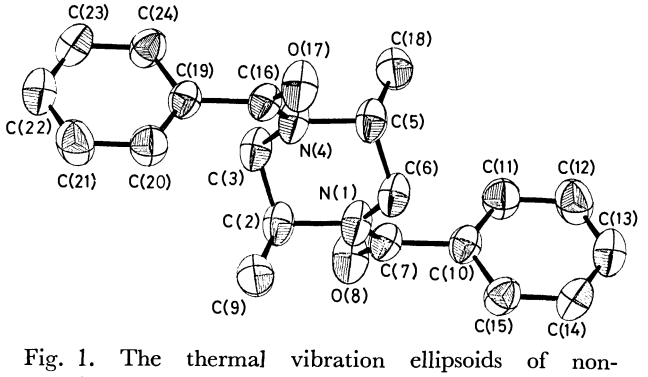

Fig. 1. The thermal vibration ellipsoids of non-hydrogen atoms drawn by ORTEP.[7]

† A preliminary report was presented at the 37th National Meeting of the Chemical Society of Japan, Yokohama, April 1978.

*** The complete F_o-F_c data are deposited as Document No. 7921 at the Office of the Editor of the Bulletin of the Chemical Society of Japan.

Table 2. Atomic coordinates ($\times 10^4$) and anisotropic thermal parameters ($\times 10^4$) of the non-hydrogen atoms

The estimated standard deviations given in parentheses, refer to the last decimal position. The anisotropic temperature factors is of the form $\exp[-(h^2\beta_{11}+k^2\beta_{22}+l^2\beta_{33}+hk\beta_{12}+hl\beta_{13}+kl\beta_{23})]$.

Atom	x	y	z	β_{11}	β_{22}	β_{33}	β_{12}	β_{13}	β_{23}
N (1)	908 (4)	1223 (4)	643 (2)	162 (2)	204 (7)	40 (1)	8 (5)	12 (2)	−19 (2)
C (2)	−1312 (5)	986 (6)	271 (2)	166 (7)	218 (8)	39 (1)	31 (6)	22 (2)	−7 (3)
C (3)	−1972 (5)	534 (5)	−553 (2)	172 (7)	204 (8)	38 (1)	15 (6)	17 (2)	−10 (3)
C (7)	1719 (5)	3030 (5)	960 (2)	190 (7)	202 (8)	28 (1)	−3 (6)	21 (2)	−7 (2)
O (8)	732 (4)	4524 (4)	946 (2)	217 (6)	213 (6)	55 (1)	11 (5)	27 (2)	−27 (2)
C (9)	−1963 (6)	−625 (7)	656 (2)	227 (9)	351 (13)	41 (1)	8 (9)	42 (3)	10 (4)
C (10)	3985 (5)	3128 (5)	1365 (2)	185 (7)	190 (7)	29 (1)	−1 (6)	21 (2)	−8 (2)
C (11)	5004 (6)	4358 (6)	1100 (2)	239 (9)	264 (10)	38 (1)	−1 (8)	37 (3)	19 (3)
C (12)	7082 (6)	4489 (7)	1479 (3)	246 (10)	325 (12)	52 (2)	−43 (9)	56 (4)	15 (4)
C (13)	8098 (5)	3427 (7)	2137 (2)	193 (8)	306 (12)	45 (2)	−17 (8)	24 (3)	−9 (4)
C (14)	7114 (6)	2239 (7)	2415 (2)	232 (9)	307 (11)	31 (1)	5 (8)	12 (3)	5 (3)
C (15)	5039 (5)	2068 (6)	2035 (2)	233 (8)	248 (9)	31 (1)	−27 (7)	26 (3)	11 (3)

Table 3. Atomic coordinates($\times 10^3$) of the hydrogen atoms

The estimated standard deviations are in parentheses.

Atom	x	y	z	B	Bonding atom
H (25)	−190 (5)	233 (6)	31 (2)	4.7 (0.8)	C (2)
H (26)	−156 (5)	177 (5)	−80 (2)	3.7 (0.7)	C (3)
H (27)	−339 (6)	21 (7)	−72 (2)	6.2 (1.0)	C (3)
H (31)	−175 (6)	−22 (7)	113 (2)	6.5 (1.0)	C (9)
H (32)	−135 (6)	−194 (7)	61 (2)	7.7 (1.2)	C (9)
H (33)	−331 (7)	−68 (8)	51 (3)	8.3 (1.3)	C (9)
H (34)	440 (6)	499 (7)	66 (2)	6.5 (1.0)	C (11)
H (35)	781 (6)	505 (7)	122 (2)	6.1 (1.0)	C (12)
H (36)	964 (7)	336 (7)	230 (2)	7.8 (1.2)	C (13)
H (37)	776 (6)	151 (7)	285 (2)	6.8 (1.1)	C (14)
H (38)	431 (5)	131 (6)	228 (2)	4.6 (0.8)	C (15)

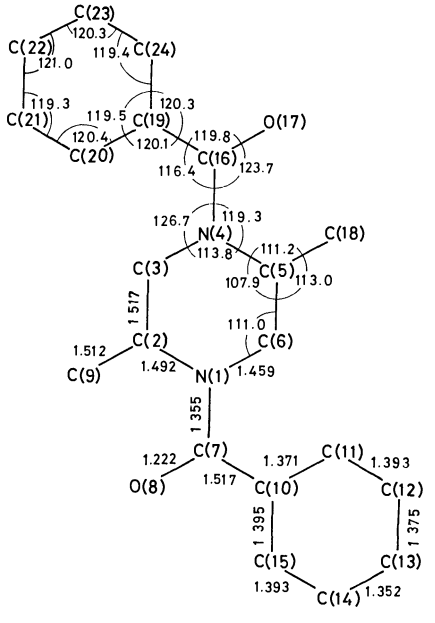

Fig. 2. Intramolecular interatomic distances and angles.

Discussion

Molecular Geometry and Conformation. Numbering scheme and the thermal ellipsoids of the non-hydrogen atoms are illustrated in Fig. 1, where thermal vibration ellipsoids are set to 50% probability. Bond distances and angles involving the non-hydrogen atoms are shown in Fig. 2. The standard deviations of these measurements are 0.004—0.008 Å for distances, and 0.1—0.4° for angles. Since the molecule is centrosymmetric, the piperazine ring has a *chair*-form.[4] The mean N–C bond length in the piperazine ring, 1.476 Å, is comparable to that of *cis*-1,4-dibenzoyl-2,5-dimethylpiperazine (*cis*-DDP).[1] The bond distances, 1.517 Å for C–C in the piperazine ring and 1.512 Å for C (piperazine)–C(methyl), are shorter than the C–C covalent bond length. The bond angles of carbon atoms in the piperazine ring are approximately tetrahedral. The value for C(5)–N(4)–C(3) is comparable to 115.7° of *cis*-DDP, or 112.6° of piperidine.[4,5]

The least-squares planes are given in Table 4 and the torsion angles in the molecule in Table 5. Exocyclic torsion angles for C(9)–C(2)–C(3)–N(4) and C(9)–C(2)–N(1)–C(6) show that C(9) is in the axial position. The shift of N(1) from the plane(1), containing C(2), C(3), C(5), and C(6), is 0.639 Å, and that of C(9) from the plane(1) is 1.383 Å.

The C–O distance of 1.222 Å is in agreement with 1.222 Å of *cis*-DDP, and 1.229 Å of *N,N'*-dibenzoyl-*p*-phenylenediamine(DPD).[6] The N–C(carbonyl) distance is 1.355 Å, corresponding to 1.357 Å in DPD, and 1.353 Å in *cis*-DDP. The C(carbonyl)–C(benzene) distance is 1.517 Å, being comparable to 1.499 Å of *cis*-DDP, and 1.502 Å of DPD.

The mean value of the C–C bond distance in the benzene ring is 1.380 Å, being shorter than 1.397 Å of benzene. The corresponding values for *cis*-DDP and DPD are both 1.386 Å.

The dihedral angle between the planes(2) and (3) is 70.5°. The angle in *cis*-DDP is about 55°. The dihedral angle between planes(1) and (2) is 56.0°, and that between planes(1) and (3) is 61.1°.

Table 4. Least-squares plane through various groups of atoms and the deviations(l/Å) of the atoms from the plane

The equation is of the form $AX+BY+CZ=D$, where X, Y, and Z are the coordinates in Å along the a, b, and c* axes, respectively. (Atoms marked by ** are not included in the least-squares calculation.)

Plane(1)			
$-0.4311X-0.8956Y+0.1096Z=0.0000$			
C (2)	0.000	C (3)	0.000
C (5)	0.000	C (6)	0.000
N (1)**	−0.639	C (7)**	−1.781
O (8)**	−2.351	C (9)**	1.383
C (10)**	−2.334		
Plane(2)			
$0.3979X+0.3280Y-0.8568Z=-0.6488$			
N (1)	−0.027	C (2)	−0.039
C (6)	0.080	C (7)	0.007
O (8)	0.063	C (10)	−0.061
Plane(3)			
$0.3591X-0.7755Y-0.5193Z=-2.2367$			
C (10)	0.010	C (11)	−0.013
C (12)	0.007	C (13)	0.001
C (14)	−0.004	C (15)	−0.001

Table 5. Torsion angles (ϕ)

Torsion angle $A(i)$-$A(j)$-$A(k)$-$A(l)$ is viewed down $A(j)$-$A(k)$ with a clockwise rotation of $A(i)$ to $A(l)$ taken to be positive.

Ring torsion angles	ϕ/°
N (1)--C (2)--C (3)--N (4)	54.7
C (2)--N (1)--C (6)--C (5)	58.1
C (3)--C (2)--N (1)--C (6)	−56.4
Exocyclic torsion angles	
C (7)--N (1)--C (6)--C (5)	−115.5
C (9)--C (2)--N (1)--C (6)	68.0
C (9)--C (2)--N (1)--C (7)	−117.8
C (3)--C (2)--N (1)--C (7)	117.8
C (9)--C (2)--C (3)--N (4)	−68.6
Bridge torsion angles	
C (6)--N (1)--C (7)--O (8)	171.5
C (2)--N (1)--C (7)--O (8)	−1.9
C (6)--N (1)--C (7)--C (10)	−9.9
C (2)--N (1)--C (7)--C (10)	176.7
N (1)--C (7)--C (10)-C (11)	114.8
N (1)--C (7)--C (10)-C (15)	−69.2
O (8)--C (7)--C (10)-C (11)	−66.6
O (8)--C (7)--C (10)-C (15)	109.4

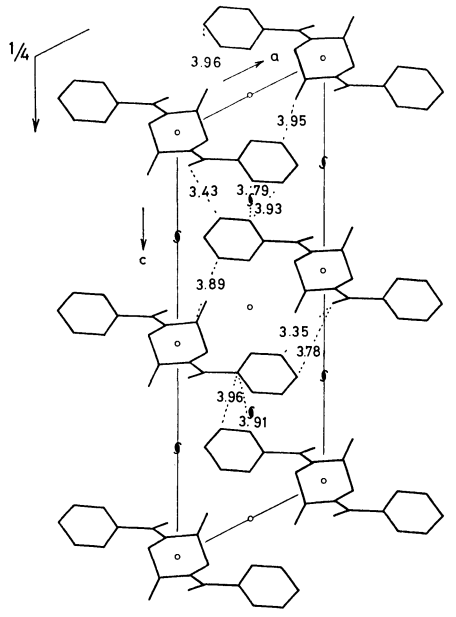

Fig. 3. The molecular packing viewed down the b axis, showing all intermolecular distances (the non-hydrogen atoms) of less than 4.00 Å.

Molecular Packing. The molecular packing in the unit cell with intermolecular distances less than 4.00 Å is shown in Fig. 3. The shortest contact of 3.35 Å is seen between C(12) and O(8) related by a translation along the a axis. The second shortest contact of 3.43 Å is seen between O(8) and C(14) related by a two-fold screw axis. No other significant contact can be seen in this structure. The molecules are held together in the crystal by the van der Waals forces.

The authors would like to thank Mr. Shigeru Hasegawa for the supply of crystals.

References

1) T. Sakurai, M. Nakamaru, S. Tsuboyama, and K. Tsuboyama, *Acta Crystallogr., Sect. B*, **33**, 3568 (1977).
2) G. Germain, P. Main, and M. M. Woolfson, *Acta Crystallogr., Sect A*, **27**, 368 (1971).
3) "International Tables for X-Ray Crystallography," The Kynoch Press, Birmingham (1959), Vol. III, pp. 201—203.
4) W. L. F. Armarego, "Stereochemistry of Heterocyclic Compounds," 1st ed, Wiley-Interscience Publication, New York (1977), pp. 189—190.
5) I. D. Blackburne, R. P. Duke, Richard A. Y. Jones, A. R. Katritzky, and K. A. F. Record, *J. Chem. Soc., Perkin Trans. 2*, **1973**, 332.
6) W. W. Adams, A. V. Fratini, and D. R. Wiff, *Acta Crystallogr., Sect B*, **34**, 954 (1978).
7) C. K. Johnson, *ORTEP*, **ORNL-3794**, Oak Ridge National Laboratory, Tennessee (1965).

Adsorptive Mechanism on Activated Carbon in the Liquid Phase. I. Free Energy Change for Adsorption of Organic Compounds from Aqueous Solution on Activated Carbon

Ikuo ABE,* Katsumi HAYASHI, Mutsuo KITAGAWA,** and Toshihiro URAHATA

Osaka Municipal Technical Research Institute, Ogimachi, Kita-ku, Osaka 530

***Society for Activated Carbon Research, Ogimachi, Kita-ku, Osaka 530*

(Received October 12, 1978)

The adsorption isotherms, from aqueous solution onto activated carbon, have been determined for the 22 aliphatic monofunctional compounds; alcohols, carboxylic acids, ketones, ethers, esters, and aldehydes. The free energy change for the adsorption process has been calculated from the adsorption equilibrium constant at infinite dilution; a linear relationship exists between the free energy change and the number of carbon atoms in the solute. The free energy of adsorption has been divided into two contributions: the hydrocarbon and the functional group contribution. The free energy change for the adsorption process has been compared with the free energy change for the precipitation process from solution into the pure liquid solute. The free energy contribution per individual methylene group to the adsorption process shows an approximate agreement with that for the precipitation process indicating that the adsorption process of the hydrocarbon portion of the solute is analogous to the precipitation process. The free energy contribution of the functional group to the adsorption process is smaller than that for the precipitation process indicating that the functional group portion of the solute is not appreciably dehydrated in the adsorption phase.

The adsorption theory in the gas phase has been extensively investigated but not in the liquid phase. In gas phase adsorption Polanyi's potential theory[1] and its modifications[2-5] have been widely used. In the theory Polanyi considered the energy processes in transferring a molecule from the gas to the adsorbed state and concluded that the free energy change in passing from the gaseous to the saturated liquid state represents a valid criterion for the free energy change of the whole process.

In liquid phase adsorption the potential theory has been applied by Hansen and Fackler[6] to the adsorption of liquid mixtures on carbon black, and by Manes[7] *et al.* to the adsorption of solids from several solvents on activated carbon. Polanyi originally supposed that the adsorption of solid solutes from solution was analogous to the adsorption of gases with precipitation of the solid taking the place of liquefaction of the gas, *i.e.*, the adsorption process was identically equal to the reverse of the solution process. This suggests that the free energy change for the adsorption process is analogous to the reverse of the solution process.

In this study, the free energy change of the adsorption process for aliphatic monofunctional compounds has been determined and compared with the free energy change of the solution process.

Experimental

Materials. The adsorbent in all instances came from a single batch of Pittsburgh Activated Carbon (grade CAL) which was ground and sieved to yield 200×350 mesh size. After sieving, the carbon was washed with distilled water to remove all fines and dried at 110 °C. The BET surface area found from nitrogen adsorption at 77 K was 1010 m²/g. The pore volume was 0.575 ml/g, when calculated from the limiting vapor adsorption at $P/P_0 \rightarrow 1$. The experimental conditions and the pore volumes determined are listed in Table 1.

All organic compounds were purchased from commercial sources and distilled, if necessary, to a minimum purity of 99% as determined by gas chromatography. All aldehydes were used without further purification.

TABLE 1. PORE VOLUME OF THE ADSORBENT CALCULATED FROM THE LIMITING VAPOR ADSORPTION AT $P/P_0 \rightarrow 1$

Adsorbate	Temperature (K)	Pore volume (ml/g)
Nitrogen[a]	77	0.586
Methanol[b]	298	0.573
2-Butanone[b]	298	0.568
Benzene[b]	298	0.572
	Av	0.575

a) Measured with BET adsorption apparatus. b) Measured by a modification of Hirata's method.[8]

Procedure. Equilibration took place in 50-ml double stoppered flasks, which were shaken for a minimum of 14 h at 25 °C in a thermostated bath; check experiments at longer shaking times established that the shaking time sufficed for equilibration. In order to eliminate loss through evaporation, pressure filtration was chosen for removing the carbon from the solution. The concentration of solute was analysed by determining the total organic carbon in a Shimadzu Model TOC-10A analyzer. The amount of adsorbed solute (mg) on carbon (grams) was calculated from the following relation:

$$X = \frac{V \cdot \Delta C}{M} \tag{1}$$

where ΔC (mg/l) is the solute concentration decrease due to adsorption and V (l) is the volume of solution added to M (g) of carbon.

Results

Figures 1—6 illustrate the 25 °C adsorption isotherms for alcohols, carboxylic acids, ketones, ethers, esters, and aldehydes, from solution, onto CAL carbon. The adsorption isotherms have been approximated by the adsorption Eqs. 2 and 3:

$$\frac{C}{X} = a_0 + a_1 C \tag{2}$$

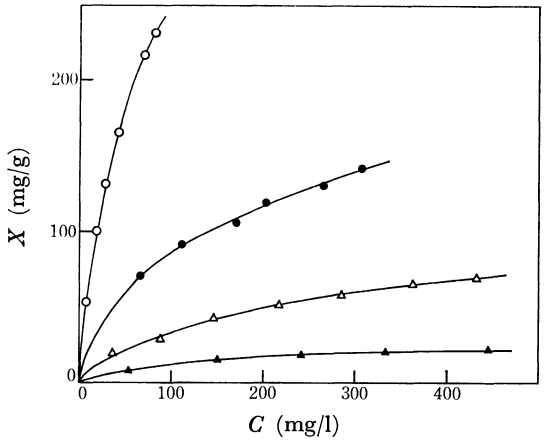

Fig. 1. Adsorption isotherms of alcohols on CAL activated carbon from aqueous solutions, 25 °C. ▲: 1-Propanol, △: 1-butanol, ●: 1-pentanol, ○: 1-hexanol.

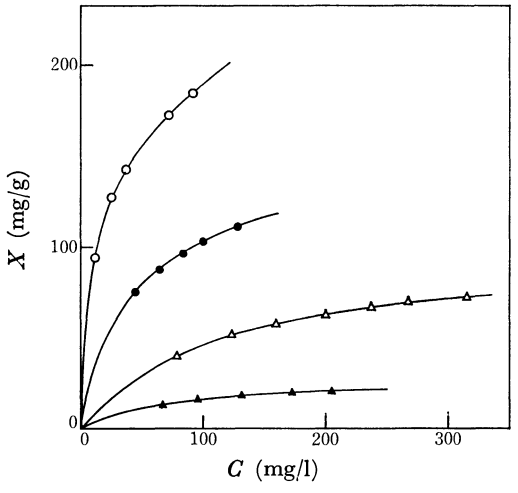

Fig. 2. Adsorption isotherms of carboxylic acids on CAL activated carbon from aqueous solutions, 25 °C. ▲: Propionic acid, △: butyric acid, ●: valeric acid, ○: hexanoic acid.

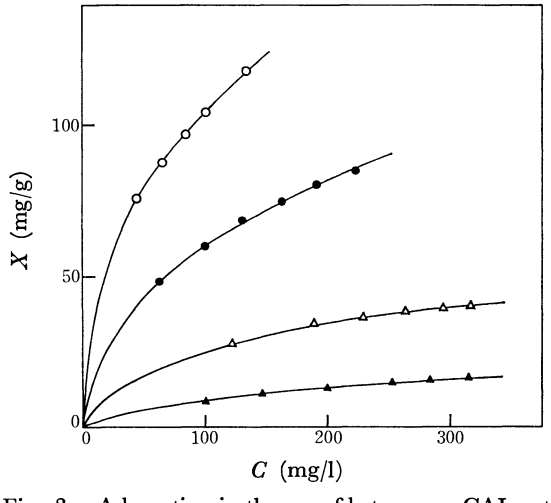

Fig. 3. Adsorption isotherms of ketones on CAL activated carbon from aqueous solutions, 25 °C. ▲: Acetone, △: 2-butanone, ●: 2-pentanone, ○: 2-hexanone.

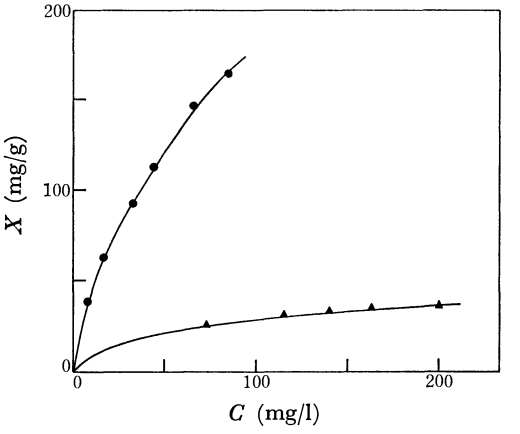

Fig. 4. Adsorption isotherms of ethers on CAL activated carbon from aqueous solutions, 25 °C. ▲: Diethyl ether, ●: dipropyl ether.

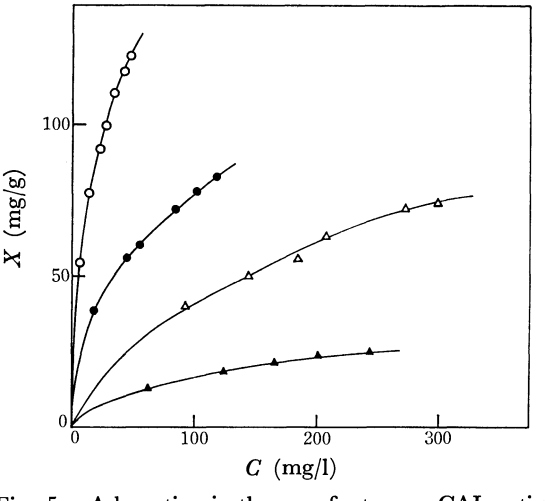

Fig. 5. Adsorption isotherms of esters on CAL activated carbon from aqueous solutions, 25 °C. ▲: Methyl acetate, △: ethyl acetate, ●: propyl acetate ○: butyl acetate.

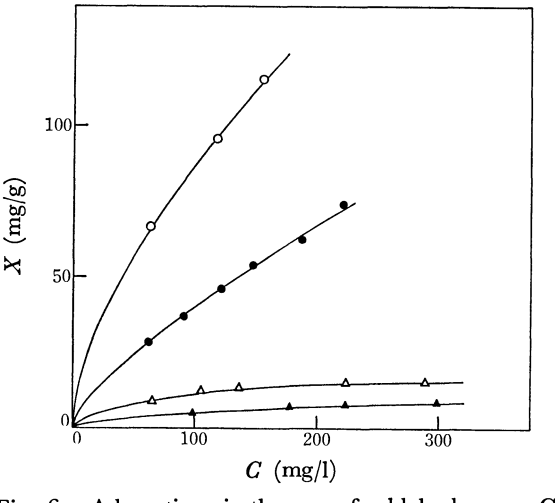

Fig. 6. Adsorption isotherms of aldehydes on CAL activated carbons from aqueous solutions, 25 °C. ▲: Acetaldehyde, △: propionaldehyde, ●: butyraldehyde, ○: valeraldehyde.

Table 2. Adsorption parameters of various organic compounds on CAL activated carbon from aqueous solutions (25 °C)

Compound	$b_2 \times 10^5$	b_1	b_0	α	a_1	a_0
[Alcohols]						
1-Propanol	−2.24	0.0407	5.43	0.184	0.0292	6.17
1-Butanol	−1.49	0.0167	1.48	0.680	0.0148	1.21
1-Pentanol	−0.794	0.00801	0.443	2.25	0.00539	0.609
1-Hexanol	−0.729	0.00356	0.110	9.08	0.00301	0.116
[Carboxylic acids]						
Propionic acid	11.7	0.00526	4.35	0.230	0.0342	2.84
Butyric acid	0.469	0.00870	1.24	0.813	0.0103	1.13
Valeric acid	−0.545	0.00770	0.260	3.84	0.00692	0.285
Hexanoic acid	−1.06	0.00569	0.0621	16.1	0.00480	0.0735
[Ketones]						
Acetone	−3.31	0.0448	7.96	0.125	0.0316	9.14
2-Butanone	1.63	0.0114	2.78	0.361	0.0180	2.20
2-Pentanone	−0.652	0.0100	0.719	1.39	0.00845	0.795
2-Hexanone	−2.01	0.00974	0.195	5.13	0.00652	0.306
[Ethers]						
Diethyl ether	2.77	0.0133	1.83	0.548	0.0203	1.43
Dipropyl ether	−3.39	0.00719	0.145	6.91	0.00531	0.152
[Esters]						
Methyl acetate	2.84	0.0196	3.65	0.274	0.0276	3.20
Ethyl acetate	−1.71	0.0148	1.10	0.913	0.00895	1.51
Propyl acetate	−3.02	0.0136	0.236	4.24	0.0103	0.295
Butyl acetate	−4.44	0.00892	0.0633	15.7	0.00711	0.0740
[Aldehydes]						
Acetaldehyde	2.84	0.0424	17.8	0.0561	0.0538	16.8
Propionaldehyde	13.3	0.00674	6.63	0.151	0.0445	4.70
Butyraldehyde	−2.44	0.0119	1.56	0.641	0.00577	1.89
Valeraldehyde	−2.64	0.00995	0.413	2.41	0.00465	0.646

$$\frac{C}{X} = b_0 + b_1 C + b_2 C^2 \tag{3}$$

where C is the equilibrium concentration; X is the amount of adsorption at C; a_0, a_1, b_0, b_1, and b_2 are constants. The results of regression analysis using Eq. 2 or Eq. 3 are presented in Table 2.

The adsorbability (α) of solute at infinite dilution has been defined as follows:

$$\alpha \equiv \lim_{C \to 0} \frac{X}{C} \tag{4}$$

In order to determine the adsorbability, C/X has been plotted against C from the data of Figs. 1—6 and the result for butyl acetate shown in Fig. 7. The intercept of the adsorption isotherm gives the value of α. It is evident from Fig. 7 that the experimental data more closely approximates to Eq. 3 than to Eq. 2 and consequently the value of α has been taken from Eq. 3. The values of α ($1/b_0$) are presented in Table 2.

Equation 2 is of Langmuir type:

$$\frac{C}{X} = \frac{1}{aX_m} + \frac{C}{X_m} \tag{5}$$

where X_m is the amount of adsorption at saturation

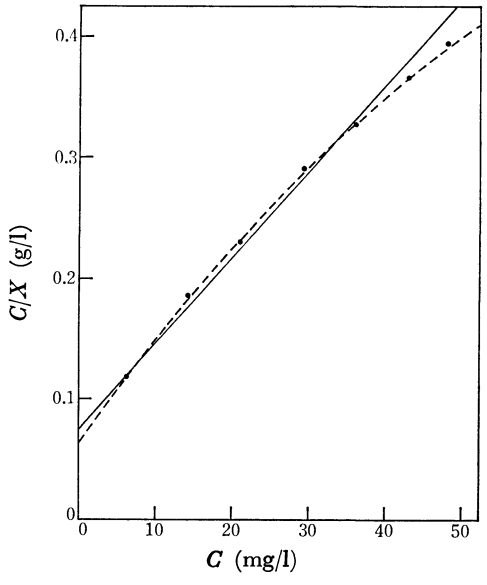

Fig. 7. Adsorption isotherm of butyl acetate on CAL activated carbon from aqueous solution, 25 °C. ●: Experimental, ——: best fitting model Eq. 2, ----: best fitting model Eq. 3.

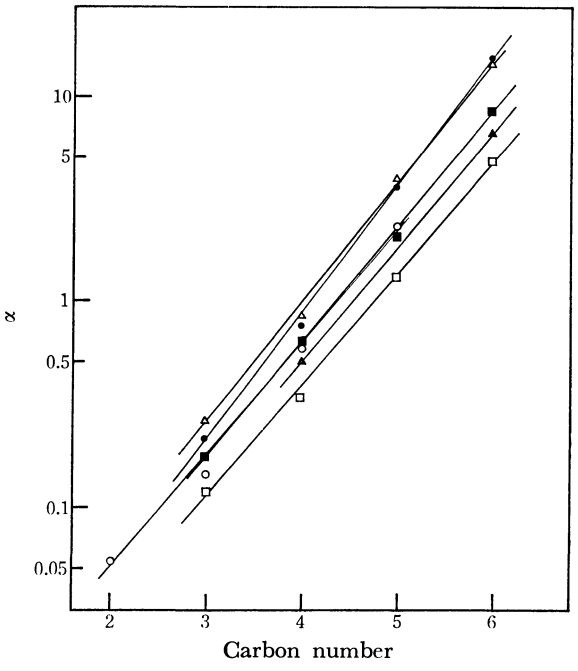

Fig. 8. Relationship between adsorption constant α and carbon atom number N. ○: Aldehydes, ●: carboxylic acids, △: esters, ▲: ethers, □: ketones, ■: alcohols.

and a is a constant. The value of α calculated by Eq. 2 is identical with X_m $(=1/a_0)$. As can be seen from Table 2, there is little difference between $1/b_0$ and $1/a_0$.

Figure 8 illustrates the relationship between log α and the number of carbon atoms in the solute. It can be seen from Fig. 8 that for a homologous series the following relation exists:

$$\log \alpha = \beta N + \gamma \tag{6}$$

where N is the number of carbon atoms and β and γ are constants. This demonstrates that Traube's rule[9] is valid in the adsorption of the homologous paraffin chain solutes.

For a thermodynamic study of adsorption from solution, it is necessary to determine the standard free energy change ΔG°. Alexander and Johnson[10] calculated ΔG° by the following equation:

$$\Delta G^\circ = -RT \ln\left(\frac{\Gamma}{tC_{bulk}}\right) \tag{7}$$

where Γ is the surface excess per unit area and t the thickness of the adsorbed layer. In this equation it is assumed that the adsorbed molecules behave ideally. Fu and Bartell[11] showed that the activity coefficient of the adsorbate on the solid greatly differed from unity, and proposed that the equilibrium constant K for the process (8) should be obtained from the limiting slope of the adsorption isotherms at zero concentration, in which the adsorbates behave ideally:

$$\text{Solute in solution} \rightleftharpoons \text{Solute in adsorption phase.} \tag{8}$$

In order to determine K, it is necessary to convert the amount of adsorption into concentration and for this purpose, the volume of the adsorption phase must be determined. Bartell[12] *et al.* used the product of the surface area of the adsorbent and the thickness of the adsorbed layer as the volume. In the case of high-porous adsorbents such as activated carbon, however, the adsorption process may be regarded as pore filling rather than monolayer coverage[13] and consequently the pore volume has been adopted as the volume of the adsorption phase. It has been assumed that the pore volume is equal to the volume calculated from the limiting vapor adsorption at $P/P_0 \rightarrow 1$, and that every pore contributes in the same manner to the adsorption of adsorbate. It may be seen from Table 1 that the volume is almost independent of the nature of vapor. Hence an average of the values obtained from four vapors has been adopted as the volume of CAL carbon (0.575 ml/g). After the volume of adsorption phase (V) has been obtained, K and ΔG° may be calculated from the following equation:

$$K = \alpha/V \tag{9}$$

$$\Delta G^\circ = -RT \ln K. \tag{10}$$

By substituting for K from Eq. 9 into Eq. 10 and for log α from Eq. 6 into Eq. 10, it may be shown that at a certain temperature:

$$\begin{aligned}\Delta G^\circ &= -RT(\ln \alpha - \ln V) \\ &= -2.303RT(\beta N + \gamma - \log V) \\ &= \beta_0 N + \gamma_0\end{aligned} \tag{11}$$

where β_0 and γ_0 are constants. The constants and the correlation coefficients calculated by regression analysis are given in Table 3. The overall statistics are excellent with an average correlation coefficient of 0.9990. The constant β_0 corresponds to the standard free energy change per individual methylene group (ΔG°_C) and γ_0 to the functional group contribution for ΔG°. Therefore, assuming that the hydrocarbon and functional portions contribute independently to the standard free energy change for monofunctional aliphatic compounds, it follows that:

$$\Delta G^\circ = \Delta G^\circ_{HY} + \Delta G^\circ_{FG}. \tag{12}$$

For the compounds examined in this study, ΔG°_{HY} may be expressed by the following equation:

$$\Delta G^\circ_{HY} = \Delta G^\circ_C \cdot N = \beta_0 \cdot N \tag{13}$$

As seen from Table 3, ΔG°_C and ΔG°_{FG} give similar values for all functional groups (the averages are -779 cal/mol and -1060 cal/mol, respectively).

Table 3. Results of regression analysis using Eq. 11

Compound	$-\beta_0$	$-\gamma_0$	Correlation coefficient r
Alcohols	764	1120	0.9996
Carboxylic acids	848	969	0.9993
Ketones	740	925	0.9987
Ethers	755	1040	1.0000
Esters	811	1190	0.9991
Aldehydes	755	1140	0.9974

Discussion

The free energy change for the solution process has been calculated by Amidon[14,15] *et al.* The molecular surface area for 158 aliphatic hydrocarbons, olefins, alcohols, ethers, ketones, aldehydes, esters, and fatty

Table 4. Free energy contribution per one methylene group to the solution process

Compound	$\Delta G^{\circ}_{C,sol}$ (cal/mol)
Alcohols	798
Carboxylic acids	759
Ketones/Aldehydes	807
Ethers	872
Esters	720
	Av 791

acids were computed and correlated with the aqueous solubilities. For monofunctional aliphatic compounds the total surface area (*TSA*) may be divided into two contributions, namely the hydrocarbon (*HYSA*) and functional group (*FGSA*) contributions.

$$TSA = HYSA + FGSA \tag{14}$$

Assuming that the hydrocarbon and functional group portions contribute independently, the following generalized equation is suggested for use in solubility correlations:

$$\log S = \Theta_1 \cdot HYSA + \Theta_2 \cdot FGSA + \Theta_3 \cdot IFG + \Theta_0 \tag{15}$$

where S is the aqueous solubility, Θ_0 is the intercept, and *IFG* is the functional group index (zero for hydrocarbons and unity for a monofunctional compound). From the coefficients for the *HYSA* term in Eq. 15, the free energy contribution per individual methylene group to the solution process ($\Delta G^{\circ}_{C,sol}$) may be calculated (assuming 31.8 Å^2 as the area per CH_2 group). The value of $\Delta G^{\circ}_{C,sol}$ for each homologous series is shown in Table 4. The average $\Delta G^{\circ}_{C,sol}$ value is 791 cal/mol and shows approximate agreement with the value of $-\Delta G^{\circ}_{C,ad}$ (779 cal/mol) obtained from the adsorption of the same homologous series on CAL carbon from aqueous solutions. This suggests that the adsorption process of the hydrocarbon portion of solute is analogous to the precipitation process from the aqueous solution into the pure liquid solute, and that the solute in the adsorption phase is in the liquid form. The Polanyi adsorption potential theory is also based on the concept that the adsorption process is identical to the precipitation process.

For the six groups of compounds included in Table 4 the general tendency is that the more polar compounds give smaller methylene group hydrophobic effects. On the other hand, Table 3 indicates that the more hydrophobic compounds have smaller hydrophobic effects caused by the methylene group. This may be due to the different effect of a methylene unit on the solute-solute interaction between the adsorption phase and the pure liquid solute phase.

The free energy contribution of the functional group to the solution process ($\Delta G^{\circ}_{FG,sol}$) may be calculated from the *FGSA* and *IFG* terms in Eq. 15. The hydroxyl group contributes −3.81 kcal/mol to the free energy of solution for the addition of a hydroxyl group to a normal hydrocarbon in the 1-position.[14] The values of $\Delta G^{\circ}_{FG,sol}$ for other functional groups are similar in magnitude to that for the hydroxyl group.[15] The free energy contribution of the functional group to the adsorption process ($\Delta G^{\circ}_{FG,ad}$) is on average −1.06 kcal/mol for the six groups of compounds in Table 3, suggesting that the adsorption of the functional group portion of the solute differs from the precipitation process. There are, however, certain factors that influence the value of $\Delta G^{\circ}_{FG,ad}$. The first is the volume of the adsorption phase. The volume of the adsorption phase in liquid phase may differ from that in the gas phase. Assuming that the volume is half the value in Table 1, the value of $\Delta G^{\circ}_{FG,ad}$ decreases from −1.06 kcal/mol to −1.47 kcal/mol. Therefore, the influence of this factor on the value of $\Delta G^{\circ}_{FG,ad}$ would not be very large.

Table 5. Free energy contribution of functional groups to the adsorption process

Compound	Functional group	Number of methyl groups	γ_1 (cal/mol)	γ_2 (cal/mol)
Alcohols	-OH	1	230	230
Carboxylic acids	-COOH	1	381	−467
Ketones	>CO	2	1775	1035
Ethers	-O-	2	1660	1660
Esters	-COOR	2	1510	699
Aldehydes	-CHO	1	210	−545

The second factor is the validity of extrapolation of the linear relationship in Eq. 11. The estimation of $\Delta G^{\circ}_{FG,ad}$ from the intercept is based on the assumption that every carbon atom in a solute compound makes the same contribution to the free energy as one methylene group. It has, however, frequently been noted that a methyl group and a methylene unit make different contributions:[16–18] the contribution to the free energy of solution for a methyl group is greater by approximately 1.35 kcal/mol than that for a methylene group.[14] The value of γ_0 in Table 3 has been corrected on the basis that the adsorption process on hydrocarbons is identical with the precipitation process, the value of the corrected γ_0 being given in the fourth column of Table 5. A similar correction must be made for the carbon atom in the functional group. The value of γ_1 does not contain the free energy contribution of the carbon atom in the functional group and it is difficult to estimate this contribution. The free energy contribution of the functional group containing the carbon atom is given in the fifth column of Table 5.

The third factor is the effect of the surface oxygen complex of activated carbon on adsorption.[19–21] The dominant component of the driving force for adsorption is the dispersion component of the Van der Waals forces. However, the polarizing component of the Van der Waals forces also contributes to adsorption for polar or polarizable substances. Consequently it is assumed that the value of γ_2 for carboxylic acids and aldehydes is smaller than that of other functional groups due to these polar effects. Aldehydes may be converted in part to carboxylic acids by oxidation in aqueous solution.

It is necessary to take into further consideration other factors in order to exactly estimate the free energy contribution of the functional group. However, in

view of these three main factors, the following conclusions may be derived. The free energy contribution of the functional group to the adsorption process is smaller than the free energy contribution of the functional group to the precipitation process, *i.e.*, the functional group of the solute molecule in the adsorption phase is appreciably hydrated.

The functional groups of alcohols, carboxylic acids, and aldehydes suffer little dehydration and be present in the solution phase, since the functional groups are situated at terminal positions in the alkyl chain. On the other hand, the functional groups of ketones, ethers, and esters would be more dehydrated and be present in the pores of the activated carbon, since the functional groups are situated between the alkyl chains.

The potential theory in liquid phase adsorption assumes that the adsorption of solute take place by precipitation of the solute in the adsorption phase. From the present investigation, however, it has become apparent that the adsorption of solute takes place by precipitation of the hydrocarbon portion of the solute and that the functional group portion of the solute is not appreciably dehydrated in the adsorption phase.

The authors wish to express their thanks to Professor Nobuhiko Kuroki and Associate Professor Joichi Koga, The University of Osaka Prefecture, for their helpful discussions.

References

1) M. Polanyi, *Verh. Deut. Phys. Ges.*, **16**, 1012 (1914); **18**, 55 (1916); *Z. Electrochem.*, **26**, 370 (1920); *Z. Phys.*, **2**, 111 (1920).
2) M. M. Dubinin, *Chem. Rev.*, **60**, 235 (1960).
3) M. M. Dubinin, E. D. Zaverina, and L. V. Radushkevich, *Zh. Fiz. Khim.*, **21**, 1351 (1947).
4) L. V. Radushkevich, *Zh. Fiz. Khim.*, **23**, 1410 (1949).
5) M. M. Dubinin and V. A. Astakhov, *Adv. Chem. Ser.*, **102**, 69 (1970).
6) R. S. Hansen and W. V. Fackler, *J. Phys. Chem.*, **57**, 634 (1953).
7) a) M. Manes and L. J. E. Hofer, *J. Phys. Chem.*, **73**, 584 (1969); b) D. A. Wohleber and M. Manes, *ibid.*, **75**, 61 (1971); c) D. A. Wohleber and M. Manes, *ibid.*, **75**, 3720 (1971).
8) M. Hirata, T. Kiryu, A. Omi, and Y. Sugiyama, *Kagaku Kogaku*, **24**, 572 (1960).
9) I. Traube, *Ann.*, **265**, 27 (1891).
10) A. E. Alexander and P. Johnson, "Colloid Science," Clarendon, Oxford (1949), Vol. 1.
11) Y. Fu, R. S. Hansen, and F. E. Bartell, *J. Phys. Colloid Chem.*, **52**, 374 (1948); **53**, 1141 (1949).
12) F. E. Bartell, T. L. Thomas, and Y. Fu, *J. Phys. Chem.*, **55**, 1456 (1951).
13) K. S. W. Sing, *Ber. Bunsenges. Phys. Chem.*, **79**, 724 (1975).
14) G. L. Amidon, S. H. Yalkowsky, and S. Leung, *J. Pharm. Sci.*, **63**, 1858 (1974).
15) G. L. Amidon, S. H. Yalkowsky, S. T. Anik, and S. C. Valvani, *J. Phys. Chem.*, **79**, 2239 (1975).
16) R. Aveyard and R. W. Mitchell, *Trans. Faraday Soc.*, **66**, 37 (1970).
17) P. Molyneux, C. T. Rhodes, and J. Swarbrick, *Trans. Faraday Soc.*, **61**, 1043 (1965).
18) G. Nemethy, I. Z. Steinberg, and H. A. Scheraga, *Biopolymers*, **1**, 43 (1963).
19) P. H. Emmett, *Chem. Rev.*, **43**, 69 (1948).
20) J. J. Kipling, *Quart. Rev.*, **10**, 1 (1956).
21) M. M. Dubinin and E. D. Zaverina, *Zh. Fiz. Khim.*, **23**, 469 (1949).

The Study of Carrier Effects on the ESR of Vanadium Ions Formed in Supported Catalysts, as Assisted by Spectrum Calculation

Hisashi UEDA

National Chemical Laboratory for Industry, 2-19-19 Mita, Meguro-ku Tokyo 153

(Received October 17, 1978)

In order to study the carrier effects on the supported catalysts of vanadium, the ESR spectra of vanadium ions supported on γ-Al_2O_3, SiO_2, ZrO_2, TiO_2, MgO, or CaO and reduced in H_2 at 500 °C were studied. When γ-Al_2O_3, SiO_2, ZrO_2, or TiO_2 were used as the carriers, the main spectral component could be assigned to the V^{4+} ion. The results of data analysis, assisted by spectrum calculation, showed that, on catalyst which had a high activity in the reduction of NO_x by NH_3, the V^{4+} ion had a highly populated d_{xy} orbital, while on catalyst of low activity, V^{4+} had a d_{xy} with a low spin density. If the carrier was MgO, the V ion was reduced to V^{2+}. If the carrier was CaO, no ESR signals due to V ions were observed. It has been suggested that an inhomogeneous and axially symmetric crystal-field model may interpret the intensity ratios among the hyperfine lines of the V^{4+} ESR absorption rather than a non-axial symmetry model of the V^{4+} unpaired electron.

A supported catalyst of vanadium can be prepared by adsorbing vanadate ions on the surface of the carrier from an aqueous solution and then calcining them to V_2O_5. The catalyst thus prepared has catalytic activities, *e.g.*, in the reduction of nitrogen oxide by NH_3. If this catalyst is placed in a reducing atmosphere, V^{4+} is formed in some cases, depending upon the carrier used. The V^{4+} ion thus formed may participate in the catalytic reaction cycles involved. The study of the supported states of the vanadium ion and its surface concentration can be important technique for elucidating the mechanism of the reaction and the catalytic activities.

There have been many reports about the ESR spectra of V^{4+} ions, including the principal values of g- and hyperfine tensors (the latter to be abbreviated simply as **A** in this paper).[1-8] Most of those data were obtained from the V^{4+} ion diluted in a diamagnetic-host single crystal. A few analyses of the ESR spectra of V^{4+} porphyrin compounds, which are found in crude petroleum, have also been reported.[8] Few detailed reports about the V^{4+} ion in supported catalysts have appeared, however. The characteristic feature of the ESR spectra of the V^{4+} ion is its approximately axial symmetry and the large differences between g_z (assumed to be the rotational axis) and g_x, and between A and B (or C).

As the vanadium nucleus, ^{51}V, has a nuclear spin of 7/2, eight spectral lines overlap each other in the ESR spectrum of a supported vanadium catalyst in which anisotropic g- and A- tensors are averaged. In addition, the ESR absorption due to some species other than V^{4+} will also overlap the V^{4+} absorption lines in most cases. In such cases, the subtraction of the calculated V^{4+} absorption from the entire spectrum observed will yield these secondary spectral components. Spectral subtraction, therefore, is an important method in spectral analysis. First derivative curves are not, to the knowledge of the present author, convenient when the addition or subtraction of two spectra is performed. Integrated curves are more easily normalized, and with them it is more easier to grasp the meaning of the spectral components. For this reason, the absorption curve obtained by the integration of a first derivative curve will hereafter be called the "true resonance curve" in this paper.

The subtraction of spectra was performed by using true resonance curves in this work. What the first derivative curve indicates is the slope of the true resonance curve. Therefore, if more than two absorption peaks partly or fully overlap each other, the precise determination of g_z and g_x (or g_y), and A and B (or C) is very difficult. In these instances, the values obtained from the peak and bottom positions of the first derivative curve are nothing more than a set of crude approximation values of g_z and g_x (or g_y). In order to get more accurate results, therefore, it is advisable to repeat the spectral simulation procedures.

In order to analyse the ESR spectra of the V^{4+} ion formed on the surface of γ-alumina powder, the spectral simulation method should be very useful for the reason stated above. However, only a little work has been done on this subject, using the type of samples described above. Campadelli and Bart analysed the line shape of the $MoO_3 \cdot Al_2O_3$ catalyst considering the g-value dispersion and the spin-spin interaction. Their calculation did not cover the entire region in which the experimental spectra had absorption intensities. It is not clear, therefore, if their assumption that the line width was caused only by the g-value dispersion and by spin-spin interactions was correct or not.[9]

Experimental, Data Processing, and Simulation

Preparation of ESR Samples. The oxides used as carriers of V_2O_5 were γ-alumina (Baikowski, A125-AS2, 148 m^2/g), silica gel (Fuji Davison, SP-No. 3, 153 cm^2/g), zirconium oxide (Mitsuwa Chemical Co., 99.9% pure, 8.5 m^2/g), titanium oxide (Kokusan Chemical Co., 7.4 m^2/g), magnesium oxide (Nihon Rikagaku, Inc., 89 m^2/g), and calcium oxide (Junsei Pure Chemicals, 3.0 m^2/g, containing alkali metals and magnesium as impurities, the sum being less than 2%). These oxides were mixed with an aqueous solution of ammonium vanadate from which mixture water was evaporated at room temperature. After drying at 100 °C, they were calcined at 550 °C in air to form V_2O_5. The final concentration in the solid mixtures obtained was 0.5%. The solid sample was then placed in a quartz tube 8 mm in inner diameter and was reduced at 500 °C with H_2 at 1 atm pressure and at the flowing rate of 50 ml/min for 1 h. Some of the V^{4+} ions contained in this sample were reduced to

some extent. The sample was cooled in the hydrogen atmosphere and was then taken out into the air. It was then placed in a ESR sample tube and ESR measurements were made while evacuating it to 10^{-5} Torr.

The results obtained are shown in Figs. 1—9, together with the simulated spectra. For the purpose of comparison, a sample of $VOSO_4$ supported on γ-alumina was prepared. In this case, 1.0 mg of $VOSO_4 \cdot 2H_2O$ was mixed with 5.0 ml of redistilled water and 1 g of γ-alumina. After the water has been evaporated, it was vacuum-dried and then used for ESR measurements. Although the official SI unit representation of the magnetic-field flux density is Tesla, T, a conventional symbol, G, is used in this report to represent 0.0001 T.

Data Processing. The output of an ESR spectrum from the spectrometer is in the form of DC voltage from 0 to 10 mV. This voltage is converted to natural numbers at the rate of 10 mV to 256. The numbers are stored in JEC-5 computer of JEOL and are then punched out on paper data tape. This spectrum is then integrated by a Fortran system of Hitac 10 II.

Spectrum Simulation. Several types of programming methods have been established to calculate the ESR spectra of the paramagnetic species existing in polycrystalline or multioriented substances.[10-13] These methods, however, have been contrived to be executed by large computers. Therefore, if one intends to handle the calculation problem simply as a matter of calculation, those past works will assist the researcher to a great extent. However, if one is intending to use the calculation as a part of his experimental system, it often happens that one cannot afford to use a large computer in his experimental system. In the present work, a calculation method which is essentially the same as those in the past reports, but which is modified so as to make it suitable for the computing system used in the present study, has been used.

The calculation was done by the Fortran system described above, and the result was displayed on a conventional paper chart recorder placed after a digital-analogue converter.[14] In the present problem, the spin Hamiltonian can be written:

$$\mathscr{H} = (g_z S_z + g_x S_x + g_y S_y)\beta H + (AS_z + BS_x + CS_y)I.$$

According to this equation, the calculation of the spectra may be carried out in three different ways. In the first case, $g_z \neq g_x \neq g_y$ and $A \neq B \neq C$. In the second case $g_z \neq g_x = g_y$ and $A \neq B = C$. In the third case $g_z = g_x = g_y$ and $A = B = C$. The third case does not have to be considered in the present work. The g-factor and coupling constant, *e.g.*, A, were surveyed in the $g \pm 0.001$ and $A \pm 0.0002$ regions, and the best combination was judged by a visual inspection.

Results

In Figs. 1—7 the spectra obtained by both experiments and calculations are shown. The true absorption of ESR is plotted, except in Fig. 1, with the magnetic field increasing from right to left. The parameters used for the calculations is shown in Table 1. The first derivative curve of the spectrum of Fig. 2 is shown in Fig. 1. The sample which gave these spectra was V_2O_5/TiO_2 reduced in H_2. The "OBS" in Fig. 1 means the observed spectrum, while "SIM" means that obtained by spectral simulation. The vertical lines shown in the figures indicate the positions of resonance, with $(h\nu/g_z\beta)+m_I A$ shown by longer lines and $(h\nu/g_x\beta)+m_I B$ shown by shorter lines, in which A and B are in the unit of the magnetic field, G. An axial symmetry is assumed, $B=C$. The z-direction is taken as the symmetry axis.

Table 1. The ESR constants found by spectral simulation

Carrier	Ion	g_z	g_x, g_y	A/cm^{-1}	B/cm^{-1}	Half-width/T[a]
TiO_2	V^{4+}	1.9400	1.9892	0.0160	0.0050	0.00632
ZrO_2	V^{4+}	1.9036	1·9735	0.0170	0.0070	0.00200
SiO_2	V^{4+}	1.9333	1.9807	0.0102	0.0048	0.00365
Al_2O_3	V^{4+}	1.9494	1.9828	0.0165	0.0055	0.00632
Al_2O_3	VO^{2+}	1.9490	1.9980	0.0174	0.0067	0.00316

a) Simulation by Lorentz function.

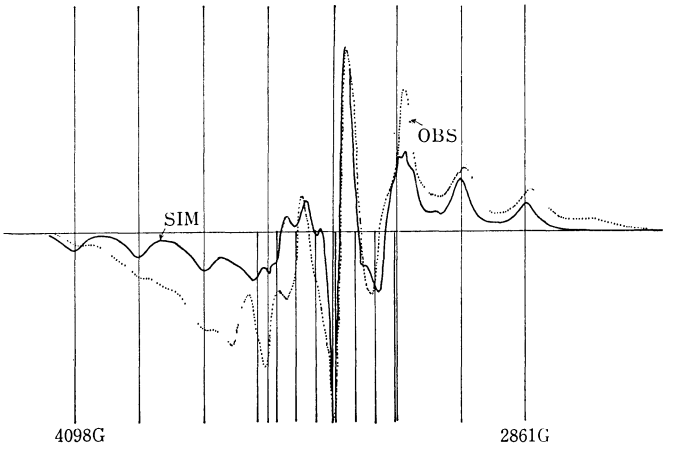

Fig. 1. The first derivative curve of ESR spectrum of hydrogen reduced 0.5% V_2O_5/TiO_2 sample. Microwave power was 0.4 mW, and at 9450 MHz. Vertical lines indicate the positions of the principal values, Table 1.

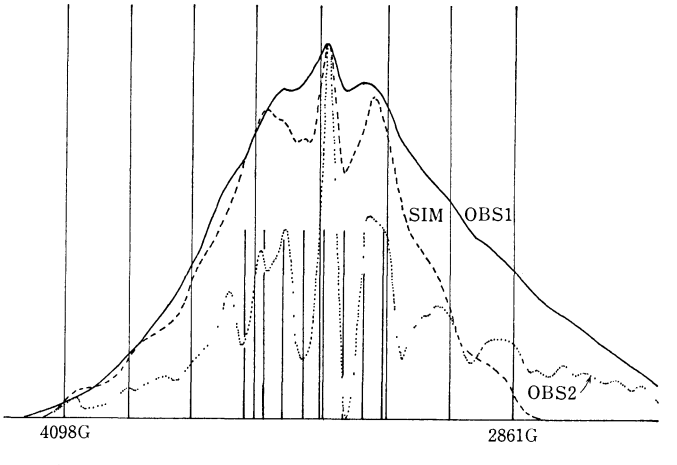

Fig. 2. True absortion curves of the spectra in Fig. 1.

The peak and the bottom positions in the outer part of the spectrum in Fig. 1 almost exactly coincide with the magnetic-field value given by the principal values of $\boldsymbol{g}$ and $\boldsymbol{A}$. Therefore, g and A may be found by solving this equation: $H=(h\nu-Am_I)/g_z\beta$ using a first derivative curve. However, the magnetic-field values for the $H=(h\nu-Bm_I)/g_x\beta$ equation are extremely difficult to find because the central part of the spectrum

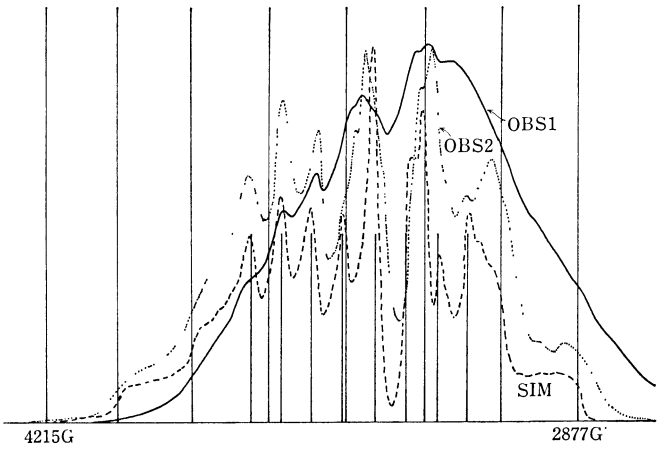

Fig. 3. 0.5% V_2O_5/ZrO_2. Other conditions identical with those of Fig. 2.

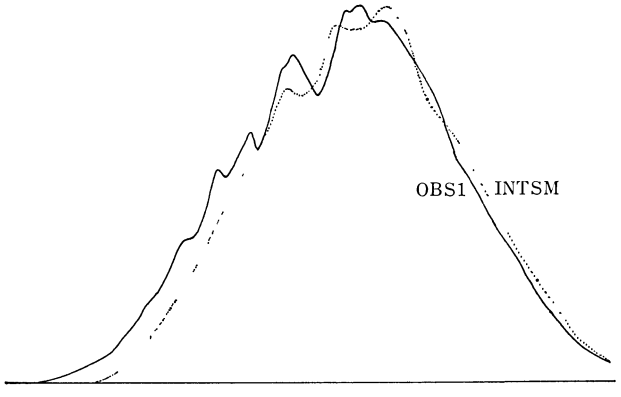

Fig. 4. Sample used was the same as that for Fig. 3.

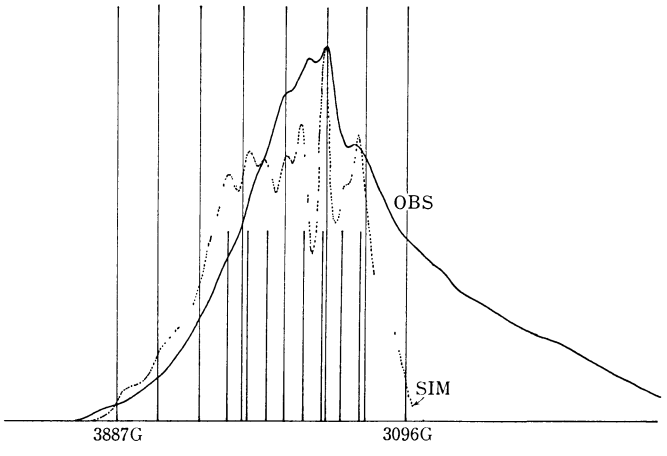

Fig. 5. 0.5% V_2O_5/SiO_2. Other conditions identical with those of Fig. 2.

is crowded overlapping spectral lines. In these cases, Kneubühl's equation is very hard to apply.[15]

In Fig. 2, OBSl is the observed spectrum. OBSSM was obtained from OBSl by the following processing method. At every magnetic-field point of the OBSl spectrum, the absorption intensities were integrated over the ±40 G region and were then averaged, the average being registered as the intensity of OBSSM at that field value. From this smoothed curve, OBS2′= OBSl−OBSSM was calculated. By the normalization

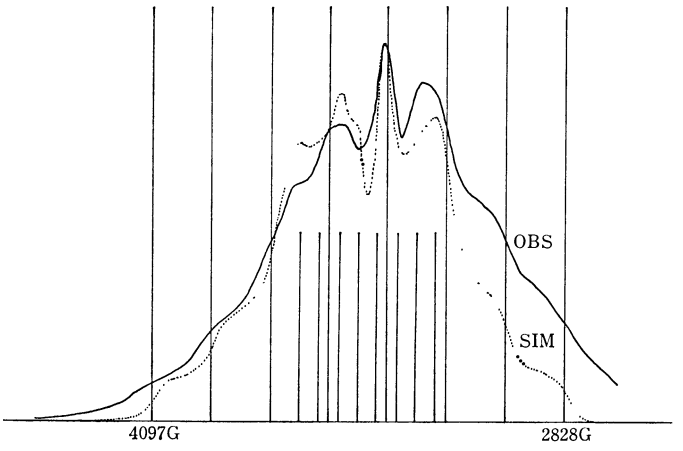

Fig. 6. 0.5% V_2O_5/γ-Al_2O_3. Other conditions are identical with those of Fig. 2.

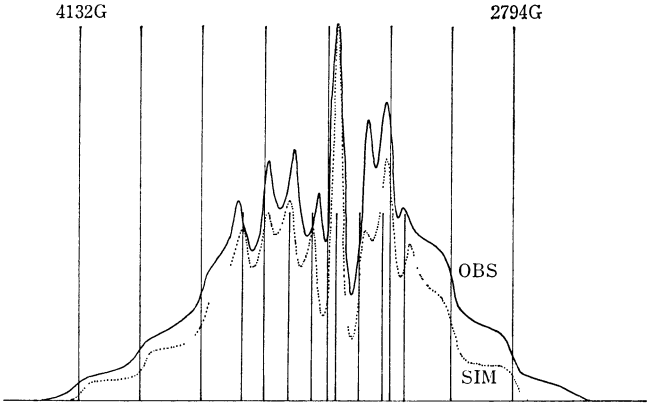

Fig. 7. 1.0 mg of $VOSO_4 \cdot 2H_2O$ dispersed on the surface of 1.0 g of γ-Al_2O_3.

of OBS2′, OBS2 was obtained. The hyperfine structures are found more clearly in OBS2, which makes the estimation of B and g easier.

The V^{4+} spectra formed in reduced V_2O_5/ZrO_2 are shown in Fig. 3. The observed spectrum is OBS1. The explanation for OBS2 will be made later. The SIM spectrum was obtained by calculations using the parameters found in OBS1. The OBS1 spectrum contains two component spectra. One of them has the hyperfine structure of the OBS2 of Fig. 2, or the normal V^{4+} hyperfine structure. The other component has a somewhat different structure. The INT spectrum, which is not shown in the figure, was made from OBS1 and SIM; INT=OBS−0.352 SIM. The INTSM spectrum was obtained by smoothing the INT spectrum in the same way as was used to get the OBS2 of Fig. 2. INTSM is shown in Fig. 4 with OBS1.

A hyperfine structure different from that of OBS1 is found in INTSM, but it was not analysed. The OBS2 spectrum of Fig. 3 was obtained as OBS1−0.813 INTSM. The parameters found in OBS2 were compared with those obtained from OBS1. Since there was some difference between these two groups of parameters, the SIM spectrum was again calculated from the data found in OBS2. By repeating the procedure described above, the INT, the INTSM, and the OBS2 spectra were again calculated. The

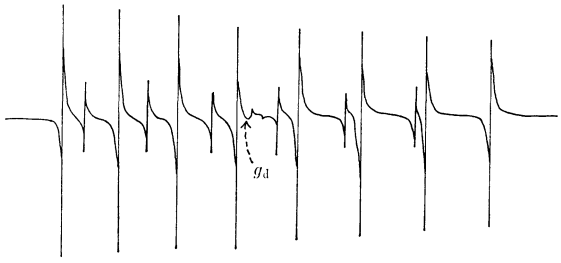

Fig. 8. 0.5% V_2O_5/MgO. Other conditions are identical with those of Fig. 3.

final agreement of OBS2 with SIM was fairly good.

The ESR spectrum of the V^{4+} ion formed in reduced V_2O_5 supported on SiO_2, OBS, and the spectrum calculated to fit it, SIM, are shown in Fig. 5. The silica gel used has some impurities. The intensity of the absorption by V^{4+} in this sample is not strong. For these two reasons, the background ESR spectrum, BG, which is not shown, was subtracted from the originally observed spectrum, OROBS, which is not shown, either. Therefore, OBS=OROBS−BG. A broad component, V, is found in the OBS spectrum in addition to the spectrum with the V^{4+} hyperfine structure. This circumstance is similar to those shown in Figs. 3 and 4.

The ESR spectra of the V^{4+} ion formed in the reduced V_2O_5 on γ-alumina are shown in Fig. 6. Since the carrier used in this sample was very pure and gave no appreciable absorption, and since the ESR absorption of V^{4+} on γ-alumina was relatively strong, the OBS spectrum itself could be fitted well by the calculated spectrum. The ESR spectrum of the VO^{2+} ion which was adsorbed on γ-alumina and the spectrum calculated to fit it are shown in Fig. 7. In Fig. 6 the half-width used for the calculation was 63.2 G, but in Fig. 7 31.6 G gave a good fit. Here the difference between VO^{2+} and V^{4+} is quite clear. No ESR spectra which are like those in Figs. 1—7 could be observed from the sample in which the carrier oxide was either CaO or MgO. If the carrier was CaO, no ESR signal due to V ions were observed. In the case of MgO, the spectrum shown in Fig. 8 was observed. It is not V^{4+} but V^{2+} that gives this spectrum.[16] The position of the magnetic field indicating $g=2.0036$ is marked by an arrow and g_d. The results obtained by CaO and MgO indicate that, on the surface of these alkaline earth oxides, V^{4+} is not stable.

Discussion

The Electronic State of the d-Electron and the Carrier Effects on It. The hyperfine splitting values observed from the V^{4+} ion have two components, the isotropic term and the anisotropic term. For the electron in a d^1 configuration, either the d_{z^2} or d_{xy} orbital is concluded to hold the unpaired electron.[5] The molecular orbital formed between the ligand orbital, $\psi_L(xy)$, and d_{xy} is denoted by π. Let β and β' be the proper coefficients, then:

$$\pi = \beta d_{xy} - \beta' \psi_L(xy).$$

Table 2. The K and β^2 values

Carrier	Ion	K/cm^{-1}	β^2
SiO_2	V^{4+}	0.0242	0.375
Al_2O_3	VO^{2+}	0.0229	0.727
ZrO_2	V^{4+}	0.0222	0.690
Al_2O_3	V^{4+}	0.0206	0.754
TiO_2	V^{4+}	0.0200	0.751

The β in this equation is different from that used in the spin Hamiltonian. The spin Hamiltonian is, if all the spectra are approximated by axially symmetric models:

$$\mathscr{H} = g_z\beta H_z S_z + g_x\beta[H_x S_x + H_y S_y] + A I_z S_z + B[I_x S_x + I_y S_y].$$

From the ESR spectrum, the hyperfine coupling constants, A and B, are obtained. A and B are shown by the following equations:[17-19]

$$A = -K - (4/7)\beta^2 P + (g-2.0023)P + (3/7)(g-2.0023)P$$

$$B = -K + (2/7)\beta^2 P + (11/14)(g-2.0023)$$

The value of P is equal to $2.0023 \cdot g_N \cdot \beta \cdot \beta_N \cdot \langle r^{-3} \rangle$, and the value for $^{51}V^{4+}$ is 0.0172 cm^{-1}.[20] Therefore, K and β^2 are solved from the above equations. Those values calculated from the data in Table 1 are shown in Table 2.

The isotropic contact term in the hyperfine interaction of paramagnetic ions has been the subject of many studies.[20-22] Abragam, Horowitz, and Pryce have observed that the quantity, χ, defined as:

$$\chi = \frac{4\pi}{S}(\psi | \sum \delta(r_1) S_{z1} | \psi)$$

is negative and nearly constant in magnitude for ions in the first transition series.[21] The χ value is related with K by means of the following equation:[21]

$$\chi = \left[-\frac{3}{2}\left(\frac{hca_0^3}{2.0023\, g_N \beta \beta_N} \right) K \right].$$

In this equation, h is Planck's constant, c is the velocity of light, a_0 is the Bohr radius, and g_N is 5.050 for ^{51}V. Therefore, the K value is proportional to the probabilities of the 2s and 3s electrons to be excited to the 3d orbital. In Table 2, the K value for V^{4+}/SiO_2 is the largest and the one for V^{4+}/TiO_2 is the smallest. The β^2 value is proportional to the spin density in d_{xy}, and the values are in a decreasing order when the samples are V^{4+}/Al_2O_3, V^{4+}/TiO_2, V^{4+}/ZrO_2, and V^{4+}/SiO_2.

The catalytic activity of V_2O_5 supported on TiO_2, ZrO_2, SiO_2, and Al_2O_3 greatly depends upon the carriers. It has been considered that the specific surface areas of these carriers are different. The TiO_2 used has only 7.4 m^2/g, while the SiO_2 used had 153 m^2/g. There are several types of reactions in which γ-alumina works as a good carrier. If used as a carrier of the supported catalyst applied to these types of reactions, the carrier effects of those oxides decrease in this order: γ-alumina, ZrO_2, TiO_2, and SiO_2. From the values of K and β^2 shown in Table 2, it may be concluded that the highly active V^{4+} ion has a d_{xy}

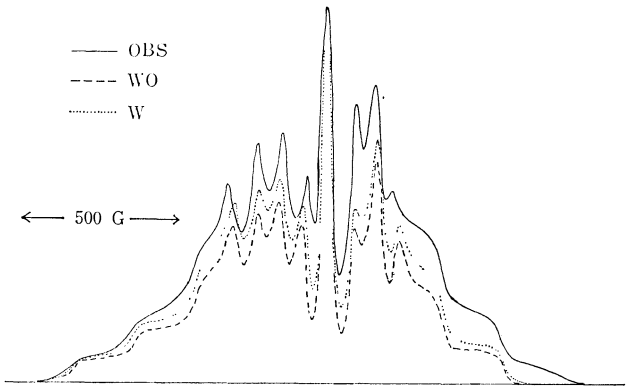

Fig. 9. True absorption curves showing the effect of axial distortion on the ESR spectrum. WO: Spectrum for the ion without axial symmetry. About parameters, see text. W: Spectrum identical with Fig. 7-SIM. OBS: Identical with Fig. 7-OBS.

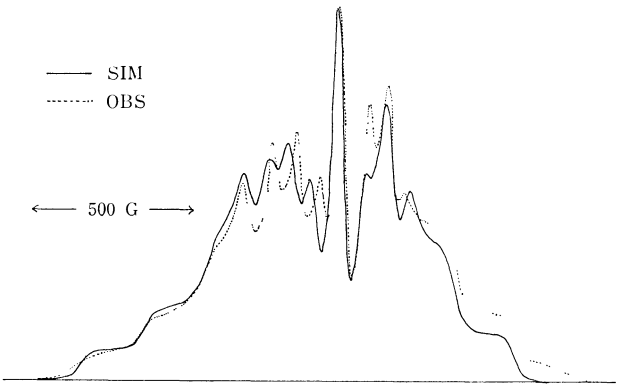

Fig. 10. True absorption curves demonstrating the effect of inhomogeneous crystal fields on the ESR spectrum. SIM: An equal mixture of two spectra, parameters are in text. OBS: Identical with Fig. 7-OBS.

orbital which extends well toward the x and y directions, as an ideal d_{xy} orbital should, or that d_{xy} has a high spin density.

Axial Distortion or Inhomogeneous Crystal Field. Broad spectral components are found in Figs. 2—5 in addition to the hyperfine spectral components. Some of them are due to some impurities in the carrier. However, many of the broad components are caused by the minor distortions and the irregular crystal fields. The V^{4+} ions on the surfaces of TiO_2, ZrO_2, and SiO_2 particles may be surrounded by these partially distorted crystal fields. Another minor irregularities of the crystal field can also be expected from the half-width value of 63 G used in the calculation of the spectrum (Table 1). Sixty-three gauss, if it is caused by the irregular g-tensor, is equivalent to $\delta g=0.036$. Therefore, if we assume a mixture of two V^{4+} ions placed in two different environments which cause the principal values of the g-tensor to differ by some 0.036, the 63 G half-width can be explained.

The approximation of the calculated spectrum SIM in Fig. 7 is not satisfactory if the intensities of the absorption peaks are considered. The first thing to be examined is if the axial symmetry assumed in this work is effective or not. Figure 9 compares two spectra with and without axial symmetry. The WO spectrum was derived by the use of $g_z=1.9490$, $g_x=1.9955$, $g_y=2.0005$, $A=0.0174$, $B=0.0068$, $C=0.0066$ cm^{-1}, and a half-width of 23.62 G. The intensity ratios, especially that of the strongest peak to those of the remaining peaks, rather deviate from that of the OBS spectrum. Therefore, it does not seem possible to interpret the large line-width in terms of the axial distortion only. Among other factors to be considered is the inhomogeneity of the crystal field surrounding the V^{4+} ions, which might be located on the edge, on the ridge, or in the valley or the deep holes existing on the surface of the carrier particles. Figure 10 shows one attempt to study this subject. The OBS spectrum is identical with the one in Figs. 7 and 9. The SIM spectrum was derived from the two spectra as an arithmetic mean. The one of the component spectra was the Fig. 7-SIM spectrum. The other component spectrum was calculated by means of $g_z=1.9599$, $g_x=g_y=2.0092$, $A=0.00174$, $B=C=0.0067$ cm^{-1}, and a half-width of 31.62 G. The agreement of the intensity ratios have been fairly well improved.

The large line-width of the paramagnetic ions located on the surface of porous powders includes many factors which it is not easy to solve or to understand fully. In the case of a nucleus which has a large nuclear spin, such as V^{4+}, the spin Hamiltonian has a nuclear quadrupole term, *e.g.*, $Q'(I_z^2-63/12)$. If the axis of the magnetization is perpendicular to the z-axis, secondary transitions can occur between energy levels; therefore, the experimental ESR spectrum may not be accounted for by simply averaging the ESR spectra which are obtained from the V^{4+} ions oriented in random directions in the magnetic field. The strongest absorption peak of the OBS spectrum in Fig. 7 is relatively weaker than that which is to be expected by the calculated spectrum, SIM. This fact might be explained if one would consider the nuclear quadrupole term. However, it seems to the present author that the angular variation of the intensity ratio of the hyperfine lines should be studied by means of a system which is simpler than the supported catalysts used in this work. For this reason, such considerations have not been undertaken here. At any rate, the inhomogeneous crystal-field approach will solve a part of this problem.

CaO and MgO as Carriers. When used as the carrier of a catalyst for a reaction in which γ-alumina works as a good carrier of the catalyst, CaO and MgO are poor carriers. It seems there are no such sites as keep the V^{4+} ion stable on the surfaces of these oxides. In the case of MgO, a Mg^{2+} vacancy will be replaced by a V^{4+} ion, which is then reduced to the +2 oxidation state if placed in a H_2 atmosphere above 500 °C. The V^{2+} ion thus formed is stable, probably because it is somehow equivalent to Mg^{2+} with respect to the electrostatic field that is produced in the surrounding crystal lattice.

References

1) F. W. Lancaster and W. Gordy, *J. Chem. Phys.*, **19**, 1181 (1952).

2) C. A. Hutchison and L. S. Singer, *Phys. Rev.*, **89**, 256 (1953).
3) K. D. Bowers and J. Owen, *Rep. Prog. Phys.*, **18**, 96 (1958).
4) C. J. Ballhausen, "Introduction to Ligand Field Theory," McGraw-Hill Book Co., New York, N. Y. (1962), p. 228.
5) C. J. Ballhausen and H. B. Gray, *Inorg. Chem.*, **1**, 111 (1962).
6) P. W. Lau and W. C. Lin, *J. Chem. Phys.*, **59**, 3998 (1973).
7) M. Marayana, S. G. Sathanaryan, and G. S. Sastry, *Mol. Phys.*, **31**, 203 (1976).
8) D. E. O'Reilly, *J. Chem. Phys.*, **29**, 1188 (1958).
9) F. Campadelli and J. C. Bart, *React. Kinet. Catal. Lett.*, **3**, 435 (1975).
10) A. C. Ling, *J. Chem. Educ.*, **51**, 174 (1974).
11) H. A. Buckmaster, R. Chatterjee, J. C. Dering, D. J. Fry, Y. H. Shing, J. D. Skirrow, and B. Venkatesan, *J. Magn. Reson.*, **4**, 113 (1971).
12) R. Lefebvre and J. Maruani, *J. Chem. Phys.*, **42**, 1480 (1965).
13) K. Kuwata, "Kagaku To Denshikeisanki," ed by T. Yonezawa and K. Osaki, Nankodo, Tokyo, Japan (1968), p. 95.
14) H. Ueda, *Bull. Chem. Soc. Jpn.*, **49**, 2343 (1976); *J. Catal.*, **47**, 284 (1976).
15) F. K. Knebühl, *J. Chem. Phys.*, **33**, 1074 (1960).
16) W. Low, *Phys. Rev.*, **101**, 1827 (1956).
17) D. Kivelson and R. Neiman, *J. Chem. Phys.*, **35**, 149 (1961).
18) H. R. Grasman and J. D. Swallen, *J. Chem. Phys.*, **36**, 3221 (1967).
19) A. H. Maki and B. R. McGarvey, *J. Chem. Phys.*, **29**, 31, 35 (1958).
20) B. R. McGarvey, *J. Phys. Chem.*, **71**, 51 (1967).
21) A. Abragam, J. Horowitz, and M. H. L. Pryce, *Proc. R. Soc. London, Ser. A*, **230**, 169 (1955).
22) A. J. Freeman and R. E. Watson, "Magnetism," ed by G. T. Rado and H. Suhl, Academic Press, New York, N. Y. (1965), Vol. IIA, p. 167.

Effect of Methyl Substitution on the Electron Spin Resonance Spectra of Yang's Biradical

Kazuo MUKAI

Department of Chemistry, Faculty of Science, Ehime University, Matsuyama 790

(Received November 4, 1978)

Mono- and dimethyl derivatives (II) and (III) of Yang's biradical (I) were prepared, and the methyl-substitution effects on the molecular symmetry and spin-density distribution of Yang's biradical have been studied. Resolved hyperfine structures were observed in the ESR spectra of liquid solutions of the biradicals (II) and (III), giving the hyperfine splitting values theoretically expected for their triplet states. In a fluid solution, the biradical molecules retain a three-fold symmetry, as has been reported for Yang's biradical, and the expected methyl-substitution effect is too small to induce any asymmetric, unpaired spin distribution. The ***g***- and ***D***-tensor values of the (II) and (III) biradicals were determined from analyses of the asymmetric ESR spectra of frozen solutions containing the biradicals. The results suggest that these biradicals must also lack a three-fold symmetry in a frozen solution, as has been observed for Yang's biradical. Essentially the same ***g***- and ***D***-tensor values as those of Yang's biradical are observed for the monomethyl derivative (II). On the other hand, the dimethyl derivative (III) shows quite different ***g***- and ***D***-tensor values.

Yang's biradical (I) is known as a fairly stable phenoxyl biradical; it has a structural three-fold symmetry and doubly degenerate non-bonding orbitals, each being half-filled.[1,2] This implies the possible existence of a triplet ground state ($S=1$), which has actually been confirmed by susceptibility measurements.[3] The fluid-solution ESR spectrum shows seven hyperfine splitting due to six equivalent *meta*-ring protons in the three benzene rings of the biradical.[4] The results of NMR[5] and ENDOR[6] studies in solution also indicate that the six *meta*-ring protons are magnetically equivalent, giving a hyperfine splitting attributable to the six *meta*-ring protons. However, the toluene rigid matrix ESR spectrum of Yang's biradical was recently reported to be a characteristic spectrum of a non-axially symmetrical triplet, with $|D|=34.1$ and $|E|=2.3$ G.[7] This result may be explained by assuming that at least one of the twist angles of the three benzene rings is different from the other two rings in the low-temperature rigid matrix. The notable solvent effects observed for the zero-field splitting parameters (D and E) suggest that the asymmetric environment due to frozen-solvent molecules contributes to the molecular distortion found for Yang's biradical.[8] In the previous papers, the effects of asymmetric deuterium and *t*-pentyl substitution on molecular distortion in Yang's biradical were also reported, indicating that the effects are negligible for the former and small for the latter.[7,9]

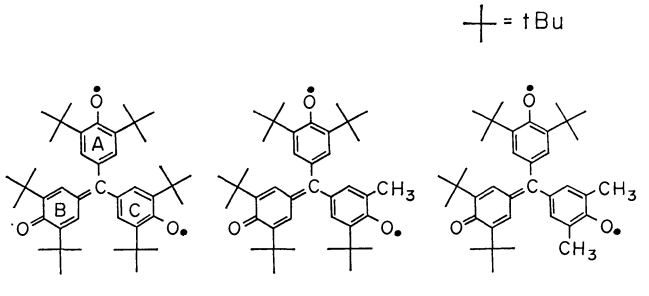

Fig. 1. Molecular structures of Yang's biradical (I), 1Me-Yang's biradical (II), and 2Me-Yang's biradical (III).

In the present work, in order to obtain further information on such molecular distortion, we have prepared the two methyl derivatives (hereafter called as the 1Me- and 2Me-Yang's biradicals (II) and (III); see Fig. 1) of Yang's biradical by the PbO_2 oxidation in toluene of the corresponding bisphenol precursors. The isotropic hyperfine splittings and ***g***- and ***D***-tensor values of these biradicals have been determined from their solution and asymmetric frozen ESR spectra respectively. The results provide direct experimental evidence for the symmetry and electronic structure of these radicals. The isotropic hyperfine splittings of the monoradical precursors of the (I), (II), and (III) biradicals have also been determined by means of their solution ESR spectra and compared with those of the corresponding biradicals.

In general, the effect of the methyl substitution on the unpaired spin distribution in free radicals, including phenoxyl radicals, is very small. However, as has been shown in ESR[10] and NMR[11] studies of the benzene anion and its methyl derivatives, the effect can be significant if the orbital ground state of the parent free radical is two-fold degenerate and if methyl substitution, by lowering the symmetry, removes the degeneracy. A notable methyl substitution effect has also been observed in ENDOR studies[12] of the pentaphenylcyclopentadienyl neutral radical, which has doubly degenerate non-bonding orbitals. By the asymmetric methyl substitution of Yang's biradical, therefore, we can expect a change in the unpaired spin distribution (the asymmetric spin distribution) and a lifting of the degeneracy.

Results and Discussion

Solution ESR Spectra of 1Me- and 2Me-Yang's Biradicals (II) and (III). As has been described in previous papers,[7-9] the oxidation product of the bisphenol precursor (bisphenol (I)) of Yang's biradical with PbO_2 in toluene in a sealed, degassed system initially gives a quintet ESR spectrum ($a_m^H=1.32\pm0.04$ G) attributable to the four equivalent *meta*-ring protons of the monoradical precursor. After further

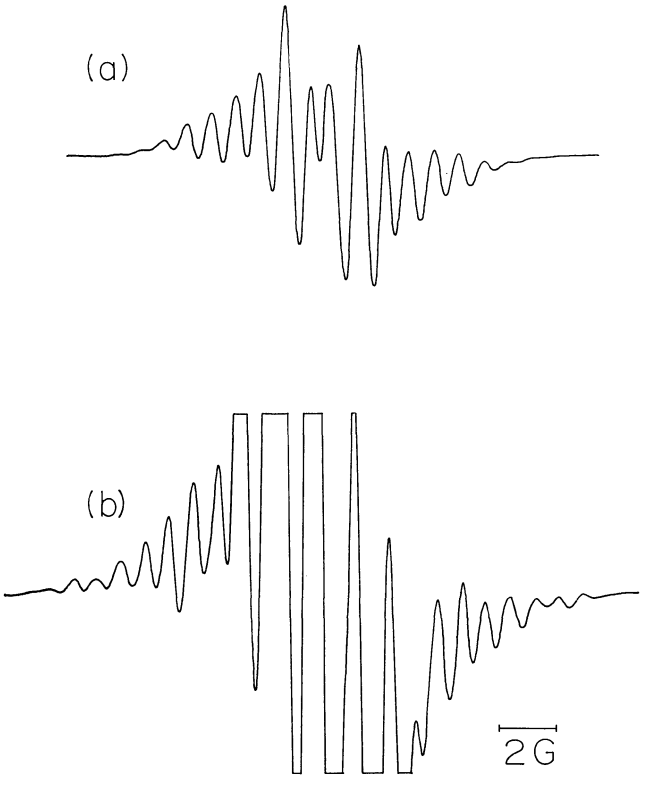

Fig. 2. Solution ESR spectra of (a) 1Me-Yang's biradical (II) and (b) 2Me-Yang's biradical (III) in toluene at 20 °C. Each spectrum includes a quintet signal due to remaining monoradical impurity.

oxidation, a five-line spectrum of the monoradical is altered to a seven-line spectrum of Yang's biradical, with an equivalent splitting constant of $a_m^H=0.91\pm0.04$ G.[4,7]

The initial partial oxidation of the bisphenol (II), the bisphenol precursor of the 1Me-Yang's biradical (II), gives ESR spectra consisting of (i) a central strong quintet and (ii) weak quartet-quintet patterns on both sides of the central quintet. The spectra are thought to be attributable to the two kinds of monoradicals (AB- and BC-types) produced when the oxidation proceeds from the A and C hydroxyphenyl rings in the bisphenol precursor respectively; the former monoradical is very stable, while the latter is unstable, disappearing within about 30 minutes at 20 °C. The spectra are readily analyzed, giving $a_m^H=1.30\pm0.04$ G for the (II-AB) monoradical and $a_{CH_3}^H=4.07\pm0.04$ G and $a_m^H=1.36\pm0.04$ G for the (II-BC) monoradical. As the oxidation proceeds further, the spectra of the two monoradicals are altered into a sixteen-line absorption signal which may be attributed to the 1Me-Yang's biradical (II). As this biradical is unstable, ESR measurements were performed on several samples, under slightly different conditions of oxidation, in order to obtain a better ESR spectrum. The best spectrum obtained is shown in Fig. 2(a). However, the spectrum indicates that a quintet signal caused by a monoradical impurity still remains. The sixteen-line absorption signal of the (II) biradical may be explained by three protons ($a_{CH_3}^H=2.59\pm0.04$ G) of a methyl group and six equivalently interacting protons ($a_m^H=0.86\pm0.04$ G) at the meta positions.

Table 1. Hyperfine splittings of Yang's biradical (I), the 1Me-Yang's biradical (II), and the 2Me-Yang's biradical (III), and their monoradical precursors (AB- and BC-types) in toluene at 20 °C (G)

	Biradical		Monoradical precursors		
			AB-type	BC-type	
	a_m^H a)	$a_{CH_3}^H$	a_m^H	a_m^H	$a_{CH_3}^H$
Yang's (I)	0.91	—	1.32	1.32	—
1Me-Yang's (II)	0.86	2.59	1.30	1.36	4.07
2Me-Yang's (III)	0.86	2.58	1.31	1.30	4.05

a) The experimental errors in the values of a_m^H and $a_{CH_3}^H$ are ±0.04 G.

Similarly, the oxidation of bisphenol (III), the bisphenol precursor of the 2Me-Yang's biradical (III), initially gives ESR spectra consisting of (i) a strong quintet and (ii) a weak septet-quintet splitting; the spectra are attributable to the two kinds of monoradicals (III-AB and -BC) produced when the oxidation proceeds from the A and C hydroxyphenyl rings in the bisphenol precursor respectively. The hyperfine splittings ($a_m^H=1.31\pm0.04$ G) and ($a_{CH_3}^H=4.05\pm0.04$ G, $a_m^H=1.30\pm0.04$ G) were observed for the (III-AB) and (III-BC) monoradicals respectively. After further oxidation, the ESR spectra of the two monoradicals were altered to an ESR spectrum, as is shown in Fig. 2(b). This spectrum may be explained by considering the contribution from both an absorption signal of the (III) biradical and a central strong quintet signal of the remaining monoradical. The stability of the (III) biradical with two methyl groups is even less than is the case for the (II) biradical, which has one methyl group, disappearing within about 20 minutes at 20 °C. The hyperfine splittings obtained for the (III) biradical are $a_{CH_3}^H=2.58\pm0.04$ G and $a_m^H=0.86\pm0.04$ G, arising from six protons of two methyl groups and six magnetically equivalent *meta*-ring protons respectively. All the hyperfine splittings are listed in Table 1. The *g*-values (g_{iso}) of these biradicals in toluene were also measured; they are listed in the last column of Table 2.

As is clear from the results listed in Table 1, the hyperfine splittings obtained for the monoradical precursors (AB- and BC-types) of Yang's biradical and its methyl derivatives in solution are equivalent to each other as resolved by the ESR experiments. The hyperfine splitting constants of Yang's biradical and its methyl derivatives in a fluid solution also show a good agreement with each other within the limits of experimental error. As has been observed for the benzene anion and its methyl derivatives,[10,11] the methyl-substitution effect can be significant if the two-fold degeneracy of the parent free radical is lifted by asymmetrical methyl substitution. Yang's biradical (I) has a structural three-fold symmetry and is orbitally degenerate.[2] By asymmetric methyl substitution, therefore, we can expect a lifting of the degeneracy, and thus a change in the unpaired spin dis-

Table 2. *D*- and *g*-tensor values of Yang's biradical (I), the 1Me-Yang's biradical (II), and the 2Me-Yang's biradical (III) in toluene at 77 K

	$\|D\|$[a]/G	$\|E\|$[a]/G	g_{xx}[b]	g_{yy}	g_{zz}	g_{av}[c]	g_{iso}[d]
Yang's (I)	34.1	2.3	2.0054	2.0054	2.0026	2.0045	2.00451
1Me-Yang's (II)	34.2	2.2	2.0052	2.0055	2.0030	2.0046	2.00447
2Me-Yang's (III)	23.3	1.4	2.0046	2.0041	2.0035	2.0040	2.00457

a) The experimental errors in the values of $|D|$ and $|E|$ are ± 0.2 and 0.4 G respectively. b) The experimental errors in the values of g_{xx}, g_{yy}, g_{zz}, and g_{av} are ± 0.0002. c) The average $g_{av}=(1/3)(g_{xx}+g_{yy}+g_{zz})$. d) The experimental errors in the values of g_{Iso} are ± 0.00005.

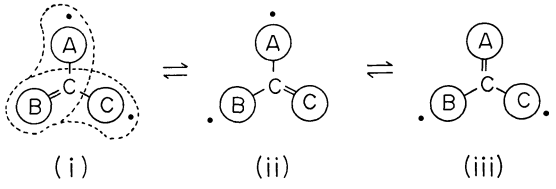

Fig. 3. Schematic representation of three valence-bond structures (i), (ii), and (iii) of the biradicals.

tribution (an asymmetric spin distribution). However, the present experimental results indicate that the expected methyl-substitution effect is too small to induce any asymmetric unpaired spin distribution in a fluid solution.

The hyperfine splitting ($a_m^H=0.91$ G) of the *meta*-ring protons of Yang's biradical is nearly two-thirds of the splitting ($a_m^H=1.32$ G) observed for the monoradical precursor. Similar results were observed for the 1Me- and 2Me-Yang's biradicals, (II) and (III). For instance, in the (III) biradical, the predicted values for the hyperfine splittings of the *meta*-ring protons and methyl protons from those of the monoradical precursor (III-BC) are 0.87 G and 2.70 G, while the observed values are 0.86 G and 2.58 G, respectively. The relative ratio (2/3) of the hyperfine splitting constants of the biradicals to the monoradicals can be predicted on the basis of simple resonance theory, as follows: one can, in principle, schematically draw three valence-bond structures, (i), (ii), and (iii) (see Fig. 3) for each biradical under study. The (i) structure is considered to be a strongly π-conjugated biradical consisting of two galvinoxyl groups (AB- and BC-types), with two unpaired electrons in a molecular orbital, in which the B ring is common to both monoradical-AB and -BC. If the nucleus, X, is in the B ring, the splitting constant ($a_{i\text{-}B}^{bi}$) in the biradical will be the arithmetic average of the splitting constants from the monoradical-AB and -BC, as was proposed by Kopf *et al.*:[13]

$$a_{i\text{-}B}^{bi}=\frac{1}{2}(a_{AB}^{mono}+a_{BC}^{mono})$$

If X is in the A ring (which is not included in the monoradical-BC), $a_{BC}^{mono}=0$, thus:

$$a_{i\text{-}A}^{bi}=\frac{1}{2}a_{AB}^{mono}$$

Similarly, for the splitting constant ($a_{i\text{-}C}^{bi}$) of the C ring,

$$a_{i\text{-}C}^{bi}=\frac{1}{2}a_{BC}^{mono}$$

For the (ii) and (iii) structures, the hyperfine splittings may be similarly represented, using the hyperfine splittings of the monoradical. If the (i), (ii), and (iii) structures are equally probable, the hyperfine splitting (for instance, a_A^{bi}) of a given nucleus, X, in the A ring of the biradical may be represented, taking the contribution from the three valence-bond structures, as:

$$\begin{aligned}a_{i\text{-}A}^{bi}&=\frac{1}{3}(a_{i\text{-}A}^{bi}+a_{ii\text{-}A}^{bi}+a_{iii\text{-}A}^{bi})\\&=\frac{1}{3}\left\{\frac{1}{2}a_{AB}^{mono}+\frac{1}{2}a_{AC}^{mono}+\frac{1}{2}(a_{AB}^{mono}+a_{AC}^{mono})\right\}\\&=\frac{2}{3}a_{AB}^{mono}\end{aligned}$$

This is what is experimentally observed for the methyl and *meta*-ring protons of the (I), (II), and (III) biradicals, as has been described above; the observed hyperfine splittings for the biradicals agree exceedingly well with those calculated from the corresponding monoradicals, thus strongly supporting the above explanation.

Rigid Matrix ESR Spectra of the 1Me- and 2Me-Yang's Biradicals (II) and (III). The observation and detailed analysis of the rigid matrix ESR spectrum of Yang's biradical have been reported in a previous paper.[7] When the bisphenol precursor (bisphenol (II)) of the 1Me-Yang's biradical (II) was oxidized with PbO_2 in toluene under a vacuum, the yellow-brown color of the phenol solution immediately became the yellow-orange of the (II-AB) and (II-BC) monoradicals. Upon further oxidation, the color was changed to yellow-green. By quickly freezing the yellow-green solution containing the (II) biradical into a rigid glass (77 K), one can observe some dipolar splittings, as is shown in Fig. 4(b). The spectrum consists of two pairs of lines disposed about $g=2$ and a weak line at $g=2$ from the monoradicals. As has been described in a previous section, the (II) biradical is unstable at 20 °C; thus, the ESR observations were performed for several samples in order to minimize the central monoradical signal and in order to get a better spectrum. The best spectrum obtained is shown in Fig. 4(b). This spectrum remained unchanged after a period of several hours at 77 K. Upon annealing at 20 °C for 30 min, however, the yellow-green color disappeared along with the biradical signal. The spectrum of the 1Me-Yang's biradical shows a shape essentially the same as that of Yang's biradical (see Fig. 4(a)), except for the difference

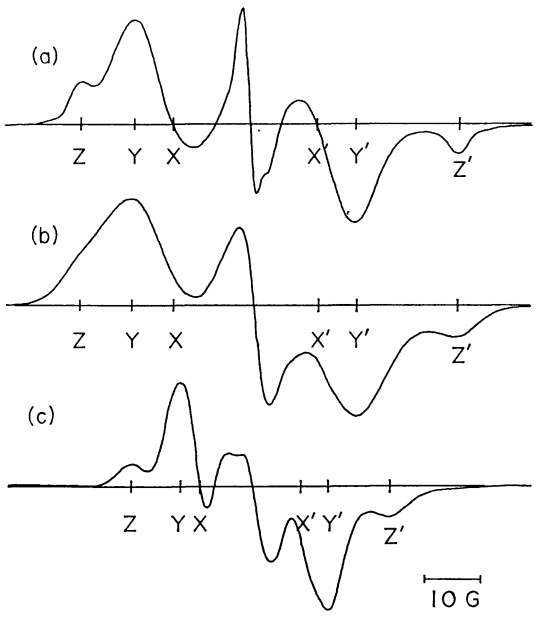

Fig. 4. Rigid matrix ESR spectra of (a) Yang's biradical (I), (b) 1Me-Yang's biradical (II), and (c) 2Me-Yang's biradical (III) in toluene at 77 K.

in the central monoradical intensity and the increase in the linewidth of each absorption line. The position and separation of the signals of the 1Me-Yang's biradical are quite similar to those of Yang's biradical. The zero-field splitting parameters (D and E) and $\boldsymbol{g}$-tensor values have been tentatively estimated from the positions of the three pairs of turning points (ZZ', YY', and XX'), as performed for Yang's biradical in a previous paper. These values are $D=34.2\pm0.2$ G, $E=2.2\pm0.4$ G, $g_{zz}=2.0030\pm0.0002$, $g_{yy}=2.0055\pm0.0002$, and $g_{xx}=2.0052\pm0.0002$. The average, $g_{av}=1/3(g_{xx}+g_{yy}+g_{zz})=2.0046\pm0.0002$, is in agreement with the isotropic $g_{iso}=2.00447\pm0.00005$ value measured at room temperature, indicating that the $\boldsymbol{g}$-tensor values obtained by the above analysis are consistent. Similarly, the toluene rigid-matrix ESR spectrum of the 2Me-Yang's biradical (III) has been measured. The ESR spectrum of the 2Me-Yang's biradical at 77 K is very different from those of Yang's biradical and the 1Me-Yang's biradical, as is shown in Fig. 4(c). The zero-field parameters and $\boldsymbol{g}$-tensor values were similarly estimated from the three pairs of turning points (ZZ', YY', and XX'), giving the values of $D=23.3\pm0.2$ G, $E=1.4\pm0.4$ G, $g_{zz}=2.0035\pm0.0002$, $g_{yy}=2.0041\pm0.0002$, $g_{xx}=2.0046\pm0.0002$, and $g_{av}=2.0040\pm0.0002$. The observed $\boldsymbol{D}$- and $\boldsymbol{g}$-tensor values of these biradicals, (II) and (III), are summarized in Table 2, together with those of Yang's biradical.

As has been described in a previous section, the results of the measurements of the solution ESR spectra of Yang's biradical (I) and its methyl derivatives (II) and (III) suggest that these radical molecules retain a three-fold symmetry in a fluid solution and show similar unpaired-spin distributions. On the other hand, since the axial spectra, *i.e.*, the spectra characterized by only one zero-field splitting parameter, D, could not be observed in any of these biradicals, (I), (II), or (III), these biradicals must lack a three-fold symmetry in a frozen solution. Yang's biradical and its methyl derivatives may be considered to have a propeller configuration, with a twist angle of about 30° in solution. Due to the delocalization of each unpaired electron, the principal Z axis of the $\boldsymbol{D}$-tensor, corresponding to the maximum $2D$ value (ZZ'), is probably parallel to the $2p_z$ orbital of the central triphenylmethyl carbon atom. Therefore, in the (I), (II), and (III) biradicals with non-zero E values, at least one of the twist angles of the three phenyl rings is different from those of the other two rings in the low-temperature rigid matrix. By substituting the methyl group for the tertiary butyl group, the steric interaction between the substituents will decrease to some extent. Consequently, the benzene ring into which the methyl groups are substituted will be twisted less than the other two benzene rings. Therefore, we can expect an increase in the D-parameter of the methyl derivatives in comparison with that of Yang's biradical.[14,15] However, in the 1Me-Yang's biradical, both the $\boldsymbol{g}$- and $\boldsymbol{D}$-tensor values are in good agreement with those of Yang's biradical. This, together with the results obtained in solution ESR spectra, gives further accurate evidence that monomethyl-substitution effects for molecular symmetry and spin-density distribution are negligible in Yang's biradical.

On the other hand, in the dimethyl derivative (III) of Yang's biradical, the change in the $\boldsymbol{D}$- and $\boldsymbol{g}$-tensor values is very remarkable. However, in contrast to the above expectation (an increase in the D-parameter), the D-parameter decreased 10.8 G compared to that (34.1 G) of Yang's biradical, suggesting an increase in the twist angle. In fact, the increase in the g_{zz} value and the decreases in the g_{yy} and g_{xx} values observed for the 2Me-Yang's biradical may also be explained by the increase in the twist angle. A notable solvent effect has been observed for the zero-field parameters of Yang's biradical; for instance, the D- and E-parameters vary from $D=34.6$ G and $E=1.5$ G in ethyl alcohol to $D=32.1$ G and $E=3.6$ G in diglyme.[8] The results suggest that the asymmetric environment due to frozen solvent molecules may contribute remarkably to a change in the conformation of the radical molecule. However, the change in the D-parameter of the 2Me-Yang's biradical is more remarkable than that due to the solvent effect. The reason why dimethyl-substitution effects are negligible in a fluid solution, while they are very remarkable in a frozen solution, is not clear at present.

Experimental

Measurements. The ESR spectra were obtained in the X band using a JES-ME-3X spectrometer equipped with a Takeda-Riken microwave frequency counter, which was used to measure the klystron frequency. The ESR splittings were determined using $(KSO_3)_2NO$ ($a^N=13.05\pm0.03$ G) as a standard. The g-values were measured relative to the value of Li-TCNQ powder, calibrated with $(KSO_3)_2NO$ ($g=2.0054$).[16] The proton magnetic reso-

nance spectra were recorded on a JEOLCO 4H-100 100 MHz spectrometer. The NMR spectra were measured in a C_6D_6 solvent, with tetramethylsilane as the internal standard.

Preparation of Specimens. The bisphenol and trisphenol precursors of Yang's biradical (I) and its methyl derivatives (II) and (III) were prepared according to a procedure similar to that used by Yang and Castro.[1] The condensation of 2,6-di-*t*-butylphenol, 2-*t*-butyl-6-methylphenol, and 2,6-dimethylphenol with 2,6-di-*t*-butyl-4-(3,5-di-*t*-butyl-4-hydroxybenzylidene)-2,5-cyclohexadien-1-one[17,18] in H_2SO_4–CH_3COOH gave a solid mixture of the bisphenol and the trisphenol, respectively. The mixture was separated by silica-gel-column chromatography (using benzene as the eluent). The subsequent removal of the benzene from bisphenol solution left a brick-red crystalline solid; this was heated at 160 °C for 5 h under a vacuum (0.1 Torr) to remove the solvent completely. The evaporation of the benzene from the trisphenol solution left pale yellow crystals, which were subsequently recrystallized twice from ethyl alcohol.

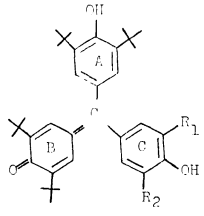

Bisphenol (I), $R_1=R_2=t$Bu
Bisphenol (II), $R_1=t$Bu, $R_2=CH_3$
Bisphenol (III), $R_1=R_2=CH_3$

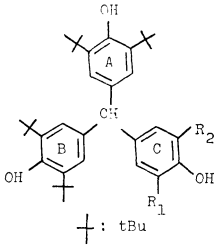

Trisphenol (I), $R_1=R_2=t$Bu
Trisphenol (II), $R_1=t$Bu, $R_2=CH_3$
Trisphenol (III), $R_1=R_2=CH_3$

Bisphenol (I). Mp 278.5—280.5 °C, brick red crystals; UV max 434 nm (log ε 4.50) in tetrahydrofuran; NMR 1.32 (36 H, s, *t*Bu, rings A and C), 1.54 (18 H, s, *t*Bu, ring B), 5.30 (2 H, s, OH), 7.53 (4H, s, aromatic H, rings A and C), 7.77 ppm (2H, s, aromatic H, ring B). Found: C, 82.30; H, 10.10%. Calcd for $C_{43}H_{62}O_3$: C, 82.83; H, 9.97%.

Trisphenol (I). Mp 241.0—242.0 °C, pale yellow crystals; UV max 278 nm (log ε 3.77) in cyclohexane; NMR 1.35 (54 H, s, *t*Bu), 4.87 (3 H, s, OH), 5.70 (1 H, s, CH), 7.43 ppm (6H, s, aromatic H). Found: C, 81.61; H, 10.54%. Calcd for $C_{43}H_{64}O_3$: C, 82.11; H, 10.26%.

Bisphenol (II). Mp 269.0—271.0 °C, brick red crystals; UV max 432 nm (log ε 4.46) in tetrahydrofuran; NMR 1.32 (18 H, s, *t*Bu, ring A), 1.47 (9 H, s, *t*Bu, ring C), 1.53 (18 H, s, *t*Bu, ring B), 1.59 (3 H, s, CH_3), 4.58 (1H, s, OH, ring C), 5.30 (1 H, s, OH, ring A), 7.10 (1 H, s, aromatic H neighboring the methyl group), 7.52 (2 H, s, aromatic H, ring A), 7.55(1 H, s, aromatic H neighboring the *t*-butyl group, ring C), 7.73 ppm (2 H, s, aromatic H, ring B). Found: : C, 82.04; H, 9.79%. Calcd for $C_{40}H_{56}O_3$: C, 82.14; H, 9.65%.

Trisphenol (II). Mp 213.5—214.5 °C, pale yellow crystals; UV max 278 nm (log ε 3.78) in cyclohexane; NMR 1.37 (36 H, s, *t*Bu, rings A and B), 1.51 (9H, s, *t*Bu, ring C), 1.64 (3H, s, CH_3), 4.12 (1 H, s, OH, ring C), 4.87 (2 H, s, OH, rings A and B), 5.62 (1 H, s, CH), 7.02 (1 H, s, aromatic H neighboring the methyl group, ring C), 7.38 (1 H, s, aromatic H neighboring the *t*-butyl group, ring C), 7.40 ppm (4H, s, aromatic H, rings A and B). Found; C, 81.60; H, 10.12%. Calcd for $C_{40}H_{58}O_3$: C, 81.86; H, 9.96%.

Bisphenol (III). Mp 270.0—271.5 °C, brick red crystals; UV max 430 nm (log ε 4.44) in tetrahydrofuran; NMR 1.33 (18 H, s, *t*Bu, ring A), 1.51 (9 H, s, *t*Bu, ring B), 1.53 (9H, s, *t*Bu, ring B), 1.90 (6 H, s, CH_3, ring C), 4.37 (1 H, s, OH, ring C), 5.28 (1 H, s, OH, ring A), 7.11 (2H, s, aromatic H, ring C), 7.50 (2 H, s, aromatic H, ring A), 7.70 ppm (2 H, s, aromatic H, ring B). Found: C, 81.77; H, 9.52%. Calcd for $C_{37}H_{50}O_3$: C, 81.87; H, 9.29%.

Trisphenol (III). Mp 170.5—172.0 °C, pale yellow crystals; UV max 278 nm (log ε 3.77) in cyclohexane; NMR 1.37 (36 H, s, *t*Bu, rings A and B), 1.91 (6 H, s, CH_3), 3.95 (1H, s, OH, ring C), 4.88 (2 H, s, OH, rings A and B), 5.59 (1 H, s, CH), 7.05 (2 H, s, aromatic H, ring C), 7.38 ppm (4H, s, aromatic H, rings A and B). Found: C. 81.58; H, 9.83%. Calcd for $C_{37}H_{52}O_3$: C, 81.57; H, 9.62%.

We are very grateful to Professor Kazuhiko Ishizu and Professor Yasuo Deguchi for their kind advice and encouragement. We are also grateful to Mr. Jun Sakamoto for his kind help in preparing the bisphenol precursors.

References

1) N. C. Yang and A. J. Castro, *J. Am. Chem. Soc.*, **82**, 6208 (1960).
2) D. Kearns and S. Ehrenson, *J. Am. Chem. Soc.*, **84**, 739 (1962).
3) K. Mukai, K. Ishizu, and Y. Deguchi, *J. Phys. Soc. Jpn.*, **27**, 783 (1969).
4) R. Kreilick, *J. Chem. Phys.*, **43**, 308 (1965).
5) P. W. Kopf and R. W. Kreilick, *J. Am. Chem. Soc.*, **91**, 6569 (1969).
6) H. V. Willigen, M. Plato, K. Möbius, K. P. Dinse, H. Kurreck, and J. Reusch, *Mol. Phys.*, **30**, 1359 (1975).
7) K. Mukai, T. Mishina, and K. Ishizu, *J. Chem. Phys.*, **66**, 1680 (1977).
8) K. Mukai, *Bull. Chem. Soc. Jpn.*, **51**, 313 (1978).
9) K. Mukai, K. Yorimitsu, and T. Mishina, *Bull. Chem. Soc. Jpn.*, **50**, 2471 (1977).
10) J. R. Bolton and A. Carrington, *Mol. Phys.*, **4**, 497 (1961).
11) E. de Boer and J. P. Colpa, *J. Phys. Chem.*, **71**, 21 (1967).
12) K. Möbius, H. Van Willigen, and A. H. Maki, *Mol. Phys.*, **20**, 289 (1971).
13) P. Kopf, K. Morokuma, and R. Kreilick, *J. Chem. Phys.*, **54**, 105 (1971).
14) A. Calder, A. R. Forrester, P. G. James, and G. R. Luckhurst, *J. Am. Chem. Soc.*, **91**, 3724 (1969).
15) K. Mukai and J. Sakamoto, *J. Chem. Phys.*, **68**, 1432 (1978).
16) J. J. Windle and A. K. Wiersema, *J. Chem. Phys.*, **39**, 1139 (1963).
17) M. S. Kharasch and B. S. Joshi, *J. Org. Chem.*, **22**, 1435 (1957).
18) A. Kosaki, H. Suga, S. Seki, K. Mukai, and Y. Deguchi, *Bull. Chem. Soc. Jpn.*, **42**, 1525 (1969).

The Combined Field Emission-Spin Trapping Method for Studying Reactions of Electrons in Organic Solutions

Shoji NODA, Yasunari OHTA, and Hiroshi YOSHIDA*

Faculty of Engineering, Hokkaido University, Kita-ku, Sapporo 060

(Received November 20, 1978)

The reactions of electrons injected by field emission into solutions have been investigated. Free radicals generated by the dissociative electron attachment to chlorinated solutes in benzene solutions were detected by the spin trapping-ESR method, using pentamethylnitrosobenzene as a spin trapping agent. Nondissociative electron attachment to styrene caused by the field emission was also evidenced by detecting the α-methylbenzyl radical generated secondarily from the styrene radical anion. The electrons field-emitted into the solutions are captured almost quantitatively by the electron scavenging solutes. The field emission method has been found to be useful for generating authentically free radicals and for studying the anionic reaction induced by electrons without interference of countercations and of any reaction intermediates from solvent molecules. As an example of the chemical utilization of the field emission technique, the ESR parameters of the spin adducts of several hydrocarbon radicals have been collected by this technique.

The reactions of electrons in solutions have been a leading subject in a variety of fields in chemistry.[1-3] The irradiation with ionizing radiations has been widely used to generate the electrons in solutions, though it simultaniously generates countercations which sometimes complicate the electron reactions to be studied. The photo-injection[4-8] and the field emission[8-10] of electrons from a metal cathode into liquids can also be used as electron sources. These methods generate the electrons in the solutions without accompanying countercations, but have been employed almost solely for studying the physical properties of the electrons in liquids, *i.e.*, electron mobility[4,8,9] and quasifree electron energy.[5-7,10] The field emission, emission of electrons from a sharp edge or a sharp tip of a metal cathode (emitter) at a high negative field, readily gives a current as high as 10^{-5} A.[11] Nevertheless, the utilization of this method in chemical reaction study has been limited to the polymerization of styrene and α-methyl-styrene.[11-13]

In order to exploit the chemical utilization of the field emission method, we have recently studied the dissociative and nondissociative attachments to organic solutes of the electrons field-emitted into benzene solutions. Free radicals, the short-lived intermediate products of the electron attachment reactions, have been detected by the spin trapping-ESR technique, in which the short-lived free radicals are transformed into stable nitroxyl radicals (to be detected readily by conventional ESR measurements) through the reactions with a proper nitroso compound or a nitrone compound (spin trap) coexisting in the solutions.[14-17]

The present investigation will give several aspects of the electron attachment in solution for some model reaction systems studied by the combined field emission-spin trapping method, and will demonstrate the general prospect of the field emission method for chemical utilizations.

Experimental

A field emission cell was made of pyrex glass tubes equipped with an emitter (a razor blade of 0.7 cm length) and a collecting electrode (a brass rod, 1.0 cm diameter) facing each other at a distance of 0.1—0.2 cm, as shown in Fig. 1.

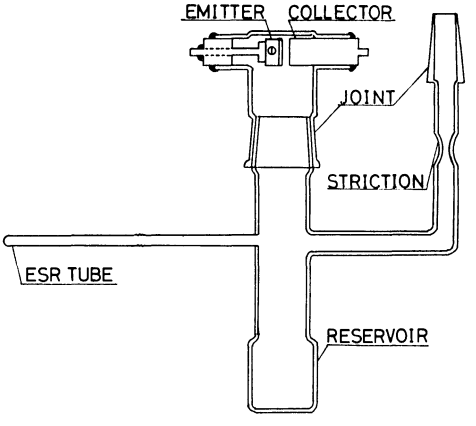

Fig. 1. Field emission cell.

The cell has a thin quartz tube (0.4 cm outer diameter) for ESR measurements. The emitter could be readily changed by disconnecting a part of the cell by means of a taper joint. The emitter and the collecting electrode could be completely covered with 3 ml of solution by turning the cell upside down. A high voltage, up to 15 kV, was applied by a stabilized high voltage supply. Typically *ca.* 5×10^{-5} F·dm^{-3} of electronic charge was field-emitted into a solution by generating for 1 h, a field emission current (monitored with an electronic microammeter) of 5 μA at a voltage of 5 to 6 kV applied to the emitter. Such a current induced a significant bulk flow of the solution, which was visible as a violent disturbance at the surface of the solution.

Benzene, ethanol, and cyclohexane of spectrograde were used as received. All organic halides used as solutes were purified by vacuum distillation. Styrene was purified as described elsewhere.[18] Pentamethylnitrosobenzene synthesized as described elsewhere[19] was used as a spin trap. The solutions were degassed by repeated freeze-pump-thaw cycles, sealed in the cell, subjected to a high applied voltage for the field emission, and examined by a conventional ESR spectrometer with a 100 kHz magnetic field modulation. All the experiments were carried out at ambient temperature.

Results and Discussion

Dissociative Electron Attachment. The dependence of the field emission current on the applied voltage is shown in Fig. 2, for the benzene solution of benzyl chloride (0.04 mol·dm^{-3}) and spin traps

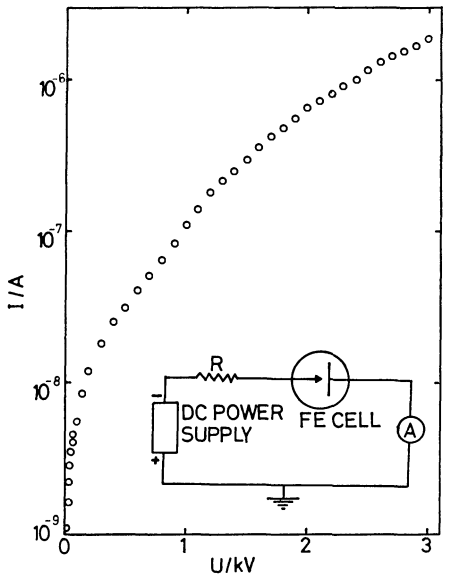

Fig. 2. Emission current-voltage curve for the benzene solution of benzyl chloride (0.04 mol·dm^{-3}) and the spin trap (0.002 mol·dm^{-3}). The electric circuit for the field emission experiment is also shown in the figure.

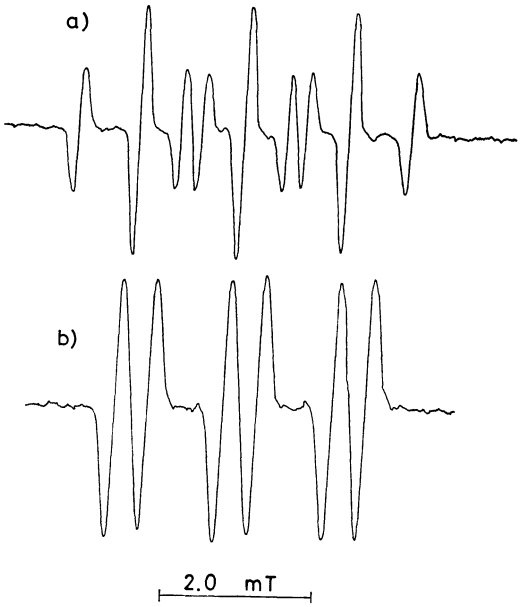

Fig. 3. ESR spectra of the spin-adduct radicals observed in a) the benzene solution of benzyl chloride (0.04 mol·dm^{-3}) and in b) the benzene solution of styrene (0.1 mol·dm^{-3}) and ethanol (0.2 mol·dm^{-3}). The concentration of the spin trap is 0.002 mol·dm^{-3} in both solutions.

(0.002 mol·dm^{-3}). The current increases with the applied voltage sharply in the low voltage region and then slowly in the higher region. The steep increase in the current indicates the onset of the field emission. The onset occurs at a high applied voltage for cyclohexane solutions. The characteristics of the current-voltage curve have been studied in detail for several liquids,[10] and the onset of the field emission has been found to depend on the quasifree electron energy in the liquids.

Spin adduct radicals were found by ESR to be generated in the solution to which electrons had been field-emitted (Fig. 3A). The spin adduct radicals indicated by hyperfine splitting due to a nitrogen nucleus (0.14 mT) and two equivalent protons (0.084 mT) have been identified to be the nitroxide radicals generated by the reaction between the spin trap and benzyl radical.[19] The latter are unquestionably the products of the dissociative electron attachment to benzyl chloride. The yield of the adduct radicals (5×10^{-5} mol·dm^{-3}) was very close to the field-emitted charge (2×10^{-7} F, or *ca.* 7×10^{-5} F·dm^{-3}). This indicates that 0.04 mol·dm^{-3} of benzyl chloride effectively scavenges all the emitted electrons. The spin trap can act as an electron scavenger.[14] In the present experiments, however, the concentration of electron-scavenging solutes is higher than that of the spin trap by one to three orders of magnitude, so that the solutes preferentially compete with the spin trap in reacting with the field-emitted electron. The field emission appears to provide a method to study selectively and quantitatively the electron reactions with the solutions.

Twelve free radicals were generated from the corresponding chlorinated compounds in benzene and studied by the combined field emission-spin trapping method. The ESR parameters of the spin adduct of these free radicals are summarized in Table 1, where some other spin adducts generated by other means[19] are also included for comparison. The spin-trapped free radicals were, in almost all the cases, those generated by the dissociative electron attachment (by the rupture of the C–Cl bond) to the solutes. No free radical from solvents was generated by field emission into benzene and cyclohexane solutions of the chlorinated compounds, whereas in γ-radiolysis the solvent radicals were also generated and spin-trapped. Field emission is a useful method to generate authentically free radicals. From *o*- and *p*-chlorotoluenes, both *o*- and *p*-chlorobenzyl radicals and *o*- and *p*-methylphenyl radicals were generated and spin-trapped. The former radicals may have been formed secondarily by the hydrogen abstraction of the latter.

Nondissociative Electron Attachment. When the benzene solution of styrene (0.1 mol·dm^{-3}), ethanol (0.2 mol·dm^{-3}), and the spin traps (0.002 mol·dm^{-3}) were subjected to the field emission, the α-methylbenzyl radical was identified by observing the ESR spectrum of its spin adduct (see Fig. 3B), which contained the hyperfine splitting due to a nitrogen nucleus (0.144 mT) and a proton (0.044 mT).[19] However, no ESR spectrum was observed in the absence of ethanol under the same conditions of measurement. Ethanol takes an essential role in the formation of α-methylbenzyl radical, which very probably results from the proton transfer from ethanol to a styrene radical anion generated by the nondissociative electron attachment to styrene. The presence of styryl radical was confirmed in the benzene–ethanol solution of phenyl acetylene. Its formation can be interpreted, in the same way, by the nondissociative electron attachment followed by the proton transfer. ESR parameters of these free radicals are also included in Table 1.

TABLE 1. HYPERFINE SPLITTING CONSTANTS AND *g*-VALUES FOR SPIN ADDUCTS (NITROXIDES) FORMED FROM PENTAMETHYLNITROSOBENZENE AS A SPIN TRAP IN BENZENE AT ROOM TEMPERATURE

Trapped radical	Radical sourse	*g*-value	a_N/mT	$a_{\beta H}$/mT
$\cdot CH_3$[a]	$CH_3I+(n\text{-}C_4H_9)_3SnH$	2.0058	1.38	1.23
$\cdot CH_2CH_3$	CH_3CH_2Br+FE	2.0062	1.40	1.16
$\cdot CH_2CH_2CH_3$[a]	$n\text{-}C_3H_7Cl+\gamma$	2.0058	1.42	1.12
$\cdot CH(CH_3)_2$[a]	$CHCl(CH_3)_2+\gamma$	2.0059	1.39	0.77
$\cdot CH(CH_3)CH_2CH_3$[a]	$CHCl(CH_3)C_2H_5+\gamma$	2.0058	1.37	0.78
$\cdot C(CH_3)_3$	$t\text{-}C_4H_9Cl+FE$	2.0060	1.35	—
$\cdot C(CH_3)_2CH_2C(CH_3)_3$	C_8H_{18}[b]	2.0060	1.35	—
$\cdot cyclo\text{-}C_6H_{11}$[a]	$cyclo\text{-}C_6H_{12}+\gamma$	2.0058	1.40	0.76
$\cdot CH_2C_6H_5$	$C_6H_5CH_2Cl+FE$	2.0062	1.40	0.84
$\cdot CH_2C_6H_4(o\text{-Cl})$	$o\text{-}ClC_6H_4CH_3+FE$	2.0061	1.40	0.88
$\cdot CH_2C_6H_4(p\text{-Cl})$	$p\text{-}ClC_6H_4CH_3+FE$	2.0062	1.40	0.84
$\cdot CH(CH_3)C_6H_5$	$CH_3CHClC_6H_5+FE$	2.0060	1.44	0.44
$\cdot CH(C_6H_5)_2$	$(C_6H_5)_2CHCl+FE$	2.0061	1.42	<0.24
$\cdot C_6H_5$	C_6H_5Br+FE	2.0058	1.03	0.28(*o*, *p*-) 0.10(*m*-)
$\cdot CH{=}CHC_6H_5$	$C_6H_5CH{=}CHBr+FE$	2.0063	1.34	0.40
$\cdot CH_2\text{-}C(Cl){=}CH_2$	$CH_2{=}C(Cl)CH_2Cl+FE$	2.0060	1.36	0.88
$\cdot C(CH_3){=}CHCH_3$	$CH_3C(Cl){=}CHCH_3+FE$	2.0061	1.37	—
$\cdot CH(CH_3)CH{=}CH_2$	$CH_3CH(Cl)CH{=}CH_2+FE$	2.0061	1.34	0.80
$\cdot CH(CH_3)OC_2H_5$[a]	$(C_2H_5)_2O+\gamma$	2.0058	1.40	0.46
$\cdot CH(CH_3)C(=O)CH_3$	$CH_3CHClC(=O)CH_3+FE$	2.0060	1.36	0.41
$\cdot C(CH_3)O$[a]	$(CH_3CO)_2+h\nu$	2.0058	1.32	—
$\cdot C(CN)(CH_3)_2$[a]	$((CH_3)_2C(CN)N{:})_2+h\nu$	2.0063	1.30	—
$\cdot CH_2Si(CH_3)_3$[a]	$Si(CH_3)_4+\gamma$	2.0060	1.38	1.58

a) Ref. 19. b) 2,2,4-Trimethylpentane.

Schnabel and Schmidt[12] have studied the field emission into bulk styrene and found no indication of its anionic polymerization. They suggested that the electron attachment to styrene does not occur because it possesses a negative electron affinity in the gas phase. In this connection, Horloyd[20] has demonstrated that an electron can be localized on a single styrene molecule in liquid hydrocarbons, whereas Shinsaka and Freeman[21] have inferred that an electron cannot be localized on a single molecule in bulk aromatic compounds, but rather moves freely and is delocalized. The present result indicates that the field-emmitted electron in the benzene solution can be localized on a styrene molecule or a phenylacetyrene molecule to form the corresponding radical anion.

Based on the possible electron localization on a styrene molecule, we attempted the anionic polymerization of styrene by the field emission method in benzene, as well as in cyclohexane and in diethyl ether, all carefully purified and dried by the standard methods in polymer chemistry.[22] A small amount of polymer was actually obtained in benzene and cyclohexane with a field-emitted charge of *ca.* 10^{-5} F, but not in diethyl ether. The polymerization was inhibited by adding triethylamine, an inhibitor for the cationic polymerization, into the benzene and the cyclohexane solutions. In addition, nitroethylene could not be polymerized by the field emission in toluene or in diethyl ether. It is a monomer polymerizable exclusively by the anionic mechanism.[23] These results seems to indicate that the radical anions generated by the field emission have a lifetime too short to grow sufficiently long polymer chains before being neutralized at the collecting electrode.

Ionization by the Injected Electrons. The field emission into the benzene solution of 0.2 mol·dm^{-3} ethanol and 0.02 mol·dm^{-3} spin traps generated the spin adduct of the phenyl radical, while no ESR spectrum was observed without ethanol. The phenyl radical adduct formation was efficiently suppressed by an electron scavenger, such a *t*-butyl chloride or styrene. The phenyl radical formation from benzene cannot be interpreted by anionic reactions initiated by the field-emitted electron, but it tentatively attributed to the cationic mechanism: the ionization of benzene by an energetic electron giving a benzene radical cation, which transfers a proton to ethanol and transforms to a phenyl radical. The emitted electron can be accelerated by a locally high electric field near the sharp edge of the emitter. Since the initial kinetic energy of the field-emitted electron is 4 to 5 eV[24] and the local electric field is thought to be 10^7—10^8 V/cm, it is probable that the electron attains a kinetic energy of *ca.* 10 eV.

The ionization energy of a molecule in condensed media is generally less than that in the gas phase by the sum of the polarization energy of a resultant positive ion, P_t, and the quasifree electron energy in the media, V_0.[25] For benzene, the gas phase ionization energy is 9.6 eV,[26] and P_t and V_0 are roughly estimated

to be -2 eV[25] and -0.1 eV[27] in liquid phase. Thus, the ionization energy is expected to be about 7.5 eV for liquid benzene, which can be ionized by the field-emitted electron after being accelerated. Such an ionization process has been demonstrated by Schnabel and Schmidt[12] for the field emission into liquid styrene.

In the presence of an electron scavenger, the emitted electrons are scavenged before being accelerated to a significant kinetic energy. This is the reason why the anionic reactions occur only in the presence of the electron scavenger.

Conclusions. The field emission into liquid solutions is a promising technique to study dissociative and nondissociative electron attachment reactions in the solutions. This is superior to the radiation chemical techniques in that the anionic reactions exclusively occur in the solutions without being interferred with the reactive intermediate coming from solvent molecules. The field emission has been used, as an example of its chemical utilization, for the authentic generation of several free radicals, whose spin adducts were examined by the ESR method. The ESR parameters of the spin adducts thus determined (Table 1) will be helpful for the spin trapping studies using pentamethylnitrosobenzene as the spin trap.

References

1) M. S. Matheson, "Physical Chemistry," ed by H. Eyring, D. Henderson, and W. Jost, Academic Press, New York (1975), Vol. VII, Chap. 10.

2) A. O. Allen and R. A. Holroyd, *J. Phys. Chem.*, **78**, 796 (1974).

3) J. C. Devins, S. J. Rzad, and R. J. Schwabe, *J. Phys. D: Appl. Phys.*, **9**, L87 (1976).

4) R. M. Minday, L. D. Schmidt, and H. T. Davis, *J. Chem. Phys.*, **54**, 3112 (1971).

5) R. A. Holroyd and M. Allen, *J. Chem. Phys.*, **54**, 5014 (1971).

6) S. Noda and L. Kevan, *J. Chem. Phys.*, **61**, 2467 (1974).

7) W. Tauchert, H. Jungblut, and W. F. Schmidt, *Can. J. Chem.*, **55**, 1860 (1977).

8) B. Halpern, J. Lekner, S. A. Rice, and R. Gomer, *Phys. Rev.*, **156**, 351 (1967).

9) B. Halpern and R. Gomer, *J. Chem. Phys.*, **51**, 1031 (1969).

10) K. Dotoku, H. Yamada, S. Sakamoto, S. Noda, and H. Yoshida *J. Chem. Phys.*, **69**, 1121 (1978).

11) W. F. Schmidt and W. Schnabel, *Ber. Bunsenges. Phys. Chem.*, **75**, 654 (1971).

12) W. Schnabel and W. F. Schmidt, *J. Polym. Sci. Symp.*, **42**, 273 (1973).

13) W. Wablat, W. F. Schmidt, and W. Schnabel, *Makromol. Chem.*, **175**, 2687 (1974).

14) M. Shiotani, S. Murabayashi, and J. Sohma, *Int. J. Radiat. Phys. Chem.*, **8**, 483 (1976).

15) K. A. Mclauchlan and R. C. Sealy, *J. Chem. Soc., Chem. Commun.*, **1976**, 115.

16) T. Kunitake and S. Murakami, *J. Polym. Sci.*, **12**, 67 (1974).

17) T. Doba, T. Ichikawa, and H. Yoshida, *Bull. Chem. Soc. Jpn.*, **50**, 3158 (1977).

18) S. Noda, Y. Fujii, and H. Yoshida, *Bull. Chem. Soc. Jpn.*, **50**, 226 (1977).

19) T. Doba, T. Ichikawa, and H. Yoshida, *Bull. Chem. Soc. Jpn.*, **50**, 3124 (1977).

20) R. A. Holroyd, *Ber. Bunsenges. Phys. Chem.*, **81**, 298 (1977).

21) K. Shinsaka and G. R. Freeman, *Can. J. Chem.*, **52**, 3495 (1974).

22) H. Yoshida, M. Irie, and K. Hayashi, ESR Applications to Polymer Research (Novel Symposium 22), ed by P. -O. Kinnel and B. Rånby, Almqvist & Wiksell, Stockholm (1973), p. 129.

23) K. Tsuji, H. Yamaoka, K. Hayashi, H. Kamiyama, and H. Yoshida, *Polym. Lett.*, **4**, 629 (1966).

24) R. Gomer, "Field Emission and Field Ionization," Harvard Univ. Press, Cambridge, Massachusetts (1961), Chap. 1.

25) R. A. Holroyd and R. C. Russell, *J. Phys. Chem.*, **78**, 2128 (1974).

26) "Handbook of Chemistry and Physics," 48th ed, by R. S. Weast, Chemical Rubber Co., Cleveland, Ohio (1967—1968).

27) R. Schiller, Sz. Vass, and J. Mandics, *Int. J. Radiat. Phys. Chem.*, **5**, 491 (1973).

The Solvent Extraction of Several Univalent Metal Picrates by 15-Crown-5 and 18-Crown-6

Yasuyuki TAKEDA* and Hiroshi GOTŌ

Department of Chemistry, Faculty of Science, Chiba University, Yayoi-chō, Chiba 260

(Received November 24, 1978)

The overall extraction equilibrium constants (K_{ex}) for 1:1:1 complexes of 15-crown-5 (15C5) and 18-crown-6 (18C6) with several univalent metal picrates between benzene and water have been determined at 25 °C. The K_{ex} sequences of the univalent metal ion with 15C5 and 18C6 are $Ag^+ > Na^+ > Tl^+ \gg K^+ > Rb^+ > Cs^+ > Li^+$ and $Tl^+ > K^+ > Rb^+ > Ag^+ > Cs^+ > Na^+ \gg Li^+$ respectively. The K_{ex} series for each same crown ether reflects the stability and the extractability of the univalent metal ion–crown ether complex in the aqueous phase. The K_{ex} sequences for the 15C5 system depends entirely on the extractability of the univalent metal ion–crown ether complex. In the case of the 18C6 system this largely depends on the stability of the univalent metal ion–crown ether complex.

It has been reported that crown ethers form stoichiometrically stable complexes with a variety of cations, especially those of the alkali and alkaline earths, and that the stability of the complexes, in which the cation is held in the center of the crown ether cavity, depends primarily on the ratio of the ionic size to the cavity size of the crown ether.[1)]

Solvent extraction is an available and convenient method for investigating the complexing ability of crown ethers for various cations, and several extraction studies have been reported to date.[2)] In some of the studies the extractability of the metal cation–crown ether complex as well as that of the metal cation have been discussed in detail.[2b,d)]

In this paper, the overall extraction equilibrium constant values for the univalent metal cation–15-crown-5 (15C5) and 18-crown-6 (18C6) systems have been determined and the overall extraction equilibria analyzed by constituent equilibria. Since a large anion is readily extracted into nonpolar solvents,[2d)] the picrate anion has been used as the counter ion. Benzene has been used as the solvent on account of its nonpolarity.

Experimental

Materials. 15C5 and 18C6 were purchased from Nisso Co., Ltd. and used without further purification. Analytical-grade benzene, HNO_3, $LiOH \cdot H_2O$, NaOH, KOH, and reagent-grade $TlNO_3$ were obtained from Wako-Pure Chemicals Ltd. $AgNO_3$ and picric acid were analytical grade reagents obtained from Koso Chemical Co., Ltd. Reagent-grade RbOH and CsOH were obtained from Mitsuwa Pure Chemicals Ltd., and Kanto Chemical Co., Inc., respectively. The purities of $AgNO_3$ and $TlNO_3$, and the concentrations of the alkali metal hydroxides and picric acid solutions were determined by means of KCl, EDTA, acid and basic titrations, respectively. Benzene was washed twice with distilled water.

Apparatus and Procedure. The organic phase of the crown ether (6.0×10^{-5}—6.6×10^{-2} M; 1 M=1 mol dm^{-3}) and the aqueous phase of the univalent metal hydroxide or nitrate (9.9×10^{-4}—3.2×10^{-2} M) and the picric acid (1.0×10^{-3}—1.1×10^{-2} M) in stoppered glass tubes (30 ml) were shaken in a thermostated water bath for approx. 30 min at 25±0.2 °C and centrifuged. The initial volume of each phase was 10 ml in all cases. A portion of the aqueous phase 8 ml was transferred to a 10 ml beaker and the hydrogen ion concentration determined by a Hitachi-Horiba F-5 pH meter. For the univalent metal hydroxide and nitrate systems the extractions were conducted at pH 9.7—12.1 and pH 2.3—2.8, respectively. For the systems of the alkali metals–15C5 and 18C6, a portion of the organic phase 8 ml was transferred to a 50 ml beaker and allowed to evaporate over several days. The residue was dissolved in 0.01 M NaOH aqueous solution 8 ml and the picrate concentration determined at 356 nm by a Shimadzu UV-200 spectrophotometer ($\varepsilon = 1.45 \times 10^4$ cm^{-1} M^{-1}). For the systems of Ag and Tl–15C5 and 18C6, the metal in the organic phase was back-extracted into 1 M nitric acid aqueous solution 8 ml and the metal concentration in the aqueous phase determined by a Seiko SAS-725 atomic absorption spectrophotometer. In control experiments in the absence of either the crown ether or picric acid, for the alkali metals and Tl–15C5 and 18C6 system, and for the Ag–15C5 and 18C6 system it was found that there was no extraction and a little extraction, respectively.

The Distribution Coefficient of the Crown Ether. A portion 13 ml of benzene solution containing the crown ether and an equal volume of distilled water were placed in a stoppered glass tube and shaken under the same conditions as above. The range of concentration of 15C5 and 18C6 were from 5.1×10^{-2} to 3.3×10^{-1} M and from 2.8×10^{-2} to 3.1×10^{-1} M, respectively. After centrifuging, a portion 12 ml of the organic phase was transferred to a 10 ml beaker, allowed to evaporate over several days, and the residue weighed. The average distribution coefficients determined in this way are given in Table 1.

Results

In an equilibrium between an aqueous solution of a univalent metal ion, M^+, a picrate ion, A^-, and a benzene solution of a crown ether, L, the equilibrium constants may be defined by the following equations:

$$K_{ex} = [MLA]_0[H^+]/[M^+][L]_0[HA]_0 \quad (1)$$

$$K_{D,L} = [L]_0/[L] \quad (2)$$

$$K_{ex}(HA) = [HA]_0/[H^+][A^-] \quad (3)$$

$$K_{ML} = [ML^+]/[M^+][L] \quad (4)$$

$$K_{ex'} = [MLA]_0/[ML^+][A^-] \quad (5)$$

where the subscript "0" and the lack of subscript designates the organic phase and the aqueous phase, respectively: square brackets indicate the molar concentrations. Thus K_{ex} can be written as follows:

$$K_{ex} = K_{D,L}^{-1}K_{ex}(HA)^{-1}K_{ML}K_{ex'} \quad (6)$$

From the mass balance, $[L]_0$, $[M^+]$, and $[A^-]$ may be given by;

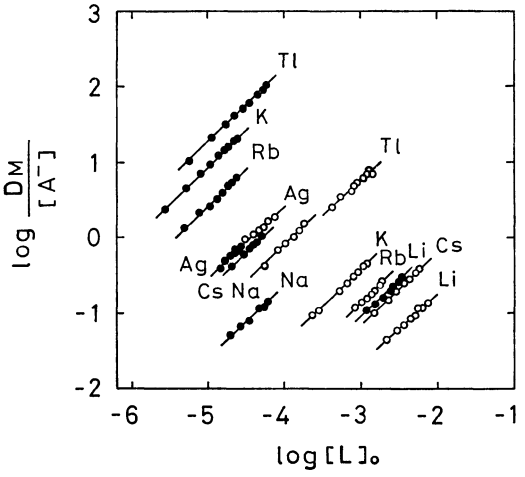

Fig. 1. Plots of log (D_M/[A$^-$]) *vs.* log[L]$_0$ for the 15C5 and 18C6 systems at 25 °C. ○: 15C5, ●: 18C6.

$$[L]_0 = ([L]_t - [MLA]_0)/(\alpha+\beta[M^+]) \quad (7)$$

$$[M^+] = ([M]_t - [MLA]_0)/(1+\beta[L]_0) \quad (8)$$

$$[A^-] = ([HA]_t - [MLA]_0)/\{1+(K_{HA}+K_{ex}(HA))[H^+]\} \quad (9)$$

where the subscript "t" denotes the total concentration, $\alpha=1+K_{D,L}^{-1}$, and $\beta=K_{ML}K_{D,L}^{-1}$. The value of K_{ex} (HA) has spectrophotometrically been determined as 247 using the association constant of picric acid ($K_{HA}=1.9_5$[3]). Substitution of Eq. 8 into Eq. 7 gives:

$$[L]_0 = [-\{\alpha+\beta([M]_t-[L]_t)\} + \sqrt{\{\alpha+\beta([M]_t-[L]_t)\}^2-4\alpha\beta([MLA]_0-[L]_t)}]/2\alpha\beta \quad (10)$$

The distribution ratio of the univalent metal may be represented by

$$D_M = [MLA]_0/([M^+] + [ML^+]) \quad (11)$$

In the case of $[M^+] \gg [ML^+]$, Eq. 11 becomes

$$D_M = K_{ex}K_{ex}(HA)[L]_0[A^-] \quad (12)$$

The log(D_M/[A$^-$]) *vs.* log[L]$_0$ plot in Fig. 1 shows a linear relationship with a slope of 1 in every case, indicating that the crown ether forms a 1:1 complex with the univalent metal ion. The values of [L]$_0$ and [A$^-$] in Eq. 12 were calculated from Eqs. 10 and 9, respectively. For the Li$^+$–15C5 and 18C6 systems, however, the value of [L]$_0$ has been calculated from Eq. 7, neglecting the term, β[M$^+$]. The equilibrium constants obtained from these data are summarized in Table 1, together with the literature values.

Discussion

From Table 1, the log K_{ex} series for 15C5 and 18C6 for the alkali metal ions are given by $Na^+ \gg K^+ > Rb^+ > Cs^+ > Li^+$ and $K^+ > Rb^+ > Cs^+ > Na^+ \gg Li^+$, respectively, indicating that the extractability of the alkali metal ion depends on the ratio of the ionic size to the cavity size of the crown ether, as can be seen in Table 2. Although the crystal radii of the Ag$^+$ and Tl$^+$ ions are nearly equal to that of the K$^+$ ion (Table 2), for the 15C5 system the log K_{ex} values for Ag$^+$ and Tl$^+$ are much larger than that for K$^+$, and for the 18C6 system the log K_{ex} value for K$^+$ is much larger than that for Ag$^+$ and a little smaller than that for Tl$^+$ (Table 1).

Table 1. Summary of equilibrium constants at 25 °C

Crown ether	$K_{D,L}$	Cation	log K_{ex}	log $K_{ex'}$	log K_{ML}[4]
15C5	0.15_6	Li$^+$	−1.10	—	—
		Na$^+$	1.51	2.40	0.70
		K$^+$	0.19	1.04	0.74
		Rb$^+$	−0.25	0.72	0.62
		Cs$^+$	−0.49	0.30	0.8
		Ag$^+$	2.06	2.71	0.94
		Tl$^+$	1.41	1.77	1.23
18C6	0.063_4	Li$^+$	−0.47	—	—
		Na$^+$	1.00	1.39	0.80
		K$^+$	3.58	2.74	2.03
		Rb$^+$	3.04	2.67	1.56
		Cs$^+$	1.99	2.19	0.99
		Ag$^+$	2.05	1.74	1.50
		Tl$^+$	3.91	2.83	2.27

Table 2. Crystal ionic radii of univalent metals and cavity radii of crown ethers (Å)

Cation	Crystal ionic radius[5]	Crown ether	Cavity radius[6]
Li$^+$	0.60	15-crown-5	0.85–1.1
Na$^+$	0.95	18-crown-6	1.3–1.6
K$^+$	1.33		
Rb$^+$	1.48		
Cs$^+$	1.69		
Ag$^+$	1.26		
Tl$^+$	1.40		

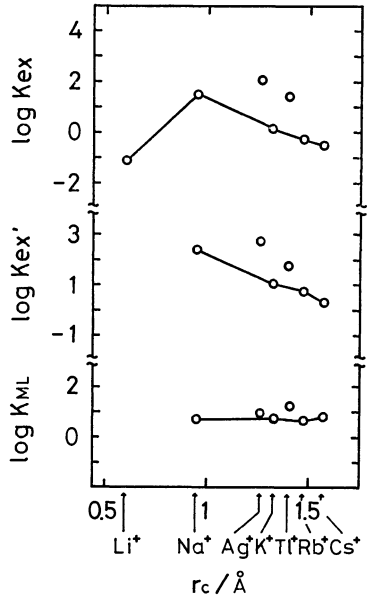

Fig. 2. Plots of logK_{ex}, log$K_{ex'}$, and logK_{ML} *vs.* crystal ionic radius, r_c, of univalent metal for the 15C5 system.

In the case of Ag$^+$ and Tl$^+$, it may be seen from Tables 1 and 2 that the univalent metal ion which has a more optimum size for the crown ether cavity shows a greater extractability, which is the same tendency for the alkali metal ions reported above.

It may be seen from Table 1 that the log $K_{ex'}$ se-

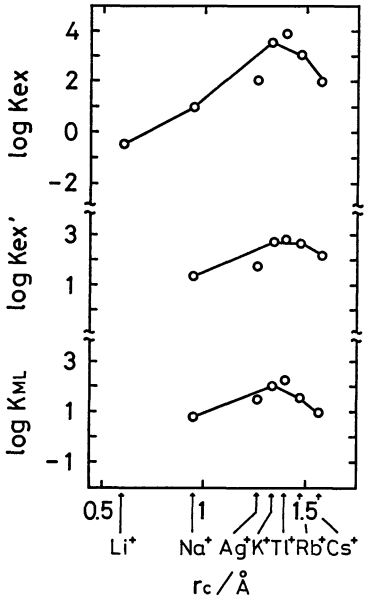

Fig. 3. Plots of $\log K_{ex}$, $\log K_{ex'}$, and $\log K_{ML}$ *vs.* crystal ionic radius of univalent metal for the 18C6 system.

quences of the alkali metal ions with 15C5 and 18C6 are $Na^+ \gg K^+ > Rb^+ > Cs^+$ and $K^+ \geq Rb^+ > Cs^+ > Na^+$, respectively. For the 15C5 system the $\log K_{ex'}$ value for Ag^+ is larger than that for Tl^+, and on the contrary for the 18C6 system (Table 1). The results show that the more closely the univalent metal ion fits into the crown ether cavity, the more extractable is the univalent metal ion–crown ether complex (Table 2). Consequently, the extractability of the univalent metal ion–crown ether complex is affected by the chemical nature of the univalent metal ion held in the cavity of the crown ether.

Equation 6 shows that the series for K_{ex} for the same crown ether for different univalent metal ions reflects the stability and the extractability of the univalent metal ion–crown ether complex in the aqueous phase. Plots of $\log K_{ex}$, $\log K_{ex'}$, and $\log K_{ML}$ *vs.* the crystal ionic radius for the 15C5 and 18C6 systems are given in Figs. 2 and 3, respectively. It may be seen from Figs. 2 and 3 that the $\log K_{ex}$ sequences for the 15C5 system depend completely on the $\log K_{ex'}$ sequences. On the other hand those for the 18C6 system largely depend on the $\log K_{ML}$ ones.

The authors would like to thank Mr. Fujio Takahashi of this laboratory for experimental assistance.

References

1) a) C. J. Pedersen, *J. Am. Chem. Soc.*, **89**, 7017 (1967); b) C. J. Pedersen, *ibid.*, **92**, 386 (1970).

2) a) C. J. Pedersen, *Fed. Proc., Fed. Am. Soc. Exp. Biol.*, **27**, 1305 (1968); b) H. K. Frensdorff, *J. Am. Chem. Soc.*, **93**, 4684 (1971); c) A. Sadakane, T. Iwachido, and K. Tōei, *Bull. Chem. Soc. Jpn.*, **48**, 60 (1975); d) P. R. Danesi, H. Meider-Gorican, R. Chiarizia, and G. Scibona, *J. Inorg. Nucl. Chem.*, **37**, 1479 (1975); e) M. Jawaid and F. Ingman, *Talanta*, **25**, 91 (1978).

3) "Dissociation Constants of Organic Acids in Aqueous Solution," ed by G. Kortün, W. Vogel, and K. Andrussov, Butterworths, London (1961).

4) R. M. Izatt, R. E. Terry, B. L. Haymore, L. D. Hansen, N. K. Dalley, A. G. Avondet, and J. J. Christensen, *J. Am. Chem. Soc.*, **98**, 7620 (1976).

5) L. Pauling, "The Nature of the Chemical Bond," 3rd ed, Cornell Univ. Press (1960).

6) H. K. Frensdorff, *J. Am. Chem. Soc.*, **93**, 600 (1971).

ESR Study of Molecular Oxygen Anion Radicals Produced on Cation-exchanged X-Type Zeolites by γ-Irradiation

Natsuko KANZAKI* and Iwao YASUMORI

Department of Chemistry, Tokyo Institute of Technology, O-okayama, Meguro-ku, Tokyo 152

(Received December 20, 1978)

Molecular Oxygen anion radicals (O_2^-) were produced on X-zeolites by γ-irradiation in the presence of O_2. Their properties were systematically investigated by means of ESR spectroscopy. Two kinds of O_2^- species with different g_z values were formed on monovalent cation-exchanged (LiX, KX, RbX, CsX) zeolites and MgX, while three and single O_2^- species were observed on divalent cation-exchanged (CaX, SrX, BaX) and trivalent cation-exchanged (LaX) zeolites, respectively. These O_2^- radicals showed different reactivities with N_2O or 1-butene, and their g_z values were classified into four groups. By considering the results from the g_z values and the effect of introduced high pressure O_2 on the O_2^- spectra, the adsorption sites for the radicals on zeolites were determined.

Many Studies have been done about O_2^- radicals adsorbed on various kinds of oxides and zeolites by the use of electron spin resonance technique.[1-11] Based on these studies, the influence of the electric charge of surface cations on the g-factor anisotropy for the adsorbed O_2^- radicals has been discussed.[1,2,5,7] Kasai found that O_2^- was formed on Y-type zeolites by γ-irradiation and the deviation of the maximum principal g value (g_z) for the adsorbed O_2^- on a monovalent zeolite NaY from that of a free electron (g_e) was twice as large as the deviation for O_2^- on a divalent zeolite BaY.[6]

Wang *et al.* have attempted to explain the change of g values for O_2^- formed on Y-type zeolites by γ-irradiation in terms of the crystal field induced by the cations.[7-8] In the case of alkaline earth cation exchanged Y-zeolites, the O_2^- radicals were found to be adsorbed on more than three different sites.[7] However, they could not clarify the nature of the respective sites. Not only on the alkaline earth Y-zeolites but also on NaY they observed three kinds of O_2^- species having different g_z values.[7] Kasai, on the other hand, reported his finding of single O_2^- species on NaY. The difference between these results has not yet been well explained. The formation of O_2^- radicals on trivalent cation-exchanged Y-type zeolites was also reported,[8] but no correlation among the changes of g values in NaY, alkaline earth Y-zeolites, and trivalent cation-exchanged Y-zeolites has yet been found.

More detailed investigations are necessary to find the correlation between the g_z values and the nature of adsorption sites for O_2^- on various kinds of cation-exchanged zeolites. Especially, studies about O_2^- on other monovalent cation-exchanged zeolites besides sodium-form zeolites should be done. In addition, no work has been carried out to examine the properties of O_2^- formed on X-type zeolites by γ-irradiation except that on NaX.[12] In this paper, O_2^- species formed on monovalent, divalent, and trivalent cation-exchanged X-type zeolites by γ-irradiation are systematically examined, and the properties of adsorption sites for the O_2^- are discussed.

Experimental

The cation-exchanged X-zeolites were prepared by immersing Linde 13X zeolite several times into the aqueous solutions of cations in the form of chloride, nitrate, or acetate. The obtained exchanged-zeolites were thoroughly washed with deionized water and dried at room temperature. The degree of ion exchange was determined by estimating the amount of sodium ions dissolved into the solution by means of flame spectrometry. The samples used and their exchange percentages are shown in Table 1.

The zeolite samples, placed in ESR quartz tubes, were degassed at 550 °C, and were exposed to oxygen after cooling to room temperature. The experimental details were similar to those described in the previous paper.[12] γ-Irradiation of samples was performed at room temperature by using a ^{60}Co source; the dose was 12 Mrad. Other samples were also irradiated by γ-rays without exposing them to oxygen. No ESR spectrum except a negligibly weak singlet line at $g=2.002$ was observed before γ-irradiation. Gaseous materials of high purity were obtained from Takachiho Chemical Co. and were used without further purification. The pressures of gases were adjusted to be within the range of 10—30 Torr when the samples were exposed to them. All gases were introduced into samples at room temperature. The ESR spectra were recorded at −196 °C with a JEOL JES-3BS X band spectrometer.

Results

Monovalent Cation-exchanged Zeolites. LiX γ-irradiated in the presence of O_2 gave a typical O_2^- ESR spectrum, as shown in Fig. 1(a).[1-12] All the spectra obtained from γ-irradiated KX, RbX, and CsX in the presence of O_2 have similar lines. Figure 1(a) also shows the low-field lines of their spectra; the estimated values of g_y and g_z are 2.009—2.007 and 2.003—2.001, respectively. The low-field lines (B and D) indicate the presence of two kinds of O_2^- species with different g_z values.[7] The spectra shapes were not changed by evacuation at room temperature.

When these alkali-cation exchanged samples were exposed to 1-butene, the O_2^-(B) spectra of the samples disappeared, whereas the other ones, O_2^-(D), were kept unchanged (Fig. 1(b)). The contact with N_2O only decreased the intensities of the O_2^-(B) spectra for RbX and CsX. All the O_2^-(B) spectra were broadened by exposing the zeolites to O_2 of 150 Torr. The γ-irradiation of LiX, KX, RbX, and CsX under vacuum gave ESR spectra almost similar to that for NaX,[12] though the relative intensity of each signal due to a V or F center was somewhat different in the respective samples.

Divalent Cation-exchanged Zeolites. Figure 2(a)

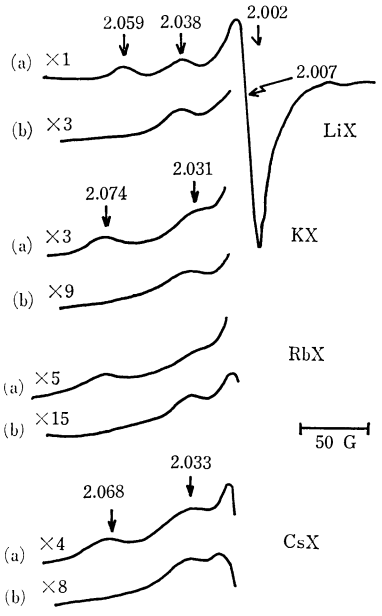

Fig. 1. ESR spectra of alkali cation-exchanged X-zeolites; (a) γ-irradiation in the presence of O_2, and (b) addition of 1-butene after (a) and evacuation.

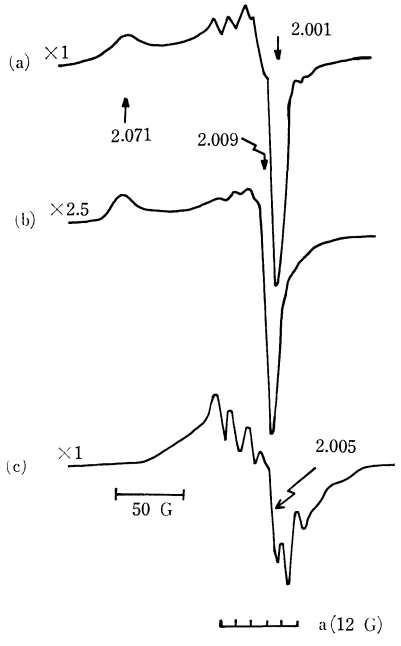

Fig. 2. ESR spectra of MgX; (a) γ-irradiation in the presence of O_2, (b) contact with N_2O after (a) and evacuation, and (c) γ-irradiation under vacuum.

shows the ESR spectrum of MgX γ-irradiated in the presence of O_2. When N_2O was added, the complicated lines in the central part ($g \approx 2.010$) of the spectrum disappeared and a typical O_2^- spectrum was observed (Fig. 2(b)). In the case of MgX γ-irradiated under vacuum, several lines due to V and F centers were observed, as is shown in Fig. 2(c). The broad asymmetric signal with six hyperfine lines ($|a(\mathrm{Al})| = 12$ G) in the figure is the same as that observed by Sogabe *et al.*[13] and can be attributed to an electron hole trapped on an oxygen atom which is bound to an aluminum atom.[9,13–16] Accordingly, the ESR spectrum shown

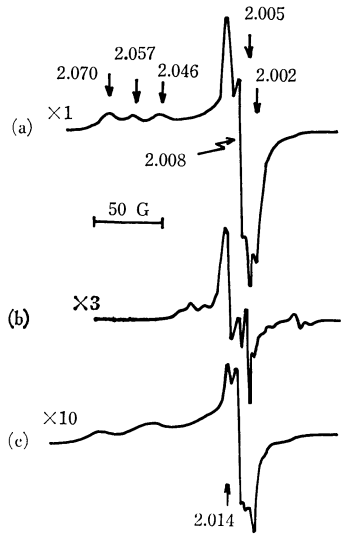

Fig. 3. ESR spectra of CaX; (a) γ-irradiation in the presence of O_2, (b) γ-irradiation under vacuum, and (c) addition of 1-butene after (a) and evacuation.

in Fig. 2(a) is recognized as this signal with hyperfine lines superposed on the signal due to O_2^-. The addition of O_2 (150 Torr) to the MgX γ-irradiated in the presence of O_2 confirmed this assignment, since the asymmetric signal with hyperfine lines became evident due to the broadening of the O_2^- signal. It was observed that the introduced 1-butene destroyed all the signals except a singlet at $g=2.005$.

When CaX was γ-irradiated in the presence of O_2, the spectrum shown in Fig. 3(a) was obtained. From the low-field shoulders ($g_z=2.070$, 2.057, and 2.046), the presence of three O_2^- species ($g_y \approx 2.008$ and $g_x \approx 2.002$) was confirmed.[1–12] Other signals ($g=2.014$, 2.005, 2.002 *etc.*) were ascribed to V and F centers,[7,9,12–16] since they were also obtained by γ-irradiation of CaX under vacuum (Fig. 3(b)). The complexity of the spectrum is due to the presence of the paramagnetic centers which interact with protons of the surface hydroxyl groups.[18,19] It was reported that the surface hydroxyl groups on alkaline earth zeolites remained even after evacuation at high temperature.[20–22]

Evacuation of the irradiated sample of CaX at room temperature decreased the intensity of the O_2^- signal with $g_z=2.070$ by 50%, but did not affect those of the other signals. When the sample was exposed to 1-butene, the intensities of the signals due to O_2^- with $g_z=2.070$ and 2.046 and the lines at $g=2.014$ and $g=2.005$ decreased, and, further, the O_2^- signal with $g_z=2.057$ disappeared (Fig. 3(c)). Upon heating at 200 °C, only the signal with $g_z=2.046$ ($g_y=2.008$ and $g_x=2.001$) remained. All the O_2^- signals were broadened by introducing O_2 of 150 Torr.

The spectrum obtained after the irradiation of SrX in the presence of O_2 was found to be composed of signals due to three O_2^- species ($g_z=2.062$, 2.054, and 2.048) and V and F centers (Fig. 4(a)). The contact with gaseous N_2O improved the resolution of the O_2^- signals, though their intensities decreased (Fig. 4(b)). By the addition of 1-butene, the O_2^- signals with $g_z=2.062$ and $g_z=2.048$ disappeared, while O_2^-

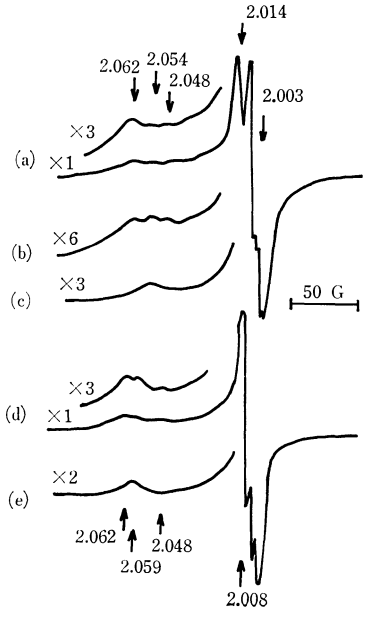

Fig. 4. ESR spectra of SrX; (a) γ-irradiation in the presence of O_2, (b) addition of N_2O after (a) and evacuation, and (c) addition of 1-butene after (a) and evacuation. ESR spectra of BaX; (d) γ-irradiation in the presence of O_2, and (e) addition of 1-butene after (a) and evacuation.

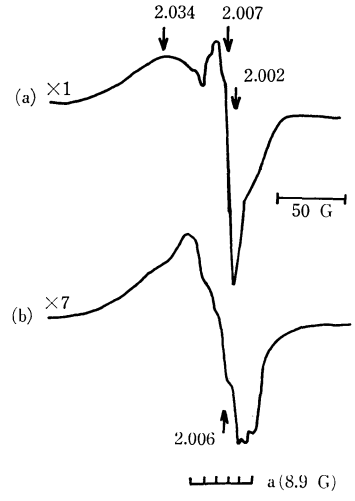

Fig. 5. ESR spectra of LaX; (a) γ-irradiation in the presence of O_2, and (b) addition of 1-butene after (a) and evacuation.

with g_z=2.054 (g_y=2.008, g_x=2.002) remained (Fig. 4(c)). The spectrum recorded at −196 °C shows that the O_2^- with g_z=2.048 was broadened by introducing O_2 (150 Torr). The broadening of other O_2^- signals (g_z=2.062 and 2.054) was not remarkable at that temperature. However, the broadening of the latter was confirmed to occur by observing the change in ESR spectra recorded at room temperature before and after the addition of O_2 (150 Torr).

The ESR spectrum of γ-irradiated BaX in the presence of O_2 indicated the formation of three O_2^- species (Fig. 4(d), g_z=2.062, 2.059, and 2.048). The shape of the O_2^- spectrum was more distinct in BaX as compared with other divalent zeolites, since the signals due to V and F centers were relatively weak. The intensity of the spectrum obtained in the γ-irradiated BaX under vacuum is about 15—20% of those obtained from the other divalent zeolites. The evacuation of O_2 attenuated the O_2^- signal with g_z=2.062 to about 65%. The O_2^- signals with g_z=2.062 and 2.048 disappeared after exposure of the zeolite to 1-butene (Fig. 4(e)). All the O_2^- signals underwent the line-broadening in the presence of O_2 (150 Torr).

Trivalent Cation-exchanged Zeolite (LaX). When LaX was irradiated in the presence of O_2, the spectrum of O_2^- with g_z=2.034, g_y=2.007, and g_x=2.002 was observed (Fig. 5(a)). Upon the addition of 1-butene, the O_2^- signal disappeared, and an asymmetric signal with 6 hyperfine lines with weak intensity became visible (Fig. 5(b)). This shows that the spectrum in Fig. 5(a) is composed of this asymmetric signal and the overlapping one due to O_2^-. The asymmetric signal was also observed by γ-irradiating LaX under vacuum. It may be attributed to electron holes similar to those produced in MgX by γ-irradiation, though the resolution of the hyperfine lines was rather lower.[9,13–16] The addition of O_2 (150 Torr) broadened the O_2^- signal.

Discussion

The ESR spectra observed on the cation-exchanged zeolites which were γ-irradiated in the presence of O_2 are sometimes complicated because of the overlapping of signals due to several O_2^- radicals which are adsorbed on different sites. The formation of V and F centers makes the spectra more complicated. For example, the presence of some O_2^-, especially those with g_z=2.035—2.040 on NaY and alkaline earth zeolites was ambiguous, since it was suggested only from the shoulders in the complicated spectrum. These O_2^- species and centers may show different stabilities on thermal treatments and reactivities with the introduced foreign gases.[12] By making use of these different reactivities and stabilities, we separated the spectrum for each individual O_2^- from the other, and provided the convincing evidence for the presence of each O_2^- species.

The g_z values for O_2^- obtained from γ-irradiated X-type zeolites in the presence of O_2 and those for NaX in our previous study[12] are classified into four groups, as is shown in Table 1. A theoretical analysis of the principal g values for O_2^- was carried out by Känzig and Cohen.[23] According to their result, the g_z component which shows the largest deviation from g_e, that of a free electron, is expressed by

$$g_z = g_e + \frac{2\lambda}{(\delta^2+\lambda^2)^{1/2}}.$$

Where λ is the spin-orbit coupling constant and is evaluated at 0.014 eV.[6] The z axis is chosen along the internuclear axis of O_2^-. The lowest electronic configuration of O_2^- is $\sigma_g^2\pi_u^4\pi_g^{*3}$. The originally degenerated π_u and π_g^* levels are split respectively into $\pi_u(2p_x)$, $\pi_u(2p_y)$ and $\pi_g^*(2p_x)$, $\pi_g^*(2p_y)$ in the adsorbed state by the asymmetric crystal field.[1,5,6,24]

TABLE 1. g_z VALUES FOR O_2^- ON CATION-EXCHANGED X ZEOLITES γ-IRRADIATED IN THE PRESENCE OF O_2 (g_y=2.007—2.009, g_x=2.000—2.003)

Cation	Exchanged %	A	B		C	D
Li	72			2.059		2.038
Na[a)]	100	2.158		2.059		2.033
K	81		2.074			2.031
Rb	67		2.074			2.031
Cs	56		2.068			2.033
Mg	67		2.071			
Ca	80		2.070	2.057	2.046	
Sr	81		2.062	2.054	2.048	
Ba	85		2.062	2.059	2.048	
La						2.034

a) The values were obtained in our previous work[12] under the same experimental conditions as used for the others.

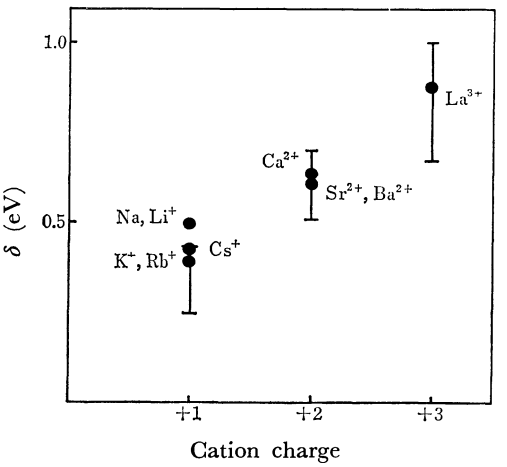

Fig. 6. Correlation between δ and the charge of metal ions. ●; cation exchanged X-zeolites: |——| ; the range of δ values previously obtained.[5]

In the above equation, δ is the energy separation between the $\pi_g^*(2p_x)$ and $\pi_g^*(2p_y)$ orbitals. When $\delta \gg \lambda$, the energy separation δ is given by $\delta=2\lambda/(g_z-g_e)$. Figure 6 shows the plot of δ values of the group B for alkali cation exchanged zeolites, the group C for alkaline earth zeolites and D for LaX against the charge of exchanged cation. The δ values summarized by Lunsford[5] are also shown in the figure as a measure of the distribution range for each value of cation charge. The δ values obtained in the present study fall almost in the ranges indicated by Lunsford. This result suggests that O_2^-(B) was adsorbed on the monovalent cation, O_2^-(C) on the divalent cation, and O_2^-(D) on the trivalent cation.

Table 1 also shows that O_2^-(D) was produced not only on LaX but also on alkali zeolites. O_2^-(D) of alkali zeolites, however, has a different character from those of the other O_2^-. In the atomosphere of O_2 (150 Torr), all the O_2^- spectra except O_2^-(D) of alkali zeolites were broadened. This indicates that the O_2^-(A, B, C, and D of LaX) are located in the supercage, while O_2^-(D) of alkali zeolites may be adsorbed on sites different from the others, possibly on those in the sodalite unit.[7] The signal of O_2^-(D) on NaX has the six hyperfine lines due to an Al nucleus,[12] and the g values for O_2^-(D) on alkali cation exchanged zeolites coincide well with those for O_2^- adsorbed on the aluminum ion in zeolite structure[8,10] and Al_2O_3.[25,26] From these facts, it can be concluded that these O_2^-(D) of the alkali zeolites were adsorbed by the lattice aluminum. The g_z value of O_2^-(D) for LaX is close to those for ScY and LaY[8] and, therefore, is characteristic of O_2^- adsorbed on the exchanged trivalent cation. The ScY and LaY have only one kind of adsorbed O_2^- species, and the observed superhyperfine structure indicates that the exchanged trivalent cations correspond to the adsorption sites.

The states of exchanged cations such as M^{2+}, $M(OH_2)_n^{2+}$, $M(OH)^+$, MO, and M^+–O–M^+ were suggested from the IR and X-ray studies of alkaline earth zeolites.[20,21,27,28] The O_2^-(B) species formed on alkaline earth zeolites have similar g_z values to those on alkali zeolites. These O_2^-(B) species may therefore be trapped on monovalent-like sites such as $M(OH)^+$ or M^+–O–M^+. It was confirmed that the $M(OH)^+$ site exists in the alkaline earth zeolites even after evacuation at high temperature.[29] The M^+–O–M^+ complexes were suggested to be formed in the sodalite unit upon mild dehydration; the M^{2+} ions located at site I′ and site II″ in the zeolite frame work are joined by an oxygen atom.[28] However, considering the movement of the cation due to dehydration at high temperature and γ-irradiation, it seems possible that the complexes with one of the M^{2+} ions in a supercage are also formed.

The O_2^-(C) species is characteristic of the divalent cation exchanged zeolites, and can be attributed to the O_2^- adsorbed on the cations in the state of M^{2+} (Fig. 6). The O_2^-(C) was not observed on MgX zeolite. It is known that the Mg^{2+} ion has a large hydration radius, and can dissociate the bound water more strongly than other divalent cations in zeolites.[13,31] The monovalent-cation like sites are formed by dissociating the bound water of hydrated cations. Most Mg^{2+} ions may take the monovalent-like form. The difference between MgX and other alkaline earth zeolites was also reported for the adsorbed states of CO_2^- and CO_2.[13,31]

Table 1 shows that the O_2^-(A) species is only obtained on NaX. Such O_2^- species with large g_z values were observed on the pretreated NaY and KY with Na and K vapor respectively.[32] The exposure of NaY to Na vapor was found to form the paramagnetic center Na_4^{3+}, and the O_2^- species is formed by taking an electron from the center. The paramagnetic center Na_4^{3+} was also formed by γ-irradiation of NaY and the adsorbed O_2^- has a large g_z value of 2.113.[6] It was suggested by Bentarrit *et al.* that the induced migration of the cation by water leads to the generation of an Na_4^{3+} center under γ-irradiation.[33] Stamires mentioned that $(Na_4)^{4+}$–$(H_2O)_x$ complex is formed in NaY zeolite after a proper degree of dehydration and is converted to $(Na_4)^{3+}$–$(H_2O)_x$ by trapping an electron.[17] As for NaX zeolite, Na_6^{5+} was found to be produced by exposing NaX to Na vapor.[34] These findings predict that the γ-irradiation produces the

$(Na_n)^{(n-1)+}$ center which become non-paramagnetic by transferring an electron to O_2; the number of atoms n depends on experimental conditions such as dehydration and γ-irradiation. The non-paramagnetic center may take the form of $(Na_n)^{n+}$ or a somewhat different configuration due to the movement of the cation after the adsorption of O_2^-, and induces a different crystal field from the usual monovalent Na^+ site. The O_2^-(A) seems to be that held at such a center. This assumption gives a reasonable explanation for the wide variety of g_z values for O_2^- on NaY. The pretreatments under different conditions may produce the sites of various configurations.[33] The O_2^-(A) species was not observed on the other alkali zeolites. The formation of $(M_n)^{n+}$ centers consisting of exchanged cations must be prevented by the remaining Na^+ cations.

By summarizing the consideration given above, the adsorption sites of O_2^- on γ-irradiated zeolites in the presence of O_2 can be assigned to the exchanged M^+ ion and the lattice aluminum cation in monovalent cation-exchanged zeolites (LiX, NaX, KX, RbX, CsX), M^{2+}, $M(OH)^+$ and M^+–O–M^+ in divalent cation-exchanged zeolites (MgX, CaX, SrX, BaX), and M^{3+} in trivalent cation-exchanged zeolites (LaX). The adsorption site $(M_n)^{n+}$ was also suggested for NaY zeolite. The lack of precise information on the electronic state and geometry of the zeolite surfaces makes the verification of these supposed adsorption sites difficult at present, but it is expected that their exact configuration and function will be revealed in the following studies using surface analytical techniques.

References

1) M. Setaka and T. Kwan, *Bull. Chem. Soc. Jpn.*, **43**, 2727 (1970).
2) I. D. Mikheikin, A. I. Mashchenko, and V. B. Kazanskii, *Kinet. Katal.*, **8**, 1363 (1967).
3) P. Meriaudeau, C. Naccache, and A. J. Tench, *J. Catal.*, **21**, 208 (1971).
4) V. A. Shvets, M. E. Sarichev, and V. B. Kazanskii, *J. Catal.*, **11**, 378 (1968).
5) J. H. Lunsford, *Catal. Rev.*, **8**, 135 (1973).
6) P. H. Kasai, *J. Chem. Phys.*, **43**, 3322 (1965).
7) K. M. Wang and J. H. Lunsford, *J. Phys. Chem.*, **74**, 1512 (1970).
8) K. M. Wang and J. H. Lunsford, *J. Phys. Chem.*, **75**, 1165 (1971).
9) J. C. Vedrine and C. Naccache, *J. Phys. Chem.*, **77**, 1606 (1973).
10) K. M. Wang and J. H. Lunsford, *J. Phys. Chem.*, **73**, 2069 (1969).
11) S. Krzyzanowski, *J. Chem. Soc., Faraday Trans. 1*, **72**, 1573 (1976).
12) N. Kanzaki and I. Yasumori, *Bull. Chem. Soc. Jpn.*, **51**, 991 (1978).
13) K. Sogabe, A. Hasegawa, Y. Yamada, and M. Miura, *Bull. Chem. Soc. Jpn.*, **45**, 3362 (1972).
14) J. C. Vedrine, A. Abou-Kais, J. Massardier, and G. Dalmai-Imelik, *J. Catal.*, **29**, 120 (1973).
15) R. R. Hentz and D. K. Wickenden, *J. Phys. Chem.* **73**, 817 (1969).
16) D. N. Stamires and J. Turkevich, *J. Am. Chem. Soc.*, **86**, 757 (1964).
17) D. N. Stamires, "Molecular Sieves," Soc. Chem. Industry, London(1968), p. 328.
18) V. B. Kazanskii, G. B. Pariiskii, and V. V. Voevodsky, *Discuss. Faraday Soc.*, **31**, 203 (1961).
19) N. Shimizu, K. Shimokoshi, and I. Yasumori, *Bull. Chem. Soc. Jpn.*, **46**, 2929 (1973).
20) J. W. Ward, *J. Catal.*, **10**, 34 (1968).
21) J. W. Ward, *J. Phys. Chem.*, **72**, 4211 (1968).
22) C. L. Angell and P. C. Schaffer, *J. Phys. Chem.*, **69**, 3463 (1965).
23) W. Känzig and M. H. Cohen, *Phys. Rev. Lett.*, **3**, 509 (1959).
24) T. Ichikawa, M. Iwasaki, and K. Kuwata, *J. Chem. Phys.*, **44**, 2979 (1966).
25) A. A. Gezalov, G. M. Zhabrova, V. V. Nikisha, G. B. Parriiskii, and K. N. Spiridonov, *Kinet. Katal.*, **9**, 462 (1968).
26) D. D. Eley and M. A. Zammitt, *J. Catal.*, **21**, 366 (1971).
27) D. H. Olson, *J. Phys. Chem.*, **72**, 1400 (1968).
28) J. B. Uytterhoeven, R. Schoonheydt, B. V. Liengme, and W. K. Hall, *J. Catal.*, **13**, 425 (1969).
29) H. Sugihara, K. Shimokoshi, and I. Yasumori, *J. Phys. Chem.*, **81**, 669 (1977).
30) R. G. Herman and D. R. Flentge, *J. Phys. Chem.*, **82**, 720 (1978).
31) J. W. Ward and H. W. Habgood, *J. Phys. Chem.*, **70**, 1178 (1966).
32) P. H. Kasai and R. J. Bishop, Jr., *J. Phys. Chem.*, **77**, 2308 (1973).
33) Y. Bentarrit, C. Naccache, M. Che, and A. J. Tench, *Chem. Phys. Lett.*, **24**, 41 (1973).
34) J. A. Rabo, C. L. Angell, P. H. Kasai, and V. Schomaker, *Discuss. Faraday Soc.*, **41**, 328 (1966).

Antiferromagnetic Spin-exchange Interaction in Mixed-spin Trinuclear Cobalt(II) Complexes with Quadridentate Schiff Bases[1)]

Visit KASEMPIMOLPORN, Hisashi OKAWA,* and Sigeo KIDA
Department of Chemistry, Faculty of Science, Kyushu University, Hakozaki, Higashi-ku, Fukuoka 812
(Received December 11, 1978)

Trinuclear cobalt(II) complexes, $[Co(R_1,R_2\text{-L})]_2CoX_2$ (R_1, R_2=H, Me; L=en, ch, ph; X=Cl^-, Br^-), have been synthesized, where $H_2(R_1,R_2\text{-L})$ denotes the Schiff bases obtained by condensing a 5(R_1), α(R_2)-substituted salicylaldehyde with a diamine ($H_2N\text{-L-}NH_2$) in a 2:1 mole ratio. From IR spectra and cryomagnetic properties, it was concluded that these complexes are in mixed-spin state of a Co(II)(s=1/2)–Co(II)(s=3/2)–Co(II)(s=1/2) system, strong antiferromagnetic spin-exchange interaction operating between low-spin and high-spin cobalt(II) ion *via* d_π(low-spin Co)-p_π(O)-d_π(high-spin Co) super pathway.

Low-spin cobalt(II) complexes have an electronic configuration of either $(d_{x^2-y^2})^2(d_{z^2})^1$ or $(d_{x^2-y^2})^2(d_{yz})^1$. In mixed-spin polynuclear cobalt(II) complexes in which high-spin and low-spin cobalt(II) ions are kept in close distance, spin-exchange interaction between the cobalt(II) ions would markedly depend upon the electronic structure of the low-spin cobalt(II) ion. We obtained mixed-spin binuclear cobalt(II) complexes, Co_2(fsaR)$(py)_3$, with *N,N'*-bis(3-carboxysalicylidene)alkanediamine(H_4fsaR) and demonstrated that no spin-exchange interaction operates between the metal ions.[2)] In these complexes low-spin cobalt(II) has an unpaired electron on the d_{z^2} orbital. Thus, it is worth while to examine spin-exchange interaction in mixed-spin polynuclear cobalt(II) complexes in which low-spin cobalt(II) has an unpaired electron on the d_{yz} orbital. However, no such mixed-spin polynuclear cobalt(II) complexes have yet been obtained.

Sinn and Harris[3)] synthesized mixed-metal trinuclear complexes of Cu(II)–M(II)–Cu(II) (M(II)=Cu(II), Ni(II), Co(II), Fe(II), Mn(II)) system by reacting copper(II) complexes of *N,N'*-disalicylideneethylenediamine or its homologues with an M(II) ion in a 2 : 1 mole ratio. Since the electronic structure of Co(salen) and its homologues was recently demonstrated to be $(d_{x^2-y^2})^2(d_{yz})^1$[1,4,5)] we have attempted to prepare Co(II)(s=1/2)–Co(II)(s=3/2)–Co(II)(s=1/2) complexes with the quadridentate Schiff bases in order to investigate their magnetic property in connection with the electronic configuration of the low-spin cobalt(II) ion.

N,N'-Disalicylidenealkanediamines are abbreviated to $H_2(R_1, R_2\text{-L})$ (R_1, R_2=H, Me; L=en, ch, ph), where R_1 and R_2 denote the substituents attached to the 5- and α-positions of salicylaldehyde moiety, respectively, and L denotes the chain combining the two nitrogen atoms.

Experimental

Preparation of Complexes. Co(H,H-en) was synthesized by the method of Bailes and Calvin.[6)] Other mononuclear cobalt(II) complexes were obtained in a similar way. The syntheses of all the trinuclear complexes, $[Co(R_1,R_2\text{-L})]_2CoX_2$, were nearly the same and are exemplified by that of $[Co(H,H\text{-en})]_2CoCl_2$ as follows.

Co(H,H-en) (500 mg) and $CoCl_2\cdot 6H_2O$ (219 mg) were dissolved in ethanol (100 ml) and the mixture was refluxed for *ca.* 2 h to give red-brown crystals. After the reaction mixture had been allowed to stand overnight, crystals were collected by filtration, washed with a small amount of ethanol and dried under reduced pressure. All operations were carried out in a nitrogen atmosphere by means of a VAC inert atmosphere & vacuum deposition equipment Model HE-43-2. Elemental analyses of $[Co(R_1,R_2\text{-L})]_2CoX_2$ are given in Table 1.

Measurements. Elemental analyses of carbon, hydrogen, and nitrogen were carried out at the Elemental Analysis Service Center, Kyushu University. Cobalt analyses were carried out with a Shimadzu atomic absorption-flame spectrophotometer Model 610S. The standard solution was prepared by decomposing Co(H,H-en) with nitric acid and diluting the decomposed mixture with water in a volumetric flask. Solutions of samples were also prepared by the same method. IR spectra were measured in the range 4000—650 cm^{-1} with a Hitachi infrared spectrophotometer Model 215 on a KBr disk. Magnetic susceptibilities were measured by the Faraday method in the temperature range 78—300 K, the apparatus being calibrated with $HgCo(NCS)_4$.[7)] Effective magnetic moments were calculated by the equation, $\mu_{eff}=2.828(\chi_M\times T)^{1/2}$, in which χ_M

Table 1. Elemental analyses of complexes

	Found (%)				Calcd (%)			
	C	H	N	Co	C	H	N	Co
$[Co(H,H\text{-en})]_2CoCl_2$	49.04	3.54	7.08	22.65	49.25	3.61	7.15	22.65
$[Co(H,H\text{-en})]_2CoBr_2$	44.02	3.26	6.37	20.33	44.21	3.24	6.44	20.34
$[Co(Me,Me\text{-en})]_2CoCl_2$	53.77	4.94	6.24	19.96	53.83	4.96	6.27	19.81
$[Co(Me,Me\text{-en})]_2CoBr_2$	48.72	4.50	5.61	17.89	48.95	4.51	5.70	18.01
$[Co(H,Me\text{-en})]_2CoBr_2$	46.66	4.18	6.11	19.11	46.73	3.92	6.05	19.10
$[Co(H,H\text{-ph})]_2CoBr_2$	49.96	2.92	5.88	18.30	49.77	2.92	5.80	18.31
$[Co(H,H\text{-ch})]_2CoBr_2$	49.17	4.22	5.61	17.91	49.15	4.12	5.73	18.09

Table 2. Color and IR skeletal band (cm^{-1}) of complexes

	Color	Skeletal[a]
$[Co(H,H\text{-}en)]_2CoCl_2$	reddish brown	1550 (1530)
$[Co(H,H\text{-}en)]_2CoBr_2$	orange	1548 (1530)
$[Co(Me,Me\text{-}en)]_2CoCl_2$	deep-orange	1540 (1515)
$[Co(Me,Me\text{-}en)]_2CoBr_2$	orange	1540 (1515)
$[Co(H,Me\text{-}en)]_2CoBr_2$	deep-orange	1540 (1515)
$[Co(H,H\text{-}ph)]_2CoBr_2$	black	1520 (1520)
$[Co(H,H\text{-}ch)]_2CoBr_2$	orange	1540 (1530)

a) Value in parentheses is the skeletal vibration for $Co(R_1,R_2\text{-}L)$.

is molar magnetic susceptibility corrected for diamagnetism for all the constituent atoms by the use of Pascal's constants.[8]

Results and Discussion

Color and IR skeletal band near 1550 cm^{-1} are given in Table 2. A skeletal band at 1515—1530 cm^{-1} found for $Co(R_1,R_2\text{-}L)$ shifts to higher frequency (1540—1550 cm^{-1}) in $[Co(R_1,R_2\text{-}L)]_2CoX_2$, except for the complex with $H_2(H,H\text{-}ph)$. The shift of the skeletal vibration to higher frequency was elucidated by Sinn *et al.*[9-12] for binuclear copper(II) complexes and is used for diagnosis of a bridging mode of phenolic oxygen in homometal polynuclear complexes,[13-18] mixed-metal polynuclear complexes[19] and Cu(II)–Cu(I) mixed-spin complexes.[20] It is likely that in the present complexes metal ions are bridged by the phenolic oxygens. Except for this skeletal band, each IR spectrum of $[Co(R_1,R_2\text{-}L)]_2CoX_2$ resembles that of the corresponding $Co(R_1,R_2\text{-}L)$.

The complexes are insoluble in most nonpolar organic solvents. They are soluble in polar solvents such as pyridine and dimethyl sulfoxide, but they decompose in these solvents. Reflectance spectra of the complexes were not well resolved. No information was available on the structure of the complexes from the electronic spectra.

As pointed out by Gruber *et al.*,[21] steric requirement of $Co(R_1,R_2\text{-}L)$ as a bidentate ligand is nearly the same as that of 2,2′-biquinolyl (biq). Because of the steric hindrance between hydrogens attached to the 8-position, two 2,2′-biquinolyl molecules can not coordinate to a metal ion in a plane; *e.g.*, the coordination geometry of $[Cu(biq)_2](ClO_4)_2$ is pseudo-tetrahedral.[22] For the same reason, two molecules of $M(R_1,R_2\text{-}L)$ should assume a pseudo-tetrahedral or cis-octahedral coordination because of the steric repulsion between the hydrogens attached to the 3-position of salicylaldehyde moiety. In fact, the configurations of Na^+ in $[Cu(H,H\text{-}en)]_2NaClO_4$[23] and the central copper(II) in $[Cu(R_1,R_2\text{-}L)]_2Cu(H_2O)_2(ClO_4)_2$[24] are cis-octahedral. Thus, we assume that the present complexes have the structure shown in Fig. 1.

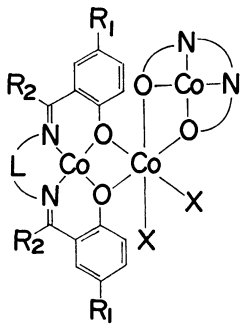

Fig. 1. Probable structure of $[Co(R_1,R_2\text{-}L)]_2CoX_2$.

Magnetic susceptibilities of the complexes were measured in the range from liquid nitrogen temperature to room temperature. Magnetic susceptibilities and magnetic moments at various temperatures are given in Table 3. Magnetic moments per molecule at room temperature fall in the range 5.83—6.02 BM, the moments decreasing with lowering of temperature. Since magnetic moments for mononuclear high-spin cobalt(II) (octahedral) and for mononuclear low-spin cobalt(II) complexes are known to be 4.5—5.2 and 2.0—2.8 BM, respectively,[25] the magnetic moment for a magnetically non-interacting Co(II)(s=1/2)–Co(II)(s=3/2)–Co(II)(s=1/2) mixed-spin system is estimated at 5.33—6.54 BM by the equation $\mu_M^2=\sum\mu_i^2$. The observed magnetic moments of $[Co(R_1,R_2\text{-}L)]_2CoX_2$ at room temperature fall in this range. On the other hand, moments near liquid nitrogen temperature are close to or less than the lowest limit 5.33 BM. Thus it is likely that $[Co(R_1,R_2\text{-}L)]_2CoX_2$ are mixed-spin trinuclear complexes, in which an antiferromagnetic spin-exchange interaction operates between the low-spin and high-spin cobalt(II) ions.

Molar magnetic susceptibility for Co(II)(s=1/2)–Co(II)(s=3/2)–Co(II)(s=1/2) system is given by

$$\chi_M=\frac{Ng^2\beta^2}{4kT}\cdot\frac{35+10\exp(-3J/kT)+10\exp(-5J/kT)+\exp(-8J/kT)}{3+2\exp(-3J/kT)+2\exp(-5J/kT)+\exp(-8J/kT)}+N\alpha,$$

which was first derived Gruber *et al.* for Cu(II)–Co(II) (s=3/2)–Cu(II) system.[26] In this equation J is the exchange integral between the low-spin and high-spin cobalt(II) ions and other symbols have their usual meanings, spin-exchange interaction between the therminal low-spin cobalt(II) ions being neglected. Magnetic susceptibilities for $[Co(R_1,R_2\text{-}L)]_2CoX_2$ can be explained by means of this equation. In Fig. 2 the best fit between empirical and theoretical inverse magnetic susceptibilities for $[Co(H,H\text{-}en)]_2CoCl_2$ is shown as an example. Magnetic parameters, J and g, obtained for $[Co(R_1,R_2\text{-}L)]_2CoX_2$ are given in Table 4; temperature independent paramagnetism, $N\alpha$, being estimated at 500×10^{-6} c.g.s./mol. It is evident that an antiferromagnetic spin-exchange interaction operates between low-spin and high-spin cobalt(II) ions. The exchange integrals (−10—−14 cm^{-1}) are appreciably large and comparable to the value (J=−16—−24 cm^{-1}) found for the Cu(II)–Co(II)(s=3/2)–Cu(II) complexes.[3,26]

TABLE 3. TEMPERATURE VARIATIONS OF MAGNETIC SUSCEPTIBILITY AND MAGNETIC MOMENT

$[Co(H,H\text{-}en)]_2CoCl_2$												
T (K)	78.8	98.3	120.2	141.5	162.7	185.3	207.7	229.9	250.7	274.3	296.6	
$\chi_M \times 10^6$	39045	33566	29383	26176	23380	21629	19698	18184	16882	15636	14476	
μ_{eff}	4.96	5.14	5.31	5.44	5.52	5.66	5.72	5.78	5.82	5.86	5.86	
$[Co(H,H\text{-}en)]_2CoBr_2$												
T (K)	81.2	101.5	119.8	139.9	159.7	178.9	199.6	219.6	238.7	259.2	279.1	298.3
$\chi_M \times 10^6$	36829	31339	28023	25551	23416	22076	20504	18956	17616	16407	15357	14461
μ_{eff}	4.89	5.04	5.18	5.35	5.47	5.62	5.72	5.77	5.80	5.83	5.85	5.87
$[Co(Me,Me\text{-}en)]_2CoCl_2$												
T (K)	82.9	103.5	129.1	149.4	169.9	190.3	213.7	235.6	257.4	275.5	297.1	
$\chi_M \times 10^6$	44703	37226	30460	26962	24218	21908	19961	18355	16948	15969	14868	
μ_{eff}	5.44	5.55	5.61	5.68	5.74	5.77	5.84	5.88	5.91	5.93	5.94	
$[Co(Me,Me\text{-}en)]_2CoBr_2$												
T (K)	83.4	103.0	122.5	142.0	161.6	180.2	199.9	219.3	238.7	258.4	278.1	297.4
$\chi_M \times 10^6$	43780	37598	32536	29103	25922	23706	21771	20202	18735	17281	16253	15229
μ_{eff}	5.40	5.57	5.65	5.75	5.79	5.85	5.90	5.93	5.98	5.98	6.01	6.02
$[Co(H,Me\text{-}en)]_2CoBr_2$												
T (K)	81.1	100.9	120.2	139.5	159.7	179.5	199.2	219.0	238.4	258.7	278.1	297.8
$\chi_M \times 10^6$	42937	36726	32319	28634	25587	23299	21233	19512	18135	16887	15811	14864
μ_{eff}	5.28	5.44	5.57	5.65	5.72	5.78	5.82	5.85	5.88	5.91	5.93	5.95
$[Co(H,H\text{-}ph)]_2CoBr_2$												
T (K)	84.6	103.3	123.3	142.8	162.7	181.9	201.4	221.1	240.4	259.5	278.1	298.0
$\chi_M \times 10^6$	40159	34940	30377	27201	24540	22172	20342	18750	17357	16204	15209	14254
μ_{eff}	5.21	5.36	5.47	5.57	5.65	5.68	5.72	5.76	5.78	5.80	5.82	5.83
$[Co(H,H\text{-}ch)]_2CoBr_2$												
T (K)	82.3	102.0	127.8	147.5	166.3	186.9	210.7	232.7	256.0	274.3	296.1	
$\chi_M \times 10^6$	44780	36999	30281	26574	23960	21754	19607	17978	16539	15611	14658	
μ_{eff}	5.43	5.49	5.56	5.60	5.65	5.70	5.75	5.78	5.82	5.85	5.89	

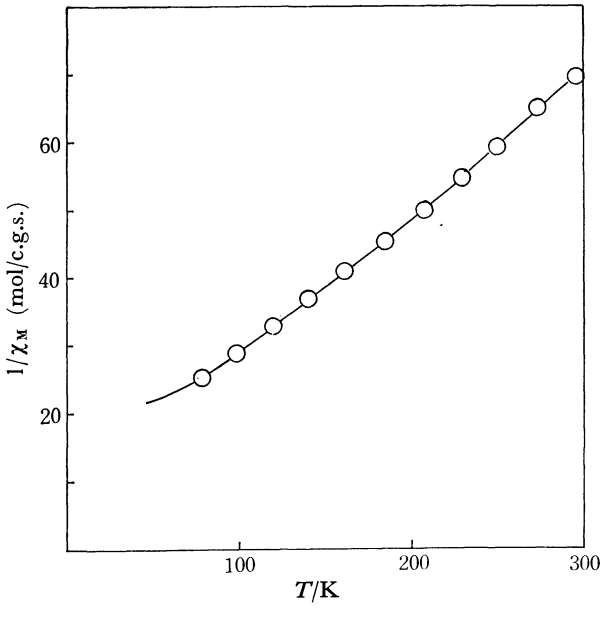

Fig. 2. Temperature variation of inverse molar magnetic susceptibility of $[Co(H,H\text{-}en)]_2CoCl_2$. The solid line represents the theoretical susceptibility with $J=-14$ cm^{-1}, $g=2.68$ and $N\alpha=500\times10^{-6}$ c.g.s./mol.

We showed that no spin-exchange interaction operates between low-spin and high-spin cobalt(II) ions in $Co_2(fsaR)(py)_3$.[2] In these complexes low-spin cobalt(II) ion has an unpaired electron on its d_{z^2} orbital. The absence of magnetic interaction may be attributed to a negligibly small overlapping between the cobalt d_{z^2} orbital and the oxygen orbital. Thus, it is important to determine the ground-state electronic configuration of the low-spin cobalt(II) in antiferromagnetic $[Co(R_1,R_2\text{-}L)]_2CoX_2$. Since $[Co(R_1,R_2\text{-}L)]_2CoX_2$ shows no well-defined ESR signal owing to high-spin cobalt(II) ion, it is desirable to prepare a complex of Co(II)($s=1/2$)–M(II)–Co(II)($s=1/2$) system, in which the central cobalt(II) is replaced by a diamagnetic M(II) ion. However, we were unsuccessful in obtaining $[Co(R_1,R_2\text{-}L)]_2MX_2$. Thus, the electronic structure of the low-spin cobalt(II) was surmised by considering binuclear complexes related to the present complexes. It was

TABLE 4. MAGNETIC PARAMETERS FOR COMPLEXES

	$-J$ (cm^{-1})	g
$[Co(H,H\text{-}en)]_2CoCl_2$	14	2.68
$[Co(H,H\text{-}en)]_2CoBr_2$	14	2.65
$[Co(Me,Me\text{-}en)]_2CoCl_2$	12	2.78
$[Co(Me\text{-}en)]_2CoBr_2$	12	2.78
$[Co(H,Me\text{-}en)]_2CoBr_2$	12	2.71
$[Co(H,H\text{-}ph)]_2CoBr_2$	12	2.66
$[Co(H,H\text{-}ch)]_2CoBr_2$	10	2.65

$N\alpha$ is estimated at 500×10^{-6} c.g.s./mol.

shown[20] that $Cu(R_1,R_2\text{-L})$ and $[Cu_2(R_1,R_2\text{-L})CH_3CN]ClO_4$ (Cu(II)–Cu(I) complex bridged by the phenolic oxygen) show ESR spectra displaying substantially identical $g_\parallel$, $g_\perp$, and $A_\parallel$ values. This indicates that the electronic property of Schiff base complexes coordinated to another metal as a bidentate ligand is almost the same as that of the original mononuclear complexes, $M(R_1,R_2\text{-L})$. This is in line with the fact that in binuclear complexes of this type the distance between the phenolic oxygen and the metal bound to the N_2O_2-donating site is nearly the same as that for the original Schiff base complex $M(R_1,R_2\text{-L})$, while the distance between the phenolic oxygen and the second metal is much elongated.[27,28] A similar trend in bond distance is observed for the binuclear complexes with 1,3,5-triketone-diamine Schiff bases.[29–31] Recently we have found that the electronic spectrum of $[Co(R_1,R_2\text{-L})]_2MnX_2$ is almost the same as that of $Co(R_1,R_2\text{-L})$.[32] Thus, it is concluded that the electronic property of the low-spin cobalt(II) in $[Co(R_1,R_2\text{-L})]_2CoX_2$ is the same as that of $Co(R_1,R_2\text{-L})$, where an unpaired electron occupies d_{yz} orbital. Since high-spin cobalt(II) has unpaired electrons in $d_{x^2-y^2}$, d_{z^2} and one of the d_π orbitals, we may conclude that in the present complexes d_π(low-spin Co)-p_π(O)-d_π(high-spin Co) super pathway plays an important role in antiferromagnetic spin-exchange interaction.

The authors are grateful to the Ministry of Education for a Scientific Research Grant-in-Aid.

References

1) Binuclear Metal Complexes. Part XXVIII. Part XXVII: Y. Numata, H. Okawa, and S. Kida, *Mem. Fac. Sci., Kyushu Univ., Ser. C*, **11**(**2**), 159 (1978).
2) N. Torihara, H. Okawa, and S. Kida, *Bull. Chem. Soc. Jpn.*, **51**, 3236 (1978).
3) E. Sinn and C. M. Harris, *Coord. Chem. Rev.*, **4**, 391 (1969).
4) Y. Nishida and S. Kida, *Chem. Lett.*, **1973**, 57; *Bull. Chem. Soc. Jpn.*, **51**, 143 (1978).
5) M. A. Hitchman, *Inorg. Chem.*, **16**, 1985 (1977).
6) R. H. Bailes and M. Calvin, *J. Am. Chem. Soc.*, **69**, 1886 (1947).
7) B. N. Figgs and R. S. Nyholm, *J. Chem. Soc.*, **1959**, 331.
8) P. W. Selwood, "Magnetochemistry," Interscience Publishers, New York (1956), pp. 78, 91.
9) S. J. Gruber, C. M. Harris, and E. Sinn, *J. Inorg. Nucl. Chem.*, **30**, 1805 (1968).
10) C. M. Harris and E. Sinn, *J. Inorg. Nucl. Chem.*, **30**, 2723 (1968).
11) C. M. Harris, J. M. James, P. J. Milham, and E. Sinn, *Inorg. Chim. Acta*, **3**, 81 (1969).
12) R. B. Coles, C. M. Harris, and E. Sinn, *Inorg. Chem.*, **8**, 2607 (1969).
13) H. Okawa, T. Tokii, Y. Nonaka, Y. Muto, and S. Kida, *Bull. Chem. Soc. Jpn.*, **46**, 1462 (1973).
14) T. Ichinose, Y. Nishida, H. Okawa, and S. Kida, *Bull. Chem. Soc. Jpn.*, **47**, 3045 (1974).
15) H. Okawa, T. Tokii, M. Nakashima, Y. Muto, and S. Kida, *Mem. Fac. Sci., Kyushu Univ., Ser. C*, **10**, 153 (1978).
16) M. Kato, K. Imai, Y. Muto, T. Tokii, and H. B. Jonassen, *J. Inorg. Nucl. Chem.*, **35**, 109 (1973).
17) T. Tokii, Y. Muto, M. Kato, K. Imai, and H. B. Jonassen, *J. Inorg. Nucl. Chem.*, **34**, 3377 (1972).
18) T. Tokii and Y. Muto, *Bull. Chem. Soc. Jpn.*, **49**, 1849 (1976).
19) H. Okawa and S. Kida, *Inorg. Chim. Acta*, **23**, 253 (1977).
20) H. Okawa, V. Kasempimolporn, and S. Kida, *Bull. Chem. Soc. Jpn.*, **51**, 647 (1978).
21) S. J. Gruber, C. M. Harris, and E. Sinn, *Inorg. Chem.*, **7**, 268 (1968).
22) C. M. Harris, H. R. H. Patil, and E. Sinn, *Inorg. Chem.*, **6**, 1102 (1967).
23) G. H. W. Hilburn, H. R. Truter, and B. L. Vickery, *Chem. Commun.*, **1968**, 1188.
24) J. M. Epstein, B. N. Figgis, A. H. White, and A. C. Willis, *J. Chem. Soc., Dalton Trans.*, **1974**, 1954.
25) A. T. Casey and S. Mitra, "Theory and Application of Molecular Paramagnetism," ed by E. A. Boudreaux and L. N. Mulay, John Wiley & Sons, New York (1976), pp. 214, 221.
26) S. J. Gruber, C. M. Harris, and E. Sinn, *J. Chem. Phys.*, **49**, 2183 (1968).
27) R. M. Countryman, W. T. Robinson, and E. Sinn, *Inorg. Chem.*, **13**, 2013 (1974).
28) M. Mikuriya, H. Okawa, I. Ueda, and S. Kida, *Bull. Chem. Soc. Jpn.*, **51**, 2920 (1978).
29) B. Tomlonovic, R. L. Hough, M. D. Glick, and R. L. Lintvedt *J. Am. Chem. Soc.*, **97**, 2925 (1975).
30) M. D. Glick, R. L. Lintvedt, D. P. Gavel, and B. Tomlonovic, *Inorg. Chem.*, **15**, 1654 (1976).
31) M. D. Glick, R. L. Lintvedt, T. J. Anderson, and J. L. Mack, *Inorg. Chem.*, **15**, 2258 (1976).
32) V. Kasempimolporn, H. Okawa, and S. Kida, Presented at the Meeting of the Chugoku-Shikoku and Kyushu Branches of the Chemical Society of Japan, Tokushima, November 1978.

Determination of Ultratrace Zinc by Enzymatic Activity of Carbonic Anhydrase

Kensei KOBAYASHI, Kitao FUJIWARA, Hiroki HARAGUCHI, and Keiichiro FUWA*

Department of Chemistry, Faculty of Science, The University of Tokyo, Hongo, Bunkyo-ku, Tokyo 113

(Received December 23, 1978)

A method for the determination of trace zinc has been investigated by using enzymatic activity of carbonic anhydrase. The recovery of enzymatic activity of apo-carbonic anhydrase was proportional to the amount of zinc in solution theoretically and experimentally, when it was monitored spectroscopically using the substrate, *p*-nitrophenyl acetate. The amount of zinc in the sample solutions was therefore determined from the curve, zinc concentration *vs.* the enzymatic activity. The limit of detection is 10 ng/ml or 2 ng. The method has been applied to the analysis of zinc in fruit juices and water samples.

Of many enzymes, the metalloenzymes have specific metal ions located at their active centers, and the metal ions play essential roles in determining the enzymatic activity and in the processes of enzymatic reactions. This allows the metalloenzymes to show their selectivity and specificity to substrates which are concerned in enzymatic reactions. Such characteristics of the metalloenzymes have been subjects of recent interest, particularly as regards their application to the determination of trace metals.[1,2]

The enzymatic activity of the metalloenzyme for substrates is determined by the amount of active metal ion in the enzyme. The assay of the metalloenzyme is performed by measuring the recovery of the enzymatic activity of the inactive metal-free apoenzyme, when the metal can be removed from the enzyme. The assay of the enzyme is very sensitive and selective to the amount and kind of metal ion added, being useful for the analysis of trace metal ions. Townshend and Vaughan reported the detection of zinc based on the re-activation of apo-alkaline phosphatase.[3] Lehky and Stein studied the determination of zinc in serum using aminopeptidase.[4] Several workers investigated the determination of zinc and copper by enzymatic activity of metalloenzymes.[5,6]

In the present paper, a theoretical consideration is given on the relationship between the recovery of enzymatic activity and the amount of zinc in the case of one active metal ion, taking into account the chemical equilibria between the apoenzyme and the metal ion. A general case, *i.e.*, one in which more than one metal ion is necessary, is given in Appendix II. The relationship is confirmed experimentally and applied to the determination of zinc in fruit juices and waters, where apo-carbonic anhydrase was used as one of the representative zinc-containing enzymes found widely in biological systems.[7]

Theoretical Consideration

The enzymatic reaction in the case of carbonic anhydrase can be described as follows (definitions of all the signs are summarized in Appendix I):

$$\mathrm{E} + \mathrm{S} \underset{k_{-1}}{\overset{k_{+1}}{\rightleftharpoons}} \mathrm{ES} \xrightarrow{k_{+2}} \mathrm{E} + \mathrm{P}. \tag{1}$$

The reaction velocity v in this system is given by the Michaelis-Menten expression:

$$v = \frac{V_{\max}[\mathrm{S}]}{K_{\mathrm{m}} + [\mathrm{S}]}, \quad \text{where} \quad K_{\mathrm{m}} = \frac{k_{-1} + k_{+2}}{k_{+1}}, \tag{2}$$

It is assumed that the following equilibrium between the apoenzyme and metal ion (zinc in the present case) exists in solution:

$$\mathrm{E_a} + \mathrm{M} \rightleftharpoons \mathrm{E} \tag{3}$$

$$K = [\mathrm{E}]/[\mathrm{E_a}][\mathrm{M}]. \tag{4}$$

Thus, the concentration of metalloenzyme is given by

$$[\mathrm{E}] = K([\mathrm{E_a}]_0 - [\mathrm{E}])([\mathrm{M}]_0 - [\mathrm{E}]). \tag{5}$$

Under the conditions $[\mathrm{S}] \gg [\mathrm{E_a}] \gg [\mathrm{M}]$, the equation is written as follows:

$$[\mathrm{E}] = \frac{K[\mathrm{E_a}]_0[\mathrm{M}]_0}{1 + K[\mathrm{E_a}]_0}. \tag{6}$$

If the concentration of substrate is sufficiently high as assumed in Eq. 6, the concentration of the product in Eq. 1 is proportional to that of the enzyme. Thus,

$$[\mathrm{P}] = k_0 t[\mathrm{E}], \tag{7}$$

where k_0 is molecular activity of enzyme and t the reaction time. Since we can assume that $K[\mathrm{E_a}]_0 \gg 1$, the following expression can be obtained from Eqs. 6 and 7.

$$[\mathrm{P}] = k_0 t \cdot \frac{K[\mathrm{E_a}]_0}{1 + K[\mathrm{E_a}]_0} \cdot [\mathrm{M}]_0 \simeq k_0 t[\mathrm{M}]_0. \tag{8}$$

Differentiating, we have

$$\frac{\mathrm{d}[\mathrm{P}]}{\mathrm{d}t} \simeq k_0[\mathrm{M}]_0. \tag{9}$$

This shows that the formation rate of the product in Eq. 1 is proportional to the initial concentration of metal ion in solution. Thus the metal concentration in the sample solution can be determined by measuring enzymatic activity, if the formation rate of the product can be obtained, for example, by absorption measurement of the product.

Since the absorption of substrate is not negligible in the present case because of the overlapped spectra, Eq. 9 should be modified. The total absorption of the substrate and product at λ is given by

$$A_\lambda = (e_{\mathrm{S}}^\lambda[\mathrm{S}] + e_{\mathrm{P}}^\lambda[\mathrm{P}])l. \tag{10}$$

By differentiation we have

$$\frac{\mathrm{d}A_\lambda}{\mathrm{d}t} = \frac{\mathrm{d}}{\mathrm{d}t}(e_{\mathrm{P}}^\lambda - e_{\mathrm{S}}^\lambda)[\mathrm{P}] \cdot l \simeq (e_{\mathrm{P}}^\lambda - e_{\mathrm{S}}^\lambda)k_0 l \cdot [\mathrm{M}]_0. \tag{11}$$

We see that the time-dependence of the total absor-

bance at λ (dA_λ/dt) is also proportional to the initial concentration of metal. The amount of zinc in the solutions can be determined from a plot of (dA_λ/dt) *vs.* $[M]_0$.

Experimental

Chemicals. Bovine carbonic anhydrase C-7500 (EC 4.2.1.1, abbreviation BCA, Sigma Chem. Co.) was used. Substrate (*p*-nitrophenyl acetate) and buffer (tris(hydroxymethyl)methanamine=Tris) were purified by means of solvent extraction using a 0.001% dithizone–chloroform solution.[8] *p*-Nitrophenyl acetate was dissolved in 0.03 M Tris buffer solution (pH 7.8).[9] (1 M=1 mol dm^{-3}.) The distilled water was prepared by a Daiken Sekiei subboiling distiller.[10] Zinc chloride was used for the preparation of standard solution of zinc.

Instruments. A Shimadzu UV-210 spectrophotometer with a SPR-5 temperature controller was used for the measurements of enzymatic activity of carbonic anhydrase, the optical path of the absorption cell being 10 mm. A Hitachi 170-50 atomic absorption spectrophotometer with a Jarrell-Ash FLA-100 carbon rod atomizer was used to determine the zinc content in the sample solutions.

Preparation of the Apoenzyme. A zinc-free enzyme (apoenzyme) was prepared by a modified method of Lindskog and Malmström[11] as follows. BCA (10 mg) was dissolved in 1 ml of water and dialyzed with 0.01 M 1,10-phenanthroline and 0.1 M of sodium acetate buffer (pH 5.0) for 5—10 days. After further dialysis with 10^{-4} M EDTA and 0.06 M Tris (pH 7.8) for half a day, the chelating reagents were eliminated by dialysis with water. The zinc content in the enzyme was reduced to less than 3% of the initial content. The concentration of enzyme protein was determined by measuring the absorbances at 260 nm and 280 nm.[12]

Measurement of Enzymatic Activity. The enzymatic reaction of BCA for the substrate, *p*-nitrophenyl acetate, proceeds as follows:

$$O_2N\text{-}C_6H_4\text{-}OCOCH_3 + H_2O \xrightarrow{BCA} O_2N\text{-}C_6H_4\text{-}OH + CH_3COOH \quad (12)$$

The absorbance of the product, *p*-nitrophenol, was measured at 348 nm.[9] We see from the Michaelis-Menten plot (reaction velocity *vs.* concentration of substrate) that 1 mM of *p*-nitrophenyl acetate is sufficient to satisfy the conditions for Eq. 6.

The procedure for enzymatic activity measurement was as follows: 2 ml of the substrate solution and 50—200 μl of the zinc-containing sample were mixed in a cuvette. 100 μl of 10^{-4} M apo-BCA was then added to the mixed solution, the time at which addition was made being taken as $t=0$. The increase in absorbance at 348 nm, which corresponds to the increase of the product in Eq. 12, was measured subsequently. All the experiments were carried out at 25 °C.

Results and Discussion

Calibration Curve for Zinc. The relationship between the change in absorbance at 348 nm (reaction rate) and the concentrations of zinc in the solution is shown in Fig. 1. The change in absorbance corresponds to the enzymatic activity. The change of absorbance per minute was adopted for measurement of enzymatic activity. The enzymatic activity was calculated from the absorbance change during the period 1—5 min after addition of enzyme.

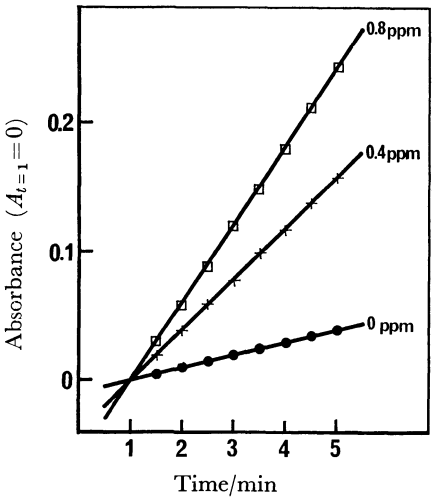

Fig. 1. Time dependence of absorbance change at several zinc concentrations. Absorbance at $t=1$ min ($A_{t=1}$) after the addition of apoenzyme was assumed zero.
Zinc solution: 100 μl, 1 mM substrate solution: 2 ml, 0.1 mM BCA solution: 100 μl. ●—●: [Zn]=0 μg/ml, ×—×: [Zn]=0.4 μg/ml □—□: [Zn]=0.8 μg/ml.

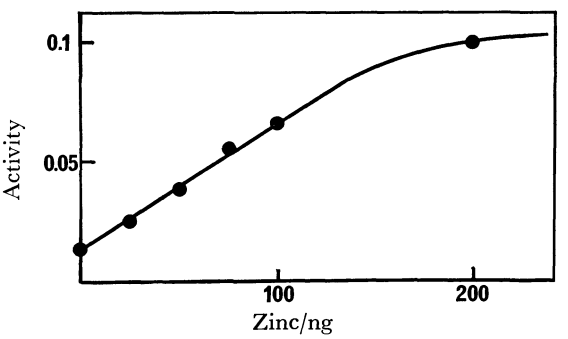

Fig. 2. Calibration curve for zinc measured by enzymatic activity of BCA. The enzymatic activity was measured as the change of absorbance (dA/dt) at 348 nm. 1 mM substrate solution: 2 ml, 0.1 mM BCA solution: 100 μl.

As shown in Fig. 2, the calibration curve is linear in the range 10—100 ng of zinc. For the amount of zinc over 100 ng, the condition $[E_a] \gg [Zn]_0$ is no longer valid and the calibration curve starts to bend. However, the dynamic range of the calibration curve can be extended by varying the amount of sample added to the buffer solution. The actual dynamic range, therefore, may be extended from 10 ng/ml to 1 μg/ml. A higher concentration of zinc ion might be determined if $[E_a]$ can be increased. However, increase of background absorption and difficulty of mixing the enzyme and sample homogeneously at the start of reaction result in poor accuracy. Thus 10 nmol enzyme is the maximum working amount for the determination of zinc under the present conditions.

The integral absorbance (A) can also be applied to the determination of zinc instead of the change in absorbance (dA/dt), as can be seen from Eq. 10.

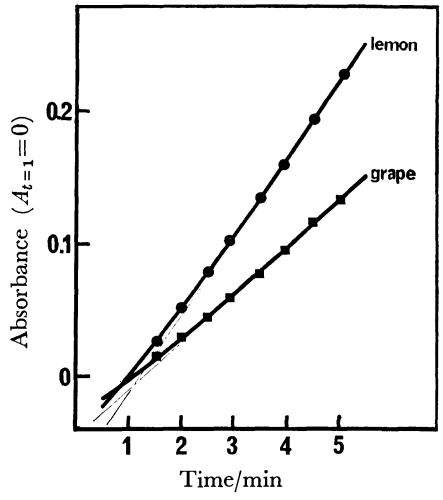

Fig. 3. Time dependence of absorbance change in grape and lemon juice samples. 1 mM substrate solution: 2 ml, 0.1 mM BCA solution: 100 μl, sample solution: 100 μl. ■—■: grape juice, ●—●: lemon juice.

However, zinc determination due to the integral absorbance causes large error in the analytical results. A typical example is shown in Fig. 3, where the absorbance changes at 345 nm are shown for grape and lemon juices. The rate of increase of absorbance is low at the initial stage of the reaction, and the amount of zinc obtained from the apparent absorbance might be less than the actual value. The slow increase of absorbance at the initial stage of the reaction might be due to the redistribution of zinc in the enzyme and sample. Measurement of the enzymatic activity should therefore be started after a few minutes (at least 1 min).

The sensitivity of the present method is *ca.* 10 ng/ml or 2 ng. As can be seen from Eq. 11, the sensitivity depends on the molecular activity (k_0) and absorption coefficient of the product (e_p). It may be improved by selection of a more appropriate substrate, although *p*-nitrophenyl acetate was used as a substrate for the sake of convenience.

In order to use the metalloenzyme method for metal determination, the following conditions should be satisfied: 1) A metal-free enzyme; 2) an enzyme stable in the metal-free state; 3) an enzyme easily obtained and convenient to work with; 4) little interference of other metal ions; and 5) linearity between the metal concentration and the rate of product formation. So far, alkaline phosphatase and aminopeptidase have been applied to zinc determination.[3,4] These enzymes can be easily obtained and are readily manipulated. The analytical sensitivity of the methods using aminopeptidase and alkaline phosphatase is comparable with that of the present method. However, more than one zinc atom is required for reactivating these enzymes from the zinc free state. As can be seen in Eqs. 2′ and 3′ in Appendix II, the relationship between zinc content and recovery of activity is complicated, not being linear. This indicates that the standard addition method may not be available, even when the interference of the matrices is large. For this reason, the use of carbonic anhydrase is preferable to these enzymes.

TABLE 1. EFFECT OF ANIONS ON ENZYMATIC ACTIVITY OF CARBONIC ANHYDRASE[a]

Anions	Amount/μmol	Relative activity[b]/%
Cl^-	1	88±18
NO_3^-	1	82±16
HSO_4^-	1	85±19
ClO_4^-	1	74±15
CN^-	0.2	12±2
CN^-	1	5±3

a) The amounts of zinc and apo-carbonic anhydrase were 1.5 nmol and 10 nmol, respectively. b) The ratio (%) of the enzymatic activities measured with and without the anions.

TABLE 2. EFFECT OF METAL IONS ON ENZYMATIC ACTIVITY OF CARBONIC ANHYDRASE[a]

Zinc amount/ng	Amount/ng		Relative activity[b]/%
0	Co(II)	0	10±3
0		100	55±12
100		20	95±18
100		100	145±22
0	Hg(II)	0	25±2
0		100	12±3
100		20	74±5
100		100	59±7
0	Cu(II)	0	6±1
0		100	7±1
100		20	87±9
100		100	88±8

a) The amounts of zinc and apo-carbonic anhydrase were 1.5 nmol and 10 nmol, respectively. b) Enzymatic activities based on the activity when only 100 ng zinc is added.

Interference of Coexistent Ions. A few studies have been made on the effect of the coexisting cations[13] and anions[14] on the activity of carbonic anhydrase. The interference of the concomitants in the present system is summarized in Tables 1 and 2. Excess amounts of cyanide and perchlorate ions interfere severely with the analytical results.

In the case of cations, Fe^{2+}, Mn^{2+}, Ca^{2+}, Na^+, and Mg^{2+} do not interfere as long as their amounts are less than twice the amount of zinc ion. Hg^{2+} reduces the enzymatic activity by 50%, and Co^{2+} at a concentration equal to that of zinc ion increases the enzymatic activity by 50%. However, the level of mercury or cobalt in real samples is generally much lower than that of zinc (in the environmental and biological samples).[15,16] Thus, the selectivity of this method is maintained at such low levels in many cases. If the interference of the concomitants can not be avoided, the standard addition method should be employed. It would improve the accuracy of the procedure.

Application to Zinc Determination. The analytical results (the standard addition method) for the

Table 3. Determination of zinc in real sample

Sample	Zn content/(ng/ml)	
	present method[a)]	atomic absorption[b)]
Grape juice	340±50	370±20
Pear juice	180±50	250±20
Lemon juice	700±50	540±30
City water	2200±100	1800±100
Drain water	260±90	190±20

a) The amount of apo-carbonic anhydrase was 10 nmol at pH 7.8. b) Determined by atomic absorption spectrometry.

fruit juices and natural waters are given in Table 3, together with the amount of zinc in the same samples determined by atomic absorption spectrometry. The analytical values obtained by the present method are in line with those obtained by atomic absorption spectrometry. This indicates that the present method can be applied to the determination of zinc in biological and environmental samples.

However, when the "metalloenzyme method" is applied to metal determination in biological samples, the same enzyme intrinsically existing in the sample interferes with the results. For example, the determination of zinc in serum would not be possible by the present method because of the high activity of carbonic anhydrase in serum. The same situation occurs in the case of other esterases, when the samples related to digestive organ are analyzed. The appropriate selection of enzyme should be made with regard to the kind of sample. Pretreatment of sample for eliminating or inactivating the intrinsic enzyme is necessary.

Conclusion

The present method shows promise for determining trace zinc. In general, biochemical amplification and specificity to the metal ion analysed are important characteristics of metal determination by the activity of metalloenzymes. In the present system, one zinc ion caught in the enzyme protein can react with many specific substrates and produce many specific products if the reaction time can be prolonged. The catalytic reaction of metalloenzyme may enhance the sensitivity of the method. This is a great advantage of the "metalloenzyme method" as compared to the usual colorimetric method. In practice, however, the present method has some limitations due to the natural hydrolysis of the substrate and incompleteness of zinc-elimination from the enzyme. Nevertheless, it is superior in selectivity and comparable in sensitivity to convenient colorimetric methods such as the dithizone method.[17] The preparation of enzyme electrodes for trace metal analysis is an interesting application of the metalloenzyme method.

The authors express their thanks to Dr. A. Ikai, Department of Biochemistry, The University of Tokyo, for helpful discussions. This research was supported by Grant-in-Aid for Scientific Research (B) under grant No. 249008 from the Ministry of Education, Science and Culture.

Appendix I

E: holoenzyme
S: substrate
P: product
ES: complex of substrate and holoenzyme
v: initial reaction rate
V_{max}: maximum reaction rate
K_m: Michaelis constant
$k_{\pm 1,+2}$: rate constant
k_0: molecular activity of enzyme
t: reaction time
E_a: apoenzyme (inactive)
M: metal ion
K: stability constant between enzyme protein and zinc
e_S^λ: absorption coefficient of substrate at λ
e_P^λ: absorption coefficient of product at λ
A^λ: absorbance at λ
l: light path length in the cuvette
$[\ ]_0$: concentration at the condition of initial stage
λ: wavelength

Appendix II

In a system where more than one zinc ion is necessary to attain recovery of enzymatic activity, Eq. 5 should be modified as follows:

i) In the case where enzymatic activity appears for n bindings of zinc ions such as in aminopeptidase:

$$[E] = K_1K_2\cdots K_n[Zn]^n[E_a] \simeq \frac{K_1K_2\cdots K_n[Zn]^n}{1+K_1[Zn]+\cdots+(K_1K_2\cdots K_n[Zn]^n)}\cdot[E_a]_0, \quad (1')$$

$$[P] \approx \frac{K_1K_2\cdots K_n[Zn]^n}{1+K_1[Zn]+\cdots+(K_1K_2\cdots K_n[Zn]^n)}[E_a]_0k_0t. \quad (2')$$

ii) In the case where the molecular activity (k_0) of the enzyme changes in terms of the binding number of zinc ions to the enzyme, such as found in alkaline phosphatase, Eq. 8 should be replaced by

$$[P] \approx \frac{K_1K_2\cdots K_n[Zn]^n}{1+K_1[Zn]+\cdots+(K_1K_2\cdots K_n[Zn]^n)}\{(K_{01}K_1[Zn]) + \cdots + (k_{0n}K_1\cdots K_n[Zn]^n)\}t[E_a]_0. \quad (3')$$

k_{0i}: molecular activity of enzyme when the binding number of zinc ions to enzyme is "i".

K_i: step-wise stability constant, $K_i = \dfrac{[E_aZn_i]}{[E_aZn_{i-1}][Zn]}$. (4')

References

1) G. G. Guilbault, "Enzymatic Methods of Analysis," Pergamon Press, Oxford (1970).
2) M. M. Fishman, *Anal. Chem.*, **50**, 261R (1978).
3) A. Townshend and A. Vaughan, *Anal. Chim. Acta*, **49**, 366 (1969).
4) P. Lehky and E. A. Stein, *Anal. Chim. Acta*, **70**, 85 (1974).
5) J. V. Stone and A. Townshend, *J. Chem. Soc., Dalton Proc.*, **1973**, 495
6) A. Townshend and A. Vaughan, *Talanta*, **17**, 289 (1970).
7) J. E. Coleman, "Inorganic Biochemistry," ed by G. L. Eichhorn, Elsevier, Amsterdam (1973), Vol. 1, p. 488.

8) B. G. Malmström, *Arch. Biochim. Biophys.*, **46**, 345 (1953).
9) J. McD. Armstrong, D. V. Myers, J. A. Verpoorte, and J. T. Edsall, *J. Biol. Chem.*, **237**, 1129 (1962).
10) T. Harada, K. Fujiwara, and K. Fuwa, *Bunseki Kagaku*, **26**, 877 (1977).
11) S. Lindskog and B. G. Malmström, *J. Biol. Chem.*, **237**, 1129 (1962).
12) E. Layne, "Methods in Enzymology," ed by S. P. Colewick and N. O. Kaplan, Academic Press, New York (1957), Vol. 3, p. 452.
13) J. E. Coleman, *Biochem.*, **4**, 2644 (1965).
14) Y. Pocker and J. T. Stone, *Biochem.*, **7**, 2936 (1968).
15) E. J. Underwood, "Trace Elements in Human and Animal Nutrition," 3rd ed, Academic Press, New York (1971).
16) J. J. Dulka and T. H. Risby, *Anal. Chem.*, **48**, 640A (1976).
17) E. B. Sandell, "Colorimetric Determination of Traces of Metals," 3rd ed, Interscience, New York (1959).

Electrochemical Behavior of Ferredoxins Adsorbed on Mercury Electrode Surface. Cyclic d.c. and a.c. Voltammetric Studies with Hanging Mercury Drop Electrode

Tokuji IKEDA,* Kazunobu TORIYAMA, and Mitsugi SENDA

Department of Agricultural Chemistry, Kyoto University, Sakyo-ku, Kyoto 606

(Received December 25, 1978)

The electrochemical behavior of *Clostridium pasteurianum* ferredoxin and spinach ferredoxin was studied by cyclic d.c. and cyclic phase-selective a.c. voltammetry with a hanging mercury drop electrode. An irreversible adsorption of these ferredoxins on the electrode surface is described. In successive cyclic voltage scans both d.c. and a.c. voltammograms of ferredoxins change gradually in both height and form until a steady state is attained, indicating that the ferredoxins adsorbed on the electrode surface decompose to cluster-free ferredoxins. Apoferredoxins give the same voltammograms as the steady state voltammograms of ferredoxins. The steady state voltammograms are assigned to RSH/RSHg redox reaction of the cysteine residues in apoferredoxin. At pH lower than 8 the d.c. waves are explained by an equation for reversible one-electron surface redox reaction. Kinetic parameters of the redox reaction were determined by a.c. voltammetry.

Ferredoxins, iron-sulfur proteins, function as electron carriers in many metabolic reactions.[1] The standard oxidation-reduction potential, E_0', and the stoichiometry of electron equivalents, n', of various ferredoxins have been measured by equilibrium techniques.[2] Attempts to measure the E_0' value directly by polarography have also been made.[3-8] Although the technique may be an advantageous means of studying the oxidation-reduction reaction of ferredoxins, the exact relationship between half-wave potential and E_0' requires further examination. In this study the electrochemical reduction and oxidation of two types of ferredoxins were examined with use of cyclic d.c. and a.c. voltammetry to gain a better understanding of their electrochemical behavior. Here we use the term "cyclic d.c. voltammetry" in place of the ordinary cyclic voltammetry in order to distinguish this technique from "cyclic a.c. voltammetry,"[9] in which alternating voltage of small amplitude is superimposed upon the cyclic sweep voltage applied to the electrode and the alternating currents (both in-phase and out-of-phase components, using a phase-selective amplifier) are measured as a function of the cyclic sweep voltage in both cathodic and anodic sweeps.

Part A. Cyclic d.c. Voltammetry

Experimental

Materials. Clostridium Pasteurianum Ferredoxin (Cl.Fd) and Spinach Ferredoxin (sp.Fd): Ferredoxins from *Clostridium pasteurianum* (ATCC 6013) and spinach were prepared according to the method of Mayhew,[10] the Cl.Fd having an absorption ratio of 0.78 or greater (390/280 nm) and sp.Fd one of 0.45 or greater (420/275 nm). The ferredoxin concentrations of stock solutions were determined spectrophotometrically with molar extinction coefficients of 3.0×10^4 at 390 nm[10] and 9.7×10^3 at 420 nm[11] for Cl.Fd and sp.Fd, respectively. The stock solutions were stored at 4 °C anaerobically.

Apoferredoxin from Clostridium Pasteurianum (apo-Cl.Fd): Iron and acid-labile sulfide were removed from Cl.Fd by treatment of the protein with an acid. Thirty microliters of *ca.* 0.5 mM Cl.Fd was acidified with 30 μl of 0.4 M hydrogen chloride. Hydrogen sulfide evolved was expelled by passing nitrogen gas through the solution. The brown color of ferredoxin disappeared completely after *ca.* 10 min, a white precipitate being formed. The solution was neutralized with 0.4 M sodium hydroxide to dissolve the precipitate and 3 μl of 0.05 M disodium ethylenediaminetetraacetate was added to the solution.

All other chemicals used were highly pure commercial products (Nakarai Chemicals Co., Ltd.). Triply distilled water was used to prepare the electrolysis solution.

Instruments. Cyclic d.c. voltammograms were recorded on a Yanagimoto PE21-TB2S potentiostat with a built-in sweep voltage generator and a Yokogawa X-Y recorder. A Metrohm E410 hanging mercury drop electrode was used, the surface area of the electrode being 0.0187 ± 0.0003 cm^2.

Electrochemical Measurements. All measurements were made with a three-electrode potentiostat. Potentials were measured against a saturated calomel electrode (SCE). Buffer solutions (0.1 M hydrogen chloride–sodium acetate for pH 1.4—4.0, 0.1 M acetic acid–sodium acetate for pH 4.0—5.5, 0.1 M sodium dihydrogenphosphate–disodium hydrogenphosphate for pH 5.5—7.0, 0.1 M hydrogen chloride–tris(hydroxymethyl)aminomethane for pH 7.0—9.2 and 0.1 M glycine–sodium hydroxide for pH 9.2—11.0) were used as the base solution. The ionic strength of the base solution was adjusted to 0.5 mol/kg with sodium chloride. To avoid possible complications associated with the foaming of the solution, 3 ml of the base solution was transferred to the cell and deaerated for *ca.* 10 min by passing nitrogen gas, which had previously been passed through a solution of the same composition as that of the base solution. An aliquot of the stock solution of ferredoxin was then introduced into the base solution with a microsyringe under nitrogen atmosphere. A fresh mercury drop from the hanging mercury drop electrode (HMDE) was exposed to the solution for a given period of time (t_{exp}), while the potential of the HMDE was kept controlled at a constant potential (E_i). The voltage scan was then started from E_i, with a scan rate $v=0.36$ V s^{-1}, unless otherwise stated. All experiments were carried out at 25 °C.

Results

Cl.Fd. Figure 1 shows a typical single sweep voltammogram of 1.2 μM Cl.Fd in pH 6.6 phosphate buffer, which was recorded after $t_{exp}=2$ min at $E_i=-0.1$ V. In addition to a catalytic wave (a presodium wave) at -1.7 V, a peak-shaped wave appeared at -0.57 V. It grew up to a certain limit with increasing concentration of Cl.Fd at a constant exposure time or with increasing exposure time at a constant

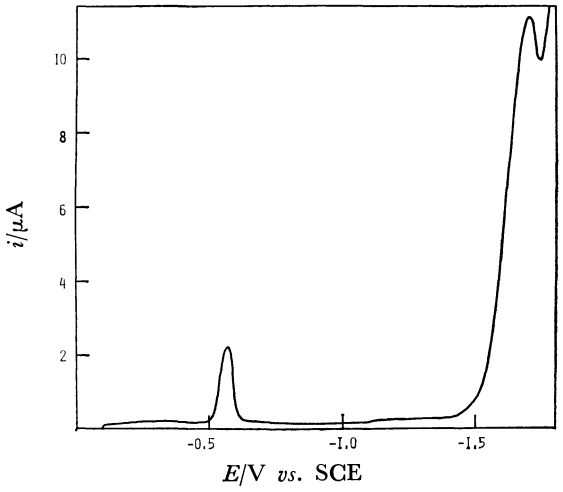

Fig. 1. d.c. voltammogram of 1.2 μM Cl.Fd in pH 6.6 phosphate buffer. Voltage scan was started from $E_i = -0.1$ V after $t_{exp} = 2$ min.

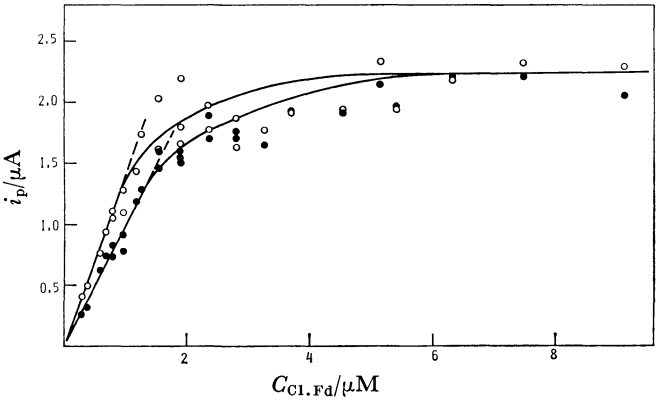

Fig. 2. The plot of i_p against $C_{Cl.Fd}$ at pH 6.9. ●: $t_{exp} = 17.5$ s, ○: $t_{exp} = 32.5$ s.

concentration of Cl.Fd, indicating that the wave is due to the Cl.Fd accumulated on the electrode surface. The dependence of peak height, i_p, of the wave on the Cl.Fd concentration, $C_{Cl.Fd}$, is shown in Fig. 2 for two t_{exp} values at pH 6.9. At lower concentrations of Cl.Fd the dependence of i_p on $C_{Cl.Fd}$ is linear, the product $C_{Cl.Fd} \times t_{exp}^{1/2}$ remaining constant for a given i_p value. This is evidence of the diffusion-controlled adsorption of Cl.Fd at the electrode surface, the current being assumed to be proportional to the surface concentration of Cl.Fd.[12-14]

Figure 3 shows cyclic voltammograms for Cl.Fd adsorbed on the HMDE at pH 9.2; the voltammograms were recorded after $t_{exp} = 1$ min at $E_i = -0.1$ V(Fig. 3A) and at -1.1 V (Fig. 3B). When the voltage scan was started from $E_i = -0.1$ V, two cathodic waves (Fig. 3A, I and II) were observed at -0.67 V and -0.78 V, respectively. Upon reversal of the scan at -1.1 V, two anodic waves(Fig. 3A, III and IV) appeared at -0.78 V and -0.63 V, respectively. In the second cycle of the voltage scan between -0.1 V and -1.1 V, the wave IV almost disappeared. In the successive voltage scans wave I decreased in height and finally disappeared, whereas the heights of waves II and III increased slightly until a steady

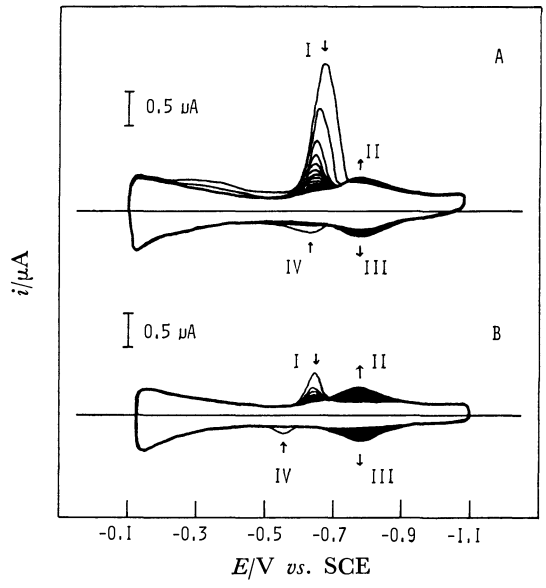

Fig. 3. Cyclic d.c. voltammograms of 1.9 μM Cl.Fd in pH 9.2 glycine buffer. Voltage scan was started from (A) $E_i = -0.1$ V and (B) $E_i = -1.1$ V after $t_{exp} = 1$ min.

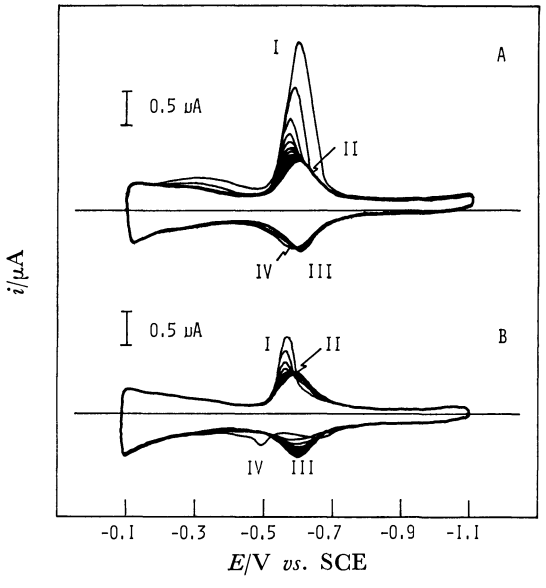

Fig. 4. Cyclic d.c. voltammograms of 1.9 μM Cl.Fd in pH 6.9 phosphate buffer. Voltage scan was started from (A) $E_i = -0.1$ V, (B) $E_i = -1.1$ V after $t_{exp} = 1$ min.

state was attained. When the voltage scan was started from $E_i = -1.1$ V after $t_{exp} = 1$ min (Fig. 3B), a small anodic wave IV was observed and a cathodic wave I in the reverse cathodic scan. However, wave IV disappeared in the second cyclic scan. In successive voltage scans, the height of wave I decreased and waves III (anodic) and II (cathodic) of nearly equal wave height appeared at -0.78 V, their heights increasing until a steady state was attained. The shape and height of the waves II and III at the steady state are independent of E_i.

Figure 4 shows cyclic voltammograms for Cl.Fd adsorbed on the HMDE surface at pH 6.9 after $t_{exp} =$

Table 1. Scan rate dependence of peak current, peak potential and half-peak width of wave II (cathodic) and wave III (anodic) at the steady state

Ferredoxin	v / V s^{-1}	$10^2\, i_p^{DC}$/μA		E_p^{DC}/V		$\Delta E_{p/2}^{DC}$/mV	
		II	III	II	III	II	III
Cl.Fd (at pH 6.9)	0.09	12	13	−0.60	−0.60	90	90
	0.18	25	25	−0.60	−0.60	85	90
	0.27	35	33	−0.60	−0.60	90	95
	0.36	45	47	−0.60	−0.60	90	95
sp.Fd (at pH 6.6)	0.09	3.2	2.9	−0.59	−0.58	95	100
	0.18	6.8	6.0	−0.59	−0.58	95	100
	0.36	14	12	−0.59	−0.58	95	105

1 min at E_i=−0.1 V (Fig. 4A) and at −1.1 V (Fig. 4B). The two cathodic waves (I and II) and the two anodic waves (III and IV), though not well separated, changed in height in successive voltage scans in nearly the same way as at pH 9.2, waves II (cathodic) and III (anodic) with identical peak potential of −0.60 V appearing on the cyclic voltammogram in the steady state.

The behavior of successive cyclic voltammograms of Cl.Fd at pH 9.2 and 6.9 indicates that the Cl.Fd adsorbed on the HMDE surface decomposes irreversibly and that waves II and III are due to the redox reaction of the decomposition product. The scan rate dependence of the peak currents, i_p(II) and i_p(III), the peak potentials, E_p^{DC}(II) and E_p^{DC}(III), and the half-peak widths, $\Delta E_{p/2}^{DC}$(II) and $\Delta E_{p/2}^{DC}$(III), of waves II and III at the steady state at pH 6.9 are summarized in Table 1. Both i_p(II) and i_p(III) are proportional to v, the ratio i_p(II)/i_p(III) being unity. E_p^{DC}(II) and E_p^{DC}(III) coincide with each other and are independent of v. The half-peak widths of these waves are 91±2 mV over the scan-rate range 0.09 V s^{-1}—0.36 Vs^{-1}. The results indicate that the reaction corresponding to waves II and III at pH 6.9 is a reversible one-electron surface redox reaction.[15] The pH dependence of E_p^{DC}(II) (=E_p^{DC}(III)) is shown in Fig. 5. E_p^{DC} shifts by −60 mV/pH at pH lower than 8 but more at pH higher than 8. The integrated current at pH 6.9 was calculated to be Q(II)=9.5± 1.0 μC cm^{-2} for wave II and Q(III)=8.0±0.5 μC cm^{-2} for wave III.

Apo-Cl.Fd. Cyclic voltammetry was performed with apo-Cl.Fd solution under experimental conditions similar to those for the native Cl.Fd. When the voltage scan was started from E_i=−1.0 V after t_{exp}=1 min, only waves II and III (Fig. 6A) appeared on the cyclic voltammogram of the first cyclic scan, remaining unchanged on the successive scans. One more cathodic wave, that is wave I in Fig. 6B, was observed when the voltage scan was started from E_i=−0.1 V after t_{exp}=1 min. However the wave almost disappeared in the second cathodic scan. The behavior of waves II and III for apo-Cl.Fd was the same as that of waves II and III for Cl.Fd in the steady state.

Sp.Fd. The same series of experiments were performed with sp.Fd. The cyclic voltammogram for sp.Fd in the steady state is shown in Fig. 7. The scan rate dependence of the peak current, peak potential and half-peak width is summarized in Table 1. The integrated current of the waves was calculated to be Q=3.2±0.4 μC cm^{-2}.

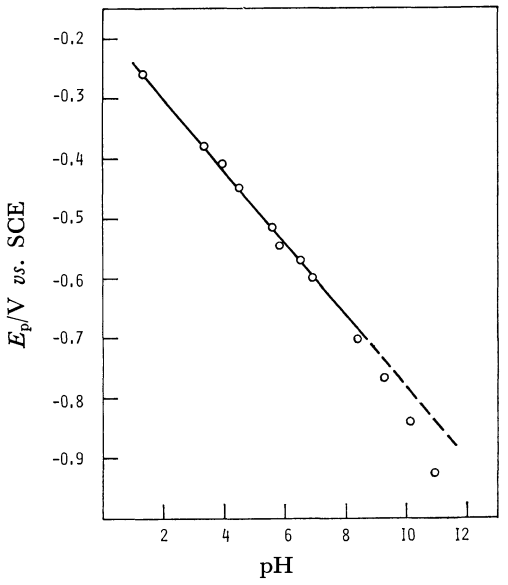

Fig. 5. Dependence of the peak potential, E_p^{DC}(II) (=E_p^{DC}(III)) on pH of the steady-state waves II and III.

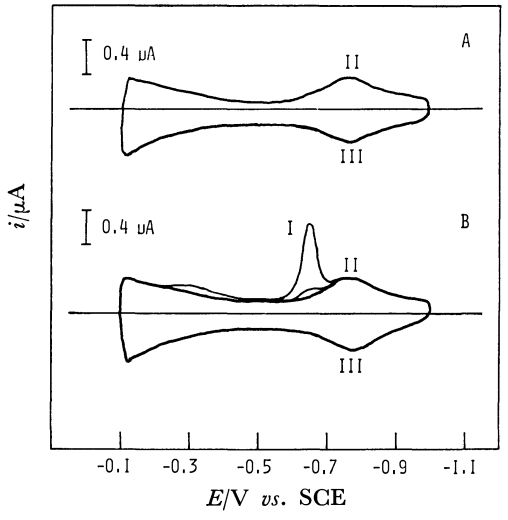

Fig. 6. Cyclic d.c. voltammograms for apo-Cl.Fd at pH 9.2. Voltage scan was started from (A) E_i=−1.0 V and (B) E_i=−0.1 V after t_{exp}=1 min.

Discussion

Adsorption of Ferredoxin on the Electrode Surface. Experimental results give evidence of an irreversible adsorption of ferredoxins on the surface of a mercury electrode. This was confirmed by the following experiment. After Cl.Fd had accumulated at the electrode surface, the electrode was removed from the protein-containing solution and washed with distilled water. The electrode was then placed in the base

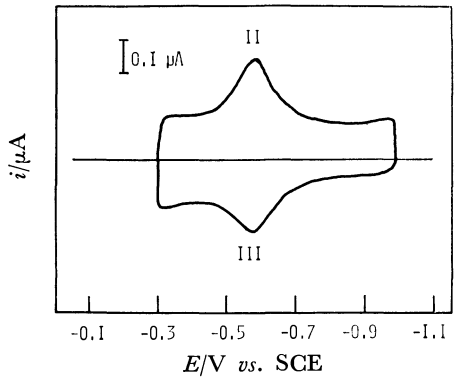

Fig. 7. Cyclic d.c. voltammogram at the steady state for sp.Fd at pH 6.6.

solution and voltammograms were recorded which were found to be the same as those in the case of an ordinary experiment with a solution containing Cl.Fd. Several workers[3,6,16] have suggested the adsorption of ferredoxins on a mercury electrode surface. Experimental results also indicate that the adsorption of ferredoxin is controlled by diffusion; at low concentrations of Cl.Fd $i_p=kq\Gamma=kq2(D_{Cl.Fd}/\pi)^{1/2}\ t_{exp}{}^{1/2}C_{Cl.Fd}$, where k is the proportionality constant, q the surface area of HMDE, Γ the surface concentration of Cl.Fd and $D_{Cl.Fd}$ the diffusion coefficient of Cl.Fd. At high concentrations a maximum current is attained, which can be given by $i_p^{max}=kq\Gamma^{max}$, where Γ^{max} is the maximum surface concentration of adsorbed Cl.Fd. Combining these two equations, we estimated the Γ^{max} value as 1.28×10^{-11} mol cm^{-2}, $D_{Cl.Fd}$ being calculated to be 1.4×10^{-6} cm^2 s^{-1} from the Svedberg equation with $s_{20.w}=1.4$ s, $v=0.63$ cm^3 g^{-1} [17] and $M.W.=6200$.[18] The value of Γ^{max} is in the order of magnitude comparable to that of other proteins.[19]

Waves I and IV. The value of integrated current of wave I was 19—30 μC cm^{-2} which is too large for this wave to be ascribed to the reduction of the biologically active cluster of Cl.Fd adsorbed on the electrode surface. A possible explanation is that the wave is due to the hydrogen evolution reaction catalyzed by the cluster of adsorbed Cl.Fd molecule, which decomposes in successive voltage scans. The large cathodic wave observed with apo-Cl.Fd in the first negative-going scan should be attributed to the residual amount of the active cluster.

The anodic wave IV may correspond to the oxidation of the cluster since it was not observed with apo-Cl.Fd. The corresponding cathodic wave may be concealed by the large cathodic hydrogen evolution current. It is difficult to study the redox reaction of the cluster by the present method.

Waves II and III. Waves II and III attain a steady state in successive voltage scans. Apo-Cl.Fd also gives the same waves as II and III of Cl.Fd in the steady state. The results indicate that waves II and III are due to the redox reaction of apoferredoxin produced by decomposition of the ferredoxin adsorbed on the electrode surface. Kuznetsov *et al.*[16] have also suggested the decomposition of the cluster of ferredoxin and the release of sulfhydryl groups on the electrode surface. The behavior of these waves (Table 1) can be explained by the equation for reversible one-electron surface redox reaction[15]

$$i = (n^2F^2/RT)qvn_c\Gamma^{max}\exp(\varphi)(1+\exp(\varphi))^{-2}, \quad (1)$$

where n is the number of electrons of the redox couple ($n=1$ in the present case), n_c the number of redox couples in one molecule of adsorbed ferredoxin and $\varphi=(nF/RT)(E-E_p^{dc})$. The results together with the pH-dependence of the peak potential indicate that the reversible one-electron wave may be assigned to RSH+Hg=RSHg+H$^+$+e$^-$. By substituting i_p values of Cl.Fd (Table 1) and $\Gamma^{max}=1.28\times10^{-11}$ mol cm^{-2} into Eq. 1 at $E=E_p^{dc}$, n_c was estimated to be 7.3±0.6. n_c was estimated to be 7.3±1.0 from the equation $Q=n_cF\Gamma^{max}$ with $Q=(1/2)(9.5+8.0)=8.7\pm1.0$ μC cm^{-2} and $\Gamma^{max}=1.28\times10^{-11}$ mol cm^{-2}. These n_c value are approximately 8, the number of cysteine residues of apo-Cl.Fd molecule. In the case of sp.Fd, n_c was estimated to be 5.2 with $Q=3.2$ μC cm^{-2} and $\Gamma^{max}=(1/2)1.28\times10^{-11}$ mol cm^{-2}, which is 5, the number of cysteine residues of apo-sp.Fd molecule. The redox mechanism corresponding to waves II and III can be assigned to (Apo-Fd(SH)$_{n_c}$)$_{ad}$+n_cHg⇌(Apo-Fd(SHg)$_{n_c}$)$_{ad}$+n_cH$^+$+n_ce$^-$, where $n_c=8$ for apo-Cl.Fd and 5 for apo-sp.Fd, at pH lower than 8.

At pH higher than 8 waves II and III become drawn out. Their wave heights decrease, the pH-dependence of the peak potential deviating from −60 mV/pH line. This indicates an involved nature of the surface redox reaction in basic solution Brown and Anson[20] have explained similar nonideal behavior of the cyclic voltammograms for reactions irreversibly attached to the surface of graphite electrode by introducing a nonideality parameter r; the surface activities used in place of the surface concentration are dependent on this parameter Another possible explanation is that the RSH/RSHg couples in apoferredoxin molecule may have different oxidation-reduction potentials which are distributed around the peak potential of the waves. Shift of the oxidation-reduction potentials associated with possible conformational changes of apoferredoxin adsorbed on the electrode surface should be taken into account.

Part B. Cyclic a.c. Voltammetry

Experimental

Experiments were performed with a Yanagimoto PE21-TB2S potentiostat with a built-in sweep voltage generator, an NF model LI572-B lock-in amplifier and a Yokogawa 3077 X-Y recorder. The amplitude of superimposed alternating voltage was adjusted to 10 mV (peak to peak) throughout the frequency range 100—700 Hz. Both resistive (in-phase) and capacitive (out-of-phase) components of the alternating currents (a.c.) were recorded against cyclic (d.c.) sweep voltage (usually $v=0.1$ V s^{-1}) applied to the HMDE For further details of the electrochemical measurements, *cf.* reference in part A.

Results

Figure 8 shows a typical cyclic in-phase a.c. voltammogram for Cl.Fd adsorbed on the HMDE surface

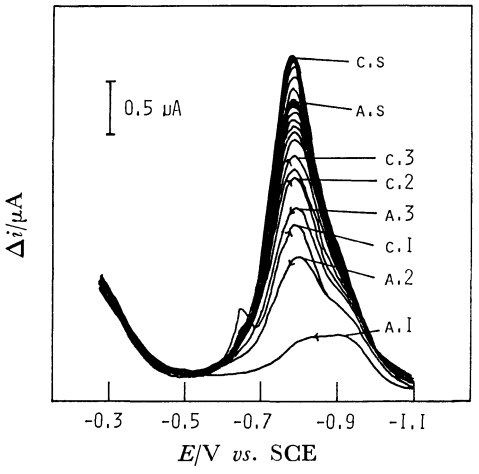

Fig. 8. Cyclic in-phase a.c. voltammogram of 1.9 μM Cl.Fd in pH 9.2 glycine buffer at f=500 Hz. d.c. voltage scan was started from E_i=−1.1 V after t_{exp}= 1 min. A1,A2,A3: Voltammograms of first, second and third anodic scan, C1,C2,C3: voltammograms of first, second and third cathodic scan and AS and CS: steady state voltammograms of positive-going (anodic) and negative-going (cathodic) scan, respectively.

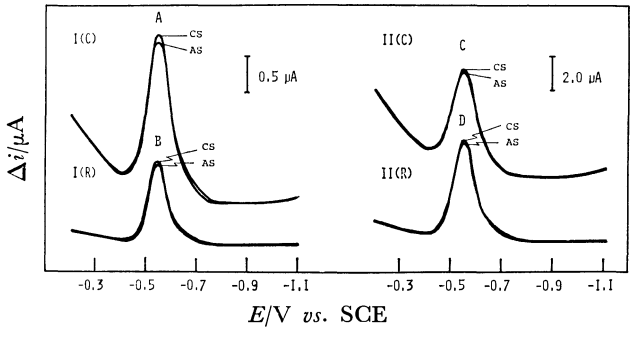

Fig. 9. Cyclic a.c. voltammograms at the steady state for Cl.Fd at pH 5.9. I(C) and I(R): Out-of-phase and in-phase component at f=100 Hz, II(C) and II(R): out-of-phase and in-phase component at f= 500 Hz. AS and CS show voltammograms of positive-going and negative-going scan, respectively.

at pH 9.2. A saturation coverage of the electrode surface with Cl.Fd was attained by exposing the electrode to the solution for one minute at E_i=−1.1 V, the voltammogram then being recorded. In the first positive-going scan a small a.c. wave appeared in the potential region −0.70 V——1.0 V. Upon reversal of the scan at −0.27 V, two a.c. waves were observed at −0.65 V and −0.78 V. The wave at −0.65 V disappeared in successive voltage scans between −0.27 V and −1.1 V, whereas the wave at −0.78 V attained a steady state in the same successive scans. Apo-Cl.Fd gave essentially the same voltammogram as that of Cl.Fd in the steady state. The results indicate that the a.c. waves of Cl.Fd in the steady state are due to the redox reaction of apo-Cl.Fd adsorbed on the electrode surface.

Figure 9 shows the cyclic a.c. voltammograms in the steady state for the adsorbed Cl.Fd at pH 5.9 at two a.c. frequencies. The peak potentials, E_p^{AC}, of the four a.c. waves (A, B, C, and D) are independent

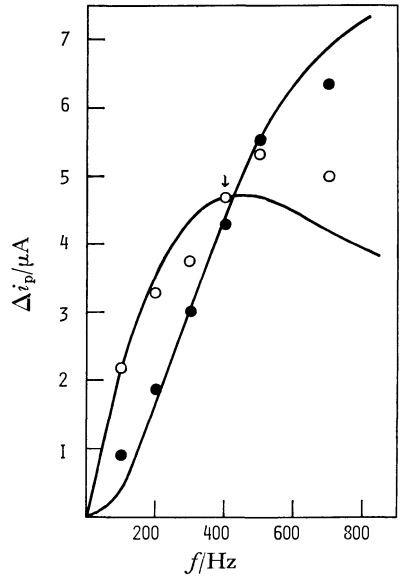

Fig. 10. Dependence of the a.c. peak currents on the a.c. frequency at pH 5.9. ○: Out-of-phase component and ●: in-phase component.

of a.c. frequency, coinciding with each other and with the peak potential of waves II and III of d.c. cyclic voltammogram at the same pH (Fig. 5). On the other hand, the peak height, Δi_p, and half-peak width, $\Delta E_{p/2}^{AC}$, of both in-phase and out-of-phase components are dependent on a.c. frequency (Fig. 10 and Table 2).

In basic solution of pH higher than 8, the a.c. voltammograms become drawn-out and decrease in height.

Discussion

According to theory of cyclic a.c. voltammetry[21] of a redox couple, ox/red, tightly adsorbed on the electrode surface, the capacitive (out-of-phase) and resistive (in-phase) components of the amplitude of a.c. currents, Δi(C) and Δi(R), are given by

$$\left.\begin{aligned}\Delta i(\mathrm{C}) &= \frac{mnF^2qn_c\Gamma_t 2\pi f\Delta E}{RT}\times\frac{\exp(\varphi)}{(1+\exp(\varphi))^2}\times\frac{1}{((2\pi f/(\vec{k}+\overleftarrow{k}))^2+1)}\\ \Delta i(\mathrm{R}) &= \frac{mnF^2qn_c\Gamma_t 2\pi f\Delta E}{RT}\times\frac{\exp(\varphi)}{(1+\exp(\varphi))^2}\times\frac{2\pi f/(\vec{k}+\overleftarrow{k})}{((2\pi f/(\vec{k}+\overleftarrow{k}))^2+1)}\end{aligned}\right\}\quad(2)$$

Here it is assumed that the redox reaction is expressed by a simple Butler-type equation $i/nFq=\overleftarrow{k}n_c\Gamma_{red}-\vec{k}n_c\Gamma_{ox}$ with $\overleftarrow{k}=k_s\exp((1-\alpha)\varphi)$, $\vec{k}=k_s\exp(-\alpha\varphi)$ and $\varphi=(nF/RT)(E^{DC}-E_0)$ and that the redox reaction is d.c.-voltammetrically reversible; $k_s/(nFv/4RT)\gg 1$. Γ_j is the surface concentration of j (j=ox and red, and $\Gamma_t=\Gamma_{ox}+\Gamma_{red}$), k_s the standard rate constant, α the transfer coefficient, m the proportionality constant,[21] in which the change of electrode charge associated with the change of Γ_j as well as n is involved, ΔE and f are the amplitude and frequency of superimposed alternating

Table 2. Peak potential and half-peak width of a.c. waves at the steady state for Cl.Fd adsorbed on mercury electrode surface at pH 5.9

f/Hz	E_p^{AC}/V	$\Delta E_{p/2}^{AC}$(R)[a]/mV		$\Delta E_{p/2}^{AC}$(C)[b]/mV	
		obsd	calcd	obsd	calcd
100	−0.55	80	74	95	92
200	−0.55	80	76	100	98
300	−0.55	85	80	110	106
400	−0.55	90	85	115	116
500	−0.55	95	90	120	126
700	−0.55	100	99	130	145

a) In-phase. b) Out-of-phase.

Table 3. Standard electron transfer rate constant of ferredoxins adsorbed on mercury electrode surface

pH	k_s[a]/10^2 s^{-1}
4.4	12.0±5.0[b]
5.9	13.4±3.7[b]
6.9	15.2±1.7[b]
6.9	10.1±3.1[c]
6.6	13.6±3.2[d]

a) Average value over the a.c. frequencies between 100 Hz and 700 Hz. b) Cl.Fd at the steady state. c) Apo-Cl.Fd. d) sp.Fd at the steady state.

voltage, respectively. At $E=E_0$, the ratio $\Delta i(\mathrm{R})/\Delta i(\mathrm{C})$ is given by

$$(\Delta i(\mathrm{R}))_{E=E_0}/(\Delta i(\mathrm{C}))_{E=E_0} = 2\pi f/2k_s \quad (3)$$

so that the k_s value can be determined experimentally provided that E_0 is known. As decribed above E_p^{AC} is independent of f and coincides with E_p^{DC} of corresponding *reversible* d.c. voltammograms, indicating that $E_p^{AC}=E_p^{DC}=E_0$ and α is at least not much different from 0.5. Application of Eq. 3 to experimental data, such as those shown in Fig. 10 gives k_s values summarized in Table 3. Solid lines in Fig. 10 are drawn by Eq. 2 at $E=E_0$ using $k_s=13.4\times10^2$ s^{-1} and $\Delta i_p(\mathrm{C})=4.7$ μA at 400 Hz. Values of $\Delta E_{p/2}^{AC}$ as calculated from Eq. 2 by assuming $n=1$ and $\alpha=0.5$ are also given in Table 2. Apparent agreement between theory and experiment is good in spite of the very simplified model of charge transfer kinetics. Kinetic study gives information on the protonation mechanism associated with the charge transfer, RSH+Hg=RSHg+H$^+$+e$^-$. When a very rapid (*i.e.* reversible) proton transfer to oxidized form is followed by the charge transfer as

$$\begin{aligned} &\mathrm{RSHg} + \mathrm{H^+} = (\mathrm{RSHg})\mathrm{H^+}, && K_\mathrm{I} \\ &(\mathrm{RSHg})\mathrm{H^+} + \mathrm{e^-} = \mathrm{RSH} + \mathrm{Hg}, && k_{s0\mathrm{I}} \end{aligned} \quad (\mathrm{I})$$

the "measured" or apparent standard rate constant k_s is given by

$$k_s = k_{s0\mathrm{I}}(1+K_\mathrm{I}/(\mathrm{H^+}))^{-(1-\alpha)} \quad (4)$$

where $k_{s0\mathrm{I}}$ is the standard rate constant and K_I the dissociation constant of (I). When the charge transfer is followed by a very rapid proton transfer to reduced form as

$$\begin{aligned} &\mathrm{RSHg} + \mathrm{e^-} = \mathrm{RS^-} + \mathrm{Hg}, && k_{s0\mathrm{II}} \\ &\mathrm{RS^-} + \mathrm{H^+} = \mathrm{RSH}, && K_\mathrm{II} \end{aligned} \quad (\mathrm{II})$$

the apparent standard rate constant k_s is given by

$$k_s = k_{s0\mathrm{II}}(1+(\mathrm{H^+})/K_\mathrm{II})^{-\alpha} \quad (5)$$

where $k_{s0\mathrm{II}}$ is the standard rate constant and K_II the dissociation constant of (II). k_s tends to increase with increasing pH (see Table 3). This supports mechanism (II). However, the change of k_s with pH is too small to be explained by Eq. 5. In view of the precision of determination of k_s value no conclusive statement can be given at present.

In a.c. voltammetry a slight difference in height between the waves of negative-going and positive-going voltage scan were observed (Fig. 9). This can be explained by assuming that there are two conformations I and II of adsorbed apoferredoxins each for oxidized form, Apo-Fd(SHg)$_{n_c}$, and reduced form, Apo-Fd(SH)$_{n_c}$,

$$\begin{array}{ccc} (\text{Apo-Fd(SHg)}_{n_c})_\mathrm{I} & \overset{n_c}{\rightleftharpoons} & (\text{Apo-Fd(SH)}_{n_c})_\mathrm{I} \\ \downarrow\uparrow & & \downarrow\uparrow \\ (\text{Apo-Fd(SHg)}_{n_c})_\mathrm{II} & \overset{n_c}{\rightleftharpoons} & (\text{Apo-Fd(SH)}_{n_c})_\mathrm{II}. \end{array}$$

The waves of negative-going and positive-going scan can be assigned to

$$(\text{Apo-Fd(SHg)}_{n_c})_\mathrm{I} \overset{n_c}{\rightleftharpoons} (\text{Apo-Fd(SH)}_{n_c})_\mathrm{I} \rightleftharpoons (\text{Apo-Fd(SH)}_{n_c})_\mathrm{II}$$

and

$$(\text{Apo-Fd(SH)}_{n_c})_\mathrm{II} \overset{n_c}{\rightleftharpoons} (\text{Apo-Fd(SHg)}_{n_c})_\mathrm{II} \rightleftharpoons (\text{Apo-Fd(SHg)}_{n_c})_\mathrm{I},$$

respectively. The difference between the two peak heights should be due to the difference between the apparant standard rate constants of the two processes.

We are grateful to Associate Professor Yoshiki Tani and Dr. Sakae Shimizu for help in growing the Clostridium pasteurianum and to Dr. Masaaki Takahashi for help in the purification of spinach ferredoxin. This work was supported by a Grant-in-Aid from the Ministry of Education.

References

1) For reviews *cf.* "Iron-Sulfur Proteins," ed by W. Lovenberg, Academic Press, New York and London, Vols. I and II(1973) and III(1977).

2) N. A. Stombaugh, J. E. Sundquist, R. H. Burris, and W. H. Orme-Johnson, *Biochemistry*, **15**, 2633 (1976) and references therein.

3) P. D. Weitzman, I. R. Kenedy, and R. A. Caldwell, *FEBS Lett.*, **17**, 241 (1971).

4) H. Dalton and J. Zubieta, *Biochim. Biophys. Acta*, **322**, 133 (1973).

5) Y. W. Chien, *J. Pharm. Sci.*, **65**, 1471 (1976).

6) B. A. Kiselev, *Biofizika*, **21**, 35 (1976).

7) C. L. Hill, J. Renaud, R. H. Holm, and L. E. Mortenson, *J. Am. Chem. Soc.*, **99**, 2549 (1977).

8) P. Bianco and J. Haladjian, *Biochem. Biophys. Res. Commun.*, **78**, 323 (1977).

9) a) W. L. Underkofler and I. Shain, *Anal. Chem.*, **37**,

218 (1965); b) A. M. Bond, R. J. O'Halloran, I. Ruzic, and D. E. Smith, *Anal. Chem.*, **48**, 872 (1976).
10) S. G. Mayhew, *Anal. Biochem.*, **42**, 191 (1971).
11) B. B. Buchanan and D. I. Arnon, *Methods Enzymol.*, **23**, 413 (1971).
12) J. Koryta, *Collect. Czech. Chem. Commun.*, **18**, 206 (1953).
13) B. A. Kuznetsov, *Experientia, Suppl.*, **18**, 381 (1971).
14) M. Senda, T. Ikeda, and H. Kinoshita, *Bioelectrochem. Bioenerg.*, **3**, 253 (1976).
15) a) E. Laviron, *J. Electroanal. Chem. Interfacial Electrochem.*, **52**, 355 (1974); b) S. Srinivasan and E. Gileadi, *Electrochim. Acta*, **11**, 321 (1966).
16) B. A. Kuznetsov, N. M. Mestechkina, and G. P. Shumakovich, *Bioelectrochem. Bioenerg.*, **4**, 1 (1977).
17) W. Lovenberg, B. B. Buchanan, and J. C. Rabinowitz, *J. Biol. Chem.*, **238**, 3899 (1963).
18) Ref. 1, Vol. II, p. 37.
19) F. Sheller, H-J. Prumke, H. E. Schmidt, and P. Mohr, *Bioelectrochem. Bioenerg.*, **3**, 328 (1976).
20) A. P. Brown and F. C. Anson, *Anal. Chem.*, **49**, 1958 (1977).
21) M. Senda and P. Delahay, *J. Phys. Chem.*, **65**, 1580 (1961).

Substituent Effect in the Ionization of *cis*-2-Substituted 1-Cyclopropanecarboxylic Acids

Yoshiaki KUSUYAMA

Department of Chemistry, Faculty of Education, Wakayama University, Masagocho 1-1, Wakayama 640

(Received August 26, 1978)

Ten *cis*-2-substituted 1-cyclopropanecarboxylic acids (substituents: H, CH_3, C_6H_5, CH_3O, C_2H_5O, Cl, Br, CH_3CO, CH_3OCO, and C_2H_5OCO) were prepared, and their pK_a values were determined in water at 25 °C, along with those of the *trans*-2-chloro and 2-methoxy derivatives. The pK_a values for cis isomers are somewhat larger than those for the corresponding trans isomers, except for the chloro and bromo derivatives. The substituent effects obtained were in the usual order in the sense of the electronic effects, except for the phenyl group, which produced a decrease in acidity relative to the unsubstituted acid. It was shown that the carbon-13 chemical shifts for the methylene carbon of the ethyl group in the ethyl *cis*-2-substituted 1-cyclopropanecarboxylate obtained in deuteriochloroform gave a reasonable linear relation with the pK_a(*cis*) values.

It is well established that the C–C bonds of cyclopropane ring have π double-bond character[1] and can extend the chain of conjugation when a cyclopropane ring is directly attached to a π system of bonds.[2] The degree of the contributions of the conjugative effect of the cyclopropane ring has been estimated by several workers.[3–6] The degree of the transmission of the electronic effects through the cyclopropane ring, however, is still uncertain, since conflicting results have been reported. For example, the effective transmission or a greater polarizability of the trans system was indicated by spectroscopic measurements[6,7] and by the chemical reactivities,[8] including the ionization of 2-phenyl-cyclopropanecarboxylic acids.[9] On the other hand, the alkaline hydrolysis of ethyl 2-phenyl-1-cyclopropanecarboxylates afforded larger Hammett's ρ values for cis isomers than for trans isomers.[10] Thus, the abilities of the cis isomer relative to the trans isomer in 1,2-disubstituted cyclopropane in transmitting electronic effects have been a continued subject of controversy.[8,11]

In attempt to resolve the contradiction in the reported results on transmitting polar effects through cyclopropylene, it appeared to be of interest to examine the effects of substituents in the ionization of 2-substituted 1-cyclopropanecarboxylic acids. In a previous paper,[12] the pK_a values of *trans*-2-substituted 1-cyclopropanecarboxylic acids and their linear relation with σ_m were reported. A study of the substituent effect in the pK_a values of *cis*-2-substituted 1-cyclopropanecarboxylic acids and in the carbon-13 chemical shifts of the methylene carbon of the ethyl group in ethyl *cis*-2-substituted 1-cyclopropanecarboxylates has been undertaken in the present study.

The system is a very interesting one from another point of view. The rigidity of the cyclopropane ring offers an interesting tool for elucidating the mechanistic problems in the acidity-structure relationship where substituents are in a close proximity to the carboxyl group. In this field of chemistry[13,14] less progress has been reported than in those concerning the effects of remote substituent groups, which have been well explained by both inductive (including the effects through both the field and bonds) and resonance effects. It appears that the data reported herein will provide useful information in order to elucidate interaction mechanisms between the proximate substituent and the carboxyl group.

Results and Discussion

Unsubstituted,[15] *cis*-2-methyl-,[13a] and *cis*-2-phenyl-1-cyclopropanecarboxylic acids[16] were synthesized by the methods described in the literature. Other substituted cyclopropanecarboxylic acids were obtained by the hydrolysis of the respective ethyl esters prepared by the appropriate methods. The cis isomers of ethyl esters were separated conveniently by a combination of fractional distillation and preparative GPLC. Cis and trans mixtures of ethyl 2-methoxy- and 2-ethoxy-1-cyclopropanecarboxylate were synthesized by the copper(I)-catalyzed decomposition of ethyl diazoacetate in methyl vinyl ether and ethyl vinyl ether respectively.[12] By using the method of McCoy,[17] diethyl and dimethyl 1,2-cyclopropanedicarboxylates were obtained. The remaining derivatives were prepared by the routes shown in the following scheme:

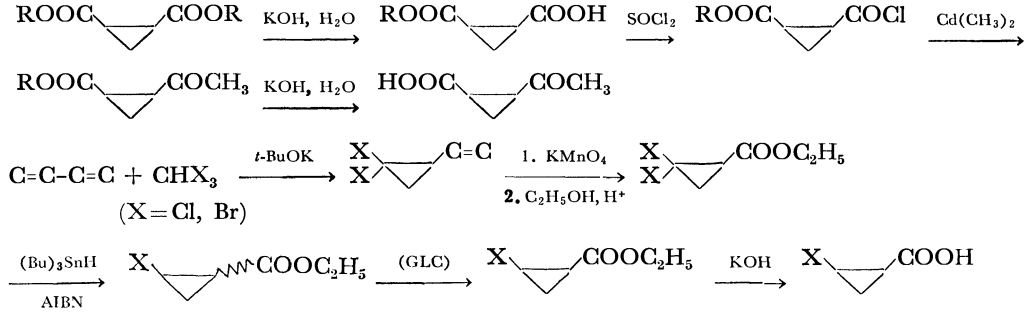

Table 1. pK_a values of 2-substituted cyclopropanecarboxylic acids in water at 25 °C

Substituent	*cis*	*trans*
H	4.83±0.01	4.84±0.01[c]
	4.83[a]	
CH_3	5.03±0.01	4.98±0.01[c]
	5.02[b]	5.00[b]
CH_3O	4.76±0.01	4.47±0.01
C_2H_5O	4.83±0.01	4.46±0.01
CH_3OCO	4.22±0.02	4.09±0.02[c]
C_2H_5OCO	4.26±0.02	4.10±0.02[c]
CH_3CO	4.19±0.01	4.08±0.01[c]
Cl	4.12±0.01	4.12±0.01
Br	4.09±0.01	4.09±0.01[c]
C_6H_5	4.95±0.02	4.57±0.02[c,d]

a) M. Kilpatric and J. O. Morse, *J. Am. Chem. Soc.*, **75**, 1854 (1953). b) Ref. 13(a). c) Ref. 12. d) Ref. 11.

Table 2. $\Delta pK_a(pK_a^X - pK_a^H)$ and $\Delta pK_a^{ct}(pK_{a_{cis}} - pK_{a_{trans}})$ values for 2-substituted cyclopropanecarboxylic acids in water at 25 °C

Substituent	$\Delta pK_a(cis)$	$\Delta pK_a(trans)$	ΔpK_a^{ct}
H	0.00	0.00	0.00
CH_3	0.20	0.14	0.05
CH_3O	−0.07	−0.37	0.29
C_2H_5O	0.00	−0.38	0.37
CH_3OCO	−0.61	−0.75	0.13
C_2H_5OCO	−0.57	−0.74	0.16
CH_3CO	−0.64	−0.76	0.11
Cl	−0.71	−0.72	0.00
Br	−0.74	−0.75	0.00
C_6H_5	0.12	−0.27	0.38

The pK_a values measured in water at 25 °C are listed in Table 1. The reproducibilities of the repeated runs are less than 0.01 pK_a unit except for the alkoxycarbonyls and the phenyl group (0.2 pK_a unit). This accuracy is considered to be sufficient for us to discuss the substituent effects. The values determined here for unsubstituted and *cis*-2-methyl derivatives showed a good agreement with those published by McCoy, within the limits of experimental error.[13a]

It is convenient to use the $\Delta pK_a^H(pK_a^X - pK_a^H)$ and $\Delta pK_a^{ct}(pK_{a_{cis}} - pK_{a_{trans}})$ values in discussing the substituent effects in comparison with various systems. These values are summarized in Table 2.

Since carbon-13 NMR chemical shifts are sensitive to changes in the electron density[18] and the stereochemical relationship of atoms in a molecule,[18,19] the application of this spectroscopic method to the methylene carbon of the ethyl group in ethyl 2-substituted 1-cyclopropanecarboxylates would provide additional insight into the substituent effect on pK_a values(*cis*) obtained here. Therefore, the substituent-induced chemical shifts(SCS)[20] for this carbon were determined under conditions essentially corresponding to an infinitive dilution in deuteriochloroform; the results are listed in Table 3, along with those of trans derivatives.[12] Both the cis and trans carbons showed "normal" substituent effects.

Table 3. ^{13}C Chemical shifts[a] for the methylene carbons of the ethyl group in ethyl 2-substituted cyclopropanecarboxylates in deuteriochloroform

Substituent	$\delta(cis)$[b,c]	$\delta(trans)$[d]	$\delta_{(cis)} - \delta_{(trans)}$
H	60.46	60.37	0.09
CH_3	60.15	60.19	−0.04
CH_3O	60.58	60.49	0.09
C_2H_5O	60.50	60.49	0.01
C_2H_5OCO	60.96	60.97	−0.01
CH_3CO	60.94	61.04	−0.10
Cl	61.04	61.04	0.00
Br	61.23	61.11	0.12
C_6H_5	60.14	60.61	−0.47
CN	61.70	61.73	−0.03

a) ppm from TMS as the internal standard. The errors are at least ±0.1 ppm. b) To be published in detail, along with the chemical shifts of cyclopropane-ring carbons. c) Measured on a Hitachi Perkin-Elmer R-22 spectrometer, with 22.6 MHz in the FT mode. d) Y. Kusuyama, *Bull. Chem. Soc. Jpn.*, **50**, 1784 (1977).

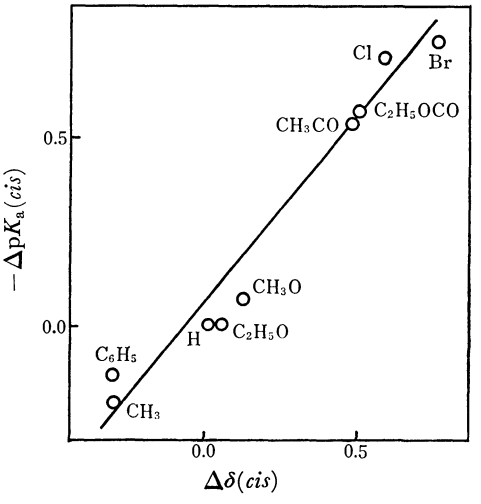

Fig. 1. Plots of ΔpK_a values for *cis*-2-substituted 1-cyclopropanecarboxylic acids at 25 °C in water *vs.* substituent induced ^{13}C chemical shifts of the methylene carbons of ethyl group in ethyl 2-substituted 1-cyclopropanecarboxylates.

The general trend of the substituent effects obtained for $pK_a(cis)$ is similar to those in such 2-substituted cyclopropane systems[6,12,13a,21] as 2-substituted 1,2-dimethyl-1-cyclopropanecarboxylic acids; they may be explained by substituent electronic effects except for the case of the phenyl group.

The $\Delta pK_a(cis)$ values showed a good linear relation with the $\Delta\delta(cis)$ values (Fig. 1). Therefore, it is reasonable to consider that the special desolvation effect by the proximate *cis*-2-substituents does not contribute to the pK_a values. In the case of 2-substituted acrylic acids, appreciable contributions of the desolvation effect to the dissociation of cis isomers have been reported.[13d]

$\Delta pK_a(cis)$ values do not afford a linear relation with those of *o*-substituted benzoic acid, where the steric

inhibition of resonance between the benzene ring and the carboxyl group by the *o*-substituents causes a acid-strengthening effect relative to *p*-substituted benzoic acids.

The cyclopropane ring is capable of overlaping with an adjacent p orbital of the substituents at the maximum in the *s-trans* or *s-cis* conformation.[6] In cyclopropanecarboxylic acid, the preferred conformation might be the *s-cis* conformer,[6] where the steric repulsion between the spherical *cis*-2-substituent and the carboxyl group is minor compared to those in ortho-substituted benzoic acids.[13c,22] Thus, spherical substituents would not prevent the resonance interaction between the cyclopropane ring and the carboxyl group. The acid-weakening effect of the *cis*-2-methyl group clearly

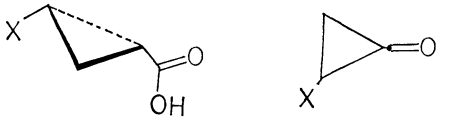

s-trans

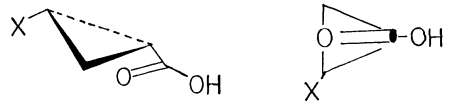

s-cis

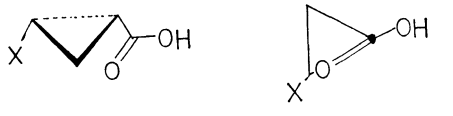

gauche

showed the same direction as that observed in the trans isomer. Moreover, it may be thought that the steric inhibition of resonance is not of major importance for chloro and bromo derivatives, although for these substituents the same acidity as in the cis and trans series respectively resulted from the compensation of contributing factors. Substituents with p-orbitals tend to have the maximum overlap with the cyclopropane ring in the bisected conformation. In *cis*-2-acetyl, methoxycarbonyl- and ethoxycarbonyl-1-cyclopropanecarboxylic acids, the steric repulsion between the substituent and the carbonyl group of the carboxyl group increases and prevents cis substituents from having the maximum overlap with the cyclopropane ring relative to the corresponding trans isomer. Such substituents could lead in the direction of acid weakening relative to the trans isomer (Table 2).

The pK_a values for alkoxy groups and phenyl group are quite high relative to that of the parent compound and the corresponding trans derivatives, if they are considered only in terms of normal electronic substituent effects. The origin for this phenomenon can not be explained clearly at the present time. Only the phenyl group deviated appreciably in the $\Delta\delta(trans)$-$\Delta\delta(cis)$ plots to the high field from the regression line (Fig. 2), while no significant difference in the plots was detected for alkoxy groups. It is considered that the methylene carbon of the ethyl group is more deshielded by the proximate phenyl group in the cis isomer.

The substituent effects can generally be analysed

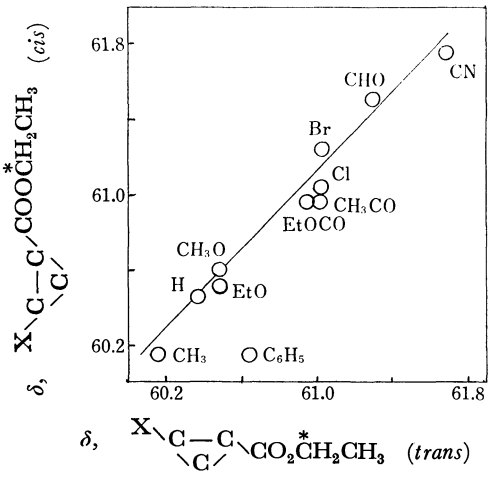

Fig. 2. Comparison of substituent-induced ^{13}C chemical shifts of the methylene carbons of ethyl group in ethyl 2-substituted 1-cyclopropanecarboxylates.

TABLE 4. THE SUBSTITUENT EFFECTS (ΔpK_a VALUES) OF METHOXYCARBONYL AND BROMINE IN THE *cis*-2-SUBSTITUTED CYCLOPROPYL FRAMEWORK

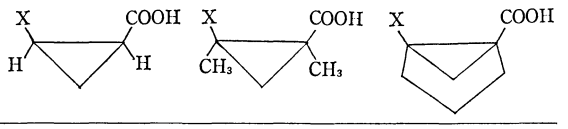

	(I)	(II)	(III)
H	0.00	0.00	0.00
CH_3OCO	−0.61	−1.019	−0.912
Br	−0.74	−1.276	−0.851

by the use of the linear free-energy relationship if only the electronic effect operates. The pK_a values for the trans series were excellently correlated by σ_m (correlation coefficient: 0.998; ρ: 1.99), indicating an appreciable contribution of the resonance effect.[12] The plots of the $\Delta pK_a(cis)$ against the substituent constants, σ^0, σ_p, and σ_I, failed to give a good linear relationship. The correlation coefficients proved to be from 0.83 to 0.89. A rather good correlation with the ρ value of 2.09 was obtained by means of σ_m with the correlation coefficient of 0.981. Although this correlation is not an excellent one, it appears that the special proximity effect is not of major importance in the dissociation of *cis*-2-substituted 1-cyclopropanecarboxylic acid.

In the series of *cis*-2-substituted 1-cyclopropanecarboxylic acids (I), the 2-substituted 1,2-dimethyl-1-cyclopropanecarboxylic acids (II), and 5-substituted bicyclo-[3.1.0]hexane-1-carboxylic acids (III)[14] effects of substituents (the values for methoxycarbonyl and bromo were available for comparison) increase in the order of I<III<II (Table 4), the same as the increasing order of the steric bulk of alkyl groups located behind the carboxyl group (hydrogen < trimethylene < two methyl groups). This order is also the same as that for the pK_a values for the parent acid of each series. Two explanations are possible for the phenomenon: (1) Bulky alkyl groups effectively desolvate the carb-

oxylate anion. The negative charge on the carboxylate does not disperse, though; accordingly, the electron density increases. (2) Alkyl groups shorten the distance between the substituent and the carboxyl group and increase the contribution of the field effect.

Experimental

The boiling points and melting points are uncorrected. The melting points were determined on a Yanaco Mp hot-stage melting-point apparatus. The ^{1}H NMR spectra were obtained on a JEOL JNM-C-60 HL spectrometer (60 MHz) and were reported in δ values relative to the internal TMS. The GLC analyses were carried out on a Yanaco GCG 550T, using a 1-m column of Silicone DC 550 or Silicone XF 1150. Preparative scale GLC separations were performed on a Yanaco G 80 aparatus equipped with an AP 11 collector.

The structure assignments for the geometrical isomers of alkyl 2-substituted 1-cyclopropanecarboxylates were made on the basis of the ^{1}H NMR spectra of ring protons by means of shift reagents, based on the generalization that the tendency of the shift of the signals of cis protons to carbonyl is larger than that of the shift of the trans protons.[23] The cis and trans isomers of alkyl 2-substituted 1-cyclopropanecarboxylates were well separated by GLC, and the cis isomer always showed a longer retention time than that of the corresponding trans isomer.

Ethyl cis-*2-Methoxy-1-cyclopropanecarboxylate.* The title compound was isolated by fractional distillation and by making two passes on the column (silicone DC 550 and silicone XF 1150) from a mixture of cis and trans isomers obtained by the reaction of ethyl diazoacetate with methyl vinyl ether.[12] Bp 81 °C/30 Torr, NMR (CCl_4) δ 0.75—1.75 (3H, m, ring), 1.24 (3H, t, J=8 Hz, CCH_3), 3.22 (3H, s, CH_3O), 3.23—3.65 (1H, m, ring), 4.05 (2H, q, J=8 Hz, CO_2CH_2C). Found: C, 58.72; H, 8.07%. Calcd: C, 58.31; H, 8.39%.

cis-*2-Methoxy-1-cyclopropanecarboxylic Acid.* Ethyl *cis*-2-methoxy-1-cyclopropanecarboxylate (1.3 g) was hydrolyzed by heating (40 °C) with sodium hydroxide (0.4 g) in 5 ml of water. After acidification to pH 3, extraction with ether, and the evaporation of the ether, *cis*-2-methoxy-1-cyclopropanecarboxylic acid was purified by short-column distillation; 0.3 g; bp 105 °C/10 Torr. NMR ($CDCl_3$) δ 0.90—2.70 (3H, m, ring), 3.34 (3H, t, J=7 Hz, CH_3), 3.30—3.7 (1H, m, ring, OCH), 7.75 (1H, s, OH). Found: C, 50.45; H, 7.55%. Calcd: C, 51.70; H, 6.94%.

Ethyl cis-*2-Ethoxy-1-cyclopropanecarboxylate.* The procedure used was the same as that employed above for the methoxy derivative; bp 103 °C/33 Torr. NMR (CCl_4) δ 0.7—1.75 (3H, m, ring), 1.10 (3H, t, J=8 Hz, $COCH_3$), 1.25 (3H, t, J=7 Hz, $COOCH_3$), 3.10—3.70 (3H, m, two methylene protons of the ethoxy group and one ring proton). Found: C, 60.76; H, 9.42%. Calcd: C, 60.74; H, 8.92%.

cis-*2-Ethoxy-1-cyclopropanecarboxylic Acid.* This compound was obtained by the alkaline hydrolysis of the corresponding ethyl ester; bp 135 °C/17 Torr. NMR ($CDCl_3$) δ 0.95—2.70 (3H, m, ring), 1.15 (3H, t, J=7 Hz, CH_3), 3.20—3.80 (3H, m, ring OCH and CH_2 of ethyl group) Found: C, 54.30; H, 7.86%. Calcd: C, 55.37; H, 7.74%.

Dimethyl and Diethyl cis-*1,2-Cyclopropanedicarboxylates.* These two esters were separated from mixtures[17] of the corresponding geometrical isomers. Dimethyl *cis*-1,2-cyclopropanedicarboxylate: bp 84 °C/4 Torr, 146—148 °C/45 Torr, lit, 110 °C/3 Torr.[24] Diethyl *cis*-1,2-cyclopropanedicarboxylate. Bp 138 °C/27 Torr, lit, bp 83—84 °C/1 Torr,[25] 124 °C/14 Torr.[24]

cis-*2-Methoxycarbonyl-1-cyclopropanecarboxylic Acid.* The alkaline hydrolysis[26] of dimethyl 1,2-cyclopropanedicarboxylate afforded *cis*-2-methoxycarbonyl-1-cyclopropanecarboxylic acid in a 30% yield; bp 147—148 °C/4.5 Torr, lit, 160 °C/3 Torr.[24]

cis-*2-Ethoxycarbonyl-1-cyclopropanecarboxylic Acid.* This compound was obtained by the alkaline hydrolysis of diethyl *cis*-1,2-cyclopropanedicarboxylate; bp 130—131 °C/3.5 Torr.

cis-*2-Ethoxycarbonyl-1-cyclopropanecarbonyl Chloride.* The treatment of *cis*-2-methoxycarbonyl-1-cyclopropanecarboxylic acid (9 g) with thionyl chloride (12 g) and subsequent distillation afforded the title compound (9 g); bp 84 °C/4 Torr. NMR (CCl_4) δ 1.00—2.00 (2H, m, ring CH_2), 1.25 (3H, t, J=7 Hz, CH_2 of the ethyl group).

Ethyl cis-*2-Acetyl-1-cyclopropanecarboxylate. A.* To dimethyl cadmium (*ca.* 0.05 mol) in benzene we added, drop by drop, 9 g (0.05 mol) of *cis*-2-ethoxycarbonyl-1-cyclopropanecarbonyl chloride in 10 ml of benzene. After a routine treatment, 3 g of crude ethyl *cis*-2-acetyl-1-cyclopropanecarboxylate were obtained. To this we then added 3 ml of water and stirred the mixture vigorously for 10 min. The organic layer was then separated and purified by distillation; 2 g; bp 95 °C/7 Torr.

Ethyl cis-*2-Acetyl-1-cyclopropanecarboxylate. B.* To a stirred mixture of 100 g of methyl vinyl ketone and 1 g of anhydrous copper(I) sulfate in 50 ml of hexane at 40 °C, 100 g of ethyl diazoacetate were added. After several minutes, the reaction took place suddenly. After the reaction was complete, the mixture was filtered and carefully distilled at atmospheric pressure in order to remove the excess methyl vinyl ketone and hexane. The residue was distilled *in vacuo* to yield 10 g of crude products; bp 70—88 °C/5.5 Torr. The fractional distillation afforded 3 g of the title compound, including 20% of impurities. Treatment with 2 ml of 0.5 M NaOH and subsequent GLC operation gave a pure material which showed essentially the same retention time in GLC and the same NMR spectrum as has been obtained by Method A.

cis-*2-Acetyl-1-cyclopropanecarboxylic Acid.* Ethyl *cis*-2-acetyl-1-cyclopropanecarboxylate (1 g) was hydrolyzed by heating (40 °C) with sodium hydroxide (0.24 g) in 6 ml of 50% ethanol to yield, after a routine treatment, *cis*-2-acetyl-1-cyclopropanecarboxylic acid (0.4 g); bp 143 °C/4 Torr. NMR ($CDCl_3$) δ 1.10—2.62 (m, 4H, ring), 2.24 (1H, s, CH_3), 8.30 (1H, s, OH). Found: C, 54.86; H, 6.62%. Calcd: C, 56.24; H, 6.30%.

1,1-Dichloro-2-vinylcyclopropane. This compound was prepared by adding potassium *t*-butoxide to a solution of 1,3-butadiene and chloroform and by a subsequent routine treatment,[27] bp 123—125 °C, lit, 122.5 °C/730 Torr.[28]

2,2-Dichloro-1-cyclopropanecarboxylic Acid. The oxidation of 1,1-dichloro-2-vinylcyclopropane with potassium permanganate in acetone gave a 2,2-dichloro-1-cyclopropanecarboxylic acid,[29] bp 92 °C/6 Torr, mp 74—75 °C, lit, mp 75—76 °C.[28]

Methyl 2,2-Dichloro-1-cyclopropanecarboxylate. This compound was obtained by the esterification of 2,2-dichloro-1-cyclopropanecarboxylic acid with methanol and sulfuric acid; bp 79 °C/23 Torr. NMR (CCl_4) δ 1.70—2.21 (2H, m, CH_2), 2.4—2.75 (1H, m), 3.76 (3H, s, CH_3).

Methyl cis-*2-Chloro-1-cyclopropanecarboxylate.* A mixture of 22 g (0.1 mol) of methyl 2,2-dichlorocyclopropane-carboxylate, 37 g (0.13 mol) of tributyltin hydride, and 1 g of AIBN was heated to about 90 °C. A vigorous reaction took place. After the mixture has then cooled to room temperature, cis and trans methyl 2-chloro-1-cyclopropane-carboxylate were obtained by fractional distillation through a small Widmer column; 8 g; bp 65—80 °C/33 Torr. A pure cis

isomer was obtained by a semi-preparative GLC operation; bp 100 °C/38 Torr. NMR (CCl_4) δ 1.10—1.68 (2H, m, CH_2), 1.73—2.15 (1H, m, CHCO), 3.00—3.45 (1H, m, CHCl), 3.70 (3H, s, CH_3). Ethyl *cis*-2-chloro-1-cyclopropanecarboxylate was prepared by the procedure described above for the methyl ester. NMR (CCl_4) δ 1.10—1.65 (2H, m, CH_2 of ring), 1.31 (3H, t, J=7 Hz, CH_3), 1.73—2.08 (1H, m, CHCO), 3.11—3.42 (1H, m, CHCl), 4.06 (2H, q, J=7 Hz, CH_2 of the ethyl group). Found: C, 48.75; H, 5.78%. Calcd: C, 48.52; H, 6.06%.

cis-*2-Chloro-1-cyclopropanecarboxylic Acid.* Ethyl *cis*-2-chloro-1-cyclopropanecarboxylate (1.1 g) was saponified by stirring with 0.4 g of sodium hydroxide in 6 ml of 30% ethanol to yield, after acidification, 0.7 g of *cis*-2-chloro-1-cyclopropanecarboxylic acid; bp 108—110 °C/5 Torr, mp 88—88.5 °C. NMR ($CDCl_3$) δ 1.2—1.6 (2H, m, CH_2), 1.6—2.27 (1H, q, J=7 Hz, CHCO), 3.13—3.57 (1H, q, J=7 Hz, CHCl), 5.5 (1H, s, OH). Found: C, 39.89; H, 3.97%. Calcd: C, 39.84; H, 4.17%.

Ethyl trans-*2-Chloro-1-cyclopropanecarboxylate.* This compound was obtained by GLC separation from a cis and trans mixture; bp 76—78 °C/36 Torr. NMR (CCl_4) δ 1.25 (3H, t, J=7 Hz, CH_3), 1.10—1.65 (2H, m, ring CH_2), 1.75—2.07 (1H, m, CHCO), 3.10—3.40 (1H, m, CHCl), 4.05 (2H, q, J=7 Hz, CH_2).

trans-*2-Chloro-1-cyclopropanecarboxylic Acid.* Ethyl *trans*-2-chloro-1-cyclopropanecarboxylate (1 g) was hydrolyzed with sodium hydroxide (0.4 g) in 40% ethanol (5 ml) to yield *trans*-2-chloro-1-cyclopropanecarboxylic acid; 0.5 g; bp 86 °C/4 Torr. Mp 59 °C. NMR ($CDCl_3$) δ 1.20—1.75 (2H, m, CH_2), 1.80—2.15 (1H, m, CHCO), 3.24—3.55 (1H, m, CHCl), 11.60 (1H, s, OH). Found: C, 40.05; H, 4.24%. Calcd: C, 39.85; H, 4.18%.

1,1-Dibromo-2-vinylcyclopropane. This compound was synthesized by the method described above for the chloro derivative; bp[30] 60 °C/22 Torr. lit, 69.5—70 °C/26 Torr[28] 53—56 °C/10 Torr.[31]

Methyl 2,2-Dibromo-1-cyclopropanecarboxylate. The oxidation of 1,1-dibromo-2-vinylcyclopropane (115 g), the same treatment as has been described for the preparation of 2,2-dichloro-1-cyclopropanecarboxylic acid, gave crude 2,2-dibromo-1-cyclopropanecarboxylic acid, which was then converted to the corresponding methyl ester by adding 200 ml of methanol and 5 ml of concentrated sulfuric acid and by refluxing the subsequent mixture for 10 h. After a routine work-up, methyl 2,2-dibromo-1-cyclopropanecarboxylate (40 g) was obtained; bp 90 °C/9 Torr. NMR (CCl_4) δ 1.76—2.70 (3H, m, ring), 3.73 (3H, s, CH_3). Found: C, 23.08; H, 2.25%. Calcd: C, 23.28; H, 2.35%.

Methyl cis-*2-Bromo-1-cyclopropanecarboxylate.* 34 g (0.13 mol) of methyl 2,2-dibromo-1-cyclopropanecarboxylate were added to 34 g (0.13 mol) of tributyltin hydride. The reaction took place immediately. After cooling to room temperature, methyl *cis*- and *trans*-2-bromo-1-cyclopropanecarboxylate were obtained by distillation; bp 65—95 °C/20 Torr. Subsequent distillation and GLC operation afforded pure methyl *cis*-2-bromo-1-cyclopropanecarboxylate; bp 108 °C/25 Torr. NMR (CCl_4) δ 1.25—1.58 (2H, m, CH_2), 1.75—2.15 (1H, q, J=8 Hz with a small splitting, CHCO), 2.95—3.33 (1H, q, J=8 Hz with a small splitting), 3.70 (3H, s, CH_3). Found: C, 33.80; H, 4.20%. Calcd: C, 33.52; H, 3.91%.

cis-*2-Bromo-1-cyclopropanecarboxylic Acid.* The alkaline hydrolysis of methyl *cis*-2-bromo-1-cyclopropanecarboxylate gave *cis*-2-bromo-1-cyclopropanecarboxylic acid; bp 120 °C/2 Torr; mp 68.5—70.5 °C. NMR ($CDCl_3$) δ 1.3—1.7 (2H, m, CH_2), 1.85—2.23 (1H, m, CHCO), 2.0—2.40 (1H, q, J=8 Hz with small spritting, CHBr), Found: C, 29.11; H, 2.82%. Calcd: C, 29.08; H, 3.05%.

The ionization constants were determined by the potentiometric titration of substituted cyclopropanecarboxylic acids (0.005 M) with sodium hydroxide (0.02 M) according to the previously outlined procedure.[3,12]

The ^{13}C NMR spectra were measured on a Hitachi Perkin-Elmer R-22 spectrometer, with 22.6 MHz in the FT mode. The measurement conditions will be described in detail elsewhere, along with the chemical shifts of the cyclopropane ring carbons.

The author wishes to thank Professor Yuho Tsuno and Dr. Masaaki Mishima (Kyushu University) for the measurements of the ^{13}C NMR spectra.

References

1) A. D. Walsh, *Nature*, **159**, 165, 712 (1947); *Trans. Faraday Soc.*, **45**, 175 (1949); C. A. Coulson and W. Moffit, *J. Chem. Phys.*, **15**, 151 (1947); R. Hoffmann, *ibid.*, **49**, 2480 (1964); N. C. Baird and M. J. S. Dewar, *J. Am. Chem. Soc.*, **89**, 3960 (1967).

2) E. P. Carr and C. P. Burt, *J. Am. Chem. Soc.*, **40**, 1590 (1918); J. M. Klotz, *ibid.*, **66**, 88 (1944); M. T. Rogers, *ibid.*, **69**, 2544 (1947); R. C. Hahn, P. H. Howard, S-M. Kong, G. A. Lorenzo, and N. L. Miller, *ibid.*, **91**, 3558 (1969).

3) Y. Kusuyama, *Bull. Chem. Soc. Jpn.*, **46**, 204 (1973).

4) L. B. Jones and V. K. Jones, *Tetrahedron Lett.*, **1966**, 1493.

5) R. G. Pews, *J. Am. Chem. Soc.*, **89**, 5605 (1967); R. G. Pews and N. D. Ojha, *ibid.*, **91**, 5769 (1969); R. C. Hahn, T. F. Corbin and H. Shechter, *ibid.*, **90**, 3404 (1968).

6) M. Charton, in "The Chemistry of Alkenes," ed by J. Zabicky, Wiley-Interscience (1970), Vol 2. Chap. 10, and the references cited therein.

7) Yu. S. Shabarov, E. S. Efremov, V. K. Potapov, and R. Ya. Levina, *Z. Org. Khimii, U.S.S.R.*, **2**, 2154 (1966).

8) T. A. Wittstruck and E. N. Trachtenberg, *J. Am. Chem. Soc.*, **89**, 3810 (1967).

9) R. Fuchs, C. A. Kaplan, J. J. Bloomfield, and L. F. Hatch, *J. Org. Chem.*, **27**, 733 (1962).

10) R. Fuchs and J. J. Bloomfield, *J. Org. Chem.*, **28**, 910 (1963).

11) E. N. Trachtenberg and G. Odian, *J. Am. Chem. Soc.*, **80**, 4018 (1958).

12) Y. Kusuyama, *Bull. Chem. Soc. Jpn.*, **49**, 724 (1976).

13) a) E. A. McCoy and L. L. McCoy, *J. Org. Chem.*, **33**, 2354 (1968); b) L. L. McCoy and E. E. Rieeke, *J. Am. Chem. Soc.*, **95**, 7407 (1973); c) M. Charton, *Prog. Phys. Org. Chem.*, **8** (1971); d) K. Bowden, *Can. J. Chem.*, **43**, 3354 (1965).

14) R. N. McDonald and R. R. Reitz, *J. Am. Chem. Soc.*, **98**, 8144 (1976).

15) C. M. McClosky and G. H. Coleman *Org. Synth.*, Coll. Vol. III, 221 (1955).

16) C. Kaiser, J. Weinstock, and M. P. Plmstead, *Org. Synth.*, **50**, 94 (1970).

17) L. L. McCoy, *J. Am. Chem. Soc.*, **80**, 6568 (1958).

18) G. C. Nelson, G. C. Levy, and J. D. Cargoli, *J. Am. Chem. Soc.*, **94**, 3089 (1972); J. B. Stothers, "Carbon-13 NMR Spectroscopy," Academic Press, New York (1972), Chap. 5.

19) N. K. Wilson and J. B. Stothers, *Top. Stereochem.*, **1974**, 8.

20) To be published in detail for the SCS of other carbons.

21) M. Charton, *J. Chem. Soc.*, **1964**, 1205.

22) Y. Yukawa, "Handbook of Organic Structural Analysis," W. A. Benjamin (1965), p. 637; H. C. Brown,

McDaniel, and O. Haflinger, in "Determination of Organic Structures by Physical Methods," ed by E. A. Brude and F. C. Nachod, Academic Press, New York, N. Y. (1955), Vol. 1.
23) Y. Kusuyama, *Bull. Fac. Edu. Wakayama Univ.*, Natural Science, **24**, 13 (1974).
24) Beilstein, **9**, II. 512.
25) G. B. Payne, *J. Org. Chem.*, **32**, 3351 (1967).
26) K. B. Wiberg, R. K. Barnes, and J. Albin, *J. Am. Chem. Soc.*, **79**, 4997 (1957).
27) Y. Kusuyama, *Bull. Chem. Soc. Jpn.*, **46**, 204 (1973).
28) R. C. Woodworth and P. S. Skell, *J. Am. Chem. Soc.*, **79**, 2542 (1957).
29) L. I. Smith and G. F. Rouault, *J. Am. Chem. Soc.*, **65**, 745 (1943).
30) Air should be introduced after the distillation apparatus has become cool, since a hot mixture of 1,1-dibromo-2-vinyl-cyclopropane and air is explosive.
31) J. A. Landgrebe and L. W. Becker, *J. Org. Chem.*, **33**, 1173 (1968).

Kinetic Studies for the Acyloxy Exchange Reactions of Acyloxytrimethylsilanes with Carboxylic Acids

Seizi KOZUKA,* Takuro KITAMURA, Noboru KOBAYASHI, and Kenji OGINO

Department of Applied Chemistry, Faculty of Engineering, Osaka City University, Sugimoto-cho, Sumiyoshi-ku, Osaka 558

(Received September 22, 1978)

The acyloxy exchange reactions of acyloxysilane with carboxylic acids have been studied kinetically. The rate of reaction has been found to proceed faster with a stronger attacking acid and more basic leaving acyloxy group. The rate was markedly accelerated by the addition of base. The steric effect due to substituents on the silicon atom and hydrogen-deuterium kinetic isotope effects have been examined. A mechanism involving the 5-coordination of the silicon atom prior to the rate-determining proton transfer has been suggested.

A number of organic synthesis recently developed have included the silylation-desilylation reactions of functional groups.[1] An advantage of this reaction is the selectivity which has been demonstrated by the monothioketalization of dicarbonyl compounds[2] and the kinetic study of the silylations of hydroxyl groups.[3] In connection with this, the greater the knowledge of the mechanism of silylation or kinetics may make the reaction more applicable to organic synthesis. Thus, a kinetic study of the proton-silyl exchange reaction *i.e.*, the acyloxy exchange reaction of acyloxysilanes with carboxylic acids as one of the most simple model reactions for the trans-silylation reaction has been carried out. The aims has been to ascertain the kinetics of the exchange reaction and to clarify the mechanism.

Results and Discussion

The acyloxy exchange reaction was found to proceed almost quantitatively if the entering carboxylic acid was stronger than the leaving acid. The rate of

$$RCOOSiR'_3 + R''COOH \longrightarrow R''COOSiR'_3 + RCOOH$$

$$pK_a\ RCOOH > R''COOH$$

acyloxy exchange for acetoxytrimethylsilane with two equivalents of formic acid in chloroform-*d* was measured by monitoring the decrease ^1H NMR trimethyl signal of the starting acetoxysilane (δ 0.28 ppm) and the increase in the product *i.e.*, formyloxytrimethylsilane (δ 0.32 ppm): the rate constant found to be second order. Under the same conditions, the rate of the reverse reaction was too small to affect the kinetics since the exchange was found to proceed almost quantitatively and the reverse reaction of formyloxytrimethylsilane with acetic acid gave no acetoxytrimethylsilane. The rate of reaction with other carboxylic acids was similarly measured and the kinetic results are given in Table 1. The reaction was found to proceed faster with a stronger acid and the rates correlated well with the σ^* parameters with a ρ^* value +1.10 as shown in Fig. 1 formic acid was the exception. The deviation in rate for the reaction of formic acid may be ascribed to the release of the steric crowding change in the acyloxy moiety from the acetoxy to the formyloxy group. The effect of the leaving acyloxy groups of acyloxytrimethylsilanes reversed the rates of exchange *i.e.*, in the trimethylsilylations of trifluoroacetic acid by various acyloxytrimethylsilanes, the rates decreased in the order acetoxy, chloroacetoxy, and dichloroace-

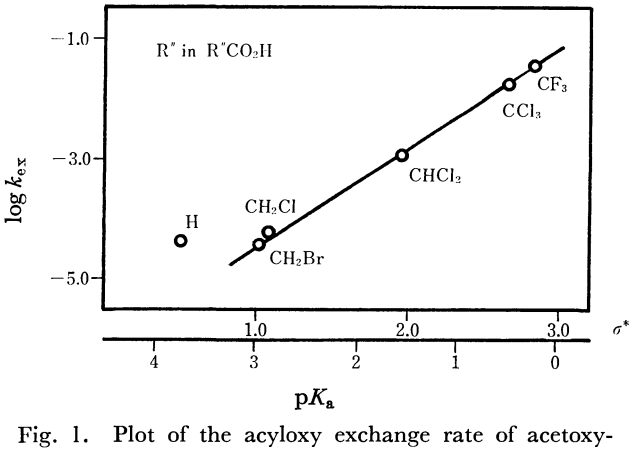

Fig. 1. Plot of the acyloxy exchange rate of acetoxytrimethylsilane *vs.* acid strength.

Table 1. Rate constants for acyloxy exchange reactions of acetoxytrimethylsilane with carboxylic acids in $CDCl_3$[a]

R'' in R''COOH	Temp °C	k_2 l mol^{-1} s^{-1}	ΔH^* kcal/mol	ΔS^* e.u.
H	34	1.32×10^{-4}		
CH_2Br	34	4.00×10^{-5}		
CH_2Cl	27	5.30×10^{-5}		
CH_2Cl	34	6.30×10^{-5}		
CH_2Cl	37	1.00×10^{-4}	11.2	−40.8
CH_2Cl	45	1.70×10^{-4}		
$CHCl_2$	34	1.30×10^{-3}		
CCl_3	34	1.8×10^{-2}		
CF_3	34	4.0×10^{-2}		

a) Concentrations are: $Me_3SiOAc = 0.58$ M, R''COOH $= 1.21$ M.

Table 2. Rate constants for the reaction of acyloxytrimethylsilane with carboxylic acids in $CDCl_3$ at 34°C[a]

R'' in the used R''COOH	k_2, l mol^{-1} s^{-1} R in the starting $RCOOSiMe_3$		
	CH_3	CH_2Cl	$CHCl_2$
CF_3	2.11×10^{-2}	3.40×10^{-3}	9.22×10^{-4}
CCl_3	1.60×10^{-2}	2.58×10^{-3}	6.61×10^{-4}
$CHCl_2$	0.13×10^{-2}	0.21×10^{-3}	

a) Concentrations are: $Me_3SiOCOR = 0.57$M, R''COOH $= 1.48$ M.

Table 3. Rate constants for the reaction of substituted acetoxysilane with $CHCl_2COOH$ and $CHCl_2COOD$[a] in $CDCl_3$ at 34 °C[b]

	R′ in the starting $Me_2R'SiOAc$			
	CH_3	C_2H_5	$C_6H_5CH_2$	C_6H_5
k_2 (H) $l\,mol^{-1}\,s^{-1}$	1.3×10^{-3}	6.9×10^{-4}	5.4×10^{-4}	4.9×10^{-4}
k_2 (D) $l\,mol^{-1}\,s^{-1}$	8.0×10^{-4}	4.3×10^{-4}	3.3×10^{-4}	
k_H/k_D	1.6	1.6	1.7	

a) 90% D content. b) Concentrations are: $Me_2R'SiOAc=0.70$ M, $CHCl_2COOH(D)=1.20$ M.

Table 4. Effect of base on the rate of reaction of acetoxytrimethylsilane with $CH_2ClCOOH$ in $CDCl_3$ at 34 °C[a]

Base	Mole ratio Base/Silane	k_2 $l\,mol^{-1}\,s^{-1}$
None	0	6.30×10^{-5}
Et_3N	0.2	very fast
C_5H_5N	0.2	4.7×10^{-2}

a) Concentrations are: $Me_3SiOAc=0.58$ M, $CH_2ClCOOH=1.21$ M.

toxytrimethylsilanes as the starting materials; similar results were obtained for the silylations of the dichloro and trichloroacetic acids. The results are given in Table 2 and together with the negative assertion to support free silicenium ion[4] would rule out prior ionization of the substrate to exchange acyloxy group.

The effect of the silyl-substituent on the rate of the exchange was examined and it was found that the rate was depressed by the bulky substituent on the silicon atom as observed in the acyloxy exchange reactions of acetoxytrimethyl-, ethyldimethyl, benzyldimethyl, and dimethylphenylsilanes with dichloroacetic acid. The results together with the hydrogen-deuterium kinetic isotope effect observed in the exchange reactions are given in Table 3. The small isotope effect is in accordance with the rate determining proton transfer reaction of the carboxylic acid by a intramolecular cyclic process.[5]

Recently, Pola *et al.* reported the equilibrium constants of proton-silyl exchange *i.e.*, for the acyloxy exchange reaction between acyloxytrimethylsilanes and phenylacetic acid in carbon tetrachloride.[6] It was

$$RCOOSiMe_3 + PhCH_2COOH \overset{K}{\rightleftharpoons} RCOOH + PhCH_2COOSiMe_3$$

reported that the silylating ability of acyloxysilanes decreased with increasing electronegativity of the R group in the acyloxy moiety and the equilibrium constants were successfully correlated with the σ^* constants of the R groups giving a ρ^* value of -0.57. On the basis of these results, it was suggested that a transition state, similar to the carboxylic acid dimer existed in which proton transfer was the rate determining step. Similar results have been observed in the present kinetic study *i.e.*, the less electronegative acyloxy groups of the starting acyloxysilanes facilitate exchange (Table 2), reactions with stronger acids proceed faster (Fig. 1) and the positive kinetic isotope effect is in accordance with the rate determining proton transfer. The base catalysis of the reaction, however, as shown in Table 4, suggests a nucleophilic attack on the silicon atom which occurrs before or at the rate determining step. Since a kinetic isotope effect was observed, nucleophilic attack would be expected to occurr before the rate determining step.

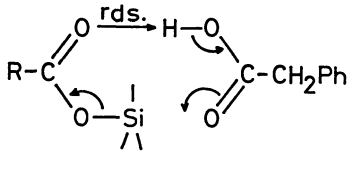

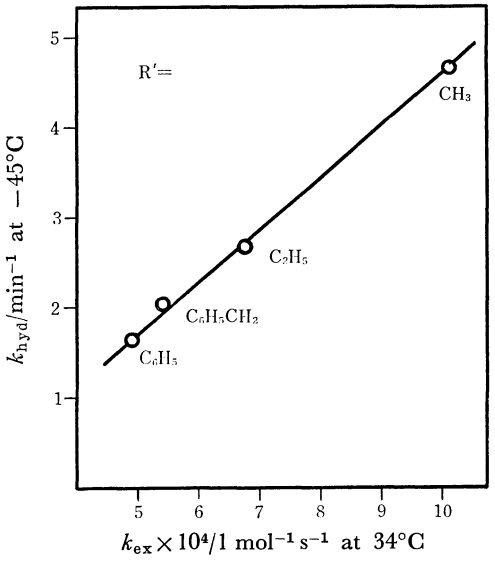

Fig. 2. Plot of rates of hydrolyses of $Me_2R'SiCl$ *vs.* rates of exchange reactions of $Me_2R'SiOAc$ with $CHCl_2CO_2H$.

Nucleophlic attack finds further support when the results given in Table 3 are compared with the rates of the hydrolyses of the corresponding chlorosilanes which proceed *via* a 5-coordinated intermediate.[7] As shown in Fig. 2, the rates of acyloxy exchange correlate linearly to the hydrolyses of the corresponding chlorosilanes. This suggests that the two reactions are very similar in mechanism *i.e.*, 5-coordination of the silicon atom. The large negative entropy value observed in the present study is also in agreement with a 5-coordination mechanism.[8]

Based on the above considerations, the most plausible mechanism for acyloxy exchange is as follows:

$$R-\overset{O}{\overset{\|}{C}}-O-SiR'_3 + R''-\overset{O}{\overset{\|}{C}}-O-H \rightleftharpoons$$

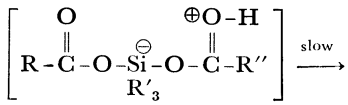

1

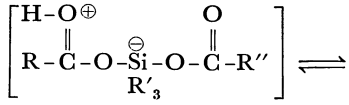

2

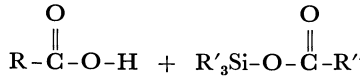

Nucleophilic attack of carboxylic acid on the substrate gives a 5-coordinated intermediate (**1**) which transfers a proton (the rate determining step) to give a second intermediate (**2**). The second intermediate collapses into the products. The latter intermediate (**2**) is expected to be more stable than **1** since the proton is bonded to a more basic site. The reverse reaction, for example, giving acetoxytrimethylsilane from formyloxytrimethylsilane and acetic acid would energetically unfavorable since an unstable intermediate would have to be formed from a stable intermediate. In the base catalyzed reaction, an intermediate **3** would be formed

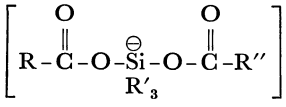

3

by the attack of a stronger nucleophile, the carboxylate ion. Thus the reaction is enhanced by the addition of base.

Experimental

Materials. Acyloxytrimethylsilanes were prepared from chlorotrimethylsilane and silver or sodium carboxylates.[9] Me_3SiOAc; bp 102 °C, (lit,[10] 103.3—105 °C), $Me_3SiOCOCH_2Cl$; bp 124—126 °C, (lit,[11] 159 °C), NMR δ (ppm) 0.32 s (9H) 4.02 s (2H), $Me_3SiOCOCHCl_2$; bp 80 °C/30 mmHg (133.322Pa), (lit,[12] 63 °C/14 mmHg). Chloro(ethyldimethyl), (benzyldimethyl), and (dimethylphenyl)silanes were prepared from dichlorodimethylsilane and the appropriate Grignard reagent.[7,13] The reactions of the chlorosilanes with sodium acetate gave the corresponding acetoxysilanes. $Me_2(Et)SiOAC$; bp 115 °C, (lit,[14] 125—126 °C), $Me_2(Ph)SiOAc$; bp 85 °C/28 mmHg, (lit,[15] 127—130 °C/44 mmHg), $Me_2(PhCH_2)SiOAc$; bp 93—94 °C/4 mmHg, NMR δ (ppm) 0.25 s (6H), 1.98 s (3H), 2.32 s (2H), 6.85—7.20 m (5H), IR (cm^{-1}) 1720, 1260, $Me_2(Ph)SiOAc$; bp 85 °C/28 mmHg, (lit,[15] 127—130 °C/44 mmHg). The deuterated carboxylic acids were obtained by the hydrolysis of the carboxylic anhydrides with deuterium oxide and purified by distillation; the deuterium contents were determined by integration of ^1H NMR signals.

Product Analysis. The reaction of acetoxytrimethylsilane (0.27 mmol) with a small excess of the carboxylic acid (0.55 mmol) was conducted in chloroform-*d* (0.37 ml) solution. The mixture was allowed to stand for 5 h. Acyloxytrimethylsilane and acetic acid were detected as products by examination of the ^1H NMR spectrum of the solution. A small amount (5—7%) of hexamethyldisiloxane (δ 0.07 ppm) was detected as a side product which was probably formed by the moisture catalyzed decomposition of the acyloxysilane.

$$RCOOSiR'_3 + H_2O \longrightarrow RCOOH + R'_3SiOH$$

$$2R'_2SiOH \rightleftharpoons R'_3SiOSiR'_3 + H_2O$$

No other compound was detected in the solution. Dichloroacetoxytrimethylsilane was isolated from the reaction mixture of acetoxytrimethylsilane (7.6 mmol) and dichloroacetic acid (15 mmol) by GLC separation and the structure confirmed by comparison with an authentic sample.

Kinetic Procedure. A typical example is as follows: acetoxytrimethylsilane (35 mg; 0.27 mmol) was dissolved in $CDCl_3$ (0.370 ml) and the solution placed in a sample tube inside a NMR probe (Hitachi-Perkin-Elmer R-20 spectrometer). Dichloroacetic acid (71 mg; 0.55 mmol) was added to the solution and the trimethyl signals recorded at specified time intervals. The reaction temperature was the same as the probe temperature (34 °C). After reaction, the volume of the reaction mixture was measured and the concentrations of the components determined. Good reproduceability for the rate constant was obtained (within ±10%). The activation parameters were obtained using a variable temperature system (JEOL PS-100 spectrometer) and the temperatures measured by observing the chemical shifts of 1,2-ethanediol at that temperatures.

References

1) S. Washburn, *J. Organomet. Chem.*, **123**, 1 (1976).
2) D. A. Evans, L. K. Tsuesdale, K. G. Grimm, and S. L. Nesbitt, *J. Am. Chem. Soc.*, **99**, 5009 (1977).
3) H. J. Schneider and R. Hornung, *Justus Liebigs Ann. Chem.*, **1974**, 1864.
4) J. B. Lambert and H. Sun, *J. Am. Chem. Soc.*, **98**, 5611 (1976) and references cited therein.
5) C. G. Swain, R. F. W. Bader, R. M. Esteve Jr., and R. G. Griffin, *J. Am. Chem. Soc.*, **83**, 1951 (1961).
6) J. Pola, A. ElAtter, and V. Chvalovsky, *Collect. Czech. Chem. Commun.*, **41**, 1772 (1976).
7) V. P. Mileshkevich, G. A. Nikolaev, V. F. Evdokimov, and A. V. Karlin, *Zh. Obshch. Khim.*, **43**, 634 (1971).
8) J. R. Chipperfield and G. E. Gould, *J. Chem. Soc., Perkin Trans. 2*, **1974**, 1324.
9) H. H. Anderson, *J. Am. Chem. Soc.*, **74**, 2371 (1952).
10) Y. Etienne, *Compt. Rend.*, **235**, 966 (1952), *Chem. Abstr.*, **47**, 10471c (1953).
11) H. H. Anderson, *J. Am. Chem. Soc.*, **74**, 2371 (1952).
12) W. McFarlane and J. H. Seaby, *J. Chem. Soc., Perkin Trans. 2*, **1972**, 1561.
13) R. N. Lewis, *J. Am. Chem. Soc.*, **69**, 1717 (1947), **70**, 1161 (1948).
14) N. F. Orlov and V. P. Mileshkevich, *Zh. Obshch. Khim.*, **36**, 699 (1966), *Chem. Abstr.*, **65**, 8954e (1966).
15) W. J. Haggerty Jr., and C. W. Breed, *J. Org. Chem.*, **26**, 2464 (1961).

The Reactions of 2-(Trimethylsiloxy)furans with Orthocarboxylic Esters, Acetals, and Acylal in the Presence of Lewis Acids

Morio ASAOKA,* Naoyuki SUGIMURA, and Hisashi TAKEI
Department of Life Chemistry, Tokyo Institute of Technology, Nagatsutacho, Midori-ku, Yokohama 227

(Received October 6, 1978)

The reaction of 2-(trimethylsiloxy)furan (**1**) with orthocarboxylic esters, acetals, and acylal in the presence of Lewis acids afforded the corresponding 4-substituted 2-buten-4-olides. The reaction of 5-methyl-2-(trimethylsiloxy)furan with orthocarboxylic esters gave unstable 2-substituted 3-penten-4-olides as major products; these gave 2,5-alkanediones upon hydrolysis. The furan (**1**) also reacted with 1,1-diacetoxy-2-butene to give a mixture of 5-acetoxy-2,6-octadien-4-olide and 7-acetoxy-5-methyl-2,6-heptadien-4-olide. From the former compound, nigrosporalactone was synthesized.

In the preceding paper, we reported the synthesis of 2-(trimethylsiloxy)furans and their Diels-Alder reaction with maleic anhydride.[1] In the present paper, we will describe the reaction of some electrophiles with the furans in the presence of Lewis acids.

Results and Discussion

It was found that the reaction of 2-(trimethylsiloxy)-furan **1** with triethyl orthoacetate **2** (R^1=Me, R^2=Et) in dichloromethane, in the presence of catalytic amounts of a Lewis acid, afforded 5,5-diethoxy-2-hexen-4-olide **3** (R^1=Me, R^2=Et).

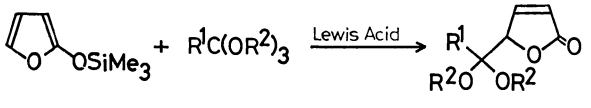

1 2 3

Scheme 1.

Among the Lewis acids examined, tin(IV) chloride and zinc chloride were found to be suitable catalysts for this reaction. That is, when the reaction was carried out at −40—10 °C for 2 h in the presence of tin(IV) chloride, **3** (R^1=Me, R^2=Et) was obtained in 71% yield, and **3** was obtained in 60% yield when the reaction was carried out at room temperature for 4.5 h in the presence of zinc chloride. But, when a stronger Lewis acid such as antimony(V) chloride or titanium(IV) chloride was used as a catalyst, the yield of **3** was low, probably because decomposition of **1** preferentially took place in contact with such a strong Lewis acid (Table 1). Next, we examined the reaction of **1** with various orthocarboxylic esters in the presence of zinc chloride or tin(IV) chloride. When triethyl orthocarboxylates were used, the yields of **3** decreased in the following order: R^1=H>Me>Et>Ph. When trimethyl orthoformate was used instead of triethyl orthoformate, **3** was obtained in higher yield. All these results suggest that the yields of **3** were markedly influenced by the size of the orthocarboxylic esters. These results are listed in Table 1.

Acetals also reacted with 2-(trimethylsiloxy)furan in the presence of tin(IV) chloride and afforded the corresponding 4-substituted 2-buten-4-olides in good yields.

Next, the reaction of 5-methyl-2-(trimethylsiloxy)-furan **6** with triethyl orthobenzoate was carried out. In this case, the formation of two compounds was confirmed by TLC, but the major product was found to be too unstable to isolate in a pure form. The acid hydrolysis of the reaction mixture afforded 1-phenyl-1,4-pentanedione as a major product and 4-benzoyl-2-penten-4-olide as a minor product. From this result, together with the NMR spectra of the crude mixture of the initially formed products, the major component of the unstable intermediate seems to possess the struc-

TABLE 1. YIELDS OF 5-SUBSTITUTED 5,5-DIALKOXY-2-PENTEN-4-OLIDES

	R^1	R^2	Lewis acid	Reaction conditions		Yield **3** (%)
				Temp (°C)	Time (h)	
3a	Me	Et	$SnCl_4$	r. t.	1	20
3a	Me	Et	$ZnCl_2$	r. t.	4.5	60
3a	Me	Et	$SnCl_4$	−40—10	2	71
3a	Me	Et	$ZnCl_2$	−40—10	2	56
3a	Me	Et	$SbCl_5$	−40—10	2	57
3a	Me	Et	$TiCl_4$	−40—10	2	30
3a	Me	Et	$BF_3{\cdot}Et_2O$	−40—10	2	38
3b	Et	Et	$SnCl_4$	−40—10	2	63
3b	Et	Et	$ZnCl_2$	r. t.	4.5	63
3c	Ph	Et	$SnCl_4$	−40—10	2	48
3c	Ph	Et	$ZnCl_2$	r. t.	4.5	44
3d	H	Et	$SnCl_4$	−40—10	2	72
3e	H	Me	$SnCl_4$	−40—10	2	91

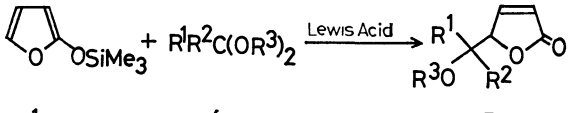

1 4 5

Scheme 2.

TABLE 2. YIELDS OF 5-SUBSTITUTED 5-ALKOXY-2-PENTEN-4-OLIDES

	R^1	R^2	R^3	Yield **5** (%)
5a	H	C_6H_5	C_2H_5	77
5b	H	p-$CH_3C_6H_4$	C_2H_5	65
5c	H	n-C_9H_{19}	C_2H_5	61
5d	CH_3	CH_3	CH_3	52
5e	C_2H_5	C_2H_5	CH_3	68
5f	$-(CH_2)_4-$		C_2H_5	77
5g	$-(CH_2)_5-$		C_2H_5	38
5h	$-(CH_2)_{11}-$		CH_3	50

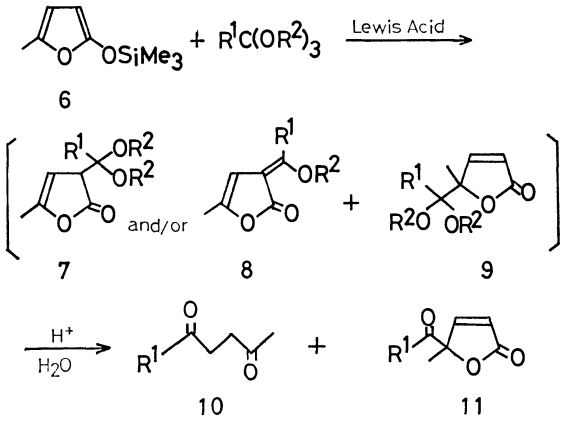

Scheme 3.

Table 3. Yields of 1,4-diketones

R^1	R^2	Lewis acid	Reaction conditions		Yield **10** (%)
			Temp(°C)	Time(h)	
Ph	Et	$SnCl_4$	r. t.	0.5	32
Ph	Et	$SnCl_4$	−5	5.5	32
Ph	Et	$ZnCl_2$	r. t.	4.5	20
Ph	Et	$SbCl_5$	r. t.	1.0	55
n-C_6H_{13}	Me	$SbCl_5$	r. t.	2.0	37

ture of **7** and/or **8**.[2] In contrast to the reaction of **1**, it is to be noted that the electrophile attacked preferentially at the 3-position of **6**. This fact can be explained by considering the steric repulsion between the methyl group at 5-position of the siloxyfuran and the electrophile. The effects of the reaction conditions, especially on the solvents and catalysts, were then examined. In this case, tin(IV) chloride was not a good catalyst. When the reaction was carried out in the presence of tin(IV) chloride, triethyl orthobenzoate still remained even after 24 h, though the other starting material, **6**, had disappeared. This suggests that the decomposition of **6** took place under the reaction conditions. When antimony(V) chloride was used instead of tin(IV) chloride, the yield was improved.

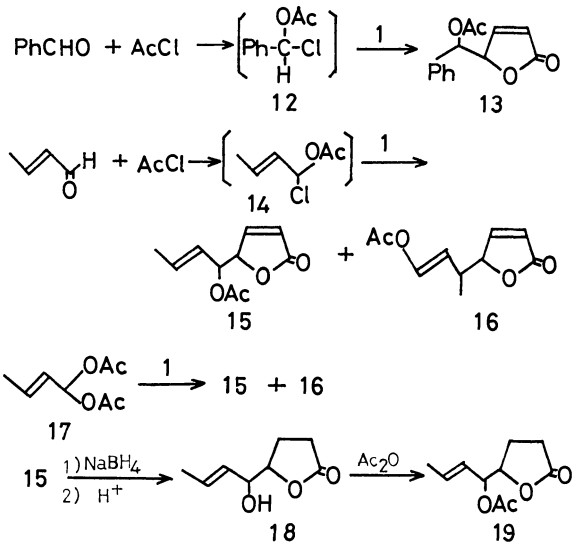

Scheme 4.

When trimethyl orthoheptanoate was used instead of orthobenzoate, 2,5-undecanedione **10**($R=C_6H_{13}$), which is known to be an important intermediate for the synthesis of dihydrojasmone,[3] was obtained in 37% yield. These results are summarized in Table 3.

Aldehydes are known to form adducts with acyl chloride.[4] So the reaction of **1** with such adducts was examined. Namely, the reaction of **1** with the mixture of benzaldehyde and acetyl chloride in the presence of a Lewis acid afforded 5-acetoxy-5-phenyl-2-penten-4-olide **13** in 57% yield. Similarly, the reaction of **1** with the mixture of crotonaldehyde and acetyl chloride afforded a 1:1 mixture of 5-acetoxy-2,6-octadien-4-olide **15** and 7-acetoxy-5-methyl-2,6-heptadien-4-olide **16** in 57% yield. When 1,1-diacetoxy-2-butene **17** was used instead of haloacetate **14**, a 1:1 mixture of **15** and **16** was obtained in 86% yield. Sodium borohydride reduction followed by acid hydrolysis of the mixture afforded threo and erythro isomers of **18** in over-all yields of 14 and 16%, respectively. The NMR spectrum of acetyl derivative of the erythro isomer

Table 4. Analytical data of 5-substituted 5,5-dialkoxy-2-penten-4-olides

Product	IR, cm^{-1}	NMR, δ	Formula	Found (Calcd), %	
				C	H
3a	1750—1800(C=O)	1.14(3H, t), 1.06(3H, s), 1.18(3H, t),	$C_{10}H_{16}O_4$	60.12	8.14
	1600(C=C)	3.50(2H, q), 3.56(2H, q), 4.98—5.06(1H, m)		(59.98	8.05)
		6.06(1H, dd), 7.44(1H, dd)			
3b	1755—1795(C=O)	0.84(3H, t), 1.12(3H, t), 1.18(3H, t),	$C_{11}H_{18}O_4$	61.47	8.43
	1600(C=C)	1.64(2H, q), 3.44(2H, q), 3.54(2H, q),		(61.66	8.47)
		4.96—5.10(1H, m), 6.02(1H, dd), 7.56(1H, dd)			
3c	1760—1790(C=O)	1.12(3H, t), 1.30(3H, t), 3.54(2H, q),	$C_{15}H_{18}O_4$	68.83	6.90
	1600(C=C)	3.70(2H, q), 5.18—5.30(1H, m), 5.66(1H, dd),		(68.68	6.92)
		7.22(5H, s), 7.34(1H, dd)			
3d	1760—1800(C=O)	1.16(3H, t), 1.24(3H, t), 3.70(2H, q),	$C_9H_{14}O_4$	58.13	7.68
	1605(C=C)	3.74(2H, q), 4.48(1H, d), 4.86—5.03(1H, m),		(58.05	7.58)
		6.10(1H, dd), 7.46(1H, dd)			
3e	1760—1800(C=O)	3.40(3H, s), 3.44(3H, s), 4.34(1H, d),	$C_7H_{10}O_4$	53.11	6.39
	1605(C=C)	6.12(1H, dd), 4.92—5.06(1H, m), 7.48(1H, dd)		(53.16	6.37)

Table 5. Analytical data of 5-substituted 5-alkoxy-2-penten-4-olides

Products	IR, cm^{-1}	NMR, δ	Formula	Found(Calcd), % C	Found(Calcd), % H	Mp, °C
5a	1765—1780(C=O) 1600(C=C)	1.02—1.36(3H, m), 3.20—3.62(2H, m), 4.40(1H, d), 4.80—5.12(1H, m), 5.76—6.04(1H, m), 7.00—7.38(1H, m), 7.14—7.30(5H, m)	$C_{13}H_{14}O_3$	71.38 (71.54	6.52 6.47)	oil
5b	1755—1780(C=O) 1605(C=C)	0.98—1.32(3H, m), 2.30(3H, s), 3.14—3.56(2H, m), 4.34(1H, d), 4.76—5.10(1H, m), 5.70—6.02(1H, m), 6.92—7.40(1H, m), 7.00—7.16(4H, m)	$C_{14}H_{16}O_3$	72.29 (72.39	6.96 6.94)	oil
5c	1760—1790(C=O) 1600(C=C)	0.68—1.82(22H, m), 3.16—3.70(3H, m), 4.64—5.04(1H, m), 5.98(1H, dd), 7.40(1H, dd)	$C_{16}H_{28}O_3$	71.62 (71.60	10.62 10.52)	oil
5d	1750—1770(C=O) 1600(C=C)	1.00(3H, s), 1.28(3H, s), 3.22(3H, s), 4.64—4.80(1H, m), 6.00(1H, dd), 7.44(1H, dd)	$C_8H_{12}O_3$	61.89 (61.52	7.84 7.75)	oil
5e	1755—1770(C=O) 1785(C=O) 1600(C=C)	0.82(3H, t), 0.92(3H, t), 1.52(2H, q), 1.64(2H, q), 3.20(3H, s), 5.98(1H, dd), 4.84—4.96(1H, m), 7.54(1H, dd)	$C_{10}H_{16}O_3$	65.01 (65.19	8.75 8.75)	oil
5f	1755—1775(C=O) 1795(C=O) 1600(C=C)	1.10(3H, t), 1.36—1.90(8H, m), 3.40(2H, q), 4.90—5.02(1H, m), 5.98(1H, dd), 7.42(1H, dd)	$C_{11}H_{16}O_3$	67.39 (67.32	8.26 8.22)	oil
5g	1750—1790(C=O) 1600(C=C)	1.00—2.10(10H, m), 1.16(3H, t), 3.48(2H, q), 4.90—5.02(1H, m), 6.10(1H, dd), 7.46(1H, dd)	$C_{12}H_{18}O_3$	68.58 (68.54	8.66 8.63)	56—57.5
5h	1750, 1790(C=O) 1600(C=C)	1.08—1.86(22H, m), 3.24(3H, s), 4.90—5.02(1H, m), 6.12(1H, dd), 7.62(1H, dd)	$C_{17}H_{28}O_3$	73.01 (72.82	10.03 10.06)	108

agreed with that of nigrosporalactone reported in the literature.[5] Thus, the natural nigrosporalactone was proved to be the erythro isomer.

In conclusion, 2-(trimethylsiloxy)furans reacted with various electrophiles similar to the silyl enol ethers[6] and afforded various substituted unsaturated lactones, which can be regarded as useful synthetic intermediates.

Experimental

A Typical Example of the Reaction of 2-(Trimethylsiloxy)-furan with Orthocarboxylates or Acetals. Triethyl orthoacetate (179 mg, 1.1 mmol) in dichloromethane (2 ml) was added to 2-(trimethylsiloxy)furan (172 mg, 1.1 mmol) and cooled to −40 °C. The reaction temperature was gradually raised to 10 °C after the addition of a few drops of tin(IV) chloride. Separation of the reaction mixture by silica gel TLC afforded 5,5-diethoxy-2-hexen-4-olide (155 mg, 71%).

1-Phenyl-1,4-pentanedione: To a solution of triethyl orthobenzoate (224 mg, 1 mmol) and 5-methyl-2-(trimethylsiloxy)furan (208 mg, 1.3 mmol) in dry dichloromethane (2.5 ml), was added one drop of antymony(V) chloride at room temperature. The reaction mixture was stirred at room temperature for 0.5 h, and the solvent was removed under reduced pressure. To the residue 5 ml of 40% of aqueous acetic acid was added and the resulting solution was refluxed for 45 min. After cooling to room temperature, the reaction mixture was extracted with three portions of ether. Removal of the solvent under reduced pressure gave a brownish oil, from which 1-phenyl-1,4-pentanedione was isolated in 55% yield by silica gel TLC (hexane–ether).

2,5-Undecanedione: The reaction of trimethyl orthoheptanoate with 5-methyl-2-(trimethylsiloxy)furan and the hydrolysis of the reaction products were carried out in a procedure similar to that mentioned above, and the isolation by TLC (hexane R_f=0.5) afforded 2,5-undecanedione in 37% yield.

5-Acetoxy-5-phenyl-2-penten-4-olide: Benzaldehyde (318 mg, 3 mmol) and acetyl chloride (238 mg, 3.03 mmol) were dissolved in 4 ml of dry dichloromethane, and the solution was stirred at room temperature for 15 min. Then the solution was cooled to −78 °C. 2-(Trimethylsiloxy)furan (515 mg, 3.3 mmol) was added to the solution and catalytic amounts of tin(IV) chloride were subsequently added. The mixture was allowed to warm to room temperature for 20 h with stirring. Ten ml of phosphate buffer (pH 7) was then added and the mixture was extracted with ethyl acetate. The organic layer was washed with water and dried over sodium sulfate. Ethyl acetate was removed under reduced pressure, and the residue was separated by silica gel column chromatography to give 5-acetoxy-5-phenyl-2-pentene-4-olide in 57% yield. IR (NaCl): 1750—1790 cm^{-1} (C=O), 1610 cm^{-1} (C=C); NMR($CDCl_3$): δ=2.10 (3H, s), 5.16—5.34 (1H, m), 5.86 (1H, d), 5.98—6.18 (1H, m), 7.10—7.60 (6H, m). Found: C, 67.24; H, 5.22%. Calcd for $C_{13}H_{12}O_4$: C, 67.23; H, 5.21%.

5-Hydroxy-6-octen-4-olide (Nigrosporalactone): To a solution of 2-(trimethylsiloxy)furan (2.43 g, 15.6 mmol) and 1,1-diacetoxy-2-butene (2.58 g, 15 mmol) in 20 ml of dry dichloromethane was added a catalytic amount of tin(IV) chloride at −40 °C. The mixture was allowed to warm to room temperature for 2 h, and was then stirred for 1 h at room temperature. Phosphate buffer (pH 7) was added to the mixture and the mixture was extracted with ethyl acetate. Ethyl acetate was removed under reduced pressure. Separation of the residue by column chromatography on silica gel gave 2.54 g of the mixture of 5-acetoxy-

2,6-octadien-4-olide and 7-acetoxy-5-methyl-2,6-heptadien-4-olide. This mixture was dissolved in 20 ml of methanol and cooled to 0 °C. Sodium borohydride(737 mg) was added to the solution in small portions and stirred for 0.5 h after the completion of the addition. The resulted mixture was acidified with 1 M hydrochloric acid (50 ml), and was stirred for 5 days. Methanol was removed under reduced pressure and the resulting mixture was extracted with ethyl acetate. The organic layer was washed with water and dried on sodium sulfate. After the removal of ethyl acetate under reduced pressure, the separation of the residue by TLC afforded erythro isomer (16%) and threo isomer (14%) of 5-hydroxy-6-octen-4-olide. Each of these were acetylated using an excess of triethyl amine and acetic anhydride. 5-Acetoxy-6-octen-4-olide (erythro): IR (NaCl): 1750 cm^{-1}, 1790 cm^{-1} (C=O); NMR ($CDCl_3$): $\delta=1.74$ (3H, d), 2.04 (3H, s), 2.20—2.54 (4H, m), 4.48 (1H, dq), 5.28 (1H, dd), 5,50 (1H, dd), 5.84 (1H, dq). Found: C, 60.10; H, 7.09%. Calcd for $C_{10}H_{14}O_4$: C, 60.59, H, 7.12%. 5-Acetoxy-6-octen-4-olide (threo); IR (NaCl): 1750 cm^{-1}, 1790 cm^{-1} (C=O); NMR ($CDCl_3$): $\delta=1.76$ (3H, d), 2.02 (3H, s), 2.00—2.54 (4H, m), 4.50 (1H, dq), 5.28 (1H, dd), 5.44(1H, dd), 5.82 (1H, dq). Found: C, 60.08; H, 6.95%. Calcd for $C_{10}H_{14}O_4$: C, 60.59; H, 7.12%.

References

1) M. Asaoka, K. Miyake, and H. Takei, *Chem. Lett.*, **1977**, 167. The syntheses and reactions of 2-(trimethylsiloxy)furans were recently reported independently. E. Yoshii, T. Koizumi, E. Kitatsuji, T. Kawazoe, and T. Kaneko, *Heterocycles*, **4**, 1663 (1976).

2) The NMR spectra of the crude mixture showed complex signals in which some signals probably due to **7** and **8** were observed. **7**: ($CDCl_3$) 1.70 (3H, s, $-CH_3$), 5.05 (1H, s, C=CH). **8**: 2.00 (3H, s, $-CH_3$), 6.00 (1H, s, C=CH), 4.33 (2H, q, $C=C-OCH_2-$). For the synthesis of 2,5-alkanediones *via* 2-ethoxyalkylidene 3-buten-4-olides, see: M. Asaoka, N. Sugimura, and H. Takei, *Chem. Lett.*, **1977**, 171.

3) H. Hunsdiecker, *Ber.*, **75**, 447, 455, 460 (1942).

4) L. H. Ulrich and R. Adams, *J. Am. Chem. Soc.*, **43**, 660 (1921).

5) R. H. Evans, Jr., G. A. Ellestad, and M. P. Kunstmann, *Tetrahedron Lett.*, **1969**, 1791.

6) a) T. Mukaiyama, K. Narasaka, and K. Banno, *Chem. Lett.*, **1973**, 1011; b) T. Mukaiyama and M. Hayashi, *ibid.*, **1974**, 15.

The Revised Structure of Dispermol and Total Synthesis of Maytenoquinone, Dispermol, and Dispermone

Takashi MATSUMOTO,* Taishi OHMURA, and Shuji USUI
Department of Chemistry, Faculty of Science, Hiroshima University, Higashisenda-machi, Hiroshima 730

(Received October 18, 1978)

Condensation of β-cyclocitral with 2-isopropyl-3,4-dimethoxybenzyl chloride afforded an alcohol (**15**) which was converted into (±)-12,13-dimethoxytotara-8,11,13-trien-6-one (**18**). Demethylation of (±)-**18** followed by air oxidation gave (±)-maytenoquinone. Reductive cleavage of the hydroxyl group in (±)-**15** produced a phenethyl derivative which was cyclized to give (±)-12,13-dimethoxytotara-8,11,13-triene (**23**) and its *cis*-isomer (**24**). Oxidation of (±)-**23** with chromium trioxide, followed by demethylation of the resulting 7-oxo compound (**25**), afforded (±)-dispermone. The Wittig reaction of (*R*)-(−)-α-cyclocitral with 2-isopropyl-3,4-dimethoxybenzyltriphenylphosphonium chloride yielded a styrene derivative. This was partially hydrogenated and then cyclized to give (+)-**23** and (−)-**24**. The *trans*-isomer (**23**) was converted into (−)-dispermone (**3**) *via* (−)-**25** and also partially demethylated to (+)-12-methoxytotara-8,11,13-trien-13-ol (**2**), the proposed structure for dispermol. Since the synthetic (+)-**2** was not identical with the natural compound, (−)-**3** was then converted into (+)-13-methoxytotara-8,11,13-trien-12-ol, which was identical with natural dispermol. (−)-**25** was also converted into (+)-maytenoquinone.

Recently, three new tricyclic diterpenes possessing a totarane skeleton, maytenoquinone, dispermol, and dispermone, have been isolated from *Maytenus dispermus* by Martin.[1] Their structures were deduced to be **1**, **2**, and **3**, on the basis of chemical and spectroscopic studies. Among these natural diterpenes, maytenoquinone (**1**) is especially of interest, because it has a unique quinone-methide chromophore, such as that in taxodione (**4**)[2-5] which has shown a significant tumor-inhibiting activity. In connection with our synthetic studies on natural diterpenes, we attempted the syntheses of these natural compounds to confirm the proposed structures and to elaborate a new synthetic route for the tricyclic diterpenes with an aromatic C ring. This paper[6] describes the revision of the structure of dispermol and the total syntheses of maytenoquinone (**1**), dispermol (**5**), and dispermone (**3**) by the new route.

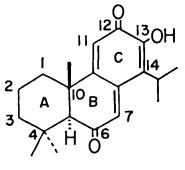

1

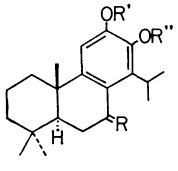

2 R=H$_2$, R'=Me, R''=H
3 R=O, R'=R''=H
5 R=H$_2$, R'=H, R''=Me

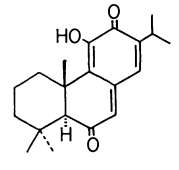

4

Our basic strategy for the synthesis of totara-8,11,13-triene skeleton (**6**) is shown in Scheme 1. That is, two C_{10} units (**8** and **9**), including A and C rings of natural compounds, were first condensed to give a C_{20} unit (**7**) and this, by intramolecular cyclization, was converted into an octahydrophenanthrene derivative (**6**) which was then transformed into the natural compounds.

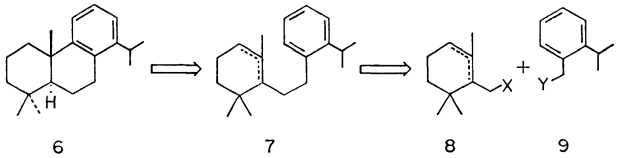

6 7 8 9

Scheme 1.

*Syntheses of (±)-Maytenoquinone (**1**) and (±)-Dispermone (**3**).* β-Cyclocitral (**10**)[7,8] and 2-isopropyl-3,4-dimethoxybenzyl chloride (**11**),[9] prepared from 2-isopropyl-3,4-dimethoxybenzoic acid (**12**)[9] *via* three steps, were chosen as the starting materials. Condensation of **10** with **11** in the presence of lithium naphthalenide afforded the desired alcohol (**15**), together with a small amount of a demethoxylated alcohol (**16**). The alcohol (**15**) was oxidized with chromium trioxide–pyridine complex to yield the corresponding α,β-unsaturated ketone (**17**), which was then submitted to intramolecular cyclization with anhydrous aluminium chloride in refluxing toluene. Because of the formation of a phenolic by-product, the crude product was immediately methylated with methyl iodide and anhydrous potassium carbonate in refluxing methyl ethyl ketone to give (±)-12,13-dimethoxytotara-8,11,13-trien-6-one (**18**). Demethylation of (±)-**18** with boron tribromide in dichloromethane afforded (±)-13-hydroxytotara-7,9(11),13-triene-6,12-dione (**1**), whose spectral data were identical with those of natural maytenoquinone. On the other hand, the demethylation of (±)-**18** with hydrobromic acid in refluxing acetic acid yielded (±)-*cis*-maytenoquinone (**19**).[10] The *cis*-configuration of the A/B ring junction in (±)-**19** was supported by its NMR spectrum, which showed a signal due to one of the *gem*-dimethyl groups at the C-4 position in very high field (δ 0.62 ppm) owing to the shielding effect of the C ring.[11]

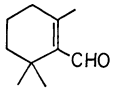

10

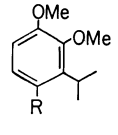

11 R=CH$_2$Cl
12 R=CO$_2$H
13 R=CO$_2$Me
14 R=CH$_2$OH

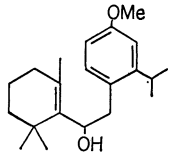

16

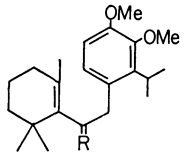

17 R=O
20 R=H_2

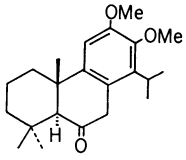

18

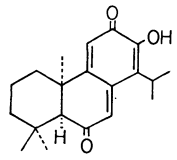

19

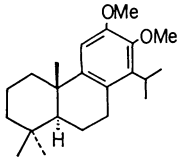

23

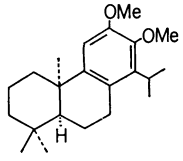

24

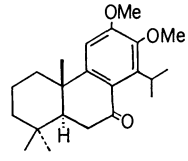

25

Our next effort was directed toward the syntheses of (±)-**2** and (±)-**3**. For reductive cleavage of the hydroxyl group, the alcohol (**15**) was treated at room temperature with dichloroaluminium hydride[12] in dry ether. Since the crude product contained a significant amount of diene compounds, it was hydrogenated over Pd–C in acetic acid to give the desired phenethyl derivative (**20**). In contrast to this result, when triethylsilane[13] was used at 0 °C in the presence of boron trifluoride etherate, the alcohol (**15**) was smoothly converted into **20** together with a small amount of (±)-12,13-dimethoxytotara-5,8,11,13-tetraene (**21**). The tetraene (±)-**21** was also obtained in moderate yield by treatment of (±)-**15** with boron trifluoride etherate at 0 °C. However, when the reaction of (±)-**15** with boron trifluoride etherate was carried out at room temperature, a rearranged product (**22**) was produced. This compound was also obtained by the similar treatment of (±)-**21**. Therefore, it is suggested that this rearrangement proceeded through the intermediate (±)-**21**. The NMR spectrum of (±)-**22** showed signals of an aromatic proton (δ 6.85), two methoxyl groups (δ 3.77 and 3.80), and an isopropyl group [δ 1.28 ppm (d, J=7 Hz)], suggesting the retention of the aromatic C ring. The compound, (±)-**22**, also showed a signal at δ 6.00 ppm (t, J=4 Hz) due to a vinylic proton attached to a trisubstituted double bond and signals at δ 0.90 (3H) and 0.93 ppm (6H) due to three tertiary methyl groups. The appearance of three tertiary methyl signals in the higher field, and of vinylic and aromatic protons in the lower field, than those in (±)-**21** suggested that the angular methyl group at the C-10 position rearranged to the C-5 position, resulting in the formation of a new trisubstituted double bond, as in Scheme 2. Thus, the structure

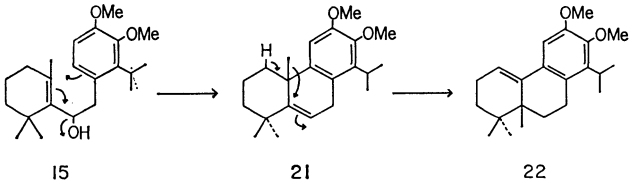

15 21 22

Scheme 2.

of (±)-**22** was tentatively assigned as 12,13-dimethoxy-5-methyl-10-nortotara-1(10),8,11,13-tetraene. Intramolecular cyclization of **20** with boron trifluoride etherate in dichloromethane afforded (±)-12,13-dimethoxytotara-8,11,13-triene (**23**) as a major product and its *cis*-isomer (**24**) as a minor one. When the cyclization was carried out with anhydrous aluminium chloride in refluxing benzene, **20** gave (±)-12-methoxytotara-8,11,13-trien-13-ol (**2**) in addition to the dimethoxy compounds, (±)-**23** and (±)-**24**. The phenol (±)-**2** was also obtained by partial demethylation of (±)-**23** with anhydrous aluminium chloride under similar conditions, and the methylation of (±)-**2** with methyl iodide and anhydrous potassium carbonate yielded (±)-**23**. The presence of a phenolic hydroxyl group at the C-13 position in (±)-**2** was supported by pyridine-induced solvent shifts[14] of the C-16 and C-17 methyls (Δ=−0.28 ppm) and an aromatic proton (Δ=−0.12 ppm) in its NMR spectrum, which was different from that of natural dispermol. This was further confirmed by the synthesis of optically active (+)-**2**, which is described later. Thus, the proposed structure (**2**) for dispermol should now be revised. Since the conversion of the optically active tetraene (**21**) into the trienes (**23** and **24**) by catalytic hydrogenation had already been reported,[1] (±)-**21** was also a useful intermediate for the present synthesis. The dimethyl ether (±)-**23** was oxidized with chromium trioxide in acetic acid to give the corresponding 7-oxo compound (**25**) and this was then demethylated with boron tribromide in dichloromethane to afford (±)-12,13-dihydroxytotara-8,11,13-trien-7-one (**3**), whose spectral data were identical with those of natural dispermone.

*Syntheses of (+)-Maytenoquinone (**1**), (+)-Dispermol (**5**), and (−)-Dispermone (**3**).* Subsequently, our attention was directed toward the total syntheses of the optically active natural maytenoquinone, dispermol, and dispermone. The starting materials chosen for these syntheses were (*R*)-(−)-α-cyclocitral (**26**)[15,16] and 2-isopropyl-3,4-dimethoxybenzyltriphenylphosphonium chloride (**27**), which was prepared from **11** and triphenylphosphine in refluxing benzene. The Wittig reaction of (−)-**26** with **27** in dry hexane in the presence of *n*-butyllithium gave the desired styrene derivative (**28**). In the NMR spectrum of (−)-**28** the vicinal coupling constant (J=15 Hz) of vinylic protons suggested the presence of a trans disubstituted double bond. Partial hydrogenation of (−)-**28** in ethanol over Pd–C afforded a phenethyl derivative (**29**), which was submitted to the intramolecular cyclization using anhydrous aluminium chloride in benzene. The crude product was then purified by column chromatography on silica gel to give (+)-**23**, $[\alpha]_D$ +50.2°, along with (−)-**24**. The conversion of (+)-**23** into (−)-dispermone (**3**) *via* the 7-oxo compound (**25**) was achieved by a method similar to that for the racemate.

(+)-**23** was partially demethylated to give (+)-**2**, mp 87—88.5 °C. The melting point of the synthetic (+)-**2** was quite different from that of natural dispermol (mp 164—166 °C). From the comparison of the NMR spectra of (+)-**2** and dispermol, the structure of natural product is expected to be 13-methoxytotara-8,11,13-trien-12-ol (**5**); this was successfully synthesized in the following manner. Partial benzylation of (−)-**3** with benzyl chloride in the presence of potassium iodide

and anhydrous potassium carbonate produced the corresponding 12-benzyl ether (**30**). The presence of a phenolic hydroxyl group at the C-13 position in (−)-**30** was supported by the solvent shifts[14] of the C-16 and C-17 methyls ($\Delta = -0.42$ ppm)[17] in its NMR spectrum. Methylation of (−)-**30** with methyl iodide and anhydrous potassium carbonate gave the 13-methyl ether (**31**) which, on hydrogenolysis over PtO_2 in ethanol containing a small amount of perchloric acid, afforded (+)-**5**, mp 166.5—167.5 °C, whose physical and spectral data were identical with those of natural dispermol. Thus, the structure of dispermol could be determined to be **5**.

(+)-Maytenoquinone (**1**) was synthesized as follows. The 7-oxo compound (−)-**25** was reduced with lithium aluminium hydride in dry ether and the resulting mixture of epimeric alcohols was dehydrated with dilute hydrochloric acid to give (−)-12,13-dimethoxytotara-6,8,11,13-tetraene (**32**). Oxidation of (−)-**32** with *m*-chloroperbenzoic acid in dichloromethane, followed by treatment with dilute hydrochloric acid in refluxing methanol, gave (+)-**18** which, on demethylation with boron tribromide in dichloromethane and subsequent oxidation with silver oxide in refluxing chloroform, afforded (+)-maytenoquinone (**1**).

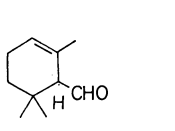

26

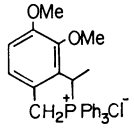

27

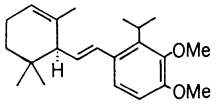

28

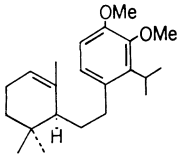

29

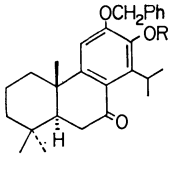

30 R=H
31 R=Me

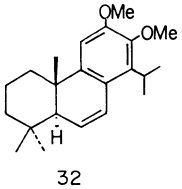

32

Experimental

All melting points are uncorrected. The IR spectra and optical rotations were measured in chloroform, and the NMR spectra in carbon tetrachloride at 60 MHz, with tetramethylsilane as an internal standard, unless otherwise stated. The chemical shifts are presented in terms of δ values; s: singlet, bs: broad singlet, d: doublet, bd: broad doublet, dd: double doublet, t: triplet, m: multiplet. Column chromatography was performed using Merck silica gel (0.063 mm).

*Methyl 2-Isopropyl-3,4-dimethoxybenzoate (**13**).* 2-Isopropyl-3,4-dimethoxybenzoic acid (**12**)[9] was methylated with diazomethane in ether to give **13**, IR: 1710 cm^{-1}; NMR: 1.31 (6H, d, J=7 Hz, $-CH(C\underline{H}_3)_2$), 3.80 (6H, s) and 3.83 (3H, s) (2-OCH_3 and $-CO_2CH_3$), 6.61 and 7.24 (each 1H, d, and J=9 Hz, aromatic protons).

*2-Isopropyl-3,4-dimethoxybenzyl Alcohol (**14**).* A solution of **13** (38.34 g) in dry ether (40 ml) was added to a stirred suspension of lithium aluminium hydride (6.11 g) in dry ether (150 ml) with cooling in an ice–water bath. The mixture was then refluxed for 2 h, cooled, poured into a mixture of ice and dilute hydrochloric acid, and extracted with ether. The ether extract was washed with brine, dried over sodium sulfate, and evaporated *in vacuo* to give **14** (33.21 g: 98%); IR: 3600, 3400 cm^{-1}; NMR: 1.29 (6H, d, J=7 Hz, $-CH(C\underline{H}_3)_2$), 1.87 (1H, s, -OH), 3.23 (1H, m, $-C\underline{H}(CH_3)_2$, 3.77 (6H, s, 2-OCH_3), 4.43 (2H, s, $-C\underline{H}_2OH$), 6.55 and 6.83 (each 1H, d, and J=9 Hz, aromatic protons).

*2-Isopropyl-3,4-dimethoxybenzyl Chloride (**11**).* A solution of thionyl chloride (17 ml) in dry ether (10 ml) was added at 5 °C to a stirred solution of **14** (33.21 g) in dry ether (40 ml) over a 30 min period. The solution was further stirred at room temperature for 1 h, diluted with dry benzene, and then evaporated *in vacuo* to give **11** (35.00 g: 97%); NMR: 1.35 (6H, d, J=7 Hz, $-CH(C\underline{H}_3)_2$), 3.23 (1H, m, $-C\underline{H}(CH_3)_2$), 3.81 (6H, s, 2-OCH_3), 4.51 (2H, s, $-CH_2Cl$), 6.57 and 6.83 (each 1H, d, and J=8 Hz, aromatic protons).

*Condensation of β-Cyclocitral (**10**) and 2-Isopropyl-3,4-dimethoxybenzyl Chloride (**11**).* A mixture of naphthalene (4.00 g) and small pieces of lithium (247 mg) in dry tetrahydrofuran (20 ml) was stirred at room temperature for 1 h in a stream of nitrogen. Into the above mixture a solution of β-cyclocitral[7,8] (1.36 g) and 2-isopropyl-3,4-dimethoxybenzyl chloride (2.250 g) in dry tetrahydrofuran (10 ml) was added at 0—5 °C over a 45 min period. The mixture was further stirred at 0—5 °C for 2 h in a stream of nitrogen diluted with ether, poured into dilute hydrochloric acid, and extracted with ether. The ether extract was washed with brine, dried over sodium sulfate, and evaporated *in vacuo*. The residue was chromatographed on silica gel (400 g) using ether–benzene (1 : 99) as the eluent to give phenolic fractions (463 mg). Further elution with ether–benzene (1 : 99 and then 3 : 97) gave an oily alcohol (**15**) (1.496 g: 48%) which was crystallized from hexane: mp 72—72.5 °C; IR: 3560 cm^{-1}; NMR: 0.94 and 1.08 (each 3H and s, $-\dot{C}(CH_3)_2$), 1.32 (6H, d, J=7 Hz, $-CH(C\underline{H}_3)_2$), 1.89 (3H, s, $=\dot{C}CH_3$), 3.23 (1H, m, $-C\underline{H}(CH_3)_2$), 3.77 and 3.79 (each 3H and s, 2-OCH_3), 4.24 (1H, dd, J=4 and 9 Hz, $-\dot{C}\underline{H}OH$), 6.60 and 6.72 (each 1H, d, and J=9 Hz, aromatic protons). Found: C, 76.41; H, 9.86%. Calcd for $C_{22}H_{34}O_3$: C, 76.26; H, 9.89%.

The above phenolic fractions (463 mg) were combined and methylated for 6 h with methyl iodide (1.0 ml) and anhydrous potassium carbonate (3.0 g) in refluxing methyl ethyl ketone (10 ml). The mixture was filtered and the filtrate was evaporated *in vacuo*. The residue was dissolved in ether, washed with brine, dried over sodium sulfate, and then evaporated to give a crude product which was purified by column chromatography on silica gel (50 g) using benzene as the eluent to yield a demethoxylated alcohol (**16**) (227 mg: 8%); IR: 3560 cm^{-1}; NMR: 0.95 and 1.09 (each 3H and s, $-\dot{C}(CH_3)_2$), 1.22 and 1.24 (each 3H, d, and J=7 Hz, $-CH(C\underline{H}_3)_2$), 1.90 (3H, s, $=\dot{C}CH_3$), 3.73 (3H, s, $-OCH_3$), 4.30 (1H, dd, J=4 and 9 Hz, $-\dot{C}\underline{H}OH$), 6.57 (1H, dd, J=2 and 8 Hz), 6.68 (1H, d, J=2 Hz), and 6.98 (1H, d, J=8 Hz) (aromatic protons). Further elution gave an additional alcohol (**15**) (168 mg: 5%).

*2,6,6-Trimethyl-1-cyclohexenyl 2-Isopropyl-3,4-dimethoxybenzyl Ketone (**17**).* A solution of (±)-**15** (1.500 g) in pyridine (3.0 ml) was added at 5—10 °C to a stirred chromium trioxide–pyridine complex prepared from chromium trioxide (2.17 g) and pyridine (30 ml). The mixture was stirred at 5—10 °C for 2 h, poured into a mixture of ice

and dilute hydrochloric acid, and filtered. The filtrate was extracted with ether and the extract was washed with brine, dried over sodium sulfate, and then evaporated *in vacuo*. The residue was chromatographed on silica gel (150 g) using benzene as the eluent to give an α,β-unsaturated ketone (**17**) (200 mg: 13%) which was recrystallized from hexane: mp 81—82.5 °C; IR: 1690 cm^{-1}; NMR: 1.07 (6H, s, $-C(CH_3)_2$), 1.30 (6H, d, J=7 Hz, $-CH(C\underline{H}_3)_2$), 1.60 (3H, s, $=CCH_3$), 3.73 (2H, s, $-COCH_2-$), 3.82 and 3.84 (each 3H and s, $2\text{-}OCH_3$), 6.58 (2H, s, aromatic protons). Found: C, 76.88; H, 9.53%. Calcd for $C_{22}H_{32}O_3$: C, 76.70; H, 9.36%. Further elution with ether–benzene (1 : 99) afforded the starting alcohol (**15**) (1.020 g: 68%).

*(±)-12,13-Dimethoxytotara-8,11,13-trien-6-one (**18**).* A mixture of **17** (93 mg) and anhydrous aluminium chloride (72 mg) in dry toluene (10 ml) was refluxed for 6 h. The mixture was diluted with ether, washed successively with dilute hydrochloric acid and water, dried over sodium sulfate, and then evaporated *in vacuo* to give a crude product, whose IR spectrum showed a band at 3540 cm^{-1} due to a phenolic hydroxyl group.

The above crude product was refluxed for 6 h with methyl iodide (0.5 ml) and anhydrous potassium carbonate (3.0 g) in methyl ethyl ketone (5.0 ml). After the usual work-up, the product was purified by column chromatography on silica gel (10 g) using hexane–benzene (1 : 4) as the eluent to give (±)-**18** (49 mg: 53%) which was recrystallized from hexane: mp 144—145 °C; IR; 1710 cm^{-1}; NMR: 1.05 and 1.12 (each 3H and s, $-C(CH_3)_2$), 1.29 (3H, s, $C_{10}-CH_3$), 1.29(6H, d, J=7 Hz, $-CH(C\underline{H}_3)_2$), 2.35 (1H, s, C_5-H), 3.06 (1H, m, $-C\underline{H}(CH_3)_2$), 3.41 (2H, d, J=5 Hz, $-COCH_2-$), 3.78 and 3.80 (each 3H and s, $2\text{-}OCH_3$), 6.66 (1H, s, $C_{11}-H$). Found: C, 76.69; H, 9.33%. Calcd for $C_{22}H_{32}O_3$: C, 76.70; H, 9.36%. Further elution with benzene gave the starting ketone **17** (29 mg: 31%).

*(±)-Maytenoquinone (**1**).* A mixture of (±)-**18** (100 mg) and boron tribromide (1.0 g) in dichloromethane (10 ml) was stirred at 0—5 °C for 1 h and then at room temperature for 30 min. The mixture was poured into ice–water, extracted with ether, and the extract was washed successively with aqueous sodium thiosulfate and brine. The dried solution was evaporated to dryness. The residue was purified by repeated column chromatography on silica gel using hexane–benzene (1 : 1) as the eluent and then recrystallized from hexane to give (±)-maytenoquinone (**1**) (63 mg: 69%), mp 173—174 °C; IR: 3370, 1660, 1630 cm^{-1}; NMR ($CDCl_3$): 1.17 and 1.26 (each 3H and s, $-C(CH_3)_2$), 1.26 (3H, s, $C_{10}-CH_3$), 1.31 and 1.37 (each 3H, d, and J=7 Hz, $-CH(C\underline{H}_3)_2$), 2.48 (1H, s, C_5-H), 3.06 (1H, m, $-C\underline{H}(CH_3)_2$), 6.37 and 6.59 (each 1H, d, and J= 2 Hz, C_7-H and $C_{11}-H$), 7.12 (1H, s, -OH). Found: C, 76.22; H, 8.42%. Calcd for $C_{20}H_{26}O_3$: C, 76.40; H, 8.34%.

*(±)-cis-Maytenoquinone (**19**).* A mixture of (±)-**18** (44.2 mg) and 47% hydrobromic acid (2.0 ml) in acetic acid (10 ml) was refluxed for 2.5 h and then evaporated *in vacuo*. The residue was extracted with ether and the extract was washed successively with aqueous sodium hydrogencarbonate and water, dried over sodium sulfate, and then evaporated. The crude product was purified by column chromatography on silica gel (10 g) using ether–benzene (1 : 99) to give (±)-**19** (33.9 mg: 82%) which was recrystallized from hexane: mp 184—187 °C (sintered at *ca.* 160 °C); IR: 3370, 1650, 1630 cm^{-1}; NMR ($CDCl_3$): 0.62 and 0.97 (each 3H and s, $-C(CH_3)_2$), 1.18 (3H, s, $C_{10}-CH_3$), 1.31 and 1.37 (each 3H, d, and J=7 Hz, $-CH(C\underline{H}_3)_2$), 2.26 (1H, s, C_5-H), 6.45 and 6.64 (each 1H, d, and J=2 Hz, C_7-H and $C_{11}-H$), 7.23 (1H, s, -OH). Found: C, 76.68; H, 8.61%. Calcd for $C_{20}H_{26}O_3$: C, 76.40; H, 8.34%.

*Reductive Cleavage of a Hydroxyl Group in the Alcohol (**15**). With Triethylsilane in the Presence of Boron Trifluoride Etherate*: A solution of boron trifluoride etherate (3.34 ml) in dichloromethane (5.0 ml) was added at −10—0 °C to a stirred solution of (±)-**15** (1.830 g) and triethylsilane (1.230 g) in dichloromethane (50 ml). The mixture was further stirred at this temperature for 1 h, diluted with ether, and then washed with water. The dried solution was evaporated *in vacuo* and the residue was chromatographed on silica gel (100 g) using hexane–benzene (7 : 3) as the eluent to give 2-(2,6,6-trimethyl-1-cyclohexenyl)-1-(2-isopropyl-3,4-dimethoxyphenyl)ethane (**20**) (1.560 g: 89%); NMR: 1.04 (6H, s, $-C(CH_3)_2$), 1.34 (6H, d, J=7 Hz, $-CH(C\underline{H}_3)_2$), 1.68 (3H, s, $=CCH_3$), 3.18 (1H, m, $-C\underline{H}(CH_3)_2$), 3.78 and 3.80 (each 3H and s, $2\text{-}OCH_3$), 6.56 and 6.74 (each 1H, d, and J= 8 Hz, aromatic protons). Found: C, 80.15; H, 10.53%. Calcd for $C_{22}H_{34}O_2$: C, 79.95; H, 10.37%. Further elution with hexane–benzene (1:1) afforded (±)-12,13-dimethoxytotara-5,8,11,13-tetraene (**21**) (132 mg: 8%); NMR: 1.16 and 1.22 (each 3H and s, $-C(CH_3)_2$), 1.26 (3H, s, $C_{10}-CH_3$), 1.27 and 1.32 (each 3H, d, and J=7 Hz, $-CH(C\underline{H}_3)_2$), 3.78 (6H, s, $2\text{-}OCH_3$), 5.83 (1H, dd, J=2.5 and 5.5 Hz, C_6-H), 6.68 (1H, s, $C_{11}-H$). Found: C, 80.67; H, 9.94%. Calcd for $C_{22}H_{32}O_2$: C, 80.44; H, 9.83%.

With Dichloroaluminium Hydride: Lithium aluminium hydride (33 mg) was added to a solution of anhydrous aluminium chloride (345 mg) in dry ether (20 ml), and the mixture was stirred at room temperature for 1 h. To the above solution was added dropwise a solution of (±)-**15** (150 mg) in dry ether (4.0 ml). The mixture was further stirred at room temperature for 1 h, poured into a mixture of ice and dilute hydrochloric acid, and extracted with ether. The ether extract was washed with brine, dried over sodium sulfate, and evaporated *in vacuo*. The residue was chromatographed on silica gel (16 g) using hexane–benzene (4 : 1) as the eluent to give an oil (121 mg: 86%), which was hydrogenated at room temperature for 6 h with 5% Pd–C (130 mg) in acetic acid (10 ml) in an atmosphere of hydrogen. After the usual work-up, the crude product was purified by column chromatography on silica gel (15 g) using hexane–benzene (4 : 1) as the eluent to afford **20** (85 mg: 60%).

*(±)-12,13-Dimethoxytotara-5,8,11,13-tetraene (**21**).* Boron trifluoride etherate (0.18 ml) was added at −10—0° C to a solution of (±)-**15** (98 mg) in dichloromethane (10 ml). The mixture was stirred at this temperature for 1 h, poured into water, and extracted with ether. The ether extract was washed with water, dried over sodium sulfate, and then evaporated *in vacuo*. The crude product was purified by column chromatography on silica gel (10 g) to give (±)-**21** (55 mg: 60%), whose IR and NMR spectra were identical with those of the sample described above.

*(±)-12,13-Dimethoxy-5-methyl-10-nortotara-1(10),8,11,13-tetraene (**22**). From the Alcohol (**15**)*: A solution of (±)-**15** (75 mg) and boron trifluoride etherate (0.14 ml) in dichloromethane (10 ml) was stirred at room temperature for 2 h, and then poured into water. The mixture was extracted with ether, dried over sodium sulfate, and evaporated *in vacuo*. The crude product was chromatographed on silica gel (10 g) using hexane–benzene (4 : 1) as the eluent to give (±)-**22** (33 mg: 45%); NMR: 0.90 (3H, s) and 0.93 (6H, s) ($-C(CH_3)_2$ and C_5-CH_3), 1.28 (6H, d, J=7 Hz, $-CH(C\underline{H}_3)_2$), 3.77 and 3.80 (each 3H and s, $2\text{-}OCH_3$), 6.00 (1H, t, J=4 Hz, C_1-H), 6.85 (1H, s, $C_{11}-H$). Found: C, 80.31; H, 9.98%. Calcd for $C_{22}H_{32}O_2$:

C, 80.44; H, 9.83%.

*From the Tetraene (**21**)*: A solution of (±)-**21** (105 mg) and boron trifluoride etherate (0.20 ml) in dichloromethane (5.0 ml) was stirred at room temperature for 1 h. After a similar treatment to that described above, the crude product was purified by column chromatography on silica gel to give (±)-**22** (54 mg).

*Intramolecular Cyclization of **20**. With Boron Trifluoride Etherate*: A solution of **20** (313 mg) and boron trifluoride etherate (0.60 ml) in dichloromethane (5.0 ml) was allowed to stand at room temperature for 13.5 h, and then poured into water. The mixture was extracted with ether and the extract was washed with water, dried over sodium sulfate, and evaporated *in vacuo*. The crude product was purified by column chromatography on silica gel (30 g) using hexane–benzene (4 : 1) as the eluent to give the *cis*-isomer (**24**) (81 mg: 26%); NMR: 0.43 and 0.94 (each 3H and s, $-\dot{C}(CH_3)_2$), 1.15 (3H, s, C_{10}–CH_3), 1.22 and 1.30 (each 3H, d, and J=7 Hz, $-CH(C\underline{H}_3)_2$), 3.80 (6H, s, 2-OCH_3), 6.66 (1H, s, C_{11}–H). Found: C, 79.87; H, 10.53%. Calcd for $C_{22}H_{34}O_2$: C, 79.95; H, 10.37%. Further elution gave (±)-12,13-dimethoxytotara-8,11,13-triene (**23**) (222 mg: 71%) which was recrystallized from methanol: mp 133.5—134 °C; NMR: 0.92 and 0.94 (each 3H and s, $-\dot{C}(CH_3)_2$), 1.19 (3H, s, C_{10}–CH_3), 1.26 (6H, d, J=7 Hz, $-CH(C\underline{H}_3)_2$), 3.73 (6H, s, 2-OCH_3), 6.58 (1H, s, C_{11}–H). Found: C, 80.22; H, 10.51%. Calcd for $C_{22}H_{34}O_2$: C, 79.95; H, 10.37%.

With Anhydrous Aluminium Chloride: A mixture of **20** (111 mg) and anhydrous aluminium chloride (51 mg) in dry benzene (4.0 ml) was refluxed for 4 h. The mixture was poured into ice–water and extracted with ether. The ether extract was washed with brine, dried over sodium sulfate, and then evaporated *in vacuo*. The crude product was chromatographed on silica gel (10 g) using hexane–benzene (4 : 1) as the eluent to give (±)-12-methoxytotara-8,11,13-trien-13-ol (**2**) (34 mg: 34%), which was recrystallized from hexane: mp 125—126 °C; IR: 3538 cm^{-1}; NMR ($CDCl_3$): 0.92 and 0.95 (each 3H and s, $-\dot{C}(CH_3)_2$), 1.20 (3H, s, C_{10}–CH_3), 1.34 (6H, d, J=7 Hz, $-CH(C\underline{H}_3)_2$), 3.84 (3H, s, $-OCH_3$), 5.62 (1H, s, C_{13}–OH), 6.70 (1H, s, C_{11}–H). NMR (C_5D_5N): 0.90 and 0.93 (each 3H and s, $-\dot{C}(CH_3)_2$), 1.21 (3H, s, C_{10}–CH_3), 1.61 and 1.63 (each 3H, d, and J=7 Hz, $-CH(C\underline{H}_3)_2$), 3.72 (3H, s, $-OCH_3$), 6.82 (1H, s, C_{11}–H). Found: C, 79.78; H, 10.38%. Calcd for $C_{21}H_{32}O_2$: C, 79.70; H, 10.19%. Further elution gave (±)-**24** (11 mg: 9%) and (±)-**23** (41 mg: 36%).

*Partial Demethylation of **23***. A mixture of (±)-**23** (102 mg) and anhydrous aluminium chloride (60 mg) in dry benzene (20 ml) was refluxed for 3 h. After the work-up described above, the crude product was chromatographed on silica gel (10 g) using hexane–benzene (4 : 1) as the eluent to give (±)-**2** (27 mg: 28%), whose IR and NMR spectra were identical with those of the sample described above. Further elution gave the starting (±)-**23** (44 mg).

*Methylation of **2***. A mixture of (±)-**2** (60 mg), methyl iodide (1.0 ml), and anhydrous potassium carbonate (3.0 g) in methyl ethyl ketone (10 ml) was refluxed for 14 h. After the usual work-up, the product was chromatographed on silica gel (6.0 g) using hexane–benzene (1 : 1) as the eluent to give (±)-**23** (51 mg: 82%), whose IR and NMR spectra were identical with those of the sample described above.

*(±)-12,13-Dimethoxytotara-8,11,13-trien-7-one (**25**)*. A mixture of (±)-**23** (209 mg) and chromium trioxide (190 mg) in acetic acid (20 ml) was stirred at room temperature for 2 h and then diluted with ether. The ether solution was washed successively with water, aqueous sodium hydrogencarbonate, and water. The dried solution was then evaporated *in vacuo* and the residue was chromatographed on silica gel (20 g) using hexane–benzene (1 : 4) as the eluent to give (±)-**25** (118 mg: 54%), which was recrystallized from methanol: mp 129—130 °C; IR: 1660 cm^{-1}; NMR (90 MHz): 0.93 and 1.02 (each 3H and s, $-\dot{C}(CH_3)_2$), 1.12 (3H, s, C_{10}–CH_3), 1.23 and 1.31 (each 3H, d, and J=7 Hz, $-CH(C\underline{H}_3)_2$), 3.76 and 3.83 (each 3H and s, 2-OCH_3), 6.58 (1H, s, C_{11}–H). Found: C, 76.98; H, 9.27%. Calcd for $C_{22}H_{32}O_3$: C, 76.70; H, 9.36%.

*(±)-Dispermone (**3**)*. Boron tribromide (0.1 ml) was added at 0—5 °C to a solution of (±)-**25** (47 mg) in dichloromethane (2.0 ml). The mixture was allowed to stand at room temperature for 4 h, poured into ice–water, and extracted with ether. The ether extract was washed successively with aqueous sodium thiosulfate and water, dried over sodium sulfate, and then evaporated *in vacuo*. The crude product was chromatographed on silica gel (5.0 g) using chloroform as the eluent to give (±)-dispermone (**3**) (38 mg: 88%), which was recrystallized from ether–hexane: mp 242—245 °C (sintered at *ca.* 230 °C); IR: 3595, 3540, 3200, 1655 cm^{-1}; NMR (90 MHz: $(CD_3)_2CO$): 0.92, 1.01, and 1.08 (each 3H and s, $-\dot{C}(CH_3)_2$ and C_{10}–CH_3), 1.30 and 1.38 (each 3H, d, and J=7 Hz, $-CH(C\underline{H}_3)_2$), 3.86 (1H, m, $-C\underline{H}(CH_3)_2$), 6.73 (1H, s, C_{11}–H). Found: C, 75.61; H, 8.72%. Calcd for $C_{20}H_{28}O_3$: C, 75.91; H, 8.92%.

*2-Isopropyl-3,4-dimethoxybenzyltriphenylphosphonium Chloride (**27**)*. A mixture of the benzyl chloride (**11**) (35.0 g) and triphenylphosphine (40.1 g) in dry benzene (35 ml) was refluxed for 5 min. The precipitated salt (**27**) (mp 243—245 °C, 29.0 g) was collected by filtration and the filtrate was further refluxed for 6 h to give some additional salt (38.5 g).

*(−)-3-(2-Isopropyl-3,4-dimethoxystyryl)-2,4,4-trimethyl-1-cyclohexene (**28**)*. A solution of *n*-butyllithium in dry hexane (15%: 2.1 ml) was added at room temperature to a stirred suspension of **27** (2.010 g) in dry hexane (6.0 ml) in a stream of nitrogen, and the mixture was stirred for 1 h. To the above mixture a solution of (*R*)-(−)-α-cyclocitral (**26**), $[\alpha]_D$ −712° (EtOH), (390 mg) in dry hexane (3.0 ml) was added at 8—10 °C over a 5 min period. The mixture was further stirred at this temperature for 4 h, exposed to air for a few min until the red solution turned yellow, then poured into dilute hydrochloric acid and extracted with ether. The ether extract was washed with brine, dried over sodium sulfate, and evaporated *in vacuo*. The residue was triturated with hexane, and the precipitated triphenylphosphine oxide was removed by filtration. The filtrate was evaporated *in vacuo*. The crude product was chromatographed on silica gel (40 g) using hexane–benzene (7:3) as the eluent to give (−)-**28** as an oil (647 mg: 77%), $[\alpha]_D$ −258°; NMR: 0.91 and 0.96 (each 3H and s, $-\dot{C}(CH_3)_2$), 1.32 (6H, d, J=7 Hz, $-CH(C\underline{H}_3)_2$), 1.67 (3H, bs, $=\dot{C}CH_3$), 3.37 (1H, m, $-C\underline{H}(CH_3)_2$), 3.77 and 3.80 (each 3H and s, 2-OCH_3), 5.42 (1H, m, $-CH=\dot{C}-$), 5.55 (1H, dd, J=9 and 15 Hz, $-\dot{C}H-C\underline{H}=CH-$), 6.61 (1H, d, J=15 Hz, $-\dot{C}H-CH=C\underline{H}-$), 6.58 and 6.90 (each 1H, d, and J=9 Hz, aromatic protons). Found: C, 80.46; H, 9.93%. Calcd for $C_{22}H_{32}O_2$: C, 80.44; H, 9.83%.

*(−)-2-(2,6,6-Trimethyl-2-cyclohexenyl)-1-(2-isopropyl-3,4-dimethoxyphenyl)ethane (**29**)*. A suspension of (−)-**28** (2.012 g) and 5% Pd–C (1.0 g) in ethanol (20 ml) was stirred at room temperature in an atmosphere of hydrogen. After

one mole equivalent of hydrogen had been absorbed (*ca.* 1.5 h), the mixture was filtered. The filtrate was evaporated *in vacuo* and the residue was purified by column chromatography on silica gel (200 g) using hexane–benzene (7:3) as the eluent to afford (−)-**29** as an oil (1.705 g: 84%), $[\alpha]_D$ −90.3°; NMR: 0.91 and 1.01 (each 3H and s, $-\dot{C}(CH_3)_2$), 1.34 (6H, d, J=7 Hz, $-CH(C\underline{H}_3)_2$), 1.73 (3H, bs, $=\dot{C}CH_3$), 3.24 (1H, m, $-C\underline{H}(CH_3)_2$), 3.80 (6H, s, 2-OCH_3), 5.30 (1H, m, $-CH=\dot{C}-$), 6.53 and 6.69 (each 1H, d, and J=9 Hz, aromatic protons). Found: C, 80.21; H, 10.11%. Calcd for $C_{22}H_{34}O_2$: C, 79.95; H, 10.37%.

*Intramolecular Cyclization of (−)-**29**.* A mixture of (−)-**29** (1.705 g) and anhydrous aluminium chloride (690 mg) in dry benzene (17 ml) was stirred at 25—30 °C for 30 min and then poured into a mixture of ice and dilute hydrochloric acid. The mixture was extracted with ether. The ether extract was washed with brine, dried over sodium sulfate, and evaporated *in vacuo*. The residue was chromatographed on silica gel (170 g) using hexane–benzene (4:1) as the eluent to give (−)-**24** (581 mg: 34%), $[\alpha]_D$ −36.4°, whose IR and NMR spectra were identical with those of (±)-**24**. Found: C, 79.77; H, 10.63%. Calcd for $C_{22}H_{34}O_2$: C, 79.95; H, 10.37%. Further elution gave (+)-**23** as a solid (739 mg: 43%), $[\alpha]_D$ +32.4°, which was recrystallized from methanol: mp 89—91 °C, $[\alpha]_D$ +50.2° (lit,[1] mp 89—90 °C, $[\alpha]_D$ +35°). The IR and NMR spectra were identical with those of (±)-**23**. Found: C, 79.93; H, 10.67%. Calcd for $C_{22}H_{34}O_2$: C, 79.95; H, 10.37%.

*(+)-12-Methoxytotara-8,11,13-trien-13-ol (**2**).* A mixture of (+)-**23** (93 mg) and anhydrous aluminium chloride (40 mg) in dry benzene (4.0 ml) was refluxed for 3 h with stirring. After the usual work-up, the crude product was purified by column chromatography on silica gel (15 g) using hexane–benzene (9:1) as the eluent to give (+)-**2** (68 mg: 77%), which was recrystallized from methanol: mp 87—88.5 °C, $[\alpha]_D$ +50.2°, whose IR and NMR spectra were identical with those of (±)-**2**. Found: C, 79.87; H, 10.32%. Calcd for $C_{21}H_{32}O_2$: C, 79.70; H, 10.19%.

*(−)-12,13-Dimethoxytotara-8,11,13-trien-7-one (**25**).* A solution of (+)-**23** (124 mg) in acetone (3.0 ml) was oxidized at 16—20 °C for 30 min with Jones reagent (8N: 0.20 ml) and then diluted with ether. The ether solution was washed with water, dried over sodium sulfate, and evaporated *in vacuo*. The crude product was purified by column chromatography on silica gel (15 g) using hexane–benzene (1:4) as the eluent to give the starting (+)-**23** (14 mg: 11%). Further elution gave (−)-**25** (95 mg: 74%), $[\alpha]_D$ −19.2°, NMR ($CDCl_3$): 0.92 and 1.01 (each 3H and s, $-\dot{C}(CH_3)_2$), 1.13 (3H, s, C_{10}–CH_3), 1.29 and 1.38 (each 3H, d, and J= 7 Hz, $-CH(C\underline{H}_3)_2$), 3.67 (1H, m, $-C\underline{H}(CH_3)_2$), 3.83 and 3.89 (each 3H and s, 2-OCH_3), 6.72 (1H, s, C_{11}–H). NMR (C_5D_5N): 0.81 and 0.89 (each 3H and s, $-\dot{C}(CH_3)_2$), 1.03 (3H, s, C_{10}–CH_3), 1.46 and 1.60 (each 3H, d, and J=7 Hz, $-CH(C\underline{H}_3)_2$), 3.85 (6H, s, 2-OCH_3), 4.17 (1H, m, $-C\underline{H}(CH_3)_2$), 6.81 (1H, s, C_{11}–H). The IR and NMR spectra were identical with those of (±)-**25**.

*(−)-Dispermone (**3**).* A solution of (−)-**25** (95 mg) and boron tribromide (0.10 ml) in dichloromethane (1.0 ml) was allowed to stand at 0—5 °C for 2 h and then treated as described for the preparation of (±)-**3**. The crude product was purified by column chromatography on silica gel using chloroform as the eluent to give (−)-dispermone (**3**) (80 mg: 92%), which was recrystallized from acetone–hexane: mp 262—267 °C, $[\alpha]_D$ −47.3° (EtOH) (lit,[1] mp 263—265 °C, $[\alpha]_D$ −48°), whose IR and NMR spectra were identical with those published.[1] Found: C, 75.75; H, 8.92%. Calcd for $C_{20}H_{28}O_3$: C, 75.91; H, 8.92%.

*(−)-12-Benzyloxy-13-hydroxytotara-8,11,13-tricn-7-one (**30**).* A mixture of (−)-**3** (204 mg), benzyl chloride (90 mg), potassium iodide (110 mg), and anhydrous potassium carbonate (1.0 g) in methyl ethyl ketone (10 ml) was refluxed for 5.5 h with stirring. After the usual work-up, the product was purified by column chromatography on silica gel (30 g) using benzene as the eluent to give (−)-**30** (260 mg: 99%), $[\alpha]_D$ −17.8°; IR: 3540, 1660 cm^{-1}; NMR ($CDCl_3$): 0.93 and 1.01 (each 3H and s, $-\dot{C}(CH_3)_2$), 1.11 (3H, s, C_{10}–CH_3), 1.33 and 1.44 (each 3H, d, and J=7 Hz, $-CH(C\underline{H}_3)_2$), 3.86 (1H, m, $-C\underline{H}(CH_3)_2$), 5.15 (2H, s, $-OCH_2-$), 5.81 (1H, s, C_{13}–OH), 6.77 (1H, s, C_{11}–H), 7.42 (5H, s, aromatic protons). NMR (C_5D_5N): 0.81 and 0.90 (each 3H and s, $-\dot{C}(CH_3)_2$), 1.07 (3H, s, C_{10}–CH_3), 1.74 and 1.87 (each 3H, d, and J=7 Hz, $-CH(C\underline{H}_3)_2$), 4.44 (1H, m, $-C\underline{H}(CH_3)_2$), 5.25 (2H, s, $-OCH_2-$), 6.93 (1H, s, C_{11}–H). Found: C, 79.75; H, 8.44%. Calcd for $C_{27}H_{34}O_3$: C, 79.76; H, 8.43%.

*(−)-12-Benzyloxy-13-methoxytotara-8,11,13-trien-7-one (**31**).* A mixture of (−)-**30** (182 mg), methyl iodide (0.10 ml), and anhydrous potassium carbonate (500 mg) in methyl ethyl ketone (5.0 ml) was refluxed for 33 h. After the usual work-up, the crude product was purified by column chromatography on silica gel (20 g) using hexane–benzene (1:1) as the eluent to give (−)-**31** (177 mg: 94%), $[\alpha]_D$ −15.1°, IR: 1660 cm^{-1}, NMR: 0.94 and 1.02 (each 3H and s, $-\dot{C}(CH_3)_2$), 1.10 (3H, s, C_{10}–CH_3), 1.28 and 1.35 (each, 3H, d, and J=7 Hz, $-CH(C\underline{H}_3)_2$), 3.83 (3H, s, $-OCH_3$), 5.10 (2H, s, $-OCH_2-$), 6.69 (1H, s, C_{11}–H), 7.38 (5H, s, aromatic protons). Found: C, 80.23; H, 8.61%. Calcd for $C_{28}H_{36}O_3$: C, 79.96; H, 8.63%.

*(+)-Dispermol (**5**).* A mixture of (−)-**31** (101 mg), PtO_2 (40 mg), and 60% perchloric acid (4 drops) in ethanol (10 ml) was stirred at room temperature for 2.5 h in an atmosphere of hydrogen. After the usual work-up, the crude product was chromatographed on silica gel (15 g) using benzene as the eluent to give (+)-dispermol (**5**) (50 mg: 66%), which was recrystallized from hexane: mp 166.5—167.5 °C, $[\alpha]_D$ +43.5° (lit,[1] mp 164—166 °C, $[\alpha]_D$ +37°); IR: 3550, 3360 cm^{-1}; NMR ($CDCl_3$): 0.95 (6H, s, $-\dot{C}(CH_3)_2$), 1.19 (3H, s, C_{10}–CH_3), 1.34 (6H, d, J=7 Hz, $-CH(C\underline{H}_3)_2$), 3.37 (1H, m, $-C\underline{H}(CH_3)_2$), 3.79 (3H, s, $-OCH_3$), 5.2 (1H, br, C_{12}–OH), 6.80 (1H, s, C_{11}–H). NMR (C_5D_5N): 0.88 and 0.94 (each 3H and s, $-\dot{C}(CH_3)_2$), 1.20 (3H, s, C_{10}–CH_3), 1.49 (6H, d, J=7 Hz, $-CH(C\underline{H}_3)_2$), 3.43 (1H, m, $-C\underline{H}-(CH_3)_2$), 4.05 (3H, s, $-OCH_3$), 7.13 (1H, s, C_{11}–H). Found: C, 79.44; H, 10.25%. Calcd for $C_{21}H_{32}O_2$: C, 79.70; H, 10.19%.

*(−)-12,13-Dimethoxytotara-6,8,11,13-tetraene (**32**).* A mixture of (−)-**25** (250 mg) and lithium aluminium hydride (30 mg) in dry ether (5.0 ml) was refluxed for 2 h. The mixture was poured into dilute hydrochloric acid, extracted with ether, and the ether extract was washed with brine, dried over sodium sulfate, and then evaporated. The residue was recrystallized from methanol to give (−)-**32** (174 mg: 73%), mp 96—97 °C, $[\alpha]_D$ −100°; NMR: 0.99 and 1.01 (each 3H and s, $-\dot{C}(CH_3)_2$), 1.06 (3H, s, C_{10}–CH_3), 1.33 (6H, d, J=7 Hz, $-CH(C\underline{H}_3)_2$), 3.46 (1H, m, $-C\underline{H}(CH_3)_2$), 3.73 and 3.81 (each 3H and s, 2-OCH_3), 5.83 (1H, dd, J= 3 and 10 Hz, C_6–H), 6.54 (1H, s, C_{11}–H), 6.76 (1H, dd, J=3 and 10 Hz, C_7–H). Found: C, 80.19; H, 9.95%. Calcd for $C_{22}H_{32}O_2$: C, 80.44; H, 9.83%. The mother

liquor of crystallization was evaporated and the residue was chromatographed on silica gel (25 g) using hexane–benzene (1:1) as the eluent to give some additional (−)-**32** (29 mg: 12%).

*(+)-12,13-Dimethoxytotara-8,11,13-trien-6-one (**18**).* A solution of (−)-**32** (202 mg) and 70% *m*-chloroperbenzoic acid (170 mg) in dichloromethane (5.0 ml) was allowed to stand at 5—7 °C for 1.5 h and then diluted with ether. The solution was washed successively with aqueous potassium iodide, aqueous sodium thiosulfate, aqueous sodium hydrogencarbonate, and water. After the solvent had been removed *in vacuo*, the residue was dissolved in methanol (5.0 ml) containing dilute hydrochloric acid (10%: 0.5 ml). The solution was refluxed for 30 min in an atmosphere of nitrogen, cooled, and extracted with ether. The ether extract was washed with water, dried over sodium sulfate, and then evaporated *in vacuo*. The crude product was chromatographed on silica gel (20 g) using benzene as the eluent to give (+)-**18** (146 mg: 69%), $[\alpha]_D$ +117°, whose IR and NMR spectra were identical with those of (±)-**18**. Found: C, 76.91; H, 9.28%. Calcd for $C_{22}H_{32}O_3$: C, 76.70; H, 9.36%.

*(+)-Maytenoquinone (**1**).* A mixture of (+)-**18** (146 mg) and boron tribromide (0.14 ml) in dichloromethane (3.0 ml) was stirred at 0—5 °C for 1 h, poured into ice–water, and extracted with ether. The ether extract was washed successively with aqueous sodium thiosulfate and water, dried over sodium sulfate, and then evaporated *in vacuo*. The residue was chromatographed on silica gel (30 g) using benzene as the eluent to give (+)-maytenoquinone (**1**) (12.2 mg: 9.1%). Further elution with ether–benzene (1:9) afforded 12,13-dihydroxytotara-8,11,13-trien-6-one (117 mg: 87%); IR: 3540, 3250, 1705 cm^{-1}; NMR ($CDCl_3$): 1.10 (6H, s, $-\underset{|}{C}(CH_3)_2$), 1.35 (3H, s, C_{10}–CH_3), 1.36 (6H, d, J=7 Hz, $-CH(C\underline{H}_3)_2$), 2.50 (1H, s, C_5–H), 3.10 (1H, m, $-C\underline{H}(CH_3)_2$), 3.55 (2H, bd, J=2 Hz, $-COCH_2-$), 5.54 (s) and 6.21 (bs) (each 1H, C_{12}–OH and C_{13}–OH), 6.80 (1H, s, C_{11}–H).

The above phenol (117 mg) was stirred and refluxed for 1 h with silver oxide (170 mg) in chloroform (10 ml). The mixture was then filtered and the filtrate was evaporated *in vacuo*. The residue was purified by column chromatography on silica gel (20 g) using benzene as the eluent to give (+)-maytenoquinone (**1**) (60 mg: 51%) (total 72.2 mg: 54% overall yield from (+)-**18**), which was recrystallized from methanol: mp 156—158 °C, $[\alpha]_D$ +407° (lit,[1] mp 158—160 °C, $[\alpha]_D$ +298°). Found: C, 76.48; H, 8.63%. Calcd for $C_{20}H_{26}O_3$: C, 76.40; H, 8.34%. The IR and NMR spectra were identical with those of (±)-**1**.

References

1) J. D. Martin, *Tetrahedron*, **29**, 2553 (1973).

2) S. M. Kupchan, A. Karim, and C. Marcks, *J. Am. Chem. Soc.*, **90**, 5923 (1968); *J. Org. Chem.*, **34**, 3912 (1969).

3) K. Mori and M. Matsui, *Tetrahedron*, **26**, 3467 (1970).

4) T. Matsumoto, Y. Tachibana, J. Uchida, and K. Fukui, *Bull. Chem. Soc. Jpn.*, **44**, 2766 (1971); T. Matsumoto, Y. Ohsuga, and K. Fukui, *Chem. Lett.*, **1974**, 297; T. Matsumoto, Y. Ohsuga, S. Harada, and K. Fukui, *Bull. Chem. Soc. Jpn.*, **50**, 266 (1977); T. Matsumoto, S. Usui, and T. Morimoto, *ibid.*, **50**, 1575 (1977).

5) Y. Ohtsuka and A. Tahara, *Chem. Pharm. Bull.*, **26**, 2007 (1978).

6) Most of the work has been reported in preliminary form: T. Matsumoto and T. Ohmura, *Chem. Lett.*, **1977**, 335; T. Matsumoto and S. Usui, *ibid.*, **1978**, 897.

7) R. N. Gedye, P. C. Arora, and K. Deck, *Can. J. Chem.*, **49**, 1764 (1971).

8) W. M. B. Könst, L. M. van der Linde, and H. Boelens, *Tetrahedron Lett.*, **1974**, 3175.

9) J. D. Edwards, Jr., and J. L. Cashaw, *J. Am. Chem. Soc.*, **78**, 3821 (1956).

10) The use of protonic acid, HBr, caused the acid-catalyzed enolization between C-6 carbonyl group and C-5 proton to form the corresponding enol compound, which was isomerized to a more stable *cis*-maytenoquinone (**19**). However, when the Lewis acid BBr_3 was used, no such enolization occurred.

11) E. Wenkert, A. Afonso, P. Beak, R. W. J. Carney, P. W. Jeffs, and J. D. McChesney, *J. Org. Chem.*, **30**, 713 (1965).

12) H. O. House, "Modern Synthetic Reactions," 2nd ed, W. A. Benjamin Inc. (1972), p. 48.

13) M. G. Adlington, M. Orfanopoulos, and J. L. Fry, *Tetrahedron Lett.*, **1976**, 2955.

14) P. V. Demarco, E. Farkas, D. Doddrell, B. L. Mylari, and E. Wenkert, *J. Am. Chem. Soc.*, **90**, 5480 (1968). $\Delta=\delta_{CDCl_3}-\delta_{C_5D_5N}$

15) C. H. Eugster, R. Buchecker, Ch. Tscharner, G. Uhde, and G. Ohloff, *Helv. Chim. Acta*, **52**, 1729 (1969).

16) T. Matsumoto and S. Usui, *Bull. Chem. Soc. Jpn.*, **52**, 212 (1979).

17) The solvent shift of the C-16 and C-17 methyls in the dimethyl ether (−)-**25** was −0.20 ppm.

The Transformations of Terpene Ketones by Oxygen. I. The Autoxidation of Fukinone

Akio HORINAKA and Keizo NAYA*

Department of Chemistry, Faculty of Science, Kwansei Gakuin University, Uegahara, Nishinomiya, Hyogo 662

(Received November 14, 1978)

Fukinone, possessing a cisoid enone system, is susceptible to air oxidation. The oxidation products have been extensively examined and have been established as including diastereomeric epoxides, a hydroxy ketone (petasitolone), a lactol (8β-hydroxyeremophilenolide), and a peroxy hemiacetal. Also, the products were compared with those derived from the autoxidation of pulegone, a monoterpenic analogue of fukinone.

A fragrant oil, fukinone (**1**),[1] $C_{15}H_{24}O$, is rather sensitive to air. Even on storage, several polar spots appear on TLC. We have been interested in the autoxidation in connection with the biogenetic-type oxidation process. Furthermore, as little is known about the autoxidation of α,β-unsaturated ketones with an exo-cyclic double bond, we have studied the autoxidation of **1** in parallel with the base-catalyzed autoxidation.[2] Pulegone (**2**), with a similar enone system, has been widely studied;[3,4] hence, the autoxidation was reinvestigated in order to compare it with the products from **1**.

The autoxidation of the title compound, **1**, was achieved by heating it at 80—90 °C under a bubbling of air for 44 h. From the reaction mixture we isolated epoxides, $C_{15}H_{24}O_2$ (**3**), a hydroxy ketone, $C_{15}H_{22}O_2$ (**4**), and a lactol, $C_{15}H_{22}O_3$ (**5**) in 24.5, 3, and 3.5% yields respectively by column chromatography on silica gel.

The epoxides, **3**, was shown by GLC analysis to be mixtures comprising approximately equal amounts of the diastereomers. **3** was separated into (**3a**) (mp 66—67 °C) and (**3b**) (mp 83—84 °C)[5] by repeated chromatogrphy on deactivated silica gel. Both the epoxides were identified by comparison with the authentic samples prepared by treating **1** with hydrogen peroxide in an alkaline solution.[6] The absolute configurations[5] previously proposed for fukinone epoxides, **3a** and **3b**, were finally settled by the X-ray analysis of the 7β-hydroxy-8-oxoeremophil-11(12)-ene (**6**)[7] prepared by the stereospecific cleavage of **3b** in the presence of *p*-toluenesufonic acid in dry benzene.[8]

The oily hydroxy ketone, **4**, was found to be identical with natural petasitolone[9] by a comparison of the IR and GLC.

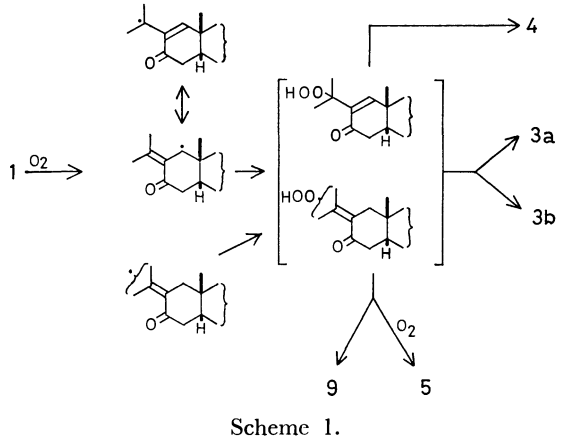

Scheme 1.

The lactol, **5**,[10] showed a wide melting range (mp 180—200 °C), even after repeated recrystallizations. Therefore, **5** was transformed into the methoxylactone (**7**) by refluxing in methanol in the presence of a catalytic amount of hydrochloric acid, which was identical with 8β-methoxyeremophilenolide[10] prepared by the photosensitized oxygenation of furanoeremophilane (**8**)[11] in methanol. Accordingly the 8-hydroxyl and 8-methoxyl groups in both the lactones can be identified as β-configurations as in the **5** and **7** formulas.

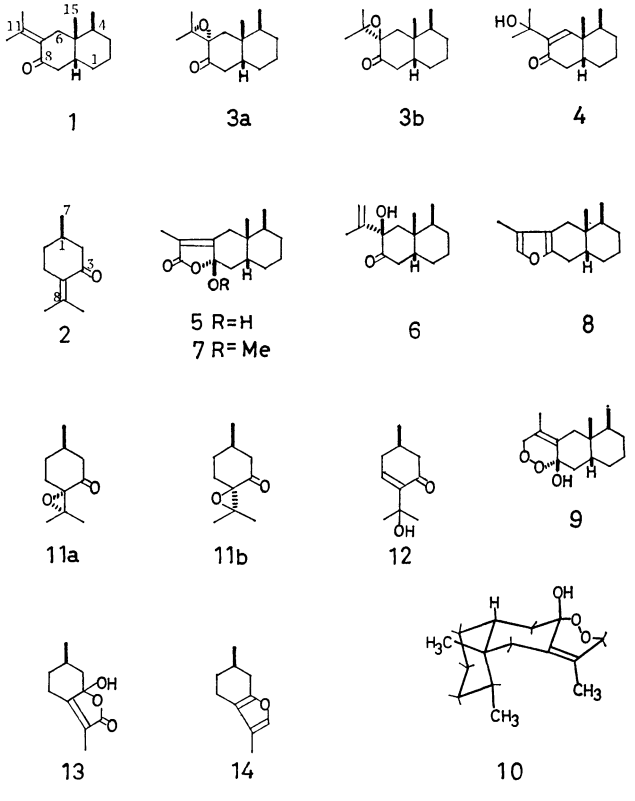

In addition, **1** left in air for a long time afforded a peroxy hemiacetal (**9**) (mp 100—103 °C) besides **3**, **4**, and **5**. The structure for **9** was readily determined from the spectral and chemical properties. In the Dreiding-model inspection, the 8α- or 8β-substituents in the peroxy hemiacetal will force the *cis*-decalin system to adopt a nonsteroidal or a steroidal A/B *cis* chair/chair configuration respectively in a manner similar to that used in the case of eremophilenolides.[10,12] Therefore, on the basis of a similar relationship between the chemical shifts of 14- and 15-methyls, the peroxy hemiacetal was tentatively assigned to the stereoformula (**10**) bearing an 8β-hydroxyl group. The reduction

of **10** with triphenylphosphine gave furanoeremophilane (**8**), which occurs with **1** in the same plant,[11] implying a biosynthetic pathway to **8** from **1**. The hemiacetal, **9**, was itself rather stable in the crystalline state at room temperature, but it decomposed considerably in solution. The isolation of **9** suggests that the primary oxidation products of **1** are hydroperoxides; hence, the epoxides, **3a** and **3b**, the main products, are probably produced by the attack of the hydroperoxides on the alternate fukinone molecule.

The reinvestigation of the autoxidation of **2** was performed in a manner similar to that used for **1** and proved to afford products similar to those from **1**. Thus, the reaction mixture was separated to give epoxides (**11**), an oily hydroxy ketone (**12**), and a lactol (**13**) in 15, 6.4, and 28% yields respectively. The absolute configurations of α-epoxide (**11a**) (mp 57—58 °C) and β-epoxide (**11b**) (mp 53—54 °C) have previously been established.[13,14] The physical properties of **12** and **13** (mp 186—187 °C) were in good agreement with those of the photooxygenation product of **2**,[15] and of the autoxidation[4] or the photooxygenation[16] product of menthofuran (**14**) respectively.

From the above results, it seems that the autoxidation of **1** and **2** should proceed in the same manner, and that the autoxidation process of **1** is as depicted in Scheme 1.

Experimental

All the melting and boiling points are uncorrected. The IR, UV, and mass spectra were taken with Hitachi EPI-G3, Shimadzu Spectronic 505, and Hitachi RMU-6 spectrophotometers respectively. The PMR spectra were recorded with a Hitachi R-20B (60 MHz) spectrometer, and the chemical shifts are reported in δ-values, with TMS as the internal reference. The optical rotations were measured with a Perkin-Elmer 141 polarimeter. The analytical and preparative GLC were performed with a Shimadzu GC-1C apparatus on a stainless steel column (ϕ=3 mm). The TLC were run on silica gel (Merck Kieselgel G). The microanalyses were carried out in the analytical section of the Research Laboratory, Toyo Jozo Co., Ltd.

Autoxidation of Fukinone (1). Fukinone (**1**) (3.759 g) was oxidized without a solvent under the bubbling of air at 80—90 °C for 44 h. The resulting mixture (3.637 g) was chromatographed on silica gel (70 g). Elution with benzene afforded, successively, the recovered fukinone (**1**), a mixture of epoxides (**3a** and **3b**) (982 mg), a hydroxy ketone (**4**) (119 mg), and a lactol (**5**) (150 mg).

Each of the epoxides, (**3a**) and (**3b**), was obtained by repeated column chromatography on deactivated silica gel (Grade II), followed by recrystallization from light petroleum. Both epoxides, **3a** (mp 66—67 °C) and **3b** (mp 83—84 °C), were identical in all respects (IR, PMR, and mixed-melting-point determination) with authentic samples.[5]

The hydroxy ketone (**4**) was found to be identical with natural petasitolone[9] by a comparison of the IR and GLC results.

Lactol (5):[10] Mp 180—200 °C, colorless prisms (from ethyl acetate), $[\alpha]_D^{28}$ +155° (*c*, 1.03, $CHCl_3$); IR($CHCl_3$): 3550, 3330, 1750, 1696, 1230 cm^{-1}; UV: λ_{max}^{MeOH} 223 nm (ε, 25000); PMR ($CDCl_3$): 3.53 (s, OH), 1.77 (d, *J*=1.5 Hz, 12-Me), 1.02 (s, 15-Me), 0.77 (d, *J*=5.0 Hz, 14-Me).

Found: C, 72.15; H, 8.72%. Calcd for $C_{15}H_{22}O_3$: C, 71.97; H, 8.86%.

Methoxy Lactone (7). A solution of the lactol (**5**) (86 mg) in methanol containing a catalytic amount of concentrated hydrochloric acid was refluxed for 2.5 h. The reaction mixture was then poured into water, and the deposited crystals (77 mg, 84%) were recrystallized from aqueous methanol; mp 99.5—100 °C as colorless needles; $[\alpha]_D^{23}$ +192° (*c*, 1.00, $CHCl_3$); MS: *m/e* 264 (M^+), *m/e* 236 (base peak); IR(KBr): 1760, 1695, 1180, 990 cm^{-1}; (CCl_4): 1763, 1700, 1177 cm^{-1}; UV: λ_{max}^{MeOH} 223 nm (ε, 15000); PMR (CCl_4): 3.07 (s, OMe), 1.80 (d, *J*=1.5 Hz, 12-Me), 1.04 (s, 15-Me), 0.80 (d, *J*=6.0 Hz, 14-Me).

Found: C, 72.84; H, 9.07%. Calcd for $C_{16}H_{24}O_3$: C, 72.69; H, 9.15%. This compound was identical with the 8β-methoxyeremophilenolide (**7**) prepared from furanoeremophilane (**8**) by photosensitized oxygenation;[10] this was determined by a comparison of the IR, UV, and PMR, and by a mixed-melting-point determination.

Isolation of Peroxy Hemiacetal (9). Fikinone (**1**) (13.591 g) was left in air and in a dark place at room temperature for several months. The resulting oil was chromatographed on silica gel, and a polar part (with R_f values less than 0.3; silica gel, benzene) was collected. The yellow viscous oil (3.164 g) was repeatedly chromatographed on silica gel, with benzene as the eluent, to give two fractions, one containing **3**, **4**, and **9**, and the other containing **4** and **5**. From each fraction, **5** and **9** were deposited as crystals in 131 mg and 107 mg yields respectively. **9** was recrystallized from light petroleum; mp 100—103 °C; long, colorless leaflets, $[\alpha]_D^{24}$ −46° (*c*, 0.98, $CHCl_3$); MS: *m/e* 252 (M^+), *m/e* 110 (base peak); IR ($CHCl_3$): 3555, 1055, 1048 cm^{-1}; PMR ($CDCl_3$): 4.74 and 3.99 (each dd, *J*=3.0 and 16 Hz, 12-CH_2), 2.90 (br s, OH), 1.67 (br s, 13-Me), 0.92 (s, 15-Me), 0.78 (d, *J*=6.0 Hz, 14-Me).

Found: C, 71.21; H, 9.46%. Calcd for $C_{15}H_{24}O_3$: C, 71.39; H, 9.59%.

Reduction of Peroxy Hemiacetal (9) with Triphenylphosphine. A solution of **9** (113 mg) and triphenylphosphine (229 mg) in benzene was refluxed for 8 h, and subsequently the solvent was evaporated *in vacuo*. The residue was extracted with light petroleum, and the extract (169 mg) was chromatographed on deactivated silica gel (Grade II, 5 g). Subsequent elution with light petroleum–ether (50:1) gave an oil (120 mg). Further purification by preparative TLC (silica gel; light petroleum–ether, 20:1) afforded furanoeremophilane (**8**) (16 mg, 17%), which was found to be identical with an authentic sample[11] by a comparison of the IR and GLC (SE-30, 2.6 m; column temperature, 155 °C; H_2-flow rate, 40 ml/min; retention time, 6.7 min).

Autoxidation of Pulegone (2). Pulegone (**2**) (1.330 g) was subjected to oxidation for 62 h in the same fashion as in the case of **1**. The resulting mixture (1.121 g) was chromatographed on silica gel (25 g) with benzene to give a mixture of epoxides (**11**) (222 mg) and a hydroxy ketone (**12**) (95 mg). Subsequent elution with benzene–ethyl acetate (50:1) gave a lactol (**13**) (44 mg).

A mixture of epoxides (**11**) was separated into two diastereomers, (**11a**) and (**11b**), by preparative GLC (PEG 20 M, 2.6 m; column temperature, 145 °C; H_2-flow rate, 45 ml/min; retention time; β-epoxide (**11b**): 12.4 min, α-epoxide (**11a**): 19.1 min). Both the epoxides, **11a** (mp 57—58 °C) and **11b** (mp 53—54 °C), were found to be identical with authentic samples[13] by a comparison of the IR, PMR, and GLC, and by a mixed-melting-point determination.

Hydroxy Ketone (12):[15] Bp 130—140 °C (bath temperature)/15 mmHg, preparative GLC (PEG 20 M, 1.1 m; column temperature, 130 °C; H_2-flow rate, 72 ml/min; reten-

tion time, 6.8 min); IR(film): 3410, 1660 cm^{-1}; UV: λ_{max}^{MeOH} 234 nm (ε, 7900); PMR(CCl_4): 6.83 (m, 5-H), 3.73 (s, OH), 1.30 (s, 9- and 10-Me), 1.06 (d, J=4.0 Hz, 7-Me).

*Lactol (**13**)*:[4] Mp 186—188 °C, colorless prisms (from acetone); IR(KBr): 3325, 1735, 1693, 1195, 1120, 960 cm^{-1}; UV: λ_{max}^{MeOH} 219 nm (ε, 16100); PMR (acetone-d_6): 2.95 (s, OH), 1.70 (d, J=1.0 Hz, Me–C=C), 0.93 (d, J=7.0 Hz, Me–CH). (Found: C, 65.75; H, 7.95%).

The authors wish to thank the staff of the Research Laboratory, Toyo Jozo Co., Ltd., for the microanalysis and for the measurement of the mass spectra.

References

1) K. Naya, I. Takagi, Y. Kawaguchi, Y. Asada, Y. Hirose, and N. Shinoda, *Tetrahedron*, **24**, 5871 (1968).
2) The details will be presented in a subsequent paper.
3) N. Seragiotto, *Gazz. Chim. Ital.*, **47**, 150 (1917).
4) R. B. Woodward and R. H. Eastmann, *J. Am. Chem. Soc.*, **72**, 399 (1950).
5) K. Kobayashi, Y. Yamamoto, H. Miyanaga, and K. Naya, 23th National Meeting of the Chemical Society of Japan, Tokyo, April 1970, Abstr. No. 18337. The hydrate of **6b** showed a mp of 69.5—70.5 °C as colorless needles (from aqueous methanol).
6) K. Naya, M. Hayashi, I. Takagi, S. Nakamura, and M. Kobayashi, *Bull. Chem. Soc. Jpn.*, **45**, 3673 (1972).
7) The details of X-ray analysis will be published soon.
8) W. Reusch, D. F. Anderson, and C. K. Johnson, *J. Am. Chem. Soc.*, **90**, 4988 (1968).
9) K. Naya, F. Yoshimura, and I. Takagi, *Bull. Chem. Soc. Jpn.*, **44**, 3165 (1971).
10) K. Naya, N. Nogi, Y. Makiyama, H. Takashina, and T. Imagawa, *Bull. Chem. Soc. Jpn.*, **50**, 3002 (1977). Though the reason for the wide range remains unexplained, **10** should be identical with 8β-hydroxyeremophilenolide, mp 212—213 °C, $[\alpha]_D$ +157°.
11) K. Naya, M. Nakagawa, M. Hayashi, K. Tsuji, and M. Naito, *Tetrahedron Lett.*, **1971**, 296.
12) K. Naya, R. Kanazawa, and M. Sawada, *Bull. Chem. Soc. Jpn.*, **48**, 3220 (1975).
13) W. Reusch and C. K. Johnson, *J. Org. Chem.*, **28**, 2557 (1963).
14) G. W. K. Cavill and C. D. Hall, *Tetrahedron*, **23**, 1119 (1967).
15) K. H. Schulte-Elte, M. Gadola, and B. L. Müller, *Helv. Chim. Acta*, **54**, 1870 (1971).
16) C. S. Foote, M. T. Wuesthoff, S. Wexler, I. G. Burstain, R. Denny, G. O. Schenck, and K. H. Schulte-Elte, *Tetrahedron*, **23**, 2583 (1967).

Nucleophilic Ion Pairs. 6. Catalytic Hydrolysis of *p*-Nitrophenyl Acetate by Zwitterionic Hydroxamate Nucleophiles in Representative Micellar Systems[1]

Toyoki KUNITAKE,* Yoshio OKAHATA, Shoichi TANAMACHI, and Reiko ANDO
Department of Organic Synthesis, Faculty of Engineering, Kyushu University, Fukuoka 812

(Received November 17, 1978)

Several surfactant-like zwitterionic hydroxamates were synthesized and their reactions with *p*-nitrophenyl acetate were studied in water in comparison with those of simple, anionic hydroxamates. The zwitterionic hydroxamates showed enhanced reactivities in cationic, zwitterionic and nonionic micelles: 20—100 times relative to the nomicellar rate at pH 8.9, 30 °C. The rate enhancement was attributed to lowered pK_a values and to activation of the hydroxamate anion in the hydrophobic domain. The rate was suppressed in an anionic micelle because of the enhanced pK_a value. Deacylation of the acetyl hydroxamate intermediate was hydroxide-catalyzed. The enhanced reactivity of the zwitterionic hydroxamate in organic media was less sensitive to the water concentration than that of the hydroxamate ion pair. These results can be explained in terms of "*hydrophobic ion pair.*"

Anionic nucleophiles such as oximates, hydroxamates, thiolates and imidazole anions possess remarkably enhanced reactivities in the presence of cationic micelles and cationic polysoaps.[2] The increase in rate cannot be attributed to the peculiar microenvironment of these aqueous micelles, and we proposed that the formation of nucleophilic ion pairs in the hydrophobic microenvironment— "*hydrophobic ion pairs*" is essential for the rate enhancement. This is supported by the extremely high reactivity of tetraalkylammonium hydroxamate ion pairs in dry aprotic solvents[3,4] and by activation of hydrophobic anionic nucleophiles in the presence of the nonmicellar (in the conventional meaning) aggregate of trioctylmethylammonium chloride.[5]

Zwitterionic nucleophiles may form hydrophobic ion pairs by themselves and could show high reactivities. Several papers describe their unexpectedly high nucleophilicities in the micellar[2,6] and polymeric[7—10] systems. However, no unified interpretation has so far been given.

In the present study, we have systematically examined the reactivity of four zwitterionic nucleophiles in representative aqueous micelles (cationic, anionic, zwitterionic, and nonionic micelles) and in organic media. The structures of the nucleophiles and surfactants used are as follows.

Nucleophile:

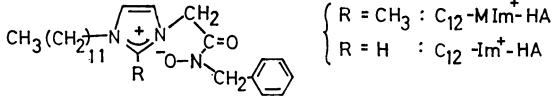

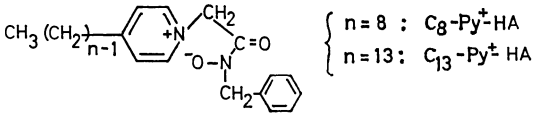

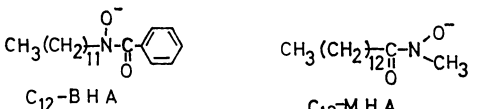

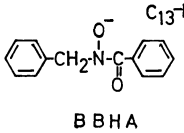

Surfactant:

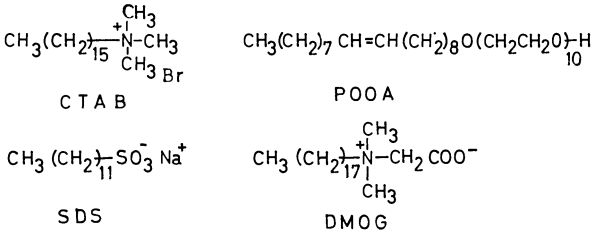

Experimental

Materials. The preparation and purification of *N*-dodecylbenzohydroxamic acid(C_{12}-BHA),[11] *N*-benzylbenzohydroxamic acid (BBHA),[12] *N*-methylmyristohydroxamic acid(C_{13}-MHA),[13] and *p*-nitrophenyl acetate[11] has been described. Commercial CTAB was recrystallized from ethanol several times. *N,N*-Dimethyl-*N*-octadecylglycine (DMOG) was prepared by the reaction of *N,N*-dimethyloctadecylamine and chloroacetic acid and recrystallized twice from ethyl acetate, mp 140—142 °C. Its IR and NMR spectra were in line with the structure. Commercial SDS and POOA were used without further purification.

N-Dodecylimidazole was prepared as follows according to the procedure of Härig:[14] Imidazole (20 g, 0.3 mol) was dissolved in a mixture of ethanol (70 ml) and aqueous 20 M (1 M=1 mol dm^{-3}) NaOH (30 ml), and 99 g (0.4 mol) of dodecyl bromide was added at 80—85 °C with stirring over 2.5 h. Stirring was continued at room temperature for 5 h. The solvent was then removed *in vacuo* and the residue was extracted twice with chloroform. The extract was dried over Na_2SO_4, solvent removed and the residue distilled: yield 65%; bp 158—168 °C/35 mmHg (1 mmHg=133.322 Pa). IR and NMR spectra were in line with the expected structure.

A similar procedure was used for preparing *N*-dodecyl-2-methylimidazole from dodecyl bromide and 2-methylimidazole: bp 147—148 °C/3 mmHg (lit,[15] bp 174—176 °C/3 mmHg).

4-Octylpyridine was obtained from pyridine and octanoic anhydride according to the procedure of Arens and Wibaut[16] in 7% yield: bp 112—114 °C/4 mmHg (lit,[16] bp 265—268 °C). 4-Tridecylpyridine was prepared from 4-pyridylmethyllithium and dodecyl bromide by the procedure of Wibaut and Hey:[17] yield 26%, mp 129—131 °C (as hydrochloride). Found: C, 67.82; H, 10.09; N, 4.57%. Calcd for $C_{18}H_{31}N \cdot HCl \cdot H_2O$; C, 68.43; H, 10.84; N, 4.43%.

These alkylamines were quaternized by benzyl *N*-benzylchloroacetohydroxamate (bp 150—155 °C/0.03 mmHg)[9] in acetone at 50 °C for 2 h, the benzyl group being removed by hydrogenation in ethanol over 5% $Pd/SrCO_3$.

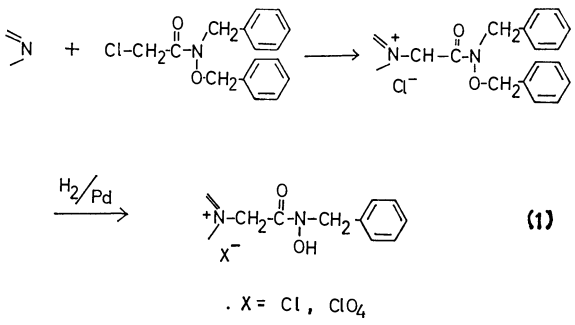

(1)

. X= Cl, ClO_4

C_{12}-Im$^+$-HA; mp 157—158 °C (from acetonitrile). Found: C, 66.03; H, 8.80; N, 9.66%. Calcd for $C_{24}H_{38}N_3O_2Cl$: C, 66.11; H, 8.78; N, 9.64%.

C_{12}-MIm$^+$-HA; mp 176—177 °C (from acetonitrile). Found: C, 66.75; H, 9.01; N, 9.29%. Calcd for $C_{25}H_{40}N_3O_2Cl$: C, 66.72; H, 8.96; N, 9.34%.

C_8-Py$^+$-HA; mp 88—89 °C (crystallized as perchlorate salt from ethanol and ether). Found: C, 57.69; H, 6.87; N, 6.12%. Calcd for $C_{22}H_{31}N_2O_6Cl$: C, 58.08; H, 6.87; N, 6.16%.

C_{13}-Py$^+$-HA; mp 176—177 °C (from acetonitrile). Found: C, 70.04; H, 8.90; N, 6.06%. Calcd for $C_{27}H_{41}N_2O_2Cl$: C, 70.33; H, 8.96; N, 6.08%.

Kinetics. The hydrolysis of PNPA in the aqueous system was conducted in 3 v/v% EtOH–H_2O at 30 °C, μ=0.01 (KCl) in the pH range 6—10. The reaction was followed by the appearance of *p*-nitrophenolate at 401 nm (Hitachi 200 UV-visible spectrophotometer with a thermostated cell compartment). In the presence of excess nucleophile the reaction followed the pseudo first-order rate law for more than 90% completion. The pseudo first-order rate constant was divided by the total nucleophile concentration to give the apparent second-order rate constant of acylation, $k_{a,obsd}$. In the case of the hydrolysis performed in organic media, the nucleophiles were neutralized by addition of 10 times excess of 1,8-diazabicyclo[5.4.0]undec-7-ene (DBU).

Burst-type kinetics were observed in the presence of excess substrate. The rate constants of acylation and deacylation were determined according to the procedure reported.[11]

Calculations were carried out with the aid of a programmable desk calculator, the least-squares procedure being applied wherever possible. The correlation coefficient was always better than 0.99. The pH measurement was carried out with a Toa Digital pH meter (Type HM-10A), pH variation of the aqueous reaction medium being confirmed to be smaller than ±0.05. The water content in the organic media was determined with a coulometric Karl-Fischer apparatus (Hiranuma Aquacounter, AQ-1).

Results

Acylation. The reaction of PNPA with excess hydroxamate nucleophiles gives the apparent rate constant of acylation as

$$k_{a,obsd} = \frac{k_{obsd} - k_{spont}}{[HA]_{total}} \quad (2)$$

where k_{obsd} and k_{spont} are pseudo first-order rate constants of *p*-nitrophenol release in the presence and absence of the nucleophile, respectively, and $[HA]_{total}$ is the total hydroxamic acid concentration.

TABLE 1. SECOND-ORDER RATE CONSTANTS OF ACYLATION IN THE MICELLAR SYSTEMS[a]

Hydroxamate	$k_{a,obsd}$ ($M^{-1}s^{-1}$)				
	Nonmicellar	SDS	CTAB	POOA	DMOG
C_{12}-Im$^+$-HA	12	1.2	1000	270	1200
C_{12}MIm$^+$-HA	13	0.8	1300	250	1100
C_{13}-Py$^+$-HA	14	1.0	1100	310	1300
C_8-Py$^+$-HA	12	—	320	45	420
C_{12}-BHA	—	0.9	1500	25	75
C_{13}-MHA	—	1.3	1300	32	45
BBHA	12	—	1500	13	23

a) 30 °C, 3 v/v% EtOH–H_2O, μ=0.01(KCl), pH 8.90 ±0.05 (0.01 M Borate). [PNPA]=9.46×10^{-6} M, [catalysts]=$(3.05—7.08)\times10^{-5}$ M. Surfactant concentrations are 1×10^{-3} M except for ([SDS]=1×10^{-2} M).

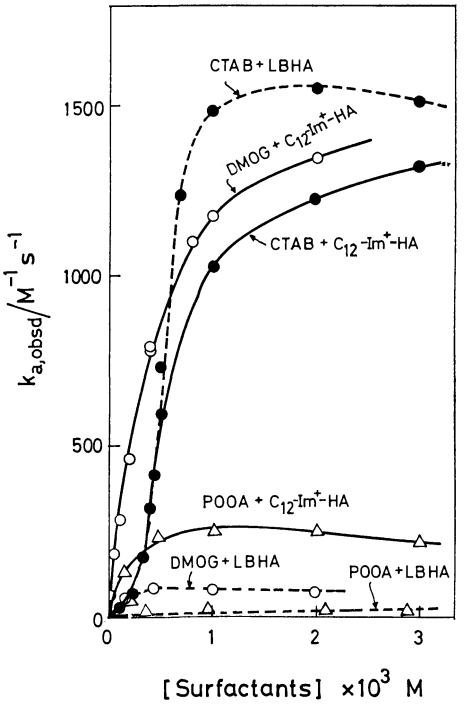

Fig. 1. Rate dependence on surfactant concentration. 30 °C, 3 v/v%EtOH–H_2O, μ=0.01 (KCl), pH 8.90± 0.05 (0.01 M Borate). [C_{12}-Im$^+$-HA]=7.08×10^{-5} M [LBHA(C_{12}-BHA)]=7.49×10^{-5} M

The $k_{a,obsd}$ values obtained in various micellar systems at pH 8.9 are summarized in Table 1. In the absence of micelles, the nucleophilic reactivity of the zwitterionic hydroxamates is similar to that of the simple hydroxamate (BBHA). $k_{a,obsd}$ of all hydroxamates was enhanced *ca.* 100 times by the cationic micelle (CTAB) and lowered to *ca.* 1/10 of the original value by the anionic micelle (SDS). As an exception, C_8-Py$^+$-HA was activated only *ca.* 30 times by the CTAB micelle because of its lower hydrophobicity. The non-zwitterionic hydroxamates (C_{12}-BHA, C_{13}-MHA, and BBHA) are not particularly activated in the nonionic and zwitterionic micelles, whereas the zwitterionic hydroxamates are activated to a greater extent. Since the nucleophiles cannot form micellar aggregates by

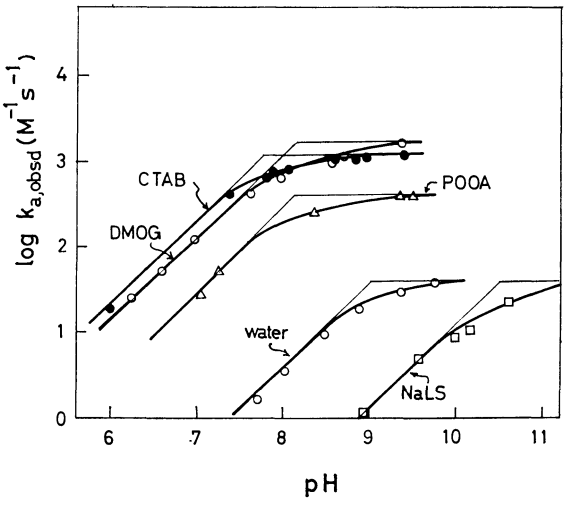

Fig. 2. pH-rate profile of the acylation of C_{12}-Im^+-HA. 30 °C, 3 v/v% EtOH-H_2O, μ=0.01 (KCl), [C_{12}-Im^+-HA]=7.08×10^{-5} M, [PNPA]=9.46×10^{-6} M. Surfactant concentration: 1×10^{-3} M for CTAB, DMOG and POOA. 1×10^{-2} M for NaLS (SDS).

themselves under these conditions, the rate enhancement is closely related to the micelle formation of added surfactants. Figure 1 shows the dependence of $k_{a,obsd}$ on the surfactant concentration for C_{12}-BHA and C_{12}-Im^+-HA, $k_{a,obsd}$ increasing rapidly at the surfactant concentration near the critical micelle concentration: 8×10^{-4} M for CTAB,[11] 3×10^{-4} M for DMOG[18] and *ca.* 10^{-6} M for POOA.[19]

C_{12}-Im^+-HA was selected as a representative zwitterionic nucleophile and its pH rate prophiles were studied in the presence of various micelles (Fig. 2). The solid curves were obtained by means of

$$k_{a,obsd}=\frac{K_a}{K_a+a_H}\cdot k_a \qquad (3)$$

where K_a and k_a are the acid dissociation constant of the hydroxamic acid and the second-order rate constant of acylation for the effective hydroxamate species, respectively, and determined by the best-fit of the theoretical and experimental curves. The results are summarized in Table 2. As compared to the nonmicellar value, the pK_a value in the anionic micelle is increased by *ca.* 1 pK unit and decreased by the nonionic, cationic and zwitterionic micelles. The k_a value in the anionic SDS micelle is similar to the nonmicellar value, but large increases are observed in other micelles: *ca.* 10 fold in POOA; 30—40 fold in CTAB and DMOG.

The influence of ionic strength on $k_{a,obsd}$ is shown in Fig. 3. $k_{a,obsd}$ decreases with increasing ionic strength in all the micellar systems studied. However, the decrease was smaller than that observed for the C_{12}-BHA–CTAB system.

Deacylation. In the reaction of C_{12}-Im^+-HA with excess PNPA, the *p*-nitrophenol release follows the burst kinetics: *i.e.*, rapid acylation and subsequent, slow deacylation.

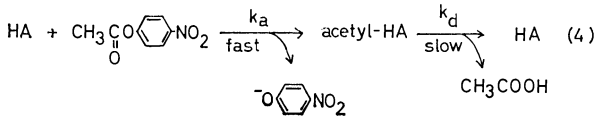

(4)

Table 2. Rate constants of acylation and dissociation constant in the reaction of PNPA and C_{12}-Im^+-HA[a]

Surfactant	C_{12}-Im^+-HA		λ_{max} of Methyl Orange in micelles (nm)
	pK_a	k_a ($M^{-1}s^{-1}$)	
None	9.03	38	465
SDS (1×10^{-2} M)	10.5	40	—
POOA (1×10^{-3} M)	8.18	420	440
CTAB (1×10^{-3} M)	7.78	1300	415
DMOG (1×10^{-3} M)	8.18	1580	420

a) 30 °C, 3 v/v% EtOH-H_2O, μ=0.01 (KCl), [C_{12}-Im^+-HA]=7.08×10^{-5} M.

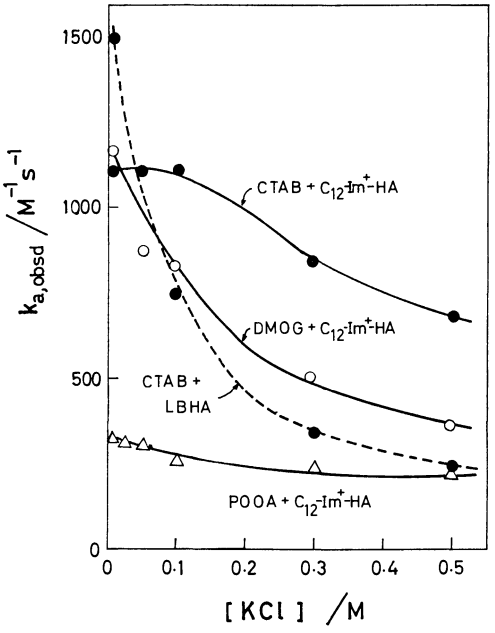

Fig. 3. Effect of ionic strength on the acylation rate. 30 °C, 3 v/v% EtOH-H_2O, pH 8.90±0.05 (0.01 M Borate). [C_{12}-Im^+-HA]=7.08×10^{-5} M, [LBHA(C_{12}-BHA)]=7.49×10^{-5} M. Surfactant concentration; 1×10^{-3} M.

The apparent rate constants of acylation and deacylation can be estimated by the following equations.

$$k_{a,obsd}=\frac{b\sqrt{B}}{[PNPA]_0\sqrt{[HA]_0}} \qquad (5)$$

$$k_{d,obsd}=b-k_a[PNPA]_0 \qquad (6)$$

where B is the extrapolation at t=0 of the steady-state *p*-nitrophenol release, and b is the pseudo first-order rate constant of the presteady state curve.[11,12]

Results obtained from analysis of the burst kinetics are given in Table 3. The $k_{a,obsd}$ values estimated by Eq. 5 agree fairly well with those obtained under the pseudo first-order conditions (Table 1).

The burst type experiment was carried out at pH 8—10. The resulting pH-rate profile of deacylation is shown in Fig. 4. In all the systems, log $k_{d,obsd}$ is a linear function of pH with the slope +1. This indicates that the deacylation process is hydroxide-catalyzed.

TABLE 3. RATE CONSTANTS OF ACYLATION AND DEACYLATION DETERMINED FROM THE BURST KINETICS[a)]

Hydroxamate	Micelle	$k_{a,obsd}$ ($M^{-1}\,s^{-1}$)	$k_{d,obsd}$ ($\times 10^2\,s^{-1}$)
C_{12}-Im^+-HA	CTAB	1030	3.50
C_{12}-Im^+-HA	DMOG	1150	0.376
C_{12}-Im^+-HA	POOA	250	0.214

a) 30 °C, pH 8.9±0.1(0.01 B Borate), 3 v/v% EtOH-H_2O, μ=0.01(KCl), [C_{12}-Im^+-HA]=1.42×10^{-5} M, [PNPA]=1.89×10^{-4} M. [Surfactant]=1×10^{-3} M.

TABLE 4. REACTION OF HYDROXAMATES WITH PNPA IN ORGANIC MEDIA[a)]

Solvent	[H_2O] (mM)	k_a ($M^{-1}\,s^{-1}$)	
		C_{12}-Im^+-HA	C_{12}-BHA
Benzene	1.0	1200	606
	10	900	105
	40	680	25
Dimethylformamide	15	3300	1000
Acetonitrile	10	*ca.* 4000	1500
Ethanol	33	160	0.1

a) 30 °C, [Hydroxamic acid]=1.42×10^{-5} M, [PNPA]=1.89×10^{-4} M, [DBU]=$(1.42—13.2)\times10^{-4}$ M.

Reaction in Organic Media. The reaction of C_{12}-Im^+-HA with PNPA was studied in dry organic solvents. The hydroxamate anion was produced by addition of strongly basic DBU. Figure 5 shows the increase in the hydroxamate absorbance at 270 nm with increasing amounts of DBU added. We see that 10 times excess of DBU is sufficient to neutralize the hydroxamic acid completely.

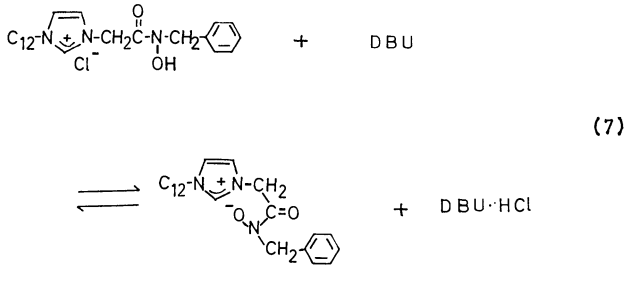

(7)

The apparent rate constant of acylation shows the same trend as that of the absorbance change. The *p*-nitrophenol release is thus effected solely by the hydroxamate anion. It was confirmed in a separate experiment that DBU alone can cause no *p*-nitrophenol release.

Values of the second-order rate constant of acylation k_a for C_{12}-Im^+-HA, determined in several organic media, are given in Table 4 together with those for C_{12}-BHA for the sake of comparison. The k_a values of these two nucleophiles differ by factors of 2—3 in dry aprotic solvents, a large reactivity difference being observed in moist benzene and in ethanol. Thus, the reactivity of the C_{12}-BHA anion in benzene decreases drastically with increase in water concentrations. However, the reactivity of the C_{12}-Im^+-HA anion is much less sensitive to the water concentration. In the same vein, k_a for C_{12}-Im^+-HA anion is 1600 times larger than that of C_{12}-BHA anion in ethanol.

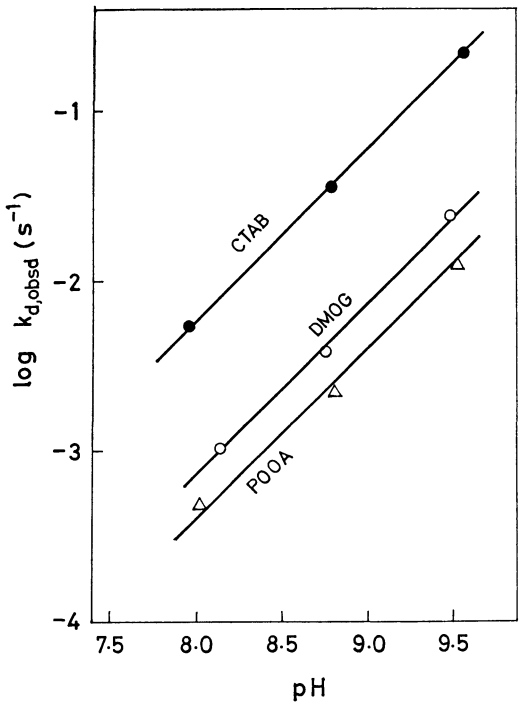

Fig. 4. pH-rate profile of the deacylation. 30 °C, 3 v/v% EtOH-H_2O, μ=0.01 (KCl). Surfactant concentration, 1×10^{-3} M.

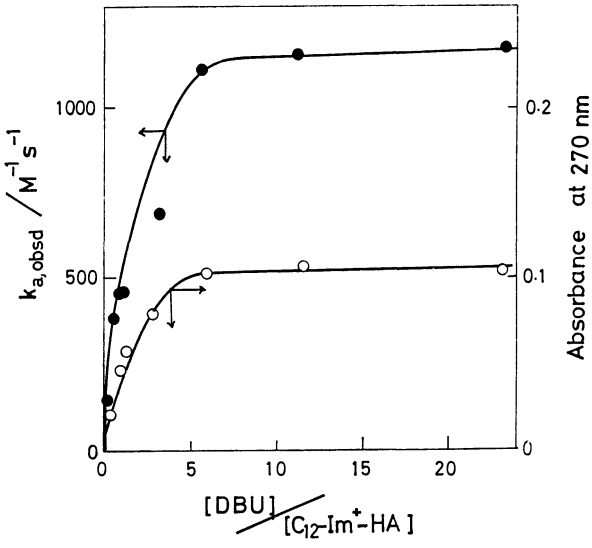

Fig. 5. Effect of DBU concentration in the reaction of C_{12}-Im^+-HA and PNPA in dry benzene. 30 °C, [H_2O]=1—3 mM, [C_{12}-Im^+-HA]=4.75×10^{-5} M, [PNPA]=6.90×10^{-6} M.

Discussion

The results on the reactivity of zwitterionic nucleophiles are wholly consistent with the concept of "*hydrophobic ion pair*." As shown in Table 1, simple hydroxamates such as C_{12}-BHA and C_{13}-MHA are highly activated in the cationic micelle due to the ion pair formation with the ammonium surfactant, but this activation mechanism cannot operate in other types of micelle. The zwitterionic hydroxamates are activat-

ed in the presence of the cationic, zwitterionic and nonionic micelles to various extents. In this case, the countercation is provided in the form of the intramolecular ammonium group. What is required is the hydrophobic microenvironment. The structure of the cationic moiety (imidazolium *vs.* pyridinium) does not affect the reactivity. The activation mechanism is better understood by examining the data in Table 2. The enhanced rate constant for C_{12}-Im$^+$-HA in the three micelles is produced by lower pK_a values and increased k_a values. The k_a value is correlated with the hydrophobic microenvironment estimated by the absorption maximum of Methyl Orange. A smaller increase in k_a in the nonionic micelle is in line with the limited hydrophobic nature of this micelle. The lowering of reactivity observed in the anionic micelle is caused by the increased pK_a value. k_a is not affected by the anionic micelle.

The reactivity of hydroxamate ammonium ion pairs in dry aprotic solvents is greatly reduced by minute amounts of water.[3,4] Similar data have been obtained in this study for C_{12}-BHA in benzene (Table 4). k_a decreases by a factor of 24 with increasing water concentrations from 1 mM to 40 mM. However, the rate-depressing effect of water is much less pronounced for the zwitterionic nucleophile; it retained more than 50% of the original reactivity during the same increase in water.

The large k_a difference (1600 fold) in ethanol between C_{12}-Im$^+$-HA and C_{12}-BHA should be related to the varied sensitivity of their reactivities to water. It is concluded that the zwitterionic hydroxamate forms a stable intramolecular ion pair which is deactivated less readily by protic solvents.

The deacylation reaction of the acetyl hydroxamate intermediate is mainly hydroxide-catalyzed. Figure 4 shows that the deacylation step is accelerated by the micellar microenvironment in the order: CTAB$\gg$ DMOG>POOA, reflecting the concentration effect of the hydroxide anion in the micellar phase.

The enhanced reactivity of the zwitterionic nucleophile has been utilized in several polymer catalysts.[7-8] In micellar catalysis, use of the well-defined zwitterionic nucleophile has been limited in number.[2,6] However, some of the reported functional micelles seem to show high reactivity because of their zwitterionic nature. The first example was reported by Tagaki *et al.* for an imidazole-containing ammonium surfactant micelle (**1**).[20] Since then several papers have appeared on the enhanced nucleophilicity of the hydroxyethyl and/or imidazole groups attached to the ammonium surfactant (**2**, **3**).[21-27]

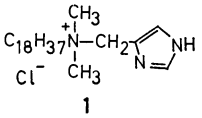

1

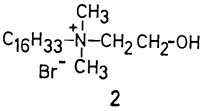

2

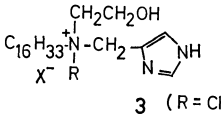

3 (R = CH_3, C_2H_5)

Rate enhancements in these examples should also arise from lowered pK_a values and activation of the anionic nucleophiles formed.[22] However, zwitterionic hydroxamates are the particularly effective nucleophile since their pK_a values are in the weakly alkaline region. The second-order rate constants of acyl transfer from PNPA to the other zwitterionic nucleophiles **1**, **2**, **3** are not quite as large, because the effective zwitterionic species are formed only in small amounts in the neutral pH region due to their high pK_a values.

References

1) Contribution No. 500 from Department of Organic Synthesis.
2) T. Kunitake, S. Shinkai, and Y. Okahata, *Bull. Chem. Soc. Jpn.*, **49**, 540 (1976) and papers cited therein.
3) S. Shinkai and T. Kunitake, *J. Chem. Soc., Perkin Trans. 2*, **1976**, 980.
4) S. Shinkai and T. Kunitake, *Chem. Lett.*, **1976**, 109; S. Shinkai, N. Nakashima, and T. Kunitake, *J. Am. Chem. Soc.*, **100**, 5887 (1978).
5) Y. Okahata, R. Ando, and T. Kunitake, *J. Am. Chem. Soc.*, **99**, 3067 (1977).
6) W. Tagaki, I. Takahara, and D. Fukushima, paper presented at the 32nd National Meeting of the Chemical Society of Japan, Tokyo, April 1975, Preprint III, p. 1308.
7) Yu. E. Kirsch, A. A. Rahmanskaya, G. M. Lukovkin, and V. A. Kabanov, *Eur. Polym. J.*, **10**, 393 (1974).
8) Yu. E. Kirsch, T. A. Lebedeva, and V. A. Kabanov, *J. Polym. Sci., Polym. Chem. Ed.*, **13**, 207 (1975).
9) Y. Okahata and T. Kunitake, *J. Polym. Sci., Polym. Chem. Ed.*, **15**, 2571 (1977).
10) Y. Okahata and T. Kunitake, *J. Mol. Cat.*, in press.
11) T. Kunitake, Y. Okahata, and T. Sakamoto, *J. Am. Chem. Soc.*, **98**, 7799 (1976).
12) T. Kunitake, Y. Okahata, and T. Tahara, *Bioorg. Chem.* **5**, 155 (1976).
13) T. Kunitake, S. Shinkai, and S. Hirotsu, *Biopolymers*, **15**, 1143 (1976).
14) M. Härig, *Helv. Chim. Acta*, **42**, 1845 (1959).
15) N. Sawa and M. Yasuda, *Chem. Abstr.*, **70**, 288 (1969).
16) J. F. Arens and J. P. Wibaut, *Recl. Trav. Chim.*, **61**, 59 (1942).
17) J. P. Wibaut and J. W. Hey, *Recl. Trav. Chim.*, **72**, 513 (1953).
18) Determined by the Wilhelmy (surface tension) method at 18 °C in 0.5 v/v% EtOH–H_2O; instrument, Kyowa Kagaku Co., DigiO-Matic ESB-IV.
19) J. H. Fendler and E. J. Fendler, "Catalysis in Micellar and Macromolecular Systems," Academic Press (1975), Chap. 2.
20) W. Tagaki, M. Chigira, T. Amada, and Y. Yano, *J. Chem. Soc., Chem. Commun.*, **1972**, 219.
21) R. A. Moss, R. C. Nahas, S. Ramaswami, and W. J. Saunders, *Tetrahedron Lett.*, **1975**, 3379.
22) K. Martinek, A. V. Lavashov, and I. V. Berezin, *Tetrahedron Lett.*, **1975**, 1215.
23) C. A. Bunton and M. McAneny, *J. Org. Chem.*, **42**, 475 (1977).
24) W. Tagaki, S. Kobayashi, and D. Fukushima, *J. Chem. Soc., Chem. Commun.*, **1977**, 29.
25) R. A. Moss, R. C. Nahas, and S. Ramaswami, *J. Am. Chem. Soc.*, **99**, 627 (1977).
26) U. Tonellato, *J. Chem. Soc., Perkin Trans. 2*, **1976**, 771.
27) U. Tonellato, *J. Chem. Soc., Perkin Trans. 2*, **1977**, 821.

Reactions of 3-Acetyltropolone and Its Methyl Ethers with Hydrazine

Akio YAMANE,† Masatoshi NAGAYOSHI,†† Kimiaki IMAFUKU,* and Hisashi MATSUMURA

Department of Chemistry, Faculty of Science, Kumamoto University, Kurokami, Kumamoto 860

(Received December 1, 1978)

3-Acetyltropolone (**1**) was synthesized from 3-isopropenyltropolone by treatment with sodium azide in concentrated sulfuric acid. Methylation of **1** by diazomethane gave two isomers, 3-acetyl-2-methoxytropone (**2a**) and 2-acetyl-7-methoxytropone (**2b**). **1**, **2a**, and **2b** reacted with hydrazine to give some 1,8-dihydrocycloheptapyrazol-8-one derivatives.

Doi reported that 4-isopropenyltropolone affords 4-acetyltropolone by treatment with one equivalent of hydrazoic acid in concentrated sulfuric acid.[1] By the application of this reaction to 3-isopropenyltropolone, we successfully obtained 3-acetyltropolone (**1**). Schenck *et al.* synthesized chloro-substituted 3-acetyltropolone by another method.[2] Since 3-acetyltropolone (**1**) has an active methyl group and β-diketone structure, several interesting reactions are expected. Its two isomeric methyl ethers, **2a** and **2b**, would behave as active troponoid. On the other hand, Matsumoto obtained 1,8-dihydrocycloheptapyrazol-8-one derivatives by the reactions of 3-formyltropolone derivatives with hydrazines.[3] We have investigated the reactions of **1**, **2a**, and **2b** with hydrazine.

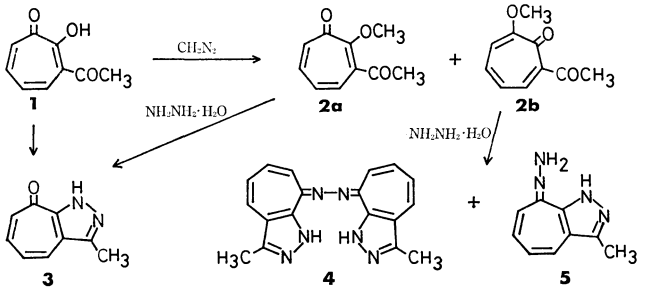

1 2a 2b 3 4 5

Scheme 1.

Results and Discussion

*Synthesis of 3-Acetyltropolone (**1**) and Its Methyl Ethers (**2a** and **2b**).* 3-Isopropenyltropolone was obtained by the method of Asao *et al.*[4] Treatment of 3-isopropenyltropolone with 1.5 equivalents of sodium azide in concentrated sulfuric acid gave 3-acetyltropolone (**1**) in a fairly good yield (70%). The structure was confirmed by means of spectral and analytical data. The IR spectrum showed a strong acetyl carbonyl band at 1715 cm^{-1} and a characteristic band for tropolone at 1620 cm^{-1}. The UV and NMR spectra also supported the structure of 3-acetyltropolone (**1**).

Being a β-diketone, 3-acetyltropolone (**1**) reacts with diazomethane to give two methyl ethers (**2a** and **2b**). As to the two methyl ethers, one is 3-acetyl-2-methoxytropone and the other 2-acetyl-7-methoxytropone. Generally, in ^1H NMR spectrum the signal of the proton situated in a β-position to a carbonyl group appears in a lower field. The NMR spectrum of **2a** showed a multiplet for seven-membered ring protons at 6.9—7.3 ppm, while that of **2b** showed a doublet of doublets for H-3 at 7.58 ppm. Thus, **2a** was assigned to 3-acetyl-2-methoxytropone and **2b** to 2-acetyl-7-methoxytropone.

*Reactions of 3-Acetyltropolone (**1**) and 3-Acetyl-2-methoxytropone (**2a**) with Hydrazine.* Refluxing of a mixture of **1** and 2 equivalents of hydrazine hydrate in methanol afforded 3-methyl-1,8-dihydrocycloheptapyrazol-8-one (**3**) in 76% yield. The reaction at room temperature also gave **3** in 62% yield. Though **3** can be considered to be another tautomeric form, 3-methylcycloheptapyrazol-8-ol, its IR, NMR, and UV spectra support the form of 3-methyl-1,8-dihydrocycloheptapyrazol-8-one. **2a** also reacted with hydrazine hydrate to give **3**, the difference between the reactivities of **1** and **2a** not being observed.

*Reaction of 2-Acetyl-7-methoxytropone (**2b**) with Hydrazine.* When a mixture of **2b** and 2 equivalents of hydrazine hydrate in methanol was refluxed, 3-methyl-1,8-dihydrocycloheptapyrazol-8-one azine (**4**) precipitated and 3-methyl-1,8-dihydrocycloheptapyrazol-8-one hydrazone (**5**) was obtained from the filtrate. The reaction with equimolar hydrazine hydrate gave only **4** (34%), **2b** being recovered (36%). The azine (**4**) was purple plates and insoluble in organic solvents except acetic acid. Nozoe *et al.*[5] obtained 3-phenyl-1,8-dihydrocycloheptapyrrol-8-one azine by the reaction of 8-chloro-3-phenylcycloheptapyrrole with hydrazine hydrate, the UV spectrum of which being very similar to that of **4**. The IR spectrum of **4** has a few absorption bands because of high symmetry but no bands at near 1600 cm^{-1} for tropone nor at near 1720 cm^{-1} for acetyl group. However, it has an absorption band near 3200 and 3400 cm^{-1} for NH. Mass spectrum of **4** shows a molecular ion peak at 326. The structure of **4** is reasonable from the above-mentioned evidence and analytical data. **5** has two tautomeric forms such as A and B. The UV spectrum of **5** in visible region shows absorption maxima at fairly shorter wavelength[6] and the NMR spectrum the signal for NH of pyrazole ring at *ca.* 12.4 ppm, indicating that **5** exists mainly in the form B.

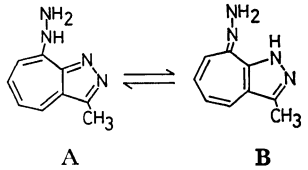

A B

Treatment of **5** with acetone yielded a tricyclic compound (**6**). The NMR spectrum of **6** showed the

† Present address: Wakunaga Pharmaceutical Co., Ltd., Koda-machi, Takata-gun, Hiroshima 729-64.

†† Present address: Iki Senior High School, Gonoura-machi, Iki-gun, Nagasaki 811-51.

presence of three methyl group [δ 1.61 (6H), 2.36 (3H)]. Two methyl groups at 1.61 ppm suggest that they exist at sp^3 carbon atom. The mass spectrum showed the parent peak at 214 and the elemental analysis also gave a satisfactory result. Accordingly, **6** was identified as 1,3,3-trimethyl-3,4-dihydro-2,2a,4,5-tetraazabenz[*cd*]azulene.

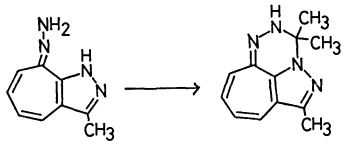

5 **6**

Experimental

The melting points were determined with a Yanagimoto hot-stage apparatus and are uncorrected. All ^1H NMR spectra were recorded with a Hitachi R-24 spectrometer (60 MHz) with TMS as an internal standard. The IR and UV spectra were recorded with a JASCO IRA-1 and a Hitachi EPS-3T spectrophotometer, respectively. The mass spectra were taken on a JEOL JMS-OI-SG-2 spectrometer.

*Preparation of 3-Acetyltropolone (**1**).* Sodium azide (10 g) was added to a stirred mixture of 3-isopropenyltropolone (16.2 g), concentrated sulfuric acid (50 ml) and chloroform (50 ml) under cooling with water. The mixture was stirred at 60—70 °C for 2 h. After removal of the chloroform layer, the acid layer was diluted with water and then left to stand overnight. The crystals deposited were recrystallized from methanol to give 11.6 g (70%) of 3-acetyltropolone (**1**) as pale yellow needles: mp 131—132 °C; λ_{max}^{MeOH} nm (log ε): 245 (4.25), 350 (3.80), 415 (3.75); IR ($CHCl_3$): 1715 (C=O), 1620 cm^{-1} (C=O); NMR ($CDCl_3$): δ 9.0 (br, s, 1H, OH), 7.76 (d, 1H, J=9.0 Hz, H-4), 6.9—7.6 (m, 4H), 2.69 ppm (s, 3H, CH_3). Found: C, 65.68; H, 4.94%. Calcd for $C_9H_8O_3$: C, 65.85; H, 4.91%.

*Methylation of 3-Acetyltropolone (**1**).* An ethereal solution of diazomethane was slowly added to a solution of **1** (11.1 g) in chloroform until the resulting mixture gave no coloration with iron(III) chloride. After removal of the solvents *in vacuo*, the residue was chromatographed on a silica gel column (Wakogel C-100, 900 g) using ethyl acetate as eluant. The former fractions were combined and recrystallized from hexane–benzene to give 5.37 g (45%) of 3-acetyl-2-methoxytropone (**2a**) as colorless needles: mp 45—46 °C; λ_{max}^{MeOH} nm (log ε): 235 (4.21), 330 (3.87); IR ($CHCl_3$): 1730 (C=O), 1587 cm^{-1} (C=O); NMR ($CDCl_3$): δ 6.9—7.3 (m, 4H), 4.00 (s, 3H, OCH_3), 2.53 ppm (s, 3H, $COCH_3$). Found: C, 67.34; H, 5.69%. Calcd for $C_{10}H_{10}O_3$: C, 67.40; H, 5.66%. The latter fractions were also combined and recrystallized from hexane–benzene to give 4.92 g (41%) of 2-acetyl-7-methoxytropone (**2b**) as pale yellow needles: mp 105—106 °C; λ_{max}^{MeOH} nm(log ε): 235 (4.24), 330 (3.84), 365 (3.83); IR ($CHCl_3$): 1716 (C=O), 1601 cm^{-1} (C=O); NMR ($CDCl_3$): δ 7.58 (dd, 1H, J=11.2 and 2.0 Hz, H-3), 6.7—7.4 (m, 3H), 3.96 (s, 3H, OCH_3), 2.53 ppm (s, 3H, $COCH_3$). Found: C, 67.22; H, 5.72%. Calcd for $C_{10}H_{10}O_3$: C, 67.40; H, 5.66%.

*Reaction of 3-Acetyltropolone (**1**) with Hydrazine.* a) A mixture of **1** (213 mg, 1.30 mmol) and 80% hydrazine hydrate (167 mg, 2.67 mmol) in methanol (10 ml) was refluxed for 1 h. After removal of the solvent the residue was recrystallized from benzene to give 158 mg (76%) of 3-methyl-1,8-dihydrocycloheptapyrazol-8-one (**3**) as orange plates: mp 183—184 °C; λ_{max}^{MeOH} nm (log ε): 235 (4.35), 296 (3.82), 308 (3.81), 365 (3.85); IR ($CHCl_3$): 3200 (NH), 1580 cm^{-1} (C=O); NMR ($CDCl_3$): δ: 12.0—13.5 (br, 1H, NH), 6.6—7.3 (m, 4H), 2.60 ppm (s, 3H, CH_3). Found: C, 67.35; H, 5.07; N, 17.74%. Calcd for $C_9H_8ON_2$: C, 67.48; H, 5.03; N, 17.49%. b) At room temperature, the reaction of **1** (205 mg, 1.25 mmol) with 80% hydrazine hydrate (80 mg, 1.28 mmol) in methanol (10 ml) gave the same product **3** (124 mg, 62%) after 48 h.

*Reaction of 3-Acetyl-2-methoxytropone (**2a**) with Hydrazine.* a) A mixture of **2a** (330 mg, 1.85 mmol) and 80% hydrazine hydrate (295 mg, 4.72 mmol) in methanol (10 ml) was refluxed for 1 h. After removal of the solvent the residue was recrystallized from benzene to give 206 mg (68%) of **3**. b) The same reaction of **2a** (206 mg, 1.26 mmol) with 80% hydrazine hydrate (67 mg, 1.07 mmol) at room temperature for 48 h also gave **3** (90 mg, 51%).

*Reaction of 2-Acetyl-7-methoxytropone (**2b**) with Hydrazine.* a) When a mixture of **2b** (722 mg, 4.05 mmol) and 80% hydrazine hydrate (496 mg, 7.92 mmol) in methanol (40 ml) was refluxed, a purple precipitate was formed. After 1 h the precipitate was filtered off and recrystallized from dimethyl sulfoxide–water to give 82 mg (13%) of 3-methyl-1,8-dihydrocycloheptapyrazol-8-one azine (**4**) as purple plates: mp >300 °C; λ_{max}^{MeOH} nm (log ε): 224 (4.32), 283 sh (3.69), 450 (4.13); IR (KBr): 3300 (NH), 1540 cm^{-1}; NMR (CF_3COOH): δ 7.4—8.1 (m, 8H), 2.98 ppm (s, 6H, $CH_3\times2$). Found: C, 67.98; H, 5.10; N, 26.28%. Calcd for $C_{18}H_{16}N_6$: C, 68.33; H, 5.10; N, 26.57%. M^+ 316. The filtrate was evaporated and the red residue was recrystallized from methanol to give 479 mg (68%) of 3-methyl-1,8-dihydrocycloheptapyrazol-8-one hydrazone (**5**) as red needles: mp 199—202 °C; λ_{max}^{MeOH} nm(log ε): 215 (4.42), 335 (3.98); IR (KBr): 3340 (NH), 3200 (NH), 1640 cm^{-1}; NMR (DMSO-d_6): δ 12.4 (br, 1H, NH), 5.6—6.7 (m, 6H), 2.28 ppm (s, 3H, CH_3). Found: C, 61.98; H, 5.81; N, 31.90%. Calcd for $C_9H_{10}N_4$: C, 62.05; H, 5.79; N, 32.17%. b) Refluxing of **2b** (409 mg, 2.30 mmol) with 80% hydrazine hydrate (137 mg, 2.19 mmol) in methanol (20 ml) for 1 h afforded **4** (130 mg, 34%), **2b** (148 mg, 36%) being recovered. c) At room temperature, the reaction of **2b** (348 mg, 1.96 mmol) with 80% hydrazine hydrate (197 mg, 3.15 mmol) in methanol (20 ml) gave **4** (61 mg, 18%) and **5** (189 mg, 51%) after 24 h. d) At room temperature, **2b** (405 mg, 2.28 mmol) reacted with 80% hydrazine hydrate (135 mg, 2.16 mmol) in methanol (20 ml) for 72 h to afford **4** (133 mg, 31%), **2b** (127 mg, 31%) being recovered.

*Reaction of 3-Methyl-1,8-dihydrocycloheptapyrazol-8-one Hydrazone (**5**) with Acetone.* Acetone (117 mg) was added to a solution of **5** (160 mg) dissolved in hot methanol (10 ml), and the mixture was refluxed for 2 h. The resulting solution was concentrated to dryness and the residue was recrystallized from benzene–petroleum ether to afford 127 mg (66%) of 1,3,3-trimethyl-3,4-dihydro-2,2a,4,5-tetraazabenz[*cd*]-azulene (**6**) as orange prisms: mp 152—155 °C; λ_{max}^{MeOH} nm(log ε): 222 (4.48), 293 (3.68), 350 (4.01); IR ($CHCl_3$): 3270 (NH), 1630, 1600 cm^{-1}; NMR ($CDCl_3$): δ 5.8—6.6 (m, 4H), 5.7 (br, 1H, NH), 2.36 (s, 3H, CH_3), 1.61 (s, 6H, $CH_3\times2$). Found: C, 67.33; H, 6.56; N, 25.96%. Calcd for $C_{12}H_{14}N_4$: C, 67.26; H, 6.59; N, 26.15%. M^+ 214.

We wish to express our thanks to Dr. Tetsuo Nozoe, Professor Emeritus of Tohoku University, for his advice and encouragement. We are also indebted to Dr. Kazu Kurosawa in this Laboratory for helpful suggestions and Mr. Shuichi Ueda of Taiho Pharmaceutical Co., Ltd. for the measurements of mass spectra.

References

1) K. Doi, *Bull. Chem. Soc. Jpn.*, **34**, 501 (1961).
2) G. O. Schenck, B. Brahler, and M. Cziesla, *Angew. Chem.*, **68**, 247 (1956).
3) S. Matsumoto, *Sci. Repts. Tohoku Univ., I*, **42**, 222 (1958).
4) T. Asao, T. Machiguchi, Y. Kitamura, and Y. Kitahara, *Chem. Commun.*, **1970**, 89.
5) T. Nozoe, Y. Kitahara, and T. Arai, *Proc. Jpn. Acad.*, **30**, 478 (1954).
6) K. Yamane, K. Fujimori, J.-K. Sin, and T. Nozoe, *Bull. Chem. Soc. Jpn.*, **50**, 1184 (1977).

The Reaction of ω-Ethoxyalkyl Bromides with Silver(I) Cyanide and Nitrite. The Participation of an Oxonium Ion

Nanao WATANABE,** Sakae UEMURA, and Masaya OKANO*
Institute for Chemical Research, Kyoto University, Uji, Kyoto 611
***Koei Chemical Co., Ltd., Joto-ku, Osaka 536*

(Received January 5, 1979)

The reaction of ω-ethoxyalkyl bromides (C_n: n=2—5) with silver(I) cyanide or nitrite in less polar solvents to give the corresponding isocyanide or a mixture of the corresponding alkyl nitrite and nitroalkane respectively, proceeded with ease only when n=4. In the latter reaction, the ratios of O- and N-attack (O/N) were 16—18/82—84 and 31—46/54—69 when $n\neq4$ and n=4 respectively. The facile reaction in both cases when n=4 and the increasing O-attack in the case of silver(I) nitrite may suggest that the reaction proceeds through the initial formation of a five-membered oxonium ion, the *O*-ethyltetrahydrofuranium ion, and a subsequent attack by CN^- and NO_2^- or their silver(I) bromide complex.

Previously, we have shown that various alkyl halides reacted with mercury(II) thiocyanate to give an isomeric mixture of alkyl thiocyanate and isothiocyanate.[1] This ambident behavior of the mercury(II) salt has also been observed in the reaction with 4-alkoxybutyl halide where the isomer ratio (N/S) of the products is nearly 1, in contrast to the results for unsubstituted primary halides (N/S=*ca.* 1/4).[2] This difference has been explained by considering the attack of an ambident anion of the mercury(II) salt upon a tetrahydrofuranium ion intermediate. In order to establish further examples of the ambident reaction of metal salt with such an oxonium ion, we have carried out the reactions of ω-alkoxyalkyl halides (C_n: n=2—5) with silver(I) cyanide and nitrite, both metal salts being well known to have an ambident reactivity on alkyl halide.[3] As a result, it was found that the reaction proceeded smoothly when n=4 and that silver(I) nitrite showed a different ambident behavior on the halide of n=4 and the halides of $n\neq4$.

Results and Discussion

The reaction of ω-alkoxyalkyl halides or butyl bromide with silver(I) cyanide was carried out by stirring a heterogeneous mixture of both reagents in dichloromethane or without a solvent at 75—85 °C for appropriate times. At least under these conditions, the reaction proceeded only in the case of 4-ethoxybutyl bromide to give the corresponding isocyanide, the formation of the cyanide being scarcely observed (Table 1 and Scheme 1).[4] Although we have already found

$$EtO(CH_2)_4Br + AgCN \longrightarrow EtO(CH_2)_4NC \quad (1)$$

that mercury(II) thiocyanate, acetate, and chloride reacted with alkyl halides in tetrahydrofuran (THF) to give the THF-incorporated compounds,[2,5] no such reaction has been observed by stirring mercury(II) or silver(I) cyanide and ethyl iodide in THF at a reflux temperature for 24 h.

The reaction of ω-ethoxyalkyl or butyl bromide with silver(I) nitrite was also carried out by stirring them in 1,2-dichloroethane, diethyl ether, or THF at 15—25 °C for 1—7 days, the mixture being heterogeneous. The products were the corresponding alkyl nitrite(**1**) and nitroalkane (**2**), the ambident character of the metal salt being clearly observed (Table 2 and Scheme 2). Here also, the reaction proceeded smoothly when

$$EtO(CH_2)_nBr + AgNO_2 \longrightarrow EtO(CH_2)_nONO + EtO(CH_2)_nNO_2 \quad (2)$$
$$\mathbf{1}(n=2-5) \qquad \mathbf{2}(n=2-5)$$

n=4. The isomer ratio (O/N) depended on the kind of alkyl bromide, an increase of the O-attack being observed in the case of n=4: namely, 31—46/54—69 from 4-ethoxybutyl bromide and 16—19/81—84 from the other halides. In contrast to the reaction with mercury(II) thiocyanate,[2] the reaction in THF as

Table 1. Reaction of RX with AgCN[a]

RX (10 mmol)	Solvent (10 ml)	React. temp (°C)	React. time (h)	Yield[b] of RNC
$EtO(CH_2)_2Br$	$(CH_2Cl)_2$	80	24	0
$EtO(CH_2)_3Br$	$(CH_2Cl)_2$	80	32	0
$EtO(CH_2)_4Br$	$(CH_2Cl)_2$	85	48	90
$EtO(CH_2)_4Br$[c]	—	80	24	75
$EtO(CH_2)_5Br$	$(CH_2Cl)_2$	85	32	trace
n-$BuO(CH_2)_4Cl$	$(CH_2Cl)_2$	85	96	0
n-BuBr	—	80	24	trace

a) AgCN, 10 mmol. b) Determined by GLC. c) RX, 30 mmol. AgCN, 20 mmol.

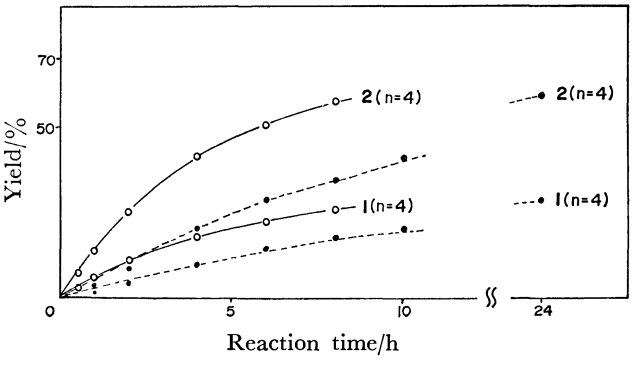

Fig. 1. The yield of **1** (n=4) and **2** (n=4) against reaction time.[a]
a) Determined by GLC using tetralin as internal standard. The reaction in 1,2-dichloroethane solvent is represented by a solid line, while that in diethyl ether by a dashed line.

Table 2. Reaction of RBr with $AgNO_2$[a]

R in RBr (10 mmol)	Solvent (10 ml)	React. time (day)	Yield[b] of **1**+**2** (%)	Isomer ratio[b] of **1**/**2** (O/N)
$EtO(CH_2)_2$	Et_2O	7	2	16/84
$EtO(CH_2)_3$	Et_2O	7	14	16/84
$EtO(CH_2)_3$	$(CH_2Cl)_2$	7	14	16/84
$EtO(CH_2)_4$	Et_2O	1	87	33/67
$EtO(CH_2)_4$	$(CH_2Cl)_2$	0.33	83	31/69
$EtO(CH_2)_4$	THF	3	54	46/54
$EtO(CH_2)_5$	Et_2O	7	8	17/83
n-C_6H_{13}	Et_2O	4	40	19/81[c]
n-C_6H_{13}	$(CH_2Cl)_2$	4	13	18/82[c]
n-C_6H_{13}	THF	4	9	16/84[c]

a) $AgNO_2$, 10 mmol. React. temp, 20—25 °C. b) Determined by GLC. c) *n*-$C_6H_{13}ONO$/*n*-$C_6H_{13}NO_2$.

Table 3. Boiling points and NMR and analytical data of new compounds

Compound	Bp (°C/mmHg)	^{1}H-NMR (δ)	Found (Calcd) C(%)	H(%)	N(%)
1(n=2)	45—46/50[a]	1.10(t. 3H), 3.45(q. 2H), 3.61(t. 2H), 4.78(t. 2H)			
1(n=3)	51—53/50	1.13(t. 3H), 1.92(quintet 2H), 3.42(q. 2H), 3.43(t. 2H), 4.71(t. 2H)	45.81(45.10)	8.70(8.33)	10.01(10.52)
1(n=4)	50—51/22	1.12(t. 3H), 1.35—2.1(m. 4H), 3.36(t. 2H), 3.39(q. 2H), 4.68 (t. 2H)	49.23(48.79)	9.27(8.90)	9.26(9.52)
1(n=5)	67—68/14	1.07(t. 3H), 1.28—2.0(m. 6H), 3.30(t. 2H), 3.36(q. 2H), 4.61(t. 2H)	52.25(52.16)	9.69(9.38)	8.97(8.69)
n-$C_6H_{13}ONO$	50—51/40[b]	0.92(t. 3H), 1.1—2.0(m. 8H), 4.61(t. 2H)			
2(n=3)	100—102/48	1.16(t. 3H), 2.17(quintet 2H), 3.43(q. 2H), 3.48(t. 2H), 4.38(t. 2H)	44.63(45.10)	8.09(8.33)	9.88(10.52)
2(n=4)	93—95/19	1.15(t. 3H), 1.4—2.4(m. 4H), 3.42(t. 2H), 3.42(q. 2H), 4.39(t. 2H)	48.35(48.97)	8.62(8.90)	9.00(9.52)
2(n=5)	105—107/11	1.14(t. 3H), 1.3—2.3(m. 6H), 3.35(t. 2H), 3.38(q. 2H), 4.35(t. 2H)	51.91(52.16)	9.61(9.38)	8.64(8.69)
n-$C_6H_{13}NO_2$	120—140/45[c]	0.90(t. 3H), 1.1—2.2(m. 8H), 4.30(t. 2H)			
$EtO(CH_2)_4NC$	90/30	1.13(t. 3H), 1.5—2.2(m. 4H), 2.9—3.9(m. 4H), 3.42(q. 2H)	65.49(66.11)	9.99(10.30)	10.71(11.01)

a) Lit,[8] bp 30—33 °C/15—20 mmHg. b) Lit,[9] bp 45 °C/30 mmHg. c) Lit,[9] bp 80°C/12 mmHg.

a solvent did not show any THF-incorporation.

It is generally known, in the reaction of alkyl halide with silver(I) nitrite, that a side reaction producing alkyl nitrate ester, alcohol, ketone, *etc.* occurs in some cases.[6] We observed, however, the formation of only a small amount of the corresponding nitrate ester and alcohol, even in the reactions continued for several days or a week. Further, when we plotted the yields of both alkyl nitrite and nitroalkane against the reaction time in the reaction with 4-ethoxybutyl bromide, the ratio between the two isomeric products was almost constant with an increase in the yield of the products (Fig. 1). These facts show that no further reaction of the initially produced alkyl nitrite occurs under these conditions and, consequently, that the O/N ratio is the kinetically controlled one in these reactions. When the reaction of ethyl iodide with silver(I) nitrite was carried out in THF at 25 °C for 6 h, an isomeric mixture of 4-ethoxybutyl nitrite and 4-ethoxy-1-nitrobutane was obtained in a 4% yield (O/N=55/45). Although the yield was low because of the rapid formation of ethyl nitrite and nitroethane, this finding shows that the THF-incorporation reaction occurs as in the cases of similar reactions with various mercury(II) salts.[2,5]

Because the silver(I) salts are almost completely insoluble in any solvent used, the reactions are generally quite slow. However, the reactions of 4-ethoxybutyl bromide proceeded smoothly. The reason for the comparatively facile reaction of this halide can be ascribed to the involvement of the *O*-ethyltetrahydrofuranium ion intermediate, as has been found in the cases of the reactions of similar halides with various mercury(II) salts.[2,5] The formation of **1** (n=4) and **2** (n=4) in the reaction of ethyl iodide in THF, though the yield was low, also supports this assumption. As to the isomer ratio of the products from the reaction of 4-ethoxybutyl bromide with silver(I) nitrite, the ratio for the O-attack was higher than that from other primary halides. This can be understood by considering that the isomer ratio is determined by the step of the attack on the intermediate oxonium ion;[2] that is, the carbon bearing a harder ligand as the leaving

group (R_2O in R_3O^+) is more apt to be attacked by a harder atom in an ambident ion, the O atom being harder than the N atom in the attacking species of NO_2^- or $AgBr(ONO)^-$. At present, the question of which is the more likely species must be left unresolved.

Experimental

The O/N ratios in mixtures of alkyl nitrites and nitroalkanes were determined by GLC. The GLC analyses were carried out on a Shimadzu 4BMPF and a Yanagimoto G800-T apparatus, using EGSS-X (1 or 3 m), Apiezon-L (1 m), and SE-30(1 m) columns(carrier gases, N_2 and H_2 respectively). The ^{1}H-NMR spectra (60 MHz) were recorded with a Varian EM-360 and a Hitachi R-24 spectrometer in CCl_4, using TMS as the internal standard.

Materials. The diethyl ether (dried over Na), 1,2-dichloroethane (over K_2CO_3), and THF (over KOH) were used after distillation, while the other organic and inorganic substances were used without further purification. The ω-alkoxyalkyl halides were prepared by a previously reported method.[6] Authentic samples of alkyl nitrite were prepared from the corresponding alcohols by a previously reported method,[7] while nitroalkanes and 4-ethoxybutyl isocyanide were separated from the reaction products by distillation and then analyzed. All the compounds except **1**(n=2), **2**(n=2), hexyl nitrite, and 1-nitrohexane are new; their boiling points and ^{1}H-NMR and analytical data are summarized in Table 3. Although **2**(n=2) could not be isolated in a pure state, the retention time in the GLC and the NMR spectrum support the assigned structure.

Reaction of 4-Ethoxybutyl Bromide with $AgNO_2$. A suspension of $AgNO_2$(1.52 g, 10 mmol) and 4-ethoxybutyl bromide(1.82 g, 10 mmol) in diethyl ether or 1,2-dichloroethane(10 ml) containing tetralin (1.07 g) as an internal standard for GLC analysis was stirred at 15—20 °C in the dark. At appropriate time intervals an aliquot was analyzed by GLC to determine the amounts of **1**(n=4) and **2**(n=4) produced (see Fig. 1). In order to isolate the products, a similar reaction was carried out without the addition of tetralin. After the precipitated AgBr had been filtered off, the filtrate was distilled to give a mixture of **1**(n=4) and **2**(n=4).

Reaction of 4-Ethoxybutyl Bromide with AgCN. A suspension of 4-ethoxybutyl bromide (3.60 g, 20 mmol) and AgCN(2.65 g, 20 mmol) in 1,2-dichloroethane (10 ml) was kept at 80—85 °C for 24 h under stirring. After being cooled down to room temperature, an aqueous KCN solution was added, the separated oil layer was extracted with ether, and the ether extract was dried over $MgSO_4$. Subsequent distillation gave 1.53 g(60% yield) of 4-ethoxybutyl isocyanide.

References

1) N. Watanabe, M. Okano, and S. Uemura, *Bull. Chem. Soc. Jpn.*, **47**, 2745 (1974).
2) N. Watanabe, S. Uemura, and M. Okano, *Bull. Chem. Soc. Jpn.*, **48**, 3205 (1975).
3) See, for example, J. March, "Advanced Organic Chemistry," 3rd ed, McGraw-Hill-Kogakusha, Tokyo (1977), p. 338.
4) It has been known in the reaction of ethyl iodide with AgCN that the relative amounts of the corresponding isocyanide and cyanide depend very much on the reaction temperature; only the isocyanide was formed at 80 °C. See, for example, P. Kurz, "Methoden der Organischen Chemie (Houben-Weyl)," ed by E. Müller, Georg Thieme Verlag, Stuttgart (1952), Vol VIII, p. 291.
5) N. Watanabe, S. Uemura, and M. Okano, *Bull. Chem. Soc. Jpn.*, **49**, 2500 (1976).
6) L. I. Smith and J. A. Sprung, *J. Am. Chem. Soc.*, **65**, 1276 (1943).
7) W. A. Noyes, *Org. Synth.*, Coll. Vol. 2, 108 (1943).
8) M. Meadow and W. M. Whaley, *J. Chem. Soc.*, **1954**, 1162.
9) H. Takayama, S. Yoneda, H. Kitano, and K. Fukui, *Kogyo Kagaku Zasshi*, **64**, 1153 (1961).

Hydrolytic Reactions of *p*-Nitrophenyl Esters in Reversed Micellar Systems

Hirotada FUJII,* Tohru KAWAI, and Hiroyasu NISHIKAWA†

Department of Polymer Technology, Tokyo Institute of Technology, Ookayama, Meguro-ku, Tokyo 152

†*Department of Physiology, Kyoto Prefectural University of Medicine, Kyoto 602*

(Received September 6, 1978)

Hydrolytic reactions of several *p*-nitrophenyl esters were studied with and without catalysts in reversed micellar systems consisting of sodium octanoate, 1-hexanol and water. Hydrolytic rate constants become very large as compared with those in aqueous solutions, increasing with decrease in the molar ratio of water to sodium octanoate (*R*-value). The results of kinetic measurements were discussed in terms of the behavior of water molecules and polar groups of sodium octanoate as revealed by means of IR and ^{1}H, ^{13}C and ^{23}Na-NMR spectroscopy. It was concluded that the decrease in the *R*-value induces the increase in the mobility of water molecules and the decrease in the polarity of the water core, which affects the partition coefficient of *p*-nitrophenyl esters between the 1-hexanol phase and the water phase, enhancing hydrolytic reactions.

A number of works[1] have been published concerning the enhancement of reaction rates at the critical micellar concentration in normal micellar systems. Attention has also been paid to reversed micellar systems, in which several reactions are much accelerated.[2–4] Fendler *et al.*[5] who extensively examined catalytic reactions in reversed micelles, pointed out that water molecules solubilized in polar cavities of reversed micellar systems are less polar than those in the bulk phase, and suggested that this is closely related to the catalytic effect. Thus, it is of interest to investigate the behavior of molecules involved in reversed micellar systems, especially the behavior of water molecules and sodium octanoate at the boundary phase between the water core and the 1-hexanol phase. This does not seem to have been fully elucidated in relation to the acceleration of chemical reactions in the systems.

We have kinetically investigated hydrolytic reactions of *p*-nitrophenyl esters in reversed micellar systems consisting of sodium octanoate, 1-hexanol and water, and also measured the catalytic activity of L-histidine and imidazole solubilized in the water core in the same system for hydrolysis of *p*-nitrophenyl acetate. The behavior of water molecules in reversed micelles was studied by means of IR and ^{1}H-NMR spectroscopy, and that of the polar group of sodium octanoate, *i.e.*, sodium ions and carbonyl groups, by ^{23}Na and ^{13}C-NMR spectroscopy. Except for the movement of the methylene group in the case of Aerosol OT in chloroform,[6] the behavior of polar groups of surfactants has scarcely been studied. The results obtained in measurements of reaction rates were discussed in terms of the characteristic behavior of molecules, ions and polar groups present at the boundary phase between the water core and the 1-hexanol phase.

Experimental

Materials. Sodium octanoate, 1-hexanol, *p*-nitrophenyl acetate (PNPA), L-histidine and imidazole (analytical grade) were used without further purification. *p*-Nitrophenyl octanoate (PNPO) and L-alanine *p*-nitrophenyl ester hydrochloride (APNP) were prepared by the condensation reaction between the corresponding acid and *p*-nitrophenol in tetrahydrofuran. Water was distilled and buffered with 0.03 M phosphate aqueous solution.

Measurements of Reaction Rates. PNPA, PNPO, and APNP were used as substrate. The initial concentration of these esters in 1-hexanol was 5×10^{-4} M. Reversed micelles were prepared by mixing three components, water (buffer solutions), 1-hexanol and sodium octanoate, and allowing them to stand at 30 °C for 24 h. 1-Hexanol solution of *p*-nitrophenyl ester was added to reversed micellar solutions, and the hydrolytic reaction rates of esters with and without catalyst were observed by measuring the absorption (OD_t) of *p*-nitrophenolate ions (400 nm) at 30 °C as a function of time with a Hitachi EPS-3T spectrophotometer. When the reaction was complete, the absorption (OD_∞) was determined from the absorption *vs.* time curve after a sufficiently long time. The results were analyzed as first order kinetics by plotting ($OD_\infty - OD_t$) in a logarithmic scale against time *t*. The slope of the line afforded the rate constant *K*. When L-histidine or imidazole was used as a catalyst, the difference in rate constants between the catalytic and noncatalytic reactions both in reversed micelles divided by the concentration of the catalyst was taken as K_c.

Spectroscopic Measurements. Infrared spectra were obtained with a Hitachi EPS-3G infrared spectrophotometer. The liquid cell used was equipped with CaF_2 windows, the optical path length being 0.05 mm. ^{1}H, ^{13}C, and ^{23}Na-NMR spectra were measured with a JEOL JNM-PS FT-NMR spectrometer operating at 100, 25 and 24 MHz, respectively. Measurement conditions for ^{13}C and ^{23}Na-NMR: spectral width 6250 and 1000 Hz, repetition 10 and 2.5 s, data point 8192 and 4096, numbers of scans 256 and 200, respectively. UV spectra of pyridine 1-oxide were observed with a Hitachi spectrophotometer model EPS-3T using a thermostated cell.

Results and Discussion

Hydrolytic Reactions of p-*Nitrophenyl Esters in Reversed Micelles.* Rate constants of hydrolysis of PNPA together with weight ratios of three components of reversed micellar systems and pH values of the phosphate buffer solution solubilized into the systems are given in Table 1. The results indicate that the rate constant increases with increase in pH. This tendency in reversed micellar systems is analogous to that in aqueous solutions.

Rate constants of hydrolysis of PNPA, PNPO, and APNP in reversed micelles are given in Table 2. When the buffer solution of the same pH is used, the hydrolytic reaction of PNPA is much more accelerated in reversed micelles as compared with that in aqueous

Table 1. Rate constants and weight ratios of the three components of reversed micelles

Water	1-Hexanol	Na Oct.	pH[a]	$K\times10^3$ (min^{-1})
2.5	6.5	1	7.7	10.3
2.5	6.5	1	7.9	14.0
2.5	6.5	1	8.0	14.5
3.0	6.0	1	7.7	9.7
3.0	6.0	1	7.9	13.0
3.0	6.0	1	8.0	13.6

a) Values of the phosphate buffer solutions solubilized into reversed micellar systems.

Table 2. Rate constants for *p*-nitrophenyl acetate (PNPA), *p*-nitrophenyl octanoate (PNPO), and L-alanine *p*-nitrophenyl ester hydrochloride (APNP) in aqueous solutions and reversed micelles

	PNPA[a]	PNPA[b]	PNPO[b]	APNP[b]	APNP[a]
$K\times10^3$ (min^{-1})	1.38	18.7	0.1	800	2.4
pH	7.9	7.9	7.9	6.5	6.5

a) In aqueous solutions. b) In reversed micelles. Concentrations of water and sodium octanoate are 12.9 and 1.38 M, respectively, in 1-hexanol ($R=9.2$).

Table 3. The catalytic rate constant of L-histidine in hydrolysis of *p*-nitrophenyl acetate in reversed micelles

R-value	$K\times10^3$ (min^{-1})	[L-his]$\times10^4$ (M)[a]	K_c ($min^{-1}\,M^{-1}$)
9.2	18.7	5.0	7.5
		20.0	7.3
13.9	16.7	5.0	6.5
18.4	13.8	5.0	3.3
		10.0	2.9

a) The concentration of L-histidine in the water core of reversed micelles. Concentrations of water and Na Oct are, respectively, 12.9 and 1.38 M in 1-hexanol for $R=9.2$, 12.9 and 0.93 M for $R=13.9$, and 12.9 and 0.69 M for $R=18.4$.

solutions. The hydrolytic reaction of APNP is remarkably accelerated, while that of PNPO is very slow. The order of rate constants for three *p*-nitrophenyl esters in the same reversed micellar systems (Table 2) is in line with the order of the solubility of these esters in water. The partition of the substrate between the water core and the 1-hexanol phase plays an important role in the acceleration of reaction. Ionic interaction between negative charges of sodium octanoate (carboxylate anion) and positive charges of L-alanine *p*-nitrophenyl ester hydrochloride (ammonium cation) is also an important factor in the prominent acceleration observed in the case of APNP. Judging from the fact that PNPO is hydrolyzed a little in spite of its very low solubility in water, the reaction is considered to take place at the boundary phase between the water core and the 1-hexanol phase.

In order to know how the structure of the water core and its surroundings affects the hydrolytic reaction, the dependency of the rate constant of hydrolysis of PNPA on the molar ratio of water to sodium octanoate, $R=[H_2O]/[Na\ Oct]$, was studied (Fig. 1). The rate constant increases linearly with decrease in *R*-value. An increase in the amount of sodium octanoate in the system seems to increase the amount of PNPA partitioned into the water core and its surrounding layer of the surfactant, accelerating the hydrolytic reaction. Reduction of the molar ratio of water to sodium octanoate at the same concentration of water decreases the diameter of the water core in reversed micelles, increasing the total surface area of the core in the system. The increase in the surface area of the water core is considered to raise the hydrolytic reaction rate.

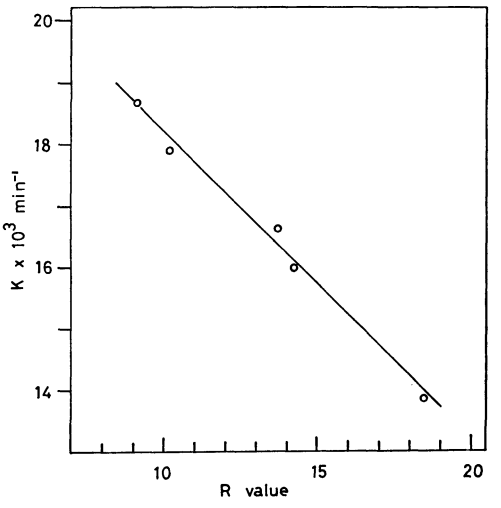

Fig. 1. Rate constant of hydrolysis of PNPA as a function of *R*-value ($[H_2O]/[Na\ Oct]$). In all cases, water concentration is 12.9 M in 1-hexanol.

Catalytic activities of L-histidine and imidazole added as a catalyst into the water core of reversed micelles were measured only in hydrolysis of PNPA. The results obtained for L-histidine are given in Table 3. The catalytic rate constant, K_c, increases with decrease in *R*-value as in the case of hydrolysis without catalyst, giving a nearly constant value in the L-histidine concentration range 5×10^{-4}—20×10^{-4} M. In the case of $R=9.2$, the catalytic rate constant is 7.5 $min^{-1}\,M^{-1}$, larger than the corresponding rate constant (5.7 $min^{-1}\,M^{-1}$) in aqueous solutions of the same pH values. In the case of $R=18.4$, however, the value of K_c (3.3 $min^{-1}\,M^{-1}$) is smaller than the catalytic rate constant (5.7 $min^{-1}\,M^{-1}$) in aqueous solutions. Thus, the probability of the presence of L-histidine at the boundary phase between the water core and the 1-hexanol phase in the above two cases would differ. Imidazole, a very active catalyst to hydrolyze PNPA in aqueous solutions, shows no catalytic activity in hydrolysis of PNPA in reversed micelles. The results reveal that the catalytic activity is dependent on the probability of the presence of the catalyst at the boundary phase in reversed micellar systems. In order to study the distribution of catalysts between 1-hexanol and water, partition coefficients, $K(C_{1\text{-hex}}/C_{aqu})$, of imidazole and L-histidine were measured and found to be 0.92 and 0, respectively. The results indicate

Table 4. Chemical shifts of protons of 1-hexanol and H_2O, and line width of H_2O peak

R-value	Chemical shift (δ)			Line width of H_2O (Hz)
	CH_3-	-CH_2-OH	H_2O	
18.4	1.24	3.90	5.18	6.61
13.6	1.24	3.90	5.20	6.45
11.6	1.25	3.90	5.24	6.31
10.3	1.27	3.90	5.24	6.01
9.2[a)]	1.28	3.90	5.26	4.95
9.2[b)]	1.28	3.90	5.27	4.95

a) Concentrations of water and sodium octanoate are 12.9 and 1.38 M, respectively. b) Concentrations of water and sodium octanoate are 14.9 and 1.61 M, respectively.

Table 5. Relative intensities of IR bands of HOD at the three wavelengths

R-value	Wavelength (cm^{-1}) of HOD band		
	3400	3550	3800
18.4	0.87	1.0	0.06
11.6	0.88	1.0	0.07
9.2	0.98	1.0	0.10

The intensity of the bond at 3550 cm^{-1} was taken as a standard.

that L-histidine molecules are concentrated at the boundary phase between the water core and the 1-hexanol phase, but not imidazole molecules due to their higher solubility into 1-hexanol. The ionic force between negative charges at the boundary phase (carboxylate anions of sodium octanoate) and positive charges of L-histidine molecules (ammonium cations) increase the probability of the presence of L-histidine at the boundary phase between the water core and the 1-hexanol phase. Thus, L-histidine molecules are concentrated at the boundary phase of reversed micelles due to their solubility and ionic force, so that L-histidine shows catalytic activity, depending on its concentration relative to that of the surfactant. This would not apply to the case of imidazole since it has higher solubility into 1-hexanol, but no positive charges.

The Structure and Behavior of Water Molecules and Polar Groups of Sodium Octanoate. In order to understand the role of the water molecule in reversed micelles in the hydrolytic reaction, their mobility and chemical environment were studied by means of ^{1}H-NMR for different values of *R*. The results are given in Table 4. The resonance peak of the water proton moves to a lower field, the line width of the water proton peak decreasing with decrease in *R*-value. For a given *R*-value, however, the line width does not change with the change in the molar ratio of water to 1-hexanol. The chemical shifts of C-1 methylene protons (-CH_2-OH) and methyl protons of 1-hexanol do not vary appreciably with *R*-value. This indicates possible structural changes in water cores of reversed micelles with change in *R*-value. The decrease in the line width of the water proton peak, *i.e.*, the increase in the mobility of water molecules in reversed micelles

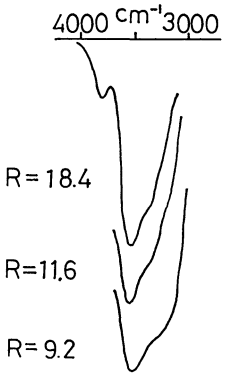

Fig. 2. Infrared spectra of HOD in reversed micelles. These spectra were taken as difference spectra between octanoic acid in 1-hexanol (reference cell) and reversed micellar solutions (sample cell).

with lowering in *R*-value seems unreasonable, since the size of the water core is considered to become smaller and consequently the relative amount of free water molecules seems to decrease with the decrease in *R*-value. For the sake of clarification, infrared spectrum due to the water molecule was taken. All the measurements were made on the uncoupled OH stretching vibration of HOD by using the solution of 5.5 M in D_2O.[7] The advantage of this approach lies in the fact that each species of water molecules gives a single, nearly gaussian absorption band. The results are shown in Fig. 2. From the absorption band due to the water molecule dispersed in pure 1-hexanol, the band at 3800 cm^{-1} is assigned to the water molecule dispersed in 1-hexanol. The band at 3400 cm^{-1} is assigned to the usual mobile (free) water by comparing the IR spectrum of pure water. Thus, the absorption band observed at 3550 cm^{-1} is due to the water molecule bound to the polar head group of the surfactant. The relative intensities of three bands, intensity of the band at 3550 cm^{-1} being taken as the standard, are given in Table 5. The relative intensity of the band at 3400 cm^{-1}, which is a measure of the mobile water molecule, increases with decrease in *R*-value. This is in line with the fact that the line width of the water proton peak decreases with decrease in *R*-value, as obtained by ^{1}H-NMR measurements.

The resonance peak of the water proton moves to a lower field with decrease in *R*-value, indicates that the property of the water molecule changes with *R*-value. Pyridine 1-oxide is a water soluble compound, the absorption maxima of which are correlated with *Z* values in several solvents.[8] The polarity of the water core of reversed micelles, measured by the absorption band shift of pyridine 1-oxide solubilized into reversed micelles (Fig. 3), depends on the ratio of water to sodium octanoate, *i.e.*, the polarity of the water core decreases with decrease in *R*-value.

In order to study the behavior of the entities at the boundary phase between the water core and the 1-hexanol phase, the mobility of the carbonyl carbon and the sodium ion of sodium octanoate was examined by means of ^{13}C and ^{23}Na-NMR, respectively. Figure 4 shows the ^{23}Na-NMR spectrum of sodium

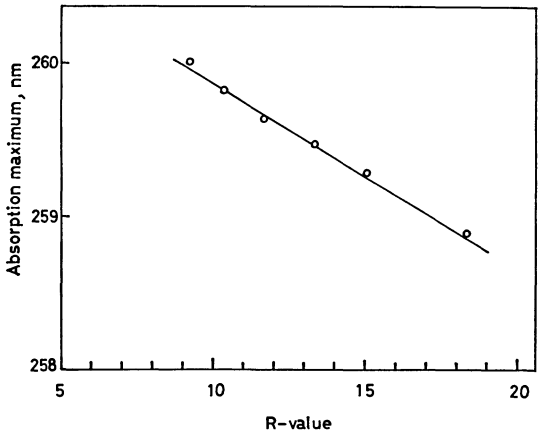

Fig. 3. Plots of absorption maxima due to pyridine 1-oxide against *R*-value. The absorption maxima due to pyridine 1-oxide in water, methanol and ethanol are 255.4, 263.3 and 265.1 nm, respectively.

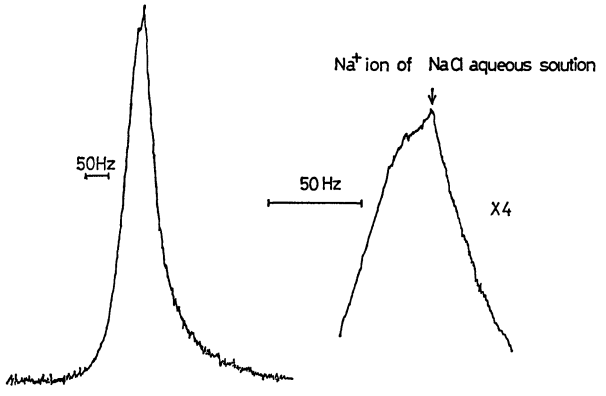

Fig. 4. ^{23}Na-NMR spectra of sodium octanoate in reversed micellar systems.

octanoate in reversed micellar system. The aqueous solution of sodium chloride was taken as an external standard, and the chemical shift of the peak due to the sodium ions in reversed micelles from the standard peak was evaluated. By using the pulse and Fourier transform technique, it has become possible to separate the resonance peak of the sodium ion in reversed micelles from that of the external standard. The chemical shifts and the line widths of the resonance peaks due to the carbonyl carbon and the sodium ion of sodium octanoate as a function of *R*-value are summarized in Table 6. When *R* is large (for instance $R=18.4$), the line width of the water proton peak in the ^{1}H-NMR spectrum (Table 4) reveals that the bound water molecules are rich. The line width and the chemical shift of the sodium ion in the ^{23}Na-NMR spectrum indicate that the mobility of the sodium ion in reversed micelles is high and the physicochemical environment of the sodium ion resembles that of a sodium ion in aqueous solutions (*i.e.*, the sodium ion is fully dissociated). When *R* is small (for instance $R=9.2$), water molecules are rather mobile, and the mobility of the sodium ion is low, so that the physicochemical environment of the sodium ion is different from that in aqueous solutions. Thus the increase in the mobility of water molecules with

Table 6. Chemical shifts and line widths of the carbonyl carbon and sodium of sodium octanoate

R-value	^{13}C-NMR[a]		^{23}Na-NMR[b]	
	Chemical shift (ppm)	Line width (Hz)	Chemical shift (ppm)	Line width (Hz)
18.4	183.4	38.4	2.08	5.4
11.6	183.1	39.7	2.79	7.3
9.2	182.6	42.7	2.97	9.8

a) Expressed in ppm using TMS as an external standard. b) Expressed in ppm using an aqueous solution of sodium chloride as an external standard.

decreasing *R*-value results from the decrease in the amount of hydrated sodium ions in the water core. The degree of dissociation of sodium ions of sodium octanoate becomes higher as *R*-value increases, and the amount of the water molecule hydrated by the sodium ion released from sodium octanoate increases with increase in *R*-value. Such a situation is also reflected in the results of ^{13}C-NMR spectra. The line width of the resonance peak of the carbonyl carbon of the surfactant decreases and the peak position is shifted to a lower field as *R* increases. The increase in the mobility and the down field shift of the carbonyl carbon signal are caused by the sodium ion released from sodium octanoate as *R* increases. Namely, the carbonyl group of the octanoate anion can move more freely and the electron density of the carbonyl group of the octanoate anion decreases by releasing the sodium ion from sodium octanoate.

In aqueous micellar systems[9] and surfactant aggregate systems in organic solvents[10] the exchange between monomers and surfactant micelles is thought to be relatively fast. However, the exchange in reversed micellar systems containing water molecules has not been clarified. The aggregation number in this system has not been measured, but from the results shown above and the fact that sodium octanoate is hardly soluble in 1-hexanol, the equilibrium constant *K* ($K=[S_m]/[S]^m$, where S_m, S, and m are the concentration of micelles, the concentration of surfactants and the aggregation number, respectively) seems to be relatively large.

Relationship between Hydrolytic Activity and the Structure of Reversed Micelles. Acceleration of the hydrolytic reaction caused by decrease in *R* may be explained as follows. The substrate becomes more soluble when the mobility of water molecules increases and the polarity of water cores decreases. The amount of substrate transferred from the 1-hexanol phase to the water core then increases. Hence, the hydrolysis is enhanced. The results of ^{23}Na and ^{13}C-NMR indicate that polar head groups of surfactants aggregate more tightly for a smaller *R*-value. Thus, the water core seems smaller for a smaller *R*-value, but this has not been confirmed by light scattering. The decrease in the diameter of the water core in reversed micelles gives rise to an increase in the specific surface area of reversed micelles, enhancing the rate of hydrolytic reaction. It was found that L-histidine is active, but not imidazole as a catalyst of hydrolysis of PNPA.

L-Histidine molecules are considered to be located at the boundary phase between the water core and the 1-hexanol phase through the ionic force between positive charges of the ammonium ion of L-histidine and negative charges of sodium octanoate and its low solubility in 1-hexanol. However, this does not apply to imidazole, since it has high solubility in 1-hexanol but no positive charge. Thus, L-histidine molecules can act as a catalyst of hydrolysis at the boundary phase of reversed micelles, but not imidazole molecules transferred from the water core to 1-hexanol phase. Hydrolytic reaction is remarkably enhanced when APNP is used as a substrate. The concentration of APNP at the boundary phase due to the ionic interaction and its high solubility in the water core may enhance the hydrolytic reaction. It is important for the reaction in reversed micellar systems to concentrate the catalyst or substrates at the boundary phase between the water core and the 1-hexanol phase.

We thank Prof. Hiroshi Watari for his interest in this work and Dr. Tetsurou Asakura for his valuable discussions.

References

1) E. F. J. Duynstee and E. Grunwald, *J. Am. Chem. Soc.*, **81**, 4540 (1959).
2) F. M. Menger, J. A Dohonue, and R. F. Williams, *J. Am. Chem. Soc.*, **95**, 286 (1973).
3) M. Seno, S. Shiraishi, K. Araki, and H. Kise, *Bull. Chem. Soc. Jpn.*, **48**, 3678 (1975).
4) K. Kon-no, K. Miyazawa, and A. Kitahara, *Bull. Chem. Soc. Jpn.*, **48**, 2955 (1975).
5) E. J. Fendler, S. A. Chang, J. H. Fendler, R. T. Medary, O. Seoud, and V. A. Woods, "Reaction Kinetics in Micelle," ed by E. H. Cordes, Plenum Press, New York, N. Y. (1973).
6) M. Ueno, H. Kishimoto, and Y. Kyogoku, *Bull. Chem. Soc. Jpn.*, **49**, 1776 (1976).
7) D. Eisenberg and W. Kauzmann, "The Structure and Properties of Water," Oxford University Press, Oxford (1969).
8) E. M. Kosower, *J. Am. Chem. Soc.*, **80**, 3253 (1958).
9) H. Inoue and T. Nakazawa, *J. Phys. Chem.*, **70**, 1108 (1966).
10) N. Muller, *J. Phys. Chem.*, **79**, 287 (1975).

Solvent Assisted Oxy-Cope Rearrangement of Diastereomeric 1,5-Hexadien-3-ols. A New Industrial Process for Polyprenyl Ketones

Yoshiji FUJITA,* Shigetoshi AMIYA, Takashi ONISHI, and Takashi NISHIDA
Central Research Laboratories, Kuraray Co. Ltd., Sakazu, Kurashiki, Okayama 710

(Received September 20, 1978)

Oxy-Cope rearrangement of diastereomeric 1,5-hexadien-3-ols, new key intermediates for terpenoids production in industrial scale, were investigated in neat systems and solvent assisted systems. Various solvents affecting the selectivity of [3,3]-shift were classified by means of NMR studies on hydroxyl proton exchange time.

The carbon-carbon elongation reactions based on [3,3]-sigmatropic rearrangement, such as the Carroll reaction[1] as well as Saucy-Marbet method[2] (C-3 extension) or Thomas[3] and Faulkner-Petersen[4] methods (C-5 extension), proceed after the loss of eliminating groups (*e.g.* CO_2, ROH) which decrease the efficiency of chain extenders particularly in lower molecules. Recently, mesityl oxide has been utilized in full as a C-6 chain extender *via* synthetically equivalent transpositions of Cope[5,6] and oxy-Cope[7] reactions.

Synthetic utility of oxy-Cope rearrangement is considerably reduced owing to the β-hydroxyolefin cleavage reaction. In order to avoid the cleavage, several modifications such as siloxy-Cope processes[8] or anionic processes[9] have been developed. On the other hand, no attention has been paid to solvent effects in oxy-Cope processes although such effects have been studied in the case of other [3,3]-sigmatropic rearrangement.[10] A report was given on a convenient solvent assisted method to increase the selectivity of [3,3]-shift of some 1,5-hexadien-3-ol systems.[7,11] We have further elaborated this method by comparing the behavior of diastereomeric dienols (**2** and **8**), and various solvents affecting the selectivity of this reaction were classified by means of NMR studies on hydroxy proton exchange time. A new process for polyprenyl ketones (**3**) useful for squalane and isophytol, which may be manufactured in the near future together with pseudoionone from intermediates **6** and **7** *via* acetylenic oxy-Cope reaction,[12] is presented in this paper.

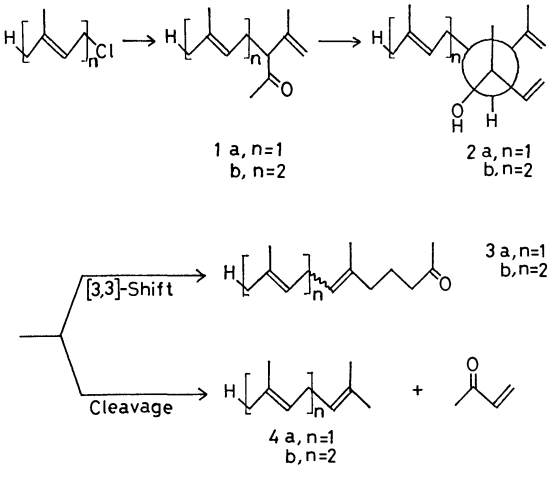

Results and Discussion

Preparation of Diastereomeric 1,5-Hexadien-3-ols and Siloxy Compound. The condensation reaction of prenyl or geranyl chloride with mesityl oxide gave the desired ketone (**1**) together with α,β-unsaturated isomer (**5**).[13,14] Reaction of **1** with vinylmagnesium bromide in tetrahydrofuran and subsequent hydrolysis afforded the only product **2** in *ca.* 80% yield. Diastereomer **2** is also obtainable by partial hydrogenation of the stoichiometric sodium acetylide ethynylation product of **1** [**1**/**5**/**6**/**7**=5/15/78/2].[13]

Semicatalytic potassium hydroxide ethynylation of **1** or **5** in liquid ammonia under pressure gave two diastereomeric alcohols in the composition **1**/**5**/**6**/**7**= 6/16/45/33. However, fractional distillation and silica gel column chromatography were ineffective for the separation of **6** and **7**. After partial hydrogenation of the mixture, careful fractional distillation gave pure dienol **8a** (50 g) from 1500 g of **2a**/**8a**=55/45.

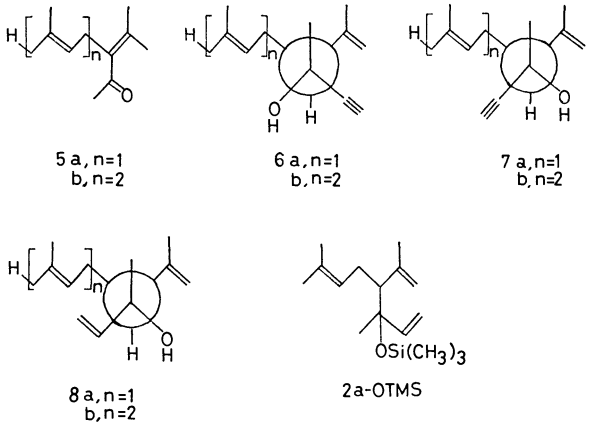

Treatment of **2a** with dry pyridine/trimethylchlorosilane in ether gave **2a**-OTMS (OTMS=trimethylsiloxy) in 78% yield.

*Thermolysis of **2**, **8a**, and **2a**-OTMS.* Thermolysis of **2a** in the temperature range 160—190 °C in neat system gave **3a** (E/Z=59.5/40.5; 170 °C) in approximately 55% yield, along with cleavage products (**4a**, methyl vinyl ketone, and polymer). Below this temperature range, the reaction was too slow for synthesis and above it the cleavage reaction occurred predominantly. The selectivity of [3,3]-shift decreased to a small extent with progress of the reaction (Fig. 3). The result of thermolysis of **2b** is similar to that of **2a**. However, dienol **8a**, in comparison to its diastereomer **2a**, shows interesting behavior: No appreciable difference in yield of **3a** was observed, but the ratio of stereoisomer of **3a** inclined to the *E*-form (E/Z=65.8/34.2; 170 °C).[15] The reaction of **8a** occurred slightly faster than **2a** [k=0.404 and 0.858 s^{-1} at 170 and 180 °C, respectively].

Table 1. Results of thermolyses of **2**, **8a**, and **2a**-OTMS

Compound	Reaction temp (°C)	E/Z ratio of **3**[a]	k[b] (s^{-1})	E_a (kcal/mol)	log A (s^{-1})
2a	160	60.0/40.0	0.107	30.34+1.78	14.35+0.87
	170	59.5/40.5	0.241		
	180	58.9/41.1	0.476		
	190	58.4/41.6	1.060		
2a/NMP=1/1[c]	160	66.8/33.2	0.192	29.45+0.55	14.16+0.27
	170	66.5/33.5	0.431		
	180	66.3/33.7	0.874		
	190	66.0/34.0	1.740		
2b/NMP=1/1[c]	170	66.2/33.8	0.494	32.59+2.53	15.78+1.21
	180	66.0/34.0	1.155		
	190	——	2.196		
	200	65.6/34.4	5.449		
8a/NMP=1/1[c]	170	60.1/39.9	0.470	——	——
	180	61.7/38.3	1.092		
	190	62.6/37.4	2.022		
2a-OTMS	150	64.0/36.0	0.120	30.86+2.38	15.06+1.18
	160	63.8/36.2	0.319		
	170	63.5/36.5	0.676		
	180	63.2/36.8	1.441		
	190	63.0/37.0	3.026		

a) E/Z ratio of **3** from **2a**-OTMS was obtained by GC analyses after the hydrolysis of **9**. b) First order rate constant [disappearance of **2**, **8a**, **2a**-OTMS]. c) By weight.

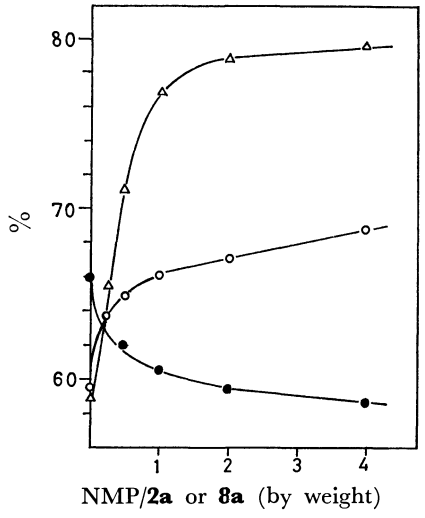

Fig. 1. Solvent effect on oxy-Cope rearrangement of **2a** and **8a** (180 °C) △: Selectivity of **3a**. ○: E-isomer of **3a** from **2a**. ●: *E*-isomer of **3a** from **8a**.

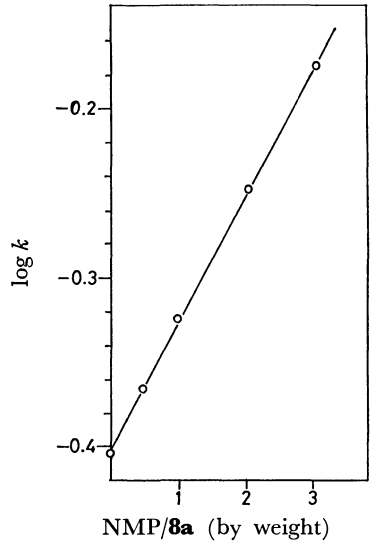

Fig. 2. Rate acceleration of **8a** by NMP (170 °C).

The siloxy-Cope rearrangement of **2a**-OTMS afforded **9** in *ca.* 97% yield, with a little rate acceleration owing to its steric factor. Hydrolysis of **9** with 1M-hydrochloric acid at 0 °C yielded **3a** quantitatively as a mixture of E/Z=63/37.

9

Ozonolysis of **3a** gave mainly 4-methyl-3-pentenal and 2,6-heptanedione, and hydrogenation of **3a** with Pd/C afforded 6,10-dimethyl-2-undecanone.

Solvent Assisted Oxy-Cope Rearrangement of 2 and 8a. Increase of the selectivity of [3,3]-shift without troublesome and costly handling is our essential problem. In this respect, the solvent assisted modification seems to be suitable for large scale production.

The use of *N*-methyl-2-pyrrolidone (NMP) as a solvent in various amounts, as shown in Fig. 1, increased the yield of **3a** to 80% with the amount of the *E*-isomer increasing from 59 to 71% in the case of **2a**, while with **8a** it decreased from 66 to 58%. A small acceleration in rate was observed (Fig. 2). Further addition of NMP, even as much as fifty-fold, caused neither increase in yield, variation in the E/Z ratio,

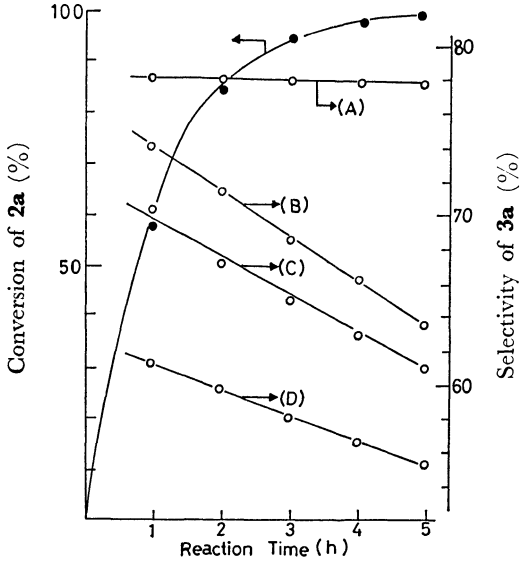

Fig. 3. Effect of the addition of *n*-decyl alcohol on selectivity of **3a** from **2a** (180 °C). ●: Conversion of **2a**. ○: Selectivity of **3a**; (A) NMP/**2a**=2/1. (B) NMP/**2a**/*n*-$C_{10}H_{21}OH$=2/1/1.5. (C) NMP/**2a**/*n*-$C_{10}H_{21}OH$=2/1/1. (D) NMP/**2a**=0 by weight.

or acceleration in rate. The decrease in the selectivity of the [3,3]-shift during the reaction observed in the neat system [initial stage 62%, end of reaction 53%] was not observed upon addition of NMP. This solvent effect was considerably reduced by the addition of primary alcohols (*e.g.* 1-decanol, ethylene glycol), even though there was no effect on the selectivity of [3,3]-shift in the neat system (Fig. 3).

A similar result was obtained by using ε-caprolactam (or 2-pyrrolidone) instead of NMP with some difference in the reaction rate and selectivity of [3,3]-shift. However, under the reaction conditions, ε-caprolactam reacted with methyl vinyl ketone derived from cleavage reaction to yield *N*-(3-oxobutyl)-ε-caprolactam which showed similar activity to that of ε-caprolactam.

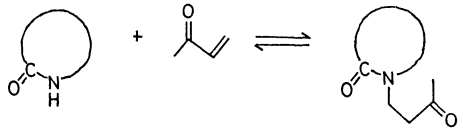

Other solvents such as glycerol, triphenylamine, decane, diethylene glycol diethyl ether[17] *etc.*, were ineffective for increasing the yield of **3** (Table 2). In the case of hydrocarbon solvent, *E*/*Z* ratio of **3** changed to 54/46. Solvents such as istain and benzotriazole were effective contrariwise for cleavage reaction.

Classification of Solvents Affecting the Selectivity of [3,3]-Shift: NMR-studies on Proton Exchange Time. The fact that the effect changes with the amount of solvent and diminishes considerably by the addition of primary alcohols indicates that there is interaction between solvent and hydroxy proton. We have studied the effect of solvent on hydroxy proton exchange by NMR wherein 10 mg of solvent was added to 0.5 ml of a solution of **2** in dimethyl-d_6 sulfoxide (DMSO-d_6) of purity higher than 99.5% and containing water as a contaminant.

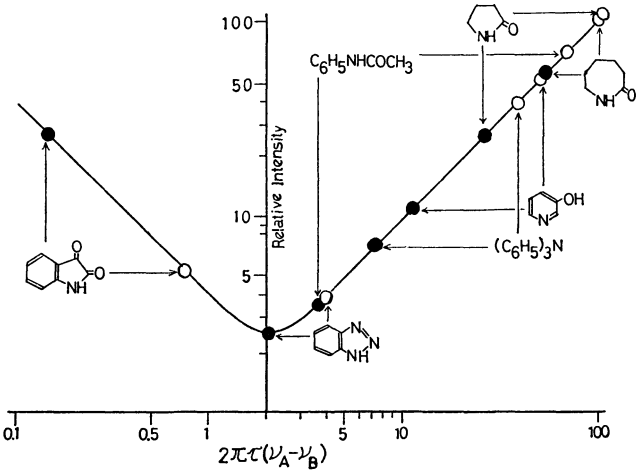

Fig. 4. Solvent effects on hydroxy proton exchange time of **2a**. ○: At 30 °C. ●: At 100 °C.

In calculating the proton exchange time (the time of exchange between the hydroxy proton of **2** and water in DMSO-d_6), the line shape [$g(\nu)$] of the NMR spectrum, chemical shift being taken into account, is theoretically a function of ν_A, ν_B, τ_A, and τ_B, where A is the change site on **2**, B is the exchange site on water; τ_A and τ_B are the times during which the protons are detained at each site, and ν_A and ν_B represent the chemical shifts. Assuming that $\tau_A=\tau_B=2\tau$ and that the line width has no broadening throughout the process except for the change, we get the following Bloch-equation.[18]

$$g(\nu) = K\frac{\tau(\nu_A-\nu_B)^2}{[1/2(\nu_A-\nu_B)-\nu]^2+4\pi^2\tau^2(\nu_A-\nu)^2(\nu_B-\nu)^2}$$

$$K = \int_{-\infty}^{\infty} g(\nu)\mathrm{d}\nu$$

The equation was solved approximately with the assumption that proton exchange occurs mainly between the hydroxyl proton of **2** and water in DMSO-d_6. The line shape was calculated with $\nu_A=\nu_B=90$ Hz and on varying the value of $2\pi\tau(\nu_A-\nu_B)$ from 100 to 0.1. The proton exchange time can be obtained by comparing the values obtained by calculation with measured line shape values. By comparing the results of thermolysis of **2** in neat system and solvent assisted system (Table 2), solvents effective for [3,3]-shift can be defined to be those for which proton exchange time is not less than 10^{-1} s at 30 °C and not less than 10^{-2} s at 100 °C. Figure 4 shows some results in which the logarithm of the value of $2\pi\tau(\nu_A-\nu_B)$ is horizontally plotted and the logarithm value of signal height based 100 with $2\pi\tau(\nu_A-\nu_B)=100$ is vertically plotted to give the curve. The relative value of the measured line shape, based on the height of hydroxyl proton of **2a** in the presence of 2-pyrrolidone, is plotted on the curve. Solvent plotted on the right of the center line of Fig. 4 would be effective for increasing the selectivity of [3,3]-shift. On the contrary, solvent plotted on the left would decrease [3,3]-shift. Benzotriazole plotted near the center at 100 °C can not be a favorable solvent for [3,3]-shift in consideration of the fact that

Table 2. Solvent effect on oxy-Cope rearrangement and on hydroxyl proton exchange time

Compound	Solvents /**2** or **8** (by weight)	Reaction conditions[a]	Conversion of **2** or **8**; %[b]	Selectivity of **3**; %[b] [*E*/*Z* of **3**]	Proton exchange time τ_0(s) at 30 °C	Proton exchange time τ_0(s) at 100 °C
2a	None	A[c]	84	55 [58.9/41.1]	——	——
	Glycerol (1.0)	B	87	52		
	Triphenylamine (1.0)	C	40	53	1.3×10^{-1}	2.4×10^{-2}
	Decane (2.0)	B	89	51 [44/46]	——	——
	Acetanilide (1.0)	C	51	55	2.4×10^{-1}	1.3×10^{-2}
	Diethylene glycol diethyl ether (2.0)	A[c]	90	55 [59/41]	——	——
	Benzotriazole (1.0)	C	78	12	1.3×10^{-2}	$>7.0\times10^{-3}$
	Isatin (1.0)	C	58	8	4.2×10^{-3}	$<5.2\times10^{-4}$
	NMP (1.0)	A[c]	98	79 [66/34]	$>4.0\times10^{-1}$	1.8×10^{-1}
	2-Pyrrolidone (2.0)	A	96	77	3.6×10^{-1}	8.8×10^{-2}
	ε-Caprolactam (1.0)	A[c]	95	77 [66.5/33.5]	$>4.0\times10^{-1}$	1.9×10^{-1}
	N-(3-Oxobutyl)-ε-caprolactam (1.0)	A[c]	92	76	$>4.0\times10^{-1}$	1.8×10^{-1}
	3-Pyridinol (1.0)	C	40	70	1.8×10^{-1}	3.8×10^{-2}
	Benzimidazole (1.0)	C	45	70	1.9×10^{-1}	7.4×10^{-2}
2b	None	A[c]	87	60 [59/41]	——	——
	3-Pyridinol (1.0)	C	46	71	2.3×10^{-1}	8.8×10^{-2}
	NMP (1.0)	A[c]	100	82 [66/34]	4.0×10^{-1}	4.5×10^{-2}
8a	None	A	87	57 [66/34]	——	——
	NMP (2.0)	A	100	79 [59/41]	——	——
10	None	A	90	58	——	——
	NMP (2.0)	A[c]	100	83 [73.5/26.5]	$>4.0\times10^{-1}$	4.9×10^{-2}
11	None	A	92	51	——	——
	NMP (2.0)	A[c]	100	78 [70/30]	3.6×10^{-1}	6.6×10^{-2}
12	None	A	90	54 [60/40]	——	——
	NMP (2.0)	A[c]	100	78 [73.6/26.4]	1.9×10^{-1}	6.2×10^{-2}

a) A; 180 °C for 4 h. B; 175 °C for 6 h. C; 170 °C for 2 h. b) Determined by GC analyses: PEG-20 M 10% on Chromosorb W (AW) or Silicone DC-550 10% on Chromosorb W (AW). c) Results of GC analyses were confirmed by isolation in large scale experiments (50—500 g).

the reaction temperature is above 160 °C. Solvent in which the hydroxyl proton exchange time largely depends upon temperature, such as acetanilide or triphenylamine, would not be preferable for [3,3]-shift. This classification is applicable to the other systems **10**—**12**.[7]

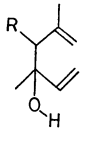

10, R=p-$CH_3C_6H_4CH_2$-
11, R=furfuryl
12, R=2-thenyl

Despite the difference in the conditions between NMR measurement and oxy-Cope reaction, it might be postulated that the added solvents effective for increasing the selectivity of [3,3]-shift fix the hydroxyl proton, slowing down the rate of proton exchange.

Synthetic utility of the process was confirmed by large scale production (semi-commercial) of geranylacetone (**3a**), and application to other naturally occurring compounds is under investigation in our laboratory.

Experimental

Boiling points are uncorrected. Infrared spectra were determined on a JASCO (DC-403G) spectrometer. NMR spectra were taken with a Varian Associate HA-100 or Varian Model A-60 spectrometer and MS with a Finnigan 9500 instrument. GC analyses were made with a Shimadzu GC-4A using 3 mm × 300 cm column. Separation of the reaction products was made with a Shimadzu GC-5A using 7 mm × 200 cm column of 10% Silicone DC-550 or 10% PEG-20M on Chromosorb W (AW). Rectification of the reaction products was carried out with a Shibata Automatic Packing Column, Model HPC-A-1500-B having 70 theoretical plates. Oxy-Cope rearrangements were carried out in nitrogen atmosphere.

*(3S)-4-Isopropenyl-3,7-dimethyl-1,6-octadien-3-ol (**2a**).* The compound was obtained according to the method reported previously[11b] by the reaction of **1a** (1 mol) with vinylmagnesium bromide (1.2 mol) in THF (1.5 l) at 40 °C for 3 h (yield 79%): bp 60—63 °C/0.5 mmHg.

*(3S)-4-Isopropenyl-3,7,11-trimethyl-1,6,10-dodecatrien-3-ol (**2b**).* The compound was obtained by the same procedure described above, from **2b** (0.5 mol) and vinylmagnesium bromide (0.6 mol): yield 81%; bp 104—106 °C 0.3 mmHg (*E*-form). IR (neat) 3480, 1640, 1450, 1375, 920, and 895 cm^{-1}. NMR (CCl_4) δ 1.15 (s, CH_3, 3H), 1.54, 1.62, 1.67 (s, CH_3, 12H), *ca.* 1.92—2.30 (m, CH_2CH and CH_2CH_2, 7H), *ca.* 4.75—5.10 (m, CH and CH_2, 4H), 5.00(dd, CH, 1H, J=2, 10 Hz), 5.18 (dd, CH, 1H, J=2, 18 Hz), and 5.90 (dd, CH, 1H, J=10, 18 Hz). MS (70 eV) *m/e* (rel intensity) 262 (M^+, 1.6), 244 (6.1), 191 (9.4), 149 (11.7),

123 (55.3), 81(41.5), and 71 (100).

Found: C, 82.62; H, 11.58%. Calcd for $C_{18}H_{30}O$: C, 82.38; H, 11.52%.

*4-Isopropenyl-3,8-dimethyl-6-octen-1-yn-3-ol (**6a**).* Acetylene gas was bubbled into a solution of sodium metal (69 g; 3 mol) in liquid ammonia (3 l) until the reaction mixture turned grey. Introduction of acetylene was then suspended and 517 g (3.1 mol) of **1a** was added over a period of 30 min. The reaction was continued for 3 h, acetylene being bubbled through the reaction system maintained at −33 °C. After removal of ammonia, the residue was neutralized with ammonium chloride, water was added, and then the mixture was extracted with ether. Distillation gave 519 g of a mixture of **1a**/**5a**/**6a**/**7a**=5/15/78/2 [analyzed by GC; PEG-20M, 160 °C], which was purified by careful fractional distillation to afford a mixture of **5a**/**6a**/**7a**=4/94/2. Pure **6a** was obtained by silica gel column chromatography (C_6H_6/*n*-C_6H_{14}=4/6; **6a**/**7a**=97/3) or preparative GC [PEG-20M, 170 °C]: bp 59—61 °C/0.5 mmHg.[13]

*4-Isopropenyl-3,7,11-trimethyl-6,10-dodecadien-1-yn-3-ol (**6b**).* The compound was obtained as a mixture of **1b**/**5b**/**6b**/**7b**=10/30/57/3 by the same procedure as described above, except for the use of **1b** (0.5 mol) in 500 ml of ether solution. Separation of **6b** by preparative GC [PEG-20M, 210 °C] was unsuccessful owing to the accompaniment of acetylenic oxy-Cope rearrangement. Pure **6b** was obtained by silica gel column chromatography (C_6H_6/*n*-C_6H_{14}=4/6): bp 120—125 °C/0.3 mmHg (**6a**/**7a**=95/5).[13]

General Procedure for Partial Hydrogenation. Hydrogen was bubbled into a mixture of **1a**/**5a**/**6a**/**7a**=5/15/78/2 (300 g) in hexane (900 ml), in the presence of 5 g of 2% Pd Lindlar catalyst at 35—40 °C for 7 h. After checking the completion of reaction by GC [PEG-20M, 160 °C], the catalyst was filtered and mother liquid evaporated under reduced pressure. Distillation gave 294 g of a mixture of **1a**/**5a**/**2a**/**8a**=6/14/78/2.

*(3R)-4-Isopropenyl-3,7-dimethyl-1,6-octadien-3-ol (**8a**).* In a 5 l autoclave, 335 g (2 mol) of **1a** was added to liquid ammonia (3.3 l) in contact with 20 wt% of aqueous KOH (45 g; 0.16 mol) as a catalyst, acetylene gas (*ca.* 260 g) being introduced with stirring at −33 °C. The reaction temperature was raised to 5 °C, stirring being continued for 32 h. The reaction mixture was cooled to −33 °C and neutralized with ammonium chloride. After removal of ammonia, water was added, and the mixture was extracted with ether. Distillation gave 319 g of a mixture of **1a**/**5a**/**6a**/**7a**=6/16/45/33: bp 59—63 °C/0.5 mmHg. Pure **7a** was obtained only by preparative GC.[13] After partial hydrogenation of the mixture (315 g) by the same method as described above, distillation [bp 82—91 °C/1.5—2 mmHg] afforded 310 g of a mixture of **1a**/**5a**/**2a**/**8a**=7/15/44/34. Careful rectification of 1500 g of a mixture [bottom temp, 128—134 °C; top temp, 94—95 °C; pess., 4 mmHg; reflux ratio=25] afforded 52 g of pure **8a**. IR (neat) 3480, 1639, 1450, 1375, 1110, 1000, 922, and 897 cm^{-1}. NMR (CCl_4) δ 1.18 (s, CH_3, 3H), 1.55, 1.60, 1.63 (s, CH_3, 9H), *ca.* 2.02—2.17 (m, CH_2CH, 3H), *ca.* 4.73—5.00 (m, CH and CH_2, 3H), 5.00 (dd, CH, 1H, J=2,10 Hz), 5.15 (dd, CH, 1H, J=2, 18 Hz), and 5.98 (dd, CH, 1H, J=10, 18 Hz). MS fragmentation pattern of **8a** was analogous to that of **2a**.

Found: C, 80.07; H, 11.18%. Calcd for $C_{13}H_{22}O$: C, 80.35; H, 11.41%.

*(3R)-4-Isopropenyl-3,7,11-trimethyl-1,6,10-dodecatrien-3-ol (**8b**).* The compound was obtained as a mixture of **1b**/**5b**/**2b**/**8b**=8/18/42/32 by the same procedure as described above. Separation and purification of **8b** by preparative GC [PEG-20 M, 210 °C] or by fractional distillation was unsuccessful owing to the occurrence of oxy-Cope rearrangement.

*3-Trimethylsiloxy-4-isopropenyl-3,7-dimethyl-1,6-octadiene (**2a**-OTMS).* The compound was obtained according to the method reported previously[11b] by the reaction of **2a** (58.2 g; 0.3 mol) with dry pyridine (28.4 g; 0.36 mol)/trimethylchlorosilane (38.9 g; 0.36 mol) in ether (200 ml) at 35 °C for 4 h; yield 78%; bp 68—70 °C/0.5 mmHg.

*6,10Dimethyl-6,9-undecadien-2-one (**3a**). General Procedure of Oxy-Cope Rearrangement in Neat System.* 800 g of **2a** (purity 93%) was placed in a 1 litre 3-necked flask and heated to 185—187 °C for 4 h in nitrogen atmosphere. The reaction mixture was cooled and distilled *in vacuo* to remove 305 g of a mixture of 2,6-dimethyl-2,5-heptadiene (**4a**)/methyl vinyl ketone, and 47 g of **5a** (impurity in the starting material, as the low-boiling fraction). As a higher boiling product [bp 77—79 °C/0.5 mmHg], 394 g (53%) of **3a** was obtained. GC analysis of **3a** [Silicone DC-550, 160 °C] showed two peaks (11.5 and 13.0 min) in the ratio 41.1 : 58.9. Separation of these compounds by fractional distillation [bottom temp, 143—147 °C; top temp, 77—83 °C; press., 0.3 mmHg; reflux ratio=30] and spectral analyses showed that the former peak is *Z*-isomer and the latter *E*-isomer.[11b]

*6,10,14-Trimethyl-6,9,13-pentadecatrien-2-one (**3b**).* The compound was obtained by the same procedure described above in 52% yield (180 °C for 3.5 h): bp 123—128 °C/0.1 mmHg (*E*/*Z*=57.5/42.5). IR (neat) 1715, 1672, 1440, 1158, 985, 970, 890, and 830 cm^{-1}. NMR (CCl_4) δ 1.50, 1.56 (s, CH_3, 12H), *ca.* 1.70—2.05 (m, CH_2CH_2, 8H), 1.92 (s, CH_3, 3H), 2.13—2.30 (m, CH_2, 2H), 2.55 (t, CH_2, 2H, J=7 Hz), and *ca.* 4.94 (broad t, CH, 3H).

Found: C, 81.99; H, 11.71%. Calcd for $C_{18}H_{30}O$: C, 82.38; H, 11.52%.

General Procedure of Oxy-Cope Rearrangement in Solvent Assisted System. A solution of 350 g of **2a** (purity 92%) in 700 g of NMP was subjected to reaction at 180 °C for 5 h with stirring. The reaction mixture was poured into water (1500 ml) and extracted with ether (500 ml×4). Distillation of the products gave 245 g (76%) of **3a** (*E*/*Z*=67/33). Quantitative analyses were carried out with gas chromatography: In the case of **2a** and **8a**, *n*-decyl alcohol was used as an internal standard to obtain the calibration curve [PEG-20M, 160 °C]. Reactions of **2b** in NMP solvent were monitored by using NMP itself as an internal standard.

We wish to express our thanks to Dr. Fumio Wada for technical assistance, and Mr. Masaya Oka for mass spectral analyses.

References

1) M. F. Carroll, *J. Chem. Soc.*, **1940**, 704, 1266.
2) G. Saucy and R. Marbet, *Helv. Chim. Acta*, **50**, 1158, 2091 (1967).
3) A. F. Thomas, *J. Am. Chem. Soc.*, **91**, 3281 (1969).
4) D. J. Faulkner and M. R. Petersen, *Tetrahedron Lett.*, **1969**, 3242.
5) G. Büchi and H. Wüest, *J. Am. Chem. Soc.*, **96**, 7573 (1974).
6) Y. Fujita, T. Onishi, and T. Nishida, *Synthesis*, **1978**, 532.
7) Y. Fujita, T. Onishi, and T. Nishida, *Synthesis*, **1978**, 612.
8) R. W. Thies, *J. Chem. Soc., Chem. Commun.*, **1971**, 237.
9) D. A. Evans and A. M. Golob, *J. Am. Chem. Soc.*, **97**, 4765 (1975).

10) D. C. Wigfield and S. Feiner, *Can. J. Chem.*, **48**, 855 (1970).
11) a) Y. Fujita, T. Onishi, and T. Nishida, *J. Chem. Soc., Chem. Commun.*, **1978**, 972; b) Y. Fujita, T. Onishi, and T. Nishida, *Synthesis*, **1978**, 934.
12) Ger. Offen, 2653646, 2705602 (1977).
13) Y. Fujita, F. Wada, T. Onishi, and T. Nishida, *Chem. Lett.*, **1977**, 943.
14) M. Matsui, T. Yoshida, and H. Mori, *Agric. Biol. Chem.*, **28**, (2), 95 (1964).
15) Previously A. Viola *et al.* reported[16] that two diastereomers of 4-methyl-1,5-hexadien-3-ol reacted at different rates.
16) A. Viola, E. J. Iorio, K. K. Chen, G. M. Glover, U. Nayak, and P. J. Kocienski, *J. Am. Chem. Soc.*, **89**, 3462 (1967).
17) Recently diglyme was used for oxy-Cope rearrangement of 1,5-hexadienol system [P. Place, M. L. Roumestant, and J. Gore, *J. Org. Chem.*, **43**, 1001 (1978)].
18) H. S. Gutowsky, D. W. McCall, and C. P. Slichter, *J. Chem. Phys.*, **21**, 279 (1953).

A Rapid Esterification by Means of Mixed Anhydride and Its Application to Large-ring Lactonization[1)]

Junji Inanaga, Kuniko Hirata, Hiroko Saeki, Tsutomu Katsuki, and Masaru Yamaguchi*

Department of Chemistry, Faculty of Science, Kyushu University, Hakozaki, Higashi-ku, Fukuoka 812

(Received September 29, 1978)

A rapid and mild esterification method using carboxylic 2,4,6-trichlorobenzoic anhydrides in the presence of 4-dimethylaminopyridine was developed. The method was also successfully applied to the synthesis of large-ring lactones, including DL-2,4,6-tridemethyl-3-deoxymethynolide.

For the preparation of large-ring lactones from the corresponding open-chain hydroxy acids, a rapid esterification reaction is necessary to overcome the unfavourable entropy factors leading to the formation of polymers. The mildness of the reaction conditions is also important if the method is to be applied to the synthesis of complex natural substances with sensitive functionalities. Most of the conventional methods have found only a limited use for this purpose. Recently, intensive studies in this field have commenced and several good lactonization methods using different types of reagents have been developed,[2)] some of them having been successfully applied to the synthesis of macrolides.[3)]

In the course of our studies of the synthesis of macrocyclic lactones, the remarkably high catalytic activity of 4-dimethylaminopyridine in acyl transfer reactions[4)] attracted our attention, and so the esterifications with combinations of this reagent and the appropriate mixed anhydrides were examined. This paper will describe the rapid and mild esterification method using 2,4,6-trichlorobenzoic carboxylic anhydride (**1**) as the anhydride counterpart in the above combination, and its successful application to the synthesis of medium- and large-ring lactones, including DL-2,4,6-tridemethyl-3-deoxymethynolide (**8**).

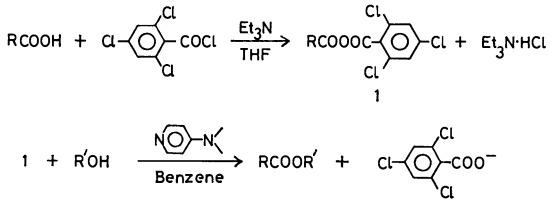

Results and Discussion

Mixed Anhydrides. The esterification by means of mixed anhydride consists of two steps: the formation of the mixed anhydride, and the alcoholysis of the anhydride. Since the first step has been well-documented,[5)] our effort was mainly directed toward the second step. In the choice of the acids to be examined as the components of the mixed anhydrides, the following two factors were considered: the component should be a good leaving group, and the carbonyl group of the component should be sterically hindered from the nucleophilic attack to some extent. The following acid chlorides which seemed to meet the above requirements were preliminarily examined by comparing the rate of the alcoholysis of the corresponding mixed anhydrides in the presence of 4-dimethylaminopyridine: 2,4,6-trichlorobenzoyl (**2**),[6)] 2,3,6-trimethyl-4,5-dinitrobenzoyl (**3**), 2,6-dichloro-3-nitrobenzoyl (**4**),[7)] 2,4,6-tribromobenzoyl (**5**),[8)] 2,6-dichloro-4-nitrobenzoyl,[9)] 2,6-dichlorobenzoyl,[10)] 2,4,6-trichloro-3-nitrobenzoyl,[11)] 2,4,6-trichloro-3,5-dinitrobenzoyl, 2,4,6-tribromo-3-nitrobenzoyl, 2,4,6-tribromo-3,5-dinitrobenzoyl, 2,6-dinitrobenzoyl,[12)] 2,4,6-trimethyl-3,5-dinitrobenzoyl,[13)] 2,3,6-trimethylbenzoyl,[11)] 2,6-dimethoxybenzoyl,[15)] and pivaloyl chloride. 2,4,6-trinitrobenzoyl[12)] and 3,5-dimethyl-2,4,6-trinitrobenzoyl chloride were also examined, but these two acyl chlorides did not give well-defined mixed anhydrides with 2-methylpentanoic acid. Among the above acid chlorides, the chlorides (**2**), (**3**), (**4**), and (**5**) gave the most promising results. Figure 1 shows the relative rates of ester formation, as followed by GLPC, in the alcoholysis of the corresponding four mixed anhydrides with 2-methylpentanoic acid by 2-methyl-2-propanol at room temperature.

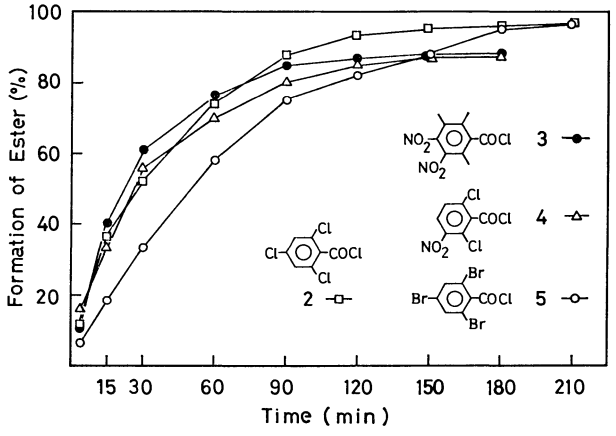

Fig. 1. Relative rates of the 2-methyl-2-propanolysis of mixed anhydrides formed from 2-methylpentanoic acid and four acid chlorides, **2**, **3**, **4**, and **5**.

2,4,6-Trichlorobenzoyl chloride (**2**) was proved to be the most satisfactory one in rate and in the yield of the alcoholysis. The reaction using the chloride (**3**) was fast but incomplete; however, it was later found that the chloride can also be used for the large-ring lactonizations.

Reaction Conditions. The following experiments were carried out by using the acid chloride (**2**) unless otherwise mentioned. Table 1 shows the relative rates of the formation of *t*-butyl 2-methylpentanoate in various solvents. Aromatic hydrocarbons, such as

benzene or toluene, were found to be the most suitable solvents for the alcoholysis step.

When the temperature of the reaction was raised, the rate of alcoholysis increased markedly without affecting the final yield; for example, *t*-butyl 2-methylpentanoate was formed almost quantitatively in 1 or 2 min in toluene at 100 °C (*cf.* entries, 1, 3, and 4 in Table 2). The amount of dimethylaminopyridine also had a significant influence on the rate of the reaction, and it was preferable to use more than one equivalent of the reagent per mole of the mixed anhydride, especially when the method was applied to large-ring lactonizations.

Table 1. Effect of solvents on the rate of ester formation[a]

Solvent	Ester formation (%)			
	4 min	15 min	30 min	60 min
Benzene	37	62	81	91
Toluene	37	59	79	95
Dioxane	20	49	71	89
Dichloromethane	10	39	59	77
Carbon tetrachloride	18	39	52	68
Pyridine	6	22	37	53
Cyclohexane	3	12	23	39
Acetonitrile	3	7	15	28

a) The formation of *t*-butyl 2-methylpentanoate was followed by GLPC.

Esterification. The results of the esterification by this method are summarized in Table 2.

As is shown in Table 2, the esters of secondary and tertiary alcohols were prepared rapidly at room temperature in good yields. In the case of primary alcohols, however, a small amount of an undesired trichlorobenzoic acid ester was formed as the by-product. The rates of the formation of benzoic acid esters were smaller than those of aliphatic acid esters. Sterically very crowded *t*-butyl pivalate could not be prepared by this method.

Lactonization. The method was then applied to

Table 2. Yields and reaction conditions of esterification using 2,4,6-trichlorobenzoyl chloride

Entry	Acid (0.3 mmol)	Alcohol[a]		Dimethyl-aminopyridine (mmol)	Time[b] (min)	Yield[c] (%)
1	2-Methyl-pentanoic acid	2-Methyl-2-propanol		0.6	90	>95
2			(2 eq.)	1.2	20	89
3			(2 eq.)	0.6	10 (80 °C)	>95
4			(2 eq.)	0.6	2 (100 °C)[d]	>95
5		2-Butanol		0.6	5	>95
6		Cyclohexanol		0.6	5	>95
7		Methanol		0.6	10	95[e]
8		Ethanol		0.6	3	95[f]
9	Cyclohexanecarboxylic acid	2-Methyl-2-propanol		0.6	20	>95
10		Cyclohexanol		0.6	20	>95
11	Benzoic acid	2-Methyl-2-propanol		0.6	270	89
12		Cyclohexanol		0.6	20	>95
13	Methyl hydrogen *meso*-2,4-dimethyl-glutarate	2-Methyl-2-propanol	(2 eq.)	0.6	60	>95[g]
14			(2 eq.)	0.6	5 (80 °C)	84[g]

a) One equivalent of alcohols to acids was used unless otherwise mentioned. b) The alcoholysis reactions were carried out at room temperature in benzene unless otherwise mentioned. c) The yields were determined by GLPC in the presence of the appropriate internal standards. d) The alcoholysis step was carried out in toluene. e) Methyl trichlorobenzoate (1.5%) was also formed. f) Ethyl trichlorobenzoate (3%) was also formed. g) No isomerization occurred at room temperature, but isomerization occurred (22%) when the reaction was carried out at 80 °C.

Table 3. Isolated yield in lactonization by trichlorobenzoyl chloride method

Hydroxy acid (Ring size)	Catalyst[a] (mol. equiv.)	Time of addition (h)	Yield (%) Monomer	Dimer
$HO(CH_2)_7CO_2H$ (9)	3	8	36	23
$HO(CH_2)_{10}CO_2H$ (12)	6	5	48	20
$C_6H_{13}CH(OH)(CH_2)_{10}CO_2H$ (13)	6	1.5	67	10
$C_6H_{13}CH(OH)CH_2CH{=}CH(CH_2)_7CO_2H$ (13)	3.3	5	57	12

a) 4-Dimethylaminopyridine.

Table 4. Isolated yield in lactonization by trimethyldinitrobenzoyl chloride method

Hydroxy acid (Ring size)	Catalyst[a] (mol. equiv.)	Time of addition (h)	Yield (%) Monomer	Dimer
$HO(CH_2)_7CO_2H$ (9)	3	7	18	41
$C_6H_{13}CH(OH)(CH_2)_{10}CO_2H$ (13)	6	8	58	8
$C_6H_{13}CH(OH)CH_2CH{=}CH(CH_2)_7CO_2H$ (13)	3	7	58	9

a) 4-Dimethylaminopyridine.

the synthesis of macrocyclic lactones. The mixed anhydrides of the long-chain hydroxy acids could be prepared in a manner similar to that used in the above esterification. After the removal of triethylamine hydrochloride, the solution of the mixed anhydride was diluted with toluene and slowly added to a refluxing solution of dimethylaminopyridine in toluene under high-dilution conditions. In this way, nine- to thirteen-membered ring lactones were prepared. They are shown in Table 3.

The results of the experiments carried out by using 2,3,6-trimethyl-4,5-dinitrobenzoyl chloride as the condensing agent are given in Table 4. As can be seen from the table, this acid chloride is as useful as 2,4,6-trichlorobenzoyl chloride, at least for the lactonization.

Finally, the method was applied to the lactonization of the seco-acid (**6**) of DL-2,4,6-tridemethyl-3-deoxymethynolide (**8**). The seco-acid has an acid-sensitive dihydroxy enone structure, and it has been shown that the compound decomposes easily to a furan derivative (**7**) and propionaldehyde on contact with a catalytic amount of hydrochloric acid.[16] When the seco-acid was cyclized under conditions similar to those used in lactonization with 2,4,6-trichlorobenzoyl chloride, the desired DL-lactone (**8**) was isolated in 46% yield, without the formation of the furan derivative.

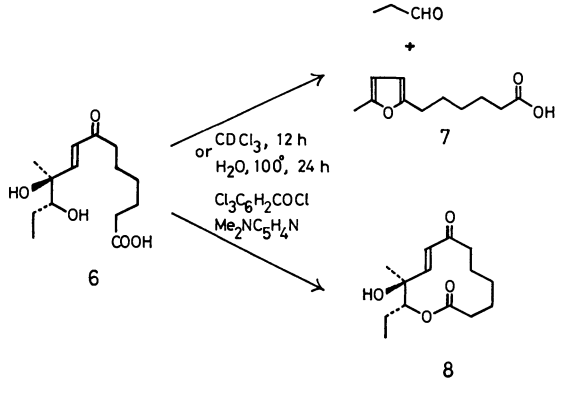

Experimental

All the procedures for the esterifications and the lactonizations were carried out under an atmosphere of nitrogen in order to exclude moisture. The melting points or boiling points are uncorrected. The IR spectra (Hitachi R-215) were obtained in liquid films or potassium bromide disks. The PMR spectra (Hitachi R-20B) were taken in deuteriochloroform solutions. The mass spectra (Hitachi RMU-6MG) were recorded with a direct-inlet system operating at 10—30 eV. The solvents were purified and dried by the standard methods.

Materials. 8-Hydroxyoctanoic acid was prepared by the hydrolysis of its methyl ester, which had been obtained by reducing methyl 7-chloroformylheptanoate with sodium borohydride in dioxane, and was purified by recrystallization from methanol. Mp 61 °C (lit, 58—58.5 °C).[17]

11-Hydroxyundecanoic acid was prepared by the sodium borohydride reduction of methyl 10-chloroformyldecanoate or by the diborane reduction of methyl hydrogen undecanedioate in THF at 0 °C, followed by the saponification of the resulting hydroxy ester, and was purified by sublimation. Mp 65—67 °C (lit, 65.5—66 °C).[18]

Commercial 12-hydroxyoctadecanoic acid and ricinoleic acid were purified by recrystallization and distillation, respectively.

*2,4,6-Trichlorobenzoyl Chloride (**2**).* According to the method in the literature, 2,4,6-trichloroaniline was converted into 2,4,6-trichlorobenzonitrile,[19] whcih was then hydrolysed to 2,4,6-trichlorobenzoic acid.[6] The acid was refluxed with thionyl chloride for 3 h. Bp 110—114 °C/9 mmHg.

*2,3,6-Trimethyl-4,5-dinitrobenzoyl Chloride (**3**).* Fuming nitric acid (4 ml) was added to a cold mixture of 2,3,6-trimethylbenzoic acid[20] (3.3 g) and concentrated sulfuric acid (12 ml), after which the mixture was kept at 40 °C for 30 min. The reaction product was then poured onto ice, and the precipitate was filtered and recrystallized from ethanol–water to give the dinitro acid (4.1 g). Mp 222 °C(dec). The acid (1.6 g) was heated with thionyl chloride (10 ml) for 12 h at 60 °C, and after the removal of thionyl chloride, the crude product was purified by sublimation. Mp 102—103 °C.

2,4,6-Trichloro-3,5-dinitrobenzoyl Chloride. 2,4,6-Trichloro-3-nitrobenzoic acid[11] (2 g) was dissolved in sulfuric acid (12 ml) heated at 85 °C, and sodium nitrate (1.7 g) was added over a period of 15 min. The mixture soon solidified. The temperature was kept at 80—90 °C for 2 h. The mixture was then worked up as usual, and the product was recrystallized from toluene. Mp 224—225 °C, 2.4 g. The dinitro acid was converted into the acid chloride by the method using phosphorus pentachloride and phosphoryl chloride and was purified by sublimation. Mp 150—152 °C.

2,4,6-Tribromo-3-nitrobenzoyl Chloride. 2,4,6-Tribromobenzoic acid[8] (3.56 g) was suspended in sulfuric acid (10 ml) and nitrated with a mixture of nitric acid (2 g) and sulfuric acid (4 g) at 0—7 °C. The mixture was kept at room temperature for 1 h, poured onto ice, filtered, and washed with dilute hydrochloric acid. Mp 186—187 °C (from toluene); 3.6 g. It was then converted into the acid chloride with phosphorus pentachloride and phosphoryl chloride. Mp 129—131 °C (from benzene–hexane).

2,4,6-Tribromo-3,5-dinitrobenzoyl Chloride. This was prepared by the method described in the case of 2,4,6-trichloro-3,5-dinitrobenzoyl chloride. 2,4,6-Tribromo-3,5-dinitroben-

Table 5. Analytical and IR data of new acids, acid chlorides, and ester

Compound (Formula)	IR (cm^{-1})	Found (Calcd) C%	H%	N%
2,3,6-Me_3-4,5-$(NO_2)_2C_6CO_2H$	1710, 1540	47.37	3.91	11.01
($C_{10}H_{10}N_2O_6$)		(47.25	3.97	11.02)
2,3,6-Me_3-4,5-$(NO_2)_2C_6COCl$	1795	44.09	3.39	10.42
($C_{10}H_9ClN_2O_5$)		(44.05	3.33	10.28)
2,4,6-Cl_3-3,5-$(NO_2)_2C_6CO_2H$	1735, 1570, 1550	26.95	0.34	8.26
($C_7HCl_3N_2O_6$)		(26.65	0.32	8.88)
2,4,6-Cl_3-3,5-$(NO_2)_2C_6COCl$	1840, 1775	25.18	0.00	8.34
($C_7Cl_4N_2O_5$)		(25.18	0	8.39)
2,4,6-Br_3-3-$(NO_2)C_6HCO_2H$	1720, 1545	20.89	0.53	3.42
($C_7H_2Br_3NO_4$)		(20.82	0.50	3.47)
2,4,6-Br_3-3-$(NO_2)C_6HCOCl$	1800, 1770	19.97	0.21	3.25
($C_7HBr_3ClNO_3$)		(19.91	0.24	3.32)
2,4,6-Br_3-3,5-$(NO_2)_2C_6CO_2H$	1720, 1545	18.90	0.19	6.22
($C_7HBr_3N_2O_6$)		(18.73	0.22	6.22)
2,4,6-Br_3-3,5-$(NO_2)_2C_6COCl$	1810, 1775	18.06	0.03	5.96
($C_7Br_3ClN_2O_5$)		(17.99	0	6.00)
3,5-Me_2-2,4,6-$(NO_2)_3C_6CO_2H$	1690, 1545	35.65	3.00	13.89
($C_9H_7N_3O_8\cdot H_2O$)		(35.65	2.99	13.86)
3,5-Me_2-2,4,6-$(NO_2)_3C_6COCl$	1760	35.49	1.93	13.83
($C_9H_6ClN_3O_7$)		(35.60	1.99	13.84)
s-Butyl 2-methylpentanoate[a]	1728	69.46	11.69	
($C_{10}H_{20}O_2$)		(69.72	11.70)	

a) Bp 88—89 °C/38 mmHg.

zoic acid; mp 275—276 °C. The acid chloride; mp 245—246 °C.

3,5-Dimethyl-2,4,6-trinitrobenzoyl Chloride. 1,3,5-Trimethyl-2,4,6-trinitrobenzene (1 g) was boiled with concentrated nitric acid (63%, 60 ml) for 80 h. The evaporation residue of the reaction mixture was then extracted with aqueous sodium carbonate, and the extract was acidified with hydrochloric acid. The acid was recrystallized from water. Mp 224—226 °C, 0.42 g. The acid chloride (phosphorus pentachloride and phosphoryl chloride) was purified by sublimation. Mp 157—159 °C.

The IR and analytical data of the new acids and acid chlorides are summarized in Table 5.

Relative Rates of Alcoholysis of Mixed Anhydrides. The acid chloride (0.3 mmol) to be examined was added to a mixture of 2-methylpentanoic acid (37 μl, 0.3 mmol) and triethylamine (42 μl, 0.3 mmol) in THF (2 ml), after which the mixture was stirred for 20 min at room temperature. After the removal of triethylamine hydrochloride by filtration, the filtrate was evaporated under nitrogen and the residue was dissolved in dichloromethane (1 ml). To this solution we added a mixture of 2-methyl-2-propanol (56 μl, 0.6 mmol) and 4-dimethylaminopyridine (73 mg, 0.6 mmol) in dichloromethane (1 ml), and the resulting mixture was stirred at room temperature. The formation of the ester was followed by GLPC by the addition of bromobenzene (50 μl) as an internal standard. The results are partly exhibited in Fig. 1.

Comparison of Solvents. The experiments were carried out in the manner described above, except that 2,4,6-trichlorobenzoyl chloride was used as the acid chloride and that dichloromethane was replaced by the other solvents (2 ml) to be examined. The results are summarized in Table 1.

Preparation of Carboxylic Esters. Carboxylic acids (0.3 mmol) and triethylamine (0.3 mmol) reacted with trichlorobenzoyl chloride (0.3 mmol) in THF (1 ml) in the same manner as above. After the removal of triethylamine hydrochloride and the solvent,[21] the resulting anhydrides were treated with alcohols (0.3—0.6 mmol) and dimethylaminopyridine (0.6—1.2 mmol) in benzene. The yields obtained by GLPC are given in Table 2. For the isolation of the esters, the reaction mixture was diluted with ether, washed successively with 3% aqueous hydrochloric acid, water, an aqueous sodium hydrogencarbonate solution, and water, dried, and distilled. They were identified by means of the PMR and IR spectra.

Preparation of Lactones. 2,4,6-Trichlorobenzoyl (or 2,3,6-trimethyl-4,5-dinitrobenzoyl) chloride (1.0 mmol) was added to a mixture of a hydroxy acid (1.0 mmol) and triethylamine (1.1 mmol) in THF (10 ml), after which the mixture was stirred for 1—2 h (or 12 h in the case of 2,3,6-trimethyl-4,5-dinitrobenzoyl chloride) at room temperature. After removal of triethylamine hydrochloride, the filtrate was diluted with toluene (500 ml) and added under the high-dilution conditions to a refluxing solution of 4-dimethylaminopyridine (3—6 mmol) in toluene (100 ml) over a period of 1.5—8 h. The reaction mixture was worked-up in a manner similar to that used in the case of the esterification and was separated by preparative TLC (silica gel G, Merck). The crude products were purified by distillation or recrystallization (Tables 3 and 4).

8-Octanolide:[22] A colorless oil; IR 1735 cm^{-1}; PMR δ 4.28 (2H, t, J=5.2 Hz, $-CH_2O-$); MS 142 (M). The dimer:[22] Colorless needles (from petroleum ether); mp 93—93.5 °C; IR 1735 cm^{-1}; PMR δ 4.15 (4H, broad t); MS 284 (M).

11-Undecanolide:[22] A colorless oil; IR 1730 cm^{-1}; PMR δ 4.2 (2H, broad t); MS 184 (M). The dimer:[22] Colorless needles (from hexane); mp 71—72 °C; IR 1730 cm^{-1}; PMR δ 3.9—4.4 (4H, broad t); MS 368 (M).

12-Octadecanolide: A colorless oil; bp 140 °C (bath temp) /20 mmHg; IR 1730 cm^{-1}; PMR δ 4.7—5.2 (H, m, –CHO–); MS 282 (M). Found: C, 76.40; H, 12.06%. Calcd for $C_{18}H_{34}O_2$: C, 76.54; H, 12.13%. The dimer: Colorless needles (from petroleum ether); mp 64—65 °C; IR 1730 cm^{-1}; PMR δ 4.6—5.2 (2H, m); MS 564 (M). Found: C, 76.55; H, 12.23%. Calcd for $C_{36}H_{68}O_4$: C, 76.54; H, 12.13%.

cis-*9-Octadecen-12-olide*: A colorless oli; bp 120 °C (bath temp)/12 mmHg; IR 1720 cm^{-1}; PMR δ 4.6—5.3 (H, m, –CHO–); 5.3—5.8 (2H, m, –CH=CH–); MS 280 (M). Found: C, 76.74; H, 11.54%. Calcd for $C_{18}H_{32}O_2$: C, 77.09; H, 11.50%. The dimer: A colorless oil; bp 160 °C (bath temp)/0.3 mmHg; IR 1720 cm^{-1}; PMR δ 4.6—5.8 (6H, m, –CHO– and –CH=CH–); MS 560 (M).

2,4,6-Tridemethyl-3-deoxymethynolide (8). A mixture of the seco-acid[16] (**6**, 272 mg, 1.0 mmol) and triethylamine (153 μl, 1.1 mmol) in THF (10 ml) was stirred for 10 min at room temperature, and then 2,4,6-trichlorobenzoyl chloride (160 μl, 1.0 mmol) was added. After stirring for 2 h at room temperature, the resulting precipitate was filtered and washed with a small amount of THF. The filtrate was diluted with benzene (500 ml) and slowly added to a refluxing solution of 4-dimethylaminopyridine (732 mg, 6 mmol) in benzene (100 ml) over a period of 40 h. The reaction mixture was washed successively with a saturated aqueous citric acid solution, water, an aqueous sodium hydrogencarbonate, and water, dried with magnesium sulfate, and evaporated. The crude product (247 mg) was separated by preparative TLC (silica gel G, Merck), with an ether–benzene mixture (2 : 1) used as the developer, to give the monomeric lactone (**8**, 116 mg, 46%), the dimer (65 mg, 26%), and the polymer (21 mg).

The Monomeric Lactone (8): Colorless needles (from dichloromethane–diisopropyl ether); mp 123 °C; IR 3520, 1725, 1680, 1620, 1225, 1150, 1085, 980 cm^{-1}; PMR δ 0.93 (3H, t, J=7.1 Hz, methyl protones of 11-ethyl), 1.2—3.0 (12H, m), 1.38 (3H, s, 10-methyl), 3.15 (H, broad s, 10-hydroxyl), 4.80 (H, dd, J=9.0 and 3.1 Hz, 11-methine), 6.29 and 6.66 (2H, q, J=16.0 Hz, 8-double bond); MS 255 (M+1), 237, 211, 196, 178, 151, 136, 135. Found: C, 65.96; H, 8.68%. Calcd for $C_{14}H_{22}O_4$: C, 66.11; H, 8.72%. Acetate (acetic anhydride and 4-dimethylaminopyridine in dichloromethane): Colorless prisms (from dichloromethane–diisopropyl ether); mp 146—147 °C; MS 296 (M), 254, 237, 225, 211, 196, 178.

The Dimer: A colorless oil; IR 3450, 1720, 1670, 1630, 975 cm^{-1}; PMR δ 0.91 (6H, t, J=7.1 Hz), 1.36 (6H, s), 1.1—3.0 (26H, m), 4.85 (2H, dd, J=9.2 and 3.2 Hz), 6.30 and 6.84 (2H, q, J=16.0 Hz); MS 508 (M), 491, 490, 237. Diacetate: Colorless needles (from dichloromethane–diisopropyl ether); mp 182.5 °C; MS 532 (M−60), 490, 472.

This work was partially supported by a Grant-in-Aid for Scientific Research from the Ministry of Education.

References

1) Presented in part at the 33rd National Meeting of the Chemical Society of Japan, Fukuoka, October, 1975.

2) a) For reviews see: K. C. Nicolaou, *Tetrahedron*, **33**, 683 (1977); T. G. Back, *ibid.*, **33**, 3041 (1977); b) T. Mukaiyama, K. Narasaka, and K. Kikuchi, *Chem. Lett.*, **1977**, 441; c) K. Narasaka, T. Masui, and T. Mukaiyama, *ibid.*, **1977**, 763.

3) a) For reviews see: Reviews cited in Ref. 2a; S. Masamune, G. S. Bates, and J. W. Corcoran, *Angew. Chem. Int. Ed. Engl.*, **16**, 585 (1977); *Angew. Chem.*, **89**, 602 (1977); b) T. Ishida and K. Wada, *J. Chem. Soc. Chem. Commun.*, **1977**, 337; c) H. Gerlach, K. Oertle, and A. Thalmann, *Helv. Chim. Acta*, **60**, 2860 (1977); d) K. Narasaka, M. Yamaguchi, and T. Mukaiyama, *Chem. Lett.*, **1977**, 959; e) S. Masamune, Y. Hayase, W. Schilling, W. K. Chan, and G. S. Bates, *J. Am. Chem. Soc.*, **99**, 6756 (1977); f) K. Narasaka, K. Maruyama, and T. Mukaiyama, *Chem. Lett.*, **1978**, 885.

4) G. Höfle and W. Steglich, *Synthesis*, **1972**, 619; H. Vorbruggen, *ibid.*, **1973**, 301.

5) N. F. Albertson, *Org. React.*, **12**, 157 (1962).

6) R. C. Fuson, J. W. Bertetti, and Wm. E. Ross, *J. Am. Chem. Soc.*, **54**, 4380 (1932).

7) Prepared from 2,6-dichloro-3-nitrobenzoic acid [K. Lehmstedt and K. Schrader, *Ber.*, **70**, 1526 (1937)] by boiling with thionyl chloride. Bp 165—168 °C/14 mmHg; IR 1800, 1770 cm^{-1}; Found: C, 33.04; H, 0.82; N, 5.57%. Calcd for $C_7H_2Cl_3O_3N$; C, 33.04; H, 0.79; N, 5.50%.

8) R. C. Fuson, J. H. Van Campen, and D. E. Wolf, *J. Am. Chem. Soc.*, **60**, 2269 (1938).

9) D. B. Cosulich, D. R. Seeger, M. J. Fahrenbach, K. H. Collins, B. Roth, M. E. Hultquist, and J. M. Smith Jr., *J. Am. Chem. Soc.*, **75**, 4675 (1953).

10) J. B. Cohen and S. H. C. Briggs, *J. Chem. Soc.*, **83**, 1213 (1903).

11) P. J. Montagne, *Chem. Centralblatt*, **1903**, I, 151.

12) J. J. Sudborough, *J. Chem. Soc.*, **67**, 587 (1895).

13) F. Kunckell and A. Hildebrandt, *Ber.*, **34**, 1826 (1901).

14) B. Luning, *Acta Chem. Scand.*, **13**, 1623 (1959).

15) J. F. Norris and V. W. Ware, *J. Am. Chem. Soc.*, **61**, 1418 (1939).

16) J. Inanaga, A. Takeda, N. Okukado, and M. Yamaguchi, *Mem. Fac. Sci., Kyushu Univ., Ser. C, Chem.*, **9**, 293 (1975).

17) P. Chuit and J. Hausser, *Helv. Chim. Acta*, **12**, 463 (1929).

18) W. H. Lycan and R. Adams, *J. Am. Chem. Soc.*, **51**, 625 (1929).

19) J. J. Sudborough, P. G. Jackson, and L. L. Lloyd, *J. Chem. Soc.*, **71**, 229 (1897).

20) H. A. Smith and J. A. Stanfield, *J. Am. Chem. Soc.*, **71**, 81 (1949).

21) In small-scale experiments like these, it is preferable to remove the THF solvent as thoroughly as possible. Otherwise, the rate of alcoholysis in benzene is retarded to some extent.

22) M. Stoll and A. Rouve, *Helv. Chim. Acta*, **18**, 1087 (1935).

Carbon-13 NMR Spectra of Stereoisomeric Substituted 2-Methylcyclohexanols and Their Acetates: A Comparison of the Observed and Predicted Chemical Shifts

Yasuhisa SENDA,* Jun-ichi ISHIYAMA, and Shin IMAIZUMI

Department of Applied Science, Faculty of Engineering, Tohoku University, Aoba, Sendai 980

(Received October 12, 1978)

The ^{13}C NMR spectra of stereoisomeric 4-*t*-butyl-2-methylcyclohexanols, 5-*t*-butyl-2-methylcyclohexanols, 2-methylcyclohexanols, and their acetates were measured. The observed chemical shifts were compared with the values estimated by using the substituent parameters of methyl, *t*-butyl, and hydroxyl groups. An appreciable deviation by vicinal substitution was found between the predicted and observed chemical shifts of C-1 and C-2. The substituent parameters of the acetoxyl group on the cyclohexane ring were estimated by means of a comparison of the chemical shifts of *cis*- and *trans*-4-*t*-butylcyclohexyl acetate, and those of *t*-butylcyclohexane.

The simple additivity relationships for carbon chemical shifts within specific families of compounds are very useful for the assignment of a certain signal to a specific carbon atom and for the prediction of the chemical shift of a certain carbon atom.[1] However, when the two substituents on a cyclohexane ring are at a geminal or vicinal position, the predicted values deviate from the observed ones.[2,3] This may be supposed to be caused by the interaction between these two groups. For two methyl groups on the adjacent or the same carbon atoms of cyclohexane, the substituent parameters of vicinal and geminal substitution were reported by Dalling and Grant.[2]

The ^{13}C NMR spectra of four stereoisomers of 5-*t*-butyl-2-methylcyclohexanols (**1**—**4**) and their acetates (**11**—**14**) were measured in order to study the effects of the steric structure of the molecule and of the vicinal substitution of the methyl and hydroxyl or acetoxyl groups on the carbon chemical shifts. The ^{13}C chemical shifts for these compounds are collected in Table 1. The assignments were based on standard methods, *i.e.*, the relative intensities, the off-resonance CW decoupling, and a comparison of the signal shift between closely related compounds. The chemical-shift differences ($\Delta\delta$) between the observed values and those calculated by using the substituent parameters of the methyl,[2] *t*-butyl, hydroxyl[3] and acetoxyl (*vide infra*) groups are also tabulated. Appreciable shift differences were found in the chemical shifts of C-1 and C-2. The chemical-shift differences of most of the other carbons were within ± 1.0 ppm.

The chemical shifts of substituted carbon atoms varied appreciably according to the orientation of the substituent. The signals of carbinol carbon and C-2 with axial substituents appeared at higher fields than those having equatorial ones. For the carbons bearing the *t*-butyl group, the signals appeared at around δ 47 when the hydroxyl or acetoxyl group was in an equa-

Table 1. Carbon-chemical shifts of stereoisomeric 2-methyl-5-*t*-butylcyclohexanols and their acetates

		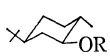				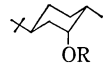		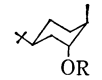	
		(**1**)	(**11**)	(**2**)	(**12**)	(**3**)	(**13**)	(**4**)	(**14**)
		(R=H)	(R=OAc)	(R=H)	(R=OAc)	(R=H)	(R=OAc)	(R=H)	(R=OAc)
C-1		77.0	78.9	73.3	76.0	71.2	74.0	72.3	75.1
	$\Delta\delta$[a]	−2.9	−4.1	−3.0	−3.4	−3.3	−4.4	1.4	−0.1
C-2		40.2	37.4	33.7	30.8	36.6	35.3	34.1	32.2
	$\Delta\delta$	−0.9	−0.3	−2.8	−2.3	−2.1	−0.9	0.0	0.6
C-3		33.7	33.4	30.9	30.7	28.9	29.5	26.6	26.9
	$\Delta\delta$	−0.5	−0.8	0.3	0.1	−0.9	−1.0	0.7	0.0
C-4		26.8	26.6	20.0	20.0	27.2	26.9	20.9	20.6
	$\Delta\delta$	0.2	−0.1	−0.1	−0.2	−0.3	−0.3	−0.1	−0.1
C-5		47.3	46.7	47.2	47.0	40.3	41.3	41.0	41.9
	$\Delta\delta$	1.2	0.6	1.0	0.8	−0.8	−1.1	−0.5	−0.6
C-6		36.9	33.2	30.0	26.8	34.8	31.9	28.9	26.1
	$\Delta\delta$	0.8	0.5	0.4	0.6	1.1	0.7	1.7	1.4
2-CH_3		18.6	18.3	10.6	11.5	18.4	18.0	16.7	16.3
	$\Delta\delta$	−4.2	−4.5	−6.9	−6.0	−4.4	−4.8	−0.8	−1.2
5-C(CH_3)$_3$		27.6	27.5	27.5	27.5	27.5	27.4	27.4	27.4
5-C(CH_3)$_3$		32.3	32.3	32.3	32.4	32.0	31.2	32.2	32.2
CH_3CO			21.2		21.3		21.1		21.4
CH_3CO			170.3		170.3		170.4		170.2

a) The observed chemical shift minus that predicted.

Table 2. Carbon-chemical shifts of *cis*- and *trans*-2-methylcyclohexanols and their acetates

	 (5) (R=H)	(15) (R=OAc)	 (6) (R=H)	(16) (R=OAc)
C-1	71.1 (71.4) [a]	73.6	76.3 (76.9)	78.2
$\Delta\delta$ [b]	−3.7	−5.2	−3.4	−4.6
C-2	36.2 (36.1)	35.0	40.4 (40.0)	37.7
$\Delta\delta$	−2.6	−2.6	−1.1	−0.4
C-3	29.2 (29.6)	29.9	34.0 (34.3)	33.9
$\Delta\delta$	−0.5	−0.6	0.0	−0.2
C-4	25.4 (24.5)	25.1	26.0 (26.1)	25.7
$\Delta\delta$	−0.5	−0.6	−0.1	−0.5
C-5	21.2 (21.8)	21.4	25.7 (25.7)	24.9
$\Delta\delta$	0.1	−0.5	0.8	0.0
C-6	32.7 (32.1)	30.0	35.7 (35.4)	32.1
$\Delta\delta$	0.1	−1.4	0.2	−0.1
2-CH_3	16.7	17.2	18.7	18.5
$\Delta\delta$	−5.3	−4.8	−4.0	−4.2
$\underline{C}H_3CO$		20.9		20.9
$CH_3\underline{C}O$		169.8		169.9

a) The values in parentheses were reported by Roberts *et al.* (J. D. Roberts, F. J. Weigert, J. I. Kroschwitz, and H. J. Reich, *J. Am. Chem. Soc.*, **92**, 1338 (1970)). b) The observed chemical shift minus that predicted.

Table 3. Carbon-chemical shifts of stereoisomeric 2-methyl-4-*t*-butylcyclohexanols and their acetates

	 (7) (R=H)	(17) (R=OAc)	 (8) (R=H)	(18) (R=OAc)
C-1	70.0	72.6	76.5	78.4
$\Delta\delta$ [a]	−4.0	−5.5	−2.9	−4.1
C-2	36.9	36.0	40.2	37.7
$\Delta\delta$	−2.3	−0.7	−1.4	−0.5
C-3	29.1	30.3	34.9	35.0
$\Delta\delta$	−0.8	−0.6	0.3	0.4
C-4	48.1	47.9	47.5	47.6
$\Delta\delta$	−0.1	0.0	0.2	0.2
C-5	20.3	20.9	26.1	25.8
$\Delta\delta$	−0.4	−0.8	0.7	0.4
C-6	33.9	31.2	35.7	32.2
$\Delta\delta$	−1.6	0.4	0.8	−0.1
2-CH_3	18.9	18.6	19.0	18.7
$\Delta\delta$	−3.9	−4.2	−3.8	−4.1
4-C($\underline{C}H_3$)$_3$	27.6	27.6	27.7	27.7
4-$\underline{C}$(CH_3)$_3$	32.5	32.5	32.2	32.2
$\underline{C}H_3CO$		21.2		20.9
$CH_3\underline{C}O$		169.9		169.8

a) The observed chemical shift minus that predicted.

Table 4. Carbon-chemical shifts of *cis*- and *trans*-4-*t*-butylcyclohexyl acetates[a] and of *t*-butylcyclohexane[b,c]

	(9) *cis*	(10) *trans*	*t*-Butyl-cyclohexane
C-1	69.2 (69.3)	73.5 (73.1)	26.9 (27.2)
C-2	30.8	32.2	27.4 (27.8)
C-3	21.8	25.6	27.8 (28.2)
C-4	47.9	47.3	48.5 (48.9)
4-C($\underline{C}H_3$)$_3$	27.5	27.7	27.6 (27.7)
4-$\underline{C}$(CH_3)$_3$	32.3	32.2	32.6 (32.7)
$\underline{C}H_3CO$	21.2	21.2	
$CH_3\underline{C}O$	169.9	169.9	

a) The values in parentheses were reported by Buchanan and Stothers (G. W. Buchanan and J. B. Stothers, *Can. J. Chem.*, **47**, 3605 (1969)). b) The carbon numbering relates, for the purposes of comparison, to the equivalent carbon in the cyclohexanol series. c) The values in parentheses were reported by Roberts *et al.* (J. D. Roberts, F. J. Weigert, J. I. Kroschwitz, and H. J. Reich, *J. Am. Chem. Soc.*, **92**, 1338 (1970)).

torial position, but at around δ 40—41 when it was in an axial position.

The NMR spectra of stereoisomeric 2-methylcyclohexanols (**5**, **6**), 4-*t*-butyl-2-methylcyclohexanols (**7**, **8**), and their acetates (**15**—**18**) were also measured (Tables 2 and 3). Most of the carbon resonances of the isomers whose hydroxyl or acetoxyl group is equatorial appeared at lower fields than those of the axial isomers.

The carbon-chemical shifts of stereoisomeric 4-*t*-butylcyclohexyl acetates (**9**, **10**) are listed in Table 4. The acetoxyl groups of *cis*- and *trans*-4-*t*-butylcyclohexyl acetates have been supposed to take exclusively an axial and an equatorial orientation respectively, judging from the confromational free energies of the acetoxyl and *t*-butyl groups.[4] Comparisons of the carbon-chemical shifts of t-butylcyclohexane, the chemical shifts of which are also tabulated in Table 4, with those of **9** and **10** give the substituent parameters for the axial and equatorial acetoxyl groups of the individual carbons of cyclohexane.

Substituent parameters of the acetoxyl group (ppm)

	Axial	Equatorial
C-1	42.3	46.6
C-2	3.4	4.8
C-3	−6.0	−2.2
C-4	−0.7	−1.2

The distribution of the conformational isomers of **5** and **15** is simply estimated from the conformational free energies[4] of the methyl, hydroxyl, and acetoxyl groups as being approximately 84% axial and 16% equatorial hydroxyl or acetoxyl conformers, while the corresponding values of **6** and **16** are 2% axial and 98% equatorial. The predicted chemical shifts of the ring carbons for each conformer are calculated using

the substituent parameters. The predicted values for these isomers can be obtained from the above conformational distribution by using the Eliel equation.[5] Similarly to the case of *t*-butylmethylcyclohexanols, appreciable shift differences between the observed and predicted values are found for the chemical shifts of C-1 and C-2.

In order to examine the correlation of the $\Delta\delta$ values with the stereochemical relationship of the methyl and hydroxyl or acetoxyl groups on the vicinal position, these values of *t*-butylmethylcyclohexanols and their acetates, the substituents of which are conformationally rigid, were compared with each other. The chemical-shift deviation of C-1 and C-2, the substituents on which are in a gauche-*cis* relation, is larger than that in gauche-*trans*, while that in anti is the smallest. These findings indicate that the dihedral angle between the methyl and hydroxyl or acetoxyl groups contributes to the magnitude of the γ-effect.

The chemical shifts for the equatorial 2-methyl groups are around δ 18—19 for **1**, **3**, **7**, **8**, and their acetates. The resonance signals for the axial methyl groups shift to higher fields, appearing at δ 10.6 for **2**, 11.5 for **12**, 16.7 for **4**, and 16.3 for **14**. The NMR spectra of stereoisomeric 1-*t*-butyl-4-methylcyclohexanes show that the chemical shift for an axial methyl group on the cyclohexane ring is δ 17.5 and that for an equatorial methyl group is δ 22.8.[6] By comparing the chemical shifts on the 2-methyl groups of **1**—**4**, **7**, **8**, and their acetates with those of the corresponding 1-*t*-butyl-4-methylcyclohexanes, the deviation can be regarded as the γ-effect parameters of the hydroxyl group on the methyl group. The values, -3.9——-6.9 ppm for gauche- and -0.8——-1.2 ppm for anti-relation, are smaller than those of the corresponding γ-effect parameters of the hydroxyl group on the cyclohexane-ring carbons, which are found to be -7.2 ppm for gauche- and -2.5 ppm for anti-relation. This is similar to the case of the methyl group, the γ-gauche effect of which has been reported to be -6.37 ppm on the cyclohexane-ring carbons and -2.82 ppm on the vicinal methyl carbon.[2] Such a difference is attributable to the situation of γ-carbons; the 2-methyl group, which can rotate freely around the carbon–carbon bond, is less restricted than the ring carbons. The predicted chemical shifts of the methyl carbons of **5**, **6**, **15**, and **16** were obtained by taking account of the conformational distributions and the carbon chemical shifts of the methyl group in stereoisomeric 1-*t*-butyl-4-methylcyclohexanes.

The ^{1}H NMR spectra of cyclohexanols **1**—**4** were also examined in search of any possible spectral correlation with their configurational structures. These compounds showed no appreciable difference in the stereochemical heterogeneity. The signals of the C-1 protons of **1** and **2**, which have an equatorial hydroxyl group, appeared at δ 3.64 and 3.67 respectively as a multiplet, while those of **3** and **4**, which have an axial hydroxyl, appeared at δ 3.77 as a broad singlet. The signals of the 2-methyl protons partially overlapped with those of the 5-*t*-butyl methyl protons, so that it is impossible to read their positions accurately from the spectra. On the other hand, the carbon-chemical shifts for the 2-methyl groups reported here have made it possible to determine the confirgurations of all the stereoisomers of the molecule.

The $\Delta\delta$ values of *t*-butylmethylcyclohexanols and their acetates are regarded as the parameters of the vicinal substitution of methyl and hydroxyl or acetoxyl groups. These values are useful for the prediction of the chemical shifts of those compounds which have 2-methylcyclohexanol or its acetate moiety.

Experimental

NMR Spectra. The ^{13}C FT-NMR spectra were obtained at 25.15 MHz with a JEOL JNM-MH-100 instrument equipped with a JNM-MFT-100 Fourier transform accessory; the instrument was controlled by means of a JEC-6 spectrum computer. The samples were dissolved in $CDCl_3$, the deuterium signal of which provided a field-frequency lock; the concentrations were 30% (w/v). The measurement conditions were as follows: pulse width, 27.5 μs (*ca.* 45°); repetition time, 4 s; spectral width, 6250 Hz; data point, 8192; acquisition time, 0.65 s. Noise-modulated proton decoupling was carried out at a nominal power of 20 W. All the chemical shifts are expressed in δ (ppm downfield from internal Me_4Si). Each observed chemical shift is estimated to be accurate to $\pm$0.1 ppm.

5-t-Butyl-2-methylcyclohexanols[7,8] ***(1)—(4) and Their Acetates***[7] ***(11)—(14).*** The hydrogenation of *cis*-5-*t*-butyl-2-methyl-2-cyclohexenol[9] over Raney Ni in ethanol gave a mixture of **1** and **2** (**1**, 73%; **2**, 27%); yield, 85%. The hydrogenation of *trans*-5-*t*-butyl-2-methyl-2-cyclohexenol[9] over PtO_2 in ethanol gave a mixture of **3** and **4** (**3**, 66%; **4**, 34%); yield, 91%. The mixtures were separated by preparative GLC. Alcohols **1** and **4** were identified by a comparison of the relative retention times of GLC with those of the hydroboration products[10] of 4-*t*-butyl-1-methylcyclohexene. Alcohols **2** and **3** were identified by a comparison of the relative retention times of GLC with those of the LAH-reduction products[11] of *cis*- and *trans*-5-*t*-butyl-2-methylcyclohexanone (**1**, 70%; **3**, 30% from *cis*-ketone: **2**, 95%; **4**, 5% from *trans*-ketone). The acetates were prepared with Ac_2O in pyridine.

4-t-Butyl-2-methylcyclohexanols,[12] ***(7) and (8), and Their Acetates,***[13] ***(17) and (18).*** The hydrogenation of 4-*t*-butyl-2-methylphenol over the Rh–Al_2O_3 catalyst in ethanol, followed by Al_2O_3 column chromatography using benzene as the eluent, gave pure **7**; yield, 42%. *cis*-4-*t*-Butyl-2-methylcyclohexanone, which had been prepared by the $Na_2Cr_2O_7$ oxidation of **7**, was reduced with LAH to give a mixture of **8**[10] (86%) and **7** (14%); yield, 89%. The mixture was separated by Al_2O_3 column chromatography, using benzene as the eluent. The acetates were prepared with Ac_2O in pyridine.

The structure of each isomer was confirmed by the ^{1}H NMR spectra and by the analytical GLC.

References

1) J. B. Stothers, "Carbon-13 NMR Spectroscopy," Academic Press, New York (1972), p. 390.
2) D. K. Dalling and D. M. Grant, *J. Am. Chem. Soc.*, **94**, 5318 (1972).
3) Y. Senda, J. Ishiyama, and S. Imaizumi, *Tetrahedron*, **31**, 1601 (1975).
4) J. A. Hirsch, "Topics in Stereochemistry," ed by N. L. Allinger and E. L. Eliel, Wiley Interscience, Vol. 1, New York (1967), Vol. 1, p. 199.

5) E. L. Eliel, *Chem. Ind. (London)*, **1959**, 568.
6) Y. Senda and S. Imaizumi, *Tetrahedron*, **31**, 2905 (1975).
7) J. Sicher and M. Tichy, *Collect. Czech. Chem. Commun.*, **32**, 3687 (1967).
8) S. Imaizumi, Y. Senda, J. Ishiyama, K. Gohke, S. Komatsu, M. Uragami, M. Satoh, and H. Nakajima, *Asahi Garasu Kogyo Gijutsu Shorei-Kai Kenkyu Hokoku*, **32**, 171 (1979).
9) Y. Senda, S. Imaizumi, S. Ochiai, and K. Fujita, *Tetrahedron*, **30**, 539 (1974).
10) D. J. Pasto and F. M. Klein, *J. Org. Chem.*, **33**, 1468 (1968).
11) N. A. LeBel and G. G. Ecke, *J. Org. Chem.*, **30**, 4316 (1965).
12) F. Sipos, J. Krupicka, M. Tichy, and J. Sicher, *Collect. Czech. Chem. Commun.*, **27**, 2079 (1962).
13) M. Pankova, J. Sicher, and M. Tichy, *J. Chem. Soc., B*, **1968**, 365.

Chemistry of *N*-Thiosulfinylanilines. I. Reactions of Sterically Hindered Anilines with Sulfur Chlorides. Preparation of *N*-Thiosulfinylanilines

Yoshio INAGAKI, Renji OKAZAKI, and Naoki INAMOTO*

Department of Chemistry, Faculty of Science, The University of Tokyo, Hongo, Tokyo 113

(Received November 7, 1978)

Reaction of 2,4-di-*t*-butyl-6-methylaniline (**3**) with disulfur dichloride afforded 2,4-di-*t*-butyl-6-methyl-*N*-thiosulfinylaniline (**4**) as a stable compound in 80% yield. Reaction of 2,4,6-tri-*t*-butylaniline (**1**) with disulfur dichloride gave in 70% yield 2,4,6-tri-*t*-butyl-7,8-dithia-9-azabicyclo[4.3.0]nona-2,4,9-triene, which in solution, exists as a tautomeric mixture with 2,4,6-tri-*t*-butyl-*N*-thiosulfinylaniline (**2b**) as a minor component. In the reactions with 2,4-di-*t*-butyl-6-isopropyl- or 2,4,6-trimethylaniline, *N*-thiosulfinylanilines obtained were unstable at ambient temperature. Aniline **1** reacted with sulfur dichloride to give **2** and the corresponding sulfur diimide and *N*-sulfinylaniline. The reaction of **4** with the dichloride afforded **4** and the corresponding sulfur diimide.

p-Dimethylamino-*N*-thiosulfinylaniline has been the only compound that has thiosulfinylamino group.[1] However, the reported yield in the reaction of *p*-dimethylaminonitrosobenzene or *p*-dimethylamino-*N*-sulfinylaniline with phosphorus pentasulfide was poor (15 or 1% respectively). Moreover, this compound could not be purified by chromatography, and appeared to be air-sensitive.[2]

Protection of a reactive group by bulky substituents often stabilizes the compounds and has an advantage over stabilization brought about by introduction of a strongly electron-donating or -withdrawing group, since the nature of a functional group to be studied is electronically less perturbed. As part of our study on poly-*t*-butylbenzene derivatives,[3] we undertook an investigation on steric protection of thiosulfinylamino group and a stable thiosulfinylamino compound was obtained in a high yield by a reaction of disulfur dichloride with a sterically hindered aniline. Although the reaction of disulfur dichloride with aniline leading to the formation of 1,2,3-benzodithiazol-2-ium chloride (Herz compound) is known as the Herz reaction[4] and has been extensively studied, there has been no report on the reaction of S_2Cl_2 with anilines bearing two ortho substituents. This paper describes the results of the reaction with such hindered anilines.

Results and Discussion

Reaction of 2,4,6-tri-*t*-butylaniline (**1**) with disulfur dichloride (S_2Cl_2) in the presence of triethylamine in ether at 0 °C for 1 h afforded a compound with a molecular formula $C_{18}H_{29}NS_2$ in 70% yield; the molecular weight was determined by mass spectrometry (M^+: *m/e* 323) and vapor pressure osmometry in benzene at 39.4 °C (323). In solution, this compound was found to be a mixture of two isomers (**2a** and **2b**) on the following basis.

1) The compound is yellow crystalline material but reddish in solution: a very weak absorption at 535 nm was observed in a fairly concentrated solution (*ca.* 2.5×10^{-2} M). This absorption around 540 nm is considered to be characteristic of the *N*-thiosulfinylanilines (see Ref. 1 and the data listed in Table 1).

2) The NMR spectrum shows the presence of two compounds; the major one (**2a**) has three singlets due to nonequivalent *t*-butyl groups at δ 0.83, 1.18, and 1.38, and two pairs of doublet due to nonequivalent olefinic protons at 5.87 and 6.39, while the minor one (**2b**) has two singlets due to *t*-butyl groups at δ 1.31 (2 and 6 positions) and 1.34 (4 position), and a singlet due to the two equivalent aromatic protons. The molar ratio of the two species was calculated based on the NMR signal intensities of the two olefinic protons of **2a** and the two aromatic protons of **2b** and found to vary reversibly with temperature. The typical results are shown in Table 2. The compound (**2**) exists only as a monomer in the solid state and the structure of **2a** was confirmed by X-ray crystallographic analysis.[5]

Table 1. Electronic spectra of *N*-thiosulfinylanilines

Compound	Solvent	λ_{max} nm, (ε)
2a+**2b**	hexane	268(2610), 292(2580), 340(2050), 410(3480), 535(weak)
4	hexane	270 sh(1470), 310 sh(1940), 343(5590), 476(2190), 536 sh(1190)
8	pentane	272 sh(2060), 305 sh(2330), 343(6960), 483(1810), 542 sh(1130)
10	pentane	336(5700), 462(1900), 540 sh(870)

Table 2. Equilibrium constant in CD_2Cl_2 (0.48 M)

Temp	[**2a**]/[**2b**]	ΔG(kcal/mol)
35 °C	14.2	1.62
0 °C	33.7	1.91

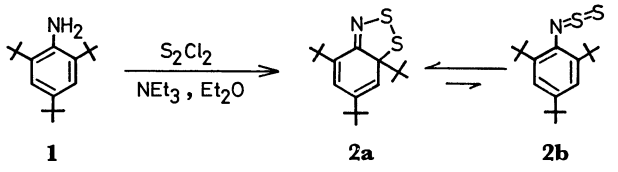

1 **2a** **2b**

Unlike the case of **1**, a similar reaction with 2,4-di-*t*-butyl-6-methylaniline (**3**) gave the corresponding *N*-thiosulfinylaniline (**4**) in 80% yield, which was deep purple crystals and stable at ambient temperature. The electronic spectra are tabulated in Tables 1 and 3; the visible part of the spectra did not show any appre-

Table 3. Solvent effect on electronic spectra of **4**

Solvent	λ_{max} nm, (ε)		
Hexane	343(5590),	476(2190),	536 sh(1190)
CCl_4	345(5830),	480(2230),	548 sh(1280)
EtOH	343(6000),	478(2170),	544 sh(1260)

ciable solvent effect (Table 3). No evidence for the ring-chain tautomerism as observed for **2** was obtained for this compound. X-Ray analysis established the structure (**4**).[5]

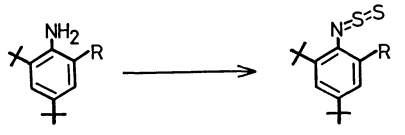

3: R=Me
7: R=*i*-Pr

4: R=Me
8: R=*i*-Pr

thus eliminating other possible structures, *i.e.*, (dithionitro)benzene (**5**) or dithiaziridine (**6**).

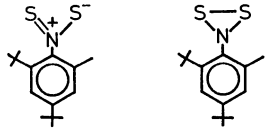

5 **6**

A similar reaction of 2,4-di-*t*-butyl-6-isopropylaniline (**7**) gave the corresponding *N*-thiosulfinylaniline (**8**) as a purple oil (14%), which decomposed slowly at room temperature. The electronic spectrum is listed in Table 1. The isolation of analytically pure specimen was difficult because of its instability. The fact that more sterically hindered *N*-thiosulfinylaniline (**7**) was less stable than **4** is noteworthy and this point will be discussed in the accompanying paper[8] in connection with the thermolysis of these *N*-thiosulfinylanilines.

The reaction of 2,4,6-trimethylaniline (**9**) with disulfur dichloride under similar conditions gave no *N*-thiosulfinylaniline. However, lowering of both reaction temperature (−78 °C, 2 h) and work-up temperature (−2 °C) enabled us to isolate **10** in 2% yield as a reddish purple oil (see Table 1 for the electronic spectrum), although satisfactory analytical data could not be obtained because of its instability.

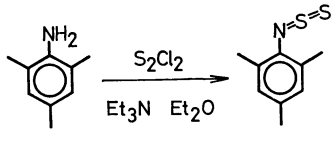

9 **10**

Unlike both aforementioned reactions and the Herz reaction, the reaction of 2,5-di-*t*-butylaniline (**11**) with disulfur dichloride under conditions similar to those for the reaction of **1** gave *N*,*N*′-bis(2,5-di-*t*-butylphenyl)sulfur diimide (**12**) in 70% yield as orange crystals.

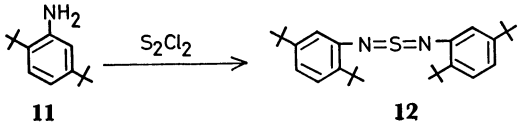

11 **12**

The above results indicate that the reactions of disulfur dichloride with anilines substituted at both ortho positions gave *N*-thiosulfinylanilines, although they are fairly unstable in the absence of bulky substituents. Therefore, existence of a highly electron-donating group (as in *p*-dimethylamino-*N*-thiosulfinylaniline)[1] is not essential for preparation of a thiosulfinylamino compound.

N-Thiosulfinylanilines were obtained also by the reactions of **1** and **3** with sulfur dichloride (SCl_2). In these cases, considerable amounts of the sulfur diimides were obtained. The *N*-sulfinylaniline (**15**) was formed as well.

$$\mathbf{1} \xrightarrow[Et_3N,\ Et_2O]{SCl_2} \mathbf{2}\ (23.7\%) + Ar^1\text{-}N{=}S{=}N\text{-}Ar^1\ (12.6\%) + Ar^1\text{-}N{=}S{=}O\ (\mathbf{14},\ 11.9\%) + \mathbf{1}\ (\mathbf{15},\ 45\%)$$

$Ar^1 = 2,4,6\text{-}(t\text{-}Bu)_3C_6H_2$

$$\mathbf{3} \xrightarrow[Et_3N,\ Et_2O]{SCl_2} \mathbf{4}\ (16.9\%) + Ar^2\text{-}N{=}S{=}N\text{-}Ar^2\ (50.1\%) + \mathbf{3}\ (26.3\%)$$

$Ar^2 = 2,4\text{-}(t\text{-}Bu)_2\text{-}6\text{-}MeC_6H_2$

Formation of **2** or **4** may be ascribed to the reactions of **1** or **3** with disulfur dichloride, because sulfur dichloride is known to dissociate partly into disulfur dichloride and chlorine molecule.[6]

Reactions of **1** and **3** with thionyl chloride gave *N*-sulfinylanilines **15** (83.0%) and **16** (72.3%), respectively. These *N*-sulfinylanilines showed no tendency to undergo intramolecular cyclization into **17** unlike the case of **2**.

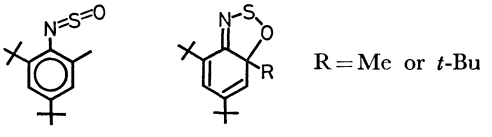

16 **17** R=Me or *t*-Bu

Experimental

All melting points were uncorrected. The IR and UV spectra were recorded with Hitachi EPI-G2 and Hitachi EPS-3 spectrophotometers, respectively. The NMR spectra were measured with a Hitachi R-20B spectrometer using tetramethylsilane as an internal standard. The mass spectra were recorded with a Hitachi RMU-6L mass spectrometer. Molecular weights were determined with a Hitachi 117 Molecular Weight Apparatus. Reactions were performed under nitrogen, and chromatographic separations were carried out by dry column chromatography (Woelm silica gel for dry column chromatography).

*Reaction of 2,4,6-Tri-t-butylaniline (**1**) with S_2Cl_2.* A solution of S_2Cl_2 (261 mg, 1.94 mmol) in ether (1.7 ml) was added dropwise to a solution of 2,4,6-tri-*t*-butylaniline[7] (500 mg, 1.91 mmol) and triethylamine (399 mg, 3.95 mmol) in ether (20 ml) with stirring at 0 °C. After being stirred for 1 h, the reaction mixture was washed with water, and dried ($MgSO_4$). Removal of the solvent gave a brown tarry material, which was chromatographed on silica gel with hexane. The first fraction gave 16 mg of sulfur. The second fraction afforded 434 mg (1.34 mmol, 70.2%) of 2,4,6-tri-*t*-butyl-7,8-dithia-9-azabicyclo[4.3.0]nona-2,4,9-triene (**2a**) as yellow crystals (mp 92.5—94 °C), which were recrystallized three times from ethanol; mp 96—97 °C; IR (KBr):

2950, 1625, 1475, 1455, 1385, 1360, 1255, 835, 665, and 638 cm^{-1}; NMR (CCl_4): the major component (**2a**) δ 0.83 (s, 9H), 1.18 (s, 9H), 1.38 (s, 9H), 5.87 (d, J=2 Hz, 1H), and 6.39 (d, J=2 Hz, 1H); the minor component (**2b**): 1.31 (s, 18H), 1.34 (s, 9H), 7.34 (s, 2H); λ_{max}^{hexane} (ε): 240 sh (4720), 268 (2610), 292 (2580), 340 (2050), 410 nm (3480), and 535 sh (very weak); *m/e* 323 (M^+, trace), 291 (4.4%), 266 (72), 251 (49), 244 (100), and 236 (49): mol wt (vapor pressure osmometry in benzene, 39.4 °C); 322.9 (Calcd: 323.55).

Found: C, 66.64; H, 8.96; N, 4.08; S, 19.72%. Calcd for $C_{18}H_{29}NS_2$: C, 66.84; H, 9.04; N, 4.33; S, 19.79%.

The third fraction gave 10 mg of orange crystals, which were identified as *N,N'*-bis(2,4,6-tri-*t*-butylphenyl)sulfur diimide (**14**)[8] by the IR spectrum and TLC. From the last fraction aniline (**1**) (52 mg, 10.4%) was recovered.

Reaction of 2,4-Di-t-butyl-6-methylaniline (3) with S_2Cl_2. A solution of S_2Cl_2 (624 mg, 4.62 mmol) in ether (4.2 ml) was added dropwise to a solution of **3**[7] (993 mg, 4.52 mmol) and triethylamine (839 mg, 8.3 mmol) in ether (40 ml) with stirring at 0 °C. After being stirred for 1 h, the reaction mixture was poured into water, and the organic layer was dried ($MgSO_4$). Removal of the solvent gave a dark purple tar, which was subjected to chromatographic separation (silica gel, hexane). The first fraction gave 27 mg of sulfur. The second purple fraction gave 1.021 g (80.1%) of 2,4-di-*t*-butyl-6-methyl-*N*-thiosulfinylaniline (**4**) as a dark purple tar, which crystallized on standing (mp 53—54 °C). Repetitive recrystallizations from aq methanol afforded analytically pure specimen, mp 67—68 °C; IR (KBr): 2950, 1590, 1455, 1360, 1222, 1169, 995, 940, 870, 780, 760, 690, 650, and 620 cm^{-1}; NMR (CCl_4): δ 1.33 (s, 18H), 2.02 (s, 3H), and 7.22 (ABq, $\Delta\delta$=0.22, J=2 Hz, 2H); λ_{max}^{hexane} (ε): 270 sh (1270), 310 (1940), 343 (5590), 476 (2190), and 536 sh nm (1190); *m/e*: 281 (M^+, 0.5%), 266 (20), 224 (100), 217 (18), 209 (18), and 204 (20); mol wt (vapor pressure osmometry in benzene at 39.4 °C): 295. Found: C, 64.01; H, 8.46; N, 5.10; S, 22.97%. Calcd for $C_{15}H_{23}NS_2$: C, 64.01; H, 8.24; N, 4.98; S, 22.78%.

The third fraction gave 86 mg of orange tar, which was treated with preparative TLC (silica gel, benzene) to give 28 mg (2.6%) of *N,N'*-bis(2,4-di-*t*-butyl-6-methylphenyl)-sulfur diimide (**13**), which was identified by comparison of the NMR, IR, and mass spectra with those of an authentic sample obtained by photolysis of **4**.[9] The fourth fraction gave 49 mg (4.9%) of **3**.

This reaction was performed in a larger scale using 20 g of **3**, where conventional column chromatography was used to separate **4** from the reaction mixture for the purpose of preparative convenience. Hexane could also be used as reaction solvent instead of ether.

Reaction of 2,4-Di-t-butyl-6-isopropylaniline (7) with S_2Cl_2. To an ice-cold solution of **7**[10] (517 mg, 2.09 mmol) and triethylamine (460 mg, 4.55 mmol) in ether (30 ml), a solution of S_2Cl_2 (294 mg, 2.18 mmol) in ether (10 ml) was added dropwise with stirring. After additional stirring for 45 min at 0 °C and then usual work up, the resulting residue was chromatographed (silica gel, pentane). A red purple part of the column was eluted with pentane to give a red purple solution, which was used for measurement of an electronic spectrum. Removal of the solvent gave 93 mg (14.4%) of 2,4-di-*t*-butyl-6-isopropyl-*N*-thiosulfinylaniline (**8**) as a purple oil. IR (neat): 1595, 1360, 1128, and 1000 cm^{-1}; NMR (CCl_4): δ 1.12 (d, J=6.5 Hz, 6H), 1.34 (s, 9H), 1.36 (s, 9H), 2.58 (sep, J=6.5 Hz, 1H), and 7.27 (ABq, $\Delta\delta$=0.13, J=2 Hz); $\lambda_{max}^{pentane}$ (ε): 272 sh (2060), 305 sh (2330), 343 (6960), 483 (1810), and 542 sh nm (1130).

Reaction of 2,4,6-Trimethylaniline (9) with S_2Cl_2. To a solution of **9** (998 mg, 7.38 mmol) and triethylamine (1.495 g, 14.8 mmol) in ether (50 ml), a solution of S_2Cl_2 (1.247 g, 9.24 mmol) in ether (30 ml) was added dropwise with stirring at −78 °C. After additional stirring for 40 min at −78 °C, an insoluble part was filtered off at −78 °C. The red-purple filtrate was condensed under reduced pressure at −10 °C. The residue was chromatographed (silica gel, pentane) at −2 °C. A red-purple fraction which contained 2,4,6-trimethyl-*N*-thiosulfinylaniline (**10**) was eluted with pentane at −2 °C to give a red solution (100 ml), which was immediately used for measurement of an electronic spectrum. The concentration of the solution was determined to be 0.3 g/l on the basis of the weight of the residue from a 5 ml-portion of the eluted solution. Thus the yield of **10** was 30 mg (2%). Removal of the solvent at −10 °C afforded a red purple oil, which was immediately subjected to NMR measurement in carbon tetrachloride. **10**; NMR (CCl_4, at 0 °C): δ 2.01 (s, 6H), 2.31 (s, 3H), and 6.90 (s, 2H); $\lambda_{max}^{pentane}$ (ε): 336 (5700), 462 (1900), and 540 sh nm (870).

The pentane solution of **10** obtained as above was decolorized by none of the following reagents suggesting no reaction: dimethyl acetylenedicarboxylate, *N*-phenylmaleimide, cyclohexene, or norbornadiene.

Reaction of 2,5-Di-t-butylaniline (11) with S_2Cl_2. A solution of S_2Cl_2 (1.001 g, 7.49 mmol) in ether (10 ml) was added to a solution of **11**[12] (996 mg, 4.85 mmol) and triethylamine (1.59 g, 15.7 mmol) in ether (50 ml) dropwise with stirring at 0 °C. After stirring for 1 h and usual work-up, the residue was chromatographed on silica gel with hexane. The first effluent (50 ml) gave 35 mg of sulfur. A red fraction gave 749 mg (70.4%) of *N,N'*-bis(2,5-di-*t*-butylphenyl)sulfur diimide (**12**) as a red tarry material, which was purified by TLC (silica gel, hexane) to give vermilion crystals, which were recrystallized three times from acetone; mp 86—87 °C; IR (KBr): 2960, 1475, 1385, 1355, 1280, 1095, and 822 cm^{-1}; NMR (CCl_4): δ 0.87 (s, 18H), 1.46 (s, 18H), 6.36 (d, J= 2 Hz, 2H), 6.89 (dd, J=8 and 2 Hz, 2H), and 7.16 (d, J= 8 Hz, 2H); λ_{max}^{hexane} (ε): 241.5 nm (14300), 252 sh (12900), 392 (9350); *m/e*: 438 (M^+, 13.7%), 381 (21), 203 (100), 188 (32), 146 (30), and 132 (39). Found: C, 76.96; H, 9.86; N, 6.38; S, 7.38%. Calcd for $C_{28}H_{42}N_2S$: C, 76.66; H, 9.65; N, 6.38; S, 7.31%. Aniline **11** (104 mg, 10.4%) was also recovered.

Reaction of 2,4-Di-t-butyl-6-methylaniline (3) with Sulfur Dichloride. To an ice-cold solution of **3** (908 mg, 4.14 mmol) and triethylamine (1.041 g, 10.31 mmol) in ether (40 ml), a solution of SCl_2 (432 mg, 4.19 mmol) in ether (10 ml) was added dropwise with stirring. After additional stirring for 1.5 h and usual work-up, the residue was chromatographed on silica gel with hexane. A red purple fraction gave 197 mg (16.9%) of 2,4-di-*t*-butyl-6-methyl-*N*-thiosulfinylaniline (**4**) as dark purple crystals (identified by IR and NMR). An orange fraction gave 484 mg (50.1%) of *N,N'*-bis(2,4-di-*t*-butyl-6-methylphenyl)sulfur diimide (**13**) as orange crystals (identified by IR and NMR).[8] From the subsequent fraction 239 mg (26.3%) of **3** was recovered.

Reaction of 2,4,6-Tri-t-butylaniline (1) with SCl_2. To an ice-cold solution of **1** (1.605 g, 6.15 mmol) and triethylamine (1.26 g, 12.5 mmol) in ether (40 ml), a solution of SCl_2 (640 mg, 6.21 mmol) in ether (10 ml) was added dropwise with stirring, and the mixture was stirred for 1.25 h at 0 °C. After usual work-up, the residue was chromatographed on silica gel with hexane. The first fraction gave 471 mg (23.7%) of **2**. The second fraction was rechromatographed (silica gel, hexane) to give 213 mg (12.6%) of *N,N'*-bis(2,4,6-tri-*t*-butylphenyl)sulfur diimide (**14**) and 224 mg (11.9%) of

2,4,6-tri-*t*-butyl-*N*-sulfinylaniline. From the third fraction, 722.4 mg (45%) of **1** was recovered.

14; mp 202.5—203.5 °C; IR (KBr): 2960, 1590, 1470, 1405, 1385, 1360, 1265, 1235, 1130, 875, and 770 cm^{-1}; NMR (CCl_4): δ 1.31 (s, 18H), 1.38 (s, 36H), and 7.26 (s, 4H); λ_{max}^{hexane} (ε): 332 (7650) and 414 nm (4960); *m/e* 550 (M^+, 3.8%), 291 (100), 259 (58), and 244 (48).

Found: C, 78.45; H, 10.37; N, 4.80; S, 6.04%. Calcd for $C_{36}H_{58}N_2S$: C, 78.49; H, 10.61; N, 5.08; S, 5.82%.

*Preparation of 2,4-Di-*t*-butyl-6-methyl-*N*-sulfinylaniline (**16**).* To an ice-cold solution of 2,4-di-*t*-butyl-6-methylaniline (**3**) (5.01 g, 22.9 mmol) and triethylamine (5.08 g, 50.3 mmol) in hexane (250 ml), a solution of thionyl chloride (2.97 g, 25 mmol) in hexane (50 ml) was added dropwise with stirring. After additional stirring for 70 min, the reaction mixture was washed with water, and dried ($MgSO_4$). Removal of the solvent afforded orange crystals, which were recrystallized once from aq. methanol to give 4.39 g (72.3%) of **16** (mp 54—55.5 °C), which was recrystallized three times from aq. methanol for an analytical specimen; mp 55.5—56.5 °C; IR (KBr): 1272 and 1182 cm^{-1} (NSO); NMR (CCl_4): δ 1.31 (s, 9H), 1.43 (s, 9H), 2.25 (s, 3H), and 7.20 (ABq, $\Delta\delta$= 0.13, J=2 Hz, 2H); λ_{max}^{hexane} (ε): 226 (10100), 255 (5390), 282 sh (2700), and 392 nm (2590); *m/e* 265 (M^+, 23%), 250 (77), 209 (42), 208 (81), 202 (32), and 57 (100). Found: C, 67.92; H, 8.92; N, 5.52; S, 11.95%. Calcd for $C_{15}H_{23}NOS$: C, 67.88; H, 8.73; N, 5.28; S, 12.08%.

*Preparation of 2,4,6-Tri-*t*-butyl-*N*-sulfinylaniline (**15**).* To an ice-cold solution of 2,4,6-tri-*t*-butylaniline (5.33 g, 20.4 mmol) and triethylamine (5.04 g, 49.9 mmol) in hexane (170 ml), a solution of thionyl chloride (2.70 g, 22.7 mmol) in hexane (30 ml) was added dropwise with stirring. After additional stirring for 40 min at 0 °C, usual work-up afforded 6.13 g (97.7%) of 2,4,6-tri-*t*-butyl-*N*-sulfinylaniline (**15**), which was recrystallized once from aq ethanol to give 5.21 g (83.0%) of **15** as orange crystals: mp 120.5—122 °C; IR (KBr): 1295 and 1180 cm^{-1} (NSO); NMR (CCl_4) δ 1.27 (s, 9H), 1.38 (s, 18H), and 7.28 (s, 2H); λ_{max}^{hexane} (ε): 230.5 (12400) and 410 nm (350); *m/e*: 307 (M^+, 13%), 292 (65), 251 (100), and 245 (90). Found: C, 70.61; H, 9.61; N, 4.86; S, 10.53%. Calcd for $C_{18}H_{29}NOS$: C 70.31; H, 9.51; N, 4.56; S, 10.43%.

References

1) D. H. R. Barton and M. J. Robson, *J. Chem. Soc., Perkin Trans. 1*, **1974**, 1245.

2) We tried to prepare *p*-dimethylamino-*N*-thiosulfinylaniline by the reported method[1] and observed a purple substance was formed in the reaction mixture. However, the purple color disappeared during the isolation procedure and only orange powder contaminated with sulfur was obtained.

3) Y. Inagaki, R. Okazaki, and N. Inamoto, *Bull. Chem. Soc. Jpn.*, **48**, 621 (1975); **48**, 3727 (1975); **49**, 1142 (1976).

4) W. K. Warburton, *Chem. Rev.*, **57**, 1011 (1957).

5) F. Iwasaki, R. Okazaki, and N. Inamoto, Abstracts of 10th Symposium on Structural Organic Chemistry (Oct., 1977, Matsuyama), 1S18.

6) K. A. Hofmann and W. Rudorff, "Anorganishe Chemie," 20, Auflage, Friedr. Vieweg & Sohn, Braunshweig (1969), p. 180.

7) J. Gueze, C. Ruinard, J. Soeterbroek, P. E. Verkade, H. Visser, and B. M. Wepster, *Recl. Trav. Chim. Pays-Bas*, **77**, 491 (1958).

8) Y. Inagaki, R. Okazaki, and N. Inamoto, *Bull. Chem. Soc. Jpn.*, **52**, 2002 (1979).

9) Y. Inagaki, R. Okazaki, and N. Inamoto, *Tetrahedron Lett.*, **1977**, 293.

10) Y. Inagaki, R. Okazaki, and N. Inamoto, *Bull. Chem. Soc. Jpn.*, **48**, 3727 (1975). 2,4-Di-*t*-butyl-6-isopropylaniline was also prepared by nitration (acetic acid-acetic anhydride-fuming HNO_3) followed by reduction (methanol-Na/Hg) of 3,5-di-*t*-butylcumene.[11] The procedure is similar to that reported for the preparation of 2,4-di-*t*-butyl-6-methylaniline.[7]

11) H.-D. Scharf and F. Döring, *Chem. Ber.*, **100**, 1761 (1967).

12) M. S. Carpenter, W. M. Easter, and T. E. Wood, *J. Org. Chem.*, **16**, 586 (1951).

Chemistry of *N*-Thiosulfinylanilines. II.[1] Thermolysis and Photolysis of *N*-Thiosulfinylanilines

Yoshio INAGAKI, Renji OKAZAKI, and Naoki INAMOTO*

Department of Chemistry, Faculty of Science, The University of Tokyo, Hongo, Tokyo 113

(Received November 7, 1978)

Thermolysis of 2,4-di-*t*-butyl-6-methyl-*N*-thiosulfinylaniline (**1**) in refluxing benzene afforded 2,4-di-*t*-butyl-8-thia-9-azabicyclo[4.3.0]nona-2,4,6,9-tetraene (**6**) and 2,4-di-*t*-butyl-6-methylaniline (**7**), while its photolysis resulted in the formation of *N*,*N*′-bis(2,4-di-*t*-butyl-6-methylphenyl)sulfur diimide (**17**) and **7**. The mechanism of the thermolysis involving 1,5-hydrogen migration and *o*-quinonoid intermediate has been proposed. The electronic spectrum of the initial intermediate in the photolysis was obtained in EPA matrix and tentatively assigned to a dithionitro compound (**42**) or a dithiaziridine (**41**). Thermolysis of 2,4,6-tri-*t*-butyl-7,8-dithia-9-azabicyclo[4.3.0]nona-2,4,9-triene (**4b**) equilibrated with 2,4,6-tri-*t*-butyl-*N*-thiosulfinylaniline (**4a**) gave 4,6-di-*t*-butyl-3*H*-1,2,3-benzodithiazole 2-oxide (**26**) and 2,4,6-tri-*t*-butylaniline (**27**). The reaction in the presence of a catalytic amount of *p*-toluenesulfonic acid improved the yield of both **26** and **27**, suggesting the ionic decomposition pathway. However, an ESR signal was observed during the thermal decomposition of **4** in the absence of oxygen, implying a concurrent homolytic pathway if not a major one. The mechanism of these reactions are briefly discussed. The photolysis of **4** led to **27** and *N*,*N*′-bis(2,4-di-*t*-butyl-6-methylphenyl)sulfur diimide (**43**).

In a previous paper,[1] we described the preparation of sterically hindered *N*-thiosulfinylanilines (**1**—**4**) by the reactions of the corresponding anilines with disulfur dichloride. Of these, **1** is a stable crystalline compound, while **2** and **3** are unstable at ambient temperature.

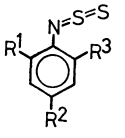

1 $R^1=R^2=t$-Bu, R^3=Me
2 $R^1=R^2=t$-Bu, $R^3=i$-Pr
3 $R^1=R^2=R^3$=Me
4a $R^1=R^2=R^3=t$-Bu

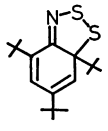

4b

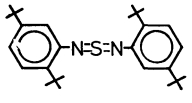

5

Furthermore, **4a** exists as a cyclized form (**4b**) in the solid state and an equilibrium between **4a** and **4b** is established in solution. In the case of 2,5-di-*t*-butylaniline, the product was not the *N*-thiosulfinylaniline but the sulfur diimide (**5**).

We disclose in this paper the thermal and photochemical behaviors of **1** and **4** and discuss the factors influencing the thermal stabilities of these *N*-thiosulfinylanilines.[2]

Results and Discussion

Thermolysis of N-*Thiosulfinylaniline (1).* Heating **1** in refluxing benzene for 21 h gave 2,1-benzisothiazole (**6**) (32%), the corresponding aniline (**7**) (26%), and sulfur. When the reaction was conducted in toluene at 70 °C (28 h), the yields of **6** and **7** were 40% and 46%, respectively.

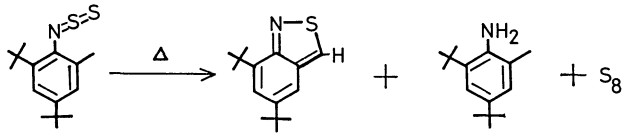

1 **6** **7**

During the reaction a trace of hydrogen sulfide was detected (as PbS). This reaction is reminiscent of the thermolysis of 2,4-di-*t*-butyl-6-methylnitrosobenzene (**8**) leading to **9** and **7**,[3] which was found by us to proceed as shown in Scheme 1.[4]

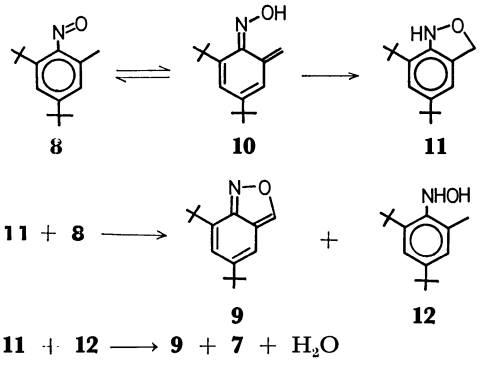

8 **10** **11**

11 + **8** → **9** + **12**

11 + **12** → **9** + **7** + H_2O

Scheme 1.

Furthermore, 2,4-di-*t*-butyl-6-ethyl- (**13**) and 2,4-di-*t*-butyl-6-isopropylnitrosobenzenes (**14**) have been found to be less stable than **8** to decompose even at 0—5 °C;[4] this order of stability is consistent with the above scheme in which the decomposition starts with 1,5-hydrogen shift, for the initially formed *o*-quinone imine (**10**) is thought to be more stable for **13** or **14** than for **8**.

Considering the similar order of stability observed in the case of *N*-thiosulfinylanilines (*i.e.*, **2** is less stable than **1**), the following mechanism (Scheme 2) starting with 1,5-hydrogen shift seems to be the most probable pathway also here.

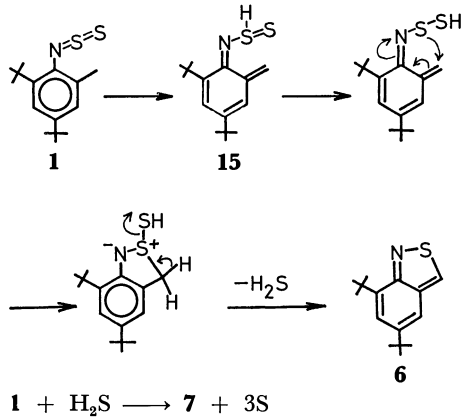

1 **15** **6**

1 + H_2S → **7** + 3S

Scheme 2.

The last step (reduction of **1** with hydrogen sulfide) was confirmed by a separate experiment.

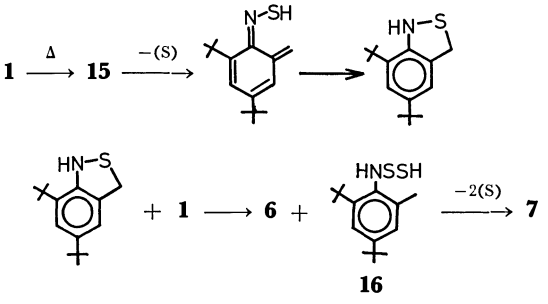

Scheme 3.

The following alternative pathway (Scheme 3) involving the thiooxime is also possible; extrusion of sulfur from such types of compounds as **15** and **16** are known.[5] However, there is no experimental evidence so far to distinguish these two mechanisms. Whichever mechanism is operative, these pathways starting with 1,5-hydrogen shift explain the instability of *N*-thiosulfinylanilines with ortho benzylic hydrogens.

Such a 1,5-hydrogen shift involving ortho benzylic hydrogens seems a general type of reaction; sulfur diimide (**17**) obtained by the photolysis of **1** (*vide infra*) cleanly disproportionated (refluxing benzene, 3 h) to yield **6** (94%) and **7** (91%). Essentially the same results were obtained also in refluxing methanol, the yields of **6** and **7** being 97 and 87% respectively.

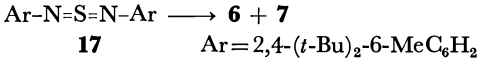

This new mode of reaction of sulfur diimide presumably proceeds also *via* 1,5-hydrogen shift from methyl group to sulfur atom followed by prototropy and cyclization as depicted in Scheme 4.

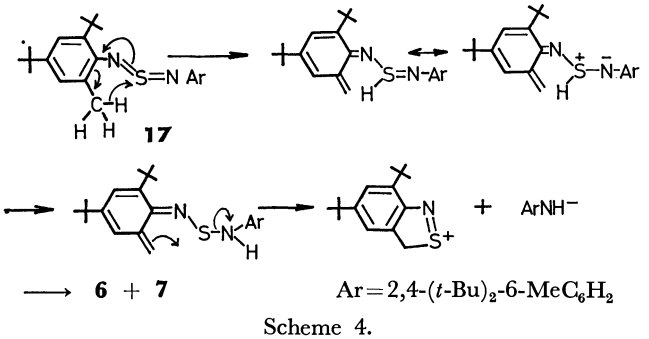

Scheme 4.

In connection with the thermal behavior of **1**, it is an interesting problem why the reaction product of 2,5-di-*t*-butylaniline with disulfur dichloride is sulfur diimide (**5**) instead of the *N*-thiosulfinylaniline **18** which would be no doubt the initial product. There are two conceivable routes leading to **5**. The one (Scheme 5) proceeds *via* three-membered ring isomer (**19**), which loses a sulfur atom to give thionitroso compound (**20**), followed by dimerization to give **21** or by cycloaddition to thiosulfinylamino group to give **22**. Subsequent extrusion of sulfur from **21** or **22** would lead to sulfur diimide (**23**). Another route consists of dimerization of the *N*-thiosulfinylaniline followed by extrusion of sulfur (Scheme 6).

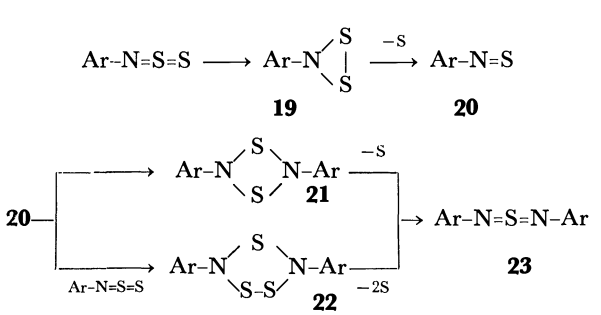

Scheme 5.

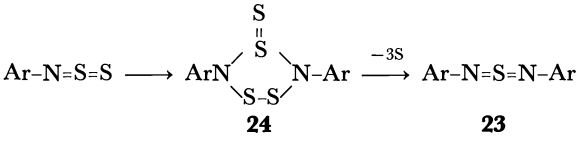

Scheme 6.

Cyclization to three-membered ring followed by extrusion of a sulfur atom has been commonly observed for other thiocumulenes: thiocarbonyl ylides give olefins,[6] thiocarbonylimines give imines,[7] a sulfine gives a ketone,[8] and *N,N'*-diphenylsulfur diimide gives azobenzene.[9] Cyclic sulfur imides such as **21** or **22** with six or less than six-membered ring appear to be unstable.[10] Bulky groups around the thiosulfinylamino group may hinder the formation of three-membered ring isomer (**19**) as well as dimerization to **24**. These considerations can thus explain the instability of **18** compared to **1**—**4**.

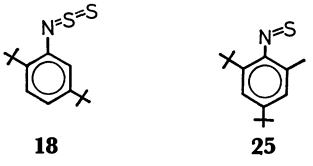

Thermolysis of **1** into **6** and **7** may be rationalized also in terms of an intermediacy of (thionitroso)benzene (**25**), which would give **6** and **7** quite similarly to the case of nitrosobenzene **8** (Scheme 1). A mercaptoamine, thio analog of **12**, is known to lose the sulfur atom to give the corresponding amine.[5a] Alternatively, formation of the sulfur diimide **17** followed by its disproportionation is also a possible route giving **6** and **7**. However, these two pathways involving the formation of **25** cannot explain the fact that 6-isopropyl derivative **2** is less stable than 6-methyl derivative **1**.

Taken together, we consider that *N*-thiosulfinylanilines decompose *via* pathways starting with 1,5-hydrogen shift if steric protection of a thiosulfinylamino group is sufficient and benzylic hydrogens are present in the ortho substituent. In the case where steric protection is insufficient, the *N*-thiosulfinylanilines would undergo decomposition into the thionitroso intermediate (**20**) *via* cyclization into the dithiaziridine (**19**) to give the sulfur diimide as the final product.

Thermolysis of N-*Thiosulfinylaniline (**4a**) Equilibrated with 1,2,3-Dithiazole (**4b**).* The above argument suggests that an *N*-thiosulfinylaniline with enough steric protection and with no ortho benzylic hydrogen would enjoy considerable thermal stability. Thus, we have examined the thermolysis of **4a** which not only

meets these requirements, but also is in equilibrium with **4b** with the latter as a major component.[1)]

Thermolysis of **4** in refluxing benzene under nitrogen for 9.7 h gave **26** (20.6%), **27** (34.2%), and sulfur (27%).

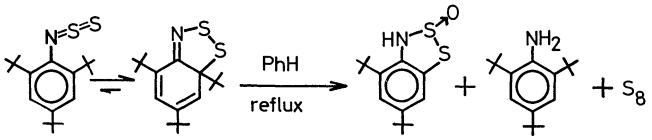

4a **4b** **26** **27**

The structure of **26** was determined by the elemental analysis, the spectral data, and the following chemical behavior. Alkaline hydrolysis of **26** followed by chromatography gave the disulfide (**28**), suggesting the 2-oxide structure of **26**; a similar hydrolysis of **30** into **31** has been reported.[11)] In the present case, **29**, a primary product, is thought to be oxidized into **28** during the work-up procedure.

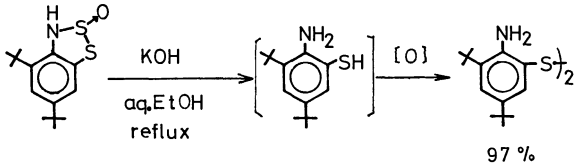

26 **29** **28**

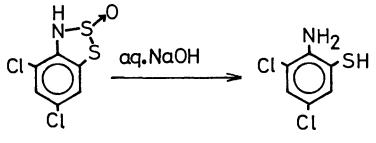

30 **31**

Thermolysis of **4** in the presence of a catalytic amount of *p*-toluenesulfonic acid improved the yield of **26** and **27** up to 39.0 and 56.1%, respectively, with 71% conversion. However, thermolysis of **4** under a stream of oxygen gave a complex reaction mixture, from which **27** (11.5%), **28** (12.2%), and **32** (9.5%) were isolated but no **26** was obtained.

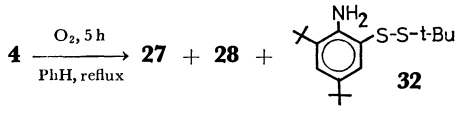

32

Thermolysis of **4** in degassed benzene at 110 °C for 5 min afforded a persistent ESR signal (a_N=8.2 G, g=2.008) as shown in Fig. 1. This signal was considered to be due to a nitrogen-centered radical **33a**, although alternative structure **33b** cannot rigorously be excluded. In any case, the large g-value (2.008) suggests that an unpaired electron is delocalized on two sulfur atoms as in the case of **34**,[12)] for which a large g-value (2.0082) was reported.

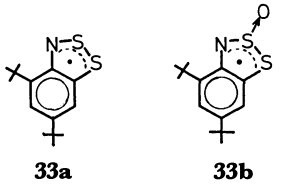

33a **33b**

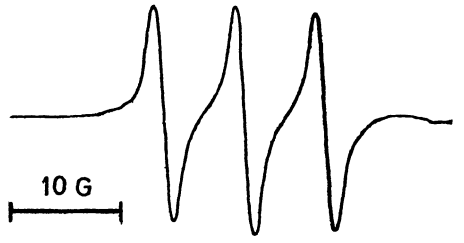

Fig. 1. An ESR spectrum of **33a**.

Table 1. ESR data of some nitrogen centered radicals

Radical	a_N (G)	g
33a	8.2	2.008
Ph-S-Ṅ-S-Ph (**34**)	11.41	2.0082
Ph-Ṅ-S-Ph (**35**)	9.59	2.0059
Ph-S-Ṅ-*t*-Bu (**36**)	11.70	2.0069

Ph-S-Ṅ-S-Ph
34

The hyperfine splitting constant (hfsc) due to a nitrogen nucleus of **33a** (8.2 G) is smaller than those of **34**,[12)] **35**,[13)] and **36**[14)] (see Table 1) suggesting the extensive delocalization of an unpaired electron into the aromatic ring and two sulfur atoms due to the planarity of the molecule.

Although the mechanism to form **26** and **27** is obscure, the following pathway shown in Scheme 7 is conceivable. Elimination of 2-methylpropene from **4b** by retro-ene reaction gives **37**, which reduces **4b** to give **38** and **39**. Then **39** may be unstable and loses the sulfur atoms to give **27** on protonation, while **38** reacts with moisture in a solvent to give **26** on deprotonation.

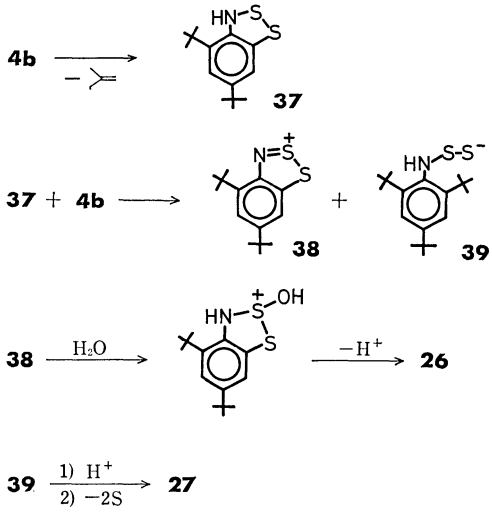

Scheme 7.

The fact that yields of **26** and **27** increased in the presence of a small amount of the acid is consistent with the above scheme, since formation of **37** appears to be catalyzed by acid.

The following free radical mechanism (Scheme 8) is also conceivable, in view of the observation of an ESR

Table 2. Yields of the photolysis products of **1**

Solvent	Concentration (g/l)	Irradiation time (h)	Isolated yields (%) **17**	**7**	S_8
Pentane	4.7	35.3[a)]	70.9	26.5	16.0
Pentane	0.7	9[b)]	42.4	17.1	11.2
Benzene	4.8	30[a)]	34.7	25.3	23.4
2-Propanol	4.7	32[a)]	36.8	28.5	19.8

a) 100 W lamp. b) 400 W lamp.

signal of what is believed to be **33a** although its importance is probably minor. The fact that the presence of oxygen did not favor the formation of **26** suggests that oxygen atom in **26** did not come from atmospheric or dissolved oxygen molecule, but from moisture in the solvent.

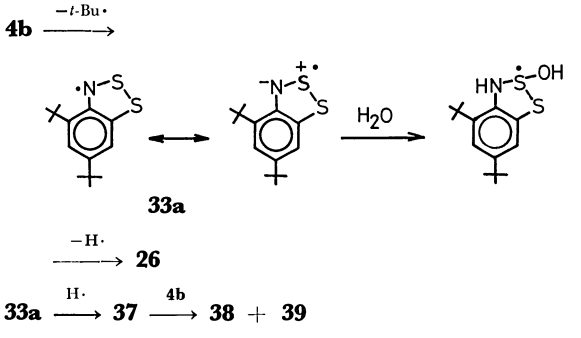

Scheme 8.

Photolysis of N-*Thiosulfinylaniline* (**1**) *and Related Compounds.* Photolysis of organic thiocumulenes of type X=S=Y has not been reported except for that of thiobenzophenone *S*-oxide, whose products are benzophenone and sulfur.[15)]

Irradiation of **1** with Pyrex-filtered light from a medium pressure mercury lamp below 25 °C afforded the sulfur diimide (**17**), aniline (**7**), and sulfur. The yields and conditions are summarized in Table 2.

$$\underset{\mathbf{1}}{\text{Ar–N=S=S}} \xrightarrow{h\nu} \underset{\mathbf{7}}{\text{ArNH}_2} + \underset{\mathbf{17}}{\text{Ar–N=S=N–Ar}} + S_8$$

$$\text{Ar} = 2,4\text{-}(t\text{-Bu})_2\text{-}6\text{-MeC}_6\text{H}_2$$

Irradition of **1** in EPA matrix was carried out at 77 K, and the change in the electronic spectra was monitored intermittently. Recorded spectra are shown in Fig. 2. During irradiation, the intensity of absorption at 340 nm decreased, while a very intense band appeared at 473 nm; isosbestic points were observed at 300 and 355 nm suggesting the species showing an absorption at 473 nm arose directly from **1**. Molar extinction coefficient of this species was estimated to be *ca.* 15000 or more on the basis of the increase of the absorption at 473 nm and the decrease of the absorption at 340 nm. Since absorption due to the nitrene **40** would be around 400 nm or below with the molar extinction coefficient of a few hundreds,[16)] and sulfur atom or its oligomers have their absorption below 420 nm,[17)] neither of these is responsible for the absorption at 473 nm. Consequently, unlike the photolysis of azides, where a nitrene is formed by elimination of nitrogen molecule, simultaneous elimination of two sulfur atoms from thiosulfinylamino group to give a nitrene can be excluded. The absorption at 473 nm may be due to one of three species (**25**, **41**, and **42**), although we have no experimental evidence to determine which is correct. In view of the well

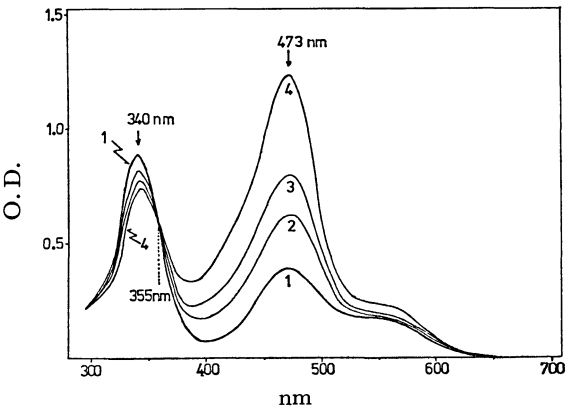

Fig. 2. Change in the electronic spectra of **1** during irradiation.

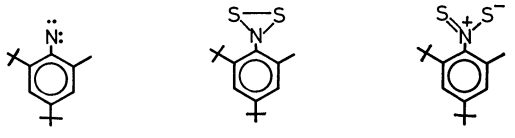

40 **41** **42**

known tendency of thiocumulenes to extrude sulfur *via* a three-membered ring in photolysis and thermolysis,[6–9,15,18)] it is reasonable to assume that **1** would change into **41** or **42** at first, then loses one sulfur to give **25**, which further reacts through pathways depicted in Scheme 5.

The aniline **7** is probably formed from photodecomposition of **17** because irradiation of **17** in pentane for 33 h gave 18.2% of **7** with recovery of **17** (68.3%). As shown in Table 3, the product ratio **7**/**17** decreases with increasing concentration. The reason for this concentration effect is not clear to us, but one explanation seems due to self quenching of **17**.

Table 3. Concentration effect of the photolysis of **1** in pentane

Concentration (g/l)	Irradiation time (h)	Molar ratio **7**/**17**
0.67	4	1.1
3.3	11.5	0.58
16.7	24.5	0.27

Photolysis of **4**. Irradiation of **4** in pentane afforded sulfur diimide (**43**) (7.5%) and aniline (**27**) (10.5%) together with some unidentified products. Since these products are very similar to those of the photoreaction of *N*-thiosulfinylaniline (**1**), the precursor of these products is considered to be the *N*-thiosulfinylaniline (**4a**).

$$\underset{\mathbf{4b}}{\overset{\mathbf{4a}}{\downarrow\uparrow}} \xrightarrow{h\nu} \underset{\mathbf{27}}{\text{Ar–NH}_2} + \underset{\mathbf{43}}{\text{Ar–N=S=N–Ar}}$$

$$\text{Ar} = 2,4,6\text{-}(t\text{-Bu})_3\text{C}_6\text{H}_2$$

Experimental

All melting points were uncorrected. The IR, UV, NMR, and mass spectra were taken with the same spectrometers as used in a previous paper.[1] ESR spectra were recorded with JEOL JES-ME spectrometer. Reactions were carried out under nitrogen unless otherwise stated.

*Thermolysis of 2,4-Di-t-butyl-6-methyl-N-thiosulfinylaniline (**1**).* *N*-Thiosulfinylaniline (**1**)[1] (404 mg, 1.44 mmol) was heated for 21 h in refluxing benzene (20 ml). Removal of the solvent followed by dry column chromatography (DCC) (silica gel, hexane) afforded 38 mg of sulfur in the first fraction. From the second fraction, 15 mg (3.7%) of **1** was recovered. The third fraction was rechromatographed (silica gel, CCl_4) to give 115 mg (32.3%) of 2,4-di-*t*-butyl-8,9-thiazabicyclo[4.3.0]nona-2,4,6,9-tetraene (**6**) which was identified by the IR, NMR, and mass spectra (mp 52—53.5 °C, recrystallized three times from methanol). Spectral and analytical data of this compound are listed in the description of thermolysis of *N,N'*-bis(2,4-di-*t*-butyl-6-methylphenyl)-sulfur diimide (**17**) (*vide infra*). The fourth fraction gave 81 mg (25.6%) of 2,4-di-*t*-butyl-6-methylaniline (**7**) which was identified by comparison of the IR and NMR spectra with those of the authentic sample.[19]

In a similar reaction, when nitrogen stream passed through the refluxing solution was led into aq lead(II) acetate, slight darkening of the solution was observed.

Heating of **1** (401 mg, 1.42 mmol) in toluene (10 ml) at 70 °C for 28 h gave 46.2% of **8**, 39.9% of **6**, and 50 mg of sulfur after a similar work-up.

*Thermolysis of N,N'-Bis(2,4-di-t-butyl-6-methylphenyl)sulfur Diimide (**17**).* Compound **17** (224 mg, 0.48 mmol) was heated for 3 h in refluxing benzene (15 ml). After removal of the solvent, the residue was chromatographed (silica gel, hexane). The first fraction gave 112 mg (94.3%) of **6** as white crystals (mp 49—52 °C), which were recrystallized three times from methanol at −78 °C to give colorless prisms, mp 52.5—53.0 °C; IR (KBr): 3080, 2900, 1358, 1245, and 745 cm^{-1}; NMR (CCl_4): δ 1.38 (s, 9H), 1.60 (s, 9H), 7.34 (ABq, J=2 Hz, $\Delta\delta$=0.14, 2H), and 8.92 (s, 1H); λ_{max}^{hexane} (ε): 232 (26900), 289.5 (8310), 300.5 (9960), and 324 nm (5230); *m/e*: 247 (M^+, 21.7%), 232 (100), 205 (12), 204 (16), 190 (15), 176 (19), 57 (16), and 41 (11). Found: C, 72.64; H, 8.64; N, 5.64; S, 12.88%. Calcd for $C_{15}H_{21}NS$: C, 72.82; H, 8.56; N, 5.66; S, 12.96%.

The second fraction gave 96 mg (91.2%) of **7**.

Thermolysis of **17** (319 mg, 0.683 mmol) in refluxing methanol (140 ml) followed by similar work-up afforded **6** (164 mg, 97.1%) and **7** (130 mg, 86.8%).

*Thermolysis of 2,4,6-Tri-t-butyl-7,8-dithia-9-azabicyclo[4.3.0]-nona-2,4,9-triene (**4b**).* Heating of **4b** (481 mg, 1.49 mmol) in refluxing benzene (25 ml) for 9.7 h gave orange solution. Removal of the solvent followed by treatment with hexane afforded 4,6-di-*t*-butyl-3*H*-1,2,3-benzodithiazole 2-oxide (**26**) as white crystals (41 mg). The filtrate was chromatographed (silica gel, hexane). The first fraction gave 15 mg of sulfur. The second fraction gave 24 mg of **4b**. The other fraction, on treatment with CCl_4 followed by filtration, gave 25 mg of **26** as white crystals, and the filtrate was chromatographed (silica gel, CCl_4). A slightly pale yellow fraction gave 133 mg (34.2%) of 2,4,6-tri-*t*-butylaniline (**27**) (identified by IR and NMR). The subsequent fraction gave 95 mg of yellow tar, which, on treatment with hexane, gave 21 mg of **26**. Thus, the total yield of **26** was 87 mg (20.6%); **26**: mp 160 °C (dec) (recrystallized four times from aq methanol); IR (KBr): 3280 (NH) and 1110 cm^{-1} (SO); NMR (CCl_4): δ 1.34 (s, 9H), 1.45 (s, 9H), 7.21 (ABq, J=1.2 Hz, $\Delta\delta$=0.12, 2H), and 7.50 (broad s); λ_{max}^{hexane} (ε): 284 sh (2130) and 294 sh nm (1560); *m/e*: 283 (M^+, 15%), 268 (23), 266 (100), 251 (39), 236 (15), 57 (21), and 41 (16); mol wt (vapor pressure osmometry, in benzene at 39.8 °C): 293.3 (calcd: 283.43). Found: C, 59.38; H, 7.69; N, 4.90; S, 22.21%. Calcd for $C_{14}H_{21}NOS_2$: C, 59.33; H, 7.47; N, 4.94; S, 22.62%.

*Thermolysis of **4b** in the Presence of p-Toluenesulfonic Acid.* A mixture of **4b** (303 mg, 0.94 mmol), *p*-toluenesulfonic acid (14 mg, 0.08 mmol), ethanol (2 ml), and benzene (20 ml) was refluxed for 3 h. Removal of the solvent followed by treatment with hexane afforded 73 mg (27.5%) of **26** as white crystals. The hexane-soluble part was chromatographed (silica gel, hexane) to give 89 mg (29.4% recovery) of **4b** and 97 mg (39.6%) of **27**.

*Thermolysis of **4b** under a Stream of Oxygen.* In refluxing benzene (20 ml), 302 mg (0.93 mmol) of **4b** was heated for 5 h under a stream of oxygen. After the solvent was removed, the residue was treated with hexane; no precipitates (**26**) were obtained. Chromatography (silica gel, CCl_4) of the residue afforded 29 mg (9.5%) of 2-amino-3,5-di-*t*-butylphenyl *t*-butyl disulfide (**32**) as a yellow tarry material, which was identified by the following spectral data: IR (neat): 3495 and 3360 cm^{-1} (NH_2); NMR (CCl_4): δ 1.27 (s, 9H), 1.35 (s, 9H), 1.43 (s, 9H), 4.45 (broad s, 2H), and 7.21 (ABq, J=2.4 Hz, $\Delta\delta$=0.08, 2H); *m/e* 325 (M^+, 2%), 293 (3), 269 (7), 254 (5), 237 (19), 236 (12), 222 (51), and 57 (100).

A crystalline material (176 mg) obtained from the second fraction was subjected to preparative TLC (silica gel, CCl_4) to give 28 mg (11.5%) of **27** and 27 mg (12.2%) of bis-(2-amino-3,5-di-*t*-butylphenyl) disulfide (**28**). These compounds were identified by comparison of the IR and NMR spectra with those of the authentic samples. Spectral and analytical data of **28** were listed in the description of hydrolysis of **26** (*vide infra*).

*Hydrolysis of 4,6-Di-t-butyl-3H-1,2,3-benzodithiole 2-Oxide (**26**).* A solution of **26** (57 mg, 0.2 mmol), potassium hydroxide (189 mg, 3.37 mmol), water (2 ml), and ethanol (7 ml) was refluxed for 2 h. The reaction mixture was neutralized by dil. HCl, and extracted with ether. The extract was washed with aq. sodium hydrogencarbonate, then with water, and dried ($MgSO_4$). After the solvent was removed, the residue was purified by preparative TLC (silica gel, CCl_4) to give 46 mg (97%) of **28** as pale yellow needles (mp 87.7—89.7 °C), which were recrystallized three times from methanol: IR (KBr): 3490 and 3370 cm^{-1} (NH_2); NMR (CCl_4): δ 1.19 (s, 18H), 1.40 (s, 18H), 4.45 (broad s, 4H), and 7.10 (ABq, $\Delta\delta$=0.08, J=2.5 Hz, 4H); *m/e*: 472 (M^+, 21%), 236 (100), 222 (48), 206 (10), 179 (10), 57 (36), and 41 (16). Found: C, 71.22; H, 9.59; N, 6.12; S, 13.67%. Calcd for $C_{28}H_{44}N_2S_2$: C, 71.13; H, 9.38; N, 5.93; S, 13.56%.

ESR Measurements. An ESR sample tube containing *ca.* 0.2 ml of benzene solution (0.05 M) was degassed by four freeze-pump-thaw cycles and heated for 5 min at 110 °C. After the sample solution was cooled to room temperature, the ESR spectra were recorded. Hyperfine splitting constants and *g*-values were determined on the base of Mn^{2+} in MnO_2.

*Photolysis of 2,4-Di-t-butyl-6-methyl-N-thiosulfinylaniline (**1**).* Typical procedures are described below. a) A pentane solution (70 ml) of **1** (329 mg, 1.17 mmol) was irradiated for 32.3 h with Pyrex-filtered light from a 100 W medium pressure mercury lamp immersed in the solution, whose temperature was controlled by external cooling with ice–water not to exceed 25 °C. After removal of the solvent, the residue was subjected to DCC (silica gel, hexane). The first fraction

gave 12 mg (16%) of sulfur. An orange fraction gave 193 mg (70.9%) of **17** as orange crystals, which were recrystallized four times from aq ethanol and once from acetone; mp 122—123 °C; IR (KBr): 2950, 1360, 1280, 1265, and 1238 cm^{-1}; NMR (CCl_4): δ 1.29 (s, 36H), 2.24 (s, 6H), 6.91 (d, J=2 Hz, 2H), and 7.17 (d, J=2 Hz, 2H); λ_{max}^{hexane} (ε): 317 (5530) and 409 nm (6560); *m/e* 466 (M^+, 0.5%), 451 (7), 247 (13), 232 (47), 219 (37), 204 (100), 57 (27), and 41 (23). Found: C, 77.05; H, 10.12; N, 5.86; S, 6.94%. Calcd for $C_{30}H_{46}N_2S$: C, 77.20; H, 9.93; N, 6.00; S, 6.87%.

The last fraction gave 83 mg of tarry metarial, which was purified by TLC (silica gel, benzene) to give 68 mg (26.5%) of 2,4-di-*t*-butyl-6-methylaniline (**7**).

b) Effect of Concentration. A solution of **1** in pentane (1.5 ml) was placed in a quartz tube, flashed with nitrogen, immersed in a water bath to keep the temperature of the solution below 20 °C, and irradiated with Pyrex-filtered light from a 400 W medium pressure mercury lamp. In this way, several solutions were irradiated at the same time. Determination of molar ratios (**7**/**17**) was performed by high speed liquid chromatography (1-m column packed with Hitachi 3010 gel, eluted with methanol). The results were shown in Table 3.

*Photolysis of **1** in EPA Matrix.* An EPA solution in a Pyrex cell was degassed by four freeze-pump-thaw cycles. This sample solution was immersed in liquid nitrogen in a Dewar vessel made of quartz which was placed in a Cary-14 spectrophotometer, and irradiated by focused light from a medium pressure mercury lamp through the Dewar vessel. Electronic spectra were recorded intermittently.

*N,N'-Bis(2,4-di-t-butyl-6-methylphenyl)sulfur Diimide (**17**).* A pentane solution (70 ml) of **17** (187 mg, 0.40 mmol) was irradiated for 33 h with a 100 W medium pressure mercury lamp immersed in the solution, whose temperature was controlled not to exceed 15 °C. The irradiated solution was examined by high speed liquid chromatography (column material: Hitachi 3010; column length: 1 m; column pressure: 45 kg/cm^2; flow rate: 1.2 ml/min; solvent: methanol) and found to show three peaks: corresponding to **7**, an unknown compound which did not correspond to **6**, and **17**. Molar ratio **7**/**17** was estimated to be 0.215. The reaction mixture was subjected to preparative TLC (silica gel, hexane, developed three times) to give 128 mg (68.3% recovery) of **17** and 28 mg of brown tarry material, which was purified by TLC (silica gel, benzene) to give 16 mg (18.2%) of **7**.

*Photolysis of **4b**.* A pentane solution (70 ml) of **4b** (402 mg, 1.24 mmol) was irradiated by Pyrex-filtered light from a 100 W medium pressure mercury lamp for 32.8 h. Temperature of the solution was controlled not to exceed 20 °C by cooling with ice-water. After removal of the solvent, the residue which was composed of many components was subjected to DCC (silica gel, hexane). From an orange fraction was obtained 38 mg of orange crystalline material, which was recrystallized from acetone to give 26 mg (7.5%) of *N,N'*-bis(2,4,6-tri-*t*-butylphenyl)sulfur diimide (**43**) (identified by comparison of the spectral data with those of an authentic sample).[1] From a pale yellow fraction, 35 mg (10.6%) of aniline (**27**) was obtained.

References

1) Part I, Y. Inagaki, R. Okazaki, and N. Inamoto, *Bull. Chem. Soc. Jpn.*, **52**, 1998 (1979).

2) Part of this work was reported in a preliminary form: Y. Inagaki, R. Okazaki, and N. Inamoto, *Tetrahedron Lett.*, **1977**, 293.

3) T. Hosogai, N. Inamoto, and R. Okazaki, *J. Chem. Soc., C*, **1971**, 3399.

4) R. Okazaki, M. Watanabe, Y. Inagaki, and N. Inamoto, *Tetrahedron Lett.*, **1978**, 3439.

5) a) D. H. R. Barton, S. V. Ley, and P. D. Magnus, *J. Chem. Soc., Chem. Commun.*, **1975**, 855; b) R. D. Baechler and S. K. Daley, *Tetrahedron Lett.*, **1978**, 101; c) R. D. Baechler, S. K. Daley, B. Daly, and K. McGlynn, *ibid.*, **1978**, 105.

6) J. Buter, S. Wassenaar, and R. M. Kellogg, *J. Org. Chem.*, **37**, 4045 (1972).

7) S. Tamagaki and S. Oae, *Bull. Chem. Soc. Jpn.*, **46**, 2608 (1973).

8) W. A. Sheppard and J. Diekmann, *J. Am. Chem. Soc.*, **86**, 1891 (1964).

9) J. L. Downie, R. Maruca, and J. R. Grunwell, *J. Chem. Soc., Chem. Commun.*, **1970**, 298.

10) Q. E. Thompson, *Quart. Reports on Sulfur Chem.*, **5**, 245 (1970).

11) L. D. Huestis, M. L. Walsh, and N. Hahn, *J. Org. Chem.*, **30**, 2763 (1965); W. K. Warburton, *Chem. Rev.*, **57**, 1101 (1957).

12) Y. Miura, M. Makita, and M. Kinoshita, *Bull. Chem. Soc. Jpn.*, **50**, 482 (1977).

13) Y. Miura and M. Kinoshita, *Bull. Chem. Soc. Jpn.*, **50**, 1142 (1977).

14) Y. Miura, H. Asada, and M. Kinoshita, *Bull. Chem. Soc. Jpn.*, **50**, 1855 (1977).

15) L. Carlsen, N. Harrit, and A. Holm, *J. Chem. Soc., Perkin Trans 1*, **1976**, 1404.

16) R. S. Berry in "Nitrene," ed by W. Lwowski, Interscience, New York (1970), p. 13.

17) C. Nishijima, N. Kanamaru, and K. Kimura, *Bull. Chem. Soc. Jpn.*, **49**, 1151 (1976) and references cited therein.

18) For a review, see Y. Inagaki and R. Okazaki, *Yuki Gosei Kagaku Kyokai Shi*, **36**, 1 (1978).

19) J. Genze, C. Ruinard, J. Soeterbroek, P. E. Verkade, and B. M. Wepster, *Recl. Trav. Chim. Pay-Bas*, **75**, 301 (1956).

Chemistry of *N*-Thiosulfinylanilines. III. Thiosulfinylamine—5*H*-1,2,3-Dithiazole Equilibrium as Studied by NMR Spectroscopy

Yoshio INAGAKI, Renji OKAZAKI, Naoki INAMOTO,* Koh-ichi YAMADA,† and Hiroshi KAWAZURA†

Department of Chemistry, Faculty of Science, The University of Tokyo, Hongo, Tokyo 113,
† *Faculty of Pharmaceutical Sciences, Josai University, Keyaki-dai, Sakado, Saitama 350-02*

(Received November 7, 1978)

Thermodynamic parameters ($\Delta H = -4.9$ kcal mol^{-1}, $\Delta S = -11.3$ cal mol^{-1} deg^{-1}) were determined for cyclization of 2,4,6-tri-*t*-butyl-*N*-thiosulfinylaniline (**1b**) (the minor component) into 2,4,6-tri-*t*-butyl-7,8-dithia-9-azabicyclo[4.3.0]nona-2,4,9-triene (**1a**) (the major component) by means of NMR spectroscopy. Using these values, π-bond of thiosulfinylamino group (–N=S=S) was estimated to be weaker than that of sulfinylamino group (–N=S=O) by, at least, 25 kcal mol^{-1}. The equilibrium ratio [**1a**]/[**1b**] is subject to considerable solvent effect, polar solvents favoring the cyclic form (**1a**). Similarity of the thiosulfinylamine–dithiazole equilibrium to that of azidoimine–tetrazole has been pointed out.

In the previous papers,[1,2] we reported that 2,4,6-tri-*t*-butyl-*N*-thiosulfinylaniline (**1b**) is in equilibrium with a cyclized form, 2,4,6-tri-*t*-butyl-7,8-dithia-9-azabicyclo[4.3.0]nona-2,4,9-triene (**1a**) in solution, while in the solid state only **1a** exists. This is, to our knowledge, the first example where aromaticity of the benzene ring is destroyed during intramolecular 1,3-dipolar cyclization, although many examples of such a ring-chain isomerization are known for azidoimine-tetrazole systems.[3] We became interested in factors influencing the equilibrium between **1b** and **1a** and this paper describes the thermodynamic properties and solvent effects of this equilibrium.

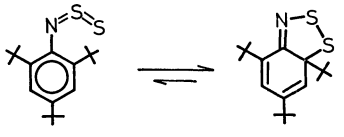

1b **1a**

Experimental

The NMR spectra were recorded with a JEOL C60-HL spectrometer (60 MHz) equipped with a variable temperature apparatus. 2,4,6-Tri-*t*-butyl-7,8-dithia-9-azabicyclo-[4.3.0]nona-2,4,9-triene (**1a**, mp 98.5—99.5 °C) was prepared as described previously.[2]

Results and Discussion

Temperature Effect. As interconversion between **1a** and **1b** was slow enough to show two sets of NMR signals due to the two tautomers (see Fig. 1), equilibrium constants were calculated based on NMR signal intensity of the two olefinic protons of **1a** and the two aromatic protons of **1b**. Table 1 shows the temperature dependence of the equilibrium constant and the free energy of isomerization measured in carbon tetrachloride solution (0.31 M) over a temperature range of 11—63 °C, where ΔG's correlate with temperatures linearly. Over the temperature range studied the major component was **1a** but the relative amount of **1b** increased with increasing temperature. Slight decomposition was observed above 60 °C. Based on the data in Table 1, the heat of isomerization (ΔH) and the entropy of isomerization (ΔS) were estimated to be -4.9 kcal mol^{-1} and -11.3 cal mol^{-1} deg^{-1}, respectively. These thermodynamic quantities bear a striking resemblance to those reported for the azidoimine–tetrazole equilibrium;[3] for instance, for the equilibrium between 2-azidopyrimidine (**2b**) and tetrazolo-

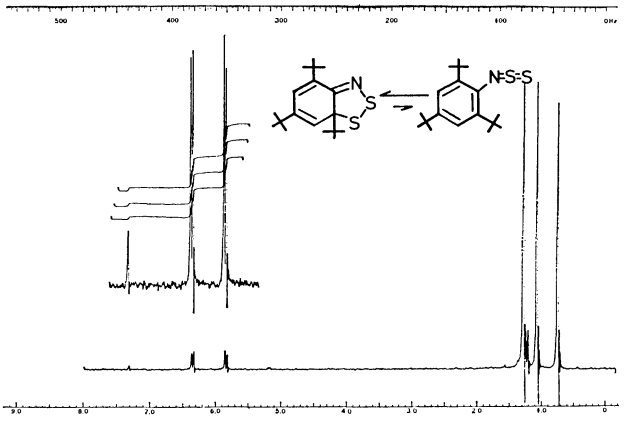

Fig. 1. NMR spectrum of an equilibribrium mixture **1a**+**1b** in CD_2Cl_2 (0.48 M) at 35 °C.

TABLE 1. TEMPERATURE DEPENDENCE OF K AND ΔG IN CCl_4

Temp (°C)	$K=\frac{[\mathbf{1a}]}{[\mathbf{1b}]}$	$-\Delta G$ (kcal mol^{-1})
11	19.5	1.68
23	14.1	1.56
30	12.0	1.50
33	10.7	1.44
38	9.9	1.42
43	9.2	1.39
48	8.2	1.34
52	6.6	1.22
58	5.7	1.14
63	5.1	1.09

At lower temperatures (*e.g.*<0 °C), linear correlation between T and ΔG did not hold because the equilibrium was reached much slower.

[1,5-*a*]pyrimidine, ΔH and ΔS have been reported to be −5.1 kcal mol^{-1} and −11.3 cal mol^{-1} deg^{-1}, respectively, in dimethyl sulfoxide-d_6.[4]

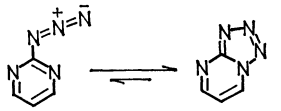

2b **2a**

For equilibria **3b**⇌**3a** and **4b**⇌**4a**, ΔH's of −4.2 and −3.4 kcal mol^{-1} have been reported.[5]

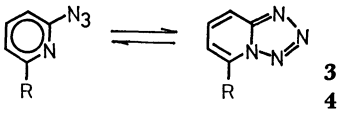

3 R=NO_2
4 R=Cl

3b, 4b **3a, 4a**

The similarity of these thermodynamic quantities, however, is somewhat surprising considering that the azidoimine–tetrazole reaction is a 6π-to-10π conversion without loss of aromaticity, at least in a formal sense, while the thiosulfinylamine–dithiazole reaction is accompanied by complete loss of aromaticity.

The exothermicity of this unusual ring formation of **1b** into **1a** may be attributable to both decreased aromaticity due to steric congestion by the three bulky groups ajacent to each other and high reactivity of the thiosulfinylamino group towards a double bond as demonstrated by 1,3-dipolar addition of *p*-dimethylamino-*N*-thiosulfinylaniline to olefins.[6] Since 2,4,6-tri-*t*-butyl-*N*-sulfinylaniline (**5**)[2] was found to have no tendency to isomerize into its cyclic form **5a**, steric congestion alone is not sufficient for ring formation. But the lack of aromaticity due to the steric congestion is an essential factor for cyclization because in the case of 2,4-di-*t*-butyl-6-methyl-*N*-thiosulfinylaniline (**6**) no evidence for the ring formation was obtained by NMR over a temperature range of −102—70 °C.

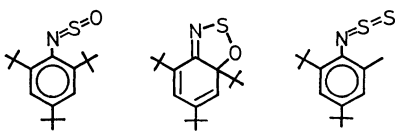

5 **5a** **6**

Difference between the π-bond energy of sulfinylamino group (–N=S=O) and that of thiosulfinylamino group (–N=S=S) can be roughly estimated using the thermodynamic data obtained above. Assuming that 1% (limit of detection) of 2,4,6-tri-*t*-butyl-*N*-sulfinylaniline (**5**) exists in its cyclic form **5a**, the free energy of isomerization of **5** into **5a** (ΔG^{NSO}) is calculated to be 2.79 kcal mol^{-1} (endothermic) at 33 °C. On the other hand, free energy of isomerization of **1b** into **1a** (ΔG^{NSS}) was −1.44 kcal mol^{-1} (exothermic) at 33 °C. If we assume that entropy changes in both isomerizations are equal and that σ bond energies of the N–S, S–O, and S–S bonds do not change through isomerization, the following equation can be given,

$$\Delta\Delta G = \Delta G^{NSO} - \Delta G^{NSS} = \Delta H^{NSO} - \Delta H^{NSS}$$
$$= (\sigma^{CO} - \pi^{NSO}) - (\sigma^{CS} - \pi^{NSS})$$
$$= 4.23 \text{ kcal mol}^{-1},$$

Table 2. Solvent effect on K at 43 °C

Solvent	ε	$K=\frac{[\mathbf{1a}]}{[\mathbf{1b}]}$
Hexane	1.89	6.3
Cyclohexane	2.02	8.6
Carbon tetrachloride	2.23	9.2
Ethyl acetate	6.02	14.5
Dichloromethane-d_2	9.08	12.2
Acetone-d_6	20.7	17.7
Acetonitrile	37.5	25

where σ^{CO} is C–O single bond energy to be gained on cyclization of **5**, σ^{CS} is C–S single bond energy to be gained on cyclization of **1b**, π^{NSO} is π bond energy of –N=S=O group, and π^{NSS} is π bond energy of –N=S=S group to be lost on cyclization. Substitution of reported values −86 and −65 kcal mol^{-1}[7] for σ^{CO} and σ^{CS}, respectively, in the above equation gives $\pi^{NSS}-\pi^{NSO}=25$ kcal mol^{-1}. Thus π-bond of –N=S=S group is weaker than that of –N=S=O group by, at least, 25 kcal mol^{-1}.

Solvent Effect. Equilibrium constants at 43 °C in various solvents are shown in Table 2, where it is demonstrated that polar solvents greatly enhance the preference of cyclic isomer **1a**, suggesting that the dipole moment of **1a** is larger than that of the *N*-thiosulfinylaniline **1b**. Actually, the dipole moment of **1a** (*ca.* 2.9 D)[8a] is larger than that of **1b** which was reasonably assumed to be nearly equal to the dipole moment of **6** (1.51 D).[8b] Interestingly, quite a similar solvent effect has been reported for azido-tetrazole equilibria;[9] in less polar solvents, the equilibrium is shifted towards the side of an azido form, suggesting that the dipole moment of an azido form is smaller than that of a tetrazole form. This situation is in line with the fact that dipole moment of phenyl azide (1.56 D)[10] is smaller than that of 1,2,3-benzotriazole (4.10 D).[10]

References

1) Y. Inagaki, R. Okazaki, and N. Inamoto, *Tetrahedron Lett.*, **1974**, 4575.

2) Y. Inagaki, R. Okazaki, and N. Inamoto, *Bull. Chem. Soc. Jpn.*, **52**, 1998 (1979).

3) For reviews, see R. N. Butler, *Chem. Ind. (London)*, **1971**, 371; M. Tisler, *Synthesis*, **1973**, 123; R. N. Butler, *Adv. Heterocyclic Chem.*, **21**, 323 (1977).

4) C. Temple, Jr., M. C. Thorpe, W. C. Coburn, Jr., and J. A. Montgomery, *J. Org. Chem.*, **31**, 935 (1966).

5) T. Sasaki, K. Kanematsu, and M. Murata, *Tetrahedron*, **27**, 5121 (1971).

6) D. H. R. Barton and M. J. Robson, *J. Chem. Soc., Perkin Trans. 1*, **1974**, 1245.

7) J. B. Hendrickson, D. J. Cram, and G. S. Hammond, "Organic Chemistry," 3rd ed, McGraw-Hill, New York (1970).

8) a) Y. Inagaki, R. Okazaki, and N. Inamoto, *Heterocycles*, **9**, 1613 (1978); b) Y. Inagaki, R. Okazaki, N. Inamoto, and T. Shimozawa, *Chem. Lett.*, 1978, 1217.

9) J. Elguero, R. Faure, J. P. Galy, and E. J. Vincent, *Bull. Soc. Chim. Belg.*, **84**, 1189 (1975); L. A. Burke, J. Elguero, G. Leroy, and M. Sana, *J. Am. Chem. Soc.*, **98**, 1985 (1976).

10) A. L. McClellan, "Tables of Experimental Dipole Moments," W. H. Feemen and Co., San Francisco (1963).

Crystal and Molecular Structure of ω-Amino Acids, ω-Aminosulfonic Acids and Their Derivatives. IX. Crystal and Molecular Structure of 3-Amino-2-hydroxy-1-propanesulfonic Acid

Yang Bae KIM,† Sachiko BANDO, Toshiyasu HOMBO, Takaji FUJIWARA, and Ken-ichi TOMITA*

Faculty of Pharmaceutical Sciences, Osaka University, Suita Osaka 565

†*College of Pharmacy, Seoul National University, Seoul, Korea*

(Received November 20, 1978)

The crystal structure of 3-amino-2-hydroxy-1-propanesulfonic acid was determined by MULTAN system with X-ray intensity data on a diffractometer and refined by the least-squares method to an *R*-value 0.087 for 1620 reflections. The crystals were orthorhombic, space group Pbca, $Z=8$, with $a=9.909$, $b=12.032$ and $c=10.251$ Å. The molecule takes the zwitterionic form, $H_3{}^+NCH_2CH(OH)CH_2SO_3{}^-$. The skeletal conformation of the molecule is planar trans zigzag. The molecules are held together by three-dimensional network of hydrogen bonds.

3-Amino-2-hydroxy-1-propanesulfonic acid acts to lower blood pressure[1] and is a hydroxy derivative of 3-amino-1-propanesulfonic acid, homotaurine, which has strong activity towards the behavior of neurones when applied extracellularly.[2]

It is of interest to investigate systematically the molecular structures of related compounds and elucidate the relationship between the molecular conformations and their physiological functions.

We previously reported the molecular and crystal structures of 3-guanidino-2-hydroxy-1-propanesulfonic acid[3] and 3-guanidino-1-propanesulfonic acid.[4]

In this paper, the authors describe the molecular and crystal structure of 3-amino-2-hydroxy-1-propanesulfonic acid.

Experimental

The compound was recrystallized from aqueous solution as colorless, transparent crystals.

Crystallographic Measurement. The space group was determined from rotation and Weissenberg photographs, and lattice constants were obtained from precise measurement on a diffractometer with Mo $K\alpha$ radiation. Density was measured by the flotation method in a mixture of 1,2-dibromoethane and carbon tetrachloride. The crystal data are listed in Table 1. Three-dimensional intensity data were collected on a computer controlled four-circle diffractometer (Rigaku Denki Co., Ltd.) with Zr-filtered Mo $K\alpha$ radiation. A total of 1749 independent reflections limited within $\sin\theta/\lambda=0.700$ Å^{-1} was scanned by ω-2θ technique at a scan speed of 2° per minute. All the reflections were recorded and corrected for usual Lorentz and polarization effects, no absorption correction being made.

TABLE 1. CRYSTAL DATA OF 3-AMINO-2-HYDROXY-1-PROPANESULFONIC ACID

Molecular formula; $C_3O_4NH_9S$	*MW* 155.17
Colorless transparent	Orthorhombic
$a=9.909(4)$ Å	$b=12.032(3)$ Å
$c=10.251(4)$ Å	
Volume of unit cell	1222.2 Å^3
D_m	1.688 Mg/m^3
D_x	1.686 Mg/m^3
$Z=8$	$F(000)=656$
Absent spectra; $hk0$ when $h=2n+1$	
$h0l$ when $l=2n+1$	
$0kl$ when $k=2n+1$	
Space group; Pbca	

Structure Determination and Refinement. The structure determination was done by MULTAN system.[5] As the average value of E^2 with h=even, k=odd and l=odd parity has significantly large one, we tried to rescale the E's so as the average E^2 value of each parity group to have unity, which revealed all the non-hydrogen atoms. Continuation of successive Fourier syntheses with overall isotropic temperature factor reduced the *R*-factor to 0.21.

Refinement was carried out for all reflections by the block-diagonal least-squares procedure with unit weight. The *R*-factor was reduced to 0.16 with isotropic temperature factors for all non-hydrogen atoms and decreased further with anisotropic temperature factors to 0.11. In this state, a difference Fourier synthesis revealed the locations of all the 9 hydrogen atoms. They were included in the final least-squares cycles with isotropic temperature factors. The final *R*-value was 0.087. The observed and calculated structure factors are listed in Table 2.**

Calculations were carried out on NEAC 2200-700 computer, Osaka University, and IBM 360, Seoul National University, Seoul, Korea. The atomic scattering factors were taken from the "International Tables for X-Rav Crystallography."[6]

Results and Discussion

The final atomic parameters are given in Tables 3 and 4, together with their estimated standard deviations. The difference Fourier map is shown in Fig. 1. As shown in Fig. 1, one hydrogen atom of sulfo group is transfered to the amino group. Thus, the molecule occurs in the zwitterionic form, $H_3{}^+NCH_2CH(OH)$-$CH_2SO_3{}^-$, as in the cases of related compounds.

Bond Distances and Angles. The interatomic distances and angles are listed in Table 5, together with their standard deviations, and those are acceptable as a whole. In the $-SO_3{}^-$ group, the average of three S–O distances, three O–S–O angles and three O–S–Cl

** Table 2 is kept as a Document at the Office of the Chemical Society of Japan (Document No. 7923).

Table 3. Final positional and thermal parameters (Estimated standard deviations in parentheses)
Anisotropic temperature factors are expressed in the form of
$\exp\{-(B_{11}h^2+B_{22}k^2+B_{33}l^2+B_{12}hk+B_{13}hl+B_{23}kl\}$.

Atom	X	Y	Z	B_{11} or B	B_{22}	B_{33}	B_{12}	B_{13}	B_{23}
S	0.7263(1)	0.5043(1)	0.7580(1)	0.0036(1)	0.0040(1)	0.0060(1)	0.0014(1)	−0.0003(1)	−0.0004(1)
C1	0.6119(4)	0.5601(4)	0.8746(5)	0.0037(4)	0.0035(3)	0.0063(3)	−0.0009(5)	0.0012(7)	−0.0007(6)
C2	0.6043(4)	0.6872(4)	0.8740(5)	0.0029(3)	0.0035(3)	0.0066(4)	−0.0004(5)	0.0006(6)	−0.0005(6)
C3	0.4998(5)	0.7205(4)	0.9757(6)	0.0050(4)	0.0038(3)	0.0092(6)	−0.0001(6)	0.0041(8)	−0.0005(7)
N	0.4876(4)	0.8444(3)	0.9818(5)	0.0039(3)	0.0040(3)	0.0086(5)	0.0011(5)	0.0006(7)	−0.0018(6)
O1	0.6825(4)	0.3885(3)	0.7406(5)	0.0068(4)	0.0037(2)	0.0113(5)	0.0012(5)	−0.0025(7)	−0.0022(6)
O2	0.8606(3)	0.5105(3)	0.8166(4)	0.0032(3)	0.0066(3)	0.0102(4)	0.0019(5)	−0.0007(6)	−0.0009(6)
O3	0.7132(4)	0.5671(3)	0.6380(4)	0.0068(4)	0.0069(3)	0.0065(3)	0.0030(6)	0.0013(6)	0.0016(6)
O4	0.7307(3)	0.7324(3)	0.9079(4)	0.0039(3)	0.0045(3)	0.0126(5)	−0.0016(5)	−0.0016(7)	−0.0000(6)

Table 4. Fractional coordinates of hydrogen atoms

Atom	X	Y	Z	
C1H1	0.516	0.527	0.855	
C1H2	0.645	0.534	0.970	
C2H1	0.578	0.721	0.774	
C3H1	0.404	0.685	0.949	Overall isotropic
C3H2	0.529	0.692	1.072	temperature factor
NH1	0.564	0.876	1.031	is 2.16 Å^2
NH2	0.433	0.863	0.903	
NH3	0.429	0.860	1.041	
O4H1	0.760	0.787	0.842	

Table 5. Bond distances(Å) and angles(°)
(Estimated standard deviations are in parentheses)

S-C1	1.779(5)	O1-S-O2	111.5(3)
S-O1	1.470(5)	O1-S-O3	111.4(3)
S-O2	1.462(4)	O2-S-O3	113.8(2)
S-O3	1.449(4)	O1-S-C1	104.5(3)
C1-C2	1.531(7)	O2-S-C1	106.5(2)
C2-C3	1.523(7)	O3-S-C1	108.4(2)
C2-O4	1.409(7)	S-C1-C2	113.9(3)
C3-N	1.497(7)	C1-C2-C3	107.1(4)
		C1-C2-O4	109.9(4)
		C3-C2-O4	109.5(4)
		C2-C3-N	110.2(4)

Table 6. Hydrogen bond lengths(Å) and angles(°)

Bond lengths		Bond angles	
O4-(O4H1)···O1(I)	2.685	C2-O4-O1(I)	113.4
N-(NH1)···O3(II)	2.949	C3-N-O3(II)	108.7
N-(NH2)···O1(III)	2.884	C3-N-O1(III)	101.4
N-(NH3)···O2(IV)	2.984[a]	C3-N-O2(IV)	130.2[a]
N-(NH3)···O4(IV)	2.935[a]	C3-N-O4(IV)	76.9[a]

(I) (1.5−X, 0.5+Y, Z); (II) (X, 1.5−Y, 0.5+Z); (III) (1.0−X, 0.5+Y, 1.5−Z); (IV) (−0.5+X, 1.5−Y, 2.0−Z).
a) Bifurcated hydrogen bond.

angles are 1.460 Å, 112.2° and 106.5°, respectively. These values are very similar to those of other compounds containing a sulfonato group. The C–H, N–H, and O–H distances are within the ranges 1.05—1.13 Å, 0.86—1.00 Å, and 0.99 Å, respectively. It is notable

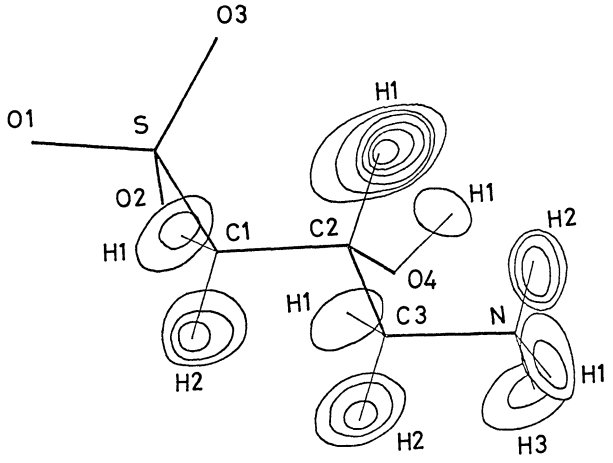

Fig. 1. Difference Fourier map of 3-amino-2-hydroxy-1-propanesulfonic acid. Contours are drawn at intervals of 0.2 e Å^{-3} starting with the contour of 0.4 e Å^{-3}.

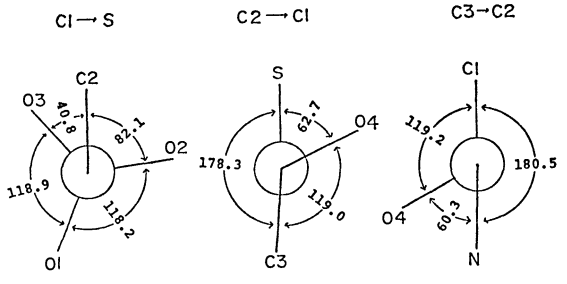

Fig. 2. Torsion angles around three bonds.

that C2–O4 distance of the hydroxyl group is 1.409 Å, slightly shorter than that found in 4-amino-3-hydroxybutyric acid[7] (1.425 Å) which is normal C–O single bond, and slightly longer than that of 3-guanidino-2-hydroxy-1-propanesulfonic acid (1.381 Å).

Conformation. The skeletal conformation of this molecule is trans-trans. The tortion angles around C1–C2 and C2–C3 are 178.3 and 180.5°, respectively. However, the corresponding values of 4-amino-2-hydroxybutyric acid and 3-guanidino-2-hydroxy-1-propanesulfonic acid, which contain β-hydroxyl group are 173.7 and 168.8°, 161.9 and 177.8°, respectively.

The torsion angles of sulfonato group are shown in Fig. 2. These values are significantly different from those of homotaurine,[8] 3-guanidino-1-propanesulfonic acid and 3-guanidino-2-hydroxy-1-propanesulfonic acid.

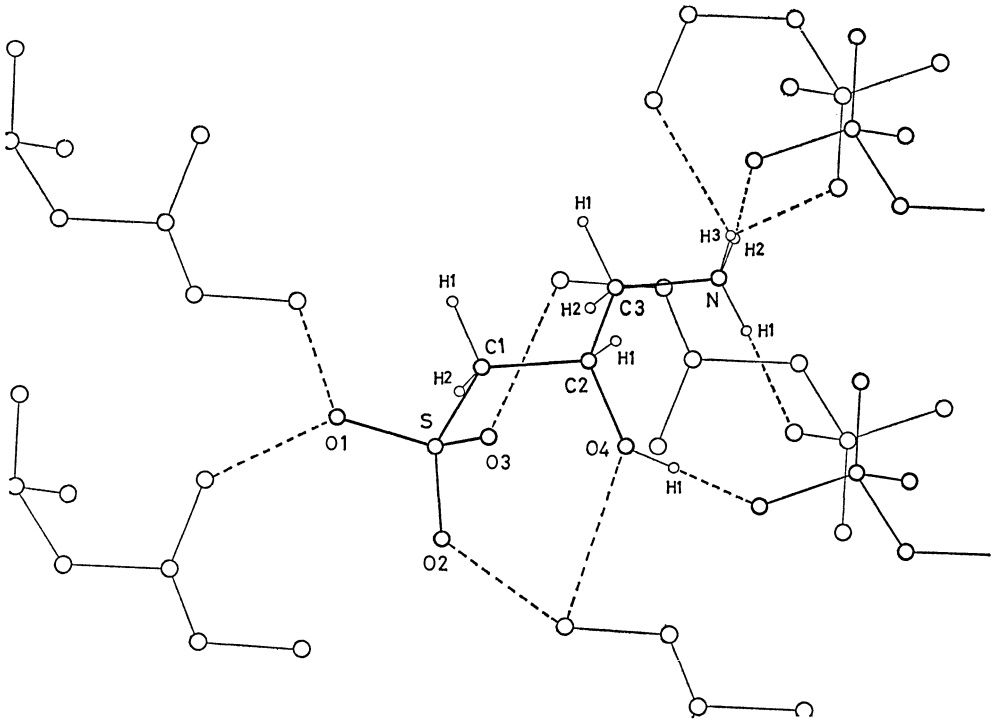

Fig. 3. Hydrogen bonds around original molecule.

Crystal Structure. Distances and angles of hydrogen bonds are listed in Table 6. All feasible hydrogen atoms in the molecule are utilized to form hydrogen bonds, in which one hydrogen atom (NH_3) on the amino group takes part in bifurcated hydrogen bond, and the molecules are held together by a three-dimensional network of NH···O and OH···O hydrogen bonds, as shown in Fig. 3.

The intermolecular contacts between adjacent molecules are in normal van der Waals distances.

This work was partly suported by a research grant from the Ministry of Education of Japan and also one of the authors, Y. B. Kim is a short-term research fellow at Osaka University sponsored by the Ministry of Education of Japan.

References

1) S. Tsunoo, K. Horisaka, H. Tanaka, T. Chida, S. Nakajima, and Z. Fukai, *J. Showa Med. Assoc.*, **30**, 521 (1970).
2) D. R. Curtis and J. C. Watkins, *J. Neurochem.*, **6**, 117 (1960).
3) Y. B. Kim, A. Wakahara, T. Fujiwara, and K. Tomita, *Bull. Chem. Soc. Jpn.*, **46**, 2194 (1973).
4) Y. B. Kim, A. Wakahara, T. Fujiwara, and K. Tomita, *Bull. Chem. Soc. Jpn.*, **46**, 2543 (1973).
5) P. Main, M. M. Woolfson, L. Lessinger, G. Germain, and J. P. Delerco, MULTAN 74. *A System of Computer Programs for the Automatic Solution of Crystal Structures from X-Ray Diffraction Data.* Univs. of York, England and Louvain-la-Neuve, Belgium.
6) "International Tables for X-Ray Crystallography," Kynoch Press, England (1974), Vol. IV.
7) M. Harada, T. Fujiwara, and K. Tomita, *Bull. Chem. Soc. Jpn.*, **46**, 2854 (1973).
8) S. Ueoka, T. Fujiwara, and K. Tomita, *Bull. Chem. Soc. Jpn.*, **45**, 3634 (1972).

A New Synthesis of Arylacetic Esters Starting from Aromatic Aldehyde by the Use of Methyl (Methylthio)methyl Sulfoxide[1)]

Katsuyuki OGURA,*,† Yoko ITO, and Gen-ichi TSUCHIHASHI*

Sagami Chemical Research Center, Nishi-Ohnuma 4-4-1, Sagamihara, Kanagawa 229

(Received January 12, 1979)

Methyl (methylthio)methyl sulfoxide was found to react with benzaldehyde in the presence of benzyltrimethylammonium hydroxide (Triton B), sodium hydroxide, or potassium hydroxide, affording 1-(methylsulfinyl)-1-(methylthio)-2-phenylethylene. Treatment of this product with hydrogen chloride in an alcohol gave the corresponding alkyl phenylacetate in high yield. The whole reaction sequence provides a new method for synthesizing phenylacetic esters starting from benzaldehyde. In a similar manner, (alkoxy-, halogen-, or alkyl-substituted phenyl)acetic esters could be synthesized from the corresponding aromatic aldehydes. The present method was shown to be also applicable to the production of (2-thienyl)acetic esters.

Methyl (methylthio)methyl sulfoxide (**1**) was first synthesized by substitution of chloromethyl methyl sulfoxide with methanethiolate anion[2)] and it was later disclosed that **1** could be more conveniently produced by oxidation of bis(methylthio)methane with hydrogen peroxide.[3)] To date, many papers on organic syntheses using **1** have been published and **1** has appeared to be a versatile reagent for making a variety of organic compounds, such as aldehydes,[4)] cyclic or acyclic ketones,[5)] α-hydroxy aldehydes,[6)] α-amino acids,[7)] and α-keto acids.[8)]

$$CH_2O + 2CH_3SH \xrightarrow{H^+} CH_2(SCH_3)_2 \xrightarrow{H_2O_2} CH_2(SCH_3)(SOCH_3)$$

1

Most of these synthetic methods involve the treatment of **1** with a strong base such as sodium hydride, potassium hydride, or butyllithium to form the carbanion which, then, is subjected to the reaction with various types of functional groups, followed by the acid-catalyzed hydrolysis, to give the product having a new functional group. For example, an aldehyde (**4**) or its acetal derivative (**5**) can be respectively synthesized by sequential treatment of **1** with sodium hydride in the coexistence of an alkyl halide (**2**) in tetrahydrofuran (THF) to form an alkylated product (**3**) followed by the acid-catalyzed decomposition of **3** either in the absence or in the presence of an orthoformate.[4)]

$$\underset{\mathbf{2}}{1} + RX \xrightarrow[THF]{NaH} \underset{\mathbf{3}}{RCH(SCH_3)(SOCH_3)} \xrightarrow{H^+} \underset{\mathbf{4}}{RCHO}\ \underset{\mathbf{5}}{[RCH(OR')_2]}$$

During the course of our investigation to search further synthetic utility of this new reagent (**1**), we observed that **1** underwent the Knoevenagel-type condensation with an aromatic aldehyde (**6**) in the presence of a base such as benzyltrimethylammonium hydroxide (Triton B), sodium hydroxide, or potassium hydroxide to give a 2-aryl-1-(methylsulfinyl)-1-(methylthio)ethylene (**7**) in high yield. Furthermore, the condensate (**7**) was found to be converted to an arylacetic ester (**8**) on treatment with hydrogen chloride in an alcohol. This whole reaction sequence provided a new synthetic route for conversion of aromatic aldehydes into the corresponding arylacetic esters. In this paper, we wish to report a full experimental detail on synthesis of arylacetic esters starting from aromatic aldehydes by the use of **1**.

$$\underset{\mathbf{6}}{ArCHO} + \mathbf{1} \xrightarrow{base} \underset{\mathbf{7}}{ArCH{=}C(SCH_3)(SOCH_3)} \xrightarrow[ROH]{HCl} \underset{\mathbf{8}}{ArCH_2COOR}$$

Results and Discussion

Transformation of Benzaldehyde into Phenylacetic Esters. When a mixture of benzaldehyde and methyl (methylthio)methyl sulfoxide (**1**) was treated with Triton B in refluxing THF, 1-(methylsulfinyl)-1-(methylthio)-2-phenylethylene (**10**) was formed: To a solution containing 2.57 g of **1** and 3 ml of benzaldehyde (**9**) in 5 ml of THF, was added 2 ml of 40% methanolic solution of Triton B, and then the resulting mixture was refluxed for 4 h. Separation by column-chromatography on silica gel gave 3.99 g (91% yield) of **10** as a colorless oil, bp 149—150 °C/0.08 Torr. When one mol-equiv of **9** was used in this condensation reaction, the yield of **10** was 80%. The structure of **10** was assigned on the basis of the following evidence.

$$\mathbf{1} + \underset{\mathbf{9}}{PhCHO} \xrightarrow{base} \underset{\mathbf{10}}{Ph(H)C{=}C(SCH_3)(SOCH_3)} \underset{h\nu}{\rightleftharpoons} \underset{\mathbf{11}}{Ph(H)C{=}C(SOCH_3)(SCH_3)}$$

Molecular formula, $C_{10}H_{12}OS_2$, for this oil was confirmed by its mass spectrum (parent peak, *m/e* 212) and elemental analysis. The NMR and IR spectra proved that it consisted of only one stereoisomer and that it had a phenyl group [NMR in CCl_4: δ=7.32 (3H, m) and 7.85 (2H, m); IR: 756 and 692 cm^{-1}], an olefinic proton [δ=7.51 (1H, s)], a methylsulfinyl group [δ=2.62 (3H, s); 1062 cm^{-1}], and a methylthio group [δ=2.26 (3H, s)]. Reduction of this oil with lithium aluminium hydride afforded 1,1-bis(methylthio)-2-phenylethane.[9)]

Another stereoisomer (**11**) was obtained by irradiation of **10** in methanol with a low-pressure mercury arc lamp (Vycor filter) as a mixture with **10**. The stereochemical structures of **10** and **11** were assigned by the comparison of the pseudo-contact effects of the shift reagent, tris(dipivaloylmethanato)europium [Eu(dpm)$_3$], which formed complexes at the oxygen atom of a sulfoxide,[10)] on the NMR chemical shifts of their olefinic protons. The singlet at δ=7.51 of **10** was shifted downfield to δ=16.49 by adding 0.51

equiv of $Eu(dpm)_3$, while the olefinic proton (δ=7.02 in CCl_4) of **11** appeared at δ=9.71 in CCl_4–$Eu(dpm)_3$ (0.51 equiv). These facts indicate that the olefinic proton and the sulfinyl group of **10** are much closer in space than those of **11**. Hence, the stereochemical structure of **10** is established to be of *E*-configuration.

The condensation reaction of benzaldehyde with **1** could be also achieved under various basic conditions. Reflux of a solution containing **1**, benzaldehyde, and potassium hydroxide (1.3 equiv) in methanol gave **10** in 44% yield. When benzaldehyde was treated with sodium hydroxide (0.6 equiv) in two mol-equiv of **1** at 70 °C, **10** was obtained in 84% yield. Furthermore, it was found that stirring a mixture of benzaldehyde, **1**, and sodium hydride either in THF at 60 °C or in *N*,*N*-dimethylformamide at room temperature gave **10** in 56% or 43% yield, respectively.

This condensation reaction is very interesting because the reaction proceeds smoothly without removal of the formed water, and even in methanol. This may be accounted for by the incapability of **10** toward the Michael-type addition of hydroxide anion, that is, the irreversible nature of the final stage of the process, *i.e.* the elimination of hydroxide anion, as shown in Scheme 1.

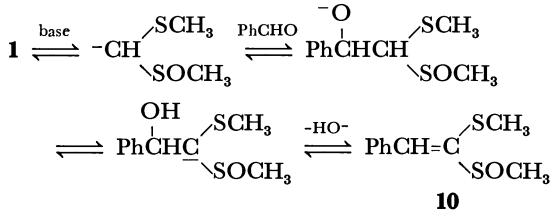

10

Scheme 1.

The degradation of **10** with hydrogen chloride took place easily in an alcohol. A solution containing 300 mg of **10** in 10 ml of ethanol was bubbled with hydrogen chloride gas under ice-cooling and then was allowed to stand at room temperature. After evaporation *in vacuo*, the residue was column-chromatographed on silica gel to give 179 mg (78% yield) of ethyl phenylacetate (**12a**).[11] In a similar manner, methyl phenylacetate (**12b**) and butyl phenylacetate (**12c**) were obtained in 75% and 79% yields by the reaction with hydrogen chloride in methanol and 1-butanol, respectively.

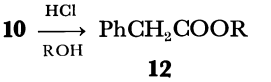

12

a	$R=C_2H_5$	78%
b	$R=CH_3$	75%
c	$R=n\text{-}C_4H_9$	79%

It should be noted that saturation of hydrogen chloride was not always necessary to the conversion of **10** into **12**. The concentration of hydrogen chloride in the system could be reduced to 0.1 M although a higher temperature was required in order to complete the reaction within a short time: Ethyl phenylacetate (**12a**) was produced in 75% yield by refluxing a solution of **10** in ethanol containing hydrogen chloride at the concentration of 0.1 M. When a solution of **10** in 1,2-dimethoxyethane was treated with conc. hydrochloric acid at room temperature, phenylacetic acid was isolated in 63% yield.

Thus, methyl (methylthio)methyl sulfoxide (**1**) was shown to be a novel reagent for the transformation of benzaldehyde into phenylacetic acid and its alkyl esters. The generality of this transformation was further investigated by examination of the reactions starting from a wide variety of aromatic aldehydes, and the results are described in the following.

Synthesis of (Alkoxy-substituted phenyl)acetic Esters. Many of (alkoxy-substituted phenyl)acetic acids are known as key-intermediates for the syntheses of isoquinoline alkaloids,[12] and it seemed very important to examine the production of these acids or their esters by using the above-mentioned procedure. The alkoxy-substituted benzaldehydes which we investigated were *p*-methoxybenzaldehyde, *p*-butoxybenzaldehyde, *p*-(benzyloxy)benzaldehyde, 3,4-dimethoxybenzaldehyde, 3,4-(methylenedioxy)benzaldehyde, and 3,4,5-trimethoxybenzaldehyde. The results are summarized in Tables 1 and 2, showing that all the aldehydes examined can be transformed in good yields into the corresponding arylacetic esters *via* the condensates with **1**.

When the condensate **13** derived from 3,4-dimethoxybenzaldehyde was treated with a saturated ethanolic solution of hydrogen chloride, ethyl (3,4-dimethoxyphenyl)(methylthio)acetate (**15**) was produced as a by-product (27% yield), resulting in formation of the expected ethyl (3,4-dimethoxyphenyl)acetate (**14**) in relatively low yield (40%). This could be overcome by reducing the concentration of hydrogen chloride: **14** was obtained in 91% yield on treatment of **13** with 0.5 M hydrogen chloride in ethanol.

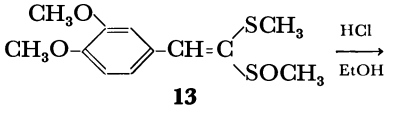

13

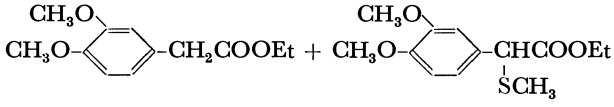

14 **15**

On the other hand, when a solution of **13** in *t*-butyl alcohol was saturated with hydrogen chloride, methanethiol ester (**16**) of (3,4-dimethoxyphenyl)(methylthio)acetic acid was isolated in 67% yield instead of *t*-butyl (3,4-dimethoxyphenyl)acetate.

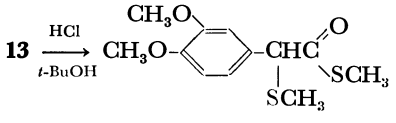

16

Miscellaneous. By the present procedure, (halogen- or alkyl-substituted phenyl)acetic esters could be synthesized. On treatment with saturated alcoholic solution of hydrogen chloride, 2-(*p*-chlorophenyl)-1-(methylsulfinyl)-1-(methylthio)ethylene which was derived from *p*-chlorobenzaldehyde and **1** was transformed into ethyl, methyl, or butyl ester of (*p*-chlorophenyl)acetic acid in 92%, 78%, or 80% yield, respectively. In analogous manners, ethyl (*o*-bromophenyl)acetate and ethyl (*p*-isopropylphenyl)acetate were also obtained, starting from *o*-bromobenzaldehyde and

TABLE 1. CONDENSATION OF AROMATIC ALDEHYDES WITH **1**

Aldehyde	Base[a]	Solvent	Temp	Yield (%)
CH_3O-C$_6$H$_4$-CHO	Triton B	THF	reflux	82 (100)[d]
	NaOH	—[b]	70 °C	93
n-BuO-C$_6$H$_4$-CHO	Triton B	THF	reflux	74
$PhCH_2O$-C$_6$H$_4$-CHO	Triton B	THF	reflux	62
	NaOH	—[c]	70—80 °C	92
PhO-C$_6$H$_4$-CHO	Triton B	THF	reflux	61
	NaOH	—[b]	70 °C	73
$(CH_3O)_2$-C$_6$H$_3$-CHO	Triton B	Dioxane	80 °C	47 (87)[d]
	Triton B	THF	reflux	66
	NaOH	—[b]	70 °C	82
1,3-benzodioxole-5-CHO	Triton B	THF	reflux	62 (81)[d]
	NaOH	—[b]	70 °C	84
$(CH_3O)_3$-C$_6$H$_2$-CHO	Triton B	THF	reflux	71
Cl-C$_6$H$_4$-CHO	Triton B	Dioxane	80 °C	51 (73)[d]
	Triton B	THF	reflux	65
	NaOH	—[b]	70 °C	70
Br-C$_6$H$_4$-CHO	Triton B	THF	reflux	51
i-Pr-C$_6$H$_4$-CHO	Triton B	THF	reflux	68
	NaOH	—[e]	60 °C	83
thiophene-2-CHO	Triton B	THF	reflux	86
	KOH	Methanol	reflux	83

a) Triton B=benzyltrimethylammonium hydroxide. b) The amount of **1** was 2.0 mol-equiv to the aldehyde. c) The aldehyde: **1**=1 : 2.56. d) Based on the unrecovered **1**. e) The aldehyde: **1**=1 : 1.5.

p-isopropylbenzaldehyde, as shown in Tables 1 and 2.

The present method was also applied to synthesis of (2-thienyl)acetic acid which was especially useful as a reagent for chemical modification of antibiotic penicillins and cephalosporins.[13] It was found that 2-thiophenecarbaldehyde underwent the condensation reaction with **1** in the presence of Triton B (86% yield) or potassium hydroxide (83% yield) in THF or methanol, respectively, under refluxing with heating, and then, on treatment of the resulting 1-(methylsulfinyl)-1-(methylthio)-2-(2-thienyl)ethylene (**17**) with 1 M hydrogen chloride in ethanol, ethyl (2-thienyl)acetate (**18**) was produced in 80% yield.[14] This method is suitable for making (2-thienyl)acetic esters, since 2-thiophenecarbaldehyde is easily available by the Vilsmeier-Haak reaction of thiophene.[15]

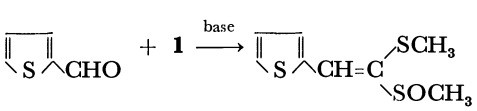

17

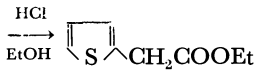

18

Experimental

*Condensation of Benzaldehyde with **1**. (a) Triton B in THF*: To a solution containing 2.572 g of **1** and 3 ml of benzaldehyde in 5 ml of THF, was added a 40% methanolic solution (3 ml) of Triton B and the resulting mixture was refluxed for 4 h. After adding 100 ml of dichloromethane, the mixture was washed with 0.5 M sulfuric acid, dried (Na_2SO_4), and evaporated *in vacuo*. The residue was separated by column-chromatography on silica gel (using dichloromethane as an eluent) to afford 3.994 g of **10** as a colorless oil which was further purified by distillation *in vacuo*: bp 149—150 °C/0.08 Torr; IR (neat) 1052 cm^{-1}; NMR (CCl_4) δ=2.26 (3H, s), 2.62 (3H, s), 7.32 (3H, m), 7.51 (1H, s), and 7.85 (2H, m); MS (70 eV), *m/e* (relative intensity), 212 (M^+, 7), 197 (5), 149 (100), 134 (96), 116 (18), 115 (14), and 89 (11). Found: C, 56.56; H, 5.70; S, 30.20%. Calcd for $C_{10}H_{12}OS_2$: C, 56.65; H, 5.72; S, 30.33%.

The above-mentioned reaction was repeated using an equimolar amount of benzaldehyde to **1**. To a solution containing benzaldehyde (1.007 g) and **1** (1.17 g) in THF (10 ml), was added a 40% methanolic solution (1.2 ml) of Triton B and the resulting mixture was refluxed for 4 h. After the addition of dichloromethane (50 ml), the solution was washed with 0.5 M sulfuric acid (20 ml) and water (50 ml×2), dried (Na_2SO_4), and evaporated *in vacuo*. The residue was column-chromatographed on silica gel (benzene–dichloro-

Table 2. Yield of alkyl arylacetate (**8**) in the reaction of 2-aryl-1-(methylsulfinyl)-1-(methylthio)ethylene (**7**) with hydrogen chloride in an alcohol

Ar	Alcohol	Concentration of HCl	Temp	Yield (%)
CH_3O-	EtOH	saturation	room temp	94
n-BuO-	EtOH	1 M	reflux	81
$PhCH_2O$-	EtOH	1 M	reflux	82
PhO-	EtOH	1 M	reflux	85
	EtOH	saturation	room temp	40[a]
CH_3O-, CH_3O	EtOH	0.5 M	—[b]	91
	t-BuOH	saturation	room temp	—
O—CH₂—O-	EtOH	saturation	room temp	91
	MeOH	saturation	room temp	80
CH_3O, CH_3O-, CH_3O	EtOH	saturation	room temp	62
	EtOH	1 M	reflux	72
Cl-	EtOH	saturation	room temp	92
	MeOH	saturation	room temp	78
	n-BuOH	saturation	room temp	80
Br	EtOH	1 M	reflux	92
i-Pr-	EtOH	1 M	reflux	96
S	EtOH	1 M	room temp	80
	EtOH	0.7 M	reflux	76

a) Methanethiol ester of (3,4-dimethoxyphenyl)(methylthio)acetic acid was isolated in 67% yield. b) Room temp → reflux.

methane (1 : 3)] to give **10** (1.606 g: 80% yield) as a pale yellow oil.

(b) KOH in Methanol: A solution containing benzaldehyde (505 mg) and **1** (585 mg) in methanol (5 ml) was refluxed for 4 days after potassium hydroxide (350 mg) was added. Dichloromethane (30 ml) was added and the resulting mixture was washed with 0.5 M sulfuric acid (10 ml) and water (30 ml×2). After being dried (Na_2SO_4) and evaporated *in vacuo*, the residue was column-chromatographed on silica gel [benzene–dichloromethane (1 : 2)] to give **10** (442 mg: 44% yield) as a pale yellow oil.

(c) NaOH and Excess of 1: After a mixture of **1** (2.34 g) and powdered sodium hydroxide (0.32 g) was stirred at 70 °C for 30 min, benzaldehyde (0.98 g) was added and then the resulting mixture was further stirred at 70 °C for 1 h. After the addition of dichloromethane (50 ml), the mixture was washed with 0.5M sulfuric acid (20 ml) and water (50 ml×2) and, the organic layer was dried (Na_2SO_4). Evaporation *in vacuo* gave a yellow oil which was column-chromatographed on silica gel [benzene–dichloromethane (1 : 3)] to afford **10** (1.654 g: 84% yield) as a pale yellow oil.

(d) NaH in DMF: To a solution containing **1** (6.00 g) in DMF (20 ml), was added sodium hydride (65% oil-dispersion; 1.80 g) and the resulting mixture was stirred at room temperature for 1.5 h. After the dropwise addition of benzaldehyde (4.80 g) over 10 min under ice-cooling, the mixture was further stirred at room temperature for 2 h, and then dichloromethane (100 ml) was added. After being washed with water (70 ml×2), the organic layer was dried ($MgSO_4$) and evaporated *in vacuo* to give an oily residue which was separated by column-chromatography on silica gel [benzene–dichloromethane (1 : 3)] to afford **10** (4.11 g: 43% yield) as a pale yellow oil.

(e) NaH in THF: To a solution of **1** (6.00 g) in THF (20 ml), was added sodium hydride (65% oil-dispersion; 1.80 g) and the resulting mixture was stirred at room temperature for 1 h. After the dropwise addition of benzaldehyde (4.90 g) over 10 min at room temperature, the reaction mixture was further stirred at 60 °C for 1.5 h and then dichloromethane (100 ml) was added. After insoluble matters were filtered off, the filtrate was washed with water (70 ml×2), dried ($MgSO_4$), and evaporated *in vacuo*. The residue was column-chromatographed on silica gel [benzene–dichloromethane (1 : 3)] to afford **10** (5.50 g: 56% yield) as a pale yellow oil.

Photochemical Isomerization of 10: A solution of the 1-(methylsulfinyl)-1-(methylthio)-2-phenylethylene (**10**, 276 mg), which was obtained by the above-mentioned reaction, in methanol (200 ml) was irradiated with a low-pressure mercury arc lamp (10 W) through Vycor filter for 2 h and 45 min. After evaporation *in vacuo*, the residue was column-chromatographed on silica gel (dichloromethane) to give a pale yellow oil (211 mg) which was shown by an NMR analysis to consist of **10** and its geometric isomer (**11**) in the ratio of 58 : 42. Found: C, 56.66; H, 5.71; S, 30.02%.

Calcd for $C_{10}H_{12}OS_2$: C, 56.56; H, 5.70; S, 30.20%.

The NMR signals of **11** appeared at δ=2.60 (3H, s), 2.47 (3H, s), 7.02 (1H, s) and 7.26 (5H, s) in CCl_4.

*Decomposition of **10** with Hydrogen Chloride (HCl). (a) In Saturated Methanolic Solution of HCl*: HCl gas was bubbled in a solution of **10** (514 mg) in methanol (5 ml) under cooling with ice–water until HCl was saturated. The resulting solution was stirred at room temperature for 19 h and then was evaporated *in vacuo*. The residue was column-chromatographed on silica gel [hexane–benzene (1 : 1)] to give methyl phenylacetate (271 mg: 75% yield) as a colorless oil which was identified by the comparison of its IR and NMR spectra with those of the authentic sample prepared from phenylacetic acid by the usual method (HCl–methanol).

(b) In Saturated Ethanolic Solution of HCl: A solution containing **10** (300 mg) in ethanol (10 ml) was saturated with HCl gas. The introduction of the gas was performed under ice-cooling. The resulting solution was stirred at room temperature for 8 h and concentrated *in vacuo*. The residue was separated by column-chromatography on silica gel (benzene) to give ethyl phenylacetate (179 mg: 77% yield) which was identified by the comparison of its IR and NMR spectra with those of the authentic sample obtained by saturation of HCl in ethanolic solution of phenylacetic acid.

(c) In 0.1M Ethanolic Solution of HCl: To a solution of **10** (505 mg) in ethanol (10 ml), was added a saturated ethanolic solution (0.1 ml) of HCl and the resulting solution was refluxed for 25 h. After evaporation *in vacuo*, the residue was subjected to column-chromatography on silica gel [hexane–benzene (1 : 1)] to afford ethyl phenylacetate (291 mg: 75% yield) as a pale yellow oil. Since a further elution with ethyl acetate afforded the starting material (**10**, 77 mg), the conversion yield of ethyl phenylacetate was calculated to be 88%.

(d) In 1-Butanol: A solution of **10** (1.763 g) in 1-butanol (10 ml) was saturated with HCl gas under cooling with ice–water and then the resulting solution was stirred at room temperature for 3 h. After evaporation *in vacuo*, the residue was column-chromatographed on silica gel [hexane–benzene (4 : 1)] to give butyl phenylacetate (1.418 g: 89% yield) as a colorless oil, which was identified by the comparison of its IR and NMR spectra with those of the authentic sample.[16]

(e) Concd Hydrochloric Acid: To a solution containing **10** (191 mg) in 1,2-dimethoxyethane (1.5 ml), was added concd hydrochloric acid (1 ml) and the resulting mixture was stirred at room temperature for 3 h. Then, dichloromethane (50 ml) and water (5 ml) were added. The aqueous layer was separated and further extracted with dichloromethane (50 ml). The organic layers were combined, dried (Na_2SO_4), and evaporated *in vacuo*. After the addition of ether (30 ml) to the residue, the solution was extracted with a saturated aqueous solution (10 ml×2) of sodium hydrogen carbonate. The aqueous layer was acidified with hydrochloric acid and extracted with dichloromethane (30 ml×3). The organic layer was dried (Na_2SO_4) and evaporated *in vacuo* to afford phenylacetic acid (77 mg: 63% yield) as colorless crystals having mp 69—75 °C. The identification was achieved by the comparison of its IR and NMR spectra with those of an authentic sample and the mixture mp.

Condensation of p-*Methoxybenzaldehyde with **1**. (a) Triton B in THF*: To a solution of **1** (951 mg) and *p*-methoxybenzaldehyde (1.17 g) in THF (10 ml), was added a 40% methanolic solution (1 ml) of Triton B and the mixture was refluxed for 5 h. Then, dichloromethane (100 ml), water (5 ml), and 4.5 M sulfuric acid (2 ml) were added and the mixture was shaken. The organic layer was separated, dried (Na_2SO_4), and evaporated *in vacuo*. The residue was subjected to column-chromatography on silica gel (dichloromethane) to obtain 2-(*p*-methoxyphenyl)-1-(methylsulfinyl)-1-(methylthio)ethylene (**19**; 1.51 g: 82% yield) as a pale yellow oil: bp 170—173 °C/0.20 Torr; IR (neat) 1059 cm^{-1}; NMR (CCl_4) δ=2.30 (3H, s), 2.63 (3H, s), 3.84 (3H, s), 6.86 (2H, d, J=8.4 Hz), 7.43 (1H, s), and 7.86 (2H, d, J=8.4 Hz); MS (70 eV), *m/e* (relative intensity), 242 (M^+, 6), 179 (87), 164 (100), 149 (41), 146 (39), and 121 (15). Found: C, 54.55; H, 5.84; S, 26.50%. Calcd for $C_{11}H_{14}O_2S_2$: C, 54.52; H, 5.82; S, 26.46%.

Further elution gave **1** (176 mg). Therefore, the conversion yield of **19** was calculated to be 100%.

*(b) NaOH and Excess of **1***: After a mixture of **1** (9.13 g) and powdered sodium hydroxide (0.45 g) was stirred at 70 °C for 30 min, *p*-methoxybenzaldehyde (4.87 g) was dropwise added and the resulting mixture was further stirred at 70 °C for 1.5 h. After the addition of dichloromethane (100 ml), the mixture was washed with 0.5 M sulfuric acid (30 ml) and water (100 ml×2) and then the organic layer was dried (Na_2SO_4). Evaporation *in vacuo*, followed by column-chromatography on silica gel [dichloromethane–ethyl acetate (4 : 1)], gave **19** (8.068 g: 93% yield) as a yellow oil.

*Decomposition of 2-(*p*-Methoxyphenyl)-1-(methylsulfinyl)-1-(methylthio)ethylene (**19**) with HCl.* A solution containing **19** (274 mg) in ethanol (10 ml) was saturated with HCl gas under cooling with ice–water and allowed to stand overnight at room temperature. After evaporation *in vacuo*, the residue was column-chromatographed on silica gel [hexane–benzene (1 : 1)] to give ethyl (*p*-methoxyphenyl)acetate (206 mg: 94% yield). This ester was identified by the comparison of its IR and NMR spectra with those of the authentic sample which was obtained by the usual esterification (HCl–ethanol) of (*p*-methoxyphenyl)acetic acid given in the following.

To a solution containing **19** (460 mg) in 1,2-dimethyoxyethane (2 ml), was added concd hydrochloric acid (1 ml) and the resulting mixture was stirred for 15 h at room temperature. After the reaction mixture was shaken with diethyl ether (50 ml), the organic layer was separated, which was extracted with an aqueous solution of potassium carbonate. The aqueous layer was acidified with concd hydrochloric acid, and then extracted with dichloromethane (50 ml×3). The organic layer was dried (Na_2SO_4) and evaporated *in vacuo* to give 62 mg of colorless crystals, which were identified as (*p*-methoxyphenyl)acetic acid by the comparison of their IR and NMR spectra with those reported in the Sadtler spectra.

Condensation of p-*Butoxybenzaldehyde with **1**.* To a solution of *p*-butoxybenzaldehyde (5.05 g) and **1** (4.26 g) in THF (50 ml), was added a 40% methanolic solution (4 ml) of Triton B and the resulting solution was refluxed for 24.5 h. Dichloromethane (50 ml) was added and the mixture was washed with 0.5 M sulfuric acid. After being dried (Na_2SO_4) and evaporation *in vacuo*, the residue was subjected to column-chromatography on silica gel [benzene–dichloromethane (1 : 1)] to give 2-(*p*-butoxyphenyl)-1-(methylsulfinyl)-1-(methylthio)ethylene (**20**; 5.94 g: 74% yield) as a pale yellow oil which soon crystallized and was further purified by recrystallization from hexane to afford colorless crystals: mp 47—48 °C; IR (KBr) 1055 cm^{-1}; NMR($CDCl_3$) δ=0.94 (3H, t, J=6 Hz), 1.20—1.88 (4H, m), 2.22 (3H, s), 2.64 (3H, s), 3.90 (2H, t, J=6 Hz), 6.84 (2H, d, J=9 Hz), 7.49 (1H, s), and 7.83 (2H, d, J=9

Hz); MS (70 eV), *m/e* (relative intensity), 284 (M^+, 13), 222 (17), 221 (100), 220 (11), 206 (37), 165 (50), 151 (11), 150 (99.7), 149 (27), 132 (40), 131 (29), 121 (24), 89 (11), 77 (12), 41 (18), and 29 (38). Found: C, 58.83; H, 7.02; S, 22.57%. Calcd for $C_{14}H_{20}O_2S_2$: C, 59.12; H, 7.09; S, 22.54%.

*Decomposition of 2-(p-Butoxyphenyl)-1-(methylsulfinyl)-1-(methylthio)ethylene (**20**) with HCl.* To a solution of **20** (492 mg) in ethanol (9 ml), was added a saturated ethanolic solution (1 ml) of HCl and the resulting solution was refluxed for 3 h. After evaporation *in vacuo*, the residue was column-chromatographed on silica gel (benzene) to give ethyl (*p*-butoxyphenyl)acetate (330 mg: 81% yield) as a pale yellow oil: IR (neat) 1783 cm^{-1}; NMR ($CDCl_3$) δ=0.93 (3H, t, J=7 Hz), 1.19 (3H, t, J=7 Hz), 1.20—1.86 (4H, m), 3.46 (2H, s), 3.86 (2H, t, J=6 Hz), 4.06 (2H, q, J=7 Hz), 6.76 (2H, d, J=9 Hz), and 7.11 (2H, d, J=9 Hz).

This ester was hydrolyzed without further purification. The ester (212 mg) was dissolved in 1,2-dimethoxyethane (5 ml) and 1 M aqueous solution (2.5 ml) of potassium hydroxide was added. The reaction mixture was stirred at room temperature for 45 h. After the addition of water (10 ml) and acidification with 0.5M sulfuric acid, the mixture was extracted with diethyl ether (30 ml×2). The organic layer was dried (Na_2SO_4) and evaporated *in vacuo* to give crude (*p*-butoxyphenyl)acetic acid as pale yellow crystals which were further purified by recrystallization from hexane to give colorless crystals: mp 87.5—88.5 °C; IR (KBr) 1701 cm^{-1}; NMR ($CDCl_3$) δ=0.94 (3H, t, J=7 Hz), 1.25—1.88 (4H, m), 3.50 (2H, s), 3.88 (2H, t, J=6 Hz), 6.78 (2H, d, J=8 Hz), 7.11 (2H, d, J=8 Hz), and 10.56 (1H, broad s). Found: C, 69.41; H, 7.72%. Calcd for $C_{12}H_{16}O_3$: C, 69.23; H, 7.68%.

Condensation of p-*(Benzyloxy)benzaldehyde with **1**. (a) Triton B in THF*: To a solution containing *p*-(benzyloxy)-benzaldehyde (999 mg) and **1** (590 mg) in THF (5 ml), was added a 40% methanolic solution of Triton B and the resulting solution was refluxed for 24 h. After the addition of dichloromethane (50 ml), the solution was washed successively with 0.5 M sulfuric acid (20 ml) and water (50 ml×2), dried (Na_2SO_4), and evaporated *in vacuo*. The residue was column-chromatographed on silica gel (dichloromethane) to give 2-(*p*-benzyloxyphenyl)-1-(methylsulfinyl)-1-(methylthio)ethylene (**21**; 935 mg: 62% yield) as a yellow oil: IR (neat) 1063 cm^{-1}; NMR ($CDCl_3$) δ=2.24 (3H, s), 2.66 (3H, s), 5.03 (2H, s), 6.94 (2H, d, J=9 Hz), 7.2—7.5 (5H, m), 7.51 (1H, s), and 7.86 (2H, d, J=9 Hz). Found: C, 63.96; H, 5.73; S, 19.87%. Calcd for $C_{17}H_{18}O_2S_2$: C, 64.12; H, 5.70; S, 20.14%.

*(b) NaOH and Excess of **1**:* A mixture of **1** (8.89 g) and sodium hydroxide (0.67 g) was stirred at 70 °C for 30 min, and then *p*-benzyloxybenzaldehyde (5.00 g) was added. The resulting mixture was further stirred at 70—80 °C for 1.5 h. After the addition of dichloromethane (100 ml), the mixture was washed with a saturated aqueous solution of sodium chloride and dried (Na_2SO_4). Evaporation *in vacuo*, followed by column-chromatography on silica gel [dichloromethane–ethyl acetate (19 : 1)], afforded **21** (6.909 g: 92% yield) as a pale yellow oil.

*Decomposition of 2-(p-Benzyloxyphenyl)-1-(methylsulfinyl)-1-(methylthio)ethylene (**21**) with HCl.* To a solution of **21** (495 mg) in ethanol (9 ml), was added a saturated ethanolic solution (1 ml) of HCl and the resulting solution was refluxed for 3 h. After evaporation *in vacuo*, the residue was column-chromatographed on silica gel [benzene-hexane (4 : 1)] to afford ethyl (*p*-benzyloxyphenyl)acetate (343 mg: 82% yield) as a colorless oil: IR (neat) 1735 cm^{-1}; NMR ($CDCl_3$) δ=1.24 (3H, t, J=7 Hz), 3.56 (2H, s), 4.15 (2H, q, J=7 Hz), 5.07 (2H, s), 6.95 (2H, d, J=9 Hz), 7.24 (2H, d, J=9 Hz), and 7.3—7.5 (5H, m); MS (70 eV), *m/e* (relative intensity), 270 (M^+, 4), 92 (7), 91(100), and 65 (6).

This ester was hydrolyzed by the usual manner: The ester (198 mg) was dissolved in 1,2-dimethoxyethane (3 ml) and 1M aqueous solution (3 ml) of potassium hydroxide was added. The resulting mixture was stirred at room temperature for 19 h and then, water (10 ml) and 0.5 M sulfuric acid (5 ml) were added. After extraction with ethyl acetate (30 ml×3), the organic layer was dried (Na_2SO_4) and evaporated *in vacuo*. The residue was column-chromatographed on silica gel [dichloromethane–ethyl acetate (2 : 1)] to give (*p*-benzyloxyphenyl)acetic acid as colorless crystals: mp 124—125 °C (from chloroform–hexane)(lit,[17] mp 120—121 °C); IR (KBr) 3200—2300 and 1688 cm^{-1}; NMR ($CDCl_3$) δ=3.48 (2H, s), 4.95 (2H, s), 6.85 (2H, d, J=9 Hz) 7.15 (2H, d, J=9 Hz), 7.2—7.4 (5H, m), and 11.44 (1H, broad s). Found: C, 74.18; H, 5.78%. Calcd for $C_{15}H_{14}O_3$: C, 74.37; H, 5.82%.

Condensation of m-*Phenoxybenzaldehyde with **1**. (a) Triton B in THF*: To a solution of *m*-phenoxybenzaldehyde (2.00 g) and **1** (1.27 g) in THF (10 ml), was added a 40% methanolic solution (1 ml) of Triton B and the solution was refluxed for 26 h. Dichloromethane (50 ml) was added and the resulting solution was washed with 1.5 M sulfuric acid. The organic layer was dried (K_2CO_3) and evaporated *in vacuo*. The residue was subjected to column-chromatography on silica gel (dichloromethane) to give 1-(methylsufinyl)-1-(methylthio)-2-(*m*-phenoxyphenyl)ethylene (**22**; 1.88 g: 61% yield) as a pale yellow oil. An analytical sample was obtained by rechromatography as a colorless oil: IR (neat) 1062 cm^{-1}; NMR ($CDCl_3$) δ=2.20 (3H, s), 2.66 (3H, s), 6.88—7.60 (9H, m), and 7.52 (1H, s); MS (70 eV), *m/e* (relative intensity), 304 (M^+, 5), 242 (19), 241 (100), 227 (13), 226 (77), 197 (12), 165 (19), 148 (35), 147 (22), 89 (30), 77 (22), 63 (11), 51 (20), and 39 (10). Found: C, 63.20; H, 5.30; S, 21.06%. Calcd for $C_{16}H_{16}O_2S_2$: C, 63.13; H, 5.30; S, 20.83%.

*(b) NaOH and Excess of **1**:* After a mixture of **1** (2.44 g) and powdered sodium hydroxide (120 mg) was stirred at 70 °C for 30 min, *m*-phenoxybenzaldehyde (1.99 g) was added and then the resulting mixture was further stirred at 70 °C for 3 h. After the addition of dichloromethane (50 ml), the mixture was washed successively with water (50 ml×2) and 0.5 M sulfuric acid (50 ml), dried ($MgSO_4$), and evaporated *in vacuo*. The residue was column-chromatographed on silica gel (dichloromethane) to give **22** (2.23 g: 73% yield) as a pale yellow oil.

*Decomposition of 1-(Methylsulfinyl)-1-(methylthio)-2-(m-phenoxyphenyl)ethylene (**22**) with HCl.* To a solution of **22** (492 mg) in ethanol (9 ml), was added a saturated ethanolic solution (1 ml) of HCl, and the solution was refluxed for 2.5 h. After evaporation *in vacuo*, the residue was subjected to column-chromatography on silica gel (benzene) to give ethyl (*m*-phenoxyphenyl)acetate (351 mg: 85% yield) as a colorless oil: IR (neat) 1736 cm^{-1}; NMR ($CDCl_3$) δ=1.14 (3H, t, J=7 Hz), 3.45 (2H, s), 4.02 (2H, q, J=7 Hz), and 6.60—7.40 (9H, m). Found: C, 74.50; H, 6.32%. Calcd for $C_{16}H_{16}O_3$: C, 74.98; H, 6.29%.

*Condensation of 3,4-Dimethoxybenzaldehyde with **1**. (a) Triton B in Dioxane*: To a solution containing 3,4-dimethoxybenzaldehyde (1.43 g) and **1** (1.078 g) in dioxane (7 ml), was added a 40% methanolic solution (1 ml) of Triton B and then the mixture was stirred for 25 h at 80 °C. After the addition of dichloromethane (100 ml), the resulting solution was washed with *ca.* 2 M hydrochloric acid (10.5

ml), dried (Na_2SO_4), and evaporated *in vacuo*. The residue was column-chromatographed on silica gel (dichloromethane) to afford 2-(3,4-dimethoxyphenyl)-1-(methylsulfinyl)-1-(methylthio)ethylene (**13**) (1.118 g: 47% yield) as a colorless oil which crystallized on standing and was further purified by recrystallization from diethyl ether–hexane to give colorless crystals: mp 61.5—62.5 °C; IR (KBr) 1057 cm^{-1}: NMR ($CDCl_3$) δ=2.31 (3H, s), 2.72 (3H, s), 6.90 (1H, d, J=8.3 Hz), 7.46 (1H, dd, J=8.3 and 2.4 Hz), 7.55 (1H, s), and 7.73 (1H, d, J=2.4 Hz). Found: C, 52.83; H, 5.88%. Calcd for $C_{12}H_{16}O_3S_2$: C, 52.91; H, 5.92%.

Since **1** (493 mg) was recovered, the yield of **13** based on the consumed **1** was calculated to be 87%.

(b) Triton B in THF: To a solution containing 3,4-dimethoxybenzaldehyde (1.007 g) and **1** (0.75 g) in THF (5 ml), was added a 40% methanolic solution (0.75 ml) of Triton B and then the resulting solution was refluxed for 48 h. After the addition of dichloromethane (50 ml), the mixture was washed with 0.5 M sulfuric acid (20 ml) and water (50 ml×2), dried (Na_2SO_4), and evaporated *in vacuo*. The residue was subjected to column-chromatography on silica gel [dichloromethane and dichloromethane–ethyl acetate (4 : 1)] to give **13** (1.085 g: 66% yield) as a yellow oil which crystallized.

*(c) NaOH and Excess of **1***: After a mixture of **1** (7.48 g) and powdered sodium hydroxide (0.36 g) was stirred at 70 °C for 30 min, 3,4-dimethoxybenzaldehyde (5.007 g) was added and then the resulting mixture was further stirred at 70 °C for 1.5 h. After the addition of dichloromethane (100 ml), the mixture was washed with 0.5 M sulfuric acid (50 ml) and water (100 ml×2), dried (Na_2SO_4), and evaporated *in vacuo*. The residue was column-chromatographed on silica gel [dichloromethane–ethyl acetate (4 : 1)] to give **13** (6.714 g: 82% yield) as a yellow oil which crystallized after a while.

*Decomposition of **13** with HCl. (a) in Saturated Ethanolic Solution of HCl*: A solution of **13** (260 mg) in ethanol (10 ml) was saturated with HCl gas at room temperature. The temperature of the solution rose up to *ca.* 50 °C. The reaction mixture was allowed to stand overnight at room temperature and then evaporated *in vacuo*. The residue was subjected to column-chromatography on silica gel (benzene) to give ethyl (3,4-dimethoxyphenyl)acetate (**14**) (86 mg: 37% yield) and ethyl (3,4-dimethoxyphenyl)(methylthio)acetate (**15**) (135 mg: 49% yield). The identification of **14** was achieved by the comparison of its IR spectrum with that of the authentic sample prepared by the usual esterification (HCl–ethanol) of commercially available (3,4-dimethoxyphenyl)acetic acid. The structure of **15** was deduced by the following physical data: IR (neat) 1727 cm^{-1}; NMR (CCl_4) δ=1.26 (3H, t, J=7.5 Hz), 2.00 (3H, s), 3.79 (3H, s), 3.83 (3H, s), 4.15 (2H, q, J=7.5 Hz), 4.28 (1H, s), and 6.55—7.05 (3H, m).

In the above reaction, when HCl gas was passed into the system under ice-cooling until the solution turned yellow, the yields of **14** and **15** were 40% and 25%, respectively.

(b) In 0.5 M Ethanolic Solution of HCl: To a solution of **13** (2.00 g) in ethanol (20 ml), was added a saturated ethanolic solution (1 ml) of HCl and the solution was stirred at room temperature for 22 h and refluxed for 2 h. After evaporation *in vacuo*, the residue was subjected to column-chromatography on silica gel (benzene) to afford **14** (1.51 g: 91% yield) as a yellow oil.

(c) In t-Butyl Alcohol: After a solution of **13** (505 mg) in *t*-butyl alcohol (5 ml) was saturated with HCl under cooling with ice-water, the resulting solution was stirred at room temperature for 2 h. After evaporation *in vacuo*, the residue was column-chromatographed on silica gel [benzene–hexane (1:4)] to give a yellow oil (338 mg: 67% yield) which was assigned as **16** from the following properties: IR (neat) 1680 cm^{-1}; NMR (CCl_4) δ=2.05 (3H, s), 2.15 (3H, s), 3.78 (3H, s), 3.82 (3H, s), 4.49 (1H, s), 6.62—6.93 (3H, m). Found: C, 53.09; H, 5.69%. Calcd for $C_{12}H_{16}O_3S_2$: C, 52.91; H, 5.92%.

*Condensation of 3,4-(Methylenedioxy)benzaldehyde with **1**. (a) Triton B in THF*: To a solution containing **1** (674 mg) and 3,4-(methylenedioxy)benzaldehyde (895 mg) in THF (5 ml), was added a 40% methanolic solution (0.7 ml) of Triton B and then the resulting mixture was refluxed for 9 h. Dichloromethane (50 ml) was added and the mixture was washed with 0.5 M sulfuric acid, dried (Na_2SO_4), and evaporated *in vacuo*. The residue was column-chromatographed on silica gel (dichloromethane) to afford 2-(3,4-methylenedioxyphenyl)-1-(methylsulfinyl)-1-(methylthio)-ethylene (**23**; 870 mg: 62% yield) as a pale yellow oil: IR (neat) 1058 cm^{-1}; NMR ($CDCl_3$) δ=2.34 (3H, s), 2.76 (3H, s), 6.05 (2H, s), 6.87 (1H, d, J=8 Hz), 7.30 (1H, dd, J=8 and 2 Hz), 7.54 (1H, s), and 7.75 (1H, d, J=2 Hz). Found: C, 51.27; H, 4.65; S, 25.20%. Calcd for $C_{11}H_{12}O_3S_2$: C, 51.54; H, 4.72; S, 25.02%.

Further elution with dichloromethane gave **1** (151 mg). Therefore, the yield based on the unrecovered **1** was calculated to be 81%.

*(b) NaOH and Excess of **1***: After a mixture of **1** (2.44 g) and powdered sodium hydroxide (0.12 g) was stirred at 70 °C for 30 min, 3,4-(methylenedioxy)benzaldehyde (1.502 g) was added and then the resulting mixture was further stirred at 70 °C for 3 h. After the addition of dichloromethane (50 ml), the mixture was washed with water (50 ml×2), dried (Na_2SO_4), and evaporated *in vacuo*. The residue was column-chromatographed on silica gel (dichloromethane) to give **23** (2.143 g: 84% yield) as a pale yellow oil.

*Decomposition of 2-(3,4-Methylenedioxyphenyl)-1-(methylsulfinyl)-1-(methylthio)ethylene (**23**) with HCl. (a) In Ethanol*: A solution of **23** (522 mg) in ethanol (10 ml) was bubbled by HCl gas under ice-cooling until the solution turned yellow (about 20 min). The reaction mixture was evaporated *in vacuo* and subjected to column-chromatography on silica gel (benzene) to afford ethyl (3,4-methylenedioxyphenyl)acetate (386 mg: 91% yield) as a pale yellow oil. Identification of the product was achieved by the comparison of its IR spectrum with that of the authentic sample prepared by the usual esterification (HCl–ethanol) of (3,4-methylenedioxyphenyl)-acetic acid which was obtained by the following procedure.

To a solution containing ethyl (3,4-methylenedioxyphenyl)-acetate (333 mg) in 1,2-dimethoxyethane (10 ml), was added 1 M aqueous solution (5 ml) of sodium hydroxide and the resulting mixture was refluxed for 2 h. After being poured into ice–water (50 ml) containing 3.5% hydrochloric acid (10 ml), the mixture was extracted with ethyl acetate (50 ml×2), dried (Na_2SO_4), and evaporated *in vacuo*. The residue was column-chromatographed on silica gel [dichloromethane–ethyl acetate (1:1)] to afford (3,4-methylenedioxyphenyl)-acetic acid (278 mg: 97% yield) as pale yellow crystals, which were further purified by recrystallization from diethyl ether–hexane to give colorless crystals: mp 132—133 °C (lit,[18] mp 128—129 °C); IR (KBr) 3300—2700 and 1703 cm^{-1}; NMR ($CDCl_3$) δ=3.50 (2H, s), 5.86 (2H, s), 6.66 (2H, diffused s), and 6.70 (1H, diffused s). Found: C, 60.10; H, 4.45%. Calcd for $C_9H_8O_4$: C, 60.00; H, 4.48%.

(b) In Methanol: A solution of **23** (309 mg) in methanol (4 ml) was saturated under ice-cooling with HCl and the resulting solution was stirred at room temperature for 15.5 h. After evaporation *in vacuo*, the residue was subjected to column-

chromatography on silica gel [benzene–hexane (1:4)] to afford methyl (3,4-methylenedioxyphenyl)acetate (183 mg: 80% yield) as a pale yellow oil which was identified by the comparison of its IR and NMR spectra with those of the authentic sample prepared by the usual esterification (HCl–methanol) of (3,4-methylenedioxyphenyl)acetic acid.

Condensation of 3,4,5-Trimethoxybenzaldehyde with ***1***. To a solution of **1** (3.353 g) and 3,4,5-trimethoxybenzaldehyde (5.016 g) in THF (50 ml), was added a 40% methanolic solution (5 ml) of Triton B and the resulting solution was refluxed for 12 h. After the addition of dichloromethane (50 ml) followed by acidification with 4.5 M sulfuric acid, the organic layer was separated, washed with water, dried (Na_2SO_4), and evaporated *in vacuo*. The residue was separated by column-chromatography on silica gel (dichloromethane) to give 2-(3,4,5-trimethoxyphenyl)-1-(methylsulfinyl)-1-(methylthio)ethylene (**24**; 5.465 g: 71% yield) as a yellow oil, which was crystallized from diethyl ether–hexane to afford colorless crystals: mp 86.5—87.5 °C; IR (KBr) 1058 cm^{-1}; NMR ($CDCl_3$) δ=2.30 (3H, s), 2.70 (3H, s), 3.83 (9H, s), 7.21 (2H, s), and 7.47 (1H, s). Found: C, 51.71; H, 6.00; S, 20.80%. Calcd for $C_{13}H_{18}O_4S_2$: C, 51.92; H, 6.00; S, 21.20%.

*Decomposition of 2-(3,4,5-Trimethoxyphenyl)-1-(methylsulfinyl)-1-(methylthio)ethylene (**24**) with HCl.* *(a) 1 M Ethanolic Solution of HCl*: To a solution of **24** (502 mg) in ethanol (9 ml), was added a saturated ethanolic solution (1 ml) of HCl and then the resulting solution was refluxed for 1.5 h. After evaporation *in vacuo*, the residue was column-chromatographed on silica gel (benzene) to give ethyl (3,4,5-trimethoxyphenyl)acetate (248 mg) as a pale yellow oil and a mixture (98 mg) which was shown to consist of ethyl (3,4,5-trimethoxyphenyl)acetate and an unknown compound in the ratio of 3:2. This unknown compound exhibits NMR signals in $CDCl_3$ at δ=1.25 (3H, t, J=7 Hz), 2.06 (3H, s), 3.81 (9H, s), 4.11 (2H, q, J=7 Hz), 4.38 (1H, s), and 6.67 (2H, s), and it was deduced to be ethyl (3,4,5-trimethoxyphenyl)(methylthio)acetate. Therefore, the total yield of ethyl (3,4,5-trimethoxyphenyl)acetate was calculated to be 72%. An analytical sample was obtained by further column-chromatography and short-path distillation (bath temperature 150 °C/0.09 Torr): IR (neat) 1737 cm^{-1}; NMR ($CDCl_3$) δ=1.23 (3H, t, J=7 Hz), 3.48 (2H, s), 3.78 (9H, s), 4.11 (2H, q, J=7 Hz), and 6.46 (2H, s); MS (70 eV), *m/e* (relative intensity), 254 (M^+, 75), 181 (100), 167 (28), and 29 (33). Found: C, 61.31; H, 7.15%. Calcd for $C_{13}H_{18}O_5$: C, 61.41; H, 7.13%.

(b) In Saturated Ethanolic Solution of HCl: A saturated ethanolic solution (10 ml) of HCl was added to **24** (495 mg) and the resulting mixture was stirred at room temperature for 1.5 h. After evaporation *in vacuo*, the residue was column-chromatographed on silica gel (benzene) to give ethyl (3,4,5-trimethoxyphenyl)acetate (34 mg) as a yellow oil and a mixture (111 mg) which was shown by an NMR analysis to consist of ethyl (3,4,5-trimethoxyphenyl)acetate and ethyl (3,4,5-trimethoxyphenyl)(methylthio)acetate in the ratio of 42:35. The yield of the ethyl (3,4,5-trimethoxyphenyl)-acetate was calculated to be 62%.

Condensation of p-*Chlorobenzaldehyde with* ***1***. *(a) Triton B in Dioxane*: To a solution containing **1** (1.17 g) and *p*-chlorobenzaldehyde (1.33 g) in dioxane (7 ml), was added a 40% methanolic solution (1 ml) of Triton B and the mixture was stirred at 80 °C for 25 h. After the addition of dichloromethane (100 ml), the resulting mixture was washed with *ca.* 2 M hydrochloric acid (10.5 ml), dried (Na_2SO_4), and evaporated *in vacuo*. The residue was column-chromatographed on silica gel (dichloromethane) to give 2-(*p*-chlorophenyl)-1-(methylsulfinyl)-1-(methylthio)ethylene (**25**; 1.19 g: 51% yield) as a colorless oil: IR (neat) 1062 cm^{-1}; NMR (CCl_4) δ=2.32 (3H, s), 2.68 (3H, s), 7.36 (2H, d, J=8.7 Hz), 7.48 (1H, s), and 7.82 (2H, d, J=8.7 Hz). Found: C, 48.63; H, 4.81%. Calcd for $C_{10}H_{12}OS_2Cl$: C, 48.67; H, 4.49%.

Since **1** (354 mg) was recovered, the yield based on the consumed **1** was calculated to be 73%.

(b) Triton B in THF: To a solution containing *p*-chlorobenzaldehyde (501 mg) and **1** (445 mg) in THF (5 ml), was added a 40% methanolic solution (0.5 ml) of Triton B, the resulting mixture was refluxed for 6 h. After the addition of dichloromethane (30 ml), the mixture was washed with 0.5 M sulfuric acid (10 ml) and water (30 ml×2), dried (Na_2SO_4), and evaporated *in vacuo*. By column-chromatography on silica gel [dichloromethane–ethyl acetate (3:1)], **25** (574 mg: 65% yield) was given as a yellow oil.

(c) NaOH and Excess of ***1***: After a mixture of **1** (8.83 g) and powdered sodium hydroxide (0.46 g) was stirred at 70 °C for 30 min, *p*-chlorobenzaldehyde (4.99 g) was added and the resulting mixture was further stirred at 70 °C for 1 h. After the addition of dichloromethane (100 ml) followed by being washed with 0.5 M sulfuric acid (20 ml) and water (100 ml×3), the organic layer was dried (Na_2SO_4) and evaporated *in vacuo*. The residue was column-chromatographed on silica gel (dichloromethane) to afford **25** (6.118 g: 70% yield) as a pale yellow oil.

*Decomposition of 2-(*p*-Chlorophenyl)-1-(methylsulfinyl)-1-(methylthio)ethylene (**25**) with HCl.* *(a) In a Saturated Ethanolic Solution of HCl*: A solution containing **25** (260 mg) was saturated with HCl gas under ice-cooling. The reaction mixture was allowed to stand at room temperature overnight. Evaporation *in vacuo*, followed by column-chromatography on silica gel [benzene–hexane (1:1)], gave ethyl (*p*-chlorophenyl)acetate (193 mg: 92% yield) which was identified by the comparison of its IR spectrum with that of the authentic sample prepared by the usual esterification (HCl–ethanol) of commercially available (*p*-chlorophenyl)acetic acid.

(b) In Saturated Methanolic Solution of HCl: After a solution of **25** (517 mg) in methanol (6 ml) was saturated with HCl under cooling with ice–water, the resulting solution was stirred at room temperature for 2.5 h. After evaporation *in vacuo*, the residue was column-chromatographed on silica gel [benzene–hexane (1:4)] to give methyl (*p*-chlorophenyl)-acetate (303 mg: 78% yield) as a colorless oil which was identified by the comparison of its IR and NMR spectra with those of the authentic sample prepared by the usual esterification (HCl–methanol) of (*p*-chlorophenyl)acetic acid.

(c) In 1-Butanol: After a solution of **25** (538 mg) in 1-butanol (5 ml) was saturated with HCl under cooling with ice–water, the resulting solution was stirred at room temperature for 2.5 h. Evaporation *in vacuo*, followed by column-chromatography on silica gel [benzene–hexane (1:4)], afforded butyl (*p*-chlorophenyl)acetate (396 mg: 80% yield) as a colorless oil: IR (neat) 1740 cm^{-1}; NMR ($CDCl_3$) δ= 0.8—1.8 (7H, m), 3.45 (2H, s), 3.99 (2H, t, J=7 Hz), and 7.19 (4H, s). Found: C, 63.80; H, 6.41%. Calcd for $C_{12}H_{15}O_2Cl$: C, 63.57; H, 6.67%.

Condensation of o-*Bromobenzaldehyde with* ***1***. To a solution of **1** (7.01 g) and *o*-bromobenzaldehyde (9.99 g) in THF (50 ml), was added a 40% methanolic solution (4 ml) of Triton B and the resulting mixture was refluxed for 46 h. After the addition of dichloromethane (100 ml), the mixture was washed with 0.5 M sulfuric acid (20 ml), dried (Na_2SO_4), and evaporated *in vacuo*. The residue was subjected to column-chromatography on silica gel (dichloromethane and

ethyl acetate) to give 2-(*o*-bromophenyl)-1-(methylsulfinyl)-1-(methylthio)ethylene (**26**; 8.026 g: 51% yield) as a pale yellow oil: bp 167—170 °C/0.15—0.2 Torr; IR (neat) 1036 cm^{-1}; NMR ($CDCl_3$) δ=2.32 (3H, s), 2.77 (3H, s), 7.0—7.8 (4H, m) and 7.98 (1H, diffused s). Found: C, 41.08; H, 3.76%. Calcd for $C_{10}H_{11}S_2OBr$: C, 41.24; H, 3.81%.

*Decomposition of 2-(o-Bromophenyl)-1-(methylsulfinyl)-1-(methylthio)ethylene (**26**) with HCl.* To a solution of **26** (505 mg) in ethanol (4.5 ml), was added a saturated ethanolic solution (0.5 ml) of HCl and the resulting solution was refluxed for 3 h. After evaporation *in vacuo*, the residue was column-chromatographed on silica gel and elution with hexane–benzene (9:1) gave ethyl (*o*-bromophenyl)acetate (390 mg: 92% yield) as a colorless oil: bp 75—80 °C/0.1 Torr; IR (neat) 1737 cm^{-1}; NMR ($CDCl_3$) δ=1.20 (3H, t, J=7 Hz), 3.49 (2H, s), 4.08 (2H, q, J=7 Hz), and 7.00—7.42 (4H, m). Found: C, 49.25; H, 4.53; Br, 33.06%. Calcd for $C_{10}H_{11}O_2Br$: C, 49.41; H, 4.56; Br, 32.87%.

Condensation of p-*Isopropylbenzaldehyde with **1**. (a) Triton B in THF*: To a solution of **1** (2.24 g) and *p*-isopropylbenzaldehyde (2.65 g) in THF (30 ml), was added a 40% methanolic solution (2 ml) of Triton B and the resulting solution was refluxed for 25 h. After the addition of dichloromethane (50 ml) and being washed with 1.5 M sulfuric acid (20 mi), the organic layer was dried (K_2CO_3) and evaporated *in vacuo*. The residue was column-chromatographed on silica gel (dichloromethane) to give 2-(*p*-isopropylphenyl)-1-(methylsulfinyl)-1-(methylthio)ethylene (**27**; 3.013 g: 68% yield) as a pale yellow oil: bp 170—172 °C/0.2 Torr; IR (neat) 1063 cm^{-1}; NMR ($CDCl_3$) δ=1.25 (6H, d, J=7 Hz), 2.28 (3H, s), 2.70 (3H, s), 2.89 (1H, septet, J=7 Hz), 7.32 (2H, d, J=7 Hz), 7.57 (1H, s), and 7.81 (2H, d, J=7 Hz). Found: C, 61.24; H, 7.14; S, 24.95%. Calcd for $C_{13}H_{18}OS_2$: C, 61.38; H, 7.13; S, 25.20%.

*(b) NaOH and Excess of **1***: To a mixture of **1** (12.6 g) and powdered sodium hydroxide (1.35 g), was added *p*-isopropylbenzaldehyde (10.1 g) dropwise over 20 min under being stirred at 60 °C, and the resulting mixture was further stirred at 60 °C for 5 h. After dichloromethane (100 ml) was added, the mixture was washed with 0.5 M sulfuric acid (25 ml) and water (100 ml×2). The organic layer was dried (Na_2SO_4), evaporated *in vacuo*, and column-chromatographed on silica gel [benzene–dichloromethane (3:1)] to give **27** (14.45 g: 83% yield) as a yellow oil.

*Decomposition of 2-(p-Isopropylphenyl)-1-(methylsulfinyl)-1-(methylthio)ethylene (**27**) with HCl.* To a solution of **27** (1.01 g) in ethanol (9 ml), was added a saturated ethanolic solution of HCl and the solution was refluxed for 3 h. After evaporation *in vacuo*, the residue was column-chromatographed on silica gel (hexane) to give ethyl (*p*-isopropylphenyl)-acetate (789 mg: 96% yield) as a colorless oil. An analytical sample was obtained by a short-path distillation (bath temperature 110—115 °C/0.3 Torr): IR (neat) 1738 cm^{-1}; NMR ($CDCl_3$) δ=1.20 (3H, t, J=7 Hz), 1.20 (6H, d, J=7 Hz), 2.83 (1H, septet, J=7 Hz), 3.50 (2H, s), 4.08 (2H, q, J=7 Hz), and 7.12 (4H, s). Found: C, 75.52; H, 8.81%. Calcd for $C_{13}H_{18}O_2$: C, 75.69; H, 8.80%.

*Condensation of 2-Thiophenecarbaldehyde with **1**. (a) Triton B in THF*: To a solution containing 2-thiophenecarbaldehyde (10.315 g) and **1** (11.42 g) in THF (50 ml), was added a 40% methanolic solution (3 ml) of Triton B and then the resulting mixture was refluxed for 6 h. After the addition of dichloromethane (100 ml), the mixture was washed with 0.5 M sulfuric acid, dried (Na_2SO_4) and evaporated *in vacuo*. The residue was distilled *in vacuo* to afford **17** (17.31 g: 86% yield) as a pale yellow oil: bp 147—152 °C/0.11—0.13 Torr; IR (neat) 1055 and 710 cm^{-1}; NMR ($CDCl_3$) δ=2.35 (3H, s), 2.70 (3H, s), 7.05 (1H, m), 7.40 (2H, m), and 7.86 (1H, s). Found: C, 43.81; H, 4.83; S, 44.00%. Calcd for $C_8H_{10}OS_3$: C, 44.00; H, 4.62; S, 44.06%.

(b) KOH in Methanol: After 2-thiophenecarbaldehyde (1.043 g) and **1** (1.221 g) were dissolved in methanol (15 ml), potassium hydroxide (440 mg) was added and the resulting solution was refluxed for 24 h. The solution was evaporated *in vacuo* and dichrolomethane (100 ml) was added. The deposited insoluble matter was filtered off and the filtrate was evaporated *in vacuo*. The residue was separated by column-chromatography on silica gel (dichloromethane) to afford **17** (1.689 g: 83% yield) as a pale yellow oil.

*Decomposition of **17** with HCl. (a) At Room Temperature*: To a solution of **17** (872 mg) in ethanol (10 ml), was added a saturated ethanolic solution (1 ml) of HCl and the resulting solution was stirred under ice-cooling for 2 h and then at room temperature for 66 h. The solution was evaporated *in vacuo* and separated by column-chromatography on silica gel [hexane–benzene (1:1)] to give ethyl (2-thienyl)acetate (544 mg: 80% yield) as a pale yellow oil. This ester was identified with the authentic sample prepared by the usual esterification (HCl–ethanol) of (2-thienyl)acetic acid.

(b) Under Refluxing: To a solution of **17** (1.762 g) in ethanol (30 ml), was added a saturated ethanolic solution (2 ml) of HCl and the solution was refluxed for 22.5 h. After evaporation *in vacuo*, the residue was column-chromatographed on silica gel [benzene–hexane (1:1)] to give a pale yellow oil (1.172 g) which was shown by an NMR analysis to consist of ethyl (2-thienyl)acetate (1.039 g: 79% yield) and ethyl (methylthio)(2-thienyl)acetate (133 mg: 8% yield).[19]

Condensation of p-*Chlorobenzaldehyde with Phenyl (Phenylthio)-methyl Sulfoxide.* To a solution containing *p*-chlorobenzaldehyde (446 mg) and phenyl (phenylthio)methyl sulfoxide[3] (545 mg) in THF (5 ml), was added a 40% methanolic solution (0.5 ml) of Triton B and the mixture was refluxed for 5.5 h. After the addition of dichloromethane (100 ml), the mixture was washed with 0.5 M sulfuric acid, dried (Na_2SO_4), and evaporated *in vacuo*. The residue was separated by column-chromatography on silica gel (dichloromethane) to give 2-(*p*-chlorophenyl)-1-(phenylsulfinyl)-1-(phenylthio)-ethylene (**28**; 708 mg: 60% yield) as colorless crystals: mp 97.5—98.5 °C; IR (KBr) 1042 cm^{-1}: NMR (CCl_4) δ=7.06 (5H, s), 7.15—7.80 (9H, m), and 7.98 (1H, s). Found: C, 64.36; H, 3.85; S, 17.47%. Calcd for $C_{20}H_{15}OS_2Cl$: C, 64.76; H, 4.08; S, 17.29%.

*Decomposition of 2-(p-Chlorophenyl)-1-(phenylsulfinyl)-1-(phenylthio)ethylene (**28**) with HCl.* A solution containing **28** (180 mg) in ethanol (10 ml) was saturated with HCl gas under ice-cooling. The reaction mixture was allowed to stand overnight at room temperature, and then evaporated *in vacuo*. The residue was separated by column-chromatography on silica gel (hexane and benzene) to give diphenyl disulfide (94 mg: 89% yield) and ethyl (*p*-chlorophenyl)-acetate (82 mg: 90% yield).

References

1) For a preliminary report see K. Ogura and G. Tsuchihashi, *Tetrahedron Lett.*, **1972**, 1383.

2) K. Ogura and G. Tsuchihashi, *J. Chem. Soc., Chem. Commun.*, **1970**, 1689.

3) K. Ogura and G. Tsuchihashi, *Bull. Chem. Soc. Jpn.*, **45**, 2203 (1972).

4) K. Ogura and G. Tsuchihashi, *Tetrahedron Lett.*, **1971**, 3151; G. R. Newkome, J. M. Robinson, and J. D. Sauer, *J. Chem. Soc., Chem. Commun.*, **1974**, 410; K. Ogura, N. Katoh,

and G. Tsuchihashi, *Bull. Chem. Soc. Jpn.*, **51**, 889 (1978).

5) K. Ogura, M. Yamashita, M. Suzuki, and G. Tsuchihashi, *Tetrahedron Lett.*, **1974**, 3653; K. Ogura, M. Yamashita, S. Furukawa, M. Suzuki, and G. Tsuchihashi, *Tetrahedron Lett.*, **1975**, 2767; K. Ogura, M. Yamashita, and G. Tsuchihashi, *Tetrahedron Lett.*, **1976**, 759; G. Schill and P. R. Jones, *Synthesis*, **1974**, 117.

6) K. Ogura and G. Tsuchihashi, *Tetrahedron Lett.*, **1972**, 2681; K. Ogura, S. Furukawa, and G. Tsuchihashi, *Chem. Lett.*, **1974**, 659.

7) K. Ogura and G. Tsuchihashi, *J. Am. Chem. Soc.*, **96**, 1960 (1974); K. Ogura, I. Yoshimura, and G. Tsuchihashi, *Chem. Lett.*, **1975**, 803.

8) K. Ogura, N. Katoh, I. Yoshimura, and G. Tsuchihashi, *Tetrahedron Lett.*, **1978**, 375.

9) K. Ogura, M. Yamashita, and G. Tsuchihashi, *Synthesis*, **1975**, 385.

10) R. R. Fraser and Y. Y. Wigfield, *J. Chem. Soc., D*, **1970**, 1471.

11) From the result that 2-(*p*-chlorophenyl)-1-(phenylsulfinyl)-1-(phenylthio)ethylene gave diphenyl disulfide in 89% yield together with ethyl (*p*-chlorophenyl)acetate (90% yield) (see Experimental section), it was suggested that the methylsulfinyl and methylthio groups of **10** were converted into dimethyl disulfide. However, the mechanism for this intriguing transformation of **10** into **12** remains unsolved.

12) For example, E. Späth and N. Lang, *Monatsh. Chem.*, **42**, 273 (1921).

13) E. H. Flynn, "Cephalosporins and Penicillins, Chemistry and Biology," Academic Press, New York, N. Y. (1972), pp 532—582.

14) Use of hydrogen chloride of higher concentration brought about the formation of a large amount of by-products, resulting in reduction of the yield of **18**.

15) E. Campaigne and W. L. Archer, *J. Am. Chem. Soc.*, **75**, 989 (1953).

16) A. I. Vogel, *J. Chem. Soc.*, **1948**, 654.

17) J. W. Corse, R. G. Jones, Q. F. Soper, C. W. Whitehead, and O. K. Behrens, *J. Am. Chem. Soc.*, **70**, 2837 (1948).

18) E. R. Shepard, H. D. Porter, J. F. Noth, and C. K. Simmans, *J. Org. Chem.*, **17**, 568 (1952).

19) Ethyl (methylthio)(2-thienyl)acetate could be also obtained on treatment of 1,1-bis(methylthio)-2-chloro-2-(2-thienyl)ethylene, which was produced by the reaction of 1-(methylsulfinyl)-1-(methylthio)-2-(2-thienyl)ethylene with thionyl chloride in the presence of triethylamine, with a catalytic amount of hydrogen chloride in refluxing ethanol: IR (neat) 1730 cm^{-1}; NMR ($CDCl_3$) 1.28 (3H, t, J=7 Hz), 2.13 (3H, s), 4.22 (2H, q, J=7 Hz), 4.75 (1H, s), and 6.8—7.4 (3H, m). The detail will be reported elsewhere in the near future.

† Present address: Department of Synthetic Chemistry, Faculty of Engineering, Chiba University, Yayoi-cho, Chiba 260.

Synthesis and Thermal Rearrangement of Homobarrelenones. Preparation of Dimethyl 1-Oxo-*cis*-3a,7a-dihydroindene-3a,7a-dicarboxylates

Tadao UYEHARA,* Shoichi MIYAKOSHI, and Yoshio KITAHARA†

Department of Chemistry, Faculty of Science, Tohoku University, Aoba, Aramaki, Sendai 980

(Received January 23, 1979)

The Diels-Alder reaction of five derivatives of 2-methoxytropone with dimethyl acetylenedicarboxylate proceeds regiospecifically giving dimethyl 1-methoxy-2-oxobicyclo[3.2.2]nona-3,6,8-triene-6,7-dicarboxylates, except in the case of 5-isopropyl-2-methoxytropone. The adducts undergo rearrangement selectively to dimethyl 7-methoxy-1-oxo-*cis*-3a,7a-dihydroindene-3a,7a-dicarboxylates, upon heating under reflux in xylene. Regiochemical aspects of the cycloaddition and mechanistic aspects of the rearrangement are discussed.

Tropone (2,4,6-cycloheptatrien-1-one, **1**) is known to react with various kinds of olefins giving Diels-Alder type 1,4-addition products.[1–12] Kinstle and Carpenter, and Uyehara *et al.* found independantly that **1** reacts with an acetylenic dienophile, dimethyl acetylenedicarboxylate (DMAD), to give dimethyl 6,7-dicarboxylate of bicyclo[3.2.2]nona-3,6,8-trien-2-one (homobarrelenone), (**2**).[13] The adduct is thermally labile, undergoing rearrangement selectively to dimethyl 1-oxo-*cis*-3a,7a-dihydroindene-3a,7a-dicarboxylate (**3**) upon heating under reflux in xylene.[13b] Dihydroindenone **3** is stable under acidic conditions, but is extreemly sensitive to the base, sodium methoxide.[14] When **3** was treated with the base in methanol at 0 °C, dimethyl 3-oxo-1,7-indandicarboxylate (**4**) was formed within a minute.

In order to know the mechanism of the rearrangement, we required a series of dimethyl 1-oxo-*cis*-3a,7a-dihydroindene-3a,7a-dicarboxylates. There are two prerequisites for the synthesis of the dihydroindenones from tropones in practical yield: regioselective Diels-Alder reaction to give homobarrelenones and selective rearrangement of the adducts to the corresponding dihydroindenones.

When 2-methoxytropone (**5**) was heated with DMAD at 90 °C, a regiospecific Diels-Alder reaction proceeded giving dimethyl 1-methoxyhomobarrelenone-6,7-dicarboxylate (**6**) in an excellent yield.[15] Similar specificity of the reaction positions of tropone **5** was observed for a reaction with methyl propiolate.[16] When the adduct **6** was heated under reflux in xylene, dimethyl 7-methoxy-1-oxo-*cis*-3a,7a-dihydroindene-3a,7a-dicarboxylate (**7**) was formed selectively.[15] These results prompted us to investigate a synthesis of the dihydroindenones from 2-methoxytropones.

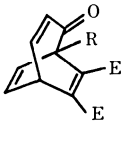

2 R=H
6 R=OCH_3

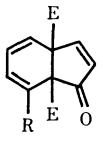

3 R=H
7 R=OCH_3

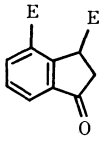

4
E=CO_2CH_3

Results and Discussion

Diels-Alder Reaction of 2-Methoxytropones with Dimethyl Acetylenedicarboxylate (DMDA). 2-Methoxytropone **5** is obtained by careful treatment of tropolone (2-hydroxy-2,4,6-cycloheptatrien-1-one) with diazomethane.[17] A series of alkyltropolones, 3-, 4-, and 5-isopropyl derivatives, is easily available.[18] Diazomethane treatment of 3-isopropyltropolone gives only 7-isopropyl-2-methoxytropone (**8d**).[19] A similar treatment of 4-isopropyltropolone gives a miture of 4- and 6-isopropyl-2-methoxytropones (**8a** and **8c**, respectively), which can not be separated from each other.[20] Compounds **8a** and **8c** have been prepared from 7-iodo-4-isopropyl and 3-iodo-6-isopropyl-2-methoxytropones, respectively, by catalytic hydrogenolysis.[21] 5-Isopropyl-2-methoxytropone (**8b**) is derived from 5-isopropyltropolone with diazomethane.[22]

Table 1. Preparation of the homobarrelenones[a]

Tropone	Product	Yield (%)	Substituent R_2	R_4	R_5	R_6	R_7
8a	**9a**	64.8[b]	OCH_3	*i*-Pr	H	H	H
8b	**9b**	96.5	H	*i*-Pr	H	H	OCH_3
8c	**9c**	63.0[c]	OCH_3	H	H	*i*-Pr	H
8d	**9d**	64.9	OCH_3	H	H	H	*i*-Pr
8e	**9e**	53.7[d]	OCH_3	H	OCH_3	H	H

a) In a sealed tube, at 90 °C for 40 h. b) With 9.7% of **12a**. c) With 4.9% of **12c**. d) In a sealed tube, at 80 °C for 100 h, with 21.4% of **12e**.

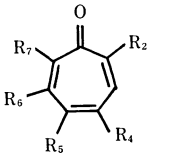

8a–e

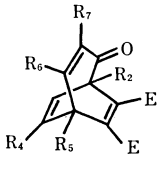

9a–e

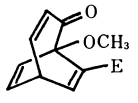

10

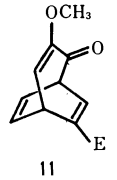

11

E=CO_2CH_3

The conditions and the results of the Diels-Alder reaction of 2-methoxytropones (**8a**—**8d**) with DMAD are given in Table 1. Each reaction temperature was kept as low as possible, since once a homobarrelenone derivative undergoes rearrangement to the corresponding dihydroindenone in the presence of DMAD, they react easily and a complex mixture of polysubstituted

† Deceased February 4, 1976.

benzenes is formed.[12b,15] The structures of the addition products (**9a**, **9b**, **9c**, and **9d**) were deduced by means of their spectral data, mainly of the ^{1}H-NMR spectra.

Regioselectivity of the 1,4-additions is surprisingly high. DMAD underwent addition to **8a**, **8c**, and **8d** only at the 2,5-position, and to **8b** only at the 4,7-position. For explanation of the regiospecificity, we propose three major factors: 1) the difference between both primary interaction energies due to the methoxyl group, an electron-donating substituent; 2) the favorable secondary interaction between the ether oxygen of the tropones and the carbonyl carbon of the dienophile (an n-pi interaction); 3) the steric repulsion between the isopropyl group and the methoxycarbonyl group, in the transition states of addition.

Ethylene, a simple and symmetrical dienophile, underwent addition to 2-methoxytropone at 2,5- and 4,7-positions in the ratio of 87.7 and 12.3.[23] No secondary interaction would take place in the transition states leading to the adducts. The preferential addition of ethylene to the 2,5-position rather than to the 4,7-position was supported by the difference between the calculated interaction energies[23] by means of PMO equation proposed by Salem.[24] Maleic anhydride, a symmetrical dienophile, reacted with **5** only at the 2,5-position.[25] Thus, Diels-Alder type 1,4-addition of symmetrical dienophiles is favorable at the 2,5-position of 2-methoxytropone. Each isopropyl-2-methoxytropone could be regarded as a perturbed 2-methoxytropone. The difference between primary interaction energies of both reaction positions of **8a**, **8b**, **8c**, and **8d** with the dienophile should be similar to that of 2-methoxytropone with the dienophile.

Low regio- and stereoselectivities have been observed for the reactions of **5** and asymmetrical oleficic dienophiles, such as acrylonitrile and methyl acrylate.[3] However, methyl propiolate, an asymmetrical acetylenic dienophile, underwent addition regioselectively to **5** giving the adduct (**10**) in 67.5% yield with a small amount of the isomer (**11**).[16] Calculated interaction energies for the four possible regiochemical combinations of **5** and methyl propiolate suggest that the major product should be **11**. Disagreement with experimental results indicates that the regioselectivity can not be explained only by primary orbital interactions. In the transition state leading to **10**, the distance between the ether oxygen and the carbonyl carbon of the dienophile should be remarkably short, because of an acetylenic dienophile, and the secondary interaction between them could not be negligible. The same interaction seems to contribute to the selective addition of DMAD to the 2,5-position of 2-methoxytropones **5**, **8a**, **8c**, and **8d**.

Reversal of regiospecificity during the addition of DMAD to **8b** may be explained by large steric repulsion between the bulky isopropyl group and the methoxycarbonyl group in the transition state leading to the addition of the 2,5-position of **8b**, again because of the linear dienophile. This steric repulsion also contributes to the preferential formation of **9a** and **9d** from **8a** and **8d**, respectively.

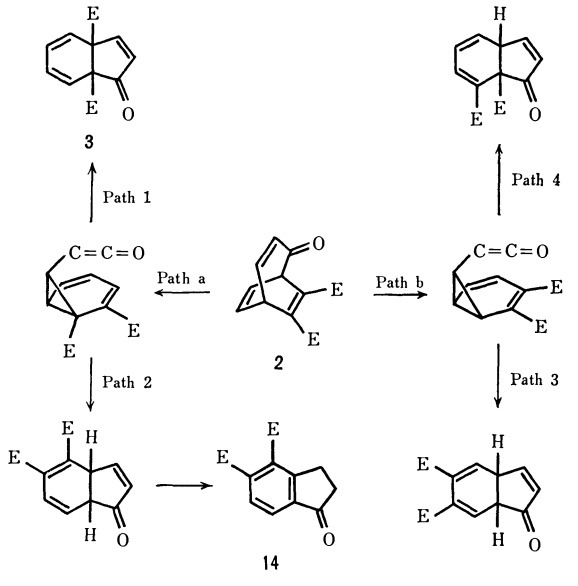

Scheme 1.

Table 2. Thermal rearrangement of the homobarrelenones

Homobarrelenone	Product	Yield (%)
8a	**12a**[a]	74.1
8b	(**8b**)[a]	90.3[b]
	(**8b**)[c]	88.8[b]
8c	**12c**[a]	73.3
8d	**12d**[a]	63.0
8e	**12e**[a]	80.0
10	**17**[c]	74.9
15	**16**[a]	60.5
	16[c]	78.9

a) Heated under reflux in xylene for 40 h. b) Recovery. c) Gas-phase thermolysis at 350 °C/0.15 Torr.

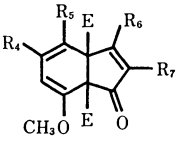

12a $R_4=i$-Rr, $R_5=R_6=R_7=H$
12c $R_4=R_5=R_7=H$, $R_6=i$-Pr
12d $R_4=R_5=R_6=H$, $R_7=i$-Pr
12e $R_4=R_6=R_7=H$, $R_5=OCH_3$

$E=CO_2CH_3$

DMAD underwent addition to the 2,5-position of 2,5-dimethoxytropone (**8e**) giving the homobarrelenone (**9e**) with dihydroindenone (**12e**) even at 80 °C. Formation of **9e** reflects the contribution of that secondary interaction.

Thermal Rearrangements of the Homobarrelenones to cis-*3a,7a-Dihydroinden-1-ones.* The process of the thermal rearrangement of **2** to the dihydroindenone **3**, proposed by Kinstle and Carpenter, involves a [3,3]-sigmatropic shift to 7-*syn*-norcaradienylketene (**13**) followed by a [3,5]-sigmatropic shift (antarapfacial or Möbius) to **3**.[13a] If the mechanism is correct, there are four possible routes, each of them giving a paticular isomer as shown in Scheme 1. Preferential formation of **3** follows path a and path 1. Dimethyl 1-oxoindan-

4,5-dicarboxylate (**14**), a minor product from **2**,[13b] should be formed through path a and path 2, followed by aromatization. Thus, preferential formation of **3** from **2** is interesting from a synthetic point of view. Study on the substituent effects for both sigmatropic rearrangements is of interest.

The rearrangement of **2** to **3** was performed by gas-phase[13a] or solution thermolysis.[13b] A concentrated solution of **2** gave many by-products, in the latter. The conditions and the results of the thermolysis of the homobarrelenones are given in Table 2. Compound **8b** was stable under the same conditions for the solution thermolysis of other isomers and at 350 °C *in vacuo*. Gas-phase thermolysis of **8b** at 450 °C gave unidentified decomposed products. The other homobarrelenones underwent rearrangement to the corresponding dihydroindenones through path a and path 1.

Thermal reactions of the monosubstituted homobarrelenone (**15**), derived from **1** and methyl propiolate,[16] yielded methyl 1-oxoindan-4-carboxylate (**16**). The process of the rearrangement involves path a and path 2 and aromatization. Gas-phase pyrolysis of **10** gave dihydroindenone (**17**). ^{1}H-NMR spectrum shows a multiplet at δ=3.97 (dddd, $J_{9,2}$=2.5 Hz, $J_{9,3}$=2.7, $J_{9,4}$=4.8, and $J_{9,5}$=1.7), a typical pattern of H_9 in *cis*-3a,7a-dihydroinden-1-ones.[26] The yield of **17** decreased when **10** was heated in a solution. The machanism of the process involves path a and path 1.

The regioselectivity of the [3,3]-sigmatropic shifts (path a is preferred) seems to be due to the electron-withdrawing substituents at the 8 and/or the 9 positions. The substituents should decrease the energy level of the HOMO of the acceptor radical fragment[27] in the transition state giving intermediates such as **13** through path a.

The other selective sigmatropic shifts (path 1 is preferred) may be caused by the differences between the pi-electron densities and the magnitude of the coefficients of each reaction position of the HOMO of the migrating framework.[27]

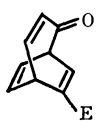

15

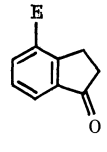

16

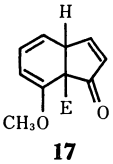

17

E=CO_2CH_3

Experimental

General. Melting points were determined on a Thomas Hoover MP Apparatus, and are uncorrected. Infrared spectra were recorded on Hitachi EPI-3 and Model 215 spectrophotometers. Ultraviolet spectra were recorded on a Hitachi EPS-2T spectrometer. NMR spectra were obtained on Varian A-60 and HA-100 spectrometers equipped with spin decouplars, using tetramethylsilane as an internal standard. The mass spectral studies were conducted using a Hitachi RMU-6D spectrometer.

*2,5-Dimethyl-2,4,6-cycloheptatrien-1-one (**8e**).* Dimethyl sulfate (3.7 g) was added to a solution of 5-hydroxytropolone[28] (1.5 g) in 2 M-sodium hydroxide (20 ml) over a period of 2.5 h at 0 °C, and the mixture was stirred at room temperature for 2 h. After being heated under reflux for 30 min, the solution was cooled to room temperature, acidified (pH 5) with 10% hydrochloric acid and extracted with three portions of dichloromethane (20 ml each). The extracts were combined, dried ($MgSO_4$) and concentrated giving brown oil (1.6 g), a mixture of methoxytropones and **8e**. The mixture was dissolved in dichloromethane and treated with an ethereal solution of diazomethane. Evaporation of the solvents and crystallization from hexane–benzene gave pale yellow prisms (1.5 g, 83% yield). **8e**: mp 74—75 °C; IR (KBr) 1630, 1595, 1563, and 1518 cm^{-1}; NMR ($CDCl_3$) δ=3.86 (3H, s, OCH_3), 3.96 (3H, s, OCH_3), and 6.35—7.27 (4H, m).

*Preparation of Homobarrelenone Derivatives (**9a**—**9e**). General Procedure*: Each 2-methoxytropone and DMAD (0.9—1.1 equiv) were placed in a Pyrex tube, sealed, and heated at 90±0.5 °C for 40 h (**8a**—**8d**) or at 80±0.5 °C for 100 h (**8e**). Isolation of each product was performed with chromatography on a silica-gel column or an alumina (neutral) column (for **9a** and **12a**) using gradient mixtures of benzene and ethyl acetate.

*Physical Properties of the New Homobarrelenones. A) Dimethyl 9-Isopropyl-1-methoxy-2-oxobicyclo[3.2.2]nona-3,6,8-triene-6,7-dicarboxylate (**9a**)*: Pale yellow oil; UV_{max} (CH_3OH) 215 (log ε 4.13), 285 (3.15)^{sh} and 345 nm (2.60); IR (film) 1740, 1722, 1692, 1666, and 1640 cm^{-1}; NMR ($CDCl_3$) δ=1.11 (6H, d, J=7.0 Hz, $CH_3\times2$), 2.46 (1H, sept of d, J=7.0 and 1.5 Hz, $CH(CH_3)_2$), 3.61 (3H, s), 3.80 (3H, s), 3.84 (3H, s), 4.32 (1H, ddd, J=8.1, 1.5 and 0.9 Hz, H_5), 5.44 (1H, dd, J=10.8 and 0.9 Hz, H_3), 6.09 (1H, dd, J=1.5 and 1.5 Hz, H_8), and 7.15 (1H, dd, J=10.8 and 8.1 Hz, H_4). Found: M$^+$, 320.

*B) Dimethyl 9-Isopropyl-3-methoxy-2-oxobicyclo[3.2.2]nona-3,6,8-triene-6,7-dicarboxylate (**9b**)*: Yellow oil; UV_{max} (CH_3OH) 227 (log ε 3.96), 289 (3.41) and 364 nm (2.58)^{sh}; IR (film) 1720, 1685, and 1640 cm^{-1}; NMR($CDCl_3$) δ=1.09 (6H, d, J=6.7 Hz, $CH_3\times2$), 2.49 (1H, broad sept, J=6.7 Hz, $CH(CH_3)_2$), 3.40 (3H, s), 3.74 (6H, s), 3.96 (1H, dd, J=9.5 and 2.3 Hz, H_5), 4.42 (1H, d, J=7.4 Hz, H_1), 5.98 (1H, ddd, J=7.3, 2.3 and 1.5 Hz, H_8), and 6.05 (1H, d, J=9.5 Hz, H_4). Found: M$^+$, 320.

*C) Dimethyl 4-Isopropyl-1-methoxy-2-oxobicyclo[3.2.2]nona-3,6,8-triene-6,7-dicarboxylate (**9c**)*: Pale yellow oil; UV_{max} (CH_3OH) 224 (log ε 4.25), 287 (3.22)^{sh} and 335 nm (2.55)^{sh}; IR (film) 1740, 1720, 1678, 1658, and 1621 cm^{-1}; NMR ($CDCl_3$) δ=1.11 (3H, d, J=6.5 Hz, CH_3), 1.13 (3H, d, J=6.5 Hz, CH_3), 2.49 (1H, sept, J=6.5 Hz, $CH(CH_3)_2$), 3.53 (3H, s), 3.71 (6H, s), 4.37 (1H, ddd, J=6.0, 1.8 and 0.9 Hz, H_5), 5.01 (1H, dd, J=0.9 and 0.9 Hz, H_3), 6.56 (1H, dd, J=8.4 and 1.8 Hz, H_8), and 6.70 (1H, dd, J=8.4 and 6.0 Hz, H_9). Found: M$^+$, 320.

*D) Dimethyl 3-Isopropry-1-methoxy-2-oxobicyclo[3.2.2]nona-3,6,8-triene-6,7-dicarboxylate (**9d**)*: Colorless needles (from CH_3OH), mp 107.5—108.5 °C; UV_{max} (CH_3OH) 222 (log ε 4.43), 292 (2.82)^{sh} and 362 nm (2.27); IR (KBr) 1729, 1715, 1672, 1657, and 1620 cm^{-1}; NMR ($CDCl_3$), δ=0.89 (3H, d, J=7.0 Hz, CH_3), 0.91 (3H, d, J=7.0 Hz, CH_3), 2.78 (1H, sept, J=7.0 Hz, $CH(CH_3)_2$), 3.59 (3H, s), 3.78 (3H, s), 3.82 (3H, s), 4.44 (1H, ddd, J=8.0, 6.5, and 1.2 Hz, H_5), 6.58 (1H, dd, J=8.5 and 1.4 Hz, H_8), 6.84 (1H, dd, J=8.0 and 1.2 Hz, H_4), and 6.88 (1H, dd, J=8.5 and 6.5 Hz, H_9). Found: C, 63.45; H, 6.29%; M$^+$, 320. Calcd for $C_{17}H_{20}O_6$: C, 63.74; H, 6.29%; M, 320.

*E) Dimethyl 1,5-Dimethoxy-2-oxobicyclo[3.2.2]nona-3,6,8-triene-6,7-dicarboxylate (**9e**)*: colorless prisms (from CCl_4), mp 101–102 °C; UV_{max} (CH_3OH) 214 (log ε 3.90), 285

(2.85)^{sh} and 360 nm (1.91); IR (KBr) 1740, 1693, 1652, and 1620 cm^{-1}; NMR ($CDCl_3$) δ=3.45 (3H, s), 3.53 (3H, s), 3.78 (3H, s), 3.83 (3H, s), 5.24 (1H, d, J=11.8 Hz, H_3), 6.55 (1H, J=9.3 Hz, H_8), 6.97 (1H, d, J=9.3 Hz, H_9), and 7.07 (1H, d, J=11.8 Hz, H_4). Found: C, 58.61; H, 5.06%; M$^+$, 308. Calcd for $C_{15}H_{16}O_7$: C, 58.44; H, 5.23%; M, 308.

Thermal Rearrangements of Homobarrellenones. General Procedure. A) Solution Thermolysis: A solution of each homobarrelenone in dry xylene (0.04—0.046 M) was heated under reflux for 40 h. After removal of the solvent, purification of the product was performed by chromatography on a silica-gel column and/or by recrystallization.

B) Gas-phase Thermolysis: A sample of each homobarrelenone was placed in a goose-necked small flask attached to a 2×15 cm oven-heated Pyrex tube, placed obliquely (45°), packed with Pyrex tips. The other end of the tube was connected to a Dry-Ice trap. The end of the trap was connected to a vacuum pump. The system was evacuated (0.15—0.2 Torr), and the Pyrex tube was heated to 350 °C. The flask containing the sample was then heated with a nichrome wound heating jacket to 100—150 °C. The pyrolysate was purified by chromatography and/or recrystallization.

Physical Properties of the New cis-*3a,7a-Dihydroindenones. A) Dimethyl 5-Isopropyl-6-methoxy-1-oxo-*cis-*3a,7a-dihydroindene-3a,7a-dicarboxylate (**12a**)*: Colorless needles (from CH_3OH), mp 149—150 °C; UV_{max} (CH_3OH) 215 (log ε 4.13), 282 (3.61) and 347 nm (2.92); IR (KBr) 1725, 1704, 1658, and 1595 cm^{-1}; NMR ($CDCl_3$) δ=1.06 (3H, d, J=7.6 Hz, CH_3), 1.07 (3H, d, J=7.6 Hz, CH_3), 2.36 (1H, sept of d, J=7.6 and 2.0 Hz, $CH(CH_3)_2$), 3.48 (3H, s), 3.66 (3H, s), 3.68 (3H, s), 5.18 (1H, d, J=1.8 Hz, H_6), 5.19 (1H, dd, J=2.0 and 1.8 Hz, H_4), 6.45 (1H, d, J=5.8 Hz, H_2), and 7.43 (1H, d, J=5.8 Hz, H_3). Found: C, 64.03; H, 6.42%; M$^+$, 320. Calcd for $C_{17}H_{20}O_6$: C, 63.74; H, 6.29%; M, 320.

*B) Dimethyl 3-Isopropyl-7-methoxy-1-oxo-*cis-*3a,7a-dihydroindene-3a,7a-dicarboxylate (**12c**)*: Colorless needles (from CH_3OH), mp 139–140 °C; UV_{max} (CH_3OH) 221 (log ε 4.16), 284 (3.57) and 338 nm (2.75); IR (KBr) 1732, 1705, 1655, and 1622 cm^{-1}; NMR ($CDCl_3$) δ=1.32 (3H, d, J=6.9 Hz, CH_3), 1.35 (3H, d, J=6.9 Hz, CH_3), 2.61 (1H, broad sept, J=6.9 Hz, $CH(CH_3)_2$), 3.67 (3H, s), 3.69 (3H, s), 3.70 (3H, s), 5.23 (1H, dd, J=6.5 and 0.8 Hz, H_6), 5.88 (1H, dd, J=10.0 and 0.8 Hz, H_4), 6.18 (1H, J=10.0 and 6.5 Hz, H_5), and 6.35 (1H, d, J=0.8 Hz, H_2). Found: C, 63.54; H, 6.38%; M$^+$, 320. Calcd for $C_{17}H_{20}O_6$: C, 63.74; H, 6.29%; M, 320.

*C) Dimethyl 2-Isopropyl-7-methoxy-1-oxo-*cis-*3a,7a-dihydroindene-3a,7a-dicarboxylate (**12d**)*: Colorless needles (from CH_3OH), mp 123.5–124.5 °C; UV_{max} 220 (log ε 4.16), 283 (3.68) and 340 nm (2.86); IR (KBr) 1739, 1720, 1651, and 1594 cm^{-1}; NMR ($CDCl_3$) δ=1.09 (3H, d, J=7.1 Hz, CH_3), 1.16 (3H, d, J=7.1 Hz, CH_3), 2.76 (1H, sept of d, J=7.1 and 1.0 Hz, $CH(CH_3)_2$), 3.68 (9H, s), 5.23(1H, d, J=6.6 Hz, H_6), 5.52 (1H, d, J=10.0 Hz, H_4), 6.07 (1H, dd, J=10.0 and 6.6 Hz, H_5), and 7.01 (1H, d, J=1.0 Hz, H_3). Found: C, 63.73; H, 6.30%; M$^+$, 320. Calcd for $C_{17}H_{20}O_6$: C, 63.74; H, 6.29%; M, 320.

*D) Dimethyl 4,7-Dimethoxy-1-oxo-*cis-*3a,7a-dihydroindene-3a,7a-dicarboxylate (**12e**)*: Pale yellow needles (from CH_3OH), mp 166—167 °C; UV_{max} (CH_3OH) 217 (log ε 4.00), 290 (3.73) and 365 nm (2.83); IR (KBr) 1746, 1712, 1662, and 1593 cm^{-1}; NMR ($CDCl_3$) δ=3.61 (3H, s), 3.66 (3H, s), 3.67 (3H, s), 3.71 (3H, s), 5.14 (2H, s, H_5 and H_6), 6.55 (1H, d, J=5.9 Hz, H_2), and 7.71 (1H, d, J=5.9 Hz, H_3). Found: C, 58.68; H, 5.09%; M$^+$, 308. Calcd for $C_{15}H_{16}O_7$: C, 58.44; H, 5.23%; M, 308.

*E) Methyl 4-Methoxy-3-oxo-*cis-*3a,7a-dihydroindene-3a-carboxylate (**17**)*: Colorless needles (from ether), mp 89—90 °C; UV_{max} (CH_3OH) 210 (log ε 4.10), 279 (3.63) and 344 nm (2.69); IR (KBr) 1736, 1704, 1651, and 1590 cm^{-1}; NMR ($CDCl_3$) δ=3.65 (3H, s) 3.72 (3H, s), 3.97 (1H, dddd, J=4.8, 2.7, 2.5, and 1.7 Hz, H_9), 5.17 (1H, d, J=6.7 Hz, H_6), 5.42 (1H, dd, J=9.7 and 4.8 Hz, H_4), 5.98 (1H, ddd, J=9.7, 6.7, and 1.7 Hz, H_5), 6.35 (1H, dd, J=5.7 and 2.5 Hz, H_2), and 7.49 (1H, dd, J=5.7 and 2.7 Hz, H_3). Found: C, 65.27; H, 5.53%; M$^+$, 220. Calcd for $C_{12}H_{12}O_4$: C, 65.44; H, 5.49%; M, 220.

*Methyl 1-Oxo-indan-4-carboxylate (**16**)*: Colorless needles (from CH_3OH), mp 102—103 °C; IR (KBr) 1710, 1580, and 760 cm^{-1}; NMR ($CDCl_3$) δ=2.70 (2H, m), 3.48 (2H, m), 3.95 (3H, s), 7.45 (1H, ddt, J=10.0, 10.0 and 0.75 Hz), 7.95 (1H, ddd, J=10.0, 1.3 and 0.5 Hz), and 8.27 (1H, dd, J=10.0 and 1.3 Hz). Found: M$^+$, 190.

*Hydrolysis of Methyl 1-Oxoindan-4-carboxylate (**16**).* A mixture of a solution of **16** (100 mg) in dioxane (5 ml) and 2 M-sodium hydroxide (30 ml) was heated under reflux for 12 h, and washed with dichloromethane. The aqueous layer was acidified with 10% hydrochloric acid, and extracted with two portions of dichloromethane. Drying over $MgSO_4$, and concentration of the solution gave a reddish solid (83 mg), which was recrystallized from hot-water. The melting point and IR spectrum of the product, colorless needles (40 mg), were identical with those of 1-oxoindan-4-carboxylic acid:[29] mp 224.5—225.5 °C; IR (KBr) 3100, 1715 and 1687 cm^{-1}.

References

1) T. Nozoe, T. Mukai, T. Nagase, and Y. Toyooka, *Bull. Chem. Soc. Jpn.*, **33**, 1146 (1960).

2) a) R. C. Cookson, B. V. Drake, J. Hudec, and A. Morrison, *Chem. Commun.*, **1966**, 15; b) S. Ito, Y. Fujise, T. Okuda, and Y. Inoue, *Bull. Chem. Soc. Jpn.*, **39**, 1351 (1966); c) S. Ito, K. Sakan, and Y. Fujise, *Tetrahedron Lett.*, **1970**, 2873; d) H. Tanida and H. R. Pfaendler, *Helv. Chim. Acta*, **55**, 3062 (1972).

3) a) S. Ito, H. Takeshita, and Y. Shoji, *Tetrahedron Lett.*, **1969**, 1815; b) Y. Shoji, Ph. D. Thesis, Tohoku University, Sendai, 1972.

4) M. Oda, M. Funamizu, and Y. Kitahara, *J. Chem. Soc., D*, **1969**, 737.

5) a) K. N. Houk and R. B. Woodward, *J. Am. Chem. Soc.*, **92**, 4145 (1970); b) T. Sasaki, K. Kanematsu, and T. Kataoka, *Chem. Lett.*, **1973**, 1183.

6) T. Uyehara and Y. Kitahara, *Chem. Ind.*, **1971**, 354.

7) S. Ito, H. Ohtani, S. Narita, and H. Homma, *Tetrahedron Lett.*, **1972**, 2223.

8) T. Uyehara, N. Sako, and Y. Kitahara, *Chem. Ind.*, **1973**, 41.

9) Y. Kashman and O. Awerbouch, *Tetrahedron*, **29**, 191 (1973).

10) Y. Fujise, Y. Chonan, H. Sakurai, and S. Ito, *Tetrahedron Lett.*, **1974**, 1585.

11) H. Takeshita, Y. Shoji, and S. Ito, *Bull. Chem. Soc. Jpn.*, **47**, 1041 (1974).

12) H. R. Pfaendler, H. Tanida, and E. Haselbach, *Helv. Chim. Acta*, **57**, 383 (1974).

13) a) T. H. Kinstle and P. D. Carpenter, *Tetrahedron Lett.*, **1969**, 3943; b) T. Uyehara, M. Funamizu and Y. Kitahara, *Chem. Ind.*, **1970**, 1500.

14) T. Uyehara, M. Funamizu, S. Miyakoshi, and Y. Kitahara, *Chem. Ind.*, **1972**, 610.

15) T. Uyehara, M. Funamizu, and Y. Kitahara, *Chem. Ind.*, **1971**, 486.
16) T. Uyehara, S. Miyakoshi, and Y. Kitahara, *Chem. Ind.*, **1972**, 607.
17) T. Nozoe, S. Seto, T. Ikemi, and T. Arai, *Proc. Jpn. Acad.*, **27**, 102, (1951); J. W. Cook, A. R. Gibb, R. A. Raphael, and A. D. Somerville, *J. Chem. Soc.*, **1951**, 503; W. von E. Doering and L. H. Knox, *J. Am. Chem. Soc.*, **73**, 828 (1951).
18) a) 3-Isopropyltropolone was derived from α-dolabrin easily prepared by the method of Asao and Kitahara: T. Asao, T. Machiguchi, T. Kitamura, and Y. Kitahara, *Chem. Commun.*, **1970**, 89. b) 4- and 5-Isopropyltropolones were obtained from Takasago Perfumery Co., Ltd.
19) S. Seto, *Sci. Repts. Tohoku Univ., I*, **37**, 292 (1953).
20) T. Nozoe, S. Seto, H. Takeda, S. Morosawa, and K. Matsumoto, *Proc. Jpn. Acad.*, **28**, 192 (1952).
21) M. Yasunami, Ph. D. Thesis, Tohoku University, Sendai, 1966.
22) T. Sato, *Tohoku Daigaku Hisuiyoeki Kenkyusho Hokoku*, **8**, 47 (1961).
23) T. Uyehara and Y. Kitahara, Abstr. No. 24-8c, 2nd International Symposium on the Chemistry of Nonbenzenoid Aromatic Compounds, Sendai, August 1970.
24) L. Salem, *J. Am. Chem. Soc.*, **90**, 543, 553 (1968).
25) T. Nozoe and Y. Toyooka, *Bull. Chem. Soc. Jpn.*, **34**, 623 (1961).
26) E. Baggldini, E. G. Herzog, S. Iwasaki, R. Scharta, and K. Schaffner, *Helv. Chim. Acta*, **30**, 277 (1967).
27) N. D. Epiotis, "Theory of Organic Reactions," Springer Verlag, New York (1978), pp. 11, 198.
28) M. Oda and Y. Kitahara, *Tetrahedron Lett.*, **1969**, 3295.
29) Y. Tomita, *Nippon Kagaku Zasshi*, **82**, 505 (1961).

A Study of the Interactions between Free Radicals and Cobalt Complexes

Kenji YOSHINO, Yasukazu OHKATSU, and Teiji TSURUTA*

Department of Synthetic Chemistry, Faculty of Engineering, The University of Tokyo, Bunkyo-ku, Tokyo 113

(Received February 10, 1979)

The interaction between free radicals and cobalt complexes (Co(II)TPP and Co(II)(sal)$_2$(*R*-CHXDA)) has been studied using (*S,S*)-(−)-, (*R,R*)-(+)-, and *meso*-1,1′-diphenylazoethane as a radical source. The decomposition of *meso*-1,1′-diphenylazoethane by heat or UV-light in the presence of Co(II)(sal)$_2$(*R*-CHXDA) having an asymmetric ligand produced an optically active (+)-2,3-diphenylbutane. The suggestion is that the α-methylbenzyl radical formed from the azo compound is stereoselectively stabilized by the Co(II)(sal)$_2$(*R*-CHXDA).

The literature cites several addition reactions of polyhaloalkanes to olefins using organometallic catalysts, 1:1 adducts being formed in good yield. In the absence of the organometallic complex, there is negligible formation of the 1:1 adducts.[1] Nagai *et al.*[2] postulated that the reaction proceeded *via* a free radical mechanism and concluded that the high selectivity in the 1:1 adduct was a direct consequence of the restricted freedom of movement of a radical which was restrained in the coordination sphere of the complex. Furthermore, Murai *et al.*[3] reported an optically active adduct in the addition reactions of bromotrichloromethane to 1-alkenes using a rhodium complex with (−)-diop as the asymmetric ligand.

It accepted that a free radical is stabilized by reacting with several metal ions (including metal complexes).[4] For example, the radicals derived from the decomposition reactions of several azo compounds are stabilized in the presence of metal complexes, especially cobalt, such as Co(II)TPP and Co(II)(sal)$_2$(*R*-CHXDA).[5]

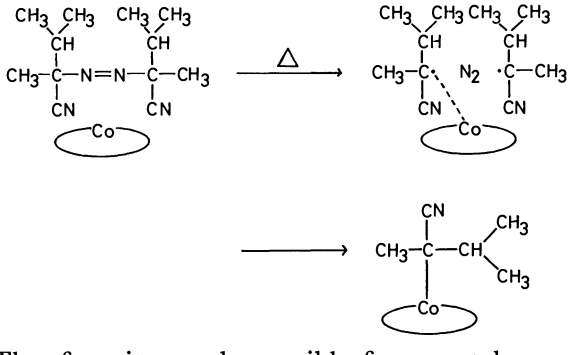

Therefore, it may be possible for a metal complex having an asymmetric ligand to stabilize radicals in two stereochemically different formes as follows:

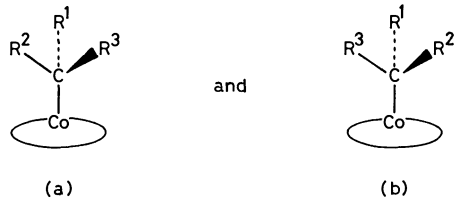

(a) and (b)

Either of these two stabilized radicals, (**a**) or (**b**), will enter a reaction preferentially owing to the difference in their reactivities resulting in the formation of an optically active product. The interactions between radicals and metal complexes, especially the effect of interaction on the yield and specific rotation of 2,3-diphenylbutane, have been studied using (*S,S*)-(−)-, (*R,R*)-(+)-, and *meso*-1,1′-diphenylazoethane as the radical source and Co(II)(sal)$_2$(*R*-CHXDA) as the asymmetric metal complex.

Experimental

Materials. The azo compounds ((*S,S*)-(−)-, (*R,R*)-(+)-, and *meso*-1,1′-diphenylazoethane[6]) and the metal complexes (Co(II)TPP and Co(II)(sal)$_2$(*R*-CHXDA)[6]) have been prepared as described in a previous paper. (−)-2,3-*O*-Isopropylidene-2,3-dihydroxy-1,4-bis(diphenylphosphino)butane ((−)-diop) has been prepared according to the method of Kagan *et al.*[7] The (−)-diop–Rh(I) has been prepared by mixing (−)-diop and di-μ-chloro-bis(π-1,5-cyclooctadiene)dirhodium(I) in benzene under nitrogen.

Decomposition of Azo Compound. The decomposition of the azo compounds in the presence or absence of metal complex has been conducted as described in a previous paper.[6] In the photo-decomposition reactions, the azo compound, contained in an ampoule under nitrogen was decomposed completely by UV-light and the volume of nitrogen released was measured.

Analysis of Decomposition Products. 2,3-Diphenylbutane, a coupling product, was separated by TLC (hexane–silica gel) and the optical rotation was measured. 2,3-Diphenylbutane was qualitatively analyzed by PMR and GC-MS.[6]

Quantitative analyses of the decomposition products were conducted by GLC (Silicone DC-550). The column temperatures were 120 °C for the non-coupling products (styrene and ethylbenzene) and 200 °C for the coupling product (2,3-diphenylbutane).

Measurement of Decomposition Rates. The decomposition rates of the azo compounds were measured as described in a previous paper.[6]

Measurement of Visible Spectra. The visible spectra of benzene solutions containing the cobalt complex (Co(II)-TPP or Co(II)(sal)$_2$(*R*-CHXDA)), (*S,S*)-(−)-1,1′-diphenylazoethane and/or nitrosobenzene were measured under nitrogen using 1 mm thick quartz glass cell.

Results and Discussion

Decomposition of 1,1′-Diphenylazoethane. According to a previous report,[6] the decomposition products from the thermolysis of 1,1′-diphenylazoethane (Azo compound) in the absence of metal complex were 2,3-diphenylbutane, styrene, and ethylbenzene. In the presence of a metal complex, an additional product, namely acetophenone α-methylbenzylhydrazone was formed.

The formation mechanism[8] of these products may be illustrated by Schemes 1 and 2.

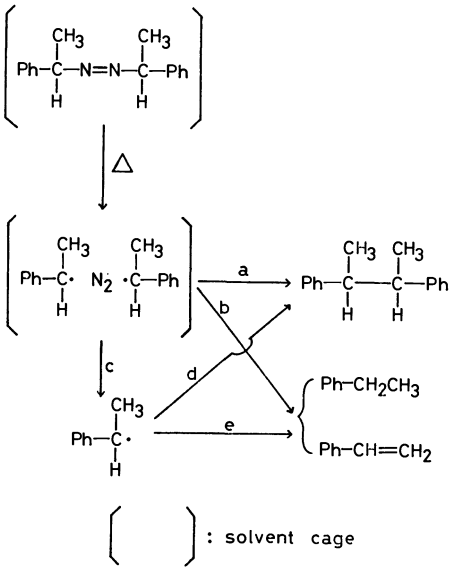

Scheme 1.

Routes **a** and **b** show the coupling and disproportionation reactions of the two radicals in a classical solvent cage, respectively. Routes **d** and **e** are, on the other hand, the corresponding reactions for radicals diffused from the cage. Scheme 2 is a possible route for the decomposition reaction in the presence of the metal complex as reported previously.[6)]

The amount of 2,3-diphenylbutane formed was less in the presence of the complex, since a part of the starting azo compound was converted into acetophenone α-methylbenzylhydrazone (Scheme 2). The complex can interact with three types of radical such as $PhCH(CH_3)$, $Ph–C(CH_3)–N=N–CH(CH_3)Ph$, and $Ph–C(CH_3)=N–\underset{\cup}{N}–CH(CH_3)Ph$. In the presence of nitrosobenzene, the only radical produced was the α-methylbenzyl radical; no acetophenone α-methylbenzylhydrazone was produced (Table 1). In order to understand the interaction between the complex and

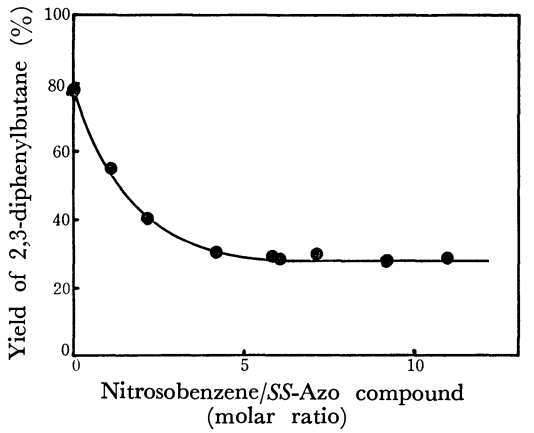

Fig. 1. Yield of 2,3-diphenylbutane in the presence of nitrosobenzene. Reaction conditions: in benzene at 104 °C for 2 days; *SS*-Azo compound: 3.7×10^{-2} M.

the α-methylbenzyl radical, the thermal decomposition has been examined in the absence and presence of nitrosobenzene.

2,3-Diphenylbutane Obtained in the Presence of Nitrosobenzene. (*S,S*)-1,1′-Diphenylazoethane (*SS*-Azo compound) was thermally decomposed in the presence of nitrosobenzene with and without the metal complex. Figure 1 illustrates the effect of nitrosobenzene on the yield of 2,3-diphenylbutane and as may be seen, the yield of 2,3-diphenylbutane decreases with the increase in the concentration of nitrosobenzene, up to six times the amount of azo compound. After this, the yield of 2,3-diphenylbutane did not vary, even in the presence of a great excess of nitrosobenzene. Twenty eight percent of 2,3-diphenylbutane is estimated to be formed in the solvent cage. Under these conditions, a trace amount of the disproportionation products was obtained and no acetophenone α-methylbenzylhydrazone was formed, even in the presence of the metal complex (Table 1).

From the result in Fig. 2, it appears there

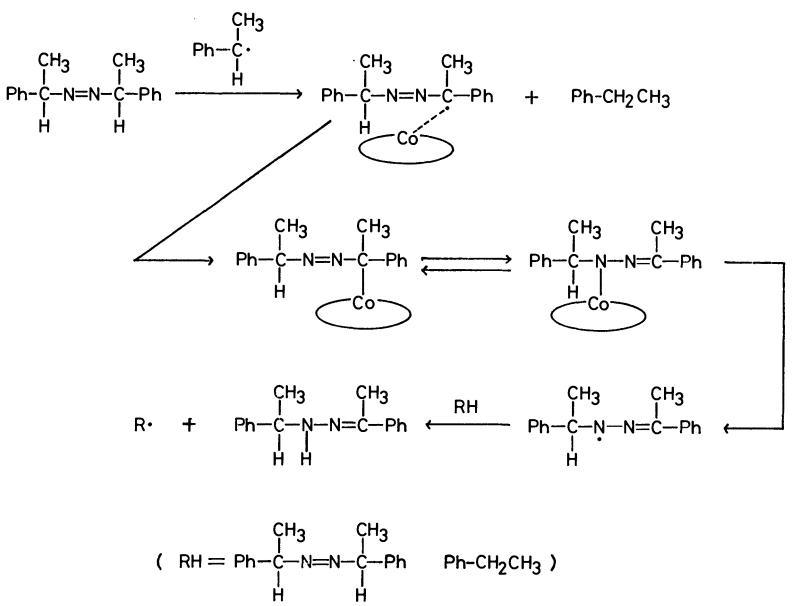

Scheme 2.

Table 1. Specific rotation and yield of 2,3-diphenylbutane formed in the presence of nitrosobenzene

Run	Azo compd ($\times 10^2$ M)	Metal complex ($\times 10^4$ M)	Nitroso-benzene ($\times 10$ M)	Products (%)				$[\alpha]_D^{b)}$ of coupling product
				$PhCH_2CH_3$	$PhCH{=}CH_2$	Ph-C(H)(Me)-C(H)(Me)-Ph	Ph-C(H)(Me)-N-N-C(H)(Me)-Ph	
1	*SS* 4.2	0	3.27	trace	trace	28.0	0	−28.4
2	*RR* 4.2	0	3.27	trace	trace	28.4	0	+28.5
3	*SS* 4.5	CoTPP 3.4	3.10	trace	trace	26.5	0	−28.5
4	*SS* 4.2	Co* 7.6	3.27	trace	trace	24.4	0	−29.0
5	*RR* 4.2	Co* 7.6	3.27	trace	trace	27.7	0	+29.3
6	*meso*[a)] 7.5	Co* 53.0	4.75	trace	trace	21.7	0	−0.9

Reaction conditions: 104 °C (a): 80 °C) in benzene for 2 days (a): 7 days).
b) Measured in benzene at 20 °C. Co*: Co(II)$(sal)_2$(*R*-CHXDA).

Table 2. Decomposition rate of azo compounds in the presence of cobalt complex in benzene at 70 °C

Azo compd	Complex	Complex/Azo compd (molar ratio)	Obsd (mol s^{-1})
SS	0	0	1.11×10^{-6}
SS	Co*	2.7×10^{-3}	1.5×10^{-6}
SS	Co(II)TPP	8.2×10^{-3}	1.4×10^{-6}

Co*: Co(II)$(sal)_2$(*R*-CHXDA).
SS-Azo compound: 2.15×10^{-1} M.

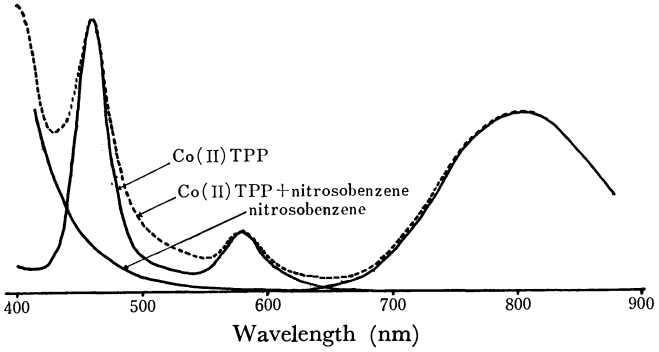

Fig. 2. Visible spectra of Co(II)TPP and/or nitrosobenzene in benzene at 20 °C. Co(II)TPP: 8.45×10^{-5} M, nitrosobenzene: 3.74×10^{-2} M.

is little, if any, interaction between nitrosobenzene and the cobalt complex, the spectrum of the binary system being a simple overlapping of the two individual spectra.

There is however, evidence which suggests a possible interaction between the metal complex and the Azo compound: (1) the visible spectra of a benzene solution of the *SS*-Azo compound and the cobalt complexes exhibited isosbestic points (Figs. 3(a) and (b)), a part of the Azo compound, at least, being thought to react with the cobalt complex, and (2) the decomposition rate of the Azo compound in the presence of a metal complex is higher than that in the absence of the metal complex (Table 2). The increase in the rate is regarded as a consequence of the increased reactivity of the Azo compound which interacts with the cobalt complex.

The specific rotation and yield of 2,3-diphenylbutane obtained from the *RR* and *SS*-Azo compounds in the

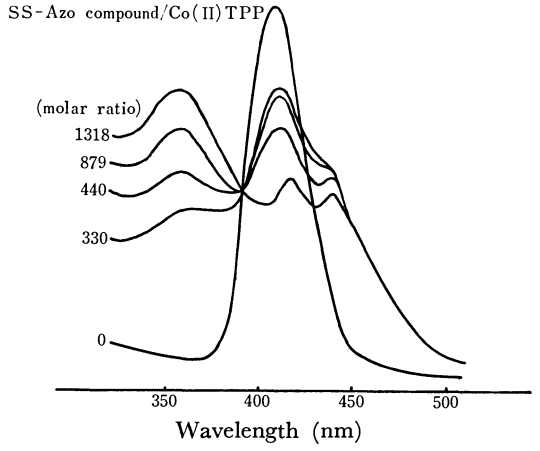

Fig. 3(a). Visible spectra of Co(II)TPP in the presence of *SS*-Azo compound in benzene at 20 °C. Co(II)TPP: 8.45×10^{-5} M.

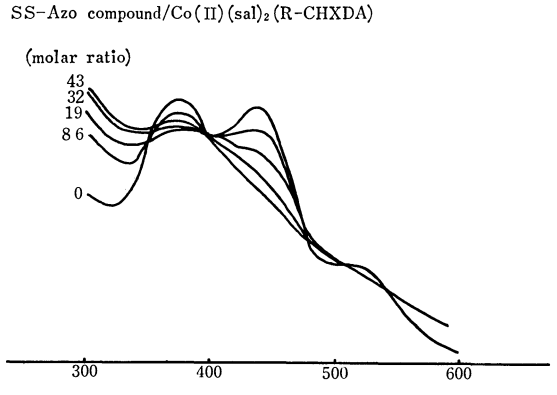

Fig. 3(b). Visible spectra of Co(II)$(sal)_2$(*R*-CHXDA) in the presence of *SS*-Azo compound in benzene at 20 °C. Co(II)$(sal)_2$(*R*-CHXDA): 5.65×10^{-4} M.

presence of both Co(II)$(sal)_2$(*R*-CHXDA) and nitrosobenzene are shown in Figs. 4 and 5, respectively. In the coupling reaction within a solvent cage, the value of $[\alpha]_D$ and the yield of 2,3-diphenylbutane, derived from the *RR*-Azo compound were negligibly changed. Little dependency upon the concentration of Co(II)-$(sal)_2$(*R*-CHXDA) was established. In the case of

the *SS*-Azo compound, however, an increase in the concentration of the metal complex caused a decrease in both the yield and the optical rotation (Fig. 4). The results may be explained by assuming the following mechanism: In the absence of the metal complex, the *SS*-Azo compound is decomposed as shown in Scheme 3, and the product consists of three coupled compounds, L-L, D-D, and L-D. Therefore, the specific rotation of the product will depend on the relative rates of coupling and inversion.[8]

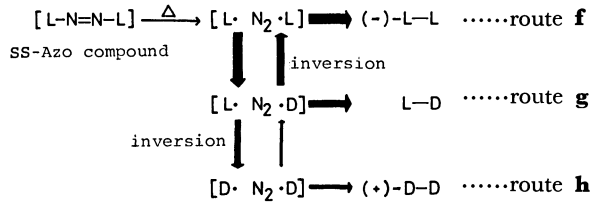

Scheme 3.

In the presence of Co(II)(sal)$_2$(*R*-CHXDA), the radicals within a solvent cage may interact with the metal complex as discussed above and consequently, the inversion and coupling reactions will be more difficult for these radicals. The results shown in Figs. 4 and 5 suggest, therefore, that the ratio of (—)-2,3-diphenylbutane ((—)-L-L) obtained from reaction route **i** is greater than that from reaction route **f** as in Scheme 3.

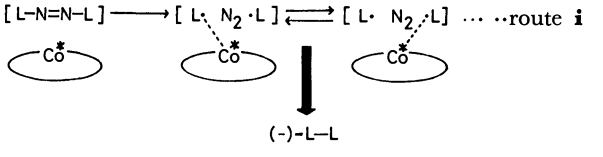

The cobalt complex, Co(II)(sal)$_2$(*R*-CHXDA), may have greater interaction with a radical from the *SS*-Azo compound compared with that from the *RR*-Azo compound, a more favorable stabilization operating in Form **A** than Form **B**.

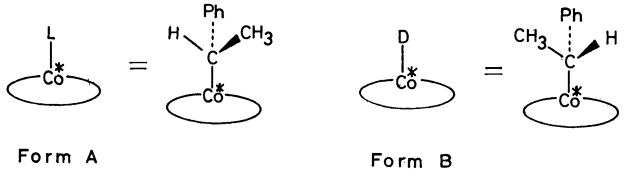

The decrease in optical rotation of 2,3-diphenylbutane from the *SS*-Azo compound (Fig. 4) may be explained by assuming that the radical formed from the *SS*-Azo compound is immediately stabilized by the Co(II)-(sal)$_2$(*R*-CHXDA) and that the inversion is suppressed. Since the stabilized radical on the complex less readily undergoes coupling, the yield of coupled product decreases.

2,3-Diphenylbutane Obtained in the Absence of Nitrosobenzene. The mechanism of formation of 2,3-diphenylbutane outside the solvent cage may be elucidated using the *meso*-Azo compound in place of the *RR* and *SS*-Azo compounds. Table 3 shows the yield and the $[\alpha]_D$ of 2,3-diphenylbutane formed from the

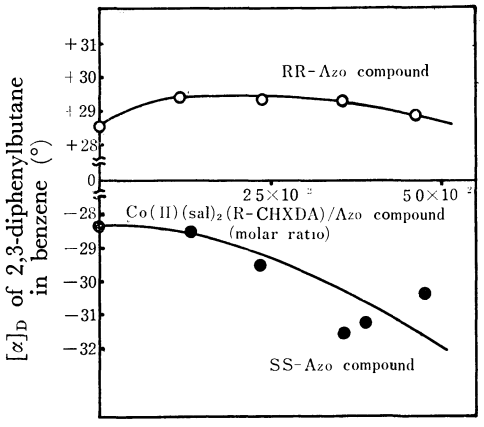

Fig. 4. The specific rotation of 2,3-diphenylbutane formed from Azo compound in the presence of Co(II)-(sal)$_2$(*R*-CHXDA) and nitrosobenzene.
Reaction conditions: Azo compound: 4.2×10^{-2} M nitrosobenzene: 3.27×10^{-1} M in benzene at 104 °C for 4 days.

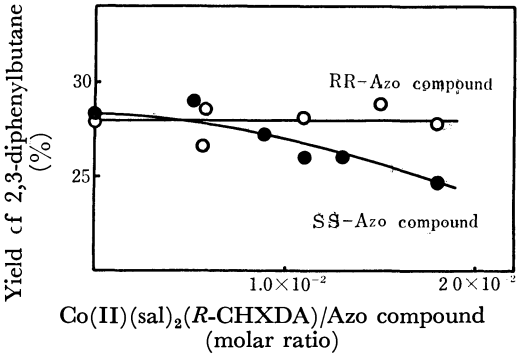

Fig. 5. Yield of 2,3-diphenylbutane formed from Azo compound in the presence of Co(II)(sal)$_2$(*R*-CHXDA) and nitrosobenzene.
Reaction conditions: Azo compound: 4.2×10^{-2} M; nitrosobenzene: 3.27×10^{-1} M, in benzene at 104 °C for 4 days.

meso-Azo compound in the presence of an optically active complex such as Co(II)(sal)$_2$(*R*-CHXDA) or (—)-diop-Rh(I). 2,3-Diphenylbutane formed in the presence of Co(II)(sal)$_2$(*R*-CHXDA) or (—)-diop-Rh(I) was optically active. With the former metal complex, the optical rotation of 2,3-diphenylbutane obtained in the absence of nitrosobenzene showed an opposite and higher absolute value compared to that obtained in the presence of nitrosobenzene (Table 1, run 6). This suggests that the major part of the optical rotation of 2,3-diphenylbutane formed in the absence of nitrosobenzene is ascribable to 2,3-diphenylbutane which was formed by the stereoselective coupling reaction of diffused radicals outside the solvent cage. The diffused radicals stereoselectively stabilized by the metal complex (probably Form **A**) are considered to undergo coupling with the other radicals with inversion of stereochemistry as shown in Scheme 4.

In the presence of nitrosobenzene, because there are relatively few diffusion radicals, the reaction in the cage predominates to form (—)-2,3-diphenylbutane as shown in route **i**.

Table 3. Specific rotation and yield of 2,3-diphenylbutane formed in the absence of nitrosobenzene

Run	*meso*-Azo compd ($\times 10^2$ M)	Metal complex ($\times 10^4$ M)	Decompn method	2,3-diphenylbutane		
				Yield (%)	$[\alpha]_D^{a)}$	e. e. (%)[8]
1	4.8	0	Δ	95.0	0 (c=0.53)	0
2	7.8	Co* 6.1	Δ	97.0	+0.8 (c=1.47)	0.8
3	4.6	Co* 3.6	Δ	98.0	+1.6 (c=1.27)	1.6
4	4.3	Co* 6.1	Δ	79.9	+2.1 (c=1.22)	2.1
5	5.4	Co* 6.1	Δ	68.3	+1.4 (c=1.50)	1.4
6	3.9	Co* 6.1	Δ	50.8	+1.6 (c=0.44)	1.6
7	5.3	Co* 3.4	*hv*	93.4	+0.2 (c=1.31)	0.2
8	5.1	Co* 6.8	*hv*	85.9	+0.3 (c=0.70)	0.3
9	4.0	Co* 6.8	*hv*	85.3	+0.3 (c=1.03)	0.3
10	8.5	Co* 16.0	*hv*	84.0	+0.9 (c=1.10)	0.9
11	4.8	(−)-diop-Rh(I) 1.2	*hv*	97.6	−0.9 (c=0.74)	0.9
12	4.2	(−)-diop-Rh(I) 2.5	*hv*	96.4	−0.5 (c=1.52)	0.5

Reaction conditions: {Δ: 82 °C in benzene for 4 days. *hv*: 30 °C in benzene by irradiating UV-light for 30 min.
Co*: Co(II)(sal)$_2$(*R*-CHXDA). a): Measured in benzene at 20 °C.

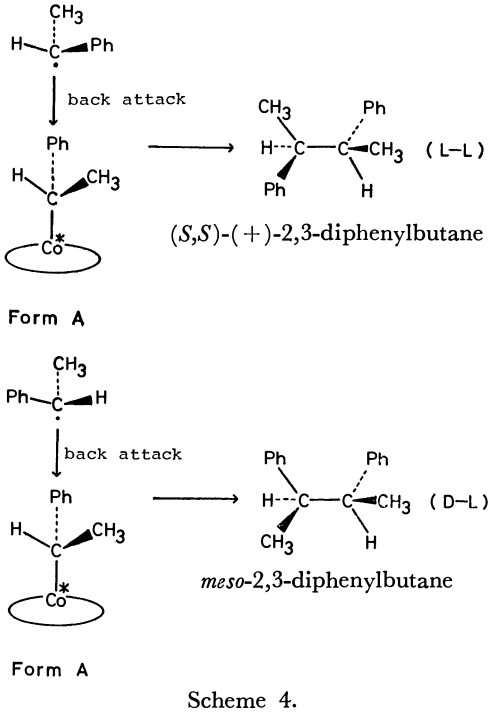

Scheme 4.

Conclusion. This study has revealed that an organometallic complex having asymmetric ligands stabilizes a free radical from an Azo compound and produces stereoselective coupling products. The optical yield of the coupling product is very low, but the optical purity may be improved by controlling the rate of decomposition of the azo compound, thereby increasing the possibility of interaction between the free radical and the complex. The use of metal complexes having more suitable chirality is another method of attaining a high value of optical purity of product.

References

1) M. Asscher and D. Vofsi, *J. Chem. Soc.*, **1963**, 1887, 3921; **1964**, 4962.
2) H. Matsumoto, T. Nakano, K. Takasu, and Y. Nagai, *J. Org. Chem.*, **43**, 1734 (1978).
3) N. Sonoda, S. Murai, R. Sugise, and K. Kondo, 26th IUPAC Congress Abstracts Session I, 93 (1978).
4) J. K. Kochi, "Free Radicals," Wiley-Interscience (1973), Vol. I, pp. 626, 627.
5) K. Yoshino, Y. Ohkatsu, and T. Tsuruta, *Polym. J.*, **9**, 275 (1977).
6) K. Yoshino, Y. Ohkatsu, and T. Tsuruta, *Bull. Chem. Soc. Jpn.*, **52**, 1738 (1979).
7) H. B. Kagan and T. -P. Dang, *J. Am. Chem. Soc.*, **94**, 6429 (1972).
8) F. D. Greene, M. A. Berwick, and J. C. Stowell, *J. Am. Chem. Soc.*, **92**, 867 (1970).

Absorption Spectra of Heterocyclic Compounds. Some 6-Hydroxy[1,3,4]thiadiazolo[2,3-*b*]benzimidazoles and Their Quaternary Derivatives

R. P. SONI and J. P. SAXENA*

Department of Chemistry, University of Jodhpur, Jodhpur, India

(Received May 1, 1978)

Some 2-alkyl-6-hydroxy[1,3,4]thiadiazolo[2,3-*b*]benzimidazoles have been synthesised. Their absorption spectra at different pH show bathochromic shift of the absorption band in the longer wavelengths, which is more pronounced in basic medium. This is ascribed to the dipolar nature of the compounds. Quaternary derivatives of the compounds show a further red shift in the absorption band in the visible region, which further corroborates their dipolar nature.

Imidazoles long considered to be cyclic amidines[1] are the most basic of the imide containing azoles.[2] Since imdazole derivatives occupy an important position with respect to the constitution of heterocyclic as well as in biochemistry, their physical properties have been investigated extensively. Although it has not been established unequivocally that the nucleus has true conjugated double bond character, imidazoles have been shown to be cyclic amidines with charges present on the nitrogen atoms in a system possessing some degree of hindered resonance. It is also apparent that the ring system possesses greater polarity than the related pyrazole but not to the extent expected from classical polar formula.

During the course of spectral study and synthesis of some donor acceptor systems in our laboratory,[3–6] benzimidazole moiety with two nitrogen atoms was selected as donors for further investigations. A perusal of literature reveals that no work has been done on the reaction of 5-alkyl-2-amino-1,3,4-thiadiazole with *p*-benzoquinone. We now report the synthesis of some new 6-hydroxy[1,3,4]thiadiazolo[2,3-*b*]benzimidazoles. The structure is of particular interest as it possesses the phenolic hydroxyl group as an acceptor and the two nitrogen atoms of the imidazole moiety as a donor, thereby facilitating the molecule to assume dipolar structure through internal charge transfer reaction. The hydroxythiadiazolobenzimidazoles were quaternized with ethyl bromide giving the corresponding 2-alkyl-9-ethyl-6-hydroxy[1,3,4]thiadiazolo[2,3-*b*]benzimidazolium bromides. The quaternary compounds gave intense yellow colour with dilute aqueous alkali due to the formation of internal charge transfer compounds, phenol betaines.[7,8]

TABLE 1. 2-ALKYL-6-HYDROXY[1,3,4]THIADIAZOLO[2,3-*b*]BENZIMIDAZOLES

Compd No.	R	Molecular formula	Mp °C	% Analysis		Yield %	UV spectra					
				Calcd	Found		Ethanol		0.1 M HCl		0.1 M NaOH	
							λ_{max} nm	log ε	λ_{max} nm	log ε	λ_{max} nm	log ε
1	H	$C_8H_5N_3SO$	285 (dec)	C, 50.2	50.1	62	237	4.33	317	3.81	310	3.62
				H, 2.6	2.4		260	3.81	382	3.75	465	3.67
				N, 21.4	20.8		365	3.62				
2	CH_3	$C_9H_7N_3SO$	337	C, 52.6	52.1	55	241	4.21	312	3.80	303	3.57
				H, 3.4	3.1		255	3.80	376	3.71	453	3.61
				N, 20.4	20.1		371	3.85				
3	C_2H_5	$C_{10}H_9N_3SO$	345	C, 54.7	54.2	48	232	4.27	305	3.73	307	3.58
				H, 4.1	3.7		251	3.75	370	3.65	460	3.61
				N, 19.1	18.8		359	3.71				
4	$CH_3(CH_2)_2$	$C_{11}H_{11}N_3SO$	360	C, 56.6	56.1	50	228	4.12	325	3.84	322	3.61
				H, 4.7	4.1		259	3.93	380	3.77	450	3.72
				N, 18.2	17.7		360	3.67				
5	$(CH_3)_2CH$	$C_{11}H_{11}N_3SO$	360	C, 56.6	55.9	35	235	4.15	315	3.73	307	3.81
				H, 4.7	4.3		315	3.83	375	3.52	435	3.54
				N, 18.2	17.9		359	3.97				
6	$CH_3(CH_2)_3$	$C_{12}H_{13}N_3SO$	360	C, 58.2	57.8	54	247	4.25	328	3.67	325	3.74
				H, 5.2	5.1		263	4.10	385	3.74	459	3.81
				N, 17.0	16.4		375	3.78				
7	$(CH_3)_2CH_2CH$	$C_{12}H_{13}N_3SO$	354—355	C, 58.2	57.9	63	271	4.07	345	3.81	351	3.57
				H, 5.2	4.9		310	4.29	397	3.72	475	3.74
				N, 17.0	16.6		364	4.31				
8	$CH_3(CH_2)_4$	$C_{13}H_{15}N_3SO$	305 (dec)	C, 59.7	58.9	49	258	4.35	330	3.62	323	3.04
				H, 5.7	5.1		302	3.97	359	3.71	445	3.34
				N, 16.0	15.3		352	4.12				

Results and Discussion

The gross structure of these compounds has been determined on the basis of infrared spectra and elemental analysis. The spectra showed the following characteristic bands at 3200, 1210 (phenolic–OH), 1610 (C=N, C=C), 1315 (C–N), 1505 cm^{-1} (aromatic ring breathing).

We see from Table 1 that the absorption spectra of various 2-alkyl-6-hydroxythiadiazolobenzimidazoles in ethanol at different pH show a characteristic bathochromic shift of the absorption maxima in the longer wavelengths in both acidic as well as alkaline medium. No zwitterionic structure is expected in strongly alkaline medium. The observed bathochromic shift might be explained by the following canonical quinoid structure (B).

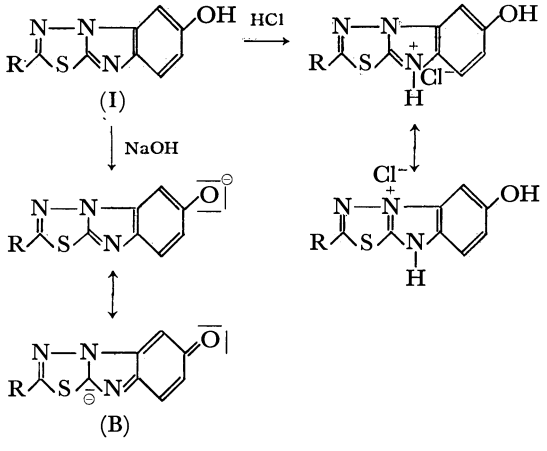

The same phenomenon is observed when these compounds are quaternized with ethyl bromide which gives rise to further red shift of absorption maxima in the visible region. This should be caused by the partial dissociation of quaternary *N*-ethylimidazoliumbromides into the dipolar betaine structure in ethanol (Table 2).

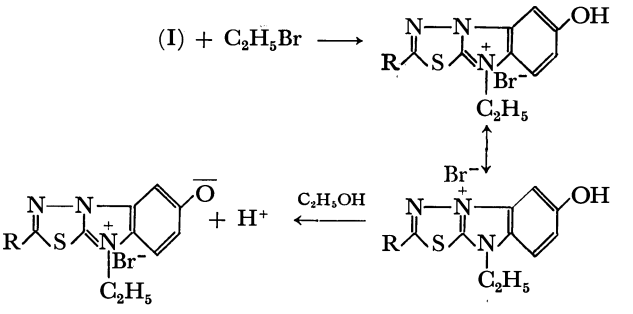

Reaction Mechanism. The following reaction mechanism is suggested for the formation.

(1) Amino group by nucleophilic addition and elimination of water gives intermediate (a)

(2) (a) on reaction with proton of acid gives (b) which causes shift of electrons, giving the final product (c).

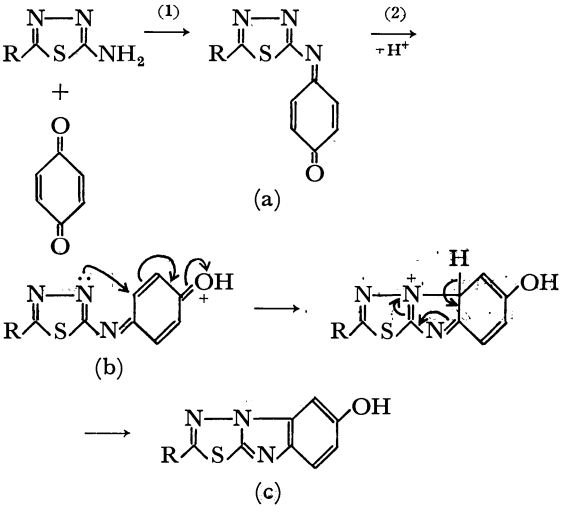

Table 2. 2-Alkyl-9-ethyl-6-hydroxy[1,3,4]thiadiazolo[2,3-*b*]benzimidazolium bromides

Compd No.	R	Molecular formula	Mp °C	Yield %	% Analysis		UV spectra Ethanol	
					Calcd	Found	λ_{max} nm	log ε
1	H	$C_{10}H_{10}N_3SOBr$	276	56	N, 14.0	13.2	285	4.15
					Br, 26.6	25.8	505	3.80
2	CH_3	$C_{11}H_{12}N_3SOBr$	308	50	N, 13.3	12.7	257	3.92
					Br, 25.4	24.8	512	3.95
3	C_2H_5	$C_{12}H_{14}N_3SOBr$	327	47	N, 12.8	12.2	263	3.84
					Br, 24.3	23.7	521	4.01
4	$CH_3(CH_2)_2$	$C_{13}H_{16}N_3SOBr$	335	45	N, 12.2	11.7	276	3.51
					Br, 23.3	22.8	515	3.84
5	$(CH_3)_2CH$	$C_{13}H_{16}N_3SOBr$	351	40	N, 12.2	11.9	258	3.62
					Br, 23.3	22.6	485	3.91
6	$CH_3(CH_2)_3$	$C_{14}H_{18}N_3SOBr$	343	48	N, 11.7	11.2	270	3.83
					Br, 22.4	21.9	495	3.95
7	$(CH_3)_2CHCH_2$	$C_{14}H_{18}N_3SOBr$	315	55	N, 11.7	11.5	265	3.93
					Br, 22.4	22.1	525	3.97
8	$CH_3(CH_2)_4$	$C_{15}H_{20}N_3SOBr$	267—268	43	N, 11.3	10.8	273	3.79
					Br, 21.6	20.9	508	3.81

Experimental

All the reagents were thoroughly dried and purified before use. Melting points were determined on a Kofler instrument and are uncorrected. IR spectra were recorded on a Perkin-Elmer 677 Spectrophotometer in KBr. UV absorption spectra were recorded on a Beckman Spectrophotometer, Model DU-2, using 1 cm path length quartz cells.

5-Alkyl-2-amino-1,3,4-thiadiazole. The compounds were prepared by known methods.[9]

*2-Alkyl-6-hydroxy[1,3,4]thiadiazolo[2,3-*b*]benzimidazoles (I).* A solution of *p*-benzoquinone (0.01 mol) in glacial acetic acid (10 ml) was added in small portions to the 5-alkyl-2-amino-1,3,4-thiadiazole (0.01 mol) in acetic acid (10 ml) with shaking. The mixture was left to stand for 2 days. To this was added 20 ml of 50% HCl and the solution was diluted with water. It was extracted with ether to remove any unreacted quinone and hydroquinone. The resulting solution was made alkaline with sodium carbonate solution when the desired compound precipitated. After treatment with charcoal in ethanol, the compound was recrystallised from ethanol. The yields, mp *etc.* are given in Table 1.

*2-Alkyl-9-ethyl-6-hydroxy[1,3,4]thiadiazolo[2,3-*b*]benzimidazolium Bromides (II).* The requisite amount of 2-alkyl-6-hydroxy[1,3,4]thiadiazolo[2,3-*b*]benzimidazole was dissolved in 1:1 ethanol–acetone solution and was boiled under reflux with excess of ethyl bromide on a water bath for 3 h, when the desired *N*-ethylimidazolium bromide was partly separated out. Excess solvent was removed by distillation on a water bath and the product was recrystallised from acetone or ethanol. The yields, mp *etc.* are given in Table 2.

Thanks are due to Prof. R. C Kapoor, Head of Chemistry Department, for providing necessary laboratory facilities and to the University Grants Commission, New Delhi, for the award of a Junior Research Fellowship to R. P. Soni.

References

1) Bamberger, *Ann.*, **273**, 300 (1893).
2) Sen and Ray, *J. Chem. Soc.*, **1926**, 646; Schwarzenbach and Lutz, *Helv. Chim. Acta*, **23**, 1162 (1940).
3) B. K. Tak and J. P. Saxena, *J. Indian Chem. Soc.*, **47**, 791 (1970).
4) B. K. Tak and J. P. Saxena, *J. Indian Chem. Soc.*, **49**, 139 (1972).
5) J. P. Saxena, B. K. Tak, and R. P. Soni, *J. Indian Chem. Soc.* Communicated.
6) R. P. Soni and J. P. Saxena, *J. Indian Chem. Soc.* Communicated.
7) J. P. Saxena, *J. Sci. Ind. Res.*, **8**, 22 (1963).
8) J. P. Saxena, W. H. Stafford, and W. L. Stafford, *J. Chem. Soc.*, **1959**, 1579.
9) Japan Patent 20944, 07 Dec., 1966; *Chem. Abstr.*, **66**, 46430f (1967).

Chemistry of Dienyl Anions. I. Crystalline Dienyl Anions by Direct Reaction of Conjugated and Non-conjugated Dienes with Alkali Metals in the Presence of Et_3N

Hajime YASUDA, Yasuo OHNUMA, Michihide YAMAUCHI, Hisaya TANI, and Akira NAKAMURA*

Department of Polymer Science, Faculty of Science, Osaka University, Toyonaka, Osaka 560

(Received December 6, 1978)

Series of acyclic and cyclic dienyl anions were prepared from both conjugated and non-conjugated dienes by direct metalation with alkali metals (Li, Na, K, Rb, and Cs) in tetrahydrofuran in the presence of triethylamine or *N,N,N′,N′*-tetramethylethylenediamine. Eight different dienyl anions of open chain or cyclic structures were isolated as crystals. All the acyclic potassium dienides of pentadienes, 2-methylpentadienes, 3-methylpentadienes, hexadienes and 2,4-dimethylpentadienes gave the corresponding 1,3-dienes upon hydrolysis, while the potassium cyclic dienide of cycloheptadienes and cyclooctadienes gave 1,4-dienes exclusively. The result of methylation of dienyl anions with methyl iodide agreed with that of hydrolysis. The reaction path for formation of these dienyl anions was studied based on the carbon skeleton and the molar ratio of the reduced diene dimers produced together with the dienyl anions. Selective oxidative coupling of the dienyl anions occurred with CuX or CuX_2 to give linear tetraenes in good yield.

Dienyl anions have been postulated as intermediates in base-catalyzed isomerization of 1,3- and 1,4-dienes[1] or in nucleophilic substitution of aromatics.[2] Their conformational stabilities have recently been studied by simple and extended Hückel MO calculations.[3] The route for preparation of dienyl monoanions has been limited to the metalation of non-conjugated 1,4-dienes with butyllithium[4] in tetrahydrofuran(THF) or with potassium in liquid ammonia.[5] Although conjugated 1,3-dienes[6] are available more readily than the 1,4-dienes, they have not yet been used for this purpose because the well-known "alkali metal catalyzed polymerization[7]" or diene dimer dianion formation[8] occurs preferentially. The only exceptional case is the reaction of cyclopentadiene with sodium to give cyclopentadienyl anion[9] whose cyclopentadienyl group was stabilized by 5π-conjugation. We wish to present here a general method for the preparation of dienyl anions from both conjugated and non-conjugated dienes. All the dienyl anions prepared were isolated as crystals for the first time and their conformation in solution were studied in order to verify the MO prediction. The present method has the advantage of performing the following: 1) preparation of special dienes such as monodeuterated and alkyl-substituted dienes, 2) interconversion reactions between *cis*- and *trans*-dienes, 3) stereoselective synthesis of di- and trisubstituted dienes, 4) selective synthesis of new type of open chain tetraenes which are useful as ligands for transition metals and 5) preparation of other dienyl metal (*e.g.*, Be, Mg, Sn, Si, *etc.*) compounds which serve as reagent for various types of selective organic syntheses.

Results and Discussion

The reaction of 1,3-pentadiene with alkali metals (Na, K, Rb, and Cs) in tetrahydrofuran gave poly(1,3-pentadiene).[10] However, we found that in the presence of an equimol of aliphatic tertiary amines, it gave pentadienyl anions **1** and reduced pentadiene dimers, $C_{10}H_{18}$, in a 2 : 1 molar ratio. The addition of a tertiary amine inhibits the polymerization completely. Trimethylamine, triethylamine, tripropylamine and *N,N,N′,N′*-tetramethylethylenediamine (TMEDA) were favorable as the tertiary amine over pyridine or 2,2′-bipyridyl with regard to yield. All the pentadiene isomers, *cis*-1,3-pentadiene, *trans*-1,3-pentadiene and 1,4-pentadiene, gave the identical pentadienyl anion $C_5H_7M\cdot THF$ **1** and $C_{10}H_{18}$ quantitatively, irrespective of the alkali metal except for lithium. Based on the molar ratio of **1** to $C_{10}H_{18}$ determined by GC and/or chemical characterization of the hydrolysis products (Tables 1 and 3), the following equation is given for the reaction.

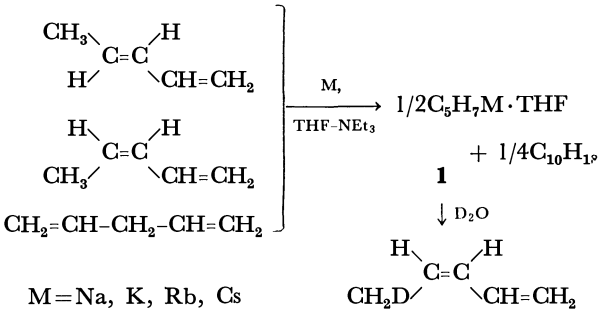

For preparation of the lithium compound, the use of 1,4-pentadiene is pertinent, since 1,3-pentadiene affords lithium pentadienide only in 30—60% yield even in the presence of two moles of TMEDA. Polymerization occurred competitively in this case. A series of pentadienyl anions thus obtained was isolated as yellow needle crystals and their structures were confirmed to be $C_5H_7M\cdot THF$ by GC and chemical characterization of the hydrolysis products (Tables 1 and 2).

The solubility of $C_5H_7M\cdot THF$ in THF decreased in the order Li>Na>K>Rb>Cs with increasing ionic characters of the metal–carbon bond. The THF molecule in $C_5H_7M\cdot THF$ (where M=K, Rb, and Cs) was easily removed by heating at 80—100 °C in a vacuum, while that of Li and Na compounds was strongly coordinated to metals even at 120 °C in a vacuum. This behavior may be explained by Pearson's principle.[11] The affinity of ligands determined by the ligand exchange reaction can also be explained by this principle; *i.e.*, the affinity of ligand to the relatively

Table 1. Characterization of alkali metal pentadienides, $C_5H_7M \cdot THF$ and THF-free C_5H_7M

M	Pentadiene[a] (mol/mol) Found	Calcd	THF[a] (mol/mol) Found	Calcd	M (%) Found	Calcd
Na[b]	1.00	(1.00)	1.00	(1.00)	13.8[d]	(14.2)
K[b]	1.05	(1.00)	0.93	(1.00)	22.0[e]	(21.9)
K[c]	0.98	(1.00)	0.03	(0.00)	35.1[e]	(36.8)
Rb[c]	0.99	(1.00)	0.01	(0.00)	53.2[e]	(55.9)
Cs[c]	1.03	(1.00)	0.00	(0.00)	66.1[e]	(66.3)

a) Determined by GC analysis of the hydrolysis products. b) $C_5H_7M \cdot THF$ system. c) THF-free C_5H_7M system. d) Titration with EDTA. e) Determined by $NaB(C_6H_5)_4$ method.

Table 2. Distribution of hydrolysis products of pentadienyl anions[a]

Counter ion	Solvent	1,3-Pentadiene (%) *trans*	*cis*	1,4-Pentadiene (%)
Li	THF	70	20	10
Li	TMEDA	66	22	12
Na	THF	62	38	0
K	THF	2	98	0
K	Isooctane[b]	98	2	0
Rb	THF	2	98	0
Rb	Isooctane	98	2	0
Cs	THF	1	99	0
Cs	Isooctane[b]	100	0	0

a) Hydrolyzed at 0 °C. b) A dispersion of THF-free carbanion was hydrolyzed in 2,2,4-trimethylpentane.

soft lithium compound falls in the order TMEDA> triethylamine>THF, while to the more electropositive K, Rb, and Cs compounds, it is reversed.

The distribution of the hydrolysis products of pentadienyl anions distinctly reflects the nature of their counter cations and the ligands. Potassium, rubidium and caesium pentadienide gave *cis*-1,3-pentadiene stereoselectively upon hydrolysis in THF, but the corresponding THF free anions gave only *trans*-1,3-pentadiene upon hydrolysis in 2,2,4-trimethylpentane or diethyl ether (Table 2). Thus interconversion between *cis*- and *trans*-diene was first accomplished by using the present method. In contrast, the lithium compound gave a mixture of three pentadiene isomers as reported by Bates *et al.*[4] and sodium compound gave a *trans-cis* mixture of 1,3-pentadiene. In the case of the lithium compound, the negative charge of the pentadienyl anion should be delocalized over terminal C_1 and internal C_3 carbon atoms. The following equilibrium is considered. The formation of both *cis*- and *trans*-1,3-pentadiene may be explained by the rotation around the inside C_2-C_3 carbon bond.

In a similar manner, hexadienyl anions having K^+ as a counter cation were prepared from *trans,trans*-2,4-hexadiene, *trans,cis*-2,4-hexadiene, *trans*-1,4-hexadiene, 1,3-hexadiene or 1,5-hexadiene. Conjugated dienes were more reactive than non-conjugated one. The reaction of 2,4-hexadiene occurred at 0 °C while 1,5-hexadiene required higher temperatures (>60 °C). The structures of **2** obtained from the four isomeric hexadienes were identical with each other, as evidenced by GC analysis of dienes obtained upon hydrolysis and the characterization of potassium with Kalignost (sodium tetraphenylborate). The most striking feature of this reaction is that **2** gave *cis,trans*-2,4-hexadiene selectively (94%) upon hydrolysis. The result of deuterolysis of **2** which gave *cis,trans*-2,4-hexadiene-1-*d* is in line with the structure of the *cis*-methylpentadienyl anion prepared from 1,4-hexadiene in liquid ammonia.[5b]

$CH_3CH{=}CHCH{=}CHCH_3$ (*trans,trans* or *trans,cis*) — 0 °C

$CH_2{=}CHCH{=}CHCH_2CH_3$ (*trans* or *cis*) — 0 °C

$CH_2{=}CHCH_2CH{=}CHCH_3$ (*trans*) — 15 °C

$CH_2{=}CHCH_2CH_2CH{=}CH_2$ — 60 °C

$\xrightarrow[\text{THF-NEt}_3]{\text{M,}}$

$$1/2C_6H_9M \cdot THF + 1/4C_{12}H_{22}$$

2

$\downarrow D_2O$

$CH_2DCH{=}CHCH{=}CHCH_3$ (*cis,trans*)

The present method is applicable to the preparation of the octadienyl anion from non-conjugated 1,7-octadiene. A mixture of 1,7-octadiene, potassium and triethylamine (3 : 2 : 2 molar ratio) was heated for 20 h at 70 °C, **3** being precipitated as orange powder in 78% yield by the addition of excess pentane. *cis*-3-Octene (76% yield), 2,6-octadiene (9% yield) and unreacted 1,7-octadiene were obtained from the pentane fraction. Based on the molar ratio, the following equation is given for the reaction.

$$3\,CH_2{=}CH(CH_2)_4CH{=}CH_2 + 2\,K \xrightarrow[\text{THF-NEt}_3]{70\,^\circ C}$$

$$2\,C_8H_{13}K \cdot THF + CH_3CH_2CH{=}CHCH_2CH_2CH_2CH_3$$

3

$$\mathbf{3} \xrightarrow{D_2O} CH_2DCH{=}CHCH{=}CHCH_2CH_2CH_3 + CH_3CH{=}CHCHDCH{=}CHCH_2CH_3$$

The resulting octadienyl anion **3** gave 2,4-octadiene-1-*d* (90%) and a small amount of 2,5-octadiene-4-*d* (10%) upon deuterolysis. No reduced octadiene dimer was obtained. The yield of 2,6-octadiene became maximum (30 mol% to 1,7-octadiene used) after the mixture had been heated at 70 °C for 8 h, decreasing with continuous heating of the solution with an increase of **3**. This strongly suggests that 1,7-octadiene isomerizes stepwise to 2,4- or 2,5-octadiene to give **3** *via* 2,6-octadiene as postulated by Birch and Phil.[12] Thus, the present method has the advantage to perform the reaction at high temperatures, at which 1,5-, 1,6-,

and 1,7-dienes can be converted into 1,3- or 1,4-dienes. Olefines, 1-octene and 2-octene, underwent no reaction under these reaction conditions.

An important feature of the present reaction is that the potassium dienides prepared from trans-conjugated dienes gave thermodynamically unfavorable *cis*-1,3-dienes selectively upon hydrolysis as shown in the hydrolysis of **1** and **2** in THF. The results led us to examine the stereoselective synthesis of di- and trisubstituted dienes by the protonation of anions. Metalation of 3-methyl-1,4-pentadiene with potassium gave 3-methylpentadienyl anion **4** and the reduced dimer, $C_{12}H_{22}$, in 93—95% yields. Deuterolysis of **4** in THF gave (*E*)-3-methyl-1,3-pentadiene-5-*d* selectively (99.5 %) in line with the hydrolysis of the corresponding lithium compound.[13] Differentiation between (*E*) and (*Z*) isomers was done chemically with maleic anhydride according to the method of Bartlett *et al.*[14]

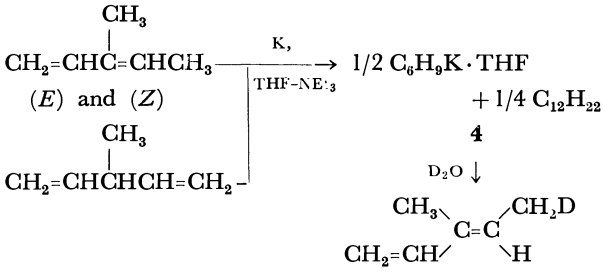

Thus, substitution with the methyl group on C_3-carbon atom of pentadiene largely effects the geometry of the product. If 3-methyl-1,4-pentadiene behaves similarly to 1,3- or 1,4-pentadiene, the hydrolysis product should be (*Z*)-3-methyl-1,3-pentadiene. This suggests that rotation around the C_2–C_3 carbon bond is inhibited by introducing the methyl group on C_3-carbon atom. A mixture of (*Z*)- and (*E*)-3-methyl-1,3-pentadiene (3 : 7 molar ratio) also gave the same products, but the yield was only 50—60% since the reaction proceeded in competition with polymerization. The substitution of methyl group on the C_3 carbon of pentadiene brings about an increased tendency to promote the polymerization since its chemical structure involves that of isoprene which gives only polymers by the reaction with alkali metals even in the presence of excess tertiary amine.[15]

Both *trans*-2-methyl- and 4-methyl-1,3-pentadiene gave the identical 2-methylpentadienyl anion **5** and reduced dimer, $C_{12}H_{22}$, by metalation with potassium in THF–triethylamine at 0 °C. Hydrolysis of **5** in THF gave *cis*-2-methyl-1,3-pentadiene and 4-methyl-1,3-pentadiene in 1 : 1 ratio. This suggests that the negative charge densities on C_1 and C_5 carbon atoms of **5** are nearly equal. No detectable amount of *trans*-2-methyl-1,3-pentadiene was obtained as evidenced by GC using a capillary column, while the corresponding lithium compound[4] gave *trans*-2-methyl-1,3-pentadiene (45%), 2-methyl-1,4-pentadiene (45%), and 4-methyl-1,3-pentadiene (10%) due to the rapid 1,3-shift present at equilibrium. The yield of **5** from 4-methyl-1,3-pentadiene (92%) is superior to that from *trans*-2-methyl-1,3-pentadiene (60%) since the latter tends to polymerize.

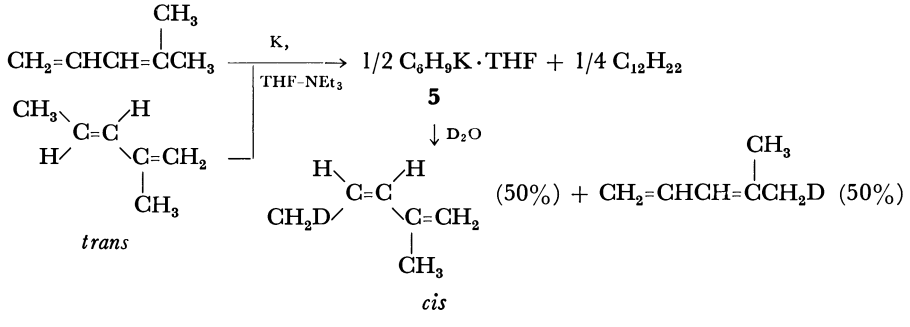

A trisubstituted diene, 2,4-dimethyl-1,3-pentadiene, gave 2,4-dimethylpentadienyl anion **6** and $C_{14}H_{26}$ in high yield (85% and 87% respectively) by the reaction with potassium in THF–triethylamine at 10 °C. The anion **6** afforded the starting diene upon hydrolysis quantitatively, no other isomer being detected. In contrast to di- and trisubstituted dienes, a tetrasubstituted diene, 2,5-dimethyl-2,4-hexadiene, was inert to the metalation even at higher temperatures (100—120 °C in a sealed tube). The acidity of its methyl group is probably not so high as to induce the reaction.

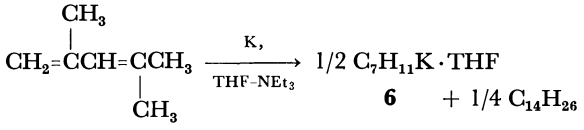

The behavior of cyclic dienes markedly differs from that of linear dienes. Although cyclopentadiene is known to give the cyclopentadienyl carbanion by the reaction with potassium or sodium evolving hydrogen,[9] both 1,3- and 1,4-cyclohexadiene gave no cyclohexadienyl anion **7** by the reaction with potassium at 0—50 °C. They isomerized completely to an equal amount of benzene and cyclohexane as was observed in the reaction with butyllithium.[16] Although no detectable amount of potassium was consumed during the course of reaction, the cyclohexadienyl anion can be considered to exist as an intermediate, since **7** was obtained by Kloosterziel and vanDrunen[17] by the reaction with potassium amide in liquid ammonia below −20 °C. At 0 °C, it decomposed thermally to benzene and cyclohexene due to the great electronic stabilization by aromatization.

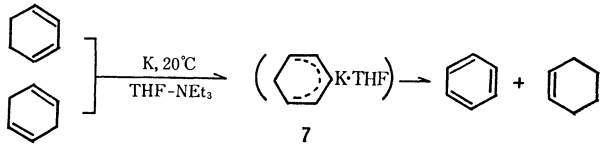

Table 3. Distribution of the reduced diene dimers obtained together with dienyl anions

Dienyl anion	Reduced diene dimer	Total yield/%
1	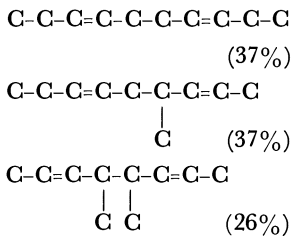 (37%) (37%) (26%)	98
2	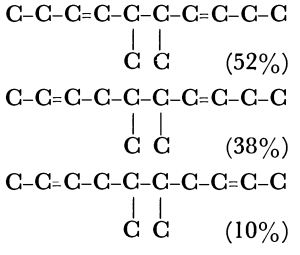 (52%) (38%) (10%)	95
4	 (96%)	92[a] 60[b]
6	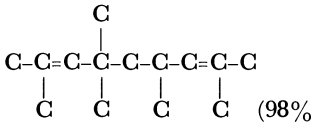 (98%)	87
5[c]	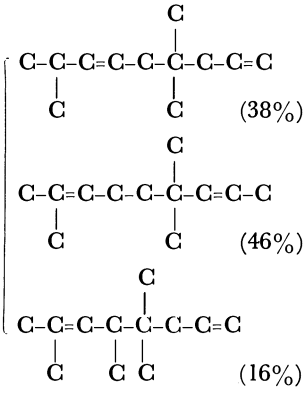 (38%) (46%) (16%)	92
5[d]	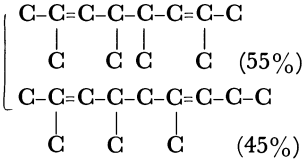 (55%) (45%)	60
8	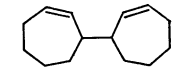 (97%)	99
9	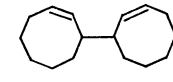 (98%)	99

a) Reaction of 3-methyl-1,4-pentadiene.
b) Reaction of 3-methyl-1,3-pentadiene.
c) Reaction of 4-methyl-1,3-pentadiene.
d) Reaction of 2-methyl-1,3-pentadiene.

By the present method, however, cycloheptadienes and cyclooctadienes gave the corresponding anions. Both 1,3- and 1,4-cycloheptadienes readily reacted with potassium in THF–triethylamine to produce cycloheptadienyl anion **8** and reduced dimers, $C_{14}H_{22}$, in 96—98% yields. The anion **8** is also prepared by the 1,6-sigmatropic rearrangement of the 1,3,5-heptatrienyl anion.[5d] The significant difference between **8**, lithium cycloheptadienide and linear dienyl carbanions observed in hydrolysis is that **8** gave a 1,4-diene predominantly (80%) but the latter two gave conjugated 1,3-dienes.

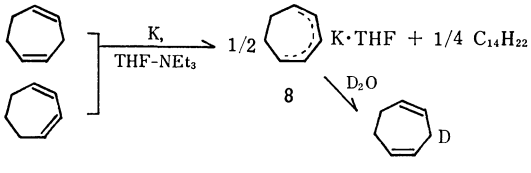

Cyclooctadienyl anion **9** was prepared from 1,3-, 1,4-, and 1,5-cyclooctadienes quantitatively (92—99% yield). Non-conjugated 1,5-cyclooctadiene requires higher temperature (>60 °C) for the completion of the reaction, while 1,3- and 1,4-dienes react with potassium at 10 °C. Cyclooctadienyl anion **9** also gave 1,4-cyclooctadiene exclusively (82%) upon hydrolysis. Thus the negative charge is concluded to be relatively large on the C_3 carbon atom of cyclic dienyl anions as postulated by Hine[18] The anion **9** is thermally stable as compared to the corresponding lithium compound[19]

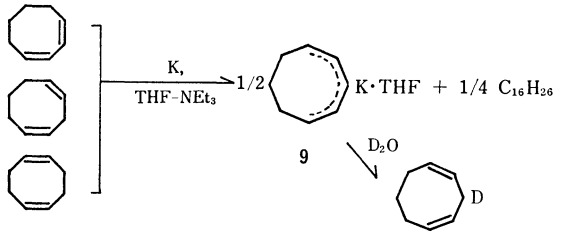

which isomerizes irreversibly to *cis*-bicyclo[3.3.0]oct-3-en-2-yl lithium at 35 °C by electrocyclization.[20] The interconversion to bicyclo[3.3.0]oct-3-en-2-yl anion should be ascribed to the equal sharing of the negative charge to C_1 and C_3 carbons of the cyclooctadienyl anion. The production of an equal amount of 1,3- and 1,4-cyclooctadienes upon the hydrolysis of the lithium compound[21] at low temperatures supports this conclusion.

As an extension of the present method, the metalation of *trans,trans,trans*- and *cis,cis,cis*-1,5,9-cyclododecatrienes was examined, 1,3,5-cyclododecatriene being obtained in 40—50% yield together with three isomeric cyclododecatrienes of unknown structures. Quantitative isomerization of these trienes into the conjugated one was unsuccessful.

Process for the Formation of Dienyl Anions. In the preparation of dienyl anions by the present method, reduced diene dimers were obtained. Although 1,3-butadiene, styrene and α-methylstyrene give their

dimer[8] or tetramer dianions[22] by the reaction with sodium, no dianions were detected by means of mass spectroscopy of the deuterolysis products. The mass number, (M^+), of reduced pentadiene dimers obtained upon deuterolysis of the reaction mixture is the same as that obtained by hydrolysis with an error of 2%. The reduced pentadiene dimers produced together with **1** are composed of three isomers (Table 3). The carbon skeleton of the dimer strongly suggests that they are formed by the homo or cross coupling of pentadiene radical anions, (I) and/or (II), and by

$$\overset{\ominus}{C}H_2CH{=}CH\underset{\displaystyle CH_3}{\underset{|}{C}}H\cdot \quad (I) \qquad \cdot CH_2CH{=}\overset{\ominus}{C}HCHCH_3 \quad (II)$$

the succeeding rapid proton abstraction from free pentadiene with the resulting dianions. As an example, the process for formation of 4-methyl-2,6-nonadiene is expressed by the following equation.

$$I + II \longrightarrow \overset{\ominus}{C}H_2CH{=}CH\underset{\displaystyle CH_3}{\underset{|}{C}}HCH_2CH{=}C\overset{\ominus}{H}CHCH_3$$

$$\downarrow 2\,C_5H_8$$

$$2\,C_5H_7^{\ominus} + CH_3CH{=}CH\underset{\displaystyle CH_3}{\underset{|}{C}}HCH_2CH{=}CHCH_2CH_3$$

The production of similar compounds by the reaction of 1,3-pentadiene with lithium naphthalene[23] may also be explained by the same concept. The radical anions corresponding to I and II were reported by Bauld.[24] The carbon skeleton and distribution of the reduced diene dimers (Table 3) strongly suggest that the mode of coupling of the radical anions is the same in principle as that of the allyl radical[25] since both of their dimers formed obey the stability of the aliphatic radical, tertiary>secondary>primary. In agreement with the behavior of pentadienes, hexadienes also gave three isomeric hexadiene dimers in a 11 : 8 : 2 ratio, the ratio being the same irrespective of the four hexadienes used. Both 2-methyl- and 4-methylpentadienes gave two or more isomeric reduced dimers but 3-methyl-1,3-pentadiene and 2,4-dimethyl-1,3-pentadiene gave only one isomer. The process for the formation of these dimers may be explained by the same principle as that described above. Cyclic dienes also gave their reduced dimers regioselectivity; 1,3-cycloheptadiene gave 3-(2-cycloheptenyl)cycloheptene and both 1,3- and 1,5-cyclooctadiene gave 3-(2-cyclooctenyl)cyclooctene. Separation of the meso-isomer from racemate by GC was unsuccessful. The structure of the reduced cyclooctadiene dimer was identical with that obtained with lithium naphthalene.[26]

Alkylation of Dienyl Anions. Alkylation with methyl iodide and *t*-butyl bromide was carried out (Table 4) to know the location of the highest negative charge density on the carbon atoms in the dienyl anions. The result of methylation is in line with that of hydrolysis and of the CNDO-II calculations[3c] of dienyl anions. In the case of the acylic dienyl anions, methylation occurs on C_1 carbon atoms in preference to the C_3 carbon atom, but, occurs exclusively on the C_3 carbon atoms for the cyclic dienyl anions. In contrast, alkylation with *t*-butyl bromide gave reversed result: *i.e.*, alkylation occurred exclusively on the C_3 carbon atom of pentadienyl carbanion. This can be explained not by the steric factor, but by considering the attack of *t*-butyl cation on the free pentadienyl anion since the result is consistent with data of Hückel MO calculations.[3a]

Table 4. Alkylation of dienyl anions on C_1 and C_3 carbon atoms with methyl iodide and *t*-butyl bromide[a]

Dienyl anion	Methyl iodide		*t*-Butyl bromide	
	C_1 (%)	C_3 (%)	C_1 (%)	C_3 (%)
1	65	35	22	78
2	62[b]	8	8[b]	92
	30			
4	85	15	3	97
5	75	25	4	96
6	42	58	3	95
8	10	90	50	50
9	5	95	47	53

a) Reaction carried out at 20 °C in THF. b) Alkylation on the C_5 carbon atoms.

Table 5. Coupling reaction of **1** or **9** with metal halides

Metal halide	Distribution (%)		Total yield/%	Distribution (%)	Total yield/%
	10	**11**		**12**	
$MgBr_2$	0	0	0	0	0
$ZnCl_2$	50	50	98	95	95
$CdCl_2$	68	32	88	90	85
CuCl	99	1	52	100	80
$CuCl_2$	98	2	50	99	73
$NiCl_2$	95	5	18	92	68
$CoCl_2$	97	3	10	91	59

Coupling Reaction of Dienyl Anions. Selective oxidative coupling of dienyl anions is an attractive organic synthesis.[27] Oxidation of alkyl mono- and dianions with metal halides or metal oxides[28] has been reported. We present here the coupling reaction of dienyl anions with a variety of metal halides using **1** as a typical acyclic dienyl anion and **9** as a cyclic dienyl anion (Table 5). The reaction of **1** with a half mol of zinc chloride or cadmium chloride gave quantitatively the tetraene composed of two isomers, **10** and **11**, in a

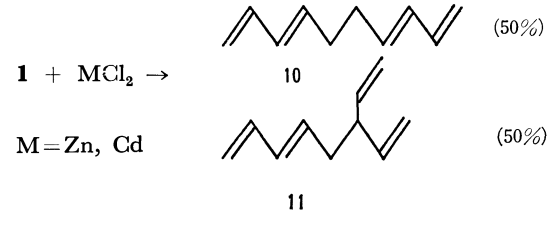

1 : 1 ratio. Thermally unstable bis(pentadienyl)zinc and bis(pentadienyl)cadmium are considered to be an intermediate in the reaction. The mechanism of these homo and cross couplings should be the same as that of allyl radicals produced by the thermal cracking of bis(allyl)zinc compounds.[29] In order to realize se-

Table 6. Tetraenes obtained by the coupling of **1** with $Br(CH_2)_nBr$

n	Tetranes (%)			Total yield/%
	14	**15**	**16**	
3	20	42	38	96
4	14	50	36	98
5	15	46	39	99

lective coupling, the reaction of **1** with various kinds of metal halides was examined.

Copper(I), copper(II), and nickel(II) halides were found to be useful for the selective production of **10**. Pentadienyl metal cluster compounds are the most possible intermediates for the coupling reaction as postulated in the alkyl coupling reaction.[30] The high selectivity should arise from the steric repulsion between the neighboring dienyl groups. The behavior of **9** differs from that of **1** giving 3-(2,7-cyclooctadienyl)-1,4-cyclooctadiene **12** regioselectively even when zinc chloride or cadmium chloride is used as an oxidant. Metal oxides, zinc oxide, and nickel oxide also assist the coupling reaction of **9** effectively. The non-conjugated dimer **12** could be easily converted into conjugated 2-(1,7-cyclooctadienyl)-1,3-cyclooctadiene **13** with a catalytic amount of $Fe_3(CO)_{12}$.

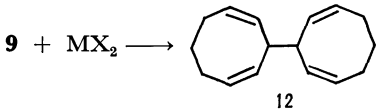

12

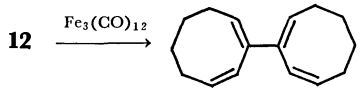

13

For the synthesis of the tetraenes separated with a carbon chain, the coupling of **1** with dibromoalkane, $Br(CH_2)_nBr$ (n=1,2,3,4,5), was examined. Coupling of two pentadienyl groups with dibromomethane and 1,2-dibromoethane was not successful since **1** was converted into **10** and **11** in a 7:3 ratio evolving ethylene. However, 1,3-dibromopropane, 1,4-dibromobutane and 1,5-dibromopentane provided the coupling compounds, **14**, **15** and **16** (Table 4).

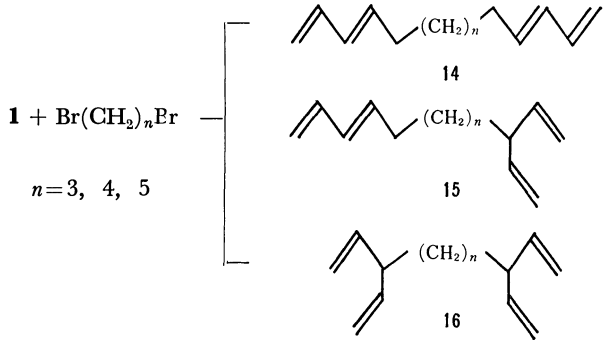

It is noteworthy that tetraene **16** was obtained though **1** did not give a tetraene with such a branched structure as **16** by the oxidative coupling with metal halides, presumably due to steric repulsion.

Experimental

All the dienes (Aldrich Chem. Inc.) and tertiary amines (Nakarai Chem. Co.) were dried over calcium hydride and distilled before use. Tetrahydrofuran was refluxed over sodium/potassium alloy and distilled under nitrogen. Finely dispersed sodium and potassium were prepared by heating them in toluene and the lithium dispersion in mineral oil. Anhydrous metal halides were prepared by heating the hydrates at prescribed temperatures. 3-Methyl-1,4-pentadiene, 1,4-cycloheptadiene, and 1,4-cyclooctadiene were obtained by the method described in this paper. All the procedures were performed under argon by means of high vacuum technique. GC analysis and separation of the reaction products were carried out with a Hitachi Model K-53 gas chromatograph using a glass capillary column (Silicone OV-101 and HB-2000) and a Varian-Aerograph Model 700 gas chromatograph using a column packed with Silicone DC-550. NMR spectra were taken with a Varian Model A-60 instrument and MS with a Hitachi RMU-7HR spectrometer. IR spectra were recorded on a Hitachi EPI-2 spectrometer. Elemental analysis of the products (bp *ca.*> 120 °C) was carried out with a Yanagimoto Model MT-2 CHN analyzer using a glass ampoule.

Preparation of Pentadienyl Anion ***1***. To the potassium (3.9 g, 0.1 g-atom) dispersed in a mixture of THF (40 ml, 0.5 mol) and triethylamine (21 ml, 0.15 mol) was added 1,3- or 1,4-pentadiene (20 ml, 0.2 mol) dropwise at 0—5 °C over a 1 h period. Vigorous stirring was necessary in order to avoid explosive reaction and polymerization. After allowing the mixture to attain room temperature in 2—4 h, THF (40 ml) was added and the mixture was heated to 60 °C for completion of the reaction and for dissolution of the suspension of **1**. Orange needle crystals of **1** were precipitated by cooling the solution to 0 °C. Typical yield of **1** was 80% (14.2 g) based on potassium. From the THF soluble fraction, 2.9 g of **1** was further obtained as crystals by addition of hexane (50 ml). The anion **1** was purified by recrystallization in 2:1 THF-hexane. From the hexane soluble fraction, a mixture of reduced pentadiene dimers (described later), $C_{10}H_{18}$, was obtained in 98% yield (6.8 g, 49% conversion based on 1,3-pentadiene). The use of trimethylamine or TMEDA instead of triethylamine also gave **1** in 90—96% yield while the use of pyridine or 2,2′-bipyridyl afforded **1** in 20—30% yield and the polymer in 70—80% yield. Rubidium and caesium compounds were prepared by the same procedure, but crystallization of the sodium compound carried out at −20——40 °C after addition of hexane (40 ml) to the resulting solution. Yield: 96—99%. Their analytical data are given in Table 1. In the metalation of 1,3-pentadiene (10 ml, 0.1 mol) or 1,4-pentadiene (10 ml, 0.1 mol) with lithium (0.7 g, 0.1 g-atom), TMEDA (30 ml, 0.2 mol) was used instead of triethylamine. The reaction was carried out in THF (20 ml) at 0 °C for 5 h and then at 30 °C for 8 h. After separating the resulting solution from unreacted lithium, hexane (40 ml) was added to the solution and the mixture was cooled to −20 °C to induce the crystallization of $C_5H_7Li \cdot TMEDA$. Yields from 1,3- and 1,4-pentadiene were 52 and 90%, respectively.

THF free alkali metal (K, Rb, Cs) pentadienides were obtained by heating **1** at 90 °C for 1 h in a vacuum (0.05 mmHg). They are explosive in the air and more unstable than the corresponding tetrahydrofuran complexes even in an argon atmosphere. A spontaneous solid state polymerization occurred gradually at room temperature, poly(3-methyl-1-butenylene) being obtained in 90% yield upon hydrolysis by keeping them for 60 days. Deuterolysis of **1** in THF

at 0 °C gave *cis*-1,3-pentadiene-5-*d* in 98% yield and that of THF free potassium pentadienide in 1,2,3,4-tetrahydronaphthalene gave *trans*-1,3-pentadiene-5-*d* in 99% yield as evidenced by GC, NMR (position of the deuterium was determined from the peak area ratio), and MS, *m/e* 69 (M^+). The purity of the *cis*- and *trans*-1,3-pentadiene-5-*d* was determined to be >97% by reference to the value of M^+ of 1,3-pentadiene.

Preparation of Hexadienyl Anion **2**. In essentially the same way as described above, the reaction of 1,3-hexadiene (5:3 *trans-cis* mixture), *trans,trans*-2,4-hexadiene, *trans,cis*-2,4-hexadiene, or *trans*-1,4-hexadiene (5.7 ml, 50 mmol) with potassium (1 g, 25 mg-atom) was carried out in a mixture of THF (9 ml) and triethylamine (5 ml) at 5—10 °C for 10 h, while that of 1,5-hexadiene was carried out at 60 °C for 20 h. After the completion of the reaction by heating the resulting suspension to 65 °C for 2 h, excess hexane (20 ml) was added and cooled to −20 °C in order to precipitate **2** as orange powder. Yield: 94% (4.5 g) for 2,4- and 1,4-hexadiene; 84% (4.0 g) for 1,3-hexadiene. The anion **2** thus obtained was washed with two portions of 20 ml hexane and then recrystallized in THF–hexane at 0 °C. Hydrolysis of **2** in 2,2,4-trimethylpentane, Found: hexadiene 43.7%; THF, 37.8% (by GC); K, 18.5% by $NaB(C_6H_5)_4$. Calcd for $C_6H_9K \cdot C_4H_8O$: hexadiene, 42.2%; THF, 37.5%; K, 20.3%. Distributions of the hydrolysis products of **2** prepared from the above four isomers were identical with each other; *trans,cis*-2,4-hexadiene (94%), *trans,trans*-2,4-hexadiene (3%) and *cis,cis*-2,4-hexadiene (3%). Purity of the deuterolysis products, *cis,trans*-2,4-hexadiene-1-*d* (or *trans, cis*-isomer), was >98% by MS. From the hexane soluble fraction, reduced hexadiene dimers were obtained by distillation (1.9 g, 95% yield).

Preparation of Dienyl Anions **4**—**9**. The reaction of 3-methyl-1,3-pentadiene, 3-methyl-1,4-pentadiene, *trans*-2-methyl-1,3-pentadiene, 4-methyl-1,3-pentadiene, 2,4-dimethyl-1,3-pentadiene, 1,3-cycloheptadiene, 1,4-cycloheptadiene, 1,3-cyclooctadiene, or 1,4-cyclooctadiene with potassium (2:1 ratio) was carried out in the same manner as in the preparation of **2**, since the solubility of their carbanions in THF is larger than that of **1**. Addition of 3-methyl-1,3-pentadiene and 2-methyl-1,3-pentadiene was made over a period of 3 h. The resulting crude crystals were recrystallized in THF–hexane at −40—0 °C. Characterization of **4**—**9** was carried out in the same way as described for **1** and **2**. Analysis of K by $NaB(C_6H_5)_4$ method, Found: 19.2, 18.8, 18.1, 17.3, and 17.8% for **4**, **5**, **6**, **8** and **9**. Calcd: 20.3, 20.3, 18.9, 19.1, and 17.9% respectively. GC analysis of dienes obtained by the hydrolysis of **4**—**9** is in line with the calculated values with errors of 2%. These dienes were identified with GC, NMR, and IR using commercial authentics amples (Aldrich Chemicals and Tokyo Kasei Co.) except for the following dienes.

(E)-3-Methyl-1,3-pentadiene: IR (neat) 1645, 1601 (C=C), 990, 894 (CH_2=CH), 764, 747 cm^{-1} (CH=CH); PMR ($CDCl_3$) δ 6.40 (d of d, 1, CH), 5.53 (q, 1, CH), 5.02 (m, 2, CH_2), 1.79 (s, 3, CH_3), 1.73 (d, 3, CH_3); MS, Found: 82 (M^+) for C_6H_{10} and 83 (M^+) for the deuterolysis product, (*E*)-3-methyl-1,3-pentadiene-5-*d* (97% purity).

cis-*2-Methyl-1,3-pentadiene*: IR (neat) 1645, 1601 (C=C), 895 (CH_2=C), 749 cm^{-1} (*cis* CH=CH); PMR ($CDCl_3$) δ 5.90 (d, 1, J=11.9, CH), 5.57 (d, of q, 1, J=11.9, CH), 4.92 (d, 2, CH_2), 1.90 (d, 3, CH_3), 1.86 (s, 3, CH_3); MS, Found: 82 (M^+) for C_6H_{10} and 83 (M^+) for the deuterolysis product, *cis*-2-methyl-1,3-pentadiene-5-*d*.

1,4-Cycloheptadiene: IR (neat) 1630 (C=C), 850, 772, 760, 711 cm^{-1} (CH=CH); PMR ($CDCl_3$) δ 5.54 (m, 4, CH), 2.79 (t, 2, CH_2), 2.23 (m, 4, CH_2); MS, Found: 94 (M^+) for C_7H_{10} and 95 (M^+) for 1,4-cycloheptadiene-3-*d*.

1,4-Cyclooctadiene: IR (neat) 1646 (C=C), 810, 790, 762, 716 cm^{-1} (CH=CH); PMR ($CDCl_3$) δ 5.73 (d of q, 2, J=6.3, CH), 5.56 (d of t, 2, J=6.3, CH), 2.77 (t, 2, CH_2), 2.23 (m, 4, CH_2), 1.46 (m, 2, CH_2); MS, Found: 108 (M^+) for C_8H_{12} and 109 (M^+) for 1,4-cyclooctadiene-3-*d*. Deuteration occurred in 98% purity.

Preparation of Octadienyl Anion **3**. 1,7-Octadiene (22 ml, 0.15 mol) was added to potassium (3.9 g, 0.1 g-atom) dispersed in a mixture of THF (40 ml, 0.5 mol) and triethylamine (21 ml, 0.15 mol). The mixture was allowed to react at 70 °C for 20 h and the resulting solution was concentrated by distillation. The anion **3** was precipitated by the addition of pentane (60 ml) to the residue. Yield: 78% (8.5 g, 52% conversion based on 1,7-octadiene). The position of deuterium in the following deuterolysis products of **3** was determined from the PMR peak area ratio by reference to the corresponding hydrolysis products.

2,5-Octadiene-4-d: IR (neat) 1658 (C=C), 963, 900, 719 cm^{-1} (CH=CH); PMR (CCl_4) δ 5.02 (m, 2, J=7.5, CH), 5.00 (m, 2, J=7.9, CH), 2.24 (m, 1, CHD), 1.59 (m, 2, CH_2), 1.22 (d, 3, CH_3), 0.53 (t, 3, CH_3); MS, Found: *m/e* 111. Calcd for $C_8H_{13}D$: M, 111.

2,4-Octadiene-1-d: IR (neat) 1650 (C=C), 945, 926, 816 cm^{-1} (CH=CH); PMR (CCl_4) δ 5.60 (d of d, 1, J=13.0, CH), 5.35 (d of d, 1, J=7.2, CH), 4.98 (m, 2, CH), 1.70 (d of t, 2, CH_2), 1.28 (d, 2, CH_2D), 1.06 (m, 2, CH_2), 0.57 (t, 3, CH_3); MS, Found: *m/e* 111. Calcd for $C_8H_{13}D$: M, 111.

3-Octene (76% yield, 25% conversion based on 1,7-octadiene), 2,6-octadiene (9% yield), and unreacted 1,7-octadiene (15%) were obtained from the distillate and pentane extract and characterized after isolation by GC.

3-Octene: IR (neat) 1658 (C=C), 964 (CH=CH); PMR (CCl_4) δ 5.00 (m, 2, J=7.9, CH), 1.60 (m, 4, CH_2), 0.95, 0.93 (m, 4, CH_2), 0.57 (t, 3, CH_3), 0.53 (t, 3, CH_3); MS, Found: *m/e* 112 (M^+). Calcd for C_8H_{16}: M, 112.

2,6-Octadiene: IR (neat) 1660 (C=C), 962, 898, 720 (CH=CH); PMR (CCl_4) δ 4.98 (m, 4, CH), 1.58 (bs, 4, CH_2), 1.16 (d, 6, CH_3); MS, Found: *m/e* 110. Calcd for C_8H_{14}: M, 110.

Reaction of Cyclohexadienes with Potassium. The reaction of 1,3-cyclohexadiene (2.4 ml, 25 mmol) or 1,4-cyclohexadiene (2.4 ml, 25 mmol) with potassium (1 g, 25 mg-atom) in a mixture of THF (10 ml) and triethylamine (5 ml) was carried out at 50 °C for 20 h. Both 1,3- and 1,4-hexadiene were converted into benzene (1.1 ml, 99%) and cyclohexene (1.2 ml, 98%), 98% of potassium used being recovered.

Alkylation of **1**, **2**, **4**, **5**, **6**, **8**, *and* **9**. A typical experiment is as follows: To potassium cyclooctadienide **9** (4.1 g, 20 mmol) in THF (20 ml) was added a THF solution (10 ml) of methyl iodide (1.3 ml, 21 mmol) at 0 °C over a 20 min period. The mixture was stirred at 0 °C for 3 h, then heated up to 50 °C for 2 h and concentrated by evaporation. The products were extracted with pentane and distilled. Yield, 99% by GC; isolated yield, 2 g (80%). Alkylation with *t*-butyl bromide was carried out under the same reaction conditions. All the alkyl-substituted dienes were obtained in 95—99% yield as evidenced by GC and separated into their respective isomers by preparative GC to determine the structure by PMR, IR, and MS. Relative ratio of the products (Table 4) was determined by a high sensitive GC using glass capillary column (Silicone OV-101). For the isolation of low boiling methyl-substituted compounds of **1**—**5**, diethylene glycol dimethyl ether was used as a solvent instead of THF since the peaks of the products and THF

overlapped each other in preparative GC.

1,3-Hexadiene from **1**: IR (neat) 1655, 1606 (C=C), 1002, 898 ($CH=CH_2$), 950, 776, 756 cm^{-1} (CH=CH); PMR ($CDCl_3$) δ 5.30—4.89 (m, 5, CH and CH_2), 2.20 (d of q, 2, CH_2), 1.02 (t, 3, CH_3).

3-Methyl-1,4-pentadiene from **1**: IR (neat) 1641 (C=C), 997, 910 cm^{-1} ($CH=CH_2$); PMR ($CDCl_3$) δ 5.63 (m, 2, CH), 4.87 (m, 4, CH_2), 2.77 (m, 1, CH), 1.03 (d, 3, CH_3); MS, Found: M^+, 82.

2,4-Heptadiene from **2**: IR (neat) 1650, 1610 (C=C), 817, 765, 720 cm^{-1} (CH=CH); PMR ($CDCl_3$) δ 5.30—6.30 (m, 4, CH), 2.20 (d of q, 2, CH_2), 1.78 (d, 3, CH_3), 1.02 (t, 3, J=7.2, CH_3); MS, Found: M^+, 96.

5-Methyl-1,3-hexadiene from **2**: IR (neat) 1655, 1605 (C=C), 1002, 898 cm^{-1} ($CH=CH_2$); PMR ($CDCl_3$) δ 6.17 (m, 1, CH), 5.80 (m, 2, J=8.6, CH), 5.38 (m, 2, CH_2), 2.15 (m, 1, CH), 0.90 (d, 6, CH_3); MS, Found: M^+, 96.

3-Methyl-1,4-hexadiene from **2**: IR (neat) 1636 (C=C), 958, 913 ($CH=CH_2$), 800, 730 cm^{-1} (CH=CH); PMR ($CDCl_3$) δ 5.64 (m, 1, CH), 5.50 (d of d, 1, J=6.9, *cis* CH), 5.31 (d of q, 1, CH), 4.89 (m, 2, CH_2), 2.76 (m, 1, CH), 1.74 (d, 3, CH_3), 0.99 (d, 3, CH_3); MS, Found: M^+, 96.

3-Methyl-1,3-hexadiene from **4**: IR (neat) 1646, 1609 (C=C), 999, 915, 892 cm^{-1} ($CH=CH_2$); PMR ($CDCl_3$) δ 6.41 (m, 1, CH), 5.53 (t, 1, J=7.0, CH), 5.06 (m, 2, CH_2), 2.17 (d of q, 2, CH_2), 1.76 (s, 3, CH_3), 1.02 (t, 3, J=7.6, CH_3); MS, Found: M^+, 96.

3,3-Dimethyl-1,4-pentadiene from **4**: IR (neat) 1642 (C=C), 995, 912 cm^{-1} ($CH=CH_2$); PMR ($CDCl_3$) δ 5.85 (m, 2, CH), 5.00 (m, 4, CH_2), 1.03 (bs, 6, CH_3).

4-Methyl-1,3-hexadiene from **5**: IR (neat) 1650, 1610 (C=C), 984, 964, 895 cm^{-1} (CH=CH, $CH=CH_2$); PMR ($CDCl_3$) δ 6.60 (m, 1, CH), 5.96 (d, 1, CH), 4.98 (m, 2, CH_2), 2.15 (q, 2, J=7.8, CH_2), 1.75 (s, 3, CH_3), 1.00 (t, 3, J=7.8, CH_3); MS, Found: M^+, 96.

2,3-Dimethyl-1,4-pentadiene from **5**: IR (neat) 1641 (C=C), 995, 915, 805 cm^{-1} (CH=CH, $CH=CH_2$); PMR ($CDCl_3$) δ 5.71 (m, 1, CH), 4.93 (m, 2, CH_2), 4.73 (bs, 2, CH_2), 2.86 (d of q, 1, CH), 1.78 (s, 3, CH_3), 1.35 (d, 3, CH_3).

2,4-Dimethyl-1,3-hexadiene from **6**: IR (neat) 1645, 1635 (C=C), 889, 850, 800 cm^{-1} (CH=CH, $CH=CH_2$); PMR ($CDCl_3$) δ 5.83 (s, 1, CH), 5.02 (d, 2, J=7.0, CH_2), 2.44 (q, 2, J=7.6, CH_2), 1.95—1.97 (two-s, 6, CH_3), 1.21 (t, 3, J=7.6, CH_3); MS, Found: M^+, 110.

2,3,4-Trimethyl-1,4-pentadiene from **6**: IR (neat) 1645 (C=C), 890 cm^{-1} ($CH=CH_2$); PMR ($CDCl_3$) δ 5.06 (bs, 4, CH_2), 3.04 (q, 1, J=7.0, CH), 1.89 (bs, 6, CH_3), 1.40 (d, 3, J=7.0, CH_3).

3-Methyl-1,4-cycloheptadiene from **8**: IR (neat) 1638 (C=C), 763, 715 cm^{-1} (CH=CH); PMR ($CDCl_3$) δ 5.62 (m, 2, CH), 5.41 (d of d, 2, J=11.5, CH), 3.30 (m, 1, CH), 2.21 (m, 4, CH_2), 1.14 (d, 3, J=7.2, CH_3); MS, Found: M^+, 108.

3-Methyl-1,4-cyclooctadiene from **9**: IR (neat) 1645 (C=C), 800, 763, 732, 717 cm^{-1} (CH=CH); PMR ($CDCl_3$) δ 5.33 (m, 2, CH), 5.09 (d of d, 2, J=10.7, CH), 2.88 (d of q, 1, CH), 1.97 (d of t, 4, CH_2), 1.19 (m, 2, CH_2), 0.85 (d, 3, CH_3); MS, Found: M^+, 122.

6,6-Dimethyl-1,3-heptadiene from **1**: IR (neat) 1655, 1602 (C=C), 1002, 896 ($CH=CH_2$), 760 cm^{-1} (CH=CH); PMR ($CDCl_3$) δ 6.05 (m, 1, CH), 5.81 (m, 2, CH), 4.89 (m, 2, CH_2), 1.85 (d, 2, CH_2), 0.79 (bs, 9, CH_3); MS, Found: *m/e* 124. Calcd for C_9H_{16}: M, 124.

3-t-Butyl-1,4-pentadiene from **1**: IR (neat) 1642 (C=C), 997, 912 ($CH=CH_2$), 780 cm^{-1} (CH=CH); PMR ($CDCl_3$) δ 6.11 (d of d of d, 2, CH), 4.94 (m, 4, CH_2), 2.78 (t, 1, CH), 0.92 (bs, 9, CH_3); MS, Found: M^+, 124.

5,6,6-Trimethyl-1,3-heptadiene from **2**: IR (neat) 1652, 1603 (C=C), 1000, 950, 899, 758 (CH=CH, $CH=CH_2$); PMR ($CDCl_3$) δ 5.82—6.03 (m, 3, CH_2), 4.88 (m, 2, CH_2), 2.15 (d of q, 1, CH), 0.90 (d, 3, CH_3), 0.81 (bs, 9, CH_3); MS, Found *m/e* 138. Calcd for $C_{10}H_{18}$: M, 138.

3-Butyl-1,4-hexadiene from **2**: IR (neat) 1640 (C=C), 995, 910 ($CH=CH_2$), 968, 788, 715, 703 cm^{-1} (CH=CH); PMR ($CDCl_3$) δ 5.79 (m, 1, CH), 5.39 (m, 2, CH), 5.00 (m, 2, CH_2), 2.75 (t, 1, CH), 1.67 (d, 3, CH_3), 0.83 (bs, 9, CH_3); MS, Found: M^+, 138.

3-Methyl-3-t-butyl-1,4-pentadiene from **4**: IR (neat) 1641 (C=C), 996, 911, 785 cm^{-1} ($CH=CH_2$); PMR ($CDCl_3$) δ 6.12 (m, 2, CH), 4.99 (m, 4, CH_2), 1.07 (s, 3, CH_3), 0.90 (bs, 9, CH_3); MS, Found: *m/e* 138. Calcd for $C_{10}H_{18}$: M, 138.

2-Methyl-3-t-butyl-1,4-pentadiene from **5**: IR (neat) 1645 (C=C), 968, 910, 890, 789 cm^{-1} (CH=CH, $CH=CH_2$); PMR ($CDCl_3$) δ 5.93 (m, 1, CH), 5.07 (bs, 2, CH_2), 4.80 (m, 2, CH_2), 2.42 (d, 1, J=10.0, CH), 1.78 (s, 3, CH_3), 0.90 (s, 9, CH_3); MS, Found: 138. Calcd for $C_{10}H_{18}$: M, 138.

2,4-Dimethyl-3-t-butyl-1,4-pentadiene from **6**: IR (neat) 1643 (C=C), 890 cm^{-1} ($C=CH_2$); PMR ($CDCl_3$) δ 4.99 (m, 4, CH_2), 1.07 (bs, 6, CH_3), 0.90 (s, 9, CH_3); Found: C, 86.52; H, 13.45%; M^+, 152. Calcd for $C_{11}H_{20}$: C, 86.76; H, 13.24%; M, 152.

3-t-Butyl-1,4-cycloheptadiene from **8**: IR (neat) 1638 (C=C), 807, 760, 715 cm^{-1} (CH=CH); PMR δ 5.79 (d of d, 2, J=7.0, CH), 5.73 (m, 2, CH), 3.00 (m, 1, CH), 2.27 (m, 4, CH_2), 0.89 (s, 9, CH_3); Found: C, 87.35; H, 12.29%; M^+, 150. Calcd for $C_{11}H_{18}$: C, 87.92; H, 12.08%; M, 150.

5-t-Butyl-1,3-cycloheptadiene from **8**: IR (neat) 1639, 1600 (C=C), 764, 715 cm^{-1} (CH=CH); PMR ($CDCl_3$) δ 5.73 (m, 4, CH), 2.43 (m, 1, CH), 1.92 (m, 2, CH_2), 1.50 (m, 2, CH_2), 0.98 (s, 9, CH_3); MS, Found: M^+, 150.

3-t-Butyl-1,4-cyclooctadiene from **9**: IR (neat) 1660 (C=C), 790, 745, 716 cm^{-1} (CH=CH); PMR ($CDCl_3$) δ 5.50 (m, 4, J=6.8, CH), 2.91 (t, 1, CH), 2.00 (m, 4, CH_2), 1.31 (m, 2, CH_2), 0.87 (s, 9, CH_3); Found: C, 87.70; H, 12.52%; M^+, 164. Calcd for $C_{12}H_{20}$: C, 87.73; H, 12.27%; M, 164.

5-t-Butyl-1,3-cyclooctadiene from **9**: IR (neat) 1650 (C=C), 815, 790, 758 cm^{-1} (CH=CH); PMR (CCl_3) δ 5.48 (m, 4, CH), 2.35 (m, 1, CH), 2.13 (m, 2, CH_2), 1.29 (m, 4, CH_2), 0.78 (s, 9, CH_3); MS, Found: M^+, 164.

Characterization of Reduced Diene Dimers. Excess pentane (50 ml) was added to the reaction solution of dienes (0.2 mol) and potassium (3.9 g, 0.1 g-atom) in order to precipitate dienyl anions. Reduced diene dimer compounds obtained from the pentane soluble fraction were separated into their respective isomers by preparative GC after distillation. Yields and distribution of the products determined by GC are given in Table 3. Isolated yields by preparative GC, 40—70% of the distillate.

3,7-Decadiene from 1,3-Pentadiene: IR (neat) 1661 (C=C), 963, 719 cm^{-1} (CH=CH); PMR (CCl_4) δ 5.36 (m, 4, CH), 1.96 (m, 8, CH_2), 0.99 (t, 6, CH_3); Found: C, 86.53; H, 13.22%; M^+, 138. Calcd for $C_{10}H_{18}$: C, 86.88; H, 13.12%; M, 138.

4-Methyl-2,6-nonadiene from 1,3-Pentadiene: IR (neat) 1660 (C=C), 718 cm^{-1} (CH=CH); PMR (CCl_4) δ 5.09 (m, 4, CH), 2.11 (m, 1, CH), 1.65 (m, 4, CH_2), 1.17 (d, 3, CH_3), 0.60 (t, 3, CH_3), 0.58 (d, 3, CH_3); Found: C, 86.50; H, 13.30%; M^+, 138.

4,5-Dimethyl-2,6-octadiene from 1,3-Pentadiene: IR (neat) 1611 (C=C), 964, 718 cm^{-1} (CH=CH). PMR (CCl_4) δ 5.00 (m, 4, CH), 1.95 (m, 2, CH), 1.23 (d, 6, CH_3), 0.52 (d, 6, CH_3). Found: C, 86.68; H, 13.08%; M^+, 138.

The above three isomers were also obtained from 1,4-pentadiene by the reaction with potassium (see Table 3) in the same ratio with an error of 5%.

5,6-Dimethyl-3,7-decadiene from 1,4-Hexadiene: IR (neat) 1660 (C=C), 965, 900, 738 cm^{-1} (CH=CH); PMR (CCl_4) δ 5.03 (m, 4, CH), 1.90 (m, 2, CH), 1.72 (m, 4, CH_2), 0.72 (d, 6, CH_3), 0.68 (t, 6, CH_3); MS, Found: *m/e* 166. Calcd for $C_{12}H_{22}$: M, 166.

5,6-Dimethyl-2,7-decadiene from 1,4-Hexadiene: IR (neat) 1688 (C=C), 963, 736 cm^{-1} (CH=CH); PMR (CCl_4) δ 5.10 (d of q, 1, J=6.2, CH), 5.07 (d of t, 1, J=6.2, CH), 5.08 (m, 2, CH), 1.85 (m, 2, CH), 1.70 (m, 4, CH_2), 1.32 (d, 3, CH_3), 0.64 (t, 3, CH_3), 0.62 (d, 6, CH_3); MS, Found: *m/e*, 166. Calcd for $C_{12}H_{22}$: M, 166.

5,6-Dimethyl-2,8-decadiene from 1,4-Hexadiene: IR (neat) 1655 (C=C), 964 cm^{-1} (CH=CH); PMR (CCl_4) δ 5.25 (d of q, 2, J=6.3, CH), 5.23 (d of t, 2, J=6.3, CH), 1.88 (m, 6, CH_2C=C and CH), 1.38 (d, 6, CH_3), 0.75 (d, 6, CH_3); MS, Found: M^+, 166.

The structure and relative ratio of reduced hexadiene dimers, $C_{12}H_{22}$, obtained from 1,5- and 2,4-hexadienes were identical with those obtained from 1,4-hexadiene.

3,4,7-Trimethyl-2,6-nonadiene from 3-Methyl-1,3-pentadiene: IR (neat) 1655 (C=C), 965, 832 cm^{-1} (CH=C); PMR ($CDCl_3$) δ 5.10 (m, 2, CH), 2.46 (t of q, 1, CH), 1.88 (m, 4, CH_2), 1.51 (s, 6, CH_3), 1.49 (d, 3, CH_3), 0.87 (d, 3, CH_3), 0.85 (t, 3, CH_3); Found: C, 86.59; H, 13.40%; M^+, 166. Calcd for $C_{12}H_{22}$: C, 86.66; H, 13.34%; M, 166.

2,4,5,7-Tetramethyl-2,6-octadiene from 2-Methyl-1,3-pentadiene: IR (neat) 1669 (C=C), 908, 842 cm^{-1} (CH=CH); PMR ($CDCl_3$) δ 4.96 (bd, 2, CH), 2.19 (m, 2, CH), 1.61 (bs, 12, CH_3), 0.83(d, 6, CH_3); Found: C, 86.20; H, 13.68%; M^+, 166. Calcd for $C_{12}H_{22}$: C, 86.66; H, 13.34%; M, 166.

2,4,6-Trimethyl-2,6-nonadiene from 2-Methyl-1,3-pentadiene: IR (neat) 1670 (C=C), 835, 735 cm^{-1} (CH=CH); PMR ($CDCl_3$) δ 5.25 (t, 1, CH), 4.93(d, 1, CH), 2.52(m, 1, CH), 2.01(m, 2, CH_2), 1.89(d, 2, CH_2), 1.62(bs, 9, CH_3), 0.91 (t, 3, CH_3), 0.87(d, 3, CH_3); MS, Found: M^+, 166.

4,4,8-Trimethyl-2,6-nonadiene from 4-Methyl-1,3-pentadiene: IR (neat) 1655 (C=C), 970, 885 cm^{-1} (CH=CH); PMR ($CDCl_3$) δ 5.34 (m, 4, CH), 2.20 (m, 1, CH), 1.89 (two-d, 2, CH_2), 1.61(d, 3, CH_3), 0.95(d, 6, CH_3), 0.89(s, 6, CH_3); Found: C, 86.58; H, 13.37%; M^+, 166. Calcd for $C_{12}H_{22}$: C, 86.66; H, 13.34%; M, 166.

2,6,6-Trimethyl-2,7-nonadiene from 4-Methyl-1,3-pentadiene: IR (neat) 1670 (C=C), 972, 832 cm^{-1} (CH=CH); PMR ($CDCl_3$) δ=5.34 (m, 2, CH), 5.10 (t, 1, CH), 1.90 (m, 2, CH_2), 1.62(m, 9, CH_3), 1.24 (m, 2, CH_2), 0.93 (s, 6, CH_3); MS, Found: M^+, 166.

2,4,5,5-Teramethyl-2,6-octadiene from 4-Methyl-1,3-pentadiene: IR (neat) 1670, 1650 (C=C), 970, 884, 830, 713 cm^{-1} (CH=CH); PMR ($CDCl_3$) δ 5.33 (m, 2, CH), 5.12 (d, 1, CH), 1.96(m, 1, CH), 1.63(bs, 6, CH_3), 1.61(d, 3, CH_3), 1.09 (s, 6, CH_3), 0.92 (d, 3, CH_3); MS, Found: M^+, 166.

2,4,4,6,8-Pentamethyl-2,7-nonadiene from 2,4-Dimethyl-1,3-pentadiene: IR (neat) 1670, 1655 (C=C), 965, 832 cm^{-1} (CH=CH); PMR ($CDCl_3$) δ 5.10 (m, 2, CH), 2.43 (m, 1, CH), 1.61 (m, 12, CH_3), 1.24 (d, 2, CH_2), 1.04 (s, 6, CH_3), 0.86 (d, 3, CH_3); Found: C, 86.10; H, 13.75%; M^+, 194. Calcd for $C_{14}H_{26}$: C, 86.51; H, 13.49%; M, 194.

3-(2-Cycloheptenyl)cycloheptene from 1,3-Cyloheptadiene: IR (neat) 1650 (C=C), 786, 684 cm^{-1} (CH=CH); PMR ($CDCl_3$) δ 5.73 (m, 4, CH), 2.38 (m, 2, CH), 2.16 (m, 4, CH_2), 1.35—1.65 (m, 12, CH_2); Found: C, 88.20; H, 11.59%; M^+, 190. Calcd for $C_{14}H_{22}$: C, 88.35; H, 11.65%; M, 190.

3-(2-Cyclooctenyl)cyclooctene from 1,3-Cyclooctadiene: IR (neat) 1650 (C=C), 762, 710, 662 cm^{-1} (CH=CH); PMR ($CDCl_3$) δ 5.42 (m, 4, J=6.3, CH), 2.42 (m, 2, CH), 2.05 (m, 4, CH_2), 1.51 (m, 16, CH_2); Found: C, 87.75; H, 11.90; M^+, 218. Calcd for $C_{16}H_{26}$: C, 88.00; H, 12.00; M, 218. The same compound was obtained also from 1,4- and 1,5-cyclooctadienes in 99 and 92% yield, respectively.

Coupling Reaction of ***1*** *and* ***9*** *with Metal Halides.* A solution of **1** (8.9 g, 50 mmol) in THF (120 ml) was added with use of a syringe to the vigorously stirred suspension of anhydrous copper(I) chloride (5.9 g, 60 mmol in THF (50 ml) at 0 °C over 30 min period. The resulting solution was quenched with water (7 ml), filtered quickly (contact of THF to the air for a long time should be avoided in order to prevent the formation of thermally unstable peroxide) and concentrated by vacuum distillation at temperatures below 30 °C after adding 1,4-benzenediol (0.18 g) to the filtrate to inhibit the radical polymerization of the tetraene. The products were separated by LCG using a column (30× 3 cm) packed with silica gel (Wako gel C-200) and using pentane as elution solvent. Separation by LCG is preferable to distillation since 10—40% of tetraenes is polymerized by heating to 150 °C. When zinc chloride or cadmium chloride was used as a coupling reagent, the resulting mixture was heated to 80 °C for 1 h in order to induce thermal cracking after **1** (50 mmol) had been added to the THF solution of the metal halide (30 mmol) at 0 °C.

1,3,7,9-Decatetraene: Bp 108 °C/48 mmHg. IR (neat) 1650, 1604 (C=C), 1004, 968, 951, 900 cm^{-1} ($CH=CH_2$, CH=CH); PMR ($CDCl_3$) δ 6.13 (m, 2, CH), 5.50—5.93 (m, 4, CH), 5.07 (m, 4, CH_2), 2.05 (t, 4, CH_2); Found: C, 89.10; H, 10.50%; M^+, 134. Calcd for $C_{10}H_{14}$: C, 89.49; H, 10.51%; M, 134.

6-Vinyl-1,3,7-octatriene: Bp 103 °C/49 mmHg. IR (neat) 1645, 1635, 1600 (C=C), 1000, 950, 915, 900, 833 cm^{-1} ($CH=CH_2$, CH=CH); PMR ($CDCl_3$) δ 5.71—6.21 (m, 5, CH), 5.01, 5.03 (m, 6, CH_2), 2.77 (t of t, 1, CH), 2.15 (t, 2, CH_2); Found: C, 89.44; H, 10.50%; M^+, 134. Calcd for $C_{10}H_{14}$: C, 89.49; H, 10.51%; M, 134.

In essentially the same way, **9** (10.9 g, 50 mmol) in THF (150 ml) was allowed to react with copper(I) chloride (5.9 g, 60 mmol) in THF (50 ml) at 0 °C for 2 h, the products being separated by LCG. Yield, 8.7 g (80%). Results of the coupling reaction with the other metal halides are given in Table 5. Zinc oxide and nickel oxide also gave **12** in 50—60% yield under the same reaction conditions.

3-(2,7-Cyclooctadienyl)-1,4-cyclooctadiene: Bp 101 °C/0.5 mmHg. IR (neat) 1640 (C=C), 718, 679 cm^{-1} (CH=CH); PMR ($CDCl_3$) δ 5.55 (m, 8, CH), 3.30 (bs, 2, CH), 3.23 (d of t, 8, CH_2), 1.52 (m, 4, CH_2); Found: C, 89.65; H, 10.20%; M^+, 214. Calcd for $C_{16}H_{22}$: C, 89.65; H, 10.53%; M, 214. Isomerization to the following conjugated tetraene occurred by keeping the compound at 180—200 °C for 3 h in 35% conversion. Complete isomerization was proceeded by the addition of $Fe_3(CO)_{12}$ (5 mol %) and heating the mixture at 170 °C for 15 h. Conversion, 97%.

2-(1,7-Cyclooctadienyl)-1,3-cyclooctadiene: Bp 103 °C/1 mmHg. IR (neat) 1642, 1697 (C=C), 920, 845, 800, 765, 690 cm^{-1} (CH=CH); PMR ($CDCl_3$) δ=5.49—5.86 (m, 6, CH), 2.15—2.35 (m, 8, CH_2), 1.50 (bs, 8, CH_2); Found: C, 89.48; H, 10.30%; M^+, 214. Calcd for $C_{16}H_{22}$: C, 89.65; H, 10.35%; M, 214.

Tetraenes Obtained by the Reaction of ***1*** *with Dibromoalkanes.* A solution of 1,3-dibromopropane (1.0 ml, 10 mmol) in THF (30 ml) was added to a solution of **1** (3.6 g, 20 mmol) in THF (60 ml) with stirring at 0 °C. The mixture was heated at 40 °C for 1 h, quenched with water (2 ml) and then filtered. The resulting teraenes were separated with GC into their

individual isomers. The reactions of 1,4-dibromobutane and 1,5-dibromopentane were carried out under the same conditions.

1,3,10,12-Tridecatetraene: IR (neat) 1640, 1605 (C=C), 988, 947, 894, 830, 784, 735 cm^{-1} (CH=CH_2, CH=CH); PMR ($CDCl_3$) δ 5.60—5.30 (m, 6, CH), 5.03, 4.88 (m, 4, CH_2), 2.17 (m, 4, CH_2), 1.44 (m, 6, CH_2); Found: C, 87.99; H, 11.42%; M^+, 176. Calcd for $C_{13}H_{20}$: C, 88.56; H, 11.44%; M, 176.

9-Vinyl-1,3,10-undecatriene: IR (neat) 1640, 1604 (C=C), 995, 912 (CH=CH_2), 949, 830, 785, 731 cm^{-1} (CH=CH); PMR ($CDCl_3$) δ 6.30 (m, 1, CH), 5.73(d of q, 2, CH), 5.64 (m, 2, CH), 5.05, 5.01, 4.87(m, 6, CH_2), 2.68(t of t, 1, CH), 2.12(m, 2, CH_2), 1.35(m, 6, CH_2); MS, Found: M^+, 176.

3,7-Dwinyl-1,8-nonadiene: IR (neat) 1637(C=C), 994, 912 cm^{-1} (CH=CH_2); PMR ($CDCl_3$) δ 5.71 (d of q, 4, CH), 5.04, 4.86 (m, 8, CH_2), 2.67 (t of t, 2, CH), 1.31 (m, 6, CH_2); MS, Found: M^+, 176.

1,3,11,13-Tetradecatetraene: IR (neat) 1640, 1603 (C=C), 1000, 987, 907 (CH=CH_2), 967, 947, 830, 783 cm^{-1} (CH=CH); PMR ($CDCl_3$) δ 5.61—6.31 (m, 6, CH), 5.08, 4.87 (m, 4, CH_2), 2.11 (d of t, 4, CH_2), 1.33 (m, 8, CH_2); Found: C, 88.30; H, 11.60%; M^+, 190. Calcd for $C_{14}H_{22}$: C, 88.35; H, 11.65%; M, 190.

10-Vinyl-1,3,11-dodecatriene: IR (neat) 1642, 1637, 1604 (C=C), 1000, 995, 912 (CH=CH_2), 949, 831, 783, 729 cm^{-1} (CH=CH); PMR ($CDCl_3$) δ 5.60—6.30 (m, 3, CH), 5.73 (d of q, 2, CH), 5.07, 4.85(m, 6, CH_2), 2.70(t of t, 1, CH), 2.12(d of t, 2, CH_2), 1.31(m, 8, CH_2); MS, Found: M^+, 190.

3,8-Divinyl-1,9-decadiene: IR (neat) 1636 (C=C), 990, 914 cm^{-1} (CH=CH_2); PMR ($CDCl_3$) δ 5.71 (d of q, 4, CH), 5.06, 4.84 (m, 8, CH_2), 2.67 (t of t, 2, CH), 1.29(s, 8, CH_2); MS, Found: M^+, 190.

1,3,12,14-pentadecatetraene: IR (neat) 1638, 1602 (C=C), 987, 910(CH=CH_2), 945, 840, 785, 764, 737 cm^{-1} (CH=CH); PMR ($CDCl_3$) δ 5.60—6.32 (m, 6, CH), 5.08, 4.88 (m, 4, CH_2), 2.08 (m, 4, CH_2), 1.33 (bs, 10, CH_2); Found: C, 88.65; H, 12.25%; M^+, 204. Calcd for $C_{15}H_{24}$: C, 88.16; H, 11.84%; M, 204.

11-Vinyl-1,3,12-tridecatriene: IR (neat) 1635, 1602 (C=C), 989 912 (CH=CH_2), 945, 785, 764, 737 cm^{-1} (CH=CH); PMR ($CDCl_3$) δ 5.60—5.32 (m, 3, CH), 5.74 (d of q, 2, CH), 5.10, 4.88 (m, 6, CH_2), 2.69 (t of t, 1, CH), 2.12 (bt, 2, CH_2), 1.34(bs, 10, CH_2); MS, Found: M^+, 204.

3,9-Dwinyl-1,10-undecadiene: IR (neat) 1635 (C=C), 995, 912 cm^{-1} (CH=CH_2); PMR ($CDCl_3$) δ 5.74 (d of q, 4, CH), 5.08, 4.86 (m, 8, CH_2), 2.68 (bt, 2, CH), 1.30 (bs, 10, CH_2); MS, Found: M^+, 204.

We are gratefull to Emeritus Prof. T. Nozoe, Tohoku University, for his valuable discussion and Prof. P. Heimbach, Max Plank Institute, for the supply of 1,5,9-cyclododecatrienes. We thank Messrs. A. Kashihara, S. Otake, T. Narita, and I. Iwase for their technical assistance.

References

1) a) D. Devaprabhakara, C. G. Cardenas, and P. D. Gardner, *J. Am. Chem. Soc.*, **85**, 1553 (1963); b) C. G. Cardenas, *J. Org. Chem.*, **35**, 264 (1970); c) R. B. Bates, R. H. Carnighan, and C. E. Staples, *J. Am. Chem. Soc.*, **85**, 3031 (1963).

2) a) A. J. Birch, *J. Chem. Soc.*, **1947**, 1642; b) A. J. Birch, E. M. A. Shoukry, and F. Stansfield, *J. Chem. Soc.*, **1961**, 5376.

3) a) R. Hoffmann and R. A. Olofson, *J. Am. Chem. Soc.*, **88**, 943 (1966); b) R. F. Hudson, *Angew. Chem. Int. Ed. Engl.*, **12**, 36 (1973); c) R. J. Bushby and A. S. Patterson, *J. Organomet. Chem.*, **132**, 163 (1977).

4) a) R. B. Bates, D. W. Gosselink, and J. A. Kaczynski, *Tetrahedron Lett.*, **1967**, 199; b) R. B. Bates, D. W. Gosselink, and J. A. Kaczynski, *ibid.*, **1967**, 205.

5) a) G. J. Heiszwolf and H. Kloosterziel, *Recl. Trav. Chim., Pays-Bas*, **86**, 807 (1967); b) G. J. Heiszwolf, J. A. A. vanDrunen, and H. Kloosterziel, *ibid.*, **88**, 1377 (1969); c) H. Kloosterziel and J. A. A. vanDrunen, *ibid.*, **89**, 270 (1970); d) H. Kloosterziel and J. A. A. vanDrunen, *ibid.*, **88**, 1084 (1969).

6) a) G. W. Wheland, "Resonance in Organic Chemistry," Wiley and Sons, Inc., New York, N. Y. (1955); b) M. J. S. Dewar and H. N. Schmeising, *Tetrahedron*, **5**, 166 (1659); c) R. S. Mulliken, *ibid.*, **6**, 68 (1959).

7) a) A. V. Tobolsky and C. E. Rogers, *J. Polym. Sci.*, **40**, 73 (1959); *ibid.*, **61**, 155 (1962); b) G. Friedman and M. Brini, *Bull. Soc. Chim. Fr.*, **4**, 1420 (1967); c) S. Bywater, *Pure Appl. Chem.*, **4**, 319 (1962).

8) a) K. Ziegler, H. Grimm, and R. Willer, *Justus Liebigs Ann. Chem.*, **542**, 90 (1940); b) C. E. Frank and W. E. Foster, *J. Org. Chem.*, **26**, 303 (1961); c) K. Suga and S. Watanabe, *Bull. Chem. Soc. Jpn.*, **40**, 1257 (1967).

9) F. G. A. Stone and R. West, "Advances in Organometallic Chemistry," Acadmic Press, (1964), Vol. 2, p. 365.

10) F. Schue, *Bull. Chem. Soc. Fr.*, **4**, 980 (1965).

11) a) R. G. Pearson, "Hard and Soft Acids and Bases," Dowden, Hutchison & Ross, Inc., Stroudsburg, Pennsylvania (1973); b) Tse-lok Ho, "Hard and Soft Acids and Bases Principle in Organic Chemistry," Academic Press, New York, N. Y. (1977).

12) A. J. Birch and M. S. D. Phil, *Quart. Rev.*, **4**, 69 (1950).

13) W. T. Ford and M. Newcomb, *J. Am. Chem. Soc.*, **96**, 309 (1976).

14) P. D. Bartlett, G. E. H. Wallbillich, and L. K. Montgomery, *J. Org. Chem.*, **32**, 1290 (1967).

15) H. Yasuda and H. Tani, unpublished work.

16) R. B. Bates, R. H. Carnighan, and C. E. Staples, *J. Am. Chem. Soc.*, **85**, 3032 (1963).

17) H. Kloosterziel and J. A. A. vanDrunen, *Recl. Trav. Chim. Pays-Bas*, **89**, 368 (1970).

18) J. Hine, *J. Org. Chem.*, **31**, 1236 (1966).

19) R. B. Bates and D. A. McCombs, *Tetrahedron Lett.*, **1969**, 977.

20) a) R. B. Woodward and R. Hoffmann, *J. Am. Chem. Soc.*, **87**, 395 (1965); b) H. Kloosterziel and E. Zwanenburg, *Recl. Trav. Chim. Pays-Bas*, **88**, 1373 (1969).

21) R. B. Bates, S. Brenner, C. M. Cole, E. W. Davidson, G. D. Forsythe, D. A. McCombs, and A. S. Roth, *J. Am. Chem. Soc.*, **95**, 926 (1973).

22) R. L. Williams and D. H. Richards, *Chem. Commun.*, **1967**, 414.

23) K. Suga, S. Watanabe, and K. Takahashi, *Bull. Chem. Soc. Jpn.*, **40**, 2432 (1967).

24) N. L. Bauld, *J. Am. Chem. Soc.*, **84**, 4347 (1962).

25) G. Boche and D. R. Schneider, *Angew. Chem. Int. Ed. Engl*, **16**, 869 (1977).

26) K. Suga and S. Watanabe, *Tetrahedron Lett.*, **1966**, 2527.

27) P. Miginiac, *Ann. Chem. (Paris)*, **7**, 445 (1962).

28) a) R. G. Harvey, L. Nazareno, and H. Cho, *J. Am. Chem. Soc.*, **95**, 2376 (1973); b) H. Yasuda, M. Walczak, W. Rhine, and G. Stucky, *J. Organomet. Chem.*, **90**, 123 (1975).

29) R. Benn, E. G. Hoffmann, H. Lehmkuhl, and H. Nehl, *J. Organomet. Chem.*, **146**, 103 (1978).

30) L. E. McCandlish, E. C. Bissell, D. Coucouvanis, J. P. Fackler, and K. Knox, *J. Am. Chem. Soc.*, **90**, 7359 (1968),

The Characterization of the Hydroxyl Surface of Silica Gel

Seiichi KONDO,* Kazuo TOMOI, and Chynryon PAK

Laboratory of Physical Chemistry, Osaka University of Education, 43 Minamikobore-cho, Tennoji-ku, Osaka 543

(Received September 4, 1978)

The properties of silica gel were studied as a function of the hydrothermal treatment of hydrogel by means of the nitrogen-adsorption isotherm, the mechanical strength, thermodilatometry, and infrared spectroscopy. As a result, the number of contact points between primary particles of silica was found to decrease, and closed pores were found to be produced, by this treatment. The analysis of the infrared absorption spectra of the OH groups of this material showed that there are three kinds of OH groups in silica gel; (1) free OH groups on the outer surface of primary particles, which can adsorb molecules easily, (2) weakly perturbed OH groups inside closed pores, and (3) strongly hydrogen-bonded OH groups on the surface around the contact points. The relative concentration of these OH groups changes drastically upon the hydrothermal treatment; this is in accord with the change in the macroscopic properties mentioned above.

The properties, such as the specific surface area and the pore-size distribution of silica gel, are highly sensitive to its history, starting from the polymerization of monomeric silicic acid to the physical and chemical treatment before and during use.[1] Many of these characteristics are controlled by surface OH groups of this material. For instance, the infrared absorption band of the OH stretching vibration is changed in shape not only by heat treatment,[2,3] but also by different methods of synthesis. However, the reason for this change is not yet fully understood. Another example is the values of the surface OH densities of various colloidal silicas, which fluctuate widely from less than 4 nm^{-2} to even more than 10 nm^{-2} from one sample to another.[4] The purpose of this paper is to try to clarify the complex nature of the OH groups of silica gel and its relation to the surface and pore structures through the infrared spectroscopy of silica gel, which has been prepared by the hydrothermal treatment of hydrogel. Three different kinds of sites have been found for OH groups on the surface in various kinds of slica gel, as will be described below.

Experimental

Fractionally distilled silicon tetraethoxide was used as the raw material for synthesizing silica gel of a high purity. Silicon tetraethoxide (1 mol) was hydrolyzed at 70 °C for 95 to 105 min with 10 mol of distilled and deionized water, whose pH has been adjusted to 2.0 with hydrochloric acid. Silica sol thus obtained was rapidly cooled to about 0 °C and then poured into flat vessels with air-tight covers in order to make a thin liquid film of the desired thickness. This sol was kept still for 24 h at 17 °C, by which time it set to hydrogel. This hydrogel was washed with water to remove the hydrochloric acid and ethanol, and was then stored in water below 10 °C. This hydrogel was sealed in Pyrex glass ampoules with distilled and deionized water of pH 5.9 and was then heated in an autoclave at various temperatures. The hydrogel thus treated was dried slowly at 10 °C for 48 h. Finally thin plates of xerogel less than 0.05 mm thick and 1—2 cm^2 wide were obtained. The influence of Pyrex glass seemed negligible, since the properties of this product were almost the same as those of substances made in ampoules of high-purity quartz glass under the same conditions.

The infrared spectra of these samples were taken after the desorption of adsorbed water at 180 °C *in vacuo* and *in situ* in a cell described elsewhere,[2]

Results and Discussion

The specific surface area and the total pore volume of this material change remarkably upon the hydrothermal reaction of hydrogel. Figure 1 shows nitrogen-adsorption isotherms of silica gel hydrothermally treated at various temperatures for 2 h. These curves indicate that this material changes from the micropore type to the macropore type with an increase in the temperature of treatment, as is well known. Figure 2 shows the curves of the specific surface area and the total pore volume against the reaction time during hydrothermal treatment at 100 °C. The specific surface area increased in the beginning, reached a maximum after a few hours, and then decreased slowly, while the pore volume increased continuously from the beginning. Figure 3 shows the change in the specific surface area and the total pore volume as a function of the temperature of the reaction for 2 h. The specific surface area increased from 10 °C, reached a maximum at about 100 °C, and then decreased gradually, while the pore volume increased continuously from 10 °C. These increases in the surface area in Figs. 2 and 3 can be explained reasonably as will be done below. Silica hydrogel is an aggregate of fine primary particles of silica loosely chained to each other with a small number of contact points per particle (coordination number). When aging is insufficient, the dehydration of water produces a xerogel with a very high packing density and with a high coordination number, since the strength of the contact points is weak and the reorientation of primary particles is easy. However, a mild hydrothermal treatment of hydrogel below 100 °C, such as is shown in the above experiments, can make the contact points stronger and does not make the size of primary particles larger, because silicic acid migrates from the convex surface of the particle to the points of contact with a concave shape and fills these narrow gaps. This produces stronger interparticle bonds than those before aging. These strong bonds make it difficult for the primary particles to reorient when hydrogel is dried, and thus give rise to a lower packing density and a smaller coordination number of xerogel. The number of coordination can be estimated from the packing density of xerogel, assuming this xerogel to be a mono-

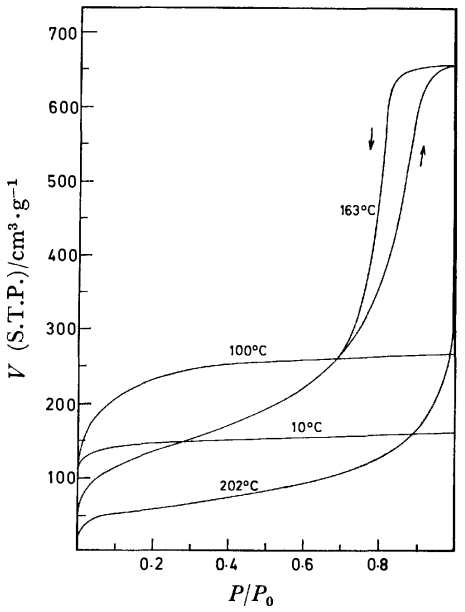

Fig. 1. The nitrogen adsorption isotherms of silica gel hydrothermally treated at various temperatures for 2 h.

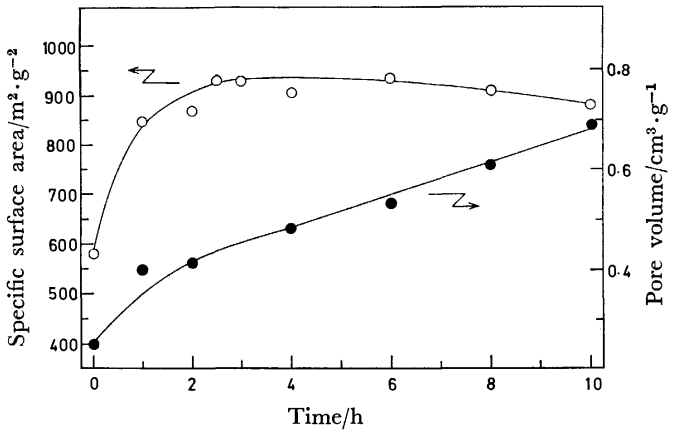

Fig. 2. The specific surface area and the pore volume of silica gel versus the time of hydrothermal reaction at 100 °C.

dispersed system of primary particles with a density of about 2.2 g/cm².[5] For example, the hydrothermal reaction at 10 °C and 100 °C for 2 h gives coordination numbers of about 9 and 6 respectively.

The reinforcement of these interparticle bonds by aging is reflected in the increase in the mechanical strength of silica gel as a bulk. Figure 4 shows the values of the strength of the silica gel per bond against the hydrothermal temperature, values obtained from the Vickers hardness (the pressure, kg/cm², neccessary to make a tiny hole of a known cross-section area on the flat surface of a specimen using a small diamond piece with a quadrangular pyramidal shape) divided by the total coordination number per unit of volume of the silica gel. In this figure, the bond strength increases as the hydrothermal temperature is raised. Another example of the increase in the bond strength is the thermodilatometric analysis of this material in Fig. 5, the experimental details of which were described

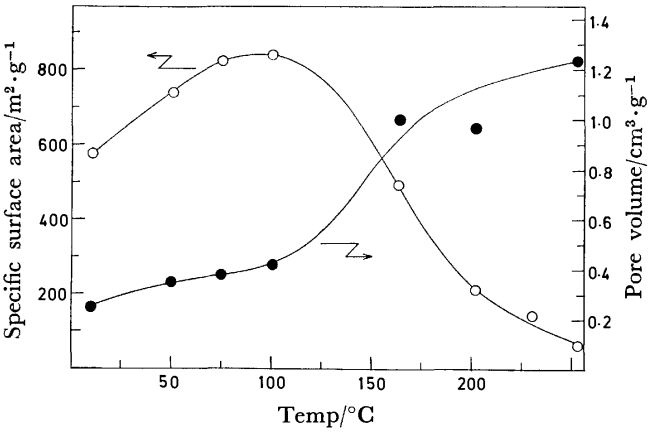

Fig. 3. The specific surface area and the pore volume of silica gel versus the temperature of hydrothermal reaction for 2 h.

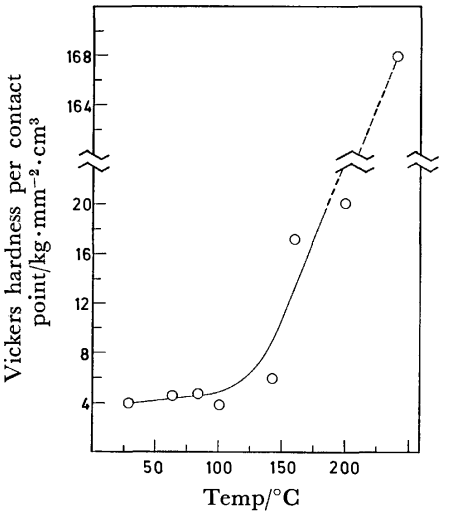

Fig. 4. The Vickers hardness per interparticle bond as a function of hydrothermal temperatures.

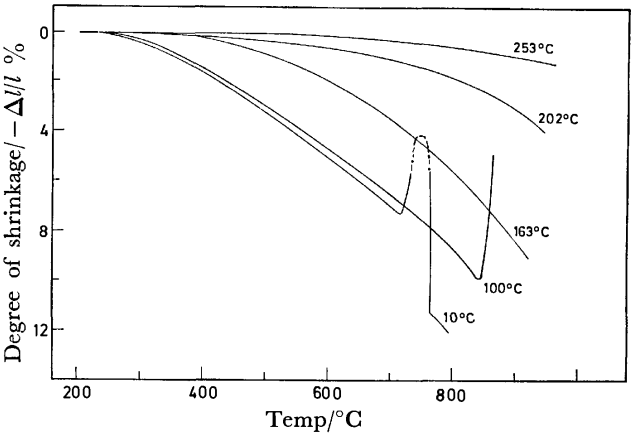

Fig. 5. The curves of thermodilatometric analysis of silica gel hydrothermally treated at various temperatures.

elsewhere.[6] This figure shows that the degree of shrinkage of silica gel by heat treatment was smaller for materials of a high hydrothermal temperature, because the deformation or the shrinkage of bulk

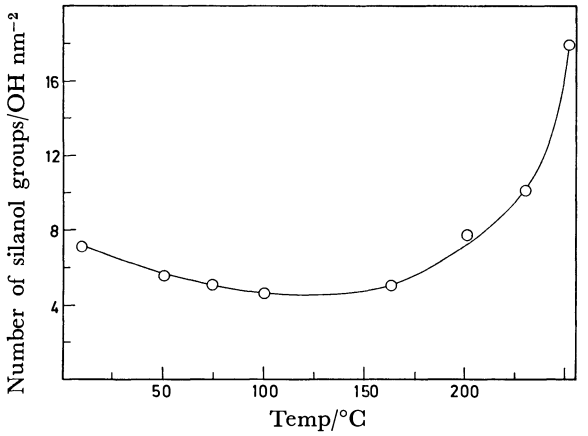

Fig. 6. The number of OH groups per nm² of silica gel hydrothermally treated at various temperatures.

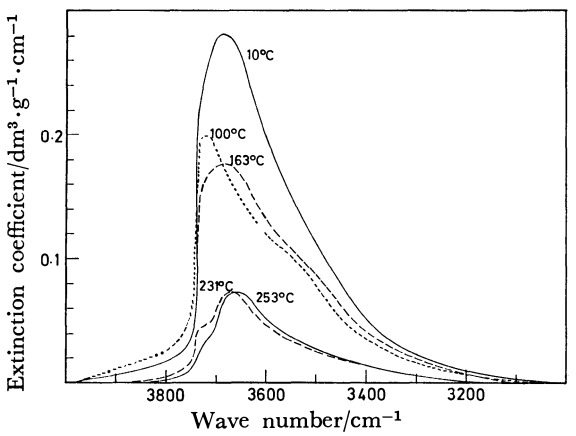

Fig. 7. The infrared spectra of OH stretching fundamental vibration of silica gel hydrothermally treated at various temperatures.

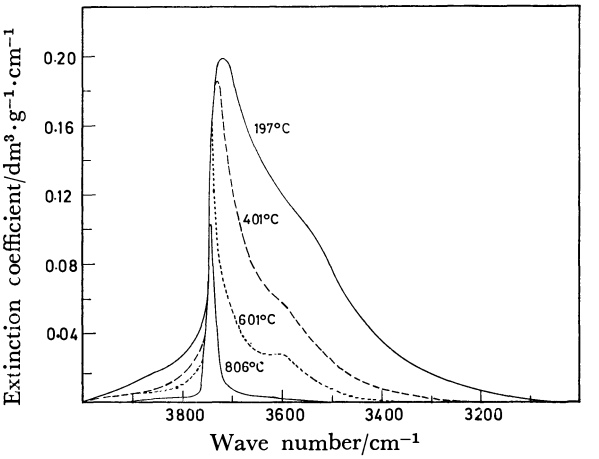

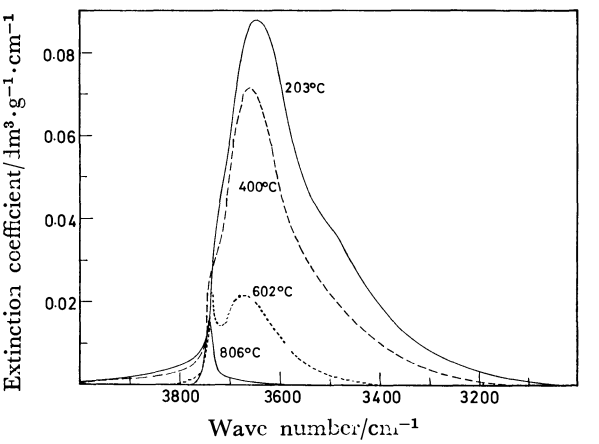

Fig. 8a and 8b. The changes of OH bands by heat treatment of silica gel hydrothermally treated at 100 °C and 250 °C, respectively.

structure by sintering would be smaller for materials with stronger interparticle bonds.

The gaps around the contact points between primary particles are so narrow that molecules such as nitrogen and water can not be adsorbed on a certain area around these points, depending upon the size of the molecules to be adsorbed. This area, which can not be measured by the adsorption of nitrogen gas, amounts to a considerable portion of the total surface area of the primary particles when these primary particles are small and possess a large number of coordination. Therefore, the specific surface area, as measured by the gas-adsorption method, will be generally larger for the materials having a smaller number of coordination when the diameters of the particles are equal, which seems to be true in case of mild hydrothermal treatment.

Figure 6 shows the number of OH groups per nm², which is obtained from the weight loss of the silica gel during heating between 180 °C (the temperature of the dehydration of adsorbed water) and 1200 °C divided by the specific surface area, as measured by the B. E. T. method using nitrogen gas. In this figure, the surface OH density is relatively larger for materials treated below 100 °C than those between 100 °C and 160 °C, because the specific surface area used for this calculation is smaller than the total surface area for the material hydrothermally treated at a lower temperature, as has been discussed in the above section. Above 100 °C, where the B. E. T. specific surface area approaches the total surface because of the decrease in coordination number, the OH density becomes smaller than 5. Surprisingly high values of OH density were obtained above 200 °C; the reason for this will be discussed below in terms of infrared spectroscopy.

Figure 7 shows the infrared spectra of the OH stretching vibration of silica gel treated hydrothermally at various temperatures for 2 h. The shapes of these OH bands changed markedly as the hydrothermal temperature was raised. As was shown in an earlier paper,[3] these bands can mainly be resolved into three component bands with absorption maxima at about 3750 cm⁻¹, 3670 cm⁻¹, and between 3500 and 3300 cm⁻¹; those maxima can be assigned to free OH groups, weakly perturbed OH groups, and strongly hydrogen-bonded OH groups respectively. As the hydrothermal temperature was raised, the intensity of free and strongly hydrogen-bonded OH components became smaller in comparison with the weakly perturbed components. The intensities and shapes of these OH bands of various

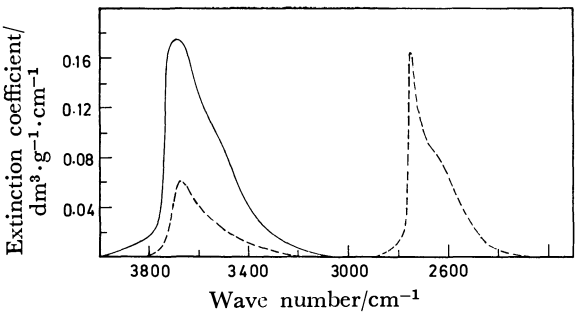

Fig. 9. The change of OH band of silica gel hydrothermally treated at 163 °C by the isotope exchange reaction by the absorption-desorption cycles of 20 times of heavy water. The full and the dotted lines show the absorption bands before and after the isotope exchange, respectively.

samples changed by heat treatment *in vacuo* as is shown in Figs. 8a and 8b. The OH band of silica gel hydrothermally treated at 100 °C in Fig. 8a became sharper when the temperature of heat treatment was raised, because of the decrease in the intensity of the strongly hydrogen-bonded component. By the heat treatment at 800 °C, the free OH component was clearly seen besides a small weakly perturbed component. On the other hand, the OH band hydrothermally treated at 250 °C in Fig. 8b obviously has two components at 3750 and 3670 cm^{-1} upon heat treatment at 600 °C, but it has almost no component below 3600 cm^{-1}. After this sample was heated at 800 °C, there remained only 3750 cm^{-1} component. The decrease in the strongly hydrogen-bonded OH component against the hydrothermal temperatures seems to be roughly parallel to that of the coordination number. Therefore, it seems reasonable to assume that most of these strongly hydrogen-bonded OH groups lie on the surface around the contact points and contribute to the formation of interparticle bonds.

The intensity of the 3670 cm^{-1} band increased as the temperature and the time of hydrothermal reaction were increased, and the shape of this component became clearly visible at higher hydrothermal temperatures. This component can also be made visible by a sufficient isotope exchange of protons of OH groups by the adsorption of heavy water, as is illustrated in Fig. 9. A similar result was reported by Abramov and others.[7] Figure 9 shows the infrared spactra after a sufficient isotope exchange of the OH band of silica gel hydrothermally treated at 163 °C. According to our qualitative observation, the 3750 cm^{-1} component seems to shift to 2750 cm^{-1} most quickly; this seems to suggest that the sites of the free OH groups are on outer convex surface, so that heavy water can be adsorbed there directly. The exchange rate of protons of the strongly hydrogen-bonded OH groups seems to be slower. This indicates that these OH groups lie on the surface near the contact points where heavy water can not be directly adsorbed, and that the H–D exchange can be carried out by the diffusion of protons and deutrons through hydrogen-bond chains of the OH groups. The exchange equilibrium was almost attained after about 20 cycles of the adsorption-desorption processes of heavy water; there remained only an OH band at about 3670 cm^{-1}. This behavior suggests that these OH groups are on the surface inside closed pores that have been produced by hydrothermal treatment, by which not only the concave surfaces at the contact points, but also small openings surrounded by a few contact points of a dense aggregate of primary particles are filled with a siloxane net work. Not even the heavy-water molecules can migrate into these closed pores.

The reason for the weak perturbation of these inner OH groups might be that the OH vibration is perturbed by a local dielectric field, which seems to be rather strong inside these small closed pores.[8] The intensity of the 3670 cm^{-1} component grew larger when the hydrothermal temperature was raised, as can be seen in Fig. 7. This suggests an increase in the area of the surface in the closed pores or an increase in the number of closed pores. There are two more pieces of evidence for the existence of the closed pores. By impregnating this material with impurities such as the sodium cations, the temperature of sintering is considerably lowered; even the free OH band disappears above about 800 °C, while the 3670 cm^{-1} band remains as it was, or its intensity even increases a little.[2] This phenomenon was interpreted as resulting from the occurence of closed pores by high-temperature sintering. Another example is the ion-exchange experiment of the OH groups of this materials with Co^{2+} ions.[9] After immersing the silica gel being hydrothermally treated at about 150 °C in a saturated aqueous solution of cobalt(II) acetate, the OH groups which were not ion-exchanged were mainly inner OH groups, together with a small part of the strongly hydrogen-bonded OH component.

The surface area inside these closed pores can not be measured by the nitrogen-adsorption method, since nitrogen molecules can not easily migrate into these pores, although the amount of OH groups can be measured by means of the weight loss of this material, as has been mentioned before, at 1200 °C, at which temperature all the OH groups including those inside the closed pores can be dehydrated by the explosion of closed pores at high temperatures, as has been mentioned elsewhere.[2] Upon hydrothermal treatment at high temperature, the fraction of the surface area inside the closed pores compared to that of the total surface increases greatly; this proves the extraordinarily large values of the OH density of silica gel at high hydrothermal temperatures. Exactly the same behavior was observed during the sintering process of this material, in which the surface area dropped to very low values, while the OH density increased highly at the same time, accompanied by the production of closed pores.[2] The amount of these inner OH groups can be estimated from the intensity of the 3670 cm^{-1} band after sufficient isotope exchange of OH group, assuming that the absorption intensity per OH group is the same for all three types of OH groups, although the degree of perturbation is different for these OH vibrations. The results of this estimation, together with the other properties of this material are shown in Table 1. In Column 5 of this table, the number

Table 1. The surface areas and the number of OH groups per nm^2 of silica gel hydrothermaly treated at various temperatures

Temperature of hydrothermal reaction, °C	Specific surface area, m^2/g	Number of OH groups per unit weight, $10^{21}/g$	Ratio of H–D exchangeable OH groups to total OH groups	Number of outer OH groups, $10^{21}/g$	OH Density of outer surface per nm^2	Total surface area, m^2/g
10	579.5	4.13	0.85	3.5	6.1	1033
50	742.1	4.13	0.84	3.5	4.7	1033
75	825.4	4.20	0.81	3.4	4.1	1050
100	839.4	3.83	0.76	2.9	3.5	958
163	495.1	2.48	0.73	1.8	3.7	620
202	214.3	1.67	0.43	0.73	3.4	418
230.5	146.6	1.49	0.27	0.40	2.7	373
253.0	63.5	1.13	0.26	0.29	4.6	283

of OH groups which can be exchanged with OD groups can be estimated from the intensity of the total OH band subtracted by that of the inner OH band. The surface densities of outer OH groups can be calculated from these values in Column 5, divided by the outer surface area, which is nearly equal to the B. E. T. specific surface area in Column 2; the results are shown in Column 6. These values of the OH surface density are less than $4/nm^2$ above 100 °C, where the surface area around the particle contacts is negligible, but are more than 4 below 100 °C, where the number of coordination is so large that the area around these points can not be neglected. It is interesting to see that the OH density of non-porous aerosil is about $3.8/nm^2$, which is almost equal to the values shown in the table.

If the bulk siloxane structure of primary particles of silica gel was homogeneous everywhere inside the particle, the surface density of OH groups would be the same all over the particle surface. Therefore, it seems possible to obtain the total surface areas of the primary particles of this material by dividing the number of the total OH groups per unit of weight in Column 3 of Table 1 by the surface OH density of $4/nm^2$. The total surface areas thus estimated are shown in the last column of Table 1. It is interesting to see that the total surface area below 100 °C is nearly equal to that calculated by taking the area around the contact points into account, as will soon be reported elsewhere.[10] The number of OH groups, $4/nm^2$, obtained here is also in good agreement with that obtained from the study of the heat of the immersion of silica gel thermally treated under various conditions.[11] The pore structure of silica gel proposed in this investigation is in fair agreement with the view given by Barby.[12]

Conclusion

The surface OH groups of silica gel are found to consist mainly of three types; the free OH groups on the outer convex surface exposed to the molecular adsorption and with an infrared absorption band at about 3750 cm^{-1}, the inner OH groups on the concave surface inside the closed pores at about 3670 cm^{-1}, and the strongly hydrogen-bonded OH groups on the surface around the contact points between primary particles with a broad absorption band at about 3500—3300 cm^{-1}. The pore structure and its change upon the hydrothermal and thermal treatment seem to influence the relative concentrations of these three types of OH groups of silica gel.

The authers are grateful to Mr. Hirofumi Fujiwara, Miss Misako Fujikawa, and to Miss Hiromi Okada of the Osaka University of Education for their discussions and experimental help.

References

1) C. Okkerse, "Physical and Chemical Aspects of Adsorbents and Catalysis," ed by B. G. Linsen, Academic Press (1970), p. 213; R. K. Iler, "The Colloid Chemistry of Silica and Silicates," Cornell University Press, New York (1955).

2) S. Kondo, H. Fujiwara, and M. Muroya, *J. Colloid Inerface Sci.*, **55**, 421 (1976).

3) S. Kondo and M. Muroya, *Bull. Chem. Soc. Jpn.*, **47**, 553 (1974).

4) B. S. Girgis, *J. Appl. Chem. Biotech.*, **26**, 683 (1976).

5) N. O. Smith, P. D. Foote, and P. F. Bunsang, *Phys. Rev.*, **34**, 1271 (1929).

6) H. Fujiwara, H. Motoki, R. Nakamura, Y. Matsuoka, and S. Kondo, *Memoirs of Osaka Univ. of Education*, **24 III**, 205 (1975).

7) N. V. Abramov, A. V. Kiselev, and V. I. Lygnin, *Zh. Fiz. Khim.*, **38**, 1044 (1964).

8) B. Crawford, A. G. Gilby, A. A. Cliford, and T. Fujiyama, *Pure Appl. Chem.*, **18**, 373 (1969).

9) S. Kondo, E. Amano, H. Kubo, M. Muroya, and I. Nakase, 30th Symposium of Colloid and Interface Chem. Jpn, Abstract, p. 64 (1977).

10) K. Naoki, C. Mineyama, K. Tomoi, and S. Kondo, *Memoirs of Osaka Univ. of Education*, **27 III**, 131 (1978).

11) S. Kondo, H. Fujiwara, T. Ichii, and I. Tsuboi, *J. Chem. Soc., Faraday Trans. 1*, **75**, 646 (1979).

12) D. Barby, "Characterization of Powder Surface," ed by G. D. Parfitt and K. S. W. Sing, Academic Press (1976), p. 353.

Determination of pH in Reversed Micelles

Hirotada FUJII,* Tohru KAWAI, and Hiroyasu NISHIKAWA**

Department of Polymer Technology, Tokyo Institute of Technology, Ookayama, Meguro-ku, Tokyo 152

***Department of Physiology, Kyoto Prefectural University of Medicine, Kyoto 602*

(Received September 21, 1978)

A new method for the determination of pH in reversed micellar systems was proposed. The degree of dissociation (α) of Phenol Red in the systems was observed spectrophotometrically. The value of pH can be obtained by use of the Henderson-Hasselbach equation with the aid of pK_a of Phenol Red measured by means of ^{31}P-NMR in the systems containing phosphate buffer solutions. The method was applied to systems consisting of sodium octanoate, 1-hexanol, and water and some buffer solutions other than phosphate buffer solutions, and found to be effective within a wide pH range. Analysis of the fluorescence spectra of 8-anilino-1-naphthalenesulfonic acid indicates that Phenol Red molecules are present at the interface between the water core and the 1-hexanol phase in reversed micelles. The hydrolytic reaction of *p*-nitrophenyl acetate was also studied kinetically and found to change slightly with pH.

The rates of the chemical reactions are drastically accelerated in the reversed micelle.[1–5] Recently, an effective energy transfer was observed in the reversed micellar system.[6]

Hydrolytic reactions of *p*-nitrophenyl esters were studied in the reversed micelle consisting of sodium octanoate, 1-hexanol, and water. It was found that the rate of the reaction is much more enhanced as compared with that in the aqueous solution. Favorable partitioning of the substrate into the water core, the orientation of the catalyst at the interface between the water core and the 1-hexanol phase and the polarity of the water molecules are important factors to accelerate the reaction. NMR studies on the behavior of water molecules and the polar headgroup of sodium octanoate in the reversed micelle showed that the mobility and polarity of water molecules change with hydration of sodium ions.

The purpose of this study is to measure the pH in the reversed micelle in order to know the effect of pH on the hydrolytic reaction. This will also be relevant to elucidating the activity of the water molecule in the reversed micelle. The pH in the reversed micelle cannot be measured with a glass electrode. The pH value in the interior of cell membranes also cannot be measured with a glass electrode, but have been determined by several alternate methods.[7–9] ^{31}P-NMR technique has been used to measure the pH values in the interior or exterior of cell membranes.[10,11] On the other hand, the acid-base indicator is useful for measuring pH of the aqueous solution. In this case, pH is determined by the Henderson-Hasselbach equation

$$\mathrm{pH} = \mathrm{p}K_a + \log \frac{\alpha}{1-\alpha} \qquad (1)$$

where K_a is the dissociation constant of the indicator, and α the degree of dissociation of the indicator. Since K_a of the indicator in the reversed micelle is not the same as that in the aqueous solution, the pH value in the reversed micelle cannot be measured only by means of indicator. The pH value in the reversed micelle consisting of the buffer solution other than the phosphate buffer solution cannot be measured by ^{31}P-NMR technique. In this study, α of Phenol Red and the pH value in the reversed micelle consisting of the phosphate buffer solution were determined by the spectrophotometry method and ^{31}P-NMR, K_a of Phenol Red being obtained by substituting α and pH in Eq. 1. Thus, the use of Phenol Red makes the pH measurement in the reversed micelle not only easier but the evaluating of the pH value in the reversed micelle consisting of any buffer solution in a wide pH range possible.

A hydrophobic probe,[12] 8-anilino-1-naphthalenesulfonic acid (ANS), is an amphiphilic compound with a chemical structure similar to that of Phenol Red. The position of Phenol Red can thus be estimated from the measurement of the fluorescence of the system.

Experimental

Materials. Analytical grade reagents of sodium octanoate, 1-hexanol, Phenol Red, adenosine-5′-triphosphate (ATP), 8-anilino-1-naphthalenesulfonic acid (ANS), and L-tryptophan were used without further purification. 2-[4-(2-hydroxyethyl)-1-piperazinyl] ethanesulfonic acid (HEPES, $pK_a = 7.5$), 3-(cyclohexylamino)-1-propanesulfonic acid (CAPS, $pK_a = 10.4$) and 3-[2-hydroxy-1,1-bis(hydroxymethyl)-ethylamino]-1-propanesulfonic acid (TAPS, $pK_a = 8.4$, DOJINDO Laboratories) were used. Reversed micellar solution was prepared by mixing three components, the buffer solution (phosphate or HEPES–TAPS–CAPS buffer solution), 1-hexanol and sodium octanoate, and allowing the mixture to stand at 30 °C for 24 h. In the measurements of the absorption spectra, ^{31}P-NMR spectra and the fluorescence spectra, the buffer solution containing Phenol Red (the concentration of Phenol Red is 10^{-4} M), adenosine-5′-triphosphate (10^{-2} M) and the fluorescence probe (10^{-4} M) was cosolubilized into the reversed micelle. The quencher, carbon tetrachloride, was added directly to the reversed micellar solution containing ANS molecules.

Measurements. ^{31}P-NMR was measured with JNM-PS type spectrometer at 40 MHz, the following setting of the pulse unit being employed; spectral width 4000 Hz, repeat time 2.5 s, pulse width 18.0 μs, 100 times accumulation. The absorption spectra were recorded on an EPS-3T Hitachi spectrophotometer at 30 °C. The fluorescence spectra were measured with a Shimadzu RF-502 type spectrofluorimeter at 30 °C.

Results and Discussion

Determination of pH *Value.* Figure 1 shows the dependence of the chemical shift of phosphorus in

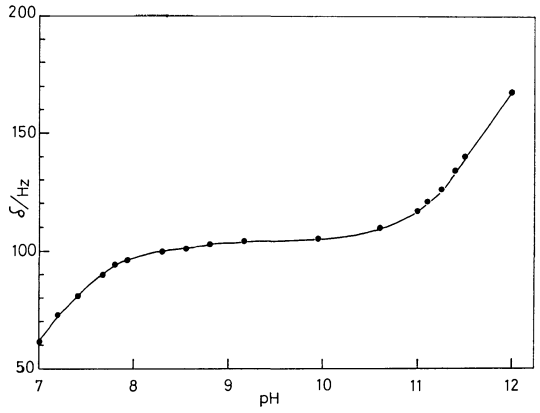

Fig. 1. The chemical shifts of phosphorus in the phosphate buffer solutions plotted as a function of pH of the buffer solution.

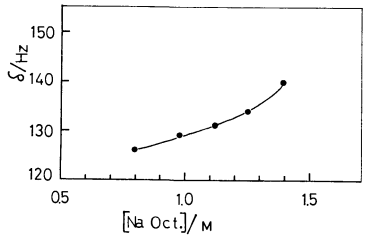

Fig. 2. Plots of the chemical shifts of phosphorus in the phosphate buffer solutions solubilized into reversed micelles against the concentration of sodium octanoate. The pH value of the phosphate buffer solution used is 7.9.

the phosphate buffer solution on the pH of the buffer solution. The steps in the chemical shift plots correspond to the processes

$$H_2PO_4^- \rightleftharpoons HPO_4^{2-} \rightleftharpoons PO_4^{3-}.$$

The chemical shifts of phosphorus were measured as a function of concentration of sodium octanoate for reversed micelles prepared by the use of phosphate buffer solutions of pH 7.9. The results are shown in Fig. 2. The chemical shift increases with increase in the concentration of sodium octanoate. This indicates that the pH value in the reversed micelle is higher than the initial pH value of the phosphate buffer solution used for the preparation of reversed micellar solutions. The activity of water molecules in the reversed micelle should decrease with increase in sodium octanoate content. However, the pH value obtained from ^{31}P-NMR method is much higher than that calculated by $[H^+]=\sqrt{K_wK_a/C}$, where K_w is the ion-product constant of water, K_a the dissociation constant of octanoic acid, and C the concentration of sodium octanoate. Such large chemical shifts of phosphorus as observed in the reversed micelle may be due to the ionic effect of the polar headgroup of sodium octanoate. Since the chemical shift of α-phosphorus of adenosine-5′-triphosphate (ATP) does not change with pH,[13] the chemical shift induced by sodium octanoate was evaluated by the following method. By means of this property of α-phosphorus of ATP, the difference between the α-P chemical shift of ATP in the aqueous solution and in the reversed micelle

Table 1. The observed chemical shift (δ), the chemical shift induced by sodium octanoate (δ′), δ−δ′ and pH obtained from (δ−δ′) for reversed micellar samples

[Sodium octanoate][a]	δ/Hz	δ′/Hz	(δ−δ′)/Hz	pH
1.38	140.0	39.0	101.0	8.6
1.24	133.7	33.0	100.7	8.5
1.10	131.7	31.3	100.4	8.4
0.97	129.9	29.5	100.4	8.4
0.69	125.5	25.4	100.1	8.3

a) The molar concentration (M) of sodium octanoate in 1-hexanol.

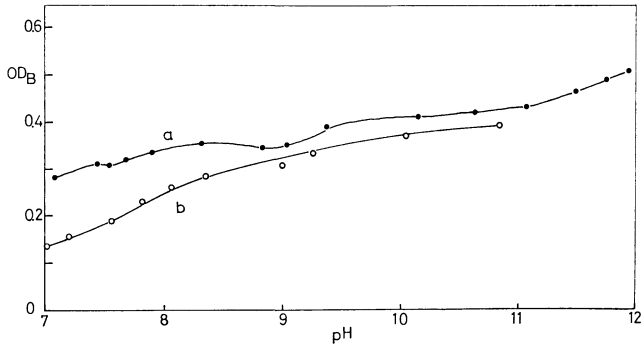

Fig. 3. Plots of the absorbance of Phenol Red due to the ionized form (OD_B) against the initial pH value of the phosphate buffer solution (a) and HEPES–TAPS–CAPS buffer solution (b) solubilized into the reversed micelle.

was measured, and used as the chemical shift induced by sodium octanoate. The real chemical shift of phosphorus in the reversed micelle should be obtained by subtracting the shift thus obtained from the chemical shift observed for the reversed micelle. From the result, the real pH value (pH′) in the reversed micelle can be obtained by means of Fig. 1. The results are given in Table 1.

The absorption spectra of Phenol Red in reversed micelles show a peak at 450 nm due to unionized form and a peak at 571 nm due to ionized form of Phenol Red and the isosbestic point at 490 nm. The absorbance at 571 nm (OD_B) due to the ionized form of Phenol Red in the reversed micelle against the initial pH value of the buffer solution (phosphate buffer or HEPES–TAPS–CAPS buffer) solubilized into the reversed micelle is plotted in Fig. 3. Although the pH values of the phosphate buffer solution containing Phenol Red vary in the range 7—12, the absorbance due to the ionized form of Phenol Red does not appreciably change with pH. This indicates that pH at the position where Phenol Red exists does not change much with pH of the phosphate buffer solution. Thus, pH in the reversed micelle is determined by the buffer capacity of sodium octanoate rather than that of the phosphate buffer solution. A similar experiment was carried out in the reversed micelle with use of another buffer solution, HEPES–TAPS–CAPS. The results are shown in Fig. 3. The transformation of Phenol Red from the acid form (unionized form) to the basic form

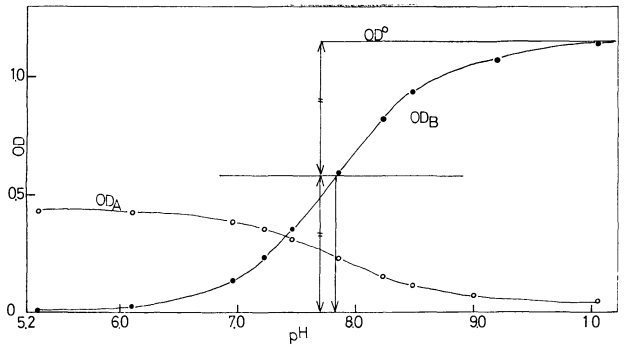

Fig. 4. Plots of the absorbance of Phenol Red due to the ionized (OD_B) and the unionized (OD_A) forms against pH of the phosphate buffer solution. This figure shows pK_a of Phenol Red in the phosphate buffer solution is 7.82.

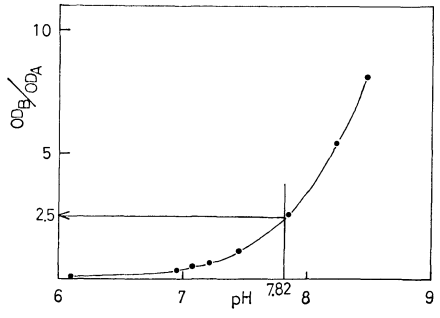

Fig. 5. Plots of OD_B/OD_A against pH of the phosphate buffer solution.

(ionized form) takes place to a greater extent than in the phosphate buffer solution, especially in the pH range 7—9. In order to estimate the degree of dissociation (α) of Phenol Red, it is necessary to measure the absorbance due to the completely ionized form of Phenol Red ($OD_B°$). However, the value of OD_B at the highest pH (pH=12) showed no constant value (Fig. 3). The following experiment was made in aqueous solutions. The absorbances of Phenol Red at 571 nm and at 450 nm were measured as a function of the pH of the buffer solution (Fig. 4). The dissociation constant *K*a of Phenol Red in this buffer solution (phosphate buffer solution) was found to be 7.82 by means of Eq. 1. The ratio of the absorbance at 571 nm (OD_B) to that at 450 nm (OD_A) is plotted against pH of the buffer solution (Fig. 5). We see that OD_B/OD_A is 2.5 for pH 7.82. The values of OD_B/OD_A were obtained for the four buffer solutions; phosphate buffer solution, HEPES–TAPS–CAPS, 90% phosphate buffer solution +10% ethanol, and 90% phosphate buffer solution +10% dioxane; the results are summarized in Table 2. The OD_B/OD_A value becomes 2.5 at the point pH=pK_a where OD_B is equal to a half of $OD_B°$. Thus, $OD_B°$ can be obtained from the value of OD_B at the pH where the value of OD_B/OD_A becomes 2.5. In the four buffer solutions, the value of $OD_B°$ thus obtained was equal to that estimated from Fig. 4. In the reversed micelle, $OD_B°$ was evaluated with the assumption that OD_B at pH of OD_B/OD_A=2.5 is also equal to a half of $OD_B°$. The following procedure was taken to determine pH

Table 2. The dissociation constant pK_a and the ratio OD_B/DA_A for four buffer solutions

	pK_a	OD_B/DA_A
Phosphate buffer	7.82	2.50±0.02
90% phosphate buffer+10% ethanol	7.90	2.50±0.02
90% phosphate buffer+10% dioxane	7.88	2.51±0.02
HEPES-TAPS-CAPS	7.82	2.48±0.02

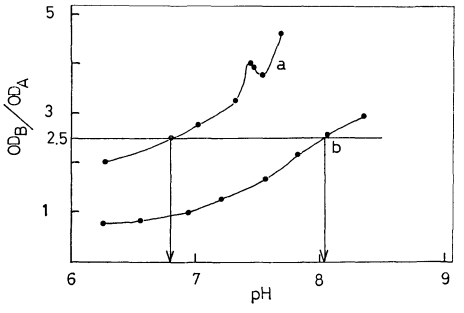

Fig. 6. Plots of OD_B/OD_A of Phenol Red against the original pH value of the buffer solution solubilized into the reversed micelle. a) Phosphate buffer, b) HEPES–TAPS–CAPS.

in the reversed micelle.

1. The values of OD_B/OD_A were determined as a function of the pH of the original buffer solution solubilized into the reversed micelle. The results are shown in Fig. 6.

2. The pH of the buffer solution giving the value OD_B/OD_A=2.5 was obtained from the OD_B/OD_A *vs.* pH curve shown in Fig. 6.

3. The OD_B value corresponding to the pH value obtained from step 2 was obtained from the OD_B *vs.* pH curve given in Fig. 3. Thus, the value of $OD_B°$ can be obtained as twice the value of OD_B.

4. The degree of dissociation (α) of Phenol Red in the reversed micelle is thus obtained as $OD_B/OD_B°$.

5. The dissociation constant K_a of Phenol Red in the reversed micelle can be calculated from the degree of dissociation of Phenol Red and the pH value obtained by ^{31}P-NMR, by means of Eq. 1. When the phosphate buffer solution of pH 7.9 was solubilized into the reversed micelle, the α and pH values were found to be 0.65 and 8.6 by spectrometric method and ^{31}P-NMR, respectively. By substituting these values into Eq. 1, the pK_a value of Phenol Red was found to be 8.3.

6. By use of α and pK_a (8.3) of Phenol Red, the real pH value (pH′) in the reversed micelle containing a buffer solution was obtained in a wide pH range. The pH′ values in the reversed micelle containing phosphate buffer solutions and HEPES buffer solutions are shown in Fig. 7.

Fluorescence Spectra. It is important to study the position of Phenol Red molecule. It may be in the water core, 1-hexanol phase or at the interface between the water core and 1-hexanol phase. Fluorescence has been used for elucidating the position. 8-Anilino-1-naphthalenesulfonic acid (ANS), which is an amphiphilic compound with a structure similar to that of Phenol Red, was used. The positions of

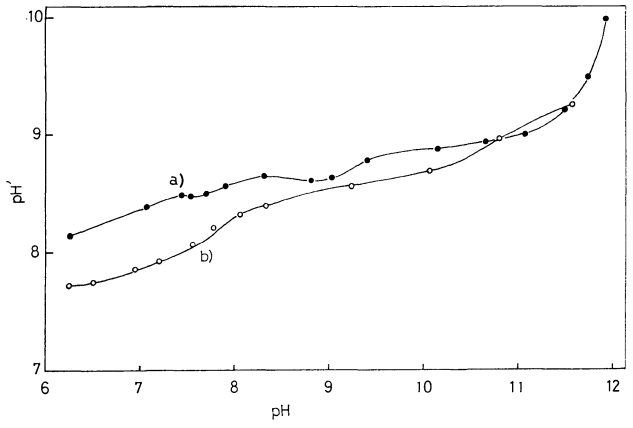

Fig. 7. Plots of the real pH value (pH') against the original pH value of the buffer solution solubilized into the reversed micelle. a) Phosphate buffer, b) HEPES–TAPS–CAPS buffer.

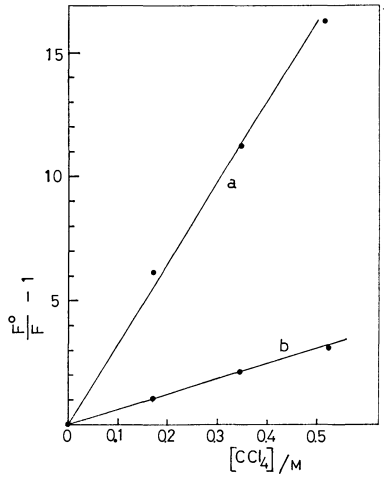

Fig. 8. The Stern-Volmer plots in 1-hexanol and the reversed micelle. The fluorescence probe used is ANS. a) 1-Hexanol, b) in the reversed micelle.

the emission maxima and the relative intensities of ANS in 1-hexanol, water, and the reversed micelle are given in Table 3. The position of the emission maximum and the very low intensity in water as compared with those in the reversed micelle indicates that ANS molecules do not exist in the water phase of the reversed micelle.

Carbon tetrachloride can quench the fluorescence of ANS in 1-hexanol. Quenching of the excited state of ANS can be quantitatively treated by the Stern-Volmer equation[14] $F^\circ/F-1=k^\circ\tau[Q]$, where F and F° are the fluorescence intensities of the probe with and without the quencher, respectively, k° the rate constant of quenching, τ° the fluorescence lifetime of the probe in the absence of the quencher, and [Q] the concentration of the quencher. Figure 8 shows the plots of the data obtained by means of this equation in 1-hexanol and in the reversed micelle. Carbon tetrachloride quenches the fluorescence of ANS in 1-hexanol to a greater extent than in the reversed micelle. The results indicate that no appreciable amount of ANS exists in the 1-hexanol phase of the reversed

Table 3. Position of emission maximum and the relative intensity of ANS in water, 1-hexanol and the reversed micelle

	Water	1-Hexanol	Reversed micelle[a]	
			A	B
Emission maximum/nm	515	460	465	470
Relative intensity	1	254	131	109

a) A; 1.38 M of sodium octanoate in 1-hexanol.
B; 0.69 M of sodium octanoate in 1-hexanol.

micelle. Thus, the probe molecules should exist at the interface between the water core and the 1-hexanol phase.

The same experiment was carried out in the reversed micellar system with use of L-tryptophan, an amphiphilic compound. L-Tryptophan is not soluble in 1-hexanol, but can be quenched a little by carbon tetrachloride in the reversed micelle. The results indicate that L-tryptophan molecules also exist at the interface between the water core and the 1-hexanol phase. Thus, the amphiphilic molecules are considered to be located at the interface between the water core and the 1-hexanol phase, due to the balance of the hydrophobic and lyophilic interactions. Phenol Red exists at the interface between the water core and the 1-hexanol phase as in the case of L-tryptophan and ANS, the real pH (pH') given in Fig. 7 being pH at the interface of the reversed micelle.

Dissociation Constant of Phenol Red and the Surface Potential in the Reversed Micelle. By substituting the pH value obtained by ^{31}P-NMR and the degree of dissociation of Phenol Red by spectrometric methods in Eq. 1, we have obtained the dissociation constant of Phenol Red as 8.3, which is larger than that in the aqueous solution (7.8). The dissociation constant of Methyl Red measured by Montal and Gitler[15] in the aqueous solution of sodium dodecyl sulfate was also larger than that in the aqueous solution. By means of the gel filtration technique, they showed that Methyl Red is influenced by the surface charges of the micelle. The concentration of H^+ ion at the surface of the micelle would differ from that in the bulk phase of the system due to the difference in electrical potential between that on the micellar surface and that in the bulk phase. The dissociation constant of Methyl Red on the micellar surface, K_s, is given by the equation $pK_s=pK_b-\varepsilon\psi/2.3\,kT$, where K_b is the dissociation constant of Methyl Red in the bulk phase, ψ the surface potential, ε the electrical charge, T the absolute temperature, and k the Boltzmann constant. For Methyl Red in the aqueous solution of sodium dodecyl sulfate, $\psi=-86$ mV, and for Phenol Red, $\psi=-30$ mV in the reversed micelle. The difference in surface potential between Methyl Red and Phenol Red would be caused by the difference in the location of the indicators and in the nature of the headgroups of the surfactants, *i.e.*, the sulfate group of sodium dodecyl sulfate and the carboxylate group of sodium octanoate.

Effect of pH *on the Reaction in the Reversed Micelle.* The rate constant of the hydrolytic reaction of *p*-

nitrophenyl acetate in the reversed micelle in which the phosphate buffer solution is solubilized is as large as that in which the HEPES buffer solution is solubilized. On the other hand, pH′ in the reversed micelle in which the phosphate buffer solution is solubilized is higher than that in which the HEPES buffer solution is solubilized (Fig. 7). Thus it appears that, although the hydrolytic reaction depends slightly on the pH in this system, it is not an important factor in the enhancement of this reaction rate in the reversed micelle.

References

1) E. J. Fendler, J. H. Fendler, R. T. Medary, and V. A. Woods, *J. Am. Chem. Soc.*, **94**, 7288 (1972).
2) F. M. Menger and A. C. Vitale, *J. Am. Chem. Soc.*, **95**, 4931 (1973).
3) C. J. O'Connor, E. J. Fendler, and J. H. Fendler, *J. Am. Chem. Soc.*, **96**, 370 (1974).
4) K. Kon-no, K. Miyazawa, and A. Kitahara, *Bull. Chem. Soc. Jpn.*, **48**, 2955 (1975).
5) O. A. EL Seoud, *J. Chem. Soc., Perkin Trans. 2*, **1976**, 1497.
6) J. H. Fendler and Li-Jen Liu, *J. Am. Chem. Soc.*, **97**, 999 (1975).
7) M. Lavallee, *Circulation Res.*, **15**, 185 (1964).
8) J. M. Severinghaus, M. Stupfel, and A. F. Bradley, *J. Appl. Phys.*, **9**, 189 (1956).
9) W. J. Waddell and T. C. Butler, *J. Clin. Invest.*, **38**, 720 (1959).
10) J. M. Salhang, T. Yamane, R. G. Shulman, and S. Ogawa, *Proc. Natl. Acad. Sci. U.S.A.*, **72**, 4966 (1975).
11) G. Navon, S. Ogawa, R. G. Shulman, and T. Yamane, *Proc. Natl. Acad. Sci. U.S.A.*, **74**, 87 (1977).
12) L. Stryer, *J. Mol. Biol.*, **13**, 482 (1965).
13) M. Cohn and T. R. Hughes Jr., *J. Biol. Chem.*, **235**, 3250 (1960).
14) W. M. Vaughan and G. Weber, *Biochemistry*, **9**, 464 (1970).
15) M. Montal and C. Gitler, *Bioenergetics*, **4**, 363 (1973).

Copper(I) Chloride Complex Containing *p*-Benzoquinone as a Ligand

Hiroko YAMAGUCHI,* Hiroshi KIMURA, and Kazuo YASUKOUCHI

Department of Industrial Chemistry, Faculty of Engineering, Kumamoto University, 2-39-1, Kurokami, Kumamoto 860

(Received October 4, 1978)

A new complex $[(NH_4)Cu_3Cl_4(C_6H_4O_2)_{3/2}\cdot H_2O]$ was synthesized from $CuCl_2$, hydroquinone, and NH_4Cl in an aqueous solution, and its structure was characterized on the bases of its UV, IR, and ESR spectra and TGA. On heating, this complex was stable up to 100 °C, but above 120 °C *p*-benzoquinone was released quantitatively. The complex was found to be a polynuclear copper(I) complex containing *p*-benzoquinone molecules and chlorides as ligands, and to be a charge-transfer complex in which π-electrons of the ring carbons of *p*-benzoquinone form coordinate bonds with Cu(I). The formation process of the complex was:

$$3CuCl_2 + 3/2(C_6H_6O_2) + H_2O + NH_4Cl = (NH_4)Cu_3Cl_4(C_6H_4O_2)_{3/2}\cdot H_2O + 3HCl$$

Deep red crystals are inadvertently obtained when $CuCl_2$, hydroquinone, and NH_4Cl are mixed in an aqueous solution. They were found to be a new-type Cu(I) complex, $[(NH_4)Cu_3Cl_4(C_6H_4O_2)_{3/2}\cdot H_2O]$ (to be called BQ-Red hereafter), in which the π-electrons of *p*-benzoquinone form coordinate bonds with Cu(I).

A complex containing a ligand of *p*-benzoquinone has been synthesized by Hashimoto *et al.*[1] In this complex, both of the oxygen atoms of *p*-benzoquinone are coordinated to Cu(I). The IR spectrum of BQ-Red, however, indicates that the oxygens can not be the donor atoms, because the shift of the C=O stretching absorption caused by complexation is only 8 cm^{-1}.

The aim of this paper is to describe a method for synthesizing this interesting complex and its chemical and spectral characteristics. The information obtained from the latter is all in harmony with its structure, which was recently established by an X-ray diffraction study.† The reaction mechanism for the formation of BQ-Red will also be discussed.

Experimental

Materials. The reagents, $CuCl_2$, hydroquinone, and NH_4Cl (Wako special grade), were used without further purification. All the solvents used were purified by repeated distillations.

Apparatus. The IR spectra were taken with Hitachi perkin Elmer Model 125(4000—400 cm^{-1}) and JASCO DS-403G grating(600—200 cm^{-1}) spectrometers. The ESR spectra were measured with a JEOL, Model JES-3BSX, X-band spectrometer. The UV and visible spectra were obtained with a Hitachi EPS-2U spectrometer. The TG and DTA measurements were carried out using a Rigaku denki DPA-001D apparatus, with α-alumina as the standard and in a quartz cell. The elemental analysis of C, H, and N was carried out by means of an auto CHN corder, Model MT-2(Yanagimoto).

Synthesis. NH_4Cl, $CuCl_2$, and hydroquinone were mixed in an aqueous solution. The total concentration of the three components in 100 ml was kept constant(2 M), while the molar ratios of the three were varied as is shown in Fig. 1. Deep red crystals separated out from the solution when 5 M NaOH (10—20 ml) was slowly added to the mixed solution with constant stirring. The crystals were obtained only when the molar ratio of the components lay inside the enclosed area shown by a dotted line (Fig. 1); no red crystals were formed outside of this area. This indicates that the formation of the red crystals depends mainly upon the amount of hydroquinone. When the amount of hydroquinone was smaller than the theoretical one (△), red crystals were easily formed. All the red crystals thus formed has the same composition. The molar ratio at which the largest amount of red crystals(BQ-Red) was formed was, $CuCl_2$: hydroquinone: NH_4Cl=3 : 1 : 1.

BQ-Red is soluble only in aqueous NH_4Cl, and the higher the concentration of NH_4Cl, the better it dissolves. The solution is reddish orange. On the other hand, when the concentration of NH_4Cl is less than 2 M, it is hardly soluble, and it decomposes gradually, forming a yellow solution after 20—30 min. In water, BQ-Red decomposes at once and becomes greenish, with the formation of $CuCl_2$. In methanol, the crystals become white CuCl, and a similar but partial decomposition occurs either in ethanol or in acetone. In 1-pentanol, benzene, ligroin, ether, or petroleum ether, however, the crystals are stable and remain deep red. Since no solvent for the recrystallization was found, the sample of BQ-Red for the analyses was purified by scrubbing it with 1-pentanol and with ether to remove all unreacted substances. Deep-red crystalline plates of BQ-Red were obtained in this way.

Analysis. The copper was determined by titrating it with EDTA after decomposition with a mixture of nitric

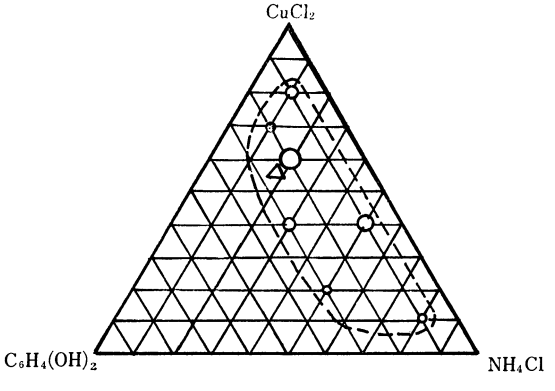

Fig. 1. Molar ratio of the three components for the formation of BQ-Red.
$[Cu]+[C_6H_4(OH)_2]+[NH_4]=2.0$ M.
△: Theoretical value of BQ-Red, $Cu:C_6H_4(OH_2):NH_4Cl=6:3:2$.
○: Formation of BQ-Red (size of the circle indicates the amount of BQ-Red formed).

† A schematic drawing of the established structure of BQ-Red is shown in Fig. A. The details of this X-ray study will be published elsewhere: H. Yamaguchi, T. Uechi, and I. Ueda, manuscript in preparation.

Table 1. Thermogravimetric analysis of BQ-Red

	(I) in air Temp (°C)	Weight loss (%)	(II) in Ar Temp (°C)	Weight loss (%)	Calcd Weight loss (%)		State
(A)	25	0	25	0	0		$Cu_3Q_{3/2}NH_4Cl_4H_2O$
(B)	103	29.3	100	28.1	30.6	$-Q_{3/2}$	$Cu_3Cl_3NH_4ClH_2O$
(C)	230	33.6	232	34.0	34.0	$-H_2O$	$(CuCl)_3NH_4Cl$
(D)	390	35.6	270	37.7	37.0	$-NH_3$	$(CuCl)_3HCl$
(E)	450	41.6	—	—	43.9	$-HCl$	$(CuCl)_3$
(F)	540	53.2	—	—	54.9	$-Cl_3+O_3$	3 (CuO)
(G)	—	—	595	83.9	81.7	$-(CuCl)_2$	(CuCl)
					or 82.0	$-Cl_3-Cu_{3/2}$	$(Cu_{3/2})$

Q: $(C_6H_4O_2)$

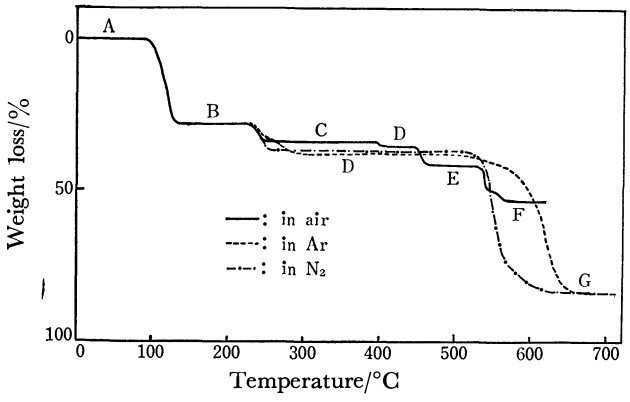

Fig. 2. TG curves of BQ-Red.

acid and perchloric acid(3 : 1).[5] The chlorine was also determined by chelate titration, after the decomposition of the BQ-Red by the Schöniger method[6] and the absorption of the evolved chlorine gas into a basic H_2O_2 solution.[7] Found: C, 20.06; H, 2.31; N, 2.62; Cl, 29.68; Cu, 35.71%. Calcd for $C_9H_{12}NCl_4O_4Cu_3$: C, 20.36; H, 2.26; N, 2.64; Cl, 26.73; Cu, 35.94%.

Results and Discussion

ESR Spectrum (Solid State). The ESR spectra of BQ-Red and $CuCl_2\cdot 2H_2O$ in the solid state were measured. Since the intensities of the obtained spectra depend upon the content of Cu(II), the content of Cu(II) in BQ-Red could be estimated from the data; it was found to be about fiftieth of the total amount of copper in BQ-Red. Thus, the copper in BQ-Red is present as a univalent ion, and BQ-Red appears to be a charge-transfer complex.

Thermogravimetric Analysis. BQ-Red decomposes, with the sublimation of the yellow crystals of *p*-benzoquinone, leaving a green copper salt, within a month at room temperature in the summer. When BQ-Red is heated, the yellow crystals of *p*-benzoquinone sublime from it at about 100 °C. Figure 2 and Table 1 show the TG curves and related data. Experiment (I) was performed in air, and (II), under flowing argon. Both sets of data show that *p*-benzoquinone sublimes endothermically at about 100 °C and that the lattice water is then lost at about 230 °C.

In air (I), the ammonium cation is lost as ammonia at about 390 °C and the chloride anion is lost as HCl at about 450 °C endothermically, and finally stable CuO (F) is obtained.

Under an inert gas, Ar (II), however, these two steps are indistinct, and the weight loss of 37.7% at the (D) point indicates that a compound with the composition of $(Cu_3Cl_3)\cdot HCl$ is formed; this compound remains stable between 270 and 595 °C. Then, at 595 °C, the weight loss suddenly increases until it becomes constant (83.9%, that is, 16.1% of the initial weight of BQ-Red); thereafter, it does not change until 800 °C. In N_2 gas, the TG curve is similar to that obtained in Ar, as is shown in Fig. 2, and the final weight of BQ-Red is 16.1% of the initial weight of BQ-Red, too. Under the inert gases, the final compound probably changes to elementary copper, corresponding to 1/2 of the initial copper content, while the rest sublimes away as chlorides.

Thus, the TG data can be explained in terms of the $[(NH_4)Cu_3Cl_4(C_6H_4O_2)_{3/2}\cdot H_2O]$ formula.

Infrared Spectrum. The IR spectrum of BQ-Red is shown in Fig. 3, while the assignments are sum-

Table 2. IR spectra of BQ-Red and *p*-benzoquinone

BQ-Red (cm^{-1})	*p*-Benzoquinone (cm^{-1})	Assignment
3500	—	ν(OH) lattice water
3140	—	$\nu(NH_4)$
—	3070	ν(CH)
3015	—	$\nu(NH_4)$
1669	—	$\delta_d(NH_4)$
1647	1655	ν(C=O)
1476	1592	ν(C=C)
1400	—	$\delta_d(NH_4)$
1288	1308	$\delta(CH_2)$ in
1056	1084	$\delta(CH_2)$ in
869	892	$\delta(CH_2)$ out

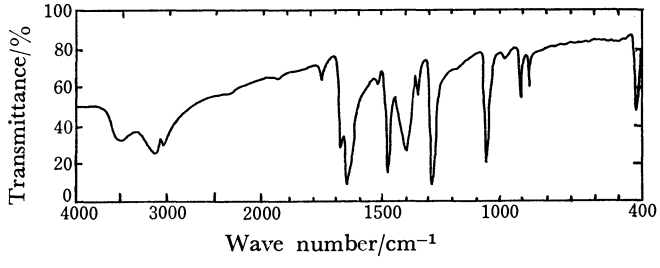

Fig. 3. IR spectrum of BQ-Red.

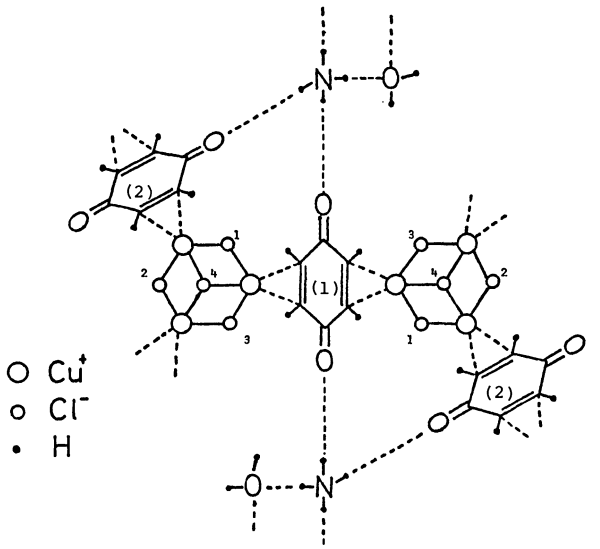

Fig. A. Schematic drawing of the molecular structure of BQ-Red.
$[(NH_4)Cu_3Cl_4(C_6H_4O_2)_{3/2}\cdot H_2O]_{2n}$.

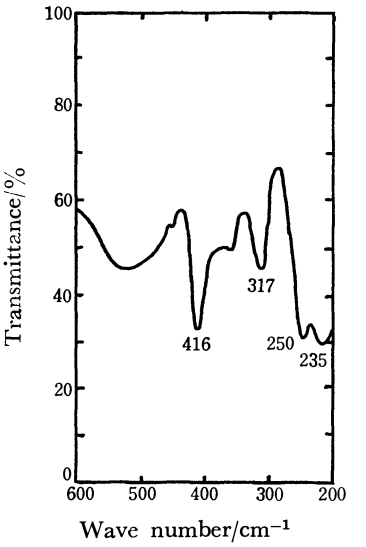

Fig. 4. Far-IR spectrum of BQ-Red.

marized in Table 2. Many bands of BQ-Red are similar to those of *p*-benzoquinone; this indicates that the starting material, hydroquinone, changes to *p*-benzoquinone upon the formation of BQ-Red. In the spectrum of BQ-Red, the C=C stretching band of *p*-benzoquinone (1592 cm^{-1}) shifts to 1476 cm^{-1}. It is interesting to note that this kind of shift to lower frequencies is more remarkable in Pt complexes.[8] For example, the C=C stretching frequency of the asymmetrical olefins observed at about 1600 cm^{-1} shifts to 1504 cm^{-1} in $K[PtCl_3(C_3H_6)]H_2O$,[9] although C=C bands of symmetrical olefins are not observed even in such complexes as $K[PtCl_3(C_2H_4)]H_2O$. This suggests that the C=C of the *p*-benzoquinone in BQ-Red is asymmetrically coordinated to Cu. In fact, the results of the X-ray structural analysis shown in Fig. A show clearly that the *p*-benzoquinone(1) has a symmetrical, but *p*-benzoquinone(2) has an asymmetrical, interaction with NH_4^+; this fact may cause some resemblance between them and symmetrical and asymmetrical olefins respectively.

On the other hand, the shift of the C=O stretching absorption caused by complexation is only 8 cm^{-1} in BQ-Red. It can thus easily be deduced that the oxygen atoms of the carbonyl groups of *p*-benzoquinone are not coordinated to Cu(I), but only make hydrogen bonds with NH_4^+. This agrees with the fact that BQ-Red readily decomposes to give *p*-benzoquinone when heated.

In addition, the intensities of the IR bands due to C–H [in-plane(1308, 1084 cm^{-1}) and out-of-plane(892 cm^{-1})] are almost equal to each other in *p*-benzoquinone, but in BQ-Red those of the latter (899 and 869 cm^{-1}) are much weaker than those of the former (1288 and 1056 cm^{-1}). Thus, in the crystals of BQ-Red, the *p*-benzoquinone molecules are arranged in a certain order, so that in-plane deformation vibration is promoted and out-of-plane deformation vibration is disturbed.

The bands of water and the ammonium cation in BQ-Red are clearly observed, as is shown in Fig. 3 and Table 2.

Far-infrared Spectrum. The characteristic band of a chloride anion bridging two metals is generally observed between 150—350 cm^{-1}, and it is slightly split into two strong bands. It is known[10] that the wave number of the stretching frequency of the bridging chloride, $\nu(M\text{–}Cl)_b$, is lower than that of terminal chloride, $\nu(M\text{–}Cl)_t$. The far-IR spectrum of BQ-Red is shown in Fig. 4. The absorption bands at 235 and 250 cm^{-1} can be assigned to those of $\nu(Cu\text{–}Cl)_b$, and the band at 317 cm^{-1}, to that of $\nu(Cu\text{–}Cl)_t$. Since the former bands are stronger than the latter, most of the chloride ions seem to be combined directly with two Cu atoms. However, the structure shown in Fig. A has no terminal chloride. Since the central Cl(4) is different from the other three (1, 2, and 3) in coordinate number, the band at 317 cm^{-1} may be assigned to the vibration of the central Cl(4).

The band at 416 cm^{-1} is due to the skeletal vibration of *p*-benzoquinone.

UV and Visible Spectra. The spectra of BQ-Red, *p*-benzoquinone, and hydroquinone in 4 M NH_4Cl solutions were also observed. The *p*-benzoquinone is characterized by maxima at 246 nm ($\log\varepsilon=3.95$) and 428 nm ($\log\varepsilon=1.4$), while hydroquinone is characterized by maxima at 222 nm and 290 nm. The spectrum of BQ-Red in the solution has maxima at 246 nm ($\log\varepsilon'=3.8$), 275 nm (shoulder, $\log\varepsilon'=3.3$), 438 nm ($\log\varepsilon'=2.5$), and 800 nm ($\log\varepsilon'=1.6$); this indicates that BQ-Red forms *p*-benzoquinone in solution. However, the red shift of the maximum at 428 nm and the presence of a shoulder at 275 nm suggest the interactions of *p*-benzoquinone with NH_4^+ and H_2O, which are in both the molecule and the solvent.

Molecular Structure. Since copper in BQ-Red is univalent, a tetrahedral arrangement of ligands like that in other Cu(I) complexes seems most probable;[11–13] this expectation conforms to the results of the X-ray analysis (Fig. A).

It is known that the coordination number of Cl is usually 1[11,14] or 2.[15] Moreover, Cu(I) complexes

with a three-coordinate chloride,[13] and a complex (Cu_4Cl_4)[12] with two two-coordinate and two three-coordinate chlorides, have been reported. However, BQ-Red is different from those reported previously,[11-15] for it contains three two-coordinated and one three-coordinated chlorides.

Although the oxygen of the carbonyl group is usually one of the well-known donor atoms, in this complex the π-electrons of the ring carbons of *p*-benzoquinone coordinate to Cu(I) as was reported in the case of a duroquinone complex,[16] in which the π-electrons of C=C of duroquinone coordinate to Ni(II). The coordination of the π-electron of C=C with Cu(I) has often been reported in aromatic complexes;[17-20] for example, the $(C_6H_6)[Cu(OSO_2CF)]_2$ complex[18] is stable up to 100 °C.

Thus, it is established that π-complexing occurs in BQ-Red, though little has been reported with regard to the fact that the copper(I) is π-bonded to a *p*-benzoquinone ring.[21]

Reaction Mechanism. The hydroquinone which is added as a starting material in the synthesis changes to *p*-benzoquinone in the complex formation, but no BQ-Red is formed when *p*-benzoquinone is used instead of hydroquinone, and Cu(II) changes to Cu(I). Thus, the formation process of BQ-Red is:

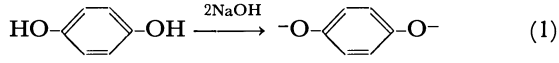

(1)

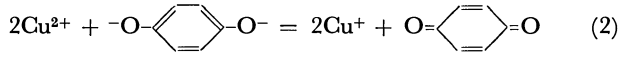

(2)

Then, three Cu(I) ions and three chloride ions make a ring:

$$3Cu^+ + 3Cl^- = \text{Ring } (-Cu-Cl-)_3 \quad (3)$$

As $Cu^+(d^{10})$ favors sp^3-hybridization, each Cu(I) accepts an electron pair from a *p*-benzoquinone around it and also combines with another chloride which is located at a center of the crown like ring (Cu_3Cl_3) (*cf.* Fig. A) to give a stable tetrahedral coordination structure:

$$\text{Ring } (Cu_3Cl_3) + NH_4Cl = (Cu_3Cl_3)Cl^- \cdot NH_4^+ \quad (4)$$

Thus, the overall reaction is:

$$3CuCl_2 + 3/2\, C_6H_4(OH)_2 + H_2O + NH_4Cl = \text{BQ-Red} + 3HCl \quad (5)$$

References

1) H. Hashimoto *et al.* prepared a reddish orange Cu(I) complex, $[Cu_2Py_2Cl_2(C_6H_4O_2)]$,[2] by means of a reaction between the Cu(II) complex $[CuPyCl(OCH_3)]_n$[3] and hydroquinone, where hydroquinone was converted to *p*-benzoquinone by the $C_6H_4(OH)_2+2Cu^{2+}=C_6H_4O_2+2Cu^+ +2H^+$ reaction,[4] in a *o*-dichlorobenzene–methanol solution.

2) H. Hashimoto, T. Noma, and T. Kawaki, *Tetrahedron Lett.*, **30**, 3411 (1968).

3) H. Finkbeiner, A. S. Hay, H. S. Blanchard, and G. F. Endres, *J. Org. Chem.*, **31**, 549(1966).

4) S. Hashimoto, M. Onohara, and H. Hashimoto, *Nippon Kagaku Kaishi*, **1976**, 468.

5) Y. Tsuchitani, Y. Tomita, and K. Ueno, *Talanta*, **9**, 1023(1962).

6) W. Schöniger, *Mikrochim. Acta*, **1955**, 123.

7) L. Erdey, L. Mázor, and T. Meisel, *Mikrochim. Acta*, **1958**, 140.

8) J. Chatt and L. A. Duncanson, *J. Chem. Soc.*, **1953**, 2939.

9) K. Nakamoto, "Infrared Spectra of Inorganic and Coordination Compounds," John Wiley & Sons, New York, London (1962), p. 228.

10) P. 121 in Ref. 9

11) Mino R. Caira and L. R. Nassimbeni, *Acta Crystallogr., Sect. B*, **31**, 1339(1975).

12) G. Nardin and L. Randaccio, *Acta Crystallogr., Sect. B*, **30**, 1377(1974).

13) I. D. Brown, *Acta Crystallogr.*, **13**, 28(1960).

14) M. E. Flect, *Acta Crystallogr., Sect. B*, **31**, 183(1975).

15) Par M. Massaux, *Acta Crystallogr., Sect. B*, **32**, 2032 (1976).

16) M. D. Glick and L. F. Dahl, *F. Organomet. Chem. (Ams.)*, **3**, 200(1965).

17) R. G. Solomon and J. K. Kochi, *J. Chem. Soc., Chem. Commun.*, **1972**, 559.

18) M. B. Dines and P. H. Bird, *J. Chem. Soc., Chem. Commun.*, **1973**, 12.

19) R. W. Turner and E. L. Amma, *J. Am. Chem. Soc.*, **85**, 4046(1963).

20) R. W. Turner and E. L. Amma, *J. Am. Chem. Soc.*, **88**, 1877(1966).

21) The fact that BQ-Red is a polymer, as is shown in Fig. A, agrees with the finding that BQ-Red is insoluble in any common solvent. The volumes of the holes in a polymer which is packed with so many molecules and ions (such as *p*-benzoquinone, Cu_3Cl_3, H_2O, NH_4^+, and Cl^-) may reasonably be said to be similar to those of the NH_4^+ and Cl^- ions; this may be the reason why it is easily soluble only in an aqueous NH_4Cl solution.

Surface Activity of Complex in Mixed Surfactant Solution

Kazuo TAJIMA*, Akio NAKAMURA, and Takao TSUTSUI

Department of Chemistry, Faculty of Science, Tokyo Metropolitan University, Setagaya-ku, Tokyo 158

(Received October 19, 1978)

The dissociation constant of the complex formed in the mixed and very dilute surfactant solution of 3-(dodecylammonio)-propionate (NDA) and sodium alkylsulfates (C_{10}, C_{12}, C_{14}) (SAS) was determined by measuring surface tension and adsorbed amounts of the solution. The composition in the surface and bulk phases did not coincide at the equimolar mixture. The adsorbed monolayer on the solution consists of the coadsorption of NDA–SAS complex (1:1) and free NDA, while the adsorption of free SAS was almost zero in various concentrations studied. Under these conditions the surface activity of the complex alone was obtained. The relationship between the surface activity and bulk concentration for each mixed solution was discussed in terms of relative adsorbability. The surface activity of the complex was one order of magnitude higher than that of NDA and two orders higher than that of SAS.

The mixed surfactant in the aqueous solution has been found to have a more surface-active character than that of each component:[1–10] in particular, the solution containing oppositely charged surfactants considerably changes by the formation of an ionic complex. There are a few papers which have described the dissociation constant of a surfactant complex, which is formed in a solution.[7,11,12] Corkill *et al.*,[2,3] who studied the solution of mixed surfactant of sodium alkyl sulfates and hexadecyltrimethylammonium bromide (HTAB), found that an adsorbed layer composed of the equimolar complex of these surfactants was independent of the bulk compositions, but that the complex formation did not take place in the bulk phase.

The surface activity of a surfactant solution is remarkably enhanced even in dilute solution when a complex is formed, but the concentration of each single species decreases only slightly. Thus a direct measurement of concentration reliable enough for determining the dissociation constant is impossible in some cases. In view of such properties of surfactant solutions, the present work was carried out to determine the dissociation constant of a surfactant complex in a mixed and very dilute solution by the surface chemical method, and to decide the surface activity due to the complex in the solution. Further, an attempt was made to elucidate the relationship between the surface activity and the bulk compositions in the solution.

Experimental

The pure and synthetic surfactants 3-(dodecylammonio)-propionate (NDA) and sodium alkyl sulfates (SAS) containing 10 (De), 12 (D), and 14 (T) carbon atoms were used. Surface tension and adsorbed amounts were measured by the Wilhelmy and the radiotracer methods, respectively. In radiometry, NDA was labelled with tritium and SAS with ^{35}S, respectively. The details of these measurements were described in previous papers.[13–15] The temperature was maintained at 30.0±0.2 °C, and the pH of the solutions was 5.8±0.2. A part of the data obtained in the present studies has been reported elsewhere.[16,17]

Results and Discussion

The complex formation in the mixed solution of NDA and SAS was confirmed by the electrophoresis study using radioactive surfactants.[17] The conductivity measurements for the solution, however, did not show any indication of complex formation in the solution, as had been found in the mixed SAS–HTAB solution,[3] probably because the concentration of complex is too low for the detection method.

In order to study the composition of the complex of NDA and SAS (*e.g.* SDS), the surface tension was measured for the single and mixed solutions of NDA and SDS. The results are shown in Fig. 1. The dotted line in the figure represents the difference in the surface tensions between the mixed and the (ideal) hypothetical mixed solutions of NDA and SDS. The maximum deviation occurred at the equimolar composition of the mixed solution. This fact leads to the conclusion that the NDA–SDS complex in the bulk phase has a stoichiometric composition in 1:1 molar ratio. This coincided with the results of elemental analysis on the precipitate which was prepared by mixing the NDA and SDS solutions at high concentrations.[17]

Determination of the Dissociation Constant of Complex. A complex, if it is surface-active, always coadsorbs at its solution surface, independently of the surface behaviors of the other species in the solution. Hence, the Gibbs adsorption isotherm may be applied to such a surface-active solution.[18] In present adsorption system, the solute species in the solution are limited

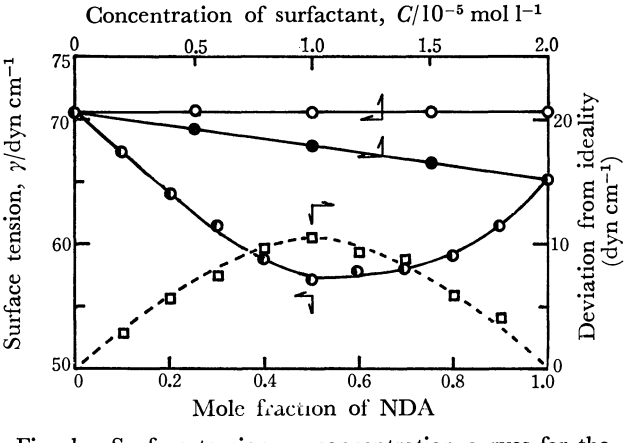

Fig. 1. Surface tension *vs.* concentration curves for the solutions of NDA(●), SDS(○) and their toatal constant mixture (◐). A dotted line shows the difference of surface pressures in the ideal and real mixed solutions.

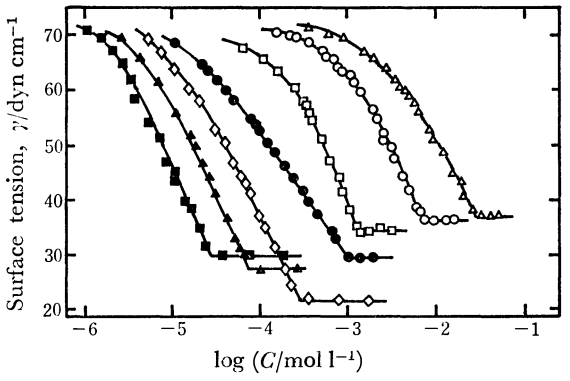

Fig. 2. Surface tension *vs.* logarithmic concentration curves for the solutions of SDeS(△), SDS(○), STS(□), NDA(●) and the equimolar mixed solutions of NDA–SDeS(◇), NDA–SDS(▲), and NDA–STS(■).

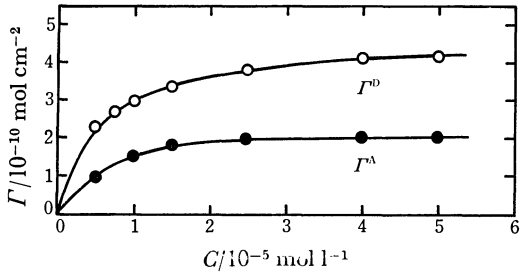

Fig. 3. Adsorption isotherms of equimolar mixed solutions. Γ^D was measured on the ^{3}HNDA–SDS solution, Γ^A on NDA–^{35}SDS.

to sodium (Na), alkyl sulfate (A), ampholyte (D), and complex (C) ions, and these are related to:

$$A^- + D^\pm \underset{K}{\rightleftharpoons} C^-$$

Previous observations[15,19] showed that the hydrolyses of the surfactants did not have to be considered under the present experimental conditions. Since the activity coefficients of these ions may be put at unity due to the low concentration, the dissociation constant of the complex, K, in the bulk phase can be defined in terms of the surface-chemical parameters as follows (see Appendix):

$$K = \frac{1}{4C}\left[\left(\frac{\Gamma^D+\Gamma^A}{2I-3\Gamma^D-\Gamma^A}\right)^2 - 1\right] \quad (1)$$

where

$$\left.\begin{aligned} I &= -(d\gamma/RT d\ln C)_{1:1}, \\ C &= C_A + C_C = C_D + C_C = C_{Na}, \\ \Gamma^D &= \Gamma_D + \Gamma_C, \end{aligned}\right\} \quad (2)$$

and

$$\left.\begin{aligned} \Gamma^A = \Gamma_A + \Gamma_C = \Gamma_{Na}. \end{aligned}\right\}$$

C is the concentration in the apparent equimolar mixed solution of NDA and SAS, γ the surface tension, Γ the surface excess, R the gas constant, and T the absolute temperature. The subscripts and superscripts mean the effective and apparent quantities for each species, respectively. K in Eq. 1 may be estimated, if the surface tension and the adsorbed amounts are

Table 1. Dissociation constant for NDA–SAS complexes in aqueous solution (30 °C)

Complex	K l/mol × 10^{-4}
NDA–SDeS	1.32
NDA–SDS	6.54
NDA–STS	33.6

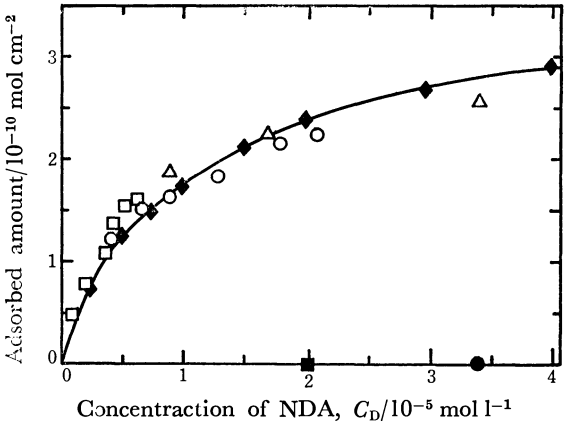

Fig. 4. Comparison of the $\Delta\Gamma$ values for each mixture with the adsorption isotherm of single NDA solution (◆). △: NDA–SDeS, ○: NDA–SDS, □: NDA–STS. Adsorbed amounts of the single SDS(●) and STS(■) solutions are plotted at the same concentration scale with NDA solution.

measured as a function of the concentration C. Figure 2 shows the γ *vs.* logarithmic concentration plot for the NDA and SAS solutions. Γ^D and Γ^A measured by radiometry are shown in Fig. 3. Similar tendencies were observed for the NDA–SDeS and NDA–STS solutions. The K values obtained are listed in Table 1. The effective concentrations, then, can be estimated for each species in the mixed surfactant solutions of NDA and SAS by using the K values.

Surface Composition. As shown in Fig. 3, the adsorption isotherms, Γ^D and Γ^A, which were independently measured with respect to each radioactive solution of ^{3}H labelled NDA–SAS and NDA–^{35}S labelled SAS at the same concentration C, did not coincide with each other even at the equimolar mixed solution. To study this difference, the surface activity was examined for each single solution of NDA and SAS at the concentrations corresponding to those which were estimated for each NDA–SAS solution by the K values. Neither surface excess nor surface tension lowering was observed for the SAS solutions, within the experimental error (see Fig. 4).[14,15,20] Then, it may be fairly asserted that Γ_A is zero at various concentrations under consideration. Since Γ_A was zero, the difference, $\Delta\Gamma$, of the Γ^D and Γ^A isotherms in Fig. 3 was compared with the surface excess, Γ^0_D, measured at the same effective concentration of the single NDA solution. The results are shown in Fig. 4. The $\Delta\Gamma$ values obtained for all NDA–SAS systems are in fairly good coincidence with the Γ^0_D values. Then $\Gamma_A \simeq 0$ and $\Delta\Gamma \simeq \Gamma^0_D$; therefore, Γ^A is Γ_C. Consequently, the difference of isotherms in Fig. 3 can be explained by

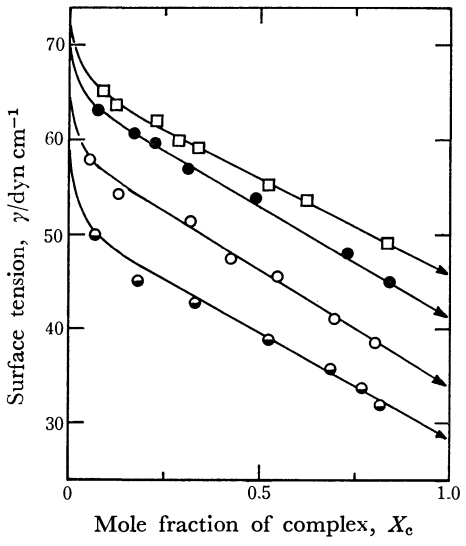

Fig. 5. Dependence of surface tension on complex concentration. Concentration of NDA ($M \times 10^5$) was kept at 0.60(□), 1.00(●), 2.00(○) and 3.60(◒). Arrows show the surface tension of complex alone.

the facts that the adsorbed monolayer from the mixed solution consists of the coadsorption of the complex of NDA–SDS and NDA, while the adsorption of SDS owing to the single dispersion in the solution is almost zero, as shown experimentally for SDS and STS in Fig. 4.

Surface Activity of Complex. Attempts were made to determine the surface activity of the complex alone, though direct measurements are of course impossible. The dependence of surface tension on composition of the film which consists of several species has not been elucidate for the adsorbed monolayer. However, the following linear relation is frequently found, in the bulk ternary system, between its surface tension and the mole fraction of solutes (1,2) at constant amount of solvent:[21]

$$\gamma = X_1\gamma_1 + X_2\gamma_2 \tag{3}$$

If γ is measured as a function of mole fraction, the extrapolated surface tensions for each single solution can be obtained at various concentrations:

$$\gamma_2^0 = (\lim_{X_2 \to 1} \gamma)_C$$

By this manner the surface tension of a complex may be obtained. The complex solutions for this purpose were prepared at various concentrations by adding varying amounts of SAS to the NDA solution of the constant concentration. The fraction of complex formation, X_C, in the solution was calculated from $X_C = C_C/C^D$ by using the K values shown in Table 1. Figure 5 is the plot of surface tension against X_c. Though the present solution contains four species, the apparent additivity expressed by Eq. 3 was well established in a wide region of mole fraction for the complex.[22] The surface tension obtained by extrapolating X_C to 1, corresponding to that for the solution of complex alone, is shown in Fig. 6 as a function of complex concentration, C_C, though only two points were obtained for SDeS and STS complexes. The surface excess, Γ_C^0, of complex was calculated from

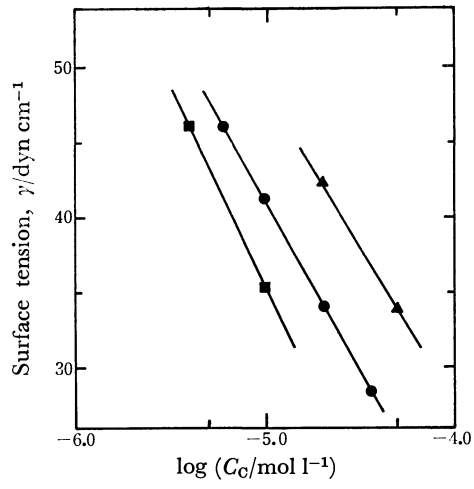

Fig. 6. Surface tension *vs.* concentration curves for the complex solutions. ▲: NDA–SDeS, ●: NDA–SDS, ■: NDA–STS.

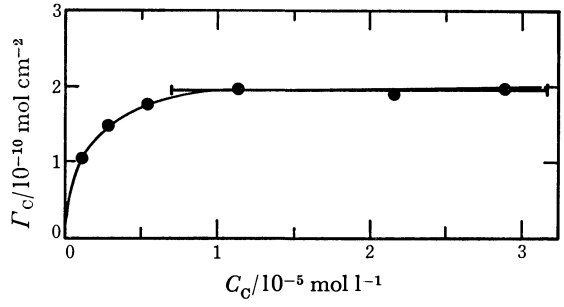

Fig. 7. Adsorption isotherm of NDA–SDS complex. Heavy solid line is the Γ_C^0 values calculated from Eq. 4.

Fig. 6 by Eq. 4, assuming an ideal solution for the complex:

$$\Gamma_C^0 = -\frac{1}{2RT}\left(\frac{\partial\gamma}{\partial \ln C_C}\right)_{NDA} \tag{4}$$

On the other hand, the Γ^A isotherm in Fig. 3 is seen to be the Γ_C isotherm, according to the argument in the previous section. The Γ_C^0 values calculated from Eq. 4 are compared with the "observed" isotherm for the NDA–SDS complex in Fig. 7. Both curves were in good agreement for either the NDA–SDeS or the NDA–STS complex. This is an experimental approval for the present approach.

In order to compare the surface activity of a complex to that of NDA, the relative adsorbability, α, was obtained by means of Eq. 5, which was defined so as to eliminate the concentration dependence near the close-packing adsorption:

$$\alpha = \lim_{C_I \to 0}\frac{\Gamma_I}{C_I} \Big/ \lim_{C_D \to 0}\frac{\Gamma_D}{C_D} \tag{5}$$

The results are shown in Table 2. It was found that the surface activity of complex is larger by one order of magnitude than that of NDA and also larger by two orders of magnitude than that of SAS. The increment of chain-length of alkyl sulfates incorporated in the complex is likely to enhance exponentially the surface activity of complex, as in free SAS. It is of interest that the increasing rate of α values for a series

Table 2. Relative adsorbability of complex and SAS to NDA

Surfactant	$\lim_{C\to 0}(\Gamma/C)$, $1/cm^2\times 10^{-5}$	α
NDA	0.313	1
SDeS	0.028	0.089
SDS	0.041	0.13
STS	0.059	0.19
NDA-SDeS	5.02	16.0
NDA-SDS	10.3	32.9
NDA-STS	20.5	65.5

of free SAS is rather less than that in the state complexed with NDA. This tendency might be reasonable, because the initial inclination in the isotherm is expected to increase more or less exponentially with increasing chain-length of surfactant.[14,23,24]

The present method will be applicable in general to the determination of the dissociation constant of a complex which is formed either by the chelation or by the association reaction, if at least one of the species in the solution is surface-active.

Appendix

The Gibbs adsorption isotherm is written for the present system as follows:

$$-\frac{d\gamma}{RT} = \Gamma_A d\ln C_A + \Gamma_D d\ln C_D + \Gamma_{Na} d\ln C_{Na} + \Gamma_C d\ln C_C \quad (A1)$$

In the equimolar mixed solution, when a complex is formed at 1 : 1 molar ratio, K is written

$$K = \frac{C_C}{C_A \cdot C_D} = \frac{C_C}{C'^2} \quad (A2)$$

where, $C'=C_A=C_D>0$. Substituting Eqs. 2 and A2 into Eq. Al, we have

$$I = (\Gamma^A+\Gamma^D)\frac{2KC}{1+4KC-(1+4KC)^{1/2}} + \Gamma^A \quad (A3)$$

By introducing the substitution $(1+4KC)^{1/2}=A$, $(A\neq 1)$, we have

$$A = \frac{\Gamma^A+\Gamma^D}{2I-3\Gamma^A-\Gamma^D} \quad (A4)$$

Then, we may obtain Eq. 1.

References

1) H. W. Hoyer, A. Marmo, and M. Zoeller, *J. Phys. Chem.*, **65**, 1804 (1961).
2) J. M. Corkill, J. F. Goodman, C. P. Ogden, and J. R. Tate, *Proc. R. Soc. London, Ser. A*, **273**, 84 (1963).
3) J. M. Corkill, J. F. Goodman, S. P. Harrold, and J. R. Tate, *Trans. Faraday Soc.*, **63**, 247 (1967).
4) H. Lange and M. J. Schwunger, *Kolloid Z. Z. Polym.*, **243**, 120 (1971).
5) M. J. Schwunger, *Kolloid Z. Z. Polym.*, **243**, 129 (1971).
6) B. W. Barry and G. M. T. Gray, *J. Colloid Interf. Sci.*, **52**, 314 (1975).
7) G. I. Mukhayer and S. S. Davis, *J. Colloid Interf. Sci.*, **53**, 224 (1975); *ibid.*, **56**, 350 (1976); *ibid.*, **59**, 350 (1977).
8) H. W. Hoyer and A. Marmo, *J. Phys. Chem.*, **65**, 1807 (1961).
9) D. G. Kolp, R. G. Langhlin, F. P. Klause, and R. E. Zimmer, *J. Phys. Chem.*, **67**, 51 (1963).
10) R. V. Scowen and R. Leja, *Can. J. Chem.*, **45**, 2821 (1967).
11) M. Mitsuishi and M. Hashizume, *Bull. Chem. Soc. Jpn.*, **46**, 1946 (1973).
12) W. P. Evans and R. A. Hudson, "4th Int. Congr. on Surface Active Substances," 725 (1964).
13) T. Okumura, K. Tajima, and T. Sasaki, *Bull. Chem. Soc. Jpn.*, **47**, 1067, 2986 (1974).
14) K. Tajima, *Nippon Kagaku Kaishi*, **5**, 883 (1973).
15) K. Tajima, M. Muramatsu, and T. Sasaki, *Bull. Chem. Soc. Jpn.*, **43**, 1991 (1970).
16) A. Nakamura, *Bull. Chem. Soc. Jpn.*, **48**, 1720 (1975).
17) A. Nakamura and M. Muramatsu, *J. Colloid Interface Sci.*, **62**, 165 (1977).
18) R. Defay and I. Prigogine, "Surface Tension and Adsorption," Longmans, London (1966), p. 85.
19) A. Nakamura, K. Tajima, and T. Sasaki, *Bull. Chem. Soc. Jpn.*, **48**, 214 (1975).
20) M. Koshinuma and T. Sasaki, *Bull. Chem. Soc. Jpn.*, **48**, 2755 (1975).
21) G. Schay, "Surface and Colloid Science," ed by E. Matijievič and F. Eirich, Wiley-interscience, N.Y. (1969), Vol. 2, p. 155.
22) Attention should be paid to the fact that the contribution of single dispersed SAS to the surface tension lowering is completely negligible in the region of these concentrations (see Fig. 2).
23) K. Shinoda, T. Nakagawa, B. Tamamushi, and T. Isemura, "Colloidal Surfactants," Academic Press, N. Y. (1963), Chapter one.
24) The initial inclination of the isotherm is approximately related to the number of carbon atoms, N, in a surfactant as follows: $\lim_{C\to 0}\Gamma/C \propto N\exp N$.

Both Oxidation and Reduction of Aromatic Hydrocarbons by an Electrolysis Cell Designed for Low-temperature ESR Studies

Hiroaki OHYA-NISHIGUCHI

Department of Chemistry, Faculty of Science, Kyoto University, Kyoto 606

(Received November 24, 1978)

A simple two-electrode cell for low-temperature electron spin resonance (ESR) measurements has been designed. A helical gold wire, the working electrode with large surface area (12 cm^2), generated *intra muros* enough positive or negative ions to measure the ESR spectra of unstable radical ions at low temperatures. To test the electrolysis conditions of the cell, the ESR spectra of about 20 aromatic compounds have been observed at temperatures as low as −90 °C. It has been shown that the cell can be applicable to the compounds with half-wave potential of 1.5 to −3.7 V SCE, provided that the ions produced are not reactive. The experimental conditions of the dimer cation generation have also been checked in polar or nonpolar solvents.

The electrochemical generation of organic radical ions for ESR studies has some advantages over the usual chemical methods.[1] The application of this method to the compounds with high ionization potential or with low electron affinity, however, has been severely limited by the following difficulties. One of the principal problems encountered in setting up an electrolysis cell inside the ESR cavity is the high dielectric loss caused by the large dielectric constants of the solvents commonly used in electrochemistry. This loss can have a very deleterious effect on the quality factor(Q) of the resonant cavity. Secondly, the conventional electrolysis cells so far used for ESR studies produced a large ohmic drop, which results in low electrolysis current. In 1975 Allendoerfer, Martinchek, and Bruckenstein[2] described a radically new design of a cell for simultaneous electrochemical-ESR(SEESR) measurements, based on a coaxial microwave cavity; this cell design has overcome the difficulties pointed out above. On the other hand, the use of low-temperature environments has proved to be of considerable value[3] for the observation of unstable species produced by electrochemical experiments. Modifying the cell developed by Allendoerfer *et al.*, Gerson, Ohya-Nishiguchi, and Wydler[4] have observed the ESR spectra of typical aromatic hydrocarbons at −90 °C to determine indirectly the half-wave reduction potentials ($E^r_{1/2}$) of benzene and paracyclophane, two compounds with low electron affinity. This modified cell was successfully used for the ESR measurements of the other compounds with high ionization potential or chemically unstable radical ions.[5] The purpose of this paper is to present a cell design which is useful for the low-temperature ESR measurements and to discuss its applicability according to the results obtained.

Cell Design

Optimum Conditions of Electrochemical ESR Measurements. We describe here the optimum conditions for electrochemical ESR measurements, assuming the linear diffusion model.[6] This assumption is not strictly applicable to our cell, but this model is adequate for qualitative understanding of the experimental conditions.

The radical concentration [R·] produced during a constant current electrolysis can be described simply by the rate equation:

$$\frac{d[R\cdot]}{dt} = \frac{i(T)}{VF} - k(T)[R\cdot] \quad (1)$$

where V is the effective volume of the diffusion layer of the radical ions produced, F the Faraday constants, and $k(T)$ and $i(T)$ are the decay constant of R· and the electric current producing R·, respectively, at temperature T. When $i(T)$ is assumed to be controlled by the linear diffusion process only, $i(T)$ can be derived from Fick's first law:

$$i(T) = \frac{D(T)A}{l(T)}nFC \quad (2)$$

where A is the surface area of the working electrode, C, $D(T)$, and $l(T)$ are the concentration, the diffusion coefficient, and the effective thickness of the diffusion layer, respectively, of parent molecules R, and n is the number of electrons involved in the electrode reaction. Hereafter n is assumed to be one, because ESR observation of the electrolysis means the one electron reaction on the electrode surface. Using the steady state condition $d[R\cdot]/dt=0$, and substituting Eq. 2 into Eq. 1, the radical concentration $[R\cdot]_s$ can be estimated from the next equation,

$$[R\cdot]_s = \frac{D(T)}{Vl(T)}\cdot\frac{AC}{k(T)} \quad (3)$$

In order to obtain high concentrations of $[R\cdot]_s$, A has to be made as large as possible without any appreciable disturbance of the microwave mode inside the cavity. Allendoerfer *et al.* succeeded in obtaining large A values by using a finely wound shallow pitched helix as a working electrode. Secondly, it can be deduced from Eq. 3 that a high concentration of the parent compound is desirable to increase $[R\cdot]_s$. High resolution ESR spectroscopy in solution requires usually a concentration not higher than 1 mmol dm^{-3}, because in the high concentration range the electron transfer effect on the ESR line width becomes predominant, in addition to the problem of the inhomogeneity of the solution.[7] Such effect, however, can be safely suppressed if the temperature of the solution is lowered below about −60 °C to the region where the electron transfer effect becomes negligible. Thirdly, Eq. 3 shows also the necessity of low temperature measurements to suppress mainly the radical decay. Strictly speaking, Eq. 3 has a maximum at a temperature (T_m) slightly higher than freezing point of the solution,

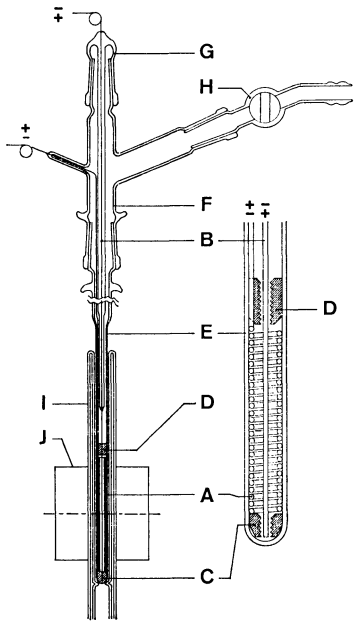

Fig. 1. Schematical diagram of the electrolysis cell mounted in a TE_{011} cylindrical cavity (J) with a temperature control dewar (I). See text about the other notations.

because of the rapid increase of viscosity and solution resistance near the melting point. This requires the development of pertinent solvent-supporting electrolyte systems possessing reasonably high conductivity over a wide low temperature range.[3] Taking such conditions into account a simple cell for the low-temperature ESR study has been designed.

Apparatus. Figure 1 shows a schematic diagram of the electrolysis cell mounted in a TE_{011} cylindrical cavity (J) with a temperature control dewar (I). The cell consists of four parts, (E) to (H): (E) contains a helical electrode wound of a 0.5 mm diameter gold wire (A) and a straight platinum wire of a 0.5 mm diameter (B) supported by two Teflon holders (C) and (D) along the tube axis. By changing the polarity of these electrodes either cations or anions can be produced on the working electrode. (F) and (G) hold the terminals for (A) and (B), respectively, which are connected to a potentiostat with a sensitive current meter. (A) is wound to fit against the inner wall of the 3.5 mm i. d. pyrex tube (E), its length and surface area being about 50 mm with 80 turns and 12 cm^2, respectively. The mercury amalgamation of (A) was carried out as required in the case of the anions. It should be noted in this figure that no reference electrode was used in order to simplify the electrolysis apparatus. If necessary one can estimates $E_{1/2}$ from a linear relationship between $E_{1/2}$ and the minimum voltages applied between two electrodes, V_a, at which the ESR spectra of the radicals appear during the electrolysis.[4]

Procedure

Each solution prepared under a nitrogen atmosphere was degassed by the freeze-pump-thaw cycles three or four times. After the cell was pumped and flushed with dry nitrogen through the stop cock in Fig. 1, the solution of about 0.7 ml was transferred into (E) through (F) with a pipette under the dry nitrogen atmosphere. Then the cell containing the solution was inserted into the cavity. After the solution temperature was decreased, the voltage was applied between two electrodes and gradually increased until ESR signals could be observed. The observation of the ESR signals was carried out with the field modulation of 1.0×10^{-4} T, which was appropriate to observe the appearance of the signals. As the voltage applied reached V_a, the electric current of the circuit also increased appreciably, its amount depending on the temperature, solvent used, and the concentration of the substrates (see Eq. 2). Several solvents were tested for the generation of both radical cations and anions. 1,2-dimethoxyethane(DME) with 0.1 mol tetrabutylammonium perchlorate (TBAP) is recommended for anions, and dichloromethane(CH_2Cl_2) including 10% trifluoroacetic acid (TFAc) and 10% trifluoroacetic anhydride(TFAn) with or without 0.01 mol TBAP[8] are recommended for cations. It should be noted in the latter case that the pertinent ratios of these solvents depend on the stability of the parent compound to be oxidized and solubility of the radical cations produced in the solvent, as will be discussed in the following section.

Experimental

DME was refluxed with $LiAlH_4$ for two days, followed by distillation onto the Na–K alloy. Dry DME was distilled into a bottle with 0.1 mol supporting reagent, and flushed with dry nitrogen gas. Spectrograde CH_2Cl_2, TFAc, and TFAn were used without further purification. ESR spectra were measured with a Varian E-9 spectrometer.

Results and Discussion

Effects of the Cell on the Cavity Properties. When this cell was inserted into the cavity, the resonance frequency became only 0.22 GHz higher than that without the cell (9.07 GHz). Such a small shift means that the cell can be treated in a similar manner to the usual sample tube containing the solution for the ESR measurements. The Q factor, on the other hand, depended on the solution to be electrolyzed as well as on the design of working electrode. Tight fitting of the helix electrode to the inner wall of (E) in Fig. 1 was most important to maintain the high Q. The loaded Q in the case of polar solvents, *i.e.* H_2SO_4, H_2O, and *N*,*N*-dimethylformamide(DMF), were measured as 2200, 2500, and 3200, respectively. Even in the case of H_2SO_4, Q was high enough to measure the ESR spectra.

Oxidation of Some Aromatic Hydrocarbons. The electrolytic oxidation of aromatic hydrocarbons was more difficult than the electrolytic reduction was, mainly because in nonpolar solvents the cations produced deposited on the surface of the electrode, while in polar solvent such as CF_3COOH, on the other hand, substrates sometimes decomposed. The most

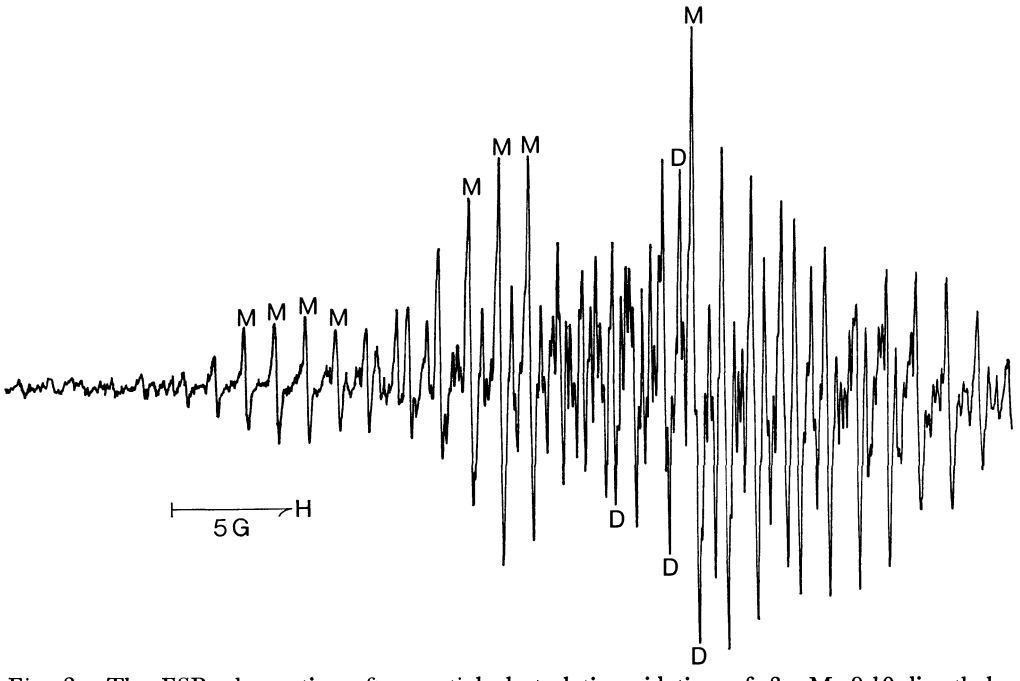

Fig. 2. The ESR observation after partial electrolytic oxidation of 3 mM 9,10-dimethylanthracene in CH_2Cl_2 with 10% CF_3COOH and 10% $(CF_3CO)_2O$ at −80 °C. Supporting reagent: Tetrabutylammonium perchlorate, field modulation: 0.1 G. M and D in the figure correspond to the representative lines due to the monomer and the dimer cation radicals, respectively. The ratio of $[DMA^{+\cdot}]$ to $[(DMA)_2^{+\cdot}]$ is about 1 : 6. Slight difference of their *g*-values leads to an asymmetric ESR spectrum.

effective solvent for electro-oxidation of aromatic hydrocarbons was the mixture CH_3NO_2 or CH_2Cl_2/TFAc/TFAn, with TBAP as a supporting reagent. The ratios of these reagents were changed, corresponding to the stability of the parent molecules and cation radicals produced. The compounds with oxidation potential ($E^{\circ}_{1/2}$) lower than *ca.* 0.9 V SCE, hereafter called Category I, were oxidized partially when dissolved in the solvent mixture (ratios: 10/(1—10)/1/0) without any application of voltage. When the voltage larger than $E^{\circ}_{1/2}$ was applied, the ESR signals increased substantially, and sometimes became highly resolved. Secondly, the compounds with $E^{\circ}_{1/2}$ between 0.9 and 1.3 V SCE (Category II) could be oxidized at temperatures as low as −60 °C in the solvent with ratios of 10/1/1/0. V_a roughly corresponded to $E^{\circ}_{1/2}$. Thirdly, the compounds of Category III having $E^{\circ}_{1/2}$ higher than *ca.* 1.3 V SCE gave the spectra at −70 to −90 °C (ratios: 10/1/1/0.01 mol dm^{-3}). Durene was the compound with the highest $E^{\circ}_{1/2}$ of all the compounds which successfully gave the resoved ESR spectra. This means that the ESR spectra of the compounds with $E^{\circ}_{1/2}$ lower than 1.5 V SCE can be observed provided that no chemical reactions of the cation produced occur. It should be pointed out here that the ESR spectra of the dimer radical cations can also be observed under the conditions a) high concentration, b) low temperature, c) nonpolar solvents, d) low voltage available, and e) the beginning of electrolysis, unlike the situation of monomer production. In some cases, i.e. pyrene, acenaphthene, and tetramethylparacyclophane, the ESR spectra due to monomer cations could not be observed even if the conditions mentioned above were changed. This means that in CH_2Cl_2, nonpolar solvent, the dimer configuration is quite stable compared with the corresponding monomer cations. The ESR observation after the oxidation of 9,10-dimethylanthracene(DMA), a typical example, showed clearly the existence of the dimer species in addition to that of the monomer under the conditions mentioned above: a) to e) (see Fig. 2). It should be noted that Van Duyne and Reilley[3] also measured the steady-state cyclic voltammograms of DMA on a platinum electrode at low temperatures. From these results they postulated an equilibrium between monomer and dimer cations of DMA:

$$DMA^{+\cdot} + DMA \underset{k_{-1}}{\overset{k_1}{\rightleftharpoons}} (DMA)_2^{+\cdot} \qquad (4)$$

which is in good agreement with our results. In Table 1 the coupling constants of the monomer and dimer cations of typical aromatic compounds are summarized, with some experimental conditions. From this table one can say roughly that V_a corresponds to $E^{\circ}_{1/2}$ in the range of the error +0.2 V, in spite of different conditions. On oxidations of benzene and naphthalene a broad line with the line width of 5 to 6 G has been observed.

Reduction of Aromatic Hydrocarbons. In order to check the applicability of the cell, the reduction of aromatic hydrocarbons, whose $E^{r}_{1/2}$ values were known by the polarographic measurements, was carried out under the same conditions (C: 5 mmol, DME/0.1 mol TBAP, −90 °C), followed by the observation of both V_a and its high-resolution ESR spectrum. The proton hyperfine coupling constants which were used for the

Table 1. The electrolysis conditions and the hyperfine coupling constants of some aromatic hydrocarbon radical cations

Substance	Voltage applied (V)	Temperature (°C)	Hyperfine coupling constants (G)[a) Monomer			Dimer		
Category I								
Naphthacene	0.5	≤25	5.09(4)	1.68(4)	1.04(4)			
Perylene	0.9	≤25	4.08(4)	3.07(4)	0.44(4)	1.96(8)	1.53(8)	0.22(8)
9,10-Dimethyl-anthracene	0.9	≤0	8.03(6)	2.48(4)	1.24(4)	3.51(12)	1.22(8)	0.66(8)
Anthracenophane	0.5	≤25	1.10(8)	0.95(8)	0.64(8)			
Category II								
Biphenylene	1.15	≤−20	3.55(4)	0.20(4)		1.75(8)	0.15(8)	
Indeno[1,2,3-*cd*]-fluoranthene	1.20	$-10 \leq T \leq +10$	2.01(4)	0.71(4)	0.19(4)			
Chrysene	1.30	≤−30	5.56(2)	2.65(2)	1.81(2)			
			1.40(2)	0.70(2)				
Pyrene	1.25	≤−30				2.68(8)	1.03(8)	0.54(4)
Anthracene	1.35	≤−30	6.61(2)	3.05(4)	1.40(4)	3.24(4)	1.45(8)	0.71(8)
Category III								
Coronene	1.3	≤25	1.50(12)			0.77(24)		
Hexamethylbenzene	1.55	≤−40	6.50(18)			3.25(36)		
Acenaphthene	1.6	≤−60				9.10(8)	2.38(4)	0.88(4)
						0.70(4)		
Tetramethyl-paracyclophane	1.7	≤−70				2.23(24)	1.67(8)	0.372(8)
						0.186(8)		
Durene	1.8	≤−90				5.0(24)	0.2(4)	

a) $G = 10^{-4}$ T. Numbers of equivalent protons giving rise to the coupling constants are indicated in parentheses.

Table 2. Appearance voltages and estimated reduction potentials of aromatic hydrocarbons with low electron affinities

Compounds	$-V_a$(V)	$-E^r_{1/2}$ *vs.* SCE(V)
Biphenyl	5.02±0.05	2.57
[2.2]Paracyclophane	5.85±0.05	3.05
Benzene	6.35±0.05	3.31
Toluene	7.0±0.1	3.7
m-Xylene	7.0±0.2	3.7

identification of the anion produced, coincided with those previously published, within the range of experimental errors. In the previous paper[4] we described the relationship between V_a and $E^r_{1/2}$. The pertinent regression line has an equation

$$V_a = (1.92 \pm 0.06) E^r_{1/2} \quad (5)$$

with a correlation coefficient of 0.991 and a deviation from the origin (0.007). V_a defined above can be alternatively described as the voltage at which [R·] reaches the minimum radical concentration detectable. If the radical decay becomes appreciably larger, i.e. irreversible in terms of cyclic voltammetry, one has to apply a voltage lower than the real one, which causes a deviation from the linear relationship of Eq. 5. Such a good relationship as in Eq. 5, therefore, has two significant meanings: One is a good correspondence of V_a and $E^r_{1/2}$, which was successfully applied to the indirect determination of $E^r_{1/2}$ of benzene and other aromatic hydrocarbons with low electron affinity (Table 2). The other is that if $E^r_{1/2}$ of a compound is higher than that of *p*-xylene (−3.7 V SCE), it is possible to observe the ESR spectrum by applying V_a corresponding to its $E^r_{1/2}$ given by Eq. 5. This is in contrast with the cell used by Levy and Myers,[9] who applied voltage as large as 110 V to reduce the pyridines and diazines.

It should be mentioned finally that DMF with 0.1 mol tetraethylammonium perchlorate(TEAP) was also a good solvent for chemically unstable radicals, because the electrolysis current is *ca.* 10 times larger than that in DME at the same temperature, although its freezing point (−60 °C) is a little high.

This work was mostly carried out at Physikalisch-Chemisches Institut der Universitaet Basel. The author would like to express his appreciation to Professor Fabian Gerson for his continual discussion and encouragement. He also wishes to thanks Drs. Jurg Bruhin, George Plattner, and Crystoph Wydler for their illuminating discussions.

References

1) C. P. Poole Jr., "Electron Spin Resonance," Interscience, New York, N. Y. (1967), p. 620.

2) R. D. Allendoerfer, G. A. Martincheck, and S. Bruckenstein, *Anal. Chem.*, **47**, 890 (1975).

3) R. P. Van Duyne and C. N. Reilley, *Anal. Chem.*, **44**, 142 (1972).

4) In the case of reduction in DME, see F. Gerson, H. Ohya-Nishiguchi, and C. Wydler, *Angew. Chem. Int. Ed. Engl.*, **15**, 552 (1976); *Angew. Chem.*, **88**, 617 (1976).

5) F. Gerson, G. Kaupp, and H. Ohya-Nishiguchi, *Angew. Chem. Int. Ed. Engl.*, **16**, 657 (1977); *Angew. Chem.*, **89**, 666 (1977); F. Gerson, R. Gleiter, and H. Ohya-Nishiguchi *Helv. Chim. Acta*, **60**, 1220 (1977); C. Elschenbroich, F. Gerson, H. Ohya-Nishiguchi, C. Wydler, and A. Nissen, *ibid.*, **60**, 2520 (1977); J. Bruhin, F. Gerson, and H. Ohya-Nishiguchi, *ibid.*, **60**, 2471 (1977).

6) I. M. Kolthoff and J. I. Lingane, "Polarography," Interscience, New York, N. Y. (1952).

7) These problems were solved by an alternative method. See, for example, J. E. Harriman and A. H. Maki, *J. Chem. Phys.*, **39**, 778 (1963); P. H. Rieger and G. K. Fraenkel, *J. Am. Chem. Soc.*, **85**, 683 (1963).

8) O. Hammerrich and V. D. Parker, *Electrochim. Acta*, **18**, 537 (1973).

9) D. H. Levy and R. J. Myers, *J. Chem. Phys.*, **41**, 1062 (1964).

The Reaction between SO_2 and MnO_2 and the Role of the Sulfato Complex in the SO_2-induced Isomerization of *cis*-2-Butene

Kiyoshi Otsuka,* Kimiaki Tanaka, and Akira Morikawa

Department of Chemical Engineering, Tokyo Institute of Technology, Ookayama, Meguro-ku, Tokyo 152

(Received January 16, 1979)

The reaction between SO_2 and MnO_2 has been studied by measuring the consumption of SO_2-gas and the infrared spectra of the wafer of MnO_2. In the low-temperature range (<200 °C) the reaction is completed within one or two surface layers of MnO_2, and the reaction products are the bidentate sulfato complex (C_{2v}) and the sulfato complex in Td symmetry. In the high-temperature range, on the other hand, the reaction progresses deep into the bulk and can be described by this stoichiometric equation; $MnO_2+SO_2\rightarrow MnSO_4$. The catalysis of MnO_2 for the SO_2-induced isomerization of *cis*-2-butene is closely related to the formation of the sulfate ion. The initiation step proposed for the isomerization is a polarization of the charge-transfer complex of SO_2 and butene under the influence of the strong electrostatic field caused by the generation of the surface sulfato complex.

The absorption of SO_2 from flue gas by an activated manganese oxide has become of interest in the field of SO_2-emission control.[1,2] In relation to this subject several kinetic studies of SO_2 absorption by manganese dioxide has been published.[3–5] However, no study of the chemistry of the reaction between SO_2 and manganese dioxide has been reported.

Otsuka *et al.* reported that, in the presence of SO_2, MnO_2 gains a very high catalytic activity in the cis-trans selective isomerization of various olefins, which is accompanied by copolymerization between SO_2 and olefins in the adsorption layer.[6] They hypothesized that the high catalytic activity of MnO_2 may be caused by a strong electrostatic field on the surface brought about by the formation of a sulfato complex.

The purpose of the present work is to investigate the reaction between SO_2 and MnO_2 by measuring the consumption of SO_2-gas and the infrared spectra of the wafer of MnO_2, and to verify the above hypothesis as to the high catalytic activity of MnO_2 in the copolymerization-accompanying isomerization of *cis*-2-butene.

Experiments

Materials. Commercial MnO_2 prepared by the reduction of $KMnO_4$ was used as the catalyst. The surface area, as determined by the BET method with nitrogen after degassing treatment at 100 °C, was 104 m^2/g. The $MnSO_4\cdot 4$—$6H_2O$ was a product of Wako Pure Chemical Ind., Ltd. The reagent SO_2 gas, of an anhydrous grade and supplied by the Matheson Chemical Co., and the *cis*-2-butene gas, a high-purity product of the Phillips Petroleum Co., were purified by trap-to-trap distillation in a vacuum apparatus.

Procedure. The catalyst in the reactor was degassed in a vacuum for 2 h at 0 or 100 °C prior to each run. The amount of the consumption of SO_2-gas by MnO_2 was determined by measuring the pressure change by means of glass Boulden Gauge attached to a conventional glass apparatus with a volume of 320 ml. The polysulfone-accompanying isomerization of *cis*-2-butene was carried out in a conventional mercury-free gas-circulation system using a mixture of SO_2 and *cis*-2-butene (1:2.5) under a total initial pressure of 175 Torr. After the addition of SO_2 to 0.05 g of MnO_2 at a required temperature for 30 min under 50 Torr of SO_2, the temperature at the catalyst bed was decreased to 20 °C or to −10 °C; then, the two reactions (the copolymerization of SO_2 and *cis*-2-butene and the isomerization of the latter) were initiated by feeding in *cis*-2-butene and circulating the gas mixture through the catalyst bed. The rate of the cis-trans isomerization was determined from the concentration of the *trans*-2-butene formed in the initial 3 min, as analyzed by gas chromatography. The amount of the copolymer generated in the 30-min period after the initiation of the reaction was estimated by measuring the infrared-absorption spectra of the MnO_2 used for the reaction. Prior to the infrared-spectra measurement, the MnO_2 sample was ground to a fine powder, and then mixed with KBr. A KBr-supporting wafer was made by pressing the mixture in 2-cm-diameter stainless steel dies at 1.9 t/cm^2. The spectra were recorded at 25 °C using a Shimadzu IR-430 grating spectrometer.

Results and Discussion

SO_2-absorption Measurement by Volumetric Method. The changes in the amount of SO_2 absorbed by MnO_2 with the time have been shown in Fig. 1; the experiment was carried out by introducing 1.38×10^{-3} mol of SO_2-gas into the system. After the initial rapid absorption of SO_2 for 1 min, a small increase in the absorbed amount is observed at the temperatures lower than 200 °C, but significant amount of SO_2 are absorbed further at 250 and 350 °C in the range

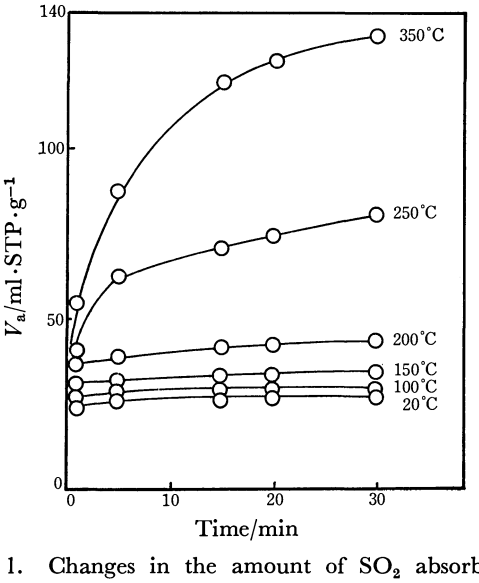

Fig. 1. Changes in the amount of SO_2 absorbed by MnO_2 with time at various experimental temperatures.

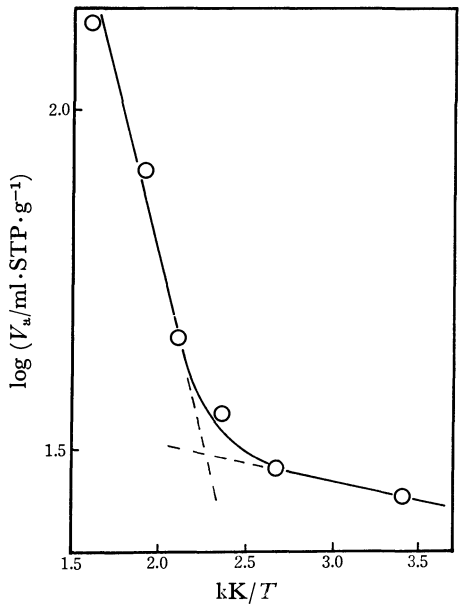

Fig. 2. log (V_a) against $1/T$ plot.

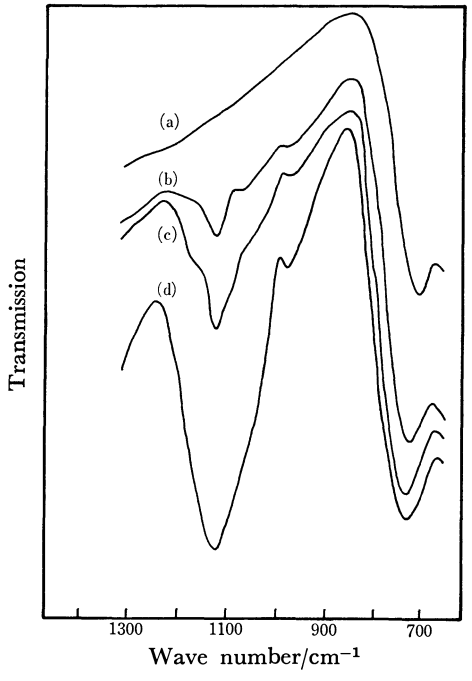

Fig. 3. Infrared spectra of the MnO_2 wafer with absorbed SO_2 at different θ_{SO_2}: (a); MnO_2 without SO_2, (b); MnO_2 with absorbed SO_2 ($\theta_{SO_2}=0.021$), (c); $\theta_{SO_2}=0.21$, (d); $\theta_{SO_2}=0.74$. The SO_2 absorption was carried out at 20 °C with MnO_2 pretreated at 100 °C.

of the absorption time from 1 to 30 min. Figure 2 shows the log (V_a) against $1/T$ plot, where V_a is the amount of SO_2 absorbed in 30 min and where T is the absorption temperature in Kelvin. The quite different slopes of the curve in the low-temperature (<150 °C) and high-temperature ranges (>200 °C) in Fig. 2 suggest that the natures of the SO_2-absorption on MnO_2 are different between the two temperature ranges. The apparent surface coverage by SO_2, θ_{SO_2}, for various absorption temperatures was

Table 1. The apparent surface coverage by SO_2, θ_{SO_2}, for the MnO_2 used in the experiments of Fig 1

Temperature (°C)	20	100	150	200	250	350
θ_{SO_2}	1.35	1.47	1.74	2.27	4.01	6.52

estimated from the amount of SO_2 absorbed in 30 min, and the BET surface area of the catalyst, from the nitrogen adsorption, where the molecular cross sections of N_2 and SO_2 were taken as 16.2 and 19.2 Å^2 respectively.[7] The results are summarized in Table 1. The large θ_{SO_2} values at the high temperatures listed in the table indicate that SO_2 penetrates into many layers of the surface.

Infrared Spectroscopic Study of the Reaction of SO_2 with MnO_2. Figure 3 shows a series of changes in the spectra of the KBr-supporting wafer of the catalyst after the absorption of the required amount of SO_2 at 20 °C for 30 min. The preparation of the wafer and the recording of the spectra were carried out in air as has been described previously. To examine the effect of air on the spectra of the SO_2-absorbing catalyst, the spectra of the air-free sample deposited on the surface of the KBr-wafer, which has been placed in a vacuum cell, has been recorded. It has been confirmed that the introduction of air into the cell does not change the absorption bands caused by the addition of SO_2. The spectra of the catalysts with a low coverage ($\theta_{SO_2}<\approx 0.21$) show four absorption bands at around 980, ≈1070, 1115, and 1180 cm^{-1}. For the catalyst with θ_{SO_2} of 0.74, however, the absorption bands at ≈1070 and 1180 cm^{-1} are obscured by the selectively developed 1115 cm^{-1} band.

Nakamoto[8] indicated that the SO_4-complex in Td symmetry shows the ν_1(very weak), ν_3(very strong), and ν_4(strong) absorption bands at 973, 1130—1140, and 617 cm^{-1}. The lowering of symmetry for the SO_4-complex caused by coordination splits the ν_3 band into two or three bands, depending on whether the unidentate or bidentate and bridging complexes respectively are involved.

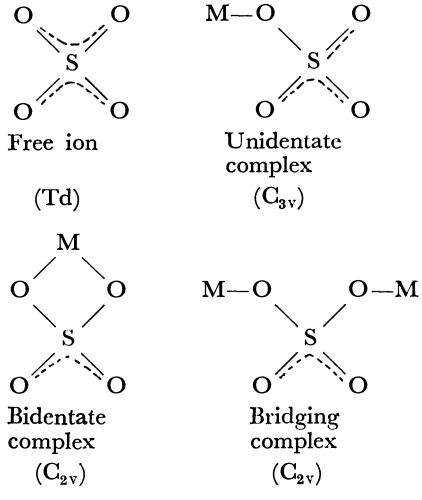

(1)

Many bidentate and bridging sulfato complexes, such as $[Cu(bpy)SO_4]\cdot 2H_2O$, $Pd(NH_3)_2SO_4$, and $[(NH_3)_4$-

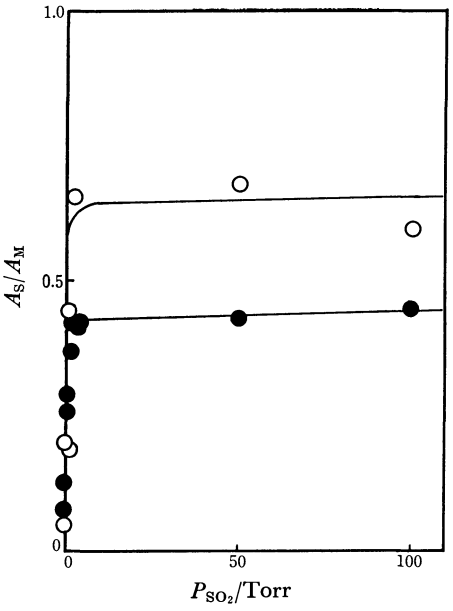

Fig. 4. Effect of SO_2-pressure on the relative amount of SO_4^{2-} complex formed at 20 °C: (○); MnO_2 degassed at 0 °C, (●); MnO_2 degassed at 100 °C.

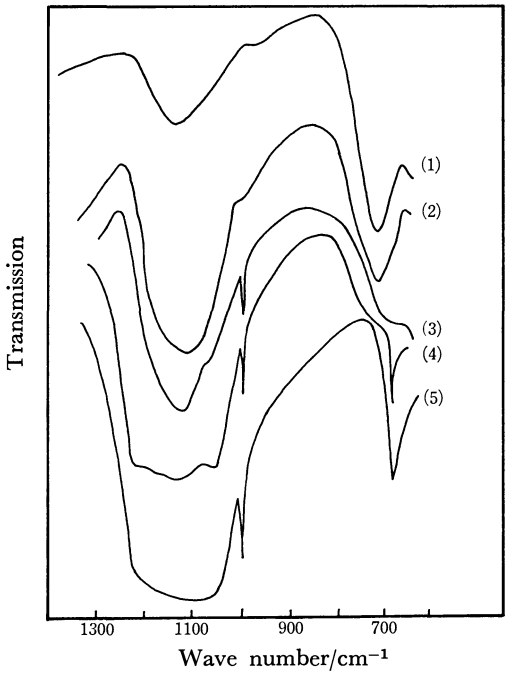

Fig. 5. Infrared spectra of SO_4-complex formed at different temperatures over MnO_2: (1); 20 °C, (2); 200 °C, (3); 300 °C, (4); 350 °C, (5); the spectra of $MnSO_4 \cdot 4—6H_2O$.

$Co\langle^{NH_2}_{SO_4}\rangle Co(NH_3)_4](NO_3)_3$, show the three bands at 1030—1060, ≈1105, and ≈1180 cm^{-1}.[8] Hence, the spectra observed at a low θ_{SO_2} in Fig. 3 can be ascribed to the bidentate or bridging SO_4^{2-}-complex on MnO_2. On the other hand, the selective increase in the intensity of the band at 1115 cm^{-1} with an increase in θ_{SO_2} indicates that SO_4^{2-}-complex in Td symmetry is a main species formed at a high θ_{SO_2}.

A_S/A_M, the optical density for the strongest absorption band at 1115 cm^{-1} divided by that for the 710 cm^{-1} band, caused by the Mn–O vibration in the MnO_2 lattice,[9] represents the relative amount of the SO_4^{2-}-complex on a unit weight of the catalyst. This value has been plotted in Fig. 4 as a function of the SO_2 pressure applied in the SO_2-absorption experiments at 20 °C for the catalysts degassed at 0 and 100 °C. The formation of the SO_4^{2-}-complex reaches a plateau at less than 1 Torr, and the amount of the SO_4^{2-}-complex formed is larger for the MnO_2 pretreated at a lower temperature.

Figure 5 shows the infrared spectra of the catalysts after SO_2 absorption under the same experimental conditions as those used to obtain the results in Fig.1. The relative amount of the SO_4^{2-}-complex increases as the absorption temperature is raised, accompanied by a decrease in the intensity of the 710 cm^{-1} band due to the Mn–O lattice vibration. The catalysts used for the experiment at the high temperatures (>300 °C) show spectra quite similar to that of $MnSO_4$. On the other hand, the spectra for the catalysts used for SO_2-absorption at low temperatures (<≈200 °C) do not show sharp bands at 1000 and 690 cm^{-1}, suggesting that the SO_4^{2-}-complex (Td symmetry) is different in its nature from the one observed on the catalyst used for the SO_2-absorption at high temperatures.

The results in Fig. 2 demonstrate that the reaction mechanism for the SO_2-absorption changes with the temperatures above ≈200 °C. At low temperatures, after a very rapid absorption of SO_2 within 1 min, only a small increment in the absorbed amount was observed (Fig. 1) and the amount of the SO_4^{2-}-complex formed did not change with the SO_2 pressure above 1 Torr (see Fig. 4). The apparent coverage of the surface by SO_2 remains less than 2.3 at low temperatures. These facts suggest that the progress of the reaction between SO_2 and MnO_2 at low temperatures (<≈200 °C) is restricted to only one or two surface layers of MnO_2. Accordingly, we consider that the initial stage of SO_2-absorption by MnO_2 may be demonstrated by the following schemes at low temperatures:

at a low θ_{SO_2},

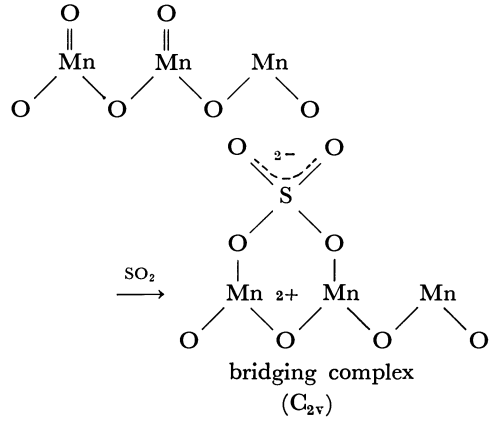

bridging complex (C_{2v}) (2)

or

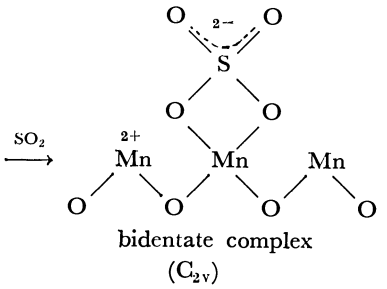

(3)

at a high θ_{SO_2},

$$MnO_2 \text{ (surface)} \xrightarrow{SO_2} SO_4^{2-}\text{-complex (surface)} \quad (4)$$
(Td)

At high temperatures, the fact that the spectra observed are quite close to that of pure $MnSO_4$ (Fig. 5) indicates that SO_2 penetrates into the bulk of MnO_2 and forms $MnSO_4$ as is shown by this stoichiometric equation:

$$MnO_2(\text{bulk}) + SO_2 \longrightarrow MnSO_4(\text{bulk}) \quad (5)^{3,5)}$$

Both the amount of SO_2 absorbed by MnO_2 and A_S/A_M, measured for the catalysts used for the SO_2-absorption experiments for 30 min in Fig. 1, have been plotted in Fig. 6 as functions of the experimental temperature; the A_S/A_M values have been corrected by considering the fraction of MnO_2 converted to $MnSO_4$, which was estimated from the amounts of SO_2 absorbed by the catalyst at each temperature. The similarity between the shapes of the two curves supports the idea that the reaction between SO_2 and MnO_2 can be described by the stoichiometric Eq. 5.

The Role of the SO_4^{2-}-complex in Butene Isomerization. The cis-trans isomerization and the copolymerization have been carried out over catalysts on which SO_2 had been preabsorbed at various temperatures (20—350 °C) for 30 min under the same experimental conditions as those used in Fig. 1. The rate of the cis-trans isomerization, $R_{c\to t}$, and the relative concentration of the formed polysulfone, A_P/A_M, the optical density for the band at 1300 cm^{-1} due to the polysulfone[6] divided by that at 710 cm^{-1} due to Mn–O, have been plotted in Fig. 7 as functions of the temperature for the SO_2 absorption. The circles and the triangles are the data obtained for the MnO_2 pretreated in a vacuum at 100 and 0 °C respectively. The dotted curve illustrates the relative amount of the SO_4^{2-}-complex (arbitrary unit), already shown in Fig. 6. The similar dependence on the absorption temperature between the rate of isomerization and the polysulfone formation illustrated in Fig. 7 can be explained by the fact that the latter reaction accompanies the former, as is demonstrated below:[6]

cis- or *trans*-2-butene + $\cdot SO_2[CH(CH_3)CH(CH_3)SO_2]_n$
$$\rightleftharpoons \cdot CH(CH_3)CH(CH_3)\text{-}SO_2[CH(CH_3)CH(CH_3)SO_2]_n \quad (6)$$

For the catalysts on which SO_2 has been preadsorbed at temperatures lower than 200 °C, the rate of the cis-trans isomerization increases in parallel with the increase in the amount of the SO_4^{2-}-complexes as the absorption temperature is raised. The catalyst outgassed at 0 °C shows a higher catalytic activity than that outgassed at 100 °C; this corresponds to the fact that the former catalyst demonstrates a higher concentration of SO_4^{2-}-complexes than the latter (Fig. 4). These results suggest that the catalytic activity of MnO_2 in the copolymerization, and accordingly for the cis-trans isomerization, is closely related to the formation of sulfate ions on the catalyst. The surface manganese must be positively charged by the

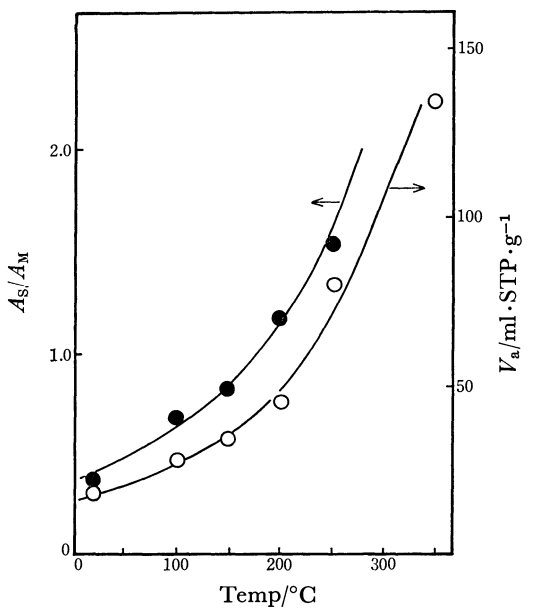

Fig. 6. Effect of temperature on the relative amount of SO_4^{2-} complex and the amount of SO_2 absorbed by MnO_2: (●); A_S/A_M, (○); V_a.

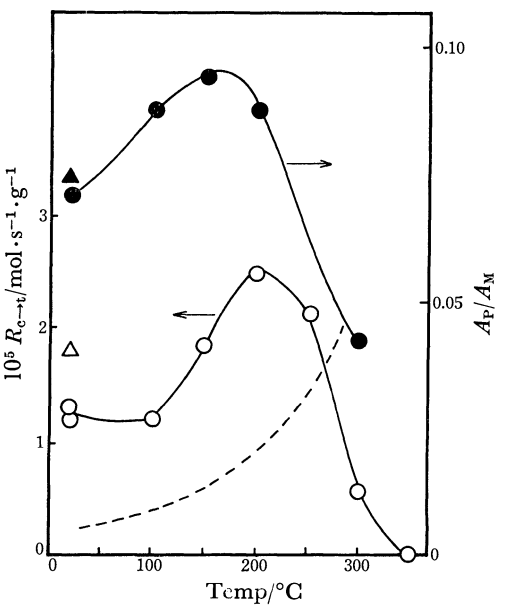

Fig. 7. The rate of isomerization, $R_{c\to t}$, and the amount of formed polysulfone, A_P/A_M, as a function of temperature for SO_2 absorption: circles; data for MnO_2 pretreated at 100 °C, triangles; data for MnO_2 pretreated at 0 °C. (●) and (▲); A_S/A_M, (○) and (△); $R_{c\to t}$. The dotted curve represents A_S/A_M (arbitrary unit) shown in Fig. 6.

formation of sulfate ions because of an electron transfer from the surface to the sulfate ions (Schemes 2—4), resulting in a generation of strong electrostatic fields on the surface. The picture of the initiation step for the reactions hypothesized previously,[6,10] *i.e.*, a polarization of the charge-transfer complex (CTC) of SO_2 and butene under the influence of the electrostatic field on the surface, can also be adopted in the present work. The CTC positioned between the manganese cation and the sulfate anion on the surface may be strongly polarized and activated by a concerted action of the anion-cation pairs, as is illustrated below:

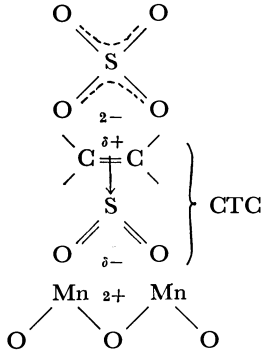

(7)

The catalytic activities of MnO_2 on which SO_2 has been preabsorbed at high temperatures ($>\approx 200$ °C) decrease, however, as the SO_2-treatment temperature is raised (Fig. 7). The catalytic activity of pure $MnSO_4$, pretreated in the presence of SO_2 at 200 °C, has been tested for the cis-trans isomerization. The activity per unit of surface area was less than 1/15 of that for MnO_2, which was tested under the same experimental conditions, implying that the decrease in the activity of MnO_2 pretreated with SO_2 at the high temperatures might result from a considerable transformation of MnO_2 to $MnSO_4$ deep into the bulk of MnO_2; eventually, then, the character of the surface becomes quite close to that of pure $MnSO_4$. The low catalytic activity of $MnSO_4$ can be attributed to a low affinity of its surface to the adsorption of SO_2 and, consequently, to a low concentration of CTC, which is necessary for the two reactions.

References

1) R. Hirose and T. Uno, *Karyoku Hatsuden*, **18**, 355 (1967).
2) T. Uno, S. Fukui, M. Atsukawa, M. Higashi, H. Yamada, and K. Kamei, *Chem. Eng. Prog.*, **66**, 61 (1970).
3) K. Itou, T. Yamada, and S. Miyoshi, *Bull. Nagoya Inst. Technol.*, **22**, 415 (1970).
4) Kun Li, R. R. Rothfus, and A. H. Adey, *Environ. Sci. Technol.*, **2**, 619 (1968).
5) Koh D. Kiang, Kun Li, and R. R. Rothfus, *Environ. Sci. Technol.*, **10**, 886 (1976).
6) K. Otsuka, T. Tanabe, and A. Morikawa, *J. Catal.*, **48**, 333 (1977).
7) D. M. Young and A. D. Crowell, "Physical Adsorption of Gases," Butterworths, London, England (1962), p. 226.
8) K. Nakamoto, "Infrared and Raman Spectra of Inorganic and Coordination Compounds," 3rd ed, Wiley-Interscience, New York, N. Y. (1977), p. 239.
9) G. A. Kolta, F. M. A. Kerim, and A. A. A. Azim, *Z. Anorg. Allg. Chem.*, **384**, 260 (1971).
10) K. Otsuka and A. Morikawa, *J. Catal.*, **56**, 88 (1979).

Photolyses of Tetraphenylcyclobutanes at 254 nm

Haruo SHIZUKA,* Ichiro SEKI,† Toshifumi MORITA, and Takeshi IIZUKA††

Department of Chemistry, Gunma University, Kiryu, Gunma 376

(Received January 22, 1979)

Photolyses of 1,2,3,4-tetraphenylcyclobutanes (TPCB) at 254 nm in hydrocarbon solvents have been studied by means of fluorometry, nanosecond time-resolved spectroscopy, and measurements of the reaction quantum yields. The photolysis of TPCB originates from the $S_1(\pi,\pi^*)$ state to give *trans*-stilbene nearly concertedly at higher temperatures (>200 K). Significant temperature and cis-effects were observed. The radiationless rate constants for the dissociation (k_r) and the other radiationless (k_n) processes decreased with lowering temperature. The value of k_r for γ-1,*t*-2,*t*-3,*c*-4-TPCB at 300 K, for example, was 4.7 times greater than that for γ-1,*t*-2,*c*-3,*t*-4-TPCB. The Arrhenius parameters of the relaxation processes were also determined. No intramolecular excimer emission was observed.

The photochemistry of four-membered rings has been extensively studied.[1] Cyclobutane photochemistry involving selectivities in cleavage orientations upon irradiation is one of the most interesting fields among them. A number of studies on photolyses of cyclobutanes have been reported.[2-10] Kaupp[3] has shown that there is a clear preference for photochemical fission of the cyclobutane bond bearing the chromophore and the substituent which sterically interacts most effectively with the chromophore (cis-effect) and that the photolysis proceeds *via* short-lived 1,4-biradicals. As for tetraphenylcyclobutanes, they undergo photochemical cycloreversion to yield *trans*-stilbene.[2,3] However no quantitative work on photolyses of tetraphenylcyclobutanes has been performed.

In the course of our studies of photochemistry of benzene derivatives,[11-13] the title compounds (see below) were chosen in the present work from the following interests:

(1) How about the reactive state and the dissociation rate?

(2) How about the relaxation processes of the excited state of tetraphenylcyclobutanes?

(3) Is there cis-effect[2,3] on photochemical and photophysical processes of the molecules?

and (4) How about intramolecular excimer formation? In a previous work,[13] an weak intramolecular excimer emission of [2.2]metacyclophane is observed, which is an exception of the $n=3$ rule.[14] A large internal conversion of [2.2]metacyclophane occurs due to a conformational change in the excited state.

This paper reports the relaxation processes of excited tetraphenylcyclobutanes (**1** and **2**) studied by means of fluorometry, nanosecond time-resolved spectroscopy, and measurements of the reaction quantum yields under various temperatures.

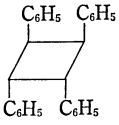

γ-1,*t*-2,*t*-3,*c*-4-tetraphenylcyclobutane
1

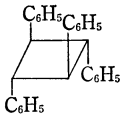

γ-1,*t*-2,*c*-3,*t*-4-tetraphenylcyclobutane
2

† Present address: The Japan Carlit Co., Ltd., Shibukawa, Gunma 377.

†† Faculty of Education, Gunma University, Aramaki, Maebashi, Gunma 371.

Experimental

Starting materials (1,2,3,4-tetraphenylcyclobutanes (**1** and **2**)) were prepared by the photodimerization of transstilbene in benzene,[15] and purified by silica-gel column chromatography using a mixture of benzene and cyclohexane (1:3) as the eluent. Methylcyclohexane, cyclohexane and isopentane (G.R.-grade products from Tokyo Kasei) were purified by passing them through a silica-gel column and then distillations. In the measurements of degassed samples, the solutions were thoroughly degassed by the freeze-pump-thaw-cycles.

A low-pressure mercury lamp (20 W) with a Vycor glass filter was used as the 254-nm radiation source. Acitnometry was carried out using a ferric oxalate solution (0.006 M).[16] The quantum yields for the product formation were measured by spectrophotometry. For the measurements of temperature effects upon the reaction quantum yields and fluorescence lifetimes, a quartz Dewar flask designed for spectrometry was used, the temperature being controlled to within ±2 °C. Measurements of absorption and fluorescence spectra were the same as reported previously.[17] The fluorescence quantum yields were measured by comparison with that of toluene in cyclohexane ($\phi_F=0.14$).[18] The fluorescence decay was recorded with a Hitachi nanosecond time-resolved spectrophotometer (pulse width 11 ns), and the lifetime was determined by the convolution method when it was shorter than 20 ns.[19]

Results

The spectrum of a 3.4×10^{-4} M cyclohexane solution of γ-1,*t*-2,*t*-3,*c*-4-tetraphenylcyclobutane (**1**) changed markedly upon irradiation with the 254-nm light at 300 K as shown in Fig. 1. A new band with maximum at 295 nm (ε: 2.74×10^4 M^{-1} cm^{-1}) appeared. The spectral change shows the formation of *trans*-stilbene as a sole photoproduct, as reported by Kaupp.[2,3] The geometric isomer (**2**) was scarcely observed by the TLC method. The quantum yields for the product formation in cyclohexane at 300 K was 0.84± 0.04. The quantum yields at 300 K did not change with variation in irradiation time (1—10 min), concentration of the starting material (10^{-4}—10^{-2} M), addition of 1,3-pentadiene ($<2\times10^{-2}$ M), and light intensity (10^{14}—10^{16} quanta ml^{-1} s^{-1}). Dissolved oxygen had no effect on the reaction quantum yields. The quantum yield Φ_r in MP (methylcyclohexane: isopentane=3:1 in volume) was the same as that in cyclohexane. Similar results were obtained in the

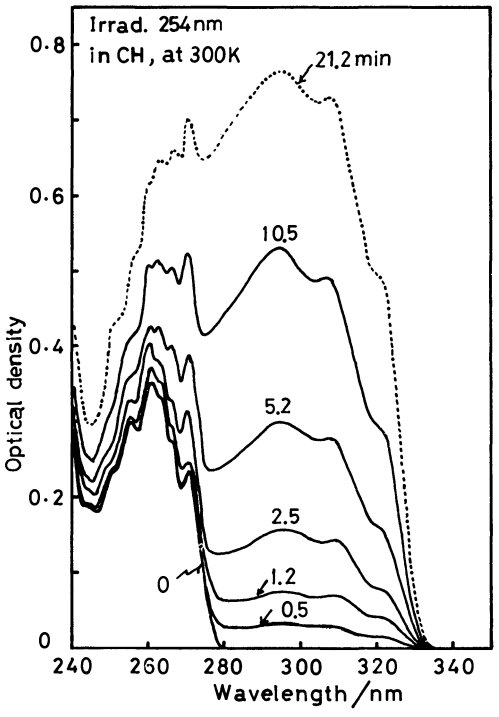

Fig. 1. The spectral change of a 3.4×10^{-4}M cyclohexane solution of No. 1 with lapse of time at 254 nm. Numbers refer to time of measurement in minutes.

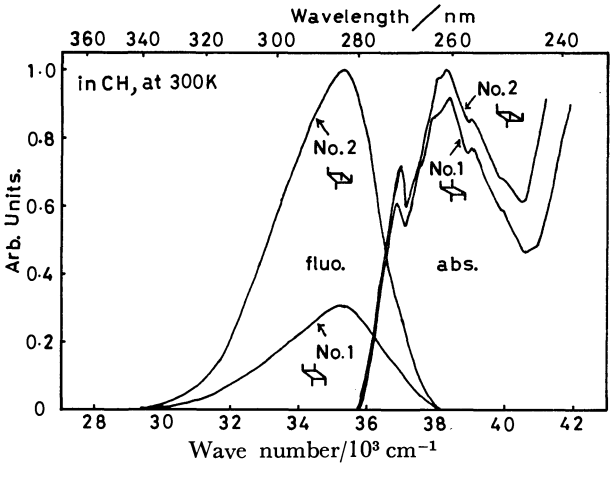

Fig. 2. Absorption and fluorescence spectra of tetraphenylcyclobutanes (No. 1 and 2) in cyclohexane.

Table 1. Experimental data of Φ_f,[a] τ_f, k_f, and Φ_r of tetraphenylcyclobutanes in MP at 300 K

Samples	$\Phi_f/10^{-2}$	τ_f/ns	$k_f/10^6$ s^{-1}	Φ_r
1	0.5±0.1	0.8±0.5	6.3	0.84±0.04
2	1.7±0.2	2.5±0.4	6.8	0.62±0.03

a) Determined by comparison with the fluorescence quantum yield of toluene ($\Phi_F=0.14$), see the Ref. 18.

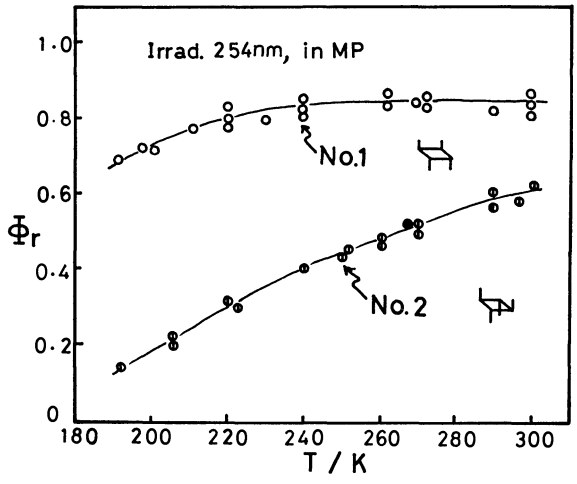

Fig. 3. The temperature dependence of the reaction quantum yields Φ_r in MP.

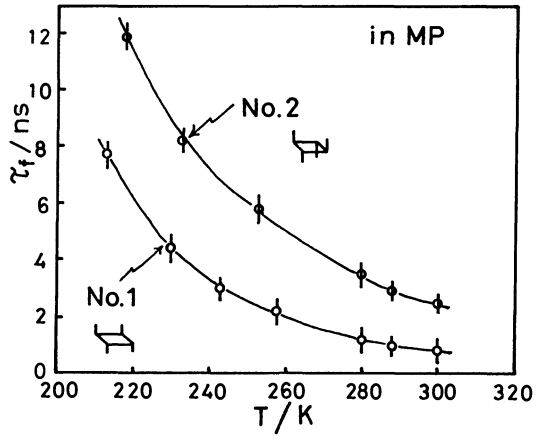

Fig. 4. The temperature dependence of the fluorescence lifetimes τ_f in MP.

case of γ-1,*t*-2,*c*-3,*t*-4-tetraphenylcyclobutane (**2**).

Figure 2 shows the absorption (**1**: $\lambda_{max}=261$ nm, $\varepsilon=1.03\pm0.02$ M^{-1} cm^{-1}; **2**: $\lambda_{max}=261$ nm, $\varepsilon=1.15\pm0.02$ M^{-1} cm^{-1}) and fluorescence ($\lambda_{max}=284$ nm for **1** and **2**) spectra of the starting materials in cyclohexane, which are very similar to those of toluene. No intramolecular excimer emission could be detected. No phosphorescence could be observed in MP at 77 K, as reported by Kaupp.[2]

The reaction quantum yields Φ_r, fluorescence quantum yields Φ_f, fluorescence lifetimes τ_f and radiative rate constants k_f in MP at 300 K are listed in Table 1. The significant temperature effects upon Φ_r and τ_f in MP were observed as shown in Figs. 3 and 4, respectively. The Φ_r values decreased with lowering temperature. In contrast, the values of τ_f increased with lowering temperature, and they were 48±3 ns (**1**) and 46±3 ns (**2**) at 77 K. The photolyses of the samples took place even at 77 K in MP rigid matrices, although the Φ_r values were very small. The Φ_r values of **1** were greater than those of **2** at various temperatures as shown in Table 1 and Fig. 3.

Discussion

Kinetic Analyses. The presence of triplet quenchers ([1,3-pentadiene]$<2\times10^{-2}$ M and [dissolved oxygen]$\approx2\times10^{-3}$ M)[20] do not affect the Φ_r values. The results indicate that the photolyses of 1,2,3,4-tetraphenylcyclobutanes (**1** and **2**) proceed *via* the

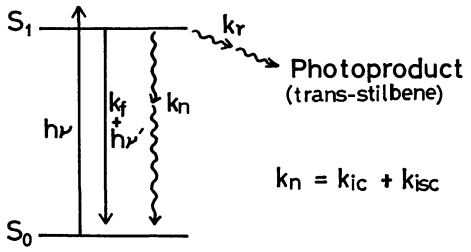

Fig. 5. A schematic energy state diagram for the photolyses of tetraphenylcyclobutanes.

excited singlet state and/or very short-lived triplet state. The fact that no phosphorescence of tetraphenylcyclobutanes could be observed suggests the existence of a relatively fast radiationless channel (probably cleavage) in the lowest triplet state. There may be two pathways of photochemical cleavage of the starting materials via the excited singlet and triplet states. However, the radiationless processes (cleavage and internal conversion) other than intersystem crossing are very predominant in the S_1 state at higher temperatures (>200 K), as will be discussed later. Accordingly, the reaction quantum yield *via* the triplet state must be small in comparison with that *via* the excited singlet state at higher temperatures (>200 K). That is, the reactive state at higher temperatures (>200 K) should be the lowest excited singlet state $S_1(\pi,\pi^*)$.

The experimental results at higher temperatures (>200 K) can be accounted for by the scheme shown in Fig. 5, where S_0 and S_1 are the ground and the lowest excited singlet states of the starting materials respectively, k_f radiative rate constant, k_r dissociation rate constant, and k_n radiationless rate constant of internal conversion k_{ic} plus intersystem crossing k_{isc}. From the usual steady-state approximation, the reaction quantum yield Φ_r is given by

$$\Phi_r = \frac{2k_r}{k_f+k_n+k_r} = 2k_r\tau_f \qquad (1)$$

The dissociation rate k_r may be expressed by Eq. 2,

$$k_r = k_r^0 + A_r\exp\left(\frac{-\Delta E_r}{RT}\right) \qquad (2)$$

where k_r^0 is the dissociation rate constant independent of temperature, A_r frequency factor of dissociation, and ΔE_r potential barrier in the dissociation process. At higher temperatures (>200 K), the value of k_r^0 is negligible compared with that of the second terms in Eq. 2, since the Φ_r values is very small at 77 K. Equation 3 is derived from Eqs. 1 and 2.

$$\log\left(\frac{\Phi_r}{2\tau_f}\right) = \log A_r - \frac{\Delta E_r}{2.303RT} \qquad (3)$$

The plot of $\log\{\Phi_r(2\tau_f)^{-1}\}$ *vs.* T^{-1} obtained experimentally, which agrees with Eq. 3, is shown in Fig. 6a. The values of A_r and ΔE_r obtained from the linear plot in Fig. 6a are listed in Table 2.

Similarly, the rate constant k_n may be written as the following equation:

$$k_n = k_n^0 + A_n\exp\left(\frac{-\Delta E_n}{RT}\right) \qquad (4)$$

where k_n^0 is the rate constant for the radiationless processes of k_{ic} plus k_{isc} independent of temperature, A_n frequency factor and ΔE_n potential barrier in the radiationless processes. The k_n^0 values for **1** and **2** are estimated to be about 1.5×10^7 s^{-1} from the data of τ_f at 77 K and k_f. Therefore, one can derive Eq. 5.

$$\log(k_n-k_n^0) = \log A_n - \frac{\Delta E_n}{2.303RT} \qquad (5)$$

where the values of k_n can be evaluated experimentally by the following equation: $k_n=\tau_f^{-1}-(k_r+k_f)$. The plot of $\log(k_n-k_n^0)$ *vs.* T^{-1} is shown in Fig. 6b, which agrees with Eq. 5. The values of A_n and ΔE_n are also summarized in Table 2.

Dissociation Process. Let us consider the dissociation process k_r in the S_1 state. It is well-known that benzene derivatives undergo the β-bond fission upon irradiation[21] and the predissociation proceeds *via* the lowest excited singlet state $S_1(\pi,\pi^*)$ $^1B_2$ to give

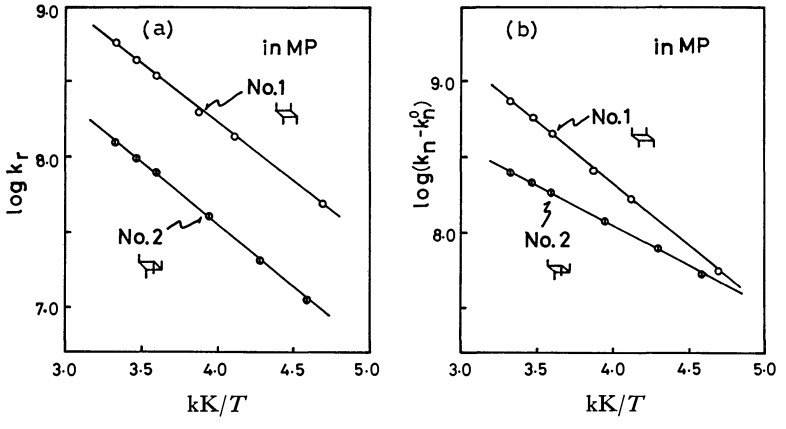

Fig. 6. (a) Plots of $\log k_r$ *vs.* T^{-1} and (b) plots of $\log(k_n-k_n^0)$ *vs.* T^{-1}.

Table 2. Frequency factors A_r and A_n and potential barriers ΔE_r and ΔE_n for k_r and k_n, respectively

Samples	$A_r/10^{11}$ s^{-1}	ΔE_r/kcal mol^{-1}	$A_n/10^{11}$ s^{-1}	ΔE_n/kcal mol^{-1}
1	2.0 (±0.3)	3.5 (±0.2)	4.2 (±0.5)	3.7_5 (±0.3)
2	0.79 (±0.07)	3.8_3 (±0.2)	0.13_8 (±0.03)	2.3_8 (±0.3)

the geminate radicals.[11,12] It seems that the photochemical cleavage of tetraphenylcyclobutanes has analogy to those of benzene derivatives. Kaupp[2,3] suggests that the photochemical reaction of tetraphenylcyclobutanes proceeds *via* a short-lived 1,4-biradical. Thus, the β-bond fission *via* the $S_1(\pi,\pi^*)$ of γ-1,*t*-2,*t*-3,*c*-4-tetraphenylcyclobutane (**1**), for example, can be expressed by Eq. 6. Of course, the β-bond fission of

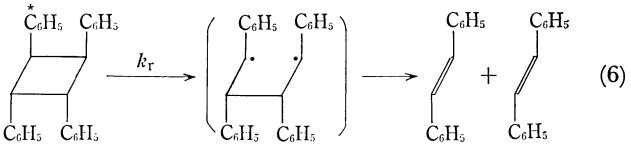

(6)

1 1,4-biradical *trans*-stilbene

the starting molecule to produce the 1,4-biradical occurs from the vibrationally relaxed S_1 state judging from the values of τ_f. It is known that the vibrational relaxation times in condensed media are of the order of 10^{-12} s.[22] If the biradical had a lifetime enough to yield the starting material *via* the back reaction, the geometrical isomer (**2**) of the starting molecule besides *trans*-stilbene would be yielded as a photoproduct resulting from rotational diffusion and subsequent recombination of the biradical. However, such photochemical isomerization was scarcely observed during the photolysis of **1**. Similar result was obtained in the case of **2**. Thus, it is reasonable to consider that the biradical is very unstable and is instantaneously broken to yield two molecules of *trans*-stilbene as shown in Eq. 6. The dissociation quantum yields are, therefore, nearly equal to $\Phi_r/2$. It can be said that the β-bond fission of tetraphenylcyclobutanes proceeds nearly concertedly to give two molecules of *trans*-stilbene. This mechanism supports the assertion that there may be a significant concerted component to the cycloreversion reaction in the excited singlet state of *cis*-1,2-diphenylcyclobutane as reported by Jones and Chow.[23]

The experimental results show quantitatively cis-effect in that **1** undergoes dissociation only to *trans*-stilbene and the values of k_r for **1** are greater than those for **2** (Fig. 6a). For instance, the dissociation rates k_r for **1** and **2** at 300 K can be estimated to be 5.5×10^8 s^{-1} and 1.2×10^8 s^{-1}, respectively. The frequency factor A_r for **1** is greater than that for **2**, and the potential barrier ΔE_r is small in comparison with that for **2** as shown in Table 2. The cis-effect may be caused by a steric strain between adjacent benzene rings of **1**. The crossing probability from the S_1 state to the repulsive state of the β-bond between proper carbon atoms in cis-form may be larger than that in trans-form.

Radiationless Processes. The rate constant k_n is comprised of k_{ic} (internal conversion $S_1\rightarrow S_0$) plus k_{isc} (intersystem crossing $S_1\rightarrow T_1$). The k_n values increase considerably with elevating temperature according to Eq. 4. At higher temperatures (>200 K), the temperature dependent rate $(k_n-k_n^0)$ becomes very much greater than that of k_n^0 and the values of $(k_n-k_n^0)$ for **1** are large compared with those for **2**, as can be seen in Fig. 6b. The values of k_n for **1** and **2** at 300 K, for example, are evaluated to be 7.8 $(\pm0.7)\times10^8$ s^{-1} and 2.5 $(\pm0.3)\times10^8$ s^{-1}, respectively. These facts indicate that steric effect is responsible for k_n as well as k_r at higher temperatures (>200 K).

The internal conversion rate constant k_{ic} is markedly enhanced due to a conformational change in the excited state.[13,24] In a similar manner, the k_n value may increase according to the enhancement of internal conversion. A conformational change among the substituted benzene rings of tetraphenylcyclobutanes in the S_1 state would be expected. However, the fact that no intramolecular excimer emission could be observed suggests the existence of large steric hindrance among the benzene rings in the S_1 state. Other possible mechanism for the large value of k_n at higher temperatures is explained by the "channel 3" decay where energy levels of isomers are incorporated as intermediate states of $S_1\rightarrow S_0$ internal conversion.[25]

The lifetimes τ_f (0.8±0.5 ns for **1** and 2.5±0.4 for **2**) are very shorter than that of toluene (34±2 ns in MP) at 300 K.

Finally, one can understand that such short lifetimes of the starting materials result from the large values of k_r and k_n (probably k_{ic}) at room temperature.

Conclusion

The photolyses of 1,2,3,4-tetraphenylcyclobutanes at higher temperatures (>200 K) proceed *via* the $S_1(\pi,\pi^*)$ state to give *trans*-stilbene nearly concertedly. The relaxation processes of the excited molecules are mainly comprised of the dissociation k_r and the other radiationless processes k_n, which are markedly dependent upon temperature. Significant cis-effect was also observed in photochemical and photophysical processes of the sample molecules.

The authors are grateful to Dr. N. Kanamaru of Nagoya University for his helpful discussion.

References

1) S. A. Martin, "Alicyclic Chemistry," The Chemical Society (1976), Vol. 4, p. 142, and references cited therein.
2) G. Kaupp, *Angew. Chem. Int. Ed. Engl.*, **13**, 817 (1974).
3) G. Kaupp and M. Stark, *Chem. Ber.*, **110**, 3084 (1977), and references cited therein.
4) M. Sauerbier, *Chem.-Ztg.* **96**, 530 (1972).
5) H. Takahashi, M. Sakuragi, M. Hasegawa, and H. Takahashi, *J. Polym. Sci., Part A-1*, **10**, 1399 (1972); M. Hasegawa and Y. Suzuki, *Chem. Lett.*, **1972**, 317.
6) C. H. Krauch, S. Farid, and G. O. Schenck, *Chem. Ber.*, **99**, 625 (1966).
7) O. Buchardt, *Angew. Chem. Int. Ed. Engl.*, **13**, 179 (1974).
8) J. Michl, *Fortschr. Chem. Forsch.*, **46**, 1 (1974).
9) K. Honda, A. Yabe, and H. Tanaka, *Bull. Chem. Soc. Jpn.*, **49**, 2384 (1976).
10) As for photolyses of cyclobutane, *e.g.*, K. Obi, H. Akimoto, Y. Ogata, and I. Tanaka, *J. Chem. Phys.*, **55**, 3822 (1971).
11) H. Shizuka and I. Tanaka, *Bull. Chem. Soc. Jpn.*, **41**, 2343 (1968); *ibid.*, **42**, 909 (1969); H. Shizuka, *ibid.*, **42**, 52, 57 (1969).
12) H. Shizuka, T. Morita, Y. Mori, and I. Tanaka,

Bull. Chem. Soc. Jpn., **42**, 1831 (1969); H. Shizuka, T. Kanai, T. Morita, Y. Ohto, and K. Matsui, *Tetrahedron*, **27**, 4021 (1971); H. Shizuka, H. Kayoiji, and T. Morita, *Mol. Photochem.*, **2**, 165 (1970); K. Tsutsumi, K. Matsui, and H. Shizuka, *ibid.*, **7**, 325 (1976).

13) H. Shizuka, T. Ogiwara, and T. Morita, *Bull. Chem. Soc. Jpn.*, **48**, 3385 (1975).

14) F. Hirayama, *J. Chem. Phys.*, **42**, 3163 (1965).

15) H. Shechter, W. J. Link, and G. V. D. Tiers, *J. Am. Chem. Soc.*, **85**, 1601 (1963).

16) C. G. Hatchard and C. A. Parker, *Proc. R. Soc. London, Ser. A*, **235**, 518 (1956); for details, see the following reference: P. de Mayo and H. Shizuka, "Creation and Detection of the Excited State," ed by W. R. Ware, Marcel Dekker, N. Y. (1976), Vol. 4, Chap. 4.

17) *E.g.* H. Shizuka, K. Matsui, Y. Hirata, and I. Tanaka, *J. Phys. Chem.*, **81**, 2243 (1977).

18) J. B. Birks, "Photophysics of Aromatic Molecules," Wiley-Interscience, London (1970), p. 122.

19) K. Tsutsumi and H. Shizuka, *Chem. Phys. Lett.*, **52**, 485 (1977).

20) S. L. Murov, "Handbook of Photochemistry," Marcel Dekker, New York, N. Y. (1973), p. 89.

21) G. Porter and E. Strachan, *Trans. Faraday Soc.*, **54**, 1595 (1958); E. J. Land, G. Porter, and E. Strachan, *ibid.*, **57**, 1885 (1961); E. J. Land and G. Porter, *ibid.*, **59**, 2016 (1963).

22) A. Laubereau, D. von der Linde, and W. Kaiser, *Phys. Rev. Lett.*, **28**, 1162 (1972); J. E. Griffiths, M. Clerc, and P. M. Rentzepis, *J. Chem. Phys.*, **60**, 3824 (1974); A. Nitzan, S. Mukamel, and J. Jortner, *J. Chem. Phys.*, **63**, 200 (1975).

23) G. Jones, Jr., and V. L. Chow, *J. Org. Chem.*, **39**, 1447 (1974).

24) G. Oster and Y. Nishijima, *J. Am. Chem. Soc.*, **78**, 1581 (1956); Th. Förster and G. Hoffmann, *Z. Phys. Chem. N. F.*, **75**, 63 (1971); D. Magde and M. W. Windsor, *Chem. Phys. Lett.*, **24**, 144 (1974); J. Kordas and M. A. El-Bayoumi, *J. Am. Chem. Soc.*, **96**, 3034 (1974).

25) N. Kanamaru, *Chem. Lett.*, **1978**, 503.

Conformational Analysis of Intramolecular Fluorescence Quenching of α-(9-Carbazolyl)-ω-[p-(methoxycarbonyl)benzoyloxy]alkanes

Toshiji KANAYA, Yoshihiko HATANO,† Masahide YAMAMOTO,* and Yasunori NISHIJIMA

Department of Polymer Chemistry, Kyoto University, Sakyo-ku, Kyoto 606

(Received February 9, 1979)

Equilibrium distribution of conformations of the series of compounds, α-(9-carbazolyl)-ω-[p-(methoxycarbonyl)benzoyloxy]alkanes in the ground state was calculated to explain the intramolecular fluorescence quenching of these compounds in a rigid medium. It was found that when the radius of active sphere R_0 for the intramolecular fluorescence quenching is taken to be 8.8—9.0 Å, the experimentally observed chain length dependence of the fluorescence quenching can be well simulated by this calculation. The active sphere for the dynamic intermolecular fluorescence quenching in solution was also discussed to compare with that of the intramolecular fluorescence quenching.

Since Leonhardt and Weller[1] first reported the intermolecular exciplex formation between perylene in its excited singlet state and *N,N*-dimethylaniline in the ground state, extensive studies have been carried out on the intermolecular exciplex formation. Recently, intramolecular exciplexes have been studied to investigate the geometry of exciplexes and their electronic structures for various exciplex systems, *e.g.*, $(CH_3)_2N$-$(CH_2)_n$-(naphthyl) (n=2—4),[2] *p*-$(CH_3)_2N$-C_6H_4-$(CH_2)_n$-(9-anthryl) (n=0—3),[3] *p*-$(CH_3)_2N$-C_6H_4-$(CH_2)_n$-(1-pyrenyl) (n=1—3),[3] (9,10-dicyanoanthryl)-$(CH_2)_3$-(naphthyl).[4] In the previous reports,[5] we have studied the intramolecular fluorescence quenching and exciplex formation for a series of α-(9-carbazolyl)-ω-[*p*-(methoxycarbonyl)benzoyloxy]alkanes (Fig. 1). It was found in these investigations that intramolecular fluorescence quenching of the system can be separated into "static quenching" and "dynamic quenching," and only the static quenching is observed in a rigid medium where the Brownian motion of the methylene chain is frozen.

The present investigation was undertaken to see if the experimentally observed chain length dependence of the static fluorescence quenching[5] can be simulated by the calculation of the equilibrium conformations of the intramolecular exciplex system. Equilibrium distribution of conformations for individual compounds in the ground state was determined by the calculation of potential energy of each conformation[6] and the degree of intramolecular static fluorescence quenching was estimated by the calculation of the probability of end-to-end encounter in all the conformations.

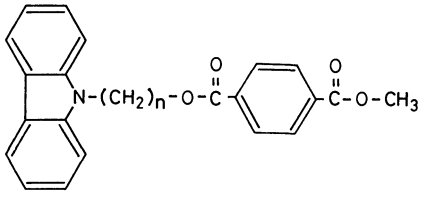

Fig. 1.

Procedures for Calculation

Structural parameters used in this calculation are shown in Figs. 2(a) and 2(b). In this calculation we assume that the ester groups are coplaner with the benzene ring and the trans conformation is predominant over the cis. This assumption has been taken routinely in conformational calculations.[7,8] Generally, conformations of methylene chain are treated by the trans(t)-gauche(g) rotational isomer model, where the statistical weight for two gauche states (g^+ and g^-) is estimated by $\exp(-500/RT)$, since the energy difference between g and t is about 500 cal/mol. However, for relatively short methylene chain having large

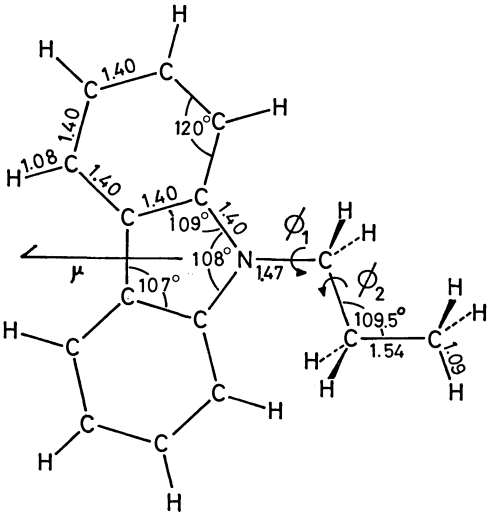

(a)

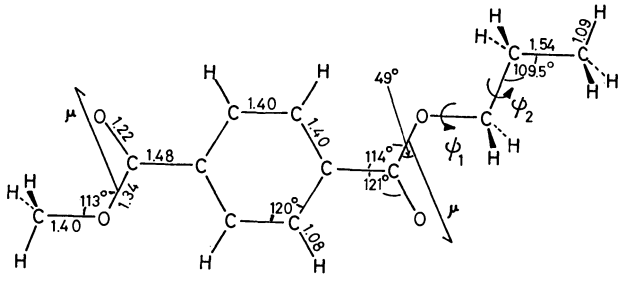

(b)

Fig. 2. Structural parameters of *N*-propylcarbazole (a) and methyl propyl terephthalate (b).

† Present address: Niigata College of Pharmacy, Kamishinei-cho, Niigata 950-21.

end groups, rotations about each C–C bond is related so strongly to one another that the statistical weight for gauche states may differ from $\exp(-500/RT)$. Hence, we calculated the conformational energy, considering that the rotations about all bonds are correlated, though we employed the t-g rotational isomer model in these calculations.

Potential energies due to the van der Waals interactions between nonbonded atoms and due to the electrostatic dipole-dipole interaction between polar end groups were calculated for all of $2\times3^{n+1}$ conformations where n denotes the number of methylene units. For the compound having $n=10$, we adopted the Monte Carlo method, since the number of possible conformation of this compound is too large. In this method we selected randomly 14500 conformations out of $2\times3^{n+1}$ conformations and calculated the potential energy of each one.

Calculation of the Potential Energy due to the Van der Waals Interaction. We adopted a potential function of the Lennard-Jones type. The potential energy P_{ij} between ith and jth nonbonded atoms is given as follows

$$P_{ij} = B_{ij}/r_{ij}^{12} - A_{ij}/r_{ij}^{6}, \tag{1}$$

where, r_{ij} is the distance of separation between ith and jth nonbonded atoms, A_{ij} and B_{ij} are parameters. The parameters A_{ij} have been estimated, using the Slater-Kirkwood equation modified by Scott and Scheraga,[9]

$$A_{ij} = \frac{(3/2)(e\hbar/m^{1/2})\alpha_i\alpha_j}{(\alpha_i/N_{\mathrm{eff}}^{(i)})^{1/2}+(\alpha_j/N_{\mathrm{eff}}^{(j)})^{1/2}}, \tag{2}$$

where, e is the charge of an electron, m is the mass of an electron, $\hbar$ is equal to $h/2\pi$ where h is the Planck's constant, α_i and $N_{\mathrm{eff}}^{(i)}$ are the polarizability and the effective number of electrons of ith atom, respectively. The values of $N_{\mathrm{eff}}^{(i)}$ were graphically determined using Pitzer's data[10] according to Scott and Scheraga.[9] The parameter B_{ij} is obtained by requiring P_{ij} to be minimum at a distance $r_{ij}=r_{ij}^{\circ}$, which is the sum of the van der Waals radii of the interacting atoms. Values of the van der Waals radius r_{w}, the polarizability α, and the effective number of electrons N_{eff} are summarized in Table 1.

Then, the potential function is modified in consideration of molecule-solvent interaction following Flory *et al.*[11] For a molecule in a solvent, intramolecular contact through alternation of conformation must occur at the expense of intermolecular interaction with the solvent. Since these latter interactions are necessarily attractive, the effect would suppress the attractive term P_{ij} occurring at the greater distance r_{ij} between the ith and the jth atoms. Thus the minimum in this function would be eliminated. Calculations have, therefore, been carried out using the potential function modified as follows

$$\begin{aligned} P_{ij}^{*} &= P_{ij} - P_{ij}^{\circ} \quad (r_{ij} < r_{ij}^{\circ}) \\ P_{ij}^{*} &= 0 \qquad\qquad (r_{ij} \geq r_{ij}^{\circ}), \end{aligned} \tag{3}$$

where P_{ij}° is the value of P_{ij} at $r_{ij}=r_{ij}^{\circ}$. We obtained the total potential energy due to the van der Waals interaction as the sum over all pairs of nonbonded atoms.

$$V_n = \sum_{i<j}\sum P_{ij}^{*} \tag{4}$$

Calculation of the Potential Energy due to the Electrostatic Dipole-Dipole Interaction. The mutual potential energy D_{ij} of two point dipoles $\vec{\mu}_i$ and $\vec{\mu}_j$ separated by the vector $\vec{r}_{ij}$ is given by

$$D_{ij} = (1/\varepsilon)[(\vec{\mu}_i\cdot\vec{\mu}_j)/r_{ij}^{3} - 3(\vec{\mu}_i\cdot\vec{r}_{ij})(\vec{\mu}_j\cdot\vec{r}_{ij})/r_{ij}^{5}], \tag{5}$$

where ε is the dielectric constant of the solvent and r_{ij} is the scalar magnitude of $\vec{r}_{ij}$. The total potential energy V_{e} due to the dipole-dipole interaction is given by the sum over all pairs of dipoles as follows.

$$V_{\mathrm{e}} = \sum_{i<j}\sum D_{ij} \tag{6}$$

In the present calculation, the dipole moments of CZ residue and ester group were taken to be 2.09 D[12] and 1.83 D, respectively; the latter value is taken from the value for the dipole moment of methyl benzoate.[13] The angle between the dipole moment (indicated by μ in Fig. 2) and the O–CO bond was taken to be 49°.

Conformations of Methylene Chain in the Neighborhood of Carbazole (CZ) and Terephthalic Acid Methyl Ester (TPM) Residues. We calculated the conformational energy applying the t-g rotational isomer model to the methylene chain. However, the location of the potential minima in the neighborhood of the large end groups might somewhat deviate from that in the t-g rotational isomer model. Hence, we have calculated the potential energies of *N*-propylcarbazole and methyl propyl terephthalate, whose structures are shown in Fig. 2, at intervals of 5° for each rotation angle, starting from conformations shown in Fig. 2 ($\phi_1=\phi_2=0$, $\psi_1=\psi_2=0$).

The potential energy, $V(\theta_i)$, associated with rotation θ_i about ith bond is given by

$$V(\theta_i) = V_{\mathrm{r}}(\theta_i) + \sum_{i<j}\sum P_{ij}, \tag{7}$$

where $V_{\mathrm{r}}(\theta_i)$ is the intrinsic torsional potential attributable to the bond itself, P_{ij} is the potential energy between nonbonded atoms given by Eq. 1 and the sum is over all pairs, i,j of atoms. For threefold rotation, V_{r} is given by

$$V_{\mathrm{r}}(\theta_i) = (V_0/2)(1-\cos 3\theta_i), \tag{8}$$

where V_0 is the torsional barrier height. In this calculation the internal rotation having a sixfold

TABLE 1. ATOMIC PARAMETERS FOR THE CALCULATION
The van der Waals radius r_{w}, the polarizability α, and the effective number of electrons N_{eff}.

Atom	r_{w}/Å [a]	α/Å^3 [b]	N_{eff}
H (arom.)	1.01	0.42	0.9
H (aliph.)	1.20	0.42	0.9
C (sp^2)	1.75	1.20	4.9
C (sp^3)	1.70	1.30	4.9
O (sp^2)	1.52	0.64	6.8
O (sp)	1.50	0.84	6.8
N (sp^2)	1.55	1.15	5.9

a) A. Bondi, *J. Phys. Chem.*, **68**, 441 (1964). b) J. Ketelaar, "Chemical Constitution," Elsevier Publishing Co., New York (1958), p. 91.

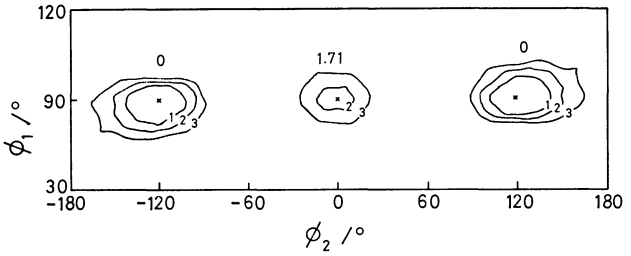

Fig. 3. Conformational energy map of *N*-propylcarbazole. Energy contours are given at interval of 1.0 kcal/mol. Numerals in the figure are the values of potential energy at its minimum position marked by X.

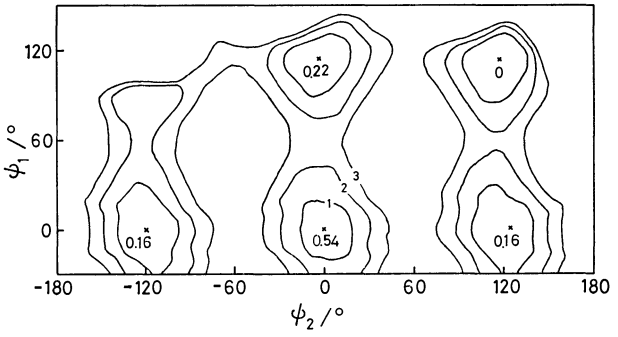

Fig. 4. Conformational energy map of methyl propyl terephthalate. Notations are the same as Fig. 3.

periodicity was neglected. Values of 2.8 kcal/mol and 1.8 kcal/mol were assigned to V_0 for C–C bond and C–O bond, respectively.[14]

Results are shown in Figs. 3 and 4. For *N*-propylcarbazole, the potential mimima are situated at rotations $\phi_1=90°$, $\phi_2=0°$, $\pm120,°$ and $\phi_1=-90°$, $\phi_2=0°$, $\pm120°$. The potential mimima for methyl propyl terephthalate are found to be about at $\psi_1=0°$, $\psi_2=0°$, $\pm120°$, $\psi_1=120°$, $\psi_2=0°$, $+120°$, and $\psi_1=-120°$, $\psi_2=0°$, $-120°$. For these two compounds, the locations of potential mimima are not so deviated from that in the t-g rotational isomer model, hence the use of the t-g rotational isomer model in the neighborhood of CZ and TPM residues appears to be justified.

Results and Discussion

The total potential energy, E, is given by the sum of the potential energy due to the van der Waals interaction and that due to the dipole-dipole interaction. Assuming that the distribution of conformations obeys the Boltzmann distribution, the fraction of ith conformation, W_i, is given by

$$W_i = \exp(-E_i/RT)/\sum_j \exp(-E_j/RT),$$

where E_i is the potential energy for ith conformation.

Distribution of End-to-end Distance. Distribution of the end-to-end distance, r, for each compound at 298 K is shown in Fig. 5, where r was defined as the distance between the center of five membered ring of CZ and the center of the benzene ring of TPM.

For the compounds having shorter methylene chains, I, II, III, the appearing conformations are so few that the distribution of end-to-end distance is very sharp. There is no conformation whose end-to-end distance

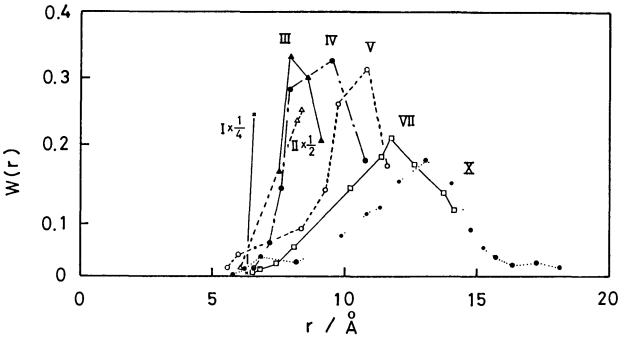

Fig. 5. Distribution of the end-to-end distance r of samples, I, II, III, IV, V, VII, and X at 298 K.

is less than 5 Å since the two end groups are large.

Static Fluorescence Quenching. We have shown[5] that the normal fluorescence of the series of compounds, I—X, is quenched by both the "static quenching" and the "dynamic quenching." The static quenching is caused by an electron transfer from CZ moiety to TPM moiety immediately after the excitation of CZ moiety regardless of the thermal motion of the methylene chain, when CZ moiety exists in the vicinity of TPM moiety. On the other hand, the dynamic quenching is diffusion controlled and reflects the frequency of intramolecular encounters between TPM moiety and the excited CZ moiety within its lifetime. We have estimated the magnitude of the static quenching from the measurement of the quantum yield of the normal fluorescence emission of CZ moiety at 77 K in a rigid 2-methyltetrahydrofuran (MTHF) matrix.

Now, the static quenching will be considered in terms of the active sphere model, in which fluorescence quenching occurs with the probability of one when the TPM moiety exists within the radius of the active sphere of CZ moiety and there is no interaction between CZ moiety and TPM moiety outside the active sphere (hard core approximation). According to this model, the static quenching occurs in the molecules having the conformation in which TPM moiety exists in the radius of the active sphere of CZ moiety immediately after the excitation of CZ moiety. In a rigid medium we observe only the static quenching, since no conformational change of molecules occurs. Therefore, the degree of the static quenching in a rigid medium reflects the distribution of conformations of these compounds immediately after the excitation of CZ moiety. In a rigid medium, it is valid to assume that the conformational distribution of these compounds in the excited state is equal to that in the ground state. Then, the magnitude of the static quenching for each compound corresponds to the fraction of conformation with the end-to-end distance, r, being shorter than the radius of the active sphere, R_0, in the conformational distribution in the ground state. So, the fraction of conformations with the end-to-end distance, r, shorter than the radius of the active sphere, R_0, for various values of R_0 was calculated for each compound. The results at 77 K and 136 K are shown in Figs. 6 and 7, respectively. At both temperatures, the best fit with experimental results was given when the value of the radius of active sphere is equal

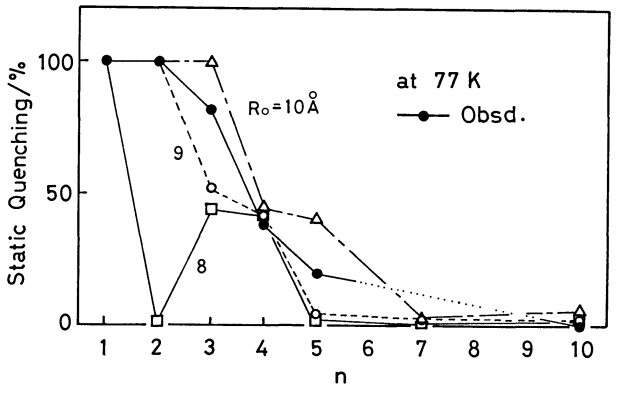

Fig. 6. Comparison of calculated fraction of the static quenching for 77 K with the observed fraction in MTHF at 77 K. (—●—): Observed value, (—△—): calculated value for $R_0=10$ Å, (--○--): calculated value for $R_0=9$ Å, (—□—): calculated value for $R_0=8$ Å.

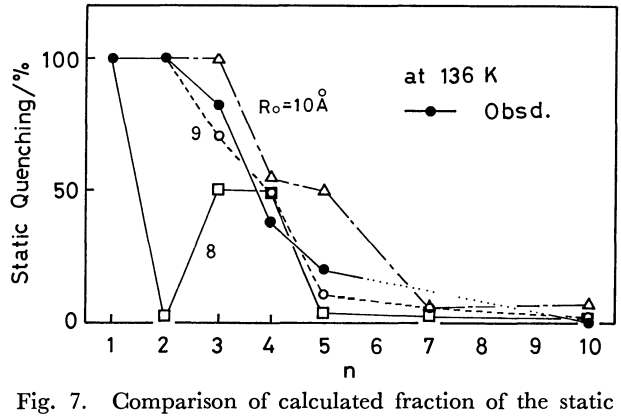

Fig. 7. Comparison of calculated fraction of the static quenching for 136 K with the observed fraction in MTHF at 77 K. Notations are the same as Fig. 6.

to 8.8—9.0 Å. The agreement between the calculated and experimental values is better at 136 K than at 77 K. This result might indicate that the equilibrium distribution of conformations at 136 K is conserved below 136 K, since the freezing point of MTHF is 136 K.

Active Sphere of the Dynamic Fluorescence Quenching in Solution. In this study, the active sphere model is used for the static fluorescence quenching of the intramolecular exciplex system. This model was first introduced by Perrin[15] for the static fluorescence quenching of the molecularly dispersed system. Smoluchowski's solution of diffusion-controlled reactions[16] are derived under the boundary condition of the hard core in the active sphere model: $c(r,0)=c_0$, $c(\infty,t)=c_0$, $c(R,t)=0$, where R is the sum of the collision radii and c_0 is the initial concentration of the diffusion species, and they have been applied to dynamic diffusion-controlled fluorescence quenching.[17]

Now, the active sphere of the dynamic fluorescence quenching of the intermolecular system: *N*-ethylcarbazole-dimethyl terephthalate will be compared with that of the static fluorescence quenching of the intramolecular exciplex system in a rigid medium. Radius of the active sphere of the dynamic fluorescence quenching of the intermolecular system was estimated in

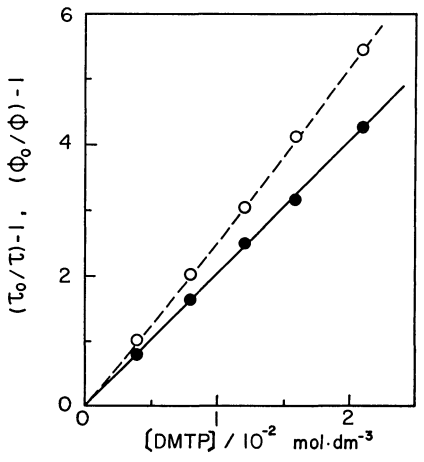

Fig. 8. Stern-Volmer plots of Φ (○) and τ (●) for the fluorescence of ECZ quenched by dimethyl terephthalate (DMTP) in THF solvent at 25 °C.

TABLE 2. RADIUS OF ACTIVE SPHERE (R') AND DIFFUSION CONSTANT (D) IN VARIOUS SOLVENTS

Solvent	Dielectric constant ε	R'/Å	$D/10^{-5}$ cm^2 s^{-1}
Toluene	2.4	5.6	2.83
Dibutyl ether	3.1	5.3	2.72
Diethyl ether	4.3	6.8	5.01
Tetrahydropyran	5.6	6.0	2.11
Tetrahydrofuran	7.6	7.3	2.32
Acetonitrile	36.7	6.4	3.34

various solvents at 25 °C by the method B of Ware and Novros,[18] *i.e.*, the Stern-Volmer plots were analyzed by the theory of diffusion-controlled fluorescence quenching including a transient term. An example of the analysis is as follows. Stern-Volmer plots of both steady-state fluorescence quantum yield Φ and fluorescence lifetime τ in THF solvent at 25 °C is shown in Fig. 8. The Stern-Volmer plot of τ gives $K_q=202$ dm^3 mol^{-1} and the lifetime in the absence of electron acceptors τ_0 was measured to be 15.8 ns, then $4\pi R'DN'=1.28\times10^{10}$ dm^3 mol^{-1} s^{-1} is obtained and furthermore, $4\sqrt{\pi D}R'^2N'=1.1\times10^5$ dm^3 mol^{-1} s$^{1/2}$ is estimated from the Stern-Volmer plot of Φ. Then the combination of these values gives $R'=7.3$ Å and $D=2.32\times10^{-5}$ cm^2 s^{-1}. The values obtained for other solvents are also shown in Table 2. As described in the previous section, the radius of active sphere $R_0=8.8$—9.0 Å was obtained for the intramolecular fluorescence quenching from the chain length dependence of the fluorescence quantum yield of CZ moiety in a rigid medium. The values of R' are slightly smaller than the intramolecular one R_0, but the agreement between the radius of active sphere for the intramolecular fluorescence quenching and the intermolecular one is fairly good.

Though we employed the hard core approximation ($c(R_0, t)=0$) for the active sphere at the present stage, neglecting the effect of the mutual orientation between CZ and TMP moieties, experimentally observed frac-

tions of the static quenching were well simulated with appropriate parameters of the radius of active sphere and the temperature of the system.

The calculations reported in this paper were carried out on the FACOM 230-75 computer at the Computer Center of Kyoto University.

References

1) H. Leonhardt and A. Weller, *Ber. Bunsenges. Phys. Chem.*, **67**, 791 (1963).

2) E. A. Chandross and H. T. Thomas, *Chem. Phys. Lett.*, **9**, 393 (1971).

3) R. Ide, Y. Sakata, S. Misumi, T. Okada, and N. Mataga, *J. Chem. Soc., Chem. Commun.*, **1972**, 1009; T. Okada, T. Fujita, J. Kubota, S. Masaki, N. Mataga, R. Ide, Y. Sakata, and S. Misumi, *Chem. Phys. Lett.*, **14**, 563 (1972); S. Masaki, T. Okada, N. Mataga, Y. Sakata, and S. Misumi, *Bull. Chem. Soc. Jpn.*, **49**, 1277 (1976); J. Hinatu, H. Masuhara, N. Mataga, Y. Sakata, S. Misumi, *Bull. Chem. Soc. Jpn.*, **51**, 1032 (1978); M. Migita, M. Kawai, N. Mataga, Y. Sakata, and S. Misumi, *Chem. Phys. Lett.*, **53**, 67 (1978).

4) M. Itoh, T. Mimura, H. Usui, and T. Okamoto, *J. Am. Chem. Soc.*, **95**, 4388 (1973).

5) M. Yamamoto, Y. Hatano, and Y. Nishijima, *Chem. Lett.*, **1976**, 351; Y. Hatano, M. Yamamoto, Y. Nishijima, *J. Phys. Chem.*, **82**, 367 (1978).

6) For examples, P. J. Flory, "Statistical Mechanics of Chain Molecules," Interscience, New York (1969), Ref. 7; M. Sisido and K. Shimada, *J. Am. Chem. Soc.*, **99**, 7785 (1977).

7) D. A. Brandt, A. E. Tonelli, and P. J. Flory, *Macromolecules*, **2**, 228 (1969).

8) M. A. Winnik, R. E. Toueman, G. Jackowski, D. S. Saunders, and S. G. Whittigon, *J. Am. Chem. Soc.*, **96**, 4843 (1974).

9) R. A. Scott and H. A. Scheraga, *J. Chem. Phys.*, **42**, 2209 (1965).

10) K. S. Pitzer, "Advance in Chemical Physics," ed by I. Prigogine, Interscience Publishers, Inc., New York, (1959), Vol. II, pp. 59.

11) D. A. Brandt and P. J. Flory, *J. Am. Chem. Soc.*, **87**, 2791 (1965).

12) L. G. Wesson, "Tables of Electric Dipole Moment," The Technology Press, Cambridge, Mass. 1948.

13) C. P. Smyth, "Dielectric Behavior and Structure," McGraw-Hill, New York 1955.

14) A. Abe and J. E. Mark, *J. Am. Chem. Soc.*, **98**, 6468 (1976).

15) F. Perrin, C. R. Acad. Sci., **178**, 1978 (1924).

16) M. v. Smoluchowski, *Z. Phys. Chem. (Frankfurt am Main)* **92**, 129 (1917).

17) See reviews, A. H. Alwattar, M. D. Lumt, J. B. Birks in "Organic Molecular Photophysics," ed by J. B. Birks, John Wiley, London (1973), Vol. 1, Chap. 8.

18) W. R. Ware and J. S. Novros, *J. Phys. Chem.*, **70**, 3246 (1966). Radius of the active sphere of intermolecular dynamic fluorescence quenching can be estimated by several ways. See, for example, T. L. Nemzek and W. R. Ware, *J. Chem. Phys.*, **62**, 477 (1975); N. Nakashima, A. Namiki, and K. Yoshihara, *J. Photochem.*, **9**, 230 (1978).

Vibrational Spectra and Normal Coordinate Analysis of *N*-Methyl Thiourea

K. DWARAKANATH and D. N. SATHYANARAYANA*

Department of Inorganic and Physical Chemistry, Indian Institute of Science, Bangalore 560012, India

(Received July 14, 1978)

The infrared spectra of *N*-methylthiourea (NMTU) and its *N*-deuterated and *S*-methylated species were measured. Assignment of the infrared and Raman spectra of NMTU has been accomplished by correlation with thiourea and by use of infrared band shifts on *N*-deuteration as well as *S*-methylation. Normal coordinate analysis was performed for all the fundamentals of NMTU and NMTU-d_3, the assignments obtained from the force field calculations being discussed in relation to those in other related thioureas and thioamides. The potential barriers to the internal rotations for the $-NH_2$, $-CH_3$, and $-CN$ groups were estimated from the force constants.

There is continued interest in the study of thiourea derivatives and their metal complexes in recent years. This may be due to some unusual spectroscopic, magnetic and structural properties shown by the metal complexes of thiourea derivatives as well as to the potential ability of thioureas for ambidentate coordination.[1-4]

N-Methylthiourea (NMTU) is the simplest alkyl-substituted thiourea. An analysis of its vibrational spectrum is necessary for the investigation of the characteristic frequencies and the force field of thiourea derivatives. Lane *et al.*[4] tentatively assigned the infrared spectra of NMTU in the region 4000—700 cm^{-1}. Of particular interest is their assignment of the C=S stretching frequency at 780 cm^{-1}. Jensen and Nielsen,[5] however, attributed a band near 635 cm^{-1} to a coupled C=S stretching mode. There are differences in the assignments also of other bands for NMTU. No complete assignment of the infrared spectra of *N*-methyl thiourea is available although quantitative vibrational assignments of thiourea,[6-8] *N,N'*-dimethyl-,[9,10] and tetramethylthioureas[10,11] have been accomplished by normal coordinate treatments. Recently, detailed vibrational assignments for thiosemicarbazide[12,13] (H_2HNH–C(=S)–NH_2) and *N*-methylurea[14] (NMU), closely related to NMTU, have been published.

An appropriate description of the fundamental vibrations of NMTU arrived at with the aid of normal coordinate analysis of NMTU and NMTU-d_3 and the infrared spectrum of the *S*-methylated NMTU is discussed herewith. The potential barriers to the internal rotation about C–N and C–C bonds are estimated from the force constants.

Experimental

NMTU was prepared by the method of Moore and Crossley[15] and purified by recrystallization from absolute ethanol. NMTU-d_3 was obtained by dissolving NMTU in D_2O and evaporating the excess D_2O in vacuo. The process was repeated several times till the infrared spectrum showed no bands due to NH vibrations. The *S*-methyl derivative of NMTU was prepared by the procedure of Brand and Brand.[16]

Spectra: Infrared spectra were measured on a Carl Zeiss UR 10 spectrophotometer between 4000 and 400 cm^{-1} in Nujol mull and KBr pellet. Far infrared spectra from 400 to 30 cm^{-1} were recorded on a Polytec FIR 30 spectrometer as polyethylene pellet. The Raman frequencies of NMTU are quoted from recent data.[17]

Normal Coordinate Treatment. The GF matrix method of Wilson[18] was employed. A trans-planar –CSNH– conformation supported by nuclear magnetic resonance studies[19] with a molecular symmetry C_s was adopted. The 27 vibrations of NMTU then divide themselves into 18 a′ (in-plane) and 9 a″ (out-of-plane) modes, all being infrared and Raman active. The following molecular parameters transferred from those of NMU[14] and Pt(II) *N*-ethyl thiourea complex[1] were used: bond distances N–H 1.00; C–H 1.08; C′–N 1.465; C–N 1.351; C–S 1.73 Å. The angles around the methyl carbon atom were taken to be tetrahedral (109.47°) and those around the nitrogen of the NH_2 group 120°. The other angles were –NCN 117°; NCS and N′CS 121.5°; C′NH and CN′H 120°. The molecular structure and the internal coordinates are shown in Fig. 1. The symmetry coordinates were the same as those employed for NMU.[14,20]

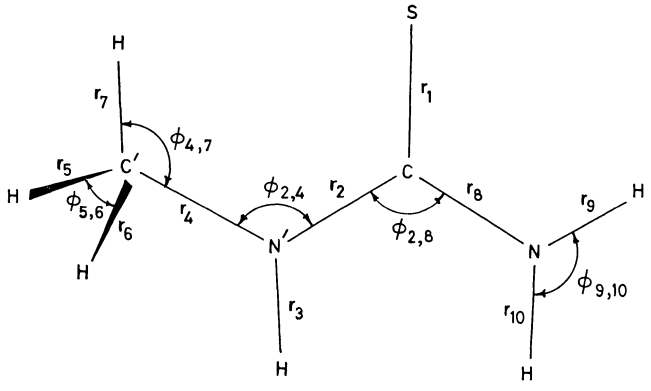

Fig. 1. Structure and internal coordinates of *N*-methyl thiourea.

The Urey-Bradley force field which gives satisfactory explanation of the spectra of thioamides[21-23] and thioureas[6,8,10] was employed. To begin with, zeroth order calculations were performed for the planar vibrations using the force constants transferred from (a) thioacetamide[21] (TAM), and (b) thiourea[6] (TU) and thioacetamide.[21] The zeroth order frequencies were similar in both cases and were reasonably close to the observed frequencies, the potential energy distributions (PED) being also comparable. For out of plane vibrations, the methyl group was treated by the Urey-Bradley force function, the valence force constants being employed for the planar molecular skeleton. The initial values of the valence force constants were taken from NMU.[14]

The force constants of set (a) were refined in order to get a good agreement between the calculated and observed frequencies for both NMTU and NMTU-d_3. The final force constants given in Table 1 are comparable with those of the initial ones, requiring only minor modifications.

Table 1. Force constants[a] for *N*-methylthiourea

Stretching		Bending		Repulsive	
K	NMTU	H	NMTU	F	NMTU
CS	4.10	HNH	0.41	HNH	0.0
CN	5.30	HNC	0.30	HNC	0.55
CN′	5.10	NCS	0.36	NCS	1.05
NH	5.60	NCN	0.74	NCN	0.65
N′H	5.10	N′CS	0.45	N′CS	1.10
C′N	2.65	CN′H	0.12	CN′H	0.50
CH	4.45	CNC	1.20	CNC	0.30
		HNC′	0.07	HNC′	0.95
		NC′H	0.27	NC′H	0.50
		HCH	0.43	HCH	0.04

Valence constants[b]

$f(wNH_2)$	0.056	$f(\pi NH)$	0.060	$f(wNH_2, \pi NH)$	−0.008
$f(\tau NH_2)$	0.110	$f(\tau CN)$	0.095	$f(\tau CN, \pi NH)$	−0.022
$f(\pi CS)$	0.090	$f(\tau CH_3)$	0.006		

a) K, H, and F are in mdyn/Å and the valence constants (f) in mdyn Å. Intramolecular tension $k(CH_3)$ −0.05 mdyn Å and interaction constant P(NH, NH) −0.12 mdyn/Å. b) w, τ, and π: As in Table 2.

The computations were carried out on an IBM 360/44 computer using programs similar to those of Schachtschneider.[24]

Results and Discussion

Agreement between the observed and calculated frequencies for NMTU-d_0 and -d_3 is satisfactory. The somewhat larger deviations for the deuterated compound can be attributed to the higher anharmonicity associated with the hydrogen-involving vibrations. As usual,[25] an interaction constant, P(NH,NH), was employed to get a better fit for the NH_2 stretching frequencies.

Band Assignments. The observed and calculated frequencies and an approximate description of the vibrations derived from the potential energy distributions amongst the symmetry coordinates are given for NMTU and NMTU-d_3 in Tables 2 and 3, respectively.

Alternate assignments for the frequencies below 700 cm^{-1} were considered by means of force field calculations. Final selection consistent with a satisfactory interpretation of all the bands was made by referring to the deuterium frequency shifts and the characteristic group frequencies in structurally related molecules.

In-plane Vibrations. Thioureide Group Vibrations. NH, NH_2 Stretching: The infrared spectrum of NMTU shows three bands in the region above 3000 cm^{-1} assignable to NH_2 and NH stretching vibrations. The bands at 3350 and 3189 cm^{-1} are easily assigned to asymmetric and symmetric NH_2 vibrations,respectively, and the band at 3280 cm^{-1} to NH stretching. On deuteration these bands are replaced by new ones at 2520, 2350, and 2415 cm^{-1}, respectively.

CN Stretching: According to the normal coordinate analysis, the band at 1567 cm^{-1} (near 1555 cm^{-1} in Raman) assigned by Lane *et al.*[4] to the thioamide II band of the –CSNH– group is due to a highly coupled vibration comprising of CN and CS stretching and NCN and CNC bending modes. The band as expected shifts to a higher frequency on *S*-methylation, being observed at 1590 cm^{-1} in the spectrum of *N*,*S*-dimethyl thiourea hydroiodide.

Table 2. Observed and calculated fundamentals and assignments for *N*-methylthiourea

Frequency, cm^{-1} Obsd Raman	Obsd IR	Calcd	D[c]	Assignment[a] (Potential energy distributions,[b] %)
a′ species				
3325	3350	3357	0.2	$\nu_a NH_2$ (100)
3293	3230	3274	0.2	νNH (99)
3166	3139	3193	0.1	$\nu_s NH_2$ (99)
2925	2970	2972	0.1	$\nu_a CH_3$ (99)
2873	2880	2888	0.3	$\nu_s CH_3$ (99)
1628	1642	1639	0.2	δNH_2 (82)
1554	1567	1573	0.4	ν_sCN (23), δNCN (22), νCS (19)
1488	1500	1503	0.2	ν_aCN (60)
1428	1462	1456	0.4	$\delta_a CH_3$ (75)
1406	1408	1394	1.0	$\delta_s CH_3$ (79)
1296	1302	1301	0.1	δNH (65)
1145	1154	1139	1.3	rNH_2 (53)
1126	1125	1122	0.3	νC′N (53), ν_sCN (25)
973	980	1000	2.0	rCH_3 (46), rNH_2 (18)
767	778	768	1.3	νCS (64)
	635	657	3.5	δSCN (27), δCNC (23), νC′N (23)
487	496	494	0.4	δNCN (52), δSCN (20)
280	300	294	2.0	δCNC (39), δSCN (38)
a″ species				
3003	2970	2969	0.0	νCH_3 (100)
	1460	1461	0.1	δCH_3 (85)
		1043		rCH_3 (82)
700	725	712	1.8	τNH_2 (99)
594	600	587	2.2	wNH_2 (91)
574	557	547	1.8	τCN (48), πNH (42)
406	400	403	0.8	πCS (75)
194	185	187	1.1	πNH (57), τCN (27)
	135	135	0.0	τCH_3 (87)

a) ν, stretching; a, asymmetric; s, symmetric; δ, bending; r, rocking; w, wagging; τ, torsion and π, out-of-plane bending. b) $100L_{ik}^2F_{ii}/\lambda_k$; those less than 20% are omitted when the individual or sum of the PED is higher than 50%. c) D is the deviation of ν as a percentage:

$$D = (|\nu_{obsd} - \nu_{calcd}|) \times 100/\nu_{obsd}.$$

The 1500 cm^{-1} band (at 1488 cm^{-1}, Raman spectrum) may be chiefly associated with C–N asymmetric stretching, which is higher than that in thiourea[6] assigned to 1472 cm^{-1}. The 1500 cm^{-1} band of NMTU is unaffected in the *S*-methyl derivative except for an increase in intensity.

NH, NH_2 Bending: Thereis a doublet in the infrared spectrum of NMTU in the 1250—1300 cm^{-1} region; the band at 1302 cm^{-1} is strong and that at 1262 cm^{-1} is medium in intensity. In the Raman spectrum also a strong band at 1296 cm^{-1} and a medium shoulder band at 1260 cm^{-1} are observed. The strong band at 1302 cm^{-1} is taken as the fundamental and the one at 1262 cm^{-1} may be due to an overtone, enhanced in intensity possibly due to Fermi resonance with the fundamental at 1302 cm^{-1}.

Table 3. Observed and calculated fundamentals and assignments for *N*-methylthiourea-d_3

Frequency, cm^{-1} Obsd	Calcd	*D*	Assignment (Potential energy distributions, %)
a′ species			
2970	2972	0.1	$\nu_a CH_3$ (99)
2880	2889	0.3	$\nu_s CH_3$ (99)
2520	2489	1.2	$\nu_a ND_2$ (98)
2415	2393	0.9	νND (97)
2350	2305	1.9	$\nu_s ND_2$ (97)
1545	1518	1.7	ν_sCN (25), δNCN (19), νCS (18)
1512	1493	1.3	ν_aCN (52)
1460	1452	0.5	$\delta_a CH_3$ (67)
1395	1381	1.0	$\delta_s CH_3$ (91)
1195	1223	2.3	δND_2 (68)
1130	1130	0.0	rCH_3 (43)
1080	1079	0.1	νC′N (51)
954	919	3.7	δND (55), rCH_2 (29)
870	860	1.1	rND_2 (62)
708	731	3.2	νCS (68)
630	630	0.0	νC′N (23), δCNC (22), ν_sCN (21), δSCN (21)
451	444	1.6	δNCN (47), δSCN (24)
292	292	0.0	δSCN (37), δCNC (39)
a″ species			
2970	2969	0.0	νCH_3 (100)
1460	1461	0.0	δCH_3 (85)
1075	1043	3.0	rCH_3 (82)
510	517	1.3	τND_2 (77)
475	495	4.2	wND_2 (50), πCS (31)
420	416	1.0	πND (41), τCN (22), wND_2 (20)
360	352	2.2	τCN (43), τCS (30)
184	178	3.2	πND (51), τCN (27)
130	135	3.8	τCH_3 (86)

The present assignment of the 1302 cm^{-1} band to thioamide II band of the –CSNH– group agrees qualitatively with that of Lane *et al.*[4] According to the potential energy distribution, the 1302 cm^{-1} band arises mainly from N–H bending (65%). This band (as also does the 1262 cm^{-1} band) disappears on N-deuteration, a new band at 954 cm^{-1} due to ND bending being found in the spectrum of NMTU-d_3. The NH bending frequency of NMTU is lower than the one at 1354 cm^{-1} in NMU.[14]

The thioamide II band of the $-CSNH_2$ group due to NH_2 bending is observed at 1642 cm^{-1}.

NH_2 Rocking: The band at 1154 cm^{-1} may be assigned to a coupled NH_2 rocking. It is compatible with the 1160 cm^{-1} band of NMU. That the 1154 cm^{-1} band of NMTU undoubtedly has its origin in the NH_2 group is confirmed by deuteration studies. It shifts to 870 cm^{-1} in the infrared spectrum of NMTU-d_3. The normal coordinate analysis shows the 1125 cm^{-1} band as due to a mixed mode mainly of H_3C–N and symmetric C–N stretching vibrations.

CS Stretching: There are two bands in the infrared spectrum of NMTU, a strong sharp band at 778 cm^{-1} and a strong somewhat broad band at 725 cm^{-1}. In the present investigation, the 778 cm^{-1} band is assigned to the C=S stretching in line with that of Lane *et al.*[4] and the 725 cm^{-1} band to an out-of-plane NH_2 bending. According to the potential energy distribution, the C=S stretching contributes nearly 65% to the 778 cm^{-1} band. A very intense Raman band at 767 cm^{-1} is observed in support of this assignment. Further, if the 778 cm^{-1} band is assigned to the NH_2 out-of-plane bending, the calculated frequency for the corresponding ND_2 mode is at 570 cm^{-1}, whereas a new strong band observed on N-deuteration is at 510 cm^{-1}.

The assignment of C=S stretching (Thioamide I band) of NMTU at 778 cm^{-1} is comparable with the C=S stretching frequency in the isoelectronic thiosemicarbazide[10,11] assigned to 800 cm^{-1}. Similarly, *N*-ethylthiourea also exhibits a strong Raman band[17] in this region at 806 cm^{-1}, which may be assigned to the C=S stretching mode. Thus the C=S stretching frequency of NMTU is higher than that in thiourea[6] and *sym*-*N*,*N*′-dimethylthiourea[9,10] assigned near 730 cm^{-1}. As in NMTU, strong Raman bands are also observed near 730 cm^{-1} in these compounds. The 778 cm^{-1} band is nearly unaffected on *S*-methylation, the behavior being similar to the *S*-methylation of thiourea. The 727 cm^{-1} band of thiourea predominantly due to C=S stretching is unaffected in the spectrum of the *S*-methyl derivative.[5]

The C=S stretching vibration has been empirically assigned to 635 cm^{-1} by Jensen and Nielsen[5] from a comparison of the spectrum of NMTU with that of it seleno analogue. This is not supported by normal coordinate analysis. However, the 635 cm^{-1} band has contribution from NCS bending and therefore shifts to a lower frequency on selenation which explains their observation.

Skeletal Bending: The band at 496 cm^{-1} is due to NCN bending, a band assigned similarly being found at 487 cm^{-1} in thiourea.[6] The NCS bending occurs as a coupled mode, contributing to the bands at 635, 496 and 300 cm^{-1}. In contrast, TAM exhibits a nearly pure NCS bending vibration[21] near 470 cm^{-1}. The zeroth order calculations clearly showed the 635 cm^{-1} band to be a coupled vibration of NCS and CNC bending modes. The lowest in-plane fundamental at 300 cm^{-1} can be assigned to CNC bending as in NMU.[14]

Methyl Group Vibrations. The band at 980 cm^{-1} can be assigned to CH_3 rocking which is coupled with NH_2 rocking as in TAM.[21] The assignment differs from that of Lane *et al.*[4] who have attributed CH_3 rocking to 1154 and 1125 cm^{-1} bands (considered as a doublet). As expected, the 980 cm^{-1} band is absent in thiourea.[6] The other CH_3 group vibrations are easily assigned as shown in Tables 2 and 3.

Out-of-plane Vibrations. There are five a″ modes for the planar skeleton. The NH_2 torsional mode of NMTU assigned to 725 cm^{-1}, which on deuteration shifts to 510 cm^{-1}, is compatible with that of NMU[14] and TAM[21,22] where it has been assigned near 710 cm^{-1}. The 600 cm^{-1} band of NMTU arises from NH_2 wagging. This is lower than the NH_2 wagging in TAM[19,20] at 709 cm^{-1} but higher than that in NMU[14] at 531 cm^{-1} and in urea[26] at 555 cm^{-1}.

The potential energy distributions show the NH bending (thioamide V band) to be highly mixed with

CN torsion, contributing to the bands at 557 and 185 cm^{-1}. A similar coupling of NH bending with CN torsion has been noted for diacetamide.[27] The band at 400 cm^{-1} of NMTU is attributed to the C=S out of plane bending (thioamide VI band). The CH_3 torsion is associated with a band at 135 cm^{-1} which is lower than that in NMU[14] at 166 cm^{-1}.

Internal Rotation. The potential barriers for the internal rotation about the C–N bonds, V_{NH_2} and V_{CH_3}, of the $-CSNH_2$ and the $-NHCH_3$ groups, respectively, can be approximated from the values of the respective torsional force constants. Using the treatment employed for NMU[14] and acetamide,[25] the barrier heights can be calculated from the relation

$$V_{NH_2} = 2f(\tau NH_2) = 30.7 \text{ kcal mol}^{-1}$$

and

$$V_{CH_3} = 3/4f(\tau CH_3) = 0.6 \text{ kcal mol}^{-1}.$$

The values of V_{NH_2} and V_{CH_3} are comparable with those of NMU[14] (31.3 and 1.7 kcal mol^{-1}, respectively). Similarly the barrier to the internal rotation about the CN bond of the –CSNH– group is given by

$$V_{CN} = 2f(\tau CN) - \Delta V/4 = 26.0 \text{ kcal mol}^{-1},$$

where ΔV is the energy difference between the *cis*- and *trans*-isomers of NMTU estimated to be 9.0 to 12.0 kcal mol^{-1} by the NMR method.[19] By taking ΔV as 9.0 kcal mol^{-1}, the value obtained for V_{CN} of NMTU is comparable with that of NMU[12] and *N*-methylformamide[28] (25.6 and 28.0 kcal mol^{-1}, respectively).

References

1) F. Bachechi, L. Zambonelli, and G. Marcotrigiano, *Inorg. Chim. Acta*, **17**, 225 (1976); and references cited therein.
2) M. V. Andreocci, M. Bossa, G. Ramunni, M. Scazzocchio, D. Gattegno, and A. M. Giuliani, *J. Chem. Soc. Dalton Trans.*, **1974**, 41.
3) E. A. Vizzini, I. F. Taylor, and E. L. Amma, *Inorg. Chem.*, **7**, 1351 (1968).
4) T. J. Lane, A. Yamaguchi, J. V. Quagliano, J. A. Ryan, and S. Mizushima, *J. Am. Chem. Soc.*, **81**, 3824 (1959).
5) K. A. Jensen and P. H. Nielsen, *Acta Chem. Scand.*, **20**, 597 (1966).
6) D. Hadzi, J. Kidric, Z. V. Knezevic, and B. Barlic, *Spectrochim. Acta, Part A*, **32**, 693 (1976).
7) G. B. Aitken, J. L. Duncan, and G. P. McQuillan, *J. Chem. Soc., A*, **1971**, 2965.
8) A. Yamaguchi, R. B. Penland, S. Mizushima, T. J. Lane, C. Curran, and J. V. Quagliano, *J. Am. Chem. Soc.*, **80**, 527 (1958).
9) R. K. Ritchie, H. Spedding, and D. Steele, *Spectrochim. Acta, Part A*, **27**, 1597 (1971).
10) R. K. Gosavi, U. Agarwala, and C. N. R. Rao, *J. Am. Chem. Soc.*, **89**, 235 (1967).
11) U. Anthoni, P. H. Nielsen, G. Borch, J. Gastausen, and P. Klaboe, *Spectrochim. Acta, Part A*, **33**, 403 (1977).
12) G. Keresztury and M. P. Marzocchi, *Spectrochim. Acta, Part A*, **31**, 275 (1975).
13) D. N. Sathyanarayana, K. Volka, and K. Geetharani, *Spectrochim. Acta, Part A*, **33**, 517 (1977).
14) Y. Saito, K. Machida, and T. Uno, *Spectrochim. Acta, Part A*, **31**, 1237 (1975).
15) M.L. Moore and P.S. Crossley, *Org. Synth.*, **3**, 617(1955).
16) E. Brand and F. C. Brand, *Org. Synth.*, **3**, 440 (1955).
17) "Raman/IR Atlas," ed by B. Schrader and W. Meiler Verlag Chemie GmbH, Weinheim/Bergstr. (1974).
18) E. B. Wilson, Jr., *J. Chem. Phys.*, **9**, 76 (1941).
19) A. S. Tompa, R. D. Barefoot, and E. Price, *J. Phys. Chem.*, **73**, 435 (1969).
20) Y. Mido and H. Murata, *Nippon Kagaku Zasshi*, **90**, 254 (1969).
21) W. Walter and P. Staglich, *Spectrochim. Acta, Part A*, **30**, 1739 (1974); and references cited therein.
22) I. Suzuki, *Bull. Chem. Soc. Jpn.*, **35**, 1286, 1449, 1456 (1962).
23) A. Ray and D. N. Sathyanarayana, *Bull. Chem. Soc. Jpn.*, **47**, 729 (1974).
24) J. H. Schachtschneider, "Technical Report 231—64 (1964)," Shell Development Company, Emeryville, U.S.A.
25) T. Uno, K. Machida, and Y. Saito, *Bull. Chem. Soc. Jpn.*, **42**, 897 (1969).
26) Y. Saito, K. Machida, and T. Uno, *Spectrochim. Acta, Part A*, **27**, 991 (1971).
27) Y. Kuroda, Y. Saito, K. Machida, and T. Uno, *Bull. Chem. Soc. Jpn.*, **45**, 2413 (1972).
28) I. Suzuki, *Bull. Chem. Soc. Jpn.*, **35**, 540 (1962).

An Alternative Method of Solving the Rose-Drago Equation for the Determination of Equilibrium Constants of Molecular Complexes†

Bejoy K. SEAL,* Ashok K. MUKHERJEE, and Dulal C. MUKHERJEE‡,††

Department of Chemistry, Burdwan University, West Bengal, India

‡*Department of Chemistry, University of Calcutta, 92 Acharya Prafulla C Road, Calcutta 700009, India*

(Received August 7, 1978)

An alternative method for solving the Rose-Drago equation for the determination of equilibrium constants of molecular complexes has been developed. It yields well-defined K values even for certain systems in which the Rose-Drago procedure for solving the R-D equation is not satisfactory. Our method is based on the transformation of the Rose-Drago equation into one involving three variables and using two linear plots. In applying the method to a wide variety of experimental data, the calculated values of the equilibrium constant have been found to be in excellent agreement with those computed by the well-known iterative procedure. With good data, the calculated values are in good agreement with those from the Benesi-Hildebrand or some other modified plots.

Molecular addition compounds formed by the interaction of electron donors and acceptors are generally characterized by intense electronic absorption attributable to neither component of the addition compound, but to a new molecular species, the compound—usually referred to as the molecular complex — itself. The interpretation of the occurrence of these absorption bands by Mulliken[1] in the light of his charge-transfer theory is now widely accepted. After the formulation of this theory, numerous workers were interested in determining the composition and stability of these complexes. Benesi and Hildebrand[2] formulated a spectrophotometric method and many investigators used it or some modification of it[3,4] to determine the equilibrium constants. Certain limitations of the Benesi-Hildebrand (B-H) method[5] became evident and new equations were derived. Of these, the most noteworthy one is the Rose-Drago equation,[6] which is perfectly general. This equation (Eq. 1; see next section) contains two unknowns, K and ε_c; they are, respectively, the equilibrium constant and the molar absorptivity of the complex. An analytical solution for ε_c could be derived by constructing two simultaneous equations, each representing different experimental trials. Alternatively Rose and Drago[6] developed a graphical procedure for solving their general equation. This consisted of random selection of ε_c values and calculation of K^{-1} from one set of experimental data, namely with one particular value of initial concentration of donor and acceptor, plotting K^{-1} as a function of ε_c, repetition of this procedure with other sets, and finally evaluating K^{-1} and ε_c values from the common point of intersection. But selection of a series of ε_c values at random for each set of experimental data renders this graphical method laborious and sometimes very difficult to employ. In addition, in many cases the Rose-Drago plot shows a wide scatter in the values of K and ε_c.[7]

In the present article, we report an alternative graphical method, based on the consideration of two linear plots, for solving the Rose-Drago equation. This procedure is straightforward, more convenient to use, and can be employed without any loss of generality of the equation.

Principle and Method

Drago and Rose[7] derived Eq. 1 relating K^{-1} and ε_c as

$$K^{-1} = \frac{C_D^\circ C_A^\circ(\varepsilon_c-\varepsilon_A)}{d-d_A^\circ} - C_D^\circ - C_A^\circ + \frac{d-d_A^\circ}{\varepsilon_c-\varepsilon_A}, \quad (1)$$

where C_D° and C_A° are the initial concentrations of the donor and acceptor respectively, ε_A is the molar absorptivity of the acceptor, d_A° is the absorbance of the initial concentration of the acceptor, and d corresponds to the total absorbance at any given wavelength for a cell of 1 cm path length.

Now, Eq. 1 can be written in the form:

$$y = L + Mx - M^2z, \quad (2)$$

where

$$y = \frac{C_A^\circ C_D^\circ}{d-d_A^\circ}, \quad x = C_A^\circ + C_D^\circ, \quad z = d - d_A^\circ,$$
$$L = K^{-1}/(\varepsilon_c-\varepsilon_A),$$

and

$$M = 1/(\varepsilon_c-\varepsilon_A).$$

Now, from definitions, it can be easily shown that z is a linear function of C_c, the equilibrium concentration of the complex, and at the lower range of donor concentration[8] or within the close range of donor concentration it is a reasonably good approximation to assume that C_c is a linear function of x in the range. Thus, to the first approximation, we can substitute $z=mx+n$ in Eq. 2, yielding

$$y = (L-M^2n) + (M-M^2m)x. \quad (3)$$

Equation 3 gives a linear plot of y *versus* x with slope,

$$S = M - M^2m, \quad (4)$$

and intercept,

$$I = L - M^2n, \quad (5)$$

where m and n can be obtained from the slope and intercept of z *vs.* x plot.

Now, from Eq. 4,

$$M = \frac{1\pm\sqrt{1-4mS}}{2m}. \quad (6)$$

The root $(1+\sqrt{1-4mS})/2m$ is discarded because its value differs widely from that given by the approximate equation $y=L+Mx$, and also because it yields inadmis-

† A preliminary account of this work was presented at the 26th Congress of the IUPAC held in September, 1977.

†† Present address: Eye Research Institute of Retina Foundation, 20 Staniford St., Boston, MA 02114, U.S.A.

sible values of ε_c. Substituting the value of M from Eq. 6 into Eq. 5, we get L, and finally $K=M/L$ and $\varepsilon_c=M^{-1}+\varepsilon_A$.

Results and Discussion

The Rose-Drago curve for the naphthalene–picric acid system, constructed from the data by Foster,[9] is shown in Fig. 1. As can be seen from the figure, well-defined values of K and ε_c are not obtainable from the plot. We also observed similar scatter in the Rose-Drago curve for the systems pyridine–iodine and 2-methylpyridine–iodine from the data of Nagchandhuri and Basu.[10]

Using our graphical procedure, we have calculated the equilibrium constant and molar absorptivity values of a large number of a wide variety of molecular complexes, using the experimental data of different investigators for different systems, such as the iodine complexes of polycyclic aromatic hydrocarbons[11] and aza-aromatics,[10] complexes of tetrachlorophthalic anhydride (TCPA) with aza-aromatics,[12] the naphthalene–picric acid complex,[9] and the chloranil–indole complex.[13] A representative linear plot of z *vs.* x and of y *vs.* x for the systems naphthalene–picric acid, iodine–pyridine, and TCPA–quinoline are shown in Figs. 2 and 3 respectively. In all other cases examined by us reasonably good linearity was obtained in these two plots. The calculated values of K and ε_c of various systems are presented in Table 1, which also contains, for comparison, the values of these quantities obtained by various authors by applying either the Benesi-Hildebrand or some other modified plot. We have also computed the values of K and ε_c of these systems with the help of the iterative technique as followed by Arnaud and Bonnier.[14] The iteratively computed values of K, computed by the IBM 1130 computer, are also presented in Table 1. In almost all the cases we examined, the values of K obtained by our procedure are in very good agreement with those obtained by the iterative procedure. Except in the case of TCPA–aza-aromatic systems we failed to obtain a reasonably good common point of intersection by the Rose-Drago procedure for the systems under consideration. In the case of the pyrene–iodine complex a K-value of 43 l mol^{-1} with a standard deviation of ± 7 was obtained by Drago and Rose[7] by applying their own procedure. Calculation by our method yields $K=42.9$ l mol^{-1}. For the biphenyl–iodine complex the Rose-Drago procedure yields $K=0.39\pm0.15$, whereas the reported value is 0.37;[11] our method gives $K=0.28$. For the naphthalene–

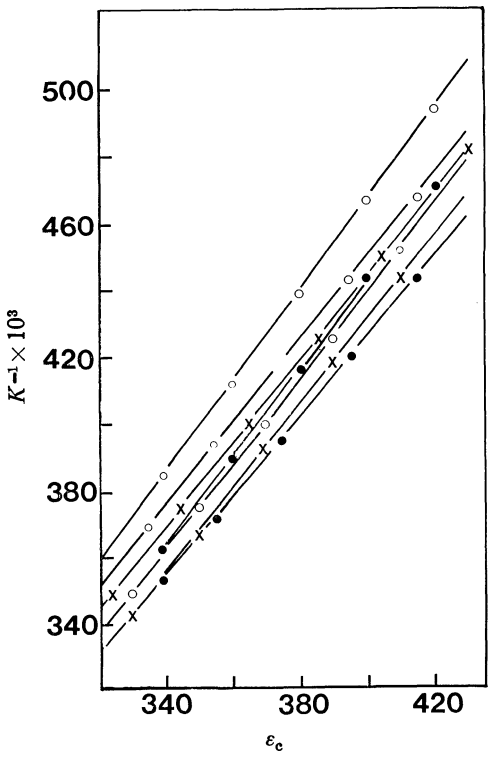

Fig. 1. Rose-Drago plot for the picric acid–naphthalene system. The different lines correspond to the different experimental trials, each a definite value of C_A° and C_D°.

Table 1. Equilibrium constants and molar extinction coefficients (ε_c) of various molecular complexes

System	K(l mol^{-1})			ε_c	
	Our method	Iterative method	B-H or modified plot	Our method	B-H or modified
TCPA+Quinoline	29.00	29.86	26.0[a]	132	—
TCPA+2-Methylquinoline	13.13	13.48	15.0[a]	226	—
TCPA+Benzo[*h*]quinoline	19.00	19.14	18.0[a]	300	—
Iodine+Pyridine	38.98	40.37	43.74[b]	1006	952[b]
Iodine+2-Methylpyridine	46.37	48.57	50.00[b]	1043	1000[b]
Iodine+2,6-Dimethylpyridine	29.64	31.95	26.23[b]	878	888[b]
Iodine+Quinoline	66.75	65.07	69.0[b]	2994	3046[b]
Iodine+Isoquinoline	40.07	39.95	39.4[b]	1551	1538[b]
Iodine+Phenanthridine	47.24	46.48	47.0[b]	852	852[b]
Indole+Chloranil	2.82	2.87	2.86[c]	1527	1510[c]
Naphthalene+Picric acid	2.38	2.40	2.29[d]	366	377[d]
Iodine+Pyrene	42.91	42.82	36.49[e]	140	161[e]
Iodine+Biphenyl	0.28	0.29	0.37[e]	5231	4000[e]
Iodine+Naphthalene	0.21	0.21	0.62[e]	6557	2395[e]
Iodine+Phenanthrene	2.67	2.61	1.06[e]	618	1492[e]

a) Ref. 12. b) Ref. 10. c) Ref. 13. d) Ref. 9. e) Ref. 11.

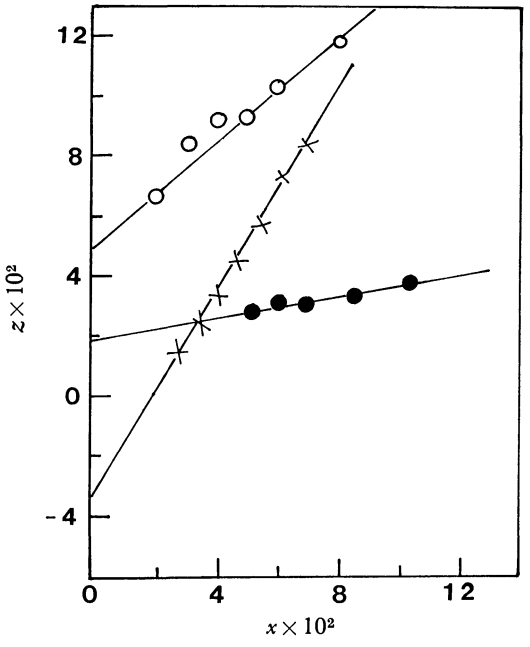

Fig. 2. z *vs.* x plot for the system TCPA–quinoline (●), picric acid–naphthalene (×), and iodine–pyridine (○).

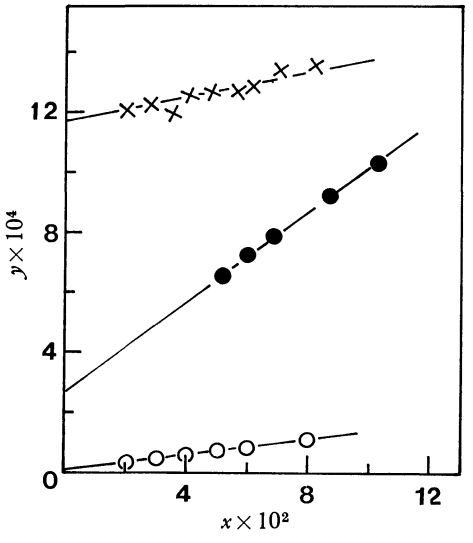

Fig. 3. y *vs.* x plot for the system TCPA–quinoline (●), picric acid–naphthalene (×), and iodine–pyridine (○).

iodine complex the recalculated K by our method is 0.21 which is close to the value, 0.25, quoted by Drago.[7] The K value of 0.62 for this system, obtained by Bhattacharya and Basu[11] from the Benesi-Hildebrand plot, is considerably higher. For the iodine–anthracene system the Rose-Drago equation, solved by our method, yields a much lower value of K than that obtained by Bhattacharya and Basu.[11] This might be due to some specific assumptions in deriving the Benesi-Hildebrand equation rendering it unsuitable for general application.[15]

Drago and Rose[7] felt that a recalculation with many reported data was necessary for yielding meaningful thermodynamic quantities from spectrophotometric investigations. These calculations can be carried out by our procedure for solving the Rose-Drago equation more easily and effectively than by their own graphical procedure.

From the excellent agreement of computed results between our procedure and the iterative procedure, it is apparent that our one-step approximation of linearity between C_c and x is somehow almost equivalent to successive approximations in the process of iteration.

The time and service made available by the Computer Center of the University of Calcutta are gratefully acknowledged. Sincere thanks are also due to Prof. S. K. Siddhanta, Head of the Department of Chemistry, Birdwan University, for constant encouragement during the progress of the work.

References

1) R. S. Mulliken, *J. Am. Chem. Soc.*, **74**, 811 (1952).
2) H. Benesi and J. H. Hildebrand, *J. Am. Chem. Soc.*, **70**, 2832 (1948); **71**, 2703 (1949).
3) J. A. A. Ketelaar, *Rec. Trav. Chim.*, **71**, 1104 (1952).
4) R. L. Scott, *Recl. Trav. Chim., Pays-Bas*, **75**, 787 (1956).
5) P. R. Hammond, *J. Chem. Soc.*, **1964**, 479.
6) N J. Rose and R. S. Drago, *J. Am. Chem. Soc.*, **81**, 6138 (1959).
7) R. S. Drago and N. J. Rose, *J. Am. Chem. Soc.*, **81**, 6141 (1959).
8) R. S. Mulliken and W. B. Person, "Molecular Complexes," Wiley, New York (1969), p. 82.
9) R. Foster, *J. Chem. Soc.*, **1957**, 5098.
10) J. Nagchaudhuri and S. Basu, *Trans. Faraday Soc.*, **55**, 898 (1959).
11) R. Bhattacharya and S. Basu, *Trans. Faraday Soc.*, **54**, 1286 (1958).
12) M. Chowdhury, *J. Phys. Chem.*, **65**, 1899 (1961).
13) R. Foster and P. Hanson, *Trans. Faraday Soc.*, **60**, 2189 (1964).
14) R. Arnaud and J. M. Bonnier, *J. Chim. Phys.*, **66**, 954 (1969).
15) J. Rose, "Molecular Complexes," Pergamon, Oxford (1967), p. 39.

Pre-exponential Factor in Semiconducting Vitamin A (Alcohol and Acetate)

Biswanath MALLIK, Alpana GHOSH, and T. N. MISRA*

Optics Department, Indian Association for the Cultivation of Science, Jadavpur, Calcutta 700032, India

(Received August 30, 1978)

The semiconductive properties of vitamin A (alcohol and acetate) on adsorption of various vapors have been studied. The adsorbed vapors increase the semiconduction currents by several orders of magnitude and decrease the semiconduction activation energies. Such change depends on the chemical nature and also on the amount of vapor adsorbed. Semiconducting vitamin A follows the three-constant equation

$$\sigma(T) = \sigma_0' \exp(E/2kT_0) \exp(-E/2kT)$$

where the conventional pre-exponential factor σ_0 has been replaced by $\sigma_0' \exp(E/2kT_0)$ (the so called compensation effect). Here T_0 and σ_0' are constants for the substance and T_0 is called the characteristic temperature. Various methods used for evaluating these constants have yielded consistent results with $T_0 \approx 402$ K and $\sigma_0' \approx 2.8 \times 10^{-9}\ \Omega^{-1}\ \mathrm{cm}^{-1}$ for vitamin A alcohol and $T_0 \approx 335$ K and $\sigma_0' \approx 1.5 \times 10^{-10}\ \Omega^{-1}\ \mathrm{cm}^{-1}$ for vitamin A acetate. Excellent correlation obtained between the relevant parameters in semiconducting vitamin A indicates that σ_0 and E are physically related. Various models for conduction mechanism leading to compensation effect have been discussed. The measured activation energies on adsorption of same amount of various vapors show a linear relationship with the ionization potential of the adsorbed molecules suggesting that charge-transfer interaction is responsible for the semiconductivity enhancement.

The electrical conductivity of conjugated π-electronic organic compounds follows the operational definition of a semiconductor

$$\sigma(T) = \sigma_0 \exp(-E/2kT) \quad (1)$$

where $\sigma(T)$ is the specific conductivity at any absolute temperature T, σ_0 is a pre-exponential factor, E the semiconduction activation energy and k is Boltzmann constant ($E/2$ is often written as E', however, we shall use the former throughout this paper). Experimentally, E is obtained from the slope of the linear plot of $\log \sigma(T)$ *vs.* $1/T$. Recently, the so called pre-exponential factor σ_0 has been the subject of much discussion[1-6] as experimental evidence accumulated shows that σ_0 contain exponential functions. Gutmann and Lyons[7] showed a linear relationship of the form

$$\log \sigma_0 = \alpha E + \beta \quad (2)$$

holds good for one entire class of organic compounds, α and β being constants. Rosenberg[2,8] *et al.* showed evidence that if E is varied by hydration or complex formation relation (2) is valid for a single organic substance as well and they suggested an expression for the specific conductivity of the form

$$\sigma(T) = \sigma_0' \exp(E/2kT_0) \exp(-E/2kT) \quad (3)$$

thus introducing an additional constant T_0, called characteristic temperature. σ_0' and T_0 for the same compound remain invariant. The linear relationship between the logarithm of the pre-exponential factor and the activation energy is called the compensation effect. σ and E change in such a manner that their effect on σ_0 are mutually compensated. It has been pointed out by Johnston and Lyons[4] that the linear relationship between $\log \sigma_0$ and E may originate solely from the calculation of these parameters and the compensation effect requires no physical interpretation. However, they have suggested that if σ_0 and E are physically related, one should get a linear relationship between $\log \sigma$ and E yielding the semiconductive parameters in agreement with the values obtained from other sources. From Eq. 3, for any particular temperature T_1, the specific conductivity is given by

$$\log \sigma(T_1) = \log \sigma_0' + \left(\frac{1}{T_0} - \frac{1}{T_1}\right)\frac{E}{2k}.$$

Thus, the plot of $\log \sigma(T_1)$ *vs.* E is expected to be linear with a slope $(1/T_0 - 1/T_1)/2k$ and an intercept of $\log \sigma_0'$. The value of σ_0' obtained from this plot should also show a good agreement with the values obtained from the $\log \sigma_0$ *vs.* E and $\log \sigma$ *vs.* $1/T$ plots. In the experiment of Johnston and Lyons[4] the $\log \sigma_0$ *vs.* E plots were linear, but a very poor correlation between $\log \sigma$ and E was observed[4] in one component crystal of anthracene by changing its purity and doping with tetracene. Some recent theoretical works[9,10] suggest that in biological semiconductors the compensation effect arises due to the dark conduction process. In view of the scanty experimental works available on this effect, it was thought worthwhile to investigate the conduction process in more biological semiconductors. To test the validity of the compensation effect, E is generally varied by various ways and $\log \sigma_0$ is plotted against E. The adsorption of gases is known[8,11] to change the activation energies of organic semiconductors. Recently, being motivated to examine the hypothesis that vitamin A is involved in olfactory transduction mechanism,[12] we have studied the effect of adsorption of gases on solid vitamin A. Such adsorption changes the activation energy and enhances the conductivity. In this paper we present experimental evidence to indicate that the compensation rule is valid for solid vitamin A and that σ_0 and E are indeed physically related. Further, the formation of donor-acceptor complex between vitamin A and the adsorbed gas molecule is shown to be responsible for the observed activation energy change.

Experimental

High purity vitamin A alcohol and vitamin A acetate were obtained from Hoffmann-La Roche and Co., Ltd., Switzerland. These were used without any further purification. Sandwich cell technique with a conducting glass and/a

stainless steel electrode was used. There was a gas inlet and an outlet in the conductivity chamber, made of brass and fashioned with Teflon, for gas adsorption study. The temperature of the sandwich cell could be controlled from outside. Temperature measurements were made using a copper-constantan thermocouple attached at the top of the metal electrode. The semiconduction currents were measured with an electrometer amplifier EA815 of the Electronic Corporation of India Ltd. Vapors of methanol, ethanol, heptane, ethyl acetate, benzene, and toluene were allowed to be adsorbed on the semiconductors. The reagent chemicals of spectrograde (E. Merck, B. D. H.) quality were used without further purification; otherwise repeated fractional distillation was done before use. To pass various vapors inside the chamber, dry nitrogen gas was used as carrier which was passed through a bubbler containing the reagent chemical. The partial pressure of the reagent vapor in the conductivity chamber was kept constant during adsorption at a pressure less than the saturation vapor pressure at the sample cell temperature by carefully adjusting the temperature of the bubbler. The partial pressure of the vapor was the saturation vapor pressure of the reagent chemical at the temperature of the bubbler. The same partial pressure (40 mm) was maintained inside the chamber for various vapors. Under this condition it is a valid assumption that the same amount of various vapors are adsorbed on the semiconductors. Repeated heating and cooling of the sample initially in vacuum and finally in dry nitrogen atmosphere ensured desorption of water vapor or any other adsorbed gases. Temperature (12.5 °C) of the sample cells and the inlet flow were kept constant during adsorption.

To determine the effect of adsorbed vapor on the semiconduction activation energy, the sample was allowed to come to a steady state in the chamber atmosphere containing the vapor with nitrogen. The pressure of the total gas mixture in the chamber was atmospheric pressure. The saturation current, after vapor adsorption was found to be almost constant even after four hours indicating that the conduction in the system is mainly electronic.[13,14] The sample cell was then rapidly cooled to about −40 °C and then the chamber was flushed gently with dry nitrogen gas. Semiconduction current was measured with increasing temperature of the sample cell. The outlet of the chamber was kept open to maintain atmospheric pressure inside the chamber.

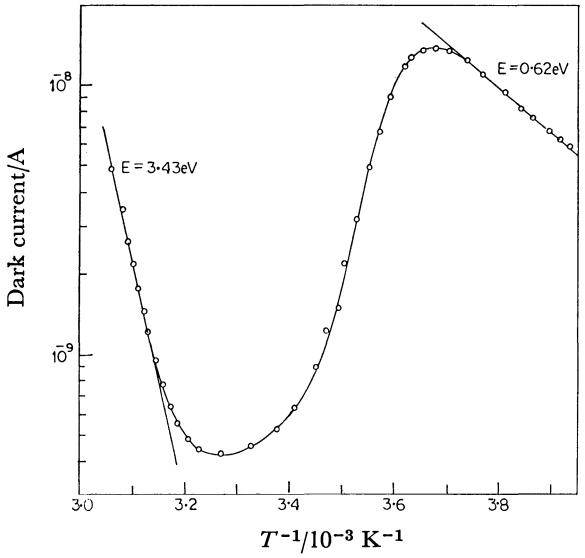

Fig. 1. Semiconductivity in a vitamin A acetate powder cell with desorption of ethyl acetate vapor as the temperature increases.

Results and Discussion

The semiconduction activation energy of crystalline powders of vitamin A (alcohol and acetate) has been measured several times in dry nitrogen atmosphere. The observed values are 2.06 and 3.50 eV (approx.) for the alcohol and acetate respectively. The adsorption of gases enhances the semiconduction current (by several orders of magnitude in some cases) and decreases the activation energy appreciably. The results of one such typical experiment is shown in Fig. 1. The straight line portion in the low temperature region shows the semiconducting properties of vitamin A acetate powder with adsorbed ethyl acetate vapor and the slope of this line gives the activation energy (0.62 eV) of this semiconducting system. The straight line portion in the high temperature region gives the activation energy of vitamin A acetate in nitrogen atmosphere. The observed value (3.43 eV) is slightly lower possibly due to incomplete desorption of adsorbed vapors. The intermediate portion shows the semiconduction behavior

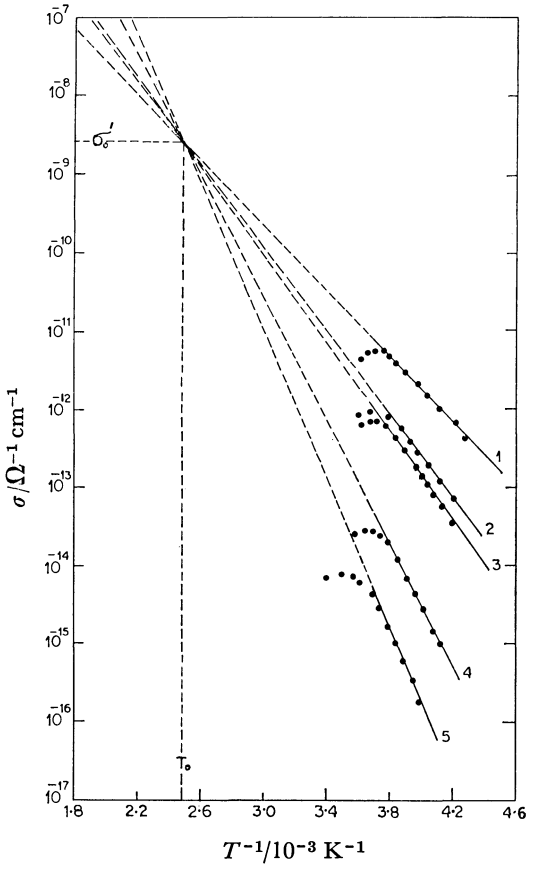

Fig. 2(a). Semiconductivity in vitamin A alcohol powder cell (steady state condition) with the adsorption of same amount of different vapors. Solid lines represent temperature region of measurements, dashed lines are extrapolations. Each line refers to a specific vapor adsorbed state. Vapors are (1) toluene; (2) ethyl acetate; (3) heptane; (4) ethanol; and (5) methanol. To avoid overlapping with (2) the line corresponding to benzene vapor is not shown. The value of $T_0 \approx 402$ K; $\sigma_0' = 2.65 \times 10^{-9}$ Ω^{-1} cm^{-1}.

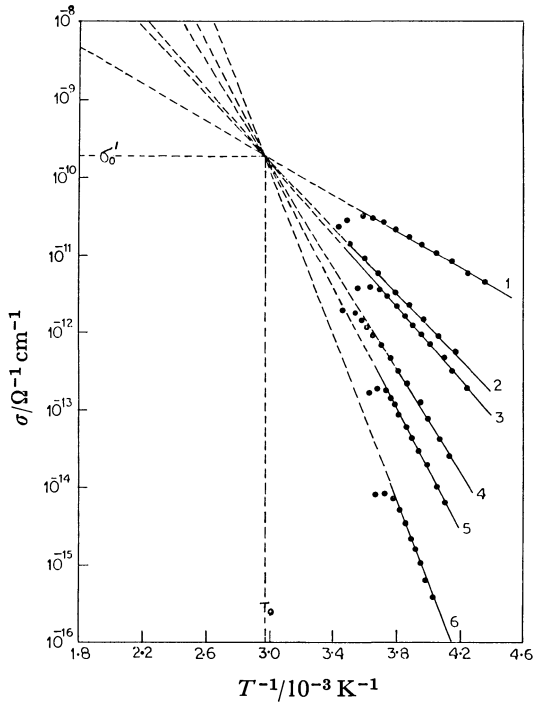

Fig. 2(b). Same as Fig. 2(a) for vitamin A acetate with adsorbed vapors (1) toluene; (2) benzene; (3) ethyl acetate; (4) heptane; (5) ethanol; and (6) methanol. $T_0 \approx 335$ K; $\sigma_0' = 1.8 \times 10^{-10}\ \Omega^{-1}\ cm^{-1}$.

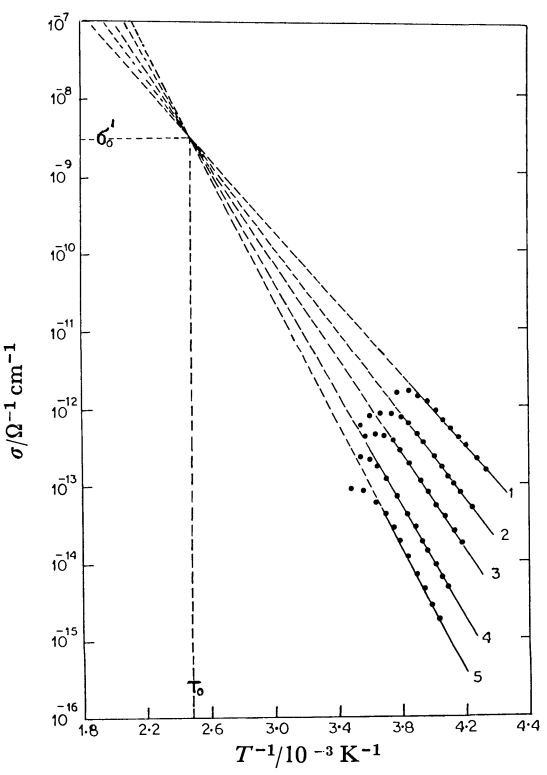

Fig. 3(a). Semiconductivity data for vitamin A alcohol powder cell (steady state condition) with adsorption of different amount of ethyl-acetate vapor. The lines (1) $\rightarrow$(5) refer to the states with the decreasing amount of adsorbed vapor. $T_0 \approx 403$ K; $\sigma_0' = 3.1 \times 10^{-9}\ \Omega^{-1}\ cm^{-1}$.

of the sandwich cell during desorption process. Similar curves were also obtained with other vapors.

The Characteristic Temperature for the Semiconducting Vitamin A. In Figs. 2(a) and 2(b) we show the straight portion in the low temperature region for a number of adsorbed vapors in vitamin A alcohol and acetate respectively. It is observed that with the same amount of vapor adsorbed, the activation energy values are different for different vapors. In this case no single value of σ_0 is found if either $T \rightarrow \infty$ or $E \rightarrow 0$ as is expected from Eq. 1. The extrapolated lines intercept the ordinate at a wide varieties of positions, but they all pass approximately through a single point at a temperature T_0, characteristic of the semiconductor. This is exactly what is expected from Eq. 3. Figs. 2(a) and 2(b) show $T_0 \approx 402$ K for vitamin A alcohol and $T_0 \approx 335$ K for vitamin A acetate. At these characteristic temperatures $\sigma(T_0) = \sigma_0'$ values of vitamin A alcohol and acetate are 2.65×10^{-9} and $1.8 \times 10^{-10}\ \Omega^{-1}\ cm^{-1}$ respectively. Adsorption of different amount of same vapor also changes the semiconduction activation energy to different extent. The plots of $\log \sigma(T)$ *vs.* $1/T$ for different amount of ethyl acetate vapor adsorbed on vitamin A alcohol and acetate semiconductors are shown in Figs. 3(a) and 3(b). These two sets also give values of T'_0's and σ'_0's [403 and 334 K and 3.1×10^{-9} and $1.65 \times 10^{-10}\ \Omega^{-1}\ cm^{-1}$ for vitamin A alcohol and acetate respectively] in good agreement with those obtained earlier.

If plotted in alternate fashion as $\log \sigma_0$ *vs.* E, the plots are linear as expected [since $\log \sigma_0 = E/(2kT_0) + \log \sigma_0'$] and are shown in Fig. 4. The value of T_0 obtained from the slopes are 404 and 333 K for vitamin A alcohol and

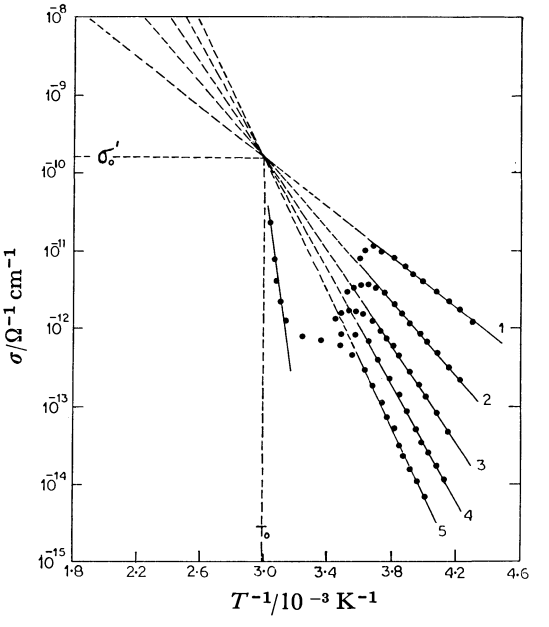

Fig. 3(b). Same as Fig. 3(a) for vitamin A acetate. Here, $T_0 \approx 334$ K; $\sigma_0' = 1.65 \times 10^{-10}\ \Omega^{-1}\ cm^{-1}$.

acetate respectively. The σ_0' values obtained from the intercepts of these plots are 2.8×10^{-9} and 1.5×10^{-10} $\Omega^{-1}\ cm^{-1}$ for vitamin A alcohol and acetate respectively. Thus the values of T_0 and σ_0' obtained from various plots are consistent and show excellent agreement.

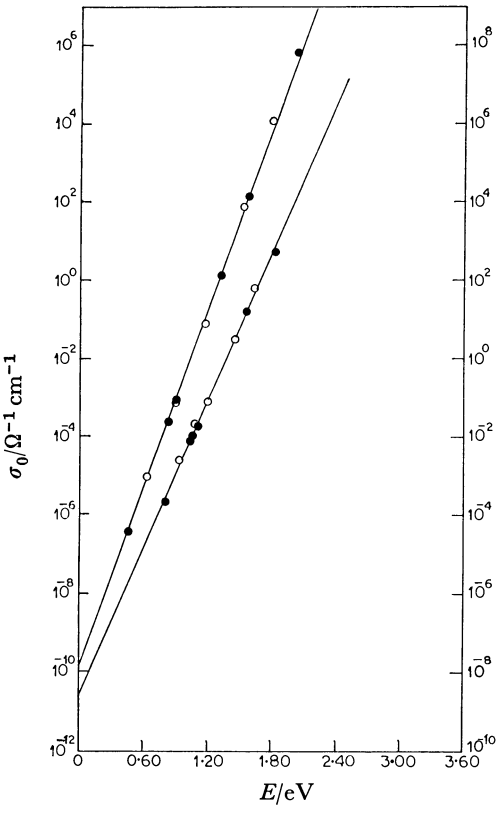

Fig. 4. Plot of the log σ_0 values [from Eq. 1] *vs.* the activation energies for vitamin A (alcohol and acetate) at a constant temperature [$1/T=3.8\times10^{-3}$ K^{-1}] The lower line is for vitamin A alcohol (right scale) and the top line is for vitamin A acetate (left scale). The dark circles refer to different vapors and the open circles to different amounts of same vapor. Slopes and σ_0' values are 14.45 eV^{-1} and 2.8×10^{-9} Ω^{-1} cm^{-1} for vitamin A alcohol and 17.52 eV^{-1} and 1.5×10^{-10} Ω^{-1} cm^{-1} for vitamin A acetate respectively.

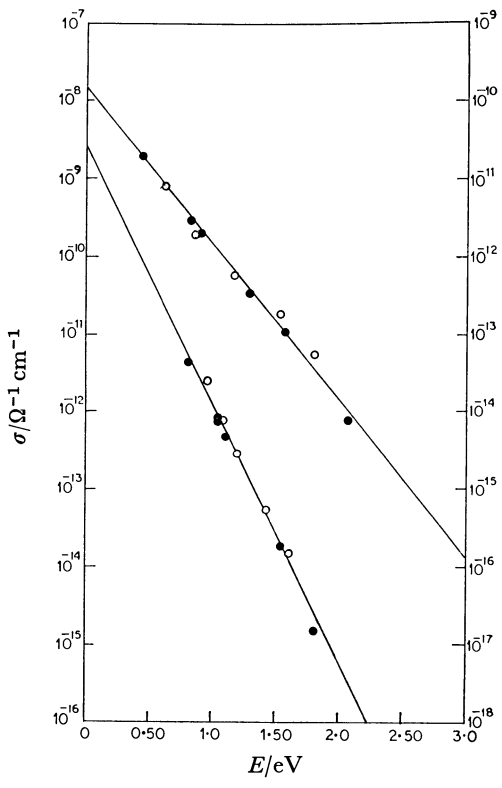

Fig. 5. Plot of the log σ values for vitamin A (alcohol and acetate) *vs.* E at a constant temperature ($1/T_1=3.8\times10^{-3}$ K^{-1}). The lower line refers to vitamin A alcohol (left scale) and the top line to vitamin A acetate (right scale). The dark circles refer to different vapors and the open circles to different amounts of same vapor. Slopes and σ_0' values are 7.70 eV^{-1} and 2.85×10^{-9} Ω^{-1} cm^{-1} for vitamin A alcohol; 4.55 eV^{-1} and 1.6×10^{-10} Ω^{-1} cm^{-1} for vitamin A acetate respectively.

Using the values of $1/2kT_0\approx14.45$ eV^{-1} and $\sigma_0'=2.8\times10^{-9}$ Ω^{-1} cm^{-1} for vitamin A alcohol, $1/2kT_0=17.52$ eV^{-1} and $\sigma_0'=1.5\times10^{-10}$ Ω^{-1} cm^{-1} for vitamin A acetate, we calculate the expected σ_0 values and compare these with experimentally measured values as obtained from the intercepts of the log σ *vs.* $1/T$ plots. These are shown in Tables 1 and 2. These data confirm the validity of Eq. 3 for vitamin A semiconductor.

The plots of log σ (T_1) *vs.* E are shown in Fig. 5 for $1/T_1\approx3.8\times10^{-3}$ K^{-1}. Taking $1/(2kT_0)\approx14.45$ and 17.52 eV^{-1} from Fig. 4, the expected slopes are 7.73 and 4.66 eV^{-1} for vitamin A alcohol and acetate respectively. The observed slopes in Fig. 5 are 7.70 and

Table 1. Semiconduction parameters for vitamin A (alcohol and acetate) on adsorption of various vapors according to Eq. 3

Vapors adsorbed	Ionization potential[a]	Vitamin A alcohol (solid state crystalline powder) $(2kT_0)^{-1}=14.45$ eV^{-1}, $\sigma_0'=2.8\times10^{-9}$ Ω^{-1} cm^{-1}			Vitamin A acetate (solid state crystalline powder) $(2kT_0)^{-1}=17.52$ eV^{-1}, $\sigma_0'=1.5\times10^{-10}$ Ω^{-1} cm^{-1}		
	eV	E / eV	$\sigma_0'\exp[E/(2kT_0)]$ / Ω^{-1} cm^{-1}	σ_0 / Ω^{-1} cm^{-1}	E / eV	$\sigma_0'\exp[E/(2kT_0)]$ / Ω^{-1} cm^{-1}	σ_0 / Ω^{-1} cm^{-1}
Toluene	8.81	0.80	2.93×10^{-4}	4.1×10^{-4}	0.448	3.84×10^{-7}	6.1×10^{-7}
Benzene	9.24	1.04	9.41×10^{-3}	7.98×10^{-3}	0.821	2.65×10^{-4}	3.8×10^{-4}
Ethyl acetate	10.11	1.06	1.26×10^{-2}	1.15×10^{-2}	0.896	9.85×10^{-4}	1.7×10^{-3}
Heptane	10.35	1.10	2.24×10^{-2}	2.6×10^{-2}	1.310	1.39×10^{0}	1.2×10^{0}
Ethanol	10.50	1.55	1.49×10^{1}	1.3×10^{1}	1.570	1.32×10^{2}	7.0×10^{1}
Methanol	10.85	1.82	7.39×10^{2}	1.25×10^{3}	2.070	8.44×10^{5}	8.0×10^{5}

a) Ref. 7, pp. 669—689.

Table 2. Semiconduction parameters for vitamin A (alcohol and acetate) on adsorption of ethyl-acetate vapor of different amounts

Vitamin A alcohol (Solid state crystalline powder) $(2kT_0)^{-1}=14.45\ eV^{-1}$; $\sigma_0'=2.8\times10^{-9}\ \Omega^{-1}\ cm^{-1}$				Vitamin A acetate (Solid state crystalline powder) $(2kT_0)^{-1}=17.52\ eV^{-1}$; $\sigma_0'=1.5\times10^{-10}\ \Omega^{-1}\ cm^{-1}$			
Curve No. from Fig. 3(a)	E / eV	$\sigma_0' \exp[E/(2kT_0)]$ / $\Omega^{-1}\ cm^{-1}$	σ_0 / $\Omega^{-1}\ cm^{-1}$	Curve No. from Fig. 3(b)	E / eV	$\sigma_0' \exp[E/(2kT_0)]$ / $\Omega^{-1}\ cm^{-1}$	σ_0 / $\Omega^{-1}\ cm^{-1}$
1	0.94	2.22×10^{-3}	2.0×10^{-3}	1	0.63	9.32×10^{-6}	1.0×10^{-5}
2	1.08	1.68×10^{-2}	2.3×10^{-2}	2	0.89	8.87×10^{-4}	1.7×10^{-3}
3	1.19	8.22×10^{-2}	1.8×10^{-1}	3	1.16	1.00×10^{-1}	1.6×10^{-1}
4	1.43	2.64×10^{0}	3.5×10^{0}	4	1.52	5.51×10^{1}	1.5×10^{1}
5	1.62	4.11×10^{1}	3.0×10^{1}	5	1.80	7.43×10^{3}	1.2×10^{3}

Curve No. 1→5 corresponds to the decreasing amount of adsorbed ethyl acetate vapor.

4.55 eV^{-1} for these two compounds respectively. The agreement is excellent. Also the intercepts give $\sigma_0' \approx 2.85\times10^{-9}\ \Omega^{-1}\ cm^{-1}$ for vitamin A alcohol and $\sigma_0' \approx 1.6\times10^{-10}\ \Omega^{-1}\ cm^{-1}$ for vitamin A acetate. These values agree well with the values obtained from the log σ_0 *vs.* E and log σ *vs.* $1/T$ plots. Thus the high correlation between the relevant parameters in semiconducting vitamin A powder on adsorption of various vapors indicates that Compensation rule is valid in these biological semiconductors and that σ_0 and E are indeed physically related.

Type of Interaction between the Adsorbed Gas and the Semiconducting Material. It needs to be pointed out that the reason for the semiconduction activation energy change is not quite settled.[8,11] However, donor-acceptor complex formation has been widely held responsible for the increase of current in some semiconductors[15-17] due to gas adsorption. As the vapors used in this present investigation are good electron donors and polyenes are known to act both as electron donor and electron acceptor,[18,19] formation of charge-transfer complexes of vitamin A (alcohol and acetate) with the adsorbed vapors may be possible. It had generally been observed[20,21] that in solid charge-transfer complexes with a particular acceptor and a number of similar type of donors, the semiconduction activation energy as obtained from relation (1) and the energy ($h\nu_{CT}$) of the lowest charge-transfer band are linearly related by the expression

$$E = h\nu_{CT} - \delta = I_D - E_A + C_1 - \delta \quad (4)$$

where, I_D is the vertical ionization potential of the donor, E_A is the vertical electron affinity of the acceptor, C_1 is a constant[22] and δ is also another constant of very low value.[20] In Fig. 6, we show a plot of E *vs.* I_D. A linear relationship is obtained as expected from Eq. 4. The slope of the line (0.6) however, is much less than unity. Such a value for the slope is a rather general observation[23,24] in $h\nu_{CT}$ *vs.* I_D plots. The intercept of this plot is −3.8 eV. The value of $-C_1$ is usually[22,25] around 3 eV. The electron affinity of anhydro vitamin A which is expected to be close to that of vitamin A (alcohol and acetate) has been reported to be[26] 0.7 eV. This gives a value of 0.1 eV for δ which is a very reasonable value.[21,23] This adds further credence to the proposed charge-transfer concept.

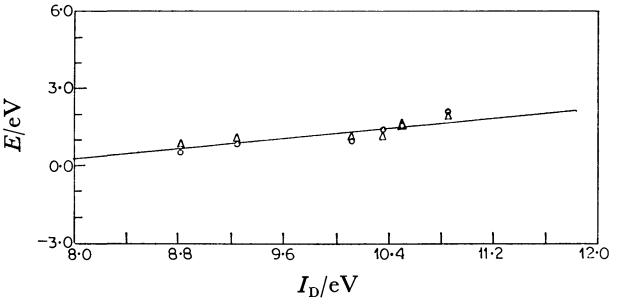

Fig. 6. Semiconductive activation energy (E) *vs.* ionization potential (I_D) of the adsorbed vapor molecules.
—△—: Vitamin A alcohol.
—○—: Vitamin A acetate.

There are number of theses about the mechanism of conduction in organic semiconductors leading to compensation effect. The carrier injection model of Green[27] produces the type of activation energy dependence of the pre-exponential factor as observed experimentally, but does not provide any physical basis for the interpretation of T_0. Significant difference in T_0 values for these two compounds suggests that T_0 is a molecular characteristic of these organic semiconductors. Kemeny and Rosenberg[28] observed compensation law in tunneling of small polaron through molecular barrier from thermally activated energy levels of molecules. Their model predicts that $T_0=\theta/2$ (where θ is the Debye temperature) and that at $T>T_0$, small polaron tunneling is not possible and compensation effect is not expected to be observed. No experimental study seems to have been reported on the semiconductive behavior of organic compounds at $T>T_0$. Debye temperature for vitamin A alcohol and acetate are not known. It has been reported[29] that the Debye temperature for a series of crystals of large aromatic molecules lie in the range 100—130 K. It seems that the T_0 values measured are far too high to justify the polaron tunneling model.

An interaction between the electrons and the vibrational motion has been thought[9,10] to be the mechanism behind compensation effect. A change in the electronic state (due to complex formation) gives rise to an activation entropy because of a change in vibrational frequencies. The variation in both the electronic energy gap

(E_g) and the activation entropy (S) can account for compensation effect if the changes in these parameters are given by

$$E_g = E_{g_0} + nE_{g_1} \text{ and } S = S_0 + nS_1$$

where n is a definite number for each system and E_{g_0}, E_{g_1}, S_0 and S_1 are same for all the systems. In this case the characteristic temperature is given by

$$T_0 = E_{g_1}/(2S_1).$$

Unfortunately due to the fact that the nature of the activated complex is not precisely known, the activation entropy S (hence S_1) is a relatively obscure quantity and any quantitative estimate of T_0 is not possible.

We thank the Council of Scientific and Industrial Research, India for a Senior Research Fellowship (to B. M.) and Prof. G. S. Kastha for his kind interest in this problem. Thanks are also due to M/s Hoffmann-La Roche and Co., Switzerland for a kind gift of the polyenes.

References

1) D. D. Eley, *J. Polym. Sci., Part C*, **17**, 73 (1967).
2) B. Rosenberg, B. Bhowmik, H. C. Harder, and E. Postow, *J. Chem. Phys.*, **49**, 4108 (1968).
3) D. D. Eley, A. S. Fawcett, and M. R. Willsis, *Trans. Faraday Soc.*, **64**, 1513 (1968).
4) G. R. Johnston and L. E. Lyons, *Aust. J. Chem.*, **23**, 2187 (1970).
5) K. Ulbert, *Aust. J. Chem.*, **23**, 1347 (1970).
6) M. Masui, H. Nagasaka, and K. Yahagi, *Jpn. J. Appl. Phys.*, **16**, 177 (1977).
7) F. Gutmann and L. E. Lyons, "Organic Semiconductors," John-Wiley, New York (1967), pp. 428—435.
8) B. Rosenberg, *J. Chem. Phys.*, **36**, 816 (1962).
9) G. Kemeny and I. M. Goklany, *J. Theor. Biol.*, **40**, 107 (1973).
10) T. A. Kaplan and S. D. Mahanti, *J. Chem. Phys.*, **62**, 100 (1975).
11) T. N. Misra, B. Rosenberg, and R. Switzer, *J. Chem. Phys.*, **48**, 2096 (1968).
12) B. Rosenberg, T. N. Misra, and R. Switzer, *Nature*, **217**, 423 (1968).
13) B. Rosenberg, *Nature*, **193**, 304 (1962).
14) B. Rosenberg, "Physical Processes in Radiation Biology," Academic Press (1969), p. 119.
15) M. M. Labes and O. N. Rudyj, *J. Am. Chem. Soc.*, **85**, 2055 (1963).
16) P. J. Reucroft, O. N. Rudyj, and M. M. Labes, *J. Am. Chem. Soc.*, **85**, 2059 (1963).
17) P. J. Reucroft, O. N. Rudyj, R. E. Salomon, and M. M. Labes, *J. Phys. Chem.*, **69**, 779 (1962).
18) B. Pullman and A. Pullman, "Quantum Biochemistry," Interscience New York (1963), p. 440.
19) J. R. Platt, *Science*, **129**, 372 (1959).
20) H. Kuroda, K. Yoshihara, and M. Akamatu, *Bull. Chem. Soc. Jpn.* **35**, 1604 (1962).
21) H. Kuroda, M. Kobayashi, M. Kinoshita, and S. Takemoto, *J. Chem. Phys.*, **36**, 457 (1962).
22) E. C. M. Chen and W. E. Wentworth, *J. Chem. Phys.*, **63**, 3183 (1975).
23) H. McConnel, J. S. Ham, and J, R. Platt, *J. Chem. Phys.*, **21**, 66 (1953).
24) R. Foster, *Tetrahedron*, **10**, 96 (1960).
25) A. L. Farragher and F. M. Page, *Trans. Faraday Soc.*, **63**, 2369 (1967).
26) V. G. Mairanovsky, A. A. Engovatov, N. T. Ioffe, and G. I. Samokhvalov, *J. Electroanal. Chem.*, **66**, 123 (1975).
27) M. E. Green, *J. Chem. Phys.*, **51**, 3279 (1969).
28) G. Kemeny and B. Rosenberg, *J. Chem. Phys.*, **53**, 3549 (1970).
29) E. I. Mukhtarov, A. A. Pichurin, and A. I. Kitaigorodskii, *Sov. Phys. Solid State (U.S.A.)*, **17**, 1871 (1975).

Diffusion Thermoeffect in Gases (The Dufour Effect)

Ali BOUSHEHRI* and A. ABBASPOUR
Department of Chemistry, Shiraz University, Shiraz, Iran

(Received July 24, 1978)

A study of the Dufour effect was made for four different gas mixtures: SF_6–N_2O, SF_6–N_2, SF_6–CO_2, and He–CO_2. Measurements were made at 300 K under 700 Torr. The values of the thermal diffusion factor were calculated for the above mixtures from experimental data on the basis of the thermodynamics of irreversible processes. A theoretical study was made also to calculate the thermal diffusion factor from kinetic theory.

The diffusion thermoeffect arises when a concentration gradient exists in a gas mixture. This gradient leads to a transient nonuniform temperature. Therefore, this effect is related to thermal diffusion, where a concentration gradient arises as a result of an initial temperature gradient. The thermal diffusion factor can be obtained from the diffusion thermoeffect which is a supplement to the more usual methods of measuring thermal diffusion factors.[1]

The Dufour effect[2] was not extensively investigated until after its rediscovery by Waldmann in 1942.[3] Although the possibility of this effect is contained in the Chapmann-Enskog theory[4] of non-uniform gases, only recently have its experimental measurements been made. For the measurement of the temperature gradient (which is a result of an initial concentration gradient) an apparatus similar to that used by Boushehri and Afrashtehfar[5] was constructed for the work discussed here. Apart from Rastogi and Madan's work,[6] and the classic studies of Waldmann, very little work in this area has been done. Mason *et al.*[7] made a study of the pressure dependence of this effect and, more recently, Sawford *et al.*[8] and Boushehri[5,9] have published more measurements. There is obviously a need for further independent studies, both to verify and to extend these few experimental studies.

Suppose two gases (labelled with subscripts 1 and 2), initially at the same temperature, diffuse into each other. On the basis of irreversible thermodynamics,[5,10] it may be shown that

$$\frac{\rho_1 RTD_{12}\alpha}{C_1\{M_1-C_1(M_1-M_2)\}}\frac{\Delta C_1}{\Delta X}+\lambda\frac{\Delta T}{\Delta X}=K, \qquad (1)$$

where ρ_1 and C_1 are the mass density and mass franction of component 1, respectively; α is the thermal diffusion factor; λ and D_{12} are heat conductivity and diffusivity coefficients, respectively; M_1 and M_2 are the molar weights; ΔX is the distance between thermocouples; and ΔT is the maximum temperature difference. K is a constant which depends on the geometry of the cell (in particular, the position of thermocouples); K has to be experimentally determined from experimental data. It is possible to leave $K=0$ as Rastogi and Madan[6] did, but this would not be the most general case.

Thermal diffusion factors have been estimated from the experimental data. Calculations for the first approximation to the thermal diffusion factor in binary mixtures was done on an IBM 370 model 135 computer for all four systems to check the values of the thermal diffusion factors deduced from Dufour effect against the values predicted by the Chapmann-Enskog kinetic theory. The experimental value for the thermal diffusion factor is comparable with its theoretical value for equimolar mixtures.

Experimental

The apparatus employed was similar to that used by Boushehri and Afrashtehfar.[5] The apparatus consisted of two double-walled glass bulbs (1, 2) of capacity 50-ml each. The two half-cells were connected by a narrow tube via stopcock having a bore of 8 mm diameter. A three junction thermocouple and a Leeds and Northrup potentiometer (± 1 μV) was used by which ΔT could be estimated to ± 0.01 °C. The thermocouples were parallel to the diffusion interface. The distance between two thermocouples was equal to 18.5 cm. The apparatus was kept in an oil bath. The temperature of bath was controlled to ± 0.1 °C. The apparatus was kept in a thermostat for two hours to insure thermal equilibrium. The annular space between the double walls of the bulbs was then evacuated to minimize heat dissipation. The apparatus was allowed to remain for further two hours to insure constancy of temperature. When the stopcock connecting the two half-cells was opened, diffusion of the gases caused a temperature gradient. This was measured as indicated above.

SF_6, N_2, and CO_2 were supplied by the Matheson Co. He and N_2O were supplied by the Fluka Co. The gases were used without further purification, since the results were not expected to be sensitive to small impurities. The purity was at least 99.9%.

Results and Discussion

The mixtures studied were: SF_6–N_2O, SF_6–N_2, SF_6–CO_2 for which the Dufour effect has not been measured previously. A CO_2–He mixture was used to determine the apparatus constant. Thermo-emf was measured using a three junction thermocouple in conjunction with the potentiometer. The temperature of the half-cell containing the lighter component always rose. The values of maximum temperature $(\Delta T)_{max}$ are given in Table 1. No measurement of $(\Delta T)_{max}$ other than for pure gases were made.

The diffusion thermoeffect is of interest in its own right and because it enables us to obtain quantitative information of the other transport coefficients, especially the thermal diffusion factor. An explicit derivation of the thermal diffusion factor on the basis of irreversible thermodynamics is given in Ref. 5. All measurements were made at 300 K and 700 Torr.

From irreversible thermodynamics the relationship between the temperature gradient and concentration gradient is shown by Eq. 1, where K is an apparatus

Table 1. Dufour effect in gaseous systems at 300 K and 700 Torr

System	$(\Delta T)_{max}$ in K($\pm$0.01)	Warm side
$He+CO_2$	0.11	He
N_2+SF_6	0.12	N_2
N_2O+SF_6	0.16	N_2O
CO_2+SF_6	0.18	CO_2

Table 2. Comparison of the values of α for different systems

System	α, from Eq. 1	α, from thermal diffusion measurement	α, from Equation (8.2—50) of Ref. 12
$He+CO_2$	0.42	0.45[a)]	0.398
N_2+SF_6	0.13	—	0.192
N_2O+SF_6	0.12	—	0.073
CO_2+SF_6	0.12	—	0.075

a) The value of α was obtained using Table 2 of Boushehri.[9)]

constant which depends on the position of thermocouples and the geometry of the cell. It may be possible to get an expression for this constant by studying variation of ΔT with both position of thermocouples and the geometry of the cell. Equation 1 can be used to estimate the value of α from the values of $(\Delta T)_{max}$ provided that ΔC_1 is known. ΔC_1 can be obtained by using the integrated form of Fick's second law of diffusion,[11)] which is given by

$$C_t = \frac{1}{2} C_0 \left[1 - erf \frac{X}{2\sqrt{Dt}} \right] \qquad (2)$$

D is the diffusion coefficient and t is the time in seconds when reaches a maximum value and is known from expcriment. C_t is the concentration of the particular component in the second chamber at time t, C_0 is the concentration of the component in the original chamber, and X is the distance from thermocouple to the plane of initial separation of components. For λ and ρ_1 in Eq. 1, we had some difficulty in assigning the values since these were not known at various concentrations. Therefore, the values for pure components were used. By setting the value of α=0.45 for carbon dioxide–helium mixture in Eq. 1, the apparatus constant K was estimated to be 3.05×10^{-5}. This point was not considered by Rastogi and Madan who left K=0 in their work. Since the distance between two thermocouples was the same in all experiments, this value of K was used for calculation for other systems. The values of α obtained in this way are recorded in the second column of Table 2. These are of the same order of magnitude as the values of thermal diffusion factors for equimolar mixture obtained from Equation (8.2—50) of the treatise of Hirschfelder *et al.*[12)] (Column 4).

In our system, a rather large concentration gradient was present which may be eliminated by taking a binary mixture in two half cells instead of pure gases. Also there was a convective mixing effect. In choosing the values of λ and ρ_1 in Eq. 1 there was some arbitrariness, the values of these parameters used being the values of the pure components.

The interpretation of the diffusion thermoeffect is more complicated than thermal diffusion since there is heat conductivity involved in the former but not in the latter. This is the disadvantage of this method compared to the thermal diffusion measurements. On the other hand, the Dufour effect gives the value of α at specific temperatures. In short, this method shows considerable promise as a means of obtaining the value of gas transport coefficients.

We thank the Iranian Ministry of Higher Education Research Foundation and the Department of Chemistry of Shiraz University for the research facilities.

References

1) K. E. Grew and T. L. Ibbs, "Thermal Diffusion in Gases," Cambridge Univ. Press, London (1952).
2) L. Dufour, *J. Chem. Soc.*, **26**, 835 (1873).
3) K. Clusius and L. Waldmann, *Naturwissenschaften*, **30**, 135 (1942).
4) S. Chapman and T. G. Cowling, "The Mathematical Theory of Non-uniform Gases," Cambridge Univ. Press, 2nd ed, London (1952).
5) A. Boushehri and S. Afrashtehfar, *Bull. Chem. Soc., Jpn.*, **48**, 2372 (1975).
6) R. P. Rastogi and G. L. Madan, *Trans. Faraday Soc.*, **62**, 3325 (1966).
7) E. A. Mason, L. Miller, and T. H. Spurling, *J. Chem. Phys.*, **47**, 1669 (1967).
8) B. L. Sawford, T. H. Spurling, and D. S. Thurley, *Aust., J. Chem.*, **23**, 1311 (1970).
9) A. Boushehri, *J. Chem. Eng. Data*, **19**, 313 (1974).
10) S. R. de Groot and J. Mazur, "Non-equilibrium Thermodynamics," North Holland Publishing Co., Amsterdam (1962).
11) W. Jost, "Diffusion in Solids, Liquids and Gases," Academic Press, Inc., New York (1960).
12) J. O. Hirschfelder, C. F. Curtiss, and R. B. Bird, "Molecular Theory of Gases and Liquids," John Wiley & Sons, Inc., 2nd ed, New York (1964).

Infrared Studies on Water Adsorption Systems with the Use of HDO. II. Na-Y Zeolite

Masao HINO* and Yasuko MIKAMI

Government Industrial Development Laboratory, Hokkaido, Higashi-tsukisamu, Toyohira-ku, Sapporo 061-01

(Received July 5, 1978)

Infrared spectra of the systems of Na-Y zeolite–H_2O, D_2O, and HDO were measured. It was shown that there are three types of adsorbed water in the zeolite–water system. Type I: adsorbed in a state in which two hydroxyl bonds are highly non-equivalent; it gives absorptions at 3695, 3400, and 1645 cm^{-1}, and is the same type as that on the Molecular sieve 13X.[1] Type II: adsorbed in another state in which the bonds are nearly equivalent; it gives bands at 3610, 3540, and 1645 cm^{-1}. Type II was more resistant to dehydration than Type I, and was irreversible for the back-adsorption of a small amount of water at room temperature, whereas Type I was almost completely reversible. Type III was observed for back-adsorption under this condition; it gives bands at 3635, 3500, and 1655 cm^{-1}. Type III can be transformed into Type II by heat treatment at a temperature which varies depending on the amount of adsorbed water. The other bands were assigned as follows: Bands at 3750 and 3645 cm^{-1} correspond to stretching of surface structural OH, and that at 3240 cm^{-1} to overtone deformation of adsorbed water. The sites of adsorbed water molecules of Types I and II were discussed.

In a previous paper[1] one of the authors showed that HDO could be effectively used for the IR analysis of water adsorption systems through the analysis of the system on Molecular sieves 13X and 4A. In the present paper, the water adsorption system on Na-Y zeolite will be analyzed by employing the same technique.

A number of IR studies have been published on the water adsorption system.[2–5] However, not all of the bands have been clarified, and there are some disagreements about the spectra observed and their assignments. The purpose of the present work is to analyze the spectra of the system on the basis of information obtained from a new technique employing HDO. The sites of the adsorbed water molecules will also be discussed.

Experimental

Linde Molecular sieve SK-40 (UNION SHOWA Co., Ltd.), which is a synthetic Na-Y zeolite, was used as the sample. Major components of the material were SiO_2 63.5, Al_2O_3 23.5, and Na_2O 13.0 in wt %. The crystallinity of the sample was confirmed to be sufficiently high by the measurements of X-ray diffraction and surface area (903 m^2/g, N_2).

Two IR spectrophotometers, a DIGILAB Model 15-B FTS and a JASCO Model 402-G, were used for recording the spectra. The latter instrument was calibrated against the former by use of ammonia, water vapor, and hydrogen bromide.

Other materials, apparatus, and procedures were the same as described before.[1]

Results

Spectra for the Desorption Process. The spectra of Na-Y zeolite–D_2O and H_2O systems after being evacuated at various temperatures are shown in Figs. 1 and 2. As seen in the Figs. various bands observed in the spectra of the two systems after the corresponding evacuation treatments can be easily matched with each other. These matching bands will be referred to using the same letters: a, b,···, and g for the spectra of both systems. Frequencies of these observed bands

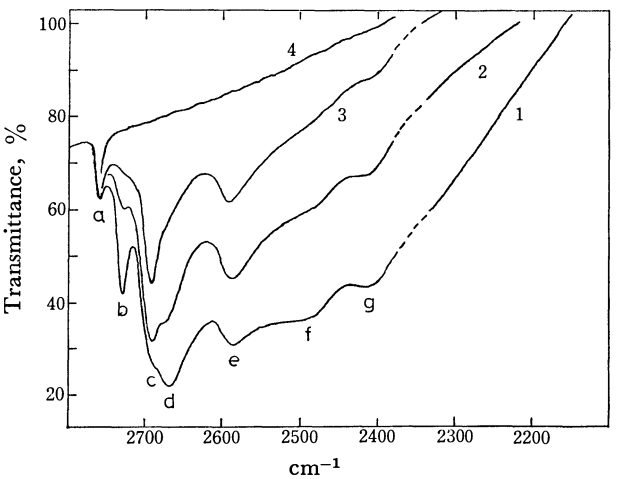

Fig. 1. Spectra of the Na-Y–D_2O system, on the desorption process.
Evacuated for (1) 1 h at 90 °C, (2) 1 h at 120 °C, (3) 30 min at 165 °C, (4) 3 h at 500 °C. "Thickness" of the sample piece was 18 mg/cm^2.

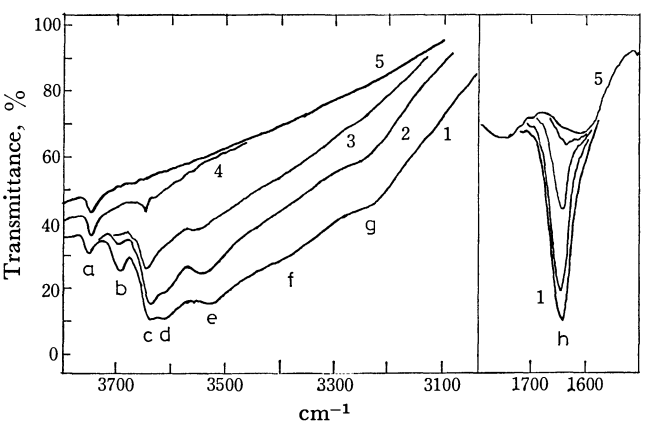

Fig. 2. Spectra of the Na-Y–H_2O system, on the desorption process.
Evacuated for (1) 1 h at 90 °C, (2) 1 h at 120 °C, (3) 30 min at 165 °C, (4) 45 min at 200 °C, (5) 3 h at 500 °C. Sample piece "thickness" 18 mg/cm^2.

Table 1. Summary of the IR bands of Na-Y zeolite–water system

Band symbol	D_2O system (cm^{-1})	H_2O system (cm^{-1})	HDO system (cm^{-1}) Stretching regions OD	OH	Deformation region	Assign
			(1) The desorption process			
a	2760	3750	2760	3750		1)
b	2730	3695	2714	3690		2)
c	2692	3645	2692	3645		3)
d	2668	3610	2647	3600		4)
e	2586	3540	2615	3540		5)
f	2490	3400	2490	3380		6)
g	2405	3240				7)
j				2940		8)
k					1460	9)
n					1422	9)
h		1645				
l					1450	10)
m					1440	10)
			(2730)			11)
			(2) The adsorption process			
a	2760	3750	2760	3750		12)
b	2730	3695	2717	3690		13)
o	2675	3635				
q			2580	3250		14)
p	2575	3500				
f	2480	3350	2465	3350		15)
g	2405	3240				16)
j				2960		17)
s		1655				18)
r					1495	18)
h		1640				
k					1460	19)
n					1422	19)

1,12), 3): OD(OH) stretching of structural deuteroxyl groups. 2,13), 6,15), 9,19): OD(OH) stretching and deformation of Type-I water. 4), 5), 10): OD(OH) stretching and deformation of Type-II water. 7,16): DOD(HOH) overtone deformation of adsorbed water. 8, 17): Overtone deformation of adsorbed HDO. 11): Arising from D_2O impurity. 14), 18): OD(OH) stretching and deformation of Type-III water.

are summarized in Table 1-(1) together with those of the corresponding bands observed for the HDO system and also with their assignments. The spectra observed for the H_2O system were similar to those reported by Ward,[2] with the exception that the band appearing at 3630 cm^{-1} in his spectra was observed to be clearly separated into two bands at 3645 (c) and 3610 cm^{-1} (d) in our spectra. Bands which were equivalent to these appeared at 2692 and 2668 cm^{-1} for the D_2O system.

Spectra observed for the HDO system in the OD, OH stretching and the HOD deformation regions are shown in Figs. 3 and 4. Those spectra shown in Figs. 3 and 4 were measured after the same evacuation treatments as those performed prior to the measurements of the spectra shown in Figs. 1 and 2, respectively, so that a comparison between the spectra of the D_2O or H_2O system and of the HDO system should be reasonable.

Correlations between the spectra in the OD stretching region of the HDO system and those of the D_2O system were analogous to those between the spectra in the OH stretching region of the HDO system and those of the H_2O system.

As in the case of the Molecular sieve 13X–water system,[1] bands a and c in the spectra of the D_2O or H_2O system appeared at just the same frequencies for the HDO system (bands a′ and c′ in Figs. 3 and 4). Band b shifted toward the lower frequency side by 16 cm^{-1} in the OD stretching region and by 5 cm^{-1} in the OH region for the HDO system. The weak absorption at 2730 cm^{-1} in Fig. 3 arises obviously from the D_2O present in the sample water mixture (about 6.3%). Band g disappeared from the spectra of the HDO system. A new band appeared for the HDO system at 2940 cm^{-1} in the OH stretching region; it can be attributed to an overtone deformation or a combination band of adsorbed HDO, like the band at 2945 or 2910 cm^{-1} which appeared in other zeolite–HDO systems.[1] Bands at 2668 (d) and at 2586 cm^{-1} (e) in the spectra of the D_2O system disappeared from the OD stretching region of the HDO system. Two

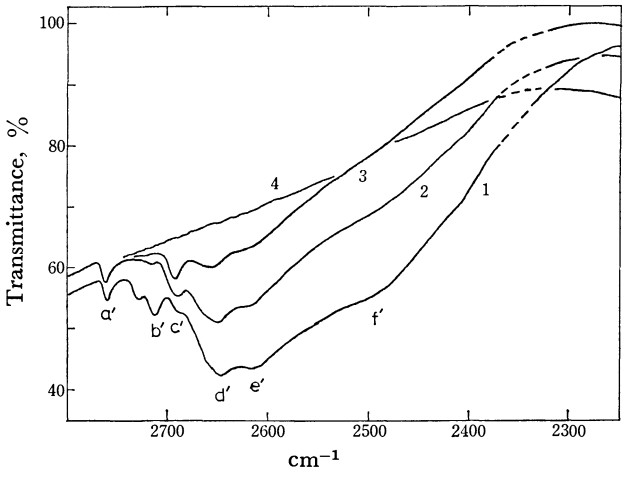

Fig. 3. Spectra of the Na-Y–HDO system in the OD stretching region, on the desorption process.
Evacuated for (1) 1 h at 90 °C, (2) 1 h at 120 °C, (3) 30 min at 165 °C, (4) 3 h at 500 °C after exposure to the vapor of H_2O–D_2O mixture of a molar ratio of 3 to 1. Sample piece "thickness" 40 mg/cm².

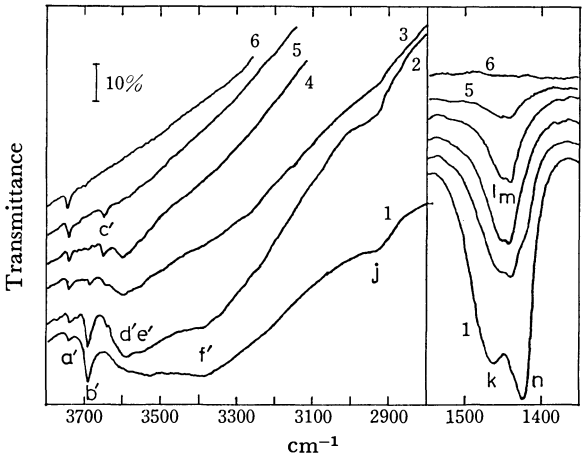

Fig. 4. Spectra of the Na-Y–HDO system in the OH stretching and deformation regions, on the desorption process.
Evacuated for (1) 10 min at 90 °C, (2) 1 h at 90 °C, (3) 1 h at 120 °C, (4) 30 min at 165 °C, (5) 45 min at 200 °C, (6) 3 h at 500 °C after exposure to the vapor of H_2O–D_2O 1 to 5 mixture. The spectra shown in the deformation region were obtained by rationing each observed spectrum against that after 500 °C evacuation of the Na-Y–H_2O system. Sample piece "thickness" was 26 mg/cm².

new bands, presumably corresponding to bands d and e, appeared at 2647 (d') and 2615 cm^{-1} (e') in the OD stretching region. In the OH region these bands d' and e' were detected in the spectra after evacuation at lower temperatures (curves 1 and 2 in Fig. 4) at 3600 and 3540 cm^{-1}, which were nearly the same frequencies as those of d and e in the spectra of the H_2O system. After the evacuation at higher temperatures, however, the band e' could not be observed, probably because the absorption was weak and broad. In the deformation region four absorptions (k, l, m, and n) appeared at 1460, 1450, 1440, and 1422 cm^{-1} in the HOD deformation region for

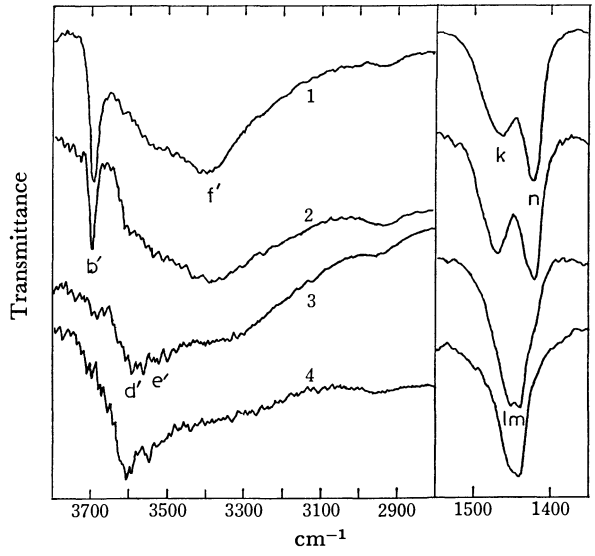

Fig. 5. Ratioed spectra of the Na-Y–HDO system in the OH stretching and deformation regions, on the desorption process. Obtained rationing (1) curves 1 and 2, (2) 2 and 3, (3) 3 and 4, (4) 4 and 5 of Fig. 4. The scale of the intensity is arbitrary as each curve is "auto expanded" into an identical hight in the frequency ranges indicated.

the HDO system, whereas only one at 1645 cm^{-1} (h) was found for the H_2O system.

On evacuation in a series where the evacuation temperature was elevated step by step, the intensity of the bands b and f for the D_2O (H_2O) system and also of the bands b', f', k, and n for the HDO system decreased preferentially in the initial steps, followed by the decrease of the bands d and e for the D_2O (H_2O) system and of d', e', l, and m for the HDO system. The intensity of band h decreased at a constant rate through the dehydration treatments. This can be seen directly in the ratioed spectra shown in Fig. 5. Those spectra were obtained for the HDO system by calculating the intensity differences between each curve shown in Fig. 4 by use of a computer system included in the FTS-15 spectrometer. Thus, it was suggested that bands b, f, and h for the H_2O (D_2O) system (corresponding bands b', f', k, and n for the HDO system) should have the same origin, while bands d, e, and the residual part of h (d', e', l, and m) came from another origin.

Spectra for the Adsorption Process. Spectral measurements on the adsorption process were also made for the systems of various kinds of water in the surface coverage of about 0—1.2 mmol/g. The general features of the spectra were almost identical irrespective of the degree of coverage in each of the systems, but were somewhat different from those of the spectra for the desorption process, as is seen in the typical examples shown in Figs. 6 and 7. Differences were found in two regions: one is the region where bands d and e appeared for the desorption process and the other is the deformation region. In the former, two relatively broad bands (o and p) appeared at 2675 and 2575 cm^{-1} for D_2O adsorption, and at 3635 and 3500 cm^{-1} for H_2O adsorption. Each of the former

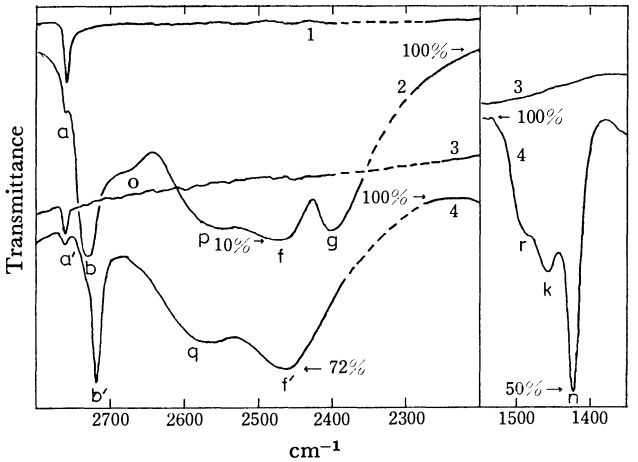

Fig. 6. Spectra of the Na-Y–D_2O and HDO systems in the OD stretching and the HOD deformation regions, on the adsorption process.
(1,3) Evacuated for 3 h at 500 °C, (2) 40 μmol of D_2O, (4) 40 μmol of H_2O–D_2O 7 to 1 mixture were readsorbed. All the curves were obtained by rationing the observed spectra against that after 500 °C evacuation of the Na-Y–H_2O system. Sample piece "thickness" 17 mg/cm².

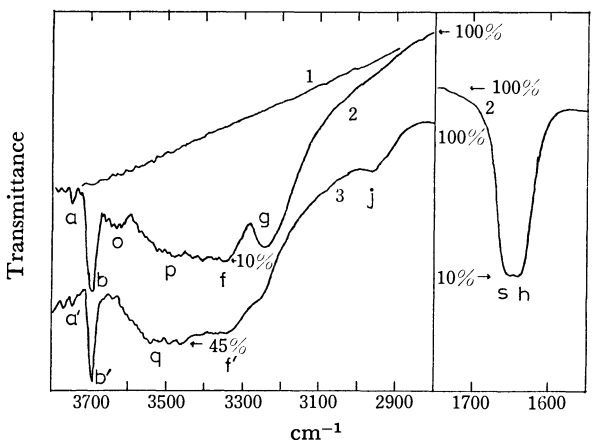

Fig. 7. Spectra of the Na-Y–H_2O and HDO systems in the OH stretching and the deformation regions, on the adsorption process. (1) Evacuated for 3h at 500 °C, (2) 24 μmol of H_2O, (3) 24 μmol of H_2O–D_2O 1 to 5 mixture were readsorbed. Curve 2 in the deformation region was obtained by rationing the observed spectra against that after 500 °C evacuation. Sample piece "thickness" was 17 mg/cm².

bands was very weak. For HDO only one broad band (q) was observed in the region around 2580 cm^{-1} for the OD region and around 3520 cm^{-1} for the OH region. Three deformation bands were observed for the HDO system, at 1495 (r), 1460 (k), and 1422 cm^{-1} (n), while two were found at 1655 (s) and 1640 cm^{-1} (h) for the H_2O system.

Observed frequencies of the various bands are summarized in Table 1-(2).

Discussion

Spectra for the Desorption Process. First, bands a and c can be assigned to the stretching vibrations of surface structural OH (OD) groups, while the remaining absorptions b, d, e, f, g, and h are attributable to some vibrations arising from adsorbed water molecules. This is because of the fact that each pair of corresponding bands, one appearing in the H_2O (D_2O) system and the other in the HDO system, of the former group appeared at the same frequency in the corresponding regions of the spectra of the H_2O, D_2O, and the HDO systems, while in the latter group the bands did not appear at the same frequency in at least one region of the spectra.

Thus there is just the same type of adsorbed water (Type I, adsorbed in a state in which its two hydroxyl bonds are highly non-equivalent) in the Na-Y zeolite–water system as the Type WX-I in the Molecular sieve 13X–water system which was reported in a previous paper.[1] That is, bands b, f, g, and h in the spectra of the present work are apparently attributed to the same vibrations as bands b, e, f, and at 1650 cm^{-1}, respectively, in the spectra of the 13X system. Each pair of these matching bands showed an almost identical behavior with the partial deuteration of the adsorption systems.

Absorptions d and e have been observed and reported only by Ward.[2] He assumed that they were due to some adsorbed water molecule, but no details were described. Our results in the present experiments support his assignment. Moreover, they give further information on the state of the adsorbed molecules as described below. When a water molecule is adsorbed in a state in which its two hydroxyl bonds are completely equivalent, the molecule is expected to give two stretching bands of ν_3 and ν_1 and one deformation band of ν_2 for H_2O (D_2O), as well as single OH and OD stretching bands which are located between the ν_3 and the ν_1 frequencies and one HOD deformation band for HDO. On the other hand, when the molecule is adsorbed in another state in which the hydroxyl bonds are not equivalent, H_A–O–H_B, it is expected that two OH stretching bands (one is rather characteristic of νOH_A and the other of νOH_B) and a single deformation band arise for H_2O and D-equivalent bands forD_2O. For HDO molecules in this state four stretching bands: νOH_A, νOH_B, νOD_A, and νOD_B and two deformation bands: $\delta H_A OD_B$ and $\delta H_B OD_A$ will occur. The degree of frequency difference between the vibrations νOH_A and νOH_B or between the two D-equivalent bands, as well as between the two deformation bands, will be larger, the larger the degree of the non-equivalency between the two hydroxyl (deuterioxyl) bonds. In the present results, bands d′ and e′, presumably corresponding to the $\nu OD_A(\nu OH_A)$ and the $\nu OD_B(\nu OH_B)$ of the HDO, appeared close to each other, being located between the frequencies of the corresponding bands d and e of the D_2O (H_2O). Thus, bands d and e can be assigned to the ν_3 and ν_1 vibrations of water molecules adsorbed in a state in which its two hydroxyl bonds are nearly equivalent (Type II). The result in the deformation region also supports this assignment. Two deformation bands (l and m) were observed to be very close to each other, with a difference of only

10 cm^{-1}, for the Type II adsorbed HDO. The corresponding difference was 38 cm^{-1} for the Type I water, in which the difference between the two OD stretching bands was 224 cm^{-1}. Hence, such a small difference of 10 cm^{-1} will be reasonable for the Type II water, in which the difference between the two OD stretching bands was 32 cm^{-1}.

In a previous paper[1] it was suggested that the weak absorption at 3590 cm^{-1} (D-equivalent band at 2645 cm^{-1}) in the spectra of the Molecular sieve 13X–water system was due to some type of adsorbed water molecule, but with no details. It is almost certain that the band arose from a similar type of adsorbed water to the present Type II water.

Spectra for the Adsorption Process. From a comparison with the spectra of the desorption process, the deformation band at 1640 cm^{-1} (h) in the H_2O system should correspond to those at 1460 (k) and 1422 cm^{-1} (n) of the HDO system, and the new band at 1655 (s) to that at 1495 cm^{-1} (r). This speculation is in harmony with the appearance of the bands in the stretching regions. Bands b, f, and g did appear at almost the same positions as those in the spectra of the desorption process; moreover, they showed similar behavior to those of the latter bands for the partial deuteration. On the other hand, bands o and p for the H_2O (D_2O) system and q for the HDO system are quite different in their spectral aspects from bands d, e, d′, and e′ of the desorption process. These facts indicate that the Type I water is almost reversible while the Type II is not, for readsorption of a small amount of water at room temperature.

The new bands o (3625, D-equivalent 2675 cm^{-1}), p (3500, D-2575 cm^{-1}), and s (1655 cm^{-1}) would be assigned to the ν_3, ν_1 and ν_2 vibrations of water adsorbed in some state with its hydroxyl groups equivalent (Type III), and bands q at 3520 and 2580 cm^{-1} and r (1495 cm^{-1}) to the OH stretching, OD stretching, and the deformation of the corresponding HDO molecules.

The state of these adsorbed molecules is obviously different from that of the Type II water, even if somewhat similar to it. In order to investigate this irreversibility a simple experiment was carried out. After 0.83 mmol/g of D_2O was back-adsorbed at room temperature, the sample piece, *in situ*, was heated up to 95 °C or 200 °C once, and then cooled slowly down to room temperature. It was found that the treatment at 200 °C gave rise to a great change in the spectrum, giving a similar spectrum to that on the desorption process with bands at 2694 (c), 2674 (d), and 2590 cm^{-1} (e). This indicates the rearrangement of the adsorbed water molecule, probably from the Type III to the Type II, and the formation of certain structural hydroxyl groups caused by dissociation of adsorbed water. And also it suggests that the Type II water is more stable than the Type III water. However, in the 95 °C treatment no spectral change occurred, whereas our spectra for the desorption process were obtained by 10 min of evacuation at 90 °C after the dried sample piece was saturated with water vapor. Thus, it is suggested that the occurrence of the rearrangement of adsorbed water and the formation of the hydroxyl groups depend on the degree of surface coverage as well as temperature. The details can not be known without further experiments.

Sites of Adsorbed Water Molecules. Mutual comparison of the results obtained for the present Na-Y zeolite and for the Molecular sieves 13-X (Na-X zeolite) and 4-A (Na-A zeolite)[1] makes it possible to discuss the sites of adsorbed water molecules.

Type I and Type II water existed on both the zeolites of Na-X and Na-Y, while on the Na-A zeolite Type I water could not be found. The single main type of adsorbed water observed on the Na-A is regarded to be similar to the Type II water in its symmetry.

Under such a condition of much lower surface coverage,[6] it is almost sure that the adsorption of water molecules occurred mainly on the zeolitic cations in such a manner that the lone pair electrons of the water oxygen atom are attracted to the positive charge of the cations, whether or not the hydrogen atoms are hydrogen bonded to the negatively charged oxygen of the zeolite lattice. Hence, it will be reasonable that the variety in the modes of adsorption should be discussed in connection with the kind of cation sites.

It is well known that the crystal structures of zeolites X and Y are essentially identical, but differ only in the number of their cations and the strength of the electrostatic force field around the cations. According to Rabo *et al.*,[7] there are three kinds of possible cation sites, S_I, S_{II}, S_{III}, in the zeolite structure. The number of each site is 16, 32, and 48, respectively, for a X type zeolite of which the ratio of Al and Si equals unity. These sites are occupied by exchangeable cations, fully or partially, depending on the type of the zeolite. On the other hand, Na-A zeolite[8] has another structure. But it includes sodalite cages similarly to the structure of the Na-X or Na-Y. There are two kinds of sites, S_1 and S_2, in the type A zeolite. For the Na-A, 12 Na cations are required per unit cell for electrical neutrality, of which 8 Na cations occupy the former site and the remaining 4 Na the other site.

Among those five kinds of sites, the site S_I can be ruled out of consideration because the cations positioned at that site will not be able to accept any adsorbate due to its small space. Site S_{II} is regarded to be similar to site S_1. Both are situated on the center of the six-membered rings of the sodalite cages facing toward the super cages of the zeolite structure, and have a C_{3v} symmetry in relation to the neighboring lattice oxygens. Site S_{III} is characteristic of zeolites X and Y, which is located on the center of four-membered rings of the sodalite cages and has a symmetry of C_{2v} in relation to the neighboring oxygens. Zeolite A has no such site.

From both the similarity and the differences among the three zeolites in the geometry around the possible cation sites and in the observed spectra, it is suggested that the Type I water is situated on the cations occupying the site S_{III}, whereas the Type II is on those of site S_{II}.

These attributions are supported by a comparison between the intensity of the spectra of each type of adsorbed water and the number of the cations occupying each site, as described below. The relative

amount of the Types I and II water on the Na-X and Na-Y zeolites can be estimated from the results shown in the present Fig. 1 or 2 and those shown in Fig. 1 or 2 of the previous report.[1] In that case, the intensity of the spectra of the 13-X water system must be compared with the other after being multiplied by a factor of 1.6, which appears from the differences in the sample thickness and the molecular weight per their unit cells.[9] Then, it can be seen that there is a much smaller amount of Type I adsorbed water on the Na-Y zeolite than on the Na-X. The Type II water is estimated to be present in much the same amount on both zeolites, or at least not so much less on the Na-X than on the Na-Y zeolite, though this is not very clear because of the overlapping of the spectra of the Types I and II water. On the other hand, according again to Rabo *et al.*,[7] the order of preference for cation occupation is $S_I > S_{II} > S_{III}$, which may lead to the conclusion that our Na-X sample (Si/Al=1.23) includes 16, 32, and 38 Na ions per unit cell for the respective sites, while the Na-Y sample (Si/Al=2.3) includes 16, 32, and 10, respectively. That is, the ratios of the cation number positioned on the same site in Na-X and Na-Y are 1:1 for the site S_{II} and 38:10 for the S_{III}. This may be comparable with the relative intensity of the spectral bands described above.

The molar absorptivity for the Type II water appears to be weaker than for the Type I water. This is probably due to the fact that the Type I water is more strongly polarized than the other. It has been shown by Dempsey[10] that the electrostatic force fields around the site S_{III} is some 50% stronger than that around site S_{II}.

It is obscure at present why and in what geometrical arrangements the Types I and II water are adsorbed on the sites, yielding such modes as described before. To answer this question, further experiments with the use of other techniques are necessary.

References

1) M. Hino, *Bull. Chem. Soc. Jpn.*, **50**, 574 (1977).
2) J. W. Ward, *J. Phys. Chem.*, **72**, 4211 (1968).
3) J. W. Ward, *J. Catal.*, **11**, 238 (1968).
4) C. L. Angell and P. C. Schaffer, *J. Phys. Chem.*, **69**, 3463 (1965).
5) G. Senkyr and H. Noller, *J. Chem. Soc., Faraday Trans. 1*, **71**, 997 (1975).
6) In the case shown in Fig. 7 the number of the adsorbed H_2O molecules corresponds to 0.05 in θ, provided that the cross section of the water molecule were 10.8 A^2, and to about one-sixth in number of the cations included to the sample.
7) J. A. Rabo, C. L. Angell, P. H. Kasai, and V. Schomaker, *Chem. Eng. Prog.*, **63**, *Sympo. Ser.*, No. **73**, 31 (1967).
8) P. A. Howell, *Acta Crystallogr.*, **13**, 737 (1960).
9) Thickness of the sample pieces were 12 mg/cm^2 and 18 mg/cm^2 respectively for the Na-X (Molecular sieve 13X) and Na-Y zeolites. Molecular weight of the zeolites per unit cells are 13423 g and 12809 g for Na-X and Na-Y, respectively.
10) Ref. 7, p. 33.

The Performance Characteristics of a Permeation Membrane Device for the Preparation of Dilute Standard Gas Mixtures

Takashi IBUSUKI,* Fumitoshi TOYOKAWA, and Kazunari IMAGAMI

National Research Institute for Pollution and Resources, Kawaguchi, Kawaguchi-shi, Saitama 332

(Received July 25, 1978)

The performance chracteristics of the permeation membrane device for the preparation of dilute standard gas mixtures developed by us was investigated in detail from the practical standpoint. By selecting a silicone-rubber and a TFE Teflon for CO or CH_4, and NO or SO_2, respectively, the steady permeation state was rapidly attained. The small quantities of the gases permeating through the membranes were precisely determined within a relative standard deviation of 1% based on a pressure-differential method. It was confirmed that the permeation rates were reproducible after repeated membrane-temperature, gas-pressure, and gas-cycle changes during an experimental period of more than five months. By changing the gas pressure and the membrane temperature, and by introducing 1—2 l min^{-1} of a diluent gas, N_2 or air, standard gas mixtures containing 0.5—10 ppm of CO or CH_4 and 0.05—0.7 ppm of NO or SO_2 were easily obtained. The standard gases concerning CO, CH_4, and NO were compared with those in cylinders prepared by the weighing method, and for SO_2 the concentration of the gas was checked by the West-Gaeke method. A good agreement in concentration was observed for CO, CH_4, and SO_2; the discrepancy found for NO was explained in terms of the decrease in the NO concentration in the cylinder.

For the accurate determination of the concentrations of gaseous pollutants at ppm and ppb levels, standard reference materials are needed to calibrate the air-monitoring instruments. Accurate gas mixtures in cylinders at 10 ppm levels have been prepared by the weighing method for various gases.[1] However, mixtures of nitrogen dioxide (NO_2) or sulfur dioxide (SO_2) change greatly in concentration with the time because of their adsorption or reaction with the cylinder wall. Permeation tubes for the condensable gases were proposed by O'Keeffe and Ortman,[2] and their performance characteristics have been widely investigated.[3—10] Unfortunately, several months or more are required to calibrate the low gas-permeation rates of the tubes by means of standard gravimetric methods at a constant, strictly controlled temperature. Dietz *et al.* recently proposed a rapid calibration method using the pressure-differential technique to measure microgram quantities of gas permeating through the plastic membrane or diffusion devices.[11,12] The device using the membrane can also be applied to non-condensable gases, such as nitrogen monooxide (NO), carbon monooxide (CO), and methane (CH_4). However, the performance characteristics of the device in the preparation of dilute standard gas mixtures have not yet been reported. We have previously studied the performance characteristics of a commercial apparatus based on the permeation method and have pointed out some of its defects from the standpoint of practical value.[13] The permeability of gaseous pollutants through various kinds of plastic membranes has, therefore, been investigated.[14] It was shown that various kinds of standard gas mixtures, ranging widely in concentration, can be prepared by selecting an appropriate combination of pure pollutant gas and membrane, together with an appropriate gas pressure and membrane temperature.

We wish to report here the performance characteristics of the permeation membrane device we have developed with regard to the following subjects: precision in the measurement of a gas-permeation rate, the dependence of the rate on the gas pressure or the membrane temperature,[13] the long-term stability of the rate under many temperature changes,[8] the procedure and the length of time to reach a steady permeation rate,[10] and, especially, whether or not the gas-permeation phenomenon will change because of the different conditions of the membrane in the measurement of the permeation rates of gas and in the preparation of dilute gas mixtures. Silicone-rubber and TFE Teflon membranes are used for CO or CH_4, and for NO or SO_2, respectively, since their permeation rates and the length of time to reach steady permeation rates have been suggested to be favorable for the precise and rapid preparation of very dilute gas mixtures.[14] Moreover, the concentrations of the dilute gases are examined by using analyzers and standard gas mixtures in cylinders for CO, CH_4, and NO, because it is important to compare the standard gases prepared by the permeation device with those in cylinders prepared by the weighing method. For SO_2, the concentration is determined by the West-Gaeke method because of the lack of reliable dilute standard gas mixtures in cylinders. The results are also discussed with respect to the development of a practical type of the permeation device.

Experimental

Apparatus. The apparatus used here is shown schematically in Fig. 1. It consists of a test cell (C), a vacuum system, a differential pressure transducer (VG), and gas-feed systems for a pure pollutant gas and a diluent gas. A flat plastic membrane (M, with an effective area for permeation of 3.14 cm^2) is held between two metal flanges and sealed with Viton-O-rings. Thin stainless steel screens are inserted between the membrane and the flanges in order to avoid the deformation of the membrane. One flange is connected to the pollutant gas source, and the other one, to the fixed-volume system (the shaded part) and the diluent-gas source. The cell is placed in a constant-temperature water bath (TB) controlled within ±0.05 °C (Riko-Kagaku Co., Model UH-1000E). The vacuum system is of Pyrex glass tubes, and the stopcocks (1—11) are made of glass and Teflon (Young Co.) in order to avoid the ad-

sorption of the pollutant gases on the grease of the usual vacuum cocks. The system can be evacuated below 5×10^{-6} mmHg (1 mmHg=133.32 Pa) by means of an oil-diffusion pump (DP), an oil-rotary pump (RP), and a liquid-nitrogen trap. The volume of the shaded part was determined to be 215 ± 2 cm^3 by using the known volume of the glass vessel (H, 1188 ± 8 cm^3). The pressure transducer is composed of an MKS Baratron 310 AH sensor head and an 170 M-7A electronic unit, measuring the pressure range from 3×10^{-5} to 1 mmHg within a 1% accuracy. The pure pollutant gas is introduced to the cell through the 1 cock, the Hg bubbler (B), and the 2 cock. The pressure is precisely read by the Hg manometer (P). The diluent gas (very purified nitrogen or air) passes through the 4 cock, the upper compartment of the cell, and the 5 cock, and is then introduced into an analyzer. The flow rate of the diluent gas is controlled by a mass-flow-rate controller (F, Ohkura Electronic Co., Model MFC-1), which is usually calibrated by means of a soap-bubble flow-meter.

Operational Procedures. Measurement of the Gas-permeation Rate: All the systems, including the cell and membrane are usually conditioned until vacuum readings of less than 5×10^{-6} mmHg are obtained, and a very low baseline drift of the shaded-part pressure with no feed gases is checked by means of the transducer. Following the baseline determination, the pollutant gas is introduced at the pressure of p_1, while simultaneously the pressure build-up (h) of the shaded part is recorded. The permeation test is carried out about four times, the time needed to reach the permeation-rate equilibrium.

Preparation of Dilute Gas Mixtures and Measurements of the Concentration: After a sufficient evacuation of the system, the diluent gas is introduced into the cell at an appropriate flow rate and is led to an analyzer. The pollutant gas is then introduced into the lower compartment of the cell in the same manner described above.

The concentrations of CO and CH_4 in the prepared dilute gases are determined by means of a total hydrocarbon analyzer(Beckmann Co., Model 6800 FID gas chromatograph equipped with a convertor of CO to CH_4). Standard gas mixtures in cylinders (7.79 ppm CH_4 in air and 9.60 ppm CO in air), prepared by the weighing method, are used for the calibration of the analyzer. An NO chemiluminescent analyzer (Bendix Co., Model 8101-B) is used for the measurements of NO in the diluent gas. The standard gas mixture in a cylinder (8.4 ppm of NO in nitrogen) is diluted to 1.68 ppm by using a STEC Model SGD-75 (Standard Technology Co.) for the calibration of the analyzer. A very purified air is used to adjust the analyzer to zero. The concentration of SO_2 is determined according to the West-Gaeke method.[15,16] The gas-flow rate of 0.5—1.5 l min^{-1} passing through the scrubber of SO_2 is controlled by means of mass-flow-rate air sampler (Milab Co., Model 69).

Reagents: All the reagents used in the West-Gaeke method were obtained from the Tokyo Kasei Co. and were used without further purification except for pararosaniline dye. TFE (tetrafluoro ethylene) Teflon and silicone-rubber membranes were obtained from the Nitto Rika Co. and the Toray Silicone Co. respectively. The pure pollutant gases in the cylinders were from the Takachiho Kagaku Co., for CH_4 (99.999%), CO (99.999%), and NO(99.8%), and from the Matheson Co. for SO_2 (99.98%).

Theoretical

According to Fick's gas-diffusion theory, q (the permeation rate of gas through a flat plastic membrane with a thickness of l and a certain area of A) is expressed as follows:[17,18]

$$q = DS(p_1-p_2)(A/l) \quad (1)$$

where D is the diffusion constant, S, the solubility coefficient, and p_1 and p_2, the partial pressures at the lower and upper compartments of the cell in Fig. 1 respectively. The permeability coefficient, P, is the product of D and S:

$$P = D \times S \quad (2)$$

The temperature dependence of the P, D, and S parameters follows an Arrhenius relationship:

$$P = P_0 \exp(-E_p/RT)$$
$$= D_0 \exp(-E_d/RT)\cdot S_0 \exp(H_s/RT) \quad (3)$$

where E_p and E_d are the activation energies for permeation and diffusion respectively, and H_s, the heat of solution.

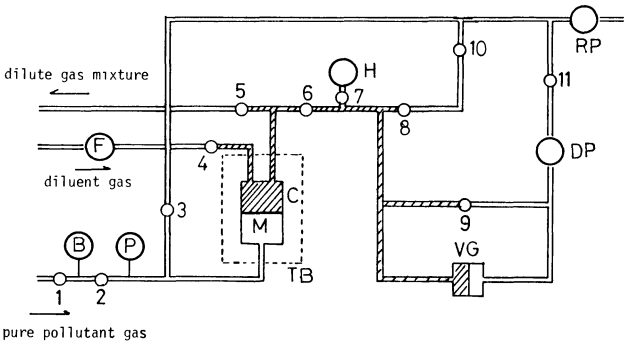

Fig. 1. Schematic diagram of permeation membrane device. M: Flat plastic membrane, C: cell, TB: constant temperature bath, B: Hg bubbler, P: Hg manometer, F: flow rate controller, H: known volume glass vessel, VG: pressure transducer, DP: diffusion pump, RP: rotary pump, 1—11: stopcocks.

Table 1. Lag-times in gas-permeation procedure for silicone-rubber–CO and CH_4 and teflon–NO and SO_2 at a gas pressure of about 70 cmHg

Membrane temp	Gas			
	CO	CH_4	NO	SO_2
30.0 °C	2.93 min	3.28 min	4.58 min	38.2 min
45.0 °C	2.43	2.48	2.64	18.9
55.0 °C	2.06	2.30	2.18	11.3

Results and Discussion

Procedure and the Length of Time to Reach a Steady State of the Permeation. The permeation procedures (time *vs.* the pressure build-up, h, of the known volume part) found for the silicone rubber (thickness l=1080 μm)–CO or CH_4 and for the Teflon (l=200 μm)–NO or SO_2 were in good accordance with the Ficksian-type permeation.[14] In Table 1, the so-called lag-time, θ, in the permeation procedure is listed for each combination of gases and membranes. Apparently the time becomes shorter with an increase in the membrane temperature. About three times as long as the lag-time is the length of time needed to reach steady

Table 2. Gas-permeation rates and their standard deviations for silicone-rubber–CO and CH_4 and Teflon-NO and SO_2 at a gas pressure of about 70 cmHg

Membrane temp	Gas			
	CO[a]	CH_4[a]	NO[b]	SO_2[b]
30.0 °C	3.55±0.02	8.58±0.03	3.03±0.01	3.73±0.05
45.0 °C	4.20±0.03	10.1±0.04	4.46±0.06	5.98±0.07
55.0 °C	4.57±0.03	10.6±0.05	5.75±0.03	7.11±0.11

a) Permeation rate [cm^3(STP) $min^{-1} \times 10^{-3}$].
b) Permeation rate [cm^3(STP) $min^{-1} \times 10^{-4}$].

Table 3. Permeability coefficients obtained for silicone-rubber–CO and CH_4 and Teflon-NO and SO_2 [cm^3(STP)·cm/cm^2·s·cmHg]

Membrane temp	Gas			
	CO ($\times 10^{-8}$)	CH_4 ($\times 10^{-8}$)	NO ($\times 10^{-10}$)	SO_2 ($\times 10^{-10}$)
30.0 °C	2.92±0.02	7.06±0.04	4.63±0.08	6.26±0.18
45.0 °C	3.44±0.01	7.86±0.02	6.95±0.11	9.74±0.25
55.0 °C	3.76±0.03	8.36±0.05	8.97±0.15	13.2±0.30

permeation rates.[13] Even for SO_2 at 30.0 °C, the time of about two hours required for calibration is much shorter than that required using conventional gravimetric or volumetric procedures for usual SO_2 permeation tubes.[11] It should further be noted that, with regard to CO, CH_4, and NO, the time needed to reach the steady-permeation state is remarkably shortened in comparison with that estimated for the use of a commercial apparatus using a FEP Teflon membrane.[13]

Precision in Measurement, Repeatability, and Long-term Stability of Permeation Rates. The permeation rates (q) were calculated from the values of dh/dt at the steady-pressure build-up state and the volume employed. The values of q obtained for CO, CH_4, NO, and SO_2 at about 70 cmHg of p_1 are summarized in Table 2, together with the standard deviations. The very small quantities of gas permeating, less than 10^{-4} cm^3 min^{-1}, were precisely measured within a relative standard deviation of 1%. It is also confirmed that the values of q obtained under various gas pressures less than 70 cmHg changed linearly with the gas pressure of p_1 in Eq. 1. This suggests that the gas pressure in the upper compartment (p_2) is negligibly small compared to p_1 [Eq. 1 can, then, be rewritten as $q = DS(p_1)(A/l)$] and that P ($D \times S$) is constant regardless of the pressure changes.

In order to ascertain the repeatability of the permeation rates, the values of q at various gas pressures of p_1 were converted to the permeability coefficients (P) according to Eqs. 1 and 2. The values of P concerning CO, CH_4, NO, and SO_2 as well as the standard deviations are summarized in Table 3. Each value of P was derived by averaging all the values of P obtained periodically for more than five months at the membrane temperatures of 30.0, 45.0, and 55.0 °C. It has been ascertained that the permeation rates are reproducible within small deviations after repeated temperature, pressure, and gas cycles for a long experimental period.

The long-term stability of the device differs in meaning from that for the conventional permeation tubes of SO_2, NO_2, *etc.* In the former device, the gas permeating through the membrane is fed and removed in each experiment, while the liquefied gases are always stored in the tubes. It is, therefore, considered that the long-term stability of the device is also confirmed by the results on the repeatability. The excellent repeatability and the long-term stability arise from the better storage condition of the membranes than in the conventional permeation tubes; that is, the membranes are in contact with the pollutant gases only at use and, moreover, can be protected from moisture or air.

The maximum uncertainty was found with respect to the SO_2–Teflon system, as can be seen from Tables 2 and 3. The precision of the temperature control of the membrane and the laboratory is considered to be an important factor in this experiment, affecting the uncertainty in the determination of q or P. The magnitude of the activation energy for permeation, E_p, is associated with the required level of the membrane-temperature control, as is suggested by Eq. 3. The values of E_p concerning CO, CH_4, NO, and SO_2 were found to be 2.0, 1.3, 5.1, and 5.9 kcal mol^{-1} (1 kcal mol^{-1}=4.184 kJ mol^{-1}), in that order, from the plots of log P *versus* the reciprocal temperature of the membrane shown in Table 3. The value for SO_2–TFE Teflon agreed well with that of 6.5 kcal mol^{-1} reported by Felder.[19] If an error of less than a 1% in the measurement of P is desired, the temperature should be maintained within ±0.36 and ±0.18 °C when the values of E_p are 5.0 and 10.0 kcal mol^{-1} respectively. The temperature control within 0.05 °C in our experiment is too much to realize less than a 1% relative standard deviation. The uncertainty can, then, be attributed to the deviation of the ambient temperature of our laboratory (±1.0 °C during 1 h). The largest uncertainty in P observed for SO_2 is related to the result shown in Table 1 that the time required to determine the permeation rate of SO_2 is much longer than those required for the other gases.

Preparation of Dilute Standard Gas Mixtures and Measurements of the Concentration. CO and CH_4 Standard Gas Mixtures: The flow rate of a diluent air (Q) was precisely measured at each experiment by means of a soap-bubble flow-meter. The air was mixed with the small quantity of CO or CH_4 (q) permeating through the silicone-rubber in the cell. The dilute gas thus prepared was then introduced into the gas chromatograph and was analyzed at intervals of 5 min. It was confirmed that the steady state of the observed concentration was achieved at the second sampling time (10 min), which is in accordance with the results shown in Table 1. The concentration of CO or CH_4 was maintained for more than four hours, long enough to calibrate the analyzer. Concentrations of CO or CH_4 ranging 0.5 to 10 ppm were easily realized by only changing the gas pressure from about 10 to 76 cmHg. The change in the membrane temperature

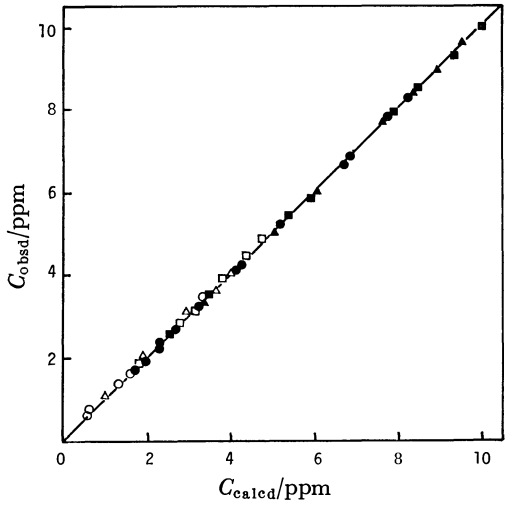

Fig. 2. Comparison of C_{calcd} with C_{obsd} for CO (unfilled symbols) and CH_4 (filled symbols)-silicone rubber. The membrane temperature were 30.0 °C (○), 45.0 °C (△), and 55.0 °C (□).

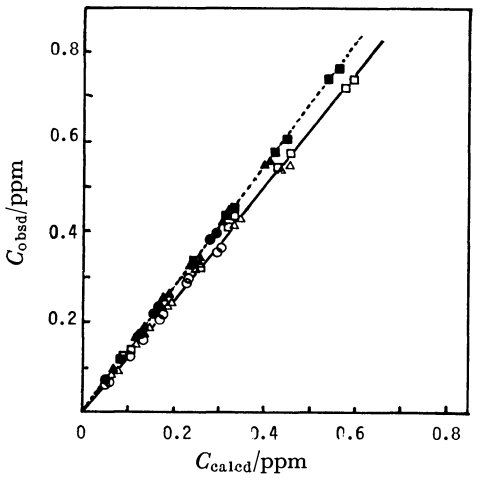

Fig. 3. Comparison of C_{calcd} with C_{obsd} for NO–Teflon at temperatures of 30.0 °C (○), 45.0 °C (△), and 55.0 °C (□). The filled symbols were obtained about two months later when the unfilled symbols were done.

was found to be less effective than that of the pressure, which reflects the very small value of E_p obtained for CO or CH_4. The observed CO or CH_4 concentrations of the dilute gas mixtures (C_{obsd}) are plotted against the calculated ones ($C_{calcd}=q/q+Q=q/Q$) in Fig. 2. By the use of the least squares method, $C_{obsd}/C_{calcd}=0.998$ and the correlation coefficient $r=0.999$ for CO and $C_{obsd}/C_{calcd}=1.01$ and $r=0.999$ for CH_4 were obtained. As has previously been pointed out, the CO or CH_4 concentrations of the dilute gas mixtures in cylinders scarcely changed with the time because of their low adsorbilities and reactivities. It is generally accepted that standard gas mixtures containing such low concentrations of CO or CH_4 prepared by the weighing method are reliable. The excellent agreement of C_{obsd} with C_{calcd} for both gases thus supports the validity of the gas-permeation rates determined here.

NO Standard Gas Mixtures: A very purified nitrogen was used as a diluent gas. By introducing less than 1 l min^{-1} of N_2, dilute gas mixtures containing 0.05—0.7 ppm NO were generated at various gas pressures and at various membrane temperatures. The steady state of the concentration of NO was reached within 20 min at the lowest temperature of 30.0 °C and was maintained more than four hours as well as both CO and CH_4. The concentrations observed by the NO analyzer (C_{obsd}) are plotted against the calculated concentration (C_{calcd}) in Fig. 3. While the correlation coefficient, r, was found to be 0.999 by the least-squares method, a large discrepancy between C_{obsd} and C_{calcd} ($C_{obsd}/C_{calcd}=1.26$) appeared. The same experiment was, therefore, performed about two months later by using the same standard cylinder gas for the span calibration of the NO analyzer. The results obtained are depicted by the dotted line in Fig. 3. The linearity ($r=0.99$) was confirmed to be good, but the C_{obsd}/C_{calcd} ratio increased from 1.26 to 1.37. This can be explained as being due to the decrease in the NO concentration in the cylinder, taking into consideration the fact that the permeability coefficient, P or q, is constant within 2% for 6 months, as has been mentioned above. NO probably adsorbs or reacts with the cylinder wall or an impurity gas such as oxygen and so decreases in concentration.[1] However, it is necessary to rule out the possibility that the discrepancy may result from the change in the quantity of gas permeating through the membrane on account of the different environmental conditions of the Teflon membrane; the determination of the permeation rate was carried out *in vacuo*, but the preparation of the dilute gas mixture was done in a diluent gas (N_2) flowing in the upper compartment of the test cell.

The values of the diffusion constant under the two environmental conditions of the membrane were, therefore, determined and were compared each other, since the diffusion constant is the factor governing the process of the permeation. The diffusion constant, D_v, in the evacuated condition can be calculated from the lag-time, θ, in Table 1 according to the following equation:

$$D_v = l^2/6\theta \quad (4)$$

The lag-time, θ, in the case of the preparation of the dilute gas mixtures can also be obtained by analyzing the change in the concentration of NO with the time.[13,20] The diffusion constants, D_d, in N_2 flowing thus were calculated according to Eq. 4. The values of both D_v and D_d, determined at the temperatures of 30.0, 45.0, and 55.0 °C, are summarized in Table 4(a). It is found that D_d agrees well with D_v within in the limits of experimental error. The possibility mentioned before can thus be excluded; the large discrepancy between C_{obsd} and C_{calcd} is attributable to the decrease of NO in the cylinder.

SO_2 Standard Gas Mixtures: A diluent nitrogen was introduced into the cell at the flow-rate of 1—2.5 l min^{-1}. As soon as the pure SO_2 was fed into the cell, the gas sampler began to operate. In Fig. 4, the observed concentration of SO_2 at the steady-permeation rate determined by the West-Gaeke method (C_{obsd}) is plotted against the calculated values (C_{calcd}).

Table 4(a). Comparison of D_v with D_d for NO-Teflon

Diffusion constant	30.0 °C	45.0 °C	55.0 °C
D_v	2.42±0.16	3.47±0.11	4.69±0.32
D_d	2.02±0.10	3.41±0.46	4.50±0.17

D_v and D_d: $cm^2/s \times 10^{-8}$

Table 4(b). Comparison of D_v with D_d for SO_2-Teflon

Diffusion constant	30.0 °C	45.0 °C	55.0 °C
D_v	2.87±0.10	5.81±0.23	8.56±0.62
D_d	2.58±0.28	5.17±0.59	7.85±1.74

D_v and D_d: $cm^2/s \times 10^{-8}$

Although some scatter is found, C_{obsd} agrees well with C_{calcd} ($C_{obsd}/C_{calcd}=0.997$ and $r=0.995$). About 6% of the relative standard deviation in the observed concentration is considered to be due to the analytical method. Although the purification of the parasoaniline dye used here was performed and a freshly prepared parasoaniline stock solution was used, the relatively large and irreproducible blank values, ranging from 0.057 to 0.078 absorbance, were not satisfactorily decreased. A better quality of the dye and a more rigorously reproducible analytical procedure will be needed to decrease the experimental error.

The diffusion constants, D_v and D_d, were also compared in the same manner as with NO; the values are listed in Table 4(b). They agreed well with each other within the limits of experimental error. The large difference in D between NO and SO_2, shown in Tables 4(a) and 4(b), is particularly noteworthy. The activation energies for diffusion (E_d) were determined to be 8.7 kcal mol^{-1} and 5.8 kcal mol^{-1} for SO_2 and NO, in that order, while those for permeation (E_p) were similar in both NO and SO_2. This reflects the difference in the gas-permeation property between SO_2 and NO. The longer time needed to reach the steady-permeation rate for SO_2 and the more rapid decrease of it with an increase in the temperature are interpreted in terms of the magnitude of D and E_d.

In conclusion, the permeation membrane device using silicone-rubber and TFE Teflon membranes shows excellent performance characteristics in the preparation of dilute standard gas mixtures. The stable and reproducible permeation rates for long periods of time are useful for the examination of the changes in the concentration of the standard gases in cylinders with time. An important characteristics of the device is that the permeation rate, *i.e.*, the concentration of the gaseous pollutants in the mixture, can easily be changed by changing the gas pressure. The calibration line and/or curve of air-monitoring instruments can be obtained more easily and rapidly than with conventional calibration devices. The use of a gas pressure lower than 76 cmHg enables us to apply the device to such condensable gases as SO_2, NO_2, H_2S, NH_3, and so on, which are not suitable for study with the commercial permeation device because of their liquefaction at 2—5 atmospheric pressures. In addition, a portable type of permeation device is expensive to fabricate. The present device consists of only a cell including a membrane whose gas-permeation rates have been measured, a simple constant-temperature oven (the precision in control is about 0.3 °C because of the small values of E_p), a flow-rate controller for a diluent gas, a pressure gauge for a pollutant gas, and a vacuum pump.

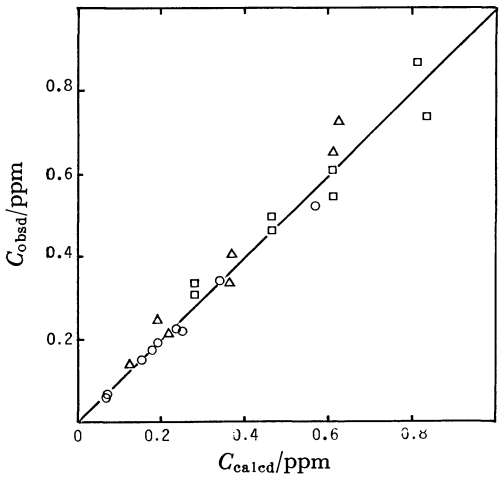

Fig. 4. Comparison of C_{calcd} with C_{obsd} for SO_2-Teflon at temperatures of 30.0 °C (○), 45.0 °C (△), and 55.0 °C (□).

References

1) E. E. Hughes, *Instr. Soc. Am., Reprint*, **1974**, 74.
2) A. E. O'Keeffe and G. C. Ortman, *Anal. Chem.*, **38**, 760 (1966).
3) B. E. Saltzman, C. R. Feldmann, and A. E. O'Keeffe, *Environ. Sci. Technol.*, **3**, 1275 (1969).
4) B. E. Saltzman, W. R. Burg, and C. Ramaswamy, *Environ. Sci. Technol.*, **5**, 1121 (1971).
5) F. P. Scaringelli, A. E. O'Keeffe, E. Rosenberg, and J. P. Bell, *Anal. Chem.*, **42**, 871 (1970).
6) F. P. Scaringelli, E. Rosenberg, and K. A. Rehme, *Environ. Sci. Technol.*, **4**, 924 (1970).
7) F. Lindqvist and R. W. Ranting, *Atmos. Environ.*, **6**, 943 (1972).
8) D. L. Williams, *Am. Soc. Test. Mater.*, **1976**, 183.
9) F. J. Debbrecht and E. M. Neel, *Am. Soc. Test. Mater.*, **1976**, 55.
10) E. E. Hughes, H. L. Rook, E. R. Deardorff, J. H. Margeson, and R. G. Fuerst, *Anal. Chem.*, **49**, 1823 (1977).
11) R. N. Dietz, E. A. Cote, and J. D. Smith, *Anal. Chem.*, **46**, 315 (1974).
12) R. N. Dietz and J. D. Smith, *Am. Soc. Test. Mater.*, **1976**, 164.
13) T. Ibusuki, M. Sakuma, and K. Imagami, *Nippon Kagaku Kaishi*, **1978**, 882.
14) T. Ibusuki, M. Sakuma, T. Hirasawa, and K. Imagami, *Kogai*, **13**, 23 (1978).
15) P. W. West and G. C. Gaeke, *Anal. Chem.*, **28**, 1816 (1956).
16) A. Cedergren, A. Wikby, and K. Bergner, *Anal. Chem.*, **47**, 100 (1975).
17) D. P. Lucero, *Anal. Chem.*, **43**, 1744 (1971).
18) J. Crank and G. S. Park, "Diffusion in Polymers," ed by J. Crank and G. S. Park, Academic Press, London and New York (**1968**), p. 1.
19) R. M. Felder, R. D. Spence, and J. K. Ferrell, *J. Chem. Eng. Data*, **20**, 235 (1975).
20) R. M. Felder, R. D. Spence, and J. K. Ferrell, *J. Appl. Polym. Sci.*, **19**, 3193 (1975).

Chemical Reaction of Electron Donor-Acceptor System: Reaction Mechanism of the Tricyanovinylation Reaction of *N,N*-Dimethylaniline with Tetracyanoethylene

Takashi Nogami,* Yoshio Nakano, Yoshiki Hasegawa,
Yasuhiko Shirota, and Hiroshi Mikawa

Department of Applied Chemistry, Faculty of Engineering, Osaka University, Yamadakami, Suita, Osaka 565

(Received August 28, 1978)

The decay of the charge-transfer (CT) absorption band in the tricyanovinylation reaction of *N,N*-dimethylaniline (DMA) with tetracyanoethylene (TCNE) in 1,2-dichloroethane was followed by the electronic absorption measurement. Primary hydrogen isotope effect was observed for the decay of the CT-band in line with the mechanism:

$$[D + A \rightleftharpoons DA] \longrightarrow I$$
$$I + D \longrightarrow NA$$
$$NA + D \xrightarrow[\text{slow}]{} P$$

D: DMA; A: TCNE; DA: CT-complex; I: zwitterionic intermediate; NA: *p*-(1,1,2,2-tetracyanoethyl)-*N,N*-dimethylaniline; P: *p*-tricyanovinyl-*N,N*-dimethylaniline.

The tricyanovinylation reaction of several aromatic amines with tetracyanoethylene (TCNE) is a typical thermal reaction involving the formation of a charge-transfer (CT) complex.[1] The reaction proceeds in two steps, (1) formation of an accumulating intermediate, and (2) slow formation of the final product. Because of the large difference in reaction rate, the steps can be followed independently by an electronic absorption measurement. Rappoport measured the decay of the CT-absorption band for the *N,N*-dimethylaniline (DMA)–TCNE system in chloroform, and found that the pseudo first order rate constant for the decay of the CT-complex (k_{obsd}) obeys the relation

$$k_{obsd} = \frac{kK[D]^2}{1+K[D]}. \quad (1)$$ [2)]

Here, k, K, and $[D]$ denote the second order rate constant for transformation from the CT-complex into a zwitterionic intermediate (I), the association constant for the formation of the CT-complex, and the initial donor concentration, respectively. The following reaction (Scheme 1) has been proposed to explain the above kinetic result, which involves the bimolecular reaction of the CT-complex with another free donor (amine) molecule to give I.

The mechanism proposed by Rappoport indicates that the CT-complex is a true intermediate in the reaction. However, it is generally recognized that kinetic data alone cannot tell whether the CT-complex is a true intermediate in chemical reactions involving the formation of the CT-complex, *e.g.*, Diels-Alder and [2+2] cycloaddition reactions.[3] From the viewpoint that this may be the case also for the tricyanovinylation reaction of aromatic amines, we have proposed an alternative mechanism (Scheme 2) which can also explain the above kinetic data.[1,4] Either the monomolecular transformation of the CT-complex or the bimolecular reaction between the free donor and acceptor molecules produces a zwitterionic intermediate (I) which reversibly returns to either the CT-complex or the component molecules,[5] and then an accumulat-

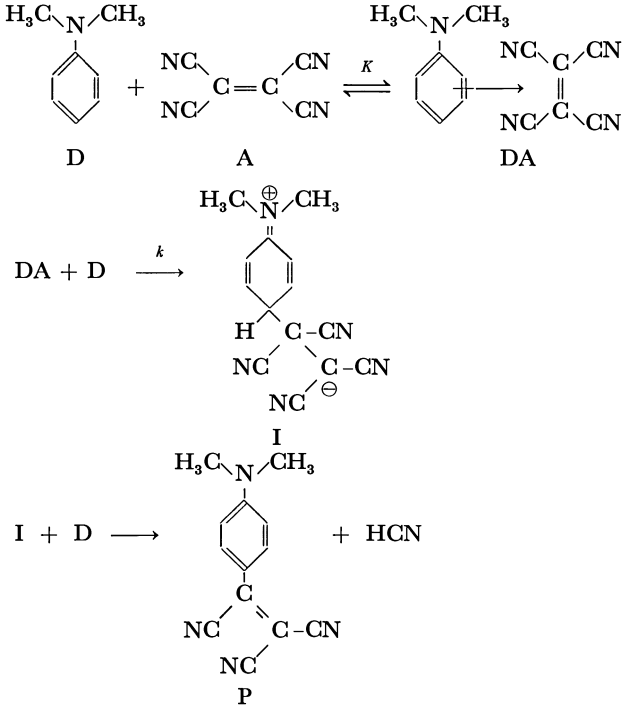

Scheme 1.

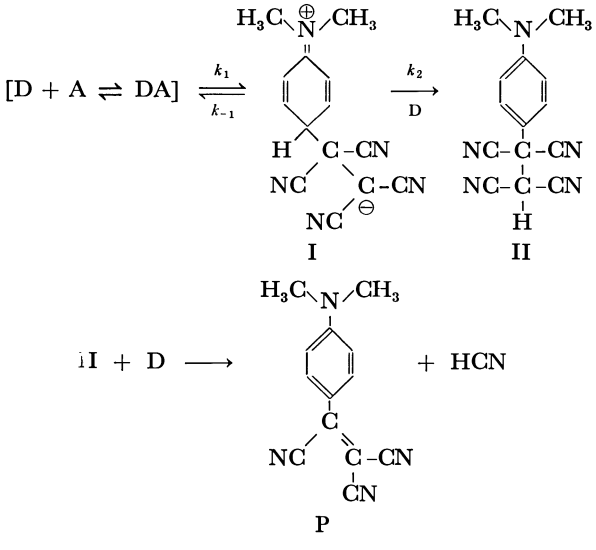

Scheme 2.

ing intermediate, *p*-(1,1,2,2-tetracyanoethyl)-*N,N*-dimethylaniline (II) (neutral adduct), is produced.[7] The formation of II is induced by the deprotonation of I with another amine (donor) molecules, followed by back proton transfer from the quarternary amine to carbanion resulting from I. The neutral adduct (II, NA) then turns gradually to the final tricyanovinylated product by another free-amine catalysed dehydrocyanation.

The kinetic result alone cannot distinguish whether the CT-complex is a true intermediate in the reaction.[11] The decay of the CT-complex following the mechanism (Scheme 2) is expressed by Eqs. 2 and 3, which are kinetically indistinguishable from each other.

$$[DA] = [DA]_0 \exp(-k_{obsd}t)$$

In the case of unimolecular transformation of the CT-complex:[12]

$$k_{obsd} = \frac{(k_1k_2/k_{-1})K[D]^2}{1+K[D]} \quad (2)$$

In the case of bimolecular reaction between free donor and acceptor molecules:[12]

$$k_{obsd} = \frac{(k_1'k_2/k_{-1}'K)K[D]^2}{1+K[D]} \quad (3)$$

In order to confirm which of Schemes 1 and 2 is more reasonable, we have carried out the measurement of the kinetic hydrogen isotope effect on the decay of the CT-complex for the DMA–TCNE and 4-deuterio-*N,N*-dimethylaniline (*d*-DMA)–TCNE systems in 1,2-dichloroethane. No primary hydrogen isotope effect will be observed for the mechanism shown in Scheme 1, since the decay process of the CT-complex involves only the exchange reaction of a complexed amine with a free amine, although a slight secondary hydrogen isotope effect might be observed. On the other hand, the primary hydrogen isotope effect will be observed for the mechanism shown in Scheme 2, since k_{obsd} involves the rate constant k_2 for the C–H and C–D bond breaking process.

Experimental

4-Deuterio-*N,N*-dimethylaniline (*d*-DMA) was synthesized according to the methods reported.[13] Purification of samples and solvents and the experimental procedures are described in a previous paper.[1]

Results and Discussion

Decay Kinetics of the CT-Band. The decay of the CT-absorption band at 675 nm was followed at 30, 35, and 40 °C for the DMA–TCNE and *d*-DMA–TCNE systems in 1,2-dichloroethane with a donor concentration much greater than that of TCNE. The measurement was made by varying the concentration of the donor (DMA and *d*-DMA), keeping that of TCNE constant. The plot of log I_{CT} (I_{CT}: absorbance of the CT-band at 675 nm) against time gave a straight line for each run. This shows that the decay of the CT-complex is of first order with respect to the concentration of the CT-complex. Typical plots of log I_{CT} against time for both DMA–TCNE and *d*-DMA–TCNE systems are shown in Fig. 1. A marked hydrogen isotope effect is observed for the decay of the CT-complex. The association constant for the formation of the CT-complex was obtained from the extrapolation of the decay of the CT-complex to time zero in order to get a Benesi-Hildebrand plot by the least squares method.[14] As expected from Eq. 1 for Scheme 1 or Eq. 2 or 3 for Scheme 2, the plot of $k_{obsd}(1+K[D])/[D]$ against $K[D]$ should give a straight line. Figures 2 and 3 show the plots of $k_{obsd}(1+K[D])/[D]$ against $K[D]$ by means of the least squares method for the DMA–TCNE and *d*-DMA–TCNE systems, respectively, both of which show a linear relation. The plots show two characteristics, *i.e.*, (1) a kinetic hydrogen isotope effect exists for the decay of the CT-complex as is evident from the marked decrease in the slope of the straight line in the *d*-DMA–TCNE system as compared with the DMA–TCNE system; (2) the plots do not pass through the origin, but have definite positive intercepts.

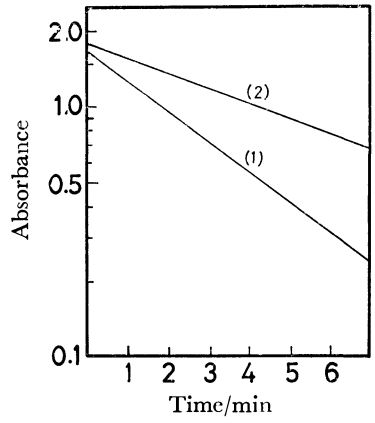

Fig. 1. The plot of log I_{CT} against t.
(1) DMA–TCNE system. [DMA]=0.2 M, [TCNE]=9.75×10^{-4} M. (2) *d*-DMA–TCNE system. [*d*-DMA]=0.2 M, [TCNE]=1.011×10^{-3} M.

Primary Hydrogen Isotope Effect. The slopes of the linear plots in Figs. 2 and 3 give the values of k (for Scheme 1) or k_1k_2/k_{-1} (for Scheme 2, in the case of monomolecular transformation of the CT-complex; hereafter, discussion will be made simply in terms of this mechanism for the sake of convenience). The ratio of the slopes of the straight lines (denoted by s^H/s^D)[15] in Figs. 2 and 3 is expressed as Eqs. 4 and 5 for the mechanism shown in Schemes 1 and 2, respectively. Since the substitution of hydrogen by deuterium at the *para*-position of DMA is assumed to give a minor effect on the rate constants k_1 and k_{-1} for the mechanism shown in Scheme 2, Eq. 5 can be approximated as Eq. 6.

$$s^H/s^D = k^H/k^D \quad \text{for Scheme 1} \quad (4)$$

$$s^H/s^D = (k_1^Hk_2^Hk_{-1}^D/k_1^Dk_2^Dk_{-1}^H) \quad \text{for Scheme 2} \quad (5)$$

$$s^H/s^D \approx k_2^H/k_2^D \quad \text{for Scheme 2} \quad (6)$$

The values of s^H/s^D obtained from Figs. 2 and 3 are 3.35, 3.32, and 3.17 at 30, 35, and 40 °C, respectively, showing a large kinetic hydrogen isotope effect. The Arrhenius plot for the observed s^H/s^D values gave an activation energy of about 1.04 kcal/mol,

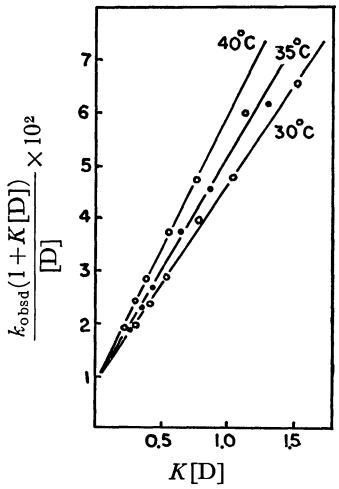

Fig. 2. The plot of $k_{obsd}(1+K[D])/[D]$ against $K[D]$ in DMA–TCNE system in 1,2-dichloroethane measured at the temperatures indicated. [TCNE]$=9.75\times10^{-4}$ M.

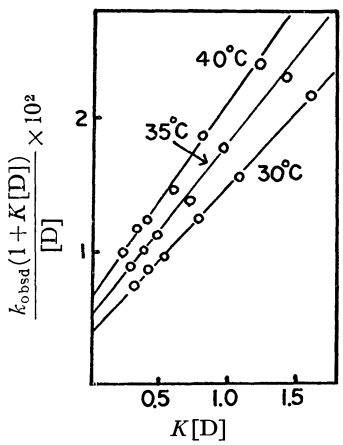

Fig. 3. The plot of $k_{obsd}(1+K[D])/[D]$ against $K[D]$ in *d*-DMA–TCNE system in 1,2-dichloroethane measured at the temperatures indicated. [TCNE]$=1.011\times10^{-3}$ M.

which is roughly equal to the zero point energy difference between the C–H and C–D stretching vibrations. The results are attributed to the primary hydrogen isotope effect. They can be explained more satisfactorily in terms of Scheme 2, since s^H/s^D roughly represents k_2^H/k_2^D,[15] the ratio of the rate constants for the C–H and C–D bond breakage.[16]

On the Positive Intercept of the Linear Plot of $k_{obsd}(1+K[D])/[D]$ *against* $K[D]$. The fact that the linear plot of $k_{obsd}(1+K[D])/[D]$ against $K[D]$ has an intercept has not so far been discussed as regards reaction mechanism. Experimental results show that the plots have negative intercepts for *e.g.*, the indole–TCNE system in dichloromethane,[17] and DMA–TCNE system in dichloromethane.[18] The present study of the DMA–TCNE system in 1,2-dichloroethane gives definite values of positive intercepts (Figs. 2 and 3), indicating that k_{obsd} is more rigorously given by Eq. 7. The k_3 term in Eq. 7 will probably arise from the following reactions: (1) the formation of unknown species X from the initial equilibrium between the CT-complex and free donor and acceptor molecules, (2) the monomolecular reaction of I to give probably NA and/or another unknown species X (Scheme 3).

$$[D + A \rightleftharpoons DA] \xrightarrow{(1)} X \qquad [D + A \rightleftharpoons DA] \xrightarrow{(2)} I \longrightarrow NA$$

$$k_{obsd} = \frac{(k_1/k_{-1})K[D]}{1+K[D]}(k_2[D]+k_3) \tag{7}$$

Scheme 3. Conceivable reactions which contribute to the k_3 term in Eq. 7.

Table 1 gives the values of k_{obsd} obtained from Fig. 1 (three plots are chosen for the sake of simplicity), and $(k_1k_2/k_{-1})K[D]^2/(1+K[D])$ (denoted by $k_{obsd(bi)}$) calculated by using the values of the slopes of the linear plots in Figs. 2 and 3. Calculation using the values of intercepts of the linear plots in Figs. 2 and 3, or substraction of $k_{obsd(bi)}$ from k_{obsd} will give $(k_1k_3/k_{-1})K[D]/(1+K[D])$ (denoted by $k_{obsd(mono)}$). It should be noted that the values of the intercepts are much less reliable than those of the slopes in Figs. 2 and 3; the values of $k_{obsd(mono)}$ are much less reliable than those of $k_{obsd(bi)}$.[19] Although no quantitative discussion on the k_3 process can be made, it is shown that the k_3 process contributes significantly under the reaction conditions of a low donor concentration ($[D]\approx0.06$ mol dm^{-3} with constant [TCNE]$\approx10^{-3}$ mol dm^{-3}). Under the reaction conditions of a high donor concentration ($[D]>0.1$ mol dm^{-3} with constant [TCNE]$\approx10^{-3}$ mol dm^{-3}), however, the contribution of the k_2 process is dominant as shown in the values of $k_{obsd(bi)}/k_{obsd}$ in Table 1, the main reaction mechanism being explained in terms of the mechanism shown in Scheme 2.

Summary. The primary kinetic hydrogen isotope effect observed for the decay of the CT-complex in the tricyanovinylation reaction of the DMA–TCNE system in 1,2-dichloroethane is explained by Scheme 2.

We are grateful to Dr. Takashi Ando, The Institute of Scientific and Industrial Research, Osaka University, for his helpful discussion.

References

1) T. Nogami, Y. Hasegawa, Y. Shirota, and H. Mikawa, *Bull. Chem. Soc. Jpn.*, **48**, 3048 (1975), and references cited therein.

2) Z. Rappoport, *J. Chem. Soc.*, **1963**, 4438.

3) Y. Shirota, J. Nagata, Y. Nakano, T. Nogami, and H. Mikawa, *J. Chem. Soc., Perkin Trans. 1*, **1977**, 14; T. Arimoto and J. Osugi, *Chem. Lett.*, **1974**, 271.

4) Y. Shirota, T. Nogami, Y. Hasegawa, and H. Mikawa, *Chem. Lett.*, **1974**, 1009.

5) The reversibility of a zwitterionic intermediate has been evidenced for the [2+2] cycloaddition reaction.[6]

6) R. Huisgen and G. Steiner, *J. Am. Chem. Soc.*, **95**, 5055 (1973).

7) The intermediate NA was actually isolated after complete disappearence of the CT-complex in the tricyanovinylation reactions of a few aromatic amines.[8–10]

Table 1. Typical kinetic data for the decay of the CT-complex in 1,2-dichloroethane

	Temp (°C)	[D] (mol dm^{-3})	$k_{obsd} \times 10^3$ (s^{-1})	$k_{obsd(bi)} \times 10^3$ a)	$k_{obsd(bi)}/k_{obsd}$
DMA-TCNE b)	30	0.295	7.69	6.87	0.89
		0.2	4.74	3.91	0.82
		0.059	0.88	0.52	0.59
	35	0.295	7.98	6.99	0.87
		0.2	4.89	3.93	0.80
		0.059	0.89	0.51	0.57
	40	0.295	8.33	7.88	0.94
		0.2	5.37	4.37	0.81
		0.059	0.88	0.55	0.62
d-DMA-TCNE c)	30	0.3	2.52	2.08	0.82
		0.2	1.53	1.17	0.76
		0.06	0.33	0.16	0.48
	35	0.3	2.85	2.22	0.77
		0.2	1.83	1.24	0.67
		0.06	0.41	0.16	0.39
	40	0.3	3.25	2.37	0.72
		0.2	2.08	1.30	0.62
		0.06	0.47	0.16	0.34

a) s^{-1}; $k_{obsd(bi)} = (k_1k_2/k_{-1})K[D]^2/(1+K[D])$. b) [TCNE] $= 9.75 \times 10^{-4}$ mol dm^{-3}. c) [TCNE] $= 1.011 \times 10^{-3}$ mol dm^{-3}.

8) Z. Rappoport and E. Shohamy, *J. Chem. Soc., B*, **1969**, 77.
9) P. G. Farrell and R. K. Wojtowski, *J. Chem. Soc., B*, **1970**, 1390.
10) Y. Shirota, S. Ezaki, S. Kusabayashi, and H. Mikawa, *Bull. Chem. Soc. Jpn.*, **45**, 836 (1972).
11) I is produced from the initial equilibrium state between D+A and DA shown symbolically as [D+A⇌DA]⇌I. In deriving the kinetic equation, however, it is assumed that the reaction proceeds either by the monomolecular transformation of the CT-complex or by the bimolecular reaction of the free donor and acceptor molecules.
12) Unimolecular transformation of the CT-complex.

$$D + A \overset{K}{\rightleftharpoons} DA$$

$$DA \underset{k_{-1}}{\overset{k_1}{\rightleftharpoons}} I \xrightarrow[k_2]{D} NA \xrightarrow[\text{slow}]{D} P$$

Bimolecular reaction between the free donor and acceptor molecules.

$$D + A \overset{K}{\rightleftharpoons} DA$$

$$D + A \underset{k'_{-1}}{\overset{k'_1}{\rightleftharpoons}} I \xrightarrow[k_2]{D} NA \xrightarrow[\text{slow}]{D} P$$

13) J. H. Billman, A. R. Radike, and B. W. Mundy, *J. Am. Chem. Soc.*, **64**, 2977 (1942); D. G. Thomas, J. H. Billman, and C. E. Davis, *ibid.*, **68**, 895 (1946); S. Baba, *Yakugaku Zasshi*, **89**, 1158 (1969).
14) Observed association constants of the CT-complex in 1,2-dichloroethane. DMA–TCNE system: K (dm^3 mol^{-1}) 5.04 (30 °C), 4.39 (35 °C), 3.89 (40 °C). *d*-DMA–TCNE system: K (dm^3 mol^{-1}) 5.31 (30 °C), 4.79 (35 °C), 4.06 (40 °C).
15) Superscripts H and D denote the rate constants for DMA–TCNE and *d*-DMA–TCNE systems, respectively.
16) P. G. Farrell and J. Newton, *J. Chem. Soc., C*, **1970**, 1630. They also observed the kinetic hydrogen isotope effect for the decay of the CT-complex in the tricyanovinylation reaction of DMA–TCNE system in chloroform.
17) R. Foster and P. Hanson, *Tetrahedron*, **21**, 255 (1965).
18) S. Garbutt and D. L. Gerrand, *J. Chem. Soc., Perkin Trans. 2*, **1972**, 782.
19) A small variation in the values of the slopes yields a large variation in the values of intercepts. This arises from the fact that the values of $k_{obsd(bi)}$ are much greater than those of $k_{obsd(mono)}$.

Magnetic and Spectral Properties of Binuclear Nickel(II) Nitrato and Acetato Complexes of Tridentate Schiff Bases Derived from Salicylaldehydes and *N*-Substituted Trimethylenediamines

Tadashi Tokii, Shuji Emori, and Yoneichiro Muto*

Department of Chemistry, Faculty of Science and Engineering, Saga University, Saga 840

(Received November 28, 1978)

A new series of binuclear Ni(II) complexes with the empirical formula Ni(5-Y-sal·pr·NRR′)X has been prepared by the reaction of the parent complexes, Ni(5-Y-sal·pr·NRR′)$_2$ with metal salts NiX_2, where 5-Y-sal·pr·NRR′=Schiff base ligand derived from 5-substituted salicylaldehyde and *N*-substituted trimethylenediamine, R=H or CH_3, R′=CH_3, Y=H or Cl and X=NO_3 or CH_3COO. The nature of the complexes has been confirmed to be dimeric on the basis of the results of molecular weight, magnetic and spectral measurements. The values of exchange integral, $J=-10$——15 cm^{-1}, have been evaluated for the Ni(II) complexes from their temperature dependences of magnetic susceptibilities. The antiferromagnetic property has been discussed in terms of structural considerations. For comparison, the corresponding Cu(II) complexes Cu(5-Y-sal·pr·NRR′)X have been prepared and investigated.

Although a large number of phenolic oxygen-bridged binuclear Cu(II) complexes with *N*-substituted salicylideneaminato ligands have been synthesized and characterized,[1,2] relatively few Ni(II) complexes analogous to the Cu(II) complexes have been prepared, the work of Butcher and Sinn[3] represents an attempt at investigation; the Ni(II) complexes are represented by the formula [Ni(bsb)NO_3·C_2H_5OH]$_2$, where bsb represents a bidentate Schiff base.

In a previous paper,[4] it was reported that bis[*N*-(3-dimethylaminopropyl)salicylideneaminato]copper(II), Cu(Sal·pr·NMe_2)$_2$, reacts with copper(II) chloride to yield a binuclear complex with the formula [Cu(Sal·pr·NMe_2)Cl]$_2$ in which the phenolic oxygen atoms act as bridges and each of the two organic ligands is tridentately coordinated to a single metal ion. Attempts to prepare the corresponding Ni(II) complex, [Ni(Sal·pr·NMe_2)Cl]$_2$, however, were unsuccessful. Six complexes with the stoichiometry of Ni(5-Y-sal·pr·NRR′)X, where X=NO_3 or CH_3COO and 5-Y-sal·pr·NRR′ represents the tridentate salicylideneaminato ligand of the general formula, have now been isolated

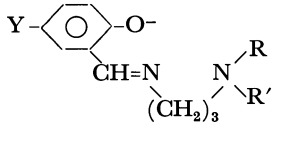

Abbreviation:
Sal·pr·NHMe; R=H, R′=CH_3, Y=H
Sal·pr·NMe_2; R=R′=CH_3, Y=H
5-Cl-sal·pr·NHMe; R=H, R′=CH_3, Y=Cl
5-Cl-sal·pr·NMe_2; R=R′=CH_3, Y=Cl

The dimeric octahedral structure has been established by comparing the IR and electronic reflectance spectra, molecular weights, and magnetic susceptibilities with those of the corresponding Cu(II) complexes, Cu(5-Y-sal·pr·NRR′)X, which have been prepared in the present study and confirmed to be monomeric. It is noteworthy that the Ni(II) complexes exhibit antiferromagnetism in contrast to [Ni(bsb)NO_3·C_2H_5OH]$_2$ which shows intramolecular ferromagnetic interaction.[3]

The results of characterization studies on the newly prepared complexes will be reported and the differences in magnetic properties between Ni(5-Y-sal·pr·NRR′)X and [Ni(bsb)NO_3·C_2H_5OH]$_2$ will be discussed from structural considerations.

Experimental

Syntheses. Ni(5-Y-sal·pr·NRR′)NO_3 Complexes: A typical synthetic method is as follows. A solution of Ni$(NO_3)_2$·$6H_2O$ (11 mmol) in ethanol (50 ml) was added to a solution of one of the parent Ni(5-Y-sal·pr·NRR′)$_2$ complexes (10 mmol) in ethanol (100 ml), and the mixture was stirred on a hot plate for 1/2 h. The green crystals thus precipitated were collected, washed repeatedly with ethanol and dried.

Ni(5-Y-sal·pr·NHMe)CH_3COO Complexes: A solution of Ni$(CH_3COO)_2$·$4H_2O$ (11 mmol) in ethanol (50 ml) was added to one of the parent Ni(5-Y-sal·pr·NHMe)$_2$ complexes (10 mmol) suspended in chloroform (50 ml). The solution was stirred at *ca.* 50 °C for 1/2 h and concentrated to one-third of the volume. After the solution had been allowed to stand overnight at *ca.* 5 °C in a freezer, the separated green crystals were collected and washed twice with a small quantity of ethanol and once with ether.

Cu(Sal·pr·NMe_2)NO_3 Complex: This complex was prepared by the reaction of Cu(Sal·pr·NMe_2)$_2$ and Cu$(NO_3)_2$·$3H_2O$ using the same procedure as for Ni(5-Y-sal·pr·NRR′)-NO_3 complexes. The purification was made by recrystallization from ethanol.

Cu(5-Y-sal·pr·NHMe)X Complexes: A solution of CuX_2·nH_2O (11 mmol) in ethanol (50 ml) was added to a mixture of bis(5-substituted salicylaldehydato)copper(II) (10 mmol) and *N*-methyl-1,3-propanediamine (20 mmol) in ethanol (50 ml). The solution was stirred at *ca.* 70 °C for 1/2 h and concentrated to one half of the volume. After the solution had been allowed to stand overnight at *ca.* 5 °C in a freezer, the separated green crystals were collected and recrystallized from ethanol.

The elemental analyses for the new compounds are summarized in Table 1.

Physical Measurements. The molecular weights of the complexes **5**—**9** listed in Table 1 were determined osmometrically with a Hitachi Molecular Weight Apparatus 117, the results of which are given in Table 2. Magnetic susceptibilities of all the complexes **1**—**10** were determined by the Gouy method in the temperature range 80—300 K. For complex **2**, the susceptibilities in the temperature range 4.2—80 K were determined by the Faraday method. Effective magnetic moments were calculated from the equation:

$$\mu_{eff} = 2.83\sqrt{(\chi_A - N_\alpha)\cdot T} \qquad (1)$$

where χ_A is the molar magnetic susceptibility corrected for the diamagnetism of the constituted atoms using Pascal's

Table 1. Analytical data

	Complex	Found (%)				Calcd (%)			
		C	H	N	Metal	C	H	N	Metal
1	Ni(Sal·pr·NHMe)NO_3	42.44	4.93	13.35	18.71	42.35	4.85	13.47	18.82
2	Ni(Sal·pr·NMe_2)NO_3	44.14	5.30	12.66	17.84	44.21	5.26	12.89	18.01
3	Ni(5-Cl-sal·pr·NHMe)NO_3	38.61	4.08	11.68	16.88	38.14	4.07	12.13	16.95
4	Ni(5-Cl-sal·pr·NMe_2)NO_3	39.82	4.49	11.44	16.43	39.99	4.48	11.66	16.29
5	Ni(Sal·pr·NHMe)CH_3COO	50.47	5.75	8.86	18.91	50.53	5.87	9.06	19.00
6	Ni(5-Cl-sal·pr·NHMe)CH_3COO	45.06	4.89	7.92	17.09	45.46	4.99	8.16	17.09
7	Cu(sal·pr·NHMe)NO_3	41.80	4.75	13.01	20.09	41.70	4.77	13.26	20.06
8	Cu(Sal·pr·NMe_2)NO_3	43.46	5.16	12.77	19.14	43.57	5.18	12.70	19.21
9	Cu(Sal·pr·NHMe)CH_3COO	49.72	5.80	8.97	20.30	49.75	5.78	8.93	20.25
10	Cu(5-Cl-sal·pr·NHMe)CH_3COO	44.78	4.93	8.07	18.22	44.83	4.92	8.04	18.24

Table 2. Molecular weight data

	Complex	Solvent	Concentration (10^{-3} mol·dm^{-3})	Molecular weight	
				Obsd	Calcd
5	Ni(Sal·pr·NHMe)CH_3COO	chloroform	2.86	558	618 (dimer)
6	Ni(5-Cl-sal·pr·NHMe)CH_3COO	chloroform	3.26	632	687 (dimer)
7	Cu(Sal·pr·NHMe)NO_3	acetone	2.86	312	317 (monomer)
8	Cu(Sal·pr·NMe_2)NO_3	acetonitrile	3.44	311	331 (monomer)
9	Cu(Sal·pr·NHMe)CH_3COO	benzene	4.67	354	314 (monomer)

Table 3. Magnetic data

	Complex	μ_{eff}/B.M. (T/K)			C	θ/K	g	J/cm^{-1}
1	Ni(Sal·pr·NHMe)NO_3	2.97 (290),	2.59 (80)		1.262	−36	2.25	−14
2	Ni(Sal·pr·NMe_2)NO_3	3.10 (299),	2.75 (80),	0.28 (4.2)	1.305	−29	2.28	−9.6[a]
3	Ni(5-Cl-sal·pr·NHMe)NO_3	3.16 (292),	2.72 (79)		1.436	−43	2.40	−14
4	Ni(5-Cl-sal·pr·NMe_2)NO_3	3.09 (302),	2.68 (78)		1.332	−35	2.31	−14
5	Ni(Sal·pr·NHMe)CH_3COO	2.98 (293),	2.64 (79)		1.229	−29	2.22	−14
6	Ni(5-Cl-sal·pr·NHMe)CH_3COO	3.02 (293),	2.58 (78)		1.334	−47	2.31	−15
7	Cu(Sal·pr·NHMe)NO_3	1.82 (300),	1.82 (78)		0.413	0	2.10	
8	Cu(Sal·pr·NMe_2)NO_3	1.82 (300),	1.80 (78)		0.414	0	2.10	
9	Cu(Sal·pr·NHMe)CH_3COO	1.83 (303),	1.80 (78)		0.410	0	2.09	
10	Cu(5-Cl-sal·pr·NHMe)CH_3COO	1.83 (303),	1.80 (78)		0.410	0	2.09	

a) The value was evaluated from the magnetic susceptibility data in the temperature range 4.2−300 K (*cf.* text).

constant[5] and N_α is the temperature-independent paramagnetism per gram-ion of Ni(II) or Cu(II). The N_α value of 200×10^{-6} and 60×10^{-6} cgs, emu were assumed for Ni(II)[6] and Cu(II),[7] respectively, and a set of the results is given in Table 3. The reflectance spectra were recorded with a Hitachi Recording Spectrophotometer 323. IR spectral measurements were made with a Hitachi EPI-G2 IR Spectrophotometer in the 400—4000 cm^{-1} region using Nujol mulls.

Results and Discussion

Molecular Weights. Molecular Weight measurements of the Ni(II) acetato complexes **5** and **6** listed in Table 1 were made osmometrically in chloroform, the results of which are given in Table 2. The molecular weights were found to be twice the empirical formula of Ni(5-Y-sal·pr·NHMe)CH_3COO, indicating the presence of a dimeric structure. The low solubility of the Ni(II) nitrato complexes **1**—**4** in chloroform or any other conventional solvents, however, did not allow an accurate determination of the molecular weights. The molecular weight determination for the Cu(II) complexes **7**—**9** showed the compounds to be monomeric (*cf.* Table 2).

Magnetic Susceptibilities. The magnetic susceptibilities of the complexes **1**—**10** were determined over the temperature range 80—300 K. The susceptibility data for complexes **1** and **3**—**10** are shown in Figs. 1 and 2 as plots of the reciprocal susceptibility corrected for diamagnetic contribution and temperature-independent magnetism, $(\chi_A-N_\alpha)^{-1}$, *vs.* temperature, T. The data for complex **2** in Fig. 3 is shown as a χ_A *vs.* T plot.

In the temperature range 80—300 K, the susceptibilities of the Ni(II) complexes **1**—**6** follow the Curie-Weiss law. The Curie (C) and Weiss constants (θ) have been evaluated from the slopes of $(\chi_A-N_\alpha)^{-1}$ *vs.* T plots, and the g values calculated from the

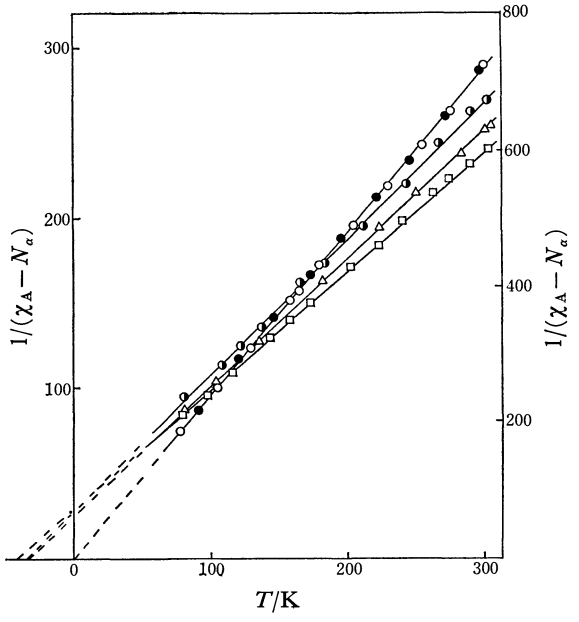

Fig. 1. Variation of magnetic susceptibilities with temperature. Left-hand scale: (◑) Ni(Sal·pr·NHMe)NO_3, (□) Ni(5-Cl-sal·pr·NHMe)NO_3, (△) Ni(5-Cl-sal·pr·NHMe$_2$)NO_3. Right-hand scale: (○) Cu(Sal·pr·NHMe)NO_3 (●) Cu(Sal·pr·NMe$_2$)NO_3.

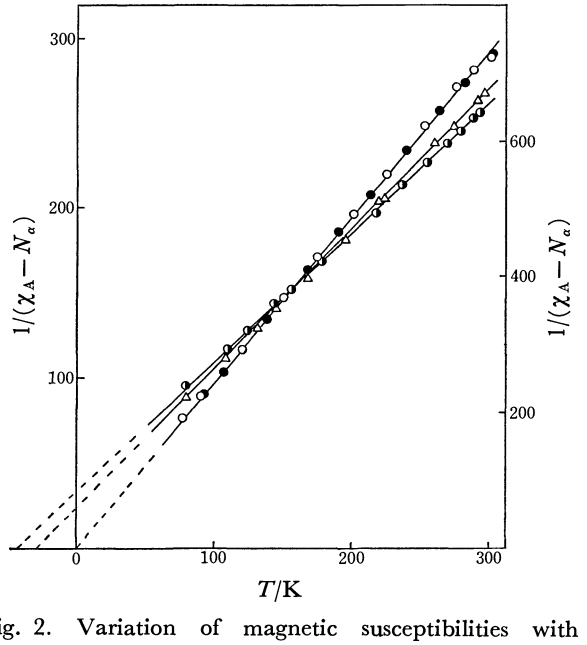

Fig. 2. Variation of magnetic susceptibilities with temperature. Left-hand scale: (△) Ni(Sal·pr·NHMe)CH_3COO, (◑) Ni(5-Cl-sal·pr·NHMe)CH_3COO. Right-hand scale: (○) Cu(Sal·pr·NHMe)CH_3COO, (●) Cu(5-Cl-sal·pr·NHMe)CH_3COO.

Curie constants using the relationship $C=N\beta^2g^2[S(S+1)]/3k$ where $S=1$; the results are listed in Table 3. The negative values of the observed Weiss constants (*ca.* −30——50 K) are indicative of the presence of antiferromagnetic coupling in the Ni(II) complexes. In order to obtain further information about the magnetic interaction, the magnetic susceptibility measurement has been extended for complex **2** from the temperature of liquid nitrogen to that of liquid helium. As can be seen in Fig. 3, the susceptibility χ_A increases with decreasing temperature until a maximum in χ_A is reached at 27 K. At temperatures below 27 K χ_A decreases markedly with decreasing temperature. It has been found that the susceptibility data could be fitted to the susceptibility equation for a Ni(II) dimer:[8]

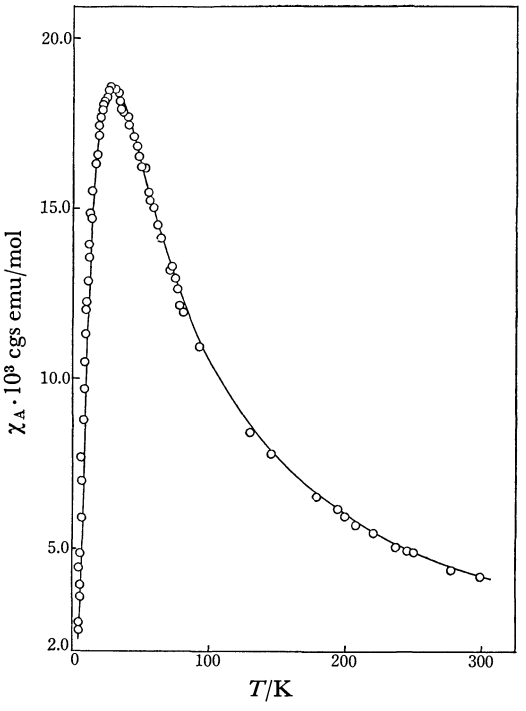

Fig. 3. Observed and calculated magnetic susceptibilities of Ni(Sal·pr·NMe$_2$)NO_3: ○, experimental; solid line, calculated by Eq. 2 (*cf.* text).

$$\chi_A = \frac{N\beta^2g^2}{kT}\left[\frac{5+\exp(-4J/kT)}{5+3\exp(-4J/kT)+\exp(-6J/kT)}\right] + N_\alpha \quad (2)$$

where J is exchange integral. The values of $J=-9.6$ cm^{-1} and $g=2.27$ have been evaluated from the best fit of the experimental data to Eq. 2, assuming $N_\alpha = 200\times10^{-6}$ cgs emu.[6] The solid line in Fig. 3 represents the susceptibility curve calculated using the parameters. The value of g agrees well with the experimental value of 2.28 determined from the $(\chi_A-N_\alpha)^{-1}$ *vs.* T plot in the temperature range 80—300 K (*cf.* Table 3). The magnetic behavior with a negative J value indicates the presence of antiferromagnetic spin coupling between the Ni(II) ions in the dimeric unit of [Ni(Sal·pr·NMe$_2$)NO_3]$_2$. For the other Ni(II) complexes **1** and **3**—**6**, the 80—300 K data gave a good fit to the theoretical curve based on Eq. 2 when the following values were used: the g value evaluated from the $(\chi_A-N_\alpha)^{-1}$ *vs.* T plot, the N_α of 200×10^{-6} cgs emu and the J value listed in Table 3.

The close agreement between the observed and calculated temperature dependences of magnetic susceptibility can be taken as evidence for the presence of a binuclear structure in the Ni(II) complexes.

The susceptibility data of the Cu(II) complexes **7**—**10** follow the Curie law as is seen in Figs. 1 and 2, indicating magnetic dilution in the crystals. Con-

Table 4. Reflectance and IR spectral data

	Complex	Ligand field band maximum, $\bar{\nu}/10^3$ cm^{-1}	IR absorption, $\bar{\nu}$/cm^{-1} band maximum[b] near 1540 cm^{-1}	$\bar{\nu}_{as}CO_2$	$\bar{\nu}_{s}CO_2$	Δ_{as-s}
1	Ni(Sal·pr·NHMe)NO_3	16.4, 10.2, 7.8 sh	1550 (+16)			
2	Ni(Sal·pr·NMe_2)NO_3	15.7, 9.8, 7.2 sh	1550 (+19)			
3	Ni(5-Cl-sal·pr·NHMe)NO_3	16.3, 10.4, 7.9 sh	1538 (+24)			
4	Ni(5-Cl-sal·pr·NMe_2)NO_3	15.7, 9.8, 7.1 sh	1537 (+17)			
5	Ni(Sal·pr·NHMe)CH_3COO	16.1, 9.9, 7.6 sh	1549 (+15)	1566	1447	119
6	Ni(5-Cl-sal·pr·NHMe)CH_3COO	15.9, 9.8, 7.6 sh	1539 (+25)	1558	1447	111
7	Cu(Sal·pr·NHMe)NO_3	15.3, 12.5	1541			
8	Cu(Sal·pr·NMe_2)NO_3	15.9, 12.8	1541 (+ 7)			
9	Cu(Sal·pr·NHMe)CH_3COO	16.4	1537	1582	1378	204
10	Cu(5-Cl-sal·pr·NHMe)CH_3COO	15.9	1525	1582	1385	197

a) sh=shoulder. b) The numerical values in parentheses indicate the increased wave numbers from the bands in the parent M(5-Y-sal·pr·NRR′)$_2$ complexes where M=Ni(II) or Cu(II).

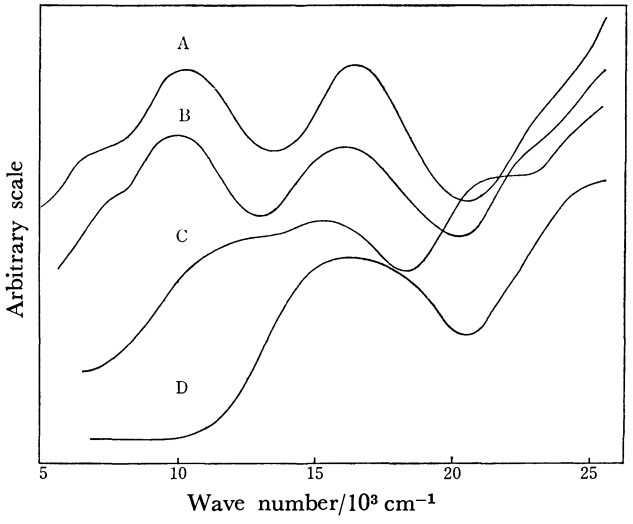

Fig. 4. Reflectance spectra of Ni(Sal·pr·NHMe)NO_3 (A), Ni(Sal·pr·NHMe)CH_3COO (B), Cu(Sal·pr·NHMe)NO_3 (C) and Cu(Sal·pr·NHMe)CH_3COO (D).

sequently in contrast to the Ni(II) complexes, the Cu(II) complexes are considered to be mononuclear.

Diffuse Reflectance Spectra. The present complexes give rise to several bands in the 5000—25000 cm^{-1} region in the diffuse reflectance spectra. The wave numbers of the band maxima are given in Table 4 and the spectral curves for complexes **1**, **5**, **7**, and **9** are shown in Fig. 4.

The Ni(II) complexes investigated all show essentially the same spectral characteristics, two well resolved maxima at *ca.* 16000 and 10000 cm^{-1} with a shoulder at *ca.* 8000 cm^{-1} (*cf.* Table 4 and Fig. 4). This type of spectra is similar to those of the distorted octahedral Ni(II) complexes,[9,10] but quite different from those of the four- or five-coordinated Ni(II) complexes.[11,12] The spectra of the Cu(II) complexes **7** and **8** show a broad band at *ca.* 15500 cm^{-1} with a shoulder at *ca.* 12500 cm^{-1} (*cf.* Table 4 and Fig. 4). This type of spectra is indicative of a five-coordination geometry around the Cu(II) ion and is to be compared with the spectra reported for some distorted square-pyramidal Cu(II) complexes.[4,13,14] The spectral feature of the Cu(II) complexes **9** and **10** is apparently that of a square planar type (*cf.* Fig. 4).

IR Spectra. The wave number of the intense band around 1540 cm^{-1} observed for complexes **1**—**10** are listed in Table 4. For all the Ni(II) complexes studied (**1**—**6**), the absorption energy of the IR band around 1540 cm^{-1} was observed to shift towards higher energies by 15—20 cm^{-1} as compared with that of the corresponding parent bis-complexes Ni(5-Y-sal·pr·NRR′)$_2$, indicating the presence of bridging phenolic oxygen atoms in the nitrato and acetato complexes (*cf.* Table 4).[1-4] No significant band shift was observed for the Cu(II) complex **8**, however, indicating that, in this complex, no phenolic oxygen-bridge exists (*cf.* Table 4). The strong band around 1540 cm^{-1} for each of the Cu(II) complexes **7**,**9**, and **10** also indicates the non-existence of any bridging phenolic oxygen in these complexes.

For the Ni(II) acetato complexes **5** and **6** and the Cu(II) acetato complexes **9** and **10**, the assignment of the IR bands due to the antisymmetric ($\bar{\nu}_{as}CO_2$) and symmetric ($\bar{\nu}_{s}CO_2$) carboxylate stretching vibrations has been made by comparing the bands of the complexes with those of the parent bis-complexes and the corresponding nitrato complexes; the wave numbers are listed in Table 4 together with the separation (Δ_{as-s}) between $\bar{\nu}_{as}CO_2$ and $\bar{\nu}_{s}CO_2$. The correlation between the carboxylate stretching frequencies and structure in Ni(II) acetato complexes has been well established by Curtis.[15] A comparison of the frequencies of $\bar{\nu}_{as}CO_2$, $\bar{\nu}_{s}CO_2$, and Δ_{as-s} for the acetato complexes in this study with those for the Ni(II) acetato complexes of known structure may yield information on the carboxylate coordination in the complexes **5** and **6**. The Ni(II) complexes exhibit $\bar{\nu}_{as}CO_2$ and $\bar{\nu}_{s}CO_2$ bands in an energy region very similar to that reported for the [Ni(tet)CH_3COO]-$ClO_4\cdot 1/2H_2O$ complex ($\bar{\nu}_{as}CO_2$ 1550 cm^{-1}, $\bar{\nu}_{s}CO_2$ 1448 cm^{-1}, Δ_{as-s} 102 cm^{-1}, tet=*dl*-5,7,7,12,14,14-hexamethyl-1,4,8,11-tetraazacyclotetradecane),[15] in which the acetato group is coordinated in a symmetrical chelating mode to the metal ion,[16] and also similar to those reported for the [Ni(en)$_2CH_3COO$] ClO_4 com-

plex ($\tilde{\nu}_{as}CO_2$ 1540 cm^{-1}, $\tilde{\nu}_{s}CO_2$ 1445 cm^{-1}, Δ_{as-s} 95 cm^{-1})[15] and the $[Ni(1,3\text{-pr})_2CH_3COO]ClO_4$ complex ($\tilde{\nu}_{as}CO_2$ 1540 cm^{-1}, $\tilde{\nu}_{s}CO_2$ 1450 cm^{-1}, Δ_{as-s} 90 cm^{-1}),[15] for both of which a symmetrical chelation of the acetato group has been assigned.[15] Thus the close similarity in absorption energy between these complexes leads to the conclusion that the carboxylate coordination mode in the Ni(II) acetato complexes in the present study is of a symmetrical chelating type.

In the case of the Cu(II) acetato complexes **9** and **10**, the $\tilde{\nu}_{as}CO_2$ and $\tilde{\nu}_{s}CO_2$ bands appear at higher and lower frequencies respectively than those of the ionic acetato ($\tilde{\nu}_{as}CO_2$ 1578 cm^{-1}, $\tilde{\nu}_{s}CO_2$ 1414 cm^{-1})[17] (*cf.* Table 4), indicating the presence of unidentate coordination of the acetato group in the complexes.[18] The unidentate coordination is consistent with their reflectance spectra showing a four-coordinated planar Cu(II) geometry.

For the nitrato coordination in the Ni(II) nitrato complexes **1**—**4**, no unambiguous assignment could be drawn from the IR spectra, since the 1200—1500 cm^{-1} region was so complicated that no NO stretching bands of the nitrato group could be recognized. The reflectance spectral feature of the complexes is very similar to those of the corresponding acetato complexes indicating a six-coordinated Ni(II) geometry and thus the nitrato coordination mode is considered to be of the symmetrical chelating type. Similarly, the nitrato coordination mode in the Cu(II) nitrato complexes **7** and **8** is presumably a symmetrical chelating type based on the reflectance spectra which show a five-coordinated Cu(II) geometry.

Structure and Magnetic Properties. On the basis of the molecular weight, magnetic and spectral data, the most probable structure for the present Ni(II) complexes **1**—**6** is considered to be I in which the phenolic oxygen atoms act as bridges between the two metal ions and the tridentate ligand 5-Y-sal·pr·NRR′ spans facially due to the long $-(CH_2)_3-$ chain in a manner similar to that in the $Ni(Sal\cdot pr\cdot NMe_2)_2$ complex.[19]

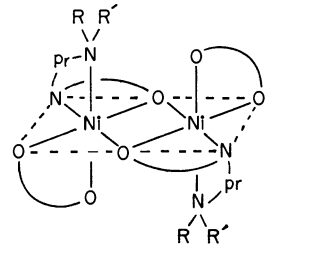

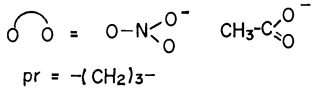

I

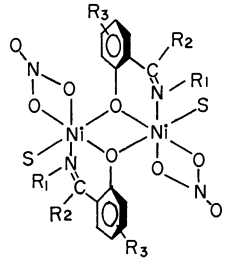

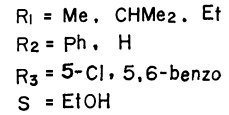

II

Structure I should be compared with that of the $[Ni(bsb)NO_3\cdot C_2H_5OH]_2$ complexes which display intramolecular ferromagnetic interaction,[3] the structure of which is shown schematically in II.[3] The most significant difference in structure between I and II is the bonding mode around the bridging phenolic oxygen atoms. As is seen from I and II, the phenolic

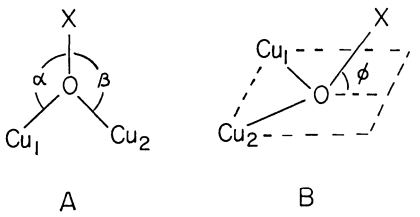

Fig. 5. Geometries around the atom bridging metal ions in phenolic oxygen-bridged binuclear copper(II) complexes.

C–O bonds in the former are coplanar with the plane of the four membered Ni_2O_2 ring due to the chelation of the 5-Y-sal·pr·NRR′ ligand with the phenolic oxygen and azomethine nitrogen atoms at the base of a distorted octahedron, whereas the C–O bonds in the latter are approximately perpendicular to the Ni_2O_2 plane, since the phenolic oxygen atom of the bsb ligand occupies one corner of the basal plane and thus the azomethine nitrogen atom takes one of the axial positions.

In previous papers,[20,21] it was reported that, in binuclear Cu(II) complexes with tridentate salicylaldehyde Schiff bases, the geometry around the atom bridging metal ions is one of the most important factors determining the strength and sign of the magnetic interaction. The structural factors which promote the antiferromagnetic interaction in the complexes are those such as the equality of the angles α and β in Fig. 5A, and the size of the angle ϕ in Fig. 5B (*i.e.*, coplanarity of the O–X bonds with the Cu_1OCu_2O coordination plane, where X is the atom linked to the bridging O atom). These factors may bring about an increase in overlap of the non-orthogonal orbitals involved in the exchange pathways. Recently, Lintvedt *et al.*[22] noted the importance of the planarity of the bridging atom in binuclear Cu(II) complexes for magnetic interaction, and Curtis *et al.*[23] reported that the weak magnetic interaction in di-μ-[4,6,6-trimethyl-3,7-diazanon-3-ene-1,9-diolato(1—)-ONN′, μ-O′]-dicopper(II) diperchlorate ($\theta\approx-25$ K) can be attributed to the nonplanarity of the bridging atom.

From the above structural considerations, the difference in magnetic properties between $[Ni(5\text{-Y-sal}\cdot pr\cdot NRR')X]_2$ and $[Ni(bsb)NO_3\cdot C_2H_5OH]_2$ is attributable to the different bonding mode of the phenolic C–O bond in the complexes, although, as is the case of $[Ni_2(en)_4Cl_2]Cl_2$,[6] the possibility of the 90° cation-anion-cation type ferromagnetic superexchange interaction as discussed by Kanamori[24] and Goodenough[25] is not excluded since the Ni–O–Ni angle has not been reported in Ref. 3.

For the Cu(II) complexes in the present study, a monomeric five-coordinated structure can be assigned for the nitrato complexes **7** and **8**, and a monomeric square planar structure for the acetato complexes **9** and **10** on the basis of the molecular weight, magnetic, and spectral data. The weaker tendency of Cu(II) to form a six-coordinated complex, as compared with Ni(II), is probably the main factor for the metal to produce the monomeric species.

The authors are grateful to Dr. Motomichi Inoue

of Nagoya University for the use of a Faraday magnetic balance. The present work was partially supported by a Grant-in-Aid for Scientific Research from the Ministry of Education.

References

1) E. Sinn and C. M. Harris, *Coord. Chem. Rev.*, **4**, 391 (1969), and references therein.
2) M. Kato, K. Imai, Y. Muto, T. Tokii, and H. B. Jonassen, *J. Inorg. Nucl. Chem.*, **35**, 109 (1973).
3) R. J. Butcher and E. Sinn, *J. Chem. Soc., Chem. Commun.*, **1975**, 832.
4) Y. Muto and T. Tokii, *Bull. Chem. Soc. Jpn.*, **51**, 139 (1978).
5) P. W. Selwood, "Magnetochemistry," Interscience Publishers, New York (1956), pp. 78, 91.
6) A. P. Ginsberg, R. L. Martin, R. W. Brookes, and R. C. Sherwood, *Inorg. Chem.*, **11**, 2884 (1972).
7) B. N. Figgis and R. L. Martin, *J. Chem. Soc.*, **1956**, 3837.
8) A. Earnshaw, "Introduction to Magnetochemistry," Academic press, London (1968), p. 77.
9) S. M. Nelson and T. M. Shepherd, *J. Chem. Soc.*, **1965**, 3276.
10) L. Sacconi, N. Nardi, and F. Zanobini, *Inorg. Chem.*, **5**, 1872 (1966).
11) L. Sacconi, P. Paoletti, and M. Ciampolini, *J. Am. Chem. Soc.*, **85**, 411 (1963).
12) L. Sacconi, P. Nannelli, N. Nardi, and U. Campigli, *Inorg. Chem.*, **4**, 943 (1965).
13) M. Ciampolini, *Struct. Bonding*, **6**, 52 (1969).
14) J. Hathaway and A. A. G. Tomlinson, *Coord. Chem. Rev.*, **5**, 1 (1970), and references therein.
15) N. F. Curtis, *J. Chem. Soc., A*, **1968**, 1579.
16) P. O. Whimp, Thesis, Victoria University of Wellington, New Zealand, 1967.
17) K. Nakamoto, J. Fujita, S. Tanaka, and M. Kobayashi, *J. Am. Chem. Soc.*, **79**, 4904 (1957).
18) K. Nakamoto and P. J. McCarthy, S. J., "Spectroscopy and Structure of Metal Chelate Compounds," John Wiley & Sons, Inc., New York (1968), p. 269.
19) M. Di Vaira and P. L. Orioli, *Inorg. Chem.*, **6**, 490 (1967).
20) Y. Muto, M. Kato, H. B. Jonassen, and L. C. Cusachs, *Bull. Chem. Soc. Jpn.*, **42**, 417 (1969).
21) T. Tokii, Y. Muto, M. Kato, K. Imai, and H. B. Jonassen, *J. Inorg. Nucl. Chem.*, **34**, 3377 (1972).
22) M. D. Glick and R. L. Lintvedt, *Prog. Inorg. Chem.*, **21**, 261 (1976).
23) N. F. Curtis, G. R. Clark, B. W. Skelton, and T. N. Waters, *J. Chem. Soc., Dalton Trans.*, **1977**, 1051.
24) J. Kanamori, *J. Phys. Chem. Solids*, **10**, 87 (1957).
25) J. B. Goodenough, "Magnetism and the Chemical Bond," Interscience Publishers, New York (1963), p. 180.

Adsorption of the Chromate Ion on Cured Diphenyl Phosphonate–Aldehyde Resins

Hidehiko MORI,* Yoshikazu FUJIMURA, and Yoshinobu TAKEGAMI†

Department of Industrial Chemistry, Chubu Institute of Technology, Matsumoto, Kasugai 487

† *Department of Hydrocarbon Chemistry, Faculty of Engineering, Kyoto University, Yoshida, Sakyo-ku, Kyoto 606*

(Received December 12, 1978)

The adsorption of the chromate ion on cured diphenyl phosphonate–aldehyde resins has been investigated. Phosphorus-containing novolak type resins, obtained from the reaction of diphenyl phosphonate with aldehydes have been cured with additional hexamethylenetetramine. The adsorption of the chromate ion on the cured resins decreased in the order: propionaldehyde≈acrylaldehyde>butyraldehyde>crotonaldehyde>acetaldehyde>furfural>formaldehyde. The optimum pH for the adsorption of the chromate ion was in the range 3.0 to 4.0. In the case of the cured diphenyl phosphonate–propionaldehyde resin, the amount of the adsorption of the chromate ion was 20.5 mg Cr/g resin. Under the same conditions, the amounts of the adsorption of molybdate and tungstate ions were 40.5 mg Mo/g resin and 80.0 mg W/g resin, respectively. The adsorbed chromate ion was recovered at approximately 80 wt% as chromium by elution with 1.0 mol/l aqueous HCl solution. The adsorbed molybdate and tungstate ions were desorbed with 2.0 and 3.0 mol/l aqueous H_2SO_4 solutions, respectively. The recovery rate for Mo and W was 100 wt%. The mechanism of adsorption of the chromate ion on the cured resins having phosphinylden groups, >P(O)H, has been discussed.

In a previous paper,[1] diphenyl phosphonate (abbreviated to DPP) was reported to react with several aldehydes, *e.g.*, formaldehyde, acetaldehyde, propionaldehyde, butyraldehyde, acrylaldehyde, crotonaldehyde and furfural to produce phosphorus-containing novolak type resins (abbreviated to DPP resin). The DPP resins were cured with additional hexamethylenetetramine at 120 to 180 °C to give insoluble resins containing phosphinylden groups, >P(O)H. In the present paper, it has been observed that the cured DPP resins selectively adsorbed Group VIB oxide ions, *e.g.*, chromate, dichromate, molybdate and tungstate ions.

The literature is extensive concerning ion exchange resins based upon organophosphorus polymers.[2–6] Organophosphorus resins have been prepared by the treatment of three-dimensional unsaturated aromatic hydrocarbon polymers with phosphorus trichloride in the presence of aluminum chloride, or by the treatment of polymers containing halogenated methyl groups with trialkyl phosphates, followed by oxidation and hydrolysis of the reaction products.[3] The phosphorus-containing ion exchange resins based on phenolic resins have also been prepared by condensing the product obtained from the reaction of *m*-hydroxyphenyl dihydrogenphosphate with formaldehyde.[4] In addition, the ion exchange resins prepared from styrene–divinylbenzene copolymers and phosphorus trichloride[6] are commercially available under the names of Duolite-62 and 63. The phosphorus-containing resins are three-dimensional high molecular weight compounds which contain free phosphonic acid [–P(O)$(OH)_2$] and phosphinic acid [>P(O)(OH)] groups. The active centers for ion exchange are the P–OH bonds and consequently the phosphorus-containing resins adsorb mainly metallic ions, behaving as cation exchangers. To date there are very few reports on phosphorus-containing anion exchangers.[7]

In this paper, the adsorption of chromate, molybdate and tungstate ions on cured DPP resins has been studied. The effect of pH on the adsorption of Group VIB oxide ions, the rate of adsorption, the amount of adsorption and elution of adsorbed Group VIB oxide ions have been examined. Furthermore, the mechanism of the adsorption of the chromate ion on the cured DPP resins has been discussed.

Experimental

Materials. All chemicals used for the preparation of the cured DPP resins were extra-pure grade reagents. Potassium chromate(GR) and dichromate(GR), potassium molybdate(GR) and potassium tungstate(GR) were used without further purification. Other chemicals used for colorimetric determination and preparation of buffer solutions were of analytical reagent-grade.

Preparation of the Cured DPP Resins. The cured DPP resins used for the adsorption were phosphorus-containing resins cured with additional hexamethylenetetramine.

DPP Resins: The phosphorus-containing novolak type resins have been prepared by a method described previously;[1] *i.e.*, DPP has been allowed to react with formaldehyde or acrylaldehyde in water at 80 °C for 3 h. Acetaldehyde, propionaldehyde, butyraldehyde and crotonaldehyde resins were prepared by the direct reaction of DPP with each aldehyde at 80 °C for 8 h. The furfural resin was produced at room temperature in 6 h.

Curing: The curing of the DPP resins was conducted by the method described previously;[1] *i.e.*, to the crude DPP resins, 10 to 15 wt% hexamethylenetetramine was added, and the mixture heated in an oil bath at 120—180 °C for 1 h to give the insoluble DPP resin. The optimum curing rates and temperatures are shown in Table 1. The products were washed with 3-pentanone, 1.0 mol/l aqueous HCl solution, and water to near the point of neutrality. The cured DPP resins were dried at 60 to 80 °C for 4 h, ground and milled to 100—150 mesh.

Procedure. The method for the adsorption of chromate, molybdate and tungstate ions was a batch type as follows; an amount of the cured DPP resin, 10—100 mg, and an aliquot of K_2CrO_4, K_2MoO_4, and K_2WO_4 solutions were added to a 100 cm^3 volumetric flask and diluted to 100 cm^3. The solutions were stirred at room temperature for 24 h. After removal of the resin, the concentrations of chromate, molybdate and tungstate ions were determined by colorimetric

Table 1. Properties of cured DPP-aldehydes resins

Compound R	Utmost curing rate wt%	Cured temp °C	P %	Amount of Cr to resin[a] mg/g	Resistance to 50 vol% H_2SO_4 Residual weight wt%
H	95.0	150	2.8	1.9	97.0
CH_3	76.0	170	3.0	7.6	75.0
C_2H_5	89.0	140	2.7	10.0	70.0
C_3H_7	69.0	170	3.1	9.1	96.0
C_3H_6	89.0	170	3.1	8.4	80.0
C_2H_3	93.0	120	2.8	10.0	86.0
C_4H_3O	92.0	120	2.6	2.8	95.0

a) Value measured for 10 ppm Cr(VI) solution.

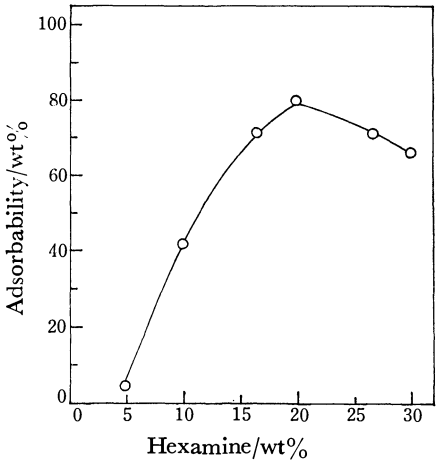

Fig. 1. Effect of amount of hexametylenetetramine in curing reaction on adsorption of chromate ion. Conditions; resin: DPP-PA, curing temp: 120 °C, curing time: 2 h.

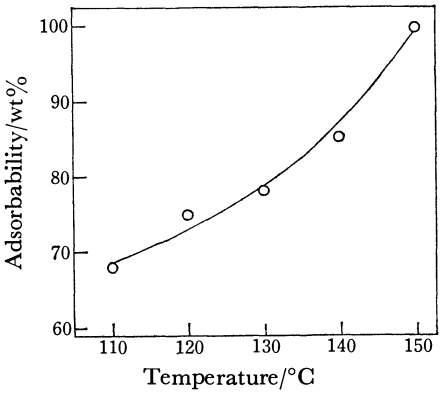

Fig. 2. Relation between adsorption of chromate ion and curing temperature. Conditions; resin: DPP-PA, curing time: 30 min, amount of hexamine: 20 wt%.

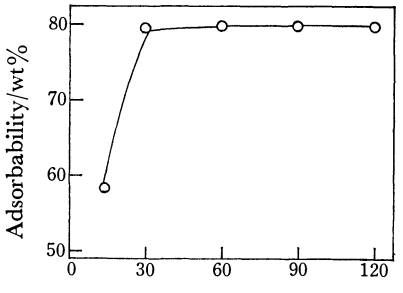

Fig. 3. Relation between adsorption of chromate ion and curing time. Conditions; resin: DPP-PA, curing temp: 120 °C, amount of hexamine: 20 wt%.

and atomic absorption. The rate of adsorption was calculated from the ratios of the concentration before and after the adsorption of each ion. The concentration of Cr(VI) was determined by the diphenylcarbazide method. The total Cr content was determined by atomic absorption. The concentrations of molybdate and tungstate ions were determined by tin(II) chloride and dithiol methods.[8]

Buffer Solution.[9] Sulfuric acid was added for the preparation of the solution bellow pH 2. The buffer solutions (pH 2.0—3.0) were prepared from chloroacetic acid and KOH, succinic acid and KOH (pH 3.0—7.0), and tris-(hydroxymethyl)methanamine and HCl (pH 7.0—9.0).

Measurements. The resin adsorbing chromate ion was washed with water, and dried under vacuum for 24 h. The IR and ESR spectra for the treated samples were recorded on JASCO IR-G, and JEOL-3BSX-ESR spectrometers.

Results and Discussion

Adsorption Characteristics of the Cured DPP Resins. For the seven DPP resins, cured at a temperature giving maximum curing, the adsorptions were conducted as follows; the cured DPP resins (100 mg) and K_2CrO_4 solution containing 1 mg Cr(VI) were added to a 100 cm^3 volumetric flask, the pH adjusted to 3.2 and then diluted to 100 cm^3. The rates of adsorption were calculated and the results are shown in Table 1. As may be seen the chromate ion is comparatively well adsorbed on the cured DPP–propionaldehyde and DPP–acrylaldehyde resins. The adsorption of the chromate ion on seven kinds of cured DPP resins decreased in the order, propionaldehyde resin≈acrylaldehyde resin > butyraldehyde resin > crotonaldehyde resin > acetaldehyde resin > furfural resin > formaldehyde resin. Therefore, subsequent adsorption experiments were conducted using the cured DPP–propionaldehyde resin (abbreviated to cured DPP–PA resin).

The Effect of Curing Conditions on the Degree of Adsorption. The DPP–PA resins have been cured under several conditions, *e.g.*, the amount of curing agent, the curing temperature and the curing time. The effect of each of the conditions on the degree of adsorption of the chromate ion has been examined. Figure

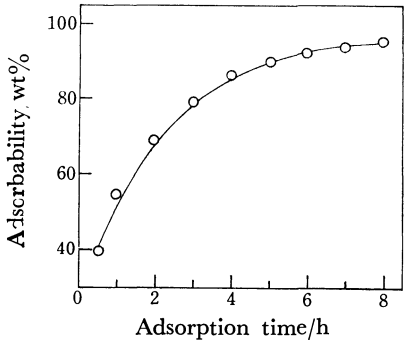

Fig. 4. Adsorption time dependence of chromate ion on cured DPP-PA resin. Conditions; amount of resin: 100 mg, pH: 3.2, concentration of CrO_4^{2-}: 1.0 mg/100 cm³, temp: 25 °C.

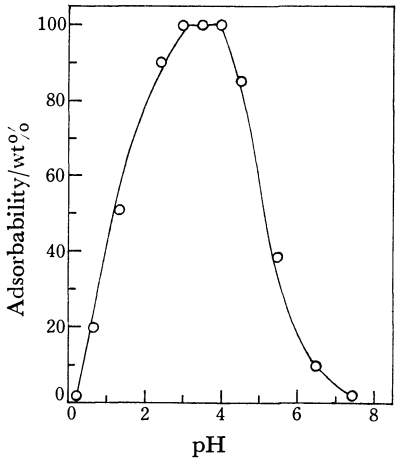

Fig. 5. Effect of pH on adsorption of chromate ion. Conditions; Amount of resin: 100 mg, Concentration of CrO_4^{2-}: 1.0 mg/100 cm³, Shaking time: 24 h, temp: 25 °C.

1 illustrates the relationship between the amount of curing agent, Fig. 2, the curing temperature and Fig. 3, the curing time and the degree of adsorption chromate ion. From these results, it has been found that the chromate ion is heavily adsorbed on the cured DPP–PA resin cured with an additional 20 wt% hexamethylenetetramine at 150 °C for up to 30 min.

The Rate of Adsorption. The rate of adsorption of the chromate ion on the cured DPP–PA resin has been examined, the results of which are shown in Fig. 4. It may be seen that the degree of adsorption of the chromate ion increases up to over 90 wt% in approximately 5 h. Subsequent adsorption proceeded slowly reaching 100 wt% after 16 h. The results of the adsorption of molybdate and tungstate ions were approximately the same.

Influence of pH. The effect of pH on the adsorption of the chromate ion has been examined by varying pH between 0 and 8.5, and the results are illustrated in Fig. 5. The residual Cr observed below pH 2.5 was Cr(III), Cr(VI) being absent. The residual Cr up to pH 4.5 was completely Cr(VI). It may be seen that the optimum pH range for the adsorption of the chromate ion 3.0—4.0. Similarly, the optimum pH range for the adsorption of molybdate and tungstate

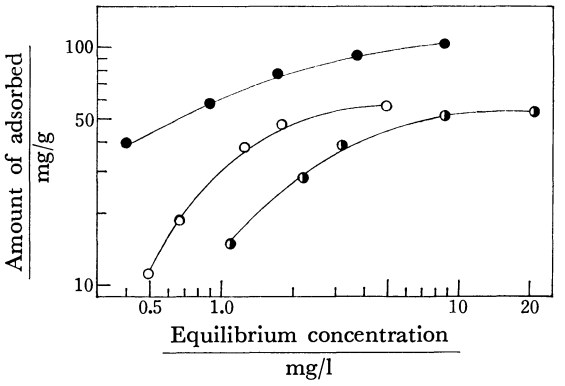

Fig. 6. Adsorption isotherm of Cr(VI), Mo(VI), and W(VI) on cured DPP–PA resin. Conditions; pH: 3.2, shaking time: 24 h, temp: 25 °C, ○: Cr(VI), ◑: Mo(VI), ●: W(VI).

Table 2. Desorption of chromium, molybdenum and tungsten from cured DPP-PA resin by aqueous HCl, H_2SO_4, and NaOH solution

Elute mol/l	Recovery of metal ion		
	Chromium wt%	Molybdenum wt%	Tungsten wt%
HCl			
0.05	46.4	0	0
0.1	60.0	10.6	2.1
0.5	63.0	21.2	10.2
1.0	80.0	26.5	25.0
4.0	81.0	42.5	40.0
H_2SO_4			
1.0	56.7	64.7	10.5
2.0	56.0	100	50.1
3.0	55.0		100
4.0	55.0		
NaOH			
0.1	100	100	100

ions was 3.0—4.0, consistent with the results for the chromate ion.

Degree of Adsorption. The degree of the adsorption of chromate ion on the cured DPP–PA resin was measured as follows; a series of K_2CrO_4 solutions containing 1.5—6.0 mg as Cr were added to the cured DPP–PA resin (100 mg). Each solution was adjusted to pH 3.2 and diluted with water to 100 cm³. Each adsorption was calculated and plotted against the equilibrium concentration of total Cr, the results of which are shown in Fig. 6. The degree of adsorption of each Cr unit to resin (1 g) was 20.5 mg. The degree of adsorption of molybdate and tungstate ions on the cured DPP–PA resin were measured in the same manner. The degree of adsorption of the Mo and W units to resin (1 g) were 40.5 and 80.0 mg, respectively.

Desorption. The desorption of chromate, molybdate and tungstate ions adsorbed on the cured DPP–PA resin were conducted using aqueous HCl, H_2SO_4 and NaOH solutions. The amounts of chromate, molybdate and tungstate ions desorbed with various concentration of acidic or basic solutions are

shown in Table 2. For the desorption of Cr it is more advantageous to use aqueous HCl rather than aqueous H_2SO_4 solution. Elution with 1.0 mol/l aqueous HCl solution, gave 80.0 wt% recovery of Cr. For the desorption of Mo and W, both ions were eluted with aqueous H_2SO_4 solution. Elution with 2.0 mol/l aqueous H_2SO_4 solution, gave 100 wt% recovery of Mo and 3.0 mol/l aqueous H_2SO_4 solution, gave 100 wt% recovery of W.

The residual weight of the cured DPP–PA resin after soaking in 50 vol% H_2SO_4 for two days was approximately 70 wt% as shown in Table 1. Consequently it has been concluded that the cured DPP–PA resin is very resistant to acid. The elution of Cr, Mo, and W by 0.1 mol/l aqueous NaOH solution, gave a recovery of 100 wt%, but as the cured DPP–PA resin was completely decomposed, elution with aqueous NaOH solution is not a suitable technique.

It has been observed that Cr eluted with HCl is recovered as Cr(III) and that Cr eluted with sodium hydroxide is Cr(VI) in 70 wt% of the total Cr content. Mo and W were recovered as Mo(VI) and W(VI) because of their lower oxidizing properties in comparison with Cr.

Mechanism of Adsorption. In order to elucidate the adsorption mechanism of the chromate ion on the cured DPP–PA resin, the IR and ESR spectra of the cured DPP–PA resin adsorbing chromate ion were measured. In the IR spectrum of the DPP–PA resin, the absorption bands assigned to the P–H and P=O bonds were observed at 2450 and 1250 cm^{-1}. In the IR spectrum of the cured DPP–PA resin adsorbing chromate ion, the absorption band of the P–H bond disappeared but the remaining absorption did not change. In the ESR spectrum, a signal with a g value of 1.97 and H_{msl} of 20, was observed together with a broad signal, the g value of which could not be determined. The two signals are thought to agree with the so-called β phase proposed by O'Reilly,[10] and thus it has been assumed that the former signal corresponds to Cr(V) while the latter corresponds to Cr(III). In the desorption of the chromate ion using aqueous sodium hydroxide solution, approximately 70 wt% in total Cr adsorbed on the cured DPP–PA resin was Cr(VI). This result does not agree with the ESR data which shows the presence of Cr(V) in the cured DPP–PA resin adsorbing chromate ion. The observed difference may be resolved assuming the β phase signal of Cr(V) is regarded as the signal associated with a three-chromium-atom center of mixed valency, Cr(VI)–Cr(III)–Cr(VI), as proposed by Spitz for the polymerization of olefins with a catalyst of chromium oxide.[11]

It has been reported[12] that the chromate ion reacts with phosphonic acid to produce the intermediate, $O_3CrO–P(OH)_2H$, and as the reaction proceeds furthermore, Cr(VI) is reduced to Cr(V) and finally to Cr(III). It is suggested that the P–H bond is broken in the rate-determining step of chromate ion reduction. It has been reported[13] that the P–H bond in the reaction of DPP with Cu(II) salts breaks as follows; $>P(O)H + H_2O \rightarrow >P(O)OH + 2H^+ + 2e$. Simultaneously the Cu(II) is reduced. It is suggested that the active center for the adsorption of the chromate ion on the cured DPP–PA resin is the P=O bond. In water solution the P=O bond reacts with a water molecule to form $>P(OH)_2H$,[1,13] and $>P(OH)_2H$ reacts with chromate ion as follows; $>P(OH)_2H + CrO_4^{2-} \rightarrow >P(H)O_2CrO_2 + 2OH^-$. At the same time the chromate ion is reduced by the P–H bond. It has been concluded that the chromate ion is adsorbed on the cured DPP–PA resin in the form of a mixed valency, Cr(VI)–Cr(III)–Cr(VI).

References

1) H. Mori, Y. Fujimura, and Y. Takegami, *Nippon Kagaku Kaishi*, **1978**, 1281.
2) J. Schubert, *Ann. Rev. Phys. Chem.*, **5**, 413 (1954).
3) R. W. Upson, U. S. Patent 2599501; *Chem. Abstr.*, **46**, 8416f (1952).
4) E. B. Trostyanskaya, A. S. Tevlina, and L. V. Bessonava, *Plast. Massay*, 1961 (11), *Chem. Abstr.*, **56**, 10391g (1962).
5) J. Kennedy, E. S. Lame, and B. K. Robinson, *J. Appl. Chem.*, **8**, 459 (1968).
6) Y. Utsunomiya, T. Tabata, E. Tsuyuki, and H. Kuyama, *Kogyo Kagaku Zasshi*, **72**, 1929 (1969).
7) N. V. Stamicarbon, Dutch Patent 75705; *Chem. Abstr.*, **49**, 71541i (1955).
8) G. Charlot, "Colorimetric Determination of the Elements," Elsevier, Amsterdam (1964), p. 226.
9) R. M. C. Dawson, D. C. Elliott, W. H. Elliott, and K. M. Jonse, "Data for Biochemical Research," Oxford, London (1969), p. 502.
10) D. E. O'Reilly, *Adv. Catal.*, **12**, 31 (1960).
11) R. Spitz, *J. Catal.*, **35**, 335 (1974).
12) G. P. Haight, J. M. Rose, and J. Preer, *J. Am. Chem. Soc.*, **90**, 4809 (1968).
13) H. Mori, Y. Fujimura, and Y. Takegami, *Nippon Kagaku Kaishi*, **1977**, 1452.

Degradation of Magnesium and Calcium Highpolyphosphate Coacervates[1)]

Takao UMEGAKI* and Takafumi KANAZAWA

Department of Industrial Chemistry, Faculty of Technology, Tokyo Metropolitan University, Fukasawa, Setagaya-ku, Tokyo 158

(Received January 20, 1979)

The degradation of highpolyphosphates in the coacervates of magnesium and calcium is discussed on the basis of the results of viscosity measurement and paper chromatographic analysis of highpolyphosphates. The initial viscosity and transparency of some magnesium coacervates were maintained with little change at 30 °C for about 2 weeks, while most calcium coacervates changed within 10 days into wet cakes containing $Ca(H_2PO_4)_2 \cdot H_2O$ and $Ca_3(HP_2O_7)_2 \cdot 4H_2O$. The formation of pyrophosphates during the course of degradation of both coacervates is remarkable as compared with that on the hydrolysis of alkali highpolyphosphates in aqueous solutions.

In dilute aqueous solutions, highpolyphosphate chain-anion undergoes degradation to produce shorter chain polyphosphates, orthophosphates and ring phosphates. Studies have been carried out on the hydrolyses of alkali highpolyphosphates and their mechanisms.[2-4)] However, only a few reports have appeared on the degradation of non-alkali highpolyphosphates.

In the preceding paper[5)] the thermal change of magnesium highpolyphosphate coacervate(MPC) was discussed on the basis of the results of thermal analysis. For the analysis, the coacervate had to be heated and partially dehydrated at 100 °C in order to avoid swelling and foaming in the sample cell. Consequently, no detail was known about the degradation of MPC below 100°C.

The present paper deals with the viscosity changes of MPC and calcium highpolyphosphate coacervate (CPC) on degradation at temperatures form 25 to 90°C. The changes of the highpolyphosphate chain length were determined by paper chromatography.

Experimental

Materials. Coacervate samples were obtained by adding ethyl alcohol to mixtures of a sodium metaphosphate solution and a solution of magnesium or calcium chloride. The coacervates were also prepared by direct addition of $MgCl_2 \cdot 6H_2O$ or $CaCl_2 \cdot 2H_2O$ powder to a sodium metaphosphate solution. The coacervate was used immediately after coacervation caused by addition of ethyl alcohol or the respective chloride powder. Conditions for the preparation of coacervates were described in detail in a previous paper.[6)]

Paper Chromatography. Since MPC and CPC contain Mg^{2+} and Ca^{2+}, respectively, ETA (about 1% in a solution) was added to each solution of the coacervates, according to the analytical method proposed by Yamazoe *et al.*[7)] Each individual spot on the filter paper was washed with ammonia water. The phosphate solutions thus obtained were strongly acidified and boiled to give rise to hydrolysis. Phosphorus in the solutions was then analyzed by heteropoly blue colorimetry.

Total absorbance due to all the phosphates was obtained by summation of the individual absorbance values. The phosphorus content of each spot is expressed as a portion of total phosphorus present as follows:

$P(\%) = (\text{absorbance for each fraction/sum of absorbance}) \times 100$

Viscosity Measurement. The viscosities of the coacervates were measured with a rotational viscometer of cone-and-plate type.[6)]

X-Ray Analysis. X-Ray powder diffraction patterns of degradation products in coacervates were obtained with a Rigaku Denki Diffractometer Model D-3F.

Results and Discussion

Linearity of the flow curves for coacervates in the present work was obtained at shearing rates 10—600 s^{-1}. Consequently, all the coacervates used were assumed to be Newtonian.

Viscosity Change with Time at 30 °C. Figure 1 shows a typical viscosity change with time in one of the MPC samples turned into a coacervate by addition of ethyl alcohol. For the first two weeks viscosity lowering was not remarkable. However, short chain-phosphates such as ortho- and pyrophosphates were detected by paper chromatography. Thus, most highpolyphosphates of long chains probably remained without cleavage, degradation of MPC initially occurring only at terminal parts of the polyphosphates. In spite of the progress of degradation of highpolyphosphates, transparency of most samples was maintained, no precipitate being found in the coacervates at 30 °C for about two months.

Most CPC were less stable than MPC. The viscosity of CPC was lowered and a small amount of white powder began to be suspended in a transparent coacervate within a week. One or two days after the first appearance of the suspension, the coacervate completely turned into a wet cake of white powder, which might consist of calcium phosphates. A calcium pyrophosphate of $Ca_3(HP_2O_7)_2 \cdot 4H_2O$[8)] was identified one or two days after the cake formation, a mixture

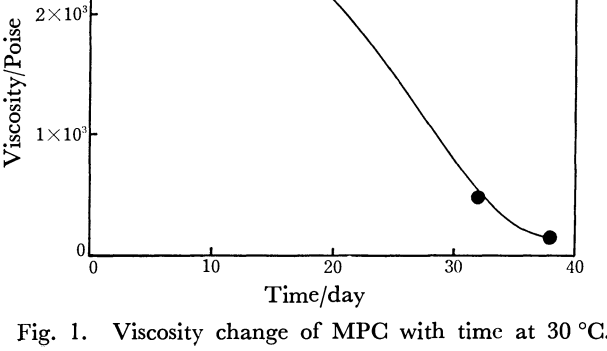

Fig. 1. Viscosity change of MPC with time at 30 °C.

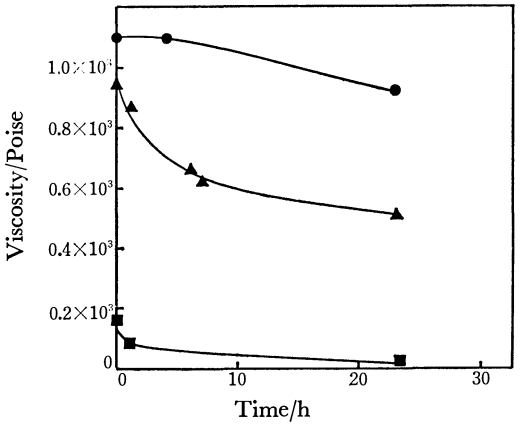

Fig. 2. Viscosity change of various MPC's with time at 50 °C. ●: Sample A, ▲: Sample B, ■: Sample C. (The initial viscosities of A, B, and C were 1.10×10^3, 0.95×10^3, and 0.16×10^3 Poise, respectively.)

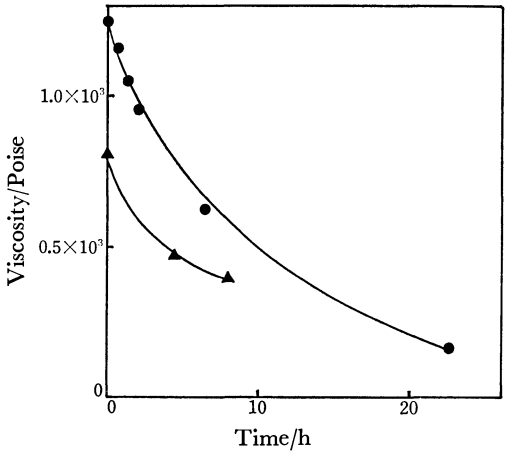

Fig. 3. Viscosity change of various CPC's with time at 50 °C. ●: Sample A, ▲: Sample B. (The initial viscosities of A and B were 1.24×10^3 and 0.80×10^3 Poise, respectively.)

of $Ca(H_2PO_4)_2\cdot H_2O$ and the pyrophosphate being obtained within 3 or 4 weeks after the beginning of degradation experiment.

The difference of stability between MPC and CPC may be interpreted in terms of solubilities of the salts of short chain-phosphates into the coacervates.

Viscosity Change of Coacervates with Various Initial Viscosities. The viscosity lowering of some MPC is slightly noticeable only at the first stage of experiments, while CPC became less viscous gradually and continually (Figs. 2 and 3). Concerning MPC, the degree of viscosity lowering decreases with increase in the initial viscosity. Highly viscous MPC is recognized to be considerably stable. From a comparison of viscosity changes in the coacervate samples with various initial viscosities, the mobility of phosphate ions in the coacervates is considered to be closely related to the rates of degradation.

Viscosity Changes at Various Temperatures. Viscosity changes with temperature of MPC and CPC are shown in Figs. 4 and 5, respectively. The viscosities of both coacervates lowered rapidly at 80—85 °C.

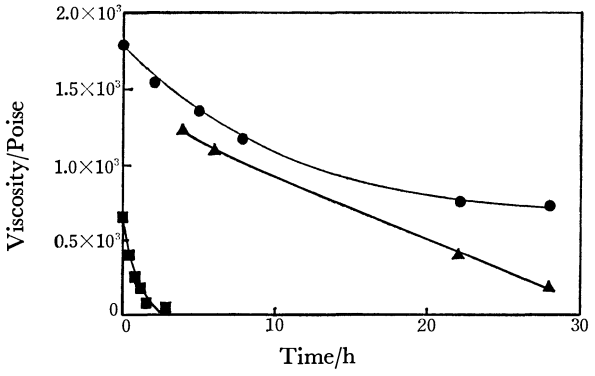

Fig. 4. Viscosity change of MPC with time at various temperatures. ●: 50 °C, ▲: 70 °C, ■: 85 °C.

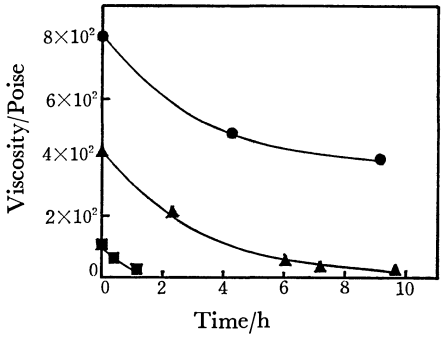

Fig. 5. Viscosity change of CPC with time at various temperatures. ●: 50 °C, ▲: 60 °C, ■: 80 °C.

The magnesium coacervates remained transparent while the calcium coacervates solidified within 10 h above 60 °C. In CPC cakes cooled to room temperature, $Ca(H_2PO_4)_2\cdot H_2O$ and $Ca_3(HP_2O_7)_2\cdot 4H_2O$ were detected by X-ray diffraction.

Short chain-phosphates formed are given in Table 1. On degradation of MPC, pyro- and tripolyphosphates appeared. On the other hand, only orthophosphates formed during the course of hydrolysis of $NaPO_3$.

As pointed out by van Wazer and his coworkers,[2] there are three alternative degradation paths of Graham's salts: Splitting of end PO_4 groups, random scission along the main chain of highpolyphosphates, and ring formation.

During the degradation of the coacervates, orthophsphates are probably formed by the cleavage of end phosphates, and pyro- and tripolyphosphates by the successive decomposition of highpolyphosphates to shorter chains. It seems difficult to give a quantitative kinetics for degradation on the basis of the results of paper chromatographic analysis since the homogeneity of coacervate samples is somewhat doubtful. However, the portion of pyrophosphates obtained on the degradation of MPC was larger than what might have been expected from the successive cleavage. The polymerization of orthophosphates into pyrophosphates is not likely to occur at low temperatures such as 30—50 °C.

Wieker[9] and Lowenstein[10] reported that pyrophosphates are formed by coupling between the terminal PO_4 of straight chain polyphosphates and orthophosphate ions in the presence of Mg ions during the

Table 1. Degradation of phosphate anions in magnesium coacervate

Sample	Temp (°C)	Time (min)	Phosphates formed on degradation (%)				
			Ortho	Pyro	Tripoly	Trimeta	Highpoly
MPC	50	0	—[a]	—	—	—	100
		210	14.9	tr.[b]	—	—	85.1
		4640	18.9	16.5	17.3	—	47.3
		6060	28.5	22.0	20.7	—	28.8
MPC	90	0	—	—	—	—	100
		20	13.3	tr.	—	—	86.7
		40	18.1	11.9	9.2	—	60.8
		60	18.5	13.0	10.8	—	57.7
$NaPO_3$[c]	90	0	—	—	—	—	100
		50	16.9	tr.	—	—	83.1
		90	22.2	tr.	—	—	77.8
		120	28.2	tr.	—	—	71.9
		210	47.9	tr.	—	—	52.1

a) Not detected. b) Trace. c) About 15% aqueous solution of $NaPO_3$.

course of hydrolysis of hexakisguanidinium tetraphosphate and adenosintriphosphate, respectively. The above reactions occurred in alkaline solutions. However, the degraded coacervates probably contained a considerable amount of hydrogen ions since calcium acid phosphates were formed during the course of CPC degradation.

In addition to the three degradation processes proposed by van Wazer and his coworkers,[2] and the coupling in alkaline solutions, there may be some other decomposition paths of coacervates and pyrophosphate formation in degraded coacervates.

Conclusion

From the results of viscosity meausrement and paper chromatography of MPC and CPC, the following conclusions were obtained:

1) Most samples of MPC are more stable than those of CPC. No precipitate in magnesium coacervates was observed at 30 °C for about two months.

2) Most samples of CPC turn into wet cakes of such calcium phosphates as $Ca(H_2PO_4)_2 \cdot H_2O$ and $Ca_3(HP_2O_7)_2 \cdot 4H_2O$ at 30 °C in about 10 days.

3) Pyrophosphate may be formed in MPC and CPC probably through a certain path differing from that of degradation of alkali highpolyphosphates in aqueous solutions and also from that of the coupling reaction in alkaline solutions.

References

1) Presented at the 34th National Meeting of the Chemical Society of Japan, Hiratsuka, April 1976.
2) J. F. McCullough, J. R. van Wazer, and E. J. Griffith, *J. Am. Chem. Soc.*, **78**, 4528 (1956).
3) E. Thilo and W. Wieker, *J. Polym. Sci.*, **53**, 55 (1961).
4) J. B. Gill and S. A. Riaz, *J. Chem. Soc., A*, **1969**, 183.
5) T. Umegaki and T. Kanazawa, *Bull. Chem. Soc. Jpn.*, **49**, 2105 (1976).
6) T. Umegaki and T. Kanazawa, *Bull. Chem. Soc. Jpn.*, **48**, 1452 (1975).
7) F. Yamazoe, N. Yoshida, and F. Tanaka, *Nippon Dojo-Hiryogaku Zasshi*, **35**, 315 (1964).
8) E. H. Brown and J. R. Lehr, *J. Agric. Food Chem.*, **12**, 201 (1967).
9) W. Wieker, *Z. Anorg. Allg. Chem.*, **355**, 20 (1967).
10) J. M. Lowenstein, *Biochem. J.*, **70**, 222 (1958).

Transpiration Study of the Reaction of Water Vapor with Barium Oxide

Tadashi SASAMOTO,* Kentarō MIZUSHIMA, and Toshiyuki SATA
Research Laboratory of Engineering Materials, Tokyo Institute of Technology, Ookayama, Meguro-ku, Tokyo 152

(Received January 23, 1979)

Barium oxide has been found to react with water vapor at temperatures from 1443 to 1593 K to form gaseous $Ba(OH)_2$ according to the reaction; $BaO(s)+H_2O(g)\rightarrow Ba(OH)_2(g)$. The standard free energy of formation is given by the equation, $\Delta G_r^\circ = 49400 - 16.6\ T$ (cal/mol) in the present temperature range. From the thermodynamic cycle the bond energy between barium and two hydroxyl groups has been found to be 196.8 kcal/mol.

The volatility of the alkaline earth oxides is greatly increased by the presence of water vapor due to the formation of volatile hydroxide vapors which result from the following reactions;

$$MO(s) + H_2O(g) \rightarrow M(OH)_2(g) \quad (1)$$

$$MO(s) + 1/2H_2O(g) \rightarrow M(OH)(g) + 1/4O_2 \quad (2)$$

where M is a Group IIa element. This has been verified for BeO,[1-3] MgO,[4,5] and BaO.[6] Stafford and Berkowitz[6] studied the $BaO-H_2O$ system mass-spectrometrically and found that dihydroxide vapor $Ba(OH)_2$, predominanted at temperatures between 1485 and 1785 K under a water pressure above 4×10^{-5} atm. The bond energy for $Ba(OH)_2$ was given by 206.3 kcal/mol. Mass-spectrometry is, however, often accompanied by errors due to the uncertainty of the relative cross section for ionization and the relative efficiency of the secondary-electron multiplier. Consequently it is necessary to confirm the value by other methods.

In the present study, the reaction of water vapor with solid barium oxide has been investigated by the transpiration method as a series of studies on the effects of water vapor upon the vaporization of alkaline earth oxides. The vapor pressures of gaseous $Ba(OH)_2$ formed according to Reaction 1 and the related thermodynamic properties have been evaluated.

Experimental

Transpiration Apparatus. Figure 1 shows a schematic drawing of the reaction zone in the apparatus used in this study. Approximately 2 g of sample was loaded into a Pt/20%Rh boat lined with magnesia. The vaporized species were collected in a condenser made of Pt/20%Rh alloy. The condenser had a capillary (0.7 mm i.d.×6 mm long) at one end. All other structual components except for those described above were made of alumina. Barium oxide reacts with alumina to form three barium aluminates, *i.e.*, $BaO\cdot 6Al_2O_3$, $BaO\cdot Al_2O_3$ and $3BaO\cdot Al_2O_3$, but the partial pressure of BaO(g) over these compounds is very small.[7,8] Therefore, it has been assumed that the formation of the barium aluminates has no effect on the equilibrium relation of the gas phase containing the barium bearing gaseous species. Temperatures were measured with a Pt/13%Rh thermocouple and regulated within ±1 °C.

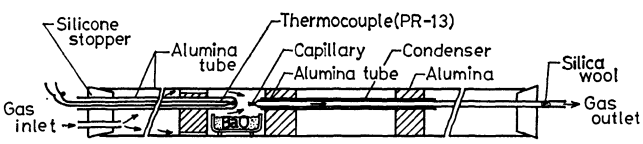

Fig. 1. Cross section of reaction zone in transpiration apparatus.

A wet gas mixture, Ar/H_2O, was obtained by passing argon gas three times through a water reservoir, the temperature of which was accurately controlled. The partial pressure of water vapor was determined from the weight increase of P_2O_5 placed in a stream of the wet gas.

Procedure. The argon carrier gas used was passed through the water reservoir described above and saturated with water vapor after passage through a KOH-column to remove carbon dioxide contained as an impurity, and then into the charge room at a given temperature. The water vapor reacted with BaO to form Ba-bearing hydroxide vapors. The carrier gas was saturated with vapors formed in the charge room at an appropriate flow rate and the vapors formed were transported by the carrier gas to the condenser. The condensate was removed into concentrated nitric acid solution and the barium in the solution was analyzed by chelatometry using EDTA and cresolphthalene complexon. The estimated analytical error is less than ±0.6% by weight of Ba.

The partial pressure of the volatile barium hydroxide compound has been calculated from the amount of collected barium, assuming that each molecule of the volatile species contains one atom of barium and that the vapor approximated to an ideal gas. Therefore, it follows that partial pressure at equilibrium is given by

$$p(Ba(OH)_{2x}) = n_v P/(n_c+n_v) \quad (3)$$

where n_c is the number of mole for the carrier gas, n_v for the sample vapor, and P the total pressure.

Sample. Guaranteed reagent-grade BaO with a 99.9% purity (supplied by Rare Metallic Co., Ltd.) was used. In order to stop dispersion of the fine particles in the carrier gas, the BaO was sintered at 1300 °C prior to use. The compacted sample was kept in a desiccator filled with pure argon to avoid reaction with water and carbon dioxide.

Results and Discussion

Effect of Flow Rate on Vapor Pressure. To determine the conditions for equilibrium a series of measurements was made at 1593 K with varying flow rates. Figure 2 illustrates the apparent vapor pressure of the assumed molecule, $Ba(OH)_{2x}$, calculated from Eq. 3 as a function of the flow rate. As can be seen from Fig. 2, the vapor pressures obtained are approximately constant in the range 1.3 up to 2.5 cm^3/s.

The decrease in vapor pressure, *i.e.*, $<1.2\ cm^3/s$, is thought due to escaping vapor from the space between the condenser and the support (alumina tube).

Water Vapor Dependence. A plot of the logarithm of the equilibrium pressure of the volatile complex as a function of the logarithm of the partial pressure

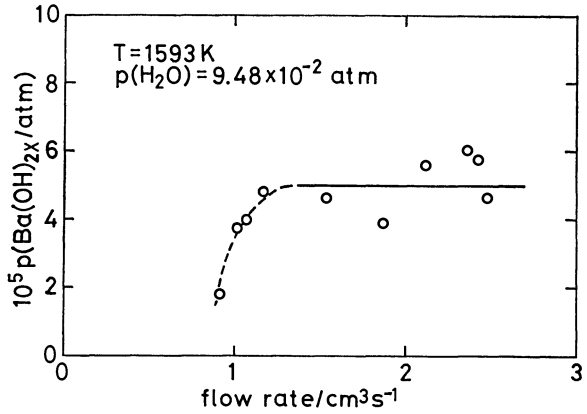

Fig. 2. Vapor pressure *vs.* the flow rate of carrier gas at $T=1593$ K and $p(H_2O)=0.0948$ atm.

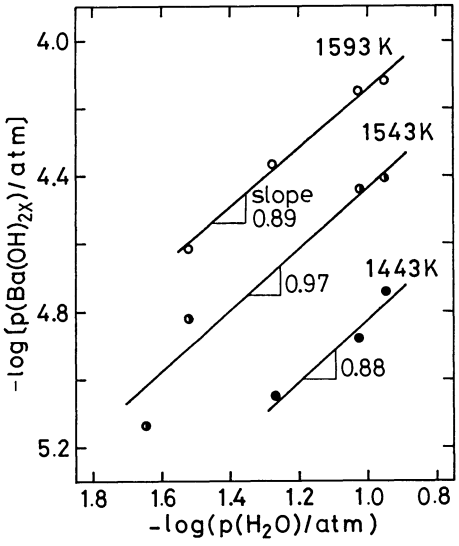

Fig. 3. Variation of log(vapor pressure of barium bearing species) *vs.* log(partial pressure of water).

of water at constant temperature and partial pressure of oxygen will indicate whether Reaction 1 or 2 occurs (this includes the correct value of x in $Ba(OH)_{2x}$) as outlined below.

Combining Reaction 1 with 2 yields the following equation for the BaO–H_2O system,

$$BaO(s) + xH_2O(g) \rightarrow Ba(OH)_{2x}(g) + \frac{(1-x)}{2}O_2(g) \quad (4)$$

The equilibrium constant k_p for the above reaction may be written as

$$k_p = \frac{p(Ba(OH)_{2x}) \cdot p(O_2)^{(1-x)/2}}{a(BaO) \cdot p(H_2O)^x} \quad (5)$$

Assuming $a(BaO)=1$ and taking logarithms of both sides;

$$\log p(Ba(OH)_{2x}) = x \log p(H_2O) - \frac{(1-x)}{2}\log p(O_2) + \log k_p \quad (6)$$

From Eq. 6 the value of x can be determined, *i.e.*, the contribution of Reactions 1 and 2 to Reaction 4.

No correction need be made for the partial pressure of BaO(g) since this is equal to only 3.54×10^{-7} atm

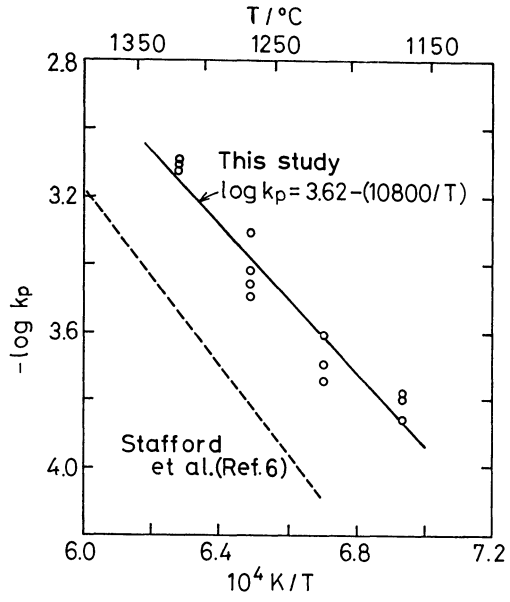

Fig. 4. Plot of equilibrium constant for the reaction $BaO(s)+H_2O(g)=Ba(OH)_2(g)$ *versus* reciprocal temperature.

at 1593 K, the highest temperature used in these measurements.

A series of measurements were made at 1443 to 1593 K with a varied vapor pressure of water at atmospheric pressure passing over the barium oxide, and the results of which are given in Table 1 are shown graphically in Fig. 3. The values of x obtained from the slopes of a $\log p(Ba(OH)_{2x})$ *versus* $\log p(H_2O)$ plot were 0.88, 0.97, and 0.89 at 1443, 1543, and 1593 K, respectively. The average value was 0.91 which was very close to unity. Considering the mass-spectrometric results of Stafford and Berkowitz,[6] the reaction form of the alkaline earth oxides with water vapor[1–6] and flame-experiment data,[9,10] the value of x has been determined as unity. Therefore the predominant reaction of water vapor with barium oxide under these conditions ($p(H_2O)=0.022$—0.112 atm) is:

$$BaO(s) + H_2O(g) \rightarrow Ba(OH)_2(g) \quad (7)$$

The selection of oxygen as the carrier gas would suppress the formation of gaseous Ba(OH) and lead to a value of x move close to unity. No examination in an oxidizing atmosphere was conducted, however, because normal barium oxide oxidizes at relatively low temperature to the per-oxide BaO_2.

The decomposition temperature of $Ba(OH)_2(s)$ is 408 °C, and hence no solid $Ba(OH)_2$ exists at the present temperature.

Vapor Pressure of $Ba(OH)_2(g)$ and Related Thermodynamic Values. The vapor pressures of gaseous $Ba(OH)_2$ and equilibrium constant k_p have been calculated from the amount of collected barium and the results are given in Table 1 and illustrated graphically in Fig. 4. The linear relationship obtained from a least squares treatment of the data corresponds to the expression,

$$\log k_p = -(10800\pm860)/T + 3.62\pm0.56 \quad (8)$$

and hence, the standard Gibbs energy for Reaction

Table 1. Equilibrium constant k_p for the reaction
$BaO(s) + H_2O(g) \rightarrow Ba(OH)_2(g)$

No.	T / K	Time / h	Flow rate / $cm^3\ s^{-1}$	$p(H_2O)$ / atm	Collected Ba / $mg\ h^{-1}$	$p(Ba(OH)_2)$ / atm	k_p	$-\Delta fef$ [a] / $cal\ mol^{-1}\ K^{-1}$	ΔH_0° / $kcal\ mol^{-1}$
1	1443	14.33	1.59	5.36×10^{-2}	0.312	8.91×10^{-6}	1.66×10^{-4}	54.56	53.78
2	1443	16.67	1.63	9.48×10^{-2}	0.475	1.32×10^{-5}	1.39×10^{-4}	54.56	53.26
3	1443	16.67	1.66	1.12×10^{-1}	0.661	1.80×10^{-5}	1.60×10^{-4}	54.56	53.71
4	1493	14.38	1.56	5.36×10^{-2}	0.335	9.76×10^{-6}	1.82×10^{-4}	51.88	51.93
5	1493	4.08	1.63	9.48×10^{-2}	0.843	2.34×10^{-5}	2.47×10^{-4}	51.88	52.82
6	1493	12.67	1.72	1.12×10^{-1}	0.869	2.28×10^{-5}	2.03×10^{-4}	51.88	52.24
7	1543	17.58	1.46	2.29×10^{-2}	0.235	7.31×10^{-6}	3.20×10^{-4}	49.49	51.71
8	1543	15.67	1.58	3.03×10^{-2}	0.527	1.51×10^{-5}	4.99×10^{-4}	49.49	53.06
9	1543	6.83	1.69	9.48×10^{-2}	1.359	3.64×10^{-5}	3.84×10^{-4}	49.49	52.26
10	1543	10.42	1.60	1.12×10^{-1}	1.387	3.91×10^{-5}	$3{\cdot}48\times10^{-4}$	49.49	51.95
11	1593	6.17	1.47	3.03×10^{-2}	0.781	2.41×10^{-5}	7.96×10^{-4}	47.01	52.31
12	1593	5.83	1.60	5.36×10^{-2}	1.534	4.35×10^{-5}	8.14×10^{-4}	47.01	52.38
13	1593	22.42	1.63	9.48×10^{-2}	2.563	7.12×10^{-5}	7.51×10^{-4}	47.01	52.12
14	1593	5.83	1.54	1.12×10^{-1}	2.595	7.62×10^{-5}	6.78×10^{-4}	47.01	51.80
									Av 52.52±0.69

a) Estimated a manner similar to that of Stafford and Berkowitz.[6]

7 is given by,

$$\Delta G_r^\circ = (49400\pm3900) - (16.6\pm2.6)T \quad (9)$$

This gives,

$$\Delta H_r^\circ(1500\ K) = 49.4\pm3.9\ kcal/mol \quad (10)$$

$$\Delta S_r^\circ(1500\ K) = 16.6\pm2.6\ cal/mol\ K \quad (11)$$

Using the ΔG_r° obtained and the JANAF data,[11] the changes in Gibbs energy, enthalpy and entropy for the following formation reaction,

$$Ba(g) + H_2(g) + O_2 = Ba(OH)_2(g) \quad (12)$$

are as follows;

$$\Delta G_f^\circ(Ba(OH)_2, (g)) = \Delta G_r^\circ + \Delta G_f^\circ(BaO, (s)) + \Delta G_f^\circ(H_2O, (g)) = 242400 \pm 4500 - (54.8\pm3.4)T \quad (13)$$

and

$$\Delta H_f^\circ(Ba(OH)_2, (g), 1500\ K) = 242.4\pm4.5\ kcal/mol \quad (14)$$

$$\Delta S^\circ(Ba(OH)_2, (g), 1500\ K) = 114.5\pm3.4\ cal/mol \quad (15)$$

The decomposition energy of $Ba(OH)_2(g)$ into two hydroxyl radicals and Ba vapor, $D_0^\circ(Ba\text{–}(OH)_2)$, has been estimated using the following thermochemical cycle;

$$\begin{array}{ccc} Ba(OH)_2(g) & \xrightarrow{D^\circ} & Ba(g) + 2(OH)(g) \\ \uparrow \Delta H_r^\circ & & \uparrow \Delta H_s^\circ \quad \uparrow \Delta H_f^\circ \\ BaO(s) + H_2O(g) & \xleftarrow{\Delta H_f^\circ} & Ba(s) + \frac{1}{2}O_2 + H_2O(g) \end{array} \quad (16)$$

whereby,

$$D_0^\circ(Ba\text{–}(OH)_2) = -\Delta H_{r,0}^\circ(Ba(OH)_2) - \Delta H_{f,0}^\circ(BaO) + \Delta H_{s,0}^\circ(Ba) + 2\Delta H_{f,0}^\circ(OH) \quad (17)$$

where $\Delta H_{r,0}^\circ(Ba(OH)_2)$ represents the heat of reaction for the Reaction 7, $\Delta H_{f,0}^\circ(BaO)$ the heat of formation for BaO(s), $\Delta H_{s,0}^\circ$ (Ba) the heat of sublimation for Ba(s) and $\Delta H_{f,0}^\circ(OH)$ the heat of formation for OH(g) from $H_2O(g)$ and O_2. The values required were 52.52 (last column in Table 1), −130.696,[12] 42.971,[13] and 37.84[11] kcal/mol at 0 K, respectively. Substitution of these values into Eq. 17 gives the value 196.8 kcal/mol as the value of $D_0^\circ(Ba\text{–}(OH)_2)$. This value differs from that of Stafford and Berkowitz[6] by 4.6%.

References

1) L. I. Grossweiner and R. L. Seifer, *J. Am. Chem. Soc.*, **74**, 2701 (1952).
2) W. A. Young, *J. Phys. Chem.*, **64**, 1003 (1960).
3) T. B. Douglas, *J. Res. Natl. Bur. Stad.*, **76A**, 511 (1972).
4) C. A. Alexander, J. S. Ogden, and A. Levy, *J. Chem. Phys.*, **39**, 3057 (1963).
5) E. Maeda, T. Sasamoto, and T. Sata, *Yogyo Kyokai Shi*, **86**, 461 (1978).
6) F. E. Stafford and J. Berkowitz, *J. Chem. Phys.*, **40**, 2963 (1964).
7) K. Hilpert, A. Naoumidis, and G. Wolff, *High Temp. Sci.*, **7**, 1 (1975).
8) K. Hilpert, H. Beske, and A. Naoumidis, *High Temp. Sci.*, **7**, 159 (1975).
9) F. W. Hoffmann and H. Kohn, *J. Opt. Soc. Am.*, **51**, 512 (1961).
10) T. M. Sugden and K. Schofield, *Trans. Faraday Soc.*, **62**, 566 (1966).
11) D. R. Stull and H. Prophed, "JANAF Thermochemical Tables," Dow Chemical Co., (1960).
12) M. W. Chase, J. L. Curnutt, H. Prophet, R. A. McDonald, and A. N. Syverud, "JANAF Thermochemical Tables, 1975 Supplement," *J. Phys. Chem. Ref. Data*, **4**, 1 (1975).
13) M. W. Chase, J. L. Curnutt, A. T. Hu, H. Prophet, A. N. Syverud, and L. C. Walker, "JANAF Thermochemical Tables, 1974," *J. Phys. Chem. Ref. Data*, **3**, 311 (1974).

Phase Relations in the Sulfur-rich Portion of the Fe–V–S System at Temperatures between 520 and 814 °C

Hiroaki WADA

National Institute for Researches in Inorganic Materials, Namiki 1-1, Sakura-mura, Niihari-gun, Ibaraki 300-31

(Received January 25, 1979)

An equilibrium study of a part of the Fe–V–S system at sections with atomic Fe:V ratios 1:1, 3:2, and 71:29 was carried out. A gravimetric method using a quartz spring balance was employed in the range of $\log(P_{S_2}/\text{atm}) = -4$ to -0.8 at temperatures between 520 and 814 °C. Phase relations in the sulfur-rich portion of the Fe–V–S system were examined on the basis of the P_{S_2}-T-X relation and X-ray analyses of the quenched specimens. The phase diagram of the Fe–V–S system was tentatively constructed at about 570 °C. The compositional dependence of the lattice parameters of the $(Fe,V)_3S_4$ solid solution was studied from the crystallographic viewpoint.

The results of an equilibrium study of a part of the Fe–V–S system at sections with atomic Fe : V ratios 1 : 19, 13 : 37, and 7 : 13 were presented in an earlier publication.[1] It has been reported that the Fe–V–S system has extensive solid solution phases, such as $(Fe,V)_5S_8$, $(Fe,V)_2S_3$, and $(Fe,V)_3S_4$, which have a lattice intermediate between the NiAs-type and the $Cd(OH)_2$ lattice. However, the solid solution fields of these phases have not yet been determined completely. The detailed phase relations in the Fe-rich portion of the composition triangle of FeS–VS–S are still obscure, in spite of the extensive studies of the binary systems FeS[2] and VS.[3]

The present study is a continuation of this work using a further series of samples in the Fe–V–S system. The author reports in this paper the results of the equilibrium study of a part of the Fe–V–S system at sections with atomic Fe : V ratios 1 : 1, 3 : 2, and 71 : 29. The main thermochemical study was carried out with a gravimetric method, which used a quartz spring balance at high temperatures, above 500°C. The P_{S_2} (equilibrium sulfur pressure)-T (temperature)-X (composition) relations and the compositional dependence of lattice constants of several phases were investigated.

Experimental

The sulfide samples with atomic Fe:V ratios 1:1, 3:2, and 71:29 were synthesized by heating the mechanical mixtures of reagent grade $VOSO_4 \cdot 3H_2O$ and $FeSO_4 \cdot (NH_4)_2SO_4 \cdot 6H_2O$ in an H_2S atmosphere at 1050 °C for 4 h and were then used as starting materials. The equilibrium study of these samples was carried out by thermogravimetry at temperatures between 520 and 814 °C. The partial pressure of sulfur was controlled within the range of the $\log(P_{S_2}/\text{atm})$, from -0.8 to -4, in an N_2–sulfur vapor system. The general experimental procedures, the apparatus, chemical analyses, and phase identification of quenched specimens are the same as those described in the previous paper.[1]

A supplemental method employed in this study was the rigid silica tube, quench-type, annealing experiment. In experiments of this type the elements or previously synthesized sulfides were used as source materials. The bulk composition of the charge was adjusted correctly to the desired proportion by weighing on an analytical balance. All weighings were made to a precision of ±0.05 mg. The empty tube was weighed first, then with metal or sulfides inserted, and finally with sulfur added to them. Tubes thus prepared were heated in horizontal furnaces for various periods of time and at fixed temperatures, controlled to within ±3 °C. At the termination of a run the charge was quenched into cold water.

Results and Discussion

Composition versus P_{S_2} *Diagram in a Part of the Fe–V–S System.* The results of equilibrium studies of the Fe–V–S system at sections with atomic Fe:V ratios 1 : 1, 3 : 2, and 71 : 29 are shown graphically in Figs. 1—2 and 4. The variation of equilibrium sulfur pressure P_{S_2} with the composition of sulfides (X=S/(Fe+V)) are given as the isothermal curves, which were drawn by a smooth fitting of data points. The phases as revealed by X-ray diffraction of the quenched specimens are also shown in the figures. Some representative results of quench-type experiments are given in Table 1. In the following text of this paper, solid solution, liquid, and vapor are abbreviated as s.s., L, and v for convenience.

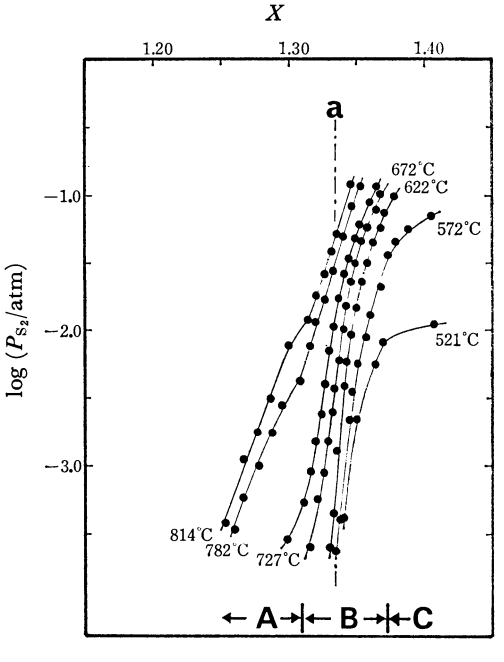

Fig. 1. P_{S_2}-composition (X=S/(Fe+V)) isotherms of $Fe_{0.50}V_{0.50}S_X$. Phase identifications of quenched specimens by X-ray powder diffraction method are shown in lower part of figure as follows A: $(Fe,V)_{1-\delta}S$ s.s.+$(Fe,V)_3S_4$ s.s. B: $(Fe_{0.50}V_{0.50})_3S_4$ s.s. C: $(Fe,V)_3S_4$ s.s.+FeS_2. The stoichiometric Fe+V: S=3:4 composition is designated as the symbol a.

Table 1. Results of X-ray identification of the quenched specimens

Composition Fe/(Fe+V)	Composition S/(Fe+V)	Method	Temp °C	Time h	Product
0.200	1.600	s. t[a)]	600	72	$(Fe, V)_5S_8$
	1.600	s. t	500	168	$(Fe, V)_5S_8+FeS_2$
0.500	1.160	s. t	700	336	$(Fe, V)_{1-\delta}S+(Fe, V)_3S_4$
	1.308	s. p. c[b)]	782	2	$(Fe, V)_{1-\delta}S+(Fe, V)_3S_4$
	1.315	s. p. c	727	5	$(Fe, V)_3S_4$
	1.366	s. p. c	622	5	$(Fe, V)_3S_4$
	1.380	s. t	570	168	$(Fe, V)_3S_4+FeS_2$
0.600	1.308	s. t	600	168	$(Fe, V)_{1-\delta}S+(Fe, V)_3S_4$
	1.317	s. t	570	168	$(Fe, V)_3S_4$
	1.357	s. t	570	168	$(Fe, V)_3S_4$
	1.377	s. t	570	408	$(Fe, V)_3S_4+FeS_2$
0.170	1.159	s. p. c	783	24	$(Fe, V)_{1-\delta}S$
	1.176	s. p. c	727	22	$(Fe, V)_{1-\delta}S+(Fe, V)_3S_4$
	1.310	s. t	570	21	$(Fe, V)_3S_4+(Fe, V)_{1-\delta}S$
	1.320	s. t	570	23	$(Fe, V)_3S_4+FeS_2$
	1.317	s. t	570	24	$(Fe, V)_3S_4$
0.800	1.250	s. t	570	82	$(Fe, V)_{1-\delta}S+(Fe, V)_3S_4$
	1.275	s. t	570	82	$(Fe, V)_{1-\delta}S+(Fe, V)_3S_4+FeS_2$
	1.300	s. t	570	83	$(Fe, V)_{1-\delta}S+(Fe, V)_3S_4+FeS_2$

a) Sealed tube method. b) Sulfur pressure control method.

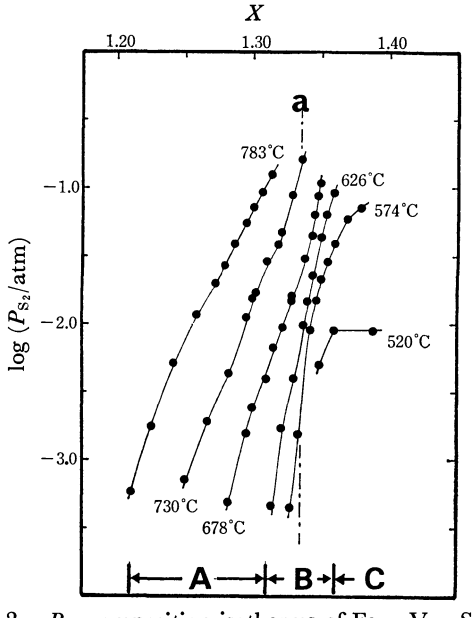

Fig. 2. P_{S_2}-composition isotherms of $Fe_{0.60}V_{0.40}S_X$. A: $(Fe,V)_{1-\delta}S$ s.s.+$(Fe,V)_3S_4$ s.s. B: $(Fe_{0.60}V_{0.40})_3S_4$ s.s. C: $(Fe,V)_3S_4$ s.s.+FeS_2. a: Stoichiometric Fe+V: S=3:4 composition.

Figure 1 shows isotherms with the composition $Fe_{0.50}V_{0.50}S_x$, where X ranges between 1.25 and 1.41 within the experimental temperature region. In this compositional range, several kinds of quenched specimens were identified by X-ray powder diffraction patterns. The following phases were found: hexagonal $(Fe,V)_{1-\delta}S$ s.s., monoclinic V_3S_4-type $(Fe,V)_3S_4$ s.s., and cubic FeS_2 (pyrite). In the range of composition between $X=1.25$ and $X=1.31$, a two-phase mixture of $(Fe,V)_{1-\delta}S$ s.s. and $(Fe,V)_3S_4$ s.s. was obtained below 814 °C. One phase of $(Fe_{0.50}V_{0.50})_3S_4$ s.s. was observed in the range $1.31 \leqq X \leqq 1.37$. Beyond $X=1.37$, FeS_2 appeared together with $(Fe,V)_3S_4$ s.s. at temperatures below 622 °C.

As shown in Fig.1, the steepest part of the isothermal curves is observed at the composition of about $X=1.33$, accompanied by the rapid change of sulfur pressure.

This feature of the isotherms in the one-phase region clearly indicates the existence of a stoichiometric (Fe+V):S=3:4 phase at temperatures below 727 °C. It is noted that isothermal curves for 814, 782, and 727 °C change their slopes slightly at about $X=1.31$. This composition corresponds to the metal-rich phase boundary of $(Fe_{0.50}V_{0.50})_3S_4$ s.s., which was determined from X-ray measurements of quenched specimens. In a two-phase field ($1.25<X<1.31$), however, the isotherms are not horizontal, as is often observed in the case of a two-phase equilibrium of binary systems, but represent rather a continuous variation of sulfur pressure with composition. The sulfur-rich limit of the $(Fe_{0.50}V_{0.50})_3S_4$ phase extends to the composition of $X=1.37$, where the isotherm becomes horizontal at 521°C due to the formation of FeS_2. However, the curvature change of the isotherm for 572 °C is observed at $X=1.38$ rather than at $X=1.37$. This suggests that the homogeneity range of $(Fe_{0.50}V_{0.50})_3S_4$ phase tends to be broadened slightly to the sulfur-rich side with increasing temperature.

A few remarks should be made here regarding the powder X-ray diffraction patterns of the FeS_2, which coexist with $(Fe,V)_3S_4$ s.s. phase. All the unit cell dimensions of FeS_2 in equilibrium with $(Fe,V)_3S_4$ s.s. are the same as those of pure FeS_2, within the limits of error. It may be concluded that FeS_2 does not take measurable amounts of vanadium or sulfur into solid solution and is a stoichiometric compound.

Figure 2 shows isotherms with the composition $Fe_{0.60}$-

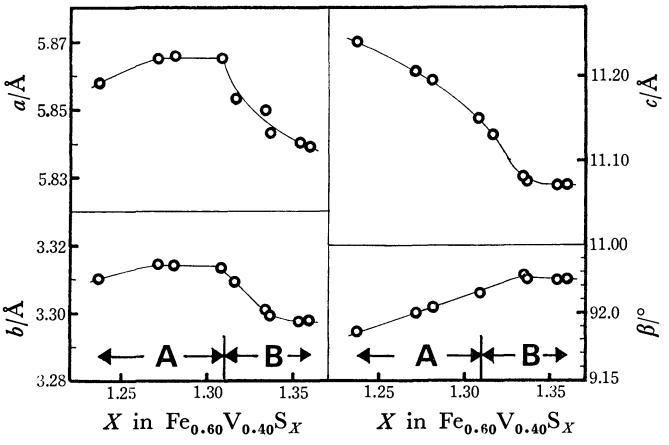

Fig. 3. Relationship between lattice constants of the coexisting phase ($(Fe,V)_3S_4$ s.s.) and the bulk composition. Region, A, is a two-phase field and region, B, a one-phase field.

$V_{0.40}S_X$, where X ranges between 1.21 and 1.39. As listed in Table 1, the following phase relations are found: a two-phase mixture of $(Fe,V)_{1-\delta}S$ s.s. and $(Fe,V)_3S_4$ s.s., $(Fe_{0.60}V_{0.40})_3S_4$ s.s. phase, and a two-phase mixture of FeS_2 and $(Fe,V)_3S_4$ s.s. in the compositional range of $X<1.31$, $1.31\leqq X\leqq 1.36$, and $1.36<X$, respectively.

Although the metal-rich phase boundary of $(Fe_{0.60}V_{0.40})_3S_4$ is determined to be about $X=1.31$ by X-ray powder diffraction of quenched specimens, no characteristic change of the curvature is observed at $X=1.31$ in the isotherms for 783, 730, and 678 °C. These isotherms exhibit rather continuous and gradual changes of sulfur pressure with composition. Within the one-phase region, a rapid increase of pressure is observed near the stoichiometric composition ($X=1.33$) at temperatures below 678 °C. This indicates the existence of the stoichiometric $(Fe_{0.60}V_{0.40})_3S_4$ phase. The isotherm for 520 °C is clearly horizontal at the composition of about $X=1.36$, due to the formation of FeS_2 in equilibrium with $(Fe,V)_3S_4$ solid solution. However, the isotherm for 574 °C does not show such an abrupt change of the slope as is observed at 520 °C.

In order to clarify the behavior of the isotherms on the metal-richer side beyond $X=1.31$, lattice parameters of several specimens quenched from 730 °C were examined by X-ray diffraction (Cu $K\alpha$). Figure 3 shows the relationships between the lattice constant of the coexisting phase ($(Fe,V)_3S_4$ s.s.) and the bulk composition within a two-phase field ($X<1.31$). The lattice constant c and β-angle of $(Fe,V)_3S_4$ s.s. in equilibrium with $(Fe,V)_{1-\delta}S$ s.s. change continuously with compositions, the lattice constants a and b remaining nearly the same in the range $1.27<X<1.31$. In general, shifts of lattice constant correspond to the compositional variation of the phase. Therefore, it may be concluded that solid solution limits of $(Fe,V)_3S_4$ phase vary smoothly with the equilibrium sulfur pressure, which is represented as the isothermal curve for 730 °C in Fig.2.

The high-temperature X-ray diffraction studies were made on a two-phase mixture of $(Fe,V)_3S_4$ s.s. and $(Fe,V)_{1-\delta}S$ s.s. with bulk composition of $X=1.28$

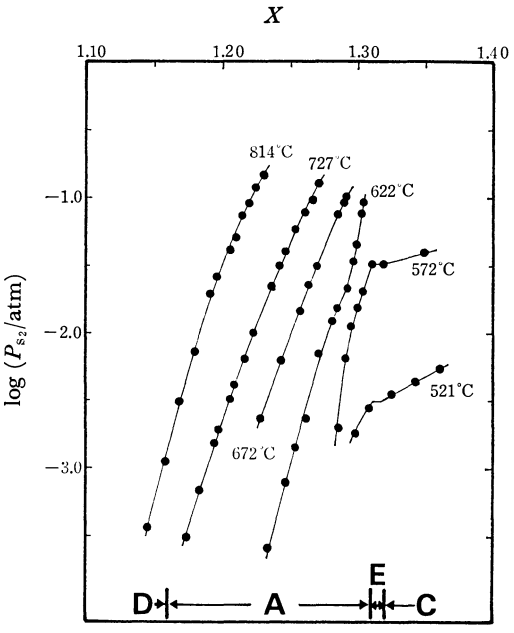

Fig. 4. P_{S_2}-composition isotherms of $Fe_{0.71}V_{0.29}S_X$. A: $(Fe,V)_{1-\delta}S$ s.s.+$(Fe,V)_3S_4$ s.s. C: $(Fe,V)_3S_4$ s.s.+FeS_2. D: $(Fe_{0.71}V_{0.29})_{1-\delta}S$ s.s. E: $(Fe,V)_{1-\delta}S$+$(Fe,V)_3S_4$ s.s.+FeS_2.

in order to observe the real phase relations directly. It was confirmed that (1) a high-temperature phase with trigonal structure is formed at temperatures above 850 °C due to the reaction of $(Fe,V)_{1-\delta}S$ s.s. with $(Fe,V)_3S_4$ s.s. and (2) the phase is unquenchable and readily inverts to the original, two different phases on quenching below 850 °C. From these results, the behavior of the isotherms for 783 and 730 °C may be interpreted as reflecting the sulfur activity change of solids at the intermediate state of phase formation or separation.

Figure 4 shows isotherms with the composition $Fe_{0.71}V_{0.29}S_X$, richer in Fe than that in Fig. 2. The region covered experimentally lies in the compositional range of $1.15<X<1.37$. From X-ray studies of the quenched specimens, the following phase relations were confirmed: $(Fe_{0.71}V_{0.29})_{1-\delta}S$ phase, a two-phase mixture of $(Fe,V)_{1-\delta}S$ s.s. and $(Fe,V)_3S_4$ s.s., and a two-phase mixture of $(Fe,V)_3S_4$ s.s. and FeS_2, in the compositional ranges of $X\leqq 1.16$, $1.16<X<1.315$, and $1.32\leqq X$, respectively.

With regard to the isotherm feature, it is noted that the isotherm for 814°C does not show any characteristic change of the curvature at the sulfur-rich limits of $(Fe_{0.71}V_{0.29})_{1-\delta}S$ phase ($X=1.16$) and exhibits continuous variations of sulfur pressure with composition in the range of $1.15<X<1.23$. This seemed to be indicative of the existence of a high-temperature phase. In this connection, X-ray studies of specimens with the bulk composition of $X=1.20$ were carried out at high temperatures. It was found that a two-phase mixture of $(Fe,V)_{1-\delta}S$ s.s. and $(Fe,V)_3S_4$ s.s. transforms to the high-temperature hexagonal $(Fe_{0.71}V_{0.29})_{0.83}S$ phase perfectly at temperatures above 800 °C. Therefore, it may be suggested that the homogeneity range of the high-temperature phase extends to $X=1.23$ under the present experimental conditions and, when quench-

ing, the specimens whose composition is richer than $X=1.16$ decompose to $(Fe,V)_{1-\delta}S$ and $(Fe,V)_3S_4$ s.s. phases.

The slope of isotherms for 572 and 521 °C changes abruptly at the composition of $X=1.31$ and a relatively small change in the pressure causes a large variation of the composition. The behavior of these isotherms may be interpreted in the same way as in the case of isotherms of $Fe_{0.60}V_{0.40}S_X$ for 520 °C. That is to say, FeS_2 begins to be formed at the composition above $X=1.31$ and the isotherms become horizontal.

However, the X-ray powder diffraction pattern of the specimen with the composition of $X=1.317$ seemed to show only the presence of one phase, $(Fe,V)_3S_4$ (Table 1); this result is inconsistent with the observation in Fig. 3. This is considered to originate from the difficulty that the small amount of $(Fe,V)_{1-\delta}S$ and FeS_2 in equilibrium with $(Fe, V)_3S_4$ can hardly be detected by X-ray powder analysis. On the basis of *in situ* observations described above, it can therefore be presumed that the three-phase field containing $(Fe, V)_{1-\delta}S$, $(Fe, V)_3S_4$, and FeS_2 occurs in the range $1.31<X<1.32$.

Tentative Phase Diagram of the Fe–V–S System at 570 °C. The isothermal tentative phase diagram in a part of the Fe–V–S system at about 570 °C was constructed mainly on the basis of the results of thermogravimetry. The phase relations and their compositional limits are summarized in Fig. 5.

Phase relations in parts of the Fe–S system at elevated temperatures have been clarified by earlier workers. Kullerud and Yoder[2] found that FeS_2 (pyrite), which has a cubic structure (Pa3), shows very little departure from the stoichiometric composition and melts incongruently at 743 °C. Arnold[4] studied equilibrium relations between $Fe_{1-\delta}S$ (pyrrhotite) and FeS_2 (pyrite) from 325 to 743 °C and determined the $Fe_{1-\delta}S$ solvus curve which represents the sulfur-rich limit of $Fe_{1-\delta}S$ coexisting with FeS_2. It is inferred from these studies that only two phases, $Fe_{1-\delta}S$ and FeS_2, are stable at about 570 °C. The sulfur-rich limit of $Fe_{1-\delta}S$ reaches about 46.2 atom%Fe at 570 °C, as can be estimated from Arnold's data.

The V–S system has recently been studied by many investigators. However, some inconsistencies exist in the reports, with respect to the phase relations and the homogeneity range of the phase. Using X-ray powder diffraction patterns of quenched specimens, de Vries and Jellinek[3] studied the V–S system, and reported that orthorhombic VS (range $VS—VS_{1.06}$), hexagonal $V_{1-\delta}S$ (range $VS_{1.06}—VS_{1.18}$), monoclinic V_3S_4 (range $VS_{1.20}—VS_{1.52}$), monoclinic V_5S_8 ($VS_{1.56}$), and trigonal V_3S_5 exist in the range $VS—VS_{1.67}$ at room temperature. Also, they found that the orthorhombic MnP-type VS transforms into hexagonal NiAs-type at about 600 °C for VS and at 350 °C for $VS_{1.05}$. Nakahira *et al.*[5] investigated the phase relations of the V–S system at 727 °C through *in situ* observations by means of a quartz spring balance and suggested the existence of sesquisulfide V_2S_3 with the homogeneity range of $VS_{1.45}—VS_{1.54}$. Recently, Wakihara *et al.*[6] examined the equilibrium phase relation between V_3S_4 and V_5S_8 in detail at temperatures from 650 to 800 °C and found that V_2S_3 appears to form below about 750 °C due to the phase separation of high-temperature V_3S_4, and that the homogeneity range of V_2S_3 extends from $VS_{1.446}$ to $VS_{1.520}$ at 650 °C. However, the existence of a V_2S_3 phase has not been confirmed at all from crystallographic viewpoint, because the X-ray diffraction pattern of the quenched V_2S_3 phase was very similar to that of the V_3S_4 phase. From the study of the chemical transport in the V–S system, Saeki *et al.*[7] found that the homogeneity range of V_5S_8 phase extends from $VS_{1.57}$ to about $VS_{1.64}$. The author showed in the previous paper[1] that the two-phase field of $(Fe,V)_2S_3$–$(Fe,V)_5S_8$ exists in the range from $X=1.55$ to $X=1.56$ at 622 °C, on the basis of experimental results of a part of the Fe–V–S system at sections with atomic Fe:V ratio 1 : 19.

A survey of the literature on the V–S system indicates that further detailed comprehensive studies are desirable to draw accurate phase diagrams at several temperatures. In the present study, the following phase relations of the V–S system are assumed for convenience: hexagonal $V_{1-\delta}S$ (range $VS—VS_{1.18}$), monoclinic V_3S_4 (range $VS_{1.20}—VS_{1.45}$), monoclinic V_2S_3 (range $VS_{1.46}—VS_{1.55}$), and monoclinic V_5S_8 (range $VS_{1.56}—VS_{1.64}$) exist at 570 °C. The trigonal V_3S_5 phase is omitted in this paper due to lack of data on its phase relation, homogeneity range, and equilibrium sulfur pressure and the possibility that it belongs to a high-pressure phase, as suggested by Nakano-Onoda *et al.*[8]

The sulfur-rich and poor limits of $(Fe,V)_3S_4$ phase are determined by a smooth fitting of the data points which are obtained in this study. The sulfur-rich boundary recedes progressively toward sulfur-poor compositions with increasing Fe content; the upper sulfur solubility limits are 58.0 and 57.8 atom % S in sections with atomic Fe : V ratio 1 : 1 and 3 : 2, respectively. On the contrary, the sulfur-poor limit of $(Fe,V)_3S_4$ phase shows a constant value of 56.7 atom % S in spite of a variation in Fe : V ratio like that described above. This boundary is drawn in Fig. 5 as a straight line in parallel with that joining VS–FeS. The Fe-rich limit of $(Fe,V)_3S_4$ s.s. phase reaches to about $0.30=V/(Fe+V)$ ratio.

Solubility of Fe in the V_5S_8 phase was determined by the supplemental, quench-type, rigid tube experiment (Table 1). The Fe-rich limit of $(Fe,V)_5S_8$ phase was confirmed to reach about 0.20, $Fe/(Fe+V)$ ratio, at 600 °C. This value is in good agreement with the Fe-rich limit of the $(Fe,V)_5S_8$ phase, which was reported by Oka *et al.*[9] As shown in Fig. 5, the phase boundary of $(Fe,V)_3S_4$, $(Fe,V)_2S_3$, and $(Fe, V)_5S_8$ on the side richer in V than $V/Fe=1$ is determined by a smooth fitting of data points. Two-phase regions of $(Fe,V)_3S_4$–$(Fe,V)_2S_3$ and $(Fe,V)_2S_3$–$(Fe,V)_5S_8$ are extended in parallel with the line joining FeS–VS from the VS–S side to the Fe-rich phase boundaries.

With respect to the lower part of the FeS–VS–S diagram, it is assumed that $Fe_{1-\delta}S$ and $V_{1-\delta}S$ phases form a complete $(Fe,V)_{1-\delta}S$ solid solution at 570 °C. With homogeneous ranges of compounds, as previ-

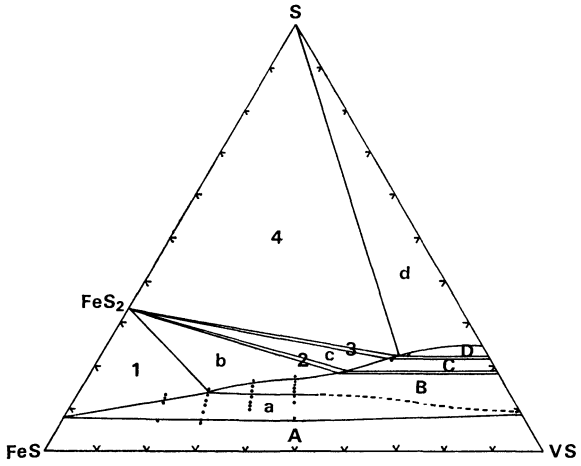

Fig. 5. Tentative phase diagram of the sulfur-rich portion of the Fe–V–S system at about 570 °C. Phase relations are represented as follows. Phase A: Monosulfide s.s. $(Fe,V)_{1-\delta}S$. B: $(Fe,V)_3S_4$ s.s. C: $(Fe,V)_2S_3$ s.s. D: $(Fe,V)_5S_8$ s.s. Two-phase regions are a: $(Fe,V)_3S_4$ s.s.+$(Fe,V)_{1-\delta}S$ s.s. b: $(Fe,V)_3S_4$ s.s.+FeS_2. c: $(Fe,V)_2S_3$ s.s.+FeS_2. d: $(Fe,V)_5S_8$ s.s.+L. Numbers in figure mean the univariant assemblages as follows. 1: FeS_2+$Fe_{1-\delta}S$+$(Fe,V)_3S_4$ s.s.+v. 2: FeS_2+$(Fe,V)_3S_4$ s.s.+$(Fe,V)_2S_3$ s.s.+v. 3: FeS_2+$(Fe,V)_2S_3$ s.s.+$(Fe,V)_5S_8$ s.s.+v. 4: FeS_2+$(Fe,V)_5S_8$ s.s.+L+v.

ously determined by Toulmin and Barton[10] and Arnold[4] for $Fe_{1-\delta}S$, and de Vries and Jellinek[3] for $V_{1-\delta}S$, it was possible to draw a monosulfide solid solution field of $(Fe,V)_{1-\delta}S$. This boundary is drawn qualitatively by a full line. The sulfur-rich limit of the monosulfide s.s. field reaches a maximum of 54.1 atom %S in the V–S side. It recedes progressively toward S-poor compositions with increasing Fe content till it reaches the middle part of the field. However, the upper sulfur solubility limits of monosulfide s.s. field are largely interpretative because of the lack of experimental data for compositions of $(Fe,V)_{1-\delta}S$ coexisting with $(Fe,V)_3S_4$.

As shown in Fig. 5, there are four univariant assemblages: $Fe_{1-\delta}S$–FeS_2–$(Fe,V)_3S_4$ s.s.-v, FeS_2–$(Fe,V)_3S_4$ s.s.–$(Fe,V)_2S_3$ s.s.–v, $(Fe,V)_2S_3$ s.s.–$(Fe,V)_5S_8$ s.s.–FeS_2-v, and FeS_2–$(Fe,V)_5S_8$ s.s.–L-v.

Relation of Lattice Parameters of $(Fe,V)_3S_4$ s.s. Phase with Composition. The $(Fe,V)_3S_4$ s.s. phase has the monoclinic V_3S_4-type structure (nonreduced space group I2/m referred to the fundamental NiAs-type cell), in which metal vacancies are ordered within alternate metal layers.[11] In the course of continuing the equilibrium study of the Fe–V–S system, several kinds of quenched specimens in the $(Fe,V)_3S_4$ s.s. field were examined by the X-ray powder diffraction technique in order to clarify the relation of lattice constant and composition. The lattice constants were calculated by the least-squares method from the data of powder diffractometer measurements using Cu $K\alpha$ radiation. Values of at least 20 reflections in the 2θ range of 10° to 70° were used in this computation. The compositional dependence of the unit cell dimensions are shown in Fig. 6—8.

It is found that the axial dimensions of the a-, b-,

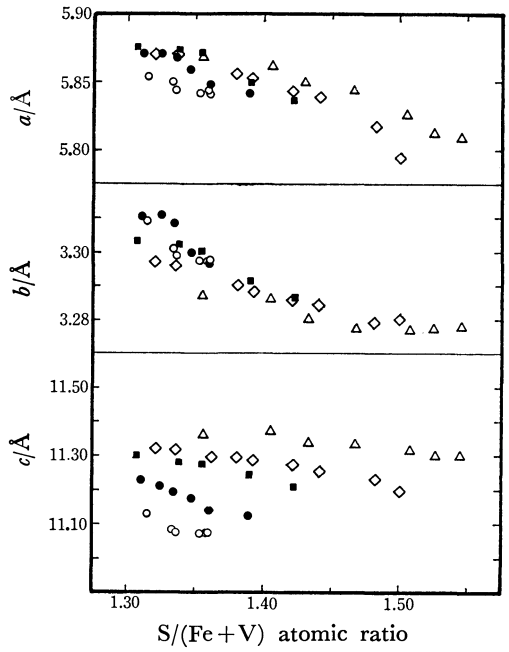

Fig. 6. Lattice constants of the unit cell of $(Fe,V)_3S_4$ s.s. phase as function of composition. △: Fe:V=1:19, ◇: Fe:V=13:37, ■: Fe:V=7:13, ●: Fe:V=1:1, ○: Fe:V=3:2.

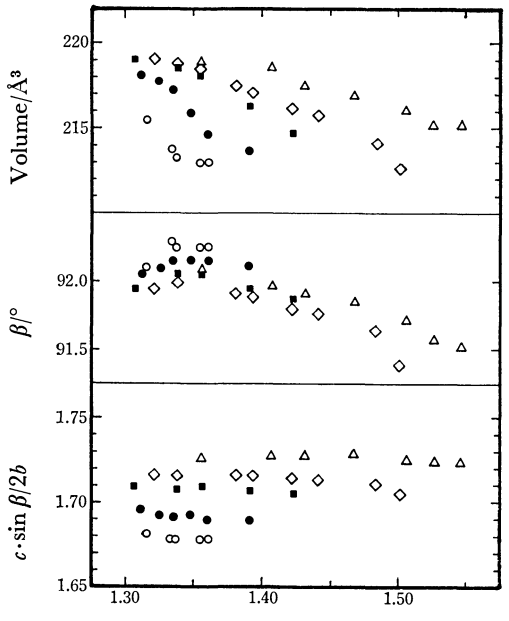

Fig. 7. Volume, β-angle and $c\cdot\sin\beta/2b$ of the unit cell of $(Fe,V)_3S_4$ s.s. phase as function of composition.

and c-axes and thus the cell volume decrease with increasing S content under the present experimental conditions. Also, the axial dimensions of the c-axis and the unit cell volume of $(Fe,V)_3S_4$ s.s. phase decrease with increasing Fe/V ratio, when the S/(Fe+V) ratio is held constant. This is in good agreement with that of $(Fe_xV_{1-x})V_2S_4$, which has been reported by Oka *et al.*[9] The c-dimensions of $(Fe,V)_3S_4$ with Fe:V=3 : 2 atomic ratio are about 2.6% smaller than that of V_3S_4.

As shown in Fig. 7, however, the behavior of the β-angle of the unit cell is quite different from those

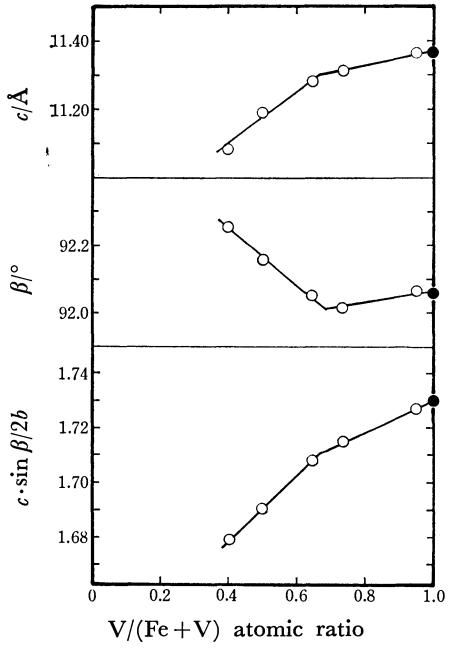

Fig. 8. Relation of c-dimension, β-angle and $c\cdot\sin\beta/2b$ of $(Fe,V)_3S_4$ compound with V/(Fe+V) atomic ratios. ●: De Vries and F. Jellinek (1974). ○: Present work.

of the a-, c-dimensions and the unit cell volume. Maximum values are observed at about $X=1.34$—1.35 in β-angle-composition relations of compounds with a constant Fe:V ratio. Also, the β-angle varies with the degree of the substitution of Fe for V in V_3S_4. It is apparent from Figs.7 and 8 that the β-angle decreases with increasing Fe content in the range of V/(Fe+V), from 1 to about 0.70, and increases with increasing Fe content in the range of V/(Fe+V), from 0.7 to 0.4.

In order to examine the directional character of the structure for several $(Fe,V)_3S_4$ s.s. phases, the $c\cdot\sin\beta/2b$ ratio in the monoclinic V_3S_4-type structure is calculated instead of the axial ratio of c/a in NiAs-type structure. As is evident in Fig. 7, the values of $c\cdot\sin\beta/2b$ of compounds with the constant Fe/V ratio are nearly equal over the whole range of composition. On the other hand, when the S content is held constant, the ratio value decreases with increasing Fe content. This result indicates that the interlayer spacing is reduced relative to the intralayer spacing by the substitution of Fe for V in V_3S_4.

Figure 8 shows the relations of c-dimension, β-angle, and $c\cdot\sin\beta/2b$ with V/(Fe+V) atomic ratio at the composition of about $X=1.33$. Data points do not fall on the same straight line and a change of the slope is observed at about V/(Fe+V)=0.67, whose composition corresponds to FeV_2S_4. From this results, it seems that the $(Fe,V)_3S_4$ s.s. phase can be divided into two types: one is the V_3S_4–FeV_2S_4 series, and the other is the FeV_2S_4–Fe_2VS_4 series. From the neutron diffraction studies of FeV_2S_4 compound,[12] it was found that all Fe atoms are confined to the partially filled metal layers and all V atoms to the filled metal layers. However, whether the $(Fe,V)_3S_4$ compound richer in Fe than FeV_2S_4 is an ordered phase or not as for the distribution of Fe and V atoms over all the metal sites is still an open question. Further detailed studies on the crystal structure and physical properties of $(Fe,V)_3S_4$ s.s. phase are necessary for a better understanding of the phase relations of the Fe–V–S system.

The author wishes to express his deep gratitude to professor Mitsuoki Nakahira of Okayama College of Science for his encouragement and helpful discussion throughout this study. Thanks are also due to Dr. H. Nakazawa for his guidance of the high-temperature X-ray measurements.

References

1) H. Wada, *Bull. Chem. Soc. Jpn.*, **51**, 1368 (1978).
2) G. Kullerud and H. S. Yoder, *Econ. Geol.*, **54**, 533 (1959).
3) A. B. De Vries and F. Jellinek, *Rev. Chim. Miner.*, **11**, 624 (1974).
4) R. G. Arnold, *Econ. Geol.*, **75**, 72 (1962).
5) M. Nakahira, K. Hayashi, M. Nakano-Onoda, and K. Shibata, "Proc. 8th Int. Symp. on the Reactivity of Solids," ed by J. Wood *et al.*, Plenum Press, New York (1977), pp. 397—401.
6) M. Wakihara, T. Uchida, and M. Taniguchi, *Metall. Trans.*, **9B**, 29 (1978).
7) M. Saeki, M. Nakano, and M. Nakahira, *J. Crystal Growth*, **24/25**, 154 (1974).
8) M. Nakano-Onoda, S. Yamaoka, K. Yukino, K. Kato, and I. Kawada, *J. Less-Common Metals*, **44**, 341 (1976).
9) Y. Oka, K. Kosuge, and S. Kachi, *Mat. Res. Bull.*, **12**, 1117 (1977).
10) P. Toulmin, III, and P. B. Barton, Jr., *Geochim. Cosmochim. Acta*, **28**, 641 (1964).
11) M. Cheverton and A. Sapet, *C. R. Acad. Sci., Paris*, **261**, 928 (1965).
12) I. Kawada, N. Niimura, M. Isobe, and H. Wada, *Res. Rep. Lab. Nucl. Sci. Tohoku Univ.*, **11**, 226 (1978).

The Thermal Decompositions of Dialkyl Peroxides

Kazuya UETAKE,* Kenji UEDA,** and Noriyuki SAKIKAWA

Department of Industrial Chemistry, College of Science and Engineering, Nihon University, Chiyoda-ku, Tokyo 101

(Received September 30, 1978)

With the purpose of obtaining information needed for hazard prevention, pure liquid dialkyl peroxides (di-*t*-butyl peroxide (**1**), bis(1-methyl-1-phenylethyl) peroxide (**2**), *t*-butyl 1-methyl-1-phenylethyl peroxide (**3**), 2,5-bis(*t*-butyldioxy)-2,5-dimethylhexane (**4**)) were subjected to thermal-decomposition experiments, in which thermal analyses were conducted by the use of a thermogravimetry (TG)-differential scanning calorimetry (DSC) apparatus equipped with a pinholed pan with a minute pinhole. From the DSC curves recorded, we obtained the decomposition temperature of Samples **2**, **3**, and **4**, as a constant value for each sample, and the maximum exothermic peaks at the optimum pinhole diameters (0.07—0.2 mm). The heats of decomposition obtained could be considered appropriate, as they roughly agreed with the estimated value, on the other hand, **1** shows no exothermic peak under these condition. Plotting by the Coats-Redfern method based on the TG-curve data (**2**, **3**, and **4**) gave reaction orders of more than unity, activation energies of 33—37 $kcal_{th}$/mol, and frequency factors of 10^{16}—10^{18} s^{-1}. It is conceivable that these results could be derived by virtue of the TG–DSC curves that were suitable in obtaining thermochemical parameters. In other words, the analysis method introduced in this paper was found to be an efficient one for liquid peroxides that are difficult to analyze by a conventional TG–DSC method.

Organic peroxides are used as polymerization initiators, curing agents, and crosslinking agents in polymer industries,[1] but they are so unstable that they readily decompose or explode when affected by heat or impact.[2] From the viewpoint of hazard prevention, it is important to have knowledge about the thermal instability of organic peroxides,[3] and one of the means to achieve this is the measurement of the activation energy[4,5] as well as the heat of decomposition.[6] However, almost all reported examples have been measurements of activation energies and frequency factors through a determination of the thermal decomposition rates either in a gas phase or in a low-concentration solution diluted in a solvent.[4,5] Furthermore, there have been hardly studies of measuring heats of decomposition.[6]

Recently, thermogravimetry (TG), differential thermal analysis (DTA), and differential scanning calorimetry (DSC) have come to be commonly used in measuring the thermal decomposition of organic peroxides.[7] Uetake *et al.* determined the activation energy and heat of decomposition of benzoyl peroxide through thermal decomposition by means of a TG–DSC apparatus.[8] Although a TG–DSC for solid materials like this is generally satisfactory, an analysis of liquid materials is extremely difficult because of the influense of the vaporization of the sample.[9,10] The difficulties in performing an acurate measurememt come from the following facts: a TG curve is a result of the overlapping of the weight change pertaining to the reaction and the weight loss caused by the vaporization of the sample, while a DSC curve is the outcome of the overlapping of the exotherm, along with its apparent decrease caused by the sample loss, and the latent heat of vaporization. As a matter of fact, most organic peroxides are in a liquid state around their decomposition temperatures; hence, examinations of either the procedure or the apparatus used for measurement are necessary in order to obtain an appropriate TG curve or DSC curve by the use of a TG–DSC apparatus. A sealed cell reportedly gives an apparently lower heat of decomposition[11] and, furthermore, cannot provide a TG curve, so that it is not suitable for our present purpose, a comprehensive evaluation. The use of a pinholed pan can, though, be proposed as a solution to this problem.[12]

This study of such organic peroxides deals with experiments using an apparatus with a pinholed pan, and intends to establish the procedure for obtaining an appropriate TG–DSC curve and derive the basic data to provide useful knowledge for hazard prevention. From an analysis of the pyrolysis experiments, an evaluation of the values of the heat of decomposition obtained is also attempted.

Experimental

Materials. Selected dialkyl peroxides are: di-*t*-butyl peroxide (**1**), bis(1-methyl-1-phenylethyl) peroxide (**2**), *t*-butyl 1-methyl-1-phenylethyl peroxide (**3**), and 2,5-bis(*t*-butyldioxy)-2,5-dimethylhexane (**4**). The commercial product (Nippon Oil and Fats Co., Ltd.) for each was used after purification. Peroxide **2** was recrystallized from ethanol.[13] Peroxide **3** was recrystallized twice at −70 °C, and the product was distilled *in vacuo* at room temperature.[14] Both **1**[15] and **4**[16] were distilled *in vacuo* at room temperature. All the samples were at least 99.0% pure.

Measurement. An aluminum sealed-type cell, with an outer diameter of 4.6 mm, 2 mm deep, and 0.1 mm thick, was utilized as a sample cell for measurement. After placing a sample in it, it was covered with an aluminum cover pinholed beforehand and was sealed by hermetical pressing by the use of a sample sealer. Hereafter, this type of sample cell will be called "a pinholed pan." After sealing, the dimensions of the pinholed pan came to be 4.6 mm in outer diameter, 2.8 mm thick, and 46.5 mm^2 in capacity. The weighing of the sample taken in was quickly carried out just after the sealing. The pinhole was bored by a needle at the center of the cover, and its diameter was measured by a microscopic scale.

The behavior on the heating of the sample in a pinholed pan was followed by a standard-type TG–DSC apparatus made by Rigaku Denki. The conditions of measurement

** Present address: Yokohama City Fire Bureau, Hodogaya-ku, Yokohama 240.

were: sample weight, 1.2—2.0 mg; heating rate, 2.5 °C/min; air atmosphere. For comparison, experiments with an open cell with no cover and those with a sealed cell with no pinhole in the cover were also conducted.

The relationships between the pinhole diameter of the pinholed pan and the TG curve as well as the DSC curve were examined, and the activation energy, the frequency factor, and the reaction order were derived from the appropriate TG curve by the use of the Coats-Redfern method.[17] The decomposition temperature and the heat of decomposition were also derived from the DSC curve.

The pyrolysis gas-chromatograph apparatus employed has been described previously.[8] The procedures used for the pyrolysis of the sample and the analysis of the pyrolysis products are essentially the same as those reported in a previous paper.[18] About 1 milligram of **4** was used for pyrolysis.[19] Samples were then pyrolyzed rapidly at 330 °C. The analytical conditions were as follows; column, Porapak Q (100—120 mesh), 3 m, 70 °C (in the case of acetone, 150 °C); detector, FID, 220 °C; N_2-flow rate, 20 ml/min; injection temperature, 150 °C.

Results and Discussion

Before proceeding to a detailed evaluation of the thermal decomposition of dialkyl peroxides by the use of the TG–DSC apparatus with a pinholed pan, let us mention that a study was made of the effects of the sample weight and the heating rate, which could conceivably have influenced the results. In the sample-weight (1—4 mg)-dependence determinations, all the runs were made at a heating rate of 2.5 °C/min, while in the heating-rate (1.25—20 °C/min)-dependence determinations, the sample weight in each case was 1.0—2.0 mg.

Consequently, it was found in the present study that the exothermic peak areas decreased with an increase in either the heating rate or the sample weight. However, there were no detectable differences in the peak areas obtained under the conditions of a sample weight of 1.0—2.0 mg, and a heating rate of 2.5 °C/min. The standard procedure described above can, therefore, be employed and is, as a matter of fact, more desirable.

Pinhole-diameter Dependence of the Thermal Properties. Figure 1 shows the relationship between the TG–DSC curve and the pinhole diameter of the pinholed pan for **2**, **3**, and **4**. The TG curves for all three samples shift to the high-temperature side, and their slopes become gentle, with a decrease in the pinhloe diameters. In the case of **2**, no change was observed in the initial decomposition temperature for the pinhole diameter range of 0.05—0.08 mm, while with an open cell the initial decomposition temperature gave rise to a small shift to the low-temperature side. Similar tendencies were observed for **3** and **4**, while, with an open cell, the plateaus of the curves were scarcely observed at all because of the drastic vaporization loss.

As for the DSC curves, all three samples showed a somewhat different pattern in relation to the decrease in the pinhole diameter. In the case of **2** with a pinhole diameter of less than 0.15 mm, we observed an endotherm trough behind the exotherm peak. As an explanation for this, we can postulate that, with a

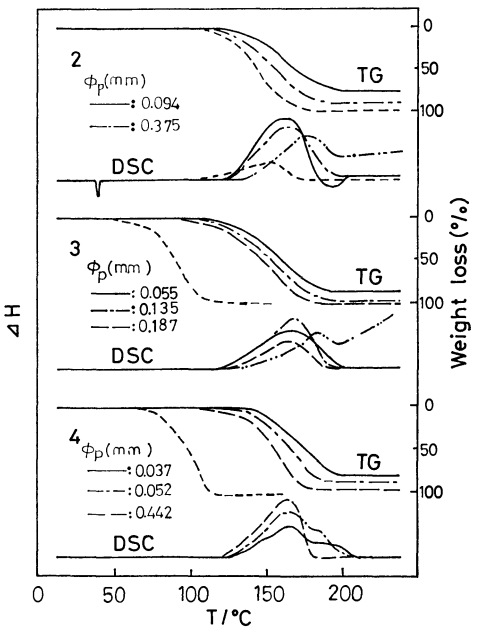

Fig. 1. Variations of TG and DSC curves for each of **2**, **3**, and **4** with various pinhole diameter (ϕ_p). ----: Open cell, ——; — — —; ——: pinholed pan —··—: closed cell.

decrease in the pinhole diameters, the high-boiling decomposition products come to remain in the cell for a longer period of time, giving rise to the appearance of an endotherm trough caused by their vaporization, accompanied by a tendency for the trough to deepen gradually. The run with a closed cell gives a reduced area of the exotherm peak. In the case with an open cell, the starting of the decomposition is obscure and the exotherm peak is small, making the analysis very difficult.

Peroxide **3** behaved very much like **2**, but it did not display a decomposition exotherm peak for the open cell. Peroxide **4** showed a similar tendency in the range down to the pinhole diameter of about 0.1 mm, but at a more reduced diameter (as low as 0.05 mm or below) a shoulder peak appeared behind the main exotherm peak; furthermore, at a diameter of 0.037 mm or below, another shoulder peak appeared before the main peak. These small peaks seem to be the outcome of the clear detection of such minute thermal changes that were not detectable with an open cell, but came to be apparent with a pinholed pan with a minute pinhole. Peroxide **1** gave neither a TG curve nor a DSC curve that could afford analysis, even with a pinholed pan with a minute pinhole (0.037 mm or below), because of its too rapid vaporization.

Figure 2, showing the DSC curve for **2**, presents the relationships of the starting of the exotherm peaks, the peak temperatures, and the end temperatures *versus* the pinhole diameters. These decomposition-related temperatures exhibit little change and are nearly constant with a decrease in the pinhole diameters. Peroxides **3** and **4** give nearly content values in a similar manner, except that the end temperature for **4** shifts almost linearly to the high-temperature side. This is understandably related to the phenomena pertaining

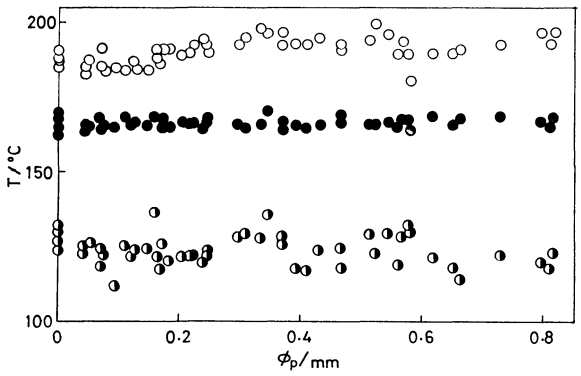

Fig. 2. The relationships of starting of exotherm peaks (◑), peak temperatures (●), and end temperatures (○) *vs.* pinhole diameters as related with the DSC curves for **2**.

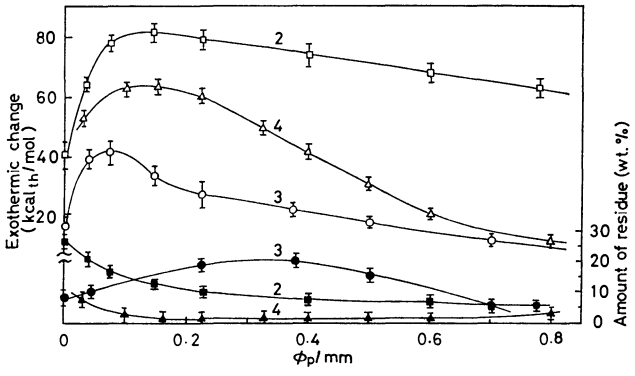

Fig. 3. Plots of exothermic change (□, ○, △) and amount of residues after decomposition (■, ●, ▲) *vs.* change in pinhole diameters for each of **2**, **3**, and **4**.

to the complicated decomposition reaction of **4** (see Fig. 1). The results of the decomposition-temperature measurements for these three samples are summarized in Table 1. The end temperature of **4** is shown for the run with a pinhole diameter of 0.1 mm (the value in the parentheses is for 0.6 mm).

Figure 3 shows the relationships of the heats of decomposition and the amounts of the residue after decomposition *versus* the change in the pinhole diameters. In the case of **2**, the heat of decomposition increases linearly with a decrease in the pinhole diameter and reaches the peak of 80.0 $kcal_{th}$/mol*** at the diameter of 0.2—0.1 mm. With a further reduction of pinhole diameter, the calorific value sharply decreases, giving the minimum value of 40.0 $kcal_{th}$/mol for the case with a closed cell. The amount of residue after the reaction increases slightly with a decrease in the pinhole diameter, while the rate of increase is enhanced by decreasing the diameter to 0.15 mm or below.

In contrast with **2**, **3**, and **4** exhibit somewhat different tendencies in both the heat of decomposition and the amount of residue after the reaction, but are similar to **2** in their maximum values of heat of decomposition: 41.5 $kcal_{th}$/mol at the pinhole diameter of 0.08 mm for **3** and 62.5 $kcal_{th}$/mol at the pinhole diameter of 0.13 mm for **4**.

*** Throughout this paper, cal_{th}=4.184 J.

Table 1. Values of the decomposition temperatures for these three samples

Compound	Starting of exothermic peak (°C)	Peak temperature (°C)	End temperature (°C)
2	123±3.8	165±3.5	186±4.0
3	126±4.0	167±3.0	196±5.0
4	123±4.0	163±3.2	200±4.0 (174±5.4)

From the above findings, it can be postulated that the increase in the apparent heat of decomposition with an early decrease in the pinhole diameter is caused by some suppression of the sample vaporization of the spreading of heat,[12] and that the decrease in the apparent heat of decomposition with a further decrease in the pinhole diameter, nearing the closed state, is the outcome of the suppression of the decomposition itself effected by the enhanced partial pressure of the produced gas.[20,21] In addition, the increased amount of tarry residue after the reaction at the smaller pinhole diameter suggests the occurrence of endothermic reactions associated with the conversion of products into high-boilers and the deposition of carbon.

Thermochemical Parameters. The results and discussion of the above experiments suggest that the TG curve best fitted for obtaining thermochemical parameters is the one obtained from a measurement using a pinholed pan with a pinhole diameter suitable for minimizing the overall effect of the sample vaporization and the partial pressure of the produced gas. From such a TG curve, the reaction order (n), activation energy (E_a), and frequency factor (A) were obtained by the Coats-Redfern method:

$$\log\left[\frac{1-(1-x)^{1-n}}{T^2(1-n)}\right] = \log\frac{AR}{\phi E_a}\left[1-\frac{2RT}{E_a}\right] - \frac{E_a}{2.3RT} \quad (1)$$

where x is the fraction of the sample decomposed at a certain time, t, and where ϕ is the heating rate. T is the absolute temperature, and R is the gas constant. This equation holds for an n-order reaction when n is not unity, and the left-hand side of the equation should be replaced by $\log[-\log(1-x)/2.3T^2]$ for a first-order reaction. Since the first term on the right-hand side of the equation can be considered nearly constant, the calculating of the left-hand side for an assumed n, followed by a plotting of this result against $1/T$, may give a straight line whose slope will give E_a and whose intercept will make possible the rough estimation of the A factor.

The results of analysis are listed in Table 2. The calculated values of the activation entropies (ΔS^*)[22] are also listed in this table. There are found in the literature some more data: for **2** in the solvent cumene,[23] A factor $10^{14.6}$ s^{-1} and E_a 34.8 $kcal_{th}$/mol; and for **3** in the solvent dodecane,[23] A factor $10^{14.4}$ s^{-1} and E_a 33.5 $kcal_{th}$/mol. The data for the two compounds under no-solvent conditions are not available. For **4**, neither data for a solution nor those for no-solvent conditions have been found in the literature. As for the reported data on various dialkyl peroxides other

Table 2. Reaction orders, activation energies, frequency factors, and activation entropies *vs.* pinhole diameter(ϕ_p) for several peroxides

Compound	ϕ_p / mm	n	E_a / $kcal_{th}\ mol^{-1}$	$\log A$ / s^{-1}	ΔS^* / $cal\ deg^{-1}\ mol^{-1}$
2	0.090—0.150	1.55±0.25	34.8±0.3	16.6±0.8	17.5
3	0.070—0.100	1.55±0.25	33.5±0.2	16.1±0.5	15.2
4	0.130—0.200	1.20±0.10	36.5±1.7	18.5±0.6	26.2

Table 3. Heats of decomposition(ΔH_d) for several peroxides

Compound	ΔH_d / $kcal_{th}\ mol^{-1}$	
	Obsd	Calcd
2	81.0±4.5	89.8
3	41.5±5.5	45.3
4	64.2±4.6	67.3

Table 4. Amounts of the products obtained by pyrolysis of several peroxides (Molar fraction)

Product	Compound		
	2[a]	**3**[b]	**4**
CH_4	0.36	trace	0.03
C_2H_4			0.09
C_2H_6	trace	0.41	0.19
$(CH_3)_2CO$	trace	0.29	0.69
$C_6H_5COCH_3$	0.57	0.30	
$C_6H_5(CH_3)_2COH$	0.06	trace	
$C_6H_5(CH_3)_2COOH$	0.01		

a) Pyrolysis temperature, 230 °C. b) Pyrolysis temperature 280 °C.

than these three peroxides, the A factors are in the range of $10^{14.0}$—$10^{16.8}\ s^{-1}$, and E_a, in the range of 31—39 $kcal_{th}$/mol.[24-28] According to Benson,[29] the unimolecular fission of a large polyatomic molecule generally gives a large A factor ($10^{16\pm1.5}\ s^{-1}$) when the mother molecule splits into two polyatomic fragments. He suggests also that the A factor will become very large when reaction order becomes large, and when the rate of decomposition decreases with a rise in the pressure in a reaction, under pressure, with positive value of the activation volume and the ΔS^*.[30,31] Huyser and Van Scoy[32] have reported that ΔS^* becomes large when the apparent rate of decomposition decreases with a reaction in a solvent.[33] It has also been reported that a thermal decomposition accompanied by an increase in the number of moles would give positive values of the activation volume and the ΔS^*.[30]

The large A factors obtained in the above experiments on the thermal decomposition without a solvent seem to be understandable when one considers, along with above arguments, the following fators: the orders of reaction $n>1$; the reactions accompanied with an increase in the number of moles; the effect of the partial pressure change in the homolysis products in the pinholed pans with a minute pinhole, and the influence of the solvent behavior of the decomposition products.

Listed in Table 3 are the values for three samples estimated by means of Eqs. 2—4; we assume an ideal thermal decomposition, based on the heats of decomposition in pinholed pans at the optimum pinhole diameters and on the data of the pyrolysis (Table 4).[18]

$$\mathbf{2} \rightarrow 1.8CH_4 + 1.8C_6H_5COCH_3 + 0.2C_6H_5C(CH_3)_2OH \quad (2)$$

$$\mathbf{3} \rightarrow C_2H_6 + (CH_3)_2CO + C_6H_5COCH_3 \quad (3)$$

$$\mathbf{4} \rightarrow 0.3CH_4 + 0.8C_2H_4 + C_2H_6 + 4(CH_3)_2CO \quad (4)$$

If available, observed values were used as the heats of formation; if they were not available, the values obtained by the method of Benson and others,[34] which applies the group-additivity rule to organic peroxides, were used. These observed values were in approximate agreement with the estimated ones, although the former values were somewhat lower. The difference in ΔH_d may be due to the decomposition temperatures[35] and other factors. In order to make this clear, however, further work is necessary.

In conclusion, it can be proposed that the use of the pinholed pans are efficient for the thermal analysis of liquid organic peroxides by means of TG–DSC.

The authors wish to thank Dr. Masahiko Kotani for his helpful discussion and Mr. Reiji Fukasawa, Mr. Hikaru Sakurai, Mr. Yoshiaki Kurimura, and Mr. Touru Asakawa for the collection of the peroxide data used in this work.

References

1) "Kagaku Benran, Oyo-hen," ed by the Chemical Society of Japan, Maruzen, Tokyo (1973), pp. 782—787.
2) D. C. Noller, S. J. Mazurowski, G. F. Linden, F. J. G. DeLeeuw, and O. L. Mageli, *Ind. Eng. Chem.*, **56**, 12, 18 (1964).
3) "Kasai Bakuhatu Kikensei No Sokuteiho," ed by T. Hikita, Nikkan Kogyo, Tokyo(1977), pp. 77—91.
4) "Yuuki Kasankabutu No Kagaku," ed by Y. Ogata, Nankodo, Tokyo (1971), p. 154.
5) "Organic Peroxides," ed by D. Swern, John Wiley & Sons, New York (1970), Vol. 1, p. 107.
6) D. H. Fine and P. Gray, *Combust. & Flame*, **11**, 71 (1967).
7) "Organic Peroxides," ed by D. Swern, John Wiley & Sons, New York(1971), Vol. 3, p. 345.
8) K. Uetake and N. Sakikawa, *Nippon Kagaku Kaishi*, **1974**, 575.
9) W. W. Wendlandt, "Thermal Method of Analysis," 2nd ed, John Wiley & Sons, New York (1974), p. 6.
10) "Netsu Bunseki," ed by H. Kambe, Koudansha, Tokyo (1975), p. 25.
11) M. Itoh, T. Yoshida, M. Nakamura, and K. Uetake,

Kogyo Kayaku Kyokaishi, **38**, 1, 17 (1977).
12) E. M. Barrall, *Thermochim. Acta*, **5**, 377 (1973).
13) M. S. Kharasch, A. Fono, and W. Nudenberg, *J. Org. Chem.*, **15**, 753 (1950).
14) M. S. Kharasch, A. Fono, and W. Nudenberg, *J. Org. Chem.*, **16**, 105 (1951).
15) N. A. Milas and D. M. Surgenor, *J. Am. Chem. Soc.*, **68**, 643 (1946).
16) Monte Catini Societa, Japan Patent 2867 (1963).
17) A. W. Coats and J. P. Redfern, *Nature*, **201**, 68 (1964).
18) M. Kotani, K. Uetake, and N. Sakikawa, *Anzen Kougaku*, **14**, 398 (1975).
19) The pyrolysis of the three samples other than **2** have been reported in a previous paper.[18]
20) W. W. Wendlandt, "Thermal Method of Analysis," 2nd ed, John Wiley & Sons, New York (1974), p. 150.
21) A. Doi and T. Katoh, *Kogyo Kagaku Zasshi*, **73**, 36 (1970).
22) M. Ohiwa, "Hanno Sokudo Keisanho," Asakura, Tokyo (1962), p. 29.
23) P. Molyneux, *Tetrahedron*, **22**, 2929 (1966).
24) P. L. Hanst, *J. Phys. Chem.*, **63**, 104 (1959).
25) E. J. Harris, *Proc. R. Soc. London, Ser. A*, **173**, 126(1939).
26) M. J. Yee Quee and J. C. J. Thynne, *Trans. Faraday Soc.*, **64**, 1296 (1968).
27) L. Blatt and S. W. Benson, *J. Chem. Phys.*, **36**, 895 (1962); **38**, 303 (1963).
28) J. H. Reley, F. F. Rust, and W. E. Vaughan, *J. Am. Chem. Soc.*, **70**, 88 (1948).
29) S. W. Benson, "Thermochemical Kinetics," 2nd ed, John Wiley & Sons, New York (1976), p. 97.
30) T. Kagia, "Kagaku Hanno No Sokudoron-Teki Kenkyu," Kagakudojin, Kyoto (1970), Jo, p. 262.
31) K. J. Laidler and D. Chen, *Trans. Faraday Soc.*, **54**, 1026 (1958).
32) E. S. Huyser and R. H. Van Scoy, *J. Org. Chem.*, **33**, 3524 (1968).
33) "Yuuki Kasankabutu No Kagaku," ed by Y. Ogata, Nankodo, Tokyo (1971), p. 156.
34) S. W. Benson and J. H. Buss, *J. Chem. Phys.*, **29**, 546 (1958).
35) T. Asakawa, Y. Fuju, Y. Inoue, M. Kotani, K. Uetake, and N. Sakikawa, 38th National Meeting of the Chemical Society of Japan, Nagoya, October 1978, Abstr (1), p. 291.

NOTES

BULLETIN OF THE CHEMICAL SOCIETY OF JAPAN, VOL. 52 (7), 2141—2142 (1979)

ENDOR Spectrum of Some Dihydro-1,4-dithiin Cation Radical

Kohji WATANABE,* Yoshimitsu NAGAO, Eiichi FUJITA, and Kazuhiko ISHIZU**

Institute for Chemical Research, Kyoto University, Uji, Kyoto 611

***Department of Chemistry, Faculty of Science, Ehime University, Matsuyama, Ehime 790*

(Received September 30, 1978)

Synopsis. The ENDOR spectrum of the 2,3-diphenyl-5,6-dihydro-1,4-dithiin cation radical, which was prepared with $AlCl_3$ in dichloromethane solution, has been observed. The spin density distribution of the new radical was also discussed and compared with the MO calculation.

ESR detections of the intermediate cation radical (g=2.0070+0.0005) formed by thallium(III) nitrate oxidation of 2,3-diphenyl-5,6-dihydro-1,4-dithiin have been previously reported.[1] Several ESR studies of 1,4-dithiin cation radicals have been published,[2] but no detailed data on the spin density distribution of the dihydro-1,4-dithiin cation radical have been given. In the present work, ENDOR observations are carried out for the intermediate cation radical produced by one electron oxidation of 2,3-diphenyl-5,6-dihydro-1,4-dithiin, and the spin density distribution of the new radical is investigated.

Experimental

The synthesis of materials has been described elsewhere.[1] Cation radicals of 2,3-diphenyl-5,6-dihydro-1,4-dithiin were prepared using thallium(III) nitrate as the oxidant. It was found, however, that the identical cation radical generated by $AlCl_3$ oxidation in CH_2Cl_2 showed a rather enhanced stability as compared with the case of thallium(III) oxidation, and no important change in the detailed hyperfine structures could be detected in the ESR spectrum. ENDOR observations were applied to this solution using a JEOL-type EX-EDX-1 spectrometer under the operating conditions similar to those described previously.[3]

Results and Discussion

Figure 1 shows the ENDOR spectrum of 2,3-diphenyl-5,6-dihydro-1,4-dithiin cation radical prepared with $AlCl_3$ oxidation in CH_2Cl_2. The four ENDOR signals (14.31, 14.76, 14.90, and 15.11 MHz) seen in the vicinity of the free proton frequency can be ascribed to the splitting due to the phenyl groups, with reference to the MO calculation of the spin densities summarized in Table 1. The ENDOR signals (17.20 and 22.73 MHz) detected at higher NMR frequency were safely assigned to either equatorial and axial protons in bridged methylene, as discussed later.

McLachlan's MO calculations (λ=1.0) were carried out using the following parameters: $\alpha(S)=\alpha(C)+1.0\beta$, $\alpha(CH_2)=\alpha(C)+2.0\beta$, $\beta(S\text{–}C)=0.6\beta(C\text{–}C)$, $\beta(S\text{–}CH_2)=0.4\beta(C\text{–}C)$, $\beta(C\text{–}\phi)=0.75\beta(C\text{–}C)$, and $\beta(CH_2\text{–}CH_2)=0$, where $\alpha(S)$ and $\alpha(CH_2)$ are the Coulomb integrals of sulfur atoms and of methylene carbon atoms, $\beta(S\text{–}C)$, $\beta(S\text{–}CH_2)$, and $\beta(C\text{–}\phi)$ are the resonance integrals defined for sulfur-ethylene carbons, sulfur-methylene carbons, and to ethylene bridging phenyl carbons, respectively. The present ENDOR measurement resolved four different hyperfine splittings, which could be assigned to the phenyl protons. An appropriate

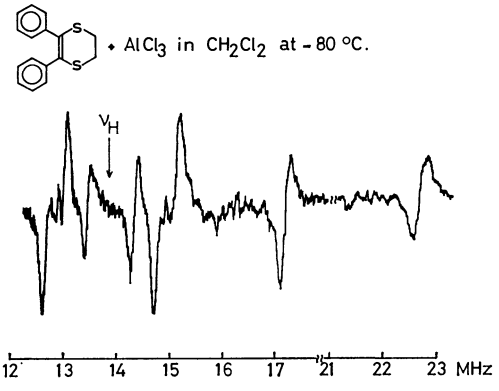

Fig. 1. Higher frequency half of ENDOR spectrum of 2,3-diphenyl-5,6-dihydro-1,4-dithiin cation radical. ν_H: free proton frequency.

TABLE 1. SUMMARY OF CALCULATIONS

	Calcd		Exptl	
	ρ_i	hfs/G	ρ_i[c]	hfs/G
1, 4	0.2195	—	—	—
2, 3	0.2241	—	—	—
5, 6	0.0084	6.336[d] 2.329[d]	—	6.339 2.383
7, 13	0.0175	—	—	—
12, 14	0.0321	0.879[c]	0.0336	0.894[a]
8, 18	0.0319	0.874[c]	0.0278	0.741[a]
10, 16	0.0296	0.810[c]	0.0241	0.643[a]
11, 15	0.0143	0.384[c]	0.0120	0.323[b]
9, 17	0.0139	0.373[c]		

a) The positions on the phenyl groups were tentatively assigned by MO calculation. b) The ENDOR spectrum can not resolve the difference in the hyperfine splittings of the meta-positions.

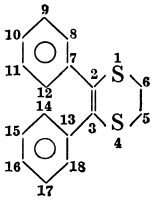

c) $a_i=|-12\rho_i^2-27\rho_i|$.

d) The axial and equatorial protons (see Text).

space filling model suggests that a steric repulsion may work between sterically approaching ortho protons (12- and 14-positions) in phenyl groups. This causes different hyperfine splittings at the positions 8 and 12, and 14 and 18. Taking account of a perturbation on the spin densities affected by the steric interaction, a slightly electro positive value was assumed for the Coulomb integrals at the ortho positions, that is, α(C-12)$=\alpha$(C-14)$=\alpha-0.1\beta$, in the same manner as has been applied to the *o*-terphenyl anion radical.[4] The MO spin densities on the phenyl groups thus calculated gave good agreement with the experimental spin densities estimated from the Colpa-Bolton's equation,[5] as shown in Table 1. It is noteworthy that the MO spin densities on the sulfur atom (0.2195) are close to those of dithiin sulfur atoms determined from the extra splitting of S^{33} (0.289).[2] This suggests that the dihydrodithiin cation radicals can be regarded to be one of the π-radicals in nature.

Both axial and equatorial proton splittings (a^{ax}, a^{eq}) are calculated in terms of the $\cos^2\theta$ rule:

$$a^{ax} = B\rho_S \cos^2\theta,$$
$$a^{eq} = B\rho_S \cos^2(60-\theta),$$

where B is the hyperconjugation parameter between the sulfur and the methylene group, ρ_S is the spin density on the sulfur atoms, and θ is the usual dihedral angle between sulsur p-orbital and sp^3-CH orbital. With the observed values for a^{ax} and a^{eq} thus determined, the dihedral angle can be obtained to be $\theta\simeq 7°$. The B-value estimated here ($\rho_S=0.2195$) is 29.4 G, which shows a good agreement with the value previously estimated for the related sulfur containing a π-radical ($B=36.8$ G).[6]

References

1) Y. Nagao, M. Ochiai, K. Kaneko, A. Maeda, K. Watanabe, and E. Fujita, *Tetrahedron Lett.*, **1977**, 1345.
2) E. A. C. Lucken, *Theor. Chim. Acta*, **1**, 397 (1963); P. D. Sullivan, *J. Am. Chem. Soc.*, **90**, 3618 (1968).
3) T. Yamamoto, K. Sato, and T. Miyamae, *J. Appl. Phys.*, **11**, 1508 (1971).
4) To be published.
5) J. P. Colpa and J. R. Bolton, *Mol. Phys.*, **6**, 273 (1963); J. R. Bolton, *J. Chem. Phys.*, **43**, 309 (1965).
6) A. Naito, K. Akasaka, and H. Hatano, *J. Magn. Reson.*, **24**, 53 (1976).

BULLETIN OF THE CHEMICAL SOCIETY OF JAPAN, VOL. 52 (7), 2143—2144 (1979)

A Theoretical Interpretation of the Half-wave Reduction Potentials of Chloronitrobenzenes

Shinichi YAMABE,* Tsutomu MINATO,** and Toshio ARAI

Department of Chemistry, Nara University of Education, Takabatake-cho, Nara 630

***Faculty of Engineering, Kyoto University, Sakyo-ku, Kyoto 606*

(Received November 16, 1978)

Synopsis. The half-wave reduction potential of chloronitrobenzenes has been studied with *ab initio* MO calculations. The relation between the energy of the lowest unoccupied MO and the reduction potential is given.

If the addition of the first electron to an aromatic hydrocarbon is the potential-determining step, there should be a relationship between the energy of the lowest unoccupied molecular orbital (LUMO) and the reduction potential.[1] We have carried out MO calculation in order to obtain possible relation between the half-wave reduction potentials ($E_{1/2}$'s) for a series of chloronitrobenzenes and the number and position of chlorine atoms attached to the benzene ring. The polarographic data are taken from the works of Fujinaga *et al.*,[2] and Kitagawa and Nakashima.[3] The MO calculation was made on the STO-3G minimal basis by use of the GAUSSIAN 70 program.[4] The coordinate and the geometrical parameters are shown in Fig. 1. For the sake of simplicity, all the bond angles in the X-Y plane are assumed to be 120° (sp^2 hybridization). The sole freedom of the geometrical change is the rotation (angle=θ°) of the nitro group around the C_1–N axis. According to X-ray analysis, pentachloronitrobenzene has θ=62°.[5] In the present study, the MO calculation is restricted to four molecules, Nos. 1, 2, 3, and 7 which are sufficient to explain the trend of $E_{1/2}$ values (Table 1).

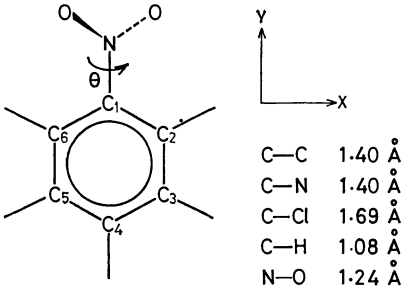

Fig. 1. The geometry taken for the MO calculation. All the bond angles are assumed to be 120°.

The values of $E_{1/2}$ are given for a variety of chloronitrobenzenes. We see a general tendency for the increase of chlorine substituents to give smaller negative values (easier reduction) except for *o*-dichloro-substituted nitrobenzenes (Nos. 7, 12, and 14). This is understandable in terms of the MO scheme, since the inclusion of hetero atoms lowers the LUMO of hydrocarbons.[1d] The greater the number of chlorine atoms attached to the benzene ring is, the more easily its anion radical is yielded through the acceptance of an electron into the LUMO. Of the three monochloronitrobenzenes

Table 1. The first half-wave reduction potential ($E_{1/2}$) and the orbital energy oe the LUMO (ε_{LUMO}) of chloronitrobenzenes

No.	Substituents	$E_{1/2}$ (V *vs.* SCE)	ε_{LUMO} (a.u.)
1	*o*-Chloro	−1.06[2]	0.1708
2	*m*-Chloro	−0.93[2]	0.1472
3	*p*-Chloro	−0.99[2]	0.1473
4	2,3-Dichloro	−0.98	
5	2,4-Dichloro	−0.99	
6	2,5-Dichloro	−0.94	
7	2,6-Dichloro	−1.15[3]	0.1715
8	3,4-Dichloro	−0.89	
9	3,5-Dichloro	−0.86	
10	2,3,5-Trichloro	−0.87[a]	
11	2,4,5-Trichloro	−0.87	
12	2,4,6-Trichloro	−1.05	
13	2,3,4,5-Tetrachloro	−0.83[b]	
14	2,3,5,6-Tetrachloro	−1.01	
15	Pentachloro	−0.89	

a) Evaluated from cyclic voltammogram of No. 14.
b) Evaluated from cyclic voltammogram of No. 15.

1, 2, and 3, the order of ease of one-electron reduction is *m*->*p*->*o*-chloronitrobenzene. In general, molecules with a greater amount of *meta*-Cl and a smaller amount of *ortho*-Cl are easily reduced. No. 9 (*m*-dichloro-substituted) is found to be most easily reduced among the series of dichloronitrobenzenes. The unfavorable role of the *ortho*-Cl against the easier reduction is observed typically in No. 7 with two Cl's. In spite of the inclusion of two hetero atoms, this molecule has a greater negative $E_{1/2}$ value (more difficult for reduction) than the parent nitrobenzene ($E_{1/2}$=−1.09). Such a trend holds also for the polychloronitrobenzenes.

The result given in Table 1 is interpreted theoretically in the MO scheme. First, the optimum θ of Nos. 1, 2, 3, and 7 is examined through a comparison of total energies. While No. 2 (*m*-Cl) and No. 3 (*p*-Cl) have a planar structure of θ=0° with the most widely spread π conjugation, No. 1 (*o*-Cl) and No. 7 (*o*-dichloro-substituted) have a nonplanar equilibrium structure with θ=54° and θ=71°, respectively. The *ortho*-Cl thus has a remarkable effect of steric hindrance on the nitro group. The question arises as to how such a nonplanar structure is related to the above mentioned result of $E_{1/2}$ of *ortho*-substituted nitrobenzenes. As θ becomes greater, the levels of LUMO 1 and 7 ascend sharply. These LUMO's are the π* orbital for θ=0°. The effect of the *ortho*-Cl on the value of $E_{1/2}$ is explained as follows. The *ortho*-Cl causes twisting of the nitro

group by steric hindrance. The subsequent nonplanar structure of the *o*-chloro-substituted nitrobenzenes raises the level of their LUMO's through the decrease of the extent of the π bonding between the benzene ring and the nitro group, resulting in the more difficult reduction, *i.e.*, a greater negative value of $E_{1/2}$. These molecules provide an interesting example of the "ortho effect" in their physical property *i.e.*, $E_{1/2}$.

Then, why does the *meta*-Cl make the reduction of nitrobenzene easier? In order to elucidate this effect, the mode of the π-MO interaction between the fragmental nitrobenzene and the chlorine atom is examined as to the planar monochloronitrobenzene. Of several π MO's of nitrobenzene, three unoccupied MO's, LUMO, (LU+1)MO, and (LU+2)MO are the most significant orbitals which contribute to the ascent or the descent of the LUMO of the monochloronitrobenzene. As for the chlorine atom, its $3p_z$ AO is the sole contributor to the LUMO of the monochloronitrobenzene. Figure 2a shows the nodal property of the π MO's of nitrobenzene and Fig. 2b the mode of the π-MO interaction between two fragmental sites. If only the LUMO of nitrobenzene interacts with the $3p_z$ AO, two kinds of orbitals, $\psi_{occ}^{o,m,p}$ and $\psi_{uno}^{o,m,p}$, are obtained. ψ_{occ} and ψ_{uno} indicate the occupied and unoccupied orbitals of the monochloronitrobenzene, respectively. The *o*, *m*, and *p* attached to the right shoulder denote the position, *ortho*, *meta*, and *para*, respectively, of the substituent. The (LUMO-$3p_z$) interaction causes the energy splitting between ψ_{occ} and ψ_{uno}, the degree of which depends entirely on the numerical value of the AO coefficients of the LUMO of nitrobenzene (Fig. 2a). Thus, the extent of energy splitting is *m*-Cl<*o*-Cl<*p*-Cl and the energy of the unoccupied level $\psi_{uno}^{m}<\psi_{uno}^{o}<\psi_{uno}^{p}$ (ψ_{uno}^{p} is highest). The secondary effect coming from the (LU+1)MO and (LU+2)MO of nitrobenzene should also be taken into account.[6] The energy levels of ψ_{occ} and ψ_{uno} produced primarily by the (LUMO-$3p_z$) interaction are lowered (Fig. 2b) according to the extent of the secondary MO interaction of (LU+1)MO and (LU+2)MO. As a result of such MO interactions, the energy level of the LUMO of nitrobenzene and monochloronitrobenzenes would have the order, *m*-Cl <*o*-Cl<*p*-Cl<nitrobenzene with no steric hindrance.

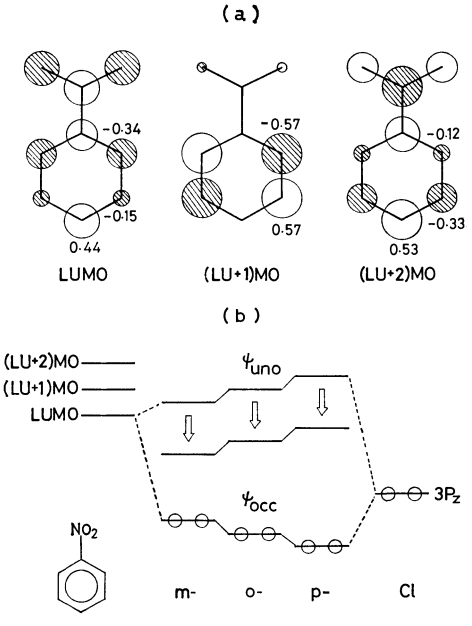

Fig. 2. (a); The AO coefficients of three π-type unoccupied MO's of nitrobenzene. (b); The mode of the orbital interaction between three unoccupied MO's of nitrobenzene and the $3p_z$ AO of Cl.

Thus, the correlation between the value of $E_{1/2}$, *i.e.*, the ε_{LUMO}, and the position of the substituent Cl is interpreted in terms of two independent factors; (a) the degree of the orbital interaction between the LUMO of nitrobenzene and the $3p_z$ AO of Cl, which depends on the numerical value of AO coefficients of the former MO, and (b) the steric hindrance caused by the *ortho*-Cl, resulting in the nonplanar structure of the *o*-chloro-substituted nitrobenzenes. In fact, the order of the experimental $E_{1/2}$ values is satisfactorily in line with that of the calculated ε_{LUMO} values.

All LUMO's of the four molecules adopted for the MO calculation are π^* (or almost π-type) orbitals. It is conceivable that, even when these molecules are reduced in one-electron step and their LUMO's accepted one electron, no dechlorination takes place. The first one-electron wave of polarography is reported to represent the reversible reduction of these compounds and the first wave corresponds to the formation of the relatively stable anion radical.

Permission to use the FACOM M-190 computer at the Data Processing Center, Kyoto University, is gratefully acknowledged. The work was carried out with Grant-in-Aid 139012 from the Ministry of Education.

References

1) a) A. Maccoll, *Nature*, **163**, 178 (1949); b) C. L. Perrin, "Organic Polarography," ed by P. Zuman and C. L. Perrin, Interscience, New York (1969); c) K. Morokuma, K. Fukui, T. Yonezawa, and H. Kato, *Bull. Chem. Soc. Jpn.*, **36**, 47 (1963); d) K. Fukui, K. Morokuma, H. Kato, and T. Yonezawa, *ibid.*, **36**, 217 (1963); e) F. A. Beland, S. O. Farwell, P. R. Callis, and R. D. Geer, *J. Electroanal. Chem.*, **78**, 145 (1977).

2) T. Fujinaga, T. Arai, and C. Kitazawa, *Nippon Kagaku Zasshi*, **85**, 811 (1964).

3) T. Kitagawa and R. Nakashima, *Rev. Polarogr.* **13**, 115 (1966).

4) W. J. Hehre, W. A. Lathan, R. Ditchfield, M. D. Newton, and J. A. Pople, program number 236 of QCPE, Indiana University (1973). The semiempirical (CNDO) MO is found to give the unreasonable equiliblium structure and is not employed here.

5) I. Tanaka, F. Iwasaki, and A. Aihara, *Acta Crystallogr., Sect. B*, **30**, 1546 (1974).

6) S. Inagaki, H. Fujimoto, and K. Fukui, *J. Am. Chem. Soc.*, **98**, 4054 (1976).

BULLETIN OF THE CHEMICAL SOCIETY OF JAPAN, VOL. 52 (7), 2145—2146 (1979)

Nonequilibrium Thermodynamics of Ionic Diffusion Coefficients in Binary Electrolyte Solutions

Eiichi KUMAMOTO* and Hideo KIMIZUKA

Department of Chemistry, Faculty of Science, Kyushu University, Fukuoka 812

(Received December 18, 1978)

Synopsis. Ionic diffusion coefficients were treated on the basis of nonequilibrium thermodynamics. They were calculated for alkali metal chloride solutions and compared with the experimental data of self-diffusion coefficients.

Miller,[1] and Paterson *et al.*[2] treated transport phenomena in terms of nonequilibrium thermodynamics and calculated the phenomenological coefficients $l_{\alpha\beta}$ from the conductance λ, salt diffusion coefficient D_s, and transference number t_α in solutions of alkali and alkaline earth chlorides. However, no mention was given of the ionic diffusion coefficient which is an important transport coefficient describing the motion of an ion in an electrolyte solution.

In this paper, the ionic diffusion coefficient has been expressed as a function of $l_{\alpha\beta}$ and related to the other transport coefficients. The ionic diffusion coefficient D_α calculated from the $l_{\alpha\beta}$ coefficients has been compared with the self-diffusion coefficient D_α^* as well as $(D_\alpha)_{\text{N.E.}}$ calculated from the ion conductance by means of the Nernst-Einstein equation. The diffusion coefficient of a salt D_s calculated from the ionic self-diffusion coefficients by means of the Nernst equation was compared with the observed one.

Results and Discussion

The independent flow J_α for the binary electrolyte system is given by

$$J_\alpha = -l_{\alpha\alpha}\nabla\bar{\mu}_\alpha - l_{\alpha\beta}\nabla\bar{\mu}_\beta, \tag{1}$$

where the subscripts α and β refer to either cation or anion, and $\nabla\bar{\mu}_\alpha$ denotes the electrochemical potential gradient for ion α. In the absence of the electric current, we find by eliminating $\nabla\bar{\mu}_\beta$

$$-J_\alpha/\nabla\bar{\mu}_\alpha = z_\beta(l_{\alpha\alpha}l_{\beta\beta} - l_{\alpha\beta}^2)/(z_\alpha l_{\alpha\beta} + z_\beta l_{\beta\beta}), \tag{2}$$

where z is the charge number of ion. The $l_{\alpha\beta}$ is related to the element of mobility matrix $u_{\alpha\beta}$ as follows[3]

$$l_{\alpha\beta} = u_{\alpha\beta}|z_\beta/z_\alpha z_\beta|c_\beta/F, \tag{3}$$

where c_β and F are the concentration of ion β and Faraday constant, respectively. Substituting Eq. 3 into the right hand side of Eq. 2, we have

$$-J_\alpha/\nabla\bar{\mu}_\alpha = c_\alpha/f_\alpha, \tag{4}$$

where f_α denotes the friction coefficient of ion α:

$$f_\alpha = F(z_\alpha|z_\beta|u_{\alpha\beta} + z_\beta|z_\alpha|u_{\beta\beta})/z_\beta(u_{\alpha\alpha}u_{\beta\beta} - u_{\alpha\beta}^2). \tag{5}$$

Defining an ionic diffusion coefficient D_α by the Einstein equation

$$D_\alpha = \frac{RT}{f_\alpha} = RT\frac{z_\beta(l_{\alpha\alpha}l_{\beta\beta} - l_{\alpha\beta}^2)}{c_\alpha(z_\alpha l_{\alpha\beta} + z_\beta l_{\beta\beta})}, \tag{6}$$

and substituting Eq. 6 into Eq. 2, we obtain the Nernst-Planck equation

$$J_\alpha = -\frac{D_\alpha c_\alpha}{RT}\nabla\bar{\mu}_\alpha. \tag{7}$$

Thus we see that the Nernst-Planck equation holds only in the limited case of no electric current in the binary electrolyte system, and that the ionic diffusion coefficient is given by Eq. 6 as a function of $l_{\alpha\beta}$. Since the equivalent conductance λ_α is given by[3]

$$\lambda_\alpha = |z_\alpha|F^2(z_\alpha l_{\alpha\alpha} + z_\beta l_{\beta\alpha})/z_\alpha c_\alpha, \tag{8}$$

we obtain by dividing Eq. 6 by Eq. 8

$$\frac{|z_\alpha|F^2 D_\alpha}{RT\lambda_\alpha} = 1 - \lambda_{\alpha\beta}\left(\frac{1}{\lambda_\alpha} + \frac{1}{\lambda_\beta}\right) \equiv F(\lambda_{\alpha\beta}), \tag{9}$$

where

$$\lambda_{\alpha\beta} = z_\alpha z_\beta F^2 l_{\alpha\beta}/|z_\beta|c_\beta. \tag{10}$$

On the other hand, the diffusion coefficient of the salt D_s is expressed in terms of $l_{\alpha\beta}$ as

$$D_s^0 \equiv \frac{D_s}{1 + \dfrac{\mathrm{d}\ln\gamma_s}{\mathrm{d}\ln m_s}} = -\frac{z_\alpha z_\beta(\nu_\alpha + \nu_\beta)(l_{\alpha\alpha}l_{\beta\beta} - l_{\alpha\beta}^2)\nu_\alpha RT}{\nu_\alpha\nu_\beta(z_\alpha^2 l_{\alpha\alpha} + 2z_\alpha z_\beta l_{\alpha\beta} + z_\beta^2 l_{\beta\beta})c_\alpha}, \tag{11}$$

where γ_s and m_s are the activity coefficient and molality of the salt, respectively.[1] Comparing Eq. 11 with Eqs. 8 and 9 and rearranging, we get

$$\nu_\alpha|z_\alpha|F^2 D_s^0/(\nu_\alpha + \nu_\beta)RT\lambda t_\alpha t_\beta = F(\lambda_{\alpha\beta}), \tag{12}$$

where λ is the equivalent conductance of the salt. Equations 9 and 12 are reduced to the Nernst-Einstein equation

$$(D_\alpha)_{\text{N.E.}} = RT\lambda_\alpha/|z_\alpha|F^2, \tag{13}$$

and the Nernst-Hartley equation

$$(D_s)_{\text{N.H.}} = \frac{(\nu_\alpha + \nu_\beta)RT\lambda t_\alpha t_\beta}{\nu_\alpha|z_\alpha|F^2}\left(1 + \frac{\mathrm{d}\ln\gamma_s}{\mathrm{d}\ln m_s}\right), \tag{14}$$

respectively, provided $l_{\alpha\beta}=0$. Substituting Eq. 13 into Eq. 9, we get

$$D_\alpha/(D_\alpha)_{\text{N.E.}} = 1 - \lambda_{\alpha\beta}/\lambda t_\alpha t_\beta = F(\lambda_{\alpha\beta}), \tag{15}$$

which relates D_α to $(D_\alpha)_{\text{N.E.}}$. Eliminating $F(\lambda_{\alpha\beta})$ from Eqs. 9 and 12, we have

$$D_s^0/(\nu_\alpha + \nu_\beta)t_\beta = D_\alpha/\nu_\alpha, \tag{16}$$

which serves to estimate D_α from D_s^0 and t_β. Since $F(\lambda_{\alpha\beta})$ is a characteristic parameter for a given system, we have from Eq. 9

$$|z_\alpha|D_\alpha/|z_\beta|D_\beta = \lambda_\alpha/\lambda_\beta = t_\alpha/t_\beta. \tag{17}$$

Further, Eq. 16 leads to the Nernst equation

$$(\nu_\alpha + \nu_\beta)/D_s^0 = \nu_\alpha/D_\alpha + \nu_\beta/D_\beta. \tag{18}$$

It should be noted that Eqs. 16—18 also hold on the basis of nonequilibrium thermodynamics, although these equations can also be derived from the Nernst-Planck equation.

In Tables 1 and 2 are listed the ionic diffusion coefficients calculated by means of Eq. 6 from $l_{\alpha\beta}$ evaluated by Miller,[1] and Paterson *et al.*,[2] the results being compared with $(D_\alpha)_{\text{N.E.}}$ and D_α^* compiled by Anderson and Paterson.[4] D_α is closer to D_α^* than $(D_\alpha)_{\text{N.E.}}$, indicating that the isotope-isotope interaction is much smaller than the cation-anion interaction. It should be also noted that D_α is greater than $(D_\alpha)_{\text{N.E.}}$. According to Eq. 15, this can be accounted for by negative $\lambda_{\alpha\beta}$ or positive $l_{\alpha\beta}$. The positive values of the interionic interaction, $l_{\alpha\beta}$, have been verified with many electrolytes.[1,2] The increase in the values of $D_\alpha/(D_\alpha)_{\text{N.E.}}$ with increase in concentration (Tables 1 and 2) indicates the increase in the cation-anion interaction. This is also reflected in the decrease in λ with increasing concentration. The difference between D_α and D_α^* shows no conspicuous concentration dependence except for Li^+ and Na^+. The D_α values are larger than the D_α^* values for these ions, the order of magnitude being reversed for the other ions. The magnitudes of cationic and anionic diffusion coefficients are in the order $D_{Li}<D_{Na}<D_K<D_{Cs}$ and $D_{Cl}(LiCl)<D_{Cl}(NaCl)<D_{Cl}(KCl)<D_{Cl}(CsCl)>D_{Cl}(RbCl)$, respectively, the same as those in the case of the self-diffusion coefficients.

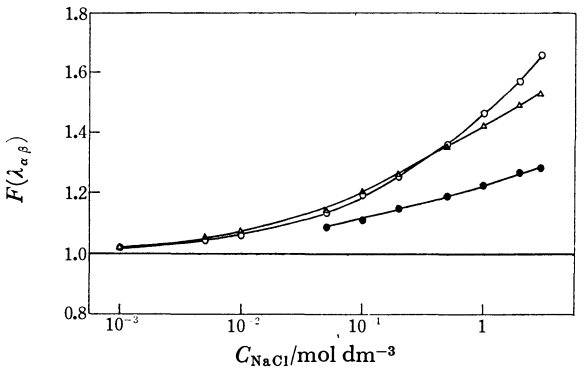

Fig. 1. $F(\lambda_{\alpha\beta})$ calculated from various origins. ○: From D_{Na}^*, ●: from D_{Cl}^*, △: from D_α. $F(\lambda_{\alpha\beta})=1$ corresponds to the calculated value from $(D_\alpha)_{\text{N.E.}}$. D_{Na}^* or D_{Cl}^* in the range 10^{-3}—10^{-1} mol/dm^3 were obtained from Mills' review.[5]

$F(\lambda_{\alpha\beta})$ in Eqs. 9 and 12 is a characteristic parameter for a given system and can be evaluated from $l_{\alpha\beta}$. Equation 9 also indicates that the values of the left hand side evaluated for both cation and anion should be the same. Since the ionic diffusion coefficient can not be measured directly, the self-diffusion coefficients were used for approximate evaluation of the value of the left hand side and the results compared with $F(\lambda_{\alpha\beta})$. An example is shown for aqueous sodium chloride solution in Fig. 1. $F(\lambda_{\alpha\beta})$ is closer to the values estimated from the self-diffusion coefficient than those predicted from the Nernst-Einstein equation or the Nernst-Hartley equation, $F(\lambda_{\alpha\beta})=1$.

Since the values of D_α are closer to those of D_α^* than $(D_\alpha)_{\text{N.E.}}$, the calculation of D_s from D_α^* by using Eq. 18 was also carried out. The difference between $(D_s)_{\text{calcd}}$ and $(D_s)_{\text{obsd}}$ is almost independent of concentration, the deviation being less than 15% for NaCl, KCl, and CsCl except for LiCl. $(D_s)_{\text{calcd}}$ is much closer to $(D_s)_{\text{obsd}}$ than $(D_s)_{\text{N.H.}}$.[6]

Table 1. Cationic diffusion coefficients

Salt	Concn / mol dm^{-3}	$D_\alpha\times10^5$ / cm^2 s^{-1} D_α^*	D_α	$(D_\alpha)_{\text{N.E.}}$	$\frac{D_\alpha}{D_\alpha^*}$	$\frac{(D_\alpha)_{\text{N.E.}}}{D_\alpha^*}$
LiCl	0.2	0.962	0.967	0.746	1.01	0.78
	0.5	0.946	0.896	0.648	0.95	0.68
	1.0	0.919	0.799	0.556	0.87	0.61
	2.0	0.868	0.653	0.442	0.75	0.51
	3.0	0.821	0.527	0.360	0.64	0.44
NaCl	0.2	1.295	1.307	1.033	1.01	0.80
	0.5	1.279	1.269	0.9350	0.99	0.73
	1.0	1.234	1.200	0.8424	0.97	0.68
	2.0	1.133	1.073	0.7187	0.95	0.63
	3.0	1.033	0.9521	0.6214	0.92	0.60
KCl	0.2	1.92	2.01	1.62	1.05	0.84
	0.5	1.87	2.03	1.53	1.09	0.82
	1.0	1.85	2.04	1.45	1.10	0.78
	2.0	1.84	2.02	1.36	1.10	0.74
	3.0	1.84	1.98	1.29	1.08	0.70
CsCl	0.5	1.947	2.197	1.565	1.13	0.80
	1.0	1.935	2.207	1.483	1.14	0.77
	1.5	1.921	2.199	1.430	1.14	0.74
	2.0	1.906	2.191	1.387	1.15	0.73
	2.5	1.888	2.185	1.345	1.16	0.71
	3.0	1.868	2.175	1.301	1.16	0.70

Table 2. Anionic diffusion coefficients

Salt	Concn / mol dm^{-3}	$D_\beta\times10^5$ / cm^2 s^{-1} D_β^*	D_β	$(D_\beta)_{\text{N.E.}}$	$\frac{D_\beta}{D_\beta^*}$	$\frac{(D_\beta)_{\text{N.E.}}}{D_\beta^*}$
LiCl	0.2	1.907	2.145	1.654	1.12	0.87
	0.5	1.817	2.099	1.518	1.16	0.84
	1.0	1.683	1.990	1.384	1.18	0.82
	2.0	1.494	1.777	1.203	1.19	0.81
	3.0	1.296	1.529	1.045	1.18	0.81
NaCl	0.2	1.925	2.117	1.673	1.10	0.87
	0.5	1.854	2.112	1.556	1.14	0.84
	1.0	1.772	2.068	1.440	1.17	0.81
	2.0	1.614	1.895	1.269	1.17	0.79
	3.0	1.449	1.722	1.124	1.19	0.78
KCl	0.2	1.966	2.097	1.686	1.07	0.86
	0.5	1.963	2.123	1.596	1.08	0.81
	1.0	1.955	2.142	1.524	1.10	0.78
	2.0	1.907	2.131	1.437	1.12	0.75
	3.0	1.835	2.095	1.360	1.14	0.74
RbCl	0.5	1.961	2.133	1.601	1.09	0.82
	1.0	1.971	2.198	1.540	1.12	0.78
	1.5	1.997	2.241	1.503	1.12	0.75
	2.0	2.042	2.264	1.471	1.11	0.72
	2.5	2.105	2.272	1.439	1.08	0.68
	3.0	2.180	2.271	1.406	1.04	0.64
CsCl	0.5	1.952	2.221	1.583	1.14	0.81
	1.0	1.963	2.274	1.527	1.16	0.78
	1.5	2.000	2.297	1.494	1.15	0.75
	2.0	2.076	2.316	1.466	1.12	0.71
	2.5	2.123	2.333	1.436	1.10	0.68
	3.0	2.189	2.345	1.403	1.07	0.64

References

1) D. G. Miller, *J. Phys. Chem.*, **70**, 2639 (1966).
2) H. S. Dunsmore, S. K. Jalota, and R. Paterson, *J. Chem. Soc., A*, **1971**, 2116; S. K. Jalota and R. Paterson, *J. Chem. Soc., Faraday Trans. 1*, **69**, 1510 (1973).
3) A. Katchalsky and P. F. Curran, "Nonequilibrium Thermodynamics in Biophysics," Harvard University Press, Cambridge, Mass. (1965), Chap. 11.
4) J. Anderson and R. Paterson, *J. Chem. Soc., Faraday Trans. 1*, **71**, 1335 (1975).
5) R. Mills, *Rev. Pure Appl. Chem.*, **11**, 78 (1961).
6) E. Kumamoto and H. Kimizuka, unpublished results.

BULLETIN OF THE CHEMICAL SOCIETY OF JAPAN, VOL. 52 (7), 2147—2148 (1979)

Scalar Coupling and Spin-rotation Interactions in the ^{13}C Nuclear Magnetic Relaxation of Methyl-d_3 Bromide

Masaru YANAGISAWA, and Osamu YAMAMOTO*

National Chemical Laboratory for Industry, 1-1-5, Honmachi, Shibuya-ku, Tokyo 151

(Received January 20, 1979)

Synopsis. ^{13}C NMR relaxation times have been obtained for methyl-d_3 bromide at room temperature, from which the spin-spin coupling constant between ^{13}C and ^{79}Br has been extracted and found to be 41.6±2.0 Hz. The contribution of the spin-rotation interaction to the ^{13}C relaxation is large in this molecule. This fact may be attributed to the presence of a methyl rotor, but cannot be satisfactorily interpreted in the framework of the present theories.

The dominant relaxation mechanism of the ^{13}C nucleus in bromomethanes has been found to be scalar coupling interaction owing to the fact that the resonance frequency of ^{13}C is close to that of bromine and that bromine has its relaxation mechanism by quadrupole interaction. We have shown that the relaxation curves for bromomethanes show non-exponential decay due to the presence of two bromine isotopes with a ratio of about 1:1.[1] By analyzing the relaxation curves we have been able to obtain the spin-spin coupling constants between ^{13}C and Br for three deuterated species, CD_2Br_2, $CDBr_3$, and CBr_4. For these species, other mechanisms contribute negligibly to ^{13}C relaxation. In methyl bromide, however, the spin-rotation mechanism may contribute to a large extent, even when the deuterated species are employed, because of the smaller size of the molecule and the presence of a methyl top. In the present paper, the spin-spin coupling constant between ^{13}C and ^{79}Br (J_{79}) for methyl-d_3 bromide has been obtained from ^{13}C relaxation time measurements, considering the contribution of the spin-rotation mechanism.

Experimental

Methyl-d_3 bromide was purchased from MSD, Canada, Ltd., and used without further purification. A high vacuum apparatus was empolyed for sampling. After several freeze-pump-thaw cycles, the sample was sealed into 8 mm dia. tube specially designed for the T_1 measurement. The sample remains in the liquid state in the sealed tube at room temperature. ^{13}C relaxation time measurements was conducted at 25.2 and 15.1 MHz with and without deuterium decoupling respectively, using a Varian XL-100-15 and a NEVA NV-14 spectrometers. Deuterium relaxation times was measured at 15.4 MHz by the XL-100-15. Other experimental details are the same as described in a previous paper.[1]

Results and Discussion

The relaxation curves obtained for ^{13}C in methyl-d_3 bromide at 15 and 25 MHz at room temperature show non-exponential decay, as predicted. The ^{13}C relaxation curve for CD_3Br is given by:[1]

$$\{I(\infty)-I(t)\}/I(\infty) = \exp(-t/T_1^s) + \exp(-t/T_1^l) \quad (1)$$

with $1/T_1^s = 1/T_1^\circ + 1/T_1^{79}$ and $1/T_1^l = 1/T_1^\circ + 1/T_1^{81}$ where T_1^{79} and T_1^{81} are the scalar relaxation (SC) times of ^{13}C bonded to a ^{79}Br and a ^{81}Br respectively, and T_1° is the relaxation time from other sources. The sum of the two exponentials in Eq. 1 may be separated into each exponetial by a nonlinear least squares fit to give T_1^s and T_1^l, the result of which is shown in Table 1.

TABLE 1. RERAXATION TIMES(S) IN CD_3Br OBSERVED AT 29.8 °C

Resonance freq.	T_1^s	T_1^l	T_1 of D
15 MHz	5.85±0.33	34.0±0.4	7.97±0.18
25 MHz	6.64±0.38	36.9±0.9	

The scalar coupling constant between ^{13}C and ^{k}Br (k=79 or 81), A_k ($=2\pi J_k$), may be obtained by solving the following set of equations.

$$1/T_1^k = (2/3)A_k^2 S(S+1)\tau_k/(1+\Delta\omega_k^2\tau_k^2) \quad (2)$$

where τ_k is the relaxation time of ^{k}Br, $\Delta\omega_k = \omega_C - \omega_{kBr}$, the resonance frequency difference, and S is the spin of bromine (3/2). T_1° includes the contributions from the dipole-dipole (DD) interaction between ^{13}C and D (T_{1D}^{CD}), from that between ^{13}C and Br (T_{1D}^{CBr}), from the spin rotation (SR) interaction (T_1^{SR}), and from intermolecular DD interactions (T_1^{inter}). Of these contributions T_{1D}^{CD} may be estimated by measuring the D relaxation time to obtain the correlation time of D using the known value of the deuterium quadrupole coupling constant in this molecule (166 kHz[2]). The contributions of T_{1D}^{CBr} ($\approx 5\times10^3$ s) and T_1^{inter} are so small that they can be neglected in the following calculation. Only the SR mechanism contributes to T_1°, and, in fact, it is a large part of $1/T_1^l$, the long component of the observed decay curve. Thus, an estimation of the SR contribution is essential for obtaining an accurate value of A_k.

T_1^{SR} and τ_k are all independent of variations in the magnetic field. Thus, the four equations such as 2 obtained from the T_1 measurements at two resonance frequencies, 15 and 25 MHz, may overdetermine the variables involved, since the independent variables are only three (A_{79}, τ_{79}, and T_{1C}^{SR}; A_{81} and τ_{81} are related to A_{79} and τ_{79} respectively). The measurements at the two fields have been carried out at 29.8 °C, and J_{79} has been determined so as to obtain agreement in τ_{79} and T_1° between the results at 15 and 25 MHz. The value of J_{79} thus obtained is 41.6 Hz, as shown in Table 2.

The values of J_{79} for methyl bromide and other bromomethanes[1] are plotted against the number of bromine atoms in Fig. 1, in which a similar plot for

Table 2. Caluculated relaxation parameters

T_{1C}^{SR} (s)	τ_{79} (μs)	T_{1D}^{CD} (s)	J_{79} (Hz)	τ_θ^{eff}(D) (ps)	τ_θ^{eff}(Br) (ps)	τ_J (ps) J-diffusion From D	J-diffusion From Br	M-diffusion From D	M-diffusion From Br
40.6	0.93	803	41.6	0.307	0.82	0.059	0.058	0.184	0.30
(±1.7)	(±0.10)	(±17)	(±2.0)	(±0.008)	(±0.10)	(±0.001)	(±0.006)	(±0.004)	(±0.03)

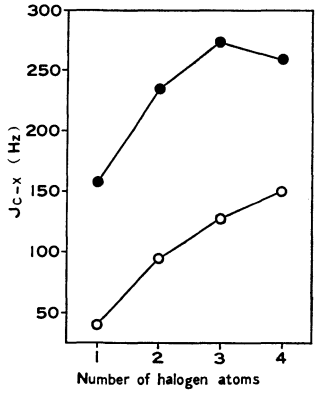

Fig. 1. Coupling Constants between ^{13}C and halogens in bromo- and fluoromethanes. ● Br, and ○ F.

fluoromethanes[3] is included for comparison. A parallelism between the two plots may be seen, *i.e.*, a monotonic increase of J_{CX} with increasing number of halogen atoms is observed. The smaller value for CF_4 than that for CHF_3 has been explained in terms of the double-bond-no-bond resonance effect.[4] In bromomethanes, such an effect seems to contribute little due to the less ionic character of Br.

McClung has developed the extended diffusion theory for molecular reorientation, in which rotational diffusion occurs through larger angle in liquid.[5] Assuming the J- or M-diffusion models, the angular momentum correlation time of the molecular reorientation, τ_θ^{eff}, which in turn, for methyl-d_3 bromide, is obtained independently from the D or Br relaxation time. Thus, the τ_J calculated from the D relaxation time should agree with that obtained from the Br relaxation time at the same temperature. As seen from Table 2, the two values well agree with each other in the J-diffusion model, but do not so in the M-diffusion model. This is consistent with the fact that the J-diffusion model also applies to CD_3CN,[6] which has nearly the same moment of inertia and approximately the same molecular geometry as CD_3Br.

The SR relaxation time in CD_3Br is *ca.* 40 s at room temperature. This value appears to be rather short, but may be compared with the values reported for CH_3CN (*ca.* 33 s at 30 °C[7]) and CH_3I (*ca.* 23.5 s at 25 °C[8]), molecules of similar size and structure, which may be roughly converted to the values for deuterated species by multiplying 1.39,[7] and then 46 and 33 s respectively. According to McClung,[5] the SR relaxation time may be calculated for τ_J and the known values of the SR coupling constants. The latter can be estimated from the relation which connects them to the average shielding value and the chemical shift anisotropy, $\Delta\sigma$.[9] Using the chemical shift data and $\Delta\sigma = -10$ ppm,[10] and taking the coupling constant of methane (−15.94 kHz[11]) as a reference, the SR coupling constant for CD_3Br is found to be $C_\perp = -0.96$ and $C_{//} = -9.86$ kHz.

The T_{1C}^{SR} calculated in this way is, however, too long to explain the experimental data, *i.e.*, 271 s at 29.8 °C, or 8 times the experimental value. This discrepancy between the experimental and estimated values is large, and a similar trend has been observed in other similar compounds. For CH_3I, the value estimated in a similar manner is 25 times the experimental value.[8] Goldammer *et al.*[7] assumed the SR coupling constants for methyl carbon which are much larger than that estimated by the chemical shift data in order to fit the experimental values of T_{1C}^{SR}. The calculations in these previous works are more or less based on the rotational diffusion theory of Hubbard[12] and Huntress,[13] which differs from that of McClung and is somewhat classical. However, the large discrepancy between the observed and the estimated values does not appear to stem from the calssical nature of the theory involved. All of the results including that of the present work suggest that the discrepancy arises from the presence of a methyl rotor, *i.e.*, the presence of a "fast internal rotation," as indicated by Gillen *et al.*[8] McClung's theory, which permits diffusive steps of arbitrary sizes, has been well adopted for reigid molecules such as benzene.[9] For the molecules with a methyl rotor, however, it appears to be still incomplete for the full description of the molecular reorientation. A more improved theory including the fast internal rotation is clearly needed.

References

1) O. Yamamoto and M. Yanagisawa, *J. Chem. Phys.*, **67**, 3803 (1977).
2) M. Rinne and J. Depireux, *Adv. Nucl. Quadrupole Reson.*, **1**, 357 (1974).
3) Data taken from J. B. Stothers, "Carbon-13 NMR Spectroscopy," Academic Press, New York (1972).
4) W. J. Considine, *Tetrahedron Lett.*, **1966**, 4923.
5) R. E. D. McClung, *J. Chem. Phys.*, **57**, 5478 (1972).
6) T. E. Bull, *J. Chem. Phys.*, **62**, 222 (1975).
7) T. K. Leipert and J. H. Noggle, *J. Magn. Reson.*, **13**, 158 (1974).
8) K. T. Gillen, M. Schwartz, and J. H. Noggle, *Mol. Phys.*, **20**, 899 (1971).
9) O. Yamamoto and M. Yanagisawa, *Chem. Phys. Lett.*, **54**, 164 (1978).
10) P. K. Bhattacharyya and B. P. Dailey, *Mol. Phys.*, **26**, 1379 (1973).
11) I. Ozier, J. A. Vitkevich, and N. F. Ramsey, Abstracts from the 27th Symposium on Molecular Structure and Spectroscopy, Ohio State University, Columbus, Ohio (1972).
12) P. S. Hubbard, *Phys. Rev.*, **131**, 1155 (1963).
13) W. T. Huntress, Jr., *J. Chem. Phys.*, **48**, 3524 (1968).

BULLETIN OF THE CHEMICAL SOCIETY OF JAPAN, VOL. 52 (7), 2149—2150 (1979)

Substitution Reactions of (Acetonitrile)chlorobis(triphenylphosphine)rhodium(I) in Benzene

Yoshimi OHTANI, Akihiko YAMAGISHI, and Masatoshi FUJIMOTO*

Department of Chemistry, Faculty of Science, Hokkaido University, Sapporo 060

(Received October 11, 1978)

Synopsis. The kinetics of the substitution reactions of $RhCl(NCCH_3)(PPh_3)_2$ in benzene was studied at 20 °C by the stopped-flow method under anaerobic conditions. The following mechanism was proposed:

$$RhCl(C_2H_4)(PPh_3)_2 \xrightarrow{H_2} RhClH_2(C_2H_4)(PPh_3)_2 \xrightarrow{C_2H_4}$$

$$RhClH_2(PPh_3)_2 \xrightarrow{CH_3CN} RhClH_2(NCCH_3)(PPh_3)_2.$$

In a previous paper we reported a kinetic study of a series of substitution reactions of Wilkinson's complex, showing that the substitution reaction, $RhCl(C_2H_4)(PPh_3)_2+H_2+PPh_3 \rightleftharpoons RhClH_2(PPh_3)_3+C_2H_4$, proceeds faster than the dissociation of C_2H_4 from $RhCl(C_2H_4)(PPh_3)_2$ as well as that of H_2 from $RhClH_2(PPh_3)_3$.[1] The results suggest an associative mechanism involving dihydrido-ethylene complex $RhClH_2(C_2H_4)(PPh_3)_2$ as a reaction intermediate, though it cannot be detected spectrophotometrically. In the present study, the substitution reaction of (acetonitrile)chlorobis(triphenylphosphine)rhodium(I) was investigated in comparison with that of chlorotris(triphenylphosphine)rhodium(I). The reaction was carried out in benzene at 20 °C.

Equilibria. The equilibrium constants $K=[RhClH_2(NCCH_3)L_2]/[RhCl(NCCH_3)L_2][H_2]$ and $K'=[RhCl(C_2H_4)L_2][CH_3CN]/[RhCl(NCCH_3)L_2][C_2H_4]$ were estimated from the measurements at $[CH_3CN]=$ 1.0, 1.9, and 3.8 mol dm^{-3} to be 2.5×10^4 mol^{-1} dm^3 and 3.4×10^2, respectively. The equilibrium constant for the substitution $K''=[RhClH_2(NCCH_3)L_2][C_2H_4]/[RhCl(C_2H_4)L_2][H_2][CH_3CN]\equiv K/K'$ was evaluated to be 74 mol^{-1} dm^3. The values of these equilibrium measurements indicate that hydrogen forms the final product $RhClH_2(NCCH_3)L_2$, but C_2H_4 cannot form the final product $RhCl(C_2H_4)(NCCH_3)L_2$. In the case of C_2H_4, substitution of CH_3CN in $RhCl(NCCH_3)L_2$ occurred to form a square planar complex $RhCl(C_2H_4)L_2$. The results may explain the low catalytic activity of Wilkinson's complex in acetonitrile solutions. The acetonitrile molecule competes with the olefin in the coordination to the central rhodium atom, as suggested by Schrock and Osborn.[3]

Kinetics. *Addition Reactions*: The addition of molecular hydrogen to $RhCl(NCCH_3)L_2$ and the substitution of the acetonitrile in $RhCl(NCCH_3)L_2$ complex by ethylene was found to proceed through both associative and dissociative paths based on the kinetic measurements:

$$\begin{array}{ccc} RhCl(NCCH_3)L_2 + S & \xrightarrow{\text{Associative path}} & RhCl(S)(NCCH_3)L_2 \\ \downarrow\uparrow & & \downarrow\uparrow \\ RhClL_2 + CH_3CN & + S \xrightarrow{\text{Dissociative path}} & RhCl(S)L_2 + CH_3CN, \end{array}$$

where S denotes hydrogen or ethylene. Though no accurate values could be obtained, the rate constant of the associative addition of hydrogen to $RhCl(NCCH_3)L_2$, k, was estimated to be *ca.* 1.4×10^2 mol^{-1} dm^3 s^{-1} from the addition rate of hydrogen obtained by extrapolating $[CH_3CN]$ to infinity. The value lies between that for $RhClL_3$ (4.8 mol^{-1} dm^3 s^{-1} at 25 °C) and that for $RhClL_2$ ($>7\times10^4$ mol^{-1} dm^3 s^{-1} at 25 °C).[4] The rate constant of the dissociation of hydrogen from $RhClH_2(NCCH_3)L_2$ is calculated to be 5.6×10^{-3} s^{-1} from k and K. The rate constant of the dissociation of C_2H_4 from $RhCl(C_2H_4)L_2$ was reported to be 0.4 s^{-1}.[1] The results indicate that the dissociation rates of H_2 from $RhClH_2(NCCH_3)L_2$ and C_2H_4 from $RhCl(C_2H_4)L_2$ are much lower than the rate of the substitution, $RhCl(C_2H_4)L_2+H_2+CH_3CN \rightleftharpoons RhClH_2(NCCH_3)L_2+C_2H_4$ (*vide infra*).

Substitution Reactions: Upon mixing a solution of $RhClH_2(NCCH_3)L_2$ with a solution containing C_2H_4, or a solution of $RhCl(C_2H_4)L_2$ with a solution containing H_2 and CH_3CN, the spectrum of the solution rapidly turned to that of an equilibrium mixture of $RhClH_2(NCCH_3)L_2$ and $RhCl(C_2H_4)L_2$. Since no hydrogenation of the coordinated C_2H_4 was observed during the course of measurement,[5] the observed process should be expressed by

$$RhCl(C_2H_4)L_2 + H_2 + CH_3CN \rightleftharpoons RhClH_2(NCCH_3)L_2 + C_2H_4.$$

Figure 1 gives the dependence of k_{obsd} for the above reaction on $[CH_3CN]$. The observed rate constant is larger than the dissociation rate constant of C_2H_4 from $RhCl(C_2H_4)L_2$ and that of H_2 from $RhClH_2(NCCH_3)L_2$, suggesting the existence of an associative intermediate. Increase in k_{obsd} with decreasing $[CH_3CN]$ suggests that, in the substitution reaction, the dihydrido complex $RhClH_2(NCCH_3)L_2$ is activated by the dissociation of CH_3CN molecule, as in the case of the dissociation of a PPh_3 molecule from Rh-

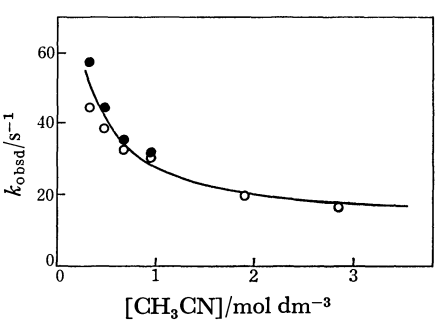

Fig. 1. The dependence of k_{obsd} on $[CH_3CN]$ for the reactions, $RhCl(C_2H_4)L_2+H_2+CH_3CN$ (○) and $RhClH_2(NCCH_3)L_2+C_2H_4$ (●). $[Rh]=1.0\times10^{-4}$, $[H_2]=1.4\times10^{-3}$, and $[C_2H_4]=7.5\times10^{-2}$ mol dm^{-3}. At 500 nm and 20 °C.

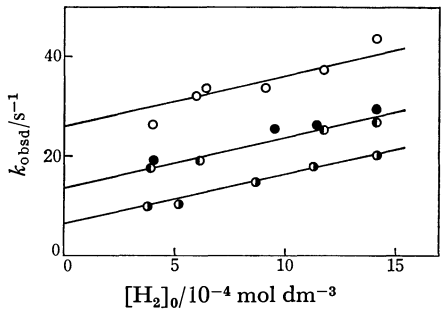

Fig. 2. The dependence of k_{obsd} on $[H_2]$, $[C_2H_4]$, and $[CH_3CN]$ for the reaction $RhCl(C_2H_4)L_2+H_2+CH_3CN$. The plot of k_{obsd} *vs.* $[H_2]$. $[Rh]=1.0\times10^{-4}$ mol dm^{-3}. $[C_2H_4]=7.5\times10^{-2}$ (○,◑,◑) or 3.8×10^{-2} (●) mol dm^{-3}. $[CH_3CN]=0.5$ (○,●), 1.0 (◐), or 1.9 (◑) mol dm^{-3}. At 500 nm and 20 °C.

ClH_2L_3.[1] Figure 2 shows the dependence of k_{obsd} on $[H_2]$, $[C_2H_4]$, and $[CH_3CN]$ for the reaction of $RhCl(C_2H_4)L_2$ with H_2 and CH_3CN. From Fig. 2 the k_{obsd} is expressed as

$$k_{obsd} = k[H_2] + k'\frac{[C_2H_4]}{[CH_3CN]}. \quad (1)$$

The following mechanism is proposed for the substitution reaction:

$$RhCl(C_2H_4)L_2 + H_2 + CH_3CN \underset{k_{-1}}{\overset{k_1}{\rightleftharpoons}} RhClH_2(C_2H_4)L_2$$
$$+ CH_3CN \underset{k_{-2}}{\overset{k_2}{\rightleftharpoons}} RhClH_2L_2 + C_2H_4 + CH_3CN \overset{K_3}{\rightleftharpoons}$$
$$RhClH_2(NCCH_3)L_2 + C_2H_4.$$

The steady-state approximation to $RhClH_2(C_2H_4)L_2$ and $RhClH_2L_2$ leads to

$$k_{obsd} = \frac{k_1k_2}{k_{-1}+k_2}[H_2] + \frac{k_{-1}k_{-2}}{(k_{-1}+k_2)K_3}\cdot\frac{[C_2H_4]}{[CH_3CN]}. \quad (2)$$

From Fig. 2, the values of $k_1k_2/(k_{-1}+k_2)$ and $k_{-1}k_{-2}/(k_{-1}+k_2)K_3$ are determined to be 9.6×10^3 mol^{-1} dm^3 s^{-1} and 1.7×10^2 s^{-1}, respectively. The value of $k_1k_2/(k_{-1}+k_2)$ agrees with that obtained previously (7.8×10^3 mol^{-1} dm^3 s^{-1}).[1]

The uni-molecular activation step $RhCl(C_2H_4)L_2\rightarrow Rh^*Cl(C_2H_4)L_2$ as observed in the case of $RhClL_3$,[1] was not observed in the present study. This would be interpreted as suppression of the reaction by acetonitrile. The proposed mechanism also suggests that the effect of acetonitrile on the catalytic activity of Wilkinson's complex is due to the formation of a catalytically inactive species $RhClH_2(NCCH_3)L_2$, the fraction of which is determined by the value of K''.

Experimental

A solution of $RhCl(NCCH_3)(PPh_3)_2$ was prepared by dissolving $RhCl(C_2H_4)(PPh_3)_2$ in oxygen-free benzene containing acetonitrile.[6] The coordinated ethylene was easily replaced by acetonitrile, leaving a pure $RhCl(NCCH_3)(PPh_3)_2$ in the solution.

$RhCl(C_2H_4)(PPh_3)_2$ was prepared from $RhCl(PPh_3)_3$ and ethylene. Benzene and acetonitrile were distilled. Commercial hydrogen and ethylene were used without further purification. Concentration and purity were determined by gas chromatography with a molecular sieve 5A.

All the measurements were carried out at 20±0.2 °C in oxygen-free benzene. The equilibrium of the reaction was measured with a Hitachi EPS-3T spectrophotometer. The kinetic measurements were made using a Union Giken RA-1300 stopped-flow apparatus under anaerobic conditions.

References

1) Y. Ohtani, M. Fujimoto, and A. Yamagishi, *Bull. Chem. Soc. Jpn.*, **50**, 1453 (1977).
2) C. A. Tolman, P. Z. Meakin, D. L. Lindner, and J. P. Jesson, *J. Am. Chem. Soc.*, **96**, 2762 (1974).
3) R. R. Schrock and J. A. Osborn, *J. Am. Chem. Soc.*, **98**, 2134 (1976).
4) J. Halpern and C. S. Wong, *J. Chem. Soc., Chem. Commun.*, **1973**, 629.
5) J. A. Osborn, F. H. Jardine, J. F. Young, and G. Wilkinson, *J. Chem. Soc., A*, **1966**, 1711.
6) Y. Ohtani, A. Yamagishi, and M. Fujimoto, *Bull. Chem. Soc. Jpn.*, **52**, 1537 (1979).

BULLETIN OF THE CHEMICAL SOCIETY OF JAPAN, VOL. 52 (7), 2151—2152 (1979)

Adduct Formation of the Mixed Copper(II) 2-Thenoyltrifluoroacetonate-3-isopropyltropolonate Chelate with Tributyl Phosphate in Solvent-extraction Systems Containing These Ligands

Tatsuya SEKINE* and Teruyuki TOSAKA

Department of Chemistry, Science University of Tokyo, Kagurazaka, Shinjuku-ku, Tokyo 162

(Received November 30, 1978)

Synopsis. From the extraction data of copper(II) in a perchlorate solution into carbon tetrachloride containing 2-thenoyltrifluoroacetone (Htta), 3-isopropyltropolone (Hipt), and tributyl phosphate (tbp), the formation of an adduct mixed chelate, Cu(tta)(ipt)(tbp), together with the $Cu(tta)_2$, $Cu(tta)_2(tbp)$, Cu(tta)(ipt), and $Cu(ipt)_2$ species, was concluded, and the formation constant of this adduct mixed chelate was calculated.

Synergism in metal chelate-extraction systems by neutral ligands is, in most cases, attributed to the adduct formation of the extracted chelate with the ligand.[1,2] It is often that the formation constants of adduct chelates of a certain metal ion with a certain given neutral ligand are very different when the chelating extractant is different.[3]

In a previous paper, this difference in the stabilities of adduct metal chelates was demonstrated by the enhancement of copper(II) extraction with 2-thenoyltrifluoroacetone (TTA) and 3-isopropyltropolone (IPT) by adding tributyl phosphate (TBP);[4] the extraction with TTA was very much enhanced by TBP, but that with IPT was not. From these results, it was concluded that the $Cu(tta)_2$ chelate formed a stable adduct, $Cu(tta)_2(tbp)$, while the $Cu(ipt)_2$ chelate formed no TBP adduct. The formation constant of the TTA-TBP adduct chelate was calculated from the enhancement of the TTA extraction, determined as a function of the concentration of TBP.

In another previous paper, the extraction of copper(II) in solvent-extraction systems containing both TTA and IPT was studied, and from the data, the extraction of the mixed chelate, Cu(tta)(ipt), together with the $Cu(tta)_2$ and $Cu(ipt)_2$ chelates, was concluded. The extraction constant of the mixed chelate was calculated from the data obtained at various molar ratios of TTA and IPT.[5]

In the present study, we have measured the distribution ratio of copper(II) in solvent-extraction systems containing TTA, IPT, and TBP; we have concluded that the mixed chelate, Cu(tta)(ipt), formed an adduct with TBP, Cu(tta)(ipt)(tbp).

Experimental

Reagents. All of the reagents were of an analytical grade. The extractants were supplied by the Dojindo Co., Kumamoto (TTA), by the Takasago Perfumery Co., Kanagawa (IPT), and by the Kanto Kagaku Co., Tokyo (TBP).

All of the experiments were made in a manner similar to that previously reported[4,5] except that the amount of copper(II) in the present study was measured by an atomic-absorption method. The temperature was 25±0.3 °C. The hydrogen-ion concentration was in stoichiometric units, as in previous studies.

Statistical

In this paper all the species in the organic phase will be denoted by the subscript "org". As has been described above, no formation of $Cu(ipt)_2(tbp)$ species was found previously. Thus, if higher adducts containing more than one TBP are negligible, the distribution ratio of copper(II) in the presence of TTA, IPT, and TBP may be written as:

$$\begin{aligned} D &= ([Cu(tta)_2]_{org} + [Cu(tta)_2(tbp)]_{org} + [Cu(tta)(ipt)]_{org} \\ &\quad + [Cu(tta)(ipt)(tbp)]_{org} + [Cu(ipt)_2]_{org})[Cu^{2+}]^{-1} \\ &= \{Kex_{2,0}[Htta]_{org}^2(1+\beta_{1(org)}^{tta}[tbp]_{org}) \\ &\quad + Kex_{1,1}[Htta]_{org}[Hipt]_{org}(1+\beta_{1(org)}^{mix}[tbp]_{org}) \\ &\quad + Kex_{0,2}[Hipt]_{org}^2\}[H^+]^{-2} \end{aligned} \quad (1)$$

where:

$$Kex_{2,0} = [Cu(tta)_2]_{org}[H^+]^2[Cu^{2+}]^{-1}[Htta]_{org}^{-2} \quad (2)$$

$$Kex_{1,1} = [Cu(tta)(ipt)]_{org}[H^+]^2[Cu^{2+}]^{-1}[Htta]_{org}^{-1}[Hipt]_{org}^{-1} \quad (3)$$

$$Kex_{0,2} = [Cu(ipt)_2]_{org}[H^+]^2[Cu^{2+}]^{-1}[Hipt]_{org}^{-2} \quad (4)$$

$$\beta_{1(org)}^{tta} = [Cu(tta)_2(tbp)]_{org}[Cu(tta)_2]_{org}^{-1}[tbp]_{org}^{-1} \quad (5)$$

$$\beta_{1(org)}^{mix} = [Cu(tta)(ipt)(tbp)]_{org}[Cu(tta)(ipt)]_{org}^{-1} \times [tbp]_{org}^{-1} \quad (6)$$

Results and Discussion

The organic solvent employed was carbon tetrachloride, and the aqueous phase contained 0.116 mol dm^{-3} of perchloric acid. The equilibrium constants defined by Eqs. 2 to 5 have already been reported in previous papers. They are given in Table 1, and they were employed for the analysis of the experimental data in the present study.

Several runs were made at various sets of concentrations of TTA, IPT, and TBP. It was found from the

TABLE 1. SUMMARY OF EQUILIBRIUM CONSTANTS[a]
Aq. phase: 0.1 mol dm^{-3} perchlorate media.
Solvent: CCl_4.

Extraction constant		Ref.	Adduct-formation constant[b]		Ref.
$\log Kex_{2,0}$	−1.08	4	$\log \beta_{1(org)}^{tta}$	2.27	4
$\log Kex_{1,1}$	0.80	5			
$\log Kex_{0,2}$	0.95	4	$\log \beta_{1(org)}^{mix}$	1.63	present work

a) The definitions of the constants are given in Eqs. 2 to 6. b) $Cu(ipt)_2$ does not form any adduct with TBP.

Table 2. Experimental data

Aq. phase: 0.116 mol dm^{-3} $HClO_4$. Org. solvent: CCl_4.

	$[TBP]_{org}$	[Cu(II)]	$[Cu(II)]_{org}$	log D	log $\beta_{1(org)}^{mix}$
	0.02	9.40×10^{-5}	1.10×10^{-4}	0.07	1.56
	0.03	8.16×10^{-5}	1.22×10^{-4}	0.20	1.60
a)	0.05	6.82×10^{-5}	1.36×10^{-4}	0.30	1.54
	0.075	5.15×10^{-5}	1.52×10^{-4}	0.47	1.63
	0.1	4.21×10^{-5}	1.62×10^{-4}	0.58	1.65
	0.02	1.28×10^{-4}	7.60×10^{-5}	−0.23	1.67
	0.03	1.14×10^{-4}	9.05×10^{-5}	−0.10	1.75
b)	0.05	1.00×10^{-4}	1.04×10^{-4}	0.02	1.69
	0.075	8.90×10^{-5}	1.15×10^{-4}	0.11	1.64
	0.1	8.11×10^{-5}	1.23×10^{-4}	0.18	1.59
	0.02	1.56×10^{-4}	4.83×10^{-5}	−0.51	1.67
	0.03	1.47×10^{-4}	5.72×10^{-5}	−0.41	1.70
c)	0.05	1.39×10^{-4}	6.52×10^{-5}	−0.33	1.62
	0.075	1.29×10^{-4}	7.49×10^{-5}	−0.24	1.59
	0.1	1.16×10^{-4}	8.81×10^{-5}	−0.12	1.63
	0.02	1.74×10^{-4}	2.96×10^{-5}	−0.76	1.78
	0.03	1.76×10^{-4}	2.81×10^{-5}	−0.80	1.53
d)	0.05	1.71×10^{-4}	3.26×10^{-5}	−0.72	1.50
	0.075	1.58×10^{-4}	4.59×10^{-5}	−0.54	1.67
	0.1	1.59×10^{-4}	4.46×10^{-5}	−0.55	1.52

a) $[Htta]_{org}=0.1$ mol dm^{-3}, $[Hipt]_{org}=0.01$ mol dm^{-3}.
b) $[Htta]_{org}=0.05$ mol dm^{-3}, $[Hipt]_{org}=0.01$ mol dm^{-3}.
c) $[Htta]_{org}=0.025$ mol dm^{-3}, $[Hipt]_{org}=0.01$ mol dm^{-3}.
d) $[Htta]_{org}=0.01$ mol dm^{-3}, $[Hipt]_{org}=0.01$ mol dm^{-3}.

results that the distribution ratio could be well explained by assuming the formation of only one adduct mixed chelate other than the four species already found. The formation constant of the adduct mixed chelate was calculated by introducing the extraction data and the values of the four constants into Eq. 1. Table 2 shows the data and the values of $\beta_{1(org)}^{mix}$ thus obtained from each set of data. In this table, the only data employed were those obtained under conditions where more than 25% of the copper(II) species in the organic phase was in the form of the adduct mixed chelate. The average value was log $\beta_{1(org)}^{mix}$ = 1.63, where the standard deviation was 0.08.

Figure 1 shows the percentage distribution of copper(II) species in the organic phase, as calculated by using the constants in Table 1. As may be seen from Fig. 1, the mixed species is always important in the high concentration range of TBP. For example, at $R=2$ and $[tbp]_{org}=0.1$ mol dm^{-3} more than 50% of the copper(II) in the organic phase is in the form of the adduct mixed chelate, Cu(tta)(ipt)(tbp).

The stability of adduct metal chelates in organic

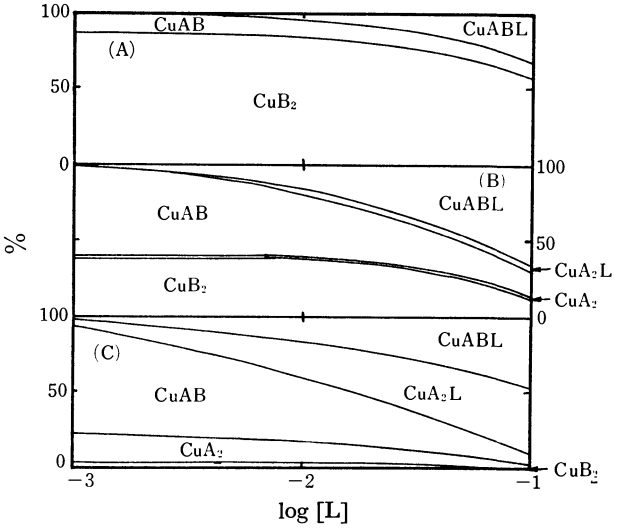

Fig. 1. The calculated percentage distribution of Cu(II) species in the organic phase as a function of the concentration ratio of the chelating extractants ($R=[HA]_{org}/[HB]_{org}$) and of L where HA is Htta, HB is Hipt, and L is tbp.
(A): $R=0.2$, (B): $R=2$, (C): $R=20$.

solvents is affected by several complicated factors, and no clear and systematic interpretation which allows a prediction of the stability of a certain given adduct metal chelate is available. Thus, we can not make any statistical estimation of the stability of the Cu(tta)(ipt)(tbp) adduct, even though we know the formation constants of the $Cu(tta)_2(tbp)$ and $Cu(ipt)_2(tbp)$ (the constant for the latter is zero). The present experimental results indicate that this adduct mixed chelate fairly stable, although it is less stable than the $Cu(tta)_2$(tbp).

No quantitative study of such adduct mixed chelate seems ever to have been made in other solvent extraction systems, but we presume that similar species would be formed in several of them containing various different sets of a metal ion, a chelating ligand, and an adduct-forming ligand.

References

1) H. M. N. H., Irving, "Solvent Extraction Chemistry," North-Holland Publ. Co., Amsterdam (1967), p. 105.
2) T. V. Healy, "Solvent Extraction Chemistry Research," Wiley Interscience, New York (1969), p. 257.
3) T. Sekine and Y. Hasegawa, "Solvent Extraction Chemistry," Marcel Dekker, New York (1977).
4) T. Sekine and D. Dyrssen, *J. Inorg. Nucl. Chem.*, **26**, 1727 (1964).
5) T. Sekine and D. Dyrssen, *J. Inorg. Nucl. Chem.*, **26**, 2013 (1964).

BULLETIN OF THE CHEMICAL SOCIETY OF JAPAN, VOL. 52 (7), 2153—2154 (1979)

Kinetics on the Formation and Decomposition of $2Al_2O_3 \cdot B_2O_3$ from Mixed Powders Prepared by the Alkoxy-method

Osamu YAMAGUCHI,* Minoru TADA, Kiyoshi TAKEOKA, and Kiyoshi SHIMIZU*

Department of Applied Chemistry, Faculty of Engineering, Doshisha University, Karasuma Imadegawa, Kamigyo-ku, Kyoto 602

(Received January 11, 1979)

Synopsis. The formation of the alkoxy-derived $2Al_2O_3.B_2O_3$ was observed in the temperature range 820—930 °C. Crystallization isotherms were best described by the contracting cube equation, the activation energy being determined as 368 kJ/mol. The kinetics on the decomposition of $2Al_2O_3.B_2O_3$ was also studied.

Aluminum boron oxide is known to exist in three forms, $9Al_2O_3 \cdot 2B_2O_3$ (orthorhombic), $2Al_2O_3 \cdot B_2O_3$ (orthorhombic), and $Al_2O_3 \cdot B_2O_3$ (hexagonal).[1-7] The former two can be prepared by the solid-liquid reaction from oxide mixtures, such as the system $\alpha \cdot Al_2O_3$–B_2O_3,[2] $\gamma \cdot Al_2O_3$–B_2O_3,[5] and $Al(OH)_3$–H_3BO_3.[3] The last one $Al_2O_3 \cdot B_2O_3$ has been recognized as a mineral, jeremejective. In a previous paper[8] dealing with the formation of $9Al_2O_3 \cdot 2B_2O_3$ from the mixed powders prepared by the simultaneous hydrolysis of aluminum and boron alkoxides, it was shown that the reaction process is similar to that of mullite($3Al_2O_3 \cdot 2SiO_2$) formed by heating a clay mineral, kaolinite($Al_2O_3 \cdot 2SiO_2 \cdot 2H_2O$). Several investigators[2,5,6] reported that $2Al_2O_3 \cdot B_2O_3$ melts incongruently at 1030—1050 °C to $9Al_2O_3 \cdot 2B_2O_3$ and liquid. No kinetic study, however, has been carried out. The present study is concerned with the kinetics of the formation and decomposition of the alkoxy-derived $2Al_2O_3 \cdot B_2O_3$.

Experimental

Boron triethoxide of guaranteed purity was used. Aluminum tris(isopentyl oxide) was synthesized by heating aluminum metal in an excess isopentyl alcohol with a small amount of mercury(II) chloride as a catalyst at 130 °C for 7 h.[9] Aluminum metal of purity 99.9% was used. A mixture of these alkoxides in the mole ratio $Al^{3+}/B^{3+}=2:1$ was prepared, and then poured into aqueous ammonia solution at 30 °C. The resulting mixed powders were washed with hot water and dried at 60 °C under reduced pressure. The average particle size of the mixed powders is *ca.* 550 Å. The X-ray diffraction(Cu $K\alpha$) pattern(Fig. 2(a)) is similar to that of the mixture whose Al^{3+}/B^{3+} mole ratio is 9:2. In view of the previous study,[8] the mixed powders are considered to be B^{3+}-substituted boemite(AlO(OH)) gel.

Results and Discussion

The TG of the mixed powders was carried out in the air from room temperature to 1000 °C(Fig. 1). The weight loss of 20.1% up to 710 °C is attributed to the loss of ammonia, absorbed water, hydrated water constitution water, and organic residue from the parent alcohol. DTA was also studied. Exothermic and endothermic reactions were observed at 820—930 °C and 1030—1250 °C, respectively. From the results of X-ray diffraction, the reactions were found to be

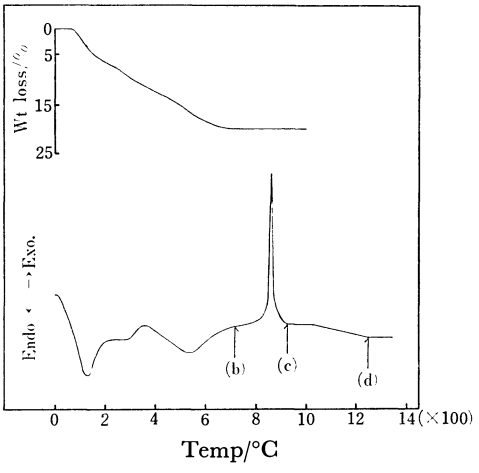

Fig. 1. TG and DTA curves of mixed powders as a raw material. Sample weight: 20 mg, heating rate: 10 °C/min.

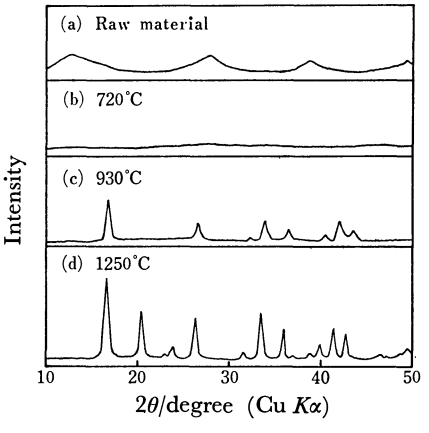

Fig. 2. X-Ray diffraction patterns of specimens with increasing temperature.
Heating rate: 10 °C/min.
(a) B^{3+}-substituted AlO(OH) gel, (b) amorphous material, (c) $2Al_2O_3 \cdot B_2O_3$, (d) $9Al_2O_3 \cdot 2B_2O_3$.

the crystallization of $2Al_2O_3 \cdot B_2O_3$ from an amorphous phase and the decomposition of $2Al_2O_3 \cdot B_2O_3$ into $9Al_2O_3 \cdot 2B_2O_3$ and liquid, respectively.

Figure 2 shows the variation of X-ray diffraction patterns of specimens with increasing temperature. The specimen heated at 720 °C after the completion of weight loss was amorphous, no significant changes being observed at 800 °C. The peaks corresponding to $2Al_2O_3 \cdot B_2O_3$ appeared at 820 °C for 25 min, the intensity increasing with increasing temperature and time. No other peaks were identified except for the $2Al_2O_3 \cdot B_2O_3$ spectrum up to 1000 °C. The peaks of $9Al_2O_3 \cdot 2B_2O_3$, as the decomposition product of

$2Al_2O_3 \cdot B_2O_3$, began to appear at 1030 °C. The specimen heated at 1250 °C showed the X-ray diffraction pattern of only $9Al_2O_3 \cdot 2B_2O_3$.

Figure 3 shows the fraction of the $2Al_2O_3 \cdot B_2O_3$ crystallization at 820, 840, and 870 °C. The mixed powders were pre-heated at 720 °C for 15 min. The average particle size of the specimen was 0.12 μm. The fraction of crystallization of each specimen was determined from the height of d=5.29 Å(2θ=16.7°) which is the strongest line of the $2Al_2O_3 \cdot B_2O_3$ spectrum. A well-crystallized specimen was obtained by heating the mixed powders at 950 °C for 30 min. Calcium fluoride was used as a standard material. Induction periods were observed, attempts being made to fit the results to kinetic laws by considering the induction periods. As shown in Fig. 4, crystallization isotherms are best described by the contracting cube equation $1-(1-\alpha)^{1/3}=k(t-t_0)$,[10] where α is the fraction of crystallization, t time and t_0 induction period. This indicates that the rate of crystallization is controlled by the rate of advance of the reaction interface. The rate constants were determined from the slopes of straight lines. The value of the activation energy calculated from the Arrhenius plot was 368 kJ/mol.

Figure 5 shows the fraction of decomposition of $2Al_2O_3 \cdot B_2O_3$ into $9Al_2O_3 \cdot 2B_2O_3$ and liquid as a function of time at different temperatures. The specimen heated at 950 °C for 30 min was used as a starting material. The fraction of decomposition of each specimen was determined by comparing the height of the d= 4.35 Å (2θ=20.4°) line with that of the same line of

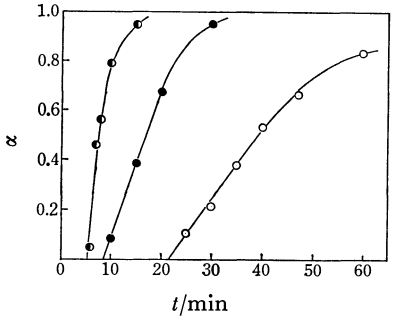

Fig. 3. Formation of $2Al_2O_3 \cdot B_2O_3$ as a function of time at different temperatures. ○: 820 °C, ●: 840 °C, ◐: 870 °C.

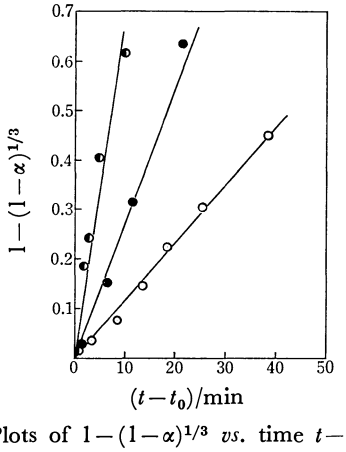

Fig. 4. Plots of $1-(1-\alpha)^{1/3}$ *vs.* time $t-t_0$ of the data shown in Fig. 3. ○: 820 °C, ●: 840 °C, ◐: 870 °C.

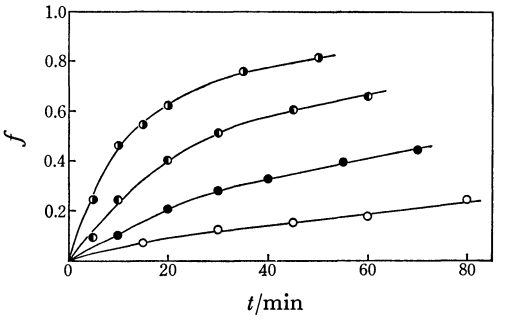

Fig. 5. Decomposition of $2Al_2O_3 \cdot B_2O_3$ as a function of time at different temperatures. ○: 1000 °C, ●: 1050 °C, ◐: 1100 °C, ◑: 1150 °C.

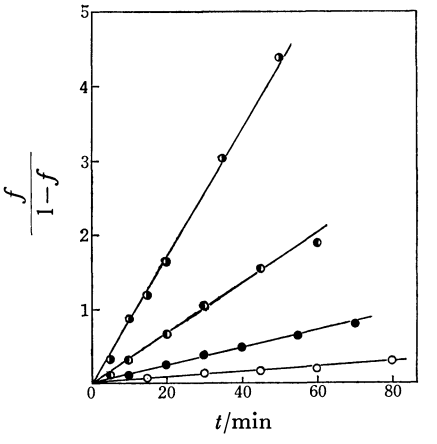

Fig. 6. Second-order plots of the data shown in Fig. 5. ○: 1000 °C, ●: 1050 °C, ◐: 1100 °C, ◑: 1150 °C.

a fully decomposed specimen, $9Al_2O_3 \cdot 2B_2O_3$. The data can be interpreted in terms of the second-order equation, as a special case of the treatment by Avrami[11] and Czanderna *et al.*[12] Figure 6 shows the plots of $f/1-f$ against t, where f is the fraction decomposed in time t. The activation energy was 301 kJ/mol, representing that employed for establishing active growth centers.

References

1) H. N. Baumann. Jr., and C. H. Moore, Jr., *J. Am. Ceram. Soc.*, **25**, 391 (1942).
2) H. Scholze, *Z. Anorg. Allg. Chem.*, **284**, 272(1951).
3) N. I. Golovastikov, E. N. Belova, and N. V. Belav, *Dokl. Akad. Nauk. S.S.S.R.*, **104**, 78 (1955).
4) A. Dietzel and H. Scholze, *Glastechn. Ber.*, **29**, 47 (1955).
5) P. J. M. Giclisse and W. R. Foster, *Nature*, **195**, 69 (1962).
6) K. H. Kim and F. A. Hummel, *J. Am. Ceram. Soc.*, **45**, 487 (1962).
7) C. Reynaud and J. T. Iiyama, *C. R. Acad. Sci. Paris*, **265**, 1105 (1967).
8) O. Yamaguchi, S. Nakamura, and K. Shimizu, *Nippon Kagaku Kaishi*, **1979**, 5.
9) For example, H. Adkins and F. W. Cox, *J. Am. Chem. Soc.*, **60**, 1151 (1938).
10) For example, R. B. Fahim and G. A. Kolta, *J. Phys. Chem.*, **74**, 2502 (1970).
11) N. Avrami, *J. Chem. Phys.*, **8**, 212 (1940).
12) A. W. Czanderna, C. N. R. Rao, and J. M. Honig, *Trans. Faraday Soc.*, **48**, 1069 (1958).

BULLETIN OF THE CHEMICAL SOCIETY OF JAPAN, VOL. 52 (7), 2155—2156 (1979)

Determination of Alkyl Thioureas, Isothiocyanates and Amines with Iodine Monochloride

Krishna K. VERMA

Department of Chemistry, University of Jabalpur, Jabalpur 482001, India

(Received August 26, 1978)

Iodine monochloride oxidizes thioureas to respective urea and sulfate in hydrogencarbonate medium. The iodine formed in the reaction is titrated with iodine trichloride to an Andrews end-point. This method has been applied to determine isothiocyanates and amines by their conversion to thioureas.

Most of the available procedures for determining thioureas by its oxidation to urea and sulfate require long standing periods in the range 5—60 min.[1-4]

A rapid and precise titrimetric method is described which requires a reaction period of about 30 s. Thioureas are reacted with iodine monochloride in hydrogencarbonate medium and the iodine formed is titrated with iodine trichloride to an Andrews end-point. This method does not require any blank determination and is unaffected by the presence of a number of concomitant substances.

This method of determining thioureas has been applied to analyze alkyl isothiocyanates involving conversion to substituted thiourea by reaction with 1-butylamine followed by oxidation with iodine monochloride. The present method has the advantage that basic or acidic impurities do not affect the results and that acid anhydrides and aldehydes, which interfere in acidimetric determination of isothiocyanates[5] by consuming amine *via* acylation and Schiff base formation respectively, can be tolerated. If the present method is coupled with acidimetry, the analysis of mixtures of isothiocyanates with isocyanates is possible since substituted ureas, formed by isocyanates, do not react with iodine monochloride.

The remarkable inertness of isothiocyanates towards several oxidizing agents, including iodine monochloride,[6] has added one more application. Primary and secondary amines react with an excess of 1-butylisothiocyanate and the substituted thiourea formed is again determined. Tertiary amines do not interfere.

Experimental

Reagents. Iodine monochloride[7] and iodine trichloride[8] solution, 0.1 mol dm^{-3} and 0.02 mol dm^{-3} respectively, were prepared in dilute hydrochloric acid and standardized iodometrically.[7]

Solutions of 1-butylamine, *ca.* 0.1 mol dm^{-3} and 1-butylisothiocyanate, *ca.* 0.1 mol dm^{-3} in dimethylformamide were used.

Test Compounds. All thioureas and amines were commercially available samples. Alkyl isothiocyanates were prepared and purified by the author.[9]

As a check independent methods were used to determine the purity of thioureas (Table 1). Solutions of amines and isothiocyanates, were prepared in dimethylformamide and the former were standardized by acidimetry[10] and the latter by the method of Vinson.[11]

Procedures. *Procedure for Thioureas*: Weigh or take an aqueous aliquot of sample containing 0.01—0.1 mmol of thiourea and dissolve or mix with 30 cm^3 of water, 2 g of sodium hydrogencarbonate and 10 cm^3 of carbon tetrachloride in a 250-cm^3 iodine flask. Introduce with swirling, 5—15 cm^3 of 0.1 mol dm^{-3} iodine monochloride, the excess being indicated by the appearance of iodine in organic layer. After swirling for 30 s, add cautiously 40 cm^3 of 6 mol dm^{-3} hydrochloric acid. When the evolution of carbon dioxide ceases, stopper the flask and shake vigorously. Titrate the liberated iodine by running in 0.02 mol dm^{-3} iodine trichloride until the solution becomes pale brown. Stopper the flask and shake well. Continue the addition of iodine trichloride in small portions, shaking vigorously after each addition, until the organic layer loses the last trace of violet color of iodine and becomes essentially colorless.

For a convenient and sharp end-point detection, invert the well-shaken-stoppered-flask and note the change from violet to colorless through the column of carbon tetrachloride at the neck of the flask.

Procedure for Isothiocyanates: Take a sample solution (5—10 cm^3) in dimethylformamide containing 0.01—0.1 mmol of isothiocyanate in a 250-cm^3 iodine flask and treat with 5 cm^3

TABLE 1. DETERMINATION OF THIOUREAS WITH IODINE MONOCHLORIDE

Thiourea, substituent	Purity, %				
	Present method	No. of detns.	Std. devn.	Comparison method	
—	99.9	8	0.08	99.8	Hypoiodite[4]
Methyl	99.7	10	0.10	99.9	Hexacyanoferrate (III)[12]
Allyl	99.5	6	0.10	99.2	Ce(IV) titration[13]
N,N'-Dimethyl	98.8	7	0.13	98.5	Bromine chloride[14]
Ethyl	98.5	6	0.09	98.7	Iodine[1]
N,N'-Diethyl	99.1	8	0.15	99.0	Iodine trichloride[15]
2-Propyl	99.0	6	0.12	99.3	Bromine[1]
1-Butyl	98.7	8	0.16	98.6	Bromine chloride[14]
2-Methyl-1-propyl	98.1	10	0.11	98.4	Ce(IV) titration[13]

of 0.1 mol dm^{-3} 1-butylamine. Swirl the solution and let stand for 10 min. Thereafter, add 30 cm^3 of water and determine the thiourea as before.

Procedure for Primary and Secondary Amines. Treat 5—10 cm^3 of sample solution in dimethylformamide containing 0.01—0.1 mmol of amine, with 5 cm^3 of 0.1 mol dm^{-3} 1-butylisothiocyanate in a 250-cm^3 iodine flask and age for 10 min. Dilute the contents with 30 cm^3 of water and determine the thiourea formed.

Results and Discussion

The iodine monochloride reacts with thiourea and its alkyl derivatives as follows:

$$RNHCSNHR + 8ICl + 5H_2O \longrightarrow RNHCONHR + 4I_2 + H_2SO_4 + 8HCl.$$

The reaction is slow in acid medium (20—30 min) but almost instantaneous and quantitative in the presence of hydrogencarbonate (Table 1). The concentration of hydrogencarbonate is not critical but it should be enough to neutralize the acid added with the reagent solution and that produced in the reaction. Iodine reacts with iodine trichloride as follows:

$$I_2 + ICl_3 \longrightarrow 3ICl.$$

The analysis of thiourea is utilized as a basis for the determination of isothiocyanate or amine if one of them is made to react with an excess of the other (Table 2):

Table 2. Determination of isothiocyanates and amines

Substance	Range determined (mg)	No. of detns.	Average % recovery	Standard deviation
Isothiocyanate				
Ethyl	0.89— 8.65	8	100.2	0.3
Propyl	1.08—10.10	6	99.8	0.2
1-Butyl	1.30—11.00	8	99.9	0.1
2-Propyl	1.45—10.28	7	98.9	0.3
2-Methyl-1-propyl	1.25— 9.65	9	99.3	0.2
Allyl	0.99— 8.29	10	99.8	0.2
Amine				
Methyl	0.42— 3.08	6	99.9	0.2
Ethyl	0.45— 4.20	6	100.1	0.1
2-Propyl	0.62— 5.46	8	99.6	0.2
1-Butyl	0.87— 6.29	10	99.8	0.1
Diethyl	0.83— 6.07	6	99.7	0.3
Piperidine	0.89— 8.46	8	99.6	0.3

$$RNCS + RNH_2 \longrightarrow RNHCSNHR.$$

Mixtures of tertiary amines with primary or secondary amines can be analyzed if the total amine is known by acidimetry.[10] Then, tertiary amine can be obtained by subtracting the amine found by iodine monochloride method. Mixtures of isothiocyanates with isocyanates can be analyzed if a total of them is determined by the method of Vinson,[11] the isothiocyanate being known by the present method.

Iodine monochloride does not react with the following substances under the conditions of determination: citric acid, oxalic acid, glucose, glycine, alanine, arabinose, serine, diphenyldisulfide, carbon disulfide, formaldehyde, and benzaldehyde. Unsaturated compounds like allyl alcohol, cinnamic, and fumaric acids, that form addition compound with iodine monochloride, also do not interfere since the final titration involves determination of the liberated iodine.

Iodide, sulfide, sulfocyanide and thiosulfate interfere severely. Arylthioureas only reacted incompletely, therefore, the present method is not recommended for them.

References

1) P. C. Gupta, *Analyst*, **88**, 896 (1963).
2) K. K. Verma, *Z. Anal. Chem.*, **275**, 287 (1975).
3) C. G. R. Nair and P. Indrasenan, *Indian J. Chem.*, **14A**, 599 (1976).
4) S. Skramovsky, *Casopis Ceskoslov. Lekarnictava*, **21**, 1 (1941).
5) S. Siggia and J. G. Hanna, *Anal. Chem.*, **20**, 1084 (1948).
6) M. R. F. Ashworth, "The Determination of Sulphur-Containing Groups," Academic Press, London (1972), Vol. I, p. 91.
7) A. Berka, J. Vulterin, and J. Zyka, "Newer Redox Titrants," Pergamon Press, Oxford (1965), p. 56.
8) Y. A. Fialkov and F. E. Kagan, *Ukrain. Khim. Zh.*, **18**, 55 (1952).
9) N. L. Drake, *Org. Synth.*, **21**, 81, 83 (1941).
10) F. E. Critchfield, "Organic Functional Group Analysis," Pergamon Press, New York (1963), p. 26.
11) J. A. Vinson, *Anal. Chem.*, **41**, 1661 (1969).
12) M. K. Joshi, *Naturwissenschaften*, **44**, 537 (1957).
13) B. C. Verma and S. Kumar, *Talanta*, **20**, 916 (1973).
14) K. K. Verma, A. Srivastava, J. Ahmed, and S. Bose, *Talanta*, **25**, 469 (1978).
15) K. K. Verma, M. P. Sahasrabuddhey, and S. Bose, *Talanta*, **24**, 515 (1977).

BULLETIN OF THE CHEMICAL SOCIETY OF JAPAN, VOL. 52 (7), 2157—2158 (1979)

The Reaction of 2,4,6-Heptanetrione with *o*-Phenylenediamine†

Akiko FURUHASHI,* Koji AOKI, and Morihito SUGIMOTO**

Department of Chemistry, College of Science and Engineering, Aoyama Gakuin University, Chitosedai, Setagaya-ku, Tokyo 157

***Department of Pollution Control, Nippon Electronics Engineering College, Nishikamata, Ota-ku, Tokyo 144*

(Received October 14, 1978)

Synopsis. 2,4,6-Heptanetrione forms 2-acetyl-4-methyl-1,5-benzodiazepine with *o*-phenylenediamine in alkaline ethanol. In acidic ethanol, it would be expected that the 2-acetyl-4-methyl-1,5-benzodiazepinium cation would be formed. Contrary to expectations, however, the cation seems to be unstable. 2,4-Dimethyl-1,5-benzodiazepinium salt was obtained instead.

2,4,6-Heptanetrione(diacetylacetone: daa) forms metal complexes through its oxygen atoms[1-2] and forms Schiff bases with ethylenediamine[3] in analogy with 2,4-pentanedione(acetylacetone), whereas it does not form dithio- or trithiodiacetylacetonato metal complexes.[4] The reaction of daa with *o*-phenylenediamine(opd) was studied.

By adding a potassium hydroxide ethanol solution to a mixture of daa and opd in ethanol, red crystals of 2-acetyl-4-methyl-1,5-benzodiazepine were obtained. On the other hand, in an ethanol solution containing hydrochloric acid, its azepinium cation seems to be destroyed and to become 2,4-dimethyl-1,5-benzodiazepinium.

Experimental

Instruments. The infrared spectra were obtained by the KBr disk or Nujol mull procedure, using a IRA-1-type infrared spectrophotometer of the Japan Spectroscopic Co., Ltd. The electronic spectra were obtained with a Shimadzu Double-beam Spectrophotometer UV-200 in 64% w/w aqueous methanol, with the ionic strength of 0.3. The NMR spectra of the $CDCl_3$ solution were obtained with a Hitachi Perkin-Elmer Model-R-20 NMR Spectrometer. Tetramethylsilane(TMS) was used as the standard. The mass spectra were obtained with a Hitachi Model-RMU-6M-GC Mass Spectrometer.

The Syntheses of the Compounds. Diacetylacetone[1] was synthesized from dehydroacetic acid by the method of Bethell and Maitland.[5] 2-Acetyl-4-methyl-1,5-benzodiazepine was synthesized from daa and opd according to the method of Thile and Steimmig[6] as follows. Daa (0.71 g, 5×10^{-3} mol) in 20 ml of an ethanol solution was added to opd(0.54 g, 5×10^{-3} mol) in 2 ml of hot ethanol containing 1 ml of acetic acid, and then potassium hydroxide in ethanol was added to the mixture. The red crystals thus formed were filtered off and recrystallized from ethanol. (Found: C, 72.88; H, 6.60; N, 13.04%. Calcd for $C_{13}H_{14}N_2O$: C, 72.90; H, 6.54; N, 13.80%). Molecular weight, 214 (from the mass spectra). The compound forms orange crystals with cadmium chloride in ethanol.

On the other hand, when gaseous hydrochloric acid was added to the mixture (daa+opd+CH_3COOH) mentioned above, the solution turned violet. By adding petroleum ether, violet-colored crystals were obtained. The results of the elemental analyses agree with those of 2,4-dimethylbenzodiazepinium chloride.[7] (Found: C, 53.56; H, 6.98; N, 11.21%. Calcd for $C_{11}H_{13}N_2\cdot2H_2O$: C, 53.99; H, 7.00; N, 11.45%).

Results and Discussion

The proton NMR spectra of the red compound are shown in Table 1. The spectra fit the structure shown in Fig. 1, 2-acetyl-4-methyl-1,5-benzodiazepine.

TABLE 1. NMR SPECTRAL DATA

δ/ppm	Integrated for	Assignment
11.75	1H	hydrogen bond
6.75	4H	phenyl
4.90	1H	methine
3.39	2H	methylene
1.98	3H	methyl
1.81	3H	methyl

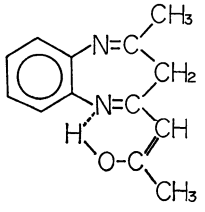

Fig. 1. 2-Acetyl-4-methyl-1,5-benzodiazepine.

The IR spectra also support the above assignment. The free C=O band which is usually expected about 1700 cm^{-1} was not observed, while three bands were observed in the 1515—1660 cm^{-1} region. These bands are likely to consist of (C=N), (C=C), and hydrogenbonded (C–O), or a mixture of them.[8]

On the other hand, the spectra of the violet compound obtained from the acidic solution are completely identical with those of the 2,4-dimethylbenzodiazepinium chloride, which does not show a peak at 1660 cm^{-1}.

The electronic spectra of the red azepine solution do not show any peak in the 350—600 nm range, whereas the addition of hydrogen chloride produced the band at 510 nm. This wavelength agrees well with that reported for the diazepinium cation.[9] (Fig. 2). The peak increased with the acid concentration, with an isosbestic point at 410 nm. It is, therefore, likely that the 2-acetyl-4-methyl-1,5-benzodiazepinium cations present in the solution. The 2,4-dimethyl-1,5-benzodiazepinium salt, however, was obtained

† A part of this work was presented at the 36th National Meeting of the Chemical Society of Japan, Osaka April 1977.

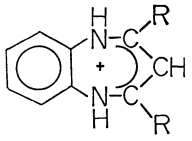

Fig. 2. Diazepinium cation.

by condensation or by adding petroleum ether. The acetyl group must interact with H^+ and be severed in an acidic solution, although the acetyl group was not determined to do so. The acetyl group seems to be relatively easily hydrolyzed because of the stabilization of the seven-membered azepinium ring, which has a resonance system.

We are pleased to acknowledge the considerable assistance of Professor Kan Kimura of Aoyama Gakuin University. The authors also wish to thank Professor Oyo Mitsunobu of Aoyama Gakuin University for his helpful advice.

References

1) F. Sagara, H. Kobayashi, and K. Ueno, *Bull. Chem. Soc. Jpn.*, **41**, 266 (1968).
2) F. Sagara, H. Kobayashi, and K. Ueno, *Bull. Chem. Soc. Jpn.*, **46**, 484 (1973).
3) T. Yano, T. Ushijima, M. Sasaki, H. Kobayashi, and K. Ueno, *Bull. Chem. Soc. Jpn.*, **45**, 2452 (1972).
4) A. Furuhashi, M. Kawano, N. Tashiro, and A. Ouchi, *J. Inorg. Nucl. Chem.*, **34**, 2960 (1972).
5) J. R. Bethell and P. Maitland, *J. Chem. Soc.*, **1962**, 3755.
6) J. Thiele and G. Steimmig, *Chem. Ber.*, **40**, 955 (1907).
7) A. Ouchi, T. Takeuchi, M. Nakatani, and Y. Takahashi, *Bull. Chem. Soc. Jpn.*, **44**, 434 (1971).
8) L. J. Bellamy, "Advances in Infrared Group Frequencies," Methuen, New York, N. Y. (1968), pp. 21—32, 49—52, 125—142.
9) J. A. Barltop, C. G. Richards, D. M. Russell, and G. Ryback, *J. Chem. Soc.*, **1959** 1132.

BULLETIN OF THE CHEMICAL SOCIETY OF JAPAN, VOL. 52 (7), 2159—2160 (1979)

The Condensation Products of Naphthanthrone

Shoji FUJISAWA,* Junji AOKI, Minoru TAKEKAWA, and Satoshi IWASHIMA†

Department of Chemistry, Faculty of Science, Toho University, Funabashi, Chiba 274

†*Department of Chemistry, Faculty of Science and Technology, Meisei University, Hino, Tokyo 191*

(Received October 28, 1978)

Synopsis Three hydrocarbons, with absorption maximum at 510 nm, 533 nm, and 567 nm respectively, have been synthesized by the condensation of naphthanthrone in a mixed flux of zinc chloride and sodium chloride with copper powder. The structures of the hydrocarbons have been determined by comparison with the products obtained by the alkali fusion and reduction of naphthanthrone and 2-bromonaphthanthrone.

On heating naphthanthrone (6*H*-benzo[*cd*]pyren-6-one) (**1**) with copper powder in a mixed flux of zinc chloride and sodium chloride, three hydrocarbons with eleven benzene rings (**2**, **3**, **4**) have been obtained. These hydrocarbons, with overcrowed hydrogen atoms, are not only stereochemically interesting, but are also very important in the field of organic semiconductors because of their high photoconductivity.[1]

Clar *et al.* reported[2] that the fusion of **1** with zinc dust gave two hydrocarbons which had absorption maximum at 510 nm and 533 nm in benzene, respectively. The former was confirmed by X-ray analysis[3] to be diphenanthro[5,4,3-*abcd*:5′,4′,3′-*jklm*]perylene (DPP) (**2**) and the latter was tentatively assigned as dibenzoviolanthrene B (**3**) by Clar *et al.* A further hydrocarbon, with an absorption maximum at 567 nm, has been found in this laboratory and an attempt to structurally analyze this new hydrocarbon and the hydrocarbon with an absorption maximum at 533 nm has been conducted.

The convenient analytical methods of NMR and IR are of little use in the case of large condensed aromatic hydrocarbons because of the existence of many similar C–H bonds. Indeed the spectra are usually very complicated and consequently cannot be used as a basis for structural analysis.

X-Ray analysis is a further tool, but considerable difficulty has been met in the growing of single crystals of sufficient size. Furthermore X-ray analysis may not be easy even with good crystals.

In this paper the structures of these two hydrocarbons, deduced from the separate synthesis of each will be presented.

On the basis of the reaction used for the synthesis of violanthrones from benzanthrone,[4] the alkali fusion of **1** is expected to give dibenzoviolanthrones (**5**, **6**). Dibenzoviolanthrone B (**6**) was reduced to the corresponding hydrocarbon, dibenzoviolanthrene B (**3**), with zinc powder, melting at 378—379 °C and with an absorption maximum at 567 nm in benzene. Thus it has been concluded that dibenzoviolanthrene B (**3**) has an absorption maximum at 567 nm and not at 533 nm as suggested by Clar *et al.*[2]

On the basis of the reaction of 3-bromobenzanthrone,[4,5] the dibenzoisoviolanthrones (**8**, **9**) were prepared from 2-bromonaphthanthrone (**7**). Dibenzoisoviolanthrone B (**9**) was reduced to the corresponding hydrocarbon, dibenzoisoviolanthrene B (**4**), with zinc powder giving a hydrocarbon with an absorption max-

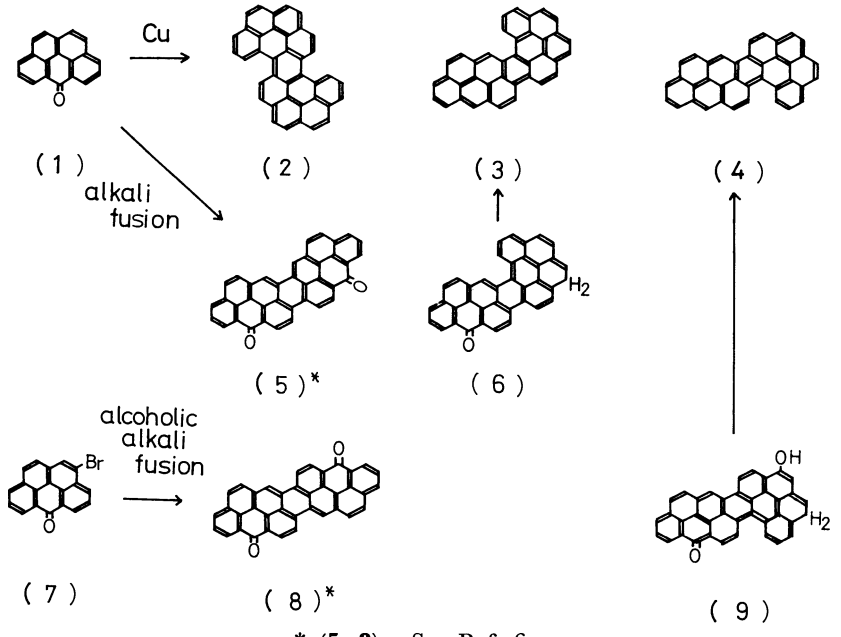

* (**5**, **8**). See Ref. 6.

Scheme.

imum at 533 nm in benzene. The absorption spectrum of this hydrocarbon was identical with that of one of the hydrocarbons obtained, and so it has been concluded that the hydrocarbon, with an absorption maximum at 533 nm, obtained both by authors and Clar *et al.* is dibenzoisoviolanthrene B (**4**), and not dibenzoviolanthrene B (**3**) as suggested by Clar *et al.*

Experimental

All melting points are uncorrected.

*Condensation of **1** with Copper Powder.* A mixture of **1** (2.0 g), copper powder (3.4 g), zinc chloride (17.0 g and sodium cholride (3.4 g) was kept at 270—280 °C for 1 h. The crude product was refluxed with benzene (100 ml) for 2 h and the insoluble residue, consisting mainly of copper powder, was removed by hot filtration. The filtrate on evaporation to dryness gave a dark brown solid (1.9 g). A benzene solution of this product was passed through a column of alumina and eluted with benzene. The absorbed layer was developed into three bands. The pale yellow band was separated and concentrated, giving red brown needles. Yield 0.5 g, mp 336—337 °C, $\lambda_{max}^{benzene}$ 510 nm. The intense yellow band was the recovered naphthanthrone. The pink band, overlapping with a small amount of the brown band, was eluted with benzene, and concentrated to give a pale brown solid (mp 379—380 °C). A benzene solution of this product had an absorption maximum at 533 nm and also a small shoulder at 567 nm. The melting point and absorption spectrum were very similar to that reported by Clar *et al.* The product was dissolved in a large amount of ethanol and the solution was put into a column of alumina. The absorbed layer was developed into two bands; the lower layer, a pale brown band, was separated, concentrated and gave pale brown needles. Yield 0.25 g; mp 362 °C; $\lambda_{max}^{benzene}$ 533 nm. The upper layer, an intense pink band, gave violet needles. Yield 0.17 g; mp 378—379 °C; $\lambda_{max}^{benzene}$ 567 nm.

*Synthesis of **6**.* To a mixture of potassium hydroxide (10.0 g) and phenol (1.0 g) heated at 260—270 °C, naphthanthrone (1.5 g) was added. The reaction mixture was maintained at the same temperature for 1 h, and then cooled and treated with water (500 ml). The insoluble residue was collected, suspended in water (300 ml) containing sodium hydroxide (10.0 g) and heated to 60 °C. In order to remove the dibenzoviolanthrone A (**5**), ethanol (100 ml) and sodium dithionite (10.0 g) were added. Compound **5** dissolved in the sodium dithionite forming a reddish purple solution, but **6** did not, thus enabling **6** to be separated from **5**. Subsequent hot filtration separated the insoluble material (0.8 g). This product was refluxed with glacial acetic acid (100 ml) for 2 h and the insoluble material was collected by hot filtration. Yield 0.7 g. This compound corresponds to **6**.

*Reduction of **6**.* A fine powder of **6** (0.7 g) was heated with zinc dust in a mixed flux of zinc chloride (5.0 g) at 270—280 °C for 1 h. In order to remove the excess zinc dust, concentrated hydrochloric acid (25 ml) was added to the solid suspended in water (100 ml), and the insoluble material was collected. Yield 0.6 g. The crude product was refluxed with trichlorobenzene (100 ml) for 2 h and the filtrate was evaporated to dryness, giving a dark violet solid (0.5 g). A toluene solution of this substance was passed through a column of alumina, and the eluent was evaporated to give deep violet needles. Yield 0.4 g; mp 378—379 °C; $\lambda_{max}^{benzene}$ 567 nm. Found: C, 95.65; H, 4.18%. Calcd for $C_{38}H_{18}$; C, 96.17; H, 3.83%.

*Synthesis of Dibenzoisoviolanthrone B (**9**).* A mixture of potassium hydroxide (10.0 g), phenol (2.0 g) and isopropyl alcohol (7.0 g) was heated at 170—180 °C. 2-Bromonaphthanthrone (**7**) (1.0 g) was added and the mixture was stirred for 4 h at the same temperature. The reaction mixture turned green immediately, then dark olive green, and finally blue green. The mixture was poured into water (100 ml) and oxidized by air. The precipitate was collected and suspended in water (200 ml) containing sodium hydroxide (10.0 g), ethanol (100 ml) and sodium dithionite (10.0 g), and maintained at 55—60 °C for 15 min. Compound **9** was collected by the same procedure used for the separation of **6** from **5** using sodium dithionite. After hot filtration, the insoluble material was collected. Yield 0.6 g. The product was boiled in glacial acetic acid (50 ml), cooled and the insoluble material was filtered. Yield 0.55 g. This product is assumed to be **9**.

*Reduction of **9**.* A fine powder of **9** (0.5 g) was treated with zinc dust (0.5 g) in a mixed flux of zinc chloride and sodium chloride at 270—280 °C for 1 h. The precipitate was filtered and dried. In order to remove the zinc dust, the precipitate was refluxed with toluene (100 ml) for 2 h and, after hot filtration, the filtrate was evaporated to dryness, giving a dark brown solid (0.4 g). Further purification was conducted by column chromatography of alumina with toluene.

The eluent was evaporated to dryness and gave pale brown needles. Yield 0.1 g; mp 362 °C; $\lambda_{max}^{benzene}$ 533 nm. Found: C, 95.85; H, 4.18%. Calcd for $C_{38}H_{18}$. C, 96.17; H, 3.83%.

References

1) Y. Kamura, H. Inokuchi, and J. Aoki, S. Fujisawa, *Chem. Phys. Lett.*, **46**, 356 (1977).
2) E. Clar, G. S. Fell, C. T. Ironside, and A. Balsillie, *Tetrahedron*, **10**, 26 (1960).
3) I. Oonishi, S. Fujisawa, J. Aoki, and T. Danno, *Bull. Chem. Soc. Jpn.*, **51**, 2256 (1978).
4) J. Aoki, M. Takekawa, S. Fujisawa, and S. Iwashima, *Bull. Chem. Soc. Jpn.*, **50**, 1017 (1977).
5) T. Maki and Y. Nagai, *Kogyo Kagaku Zasshi*, **37**, 493 (1934).
6) W. Bradley and F. K. Sutcliffe, *J. Chem. Soc.*, **1951**, 2118.

BULLETIN OF THE CHEMICAL SOCIETY OF JAPAN, VOL. 52 (7), 2161—2162 (1979)

Structure of the Rearrangement Product of Dihydromayurone with Boron Trifluoride in Acetic Acid–Acetic Anhydride at 50 °C

Haruo SEKIZAKI,* Masaaki ITO, and Shoji INOUE**

Chemistry Laboratory, Department of General Education, Higashi Nippon Gakuen University, Onbetsu-cho, Hokkaido 088-01

***Faculty of Pharmacy, Meijo University, Tenpaku-ku, Nagoya 468*

(Received November 24, 1978)

Synopsis. The structure of the second main product, 4-acetoxy-1,7,8-trimethyltricyclo[5.4.0.0^{4,8}]undec-9-ene, in the rearrangement reaction of dihydromayurone with boron trifluoride in acetic acid–acetic anhydride at 50 °C, and reaction mechanism is presented and discussed.

In a preceding communication,[1] the formation of four kinds of corresponding acetates in the rearrangement reaction of dihydromayurone with boron trifluoride in acetic acid–acetic anhydride, has been described and related to the reaction temperature. The reaction at 50 °C afforded 7-acetoxy-2,2,3-trimethyltricyclo[5.2.2.0^{1,6}]undec-3-ene (**1**) in 45% yield. Chromatographic analysis of the reaction mixture over silica gel using benzene as the eluant gave compound **1**[1] as a fast eluent in 45% yield, and an oily product (**2**) as slow eluent in 30% yield. The IR spectrum bands at 3060 and 1690 cm^{-1} disappeared indicating the presence of a cyclopropyl and carbonyl group, and the band at 1738 cm^{-1} indicated the presence of an ester group. The PMR spectrum contained signals at δ 1.95, 5.21, and 5.81 ppm, indicating the presence of one acetyl group and two vinyl protones. And the mass spectrum showed a molecular ion peak at *m/e* 248 (M^+), and fragment of this at *m/e* 206 (M—42). Thus, the structture of **2** has been assumed to be a isomeric acetate in which the cyclopropane ring was cleaved.

Hydrolysis of **2** with ethanolic potassium hydroxide gave the alcohol (**3**), the IR spectrum of which exibited a strong band at 3355 cm^{-1}, indicating the presence of a hydroxyl group. The PMR spectrum of one vinyl proton shows a doublet of doublets of doublets (J= 10.8, 2.5, and 2.5 Hz) at 5.18, and the other vinyl proton shows a doublet of doublets of doublets (J= 10.8, 5.0, and 3.5 Hz) at 5.78 ppm. Analysis was conducted by the decoupling technique. The C^{13}-NMR spectrum exibited the presence of C–O (δ 80.6 ppm (s)), and –CH=CH– (δ 127.8 (d) and 130.0 ppm (d)) linkages (Fig. 1).

Thus, the structure of **3** has been assigned to be a tertiary alcohol including the partial structure (**a**)

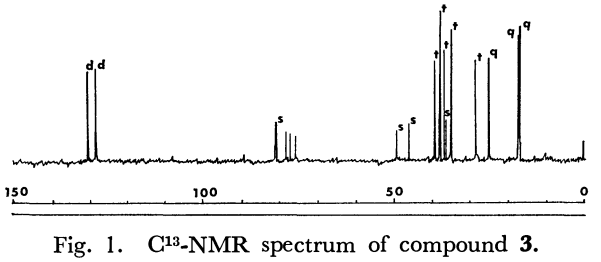

Fig. 1. C^{13}-NMR spectrum of compound **3**.

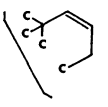

a

and tricyclic compound. This partial structure was unambiguously substantiated by the following chemical evidences. Oxidation of **3** with osmium tetraoxide in ether afforded a diol (**5**) and subsequent oxidation of **5** with lead tetraacetate gave a dialdehyde (**6**). The PMR spectrum showed signals at δ 9.73 (t, 1, J=3.0 Hz) and 9.75 ppm (s, 1), indicating the presence of two formyl groups.

An attempt was made to obtain the acetate (**2**) from the acetate (**4**)[1] under the above reaction conditions and the results indicate that **4** may be the precursor of **2**. The structure of **2** has been assumed to be 4-acetoxy-1,7,8-trimethyltricyclo[5.4.0.0^{4,8}] undec-9-ene on the basis of the above spectral data, the chemical evidence, and the reaction mechanism (Scheme 1).

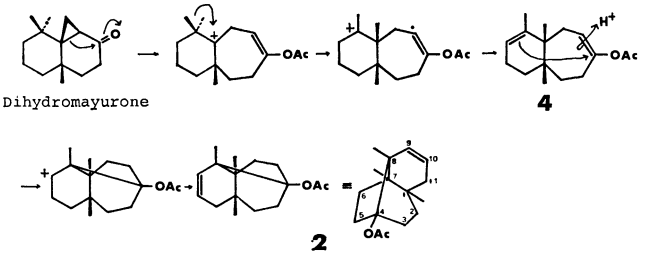

Scheme 1.

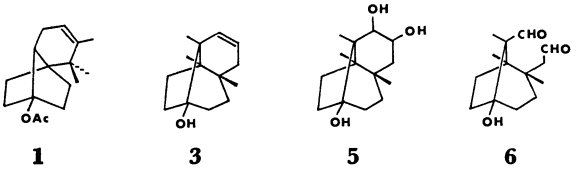

1 **3** **5** **6**

Experimental

The melting points were determined on a Yanagimoto micro melting point apparatus and are uncorrected. The PMR spectra were recorded at 60 MHz and 100 MHz on a JEOL PMX-60 and a JEOL PS-100 spectrometer respectively, using Me_4Si as an internal standard. The C^{13}-NMR spectra were recorded on a JEOL FX-100 spectrometer, using Me_4Si as an internal standard. The IR spectra were determined on a Shimadzu IR-400 spectrometer. The elemental analyses were performed on a Hitachi 026 CHN analyzer.

Isomerization of Dihydromayurone. A mixture of dihydromayurone (2.06 g, 10 mmol), acetic acid (10 ml), acetic anhydride (10 ml), and boron trifluoride etherate (2 ml, 4.5 mmol) was heated at 50 °C for 2 h. The dark brown reaction mixture was poured into ice-water (20 ml) and extracted with ether. The extract was washed with aqueous $NaHCO_3$ solution, water, dried (Na_2SO_4), and evaporated to give an oily residue (2.87 g). The products were separated by column chromatography using silica gel. Elution with benzene gave **1** (1.11 g) and **2** (0.8 g) as colorless liquids, respectively. **2**: MS *m/e* 248 (M^+) and 206 (M−42); IR (neat) ν 1738 cm^{-1}; PMR ($CDCl_3$) δ 0.81 (s, 6, $2CH_3$), 1.01 (s, 3, CH_3), 1.95 (s, 3, CH_3), 5.21 (ddd, 1, J=10.8, 2.5, and 2.5 Hz), and 5.81 (ddd, 1, J=10.8, 5.0, and 3.5 Hz).

Hydrolysis of 2. Compound **2** (1.24 g, 5 mmol) was hydrolyzed in alcohol (15 ml) with potassium hydroxide (560 mg, 10 mmol) at room temperature for 2 h. After the usual work-up a crude product (992 mg) was obtained. Recrystallization from hexane gave pure **3** (876 mg). **3**: Mp 145—148 °C; MS *m/e* 205 (M^+); IR (KBr) ν 3355 cm^{-1}; PMR ($CDCl_3$) δ 0.80 (s, 6, $2CH_3$), 1.02 (s, 3, CH_3), 5.18 (ddd, 1, J=10.8, 2.5, and 2.5 Hz), and 5.78 (ddd, 1, J=10.8, 5.0, and 3.5 Hz); C^{13}-NMR ($CDCl_3$) δ 17.0 (q), 17.2 (q), 24.9(q) 28.4(t), 34.6 (t), 35.7 (s), 36.3 (t), 37.4 (t), 39.3 (t), 45.9 (s), 49.0 (s), 80.6 (s), 127.8 (d), and 130.0 ppm (d). Found: C, 81.59; H, 10.66%. Calcd for $C_{14}H_{22}O$: C, 81.50; H, 10.75%.

Oxidation of 3 with Osmium Tetraoxide. To a stirred solution of **3** (782.8 mg, 3.8 mmol) in pyridine (2 ml) and ether (35 ml) was added dropwise a solution of osmium tetraoxide (1.0 g, 4.0 mmol) in ether (35 ml) under nitrogen at room temperature in 10 min. The mixture was subsequently stirred for 2 days. After the usual work-up a crude product (856 mg) was obtained. Recrystallization from ethyl acetate gave pure **5** (781 mg). **5**: Mp 210—212 °C; IR (KBr) ν 3350 cm^{-1}; PMR (DMSO-d_6) δ 0.72 (s, 3, CH_3), 0.97 (s, 3, CH_3), 1.05 (s, 3, CH_3), 3.57 (m, 1), and 4.61 (d, 1, J=6.0 Hz). Found: C, 70.42; H, 9.83%. Calcd for $C_{14}H_{24}O_3$: C, 69.96; H, 10.07%.

Oxidation of 5 with Lead Tetraacetate. To a stirred solution of **5** (141.2 mg, 0.6 mmol) in acetic acid (5 ml), kept at 15 °C, was added lead tetraacetate (285 mg, 0.65 mmol) in portions over 20 min. The mixture was stirred for 5 h at room temperature. The usual work-up gave a crude product (140 mg), which was chromatographed on a sillica-gel column. Elution with ethyl acetate and benzene (10:1) gave **6** (126 mg). Recrystallization from benzene gave pure **6** (105 mg) as colorless crystals. **6**: Mp 186—189 °C; IR (KBr) ν 3500, 2700, and 1703 cm^{-1}; PMR ($CDCl_3$) δ 1.02 (s, 3, CH_3), 1.10 (s, 3, CH_3), 1.15 (s, 3, CH_3), 9.73 (t, 1, -CHO, J=3.0 Hz), and 9.75 (s, 1, -CHO). Found: C, 71.08; H, 9.01%. Calcd for $C_{14}H_{22}O_3$: C, 70.55; H, 9.31%.

Isomerization of 4. A mixture of **4** (248 mg, 1 mmol), acetic acid (1.5 ml), acetic anhydride (1.5 ml), and boron trifluoride etherate (0.2 ml, 0.45 mmol) was heated at 50 °C for 2 h. The usual work-up as reported above gave **2** (178.6 mg).

Reference

1) H. Sekizaki, M. Ito, and S. Inoue, *Chem. Lett.*, **1978**, 1191.

BULLETIN OF THE CHEMICAL SOCIETY OF JAPAN, VOL. 52 (7), 2163—2164 (1979)

A Hydroxyl Proton Magnetic Resonance Study of 2-Cyclohexen-1-ols, 1-Tetralols, 4-Chromanols, and 4-Thiochromanols in Dimethyl Sulfoxide

Kaoru HANAYA,* Hideaki KUDŌ, Kazuo GOHKE,** and Shin IMAIZUMI**

Department of Chemistry, Faculty of Science, Yamagata University, Koshirakawa-cho, Yamagata 990

***Department of Applied Science, Faculty of Engineering, Tohoku University, Aramaki-Aoba, Sendai 980*

(Received January 12, 1979)

Synopsis. The proton magnetic spectra in dimethyl sulfoxide of 2-cyclohexen-1-ols, 1-tetralols, 4-chromanols, and 4-thiochromanols have been determined. In all cases, the pseudoaxial OH proton resonates at a higher field than the pseudoequatorial one. The spin-spin coupling between the hydroxyl and carbinyl protons is found to be greater for the pseudoequatorial epimer.

Dimethyl sulfoxide (DMSO) is known to be an excellent solvent for the facile observation of H–C–O–H splitting.[1] Recently two studies of the OH proton chemical shifts and coupling constants for a series of epimeric saturated cyclic alcohols have been reported.[2,3] The axial and equatorial hydroxyl groups in a saturated cyclanols can be clearly distinguished from the equatorial hydroxyl resonance at a lower field and a larger coupling constant.

However, no systematic study of the PMR spectra of α,β-unsaturated cyclanols in DMSO has yet appeared in the literature. In order to examine whether or not a relationship similar to those found in the case of the saturated cyclanols exists between the chemical shifts, coupling constants, and conformations of α,β-unsaturated cyclanols, we investigated the ^1H NMR spectra in DMSO of epimeric 2-cyclohexen-1-ols, 1-tetralols, 4-chromanols, and 4-thiochromanols in the low-concentration region, in which the chemical shift has been established as invariant. The results are summarized in Table 1. Table 1 shows the clear correlation that, in each epimeric set, the pseudoaxial OH proton resonates at a significantly higher field than its pseudoequatorial counterpart, as has previously been noted for the saturated cyclanols.[2,3] The chemical shift difference between the epimeric alcohols may be related to the solute-solvent hydrogen bonding. Hydrogen bonding is known to influence profoundly the chemical shift of a participating proton.[3] The coupling constant data in Table 1 also lend themselves to ready correlation with the conformation. In each set of epimers, the pseudoequatorial OH coupling constant is greater than that of its pseudoaxial epimers. The difference between the hydroxyl-carbinyl proton coupling constants for epimeric α,β-unsaturated cyclanols may be understood from a consideration of the conformational equilibria resulting from rotation about

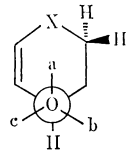

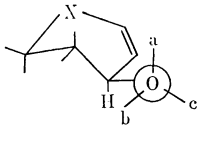

Table 1. Hydroxyl proton chemical shifts and coupling constants of epimeric α,β-unsaturated cyclanols in DMSO

Compound	Pseudoaxial alcohol		Pseudoequatorial alcohol	
	Chemical shift τ	Coupling constant J (Hz)	Chemical shift τ	Coupling constant J (Hz)
1	5.54	6.0	5.45	6.9
2	5.32	4.7	5.24	5.4
3	4.86	5.3	4.63	7.1
4	5.04	5.4	4.81	7.1
5	5.14	6.2	5.13	7.9
6	4.54	5.0	4.47	6.7
7	4.72	5.3	4.61	6.9
8	4.66	6.6	4.52	7.5
9	4.83	5.7	4.65	6.6
10	4.68	5.4	4.49	6.3
11	4.79	5.8	4.04	7.8
12	4.12	6.0	3.89	7.3
13	4.26	5.9	4.05	8.1

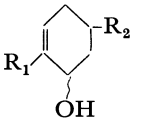

1 $R_1=CH_3$, $R_2=t$-Bu
2 $R_1=H$, $R_2=C_6H_5$

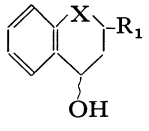

3 $X=CH_2$, $R_1=C_6H_5$
4 $X=CH_2$, $R_1=CH_3$
6 $X=O$, $R_1=C_6H_5$
7 $X=O$, $R_1=CH_3$
10 $X=S$, $R_1=CH_3$
12 $X=SO_2$, $R_1=CH_3$

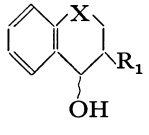

5 $X=CH_2$, $R_1=C_6H_5$
8 $X=O$, $R_1=C_6H_5$
9 $X=O$, $R_1=CH_3$
11 $X=S$, $R_1=CH_3$
13 $X=SO_2$, $R_1=CH_3$

the C–O bond.[2-4] The contribution of the **a**-type conformation, in which the OH bond is directed towards the center of the cyclohexene, dihydropyran, or dihydrothiopyran ring, may be smaller in the OH pseudoaxial epimer because of the 1,3-diaxial interaction.[5] Assuming that the H–C–O–H coupling constants vary with the dihedral angle in a manner similar to that for the H–C–C–H system, Rader *et al.*,[2] Sehgal *et al.*,[3] and Fraser *et al.*[6] were led to the conclusion that an equatorial alcohol should have a larger coupling constant than its axial epimer because of the greater contribution of the anti conformer, **a**, in the former.

From the present study, it is significant that, in view of the characteristic chemical shift differences and coupling constants, the NMR technique in DMSO can be used to distinguish not only the epimers of saturated cyclanols, but also those of α,β-unsaturated cyclanols. These observations appear to provide direct experimental evidence for the configuration and conformations of these epimers.

Experimental

Materials. All the compounds employed in this work have been previously reported: **1**,[7] **2**,[8] **3**,[9] **4**,[9] **5**,[10] **6**,[11] **7**,[12] **8**,[13] **9**,[14] and **10**—**13**.[15] The conformations of 2-cyclohexen-1-ols,[7] 1-tetralols,[5,16,17] 4-chromanols,[5,12,13,15,16] and 4-thiochromanols[15] were examined by means of their ^{1}H NMR, ^{13}C NMR, and IR spectra.

NMR Spectra. All the ^{1}H NMR spectra were taken with either a Hitachi H-60 or R-24B spectrometer at a probe temperature of 30 °C, unless otherwise noted. Tetramethylsilane was used as the internal standard; the concentrations were *ca.* 2×10^{-2} in the mole fraction.

References

1) O. L. Chapman and R. W. King, *J. Am. Chem. Soc.*, **86**, 1256 (1964).
2) C. P. Rader, *J. Am. Chem. Soc.*, **88**, 1713 (1966).
3) R. K. Sehgal, R. U. Koenigsberger, and T. J. Howard, *Tetrahedron Lett.*, **1974**, 4173.
4) J. J. Uebel and H. W. Goodwin, *J. Org. Chem.*, **31**, 2040 (1966).
5) H. Iwamura and K. Hanaya, *Bull. Chem. Soc. Jpn.*, **43**, 3901 (1970).
6) R. R. Fraser, M. Kaufman, and P. Morand, *Can. J. Chem.*, **47**, 403 (1969).
7) Y. Senda, S. Imaizumi, S. Ochiai, and K. Fujita, *Tetrahedron*, **30**, 539 (1974).
8) K. Hanaya, *Nippon Kagaku Zasshi*, **91**, 82 (1970).
9) K. Hanaya, *Nippon Kagaku Zasshi*, **87**, 995 (1966).
10) K. Hanaya, *Nippon Kagaku Zasshi*, **87**, 745 (1966).
11) S. Mitsui and A. Kasahara, *Nippon Kagaku Zasshi*, **79**, 1382 (1958).
12) K. Hanaya and K. Furuse, *Nippon Kagaku Zasshi*, **89**, 1002 (1968).
13) S. Yamaguchi, S. Ito, A. Nakamura, and N. Inoue, *Bull. Chem. Soc. Jpn.*, **38**, 2187 (1965).
14) K. Hanaya, *Bull. Chem. Soc. Jpn.*, **43**, 442 (1970).
15) K. Hanaya, S. Onodera, S. Awano, and H. Kudo, *Bull. Chem. Soc. Jpn.*, **47**, 509 (1974).
16) Y. Senda, J. Ishiyama, S. Imaizumi, and K. Hanaya, *J. Chem. Soc., Perkin Trans. 1*, **1977**, 217.
17) S. Mitsui, A. Kasahara, and K. Hanaya, *Bull. Chem. Soc. Jpn.*, **41**, 2526 (1968).

BULLETIN OF THE CHEMICAL SOCIETY OF JAPAN, VOL. 52 (7), 2165—2166 (1979)

Asymmetric Reactions. IV. Asymmetric, Catalytic Activity of Poly(2-quinuclidinylmethyl acrylate)

Tetsushi YAMASHITA,* Hiroshi YASUEDA, and Nobuo NAKAMURA

Department of Chemistry, Faculty of Science, Osaka City University, Sugimoto-cho, Sumiyoshi-ku, Osaka 558

(Received January 12, 1979)

Synopsis. The asymmetric addition of methanol to phenylmethylketene has been conducted in the presence of poly(2-quinuclidinylmethyl acrylate) and 2-quinuclidinylmethyl propionate derived from (*S*)-2-quinuclidinylmethanol. The asymmetric functions of the above catalysts were similar to those of poly(*O*-acryloylquinine) and *O*-propionylquinine, which contain a quinoline ring and a vinyl group as additional groups to the quinuclidine ring.

Several workers[1-3] have recently studied asymmetric, catalytic reactions using chiral polymers derived from cinchona alkaloids. Cinchona alkaloids (**A**) consist of four asymmetric carbons (C_3, C_4, C_8, and C_9) and three main functional groups (a quinuclidinyl, a vinyl and a quinolyl group). In this paper, poly(2-quinuclidinylmethyl acrylate) (**HB**) and 2-quinuclidinylmethyl propionate (**LB**) were used to clarify the role of the quinuclidinyl group as an active site in cinchona alkaloid catalysts.

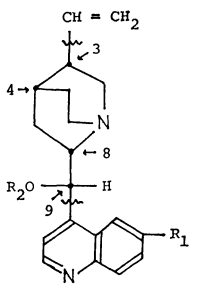

(A)

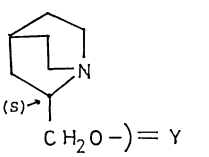

HB; $-(CH_2-CH)_n-CO-Y$
MB; $CH_2=CH-CO-Y$
LB; CH_3CH_2-CO-Y

(B)

High- or low-molecular-weight catalysts (**HB** or **LB**) have been prepared by the acylation of (*S*)-2-quinuclidinylmethanol, which was obtained by reduction of (*S*)-2-(ethoxycarbonyl)quinuclidine with lithium aluminum hydride; (*S*)-2-(ethoxycarbonyl)quinuclidine was obtained by optical resolution[4] of the racemic mixture[5,6] derived from 4-methylpyridine.

(*S*)-2-Quinuclidinylmethanol was allowed to react with propionic anhydride or acryloyl chloride giving 2-quinuclidinylmethyl propionate (**LB**) or 2-quinuclidinylmethyl acrylate (**MB**) respectively. A soluble polymer (**HB**) was obtained by the polymerization of **MB** using a catalytic amount of azobisisobutyronitrile as initiator. The catalytic activities of **LB** and **HB** have been examined for the asymmetric synthesis of methyl 2-phenylpropionate. The addition of methanol to phenylmethylketene has been conducted according to an earlier report.[1]

$$\mathrm{Ph-\underset{\displaystyle CH_3}{\underset{|}{C}}=C=O + CH_3OH \xrightarrow{\text{Catalyst}} Ph-\underset{\displaystyle CH_3}{\underset{|}{CH}}-COOCH_3}$$

Figure 1 shows plots of the optical purities (O.P.) of the addition products against reaction temperatures (T °C) for **HB** and **LB**. The results[1a] obtained previously with poly(*O*-acryloylquinine) (**HA**) and *O*-propionylquinine (**LA**) are also shown in Fig. 1 [Quinine catalysts (**A**): C_8, *S*-configuration; $R_1=OCH_3$; $R_2=$ acyl group].

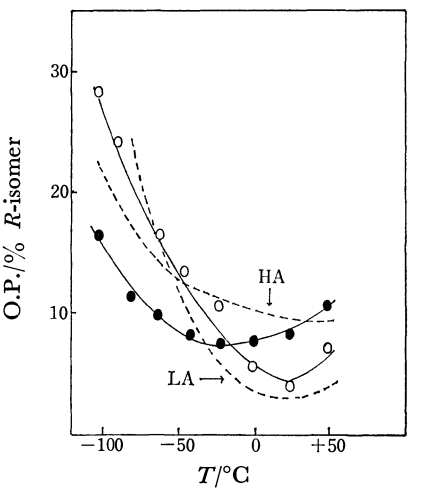

Fig. 1. Plots of optical purities[a] (O. P.) against reaction temperatures (T °C) in case of **HB** (●) and **LB** (○) (catalyst[b]: 0.025 mmol, phenylmethylketene: 2.500 mmol, methanol: 2.600 mmol, solvent: 25 ml of dry toluene).
a) The optical purity was calculated from the specific rotation of the product and that of optically pure methyl 2-phenylpropionate[1a] (*S*-form, $[\alpha]_D^{22}$ +109° in toluene). b) The molar equivalent amount of the polymeric catalyst was calculated on the basis of that of the monomer used in the polymerization.

All of the catalysts described above gave the addition products showing preference to the *R*-isomer in the range from −100 °C to +50 °C. Figure 1 also indicates that **HB** yielded a higher predominance of addition products with *R*-configuration than did **LB** above 0 °C. This sort of polymer effect was similar to that observed with quinine catalysts (**HA** and **LA**) above −50 °C.

Figure 1 suggests that the asymmetric functions of 2-quinuclidinylmethanol catalysts do not greatly differ from those of the quinine catalysts.

These results suggest that the configuration at C_8 of the quinuclidinyl group in cinchona alkaloid catalysts is very important in determining the configuration of products.

Experimental

A JASCO IRA-1 (IR) apparatus, a JEOL-60 MC (NMR)

apparatus, a Hitachi M52 (MS) apparatus, a Rex-automatic polarimeter (optical rotation, 10 cm cell) and a Knauer vapor pressure osmometer (molecular weight) were used.

*(S)-2-Quinuclidinylmethyl Acrylate (**MB**).* Powdered sodium hydroxide (2.25 mmol) was suspended in a solution of (*S*)-2-quinuclidinylmethanol[6] (1.50 mmol) in dry dichloromethane (15 ml) in argon at −10 °C. To the mixture was added a solution of acryloyl chloride (1.80 mmol) in dry dichloromethane (5 ml). The reaction mixture was stirred for 20 h at the same temperature and the precipitate filtered. The filtrate was dried and evaporated to dryness and the residue subjected to column chromatography on alumina (2×10 cm, 200 mesh, neutral). Elution with chloroform gave **MB** as an oily material which was distilled to give a colorless oil. Yield, 60%. Bp 100 °C at 1 mmHg. $[\alpha]_D^{24}$ −60° (*c* 1.23, benzene); IR (neat): 1727, 1632, 995 cm^{-1}; ^1H NMR ($CDCl_3$) δ=5.64—6.46 ppm; MS *m/e* 195 (M^+).

*Poly(2-quinuclidinylmethyl acrylate) (**HB**).* A solution of 2-quinuclidinylmethyl acrylate (80 mg) and azobisisobutyronitrile (3 mg) in dry benzene (0.4 ml) was polymerized at 80 °C for 40 h in a sealed tube filled with argon. The product was poured into ether, and the precipitate filtered and washed with ether. Yield, 60%. $[\alpha]_D^{16}$ −47° (*c* 1.3, benzene); mol wt 5850 (benzene).

*(S)-2-Quinuclidinylmethyl Propionate (**LB**).* **LB** was obtained in 75% yield as a colorless oil by the reaction of (*S*)-2-quinuclidinylmethanol with propionic anhydride in the presence of triethylamine. Bp 105 °C at 3 mmHg. $[\alpha]_D^{20}$ −50.8° (*c* 0.96, benzene); IR (neat): 1740, 1188, 1058 cm^{-1}; ^1H NMR ($CDCl_3$) δ=2.37, 1.13 ppm; MS *m/e* 197 (M^+).

References

1) a) T. Yamashita, H. Yasueda, and N. Nakamura, *Chem. Lett.*, **1974**, 585; b) T. Yamashita, H. Yasueda, Y. Miyauchi, and N. Nakamura, *Bull. Chem. Soc. Jpn.*, **50**, 1532 (1977); c) T. Yamashita, H. Yasueda, N. Nakatani, and N. Nakamura, *ibid.*, **51**, 1183 (1978); d) T. Yamashita, H. Yasueda, and N. Nakamura, *ibid.*, **51**, 1247 (1978).

2) K. Hermann and H. Wynberg, *Helv. Chim. Acta*, **60**, 2208 (1977).

3) N. Kobayashi and K. Iwai, *J. Am. Chem. Soc.*, **100**, 7071 (1978).

4) H. Pracejus and G. Kohl, *Ann. Chem.*, **722**, 1 (1969).

5) a) E. Renk and C. A. Grob, *Helv. Chim. Acta*, **37**, 2119 (1954); b) M. Kleinman and S. Weinhouse, *J. Org. Chem.*, **10**, 562 (1945).

6) a) B. Langstrom, *Chem. Scr.*, **5**, 170 (1974); b) B. Langstrom and G. Gergson, *Acta Chim. Scand.*, **27**, 3118 (1973).

BULLETIN OF THE CHEMICAL SOCIETY OF JAPAN, VOL. 52 (7), 2167—2168 (1979)

Synthesis of (*S,S*)-2-Amino-3-phenylbutyric Acid

Gen-ichi TSUCHIHASHI,* Shuichi MITAMURA, and Katsuyuki OGURA

Sagami Chemical Research Center, Nishi-Ohnuma, Sagamihara, Kanagawa 229

(Received January 20, 1979)

Synopsis. (*S,S*)-2-Amino-3-phenylbutyric acid was synthesized starting from diethyl (*R*)-(1-phenylethyl)malonate which was obtained by desulfurization of the adduct in the stereoselective Michael reaction of (*R*)-styryl *p*-tolyl sulfoxide with diethyl malonate. This synthetic amino acid was identical with the 2-amino-3-phenylbutyric acid obtained by degradation of bottromycin and thus the absolute configuration of the naturally occurring amino acid was proved to be (*S,S*).

In 1957, (—)-2-amino-3-phenylbutyric acid [(—)-**1**] was reported to be a component of bottromycin which was isolated from a culture of *Streptomyces bottropensis*.[1]

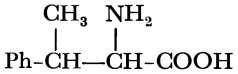

1

Since this amino acid contains two chiral centers, four isomers [(2*R*,3*R*), (2*R*,3*S*), (2*S*,3*R*), and (2*S*,3*S*)] are possible. As to the absolute configuration at the 2-position, (*S*) was suggested, based on the positive Cotton effect in the ORD of its *N*-ethylthiothiocarbonyl derivative, the resistance against a D-amino acid oxidase,[2] and the application of the Clough, Lutz, and Jirgensons rule to the optical rotatory powers of the amino acid and its derivatives.[3] Later, the diastereomeric relationship between the 2- and 3-positions was determined to be erythro by the chemical transformation[3] and the NMR study.[4]

We previously synthesized diethyl (*R*)-(1-phenylethyl)malonate [(*R*)-**2**] by desulfurization of diethyl (*R,R*)-[1-phenyl-2-(*p*-tolylsulfinyl)ethyl]malonate, which was obtained by the stereoselective Michael reaction of (*R*)-styryl *p*-tolyl sulfoxide with diethyl malonate.[5,6] Now, we have synthesized (*S,S*)-**1** starting from this (*R*)-**2** according to the Fischer's method[7-9] as shown in Scheme 1 and have found that the naturally occurring **1** is identical with this (*S,S*)-**1**.

(*R*)-(1-Phenylethyl)malonic acid [(*R*)-**3**], which was obtained by hydrolysis of (*R*)-**2** in 88% yield, was subjected to bromination with bromine–red phosphorus to give (*S*)-bromo(1-phenylethyl)malonic acid [(*S*)-**4**]. Thermal decarboxylation of (*S*)-**4** afforded a crystalline product which was recrystallized from benzene to give pure (*S,S*)-2-bromo-3-phenylbutyric acid [(*S,S*)-**5**; 40% overall yield from (*R*)-**3**]:[9] mp 167—168 °C; $[\alpha]_D^{30}$ −31.4° (*c* 0.327, benzene). Treatment of (*S,S*)-**5** with aqueous ammonia gave a mixture of (*S,S*)-2-amino-3-phenylbutyric acid [(*S,S*)-**1**] and ammonium bromide. This mixture was subjected to the reaction with acetic anhydride–1 M aqueous sodium hydroxide[1b] to afford (*S,S*)-2-acetylamino-3-phenylbutyric acid [(*S,S*)-**6**; 95% yield from (*S,S*)-**5**]: mp 188—190 °C (from 20% ethanol); $[\alpha]_D^{29}$ +34.8° (*c* 0.810, 96% ethanol). These values agree well with those reported

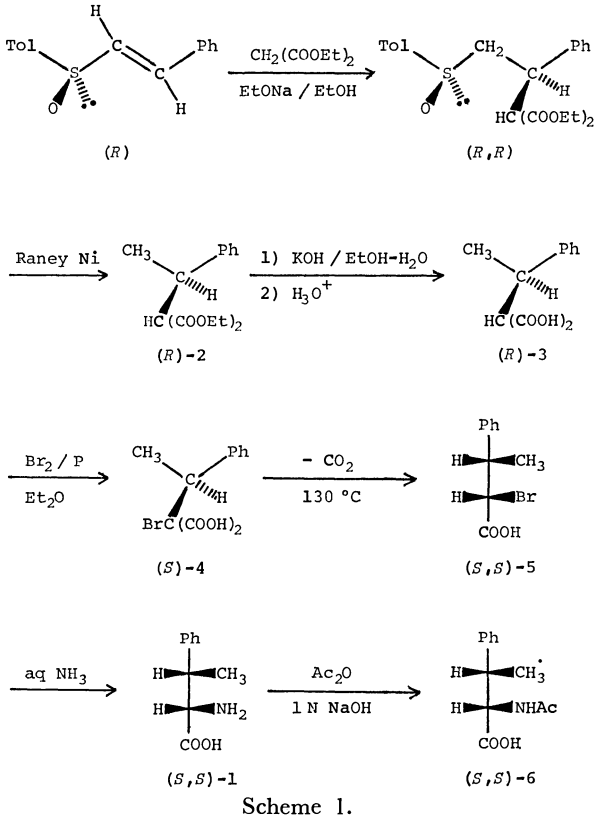

Scheme 1.

for the *N*-acetyl derivative of the naturally occurring **1** [mp 177—185 °C (from 20% ethanol) and $[\alpha]_D^{25}$ +35.0° (*c* 2%, 96% ethanol)].[1b]

The starting material of the present synthesis, (*R*)-**2**, was already connected to (—)-3-phenylbutyric acid,[5] whose absolute configuration was determined as (*R*) by the comparison with the authentic specimen synthesized from (*S*)-hydratropic acid.[10] Based on these relations, the present synthesis clearly established that the absolute configuration of the 2-amino-3-phenylbutyric acid from bottromycin is (*S,S*).

Experimental

All melting points were measured by a Yanagimoto micro melting point apparatus and uncorrected. Infrared spectra were taken on a Hitachi EPI-G3 spectrophotometer. NMR spectra were recorded on Varian T-60 and Varian HA-100 spectrometers. Optical rotations were measured on a Yanagimoto polarimeter OR 50.

Hydrolysis of (R)-*2*. To a solution of 472 mg (1.79 mmol) of (*R*)-**2** having $[\alpha]_D^{26}$ −21.0° (*c* 2.365, $CHCl_3$)[11] in 6 ml of ethanol, were added 3 ml of water and 550 mg of potassium hydroxide and the reaction mixture was stirred at 100 °C for 3 h. After cooling, 20 ml of water was added and the mixture was washed with dichloromethane (10 ml). The aqueous layer was acidified by adding concd hydrochloric

acid and extracted with diethyl ether (20 ml×4). The extract was washed with water (10 ml) and dried (Na_2SO_4). After evaporation *in vacuo*, the crystalline residue was recrystallized from benzene to afford 328 mg (88% yield) of (*R*)-**3** as colorless crystals: mp 94—96 °C; $[\alpha]_D^{21}$ −30.1° (*c* 0.866, methanol); IR (KBr): 3500—2800, 1740, 1695, 1220, 1200, 1155, 760, and 700 cm^{-1}; NMR ($CDCl_3$): δ=1.34 (3H, d, J=6 Hz), 3.2—3.8 (2H, m), 7.27 (5H, s), and 12.70 (2H, s). The NMR spectrum was identical with that of the racemic compound.[5,7]

Transformation of (R)-***3*** *into* (S,S)-***5*** via (S)-***4***. To a solution of 237 mg (1.14 mmol) of (*R*)-**3** in 5 ml of diethyl ether, were added a solution of 184 mg of bromine in 0.8 ml of dichloromethane and 1 mg of red phosphorus and the mixture was stirred for 45 min at room temperature. After reduction of remaining bromine by adding aqueous sodium thiosulfate, the mixture was extracted with diethyl ether (15 ml×4). The extract was dried ($MgSO_4$) and evaporated *in vacuo* to give crude (*S*)-**4** as an oil: NMR ($CDCl_3$): δ= 1.62 (3H, d, J=7 Hz), 3.77 (1H, q, J=7 Hz), 7.32 (5H, m), and 10.50 (2H, broad s). This oil was heated at 130 °C for 15 min under reduced pressure (*ca.* 20 Torr). The resulting crystalline product was recrystallized from benzene to give 105 mg (40% yield[9]) from (*R*)-**3**) of (*S,S*)-**5** as colorless crystals: mp 167—168 °C; $[\alpha]_D^{30}$ −31.4° (*c* 0.327, benzene); NMR (acetone-d_6): δ=1.43 (3H, d, J=7 Hz), 3.41 (1H, dq, J=10 and 7 Hz), 4.57 (1H, d, J=10 Hz), and 7.2—7.5 (5H, m). The NMR spectrum was identical with that of the racemic specimen.[7]

Synthesis of (S,S)-***6***. A mixture of 105 mg (0.43 mmol) of (*S,S*)-**5** and 4 ml of 28% aqueous ammonia was heated in a sealed tube at 90 °C for 2.5 h and then concentrated *in vacuo* to yield a mixture of (*S,S*)-**1** and ammonium bromide. After addition of 2.5 ml of 1 M aqueous sodium hydroxide to the above mixture, 0.15 ml of acetic anhydride and 1.3 ml of 1 M aqueous sodium hydroxide were simultaneously added over 5 min and the mixture was stirred for 1 h under ice-cooling. After simultaneous addition of 0.15 ml of acetic anhydride and 3 ml of 1 M aqueous sodium hydroxide, the resulting mixture was further stirred for 30 min under ice-cooling, acidified to pH 1 with concd hydrochloric acid, and extracted with ethyl acetate (15 ml×4). The extract was dried ($MgSO_4$) and evaporated *in vacuo* to afford 91 mg (95% yield) of (*S,S*)-**6** as colorless crystals: mp 188—190 °C (from 20% ethanol), $[\alpha]_D^{29}$ +34.8° (*c* 0.810, 96% ethanol) [lit,[1b] mp 177—185 °C (from 20% ethanol), $[\alpha]_D^{25}$ +35.0° (*c* 2%, 96% ethanol)]; IR (KBr): 3330, 1710, 1610, 1550, 1265, 765, 705, and 695 cm^{-1}; NMR (DMSO-d_6): δ=1.19 (3H, d, J=7 Hz), 1.68 (3H, s), 2.9—3.3 (1H, m), 4.42 (1H, t, J=8 Hz, 7.19 (5H, s), and 7.85 (1H, diffused d, J=8 Hz, NH). The NMR spectrum was identical with that of the racemic compound.[1c]

References

1) a) J. M. Waisvisz, M. G. van der Hoeven, J. van Peppen, and W. C. M. Zwennis, *J. Am. Chem. Soc.*, **79**, 4520 (1957); b) J. M. Waisvisz, M. G. van der Hoeven, J. F. Hölscher, and B. te Nijenhuis, *ibid.*, **79**, 4522 (1957); c) J. M. Waisvisz, M. G. van der Hoeven, and B. te Nijenhuis, *ibid.*, **79**, 4524 (1957).

2) S. Nakamura, T. Chikaike, H. Yonehara, and H. Umezawa, *Chem. Pharm. Bull.*, **13**, 599 (1965).

3) a) H. Arold, M. Eule, and S. Reissmann, *Z. Chem.*, **9**, 447 (1969); b) H. Arold, S. Reissmann, and M. Eule, *J. Prakt. Chem.*, **316**, 93 (1974).

4) Y. Kataoka, Y. Seto, M. Yamamoto, T. Yamada, S. Kuwata, and H. Watanabe, *Bull. Chem. Soc. Jpn.*, **49**, 1081 (1976).

5) G. Tsuchihashi, S. Mitamura, S. Inoue, and K. Ogura, *Tetrahedron Lett.*, **1973**, 323.

6) G. Tsuchihashi, S. Mitamura, and K. Ogura, *Tetrahedron Lett.*, **1976**, 855.

7) a) E. Fischer and W. Schmitz, *Chem. Ber.*, **39**, 351 (1906); b) E. Fischer and W. Schmitz, *ibid.*, **39**, 2208 (1906); c) F. Knoop and H. Hoessli, *ibid.*, **39**, 1477 (1906).

8) The identification of the synthetic **1** obtained by Fischer and Schmitz[7] with the naturally occurring **1** was unequivocally established.[1,3]

9) Fischer and Schmitz reported that the decarboxylation of racemic **4** resulted in the formation of a single compound (75% yield) which melted at 188—190 °C.[7] This compound was determined to have erythro, *i.e.* (*S,S*/*R,R*), configuration.[3] We traced Fischer's experiment and obtained the following results. When racemic **4** was heated at 130 °C under reduced pressure (*ca.* 20 Torr), carbon dioxide gas evolved, giving a crystalline material which was recrystallized from benzene to afford (*S,S*/*R,R*)-**5** (53% yield): mp 187—189 °C. Its NMR spectrum was in complete agreement with that of (*S,S*)-**5**. The mother liquor was concentrated *in vacuo* to give an oily residue (44% yield), which was shown by an NMR analysis to consist of (*S,S*/*R,R*)-**5** and (*S,R*/*R,S*)-**5** in a ratio of 1:2 [NMR of (*S,R*/*R,S*)-**5** (acetone-d_6): δ=1.53 (3H, d, J=7 Hz), 3.41 (1H, dq, J=10 and 7 Hz), 4.61 (1H, d, J=10 Hz), and 7.2—7.5 (5H, m)]. Thus, the ratio of (*S,S*/*R,R*)-**5**: (*S,R*/*R,S*)-**5** in the crude product can be calculated to be *ca.* 7:3.

10) V. Prelog and H. Scherrer, *Helv. Chim. Acta*, **42**, 2227 (1959).

11) This material was synthesized according to the previously reported method.[5]

BULLETIN OF THE CHEMICAL SOCIETY OF JAPAN, VOL. 52 (7), 2169—2170 (1979)

A Facile Synthesis of 4,5-Dialkoxy-*o*-benzoquinones by the Oxidation of Catechol with Iodates in Alcohol

Yuji ITOH, Takuya KAKUTA, Masao HIRANO, and Takashi MORIMOTO*

Department of Industrial Chemistry, Faculty of Engineering, Tokyo University of Agriculture and Technology, Koganei, Tokyo 184

(Received January 27, 1979)

Synopsis. 4,5-Dimethoxy-*o*-benzoquinone has been prepared by the oxidation of catechol with sodium iodate in methanol. In higher alcohols, the same oxidation occurs in the presence of a crown ether to give the corresponding 4,5-dialkoxy-*o*-benzoquinones. In the latter cases using 18-crown-6, the potassium salt is more effective than the sodium salt.

o-Benzoquinone derivatives are conventionally prepared by the oxidation of the corresponding catechols. Wanzlick and Jahnke have reported the preparation of 4,5-dimethoxy- and 4,5-diethoxy-*o*-benzoquinones by the oxidation of catechol with lead(IV) oxide in methanol and ethanol, respectively, in the presence of alkoxide.[1]

In this note, a novel and simple method for the synthesis of 4,5-dialkoxy-*o*-benzoquinones from catechol will be reported using potassium and sodium iodates as oxidizing agents in alcohols from methyl to pentyl alcohol as solvents in the presence or absence of a crown ether. The products, except for dimethoxy and diethoxy derivatives, are unknown. 4-Substituted catechols have been oxidized with iodates to the corresponding quinones,[2,3] but to date there has been no report on the oxidation of unsubstituted catechol with the oxidants.

Results and Discussion

A mixture of catechol and two equivalents of sodium iodate in absolute methanol at 60 °C gradually darkened and became black after 20 h. Isolation by column chromatography gave 4,5-dimethoxy-*o*-benzoquinone (**2a**) in 58.3% yield. The structure of the quinone was elucidated from the spectral data and elemental analysis. The NMR spectrum of **2a** showed a singlet at τ=4.2 (2H; olefinic protons at C-3 and C-6) and a singlet at τ=6.1 (6H; methyl protons). The UV spectrum showed peaks at 413 nm (ε=560) and 287 nm (ε=12500). These data are consistent with those reported by Wanzlick and Jahnke.[1]

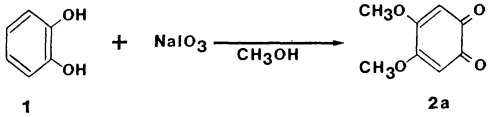

1 2a

The use of potassium iodate as the oxidant decreased the yield of the quinone to 36.9%.

The oxidation of catechol with sodium or potassium iodate in ethanol gave 4,5-diethoxy-*o*-benzoquinone (**2b**) in very low yield (less than 2% in both cases). No reaction occurred in propyl and higher alcohols.

The observation that the yield of the quinone decreases with the length of the alcohol chain is ascribed to the decrease in the solubility of the iodates in alcohols. Crown ethers have been well-known to enhance the solubility of inorganic salts in organic solvents,[4,5] and consequently the effect of 18-crown-6 has been examined using potassium iodate as the oxidant. The addition of 18-crown-6 (2.33 mmol) to the mixture of catechol (10 mmol) and potassium iodate (20 mmol) in absolute methanol (100 ml) increased the yield of **2a** to 49.2%. The effect was more dramatic in ethanol. Under similar conditions, the addition of 1.25 and 2.73 mmol of the crown ether gave **2b** in 20.7 and 44.4% yields, respectively.

The same method was employed for the preparation of several 4,5-dialkoxy-*o*-benzoquinones in higher alcohols.

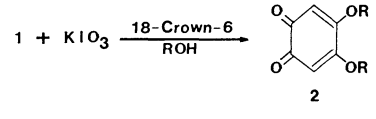

2

a, R=CH_3 (49.2%)
b, R=C_2H_5 (44.4%)
c, R=n-C_3H_7 (35.3%)
d, R=n-C_4H_9 (31.1%)
e, R=i-C_4H_9 (30.7%)
f, R=n-C_5H_{11} (26.4%)
g, R=i-C_5H_{11} (43.3%)

In primary alcohols, catechol reacted with iodate to give the corresponding dialkoxy-quinones. All of the quinones exhibited a singlet at τ=4.2 in the NMR spectra and two peaks in the 413—416 and 289—291 nm region of the UV spectra.

In the alcohols which branched at the α-position of the hydroxyl group, *e.g.*, isopropyl and *t*-butyl alcohols, however, the reaction did not give the corresponding dialkoxy-*o*-benzoquinone derivative but a red amorphous solid. A similar product was obtained from the reaction in acetonitrile. In both cases, the IR spectrum of the product showed two absorption bands in the region of 1600—1700 cm^{-1}, possibly due to carbonyl groups. The solid however could not be purified because of the low solubility in organic solvents and a broad melting range.

There are few reports of the oxidation of substituted catechols by iodates to quinone derivatives in water and in water–alcohol mixtures during a short reaction period.[2,3] In such experiments here the products were complex substances which could not be separated.

Experimental

Melting points were determined with a Yamato Capillary Melting Point apparatus and are uncorrected. Proton magnetic resonance spectra were obtained on a JEOL Model JNM-C-HL spectrometer in deuterated chloroform. Electronic spectra were recorded on a Hitachi 124 spectrophotometer in ethanol. The alcohols were purified by distillation after drying over molecular sieves 4A. All other materials

were commercially available.

*Preparation of 4,5-Dimethoxy-o-benzoquinone (**2a**).* Sodium iodate (4.0 g, 20 mmol) was suspended in a solution of catechol (1.1 g, 10 mmol) in dry methanol (100 ml) and the mixture vigorously stirred for 20 h at 60 °C. After filtration, the filtrate was condensed on a rotary evaporator under reduced pressure to a volume of *ca.* 30 ml and cooled to −15 °C. The precipitate formed was filtered and washed with diethyl ether (50 ml). The precipitate was separated by column chromatography using silica gel (*ca.* 11 g) and chloroform. Evaporation of the solvent from the first orange elute gave orange needles (0.98 g, 58.3%), which were recrystallized from methanol: mp 230—233 °C (lit, 225—227 °C).[1] Found: C, 57.85; H, 4.74%. Calcd for $C_8H_8O_4$: C, 57.15; H, 4.80%.

*Preparation of 4,5-Diethoxy-o-benzoquinone (**2b**).* Potassium iodate (4.3 g, 20 mmol) was suspended in a solution of catechol (1.1 g, 10 mmol) and 18-crown-6 (0.72 g, 2.73 mmol) in absolute ethanol (100 ml) and the mixture vigorously stirred for 20 h at 65 °C. After filtration, the alcohol was evaporated under reduced pressure and the residue extracted twice with benzene (100 ml). The combined extracts were filtered and concentrated. The residual red-brown substance was further extracted with diethyl ether (150 ml). The residue was separated by column chromatography using silica gel and chloroform. Evaporation of the solvent from the first orange elute gave orange needles (0.87 g, 44.4%), which were recrystallized from ethanol: mp 172—174.5 °C (lit, 175 °C).[1] NMR ($CDCl_3$) τ=8.5 (6H, t), 5.9 (4H, q) and 4.25 (2H, s); UV_{max} (C_2H_5OH) 289 (ε=13700) and 416 nm (ε=535). Found: C, 61.60; H, 5.75%. Calcd for $C_{10}H_{12}O_4$: C, 61.22; H, 6.17%.

Preparation of the 4,5-Dialkoxy-o-benzoquinones. The method described for the preparation of diethoxy derivative (**2b**) was employed except that the reaction was conducted in the corresponding alcohol at 90—95 °C. The physical properties are as follows;

*4,5-Dipropoxy-o-benzoquinone (**2c**).* Mp 153—154.5 °C from CCl_4. NMR ($CDCl_3$) τ=8.95 (6H, t), 8.1 (4H, m), 6.0 (4H, t), and 4.25 (2H, s); UV_{max}(C_2H_5OH) 290 (ε=14000) and 415 nm (ε=532). Found: C, 65.20; H, 7.25%. Calcd for $C_{12}H_{16}O_4$: C, 64.29; H, 7.19%.

*4,5-Dibutoxy-o-benzoquinone (**2d**).* Mp 140.5—142 °C from CCl_4. NMR ($CDCl_3$) τ=9.0 (6H, t), 8.1 (8H, m), 6.0 (4H, t), and 4.3 (2H, s); UV_{max}(C_2H_5OH) 291 (ε=12800) and 414 nm (ε=487). Found: C, 67.18; H, 8.20%. Calcd for $C_{14}H_{20}O_4$: C, 66.65; H, 7.99%.

*4,5-Diisobutoxy-o-benzoquinone (**2e**).* Mp 157.5—159 °C from CCl_4. NMR ($CDCl_3$) τ=8.95 (12H, d), 7.95 (2H, m), 6.25 (4H, t), and 4.3 (2H, s); UV_{max}(C_2H_5OH) 290 (ε=13800) and 414 nm (ε=512). Found: C, 66.29; H, 7.89%. Calcd for $C_{14}H_{20}O_4$: C, 66.65; H, 7.99%.

*4,5-Bis(pentyloxy)-o-benzoquinone (**2f**).* Mp 130—131 °C from CCl_4–petroleum ether. NMR ($CDCl_3$) τ=9.0 (6H, t), 8.4 (12H, m), 6.0 (4H, t), and 4.3 (2H, s); UV_{max}(C_2H_5OH) 291 (ε=13400) and 413 nm (ε=496). Found: C, 68.36; H, 8.99%. Calcd for $C_{16}H_{24}O_4$: C, 68.55; H, 8.63%.

*4,5-Bis(isopentyloxy)-o-benzoquinone (**2g**).* Mp 119—120 °C from CCl_4–petroleum ether. NMR ($CDCl_3$) τ=9.0 (12H, d), 8.25 (6H, m), 5.95 (4H, t), and 4.3 (2H, s); UV_{max} (C_2H_5OH) 290 (ε=13800) and 414 nm (ε=512). Found: C, 68.61; H, 8.72%. Calcd for $C_{16}H_{24}O_4$: C, 68.55; H, 8.63%.

The authors wish to thank Mrs. Junko Takizawa and Mrs. Michiko Asuke of Tokyo University of Agriculture and Technology for the NMR measurements and elemental analysis.

References

1) H-W. Wanzlick and U. Jahnke, *Chem. Ber.*, **101**, 3744 (1968).
2) J. M. Bruce, *J. Chem. Soc.*, **1959**, 2366.
3) J. D. Bu'Lock and J. Harley-Mason, *J. Chem. Soc.*, **1951**, 2248.
4) C. J. Pedersen and H. K. Frensdorff, *Angew. Chem.*, **84**, 16 (1972).
5) J. J. Christensen, D. J. Eatough, and R. M. Izatt, *Chem. Rev.*, **74**, 351 (1974).

BULLETIN OF THE CHEMICAL SOCIETY OF JAPAN, VOL. 52 (7), 2171—2172 (1979)

Kinetics of the Aminolysis of α-Chloropropionic Acid. Reactivity of Aliphatic Amines[1)]

Yoshiro OGATA* and Yuya YAMAUCHI

Department of Applied Chemistry, Faculty of Engineering, Nagoya University, Chikusa-ku, Nagoya 464

(Received January 31, 1979)

Synopsis. The kinetics for the reaction of α-chloropropionic acid with some amines (methylamine, dimethylamine, trimethylamine, ethylamine, and diethylamine) and ammonia have been studied in an aqueous solution. The reactivity of amines is discussed on the basis of the Swain-Scott and Taft equations.

The steric as well as polar effect was found to be important in the reaction of ammonia, alanine, and α,α′-iminodipropionic acid with α-chloropropionic acid.[2)] Hall Jr.[3)] reported that the data for the reaction of 30 amines with 15 substrates including chloroacetic acid are correlated by the Swain-Scott equation. We have studied the rate of the reaction of some amines with α-chloropropionic acid (CPA), forming *N*-alkylated alanine.

Discussion is given on the reactivity of amines on the basis of the Swain-Scott[4)] and Taft equations.[5)]

Results and Discussion

$$CH_3CHClCO_2H + R^1R^2R^3N \xrightarrow[-Cl^-]{\text{in } H_2O} CH_3\underset{\displaystyle N^+R^1R^2R^3}{\underset{|}{C}}HCO_2H + CH_3\underset{OH}{\underset{|}{C}}HCO_2H \quad (1)$$

	2a	**2b**	**2c**	**2d**	**2e**	**2f**
R^1	H	Me	Me	Me	Et	Et
R^2	H	H	Me	Me	H	Et
R^3	H	H	H	Me	H	H

Aminolysis was conducted at 60 °C in an aqueous solution and the chloride ion produced was measured in order to follow the rate of reaction. The pseudo-first-order rate constants (k_{obsd}) were measured at various concentrations of amines. The plot of the pseudo-first-order rate constants against the initial concentrations of amines gives a straight line with an intercept. The rate equation fits the equation,

$$\frac{d}{dt}[Cl^-] = (k_1 + k_2[\text{Amine}]_{ex})[\text{CPA}]. \quad (2)$$

Where $[\text{Amine}]_{ex}$ is the excess concentration of amine to that of α-chloropropionic acid, *i.e.*, effective amine concentration. Rate constants, k_1 and k_2, evaluated from the intercept of the plot and the slope, are given in Table 1.

Independent experiments for pure hydrolysis of CPA were carried out. The first- and second-order rate constants thus obtained for the hydrolysis of CPA are $0.35\times10^{-5}\,s^{-1}$ (S_N1) and $0.76\times10^{-5}\,s^{-1}\,M^{-1}$ (S_N2), respectively (60 °C).

Thus, in the case of methylamine (**2b**), dimethylamine (**2c**), trimethylamine (**2d**), and ethylamine (**2e**), the hydrolysis is negligible, the rate equation being of second-order: $v=k_2[\text{Amine}]_{ex}[\text{CPA}]$.

In order to examine the effect of substituent on amines, Taft equations[5)] with $\log k_{2rel}=\rho_s E_s+\delta E_s$ and $\log k_{2rel}=\rho^*\sigma^*$ were applied, where k_{2rel} is the relative rate constant. The former equation including a steric term, δE_s, gave poor correlation (ρ_s ranging −2.50—59.5 and δ ranging −58.1—2.76), and we could not determine values of ρ_s and δ, whereas the latter equation including only a polar term gave ρ^* value of −1.8 from the plot of $\log k_{2rel}$ against $\Sigma\sigma^*$ (summation of Taft polar substituent constants), except **2d** and **2f** (Fig. 1). In other words, electron-releasing groups promote the reaction. This is expected from the nucleophilic nature of amines, but the steric effect becomes important for the reaction of **2d** and **2f**.

The Swain-Scott equation[4)] is given by

$$\log(k/k_0) = sn \quad (3)$$

where s is the sensitivity to nucleophiles and n is the nucleophilic parameter. The plot of $\log k_2$ against n gave a straight line except for **2d** and **2f**. The s value of 1.05 was obtained for the reaction of CPA

Table 1. Rate constants for the reaction of α-chloropropionic and chloroacetic acids with amines $R^1R^2R^3N$ in an aqueous solution

	R^1	R^2	R^3	$CH_3CHClCO_2H$ (60 °C) $k_1\times10^{-5}\,s^{-1}$	$CH_3CHClCO_2H$ (60 °C) $k_2\times10^{-5}\,s^{-1}\,M^{-1}$	$ClCH_2CO_2H$ (25 °C)[6)] $k_2\times10^{-5}\,s^{-1}\,M^{-1}$	n[a)]
2a	H	H	H	0.67	0.97	0.633	4.13
2b	Me	H	H	0.00	10.0	11.5	5.18
2c	Me	Me	H	0.00	43.0	47.0	5.63
2d	Me	Me	Me	0.00	12.1	58.3	5.98
2e	Et	H	H	0.00	8.0	7.0	5.03
2f	Et	Et	H	0.40	1.5	5.0	4.83

a) *n*-Values are the average of the caluculated values from Ref. 3.

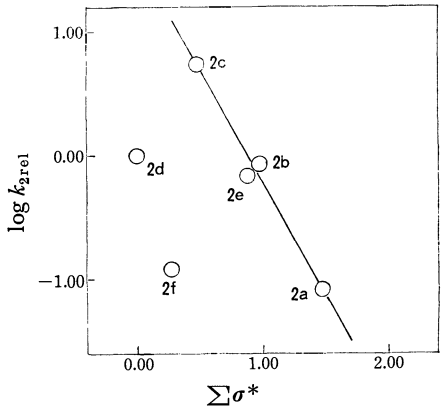

Fig. 1. Plot of k_{2rel} against $\sum\sigma^*$ for the reaction of α-chloropropionic acid with some amines in an aqueous solution at 60 °C.

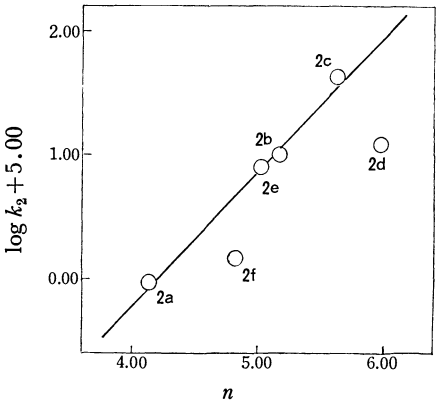

Fig. 2. Swain-Scott plot for the reaction of α-chloropropionic acid with some amines in an aqueous solution at 60 °C.

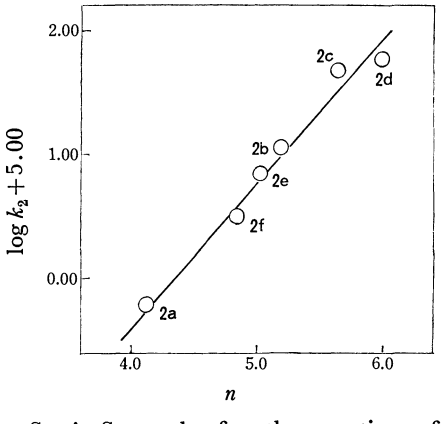

Fig. 3. Swain-Scott plot for the reaction of chloroacetic acid with some amines in an aqueous solution at 25 °C.

with some amines. Deviation from the straight line is larger with CPA (Fig. 2) than with chloroacetic acid (Fig. 3, $s=1.2$), especially with **2d** and **2f**. Since **2d** is tertiary and **2f** is secondary, the deviation may be due to the steric hindrance in the transition state. In aminolysis of phenethyl nitrite,[7] successive substitution of hydrogen by the methyl group in NH_3 leading to Me_3N always increases the relative rate, whereas in the reactions with CPA bearing α-methyl group, there is more interaction between substituent of amines than in those with chloroacetic acid or phenethyl nitrite, so that steric requirement decreases not only the reactivity of trimethylamine but also that of diethylamine.

Experimental

Materials. α-Chloropropionic acid bp 92—93 °C/15 Torr (lit,[8] 82.5—83.5 °C/12 Torr), aqueous 40% methylamine, 50% dimethylamine, 50% trimethylamine, 70% ethylamine, and 28% ammonia, and diethylamine of guaranteed reagent grade were used.

Kinetics. A solution of α-chloropropionic acid (1 M, 5 ml) was added to an aqueous solution of amines (1.2—3.5 M, 45 ml) in a glass-stoppered flask, which had attained thermal equilibrium at 60±0.1 °C in a thermostat. Aliquots (5 ml) were pipetted out at regular intervals and cold dil. HNO_3 was added to stop the reaction. The chloride ion concentration was determined by the Volhard method.[9] The pseudo-first-order rate was measured up to 30—60% conversion.

Products. NMR spectra were recorded on a Hitachi R-24B spectrometer. Under the kinetics conditions, the main product was *N*-alkylated alanine. On the basis of NMR spectra, the reaction products of α-chloropropionic acid with ammonia were found to be a mixture of alanine and lactic acid, and the products from diethylamine a mixture of *N,N*-diethyl alanine and lactic acid. They were produced by competitive aminolysis and hydrolysis, respectively. On the other hand, no lactic acid was detected in the case of the other amines.

References

1) Contribution No. 262.
2) Y. Ogata, A. Kawasaki, Y. Sawaki, and Y. Yamauchi, *Bull. Chem. Soc. Jpn.*, **52**, 1473 (1979).
3) H. K. Hall Jr., *J. Org. Chem.*, **29**, 3539 (1964).
4) C. G. Swain and C. B. Scott, *J. Am. Chem. Soc.*, **75**, 141 (1953).
5) a) R. W. Taft Jr., *J. Am. Chem. Soc.*, **75**, 4534 (1953); b) J. A. MacPhee, A. Panaye and J. E. Dubois, *Tetrahedron*, **34**, 3553 (1978).
6) T. S. Moore, D. B. Somevervell, and J. N. Derry, *J. Chem. Soc.*, **101**, 2459 (1912).
7) S. Oae, N. Asai, and K. Fujimori, *J. Chem. Soc., Perkin Trans. 2*, **1978**, 1124.
8) A. Michael, *Ber.*, **34**, 4049 (1901).
9) J. R. Coldwell and H. V. Meyer, *Ind. Eng. Chem. Anal. Ed.*, **7**, 38 (1935).

BULLETIN OF THE CHEMICAL SOCIETY OF JAPAN, VOL. 52 (7), 2173—2174 (1979)

Syntheses of 3,5-Dimethylspiro[5.5]undeca-2,4-diene-1,8-dione and 7,11-Dimethylspiro[5.5]undeca-7,10-diene-2,9-dione

Kalyan Kumar BHATTACHARYA and Parimal Krishna SEN*

Department of Chemistry, Presidency College, Calcutta 700073, India

(Received July 8, 1978)

Synopsis. Syntheses of 1-diazo-5-(2-hydroxy-4,6-dimethylphenyl)-2-pentanone and 1-diazo-5-(4-hydroxy-2,6-dimethylphenyl)-2-pentanone and their acid catalysed spiroannulation to 3,5-dimethylspiro[5.5]undeca-2,4-diene-1,8-dione and 7,11-dimethylspiro[5.5]undeca-7,10-diene-2,9-dione respectively *via* Ar_1-6 participation are described. Succinylation of 3,5-dimethylanisole is also discussed.

Aryl participation of phenolic diazo ketones toward the formation of spirodienone have recently been developed. Mander and Beams[1] reported a spectral indication of the formation of spirodienone *via* Ar_1-6 participation route in connection with their study on intramolecular alkylation of phenolic diazo ketones. Here we report the syntheses of two intermediate phenolic diazo ketones, 1-diazo-5-(2-hydroxy-4,6-dimethylphenyl)-2-pentanone (**8**) and 1-diazo-5-(4-hydroxy-2,6-dimethylphenyl)-2-pentanone (**18**) and their conversion into the spirodienones, 3,5-dimethylspiro[5.5]undeca-2,4-diene-1,8-dione (**1**) and 7,11-dimethylspiro[5.5]undeca-7,10-diene-2,9-dione (**2**), respectively. The spirodienones were isolated and characterized by spectral analyses.

Succinylation of 3,5-dimethylanisole at −5 °C in 1,1,2,2-tetrachloroethane–nitrobenzene mixture afforded the ortho-isomer, 3-(2-methoxy-4,6-dimethylbenzoyl) propanoic acid (**3**), mp 101 °C, in an excellent yield. The NMR spectrum of the keto acid **3** showed two sets of distinct singlets at δ 2.08, 2.25 (aromatic methyls) and at δ 6.61, 6.71 (aromatic protons). Clemmensen reduction of **3** and subsequent demethylation gave the hydroxy acid **5**, mp 130 °C. The same compound was synthesised by Brown and McCall[2] from a different route, mp 130—132 °C. The hydroxy acid was converted into the hydroxy diazo ketone **8** *via* acetylation, diazo ketone formation and deacetylation. Consistency in spectral data due to non-equivalent aromatic protons and methyls has also been observed in each step reaction product in the synthesis of **7** starting from the succinylated product **3** (*vide* Experimental). Aryl participation of the phenolic diazo ketone **8** was carried out in thoroughly dried nitromethane in presence of boron trifluoride etherate catalyst in an atmosphere of dry nitrogen at room temperature. Two products **1** and **9** were isolated by column chromatography from the crude reaction mixture. The formation of **9** during spiroannulation can be explained simply by SN_2 attack of ambident nitromethane on protonated[3] diazo ketone **8**.

Uneyama *et al.*[4] succinylated 3,5-dimethylanisole under almost identical conditions, but they reported the formation of the para-isomer, 4-(4-methoxy-2,6-dimethylbenzoyl) propanoic acid (**20**), mp 102—102.5 °C, and further converted it into **14**. Their claim for the above para products is untenable on the ground of non-equivalent aromatic protons and methyls shown in their NMR spectra. Moreover, we have synthesised the para-isomer **14** independently from authentic 3-(4-methoxy-2,6-dimethylphenyl) propanoic acid[5] (**12**) by the Arndt-Eistert reaction. The product gave a singlet (δ 2.28) for two aromatic methyls and a singlet (δ 6.46) for two aromatic protons in the NMR spectrum suggesting the para structure. The mp and NMR data reported by Uneyama *et al.* for the same compound **14** are different. Following exactly their method we also succinylated 3,5-dimethylanisole and obtained the same ortho acid **3** (undepressed mixed mp and identical NMR spectra). We presume that Uneyama *et al.* also obtained the ortho-isomer **3** by succinylation of 3,5-dimethylanisole but reported it as the para-isomer **20**.

Cyanoethylation of 3,5-dimethylanisole gave a mixture of propionitriles where the para-isomer **10** predominated. The hydroxy propanoic acid **11** was prepared from the crude propionitrile by refluxing with hydrobromic acid–acetic acid mixture and subsequent separation from the δ-lactone produced from the ortho-isomer. Methylation, homologation by the Arndt-Eistert method, demethylation, acetylation, diazo ketone formation, deacetylation and finally acid-catalysed Ar_1-6 participation starting from **11** afforded **2** and **19** (*vide* Experimental).

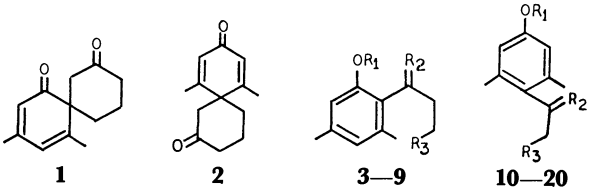

1 **2** **3—9** **10—20**

	R_1	R_2	R_3
3	CH_3	O	CO_2H
4	CH_3	H_2	CO_2H
5	H	H_2	CO_2H
6	Ac	H_2	CO_2H
7	Ac	H_2	$COCHN_2$
8	H	H_2	$COCHN_2$
9	H	H_2	$COCH_2OH$
10	CH_3	H_2	CN
11	H	H_2	CO_2H

	R_1	R_2	R_3
12	CH_3	H_2	CO_2H
13	CH_3	H_2	CO_2H
14	CH_3	H_2	$COCHN_2$
15	H	H_2	CH_2CO_2H
16	Ac	H_2	CH_2CO_2H
17	Ac	H_2	CH_2COCHN_2
18	H	H_2	CH_2COCHN_2
19	H	H_2	CH_2COCH_2OH
20	CH_3	O	CH_2CO_2H

Experimental

Light petrol and petroleum refer to the fraction of bp 40—60 °C and 60—80 °C, respectively. NMR spectra were recorded with a Varian EM 390 instrument.

3-(2-Methoxy-4,6-dimethylbenzoyl)propanoic Acid (3). Friedel-Crafts reaction of 3,5-dimethylanisole (2.7 g) with succinic anhydride (2.1 g) and anhydrous aluminium chloride (5.6 g) in dry 1,1,2,2-tetrachloroethane (23 ml) and nitrobenzene (6 ml) at −5 °C for 3 days yielded **3** (3.9 g, 84%) as

colorless cubes, mp 101 °C (ethanol–water); IR(KBr) 1710—1695 cm^{-1}; NMR [$(CD_3)_2SO$] δ 2.08 (s, 3H), 2.25 (s, 3H), 2.48 (t, 2H), 2.93 (t, 2H), 3.72 (s, 3H), 6.61 (s, 1H), 6.71 (s, 1H). Found: C, 65.91; H, 6.90%. Calcd for $C_{13}H_{16}O_4$: C, 66.10; H, 6.78%.

4-(2-Methoxy-4,6-dimethylphenyl)butanoic Acid (4). Clemmensen reduction of **3** (2.3 g) gave **4** (2 g, 90%) as colorless crystals, mp 99 °C (petroleum–benzene): IR(KBr) 1705 cm^{-1}; NMR($CDCl_3$) δ 1.74—1.96 (m, 2H), 2.26 (s, 3H), 2.28 (s, 3H), 2.40—2.76 (m, 4H), 3.76 (s, 3H), 6.54 (s, 1H), 6.61 (s, 1H). Found: C, 70.13; H, 7.94%. Calcd for $C_{13}H_{18}O_3$: C, 70.27; H, 8.11%.

4-(2-Hydroxy-4,6-dimethylphenyl)butanoic Acid (5). Demethylation of **4** (2.2 g) with pyridine hydrochloride (7 g) at 210 °C under dry nitrogen gave **5** (1.9 g, 90%) as colorless crystals, mp 130 °C (benzene) (lit,[2]) mp 130—132 °C): IR-(KBr) 3250, 1705 cm^{-1}; NMR ($CDCl_3$) δ 1.75—1.96 (m, 2H), 2.20 (s, 3H), 2.22 (s, 3H), 2.32—2.78 (m, 4H), 6.46 (s, 1H), 6.52 (s, 1H). Found: C, 69.37; H, 7.48%. Calcd for $C_{12}H_{16}O_3$: C, 69.23; H, 7.69%.

4-(2-Acetoxy-4,6-dimethylphenyl)butanoic Acid (6). Acetylation of the phenolic acid **5** with acetic anhydride in aqueous sodium hydroxide at −5 °C gave **6** (65%) as colorless crystals, mp 93 °C (petroleum–benzene): IR(KBr) 1750, 1705 cm^{-1}; NMR (CCl_4) δ 1.56—1.88 (m, 2H), 2.20 (s, 3H), 2.26 (s, 6H), 2.32—2.68 (m, 4H), 6.60 (s, 1H) 6.80 (s, 1H), 11.26 (s, 1H). Found: C, 66.97; H, 7.31%. Calcd for $C_{14}H_{18}O_4$: C, 67.20; H, 7.22%.

1-Diazo-5-(2-acetoxy-4,6-dimethylphenyl)-2-pentanone (7). Acid chloride was prepared from **6** by the oxalyl chloride method. It was transformed into **7** (80%) by diazomethane as a light yellow oil: IR(neat) 2110, 1750, 1630 cm^{-1}; NMR ($CDCl_3$) δ 1.64—1.92 (m, 2H), 2.20 (s, 3H), 2.28 (s, 6H), 2.32—2.70 (m, 4H), 5.24 (s, 1H), 6.60 (s, 1H), 6.80 (s, 1H).

1-Diazo-5-(2-hydroxy-4,6-dimethylphenyl)-2-pentanone (8). Deacetylation of **7** by Na_2CO_3–$NaHCO_3$ solution gave **8** (75%) as a pale yellow oil: IR (neat) 3300, 2110, 1620 cm^{-1}; NMR ($CDCl_3$) δ 1.70—1.98 (m, 2H), 2.26 (s, 6H), 2.34—2.70 (m, 4H), 5.30 (s, 1H), 6.56 (s, 2H).

3,5-Dimethylspiro[5.5]undeca-2,4-diene-1,8-dione (1). A mixture of **8** (500 mg) and BF_3–etherate (5 drops) in thoroughly dried nitromethane (40 ml) was stirred for 15 min at 20 °C to afford a red oil after the usual work-up. It was purified by column chromatography. Petroleum eluted **7** (85 mg) as semi-solid mass: UV (MeOH) 232 (log ε 4.31), 280 (log ε 3.52), 312 nm (log ε 4.28); IR ($CHCl_3$) 1710, 1660, 1620, 1575 cm^{-1}; NMR ($CDCl_3$) δ 1.70—2.04 (m, 2H), 2.22 (s, 6H), 2.62—2.96 (m, 4H), 4.40 (s, 2H), 6.78 (s, 2H). Benzene eluted **9** (130 mg) as colorless crystals, mp 95 °C (light petrol–ether): IR(KBr) 3350—3250, 1715, 1600 cm^{-1}; NMR ($CDCl_3$) δ 1.64—1.96 (m, 2H), 2.16 (s, 3H), 2.18 (s, 3H), 2.36—2.62 (m, 4H), 2.98 (t, 1H, J 5 Hz), 4.20 (d, 2H, J 5 Hz), 5.36 (s, 1H), 6.42 (s, 1H), 6.50 (s, 1H). Found: C, 70.41; H, 8.02%. Calcd for $C_{13}H_{18}O_3$: C, 70.27; H, 8.11%.

3-(4-Hydroxy-2,6-dimethylphenyl)propanoic Acid (11). Cyanoethylation of dimethylanisole with acrylonitrile in 1,1,2,2-tetrachloroethane by use of anhydrous $AlCl_3$ and dry HCl gas gave **10** (62%), contaminated with a trace of ortho-isomer. Reaction of crude propionitrile **10** with HOAc–HBr mixture gave **11** (68%) as colorless needles, mp 125 °C (benzene) (lit,[5] mp 126—127 °C): IR (Nujol) 3450, 1705 cm^{-1}; NMR ($CDCl_3$) δ 2.30 (s, 6H), 2.50 (t, 2H), 3.0 (t, 2H), 6.50 (s, 2H) 8.50 (s, 2H). Found: C, 67.75; H, 6.86%. Calcd for $C_{11}H_{14}O_3$: C, 68.04; H, 7.22%.

3-(4-Methoxy-2,6-dimethylphenyl)propanoic Acid (12). Methylation of **11** with $(CH_3)_2SO_4$ gave **12** (82%) as colorless needles, mp 95 °C (petroleum): NMR ($CDCl_3$) δ 2.30 (s, 6H), 2.50 (t, 2H), 3.0 (t, 2H), 3.80 (s, 3H), 6.50 (s, 2H), 11.50 (s, 1H). Found: C, 68.94; H, 7.46%. Calcd for $C_{12}H_{16}O_3$: C, 69.23; H, 7.69%.

4-(4-Methoxy-2,6-dimethylphenyl)butanoic Acid (14). Diazo ketone **13** was prepared from **12** and the crude product was treated with Ag_2O in methanol. After saponification of the intermediate ester, methoxy acid **14** (75%) was obtained as colorless crystals, mp 108 °C (petroleum–benzene): NMR (CCl_4) δ 1.62—1.90 (m, 2H), 2.28 (s, 6H), 2.37—2.68 (m, 4H), 3.68 (s, 3H), 6.46 (s, 2H), 11.54 (s, 1H). Found: C, 70.39; H, 7.99%. Calcd for $C_{13}H_{18}O_3$: C, 70.27; H, 8.11%.

4-(4-Hydroxy-2,6-dimethylphenyl)butanoic Acid (15). Demethylation of **14** gave **15** (90%) as colorless crystals, mp 125 °C (benzene): IR ($CHCl_3$) 3250, 1705 cm^{-1}; NMR ($CDCl_3$) δ 1.60—1.92 (m, 2H), 2.32 (s, 6H), 2.38—2.70 (m, 4H), 6.50 (s, 2H). Found: C, 69.10; H, 7.51%. Calcd for $C_{12}H_{16}O_3$: C, 69.23; H, 7.69%.

4-(4-Acetoxy-2,6-dimethylphenyl)butanoic Acid (16). Acetylation of **15** gave **16** (60%) as colorless crystals, mp 96 °C (petroleum–benzene): IR ($CHCl_3$) 1750, 1715 cm^{-1}; NMR ($CDCl_3$) δ 1.62—1.90 (m, 2H), 2.25 (s, 3H), 2.32 (s, 6H), 2.38—2.72 (m, 4H), 6.72 (s, 2H), 11.30 (s, 1H). Found: C, 66.91; H, 7.08%. Calcd for $C_{14}H_{18}O_4$: C, 67.20; H, 7.20%.

1-Diazo-5-(4-acetoxy-2,6-dimethylphenyl)-2-pentanone (17). Diazo ketone **17** (91%) was prepared from **16** following the usual procedure as a pale yellow oil: IR ($CHCl_3$) 2100, 1750, 1635 cm^{-1}; NMR ($CDCl_3$) δ 1.62—1.90 (m, 2H), 2.26 (s, 3H), 2.32 (s, 6H), 2.40—2.82 (m, 4H), 5.20 (s, 1H), 6.75 (s, 1H).

1-Diazo-5-(4-hydroxy-2,6-dimethylphenyl)-2-pentanone (18). Deacetylation of **17** afforded **18** (90%) as a light yellow oil: IR ($CHCl_3$) 3300, 2100, 1630 cm^{-1}; NMR ($CDCl_3$) δ 1.62—1.92 (m, 2H), 2.32 (s, 6H) 2.40—2.78 (m, 4H), 5.20 (s, 1H), 6.48 (s, 2H).

7,11-Dimethylspiro[5.5]undeca-7,10-diene-2,9-dione (2). Ar_1-6 participation of **18** (500 mg) with BF_3–etherate gave a red oil. Dienone **2** (90 mg) was obtained from benzene elute as colorless needles, mp 128 °C (light petrol–ether): UV (MeOH) 246 nm (logε 4.40); IR ($CHCl_3$) 1710, 1660, 1625 cm^{-1}; NMR ($CDCl_3$) δ 1.67—1.87 (m, 4H), 2.06 (s, 6H), 2.23—2.48 (m, 4H), 6.05 (s, 2H); MS (50 eV) 204 (M^+), 176 (M−CO), 161 (M−CH_2CO), 134 [M−(C_2H_4, CH_2CO)], 91 [M−(C_2H_4, CH_2CO, CO, CH_3)] (100%). Found: C, 76.29; H, 7.96%. Calcd for $C_{13}H_{16}O_2$: C, 76.47; H, 7.84%. The hydroxy ketone **19** (120 mg) was obtained from benzene–ethyl acetate elute as colorless crystals, mp 100 °C (ether–light petrol): IR ($CHCl_3$) 3340—3250, 1715, 1600 cm^{-1}; NMR ($CDCl_3$) δ 1.64—1.90 (m, 2H), 2.30 (s, 6H), 2.36—2.64 (m, 4H), 4.20 (d, 2H), 5.0 (t, 1H), 6.50 (s, 2H). Found: C, 70.06; H, 8.10%. Calcd for $C_{13}H_{18}O_3$: C, 70.27; H, 8.11%.

References

1) L. N. Mander and D. J. Beams, *Aust. J. Chem.*, **27**, 1257 (1974).

2) J. B. Brown and E. B. McCall, *J. Chem. Soc.*, **1957**, 3875.

3) Lewis acid-base complex generated from BF_3 and the diazo ketone might be the reacting electrophile. However, we favor protonation[1] by Brönsted acid which could be formed by complexing BF_3 with the phenolic hydroxyl group.

4) K. Uneyama, H. Sakumoto, and S. Torii, *Bull. Chem. Soc. Jpn.*, **49**, 2649 (1976).

5) A. Ogiso, M. Kurabayashi, H. Nagahori, and H. Mishima, *Chem. Pharm. Bull.*, **18**, 1283 (1970).

Empirical Formula for Mass Transfer across the Boundary between Convections in a Two-layer System

Katsuyoshi KAMAKURA

Department of Industrial Chemistry, Toyama Technical College, Hongo-cho, Toyama 930-11

(Received April 7, 1978)

When a two-layer system which consists of water (upper layer) and an aqueous solution (lower layer) is heated from one side and cooled from the opposite side, a convection starts in each layer and a sharp horizontal boundary is formed by the two flows in opposite directions. The empirical formula for the transfer of a solute across the boundary was obtained by measuring the change in the concentration of a solute in the upper layer. The flux, W_A, of a solute, A, was expressed by

$$W_A = a_3(\Delta\rho_1 - \Delta\rho_0)D^{0.5}(\Delta c_I/\Delta\rho_2).$$

Here, a_3 is the mass-transfer coefficient; $\Delta\rho_1$, the density difference between the liquid on the heated wall and that on the cooled wall; $\Delta\rho_0$, the value of $\Delta\rho_1$ at which the convections start; D, the diffusion coefficient of a solute; and Δc_I and $\Delta\rho_2$, the concentration difference and the density difference, respectively, between the solution of the upper layer and that of the lower layer.

When a two-layer system which consists of water (A) and an aqueous solution (B) is heated from one side and cooled from the opposite side, the liquid adjacent to the hot vertical surface moves upward, while that adjacent to the cool vertical surface moves downward. A convection starts in each layer, and a sharp horizontal boundary is formed by the two flows in opposite directions, as is shown in Fig. 1. Two papers[1,2] have been published on this phenomenon, but no attempts have been made to estimate the rate of transfer of a solute across the boundary. This paper will describe the empirical formula of mass transfer in our model.

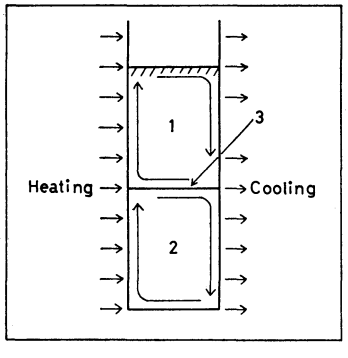

Fig. 1. Schematic illustration of the convections in two-layer system.
1: Upper layer (water), 2: lower layer (aqueous solution), 3: boundary.

Experimental

Materials. All the chemicals were reagent grade and were used without further purification. The sodium chloride was dried at 280 °C for 1 h, the copper sulfate and sucrose were used without drying, and the other salts were dried at 105—110 °C for 5 h.

Apparatus and Method. Figure 2 shows the apparatus used for measuring convections in the two-layer system; it is made of 200×50×3 mm glass plates joined by the use of epoxide resin as adhesive. Two glass rods, 3 mm in diameter and 50 mm in length, were fixed on both sides at a distance of 7 cm above the bottom in order to make the flows of the convections stable.

Water (63 cm³) was gradually poured over an aqueous solution (63 cm³) previously placed in the vessel at the flow speed of 2 cm³/min by the use of a micropump; the two-layer system was thus made. The temperature of the circulating water used for heating or cooling the wall was kept constant within ±0.05 °C.

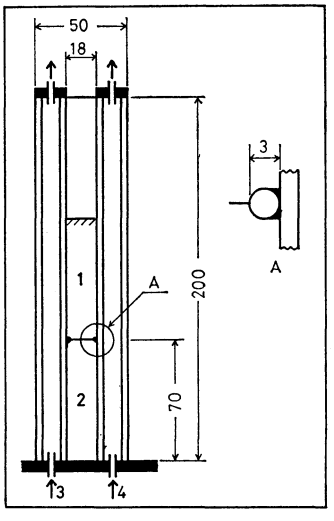

Fig. 2. Apparatus for measuring convections in two-layer system.
1: Upper layer, 2: lower layer, 3: hot water, 4: cold water.

The concentration of electrolytes was determined by the electric-conductance method. The conductance was measured with a conductometer (Toa Electronics CM-6A) equipped with electrodes formed of platinized platinum wires which were sealed at one end of a glass tube 6 mm in diameter. The electrodes were placed in the middle of the upper layer.

The concentration of sucrose was determined by colorimetry as reported by Dubois *et al.*[3] The samples (50 mm³) for the determination of the solute concentration were taken out from the solution in the middle of an upper layer.

Results and Discussion

Phenomenon of Mass Transfer. In a previous paper[2] it was shown that the concentration in each layer is uniform. Therefore, the rate of mass transfer across the boundary can be calculated from the incre-

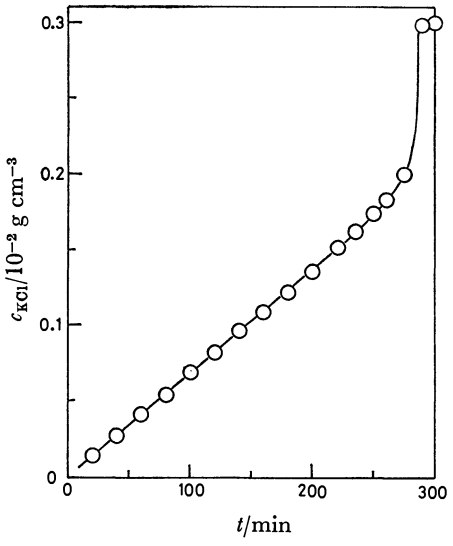

Fig. 3. Variation of the concn c_{KCl} in the upper layer with time t.
Concn of the lower layer at the start of the convections: 0.6 g/(100 cm^3), temps of heating and cooling water: 36 and 26 °C.

ment in the concentration of a solute in the upper la er. Figure 3 shows the variation in the concentration of a solute in the upper layer with the lapse of time. Within ten minutes from the beginning of the convections, each convection becomes a steady current; then the concentration in the upper layer increases linearly with the time. When the time has elapsed, the concentration difference between the two layers becomes small and the boundary unstable. Then, the boundary is destroyed and the two-layer system changes into a one-layer system. The flux (g cm^{-2} min^{-1}), W_A, of a solute, A, across the boundary was calculated by means of

$$W_A = \frac{V}{100S}\frac{\Delta c_A}{\Delta t}. \quad (1)$$

Here, c_A, S, t, and V are the concentration {g/(100 cm^3)} of a solute, A, in the upper layer, the area (cm^2) of the boundary, the time (min), and the volume (cm^3) of the upper layer, respectively.

Figure 4 shows the relation between W_{KCl} and the concentration in the lower layer at the start of the convections. It can be seen that W_{KCl} is independent of the concentration difference.

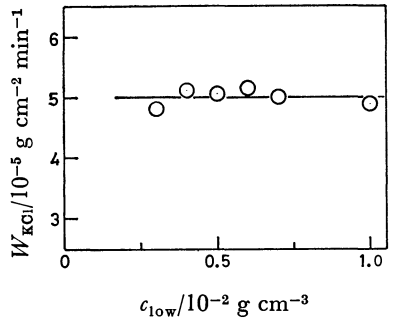

Fig. 4. Relation between W_{KCl} and concn c_{low} of KCl in the lower layer at the start of the convections.
Temps of heating and cooling water: 30 and 20 °C.

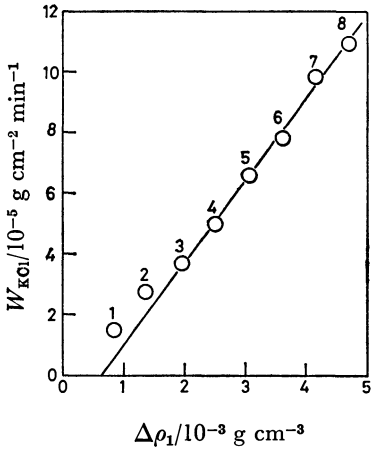

Fig. 5. Dependence of the flux W_{KCl} on the density difference $\Delta\rho_1$ between the liquids on the heated and the cooled wall.
Concns in the lower layer at the start of convections: 0.2—1.0 g/(100 cm^3).
Temps of heating and cooling water—1: 29 and 26 °C, 2: 30 and 25 °C, 3: 31 and 24 °C, 4: 32 and 23 °C, 5: 33 and 22 °C, 6: 34 and 21 °C, 7: 35 and 20 °C, 8: 36 and 19 °C.

Effect of Density Difference Caused by the Temperature. Figure 5 shows the dependence of W_{KCl} on the density difference, $\Delta\rho_1$, between the liquid on the heated wall and that on the cooled wall. This plot shows a straight line except for small values of the density difference. The value of $\Delta\rho_0 = 0.63 \times 10^{-3}$ g cm^{-3} was obtained by extrapolation of the linear portion of the plot to $W_{KCl} \to 0$. The convections in our two-layer system can be considered to occur above this value of $\Delta\rho_0$. Therefore, the following equation can be obtained:

$$W_A = a_1(\Delta\rho_1 - \Delta\rho_0). \quad (2)$$

Here, a_1 is the mass-transfer coefficient.

Effect of the Kind of Solute. The values of W_A may depend on the kind of solute through a variety of factors: (1) the diffusion coefficient of the solute; (2) the density difference between the liquid in the upper layer and that in the lower layer; and (3) the viscosity of the fluid. However, the rate of mass transfer may be expected to be practically unaffected by the viscosity, because this experiment was performed in dilute solutions. Therefore, the results were discussed from the viewpoints of the diffusion coefficient, D (cm^2 s^{-1}), and the density difference, $\Delta\rho_2$ (g cm^{-3}). The rate of mass transfer may be proportional to the x-th power of D with $0 \leqq x \leqq 1$, because the solute is transported across the boundary by eddy or by molecular diffusion.[4] The concentration difference, Δc_I {g/(100 cm^3)}, should be a driving force for this mass transfer. However, it has already been described that W_A is independent of Δc_I. Δc_I is proportional to $\Delta\rho_2$, so that the $\Delta c_I/\Delta\rho_2$ ratio should be constant for a given solute. Therefore, it is likely that W_A is proportional to $\Delta c_I/\Delta\rho_2$, and that, thus:

$$W_A = a_2 D^x \frac{\Delta c_I}{\Delta\rho_2}. \quad (3)$$

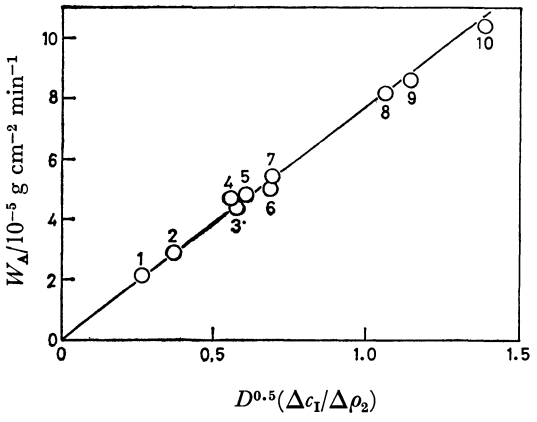

Fig. 6. Relation between W_A and $D^{0.5}(\Delta c_I/\Delta\rho_2)$.
Temps of heating and cooling water: 30 and 20 °C.
Solutes—1: $CuSO_4$, 2: Na_2SO_4, 3: CsCl, 4: NaCl, 5: sucrose, 6: KCl, 7: KNO_3, 8: NH_4NO_3, 9: HCl, 10: NH_4Cl.

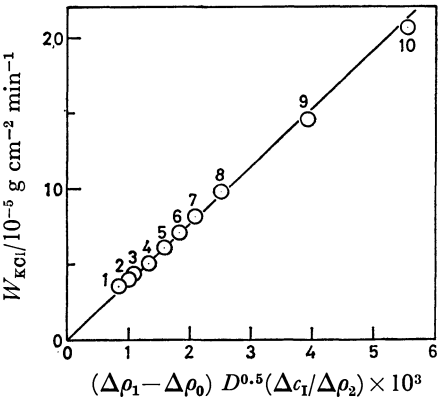

Fig. 7. Relation between W_{KCl} and $(\Delta\rho_1-\Delta\rho_0)D^{0.5}\cdot(\Delta c_I/\Delta\rho_2)$.
Concn in the lower layer at the start of convections: 0.25—1.00 g/(100 cm^3).
Temps of heating and cooling water—1: 24 and 14 °C, 2: 16 and 26 °C, 3: 27 and 17 °C, 4: 30 and 20 °C, 5: 23 and 33 °C, 6: 26 and 36 °C, 7: 29 and 39 °C, 8: 20 and 35 °C, 9: 20 and 40 °C, 10: 20 and 45 °C.

Here, a_2 is the mass-transfer coefficient. The value of $\Delta c_I/\Delta\rho_2$ was calculated approximately from

$$\frac{\Delta c_I}{\Delta\rho_2}=\left(\frac{\Delta\rho_2}{\Delta c_I}\right)^{-1}\approx((d_4^t)_s-(d_4^t)_w)^{-1}, \tag{4}$$

where $(d_4^t)_s$ is the specific gravity of the solution of 1 wt %, $(d_4^t)_w$ that of water, and t the mean temperature in the upper layer. For a number of solutes we measured W_A and made a plot of log $\{W_A/(\Delta c_I/\Delta\rho_2)\}$ *vs.* log D, from the slope of which we obtained $x=0.5$. Thus, W_A was found to be proportional to $D^{0.5}(\Delta c_I/\Delta\rho_2)$, as be shown in Fig. 6.

Empirical Formula for Mass-transfer Rate. Combining Eq. 2 with Eq. 3 yields the following final expression for W_A:

$$W_A=a_3(\Delta\rho_1-\Delta\rho_0)D^{0.5}\frac{\Delta c_I}{\Delta\rho_2}. \tag{5}$$

Here, a_3 is the mass-transfer coefficient. Figure 7 shows the plot of W_{KCl} *vs.* $(\Delta\rho_1-\Delta\rho_0)D^{0.5}(\Delta c_I/\Delta\rho_2)$ at different pairs of temperatures. This plot is linear except for the points obtained at low temperatures.

References

1) W. Schaaffs, *Kolloid Z. Z. Polym.*, **227**, 131 (1967).
2) K. Kamakura, Y. Nakamoto, and A. Yanagihara, *Denki Kagaku*, **41**, 884 (1973).
3) M. Dubois, K. A. Gilles, J. K. Hamilton, P. A. Rebers, and F. Smith, *Anal. Chem.*, **28**, 350 (1956).
4) T. K. Sherwood, R. L. Pigford, and C. R. Wilke, "Mass Transfer," McGraw-Hill, New York (1975), Chap. 5.

Vibrational Spectra and Rotational Isomerism of Isopropyl Methyl Selenide and Diisopropyl Selenide

Keiichi OHNO,* Akitoshi MITSUI, and Hiromu MURATA

Department of Chemistry, Faculty of Science, Hiroshima University, Higashisenda-machi, Hiroshima 730

(Received November 8, 1978)

The infrared and Raman spectra of isopropyl methyl selenide and diisopropyl selenide were measured for the liquid and solid states. The fundamental vibrations were assigned and the rotational isomerism was studied on the basis of the spectral observations and the normal coordinate treatment. For isopropyl methyl selenide, the C_1 and C_s forms coexisted in the liquid state and the enthalpy difference between them was obtained as $\Delta H(C_1-C_s)=-0.52\pm0.05$ kcal mol^{-1}. For diisopropyl selenide, it was presumed that only the C_2 form persisted in the solid state while the C_2, C_s, and C_1 forms coexisted in the liquid state, the C_2 form being the most stable.

The vibrational spectra of unbranched dialkyl ethers and sulfides have been studied extensively in relation to the rotational isomerism.[1] Recently, we have reported the existence of the rotational isomers about the C–Se axis[2] and the correlations of the C–Se stretching wave numbers to the molecular conformations.[3] Among the most simple molecules with the C–Y (Y= O, S, and Se) internal rotation axis, the T form is more stable than the G form for ethyl methyl ether,[4] but the reverse is true for ethyl methyl sulfide[5] and selenide.[2,6] Therefore, we have taken an interest in studying these molecules, in which the hydrogen of the methylene group is replaced by a methyl group, in order to obtain information on the stability of the molecular conformations. The studies for isopropyl methyl ether[7] and sulfide[8] have already been reported. In this paper, we will deal in detail with the molecular vibrations and rotational isomerism of isopropyl methyl selenide and diisopropyl selenide by treating their normal coordinates.

Experimental

The samples were prepared by the treatment of alkylhalides with selenium[9] and were purified by fractional distillation. The purities of the samples were checked by means of NMR and gas chromatography.

The Raman spectra in the region below 4000 cm^{-1} were recorded on a JEOL spectrophotometer (Model JRS 400D) with a Coherent Radiation CR-2 argon-ion laser. The Raman spectra were measured for the liquid state at various temperatures and for the solid state at liquid nitrogen temperature. For the determination of the enthalpy difference between isomers, the integrated intensities of the Raman lines were measured in the liquid state; each experiment was repeated several times after attaining a constant temperature. The infrared spectra in the 300—4000 cm^{-1} region were recorded on a Perkin-Elmer spectrophotometer (Model 621). The solid state was obtained by depositing vapor of the sample onto a CsI window cooled with liquid nitrogen and annealing it repeatedly.

Results and Discussion

Normal Coordinate Treatment. For isopropyl methyl selenide, the existence of the rotational isomers has already been reported[2] and the molecular forms have been determined from the calculation of the skeletal vibrations.[3] Thus, the normal vibrations were calculated in order to obtain a reasonable set of the force constants for the branched dialkyl selenide and information on the molecular forms and the vibrational assignment of diisopropyl selenide. The Urey-Bradley force field was used in the calculation. The structural parameters used were the same as those reported previously.[3] The force constants were initially transferred from those of isopropyltrichlorosilane[10] and dimethyl selenide[11] and some of them were adjusted by the least-squares method to reproduce better the observed wave numbers of isopropyl methyl selenide. The force constants obtained were then transferred to those of diisopropyl selenide. The accuracy of the calculation was good enough for analyzing the observed spectra. The observed and calculated wave numbers are given in Tables 1 and 2, together with the assignment based on the predominant potential energy distributions. The force constants used are listed in Table 3.

Vibrational Assignment. Figures 1—4 show the infrared and Raman spectra of isopropyl methyl selenide and diisopropyl selenide in the region below 1500 cm^{-1}. The observed wave numbers above 800 cm^{-1} resemble very closely those of the corresponding sulfides. In the region below 800 cm^{-1}, only the C–Se stretching, skeletal deformation, and torsional vibrations are expected. Therefore, the fundamental vibrations are easily assigned by comparing the spectra with those of the sulfides and the relative intensities between the infrared bands and the Raman lines. Table 4 lists the isopropyl group vibrations of the selenides, together with those of the corresponding ethers[7] and sulfides.[8] It is noteworthy that the wave numbers of the isopropyl group vibrations of isopropyl methyl selenide are nearly

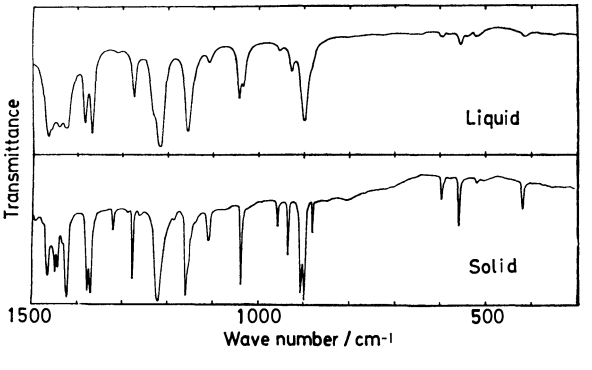

Fig. 1. Infrared spectra of isopropyl methyl selenide in the liquid and solid states in the 300—1500 cm^{-1} region.

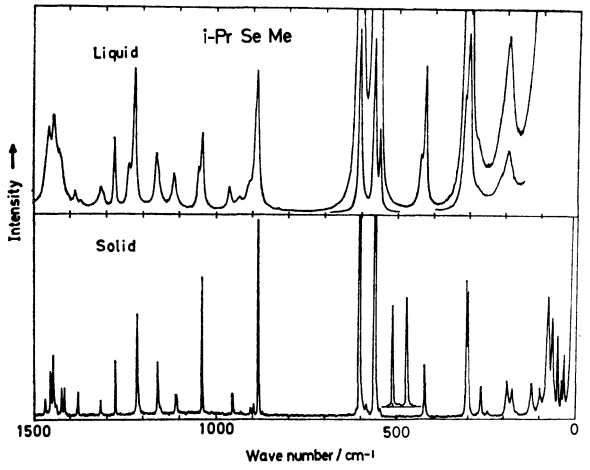

Fig. 2. Raman spectra of isopropyl methyl selenide in the liquid and solid states in the region below 1500 cm^{-1}.

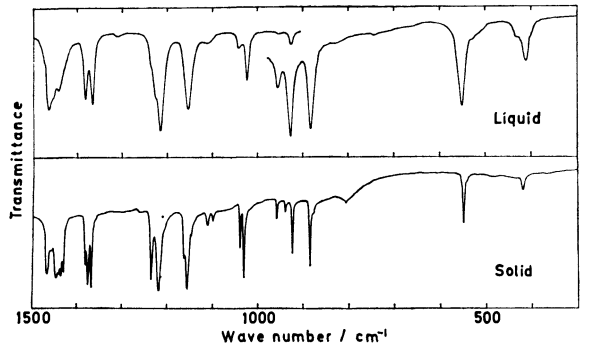

Fig. 3. Infrared spectra of diisopropyl selenide in the liquid and solid states in the 300—1500 cm^{-1} region.

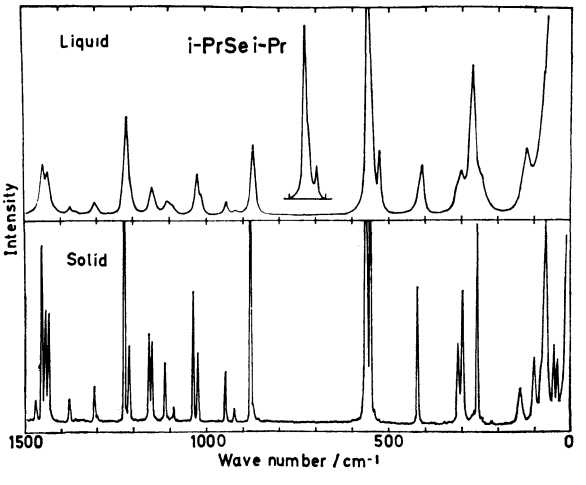

Fig. 4. Raman spectra of diisopropyl selenide in the liquid and solid states in the region below 1500 cm^{-1}.

the same as those of diisopropyl selenide and those of the sulfides.

Rotational Isomers. Isopropyl methyl selenide has one C–Se axis and has two possible rotational isomers, with the C_1 or C_s symmetry (the C_1 and C_s forms). Useful information on the rotational isomers has been obtained from the C–Se stretching vibrations. For isopropyl methyl selenide, the very intense Raman lines at 557 and 597 cm^{-1} in the solid state were assigned to the C–Se stretching vibrations of one isomer. The Raman line at 539 cm^{-1} in the liquid state was assigned to the C–Se stretching vibration of the other isomer. It has been reported[2] from the calculation of the skeletal vibrations that the Raman lines at 557 and 597 cm^{-1} can be assigned to the CH–Se and CH_3–Se stretching vibrations, respectively, of the C_1 form and the Raman lines at 539 and 597 cm^{-1} to those of the C_s form. This conclusion is also confirmed from the present normal coordinate treatment.

Diisopropyl selenide has two C–Se axes and has four possible isomers with the C_{2v}, C_2, C_s, or C_1 symmetry (the C_{2v}, C_2, C_s, and C_1 forms). All the fundamental vibrations for these molecular forms are infrared and Raman active, except for the vibrations of the A_2 species of the C_{2v} symmetry which are infrared inactive. For diisopropyl selenide, information of the rotational isomers is obtained only from the C–Se stretching and skeletal deformation vibrations. The comparison of the observed wave numbers with the calculated ones indicates that the Raman lines at 555 and 529 cm^{-1} are to be assigned to the CH–Se stretching vibration of the C_2 and C_s forms and the C_1 and C_{2v} forms, respectively. In the solid state, the former line persists but the latter disappears. However, the molecular form persisting in the solid state cannot be determined from the calculation, because the C_2 and C_s forms have nearly the same calculated wave numbers, as in the case of diisopropyl sulfide.[12] For diisopropyl selenide, the magnitude of the H···H nonbonded repulsion between the methyl groups is in the order: the C_{2v} form>the C_1 form$\gtrsim$the C_s form>the C_2 form. On the assumption that the stability of the molecular forms is mainly due to the nonbonded repulsion, it is expected that only the C_2 form persists in the solid state and that the C_2, C_s, and C_1 forms coexist in the liquid state. However, the existence of the C_{2v} form is unlikely, because the GG′ form, with the large H···H nonbonded repulsion between the methyl groups, has not been reported to exist for diethyl ether,[1] diethyl sulfide,[1] or diethyl selenide.[6]

Enthalpy Difference between Isomers. The enthalpy difference can be determined from the intensity ratios of the Raman lines belonging to different isomers. The relative intensities of the Raman lines assigned to the CH–Se stretching vibration were measured in the liquid

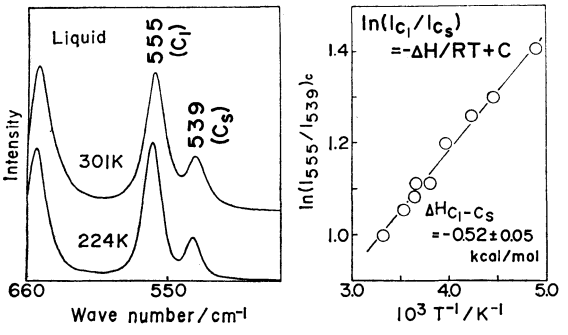

Fig. 5. Observed Raman spectra in the 510—600 cm^{-1} region and a plot of $\ln(I_{555}/I_{539})_c$ *vs.* $1/T$.

Table 1. Observed and calculated wave numbers of isopropyl methyl selenide (cm^{-1})[a]

Liquid			Solid		Calcd[b]		Assignment[c]
IR	Raman		IR	Raman	C_s	C_1	
1465s			1465m	1473vw	1451A′	1452	$\delta_a CCH_3$
1457s	1455w	dp		1458w	1449A″	1450	
			1449m	1450w	1449A′	1449	
1440s	1441w	dp	1444m	1442vw	1449A″	1449	
			1433w	1430vw	1425A′	1425	$\delta_a SeCH_3$
1425s	1426vw, sh	dp	1423s	1420vw	1424A″	1424	
1382s	1382vw		1378s	1382vw	1379A′	1380	$\delta_s CCH_3$
1366s	1367vvw		1370s		1379A″	1380	
1310vvw	1311vw		1320w	1319vw		1297	δCH o.p., $r_s CCH_3$
	1304vw, sh				1296A″		
1274m	1275m	p	1278s	1279w	1277A′	1276	$\delta_s SeCH_3$
1230s, sh	1233w	p			1224A′		δ CH i.p., $r_s CCH_3$
1217vs	1219s	p	1221vs	1218m		1224	
1154s	1156vw		1159s	1162w	1137A′	1136	$r_a CCH_3$, ν_sC–C
1108w	1108vw	dp	1109w	1111vw	1098A″	1101	ν_aC–C, $r_a CCH_3$
1040m	1040vw	p	1037s	1040s		1035	$r_s CCH_3$, δ CH i.p.
1031m	1031w	p			1036A′		
952vw	953vw	dp	956w	953vw	973A″	973	$r_a CCH_3$, ν_aC–C
925w	925vw		933m	932vw	922A″	924	$r_s CCH_3$, δCH o. p.
			904s	904vw	897A′	895	$r_s SeCH_3$
897s	894vw, sh		895vs	895w	893A″	893	$r_a SeCH_3$
884w, sh	876m		878w	881vvs	878A′	877	ν_sC–C, $r_a CCH_3$
594vw	596vvvs	p	594w	597vvvs	599A′	595	νCH_3–Se
				580vw			
552w	555vvvs	p	555m	557vvvs		554	νCH–Se
538vw	539vvs	p			550A′		
	421w	p	416w	417m		411	$\nu_s C_2CSe$
409vw	410s	p			419A′		$\delta_s C_2CSe$, $\delta_a C_2CSe$
	301vs, sh	p		302s 298s		300	$\delta_a C_2CSe$
	292vs	p			288A′		$\delta_a C_2CSe$
					287A″		$\delta_a C_2CSe$
	265w, sh			261vw		267	$\delta_a C_2CSe$, $\delta_s C_2CSe$
				242vvw			
	198w, sh			187vw	203A′	204	$\tau_s CCH_3$
					202A″	201	$\tau_a CCH_3$
	178m	dp		175vw	167A′	178	δCSeC
				120vw	159A″	159	$\tau SeCH_3$
				97vw			
				74s	75A″	75	τCHSe and lattice vibrations
				63m			
				48m			
				37vw			
				30w			

a) Wave numbers above 1500 cm^{-1} are not included and infrared spectra below 300 cm^{-1} are not recorded. s: Strong, m: medium, w: weak, v: very, sh: shoulder, b: broad, p: polarized, and dp: depolarized. b) A′, A″: A′ and A″ species in the C_s symmetry. c) ν: stretching, s: scissoring, w: wagging, t: twisting, r: rocking, δ: deformation, τ: torsion, i.p.: in-plane mode, o.p.: out-of-plane mode, a: asymmetric mode, and s: symmetric mode.

state at different temperatures. For isopropyl methyl selenide, Fig. 5 gives the intensity ratio of the Raman line at 555 cm^{-1} (the C_1 form) to that at 539 cm^{-1} (the C_s form). From the slope of the straight line of $\ln(I_{555}/I_{539})_c$ *vs.* $1/T$, the enthalpy difference $\Delta H(C_1-C_s)$ was obtained as -0.52 ± 0.05 kcal mol^{-1}.

For diisopropyl selenide, the relative intensity of the Raman line at 555 cm^{-1} belonging to the C_2 and/or C_s forms increases with decreasing temperature, as compared with that of the Raman line at 529 cm^{-1} belonging to the C_1 form. Therefore, for these compounds the molecular form with more C_1 conformations of the isopropyl parts is more stable than the others.

Stability of Molecular Conformation. For isopropyl methyl selenide, the C_1 form is found to be more stable than the C_s form by 0.52 ± 0.05 kcal mol^{-1} in the liquid

Table 2. Observed and calculated wave numbers of diisopropyl selenide (cm^{-1})[a)]

Liquid			Solid		Calcd[b)]				Assignment[c)]
IR	Raman		IR	Raman	C_2	C_s	C_1	C_{2v}	
1466s			1468s	1477vw					
1456s, sh	1457w	dp	1458m	1459vs	1451A,B	1451A′,A″	1451	$1451A_1,B_1$	$\delta_a CCH_3$
			1447s	1450m					
1443s	1442w	dp	1443s	1441m	1449A,B	1449A′,A″	1449	$1449A_1,B_1$	$\delta_a CCH_3$
			1437s					A_2,B_2	
			1431s						
1382s	1383vw	p	1382s	1384vw	1379A,B	1379A′,A″	1379	$1379A_1,B_1$	$\delta_s CCH_3$
			1376vs					A_2,B_2	
1366s	1368vvw		1368vs	1369vvw					
1313vw, b	1314vw	dp		1314w	1299A	1300A′	1298	$1298A_2$	δCH o.p., $r_s CCH_3$
	1307vvw, sh			1307vvw	1297B	1295A″	1296	$1294B_2$	
1224s, sh	1226m	p	1235vs	1231vs	1224A	1224A′	1225	$1225A_1$	δCH i.p., $r_s CCH_3$
1214vs	1218w, sh	p	1219vs	1218m	1224B	1224A″	1223	$1224B_1$	
			1163m	1164m	1137A	1137A′	1139	$1139A_1$	$r_a CCH_3$, ν_sC–C
1153s	1156vw		1156vs	1156m	1136B	1136A″	1135	$1136B_1$	
			1147w						
1121vw, b	1114vw	dp		1120w	1106A				
	1109vw, sh		1111vw			1104A′	1101	$1100B_2$	ν_aC–C, $r_a CCH_3$
	1100vw, sh		1100vw	1097vw	1097B	1098A″	1098	$1096A_2$	
1041vw			1039m	1043s	1036A	1037A′	1038	$1038B_1$	
	1033w	p	1030vs	1031w	1035B			$1035A_1$	$r_s CCH_3$, δCH i.p.
1023m	1022vw	p				1033A″	1034		
954vw	952vw	dp	958w	952w	975A	974A′	973	$973B_2$	$r_a CCH_3$, ν_aC–C
			939vw		972B	973A″	973	$972A_2$	
925vw	928vvw		923s	927vw	925A	926A′	924	$923A_2$	$r_s CCH_3$, δCH o.p.
					923B	922A″	922	$921B_2$	
881vw	879m		885s	882vvs	877A	877A′	879	$881A_1$	ν_sC–C, $r_a CCH_3$
			877vw, sh	874vw	876B	876A″	876	$876B_1$	
	564vvs	p		563vvs	560B	558A″	568	$570B_1$	ν_aCH–Se
549vw	555s,sh	p	548m	552vvs	553A	554A′			ν_sCH–Se
	529m	p					545	$543A_1$	
424vw	422vw, sh	p	418vw	423s	414A	415A′	422	$430A_1$	δC_2CSe
410vw	413w	p			408B	407A″	407	$407B_1$	
	315w, sh			313m	307A	316A′	318	$304A_1$	
	305w			300s	299B	299A″		$302B_2$	
	275s	p					289		
				268vvw	274B	260A″	264	$272A_2$	
	252w, sh	p		258vs	243A	246A′	254	$252B_1$	
				247vvw	203A	203A″	202	$203A_2$	τCCH_3
				219vvw	202A	202A′	202	$202A_1$	
					201B	202A′	201	$202B_2$	
					199B	200A″	200	$199B_1$	
	125w	dp		139vw	116A	118A′	111	$104A_1$	δCSeC
				99w					τCHSe and lattice vibrations
				80w, sh					
				69vs	59A	56A″	63	$69A_2$	
				45w	55B	56A′	50	$46B_2$	
				36w					

a), b), c) See a), b), and c) of Tabel 1.

state. For isopropyl methyl sulfide, which is one of the $(CH_3)_2CHYCH_3$-type molecules (Y=O, S, and Se), the C_1 form is also more stable than the C_s form by 1—1.5[8a)] and 0.19 ± 0.03 kcal mol^{-1} [8b)] in the liquid state. However, for isopropyl methyl ether the C_1 form has predominantly existed in the liquid state.[7)] On the other hand, in the $CH_3CH_2YCH_3$-type molecules (Y=O, S, and Se), the T form has been more stable than the G form by 1.1—1.5 kcal mol^{-1} in the gaseous and liquid states for ethyl methyl ether,[4)] but the reverse is true for ethyl methyl sulfide ($\Delta H(T-G)=-0.03\pm0.05$ kcal mol^{-1} in the gaseous state[5a)] and -0.14 ± 0.05 kcal mol^{-1} in the liquid state[5b)]) and ethyl methyl selenide ($\Delta H(T-G)=-0.28\pm0.05$ kcal mol^{-1} in the

Table 3. Force constants for branched dialkyl selenides[a)]

Force constant	Value	Force constant	Value
K(C–H),CCH_3	4.198	F(C·C·C)	0.355
K(C–H),CH	4.100	F(C·C·Se)	0.290
K(C–H),$SeCH_3$	4.379	F(C·Se·C)	0.060
K(C–C)	2.144	$\kappa(CCH_3)$	0.024
K(C–Se)	1.356	κ(CH)	−0.053
H(H–C–H),CCH_3	0.370	$\kappa(SeCH_3)$	0.029
H(H–C–H),$SeCH_3$	0.355	$Y(C–CH_3)$	0.076
H(C–C–H),CCH_3	0.194	$Y(Se–CH_3)$	0.047
H(C–C–H),CH	0.177	Y(Se–CH)	0.095
H(Se–C–H),CH	0.044	p(C–H),CCH_3	−0.122
H(Se–C–H),$SeCH_3$	0.035	p(C–H),$SeCH_3$	−0.094
H(C–C–C)	0.358	p(C–Se)	−0.075
H(C–C–Se)	0.208	$n(CCH_3)$	0.021
H(C–Se–C)	0.219	$n(SeCH_3)$	0.014
F(H·C·H)	0.200	$t(CCH_3,CCH)$	0.122
F(C·C·H)	0.540	$g(CCH_3,CCH)$	−0.029
F(Se·C·H)	0.617		

a) The Urey-Bradley force field; the units of the force constants are in mdyn/Å for stretching, K; bending, H; repulsion, F; bond interaction, p; and in mdyn·Å for intramolecular tension, k; torsion, Y; angle interaction between the CCH and HCH angles of methyl group, n; *trans* coupling, t; *gauche* coupling, g.

liquid state[6]).

The above results indicate that for isopropyl methyl sulfide and selenide the C_1 form with fewer methyl-methyl *gauche*-dispositions is more stable than the C_s form with more methyl-methyl *gauche*-dispositions, although for ethyl methyl sulfide and selenide the conformation with the methyl-methyl *gauche*-disposition (the G form) is more stable than the other (the T form). This inconsistency suggests the following. The H···H nonbonded repulsion between the methyl groups may affect the stability of the molecular forms and so the dihedral angles for the *gauche* $CH_3CH_2YCH_3$-type molecules (Y=O, S, and Se) and the C_1 form of the $(CH_3)_2CHYCH_3$-type molecules would be slightly larger than the 60° of the original *gauche* position. The C_s form of the $(CH_3)_2CHYCH_3$-type molecules (Y=O, S, and Se) inevitably has the dihedral angle of 60°. Therefore, the C_1 form may be more stable than the C_s form because of the H···H nonbonded repulsion. For ethyl methyl ether and isopropyl methyl ether with the shorter C–O bond length, the stability of the molecular forms can be interpreted in terms of the larger H···H nonbonded repulsion between the methyl groups.

Recently, Oyanagi and Kuchitsu[13] have reported from an electron diffraction study that the G form of ethyl methyl ether has the dihedral angle of 84±6°, far away from the original *gauche* position, and that the G form of ethyl methyl sulfide has an angle of 66±9°. For the *gauche* $CH_3CH_2YCH_3$-type molecules (Y=O, S, and Se), the nearest H···H nonbonded distances between the methyl groups were calculated by using the structural parameters determined by the electron diffraction study, where the values of ethyl methyl selenide were assumed to be the same as those of ethyl methyl sulfide, except for the C–Se bond of 1.943 Å and the CSeC valence angle of 96° 11′. The dihedral angle ϕ used in the calculation was taken as 60°, the original *gauche* position, and the values determined by the electron diffraction study. The H···H distance calculated is 1.74 Å (ϕ=60°) and 2.09 Å (ϕ=85°) for ethyl methyl ether, 1.95 Å (ϕ=60°) and 2.03 Å (ϕ=66°) for ethyl methyl sulfide, and 2.09 Å (ϕ=60°) and 2.17 Å (ϕ=66°) for ethyl methyl selenide. Therefore, the H···H nonbonded repulsion may rapidly decrease with increasing values of the dihedral angle under a potential such as the Lennard-Jones type. On the other hand, trithia[5]heterohelicene has been shown to have a spiral configuration because of the steric repulsion between the terminal atoms by the X-ray study.[14] The nearest H···H nonbonded distance of the terminal rings has been reported to be 2.15 Å. It should be noted that the nearest H···H nonbonded distance is in the range of about 2.03 to 2.15 Å for ethyl methyl ether with the dihedral angle of 85°, ethyl methyl sulfide with the dihedral angle of 66°, and trithia[5]heterohelicene.

The authors wish to express their thanks to Dr. Hiroatsu Matsuura for his valuable discussion.

Table 4. Observed wave numbers of isopropyl group vibrations[a)]

Description	Ethers[b)]			Sulfides[c)]			Selenides[d)]		
	i-PrOMe	$(i\text{-Pr})_2O$		*i*-PrSMe	$(i\text{-Pr})_2S$		*i*-PrSeMe	$(i\text{-Pr})_2Se$	
CH_3 symmetric deformation	1381	1379		1383	1382		1382	1383	
	1372	1365		1366	1367		1367	1368	
CH out-of-plane bending	1345	1337	1326	1312	1312	1301	1311	1314	1307
CH in-plane bending	1338	1326	1313	1244	1251	1239	1219	1226	1218
CH_3 rocking and C–C stretching	1214	1169	1162	1159	1158	1152	1156	1156	
	1136	1127	1100	1113	1113	1096	1108	1114	1100
	1115	1018	994	1064	1064	1045	1040	1043	1033
	938	938	932	952	952		953	952	
	921	919	908	927	927		925	928	
	799	852	798	884	882		876	879	

a) The vibrations of the C–H stretchings and the CH_3 asymmetric deformations are not included. b) Infrared wave numbers in the solid state. From Ref. 7. c) Infrared wave numbers belonging to the C_1 form in the liquid state. From Ref. 8. d) Raman wave numbers belonging to the C_1 form in the liquid state.

References

1) T. Shimanouchi, Y. Ogawa, M. Ohta, H. Matsuura, and I. Harada, *Bull. Chem. Soc. Jpn.*, **49**, 2999 (1976); M. Ohta, Y. Ogawa, H. Matsuura, I. Harada, and T. Shimanouchi, *ibid.*, **50**, 380 (1977).

2) K. Ohno, T. Hirokawa, S. Aono, and H. Murata, *Chem. Lett.*, **1976**, 1221.

3) K. Ohno, T. Hirokawa, S. Aono, and H. Murata, *Bull. Chem. Soc. Jpn.*, **50**, 305 (1977).

4) T. Kitagawa, K. Kusaki, and T. Miyazawa, *Bull. Chem. Soc. Jpn.*, **46**, 3685 (1973).

5) a) M. Sakakibara, H. Matsuura, I. Harada, and T. Shimanouchi, *Bull. Chem. Soc. Jpn.*, **50**, 111 (1977); b) N. Nogami, H. Sugeta, and T. Miyazawa, *ibid.*, **48**, 3573 (1975).

6) H. Matsuura, K. Ohno, and H. Murata, to be published.

7) A. D. H. Clague and A. Danti, *Spectrochim. Acta, Part A*, **24**, 439 (1968); R. G. Snyder and G. Zerbi, *ibid.*, **23**, 391 (1967).

8) a) M. Ohsaku, Y. Shiro, and H. Murata, *Bull. Chem. Soc. Jpn.*, **45**, 3480 (1972); b) M. Sakakibara, I. Harada, H. Matsuura, and T. Shimanouchi, *J. Mol. Struct.*, **49**, 29 (1978).

9) T. Hashimoto, M. Sugita, H. Kitano, and K. Fukui, *Nippon Kagaku Zasshi*, **88**, 991 (1967); F. Challenger and M. L. Brid, *J. Chem. Soc.*, **1942**, 570.

10) K. Ohno, K. Taga, I. Yoshida, and H. Murata, to be published.

11) Y. Shiro, M. Ohsaku, M. Hayashi, and H. Murata, *Bull. Chem. Soc. Jpn.*, **43**, 619 (1970).

12) D. W. Scott and M. Z. El-Sabban, *J. Mol. Spectrosc.*, **30**, 317 (1969).

13) K. Oyanagi and K. Kuchitsu, *Bull. Chem. Soc. Jpn.*, **51**, 2237; 2243 (1978).

14) M. Imano, Y. Saito, K. Yamada, and H. Kawamo, Molecular Structure Symposium, October 1978, Hiroshima, Japan.

Interaction of Excited Lithium Atom with Molecular Hydrogen. I. Preliminary Potential Energy Surfaces in an OVC MCSCF Approximation

Kimiko MIZUTANI,* Yoshihiro KURIBARA, Kazuko HAYASHI, and Shiro MATSUMOTO

Department of Chemistry, College of Science and Engineering, Aoyama Gakuin University, Chitosedai, Setagaya-ku, Tokyo 157

(Received November 16, 1978)

Potential energy surfaces were computed for the Li–H_2 system of C_{2v} symmetry, which dissociates to a normal hydrogen molecule and a lithium atom either in its ground state or in the ^2P excited state, in order to get an idea of the quenching process of the atom by the molecule. The potential surfaces crossed in a line and two shallow minima appeared on the $^2B_2$ surface. Natural orbital analysis and electron density maps gave information on the charge transfer character of the interaction of the excited atom with the molecule.

Quenching of excited atoms by diatomics is of interest as a prototype of elementary processes involving crossovers between adiabatic potential energy surfaces, *e. g.*, the processes involving the conversion of electronic excitation energies to those of chemical bonds. The present work was undertaken with the view that detailed understanding of the representative case would be an essential step in the clarification of these attractive molecular phenomena.

Bauer and his coworkers[1] published detailed calculations of the quenching process. They described a scheme which could be adjusted to yield results in substantial agreement with experiments in certain important aspects; the gross features of the scheme appeared reasonable from general theoretical points of view. The method they used to construct potential curves, though, involved many arbitrary and *ad hoc* assumptions.

Krauss[2] seems to be the first who undertook to calculate directly the potential curves for the simplest system of the class —Li–H_2. His results contained many important conclusions about the features of the system, which are in agreement with those of the present more comprehensive calculations. A few published[3] and unpublished[4] calculations have been performed for the system since then. Unfortunately, although they used elaborate extended bases and configurational interactions, they were restricted to special geometries of the system. The general description of the processes which occur in the electronic environment when the components come to interact seems, as far as we know, to be undocumented to date.

MCSCF calculations using OVC approximation[5] seem to be one of the reliable means to compute at least qualitatively the electronic structures of simpler systems, when the nuclear geometry is varied. As is well known, however, MCSCF calculations often suffer convergence difficulties, especially when the geometry changes greatly. A number of procedures[6] have been reported to overcome these difficulties. Some earlier calculations in this work were done by a method of direct minimization of the energy functional,[6a] which showed excellent stabilities toward iterations. The convergence of the method was rather slow, however, and most of the later calculations were performed using the coupling operator method proposed by Hirao and Nakatsuji[7] and Carbo,[8] into which quadratic convergency was incorporated.

The present paper reports the preliminary potential energy surfaces of the lowest $^2A_1$ and $^2B_2$ states of the Li–H_2 system in the C_{2v} symmetry. These states seem to be appropriate in describing the quenching process of Li(^2P) by H_2. Some features of the electronic structure of the system at several representative points on the surfaces are given also. The surfaces cross in a line; somewhere around this crossing, non-adiabatic transitions will occur as the result of perturbations. Two shallow minima appear on the $^2B_2$ surface, which may lead to exciplex formation.

Preliminary calculations showed that the potential energy surfaces of two linearly arranged Li–H_2 systems, which correlated to the isolated Li(^2S)+H_2 and to the isolated Li(^2P)+H_2, did cross as in the case of C_{2v} geometry. The lowest point of the crosssection, however, had a much higher (*ca.* 50 kcal/mol) energy than the point for the isolated Li(^2P)+H_2 system. A process *via* such arrangements seems to be inefficient in the quenching of Li(^2P) compared with the process presented above (activation energy≈4 kcal/mol). The results for linear geometry and for the general C_s geometries will be reported later, together with more detailed calculations near the crossing region using extended basis sets.

Method of Calculation

Geometry was restricted to the C_{2v} symmetry shown in Fig. 1. The bases were minimal STO-3G functions, as suggested by Pople *et al.*[9] and full CI was

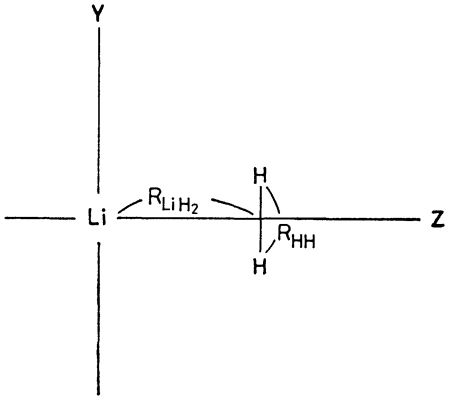

Fig. 1. Geometry of the system.

taken into account.

We take the OVC approximation[5] and express the electronic wavefunction Ψ as a linear combination of configurational wavefunctions differing only in the way the valence electrons occupy the molecular orbitals (MO):

$$\Psi = \sum_i A_i \Psi_{p_i r_i q_i}.$$

Of the five electrons of the system, two are assumed to occupy the core orbital and the remaining three are taken as valence electrons. In Ψ_{prq}, these electrons occupy p, r, and q valence orbitals with α, β, and α spin, respectively. When either p or q coincides with r, there is only one way of constructing a doublet configuration state function (CSF). If this is not the case, there arise two independent doublet CSF's of the same electronic configuration, and their forms are assumed to be

$$\Psi^{(1)}_{prq} = (D_{prq}+D_{rpq})/\sqrt{2}$$
$$\Psi^{(2)}_{prq} = (D_{prq}-D_{rpq}+2D_{pqr})/\sqrt{6},$$

where D_{prq} is the Slater determinant $(5!)^{-1/2}\,|\phi_1(1)\phi_{\bar{1}}(2)\phi_p(3)\phi_{\bar{r}}(4)\phi_q(5)|$. The energy expression for the OVC wave function is written:

$$E=\sum_{m,n}(h_{mn}+H^{core}_{mn})D^{core}_{mn}+\sum_{m,n}^{val.}\sum_{p,q}(C^{pq}h_{mn}+H^{pq}_{mn})b^p_m b^q_n,$$

where b^p_m are the expansion coefficients of the p-th orbital, h_{mn} are the matrix elements of the bare-nucleus Hamiltonian, and D^{core}_{mn} are the elements of the core density matrix $\sum_r^{core} b^r_m b^r_n$. H^{core}_{mn} and H^{pq}_{mn} are defined as

$$H^{core}_{mn} = h_{mn} + \sum_{k,l}\{D^{core}_{kl}+\sum_{p,q}^{val.} C^{pq}b^p_k b^q_l\}(2J_{mnkl}-K_{mnkl}),$$
$$H^{pq}_{mn} = C^{pq}\{h_{mn}+\sum_{k,l}D^{core}_{kl}(2J_{mnkl}-K_{mnkl})\} + \sum_{k,l}\sum_{r,s}^{val.} R^{pq}_{rs}b^r_k b^s_l J_{mnkl},$$

where J_{mnkl} and K_{mnkl} are the coulombic and the exchange repulsion integrals. C^{pq} and R^{pq}_{rs} are the coefficients of averaged occupancies of valence orbitals and have similar meanings to the terms $P^{(s)AO}_{1AB}$ and $P^{(s)AO}_{2ABCD}$ of Ref. 6a. In this special case, they are written as

$$R^{pq}_{rs} = 2\{\sum_{t(\neq r,s)} A_{tpr}A_{tqs}+\sum_{t(\neq p,q)} A_{prt}A_{qst}+\sum_t A_{ptr}A_{qts}\},$$
$$C^{pq} = \sum_t^{val.} R^{tt}_{pq}/2,$$

where A_{prq} are the expansion coefficients in $\Psi = \sum_{p,r,q} A_{prq}D_{prq}$. According to the formulation of Carbo,[8] every molecular orbital wavefunction ϕ^p is an eigenfunction of a coupling operator $\mathbf{R}$.

$$\mathbf{R}|\phi^p\rangle = |\phi^p\rangle\varepsilon^p \qquad (1)$$

When approximate orbital functions given by the last iteration are used as a temporary basis, the matrix elements of $\mathbf{R}$ are given as follows. For diagonal elements:

$$R_{rr} = \sum_i b^r_i F^r_i + \beta_r, \quad R_{vv} = \sum_{i,j} b^v_i H^{occ}_{ij} b^v_j + \beta_v$$

and for non-diagonal elements:

$$R_{rs} = \lambda_{rs}\sum_i (b^r_i F^s_i - b^s_i F^r_i), \quad R_{vr} = \sum_i b^v_i F^r_i,$$

$$R_{vv'} = \sum_{i,j} b^v_i H^{occ}_{ij} b^{v'}_j,$$

where $F^r_i = \sum_{s,j} H^{rs}_{ij} b^s_j$ (r,s: valence), $F^r_i = \sum_j H^{core}_{ij} b^r_j$ (r: core), and $\mathbf{H}^{occ} = 1/2\sum_{p,q}^{occ}(\mathbf{H}^{pq}+\mathbf{H}^{qp})$. Superfixes r and s refer to occupied orbitals and v and v' refer to vacant orbitals. The value β_p is the level shift given to the MO p. The absolute values of the nondiagonal matrix element λ_{rs} were usually taken to be unity. At later stage of iteration using Eq. 1 alone, the convergence was often slow, and quadratic convergency was incorporated into the computing program along with the Newton-Raphson procedure, as done by Hunt, Goddard, and Dunning.[10] The resultant formulation appears to be similar to that given by Hinze.[6b]

Results and Discussion

Potential Energy Surface. The computed energies of the ground state ($^2A_1$) and the first excited state ($^2B_2$) are shown in the contour maps of Figs. 2 and 3, respectively, as functions of two distances R_{HH} and R_{LiH_2}. The first state dissociates to a normal lithium

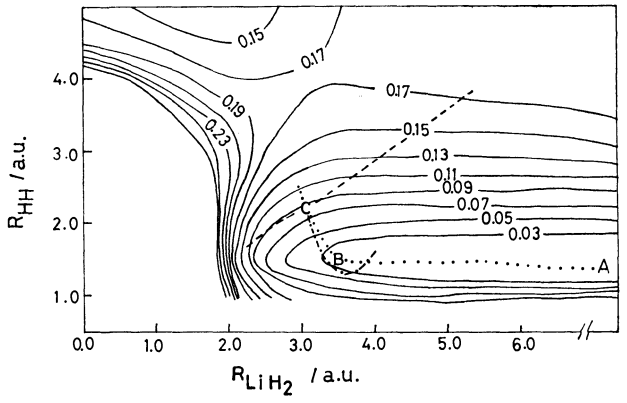

Fig. 2. Potential energy surface for $^2A_1$ ground state. R_{LiH_2} is the distance in bohrs from the Li nucleous to the midpoint of the line connecting the two hydrogens. R_{HH} is the distance between the hydrogens. The figures beside contours are energies in hartrees minus −8.47.

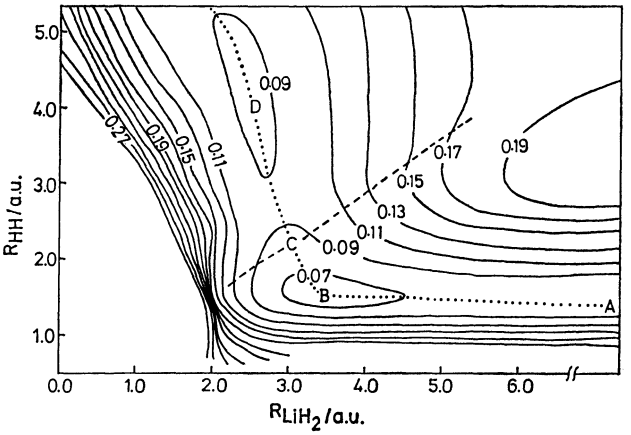

Fig. 3. Potential energy surface for the lowest $^2B_2$ state. The figures beside contours are energies in hartrees minus −8.47.

atom and a hydrogen molecule, while the latter is seen to dissociate to an excited lithium (^2P) atom and a hydrogen molecule in the ground state. The energy surface of the $^2B_2$ state is seen to have two minima, one at $R_{LiH_2}\approx3.5$ a.u., $R_{HH}\approx1.5$ a.u., and the other at $R_{LiH_2}\approx2.5$ a.u., $R_{HH}\approx4.0$ (a.u.). The calculated depth of the former was 9.5 kcal/mol, with respect to the isolated system of Li(^2P) and H_2 ($^1\Sigma_g$). The bottom of the latter was calculated to lie 6.2 kcal/mol above the isolated system, and to be separated by some potential barrier (see below). These minima might correspond to exciplexes, if any exist, between an excited Li atom and a hydrogen molecule. The general appearance of the $^2A_1$ surfaces is similar to that of the $^2B_2$ surface, but no minima appear in the lower-right valley, and the surface in Fig. 2 is more steeply ascending toward the upper-left region than is the $^2B_2$ surface in Fig. 3. The two potential surfaces intersect in a curve, which is shown by broken lines in Figs. 2 and 3.

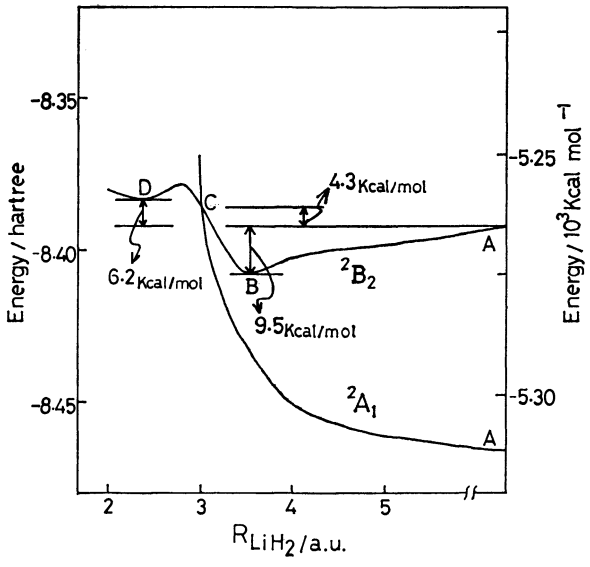

Fig. 4. Energies along minimum energy path.

On these potential surfaces, we might picture the quenching process of excited lithium atoms by hydrogen molecules through geometries close to C_{2v}. Starting from point A in Fig. 3, the path of energetically most favorable approach, *i.e.* the path of quasi-static approach, is shown by the dotted lines in Figs. 2 and 3, and the change of energy along the path is shown schematically in Fig. 4.** The crossing point of $^2A_1$ and $^2B_2$ curves in Fig. 4 is the point of lowest energy on the broken line of Fig. 3. The geometry was found to be $R_{HH}\approx3.0$ a.u. and $R_{LiH_2}\approx2.2$ (a.u.). Activation energy was 4.3 kcal/mol. Transitions at nearby geometries between the surfaces may become possible by contributions of vibrations of appropriate symmetry or by proper

** In actuality, the path would wander somewhat, as is shown partly by the chain line in Fig. 2, thus resulting in a vibrationally excited H_2 molecule. Some coupling of vibrational motion to the translational motion should also exist in the ascending path on the $^2B_2$ surface. To get actual reaction paths is, however, not in the scope of this paper.

TABLE 1. CI WAVE FUNCTIONS OF THE $^2B_2$ STATE AT FOUR TYPICAL GEOMETRIES: A, B, C, AND D, IN Fig. 3

CSF[a]	CI coefficient Geometry			
	A[b]	B[c]	C[d]	D[e]
$1a_1^2 2a_1^2 1b_2$	0.9937	0.9921	0.9823	0.9695
$1a_1^2 3a_1^2 1b_2$	0.0	−0.0320	−0.0422	−0.0685
$1a_1^2 1b_2 1b_1^2$	0.0	0.0023	0.0076	0.0231
$1a_1^2 1b_2 2b_2^2$	0.1121	0.1039	0.1137	0.0475
$1a_1^2 2b_2 1b_1^2$	0.0	0.0008	0.0031	−0.0036
$1a_1^2 2a_1^2 2b_2$	0.0	−0.0039	−0.0122	0.0183
$1a_1^2 3a_1^2 2b_2$	0.0	−0.0032	−0.0120	0.0227
$1a_1^2 4a_1^2 1b_2$	0.0	−0.0006	−0.0007	−0.0059
$1a_1^2 4a_1^2 2b_2$	0.0	0.0	−0.0003	0.0015
$1a_1^2 1b_2^2 2b_2$	0.0	0.0350	0.0924	−0.1227
$1a_1^2 2a_1 3a_1 1b_2$	0.0	−0.0230	−0.0129	−0.1667
$1a_1^2 2a_1 3a_1 1b_2$	0.0	0.0003	−0.0024	−0.0032
$1a_1^2 2a_1 3a_1 2b_2$	0.0	0.0444	−0.0937	0.0702
$1a_1^2 2a_1 3a_1 2b_2$	0.0	−0.0035	−0.0461	0.0602
$1a_1^2 2a_1 4a_1 1b_2$	0.0	0.0	−0.0001	−0.0003
$1a_1^2 2a_1 4a_1 1b_2$	0.0	0.0098	0.0164	0.0071
$1a_1^2 2a_1 4a_1 2b_2$	0.0	−0.0007	−0.0065	0.0139
$1a_1^2 2a_1 4a_1 2b_2$	0.0	0.0064	0.0048	0.0024
$1a_1^2 3a_1 4a_1 1b_2$	0.0	−0.0061	0.0033	0.0003
$1a_1^2 3a_1 4a_1 1b_2$	0.0	−0.0014	0.0010	−0.0006
$1a_1^2 3a_1 4a_1 2b_2$	0.0	−0.0001	−0.0011	0.0025
$1a_1^2 3a_1 4a_1 2b_2$	0.0	0.0004	−0.0019	0.0015

a) Configuration state function. The last twelve CSF's represent six pairs, the two members of each pair corresponding to two different spin states of same configuration. b) $R_{LiH_2}=100$ a.u., $R_{HH}=1.4$ a.u. c) $R_{LiH_2}=3.5$ a.u., $R_{HH}=1.5$ a.u. d) $R_{LiH_2}=3.02$ a.u., $R_{HH}=2.2$ a.u. e) $R_{LiH_2}=2.5$ a.u., $R_{HH}=4.0$ a.u.

TABLE 2. NATURAL ORBITALS CONSTITUTING CONFIGURATIONS IN TABLE 1

Molecular orbital	Basis function	Molecular orbital coefficient Geometry			
		A	B	C	D
ϕ_{1a_1}	H_2 $1\sigma_g$	0.0	−0.0122	0.0037	0.0005
	Li 1s	0.9950	0.9955	0.9950	0.9960
	Li 2s	0.0267	0.0268	0.0253	0.0212
	Li $2p_z$	0.0	0.0002	−0.0023	−0.0055
ϕ_{2a_1}	H_2 $1\sigma_g$	1.0	0.9578	0.8362	0.6164
	Li 1s	0.0	−0.0465	−0.0996	−0.1298
	Li 2s	0.0	0.0464	0.1614	0.4030
	Li $2p_z$	0.0	0.0486	0.1509	0.2488
ϕ_{3a_1}	H_2 $1\sigma_g$	0.0	−0.8300	1.1018	1.2298
	Li 1s	−0.1967	−0.1517	0.1253	0.1181
	Li 2s	0.9819	0.9657	−1.0672	−1.1571
	Li $2p_z$	−0.2542	0.8351	−0.8719	−0.6216
ϕ_{4a_1}	H_2 $1\sigma_g$	0.0	−0.2274	−0.2984	−0.4562
	Li 1s	−0.0517	0.1271	0.1265	0.0936
	Li 2s	0.2581	−0.5766	−0.5100	−0.2526
	Li $2p_z$	0.9671	0.8521	0.9099	1.0591
ϕ_{1b_2}	H_2 $1\sigma_u$	0.0	0.1260	0.3937	0.7666
	Li $2p_y$	1.0	0.9632	0.8030	0.3778
ϕ_{2b_2}	H_2 $1\sigma_u$	1.0	1.0204	0.9780	−0.8300
	Li $2p_y$	0.0	−0.3597	−0.6832	1.0648
ϕ_{1b_1}	Li $2p_x$	1.0	1.0	1.0	1.0

TABLE 3. CI WAVE FUNCTIONS OF THE $^2A_1$ GROUND STATE AT FOUR TYPICAL GEOMETRIES: A, B, C, AND D, IN Fig. 2

CSF	CI coefficient Geometry			
	A	B	C	D
$1a_1^2 2a_1^2 3a_1$	0.9937	0.9921	0.9776	0.3540
$1a_1^2 2a_1 3a_1^2$	0.0	−0.0016	−0.0053	−0.0780
$1a_1^2 2a_1 1b_2^2$	0.0	0.0115	0.0249	0.8903
$1a_1^2 3a_1 1b_2^2$	0.1121	0.1185	0.2033	0.0525
$1a_1^2 2a_1 1b_1^2$	0.0	−0.1160	−0.0181	−0.0187
$1a_1^2 3a_1 1b_1^2$	0.0	0.0024	0.0052	0.0059
$1a_1^2 2a_1 4a_1^2$	0.0	0.0076	0.0088	−0.0169
$1a_1^2 3a_1 4a_1^2$	0.0	0.0254	0.0263	0.0040
$1a_1^2 2a_1 2b_2^2$	0.0	−0.0105	−0.0144	−0.1056
$1a_1^2 3a_1 2b_2^2$	0.0	0.0019	0.0037	0.0452
$1a_1^2 4a_1 1b_2^2$	0.0	−0.0005	−0.0016	0.0050
$1a_1^2 4a_1 2b_2^2$	0.0	0.0015	0.0021	0.0017
$1a_1^2 4a_1 1b_1^2$	0.0	0.0015	0.0021	−0.0005
$1a_1^2 2a_1^2 4a_1$	0.0	−0.0002	0.0001	−0.0076
$1a_1^2 3a_1^2 4a_1$	0.0	0.0091	0.0090	0.0020
$1a_1^2 2a_1 3a_1 4a_1$	0.0	0.0030	0.0026	−0.0035
$1a_1^2 2a_1 3a_1 4a_1$	0.0	0.0018	0.0015	−0.0058
$1a_1^2 2a_1 1b_2 2b_2$	0.0	−0.0197	−0.0298	−0.1716
$1a_1^2 2a_1 1b_2 2b_2$	0.0	−0.0042	−0.0073	0.1152
$1a_1^2 3a_1 1b_2 2b_2$	0.0	0.0001	0.0010	−0.0026
$1a_1^2 3a_1 1b_2 2b_2$	0.0	0.0001	0.0007	−0.1276
$1a_1^2 4a_1 1b_2 2b_2$	0.0	−0.0001	−0.0017	0.0095
$1a_1^2 4a_1 1b_2 2b_2$	0.0	0.0003	0.0007	−0.0115

TABLE 4. NATURAL ORBITALS CONSTITUTING CONFIGURATIONS IN TABLE 3

Molecular orbital	Basis function	Molecular orbital coefficient Geometry A	B	C	D
ϕ_{1a_1}	H_2 $1\sigma_g$	0.0	−0.0060	−0.0022	0.0050
	Li 1s	0.9952	0.9954	0.9957	0.9948
	Li 2s	0.0257	0.0262	0.0239	0.0253
	Li $2p_z$	0.0	0.0031	0.0011	−0.0017
ϕ_{2a_1}	H_2 $1\sigma_g$	1.0	0.9713	0.9033	0.7148
	Li 1s	0.0	−0.0512	−0.0864	−0.1383
	Li 2s	0.0	0.0295	0.0915	0.3538
	Li $2p_z$	0.0	0.0357	0.0988	0.1391
ϕ_{3a_1}	H_2 $1\sigma_g$	0.0	−0.1829	−0.1779	−0.7938
	Li 1s	−0.2024	−0.1820	−0.1683	−0.1512
	Li 2s	1.0152	0.9646	0.9236	1.1191
	Li $2p_z$	0.0	−0.3565	−0.4422	−0.0323
ϕ_{4a_1}	H_2 $1\sigma_g$	0.0	−0.8254	−1.0746	−0.9795
	Li 1s	0.0	−0.0760	−0.0661	0.0033
	Li 2s	0.0	0.5796	0.7509	0.4328
	Li $2p_z$	1.0	1.1391	1.1856	1.2448
ϕ_{1b_1}	H_2 $1\sigma_u$	1.0	1.0045	0.9958	0.7039
	Li $2p_y$	0.0	−0.0202	0.0129	0.4546
ϕ_{2b_1}	H_2 $1\sigma_u$	0.0	−0.2193	−0.3462	−0.8838
	Li $2p_y$	1.0	1.0279	1.0542	1.0344
ϕ_{1b_2}	Li $2p_x$	1.0	1.0	1.0	1.0

deformations from C_{2v} symmetry. Thus the way in which the elcctronic energy is converted to the vibrational and translational energies of the hydrogen molecule may easily be visualized.

Some Remarks on the Wave Function. Tables 1 and 2 show the computed $^2B_2$ wave functions as expressed by natural orbital expansions at four typical geometries on the dotted line in Fig. 3. Tables 3 and 4 show, for comparison, the corresponding $^2A_1$ wave functions at these geometries. As is seen in Table 1, the predominant CSF in the expansion of the $^2B_2$ wave function is always $\Psi_{2a_1 2a_1 1b_1}$. Table 2 shows that the orbitals ϕ_{2a_1} and ϕ_{1b_1} are always bonding in the sense that they pile up electron densities between the Li atom and the H_2 molecule. They are seen, however, to cause electrons to migrate in opposite directions. The occupation of ϕ_{1b_1} means more and more electron migrations from the Li $2p_y$ atomic orbital to the $1\sigma_u$ hydrogen molecular orbital, as we go down the series of geometries from A to D. The occupation of ϕ_{2a_1} means, on the contrary, electron migrations from the fully occupied $1\sigma_g$ hydrogen MO to the nearly sp hybridized Li 2s and $2p_z$ atomic orbitals, though the extent of charge migration is less remarkable than in the case of ϕ_{1b_1}.

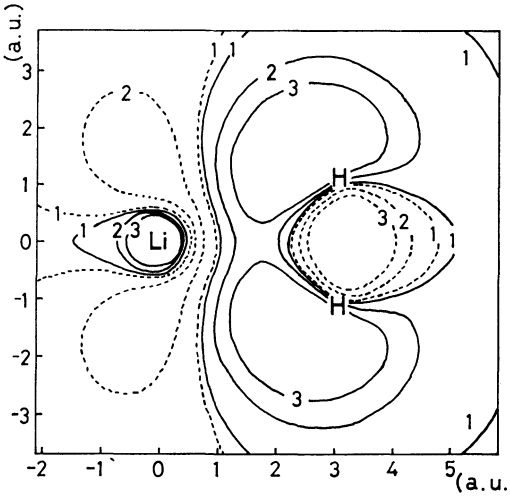

Fig. 5. Contour plots of total electron density of $^2B_2$ state at the geometry C in Fig. 3 minus the density of hypothetical $^2B_2$ state lacking in the interaction between Li and H_2. Full lines correspond to positive and broken lines to negative values of difference. The numbers 1, 2, 3 beside the contours indicate electron density change of 2.0×10^{-4}, 2.0×10^{-3}, 4.0×10^{-3} electrons/a.u.^{3}, respectively.

The predominant configuration in the $^2A_1$ state is $\Psi_{2a_1 2a_1 3a_1}$ for the geometries A, B, and C, but is $\Psi_{2a_1 1b_1 1b_1}$ for the geometry D. In the three former cases, double occupation of ϕ_{2a_1} effects a similar charge migration to that in the $^2B_2$ state and the occupation of ϕ_{3a_1} is seen to affect the charge migration only slightly. The net effect is that the electron transfer in the $^2A_1$ complex is in the opposite direction (from hydrogen toward lithium) to that in the $^2B_2$ complex. This may be important in the stabilization of the $^2B_2$ complex relative to the $^2A_1$ state. The situation at the C geometry is made more visual in Fig. 5, where the electron densities of the $^2B_2$ state minus the electron densities of a hypothetical system, in which the interactions between Li and H_2 have been artificially removed, are

plotted as contour lines: full-lines indicate an increase and dotted lines indicate a decrease in electron densities upon interaction. As noted above, the predominant configurations of the $^2A_1$ state at the D geometry has changed to $\Psi_{2a_1 1b_1 1b_1}$. In this case, the occupation of ϕ_{1b_1} also causes electrons to migrate from H_2 to Li, though the region of charge redistribution is different from that in the ϕ_{2a_1}. Fuller account of the analysis of the situation will be given in a succeeding paper.

The potential surfaces and electronic wave functions given here are preliminary in that the basis functions used are limited. It is hoped, however, that the results are at least qualitatively correct[4] and will be a useful starting point for more quantitative investigations. Work is going on to extend the bases to reach wave functions which could be used in a quantitative description of the non-adiabatic transitions in the interaction of excited atoms with molecules.

The authors wish to thank Dr. S. Iwata of the Institute of Physical and Chemical Research for his helpful discussions. They also express their gratitude to the Aoyama Gakuin Computing Center, where all computations were carried out on an IBM 370-138. Thanks are due to Miss J. Okamura, Miss J. Oga, Miss K. Yahata, and Mr. H. Miyoshi for their help in these computations.

References

1) E. Bauer, E. R. Fisher, and F. R. Gilmore, *J. Chem. Phys.*, **51**, 4173 (1969).
2) M. Krauss, *J. Res. Natl. Bur. Stand., Sect. A* **72**, 553 (1968).
3) P. J. A. Ruttink and J. H. van Lenthe, *Theor. Chim. Acta*, **44**, 97 (1977).
4) H. F. Schaefer III, "Method of Electronic Structure Theory," Plenum Pub. Corp., New York (1976), p. 51.
5) A. C. Wahl and G. Das, *Adv. Quant. Chem.*, **5**, 261 (1970); G. Das and A. C. Wahl, *J. Chem. Phys.*, **44**, 87 (1966); *ibid.*, **56** 3532 (1972).
6) a) S. Polezzo, *Theor. Chim. Acta*, **40**, 245 (1975); P. Fantucci and S. Polezzo, *ibid.*, **44**, 421 (1977); b) J. Hinze, *J. Chem. Phys.*, **59**, 6424 (1973); c) G. Das and A. C. Wahl, *ibid.*, **56** 1769 (1972).
7) K. Hirao and H. Nakatsuji, *J. Chem. Phys.*, **59**, 1457 (1973).
8) R. Carbo, R. Gallifa, and J. M. Riera, *Chem. Phys. Lett.*, **33**, 545 (1975).
9) W. J. Hehre, R. F. Stewart, and J. A. Pople, *J. Chem. Phys.*, **51**, 2657 (1969).
10) W. J. Hunt, W. A. Goddard, III, and T. H. Dunning, Jr., *Chem. Phys. Lett.*, **6**, 147 (1970).

Deuterium Tracer Study on Isomerization of Cyclopropane over Thorium Sulfate

Yuzo IMIZU, Hideshi HATTORI,* Kozo TANABE, and Toshihiko KONDO**

Department of Chemistry, Faculty of Science, Hokkaido University, Sapporo 060
***Sagami Chemical Research Center, Nishi-Ohnuma 4-4-1, Sagamihara 229*

(Received December 4, 1978)

Mechanistic study on the isomerization of cyclopropane into propene was made over $Th(SO_4)_2$ catalyst. With a fresh catalyst, an induction period was observed, disappearing in successive runs. Coisomerization of cyclopropane d_0/d_6 reveals that the reaction involves an intermolecular H(or D) transfer. Nearly random location of the H(or D) atom in the mono-exchanged propene-d_1, and -d_5 indicates that the isomerization proceeds *via* nonclassical carbonium ion in which seven hydrogen atoms are equivalent.

The isomerization of cyclopropane to propene is catalyzed by acidic oxides[1] and crystalline zeolites.[2] Deuterium tracer studies have been made over silica–alumina[3,4] and sodium Y zeolite.[5] On the basis of deuterium distributions in the reactant and product together with the kinetic data over silica–alumina, Hightower and Hall presented the non-classical carbonium ion of cyclopropane as an intermediate in which seven hydrogen atoms are equivalent.[3,4] Bartley *et al.* proposed a different type of nonclassical carbonium ion intermediate in which the hydrogen atom added is not equivalent to the original six hydrogen atoms.[5] They suggested that an intramolecular hydrogen transfer occurs after the ring of the nonclassical carbonium ion is opened, since the reaction partly involves an intramolecular hydrogen transfer.

However, the above discussions are based primarily on the deuterium contents of the reactant and product. The location of deuterium and hydrogen atoms in propene would provide important information as to whether the hydrogen atom added in the intermediate is equivalent to the original hydrogen atoms.

The present study was undertaken to elucidate the intermediate of the isomerization of cyclopropane over an acidic catalyst, thorium sulfate, by deuterium tracer studies. The locations of hydrogen and deuterium atoms in propene were determined by microwave spectroscopy.[6]

Experimental

Catalyst and Reactants. Thorium sulfate was obtained by heating its hydrated form (Wako Pure Chemical Ind., Ltd.) at 500 °C for 3 h in air. Prior to reaction, the catalyst was pretreated with O_2 at 500 °C followed by evacuation at 500 °C for more than 3 h. The BET surface area was 5 m^2/g.

Cyclopropane of 99.8% purity was supplied by Tokyo Kasei Ind., Ltd. Perdeuteriocyclopropane was prepared by repeated exchange reactions of cyclopropane with D_2 over aluminum oxide (Nishio AE 11) at 100 °C.[7] The isotopic purity was higher than 98.0%. The reactants were purified by passage through 4A molecular sieves at −94 °C.

Apparatus and Procedure. A 47 Torr of cyclopropane was allowed to react over 0.1—1 g of catalyst at 80—200 °C in *ca.* 400 ml of a recirculation reactor. The products were separated by gas chromatographic column of VZ-7 (5 m), collected in a liquid N_2 trap, and subjected to mass and microwave spectroscopic analyses in order to determine the deuterium content and the location of deuterium atoms in the product, respectively.

Results and Discussion

Cyclopropane underwent isomerization at 80 °C to yield only propene over a freshly pretreated catalyst with an induction time of 20 min. In the subsequent experiment carried out after brief evacuation at the reaction temperature, isomerization occurred without the induction time, a decrease in rate to some extent being observed (Fig. 1). The isomerization rate was of zero order in cyclopropane. The induction time was prolonged with lowering of reaction temperature. This indicates that the active sites are formed by the interaction of the substrate with a freshly pretreated surface. As observed for the other solid acid catalysts,[3,4] it is suggested that the active sites on $Th(SO_4)_2$ are polymeric residues which supply the protons to act as the Brönsted acid sites.

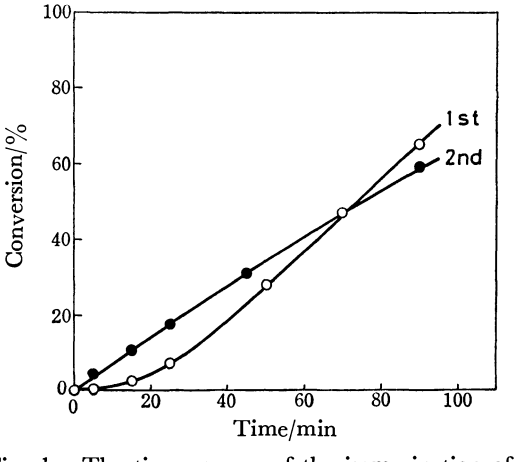

Fig. 1. The time courses of the isomerization of cyclopropane over $Th(SO_4)_2$ at 80 °C in the initial run (○) and in the successive run (●).

Coisomerization experiments were carried out at 100 °C and 200 °C with a mixture containing equal amounts of nondeuterio and perdeuteriocyclopropanes. Isotopic distributions at the two reaction temperatures were similar, those at 100 °C being given in Table 1. The product consisted primarily of non-exchanged isotopic species, d_0 and d_6, and mono-exchanged isotopic species, d_1 and d_5. The numbers of hydrogen atoms

Table 1. Coisomerization of cyclopropane-d_0 and -d_6 over thorium sulfate[a)]

Reaction time, h	Product	% each product	% isotopic species d_0	d_1	d_2	d_3	d_4	d_5	d_6	Atoms exchanged/ molecule[b)]	Ratio of light molecule/ heavy molecule[c)]
0.00	Cyclopropane	100.0	49.5	0	0	0	0	0.9	49.6	0.009	0.980
0.33	Propene	0.7	35.6	14.0	0	0	0	21.3	29.1	0.353	0.984
	Cyclopropane	99.3	50.8	0	0	0	0	1.0	48.2	0.010	1.033
1.00	Propene	2.9	26.7	15.7	0	0	0.5	23.7	33.4	0.404	0.736
	Cyclopropane	97.1	49.5	0	0	0	0	1.3	49.2	0.013	0.980
2.00	Propene	7.7	26.2	17.1	0.3	0	0.7	23.3	32.4	0.424	0.773
	Cyclopropane	92.3	47.6	1.2	0	0	0	1.9	49.3	0.031	0.953
3.00	Propene	12.2	24.5	16.9	0.6	0	0.9	24.0	33.1	0.439	0.724
	Cyclopropane	87.8	48.2	2.1	0	0	0	2.7	47.0	0.048	1.012
6.00	Propene	24.6	22.2	16.9	1.2	0	1.6	25.0	33.1	0.475	0.675
	Cyclopropane	75.4	46.3	5.0	0	0	0	4.5	44.2	0.095	1.053

a) 45.4 Torr of cyclopropane, 100 °C, 150.7 mg of catalyst. b) Calculated from $\sum_{i=0}^{2} i \cdot N_i + \sum_{i=3}^{6} (6-i) \cdot N_i$, N_i; mole fraction of isotopic species containing i deuterium atoms.[3)] c) Calculated from $(\sum_{i=0}^{2} N_i + N_3/2)/(\sum_{i=4}^{6} N_i + N_3/2)$[3)]

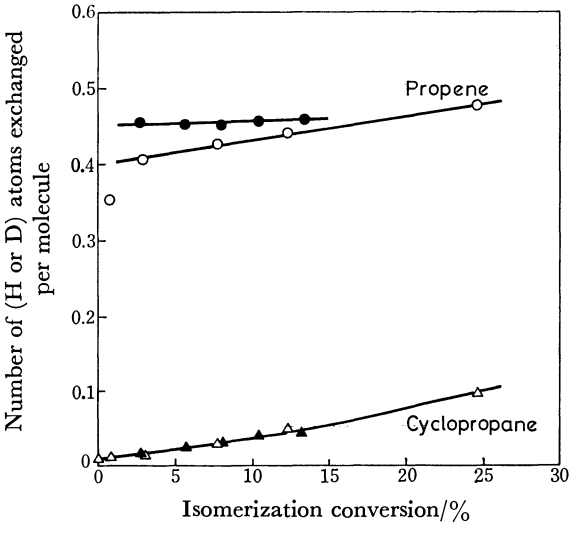

Fig. 2. Exchange concentration curves for coisomerization of cyclopropane-d_0 and -d_6 over $Th(SO_4)_2$. Open symbol: 100 °C, solid symbol: 200 °C.

exchanged per molecule at 100 °C and 200 °C are plotted against conversion in Fig. 2. Hydrogen atoms were exchanged into the unisomerized cyclopropane as well as the product. The superposition of the exchanged concentration curves for cyclopropane at the different reaction temperatures indicates that the activation energy for the exchange process is close to that for isomerization. A similar slope of the curves for cyclopropane and propene indicates that there is little further intermolecular scrambling of hydrogen atom among the propene molecules produced; this is consistent with the limitation of hydrogen exchange mainly to the mono-exchanged isotopic species. The zero conversion intercept of nearly 0.5 for propene demonstrates that one hydrogen atom per molecule is transferred intermolecularly during the course of isomerization.

If the reaction proceeds *via* classical carbonium ions in which no intramolecular hydrogen exchange occurs, the hydrogen atom added would be always left in the product molecule and the original hydrogen atom would be lost on the surface. The intercept for the exchange concentration curve for the product in the coisomerization experiment is expected to be 1/2. On the other hand, if the proton attacks the cyclopropane molecule to form a protonated nonclassical carbonium ion in which seven hydrogen atoms are equivalent, the hydrogen atom added has the same probability of being lost as the original hydrogen atoms when the reaction is completed. As a result, the intercept of the exchange concentration curve will be 6/14. The observed values of 0.45 and 0.40 at 200 °C and 100 °C, respectively, are close to 6/14. The ratio of light molecule (d_0—d_2) to heavy molecule (d_4—d_6) is plotted against conversion in Fig. 3. The zero conversion intercept divided by the initial ratio of light molecule to heavy molecule of reactant gives a kinetic isotope effect. The isotope effect was small or slightly inverse.

The locations of the deuterium atom in propene-d_1

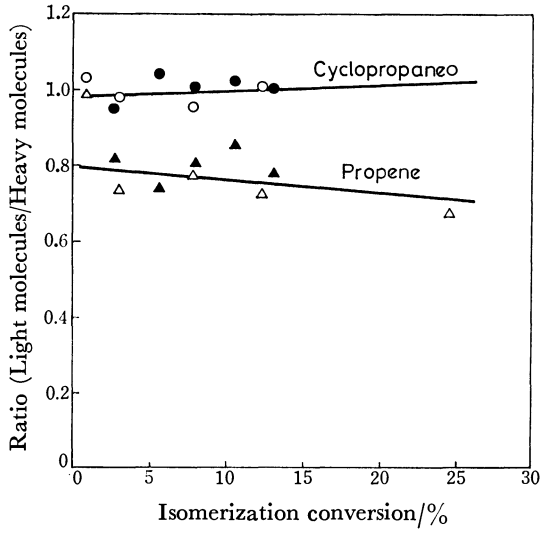

Fig. 3. The ratios of "light molecules" to "heavy molecules" with the conversion in the coisomerization of cyclopropane-d_0 and -d_6 over $Th(SO_4)_2$. Open symbol: 100 °C, solid symbol: 200 °C.

Table 2. Mass spectrometric and microwave spectroscopic analyses of products formed in the coisomerization of cyclopropane-d_0 and -d_6 at 100 °C

	Product	% each isotopic species						
		d_0	d_1	d_2	d_3	d_4	d_5	d_6
3.9% conversion	Propene	28.4	17.2	0.1	0	0.5	22.9	30.9
	Cyclopropane	50.0	0.2	0	0	0	1.1	48.7
	Location of D in propene-d_1	%		Location of H in propene-d_5		%		Random distribution %
	(Z)-1-d_1 [a)]	14.4		(Z)-1-h_1 [a)]		—		33.3
	(E)-1-d_1 [a)]	13.8		(E)-1-h_1 [a)]		—		
	2-d_1	13.0		2-h_1		—		16.7
	3-d_1	58.8		3-h_1		—		50.0
	Product	% each isotopic species						
		d_0	d_1	d_2	d_3	d_4	d_5	d_6
21.2% conversion	Propene	24.4	17.7	1.1	0	1.4	23.3	32.1
	Cyclopropane	47.9	3.3	0	0	0	3.3	45.5
	Location of D in propene-d_1	%		Location of H in propene-d_5		%		Random distribution %
	(Z)-1-d_1 [a)]	14.7		(Z)-1-h_1 [a)]		15.9		33.3
	(E)-1-d_1 [a)]	15.6		(E)-1-h_1 [a)]		19.1		
	2-d_1	11.8		2-h_1		9.2		16.7
	3-d_1	57.9		3-h_1		55.8		50

a); (Z)-1-d_1 (E)-1-d_1 (Z)-1-h_1 (E)-1-h_1

and of the hydrogen atom in propene-d_5 produced in the coisomerization are given in Table 2. The deterium or hydrogen atom was distributed throughout almost all positions instead of being localized at a certain carbon atom. This strongly suggests that the reaction proceeds *via* the nonclassical carbonium ion in which seven hydrogen atoms are equivalent.

If the reaction proceeded *via* classical carbonium ion, the distribution of hydrogen and deuterium atoms might be as follows. 1) A fast intramolecular H transfer occurs after the ring is opened. 2) An intermolecular hydrogen exchange occurs among the propene molecules produced. However, case 1) can be eliminated since the hydrogen transfer should involve the conversion of a stable secondary propyl cation into an unstable primary propyl cation, while in case 2), an extensive hydrogen scrambling among the products should proceed, which was not observed.

Thus, the reaction mechanism is suggested to be as follows: the nonclassical carbonium ion (protonated cyclopropane) is formed by the interaction of cyclopropane with a proton supplied by the surface residue followed by the opening of the ring to yield propene *via* primary propyl cation. The same intermediate, which discharges a proton to the surface and returns to the gas phase without the ring being opened, accounts for the incorporation of hydrogen or deuterium atoms into unisomerized cyclopropane.

This mechanism has been proposed for the reaction over silica–alumina[3,4] without determination of the location of hydrogen or deuterium atom in the product. By analysis of the position of deuterium and hydrogen

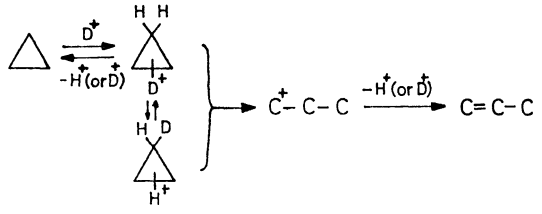

atoms in the product by microwave spectroscopy, the proposed mechanism became more plausible.

Neither kinetic isotope effect nor slightly reverse isotope effect appeared for the formation of propene. The cleavage of C–H bond should be fast. The slow step involves either the protonation to cyclopropane or the C–C bond cleavage of the protonated cyclopropane. Since, in both cases, the exchange concentration curves for cyclopropane at different temperatures are on the same line, the energy barriers to cyclopropane and to primary propyl cation from the nonclassical carbonium ion are similar.

References

1) R. M. Roberts, *J. Phys. Chem.*, **63**, 1400 (1959).
2) D. W. Bassett and H. W. Habgood, *J. Phys. Chem.*, **64**, 769 (1960).
3) J. W. Hightower and W. K. Hall, *J. Am. Chem. Soc.*, **90**, 851 (1968).
4) J. W. Hightower and W. K. Hall, *J. Phys. Chem. Soc.*, **72**, 4555 (1968).
5) B. H. Bartley, H. W. Habgood, and Z. M. George, *J. Phys. Chem.*, **72**, 1689 (1968).
6) T. Kondo, S. Saito, and K. Tamaru, *J. Am. Chem. Soc.*, **96**, 6857 (1974).
7) J. G. Larson, J. W. Hightower, and W. K. Hall., *J. Org. Chem.*, **31**, 1225 (1966).

Singlet Excitation Energy Migration in the Glassy Organics Blended with Polymer

Yumiko SANO, Yasuhiko SHIROTA, and Hiroshi MIKAWA*

Department of Applied Chemistry, Faculty of Engineering, Osaka University, Yamadakami, Suita, Osaka 565

(Received December 6, 1978)

Studies have been made of the singlet excitation energy migration of 1,3-diphenyl-5-(*p*-chlorophenyl)-2-pyrazoline in a glassy state blended with an ethylene–vinyl acetate copolymer by the fluorescence quenching method. The results are discussed in terms of the simple random energy migration model, showing that the efficiency of the singlet excitation energy migration does not differ between the glassy state and the polymer blend system.

Many organic photoconductors have been reported to function as photosensitive material for use in electrophotography. Among others, poly(*N*-vinylcarbazole) (PVCz) films sensitized with dyes such as benzopyrylium dyes[1–3] and the charge-transfer complex of PVCz with 2,4,7-trinitro-9-fluorenone (TNF)[4] are in commercial use. For the application of organic photoconductors to electrophotography, they are usually used as a blend system with an appropriate polymer which acts as a binder. Poly(*N*-vinylcarbazole) is also mixed with an appropriate polymer in order to improve the mechanical properties of the film. In the layered photoconductive system recently developed, organic photoconductors are dispersed in polymer materials.[5,6] Other blend systems of organic photoconductors with polymers have also been reported.[7]

From both scientific and practical aspects, it is of interest to investigate the transport phenomena in the photoconductor-polymer blend system. Studies have been carried out in detail on the carrier transport in the PVCz–TNF system.[8] The migration of the excitation energy in polymer blend systems has not been much investigated,[9–11] but it is an important precursory process for the photocarrier generation.

1,3,5-Triaryl-2-pyrazolines form a glassy state near room temperature, which is kept for quite a long period of time.[12,13] They have an intense fluorescent characteristic[14] and a photoconductive property.[15] We have made comparative studies of the singlet excitation energy migration of 1,3-diphenyl-5-(*p*-chlorophenyl)-2-pyrazoline in the glassy and single crystalline states.[16] This compound is miscible with ethylene–vinyl acetate copolymer giving a transparent material over a wide blend ratio from the excess of pyrazoline to the excess of polymer. Thus the system may be appropriate for investigating the singlet excitation energy migration in the photoconductor-polymer blend system.

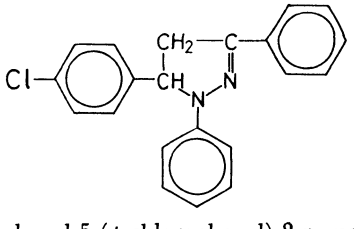

1,3-diphenyl-5-(*p*-chlorophenyl)-2-pyrazoline

Experimental

Materials. 1,3-Diphenyl-5-(*p*-chlorophenyl)-2-pyrazoline (glass transition point 16.5 °C) was prepared and purified by the zone refining technique. Dimethyl terephthalate was purified by repeated recrystallization from ethanol and then by sublimation.

Evaflex 210, a random copolymer of ethylene (*ca.* 72 wt %) and vinyl acetate (*ca.* 28 wt %) which softens at 80 °C (Mitsui Polychemicals Co., Ltd.) was reprecipitated four times from benzene with methanol. The polymer has low viscosity and is transparent after cycles of melting and cooling, the glass transition temperature being below −50 °C.

*Preparation of the Blend of 1,3-Diphenyl-5-(*p*-chlorophenyl)-2-pyrazoline and the Polymer.* 1,3-Diphenyl-5-(*p*-chlorophenyl)-2-pyrazoline doped with dimethyl terephthalate was prepared in a high vacuum. The doped material was diluted further with pure 1,3-diphenyl-5-(*p*-chlorophenyl)-2-pyrazoline and blended with the polymer in a pyrex glass tube (diameter 1.5 mm) by melting them together under a nitrogen atmosphere, degassed and sealed in a high vacuum (3×10^{-6} mmHg). The samples thus prepared were immediately cooled down to a liquid nitrogen temperature (77 K). This is a convenient method for keeping the samples transparent at room temperature.

Measurement. The degassed samples were subjected to measurement without being taken out from the pyrex glass tube in order to avoid exposure of the samples to oxygen. The fluorescence intensity was measured with a Hitachi fluorescence spectrophotometer MPF-3 by using a special sample holder which can hold the sample tube in a fixed position at constant temperature (10 °C).

Results and Discussion

The absorption and fluorescence spectra of 1,3-diphenyl-5-(*p*-chlorophenyl)-2-pyrazoline in the glassy state are shown in Figs. 1(a) and (b), respectively. Even when the pure 1,3-diphenyl-5-(*p*-chlorophenyl)-2-pyrazoline glass is mixed with an equal amount of ethylene–vinyl acetate copolymer, the shape of the fluorescence spectrum remains unchanged (curve c). When pure 1,3-diphenyl-5-(*p*-chlorophenyl)-2-pyrazoline is mixed with a small amount of dimethyl terephthalate, the fluorescence of 1,3-diphenyl-5-(*p*-chlorophenyl)-2-pyrazoline is partially quenched. Figure 1(d) shows the reduced fluorescence of pure 1,3-diphenyl-5-(*p*-chlorophenyl)-2-pyrazoline when $\approx10^{-3}$ mol/mol of dimethyl terephthalate is doped. The copolymer does not work as a trapping center of the pyrazoline excitation energy.

In the present study, the quenching of the fluorescence of 1,3-diphenyl-5-(*p*-chlorophenyl)-2-pyrazoline in the polymer matrix was investigated by doping dimethyl terephthalate as a quencher. When the polymer

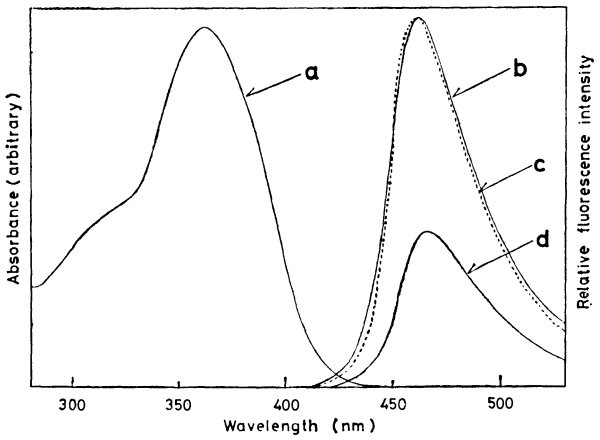

Fig. 1. Absorption and fluorescence spectra of 1,3-diphenyl-5-(*p*-chlorophenyl)-2-pyrazoline in the glassy state. (a) Absorption spectrum; (b) fluorescence spectrum; (c) fluorescence spectrum when mixed with an equal amount of ethylene–vinyl acetate copolymer, the spectrum being normalized at the fluorescence peak of curve (b); (d) fluorescence quenching by 10^{-3} mol/mol dimethylterephthalate.

content is less than 20%, *viz.*, the content of 1,3-diphenyl-5-(*p*-chlorophenyl)-2-pyrazoline exceeds 80%, no perfectly homogeneous transparent samples can be prepared, apparently due to the phase separation in the micro scale. Examination was therefore made with polymer content of more than 20%.

For such a homogeneous system, the Stern-Volmer type equation is expected to hold for the fluorescence quenching:

$$\frac{F_0(p)}{F(p)} = 1 + K_{sv}(p)\frac{(1-p)N_g}{N_h} \qquad (1)$$

where $F_0(p)$ and $F(p)$ are the fluorescence intensity of the pyrazoline in the absence and presence, respectively, of the quencher, in a system containing the polymer of the fraction p of the total. $K_{sv}(p)$ is the quenching constant, and N_h and N_g are the number of host and guest molecules, respectively. Since p stands for the volume fraction of the polymer, the quencher concentration is $N_g/[(N_h+N_g)/(1-p)] \fallingdotseq (1-p)N_g/N_h$. Figure 2 shows the Stern-Volmer plot for a system containing 80% polymer. As expected, the plot shows approximate linearity.

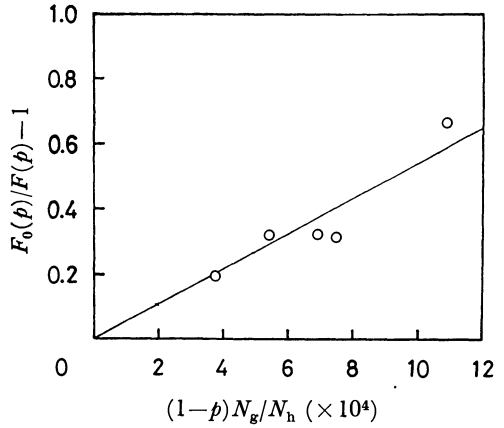

Fig. 2. Fluorescence quenching of 1,3-diphenyl-5-(*p*-chlorophenyl)-2-pyrazoline in the ethylene–vinyl acetate copolymer matrix with dimethylterephthalate as a quencher. The polymer content is 80% by weight, which is almost equal to the volume %, if the specific volume of the polymer is assumed to be approximately equal to that of the pyrazoline. Based on this approximation, p represents the volume fraction of the polymer, $p=0.8$.

Equation 1 can be derived also in terms of a simple model of random energy migration. In the present system, energy migration from pyrazoline molecules to the polymer is energetically impossible. Thus the excitation energy migration should take place only from pyrazoline to pyrazoline. The probability of some site being the guest molecule should be $N_g/(N_h+N_g)/(1-p)$. Since the probability of an excited state at some site to migrate to the next site during the course of energy dissipation is $k_m(p)/(k_f(p)+k_i(p)+k_m(p))$, the probability $P_m(p)$ of the excited state reaching the guest molecule is

$$P_m(p) = \sum_{n=1}^{\infty}\left(\frac{k_m(p)}{k_f(p)+k_i(p)+k_m(p)}\right)^{n-1}\left(1-\frac{N_g}{N_h+N_g}\right)^{n-1}_{1-p} \times \frac{k_t(p)}{k_f(p)+k_i(p)+k_m(p)+k_t(p)}\frac{N_g}{N_h+N_g}_{1-p}$$

where $k_f(p)$, $k_i(p)$, and $k_m(p)$ are the rate parameters for radiative decay, non-radiative decay and migration, respectively, of the excitation energy in the pyrazoline-polymer blend system. $k_t(p)$ is the rate parameter for energy trapping by the guest molecule. In the case $k_t(p) \gg k_m(p)$, the above equation is written as

$$P_m(p) = \sum_{n=1}^{\infty}\left(\frac{k_m(p)}{k_f(p)+k_i(p)+k_m(p)}\right)^{n-1}\left(\frac{N_h+pN_g}{N_h+N_g}\right)^{n-1} \times \frac{(1-p)N_g}{N_h+N_g}.$$

The probability $P_f(p)$ with which the excited state releases the energy as fluorescence would be $P_f(p)=(1-P_m(p))k_f(p)/(k_f(p)+k_i(p))$. Since $F_0(p)/F(p)$ is the ratio of the fluorescence intensities for $N_g=0$ and $N_g=N_g$, which should be proportional to the probability $P_f(p)$, we can get Eq. 2 which is the same as Eq. 1 with $K_{sv}(p)=k_m(p)/(k_f(p)+k_i(p))$.

$$\frac{F_0(p)}{F(p)} = 1 + \frac{k_m(p)}{k_f(p)+k_i(p)}\frac{(1-p)N_g}{N_h} \qquad (2)$$

Since $1/(k_f(p)+k_i(p))$ is lifetime (τ_0) of the excited state of the pyrazoline in the absence of the quencher molecule, $k_m(p)/(k_f(p)+k_i(p))=n(p)$ is the number of hops of the singlet excitation energy over the pyrazoline molecules within its lifetime. The experimental results shown in Fig. 2 give the value $n(0.8)=538\pm32$. This does not differ within experimental errors from the value obtained for the pure glassy state of the pyrazoline $n(0)=523\pm9$.[16] This indicates that the number of hops $n(p)$ of the singlet excitation energy within its lifetime does not differ between the pure glassy state and the polymer blend system ($p=0.8$). In order to

confirm this for a wider range of the polymer content, it is necessary to carry out a series of similar fluorescence quenching experiments over various polymer contents; however, the following simple method was employed instead.

$F_0(p)/F(p)$ is plotted against the varying $(1-p)$ for Eq. 2 by keeping N_g/N_h constant and varying only the amount of the polymer (p). The amount of quencher molecule in the system is thus continuously varied by a factor $(1-p)$. Consequently, if $n(p)$ is independent of the polymer content as actually found to be the case for $p=0.8$, the plot of $F_0(p)/F(p)$ *vs.* varying $(1-p)$ (more strictly *vs.* $(1-p)N_g/N_h$ with constant N_g/N_h) for Eq. 2 would give a straight line; if $n(p)$ varies with polymer content the plot would not be linear.

1,3-Diphenyl-5-(*p*-chlorophenyl)-2-pyrazoline containing 2.70×10^{-3} mol/mol of dimethyl terephthalate was prepared first and the doped pyrazoline was mixed with various amounts of the ethylene–vinyl acetate copolymer. The intensity of the fluorescence of the samples, $F(p)$, and that of each corresponding mixture of the undoped pyrazoline with the polymer, $F_0(p)$, were measured, the values of $F_0(p)/F(p)-1$ being plotted against $(1-p)$. As shown in Fig. 3, the results (open circles) lie on a straight line over the polymer content range from 90% $(1-p=0.1)$ to pure pyrazoline $(1-p=1.0)$. The black circle represents the value for the pure pyrazoline glass. The linearity indicates that $n(p)=k_m(p)/(k_f(p)+k_i(p))$ remains unchanged irrespective of the difference in polymer content. The results indicate that $k_m(p)$ is independent of polymer content, since the lifetime of the excited state, $\tau_0=1/(k_f(p)+k_i(p))$, is practically independent of polymer content.

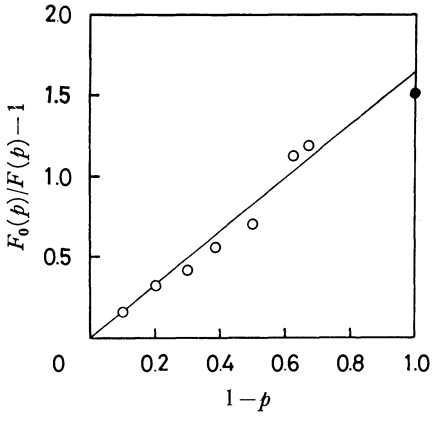

Fig. 3. Plot of $F_0(p)/F(p)-1$ as a function of $1-p$. $F_0(p)$ and $F(p)$ are the fluorescence intensities of the undoped and the doped materials, respectively, when the ethylene–vinyl acetate copolymer is blended with the fraction of p.

The efficiency of the singlet energy migration of 1,3-diphenyl-5-(*p*-chlorophenyl)-2-pyrazoline was found to be invariable between the pure glassy state and the polymer blend system over a wide range of polymer content when suitable polymers inert to excited molecules are chosen.

References

1) Y. Murakami and K. Morimoto, U. S. Patent 3 526 502 (1970).
2) Y. Murakami and K. Morimoto, U. S. Patent 3 712 811 (1972).
3) Y. Murakami and K. Morimoto, Brit. Patent 1 353 264 (1974).
4) R. M. Schaffert, *IBM J. Res. Develop.*, **75**, Jan (1971).
5) Y. Hayashi, M. Hasegawa, and E. Ando, *SPSE 25 Ann. Conf.*, April, 1972.
6) P. J. Melz, R. B. Champ, L. S. Chang, C. Chiou, G. S. Keller, L. C. Liclican, R. R. Neiman, M. D. Shattuck, and W. J. Weiche, *Photogr. Sci. Eng.*, **21**, 73 (1977).
7) P. Borsenberger, A. Chowdry, W. Dulmage, D. Hoesterey, W. Light, S. Marino, W. Mey, C. Salzberg, D. Smith, and W. Staudenmayer, Third International Conference on Electrophotography, November 15—18, 1977, Washington D. C., preprint p. 31.
8) W. D. Gill, *J. Appl. Phys.*, **43**, 5033 (1972).
9) R. Katraro, A. Ron, and S. Speiser, *Chem. Phys. Lett.*, **52**, 16 (1977).
10) R. D. Burkhart and E. R. Lonson, *Chem. Phys. Lett.*, **54**, 85 (1978).
11) N. J. Turro, I. E. Kochevar, Y. Noguchi, and M. Chow, *J. Am. Chem. Soc.*, **100**, 3170 (1978).
12) K. Kato, M. Yokoyama, Y. Shirota, H. Mikawa, M. Sorai, H. Suga, and S. Seki, "Energy and Charge Transfer in Organic Semiconductors," ed by K. Masuda and M. Silver, Plenum Publishing Corp. (1972), p. 77.
13) Y. Sano, K. Kato, M. Yokoyama, Y. Shirota, and H. Mikawa, *Mol. Cryst. Liq. Cryst.*, **36**, 137 (1976).
14) I. H. Leaver, *Mol. Photochem.*, **5**, 411 (1973) and references cited therein.
15) Japanese Patent Application Disclosure No. 5466 of 1959, Kalle and Company, A. G.
16) Y. Sano, M. Yokoyama, Y. Shirota, and H. Mikawa, *Mol. Cryst. Liq. Cryst.*, in press (1979).

Determination of Heats of Adsorption of Triphenylchloromethane from Its Hexane Solution onto Dehydrated Silica-Alumina Surface

Hitofumi TANIGUCHI,* Tatsuo MASUDA, Kazuo TSUTSUMI, and Hiroshi TAKAHASHI
Institute of Industrial Science, The University of Tokyo, 7-22-1 Roppongi, Minato-ku, Tokyo 106
(Received December 15, 1978)

Heats of adsorption of gaseous triphenylchloromethane (TPC) onto silica–alumina surface were determined from the heat evolved with the immersion of silica–alumina into TPC–hexane solution. The heat of dissolution and the heat of sublimation of TPC and the heat of immersion of the sample into hexane were considered for their determination. It became clear that TPC molecules interacted with silica–alumina surface in two manners. The one was observed in smaller adsorbed amount (below 45 μmol/g), and the other in adsorbed amount from 45 to 100 μmol/g. The former could be attributed to the interaction between TPC and Lewis or oxidizing sites and the latter to the attractive interaction between the adsorbed molecules. The adsorbed amount in the first stage (4.7×10^{12} molecules/cm^2) agreed closely with the number of Lewis acid sites (5.0×10^{12} sites/cm^2) measured by Leftin and Hall.

Although the existence of two types of acid sites (Lewis and Brönsted type) on dehydrated silica–alumina surface has been known by IR spectroscopy,[1,2] the method of their quantitative determination has not yet been established. A great number of techniques has been reported for specific adsorption on each kind of acid sites. Okuda and Tachibana[3] observed that the cation radical $[NH_2C_6H_4NH_2\cdot]^+$ derived from adsorbed *p*-phenylenediamine $[NH_2C_6H_4NH_2]$ on silica–alumina surface appears under the existence of electron-acceptor sites. Leftin and Hall[4] reported that the amount of Lewis acid sites can be determined from the amount of triphenylmethylium ions formed when the acid center abstracts a hydride ion from triphenylmethane (TPM). The method was modified by Shiba and coworkers[5] who used triphenylchloromethane (TPC) instead of TPM. The adsorption equilibrium is much more readily attained for the former than for the latter. Besides above-mentioned methods, polycyclic condensed aromatics such as perylene and anthracene were used as the reagents for the specific adsorption on Lewis acid sites. The determinations of Lewis acidity in these methods were carried out by gravimetry, spectroscopy or electron-spin-resonance. Calorimetric studies for this purpose have hardly been done. If the reagents above-mentioned had sufficiently high vapor pressure at room temperature, the gas-adsorption-calorimetry[6–9] could be applied. In this study, the heat of adsorption was measured from TPC–hexane solution.

Experimental

Silica–alumina cracking catalyst (Al_2O_3: 13 wt %) was supplied by Catalysts and Chemicals Ind. Co., Ltd. Each sample was evacuated at 600 °C under 10^{-5} Torr for 5 h before measurement. Triphenylchloromethane and hexane were special grade reagents supplied by Wako Pure Chemical Industries, Ltd.

Calorimetric studies were carried out by a twin-conduction type calorimeter (Tokyo Riko Co., Ltd.).

Specific surface area of the sample was measured to be 575 m^2/g by the BET nitrogen method. Chemisorbed amount of TPC was determined spectroscopically after the extraction with dry hexane for 2 h.

Results and Discussion

The measurements of heats of adsorption of solute onto solid surface from the solution were extensively reported.[10–12] In these papers, heats of adsorption were determined by considering the heat of immersion of solid into solvent or the heat of dissolution of solute into solvent.

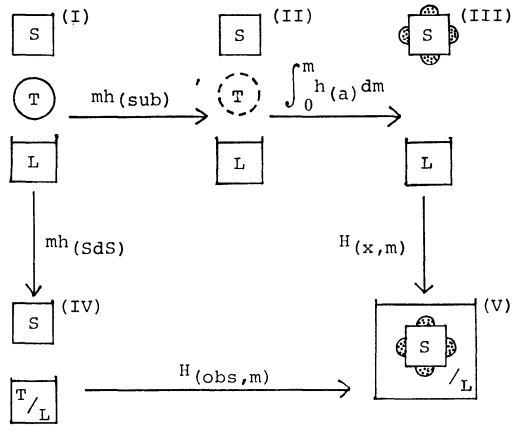

Fig. 1. Diagrammatic representation of the relation between the calorimetrically measured heat and the heat of adsorption of TPC.
S: Silica–alumina, T: TPC(triphenylchloromethane), L: hexane, T/L: TPC–hexane solution.
○: Solid, ○: gas.

Figure 1 shows the diagrammatic representation of the relation between the calorimetrically measured heat and the heat of adsorption of gaseous TPC, where $h_{(a)}$ is the enthalpy change with the adsorption of TPC(gas) onto silica–alumina surface (differential heat of adsorption), $H_{(obs,m)}$ the enthalpy change with the immersion of the sample into TPC–hexane solution, $h_{(SdS)}$ the molar enthalpy change with the dissolution of TPC-(solid) into hexane, $h_{(sub)}$ the molar enthalpy change with the sublimation of TPC(solid) and $H_{(x,m)}$ the enthalpy change with the change of state from (III) to (V). The additivity of these enthalpy changes is to be hold

for this cycle, therefore, if $h_{(sub)}$, h_{SdS}, and $H_{(x,m)}$ are obtained, $h_{(a)}$ can be derived from $H_{(obs,m)}$.

The $h_{(SdS)}$ was measured with a twin-conduction type calorimeter, and was positive value (endothermic) as shown in Fig. 3. The $h_{(sub)}$ was calculated from the temperature dependence of the vapor pressure of TPC by using Clausius-Clapeyron's equation. At the step (III) the sample is preadsorbed with gaseous TPC, hence $H_{(x,m)}$ must be obtained by the measurement of the heat evolved with the immersion of the sample partially preadsorbed with gaseous TPC into hexane. The vapor pressure of TPC is, however, extremely low and the stability of TPC molecules depends on the temperature very sensitively. Therefore, the partial preadsorption with TPC in gas phase was very difficult. The step from (III) to (V) consists of both the change of the adsorbed state of TPC and the immersion of the sample with the preadsorbed TPC into hexane. In this study, $H_{(x,m)}$ was calculated by using the following equation under the assumption that the former might be energetically negligible,

$$H_{(x,m)} = H_I \times (1-\theta(m)), \quad (1)$$

where H_I is the heat of immersion of bare silica–alumina into hexane and $\theta(m)$ the surface coverage of TPC. The relationship among these heat values is expressed as

$$mh_{(SdS)} + H_{(obs,m)} = mh_{(sub)} + \int_0^m h_{(a)}dm + H_{(x,m)} \quad (2)$$

which leads to

$$\int_0^m h_{(a)}dm = m[h_{(SdS)} - h_{(sub)}] + [H_{(obs,m)} - H_{(x,m)}]. \quad (3)$$

The term, $\int_0^m h_{(a)}dm$, will be refered to the cumulative heat of adsorption. The differential heat of adsorption, q, of gaseous TPC onto silica–alumina surface can be expressed by

$$q = -h_{(a)} = h_{(sub)} - h_{(SdS)} + \frac{\partial}{\partial m}[H_{(x,m)} - H_{(obs,m)}]. \quad (4)$$

If the variation of m is sufficiently small, in other words, if each difference of concentrations of solutions in the experiment is sufficiently small, q can be determined by graphical differentiation of the plot of $\int_0^m h_{(a)}dm$ against m.

When the pretreated silica–alumina was immersed into TPC–hexane solution, the heat was evolved as shown in Fig. 2. Two steps are observed in the heat curve, which suggests the existence of two kinds of surface reaction with TPC. On the other hand, the curve showing the relation between the chemisorbed amount and the concentration of solution has three steps, and first two correspond to the steps of heat curve. After the initial stage, the adsorbed amount gradually increased. The nature of Lewis acid sites has been characterized by the adsorption of TPC or TPM and their number has been determined after the extraction of physically adsorbed species by use of dry benzene.[4] While in this study the extraction was carried out with hexane because it dissolved TPC much more than benzene did and the heat of immersion of silica–alumina into it was lower, which were important factors in

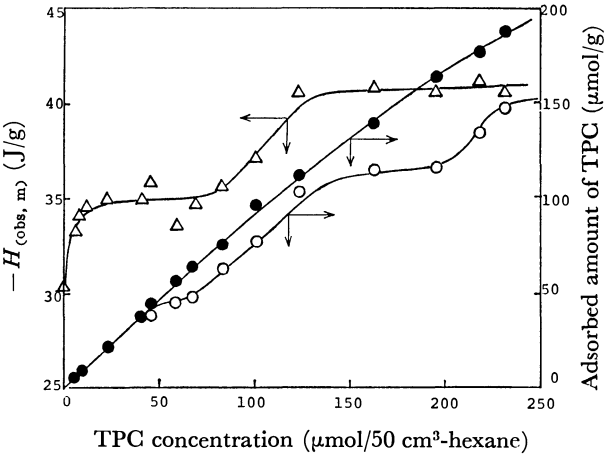

Fig. 2. The calorimetrically measured heats (△), the total adsorbed amount (●) and the chemisorbed amount of TPC (○) *vs.* the concentration of TPC–hexane solution. (The chemisorbed amount was equal to the total adsorbed amount below 45 μmol/g of adsorbed amount.)

calorimetric measurements. The extraction with benzene showed here that the chemisorbed amount was 43 μmol/g even at the solution concentration of 150 μmol/50 cm³ hexane. This value was in good agreement with that at the end point of the first stage in case of hexane extraction. However, the amount obtained after hexane extraction will be called "chemisorbed" one hereafter. In order to obtain the heat of adsorption of TPC, other enthalpy changes were measured or calculated as follows.

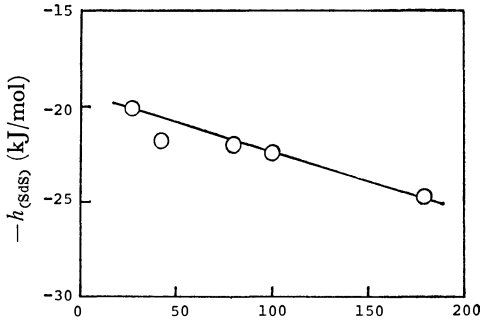

Fig. 3. Molar enthalpy change with the dissolution of TPC (solid) into hexane.

Figure 3 shows the integral heat of dissolution of TPC into hexane ($h_{(SdS)}$). A slite change was observed against the concentration of solutions, which seemed to be due to heat of dilution. The value corresponding to the amount adsorbed was applied for Eq. 3. The heat of sublimation of TPC ($h_{(sub)}$) was determined as mentioned above to be 34.6 kJ/mol. The heat of immersion of bare silica–alumina into hexane (H_I) was measured to be −30.3 J/g. $H_{(x,m)}$ was determined by use of Eq. 1 under the assumption that the surface coverage of TPC increased linearly with the adsorbed amount below 45 μmol/g and that it did not, however, change any

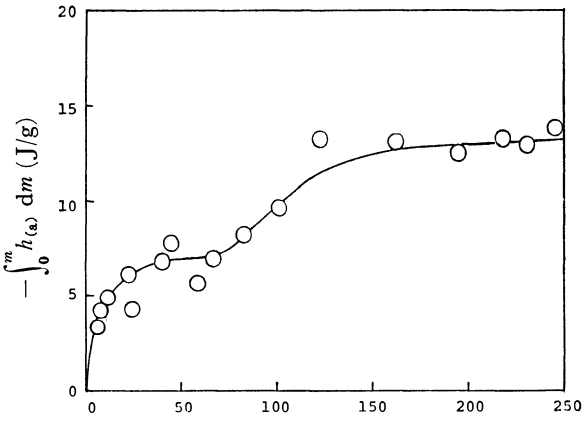

Fig. 4. Cumulative heat of adsorption of TPC *vs.* concentration of TPC–hexane solution.

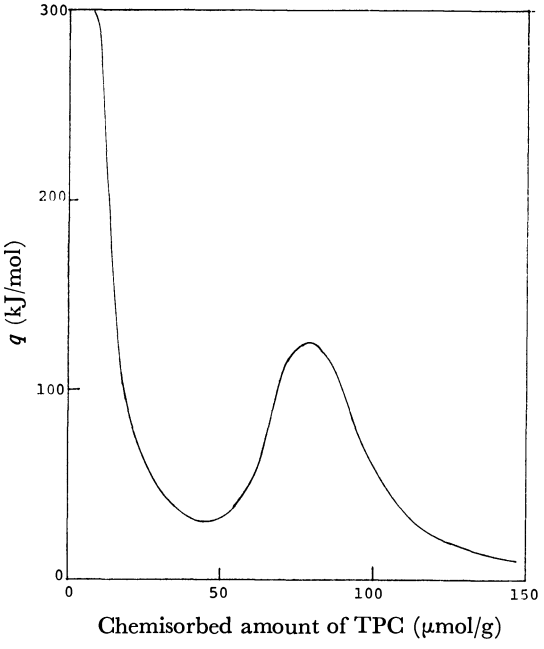

Fig. 5. Differential heat of adsorption of gaseous TPC onto silica–alumina surface.

more above 45 μmol/g. The reason for this assumption will be mentioned in the later section. The cross-sectional area of TPC molecule was taken as 1.54 nm².[13] The cumulative heat of adsorption against the solution concentration and the differential heat of adsorption are shown in Figs. 4 and 5, respectively. The determination of the differential heat of chemisorption was based on the assumption that the heat of physical adsorption was equal to the heat of sublimation of TPC, 34.6 kJ/mol. As shown in Figs. 4 and 5, two types of adsorption occured: the one was observed in the first stage where the chemisorbed amount of TPC was lower than 45 μmol/g, and the other was in the second stage where the chemisorbed amount was between 45 and 100 μmol/g. The visible reflection spectrum of the sample of the former type consisted of only 400—420 nm absorption band which was the same as that obtained with concentrated sulfuric acid–triphenylmethanol system (Fig. 6). Considered together with the results of Leftin and Hall, these species could be assigned to carbonium ions derived from TPC by its interaction with silica–alumina surface. The formation of triphenylmethyl radical by the interaction with oxidizing sites may be possible as reported by Arai and coworkers.[14] In the second stage, the new absorption bands (540, 640 nm) appeared besides that of carbonium ion. Since the adsorbed amount in this stage was nearly equal to that in the first one, this might be attributed to the interaction between carbonium ion or triphenylmethyl radical which had been formed on the surface and TPC molecules, and to the lateral interaction among adsorbed molecules. A maximum in the second stage of the plot of the heat of adsorption must be satisfactorily explained on the basis of these interactions. The chemisorbed species of this stage were removed by benzene extraction, but their chemical identification is not yet made.

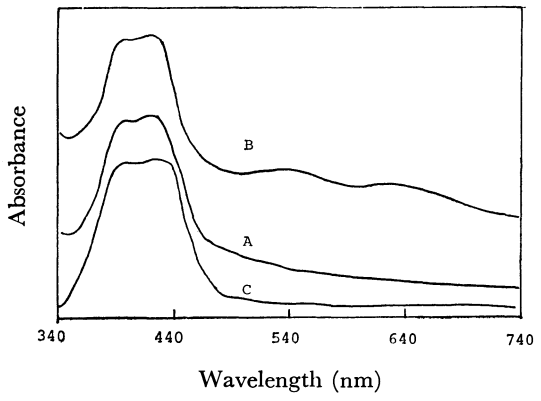

Fig. 6. Visible reflection spectrum of TPC adsorbed on silica–alumina surface.
A: Chemisorbed amount of TPC was less than 45 μmol/g, B: chemisorbed amount was more than 45 μmol/g, C: triphenylcarbinol in concd H_2SO_4.

Consequently, it was clarified by calorimetric measurement that the adsorption of TPC onto silica–alumina surface from its hexane solution consisted of at least two steps. At the intial stage, TPC molecules were chemisorbed on Lewis acid sites or oxidizing sites. The initial differential heat of adsorption was about 300 kJ/mol and the decrease hereafter was considerably steep. The adsorbed amount in this stage was about 45 μmol/g (4.7×10^{12} molecules/cm²), which agrees closely with the number of Lewis acid sites, 5.0×10^{12}/cm², measured by Leftin and Hall. After the initial stage, a rise in the heat of adsorption to give a maximum was observed, which must be ascribed to the attractive interactions between adsorbed molecules.

This work was partly supported by a Grant-in-Aid for Science Research from the Ministry of Education.

References

1) M. R. Basila and T. R. Kantner, *J. Phys. Chem.*, **71**, 467 (1967).
2) E. P. Parry, *J. Catal.*, **2**, 371 (1963).
3) N. Okuda and T. Tachibana, *Bull. Chem. Soc. Jpn.*, **33**, 863 (1960).

4) H. P. Leftin and W. K. Hall, Actes Congr. Intern. Catalyse, 2e, Paris, II, No. 65 (1960).
5) A. Nakamura, K. Sato, K. Takemura, and T. Shiba, *Shokubai*, **4**, 58 (1962).
6) T. Masuda, H. Taniguchi, K. Tsutsumi, and H. Takahashi, *Bull. Chem. Soc. Jpn.*, **51**, 633 (1978).
7) T. Masuda, H. Taniguchi, K. Tsutsumi, and H. Takahashi, *Bull. Chem. Soc. Jpn.*, **51**, 1965 (1978).
8) H. Taniguchi, T. Masuda, K. Tsutsumi, and H. Takahashi, *Bull. Chem. Soc. Jpn.*, **51**, 1970 (1978).
9) T. Masuda, H. Taniguchi, K. Tsutsumi, and H. Takahashi, *Bull. Jpn. Petrol. Inst.*, **22**, 67 (1979).
10) P. Roy and D. W. Fuerstenau, *J. Colloid Interface Sci.*, **26**, 102 (1968).
11) C. G. Armisted, A. J. Tyler, and J. A. Hockey, *Trans. Faraday Soc.*, **67**, 500 (1971).
12) M. Miura, Y. Kubota, T. Iwaki, K. Takimoto, and Y. Muraoka, *Bull. Chem. Soc. Jpn.*, **42**, 1476 (1969).
13) A. E. Hirschler and J. O. Hudson, *J. Catal.*, **3**, 239 (1964).
14) H. Arai, Y. Saito, and Y. Yoneda, *Bull. Chem. Soc. Jpn.*, **40**, 312 (1967).

Ultraviolet Photoelectron Spectra of Crown Ethers

Masatsugu KAJITANI, Akira SUGIMORI, Naoki SATO,† Kazuhiko SEKI,†
Hiroo INOKUCHI,† and Yoshiya HARADA*,††

Department of Chemistry, Faculty of Science and Technology, Sophia University, Kioi-cho, Chiyoda-ku, Tokyo 102
†*Institute for Molecular Science, Myodaiji, Okazaki 444*
††*Department of Chemistry, College of General Education, The University of Tokyo, Komaba, Meguro-ku, Tokyo 153*

(Received December 18, 1978)

The He I spectra of 12-crown-4, 15-crown-5, 18-crown-6, dicyclohexyl-18-crown-6, and dibenzo-18-crown-6 have been measured. The features of the spectra are similar except for the case of dibenzo-18-crown-6, where two lower IP bands correlated with the highest occupied π-orbitals of benzene are observed together with the bands due to the polyether ring. By the aid of the CNDO/2 calculation, the lower IP bands of the spectra have been assigned to the MO's mainly due to the equatorial or axial type non-bonding orbitals of the oxygen atoms of the polyether rings.

There has been considerable interest in macrocyclic "crown" ethers since Pedersen reported their syntheses in 1967.[1,2] They are capable of binding with a wide variety of salts to form complexes and can thereby solubilize many inorganic reagents in nonaqueous solvents, in which the reagents exhibit enhanced anion activity.[3,4] Thus, crown ethers have been found to be very useful reagents in organic chemistry. In life sciences, they are also used as models for carrier molecules in the study of cation transport through membranes.[5]

In order to study the electronic structure of crown ethers, we have measured the He I spectra of 12-crown-4 (I), 15-crown-5 (II), 18-crown-6 (III), dicyclohexyl-18-crown-6 (IV), and dibenzo-18-crown-6 (V) (Fig. 1), and tried to assign the observed bands with the aid of molecular orbital calculations.

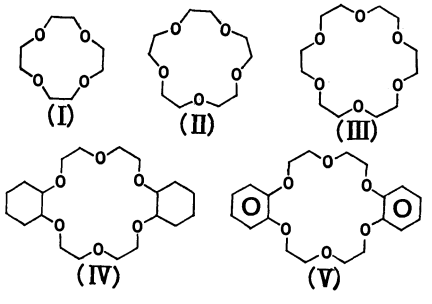

Fig. 1. Crown ethers.
(I) 12-Crown-4, (II) 15-crown-5, (III) 18-crown-6, (IV) dicyclohexyl-18-crown-6, (V) dibenzo-18-crown-6.

Experimental

Commercial crown ethers were purified by vacuum sublimation. He I spectra were recorded on a Perkin-Elmer PS-18 photoelectron spectrometer using the Ar and Xe doublets as internal standards. The resolution was less than 30 meV. The spectra of I and II were measured at room temperature, and those of the larger crown ethers at 70 °C (III), 150 °C (IV), and 190 °C (V).

Results and Discussion

Figure 2 shows the He I spectrum of 12-crown-4. Four broad peaks appear around 9.3, 9.9, 11.4, and 12.5 eV. In the higher IP region the spectrum is diffuse, as is frequently the case in large molecules.

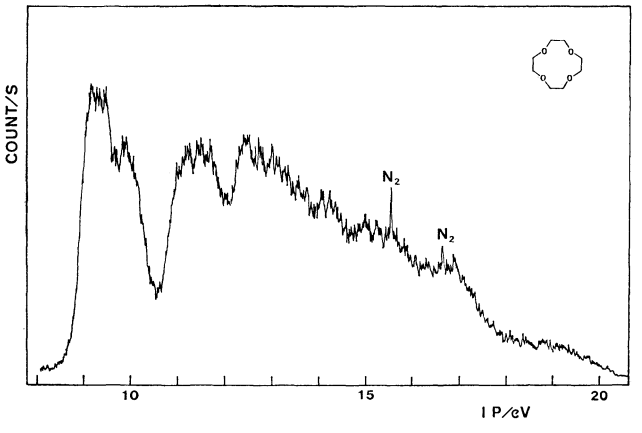

Fig. 2. He I spectrum of 12-crown-4.

The molecular structure of 12-crown-4 has not been determined experimentally. Pullman *et al.*[5] calculated the energies of two types of conformations, maxidentate (crown) and alternate forms (Fig. 3), using an *ab initio* LCAO MO method. According to them, the most stable conformer is a deformed alternate one; the value of its torsion angle τ about the C_2C_3 bond is 70°, while the symmetric alternate conformer (Fig. 3) has τ= 48.65°. We calculated the molecular orbitals of these alternate conformers by the CNDO/2 method. The energies of the upper occupied levels and the shapes of the corresponding wave functions are illustrated schematically in Fig. 4. The symmetric alternate conformer

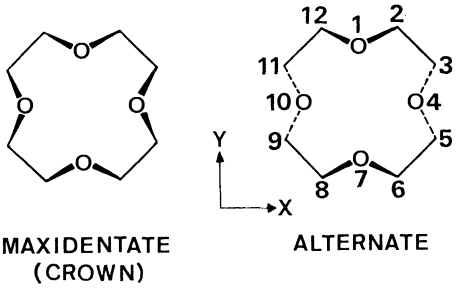

Fig. 3. Conformations of 12-crown-4. All the carbon atoms lie on the same plane.

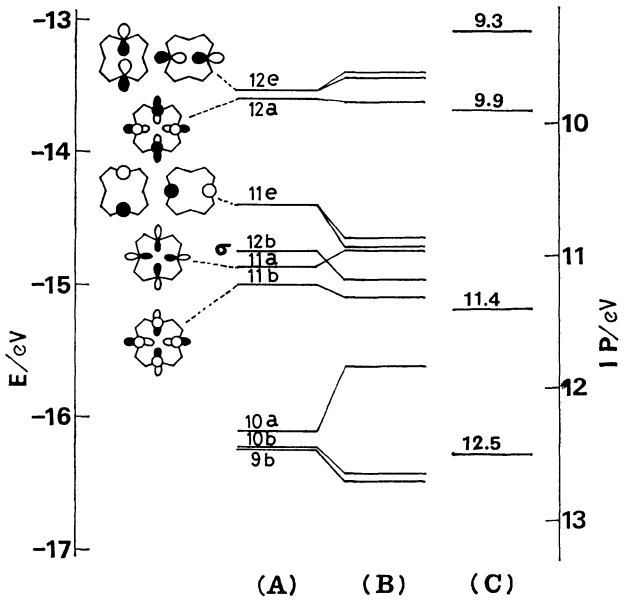

Fig. 4. The energies of the upper occupied levels and the shapes of the corresponding wave functions of 12-crown-4.
(A) Calculated energies for the symmetric alternate conformer. (B) Calculated energies for the most stable conformer. (C) Observed IP values (peak positions in the spectrum).

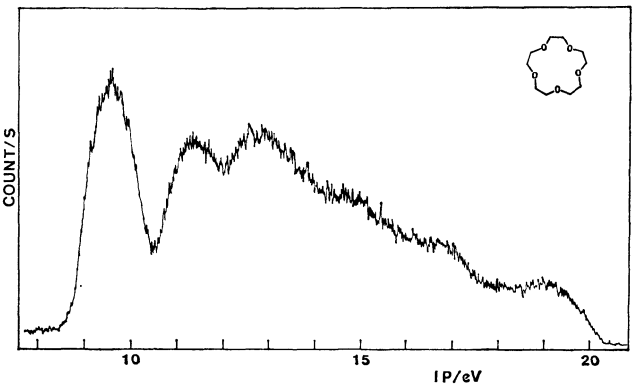

Fig. 5. He I spectrum of 15-crown-5.

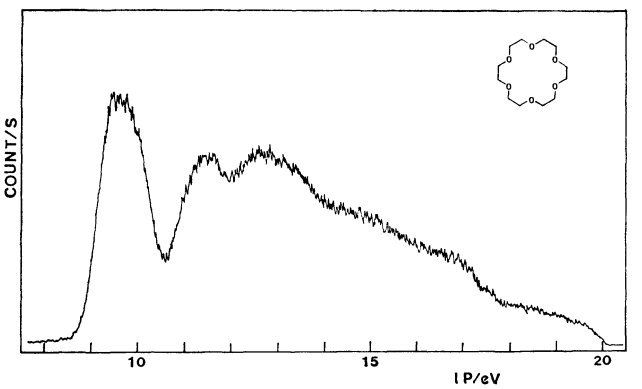

Fig. 6. He I spectrum of 18-crown-6.

belongs to the symmetry group S_4, having degenerate e orbitals, whereas the degeneracy is lifted in the stable one. The CNDO/2 calculation shows that the highest occupied e orbitals of the symmetric conformer (12e in Fig. 4) are mainly due to the non-bonding combination of the equatorial type lone pair orbitals (N_{eq}) of two oxygen atoms and the second highest (12a) to the bonding combination of four N_{eq} orbitals together with the anti-bonding combination of four axial type lone pair orbitals (N_{ax}). For the deformed form, the splitting of the 12e orbital is calculated to be only 0.04 eV (Fig. 4). Therefore, they may not be resolved in the observed photoelectron spectrum. Since the integrated intensity of the first (9.3 eV) band of 12-crown-4 is about twice as large as that of the second (9.9 eV) one, the first and second bands can be assigned to the 12e and 12a orbitals, respectively. Both these orbitals are due to lone pair type orbitals of oxygen atoms, having a similar localized nature. Thus the intensity ratio of the two bands due to the 12e and 12a orbitals can be expected to be 2 to 1, the ratio of their degeneracies.** Further, the assignment of the second band to the 12a orbital can be supported from a comparison of the spectrum of 12-crown-4 with spectra of the other crown ethers (see below). The intensity of the 11.4 eV band, as compared to those of the first and second bands, suggests that it corresponds to the removal of electrons from two or three occupied orbitals. Judging from the results of the calculation shown in Fig. 4, electrons from the 11e orbital, the anti-bonding combination of two N_{ax} orbitals, may contribute to this band.

Figures 5 and 6 show the He I spectra of 15-crown-5 and 18-crown-6, respectively. The appearance of the spectra is similar to that of 12-crown-4 (Fig. 2), except for the portion of the spectra between 8.5 and 10.5 eV. In the former spectra the 9.3 and 9.9 eV bands of 12-crown-4 appear to be mixed into one band located at intermediate positions: 9.58 eV for 15-crown-5 and 9.7 eV for 18-crown-6. This can be interpreted by assuming that orbitals having shapes similar to those of the 12e and 12a of 12-crown-4 are responsible for the first band in its higher homologs. Since 12e type orbitals due to anti-bonding combinations of N_{eq}'s become more stable and 12a type orbitals due to bonding combination of N_{eq}'s become less stable with increasing ring size of polyethers, the bands due to these two orbitals may not be resolved for 15-crown-5 and 18-crown-6. As for the second bands in Figs. 5 and 6, the peak positions (11.4 eV for 15-crown-5, 11.5 eV for 18-crown-6) are nearly the same as that in 12-crown-4. This is considered to be consistent with the previous assignment that the 11.4 eV band in 12-crown-4 is related to the 11e orbital, since the energy of the 11e type orbitals may not shift much with increasing ring size owing to the small interaction among N_{ax} orbitals.

** A similar intensity relation has been found in the photoelectron spectrum of biphenyl, in which the lowest three ionization bands are associated with the highest occupied π-orbitals of the benzene rings (J. P. Maier and D. W. Turner, *Faraday Discuss. Chem. Soc.*, **54**, 149 (1972)). The intensity ratio of approximately 1:2:1 has been observed for these three bands, of which the second one is due to almost doubly degenerate orbitals.

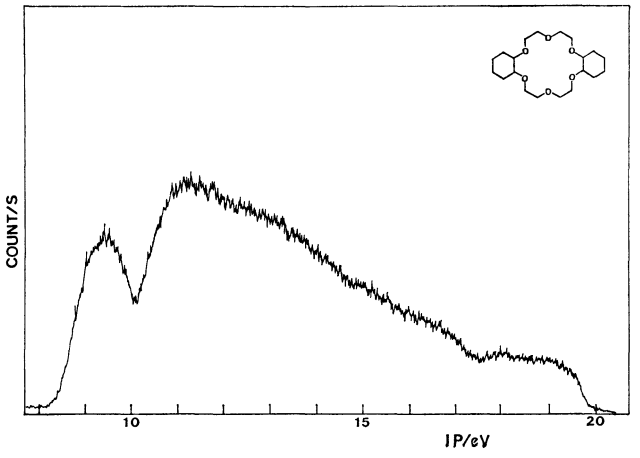

Fig. 7. He I spectrum of dicyclohexyl-18-crown-6.

Figure 7 shows the He I spectrum of dicyclohexyl-18-crown-6. With the introduction of two cyclohexane rings, the peak position of its first band (9.45 eV) is lowered by 0.25 eV as compared with that of 18-crown-6. Furthermore, in the 10—13 eV region the feature of the spectrum is different from those of the spectra of unsubstituted crown ethers. This may be due to the effect of the σ-orbitals of cyclohexane, the adiabatic IP of which is around 10.0 eV.[6]

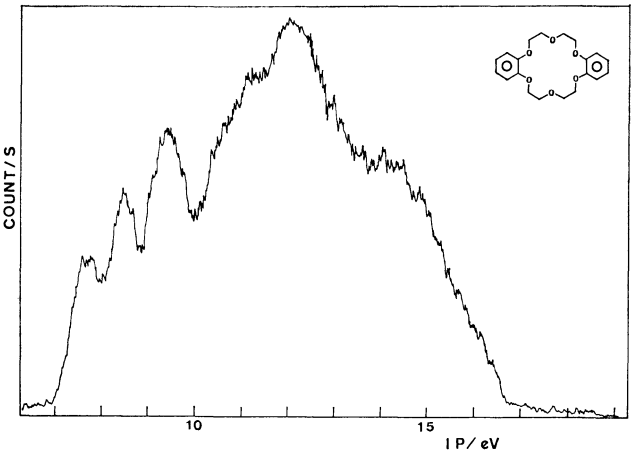

Fig. 8. He I spectrum of dibenzo-18-crown-6.

The He I spectrum of dibenzo-18-crown-6 is shown in Fig. 8. The third band located at 9.45 eV can be correlated to the first band of 18-crown-6. The first and second bands (vertical IP 7.70 eV, 8.50 eV) may be related to electrons from the highest occupied doubly degenerate π-orbitals (e_{1g}) of benzene rings. This assignment is supported by the fact that the *o*-dimethoxybenzene gives the first and second bands at vertical IP 8.20 and 8.91 eV,[7] which are associated with the e_{1g} orbitals of the benzene ring. Since there is interaction in this molecule, among the e_{1g} orbitals of the benzene ring (IP 9.24 eV for benzene) and the non-bonding orbitals of the oxygen atoms (IP 10.96 eV for methanol), the former orbitals are considered to split and give two bands in the lower IP region of the spectrum.*** The vertical IP's relating to these bands are further lowered by 0.4—0.5 eV for dibenzo-18-crown-6, where the π-conjugated system is larger than that of *o*-dimethoxybenzene.

As for the IP region higher than 10 eV the appearance of the spectrum in dibenzo-18-crown-6 is quite different from that of 18-crown-6 owing to the introduction of two benzene rings. However, the shoulder at 11.2 eV may be correlated to the second band of 18-crown-6.

The authors wish to thank Prof. A. Pullman, Institut de Biologie Physico-Chimique, C. N. R. S., for sending them the data on the atomic cordinates of the most stable conformer for 12-crown-4.

References

1) C. J. Pedersen, *J. Am. Chem. Soc.*, **89**, 2495 (1967).
2) C. J. Pedersen, *J. Am. Chem. Soc.*, **89**, 7017 (1967).
3) J. J. Cristensen, D. J. Eatough, and R. M. Izatt, *Chem. Rev.*, **74**, 351 (1974).
4) A. C. Knipe, *J. Chem. Educ.*, **53**, 618 (1976).
5) A. Pullman, C. Giessner-prettre, and Yu. Y. Kruglyak, *Chem. Phys. Lett.*, **35**, 156 (1975).
6) A. W. Potts and D. G. Streets, *J. Chem. Soc., Faraday Trans. 2*, **70**, 875 (1974).
7) N. Sato, unpublished results.

*** We can correlate the 8.20 and 8.91 eV bands of *o*-dimethoxybenzene with the π_2 and π_3 orbitals of the benzene ring, respectively, because, in *o*-dimethoxybenzene, the π_2 orbital of the ring having its maximun electron density at both points of substitution is more affected than the π_3 orbital.

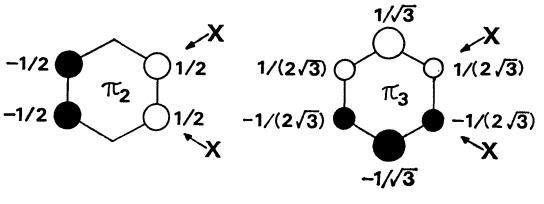

Stability of Multi-center Bonds in Inorganic Cluster Compounds

Jun-ichi AIHARA

Department of Chemistry, Faculty of Science, Hokkaido University, Sapporo 060

(Received December 19, 1978)

An ideal multi-center bond is a bond in which three or more atomic orbitals of the same kind, each from a different atom, interact equally with each other. Since such a multi-center bond can be regarded as a cyclic conjugated system, the graph theory of aromaticity can be applied to it. It was then found that multi-center bonds are aromatically stabilized to a great extent. Most inorganic cluster compounds are polyhedral in shape. This might be rationalized by the fact that polyhedrons are favorable to a formation of a multi-center bond or the like at the core.

Boranes and metal carbonyl clusters were once regarded as obscure chemical rule-breakers because of their unfamiliar bonding patterns. During the last decade a great deal of effort has been devoted to an understanding of chemical bonds in such non-classical cluster compounds.[1] The present-day situation can adequately be expressed by the following sentence: Gather any large group of inorganic chemists and they will start talking about metal clusters.[2] Pauling also pointed out that the bonding principle of metal carbonyl clusters is one of the most important problems yet to be solved.[3] In line with this, several skeletal electron-counting rules have been proposed as a theoretical basis for rationalizing the bonding pattern of cluster compounds.[4–8] However, these rules rarely provide explicitly for a measure of stabilization of the molecular clusters. In this paper, I would like to stress that a multi-center bond formation might often play a significant role in stabilizing non-classical molecular clusters.

Theoretical

Consider a multi-center bonding system in which three or more atomic orbitals of the same kind, each belonging to a different atom, interact equally with each other. The simplest multi-center bond is a central three-center BBB bond, in which each of the three boron atoms interacts equally with the other two.[9] When ten atomic orbitals interact in this manner to form a ten-center bond, its bonding pattern can be expressed as in Fig. 1. This is identical with a complete graph of degree ten, K_{10}, where the vertices indicate the atomic orbitals concerned. In general, a complete graph of degree n, K_n, is a graph in which each of the n vertices is connected to all the other vertices.[10] A conjugated system of the type K_n gives only one bonding molecular orbital,[8] the energy of which is equal to $(n-1)\beta$. All the other molecular orbitals are antibonding, and the energies are equal to $-\beta$. Therefore, any ideal multi-center bond has two bonding electrons with the bonding energy of $2(n-1)\beta$.

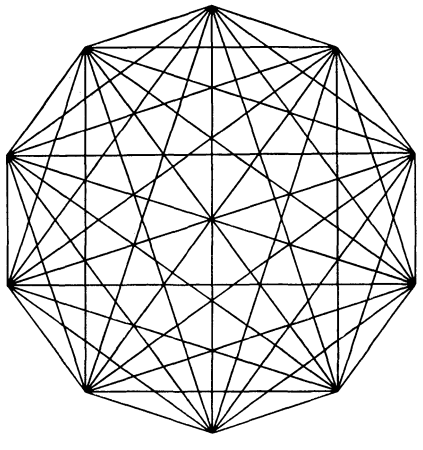

Fig. 1. A complete graph of degree ten, K_{10}.

Table 1. Resonance energies of K_n-type bonding systems

n	SC	RE/β	$\%RE$
3	3	0.536	15.5
4	3	1.331	28.5
5	15	2.286	39.6
6	15	3.351	50.4
7	105	4.499	60.0
8	105	5.711	68.9
9	945	6.975	77.3
10	945	8.281	85.2
11	10395	9.624	92.8
12	10395	10.998	100.0

In order to estimate stabilities of such multi-center bonding systems, it is instructive to examine the resonance energies calculated by means of the graph theory of aromaticity.[11] Resonance energies calculated for a series of K_n-type conjugated systems[12] are listed in Table 1. This type of resonance energy has been interpreted as an extra stabilization energy due to aromaticity.[11]

Results and Discussion

First of all, it is noteworthy that the resonance energy of any K_n-type bonding system is positive, indicating its aromaticity. The resonance energy (RE) is proportional to the logarithm of the Kekulé structure count (SC), *i.e.*, the number of Kekulé structures allowed for K_n. An analogous feature of resonance energies has already been reported for benzenoid hydrocarbons[13] and polyhedral boranes.[14] However, the situation is somewhat different from that for these compounds. As shown in Fig. 2, a correlation line for K_n with $n=2m-1$ obviously deviates downward from that for K_n with $n=2m$. Here, m is an arbitrary integer. For K_{2m}-type bonding systems

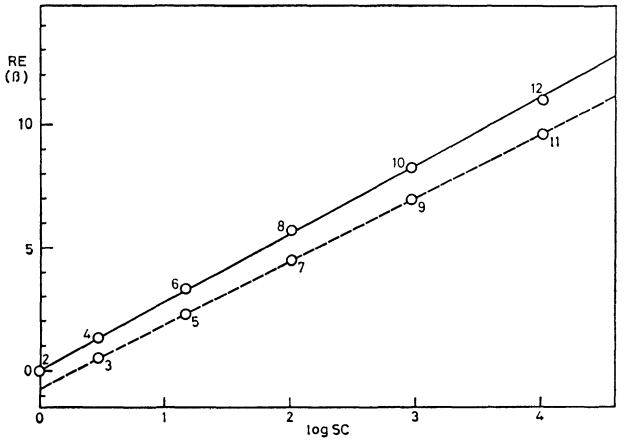

Fig. 2. *SC* Dependence of resonance energy for a series of K_n-type bonding systems.

$$RE = 2.768 \log SC, \quad (1)$$

and for K_{2m-1}-type bonding systems

$$RE = 2.573 \log SC - 0.710. \quad (2)$$

These relations hold well at least up to $m=6$.

One of the characteristics of such a multi-center bonding system is that its resonance energy is unusually large as compared with the energy of its olefinic reference structure, *i.e.*, the reference energy,[11] In order to see this aspect, a new quantity is defined as 100 times the resonance energy, divided by the reference energy, and it will be called the percent resonance energy (%*RE*). The %*RE* can be regarded as a practical index suitable for estimating aromatic stabilization of a conjugated system. The two largest %*RE*'s so far known among familiar compounds are 15.5 for a cyclopropenyl cation and 3.5 for benzene.[11] Note that a conjugated system of a cyclopropenyl cation is another example of a three-center bonding system.

In contrast to them, even for the next smallest multi-center bond, K_4, the %*RE* amounts to 28.5. The %*RE* increases as the degree of a complete graph increases. Such large %*RE* values cannot be imagined for any other kind of conjugated system. This means that a larger multi-center bonding system fixes itself more tightly, as long as the resonance integrals between the atomic orbitals remain almost unchanged.

From the above energy consideration, we can fully expect the formation of bonding systems analogous to multi-center bonds in some way or other. When atoms M, each with an s-type atomic orbital, are employed for simplicity, molecular clusters with a general formula of M_n^{n-2} can be constructed so as to form K_n-type conjugated systems. The simplest example is a triangular H_3^+ ion.[15] When the size of such a cluster increases, an increased excess $(n-2)$ charge must be overcome either by some intramolecular balance or by the environment. In this sence, the realistic clusters of this type must be relatively small. The next promising species is of the type M_4^{2+}, where M is either an alkali or a coinage metal atom.

On the other hand, King and Rouvray presented a new bonding model of polyhedral systems, such as boranes $B_nH_n^{2-}$ and carboranes $B_{n-2}C_2H_n$.[8] According to it, the skeletal boron (or carbon) atom can be regarded as sp hybridized. The remaining two p orbitals, which are tangentially oriented with respect to the pseudo-polyhedron surface, are used for surface bonding. One sp hybrid orbital is used to bond the terminal hydrogen. The other sp hybrid orbital points radially in toward the center of the cluster. Such inward pointing sp hybrid orbitals emanating from all vertex atoms interact at the core of the polyhedral cluster. King and Rouvray assumed that the bonding pattern of these sp hybrid orbitals can roughly be represented by a complete graph.[8] In other words, all the inward pointing sp hybrid orbitals form a single multi-center bonding orbital with two electrons.

In a previous paper,[14] I calculated resonance energies of polyhedral boranes on the basis of the Kettle-Tomlinson bonding model,[16] in which borane molecular orbitals are depicted as a linear combination of localized three-center BBB bonding orbitals. The resonance energy obtained for every borane correlated well with the energy separation between the lowest unoccupied molecular orbital (LUMO) and the highest occupied molecular orbital (HOMO). We must, however, say that these resonance energies reflect primarily the stability of the surface bonding of the cluster because both LUMO and HOMO belong mostly to the surface bonding[1] and because the Kettle-Tomlinson model cannot fully express the multi-center bonding at the core of the cluster.[16] The weight of a core bonding system is obviously underestimated in this model.

On the contrary, the most distinct aspect of the King-Rouvray model is that a K_n-type core bonding system is factored out from an entire molecular cluster.[8] In accord with this, it has been shown that the core bonding can be factored out with some precautions to obtain an approximate picture of the valence structure.[17] Therefore, this model can be considered as a complement to the Kettle-Tomlinson model. The core bonding system is totally symmetric, and hence constitutes the lowest molecular orbital in a molecular cluster. It is often much lower in energy than the second lowest orbital.[18] Consequently, it naturally follows that, even if an actual core bonding system deviates more or less from a complete graph,[19] it should still contribute much to the stability of an entire cluster compound because an ideal multi-center core bonding orbital has both the largest bonding energy in the cluster and quite a large %*RE* value. This view is consistent, at least, with synthetic accessibility to many polyhedral boranes and metal carbonyl clusters and their stability. In these compounds, the overall charge which a cluster bears is generally small because most of the excess $(n-2)$ charge due to the K_n-type core bonding is cancelled by the polyhedral surface bonding.[8]

Conversely, we might safely say that an inorganic compound often tends to become polyhedral in shape so as to form a K_n-like core bonding system. This gives the major reason why shapes of most inorganic cage compounds are polyhedrons or polyhedral fragments. A multi-center bond formation thus appears to be one of the most workable ways to stability. Figure 3 shows typical shapes of polyhedral compounds (*e.g.*, closo-

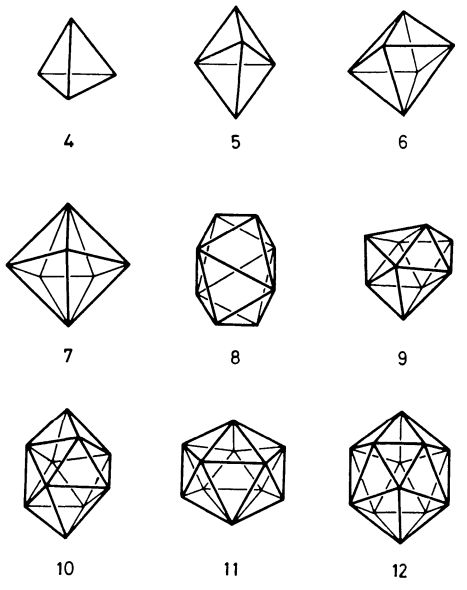

iFg. 3. Shapes of typical polyhedral compounds.

boranes) which contain such multi-center core bonding systems. The number given below each polyhedron indicates the degree of a complete graph related to the core bonding,[19] and this is equal to the number of vertices of the polyhedron.

The present approach thus provides a convenient rationale for the existence and stability of polyhedral non-classical compounds, although it is simple and based on approximate bonding models. It goes without saying that the surface bonding may modify the degree of stability of an entire conjugated system to some extent. Considering that a surface bonding system is often a network of three-center bonds,[16] I feel confident that the concept of a multi-center bond is in some way essential to the stability consideration of not only homopolyatomic clusters formed by the s-like atomic orbitals but also general inorganic cage compounds including mixed clusters.[1]

The author expresses his gratitude to Professor R. B. King of the University of Georgia for critical but encouraging comments. The use of the facilities of the Hokkaido University Computing Center is acknowledged.

References

1) K. Wade, *Adv. Inorg. Chem. Radiochem.*, **18**, 1 (1976); *Chem. Brit.*, **11**, 177 (1975).
2) See, *e.g.*, *Chem. Eng. News*, **56**, 20 (April 3, 1978).
3) L. Pauling and D. Ridgway, *J. Chem. Educ.*, **53**, 471 (1976).
4) K. Wade, *Chem. Commun.*, **1971**, 792; *Inorg. Nucl. Chem. Lett.*, **8**, 559 (1972).
5) D. M. P. Mingos, *Nature (London), Phys. Sci.*, **236**, 99 (1972).
6) R. W. Rudolph and W. R. Pretzer, *Inorg. Chem.*, **11**, 1974 (1972); R. W. Rudolph, *Acc. Chem. Res.*, **9**, 446 (1976).
7) C. J. Jones, W. J. Evans, and M. F. Hawthorne, *J. Chem. Soc., Chem. Commun.*, **1973**, 543.
8) R. B. King and D. H. Rouvray, *J. Am. Chem. Soc.*, **99**, 7834 (1977); *Theor. Chim. Acta*, **48**, 207 (1978).
9) W. N. Lipscomb, *Acc. Chem. Res.*, **6**, 257 (1973); *Science*, **196**, 1047 (1977).
10) F. Harary, "Graph Theory," Addison-Wesley, Reading, Mass. (1969), Chap. 2.
11) J. Aihara, *J. Am. Chem. Soc.*, **98**, 2750, 6840 (1976); I. Gutman, M. Milun, and N. Trinajstić, *ibid.*, **99**, 1692 (1977).
12) In this context, Gutman and Hosoya recently derived an analytical form of a reference polynomial for K_n-type conjugated systems: I. Gutman and H. Hosoya, *Theor. Chim. Acta*, **48**, 279 (1978). Here, a reference polynomial signifies a characteristic polynomial defined for an olefinic reference structure of a conjugated system; it is needed to calculate the resonance energy.[11]
13) R. Swinborne-Sheldrake, W. C. Herndon, and I. Gutman, *Tetrahedron Lett.*, **1975**, 755.
14) J. Aihara, *J. Am. Chem. Soc.*, **100**, 3339 (1978).
15) M. J. Gaillard, D. S. Gemmell, G. Goldring, I. Levine, W. J. Pietsch, J. C. Poizat, A. J. Ratkowski, J. Remillieux, Z. Vager, and B. J. Zabransky, *Phys. Rev. A*, **17**, 1797 (1978).
16) S. F. A. Kettle and V. Tomlinson, *J. Chem. Soc., A*, **1969**, 2002, 2007.
17) R. Hoffmann and W. N. Lipscomb, *J. Chem. Phys.*, **36**, 2179 (1962).
18) M. J. S. Dewar and M. L. McKee, *Inorg. Chem.*, **17**, 1569 (1978).
19) When the size of a molecular cluster increases, the geometry of the core bonding system will necessarily deviate from that of a complete graph. The β values in it will then be diversified, the absolute values being decreased to a varying extent. Such modification of the core bonding system will somewhat diminish both the resonance energy and the $\%RE$. This might be partially responsible for the fact that there are few polyhedral compounds which have more than eleven vertex atoms.[1]

Raman Spectra of Alkali Metal Oxalates in Aqueous Solution. Evidence for Ion-pair Formation

Kan KANAMORI,* Masamitsu MIHARA, and Kiyoyasu KAWAI

Department of Chemistry, Faculty of Science, Toyama University, Gofuku, Toyama 930

(Received December 23, 1978)

Laser Raman spectra of aqueous solutions of lithium, potassium, and caesium oxalates have been obtained; their band contours were examined by curve analysis. The intensities of several bands show distinct concentration and cation dependences. This behavior is connected with the ion-pair formation of oxalate ions with alkali metal cations. The assignments of C=O stretching vibrations are also discussed.

Laser Raman spectroscopy has been widely used to explore the properties of ion-pairs formed in aqueous solutions of electrolytes. For the Raman spectra of aqueous solutions of metal sulfates or nitrates, many authors[1] have reported some additional bands which can give direct information on the ion-pairing. However, vibrational spectroscopic evidence for ion-pairing of carboxylate ions with metal cations is rarely found in earlier works, although thermodynamic evidence is presented by several authors.[2]

The oxalate ion has the simplest structure among the dicarboxylate ions. This anion is expected to have a comparatively large association constant owing to the formation of a chelate-like structure with metal cations in aqueous solutions.

The Raman spectra of aqueous oxalate solutions were studied by several authors in order to assign the symmetry of the free oxalate ion. Murata and one of us (K.K)[3] assumed that the oxalate ion had a planar D_{2h} symmetry because of the inconsistency between the IR and Raman frequencies for the potassium salt. The same symmetry was also assumed by Ito and Bernstein[4] for the ion, while a staggered form of D_{2d} symmetry was proposed by Begun and Fletcher[5] and Bardet and Fleury[6] on the basis of the aqueous IR and Raman spectra. Schmelz, Miyazawa, Mizushima, Lane, and Quagliano[7] assumed the ion to have a D_2 symmetry by comparing the infrared data of the solid salt with the Raman data of an aqueous solution reported by Edsall.[8]

In the present work Raman spectra of aqueous alkali metal oxalate solutions are interpreted in terms of coexistence of the free and the ion-paired oxalate ions. The assignment for the Raman bands of the free oxalate ion is also reexamined.

Experimental

The $Li_2C_2O_4$ and $K_2C_2O_4 \cdot H_2O$ used were reagent grade chemicals. $Cs_2C_2O_4$ was prepared by the reaction of Cs_2CO_3 with $H_2C_2O_4$; the crude product was purified by recrystallization. Aqueous solutions were prepared by dissolving a determined amount of these oxalates in distilled water. The solution were filtered through sintered glass filters prior to measurements of Raman spectra.

The Raman spectra were recorded on a JASCO Laser-Raman spectrometer (model R-800) using an Ar^+ ion (514.5 nm) laser as a excitation source at room temperature (20±1 °C). The frequencies of observed bands are accurate within ±2 cm^{-1}.

The band decomposition was carried out using the FACOM 230 computer at Toyama University Computer Center, with a Voight function[9] taken as the spectral distribution of a single band.

Results and Discussion

Polarized Raman spectra observed for a saturated solution of potassium oxalate are shown in Fig. 1. The isotropic spectrum in Fig. 1 is the same in general spectral features as that given previously by Begun and Fletcher,[5] except that two very weak polarized bands at 1750 and 1360 cm^{-1} were recognized in the present study. However, it was found that some of the observed bands have obvious asymmetries and some features show distinct dependence on stoichiometric concentration.

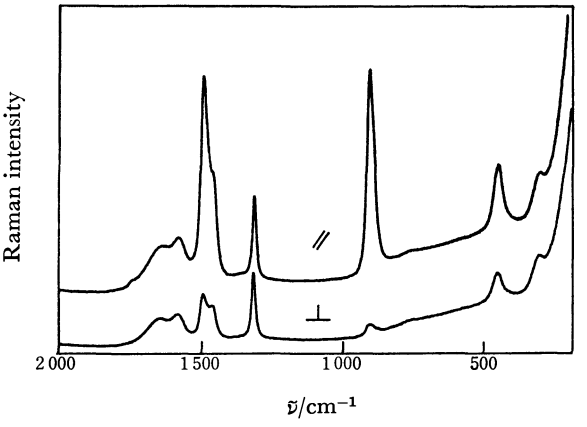

Fig. 1. Polarized Raman spectra of a satulated aqueous solution of potassium oxalate.

In previous works,[3-7] the band at *ca.* 900 cm^{-1} was assigned to the C–C stretching vibration as a single band. As shown by the solid line in Fig. 2, however, the isotropic and anisotropic band shapes observed for a saturated solution of potassium oxalate suggest that these bands consist of more than two components. We analyzed both the isotropic and anisotropic spectra, assuming that the components resolved in the isotropic spectrum are at the same frequencies as the corresponding ones in the anisotropic spectrum. As shown by broken lines in Fig. 2, both spectra can be resolved into three bands at 906, 891, and 872 cm^{-1}, of which the two high frequency bands are apparently polarized,

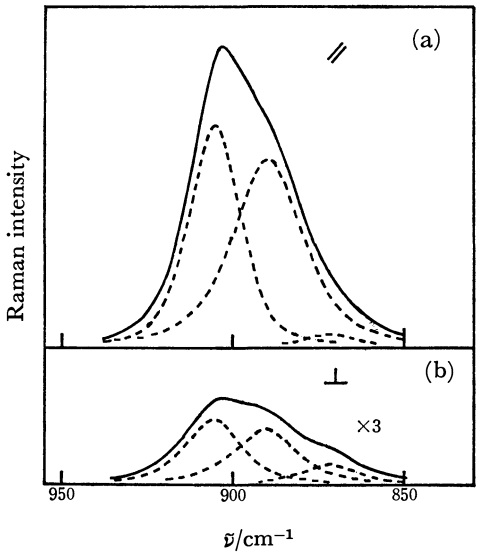

Fig. 2. The observed Raman contour (——) and the computer-analyzed components (----) in C–C stretching region of a saturated aqueous potassium oxalate. (a) Isotropic spectrum; (b) anisotropic spectrum.

while the low frequency weak one is depolarized. This depolarized band is irrelevant to the discussion on the C–C stretching vibration and may be assigned to a combination band of the two IR frequencies[5] (525+351=876 cm^{-1}), because regardless of the symmetry of the oxalate ion the C–C stretching vibration belongs to a totally symmetric species and no band was observed near 872 cm^{-1} in the infrared spectra of either aqueous solution or solid state.[5] The Raman contours observed in this region for solutions of different concentrations of $K_2C_2O_4$ or for the $K_2C_2O_4$–KCl–H_2O solution were satisfactorily decomposed into the three bands, but the relative intensities of the two polarized bands showed a marked stoichiometric concentration dependence. Integrated intensity ratios of the 891 cm^{-1} band to the 906 cm^{-1} one for these systems are shown in Table 1. One notices from Table 1 that the ratio (I_{891}/I_{906}) increases with increasing stoichiometric concentration of potassium oxalate or by the addition of potassium chloride. From this behavior, the band at 891 cm^{-1} can be reasonably assigned to the C–C stretching vibration

TABLE 1. INTENSITY RATIOS OF THE 891 TO 906 cm^{-1} BANDS[a]

System	I_{891}/I_{906}
0.1 M $K_2C_2O_4$	0.44
0.5 M $K_2C_2O_4$	0.51
0.7 M $K_2C_2O_4$	0.54
1.0 M $K_2C_2O_4$	0.58
1.5 M $K_2C_2O_4$	0.63
1.8 M $K_2C_2O_4$	0.69
0.5 M $K_2C_2O_4$+2.5 M KCl	0.73
0.5 M $Li_2C_2O_4$	0.88
0.5 M $Cs_2C_2O_4$	0.48

a) The *ca.* 900 cm^{-1} contour has been assumed to consist of three bands whose widths are invariant for the different systems.

of ion-paired oxalate and the band at 906 cm^{-1} to that of the free oxalate ion.

The Bjerrum theory[10] on ion association suggests that, in the systems which contain a common ion, the smaller the radius of the counter ion is, the larger the association constant which can be expected. In order to examine the effect of metal cations on the ion-pair formation, the Raman spectrum of an aqueous solution of lithium or caesium oxalate was also observed. The Raman contours of the C–C stretching region of these systems were also resolved into three bands. The frequency shifts of these bands with the variation of cations were about ± 3 cm^{-1}, and within the error estimated from both the measurements and the curve analysis. However, some cation dependence was found in the relative intensities of the two polarized bands. At the same stoichiometric concentration (0.5 M) the value of the I_{891}/I_{906} ratio, which is a measure of the degree of ion-pair formation, decreases in the order of lithium>potassium>caesium oxalate (see Table 1). This order also supports the above assignment of the C–C stretching region.

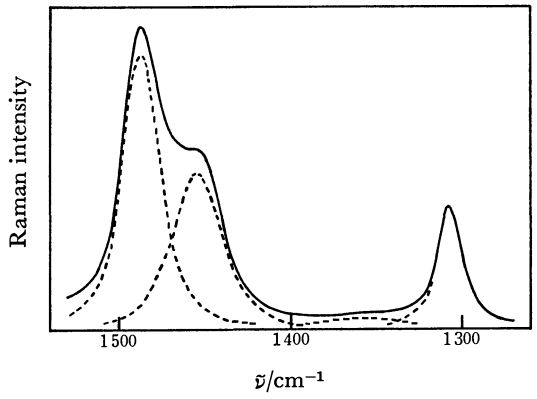

Fig. 3. The observed Raman contour (——) and the computer-analyzed components (----) from 1270 to 1530 cm^{-1} of a saturated aqueous potassium oxalate.

The spectrum in the C=O stretching region for a saturated solution of potassium oxalate is shown in Fig. 3 (solid line). The resolution of the band contour into components is also shown in Fig. 3 (broken line). The resulting bands are situated at 1308, 1360, 1456, and 1488 cm^{-1}. The very weak and broad band at 1360 cm^{-1} is polarized and may be assigned to a combination band such as the C–C stretching and the CO_2^- bending modes (906+450=1356 cm^{-1}). The two bands at 1456 and 1488 cm^{-1} are clearly polarized, as is seen in Fig. 1. As shown in Table 2, there is some confusion in the assignments of the bands in this region, particularly of the band at 1456 cm^{-1}, depending on the symmetry of the free oxalate ion in the previous studies.[3–7] The Raman contours from 1400 to 1550 cm^{-1} in various systems are shown in Fig. 4. The relative intensity of the 1456 cm^{-1} band distinctly depends on both the stoichiometric concentration of oxalate and the variation of cations, just as that of the 891 cm^{-1} band does.

Figure 5 shows integrated intensity ratios of the 1308, 1456, and 1488 cm^{-1} bands to the 906 or 891 cm^{-1}

Table 2. Observed Raman frequencies (cm^{-1}) and their assignments of the C=O stretching region of aqueous potassium oxalate and of the symmetry (point group) of the free oxalate ion

D_{2h}				D_{2d}				D_2		D_2 or D_{2d}	
M.K.[3]		I.B.[4]		B.F.[5]		B.F.[6]		S.M.M.L.Q.[7]		This work	
Obsd	Assign.	Obsd	Assign.[a]	Obsd	Assign.	Obsd	Assign.	Obsd[c]	Assign.	Obsd	Assign.
		1305	ν_8	1309	ν_7	1310	ν_7	1310	ν_{11}	1308	ν_{11} for D_2 or ν_5 for D_{2d}
1450		1452	$\nu_{10}+\nu_{11}$	1458[b]	$2\nu_8$	1456[b]	$2\nu_8$	1457		1456	ν_1 for ion-pair
1485	ν_1	1488	ν_1	1487	ν_1	1486	ν_1	1489	ν_1	1488	ν_1 for D_2 or D_{2d}
				1577[b]	ν_5	1581[b]	ν_5	1580		1575	ν_5 and ν_9 for D_2 or ν_7 for D_{2d}
1664	ν_5	1660	ν_5					1647			ν_5 for ion-pair

a) The numbering of the fundamentals is in accord with that of Schmelz *et al.*[7] b) These frequencies were interpreted to be a result of Fermi resonance. c) These data were obtained by Edsall.[8]

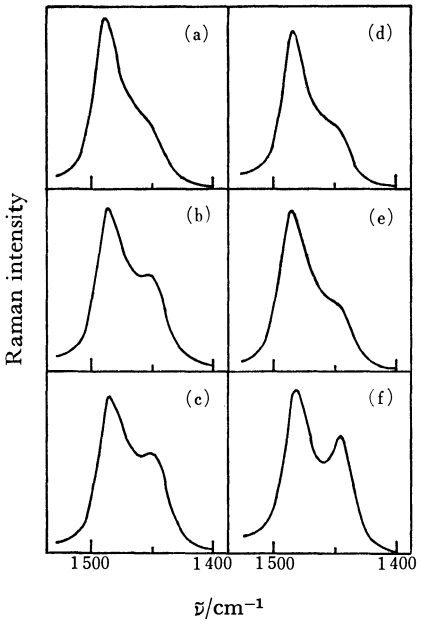

Fig. 4. The observed Raman bands from 1400 to 1500 cm^{-1} in various systems (a) 0.1 M $K_2C_2O_4$ (b) 1.8 M $K_2C_2O_4$ (c) 0.5 M $K_2C_2O_4$ +2.5 M KCl (d) 0.5 M $Cs_2C_2O_4$ (e) 0.5 M $K_2C_2O_4$ (f) 0.5 M $Li_2C_2O_4$.

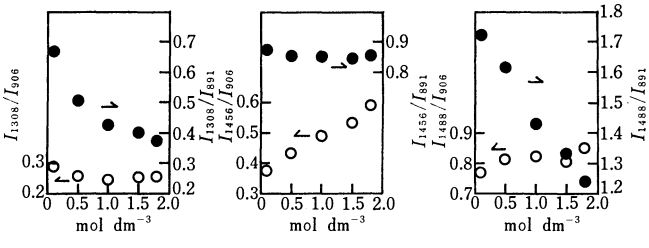

Fig. 5. Plots of the intensity ratios of C=O stretching bands to C–C stretching bands against the stoichiometric concentrations of potassium oxalate.

band *vs.* the stoichiometric concentration of potassium oxalate. Unfortunately, the integrated intensity of the band at 1575 cm^{-1} could not be obtained with enough accuracy for a quantitative discussion, because of its weakness and the overlapping with water bands. The independencies of the stoichiometric concentration are found for the intensity ratios of the 1308 and 1488 cm^{-1} bands to the 906 cm^{-1} band in Fig. 5. The same is true for the ratio of the 1456 cm^{-1} band to the 891 cm^{-1} band. The bands at 906, 1308, and 1488 cm^{-1} thus belong to the vibrations of the free oxalate, while the bands at 891 and 1456 cm^{-1} belong to those of the ion-paired oxalate.

Earlier studies on the vibrational spectrum of the oxalate ion were based mainly on the number of Raman active C=O stretching modes in the determination of the symmetry of the ion. The free oxalate ion in an aqueous solution should have one of three conformations: D_{2h} (planar), D_{2d} (two CO_2^- planes are at right angles), and D_2 (two CO_2^- planes are rotated with respect to each other by an angle which is not 90°). Symmetry correlations and vibrational activities related to the C=O stretchings are as follows.

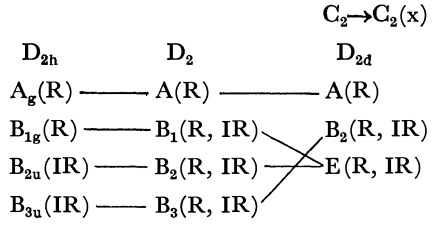

An oxalate ion in solid $K_2C_2O_4 \cdot H_2O$ has a planar symmetry[11] and so the Raman and IR activities are mutually exclusive. Recently, Eriksson and Nielsen[12] found the Raman active antisymmetric and symmetric C=O stretching vibrations (A_g and B_{1g} modes) for polycrystalline and single crystal $K_2C_2O_4 \cdot H_2O$ at *ca.* 1600 and 1444 cm^{-1}, respectively. Two IR active stretching vibrations were observed for the salt at 1600 and 1310 cm^{-1} by Schmelz *et al.*[7] and at 1610 and 1312 cm^{-1} by Begun and Fletcher.[5] These vibrations were also examined in detail by Fukushima[13] in terms of the lattice vibrations of hydrated potassium oxalates. Schmelz *et al.*[7] have assigned the former to the antisymmetric vibration and the latter to the symmetric one. These assignments have been regarded as reasonable by the comparison of the frequencies with the Raman data,[12] though the opposite assignments had been given by Begun and Fletcher.[5] Cadene and Fournel[14] observed bands at *ca.* 1600 and *ca.* 1300 cm^{-1} in both the IR and Raman spectra of single crystal $(NH_4)_2C_2O_4 \cdot H_2O$, where the dihedral angle between two CO_2^- planes is 26.6°.[15] They have assigned the two bands to

the antisymmetric and symmetric (not totally) C=O stretching vibrations, respectively, though their assignments were made on the basis of the D_{2d} symmetry for the oxalate ion. By comparing the two antisymmetric C=O stretching vibrational frequencies obtained in the previous studies,[5,7,12,14] little difference was found between the two vibrational frequencies for the ion whose symmetry is D_{2h} or D_2. There may be an accidental degeneracy in some cases. If the ion has a D_{2d} symmetry, the two antisymmetric C=O stretching frequencies are degenerate. For the structure of the free oxalate ion in aqueous solution, Begun and Flecher[5] pointed out that the ion has D_{2d} symmetry, because they found the existence of three coincidences between the IR and the Raman bands in the C=O stretching region of the spectra for aqueous solutions of alkali metal oxalates. Because of the appearance of the *ca.* 1300 cm^{-1} Raman band, which is reasonably assigned to the symmetric C=O stretching vibration, we conclude that the free ion does not have a planar structure. The assignment of the proper symmetry (D_2 or D_{2d}) of free oxalate, however, is difficult, because of the possibility of the accidental degeneracy in the two antisymmetric C=O stretching vibrations or the serious overlapping of several bands at *ca.* 1600 cm^{-1}. The tentative assignments of C=O stretchings are shown in Table 2.

The reason why only a Raman band which belongs to the C=O stretching vibrations has been detectable for the ion-paired oxalate may be discovered on the assumption that the oxalate ion has a planar and quasi-centrosymmetric structure. If the symmetry of the ion-paired oxalate is closer to D_{2h}, the intensity of the Raman band due to the symmetric vibration at *ca.* 1310 cm^{-1} will be less intense. This assumption may be supported by the low frequency shifts of the C–C stretching and the totally symmetric C=O stretching vibrations for ion-paired oxalate, compared with those for free oxalate in aqueous solutions; these vibrations were observed at 881 and 1444 cm^{-1} for polycrystalline $K_2C_2O_4 \cdot H_2O$.[12] Some planarity of ion-paired oxalate will be brought preferably by the formation of a chelate-like structure; because the interaction between oxalate and alkali metal ions will be mainly ionic, the oxalate ion is also expected to be kept in a quasi-centrosymmetric structure. Even if the interaction between cation and anion were covalent to some degree and thus the oxalate ion lost its quasi-centrosymmetric structure, the Raman band due to the (not totally) symmetric C=O stretching vibration would not be detectable in the range 1300—1400 cm^{-1}; this result is suggested by the fact that no Raman band was detected in the range 1300—1400 cm^{-1} for oxalato aluminium[16] or beryllium complex.[17] The Raman active antisymmetric C=O stretching vibrations for ion-paired oxalate will be expected at *ca.* 1600 cm^{-1}. Serious overlapping of the bands with the free oxalate or water bands will then occur. No useful information on band overlapping has yet been provided by Raman spectral measurements in D_2O, but the broad Raman band at 1575 cm^{-1} may reflect such a situation.

The authors are indebted to Professor Yoichi Shimura of Osaka University and Dr. Isao Kanesaka of our university for their valuable discussions.

References

1) a) R. M. Chatterjee, W. A. Adams, and A. R. Davis, *J. Phys. Chem.*, **89**, 246 (1974); b) F. P. Daly, C. W. Brown, and D. R. Kester, *ibid.*, **76**, 3664 (1972); c) M. Peleg, *ibid.*, **76**, 1019 (1972); d) D. L. Nelson and D. E. Irish, *J. Chem. Phys.*, **54**, 4479 (1971); e) J. Janz, K. Balasubrahmanyam, and B. G. Oliver, *ibid.*, **51**, 5723 (1969); f) R. P. Oertel and R. A. Plane, *Inorg. Chem.*, **7**, 1192 (1968).

2) a) U. K. Kläning and O. Østerby, *J. Chem. Soc., Faraday Trans. 1*, **72**, 513 (1976); b) H. S. Dunsmore and D. Midgley, *J. Chem. Soc., Dalton Trans.*, **1972**, 64; c) C. E. Evans and C. B. Monk, *Trans. Faraday Soc.*, **66**, 1491 (1970).

3) H. Murata and K. Kawai, *J. Chem. Phys.*, **25**, 589 (1956).

4) K. Ito and H. J. Bernstein, *Can. J. Chem.*, **34**, 170 (1956).

5) G. M. Begun and W. H. Fletcher, *Spectrochim. Acta*, **19**, 1343 (1963).

6) L. Bardet and G. Fleury, *C. R. Acad. Sci., Ser. B*, **265**, 983 (1967).

7) M. J. Schmelz, T. Miyazawa, S. Mizushima, T. J. Lane, and J. V. Quagliano, *Spectrochim. Acta*, **9**, 51 (1957).

8) J. T. Edsall, *J. Chem. Phys.*, **5**, 508 (1937).

9) I. F. Kielkopf, *J. Opt. Soc. Am.*, **63**, 987 (1973).

10) N. Bjerrum, *K. Danske Vidensk. Selk.*, **9**, 7 (1926).

11) a) S. B. Hendricks, *Z. Krist.*, **91**, 48 (1935); b) G. A. Jeffrey and G. S. Parry, *J. Am. Chem. Soc.*, **76**, 5283 (1954); c) B. F. Pedersen, *Acta Chem. Scand.*, **18**, 1635 (1964).

12) A. Eriksson and O. F. Nielsen, *J. Mol. Struct.*, **48**, 343 (1978).

13) K. Fukushima, *Bull. Chem. Soc. Jpn.*, **43**, 39.1313 (1970).

14) M. Cadene and A. Fournel, *J. Mol. Struct.*, **37**, 35 (1977).

15) J. H. Robertson, *Acta Crystallogr.*, **18**, 410 (1965).

16) M. Jaber, F. Bertin, and G. Thomas-David, *Can. J. Chem.*, **55**, 3689 (1977).

17) M. Jaber, F. Bertin, and G. Thomas-David, *Can. J. Chem.*, **56**, 777 (1978).

The Transport of Metal Ions against Their Concentration Gradients through a 1,2-Dichloroethane Membrane

Masaaki SUGIURA* and Toshio SHINBO

National Chemical Laboratory for Industry, Nishiyawata, Hiratsuka 254

(Received January 6, 1979)

The uphill transport of metal ions such as copper, zinc, cobalt, and iron(II) ions through a bulk 1,2-dichloroethane membrane in the presence of various chelating agents has been studied. The membrane separated two aqueous phases, one containing the metal ion and potassium or lithium sulfate, and the other containing the metal ion and lithium nitrate or chloride. The chelating agents used were derivatives of 1,10-phenanthroline and acetylacetone. The accumulation of the metal ions in the aqueous phase containing the potassium or lithium sulfate was observed for only the following chelating agents: copper: 4,7-diphenyl-2,9-dimethyl- and 4,7-diphenyl-1,10-phenanthroline; zinc: 4,7-diphenyl-, 3,8-diphenyl-, 2,9-dimethyl-, and 4,7-diphenyl-2,9-dimethyl-1,10-phenanthroline; cobalt: 3,8-diphenyl- and 4,7-diphenyl-1,10-phenanthroline; and iron(II): 3,8-diphenyl-1,10-phenanthroline. In the system containing lithium sulfate in the aqueous phase, the rate of transport of the metal ions was slightly higher than that in the system containing potassium sulfate. The reduction of the nitrate ion in the aqueous phase brought about a lowering of the rate of transport of the metal ions. The transport of the metal ions was, however, unaffected by the electrostatic effect. The metal ion complexed by the chelating agent may be transferred in the 1,2-dichloroethane phase, thus forming an ion-pair with the nitrate or chloride ion.

In a previous paper,[1] the present authors studied the uphill transport of the picrate anion through a bulk 1,2-dichloroethane membrane. The picrate anion was transported against its concentration gradient by coupling to a diffusion of potassium ions *via* various potassium ionophores.

Using a membrane system similar to that used for the picrate transport and various chelating agents, we have now made an attempt to make metal ions move against their concentration gradient. This report will concern the uphill transport of some metal ions, such as copper, zinc, cobalt, and iron(II) ions.

Experimental

Apparatus. The apparatus used for measuring the transport of the metal ions was the same as that used in the previous paper.[1] In the transport cell (cylindrical glass vessel:[2] 7 cm i.d.,; height, 7 cm), the dichloroethane phase (100 ml), containing a 10^{-3} M chelating agent, separated two aqueous phases (50 ml each), one (Phase I) containing 5×10^{-4} M metal sulfate and 0.05 M potassium or lithium sulfate, and the other (Phase II) containing 5×10^{-4} M metal sulfate and 0.1 M lithium nitrate or chloride.

Materials. As lipophilic chelating agents, derivatives of 1,10-phenanthroline and acetylacetone were used: the 5-methyl-, 5-nitro-, 5-chloro-, 2,9-dimethyl-, 4,7-dimethyl-, and 3,8-diphenyl-1,10-phenanthroline, dibenzoylmethane, benzoyltrifluoroacetone, and benzoylacetone were commercial products from the Tokyo Kasei Kogyo Co., Ltd., while the 4,7-diphenyl- and 4,7-diphenyl-2,9-dimethyl-1,10-phenanthroline and 2-thenoyltrifluoroacetone were from the Dojindo Lab. The metallic salts, copper, zinc, cobalt, and iron(II) sulfate and the other chemicals were reagent-grade and were not subsequently purified.

Procedure. The technique used for measuring the rate of transport of the metal ions and the membrane potential was the same as that described in the previous paper.[1] The measurements were carried out at 25 °C. The dichloroethane used as the liquid membrane was pre-equilibrated with a 5×10^{-4} M metal sulfate solution containing a potassium or lithium sulfate and lithium nitrate or chloride, whose concentrations were equal to those in the two aqueous phases, I and II. After this treatment, the membrane system was constructed in the transport cell as has been described above. The determination of the metal-ion concentration in Phases I and II at regular time intervals was carried out by a colorimetric method, after a small volume of the aqueous solutions had been pipetted off (copper; 0.5 ml, zinc; 0.2 ml, cobalt; 0.5 ml, iron(II); 0.5 ml); the concentration of copper was determined by the neocuproine method,[3] the zinc, by the zincon method,[4] the cobalt, by the 2-nitroso-1-naphthol method,[5] and the iron(II), by the 1,10-phenanthroline method.[6]

Results

Uphill Transport of Various Metal Ions. The rates of transport of the metal ions across the dichloroethane membrane in the presence of various chelating agents were measured. The uphill transport was, however, observed for only the following chelating agents: copper: 4,7-diphenyl-2,9-dimethyl-, and 4,7-diphenyl-1,10-phenanthroline; zinc: 4,7-diphenyl-, 3,8-diphenyl-, 2,9-dimethyl-, and 4,7-diphenyl-2,9-dimethyl-1,10-phenanthroline; cobalt: 3,8-diphenyl- and 4,7-diphenyl-1,10-phenanthroline; iron(II): 3,8-diphenyl-1,10-phenanthroline. The curves of the concentrations of the metal ions in both aqueous phases and the membrane potential against the time for these chelating agents are shown in Figs. 1 to 3. The solid and dotted lines in each figure (a) represent the concentration curves in Phases I and II respectively. The polarity of the membrane potential was positive in Phase II with respect to Phase I. In these systems, Phase I contained 0.05 M potassium sulfate, and Phase II, 0.1 M lithium nitrate.

In the present experiment, 10^{-3} M was chosen as the concentration of the chelating agents in the dichloroethane phase. It was the most effective concentration for the transport of the metal ions. As an example of the effect of concentration of the chelating agents on the transport of the metal ions, the curves of the copper concentrations in both aqueous phases and the membrane potential against the time for various concentrations of 4,7-diphenyl-2,9-dimethyl-1,10-phenanthroline are shown in Fig. 4.

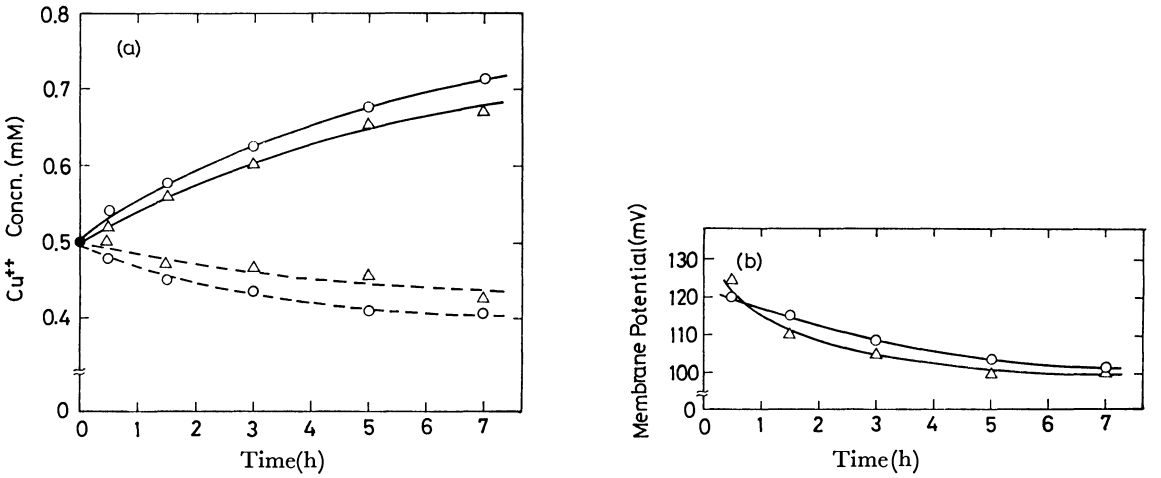

Fig. 1. (a) Copper concentrations in both aqueous phases against time curves. The solid and dotted lines represent the copper concentrations in Phases I and II respectively.
(b) Membrane potential against time curves for the copper.
Chelating agent;
○: 4,7-diphenyl-2,9-dimethyl-1,10-phenanthroline, △: 4,7-diphenyl-1,10-phenanthroline.
Phases I and II contained 0.05 M K_2SO_4 and 0.1 M $LiNO_3$ respectively.

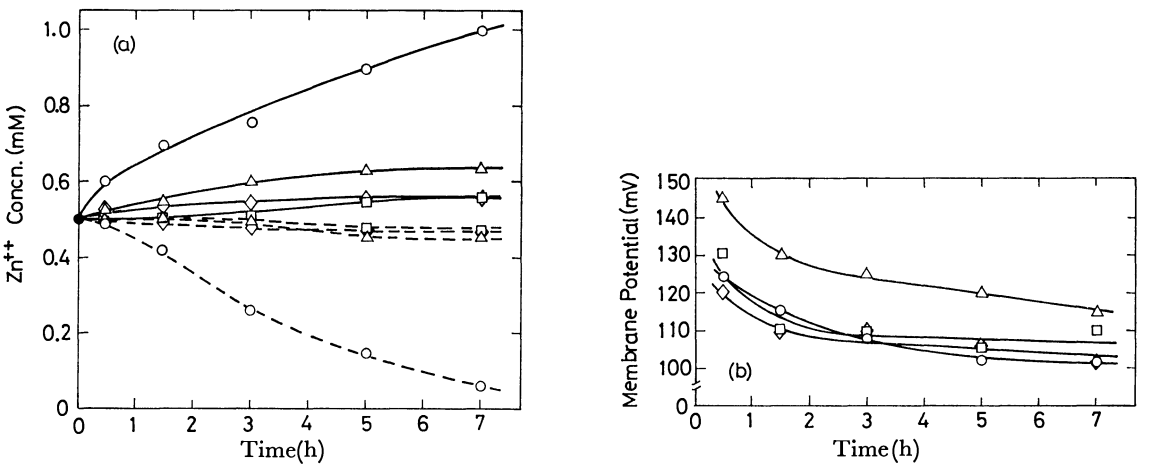

Fig. 2. (a) Zinc concentrations in both aqueous phases against time curves.
The curves have the same meanings as in Fig. 1.
(b) Membrane potential against time curves for the zinc.
Chelating agent;
○: 4,7-diphenyl-1,10-phenanthroline, △: 3,8-diphenyl-1,10-phenanthroline, ◇: 2,9-dimethyl-1,10-phenanthroline, □: 4,7-diphenyl-2,9-dimethyl-1,10-phenanthroline.
Phases I and II contained 0.05 M K_2SO_4 and 0.1 M $LiNO_3$ respectively.

In the case of the other phenanthroline and acetylacetone derivatives used, no transfer of the metal ions across the membrane was observed, though a membrane potential ranging from 100 to 200 mV was developed.

Effect of Potassium Ion and Lithium Counter-ions. When the lithium sulfate was added to Phase I in place of the potassium sulfate, the rate of transport of the metal ions increased slightly. The decrease in the concentration of the nitrate ion in Phase II brought about a lowering of the rate of transport of the metal ions. In the system containing the chloride in Phase II in place of the nitrate, a considerable high rate of transport of the metal ions was also observed. These results are illustrated in Fig. 5, which shows the data for the copper-4,7-diphenyl-2,9-dimethyl-1,10-phenanthroline system.

In the system containing the potassium and lithium sulfates in Phases I and II respectively, a membrane potential of approximately 60 mV was developed by the addition of a potassium ionophore such as dicyclohexyl-18-crown-6. No transfer of the metal ions across the membrane was, however, observed in this system.

Effect of Membrane Potential. In order to examine the role of the membrane potential, the potential difference between Phases I and II was clamped at 0 mV by means of a short-circuit method.[7] The results obtained are shown in Fig. 6. The data for the transport of the metal ions obtained with the voltage clamp

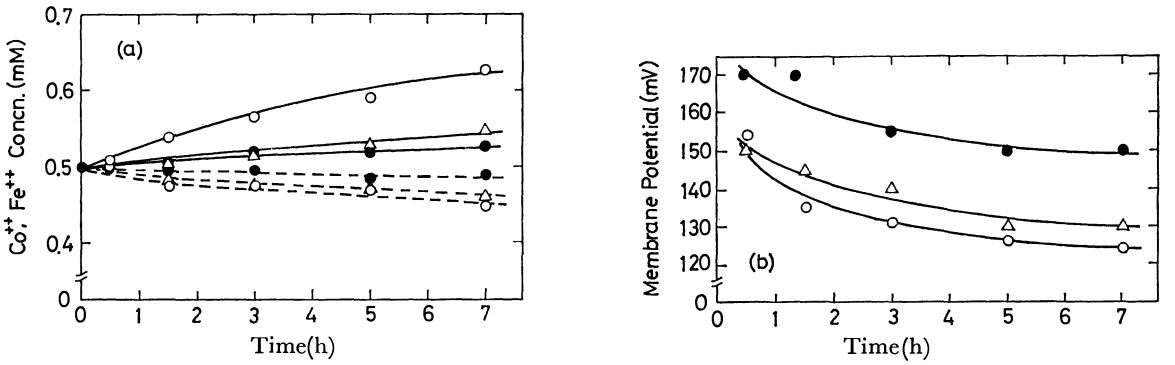

Fig. 3. (a) Cobalt and iron(II) concentrations in both aqueous phases against time.
The curves have the same meanings as in Fig. 1.
(b) Membrane potential against time for the cobalt and iron(II).
Chelating agent for cobalt; ○: 3,8-diphenyl-1,10-phenanthroline, △: 4,7-diphenyl-1,10-phenanthroline, for iron(II); ●: 3,8-diphenyl-1,10-phenanthroline.
Phases I and II contained 0.05 M K_2SO_4 and 0.1 M $LiNO_3$ respectively.

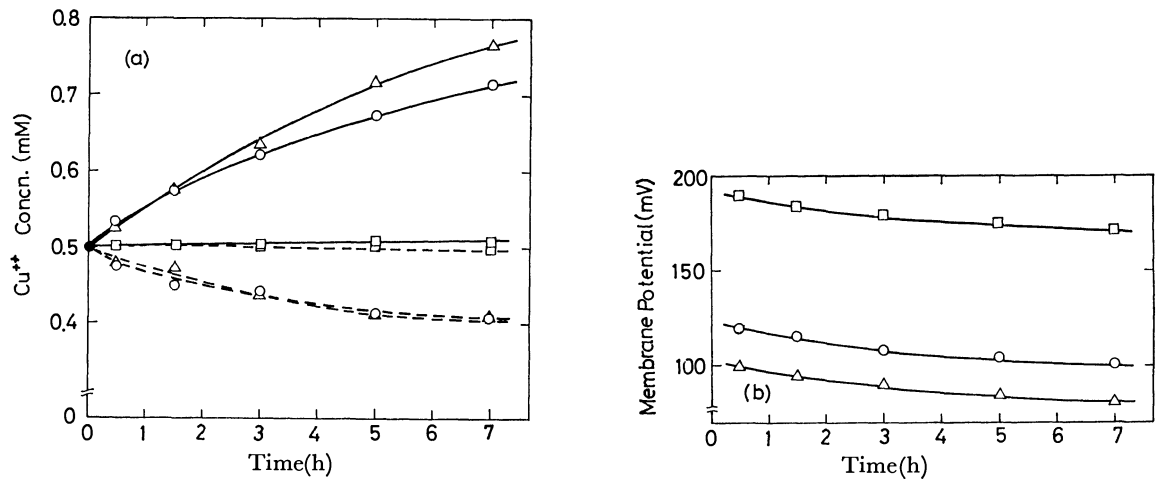

Fig. 4. Effect of concentration of chelating agent on the transport of copper.
(a) Copper concentrations in both aqueous phases against time for various concentrations of 4,7-diphenyl-2,9-dimethyl-1,10-phenanthroline.
The curves have the same meanings as in Fig. 1.
(b) Membrane potential against time for the chelating agent.
Concentration of chelating agent; □: 10^{-4} M, ○: 10^{-3} M, △: 10^{-2} M.
Phases I and II contained 0.05 M K_2SO_4 and 0.1 M $LiNO_3$ respectively.

agreed almost entirely with those obtained without the voltage clamp.

Discussion

In the previous paper,[1] the highest rate of picrate transport was observed in the system containing potassium sulfate and lithium nitrate in Phases I and II respectively. The membrane potential in this system was higher than that in the other systems used. Using the membrane system and various chelating agents, the present authors first attempted to make the metal ions move against their concentration gradient. As may be seen in Figs. 1 to 3, however, the uphill transport of the metal ions occurred for only some phenanthroline derivatives. In addition, the rate of transport of the metal ions differed from one another in the combination of chelating agent and metal ion.

The phenanthroline derivatives which can move the metal ions form complexes with the metal ions. However, they do not necessarily have a high stability constant for the formation of the complexes. Although some of the phenanthroline derivatives used form a stable complex with the metal ion,[8] they cannot move the metal ion. On the other hand, the metal ions which can be moved by the phenanthroline derivatives have almost constant ionic radii:[9] copper, 0.72 Å; zinc, 0.74 Å; cobalt, 0.72 Å; iron(II), 0.74 Å. The nickel and iron(III) ions whose ionic radii were 0.69 and 0.64 Å respectively could not be moved in the system used in the present experiment. It is assumed that the chelating agents can move the metal ions only when they form complexes with a specific structure which facilitates the transfer of the metal ions at the aqueous phase-

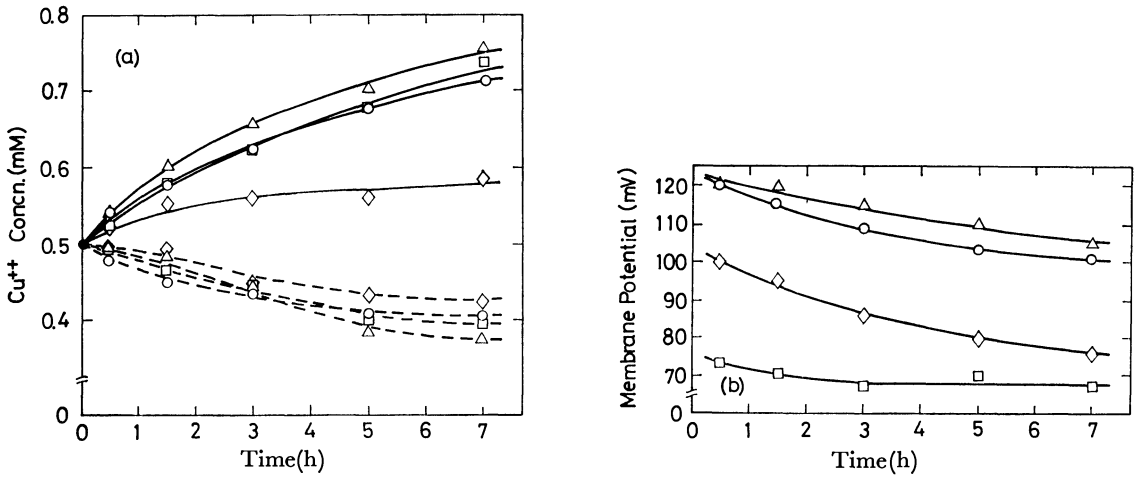

Fig. 5. Effect of potassium ion and lithium counter-ions on the transport of copper.
(a) Copper concentrations in both aqueous phases against time for various potassium and lithium salts systems. The curves have the same meanings as in Fig. 1.
(b) Membrane potential against time curves for the systems.
K and Li salts in Phases I and II; ○: 0.05 M K_2SO_4 (I)–0.1 M $LiNO_3$ (II), △: 0.05 M Li_2SO_4 (I)–0.1 M $LiNO_3$ (II), □: 0.05 M Li_2SO_4 (I)–0.1 M LiCl (II), ◇: 0.05 M Li_2SO_4 (I)–0.01 M $LiNO_3$, 0.045 M Li_2SO_4 (II).
Chelating agent; 4,7-diphenyl-2,9-dimethyl-1,10-phenanthroline.

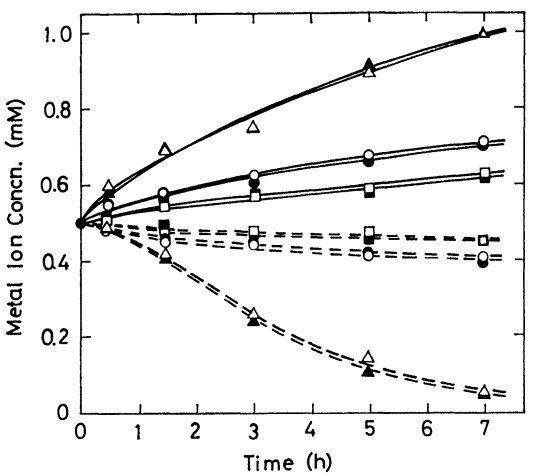

Fig. 6. Effect of membrane potential on the transport of metal ions.
Concentrations of metal ions in both aqueous phases against time.
The curves have the same meanings as in Fig. 1.
●,▲,■: Maintained at 0 mV with a voltage clamp, ○,△,□: without the voltage clamp.
Metal-chelating agent system; ○,●: copper–4,7-diphenyl-2,9-dimethyl-1,10-phenanthroline, △,▲: zinc–4,7-diphenyl-1,10-phenanthroline, □,■: cobalt–3,8-diphenyl-1,10-phenanthroline.
Phases I and II contained 0.05 M K_2SO_4 and 0.1 M $LiNO_3$ respectively.

membrane interfaces; the formation of a more stable metal-complex brings about a lowering of the rate of dissociation of the metal-complex.[10]

The phenanthroline derivatives which can move the metal ions are composed of lipophilic groups with a high solubility in the organic solvent. The partition coefficients of their metal-complexes between the aqueous and membrane phases must, therefore, be higher than that of the other phenanthroline derivatives. This high solubility in the membrane phase may also facilitate the transfer of the metal ions.

The acetylacetone derivatives could not move the metal ions. These compounds form fairly stable complexes with potassium and lithium ions as well as with the metal ions;[11,12] in this respect, they differ from the phenanthroline derivatives. The transfer of the metal ions in the membrane may be prevented by the formation of complexes with the potassium and lithium ions.

In the system containing lithium sulfate in Phase I, the rate of transport of the metal ions was slightly higher than that in the system containing potassium sulfate. In the case of the potassium sulfate, the transfer of the metal ions from Phase II to Phase I may be somewhat depressed by the diffusion of lithium ions from Phase II to Phase I, whereas in the case of the lithium sulfate the diffusion of the lithium ions does not occur.

The reduction of the nitrate ion in Phase II brought about a lowering of the rate of transport of the metal ions. In addition, in the potassium sulfate–lithium sulfate system containing a potassium ionophore, the transfer of the metal ions was not observed. The data for the transport of the metal ions with the voltage clamp agreed almost entirely with those for the ions without the voltage clamp. These facts show that the transfer of the metal ions occurs only in combination with the diffusion of nitrate ions (or chloride ions), which can penetrate the membrane.

In the previous paper,[1] the picrate anion in Phase I was dissolved in the dichloroethane phase, forming an ion-pair with a complexed cation consisting of an ionophore and the potassium ion, and then liberated into phase II by the dissociation of the ion-pair. The

metal ions may also be transported by the same mechanism; the metal ion, complexed by the chelating agent in Phase II, was dissolved in the dichloroethane phase, thus forming an ion-pair with a nitrate ion (or a chloride ion), and then liberated into Phase I by the dissociations of the ion-pair and the complex.

References

1) M. Sugiura and T. Shinbo, *Bull. Chem. Soc. Jpn.*, **52**, 684 (1979).
2) J. P. Behr and J. M. Lehn, *J. Am. Chem. Soc.*, **95**, 6108 (1973).
3) "Shin-Jikken-Kagaku-Koza, Bunseki-Kagaku I," ed by The Chemical Society of Japan, Maruzen, Tokyo (1976), p. 383.
4) R. M. Rush and J. H. Yoe, *Anal. Chem.*, **26**, 1345 (1954).
5) L. J. Clark, *Anal. Chem.*, **30**, 1153 (1958).
6) "Shin-Jikken-Kagaku-Koza, Bunseki-Kagaku I," ed by The Chemical Society of Japan, Maruzen, Tokyo (1976), p. 331.
7) "Seitaimaku Jikken-Gijutsu," ed by T. Onishi and Nankodo, Tokyo (1967), p. 301; H. H. Ussing and K. Zerahn, *Acta Physiol. Scand.*, **23**, 111 (1951).
8) "Kinzoku-Chelate, (III)," ed by B. Sakaguchi and K. Ueno, Nankodo, Tokyo (1967), Table, p. 69.
9) "Kagaku-Benran, Kiso-hen II," ed by The Chemical Society of Japan, Maruzen, Tokyo (1966), p. 1264.
10) "Membranes," ed by G. Eisenman, Marcel Dekker, New York (1975), Vol. 3, p. 3.
11) "Kinzoku-Chelate, (III)," ed by B. Sakaguchi and K. Ueno, Nankodo, Tokyo (1967), Table, p. 62.
12) "Membranes," ed by G. Eisenman, Marcel Dekker, New York (1975), Vol. 3, p. 72.

A Study on Electronic Excited States of Iridium(III) Complexes Containing Bipyridine and Phenanthroline Ligands. Solvent Effect on Triplet-Triplet Absorption Spectra

Yukako OHASHI*,† and Takayoshi KOBAYASHI

The Institute of Physical and Chemical Research, Hirosawa, Wako 351

(Received January 26, 1979)

In order to study the solvent effect on the lowest excited state of *cis*-$[IrCl_2L_2]Cl$ (L=2,2′-bipyridine, 1,10-phenanthroline, and 4,7-dimethyl-1,10-phenanthroline), the triplet-triplet absorption spectra (15000 cm^{-1}—27000 cm^{-1}) were measured by the use of *N,N*-dimethylformamide–water mixed solvents. For the triplet-triplet spectra of the three iridium complexes, remarkable spectral changes were observed with the change of the solvent polarity. An SCF calculation of the triplet-triplet transitions was carried out for free bipyridine and free phenanthroline. By comparing the calculated results and the observed spectra, the solvent effect can be interpreted in terms of a model invoking $d\pi^*$-$\pi\pi^*$ interaction, as proposed by Crosby. The lowest triplet state of $[IrCl_2(phen)_2]Cl$ is predominantly a $d\pi^*$ state in 95% v/v DMF–water, but in water, by the reversal of the state ordering, the lowest state becomes a $\pi\pi^*$ state. Furthermore, a quite similar solvent effect which was observed on the lowest triplet state of $[IrCl_2(bpy)_2]Cl$ is discussed; this state is not expected to have a $d\pi^*$-$\pi\pi^*$ interaction.

It has been pointed out that, in contrast to the ruthenium(II) complexes,[1–4] the character of the lowest excited state of *cis*-$[IrCl_2(phen)_2]Cl$ (phen: phenanthroline) is very sensitive to the solvent. The emission spectra and lifetimes at 77 K show a distinct solvent effect as the solvent polarity changes. This effect has been interpreted in terms of a change in the character of the lowest excited state.[1–3] Since the lowest $d\pi^*$ state (metal-to-ligand charge transfer excited state) and the lowest $\pi\pi^*$ state (locally excited state of a ligand) lie very close to each other, the solvent polarity affects their energy separation, which changes the electronic character of the lowest excited state. Recently, the contribution of the lowest d-d (locally excited state of a metal) level to the lowest excited state was also shown to be important by photochemical measurements[4] and the temperature dependence of the emission spectra.[5]

Since the excited-state absorption spectrum is assumed to change sharply, as the character of the lowest excited state changes, we measured the triplet-triplet absorption spectra of three *cis*-biscoordinated complexes($[IrCl_2(phen)_2]Cl$, $[IrCl_2(4,7\text{-Mephen})_2]Cl$, and $[IrCl_2(bpy)_2]Cl$) (bpy: bipyridine) and one triscoordinated complex ($[Ir(bpy)_3](NO_3)_3$) at room temperature, by using the mixed solvents of *N,N*-dimethylformamide (DMF) and water. Large solvent effects on the triplet-triplet absorption spectra were observed for the three biscoordinated complexes, but almost no solvent effect was seen for the triscoordinated complex. Using these results, we discuss the electronic structure of these biscoordinated complexes.

Experimental

Materials. *cis*-Dichlorobis(1,10-phenanthroline)iridium(III) chloride trihydrate, $[IrCl_2(phen)_2]Cl\cdot 3H_2O$, was prepared by following the procedure of Broomhead and Grumly.[6] *cis*-Dichlorobis(4,7-dimethyl-1,10-phenanthroline)iridium(III) chloride pentahydrate, $[IrCl_2(4,7\text{-Mephen})_2]Cl\cdot 5H_2O$, wa prepared by the same procedure. *cis*-Dichlorobis(2,2′-bipyridine)iridium(III) chloride dihydrate, $[IrCl_2(bpy)_2]Cl\cdot 2H_2O$, was synthetized by the method of Watts and Crosby.[7] Tris(bipyridine)iridium(III) nitrate, $[Ir(bpy)_3](NO_3)_3$, was prepared by the method of Flynn and Demas.[8] The purity of the complexes was checked by measuring the phosphorescence spectra, decay times, and the excitation spectra. Dimethylformamide was of spectrophotometric grade and water was distilled four times.

Apparatus. The triplet-triplet absorption spectra were obtained at room temperature using a nitrogen laser as an exciting light source and a pulsed xenon flash as a monitoring light source.[9] In order to discuss the relative absorbance of the triplet-triplet spectrum, we made a correction for the concentration of the excited molecules. Since in iridium(III) complexes no fluorescence was observed and the phosphorescence quantum yield does not depend on the exciting wavelength, we can assume that the quantum yield of triplet formation is very close to unity. Then, the absorbance at 337 nm of the ground-state absorption of each sample is proportional to the concentration of the excited triplet molecules. The ethanol–methanol solution (4: 1, v/v) of $[IrCl_2(phen)_2]Cl$ was used as a standard sample. The absorbance of the standard solution was measured in the same laser conditions as that for each sample solution. With the use of the relative concentration of the excited molecules estimated by the 337 nm absorbance, we obtained the corrected triplet-triplet absorption spectra corresponding to the same concentration of the excited molecules.

Results and Discussion

Figure 1 shows the triplet-triplet absorption spectra of $[IrCl_2(bpy)_2]Cl$ in water, 45% v/v DMF–water and 95% v/v DMF–water, and the triplet-triplet spectrum of $[Ir(bpy)_3](NO_3)_3$ in ethanol–methanol (4: 1, v/v).

In our present experiment, the measurements were carried out at concentrations of $\approx 10^{-3}$ mol dm^{-3}. An absorbance of less than 0.01 could not be measured.

In the case of $[IrCl_2(bpy)_2]Cl$, the absorbance in the spectral region below 21000 cm^{-1} decreases and the absorbance above 23000 cm^{-1} increases, as the solvent becomes more polar. However, for $[Ir(bpy)_3](NO_3)_3$, no solvent effect on the absorption spectra was observed for water, 95% v/v DMF–water, and ethanol–methanol (4: 1, v/v). Figures 2 and 3 show the triplet-triplet

† Present address: Bunkyo University, Minamiogishima, Koshigaya 343.

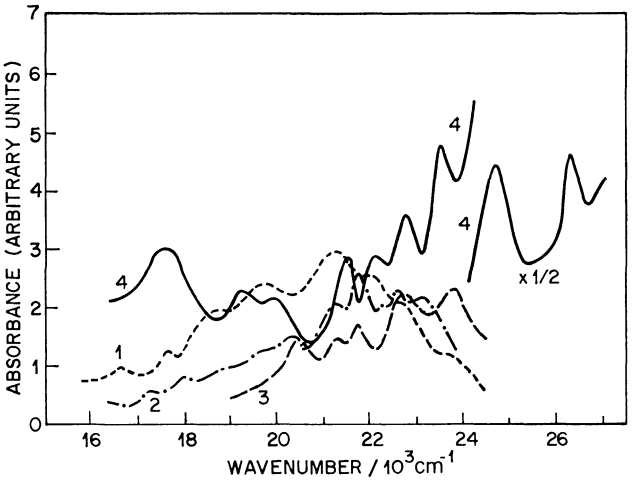

Fig. 1. Triplet-triplet absorption spectrum of $[IrCl_2(bpy_2)]Cl$ in 95% v/v DMF–water(curve 1), in 45% v/v DMF–water(curve 2) and in water(curve 3). The triplet-triplet spectrum of $[Ir(bpy)_3](NO_3)_3$ in ethanol–methanol(4: 1, v/v)(curve 4).

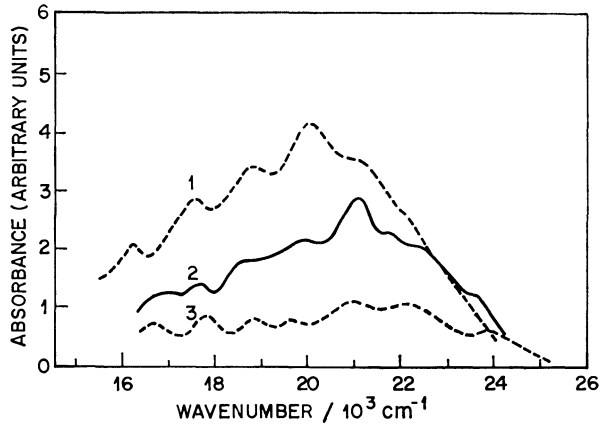

Fig. 2. Triplet-triplet absorption spectrum of $[IrCl_2(phen)_2]Cl$ in 95% v/v DMF–water(curve 1), in 45% v/v DMF–water(curve 2) and water(curve 3).

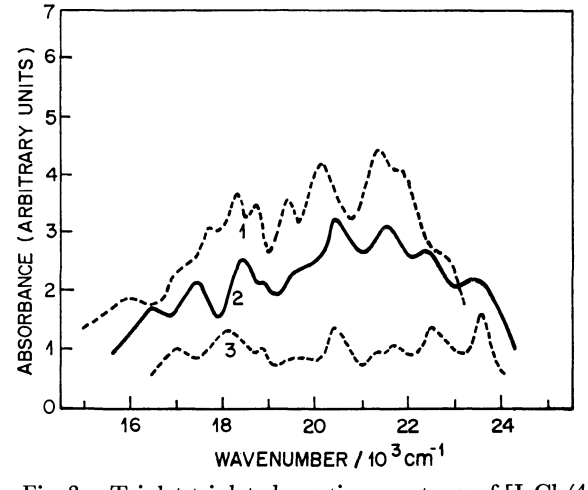

Fig. 3. Triplet-triplet absorption spectrum of $[IrCl_2(4,7\text{-Mephen})_2]Cl$ in 95% v/v DMF–water(curve 1), in 45% v/v DMF–water(curve 2) and water(curve 3).

absorption spectra of $[IrCl_2(phen)_2]Cl$ and $[IrCl_2(4,7\text{-Mephen})_2]Cl$ in DMF–water mixed solvents. In both complexes, the absorbance decreases remarkably as the solvent polarity increases. Furthermore, the same shift of the spectra was observed as for the bis(bipyridine) complex.

Assignment of Excited States. The absorption spectrum of $[Ir(bpy)_3](NO_3)_3$ has no low-energy $^1d\pi^*$ band and resembles that of free bipyridine molecules.[8] Since the singlet-triplet energy separation of a $\pi\pi^*$ state is generally much larger than that of a $d\pi^*$ state, the emitting level of the tris(bipyridine) complex(E_0= 22350 cm^{-1}) was assigned to a $^3\pi\pi^*$ state. The phosphorescence lifetime we observed is 49 μs at 77 K in degassed methanol. This value is ten times as long as the typical lifetimes of $d\pi^*$ phosphorescence.[10]

From the absorption spectrum measurements,[1] the lowest singlet state of $[IrCl_2(bpy)_2]Cl$ at 21900 cm^{-1} and $[IrCl_2(phen)_2]Cl$ at 21700 cm^{-1} was assigned to a $^1d\pi^*$ state. The singlet-triplet energy separation is generally small for a $d\pi^*$ state, hence the $^3d\pi^*$ level lies just below the $^1d\pi^*$ level. On the other hand, both of the free ligands also have a $^3\pi\pi^*$ emission in this region: E_0=23500 cm^{-1} for free bipyridine and 22200 cm^{-1} for free phenanthroline, at 77 K in ethanol–methanol (4: 1, v/v). Thus, the energy separation between the lowest $^3d\pi^*$ state and the lowest $^3\pi\pi^*$ state is expected to be small. The stabilization energy by solvent polarization is different depending upon the types of the electronic structures, that is, the ground state, $d\pi^*$ states, and $\pi\pi^*$ states. These differences of polarization energy are assumed to be of the same order as the energy separation between the lowest $^3d\pi^*$ and $^3\pi\pi^*$ states. Therefore, the character of the observed lowest triplet state of biscoordinated complexes is sensitive to the environment, as is seen from Figs. 1 and 2. The emitting state of $[IrCl_2(bpy)_2]Cl$ is 21400 cm^{-1} and that of $[IrCl_2(phen)_2]Cl$ is 21000 cm^{-1}, in ethanol–methanol (4: 1, v/v). Since the $^3\pi\pi^*$ energy of free bipyridine is 1300 cm^{-1} higher than that of free phenanthroline, the interaction in $[IrCl_2(bpy)_2]Cl$ between $^3d\pi^*$ and $^3\pi\pi^*$ states is thought to be small, in contrast to the case of $[IrCl_2(phen)_2]Cl$.[2] However, the lowest $^3\pi\pi^*$ state of $[Ir(bpy)_3](NO_3)_3$ appears at 22350 cm^{-1}, 1200 cm^{-1} lower than that of free bipyridine. The red shift of the $\pi\pi^*$ peak upon complex formation is thus large for a bipyridine complex but very small for a phenanthroline complex. Therefore, the energy separation between the lowest $^3\pi\pi^*$ and $^3d\pi^*$ of $[IrCl_2(bpy)_2]Cl$ is very similar to that of $[IrCl_2(phen)_2]Cl$.

For the bis(phenanthroline) complex, the emission lifetime at room temperature decreases from 270 ns[4] to 13 ns(our data), when the solvent is changed from 95% v/v DMF–water to water. This rapid decrease of the lifetime is also observed for bis(bipyridine) complex. From this similarity we can conclude that the character of the lowest triplet state of $[IrCl_2(bpy)_2]Cl$ is analogous to $[IrCl_2(phen)_2]Cl$.

Recently, from the large temperature dependence of the emission spectra in glycerol, the lowest triplet state of $[IrCl_2(phen)_2]Cl$ and $[IrCl_2(5,6\text{-Mephen})_2]Cl$ was assigned to an excited state localized on the metal(dd).[5]

However, in ethanol–methanol (4: 1, v/v), we observed no shift between the emission spectra at 77 K and 300 K for $[IrCl_2(phen)_2]Cl$. Furthermore, in water and 95% v/v DMF–water, the emission of $[IrCl_2(phen)_2]Cl$ and $[IrCl_2(5,6\text{-Mephen})_2]Cl$ at room temperature also does not show any shift from the low-temperature emission.[4] Therefore, in the solvents used in our experiments, the contribution of a dd level to the lowest triplet state can be neglected.

Solvent Effect of Triplet-Triplet Absorption Spectra. For the three biscoordinated complexes, the ground-state absorption peaks show a blue shift of 400—1000 cm^{-1}, when the solvent is changed from 95% v/v DMF–water to water. The observed stabilization of the singlet energy levels in polar solvents were almost equal for the same type of transition. On the other hand, the observed strong triplet-triplet transitions are primarily assigned to the transitions between electronic states of the same type($d\pi^*$-$d\pi^*$ or $\pi\pi^*$-$\pi\pi^*$). For the triplet-triplet transition the solvent effect on both states is almost counterbalanced. Therefore, the observed solvent effects on the triplet-triplet absorption spectra shown in Figs. 1, 2, and 3 can not be explained only by the above-mentioned solvent shifts of the energy levels.

The lowest triplet state in a tris(bipyridine) complex is $^3\pi\pi^*$; hence the observed triplet-triplet absorption spectrum is assigned to a $\pi\pi^*$-$\pi\pi^*$ transition. In a bis(bipyridine) complex, since the $^3d\pi^*$-$^3\pi\pi^*$ energy separation is of the same order as the solvent shift of the energy levels, a reversal of the states can occur by changing the solvent polarity. If the lowest triplet state(T_1) is denoted as $T_1 = A_{CT}\Psi(d\pi^*) + A_{LE}\Psi(\pi\pi^*)$, where A_{CT} and A_{LE} are coefficients of the wave function, the observed triplet-triplet absorption spectrum changes from T_1-higher $d\pi^*$ transitions to T_1-higher $\pi\pi^*$ transitions, as the coefficient A_{LE} increases.

We carried out an SCF-CI calculation on the triplet-triplet transitions for free bipyridine and free phenanthroline molecules. Figure 4 shows the calculated transition energies. The observed triplet-triplet absorption spectrum of free phenanthroline and the $^3\pi\pi^*$-$^3\pi\pi^*$ absorption spectrum of $[Ir(bpy)_3](NO_3)_3$ in ethanol–methanol (4: 1, v/v) are shown in Fig. 4. SCF-CI calculations generally gives an over-estimate of the transition energy, so the observed spectrum of tris-(bipyridine) complex can be assigned to one strong and three weak $^3\pi\pi^*$-$^3\pi\pi^*$ transitions, and the observed one of free phenanthroline to several weak $^3\pi\pi^*$-$^3\pi\pi^*$ transitions. With respect to the $^3d\pi^*$-$^3d\pi^*$ transitions, the energies can be estimated from the differences in orbital energies. Using the orbital energies of our calculation, for a bipyridine complex, two bands at 16200 cm^{-1} and 29500 cm^{-1} are expected; for a phenanthroline complex, two bands at 20200 cm^{-1} and 30200 cm^{-1} are expected. Thus from our SCF-CI calculations, we conclude that the triplet-triplet transitions both to the higher $^3d\pi^*$ states and to higher $^3\pi\pi^*$ states from the lowest triplet state are expected in the wave number range of our experiment.

It was pointed out that in the bis(bipyridine) complex the lowest $^3\pi\pi^*$ state lies a little higher than the lowest $^3d\pi^*$ state in ethanol–methanol (4: 1, v/v).[1] 95% DMF–water has a similar polarity to that of ethanol–methanol, so spectrum 1 in Fig. 1 is assigned to $^3d\pi^*$-$^3d\pi^*$ transition. On the other hand, spectrum 3 in Fig. 1 shows the vibrational structure, which resembles closely that of a tris(bipyridine) complex. Therefore, in water the $\pi\pi^*$ component of the lowest triplet state is predominant. The spectrum in 45% v/v DMF–water is interpreted as a superposition of almost equal contributions from the T_1-$^3\pi\pi^*$ and T_1-$^3d\pi^*$ transitions.

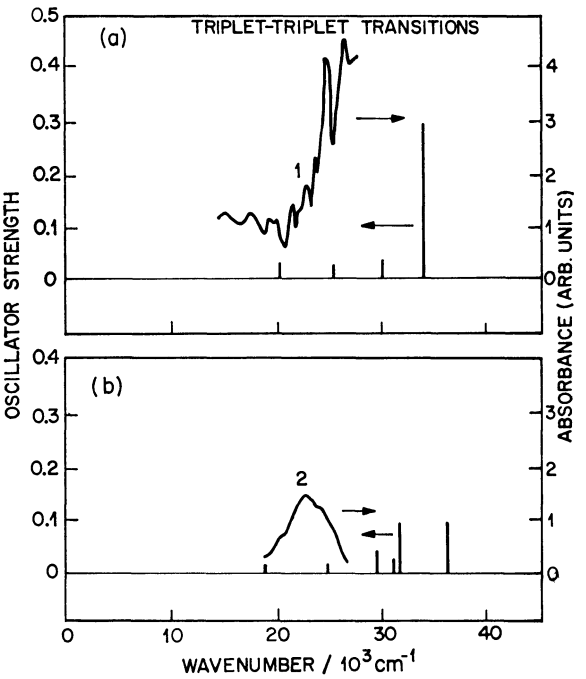

Fig. 4. Calculated triplet-triplet transition energies and their oscillator strength. (a) Free bipyridine, (b) free phenanthroline. Curves are the observed triplet-triplet absorption spectra of $[Ir(bpy)_3](NO_3)_3$ in 95% v/v DMF–water (curve 1) and free phenanthroline in ethanol–methanol(4: 1, v/v)(curve 2).

In the bis(phenanthroline) complex, the most distinct characteristics of the solvent effect on the triplet-triplet absorption spectrum is the large change in the absorption intensity. In 95% v/v DMF–water, the lowest triplet state is assigned to mainly $^3d\pi^*$, as in the bis(bipyridine) complex.[1] As the solvent becomes polar, the absorption intensity decreases rapidly and the peak maxima shift to slightly higher energy. This intensity decrease can be interpreted as a change in the character of T_1. In a bipyridine complex, the solvent affects only the absorption frequency, so the observed T_1-$^3\pi\pi^*$ transitions and T_1-$^3d\pi^*$ transitions have almost equal intensity. However, as is shown in Fig. 4, $^3\pi\pi^*$-$^3\pi\pi^*$ transitions of phenanthroline are weaker than the strong band of bipyridine. Therefore, an increase in the $\pi\pi^*$ component of T_1 results in a decrease of the intensity of the triplet-triplet absorption. Spectrum 3 in Fig. 2 can be assigned mainly to $^3\pi\pi^*$-$^3\pi\pi^*$ transitions. An analogous solvent effect was observed for bis(4,7-dimethyl-1,10-phenanthroline) complex (Fig. 3).

In conclusion, the excited states of the iridium(III) complexes with such ligands as bipyridine, phenanthroline, and their derivatives are very sensitive to the

environment. Changing the mixing ratio of DMF and water can cause changes in the character of the lowest triplet state as well as a reversal in the order of the state. Such solvent effects may become an important factor in the reactivity of these complexes in various solvents.

The authors are grateful to Professor Saburo Nagakura of the Institute for Solid State Physics for his kind support and valuable suggestions.

References

1) M. K. DeArmond and J. E. Hills, *J. Chem. Phys.*, **54**, 2247 (1971).
2) R. J. Watts, G. A. Crosby, and J. L. Sansregret, *Inorg. Chem.*, **11**, 1474 (1972).
3) R. J. Watts and G. A. Crosby, *Chem. Phys. Lett.*, **13**, 619 (1972).
4) R. Ballardini, G. Varani, L. Moggi, V. Balzani, K. R. Olson, F. Scandola, and M. Z. Hoffman, *J. Am. Chem. Soc.*, **97**, 728 (1975).
5) R. J. Watts, T. P. White, and B. G. Griffith, *J. Am. Chem. Soc.*, **97**, 6914 (1975).
6) J. A. Broomhead and W. Grumly, *Inorg. Chem.*, **10**, 2002 (1971).
7) R. J. Watts and G. A. Crosby, *J. Am. Chem. Soc.*, **93**, 3184 (1971).
8) C. M. Flynn, Jr., and J. N. Demas, *J. Am. Chem. Soc.*, **96**, 1959 (1974).
9) R. Nakagaki, T. Kobayashi, J. Nakamura, and S. Nagakura, *Bull. Chem. Soc. Jpn.*, **50**, 1909 (1977).
10) R. J. Watts and G. A. Crosby, *J. Am. Chem. Soc.*, **94**, 2606 (1972).

Photo-oxidation Effect of Poly(*N*-vinylcarbazole) Film on Photoconductivity and Electronic Spectra[1)]

Akira ITAYA,* Ken-ichi OKAMOTO, and Shigekazu KUSABAYASHI

Department of Chemical Engineering, Faculty of Engineering, Yamaguchi University, Tokiwadai, Ube 755

(Received January 26, 1979)

The photo-oxidation effect on poly(*N*-vinylcarbazole) (PVCz) and amorphous 1,3-di(*N*-carbazolyl)propane films was studied by means of ultraviolet absorption, infrared absorption, and fluorescence spectra. The photoconductivity of the photo-oxidized PVCz films was also measured as a function of photoirradiation time. A photo-oxidation product which formed near the surface of films had a carbonyl substituent group, acted as a singlet exciton trap in competition with the excimer-forming sites, and formed an exciplex with an excited carbazolyl chromophore. The very slight amount of the photo-oxidation product enhanced the photoconductivity of PVCz films by a factor of *ca.* 15, suggesting that the product acted as an electron-accepting impurity in the photo-carrier-generation mechanism in the lowest π-π^* absorption region of PVCz films.

There have been many investigations concerning the photo-carrier-generation mechanism in the lowest π-π^* absorption region of poly(*N*-vinylcarbazole) (PVCz) film.[2-7)] The following mechanism is considered to be most appropriate at the present stage:[6,7)]

$$D^* + A \longrightarrow (D^*\cdots A) \longrightarrow {}^1(D^+\cdots A^-)$$

encounter complex; nonrelaxed exciplex state

$$^1(D^+\cdots A^-) \xrightarrow{F} D^+ + A^-$$

$$^1(D^+\cdots A^-) \longrightarrow (D^+\text{—}A^-)^*$$

$(D^+\cdots A^-)$: geminate ion pair; $(D^+\text{—}A^-)^*$: exciplex state

Scheme 1.

The singlet excited state(D*) (singlet exciton) of PVCz migrates effectively through the carbazole(Cz) chromophores and encounters some electron-accepting impurity (A) during its lifetime to form an encounter complex ($D^*\cdots A$). The complex goes through a rapid electron transfer and changes to a nonrelaxed exciplex state $^1(D^+\cdots A^-)$. The nonrelaxed exciplex state has some excess kinetic energy and undergoes a thermalization of the excess energy to give an electron-hole ion pair ($D^+\cdots A^-$) at a separation r_0. The electron-hole pair will either recombine geminately to give a relaxed fluorescence exciplex state $(D^+\text{—}A^-)^*$, or dissociate into free carriers (D^+, A^-) when it is assisted by an external electric field *F*. Taking account of the ionization potential (6.1 eV) and the electron affinity (1.5 eV) of PVCz in film, the electron affinity of the compound acting as an electron acceptor should be higher than 0.6—0.8 eV. Some unknown impurities contaminated in course of synthesis of the monomer and/or polymer, dissolved oxygen, or a photo-oxidation product of the polymer can be considered as the electron-accepting impurities in a PVCz film. Judging from the migration efficiency of the singlet exciton,[8-10)] a concentration of the electron-accepting impurity of about 10^{-3} mol/mol monomer unit seems to be necessary to interpret the high yield of photo-carrier-generation (*ca.* 0.1). Contamination by such a concentration of the impurity is improbable in course of the synthesis. In the case of triplet oxygen in the ground state, of which the electron affinity is *ca.* 0.42 eV,[11)] considerable thermal activation should be necessary to give the electron-hole ion pair. Therefore, it is impossible to explain the high yield of the photo-carrier-generation in PVCz films by considering only the unknown contaminating impurity and the oxygen. Then, a photo-oxidation product of PVCz should be considered as an electron-accepting impurity which might be effective for the photo-carrier-generation. Therefore, detailed information on the photo-oxidation of a PVCz film is very important in understanding the origin of the high photoconductive properties of the polymer. It has been briefly reported that photo-oxidation products were obtained by irradiation of PVCz suspended in sulfuric acid–ethanol solution in a stream of air[12)] and of a PVCz film in air.[6)] However, no detailed study has been reported on the photo-degradation of a PVCz film.

In the present research, we have investigated the photo-oxidation of an amorphous PVCz film and an amorphous 1,3-di(*N*-carbazolyl)propane (DCzP(a)) film,[13)] which is a dimeric model compound of PVCz, by measuring the change in the absorption and fluorescence spectra caused by photoirradiation and have compared the difference in behavior of the photo-oxidation between these two films. We have also investigated how the photo-oxidation affects the photoconductivity of a PVCz film.

Experimental

The PVCz was prepared by free-radical polymerization (initiator; AIBN) and was reprecipitated from benzene solution with methanol. Thin PVCz films used for measuring the absorption and fluorescence spectra were cast on quartz plates from benzene solution and dried *in vacuo*. Films of PVCz 10 μm thick for electrical measurements were cast on nesa-coated conductive quartz plates from benzene solution. A semitransparent gold main electrode was evaporated on the film to prepare a sandwich-type cell. The DCzP(a) films were prepared by the methods described previously.[13)]

The absorption and fluorescence spectra were measured with the apparatus described in a previous paper.[14)] The electrical measurements (photoconductivity and magnetic field effect on the photoconductivity) were carried out under a vacuum of 10^{-2} Torr at 20 °C by a DC method. Films were irradiated in air at atmospheric pressure though a water filter (21 cm) with the full spectrum of a 500 W high pressure mercury lamp. The radiation density ($\lambda < 350$ nm) was about 1×10^{17} photons/cm^2 s.

Results and Discussion

Electronic Spectra. Figure 1 shows the change in the absorption spectra of PVCz films caused by photo-irradiation. With irradiation time, the absorption intensity of Cz chromophores decreased and new absorption (300—340 nm and 350—420 nm) appeared and increased. Three isosbestic points were observed at 348, 341, and 303 nm. These new bands are attributed to a photo-oxidation product, because no change in the absorption was observed for a PVCz film irradiated under a vacuum of 10^{-1} Torr. The further irradiation caused a deviation from these isosbestic points and also a decrease of the absorption intensities of the photo-oxidation product, as is shown in Fig. 2. Similar phenomena (decrease in the absorption intensity of Cz chromophores and appearance of new absorption bands) were also observed for DCzP(a) film, although five isosbestic points were observed. The dependence of the absorption intensity (370 nm) due to the photo-oxidation product on irradiation time is shown in Fig. 2. Assuming that there is no remarkable difference in the molar extinction coefficient of the photo-oxidation product between PVCz and DCzP(a), Fig. 2 shows that the formation rate of the photo-oxidation product observed for a PVCz film is larger than that for a DCzP(a) film by a factor of *ca.* 4. This may be attributed to the presence in the polymer film of sites which are susceptible to photo-oxidation. Judging from the fact that the concentration of the sandwich-like excimer-forming sites in a PVCz film is higher than that in a DCzP(a) film, the sandwich-like excimer-forming sites seem to be susceptible in such a way. This would be supported by the fact that the decrease of the sandwich-like excimer fluorescence (*ca.* 23900 cm^{-1}) caused by photo-oxidation is larger than that of the second excimer fluorescence (*ca.* 26500 cm^{-1}), as is clearly shown in Fig. 4.

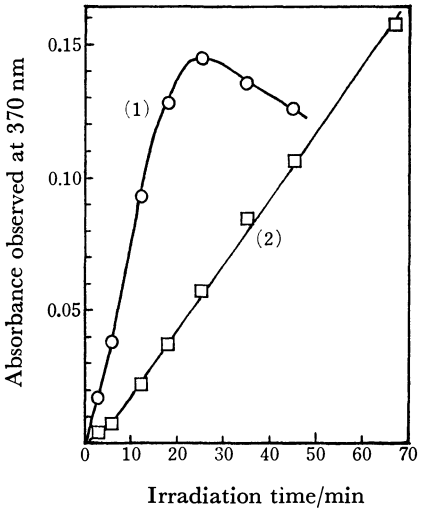

Fig. 2. Dependence of the absorption intensity at 370 nm on photoirradiation time for (1) PVCz and (2) DCzP(a) films.

Infrared spectra of photo-oxidized PVCz films are shown in Fig. 3. The increasing absorption observed at around 1700 cm^{-1} is attributable to carbonyl groups. A similar phenomenon was also observed for a DCzP(a) film. These results show that the photo-oxidation products formed in both PVCz and DCzP(a) films have carbonyl groups, which are electron-accepting substituents. The formation of the carbonyl group in a PVCz film by photo-oxidation is similar to the phenomenon observed for a photo-oxidized polystyrene (PSt) film.[15]

It has been reported that a PSt film becomes brittle by photo-oxidation, although extraction of the photo-oxidized PSt film with chloroform leaves a very small

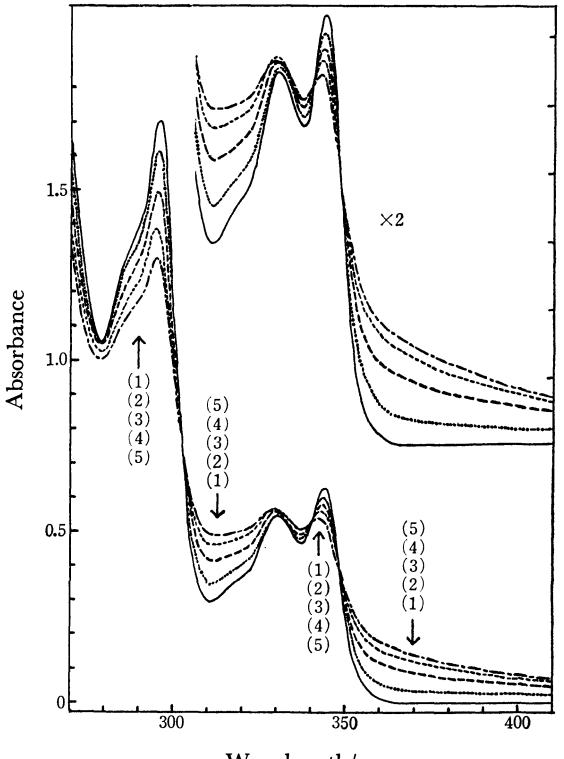

Fig. 1. Change in the absorption spectra of a PVCz film caused by photoirradiation. Irradiation time; (1) 0, (2) 6, (3) 12, (4) 18, and (5) 25 min.

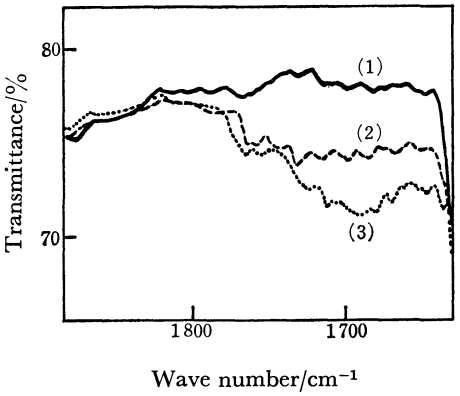

Fig. 3. Change in the infrared absorption spectra of a PVCz film caused by photoirradiation. Irradiation time; (1) 0, (2) 20, and (3) 100 min.

amount of residue.[15] On the other hand, the heavily photo-oxidized PVCz film becomes insoluble in most solvents, such as benzene and 1,2-dichloroethane. This fact suggests that the disruption of the Cz chromophore and a crosslinking reaction seems to take place at the same time in a PVCz film.

The change in the fluorescence spectra of PVCz films caused by photoirradiation in air is shown in Fig. 4. Little change was observed in the fluorescence spectra of PVCz films by photoirradiation under a vacuum of 10^{-1} Torr. Remarkable changes in the fluorescence spectra were observed for very weakly photo-oxidized PVCz films, compared with the case of absorption spectra. With irradiation time, the excimer fluorescence of PVCz films decreased and a new fluorescence band in the longer-wavelength region ($\nu<20000$ cm^{-1}) appeared. Further irradiation caused a decrease of the excimer and the new fluorescence intensities. A quite similar phenomenon was observed for DCzP(a) films, as is shown in Fig. 5. The broad and structureless emission band with a peak (or shoulder) at 19000—20000 cm^{-1} of the weakly photo-oxidized PVCz and DCzP(a) films may be assigned to the exciplex fluorescence, which is formed between an excited Cz chromophore and the photo-oxidation product with the carbonyl substituent group. This assignment is supported by the following observation. The fluorescence observed at 515 nm for the weakly photo-oxidized PVCz film was partly quenched by applying an electric field and the decrease in the fluorescence showed a quadratic dependence on the field strength, as is shown in Fig. 6. It has been reported by Yokoyama *et al.* that a similar phenomenon is observed for the exciplex fluorescence of PVCz films doped with dimethyl terephthalate (DMTP).[6,16]

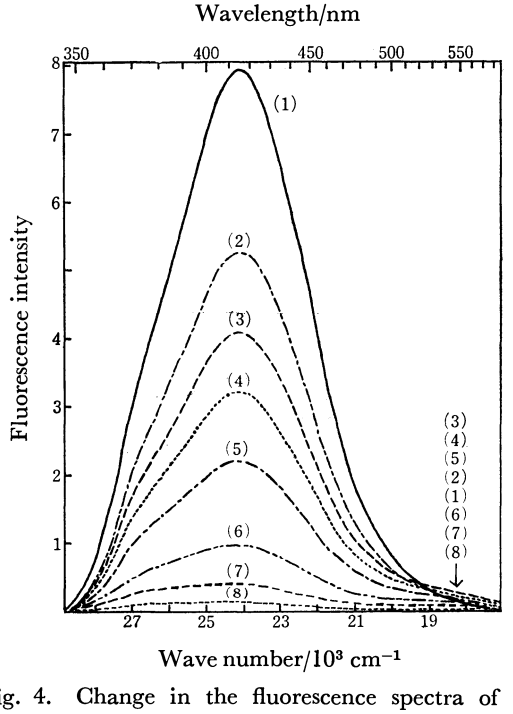

Fig. 4. Change in the fluorescence spectra of PVCz films caused by photoirradiation. Irradiation time; (1) 0, (2) 0.5, (3) 1, (4) 1.5, (5) 2.5, (6) 4.5, (7) 9, and (8) 15 min.

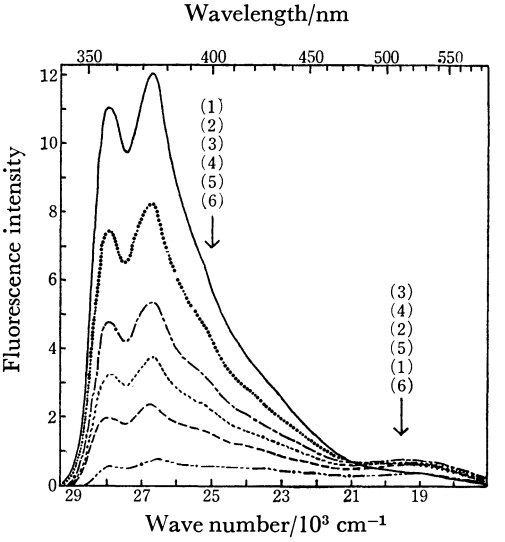

Fig. 5. Change in the fluorescence spectra of DCzP(a) films caused by photoirradiation. Irradiation time; (1) 0, (2) 0.17, (3) 0.5, (4) 1, (5) 1.5, and (6) 10 min.

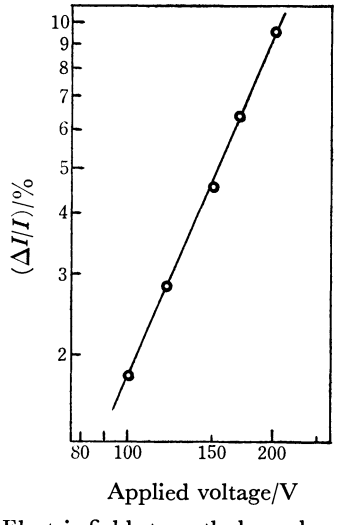

Fig. 6. Electric field-strength dependence of the fluorescence decrease observed at 510 nm for the weakly photo-oxidized PVCz film (≈0.5 μm thick). Irradiation time; 25 s. Excitation wavelength; 335 nm.

In order to represent the decrease of fluorescence, a quenching factor, Q, which has frequently been used in investigations of energy migration in polymer films,[8-10,17] is defined for convenience by the following equation:

$$Q_t = (I_0 - I_t)/I_t$$

where I_0 and I_t are fluorescence peak intensities before and after photo-irradiation, respectively. The dependence of the quenching factor of photo-oxidized PVCz and DCzP(a) films on the irradiation time is shown in Fig. 7. The value of Q obtained for thin films was larger than that obtained for thick films. This result suggests that the process of the photo-oxidation proceeds near the surface of films. Therefore, the photo-oxidation product is not formed in the bulk of film uniformly.

However, an approximately linear relationship existed between the quenching factor, Q, and the irradiation time, t, in an early stage of photoirradiation. This phenomenon seems to suggest that the photo-oxidation product acts as an exciton trap in competition with the excimer-forming sites. The value of Q obtained for DCzP(a) films was larger than that obtained for PVCz films. Considering that the concentration of the photo-oxidation product formed in PVCz films is higher than that formed in DCzP(a) films, as mentioned above, this fact suggests that the number of Cz chromophores covered by a singlet excition during its lifetime in a DCzP(a) film is larger than that in a PVCz film. This fact is consistent with the result obtained by investigation of the excitation energy migration, in which the fluorescence quenching by a guest molecule such as DMTP in PVCz and DCzP(a) films was investigated.[18]

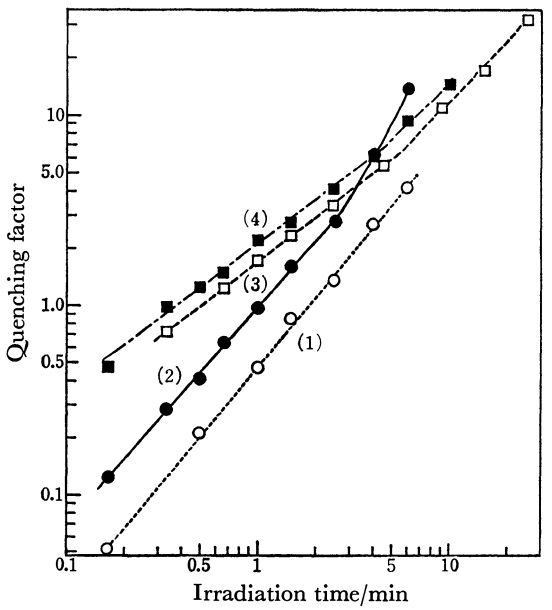

Fig. 7. Quenching factor *vs.* irradiation time. (1) PVCz film (≈0.7 μm thick), (2) PVCz film (≈0.2 μm thick), (3) DCzP(a) film (≈0.3 μm thick), and (4) DCzP(a) film (≈0.2 μm thick). Excitation wavelength; 330 nm.

The host fluorescence was depressed to half its original intensity ($Q=1$) at a guest concentration equal to the concentration of excimer-forming sites, in the case of PVCz films.[8–10] The concentration of excimer-forming sites in the PVCz film used in the present investigation was *ca.* 3×10^{-3} mol/mol basic unit.[10] Therefore, the concentration of the photo-oxidation product in a thin PVCz film (≈0.2 μm), where the product might be formed comparatively uniformly, became *ca.* 3×10^{-3} mol/mol basic unit by the irradiation for one minute, as is shown in Fig. 7. Considering the number of absorbed photons, the yield of the formation of the photo-oxidation product was estimated to be *ca.* 10^{-4}.

Photoconductivity. Dependence of the photocurrent of the photo-oxidized PVCz films on irradiation time is shown in Fig. 8. The photocurrent observed in the π-π^* absorption region increased steeply, by a factor of about 15, with photo-oxidation. It decreased when the film was exposed to radiation until a change in the absorption spectra by photo-oxidation could be observed. Voltage, spectral, light-intensity, and temperature dependence of the photocurrent of the photo-oxidized PVCz film were almost the same as those of the unirradiated PVCz film.[19]

It has been reported that an external magnetic field increased the photocurrent in a PVCz film and that this magnetic filed effect was enhanced by doping with a weak acceptor such as DMTP.[7] Figure 9 shows the dependence of the positive magnetic field effect of the photo-oxidized PVCz films on irradiation time. The effect was enhanced by a factor of about 3 by weak photo-oxidation.

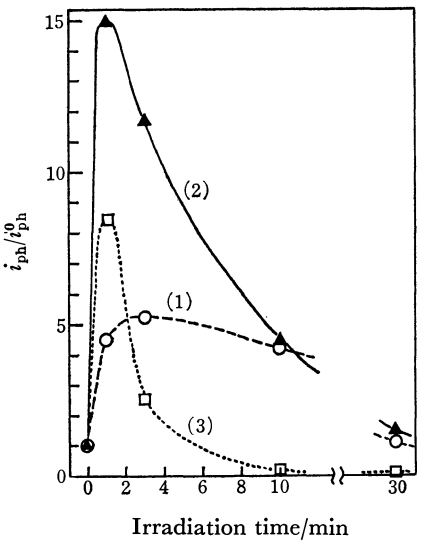

Fig. 8. Irradiation time dependence of the relative photocurrent(i^+_{ph}) of a photo-oxidized PVCz film under 35000 V/cm.
(1) 400, (2) 360, and (3) 330 nm.

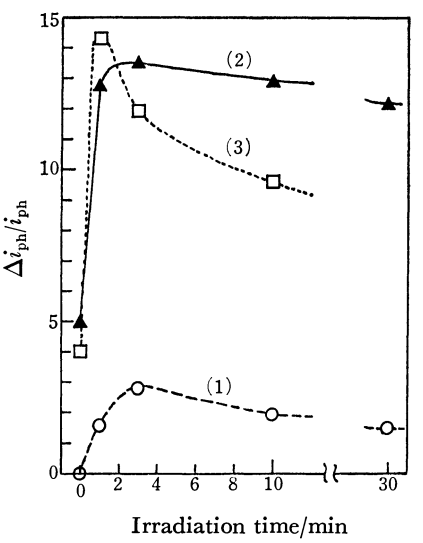

Fig. 9. Dependence of the positive magnetic field effect of a photo-oxidized PVCz film on irradiation time. Magnetic field; 1000 G. Applied voltage; 35000 V/cm.
(1) 400, (2) 360, and (3) 330 nm.

It is clear from the above-mentioned results that the yield of photo-carrier-generation of the weakly photo-oxidized PVCz films is much higher than the yield of the unirradiated PVCz films. That is, even if the concentration of the photo-oxidation product is too low to be detected by the absorption spectra, the product acts effectively as an electron-accepting impurity(A) in the Scheme 1 to enhance effectively the yield of photo-carrier-generation of a PVCz film. A high yield of photo-carrier-generation is obtained by a xerographic method,[5,20] where the surface of samples is exposed to a corona-charge under an ambient condition, and by measuring the photoconductivity of polymer films dried for a prolonged time under an ambient condition at a high temperature.[21] Such yields might be attributable to the mechanism of photo-carrier-generation described in Scheme 1, in which the electron-accepting impurity(A) seems to be a photo-oxidation product formed near the surface of PVCz films.

The present work was supported in part by a Grant-in-Aid for Scientific Research from the Ministry of Education.

References

1) A part of this paper was presented at the 25th Symposium on Macromolecules, Nagoya, October, 1976.
2) M. Lardon, E. Loll-Doller, and J. W. Weigl, *Mol. Cryst.*, **2**, 241 (1967).
3) P. J. Melz, *J. Chem. Phys.*, **57**, 1694 (1972).
4) K. Okamoto, S. Kusabayashi, and H. Mikawa, *Bull. Chem. Soc. Jpn.*, **46**, 2613 (1973).
5) G. Pfister and D. J. Williams, *J. Chem. Phys.*, **61**, 2416 (1974).
6) M. Yokoyama, Y. Endo, and H. Mikawa, *Bull. Chem. Soc. Jpn.*, **49**, 1538 (1976).
7) K. Okamoto, M. Oda, A. Itaya, and S. Kusabayashi, *Chem. Phys. Lett.*, **35**, 483 (1975).
8) W. Klöpffer, *J. Chem. Phys.*, **50**, 2337 (1969).
9) K. Okamoto, A. Yano, S. Kusabayashi, and H. Mikawa, *Bull. Chem. Soc. Jpn.*, **47**, 749 (1974).
10) A. Itaya, K. Okamoto, and S. Kusabayashi, *Bull. Chem. Soc. Jpn.*, **50**, 22 (1977).
11) W. T. Zemke, G. Das, and A. C. Wahl, *Chem. Phys. Lett.*, **14**, 310 (1972).
12) G. N. Ivanov, Y. Ya. Tolwacheve, V. P. Lopatinski, O. V. Rotar, T. G. Vedevnikova, and G. S. Yakusheve, *Chem. Abstr.*, **81**, 162019 (1974).
13) A. Itaya, K. Okamoto, and S. Kusabayashi, *Chem. Lett.*, **1978**, 131.
14) A. Itaya, K. Okamoto, and S. Kusabayashi, *Bull. Chem. Soc. Jpn.*, **49**, 2039 (1976).
15) J. F. Rabek and B. Rånby, *J. Polym. Soc., Polym. Chem. Ed.*, **12**, 273 (1974).
16) M. Yokoyama, Y. Endo, and H. Mikawa, *Chem. Phys. Lett.*, **34**, 597 (1975).
17) R. C. Powell, *J. Chem. Phys.*, **55**, 1871 (1971).
18) A. Itaya, K. Okamoto, and S. Kusabayashi, Symposium on Molecular Structure, Hiroshima, October, 1978.
19) K. Okamoto, S. Kusabayashi, and H. Mikawa, *Bull. Chem. Soc. Jpn.*, **46**, 2324 (1973).
20) P. J. Regensburger, *Photochem. Photobiol.*, **8**, 429 (1970).
21) D. M. Pai, *J. Chem. Phys.*, **52**, 2285 (1970).

Molecular Structures of Adducts of Benzoyl Isothiocyanate and Hydrazones Determined by the X-Ray Diffraction Method

Yasuhide FUKUTANI, Kumiko TSUKIHARA, Yukio OKUDA, Keiichi FUKUYAMA,*
Yukiteru KATSUBE, Iwao YAMAMOTO,** and Haruo GOTOH**

Faculty of Engineering, Tottori University, Koyama, Tottori 680
***Department of Chemistry, Shinshu University at Ueda, Ueda, Nagano 386*

(Received January 30, 1979)

X-Ray diffraction analysis was used to establish the molecular structures of some adducts of benzoyl isothiocyanate with hydrazones: benzaldehyde 4-benzoyl-2-phenylthiosemicarbazone (**1**), 2-benzoylimino-3,5-diphenyl-2,3-dihydro-1,3,4-thiadiazole (**2**), and 5-benzoylimino-2,2-dimethyl-4-phenyl-1,3,4-thiadiazolidine (**3**). In adducts **2** and **3**, a strong intramolecular interaction between sulfur and carbonyl oxygen atoms has been found. The S···O distance is 2.56 Å for **2** and 2.76 Å for **3**, and the oxygen atom lies approximately in the plane defined by the sulfur atom and the two carbon atoms bonded to the sulfur atom. The absence of a characteristic absorption due to a carbonyl group in the IR spectra of **2** and **3** reflects the intramolecular interaction. The crystal of **1** is triclinic, space group $P\bar{1}$, with $a=12.041$, $b=8.414$, $c=11.298$ Å, $\alpha=116.13$, $\beta=103.39$, $\gamma=103.27°$; that of **2** is monoclinic, space group $P2_1/c$, with $a=20.842$, $b=3.977$, $c=21.120$ Å, $\beta=103.55°$; and that of **3** is monoclinic, space group $P2_1$, with $a=12.559$, $b=6.910$, $c=10.283$ Å, $\beta=115.46°$. The structure has been refined by the block-diagonal least-squares method to $R=0.089$ with 2508 reflections for **1**, to $R=0.088$ with 1872 reflections for **2**, and to $R=0.098$ with 1031 reflections for **3**.

Previously Yamamoto *et al.* reported the reaction of benzoyl isothiocyanate with hydrazones and discussed the reaction mechanism; the reaction of benzoyl isothiocyanate with the derivatives of hydrazone yielded seven-membered ring compounds whose structures were assigned on the basis of their spectroscopic results.[1] In view of the novelty of their structures we have reexamined the molecular structures of the products by the X-ray diffraction method. We now report investigations leading to a revised structure **3**, together with establishment of the structures **1** and **2**.

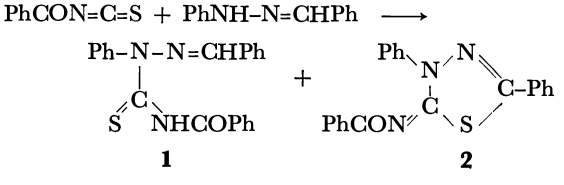

1 **2**

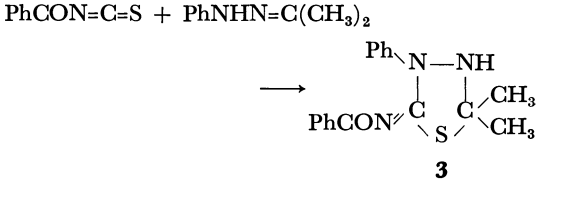

3

Experimental

The space group and preliminary unit cell constants for each crystal were determined by oscillation and Weissenberg photographs. The accurate cell constants for each crystal were determined by the least-squares method using at least 39 reflections measured on a four-circle diffractometer. The density of each crystal was obtained by the flotation method.

Crystal Data. (a) Product (**1**), $C_{21}H_{17}N_3OS$: $M=359.4$, triclinic, $P\bar{1}$, $a=12.041$, $b=8.414$, $c=11.298$ Å, $\alpha=116.13$, $\beta=103.39$, $\gamma=103.27°$, $V=924.9$ Å^3, $Z=2$, $D_m=1.30$ g·cm^{-3}, $D_x=1.29$ g·cm^{-3}. (b) Product (**2**), $C_{21}H_{15}N_3OS$: $M=357.4$, monoclinic, $P2_1/c$, $a=20.842$, $b=3.977$, $c=21.120$ Å, $\beta=103.55°$, $V=1701.9$ Å^3, $Z=4$, $D_m=1.40$ g·cm^{-3}, $D_x=1.39$ g·cm^{-3}. (c) Product (**3**), $C_{17}H_{17}N_3OS$: $M=311.4$, monoclinic, $P2_1$, $a=12.559$, $b=6.910$, $c=10.283$ Å, $\beta=115.46°$, $V=805.7$ Å^3, $Z=2$, $D_m=1.28$ g·cm^{-3}, $D_x=1.28$ g·cm^{-3}.

Intensity Measurements of 1 and 3. The intensities were measured on a Rigaku tape-controlled four-circle diffractometer with Ni-filtered Cu $K\alpha$ radiation. The approximate crystal size used for these intensity measurements was $0.1\times0.1\times0.4$ mm for **1** and $0.3\times0.06\times0.1$ mm for **3**. The θ-2θ scan technique was employed with a scan speed of 4°/min for 2θ. The backgrounds were counted for 6 s at both sides of the scan range. The intensities of 2677 independent reflections were measured in the range $0<\sin\theta/\lambda<0.56$ for **1**, and those of 1031 independent reflections in the range $0<\sin\theta/\lambda<0.53$ for **3**.

Intensity Measurement of 2. The intensities of reflections with $\sin\theta/\lambda$ less than 0.53 were measured from a crystal with dimensions of $0.5\times0.1\times0.05$ mm with Ni-filtered Cu $K\alpha$ radiation. The stationary-crystal stationary-counter technique was applied using a Toshiba four-circle diffractometer. A background for each reflection was taken from a curve which was determined by a plot of the backgrounds measured at several values of 2θ against their 2θ values. A total of 2132 reflections were measured, of which 1872 were recorded as non-zero intensity.

The intensities were corrected for the Lorentz and polarization factors, but were not corrected for absorption.

Structure Determination of 1. The structure was solved by an application of the direct method.[2] An E map based on the phases of 207 reflections revealed the positions of all non-hydrogen atoms. The structure was refined by the block-diagonal least-squares method,[3] initially with isotropic temperature factors and subsequently with anisotropic ones. The atomic species were assigned by inspection of temperature factors as well as interatomic distances and angles. All hydrogen atoms were revealed on a difference Fourier synthesis. Final refinement, by including these hydrogen atoms with isotropic temperature factors, reduced the R value to 0.089 for 2508 non-zero reflections. In the final refinement, the following weighting scheme was adopted: $w=0.0$ for $F_o=0$, $w=1.0$ for $0\leqq F_o<10$, and $w=[1.0+0.15(F_o-10)]^{-1}$ for $10<F_o$. The final atomic coordinates are given in Table 1.

Structure Determination of 2. The structure was solved by the heavy atom method, and refined by the block-diagonal least-squares method in the same way as for **1**. Including the hydrogen atoms revealed on a difference Fourier synthesis,

Table 1. Final atomic coordinates of **1** with estimated standard deviations in parentheses

	x	y	z		x	y	z
S(1)	−0.0227(1)	−0.3150(2)	−0.0918(1)	C(23)	0.6618(5)	0.4371(9)	0.6391(6)
C(2)	0.3805(4)	0.1129(7)	0.3058(5)	C(24)	0.6305(6)	0.4005(8)	0.7366(6)
N(3)	0.2680(3)	0.0038(6)	0.2621(4)	C(25)	0.5133(6)	0.2729(9)	0.6948(6)
N(4)	0.1941(3)	−0.0879(6)	0.1184(4)	C(26)	0.4307(5)	0.1746(8)	0.5542(6)
C(5)	0.0734(4)	−0.1952(7)	0.0758(5)	H(C2)	0.414(6)	0.166(9)	0.254(7)
N(6)	0.0451(3)	−0.1945(6)	0.1873(4)	H(N6)	0.106(6)	−0.129(9)	0.268(7)
C(7)	−0.0655(4)	−0.2836(7)	0.1911(5)	H(C10)	0.141(6)	−0.250(9)	0.390(6)
O(8)	−0.1644(3)	−0.3588(5)	0.0926(4)	H(C11)	0.159(7)	−0.229(10)	0.611(8)
C(9)	−0.0514(5)	−0.2747(7)	0.3284(5)	H(C12)	−0.024(7)	−0.234(10)	0.680(8)
C(10)	0.0574(5)	−0.2598(8)	0.4157(6)	H(C13)	−0.210(7)	−0.275(11)	0.533(8)
C(11)	0.0644(6)	−0.2543(10)	0.5439(7)	H(C14)	−0.228(7)	−0.318(10)	0.296(7)
C(12)	−0.0356(7)	−0.2590(9)	0.5820(7)	H(C16)	0.225(5)	0.171(8)	0.047(6)
C(13)	−0.1451(7)	−0.2757(9)	0.4945(7)	H(C17)	0.296(6)	0.171(9)	−0.135(7)
C(14)	−0.1513(5)	−0.2837(8)	0.3678(6)	H(C18)	0.404(6)	−0.027(10)	−0.225(7)
C(15)	0.2469(4)	−0.0788(7)	0.0179(5)	H(C19)	0.394(5)	−0.298(8)	−0.180(6)
C(16)	0.2511(5)	0.0661(7)	−0.0098(6)	H(C20)	0.289(6)	−0.329(9)	−0.028(7)
C(17)	0.3102(5)	0.0792(8)	−0.0988(6)	H(C22)	0.605(5)	0.385(8)	0.427(6)
C(18)	0.3597(5)	−0.0530(9)	−0.1607(6)	H(C23)	0.755(6)	0.532(9)	0.664(7)
C(19)	0.3538(5)	−0.1982(8)	−0.1331(6)	H(C24)	0.702(6)	0.480(9)	0.843(7)
C(20)	0.2962(5)	−0.2129(7)	−0.0437(6)	H(C25)	0.482(6)	0.235(9)	0.760(7)
C(21)	0.4628(4)	0.2117(7)	0.4559(5)	H(C26)	0.339(6)	0.068(9)	0.518(7)
C(22)	0.5795(5)	0.3424(8)	0.4994(6)				

Table 2. Final atomic coordinates of **2** with estimated standard deviations in parentheses

	x	y	z		x	y	z
S(1)	0.1462(1)	0.0855(4)	0.2217(1)	C(22)	−0.0064(3)	0.0244(16)	0.1743(3)
C(2)	0.1017(2)	−0.0802(14)	0.1481(2)	C(23)	−0.0746(3)	−0.0026(16)	0.1586(3)
N(3)	0.1369(2)	−0.2005(12)	0.1097(2)	C(24)	−0.1069(3)	−0.1427(17)	0.1009(3)
N(4)	0.2033(2)	−0.1599(12)	0.1384(2)	C(25)	−0.0719(3)	−0.2606(16)	0.0571(3)
C(5)	0.2191(2)	−0.0143(14)	0.1978(2)	C(26)	−0.0035(3)	−0.2395(15)	0.0724(3)
N(6)	0.2799(2)	0.0471(12)	0.2299(2)	H(C10)	0.399(3)	0.111(20)	0.248(3)
C(7)	0.2870(3)	0.2083(16)	0.2890(2)	H(C11)	0.512(3)	0.200(16)	0.300(3)
O(8)	0.2413(2)	0.2832(13)	0.3141(2)	H(C12)	0.536(3)	0.466(17)	0.413(3)
C(9)	0.3571(3)	0.2902(15)	0.3210(2)	H(C13)	0.443(3)	0.638(19)	0.460(3)
C(10)	0.4086(3)	0.2089(16)	0.2926(3)	H(C14)	0.330(3)	0.514(17)	0.403(3)
C(11)	0.4727(3)	0.2828(18)	0.3252(3)	H(C16)	0.179(3)	−0.167(16)	0.010(3)
C(12)	0.4856(3)	0.4326(19)	0.3858(3)	H(C17)	0.250(3)	−0.367(17)	−0.057(3)
C(13)	0.4344(3)	0.5173(18)	0.4137(3)	H(C18)	0.360(3)	−0.571(17)	−0.009(3)
C(14)	0.3694(3)	0.4447(16)	0.3815(3)	H(C19)	0.399(3)	−0.571(16)	0.114(3)
C(15)	0.2480(2)	−0.2676(14)	0.0998(2)	H(C20)	0.325(3)	−0.358(16)	0.182(3)
C(16)	0.2266(3)	−0.2612(16)	0.0331(3)	H(C22)	0.016(3)	0.143(15)	0.216(3)
C(17)	0.2676(3)	−0.3732(18)	−0.0055(3)	H(C23)	−0.100(3)	0.101(15)	0.190(3)
C(18)	0.3302(3)	−0.4843(18)	0.0226(3)	H(C24)	−0.155(3)	−0.168(16)	0.093(3)
C(19)	0.3510(3)	−0.4937(18)	0.0899(3)	H(C25)	−0.099(3)	−0.381(20)	0.013(3)
C(20)	0.3107(3)	−0.3857(16)	0.1299(3)	H(C26)	0.022(3)	−0.289(16)	0.038(3)
C(21)	0.0294(2)	−0.0945(14)	0.1312(2)				

final refinement was carried out using the following weighting scheme: $w=0.0$ for $F_o=0$, $w=1.0$ for $0<F_o\leqq 24$, and $w=[1.0+0.67(F_o-24)]^{-1}$ for $24<F_o$. The final R value was 0.088 for 1872 non-zero reflections. The final atomic coordinates are given in Table 2.

Structure Determination of 3. The structure was solved by the direct method[2] followed by successive Fourier synthesis, and refined in the same way as for **1**. The final refinement, including the contribution of the hydrogen atoms and anomalous scattering of sulfur atom, reduced R to 0.098 for 1031 reflections ($R=0.088$ for non-zero reflections). The weighting scheme adopted in the final refinement was: $w=0.2$, for $F_o=0$, $w=1.0$ for $0<F_o\leqq 24$, and $w=[1.0+0.43(F_o-24)]^{-1}$ for $24<F_o$. The final atomic coordinates are given in Table 3.

The atomic scattering factors were taken from the International Tables for X-Ray Crystallography.[4] The temperature factors and the list of observed and calculated structure factors for each compound are kept as Document No. 7924 at the Chemical Society of Japan.

Table 3. Final atomic coordinates of **3** with estimated standard deviations in parentheses

	x	*y*	*z*
S(1)	0.4879(2)	0.0000(7)	0.5865(3)
C(2)	0.5000(9)	0.0443(19)	0.7734(9)
N(3)	0.4556(7)	0.2379(15)	0.7660(8)
N(4)	0.3601(7)	0.2645(17)	0.6260(9)
C(5)	0.3662(9)	0.1551(17)	0.5199(11)
N(6)	0.2831(7)	0.1743(16)	0.3844(8)
C(7)	0.3038(9)	0.0809(18)	0.2800(11)
O(8)	0.4002(6)	0.0286(18)	0.2907(8)
C(9)	0.1953(9)	0.0673(17)	0.1391(9)
C(10)	0.0843(10)	0.0791(25)	0.1353(11)
C(11)	−0.0144(13)	0.0611(32)	0.0022(17)
C(12)	0.0003(13)	0.0300(32)	−0.1212(13)
C(13)	0.1106(14)	0.0188(27)	−0.1153(13)
C(14)	0.2132(11)	0.0340(23)	0.0167(11)
C(15)	0.2720(9)	0.4015(19)	0.6114(10)
C(16)	0.2201(10)	0.3900(24)	0.7097(12)
C(17)	0.1311(10)	0.5195(34)	0.6896(14)
C(18)	0.0991(12)	0.6609(27)	0.5886(14)
C(19)	0.1528(13)	0.6727(28)	0.4975(13)
C(20)	0.2380(10)	0.5471(23)	0.5070(12)
C(21)	0.6335(10)	0.0428(26)	0.8798(12)
C(22)	0.4280(11)	−0.1060(21)	0.8062(12)
H(N3)	0.508(12)	0.330(24)	0.760(15)
H(C10)	0.077(11)	0.116(23)	0.230(14)
H(C11)	−0.100(10)	0.073(21)	−0.006(13)
H(C12)	−0.071(12)	0.006(29)	−0.220(15)
H(C13)	0.128(11)	0.006(27)	−0.207(14)
H(C14)	0.286(12)	−0.042(24)	0.030(15)
H(C16)	0.243(11)	0.279(25)	0.781(14)
H(C17)	0.093(12)	0.490(29)	0.766(16)
H(C18)	0.039(10)	0.763(21)	0.584(12)
H(C19)	0.132(12)	0.779(26)	0.422(15)
H(C20)	0.281(10)	0.533(23)	0.430(12)
H(C21a)	0.649(10)	−0.093(22)	0.906(13)
H(C21b)	0.626(9)	0.114(19)	0.941(12)
H(C21c)	0.674(11)	0.052(23)	0.829(14)
H(C22a)	0.455(12)	−0.258(24)	0.799(15)
H(C22b)	0.338(9)	−0.073(18)	0.731(11)
H(C22c)	0.440(9)	−0.087(18)	0.901(11)

Table 4. Selected bond lengths (*l*/Å) and angles (*φ*/°) for non-hydrogen atoms

(a) Adduct **1**

S(1)–C(5)	1.646(6)	C(2)–N(3)	1.281(8)
C(2)–C(21)	1.467(8)	N(3)–N(4)	1.391(7)
N(4)–C(5)	1.361(8)	N(4)–C(15)	1.445(7)
C(5)–N(6)	1.376(8)	N(6)–C(7)	1.390(8)
C(7)–O(8)	1.216(7)	C(7)–C(9)	1.487(8)
N(3)–C(2)–C(21)	120.9(5)	C(2)–N(3)–N(4)	118.6(5)
N(3)–N(4)–C(5)	117.5(5)	N(3)–N(4)–C(15)	120.5(5)
C(5)–N(4)–C(15)	121.8(5)	S(1)–C(5)–N(4)	122.2(4)
S(1)–C(5)–N(6)	125.7(5)	N(4)–C(5)–N(6)	112.0(5)
C(5)–N(6)–C(7)	130.9(5)	N(6)–C(7)–O(8)	123.3(5)
N(6)–C(7)–C(9)	113.5(5)	O(8)–C(7)–C(9)	123.2(5)

(b) Adduct **2**

S(1)–C(2)	1.743(6)	S(1)–C(5)	1.757(6)
C(2)–N(3)	1.305(7)	C(2)–C(21)	1.467(8)
N(3)–N(4)	1.384(7)	N(4)–C(5)	1.351(7)
N(4)–C(15)	1.437(7)	C(5)–N(6)	1.312(7)
N(6)–C(7)	1.379(8)	C(7)–O(8)	1.230(8)
C(7)–C(9)	1.495(9)	S(1)···O(8)	2.558(6)
C(2)–S(1)–C(5)	88.4(3)	S(1)–C(2)–N(3)	115.8(4)
S(1)–C(2)–C(21)	122.2(4)	N(3)–C(2)–C(21)	122.0(5)
C(2)–N(3)–N(4)	109.6(5)	N(3)–N(4)–C(5)	117.2(5)
N(3)–N(4)–C(15)	115.5(4)	C(5)–N(4)–C(15)	127.2(5)
S(1)–C(5)–N(4)	109.0(4)	S(1)–C(5)–N(6)	127.1(4)
N(4)–C(5)–N(6)	123.8(5)	C(5)–N(6)–C(7)	116.2(5)
N(6)–C(7)–O(8)	125.0(6)	N(6)–C(7)–C(9)	113.4(5)
O(8)–C(7)–C(9)	121.6(6)	O(8)···S(1)–C(2)	162.2(4)
O(8)···S(1)–C(5)	73.8(4)		

(c) Adduct **3**

S(1)–C(2)	1.89(1)	S(1)–C(5)	1.75(1)
C(2)–N(3)	1.44(2)	C(2)–C(21)	1.56(2)
C(2)–C(22)	1.51(2)	N(3)–N(4)	1.44(2)
N(4)–C(5)	1.36(2)	N(4)–C(15)	1.41(2)
C(5)–N(6)	1.34(2)	N(6)–C(7)	1.37(2)
C(7)–O(8)	1.22(2)	C(7)–C(9)	1.51(2)
S(1)···O(8)	2.76(1)		
C(2)–S(1)–C(5)	89(1)	S(1)–C(2)–N(3)	104(1)
S(1)–C(2)–C(21)	108(1)	S(1)–C(2)–C(22)	109(1)
N(3)–C(2)–C(21)	109(1)	N(3)–C(2)–C(22)	113(1)
C(21)–C(2)–C(22)	114(1)	C(2)–N(3)–N(4)	108(1)
N(3)–N(4)–C(5)	115(1)	N(3)–N(4)–C(15)	118(1)
C(5)–N(4)–C(15)	127(1)	S(1)–C(5)–N(4)	112(1)
S(1)–C(5)–N(6)	129(1)	N(4)–C(5)–N(6)	119(1)
C(5)–N(6)–C(7)	116(1)	N(6)–C(7)–O(8)	126(1)
N(6)–C(7)–C(9)	113(1)	O(8)–C(7)–C(9)	121(1)
O(8)···S(1)–C(2)	158(1)	O(8)···S(1)–C(5)	70(1)

Results and Discussion

The present X-ray analysis has determined the molecular structures of the adducts unambiguously, showing the benzoyl isothiocyanate adducts with benzaldehyde phenylhydrazone to be benzaldehyde 4-benzoyl-2-phenylthiosemicarbazone (**1**) and 2-benzoyl-imino-3,5-diphenyl-2,3-dihydro-1,3,4-thiadiazole (**2**), and that with acetone phenylhydrazone to be 5-benzoyl-imino-2,2-dimethyl-4-phenyl-1,3,4-thiadiazolidine (**3**). Thus the structural formula (16a) which was given in Ref. 1 should be revised to **3**. The molecular structures and the numbering scheme used in the present paper are shown in Fig. 1, and the crystal structure of **3** in Fig. 2. Selected bond lengths and angles are given in Table 4, and the equations of the least-squares planes, deviations of atoms from each plane, and selected torsion angles in Table 5. The molecules of **2** are stacked along the b axis, with interplanar distances of about 3.6 Å. Except for the intermolecular hydrogen bond in the crystal of **3**, there is neither an intermolecular hydrogen bond nor any abnormally short intermolecular contact in the crystals of **1** and **2**.

Molecular Structure of ***1***. The S(1)–C(5) length of 1.646 Å is reasonable, compared with the thione bond lengths observed in various compounds, although these lengths differ from compound to compound.[6] The distribution of the bond lengths among the C(2), N(3), N(4), C(5), and C(7) atoms and the fact that these

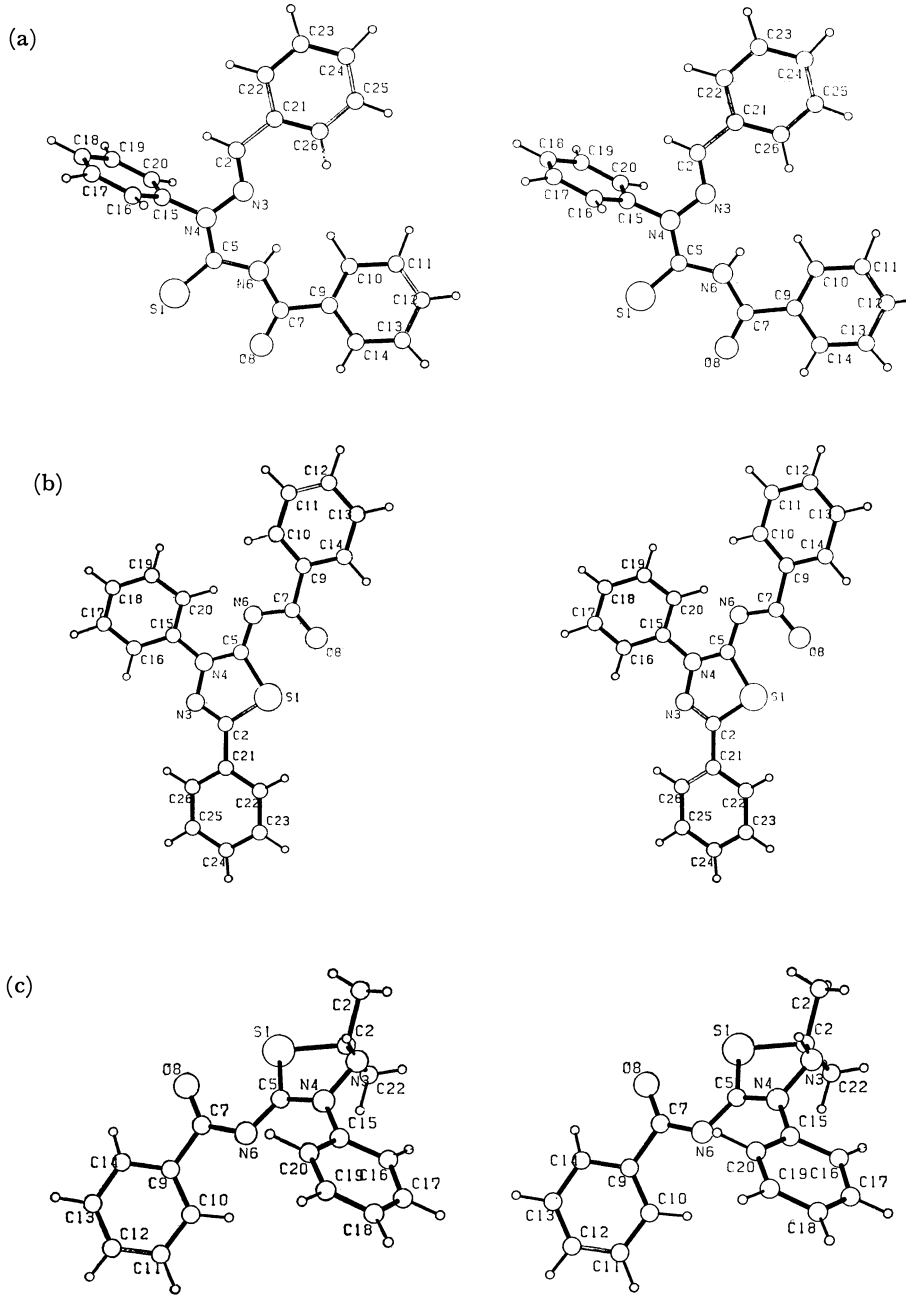

Fig. 1. Molecular structures and numbering schemes of (a) adduct **1**, (b) adduct **2**, and (c) adduct **3**.

atoms are nearly coplanar suggest appreciable delocalization of π electrons.

*Molecular Structures of **2** and **3** and S···O Interaction.* The benzoylimino group, the thiadiazoline ring, and the phenyl group of C(21)–C(26) in **2** are substantially coplanar. The geometry and the bond lengths of these groups indicate that a conjugated system exists among these groups. The five-membered ring of **3** has an envelope conformation with the C(2) atom deviating significantly from the plane through the S(1), N(3), N(4), and C(5) atoms; its conjugated system is disrupted by the C(2) and N(3) atoms, as expected from structural formula **3**.

The noteworthy feature of the molecular structures of **2** and **3** is the intramolecular S···O interaction; the distance between these atoms is 2.56 Å for **2** and 2.76 Å for **3**, which is significantly shorter than the sum of the van der Waals radii of the atoms. The oxygen atom of **3**, as well as that of **2**, lies approximately in the plane defined by S(1), C(2), and C(5) atoms. In the case of **3**, twists occur around the C(5)–N(6) double bond by 10° and the N(6)–C(7) bond by 21° such that the oxygen atom lies in the plane. Otherwise the deviation of the oxygen atom from the plane amounts to 0.7 Å, since the C(5)–N(6) bond deviates from the plane. The length of the intermolecular hydrogen bond between

TABLE 5. LEAST-SQUARES PLANES, DEVIATIONS OF ATOMS FROM EACH PLANE, (d/Å) AND SELECTED TORSION ANGLES (φ/°)

(a) Adduct **1**

(I) Plane through the atoms of S(1), N(4), C(5), and N(6) $0.534X-0.829Y-0.164Z=2.148$

S(1)	−0.004	N(4)	−0.004
C(5)	0.011	N(6)	−0.004
N(3)[a]	−0.023	C(7)[a]	0.004
O(8)[a]	0.231	C(15)[a]	−0.090

(II) Plane through the atoms of N(6), C(7), O(8), and C(9) $0.490X-0.791Y-0.366Z=1.679$

N(6)	0.002	C(7)	−0.006
O(8)	0.002	C(9)	0.002
S(1)[a]	−0.543	C(5)[a]	−0.190

The atoms of each benzene ring are coplanar, with r.m.s. of deviations being about 0.01 Å. The dihedral angle between the plane (I) and the benzene ring of C(15)–C(20) is 89.2°and that between the plane (II) and the benzene ring of C(9)–C(14) is 26.3.°

(III) Torsion angles

C(21)–C(2)–N(3)–N(4)	−179.4
N(3)–N(4)–C(5)–N(6)	− 0.4
N(4)–C(5)–N(6)–C(7)	180.0
C(5)–N(6)–C(7)–O(8)	− 11.5
N(6)–C(7)–C(9)–C(10)	− 26.8

(b) Adduct **2**

(I) Plane through all non-hydrogen atoms except the atoms of C(15)–C(20) $0.056X+0.893Y-0.446Z=-1.590$

S(1)	−0.028	C(2)	0.026
N(3)	0.002	N(4)	−0.047
C(5)	−0.072	N(6)	−0.087
C(7)	−0.063	O(8)	−0.087
C(9)	0.007	C(10)	0.045
C(11)	0.075	C(12)	0.050
C(13)	0.028	C(14)	−0.001
C(21)	0.051	C(22)	0.026
C(23)	−0.001	C(24)	0.008
C(25)	0.043	C(26)	0.053

The atoms of each of two six-membered and five-membered rings are coplanar, with the r.m.s. deviation being less than 0.01 Å. The dihedral angle between the above plane and the plane defined by the atoms of C(15)–C(20) is 31.3.°

(c) Adduct **3**

(I) Plane through the atoms of S(1), N(3), N(4), and C(5) $0.687X+0.702Y-0.188Z=1.415$

S(1)	0.01	N(3)	−0.01
N(4)	0.02	C(5)	−0.01
C(2)[a]	0.58	C(21)[a]	−0.06
C(22)[a]	2.09	N(6)[a]	−0.04
C(15)[a]	0.04		

The r.m.s. of the deviations of the atoms of benzene ring is about 0.01 Å.

(II) Torsion angles

C(5)–S(1)–C(2)–N(3)	−30.3
S(1)–C(2)–N(3)–N(4)	36.7
C(2)–N(3)–N(4)–C(5)	−27.9
N(3)–N(4)–C(5)–S(1)	3.0
S(1)–C(5)–N(6)–C(7)	−10.1
C(5)–N(6)–C(7)–O(8)	−21.1
N(6)–C(7)–C(9)–C(10)	−23.0
N(3)–N(4)–C(15)–C(16)	−50.5

a) Not included in the least-squares calculations.

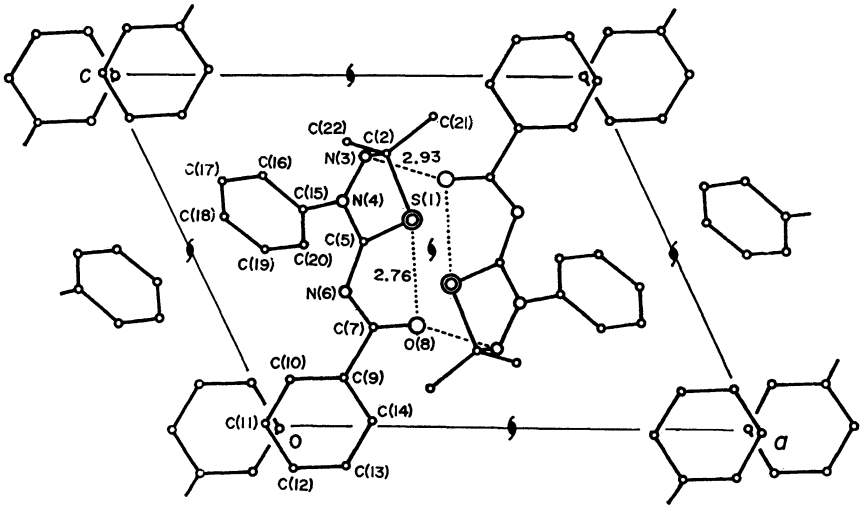

Fig. 2. Crystal structure of **3** viewed along the b axis. Broken lines indicate intermolecular hydrogen bond, and dotted lines S···O interaction (see text). Hydrogen atoms are omitted from the figure for the sake of clarity.

the N(3) and O(8) atoms is lengthened by the twists. A similar geometrical feature, where the oxygen atom lies in the plane defined by the sulfur atom and two adjacent atoms bonded to the sulfur atom, has been reported in other compounds.[7–11] The absence of a characteristic absorption due to C=O stretching in the IR spectra of **2** and **3** should be associated with the S···O interaction.[12]

We wish to thank Dr. Tomitake Tsukihara for his fruitful discussions. We are also grateful to Mr. Hiroshi Kuroda, Mr. Susumu Fujii, Mr. Keisuke Ohgitani, and Mr. Eiichi Waki for valuable assistance in X-ray work.

References

1) I. Yamamoto, A. Mamba, and H. Gotoh, *J. Chem. Soc., Perkin Trans. 1*, **1976**, 2243. The compounds (18), (19), and (16a) in the Journal correspond to **1**, **2**, and **3** in this Bulletin respectively.

2) G. Germain, P. Main, and M. M. Woolfson, *Acta Crystallogr., Sect. A*, **27**, 368 (1971).

3) T. Ashida, HBLS-V, The Universal Crystallographic Computing System-Osaka, The Computing Center, Osaka University, 1973, p. 55.

4) "International Tables for X-Ray Crystallography," Kynoch Press, Birmingham (1974), Vol. IV.

5) S. Motherwell, PLUTO, a Program for Plotting Molecular and Crystal Structures, Cambridge Crystallographic File User Manual, May 1976.

6) The geometries of thione groups in various compounds have been determined and compared with each other by many authors. For example: T. C. Downie, W. Harrison, E. S. Raper, and M. A. Hepworth, *Acta Crystallogr., Sect. B*, **28**, 1584 (1972); H. R. Luss and D. L. Smith, *ibid., Sect. B*, **29**, 998 (1973); C. D. Shirrell and D. E. Williams, *ibid., Sect. B*, **29**, 1648 (1973); S. Pérez-Garrido, A. Conde, and R. Márquez, *ibid., Sect. B*, **30**, 2348 (1974); G. J. Palenik, D. F. Rendle, and W. S. Carter, *ibid., Sect. B*, **30**, 2390 (1974).

7) J. A. Kapecki, J. E. Baldwin, and I. C. Paul, *J. Am. Chem. Soc.*, **90**, 5800 (1968), and references cited therein.

8) F. S. Stephenes, *J. Chem. Soc., A*, **1970**, 1843.

9) P. L. Johnson, K. I. G. Reid, and I. C. Paul, *J. Chem. Soc., B*, **1971**, 946; K. I. G. Reid and I. C. Paul, *ibid.*, **1971**, 952.

10) T. R. Lynch, I. P. Mellor, and S. C. Nyburg, *Acta Crystallogr., Sect. B*, **27**, 1948 (1971) and references cited therein; I. P. Mellor and S. C. Nyburg, *ibid., Sect. B*, **27**, 1954, 1959 (1971).

11) E. Adman, L. H. Jensen, and R. N. Warrener, *Acta Crystallogr., Sect. B*, **31**, 1915 (1975).

12) W. Walter, B. Krische, G. Adiwidjaja, and J. Voß, *Chem. Ber.*, **111**, 1685 (1978).

Crystal Structures of Mixed Ligand Copper(II) Complexes Containing L-Amino Acids. I. L-Asparaginato-L-histidinato-copper(II) and Its Hydrate

Taizo ONO, Hirotaka SHIMANOUCHI, Yoshio SASADA,* Takeshi SAKURAI,†
Osamu YAMAUCHI,† and Akitsugu NAKAHARA†

Laboratory of Chemistry for Natural Products, Tokyo Institute of Technology, Nagatsuta, Midori-ku, Yokohama 227

†*Institute of Chemistry, College of General Education, Osaka University, Toyonaka, Osaka 560*

(Received February 8, 1979)

Two copper complexes containing L-histidine and L-asparagine crystallize from aqueous solution at pH 7.0. Both crystals are monoclinic, space group $P2_1$. L-Asparaginato-L-histidinatocopper(II): $a=10.913(3)$, $b=12.911(4)$, $c=10.206(3)$ Å, $\beta=113.83(2)°$, $Z=4$. L-Asparaginato-L-histidinatoaquacopper(II) trihydrate: $a=12.654(4)$, $b=11.623(4)$, $c=5.931(2)$ Å, $\beta=100.47(3)°$, $Z=2$. In both structures, four coordinating atoms in an approximately planar arrangement around copper are the α-amino and imidazole δ-nitrogen atoms of L-histidine and α-amino nitrogen and α-carboxyl oxygen of L-asparagine. The fifth coordination site is occupied by the α-carboxyl oxygen of L-histidine. Difference between the two complex crystals is found at the sixth coordination site; a water molecule is coordinated in the hydrated crystal to complete a distorted octahedral environment, while in the anhydrous crystal this site is unoccupied so that the geometry of the complex is square-pyramidal.

Studies of copper ion in normal human serum suggested that the complexes of copper and amino acids may play a part in the transport of Cu(II) between blood and tissues. Under physiological conditions, some copper complexes with mixed amino acid ligands are identified, in which histidine is primarily involved. When the second amino acid is asparagine, glutamine, or threonine, the stability of the complexes seems to be high by some cooperativity.[1,2] It is interesting to explore the coordination of these ternary complexes consisting of copper, histidine and the other amino acids at the physiological pH.

We have succeeded in preparing the single crystals of L-asparaginato-L-histidinatocopper(II) and its hydrate. The present paper deals with the structures of these two mixed ligand complexes determined by X-ray method.

Experimental

Copper hydroxide was obtained by the usual method from copper sulphate, 35% ammonia and sodium hydroxide. 1 mmol of L-asparagine (0.1311 g) and 1 mmol of L-histidine (0.1552 g), both of which were of reagent grade and purchased from Nihon Rigaku Corporation, were dissolved in 10 ml of ion-exchanged water. To this solution, 1 mmol of copper hydroxide (0.097 g) was added and the mixture was stirred for a few minutes, until intense blue colour developed. This solution was filtered to remove some copper oxide deposited in the bottom. The pH of the solution was about 7.0.

Anhydrous Crystal. Intense blue crystals with various polyhedral shapes were obtained from the filtrate by the vapor diffusion method using methanol, ethanol, or acetone. Elementary analysis. Calcd: C, 34.43; H, 4.33; N, 20.08% for $C_{10}H_{15}N_5O_5Cu$. Found: C, 34.23; H, 4.25; N, 20.04%.

Hydrated Crystal. *N,N*-Dimethylformamide was poured into the above-mentioned filtrate. Light blue single crystals were grown by standing it overnight at room temperature. The crystals were boat-shaped, the crystallographic c axis being parallel to the length of the boat. Elementary analysis. Calcd: C, 28.53; H, 5.51; N, 16.64% for $C_{10}H_{23}N_5O_9Cu$. Found: C, 28.37; H, 5.52; N, 16.58%.

Crystal Data

Anhydrous Crystal. Monoclinic, $a=10.913(3)$, $b=12.911(4)$, $c=10.206(3)$ Å, $\beta=113.83(2)°$, $D_m=1.76$ (by flotation), $D_x=1.76$ g·cm^{-3}, $Z=4$.

Hydrated Crystal. Monoclinic, $a=12.654(4)$, $b=11.623(4)$, $c=5.931(2)$ Å, $\beta=100.47(3)°$, $D_m=1.64$ (by flotation), $D_x=1.63$ g·cm^{-3}, $Z=2$.

Systematic absences for both crystals; $0k0$ for odd k. Space group $P2_1$; alternative space group $P2_1/m$ was excluded, since these crystals contain L-amino acids.

Accurate unit cell dimensions were obtained from a least-squares fit to the 2θ values measured by a diffractometer. Intensity data were collected on the Rigaku automated four-circle diffractometer with graphite-monochromated Mo $K\alpha$ radiation at room temperature. A θ-2θ scan technique was employed, and reflexions for $2\theta \leqq 55°$ were recorded. A total of 2933 and 2067 non-zero reflexions out of 3154 and 2190 recorded ones were obtained for the anhydrous and hydrated crystals, respectively. Intensities were corrected for the Lorentz and polarization effects but not for absorption and secondary extinction.

Structure Determination

Anhydrous Crystal. Since Z is 4 in the space group $P2_1$, there are two molecules in an asymmetric unit. From two high peaks on the Harker section and two cross-vector peaks in general positions of the sharpened Patterson map, the coordinates of two copper atoms were deduced, the y coordinate of one copper atom being taken as 0.25. Ten light atoms around copper were located from the Fourier map phased with two copper atoms. The remaining non-hydrogen atoms were found on the next Fourier map. The structural parameters were refined by the block-diagonal least-squares method. The final R factor was 0.061 for all the reflexions and 0.049 for the non-zero reflexions.

Hydrated Crystal. The x and z coordinates of

copper were obtained from the Harker section and y was taken arbitrarily as 0.25. The Fourier map phased with the copper atom has shown a pseudo-mirror symmetry at $y=0.25$. Therefore, the positions of the nearest four atoms coordinating to the central copper atom were chosen appropriately. The other non-hydrogen atoms were obtained by successive Fourier syntheses. After the block-diagonal least-squares refinement, the final R factor was 0.093 for all the reflexions and 0.066 for the non-zero reflexions.

Atomic scattering factors were taken from "International Tables for X-Ray Crystallography."[3] The final atomic parameters are listed in Tables 1 and 2.[4]

Description of the Structure and Discussion

Crystal Structure. Figures 1 and 2 show the structures of the anhydrous and hydrated crystals, respectively, where hydrogen bonds are indicated by broken lines. Hydrogen bond lengths are listed in Table 3. In the hydrated crystal, the molecules are connected mainly through water molecules to form a three-dimensional hydrogen bond network. In the anhydrous crystal, many of the hydrogen bond lengths exceed 3 Å, suggesting that a three-dimensional

Table 1. The final fractional coordinates ($\times 10^4$) and thermal parameters ($\times 10^5$) for L-asparaginato-L-histidinatocopper(II)

Anisotropic thermal parameters are in the form: $\exp[-(h^2\beta_{11}+k^2\beta_{22}+l^2\beta_{33}+hk\beta_{12}+hl\beta_{13}+kl\beta_{23})]$.
Estimated standard deviations are in parentheses.

Atom	x	y	z	β_{11}	β_{22}	β_{33}	β_{12}	β_{13}	β_{23}
Cu(A)	2363(1)	2500(1)	352(1)	427(7)	288(4)	660(8)	−97(11)	292(12)	−23(12)
Cu(B)	7510(1)	1735(1)	2594(1)	379(6)	383(5)	593(8)	63(11)	267(12)	12(13)
C(1A)	3407(8)	1184(6)	−1442(8)	752(77)	209(39)	974(93)	269(93)	492(140)	162(100)
C(2A)	2025(7)	1614(6)	−2366(7)	513(61)	378(46)	567(68)	−117(93)	79(106)	−142(98)
C(3A)	2166(7)	2640(6)	−3023(8)	726(72)	280(45)	827(83)	−56(95)	424(127)	133(99)
C(4A)	2968(7)	3442(5)	−1970(8)	689(73)	172(37)	825(84)	100(84)	268(128)	179(91)
C(5A)	3762(7)	4340(6)	−9(9)	529(69)	391(48)	994(95)	−125(96)	334(130)	−146(113)
C(6A)	3826(7)	4146(7)	−2128(8)	578(71)	434(49)	898(90)	59(100)	575(132)	289(112)
C(11A)	3216(7)	2740(5)	3290(8)	568(65)	271(43)	895(85)	55(81)	641(125)	−50(92)
C(12A)	2153(7)	1890(6)	2963(8)	519(61)	387(48)	811(78)	53(91)	618(116)	44(103)
C(13A)	2539(8)	1032(6)	4093(9)	934(88)	359(46)	975(96)	−12(109)	1124(155)	116(112)
C(14A)	3743(7)	371(6)	4215(8)	570(68)	302(41)	785(81)	−186(87)	616(124)	−131(96)
N(1A)	1227(5)	1772(6)	−1508(6)	515(52)	371(36)	794(66)	−85(86)	416(96)	−224(98)
N(2A)	2932(6)	3563(5)	−631(6)	586(59)	288(35)	708(68)	−158(75)	287(103)	−174(80)
N(3A)	4303(6)	4732(6)	−883(7)	689(66)	377(40)	1051(85)	−105(89)	647(123)	262(101)
N(11A)	1812(5)	1495(5)	1496(6)	466(52)	297(36)	717(65)	−35(68)	337(97)	0(76)
N(12A)	4310(7)	−160(6)	5431(7)	861(75)	471(47)	851(80)	−71(100)	539(127)	209(104)
O(1A)	3838(5)	1322(4)	−108(5)	714(55)	460(36)	617(56)	322(74)	122(90)	−9(74)
O(2A)	4030(7)	752(6)	−2067(7)	1094(76)	781(55)	1070(79)	944(108)	670(128)	−47(109)
O(11A)	3389(5)	3126(5)	2217(6)	713(56)	503(39)	790(62)	−289(78)	463(97)	19(82)
O(12A)	3839(6)	3032(5)	4540(6)	790(61)	677(47)	854(68)	−337(88)	469(105)	−345(94)
O(13A)	4104(5)	332(5)	3228(6)	653(54)	532(39)	907(66)	249(77)	867(100)	169(85)
C(1B)	8101(7)	2963(6)	5151(8)	589(69)	329(42)	775(82)	1(90)	468(124)	41(100)
C(2B)	6882(7)	2270(6)	4949(7)	490(60)	410(50)	623(73)	27(84)	465(110)	−78(92)
C(3B)	7283(7)	1273(6)	5826(8)	618(69)	338(42)	835(84)	51(91)	788(129)	159(100)
C(4B)	8244(7)	640(6)	5462(7)	516(64)	343(42)	606(74)	−73(87)	229(115)	−63(93)
C(5B)	9343(7)	53(6)	4238(9)	505(69)	348(45)	1091(100)	89(92)	428(136)	−103(111)
C(6B)	9097(7)	−124(6)	6231(8)	530(68)	376(47)	830(87)	1(94)	117(126)	209(107)
C(11B)	8346(7)	1550(6)	375(8)	447(61)	451(51)	863(84)	44(92)	544(120)	−53(107)
C(12B)	7098(7)	2233(7)	−297(8)	450(62)	581(58)	721(81)	−43(96)	221(116)	−216(108)
C(13B)	7331(7)	3132(7)	−1173(7)	552(70)	659(62)	540(74)	59(109)	287(119)	−78(113)
C(14B)	8443(8)	3853(7)	−289(9)	830(84)	439(51)	810(89)	−231(109)	627(143)	−81(112)
N(1B)	6140(6)	2020(5)	3416(6)	486(54)	435(42)	625(64)	77(75)	247(96)	102(82)
N(2B)	8422(6)	753(5)	4201(6)	385(51)	344(36)	765(70)	44(71)	196(98)	47(84)
N(3B)	9757(6)	−471(5)	5439(8)	648(65)	293(37)	1155(90)	151(81)	497(123)	−126(95)
N(11B)	6646(6)	2575(6)	821(7)	691(60)	504(44)	909(74)	425(101)	906(112)	29(110)
N(12B)	9356(7)	4077(6)	−805(8)	935(81)	517(49)	1300(102)	−254(109)	1161(152)	−74(121)
O(1B)	8297(6)	3139(5)	4058(6)	1098(70)	533(41)	727(62)	−702(91)	704(109)	−186(84)
O(2B)	8811(6)	3240(5)	6400(6)	791(60)	603(43)	850(66)	−352(88)	518(104)	−518(93)
O(11B)	8710(5)	1317(5)	1691(6)	598(53)	772(49)	711(61)	623(84)	334(93)	326(89)
O(12B)	8945(6)	1266(5)	−362(6)	713(58)	676(46)	963(70)	361(86)	726(106)	90(94)
O(13B)	8464(8)	4261(7)	830(7)	1556(99)	890(62)	1134(87)	−807(134)	1300(155)	−927(125)

TABLE 2. THE FINAL FRACTIONAL COORDINATES ($\times 10^4$) AND THERMAL PARAMETERS ($\times 10^5$) FOR L-ASPARAGINATO-L-HISTIDINATOAQUACOPPER(II) TRIHYDRATE

Anisotropic thermal parameters are in the form: $\exp[-(h^2\beta_{11}+k^2\beta_{22}+l^2\beta_{33}+hk\beta_{12}+hl\beta_{13}+kl\beta_{23})]$. Estimated standard deviations are in parentheses.

Atom	x	y	z	β_{11}	β_{22}	β_{33}	β_{12}	β_{13}	β_{23}
Cu	2331(1)	2500(2)	4238(2)	375(5)	239(5)	1370(22)	60(15)	586(17)	81(30)
C(1)	4106(6)	4239(9)	4509(16)	190(47)	504(70)	2387(290)	203(95)	230(184)	−134(239)
C(2)	3464(7)	4159(8)	2033(14)	380(54)	426(66)	1435(231)	−421(100)	547(182)	−519(210)
C(3)	2570(7)	5043(8)	1569(16)	527(65)	298(61)	2049(271)	122(106)	619(215)	485(216)
C(4)	1818(6)	4993(7)	3290(15)	273(49)	305(57)	1975(258)	81(89)	44(180)	−203(207)
C(5)	910(7)	4257(8)	5682(15)	385(55)	427(66)	1836(266)	223(101)	244(194)	−174(220)
C(6)	1274(7)	5871(8)	4046(17)	257(51)	407(67)	3105(337)	119(96)	327(210)	1029(250)
N(1)	3029(6)	2975(6)	1605(11)	457(48)	376(50)	1106(183)	18(86)	558(154)	−119(163)
N(2)	1607(5)	3981(6)	4308(12)	298(43)	283(49)	1783(215)	−37(77)	165(151)	−142(169)
N(3)	705(6)	5386(7)	5568(13)	318(46)	467(60)	2410(257)	65(86)	432(171)	−332(204)
O(1)	3938(5)	3452(6)	5899(11)	478(44)	613(59)	1769(192)	−74(86)	−12(149)	−41(174)
O(2)	4683(6)	5115(6)	4982(14)	423(49)	430(53)	3613(252)	6(90)	198(196)	−518(196)
C(11)	1807(7)	891(8)	7322(13)	360(53)	494(68)	1090(216)	152(100)	624(174)	−132(201)
C(12)	2233(6)	130(7)	5605(13)	320(47)	206(52)	1414(225)	48(86)	512(165)	157(178)
C(13)	2824(7)	−932(7)	6784(14)	484(58)	302(60)	1168(222)	294(98)	336(180)	38(190)
C(14)	3140(6)	−1782(7)	5094(15)	347(49)	164(50)	2200(265)	−54(84)	927(191)	−341(195)
N(11)	2879(5)	839(6)	4286(12)	295(43)	262(48)	2110(225)	52(74)	840(156)	249(168)
N(12)	3866(6)	−2570(9)	6062(11)	624(50)	298(50)	1818(190)	327(123)	686(159)	171(244)
O(11)	1827(5)	1986(5)	7031(10)	604(45)	192(37)	1444(171)	291(72)	772(141)	−87(133)
O(12)	1460(5)	445(6)	8933(11)	627(49)	408(48)	2175(204)	276(82)	1491(163)	177(164)
O(13)	2746(5)	−1792(6)	3042(10)	448(42)	556(53)	1618(184)	144(81)	2(144)	−298(165)
O(1′)	520(5)	1681(6)	1851(11)	496(44)	383(46)	2109(196)	189(74)	840(151)	23(161)
O(2′)	5524(5)	2597(9)	9093(9)	516(41)	957(71)	1481(159)	−510(123)	25(130)	662(247)
O(3′)	660(6)	−1542(7)	500(13)	611(55)	655(67)	3548(280)	−535(102)	295(197)	810(223)
O(4′)	4324(6)	805(7)	632(13)	509(47)	697(64)	2891(246)	−87(92)	574(168)	384(210)

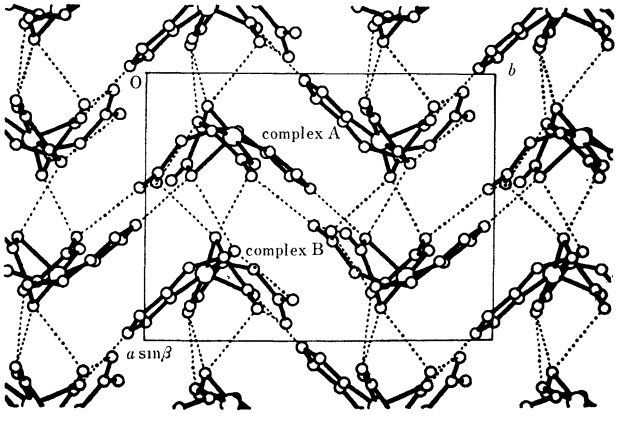

Fig. 1. Structure of the anhydrous crystal projected along c.

hydrogen bond network is not so well constructed, probably owing to the absence of water of crystallization.

Molecular Structure. The anhydrous crystal contains two crystallographically independent complexes; they are abbreviated hereafter complexes A and B, respectively. Similarly, the complex in the hydrated crystal is called as aqua complex. Figure 3 shows the stereoviews of the structures of these complexes. The bond lengths and angles are given in Fig. 4 and Table 4, respectively. Fairly good agreement among the values for corresponding bonds is observed, except for the

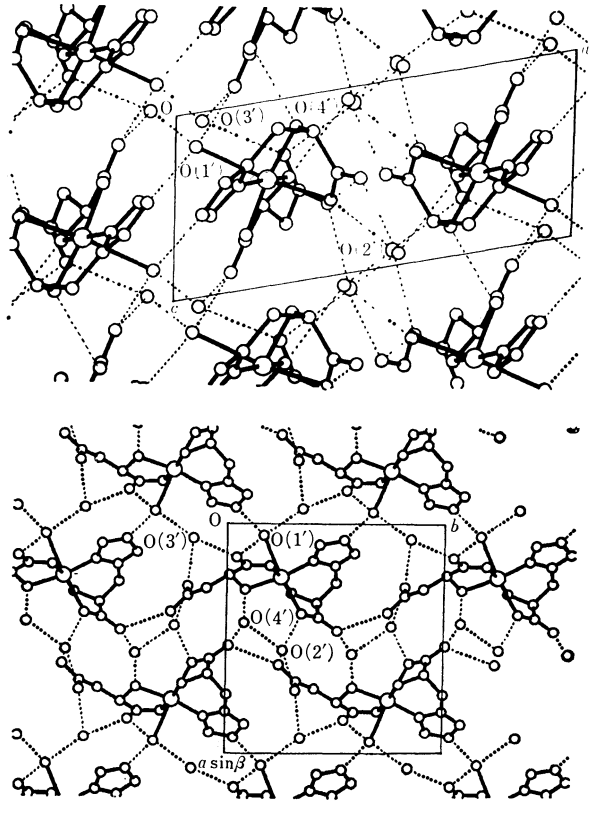

Fig. 2. Structure of the hydrated crystal projected along b (upper) and c (lower).

Table 3. Distances of hydrogen bonds(X–H···Y)

a) *Anhydrous Crystal*

X at a	Y	at	Distance X···Y (*l*/Å)
N(1A)	O(2B)	e	3.249(10)
N(1A)	O(12B)	b	3.217(10)
N(3A)	O(1A)	f	2.774(9)
N(11A)	O(13A)	a	2.840(9)
N(11A)	O(12B)	b	2.946(9)
N(12A)	O(2A)	c	2.937(11)
N(12A)	O(12A)	g	3.079(10)
N(1B)	O(11A)	a	3.095(9)
N(3B)	O(13A)	a	3.062(9)
N(3B)	O(1B)	h	2.667(10)
N(11B)	O(13B)	a	2.943(11)
N(11B)	O(1A)	a	3.250(10)
N(12B)	O(2B)	d	2.879(11)

Code of symmetry related position

a: x, y, z
b: $-1+x, y, z$
c: $x, y, 1+z$
d: $x, y, -1+z$
e: $-1+x, y, -1+z$
f: $1-x, 0.5+y, -z$
g: $1-x, -0.5+y, 1-z$
h: $2-x, -0.5+y, 1-z$

b) *Hydrated Crystal*

X at a	Y	at	Distance X···Y (*l*/Å)
O(1′)	O(3′)	d	2.772(10)
O(1′)	O(12)	c	2.687(9)
O(2′)	O(1)	a	2.688(13)
O(2′)	O(13)	f	2.812(13)
O(3′)	O(12)	c	2.750(10)
O(3′)	O(13)	a	2.807(11)
O(4′)	O(2)	g	2.792(11)
O(4′)	O(2′)	c	2.825(13)
N(1)	O(11)	c	3.081(10)
N(3)	O(1′)	e	2.806(10)
N(11)	O(4′)	a	3.080(11)
N(12)	O(2′)	h	2.844(15)
N(12)	O(2)	b	2.993(13)

Code of symmetry related position

a: x, y, z
b: $x, -1+y, z$
c: $x, y, -1+z$
d: $-x, 0.5+y, -z$
e: $-x, 0.5+y, 1-z$
f: $1-x, 0.5+y, 1-z$
g: $1-x, -0.5+y, 1-z$
h: $1-x, -0.5+y, 2-z$

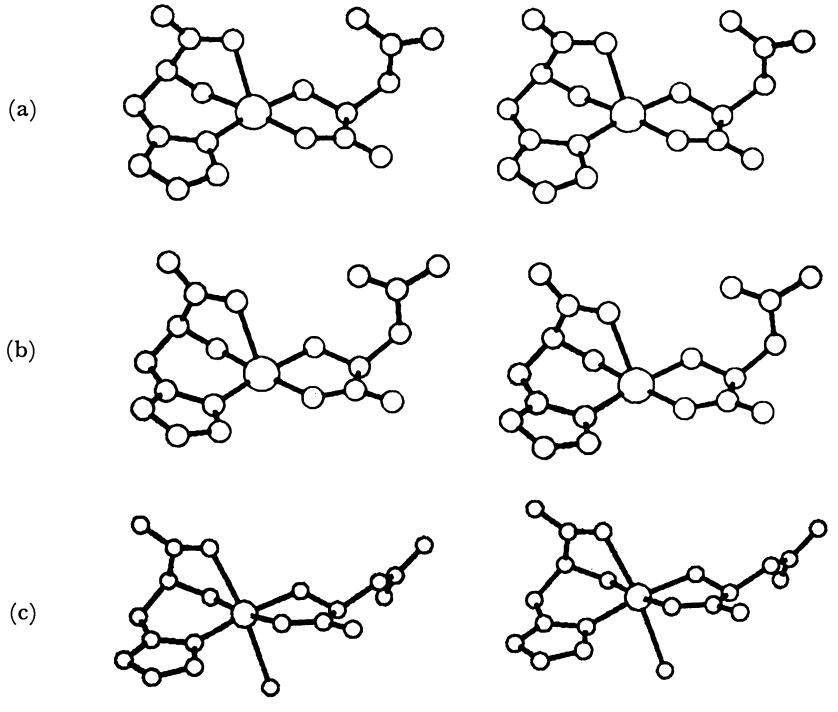

Fig. 3. Stereoviews of the structures of complex A (a), complex B (b), aqua complex (c).

values relating to the metal chelation.

For three kinds of complexes in common, L-asparagine molecule coordinates to copper through the α-amino nitrogen and α-carboxyl oxygen, and L-histidine through the α-amino nitrogen, imidazole δ-nitrogen, and α-carboxyl oxygen. These atoms except the last one occupy the corners of the planar coordination square. The coordination distances, especially for Cu–N(2) and Cu–N(11), vary significantly among three kinds of complexes (the maximum difference is 0.058 Å). But

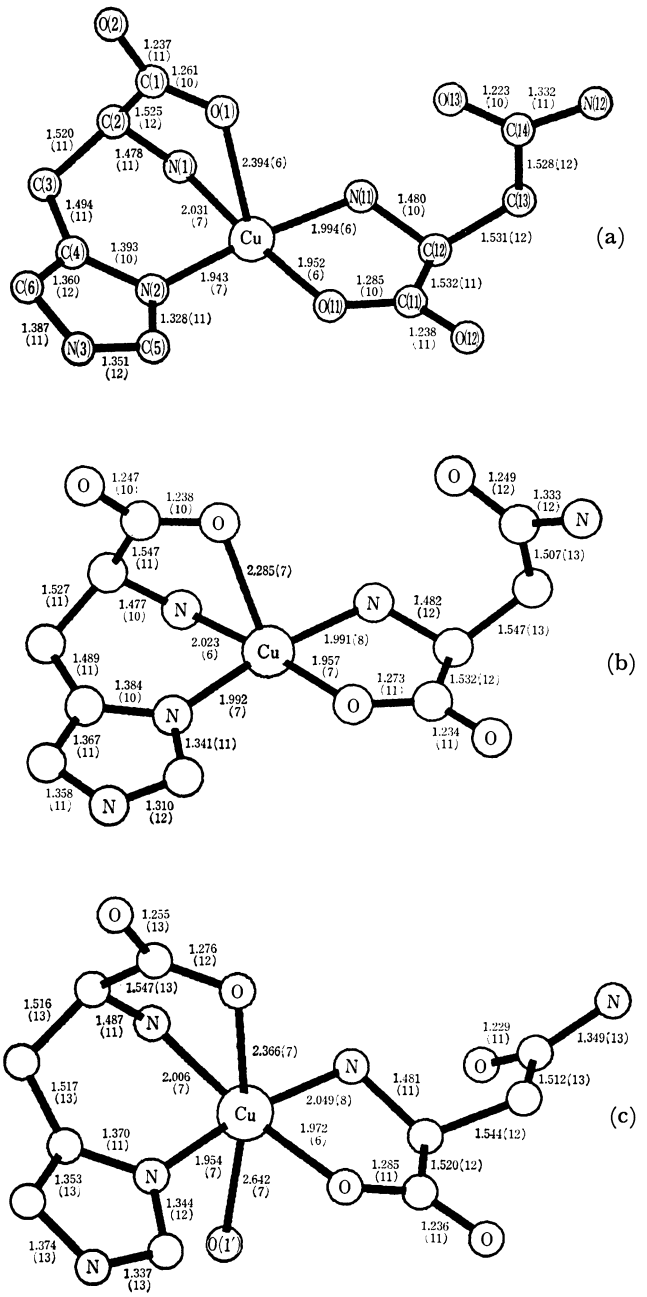

Fig. 4. Bond lengths (l/Å) in complex A (a), complex B (b), and aqua complex (c).
Estimated standard deviations in the last digits are in parentheses.

there are no correlation between the distances and any other geometrical features. The α-carboxyl oxygen atom in L-histidine deviates from the normal axial position, the angle N(1)–Cu–O(1) being 74.2, 74.3, and 74.3° for A, B, and aqua complexes, respectively. Such deviations may be due to the constraint of the histidine molecule. Axial bond length in complex B, 2.285 Å, is the shortest among the copper complexes containing amino acids or peptides.[5] The coordination geometry of these three complexes is the same as that of L-histidinato-L-threoninatoaquacopper(II) hydrate reported by Freeman *et al.*[6] Since the N(1)–Cu–O(1) angle in this complex is 68.3°, overlapping between d_{z^2} of copper and

Table 4. Bond angles (θ/°)

	Complex A	Complex B
a) *Anhydrous Crystal*		
O(1)–Cu–O(13)	106.7(2)	112.4(3)
O(1)–Cu–N(1)	74.2(3)	74.3(3)
O(1)–Cu–N(2)	88.1(2)	92.0(3)
O(1)–Cu–N(11)	95.0(2)	94.4(3)
N(1)–Cu–N(2)	92.7(3)	88.9(3)
N(1)–Cu–N(11)	91.8(3)	96.9(3)
N(1)–Cu–O(11)	175.3(3)	173.3(3)
N(2)–Cu–O(11)	91.9(3)	90.4(3)
N(2)–Cu–N(11)	175.1(3)	172.3(3)
O(11)–Cu–N(11)	83.6(3)	83.3(3)
O(1)–C(1)–O(2)	125.3(8)	127.3(8)
O(1)–C(1)–C(2)	117.4(7)	116.0(7)
O(2)–C(1)–C(2)	117.3(8)	116.6(7)
C(1)–C(2)–C(3)	109.9(8)	112.4(6)
C(1)–C(2)–N(1)	110.9(7)	110.0(6)
N(1)–C(2)–C(3)	109.3(7)	110.0(6)
C(2)–C(3)–C(4)	114.9(7)	112.4(7)
C(3)–C(4)–C(6)	127.6(8)	129.7(7)
C(3)–C(4)–N(2)	122.9(7)	123.5(7)
N(2)–C(4)–C(6)	109.6(7)	106.9(7)
N(3)–C(5)–N(2)	111.3(8)	110.2(8)
C(4)–C(6)–N(3)	106.2(7)	107.4(7)
C(5)–N(3)–C(5)	107.3(7)	108.7(8)
C(4)–N(2)–C(5)	105.6(7)	106.8(7)
C(4)–N(2)–Cu	124.7(5)	128.4(5)
C(5)–N(2)–Cu	125.8(6)	124.8(6)
C(2)–N(1)–Cu	109.5(5)	107.4(5)
O(11)–C(11)–O(12)	123.4(8)	123.8(8)
O(11)–C(11)–C(12)	116.9(7)	116.7(7)
O(12)–C(11)–C(12)	119.7(7)	119.5(7)
C(11)–C(12)–N(11)	109.0(6)	109.8(7)
C(11)–C(12)–C(13)	113.6(7)	111.5(7)
N(11)–C(12)–C(13)	113.1(6)	113.9(7)
C(12)–C(13)–C(14)	115.6(7)	113.5(8)
C(13)–C(14)–O(13)	120.6(7)	121.4(9)
C(13)–C(14)–N(12)	115.1(7)	116.6(8)
O(13)–C(14)–N(12)	124.3(8)	121.9(9)
C(11)–O(11)–Cu	116.5(5)	116.7(6)
C(12)–N(11)–Cu	110.9(5)	110.8(6)
b) *Hydrated Crystal*		
O(1)–Cu–N(1)	74.3(3)	
O(1)–Cu–N(2)	87.1(3)	
O(1)–Cu–N(11)	99.9(3)	
O(1)–Cu–O(11)	100.2(3)	
O(1)–Cu–O(1′)	170.8(2)	
O(1′)–Cu–N(1)	98.3(3)	
O(1′)–Cu–N(2)	88.0(3)	
O(1′)–Cu–N(11)	85.8(3)	
O(1′)–Cu–O(11)	87.7(2)	
N(1)–Cu–N(2)	92.8(3)	
N(1)–Cu–N(11)	94.3(3)	
N(1)–Cu–O(11)	172.9(3)	
N(2)–Cu–O(11)	91.4(3)	
N(2)–Cu–N(11)	171.2(3)	
O(11)–Cu–N(11)	82.2(3)	
O(1)–C(1)–O(2)	126.6(9)	
O(1)–C(1)–C(2)	116.7(8)	
O(12)–C(11)–C(12)	119.5(8)	
C(11)–C(12)–C(13)	111.3(7)	
C(11)–C(12)–N(11)	109.1(7)	
N(11)–C(12)–C(13)	114.6(7)	
C(12)–C(13)–C(14)	112.8(7)	
O(2)–C(1)–C(2)	116.4(9)	
C(1)–C(2)–C(3)	112.2(8)	
C(1)–C(2)–N(1)	109.4(7)	
N(1)–C(2)–C(3)	110.8(7)	
C(2)–C(3)–C(4)	113.0(8)	
C(3)–C(4)–C(6)	127.8(8)	
C(3)–C(4)–N(2)	121.7(8)	
N(2)–C(4)–C(6)	110.5(8)	
N(3)–C(5)–N(2)	110.2(8)	
C(4)–C(6)–N(3)	105.5(9)	
C(5)–N(3)–C(6)	108.4(8)	
C(4)–N(2)–C(5)	105.4(7)	
C(4)–N(2)–Cu	128.1(6)	
C(5)–N(2)–Cu	125.8(6)	
C(2)–N(1)–Cu	108.9(5)	
O(11)–C(11)–O(12)	122.6(8)	
O(11)–C(11)–C(12)	117.9(8)	
C(13)–C(14)–N(12)	113.8(8)	
C(13)–C(14)–O(13)	123.6(8)	
O(13)–C(14)–N(12)	122.6(9)	
C(11)–O(11)–Cu	115.5(6)	
C(12)–N(11)–Cu	108.3(5)	

lone-pair orbital of oxygen is less, so that the Cu–O (axial) length (2.58 Å) is longer than the values in the present three complexes.

In the hydrated crystal, the copper coordination is octahedral; water molecule occupies the sixth coordination site at a distance of 2.642 Å. It is noted that this also occurs in rather oblique direction, O(water)–Cu–O(11) being 87.7°, perhaps owing to the trans effect. The atoms forming the coordination square are not precisely coplanar. Their deviations may be described as a very flattened tetrahedron. The dihedral angle between the two planes, N(1)–Cu–N(2) and N(11)–Cu–O(11), is 8.5(3)°. Such deformation from the square planar coordination is attributed to the geometrical constraint owing to the chelation of L-histidine as a tridentate ligand, since bishistaminocopper(II) perchlorate[7] has exactly and bis(L-asparaginato)copper(II)[8] has almost square-planar coordination.

In the anhydrous crystal, the copper atom is five-coordinated, forming a square pyramid. The copper atoms in A and B complexes are out of the best plane for the equatorial coordinating atoms toward the top of the pyramid (0.023 and 0.099 Å, respectively). This is because of the disproportion of the charge, and is the general trend for the square-pyramidal environment of copper complexes. The sixth sites are blocked by carbonyl oxygen O(12B) and amino nitrogen N(12B) for complex A and imidazole nitrogen N(3A) for complex B. The distances from these atoms to copper are 3.846(7), 3.631(9), and 3.295(7) Å, respectively.

The imidazole rings in these complexes are planar within the experimental errors. The ring planes make dihedral angles of 19.9(3), 11.5(3), and 13.1(3)° with the copper square planes for A, B, and aqua complexes, respectively.

Side chains of asparagine in anhydrous complexes have a compact form puckered onto the coordination square, as shown in Fig. 3, while that in aqua complex has an extended one. As for the conformation around C(12)–C(13), C(14) is gauche to C(11) and N(11) in the former, and C(14) is trans to C(11) in the latter. The conformation of the former may be stabilized by the intramolecular hydrogen bond O(13)···N(11) in both of A and B complexes.

For mixed ligand copper(II) complexes involving an acidic amino acid and a basic amino acid, the electrostatic ligand-ligand interaction between their charged side chains has been proposed on the basis of the synthetic and CD spectral studies.[9,10] Also, successful optical resolution of DL-histidine *via* formation of the ternary complex with L-asparagine has been inferred to be due to the intramolecular hydrogen bonding between the polar side chains[11] in solution. Although such ligand-ligand interactions have not been realized in the structures of the present three complexes, they may occur under favourable conditions by the conformational change around C(12)–C(13) and C(13)–C(14) of asparagine, and the present study has revealed that the conformation around these bonds is flexible for the change of crystalline environment.

The authors are grateful to Dr. Akio Takenaka of Tokyo Institute of Technology for his assistance in drawing the diagrams by the computer graphics. The present work was partially supported by a Grant-in-Aid for Scientific Research from the Ministry of Education, to which the author's thanks are due.

References

1) P. Z. Neuman and A. Sass-Kortsak, *J. Clin. Invest.*, **46**, 646 (1967).

2) B. Sarker and T. P. A. Kruck, "The Biochemistry of Copper," ed by J. Peisach, P. Aisen, and W. E. Blumberg, Academic Press, New York (1966), p. 183.

3) "International Tables for X-Ray Crystallography," The Kynoch Press, Birmingham (1974), Vol. IV, p. 72.

4) Atomic coordinates of hydrogen atoms and a list of the observed and calculated structure factors are kept in the Office of the Chemical Society of Japan (Document No. 7926).

5) H. C. Freeman, J. M. Guss, M. J. Healy, R-P. Martin, C. E. Nockolds, and B. Sarker, *Chem. Commun.* **1967**, 225.

7) P. J. J. Bonnet and Y. Jeannen, *Acta Crystallogr. Sect. B*, **26**, 318 (1970).

8) F. S. Stephen, R. S. Vagg, and P. A. Williams, *Acta Crystallogr. Sect. B*, **31**, 841 (1975).

9) O. Yamauchi, Y. Nakao, and A. Nakahara, *Bull. Chem. Soc. Jpn.*, **48**, 2572 (1975).

10) T. Sakurai, O. Yamauchi, and A. Nakahara, *Bull. Chem. Soc. Jpn.*, **49**, 169 (1976).

11) T. Sakurai, O. Yamauchi, and A. Nakahara, *J. Chem. Soc., Chem. Commun.* **1977**, 718.

Solvent Effects on Raman Intensity and the Determination of Transition Hyperpolarizability Tensor Element

Tsunetake FUJIYAMA,* Haruo HATAKEYAMA, and Shi-aki HYODO

Department of Chemistry, Faculty of Science, Tokyo Metropolitan University, Fukazawa, Setagaya-ku, Tokyo 158

(Received February 14, 1979)

Raman intensities of methyl iodide were observed in carbon tetrachloride solution at various concentrations. The observed lines were ν_1, ν_2, ν_3, ν_5, and ν_6. From the observed data, the transition polarizabilities were determined for the ν_1, ν_2, and ν_3 fundamentals of methyl iodide and the transition hyperpolarizabilities were obtained for the ν_3 fundamental of methyl iodide in the form of tensor elements.

In preceding reports,[1,2] the solvent effects on the absolute infrared intensities and on the absolute Raman scattering cross-sections have been discussed quantitatively from the view-point of dipole-dipole interaction. It has been shown that the interaction of the dipole-dipole type is quite a reasonable model for explaining the spectroscopic information observed in various binary solutions. It has also been shown in these reports that the polarizability derivatives can be determined by observing the solvent effects on the infrared-absorption intensities and that the hyperpolarizability derivatives can be determined by observing the solvent effects on the Raman scattering cross-sections. In the report,[2] however, we could not obtain the hyperpolarizability derivatives in the form of a tensor element, but in the form of a linear combination of the products of polarizability and hyperpolarizability derivatives.

The present report will concern itself with the observation of the Raman intensities of methyl iodide in carbon tetrachloride solutions. Our interest lies in the possibility of determining the magnitude of polarizability and hyperpolarizability derivatives in the form of tensor elements through the observation of solvent effects on Raman intensities.

Experimental

The spectrometer used for the present work was designed and constructed by the authors. The instrument is composed of a He–Ne gas laser source (NEC, GLF-105, 15 mW), a JSG-125 grating monochromator (JEOL), a HTV R-374 photomultiplier (S-20 response), a lock-in amplifier (LI-573, NF), and a recorder. The linearity of the whole system with respect to an intensity axis was ascertained to be better than 1 percent of the full scale, as long as the output voltage was less than 10 V.

Attention was paid to the output power of the laser source. The stability of the laser output during the individual spectral measurements was observed by monitoring the light energy which penetrated through the 100 percent reflectance mirror of the laser cavity. When the power of the laser source drifted more than 1 percent during the measurements, the data observed were completly discarded.

The light scattered at 90° within a solid angle of 8×10^{-3} steradians was observed. The electric polarization of the incident light was rotated by the use of a half-wave plate (1419PA polarization rotator, Spex). The polarization characteristics of the monochromator and the frequency dependence of the photomultiplier sensitivity were calibrated by the use of a standard halogen lamp.

All the chemicals were commercial products of spectroscopic grade. Carbon tetrachloride and methyl iodide were doubly distilled following the directions given in the literature.[3]

The Raman intensities were observed for the ν_1, ν_2, ν_3, ν_5, and ν_6 bands of methyl iodide relative to the intensity of the ν_1 band of carbon tetrachloride for various concentrations.

Results and Discussion

Concentration Dependence of Relative Intensity. Consider the observation of the relative intensities of two Raman lines arising from two components of a binary solution. The quantities related to two Raman lines will be distinguished by the suffixes a and b. The observed intensity area I is proportional to the molar concentration c_m, the scattering cross section per molecules Ω, the instrumental factors $S\beta$, and the factor for the internal field effect:[4]

$$I_a = C\cdot c_{ma}\Omega_a\frac{1}{n_s}\left(\frac{n_a^2+2}{(n_a/n_s)^2+2}\right)^4 S_a\beta_a \quad (1)$$

$$I_b = C\cdot c_{mb}\Omega_b\frac{1}{n_s}\left(\frac{n_b^2+2}{(n_b/n_s)^2+2}\right)^4 S_b\beta_b \quad (2)$$

where C is a constant, S the relative sensitivity of the photomultiplier, β the transmittance of the monochromator for the light whose electric vector is polarized perpendicularly to the slit, and where n_a, n_b, and n_s are, respectively, the refractive indices of the a component, the b component, and the mixture of the a and b components. It can immediately be concluded from these equations that:

$$\frac{\Omega_a}{\Omega_b} = \frac{I_a}{I_b}\cdot\frac{c_{mb}}{c_{ma}}\left(\frac{n_b^2+2}{n_a^2+2}\,\frac{(n_a/n_s)^2+2}{(n_b/n_s)^2+2}\right)^4\cdot\frac{S_b\beta_b}{S_a\beta_a} \quad (3)$$

Thus we can obtain the ratio, Ω_a/Ω_b, of the scattering cross sections from the observed intensity ratio, I_a/I_b, because c_m, S, and β are known from the experimental conditions and because the refractive indices can be measured by the use of a refractometer.

In the previous report,[2] the expression for Raman intensity has been given for the case where the existence of the non-zero averaged molecular field introduces non-linear effects to the molecular polarizability. For the binary mixture of methyl iodide and carbon tetrachloride, the ratio of the scattering cross section of the ν_i band of methyl iodide, $\Omega(CH_3I;\nu_i)$, can be expressed by the equation:

$$\frac{\Omega(CH_3I;\nu_i)}{\Omega(CCl_4;\nu_1)} = \left(\frac{\lambda_1^4}{\lambda_i^4}\right)\frac{B+A\langle F_{0z}\rangle_{av}}{\varrho_1(\alpha_1^\circ)^2_{CCl_4}} \quad (4)$$

where λ_1 is the wavelength of the ν_1 line of carbon

tetrachloride, λ_i the wavelength of the ν_i line of methyl iodide, and ${}^{q_i}(\alpha_1^\circ)_{CCl_4}$ the transition polarizability of carbon tetrachloride related to the normal coordinate, Q_1.

$\langle F_{0z}\rangle_{av}$ of Eq. 4 is an averaged molecular field which is produced at the position of a methyl iodide molecule by the surrounding molecules. There are many types of intermolecular interactions which produce electric fields at the position of a given molecule in liquids or solutions. The simplest and most important of these is the interaction of a dipole-dipole type. Taking into account this type of interaction, $\langle F_{0z}\rangle_{av}$ for a binary solution has been calculated to be[5]

$$\langle F_{0z}\rangle_{av} = \frac{4\pi^2}{27}N_A{}^2\mu_0\left[\left(\frac{\mu_0{}^2}{kT}+3\bar{\alpha}\right)\frac{\rho c_m}{W_m}+\left(\frac{\mu_{0s}^2}{kT}+3\bar{\alpha}_s\right)\frac{8}{K}c_{ms}\right] + \frac{2\pi^4}{25\times 243}N_A{}^4\frac{\mu_0{}^3}{(kT)^3}\left[\mu_0{}^4\left(\frac{\rho}{W_m}\right)^3 c_m+\mu_{0s}^4\left(\frac{8}{K}\right)^3 c_{ms}\right]$$

with

$$K=\left[\left(\frac{W_m}{\rho}\right)^{1/3}+\left(\frac{W_{ms}}{\rho_s}\right)^{1/3}\right]^3 \qquad (5)$$

where μ_0 is a permanent dipole moment; $\bar{\alpha}$, the averaged polarizability defined by $3\bar{\alpha}=(\alpha_{xx}+\alpha_{yy}+\alpha_{zz})$; c_m, the molar concentration; ρ, the density; W_m, the molecular weight; T, the absolute temperature; k, the Boltzmann constant; and N_A, Avogadro number. The symbols suffixed by "s" correspond to the solvent molecule. As the $\langle F_{0z}\rangle_{av}$ is concentration dependent, we can determine the A and B values by plotting the observed $\mathcal{R}(CH_3I;\nu_i)/\mathcal{R}(CCl_4;\nu_1)$ values against the calculated $\langle F_{0z}\rangle_{av}$ values. In Table 1, the A and B values thus obtained are summarized. The value of 1.99×10^{-50} cm^6 observed by Kato *et al.*[6] was used for the ${}^{q_i}(\alpha_1^\circ)^2$ of carbon tetrachloride. As for the ν_1 and ν_2 lines of methyl iodide, accurate A values could not be obtained because their intensities were not strong enough for our instrument.

Table 1. The observed A and B values for methyl iodide in carbon tetrachloride solution

Line	$B_{//}$ / 10^{-50} cm^6	$A_{//}$ / 10^{-55} cm^6 dyn esu^{-1}	$B_\perp$ / 10^{-51} cm^6	$A_\perp$ / 10^{-55} cm^6 dyn esu^{-1}
ν_1	2.31	—	1.50	—
ν_2	0.16	—	0.23	—
ν_3	2.38	−1.97	7.84	−1.61
ν_5	0.10	—	—	—
ν_6	0.27	—	—	—

Calculation of Transition Polarizabilities. The parameters A and B of Eq. 4 can be expressed in terms of transition polarizability and transition hyperpolarizability.[2] In the case of a molecule belonging to a C_{3v} symmetry, A and B are expressed as:

1) an a_1-type vibration

1-a) for a parallel component,

$$A_{//}=\frac{1}{15\gamma(\lambda_i)}[(16\gamma(\lambda_i)+2){}^{q_i}(\alpha_1^\circ)_{xx}{}^{q_i}(\beta_1^\circ)_{xxz} +(6\gamma(\lambda_i)+2){}^{q_i}(\alpha_1^\circ)_{zz}{}^{q_i}(\beta_1^\circ)_{zzz} +(4\gamma(\lambda_i)-2){}^{q_i}(\alpha_1^\circ)_{xx}{}^{q_i}(\beta_1^\circ)_{zzz} +(4\gamma(\lambda_i)-2){}^{q_i}(\alpha_1^\circ)_{zz}{}^{q_i}(\beta_1^\circ)_{xxz}] \qquad (6a)$$

$$B_{//}=\frac{1}{15\gamma(\lambda_1)}[(8\gamma(\lambda_1)+1){}^{q_i}(\alpha_1^\circ)_{xx}^2 +(3\gamma(\lambda_1)+1){}^{q_i}(\alpha_1^\circ)_{zz}^2 +(4\gamma(\lambda_1)-2){}^{q_i}(\alpha_1^\circ)_{xx}{}^{q_i}(\alpha_1^\circ)_{zz}] \qquad (6b)$$

1-b) for a perpendicular component,

$$A_\perp=\frac{2(15\gamma(\lambda_1)+15)}{15\gamma(\lambda_1)}({}^{q_i}(\alpha_1^\circ)_{xx}-{}^{q_i}(\alpha_1^\circ)_{zz}) \times({}^{q_i}(\beta_1^\circ)_{xxz}-{}^{q_i}(\beta_1^\circ)_{zzz}) \qquad (7a)$$

$$B_\perp=\frac{1+\gamma(\lambda_1)}{15\gamma(\lambda_1)}({}^{q_i}(\alpha_1^\circ)_{xx}-{}^{q_i}(\alpha_1^\circ)_{zz})^2 \qquad (7b)$$

2) for an e-type vibration, and for a parallel component

$$A_{//}=\frac{4\gamma(\lambda_1)+3}{15\gamma(\lambda_1)}\cdot 4({}^{q_i}(\alpha_1^\circ)_{xy}{}^{q_i}(\beta_1^\circ)_{xyz}+{}^{q_i}(\alpha_1^\circ)_{yz}{}^{q_i}(\beta_1^\circ)_{yzz}) \qquad (8a)$$

$$B_{//}=\frac{4\gamma(\lambda_1)+3}{15\gamma(\lambda_1)}\cdot 2({}^{q_i}(\alpha_1^\circ)_{xy}^2+{}^{q_i}(\alpha_1^\circ)_{yz}^2) \qquad (8b)$$

where the molecular fixed Cartesian coordinates, x, y, and z, are defined so that the z-axis coincides with the molecular axis. For e-type lines, $A_\perp$ and $B_\perp$, which correspond to the perpendicular components, are: $A_\perp=(3/4)A_{//}$ and $B_\perp=(3/4)B_{//}$. In the above equations, $\gamma(\lambda_i)=\beta_\perp(\lambda_i)/\beta_{//}(\lambda_i)$, represents the ratio of the transmittances of the monochromator for the light whose electric vector is being polarized perpendicular to the slit, $\beta_\perp(\lambda_i)$, and that parallel to the slit, $\beta_{//}(\lambda_i)$, at the wavelength λ_i. In the case of an a_1-type vibration of a molecule belonging to a C_{3v} symmetry, the transition polarizability tensor can be completely determined if we know the elements ${}^{q}(\alpha_1^\circ)_{zz}$ and ${}^{q}(\alpha_1^\circ)_{xx}$, because the relations between the tensor elements are:

$${}^{q_i}(\alpha_1^\circ)_{xx}={}^{q_i}(\alpha_1^\circ)_{yy}\neq 0,\quad {}^{q_i}(\alpha_1^\circ)_{zz}\neq 0,$$
$${}^{q_i}(\alpha_1^\circ)_{xy}={}^{q_i}(\alpha_1^\circ)_{xz}={}^{q_i}(\alpha_1^\circ)_{yz}=0.$$

For an e-type vibration, it is necessary to know the elements ${}^{q}(\alpha_1^\circ)_{xy}$ and ${}^{q}(\alpha_1^\circ)_{yz}$, because the relations which hold in this case are:[7]

$${}^{q_i}(\alpha_1^\circ)_{xx}={}^{q_i}(\alpha_1^\circ)_{yy}={}^{q_i}(\alpha_1^\circ)_{zz}={}^{q_i'}(\alpha_1^\circ)_{zz}=0,$$
$${}^{q_i'}(\alpha_1^\circ)_{xy}={}^{q_i'}(\alpha_1^\circ)_{yz}={}^{q_i}(\alpha_1^\circ)_{xz}=0,$$
$${}^{q_i}(\alpha_1^\circ)_{xy}=-{}^{q_i'}(\alpha_1^\circ)_{yy}={}^{q_i'}(\alpha_1^\circ)_{xx},$$
$${}^{q_i}(\alpha_1^\circ)_{yz}=-{}^{q_i}(\alpha_1^\circ)_{xz}.$$

where Q_i and Q_i' refer to the doubly degenerated normal coordinate pair. Similar relations hold between transition hyperpolarizabilities, as has been shown in the previous report.[7]

Using the A and B values obtained for the a_1-type vibrations, we can obtain the transition polarizabilities and hyperpolarizabilities, ${}^{q}(\alpha_1^\circ)_{xx}$, ${}^{q}(\alpha_1^\circ)_{zz}$, ${}^{q}(\beta_1^\circ)_{xxz}$, and ${}^{q}(\beta_1^\circ)_{zzz}$. First, we can determine ${}^{q}(\alpha_1^\circ)_{xx}$ and ${}^{q}(\alpha_1^\circ)_{zz}$ by solving the simultaneous equation which is composed from Eqs. 6b and 7b. Then, the ${}^{q}(\beta_1^\circ)_{xxz}$ and ${}^{q}(\beta_1^\circ)_{zzz}$ values can be determined by putting the ${}^{q}(\alpha_1^\circ)_{xx}$ and ${}^{q}(\alpha_1^\circ)_{zz}$ values into Eqs. 6a and 7a and by solving the resultant simultaneous equation composed from Eqs. 6a and 7a. The polarizability derivative, $\partial\alpha^\circ/\partial Q$, is related to the transition polarizability, ${}^{q}(\alpha_1^\circ)$, as

$${}^{q}(\alpha_1^\circ)_{ij}=\left(\frac{\partial\alpha_{ij}^\circ}{\partial Q}\right)\langle I|Q|F\rangle$$

TABLE 2. PLAUSIBLE SETS OF POLARIZABILITY DERIVATIVES FOR a_1-TYPE LINES OF METHYL IODIDE (10^{-5} g$^{-1/2}$ cm^2)

#	$\partial\alpha_{xx}/\partial Q_1$	$\partial\alpha_{zz}/\partial Q_1$	$\partial\alpha_{xx}/\partial Q_2$	$\partial\alpha_{zz}/\partial Q_2$	$\partial\alpha_{xx}/\partial Q_3$	$\partial\alpha_{zz}/\partial Q_3$
1	10.74	23.42	3.49	0.36	9.02	−2.46
2	10.74	23.42	3.49	0.36	1.37	12.84
3	10.74	23.42	3.49	0.36	−9.02	2.46
4	10.74	23.42	3.49	0.36	−1.37	−12.84
5	10.74	23.42	1.41	4.54	9.02	−2.46
6	10.74	23.42	1.41	4.54	1.37	12.84
7	10.74	23.42	1.41	4.54	−9.02	2.46
8	10.74	23.42	1.41	4.54	−1.37	−12.84
9	10.74	23.42	−3.49	−0.36	9.02	−2.46
10	10.74	23.42	−3.49	−0.36	1.37	12.84
11	10.74	23.42	−3.49	−0.36	−9.02	2.46
12	10.74	23.42	−3.49	−0.36	−1.37	−12.84
13	10.74	23.42	−1.41	−4.54	9.02	−2.46
14	10.74	23.42	−1.41	−4.54	1.37	12.84
15	10.74	23.42	−1.41	−4.54	−9.02	2.46
16	10.74	23.42	−1.41	−4.54	−1.37	−12.84
17	19.19	6.51	3.49	0.36	9.02	−2.46
18	19.19	6.51	3.49	0.36	1.37	12.84
19	19.19	6.51	3.49	0.36	−9.02	2.46
20	19.19	6.51	3.49	0.36	−1.37	−12.84
21	19.19	6.51	1.41	4.54	9.02	−2.46
22	19.19	6.51	1.41	4.54	1.37	12.84
23	19.19	6.51	1.41	4.54	−9.02	2.46
24	19.19	6.51	1.41	4.54	−1.37	−12.84
25	19.19	6.51	−3.49	−0.36	9.02	−2.46
26	19.19	6.51	−3.49	−0.36	1.37	12.84
27	19.19	6.51	−3.49	−0.36	−9.02	2.46
28	19.19	6.51	−3.49	−0.36	−1.37	−12.84
29	19.19	6.51	−1.41	−4.54	9.02	−2.46
30	19.19	6.51	−1.41	−4.54	1.37	12.84
31	19.19	6.51	−1.41	−4.54	−9.02	2.46
32	19.19	6.51	−1.41	−4.54	−1.37	−12.84

where $\langle I|Q|F\rangle$ is a transition matrix element corresponding to the transition between the vibrational levels I and F.

As the Eqs. 6b and 7b are quadratic with respect to the polarizability derivatives, there are four possible sets of polarizability derivative values for each normal mode, Q_1, Q_2, and Q_3. Therefore, there can be obtained $4^3=64$ possible combinations of polarizability derivatives, which are summarized in Table 2. The sixty-four sets of polarizability derivatives can be classified into two groups whose polarizability derivatives have exactly the same absolute values with an opposite sign. As we have no way to distinguish these two groups at present, we assume that all the polarizability derivatives related with the normal mode Q_1 are positive.[8] Therefore, we consider only thirty-two sets of polarizability derivatives hereafter.

Determination of Transition Polarizability. In order to select the most reliable set of polarizability derivatives out of the thirty-two, we introduce the so-called bond polarizability theory which was proposed first by Wolkenstein[9] and Eliashevich[10] and was modified later by Long.[11] The basic idea of this theory is the assignment of a characteristic bond polarizability to each bond in the molecule. This bond polarizability is then defined completely in terms of a polarizability ellipsoid having the major axis coincident with the bond direction. Instead of an irreducible tensor expression which is used in Long's theory, we focus our attention on a reducible tensor, simply because it is more convenient for determining the elements of a transition polarizability tensor. The polarizability derivative, $\partial\alpha/\partial Q$, is expressed as a linear combination of the bond polarizability parameters:[12]

$$\frac{\partial\alpha}{\partial Q} = (J(\gamma_1')K^*L_x)\gamma_1' + (J(\delta_1')K^*L_x)\delta_1' + (J(\varepsilon_1)K^*L_x)\frac{\varepsilon_1}{r_{CI}} + (J(\gamma_2')K^*L_x)\gamma_2' + (J(\delta_2')K^*L_x)\delta_2' + (J(\varepsilon_2)K^*L_x)\frac{\varepsilon_2}{r_{CH}} \quad (9)$$

where $(\gamma_1', \delta_1', \varepsilon_1/r_{CI})$ and $(\gamma_2', \delta_2', \varepsilon_2/r_{CH})$ are the bond polarizability parameters related with the C–I and C–H bonds, respectively. The matrices J and K are determined only from the molecular geometry. The matrix L_x is the transformation matrix between the Cartesian displacement coordinates fixed in the molecule and the normal coordinates, and therefore can be calculated from the molecular force field. In the case of the a_1-type vibrations of methyl iodide, the transformation matrix (JKL_x) is 6×6, because the number of the bond

polarizability parameters is six, while the six elements of the bond polarizability derivative contribute to the scattering cross-section of the a_1-type vibrations. Therefore, we can in principle calculate the bond polarizability parameters by the use of the polarizability derivative values of Table 2. The transformation matrix (JKL_x), which was calculated by the use of the force constants reported by Crawford *et al.*,[8] relates the polarizability derivatives and the bond polarizability parameters:

$$\begin{bmatrix} \partial\alpha^\circ_{xx}/\partial Q_1 \\ \partial\alpha^\circ_{zz}/\partial Q_1 \\ \partial\alpha^\circ_{xx}/\partial Q_2 \\ \partial\alpha^\circ_{zz}/\partial Q_2 \\ \partial\alpha^\circ_{xx}/\partial Q_3 \\ \partial\alpha^\circ_{zz}/\partial Q_3 \end{bmatrix} = \begin{bmatrix} 0 & a & 0 & d & i & m \\ a & a & 0 & e & j & n \\ 0 & b & 0 & f & k & p \\ b & b & 0 & g & k & q \\ 0 & c & 0 & h & l & r \\ c & c & 0 & i & l & s \end{bmatrix} \begin{bmatrix} \gamma_1' \\ \delta_1' \\ \varepsilon_1/r_{CI} \\ \gamma_2' \\ \delta_2' \\ \varepsilon_2/r_{CH} \end{bmatrix} \quad (10)$$

Eq. 10 shows that the parameter ν_1 does not contribute to any polarizability derivatives and, therefore, the inverse matrix $(JKL_x)^{-1}$ does not exist. However, we can reduce the transformation matrix of Eq. 10 into:

$$\begin{bmatrix} \partial\alpha^\circ_{xx}/\partial Q_1 - \partial\alpha^\circ_{zz}/\partial Q_1 \\ \partial\alpha^\circ_{xx}/\partial Q_2 - \partial\alpha^\circ_{zz}/\partial Q_2 \\ \partial\alpha^\circ_{xx}/\partial Q_3 - \partial\alpha^\circ_{zz}/\partial Q_3 \end{bmatrix} = \begin{bmatrix} -a & d-l & m-n \\ -b & f-g & p-q \\ -c & h-i & r-s \end{bmatrix} \begin{bmatrix} \gamma_1' \\ \delta_2' \\ \varepsilon_2/r_{CH} \end{bmatrix} \quad (11)$$

Thus we can calculate the bond polarizability parameters, γ_1', γ_2', and ε_2/r_{CH}, by solving Eq. 11. By putting back the calculated bond polarizability parameters into Eq. 10 and by solving the linear equations composed from the first and the third columns of Eq. 10, we can obtain the remaining bond polarizability parameters, δ_1' and δ_2'. In other words, we can calculate the thirty-two sets of bond polarizability parameters, γ_1', γ_2', δ_1', δ_2', and ε_2/r_{CH}, which correspond to the thirty-two sets of polarizability derivatives. Finally, we calculate the polarizability derivatives, $\partial\alpha^\circ{}_{xx}/\partial Q_3$ and $\partial\alpha^\circ{}_{zz}/\partial Q_3$, using the fifth and sixth columns of Eq. 10: the results are summarized in Table 3. By comparing the calculated values of $\partial\alpha^\circ{}_{xx}/\partial Q_3$ and $\partial\alpha^\circ{}_{zz}/\partial Q_3$ with the observed values of Table 2, we can select the eight possible sets of molecular polarizability derivatives (#11, 12, 15, 16, 27, 28, 31, and 32) out of the thirty-two sets of Table 2.

The next step is to select more reliable sets of polarizability derivatives out of the eight sets. This can be done by calculating the remaining undetermined bond polarizability parameter, ε_1/r_{CH}, from the observed intensities related with the e-species Raman lines. For the e-type vibrations, the transformation matrix (JKL_x), which was calculated by the use of the force constants of Crawford,[8] relates the polarizability derivatives and the bond polarizability parameters:

$$\begin{bmatrix} \partial\alpha^\circ_{xy}/\partial Q_1 \\ \partial\alpha^\circ_{yz}/\partial Q_1 \end{bmatrix} = \begin{bmatrix} 0 & a & b \\ c & d & e \end{bmatrix} \begin{bmatrix} \varepsilon_1/r_{CI} \\ \gamma_2' \\ \varepsilon_2/r_{CH} \end{bmatrix} \quad (12)$$

By putting the eight possible sets of polarizability parameters previously calculated, γ_2' and ε_2/r_{CH}, into Eq. 12 and by putting Eq. 12 into Eq. 8b, we can derive the quadratic equation with respect to the remaining bond polarizability parameter, ε_1/r_{CI}. Thus the remaining bond polarizability parameter, ε_1/r_{CI}, can be calculated for both ν_5 and ν_6 lines corresponding to the eight possible sets of bond polarizability parameters. The results are summarized in Table 4. As the bond polarizability parameters should be real, the sets #11, 12, 15, 28, 31, and 32, can be discarded, because the calculated ε_1/r_{CI} values are imaginary. The remaining sets #16 and 27 are considered to be reasonable, because the ε_1/r_{CI} values which have been obtained are similar in magnitude for ν_5 and ν_6: 2.54×10^{-16} cm^2 (ν_5) and 2.24×10^{-16} cm^2 (ν_6) for #16, and -2.54×10^{-16} cm^2 (ν_5) and -2.24×10^{-16} cm^2 (ν_6) for #27. There is no way to distinguish these two sets of polarizability derivatives within the bond polarizability hypothesis. Fortunately, however, we can choose sets #16 as the most reliable set of molecular polarizability derivatives, because of the following reason.

In the preceding discussion, the transition polarizability related with the Q_3 normal mode, $^{0_1}(\alpha_1^\circ)_{zz}$, was obtained to be 2.94×10^{-25} cm^3 (for #16) or -2.94×10^{-25} cm^3 (for #27). According to our previous work

TABLE 3. POLARIZABILITY DERIVATIVES FOR Q_3 OF METHYLIODIDE CALCULATED FROM BOND POLARIZABILITY PARAMETERS (10^{-5}g$^{-1/2}$ cm^2)

#	$\partial\alpha_{xx}/\partial Q_3$	$\partial\alpha_{zz}/\partial Q_3$	#	$\partial\alpha_{xx}/\partial Q_3$	$\partial\alpha_{zz}/\partial Q_3$
1	6.14	−5.33	17	6.11	−5.36
2	−1.50	9.97	18	−1.53	9.94
3	−1.50	9.97	19	−1.53	9.94
4	6.14	−5.33	20	6.11	−5.36
5	6.14	−5.33	21	6.12	−5.35
6	−1.50	9.97	22	−1.52	9.94
7	−1.50	9.97	23	−1.52	9.94
8	6.14	−5.33	24	6.12	−5.35
9	−1.87	−13.34	25	−1.89	−13.36
10	−9.51	1.96	26	−9.53	1.94
11	−9.51	1.96	27	−9.53	1.94
12	−1.87	−13.34	28	−1.89	−13.34
13	−1.87	−13.34	29	−1.89	−13.37
14	−10.00	1.48	30	−9.54	1.93
15	−10.00	1.48	31	−9.54	1.93
16	−1.87	−13.34	32	−1.89	−13.37

TABLE 4. e_2/r_{CH} VALUES CALCULATED FOR ν_5 AND ν_6 LINES (10^{-16} cm^2)

#	11	12	15	16
ν_5	$3.61\pm1.96i$	$7.93\pm10.2i$	$8.12\pm13.0i$	$\begin{cases} 2.54 \\ -7.98 \end{cases}$
ν_6	$\begin{cases} -0.67 \\ -2.70 \end{cases}$	$3.35\pm9.39i$	$3.93\pm1.26i$	$\begin{cases} 2.24 \\ -0.05 \end{cases}$
#	27	28	31	32
ν_5	$\begin{cases} -2.54 \\ 7.98 \end{cases}$	$8.12\pm13.0i$	$7.93\pm10.2i$	$3.61\pm1.96i$
ν_6	$\begin{cases} -2.24 \\ 0.05 \end{cases}$	$3.93\pm1.26i$	$3.35\pm9.39i$	$\begin{cases} -0.67 \\ -2.70 \end{cases}$

on the solvent effect on the infrared absorption intensity for the ν_3 band of methyl iodide,[1] the $^{Q_1}(\alpha_1^\circ)_{zz}$ has been obtained to be -1.1×10^{-25} cm^3. We should not attach too much importance to the absolute values of these results, because the frequency region of the infrared measurement belongs to the resonant region, while that of the Raman measurement belongs to the off-resonant region. However, the minus sign attached to the $^{Q_1}(\alpha_1^\circ)_{zz}$ value is of much importance, because the signs attached to the $^{Q_1}(\alpha_1^\circ)_{zz}$ values of the Raman and infrared results should be the same. Thus we can say that set #16 is more reliable than set #27.

Determintaion of Transition Hyperpolarizability. Using the finally determined set of polarizability derivatives, that is,

$$^{Q_1}(\alpha_1^\circ)_{xx} = 1.05\times10^{-25} \quad (\text{cm}^3)$$
$$^{Q_1}(\alpha_1^\circ)_{zz} = 2.28\times10^{-25} \quad (\text{cm}^3)$$
$$^{Q_1}(\alpha_1^\circ)_{xx} = -2.10\times10^{-26} \quad (\text{cm}^3)$$
$$^{Q_1}(\alpha_1^\circ)_{zz} = -6.76\times10^{-26} \quad (\text{cm}^3)$$
$$^{Q_1}(\alpha_1^\circ)_{xx} = -3.14\times10^{-26} \quad (\text{cm}^3)$$
$$^{Q_1}(\alpha_1^\circ)_{zz} = -2.94\times10^{-25} \quad (\text{cm}^3)$$

and using Eqs. 6a and 7a, we can calculate the transition hyperpolarizability elements for Q_3:

$$^{Q_1}(\beta_1^\circ)_{xxz} = 7.07\times10^{-31} \quad (\text{cm}^3\ \text{dyn}^{-1}\ \text{esu})$$
$$^{Q_1}(\beta_1^\circ)_{zzz} = 8.88\times10^{-31} \quad (\text{cm}^3\ \text{dyn}^{-1}\ \text{esu})$$

which are certainly of the correct order of magnitude. The magnitude of the transition hyperpolarizability has been considered to be of the order of 10^{-31}—10^{-32} (cm^3 dyn^{-1} esu), although no direct measurement of transition hyperpolarizability has actually been reported yet.

Concluding Discussion. From the discussion of the previous paragraphs, a few important conclusions can be drawn.

1) It was shown that the hyperpolarizability, which is a higher order term of the polarizability, does change the Raman intensities through the existence of the averaged molecular field, $\langle \boldsymbol{F}_{0z} \rangle_{av}$, in solution. If the averaged molecular field is properly estimated, the transition polarizability and transition hyperpolarizability can be determined simultaneously in the form of tensor elements by observing the solvent effect on Raman intensity.

2) For determining the sign of the transition polarizability, the bond polarizability theory has been shown to be quite helpful. At the same time, the information about the sign of the transition polarizability which is observed in the solvent effect on infrared intensity is very important and convincing.

3) Incidentally, this seems to be the first work in which the transition hyperpolarizability is obtained in the form of a tensor element. The examination of the reliability of the resultant transition hyperpolarizability, however, will be left for future studies in which the transition hyperpolarizability will be directly observed by, for example, the intensity measurement of a hyper-Raman line.

References

1) M. Kakimoto and T. Fujiyama, *Bull. Chem. Soc. Jpn.*, **48**, 2258 (1975).

2) J. Koike, T. Suzuki, and T. Fujiyama, *Bull. Chem. Soc. Jpn.*, **49**, 2724 (1976).

3) J. A. Riddick and B. Bunger, "Organic Solvents, Techniques of Chemistry Vol. II," 3rd ed, John Wiley and Sons, New York (1970).

4) G. Eckhardt and W. G. Wagner, *J. Mol. Spectrosc.*, **19**, 407 (1966); G. Fini, P. Mirone, and P. Patella, *ibid.*, **28**, 144 (1968); P. Mirone, *Chem. Phys. Lett.*, **4**, 323 (1969); G. Fini, M. G. Giorgini, and P. Mirone, *Gaz. Chim. Ital.*, **102**, 288 (1972); T. Fujiyama, *Bull. Chem. Soc. Jpn.*, **46**, 87 (1973); H. Hatakeyama and T. Fujiyama, *ibid.*, **51**, 431 (1978).

5) In our previous reports (Ref. 1 and Ref. 2), the terms corresponding to the dipole-induced dipole interaction have been under-estimated. Readers are invited to have more confidence in Eq. 5 of the present report.

6) Y. Kato, Thesis submitted to the University of Tokyo (1969).

7) These relations have been mis-printed in Appendix II of Ref. 2. Readers are invited to read Eq. A25 and Eq. A22 of Ref. 2 as:

$$^{Q_1}(\beta_1^\circ)_{xyz} = -{}^{Q_1}(\beta_1^\circ)_{yyz} = {}^{Q_1}(\beta_1^\circ)_{xxz}$$
$$^{Q_1}(\beta_1^\circ)_{yzz} = -{}^{Q_1}(\beta_1^\circ)_{xzz} \quad (\text{A25})$$
$$^{Q_1}(\alpha_1^\circ)_{xy} = -{}^{Q_1}(\alpha_1^\circ)_{yy} = {}^{Q_1}(\alpha_1^\circ)_{xx}$$
$$^{Q_1}(\alpha_1^\circ)_{yz} = -{}^{Q_1}(\alpha_1^\circ)_{xz} \quad (\text{A22})$$

8) This assumption has been widely accepted in previous works: A. D. Dickson, I. M. Mills, and B. L. Crawford, Jr., *J. Chem. Phys.*, **27**, 445 (1957); D. A. Long, *Trans. Faraday Soc.*, **59**, 43 (1963).

9) M. Volkenstein, *C. R. Acad. Sci. USSR*, **30**, 791 (1941).

10) M. Eliashevich and M. Volkenstein, *J. Phys. USSR*, **9**, 101; 326 (1945).

11) D. A. Long, *Proc. R. Soc. London, Ser. A*, **217**, 203 (1953).

12) For the detailed notations, see R. E. Hester in: "Raman Spectroscopy," ed by Szymanski, Plenum Press, New York (1967), Chap. 4.

Calculations of the Solvent Effects on Some Nitrogen Chemical Shifts

Isao ANDO,* M. JALLALI-HERAVI,** Masahiro KONDO, Shosuke WATANABE, and G. A. WEBB**

Department of Polymer Chemistry, Tokyo Institute of Technology, Ookayama, Meguro-ku, Tokyo 152
***Department of Chemical Physics, University of Surrey, Guildford, Surrey GU2 5XH, England*

(Received March 2, 1979)

Nitrogen screening constants are calculated by the sum-over-states method using INDO/S parameters and by the finite perturbation procedure employing INDO parameters. The solvaton model is employed to describe changes in nuclear screening as a function of the dielectric constant of the medium. The calculated variations of nitrogen screening are in reasonable agreement with the available experimental data. The effects on screening of hydrogen bonding are included in the sum-over-states calculations by means of dimer models.

In order to obtain a close comparison between theoretical and experimental estimates of nuclear screening some allowance should be made for medium effects. Contributions from the bulk magnetisation and the diamagnetic anisotropy of the solvent to the total screening can be effectively removed by a suitable choice of solvent and the use of an internal standard. Account should also be taken of van der Waals interactions between solute and solvent, which usually deshield the nucleus of interest,[1,2] polar effects due to the charge distribution in neighbouring solvent molecules and specific solute solvent interactions such as hydrogen bonding and complex formation.

The influence of van der Waals interactions are likely to be most pronounced in the case of relatively nonpolar systems. For polar molecules it seems reasonable to suppose that effects due to solvent-charge distribution and specific solute-solvent interactions will dominate.

The polar effects of solvents on nuclear screening may be accounted for by means of the solvaton model.[3] This has been successfully employed in the calculation of solvent effects on ^{13}C chemical shifts in a number of molecules.[4,5]

In the present study these investigations are extended to nitrogen chemical shifts. Since these are more sensitive to medium effects than ^{13}C chemical shifts,[6] it is anticipated that they may provide a closer insight into the effects of solute-solvent interactions on chemical shifts.

As discussed elsewhere[7] Pople's model[8,9] appears to provide the most acceptable basis for satisfactory discussions of nuclear screening. Calculations using semi-empirical MO parameter sets are often inadequate due to the difficulties involved in accurately determining the contributions to the paramagnetic component of the screening tensor from the excited states. Two approaches to this problem are currently available. The sum-over-states method incorporating parameter sets which provide a realistic description of the excited states. In addition, there is the finite perturbation procedure which does not explicitly involve the estimation of excited state eigenfunctions.

Both of these approaches are employed in the present work. The sum-over-states calculations use INDO/S parameters which have been demonstrated to provide a satisfactory account of nitrogen chemical shifts[10] and the finite perturbation method employs INDO parameters within a revised formulation.[11] In the latter case, the values of the bonding parameters β_H° and β_C°, for the hydrogen and carbon atoms respectively, are taken to be -13 eV and -15 eV. The correction factor K for π-π interactions takes the value of 0.85. Calculations incorporating these values provide a reasonable account of some ^{13}C chemical shifts.[11]

Results and Discussion

The results of the calculations of the total charge density on the nitrogen atom, q, the averaged value of its screening tensor, σ, and the relative chemical shift, δ, as a function of the dielectric constant of the medium, ε, for both the sum-over-states (SOS) and finite perturbation (FPT) calculations are presented in Table 1.

The decrease in screening of the nitrogen nucleus in nitromethane as ε increases is almost entirely due to changes in the paramagnetic contribution to the screening tensor. As ε increases from 1 to 80 the diamagnetic term reduces by 1.83 ppm in the sum-over-states calculations and 0.95 ppm in the finite perturbation results. This follows a reduction in the nitrogen charge density. In general, it is found that the calculated changes in the diamagnetic term, as a function of ε, are very small when compared with those in the paramagnetic contribution. Consequently only changes in the total nuclear screening are reported in Table 1.

The data reported in Table 1 imply that changes in q, as a function of ε, do not always follow in the same direction as variations in σ. This is most probably due to the fact that differences in σ are controlled by changes in the paramagnetic contribution which, in general, are not expected to depend linearly on charge density differences.[7]

Both sets of calculations qualitatively follow the trend of changes in nitrogen screening with ε for nitromethane reported experimentally.[6] More quantitative data would reveal whether the large change in σ, predicted by the sum-over-states calculations, or the smaller change indicated by the finite perturbation results is the more accurate.

The finite perturbation results reported in Table 1 do not contain the contribution to the diamagnetic term arising from the 1s electrons. Thus the values of σ reported are smaller than those obtained from the sum-over-states calculations. However, this should not influence the calculated changes in σ as a function of ε.

The sum-over-states results indicate a value of about -141 ppm for the nitrogen screening of neat nitromethane which is in reasonable agreement with the estimated

TABLE 1. SOME SUM-OVER-STATES (SOS) AND FINITE PERTURBATION (FPT) CALCULATIONS OF THE DEPENDENCE OF SOME NITROGEN CHARGE DENSITIES (q), SCREENING CONSTANTS (σ) IN ppm AND CHEMICAL SHIFTS (δ) IN ppm UPON DIELECTRIC CONSTANT

Species	Method	Data	Dielectric constant						
			1	2	6	10	20	40	80
CH_3NO_2	SOS	q	4.519	4.438	4.383	4.372	4.363	4.359	4.357
		σ	−112.46	−126.26	−136.93	−138.94	−140.45	−141.20	−141.57
		δ	0.0	13.80	24.97	26.48	27.99	28.74	29.11
	FPT	q	4.448	4.406	4.378	4.372	4.368	4.366	4.365
		σ	−444.46	−446.91	−448.41	−448.70	−448.92	−448.96	−449.07
		δ	0.0	2.45	3.95	4.24	4.46	4.50	4.61
NH_3	SOS	q	5.282	5.337	5.373	5.381	5.386	5.389	5.390
		σ	112.12	120.62	125.78	126.88	127.80	128.20	128.40
		δ	0.0	−8.50	−13.66	−14.76	−15.68	−16.08	−16.28
	FPT	q	5.276	5.286	5.293	5.295	5.296	5.296	5.297
		σ	−127.24	−126.04	−125.24	−125.07	−124.96	−124.91	−124.86
		δ	0.0	−1.20	−2.00	−2.17	−2.28	−2.33	−2.38
Pyridine	SOS	q	5.297	5.308	5.316	5.317	5.318	5.319	5.319
		σ	−20.40	−20.27	−20.17	−20.14	−20.12	−20.11	−20.11
		δ	0.0	−0.13	−0.23	−0.26	−0.28	−0.29	−0.29
	FPT	q	5.206	5.221	5.227	5.231	5.231	5.231	5.232
		σ	−465.82	−451.63	−444.33	−442.88	−441.80	−441.24	−441.11
		δ	0.0	−14.19	−21.49	−22.94	−24.02	−24.58	−24.71
CH_3CN	SOS	q	5.294	5.304	5.311	5.313	5.314	5.315	5.315
		σ	35.51	35.47	35.23	35.12	35.08	35.06	35.04
		δ	0.0	0.04	0.28	0.39	0.43	0.45	0.47
	FPT	q	5.202	5.235	5.250	5.255	5.258	5.260	5.261
		σ	−349.77	−337.41	−329.59	−327.99	−326.81	−326.18	−325.92
		δ	0.0	−12.36	−20.18	−21.78	−22.96	−23.59	−23.85
CH_3NC	SOS	q	5.118	5.124	5.131	5.132	5.133	5.134	5.134
		σ	91.50	93.79	94.10	94.09	94.16	94.13	94.11
		δ	0.0	−2.29	−2.60	−2.59	−2.66	−2.63	−2.61
	FPT	q	5.029	5.004	4.987	4.984	4.981	4.980	4.979
		σ	−144.05	−149.37	−153.06	−153.80	−154.37	−154.65	−154.79
		δ	0.0	5.32	9.01	9.75	10.32	10.60	10.74
NO_3^-	SOS	q	4.477	4.359	4.281	4.263	4.250	4.235	4.231
		σ	−94.98	−192.14	−237.36	−291.83	−306.17	−316.26	−320.03
		δ	0.0	97.16	178.38	196.85	211.19	221.28	225.05
	FPT	q	4.323	4.260	4.219	4.211	4.206	4.203	4.201
		σ	−537.91	−465.39	−413.88	−406.70	−401.43	−398.83	−397.54
		δ	0.0	−72.52	−124.03	−131.21	−136.48	−139.08	−140.37
NH_4^+	SOS	q	4.822	4.817	4.814	4.814	4.813	4.813	4.813
		σ	137.56	175.30	192.42	195.47	197.54	199.47	199.99
		δ	0.0	−37.74	−54.86	−57.91	−59.98	−61.91	−62.43
	FPT	q	4.965	4.986	5.002	5.005	5.008	5.009	5.010
		σ	−66.32	−88.19	−107.22	−111.44	−114.72	−116.38	−117.24
		δ	0.0	21.87	40.90	45.12	48.40	50.06	50.92

a) The chemical shifts are reported with respect to the isolated molecule, $\varepsilon=1$, shifts to higher frequency being positive.

value of −130 ppm.[6]

In the case of ammonia both sets of calculations predict an increase in nitrogen screening as ε increases. This appears to be in contradiction to the available experimental data which show a nitrogen screening decrease by up to 21 ppm when gaseous ammonia is dissolved in various solvents.[6] However, the nitrogen screening of the ammonium ion can be 40 to 50 ppm less then in ammonia[6] and since the available experimental solution data on ammonia involves media conductive to protonation and/or hydrogen-bonding the comparison with the theoretical results in Table 1 may not be a valid one.

The small increase in the nitrogen screening of pyridine as ε increases, from the sum-over-states calculations, follows the trend of the available experimental data for non-hydrogen bonding media.[6,12] In hydrogen-bonding solvents large increases in the nitrogen screening are reported which are dominated by changes in the paramagnetic term.[12] To investigate this we have calculated the nitrogen screening constant for the hydrogen-bonded pyridine–water dimer in a minimum

Table 2. Sum-over-states calculated values of the charge and contributions to the nuclear screening tensor (ppm) of some nitrogen nuclei in cases where hydrogen bonding is significant

Compound	q	Average weighted value of transition energies (eV)	σ^d	σ^p (loc)	σ^p (nonloc)	σ	δ
NO_3^- (isolated)	4.4770	14.08	318.48	−416.29	2.83	−94.98	0.0
Hydrated NO_3^- [14]	4.4879	14.33	318.62	−408.35	2.34	−87.39	−7.59
Pyridine (isolated)	5.2973	11.82	327.11	−349.80	2.30	−20.40	0.0
Pyridine/Water[a]	5.2775	12.37	326.93	−334.04	2.50	−4.61	−15.79
CH_3CN (isolated)	5.2944	11.510	327.15	−289.45	−5.19	35.51	0.0
CH_3CN/CH_3OH[b]	5.2593	13.075	326.82	−256.14	−1.13	69.56	−34.05

a)

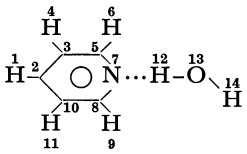

$C_2H_1=C_3H_4=C_{10}H_{11}=1.105$ Å
$C_5H_6=C_8H_9=1.114$ Å
$C_2C_3=C_3C_5=C_8C_{10}=C_2C_{10}=1.407$ Å
$C_5N_7=C_8N_7=1.334$ Å
$N_7H_{12}=4.626$ Å
$H_{12}O_{13}=H_{14}O_{13}=0.949$ Å

$H_1\hat{C}_2C_3=H_4\hat{C}_3C_2=120.3°$
$C_2\hat{C}_3C_5=C_2\hat{C}_{10}C_8=118.1°$
$C_3\hat{C}_5N_7=C_{10}\hat{C}_8N_7=121.8°$
$C_3\hat{C}_5H_6=121.7°$
$C_5\hat{N}_7C_8=120.7°$
$N_7\hat{C}_8H_9=116.6°$
$C_5\hat{N}_7H_{12}=118.0°$
$N_7H_{12}O_{13}=180.6°$
$H_{12}\hat{O}_{13}H_{14}=103.7°$

b)

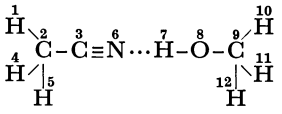

$H_1C_2=H_4C_2=H_5C_2=1.121$ Å
$C_2C_3=1.424$ Å
$C_3N_6=1.196$ Å
$N_6H_7=1.406$ Å
$H_7O_8=1.072$ Å
$O_8C_9=1.362$ Å
$C_9H_{10}=C_9H_{11}=C_9H_{12}=1.126$ Å

$H_1\hat{C}_2C_3=110.9°$
$C_2\hat{C}_3N_6=179.5°$
$H_7\hat{N}_6C_3=175.0°$
$O_8\hat{H}_7N_6=174.6°$
$C_9\hat{O}_8H_7=111.6°$
$H_{10}\hat{C}_9O_8=111.6°$

energy conformation obtained from an INDO geometry optimization procedure.

The results given in Table 2 reveal an increase in nitrogen screening of 15.79 ppm due to hydrogen-bond formation. This compares with a measured increase of about 25 ppm.[12] The increase arises from a reduction in the paramagnetic contribution to the screening as a result of increases of energy denominators weighted by transition elements in various transitions.[10] The major transition changes result from the effective removal of the nitrogen lone pair due to hydrogen-bond formation.

The finite perturbation results (Table 1) show a much larger increase in the nitrogen screening of pyridine, with an increase in ε, without specifically incorporating the formation of a hydrogen bond.

A similar situation arises in the case of acetonitrile. The observed increase in the nitrogen screening in methanol appears to be accounted for by the finite perturbation calculations on the solvaton model, whereas the sum-over-states method requires the acetonitrile-methanol dimer as a model (Table 2) to reproduce the experimental trend. The structure used in this calculation again corresponds to a minimum energy conformation as obtained from INDO calculations.

The available experimental data on the nitrogen resonance of methyl isocyanide[13] indicate that it is far less sensitive to changes in solvent than is its counterpart for acetonitrile. The calculations reported here support this conclusion. However, the opposing trends predicted by the two sets of calculations are probably indicative of medium effects which are not specifically incorporated in the solvaton model.

The sum-over-states calculations for the nitrate ion indicate that the nitrogen atom in the free ion suffers a large decrease in screening as ε increases. However, in the presence of water a hydrogen-bonded structure has been reported.[14] Calculations on this structure (Table 2) reveal an increase of nitrogen screening. The increase in nitrogen screening, as a function of ε, is predicted by the finite perturbation calculation without invoking hydrogen-bonding.

Since nitrate ion is usually used in aqueous media the opposing screening trends due to the solvaton and hydrogen-bonding interactions renders its nitrogen resonance position very susceptible to changes in concentration and pH. Taken together these effects make nitrate ion unsatisfactory as a reference standard for nitrogen NMR.[6]

The trend obtained (Table 1) by the sum-over-states calculations for the nitrogen screening of the ammonium ion, as a function of ε, is in reasonable agreement with the available experimental data.[6] The opposing trend suggested by the finite perturbation calculations implies that interactions other than those described by the solvaton model are operative.

For use as a nitrogen NMR reference material the position of a nitrogen signal should be relatively insensitive to solvent changes in order to compare results between different laboratories. The calculations reported here indicate that the ammonium ion is not to be recommended as a nitrogen standard.[6]

At present it is not clear why the sum-over-states calculations for pyridine, acetonitrile and nitrate ion require both solvaton and hydrogen bonding effects to reproduce experimental trends, whereas only solvaton interactions are necessary in the finite perturbation approach. However, in general, the effects of the medium on nitrogen chemical shifts appear to be reasonably well accounted for by the calculations reported here involving both the solvaton model and specified hydrogen-bonding interactions. To examine these data more searchingly further experimental results of changes in nitrogen screening as a function of ε are required.

Experimental

The sum-over-states calculations were performed on the CDC 7600 systems of the Universities of London and Manchester using a modified version of QCPE 174. Standard geometries[15] were used in the calculations. The finite perturbation calculations were performed on the HITAC M180 system of the Tokyo Institute of Technology.

M. Jallali-Heravi acknowledges receipt of an Iranian Government Scholarship. G. A. Webb is grateful for Royal Society support under its Japan programme.

References

1) A. D. Buckingham, T. Schaefer, and W. G. Schneider, *J. Chem. Phys.*, **32**, 1227 (1960).
2) I. D. Gay and J. F. Kriz, *J. Phys. Chem.*, **82**, 319 (1978).
3) H. A. Germer, *Theor. Chim. Acta*, **34**, 145 (1974).
4) I. Ando, A. Nishioka, and M. Kondo, *J. Magn. Reson.*, **21**, 429 (1976).
5) I. Ando, Y. Kato, M. Kondo, and A. Nishioka, *Makromol. Chem.*, **178**, 803 (1977).
6) M. Witanowski, L. Stefaniak, and G. A. Webb, "Annual Reports on NMR Spectroscopy," ed by G. A. Webb, Academic Press, London (1977), **7**, 117.
7) K. A. K. Ebraheem and G. A. Webb, "Progress in NMR Spectroscopy," ed by J. W. Emsley, J. Feeney, and L. H. Sutcliffe, Pergamon Press, Oxford (1977), **11**, 149.
8) J. A. Pople, *J. Chem. Phys.*, **37**, 53 (1962).
9) J. A. Pople, *J. Chem. Phys.*, **37**, 60 (1962).
10) M. Jallali-Heravi and G. A. Webb, *J. Magn. Reson.*, in the press.
11) M. Kondo, I. Ando, R. Chujo, and A. Nishioka, *J. Magn. Reson.*, **24**, 315 (1976).
12) R. O. Duthaler and J. D. Roberts, *J. Am. Chem. Soc.*, **100**, 4969 (1978).
13) A. Loewenstein and Y. Margalit, *J. Phys. Chem.*, **69**, 4152 (1965).
14) R. Caminiti, G. Licheri, G. Piccaluga, and G. Pinna, *J. Chem. Phys.*, **68**, 1967 (1978).
15) J. A. Pople and M. S. Gordon, *J. Am. Chem. Soc.*, **89**, 4253 (1967).

Film Dichroism. III. Linearly-polarized Absorption Spectra of Highly Symmetric Triphenylmethane Dyes in the Stretched Poly(vinyl alcohol) Films

Yukio MATSUOKA and Kiwamu YAMAOKA*

Faculty of Science, Hiroshima University, Higashisenda-machi, Hiroshima 730

(Received March 9, 1979)

The linear dichroic absorption spectra of Pararosaniline (PR), Crystal Violet (CV), and Ethyl Violet (EV) were measured in the UV and visible regions by the stretched film technique. Poly(vinyl alcohol) was used as the film matrix. A method, which is expressed in the forms of reduced dichroism and dichroic ratio, was proposed for the analysis of the linear dichroism of disk-like molecules. The dyes PR, CV, and EV were shown to behave like disks regarding their orientation in the polymer matrix. The isotropic absorption spectra of PR, CV, and EV were resolved into the in-plane and out-of-plane polarized components by the reduction procedure. In each isotropic spectrum the out-of-plane component was found to overlap with the intense in-plane component in the UV and visible wavelength regions.

Crystal Violet (CV) has attracted considerable attention in the last decade because it is a typical non-intercalative dye which binds to biopolymers.[1,2] Measurements of the optical rotatory dispersion[1] and linear flow dichroism[2,3] of CV bound to deoxyribonucleic acid (DNA) were carried out to elucidate the binding mode of the dye. In order to obtain useful information on the optical properties of the DNA–CV complexes, however, it is of utmost importance to know the polarization direction of the electronic absorption bands of CV itself in detail, as pointed out in a previous paper.[4] In the assignment of the polarization direction for the disk-like molecules which belong to a D_{nh} or C_{nv} ($n \geqq 3$) point symmetry, a transition polarized perpendicularly to the molecular plane (*i.e.*, out-of-plane transition) should not be ignored. Since CV is most likely to belong to the D_{3h} or C_{3v} point symmetry, the out-of-plane transition must be taken into account in the analysis of its dichroic data.

Recently, Yogev *et al.*[5] reported the expressions for the linear dichroism of disk-like molecules in some special cases and thereby resolved the isotropic absorption spectra of penta- and hexahelicenes into the in-plane and out-of-plane polarized absorption components. For the triphenylmethane dyes such as CV and Malachite Green, both the measurements of dichroic absorption spectra and the interpretations of the dichroic ratio have been carried out.[6,7] Tanizaki[6] first determined the relative directions of the transition moments of CV for the visible absorption bands. Nordén[7] measured the dichroic ratios of some triphenylmethane dyes in the visible region and explained them qualitatively. Both of these workers have suggested the possibility of the presence of an out-of-plane polarized absorption component in the isotropic spectrum of CV, but they have failed to show the location and band shape of the component.

The main objects of this paper are, first, to determine the in-plane and out-of-plane polarized absorption components (the reduced spectra) of CV from its dichroic absorption spectra by the *reduction procedure*;[8] second, to apply the same procedure to the dichroic spectra of Pararosaniline (PR) and Ethyl Violet (EV), which belong to the same point symmetry as CV (*i.e.*, D_{3h}[7,9] or C_{3v}[2,10]); and finally, to compare their reduced spectra. The three dyes are all derivatives of triphenylmethane differing only in the amino substitution and, therefore, are expected to have closely related spectral properties. The evaluation of the reduced spectra of those disk-like triphenylmethane dyes must differ from the previous case for the acridine dyes of C_{2v} point symmetry,[4] because PR, CV, and EV all lack the longest dimension in the molecular shape but possess several symmetrically distributed axes of equivalence. A new formalism of the linear dichroism of these disk-like molecules is necessary for the interpretation of the dichroic results.

The resultant reduced spectra of each dye show both the in-plane and out-of-plane polarized absorption components in the visible and UV regions. The presence of the out-of-plane component in the visible region indicates that the effective symmetry of PR, CV, and EV is not D_{3h} but rather C_{3v} or D_3 in the poly(vinyl alcohol) (PVA) film.

Experimental

Materials. Dyes used were all in the monocationic form, the anion being chloride. CV was purified as described before,[11] and PR and EV were purified by the method of preparative thin-layer chromatography. The powdered PVA sample with a nominal degree of polymerization of 1750 was obtained from Tokyo Kasei Co., Ltd. The concentration of each dye was *ca.* 20 μM (1 μM = 1×10^{-6} mol dm^{-3}) in the 9.1 w/w % aqueous PVA solution prior to casting. Both sample and reference films were prepared as described before.[4]

Apparatus. The linear dichroic absorption spectra ($A_{\parallel}$- and $A_{\perp}$-spectra) of PR, CV, and EV were measured on a Hitachi EPS-3T double beam recording spectrophotometer equipped with a mechanical stretcher designed and constructed in this laboratory.[12] The sample and reference films were stretched simultaneously in the cell compartment of the instrument at about 80 °C. The stretch ratio (S) was defined as described elsewhere.[4,6]

Evaluation of Reduced Spectra. All PR, CV, and EV belong to a D_{3h} or C_{3v} point symmetry and possess no uniquely defined axis of orientation (the longest axis). However, they have several axes equally distributed in the molecular plane, according to the definitions of the axes for the disk-like molecule given in Ref. 8 (see Fig. 3). The experimental fact is that each dye in the stretched PVA film can be oriented; the

orientation should be ascribed to the redistribution of the "circular"plane from its random distribution before stretching. Therefore, the orienting property of all those dyes may be represented by the behavior of a disk molecule. When the in-plane or the out-of-plane polarized transitions are assumed in the isotropic spectrum of the disk-like molecule, the reduction procedure for the molecule will be employed to evaluate the reduced spectra, namely, the (A_y+A_z)-spectrum for the in-plane polarized absorption component of the isotropic spectrum and the A_x-spectrum for the out-of-plane polarized component.

If the disk-like molecules are oriented unidirectionally in the PVA film, the formulas necessary for the procedure are as follows:[8]

$$A_\perp - \frac{1}{d}A_\parallel = \frac{d-1}{d}A_x \quad (1)$$

$$A_\parallel - d_x A_\perp = \frac{d-1}{d}(A_y+A_z) \quad (2)$$

where d_x and d ($d=d_y=d_z$ for the disk-like molecule) are the *reduction factors*[8] which should be determined by the procedure. The *orientation factors*[8] K_x and K ($K=K_y=K_z$) are given by

$$K_x = \frac{d_x}{2+d_x} \quad \text{and} \quad K = \frac{d}{2+d} \quad (3)$$

Results and Discussion

Isotropic, Dichroic, and R_d-Spectra.[4] Figures 1a—1c show two kinds of isotropic spectra, *i.e.*, $\bar{k}\times A_0(S=1)$ (open circles) and $A=(A_\parallel+2A_\perp)/3$ (solid curve), for PR, CV, and EV in the PVA film at an S value of 3.7. A good agreement between these two isotropic spectra in each case suggests that the dye molecules are oriented unidirectionally in the stretched film. The observed isotropic spectrum of each dye in the film was similar to the spectrum in the corresponding aqueous PVA solution, except that the film spectrum was slightly shifted toward the long-wavelength side. There appear three peaks (designated as **A**, **C**, and **D**), shoulder(s) in the 340—400 nm region, and a shoulder (designated as **B**) in each film spectrum. These apparent wavelength positions are given for PR, CV, and EV in Table 1.

PR: Figure 2a shows the dichroic, $\Delta A/A$, and R_d-spectra of PR in the UV and visible regions. The $A_\parallel$-spectrum is always more intense than the $A_\perp$-spectrum over the entire wavelength. The R_d-spectrum decreases slightly on the long-wavelength side of the visible peak, but changes irregularly in the UV region. The R_d-spectrum becomes highest near the shoulder band at *ca.* 510 nm and the UV peak at 294 nm.

CV: Figure 2b shows the dichroic, $\Delta A/A$, and R_d-spectra of CV in the UV and visible regions. The

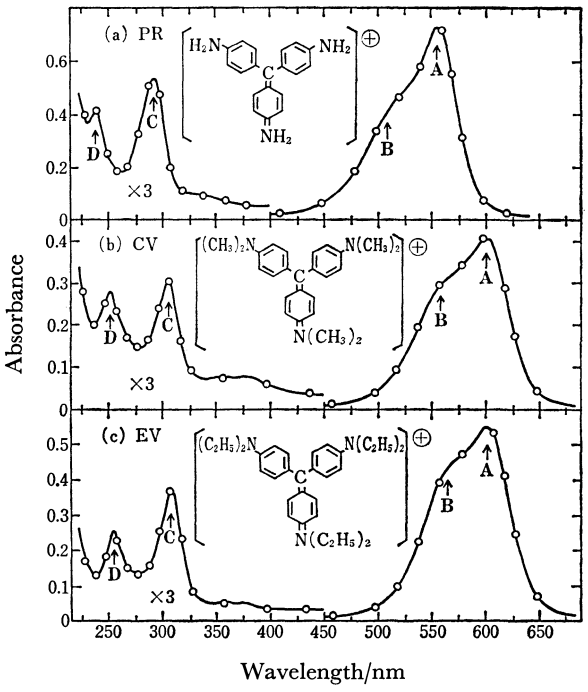

Fig. 1. Isotropic spectra of PR, CV, and EV in the stretched PVA film at $S=3.7$. The solid line (——) is the isotropic spectrum calculated from $A_\parallel$ and $A_\perp$ by the use of the relation, $A=(A_\parallel+2A_\perp)/3$. Circles (-o-o-) are the normalized isotropic absorbance calculated from $\bar{k}\times A_0(S=1)$. For the definition of these quantities, see Ref. 4. The values of $\bar{k}$ were 0.65 for PR and 0.61 for CV and EV. Letters **A** to **D** indicate the apparent peak or shoulder positions in each isotropic spectrum.

$A_\parallel$-spectrum is more intense than the $A_\perp$-spectrum except in the 280 nm region. There are two peaks in the 340—400 nm region, which were obscure in the dichroic spectra of PR. In spite of the simple profile of the isotropic absorption spectrum in the visible and UV regions, the R_d-spectrum is not flat but changes irregularly. The R_d-spectrum gives the highest value near the shoulder band at *ca.* 556 nm and the lowest value near 280 nm. A gradual decrease of the R_d-spectrum is noted near the principal peak in the visible region (570—670 nm). Those apparent dichroic features in the visible region are in excellent agreement with previous reports.[6,7]

EV: Figure 2c shows the dichroic, $\Delta A/A$, and R_d-spectra of EV. The $A_\parallel$-spectrum is always more intense than the $A_\perp$-spectrum in the UV and visible regions. The R_d-spectrum of EV behaves very much

Table 1. The apparent band positions (**A**—**D**) in the isotropic spectra and the transition moment angles (θ_A–θ_C) at the corresponding band positions of PR, CV, and EV

Dyes	Apparent positions[a] (nm)				Angles (deg)		
	A	**B**	**C**	**D**	θ_A	θ_B	θ_C
PR	557(549)	510(500)	294	241	48±1	48±1	49±1
CV	600(594)	560(550)	308(304)	252(251)	48±1	46±1	49±1
EV	603(601)	565(555)	310(308)	256(254)	49±1	47±1	47±1

a) The values in the parentheses are the corresponding positions in the aqueous PVA solution.

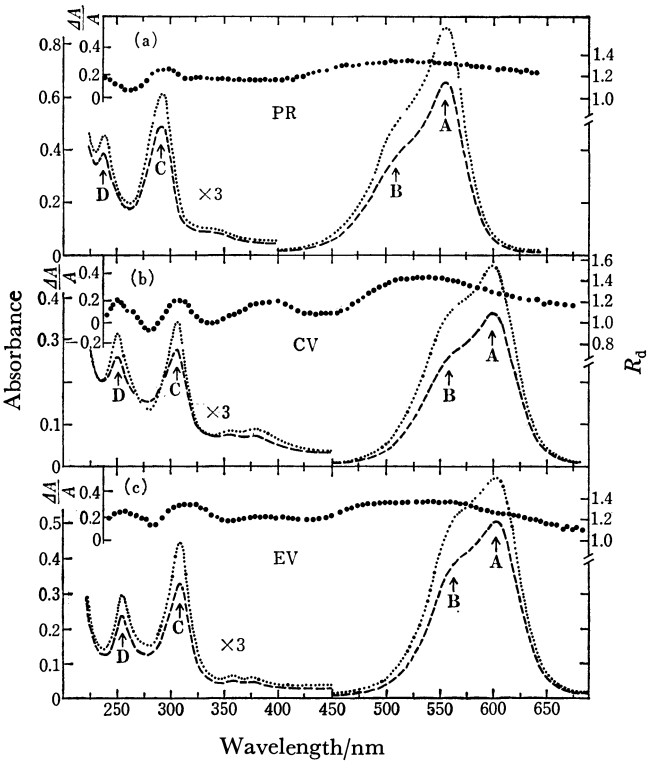

Fig. 2. Dichroic spectra and R_d-spectra of PR, CV, and EV in the stretched PVA film at $S=3.7$. The R_d-value can be converted into the reduced dichroism, $\Delta A/A$, which is referred to the left ordinate of each figure, by the use of Eq. 6 in Ref. 4. Symbols are: the parallel $A_{\parallel}$ (·····) and perpendicular $A_{\perp}$ (------) polarized spectra, and $\Delta A/A$ or R_d-spectrum (••••••). Letters **A** to **D** are the same as in Fig. 1.

like that of CV, although the R_d-values of EV at the UV peaks (**C** and **D**) are larger than those of CV at the corresponding positions.

Determination of Transition Moment Angles. In a previous paper we have dealt with the acridine dyes of C_{2v} point symmetry, each of which has a unique axis of orientation in the molecular plane (*i.e.*, the orientation axis). In that treatment the transition moment angles relative to the orientation axis were determined by the method of Tanizaki.[6] However, in the case of the disk-like molecule, such an orientation axis can not be assigned uniquely in the molecular plane because of its possible distribution in any direction. Nevertheless, if we presume an orientation axis (OA) in the molecular plane of the disk-like molecule, we can estimate the direction of a transition moment μ as the angle θ relative to the OA (Fig. 3a) by the method of Tanizaki. However, since this value of θ results from the averaging over μ around the out-of-plane axis (x-axis), it is only an apparent angle.

In the radially symmetrical molecules such as PR, CV, and EV, all in-plane polarized transitions will show a constant dichroic ratio at a given value of S.[5] Moreover, in the absence of the out-of-plane polarized transitions, the values of θ for the in-plane transitions of the disk-like molecule will become 45°.[5-7] In order to determine the values of θ, the dependence of R_d on S

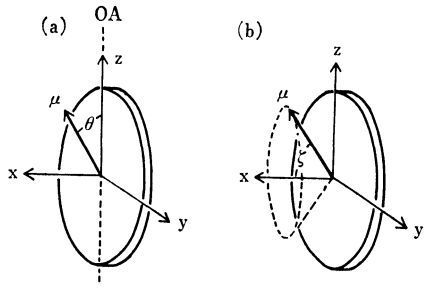

Fig. 3. Schematic illustration of the perfect orientation of a disk-like molecule in the stretched PVA film. The molecule has a transition dipole moment μ taking an arbitrary direction. The molecular coordinates are the y- and z-axes (in-plane) and the x-axis (out-of-plane), where the z-axis is tentatively taken along the stretching direction. (a) The direction of μ is measured by an angle θ relative to an orientation axis (OA) in the molecular plane. (b) The direction of μ is measured by an angle ζ with respect to the out-of-plane x-axis.

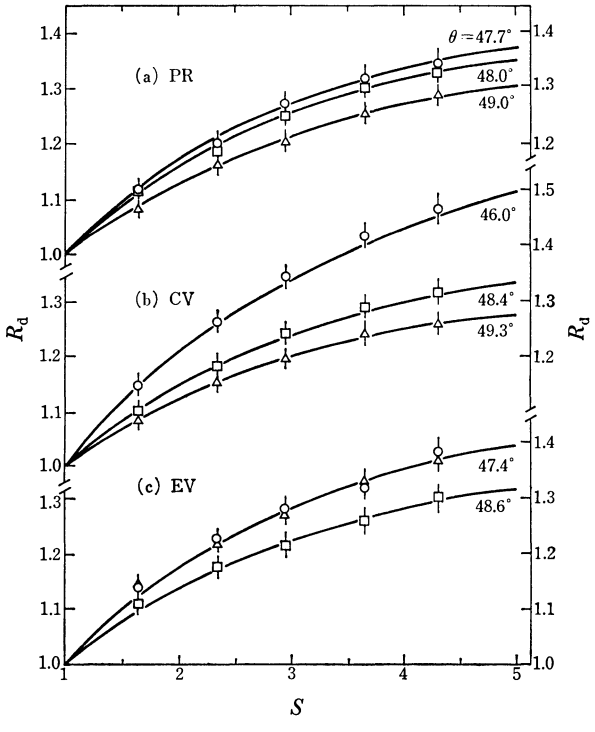

Fig. 4. Dependence of R_d on S for PR, CV, and EV. Symbols (□, ○, and △) denote the R_d-values at the wavelength positions of **A**, **B**, and **C** at five different S-values. Each solid curve is a theoretical one which fits best to those observed points. The value of the angle θ specifying each curve was determined by the method of Tanizaki.

was examined at the positions of **A**, **B**, and **C** for PR, CV, and EV. The results are shown in Fig. 4, where the values of θ were determined by the method of Tanizaki.[4,6] The observed values of R_d appear to fall on the respective theoretical curves indicated by the angle θ within experimental errors. As shown in Fig. 4, Tanizaki's method is applicable for the molecules which give rise to a small dichroic ratio. All values of θ for

PR, CV, and EV are given in Table 1. It should be noted that each θ is determined relative to an arbitrary and unspecified axis in the molecular plane and, hence, that the angle θ is only apparent. It is now clear that the values of θ are not equal to, but always larger than, 45° at the positions of **A**, **B**, and **C**, and that they differ from each other. These results are indeed strong and direct evidence that the apparent bands **A**, **B**, and **C** each contain not only the in-plane but also the out-of-plane transitions. The presence of the out-of-plane polarized transition(s) in those wavelength positions will be shown below.

The in-plane polarized transitions of the disk-like molecule can not be divided uniquely into the so-called y- and z-axis polarized components[4] because of the flatness of the R_d-spectrum. However, the isotropic spectrum should be divided into the in-plane and the out-of-plane polarized absorption components, as carried out by Yogev *et al.*[5] In order to determine these absorption components, it is necessary to differentiate the out-of-plane polarized transition from the in-plane polarized one in the same overlapping wavelength region in the isotropic spectrum. For this purpose, Yogev *et al.* have attempted to determine the direction of the out-of-plane transition moment by two angles of α and β relative to two particular axes in the molecular plane.[5] However, this determination of the direction is not well suited for the disk-like molecule of high symmetry, because the out-of-plane transition moment vector is generally distributed equally and evenly around the x-axis when the molecules are oriented unidirectionally. In order to find the in-plane and out-of-plane polarized transitions more convincingly, a new analysis of the linear dichroism for a disk-like molecule will be presented in the next section.

Analysis of Linear Dichroism for Disk-like Molecules. As a representative disk-like molecule, CV is chosen for illustration of procedures. Since CV does not possess a defined axis of orientation lying in the molecular plane, it will orient itself in the stretched PVA film preferentially with its plane parallel to the stretching direction. The definition of the molecular axes x, y, and z is shown in Fig. 3b, where a transition moment $\boldsymbol{\mu}$ of the molecule is directed along an arbitrary direction. The direction of the moment is measured with the angle ζ relative to the x-axis. According to this scheme, the reduced dichroism and the dichroic ratio ($\Delta A/A$ and R_d) for an assembly of like molecules are represented by Eqs. 4 and 5, respectively, by analogy with the case for the rod-like molecules:[13]

$$\frac{\Delta A}{A} = \frac{3(A_{\parallel}-A_{\perp})}{A_{\parallel}+2A_{\perp}} = \frac{3}{2}(3\cos^2\zeta-1)\varPhi \tag{4}$$

and

$$R_d = \frac{A_{\parallel}}{A_{\perp}} = \frac{2+2(3\cos^2\zeta-1)\varPhi}{2-(3\cos^2\zeta-1)\varPhi} \tag{5}$$

where $\varPhi$ is the orientation function[14] and takes any value between 0 and -0.5 depending on the orientability of a particular kind of dye embedded in the PVA film. The detailed discussion will be given later.[13] A very closely related orientation function has already been derived for the disk-shaped molecule in the study of electric dichroism.[15] The function $\varPhi$ may be connected to the degree of orientation, f ($0 \leqq f \leqq 1$), of the assembly of dye molecules in such a way that $f=-2\varPhi$. The value of f then represents a hypothetical fraction of the disk-like molecules having their planes in the direction of stretch at a given S. It should be noted that, at the limiting stretch ratio ($S\to\infty$), $\varPhi$ takes a value of -0.5 if the orientation is such that the y- or z-axis is parallel to the stretching direction, but it takes a value of 1 if the orientation is such that the x-axis is parallel to the stretching direction. (The latter is the case of a cylindrical molecule for which the x-axis is the longest.) Thus the general behavior of $\varPhi$ for the disk-like molecule differs from that for the rod-like molecule.[13]

On the basis of Eqs. 4 and 5, the analysis of the linear dichroism for the disk-like molecule will be shown below in order to differentiate the out-of-plane polarized transition from the in-plane polarized one. When dichroic absorption spectra are measured for a disk-like molecule, they should show that a transition moment with $\zeta=0°$ will preferentially absorb the light polarized perpendicularly to the direction of stretch. (In this case a negative linear dichroism should be observed.) If all molecules are oriented with their molecular plane perfectly parallel to the stretching direction (*i.e.*, $\varPhi=-0.5$ or $f=1$), the reduced dichroism, $\Delta A/A$, and the dichroic ratio, R_d, for the transition moment with $\zeta=0°$ would have the limiting values of -1.5 and 0 in Eqs. 4 and 5, respectively. If the molecules are partially oriented, the reduced dichroism and the dichroic ratio for the same transition moment would be a function of $\varPhi$ or f only and may be obtained from Eqs. 4 and 5 by substituting $\zeta=0°$:

$$\frac{\Delta A}{A} = 3\varPhi = -\frac{3}{2}f \tag{6}$$

$$R_d = \frac{1+2\varPhi}{1-\varPhi} = \frac{2(1-f)}{2+f} \tag{7}$$

Since $\varPhi$ varies between 0 and -0.5 (f varies between 0 and 1), $-1.5 \leqq \Delta A/A \leqq 0$ and $0 \leqq R_d \leqq 1$. On the other hand, the reduced dichroism and the dichroic ratio due to a transition moment polarized in the molecular plane may be given by substituting $\zeta=90°$ into Eqs. 4 and 5:

$$\frac{\Delta A}{A} = -\frac{3}{2}\varPhi = \frac{3}{4}f \tag{8}$$

$$R_d = \frac{2-2\varPhi}{2+\varPhi} = \frac{4+2f}{4-f} \tag{9}$$

In this special case, $0 \leqq \Delta A/A \leqq 3/4$ and $1 \leqq R_d \leqq 2$. Equations 7 and 9 are now reduced to the same expressions which have been derived by Yogev *et al.* (Eqs. 2 and 9 in Ref. 5). Thus, Eqs. 4 and 5 are more general and appropriate to the analysis of the dichroic spectra containing both the in-plane and out-of-plane polarized transitions.

The dependence of $\Delta A/A$ or R_d on wavelength makes it possible to distinguish between the in-plane and the out-of-plane transitions of the disk-like molecule. If only the in-plane or the out-of-plane polarized transitions are present in the observed wavelength region, the wavelength dependence of $\Delta A/A$ or R_d becomes flat throughout the region concerned at a given value of S. The

absolute values of $\Delta A/A$ or R_d depend only on the degree of orientation, as indicated by Eqs. 6 and 7 for the out-of-plane transition or by Eqs. 8 and 9 for the in-plane transition. If both the in-plane and the out-of-plane transitions are overlapped, the wavelength dependence is not constant any longer in a particular wavelength region, the former being located in the region with the large $\Delta A/A$ or R_d-value and the latter being located in the region with the small $\Delta A/A$ or R_d-value. This is because the values of $\Delta A/A$ and R_d of the out-of-plane transition should be smaller than those of the in-plane transition at a given value of S (for the details, see the next section).

Reduced Spectra of PR, CV, and EV. The following analysis is based on the assumption that the dyes PR, CV, and EV in the PVA film can be treated as disk-like molecules oriented with their molecular planes parallel to the stretching direction (see Fig. 3b). Since the structure of those dyes belong to a D_{3h} or C_{3v} point symmetry, the assumption is probably quite appropriate. Their absorption spectra then consist of the transitions which are allowed in the plane (yz-plane) perpendicular to the three-fold symmetry axis and possibly along the three-fold symmetry axis (x-axis), *i.e.*, the out-of-plane polarized transitions. The in-plane polarized transitions may lie along either the y- or z-axis. From the changes in each $\Delta A/A$ or R_d-curve of PR, CV, and EV (Figs. 2a—2c), the absorption band near the **B** position appears to be mainly composed of the in-plane transition because of the largest $\Delta A/A$ or R_d-value, whereas the absorption band near the **A** position appears to be composed of the intense in-plane and weak out-of-plane transitions because of the smaller $\Delta A/A$ or R_d-value.

On the basis of the apparent spectral features, the reduction procedure was applied to the dichroic absorption spectra of PR, CV, and EV measured at $S=3.7$. The reduction factors d_x and d in Eqs. 1 and 2 were sought out by means of the trial-and-error reduction search.[8] The best values are given in Table 2, together with the values of the orientation factors K_x and K calculated from Eq. 3. The resultant reduced spectra of those dyes are shown in Figs. 5a—5c. As expected from the R_d data in Figs. 2a—2c, an out-of-plane polarized transition is clearly unmasked in the visible band at *ca.* 577 nm for PR, 608 nm for CV, and 613 nm for EV in each A_x-spectrum (solid curve). The in-plane polarized transitions, probably y- and z-axis polarized, are dominant in the visible region, as indicated by the (A_y+A_z)-spectrum (dotted curve).

The isotropic spectrum of each dye in the visible region may contain three different electronic transitions: two lie in the molecular plane (the A_y- or A_z-component near the **B** position and the A_z- or A_y-component near the **A** position) and one lies out of the molecular plane (the A_x-component near the **A** position). The present analysis for CV is in good agreement with the qualitative interpretation proposed by Tanizaki[6] and Nordén.[2,7] Hidden in the isotropic spectrum in the visible region, the out-of-plane polarized transition is responsible for the decrease in the R_d-values near the principal band at **A** position (Figs. 2a—2c). The weak isotropic band in the 340—420 nm region mostly consists of the in-plane transitions, while the bands in the 220—340 nm region contain both the out-of-plane and intense in-plane transitions (see Fig. 5). Thus, the isotropic spectra of the highly symmetric triphenylmethane dyes such as PR, CV, and EV could now be resolved into their in-plane and out-of-plane components by the reduction procedure. The presence of the out-of-plane component may give a key for elucidating the configuration of triphenylmethane dyes[16] and, consequently, the metachromatic changes caused by interaction with various polyelectrolytes and biopolymers.[11,17,18]

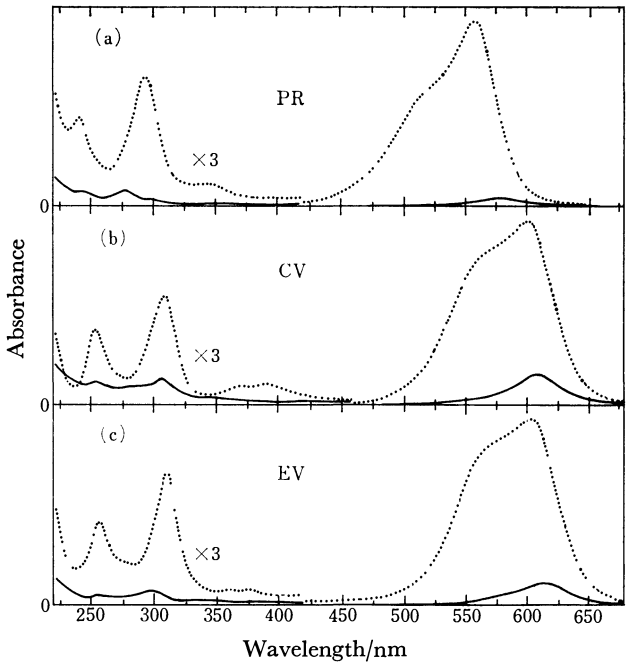

Fig. 5. The reduced (A_y+A_z)- and A_x-spectra of PR, CV, and EV. The in-plane (yz-plane) and the out-of-plane (x-axis) polarized absorbances (arbitrary units) are shown by the dotted and the solid curves, respectively.

Table 2. The average values of the reduction factors (d_x and d) and the orientation factors (K_x and K) of PR, CV, and EV at $S=3.7$

Dyes	d_x	$d=d_y=d_z$	K_x	$K=K_y=K_z$
PR	0.48	1.35	0.194	0.403
CV	0.30	1.54	0.130	0.435
EV	0.38	1.45	0.160	0.420

If triphenylmethane has a triangular and planar configuration with three benzene rings toward the corners (D_{3h} point symmetry), the resolved out-of-plane component may have to be attributed to n-π^* transitions. However, the presence of numbers of n-π^* transitions is unrealistic in the visible and near UV regions. The structure of the triphenylmethane skelton is probably distorted in such a way that the central carbon-phenyl ring bonds either form a pyramidal structure (C_{3v} point symmetry), remain co-planar with three phenyl rings being tilted (D_3 point symmetry), or a pyramidal structure with the tilted rings (C_3 point symmetry). In order to discuss the configuration of

the triphenylmethane dyes more in detail, a complete assignment of each absorption band may be necessary by taking into account both the in-plane and out-of-plane polarized transitions. Nevertheless, the optical properties now available for biologically important triphenylmethane dyes will facilitate the structural studies of the complexes between biopolymers and these dyes.[1,2,18–20]

Conclusions

Since the R_d-values of triphenylmethane dyes PR, CV, and EV were not large as compared with those of acridine dyes,[4] the values of the transition moment angles θ at the absorption band centers of each dye could be evaluated by the method of Tanizaki.[6] However, these values give rise to only the apparent angles for disk-like triphenylmethane dyes. The orientation of those highly symmetric dyes originates from a mechanism which differs from that of acridine dyes. To evaluate the reduced spectra of the disk-like molecule, a new analysis of the linear dichroism was presented (Eqs. 4 and 5). In this analysis the transition moment angle is measured relative to the x-axis, which is perpendicular to the molecular plane. This method differs from the one proposed by Yogev *et al.*[5] The major findings in this work are as follows: (1) In the isotropic spectra of PR, CV, and EV, both the out-of-plane and in-plane polarized electronic transitions are present and overlap each other in the UV and visible regions. In particular, the intense visible band is a composite of one out-of-plane and two in-plane transitions. (2) The behavior of the orientation function Φ for the disk-like molecule can be related to the degree of orientation f by $f=-2\Phi$, which differs from the relation $f=\Phi$ for the rod-like molecule.

The authors wish to thank Mrs. Mayumi Masujima for the purification of PR.

References

1) K. Yamaoka, *Biopolymers*, **11**, 2537 (1972).
2) B. Nordén, F. Tjerneld, and E. Palm, *Biophys. Chem.*, **8**, 1 (1978).
3) K. Yamaoka and H. Hashimoto, *Chem. Lett.*, **1976**, 465.
4) Y. Matsuoka and K. Yamaoka, *Bull. Chem. Soc. Jpn.*, in press.
5) A. Yogev, L. Margulies, B. Strasberger, and Y. Mazur, *J. Phys. Chem.*, **78**, 1400 (1974).
6) Y. Tanizaki, *Bull. Chem. Soc. Jpn.*, **32**, 75 (1959).
7) B. Nordén, *Chem. Scr.*, **1**, 145 (1971).
8) J. Michl and E. W. Thulstrup, *Spectrosc. Lett.*, **10**, 401 (1977); E. W. Thulstrup, J. Michl, and J. H. Eggers, *J. Phys. Chem.*, **74**, 3868 (1970).
9) G. N. Lewis and J. Bigeleisen, *J. Am. Chem. Soc.*, **65**, 2102 (1943).
10) C. W. Looney and W. T. Simpson, *J. Am. Chem. Soc.*, **76**, 6293 (1954); F. C. Adam and W. T. Simpson, *J. Mol. Spectrosc.*, **3**, 363 (1959).
11) K. Yamaoka, M. Takatsuki, K. Yaguchi, and M. Miura, *Bull. Chem. Soc. Jpn.*, **47**, 611 (1974).
12) K. Yamaoka and Y. Matsuoka, *J. Sci. Hiroshima Univ., Ser. A*, **40**, 105 (1976).
13) A manuscript in preparation. The detail on the generalized treatment of planar, disk-like, and rod-like molecules will be reported.
14) This quantity will be represented by the orientation factors K_i (i=x, y, z) as $\Phi=(3K_x-1)/2=1-3K_y=1-3K_z$.
15) a) C. T. O'Konski, "Molecular Electro-Optics. Part I," Marcel Dekker, Inc. (1976), pp. 247—249; b) M. J. Shah, *J. Phys. Chem.*, **67**, 2215 (1963).
16) a) D. W. A. Sharp and N. Sheppard, *J. Chem. Soc.*, **1957**, 674; b) R. Itoh, *J. Phys. Soc. Jpn.*, **12**, 644 (1957).
17) M. Schubert and A. Levine, *J. Am. Chem. Soc.*, **77**, 4197 (1955).
18) K. Yamaoka and M. Takatsuki, *Bull. Chem. Soc. Jpn.*, **51**, 3182 (1978).
19) R. W. Armstrong and N. M. Panzer, *J. Am. Chem. Soc.*, **94**, 7650 (1972).
20) W. Müller and F. Gantier, *Eur. J. Biochem.*, **54**, 385 (1975).

Thermodynamic Study of the Self-association of 6-Methylpurine in Water–1,4-Dioxane Solvent

Satoshi MORIMOTO

Research Institute for Polymers and Textiles, 1-1-4 Yatabe-Higashi, Tsukuba, Ibaraki 300-21

(Received May 29, 1978)

Determination of the thermodynamic quantities of the self-association of 6-methylpurine in water(1)–1,4-dioxane(2) ($x_2=0$—0.36) mixed solvent has been made from heat of dilution measurements in various organic contents, at 25 °C. It was confirmed experimentally that the dissociation process of associating purine bases in solution is very fast by dilution. It was characteristic of this solvent system that the standard enthalpy and entropy changes, $\Delta H°$ and $\Delta S°$, of the association exhibited an abrupt behavior. These values decrease remarkably with 1,4-dioxane content up to a water-rich solvent composition below $x_2=0.012$. After that, they approach their relatively high values for the pure organic component, at first with a steep slope, later more gradually. This behavior is related to the structural changes of the solvent in an extremely sensitive way. In the case of water(1)–methanol(2) ($x_2<0.19$) mixed solvent system which has been investigated for comparison with the above system, minimum values of the same kind were found in the vicinity of $x_2=0.12$, at 25 °C.

There have been a number of studies of the self-association of purine bases in aqueous solution. So far, however, there appears to be little work[1–4] with emphasis on the solvent effects in various aqueous media. To obtain the relationships between the thermodynamic quantities of the association and the solvent characters or effects, the quantities of 6-methylpurine in water–1,4-dioxane solvent system were evaluated from directly measured integral heats of dilution and were investigated in relation to solvent composition. As the result, a characteristic behavior was found as a function of dioxane content in this system and is discussed in terms of the solvent characters.

Experimental

Materials. 6-Methylpurine from Sigma Chemical Co. (product No. M6502) was vacuum dried over P_2O_5 for about 48 h before use. The infrared spectrum of this sample agreed with the reported one.[5] The other purine derivatives, purine (No. P6880) and purine-riboside (No. P7005), were from the same source and they were subjected to the same drying and identification. Solvent water was obtained by distilling ion-exchange water from an alkaline potassium permanganate solution. 1,4-Dioxane and methanol were spectro-grade reagents of Wako Junyaku Co. Trace amounts of water remaining in them were removed by fractional distillation before use.

Heat of Dilution. The heat of dilution was measured at 25 °C by using a 8721-l solution calorimeter of the precision calorimetry system (LKB produkter AB). At the temperature, the enthalpy of solution of tris(hydroxymethyl)-aminomethane (NBS, 724a sample) in 0.100 M HCl was found to be -29.7704 ± 0.0264 kJ/mol; this agrees well with the reported values.[6] By this calibration, it was confirmed that this calorimeter was operating normally. In measuring the heat of dilution of each purine derivative solution, about 1 cm³ of sample solution was diluted in about 100 cm³ solvent with stirring at 500 r.p.m. Integral heats of dilution ΔH_∞ to zero concentration were obtained by normalizing the heats of dilution $\Delta h/n_i$ to finite dilution, where Δh is the actually observed heat and n_i is the number of moles in the initial solution. Assuming that the value $\Delta h/n_i$ at low concentrations would decrease linearly, it is regarded that the corrected heat of dilution to zero concentration added to the $\Delta h/n_i$ value is equal to the ΔH_∞ value. The calorimetric result in a typical system is shown in Table 1. Here, in the highest dilution process No. 7, the heat of dilution from $m_f=0.000367$ to zero concentration was obtained by extrapolating the two $\Delta h/n_i$ values at $m_i=0.03977$ and 0.000367 to zero concentration; all the ΔH_∞ values in this series were calculated on the basis of this corrected value, where m is molarity (mol/kg solvent) and suffixes i and f are for the initial and final situations. The heats of solution were measured at 25 °C by means of the same calorimeter and the values at infinite dilution were determined according to the same procedure.

Results

It should be noted, at first, that the dissociation process of associating purine bases in solution is very fast by dilution. It is therefore suitable to measure the dissociation enthalpy by using this calorimeter with a

TABLE 1. AN EXAMPLE OF VALUES OF THE HEAT OF DILUTION OF 6-METHYLPURINE IN WATER–1,4-DIOXANE (6.166 mol kg^{-1}) MIXED SOLVENT AT 25 °C

No.	Weight of solution / g	$m_i \cdot 10$ / mol kg^{-1}	$m_f \cdot 10^3$ / mol kg^{-1}	Δh / J	$\Delta h/n_i$ / kJ mol^{-1}	ΔH_∞ / kJ mol^{-1}
1	0.93085	6.6769	5.704	3.0449	5.2661	5.3115
2	0.48915	5.4221	2.408	1.1786	4.6012	4.6217
3	0.97957	4.2733	3.820	1.6293	4.0120	4.0482
4	0.95154	3.1753	2.794	0.9994_2	3.3073	3.3367
5	0.93990	1.6280	1.444	0.3581_9	2.1184	2.1374
6	0.84212	0.7081	0.570	0.1142_1	1.2398	1.2499
7	0.96375	0.3977	0.367	0.0704_1	0.7723	0.7795

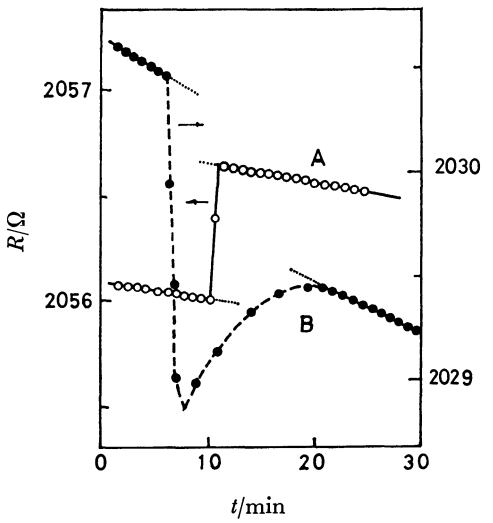

Fig. 1. Examples of thermistor resistance-time curves of dilution process, $55\Omega/K$ ($=\Delta R/\Delta T$) at 25 °C.
A: 6-Methylpurine in water–1,4-dioxane, B: 2-Pyridinol in 1,4-dioxane.

constant environment temperature. An example of the measured thermistor resistance of the dilution process for the 1,4-dioxane aqueous solution of 6-methylpurine against time is shown in Fig. 1 as curve A; the fast dissociation rate can be recognized from this curve.

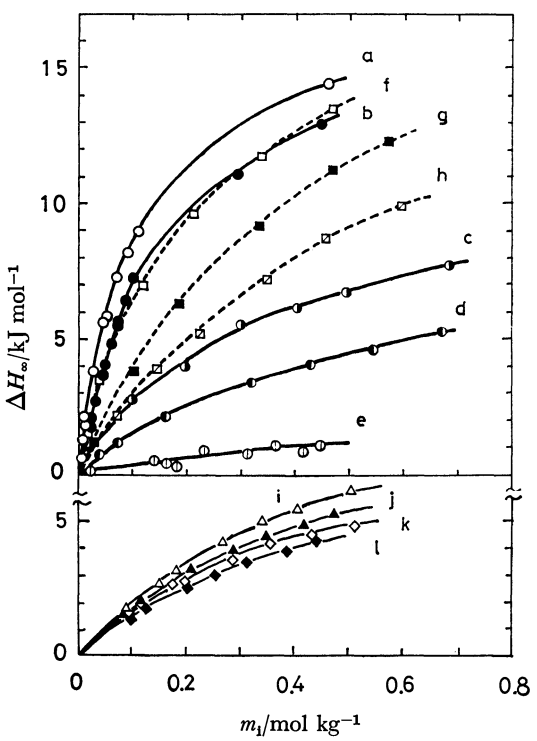

Fig. 2. Concentration dependence of the integral heats of dilution, at 25 °C.
Molarity of organic component (mol/kg water) in aqueous solvent: for 6-methylpurine solute systems; 1,4-dioxane aqueous, (a) 0, (b) 0.6400, (c) 2.761, (d) 6.166, (e) 19.58; methanol aqueous, (f) 1.423, (g) 5.359, (h) 10.67; for purine solute systems; 1,4-dioxane aqueous, (i) 0, (j) 0.6400; for purine–riboside solute systems; 1,4-dioxane aqueous, (k) 0, (l) 0.6400.

In the same figure, another example is shown: this is the dilution curve (B) of 2-pyridinol in 1,4-dioxane solvent, which can be ascribed to the association forming of the hydrogen-bonded dimers.[7] This may be compared with the above 6-methylpurine solution system. Curve B appears to reflect two thermal effects, which consist of exothermic dilution and endothermic dissociation enthalpies, and to have a time lag. The dissociation process of associating purine bases in organic aqueous solution by dilution was shown to be monotonous and very fast in this study.

In Fig. 2, the ΔH_∞ data in this work are all plotted against initial solute molarity m_i of solution. All the values are endothermic and gradually decrease with the ratio of organic component in mixed solvent, and all the curves intersect at the point zero. Curves k and l of solute purine-riboside have lower ΔH_∞ values, as compared with curves i and j of solute purine. This is probably an effect of steric hindrance from the association due to the large ribosil groups, as has been suggested by Marenchic and Sturtevant.[3]

Ts'o and Chan[8] have shown that 6-methylpurine is uncharged and that the equilibrium between various associated species in water can be characterized by a single equilibrium constant. Furthermore, the association of this monomeric solute has been supposed to proceed to an indefinite degree.[8,9] For an ideal self-association process, the ΔH_∞ values per mol of solute monomer would follow Eq. 1, as Stoesser and Gill have shown.[9] The data in Fig. 2 were all fitted

$$\Delta H_\infty = -\Delta H^\circ + (-\Delta H^\circ/K)^{1/2}(\Delta H_\infty/m_1)^{1/2} \qquad (1)$$

in Fig. 3 according to this equation, where K is the equilibrium constant, and ΔH° the standard enthalpy change of association. As shown by the straight lines

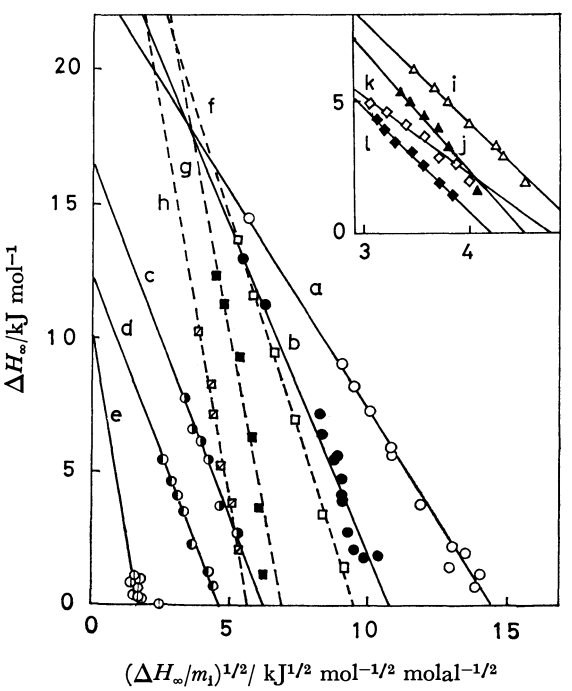

Fig. 3. Integral heat of dilution ΔH_∞ plotted against $(\Delta H_\infty/m_1)^{1/2}$, according to Eq. 1. All symbols are referred to Fig. 1.

Table 2. Evaluated thermodynamic quantities of the self-association of 6-methylpurine in water–1,4-dioxane and –methanol solvents, at 25 °C

Organic component in solvent		K	$-\Delta G^\circ$	$-\Delta H^\circ$	$-\Delta S^\circ$
mol kg^{-1}	x_2[a]	mol^{-1}	kJ mol^{-1}	kJ mol^{-1}	J deg^{-1} mol^{-1}
0	0	8.55±0.81	5.31±0.21	23.6±0.6	61.1±1.3
0	0	(8.6 ±1.1)	(5.36±0.42)	(23.4±0.8)	(60.7±2.9)[9]
0	0	(7.75±1.6)	(5.06±0.29)	(23.3±0.2)	(61.1±0.4)[3]
[1,4-Dioxane]					
0.6400	0.0115	4.42±1.00	3.68±0.50	26.1±1.7	75.3±2.9
2.761	0.0497	2.27±0.27	1.72±0.04	16.8±1.1	50.6±3.8
6.166	0.1111	1.74±0.14	1.38±0.20	12.3±0.6	36.8±1.7
19.58	0.3527	0.42±0.24	2.30±1.26	10.4±2.9	27.2±13.8
[Methanol]					
1.423	0.0256	3.12±0.12	2.76±0.04	30.3±0.3	92.5±1.3
5.359	0.0965	1.09±0.15	0.21±0.33	41.5±1.7	139 ±7
10.67	0.1922	1.05±0.13	0.08±0.42	40.8±1.4	136 ±6

a) Mole fraction of organic component.

Table 3. Evaluated thermodynamic quantities of the self-association of purine derivatives in water–1,4-dioxane solvents, at 25 °C

Organic component in solvent		K	$-\Delta G^\circ$	$-\Delta H^\circ$	$-\Delta S^\circ$
mol kg^{-1}	x_2[a]	mol^{-1}	kJ mol^{-1}	kJ mol^{-1}	J deg^{-1} mol^{-1}
[Purine]					
0	0	1.28±0.11	0.63±0.21	19.5±0.42	47.7±16.7
0.6400	0.0115	1.04±0.13	0.08±0.29	20.4±0.62	65.3± 1.1
[Purine–Riboside]					
0	0	1.60±0.31	1.17±0.42	13.9±0.6	42.7± 0.6
0.6400	0.0115	1.05±0.12	0.13±0.25	16.6±0.5	55.2± 0.8
[6-Dimethylaminopurine][3]					
0	0	61.7±1.0	10.2±0.04	38.1±0.42	94.1± 1.3
0.64	0.012	26.3±0.03	8.08±0.04	39.3±0.42	105 ± 0.8

a) Mole fraction of organic component.

in Fig. 3, the ΔH_∞ values determined for all systems in this study satisfy the equation under the assumption of the ideal process. Values of K and ΔH° were obtained from Eq. 1, and values of standard free energy change ΔG° and of entropy change ΔS° of association which were derived from these are shown in Tables 2 and 3 with the values for a few reported systems. These values in 6-methylpurine–water system in Table 2 agree well with the reported values determined by flow calorimetry[3,9] and the results in purine and purine–riboside–water systems in Table 3 agree approximately with reported values[10–13] determined by other methods, although the concentration ranges were slightly different.

Discussion

All the integral heats of dilution were in good agreement with ideal solution behavior, as is evident from Fig. 3. However, this result contains two problems, at least. One of them is the concentration range. It is better to measure the heat of dilution at very low concentrations[9] where more ideal solution behavior always occurs and dimerization becomes predominant. However, this could not be done here because it was difficult to obtain the heat of dilution at very low concentrations in this mixed solvent system. The other problem is the heat effect, which is the heat of dilution of solute species in each solvent. However ,as shown earlier,[14,15] the heat effect in this study can be taken to be insignificant compared with the experimental ΔH_∞ values. From Eq. 9 in Ref. 16, this effect is sufficiently less than 1% of each ΔH_∞ value even if the enthalpy parameter χ_H, for example, equals 2, which is quite large for a solute-solvent system which does not have particular interactions. This discussion will be done, therefore, on the basis of the thermodynamic quantities in Tables 2 and 3; we wish to focus attention on their solvent composition dependence.

Thermodynamic quantities evaluated in this study are shown in Fig. 4, including the values reported in references, as a function of solvent composition. The higher organic component systems were impossible to measure due to their solubilities. Our result, which covers a more extensive organic composition range in aqueous solvent, therefore helps to clarify the solvent effects of the association. In Fig. 4, thermodynamic values of the association in the same solvent system vary with the kinds of purine derivatives. The absolute values of 6-methylpurine are smaller than those of the other purine derivatives in the figure, *e.g.* 6-dimethylaminopurine, and they

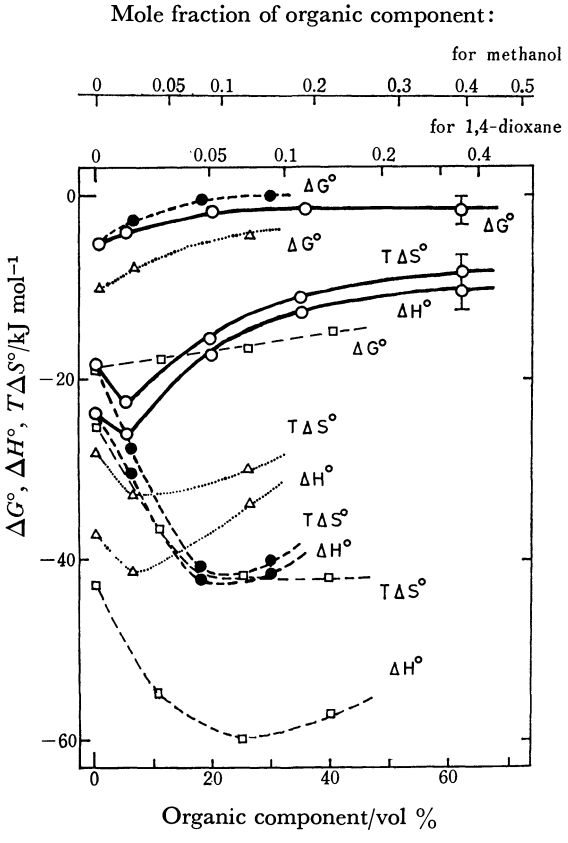

Fig. 4. Evaluated thermodynamic quantities of association plotted against organic component in aqueous solvent: (-○-) 6-methylpurine in 1,4-dioxane–, (-●-) 6-methylpurine in methanol–, (-□-) actinomycin-deoxyguanosine in methanol–[2], and (-△-) 6-dimethylaminopurine in acetonitrile–water[3] systems.

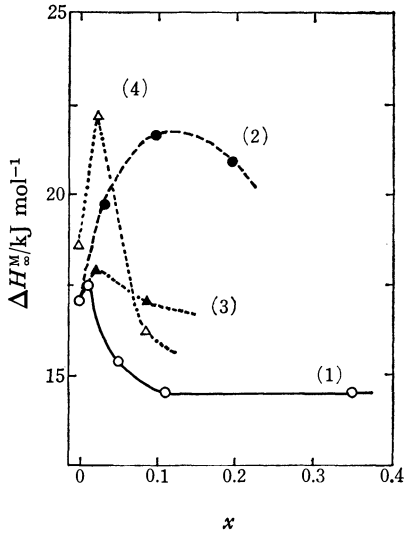

Fig. 5. Heats of solution ΔH_∞^M in purine derivatives–aqueous solvent systems, at 25 °C, plotted against mole fraction x of organic component in aqueous solvent: (1) 6-methylpurine–1,4-dioxane–, (2)–methanol–, (3)–acetonitrile– and (4) 6-dimethylaminopurine–acetonitrile–aqueous solvent systems.

are larger than those of purine in Table 3. These decreased and increased associations, as described by Marenchic and Sturtevant,[3] can be attributed mainly to the decreased and increased polarizabilities of the π-electron system[16] of these purine derivatives. Some part of the increasing and decreasing associations with variety of solvent system is presumed to be attributed to hydrophobic interactions,[17] which supposedly promote the stacking reactions of purine bases in aqueous solutions. Quantitative details of these phenomena must be left for a future study, which will compare the theoretical aspects[18–20] and the needed experimental quantities.

Recently, Leifer *et al.*[4] have studied aqueous purine solutions in the absence and presence of NaCl by vapor-pressure osmometry and high-resolution proton-magnetic-resonance spectroscopy. They have found that there is a sharp decrease in purine stacking at temperatures above 42 °C in the presence of NaCl; this salt-induced destacking of purine is consistent with the salt-induced breaking of the structure of solvent bulk water at the higher temperatures. This phenomenon is suggestive of biological systems and it must be emphasized that the solvent structure plays an important role in the association behavior. From our result, such a characteristic behavior is disclosed in the water–1,4-dioxane system. The values of $\Delta H°$ and $\Delta S°$ decrease remarkably with 1,4-dioxane content in the aqueous solvent until a water-rich binary solvent composition is reached. After the decrease, the values increase steeply, then approach gradually to their relatively high values, *i.e.*, low negative values, for pure dioxane. This tendency resembles the tendency of heat effects which occur from the solute-solvent interactions due to adding a third component to aqueous binary solvents,[21–24] although the decreasing and increasing tendencies of this study are of course opposite to the latter.

The heats of solution, *i.e.*, heats of mixing ΔH_∞^M at infinite dilution, of 6-methylpurine and 6-dimethylaminopurine in water or in some water-organic component solvents have thus been measured at the same temperature to determine the solvation effects on the $\Delta H°$ behavior. The results are shown in Fig. 5 as a function of mole fraction x of organic component in aqueous solvent. One can recognize the abrupt behavior similar to that of $\Delta H°$. Values of ΔH_∞^M do not agree, of course, with those of $\Delta H°$ even if their absolute values are compared. Fig. 6 shows a comparison of $\Delta H°$ with $-\Delta H_\infty^M$ in 6-methylpurine–1,4-dioxane aqueous solvent system. The heats of solution ΔH_∞^M would be more subjected to effects of solvation than the $\Delta H°$ because of the surface dimensions of the solute molecule. In the case of ΔH_∞^M, the solvation would be done all over the molecular surface including the hydrophilic part of solute, which is outside of the hydrophobic part which participates in the self-association. The difference between $\Delta H°$ and $-\Delta H_\infty^M$, consequently, indicates the contribution to the interaction energy of the hydrophilic part of solute. Some problems, for example, with the cavity term, the entropy term, and the relaxation term of association in the theoretical treatments[18,20] can be eliminated by this comparison between the two values, $\Delta H°$ and ΔH_∞^M. In Fig. 6, the difference between two curves appears to change the contribution from exother-

mic in water or water-rich binary solvent to endothermic in the higher organic contents. Therefore, the dependence of ΔH° on solvent composition is more remarkable than that of ΔH^M_∞. For the dissociation process of a third component, the maxima of enthalpy and entropy changes in water-rich binary solvents occur in the position of maximum structuredness of the solvent and, at this position, the interactions with solvent or the solvations of solvent molecules are minimized as a result of the solvent structure. The data of heat of mixing show that addition of 1,4-dioxane[25] or methanol[26] to pure water causes at first an increase in the solvent structuredness. The ΔH° and $T\Delta S^\circ$ curves in 1,4-dioxane, or methanol aqueous solution systems in Fig. 4, may be closely related to such variation of solvent structures.

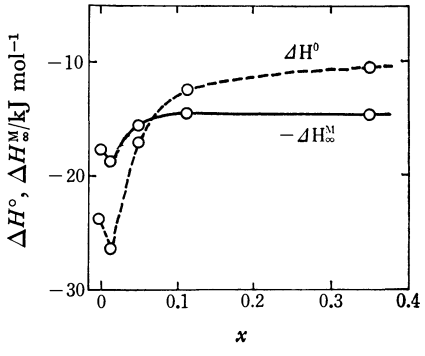

Fig. 6. Comparison of ΔH° with $-\Delta H^M_\infty$ in 6-methylpurine–1,4-dioxane aqueous solvent system, at 25 °C.

The heats of vaporization of purine derivatives have been reported to be about 80—130 kJ/mol.[27] That of 6-methylpurine has not yet been made clear, but the association heat of 6-methylpurine in gas phase will probably exhibit a similarly large negative value. From the trends shown in Figs. 5 and 6, it is assumed in this 6-methylpurine aqueous solution that the contributions of solvation or de-solvation due to hydrophobic interactions are strongly connected with the ΔH° values. The ΔH° behavior with organic component seems to be more influenced by the behavior of the other contributions, which reflect the variation of solvent structure. It could be considered that the characteristic behavior of ΔH° and ΔS° with the organic content generally come from the nature or the structure of the bulk solvent itself. The effects of solvent atmosphere, and especially the effects of the variation of solvent structures on the association, would considerably affect both ΔH° and ΔS° behaviors.

From Tables 2 and 3, a characteristic feature is recognized for purine and three purine derivatives: 6-methylpurine, 6-dimethylaminopurine, and purine-riboside, in water and 0.64 mol kg^{-1} 1,4-dioxane–water systems. Although the hydrophobic strength of the purine rings is considered to be different for each purine derivative, the thermodynamic values of association ΔH° and ΔS° in both solvent systems were almost identical, irrespective of the sort of purine derivatives. In all four systems, the entropy changes in aqueous solution of 0.64 mol kg^{-1} of 1,4-dioxane showed a decrease of about 12 to 17 J/deg mol, and the enthalpy changes showed a decrease of about 2.5 kJ/mol, in comparison with the ones of the system in pure water. These significant differences may be ascribed to the solvation changes of purine rings, and to the variation of bulk solvent structures around the dissolved purine derivative solutes. As a result, a characteristic abrupt change in thermodynamic quantities was found to be expressible as a function of 1,4-dioxane content in this solution system.

The author wishes to thank Mr. Yoshio Tani of Professor Masao Nakamura's Laboratory of Tokai University for his experimental help.

References

1) S. I. Chan, M. P. Schweizer, P. O. P. Ts'o, and G. K. Helmkamp, *J. Am. Chem. Soc.*, **86**, 4182 (1964).
2) D. M. Crothers and D. I. Ratner, *Biochemistry*, **7**, 1823 (1968).
3) M. G. Marenchic and J. M. Sturtevant, *J. Phys. Chem.*, **77**, 544 (1973).
4) G. P. Kreishman, D. A. Foss, K. Inoue, and L. Leifer, *Biochemistry*, **15**, 5431 (1976).
5) C. J. Pouchert, "The Aldrich Library of Infrared Spectra," 2nd ed, Aldrich Chemical Co., Milwaukee (1975), p. 1118.
6) G. Gunn, *J. Phys. Chem.*, **69**, 2902 (1965); J. O. Hill, G. Oejelund, and I. Wadsoe, *J. Chem. Thermodyn.*, **1**, 111 (1969); A. P. Brunetti, E. D. Prosen, R. N. Goldberg, and M. V. Kilday, *J. Res. Nat. Bur. Stand.*, **77A**, 581, 599 (1973).
7) M. H. Krackov, C. M. Lee, and H. G. Mautner, *J. Am. Chem. Soc.*, **87**, 892 (1965).
8) P. O. P. Ts'o and S. I. Chan, *J. Am. Chem. Soc.*, **86**, 4176 (1964).
9) P. R. Stoesser and S. I. Gill, *J. Phys. Chem.*, **71**, 564 (1967).
10) P. O. P. Ts'o, I. S. Melvin, and Ac.Olson, *J. Am. Chem. Soc.*, **85**, 1289 (1963).
11) S. J. Gill, M. Downing, and G. F. Sheats, *Biochemistry*, **6**, 272, (1967).
12) A. D. Broom, M. P. Schweizer, and P. O. P. Ts'o, *J. Am. Chem. Soc.*, **89**, 3612 (1967).
13) E. L. Farquhar, M. Downing, and S. J. Gill, *Biochemistry*, **7**, 1224 (1968).
14) A. Kagemoto, S. Murakami, and R. Fujishiro, *Bull. Chem. Soc. Jpn.*, **39**, 15 (1966).
15) S. Morimoto, *Bull. Chem. Soc. Jpn.*, **44**, 879 (1971).
16) H. DeVoe and I. Tinoco, Jr., *J. Mol. Biol.*, **4**, 500 (1962).
17) W. Kauzmann, *Adv. Protein Chem.*, **14**, 1 (1959).
18) A. Ben-Naim, "Water and Aqueous Solutions," Plenum Press, N. Y. (1974), Chap. 8.
19) A. Ben-Naim, *Biopolymers*, **14**, 1337 (1975).
20) O. Sinanoglu, "Molecular Association in Biology," ed by B. Pullman, Academic Press, N. Y. (1968), pp. 427—445.
21) E. M. Arnett, P. McC. Duggleby, and J. J. Barke, *J. Am. Chem. Soc.*, **85**, 1350 (1963).
22) E. M. Arnett, W. G. Bentrude, J. J. Barke, and P. McC. Duggleby, *J. Am. Chem. Soc.*, **87**, 1541 (1965).
23) A. Ben-Naim, *J. Phys. Chem.*, **71**, 4002 (1967).
24) A. Ben-Naim and M. Yaacobi, *J. Phys. Chem.*, **79**, 1263 (1975).
25) Z. Vierk, *Anorg. Chem.*, **261**, 283 (1950).
26) G. L. Bertrand, F. J. Millero, C. Wu, and L. G. Hepler, *J. Phys. Chem.*, **70**, 699 (1966).
27) L. B. Clark, G. G. Peschel, and I. Tinoco, Jr., *J. Phys. Chem.*, **69**, 3615 (1965).

On the Critical Phenomena in the Decomposition of Hydroperoxides and in the Autoxidation of Cumene with Bis(acetylacetonato)manganese(II)

Shun-ichi FUKUZUMI and Yoshio ONO*

Department of Chemical Engineering, Tokyo Institute of Technology, Ookayama, Meguro-ku, Tokyo 152

(Received November 22, 1978)

The decomposition of 1-methyl-1-phenylethyl hydroperoxide and *t*-butyl hydroperoxide with $Mn(II)(acac)_2$ and the autoxidation of cumene with $Mn(II)(acac)_2$, $Mn(III)(acac)_3$, and $MnCO_3$ have been studied at 323 K. In the decomposition of the hydroperoxides with $Mn(II)(acac)_2$, the peroxyl radicals are observed only when the initial ratio of hydroperoxide to catalyst amount exceeds a certain value. The critical phenomenon is observed in the oxidation of cumene with $Mn(II)(acac)_2$ and also with $MnCO_3$. A scheme for the cause of the critical phenomena has been proposed.

It has been reported that, in the liquid phase oxidation of hydrocarbons with metal oxides, there is a critical amount of catalyst above which the reaction does not proceed.[1–10] A similar critical phnomenon was observed in the autoxidation with homogeneous catalysts.[11,12] Decrease of the oxidation rate at a high catalyst amount indicates that the solid acts as an inhibitor rather than as a catalyst. However, causes for the same substance having dual functions, *i.e.* it accelerates the oxidation rate at lower catalyst amount and inhibits the reaction at higher catalyst amount, and for the change from catalysis to inhibition occurring abruptly, have not been clarified.

As regards catalysis, it is accepted that the decomposition of the hydroperoxide on solid surface produces free radicals, which in turn, propagate the chain reactions in liquid phase.[1–10]

Interaction of hydroperoxide with surfaces also seems to cause the critical phenomena. Thus, a critical catalyst amount has been reported to depend on the initial concentration of the hydroperoxide.[1,3,7] Mukherjee and Graydon[1] found that there is a critical hydroperoxide to catalyst ratio, below which no reaction takes place in the oxidation of tetraline with Mn_2O_3. They assumed that there are two distinct sites on the catalyst, one preferentially adsorbing the hydroperoxide and the other taking part in the production of free radicals. When the amount of hydroperoxide is small, no reaction takes place, since all of it is consumed to saturate the inactive sites which do not contribute to radical formation.

The inhibiting action of the surface might depend also on the oxidation state of the metal cations. Manganese-catalyzed autoxidation was observed to start when Mn(II) was converted into Mn(III).[13] Inhibition of autoxidations by transition metals in low oxidation states such as Co(II) or Mn(II) was reported.[11,14–16] In cyclohexene oxidation with manganous heptanoate, Chalk and Smith[17] observed long induction periods, which do not terminate until sufficient hydroperoxide is formed to convert nearly all the manganous manganese into manganic state. The reaction of metal cations with peroxyl radicals has been postulated as one of the termination reactions also in the autoxidation with metal oxides.[7,10]

In the present work, we have found a critical phenomenon in the decomposition of hydroperoxides with bis(acetylacetonato)manganese(II), $Mn(II)(acac)_2$, and also in the oxidation of cumene with $Mn(II)(acac)_2$. No such phenomenon is observed in the oxidation with tris(acetylacetonato)manganese(III), $Mn(III)(acac)_3$, indicating the importance of the oxidation state of the cations for critical phenomena. The critical phenomenon in the oxidation and that in the hydroperoxide decomposition are closely related. A scheme for the cause of the critical phenomena is proposed. The critical phenomenon in the oxidation of cumene with $MnCO_3$ is also mentioned.

Experimental

Materials. Commercial cumene (reagent grade) was distilled and percolated through an activated alumina column three times prior to use in order to remove any trace of hydroperoxide. *t*-Butyl hydroperoxide and 1-methyl-1-phenylethylhydroperoxide(Nakarai Chem. Ltd.), were purified by vacuum distillation. Commercial $Mn(II)(acac)_2$, $Mn(III)(acac)_3$, and $MnCO_3$ were used.

Apparatus and Procedure. The apparatus has been described in detail.[18–20] Carbon tetrachloride was used as a solvent, since it is an inert solvent in autoxidation or hydroperoxide decomposition.[16–19] For example, the decay rate of 1-methyl-1-phenylethylperoxyl radical in CCl_4 was the same as that in cumene.[21] Measurements of the peroxyl radical concentration during the course of decomposition of hydroperoxide were performed as follows. The solvent (CCl_4 70 cm^3) and the catalyst ($Mn(II)(acac)_2$) were stirred in a flask and the part of the solution with the colloidal catalyst was circulated with use of a roller pump through the ESR cavity. The reaction was started by the addition of hydroperoxide (20—123 μl). ESR intensity of the peroxyl radicals was monitored with time by use of a JEOL-X-band spectrometer (JEOL-PE-1X) with 100 kHz magnetic modulation. The radical concentration was determined using 1,1-diphenyl-2-picrylhydrazyl in benzene as a reference.

The rates of oxygen absorption during the course of autoxidation of cumene with $Mn(II)(acac)_2$, $Mn(III)(acac)_3$, and $MnCO_3$ were measured with a gas burette or a gasometer. The radical concentration during the course of oxidation was determined in the same manner as above.

Results

Critical Phenomena in the Decomposition of Hydroperoxides by $Mn(II)(acac)_2$. The ESR spectrum of the

1-methyl-1-phenylethyl-peroxyl radical($RO_2\cdot$, $g=2.015\pm0.0002$) or the *t*-butylperoxyl ($BO_2\cdot$, $g=2.0144\pm0.0002$) was observed, when an amount of 1-methyl-1-phenylethyl hydroperoxide (ROOH) or *t*-butyl hydroperoxide (BOOH) exceeding a certain value was added to 70 cm^3 of CCl_4 solution containing 0.2 g of Mn(II)-$(acac)_2$, indicating the decomposition of hydroperoxide. The radical concentration increased markedly with reaction time, reaching a maximum, then decreasing. Typical examples are shown in Fig. 1.

The maximum concentration of the peroxyl radicals, $[RO_2\cdot]_{max}$, are plotted against the initial concentration of the hydroperoxides in Fig. 2. For concentrations of the hydroperoxides lower than 4.0×10^{-3} M, no peroxyl radicals were observed. By a slight increase of hydroperoxide concentration above 4.0×10^{-3} M, the peroxyl radicals were observed, the maximum radical concentration increasing linearly with an increase in initial hydroperoxide concentration. It is evident that critical phenomenon exists in the decomposition of hydroperoxides. The critical concentration of the hydroperoxides is the same (4.0×10^{-3} M) for ROOH and BOOH, the critical ratio of hydroperoxide to Mn(II)$(acac)_2$ amount being 1.4×10^{-3} mol/g-Mn(II)$(acac)_2$.

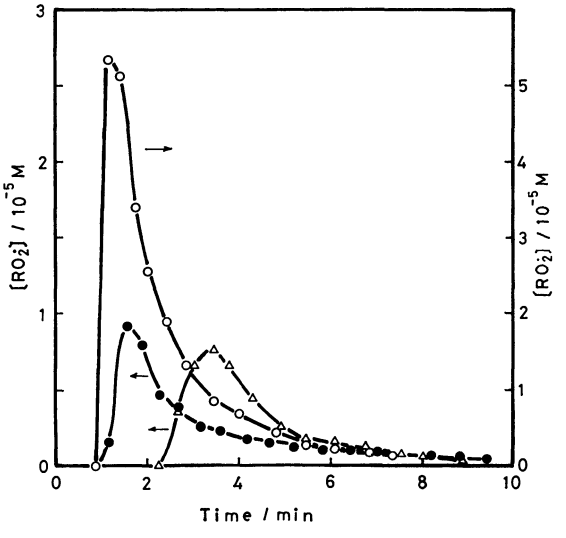

Fig. 1. Concentration of peroxyl radicals during the decomposition of *t*-butyl hydroperoxide and cumene hydroperoxide with Mn(II)(ffcac)$_2$ at 323 K plotted against reaction time; Mn(II)$(acac)_2$ 2.86 g l^{-1}, △ [BOOH] 4.47×10^{-3} M, ● [BOOH] 7.83×10^{-3} M, ○ [ROOH] 8.18×10^{-3} M.

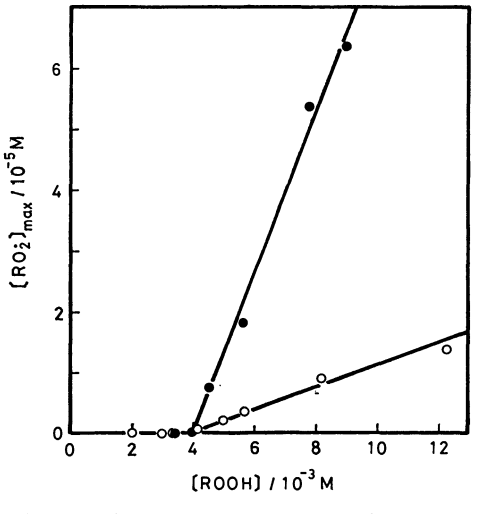

Fig. 2. Maximum concentration of peroxyl radicals during the decomposition of *t*-butyl hydroperoxide and cumene hydroperoxide with Mn(II)$(acac)_2$ at 323 K plotted against initial hydroperoxide concentration; Mn(II)$(acac)_2$ 2.86 g l^{-1}, solvent CCl_4, ● BOOH, ○ ROOH.

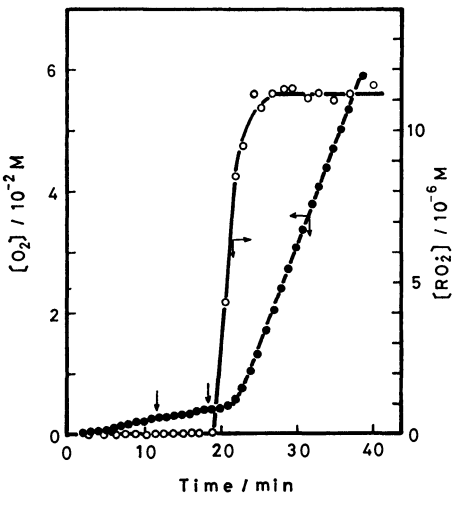

Fig. 3. Cumulative amount of oxygen absorbed and the concentration of cumylperoxyl radical during the autoxidation of cumene with Mn(II)$(acac)_2$ at 323 K plotted against reaction time; Mn(II)$(acac)_2$ 1.54 g l^{-1}, cumene 65 cm^3; Initial ROOH concentration is zero, 10 l of ROOH was added at 12 min (↓) and another 10 l of ROOH was added at 19 min (↓).

Critical Phenomena in the Autoxidation of Cumene with Mn(II)$(acac)_2$. In order to see whether the critical phenomenon is also observed in autoxidation with Mn-

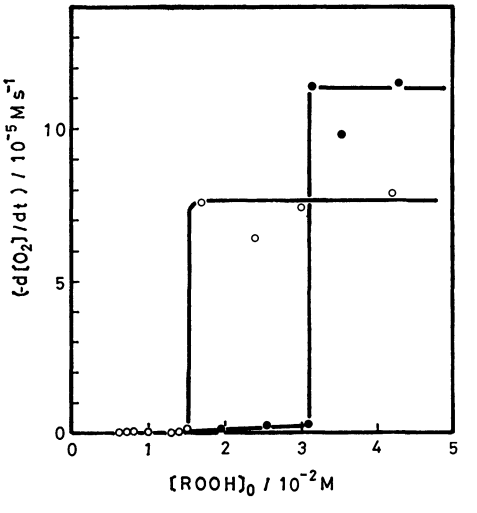

Fig. 4. Rate of oxygen absorption during the autoxidation of cumene with Mn(II)$(acac)_2$ at 323 K plotted against initial hydroperoxide concentration; Mn(II)-$(acac)_2$; ○ 10.34 g l^{-1}, ● 20.7 g l^{-1}.

(II)$(acac)_2$, the autoxidation of cumene with Mn(II)-$(acac)_2$ was studied at 323 K. As shown in Fig. 3, no peroxyl radicals were observed when no hydroperoxide was added, though a slow oxygen uptake was observed. Addition of 10 μl of ROOH caused no change in the situation. However, when another 10 μl of ROOH was added, peroxyl radicals were observed, the radical concentration and rate of oxygen absorption increasing markedly with time to reach a steady concentration and a steady rate, respectively.

Figure 4 shows the steady rate of oxygen absorption as a function of the initial hydroperoxide concentration. The rate of oxygen absorption is almost zero when the initial hydroperoxide concentrations are lower than 1.6×10^{-2} M and 3.1×10^{-2} M for 10.3 and 20.7 g l^{-1} of [Mn(II)$(acac)_2$], respectively. A slight increase in hydroperoxide concentration in excess of these values causes an abrupt increase in the oxidation rate, which does not change significantly by further increase in the hydroperoxide concentration (Fig. 4). The critical ratio of hydroperoxide to catalyst amount is 1.5×10^{-3} mol/g-Mn(II)$(acac)_2$.

It should be noted that the critical hydroperoxide concentration is doubled by doubling the amount of the catalyst, indicating that the parameter determining critical phenomenon is not hydroperoxide concentration but the ratio of the concentration to the catalyst amount, in agreement with the results of Mukherjee and Graydon,[1] and Neuberg *et al.*[3] This was confirmed also by examining the effect of catalyst amount on the rate of oxidation and on the concentration of peroxyl radical at a constant hydroperoxide concentration (1.56×10^{-2} M). The maximum rate of oxygen absorption and the maximum concentration of the peroxyl radical are plotted against the catalyst amount in Fig. 5. The rate of oxygen absorption increases with increases in the catalyst amount, reaching a constant value, and decreasing drastically above 12.1 g l^{-1} of Mn(II)-$(acac)_2$. The critical ratio of hydroperoxide to catalyst amount is 1.3×10^{-3} mol/g-Mn(II)$(acac)_2$, which is very close to that given in Fig. 4.

It should be noted that the critical ratio of hydroperoxide to catalyst ($1.3—1.5\times10^{-3}$ mol/g) in cumene autoxidation with Mn(II)$(acac)_2$ is the same as that in the decomposition of hydroperoxides with the same catalyst (1.4×10^{-3} mol/g).

As shown in Fig. 5, the rate of oxygen absorption and radical concentration behave in exactly the same manner, *viz.*, the rate of oxygen absorption is proportional to the concentration of peroxyl radical. This indicates that oxygen is absorbed mainly by the elementary reactions, $R\cdot+O_2\rightarrow RO_2\cdot$, and $RO_2\cdot+RH\rightarrow ROOH+R\cdot$.

Autoxidation of Cumene with Mn(III)$(acac)_3$. In order to find the effect of the oxidation state of manganese cation, the oxidation of cumene was studied with Mn(III)$(acac)_3$. The concentration of the peroxyl radical and the rate of oxygen absorption were measured simultaneously at 323 K. In the oxidation with Mn-(III)$(acac)_3$, the reaction proceeds even when the initial hydroperoxide concentration is much lower than the critical concentration in the oxidation with Mn(II)-$(acac)_2$. Figure 6 shows typical examples of the change in the rate of oxygen absorption and the peroxyl radical concentration with reaction time. When 4 μl of ROOH was added to 70 cm^3 of CCl_4 solution containing 0.60 g of Mn(III)$(acac)_3$, the peroxyl radical and the absorption of oxygen were observed after standing for 30 min. The hydroperoxide formed after prolonged standing might cause the reaction to proceed. When 150 μl of ROOH was added, the reaction proceeded immediately. In the case of Mn(II)$(acac)_2$, the reaction does not proceed when the initial ratio of hydroperoxide to catalyst amount is less than 1.5×10^{-3} mol/g-Mn(II)-

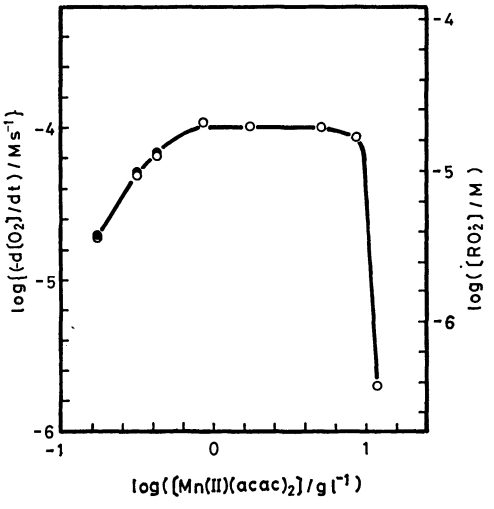

Fig. 5. The rate of oxygen absorption and the concentration of cumylperoxyl radical as a function of the catalyst weight to liquid volume ratio in the autoxidation of cumene with Mn(II)$(acac)_2$ at 323 K; ROOH 1.56×10^{-2} M, ● $[RO_2\cdot]$, ○ $-d[O_2]/dt$.

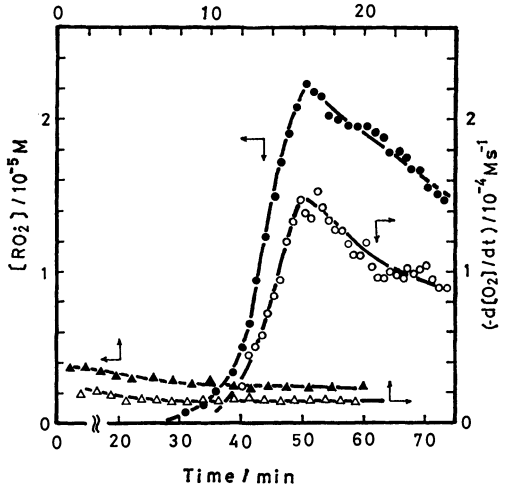

Fig. 6. Change in the rate of oxygen absorption and the concentration of cumylperoxyl radical with time in the autoxidation of cumene with Mn(III)$(acac)_3$ at 323 K. ○ ● Mn(III)$(acac)_3$ 8.57 g l^{-1}, ROOH 4.0×10^{-4} M, RH 7.18 M; △ ▲ Mn(III)$(acac)_3$ 0.17 g l^{-1}, ROOH 1.56×10^{-2} M, RH 7.18 M.

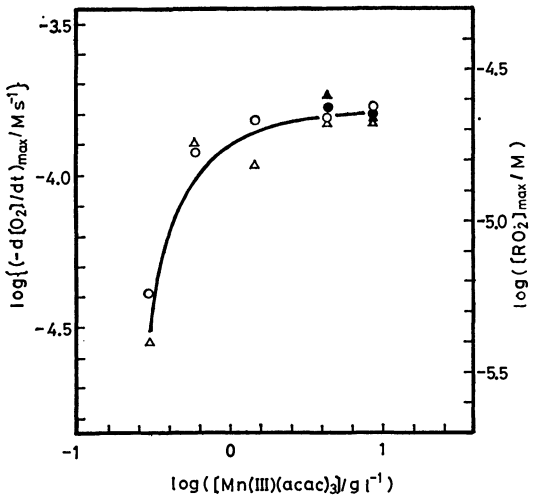

Fig. 7. The naximum rate of oxygen absorption and the maximum concentration of cumylperoxyl radical as a function of the catalyst weight to liquid volume ratio in the autoxidation of cumene with Mn(III)(acac)$_3$; $-d[O_2]/dt$: △ ROOH 4.0×10^{-4} M, ▲ ROOH 1.50×10^{-2} M; $[RO_2]$: ○ ROOH 4.0×10^{-4} M, ● ROOH 1.50×10^{-2} M.

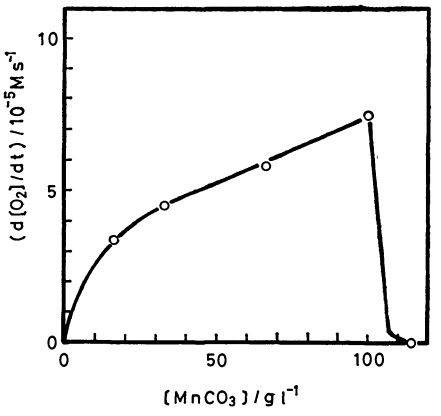

Fig. 8. Rate of oxygen absorption during the autoxidation of cumene by $MnCO_3$ at 323 K plotted against the ratio of catalyst weight to liquid volume; RH 7.18 M, ROOH 2.33×10^{-3} M.

(acac)$_2$; *e.g.*, ROOH 120 μl for Mn(II)(acac)$_2$ 0.60 g

The radical concentration and the rate of oxygen absorption increase with reaction time, reaching a maximum, then decreasing (Fig. 6). This might be due to the deactivation of catalyst. The effects of catalyst amount on the maximum rate of oxygen absorption and the maximum concentration of $RO_2\cdot$ are shown in Fig. 7. The rate of oxygen absorption and the radical concentration increase with increase in catalyst amount and reach a constant value, independent of the initial hydroperoxide concentration. As is the case of Mn(II)-(acac)$_2$, the rate of oxygen absorption and the radical concentration behave in the same manner, showing that the rate of oxygen absorption is proportional to the radical concentration in the case of Mn(III)(acac)$_3$ as well.

ESR Spectra during Autoxidation of Cumene with Mn(II)-(acac)$_2$ and Mn(III)(acac)$_3$. The ESR spectrum during the course of autoxidation of cumene with Mn-(II)(acac)$_2$ was measured. When the concentration of the hydroperoxide is below the critical concentration, the broad signal due to Mn(II) is observed. When a sufficient amount of hydroperoxide is introduced to start the oxidation, the intensity due to Mn(II) decreases with time and becomes constant, a sharp signal due to peroxyl radical being observed. The essentially same ESR spectrum was observed during cumene oxidation with Mn(III)(acac)$_3$, indicating that the state of manganese ion is the same irrespective of the valency of the starting complexes, once oxidation is started.

Critical Phenomenon in the Autoxidation of Cumene by $MnCO_3$. The autoxidation of cumene by $MnCO_3$ was studied for 2.33×10^{-3} M of initial hydroperoxide concentration at 323 K. As shown in Fig. 8, the rate of oxygen absorption increases with an increase in the catalyst amount, the rate declining drastically at high catalyst amount. The critical ratio of hydroperoxide to catalyst amount is 2.1×10^{-5} mol/g-$MnCO_3$, much less than the value in the case of oxidation with Mn(II)-(acac)$_2$.

Discussion

Resutts. The results in this study can be summarized as follows.

1. In the decomposition of ROOH and BOOH with Mn(II)(acac)$_2$ there is a critical ratio of hydroperoxide to catalyst amount (1.4×10^{-3} mol/g-Mn(II)(acac)$_2$) below which no peroxyl radicals are observed during the course of reaction.
2. In the autoxidation of cumene with Mn(II)-(acac)$_2$, there is a critical ratio of hydroperoxide to catalyst amount below which the oxidation does not proceed, the ratio being the same as that found in the hydroperoxide decomposition.
3. In the autoxidation of cumene with Mn(III)-(acac)$_3$, no critical phenomenon is observed.
4. The ESR signals due to manganese ion during the course of autoxidation of cumene with Mn(II)-(acac)$_2$ are the same as those with Mn(III)(acac)$_3$.
5. In the autoxidation of cumene by $MnCO_3$, there is also a critical ratio of hydroperoxide to catalyst amount (2.1×10^{-5} mol/g-$MnCO_3$), the critical value being much smaller than that in the case of Mn(II)(acac)$_2$.

Reaction Mechanism. Agreement of critical ratios in the hydroperoxide decompositions and in cumene oxidation (observations 1 and 2) indicates that the critical phenomenon in the autoxidation is substantially identical to the critical phenomenon in the hydroperoxide decomposition. Inhibition of oxidation below a critical hydroperoxide concentration might be caused by the fact that the hydroperoxide decomposition gives no peroxyl radicals available for chain propagation.

From the results given in 3, we see that the Mn(II) and not Mn(III) species play an essential role in the appearance of the critical phenomena. 4 suggests that there is a redox interconversion between Mn(II) and Mn(III) during the course of reaction. The mechanism for the autoxidation of cumene with Mn(II)(acac)$_2$ and

$Mn(III)(acac)_3$ can be written as follows:

Initiation

$$ROOH + Mn(II) \xrightarrow{fast} RO\cdot + Mn(III) + OH^- \quad (1)$$

$$ROOH + Mn(III) \longrightarrow RO_2\cdot + Mn(II) + H \quad (2)$$

Propagation

$$RO_2\cdot + RH \longrightarrow ROOH + R\cdot \quad (3)$$

$$R\cdot + O_2 \xrightarrow{fast} RO_2\cdot \quad (4)$$

$$RO_2\cdot + RO_2 \longrightarrow 2RO\cdot + O_2 \quad (5)$$

$$RO\cdot + ROOH \xrightarrow{fast} ROH + RO_2\cdot \quad (6)$$

Termination

$$RO_2\cdot + Mn(II) \longrightarrow (RO_2\cdot \cdots Mn(II)) \longrightarrow \text{inactive product} \quad (7)$$

$$RO_2\cdot,\ RO\cdot \longrightarrow \text{decay} \quad (8)$$

The reaction mechanism is the same as that proposed for the cumene oxidation with PbO_2,[16] except for elementary Reactions 1, 2, and 7. The initiation Reactions 1 and 2 are accepted for homogeneous systems.[22,23] Reaction 7 is included to account for the inhibiting action of the catalyst. The radical scavenging action of the lower oxidation state of metal cation has been postulated by several authors,[7,11,14,16,17,24] and the rate constants for reactions of peroxyl radicals and the metal cations have been estimated.[15,25,26]

Origin of Critical Phenomena. In order to confirm the origin of the critical phenomena in oxidation and hydroperoxide decomposition, we should consider relative rates of elementary reactions. Reaction 1 is much faster than Reaction 2 in the manganese system.[23] Reaction 7 is much faster than Reaction 3, hydrogen abstraction from RH by RO_2. Thus, the rate constant for the reaction of cumylperoxyl radical with manganous cation is $4.3\times10^4\ M^{-1}\ s^{-1}$ at 308 K,[15] while the rate constant for the reaction of the same radical and cumene is estimated to be $7.6\ M^{-1}\ s^{-1}$ at the same temperature.[17] Thus, in the presence of sufficient amount of Mn(II), the peroxyl radicals formed by Reactions 1 and 6 are scavanged by Mn(II), the autoxidation being inhibited. Above the critical ratio of hydroperoxide to Mn(II) amount, most of Mn(II) species are converted into Mn(III) by Reaction 1 and the remaining ROOH molecules are converted into peroxyl radicals by Reaction 2 and the oxidation can proceed through Reactions 4 and 5. Under these conditions, Reaction 7 is negligible because of low concentration of Mn(II). For the same reason, no critical phenomena would be observed if Mn(III) is used as a catalyst from the beginning.

Reactions 1 and 7 are only known in the case of transition metal cations which have variable oxidation states, such as Co(II)/Co(III) and Mn(II)/Mn(III). The fact that critical phenomena in the autoxidation of hydrocarbons have been observed only with such transition metal ions[1–10] also supports the view that the cause of critical phenomena can be attributed to Reactions 1 and 7.

Elimination of the elementary Reactions 3 and 4 from the above oxidation mechanism should give the mechanism for the hydroperoxide decomposition.[19,27] Since the mechanisms of initiation and chain scavenging remain identical to those in the autoxidation, the origin of the critical phenomena both in the hydroperoxide decomposition and the autoxidation should be common. This explains why both critical phenomena occur at the same ratio of the hydroperoxide to catalyst amount.

The critical molar ratio of hydroperoxide to Mn(II), expected from Reactions 1 and 7, is unity. But the experimental critical ratio of hydroperoxide to $Mn(II)(acac)_2$ amount is 1.5×10^{-3} mol/g-$Mn(II)(acac)_2$, that is, the critical molar ratio is 0.38, smaller than unity, probably because of the fact that $Mn(II)(acac)_2$ is partly heterogeneous during the course of reaction.

The critical phenomenon in the autoxidation of cumene by $MnCO_3$ can be explained similarly. Since $MnCO_3$ is a heterogeneous catalyst, and only Mn(II) on the surface is available for the initiation, the effective Mn(II) species in $MnCO_3$ are much less than those in $Mn(II)(acac)_2$, resulting in a much smaller critical ratio of hydroperoxide to catalyst amount.

We are very grateful to Professor T. Keii for helpful discussions.

References

1) A. Mukherjee and W. F. Graydon, *J. Phys. Chem.*, **71**, 4232 (1967).
2) N. J. Neuberg, J. M. Basset, and W. F. Graydon, *J. Catal.*, **25**, 425 (1972).
3) N. P. Evmenenko, Ya. B. Gorokhovatsky, and Yu. I. Pylenko, *Dokl. Akad. Nauk USSR*, **202**, 1117 (1972).
4) Ya. B. Gorokhovatsky and A. I. Pyatnitskaya, *Kinet. Katal.*, **13**, 1527 (1972).
5) Ya. B. Gorokhovatsky, *Proc. Congr. Catal.*, 5th, 1972, **2**, 879 (1973).
6) G. R. Varma and W. F. Graydon, *J. Catal.*, **28**, 236 (1973).
7) H. J. Neuberg, M. J. Phillips, and W. F. Graydon, *J. Catal.*, **38**, 33 (1975)
8) R. K. Srivastava and R. D. Srifastava, *J. Catal.*, **39**, 317 (1975).
9) D. L. Allara and R. F. Roberts, *J. Catal.*, **45**, 54 (1976).
10) L. V. G. Krishma, M. S. Rao, and R. D. Srivastava, *J. Catal.*, **49**, 109 (1977).
11) Y. Kamiya and K. U. Ingold, *Can. J. Chem.*, **42**, 2424 (1964).
12) A. T. Betts and N. Uri, *Adv. Chem. Ser.*, **76**, 160 (1968).
13) E. T. Denisov and N. M. Emanuel, *Russ. Chem. Rev.* **29**, 645 (1960).
14) A. T. Betts and N. Uri, *Makromol. Chem.*, **95**, 22 (1966).
15) D. G. Hendry and D. Schueltzle, *Am. Chem. Soc., Div. Petrol. Chem. Prepr.*, **14**, (4), A31 (1969).
16) E. Niki and Y. Kamiya, *Bull. Chem. Soc. Jpn.*, **39**, 1095 (1966).
17) A. J. Chalk and J. F. Smith, *Trans. Faraday Soc.*, **53**, 1214 (1957).
18) S. Fukuzumi and Y. Ono, *J. Phys. Chem.*, **80**, 2973 (1976).
19) S. Fukuzumi and Y. Ono, *J. Chem. Soc., Perkin Trans. 2*,

1977, 784.
20) S. Fukuzumi and Y. Ono, *J. Phys. Chem.*, **81**, 1895 (1977).
21) S. Fukuzumi and Y. Ono, *J. Chem. Soc., Perkin Trans. 2*, 622 (1977).
22) J. K. Kochi, "Oxidation-Reductions of Free Radicals and Metal Complexes," in "Free Radicals," ed by J. K. Kochi, John-Wiley and Sons, New York (1973), Vol. 1, Part 1, Chap. 11, pp. 591—684.
23) R. A. Sheldon and J. K. Kochi, "Metal Catalyzed Oxidations of Organic Compounds in the Liquid Phase: A Mechanistic Approach," in "Advances in Catalysis," ed by D. D. Eley, H. Pines, and P. B. Weisz, Academic Press, New York (1976), Vol. 25, pp. 274—414.
24) J. F. Black, *J. Am. Chem. Soc.*, **100**, 527 (1978).
25) V. M. Goldberg and L. K. Obukhova, *Dokl. Akad. Nauk USSR*, **165**, 860 (1965).
26) W. J. De Klin and K. C. Kooyman, *J. Catal.*, **4**, 626 (1965).
27) S. Fukuzumi and Y. Ono, *J. Chem. Soc., Perkin Trans. 2*, 625, (1977).

Solubility Isotherm of Reciprocal Salt-Pairs Containing Bis(ethylenediamine)oxalatocobalt(III) (1*R*,3*S*,4*S*,7*R*)-3-Bromocamphor-9-sulfonate

Akira FUYUHIRO,* Kazuaki YAMANARI, and Yoichi SHIMURA

Department of Chemistry, Faculty of Science, Osaka University, Toyonaka, Osaka 560

(Received January 30, 1979)

Four-component solubility isotherm of reciprocal salt-pairs consisting of (Λ-[Co(ox)(en)$_2$]$^+$, Δ-[Co(ox)(en)$_2$]$^+$)–(Cl$^-$, *d*-$C_{10}H_{14}OBrSO_3^-$)–H_2O has been determined experimentally at 25 °C. It was found that a pseudoracemate, Λ-[Co(ox)(en)$_2$]·Δ-[Co(ox)(en)$_2$](*d*-$C_{10}H_{14}OBrSO_3)_2\cdot 2H_2O$, is present as the only double salt, optical resolution of the bis(ethylenediamine)oxalatocobalt(III) ion in this system at 25 °C being impossible as in the case of the ternary system, Λ-[Co(ox)(en)$_2$](*d*-$C_{10}H_{14}OBrSO_3$)–Δ-[Co(ox)(en)$_2$](*d*-$C_{10}H_{14}OBrSO_3$)–H_2O, at 25 °C.

The (1*R*,3*S*,4*S*,7*R*)-3-bromocamphor-9-sulfonate(1—) anion, *d*-$C_{10}H_{14}OBrSO_3^-$ (abbreviated to *d*-bcs$^-$) is known as one of the most effective resolving agents for metal complexes. It was concluded from a study on the solubility isotherm of a ternary system, Λ-[Co(ox)(en)$_2$](*d*-bcs)–Δ-[Co(ox)(en)$_2$](*d*-bcs)–H_2O, that the resolving agent is unsuitable to the optical resolution of bis(ethylenediamine)oxalatocobalt(III) complex, [Co(ox)(en)$_2$]$^+$, at 25 °C because of the formation of a pseudoracemate, Λ-[Co(ox)(en)$_2$]·Δ-[Co(ox)(en)$_2$]-(*d*-bcs)$_2\cdot 2H_2O$.[1] Recently, we have found that the optical resolution is possible at temperatures lower than 19 °C, in spite of the existence of the pseudoracemate in the ternary system.[2] Nevertheless, it is interesting to see in which way the pseudoracemate behaves to prevent the optical resolution in a four-component system, since no four component system containing a pseudoracemate has been studied in view of solubility phase diagrams and their application to a practical optical resolution.

This paper deals with the determination of the solubility isotherm of the reciprocal salt-pairs, (Λ-[Co(ox)(en)$_2$]$^+$, Δ-[Co(ox)(en)$_2$]$^+$)–(Cl$^-$, *d*-bcs$^-$)–H_2O, at 25 °C. Discussion is given on the possibility of the optical resolution of the bis(ethylenediamine)-oxalatocobalt(III) ion as compared with two other successful cases of optical resolution of the complex.[3]

Experimental

Materials. [*Co*(*ox*)(*en*)$_2$]*Cl*·H_2O: The Λ- and Δ-complex chloride monohydrates were the same as reported.[3]

[*Co*(*ox*)(*en*)$_2$](d-*bcs*)·nH_2O: The Λ-diastereomeric salt monohydrate, Δ-diastereomeric salt 1.5-hydrate, and the pseudoracemate dihydrate, Λ-[Co(ox)(en)$_2$]·Δ-[Co(ox)(en)$_2$]-(*d*-bcs)$_2\cdot 2H_2O$, were the same as reported.[2]

Measurements. Solubility in water at 25 °C was determined in molality.[3] Optical densities were measured at 497 nm, and CD at 523 and 310 nm. The concentrations of {Λ-[Co(ox)(en)$_2$]$^+$+Δ-[Co(ox)(en)$_2$]$^+$} were determined from the observed optical densities, referring to the established molar absorption coefficients of the component ions; ε(497 nm) =120 for Λ- and Δ-[Co(ox)(en)$_2$]$^+$, and ε(497 nm)=0 for *d*-bcs$^-$. The concentrations of {Λ-[Co(ox)(en)$_2$]$^+$—Δ-[Co(ox)(en)$_2$]$^+$} were determined from the observed CD values in 523 nm, referring to the following data; $\Delta\varepsilon$(523 nm)= +2.71, −2.71, and 0 for Λ-[Co(ox)(en)$_2$]$^+$, Δ-[Co(ox)(en)$_2$]$^+$, and *d*-bcs$^-$, respectively. The concentrations of Λ- and Δ-[Co(ox)(en)$_2$]$^+$ were separately calculated from the concentrations of {Λ-[Co(ox)(en)$_2$]$^+$+Δ-[Co(ox)(en)$_2$]$^+$} and {Λ-[Co(ox)(en)$_2$]$^+$—Δ-[Co(ox)(en)$_2$]$^+$}. The concentrations of *d*-bcs$^-$ were determined from the observed CD values in 310 nm; $\Delta\varepsilon$(310 nm)=+3.23 for *d*-bcs$^-$ and $\Delta\varepsilon$(310 nm) =0 for Λ- and Δ-[Co(ox)(en)$_2$]$^+$.

The solid phases were identified from elemental analyses, absorption and CD spectra. Optical densities were measured with a JASCO UVIDEC-1 spectrophotometer and CD with a JASCO MOE-1 spectropolarimeter.

Results and Discussion

The solubility data are given in Table 1, and Figs. 1 and 2. Solubility is expressed in molalities of component ions and are attributed to the molalities of

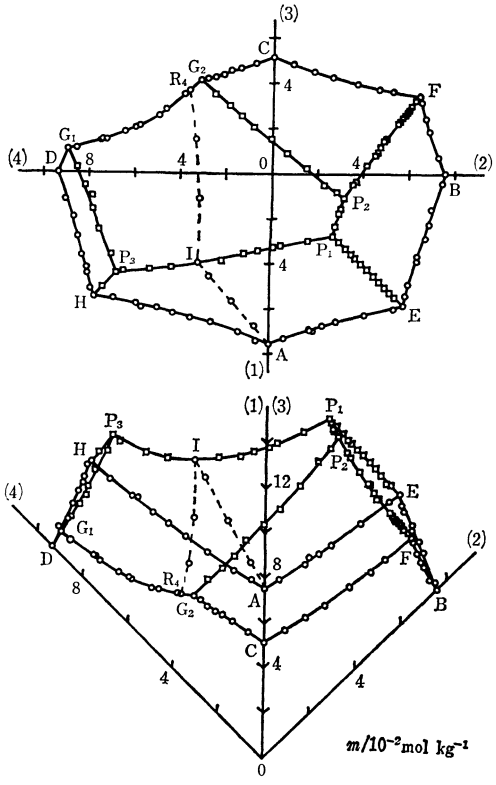

Fig. 1. The plane projection (upper) and the side elevation of the solubility isotherm of the system, (Λ-[Co(ox)(en)$_2$]$^+$, Δ-[Co(ox)(en)$_2$]$^+$)–(Cl$^-$, *d*-bcs$^-$)–H_2O, at 25 °C. Solubility is presented in molality *m* of anhydrous salt: (1) Λ-[Co(ox)(en)$_2$]Cl, (2) Δ-[Co(ox)(en)$_2$]-Cl, (3) Δ-[Co(ox)(en)$_2$](*d*-bcs), and (4) Λ-[Co(ox)-(en)$_2$](*d*-bcs); □, solubility of four-components; ○, solubility of two- or three-components.

Table 1. Equilibrium of (Λ-[Co(ox)(en)$_2$]$^+$, Δ-[Co(ox)(en)$_2$]$^+$)-(Cl$^-$, d-bcs$^-$)-H_2O system at 25 °C

In liquid phases, solubility is presented in molalities m of the component ions. Abbreviations are as follows: Λ-[Co(ox)(en)$_2$]$^+$=Λ^+, Δ-[Co(ox)(en)$_2$]$^+$=Δ^+, Λ-[Co(ox)(en)$_2$]Cl·H_2O=ΛCl, Δ-[Co(ox)(en)$_2$]Cl·H_2O=ΔCl, Δ-[Co(ox)(en)$_2$](d-bcs)·$4H_2O$=Δ(d-bcs), Λ-[Co(ox)(en)$_2$](d-bcs)·H_2O=Λ(d-bcs), and Λ-[Co(ox)(en)$_2$]·Δ-[Co(ox)(en)$_2$](d-bcs)$_2$·$2H_2O$=$\Lambda\Delta$(d-bcs)$_2$.

a)	b)	Liquid phase[c] $m/10^{-2}$ mol kg^{-1} Λ^+	Δ^+	d-bcs$^-$	Solid phase
G_1 ↕ P_3	4	9.49 9.97 10.26 10.77 11.43 12.10	1.18 1.26 1.36 1.31 1.39 1.52	9.71 9.44 9.25 9.16 8.94 8.50	Λ(d-bcs) +$\Lambda\Delta$(d-bcs)$_2$
P_3	4	12.76 (±0.20)	1.57 (±0.10)	8.33 (±0.16)	ΛCl +Λ(d-bcs) +$\Lambda\Delta$(d-bcs)$_2$
G_2 ↕ P_2	4	3.50 3.68 3.90 4.25 4.47 4.76 5.20 5.73 5.88	4.48 4.80 5.10 5.46 5.92 6.32 6.93 7.53 7.94	6.99 6.68 6.44 6.29 5.98 5.65 5.43 5.24 5.09	Δ(d-bcs) +$\Lambda\Delta$(d-bcs)$_2$
P_2	4	6.14 (±0.17)	8.19 (±0.10)	5.05 (±0.08)	ΛCl +Δ(d-bcs) +$\Lambda\Delta$(d-bcs)$_2$
A ↕ H	3	7.95 8.35 9.14 9.82 10.39 10.88 11.57 11.61 12.38		0.56 1.34 2.55 3.44 4.22 4.92 5.61 5.82 6.85	ΛCl
D ↕ H	3	10.22 10.60 11.25 11.84 12.21 12.45 12.99		9.03 8.65 8.45 8.22 8.01 7.99 7.84	Λ(d-bcs)
H	3	13.16 (±0.10)		7.68 (±0.04)	ΛCl +Δ(d-bcs)
H ↕ P_3	4	12.95	0.57	7.91	ΛCl +Λ(d-bcs)
B ↕ F	3		7.99 8.72 9.12 9.63	0.73 1.89 2.43 3.18	ΔCl
C ↕ F	3		5.71 6.30 6.85 7.66 8.33 8.89	4.83 4.50 4.23 3.96 3.71 3.65	Δ(d-bcs)
F	3		9.83 (±0.04)	3.41 (±0.03)	ΔCl +Δ(d-bcs)
F ↕ P_2	4	0.27 0.57 0.78 0.92 1.04 1.19 1.37 1.43 1.58 2.55 2.62 2.98 3.31 3.46 4.15 5.02 5.23	9.80 9.64 9.59 9.57 9.48 9.39 9.38 9.35 9.33 9.07 8.93 8.88 8.83 8.77 8.60 8.36 8.36	3.52 3.57 3.62 3.68 3.69 3.71 3.77 3.76 3.84 4.08 4.05 4.14 4.22 4.27 4.48 4.67 4.79	ΛCl +Δ(d-bcs)
E ↕ P_1	4	6.10 6.12 6.30 6.46 6.59 6.75 6.87 7.00 7.10 7.23 7.40	6.10 6.12 6.30 6.46 6.59 6.75 6.87 7.00 7.10 7.23 7.40	0.61 0.84 1.24 1.65 2.05 2.49 2.89 3.26 3.54 3.92 4.39	ΛCl +ΔCl
P_1	4	7.58 (±0.03)	7.58 (±0.03)	4.86 (±0.09)	ΛCl +ΔCl +$\Lambda\Delta$(d-bcs)$_2$
P_1 ↕ P_2	4	7.17 6.73 6.55	7.77 7.93 7.99	4.96 5.00 4.98	ΔCl +$\Lambda\Delta$(d-bcs)$_2$
P_3 ↕ I	4	12.42 11.51 10.91	1.59 1.98 2.42	8.07 7.26 6.74	ΛCl +$\Lambda\Delta$(d-bcs)$_2$
I	3	10.17 (±0.12)	3.07 (±0.02)	6.20 (±0.07)	ΛCl +$\Lambda\Delta$(d-bcs)$_2$
I ↕ P_1	4	9.63 9.05 8.78 8.47 8.39 7.92	3.71 4.41 4.86 5.36 5.66 6.59	5.80 5.53 5.39 5.25 5.23 4.97	ΛCl +$\Lambda\Delta$(d-bcs)$_2$
R_4 ↕ I	3	5.25 7.45	3.40 3.18	6.74 6.35	$\Lambda\Delta$(d-bcs)$_2$
A ↕ I	3	8.05 8.89 9.80	0.66 1.62 2.68	1.32 3.26 5.35	ΛCl

a) Positions of points shown in Figs. 1 and 2. G_1↔P_3, for example, does not contain points G_1 and P_3. Reported data for A, B, E, A↔E, and B↔E[3] and for C, C↔G_2, R_4, R_4↔G_1, G_1, and D[2] not shown. b) Number of components. c) Values in parentheses are estimated errors and calculated from twice the standard deviations of experimental measurements repeated 4—7 times. At a point in A↔I, I, and R_4↔I, the molality of d-bcs$^-$ ideally becomes twice those of Δ^+.

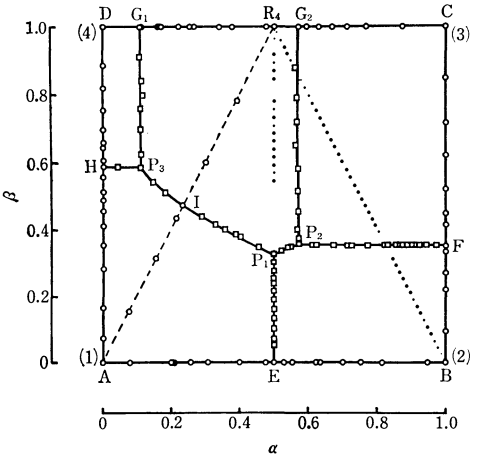

Fig. 2. The clinographic projection of the solubility isotherm of the system, (Λ-[Co(ox)(en)$_2$]$^+$, Δ-[Co(ox)-(en)$_2$]$^+$–(Cl$^-$, d-bcs$^-$)–H_2O, at 25 °C: α, mole fraction of Δ-[Co(ox)(en)$_2$]$^+$ to all the cations; β, mole fraction of d-bcs$^-$ to all the anions; (1) Λ-[Co(ox)(en)$_2$]Cl, (2) Δ-[Co(ox)(en)$_2$]Cl, (3) Δ-[Co(ox)(en)$_2$](d-bcs), and (4) Λ-[Co(ox)(en)$_2$](d-bcs); □, solubility of four-components; ○, solubility of two- or three-components.

three salts.[3] Thus the solubility isotherm can be drawn in a space according to the definition of solubility diagrams of reciprocal salt-pairs; Figure 1 represents the plane projection and the side elevation, and Fig. 2 the clinographic projection.[3]

The isotherm shows that the pseudoracemic compound, Λ-[Co(ox)(en)$_2$]·Δ-[Co(ox)(en)$_2$](d-bcs)$_2$·$2H_2O$, is present as the only double salt, no solid solution existing in this system. In the areas of AEP_1IP_3H, $EBFP_2P_1$, CG_2P_2F, $G_2R_4G_1P_3IP_1P_2$, and DHP_3G_1 in Figs. 1 and 2, which contain their boundaries, the saturated solutions are in equilibrium with the solids Λ-[Co(ox)(en)$_2$]Cl·H_2O, Δ-[Co(ox)-(en)$_2$]Cl·H_2O, Δ-[Co(ox)(en)$_2$](d-bcs)·$4H_2O$, Λ-[Co-(ox)(en)$_2$]·Δ-[Co(ox)(en)$_2$](d-bcs)$_2$·$2H_2O$, and Λ-[Co-(ox)(en)$_2$](d-bcs)·H_2O, respectively. Points A, B, C, R_4, and D denote the solubility of binary systems, and the faces AEB, BFC, $CG_2R_4G_1D$, DHA, and AIR_4 that of ternary systems. The lines of EP_1, FP_2, G_2P_2, G_1P_3, and HP_3 in Fig. 2 are almost parallel to the abscissa or ordinate. This shows that the mole ratio of Λ-[Co(ox)(en)$_2$]$^+$ to Δ-[Co(ox)(en)$_2$]$^+$ or Cl$^-$ to d-bcs$^-$ is constant on these lines.[3]

On the "racemic line" ER_4 (Fig. 2) where the amounts of Λ- and Δ-[Co(ox)(en)$_2$]$^+$ ions are equal, the saturated solution is in equilibrium with the pseudoracemate, Λ-[Co(ox)(en)$_2$]·Δ-[Co(ox)(en)$_2$](d-bcs)$_2$·$2H_2O$ (on P_1R_4), or the racemic mixture, [Co-(ox)(en)$_2$]Cl·H_2O (on EP_1). Thus, the system at 25 °C can not be applied successfully to practical optical resolution. One mole of *rac*-[Co(ox)(en)$_2$]Cl is dissolved in an excess of water and x mol of Ag(d-bcs) is added ($0<x<1$). The resulting precipitate AgCl is filtered off and the filtrate then concentrated at 25 °C. If we ignore the dissolved AgCl, this operation gives just the same conditions as the isotherm, (Λ-[Co(ox)(en)$_2$]$^+$, Δ-[Co(ox)(en)$_2$]$^+$)–(Cl$^-$, d-bcs$^-$)–H_2O, at 25 °C. In the case of $0<x<0.32$, the situation corresponds to the region of $E \leftrightarrow P_1$, giving the first precipitation of the racemic mixture, [Co(ox)(en)$_2$]Cl·H_2O, on concentrating at 25 °C. In the case of $x=0.32$ which corresponds to point P_1, the racemic mixture, [Co(ox)(en)$_2$]Cl·H_2O, and the pseudoracemate, Λ-[Co(ox)(en)$_2$]·Δ-[Co(ox)(en)$_2$](d-bcs)$_2$·$2H_2O$, will precipitate simultaneously. In the case of $0.32<x<1$ which is related to the region of $P_1 \leftrightarrow R_4$, the pseudoracemate deposits at first. The final liquid phase composition in this operation corresponds to point P_1 regardless of the value of x. Thus, optical resolution is impossible in this isotherm because of the formation of the racemic mixture or the pseudoracemic compound. No tie-line intersects the "racemic line".

There are three invariant points, P_1, P_2, and P_3, in the four-component system at 25 °C. When the unsaturated solution composition is in the region of AR_4D except for its boundary in Fig. 2, the concentration of this solution would bring the solution composition to point P_3. Thus, point P_3 represents the final liquid phase composition for the region AR_4D. Both points P_1 and P_2 also represent the final liquid phase compositions for the regions ABR_4 and BCR_4, respectively. Point P_2 is a kind of "pseudo invariant point,"[2] since the composition of P_2 exists not in the region BCR_4 but in ABR_4.

References

1) Y. Shimura and K. Tsutsui, *Bull. Chem. Soc. Jpn.*, **50**, 145 (1977).

2) A. Fuyuhiro, K. Yamanari, and Y. Shimura, *Chem. Lett.*, **1978**, 1393; A. Fuyuhiro, K. Yamanari, and Y. Shimura, *Bull. Chem. Soc. Jpn.*, **52**, 1420 (1979).

3) A. Fuyuhiro, K. Yamanari, and Y. Shimura, *Bull. Chem. Soc. Jpn.*, **52**, 90 (1979).

The Thermochemical Behavior of Pentaamminedinitrogenruthenium(II) Complexes and the Kinetics of the Liberation of Ammonia from the Complex in the Solid State

Susumu KOHATA,* Noriko ITOH,** Hitoshi KAWAGUCHI,** and Akira OHYOSHI**

Yatsushiro College of Technology, Hirayamashin-machi, Yatsushiro 866

***Department of Industrial Chemistry, Faculty of Engineering, Kumamoto University, Kurokami, Kumamoto 860*

(Received March 9, 1978)

The thermochemical reactions of $[Ru(NH_3)_5N_2]X_2$ (X=Cl, Br, I) were investigated in the solid state. The ammonia ligand was liberated at a lower temperature (165—213 °C) than the nitrogen ligand (243—270 °C). The isothermal measurement reveals that the first step of the degradation of the complex can be expressed as: $[Ru(NH_3)_5N_2]X_2(s) \rightarrow [RuX(NH_3)_4N_2]X(s) + NH_3(g)$ (X=Cl, Br, or I). The rate of the reaction is first-order to $[Ru(NH_3)_5N_2]X_2$, and the first-order rate constant increased in the order of: chloride<bromide<iodide. The activation energies and the activation entropies (E/kJ mol^{-1} and ΔS^*/J K^{-1} mol^{-1} respectively) for the reaction were as follows: chloride (181 ± 1, 62 ± 1), bromide (99 ± 1, -95 ± 2), and iodide (89 ± 1, -102 ± 3). The values of ΔS^* suggest that the salt with Cl^- degrades through an S_N1-like mechanism, while those with Br^- and I^- degrade through an S_N2-type mechanism. The thermochemistry of $[Ru(NH_3)_5N_2]X_2$ has been discussed on the basis of the strong π-backbonding ability of the nitrogen ligand and the electronegativity of the outer-sphere ions.

After the isolation of Ru(II)–N_2 compounds by Allen and Senoff,[1] a number of nitrogen compounds of the transition metals (Co, Ir, Os, *etc.*)[2-4] have been synthesized. These nitrogen compounds have been energetically studied because they are known to play an important part in the fixation of the N_2 molecule. The X-ray analysis of the Ru(II)–N_2 compound has revealed that the Ru–N–N group is linear.[5] The Ru–N_2 bond is known to be stable because of the π-backbonding between the Ru d_π-orbital and the p_π-orbital of the N_2 ligand.[6] In an aqueous solution, however, the N_2 molecule is easily replaced by a water molecule. Therefore, it is worthwhile to investigate the nature of the Ru–N_2 bond. Some properties of $Ru(NH_3)_5N_2^{2+}$ in an aqueous solution have been reported,[7] but these seem to have been no report in the solid-state reaction.

In this work, the thermochemical behavior of the Ru(II)–ammine compounds containing molecular nitrogen has been studied in the solid state in order to obtain information about the lability of the Ru–N_2 and Ru–NH_3 bonds. The kinetics of the deammonation-anation reaction have also been studied. Furthermore, the application of the solid-state thermal reaction in convenient syntheses of dinitrogen compounds with various substituents has been researched.

Experimental

Materials. The $[Ru(NH_3)_5N_2]Cl_2$ complex was prepared according to the method described in the literature,[1] with caution taken, to avoid contamination with the binuclear species.[8] The bromide and the iodide were prepared by exchanging the chloride ion with the corresponding ions in an aqueous solution of sodium bromide and sodium iodide. The *cis*-$[Ru(NH_3)_4(OH_2)(N_2)]Br_2$ complex was prepared by the reaction of *cis*-$[RuBr_2(NH_3)_4]Br$ with sodium azide and methanesulfonic acid.[9] The purity of the compounds was confirmed by elemental analysis and by UV-spectral measurements.

Derivatographic and Isothermal Measurements. The derivatograms (TG and DTA) were obtained by using a Shimadzu DTG-20-type micro-differential thermobalance. The experiments were made in a constant nitrogen stream (50 ml/min) at a constant heating rate (5 °C/min), using about 10 mg of the sample in each run. The isothermal kinetic measurements were carried out as has been described in a previous report.[10] The UV and IR spectra of the initial compound and the reaction product were measured with a Shimadzu UV-200-type Spectrophotometer and a JASCO Model DS-403G Grating Infrared Spectrophotometer respectively.

Results and Discussion

Derivatographic Studies. The TG and DTA curves of $[Ru(NH_3)_5N_2]X_2$ (X=Cl, Br, and I) are given in Fig.

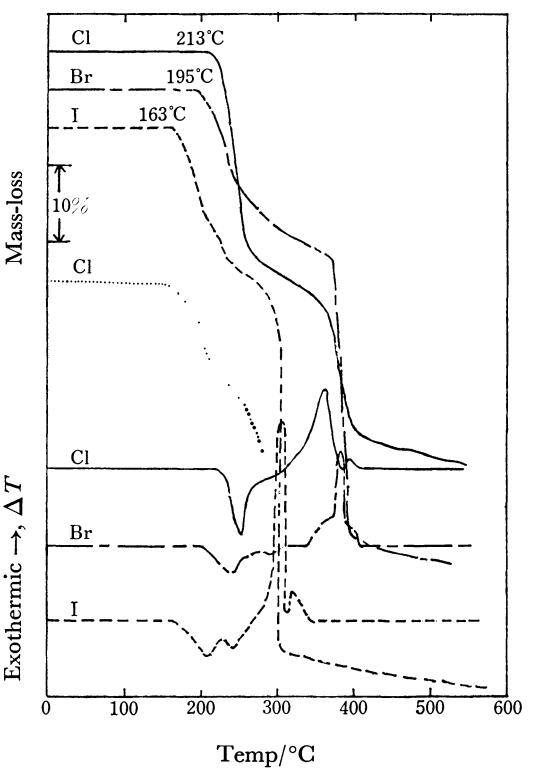

Fig. 1. TG and DTA curves of $[Ru(NH_3)_5N_2]X_2$ (heating rate 5 °C/min; —— chloride, ——— bromide, ---- iodide), (heating rate 2 °C/min; ····· chloride).

Table 1. DTA and mass-loss data for $[Ru(NH_3)_5N_2]X_2$

Compound	DTA peak (Temp/°C)		TG stage (Temp/°C)	Mass-loss/% Obsd/Theo.	
$[Ru(NH_3)_5N_2]Cl_2$	P_1(252)	Endo[a]	213—255	24/23.8	$-4NH_3$
	Sh.(280—309)	Endo	255—362	10/9.8	$-N_2$
	P_2(362), P_3(394)	Exo[b]	<362	20/31.6	$-0.5Cl_2$, NH_4Cl, *etc.*
$[Ru(NH_3)_5N_2]Br_2$	P_1(243)	Endo	195—270	15/14.2	$-4NH_3$
	P_2(286)	Endo	270—370	8/7.5	$-N_2$
	Sh.(340—369), P_3(379), P_4(390)	Exo	<370	40/47.8	$-0.5Br_2$, NH_4Br, *etc.*
$[Ru(NH_3)_5N_2]I_2$	P_1(211)	Endo	165—243	18/18.2	$-5NH_3$
	P_2(240)	Endo	243—301	6/6.0	$-N_2$
	P_3(308), P_4(318)	Exo	<301	48/54.2	$-I_2$

a) Endotherm. b) Exotherm.

Table 2. Analysis of the isothermal-reaction products of pentaamminedinitrogenruthenium(II)

Initial compound	$[Ru(NH_3)_5N_2]Cl_2$	$[Ru(NH_3)_5N_2]Br_2$	$[Ru(NH_3)_5N_2]I_2$
Sample color	brown	dark brown	black
Chemical formula assigned	$[RuCl(NH_3)_4N_2]Cl$	$[RuBr(NH_3)_4N_2]Br$	$[RuI(NH_3)_4N_2]I$
Elemental analysis (H%, N%) Found	(3.93, 31.29)	(3.66, 22.97)	(2.36, 18.11)
Calcd	(4.48, 31.34)	(3.36, 23.54)	(2.66, 18.63)
Electronic spectrum (λ_{max}/nm, ε/cm^{-1} mol^{-1} dm^{-3})	(225, 6.5×10^3)	(218, 5.8×10^3)	(232, 1.16×10^4)

1, while their data are summarized in Table 1. All the TG curves show three steps in the mass-loss stage. The initial mass-loss temperatures are 213, 195, and 165 °C for chloride, bromide, and iodide respectively. The DTA curves show endothermic peaks at the two initial mass-loss stages: P_1, Sh./252, 280 °C (chloride), P_1, P_2/243, 286 °C (bromide), and P_1, P_2/211, 240 °C (iodide). The curves show also two exothermic peaks in the succeeding, third mass-loss stage: P_2, P_3/362, 394 °C (chloride), P_3, P_4/379, 390 °C (bromide), and P_3, P_4/308, 318 °C (iodide). The magnitude of the mass-loss in the first stage corresponds to the liberation of four or five molecules of NH_3, and that in the second stage, to the liberation of N_2.

In order to obtain more detailed information on the first mass-loss stage, the isothermal pyrolysis was carried out. The compound was heated for 20—60 min at a constant temperature just below the initiation point of the mass-loss; the temperatures chosen were 201, 183, and 155 °C for chloride, bromide, and iodide respectively.

The analytical data of the isothermal-reaction products (Table 2) clearly indicate that the product has the $[RuX(N_2)(NH_3)_4]X$ formula; that is, the product is a substituent of one molar ammonia of the initial compound by one molar of the halide ion. Thus, the main reaction through the first endothermic peak can be expressed by Eq. 1:

$$[Ru(NH_3)_5N_2]X_2(s) \xrightarrow{\Delta T} [RuX(N_2)(NH_3)_4]X(s) + NH_3(g) \quad (X=Cl, Br, I) \quad (1)$$
$$[A]$$

The IR spectral data are shown in Table 3. The

Table 3. Infrared frequencies (cm^{-1}) of Ru(II)–nitrogen compounds

Compound	ν(N–N)	$\delta(NH_3)$ deg	$\delta(NH_3)$ sym	$\rho(NH_3)$	ν(Ru–N_2)	ν(Ru–NH_3)	δ(N–Ru–N)	
$[Ru(NH_3)_5N_2]Cl_2$	2105	1622	1270	798	508	435	260[d]	(a)
$[RuCl(NH_3)_4N_2]Cl$	2129	1606	1272	801	510	440	257 (304)[e]	(b)
$[Ru(NH_3)_5N_2]Br_2$	2114	1618	1266	788	499	423	256[d]	(a)
$[RuBr(NH_3)_4N_2]Br$	2133	1607	1300	793	494	437	—	(b)
cis-$[RuBr(NH_3)_4N_2]Br$	2130	1609	1300	791	*	*	*	(c)
$[Ru(NH_3)_5N_2]I_2$	2129	1605	1276	775	489	412	248[d]	(a)
$[RuI(NH_3)_4N_2]I$	2152	1617	1294	777	474	400	241	(b)

a) Initial compounds from Ref. 5a). b) Thermal reaction products of (a). c) Thermal reaction product from *cis*-$[Ru(NH_3)_4(OH_2)(N_2)]Br_2$. *Not measured. d) Ref. 14. e) ν(Ru–Cl). Ref. 11.

absorption bands of the [A] product in the regions of 2152—2129 cm^{-1} and 510—474 cm^{-1} have been assigned to the stretching frequencies of ν(N–N) and ν(Ru–N_2) respectively. The N–N stretching shifted to a frequency higher by *ca.* 20 cm^{-1} on the deammonation. The Ru–N_2 stretching, on the contrary, shifted to a frequency lower by about 5—10 cm^{-1} on the reaction, whereas the Ru–NH_3 stretching shifted to a frequency higher by 5—15 cm^{-1} except for the chloride. Only in the chloride of [A] was a new absorption band, which can be assignable to ν(Ru–Cl),[11] observed in the lower region of 304 cm^{-1}. The ν(Ru–X) stretching frequency (X=Br, I) could not observed, but it can be expected to appear in a much lower region. The shifts may be caused by the deammonation and anation of the halide ion.

From the isothermal study described above, the first mass-loss stage have been ascribed to the quantitative liberation of ammonia as seen in amminehalogenoruthenium(III) complexes.[10,12] The second mass-loss stage seems due to the liberation of molecular nitrogen. The succeeding mass-loss stage, which shows exothermic peaks, might correspond to the continuous degradation reactions, such as the sublimation of ammonium halide and the evolution of free halogen.

As is pictured in Fig. 1, however, the non-isothermal (heating rate of 5 °C/min) derivatograms do not reveal the mass-loss stage of the liberation corresponding to the release of one molar ammonia. The TG curve of $[Ru(NH_3)_5N_2]Cl_2$ was obtained with a heating rate of 2 °C/min; it is shown again in Fig. 1. In this case, the initial mass-loss stage cleary corresponds to the liberation of one molar ammonia.

In order to confirm the stereochemical configuration of the [A] product, *cis*-type tetraamminebromodinitrogenruthenium(II) bromide [B] was prepared by employing a thermal-substitution reaction in the solid state:

$$cis\text{-}[Ru(NH_3)_4(OH_2)(N_2)]Br_2(s) \xrightarrow{\Delta T} cis\text{-}[RuBrN_2(NH_3)_4]Br(s) + H_2O(g)$$
[B]

The UV (218 nm) and IR spectra of [A(X=Br)] both agreed with those of [B]; this fact indicates that the thermal-reaction product [A] has a *cis*-configuration (Tables 2 and 3).

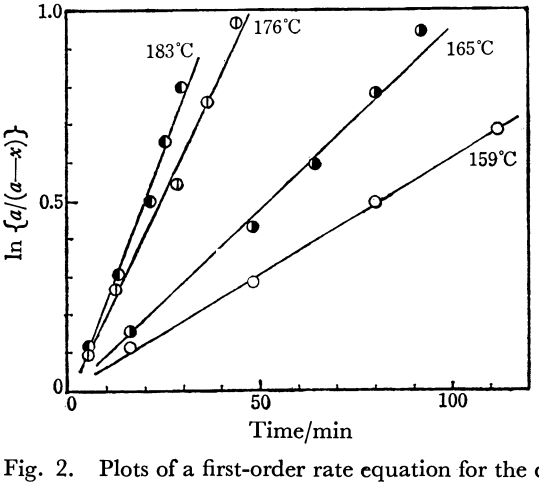

Fig. 2. Plots of a first-order rate equation for the deammonation-anation reaction of $[Ru(NH_3)_5N_2]Br_2$.

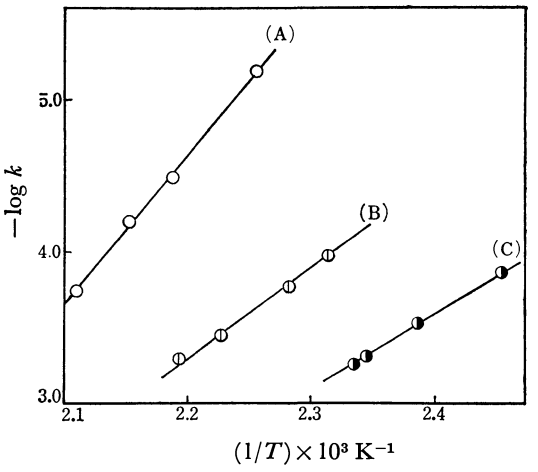

Fig. 3. Arrhenius plots of the substitution reactions for pentaamminedinitrogenruthenium(II). $[Ru(NH_3)_5N_2]X_2$; chloride(A), bromide(B), iodide(C).

Table 4. Kinetic parameters for the deammonation-anation reaction of Ru(II) and Ru(III) compounds

Compound	$k\times10^5$/s^{-1} (Temp/°C)	$E^{a)}$/kJ mol^{-1}	$\Delta S^{\ddagger,a)}$ /J K^{-1} mol^{-1}
$[Ru(NH_3)_5N_2]Cl_2$	0.68(170)	181±1	62±1
	3.33(184)		
	6.48(192)		
	18.7(201)		
$[Ru(NH_3)_5N_2]Br_2$	10.9(159)	99±1	−95±2
	17.2(165)		
	35.1(177)		
	48.7(183)		
$[Ru(NH_3)_5N_2]I_2$	14.2(134)	89±1	−102±3
	30.1(146)		
	49.1(154)		
$[Ru(NH_3)_6]Cl_3$[b)]	0.42(200)	122	−93
$[Ru(NH_3)_6]Br_3$[c)]	4.17(177)	97	−123
$[Ru(NH_3)_6]I_3$[c)]	6.02(151)	87	−132

a) Error recorded is e.s.d. b) Unpublished work; see Ref. 15. c) Ref. 12.

In conclusion, it is interesting to note that the Ru(II)–N_2 bond is more stable than the Ru(II)–NH_3 bond in this reaction.

Isothermal Kinetic Study. The kinetic measurements for the deammonation-anation reaction (1) (Fig. 2) show that Reaction (1) can be regarded as first-order with respect to the reactant. The first-order rate constants obtained and the activation parameters evaluated from the Arrhenius plot (Fig. 3) are given in Table 4. The rate constant of the bromide is about eleven times greater than that of the chloride. The rate constant of the iodide is about five times greater than that of the bromide. Consequently, the rate constant increases in this order: chloride<bromide<iodide; this relation is in accord with that among the Ru(III)–ammine compounds.[12] A more detailed discussion of this relation will be presented in the following section.

Reaction Mechanism. If the deammonation-anation reaction proceeds *via* an S_N1-like mechanism, the rate-

determinant step can be expected to be the Ru–NH_3 bond-rupture. Then, the rate constants may be practically independent of the nucleophilicity of the outer-sphere ions. On the contrary, if it proceeds through an S_N2-type mechanism, the rate constants might depend strongly on the outer-sphere ions. As may be seen in Table 4, the rate constants obtained largely depend on the outer-sphere ions; this suggests, then, that the deammonation-anation reactions proceed according to an S_N2-type mechanism.

The chloride, however, shows the smallest value of the rate constant among these three nitrogen compounds, while also revealing the largest value of the activation energy, E (181 kJ mol^{-1}), and the most positive value of the activation entropy, ΔS^* (62 J K^{-1} mol^{-1}). These results imply that the rate-determinant step is the Ru–NH_3 bond-breaking. In this case, a large activation energy is needed for bond-breaking; the increased activation entropy as a transitions-state complex can, therefore, be expected to be a five-coordinated intermediate. Therefore, the reaction of the pentaamminedinitrogenruthenium(II) chloride belongs to an S_N1-like mechanism.

On the other hand, the bromide and iodide reveal small values of E (99, 89 kJ mol^{-1}) and negative values of ΔS^* (−95, −102 J K^{-1} mol^{-1}). It is reasonable to consider that the mechanisms of the bromide and iodide of pentaamminedinitrogenruthenium(II) belong to an S_N2 category, because the values of E and ΔS^* obtained in the deammonation of $[Ru(NH_3)_5N_2]X_2$ [I] and $[Ru(NH_3)_6]X_3$ [II] (X=Br and I) are comparable with each other, and as the latter compounds are known to proceed through an S_N2 mechanism. The finding that the two types of complexes, [I] and [II], reveal comparable activation parameters might be explained by the π-backbonding of the N_2 ligand; that is, the effective charge on Ru(II) increases because the N_2 ligand is bound to the ruthenium, with the $3\sigma_g$-orbital as a σ-donor and with the $1\pi_g$*-orbital as a π-acceptor.[13]

Influence of Outer-sphere Ion. The rate constants of these compounds have revealed larger differences (*ca.* 8 (iodide) and 9 (bromide) times larger) in the $Ru(NH_3)_5N_2^{2+}$ compound than in the $Ru(NH_3)_6^{3+}$ compound. If the reactions proceed *via* an S_N2 mechanism, the increase in the nucleophilicity of the outer-sphere ion can be expected to give rate constants in the order of: I<Br<Cl. The rate constants, however, increased in the reverse order of: Cl<Br<I. This contradiction might be explained as follows. In the solid-state reaction, halogen's larger electronegativity in the outer-sphere might result in an increase in the net charge of the complex ion. In fact, ν(Ru–NH_3) and ν(Ru–N_2) in $[Ru(NH_3)_5N_2]X_2$ become higher with halogen's larger electronegativity (Table 3): I<Br<Cl. The smallest value of the rate constant in the chloride might be one of the supports for an S_N1-like mechanism. The difference in the rate constant between Ru(II) and Ru(III) complexes mentioned above might be contributed to by the difference in the number of halogen ions in the outer-sphere.

In conclusion, the thermochemical behavior of the pentaamminedinitrogenruthenium(II) compounds has been characterized by a stable Ru(II)–N_2 bond including a strong π-backbonding and by the electronegativity of the outer-sphere ions. Moreover, it might be due to the "*cis*-effect" of the N_2 ligand that the reaction product has a *cis*-form configuration, though this point needs a more detailed investigation. An isothermal reaction can be used for a convenient synthesis of the dinitrogenruthenium(II) compound with various substituents.

References

1) A. D. Allen and C. V. Senoff, *Chem. Commun.*, **1965**, 621.
2) A. Yamamoto, S. Kitazume, L. S. Pu, and S. Ikeda, *Chem. Commun.*, **1967**, 79.
3) J. P. Collman and J. W. Kang, *J. Am. Chem. Soc.*, **88**, 3459 (1969).
4) J. Chatt, G. J. Leigh, and R. L. Richards, *J. Chem. Soc., A*, **1970**, 2243.
5) a) A. D. Allen, F. Bottomley, R. O. Harris, V. P. Reinsalu, and C. V. Senoff, *J. Am. Chem. Soc.*, **89**, 5595 (1967); b) J. N. Armor and H. Taube, *J. Am. Chem. Soc.*, **92**, 6170 (1970).
6) F. Bottomley and S. C. Nyburg, *Chem. Commun.*, **1966**, 899, *Acta Crystallogr.*, **324**, 1289 (1968).
7) P. C. Ford, *Coordin. Chem. Rev.*, **5**, 75 (1970).
8) The solution was heated at 75—80 °C about 15 min, until the red color of solution became slightly red-yellow.
9) A. D. Allen, T. Eliades, R. O. Harris, and V. P. Reinsalu, *Can. J. Chem.*, **47**, 1605 (1969).
10) A. Ohyoshi, S. Kohata, M. Nishimori, Y. Shimura, and N. Iwasaki, *Bull. Chem. Soc. Jpn.*, **49**, 1284 (1976).
11) M. W. Bee, S. F. A. Kettle, and D. B. Powell, *Spectrochim. Acta, Part A*, **30**, 139 (1974).
12) A. Ohyoshi, S. Hiraki, T. Odate, S. Kohata, and J. Oda, *Bull. Chem. Soc. Jpn.*, **48**, 230 (1975).
13) S. S. Isied and H. Taube, *Inorg. Chem.*, **15**, 3070 (1976).
14) M. W. Bee, S. F. A. Kettle, and D. B. Powell, *Spectrochim. Acta, Part A*, **30**, 585 (1974).
15) The reaction mechanism of this compound seems to belong to the S_N2 category.

Equilibria of Imidazole Derivatives with (Protoporphyrin IX dimethyl ester)iron(III) Chloride

Tetsuhiko YOSHIMURA* and Tomio OZAKI

The Environmental Science Institute of Hyogo Prefecture, Yukihira-cho Suma-ku, Kobe 654

(Received September 1, 1978)

The equilibria of sterically hindered and unhindered imidazoles (B) with (protoporphyrin IX dimethyl ester)-iron(III) chloride (Fe(PPDME)Cl) have been spectrophotometrically investigated in chloroform and 1,2-dichloroethane. The addition reaction of hindered imidazole with Fe(PPDME)Cl proceeds in two steps to give $Fe(PPDME)B_2Cl$, with a formation constant, K_1, greater than K_2. The mono-adduct of hindered imidazoles exhibits an absorption band at around 590 nm, which shifts to longer wavelengths as the formation constant K_1 decreases in this order; 2,4-dimethyl-$>$2-methyl-$>$2-ethyl-$>$2-phenyl-$>$1,2-dimethylimidazole. The addition reaction of an unhindered imidazole with Fe(PPDME)Cl proceeds in an apparent one step to give $Fe(PPDME)B_2Cl$, with an overall formation constant of β_2. The log β_2 linearly increases with the basicity, $pK_a(BH^+)$, of unhindered imidazoles. The log β_2 for the system with NH-containing imidazoles is greater than that for the system with *N*-substituted imidazoles by about 3.1 log units, on the average, based on the stabilization of the positive charge on iron(III) through NH···Cl hydrogen bonding. The solvent effect on the formation constants is also discussed.

Imidazole is known to coordinate axially to heme iron in such hemoproteins as hemoglobin, myoglobin, cytochromes, peroxidases, and catalases.[1] The proximal and the distal histidine imidazoles play an important role in the heme-heme interaction and the Bohr effect in hemoglobin.[2] The state and the nature of the heme iron–imidazole bonds in the other hemoproteins are also closely related to the function of hemoproteins; thus, many investigations have been directed toward elucidating the thermodynamic properties of porphyrin iron model complexes with the imidazole derivatives.[3–21,23,25,26] La Mar and his coworkers have systematically investigated the kinetics and the thermodynamics of axial ligation in iron(III) complexes with synthetic porphyrins on the basis of proton NMR results.[21–26] Walker *et al.* followed the reaction of iron(III) para-substituted tetraphenylporphyrins with various imidazole derivatives by measuring the visible absorption spectrum in such noncoordinating solvents as chloroform, dichloromethane, and benzene; the effects of the solvent and the base on the equilibrium constant were also discussed.[14] The reaction of porphyrin iron(III) with imidazole in such coordinating solvents as dimethyl sulfoxide[18,19] and aqueous ethanol has also been studied.[5,6,12] The formation of a hemin complex with a mixed ligand of cyanide and imidazole in dimethyl sulfoxide has recently been studied by means of proton NMR.[20] Generally, the thermodynamics in coordinating solvents as compared with that in noncoordinating solvents is complicated by the solvation or the coordination of the solvent which remains unidentified.[19]

The imidazole derivatives are classified into two groups for steric reasons. They are sterically hindered imidazoles (2-methyl-, 1,2-dimethylimidazole, *etc.*), with significant steric interaction between the porphyrin core and the substituent adjacent to the bonding nitrogen, and unhindered imidazoles (imidazole, 4-methyl-, 1-methylimidazole, *etc.*). The majority of studies of porphyrin iron complexes with the imidazole derivatives as axial ligand(s) have been of unhindered imidazoles; there have been only a few of hindered imidazoles. The porphyrin iron complexes with unhindered imidazoles have been isolated as bis-adducts,[27–29] whereas those with hindered imidazoles have been isolated as mono-adducts.[30,31]

The reaction of porphyrin iron(III) chloride (FePCl) with nitrogenous bases (B) in solution is considered to proceed in two steps:

$$FePCl + B \overset{K_1}{\rightleftharpoons} FePBCl \quad (1)$$

$$K_1 = [FePBCl]/[FePCl][B] \quad (2)$$

$$FePBCl + B \overset{K_2}{\rightleftharpoons} FePB_2Cl \quad (3)$$

$$K_2 = [FePB_2Cl]/[FePBCl][B] \quad (4)$$

The overall reaction is:

$$FePCl + 2B \overset{\beta_2}{\rightleftharpoons} FePB_2Cl \quad (5)$$

$$\beta_2 = [FePB_2Cl]/[FePCl][B]^2 \quad (6)$$

$$(\beta_2 = K_1K_2)$$

Whether the chloride in the mono-adduct FePBCl is in the inner (six-coordinated) or outer coordination sphere (five-coordinated, ion-pair) is unknown, but in the former case the chloride ligand is considered to coordinate weakly to iron(III) because no change in the spin state ever occurs upon the addition of the first axial base.[11]

When unhindered imidazole is added to a porphyrin iron(III) chloride solution, the change in the visible absorption spectrum apparently exhibits the bis-adduct formation in general, though the isosbestic points indicating the mono-adduct formation are rarely found in the lower concentration of the imidazole.[14] Thus, the stepwise formation constant, K_2, is found to be much greater than K_1, so that only the overall formation constant, β_2, can be estimated from the finding regarding the spectral change. In the NMR spectrum of the porphyrin iron(III)–unhindered imidazole system, only the signals arising from the porphyrin iron(III) and the bis-adduct are detectable in solution.[21]

Upon the addition of hindered imidazole to a porphyrin iron(III) chloride solution, the NMR spectra exhibit only the bis-adduct formation for synthetic porphyrins,[25] whereas the visible absorption spectra exhibit the mono-adduct formation intermediately.[14]

It is known that the thermodynamics of metallopor-

phyrin complexes is highly sensitive to the porphyrin basicity[32] and that the basicity of the protoporphyrin IX, which occurs naturally, is different from that of such synthetic porphyrins as tetraphenyl- and octaethylporphyrin.[33] For understanding the nature of the iron–imidazole bond in the hemoproteins it is, therefore, considered useful to investigate the thermodynamics of the protoporphyrin iron complex with imidazole. In this paper we wish to report on our spectroscopic studies of the equilibria of sterically hindered and unhindered imidazoles with (protoporphyrin IX dimethyl ester) iron(III) chloride in chloroform and 1,2-dichloroethane, and to discuss the effect of the solvent and the base on the formation constant and the visible absorption spectra. Furthermore, the steric interaction of the porphyrin core with the base will be discussed.

The abbreviations used are as follows: (protoporphyrin IX dimethyl ester)iron(III) chloride, Fe(PPDME)-Cl. Unhindered imidazoles: imidazole, Im; 4-methylimidazole, 4MeIm; 4-phenylimidazole, 4PhIm; histamine, Him; 1-methylimidazole, NMeIm; 1-ethylimidazole, NEtIm; 1-acetylimidazole, NAcIm; 5-chloro-1-methylimidazole, 5ClNMeIm. Hindered imidazoles: 2-methylimidazole, 2MeIm; 2-ethylimidazole, 2EtIm; 2-phenylimidazole, 2PhIm; 2,4-dimethylimidazole, 2,4DMeIm; 1,2-dimethylimidazole, 1,2DMeIm.

Experimental

The Fe(PPDME)Cl was prepared as described before.[34] The Im, 4PhIm, NAcIm, 2MeIm, 2PhIm, and Him were recrystallized three times from chloroform–petroleum ether or acetone–petroleum ether and dried *in vacuo*. The 4MeIm, 2EtIm, and 2,4DMeIm were purified three times by vacuum sublimation and dried *in vacuo*. The NMeIm, NEtIm, 5ClNMeIm, and 1,2DMeIm were distilled four times at reduced pressure under N_2. Chloroform and 1,2-dichloroethane of an analytical grade were purified by the usual method. The ethanol was of a spectro-grade. The other reagents were of an analytical grade and were used without further purification.

The visible absorption spectrum was recorded on a Shimadzu MPS-5000 spectrophotometer at 25.0±0.2 °C. The plot of the absorbance at several wavelengths against the concentration of Fe(PPDME)Cl in chloroform was found to be linear in the concentrations below 0.3 mM; thus, the concentration of Fe(PPDME)Cl in measurements of the formation constants was maintained at 0.15 mM unless otherwise stated. The measurements of the spectral change upon the addition of bases to the Fe(PPDME)Cl solution were repeated several times in order to confirm the reproducibility.

Results

Absorption Spectra and Equilibria of the Fe(PPDME)Cl–Unhindered Imidazole System. The addition of imidazole to Fe(PPDME)Cl in chloroform resulted in the spectral changes shown in Fig. 1, which illustrates six concentrations of imidazole out of the 18 measured. The absorption maxima for the (protoporphyrin IX dimethyl ester)iron(III) complex with imidazole were 356.2 (26.1×10^3), 414.3 (124×10^3), 480.1 sh(7.65×10^3), 538.5 (10.8×10^3), and 563.4 sh(8.75×10^3), nm where sh is an absorption as a shoulder and where the

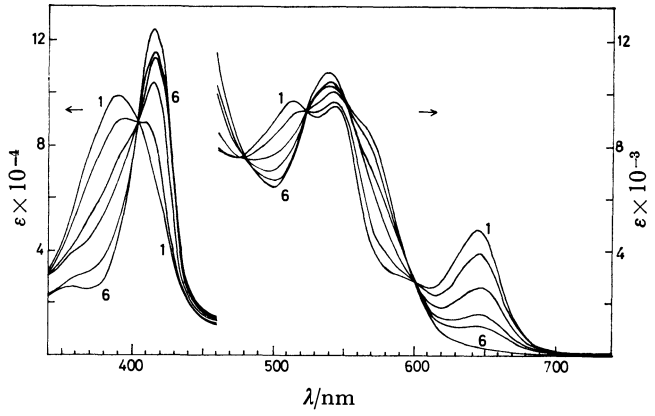

Fig. 1. Spectral changes observed upon addition of imidazole (0—12 mM) to an 0.15 mM solution of Fe(PPDME)Cl in chloroform (illustrated for 6 concentrations out of 18 ones measured). Imidazole concentrations: 1, 0 mM; 2, 0.3 mM; 3, 0.6 mM; 4, 0.9 mM; 5, 1.2 mM; 6, 12 mM.

values in parentheses are the molar extinction coefficients. The wavelengths of the absorption maxima in the case of the addition of the other seven unhindered imidazoles agreed with those of imidazole within ±2 nm. As is shown in Fig. 1, the isosbestic points were observed at 402, 480, 524, and 596 nm. For the molar ratios lower than [Im]/[Fe(PPDME)Cl]=2, the isosbestic point at 480 nm shifted slightly to the shorter wavelength side and the absorbance of the band at 540 nm was slightly lowered relative to that for Fe(PPDME)Cl; this behavior was found also in the case of the addition of the other seven unhindered imidazoles and was, indeed, even more distinct in the system with a smaller formation constant.

The spectral changes in Fig. 1, where the spectra of free Fe(PPDME)Cl changed to low-spin spectra,[35] indicate that the reaction of imidazole with Fe(PPDME)Cl proceeds in an apparent one step, based on the overall process of Eq. 5. Plots of A_0-A at 645 nm against log [B] are shown in Fig. 2, where A is the observed absorbance at a given wavelength, A_0 is the absorbance of Fe(PPDME)Cl in the absence of a base, and [B] is the

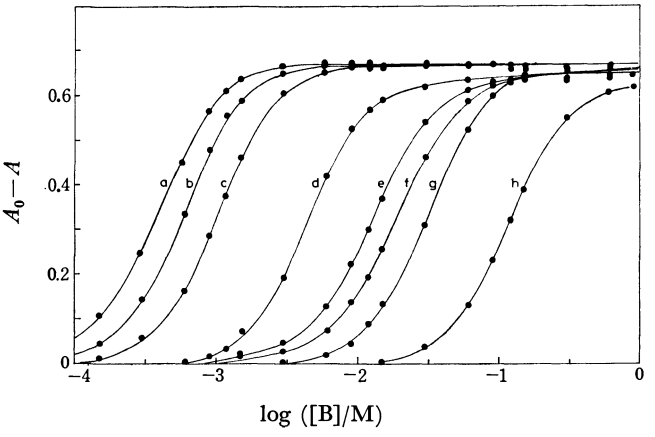

Fig. 2. Plots of A_0-A at 645 nm against log [B] for the addition of various unhindered imidazoles: a, Him; b, Im; c, 4MeIm; d, 4PhIm; e, NMeIm; f, NEtIm; g, NAcIm; h, 5ClNMeIm.

Table 1. Formation constants of (protoporphyrin IX dimethyl ester)iron(III) complexes with unhindered imidazoles at 25 °C

Solvent	Base	$pK_a(BH^+)$[a]	[Fe(PPDME)Cl]/mM	log K_1[b]	log β_2[b]
$CHCl_3$	4MeIm	7.22	0.15	2.7	6.68±0.03
	Im	6.65	0.15	2.8	6.72±0.04
	Him	5.73	0.15	3.3	7.17±0.06
	4PhIm	5.70	0.15	2.2	5.40±0.05
	NMeIm	7.33	0.15	1.6	3.77±0.05
			0.015	1.5	3.80±0.13
			0.0075	1.6	3.88±0.37
	NEtIm	7.30	0.15	1.5	3.65±0.07
	5ClNMeIm	4.75	0.15	0.6	1.86±0.05
	NAcIm	3.6	0.15	1.2	2.90±0.05
$ClCH_2CH_2Cl$	Im	6.65	0.15	2.1	5.20±0.04
	NMeIm	7.33	0.15	2.0	4.19±0.04
	NAcIm	3.6	0.15	0.9	2.13±0.02

a) A. Albert, *Phys. Methods Heterocycl. Chem.*, **1**, 1 (1963). A. R. Katritzky and A. J. Boulton, *Adv. Heterocycl. Chem.*, **12**, 103 (1970). Corrected for the presence of two protons in the conjugate acid (log 2) for NH imidazoles.[14] b) β_2, in units of M^{-2}; K_1, in units of M^{-1}.

Table 2. Formation constants of various porphyrin iron(III) complexes with unhindered imidazoles in chloroform

Porphyrin complex[a]	Base	T/°C	log β_2	References
Fe(PPDME)Cl	Im	25	6.72	This work
	NMeIm	25	3.77	This work
Fe(TPP)Cl	Im	25	6.20	14
	NMeIm	25	3.18	14
Fe(OEP)Cl	Im	25	6.03	14
	NMeIm	25	3.83	14
Fe(DPDME)Cl	Im	30	6.45	8

a) PPDME, protoporphyrin IX dimethyl ester; TPP, tetraphenylporphyrin; OEP, octaethylporphyrin; DPDME, deuteroporphyrin IX dimethyl ester.

concentration of the base. A_0-A for all the unhindered imidazoles varies with log [B] with a similar tendency, showing that the reaction of the unhindered imidazole with Fe(PPDME)Cl proceeds in an apparent one step. Then, the overall formation constant (β_2) is given by

$$\beta_2 = \frac{[FePB_2Cl]}{([FePCl]_T-[FePB_2Cl])([B]_T-2[FePB_2Cl])^2} \quad (7)$$

where $[FePCl]_T$ and $[B]_T$ are the total concentrations of Fe(PPDME)Cl and a base respectively. Since $[FePB_2Cl]=(A-A_0)/(\varepsilon_2-\varepsilon_0)$[36] where ε_0 is the molar extinction coefficient of Fe(PPDME)Cl in the absence of a base and where ε_2 is that of $Fe(PPDME)B_2Cl$ in the presence of a large excess of a base, Eq. 7 becomes:

$$\beta_2 = \frac{(A-A_0)/(\varepsilon_2-\varepsilon_0)}{\{[FePCl]_T-(A-A_0)/(\varepsilon_2-\varepsilon_0)\}\{[B]_T-2(A-A_0)/(\varepsilon_2-\varepsilon_0)\}^2} \quad (8)$$

By the method of Momenteau,[8] $1/(A_0-A)$ was plotted against $1/[B]_T^2$ at the wavelengths at 500, 540, 560 (or 570), and 645 nm. From the data in the linear part of the plots, β_2 was calculated by means of Eq. 8, and then the mean values and the standard deviations were evaluated (Table 1). From the data in the nonlinear part of the plot at 500 nm in the lower base concentrations, in which the isosbestic point at 480 nm shifts as described above, the formation constant, K_1, could be estimated. From Eq. 2 and the relation $[FePBCl]=(A-A_0)/(\varepsilon_1-\varepsilon_0)$,[36] K_1 is given by

$$K_1 = \frac{(A-A_0)/(\varepsilon_1-\varepsilon_0)}{\{[FePCl]_T-(A-A_0)/(\varepsilon_1-\varepsilon_0)\}\{[B]_T-(A-A_0)/(\varepsilon_1-\varepsilon_0)\}} \quad (9)$$

where ε_1 is the molar extinction coefficient of Fe(PPDME)BCl. Assuming that the spectra of mono- and bis-adducts are similar at 500 nm, the value of ε_2 in the calculation of β_2 was used as that of ε_1 in Eq. 9.[14] Thus, the values of K_1 in Table 1 are only approximate, but they are, nevertheless, of the correct order of magnitude.

Absorption Spectra and Equilibria of the Fe(PPDME)Cl–Hindered Imidazole System. The addition of hindered imidazoles to Fe(PPDME)Cl in chloroform resulted in the spectral changes summarized in Figs. 3 (base: 2-methylimidazole) and 4 (base: 2-ethylimidazole). The absorption maxima of the product obtained were 360.0

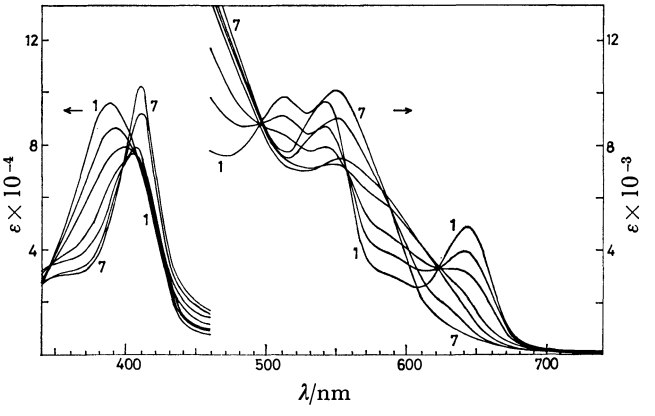

Fig. 3. Spectral changes observed upon addition of 2-methylimidazole (0—1.2 M) to an 0.15 mM solution of Fe(PPDME)Cl in chloroform (illustrated for 7 concentrations out of 18 ones measured). 2-Methylimidazole concentrations: 1, 0 mM; 2, 9 mM; 3, 15 mM; 4, 30 mM; 5, 90 mM; 6, 0.3 M; 7, 1.2 M.

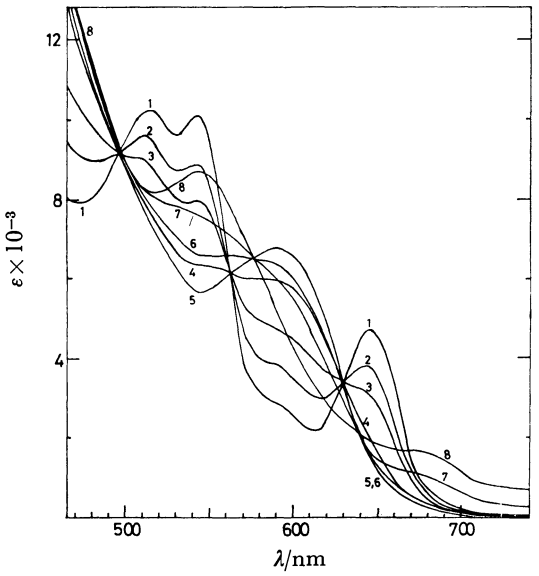

Fig. 4. Spectral changes observed upon addition of 2-ethylimidazole (0—3 M) to an 0.015 mM solution of Fe(PPDME)Cl in chloroform (illustrated for 8 concentrations out of 17 ones measured). 2-Ethylimidazole concentrations: 1, 0 mM; 2, 9 mM; 3, 15 mM; 4, 30 mM; 5, 0.12 M; 6, 0.6 M; 7, 1.2 M; 8, 3 M.

sh, 410.6, 451.0 sh, and 550.0 nm for 2-methylimidazole, and 410.8, 450.0 sh, and 544 nm for 2-ethylimidazole. In the case of the addition of 2,4-dimethylimidazole, the spectral changes were similar to those in Fig. 3. In the case of the addition of 1,2-dimethyl- and 2-phenylimidazole, however, even when the base was added up to the solubility limit, the spectrum was not further changed from that similar to the intermediate spectrum in Fig. 3 and in Fig. 4 respectively. The isosbestic points for 2-methylimidazole (Fig. 3) were observed at 496, 558, and 625 nm for the lower molar ratios of [2MeIm]/[Fe(PPDME)Cl] and at 586 nm for the higher ratios, while those for 2-ethylimidazole (Fig. 4) were observed at 494, 563, and 628 nm for the lower molar ratios of [2EtIm]/[Fe(PPDME)Cl] and at 582 and 643 nm for the higher ratios. No distinct isosbestic points were present in the range of the Soret band, as is shown in Fig. 3. These spectral changes appear to be markedly different from those for unhindered imidazoles. The two sets of isosbestic points indicate that the equilibria involve mono- and bis-adducts.

This spectral behavior shows that the addition of hindered imidazoles to Fe(PPDME)Cl occurs in two steps. Since the equilibrium involve mono- and bis-adducts, the following relation can be derived:

$$[\mathrm{FePCl}]_T = [\mathrm{FePCl}] + [\mathrm{FePBCl}] + [\mathrm{FePB_2Cl}] \quad (10)$$

$$[\mathrm{B}]_T = [\mathrm{B}] + [\mathrm{FePBCl}] + 2[\mathrm{FePB_2Cl}] \quad (11)$$

$$A = \varepsilon_0[\mathrm{FePCl}] + \varepsilon_1[\mathrm{FePBCl}] + \varepsilon_2[\mathrm{FePB_2Cl}] \quad (12)$$

where the absorbances are for a 1-cm light path. In the second step of the reaction, $[\mathrm{FePCl}]_T$ can be approximately equal to $[\mathrm{FePBCl}]+[\mathrm{FePB_2Cl}]$, A, to $\varepsilon_1[\mathrm{FePBCl}]+\varepsilon_2[\mathrm{FePB_2Cl}]$, and $[\mathrm{B}]_T$, to $[\mathrm{B}]$, because a base was present in a large excess relative to $[\mathrm{FePCl}]_T$. Thus, K_2 is given by

$$K_2 = \frac{[\mathrm{FePB_2Cl}]}{([\mathrm{FePCl}]_T - [\mathrm{FePB_2Cl}])[\mathrm{B}]_T} \quad (13)$$

Then,

$$A = \varepsilon_1([\mathrm{FePCl}]_T - [\mathrm{FePB_2Cl}]) + \varepsilon_2[\mathrm{FePB_2Cl}],$$

and letting

$$A_1 = \varepsilon_1[\mathrm{FePCl}]_T, \quad (14)$$

we obtain:

$$[\mathrm{FePB_2Cl}] = (A - A_1)/(\varepsilon_2 - \varepsilon_1) \quad (15)$$

From Eqs. 13 and 15, the following equation is derived:

$$\frac{[\mathrm{FePCl}]_T}{A - A_1} = \frac{1}{K_2(\varepsilon_2 - \varepsilon_1)}\frac{1}{[\mathrm{B}]_T} + \frac{1}{\varepsilon_2 - \varepsilon_1} \quad (16)$$

Such a value of A_1 that a plot of $[\mathrm{FePCl}]_T/(A-A_1)$ against $1/[\mathrm{B}]_T$ gives a straight line at a given wavelength was convergently computed by the use of the least-squares method. From this straight line (its slope and intersection with the ordinate), the A_1 value, and Eq. 14, the values of ε_1, ε_2, and K_2 were obtained. Such a calculation was made on three or four wavelengths; the mean of the K_2 values thus obtained given in Table 2. The ε_1 value evaluated from the above calculation agreed reasonably well with that estimated directly from the results of spectral changes at some wavelengths (*e.g.*, at 586 nm in Fig. 3).

Further, by the use of the ε_1 value thus obtained, K_1 in the first step of the reaction was calculated by means of Eq. 9; then, the mean values and the standard deviations were evaluated (Table 3). In the case of 1,2-dimethyl- and 2-phenylimidazole, K_1 was calculated by the use of the ε_1 value estimated from the spectral changes.

Dissociation of Fe(PPDME)B_2Cl and Equilibria in a Chloroform–Ethanol Mixed Solvent. When the

Table 3. Formation constants of porphyrin iron(III) complexes with hindered imidazoles at 25 °C

Porphyrin complex	Solvent	Base	pK_a(BH$^+$)[a]	log K_1[b]	log K_2[b]	log β_2[b]	References
Fe(PPDME)Cl	$CHCl_3$	2,4DMeIm	8.06	1.78±0.07	0.77		This work
		1,2DMeIm	7.85	0.71±0.04	<-0.6		
		2EtIm	7.70	1.31±0.04	0.02		
		2MeIm	7.56	1.75±0.07	0.78		
		2PhIm	6.09	1.04±0.05			
	$ClCH_2CH_2Cl$	2MeIm	7.56	1.24±0.07	0.66		
Fe(TPP)Cl	$CHCl_3$	1,2DMeIm	7.85	0.53		0.97	14
		2MeIm	7.56	1.20		3.52	14

a) See Footnote a of Table 1. b) β_2, in units of M^{-2}; K_1 and K_2, in units of M^{-1}.

reaction of (tetraphenylporphyrinato)iron(III) chloride (Fe(TPP)Cl) with 1-methylimidazole in chloroform was examined under a low concentration of Fe(TPP)Cl (7.6×10^{-7} M), the following equilibrium was observed in the system[14]

$$Fe(TPP)Cl + 2NMeIm \rightleftarrows Fe(TPP)(NMeIm)_2^+ + Cl^- \quad (17)$$

In this study, a similar examination was made in [Fe(PPDME)Cl] $= 7.5 \times 10^{-6}$ M. As is shown in Table 1, the value of β_2 was essentially independent of [Fe(PPDME)Cl], though the value and the deviation increased only slightly with lowering of [Fe(PPDME)Cl]. Thus, for Fe(PPDME)Cl in chloroform the influence of the equilibrium of Eq. 17 is considered to be negligible in concentrations higher than [Fe(PPDME)Cl] $= 7.5 \times 10^{-6}$ M.

The effects of the polar and hydrogen-bonding solvent on the formation constant were investigated in chloroform containing 1, 5, and 10 vol % ethanol for the three bases of imidazole, 1-methyl-, and 2-methylimidazole. For the addition of imidazole and 1-methylimidazole, the overall spectral changes in the mixed solvents were similar to those for imidazole in chloroform (in Fig. 1), whereas for the addition of 2-methylimidazole they were similar not to those for 2-methylimidazole in chloroform (in Fig. 3), but to those for 2-ethylimidazole in chloroform (in Fig. 4). As is shown in Table 4, β_2 decreased for imidazole, but increased for 1-methylimidazole, with an increase in the ethanol content. For 2-methylimidazole, as the ethanol content increased, K_1 markedly increased, whereas K_2 slightly decreased.

Table 4. Formation constants of (protoporphyrin IX dimethyl ester)iron(III) complexes in chloroform–ethanol mixed solvents at 25 °C

Solvent	Base	log K_1[a]	log K_2[a]	log β_2[a]
$CHCl_3$	Im	2.8		6.72±0.04
	NMeIm	1.6		3.77±0.05
	2MeIm	1.75±0.07	0.78	
$CHCl_3$–1%EtOH	Im	3.0		6.79±0.07
	NMeIm	1.7		3.94±0.04
	2MeIm	2.05±0.07	0.3	
$CHCl_3$–5%EtOH	Im	2.7		6.50±0.11
	NMeIm	1.6		3.99±0.21
	2MeIm	3.11±0.06	<0.03	
$CHCl_3$–10%EtOH	Im	2.6		6.35±0.14
	NMeIm	1.8		4.48±0.26

a) See Footnote b of Table 3.

The spectra of Fe(PPDME)Cl in these mixed solvent was unchanged at the content of ethanol lower than 20 vol %, whereas above that point spectral changes which seemed to originate from ethoxo coordination were observed.

Discussion

Absorption Spectra of the Fe(PPDME)Cl–Imidazoles System. Upon the addition of unhindered imidazole to a Fe(PPDME)Cl solution, the spectra changed from those of free Fe(PPDME)Cl (high-spin) to those of the bis-adduct, Fe(PPDME)B_2Cl (low-spin). These overall spectral changes are very similar to those for the (deuteroporphyrin IX dimethyl ester)iron(III)–imidazole system.[8] The fact that the low-spin bis-adducts formed have essentially identical spectra for the eight unhindered imidazoles indicates that the stereochemistry of the bis-adducts is not appreciably dependent on the nature of these axial bases.

Upon the addition of hindered imidazole to a Fe(PPDME)Cl solution, the spectra of mono-adduct Fe(PPDME)BCl was intermediately obtained in the course of spectral changes from Fe(PPDME)Cl to Fe(PPDME)B_2Cl, as is shown in Figs. 3 and 4.[37] The spectra of a bis-adduct with hindered imidazoles are similar to those with unhindered imidazoles, but the wavelengths of the absorption maxima at around 545 and 570 nm for the former were found to change with the degree of steric hindrance. It has been pointed out by Smith and Williams that these absorption bands in the low-spin spectra of the porphyrin iron(III) complex are sensitive to the nature of the axial ligands.[35] The wavelengths of the Soret and the characteristic bands (around 590 nm) in the mono-adduct spectra are given in Table 5. The wavelength of this Soret band is intermediate between that for Fe(PPDME)Cl and Fe(PPDME)B_2Cl. The band at around 590 nm is considered to be a charge-transfer band characteristic of high-spin five-coordinated porphyrin iron(III) complexes.[35,38] These mono-adducts may be either five-coordinated ion-pairs, in which chloride is in the outer coordination sphere, or

Table 5. Absorption maxima for high-spin five-coordinated porphyrin iron(III) complexes

Porphyrin[a] complex	Solvent	Base or ligand	λ max/nm		References
Fe(PPDME)	$CHCl_3$	Cl^-	389	644	This work
		1,2DMeIm	405	595 sh	
		2PhIm	401	593	
		2EtIm	400	586	
		2MeIm	406	580 sh	
		2,4DMeIm	405	577	
	CH_2Cl_2–10%EtOH	Ethoxo	400	580, 598 sh	39
Fe(DPDME)	benzene	F^-	393	587	38
		Cl^-	373	628	38
		I^-	368	641	38
μ-oxo[Fe(PPDME)]$_2$			397	573, 599	40

a) See Footnote a of Table 2.

six-coordinated complexes in which the interaction of chloride with iron(III) is considerably weak. The wavelength of this characteristic band is comparable to those of the following complexes: (deuteroporphyrin IX dimethyl ester)iron(III) with fluoride,[38] ethoxo(protoporphyrin IX dimethyl ester)iron(III),[39] and μ-oxo-bis-(protoporphyrin IX dimethyl ester iron(III))[40] (Table 5). In these complexes, it is known that the interaction of iron with the axial ligand is relatively strong and that the iron atom is displaced from porphyrin plane toward the axial ligand[38]; thus, it seems that the second axial ligand can not readily coordinate to iron(III).

Effect of the Base on Formation Constant. In the case of hindered imidazoles, no correlation between the basicity of these bases and the formation constants is found, as is shown in Table 3. On the contrary, in the case of unhindered imidazoles such a correlation is clearly found, as is shown in Fig. 5; that for NH imidazoles (Im, 4MeIm, 4PhIm) is different from that for NR imidazoles (NMeIm, NEtIm, 5ClNMeIm), though the plots for histamine and 1-acetylimidazole in Fig. 5 deviate from straight lines.

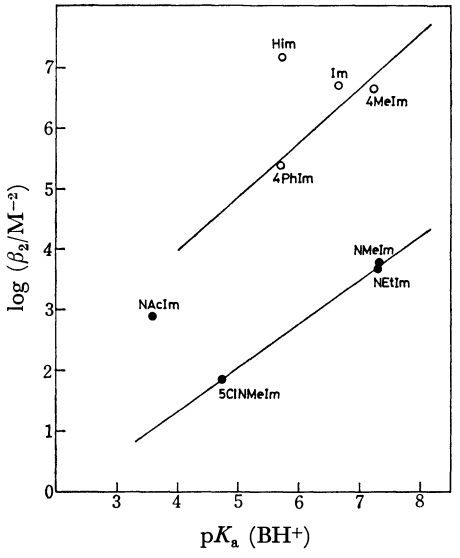

Fig. 5. Relationships between log β_2 and the basicity of unhindered imidazoles: ○, β_2 for NH imidazoles; ●, β_2 for NR imidazoles.

For the (protoporphyrin IX dimethyl ester)iron(III) and the (tetraphenylporphyrinato)iron(III) complexes, the log β_2 values for NH imidazole are larger than that for NR imidazole by about 3.1 and 3.3 log units on the average respectively. The larger value of β_2 for NH imidazole is considered to be based on the stabilization by the delocalization of the positive charge on iron(III) through Interaction I[14] or II.[25,26] In the case of the Interaction I, the delocalization of the positive charge on iron(III) leads to an increase in β_2, whereas the association between coordinated and free NH imidazole may lead to a decrease in β_2. Thus, it seems unlikely that the Interaction I contributes to the increase of about 3 log unit in β_2. The interaction of chloride with the NH group of imidazole has been suggested in a study of the crystal structure of bis(imidazole)tetraphenylporphyrinatoiron(III) chloride.[27] Furthermore, the appreciable

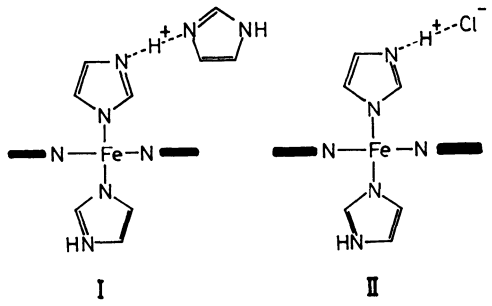

interaction of halide with the NH group of coordinated NH imidazoles has been confirmed by EPR and NMR measurements of the deuteroporphyrin IX dimethyl ester[9] and teraphenylporphyrin iron(III) complexes with NH imidazoles in solution.[26] Accordingly, the stabilization of the complex with NH imidazoles may be mainly due to Interaction II. Thus, it seems unreasonable that the complexes with NH imidazoles are represented by the formula of the ion-pair, Fe(PPDME)-$B_2^+Cl^-$.

The log β_2 for histamine is larger than that which would be predicted from the straight line of NH imidazole in Fig. 5, which is probably based on the additional stabilization of the complex by intramolecular hydrogen bonding between the amino group and the carbonyl group at the porphyrin periphery.[31] The log β_2 for 1-acetylimidazole is also larger than that which would be predicted from the straight line of NR imidazole in Fig. 5. In 1-acetylimidazole, which is known to be a good acetylating reagent, the nitrogen atom at the 1-position of the imidazole ring is susceptible to nucleophilic attack because the acetyl group with an electron-withdrawing ability attracts the electron on the nitrogen atom.[41] In this case, the chloride of the nucleophilic reagent in Fe(PPDME)Cl can interact with the nitrogen atom. Thus, through such interaction the positive charge on iron(III) is delocalized and stabilized; consequently, the formation constant may increase relatively.

In these cases, the two axial imidazoles of the bis-adduct are nonequivalent, because only one chloride is present in a bis-adduct molecule.[25] For both NH and NR imidazoles, the ratios of log K_1/log β_2 are in the narrow range of 0.3—0.4. Thus, it is not possible to specify whether the stabilization of the complex based on the interaction with chloride is accompanied by the axial coordination of NH imidazole in the first step, in the second step, or in the intermediate state.

The coordination of 4-substituted imidazoles to iron-(III) may be equivalent to that of 5-substituted ones caused by rapid tautomerism, for no lowering of the formation constants based on the steric effect was observed.

The basicity of the protoporphyrin IX dimethyl ester is higher than that of tetraphenylporphyrin and lower than that of octaethylporphyrin;[33] therefore the decreasing order of the formation constant for these porphyrin iron(III) complexes can be expected to be: TPP> PPDME>OEP.[21,22,32,42] Such a trend, however, is not clearly found in Table 2. The formation constants for (protoporphyrin IX dimethyl ester)iron(III) complexes should be compared with those for substituted deutero-

porphyrin iron(III) complexes, for which few data have been reported.

Solvent Effect on Formation Constants. The solvent effect on formation constants may be described in terms of the polarity and the hydrogen-bonding ability of the solvents. When the forms of mono- and bis-adducts are the ion-pairs of $Fe(PPDME)B^+Cl^-$ and $Fe(PPDME)B_2^+Cl^-$ respectively, these formation constants can be expected to increase with the polarity of the solvents.[10,11,15] The hydrogen bonding between base and solvent complicates the situation. As for the thermodynamics of the (tetraphenylporphyrinato)iron(III) complex with imidazole in various solvents (acetone, ethyl acetate, DMF, $CHCl_3$, and CH_2Cl_2), it has been reported by Ciaccio *et al.* that the hydrogen-bonding solvents combine with free imidazole to decrease the formation constants,[15] while Walker *et al.* have reported that chloroform, with a weak hydrogen-bonding ability, reduces the self-association of NH imidazole and thus allows the formation constants to be larger than in other solvents.[14]

NR imidazoles are not capable of self-association, but the nitrogen at the 3-position of free NR imidazole can hydrogen-bond to the hydrogen-bonding active group such as NH, OH, and CH in solvent molecules. Such a hydrogen bonding can decrease the formation constants, as has been pointed out by Ciaccio *et al.*[15] Since chloroform is stronger in hydrogen-bonding ability[43] and lower in polarity than 1,2-dichloroethane, β_2 ($CHCl_3$) $<\beta_2$ ($C_2H_4Cl_2$) for 1-methylimidazole in Table 1 seems to be reasonable.

On the contrary, for imidazole, 2-methyl-, and 1-acetylimidazole the formation constants in chloroform are larger than in 1,2-dichloroethane (Tables 1 and 2). The explanation for NH imidazole that the self-association is reduced with the hydrogen-bonding ability of solvents and that, thus, the formation constants are: in $CHCl_3$ $<$in $C_2H_4Cl_2$ is inapplicable to that for the 1-acetylimidazole of the NR imidazole.[44] A feature common to the complexes with these three imidazole bases is that the chloride strongly interacts with the coordinated base; thus, the complex is markedly stabilized, as described above. This interaction between the chloride and the coordinated base may be weakened with the solvent polarity because of a concomitant slight dissociation of the chloride ion; consequently, the formation constants of the complexes may decrease with the solvent polarity. To the solvent effect on the complex formation with these imidazole bases, the contribution of the polarity is considered to surpass that of the hydrogen-bonding ability.

Ethanol is the polar and the hydrogen-bonding solvent. The polarity of a chloroform–ethanol mixed solvent can increase with the ethanol content. The fact that β_2 for imidazole decreases with the ethanol content suggests that the interaction between the chloride and the imidazole NH group is weakened with the polarity of the solvent, thus lowering the stability of the complex (Table 4). Since the complex with 1-methylimidazole is an ion-pair in contrast to that with imidazole, the β_2 increases with the polarity of the solvent. Thus, for the system of imidazole and 1-methylimidazole, the effect of the addition of ethanol to the chloroform solution may be explained on the basis of the increase in polarity. The fact that K_1 for 2-methylimidazole markedly increases with the ethanol content, whereas K_2 slightly decreases, indicates that the stability of the mono-adduct is remarkably enhanced with the ethanol content; the reason for this remains to be clarified.

In the (protoporphyrin IX dimethyl ester)iron(III) complexes, the solvent effect is further complicated by the possibility of the hydrogen bonding of the solvent molecule with the ester carbonyl group at the porphyrin periphery relative to the cases of the tetraphenylporphyrin and octaethylporphyrin iron(III) complexes.

Steric Effect on Formation Constants. As is shown in Table 3, the formation constants of the complexes with hindered imidazoles are found to decrease with the degree of steric hindrance provided by the 2-substituent. The formation constant, K_1, for 1,2-dimethylimidazole is the smallest in the systems studied here, for the 1-methyl group hinders the bending of the 2-methyl group to avoid the steric interaction with the porphyrin plane.[25] The plot of log K_1 against the wavelength of the absorption maximum at around 590 nm characteristic of the mono-adduct is found to be linear, as is shown in Fig. 6. In the mono-adduct which exhibits this band on the longer-wavelength side, the displacements of the iron atom from the porphyrin plane are considered to be larger.

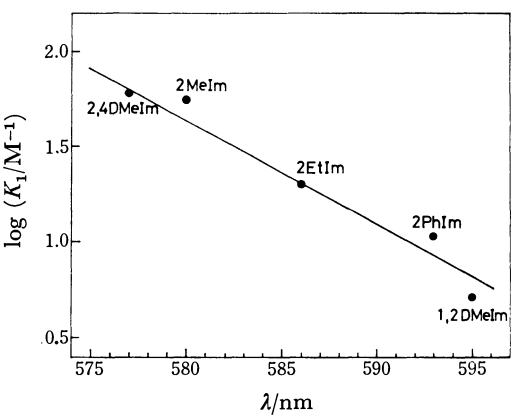

Fig. 6. Relationships between log K_1 and the wavelength of absorption maxima for the mono-adduct with hindered imidazole.

In the porphyrin iron(III) complex, in which a change in the spin state from high- to low-spin occurs upon the addition of the second axial base, the formation constant, K_1, can be smaller than K_2. Accordingly, the relation of $K_1>K_2$ for the complexes with hindered imidazoles is probably based on the steric reason. On the contrary, for the tetraphenylporphyrin iron(III) complex with 2-methylimidazole it is reported to be $K_1 <\beta_2/K_1$ ($=K_2$).[14] It seems that the bis-adduct of (protoporphyrin IX dimethyl ester)iron(III) with hindered imidazoles is not readily isolated because $K_1<K_2$.

References

1) "Inorganic Biochemistry," ed by G. L. Eichhorn,

Elsevier, Amsterdam (1973).
2) M. F. Perutz, *Nature*, **228**, 726 (1970).
3) R. W. Cowgill and W. M. Clark, *J. Biol. Chem.*, **198**, 33 (1952).
4) H. S. Olcott and A. Lukton, *Arch. Biochem. Biophys.*, **93**, 666 (1961).
5) N. S. Angerman, B. B. Hasinoff, H. B. Dunford, and R. B. Jodan, *Can. J. Chem.*, **47**, 3217 (1969).
6) B. B. Hasinoff, H. B. Dunford, and D. G. Horne, *Can. J. Chem.*, **47**, 3225 (1969).
7) P. Hambright, *Coord. Chem. Rev.*, **6**, 247 (1971).
8) M. Momenteau, *Biochim. Biophys. Acta*, **304**, 814 (1973).
9) M. Momenteau, J. Mispelter, and D. Lexa, *Biochim. Biophys. Acta*, **320**, 652 (1973).
10) J. M. Duclos, *Bioinorg. Chem.*, **2**, 263 (1973).
11) C. L. Coyle, P. A. Rafson, and E. H. Abbot, *Inorg. Chem.*, **12**, 2007 (1973).
12) T. H. Davies, *Biochim. Biophys. Acta*, **329**, 108 (1973).
13) E. H. Abbot and P. A. Rafson, *J. Am. Chem. Soc.*, **96**, 7378 (1974).
14) F. A. Walker, M-W. Lo, and M. T. Ree, *J. Am. Chem. Soc.*, **98**, 5552 (1976).
15) P. R. Ciaccio, J. V. Ellis, M. E. Munson, G. L. Kedderis, F. X. McConville, and J. M. Duclos, *J. Inorg. Nucl. Chem.*, **38**, 1885 (1976).
16) E. v. Goldammer and H. Zorn, *Z. Naturforsch.*, **31b**, 242 (1976).
17) M. Nappa, J. S. Valentine, and P. A. Snyder, *J. Am. Chem. Soc.*, **99**, 5799 (1977).
18) R. F. Pasternack and J. R. Stahlbush, *J. Chem. Soc., Chem. Commun.*, **1977**, 106.
19) R. F. Pasternack, B. S. Gillies, and J. R. Stahlbush, *J. Am. Chem. Soc.*, **100**, 2613 (1978).
20) J-T. Wang, H. J. C. Yeh, and D. F. Johnson, *J. Am. Chem. Soc.*, **100**, 2400 (1978).
21) G. N. LaMar and F. A. Walker, *J. Am. Chem. Soc.*, **94**, 8607 (1972).
22) G. N. LaMar, *J. Am. Chem. Soc.*, **95**, 1662 (1973).
23) G. N. LaMar, J. D. Satterlee, and R. V. Snyder, *J. Am. Chem. Soc.*, **96**, 7137 (1974).
24) R. V. Snyder and G. N. LaMar, *J. Am. Chem. Soc.*, **98**, 4419 (1976).
25) J. D. Satterlee, G. N. LaMar, and J. S. Frye, *J. Am. Chem. Soc.*, **98**, 7275 (1976).
26) J. D. Satterlee, G. N. LaMar, and T. J. Bold, *J. Am. Chem. Soc.*, **99**, 1088 (1977).
27) D. M. Collins, R. Country, and J. L. Hoard, *J. Am. Chem. Soc.*, **94**, 2066 (1972).
28) A. Takenaka, Y. Sasada, E. Watanabe, H. Ogoshi, and Z. Yoshida, *Chem. Lett.*, **1972**, 1235.
29) R. G. Little, K. R. Dymock, and J. A. Ibers, *J. Am. Chem. Soc.*, **97**, 4532 (1975).
30) J. P. Collman and C. A. Reed, *J. Am. Chem. Soc.*, **95**, 2048 (1973).
31) T. Yoshimura, T. Ozaki, Y. Shintani, and H. Watanabe, *J. Inorg. Nucl. Chem.*, **38**, 1879 (1976).
32) J. E. Falk, "Porphyrins and Metalloporphyrins," Elsevier, Amsterdam (1964).
33) K. M. Kadish and G. Larson, *Bioinorg. Chem.*, **7**, 95 (1977).
34) T. Yoshimura, T. Ozaki, and Y. Shintani, *J. Inorg. Nucl. Chem.*, **39**, 185 (1977).
35) D. W. Smith and R. J. P. Williams, *Struct. Bonding (Berlin)*, **7**, 1 (1970).
36) S. Nagakura, *J. Am. Chem. Soc.*, **80**, 520 (1958).
37) The spectra of the mono-adduct are similar to those of μ-oxo-bis[Fe(PPDME)].[40] The μ-oxo dimer is known to form in the presence of an aqueous base.[10] In this study, bases and solvents were sufficiently dried; the absence of water was confirmed by a study of the infrared spectrum; sample preparation and measurements were carried out rapidly and carefully.
38) W. S. Caughy, "Inorganic Biochemistry," ed by G. L. Eichhorn, Elsevier, Amsterdam (1973), Vol. 2, p. 797.
39) S. C. Tang, S. Koch, G. C. Papaefthymiou, S. Foner, R. B. Frankel, J. A. Ibers, and R. H. Holm, *J. Am. Chem. Soc.*, **98**, 2414 (1976).
40) G. A. Smythe, W. H. Fuchsman, T. H. Moss, H. R. Lilienthal, and W. S. Caughey, *Bioinorg. Chem.*, **5**, 125 (1975).
41) H. A. Staab, *Angew. Chem., Int. Ed. Engl.*, **1**, 351 (1962).
42) "Porphyrins and Metalloporphyrins," ed by K. M. Smith, Elsevier, Amsterdam (1975).
43) G. C. Pimentel and A. L. McClellan, "The Hydrogen Bond," W. H. Freeman, San Francisco (1960), Chap. 6.
44) The hydrogen bonding between the acetyl carbonyl group of 1-acetylimidazole and the CH group of chloroform is not observed from the IR spectra, in which the carbonyl stretching frequencies of 1-acetylimidazole in carbon tetrachloride, chloroform, dichloromethane, and 1,2-dichloroethane are essentially identical.

Differential Determination of Tellurium(IV) and Tellurium(VI) by Atomic Absorption Spectrophotometry after Hydride Generation. Combined Use of Titanium(III) Chloride as a Prereductant and Sodium Borohydride Solution

Kazuo JIN,* Mitsuhiko TAGA,* Hitoshi YOSHIDA, and Seiichiro HIKIME

Department of Chemistry, Faculty of Science, Hokkaido University, Nishi-8-chome, Kita 10-jo, Kita-ku, Sapporo, 060

(Received September 2, 1978)

Sensitive determination of tellurium was investigated by atomic absorption spectrophotometry after hydride generation and differential determination of tellurium(IV) and tellurium(VI) in acidic solution was carried out. When sodium borohydride solution is used without any prereductant, only the signal from tellurium(IV) is obtained. On the other hand, when titanium(III) chloride solution is added before the addition of borohydride solution, total signal from tellurium(IV) and tellurium(VI) can be obtained; 30—60 s of prereduction is required. The effectiveness of the titanium(III) chloride–borohydride reduction system is shown in the interference study. The interference of selenium(IV) is eliminated up to 200 fold *vs.* 0.25 μg of tellurium(IV) in 20 cm^3 of 3 mol dm^{-3} hydrochloric acid by the use of 2 cm^3 of 5% w/v titanium(III) chloride solution as a prereductant. Tellurium in steel and sulfur (commercial reagent) can be determined satisfactorily without isolation of tellurium from matrix by this method. Detection limit of the method is 8 ng. The coefficient of variation of the method is 2.4% in the ten determinations of 0.25 μg of tellurium.

Determination of a trace amount of tellurium has become of interest in recent years. Tellurium is harmful to the strength of steel[1,2] and high temperature alloys[3] even in a low concentration; in geochemical aspects it is useful as an indicator element.[4–6] Bismuthiol-II is one of the most sensitive reagents in the spectrophotometric determination of tellurium(IV),[7–9] but complete separation of tellurium from interfering ions, *e.g.*, selenium, copper, vanadium, and palladium is required. Although flame atomic absorption spectrophotometry is especially convenient method for the determination of tellurium containing selenium,[10–12] the sensitivity is not yet sufficient for the determination of tellurium in concentration below ppm, and tellurium should be concentrated by solvent extraction[2,10] or coprecipitation with arsenic.[9,10] Hydride generation-atomic absorption spectrophotometry has also been applied to determine tellurium because of its high sensitivity.[13–15] In the method titanium(III) chloride together with magnesium[13] or sodium borohydride[14,15] has been used as a reductant to generate tellurium hydride. There have been no reports, however, on the differential determination of tellurium(IV) and tellurium(VI) in the same solution by atomic absorption spectrophotometry. In order to find suitable experimental conditions for determining tellurium by hydride generation-atomic absorption spectrophotometry, experiments have been carried out.

It was found that sodium borohydride reduces tellurium(IV) to tellurium hydride and is not effective for the reduction of tellurium(VI), and that titanium(III) chloride reduces tellurium(VI) to tellurium(0) *via* tellurium(IV). By utilizing the differences in ability of reduction for tellurium spieces, differential determination of tellurium(IV) and tellurium(VI) in the solution was satisfactorily carried out. When sodium borohydride solution was added alone to the mixed solution of tellurium(IV) and tellurium(VI), only the signal from tellurium(IV) was obtained and not from tellurium(VI). On the other hand, when titanium(III) chloride solution was added to the solution as a prereductant prior to the addition of borohydride solution, total signal from tetravalent and hexavalent tellurium was obtained. Both the concentration of titanium(III) chloride and the prereduction time affected the sensitivity of this method.

This procedure was applied to the determination of trace amounts of tellurium in steel and sulfur.

Experimental

Apparatus. A Hitach Model 170-50 type atomic absorption spectrophotometer with deuterium background corrector and a tellurium hollow-cathode lamp (Hamamatsu TV) were used. A modified Hitachi arsenic determination unit was used for the generation of tellurium hydride; a reaction vessel (vol 115 cm^3) was connected to a dispenser (REBURET, Nippon Garasu Ryoki Co., Ltd.) with a silicone tube (ϕ=1.5 mm) attached firmely to a teflon cap as shown in Fig. 1. A prescribed volume of borohydride solution was introduced

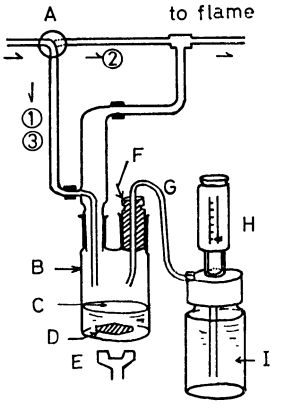

Fig. 1. Reaction vessel and piping diagram used for the evolution of tellurium hydride.
A: Electric valve, ①~③ flow paths of nitrogen; B: reaction vessel; C: sample solution; D: spin bar E: magnetic stirrer; F: Teflon cap; G: silicone tube; H: dispenser; I: sodium borohydride solution.

Table 1. Conditions for nitrogen-hydrogen flame

Wavelength		214.3 nm
Lamp current		4 mA
Slit width	inlet	0.4 mm
	outlet	0.5 mm
Nitrogen flow rate		8 dm^3 min^{-1}
Hydrogen flow rate		7 dm^3 min^{-1}
Aux. nitrogen flow rate		2.5 dm^3 min^{-1}
Height of beam above burner tip		20 mm

instantly from the dispenser into the reaction vessel through the silicone tube. Generated tellurium hydride was carried into a nitrogen-hydrogen flame (one slot burner with 10 cm) and atomic absorption signals were recorded with a Hitachi 056 type recorder. Conditions for the nitrogen-hydrogen flame are given in Table 1.

Reagents. Standard tellurium(IV) solution (1000 ppm Te(IV)–3 mol dm^{-3} hydrochloric acid): 2.000 g of metallic tellurium (99.999%) was dissolved in 8 cm^3 of nitric acid and 10 cm^3 of hydrochloric acid, and the solution was dried up on a water bath. Ten cm^3 of hydrochloric acid was added and the solution was dried up, the procedure being repeated three times. After addition of 500 cm^3 of hydrochloric acid, the solution was diluted exactly to 2000 cm^3 with water. The solution was used by sequential dilution. Standard tellurium(VI) solution: 1.072 g of sodium tellurate ($Na_2TeO_4 \cdot 2H_2O$) was dissolved in hydrochloric acid and diluted exactly to 500 cm^3 with water (1000 ppm Te(VI)–3 mol dm^{-3} hydrochloric acid). The solution was also used by sequential dilution. Titanium chloride(III) solution (5% w/v): 12.5 g of titanium(III) chloride was dissolved in 125 cm^3 of 6 mol dm^{-3} hydrochloric acid, and diluted to 250 cm^3. Sodium borohydride solution (5% w/v, 1% sodium hydroxide): Five grams of sodium borohydride was dissolved in 100 cm^3 of 1% w/v sodium hydroxide. Other reagents were of analytical reagent grade. Deionized water was twice distilled.

Procedure. Transfer a prescribed volume of sample solution containing less than 0.8 μg of tellurium into a reaction vessel, add 5 cm^3 of hydrochloric acid, and dilute the solution to 20 cm^3 with water. Put spin bar into the vessel and set up it on hydride generation unit. Pass nitrogen gas in the vessel for 20 s. Turn electric valve to pass nitrogen through bypass to burner, and start magnetic stirrer. Pour 5 cm^3 of 5% w/v borohydride solution into the vessel from a dispenser when stirring becomes stationary, and lead the generated tellurium hydride to burner with hydrogen generated at the same time and record the signal of tellurium on the recorder. Pass nitrogen through the vessel for cleaning when the signal returns to baseline. Then, exchange the reaction vessel for another one. Determination of one sample can be done within about 1 min.

Results and Discussion

For hydride generation-atomic absorption method, the geometry of reaction vessel, atomizer unit, flow rate of auxiliary nitrogen (or argon), volume and concentration of borohydride solution, volume of sample solution and its acidity play important roles in determining the detection limit and sensitivity. These factors were studied independently in order to elucidate individual effects.

Effect of the Concentration of Sodium Borohydride Solution. Effects of sodium borohydride solution in the concentration range 3—8% w/v and of the solution volume on the sensitivity were examined in 3 mol dm^{-3} hydrochloric acid. The use of low concentration of borohydride resulted in low sensitivity of the method and the solution of high concentration was less stable than that of low concentration. Increase of the volume of borohydride solution up to 8 cm^3 increased sensitivity of the method. On the other hand, the accuracy of the method decreased apparently when more than 5 cm^3 of borohydride was used. Because of these limitations, 5 cm^3 of 5% w/v sodium borohydride was used throughout this study in view of sensitivity and accuracy of the method.

Flow Rate of the Auxiliary Nitrogen. The flow rate of auxiliary nitrogen, which was made to flow through the reaction vessel, was chosen to be 0—5 dm^3 min^{-1}. With increase of the flow rate of nitrogen, the peak height of tellurium decreased gradually. Therefore, nitrogen was made to flow through a bypass after the removal of oxygen from the system. No significant difference in sensitivity appeared between nitrogen-hydrogen flame and argon-hydrogen flame.

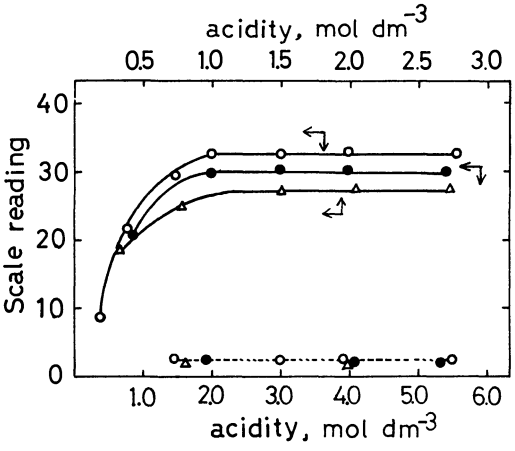

Fig. 2. Effect of acids on the sensitivity.
Te(IV): 0.25 μg/20 cm^3; 5% w/v $NaBH_4$: 5 cm^3.
-○- HCl, -●- HNO_3, -△- H_2SO_4.
Broken line indicates blank values for acids.

Effect of Acid. The sensitivity of this method was examined with use of a borohydride solution in hydrochloric acid, nitric acid, or sulfuric acid. The results are shown in Fig. 2. The absorption peaks of tellurium are slightly less in the cases of nitric acid and sulfuric acid media than in the case of hydrochloric acid medium, but in each case constant signals were obtained in the acid concentration range 2—5.5 mol dm^{-3}.

When the reaction vessel was replaced by a small one (vol 50 cm^3), the difference in peak height decreased, almost the same signal being obtained in hydrochloric acid and nitric acid media.

Volume of Solution in the Reaction Vessel. The efficiency of the reduction of tellurium(IV) to tellurium hydride decreased almost linearly with increase of the volume of solution in the reaction vessel from 10 to 50 cm^3; *e.g.*, the peak height of 0.25 μg of tellurium in 50 cm^3 was about one fourth of that in 10 cm^3. Therefore the volume of sample solution was chosen to be 20 cm^3 in order to attain best detection limit and precision of the method.

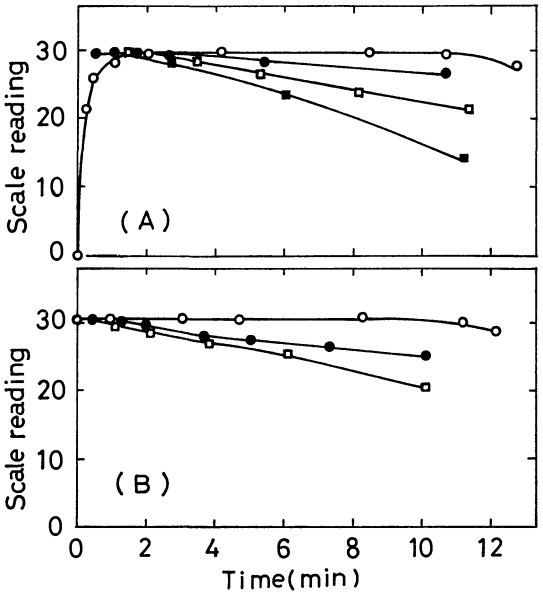

Fig. 3. Effect of the amount of titanium(III) chloride as a function of prereduction time.
(A) Te(VI), 0.25 μg/3 mol dm^{-3} HCl, (B) Te(IV), 0.25 μg/3 mol dm^{-3} HCl. 5% w/v $NaBH_4$: 5 cm^3, 5% w/v $TiCl_3$: -○- 1 cm^3, -●- 2 cm^3, -□- 4 cm^3, -■-5 cm^3.

Addition of Titanium(III) Chloride as a Prereductant of Tellurium(VI). Tellurium(VI) could not be reduced to tellurium hydride with borohydride alone (Fig. 3). Reduction of tellurium(VI) was carried out satisfactorily by the use of titanium(III) chloride together with borohydride. However, the peak height changes apparently with the concentration of titanium chloride(III) and prereduction time. In order to attain constant reduction of tellurium(VI) to tellurium(IV), the concentration of titanium(III) chloride and prereduction time, time from addition of the reagent to the injection of borohydride solution, were examined. The results are shown in Fig. 3. More than 120 s of prereduction time is required to obtain constant peak height when 1 cm^3 of 5% w/v titanium(III) chloride is used. When 2 cm^3 of 5% w/v titanium(III) chloride is used together with borohydride, almost constant peak height is obtained within 20—120 s of prereduction time. The peak height of tellurium is reduced considerably with increase in the volume of titanium(III) chloride and the prereduction time. This suggests that tellurium(VI) is reduced gradually to tellurium(0) *via* tellurium(IV) by titanium(III) chloride and precipitates in the reaction vessel. The same phenomenon is observed for tellurium(IV) as shown in Fig. 3. Within 90 s of prereduction time, addition of 2 cm^3 of 5% w/v titanium(III) chloride to the acidic tellurium(IV) solution before addition of borohydride solution does not reduce the peak height and gives satisfactory result.

Differential Determination of Tellurium(IV) and Tellurium(VI). Figure 3 suggested the possibility of differential determination of tellurium(IV) and tellurium(VI). Tellurium(IV) was determined by reduction with borohydride alone, and total amount of tellurium was determined by the reduction of tellurium using 2 cm^3 of 5% w/v titanium(III) chloride for one min, followed by addition of 5% w/v sodium borohydride. The results are shown in Fig. 4, in which total amount of tellurium is kept 0.4 μg and the mixing degree of tellurium(IV) and tellurium(VI) is varied. Tellurium(IV) can be determined regardless of tellurium(VI) by borohydride alone as a reductant.

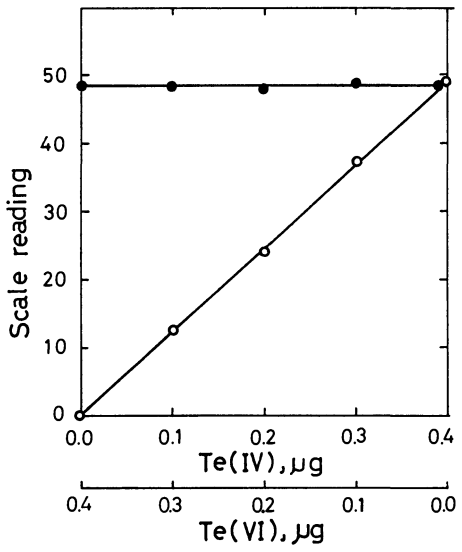

Fig. 4. Differential determination of tellurium(IV) and tellurium(VI).
Total tellurium: 0.4 μg; -○- 5% w/v $NaBH_4$: 5 cm^3, -●- 5% w/v $TiCl_3$: 2 cm^3 (prereduction time: 1 min), 5% w/v $NaBH_4$: 5 cm^3.

Influence of Diverse Ions. The influence of diverse

Table 2. Comparison of permissible amounts of foreign ions for tellurium determination (within 10% negative error, ion (μg) *vs.* 0.25 μg of Te(IV))

Ion	Reduction system			
	$NaBH_4$[a)]	KI–$NaBH_4$[b)]	$TiCl_3$–$NaBH_4$[c)]	$TiCl_3$–Mg[d)]
Ag(I)	1.0	5.0	1.25	6.25
As(III)	0.75	2.5	5.0	7.5
As(V)	25	15	75	7.5
Bi(III)	5.0	5.0	3.75	50
Cu(II)	25	75	25	27.5
Hg(II)	1.25	1.25	2.5	1.25
Se(IV)	5.0	75	50	35
Sb(III)	5.0	5.0	5.0	7.5
Ni(II)	25	25	25	50
Co(II)	50	250[e)]	250[e)]	50
Pb(II)	125	250[e)]	250[e)]	125
Cd(II)	50	250[e)]	200	250[e)]

a) The following ions does not influence in excess amount (2500 μg): Na, K, Mg, Ca, Sr, Ba, Zn(II), Cr(III), Al(III), Fe(III), Mo(VI), Mn(II), V(V), SO_4^{2-}, NO_3^-, $C_2O_4^{2-}$, Br^-, SiO_3^{2-}, CH_3COO^-, ClO_4^-; Te(IV) 0.25 μg/3 mol dm^{-3}–HCl, 20 cm^3; 5% w/v $NaBH_4$, 5 cm^3. b) 20% KI, 1 cm^3, prereduction: 5 min. c) 5% w/v $TiCl_3$, 2 cm^3. d) 5% $TiCl_3$, 1 cm^3+0.5 g Mg, 6 mol dm^{-3} HCl. e) No influence.

ions on the determination of tellurium(IV) is given in Table 2. When borohydride alone is used as a reductant, relatively large interference arises in the order: arsenic(III)>silver(I)>mercury(II)>bismuth(III)>selenium(IV), antimony(III)>arsenic(V), copper(II), and nickel(II). Various reductants were used together with borohydride in order to eliminate the interference. Tin(II) chloride cannot be used because of uncorrectable background absorption. Potassium iodide is useful for eliminating the interference of some coexisting ions, especially selenium(IV); coexisting 200 fold of selenium(IV) *vs.* tellurium(IV) does not interfere when 2 cm^3 of 20% w/v potassium iodide is used as a prereductant (5 min of prereduction time). Titanium(III) chloride is also useful for eliminating the interference of selenium(IV) (Table 2).

Titanium(III) chloride–magnesium system[13] was also reexamined as regards the generation of tellurium hydride, and the results were compared with that of titanium(III) chloride–borohydride reduction system. Granular magnesium, wrapped in a wafer sheet, was added to sample solution containing titanium(III) chloride (6 mol dm^{-3} hydrochloric acid). The effect of diverse ions on the determination of tellurium is almost the same in these two reduction systems. However, reduction of tellurium by borohydride is superior to titanium(III) chloride–magnesium system in sensitivity, reproducibility, and handling.

In each reduction system, anions listed in Table 2 do not interfere in 10000 fold excess of tellurium in the determination.

Detection Limit and Precision of the Method. Calibration curves for tellurium(IV) determination by borohydride reduction and for tellurium(VI) by titanium(III) chloride–borohydride reduction are both linear up to 0.8 μg of tellurium. The coefficients of variation in the determinations of 0.25 μg tellurium(IV) and the same amount of tellurium(VI) were 2.4% and 2.9%, respectively. Detection limit of the method is 8 ng (S/N=2).

Determination of Tellurium in Steel. Prior to application of the method, the effect of iron(III) matrix on the determination of tellurium was examined (Fig. 5). Iron(III) does not interfere up to 40 mg *vs.* 0.25 μg of tellurium(IV) by sodium borohydride, or 0.25 μg tellurium(VI) by titanium(III) chloride–sodium borohydride reduction system. No separation or preconcentration technique is required for the determination of ppm level of tellurium in iron matrix, if there is no other interfering ion. The standard steel was dissolved by the following procedure; 0.1 g steel was weighed precisely in a 50 cm^3 beaker. After addition of 3 cm^3 of hydrochloric acid and 1 cm^3 of nitric acid, the mixture was heated on a water bath, and the steel was dissolved. The solution was diluted to 50 cm^3 with water in a measuring flask after cooling. A prescribed volume of this solution was transferred to the reaction vessel and determination was carried out by means of the titanium(III) chloride–borohydride reduction(Table 3). The procedure could be completed within 30 min. Almost the same results were obtained in the standard addition and calibration curve techniques.

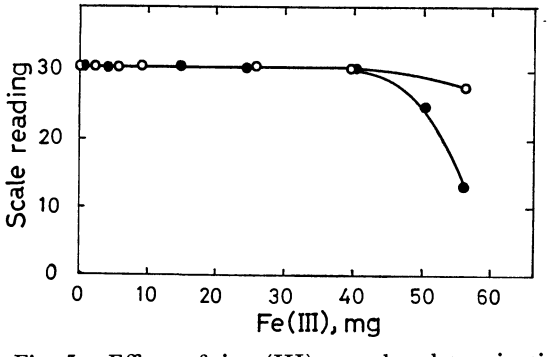

Fig. 5. Effect of iron(III) on the determination of tellurium.
-○- Te(IV) 0.25 μg/3 mol dm^{-3} HCl, 5% w/v $NaBH_4$, 5 cm^3. -●- Te(VI) 0.25 μg/3 mol dm^{-3} HCl, 5% w/v $TiCl_3$, 2 cm^3 (prereduction time, 40 s) 5% w/v $NaBH_4$, 5 cm^3.

Determination of Tellurium in Sulfur. The proposed technique was also applied to the determination of tellurium in commercial reagent sulfur. The results are given in Table 4. The modified procedure of Arikawa[12] was used: Sulfur powder (*ca.* 0.1 g) was weighed in a teflon beaker; 5 cm^3 of 3 mol dm^{-3} sodium hydroxide solution was added, and the mixture was heated on a hot plate (*ca.* 150 °C) in order to dissolve the powder. After cooling, 20 cm^3 of water was added, followed by 4 cm^3 of 30% w/v hydrogen peroxide solution to oxidize sulfur to hexavalent (tellurium is also oxidized to hexavalent). Excess hydrogen peroxide was then decomposed by careful heating. Finally, 10 cm^3 of hydrochloric acid was added, and the solution was diluted to 100 cm^3 with

Table 3. Determination of tellurium in steel

Sample	Taken(g)	Te Found (g)[a]	Te %	Certified %
Tellurium-1[b]	0.0585	3.5	0.0059	0.0056_3
	0.1040	5.8	0.0056	
	0.1255	6.9	0.0055	
		average	0.0056_7	
Tellurium-2[b]	0.1052	8.0	0.0076	0.0075_3
	0.1140	8.2	0.0072	
	0.1088	8.1	0.0074	
		average	0.0074	
A[b]	0.1095	22	0.020	0.02[c]
	0.1070	21	0.020	
	0.4456	85	0.019	
	0.3588	75	0.021	
	1.0239	200[d]	0.020	
	1.0107	208[d]	0.021	
	2.0122	390[d]	0.019	
		average	0.020	
B[b]	0.3390	332	0.098	0.10[c]
	0.5233	512	0.098	
	0.3524	573	0.103	
		average	0.099_7	

a) Average of three determinations. b) Supplied by Japan Steel Works, Ltd. (Muroran Plant). c) Tellurium content of the sample. d) Separated from iron matrix by tin(II) chloride precipitation procedure.

TABLE 4. DETERMINATION OF TELLURIUM IN REAGENT SULFUR

Sample		Te		
Form	Taken(g)	Found(μg)	%	
Powder	0.1047	3.8_1	0.003_6	
	0.0664	2.5_3	0.003_8	mean=
	0.1103	4.3_0	0.004_0	
	0.0616	2.0_9	0.003_4	0.003_6
	0.1015	3.4_5	0.003_4	
	0.1014	7.7	(4 μg of Te was added)	
	0.0983	10.1	(6 μg of Te was added)	
Sublimed	0.1017	1.9_0	0.001_9	0.002_0
	0.1044	2.1	0.002_0	
Colloidal	0.5041	0.08	0.00002	
	0.3172	0.07	0.00002	
Crystalline	0.6718		<0.00001	
	0.5108		<0.00001	

a) Average of three determinations

water. An adequate volume of the solution was transferred to the vessel and the tellurium was determined by titanium(III) chloride–borohydride reduction system (2 cm^3 of 5% w/v titanium(III) chloride for 1 min of prereduction time). Though the titanium(III) chloride–borohydride reduction system cannot be applied to sulfuric acid medium, the presence of 2 mmol sulfuric acid in 3 mol dm^{-3} hydrochloric acid caused no interference. The standard addition technique and calibration technique gave almost the same results.

References

1) H. D. Fleming and R. G. Ide, *Anal. Chim. Acta*, **83**, 323 (1976).
2) M. V. Marcec, K. Kinson, and C. B. Belcher, *Anal. Chim. Acta*, **41**, 447 (1968).
3) G. G. Welcher, O. H. Kriege, and J. Y. Marks, *Anal. Chem.*, **46**, 1227 (1974).
4) B. C. Severner and R. R. Brooks, *Talanta*, **19**, 1467 (1972).
5) L. P. Greenland and E. Y. Campbell, *Anal. Chim. Acta*, **87**, 323 (1976).
6) J. A. Corbett and W. C. Godbeer, *Anal. Chim. Acta*, **91**, 209 (1977).
7) H. Yoshida and S. Hikime, *Bunko Kenkyu*, **14**, 131 (1966).
8) H. Yoshida, M. Taga, and S. Hikime, *Talanta*, **13**, 185 (1966).
9) S. Maekawa and K. Katho, *Bunseki Kagaku*, **19**, 10 (1970).
10) C. L. Chakrabarti, *Anal. Chim. Acta*, **39**, 293 (1967).
11) S. Musha, S. Munemori, and T. Nakahara, *Nippon Kagaku Kaishi*, **89**, 495 (1968).
12) Y. Arikawa, *Bunseki Kiki*, **14**, 477 (1976).
13) E. N. Pollock and S. J. West, *At. Abs. Newslett.*, **12**, 6 (1973).
14) K. C. Thompson and D. R. Thomerson, *Analyst*, **99**, 595 (1974).
15) J. A. Fiorino, J. W. Jones, and S. G. Capar, *Anal. Chem.*, **48**, 120 (1976).

Curve Fitting Methods Applied to the Elucidation of Asymmetric Gas-Liquid Chromatographic Peaks

Koji TAKEUCHI and Tomihito KAMBARA*

Department of Chemistry, Faculty of Science, Hokkaido University, Sapporo 060

(Received September 8, 1978)

It was shown that the shape of gas-liquid chromatographic peak is expressed by the Gaussian distribution multiplied by a higher order algebraic equation of time. Application of the curve fitting methods, *i.e.*, the Newton's divided-difference formula and the orthogonal polynomials method, could well clear up the experimentally observed gas-liquid chromatograms of trailing and leading types, respectively. The asymmetric shapes of gas-liquid chromatographic peaks are attributed to the slowness of vaporization or dissolution in the partition process.

Although one observes in general the trailing type peaks in gas-solid adsorption chromatography, in gas-liquid partition chromatography the peaks of trailing and leading shapes[1–3] are observed at higher and lower column temperatures, respectively.

As to the asymmetric shapes of gas chromatographic peaks, there has been given only a qualitative explanation that the partition isotherm of a solute component between the mobile and stationary phases is nonlinear, as described in the several monographs.[4–6] A mathematical model for nonlinear partition based on the numerical solution by means of computer was proposed.[7] The theory by Schmauch[8] explains only the leading type peak, and on the contrary the papers by the Littlewood school[9,10] and others[11,12] deal with only the trailing peak expressed as the convolution of exponential decay constant. The derivative method for gas chromatograph developed by Saitoh *et al.*[2,13–17] is not only very useful in trace analysis but also gives important knowledges about the asymmetric shapes.

It is pointed out that the rate of vaporization is slow at lower temperature and on the other hand the rate of dissolution into stationary phase becomes too small at higher temperature, hence the partition equilibrium does hold no more. In this case a new theory dealing with the kinetically irreversible partition process between both phases is required.

As reported in our previous paper[18] the asymmetric gas-liquid chromatographic peaks are expressed by the series consisting of the Gaussian distribution G and its derivatives. In this paper the familiar curve fitting methods are applied to the mathematical analysis of the experimentally observed gas-liquid chromatograms of leading and trailing shapes.

Theoretical

The system of differential equations given by Kambara and Ohzeki[19] is as follows:

$$F\frac{\partial C}{\partial t} = -F\frac{\partial}{\partial x}\left(-\frac{D^*}{P}\frac{\partial C}{\partial x}+uC\right) + \alpha(K^{-1}C_s - C) \quad (1)$$

$$F_s\frac{\partial C_s}{\partial t} = -\alpha(K^{-1}C_s - C) \quad (2)$$

Equations 1 and 2 represent the concentration changes of the injected solute with time in the mobile and stationary phases, respectively. The meanings of symbols are summarized in Table 1. When the column temperature is lower than the optimum temperature, the rate of vaporization $\alpha K^{-1} C_s$ may be much smaller than that of dissolution αC. On the contrary, αC may be much smaller compared with $\alpha K^{-1} C_s$ at higher temperature. It is thus considered that the partition equilibrium would not hold at the column temperature much higher or lower than the optimum one.

The approximate solution of Eqs. 1 and 2 has been already presented as[19]

$$C(l, t) = \frac{p_o C_0 t_0}{p_l\sqrt{2\pi}\sigma}\exp\left\{-\frac{(t-t_R)^2}{2\sigma^2}\right\}. \quad (3)$$

On the basis of this expression the dependences of HETP on the flow rate of carrier gas,[20] on the column temperature[21] and on the column length[22] are elegantly clarified. For the convenience of the following treatment, one writes

$$\frac{p_o C_0 t_0}{p_l} = A, \quad (4)$$

$$t - t_R = \xi, \quad (5)$$

$$G(\xi) = \frac{1}{\sqrt{2\pi}\sigma}\exp\left(-\frac{\xi^2}{2\sigma^2}\right). \quad (6)$$

Therefore, Eq. 3 can be written as the product of peak area A and the normal or Gaussian distribution $G(\xi)$:

$$C(l, \xi) = AG(\xi) \quad (7)$$

At the appropriate temperature, both the rates of dissolution and vaporization being great, the term in the left-hand side of Eq. 2 is negligibly small compared with the two terms in the right-hand side. Then, one has

$$C_s(l, \xi) = KC = KAG(\xi). \quad (8)$$

Namely, the equilibrium holds at every position in the column. At higher or lower temperature, the concentrations in both phases are no more equilibrated. In this case one should treat the problem kinetically. As derived in our previous paper[18] the outlet concentration is shown by

$$C(l, \xi) = A(G \pm zG^{(1)} + z^2G^{(2)} \pm z^3G^{(3)} + z^4G^{(4)} \pm z^5G^{(5)} + \cdots), \quad (9)$$

where plus sign holds for trailing peak and minus sign for leading peak, respectively.

Furthermore, Eq. 9 can be rewritten in the alternative form. Derivatives of Gaussian distribution $G^{(n)}$ are calculated as

$$G^{(1)} = -\frac{\xi}{\sigma^2}G(\xi) \quad (10)$$

TABLE 1. LIST OF SYMBOLS

Symbol	Meaning	Units
A	peak area	mol s cm^{-3}
a_i	coefficient in Eq. 12	s^{-i}
b	z/σ	dimensionless
C	solute concentration in mobile phase	mol cm^{-3}
$C(l, \xi)$	outlet concentration in mobile phase, dependent on ξ	mol cm^{-3}
C_s	solute concentration in stationary phase	mol cm^{-3}
$C_s(l, \xi)$	outlet concentration in stationary phase, dependent on ξ	mol cm^{-3}
C_0	initial solute concentration injected	mol cm^{-3}
D^*	diffusion constant at unit pressure	cm^2 s^{-1} atm
F	volume fraction occupied by mobile phase	dimensionless
F_s	volume fraction occupied by stationary phase	dimensionless
$G(\xi)$	Gaussian distribution described by Eq. 6	s^{-1}
$G^{(n)}$	n-th derivative of $G(\xi)$	s$^{-(n+1)}$
h	peak height	mol cm^{-3}
K	partition coefficient (C_s/C at equilibrium)	dimensionless
l	column length	cm
p	pressure of carrier gas dependent on x	atm
p_1	pressure of carrier gas at column inlet	atm
p_0	pressure of carrier gas at column outlet	atm
R	skew ratio	dimensionless
t	time elapsed after solute fed	s
t_R	retention time of solute component	s
t_0	duration of concentration pulse injected	s
u	linear gas velocity dependent on x	cm s^{-1}
x	distance from inlet along the column	cm
y	a function expressed by $C(l, \xi)/AG(\xi)$	dimensionless
z	F_sK/α	s
α	rate constant of dissolution of solute	s^{-1}
σ^2	peak variance	s^2
ξ	time measured from retention time defined by Eq. 5	s

$$G^{(2)} = \frac{1}{\sigma^2}\left(\frac{\xi}{\sigma^2} - 1\right)G(\xi). \tag{11}$$

Insertion of these derivatives into Eq. 9 gives the following Eq. 12 in which the elution profile $C(l, \xi)$ is a product of $AG(\xi)$ and a high-order algebraic equation of ξ.

$$C(l, \xi) = AG(\xi)(a_0 + a_1\xi + a_2\xi^2 + a_3\xi^3 + a_4\xi^4 + a_5\xi^5 + \cdots) \tag{12}$$

The coefficient a_i (i=0, 1, 2, $\cdots$) is given by

$$\begin{aligned} a_0 &= 1 - b^2 + 3b^4 - \cdots \\ a_1 &= \pm\sigma^{-1}(b - 3b^3 + 15b^5 - \cdots) \\ a_2 &= \sigma^{-2}(b^2 - 6b^4 + 45b^6 - \cdots) \\ a_3 &= \pm\sigma^{-3}(b^3 - 10b^5 + 105b^7 - \cdots) \\ a_4 &= \sigma^{-4}(b^4 - 15b^6 + 210b^8 - \cdots) \\ a_5 &= \pm\sigma^{-5}(b^5 - 21b^7 + 378b^9 - \cdots) \end{aligned} \tag{13}$$

where

$$b = \frac{z}{\sigma} \tag{14}$$

Thus, a theoretical expression for the asymmetric elution profiles in partition chromatography is shown by Eq. 9 or 12, which is reduced to Eq. 3 when z tends to zero.

According to Eq. 12, $C(l, \xi)$ divided by $AG(\xi)$ is defined as

$$y = \frac{C(l, \xi)}{AG(\xi)} = a_0 + a_1\xi + a_2\xi^2 + a_3\xi^3 + a_4\xi^4 + a_5\xi^5 + \cdots \tag{15}$$

Experimental

Reagents and Apparatus. Helium was used as the carrier gas. Benzene and diethyl ether (Wako Pure Chemicals Co.) were used as solute and diluent, respectively. A Hitachi gas chromatograph, Model 063, with a flame ionization detector was employed. The output current of FID was amplified and then recorded with a Hitachi 056 recorder. The packing of 25% dinonyl phthalate on 60/80 mesh Shimalite supplied by Shimadzu Seisakusho Ltd. was packed into a stainless steel column of 4 mm i.d. and 1 m in length. A soap-film flowmeter was used for the measurement of flow rate.

The column temperature was varied in the range of 45.7—93.0 °C and maintained within ±0.1 °C of the set temperature. The temperatures of injection port and detector were fixed at 105 °C. Carrier gas flow rate was adjusted to 30.0±0.3 ml min^{-1}.

The solute amount smaller than 0.8 μl was confirmed to have no effect on the number of theoretical plates for benzene. Therefore, a 5-μl portion of benzene diluted 10-fold with diethyl ether was injected. The gas chromatograms are reproduced in Fig. 1.

Estimation of t_R and σ. The apparent retention time as measured at the peak maximum depends slightly on the solute amount fed when the column temperature deviates from the optimum one. The chromatograms with varying amounts of

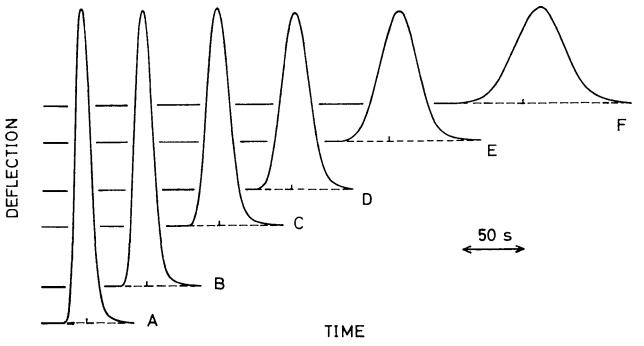

Fig. 1. Gas chromatograms of benzene at various temperatures. Sample size injected was 0.5 μl and detected by FID. Each peak was corrected for the temperature dependence of detector sensitivity to have the same peak area. Column temperature: A 93.0, B 83.3, C 74.1, D 64.8, E 55.0, F 45.7 °C. The mark on the base line indicates the corrected retention time. The other data are shown in Table 5.

benzene smaller than 0.5 μl were accurately superimposed on the one with 0.5 μl so as to give the true retention time. Retention time was determined by extrapolating the solute amount to zero, *i.e.*, at the point on which the line connecting the maxima of the peaks intersects the base line, as Fig. 2 shows.

The standard deviation σ, namely, the square root of the peak variance needs to be estimated. It was presumed that the quantity 2σ is given by the peak width at the peak height of $e^{-1/2} \cdot h$, where h is the maximum peak height. Peak area A was calculated by the so-called trapezoidal rule with the known $C(l, \xi)$ values at equi-spaced points. Skew ratio R is defined as the ratio of the slopes of tangents at the inflection points on both sides of the peak,[24] and calculated for each chromatogram as a measure of asymmetry.

Curve Fitting Methods. The mathematical expression for the experimentally observed y-function shown by Eq. 15 was determined by means of the familiar curve fitting methods. One is the Newton's divided-difference formula[25] and the other is the orthogonal polynomials.[25,26] The former is one of the interpolation formula which is advantageous in treating with a curve of the complicated form such as the results observed at higher temperatures (curves d and d′ in Fig. 2). The latter is the most general method of curvilinear regression by the method of least squares and suitable for the simple and monotone function as seen in the case obtained at lower temperatures (curves c and c′ in Fig. 2). Another advantage of the orthogonal polynomials is that one can easily decide what order of polynomials should be statistically significant when the analysis of variance table is constructed. The algebraic equations determined are plotted and this operation is repeated until the satisfactory fitting is confirmed.

Results and Discussion

The theoretical elution profiles were calculated with the derivative series including the fifth order derivative shown by Eq. 9, as reported before. When the value z was smaller than 0.45σ, Eq. 9 was found to fit well. A symmetric Gaussian peak is obtained when $z=0$ and the distortion of peak becomes more remarkable with increasing value of z. Skew ratio R was evaluated as 1.06 (leading), 0.94 (trailing) with $z=0.40\sigma$; 1.68 (leading), 0.60 (trailing) with $z=0.45\sigma$. With z-value greater than 0.45σ, Eq. 9 represents an inadequate curve, the concentration $C(l, \xi)$ showing negative values at the feet of the peak.

Thus Eq. 9 was confirmed to express well the asymmetric curves of both leading and trailing types. Furthermore, another verification of Eq. 9 with experimental chromatograms was attempted. Chromatograms with varying solute amounts of 0.1—0.5 μl were carefully superimposed on a chart. Figure 2 shows the typical leading and trailing chromatograms of benzene and the mathematical analysis of y-function.

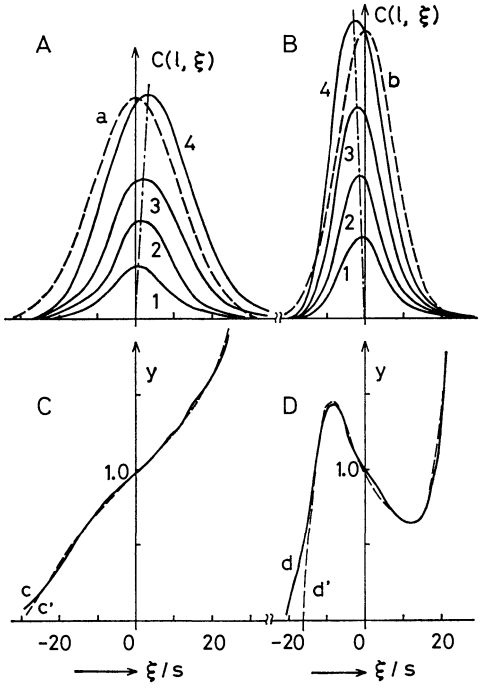

Fig. 2. Comparison of the experimentally recorded leading (curves A, 64.8 °C) and trailing (curves B, 83.3 °C) gas chromatograms of benzene (solid line) with the Gaussian peaks of the same σ-values (dashed line, curves a and b). The amount of benzene injected: 1 0.1, 2 0.2, 3 0.3, 4 0.5 μl. Curves C and D show the y-functions given by Eq. 15. Curves c and d (solid line): experimental value; curves c′ and d′ (dashed line): calculated value.

With increasing solute amount injected, the apparent rentention time of the peak maximum becomes longer in the case of leading peak, and on the contrary, it becomes shorter in the case of trailing peak (A and B in Fig. 2). The values of t_R, σ, and A were evaluated and the curves $AG(\xi)$ (dashed line, a and b in Fig. 2), which might be considered as a well-equilibrated elution profile of Gaussian type, were plotted for reference. The ratio of $C(l, \xi)$ to $AG(\xi)$ defined as y in Eq. 15 was then evaluated from experimental data (solid line, curves c and d in Fig. 2). The theoretical equations for these experimentally obtained y-functions were determined by the curve fitting methods (dashed line, curves c′ and d′). In the case of data at 83.3 °C, the Newton's divided-difference formula was applied as shown in Table 2. Several characteristic points including maximum, mini-

Table 2. Curve fitting method. Newton's divided-difference formula[a)]

ξ/s	y	Divided difference[b)]				
−12	1.2153					
		0.05308				
−8	1.4276		−0.01119			
		−0.0588		$6.936\cdot10^{-4}$		
−2	1.0748		0.001296		$-2.83\cdot10^{-5}$	
		−0.0407		$1.369\cdot10^{-5}$		$1.245\cdot10^{-6}$
6	0.7496		0.001570		$6.534\cdot10^{-6}$	
		−0.0187		$1.705\cdot10^{-4}$		
12	0.6367		0.004639			
		0.02773				
16	0.7485					

a) Data of 83.3 °C were analysed. b) The y-function is expressed as follows. $y=1.2153+0.05308\,(\xi+12)-0.01119\,(\xi+12)\,(\xi+8)+6.936\cdot10^{-4}\,(\xi+12)\,(\xi+8)\,(\xi+2)-2.833\cdot10^{-5}\,(\xi+12)\,(\xi+8)\,(\xi+2)\,(\xi-6)+1.245\cdot10^{-6}\,(\xi+12)\,(\xi+8)\,(\xi+2)\,(\xi-6)\,(\xi-12)$
$=0.9612-0.0508\,\xi+0.003121\,\xi^2+6.243\cdot10^{-6}\,\xi^3-2.3347\cdot10^{-5}\,\xi^4+1.245\cdot10^{-6}\,\xi^5$.

Table 3. Curve fitting method. Orthogonal polynomials and the calculation table[a)]

		Polynomials from zero to fifth order[b)]						y	y^2
		P_0	P_1	P_2	P_3	P_4	P_5		
ξ	−26	1	−13	325	−130	2990	−16445	0.1488	0.0221
	−24	1	−12	250	−70	690	2530	0.2196	0.0483
	−22	1	−11	181	−22	−782	10879	0.2877	0.0828
	0	1	0	−182	0	1638	0	0.9748	0.9502
	26	1	13	325	130	2990	16445	2.0727	4.2961
a_{ii}		27	1638	712530	101790	56448210	2032135560	$\sum y^2$	34.0625
λ_i		1	1	3	1/6	7/12	21/40		
β_i		1.0016	0.064735	$5.244\cdot10^{-4}$	$1.4291\cdot10^{-4}$	$7.1918\cdot10^{-6}$	$4.47\cdot10^{-8}$		

		P_0y	P_1y	P_2y	P_3y	P_4y	P_5y
ξ	−26		−1.9344	48.36	−19.34	444.91	−2447.0
	−24	equal to y	−2.6352	54.90	−15.37	151.52	555.6
	−22		−3.1647	52.07	−6.33	−224.98	3129.9
	0		0	−177.41	0	1596.72	0
	26		26.9451	673.63	269.45	6197.37	34085.6
$\sum P_iy$		27.0442	106.0365	124.5588	87.2792	695.9422	173.0

a) Data of 64.8 °C, sample number $n=27$, sample space $h=2$. b) Values of orthogonal polynomials (P_i), its sum of squares (a_{ii}) and coefficient (λ_i) are quoted from Ref. 26. $\beta_i=\frac{\lambda_i\sum P_iy}{a_{ii}}$, $P_0(d)=1$, $P_1(d)=d$, $P_2(d)=d^2-\frac{1}{12}(n^2-1)$, $P_3(d)=d^3-\frac{1}{20}(3n^2-7)d$, $P_4(d)=d^4-(3n^2-13)d^2+\frac{3}{560}(n^2-1)(n^2-9)$, $P_5(d)=d^5-\frac{5}{18}(n^2-7)d^3+\frac{1}{1008}(15n^2-230n^2+407)d$ where $d=\frac{\xi-\bar{\xi}}{h}$. The regression equation is given by $y=\beta_0P_0(d)+\beta_1P_1(d)+\beta_2P_2(d)+\beta_3P_3(d)+\cdots$ Thus, in this case, the following regression equation is obtained.
$y=0.9900+0.02458\xi-1.481\cdot10^{-4}\xi^2+1.786\cdot10^{-5}\xi^3+4.495\cdot10^{-7}\xi^4$.

mum and inflection points are picked up and the difference between the adjacent y values is divided by the difference in ξ. Upon repeating this calculation, the interpolation equation is obtained as shown in Table 2.

In the case of data at 64.8 °C, the method of orthogonal polynomials was applied and the result is given in Table 3. In the calculation table the values of orthogonal polynomials P_i are cited, and the values of y, y,^{2} and P_iy are evaluated from the experimental data. Then the product of the coefficient λ_i and $\sum P_iy$ is divided by a_{ii} to give β_i which is the coefficient of the orthogonal polynomial of i-th order. The orthogonal polynomials can be added to an arbitrary higher order until the satisfactory fitting is obtained. The analysis of variance table given in Table 4 shows that for the data of 64.8 °C the fifth order polynomial is not significant since the sum of squares contributed by the fifth order term is smaller than the residual. Therefore, the use of polynomials until fourth order is sufficient in this case.

An excellent agreement between the experimental

Table 4. Analysis of variance in orthogonal polynomials

Source of variance	Sum of squares[a] 55.0 °C	64.8 °C
1st order	13.280504	6.864310
2nd	1.174419	0.021774
3rd	0.083573	0.074837
4th	0.001454	0.008580
5th	0.000634	0.000015
Residual	0.005212	0.004542
Total	14.545796[b]	6.974058

a) Calculated by $\frac{(\sum P_i y)^2}{a_{ii}}$. b) Calculated by $\sum y^2 - \frac{(\sum y)^2}{a_{00}}$.

values and the calculated y-function was seen in Fig. 2. This treatment shows that curves c and d were fourth and fifth order algebraic equations of ξ, respectively. The deviations in the feet of a peak where the absolute value of ξ is large, may be caused by the measuring error.

Thus, the actual chromatograms of leading and trailing types were found to be reasonably expressed by Eq. 12. Consequently, the present theoretical treatment can well clear up the asymmetric peak shapes. The results successfully obtained by the curve fitting methods for chromatograms at various temperatures were tabulated in Table 5.

The retention time as well as the standard deviation decreases with increasing temperature. Although the skew ratio R also decreases with increasing temperature, it lies at about 0.87 at the optimum temperature of 73.7 °C, deviating a little from unity. As for the coefficients in Eq. 12, the first term a_0 shows its maximum value near the optimum temperature, since the degree of symmetry is mainly governed by a_0.

Development of the Kinetic Theory. Proposal of the present theory is quite similar to the development of the polarographic theory. In 1935 Heyrovsky and Ilkovic postulated the dynamic equilibrium of oxidant and reductant concentrations at the surface of dropping mercury electrode depending on the potential. Thus they succeeded in elucidating the reversible wave, as described in several monographs.[27–29] Later in 1950's several kinetic theories were proposed dealing with the irreversible reduction in which the concentrations of oxidant and reductant are not equilibrated at the electrode surface.

Thanks are due to Dr. Kunio Ohzeki for his kind discussions.

References

1) T. Kambara and H. Kodama, *J. Chromatogr.*, **17**, 66 (1965).
2) T. Kambara, and K. Saitoh, *J. Chromatogr.*, **35**, 318 (1968).
3) K. Saitoh and T. Kambara, *Bunseki Kagaku*, **20**, 1375 (1971).
4) A. B. Littlewood, "Gas Chromatography," Academic Press, London (1962), p. 12.
5) H. Purnell, "Gas Chromatography," John Wiley and Sons, New York (1962), p. 82.
6) A. I. M. Keulemans, "Gas Chromatography," 2nd ed, ed by C. G. Verver, Reinhold, New York (1959), Chap. 4.
7) J. E. Funk and G. Houghton, *Nature*, **188**, 389 (1960).
8) L. J. Schmauch, *Anal. Chem.*, **31**, 225 (1959).
9) A. H. Anderson, T. C. Gibb, and A. B. Littlewood, *Anal. Chem.*, **42**, 434 (1970).
10) A. H. Anderson, T. C. Gibb, and A. B. Littlewood, *J. Chromatogr. Sci.*, **8**, 640 (1970).
11) W. W. Yau, *Anal. Chem.*, **49**, 395 (1977).
12) R. E. Pauls and L. B. Rogers, *Anal. Chem.*, **49**, 625 (1977).
13) T. Kambara, K. Saitoh, and K. Ohzeki, *Bunseki Kagaku*, **15**, 517 (1966).
14) T. Kambara, K. Saitoh, and K. Ohzeki, *Anal. Chem.*, **39**, 409 (1967).
15) T. Kambara, K. Saitoh, and K. Ohzeki, *Bunseki Kagaku*, **16**, 721 (1967).
16) T. Kambara, S. Katada, and K. Saitoh, *Bunseki Kagaku*, **18**, 1225 (1969).
17) K. Saitoh and T. Kambara, *Kagaku No Ryoiki*, **23**, 11 (1969).
18) K. Takeuchi and T. Kambara, *Chem. Lett.*, **1978**, 1081.
19) T. Kambara and K. Ohzeki, *J. Chromatogr.*, **21**, 383 (1966).
20) T. Kambara, K. Ohzeki, and K. Saitoh, *J. Chromatogr.*, **27**, 33 (1967).
21) T. Kambara, K. Hata, and K. Ohzeki, *J. Chromatogr.*, **37**, 304 (1968).
22) K. Ohzeki, T. Kambara, and K. Kodama, *J. Chromatogr.*, **121**, 199 (1976).
23) Ref. 4, p. 166, Eqs. 5.55 and 5.56.

Table 5. Characteristics of gas chromatograms observed with varying temperatures[a]

Temp °C	t_R/s	σ/s	R	Method[b]	Coefficients in Eq. 12 determined a_0	10^2a_1	10^3a_2	10^5a_3	10^5a_4	10^6a_5
45.7	591.9	20.0	1.084	o.p.	0.7745	2.624	0.522	0.572	0	0
55.0	430.8	14.85	1.067	o.p.	0.8587	3.114	0.582	0.815	0	0
64.8	305.7	11.1	0.940	o.p.	0.9900	2.458	−0.148	1.786	0.045	0
73.3	237.2	8.9	0.923	o.p.	1.0645	1.776	−1.306	3.467	0.199	0
74.1	234.0	9.1	0.812	N	1.0755	−1.411	−0.988	7.622	0.059	0
83.3	183.2	7.25	0.698	N	0.9612	−5.079	3.121	0.624	−2.335	1.245
93.0	145.6	6.35	0.638	N	0.9078	−7.090	4.260	−4.703	−2.193	1.537

a) 25% DNP on 60/80 mesh Shimalite in 4 mm i.d., 1 m stainless column; carrier gas He 30 ml min^{-1}; detector FID. b) o.p.=orthogonal polynomials, N=Newton's divided-difference formula.

24) A. J. B. Cruickshank and D. H. Everett, *J. Chromatogr.*, **11**, 289 (1963).
25) C. R. Wylie, Jr., "Advanced Engineering Mathematics," McGraw-Hill, New York (1966), Chap. 4.
26) "Statistical Tables and Formulas with Computer Applications. JSA-1972," ed by Z. Yamauti, Japan Standards Association, Tokyo (1972), pp. 407—417.
27) P. Delahay, "New Instrumental Methods in Electrochemistry," Interscience Publishers, Inc., New York (1954), Chaps. 3 and 4.
28) J. Heyrovsky and J. Kuta, "Principles of Polarography," Academic Press, New York (1965), Chaps. 9 and 13.
29) G. Charlot, J. Badoz-Lambling and B. Trémillon, "Les Réactions Electrochimiques. Méthodes Electrochimiques d'Analyse," Masson, Paris (1959), Chaps. 3 and 4. English translation: "Electrochemical Reactions. The Electrochemical Methods of Analysis," Elsevier, Amsterdam (1962).

Measurement of Ambient Nitrogen Oxides over an Extended Period of Time by Means of a Solid Absorber Technique

Takashi YASUOKA* and Shunmei MITSUZAWA

Department of Chemistry, Faculty of Science, Tokai University, Kitakaname, Hiratsuka 259-12

(Received October 27, 1978)

A new technique using a solid substance for the absorption of nitrogen oxides in the atmosphere was developed in order to obtain an average concentration of nitrogen oxides over a period of several weeks. Nitrogen oxides is absorbed by an absorbent (alkaline earth metal peroxide), and the nitrate produced in the absorber is extracted into water to determine the amount of nitrate by the ion-selective electrode method. The concentration of atmospheric nitrogen oxides is calculated from the amount of nitrate in the extract. A quantitative relation was found between the amount of nitrogen oxides collected on the absorber and that of nitrate in the extract. Hydrogen peroxide produced by the reaction of the absorber and water did not interfere with the measurement of nitrate by the ion-selective electrode technique. Practicability of this technique was demonstrated in comparison with the automatic recording analyzer (NO_x meter) with the Saltzman reagent.

Liquid absorber techniques using absorption bottles and impingers are the most popular and convenient for analysis of gaseous pollutants in the atmosphere.[1,2] These methods are suitable for obtaining hourly or short term concentrations of air pollutants. However, they require a tedious averaging process for weekly or monthly averages. A filter paper impregnated with some reagents can also be used for sampling gaseous pollutants, such as fluorides, sulfur dioxide and nitrogen dioxide, but no report seems to have apeared on the measurement of nitrogen oxides by this method. Cuddeback *et al.*[3] reported on the use of copper shot for the collection of nitrogen dioxide, but the sampling time of this method is 24 h or less. Measurement of average concentration over a long duration of time is often necessary for practical purposes such as the biological evaluation of air pollution and studies of the corrosion of metals.

In this investigation, we attempted to develop a technique to obtain an average concentration of nitrogen oxides over a period of several weeks, using a solid substance for the absorption of nitrogen oxides in the atmosphere. Peroxides of alkaline earth metals were chosen as absorbents since (1) they absorb nitrogen dioxide and (2) they oxidize the nitrogen oxide to dioxide in the presence of humidity and the resulting nitrogen dioxide is absorbed. The nitrate produced in the absorber is extracted into water for determination of the amount of nitrate by the ion-selective electrode method. The concentration of nitrogen oxides in the air can be calculated from the concentration of nitrate.

Experiments were carried out to study the possible interference by hydrogen peroxide in the determination of nitrate, to determine the capacity of the peroxide agents in the absorption of nitrogen oxides, and to examine relevant parameters. Among the peroxides of alkaline earth metals, barium peroxide was found to be the most suitable, and was rested over a period of two weeks. The practicability of this technique was demonstrated in comparison with the automatic recording analyzer (NO_x meter) with the Saltzman reagent.

Experimental

Apparatus and Reagents. Ion-selective electrode for nitrate: Type 93-07 (Orion Co.) electrode was used and the electrode potential was measured with a pH-mV meter (Type M-5, Hitachi-Horiba Co.) against a reference electrode, type 90-02 (Orion Co.), which has a double-junction reference electrode filled with the Orion filling solution (Cat. No. 90-00-02) in the inner chamber. The response of the (pH-mV) meter was recorded on a QPD-54 recorder (Hitachi Co.).

Absorbents for nitrogen oxides: Magnesium peroxide (Kyowa-Kagaku Co.) and commercial calcium peroxide, strontium peroxide and barium peroxide of the first grade were used. They were formed into tablets of $3\phi \times 5$ mm.

Autoanalyzer of nitrogen oxides: Type GP-5B, Denki-Kagaku-Keiki Co. using the Saltzman reagent.

Calibration Curve. The calibration curve of nitrate concentration was made with potassium nitrate (1—100 ppm). Calibration curves were prepared for each absorbent (MgO_2, CaO_2, or SrO_2) by dissolving 5 g of each in water and then adding a fixed amount of nitrate to the solution followed by dilution to 50 ml with water. A series of standard solutions thus prepared were passed through a filter paper to remove the peroxide and oxide from the solution, and the nitrate and a small amount of hydroxide of alkaline earth metals produced in the absorbent during the sampling were filtered off. 2 ml of 2M-$(NH_4)_2SO_4$ and 1 ml of 1M-H_3BO_3 were then added to the filtrate in order to adjust the ionic strength and to keep the stability of the nitrate in the measurement by an ion-selective electrode.[4] For the standard solution with barium peroxide, a procedure to remove the barium ions was necessary before the addition of $(NH_4)_2SO_4$ and H_3BO_3. For this purpose, excess 2M-$(NH_4)_2SO_4$ (2 ml) was added to the solution and the resulting $BaSO_4$ was filtered off. The volume of the solution was then made to 50 ml by adding water, with the addition of 1M-H_3BO_3 for the measurement of nitrate.

Capability Tests of Absorbents. The 1 ppm nitrogen dioxide gas was prepared by the nitrogen dioxide permeation tube technique with clean air, and the 1 ppm nitrogen oxide was prepared by the dilution of 50 ppm nitrogen oxide from the tank with clean air. Concentrations of these gases were measured with an automatic recording spectrometer using the Saltzman reagent. The amount of absorption of nitrogen oxide and nitrogen dioxide was determined by the difference in concentrations of these gases in the air flow before and after exposure to the absorbents, and the amount was compared with that of nitrate measured by the ion-selective electrode technique.

Results and Discussion

Calibration Curve. The calibration curves of nitrate for each absorbent are shown in Fig. 1. The

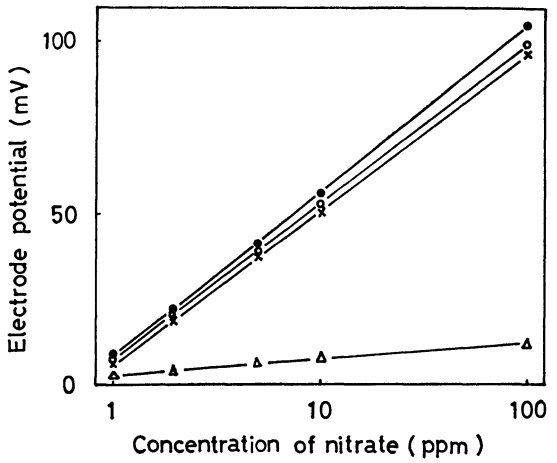

Fig. 1. Calibration curve of nitrate with each absorbent.
●: BaO_2, ○: CaO_2, ×: MgO_2, △: SrO_2.

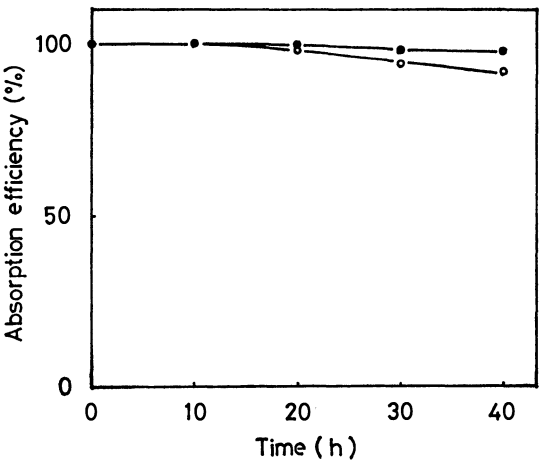

Fig. 2. Change in absorption efficiency of barium peroxide with time.
Weight of absorbent: 5 g, temperature: 25 °C, relative humidity: 50%, flow rate of gas: 300 ml/min.
Concentration of nitrogen oxide and dioxide: 1 ppm each.
●: NO_2, ○: NO.

sensitivity of nitrate measurement varies with peroxide, the order of sensitivity being $BaO_2 > CaO_2 > MgO_2 > SrO_2$. BaO_2, CaO_2, MgO_2 can be used, but BaO_2 was chosen for practical use because of its longer life as compared to that of the other peroxides.

Effect of Hydrogen Peroxide on the Nitrate Measurement by Ion-selective Electrode. Hydrogen peroxide is produced by dissolving the alkaline earth metal peroxides in water in a reaction as follows.

$$MO_2 + 2H_2O = M(OH)_2 + H_2O_2$$

where M denotes the atom of alkaline earth metal. The possible interference of hydrogen peroxide on the nitrate solutions of 10 and 100 ppm was examined by the addition of 30% hydrogen peroxide. The electrode potential generated by nitrate ions was not affected by hydrogen peroxide in the range 0.001—0.1%. This indicates that the influence of hydrogen peroxide is negligible in a solution containing 10—20 ppm of hydrogen peroxide. Kuroda endorsed this by an experiment in which he used a hydrogen peroxide solution containing phosphoric acid in the sampling of nitrogen oxides in the analysis of gaseous industrial effluents.[5] He reported that the presence of hydrogen chloride and sulfur dioxide does not interfere with analysis of nitrogen oxides. No examination of the interferences was carried out.

Absorption of Nitrogen Oxides by Barium Peroxide. The time variation of the absorption efficiency of nitrogen oxides to barium peroxide is shown in Fig. 2. Nitrogen oxide and dioxide each of concentration 1 ppm and 5 g of barium peroxide were used. The absorption efficiency of nitrogen dioxide did not change throughout 40 h, but that of nitrogen oxide decreased slightly with time, being higher than 90% after 40 h. The decrease of absorption might be attributed to a decrease in the power of the peroxide to oxidize the nitrogen oxide to dioxide.

It has been shown that 50 g of barium peroxide can remove more than 90% of nitrogen oxide from the air one month under sampling conditions of flow rate 300 ml/min and relative humidity<40%.[6] The absorption capacity of barium peroxide was demonstrated by the removal of nitrogen oxides from the air at the air inlet of an automatic NO_x meter; 50 g of barium peroxide showed complete removal of nitrogen oxides of background levels for two weeks. If an alkaline layer is placed before the peroxide layer, the former absorbs only nitrogen dioxide and the latter only nitrogen oxide. This could be utilized in a simultaneous measurement of nitrogen oxide and dioxide.

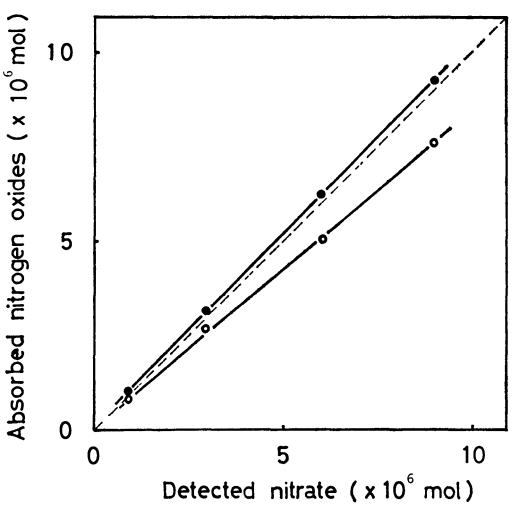

Fig. 3. Comparison of the amounts of absorbed nitrogen oxides and detected nitrate.
●: NO_2, ○: NO.
(Dotted line shows an ideal equivalent line.)

Relations between the amount of nitrogen oxides measured by NO_x meter and that of nitrate measured by the ion-selective electrode are shown in Fig. 3, where the amount of nitrate is 20% higher than that of nitrogen dioxide. The difference might be caused by the lower estimation of nitrogen oxide by the NO_x meter resulting

from the low oxidation efficiency of the $KMnO_4$–H_2SO_4 solution. If the low efficiency (80%) is corrected, the ratios of the amount of absorbed nitrogen oxides to the amount of nitrate measured by use of the peroxide become almost 1 both for nitrogen oxide and dioxide (Fig. 3). The amount of nitrogen oxides was controlled by changing the absorption time, keeping the concentration of nitrogen oxides constant.

Table 1. Comparison of data obtained by the solid sampling technique and by NO_x according to the conventional method

Date	From '78 Jan. 1st till '78 Jan. 14th		From '78 Jan. 15th till '78 Jan. 28th	
Analytical method	Solid absorbent method	Auto-analyzer	Solid absorbent method	Auto-analyzer
Concentration of NO_x in the atmosphere	0.061	0.048	0.052	0.045

Comparison of the Present Method with an Automatic NO_x *Meter.* Tests of our technique were made by setting up the barium peroxide samplers and an automatic recording analyzer for nitrogen oxides by absorption spectrometry with the Saltzman reagent for field measurements. These apparatus were operated together for two weeks, and data obtained from them were compared. Average concentrations of nitrogen oxide and dioxide during two weeks were calculated from the hourly values by the NO_x meter. The peroxide absorbent was pulverized in a mortar; 5.0 g out of the 50 g absorber was treated by the same procedure as that for the preparation of the calibration curve. The average concentrations during this period, in the first half and the latter half of January in 1978, were 0.061 and 0.052 ppm by the present method, and 0.048 and 0.045 ppm by the NO_x meter. If corrections owing to the low conversion efficiency of nitrogen oxide to dioxide were made on the latter, the data by NO_x meter would be 0.054 and 0.051. Real comparison would not be made in this way, but the concentrations obtained by the present technique are close to those by the NO_x meter. Advantages of the solid absorber technique are: (1) the size of sampling device is small, convenient for transport, (2) preparation and handling of the sampling tube is simple, (3) adjustment of the flow rate is simpler than that in the bubbling system, the shape and grain size of the peroxide being unchanged throughout the sampling period.

Conclusion

In a long run measurement, the average concentration of the nitrogen oxides can be obtained by a simple technique using a solid absorber of barium peroxide. The measurement was made by means of nitrate determination in the peroxide absorber by the use of an ion-selective electrode technique. Since the sensitivity of the ion-selective electrode, which requires 50 ml of an aliquot, is 1 ppm for the solution to be measured, the practical sensitivity of this technique for nitrogen oxides determination is 10^{-6} mol. No special cases or adjustments were required in two weeks sampling. The values of concentration of nitrogen oxides in the atmosphere were very close to those found by the NO_x meter. Advantages of this solid absorber technique are simplicity in operation and stability of air flow rate in sampling.

References

1) M. B. Jacoks and S. Hocheiser, *Anal. Chem.*, **30**, 426 (1958).
2) T. Nash, *Atmos. Environ.*, **4**, 661 (1970).
3) J. E. Cuddeback, B. E. Saltzman, and W. R. Burg, *J. A. P. C. A.*, **25**, 725 (1975).
4) P. J. Milham, A. S. Awad, R. E. Paull, and J. E. Bull, *Analyst*, **95**, 751 (1970).
5) T. Kuroda, *Bunseki Kagaku*, **22**, 1191 (1973).
6) T. Yasuoka and S. Mitsuzawa, *Nippon Kagaku Kaishi*, **1978**, 1032.

The Halomercury(II)-assisted Aquation of the Bromopentacyanocobaltate(III) Anions

Masayasu IIDA* and Hideo YAMATERA**

Department of Chemistry, Faculty of Science, Nara Women's University, Nara 630
***Department of Chemistry, Faculty of Science, Nagoya University, Chikusa-ku, Nagoya 464*

(Received November 8, 1978)

The aquation of the bromopentacyanocobaltate(III) ion was carried out in the presence of several kinds of hard acids or halomercury(II) complexes. The hard acids(H^+, Na^+, and Mg^{2+}) had small effects, while the addition of mercury(II) halides significantly accelerated the aquation. The effect of mercury(II) halides was attributed to the monohalomercury(II) cations, which were formed in a small amount by the dissociation of the dihalomercury(II) complexes. The effect of the dihalomercury(II) complexes was also studied in the presence of an excess of sodium halide. The rate constant for halomercury(II)-assisted aquation was expressed by:

$$k_{obsd} = k_0 + k_1[HgX^+] + k_2[HgX_2], \quad X^- = Cl^-, Br^-.$$

The values of k_1 and k_2 obtained ($k_1 = 1.6 \times 10^4$ mol^{-1} dm^3 s^{-1}, $k_2 = 1.0$ mol^{-1} dm^3 s^{-1}, for $X^- = Cl^-$; $k_1 = 2.0 \times 10^4$ mol^{-1} dm^3 s^{-1}, $k_2 = 1.6 \times 10^{-1}$ mol^{-1} dm^3 s^{-1}, for $X^- = Br^-$) were compared with the stability constants for the mercury(II) complexes formed by the combination with Br^-.

The metal ion-assisted aquation of halo-cobalt(III) and chromium(III) complexes has been extensively studied, and attempts have been made to correlate the rate constants with the stability constants for the respective halo complexes of the metal ions and with the electrostatic force between the reactants.[1] However, the mechanism of the reaction and the nature of the intermediate are not yet well characterized, and only cationic complexes have hitherto been studied, with a few exceptions.[2] Therefore, studies of the reaction of different types are necessary in order to generalize the reaction mechanism.

In this study, the anionic complex, $[CoBr(CN)_5]^{3-}$, was allowed to aquate in the presence of such metal ions as Na^+, Mg^{2+}, and Hg^{2+} or of the halomercury(II) complexes ($HgCl^+$, $HgBr^+$, $HgCl_2$, and $HgBr_2$). The results will be discussed in the light of those obtained for the halopentaamminecobalt(III) complexes.

Experimental

Materials. *Potassium Bromopentacyanocobaltate(III)*: The complex was prepared by Adamson's method.[3] The visible absorption spectrum of the product agreed with the published data.[3,4] Found: C, 15.39; N, 18.82%. Calcd for $K_3[CoBr(CN)_5]$: C, 15.55; N, 18.13%.

Magnesium Perchlorate Solution: Hydrous magnesium perchlorate, a guaranteed reagent of Wako Pure Chemical Industries, Ltd., was dissolved in a perchloric acid solution ($[HClO_4] = 0.05$ mol dm^{-3}) and was used as the stock solution. The magnesium concentration of this solution was determined by direct titration with EDTA (= ethylenediaminetetraacetic acid), using EBT (= Eriochrome Black T) as the indicator.

Mercury(II) Perchlorate Solution: Mercury(II) oxide was dissolved in a 5-mol dm^{-3} perchloric acid solution, and the mercury(II) perchlorate was crystallized out by cooling. The hygroscopic crystals were dissolved in a perchloric acid solution ($[HClO_4] = 0.05$ mol dm^{-3}) and thereafter used as the stock solution. The mercury(II) concentration was determined by back titration with EDTA in the presence of excess $Mg(edta)^{2-}$ ($EDTA = H_4edta$), using EBT as the indicator.

Mercury(II) Halides: Guaranteed reagents of E. Merck AG were used.

Solutions of Halomercury(II) Complexes: Proper amounts of mercury(II) halide and sodium halide were dissolved in a perchloric acid ($[HClO_4] = 0.05$ mol dm^{-3}) solution. The sodium halides used were guaranteed reagents of Wako Pure Chemical Industries, Ltd., and were dried at 110 °C before use.

Kinetic Runs. The rate of the absorbance change was measured at 35 °C for the solutions containing the complex (4.5×10^{-4} mol dm^{-3}) and the other salts. The change in absorbance was observed at 290 nm for all the solutions except for those containing tribromo- and tetrabromomercurate(II) ions, which were measured at 360 nm because of the strong absorption in the ultraviolet region.

A Hitachi 200-10 spectrophotometer was used for the slow reactions (with half-lives greater than 1 min) and a UNION RA-1300 stopped-flow spectrophotometer for the fast reactions (with half-lives less than 10 s).

The rates were determined by plotting $\ln(D_t - D_\infty)$ against the time, t, D_t, and D_∞ being the absorbances at the time t and at an infinite time respectively. The slope of this plot gives the pseudo-first-order rate constant, k_{obsd}.

Results and Discussion

Catalysis by Hard Acids. We first studied the effects of hard acids, such as protons, sodium ions, and magnesium ions, on the aquation rate of the bromopentacyanocobaltate(III) anion. The results given in Table 1 show that protons and sodium ions (ionic strength) have little effect, whereas magnesium ions slightly retard the aquation. This effect can be explain-

Table 1. Effect of hard acids on the rate of the aquation of $[CoBr(CN)_5]^{3-}$

Run	Medium (concentrations/mol dm^{-3})	$k_{obsd} \times 10^4$/s^{-1}
1	$HClO_4$ (0.084)	1.05
2	NH_4ClO_4(0.05)–NH_3(0.05) buffer pH *ca.* 9	1.12
3	NaOH (0.10)	1.09
4	$NaClO_4$ (0.14)	1.03
5	$NaClO_4$ (0.34)	1.02
6	$NaClO_4$ (0.54)	1.03
7	$NaClO_4$ (0.74)	1.02
8	$NaClO_4$ (0.97)	1.00
9	$Mg(ClO_4)_2$ (0.14)	0.85
10	$Mg(ClO_4)_2$ (0.28)	0.81

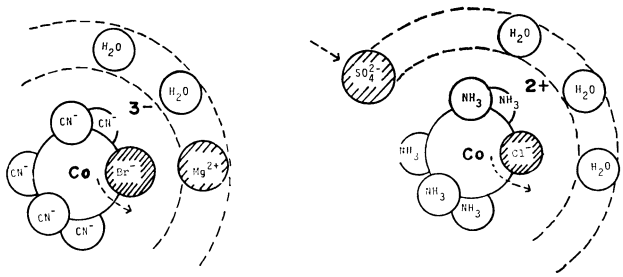

a) $CoBr(CN)_5^{3-}\cdot Mg^{2+}$ b) $CoCl(NH_3)_5^{2+}\cdot SO_4^{2-}$

Fig. 1. Structures of ion-pairs.

ed on the basis of the postulate that the spontaneous aquation of the complex proceeds by means of the "D mechanism"[5] and that the formation of ion-pairs between the complex anion and magnesium cations suppresses the dissociation of the bromide ion (Fig. 1a). It is interesting to compare this slight retardation with the appreciable acceleration of the aquation of the pentaamminechlorocobalt(III) cation caused by ion-pairing with sulfate ions.[6] The latter reaction is also known to proceed dissociatively. When a multivalent anion associates with the complex cation, it will preferentially occupy a site opposite to the chloride ligand as a result of electrostatic repulsion, and will effectively push the chloride ion out of the complex (Fig. 1b). In the present reaction systems, however, all the ligands attached to the cobalt(III) are anionic, and so little preference is shown by the magnesium ion as to the site of association with the complex anion. Thus, the effect of magnesium ions on the complex anion spreads over all the ligands, resulting in only a slight retardation of the dissociation of the bromide ligand.

Interactions with Mercury(II) Ions. Bromopentacyanocobaltate(III) anions form a pale yellow precipitate with mercury(II) cations. This reaction appears to include a mercury(II)-assisted aquation, but the follow-up of the aquation was prevented by the formation of a precipitate even if the stopped-flow technique was used. An elemental analysis of this precipitate gave a composition suggesting a mixture of $Hg[Co(OH_2)(CN)_5]$ and $Hg_3[CoBr(CN)_5]_2$.

In order to gain further information, the infrared spectrum of the precipitate was compared with that of the reactant, $K_3[CoBr(CN)_5]$. The bromo complex has a strong absorption maximum at 2140 cm^{-1} assigned to the terminal C≡N stretching, while the precipitate exhibits two absorption maxima, at 2200 cm^{-1} (strong) and 2140 cm^{-1} (medium), assigned respectively to the bridging and to the terminal C≡N stretching. In the lower-frequency region, the bromo complex exhibits Co–C stretching bands at 550 and 570 cm^{-1} (shoulder) and a precipitate at 625 cm^{-1}. This shift can be attributed to the conversion of the terminal C≡N into the bridging C≡N.[7]

These infrared results show that mercury(II) ions reacted with both cyano and bromo ligands to form cyano-bridged and partially aquated polymers. This kind of bridging polymerization of the cyano complexes by heavy metals is well known in the formation of $KFe^{III}Fe^{II}(CN)_6$, $KFe^{II}Cr^{III}(CN)_6$, *etc.*[8]

Interactions with Chloromercury(II) Complexes. On the addition of mercury(II) chloride to a dilute perchloric acid solution containing bromopentacyanocobaltate(III) ions ($[HClO_4]=0.05$ mol dm^{-3}), a rapid change in the spectrum of the complex occurred, with isosbestic points at 340 nm and 400 nm. This spectral change can reasonably be associated with the aquation of bromopentacyanocobaltate(III) ions, forming aquapentacyanocobaltate(III) ions and no other cobalt complexes. The absorbance change at 290 nm was observed by means of the stopped-flow technique and was found to follow a pseudo-first-order law in the presence of a large excess of mercury(II) chloride(more than ten times the concentration of the cobalt(III) complex). At low concentrations of mercury(II) chloride near that of the cobalt(III) complex, the $\ln(D_t-D_\infty)$ *vs.* t plots showed deviations from linear relationships. Therefore, under such conditions, the linear portions of the plots were used to obtain the rate constants. The observed pseudo-first-order rate constants, k_{obsd}, depend on the $HgCl_2$ concentration (Table 2).

Table 2. Effect of mercury(II) chloride on the rate of the aquation of $[CoBr(CN)_5]^{3-}$ $[CoBr(CN)_5^{3-}]=4.5\times10^{-4}$ mol dm^{-3}, $[HClO_4]=0.05$ mol dm^{-3}, ionic strength $=1.0$ mol dm^{-3} ($NaClO_4$).

$[HgCl_2]$/ mol dm^{-3}	$[HgCl^+]$/ mol dm^{-3}	$[HgCl_3^-]$/ mol dm^{-3}	k_{obsd}/s^{-1}
1.00×10^{-1}	2.35×10^{-4}	8.45×10^{-5}	3.00
4.98×10^{-2}	1.51×10^{-4}	3.29×10^{-5}	2.15
2.99×10^{-2}	1.12×10^{-4}	1.60×10^{-5}	1.96
9.94×10^{-3}	6.12×10^{-5}	3.26×10^{-6}	0.956
4.96×10^{-3}	4.27×10^{-5}	1.17×10^{-6}	0.668
2.47×10^{-3}	3.00×10^{-5}	4.16×10^{-7}	0.410

Table 3. Dependence of the rate on the ionic strength for the mercury(II) chloride-assisted aquation of $[CoBr(CN)_5]^{3-}$ $[CoBr(CN)_5^{3-}]=4.5\times10^{-4}$ mol dm^{-3}, $[HClO_4]=0.05$ mol dm^{-3}, $[HgCl_2]=0.01$ mol dm^{-3}, at 35 °C.

$[NaClO_4]$/ mol dm^{-3}	Ionic strength /mol dm^{-3}	k_{obsd}/s^{-1}
0	0.05	1.89
0.20	0.25	1.48
0.40	0.45	1.15
1.00	1.05	0.96

The rate constant also depends on the ionic strength, as is shown in Table 3. This suggests that the reactions occur between the ions of opposite signs and, therefore that $HgCl^+$, produced through the dissociation of $HgCl_2$, may participate in the reaction rather than the $HgCl_2$ molecule. While the formation of chloromercury(II) complexes has been studied by many workers, the stability constants obtained by Sillén *et al.*[9] at 25 °C and at an ionic strength of 0.5 are adopted here:

$$Hg^{2+} + Cl^- \rightleftharpoons HgCl^+ \qquad \log K_1 = 6.74,$$

$$HgCl^+ + Cl^- \rightleftharpoons HgCl_2 \qquad \log K_2 = 6.48,$$

$$HgCl_2 + Cl^- \rightleftarrows HgCl_3^- \qquad \log K_3 = 0.85,$$
$$HgCl_3^- + Cl^- \rightleftarrows HgCl_4^{2-} \qquad \log K_4 = 1.00.$$

The correction of these values to the present condition of $I=1.0$ and 35 °C was made as follows.

According to the results of Scaife and Tyrrell[10] and of Vasil'kevich and Shilov[11] for halomercury(II) complexes, the logarithm of the formation constant decreased by 0.1 unit with the rise in temperature from 25 °C to about 35 °C. Therefore, the values at 35 °C were estimated to be Sillén's values minus 0.1. The resulting values were then corrected to the ionic strength of 1.0 by using the Davies equation:

$$\log y_i = -0.521 z_i^2 \left(\frac{\sqrt{I}}{1+\sqrt{I}} - 0.3I \right),$$

where y_i is the activity coefficient of the i ion; z_i, its charge number, and I, the ionic strength. The corrected values are $\log K_1' = 6.77$, $\log K_2' = 6.45$, $\log K_3' = 0.75$, and $\log K_4' = 0.83$. Using these values, one can calculate the concentrations of the halomercury(II) complexes existing in the mercury(II) chloride solutions. Among them, Hg^{2+} and $HgCl_4^{2-}$ are present only in trace amounts and can be neglected.

Table 2 shows the calculated concentrations of each chloromercury(II) complex and the observed rate constants. Whereas the values of k_{obsd} show an apparent dependence on $[HgCl_2]$ to the 0.6 power, their dependence on $[HgCl^+]$ is approximately linear.

In view of the fact that reaction rates of the first order with respect to the metal-ion concentrations have been observed in many metal-ion-assisted aquations,[12] the present results can be taken as suggesting that the catalyst in the present reaction system is actually $HgCl^+$.

In order to substantiate this view, the aquation was examined in solutions containing mercury(II) chloride and an excess of sodium chloride. The concentrations of the respective chloromercury(II) complexes were calculated for each run by the use of four equilibrium constants, K_1', K_2', K_3', and K_4'. In order to see how k_{obsd} depends on the concentration of each chloromercury(II) complex, $\log(k_{obsd}-k_0)$ is plotted against $\log[HgCl_n^{2-n}]$ ($n=1$—4) in Fig. 2. The observed value of 1.0×10^{-4} s^{-1} was used for the spontaneous aquation rate constant, k_0. Figure 2 shows that the $\log(k_{obsd}-k_0)$ values have no simple correlations with the $\log[HgCl_n^{2-n}]$ values in any case except for $n=2$. This can be taken as evidence that only $HgCl_2$ molecules effectively assisted the aquation in these runs. Therefore, the results were analyzed by using this equation:

$$k'_{obsd} = k_0 + k_2[HgCl_2]$$

(in solutions containing mercury(II) chloride and an excess of sodium chloride)

which gave $k_2=(1.0\pm0.1)$ mol^{-1} dm^3 s^{-1}. This value of k_2 shows that the contribution of $HgCl_2$ to the reaction can be neglected when mercury(II) chloride reagent is added. Therefore, from Table 2 the second-order rate constant, k_1, of the $HgCl^+$-assisted reaction was found to be $(1.6\pm0.2)\times10^4$ mol^{-1} dm^3 s^{-1}. Thus, the pseudo-first-order rate constant for the chloromercury(II)-assisted aquation can be expressed by this equation:

$$k_{obsd} = k_0 + k_1[HgCl^+] + k_2[HgCl_2].$$

An additional term, $k[Hg^{2+}]$, may be included when $[Hg^{2+}]$ is present in an appreciable concentration; however, this term could not be well characterized because of the strong interaction of the mercury(II) ions with the cyano ligands.

Interactions with Bromomercury(II) Complexes. The addition of mercury(II) bromide also accelerated the aquation of $[CoBr(CN)_5]^{3-}$, but to a smaller degree than in the case of mercury(II) chloride. This is reasonable if $HgBr^+$, by analogy with $HgCl^+$, acts as a virtual reacting species, since the dissociation constant of $HgBr_2$ is much smaller than that of $HgCl_2$. The $\ln(D_t-D_\infty)$ *vs.* t plot was not linear, not even at $HgBr_2$ concentrations as high as 1.0×10^{-2} mol dm^{-3}, nearly the highest one experimentally attainable. (The solubility is 2.2×10^{-2} mol dm^{-3} at 35 °C). Therefore, the rate constant was not obtained directly, but from the analysis of the results according to the following reaction scheme:

$$CoBr(CN)_5^{3-} + HgBr^+ \xrightarrow[\text{slow}]{k_{1(Br)}} Co(CN)_5^{2-} + HgBr_2 \qquad (1)$$
$$\xrightarrow[\text{fast}]{} Co(OH_2)(CN)_5^{2-} + HgBr_2$$

$$HgBr^+ + Br^- \overset{K_{2(Br)}}{\rightleftarrows} HgBr_2 \qquad (2)$$

$$HgBr_2 + Br^- \overset{K_{3(Br)}}{\rightleftarrows} HgBr_3^- \qquad (3)$$

where $\log K_{2(Br)}=8.28$ and $\log K_{3(Br)}=2.41$ ($I=0.5$), as has been reported by Sillén.[13]

The reaction rate can be expressed by

$$-\frac{d[CoBr]}{dt} = k_{1(Br)}[CoBr][HgBr^+], \qquad (4)$$

where $CoBr(CN)_5^{3-}$ is abbreviated as CoBr.

The expressions for Equilibria 2 and 3 are

$$K_{2(Br)} = \frac{c_{HgBr_2}}{[HgBr^+][Br^-]}, \qquad (5)$$

$$K_{3(Br)} = \frac{[HgBr_3^-]}{c_{HgBr_2}\cdot[Br^-]}, \qquad (6)$$

where c_{HgBr_2} represents the analytical concentration of $HgBr_2$ and is practically equal to its actual concentration

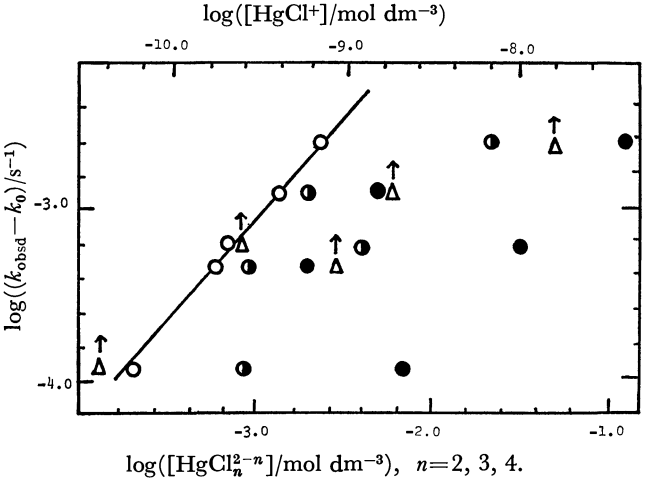

Fig. 2. Effect of chloromercury(II) complexes on the aquation rate of $[CoBr(CN)_5]^{3-}$.
$HgCl_4^{2-}$: ●, $HgCl_3^-$: ◑, $HgCl_2$: ○, $HgCl^+$: △.

at any stage of the reaction. At time 0, the following expression should hold in order for the system to be electrically neutral:

$$[HgBr^+]_0 = [Br^-]_0 + [HgBr_3^-]_0.$$

At time t this becomes

$$[HgBr^+] = [Br^-] - [CoBr]_0 + [CoBr] + [HgBr_3^-]. \quad (7)$$

Equations 6 and 7 are combined to give

$$[Br^-] = \frac{[HgBr^+]+[CoBr]_0-[CoBr]}{1+K_{3(Br)}c_{HgBr_4}}.$$

By substituting this expression for $[Br^-]$ in Eq. 5, one obtains

$$K_{2(Br)}[HgBr^+]^2 + K_{2(Br)}([CoBr]_0-[CoBr])[HgBr^+] - (K_{3(Br)}c_{HgBr_4}+1)c_{HgBr_4} = 0. \quad (8)$$

The elimination of $[HgBr^+]$ from Eqs. 4 and 8 gives a differential equation with respect to [CoBr]. From this equation, a reasonable $k_{1(Br)}$ value can be determined so as to fit the experimental results. The $K_{2(Br)}$ and $K_{3(Br)}$ values given for $I=0.5$, 25 °C were corrected to the present conditions in the same way as has been described above for the case of chloro complexes; then, with the corrected $K'_{2(Br)}$ and $K'_{3(Br)}$ values and an arbitrarily chosen $k_{1(Br)}$ values, the concentration of $[CoBr(CN)_5]^{3-}$ denoted by [CoBr] was calculated as a function of the time for each system. The best fit to the experimental values was obtained when $k_{1(Br)}$ was assumed to be 2.5×10^4 mol^{-1} dm^3 s^{-1} (Fig. 3). The calculations were carried out on a FACOM 270-20 computer for the two systems, with $[CoBr]_0=4.5\times10^{-4}$ mol dm^{-3} and $c_{HgBr_4}=7.63\times10^{-3}$ and 3.81×10^{-3} mol dm^{-3}.

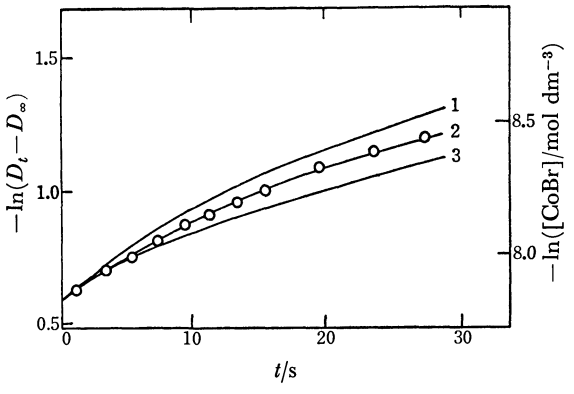

Fig. 3. Comparison of the experimental results(○) and the computational ones(—, scaled on the right-hand oridinate). $c_{HgBr_4}=7.63\times10^{-3}$ mol dm^{-3}. $[CoBr(CN)_5^{3-}]_0=4.5\times10^{-4}$ mol dm^{-3}, at 35 °C. $k_{1(Br)}$ was assumed to 3.0×10^4 mol^{-1} dm^3 s^{-1} (curve 1), 2.5×10^4 mol^{-1} dm^3 s^{-1}(curve 2), and 2.0×10^4 mol^{-1} dm^3 s^{-1} (curve 3).

Another indirect way of obtaining the second-order rate constant, $k_{1(Br)}$, is to carry out the aquation in the presence of an excess of $HgBr^+$ and Hg^{2+}. Under such conditions, the decrease in the concentration of $HgBr^+$, accompanies by the progress of the reaction can be neglected, and the $\ln(D_t-D_\infty)$ *vs.* t plots give straight lines. Since this disproportionation reaction:[13]

Table 4. Rapid aquation of $[CoBr(CN)_5]^{3-}$ in the presence of $HgBr^+$ (with Hg^{2+} and Br^- added in equal analytical concentrations)

[Hg(II)]/mol dm^{-3}	k_{obsd}/s^{-1}
9.83×10^{-3}	92.5
4.91×10^{-3}	41.9
1.96×10^{-3}	22.5

$2\,HgBr^+ \overset{K}{\rightleftarrows} HgBr_2+Hg^{2+}$ (log $K=-0.83$ at $I=0.5$) occurs, the rate constant for the $HgBr^+$-assisted aquation cannot be estimated independently of the effect of Hg^{2+}. As has been described above, Hg^{2+} interferes with the measurement of aquation by forming a precipitate. However, if $HgBr^+$ is present in excess of Hg^{2+}, the stopped-flow technique enables us to observe the aquation before the precipitation begins. Table 4 shows the results. In order to obtain the first-order rate constant, $k_{1(Br)}$, a certain magnitude of the relative effect of Hg^{2+} on the aquation has to be assumed. If Hg^{2+} has no effect, $k_{1(Br)}$ will be 1.8×10^4 mol^{-1} dm^3 s^{-1}, and if Hg^{2+} has an effect as large as that of $HgBr^+$, $k_{1(Br)}$ will be 1.3×10^4 mol^{-1} dm^3 s^{-1}. These values are somewhat smaller than that obtained from the other experiment described above (2.5×10^4 mol^{-1} dm^3 s^{-1}), but are comparable to that for $HgCl^+$. Therefore, the rate constant due to $HgBr^+$ can be $k_{1(Br)}=(2.0\pm0.5)\times10^4$ mol^{-1}dm^3 s^{-1}.

Table 5. Effect of bromomercury(II) complexes on the rate of aquation of $[CoBr(CN)_5]^{3-}$

$[HgBr_4^{2-}]$/ mol dm^{-3}	$[HgBr_3^-]$/ mol dm^{-3}	$[HgBr_2]$/ mol dm^{-3}	$(k_{obsd}-k_0)$/ s^{-1}
7.54×10^{-3}	1.09×10^{-2}	1.29×10^{-3}	2.28×10^{-4}
5.70×10^{-3}	3.95×10^{-2}	1.81×10^{-3}	2.66×10^{-4}
2.11×10^{-2}	2.58×10^{-2}	2.24×10^{-3}	3.50×10^{-4}

The effect of $HgBr_2$ was also examined in a manner similar to that described for the case of $HgCl_2$. Table 5 gives the results, from which the second-order rate constant, $k_{2(Br)}=(1.6\pm0.2)\times10^{-1}$ mol^{-1} dm^3 s^{-1}, was obtained.

The pseudo-first-order rate constant for the bromomercury(II)-assisted aquation can, then, be expressed by

$$k_{obsd}^{(Br)} = k_0 + k_{1(Br)}[HgBr^+] + k_{2(Br)}[HgBr_2].$$

Comparisons of $k_{1(Br)}$ and $k_{2(Br)}$ with k_1 and k_2 show that the effect of $HgBr^+$ is comparable to that of $HgCl^+$ and that $HgCl_2$ is a somewhat better catalyst than $HgBr_2$.

Table 6 summarizes the results obtained for the present systems as well as for the $CoBr(NH_3)_5^{2+}$–Hg^{2+} system.[14] The last column shows the stability constants for the mercury(II) complexes formed by the combination with Br^-. The constant for HgClBr has not been directly obtained, so we estimated it in the following manner.

These equilibria

$$Hg^{2+} + Br^- \rightleftarrows HgBr^+ \qquad \log K'_{1(Br)} = 9.08 \quad (9)$$

$$HgBr^+ + Br^- \rightleftarrows HgBr_2 \qquad \log K'_{2(Br)} = 8.22 \quad (10)$$

TABLE 6. HALOMERCURY(II)-ASSISTED AQUATION OF BROMOCOBALT(III) COMPLEXES

Ionic strength=1.0 mol dm^{-3} ($NaClO_4$), at 35 °C.

Complex		$\log k_i/k_0$	$\log K_i'$
$[CoBr(NH_3)_5]^{2+}$	Hg^{2+}	6.51[a]	9.08
$[CoBr(CN)_5]^{3-}$	$HgCl^+$	8.18	9.1[b]
	$HgBr^+$	8.3[b]	8.22
	$HgCl_2$	4.00	—
	$HgBr_2$	3.30	2.31

a) Unpublished result. Brønsted and Livingston obtained $\log k_i/k_0=6.28$ at the ionic strength of 0.03 and at 25 °C.[14] b) These values may contain larger errors than the others.

$$Hg^{2+} + Cl^- \rightleftharpoons HgCl^+ \qquad \log K_1' = 6.77 \qquad (11)$$

$$HgCl^+ + Cl^- \rightleftharpoons HgCl_2 \qquad \log K_2' = 6.44 \qquad (12)$$

$$\frac{1}{2}HgCl_2 + \frac{1}{2}HgBr_2 \rightleftharpoons HgClBr \qquad \log K' = 0.6[15] \qquad (13)$$

were considered.

From Eqs. 9 and 11,

$$\frac{[HgBr^+][Cl^-]}{[HgCl^+][Br^-]} = \frac{K_{1(Br)}'}{K_1'}. \qquad (14)$$

From Eqs. 10, 12, and 13,

$$\frac{[HgClBr]}{[HgCl^+][Br^-]}\frac{[HgClBr]}{[HgBr^+][Cl^-]}K_{2(Br)}'^{-1}K_2'^{-1} = (K')^2. \qquad (15)$$

Eliminating the $[HgBr^+][Cl^-]$ term in Eqs. 14 and 15, one obtains

$$\frac{[HgClBr]}{[HgCl^+][Br^-]} = K'K_2'^{1/2}K_{2(Br)}'^{1/2}K_{1(Br)}'^{1/2}K_1'^{-1/2} = 10^{9.1}.$$

The results listed in Table 6 show a roughly linear relation between the ratios of the second-order rate constant for each assisted aquation to the first-order rate constant for the spontaneous aquation (k_i/k_0) and the related stability constants (K_i').

The ratios of the rate constants for $CoBr(CN)_5^{3-}$ are significantly larger than that for $CoBr(NH_3)_5^{2+}$ in spite of the similar magnitudes of the stability constants. This difference may be attributed partially to the opposite sign of the electrostatic long-range interactions between the reactants and partially to the dissimilar short-range interactions; the latter is to be expected, since the two complexes differ greatly in their dipolar properties.

Two molecular species, $HgCl_2$ and $HgBr_2$, also showed appreciable effects on the rate of aquation of $[CoBr(CN)_5]^{3-}$. Although these effects are much smaller than those of $HgCl^+$ and $HgBr^+$, the present results show rare cases in which the effects of $HgCl_2$ and $HgBr_2$ on the aquations of metal complexes were experimentally detected. In these cases, the values of k_i/k_0 were greater than would be expected from the related equilibrium constants, K_i'. This also suggests that there exists a kind of short-range interaction between $[CoBr(CN)_5]^{3-}$ and dihalomercury(II) complexes.

We are grateful to Professor Shinichi Kawaguchi of Osaka City University for the use of the stopped-flow apparatus.

References

1) I. V. Kozhevnikov and E. S. Rudakov, *Inorg. Nucl. Chem. Lett.*, **8**, 571 (1972).
2) S. P. Tanner and W. C. E. Higginson, *J. Chem. Soc., A*, **1969**, 1164; J. Burgess and S. J. Cartwright, *J. Chem. Soc., Dalton Trans.*, **1976**, 1561.
3) A. W. Adamson, *J. Am. Chem. Soc.*, **78**, 4260 (1956).
4) S. Misumi and S. Kida, "Sakuen Kagaku," Gihodo, Tokyo (1974), p. 115.
5) R. Grassi, A. Haim, and W. K. Wilmarth, *Inorg. Chem.*, **6**, 237 (1967).
6) S. H. Laurie and C. B. Monk, *J. Chem. Soc.*, **1965**, 724.
7) K. Nakamoto, "Infrared Spectra of Inorganic and Coordination Compounds," 2nd ed, John Wiley & Sons, New York (1970), p. 186.
8) J. E. Huheey, "Inorganic Chemistry," Harper and Row, New York (1972), p. 414.
9) B. Lindgren, A. Jonsson, and L. G. Sillén, *Acta Chem. Scand.*, **1**, 479 (1947).
10) D. B. Scaife and H. J. V. Tyrrell, *J. Chem. Soc.*, **1958**, 392.
11) I. M. Vasil'kevich and E. A. Shilov, *Ukr. Khim. Zh.*, **32**, 947 (1966).
12) R. G. Wilkins, "The Study of Kinetics and Mechanism of Reactions of Transition Metal Complexes," Allyn and Bacon, Boston (1974), p. 212.
13) P. O. Bethge, I. Jonevall-Westöö, and L. G. Sillén, *Acta Chem. Scand.*, **2**, 828 (1948).
14) J. N. Brønsted and R. Livingston, *J. Am. Chem. Soc.*, **49**, 435 (1927).
15) I. Eliezer, *J. Phys. Chem.*, **68**, 2722 (1964).

Thermodynamics of 1:1 Adduct-formation of Bis(trifluoroacetylacetonato)copper(II) with Lewis Bases

Yoshihiro SASAKI,* Matsujiro SAKURADA, Masakazu MATSUI, and Tsunenobu SHIGEMATSU

Institute for Chemical Research, Kyoto University, Uji, Kyoto 611

(Received November 27, 1978)

Formation constants and thermodynamic parameters for the 1:1 adduct-formation reactions of bis(trifluoroacetylacetonato)copper(II), $Cu(tfac)_2$, with alkylamines, α-picoline, 2,6-lutidine, and THF have been determined spectrophotometrically. The $\Delta H°-\Delta S°$ plots for primary and secondary alkylamines gave a linear relationship for the thermodynamic parameters of the $Cu(tfac)_2$–heterocyclic base systems. The plots for the 2,6-lutidine, THF and tertiary alkylamine systems have been found consistent with a correlation between $\Delta H°$ and $\Delta S°$ values for bis(acetylacetonato)copper(II)–heterocyclic base systems. It has been subsequently deduced that the 1:1 adducts of $Cu(tfac)_2$ with Lewis bases possess a square-pyramidal structure on the basis of the ESR data for the $^{63}Cu(tfac)_2$–Lewis base systems.

The 1:1 adduct-formation constants of copper(II) complexes of β-diketonates with pyridine and its derivatives have been reported.[1] The systematic studies reveal that (i) substitution of one or both terminal methyl groups in acetylacetone by the trifluoromethyl group increases the formation constant, (ii) the greater the basicity of the donor atom, the greater the stability of the adduct formed, and (iii) the stability of the adducts of α-picoline and 2,6-lutidine are lower than that of the pyridine adduct. The explanation for (i) has been ascribed to the decrease in electron density around the central copper ion by the electron-withdrawing trifluoromethyl group and in (iii) to the steric hindrance of the methyl group in α-positions.

Graddon *et al.* measured the thermodynamic parameters for the 1:1 adduct-formation reactions of copper(II) complexes of fluorinated β-diketonates with heterocyclic bases and noted that the high stability of the bis(trifluoroacetylacetonato)copper(II) ($Cu(tfac)_2$) adduct with pyridine was largely due to an entropy factor.[2,3] Drago *et al.* found that the enthalpy change of 1:1 adduct-formation reactions of bis(hexafluoroacetylacetonato)-copper(II) with several Lewis bases did not obey the double-scale enthalpy equation proposed and brought this into close connection with the formation of different isomers in solution.[4] The 1:1 adduct of bis(3-trifluoromethyl-*d*-camphorato)copper(II) with α-picoline has been shown by the authors to be more stable than the pyridine adduct.[5] These results suggest that the factors affecting 1:1 adduct-formation equilibria of bis(β-diketonato)copper(II) with Lewis bases need further investigation. In this paper the 1:1 adduct-formation constants and thermodynamic parameters for the 1:1 adduct-formation reactions of $Cu(tfac)_2$ with alkylamines, THF, α-picoline and 2,6-lutidine will be reported together with an ESR investigation of the 1:1 adducts of $^{63}Cu(tfac)_2$ in an attempt to elucidate the geometries in solution. The adduct-formation constants have been determined spectrophotometrically.

Experimental

Materials and Measurements. $Cu(tfac)_2$ was prepared by the addition of an ethanol solution of trifluoroacetylacetone to an aqueous solution of copper acetate. The solution upon recrystallization from toluene gave dark blue crystals (Found: C, 32.67; H, 2.36; F, 31.14%). In the ESR spectra of $Cu(tfac)_2$, $^{63}Cu(tfac)_2$ was prepared from isotopically pure ^{63}CuO (99.8%). The bases were obtained commercially and distilled at reduced pressure. Dodecylamine and tertiary alkylamines were used without further purification. Reagent grade benzene was used without further purification as the solvent. Optical absorption measurements were made on a Hitachi 323 automatic recording spectrophotometer equipped with a water cooled cell holder. The temperature of the samples was maintained constant within ±0.1 °C. The absorbances were measured at 540 nm for THF and at 700 nm for the other bases. ESR measurements were made with a JEOL-ME-3X X-band ESR spectrometer at 77 K. The spectra were calibrated with Mn^{2+} in MgO and DPPH.

Calculation of 1:1 Adduct-formation Constant. The 1:1 adduct-formation constants in the primary alkylamine systems were determined graphically from the following equation:[6]

$$1/K_1 = \frac{A-A_0}{\varepsilon_2-\varepsilon_1} - a_0 - b_0 + a_0 b_0 \frac{\varepsilon_2-\varepsilon_1}{A-A_0} \quad (1)$$

where ε_1 and ε_2 are the molar extinction coefficients of $Cu(tfac)_2$ and the adducts formed, and a_0 and b_0 are the initial concentration of $Cu(tfac)_2$ and that of the primary alkylamine added, respectively, and $A_0=\varepsilon_1 a_0$, for the 1 cm cells were used in this study. The formation constants in secondary alkylamine systems are given by:

$$K_1 = \frac{A-A_0}{A_\infty-A} \times \frac{1}{b_0-a_0(A-A_0)/(A_\infty-A_0)} \quad (2)$$

where $A_\infty=\varepsilon_2 a_0$. K_1 and ε_2 cannot be experimentally evaluated at the same time. Thus the K_1 value giving the smallest standard deviation was found using various A_∞ values.[7] In the case that a_0 and b_0 are much greater than the concentration of adduct formed, Eq. 1 transforms into Eq. 3:

$$\frac{a_0}{A-A_0} = \left(a_0+\frac{1}{K_1}\right) \times \frac{1}{(\varepsilon_2-\varepsilon_1)} \times \frac{1}{b_0} + \frac{1}{\varepsilon_2-\varepsilon_1}. \quad (3)$$

Under the experimental conditions that $b_0-c \fallingdotseq b_0$, where c is the concentration of adduct formed, Eq. 1 transforms into a modified Benesi equation:[6]

$$\frac{a_0}{A-A_0} = \frac{1}{K_1(\varepsilon_2-\varepsilon_1)} \times \frac{1}{b_0} + \frac{1}{\varepsilon_2-\varepsilon_1}. \quad (4)$$

K_1 and ε_2 of α-picoline and 2,6-lutidine were determined from the plots of $a_0/(A-A_0)$ *vs.* $1/b_0$ according to Eq. 3, and those of the tertiary alkylamines and THF according to Eq. 4.

Results and Discussion

1:1 Adduct-formation Constant and Thermodynamic Param-

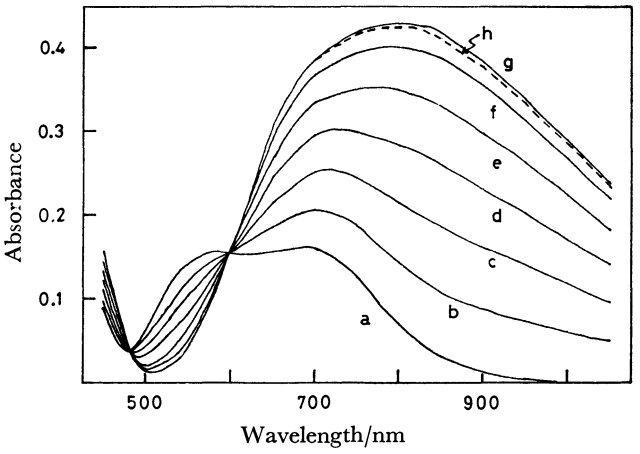

Fig. 1. Spectral change of $Cu(tfac)_2$ in benzene by the addition of octylamine at 20 °C. $a_0=5.43_4\times10^{-3}$ M, b_0/a_0; a: 0.0, b: 0.2, c: 0.4, d: 0.6, e: 0.8, f: 1.0, g: 3.0, h: 5.0 (1 M=1 mol dm^{-3}).

eters. The spectral change of $Cu(tfac)_2$ by the addition of octylamine at 20 °C is shown in Fig. 1 as an example. In the concentration-ratio range of 0—5.0 of the amine to $Cu(tfac)_2$ (b_0/a_0), three isosbestic points were observed at 426, 479, and 598 nm. The absorbance in the near-infrared region decreases at high concentration-ratio. The change in absorbance at 700 nm is large when $b_0/a_0<1$, but extremely small when $b_0/a_0>2$. Thus it has been concluded that only the 1 : 1 adduct is formed when the concentration-ratio is less than 1. Figure 2 shows a set of curves of $1/K_1$ *vs.* $\varepsilon_2-\varepsilon_1$ for the $Cu(tfac)_2$–octylamine system at 20 °C. Each curve was calculated from the observed $A-A_0$ value at one of the base concentrations according to Eq. 1. The coordinates for the intersection on the curves give the common solution for K_1 and ε_2. The set of curves calculated from Eq. 1 for the secondary alkylamine systems give only a dull intersecting point in a range of concentration-ratio (b_0/a_0) exhibiting isosbestic points. Thus the formation constants for the systems have been estimated according to the method described above.

Table 1 shows the 1 : 1 adduct-formation constants and the thermodynamic parameters calculated from the

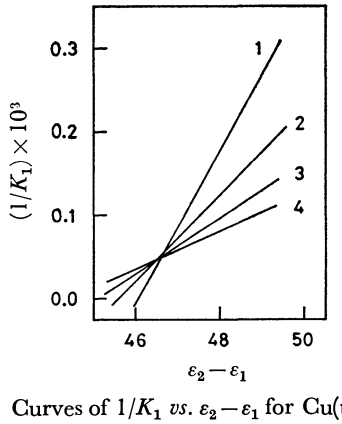

Fig. 2. Curves of $1/K_1$ *vs.* $\varepsilon_2-\varepsilon_1$ for $Cu(tfac)_2$–octylamine system at 20 °C. $a_0=5.12_7\times10^{-3}$ M, b_0; 1 : $1.01_0\times10^{-3}$ M, 2 : $3.03_0\times10^{-3}$ M, 3 : $4.03_9\times10^{-3}$ M, 4 : $5.04_9\times10^{-3}$ M (1 M=1 mol dm^{-3}).

Table 1. 1:1 Adduct-formation constants and thermodynamic parameters for 1 : 1 adduct-formation reactions of $Cu(tfac)_2$ with Lewis bases in benzene

Base	log K_1 at 20 °C (1/mol)	$\Delta H°$ (kJ/mol)	$\Delta S°$ (J/mol K)
Butylamine	4.64±0.05	−54±6	−96±20
Hexylamine	4.50±0.16		
Octylamine	4.30±0.02	−58±2	−116±6
Dodecylamine	4.32±0.02		
Dibutylamine	3.35±0.02	−37±3	−61±10
Dihexylamine	3.55±0.07		
Dioctylamine	3.50±0.02	−36±3	−57±9
Tributylamine	K_1=3.9±0.1	−20±2	−55±12
Trioctylamine	K_1=3.5±0.1	−14±2	−39±13
Pyridine[a)]	3.00	−30.9	−48
γ-Picoline[a)]	3.33	−30.7	−41
α-Picoline	K_1=83±4	−33±4	−75±15
2,6-Lutidine	K_1=9.5±0.7	−40±3	−118±11
THF	K_1=5.4±0.3	−17±3	−43±11

a) From Ref. 3. log K_1 at 20 °C was calculated from the thermodynamic parameters.

van't Hoff plots of ln K_1, together with the K_1 values and the thermodynamic data of the pyridine and γ-picoline systems reported by Graddon and Ong.[3] The effect of self-association of primary alkylamine has not been taken into account because of the low concentration of the amines.[8] The 1 : 1 adducts of primary alkylamines are more stable than that of pyridine. The formation constants of the alkylamines increase in the order: primary alkylamine>secondary alkylamine≫tertiary alkylamine. The number of carbon atoms in the alkyl chains do not significantly affect the value of the formation constant. The formation constants of the bulky heterocyclic bases and THF, which is a weak base, are remarkably small, as previously reported. The enthalpy term for 2,6-lutidine which exhibits steric hindrance is smaller than that of pyridine. The magnitude of the enthalpy change for the pyridine and α-picoline systems is approximately equal. The thermodynamic data for the heterocyclic base systems show that the remarkably small formation constants of the α-picoline and 2,6-lutidine systems may be ascribed to the decrease in the entropy term. The enthalpy term of the primary alkylamines is smaller than that of the heterocyclic bases due to the strong basicity and the enthalpy change of the secondary alkylamines is larger than that of the primary alkylamines due to steric effects.

ESR Measurements. The ESR spectral change of isotopically enriched $^{63}Cu(tfac)_2$ in frozen toluene was measured by the addition of Lewis bases. Figure 3 illustrates the spectral change in the $g_{//}$ region by the addition of octylamine, which shows that only the 1 : 1 adduct is formed when $b_0/a_0<1$. The ESR data of the 1 : 1 adducts are given in Table 2. Trigonal-bipyramidal complexes of copper have a d_{z^2} ground state which gives rise to $g_\perp\simeq2.2$ and to $g_\perp<g_{//}$.[9,10] In the adducts studied here $g_{//}\simeq2.3$ and $g_\perp\simeq2.04$, which are typical values for square-pyramidal complexes with a $d_{x^2-y^2}$ ground state. Thus it has been assumed that the adducts possess a square-pyramidal structure. There are two

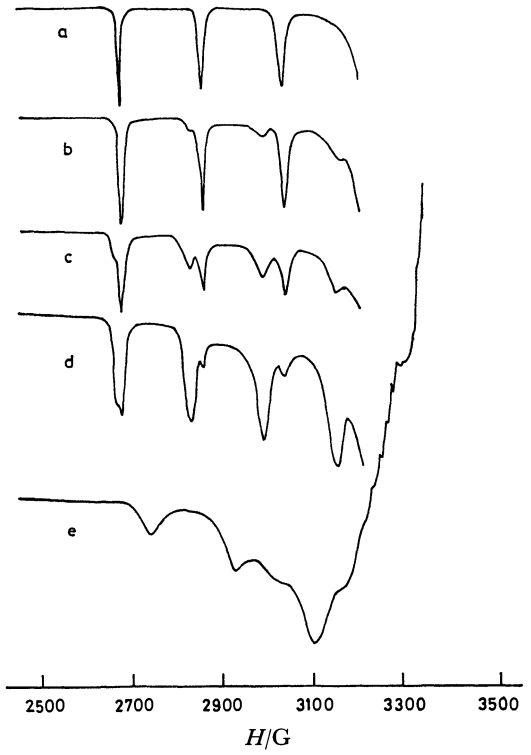

Fig. 3. ESR spectral change of $^{63}Cu(tfac)_2$ in toluene by the addition of octylamine at 77 K. $a_0=2.31_7\times10^{-3}$ M, b_0/a_0; a: 0.0, b: 0.3, c: 0.6, d: 0.9, e: 9.0 (1 M=1 mol dm^{-3}).

Table 2. ESR parameters for 1:1 adducts of $^{63}Cu(tfac)_2$ with Lewis bases in frozen toluene

Base	$g_{//}$	$g_\perp$	$A_{//}$	$A_\perp$
—	2.266	2.044	193	15.7
Octylamine	2.303	—	171	—
Dibutylamine	2.292	—	167	—
Tributylamine	2.300	2.019	164	34
Pyridine	2.296	—	182	—
α-Picoline	2.319	2.043	162	—
2,6-Lutidine	2.303	2.014	134	48
THF	2.296	—	180	—

A: 10^{-4} cm^{-1}.

isomers for the limiting square-pyramidal structure. One involves apical coordination of a Lewis base molecule and the other involves basal coordination. ^{14}N ligand hyperfine structure was found in the frozen solution ESR spectrum of the 1:1 adduct of $Cu(hfac)_2$ with pyridine and it has been proposed that the adduct has a basal structure.[4,11] In the spectra of the adducts studied such ligand hyperfine splitting was not observed. This, however, does not necessarily indicate that the structure of the adducts is of an apical type.

Correlation between Thermodynamic Parameters. Figure 4 shows the relationship between $\Delta H°$ and $\Delta S°$ values. The $\Delta H°-\Delta S°$ plots of the primary and secondary alkylamines fit a linear relationship for the thermodynamic parameters of $Cu(tfac)_2$–heterocyclic base systems. The plots for THF and the bulky heterocyclic bases except α-picoline are consistent with a correlation between the thermodynamic parameters of bis(acetylacetonato)-

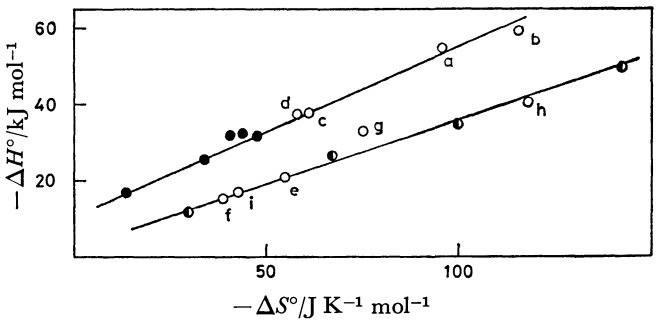

Fig. 4. Relationships between $\Delta H°$ and $\Delta S°$ values.
● Plots for $Cu(tfac)_2$–heterocyclic base systems from Ref. 3. ◐ Plots for $Cu(acac)_2$–heterocyclic base systems from Ref. 1 (b). ○ Present work; a: butylamine, b: octylamine, c: dibutylamine, d: dioctylamine, e: tributylamine, f: trioctylamine, g: α-picoline, h: 2,6-lutidine, i: THF.

copper(II) ($Cu(acac)_2$)–heterocyclic base systems. One of the conditions for the existence of a set of reactions having such a linear relationship is that they should share a common interaction mechanism.[12] The fact that $\Delta H°$ of 2,6-lutidine is smaller than that of pyridine may also mean that the interaction mechanism in the 2,6-lutidine and pyridine systems is different. The ESR data show that the 1:1 adducts in this study exist in two square-pyramidal structures. The adduct of $Cu(acac)_2$ with quinoline is of an apical type.[13] Therefore, Fig. 4 suggests that the 1:1 adducts of $Cu(tfac)_2$ with THF and the bulky heterocyclic bases except α-picoline possess an apical structure and that those of pyridine and the primary and secondary alkylamines have a basal structure. It is known that in 1:1 adducts of bis(β-diketonato)copper(II) with Lewis bases, which have a square-pyramidal structure, the axial bond length is longer than the equatorial bond length.[13-15] Thus the axial ligation of a Lewis base molecule to $Cu(tfac)_2$ results in the formation of new, relatively longer Cu–N or Cu–O bonds normal to the almost undisturbed CuO_4 plane. The steric hindrance of the bulky heterocyclic bases may be weakened by this interaction mechanism. The structure of the adduct of α-picoline cannot, however, be presumed on the basis of the data in this study. It is reported that the 1:1 adduct of bis(α-nitroacetophenonato)copper(II) with α-picoline has a basal structure in which the methyl group in the α-position sticks out toward the sixth coordination position.[16]

There is a linear relationship between the log K_1 values of pyridine, γ-picoline and butylamine and the log K_H values in the aqueous solutions, while the plots for the secondary alkylamines lie below the line due to steric effects. This linear relationship is explainable by the fact that the strength of the bond between a ligand and a metal ions is determined to a first approximation by the same factors as those which determine the strength of protonation of the ligand. Butylamine is a σ-donor and γ-picoline has a considerably stronger σ-donor property. Thus it is suggested that in the adduct-formation of $Cu(tfac)_2$ with the heterocyclic bases, the σ-bond may play a more important role than the π-bond.

References

1) a) D. P. Graddon, *Coord. Chem. Rev.*, **4**, 1 (1969); b) W. R. May and M. M. Jones, *J. Inorg. Nucl. Chem.*, **25**, 507 (1963); c) D. P. Graddon and E. C. Watton, *ibid.*, **21**, 49 (1961); d) W. R. Walker and N. C. Li, *ibid.*, **27**, 2255 (1965); e) T. Shigematsu, M. Tabushi, M. Matsui, and M. Munakata, *Bull. Chem. Soc. Jpn.*, **41**, 2656 (1968); f) A. F. Garito and B. B. Wayland, *J. Am. Chem. Soc.*, **91**, 866 (1969); g) W. Partenheimer and R. S. Drago, *Inorg. Chem.*, **9**, 47 (1970); h) N. S. Al-Niaimi and H. A. A. Rasoul, *J. Inorg. Nucl. Chem.*, **36**, 2051 (1974); i) E. Kwiatkowski and J. Trojanowski, *ibid.*, **38**, 131 (1976).

2) D. P. Graddon and K. B. Heng, *Aust. J. Chem.*, **24**, 1781 (1971).

3) D. P. Graddon and W. K. Ong, *Aust. J. Chem.*, **27**, 741 (1974).

4) D. R. McMillin, R. S. Drago, and J. A. Nusz, *J. Am. Chem. Soc.*, **98**, 3120 (1976).

5) T. Shigematsu, M. Matsui, Y. Sasaki, and M. Sakurada, *Bull. Chem. Soc. Jpn.*, **49**, 2325 (1976).

6) N. J. Rose and R. S. Drago, *J. Am. Chem. Soc.*, **81**, 6138 (1959).

7) P. Gans and H. M. N. Irving, *J. Inorg. Nucl. Chem.*, **34**, 1885 (1972).

8) H. Wolff and A. Höpfner, *Z. Electrochem.*, **66**, 149 (1962).

9) B. J. Hathaway and D. E. Billing, *Coord. Chem. Rev.*, **5**, 143 (1970).

10) J. Pradilla-Sorzano and J. P. Fackler, Jr., *Inorg. Chem.*, **13**, 38 (1974).

11) B. B. Wayland and M. D. Wisniewski, *J. Chem. Soc., Chem. Commun.*, **1971**, 1025.

12) J. E. Leffler and E. Grunwald, "Rates and Equilibria of Organic Reactions," John Wily & Sons Inc. (1963), p. 315.

13) P. Jose, S. Ooi, and Q. Fernando, *J. Inorg. Nucl. Chem.*, **31**, 1971 (1969).

14) G. W. Bushnell, *Can. J. Chem.*, **49**, 555 (1971).

15) V. F. Duckworth, D. P. Graddon, G. M. Mockler, and N. C. Stephenson, *Inorg. Nucl. Chem. Lett.*, **3**, 1471 (1976).

16) M. Bonamico and G. Dessy, *J. Chem. Soc., Chem. Commun.*, **1970**, 1218.

A Possible Method for Obtaining Precise Isotope Ratio of the Element Having Only Two Isotopes

Hitoshi KANNO
Department of Chemistry, Meisei University, Hino, Tokyo 191
(Received November 27, 1978)

As an extension of the atomic/molecular vaporization model, a new method is presented for correcting the isotopic fractionation effects in the multiple filament thermal ionization source (MFTIS). It is applicable to the isotope ratio measurements of the element having only two observable isotopes.

It is well known that the isotope ratio observed in a thermal ionization mass spectrometry is "fractionated"[1-7] due to the isotope effects in the vaporization process of the sample. As the correction methods for elements having more than three isotopes, normalization and double spike techniques[8-12] are usually adopted to obtain "precise" isotope ratio capable to interlaboratory comparison and geochemical uses. However, when the element in question has only two stable isotopes, it is almost impossible to estimate the extent of isotopic fractionation in an observed isotope ratio.

In this paper I propose a new method which may be used to overcome the limitation inherent to the element having only two isotopes for obtaining precise isotope ratio.

Theoretical

In a multiple filament thermal ionization source (MFTIS), sample evaporates in both atomic and molecular species

$$MX_{(s)} \longrightarrow M_{(g)} + X_{(g)}$$
$$MX_{(s)} \longrightarrow MX_{(g)}$$

and ionization occurs at or near the ionizing filament,

$$M \longrightarrow M^+$$
$$MX \longrightarrow M^+ + X^{(0,-)}$$
$$\searrow\ MX^+.$$

If molecular ions are stable enough to be observed as mass spectra and if metal counterpart (X in this case) consists of more than two isotopic species, we will observe (at least) following four peaks in the mass spectra of molecular ions

$$M_lX_l^+,\ M_lX_h^+,\ M_hX_l^+,\ \text{and}\ M_hX_h^+$$

where h and l denote heavy and light isotopes of the element M and its counterpart X. It is to be noted that the overlapping of mass peaks may sometimes occur due to the particular combination of mass numbers of M and X. In addition to these mass peaks, we can also get isotope ratio of the element M as usual from mass peaks of M^+ ions. Combination of isotope ratios of molecular ions and atomic ions may resolve the fractionation problem. This is shown in the following way. As in the previous analysis,[5] we assume that the molar quantity of MX (vapor B) is always k_m times as much as $M^{(0,+)}$ (vapor A) and k_x times as much as $X^{(0,+,-)}$(vapor C). Thus we get

$$\begin{aligned} d[B] &= k_m d[A] \\ d[B] &= k_x d[C] \end{aligned} \qquad (1)$$

where [Y] is the molar quantity of the vapor Y. It is easily seen from Eq. 1 that k_m is equal to k_x in the ideal case. For the simplicity of the discussion, we further assume that (1) the residual sample on the filament undergoes complete and continuous mixing and there is no isotopic fractionation between the compounds (chemical species) on the filament and (2) the residence time of the vapor in the ion source is short so that there are no isotopic exchanges in the successively evaporating chemical species. Here we assume that the element M and its counterpart X consist each of only two isotopes (isotopic species). The isotopic fractionation factors are defined as follows;

$$\begin{aligned} &\alpha = (M_h/M_l)^{1/2},\quad \beta = (M_h\bar{X}/M_l\bar{X})^{1/2}, \\ &\gamma_1 = (\bar{M}X_h/\bar{M}X_l)^{1/2},\quad \gamma_2 = (X_h/X_l)^{1/2} \end{aligned} \qquad (2)$$

where $\bar{M}$ and $\bar{X}$ are the average mass of the element M and its counterpart X, respectively. The isotope ratios R_a and R_b of the element M in the vapor A and vapor B evaporating from the filament are given by

$$R_a = \alpha R \text{ and } R_b = \beta R \qquad (3)$$

where R is the isotope ratio of the element M in the sample remaining on the filament.

The differential equation describing the change in the isotope ratio R in the course of evaporation is

$$\frac{1}{k_m+1}\left(\frac{\alpha R}{1+\alpha R}+\frac{\beta k_m R}{1+\beta R}\right)dQ = \frac{R\,dQ}{1+R} + \frac{Q\,dR}{(1+R)^2} \qquad (4)$$

where Q is the amount of sample on filament. The integration of Eq. 4 gives

$$\ln\left(\frac{Q}{Q_0}\right) = a_m \ln\left(\frac{R}{R_0}\right) + \ln\left(\frac{R+1}{R_0+1}\right) + b_m \ln\left(\frac{c_m+d_mR}{c_m+d_mR_0}\right) \qquad (5)$$

where Q_0: amount of sample originally on filament,
R_0: true isotope ratio of the sample at Q_0,

$$a_m = (k_m+1)/c_m,\quad b_m = (\alpha-\beta)^2k_m/(c_md_m),$$
$$c_m = (\alpha-1) + (\beta-1)k_m,$$
$$d_m = (\alpha-1)\beta + \alpha(\beta-1)k_m.$$

When we measure the metal ions M^+ for obtaining isotope ratio of the element M, the observed isotope ratio (R_{ob}) will be the mean isotope ratio of the vapor A and vapor B as expressed by

$$R_{ob} = \frac{(\alpha+\beta k_m I_m)R + \alpha\beta(k_mI_m+1)R^2}{(k_mI_m+1)+(\beta+\alpha k_mI_m)R} \qquad (6)$$

where $I_m = I_a/I_b$ and I_a and I_b are the ionization efficiencies (production rate of metal ion M^+) of the vapor A and vapor B, respectively.

Next we consider the change of isotope ratio of X during the course of evaporation of the sample MX. The isotope ratios r_b and r_c of X in the vapor B and vapor C (MX and X) are given by

$$r_b = \gamma_1 R_x \text{ and } r_c = \gamma_2 R_x \tag{7}$$

where R_x is the isotope ratio of X in the sample remaining on the filament. The equation corresponding to Eq. 4 is

$$\frac{1}{k_x+1}\left(\frac{\gamma_1 R_x}{1+\gamma_1 R_x}+\frac{\gamma_2 k_x R_x}{1+\gamma_2 R_x}\right)dQ_x = \frac{R_x dQ_x}{1+R_x} + \frac{Q_x dR_x}{(1+R_x)^2} \tag{8}$$

where Q_x is the amount of the sample (X-containing chemical species) remaining on the filament, and Eq. 8 is integrated to give

$$\ln\left(\frac{Q_x}{Q_0}\right) = a_x \ln\left(\frac{R_x}{R_x^\circ}\right) + \ln\left(\frac{R_x+1}{R_x^\circ+1}\right) + b_x \ln\left(\frac{c_x+d_x R_x}{c_x+d_x R_x^\circ}\right) \tag{9}$$

where R_x°: the initial isotope ratio of X on the sample filament,

$a_x = (k_x+1)/c_x$, $b_x = (\gamma_1-\gamma_2)^2 k_x/(c_x d_x)$,

$c_x = (\gamma_1-1) + (\gamma_2-1)k_x$,

$d_x = (\gamma_1-1)\gamma_2 + \gamma_1(\gamma_2-1)k_x$.

Thus the observed isotope ratio of X in the vapor of molecular ions MX^+ will be

$$r_{ob} = \frac{[M_l X_h^+]+[M_h X_h^+]}{[M_l X_l^+]+[M_h X_h^+]} = \gamma_1 R_x. \tag{10}$$

Here [Z] represents the peak height of mass spectrum at the mass number Z. If we use the sample MX as a working material in which the initial isotope ratio of X is precisely known, we can monitor the amount of the sample remaining on the filament Q_x (or Q) from the measured r_{ob} value, initial isotope ratio R_x° and the k_x value using Eqs. 7 and 9. Evaluation of k_m and k_x may be achieved by either calibration curve or thermodynamic studies on vapor composition in a thermal ion source. Recently Heald has attempted the computer calculation of equilibrium compositions of vapor species in a thermal ionization mass spectrometer.[13] Once we get Q_x ($Q_x \simeq Q$) value, it is easy to get the "precise" isotope ratio R_0 of the element M by use of Eqs. 5 and 6, evaluated k_m value and observed R_{ob} value.

Discussion

The crucial point of this method is whether the sample MX can form stable molecular ions to be observed as mass spectra. There have been only a few studies on the stability and intensity of molecular ions in a thermal ionization ion source as atomic ions have exclusively been the only target for observations in most isotope ratio measurements.[14-16] However, there is much evidence for the existence of molecular ions as well as atomic metal ions in a thermal ionization ion source.[14-18] Together with the high-temperature vaporization data of inorganic salts by Knudsen-cell effusion method,[19,20] recent extensive studies by NBS group[7] support the above contention. It is very common to observe not only atomic ions M^+ but also oxide ions such as MO^+ in the isotope ratio measurements of rare earth elements when nitrates or perchlorates are used as a chemical form of the sample.[14,15] In the experimental work by Gensho and Honda,[18] they used M_2BO_3 (M=Li, Na, K, and Rb) as a working material for obtaining precise isotopic abundance ratio of boron ($^{11}B/^{10}B$). When the metal M consists of more than two isotopes such as Li, K, and Rb, we can obtain more than three $M_2BO_2^+$ ion peaks. This makes it possible to evaluate the discrimination factor which would otherwise be unobtainable from only two peaks ($M_2{}^{10}BO_2^+$ and $M_2{}^{11}BO_2^+$). The merits of using M_2BO_3 (M=Li, K, and Rb) instead of Na_2BO_3 as a sample in measuring isotope ratio of boron are summarized by Gensho and Honda as follows: (a) three or more mass peaks are observable from the combination of isotopes of boron and alkali metal (Li, K, and Rb), (b) the discrimination factor (including fractionation effect) may be obtained using a synthetic mixture of isotopes of alkali metal, and (c) the relative peak heights can be adjusted by using a synthetic isotope mixture so as to minimize the reading error (the error arising from using different ranges for recordings of two peaks having a large difference in intensities).

It is important to know how high precision we have to evaluate Q_x (Q) for getting "precise" isotope ratio R_0 of M. The main sources for errors possibly caused in evaluating Q_x come from the evaluation of k_x and the measurement of R_x. From Eqs. 4 and 8, we obtain

$$\frac{\Delta Q}{Q} = \frac{(k_m+1)(\alpha R+1)(\beta R+1)}{(R+1)(c+dR)}\frac{\Delta R}{R},$$

$$\frac{\Delta R_x}{R_x} = \frac{(R_x+1)(c_x+d_x R_x)}{(k_x+1)(\gamma_1 R_x+1)(\gamma_2 R_x+1)}\frac{\Delta Q_x}{Q_x}.$$

Combination of these two equations with Eqs. 5 and 9 gives the magnitude of error permissible to the observed R_x or to the evaluation of Q as a function of Q (or Q_x). Table 1 shows an example of calculations for ΔR_x and ΔQ under the conditions: $k_m=k_x=1$, $Q=Q_x$, and $\Delta R/R=0.05\%$.

Remarkable points of the calculations are that relative

Table 1. The relative error permissible to the evaluation of Q or R_x as a function of Q

Q/Q_0	R ($^{39}K/^{41}K$)	$\Delta Q/Q$ (%)	R_x ($^{35}Cl/^{37}Cl$)	$\Delta R_x/R_x$ (%)
1.00	13.850	—	3.1248	—
0.95	13.837	2.64	3.1215	0.05_4
0.90	13.822	2.64	3.1181	0.05_4
0.80	13.792	2.64	3.1106	0.05_4
0.70	13.757	2.64	3.1021	0.05_4
0.60	13.717	2.64	3.0924	0.05_4
0.50	13.669	2.64	3.0809	0.05_4
0.40	13.612	2.64	3.0669	0.05_4
0.30	13.537	2.64	3.0489	0.05_4
0.20	13.434	2.64	3.0238	0.05_4
0.10	13.258	2.64	2.9813	0.05_4
0.05	13.085	2.64	2.9394	0.05_4

R_0 ($^{39}K/^{41}K$)=13.850, R_x° ($^{35}Cl/^{37}Cl$)=3.1248, α=1.02532, β=1.01334, γ_1=1.01339, γ_2=1.02816, $Q=Q_x$, $k_m=k_x$=1.0, $I_m=I_x$=1.0, $\Delta R/R$=0.05%.

error permissible to the evaluation of Q is rather constant and large as expected and that the precision required to the measurement of R_x is comparable to the precision of the isotope ratio of M which we intend to obtain. The accuracy of the evaluation of Q_x (Q) can be improved by the least-squares curve fitting of several sets of Q and R_x data so that a lower accuracy for each R_x may be tolerable to get the required accuracy of Q. Probably the calibration curve which may be constructed by use of the synthetic isotope mixtures of both metal M and its counterpart X suffices this object because most accurate Q value is obtainable from the comparison of the calibration curve and observed R_x of the sample.

When molecules or molecular ions are the only entity of vaporizing species from sample filament, calculations become much simpler and easier. Equation 5 is reduced to

$$(\beta-1)\ln\left(\frac{Q}{Q_0}\right)=\ln\left(\frac{R}{R_0}\right)+(\beta-1)\ln\left(\frac{R+1}{R_0+1}\right)$$

and the observed isotope ratio of metal ions will be $R_{ob}=\beta R$. Equation 9 is also simplified to be

$$(\gamma_1-1)\ln\left(\frac{Q_x}{Q_0}\right)=\ln\left(\frac{R_x}{R_x^\circ}\right)+(\gamma_1-1)\ln\left(\frac{R_x+1}{R_x^\circ+1}\right)$$

and the observed isotope ratio of X in molecular ions MX^+ is $\gamma_1 R_x$. If we can observe X^{+or-} ions as mass peaks, the isotope ratio of X^{+or-} ions should be $\gamma_1 R_x$. The observation of X^{+or-} ions may be advantageous from the practical stand point as will be discussed later in more details.

In recent high precision mass spectroscopic studies, the synthetic mixture of isotopes from highly enriched isotopes plays an important role in getting high accuracy.[6] The use of a synthetic isotope mixture makes it feasible to apply the present method to various isotope ratio measurements. In fact, it is almost straightforward to make a rough estimation of Q value from the precisely known R_x° value and observed isotope ratio R_x of X. Furthermore, the isotope mixture of an appropriate composition can greatly improve the accuracy of isotope ratio of molecular ions, *e.g.*, if we use the sample of La_2O_3 in which the isotope ratio of $^{18}O/^{16}O$ is about 1122, we will have the comparable intensities for $^{139}La^{16}O^+$ ($m=155$) and $^{138}La^{18}O^+$ ($m=156$) peaks so that recording error will be minimized.

An alternative method for estimating Q is the measurements of isotope ratio of X by observing mass spectra of X ions. It is to be noticed that isotope ratios of chlorine and bromine can be obtained by measuring negative ions of these elements ionized in a thermal ionization ion source.[21,22] Chloride and bromide are the most common chemical form of the sample in a MFTIS. The advantage of measuring chloride or bromide ions is the possible applicability of the present method to most metal elements by adopting chloride or bromide as a chemical form of the sample. The simultaneous determinations of isotope ratios of M^+ and X^- in the same sample are attainable by simply changing polarity of the accerating voltage and magnetic current of a mass spectrometer. Instead of Eq. 10, the equation relating R_x and observed isotope ratio r_x in the vapor X^{-or+} is given by

$$r_x=\frac{(\gamma_1+\gamma_2 k_x I_x)R_x+\gamma_1\gamma_2(k_x I_x+1)R_x^2}{(k_x I_x+1)+(\gamma_2+\gamma_1 k_x I_x)R_x}$$

where $I_x=I_{xb}/I_{xc}$, and I_{xb} and I_{xc} are the ionization efficiencies of the vapor B and vapor C, respectively.

It is expected that the fractionation factor of $M\overline{X}$ (or $\overline{M}X$) varies according to the change in the average mass of $\overline{X}$ (or $\overline{M}$) as the sample evaporation proceeds. However, the change is usually so small that fractionation factors can be regarded constant in most cases without causing any detectable errors (Table 2).

Table 2. Fractionation factors of KCl as a function of average mass of potassium or chlorine

$R(^{39}K/^{41}K)$	$\overline{M}(K)$	$\gamma_1=(\overline{M}^{37}Cl/\overline{M}^{35}Cl)^{1/2}$
13.850	39.098_3	1.01339_2
13.700	39.099_6	1.01339_1
13.300	39.103_4	1.01339_1
12.900	39.107_4	1.01339_0
12.000	39.129_8	1.01338_5
$R_x(^{35}Cl/^{37}Cl)$	$\overline{X}(Cl)$	$\beta=(^{41}K\overline{X}/^{39}K\overline{X})^{1/2}$
3.1248	35.453_0	1.01333_9
3.0000	35.468_1	1.01333_6
2.8000	35.494_4	1.01333_2
2.5000	35.539_4	1.01332_4

As implicitly implied in the previous paper[5] and extensively studied by Moore *et al.*,[7] the change of k must be admitted during the vaporization process. In fact, not only k but also I varies in the actual experimental situation. In addition to the fractionation pattern, most anomalous phenomena associated with MFTIS may be explained by admitting the change in either k or I (or both) during analysis.[5,7] From the practical stand point, the entire fractionation curve can be constructed experimentally on a point-by-point basis with a standard sample in which initial isotope ratios of both M and X are precisely known. With experimental data of k and I (or the combination factor $L=k\,I$), incorporation of the changes of k and I will be made case by case by using Eqs. 4 and 8 as a starting point. Some examples of such attempts have been presented by Moore *et al.*[7]

References

1) A. K. Brewer, *J. Chem. Phys.*, **4**, 350 (1936).
2) S. Taniguchi, O. Toyama, and T. Hayakawa, *Mass Spectroscopy*, **10**, 91 (1962).
3) W. R. Shields, E. L. Garner, C. E. Hedge, and S. S. Goldich, *J. Geophys. Res.*, **68**, 2331 (1963).
4) A. Eberhardt, R. Delwiche, and J. Geiss, *Z. Naturforsch., Teil A*, **19**, 736 (1964).
5) H. Kanno, *Bull. Chem. Soc. Jpn.*, **44**, 1808 (1971); H. Kanno, *Mass Spectroscopy*, **19**, 118 (1971).
6) Paul de Biévre, *Adv. Mass Spectrom.*, **7**, 395 (1978).
7) L. J. Moore, E. F. Heald, and J. J. Filliben, *Adv. Mass Spectrom.*, **7**, 448 (1978).
8) M. H. Dodson, *J. Sci. Instrum.*, **40**, 288 (1963); M. H. Dodson, *Geochim. Cosmochim. Acta*, **34**, 1241 (1970).
9) W. Compston and V. M. Oversby, *J. Geophys. Res.*, **74**, 4338 (1969).

10) J. A. Cooper, P. H. Reynolds, and J. R. Richards, *Earth Planet. Sci. Lett.*, **6**, 467 (1969).
11) M. L. Coleman, *Earth Planet. Sci. Lett.*, **12**, 399 (1971).
12) L. J. Moore, L. A. Machlan, W. R. Shields, and E. L. Garner, *Anal. Chem.*, **46**, 1082 (1974).
13) E. F. Heald, private communication obtained from Dr. L. J. Moore.
14) G. H. Palmer, *Adv. Mass Spectrom.*, **1**, 89 (1959).
15) M. G. Inghram, R. J. Hayden, and D. C. Hess, *Phys. Rev.*, **79**, 271 (1950).
16) C. M. Gray and W. Compston, *Nature*, **251**, 495 (1974).
17) A. H. Turnbull, "U. K. Atomic Energy Authority Research Group Report," AERE Report 4295, Harwell (1963).
18) R. Gensho and M. Honda, *Mass Spectroscopy*, **19**, 134 (1971).
19) "The Characterization of High Temperature Vapors," ed by John L. Margrave, Wiley, New York (1967); S. H. Bauer and R. F. Porter, "Molten Salt Chemistry," ed by M. Blander, Wiley Interscience, New York (1964), p. 607.
20) John W. Hastie, "Advances in Molten Salt Chemistry," Plenum Press, New York (1971), Vol. 1, p. 225.
21) W. R. Shields, T. J. Murphy, E. L. Garner, and V. H. Dibeler, *J. Am. Chem. Soc.*, **84**, 1519 (1962).
22) K. G. Heumann and R. Hoffmann, *Adv. Mass Spectrom.*, **7**, 610 (1978).

Spectrophotometric Determination of Cobalt(II) with Eriochrome Black T after Extraction as Methyltrioctylammonium Tetrathiocyanatocobaltate(II)

Yuh'ichi ROKUGAWA, Masao SUGAWARA, and Tomihito KAMBARA*
Department of Chemistry, Faculty of Science, Hokkaido University, Sapporo 060
(Received December 20, 1978)

A sensitive extraction-spectrophotometric method for determination of cobalt(II) with Eriochrome Black T is described, which involves the preliminary separation of cobalt from aqueous solution by the benzene extraction of methyltrioctylammonium tetrathiocyanatocobaltate(II). The quantitative formation of ion pair between cobalt–Eriochrome Black T complex anion and the quaternary ammonium cation is attained by shaking the resulting extract with aqueous Eriochrome Black T solution of pH 5.5—8.2. Beer's law holds for 0.57—4.0 μg cobalt in 5 ml of the extract with the molar absorption coefficient of $\varepsilon_{587}=6.62\times10^4$ cm^{-1} mol^{-1} l (Sandell sensitivity 8.90×10^{-4} μg cm^{-2}). The composition of the extracted ion pair is estimated to be cobalt: Eriochrome Black T: methlytrioctylammonium ion = 1 : 2 : 3.

The use of 1-(1-hydroxy-2-naphthylazo)-6-nitro-2-naphthol-4-sulfonic acid, sodium salt (Eriochrome Black T, abbreviated to EBT) for extraction-spectrophotometric determination of metal ions has been described by several authors.[1–5] Fukamachi *et al.*[3] and Pyatnitskii *et al.*[5] reported that the color intensity of magnesium(II) complex in the organic phase is higher than that in the aqueous solution.

In the present paper a sensitive method for extraction-spectrophotometric determination of cobalt(II) with EBT is described, in which cobalt(II) is first separated into benzene as the methyltrioctylammonium tetrathiocyanatocobaltate(II) and the resulting extract, without stripping, is subjected to the procedure for color development.

Experimental

Reagents. Commercial Eriochrome Black T(Dojindo Laboratories Ltd.) was used without further purification. The solution (0.1 mM nominal, 1 M = 1 mol dm^{-3}) was daily prepared by dissolving the reagent in water and the concentration was corrected. The purity of EBT was evaluated as described in a previous paper[6] and found to be 52.6%.

A 5% benzene solution of methyltrioctylammonium chloride (Capriquat, Dojindo Laboratories Ltd., abbreviated as Q^+Cl^-) was converted into its thiocyanate form according to the method of Wilson and McFarland.[7] The stock solution was diluted with benzene as required.

A 0.01 M standard solution of cobalt(II) was prepared from its nitrate and standardized by means of the conventional chelatometric titration.

A mixture of 5 (v/v)% hydrogen peroxide and 10 μM manganese(II) buffered at pH 8.0 was freshly prepared before use by mixing the appropriate amounts of 30 (w/w)% hydrogen peroxide and 0.01 M manganese(II) chloride solutions and satd sodium tetraborate–0.1 M hydrochloric acid buffer solution.

Saturated sodium tetraborate–0.1 M hydrochloric acid or 0.1 M sodium hydroxide buffer and 0.2 M acetic acid–0.2 M sodium acetate buffer solutions were used. Deionized water was used. Other reagents used were all of analytical grade.

Apparatus. A Hitachi two-wavelength and double beam spectrophotometer 356 and a Shimadzu spectrophotometer, Model QV-50, 10-mm cells were used for absorptiometric measurements. A Yamato shaker, Model SA-31, was used for extraction. A Hitachi-Horiba glass electrode pH meter, Model F-5, was used for pH measurements.

Procedure. In a 100-ml separating funnel are taken 10 ml of the solution containing less than 4.0 μg of cobalt(II), 7 ml of a mixture of 1.5 M potassium thiocyanate, 1 M sodium citrate solutions and 0.15 M tris(hydroxymethyl)aminomethane–sulfuric acid buffer solution (pH 8.0). The mixture is shaken for 15 min with 5 ml of 0.5% benzene solution of methyltrioctylammonium thiocyanate(Q^+SCN^-). The organic phase is washed with 5 ml of a mixture of 0.5 M potassium thiocyanate, 0.7 M sodium citrate and 0.9 M sodium thiosulfate. After addition of 5 ml of 52.6 μM EBT solution and 10 ml of satd sodium tetraborate–0.1 M hydrochloric acid buffer solution (pH 7.5), the two phases are shaken for 5 min. The organic phase is washed twice with water and then shaken for 50 min with 15 ml of 5% hydrogen peroxide–10 μM manganese(II) solution of pH 8.0. The organic phase is transferred into a beaker containing anhydrous sodium sulfate and the absorbance of the extract is measured at 587 nm against a reagent blank.

Results and Discussion

Decomposition of the Excess EBT. The use of manganase(II)-catalyzed discoloration reaction for the decomposition of the excess *o,o'*-dihydroxy azo reagents was investigated in order to improve the sensitivity and selectivity of spectrophotometric determination of copper(II).[6,8,9] To apply this reaction to decompose the excess EBT in the benzene phase, effects of pH and shaking time were investigated. The decomposition of EBT proceeds efficiently (Fig. 1), when the extract is shaken for longer than 40 min with the aqueous solution of pH higher than 7.5 (5% in hydrogen peroxide and 10 μM in manganese(II)). Washing of the extract with water before this procedure is necessary for the complete decomposition of EBT.

Separation of Cobalt(II). A large number of metal ions such as copper(II), nickel(II), iron(III), and chromium(III) cause serious interference with the determination of cobalt(II) by forming colored, benzene-extractable complexes with EBT. In order to remove the interference a prior separation of cobalt(II) by means of the modified Vogel reaction was found to be useful. The procedure given here is based on the suggestion given by Wilson and McFarland,[7] except that the

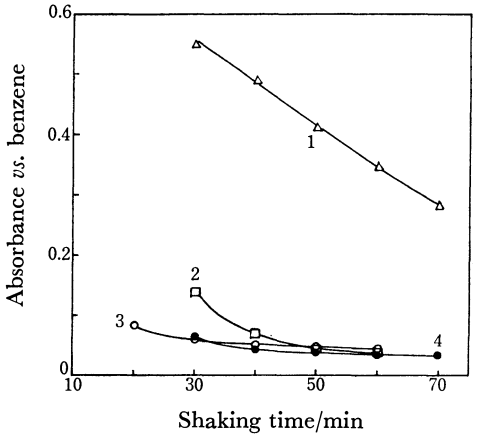

Fig. 1. Effects of pH and shaking time on the decomposition of 52.6 μM EBT in benzene with the aqueous solution of 5% hydrogen peroxide and 12 μM manganese(II).
$[QSCN]_0$=0.01 M, 587 nm, benzene as reference. pH (1): 7.0, (2): 7.5, (3): 8.0, (4): 9.0.

concentration of methyltrioctylammonium thiocyanate in benzene is lower than that recommended. The thiocyanate system is useful for the spectrophotometric determination of 1.2—59 μg of cobalt per milliliter. However, the extraction of smaller amounts of cobalt has not been reported. In order to determine the extractability of cobalt(II) at a few hundred ppb levels, the aqueous phase was repeatedly extracted with the benzene solution of methyltrioctylammonium thiocyanate and the extract was subjected to absorbance measurement. It was found that 2.3 μg of cobalt(II) is almost completely extracted by a single extraction with the 0.5% quaternary ammonium salt solution in benzene.

Absorption Spectra. Based on the observation that the methyltrioctylammonium cobaltothiocyanate in the benzene extract reacts with EBT forming an ion-pair of cobalt–EBT complex anion and the quaternary ammonium cation, the procedure for color development was determined as above. Absorption spectra of cobalt(II)–EBT complex in the aqueous solution and the ternary complex in the extract after the decomposition of excess EBT are shown in Fig. 2. A bathochromic shift of the absorption maxima, accompanied by the enhancement of the absorption intensity, is observed when the cobalt(II)–EBT complex anion is extracted as an ion-pair with the quaternary ammonium cation. The red-purple coloration of the ternary complex, the absorption maxima being 544 and 587 nm, is stable for at least 20 min.

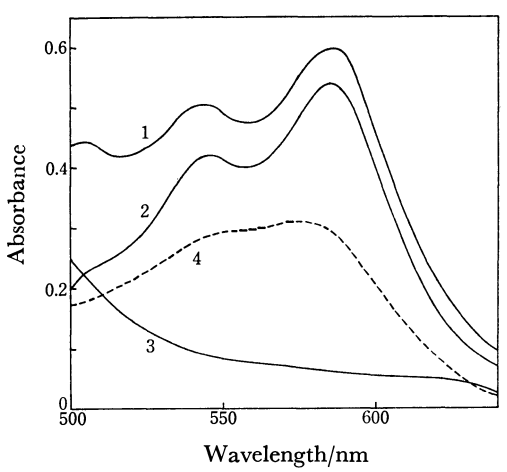

Fig. 2. Absorption spectra of cobalt–EBT complex in aqueous solution and the ternary complex in organic phase after decomposition of excess EBT.
1: Ternary complex *vs.* benzene; 2: ternary complex *vs.* reagent blank; 3: reagent blank *vs.* benzene; $[Co(II)]_0$=7.79 μM, $[EBT]_0$=52.6 μM, pH 8.0; 4: cobalt–EBT complex in aqueous solution *vs.* reagent blank; $[Co(II)]_w$=7.79 μM, $[EBT]_w$=40 μM, pH 10.5.

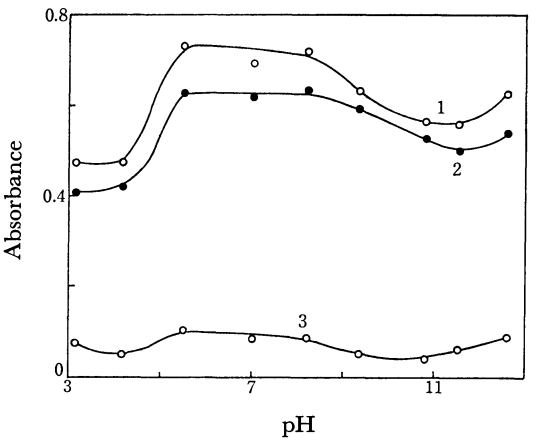

Fig. 3. Effect of pH on the absorbance of cobalt–EBT–Q ternary complex at 587 nm after decomposition of excess EBT. 1: Ternary complex *vs.* benzene; 2: ternary complex *vs.* reagent blank; 3: reagent blank *vs.* benzene; $[Co(II)]_0$=9.73 μM, $[EBT]_w$=17.53 μM, $[QSCN]_0$=0.01 M. Volume ratio of aqueous-to-organic phase is 3: 1.

Effects of pH *and EBT Concentration.* A constant and stable absorbance of cobalt–EBT–Capriquat ternary complex is obtained by shaking the extract with the EBT solution of pH 5.5—8.2 as shown in Fig. 3. For full development of color, addition of EBT in a small excess of the stoichiometrically necessary amount is sufficient.

Effect of Methyltrioctylammonium Thiocyanate Concentration. As described above, 0.5% methyltrioctylammonium thiocyanate in benzene is sufficient for the quantitative extraction of microgram amounts of cobalt(II) as the thiocyanate complex. It was found that the red-purple coloration of the ion-pair of cobalt–EBT complex anion and the quaternary ammonium cation is fully developed by shaking the extract for longer than 3 min with EBT solution. The ion-pair, once formed, is not stripped even by shaking with water and the mixture of hydrogen peroxide and manganese(II).

Calibration Curve and Sensitivity. The calibration curve conforms to Beer's law in the concentration range 0.57—4.0 μg cobalt in 5 ml of the extract, with the molar absorption coefficient of 6.62×10^4 cm^{-1} mol^{-1} l at 587 nm, which is higher than 4.04×10^4 cm^{-1} mol^{-1} l at 573 nm in the aqueous solution. The average of absorbance

Table 1. Effect of various ions

Ion added (X)	Amount μg	Cobalt(II) found μg	Error %
Al(III)	458	2.34	+2.2
Cd(II)	458	2.26	−1.3
Cr(III)	115	2.28	−0.4
Cu(II)	458	2.34	+2.2
Fe(III)	687	2.34	+2.2
Mn(II)	22.9	2.21	−3.5
Ni(II)	11.5	2.38	+3.9
Pb(II)	458	2.27	+0.9
Sn(II)	458	2.25	−1.7
Zn(II)	458	2.35	+2.6
MoO_4^{2-}	756	2.28	−0.4
VO_3^-	46	2.24	−2.2
WO_4^{2-}	618	2.21	−3.5
Cl^-	4580	2.26	−1.3
ClO_4^-	11450	2.28	−0.4
HPO_4^{2-}	2314	2.24	−2.2
SO_4^{2-}	6870	2.29	±0

Cobalt(II) taken: 2.29 μg.

obtained by three determinations was 0.386 and the range was 0.009 for 1.72 μg of cobalt(II) in the extract.

Effect of Foreign Ions. The results of tolerance test according to the above procedure are given in Table 1. The cations were added as nitrates, chlorides or sulfates and anions as sodium, potassium, or ammonium salts. Iron(III), copper(II), and nickel(II) form thiocyanate complexes which are extracted into benzene as the quaternary ammonium salts, interfering with the subsequent photometric analysis. The interference by these ions is removed by washing with the scrub solution mentioned above. Zinc(II) is extracted as the thiocyanate complex and reacts with EBT, forming a deep red complex. However, the complex is unstable and decomposed by shaking with the hydrogen peroxide–manganese(II) mixture.

Composition of the Extracted Species. Extraction of cobalt(II)–thiocyanate complex anion with amines and quaternary ammonium compounds has been investigated by many authors.[7,10–15] The blue color of the nonaqueous cobaltothiocyanate solution is attributable to $[Co(SCN)_4]^{2-}$ ion.[10,11,14,15] We might conclude that the faintly blue extract obtained with methyltrioctylammonium thiocyanate is due to the ion-pair of tetrathiocyanatocobaltate(II) anion with the methyltrioctylammonium cation. By using the familiar mole-ratio method, the molar ratio of EBT to cobalt(II) was found to be 2: 1 (Fig. 4). The molar ratio of methyltrioctylammonium cation to cobalt(II)–EBT chelate anion was determined by the method of equilibrium shift (Fig. 5). The distribution ratio D of cobalt(II) was evaluated from the molar absorption coefficient and the absorbance at 587 nm. The slope of the plot evaluated by the method of least squares is 2.87, indicating that the ternary complex has the composition of Co: EBT: Q=1: 2: 3. According to Kodama,[16] cobalt(II) ion forms a 1 to 1 complex with EBT in a weakly alkaline aqueous solution. If we assume that cobalt(II) ion forms the chelate anion

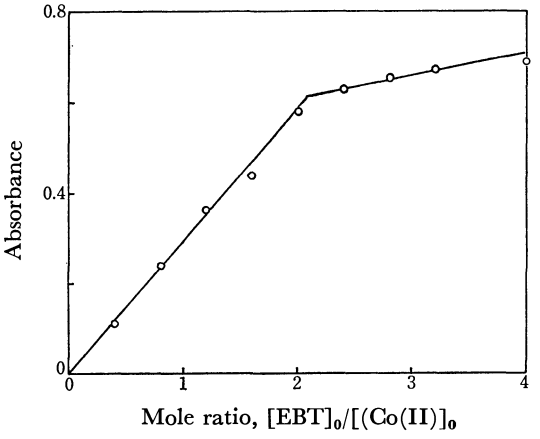

Fig. 4. Mole-ratio method applied to cobalt–EBT system in the extract. $[Co(II)]_w=9.73$ μM, $[KSCN]_w=0.6$ mM, $[QSCN]_0=0.01$ M, pH 8.9, 587 nm *vs.* benzene. The excess EBT was decomposed as above.

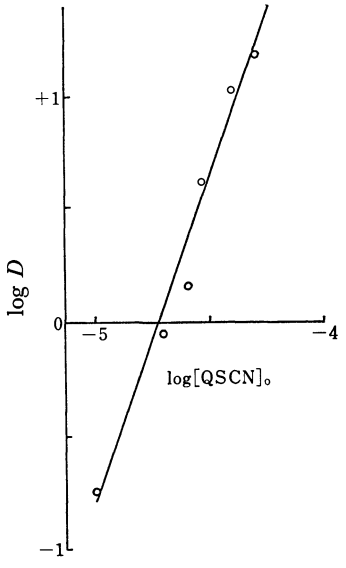

Fig. 5. The logarithm of distribution ratio D plotted *vs.* log $[QSCN]_0$ at pH 9.0 in the presence of 9.73 μM cobalt(II), 19.5 μM EBT and 0.5 mM KSCN.

with EBT which is extracted as the ion-pair with methyltrioctylammonium cation, the composition can be expressed by $[Co^{2+}(HEBT^{2-})(EBT^{3-})(Q^+)_3]_0$. The composition is comparable with $[Mg^{2+}(HEBT^{2-})(EBT^{3-})(Z^+)_3]_0$, that of magnesium complex reported by Pyatnitskii *et al.*,[5] where Z^+ indicates trioctylammonium ion. However, the possibility of +3 oxidation state of cobalt in the extract can not be excluded.

The present work was partially supported by a Grant-in-Aid for Scientific Research from the Ministry of Education (No. 347025).

References

1) M. Nishimura and S. Nakaya, *Bunseki Kagaku*, **16**, 463 (1967).
2) C. Woodward and H. Freiser, *Talanta*, **15**, 321 (1968).
3) K. Fukamachi, H. Kohara, and N. Ishibashi, *Bunseki Kagaku*, **19**, 1529 (1970).

4) C. Woodward and H. Freiser, *Talanta*, **20**, 417 (1973).
5) I. V. Pyatnitskii, S. G. Pinaeva, and N. V. Pospelova, *Zh. Anal. Khim.*, **12**, 2316 (1975).
6) M. Sugawara, Y. Rokugawa, and T. Kambara, *Bull. Chem. Soc. Jpn.*, **50**, 3206 (1977).
7) A. M. Wilson and O. K. McFarland, *Anal. Chem.*, **35**, 302 (1963).
8) M. Sugawara, Y. Ozawa, and T. Kambara, *Bunseki Kagaku*, **23**, 1058 (1974).
9) M. Sugawara, Y. Sato, and T. Kambara, *Bunseki Kagaku*, **26**, 346 (1977).
10) A. R. Selmer-Olsen, *Anal. Chim. Acta*, **31**, 33 (1964).
11) H. Matsuo, S. Chaki, and S. Hara, *Bunseki Kagaku*, **14**, 935 (1965).
12) A. W. Ashbrook, *Analyst*, **84**, 177 (1959).
13) M. Fujimoto and Y. Nakatsukasa, *Anal. Chim. Acta*, **27**, 373 (1962).
14) H. Watanabe and K. Akatsuka, *Anal. Chim. Acta*, **38**, 547 (1967).
15) N. Gundersen and E. Jacobsen, *Anal. Chim. Acta*, **42**, 330 (1968).
16) M. Kodama, *Bull. Chem. Soc. Jpn.*, **40**, 2575 (1967).

The Electrochemical Oxidation of Aminopurines and Their Hydroxy Derivatives at the Glassy Carbon Electrode

Toshio YAO* and Soichiro MUSHA

Department of Applied Chemistry, College of Engineering, University of Osaka Prefecture, Mozuumemachi, Sakai 591

(Received January 20, 1979)

The electrochemical oxidation of aminopurines and their hydroxy derivatives, which gave a single voltammetric peak at the glassy carbon electrode, was investigated by means of linear-sweep voltammetry, cyclic voltammetry, coulometry, and macroscale controlled-potential electrolysis. In general, the ease of oxidation of these compounds increased in proportion to the number of hydroxyl or amino groups on the molecule. The coulometric *n*-values for monosubstituted purines were 5.86—6.08, for disubstituted purines they were 3.90—4.20, and for trisubstituted purines they were 2.07—2.33. The electrochemical oxidation of the different aminopurines appeared to follow initially the same path as the enzymatic oxidation; *i.e.*, the primary attack for the electrochemical oxidation occurred first at the C-8 position, and then the C-2 position. Thus, aminopurines were oxidized in two sequential two-electron processes to give first 8-hydroxy and then 2,8-dihydroxy(or 6,8-dihydroxy) intermediates. Then, this latter intermediate was further oxidized in a two-electron process to produce a diimine intermediate, which was unstable and which then broke down to the ultimate products, such as parabanic acid, oxaluric acid, urea, ammonia, allantoin, and guanidine.

Aminopurines, especially the two bases of adenine and guanine, are important components of nucleic acids and play an important role in many metabolic processes. Several works[1–3] have suggested a possible parallelism between the modes of electrochemical process and the biological transformation, *e.g.*, the enzymatic oxidation. The enzymatic and biological oxidation of adenine and guanine have been examined; they are covered in part in the reviews by Lister[4] and Robins.[5] The oxidation of adenine by the enzyme xanthine oxidase gives 6-amino-8-hydroxypurine as an intermediate in the formation of 6-amino-2,8-dihydroxypurine.[6] Also, guanine is slowly oxidized to uric acid in the presence of very large excesses of xanthine oxidase;[7] this process may be brought about by traces of guanine present in the xanthine oxidase.

Most of the aminopurines were not reduced easily at the dropping mercury electrode(DME) in aqueous solutions. However, some aminopurines can be voltammetrically oxidized at the pyrolytic graphite electrode[2,8,9] and the glassy carbon electrode (GCE).[10–12]

In this paper, the electrochemical oxidation of the aminopurines and their hydroxy derivatives was investigated by means of linear-sweep voltammetry, cyclic voltammetry, controlled-potential coulometry, and the polarography of the oxidation products. On the basis of the data reported here, different and plausible oxidation products were proposed; the mechanisms for the electrochemical oxidation were also proposed. In order to compare the mechanisms and products of oxidation of aminopurines with those of previously known biological oxidations, these studies were carried out in some detail.

Experimental

Chemicals. The 6-aminopurine (adenine), 2-aminopurine, and 2-amino-6-hydroxypurine (guanine) were obtained from the Wako Pure Chemical Co. The 6-amino-2-hydroxypurine (isoguanine) and 2,6-diaminopurine were obtained from the Sigma Chemical Co. The 6-amino-8-hydroxypurine, 6-amino-2,8-dihydroxypurine, 2-amino-8-hydroxypurine, 2-amino-6,8-dihydroxypurine, and 2,6-diamino-8-hydroxypurine were all synthesized according to methods previously described.[13] All the products were recrystallized three times from distilled water before drying *in vacuo* at 60 °C, and their purities were checked by both elemental analysis and linear-sweep voltammetry.

Apparatus. The polarograms and anodic voltammograms were recorded using a Yanagimoto P-8 type Polarograph. The cyclic voltammograms were obtained with a versatile solid-state instrument constructed in this laboratory, with triangular voltage sweeps supplied by a NF Circuit Design Block Co. Model FG-104T function generator. The current-voltage curves were recorded on an IWATSU Model DS-5016 dual-beam oscilloscope equipped with a camera or on a Hewlett Packard Model 7045A X-Y recorder.

A three-electrode cell was used for all the experiments. A saturated calomel electrode (SCE) was used as a reference electrode, while a platinum wire was used as a counter electrode.

The DME used had the following characteristics: mercury flow rate, $m=2.32$ mg/s and drop time, $t=3.32$ s at an open circuit with a mercury head of 70 cm in 1 M H_3PO_4.

The working electrode used for anodic voltammetry, GCE, was constructed as has been described before.[10] The GCE was polished for about 30 s with 1500-grade emery paper and then a paste of CeO_2 on asphalt pitch until the surface of the electrode was brought to a mirror finish. Also, in order to obtain reproducible results, the standard pretreatment procedure described previously was applied before recording each voltammogram.[10]

Controlled-potential electrolysis was done at the potentials on the crest of the anodic peaks, with a NICHIA Model NP-1 potentiostat. A glassy carbon beaker (40 ml in volume; Tokai Electrode Co.) was used as the working electrode. The colorimetric determinations of oxidation products were done using a Shimadzu Model Spectronic 20.

Colorimetric Methods for the Determination of Oxidation Products. The urea was determined by a modification of Rosenthal's method.[14,15] The ammonia was determined by the Nessler method, following King and Faulconer.[16] The allantoin was determined by a modification of the Young and Conway procedure.[17] The guanidine was determined by the procedure described by Staron and Allard.[18]

Polarographic Methods for the Determination of Parabanic and

TABLE 1. VOLTAMMETRIC DATA FOR THE OXIDATION PEAKS OF AMINOPURINES AND THEIR HYDROXY DERIVATIVES AT THE STATIONARY GCE

Compound[a)]	pH range	$E_{p/2}$ (V *vs.* SCE)	$(i_p/ACV^{1/2})$[b),c)]	$E_p-E_{p/2}$[c)] (mV)
6-Aminopurine	0—12	1.45—0.064pH	145	60
6-Amino-8-hydroxypurine	0—13	1.01—0.067pH	95	45
6-Amino-2-hydroxypurine	0—13	1.03—0.057pH	103	35
6-Amino-2,8-dihydroxypurine	0—13	0.77—0.072pH	46	52
2-Aminopurine	0—12	1.34—0.087pH	130	37
2-Amino-6-hydroxypurine	0—13	1.13—0.059pH	93	29
2-Amino-8-hydroxypurine	0—13	1.11—0.068pH	87	32
2-Amino-6,8-dihydroxypurine	0—13	0.79—0.077pH	51	27
2,6-Diaminopurine	0—13	1.03—0.054pH	93	30
2,6-Diamino-8-hydroxypurine	0—13	0.76—0.074pH	49	33

a) Concentration of each compound: 0.05 mM. b) Peak current function: $\mu A\ (cm^2 \cdot mM)^{-1}(mV/s)^{-1/2}$.
c) In 1M H_2SO_4.

Oxaluric Acids. The parabanic acid was determined on the completion of the electrolysis by transferring about 10 ml of the electrolyzed solution (1 M H_2SO_4) into a polarographic cell, deaerating it, running a polarogram between 0 and −1.1 V *vs.* SCE, and then comparing the height of the wave at −0.53 V *vs.* SCE with a calibration curve prepared from authentic parabanic acid. The oxaluric acid was determined on the completion of the electrolysis in the same way, using the height of the wave at −0.87 V *vs.* SCE.

Results and Discussion

Anodic Voltammetry. Each of the aminopurines and their derivatives studied gave a voltammetric oxidation peak at a stationary GCE over a wide pH range. The half-peak potentials ($E_{p/2}$) of their oxidation peaks shifted linearly towards negative potentials with the increase in the pH, as is summarized in Table 1. Also, the peak current function, $i_p/ACV^{1/2}$, decreased gradually with the increase in the pH, but in the electrolytes with pH values below 2.8 the peak current functions for all the aminopurines studied remained almost constant in spite of the variations in the pH values. In 1 M H_2SO_4, good linear relationships were observed between the peak current and the concentration, and the peak current functions were almost independent of the scan rate. These facts imply that, in 1 M H_2SO_4, these voltammetric oxidations are diffusion-controlled processes. Accordingly, the peak current functions for all the compounds studied were determined in 1 M H_2SO_4; these results are shown in Table 1.

It was proved in the previous report[12)] that uric acid (2,6,8-trihydroxypurine) gives a well-defined oxidation peak when in acidic solutions, but the peak tends to be ill-defined because of the adsorption of a depolarizer on the electrode surface when in neutral or alkaline solutions, and that the oxidation peak obtained in acid solutions, such as 1M H_3PO_4 and H_2SO_4, is attributable to a two-electron, diffusion-controlled process. The value of the peak current function for uric acid was 47.1 $\mu A(cm^2 \cdot mM)^{-1}(mV/s)^{-1/2}$ in 1 M H_2SO_4. This value was compared with the values for all the compounds studied by assuming that their diffusion-constant values are equal to that of uric acid. The results indicated that the values of the peak current function for the oxidation peaks of monosubstituted purines were *ca.* 130—145 $\mu A(cm^2 \cdot mM)^{-1}(mV/s)^{-1/2}$, corresponding to a six-electron process. Similarly, it is feasible that disubstituted purines are oxidized in a four-electron process, and that trisubstituted purines are oxidized in a two-electron process.

Coulometry. The coulometric measurements at the controlled potentials were performed in order to determine the number of electrons involved in the overall electron-transfer reactions. In 1 M H_2SO_4, the time taken to oxidize completely all of the depolarizer was from one to two hours. However, in the Britton-Robinson buffers with pH values above 4, exhaustive electrolysis required a much longer time and the electrolytic current remained at a low value throughout the electrolysis; this is indicative of a very slow intermediate step in the oxidation, the deposition of an insoluble reaction product, film formation on the electrode surface, or a combination of these phenomena.

Consequently, the coulometric *n*-values were determined in 1 M H_2SO_4. The results are presented in Table 2; the *n*-values for monosubstituted purines were 5.86—6.08, for disubstituted purines they were 3.90—4.20, and for trisubstituted purines they were 2.07—2.33. These results were consistent with the *n*-values determined from the peak current functions of the voltammetric peaks.

TABLE 2. COULOMETRIC *n*-VALUES FOR THE CONTROLLED-POTENTIAL ELECTROLYSIS OF AMINOPURINES AND THEIR HYDROXY DERIVATIVES IN 1M H_2SO_4

Compound	Applied potential (V *vs.* SCE)	n[a)]
6-Aminopurine	1.55	5.86
6-Amino-8-hydroxypurine	1.05	3.90
6-Amino-2-hydroxypurine	1.03	4.20
6-Amino-2,8-dihydroxypurine	0.75	2.28
2-Aminopurine	1.30	6.08
2-Amino-6-hydroxypurine	1.15	4.11
2-Amino-8-hydroxypurine	1.15	4.18
2-Amino-6,8-dihydroxypurine	0.75	2.33
2,6-Diaminopurine	1.05	3.92
2,6-Diamino-8-hydroxypurine	0.75	2.07

a) Average value of three determinations.

Table 3. Effect of pH on the peak potential[a] of anodic peaks observed on the cyclic voltammograms of aminopurines and their hydroxy derivatives

A, Original peak; B, anodic peaks of intermediates.

Compound	1M H_2SO_4		Britton-Robinson buffer					
			pH 2.1		pH 3.0		pH 4.1	
	A	B	A	B	A	B	A	B
6-Aminopurine	1.45	0.99 0.76	1.37	0.92 0.66	1.31	0.86 0.61	1.24	0.78 0.54
6-Amino-8-hydroxypurine	0.99	0.76	0.91	0.68	0.85	0.61	0.78	0.53
6-Amino-2-hydroxypurine	1.01	0.76	0.95	0.68	0.89	0.61	0.83	0.54
6-Amino-2,8-dihydroxypurine	0.76		0.67		0.61		0.53	
2-Aminopurine	1.30	1.08 0.75	1.19	1.00 0.79	1.12	0.94 0.59	1.02	0.88 0.52
2-Amino-6-hydroxypurine	1.10	0.76	1.03	0.79	0.98	0.59	0.91	0.52
2-Amino-8-hydroxypurine	1.08	0.75	0.99	0.79	0.94	0.58	0.88	0.51
2-Amino-6,8-dihydroxypurine	0.75		0.79		0.59		0.51	
2,6-Diaminopurine	1.01	0.73	0.95	0.64	0.90	0.58	0.84	0.50
2,6-Diamino-8-hydroxypurine	0.73		0.63		0.57		0.50	

a) in V *vs.* SCE.

Cyclic Voltammetry. Cyclic voltammograms at fast scan rates were recorded in 1 M H_2SO_4 for each of the four 6-aminopurines. The results are shown in Fig. 1. When scanning was done from 0.0 V at a clean electrode toward a positive potential, only a single anodic peak was observed for 6-aminopurine (Curve A). The principal point of interest in this voltammogram is that two new, small anodic peaks (Peaks I and II) were observed on the second sweep toward the positive potential at a fast scan rate of more than 0.25 V/s. Peak I appeared at almost the same peak potential as the original anodic peak of 6-amino-8- or 6-amino-2-hydroxypurine. Also, the peak potential of Peak II was the same as that of the anodic peak of 6-amino-2,8-dihydroxypurine. Each of 6-amino-8- and 6-amino-2-hydroxypurine gave a new anodic peak on the second sweep toward the positive potential; the peak potential of this new peak was consistent with that of the original peak of 6-amino-2,8-dihydroxypurine.

However, since the peak potentials of these new peaks were dependent on the pH of the electrolyte solutions, cyclic voltammograms were recorded in electrolyte solutions of various pH values. The results are shown in Table 3. At various pH values, Peak I and Peak II of 6-aminopurine coincided in potential with the original peak of 6-amino-8-hydroxypurine and 6-amino-2,8-dihy-

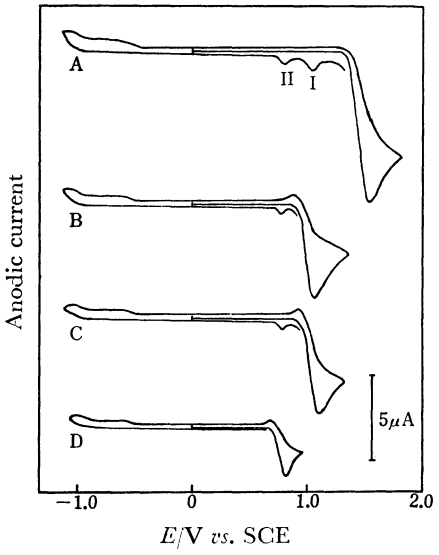

Fig. 1. Cyclic voltammograms of 6-aminopurines in 1 M H_2SO_4.
(A), 6-Aminopurine; (B), 6-amino-8-hydroxypurine; (C), 6-amino-2-hydroxypurine; (D), 6-amino-2,8-dihydroxypurine. Concn of all the compounds: 0.5 mM. GCE geometric area: 0.071 cm^2. Scan rate: (A), 0.64 V/s; (B), (C), (D), 0.56 V/s.

Table 4. Comparison of polarographic behavior of parabanic and oxaluric acids with products of the electrolytic oxidation of 6-aminopurine

pH	Oxidation products[a]				Parabanic acid[b]		Oxaluric acid[b]	
	1st wave		2nd wave					
	$E_{1/2}$ (V *vs.* SCE)	i_d (μA)	$E_{1/2}$ (V *vs.* SCE)	i_d (μA)	$E_{1/2}$ (V *vs.* SCE)	i_d (μA)	$E_{1/2}$ (V *vs.* SCE)	i_d (μA)
1M H_2SO_4	−0.566	0.56	−0.957	0.32	−0.569	1.25	−0.955	1.06
Britton-Robinson buffer								
2.1	−0.652	0.55	−1.077	0.35	−0.655	1.26	−1.080	1.12
3.0	−0.715	0.49	−1.165	0.30	−0.717	1.32	−1.171	1.00
4.1	−0.795	0.51	−1.287	0.26	−0.793	1.28	−1.283	0.95

a) Exhaustive electrolysis of 1.0 mM 6-aminopurine. b) Concentration: 0.2 mM.

TABLE 5. DETERMINATION OF OXIDATION PRODUCTS AFTER EXHAUSTIVE ELECTROLYSIS

Compound[a)]	Polarographic method		Colorimetric method			
	Parabanic acid (mM)	Oxaluric acid (mM)	Urea (mM)	Ammonia (mM)	Allantoin (mM)	Guanidine (mM)
6-Aminopurine	0.09	0.06	0.25	2.36	0.24	—
6-Amino-2-hydroxypurine	0.04	0.05	0.21	2.98	0.30	—
6-Amino-8-hydroxypurine	0.05	0.03	0.16	3.36	0.34	—
6-Amino-2,8-dihydroxypurine	0.05	0.03	0.32	3.48	0.29	—
2-Aminopurine	0.02	0.01	0.29	0.93	0.55	0.60
2-Amino-6-hydroxypurine	0.01	0.01	0.20	0.52	0.78	0.63
2-Amino-8-hydroxypurine	0.01	0.01	0.30	0.82	0.60	0.61
2-Amino-6,8-dihydroxypurine	0.01	0.01	0.32	1.00	0.48	0.64
2,6-Diaminopurine	0.04	0.03	0.25	2.50	0.52	0.55
2,6-Diamino-8-hydroxypurine	0.03	0.03	0.21	2.75	0.60	0.51

a) Exhaustive electrolysis of 1 mM aminopurines in 1M H_2SO_4.

droxypurine respectively. Also, the new anodic peaks of 6-amino-8- and 6-amino-2-hydroxypurine were observed at almost the same potentials at various pH values, and their peak potentials were in very close agreement with that of the original peak of 6-amino-2,8-dihydroxypurine.

Similarly, 2-aminopurine gave two new, small anodic peaks on the second sweep toward the positive potential. At various pH values, the peak potentials for these two peaks were the same as those of the anodic peaks for the oxidation of 2-amino-8-hydroxypurine and 2-amino-6,8-dihydroxypurine, as is shown in Table 3. Also, 2,6-diaminopurine gave a new anodic peak corresponding to an oxidation peak of 2,6-diamino-8-hydroxypurine on the second sweep toward the positive potential.

Controlled-potential Electrolysis. After the exhaustive electrolysis of 1 mM aminopurines, linear-sweep voltammetry at the GCE showed no anodic peak, but polarography at the DME showed two reduction waves. These waves were probably due to the reduction of the ultimate products produced by the oxidation; their half-wave potentials shifted toward negative potentials with the increase in the pH values of the electrolyte solutions. The polarographic behavior of the products in the electrolyzed solutions was compared with those of parabanic and oxaluric acids. In the case of 6-aminopurine,

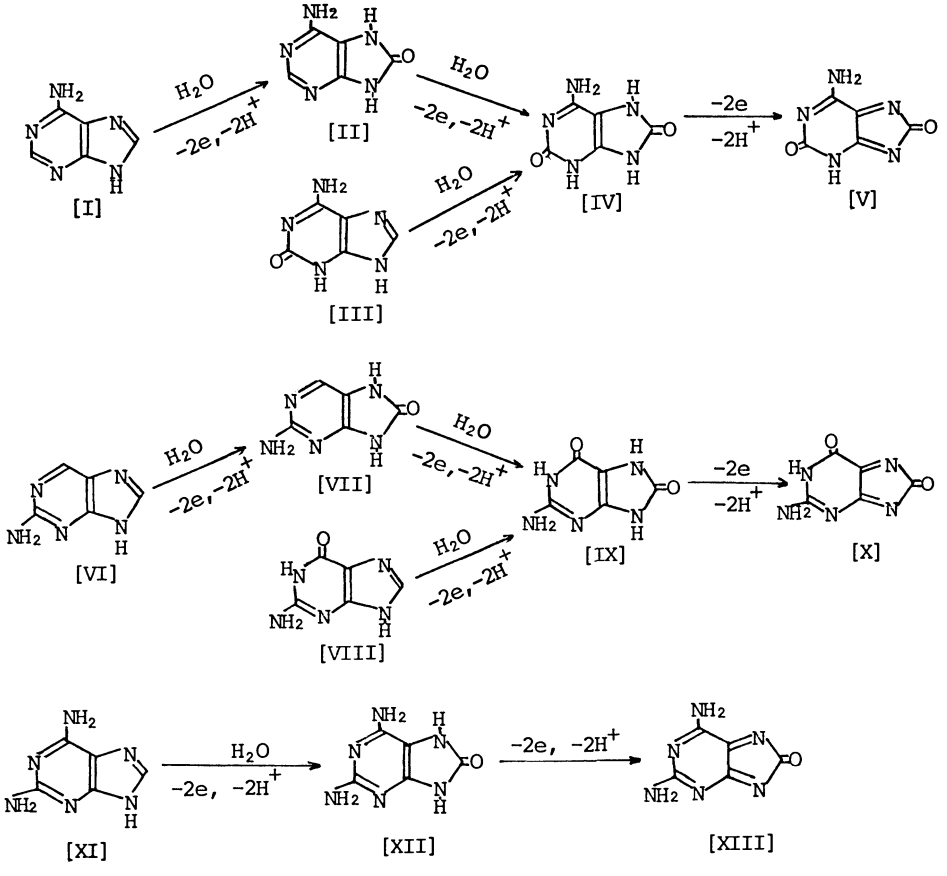

Fig. 2. Proposed primary electrochemical pathways for electrooxidation of different aminopurines.

the experimental results are summarized in Table 4. The $E_{1/2}$ values of the first and second waves agreed very closely with those of parabanic and oxaluric acids respectively.

The ultimate electroinactive products (urea, ammonia, allantoin, and guanidine) were determined by the colorimetric methods given in the Experimental section. The results are shown in Table 5.

Mechanisms. The characteristic ultraviolet absorption spectra of the aminopurines (λ_{max}=260—270 nm) are attributable mainly to the –C(4)=C(5)–C(6)=N(1)– chromophoric group.[19,20] The disappearance of these peaks after exhaustive electrolysis indicates that the –C(4)=C(5)– bond is ultimately oxidized and cleaved. In addition, an analysis of the product solutions after exhaustive electrolysis suggested the presence of parabanic acid, oxaluric acid, urea, ammonia, allantoin, and guanidine. The cyclic voltammetric data also suggested the presence of various intermediates which were more easily oxidized than their parent compounds. The presumed mechanisms of the primary oxidations of the different aminopurines studied at the GCE are summarized in Fig. 2.

The coulometric *n*-value for the oxidation of 6-aminopurine was *ca.* 5.86. Also, cyclic voltammetric experiments revealed the presence of both 6-amino-8-hydroxypurine(II) and 6-amino-2,8-dihydroxypurine(IV) as the electrochemical intermediates, both of which were more easily oxidized than 6-aminopurine(I). The coulometric *n*-values for the oxidation of Compounds II and IV were *ca.* 3.90 and 2.28 respectively. These facts supported the idea that the electrochemical oxidation of 6-aminopurine proceeds initially by two sequential two-electron steps to give first Compound II and then Compound IV. The latter compound was similar to uric acid except for the presence of an amino group in place of an hydroxyl group at the 6-position; then it was probably oxidized in a further two-electron step to produce a diimine intermediate(V) of the same type as that proposed for the electrochemical oxidation of uric acid.[1] The continuous oxidation to the diimine intermediate, as soon as the initial two-electron oxidation had occurred, was caused by the fact that the ease of oxidation generally increased with the number of hydroxyl groups on the molecule (see Table 1). Compounds II and IV were easily oxidized electrochemically than was 6-aminopurine itself and, consequently, were unstable with respect to the oxidation at the potential at which 6-aminopurine was oxidized. Also, an intermediate for the two-electron oxidation of 6-aminopurine was 6-amino-8-hydroxypurine, and no evidence for the presence of 6-amino-2-hydroxypurine(III) was given by cyclic voltammetry. In addition, both Compounds II and III were oxidized in a two-electron step to produce the same intermediate, Compound IV. Thus, under electrochemical conditions oxidation occurred first at the C-8 position and then at the C-2 position.

Similarly, 2-aminopurine(VI) was electrochemically oxidized to 2-amino-6,8-dihydroxypurine(IX) *via* 2-amino-8-hydroxypurine(VII). Also, 2,6-diaminopurine(XI) was oxidized in a two-electron step to produce 2,6-diamino-8-hydroxypurine(XII), as was shown by cyclic voltammetric experiments. Compounds IV, IX, and XII were oxidized in a two-electron step to produce the corresponding unstable diimine intermediates (V, X, and XIII), which were then hydrolyzed in water to the ultimate compounds, such as parabanic acid, oxaluric acid, urea, ammonia, allantoin, and guanidine.

Conclusions

The different aminopurines studied were electrochemically oxidized by a mechanism very similar to that observed for other naturally occurring purines, such as uric acid and xanthine. The evidence put forward supported the view that the locus of the initial electron removal was the same for enzymatic and electrochemical processes, *i. e.*, in both the enzymatic and electrochemical oxidations the attack was first at the C-8 position and then at the C-2 position. Unlike most enzyme reactions, where the 2-amino group of guanine is removed, this group remained intact under electrochemical oxidations, and further electrochemical reaction occurred at the –C(4)=C(5)– bond.

References

1) W. A. Struck and P. J. Elving, *Biochem.*, **4**, 1343 (1965).
2) G. Dryhurst and P. J. Elving, *J. Electrochem. Soc.*, **115**, 1014 (1968).
3) G. Dryhurst, *J. Electrochem. Soc.*, **116**, 1097 (1969).
4) J. H. Lister, "Advances in Heterocyclic Chemistry," Interscience, New York (1966), p. 1.
5) R. K. Robins, "Heterocyclic Compounds," Interscience, New York (1967), p. 162.
6) J. B. Wyngaarden and J. T. Dunn, *Arch. Biochem. Biophys.*, **70**, 150 (1957).
7) J. B. Wyngaarden, *J. Biol. Chem.*, **224**, 453 (1957).
8) G. Dryhurst and P. J. Elving, *Talanta*, **16**, 855 (1969).
9) G. Dryhurst and G. F. Pace, *J. Electrochem. Soc.*, **117**, 1259 (1970).
10) T. Yao, T. Wasa, and S. Musha, *Bull. Chem. Soc. Jpn.*, **50**, 2917 (1977).
11) T. Yao, T. Wasa, and S. Musha, *Bull. Chem. Soc. Jpn.*, **51**, 1235 (1978).
12) T. Yao, Y. Taniguchi, T. Wasa, and S. Musha, *Bull. Chem. Soc. Jpn.*, **51**, 2937 (1978).
13) L. F. Cavalieri and A. Bendich, *J. Am. Chem. Soc.*, **72**, 2587 (1950).
14) H. L. Rosenthal, *Anal. Chem.*, **35**, 1770 (1963).
15) D. L. McAllister and G. Dryhurst, *J. Electroanal. Chem.*, **55**, 69 (1974).
16) R. W. King and W. B. N. Faulconer, *Anal. Chem.*, **28**, 255 (1956).
17) E. G. Young and C. F. Conway, *J. Biol. Chem.*, **142**, 839 (1942).
18) T. Staron, C. Allard, M. M. Chambre, and D. W. Xuong, *C. R. Acad. Sci.*, **257**, 2552 (1963).
19) F. Bergmann and S. Dikstein, *Biochem. J.*, **77**, 691 (1955).
20) L. F. Cavalieri, A. Bendich, J. F. Tinker, and G. B. Brown, *J. Am. Chem. Soc.*, **70**, 3875 (1948).

The Isolation of ^{227}Ac from ^{231}Pa and the Gamma-ray Spectra of ^{231}Pa, ^{227}Th, and ^{223}Fr

Toshiaki MITSUGASHIRA,* Hajimu YAMANA, and Shin SUZUKI

The Research Institute for Iron, Steel, and Other Metals, Tohoku University, Katahira 2-chome, Sendai 980

(Received January 20, 1979)

A method for the isolation of ^{227}Ac and its daughter nuclides from ^{231}Pa was established. The γ-ray spectra of ^{231}Pa, ^{227}Th, and ^{223}Fr were investigated, and the γ-ray tables of these nuclides were presented. A decay scheme of ^{223}Fr was corrected so as to explain these γ-ray data.

Several handicaps for the radiochemical study of the natural actinium series are known. Some of them are as follows:

1. It is difficult to keep enough ^{231}Pa or ^{227}Ac.
2. No confidential method for the separation of ^{231}Pa and ^{227}Ac has been established.
3. The exact information about the complex γ-rays of the nuclides of the actinium series is not enough for the γ-ray spectrometries of these nuclides.

From the standpoint of radiochemical common sense, ^{231}Pa is a precursor of ^{227}Ac. However, it is widely believed that the radiochemical purity of ^{227}Ac isolated from ^{231}Pa is not enough, because the complete removal of the colloidal or polymeric species of ^{231}Pa is very difficult. ^{227}Ac is almost non-γ-radioactive. The decay chain is complicated. Also ^{231}Pa, ^{227}Th, and ^{223}Fr have many γ-rays of approximately equal energies. Therefore, it is difficult to certify the radiochemical purity by γ-ray spectrometry in spite of the recent development of solid-state detectors. On the other hand, ^{227}Ac is produced as the daughter of ^{227}Ra, which is produced by means of the ^{226}Ra(n, γ) ^{227}Ra reaction. This method is recommended today. However, we do not think that the production of ^{227}Ac from ^{226}Ra is a popular technique or a conventional method, considering that the geochemical abundance of ^{231}Pa is of the same order as that of ^{226}Ra. Therefore, we tried to isolate ^{227}Ac from ^{231}Pa. Recently, we presented a method for the mutual separation of ^{227}Ac, ^{227}Th, ^{223}Ra, and ^{223}Fr.[1] The combination of these two methods will be an answer to the second difficulty with the radiochemistry of the actinium series mentioned above.

Then we determined the γ-ray spectra of ^{231}Pa, ^{227}Th, ^{223}Ra, and ^{223}Fr by means of a high-resolution Ge(Li) detector or an intrinsic germanium detector with a higher resolution. Moreover, we will present the data on the γ-rays of these nuclides for the sake of the γ-ray spectrometric determination of these nuclides.

Experimental

Radioisotopes. ^{231}Pa was supplied by The Radiochemical-Centre (Amersham, England). A 10-mg portion of the ^{231}Pa was purified by the method reported by Suzuki and Inoue.[2] The purified ^{231}Pa was left to stand for seven years to grow enough ^{227}Ac and then used for the experiment.

Reagents. All the chemicals used were of an analytical grade. HBEHP (bis(2-ethylhexyl) phosphate) was purified by the method reported previously.[3]

Apparatus. The apparatuses used were as follows. Separatory funnel shaker: IWAKI KM type(200—400 min^{-1}); coaxial Ge(Li) detector: ORTEC model 8101—1820 (effective volume, *ca.* 60 cm^3); planar intrinsic germanium detector: ORTEC model 16300-1000 (Be window 25 μm thick; effective volume, *ca.* 1.4 cm^3); silicon surface-barrier α-ray detector: ORTEC model BE-16-160-100 (active area, 160 mm^2; depletion depth, 100 μm); multichannel pulse-height analyzer: TOSHIBA USC-1 model 10 4096 ch. (controlled by a minicomputer TOSBAC-40A); linear amplifier: ORTEC model 472 spectroscopy amplifier (the shaping time constant was fixed to 2 μs throughout the spectrum accumulation).

The dead-time ratio was monitored by USC-1 and was found to be less than 10%.

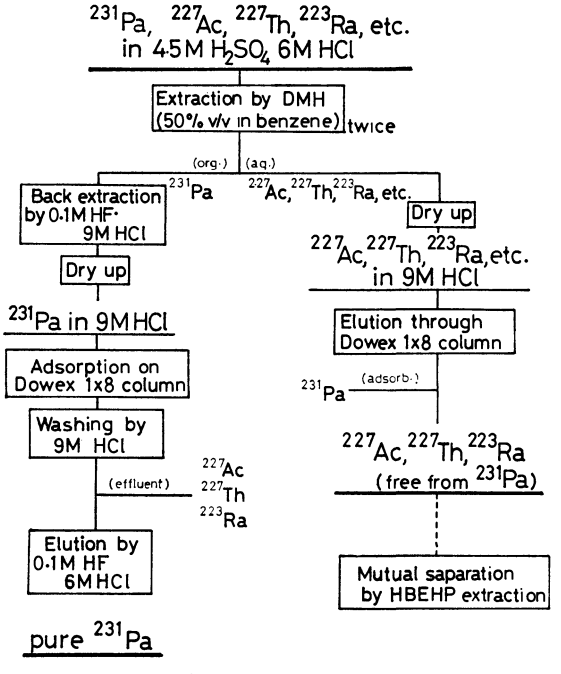

Fig. 1. The separation method for ^{231}Pa and ^{227}Ac.
In this figure 1 M=1 mol/dm^3.

Procedures. *Separation of ^{231}Pa and Its Daughter Nuclides*: A flow chart for the chemical separation of ^{231}Pa and ^{227}Ac is shown in Fig. 1. The meaning and the performance of the separation method will be described in the next section. From the isolated ^{227}Ac fraction, ^{227}Ac, ^{227}Th, and ^{223}Ra were purified by the method reported in Ref. 1. ^{223}Fr was milked from the purified ^{227}Ac by the method reported in Ref. 1.

Alpha-ray Spectrometry: In order to examine the radiochemical purity of the purified ^{231}Pa and ^{227}Ac, the α-ray spectra were compared. Thin sources for good resolution in the α-ray spectrum were prepared by the evaporation of aliquots of solutions of these nuclides onto glass plates. The apparent resolution of an α-ray peak was less than 20 keV in FWHM.

Gamma-ray Spectrometry: The γ-ray spectra of ^{231}Pa, ^{223}Fr,

and ^{223}Ra were determined by means of the Ge(Li) detector. The γ-ray spectrum of ^{227}Th was determined by the intrinsic germanium detector, because the spectrum is too complex to resolve each γ-ray by the Ge(Li) detector. For the calibration of energy and the efficiency of the acquisition system, the standard sources of ^{241}Am, ^{109}Cd, ^{144}Ce, ^{133}Ba, ^{22}Na, ^{106}Ru, ^{137}Cs, ^{54}Mn, and ^{60}Co were used. In addition, KX-rays of Ac, Ra, Rn, Po, Bi, and Pb were applied to the inner calibration. The highest resolution observed for the Ge(Li) detector was 1.2 keV in FWHM for 300 keV γ-ray of ^{231}Pa. The resolution of the intrinsic germanium detector was 300 eV at 20 keV, 400 eV at 50 keV, 500 eV at 100 keV, and 800 eV at 300 keV.

Plate sources of ^{231}Pa, ^{227}Th, and ^{223}Ra were prepared by the evaporation of aliquots of the purified stock solutions onto stainless steel plates. Liquid sources of ^{223}Fr were prepared by pipetting aliquots of the purified solution into polyethylene test tubes. The calibration factor for the self-absorption by the liquid sources was calculated by comparing the relative intensities determined with respect to the two kinds of sources of ^{227}Th, which has many γ-rays identical with ^{223}Fr.

All the spectra were analyzed by means of a nonlinear least-mean-squares fitting method to evaluate the peak position and the peak area. The least-mean-squares fitting method is based upon peak response functions rather than analytical functions in order to account for the histogram nature of the γ-ray spectrum accumulated by a multichannel pulse-height analyzer. Moreover, the peak response functions were determined from the γ-ray peak shapes of the γ-rays of the standard sources.

The relative intensities of the γ-rays of ^{227}Th, ^{223}Fr, and ^{223}Ra were determined by the decay analysis of the calculated peak areas. The abundances of the γ-rays of ^{223}Fr were calculated by normalizing the relative intensities to the α-disintegration rate of ^{227}Ac, which was in radioequilibrium with ^{223}Fr.

Results and Discussion

Radiochemical Purity of the Purified ^{231}Pa and ^{227}Ac. From the point of view of the decontamination of ^{227}Ac for ^{231}Pa, the anion-exchange chromatographic separation method reported by Suzuki and Inoue[2] is the best method if we can suppress the irreversible formation of colloidal or polymeric species of Pa(V), which is not adsorbed by the anion-exchange resin column. Therefore, we applied this method to the final stage of the separation of ^{227}Ac and ^{231}Pa, as is shown in Fig. 1. However, it was often observed that a small fraction of ^{231}Pa was eluted out with a loading solution when more than 1 mg of ^{231}Pa was introduced into the separation column. The fast, irreversible polymerization of Pa(V) in a hydrochloric acid solution has been reported.[4] Therefore, this eluted fraction of ^{231}Pa can be considered to be the polymeric species.

To get enough ^{227}Ac from ^{231}Pa, we must chemically process a weighable amount of ^{231}Pa. Quantitative information has not yet been obtained about the chemical behavior of polymeric Pa(V) in an aqueous solution. However, it is known that the polymerization of Pa(V) in an aqueous solution is negligible unless the solution is left to stand too long after the preparation and unless the concentration of Pa(V) is more than 10^{-7} mol/dm^3.[4-6] These facts show that, in order to suppress the formation of polymeric Pa(V) in a hydrochloric acid solution, the concentration of Pa(V) should be lower than 10^{-7} mol/dm^3.

On the basis of these considerations, we applied a preliminary separation based on the DMH(2,6-dimethyl-4-heptanol)-extraction of ^{231}Pa from a mixed acid solution of a sulfuric acid and a hydrochloric acid in order to lower the concentration of ^{231}Pa in the ^{227}Ac fraction. Pa(V) forms stable anionic complexes in a concentrated sulfuric acid solution and does not show the tendency to polymerize. Moreover, the extraction of macro amount of Pa(V) from the mixed acid gives very reproducible results. The extraction ratio of Pa(V) exceeds 99.95% by the use of DMH-extraction process shown in Fig. 1, while Ac is not extracted. The isolated ^{227}Ac fraction was processed by the HBEHP-extraction method to get the purified ^{227}Ac, ^{227}Th, ^{223}Ra, and ^{223}Fr.[1]

An α-ray spectrum of the purified ^{231}Pa is compared with a spectrum of ^{231}Pa before the separation in Fig. 2.

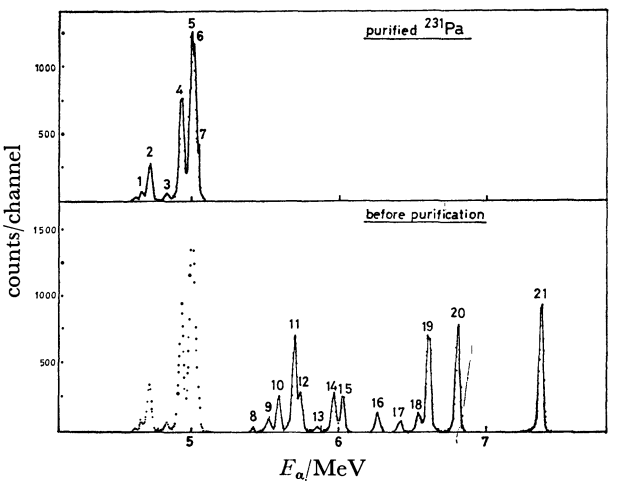

Fig. 2. Alpha-ray spectra of ^{231}Pa.
1, 4.671 MeV ^{231}Pa; 2, 4.727 MeV ^{231}Pa; 3, 4.844 MeV ^{231}Pa; 4, 4.943 MeV ^{231}Pa; 5, 5.007 MeV ^{231}Pa; 6, 5.023 MeV ^{231}Pa; 7, 5.052 MeV ^{231}Pa; 8, 5.432 MeV ^{227}Th; 9, 5.538 MeV ^{227}Th; 10, 5.605 MeV ^{223}Ra; 11, 5.71 MeV (complex) ^{227}Th and ^{223}Ra; 12, 5.755 MeV ^{227}Th; 13, 5.864 MeV ^{227}Th; 14, 5.976 MeV ^{227}Th; 15, 6.037 MeV ^{227}Th; 16, 6.278 MeV ^{211}Bi; 17, 6.423 MeV ^{219}Rn; 18, 6.551 MeV ^{219}Rn; 19, 6.622 MeV ^{211}Bi; 20, 6.817 MeV ^{219}Rn; 21, 7.384 MeV ^{215}Po.

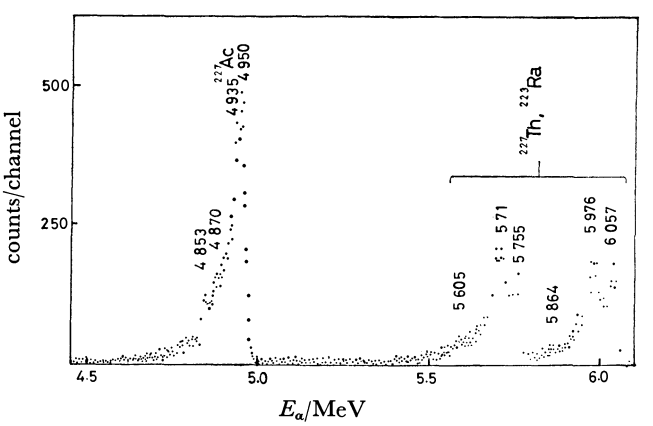

Fig. 3. Alpha-ray spectrum of the purified ^{227}Ac.

An α-ray spectrum of ^{227}Ac is also shown in Fig. 3. In Fig. 3, no α-rays of ^{231}Pa are observed, while α-rays of ^{227}Th and ^{223}Ra are observed. These daughter nuclides grow fast during the sample preparation and the spectrum acquisition. The branching ratio of the α-decay of ^{227}Ac is only 1.38%.[7] Therefore by comparing these three α-ray spectra, it can be concluded that the purified ^{227}Ac is completely free from the contamination of ^{231}Pa. On the other hand, no α-rays of ^{227}Th, ^{223}Ra, and their daughter nuclides appeared in the purified ^{231}Pa sample. This is evidence that the purified ^{231}Pa is free from any contamination of the daughter nuclides.

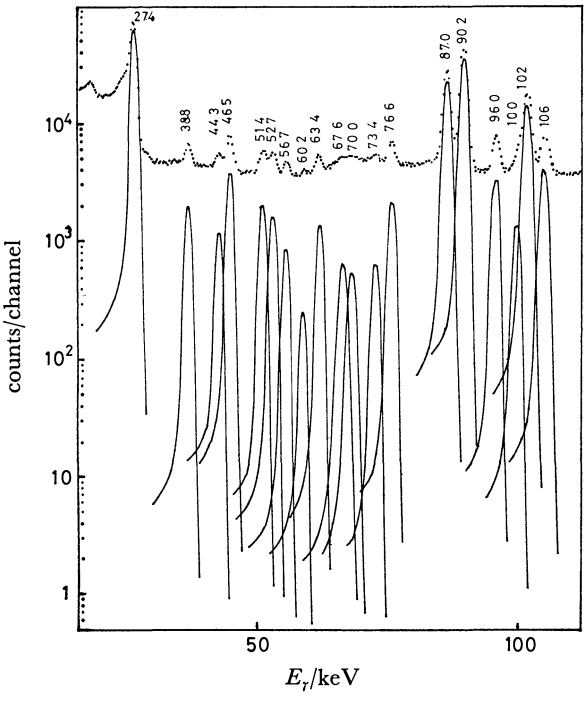

Fig. 4. Gamma-ray spectrum of ^{231}Pa, from 20 keV to 110 keV.

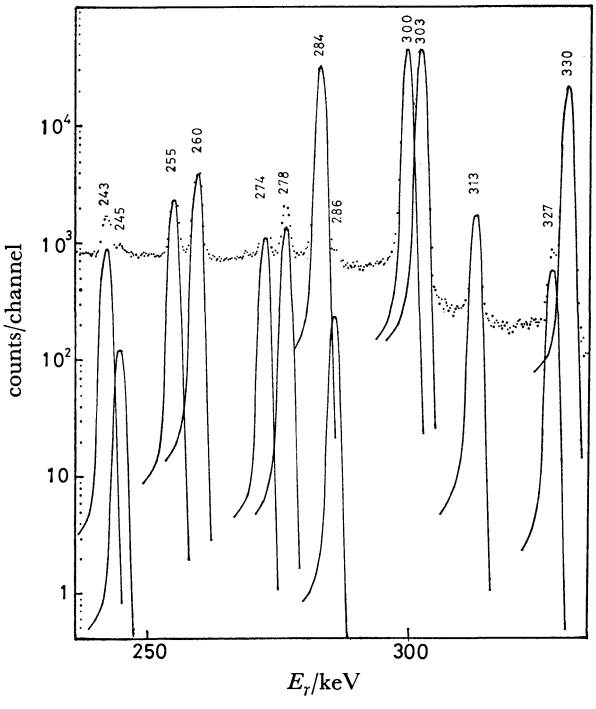

Fig. 5. Gamma-ray spectrum of ^{231}Pa, from 240 keV to 335 keV.

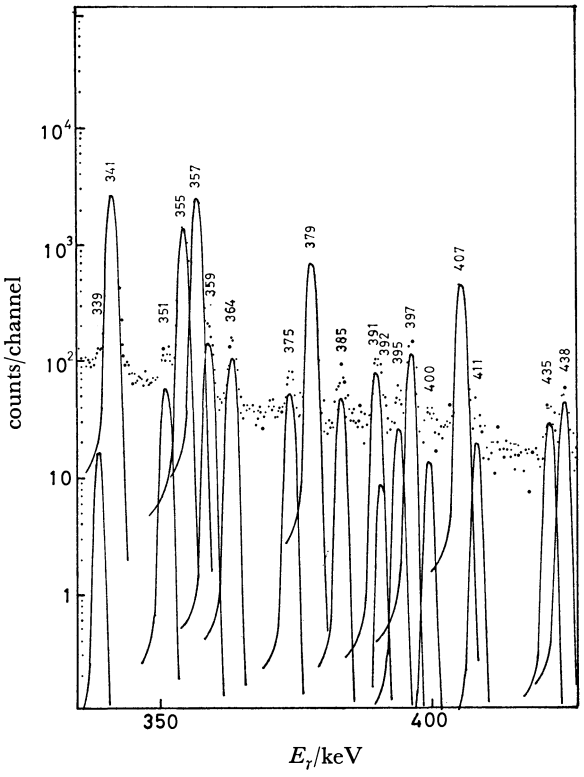

Fig. 6. Gamma-ray spectrum of ^{231}Pa, from 335 keV to 440 keV.

Gamma-ray Spectrum of ^{231}Pa. The γ-ray spectra of ^{231}Pa are shown in Figs. 4—6. In these figures, the peak components are shown as the peak shapes to illustrate the analysis of the γ-ray spectrum described in the Experimental section. The relative intensities of some γ-rays are shown in Table 1.

It is worthwhile to point out the following facts from Table 1:

1. Our data show the best correlation with the data of de Pinho *et al.*[8] The correlation is almost complete for the γ-rays whose intensities relative to that of 303

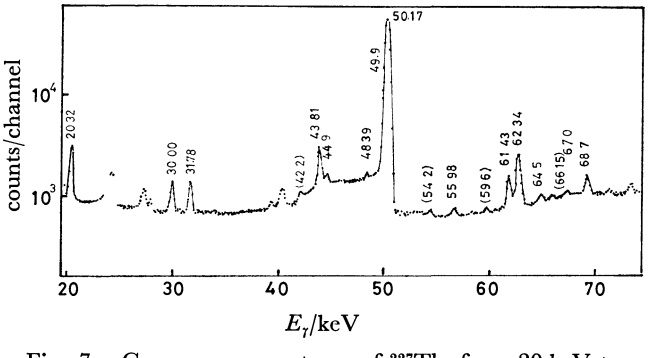

Fig. 7. Gamma-ray spectrum of ^{227}Th, from 20 keV to 73 keV.
The γ-rays in parentheses are decayed also but the intensities are not certain.

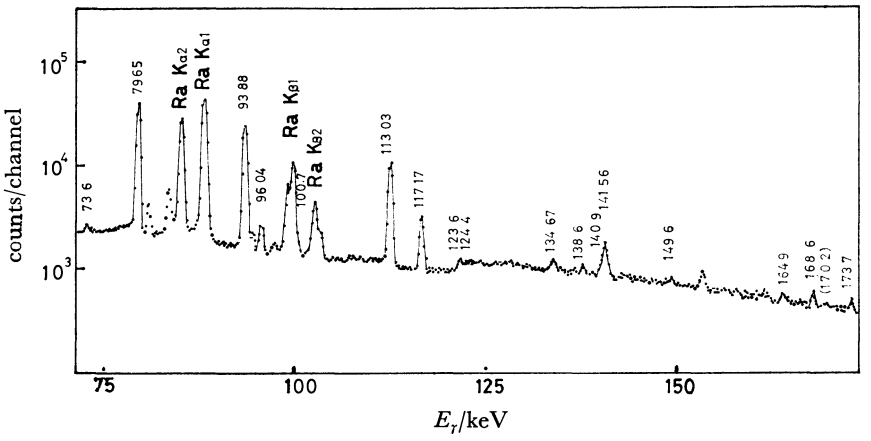

Fig. 8. Gamma-ray spectrum of ^{227}Th, from 72 keV to 175 keV. The γ-rays in parentheses are decayed also but the intensities are not certain.

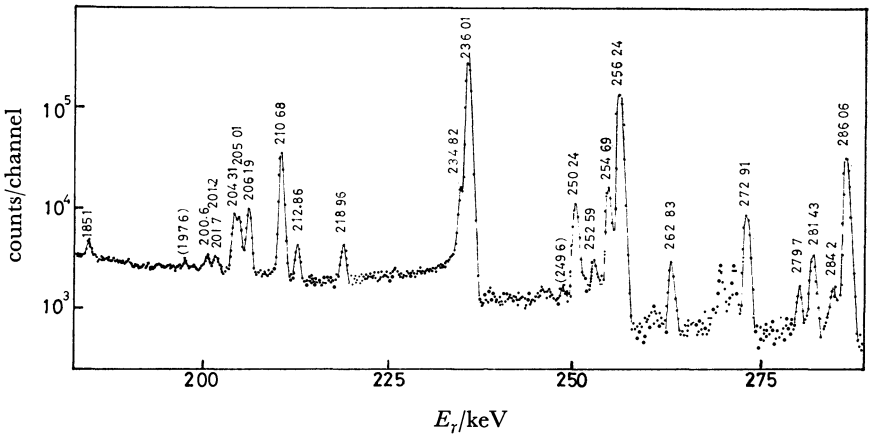

Fig. 9. Gamma-ray spectrum of ^{227}Th, from 180 keV to 288 keV. The γ-rays in parentheses are decayed also but the intensities are not certain.

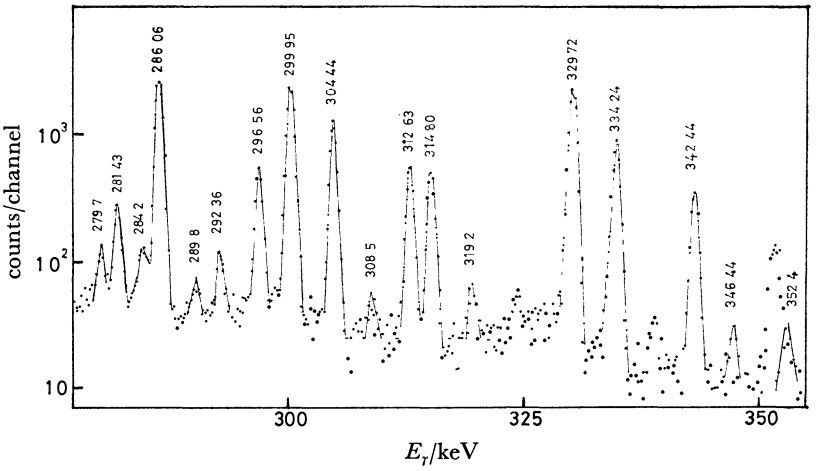

Fig. 10. Gamma-ray spectrum of ^{227}Th, from 278 keV to 355 keV.

keV γ-ray are greater than 0.01.

2. The data of Lange and Hagee[9] are quite erroneous, though they were employed in the γ-ray catalogue of Wakat.[10]

3. The data of Zaddach[11] are the latest. His data about abundances are identical with the data of Leang and since Zaddach did not describe his experimental technique, we considered the data of Leang. As will be described below, Leang's data are not very accurate and the intensities of the 255 keV, 284 keV, 300 keV,

TABLE 1. TABLE OF γ-RAYS OF ^{231}Pa

E_γ/keV	Relative intensity: This work	References: 9, 10[a]	8	11, 12
27.4	4.1	(obsd)[b]	3.97	2.98
38.8	0.044	(obsd)	0.063	0.043
44.3	0.027	(obsd)	0.026	
46.5	0.077	(obsd)	0.089	0.077
52.7	0.035	(obsd)	0.036	
56.7	0.018		0.016	
63.4	0.016		0.021	
73.4	0.015		0.011	
76.7	0.036	(obsd)	0.029	(obsd)
96.0	0.039		0.038	0.030
100	0.017		0.013	
243	0.017	0.025	0.015	(obsd)
255	0.043	0.027	0.043	0.057
260	0.076	0.082	0.074	0.078
274	0.021	(obsd)	0.025	0.03
278	0.025	(obsd)	0.029	0.03
284	0.67	0.43	0.67	0.70
300	0.97	1.00	0.97	1.00
303	1.00		1.00	1.00
313	0.039	0.018	0.040	0.047
327	0.016		0.013	
330	0.55	0.15	0.56	0.57
341	0.070	0.016	0.070	(obsd)
355	0.038		0.040	0.043
357	0.066	0.020	0.075	0.065
379	0.019	0.003	0.021	0.017
407	0.018	(obsd)	0.015	0.009

The γ-rays which are important for the γ-ray spectrometry of the actinium series are tabulated in this table.
a) Intensities relative to the doublet of 300 keV and 303 keV. b) Observed.

and 313 keV γ-rays are obviously overcounted. These deviations, except that of the γ-ray of 255 keV, can be explained as resulting from the contamination of ^{233}Pa, which was spiked as a tracer in his experiment. Indeed, this contamination was mentioned by Leang in his raw γ-ray spectrum.[12]

As has been described above, we can conclude that our data and de Pinho's data about the relative intensity have a higher reliability than the other data. The abundances of the γ-rays of ^{231}Pa were determined by Leang; the abundance of 303 keV γ-ray is 2.3%.[12] As will be described below, the abundance of the γ-rays of ^{231}Pa are much smaller than those of ^{227}Th. Also, the measurement of the intensities of the main γ-rays of ^{231}Pa, *i.e.*, 284 keV, 300 keV, 303 keV, 341 keV, and 357 keV, is almost impossible if ^{227}Ac, ^{227}Th, or ^{223}Ra is in the sample of ^{231}Pa. Especially, it should be remenbered that 300 keV γ-rays of ^{231}Pa and ^{227}Th appear as a singlet peak even when a high-resolution Ge(Li) detector is used. Therefore, it is necessary to separate completely ^{227}Ac and its daughter nuclides from ^{231}Pa for the γ-ray spectrometric determination of ^{231}Pa. It is also necessary to certify the correlation between the relative intensities of the observed γ-rays and our data.

Gamma-ray Spectrum of ^{227}Th. The γ-ray spectra of ^{227}Th, as obtained by the intrinsic germanium detector, are shown in Figs. 7—10. Even in an initially pure ^{227}Th sample, ^{223}Ra and its daughter nuclides grow rather fast. Therefore, as has been described in the Experimental section, the decay in the γ-rays was examined until the transient equilibrium was attained between ^{227}Th, ^{223}Ra, and their daughter nuclides. Some examples of the decay curves are shown in Fig. 11. As is shown in Fig. 11, γ-rays of ^{227}Th can be easily determined to be monotonously decaying γ-rays. In Table 2, the relative intensities are shown along with the literature values.[13,14]

The data of Hesselink *et al.*[14] are the latest and were obtained by α,γ coincidence employing a Ge(Li) detector with a resolution of 2.3 keV at 120 keV and a silicon surface-barrier detector with a resolution of 30 keV. It is clear from Figs. 2 and 7—10 that the Ge(Li) detector and the silicon surface-barrier detector do not have efficient enough resolutions for the γ-ray spectroscopy of ^{227}Th. On the other hand, the works of Briancon *et al.*[13] consist of γ,γ coincidence and conversion electron spectroscopy. They also employed two Ge(Li) detectors with resolutions of 0.9 keV and 2.5 keV for 100 keV γ-ray. The resolutions of the Ge(Li) detectors employed by Briancon *et al.* were not good enough to resolve the complex structure of the γ-ray spectrum of ^{227}Th at the energy regions of 40 keV to 50 keV, 80 keV to 100 keV, 200 keV to 213 keV, 234 keV to 236 keV, 250 keV to 257 keV, 269 keV to 273 keV, 279 keV to 305 keV, 312 keV to 315 keV, and 350 keV to 353 keV. In spite of these difficulties, the two works agree well about existence of the main γ-rays. However, about the intensities of almost all the γ-rays and the existence of some weak γ-rays, the agreement between the two works is far from satisfactory. For the γ-ray spectrometry of ^{227}Th, the

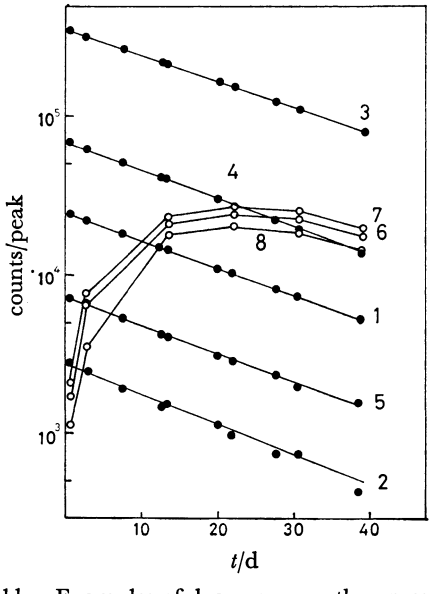

Fig. 11. Examples of decay or growth curves of some γ-rays found in initially pure ^{227}Th. 1, 20.32 keV; 2, 30.00 keV; 3, 50.17 keV; 4, 236.01 keV; 5, 299.95 keV; 6, 72.86 keV; 7, 269.46 keV; 8, 351.1 keV.

Table 2. Table of γ-rays of ^{227}Th

E_γ/keV	Relative intensity[a] This work	Ref. 14	Ref. 13	Transition
20.32(5)	0.030(2)[b]		0.037	50.2—29.9
30.00(5)	0.005(1)		0.007	29.9—0
31.78(8)	0.005(1)		0.006	61.5—29.9
43.81(9)	0.017(3)	0.002	0.017	329.8—286.1
44.5(1)	0.002(1)	0.001		174.6—130.0
48.39(8)	0.003(1)	0.004	0.0007	334.2—286.1
49.9(2)	0.062(9)	0.002	0.04	79.8—29.9
50.17(6)	0.59(2)	0.72	0.59	50.2—0
55.98(8)	0.0006(1)	0.0002	0.0004	432.4—376.4
61.43(8)	0.007(1)		0.006	61.5—0
62.34(7)	0.017(1)	0.021	0.015	123.9—61.5
64.5(1)	0.0011(6)	0.002	0.001	350.5—286.1
67.0(1)	0.0016(5)			
68.7(1)	0.0061(3)	0.002	0.004	130.3—61.5
73.6(1)	0.0012(2)	0.0014	0.0015	123.9—50.2
79.65(2)	0.162(4)	0.15	0.15	79.8—0
93.88(9)	0.127(4)	0.11	0.10	123.9—29.9
96.04(8)	0.007(1)	0.004	0.005	376.4—280.5
100.7(1)	0.0028(5)	0.007	0.006	130.0—29.9
113.03(1)	0.067(1)	0.045	0.053	174.6—61.5
117.17(1)	0.016(1)	0.013	0.013	247.5—130.3
123.6(2)	0.0011(6)	0.0007	0.0007	247.3—123.9
124.4(4)	0.0009(1)	0.0002	0.0004	174.6—50.2
134.67(9)	0.0022(4)	0.002	0.002	369.4—234.8
138.6(6)	0.001			
140.9(2)	0.0023(3)	0.003		314.8—174.6
141.56(6)	0.0086(6)	0.005	0.01	376.4—234.8
149.6(1)	0.0007(4)	0.002	0.0007	280.5—130.5
164.9(7)	0.0009(1)		0.001	445.1—280.5
168.6(2)	0.0010(3)	0.001	0.001	342.9—174.6
173.7(2)	0.0014(3)	0.0009	0.001	234.8—61.5
185.1(4)	0.0029(5)	0.0022	0.003	234.8—50.2
200.6(2)	0.0017(6)	0.0004	0.003	280.5—79.8
201.2(2)	0.0017(6)			
201.7(2)	0.0017(6)	0.0018	0.003	376.4—174.6
204.31(3)	0.015(1)	0.019	0.016	334.2—130.2
205.01(5)	0.011(1)	0.014	0.011	234.8—29.9
206.19(3)	0.018(1)	0.022	0.016	329.9—123.9 or 286.1—79.8
210.68(2)	0.089(2)	0.10	0.082	334.2—123.9
212.86(4)	0.0062(5)	0.007	0.006	342.9—130.3
218.96(5)	0.0069(8)	0.004	0.005	342.9—123.9
234.82(6)	0.040(2)	0.05	0.04	234.8—0
236.01(1)	0.96(1)	0.95	0.97	286.1—50.2
250.24(2)	0.037(2)	0.023	0.031	329.8—79.8
252.59(6)	0.007(1)	0.009	0.007	376.4—123.9
254.69(2)	0.058(2)	0.075	0.052	334.2—79.8
256.24(2)	0.522(9)	0.52	0.54	286.1—29.9
262.83(6)	0.0054(3)	0.008	0.007	342.4—79.8
272.91(3)	0.038(1)	0.041	0.037	334.2—61.5
279.7(1)	0.0043(8)	0.008	0.005	329.8—50.2
281.43(6)	0.014(1)	0.012	0.012	342.9—61.5
284.2(3)	0.0045(4)	0.002	0.004	334.2—50.2
286.06(2)	0.157(2)	0.14	0.11	286.1—0
289.8(3)	0.0018(6)	0.0003	0.0005	369.4—79.8
292.36(5)	0.0045(6)	0.005	0.005	342.4—50.2
296.56(3)	0.037(5)	0.032	0.036	376.4—79.8
299.95(3)	0.172(4)	0.16	0.16	329.8—29.9
304.44(3)	0.085(1)	0.11	0.075	334.2—29.9
308.5(1)	0.0016(4)	0.001	0.001	432.4—123.9
312.63(2)	0.041(2)	0.043	0.037	342.4—29.9
314.80(3)	0.038(1)	0.047	0.035	376.4—61.5
319.2(3)	0.0025(5)	0.002	0.003	369.4—50.2
329.72(3)	0.212(6)	0.24	0.21	329.8—0
334.24(2)	0.083(3)	0.095	0.082	334.2—0
342.44(5)	0.036(4)	0.016	0.031	342.4—0
346.44(5)	0.0018(3)	0.0007	0.0007	376.4—29.9
352.4(1)	0.0008(3)	0.0007	0.001	432.4—79.8
384.5(1)	0.0038(9)	0.0002	0.004	424.0—61.5

a) Intensities relative to the doublet of 234.82 keV and 236.01 keV. b) Numbers in parentheses are estimated standard deviations in units of the last significant digit.

relative intensities of the γ-rays of 50 keV, 236 keV, 286 keV, and 300 keV are very important parameters as measures of the radiochemical purity of the sample, because the contamination by ^{231}Pa or ^{227}Ac influences the relative intensities of these γ-rays. These γ-rays are observed as multiplet γ-ray peaks, and the multiplicity depends on the resolution of the detector employed. Therefore, it is necessary to get data about the intensities of these γ-rays based upon more accurate basis than the two works in the literature in order to improve the accuracy of the γ-ray spectrometry of ^{227}Th.

On the other hand, the excellency of our measurement depends on the highest resolution of the detector employed. As is shown in Figs. 7—10, we obtained well-resolved γ-ray spectra, and so we can now consider the reason for the disagreement between the literature data.

Obviously, there is no doubt about the existence of

Table 3. Table of γ-rays of ^{223}Ra

E_γ/keV	Relative intensity This work	Ref. 15	Nuclide
123	0.105	0.082	^{223}Ra
132	0.017	0.009	^{219}Rn
144	0.267	0.221	^{223}Ra
154	0.459	0.386	^{223}Ra
159	0.058	0.050	^{223}Ra
180	0.015	0.011	^{223}Ra
269	1.00	1.00	^{223}Ra
271	0.818	0.786	^{219}Rn
324	0.265	0.264	^{223}Ra
328	0.013	0.014	^{223}Ra
338	0.186	0.193	^{223}Ra
343	0.011	0.014	^{223}Ra
351	0.951	0.950	^{211}Bi
372	0.037	0.039	^{223}Ra
402	0.457	0.479	^{219}Rn
405	0.271	0.293	^{211}Pb
427	0.122	0.136	^{211}Pb

Only the γ-rays, which are important for γ-ray spectrometry of the actinium series, are tabulated.

the three γ-rays of 20.32 keV, 30.00 keV, and 31.78 keV reported by Briancon *et al.*[13] However, we could not find any γ-rays except the KX escape peaks of 50.17 keV γ-ray at 39.22 keV and 40.32 keV. It was found the intensity ratio of these two peaks in identical to that of the K_α and K_β rays of Ge. Thus, the intensity of the γ-ray of 40.1 keV reported in Ref. 13 seems to be doubtful. Similarly, we did not observe the 224.7 keV and 246.4 keV γ-rays except the KX escape peaks of the 236.01 keV and 256.24 keV γ-rays respectively, while these two γ-rays were reported in Ref. 14. For the sake of further consideration, a γ-ray table of ^{223}Ra and its daughter nuclides is shown in Table 3. In the γ-ray spectrum of ^{223}Ra, KX-rays of the daughter elements are also observed. In ^{227}Th, we observed rapidly growing KX-rays and γ-rays of 69.8 keV, 72.9 keV, 75.3 keV, 89.9 keV, 95.0 keV, 269.5 keV, 271.2 keV, 324.2 keV, 338.3 keV, and 351.1 keV. Many γ-rays with energies approximately equal to these KX-rays and γ-rays were reported in Refs. 13 and 14. For the γ-ray spectrometry of ^{227}Th, these γ-rays are not important because the many other intense γ-rays can be utilized. However for ^{223}Ra, 269 keV, 324 keV, and 338 keV γ-rays are important for the γ-ray spectrometry. According to Refs. 13 and 14, it seems necessary to correct the contribution by the interfering γ-rays in order to evaluate the intensities of these γ-rays accurately when the sample is contaminated with ^{227}Ac or ^{227}Th. However as is shown about the 269.46 keV γ-ray in Fig. 11, the correction is negligibly small.

According to Refs. 13 and 14, the abundances of the 50 keV, 236 keV, 256 keV, 286 keV, 300 keV, 304 keV, and 330 keV γ-rays of ^{227}Th are large enough to apply these γ-rays to the γ-ray spectrometry of ^{227}Th. We measured the abundance of the overlapped γ-rays of 234.82 keV and 236.01 keV and got a value of $(12.1\pm 0.6)\%$.[16] However, it should be mentioned that all these seven γ-rays are observed as complex overlapping peaks even when the spectrum is determined by a detector with the highest resolution. Therefore, it is very important to take into account the complex nature of the γ-ray spectrum of ^{227}Th in order to apply the γ-ray spectrometric technique to the determination of ^{227}Th. Today, ^{227}Th is often used as a radiochemical tracer for ^{231}Pa or ^{227}Ac in geochemical application. It should be mentioned that measurement by a few γ-rays, such as 50 keV, 236 keV, or 256 keV, can not be correct because of the complex nature of the decay chain and the γ-ray spectrum of ^{227}Th. The relative intensities of the observed γ-rays should be carefully examined to account for the radiochemical purity of the sample.

Gamma-ray Spectrum and Decay Scheme of ^{223}Fr. A γ-ray spectrum of ^{223}Fr is shown in Fig. 12. We observed 16 γ-rays which decayed with a half-life of ^{223}Fr in the energy region from 50 keV to 876 keV. Our observation is an additional proof of the characteristics of the γ-ray spectrum of ^{223}Fr, *i.e.*, the existence of two grounps of γ-rays, one in an energy region below 369 keV and the other in a region higher than 700 keV.[17,18] In Table 4, the relative intensities, abundances, and characteristics of the γ-rays are shown.

Among the works done previously, the work of Maria *et al.*[18] is the most comprehensive. However, we found some disagreements between the results. We found the relative intensity of the 50 keV γ-ray and the 235 keV γ-ray to be 13.9 whereas their value is only 10.[18] Another difference is in the point that they assigned the very weak γ-rays to ^{223}Fr. They used a large amount of ^{227}Ac precursor (740 MBq). Their experimental conditions are more suitable for the detection of weak γ-rays than our experimental conditions. Even so, an ambiguity remains with regard to the γ-rays of 256 keV and 286 keV, which were reported in Ref. 18. As has already been shown in Table 2, it is well known that the three γ-rays of 236 keV, 256 keV, and 286 keV are emitted from the same excited state of ^{223}Ra. Therefore, their result is erroneous in the point that they missed the 236 keV γ-ray, which is the most intense γ-ray among the three γ-rays. We did not observe any γ-rays between 240 keV and 289 keV which decayed with the half-life of ^{223}Fr. A possible explanation for these disagreements

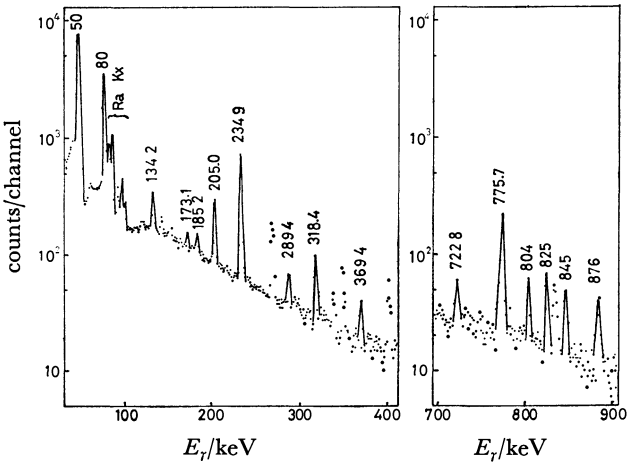

Fig. 12. Gamma-ray spectrum of ^{223}Fr.

TABLE 4. TABLE OF γ-RAYS OF ^{223}Fr

E_γ/keV	Transition	Relative intensity		Abundance (%)
		This work	Ref. 18	
50.0(2)[a]	50.2—0; El	13.9(5)	10	47(1)
80.0(3)	79.8—0; El	3.3(2)	2.4	10.9(5)
134.2(6)	369—235; El	0.17(3)	0.16	0.6(1)
173.1(6)	235—61.5; Ml, El	0.044(3)	0.04	0.15(2)
185.2(5)	235—50.2; El	0.075(6)	0.09	0.25(2)
205.0(5)	235—29.9; Ml, El	0.33(2)	0.34	1.1(1)
234.9(4)	235—0; Ml	1.00	1.00	3.4(1)
289.4(6)	369—79.8; Ml	0.08(1)	0.072	0.27(1)
318.4(5)	369—50.2; Ml	0.14(1)	0.162	0.47(2)
369.4(4)	369—0; El	0.041(4)	0.032	0.14(1)
722.8(6)	804—79.8	0.022(5)	0.015	0.07
775.7(7)	824—50.2	0.14(1)	0.123	0.46(3)
804(1)	804—0	0.025(5)	0.017	0.08(2)
825(1)	824—0	0.027(5)	0.014	0.09(2)
845(1)	908—61.5	0.018(7)	0.014	0.06(2)
876(1)	908—29.9	0.014(6)	0.013	0.05(2)

a) Numbers in parentheses are estimated standard deviations in units of the last significant digit.

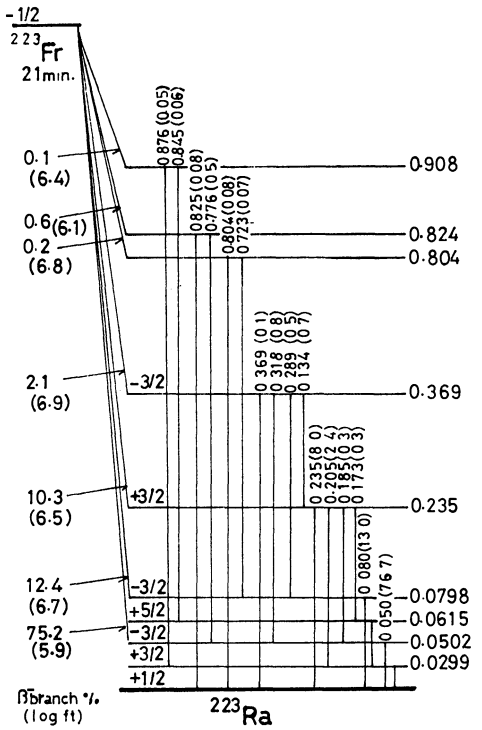

Fig. 13. Decay scheme of ^{223}Fr. Energies are given in MeV unit. Probabilities of γ-transitions per 100 β^- disintegrations are given in parentheses.

is as follows. As has been described before, the four γ-rays of 236 keV, 256 keV, 286 keV, and 50 keV are the main γ-rays of ^{227}Th. Moreover, the intensity of the overlapped γ-rays at 50 keV relative to the overlapped γ-rays at 236 keV is 0.65 for ^{227}Th. Therefore, it is reasonable to assume a trace contamination of ^{227}Th or ^{227}Ac in ^{223}Fr as an explanation of the low value of the relative intensity and of the exitence of the 256 keV and 286 keV γ-rays in the γ-ray spectrum of ^{223}Fr.

By investigations of the α-decay of ^{227}Th, we can utilize much information about the level structure of ^{223}Ra.[19] On this basis, we can conclude that all the γ-rays can be explained by the seven β^--transitions to the 50 keV (−3/2), 79.8 keV (+3/2), 235 keV (+3/2), 368 keV (+1/2), 804 keV, 824 keV, and 908 keV levels of ^{223}Ra. The decay scheme thus constructed is shown in Fig. 13. In this figure, the 29.9 keV (+3/2) and 61.5 keV (+5/2) levels are assumed to be the rotational excited states.[18,19] The classfications of the six γ-transitions from the 908 keV, 824 keV, and 804 keV levels are not known. However, the contribution of the conversion process to these γ-transitions can be neglected because of the high transition energies. For the other ten γ-transitions, the conversion coefficients were calculated by the use of the table of Hager and Seltzer.[20] Maria *et al.* also proposed a decay scheme.[18] Our modification involves the branching ratio of the most intense β^--transition to the 50 keV level.

As a conventional rapid method for the determination of non-γ-radioactive ^{227}Ac, γ-ray spectrometry of ^{223}Fr which is in radioequilibrium with ^{227}Ac is considered to be promising. Practically the methods can be classified into two types. One type is based on the measurement of the purified ^{223}Fr. The other type is based on the measurement of ^{223}Fr which is in the partial radioequilibrium with ^{227}Ac, when the other daughter nuclides has been removed from the sample. And then, the γ-ray spectrum of almost pure ^{223}Fr will be determined. In order to apply the former method, ^{223}Fr should be isolated from ^{227}Ac by a method which has a definite mean retention time for ^{223}Fr. Also, the mean retention time should be less than 1 min in the cow phase of ^{227}Ac to get more than 95% of ^{223}Fr. Therefore, the latter method seems to be more reliable. Of course, it is necessary to correct the contribution by ^{227}Th when the intensity of the sample is not large enough. However, the correction can be done with a high precision by referring to the relative intensities of the γ-rays of ^{227}Th tabulated in Table 2. Moreover, whether or not there is a necessity to correct can be easily desided when an abnormally low value of the relative intensity of the 50 keV γ-ray is measured.

The authors would like to thank Professor Kiyoteru Otozai, the Osaka University, for his helpful discussion of the γ-ray spectrometry and the decay scheme of ^{223}Fr.

References

1) T. Mitsugashira, H. Yamana, and S. Suzuki, *Bull. Chem. Soc. Jpn.*, **50**, 2913 (1977).
2) S. Suzuki and Y. Inoue, *Bull. Chem. Soc. Jpn.*, **39**, 490 (1966).
3) T. Mitsugashira and S. Suzuki, *J. Radioanal. Chem.*, **34**, 309 (1976).
4) A. T. Casey and G. Maddock, *J. Inorg. Nucl. Chem.*, **10**, 58 (1959).
5) S. Suzuki and Y. Inoue, *Bull. Chem. Soc. Jpn.*, **39**, 1705 (1966).
6) R. Guillaumont, *Actinide Rev.*, **1**, 125 (1968).
7) H. W. Kirby, *J. Inorg. Nucl. Chem.*, **32**, 2823 (1970).
8) A. G. de Pinho, E. F. de Silveira, and N. L. da Costa, *Phys. Rev. C*, **2**, 572 (1970).
9) R. C. Lange and G. R. Hagee, *Nucl. Phys. A*, **124**, 412 (1968).
10) M. A. Wakat, *Nucl. Data Table*, **8**, 445 (1971).
11) G. Zaddach, "Katalog von Ge(Li)-γ-Spectren," JUL-914-DE, **1973**.
12) C. F. Leang, *J. Phys. (Paris)*, **31**, 269 (1970).
13) C. Briancon and C. Vieu, *J. Phys. (Paris)*, **32**, 373 (1971); C. Briancon and R. Walen, *ibid.*, **32**, 373 (1971).
14) W. H. A. Hesselink, A. H. Wapstra, J. G. Kromme, E. J. Haighton, M. von Kampen, W. Hutjes, and K. E. M. Dijkman, *Nucl. Phys. A*, **191**, 283 (1972).
15) C. Briancon, C. F. Leang, and R. Walen, *C. R. Acad. Sci., Ser. B*, **266**, 1533 (1968).
16) Result of γ-ray spectrometry using the Ge(Li) detector.
17) C. Ythier, G. Mazzone, and P. W. F. Louwrier, *Physica*, **30**, 2143 (1964).
18) H. Maria, C. Ythier, P. Polak, and A. H. Wapstra, *Physica*, **34**, 571 (1967).
19) C. Malpes, *Nucl. Data Sheets*, **22**, 243 (1977).
20) R. S. Hager and E. C. Seltzer, *Nucl. Data Table A*, **4**, 1 (1968).

Studies of the Metal Complexes of Cyclohexane Derivatives. VI.[1] The Thermal Transformation of Nickel(II) Complexes of 1,2-Cyclohexanediamine Isomers

Reiko SAITO* and Yoshinori KIDANI†

Aichi Junior College of Nursing, Kamishidanmi, Moriyama-ku, Nagoya 463

†*Faculty of Pharmaceutical Sciences, Nagoya City University, Tanabedori, Mizuho-ku, Nagoya 467*

(Received January 25, 1979)

The thermal transformations of the following three types of nickel(II) complexes were investigated by means of TG-DSC analyses: $[Ni(t\text{-chxn})_2(H_2O)_2]X_2$, $[Ni(c\text{-chxn})_3]X_2\cdot nH_2O$, and $[Ni(t\text{-chxn})_3]X_2\cdot nH_2O$ ($X=Cl^-$, Br^-, and NO_3^-), where *c*- and *t*-chxn denote *cis*- and *trans*-1,2-cyclohexanediamine respectively. The distorted octahedral $[Ni(t\text{-chxn})_2(H_2O)_2]X_2$ complexes ($X=Cl^-$ and Br^-) are thermally deaquated to form yellow complexes, which then turn into parental diaquabis-complexes in the air at room temperature. $[Ni(t\text{-chxn})_2(H_2O)_2](NO_3)_2$ undergoes a thermal deaquation-anation reaction. The octahedral tris(*c*-chxn) complex is converted into a square planar bis(*c*-chxn) one by the evolution of one molecule of the ligand upon heating, whereas tris(*t*-chxn) complex became a distorted octahedral bis(*t*-chxn) one with anion coordination. In this paper, the stereochemical thermal changes of the complexes in the solid state will be discussed with regard to the steric configuration of the ligands.

The present authors reported earlier the preparations of the copper(II) and the nickel(II) complexes of *cis*- and *trans*-1,2-cyclohexanediamine (abbreviated as *c*-chxn and *t*-chxn), and showed that the structures of the bis-complexes were greatly affected by the steric configurations of these diamines.[2] The ligand, *t*-chxn, whose amino groups bonded to the cyclohexane ring in the diequatorial conformation(b), as is shown below, can be expected to have a coordination ability closely related to that of ethylenediamine.[3-5] It affords violet paramagnetic bis-complexes such as $[Ni(t\text{-chxn})_2(H_2O)_2]Cl_2$. On the other hand, since the *c*-chxn has two amino groups in the axial and the equatorial positions (a), it preferentially forms yellow diamagnetic bis-complexes such as $[Ni(c\text{-chxn})_2]Cl_2$. The distances between N atoms of the diamine isomers are nearly equal, therefore, the structural differences among the complexes seem to be due to the degree of the steric hindrance of the cyclohexane ring. In this paper, the results of thermal reactions of the nickel(II) complexes in the solid state will be described and the steric influence of these ligands on coordination will be shown.

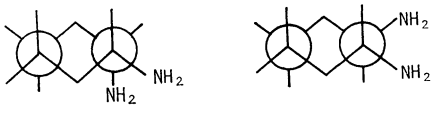

(a) *c*-chxn (b) *t*-chxn

Experimental

Measurements. Thermogravimetric(TG) and differential scanning calorimetric(DSC) curves were obtained with a Rigaku Denki 8185 DI apparatus at a 1.25 °C min^{-1} heating rate and with a 50 cm^3 min^{-1} flow rate of nitrogen gas. The reflectance spectra were measured with a Hitachi EPS-3T spectrophotometer. The infrared spectra were recorded with a JASCO IRA-2 spectrophotometer by means of the HCB mull and the KBr disc method.

Preparations. The ligands, *c*-chxn and racemic *t*-chxn, were obtained in the manner reported previously.[6] $[Ni(t\text{-chxn})_2(H_2O)_2]Br_2$, $[Ni(c\text{-xhn})_3]Cl_2\cdot 1.5H_2O$, $[Ni(c\text{-chxn}_3)]Br_2\cdot H_2O$, and $[Ni(c\text{-chxn})_3](NO_3)_2\cdot 0.5H_2O$ were prepared by means of the previously described procedures.[2] $[Ni(t\text{-chxn})_2(H_2O)_2]X_2$ ($X=Cl^-$ and NO_3^-), $[Ni(t\text{-chxn})_3]Cl_2\cdot 2H_2O$, and $[Ni(t\text{-chxn})_3]Br_2\cdot 3H_2O$ were synthesized with reference to the methods described in the literature.[7,8] The chemical formulae were confirmed by elemental analyses.

Results and Discussion

The TG-DSC curves of the following three types of complexes, $[Ni(t\text{-chxn})_2(H_2O)_2]X_2$, $[Ni(c\text{-chxn})_3]X_2\cdot nH_2O$, and $[Ni(t\text{-chxn})_3]X_2\cdot nH_2O$ ($X=Cl^-$, Br^- and NO_3^-), are shown in Figs. 1, 2, and 3 respectively, while the results are summarized in Table 1. It was confirmed that the colors of $[Ni(c\text{-chxn})_2]X_2$ complexes did not change in the temperature range from *ca.* 25 °C to 250 °C. Therefore, the square planar structures of these complexes are regarded as very stable. The *c*-chxn molecules in this structure make it unfavorable for water molecules or anions to approach the nickel(II) ion along

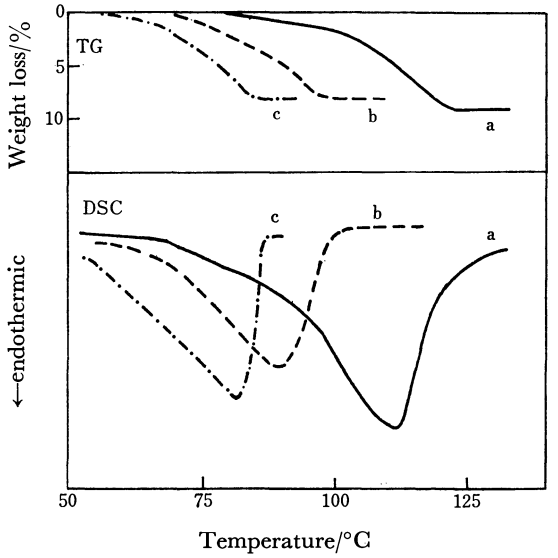

Fig. 1. TG and DSC curves of (a) $[Ni(t\text{-chxn})_2(H_2O)_2]Cl_2$, (b) $[Ni(t\text{-chxn})_2(H_2O)_2]Br_2$, and (c) $[Ni(t\text{-chxn})_2(H_2O)_2](NO_3)_2$.

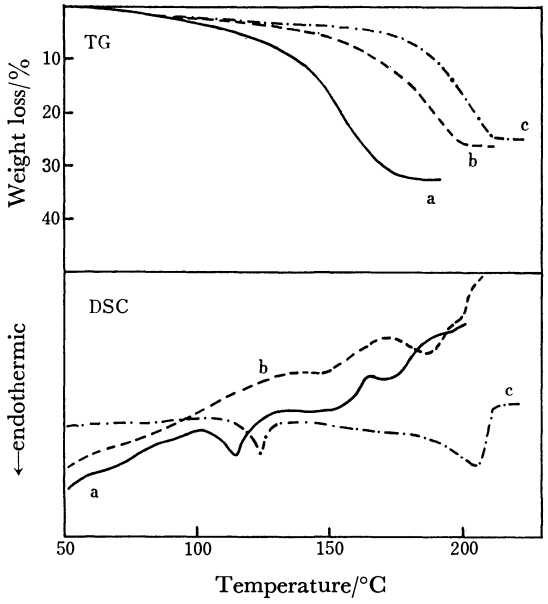

Fig. 2. TG and DSC curves of (a) $[Ni(c\text{-chxn})_3]Cl_2 \cdot 1.5H_2O$, (b) $[Ni(c\text{-chxn})_3]Br_2 \cdot H_2O$, and (c) $[Ni(c\text{-chxn})_3](NO_3)_2 \cdot 0.5H_2O$.

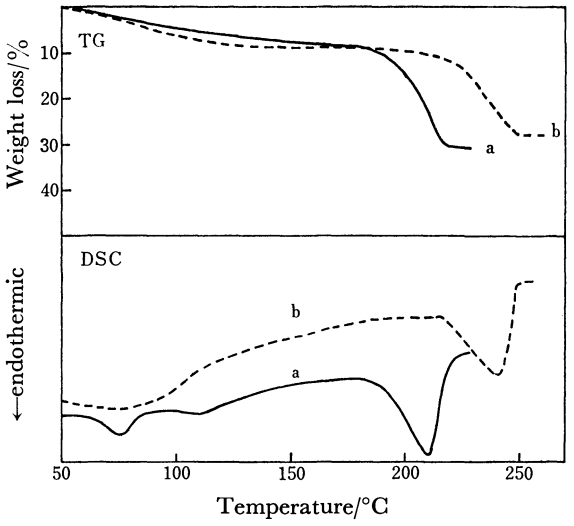

Fig. 3. TG and DSC curves of (a) $[Ni(t\text{-chxn})_3]Cl_2 \cdot 2H_2O$ and (b) $[Ni(t\text{-chxn})_3]Br_2 \cdot 3H_2O$.

the z axes because of the steric hindrance caused by the cyclohexane rings, which are located obliquely above the chelate ring.

The diaquabis(*t*-chxn) complexes of three kinds of X anions liberated two molecules of coordinated water in the following order of increasing deaquation temperature; $X = NO_3^- < Br^- < Cl^-$, giving similar DSC curves. A few qualitative observations of this thermal behavior have been reported by Tsuchida.[7] The temperature at which thermal deaquation occurs seems to be dependent upon the degree of interaction between a water molecule and an anion, and also upon the degree of axial perturbation of the anions. The present authors have presumed on the basis of the infrared spectra, that, in the structures of these complexes, not anions, but water molecules are coordinated in the apical positions.[2] The coordination of water molecules is also suggested by the large endothermic peak of the DSC curves.

The complexes of this type are found to undergo thermal transformation in two ways with a variety of anions, like diaquabis(*N*,*N*-diethylethylenediamine)nickel(II) complexes.[9,10] In the cases of the chloride and the bromide, yellow complexes were obtained after deaquation, but they turned blue violet again when they were kept in the air at room temperature. The resultant blue violet complexes are assumed to be the initial diaquabis-complexes because the former exhibit infrared and electronic spectra almost identical with those of the latter. This indicates the reversible transformation from a square planar structure to a distorted octahedron by the coordination of water molecules in the apical positions in the solid state. On the other hand, the color of $[Ni(t\text{-chxn})_2(H_2O)_2](NO_3)_2$ did not change on deaquation. Figure 4 shows the infrared spectra of the nitrate complex and the sample obtained by heating. The broad ν_{NO} of the initial diaquabis-complex splits into two peaks, at 1310 and 1432 cm^{-1}, after deaquation. They can reasonably be assigned to the ν_{NO} stretching

Table 1. DSC peak temperature (t_m/°C), weight-losses ($-\Delta W$/%), and color changes in thermal analyses

Complexe	Deaquation				Liberation of ligand				Color change
	t_m/°C	DSC	$-\Delta W$/% Obsd	Calcd	t_m/°C	DSC	$-\Delta W$/% Obsd	Calcd	
$[Ni(t\text{-chxn})_2(H_2O)_2]Cl_2$	112	endo	9.2	9.1					BV→Y
$[Ni(t\text{-chxn})_2(H_2O)_2]Br_2$	90	endo	8.3	7.5					BV→Y
$[Ni(t\text{-chxn})_2(H_2O)_2](NO_3)_2$	82	endo	8.1	8.2					BV→BV
$[Ni(c\text{-chxn})_3]Cl_2 \cdot 1.5H_2O$	—[a]	endo	—[b]		115, 156, 174	endo	32.8	28.3	V→Y
$[Ni(c\text{-chxn})_3]Br_2 \cdot H_2O$	—[a]	endo	—[b]		149, 188, 197	endo	26.0	22.8	V→Y
$[Ni(c\text{-chxn})_3](NO_3)_2 \cdot 0.5H_2O$	—[a]	endo	—[b]		124, 206	endo	25.1	24.0	V→Y
$[Ni(t\text{-chxn})_3]Cl_2 \cdot 2H_2O$	77, 112	endo	7.9	7.1	211	endo	22.5	22.5	V→BV
$[Ni(t\text{-chxn})_3]Br_2 \cdot 3H_2O$	—[a]	endo	8.9	8.8	240	endo	19.1	18.6	V→BV

endo=endothermic, BV=blue violet, V=violet, Y=yellow

a) The deaquation change occurred so gradually that the DSC peak temperature could not be measured exactly. b) The weight-losses in the deaquation step could not be measured independently, so the ΔW values in the Liberation of ligand column contain ΔW in the deaquation step.

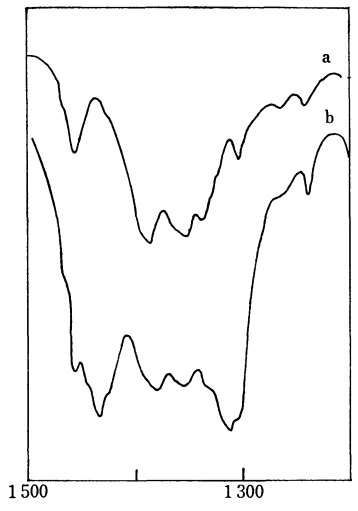

Fig. 4. Infrared spectra of $[Ni(t\text{-chxn})_2(H_2O)_2](NO_3)_2$: (a) before heating, (b) after heating.

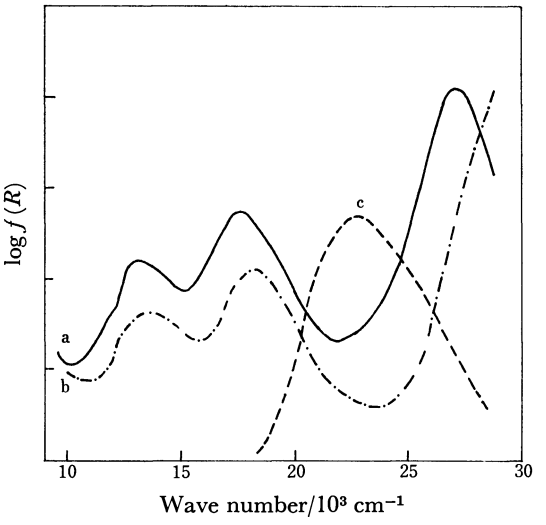

Fig. 5. Reflectance spectra of the samples, after heating, (a) $[Ni(t\text{-chxn})_3]Br_2 \cdot 3H_2O$ at 260 °C, (b) $[Ni(t\text{-chxn})_2(H_2O)_2](NO_3)_2$ at 100 °C, and (c) $[Ni(c\text{-chxn})_3]Cl_2 \cdot 1.5H_2O$ at 220 °C.

of the unidentate nitrate anion.[11] In the reflectance spectrum of the corresponding anhydrous complex, three characteristic maxima, at 12300 (sh), 13500, and 17200 cm^{-1}, were observed (Fig. 5), they are ascribable to the trans tetragonal structure, although the band near 28000 cm^{-1} could not be observed due to the charge-transfer band of a nitrate anion. Therefore, in the case of nitrate, deaquation-anation seems to take place simultaneously. This thermal reaction is parallel to that found by Inoue[12] and Curtis[11] for $[Ni(en)_2(H_2O)_2](NO_3)_2$.

The tris-complexes of *c*-chxn changed to yellow complexes, liberating some water of crystallization and one molecule of ligand on heating, although no distinct plateau on the TG curves for the deaquation process were observed. The spectral patterns of the yellow complexes are in good agreement with those of the corresponding diamagnetic $[Ni(c\text{-chxn})_2]X_2$.[2] Nishimoto reported the thermal transformation from the octahedral structure of tris(*meso*-2,3-butanediamine)nickel(II) halide to a square planar structure.[13] It was revealed that the cyclohexane ring of *c*-chxn had steric effects on the configuration of the nickel(II) complexes similar to those of the ethylenediamine derivative with substituents on the C atoms.

The tris-complexes of *t*-chxn with halide ions gave blue violet bis-complexes, releasing one molecule of a ligand, upon heating. The visible reflectance spectra of the resultant bis-complexes show ν_{max} at 12100 (sh), 13500, 17500, and 27400 cm^{-1} ($X=Cl^-$), and at 11800 (sh), 13200, 17500, and 27500 cm^{-1} ($X=Br^-$), respectively (Fig. 5). The resemblance of these spectra to those of dihalogenobis(*N,N'*-dimethylethylenediamine)nickel(II)[14] suggests that the bis-complexes have a tetragonally distorted octahedral structure, with halide ions coordinated in the apical positions. The *t*-chxn is assumed to prefer the above structure because of the ample spaces in the z axes. The corresponding nitrate released a ligand at higher temperatures and gave a brown material as a result of the successive decomposition. It is of interest to note that the temperatures of the eliminating ligand for each type of tris-complex, *c*-chxn and *t*-chxn, increase in the following order; $X=Cl^-<Br^-<NO_3^-$, the reverse of that in the case of the deaquation of diaquabiscomplexes.

References

1) Part V of this series: R. Saito and Y. Kidani, *Bull. Chem. Soc. Jpn.*, **52**, 57 (1979).
2) R. Saito and Y. Kidani, *Bull. Chem. Soc. Jpn.*, **51**, 159 (1978).
3) R. D. Gillard and H. M. Irving, *Chem. Rev.*, **65**, 603 (1965).
4) A. E. Martell, *J. Phys. Chem.*, **59**, 308 (1955).
5) E. J. Corey and J. C. Bailar, Jr., *J. Am. Chem. Soc.*, **81**, 2620 (1959).
6) R. Saito and Y. Kidani, *Chem. Lett.*, **1976**, 123.
7) M. Tsuchida, *Natural Science Report Ochanomizu Univ.*, **24**, 13 (1972).
8) R. S. Treptow, *Inorg. Chem.*, **7**, 1229 (1968).
9) R. Tsuchiya, S. Joba, A. Uehara, and E. Kyuno, *Bull. Chem. Soc. Jpn.*, **46**, 1454 (1973).
10) D. M. L. Goodgame and L. M. Venanzi, *J. Chem. Soc.*, **1963**, 616.
11) N. F. Curtis and Y. Curtis, *Inorg. Chem.*, **4**, 804 (1965).
12) T. Inoue, *Nippon Kagaku Zasshi*, **54**, 65 (1933).
13) H. Nishimoto, T. Yoshikuni, A. Uehara, E. Kyuno, and R. Tsuchiya, *Bull. Chem. Soc. Jpn.*, **51**, 1068 (1978).
14) D. A. Rowley and R. S. Drago, *Inorg. Chem.*, **4**, 795 (1968).

Region of Formation of Iron(III) Hydrogen Orthophosphate and Structural Changes in Humid Atmospheres

Mitsutomo Tsuhako,* Chinuyo Oyama, Tsuneo Matsuo,
Itaru Motooka,† and Masamitsu Kobayashi†

Kobe Women's College of Pharmacy, Motoyama, Higashinada-ku, Kobe 658
†*Department of Chemistry, Faculty of General Education, Kobe University, Tsurukabuto, Nada-ku, Kobe 657*

(Received February 8, 1979)

The conditions of formation of the A and B forms of $Fe(H_2PO_4)_3$ by the reaction of Fe_2O_3 and H_3PO_4 have been established, and the thermal changes and structural changes in humid atmospheres investigated. 1) The A and B forms of $Fe(H_2PO_4)_3$ were readily formed by secondary heat treatment at 150 °C and 125 °C, respectively. 2) The forms of $Fe(H_2PO_4)_3$ were largely dependent on the heating rate in the primary heat treatment, *i.e.*, at a mean heating rate less than 7 °C/min the A form predominated, whereas above 60 °C/min the B form predominated. A heating rate between 7 and 60 °C/min gave a mixture of the A and B forms. 3) A close relationship between the water content of the primary product and yields of the A and B forms of $Fe(H_2PO_4)_3$ was found, *i.e.*, only the B form was obtained when the water content of the primary product was less than 7%, while the A form was readily formed when the water content was greater than 11%. 4) Heating the primary product under various degrees of humidity enabled the formation of $Fe(H_2PO_4)_3$ to be investigated. The effect of heating atmosphere was small except under vacuum. 5) The structural changes of the A and B forms of $Fe(H_2PO_4)_3$ under several humid atmospheres are summarized as follows:

$$Fe(H_2PO_4)_3\ \text{B form} \underset{P_2O_5}{\overset{\text{air}}{\rightleftarrows}} FeH_6(PO_4)_3 \overset{\text{wet air}}{\underset{P_2O_5}{\rightleftarrows}} \text{amorphous}$$

$$\text{iron phosphate} \xrightarrow{\text{air}} FeH_3(PO_4)_2\cdot 2.5H_2O$$

$$Fe(H_2PO_4)_3\ \text{B form} \quad \text{air} \uparrow\downarrow P_2O_5$$

$$Fe(H_2PO_4)_3\ \text{A form} \xrightarrow{\text{air}} FeH_6(PO_4)_3 \overset{\text{wet air}}{\underset{SiO_2}{\rightleftarrows}} \text{amorphous}$$

$$\text{iron phosphate} \xrightarrow{\text{air}} FeH_3(PO_4)_2\cdot 2.5H_2O$$

Iron phosphates have been studied for several years and already in 1878 several iron phosphates had been synthesized by Erlenmeyer.[1] Since then the structural chemistry of several natural iron phosphates, such as strengite $FePO_4\cdot 2H_2O$,[2] vivianite $Fe_3(PO_4)_2\cdot 8H_2O$,[3] ludlamite $Fe_3(PO_4)_2\cdot 4H_2O$[4] and the like,[5–7] have been conducted by many researchers. Carter,[8] Jameson[9] and Kobayashi[10] have studied the phase diagram of the Fe_2O_3–P_2O_5–H_2O system at 25 °C and several iron phosphates synthesized. d'Yvoire[11] has studied in detail the similarity of structure between iron phosphate and aluminum phosphate.

Recently, fundamental studies of iron phosphate as an inorganic ion exchanger have been published,[10,12–14] but a systematic study of the preparation of iron phosphates remains absent. Consequently it is difficult to obtain iron phosphates with fine reproducibility. In the present study, the authors investigated the preparative methods for the A and B forms of iron hydrogen orthophosphate $Fe(H_2PO_4)_3$, and established the preparative conditions in the reaction of Fe_2O_3 and H_3PO_4. The thermal changes of the A and B forms of $Fe(H_2PO_4)_3$ as well as the structural changes under several different humid atmospheres were also investigated.

Experimental

Preparation of Iron Phosphate. Ferric oxide Fe_2O_3 (E. Merck) and 85% orthophosphoric acid were mixed in a gold or porcelain crucible in molar ratios Fe_2O_3/P_2O_5 (R) of 1/3 and 1/4. The mixture was heated at various heating rates by a weak flame with vigorous agitation to obtain a grey, highly viscous product. (This is designated as the primary heat treatment, giving the primary products.) A small amount (0.5—0.6 g) of the primary product was accurately weighed, and the water content determined by the Karl-Fischer method at 150 °C. Another portion was heated at 150 °C for 5 h in a thermostated electric furnace, under vacuum (0.01 mmHg), in dry air (50 ml/min, vapor pressure 0—1 mmHg), and in water vapor (500 g H_2O/h, vapor pressure 760 mmHg). (This is designated as the secondary heat treatment, giving the secondary products.) The experimental method may be shown schematically as follows:

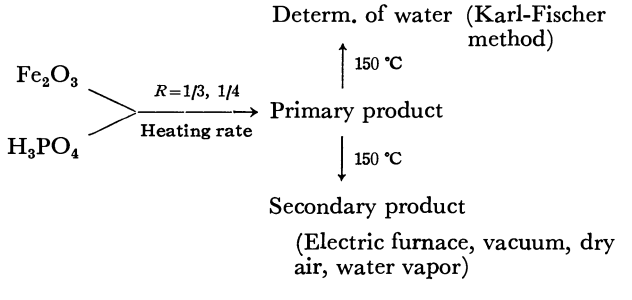

The temperature of the primary heat treatment is affected by the amount of starting material, the molar ratio R and the heating rate; the temperature being generally approximately 70—170 °C.

The iron phosphates prepared at 150 °C were relatively hard, but absorbed moisture on standing in air. Thus, X-ray

analysis, differential thermal analysis (DTA), and thermogravimetry (TG) of iron phosphates were conducted immediately after preparation.

Apparatus and Methods. The X-ray analysis was conducted with a Rigaku Denki Geigerflex X-ray diffractometer, using Ni filtered Cu $K\alpha$ radiation. A Kyoto Denshi Karl-Fischer Titrator was used for the determination of water. A Rigaku Denki Differential Thermogravimetric Analyzer, 8076E1, was used for the DTA and TG. The X-ray analysis, differential thermal analysis, and thermogravimetry of iron phosphates were conducted by the methods described in a previous paper.[15]

The yields of the A and B forms of $Fe(H_2PO_4)_3$, $FeHP_2O_7$, $Fe_4(P_2O_7)_3$ and $FeH_6(PO_4)_3$ were determined from the integrated intensities of the characteristic X-ray diffraction peaks; *i.e.*, type A of $Fe(H_2PO_4)_3$ by the peak at $d=3.634$ Å; type B of $Fe(H_2PO_4)_3$, by that at 7.724 Å; $FeHP_2O_7$, by that at 3.860 Å; $Fe_4(P_2O_7)_3$, by that at 5.336 Å; and $FeH_6(PO_4)_3$, by that at 8.776 Å.

Results and Discussion

Relationship between Yields of Iron(III) Phosphates and Heating Temperature. Figure 1 shows the relationship between the heating temperature and the yields of iron phosphates in the reaction of Fe_2O_3 and H_3PO_4 at a molar ratio P_2O_5/Fe_2O_3 ($1/R$) of 3. As seen, the crystalline iron phosphates formed at temperature below 250 °C were four, namely, the A and B forms of $Fe(H_2PO_4)_3$, $FeHP_2O_7$, and $Fe_4(P_2O_7)_3$. At temperatures below 200 °C, iron hydrogen orthophosphate predominated, whereas above 225 °C pyrophosphate predominated. The A form of $Fe(H_2PO_4)_3$ was formed at temperatures below 200 °C, and especially at 150 °C. The B form was formed at temperatures below 175 °C, particularly readily at 125 °C. At temperatures above 225 °C $FeHP_2O_7$ and $Fe_4(P_2O_7)_3$ were obtained in a mixture, but in the temperature range 200—250 °C, the presence of large quantity of amorphous iron phosphate was proved by X-ray diffraction. The poor yields of $FeHP_2O_7$ and $Fe_4(P_2O_7)_3$ may be explained in terms of the mixing rate (R) of phosphoric acid and Fe_2O_3. $R=1/3$ corresponds to the meta-composition, and the quantity of phosphoric acid is too large to form iron pyrophosphate. No distinct difference could be established between the temperature of formation of $FeHP_2O_7$ and that of $Fe_4(P_2O_7)_3$, while considerable difference was observed between the temperature of formation of the A form of $Fe(H_2PO_4)_3$ and that of the B form. This establishes that the B form is prefered at low temperatures. At 150 °C, however, both forms were obtained in a mixture, and the reproducibility of yield was poor. It was also discovered that the yields were affected not only by the heating temperature but also by the conditions of the primary heat treatment. Maintaining the molar ratios and the temperatures of the primary and secondary heat treatments did not always give the same form of $Fe(H_2PO_4)_3$. Thus, the primary heat treatment, heating rate, the state of the primary product, the water content and heating atmosphere in the secondary heat treatment were further investigated. With molar ratios $1/R$ of 4 and 3, almost the same results were obtained. At a secondary heat treatment temperature below 110 °C, the product did not solidify and crystalline iron phosphate could not be obtained.

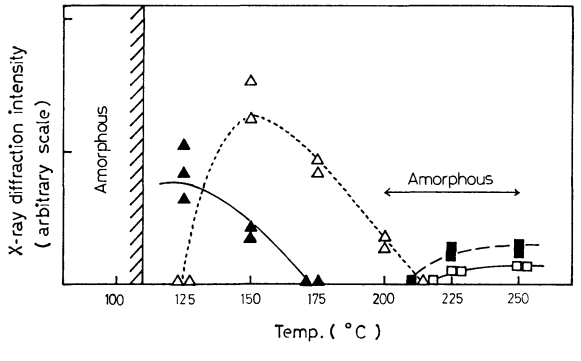

Fig. 1. Relationship between heating temperature and the yields of iron phosphates at $P_2O_5/Fe_2O_3=3$.
-△-: $Fe(H_2PO_4)_3$(A), -▲-: $Fe(H_2PO_4)_3$(B),
-■-: $FeHP_2O_7$, -□-: $Fe_4(P_2O_7)_3$.

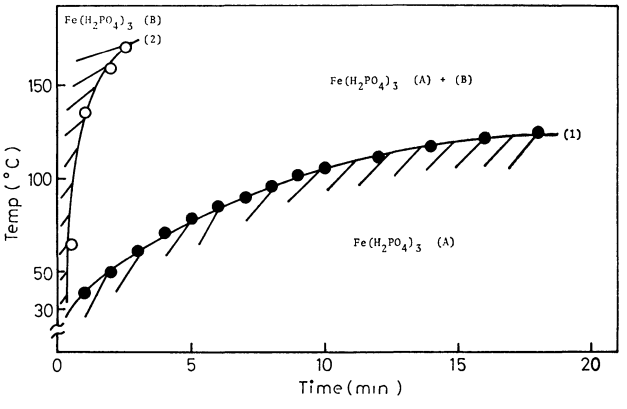

Fig. 2. Relationship between the formation of $Fe(H_2PO_4)_3$ (A), (B) and heating rate in the primary heat treatment. Molar ratio (P_2O_5/Fe_2O_3);3, heating rate; (1): 7 °C/min, (2): 60 °C/min, secondary heat treatment; 150 °C, 5 h.

Relationship between the Formation of the A and B Forms of $Fe(H_2PO_4)_3$ and the Heating Rate. Figure 2 illustrates the change in formation of the A and B forms of $Fe(H_2PO_4)_3$ with changes in the heating rate in the primary heat treatment. As shown by curve (1) in Fig. 2, slow heating at a mean heating rate less than 7 °C/min results in the exclusive formation of the A form. As can be seen from curve (2), rapid heating at a rate in excess of 60 °C/min produces exclusively the B form. Heating at a rate between 7 and 60 °C/min (the region surrounded by curves (1) and (2) in Fig. 2) results in a mixture. The A form, however, predominates at a lower heating rate (10—20 °C/min), whereas the B form predominates at a higher heating rate (40—60 °C/min). The above results were highly reproducible, there being only a few exceptions in 80 experiments. These results are only applicable for highly viscous primary products. Further heating of the viscous primary product and subsequent solidification in the course of the primary heat treatment, however, gave a different relationship, the results of which are shown in Fig. 3. At a primary heat treatment of heating rate below 2.5 °C/min (curve (1) in

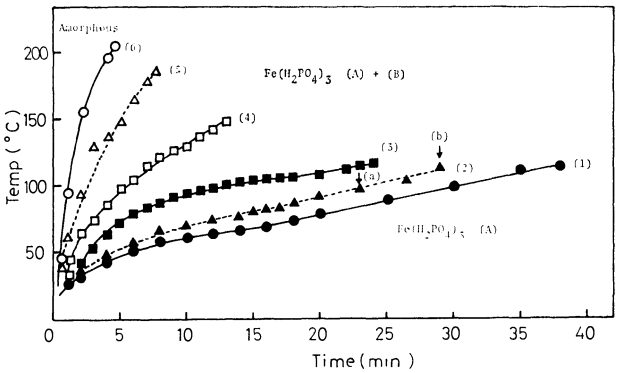

Fig. 3. Relationship between the formation of $Fe(H_2PO_4)_3$ (A), (B) and heating rate in the primary heat treatment. Molar ratio (P_2O_5/Fe_2O_3): 3, secondary heat treatment: 150 °C, 5 h, heating rate; (1): 2.5 °C/min, (2): 3.7 °C/min, (3): 4.2 °C/min, (4): 9.6 °C/min, (5): 21.7 °C/min, (6): 40.2 °C/min.

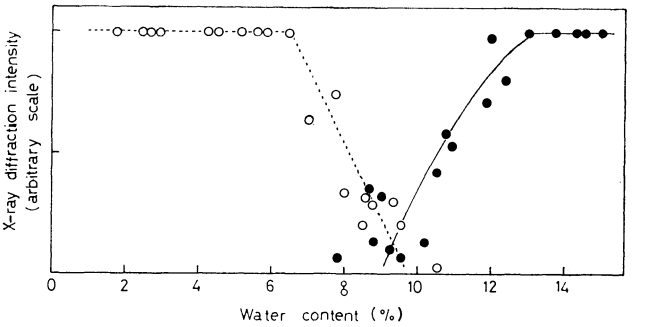

Fig. 4. Relationship between water content of the primary product and the yields of the A and B types of $Fe(H_2PO_4)_3$.
-●-: $Fe(H_2PO_4)_3$ A type, -○-: $Fe(H_2PO)_3$ B type, Molar ratio (P_2O_5/Fe_2O_3): 3, secondary heat treatment: 150 °C, 5 h.

Fig. 3), only the A form of $Fe(H_2PO_4)_3$ was obtained. At a primary heat treatment of heating rate above 40 °C/min (curve (6)), no crystalline iron phosphate was formed. At a primary heat treatment of heating rate of 3—40 °C/min (curves (2)—(5)), a mixture of the A and B forms was produced. Thus, only the B form of $Fe(H_2PO_4)_3$ could not be obtained from the solidified primary products. Two samples of the primary product obtained at a mean heating rate of about 3.7 °C/min (curve (2)), one of which was a highly viscous nature corresponding to point (a) and other the solidified state corresponding to point (b), were submitted for secondary heat treatment at 150 °C for 5 h. The iron phosphate formed from the former was the A form of $Fe(H_2PO_4)_3$, while that from the latter was a mixture of both A and B forms. The amounts of water liberated on heating the primary products corresponding to points (a) and (b) at 150 °C were 13.5% and 9.4%, respectively, indicating that since the primary product of the solidified state which was subjected to primary heat treatment at a higher temperature than that of the highly viscous state, the water content of the latter, corresponding to point (a), may be more than that of the former, corresponding to point (b). Based on this, it may be seen that the formation of both forms is strongly dependent on the state of the primary products, *i.e.*, at the same heating rate, the formation regions of the A and B forms for the highly viscous primary products differ from those for the solidified primary products. Furthermore, as can be seen from Figs. 2 and 3, the formation region of the mixture of both forms in the solidified primary product is greater than that in the highly viscous primary product.

Relationship between Water Content of the Primary Product and Yields of Iron(III) Hydrogen Orthophosphate. As described above, the formation of the A and B forms of $Fe(H_2PO_4)_3$ strongly depend on the heating temperature, heating rate and the state of the primary product. Thus, the relationship between the water content of the primary product and yields of the A and B forms of $Fe(H_2PO_4)_3$ was investigated, the results of which are shown in Fig. 4. From a primary product containing approximately 7% or less of water, only the B form of $Fe(H_2PO_4)_3$ was obtained, while from a primary product containing 11% or more of water, only the A form was obtained. From primary products having between 7.5 and 10.5% water content, a mixture of both A and B forms was obtained. The results of DTA and TG of the primary products suggest that the water liberated on heating the primary product at 150 °C may be water loosely bound on the solid surface, and not the structural water (P–OH) of iron phosphate. It is evident, therefore, that the water content (loosely bound water) of the primary product strongly affects the formation of the A and B forms of $Fe(H_2PO_4)_3$. It was also estab-

Table 1. Formation of iron phosphates at a molar ratio (Fe_2O_3/P_2O_5) of 1/3 under various heating atmospheres at 150 °C

Heating rate (°C/min)	Water content (%)	Electric furnace	Water vapor	Dry air	Vacuum
2.4	12.7	A(s)	A(m)	A(m)	A(s)
6.6	11.7	A(vs)	A(vs)	A(vs)	A(vs)
17.9	10.2	A(w)	A(w)	A(vw)	A(w)
		B(vs)	B(m)	B(m)	
55.6	5.8	A(w)	A(vw)	A(vw)	Amorphous
		B(vs)	B(m)	B(w)	
62.2	4.4	B(vs)	B(vs)	B(s)	Amorphous
87.2	2.5	B(vs)	B(m)	B(w)	Amorphous

X-Ray diffraction intensity, vs: very strong, s: strong, m: medium, w: weak, vw: very weak.
Product, A: $Fe(H_2PO_4)_3$ A form, B: $Fe(H_2PO_4)_3$ B form.

lished that the water content was inversely proportional to the heating rate of the primary heat treatment, *i.e.*, the water content decreased with increase in the heating rate.

In conclusion the A form of $Fe(H_2PO_4)_3$ is formed more readily at a low rate of heating, namely in the region in which the water content of the primary product was high. The B form is prefered at a higher heating rate, *i.e.*, at lower water content of the primary product.

Formation of Iron(III) Phosphates in Several Heating Atmospheres. The primary products prepared by the above-mentioned methods at various heating rates, *i.e.*, primary products containing various water contents were heated at 150 °C for 5 h in various water vapor pressures and the formation of iron phosphate investigated. The results are summarized in Table 1. As can be seen from Table 1, the formation of iron hydrogen orthophosphate is only slightly dependent on the heating atmosphere, but strongly affected by the heating rate of the primary heat treatment and consequently, by the water content of the primary product. This strongly supports the relationship reported above between the water content of the primary product and yields of the A and B forms of $Fe(H_2PO_4)_3$, *i.e.*, at a low heating rate the A form predominates, while at a high heating rate, the B form predominates. In vacuum, the formation of the B form of $Fe(H_2PO_4)_3$ was not observed, amorphous iron phosphate being obtained at low water content.

DTA and TG of the A and B Forms of $Fe(H_2PO_4)_3$.

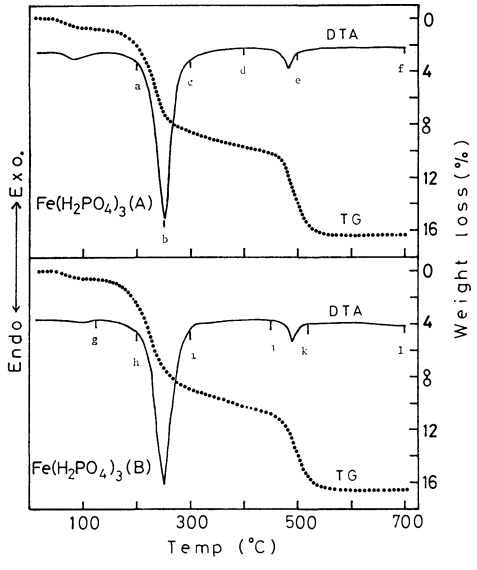

Fig. 5. DTA and TG of $Fe(H_2PO_4)_3$ (A), (B). Sample; 20—22 mg, heating rate; 10 °C/min.

Figure 5 illustrates the results of DTA and TG for the A and B forms of $Fe(H_2PO_4)_3$. For the A form, endothermic peaks were observed at approximately 75—80, 250, and 475 °C. The products corresponding to each point, a (200 °C), b (250 °C), c (300 °C), d (400 °C), e (500 °C), and f (700 °C) on the DTA curve were investigated by powder X-ray diffraction. At point a, only the starting material, the A form of $Fe(H_2PO_4)_3$ was observed. Thus, the small endothermic peak at approximately 75—80 °C, which is accompanied by a slight weight loss (0.9—1.2%), may be attributed to the removal of water adhering to the solid surface, namely adhesive water. Furthermore, from the X-ray diffraction patterns of the products corresponding to points b and c, it was shown that the A form of $Fe(H_2PO_4)_3$ is transformed into amorphous iron phosphate through the strong endothermic reaction with a weight loss caused by dehydration at about 250 °C. At point d, the amorphous iron phosphate was partially transformed into the B and C forms of $Fe(PO_3)_3$. Furthermore, the endothermic reaction at approximately 475 °C (point e), the amorphous iron phosphate was completely transformed into the C form of $Fe(PO_3)_3$, which did not change at 700 °C (point f). The results of the DTA and TG of the B form of $Fe(H_2PO_4)_3$ were almost identical with those of the A form. For the B form of $Fe(H_2PO_4)_3$, a small endothermic peak, accompanied by a 0.5—0.8% weight loss, was observed at approximately 75—80 °C. This weak endothermic reaction may be considered as the removal of adhesive moisture, since the X-ray diffraction patterns of the products at points g (120 °C) and h (200 °C), the B form of $Fe(H_2PO_4)_3$ did not change due to this endothermic reaction. Furthermore, a large endothermic peak with an accompanying weight loss was observed at 250 °C. In this endothermic reaction, the B form of $Fe(H_2PO_4)_3$ was dehydrated and transformed into amorphous iron phosphate, as shown by the X-ray diffraction patterns of the product corresponding to point i (300 °C). At point j (450 °C), the amorphous iron phosphate was partially transformed into a mixture of the A, B, and C forms of $Fe(PO_3)_3$. At approximately 500 °C, and endothermic peak with a weight loss due to dehydration of structural water (P–OH) was observed. It was shown by the X-ray diffraction pattern of the product corresponding to point k (520 °C) that in this endothermic reaction, the amorphous iron phosphate was completely transformed into a mixture of the A, B, and C forms of $Fe(PO_3)_3$. In the temperature range from 520 to 700 °C, no changes were observed on the DTA curve, but the X-ray diffraction pattern of the product corresponding to point l (700

Table 2. Thermal changes of the A form of $Fe(H_2PO_4)_3$ in various heating atmospheres

Temp (°C)	Electric furnace	Water vapor	Vacuum
200	$Fe(H_2PO_4)_3$ A(s)	$FeHP_2O_7$(vw)	Amorphous
250	Amorphous	$FeHP_2O_7$(m)	Amorphous
300	Amorphous	$FeHP_2O_7$(m)	$Fe(PO_3)_3$ B(m), C(vs)
400	$Fe(PO_3)_3$ B(w), C(vs)	$Fe(PO_3)_3$ A(m), C(vs)	$Fe(PO_3)_3$ A(m), B(w), C(s)
500	$Fe(PO_3)_3$ C(vs)	$Fe(PO_3)_3$ C(vs)	$Fe(PO_3)_3$ A(w), C(vs)
700	$Fe(PO_3)_3$ C(vs)	$FePO_4$(vs)	$Fe(PO_3)_3$ C(vs)

X-Ray diffraction intensity, vs: very strong, s: strong, m: medium, w: weak, vw: very weak.

Table 3. Thermal changes of the B form of $Fe(H_2PO_4)_3$ in various heating atmospheres

Temp (°C)	Electric furnace	Water vapor	Vacuum
120	$Fe(H_2PO_4)_3$ B(vs)	$FePO_4 \cdot 2H_2O$(m)	$Fe(H_2PO_4)_3$ B(m)
200	$Fe(H_2PO_4)_3$ B(m)	$FeHP_2O_7$(m)	Amorphous
300	Amorphous	$FeHP_2O_7$(s)	$Fe(PO_3)_3$ A(m), B(vs)
450	$Fe(PO_3)_3$ A(m), B(m), C(s)	$Fe(PO_3)_3$ A(w), C(vs)	$Fe(PO_3)_3$ A(m), B(s), C(m)
520	$Fe(PO_3)_3$ A(m), B(m), C(s)	$Fe(PO_3)_3$ C(vs)	$Fe(PO_3)_3$ A(w), C(vs)
700	$Fe(PO_3)_3$ C(vs)	$Fe_4(P_2O_7)_3$(vs) $FePO_4$(vs)	$Fe(PO_3)_3$ A(w), C(vs)

X-Ray diffraction intensity, vs: very strong, s: strong, m: medium, w: weak.

°C) showed that both the A and B forms of $Fe(PO_3)_3$ had already transformed into the C form of $Fe(PO_3)_3$.

The thermal changes of $Fe(H_2PO_4)_3$ at temperatures corresponding to points a—l on the DTA curves of the A and B forms of $Fe(H_2PO_4)_3$ were also investigated, the results of which are summarized in Tables 2 and 3. In all experiments, the samples were heated for 5 h. The results of the thermal changes of the A and B forms of $Fe(H_2PO_4)_3$ in an electric furnace largely support the results of the DTA study described above. The results of the thermal changes of both A and B forms in an atmosphere of water vapor differ considerably from those in other heating atmospheres, *i.e.*, in an atmosphere of water vapor below 300 °C, the A form of $Fe(H_2PO_4)_3$ gives $FeHP_2O_7$ and is transformed into $Fe(PO_3)_3$ at 400 °C. At a temperature above 700 °C, $Fe(PO_3)_3$, liberating white P_2O_5 fumes, decomposes to form $FePO_4$. The formation of $FePO_4$ may be interpreted in terms of evaporation of the P_2O_5 component caused by the flow of water vapor at high temperature. Under vacuum, both A and B forms of $Fe(H_2PO_4)_3$ begin to transform into amorphous iron phosphate at 200 °C. This transformation temperature is approximately 50—100 °C lower than in the electric furnace. Under vacuum, furthermore, the formation of $Fe(PO_3)_3$ was observed at 300 °C. Thus, it may be concluded that the thermal changes shift to lower temperatures under vacuum.

From the above experimental results, the thermal changes in air of the A and B forms of $Fe(H_2PO_4)_3$ may be given by:

$$Fe(H_2PO_4)_3 \text{ A form} \xrightarrow{250\,^\circ C} \text{amorphous iron phosphate}$$

$$\xrightarrow{400\,^\circ C} Fe(PO_3)_3 \text{ B + C form} \xrightarrow{500\,^\circ C} Fe(PO_3)_3 \text{ C form}$$

$$Fe(H_2PO_4)_3 \text{ B form} \xrightarrow{250\,^\circ C} \text{amorphous iron phosphate}$$

$$\xrightarrow{450\,^\circ C} Fe(PO_3)_3 \text{ A+B+C form} \xrightarrow{700\,^\circ C} Fe(PO_3)_3 \text{ C form}$$

Changes of the A and B Forms of $Fe(H_2PO_4)_3$ in Various Humid Atmospheres. The structural changes of the A and B forms of $Fe(H_2PO_4)_3$ after standing in various humid atmospheres are shown in Figs. 6a—6c. As may be seen from Fig. 6a, the B form of $Fe(H_2PO_4)_3$ was completely transformed into $FeH_6(PO_4)_3$, on standing in air for 4 days. The X-ray diffraction pattern of the product was in fair agreement with that of $FeH_6(PO_4)_3$ already reported by Kobayashi.[10] The compound $FeH_6(PO_4)_3$ obtained under the above conditions, on standing in a desiccator with P_2O_5, was transformed into the B form of $Fe(H_2PO_4)_3$ starting from the third day. The amount of $FeH_6(PO_4)_3$ gradually decreases with time, virtually disappearing on the seventh day. Thus, the B form of $Fe(H_2PO_4)_3$, on standing in air, absorbs moisture to form $FeH_6(PO_4)_3$, but the latter is dehydrated in a desiccator with P_2O_5, reverting to the former again. As may be seen from Fig. 6b, on standing in wet air (water vapor 20—25 mmHg) for 2 h, the B form is completely transformed into amorphous iron phosphate. This amorphous iron phosphate is transformed into $FeH_6(PO_4)_3$ on standing in a desiccator with P_2O_5 for 24 h. On standing in a desiccator with P_2O_5 for more than 7 days, $FeH_6(PO_4)_3$ is further dehydrated to give the B form of $Fe(H_2PO_4)_3$. This suggests that the changes of the B form of $Fe(H_2PO_4)_3$ into $FeH_6(PO_4)_3$ and amorphous iron phosphate caused by moisture absorption may be reversible. The A form of

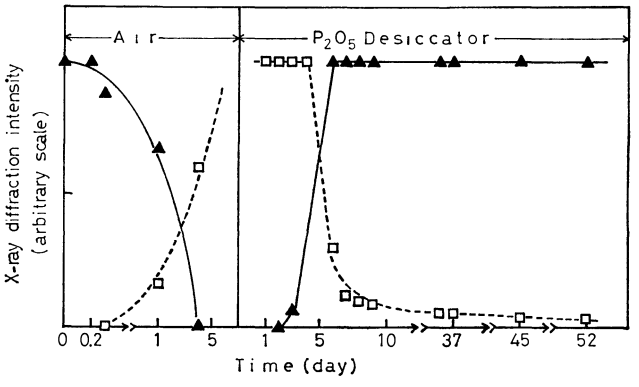

Fig. 6a. Structural change of iron phosphate in various humid atmospheres.
—▲—: $Fe(H_2PO_4)_3$(B), ···□···: $FeH_6(PO_4)_3$.

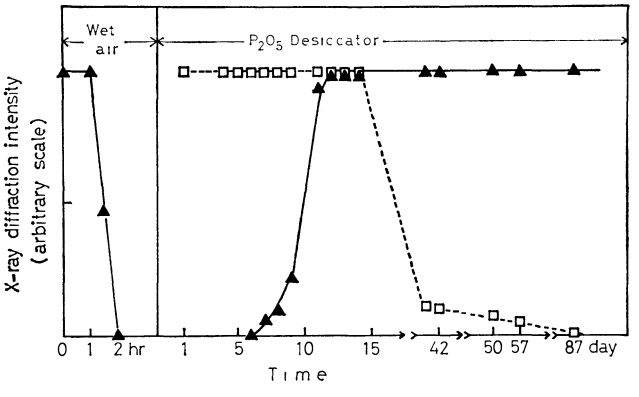

Fig. 6b. Structural change of iron phosphate in various humid atmospheres.
—▲—: $Fe(H_2PO_4)_3$(B), ···□···: $FeH_6(PO_4)_3$.

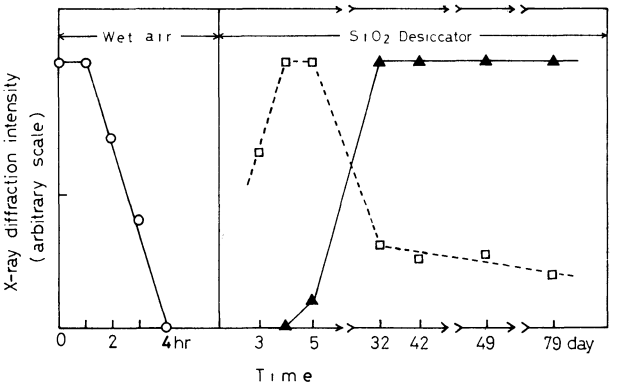

Fig. 6c. Structural change of iron phosphate in various humid atmospheres.
—○—: $Fe(H_2PO_4)_3$ (A), --▲--: $Fe(H_2PO_4)_3$ (B), —□—: $FeH_6(PO_4)_3$.

$Fe(H_2PO_4)_3$, as seen from Fig. 6c, is rapidly transformed into amorphous phosphate on standing in wet air, a result similar to that for the B form. Amorphous iron phosphate, on standing in a desiccator with silica gel, is transformed into $FeH_6(PO_4)_3$, which, beginning on the fifth day, is gradually transformed into the B form of $Fe(H_2PO_4)_3$ over a long time. $FeH_6(PO_4)_3$, on standing in a desiccator with P_2O_5, is transformed into the B form of $Fe(H_2PO_4)_3$, beginning on the third day and almost completely within two weeks. It is of interest that the A form of $Fe(H_2PO_4)_3$ is transformed into amorphous iron phosphate or $FeH_6(PO_4)_3$ with moisture absorption, and by dehydration of $FeH_6(PO_4)_3$ in a desiccator with P_2O_5 or silica gel, the B form and not the A form of $Fe(H_2PO_4)_3$ is directly obtained. From these facts, it is suggested that changes in the structures of the A and B forms of $Fe(H_2PO_4)_3$ caused by moisture absorption are completely different from each other.

From the results shown in Fig. 6, it is suggested that $FeH_6(PO_4)_3$ may contain more water than the A and B forms of $Fe(H_2PO_4)_3$. Based on the reversible change between $FeH_6(PO_4)_3$ and $Fe(H_2PO_4)_3$ structures caused by moisture absorption, it may be more reasonable to regard $FeH_6(PO_4)_3$ as another form of $Fe(H_2PO_4)_3$ since the A and B forms of $Fe(H_2PO_4)_3$ are isomorphous with the A and B forms of $Al(H_2PO_4)_3$, respectively. The existence of the C and D forms of $Al(H_2PO_4)_3$ other than the A and B forms has been reported,[11] while the C and D forms of $Fe(H_2PO_4)_3$, isomorphous with those of $Al(H_2PO_4)_3$, are unknown. Consequently, $FeH_6(PO_4)_3$ may be tentatively assigned the E form of $Fe(H_2PO_4)_3$. The experimental results are summarized schematically as follows:

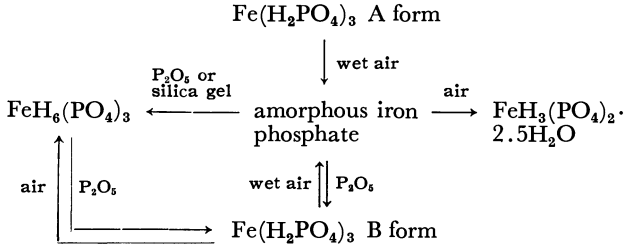

Amorphous iron phosphate obtained from the A and B forms of $Fe(H_2PO_4)_3$ and $FeH_6(PO_4)_3$ by moisture absorption gave crystalline $FeH_3(PO_4)_2 \cdot 2.5H_2O$ on standing in air over 20 days. This product may be formed by the hydrolysis of amorphous iron phosphate.

References

1) E. Erlenmeyer, *Ann.*, **194**, 176 (1878).
2) D. McConnell, *Am. Mineralogist*, **25**, 719 (1940).
3) H. Mori and T. Ito, *Acta Crystallogr.*, **3**, 1 (1950).
4) T. Ito and H. Mori, *Acta Crystallogr.*, **4**, 412 (1951).
5) L. Katz and W. N. Lipscomb, *Acta Crystallogr.*, **4**, 345 (1951).
6) M. L. Lindberg and C. L. Christ, *Acta Crystallogr.*, **12**, 695 (1959).
7) R. J. Meyer, "Gmelins Handbuch der Anorganischen Chemie," Verlag Chemie·Gmbh·Weimheim/Bergstr. Teil A, 1965, pp. 306—308, 316.
8) S. R. Carter and N. Holt, *J. Chem. Soc.*, **123**, 2223 (1923).
9) R. F. Jameson and J. E. Salmon, *J. Chem. Soc.*, **1954**, 28.
10) E. Kobayashi, *Kogyo Kagaku Zasshi*, **73**, 1797 (1970).
11) F. d'Yvoire, *Bull. Soc. Chim. Fr.*, **1961**, 1762, 2277, 2283; **1962**, 1224, 1237, 1243; *C. R. Acad. Sci.*, **250**, 2213 (1960); **251**, 2182, 2958 (1960).
12) E. Kobayashi and T. Goto, *Kogyo Kagaku Zasshi*, **73**, 692 (1970).
13) M. Abe, *Bunseki Kagaku*, **23**, 1561 (1974).
14) J. P. Rawat and P. S. Thind, *Can. J. Chem.*, **54**, 1892 (1976).
15) M. Tsuhako, K. Hasegawa, T. Matsuo, I. Motooka, and M. Kobayashi, *Bull. Chem. Soc. Jpn.*, **48**, 1830 (1975).

Solvation of Anions in Solvent Mixtures as Deduced from the Rates of the Finkelstein Reaction

Yasuhiko KONDO,* Akira NISHIKATA, Akiteru YOSHIOKA, and Niichiro TOKURA

Department of Applied Chemistry, Faculty of Engineering, Osaka University, Suita, Osaka 565

(Received July 19, 1978)

The Finkelstein reaction has been studied in five dipolar aprotic–dipolar aprotic solvent mixtures and one protic–dipolar aprotic solvent mixture. The theoretical equations for the rate constant as a function of solvent composition derived previously have been reformulated in terms of the solvent exchange model on the solvation site, taking into account the two main features of solvation: the number of the solvation sites on the solvent molecule and the equilibrium constant for the solvent exchange process. The results obtained previously, together with present results, are comprehensively discussed and the solvent mixtures are classified into four groups from the viewpoint of solute-solvent interaction in the region near the ion, using derived theoretical equations.

Thermodynamics of transfer of a single ion from one solvent to another as expressed in terms of a solvent activity coefficient has been accepted as an important criteria, when discussing solvent effects on reaction rates and mechanisms in solution.[1,2] In the course of the development of the concept, most attention seems to have been paid to the hydrogen bonding interaction, and polarizability effects, between solute and solvent. Even though this is quite useful in discussing the gross features of a solute in pure solvents, more sophisticated versions on the solute-solvent interactions in the vicinity of an ionic solute are required, when analyzing chemical phenomena in mixed solvents.[3,4]

In previous papers[5,6] we have dealt with the analysis of reaction rates of the Finkelstein reaction in acetonitrile–protic solvent mixtures from the viewpoint of the specific solvation of the anion in the solvent mixtures. In the present work we set up a generalized model for describing the cluster distribution of anion solvates in solvent mixtures, and derive the theoretical equations for the reaction rate in solvent mixtures on the basis of the model. By the mathematical analysis of reaction rates in solvent mixtures, solvent mixtures are classified into four groups from the viewpoint of ion-solvent interactions in the region near the ion.

Experimental

Materials: *N,N*-Dimethylacetamide, Wako's guaranteed reagent, was distilled from barium oxide and from calcium hydride under reduced pressure. Ethyl methyl ketone, Wako's extra pure reagent, was distilled twice after storage over anhydrous sodium sulfate. γ-Butyrolactone, Wako's extra pure reagent, was distilled twice under reduced pressure after storage over calcium hydride. Sulfolane, Wako's reagent, was distilled three times under reduced pressure after storage over sodium hydroxide. Propylene carbonate, Wako's extra pure reagent, was stored over freshly activated molecular sieves and distilled twice under reduced pressure. Other materials were treated as described elsewhere.[5]

Kinetic measurements and calculations were carried out as described elsewhere.[5]

Density measurements were performed with a glass dilatometer consisting of a bulb and two graded stems (*ca.* 40 ml capacity).

Densities and rate constants are summarized in Tables 1 and 2.

Results and Discussion

Activation Parameters in Pure Solvents and the Solvent Activity Coefficients of Bromide Ion. Rate constants and activation parameters in pure solvents are summarized in Table 3. They change according to solvents

TABLE 1. DENSITIES OF SOLVENT MIXTURES (30 °C)

N,N-Dimethylacetamide–acetonitrile mixtures		Ethyl methyl ketone–sulfolane mixtures		Ethyl methyl ketone–propylene carbonate mixtures		Ethyl methyl ketone–acetonitrile mixtures		Ethyl methyl ketone–γ-butyrolactone mixtures	
x_{DMA}	d	x_{EMK}	d	x_{EMK}	d	x_{EMK}	d	x_{EMK}	d
1.0	0.9319	1.0	0.7948	1.0	0.7948	1.0	0.7948	1.0	0.7948
0.90	0.9232	0.90	0.8487	0.90	0.8345	0.80	0.7927	0.90	0.8251
0.80	0.9133	0.75	0.9262	0.75	0.8952	0.65	0.7906	0.75	0.8716
0.70	0.9022	0.50	1.0480	0.50	0.9951	0.50	0.7878	0.50	0.9516
0.60	0.8899	0.25	1.1604	0.25	1.0951	0.35	0.7842	0.25	1.0341
0.50	0.8761	0.0	1.2622	0.0	1.1945	0.15	0.7778	0.0	1.1192
0.40	0.8604					0.0	0.7713		
0.30	0.8426								
0.20	0.8221								
0.10	0.7986								
0.0	0.7713								

TABLE 2. RATE CONSTANTS IN SOLVENT MIXTURES (30 °C)

Acetonitrile–methanol mixtures			*N*,*N*-Dimethylacetamide –acetonitrile mixtures		
x_{AN}	EtI+Br⁻ $k\times10^5$	EtBr+I⁻ $k\times10^5$	x_{DMA}	EtI+Br⁻ $k\times10^2$	*i*-PrI+Br⁻ $k\times10^4$
1.0	1050	59.3	1.0	62.5	154.2
0.90	70.7	18.5	0.90	—	107.4
0.80	24.1	9.67	0.80	27.8	—
0.60	7.60	5.42	0.70	—	45.0
0.40	3.78	3.69	0.60	12.1	—
0.20	1.89	2.39	0.50	—	22.3
0.0	1.01	2.05	0.40	5.01	—
			0.30	—	10.6
			0.20	2.37	—
			0.10	—	5.42
			0.0	1.05	3.98

Ethyl methyl ketone –propylene carbonate mixtures		Ethyl methyl ketone –sulfolane mixtures	
x_{EMK}	EtI+Br⁻ $k\times10^2$	x_{EMK}	EtI+Br⁻ $k\times10^2$
1.0	58.1	1.0	58.1
0.90	19.2	0.90	34.5
0.75	7.98	0.75	24.9
0.50	3.84	0.50	16.9
0.25	2.92	0.25	13.0
0.0	2.21	0.0	10.5

Ethyl methyl ketone –acetonitrile mixtures		Ethyl methyl ketone –γ-butyrolactone mixtures	
x_{EMK}	EtI+Br⁻ $k\times10^2$	x_{EMK}	EtI+Br⁻ $k\times10^2$
1.0	58.1	1.0	58.1
0.80	23.2	0.90	37.0
0.65	11.6	0.75	26.2
0.50	5.98	0.50	16.2
0.35	3.57	0.25	13.1
0.15	1.80	0.0	8.83
0.0	1.05		

k; 1.0 mol^{-1}·s^{-1}.

without any clear pattern, except for methanol solvent, in which the enthalpy term is the predominant factor responsible for the much reduced rate.

As summarized in Table 4, logarithmic relative rates are well correlated with the single ion solvent activity coefficient of bromide ion, for both protic and dipolar aprotic solvents.[7–9] The transition state anion-neutral molecule assumption[1,7] was used to obtain the bromide ion activity coefficient.[1]

The sensitivity of a bulky transition state to a change in solvent is believed to be less than that of a compact reactant anion in solvent mixtures as well as in pure solvents.[1] The principal feature of the log k_{mix} *vs.* composition profile (Figs. 1, 2, and 3) should be ascribed to the change in the solvation of a reactant anion, even though there must be differences in the solvent activity coefficient of the transition state.

TABLE 3. RATE CONSTANTS AND ACTIVATION PARAMETERS FOR THE REACTION OF ETHYL IODIDE WITH BROMIDE ION (30 °C)

Solvents	k (l·mol^{-1}·s^{-1})	$\Delta H^{\neq}$ (kcal·mol^{-1})	$\Delta S^{\neq}$ (cal·K^{-1}·mol^{-1})
N,*N*-Dimethylacetamide	6.25×10^{-1}	16.6	−4.74
Ethyl methyl ketone	5.81×10^{-1}	17.4	−2.25
γ-Butyrolactone	8.83×10^{-2}	16.3	−9.62
Propylene carbonate	2.21×10^{-2}	17.0	−10.06
Acetonitrile	1.05×10^{-2}	18.3	−7.25
Methanol	1.01×10^{-5}	22.7	−6.54

TABLE 4. RELATIVE RATES AND SOLVENT ACTIVITY COEFFICIENTS

Solvents	$\log(k/k_{AN})$	$\log {}^{0}\gamma^{S}_{Br^-}$
N,*N*-Dimethylacetamide	1.77	2.0[7]
Ethyl methyl ketone	1.74	2.5,[a,7] 2.35[a,8] 1.90,[a,9] 2.93[b]
Sulfolane	1.00	0.4,[7] 1.90[9]
γ-Butyrolactone	0.925	—
Propylene carbonate	0.323	0.5,[7] 0.367[9]
Acetonitrile	0	0
Methanol	−3.01	−2.3[7]

a) $\log {}^{0}\gamma^{S}_{Br^-}$ for acetone. b) Private communication from Dr. M. H. Abraham.

Reaction Rates in Binary Mixed Solvents. Thermodynamic Treatments: In the previous papers of this series[5,6] it was shown that the chemical equilibria and the reaction rates in binary mixed solvents could be reproduced by treating the solvation change of the respective solute in terms of *m* successive solvent exchange processes.

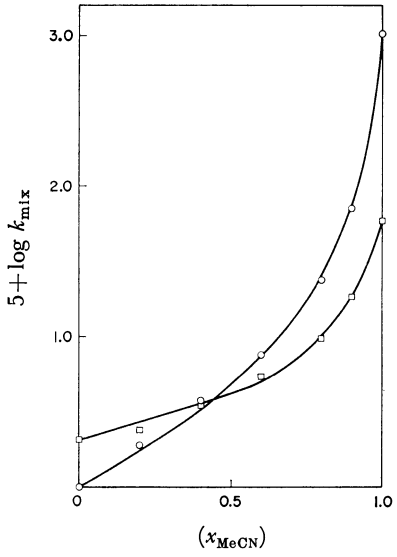

Fig. 1. Plots of log k_{mix} *vs.* mole fraction of acetonitrile (in MeOH–MeCN mixtures).
○; Experimental results for EtI+Br⁻, ——; calculated at $K_{se,1}=75.0$, $K_{se,2}=7.16$, $K_{se,3}=1.49$ in Eq. 5. □; Experimental results for *i*-PrI+I⁻, ——; calculated at $K_{se,1}=22.3$ in Eq. 5.

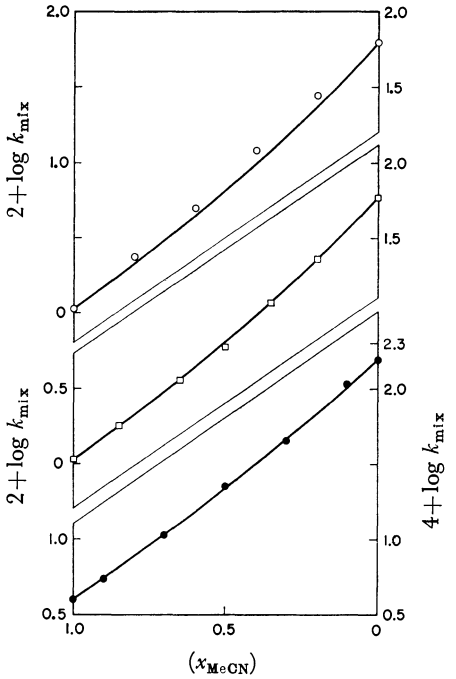

Fig. 2. Plots of log k_{mix} *vs.* mole fraction of acetonitrile. ○: Experimental results for EtI+Br^- in DMA–AN mixtures, ——: calculated at $K_{se,1}=1.80$ in Eq. 7. □: Experimental results for EtI+Br^- in EMK–AN mixtures, ——: calculated at $K_{se,1}=1.79$ in Eq. 7. ●: Experimental results for *i*-PrI+Br^- in DMA–AN mixtures, ——: calculated at $K_{se,1}=1.68$ in Eq. 7.

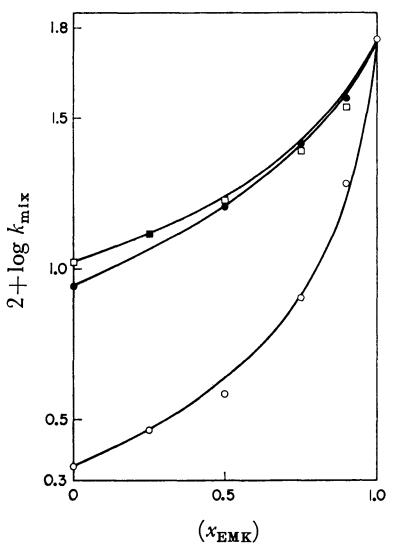

Fig. 3. Plots of log k_{mix} *vs.* mole fraction of methyl ethyl ketone.
□: Experimental results for EtI+Br^- in EMK–$TMSO_2$ mixtures, ——: calculated at $K_{bs,2}=4.81$ in Eq. 11. ●: Experimental results for EtI+Br^- in EMK–γ-BL mixtures, ——: calculated at $K_{bs,2}=4.58$ in Eq. 11. ○: Experimental results for EtI+Br^- in EMK–PC mixtures, ——: calculated at $K_{bs,2}=23.8$ in Eq. 11.

For formal simplicity of the derived equations it is necessary to assume that the true solvation number of a solute,[5] or the number of a solvation site Z° is an even integral value and that these sites are grouped into

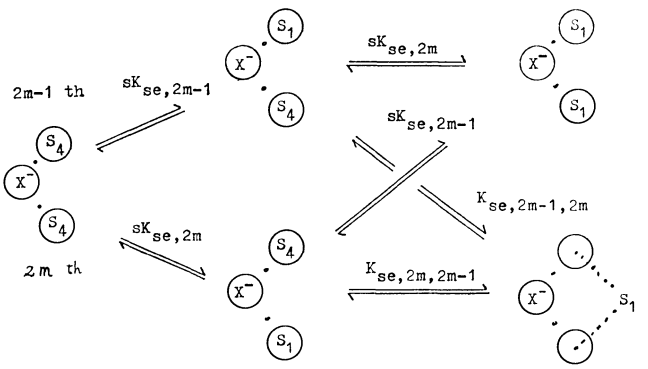

Scheme 1. Solvent exchange scheme on $2m-1$ th and $2m$ th solvation sites.

adjacent pairs of sites which are independent of each other in the respective pair, as well as of the members of other pairs.

As was suggested previously[6] and will be suggested also later, in some cases it is feasible that a solvent molecule can interact with a solute by simultaneously occupying a pair of solvation sites, if the solvent molecule contains multiple functional solvating groups. In the following treatment we will deal with the cluster distribution in solvent mixtures in which a component solvent, 4, has only one functional group, whereas a solvent, 1, has s equivalent functional groups.

Consider the frequencies of occupation of a given pair of sites which are referred to as $2m-1$ th and $2m$ th solvation site on the basis of the above solvent exchange scheme, where $K_{se,2m-1}$ and $K_{se,2m}$ refer to the equilibrium constants for the solvent exchange process on the $2m-1$ th and the $2m$ th solvation site, and $K_{se,2m-1,2m}$ refers to that of the bidentate solvent exchange process.

The number of ways of occupation of the solvation site is given as follows:

S_4 on both $2m-1$ th and $2m$ th site; x_4^2

S_4 on $2m-1$ th and S_1 on $2m$ th site; $sK_{se,2m}x_1x_4$

S_1 on $2m-1$ th and S_4 on $2m$ th site; $sK_{se,2m-1}x_1x_4$

different S_1 molecules on both $2m-1$ th and $2m$ th site; $s^2K_{se,2m-1}K_{se,2m}x_1^2$

same S_1 molecule on both $2m-1$ th and $2m$ th site; $sK_{se,2m-1}K_{se,2m-1,2m}x_1=sK_{se,2m}K_{se,2m,2m-1}x_1$

When the average monodentate and bidentate solvation equilibrium constants, $K_{ms,2m}$ and $K_{bs,2m}$ are defined by the equations,

$$K_{ms,2m} = (K_{se,2m-1}K_{se,2m})^{1/2}$$

$$K_{bs,2m} = (K_{se,2m-1,2m}K_{se,2m,2m-1})^{1/2}$$

the distribution of cluster as defined by the way of occupation of Z° solvation sites on a solute, M, is given by the equation,

$$\prod_{m=1}^{Z^\circ/2}\{(x_4+sK_{se,2m-1}x_1)(x_4+sK_{se,2m}x_1)+sK_{ms,2m}K_{bs,2m}x_1\}. \quad (1)$$

The activity coefficient of a solute, M, in the solvent mixture, $\beta_{M,mix}$, is given by the equation derived in the previous paper,[5]

$$\lim_{x_M\to 0}\beta_{M,mix} = f_M^\circ/[1+K_0\prod_{m=1}^{Z^\circ/2}\{(x_4+sK_{se,2m-1}x_1)(x_4+sK_{se,2m}x_1) + sK_{ms,2m}K_{bs,2m}x_1\}](V_{mix}/RT) \quad (2)$$

where f_M° is the fugacity of equibrated vapor of a pure solute, M,[5] and V_{mix} is the mean molar volume of the mixed solvent; K_0 is the equilibrium constant for the reaction,

$$M + Z^\circ S_4 = M\cdot(S_4)_{Z^\circ}.$$

As was mentioned above and discussed elsewhere,[1,5] the rate of the Finkelstein reaction seems to be predominantly controlled by the solvation of a nucleophile. Thus, by the same procedure as described in the previous paper,[5] the rate constants in solvent mixtures, k_{mix}, and the ratio of the rate constants in solvent 4 and 1, (k_4/k_1), are given by the equations,

$$\ln k_{mix} = \ln k_1 + \ln \prod_{m=1}^{Z^\circ/2} (s^2K_{se,2m-1}K_{se,2m} + sK_{ms,2m}K_{bs,2m}) - \ln \prod_{m=1}^{Z^\circ/2} \{(x_4 + sK_{se,2m-1}x_1)(x_4 + sK_{se,2m}x_1) + sK_{ms,2m}K_{bs,2m}x_1\} + \ln (V_{mix}/V_1) \quad (3)$$

$$(k_4/k_1) = \prod_{m=1}^{Z^\circ/2} (s^2K_{se,2m-1}K_{se,2m} + sK_{ms,2m}K_{bs,2m}) \times (V_4/V_1) \quad (4)$$

where V_4 and V_1 stand for the molar volumes of solvents 4 and 1.

Comparisons with the Experimental Results. Case I. Alcohol and Acetonitrile Mixtures (Fig. 1): Both alcohol and acetonitrile contain only one functional group each. Thus, by setting s equal to unity, and $K_{bs,2m}$ equal to zero, Eqs. 3 and 4 reduce to Eqs. 5 and 6, which are the same formulae as derived previously.[5]

$$\ln k_{mix} = \ln k_1 + \ln \prod_{m=1}^{Z^\circ} K_{se,m} - \ln \prod_{m=1}^{Z^\circ} (x_4 + K_{se,m}x_1) + \ln (V_{mix}/V_1) \quad (5)$$

$$(k_4/k_1) = \prod_{m=1}^{Z^\circ} K_{se,m}(V_4/V_1) \quad (6)$$

Equation 6 gives the boundary conditions for $\prod_{m=1}^{Z^\circ} K_{se,m}$. Under these conditions, the theoretical values of the rate constants were obtained as a function of the solvent compositions on the basis of Eq. 5 for a definite set of Z° and $K_{se,2m}$'s. The calculations were repeated by a trial and error-method, systematically changing the equilibrium constants for the respective solvation number and afterwards for the different values of Z°.

In applying Eqs. 5 and 6 to the experimental data, only those equilibrium constants which are larger than unity are detectable from the solvent exchange studies,[5] since the term $x_4 + K_{se,m}x_1$ reduces to unity when $K_{se,m}$ becomes unity.[5]

One noticeable trend observed in the solvent mixtures is a large attenuation effect in $K_{se,m}$ as described previously.[5] Similar effects were observed in Ag^+ solvation exchange studies in *N,N*-dimethylthioformamide–propylene carbonate, $-H_2O$, and –acetonitrile mixtures.[10] Similar but rather smaller attenuation effects were also observed in NMR chemical shift studies in solvent mixtures.[11] Throughout these studies, the solvent exchange processes with up to four steps are sufficient to reproduce the data.[5,10,11]

In alcoholic and dipolar aprotic solvents, only proton and first row elements can interact with the anion. These have respective Slater orbital exponents which crucially effect the interaction distances between ion and solvents. The variation in the interaction distances, which would alternatively be stated as a change in the degree of covalency in the interaction,[10] is the predominant feature with regard to the inequivalence of the respective solvation sites.

Case II. Acetonitrile–Ethyl Methyl Ketone, and N,N-*Dimethylacetamide Mixtures (Fig. 2)*: These component solvents contain only one solvation site each as in case I. In contrast, experimental results were reproduced by taking the same equilibrium constant throughout the solvent exchange processes concerned and by taking the number of solvation site as equal to a normal coordination number, *i.e.*, six,[12] as expressed in Eqs. 7 and 8.

$$\ln k_{mix} = \ln k_1 + \ln (K_{se,1})^6 - \ln (x_4 + K_{se,1}x_1)^6 + \ln (V_{mix}/V_1), \quad (7)$$

$$(k_4/k_1) = (K_{se,1})^6(V_4/V_1). \quad (8)$$

Similar patterns of solution phenomena *vs.* composition profile were observed previously,[10,13] where the pattern was designated as binomial distribution of cluster.

In the solvent mixtures of this class, all the component solvents retain first row elements as a binding site with the anion. Their Slater orbital exponents resemble each other in magnitude, thus leading to a similar interaction distance with the anion. This can be considered as a major factor in indiscriminating the essentially inequivalent solvation sites.

Case III. Glycol–Acetonitrile Mixtures: In glycol two hydroxyl groups are available for interaction with the anion, so that s is equal to 2. When a pair of sites are considered as approximately equivalent to one another, and only one pair of sites contribute predominantly to the total solvation exchange, that is to say the contributions from the remaining sites are minor and masked by the much larger terms from the first pair of sites, then Eqs. 3 and 4 reduce to Eqs. 9 and 10, since for the other pair of sites, the term, $\{(x_4 + 2K_{ms,2m}x_1)^2 + 2K_{ms,2m}K_{bs,2m}x_1\}$, should be equal to unity irrespective of the value, x_1.

$$\ln k_{mix} = \ln k_1 + \ln \{2K_{ms,2}(2K_{ms,2} + K_{bs,2})\} - \ln \{(x_4 + 2K_{ms,2}x_1)^2 + 2K_{ms,2}K_{bs,2}x_1\} + \ln (V_{mix}/V_1). \quad (9)$$

$$(k_4/k_1) = 2K_{ms,2}(2K_{ms,2} + K_{bs,2})(V_4/V_1). \quad (10)$$

Equations 9 and 10 are equivalent to those derived previously on a less sophisticated basis.[6] Rates *vs.* composition profile in five glycol–acetonitrile mixtures were satisfactorily reproduced by these equations.[6]

Case IV. Propylene Carbonate–, Sulfolane–, and γ-Butyrolactone–Ethyl Methyl Ketone Mixtures (Fig. 3): Propylene carbonate, sulfolane and γ-butyrolactone each have multiple solvation sites. When the same conditions as mentioned in case III also hold for the solvent mixtures of this class, Eqs. 9 and 10 would apply to the present cases. As a matter of fact, experimental results were satisfactorily reproduced by the simplest formulae *i.e.*, Eqs. 11 and 12 as obtained by setting $sk_{ms,2m}=1$ for $m \geqq 1$ in Eqs. 9 and 10.

$$\ln k_{mix} = \ln k_1 + \ln (1+K_{bs,2}) - \ln (1+K_{bs,2}x_1) + \ln (V_{mix}/V_1), \quad (11)$$

$$(k_4/k_1) = (1+K_{bs,2})(V_4/V_1). \quad (12)$$

They are formally equivalent to the formulae as derived from Eqs. 5 and 6 under the conditions, $K_{se,m}=1$ for $m \geqq 2$. Thus, on purely mathematical grounds, the present systems are indistinguishable from the systems stet case I. Other mechanistic criteria are necessary in order to establish the solvation pattern. On the basis of the results of model CNDO/2 calculations,[14] the present systems would preferably be classified as a special case of a concurrent monodentate-bidentate solvation system, *i.e.*, the special case of case III.

In acetonitrile and propylene carbonate, rate constants and activation parameters are quite similar in value (Table 3), and do not indicate any marked mechanistic difference for Finkelstein reactions in the two solvents; the activity coefficient for bromide ion (Table 4) is also nearly the same in these solvents.

However, logarithmic rate *vs.* composition profiles are quite different for systems containing acetonitrile or propylene carbonate (*e.g.* for the acetonitrile–ethyl methyl ketone and propylene carbonate–ethyl methyl ketone systems). The use of solvent mixtures and the mathematical analysis of the results have thus provided information on solute-solvent interactions in the vicinity of the bromide ion that cannot be obtained from studies of data in the two pure single solvents.

We wish to thank Dr. M. H. Abraham, University of Surrey, England for his discussions and for his comments on the original version of the manuscript.

References

1) A. J. Parker, *Chem. Rev.*, **69**, 1 (1969).
2) M. H. Abraham, "Progress in Physical Organic Chemistry," Wiley-Interscience, New York (1974), Vol. 11, p. 1.
3) J. Padova, "Modern Aspects of Electrochemistry," No. 7 ed by B. E. Conway and J. O'M. Bockris, Plenum Press, New York (1972), p. 1.
4) W. L. Marshall, *J. Phys. Chem.*, **76**, 720 (1972).
5) Y. Kondo, T. Kato, and N. Tokura, *Bull. Chem. Soc. Jpn.*, **48**, 285 (1975).
6) Y. Kondo, K. Tanaka, and N. Tokura, *ibid.*, **49**, 3100 (1976).
7) R. Alexander, A. J. Parker, J. H. Sharp, and W. E. Waghorne, *J. Am. Chem. Soc.*, **94**, 1148 (1972).
8) M. H. Abraham, and A. F. D. de Namor, *J. Chem. Soc., Faraday Trans. 1*, **72**, 955 (1976).
9) M. Salomon, *J. Phys. Chem.*, **79**, 2000 (1975).
10) G. Clune, W. E. Waghorne, and B. G. Cox., *J. Chem. Soc., Faraday Trans. 1*, **72**, 1294 (1976).
11) A. K. Covington, and J. M. Thain, *J. Chem. Soc., Faraday Trans. 1*, **70**, 1879 (1974).
12) H. G. Hertz, *Angew. Chem.*, **82**, 91 (1970).
13) A. K. Covington, K. E. Newman, and T. H. Lilly, *J. Chem. Soc., Faraday Trans. 1*, **69**, 973 (1973).
14) Y. Kondo, unpublished results.

Crystal and Molecular Structure of Mitomycin C, an Anticancer Antibiotic

Keizo OGAWA,* Akiko NOMURA, Takaji FUJIWARA, and Ken-ichi TOMITA

Faculty of Pharmaceutical Sciences, Osaka University, Yamada-kami, Suita, Osaka 565

(Received August 28, 1978)

The crystal structure of mitomycin C was determined by means of X-ray diffraction. Mitomycin C was crystallized in the orthorhombic space group $P2_12_12_1$, with $a=12.887$, $b=13.851$, $c=9.718$ Å, and $Z=4$, and its structure solved by the trial and error method using the rigid-body approximation. The absolute configuration was determined by referring to that of *N*-(*p*-bromobenzoyl)mitomycin C. The carbamoyloxymethyl side chain participates in hydrogen bonds as in the case of other mitomycins in the crystalline state.

Mitomycins extracted from Streptomyces species, known to be antibiotics having anticancer activity, have the chemical structures shown in Fig. 1. Mitomycins were found to crosslink to double-stranded DNA by covalent bonds and to inhibit a duplication of DNA.[1] Szybalski and Iyer proposed that atoms C1 and C10 of mitomycin bind covalently to atoms O6 of guanine bases of the DNA duplex after enzymic reduction.[2] An intercalative model of mitomycin with DNA in the form of a semiquinone radical followed by the covalent bond formation was proposed by Tomatz *et al.*,[3] who stated that mitomycin might interact specifically with double-stranded polynucleotides, since no complex formation of the antibiotic with monomeric nucleotides or guanylyl(3′,5′)cytidine was observed. A recent CD study showed that mitomycin might interact with the fragment having the GpC(deoxyguanosine-phosphate-deoxycytidine) base sequence in DNA.[4]

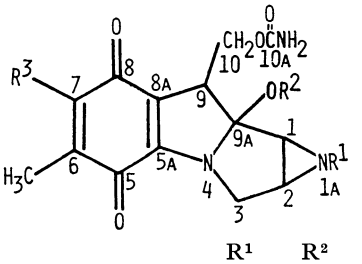

	R^1	R^2	R^3
mitomycin A	H	CH_3	OCH_3
N-methyl-mitomycin A	CH_3	CH_3	OCH_3
mitomycin B	CH_3	H	OCH_3
mitomycin C	H	CH_3	NH_2
porfiromycin	CH_3	CH_3	NH_2
7-hydroxyl-porfiromycin	CH_3	CH_3	OH

Fig. 1. Structures of mitomycins and porfiromycins.

This paper deals with the three-dimensional structure analysis of mitomycin C, and a structural comparison with *N*-brosylmitomycin A,[5] 7-demethoxy-7-(*p*-bromoanilino)mitomycin B[6] and *N*-(*p*-bromobenzoyl)mitomycin C.[7]

Experimental

Mitomycin C crystallized in the form of dark violet plates from a 50% aqueous ethanol solution. Oscillation and Weissenberg photographs showed the crystal to be orthorhombic with the space group $P2_12_12_1$. The crystallographic data are given in Table 1. The density measurement made by a floatation method using a benzene–carbon tetrachloride mixture revealed that an asymmetric unit contains one mitomycin C and two water molecules.

Table 1. Crystal data

Formula	$C_{15}H_{18}N_4O_5\cdot 2H_2O$
Formula weight	370.37
Crystal system	Orthorhombic
Space group	$P2_12_12_1$
a	12.887(2) Å
b	13.851(2) Å
c	9.718(1) Å
V	1734.6(3) Å^3
Z	4
D_m	1.423(4) Mg/m^3
D_x	1.418 Mg/m^3

Three-dimensional intensity data were collected on a computer-controlled four-circle diffractometer using Ni-filtered Cu $K\alpha$ radiation. Employing ω-2θ scan technique with a scan speed of 4°/min(2θ) and 10 s. background measurement at each end of the scan, 1145 independent structure factor magnitudes greater than three times their standard deviations were obtained within $\sin\theta/\lambda=0.547$ Å^{-1}.

Structure Determination and Refinement

Orientation of the molecule in the crystal was determined by the rigid group convolution and search method (RICS).† The coordinates of 17 atoms involving ring portion in 7-demethoxy-7-(*p*-bromoanilino)mitomycin B solved by Yahashi and Matsubara[6] were utilized as a model. The convolution calculated from the model having the benzoquinone ring vertical to the b-axis showed good agreement with the three-dimensional Patterson peaks around the origin. However, the translation search procedure failed to find the correct position in the crystal by employing the resultant model. This might be due to the peculiar molecular packing. Thus the R-map method was tried using a program written by one of the authors (K. O.). The minimum *R*-value (0.51) was obtained by translating the model having the C5A–C6 vector parallel to the c-axis. Using the coordinates of 17 atoms obtained by the above method, an electron density map was constructed to find all nonhydrogen atoms.

† The rigid group convolution and search programs were written by Dr. I. Tanaka.

Table 2. Final positional and thermal parameters with their estimated standard deviations in parentheses ($\times 10^4$)

Anisotropic temperature factors are of the form; $\exp[-(B_{11}h^2+B_{22}k^2+B_{33}l^2+B_{12}hk+B_{13}hl+B_{23}kl)]$.

	x	y	z	B_{11}	B_{22}	B_{33}	B_{12}	B_{13}	B_{23}
C1	3874(7)	5655(7)	2883(10)	43(6)	33(5)	91(12)	16(11)	0(16)	8(15)
C2	5019(8)	5500(7)	3045(10)	48(6)	42(6)	77(11)	1(11)	28(16)	26(15)
C3	5463(7)	6292(7)	3958(11)	32(6)	49(6)	87(12)	4(11)	31(16)	−14(15)
C5A	4194(6)	6769(6)	5880(9)	29(5)	30(5)	40(9)	−4(9)	8(12)	0(12)
C5	4919(7)	6867(7)	7043(9)	32(5)	46(6)	70(11)	1(10)	−7(15)	16(15)
C6	4464(7)	6941(7)	8441(9)	39(5)	44(6)	62(10)	−12(11)	−18(15)	17(14)
C7	3392(7)	6941(6)	8564(9)	40(6)	35(5)	54(10)	3(10)	−11(14)	−8(13)
C8	2681(7)	6841(6)	7341(9)	34(5)	33(5)	58(10)	−9(9)	−10(14)	11(13)
C8A	3141(6)	6741(6)	6013(9)	32(5)	34(5)	40(9)	−3(9)	−6(13)	1(12)
C9	2631(8)	6610(7)	4615(9)	30(6)	39(6)	51(9)	−1(10)	−8(13)	3(13)
C9A	3602(7)	6587(6)	3654(8)	44(6)	26(5)	35(9)	0(9)	−9(13)	−13(11)
C10	1965(7)	5688(8)	4636(10)	42(7)	54(6)	57(10)	−29(12)	−27(14)	3(16)
C10A	497(7)	5631(7)	3125(10)	34(6)	50(6)	75(11)	−3(11)	−9(15)	−19(16)
C11	5155(8)	7029(9)	9667(10)	53(7)	80(8)	58(11)	−23(14)	−41(16)	22(18)
C12	3544(9)	8296(7)	3020(11)	84(9)	35(5)	101(13)	−20(13)	−13(21)	3(16)
N1A	4255(6)	4882(6)	3835(9)	50(6)	45(5)	98(11)	4(9)	−16(14)	−1(13)
N4	4503(5)	6733(5)	4550(8)	27(4)	39(4)	63(9)	0(8)	−3(11)	1(11)
N7	2876(7)	7051(7)	9746(8)	53(6)	68(6)	56(9)	−1(11)	12(13)	−1(13)
N14	177(6)	5515(6)	1800(8)	51(6)	55(5)	72(9)	1(10)	−21(13)	1(11)
O5	5859(5)	6915(5)	6873(7)	36(4)	74(5)	91(9)	−21(8)	−16(11)	3(12)
O8	1734(4)	6830(5)	7548(7)	35(4)	51(4)	70(7)	8(7)	11(10)	0(10)
O9	3553(5)	7289(4)	2583(6)	56(4)	31(3)	61(7)	2(7)	−11(11)	10(9)
O10	1531(5)	5584(5)	3218(6)	35(4)	59(4)	59(7)	−11(8)	−8(10)	−14(10)
O13	−68(6)	5776(6)	4093(8)	58(5)	99(7)	90(9)	7(11)	−6(12)	−59(14)
OW1	−2172(6)	5436(7)	3855(9)	54(5)	104(7)	147(11)	−19(11)	30(15)	−13(16)
OW2	−2111(7)	5671(7)	935(9)	87(7)	71(6)	161(12)	1(12)	−48(17)	10(16)

The structure was refined by the full-matrix least-squares method with isotropic temperature factors, and then by the block-diagonal least-squares method with anisotropic temperature factors for all nonhydrogen atoms. At this stage, difference Fourier synthesis was carried out, the result being unsatisfactory for full detection of hydrogen atoms. At the final refinement, following weighting scheme was employed; $w=0.0$ for $F_o=0.0$, $w=1.0$ for $F_o \leqq 45.0$, and $w=1.0/(1.0+0.235(F_o-45.0))$ for $F_o \leqq 45.0$. The final R-value is 0.080 for all reflections. The final atomic parameters are given in Table 2 with their estimated standard devia-

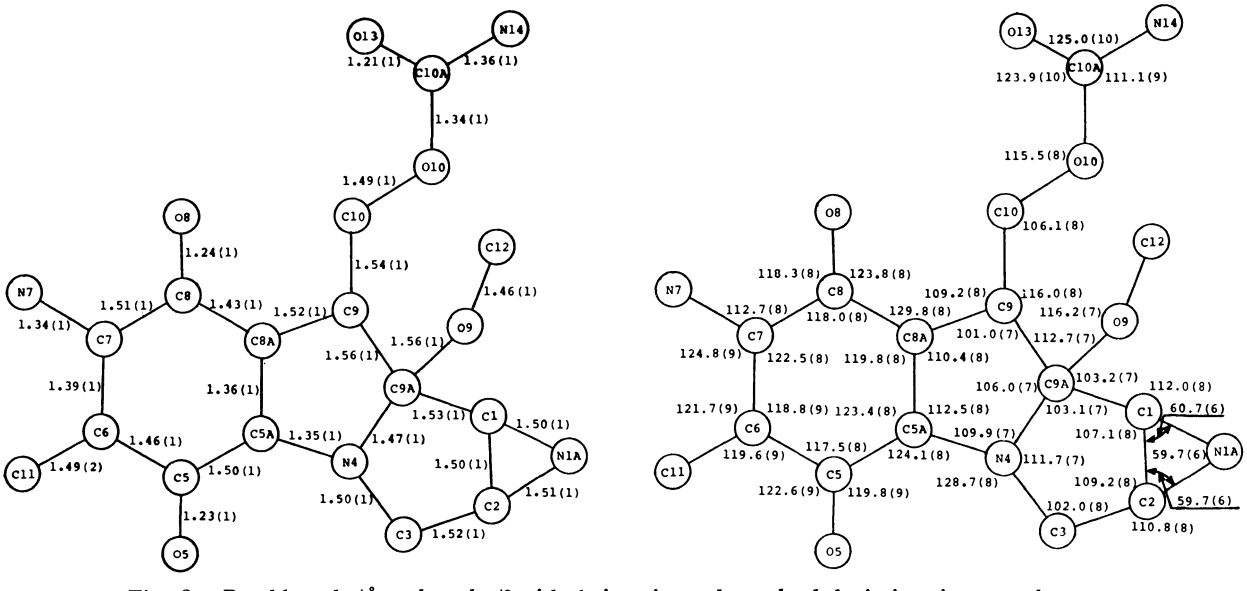

Fig. 2. Bond lengths/Å and angles/° with their estimated standard deviations in parentheses.

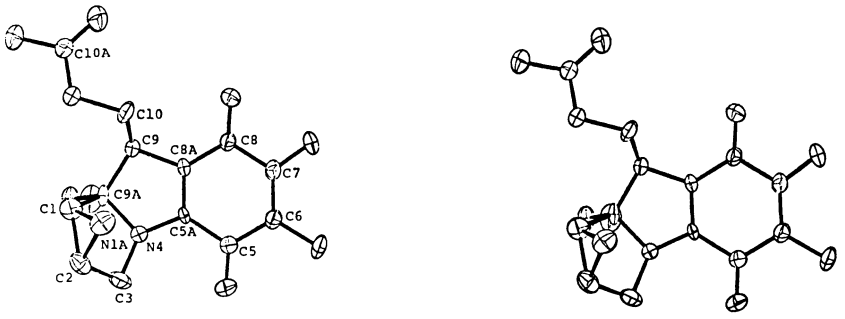

Fig. 3. Stereoscopic view of mitomycin C molecule.

tions. The observed and calculated structure factors are given in Table 3.†† The absolute configuration of mitomycin C was determined by referring to that of *N*-(*p*-bromobenzoyl)mitomycin C.[7]

The computations were performed on a NEAC 2200-700 computer at the Computing Center of this University, using Universal Crystallographic Computing System-Osaka.[8]

Results and Discussion

The bond lengths and angles are given in Fig. 2. A stereoscopic view of the mitomycin C molecule is shown in Fig. 3. The molecular geometry is essentially similar to that of the bromo derivative of mitomycin A,[5] exclusive of the conformation of the carbamoyloxymethyl side chain. The torsion angles of the side chain in four kinds of mitomycins are shown in Table 4. The variance among these torsion angles may be due to the difference in packing force acting on each molecule in the crystal, suggesting that the group is flexible in solution. The fact that the carbamoyl group of the side chain participates in intermolecular hydrogen bond formations, and the configuration of C9(R) is invariant in all cases,[5-7] seems to give valuable information on the interaction mechanism of mitomycin with DNA.

The strain of the indolequinone ring in mitomycins is dependent on the side chain configurations at positions C9 and C9A, *viz.*, the trans-arrangement of carbamoyloxymethyl and methoxy groups in mitomycins A and C

Table 4. Torsion angles in carbamoyloxymethyl side chain

	θ (C8A–C9–C10–O10)	ϕ (C9–C10–O10–C10A)	ψ (C10–O10–C10A–O13)
Br-A	179.5°	166.2°	1.8°
Br-B	298.5	160.1	344.8
Br-C	180.5	280.7	353.9
C	182.4	244.0	2.3

a) Angles are measured in the clockwise sence, faking the cis position as 0°. The notations θ, ϕ, and ψ are shown in Fig. 5. Br-A; *N*-brosylmitomycin A[5] Br-B; 7-demethoxy-7-(*p*-bromoanilino)mitomycin B[6] Br-C; *N*-(*p*-bromobenzoyl)mitomycin C[7] C; mitomycin C.

†† Table 3 is kept as a Document at the Office of The Chemical Society of Japan(Document No. 7925).

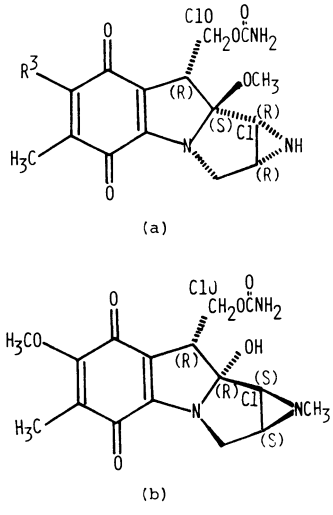

Fig. 4. Absolute configurations.
(a) Mitomycins A and C, (b) mitomycin B.

may release the intramolecular short contacts between these groups. The least-squares plane through the indolequinone ring including atoms C11 and N7 is represented by $-0.035x-0.994y-0.106z+5.225=0.0$. The mean deviation of the atoms from this plane is 0.024 Å, smaller than in mitomycin B (0.079 Å)[6] and close to that in mitomycin A(0.026 Å).[5] The configurations at C9A, C1, and C2 are, respectively, (S), (R), and (R) in mitomycins A[5] and C,[7] differing from those in mitomycin B[6] as shown in Fig. 4. Consequently, significant differences can be seen between the molecular structures of mitomycin B and mitomycins A or C,

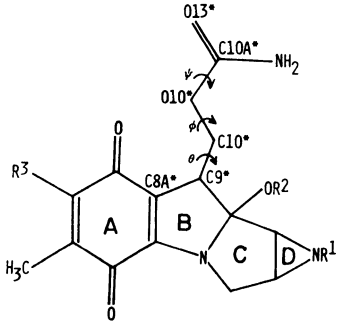

Fig. 5. Notations of torsion angles in carbamoyloxymethyl side chain and of the least-squares planes.

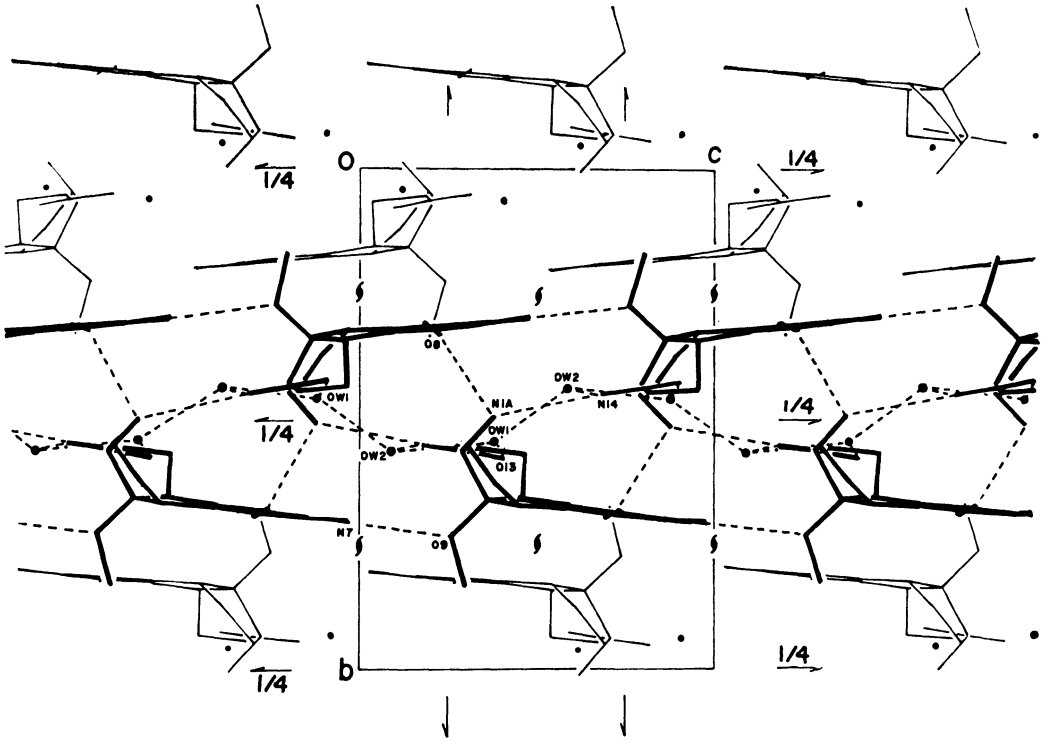

Fig. 6. Crystal structure of mitomycin C projected along the a-axis. Dashed lines and black circles indicate the hydrogen bonds and water oxygen atoms, respectively.

Table 5. Dihedral angles between the least-squares planes

Plane	Plane	Br-A[5]	Br-B[6]	Br-C[7]	C
A	B	3.7°	9.9°	4.4°	3.0°
A	C	133.9	115.7	137.8	135.3
A	D	54.0	41.0	57.4	54.8
B	C	131.1	123.5	133.4	134.2
B	D	53.4	47.2	54.4	53.5
C	D	98.4	100.0	97.4	97.9

The notations A, B, C, and D are shown in Fig. 5.

Table 6. Hydrogen bond distances and short contacts

Hydrogen bonds		Short contacts	
O13–OW1	2.76 Å	C5A–N14[a]	3.40 Å
N14–OW2	3.07	C5–N14[a]	3.30
OW1–OW2	2.86	O5–C10A[d]	3.44
O8–N1A[a]	2.96	O5–O9[d]	3.40
O9–N7[b]	2.92	C7–OW2[d]	3.41
N1A–N14[a]	3.03	N7–OW2[d]	3.23
OW1–OW2[e]	2.70	O13–C5[e]	3.46

Symmetry codes;

a) $\frac{1}{2}-x, 1-y, \frac{1}{2}-z$ b) $x, y, -1+z$

c) $-\frac{1}{2}-x, 1-y, \frac{1}{2}+z$ d) $\frac{1}{2}+x, \frac{3}{2}-y, 1-z$

e) $-\frac{1}{2}+x, \frac{1}{2}-y, 1-z$

especially in the dihedral angles between the least-squares planes given in Table 5. For example, in mitomycins A and C, the dihedral angles between planes B and C and between B and D become larger than those in mitomycin B, probably to avoid the short contact between C1 and C10.

The crystal structure is shown in Fig. 6. The molecules at the positions (x, y, z), $(x, y, 1+z)$, and $(1/2-x, -y, 1/2+z)$ are linked by seven intermolecular hydrogen bonds to form a double layered structure (Table 6 and Fig. 6). These layers are held together mainly by van der Waals forces. The indolequinone ring and carbamoyl group with atom O10 are almost vertical to the b-axis, the interplanar spacing being about one-eight of the b-axis dimesion.

A discussion on the interaction between mitomycin and the double-stranded DNA was given in a previous paper.[9] The intercalative model for the interaction of mitomycin with DNA could be built by using the space-filling model and the Kendrew-Watson skeletal model. As the atomic coordinates of base-pair and sugar-phosphate backbone of DNA, the structural data of B-DNA[10] and the crystalline complex of ethidium bromide (2,7-diamino-9-phenyl-10-ethylphenanthridinium bromide) and iodoCpG(5-iodocytidylyl(3′,5′)-guanosine)[11] were referred to.

Although a favorable intercalation model of mitomycin with the GpC fragment of the double-stranded DNA was obtained by examining the stacking and hydrogen bonding, further evidence is necessary before the validity of the intercalative model is discussed.

We thank Dr. Kazuo Yamaguchi for supplying atomic coordinates of *N*-(*p*-bromobenzoyl)mitomycin C.

References

1) W. Szybalski and V. N. Iyer, *Federation Proc.*, **23**, 946 (1964).
2) W. Szybalski and V. N. Iyer, "Antibiotics I. Mechanism of Action," ed by D. Gottlieb and P. D. Shaw, Springer Verlog, New York (1967), p. 211.
3) M. Tomatz, C. M. Mercado, J. Olson, and N. Chatterjie, *Biochemistry*, **13**, 4878 (1974).
4) C. M. Mercado and M. Tomatz, *Biochemistry*, **16**, 2040 (1977).
5) A. Tulinsky and J. H. Van den Hende, *J. Am. Chem. Soc.*, **89**, 2905 (1967).
6) R. Yahashi and I. Matsubara, *J. Antibiot.*, **29**, 104 (1976).
7) K. Yamaguchi *et al.*, private communication.
8) T. Ashida, "The Universal Crystallographic Computing System-Osaka," (1973).
9) K. Ogawa, A. Nomura, T. Fujiwara, and K. Tomita, *Nucl. Acids Res. Special Publication*, No. 3, s79 (1977).
10) S. Arnott and D. W. L. Hukins, *Biochem. Biophys. Res. Commun.*, **47**, 1504 (1972).
11) S. C. Jain, C. Tsai, and H. M. Sobell, *J. Mol. Biol.*, **114**, 317 (1977).

Relative Spin-trapping Ability of *N*-Benzylidene-*t*-butylamine Oxide, *N*-Benzylideneaniline Oxide, and 2,3,5,6-Tetramethylnitrosobenzene towards Phenyl and Phenylcyclohexadienyl Radicals

Mariko KAMIMORI,* Hirochika SAKURAGI, Katsuhiko SAWATARI,† Tadashi SUEHIRO,††
Katsumi TOKUMARU, and Masayuki YOSHIDA†

Department of Chemistry, The University of Tsukuba, Sakura-mura, Ibaraki 300-31
†*Department of Chemistry, Faculty of Science, The University of Tokyo, Hongo, Bunkyo-ku, Tokyo 113*
††*Faculty of Sciences, Gakushuin University, Mejiro, Toshima-ku, Tokyo 171*

(Received September 27, 1978)

N-Benzylidene-*t*-butylamine oxide (PBN), *N*-benzylideneaniline oxide (DPN), and 2,3,5,6-tetramethylnitrosobenzene (ND) trap phenyl radicals in a relative rate of 1: 0.72: 2.6, whereas they trap phenylcyclohexadienyl radicals in a relative rate of 1: 2.3: 130. The origin of such different spin-trapping abilities of these spin traps towards phenylcyclohexadienyl radicals is discussed.

The spin-trapping technique has been widely employed for the characterization of transient reactive free radicals, and various kinds of spin traps have been reported.[1] However, the spin-trapping abilities of various spin traps towards a given free radical have remained obscure.

It is well known that the thermal decomposition of phenylazotriphenylmethane (PAT) in benzene produces triphenylmethyl and phenyl radicals. The latter radicals add to benzene to give phenylcyclohexadienyl radicals, which subsequently either recombine or disproportionate with triphenylmethyl radicals, thus leading to 1,4-dihydro-4-triphenylmethylbiphenyl or triphenylmethane and biphenyl.[2] We have reinvestigated this reaction in the presence of such spin traps as *N*-benzylidene-*t*-butylamine oxide (*N*-*t*-butyl-α-phenylnitrone, PBN), *N*-benzylideneaniline oxide (α,*N*-diphenylnitrone, DPN), and 2,3,5,6-tetramethylnitrosobenzene (nitrosodurene, ND), and have found that while all these spin traps gave their spin adducts with phenyl radicals, only ND afforded the spin adduct with phenylcyclohexadienyl radicals also.[3] Obviously, these facts indicate that spin traps have different reactivities towards phenyl and phenylcyclohexadienyl radicals. In order to confirm this, we have undertaken to determine the relative spin-trapping ability of the spin traps towards phenyl and phenylcyclohexadienyl radicals by competitive methods; our results are described in this paper.

Results

Relative Reactivity of PBN, DPN, and ND towards Phenyl Radicals. PAT was allowed to decompose at a low conversion rate in carbon tetrachloride in the presence of PBN, DPN, and ND under an argon atmosphere at 80 °C. The subsequent examination of the reaction solution by ESR showed signals attributable to phenyl spin adducts of the respective spin traps,[4] along with those attributable to triphenylmethyl radicals. The signals attributable to the triphenylmethyl radicals disappeared on the exposure of the reaction solution to oxygen, but the signals of the nitroxides remained. With authentic specimens of the nitroxides, their stability against oxygen, prolonged heating, and the spin traps was confirmed. Since the nitroxides were produced only in minor amounts (*ca.* 10^{-7} mol l^{-1}), their scavenging by phenyl radicals under the present reaction conditions is very inconsiderable. These results enabled us to determine the relative reactivity of the spin traps towards phenyl radicals by the competitive method.

When PAT was decomposed in the presence of a mixture of PBN (1.5×10^{-2} mol l^{-1}) and DPN (5.0×10^{-3} mol l^{-1}) in carbon tetrachloride at 80 °C, the ESR signals due to the phenyl spin adducts of PBN and DPN (**1** and **2**) were observed (Scheme 1) (Fig. 1). The ratio

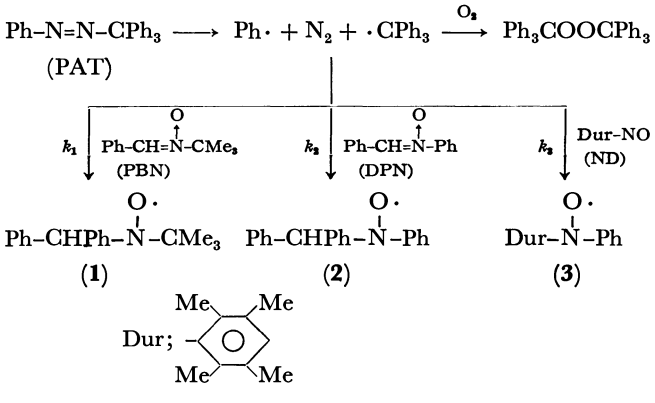

Scheme 1.

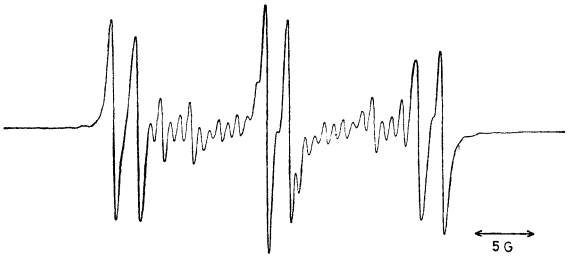

Fig. 1. The ESR spectrum of **1** and **2** obtained from the decomposition of PAT in carbon tetrachloride at 80 °C in the presence of PBN (5.0×10^{-3} M) and DPN (1.5×10^{-2} M). For **1**, a_N=14.1, $a_{\beta\text{-H}}$=2.1 G; for **2**, a_N=10.1, $a_{\beta\text{-H}}$=3.4, $a_{o,p\text{-H}}$=2.5, $a_{m\text{-H}}$=0.9 G.

of the concentrations of the two spin adducts ([**2**]/[**1**]) was obtained as 0.24 by means of the double integration of the ESR signals. Combining this value with the concentrations of PBN and DPN, the ratio of the rate constants of the addition of phenyl radicals to PBN (k_1) and DPN (k_2) was obtained as $k_2/k_1=0.72$ at 80 °C by the use of this equation: $[\mathbf{2}]/[\mathbf{1}]=k_2[\mathrm{DPN}]/k_1[\mathrm{PBN}]$. Triplicated runs afforded the same value within the limits of experimental error. At the concentrations of DPN$=5.0\times10^{-2}$ mol l^{-1} and PBN$=1.5\times10^{-2}$ mol l^{-1}, k_2/k_1 is 0.68 and is almost unchanged as to the relative concentrations of the spin traps.

The decomposition of dibenzoyl peroxide (BPO) in the presence of DPN (5.0×10^{-3} mol l^{-1}) and PBN (1.5×10^{-2} mol l^{-1}) in carbon tetrachloride gave their phenyl spin adducts in a ratio of [**2**]/[**1**]$=0.23$, which led to the value of k_2/k_1 ($=0.69$), similar to that obtained from PAT. Apparently, the relative reactivity towards phenyl radicals (k_2/k_1) is independent of the sources of phenyl radicals. Thus, the possibility that the nitroxides are scavenged by triphenylmethyl radicals concurrently formed in the decomposition of PAT can be disregarded. Accordingly, it is concluded that PBN traps phenyl radicals 1.4 times faster than does DPN.

Likewise, the decomposition of PAT in the presence of ND (4.9×10^{-3} mol l^{-1}) and PBN (5.2×10^{-3} mol l^{-1}) in carbon tetrachloride at 80 °C gave the phenyl spin adducts of ND (**3**) and PBN (**1**) in a ratio of [**3**]/[**1**]$=$ 2.5 (Fig. 2). This value leads to this ratio of the rate constants: $k_3/k_1=2.6$, in which k_3 is the rate constant for the addition of phenyl radicals to ND. The same value was obtained in the decomposition of BPO in the presence of ND (4.5×10^{-3} mol l^{-1}) and PBN (5.5×10^{-3} mol l^{-1}). Therefore, the rate constant for the addition of phenyl radicals to ND (k_3) is approximately 3 times larger than that to PBN (k_1) at 80 °C.

All the above reactions were carried out in carbon tetrachloride, from which phenyl radicals are known to abstract a chlorine atom to yield trichloromethyl radicals. However, none of the spectrum caused by the trichloromethyl spin adduct was hitherto observed. This finding suggests either that phenyl radicals add to the spin traps more rapidly than they abstract a chlorine atom from carbon tetrachloride or that trichloromethyl radicals are not efficiently captured by the spin traps. Therefore, it can safely be said that this side reaction, even if it occurs concurrently, does not affect the rate ratios, k_2/k_1 and k_3/k_1.

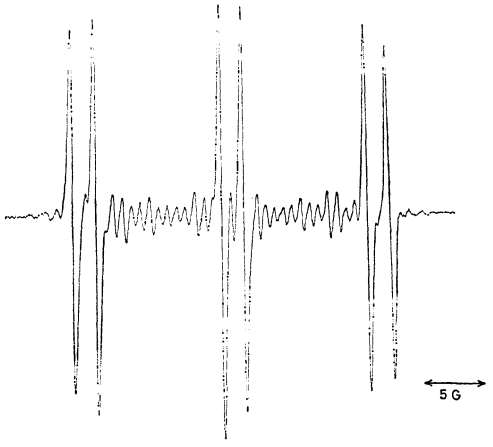

Fig. 2. The ESR spectrum of **1** and **3** obtained from the decomposition of PAT in carbon tetrachloride at 80 °C in the presence of PBN (5.2×10^{-3} M) and ND (4.9×10^{-3} M). For **1**, $a_N=14.4$, $a_{\beta\text{-H}}=2.1$ G; for **3**, $a_N=9.5$, $a_{o,p\text{-H}}=2.7$, $a_{m\text{-H}}=0.9$ G.

Relative Reactivity of PBN, DPN, and ND towards Phenylcyclohexadienyl Radicals. In an attempt to determine the relative reactivities of the spin traps towards phenylcyclohexadienyl radicals, 1,4-dihydro-4-triphenylmethylbiphenyl (DTB) was used as the source of this radical. The thermal decomposition of 2-chloro-1,4-dihydro-4-triphenylmethylbiphenyl in benzene was previously shown to generate triphenylmethyl and 1-chloro-6-phenyl-2,4-cyclohexadienyl radicals, which subsequently disproportionate into 2-chlorobiphenyl and triphenylmethane.[5]

The decomposition of DTB in benzene at 80 °C in the presence of PBN, DPN, and ND under an argon atmosphere produced their phenylcyclohexadienyl spin adducts (**5**, **6**, and **9**) and biphenylyl spin adducts (**7**, **8**, and **10**) along with triphenylmethyl radicals (Scheme 2). On the exposure of the reaction mixture to atmospheric oxygen, the triphenylmethyl radicals were eliminated and the phenylcyclohexadienyl spin adducts were converted to the biphenylyl spin adducts, the concentration of which was subsequently determined quantitatively. The stability of the biphenylyl spin adducts to oxygen, prolonged heating, and spin traps was previously confirmed.[2,6]

The thermal decomposition of DTB in benzene in the presence of a mixture of PBN (3.0×10^{-2} mol l^{-1}) and DPN (3.0×10^{-2} mol l^{-1}) under an argon atmosphere at 80 °C produced triphenylmethyl radicals and nitroxides (**5**, **6**, **7**, and **8**). When oxygen was passed into the reaction mixture, two nitroxides (**5** and **6**) were completely oxidized to **7** and **8** respectively. The ratio of their concentrations ([**8**]/[**7**]) was determined to be 2.3, which gives the realtive reactivity of DPN (k_6) and PBN (k_5) towards phenylcyclohexadienyl radicals as $k_6/k_5=2.3$ in benzene at 80 °C.

Likewise, the decomposition of DTB in benzene in the presence of PBN (9.8×10^{-2} mol l^{-1}) and ND (4.9×10^{-3} mol l^{-1}) at 80 °C, followed by treatment with oxygen, gave their biphenylyl spin adducts (**7** and **10** respectively). The ratio of their concentrations, [**7**]/[**10**], was determined to be 0.15, from which the relative reactivity of PBN (k_5) and ND (k_9) towards phenylcyclohexadienyl radicals was obtained as $k_5/k_9=7.7\times10^{-3}$ at 80 °C. Therefore, ND traps phenylcyclohexadienyl radicals 130 times faster than does PBN.

Discussion

The present results indicate that the nitrones (PBN and DPN) and ND trap phenyl radicals with similar rate constants. Janzen and Evans reported that phenyl radicals add to PBN in methanol at a rate constant of 1.2×10^7 mol l^{-1} at 80 °C.[7] The activation energy for the above reaction probably does not exceed that for the addition of benzoyloxyl radicals to benzene, which

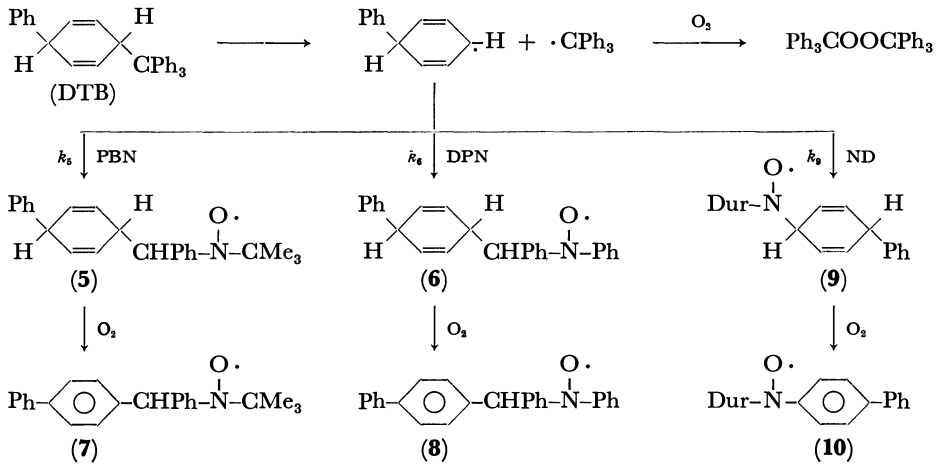

Scheme 2.

has been found to be 6 kcal mol^{-1}.[8] If it is assumed that the rate constant for the spin trapping in carbon tetrachloride is the same as in methanol, and that the activation energy is equal to 6 kcal mol^{-1}, the rate constant for the addition of phenyl radicals to PBN (k_1) in carbon tetrachloride at 80 °C can be estimated as 1.0×10^8 mol l^{-1} s^{-1}. The combination of this value with the observed rate ratios (k_2/k_1 and k_3/k_1) gives k_2 and k_3 as 7.2×10^7 and 2.6×10^8 mol l^{-1} s^{-1} respectively at 80 °C. The above large rate constants for the spin-trapping processes, as much as 10^8 mol l^{-1} s^{-1}, may be responsible for the lower selectivity between the spin traps in these reactions.

On the other hand, ND is now found to trap phenylcyclohexadienyl radicals nearly 130 times faster than the nitrones. A triphenylmethyl radical does not add at all to PBN,[9] DPN,[6] and ND,[10] probably because its addition to the spin traps is highly endothermic. The absolute rate constants for the addition of phenylcyclohexadienyl radicals to the spin traps cannot be estimated. However, as phenylcyclohexadienyl radicals are stabilized, though to a lesser extent, like triphenylmethyl radicals through the delocalization of the unpaired electron, it is suspected that phenylcyclohexadienyl radicals do not react with the spin traps so rapidly as do phenyl radicals.

Recently, Schmid and Ingold reported that 5-hexenyl radicals react with PBN at a rate constant of 1.3×10^5 mol l^{-1} s^{-1} at 40 °C in benzene and more rapidly with ND (3.9×10^7 mol l^{-1} s^{-1} at 40 °C).[11] It is worthwhile noting that ND tends to trap phenylcyclohexadienyl radicals and 5-hexenyl radicals more rapidly than the nitrones, whereas ND and the nitrones capture phenyl radicals with similar rate constants. The above fact may be interpreted in terms of the fact that phenylcyclohexadienyl radicals and 5-hexenyl radicals would suffer more steric hindrance on approaching to the nitrones to give the spin adducts than would phenyl radicals, whereas none of these radicals would suffer any serious steric hindrance in the reaction with ND.

Experimental

Materials. Nitrosodurene (ND),[12] *N*-*t*-butyl-α-phenylnitrone (PBN),[13] α,*N*-diphenylnitrone (DPN),[14] phenylazotriphenylmethane (PAT),[15] and 1,4-dihydro-4-triphenylmethylbiphenyl (DTB)[2] were prepared according to the methods in the literature.

Examination of the Stability of the Nitroxides, 1, 2, and 3. Benzhydrylphenylnitroxide (**2**) was prepared by the oxidation of benzhydrylphenylhydroxylamine[16] with silver oxide in carbon tetrachloride. A mixture of the precipitates was removed by filtration, and the filtrate was used in situ for examining the stability of **2**.

2,3,5,6-Tetramethyldiphenylnitroxide (**3**) was prepared by the complete decomposition of PAT in carbon tetrachloride at 80 °C in the presence of ND; oxygen was passed through the solution to eliminate triphenylmethyl radicals.

Benzhydryl-*t*-butylnitroxide (**1**) was prepared according to the method in the literature.[17]

Each nitroxide solution in carbon tetrachloride was heated for 30 min at 80 °C, was treated with oxygen by passing it in for 3 min, or was mixed with the corresponding spin traps. The intensity of the ESR signals of each nitroxide did not vary under the above conditions.

Decomposition of PAT, DTB, and BPO in the Presence of the Spin Traps. A solution (0.3—0.4 ml) of PAT (2.0×10^{-3} mol l^{-1}) and the spin traps (PBN, 5.0×10^{-3}—5.0×10^{-2} mol l^{-1}; DPN, 1.5×10^{-2} mol l^{-1}; ND, 4.9×10^{-3} mol l^{-1}) in carbon tetrachloride was heated at 80 °C for 3 min under an atmosphere of argon, and then oxygen was passed through the solution in order to remove the triphenylmethyl radicals. The reaction mixture was subsequently purged with argon, and the ESR spectra were recorded.

DTB (8.0×10^{-3} mol l^{-1}) was similarly decomposed in benzene in the presence of the spin traps (PBN, 3.0—9.8×10^{-2} mol l^{-1}; DPN, 3.0×10^{-2} mol l^{-1}; ND, 4.9×10^{-2} mol l^{-1}) at 80 °C for 30 min. The reaction mixture was then treated similarly.

The decomposition of BPO (2.0×10^{-3} mol l^{-1}) was carried out in carbon tetrachloride in the presence of the spin traps (PBN, 5.0×10^{-3} mol l^{-1}; DPN, 1.5×10^{-2} mol l^{-1}; ND, 4.5×10^{-3} mol l^{-1}) at 80 °C for 3 min. Thereafter, the ESR spectra were measured immediately.

The ESR spectra were recorded on a JEOL JES-ME-1X spectrometer. The peak heights were converted to area units by the use of a double integrator. The ratio of the concentrations of the two spin adducts was determined by double integration.[18] The peak-overlap effects of two nitroxides were taken into account by a computer simulation of the summed spectra.

The authors are grateful to Professors Kunio Nakano and Hiroshi Tadano of Rikkyo University for their suggestions regarding the construction of the double integrator.

References

1) For Example, E. G. Janzen, *Acc. Chem. Res.*, **4**, 31 (1971).
2) D. H. Hey, M. J. Perkins, and G. H. Williams, *J. Chem. Soc.*, **1965**, 110.
3) T. Suehiro, M. Kamimori, K. Tokumaru, and M. Yoshida, *Chem. Lett.*, **1976**, 531.
4) The identification and assignment of all the nitroxides in this paper were described in previous papers.[3,6]
5) D. J. Atkinson, M. J. Perkins, and P. Ward, *J. Chem. Soc., C*, **1971**, 3240.
6) M. Kamimori, H. Sakuragi, T. Suehiro, K. Tokumaru, and M. Yoshida, *Bull. Chem. Soc. Jpn.*, **50**, 1195 (1977).
7) E. G. Janzen and C. A. Evans, *J. Am. Chem. Soc.*, **97**, 205 (1975).
8) T. Suehiro and M. Ishida, *Bull. Chem. Soc. Jpn.*, **44**, 1692 (1971).
9) E. G. Janzen and B. J. Blackburn, *J. Am. Chem. Soc.*, **91**, 4481 (1969).
10) Unreported results in our laboratory.
11) P. Schmid and K. U. Ingold, *J. Am. Chem. Soc.*, **100**, 2493 (1978).
12) S. Terabe, K. Kuruma, and R. Konaka, *J. Chem. Soc., Perkin Trans. 2*, **1973**, 1252.
13) W. D. Emmons, *J. Am. Chem. Soc.*, **79**, 5739 (1957).
14) O. H. Wheeler and P. H. Gore, *J. Am. Chem. Soc.*, **78**, 3363 (1956).
15) H. Wieland, F. Popper, and H. Seefried, *Ber.*, **55**, 1816 (1922).
16) C. E. Griffin, N. F. Hepfinger, and B. L. Shapiro, *Tetrahedron*, **21**, 2735 (1965).
17) A. K. Hoffman and E. G. Abraham, U. S. Patent 3422144 (1969); *Chem. Abstr.*, **70**, 67880a (1969).
18) K. Nakano, H. Tadano, and M. Oshima, *Nippon Kagaku Kaishi*, **1972**, 2453.

A Comparative Study of Nickel and Cobalt Catalysts in the Hydrogenation of Substituted Acetophenones. Dependence of Hydrogenation Rate and Adsorption Strength on Substituents and Solvents

Masatsugu KAJITANI,* Naoki SUZUKI, Tsutomu ABE, Yoshimitsu KANEKO, Kazuhiko KASUYA, Kazunori TAKAHASHI, and Akira SUGIMORI

Department of Chemistry, Faculty of Science and Technology, Sophia University, Kioi-cho 7, Chiyoda-ku, Tokyo 102

(Received October 4, 1978)

The difference in the nature of nickel and cobalt catalysts has been investigated by a comparative study of the competitive hydrogenation of substituted acetophenones. The electronic and steric effects of substituents and the effects of solvents on the adsorption strength of acetophenones are greater for the reactions over R-Ni than for those over R-Co. On R-Co catalyst acetophenones substituted with electron attracting groups (3-methoxyl, 3-hydroxyl, and 4-fluoro groups with $\sigma^0>0$) are adsorbed more strongly than those with electron donating groups (2-, 3-, and 4-alkyl and 4-methoxyl groups with $\sigma^0<0$). Over R-Ni catalyst the adsorption of acetophenone is greater than that of any substituted acetophenones. The rates of hydrogenation over R-Ni are more susceptible to the effects of substituent and solvent than those over R-Co. Over both R-Ni and R-Co the rates of hydrogenation of unsubstituted acetophenones are greater than those of substituted acetophenones with either electron donating or electron attracting groups.

Heterogeneously catalyzed reactions involve the adsorption of substrates on the catalyst surface and the reaction on the catalyst surface. Solvents can affect both processes in different ways.

In recent years, it has become possible to examine the adsorption step by a method of competitive reaction. The following systems have been studied by the competitive reaction: cyclohexanone–its 4-alkyl derivatives,[1] cyclohexanone–its alkyl-substituted derivatives,[2] acetone–alkyl methyl ketones,[3] acetophenone–its substituted derivatives,[4] benzene–polymethylbenzenes,[5,6] cyclohexene–cyclooctene,[7,8] 1-hexene–olefinic substrates,[9,10] 2-phenyl-3-methyl-2-butene–its substituted derivatives,[11] cyclohexene–cycloalkenes,[12] 1-phenyl-2-propane–4-nitrotoluene,[13] and nitrobenzene–its substituted derivatives.[14]

Reports appeared on the effects of substituents and ring size on the strength of adsorption in the hydrogenation of cycloalkenes[7] and *p*-substituted nitrobenzenes[14] over various nickel catalysts. Bekkum and his coworkers reported that in the hydrogenation over palladium catalyst the adsorption of acetophenones in an alkaline ethanol solution is influenced to a lesser extent by electronic and steric substituent effects than the rate of hydrogenation and that the hydrogenation is accelerated by electron attracting groups and retarded by electron donating groups.[4]

In this work, the effectiveness of nickel and cobalt catalysts in the individual and competitive hydrogenation of substituted acetophenones in various solvents are compared. In order to confirm that the observed differences are attributable to the difference in metallic properties of nickel and cobalt, the effects of substituents (electronic and steric) on the rate of hydrogenation and on the strength of adsorption were examined mainly over Raney nickel (R-Ni) and Raney cobalt (R-Co) catalysts. The solvent effects were also investigated.

Experimental

Materials and Solvents. Commercial reagent grade R-Ni alloy (Ni;48 %), R-Co alloy (Co; 48—50%), zinc dust, nickel(II) chloride hexahydrate, cobalt(II) chloride hexahydrate (Guaranteed Reagent grade; GR), sodium tetrahydroborate (Wako Pure Chemical Industries) were used without further purification.

Acetophenone (GR), 4-methyl-(Extra Pure grade; EP), and 4-carboxyacetophenone (GR) (Wako Pure Chemical Industries Co.) and 4-amino-(GR), 2-methyl-(GR), 3-methyl-(GR), 4-chloro-(EP), and 4-methoxyacetophenone (EP) (Tokyo Kasei Kogyo Co.) were purified by fractional distillation or recrystallization.

4-Ethyl-, 4-isopropyl-, and 4-*t*-butylacetophenone[15] and 4-fluoroacetophenone[16] were synthesized from the corresponding alkylbenzenes and fluorobenzene by Friedel-Crafts reactions. After distillation, 4-methyl-, 4-ethyl-, and 4-*t*-butylacetophenone were purified as the corresponding oximes by fractional crystallization in aqueous methanol. The purified oximes were hydrolyzed in an aqueous solution of 25% hydrochloric acid, the ketones being again purified by fractional distillation.

Commercial reagent grade isopropyl alcohol (*i*-PrOH), methyl alcohol (MeOH), ethyl alcohol (EtOH), propyl alcohol (*n*-PrOH), *t*-butyl alcohol (*t*-BuOH), cyclohexane, benzene, and toluene were purified by the methods given in literature.[17] Each alcohol was dehydrated by refluxing with calcium hydride and then distilled.

Both the ketones and the solvents thus purified were gas-chromatographically pure.

Catalysts. R-Ni and R-Co were prepared by the modified method of Adkins and Billica[18] described in the preceding paper.[19] Urushibara nickel B (U-Ni-B) and Urushibara cobalt B (U-Co-B) catalysts were prepared by the simplified methods.[20] Nickel boride (Ni_2B) and cobalt boride (Co_2B) catalysts were prepared as reported by Paul *et al.*, by reducing nickel(II) chloride or cobalt(II) chloride with sodium tetrahydroborate in aqueous solutions.[21]

The catalysts were washed thoroughly with water until the washings were neutral to phenolphthalein. When a solvent immiscible with water was used, the catalysts were further washed with *i*-PrOH to remove water and finally with the solvent.

Urushibara catalysts, metal boride catalysts, and R-Co catalysts each containing 1 g of Ni or Co, and R-Ni containing

0.5 g of Ni were used for hydrogenation.

Hydrogenation. For individual hydrogenation, the substrate (5.2×10^{-3} mol) was hydrogenated with various nickel and cobalt catalysts in 10 cm^3 of solvent at 30 °C and under atmospheric pressure of hydrogen in a glass reaction vessel shaken at 350—400 strokes per minute.

For competitive hydrogenation, an equimolar mixture of two substrates (5.2×10^{-3} mol of acetophenone and of substituted acetophenone) was used. Hydrogenation was pseudo zero order with respect to the substrate and first order with respect to catalyst. The rate of hydrogenation is expressed in terms of the initial rate of hydrogen uptake per g catalyst (mol min^{-1} g^{-1}).

Analysis. The products were identified by comparison of their NMR spectra recorded on a Hitachi R-24 (60 MHz), IR spectra recorded on a Hitachi 215, melting point, boiling point, and retention time in gas chromatography with those of authentic samples prepared by the sodium tetrahydroborate reduction.[22]

In the course of competitive hydrogenation, samples of 0.1—0.2 cm^3 were withdrawn at appropriate intervals of hydrogen uptake (0—30%) for gas-chromatographic analysis.

Gas-chromatographic analyses of the reaction mixtures were performed with Shimadzu GC6A (detector, FID; carrier gas, N_2) and Shimadzu GC5A (detector, TCD; carrier gas, He) equipped with a column of 5% Silicone OV-17 on Uniport B (80/100 mesh) and of 10% PEG 20M on Celite 545 (60/80 mesh) (Gasukuro Kogyo Co.). The column temperatures employed in the case of OV-17 were 125—150 °C for acetophenone–alkylacetophenones, 170 °C for acetophenone–3-hydroxyacetophenone and acetophenone–4-fluoroacetophenone, and 200 °C for acetophenone–4-methoxyacetophenone.

Results and Discussion

Behavior of Substituted Acetophenones for the Catalytic Hydrogenation with Nickel and Cobalt. Alkyl-, methoxyl-, hydroxyl-, and fluoro-substituted acetophenones were hydrogenated to the corresponding 1-arylethanols in alcohol or hydrocarbon solutions over Ni and Co.

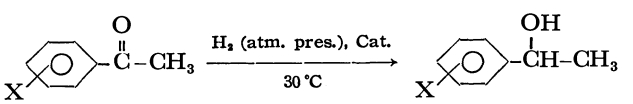

X=–H, –CH_3, –CH_2CH_3, –$CH(CH_3)_2$, –$C(CH_3)_3$, –OCH_3, –OH, –F

Neither hydrogenolysis of the carbonyl group nor hydrogenation of the aromatic ring was observed at the initial stage of reaction of these substrates.

4-Chloro-, 4-carboxy-, and 4-aminoacetophenone were not studied in detail because of their abnormal behavior during the course of hydrogenation. When 4-chloroacetophenone was subjected to catalytic hydrogenation, the reaction stopped after a slight hydrogen uptake, and the reaction mixture turned green, indicating nickel ion formation. Hydrogenation of 4-aminoacetophenone over nickel catalysts was accompanied by hydrogenolysis.

Kinetics. Kinetic measurements were performed under conditions at which the reaction rates are independent of mass transfer. The rate of hydrogenation was found to be first order with respect to catalysts.

The dependence of the initial reaction rate of hydrogenation of acetophenone on its concentration over R-Ni and R-Co in *i*-PrOH solutions is shown in Fig. 1. The

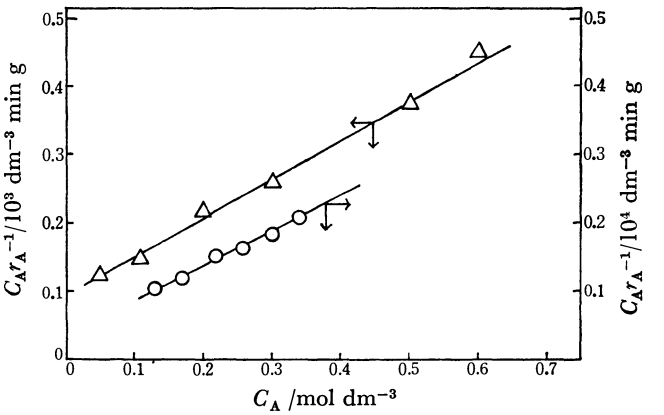

Fig. 1. Langmuir plot for hydrogenation of acetophenone in *i*-PrOH solution over R-Ni and R-Co catalysts.
△: R-Ni, ○: R-Co.

linear correlation of the reciprocals of the hydrogenation rate (r_A) *vs.* the concentration of the substrate (C_A) satisfies the Langmuir isotherm

$$r_A = -\frac{dC_A}{dt} = k_A\theta_A = \frac{k_A K_A C_A}{1+K_A C_A}$$

where k_A is the reaction rate constant of A, θ_A the fractional surface coverage of A, and K_A the adsorption equilibrium constant of A. In the region of [acetophenone]>0.2 mol dm^{-3}, the rate of hydrogen uptake is zero order with respect to the concentration of acetophenone, thus, $r_A=k_A$. The hydrogenation was carried out by using a solution of [ketone]≥0.52 mol dm^{-3} in which the reaction rates are independent of the concentration of substrate.

In the competitive hydrogenation of substrates A and B, assuming that the rate of hydrogenation of A (or B) is proportional to the amount of adsorbed A (or B) and that the adsorption of A (or B) follows the Langmuir isotherm, the following equation is obtained:[1,4]

$$K_{B,A} = S_{B,A}/r_{B,A}$$

where $K_{B,A}$ is the relative adsorption coefficient of B to A and used as a measure for the strength of adsorption, $r_{B,A}$ the ratio of the rates in the individual reaction and $S_{B,A}$ the ratio of the product concentration formed in the competitive hydrogenation between A and B. $S_{B,A}$ was determined in the range where the relative rate is independent of time. Thus, $S_{B,A}$ is unaffected by C_A and C_B.

Substituents Effects on the Hydrogenation of Acetophenones over R-Ni and R-Co. The results of hydrogenation (individual and competitive) of acetophenones over R-Ni and R-Co in *i*-PrOH solutions are shown in Table 1. The rate of hydrogenation and the strength of adsorption of acetophenones over R-Ni and R-Co are affected by the nature (electronic and steric effects) of the substituents. In view of substituent effects, the differences in the characteristics of nickel and cobalt catalysts can be summarized as follows:

(1) Electronic Effects of Substituents. The electronic effects of substituents on the strengths of adsorption and the rates of reaction over R-Ni and R-Co in *i*-PrOH solution are shown in terms of Hammett's relationship

Table 1. Substituent effects on the hydrogenation of acetophenone and substituted acetophenone over R-Ni and R-Co catalysts (solv.: *i*-PrOH 10 cm³)

Substituent (X=)	R-Ni $K_{X,H}(S_{X,H}/r_{X,H})$	R-Co $K_{X,H}(S_{X,H}/r_{X,H})$
H	1	1
2-Me	0.21(0.16/0.76)	0.27(0.18/0.66)
3-Me	0.50(0.44/0.88)	0.95(0.80/0.84)
4-Me	0.37(0.29/0.78)	0.93(0.71/0.76)
4-Et	0.36(0.24/0.67)	0.54(0.39/0.72)
4-*i*-Pr	0.42(0.21/0.50)	0.58(0.36/0.62)
4-*t*-Bu	0.37(0.11/0.30)	0.59(0.33/0.56)
4-OMe	0 (≈0/0.54)	0 (≈0/0.56)
3-OMe	0.99(0.83/0.84)	1.52(1.32/0.87)
3-OH	0 (≈0/0.49)	4.07(2.36/0.58)
4-F	0.48(0.29/0.60)	1.35(0.97/0.72)

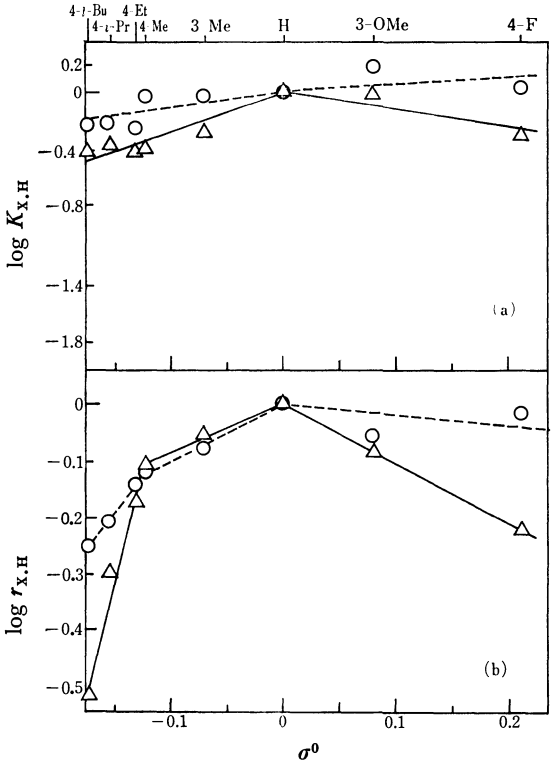

Fig. 2. log $K_{X,H}$ and log $r_{X,H}$ plotted against σ^0 values for the competitive hydrogenation of substituted acetophenones in *i*-PrOH solution over R-Ni and R-Co catalysts.
-△-: R-Ni, -○-: R-Co.

using σ^0[11,23] in Figs. 2a and 2b, respectively.

Strength of Adsorption: Over R-Co the strength of adsorption is greater for the acetophenones with electron attracting groups and smaller for those with electron donating groups than for unsubstituted acetophenone. The ρ value of Hammett plot in the region $\sigma^0<0$ is somewhat higher than that in the region $\sigma^0>0$.

Over R-Ni the adsorption of acetophenone is the strongest. On the two sides of $\sigma^0>0$ and $\sigma^0<0$, the Hammett plot forms approximately straight lines with different slopes. The adsorption over R-Co is affected by substituents to a lesser extent as compared with that over R-Ni.

In the competitive hydrogenation of acetophenone and 3-methoxyacetophenone or 4-fluoroacetophenone, the $K_{X,H}$ values are always larger over R-Co than over R-Ni. The values for 3-methoxyacetophenone over R-Co are much greater than unity (Table 2b). 3-Methoxyacetophenone is more strongly adsorbed on R-Co than acetophenone.

Rate of Hydrogenation: Over both R-Ni and R-Co, the rate of hydrogenation of unsubstituted acetophenone is greater than that of substituted acetophenones with either electron donating or electron attracting groups (Fig. 2b). The Hammett plot for the reaction rates shows greater deviation from the linear relationship than that for the adsorption coefficients. The hydrogenation over R-Ni was affected to a greater extent by substituents than that over R-Co.

Table 2. Solvent effects on competitive hydrogenation over R-Ni and R-Co catalysts (solv.: 10 cm³)

(a) Hydrogenation of acetophenone and 3-hydroxyacetophenone.

Solvent	$K_{3\text{-OH},H}(S_{3\text{-OH},H}/r_{3\text{-OH},H})$ R-Ni	R-Co
MeOH	0(≈0/1.08)	2.05(1.17/0.57)
EtOH	0(≈0/1.00)	2.51(1.53/0.61)
n-PrOH	0(≈0/0.87)	2.80(1.26/0.45)
i-PrOH	0(≈0/0.67)	3.00(1.68/0.56)

(b) Hydrogenation of acetophenone and 4-alkylacetophenones.

Solvent	$K_{X,H}(r_{X,H})$ X=4-Me R-Ni	X=4-Me R-Co	X=4-*t*-Bu R-Ni	X=4-*t*-Bu R-Co
MeOH	0.16 (0.89)	1.26 (0.52)	0.063 (0.26)	
EtOH	0.17 (0.80)	0.91 (0.70)	0.070 (0.47)	0.59 (0.68)
n-PrOH	0.31 (0.59)	0.85 (0.72)		
i-PrOH	0.37 (0.78)	0.93 (0.76)	0.37 (0.11)	0.59 (0.56)
Cyclohexane	0.25 (1.00)	0.51 (0.88)	0.40 (0.30)	

(c) Hydrogenation of acetophenone and 3-methoxyacetophenone or 4-fluoroacetophenone.

Catalyst	Solvent	$K_{X,H}(S_{X,H}/r_{X,H})$ X=3-OMe	X=4-F
R-Ni	MeOH	0.23(0.10/0.44)	0.19(0.05/0.26)
	EtOH	0.23(0.15/0.65)	0.28(0.11/0.39)
	n-PrOH	0.31(0.24/0.77)	0.31(0.17/0.55)
	i-PrOH	0.99(0.83/0.84)	0.48(0.29/0.60)
	Cyclohexane	0.96(0.74/0.77)	0.55(0.32/0.58)
R-Co	MeOH	1.40(1.27/0.91)	1.02(1.26/1.23)
	EtOH	1.73(1.59/0.92)	1.01(0.87/0.86)
	n-PrOH	1.30(1.13/0.87)	0.92(0.67/0.73)
	i-PrOH	1.52(1.32/0.87)	1.00(0.92/0.92)
	Cyclohexane	1.92(1.82/0.95)	0.80(0.82/1.02)

Concerning the rates of hydrogenation over nickel catalysts, similar effects of substituents have been recently reported in the reaction of substituted acetophenones by Nitta *et al.*[24] In the hydrogenation of substituted acetophenones over carbon-supported palladium catalyst, Bekkum *et al.* obtained $\rho=0.7$.[4]

The $S_{X,H}$ values of 3-hydroxyacetophenone and 4-methoxyacetophenone are exceptionally low (Table 1). The deactivating effects of substituents are particularly noticeable with 3-hydroxyacetophenone (over R-Ni in Table 2a) and 4-methoxyacetophenone (over R-Ni and R-Co) which is not hydrogenated at all before acetophenone is completely consumed in alcoholic solutions.

(2) Steric Effects of Substituents. Strength of Adsorption: Both over R-Ni and R-Co, the effects of increase in size of alkyl groups at the 4-position of acetophenone on the strength of adsorption are not significant. However, the alkyl group (methyl-) at the 2-positions brings about a decrease in the strength of adsorption.

Rate of Hydrogenation: The rate of hydrogenation (Table 1) of 4-alkylacetophenones over R-Ni and R-Co in *i*-PrOH solution decreases in the order: H>4-Me>4-Et>4-*i*-Pr>4-*t*-Bu. This indicates that the bulkiness of the substituents at the 4-position plays an important role in the reaction rates, which depend on steric effects rather than electronic effects.

The reaction over R-Ni is more sensitive to the steric substituent effects than that over R-Co, with respect to both the hydrogenation rate and the adsorption strength.

(3) Solvent Effects. The hydrogenation of acetophenones is strongly affected by the solvent used, particularly on the adsorption strength of acetophenones over Ni catalysts.

From the results (Tables 2b and 2c), the differences between R-Ni and R-Co became apparent by varying the solvents. In general, in the hydrogenation of acetophenones both the rate of hydrogenation and the strength of adsorption over R-Ni are susceptible to solvents to a greater extent than over R-Co.

The adsorption of 4-alkylacetophenones over R-Ni in MeOH and EtOH solvents is very weak, as compared with that of acetophenone (Table 2b). The selectivity of adsorption in MeOH and EtOH solutions is higher for 4-*t*-Bu ($K_{X,H}=0.06$—0.07) than for 4-Me ($K_{X,H}=0.16$—0.17). On the other hand, the adsorption strengths of 4-methylacetophenone and 4-*t*-butylacetophenone over R-Co are hardly affected by solvent, as can be seen from the values of EtOH and *i*-PrOH solvents.

The solvent effects on the rate of hydrogenation and strength of adsorption can be correlated with the relative dielectric constant ε_r (Figs. 3a and 3b). In the case of R-Ni, both $r_{X,H}$ and $K_{X,H}$ values decrease with increase in the dielectric constant ε_r. In the case of R-Co, both $r_{X,H}$ and $K_{X,H}$ values are affected to a lesser extent by ε_r.

Effects of the Method of Catalyst Preparation. In order to know whether the above differences between Ni and Co catalysts are essential or not, the effects of the method of catalyst preparation were studied.

The results of competitive hydrogenation of acetophenone and 4-methylacetophenone over the catalysts obtained by three methods are given in Table 3. The $K_{X,H}$ values of R-Ni, U-Ni-B, and Ni_2B catalysts agree

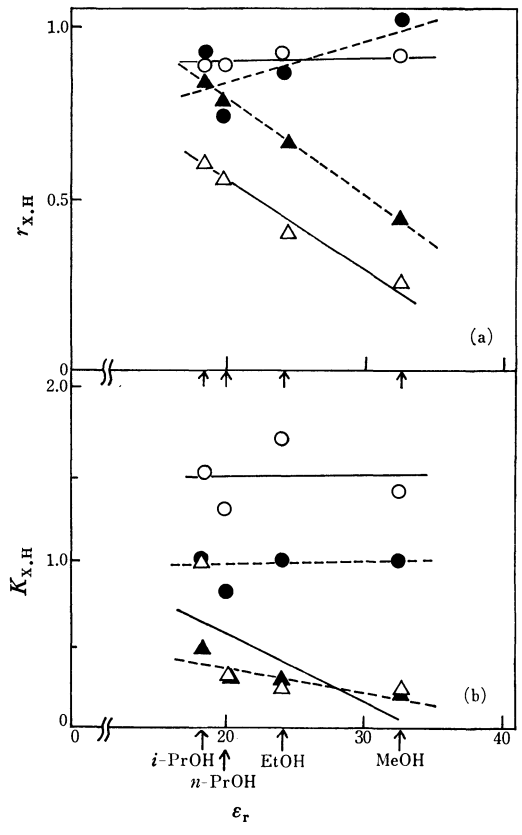

Fig. 3. Relationship between $K_{X,H}$ and $r_{X,H}$ and relative dielectric constants (ε_r) in the hydrogenation of 3-methoxyacetophenone and 4-fluoroacetophenone over R-Ni and R-Co catalysts.
△, ▲: R-Ni, ○, ●: R-Co, ——: X=3-Me, ——: X=4-F.

TABLE 3. COMPETITIVE HYDROGENATION OF ACETOPHENONE AND 4-METHYLACETOPHENONE OVER VARIOUS Ni AND Co CATALYSTS IN EtOH SOLVENT

Catalyst	$K_{4\text{-Me},H}(S_{4\text{-Me},H}/r_{4\text{-Me},H})$
R-Ni	0.17(0.14/0.80)
U-Ni-B	0.17(0.15/0.90)
Ni_2B	0.16(0.10/0.61)
R-Co	0.91(0.91/0.70)
U-Co-B	0.94(0.85/0.90)
Co_2B	0.63(0.60/0.76)

TABLE 4. $S_{3\text{-OMe},H}$ VALUES ON THE COMPETITIVE HYDROGENATION OF ACETOPHENONE AND 3-METHOXYACETOPHENONE

Catalyst	Solvent	
	MeOH	*i*-PrOH
Ni_2B	0.09	0.86
Co_2B	0.86	0.91
R-Ni	0.10	0.83
R-Co	1.27	1.32

within the range 0.16—0.17, as is the case for the three cobalt catalysts.

A comparison between Ni_2B and Co_2B with respect to the $S_{X,H}$ values in the competitive hydrogenation of acetophenone and 3-methoxyacetophenone shows nearly the same tendency as shown by Raney catalysts (Table 4).

Dependence of $S_{X,H}$ values on the conditions of catalyst preparation was examined in the competitive hydrogenation between acetophenone and 3-methoxyacetophenone. Concerning the effect of aging time in *i*-PrOH solution on the $S_{X,H}$ values, R-Ni is somewhat more susceptible to aging as compared with R-Co (Fig. 3b).[25] The digestion time of Raney alloy by 20% NaOH solution has no influence on the $S_{X,H}$ values, despite the presumed gradual decrease in Al content with digestion time. The effect of Al components on $S_{X,H}$ values seems negligible.

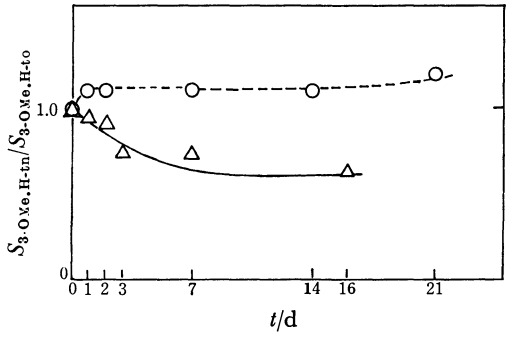

Fig. 4. Relationship between aging time of catalyst in *i*-PrOH solution and relative $S_{3\text{-OMe,H}}$ value.
-△-: R-Ni, -○-: R-Co.

Difference between Ni and Co Catalysts. The above results suggest that the characteristic difference between R-Ni and R-Co can be essentially attributed to the difference between Ni and Co metals. Ni is more susceptible to the effects of substituent groups and solvents as compared with Co. The difference between the two catalysts is in line with our observation that the selectivity over Co catalysts in the selective hydrogenation of 2-naphthol is influenced to a lesser extent by the solvents, as compared with Ni catalysts.[19] In their study of infrared spectra, Blyholder and Shihabi reported that acetone undergoes chemisorption on silica-supported Ni and Co at 25 °C, the amount on Ni being less than that on Co, and that a metal–oxygen bond rather than a metal–carbon bond is responsible for the bonding between acetone and the metal surfaces.[26] In the hydrogenation of acetophenones over various Ni catalysts, Nitta *et al.* reported that the rate of hydrogenation is proportional to the surface d-electron density of catalysts, whereas the strength of adsorption of the reactants on the catalyst is inversely proportional to the surface d-electron density of catalysts.[24]

The reaction over Co catalyst is not very susceptible to the effects of substituents and the strength of adsorption, as compared with that over Ni catalyst. This suggests that the carbonyl group of acetophenone is adsorbed more strongly over Co than over Ni. The characteristic difference between Ni and Co catalysts can be attributed to the difference of the surface d-electron density between the two metals; the surface d-electron density of Co is smaller than that of Ni. The results support observations concerning the relationship between the strength of adsorption and the surface d-electron density.[24] However, the effects of substituents on the strength of adsorption and the rate of hydrogenation are still not completely explained on the basis of only this relationship. The difference between Ni and Co catalysts should be further discussed from the standpoint of their difference in physical properties as related to the mechanisms of hydrogenation.

We wish to thank Professor Shigeo Nishimura, the Tokyo University of Agriculture and Technology, for his valuable discussion.

The present work was partially supported by a Grant-in-Aid for Scientific Research No. 274161 from the Ministry of Education, Science and Culture.

References

1) T. Chihara and K. Tanaka, *Chem. Lett.*, **1977**, 843.
2) K. Tanaka, Y. Takagi, O. Nomura, and I. Kobayashi, *J. Catal.*, **35**, 24 (1974).
3) I. Iwamoto, T. Yoshida, and T. Aonuma, *Nippon Kagaku Zasshi*, **92**, 504 (1971).
4) H. van Bekkum, A. P. G. Kieboom, and K. J. G. van de Putte, *Recl. Trav. Chim. Pays-Bas*, **88**, 52 (1969).
5) C. P. Rader and H. A. Smith, *J. Am. Chem. Soc.*, **84**, 1443 (1962).
6) H. A. Smith and W. E. Cambell, "Proc. Third Intern. Congr. Catalysis," ed by Sachtler, Schuit, and Zwietering, North-Holland, Amsterdam (1965), p. 1373.
7) M. Kajitani, Y. Sasaki, J. Okada, K. Omura, A. Sugimori, and Y. Urushibara, *Bull. Chem. Soc. Jpn.*, **47**, 1203 (1974).
8) Y. Nitta, T. Imanaka, and S. Teranishi, *Nippon Kagaku Zasshi*, **1976**, 1362.
9) L. Cerveny, F. Urbanova, and V. Ruzicka, *Collect. Czech. Chem. Commun.*, **40**, 3659 (1975).
10) L. Cerveny, V. Nevrkala, and V. Ruzicka, *Collect. Czech. Chem. Commun.*, **42**, 2590 (1977).
11) A. P. G. Kieboom and H. van Bekkum, *J. Catal.*, **25**, 342 (1972).
12) A. S. Hussey, *J. Catal.*, **10**, 258 (1968).
13) L. Cerveny and V. Ruzicka, *Collect. Czech. Chem. Commun.*, **41**, 1894 (1976).
14) A. Sugimori, *Bull. Chem. Soc. Jpn.*, **34**, 407 (1961).
15) D. T. Mowry, M. Renoll, and W. F. Huber, *J. Am. Chem. Soc.*, **68**, 1105 (1946).
16) R. Adams and C. R. Noller, *Org. Synth.*, Coll. Vol. I, 109 (1941).
17) "Technique of Organic Chemistry, Vol. VII, Organic Solvents," ed by A. Weissberger, Interscience, New York (1955).
18) H. Adkins and H. R. Billica, *J. Am. Chem. Soc.*, **70**, 195 (1948).
19) M. Kajitani, Y. Watanabe, Y. Iimura, and A. Sugimori, *Bull. Chem. Soc. Jpn.*, **48**, 2848 (1975).
20) S. Taira, *Bull. Chem. Soc. Jpn.*, **34**, 1294 (1961).

21) R. Paul, P. Busson, and N. Joseph, *Ind. Eng. Chem.*, **44**, 1006 (1952).
22) S. H. Wilen, C. B. Kremer, and I. Waltcher, *J. Chem. Educ.*, **38**, 304 (1961).
23) Y. Yukawa and Y. Tsuno, *Nippon Kagaku Zasshi*, **86**, 873 (1965).
24) Y. Nitta, Y. Okamoto, T. Imanaka, and S. Teranishi, *Nippon Kagaku Zasshi*, **1978**, 634.
25) M. Maruoka, K. Isagawa, and Y. Fushizaki, *Nippon Kagaku Zasshi*, **82**, 913 (1961).
26) G. Blyholder and D. Shihabi, *J. Catal.*, **46**, 91 (1977).

Effect of Hydration on the Thermal Stability of Protein as Measured by Differential Scanning Calorimetry. Lysozyme-D_2O System

Yukihisa FUJITA* and Yukinao NODA

Department of Chemistry, Hyogo College of Medicine, Mukogawa, Nishinomiya, Hyogo 663

(Received October 9, 1978)

The thermal denaturation of the deuterated lysozyme has been investigated by differential scanning calorimetry in the range of deuterium oxide (D_2O) content from 0.03 to 1.6 g of D_2O per g of protein. At D_2O contents above 0.55 g/g, the temperature, T_d, and enthalpy change, ΔH_d, of denaturation were almost independent of the degree of hydration. At lower D_2O contents, however, both T_d and ΔH_d showed marked dependence on the degree of hydration. The values of T_d increased with a decrease in the D_2O content. Whereas the values of ΔH_d decreased with a decrease in the D_2O content in the same region. The degree of hydration dependency of ΔH_d exhibited a break at approximately 170 mol/mol, which indicates that at least two types of hydration contributes to the thermal stability of the protein. The conformational enthalpy change of the protein and the enthalpy change of the hydration layer have also been estimated from the degree of hydration dependency of ΔH_d. The results have been compared with those of the lysozyme–H_2O system.

There has been a great deal of experimental evidence which has established that the interaction of water with proteins has an important role in determining the structure and biological function of the protein. This role, however, is poorly understood. The physical properties of water in the protein solution have been extensively investigated by several techniques, such as dielectric relaxation measurement,[1] NMR spectroscopy,[2] and calorimetry.[3] The studies have revealed that the properties of the interacting water are evidently different from those of pure water *e.g.*, lower mobility and reduced freezing point. It has been also observed that the hydration values in globular proteins do not differ greatly, being approximately 0.3 g of water per g of protein.[4]

In a previous paper,[5] the effect of hydration on the thermal stability of lysozyme was investigated by differential scanning calorimetry (DSC). It was observed that the essential hydration for stabilizing the spatial structure of lysozyme in water was completed at about 0.75 g/g. Below this water content, both the temperature and enthalpy change of denaturation showed a marked dependence on the degree of hydration. It was further suggested that at least two types of hydration contributed to the thermal stability of the protein, the threshold water content being approximately 0.33 g/g.

The present work was undertaken to investigate the effect of hydration of deuterium oxide (D_2O) on the thermal stability of deuterated lysozyme by DSC and to compare the results with those of the lysozyme–H_2O system.

Experimental

Materials. The hen egg-white lysozyme used in the present study was a recrystallized ($\times 6$) sample from Seikagaku Kogyo Co. The deuterium oxide (D_2O, purity 99.8%) was purchased from Aldrich Chemical Co.

Methods. Prior to calorimetric measurement, the lysozyme sample was deuterated as follows: the lysozyme was dissolved in D_2O(approximately 3% concentration), shaken for 50 h at 313 K, and lyophilized. After reaction, the extent of hydrogen-deuterium exchange was estimated by IR absorption according to the methods described by Blout *et al.*[6] and Nakanishi *et al.*[7] The amount of undeuterated peptide group was taken as proportional to the ratio of the absorbance of the amide II (at 1540 cm^{-1}) to that of the amide I (at 1650 cm^{-1}). In the absorbance measurement, the baseline for the amide I band was drawn parallel to the 100% transmittance at 1800 cm^{-1}, and the baseline of the amide II band taken as the absorption of the completely deuterated lysozyme. Complete deuteration was achieved by heating a solution of the exchanging protein at 353 K. From the IR measurements, approximately 83% of the total hydrogen atoms of the peptide exchanged, this amount corresponding to 106 peptide groups per molecule. It is a valid assumption that the hydrogen atoms of the protein side chain more rapidly exchange compared with those of the peptide group. In the lysozyme molecule there are in all 260 exchangeable hydrogen atoms.[8] The degree of deuteration which accounted for the number of deuterium atoms in the side chain was 92%, therefore, the molecular weight of the deuterated lysozyme has been taken as 14500.

The D_2O content of the sample was adjusted by conditioning in constant humidity apparatus at the appropriate relative humidity for 7 days. Higher D_2O contents were adjusted either by directly adding D_2O or by placing the sample in the saturated vapor at 293 K for an appropriate period. The relative humidity was maintained by a saturated aqueous solution in contact with an excess of solute at 293 K.[9]

The thermal denaturation of lysozyme was measured with a Rigaku Denki standard-type differential scanning calorimeter. For calorimetric measurements, the heating rate was 2.5 K/min.

The exact dry weight and D_2O content of sample were determined gravimetrically by drying the punctured sample pan at 378 K *in vacuo* for 24 h.

Results and Discussion

The thermal denaturation of deuterated lysozyme has been measured in the D_2O content range from 0.03 to 1.6 g/g. The temperature, T_d, and the enthalpy change, ΔH_d, of denaturation have been estimated from the temperature of the peak and the peak-area of the thermogram obtained, and plotted as a function of the D_2O content as shown in Figs. 1 and 2, respectively.

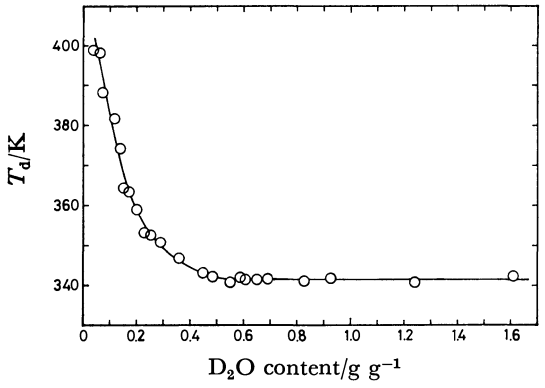

Fig. 1. The temperature of denaturation, T_d, of deuterated lysozyme as a function of the D_2O content.

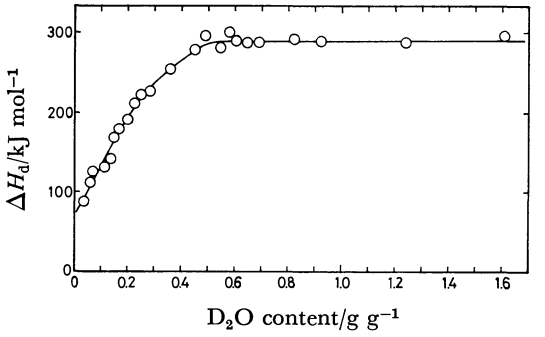

Fig. 2. The enthalpy change of denaturation, ΔH_d, deuterated lysozyme as a function of the D_2O content.

The data shows a marked dependency on the D_2O content, and the behavior has a resemblance to that for the lysozyme–H_2O system.

Both T_d and ΔH_d were slightly dependent on the D_2O content above 0.55 g/g which was a lower value than that reported for the lysozyme–H_2O system. The mean values in this region were 341.4 K and 298 kJ/mol, values which are almost identical not only with those for the lysozyme–H_2O system above 0.75 g/g, but also with those for lysozyme in aqueous solution.[10,11] The thermal denaturation of several proteins has been investigated in both H_2O and D_2O solutions and differences in the thermal stability of proteins in H_2O and D_2O solutions have been reported.[12,13] Nakanishi *et al.*[14] have, however, reported from UV measurements that the temperature of denaturation of lysozyme in D_2O solution was identical with that in H_2O solution. From NMR spectroscopic studies, McDonald *et al.*[15] also observed that the extent of denaturation of lysozyme in D_2O exhibited the same temperature dependency as that in H_2O. It appears reasonable to assume that a similar conformational change which takes place in solution occurs in the solid state containing a lot of water and that the conformational change of lysozyme by thermal denaturation makes little difference in H_2O and D_2O. In addition, the indication is that the hydration, an essential process for stabilizing the spatial structure of lysozyme in water, is completed at about 0.55 g/g for the lysozyme–D_2O system, which is a smaller value than that reported for the lysozyme–H_2O system, namely 0.75 g/g.

Below a D_2O content of 0.55 g/g, the T_d increased gradually with decrease in the D_2O content. The increase became much more marked at D_2O contents lower than 0.2 g/g. The ΔH_d, on the other hand, decreased with decrease in the D_2O content in the same region. In order to analyze the experimental data in this region of D_2O content it has been assumed that the observed enthalpy change of denaturation, ΔH_d, may be expressed as follows:

$$\Delta H_d = \Delta H_{conf} + n_{hyd}\Delta H_{hyd}$$

where ΔH_{conf} is the enthalpy change due to conformational changes in the protein, n_{hyd} is the degree of hydration, expressed by the number of mol of water adsorbed per mol of protein, and ΔH_{hyd} is the enthalpy change of the hydration layer, expressed on the basis of one mol of water per mol of protein. A plot of ΔH_d against n_{hyd} is shown in Fig. 3 together with that for the lysozyme–H_2O system. As may be seen, the relationship may be represented by two segments of a straight line, with the break occurring at 170 mol/mol which is a lower value than that for the lysozyme–H_2O system, namely 260 mol/mol. This indicates that at least two types of hydration exist and contribute to the thermal stability of the protein.

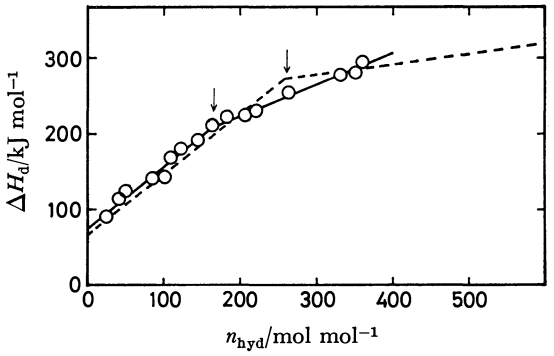

Fig. 3. The plots of the enthalpy change of denaturation, ΔH_d, of lysozyme against the degree of hydration, n_{hyd}, for lysozyme–D_2O system(solid line) and lysozyme–H_2O system (broken line).

Calorimetric studies of frozen protein solutions have revealed that water in protein solutions may be classified into four different states.[16,17] The four states are described as (1) non-freezable water, (2) freezable water with both heat and temperature of fusion different from the values for bulk water, (3) freezable water with the heat of fusion of bulk water, but a temperature of fusion lower than that of bulk water, and (4) bulk water. From recent NMR studies of aqueous protein solutions, Grosch and Noack[18] have suggested that at least three types of water which may be distinguished: (a) "rotationally bound" water, the rotational motion of which is considerably hindered by strong interactions with the protein, (b) "translationally hindered" water, the translational diffusion of which is hindered by interaction with the protein surface, and (c) "free bulk" water, the motion of which is not appreciably altered by interaction with the protein.

It has been assumed here that the hydration may be classified into two types as follows: (1) primary hydration *i.e.*, below n_{hyd} of 170 mol/mol for the lysozyme–D_2O system and 260 mol/mol for the lysozyme–H_2O system, and (2) secondary hydration *i.e.*, the range of n_{hyd} from 170 to 400 mol/mol for the lysozyme–D_2O system and from 260 to 600 mol/mol for the lysozyme–H_2O system. The values of ΔH_{hyd} and ΔH_{conf} have been estimated from the slopes and the intercepts, respectively, and are summarized in Table 1.

Table 1. The enthalpy change due to conformational changes of the protein, ΔH_{conf}, and the enthalpy change of hydration layer, ΔH_{hyd}, in primary and secondary hydration

Hydration	Water content	n_{hyd}	ΔH_{conf}	ΔH_{hyd}
	g g^{-1}	mol mol^{-1}	kJ mol^{-1}	kJ mol^{-1}
Lysozyme–D_2O system				
primary	0.23	170	72	0.83
secondary	0.55	400	140	0.43
Lysozyme–H_2O system				
primary	0.33	260	66	0.80
secondary	0.75	600	240	0.14

Primary hydration was completed at about 170 mol/mol for the lysozyme–D_2O system and 260 mol/mol for the lysozyme–H_2O system. The values of ΔH_{hyd} in the primary hydration region for both systems were considerably larger compared with those in the secondary hydration region. This indicating that the water molecules in this region contribute significantly to the stability of the protein compared with those in the secondary hydration region. The values of 170 mol/mol and 260 mol/mol correspond approximately to 1.0 and 1.5 molecules of water per hydrogen-bonding site, polar amino acid residue and peptide group, on the lysozyme molecule, respectively.[8] In this region, the water molecules are assumed to be tightly bound to the hydrogen-bonding sites, probably corresponding to the "rotationally bound" water molecules or state (1) in the calorimetric studies. It appears probable that the water molecules are selectively arranged in the vicinity of the polar regions of the protein by hydrogen bonds and form part of a first hydration monolayer.

The values of ΔH_{hyd} were almost identical for D_2O and H_2O in the primary hydration region. It is suggested that the primary hydration for D_2O contributes to the thermal stability of lysozyme in a similar manner to that for H_2O: the strength of interaction between the protein and D_2O are the almost identical to that between the protein and H_2O. The amount of primary hydration for the lysozyme–D_2O system, however, was considerably smaller than that for the lysozyme–H_2O system.

Secondary hydration was completed at about 400 mol/mol for the lysozyme–D_2O system and 600 mol/mol for the lysozyme–H_2O system. These values are comparable to approximately 3 and 5 molecules of water per amino acid residue on the lysozyme molecule, respectively. In the secondary hydration region, it is probable that the water molecules interact with the surface of the protein by repulsive hydrophobic interactions with the nonpolar parts of the protein and by hydrogen bonds on the some polar groups of the protein, correspond to the "translationally hindered" water molecules or states (2) and (3) in the calorimetric studies. It has also been assumed that the water molecules form parts of second and higher hydration layers which ambivalently interact not only with the water molecules in the primary hydration region, but with the normal bulk water.

The differences in ΔH_{hyd} between the lysozyme–D_2O system and the lysozyme–H_2O system in the secondary hydration region were considerable by a factor of approximately 3. It is suggested that the contribution of secondary hydration to the thermal stability of lysozyme is larger for D_2O than for H_2O. In this region, the D_2O molecules may interact more strongly with the protein compared with the H_2O molecules. The amount of secondary hydration for the lysozyme–D_2O system was smaller than that for the lysozyme–H_2O system. The differences in degree of hydration between D_2O and H_2O are too large to explain purely in terms of molecular size. Nemethy and Scheraga[19] compared the structures of H_2O and D_2O and noted that the hydrogen bond was stronger in D_2O than in H_2O and, therefore, more structural order existed in D_2O than in H_2O. One of the reasons for the lower degree of hydration and the higher value of ΔH_{hyd} in the secondary hydration region for the lysozyme–D_2O system may arise from the stronger intermolecular interaction for D_2O. It appears probable that the increase in strength of the hydrophobic interaction of the protein results from the increasing strength of interaction between the D_2O molecules. Secondary hydration may be affected markedly by the strength of the intermolecular interactions.

In primary hydration, the value of ΔH_{conf} for the lysozyme–D_2O system was slightly larger than that for the lysozyme–H_2O system. The ΔH_{conf} in this region may be associated with the intramolecular interactions, probably hydrogen bonds, in the protein molecule. Presumably, the small difference in ΔH_{conf} reflects the increase in strength of the intramolecular hydrogen bond of the protein by deuteration. A more accurate measurement, however, is necessary in order to discuss the structure of the protein in detail from the value of ΔH_{conf}. The variation of ΔH_{conf} in primary and secondary hydration regions suggests that the exhaustive removal of the water molecules associated with the protein brings about changes in the structure of the protein, as reported by Hanafusa.[20]

The higher contribution of hydration to the stabilization of the protein in the secondary hydration region may compensate for the lower degree of hydration in the lysozyme–D_2O system compared with the lysozyme–H_2O system. The thermal stabilities of lysozyme in H_2O and in D_2O are, therefore, almost identical.

References

1) B. E. Pennok and H. P. Schwan, *J. Phys. Chem.*, **73**, 2600 (1969).

2) H. E. Grant, S. E. Keefe, and S. Takashima, *J. Phys.*

Chem., **72**, 4373 (1968).
3) P. L. Privalov and G. M. Mrevlishvili, *Biofizika*, **12**, 22 (1967).
4) I. D. Kuntz, Jr., and W. Kauzumann, *Adv. Protein Chem.*, **28**, 239 (1974).
5) Y. Fujita and Y. Noda, *Bull. Chem. Soc. Jpn.*, **51**, 1567 (1978).
6) E. R. Blout, C. deLoze, and A. Asadourian, *J. Am. Chem. Soc.*, **83**, 1895 (1961).
7) M. Nakanishi, M. Tsuboi, and A. Ikegami, *J. Mol. Biol.*, **70**, 351 (1972).
8) R. E. Canfield, *J. Biol. Chem.*, **238**, 2698 (1963).
9) "Kagaku Benran," ed by the Chemical Society of Japan, Maruzen, Tokyo (1960), p. 66.
10) F. Delben and V. Creascenji, *Biochim. Biophys. Acta*, **194**, 615 (1969).
11) J. M. O'Reilly and F. E. Karasz, *Biopolymers*, **9**, 1429 (1970).
12) H. Takesada, M. Nakanishi, and M. Tsuboi, *J. Mol. Biol.*, **77**, 605 (1973).
13) M. Nakanishi and M. Tsuboi *Biochim. Biophys. Acta*, **434**, 365 (1976).
14) M. Nakanishi, M. Tsuboi, and A. Ikegami, *J. Mol. Biol.*, **75**, 673 (1973).
15) C. C. McDonald, W. D. Philips, and J. D. Glickson, *J. Am. Chem. Soc.*, **93**, 235 (1971).
16) A. R. Haly and J. W. Snaith, *Biopolymers*, **10**, 1681 (1971).
17) M. Ruegg, U. Moor, and B. Blanc, *Biochim. Biophys. Acta*, **400**, 334 (1975).
18) L. Grosch and F. Noack, *Biochim. Biophys. Acta*, **453**, 218 (1976).
19) G. Nemethy and H. A. Scheraga, *J. Chem. Phys.*, **41**, 680 (1964).
20) N. Hanafusa, *Teion Kagaku, B*, **27**, 11 (1969).

Stereochemistry in the Hydrosilylation of Substituted Cyclohexanones Catalyzed by Chlorotris(triphenylphosphine)rhodium and the Silica-linked Rhodium(I) Complex

Jun-ichi ISHIYAMA,* Yasuhisa SENDA, Isamu SHINODA, and Shin IMAIZUMI
Department of Applied Science, Faculty of Engineering, Tohoku University, Aoba, Sendai 980
(Received November 13, 1978)

The homogeneous and heterogeneous hydrosilylation of simple substituted cyclohexanones catalyzed by chlorotris(triphenylphosphine)rhodium, $RhCl(PPh_3)_3$, and the silica-linked rhodium(I) complex, $(\equiv Si\text{–}O\text{–}\overset{|}{\underset{|}{Si}}CH_2CH_2PPh_2)_3RhCl$, was examined. The stereoselectivity exhibited by the homogeneous catalyst was found to be nearly the same as that exhibited by the heterogeneous catalyst. The silica-linked rhodium catalyst could be re-used several times without any significant loss of the catalytic activity.

Although the homogeneous hydrosilylation of terpene ketones catalyzed by $RhCl(PPh_3)_3$ has been reported in detail by Ojima *et al.*,[1,2] that of simple cyclohexanones with alkyl substituents has not yet been studied. In order to shed further light on the reaction mechanism, we have now undertaken an investigation of the hydrosilylation of some simple substituted cyclohexanones by Et_3SiH, Ph_2SiH_2, and $PhSiH_3$ with the homogeneous rhodium(I) and the heterogeneous silica-linked rhodium(I) complexes. We have examined how the stereoselectivity is dependent on substrates, reagents, and catalysts. The stereoselectivity in the hydrosilylation effected by the recovered heterogeneous catalyst was also checked.

Results and Discussion

The results of the hydrosilylation of alkyl-substituted cyclohexanones with three kinds of hydrosilanes catalyzed by $RhCl(PPh_3)_3$ are presented in Table 1. In the reaction of 4-methyl- (**2**), 4-*t*-butyl- (**3**), 3-methyl- (**4**), and 3-*t*-butylcyclohexanone (**5**), the bulkiness of the silanes was not an important factor in controlling the stereoselectivity. However, the effects of the bulkiness of the silanes on the stereochemical course of the reduction became significant in the hydrosilylation of 2-methyl- (**6**) and 2-*t*-butylcyclohexanone (**7**). The relative amount of the more stable alcohol increased with an increase in the bulkiness of the hydrosilanes used. This trend was also realized in 3,3,5-trimethylcyclohexanone (**8**), which bears an axial methyl substituent at the 3-position. Thus, the results of **6**—**8** are in good agreement with those of menthone (**9**) and camphor (**10**).[1]

The relative rates of the hydrosilylation for alkyl-substituted cyclohexanones catalyzed by $RhCl(PPh_3)_3$ were estimated by a comparison of conversion in competitive reactions employing a binary mixture of cyclic carbonyl compounds. The results are listed in Table 2. With each hydrosilane, the relative rates of unhindered cyclohexanones, such as **1**—**5**, were not very different from each other, while those of hindered cyclohexanones, such as **6**—**8**, were found to be smaller than those of unhindered ones. These differences in relative rates seem to be due to the steric interaction between substituents at the 2- or 3-position and hydrosilanes in the transition state. It has previously been reported that the relative rate of $PhSiH_3$ or Ph_2SiH_2 increases remarkably compared to that of Et_3SiH in the cases of terpene ketones and other acyclic carbonyl

TABLE 1. STEREOSELECTIVITIES IN HYDROSILYLATION OF SUBSTITUTED CYCLOHEXANONES CATALYZED BY $RhCl(PPh_3)_3$ (% less stable alcohol)

	 (**2**)	 (**3**)	 (**4**)	 (**5**)	 (**6**)	 (**7**)	 (**8**)	 (**9**)	 (**10**)
$PhSiH_3$	34	27	39	38	67	84	80	—(90)[b]	—(90)[b]
Ph_2SiH_2	39	30	38	40	64	65	79	75(85)[b]	65(73)[b]
Et_3SiH	40	35[a]	42	40	35	54	63	59(64)[b]	29(30)[b]

a) Hexane was employed as the solvent. b) See Ref. 1.

TABLE 2. COMPARISON OF CONVERSION IN COMPETITIVE HYDROSILYLATION OF CYCLOHEXANONES CATALYZED BY $RhCl(PPh_3)_3$

	(**1**)	(**2**)	(**3**)	(**4**)	(**5**)	(**6**)	(**7**)	(**8**)
$PhSiH_3$	1.00[a]	1.06	0.94	1.16	0.95	0.38	0.06	0.63
Ph_2SiH_2	1.00[a]	—	1.01	—	1.05	—	0.27	0.90
Et_3SiH	1.00[a]	1.05	1.00	1.11	1.00	0.27	0.16	0.42

a) For each hydrosilane, the relative rates of hydrosilylation are normalized to 1.00 for the parent cyclohexanone (**1**).

Table 3. Stereoselectivities in hydrosilylation of substituted cyclohexanones catalyzed by (≡Si–O–SiCH$_2$CH$_2$PPh$_2$)$_3$RhCl

(% less stable alcohol)

		(2)	(3)	(4)	(5)	(6)	(7)	(8)	(9)	(10)
$PhSiH_3$	I	46	25	43	47	67	80	82		
	II[a]		39		46		80			
	III[b]		42		44		78			
Ph_2SiH_2	I	39	38	41	52	65	69	80	69	69
	II[a]	45	44	49			71			
	III[b]	49	47	54			64			
Et_3SiH	I	35	32[c]	29	34	37	X[d]	73	26	17[c]
	II[a]	32	35[c]	27	34	X[d]	X[d]	77		
	III[b]	32	34[c]			X[d]	X[d]	85		

a) II shows stereoselectivities by the re-used catalyst of I. b) III shows stereoselectivities by the re-used catalyst of II. c) Hexane was employed as the solvent. d) Cyclohexanone was recovered without any hydrosilylation.

compounds.[5,6] In this study, for example, the conversion of **8** employing $PhSiH_3$ or Ph_2SiH_2 was over 90% in 15 min, but that employing Et_3SiH was 60% in 3 h. Our results also showed that the relative rate of trihydro or dihydro-silane increased compared to that of monohydro-silane in the reaction of alkyl-substituted cyclohexanones.

The hydrosilylation using (≡Si–O–SiCH$_2$CH$_2$PPh$_2$)$_3$RhCl showed stereoselectivities similar to those using $RhCl(PPh_3)_3$. These results are summarized in Table 3. The stereoselectivity exhibited by the re-used catalyst was not significantly different from that of the original one.

The effect of repeated use on the catalytic activity of this heterogeneous catalyst was examined employing cyclohexanone (**1**) as a standard substrate (Table 4). The conversion of **1** was 70% at room temperature using the original heterogeneous catalyst, but it went up to 83% at 50 °C. As can be seen in Table 4 (Entry Nos. 1—5), the activity gradually deteriorated upon repeated use, apparently because of the repeated contact with the air. Practically speaking, however, the results of Entry Nos. 1—4 (conversion 70—44%) suggest that the silica-linked catalyst could be re-used several times. Although a closer examination is still needed of the effect of the temperature in repeated use, it should be noted that, judging from the above results, this heterogeneous rhodium complex catalyst has the advantage that the separation of the products from the catalyst is easier than in homogeneous metal complexes and that the re-use is possible.

Table 4. Change by repeated use in silica-linked catalyst[a]

Substrate	Entry[b] No.	Reaction time/h	Conversion /%
 (**1**)	1	3	70(83)[c]
	2	3	69
	3	3	54
	4	3	44
	5	3	13

a) Et_3SiH was employed as the hydrosilane. b) The entry number also represents the time of repeated use. c) At 50 °C.

In order to examine the regioselectivity, the competitive hydrosilylation of a binary mixture of heptanal, 2-heptanone, and 4-heptanone with Et_3SiH was performed employing the two rhodium(I) complex catalysts. The results are shown in Table 5. The rate difference between the reaction with (≡Si–O–SiCH$_2$CH$_2$PPh$_2$)$_3$RhCl was notably greater than between those with $RhCl(PPh_3)_3$. The relative rates for 2- and 4-heptanone were 0.11 and 0.074 on respectively $RhCl(PPh_3)_3$, while the values changed to 0.02 and 0.008 with (≡Si–O–SiCH$_2$CH$_2$PPh$_2$)$_3$RhCl. These results show that the reactivity toward the internal carbonyl group in the heterogeneous catalyst is very low compared to that in the homogeneous one. The observed difference in regioselectivity between the reactions catalyzed by the two catalysts suggests that the silica support acts as a steric bulk.

Ojima *et al.* reported that the stereoselectivity in the hydrosilylation is governed only by the size of the silyl

Table 5. Regioselectivities in hydrosilylation by triethylsilane–rhodium(I) complex combination

	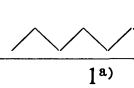	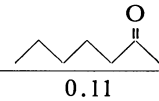	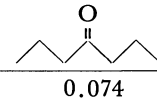
$RhCl(PPh_3)_3$	1[a]	0.11	0.074
(≡Si–O–SiCH$_2$CH$_2$PPh$_2$)$_3$RhCl	1[a]	0.02	0.008

a) For each catalyst, the relative rates of hydrosilylation are normalized to 1.00 for heptanal.

moiety. Consequently, it has been mentioned that the bulkier the substituents on silicon, the more pronounced may be the formation of the α-silyloxyalkylrhodium complex IIIa, which is a precursor of the more stable alcohol.[1,6] Although a similar change in the stereoselectivity depending on hydrosilanes was also observed in the reaction of hindered cyclohexanones (**6**—**8**), no change was found in the reaction of unhindered cyclohexanones (**2**—**5**), which gave equatorial alcohols predominantly. *A priori*, the stereoselectivity in the hydrosilylation of alkyl-substituted cyclohexanones is governed kinetically by the insertion step from II to III. Our results clearly show that, in the reaction of unhindered cyclohexanones (**2**—**5**), the axial attack of Rh predominates at the insertion step. Klein and others[7-9] have proposed a stereochemical control based on orbital-symmetry arguments. On the basis of the orbital-distortion theory, Klein[9,10] has reported that, in the absence of steric factors, an electrophilic reagent attacks the cyclohexanone from the equatorial side and a nucleophile attacks from the axial side. As is envisioned in the scheme, the transfer of Rh is supposed to be a nucleophilic reaction; hence, the predominant formation of equatorial alcohol can be accounted for in terms of Klein's criterion. On the other hand, the axial attack of Rh on hindered cyclohexanones (**6**—**8**) is restricted by the substituents at the 2- or 3-position. Consequently, the equatorial attack of Rh predominates in the reaction of hindered cyclohexanones (**6**—**8**), supporting results presented by previous workers.[1,6]

The influence of the bulkiness of silanes was thus significant only in the reaction of hindered cyclohexanones, such as **6**—**10**. These changes in the product distribution may be attributed to the equilibrium between IIIa and IIIb originating in the large interaction between the axial silyloxyl group and the substituents in the IIIb complex.[1] Therefore, the bulky silyloxyl group may occupy the less-hindered position when the silyloxyl group becomes larger than the rhodium moiety, which is kept constant in the III complex.

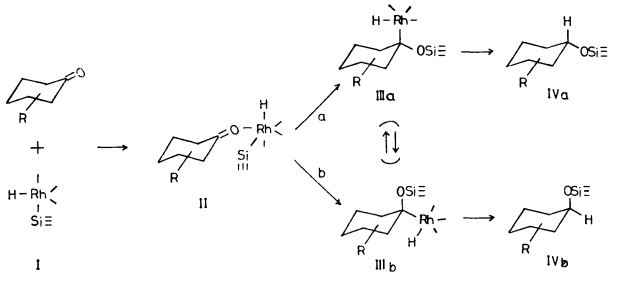

Experimental

A typical procedure will be described for the hydrosilylation of 4-methylcyclohexanone (**2**): To a mixture of 2 mmol of **2** and hydrosilanes, 5.2×10^{-3} mmol of $RhCl(PPh_3)_3$ or 0.1 g of $(\equiv Si-O-\overset{|}{Si}CH_2CH_2PPh_2)_3RhCl$ was added. The amount of $RhCl(PPh_3)_3$ was equalized in Rh content to that of $(\equiv Si-O-\overset{|}{Si}CH_2CH_2PPh_2)_3RhCl$, which had been found to contain 0.54 wt % of Rh. The mixture was stirred for 15 min ($PhSiH_3$), for 30 min (Ph_2SiH_2), and for 3 h (Et_3SiH) at room temperature under a nitrogen atmosphere. The silyl ether thus obtained was hydrolyzed by a MeOH–KOH–H_2O soln. to afford cyclohexanol quantitatively. The worked-up mixture was analyted by GLC.

Silica-linked Rhodium (I) Complex.[3,4] $(\equiv Si-O-\overset{|}{Si}CH_2CH_2PPh_2)_3RhCl$ was prepared from chlorotris[diphenyl[2-(triethoxysilyl)ethyl]phosphine]rhodium, $[(EtO)_3SiCH_2CH_2PPh_2]_3RhCl$, and silica gel (pore radius, 150 Å; surface area, 270 m^2/g; surface OH concentration, *ca.* 4 mmol/g) by refluxing with anhydrous benzene. The heterogeneous catalyst used was washed several times with pentane and dried under reduced pressure. This catalyst was then re-used.

Competitive Hydrosilylation. In a flask containing 5.2×10^{-3} mmol of $RhCl(PPh_3)_3$, 0.05 mmol each of two carbonyl compounds and 0.1 mmol of a hydrosilane were stirred at room temperature under a N_2 atmosphere. The composition of the mixture was checked in order to stop the reaction when half of the hydrosilane had been consumed. Water and crushed ice were added, and the resultant silyloxy compounds were hydrolyzed with a sufficient quantity of the MeOH–KOH–H_2O solution. The aqueous layer was extracted with ether, which had been washed with brine and dried over Na_2SO_4. The soln. was concentrated by removing a part of the ether, and the residual solution was subjected to GLC.

References

1) I. Ojima, M. Nihonyanagi, and Y. Nagai, *Bull. Chem. Soc. Jpn.*, **45**, 3722 (1972).
2) I. Ojima, T. Kogure, and Y. Nagai, *Tetrahedron Lett.*, **1972**, 5035.
3) K. G. Allum, R. D. Hancock, I. V. Howell, S. McKenzie, R. C. Pitkethly, and P. J. Robinson, *J. Organomet. Chem.*, **87**, 203 (1975).
4) K. G. Allum, R. D. Hancock, I. V. Howell, T. E. Lester, S. Mackenzie, R. C. Pitkethly, and P. J. Robinson, *J. Catal.*, **43**, 331 (1976).
5) I. Ojima, M. Nihonyanagi, T. Kogure, M. Kumagai, S. Horiuchi, K. Nakatsugawa, and Y. Nagai, *J. Organomet. Chem.*, **94**, 449 (1975).
6) I. Ojima, T. Kogure, M. Kumagai, S. Horiuchi, and T. Sato, *J. Organomet. Chem.*, **122**, 83 (1976).
7) N. T. Anh, O. Eisenstein, J.-M. Lefour, and M.-E. Tran Huu Dau, *J. Am. Chem. Soc.*, **95**, 6146 (1973); C. Liotta, *Tetrahedron Lett.*, **1975**, 519.
8) J. Klein and H. Stollar, *Tetrahedron*, **30**, 2541 (1974).
9) J. Klein, *Tetrahedron Lett.*, **1973**, 4307.
10) J. Klein, *Tetrahedron*, **30**, 3349 (1974).

Solvolysis in Carboxamides. VI.[1] Kinetic, Product, and Deuterium Tracer Studies on the *N,N*-Dimethylacetamide Solvolysis of *threo*-2-(*p*-Methoxyphenyl)-1-methylpropyl Brosylate. Nature of the k_Δ Pathway

Seiki SAITO,* Kenji DOIHARA, Toshio MORIWAKE, and Kunio OKAMOTO**

Department of Synthetics Chemistry, School of Engineering, Okayama University, Tsushima, Okayama 700
***Department of Hydrocarbon Chemistry, Faculty of Engineering, Kyoto University, Sakyo-ku, Kyoto 606*

(Received November 13, 1978)

Solvolysis of *threo*-2-(*p*-methoxyphenyl)-1-methylpropyl brosylate (**1**) and its deuterium derivative (**1**-2-*d*) has been carried out in *N,N*-dimethylacetamide (DMA) as solvent at 50.0 and 75.0 °C. Product examination revealed that in the presence of water (0.17 mol/dm^3) the main product is *threo*-2-(*p*-methoxyphenyl)-1-methylpropyl acetate (73% at 50 °C), but in the absence of water (*Z*)-2-(*p*-methoxyphenyl)-2-butene (**5**) (*ca.* 70% at 50 °C). Both of these products are derived from a *threo*-imidatonium ion [*threo*-R-Amide]$^+$ which is produced by DMA capture of the tight ion-pair [R$^+$OBs$^-$] (**2**) from the front-side. A part (*ca.* 14% yield) of the (*Z*)-olefin **5** is directly led from the tight ion-pair **2**. The formation of the olefin **5** can not be explained by intervention of the phenyl-bridged ion. Although the rate of the brosylate **1** exhibits the k_Δ portion deviating upwards from the Hammett plot for **a** series of *threo*-2-aryl-1-methylpropyl brosylates, the Schleyer's k_Δ-k_s treatment for the rate-(retained)product correlation was unsatisfactory. The classical simple S_N1 mechanism can preferably elucidate the product distribution, including the isotope distribution, without intervention of the phenyl-bridged ion intermediate.

Neighboring β-aryl participation in solvolytic reaction has received considerable attention in recent years.[2] The parent phenyl derivative among a series of substituted 1-methyl-2-phenylpropyl system exhibited remarkable stereospecificity in acetolysis[3] but its rate was unexpectedly slow.[4] This apparent discrepancy has been a starting point of the controversy[2,5] with regard to the role of β-aryl groups and the existence of a phenyl-bridged intermediate in solvolytic reactions.

Schleyer and his collaborators[6] have recently suggested a dual-mechanism in that the solvolysis of β-arylalkyl systems proceeds through aryl-assisted (k_Δ) and/or aryl-unassisted (k_s) pathways; they have divided the observed rate constant (k_t) into discrete Fk_Δ and k_s components, and the Fk_Δ was estimated from the upward deviation from the normal line in Hammett correlation. They have also postulated that the k_Δ pathway prodeeds *via* a phenyl-bridged ion giving a retained product (Scheme 1[6h]).

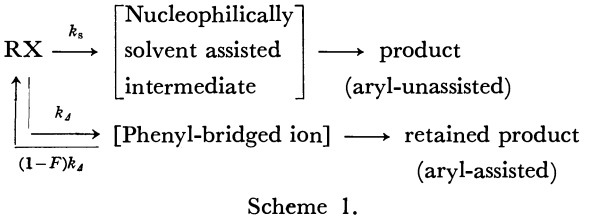

Scheme 1.

Although this dissection has been followed in 2-aryl-1-methylpropyl system by Brown and Kim,[7a] these investigators have proposed another mechanism which postulates prior formation of a tight ion-pair followed by subsequent k_p and k_2 pathways,[7a,b] which are respectively designated as aryl-assisted and aryl-unassisted pathways (Scheme 2[7a]). In addition, there still remains an original controversy as regards intervention of the phenyl-bridged ion in the k_Δ pathway.[7b]

In connection with our previous studies,[1,8-11] which disclosed several characteristics of carboxamide solvolysis, it was tempting to speculate that carboxamide solvolysis serves as a probe to scrutinize the reaction scheme (dual[6h] or single[7a]) and to examine the nature of so-called k_Δ pathway, especially as regards the intervention of the phenyl-bridged ion.

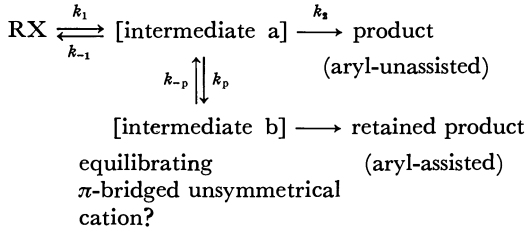

Scheme 2.

In the previous trial[1] of dissection of the observed rate (k_t) of *N,N*-dimethylacetamide (hereafter DMA) solvolysis into k_s and k_Δ components, it has been disclosed that the solvolysis of *threo*-1-methyl-2-phenylpropyl brosylate proceeds by complete (100%) k_s pathway, but the methoxy derivative, *threo*-2-(*p*-methoxyphenyl)-1-methylpropyl brosylate (**1**), predominantly reacts by the k_Δ route. As a model reaction to scrutinize k_Δ process the DMA solvolysis of the methoxyl derivative **1** was selected.

Results and Discussion

Product Distribution in the Presence of Water. In a series of our previous investigation for typical secondary cycloalkyl systems (4-*t*-butylcyclohexyl,[8] 7β-methylbicyclo[3.3.1]non-3β-yl,[9] and *exo*-2-norbornyl[11] systems), it has been revealed that the carboxamide solvolysis proceeds through an intermediate, characterized as a tight ion-pair [R$^+$X$^-$] (classical), and subsequently the intermediate undergoes a variety of processes such as *E*1 deprotonation, solvent capture (formation of an imidatonium ion), and rearrangements (Scheme 3).

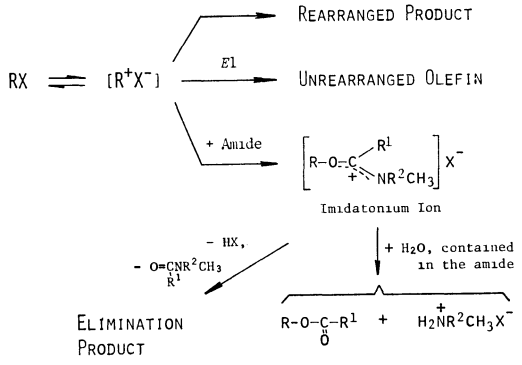

Scheme 3.

The unstable imidatonium ion, which otherwise decomposes to give elimination products, can be readily trapped by water to yield the carboxylic ester (Scheme 3); the efficient trapping with sufficient amounts of water has been successfully utilized in the previous works[1,9,11] to estimate the amount of the imidatonium ion and also to investigate the stereochemistry of its formation from the tight ion-pair.

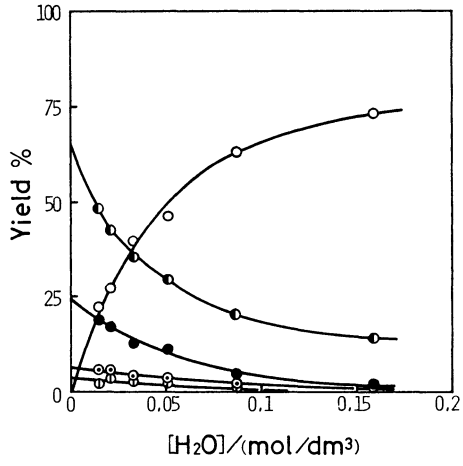

Fig. 1. Effect of water content of DMA on the formations of (*Z*) olefin **5** (◐), (*E*)-olefin **6** (●), 2-(*p*-$MeOC_6H_4$)-1-butene **7** (⊙), 3-(*p*-$MeOC_6H_4$)-1-butene **8** (⊕), and *threo*-acetate **9** (○), at 50 °C.

Table 1. Effect of added water on product distribution for the DMA solvolysis of *threo*-2-(*p*-methoxyphenyl)-1-methylpropyl brosylate **1**[a]

T / °C	$[H_2O]$ / mol/dm³	Yield/%							
		Olefin				Ester		Alcohol	
		5	**6**	**7**	**8**	**9**	**10**	**11**	**12**
50	0.015	48.2	18.4	5.7	1.9	22.1	2.1	1.5	0.1
	0.021	42.5	17.0	5.8	3.4	27.1	2.4	1.7	0.1
	0.033	35.0	12.6	4.1	2.7	39.9	3.7	1.8	0.2
	0.051	29.5	11.2	3.8	2.3	46.2	3.7	3.1	0.2
	0.087	20.0	4.9	2.0	1.5	63.2	3.5	4.6	0.3
	0.159	14.4	2.2	1.0	0.6	73.1	3.1	5.3	0.3
75	0.170	17.1	5.2	5.1	2.3	60.1	2.6	7.3	0.3

a) [**1**]=0.075 mol/dm³; [C_5H_5N]=0.077 mol/dm³.

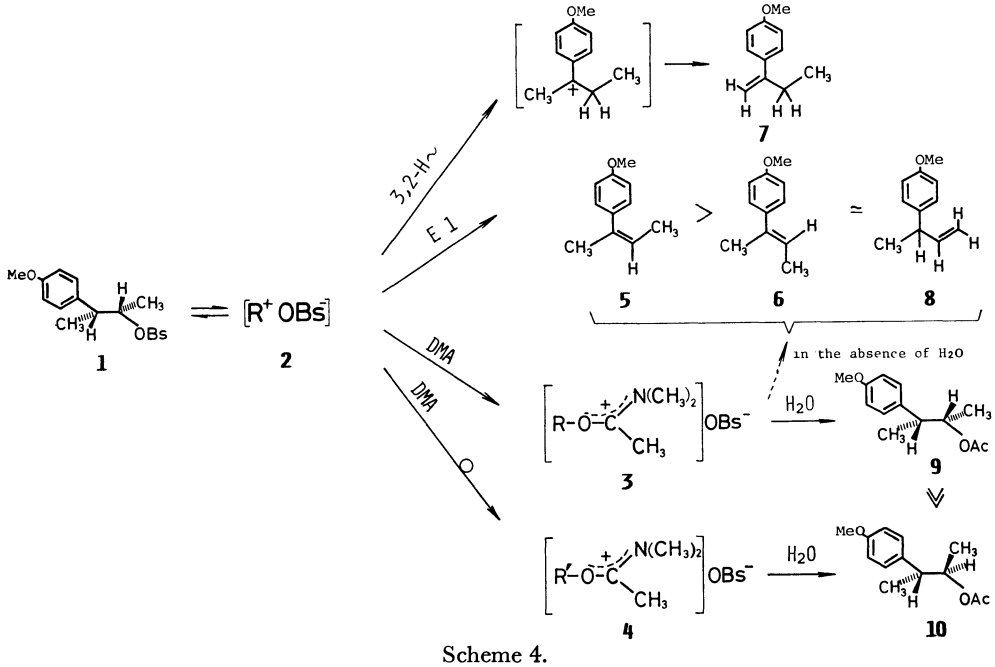

Scheme 4.

Thus the product distribution was determined in the presence of water, sufficient (0.16—0.17 mol/dm^3) to trap the imidatonium ion at 50.0 and 75.0 °C. The results are summarized in Table 1 and illustrated in Fig. 1 and Scheme 4.

The retained acetate, *threo*-2-(*p*-methoxyphenyl)-1-methylpropyl acetate (**9**), was a major product (60% at 75 °C; 73% at 50 °C), indicating that the most of the tight ion-pair (**2**) is captured by DMA from the retentive site to give a *threo*-imidatonium ion [*threo*-R-Amide]$^+$ (**3**). The rest of the tight ion-pair **2** undergoes 2,1-hydride shift and elimination. It is clear from attenuation of increase in the *threo*-acetate yield (Fig. 1) that 0.16—0.17 mol/dm^3 of water is almost sufficient to convert all imidatonium ion to the acetate.

As another retained product *threo*-3-(*p*-methoxyphenyl)-2-butanol (**11**) was obtained, though in a small amount (7% yield at 75 °C), indicating that the hydrolysis of the *threo*-brosylate **1** also proceeds with predominant retention of configuration (*cf.* the *erythro*-alcohol (**12**) in Table 1).

As regards these retentive pathways, it has been reported that in the acetolysis of various *threo*-2-aryl-1-methylpropyl brosylates the amount of retained product, *i.e.*, the *threo*-acetates, agrees well with the predicted value which was calculated by 100 (Fk_Δ/k_t) provided that the k_Δ pathway leads solely to the retained acetate.[7a] Furthermore, as shown in a recent tabulation of the rate-(retained)product correlations for β-arylalkyl systems,[12] satisfactory rate-(retained)product correlation has been observed for acetolysis of many other primary and secondary β-arylalkyl substances.

Therefore, the predominant formation of the retained product might predict a satisfactory rate-(retained)-product correlation in DMA solvolysis. However, the observed amounts of the retentive products (7%+60%, at 75 °C, Table 1) does not agree with the one (83%) calculated by 100(Fk_Δ/k_t) from the Fk_Δ and k_t in the previous work.[1] This discrepancy implies existence of a mechanism different from the acetolysis and also a need to consider about a reaction pathway which affords the retained product without intervention of a phenyl-bridged ion.

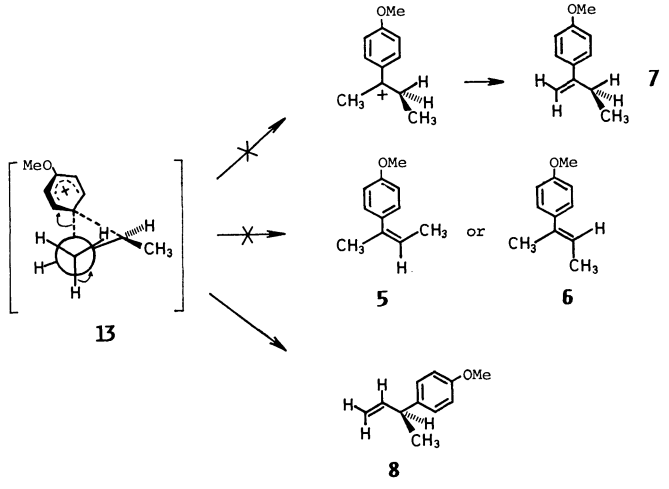

Scheme 5.

Besides the retained substitution products, **9** and **11**, (*Z*)-2-(*p*-methoxyphenyl)-2-butene (**5**), albeit in low yield (17% at 75 °C; 14% at 50 °C), was obtained. This olefin must be derived by *anti*-elimination from the tight ion-pair **2**, competing with DMA capture. Direct formation of the olefin **5** by the *E*2 reaction is less probable in view of the low basicity of DMA. When this olefin is derived from the tight ion-pair **2**, the ion-pair can not have a phenyl-bridged structure, because it has been suggested that the formation of the conjugated olefin such as **5** may be forbidden from the bridged ion **13**, because of the rigid and unfavorable dihedral angle (120°) between the C(1) and C(2) hydrogen and the departing aryl ring (Scheme 5).[13]

Another minor product, (*E*)-2-(*p*-methoxyphenyl)-2-butene (**6**), can not be derived from the bridged ion **13** either for the same reason (Scheme 5).

A terminal olefin, 2-(*p*-methoxyphenyl)-1-butene (**7**), which must be derived *via* 1-(*p*-methoxyphenyl)-1-methylpropyl cation, a 2,1-hydride shift product, can not obviously be led from the bridged ion **13** (Scheme 5).

The sole olefin, which can be derived from the phenyl-bridged ion **13**, is 3-(*p*-methoxyphenyl)-1-butene (**8**) (Scheme 5). This is actually found in the products, but is in very minor amount (less than 2%).

From these results it is concluded that the tight ion-pair can not be a phenyl-bridged ion, although it affords the retained imidatonium ion **3** and also the

Table 2. Isotopic scrambling of the products for the DMA solvolysis of *threo*-2-(*p*-methoxyphenyl)-1-methylpropyl-2-*d* brosylate **1**-2-*d*[a]

Product		Yield/% (Composition/%)[b] 50 °C	75 °C
Butene:			
(*Z*)-2-(*p*-$CH_3OC_6H_4$)-2-		12.0	16.0
(3-H: 3-D)	**5**	(52: 48)	(65: 35)
(*E*)-2-(*p*-$CH_3OC_6H_4$)-2-		1.8	3.7
(3-H: 3-D)	**6**	(57: 43)	(76: 24)
2-(*p*-$CH_3OC_6H_4$)-1-		0.6	2.4
(3-D,H: 3-H)	**7**	(90: 10)	(62: 38)
3-(*p*-$CH_3OC_6H_4$)-1-		0.8	3.2
(3-D: 2-D)	**8**	(50: 50)	(50: 50)
Acetate:			
threo-2-(*p*-$CH_3OC_6H_4$)-1-methyl-		75.8	60.2
propyl (2-D: 1-D)	**9**	(50: 50)	(50: 50)
erythro-2-(*p*-$CH_3OC_6H_4$)-1-methyl-		3.2	3.5
propyl (2-D: 1-D)	**10**	(49: 51)	(51: 49)
Alcohol:			
threo-3-(*p*-$CH_3OC_6H_4$)-2-butanol		5.3[c]	10.3
(3-D: 2-D)	**11**		(54: 46)
erythro-3-(*p*-$CH_3OC_6H_4$)-2-butanol		0.5[c]	0.7
(3-D: 2-D)	**12**		(58: 42)

a) [**1**-2-*d*]=0.075 mol/dm^3; [C_5H_5N]=0.077 mol/dm^3; [H_2O]=0.17 mol/dm^3. b) The accuracy for NMR measurement of isotopic content was $\leq$1%; reproducibility=$\pm$3%. c) Precise determination of an isotopic distribution was not made: the label would be scrambled more extensively than in the case at 75 °C, in view of the trend found in the other products **5**, **6**, **7**, and **8** at 50 and 75 °C.

retained alcohol **11**. Possible and the simplest reaction pathways for the formation of these olefins can be depicted as illustrated in Scheme 4 along with those for the imidatonium ion formation and its water trapping pathway.

Product Distribution in the Absence of Water. From variation in the yield at 50 °C (Fig. 1), caused by change in water concentration in DMA, it is indicated that in completely dried DMA the olefins are sole products and among them (*Z*)-2-(*p*-methoxyphenyl)-2-butene (**5**) is a major product (65% yield) along with minor amounts of olefins **6**, **7**, and **8**. Thus it is clear that the imidatonium ion **3**, which gave the retained acetate **9** in the presence of water, can afford mainly the 2-butenes (Saytzeff products) as the final product in the absence of water.

As mentioned above, in the presence of water (0.16 mol/dm^3) the small amounts (3.8% in composite yield) of olefins **6**, **7**, and **8** were produced besides the olefin **5**. However, in the absence of water a fair amounts (*ca.* 30% in composite yield) of these olefins have been obtained. Consequently, most of these olefins (30%—3.8%=26.2% in composite yield) must have come from the imidatonium ion **3** (Fig. 1).

The (*Z*)-olefin **5** was produced in 14% yield from the tight ion-pair **2** in the presence of water (Table 1), but in the absence of water it should be led also from the imidatonium ion **3** in about 51% (*ca.* 65%—14%) yield.

Among these olefins only **8** (*ca.* 3% yield) can be derived from the phenyl-bridged ion. Therefore in the course of the olefin formation from the *threo*-imidatonium ion **3** a possibility of intervention of the phenyl-bridged ion is mostly ruled out.

Deuterium Distribution in the Products. In order to examine the reaction pathways thoroughly, the deuterium scrambling in the products **5**—**12**, which were isolated from the wet DMA solvolysis mixture of *threo*-2-(*p*-methoxyphenyl)-1-methylpropyl-2-*d* brosylate (**1**-2-*d*), was examined by the use of previously reported ^{1}H NMR spectroscopic method.[1] The results are summarized in Table 2 and illustrated in Scheme 6.

The rearrangement in the product amounts to 50% (complete scrambling) for the acetates **9** and **10** (64% in composite yield), but for the elimination products (**5**, **6**, and **7**, except for **8**) and the hydrolysis products (**11** and **12**) it does not reach complete scrambling. The incomplete scrambling in the elimination and the hydrolysis clearly indicates that the tight ion-pair **2** does not have such symmetrical structure as a phenyl-bridged ion structure.

When the scrambling in the tight ion-pair **2** is so incomplete, the scrambling in the imidatonium ion **3** should also be incomplete, because the imidatonium ion is a primary product from the ion-pair **2** as illustrated in Scheme 4. This indicates in turn that the scrambling in the acetate **9** would not be complete. However, it is not the case.

Thus, the complete scrambling in the acetate **9** implies that it must occur in the process of the hydrolysis of the imidatonium ion **3**. Since the hydrolysis does not proceed on the carbenium ion center of the imidatonium ion **3** but on the carbonyl carbon, it seems difficult to find a reasonable explanation for the scrambling in the imidatonium-ion hydrolysis. However, as one of possible explanations, it might be helpful to consider about a hidden scrambling process during the hydrolysis as illustrated in Scheme 7.

Since in the absence of water the imidatonium ion **3** can give rise to the olefins, these olefins should be produced *via* a new ionized intermediate **14** (Scheme 7). This ionization process might be hidden in the presence of water, because the rate of hydrolysis might overwhelmingly exceed the elimination rate in spite of rapid equilibration between the imidatonium ion **3** and the

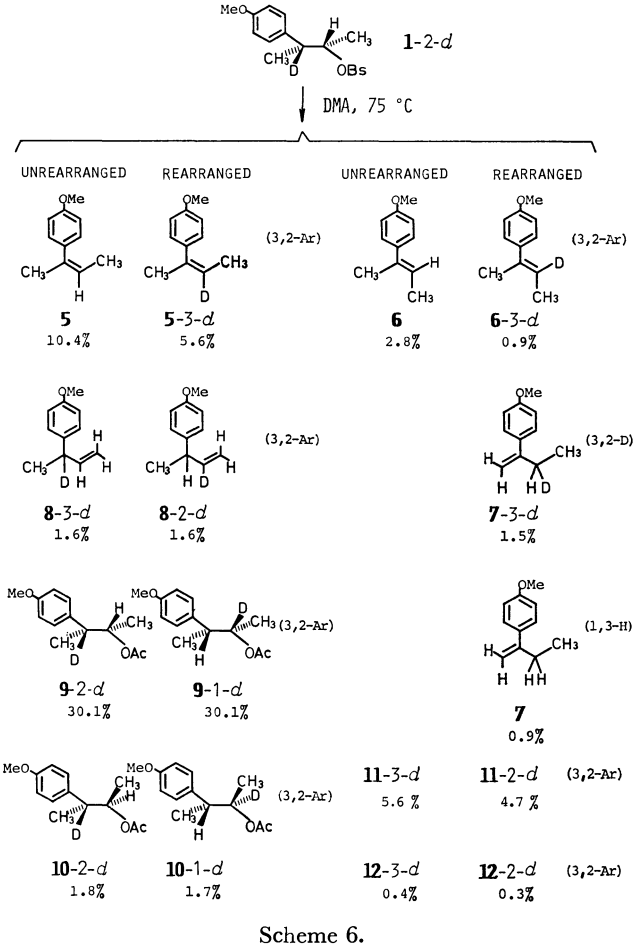

Scheme 6.

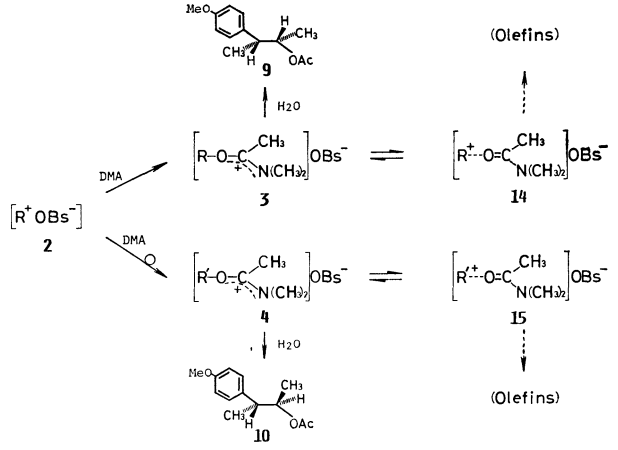

Scheme 7.

new ionized intermediate **14**. Conceivably, the hidden ionization would bring about the complete scrambling in the acetate **9**. As mentioned above, most of the olefins formed from the imidatonium ion **3** (in the absence of water) can not be derived from a phenyl-bridged ion. This indicates, consequently, that the intermediate **14** does not have the phenyl-bridged ion structure either.

Furthermore, it is notable that the inverted *erythro* acetate **10**, albeit in very low yield (3% at 50 °C and 2% at 75 °C), also undergoes complete scrabling of deuterium at C(2) and C(3) at 50 °C. The inverted acetate **10** can not be led from the *threo*-phenyl-bridged ion. Therefore, when we follow the reaction schemes shown in Scheme 1, it must be derived *via* k_s route[6h] starting from the *threo*-brosylate **1**. If it is derived *via* k_s route, complete scrambling in the *erythro* acetate **10** is possible only when the scrambling in the unchanged *threo*-brosylate **1**-2-*d* is complete at an early stage of the solvolysis. However, when unchanged brosylate was reclaimed at a half-life, only 30% of deuterium was found at C(2). Consequently, the formation of the *erythro*-acetate **10** *via* k_s route would be ruled out. The rear-side attack of DMA on the tight ion-pair **2** could explain the formation of completely scrambled *erythro*-acetate **10**, if we assume a rapid equilibration between **4** and **15** (Scheme 7). The cross-over between *threo* and *erythro* open carbenium ions in the tight ion-pair **2** or the intermediates **14** and **15** is conceivable, but it is not clear since in the reclaimed brosylate **1** scarecely was contained the *erythro* brosylate.

In conclusion, so far as the DMA solvolysis of *threo*-2-(*p*-methoxyphenyl)-1-methylpropyl brosylate is concerned, the intervention of the bridged ion is mostly improbable and the discrete k_Δ-k_s dual mechanism does not give a satisfactory explanation for the rate-(retained)product correlation but the usual S_N1 mechanism, *i.e.*, the prior formation of a tight ion-pair intermediate followed by various subsequent routes such as 2,1-aryl shift, 2,1-hydride shift, *anti*-elimination, and DMA capture, can account for the product and deuterium distributions. For elucidation of the excessive rate enhancement by methoxyphenyl or by the aryl participation, an examination of the linear free-energy relationship, especially reactivity-selectivity correlation, may served as a new probe and this is the subject of the succeeding paper.

Experimental

Melting points determined on a Yamato Model MP-1 apparatus were uncorrected. NMR spectra were recorded on either a Hitachi R-24, JEOL JNM-MH 100, or JEOL JNM-FX 100 instrument, and spectral data were obtained in $CDCl_3$ solution. Both analytical and preparative GLC's were conducted on a Hitachi K-53 gas chromatograph attached with a thermal conductivity detector by the use of helium as carrier gas. The following column was used: 3 m×3 mm 10% PEG 6000 on 60—80 mesh Chromosorb W (NAW).

Materials. DMA was purified in the identical manner as described in the previous paper.[9] $NaBD_4$ (97.0 D-atom %) was supplied from CEA. Ether, THF, diglyme, and pentane, used as reaction medium or solvent for recrystallization, were distilled from sodium–benzophenone ketyl before use. Reagent grade chemicals were used without further purification unless otherwise noted.

threo-*3-(*p*-Methoxyphenyl)-2-butanol-3*-d *and Its Brosylate* **1***-2*-d. Deuterium at C(3) position was introduced by deuterioboration of (*E*)-2-(*p*-methoxyphenyl)-2-butene prepared in the same manner as reported.[1] Deuterioboration–oxidation was carried out according to the published method.[14] Diborane-d_6 was generated externally from $NaBD_4$ and boron trifluoride etherate in diglyme and introduced into THF solution of the olefin. The deuterated alcohol was obtained in 83% yield after the purification by column chromatography (Al_2O_3). The brosylate **1**-2-*d* was synthesized from this alcohol in the usual manner[15] in 87% yield. **1**-2-*d*: mp 100—101 °C (lit,[16] 97.5—98.5 °C for the unlabeled sample); NMR (100 MHz) δ=1.19 (3H, s, C(4)H_3). 1.30 (3H, d, C(1)H_3), 3.79 (3H, s, OCH_3), 4.70 (1H, quartet, C(2)H), 6.88 (4H, d of d, Ar–H), and 7.55 ppm (4H, s, Ar–H). ^1H and ^{13}C NMR spectra showed the absence of deuterium scrambling during the synthesis and an isotopic purity of 97%.

Product Analysis. The method employed was identical with that used in the preceding work.[1] Unlike the parent phenyl derivative, the acetates **9** and **10**, obtained from the DMA solvolysis of **1** or **1**-2-*d*, could not be separated on GLC. Therefore, the ratio (**9**: **10**) was determined by means of GLC with the corresponding alcohols which was derived from the esters by hydrogenolysis with $LiAlH_4$ in ether: the ester mixture was isolated from the product mixture by column chromatography (SiO_2).

Partial Solvolysis and Isolation of Unchanged Brosylate. The brosylate recovered from half-life solvolysis of **1**-2-*d* in DMA solvent was isolated from the reaction mixture by repeated recrystallization from ether–pentane at −78 °C. Colorless crystalline brosylate was obtained almost quantitatively based on theoretical amount. The sample was dried by keeping under high vacuum over P_2O_5 at room temperature overnight. ^1H NMR spectrum (100 MHz) of the sample exhibited no sign of contamination with the solvolysis products and also of an existence of *erythro*-isomer.

Deuterium Distribution Analysis. The deuterium distribution was determined by means of ^1H NMR spectroscopy (100 MHz) in the Fourier transform mode. The operating parameters employed in NMR works were identical with those reported in the preceding paper.[1] Analytical procedures and sample preparations were performed in the same manner as described in the paper,[1] except for the sample of the acetate **9** or **10**.

The mixture of the acetates **9** and **10** was isolated by column chromatography (SiO_2) and was hydrogenolyzed ($LiAlH_4$ in ether) into the corresponding mixture of alcohols from which each isomer was separated by preparative GLC. Each isomeric alcohol was transformed again into the corresponding acetate **9** or **10** in the usual manner (acetic anhydride–pyridine) in order to avoid an overlapping of NMR signals due to *O*-methyl and C(1)–H protons.

Kinetic Measurements. All kinetic runs were carried out in the same way as described in the previous papers.[1,11]

References

1) S. Saito, K. Doihara, T. Moriwake, and K. Okamoto, *Bull. Chem. Soc. Jpn.*, **52**, 1478 (1979): Part V.

2) For a review, see C. J. Lancelot, D. J. Cram, and P. v. R. Schleyer in "Carbonium Ions," ed by G. A. Olah and P. v. R. Schleyer, Wiley-Interscience, New York, N. Y. (1972), Vol. 3, Chap. 27.

3) D. J. Cram, *J. Am. Chem. Soc.*, **71**, 3863 (1949); *ibid.*,

74, 2129 (1952).

4) S. Winstein, B. K. Morse, E. Grunwald, K. C. Schreiber, and J. Corse, *J. Am. Chem. Soc.*, **74**, 1113 (1952).

5) a) H. C. Brown, "The Transition State," Special Publication No. 16, The Chemical Society, London, 1962, p. 140 ff.; b) H. C. Brown, K. J. Morgan, and F. J. Chloupek, *J. Am. Chem. Soc.*, **87**, 2137 (1965); c) H. C. Brown, R. Bernheimer, C. J. Kim, and S. E. Scheppele, *ibid.*, **89**, 370 (1967); d) H. C. Brown and C. J. Kim, *ibid.*, **90**, 2082 (1968).

6) a) C. J. Lancelot and P. v. R. Schleyer, *J. Am. Chem. Soc.*, **91**, 4291 (1969); b) *ibid.*, **91**, 4296 (1969); c) C. J. Lancelot, J. J. Harper, and P. v. R. Schleyer, *ibid.*, **91**, 4294 (1969); d) P. v. R. Schleyer and C. J. Lancelot, *ibid.*, **91**, 4297 (1969); e) J. M. Harris, F. L. Schadt, P. v. R. Schleyer, and C. J. Lancelot, *ibid.*, **91**, 7508 (1969); f) D. J. Raber, J. M. Harris, and P. v. R. Schleyer, *ibid.*, **93**, 4829 (1971); g) H. C. Brown, C. J. Kim, C. J. Lancelot, and P. v. R. Scheleyer, *ibid.*, **92**, 5244 (1970); h) F. L. Schadt III, C. J. Lancelot, and P. v. R. Schleyer, *ibid.*, **100**, 228 (1978).

7) a) H. C. Brown and C. J. Kim, *J. Am. Chem. Soc.*, **93**, 5765 (1971); b) C. J. Kim and H. C. Brown, *ibid.*, **94**, 5051 (1972).

8) S. Saito, T. Yabuki, T. Moriwake, and K. Okamoto, *Bull. Chem. Soc. Jpn.*, **46**, 1795 (1973).

9) S. Saito, T. Yabuki, T. Moriwake, and K. Okamoto, *Bull. Chem. Soc. Jpn.*, **51**, 529 (1978).

10) S. Saito, K. Doihara, T. Moriwake, and K. Okamoto, *Bull. Chem. Soc. Jpn.*, **51**, 1565 (1978).

11) S. Saito, T. Moriwake, K. Takeuchi, and K. Okamoto, *Bull. Chem. Soc. Jpn.*, **51**, 2634 (1978).

12) See Table XI in Ref. 2; see also Ref. 7.

13) a) D. J. Cram, *J. Am. Chem. Soc.*, **74**, 2137 (1952); b) J. E. Nordlander and W. J. Kelly, *ibid.*, **91**, 996 (1969).

14) G. Zweifel and H. C. Brown, *Org. React.*, **13**, 1 (1963).

15) R. S. Tipson, *J. Org. Chem.*, **9**, 235 (1944); see also, H. C. Brown and G. Ham, *J. Am. Chem. Soc.*, **78**, 2735 (1956).

16) S. Winstein, E. Clippinger, A. H. Fainberg, R. Heck, and G. C. Robinson, *J. Am. Chem. Soc.*, **78**, 328 (1956).

Solvolysis in Carboxamides. VII.[1] Carboxamide Solvolysis of *threo*-2-Aryl-1-methylpropyl Brosylates. Reactivity-Selectivity Relationships as a Mechanistic Probe

Seiki SAITO,* Kenji DOIHARA, Toshio MORIWAKE, and Kunio OKAMOTO**

Department of Synthetics Chemistry, School of Engineering, Okayama University, Tsushima, Okayama 700
***Department of Hydrocarbon Chemistry, Faculty of Engineering, Kyoto University, Sakyo-ku, Kyoto 606*

(Received December 1, 1978)

Solvolysis of a series of *threo*-2-aryl-1-methylpropyl brosylates (*p*-MeO, *p*-Me, H, *p*-Cl, *m*-Cl, *m*-CF_3, and *p*-NO_2; **1a**—**g**) has been carried out in four carboxamides, *N*-methylformamide (NMF), *N*-methylacetamide (NMA), *N*,*N*-dimethylformamide (DMF), and *N*,*N*-dimethylacetamide (DMA), as solvent. Fractions of k_s and Fk_Δ pathway were determined on the basis of the upward drift from the Hammett plot of the rate constant (k_t); the extra acceleration by *p*-MeO and *p*-Me substituents was assigned to the Fk_Δ fraction. The Fk_Δ/k_t values were not in agreement with the amount of retained products (*threo*-acetate and *threo*-alcohol) obtained in NMA and DMA solvolysis of **1a**—**c**, although they should be in line with each other on the basis of the bridged-ion theory. The C(2)-deuterated phenyl derivative (**1c**-2-*d*) was solvolyzed in NMF, NMA, and DMF to give retained carboxylates (acetate or formate). However, the isotope scrambling at C(2) and C(1) of the carboxylates is incomplete, indicating that a symmetrical ion, such as a phenyl-bridged ion, can not be the intermediate of the carboxamide solvolysis. A good correlation of log k_t for substrates (**1a**—**g**) with log (% *threo*-acetate/% *erythro*-acetate) or with log (% *threo*-acetate/% olefinic products) was found for solvent systems such as NMA, DMA, and acetic acid, indicating that the reactions of all substituted substrates can be explained by intervention of a common intermediate [R^+X^-], a classical tight ion-pair from which the final products are derived. Such reactivity-selectivity relationship also holds between log k_t's of **1c** in a series of carboxamide and logarithms of *threo-erythro* ratio in acetate or formate. Through-space interaction between a face of aryl ring and carbenium ion center in the transition state is considered as a possible cause for the anomalous acceleration by the activating aryl groups.

Although a phenyl-bridged ion has been postulated as an intermediate in acetolysis of diastereomeric 2-aryl-1-methylpropyl tosylates accounting for remarkably high stereospecificity of the substitution,[2] the rate enhancement expected in such participation phenomena is not significant in this system.[3] This apparent discrepancy between rate and product stereochemistry has long been a subject of dispute.[4-16]

Brown and Kim[7a] carried out acetolysis of a series of ring substituted *threo*-1-methyl-2-phenylpropyl brosylates and found that this system displays excellent rate-(retained)product correlation. They pointed out that the nature of the k_s pathway in the acetolysis can be recongnized as S_N1 mechanism, and proposed the following mechanism (Scheme 1)[7a] in which the reaction proceeds *via* a tight ion-pair followed by k_p and k_2 processes, denoting aryl-assisted and aryl-unassisted pathways, respectively.

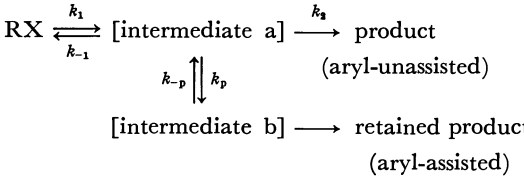

Scheme 1.

Schleyer and his collaborators[6] suggested that solvolysis of all primary and most of secondary β-arylalkyl systems proceeds through discrete aryl-assisted (k_Δ) and/or aryl-unassisted, *i.e.*, nucleophilically solvent-assisted (k_s), pathways (dual mechanism, Scheme 2).[6h] They considered the rate enhancement due to activated phenyl groups to result from the incursion of the k_Δ process with a phenyl-bridged ion, and the substrate containing a deactivated phenyl group to be a good model for the anchimerically unassisted route (k_s). They showed that the values of Fk_Δ/k_t determined independently from the rate data and product stereochemistry (rate-product correlation) are in agreement with each other for several β-arylalkyl solvolyses.[4]

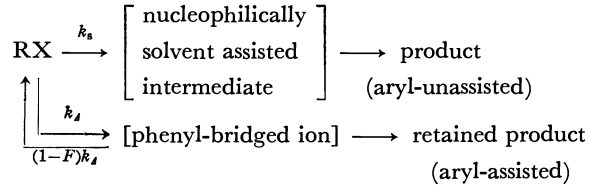

Scheme 2.

In our effort to scrutinize the nature of carboxamide solvolysis of secondary substrates,[1,17-20] it was found that solvolysis of *threo*-1-methyl-2-phenylpropyl brosylate (**1c**)[20] and that of its *p*-methoxyphenyl derivative (**1a**)[1] in *N*,*N*-dimethylacetamide (DMA) are represented respectively by 100% k_s and 83% k_Δ (17% k_s) solvolysis in the k_Δ-k_s dissection method.[6] However, on the basis of the lack of rate-product correlation, and from an examination of deuterium distribution in the reaction products or unchanged starting brosylates and the nature of the olefinic products, it was disclosed that the solvolysis of these 1-methyl-2-phenylpropyl systems proceeds without intervention of a phenyl-bridged ion but a classical tight ion-pair intermediate, subsequent processes such as *E*1 reaction, phenyl- or hydride-shift, and solvent capture occurring competitively (Scheme 3).[1,20]

In order to obtain further information on such mechanism, we extended the investigation to a series of ring substituted *threo*-1-methyl-2-phenylpropyl brosylates (**1a**—**g**) and other carboxamide solvents such as

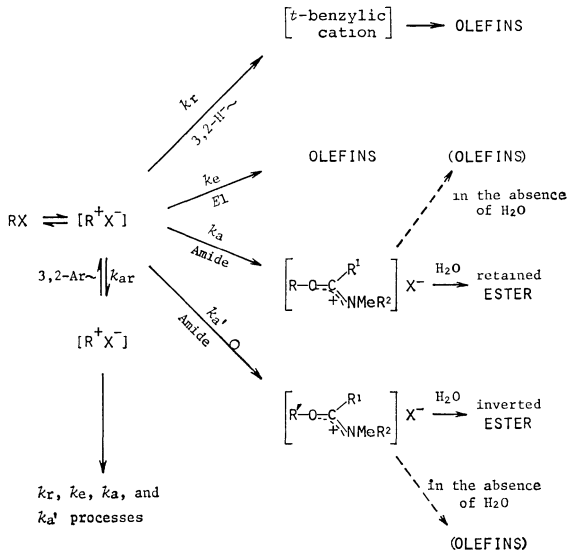

Scheme 3.

N-methylformamide (NMF), *N*-methylacetamide (NMA), and *N*,*N*-dimethylformamide (DMF).

The present paper describes the results of the examinations of the Hammett correlation for the solvolysis of **1a**—**g** in NMF, NMA, and DMF as solvent, the product distribution in NMA and DMA solvolyses, deuterium distribution in the products for NMF, NMA, and DMF solvolyses of C(2)-deuterated parent phenyl derivative (**1c**-2-*d*), and the reactivity-selectivity relationships. The mechanistic implications of the results, especially in the light of classical solvolysis mechanism, are also discussed.

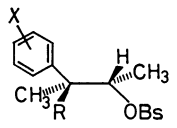

1a R=H, X=*p*-MeO
1b R=H, X=*p*-Me
1c R=H, X=H
1c-2-*d* R=D, X=H
1d R=H, X=*p*-Cl
1e R=H, X=*m*-Cl
1f R=H, X=*m*-CF_3
1g R=H. X=*p*-NO_2

Results and Discussion

Unsatisfactory Rate-product Correlation. First-order rate constant (k_t) for the respective carboxamide solvolyses (NMF, NMA, and DMF) of the substrates **1a**—**g** have been determined titrimetrically.[19,20] The results are summarized in Table 1. The Hammett plot for each carboxamide solvolysis, including DMA solvolysis,[1,20] is given in Fig. 1.

A satisfactory linear correlation holds solely for the substrates containing deactivating and, partly, activating phenyl groups with ρ-values, −0.69, −0.64, −0.57,

Table 1. Kinetic data for the solvolysis of *threo*-2-aryl-1-methylpropyl brosylates **1a**—**g** in various carboxamides

Amide	Substituent	$10^5 k_t$/s^{-1}[b]				$\Delta H^{\ddagger}$[c]/*A*	$\Delta S^{\ddagger}$[d]/*B*
		25.0 °C[e]	50.0 °C	75.0 °C	100.0 °C		
DMF	*p*-MeO	0.327	6.25	78.1		21.3	−11.7
	p-Me	0.0187		7.64	84.4	24.2	−8.2
	H	0.0138		4.79	49.5	24.1	−11.0
	p-Cl	0.00794		2.81	29.3	24.2	−11.9
	m-Cl	0.00764		2.65	27.4	24.1	−12.2
	m-CF_3	0.00622		2.48	27.1	25.1	−10.7
	p-NO_2	0.00372		1.63	18.5	25.4	−10.4
NMA	*p*-MeO	1.15[f]	25.7	371		23.2	−3.2
	p-Me	0.0575	1.78	33.6		25.7	−1.0
	H	0.0381	1.06	18.1		24.8	−4.7
	p-Cl	0.0205		8.92	101	24.4	−7.1
	m-Cl	0.0192		8.26	93.1	24.4	−7.4
	m-CF_3	0.0170		7.07	78.7	24.3	−8.1
	p-NO_2	0.00875		4.13	48.3	24.8	−7.7
NMF	*p*-MeO	3.27[f] 13.0[g]	72.3	1020		23.1	−1.6
	p-Me	0.246	6.49	107		24.4	−2.2
	H	0.0735	2.17	38.5		25.1	−2.3
	p-Cl	0.0399		16.3	180	24.2	−6.7
	m-Cl	0.0267	0.743	12.8		24.8	−5.3
	m-CF_3	0.0245	0.680	11.7		24.8	−5.5
	p-NO_2	0.0155		6.79 3.95[h]	29.8[i]	24.4	−7.8

a) [ROBs]=0.075 mol/dm^3; [C_5H_5N]=0.077 mol/dm^3; [H_2O]=0.003 (for DMF), 0.01 (for NMA), or 0.02 (for NMF) mol/dm^3. b) Mean deviations for k_t's are ±2%. c) At 25.0 °C; A=4.184 kJ/mol. d) At 25.0 °C; B=4.184 J/K mol. e) Extrapolated from data at other temperatures. f) Determined at 25.0 °C. g) Determined at 35.0 °C. h) Determined at 70.0 °C. i) Determined at 90.0 °C.

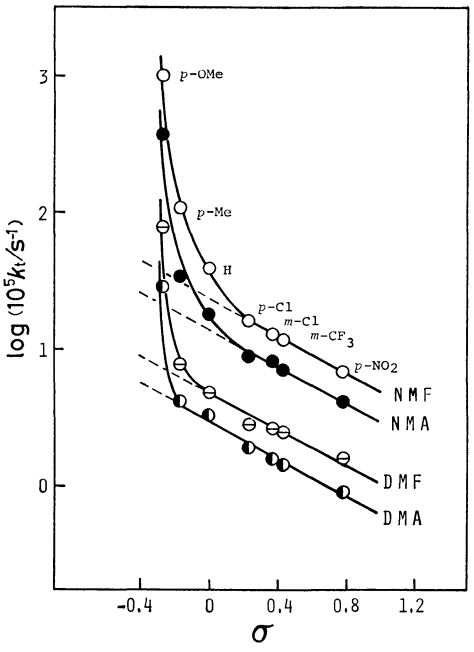

Fig. 1. Plot of log k_t (**1a**—**g**) for the carboxamide solvolysis *vs.* σ at 75 °C; ρ-value and correlation coefficient for DMA, DMF, NMA, and NMF are −0.72 and 0.991, −0.57 and 0.974, −0.64 and 0.986, and −0.69 and 0.999, respectively; for the rate constant in DMA, see Ref. 20.

Table 2. Effect of aryl participation on the rate of solvolysis of *threo*-2-aryl-1-methylpropyl brosylates at 75 °C

Substrate	Amide	Rate const/10^{-5} s^{-1}		$100Fk_\Delta$[c] / k_t
		k_t[a]	k_s[b]	
1a (OCH_3)	DMA[d]	28.8	4.77	83
	DMF	78.1	6.17	92
	NMA	371	19.6	95
	NMF	1020	35.5	97
1b (CH_3)	DMA[d]	4.15	4.15	0
	DMF	7.64	5.43	29
	NMA	33.6	16.9	50
	NMF	107	30.4	72
1c (H)	DMA	3.34	3.34	0
	DMF	4.79	4.79	0
	NMA	18.1	13.2	27
	NMF	38.5	23.2	40

a) Data in Table 1. b) Calculated from the least-squares line (k_s line) in Fig. 1. c) $Fk_\Delta=k_t-k_s$. d) See Ref. 20, Table 1.

and −0.72, respectively, for NMF, NMA, DMF, and DMA solvent. Such linear portions of the Hammett plot give the k_s values for **1a**—**c** by the least-squares treatment, from which the predicted amounts of retained product arising from the so-called k_Δ route was calculated by $100Fk_\Delta/k_t$, where $Fk_\Delta=k_t-k_s$. The results are given in Table 2.

The rate-(retained)product correlation is used as a probe for the dual mechanism concept and the phenyl-bridged ion intervention.[6] However, there are cases in which the agreement between the predicted and observed values is less satisfactory.[4,7] Acetolysis of a series of *threo*-2-aryl-1-methylpropyl brosylates has provided a representative example in which the agreement between the predicted and observed values is excellent.[7a]

Table 3. Comparison of the predicted and observed amounts of retained product arising from the carboxamide solvolysis of *threo*-2-aryl-1-methylpropyl brosylates at 75 °C

Substrate	Amide	Retained product yield/%	
		Predicted	Obsd
1a (OCH_3)	DMA[c]	83	67
	NMA[d]	95	91
1b (CH_3)	DMA[d]	0	16
	NMA[d]	50	43
1c (H)	DMA[e]	0	4
	NMA[d]	27	13

a) See Table 2. b) Amounts of sum of *threo*-acetate and *threo*-alcohol. c) Ref. 1. d) See Table 5. e) Ref. 20.

When the correlation was examined on the NMA and DMA solvolysis (Table 3), the results were far less satisfactory, a gap between predicted and observed values clearly existing. This suggests that a dual mechanism (Scheme 2) can not be applied to the carboxamide solvolysis; the mechanism shown in Scheme 3, postulated for the DMA solvolysis of **1a**[1] or **1c**,[20] is applicable to the NMA solvolysis and the other carboxamide solvolysis in NMF and DMF.

Incomplete Scrambling of Deuterium in the Products of Carboxamide Solvolysis of ***1c****-2*-d. In order to test whether Scheme 3, which does not need the intervention of the phenyl-bridged ion, can serve as a generalized reaction scheme in carboxamide solvolysis, the deuterium distribution in the products of the NMF, NMA, and DMF solvolysis of **1c**-2-*d* was examined by means of ^{1}H NMR spectroscopic method.[20] The results are summarized in Table 4.

Although the amounts of the retained products, *i.e.*, the sum of *threo*-ester and *threo*-alcohol, increase in the order NMF>NMA>DMF>DMA[20] in accord with the order of increase in the amount of Fk_Δ component (Table 2), the deuterium label is situated more at position C(2) than C(1) in the retained *threo*-1-methyl-2-phenylpropyl acetate or formate. This indicates that a symmetrical intermediate such as a phenyl-bridged ion is ruled out as a precursor of the retained products.

Linear Reactivity-Selectivity Relationship in Carboxamide Solvolysis. The product distribution, rearrangement, and steric course in carboxamide solvolysis can not be explained by means of the k_Δ-k_s rate treatment.[1,20] The linear reactivity-selectivity relationship[21] in the solvolysis of a series of substrates in a series of solvents has been utilized to prove the existence of a common intermediate which produces more than two products.[22] The relationship was examined for a series of the 1-methyl-2-phenylpropyl system (**1a**—**g**) independent of the k_Δ-k_s analysis.[6]

When the log k_t values are plotted against the

Table 4. Isotope distribution in the products for the carboxamide solvolysis of *threo*-1-methyl-2-phenylpropyl-2-*d* brosylate at 75 °C[a]

Product	Yield/% (Composition/%)			
	DMA[c]	DMF	NMA	NMF
Butene:				
(*Z*)-2-Ph-2- (3-H: 3-D)	54.9(82: 18)	43.5(75: 25)	43.0(74: 26)	35.5(70: 30)
(*E*)-2-Ph-2- (3-H: 3-D)	8.6(64: 36)	5.8(57: 43)	5.3(53: 47)	4.9(48: 52)
3-Ph-1- (3-D: 2-D)	6.7(100: ≈0)	7.1(87: 13)	6.2(83: 17)	4.2(80: 20)
2-Ph-1- (3-D,H: 3-H_2)	5.1(100: ≈0)	4.9(100: ≈0)	5.2(100: ≈0)	5.9(100: ≈0)
Ester:[d]				
erythro-1-Me-2-Ph-propyl (2-D: 1-D)	21.0(87: 13)	26.3(82: 19)	22.9(80: 20)	17.3(75: 25)
threo-1-Me-2-Ph-propyl (2-D: 1-D)	3.7(65: 35)	6.6(60: 40)	16.5(55: 45)	23.2(53: 47)
Alcohol:[e]				
erythro-3-Ph-2-butanol	trace	4.1	0.5	3.6
threo-3-Ph-2-butanol	0	1.7	0.4	5.4[f]

a) [**1c**-2-*d*]=0.075 mol/dm³; [C_5H_5N]=0.077 mol/dm³; [H_2O]=0.17 mol/dm³. b) Accuracy for NMR measurement of isotopic content was ≲1%; reproducibility=±3%. c) Ref. 20. d) Acetate for DMA or NMA and formate for DMF or NMF. e) Deuterium distribution not determined unless otherwise noted. f) The ratio 3-D: 2-D=55: 45.

Table 5. Rates and product distributions for the DMA and NMA solvolysis of *threo*-2-aryl-1-methylpropyl brosylates at 75 °C[a]

Substrate	Amide	k_t[b] / 10^{-5} s^{-1}	Product yield/%			
			Olefins	Acetate		Alcohol
				erythro	*threo*	
1a	DMA[c]	28.8	29.7	2.6	60.1	7.6
	NMA	371	8.6	0.3	79.4	11.7[e]
1b	DMA	4.15	72.0	10.4	13.4	4.2
	NMA	33.6	48.3	6.7	35.5	9.5[f]
1c	DMA[d]	3.34	83.2	13.3	2.4	1.1
	NMA	18.1	62.3	18.6	9.8	9.3[g]
1d	DMA	1.90	—	(87.6	12.4)[h]	—
1e	DMA	1.59	—	(89.4	10.6)[h]	—
	NMA	8.26	68.9	28.9	1.1	1.1[i]
1f	DMA	1.44	72.5	25.2	1.5	0.8[i]
	NMA	7.07	70.9	28.5	0.6	trace
1g	DMA	0.916	71.0	28.5	0.5	trace
	NMA	4.13	68.3	31.5	0.2	trace

a) [ROBs]=0.075 mol/dm³; [C_5H_5N]=0.077 mol/dm³; [H_2O]=0.17 for DMA and 0.34 mol/dm³ for NMA. b) See Table 1 for NMA; Ref. 20 for DMA. c) Ref. 1. d) Ref. 20. e) *threo*: *erythro*=99.6: 0.4. f) *threo*: *erythro*=81.4: 18.6. g) *threo*: *erythro*=44.1: 55.9. h) Isomer composition. i) Isomer composition not determined.

logarithms of the ratio (% yield of the retained acetate: % yield of the inverted acetate) or (% yield of the retained acetate: % yield of the olefinic products) for the DMA or NMA solvolysis of a series of *threo*-2-aryl-1-methylpropyl brosylates, a good reactivity-selectivity relationship was found. The results are shown in Figs. 2.1, 2.2 with use of the data in Table 5.

The linear relationships observed between log k_t and log (% *threo*-ROAc/% olefin) suggest that such processes as k_a, k_r, and k_e, (Scheme 3) result from a single intermediate [R^+X^-]. The proposed classical *E*1-S_N1 competition mechanism is substantiated from the carboxamide solvolysis.

An examination of these treatments was also carried out for the log k_t's of the acetolysis of a series of *threo*-2-aryl-1-methylpropyl brosylates using the data of Brown and Kim.[7a] As in the case of the DMA or NMA, solvolysis, excellent linear relationships were observed (Fig. 3), indicating that even for the acetolysis, in which the rate-(retained)product correlation satisfactorily holds the reaction proceeds through a single intermediate, the open ion-pair (Scheme 1).

When the log k_t values of the brosylate **1c** in a series of amide solvents are plotted against the logarithm of the ratio (% yield of the retained ester: % yield of the inverted ester), an excellent linear relationship is observed (Fig. 4, correlation coefficient=0.990). Pertinent data for the test are given in Table 6.

On the basis of this linear relationship, it is deduced that both the retained and inverted esters stem from a

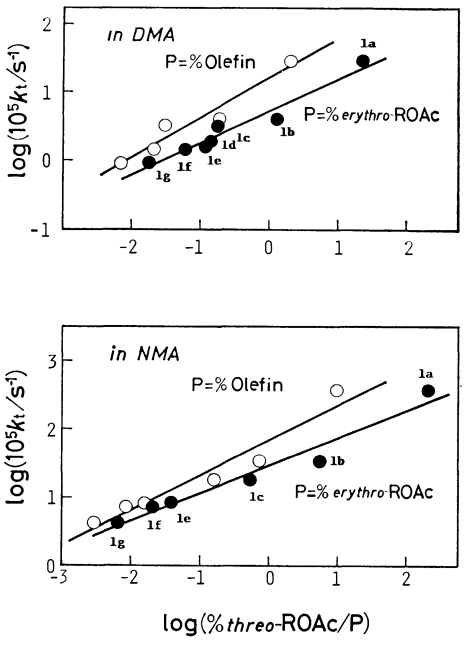

Fig. 2. Linear reactivity-selectivity relationship between log k_t and log (% *threo*-acetate/% *erythro*-acetate) or log (% *threo*-acetate/% olefin) for the DMA (upper) and NMA (bottom) solvolyses of *threo*-2-aryl-1-methylpropyl brosylates at 75 °C; correlation coefficient=0.976 (P=% *erythro*-acetate, DMA), 0.970 (P=% olefin, DMA), 0.981 (P=% *erythro*-acetate, NMA), and 0.969 (P=% olefin, NMA).

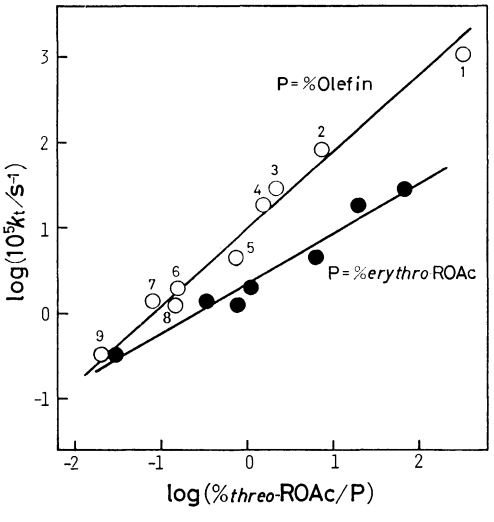

Fig. 3. Linear reactivity-selectivity relationships between log k_t and log (% *threo*-acetate/% *erythro*-acetate) or log (% *threo*-acetate/% olefin) for the acetolysis of *threo*-2-aryl-1-methylpropyl brosylates at 75 °C (data from Ref. 7a); 1=**1a**, 2=**1b**, 3=*m*-MeC_6H_4- derivative, 4=**1c**, 5=**1d**, 6=**1e**, 7=**1f**, 8=*p*-$CF_3C_6H_4$- derivative, and 9=**1g**; correlation coefficient=0.982 (P=% *erythro*-acetate) and 0.991 (P=% olefin).

single solvolytic species, a tight ion-pair intermediate, as shown in Scheme 3. The *threo*-type imidatonium ion (retained), which leads to *threo*-ester by hydrolysis, is formed by the front-side attack of the carboxamide on the tight ion-pair. A front-side solvent capture may

Table 6. Solvolysis rates and retention/inversion ratios for the carboxamide solvolysis of *threo*-1-methyl-2-phenylpropyl brosylate **1c** at 75 °C

Amide	$\frac{k_t}{10^{-5}\,s^{-1}}$ [a]	Yield of *threo* ester [b]	Ratio $\left(\frac{\text{retention}}{\text{inversion}}\right)$
DMA [c]	3.34	2.4%	0.179
DMF [d]	4.79	4.5%	0.251
NMA [e]	18.1	9.8%	0.526
NMF [d]	38.5	19.9%	1.18

a) See Table 1. b) Acetate for DMA or NMA and formate for DMF or NMF. c) Ref. 20. d) The solvolysis was conducted under the same conditions as those described in Ref. 20. e) See Table 5.

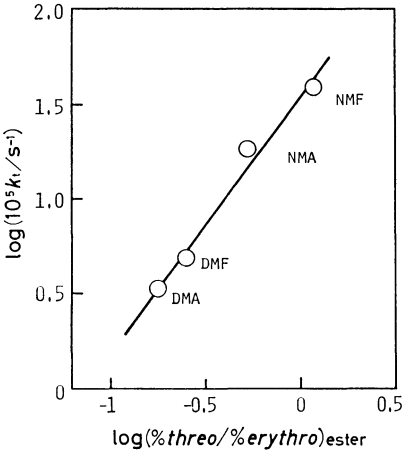

Fig. 4. Linear reactivity-selectivity relationship between log k_t and log (% *threo*-ester/% *erythro*-ester) for the carboxamide solvolysis of **1c** at 75 °C; correlation coefficient=0.990.

have an advantage over a rear-side solvent capture when the rate of 2,1-phenyl migration becomes fast enough to shield the rear-side effectively. Thus, as the selectivity increases on going from DMA solvolysis to NMF solvolysis (Table 6), the extent of deuterium scrambling in the ester products becomes greater (Table 4). This might explain why the DMF solvolysis produces retained ester in a larger amount with more scrambling of the deuterium label than the DMA solvolysis (Table 4). The dual mechanism (Scheme 2) gives no explanation.

Possible Origin of the Rate Enhancement. From a kinetic point of view, there is another mechanistic feature for the solvent effect on the carboxamide solvolyses. When the log k_t values for the NMF, NMA, and DMF solvolysis, or the acetolysis[7a] of a series *threo*-2-aryl-1-methylpropyl brosylates **1a**—**g** are plotted against those for the DMA solvolysis,[20] satisfactory linear free-energy relationships are observed (Fig. 5): correlation coefficients are 0.988, 0.997, 0.995, and 0.971, respectively.

If the observed titrimetric rate constant (k_t) is represented by the sum of two independent processes, k_s and Fk_Δ, no such linear correlation would hold. Consequently, the deviation of the points for the

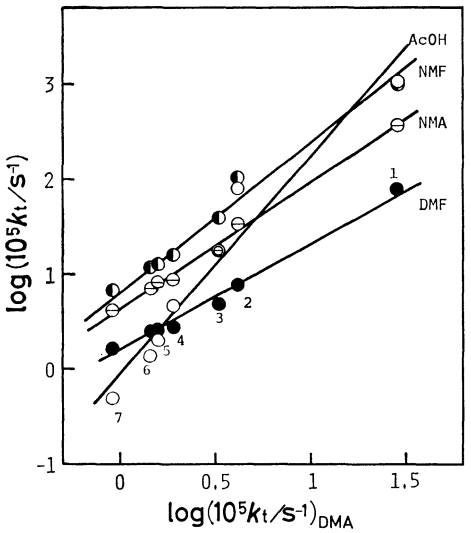

Fig. 5. Linear free-energy relationships between log k_t (DMA) and log k_t (DMF (●), NMA (⊖), NMF (◐), or AcOH (○)) for **1a**—**g** (1=**1a**, 2=**1b**, 3=**1c**, 4=**1d**, 5=**1e**, 6=**1f**, and 7=**1g**) at 75 °C; slope and correlation coefficient are 1.11 and 0.995 (DMF), 1.29 and 0.997 (NMA), 1.47 and 0.988 (NMF), and 2.27 and 0.971 (AcOH); for the rate constants in DMA and AcOH, see Refs. 20 and 7a, respectively.

substrates containing activating phenyl groups in the Hammett plot (Fig. 1) should be attributed to cause other than the intrusion of the Fk_Δ component and of the phenyl-bridged ion.

According to Tabushi *et al.*,[23] the remarkable rate enhancement is observed in the solvolysis of pseudo-axial system of [2.2.2]paracyclophane derivative (**2**) in which the developing carbenium ion center can advantageously interact with the face of benzene ring through space; solvolysis rate of the pseudo-axial substrate was accelerated by a factor of $10^{14.7}$ as compared with corresponding pseudo-equatorial substrate. The same type of interaction, therefore, might be operative between the β-aryl group and the carbenium ion center. The proposal is, however, qualitative. Confirmation of the cause of the deviation in the Hammett plot (Fig. 1) would be achieved by a precise estimation of the intrinsic magnitude of such a transannular interaction between the individual β-aryl group and a p-orbital of the cationic carbon in the transition state.

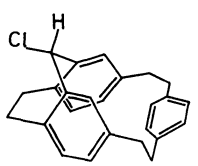

2

In conclusion, the mechanism which formulates the initial ionization as formation of tight ion-pair (open or classical), followed by a variety of competing processes (k_r, k_e, k_a, k_a', and k_{ar} pathways, Scheme 3), can explain the results of carboxamide solvolysis. This is essentially the same as that proposed by Brown *et al.*[5b] No intervention of a phenyl-bridged ion is necessary for the carboxamide solvolysis.

Experimental

The four carboxamides were purified in the same way as described.[18] The substrates **1a**—**g** and **1c**-2-*d* were the products from the same lot employed in the previous work; product analysis and deuterium distribution analysis were performed in the same manner as reported.[20] Kinetic measurements were carried out following the method described previously.[19]

References

1) S. Saito, K. Doihara, T. Moriwake, and K. Okamoto, submitted for publication in *Bull. Chem. Soc. Jpn.*, **52**, 2356 (1979): Part VI.

2) a) D. J. Cram, *J. Am. Chem. Soc.*, **71**, 3863 (1949); b) D. J. Cram, *ibid.*, **74**, 2129 (1952).

3) S. Winstein, B. K. Morse, E. Grunwald, K. C. Schreiber, and J. Corse, *J. Am. Chem. Soc.*, **74**, 1113 (1952).

4) For a leading review, see C. J. Lancelot, D. J. Cram, and P. v. R. Schleyer in "Carbonium Ions," ed by G. A. Olah and P. v. R. Schleyer, Wiley-Interscience, New York, N. Y. (1972), Vol. 3, Chap. 27.

5) H. C. Brown, "The Transition State," Special Publication No. 16, The Chemical Society, London, 1962, p. 140 ff.; b) H. C. Brown, K. J. Morgan, and F. J. Chloupek, *J. Am. Chem. Soc.*, **87**, 2137 (1965); c) H. C. Brown, R. Bernheimer, C. J. Kim, and S. E. Scheppele, *ibid.*, **89**, 370 (1967); d) H. C. Brown and C. J. Kim, *ibid.*, **90**, 2082 (1968).

6) a) C. J. Lancelot and P. v. R. Schleyer, *J. Am. Chem. Soc.*, **91**, 4291 (1969); b) C. J. Lancelot and P. v. R. Schleyer, *ibid.*, **91**, 4296 (1969); c) C. J. Lancelot, J. J. Harper, and P. v. R. Schleyer, *ibid.*, **91**, 4294 (1969); d) P. v. R. Schleyer and C. J. Lancelot, *ibid.*, **91**, 4297 (1969); e) J. M. Harris, F. L. Schadt, P. v. R. Schleyer, and C. J. Lancelot, *ibid.*, **91**, 7508 (1969); f) D. J. Raber, J. M. Harris, and P. v. R. Schleyer, *ibid.*, **93**, 4829 (1971); g) H. C. Brown, C. J. Kim, C. J. Lancelot, and P. v. R. Schleyer, *ibid.*, **92**, 5244 (1970); h) F. L. Schadt III, C. J. Lancelot, and P. v. R. Schleyer, *ibid.*, **100**, 228 (1978).

7) a) H. C. Brown and C. J. Kim, *J. Am. Chem. Soc.*, **93**, 5765 (1971); b) C. J. Kim and H. C. Brown, *ibid.*, **94**, 5051 (1972).

8) a) D. J. Cram, *J. Am. Chem. Soc.*, **86**, 3767 (1964); b) D. J. Cram and J. A. Thompson, *ibid.*, **89**, 6766 (1967); **91**, 1778 (1969).

9) B. G. Ramsey and N. K. Das, *J. Am. Chem. Soc.*, **94**, 4233 (1972).

10) J. A. Cramer and J. G. Jewett, *J. Am. Chem. Soc.*, **94**, 1377 (1972).

11) A. Diaz, I. Lazdins, and S. Winstein, *J. Am. Chem. Soc.*, **90**, 6546 (1968).

12) M. D. Bentley and M. J. S. Dewar, *J. Am. Chem. Soc.*, **90**, 1075 (1968).

13) J. E. Nordlander and W. G. Deadman, *J. Am. Chem. Soc.*, **90**, 1590 (1968).

14) R. J. Jablonski and E. I. Snyder, *Tetrahedron Lett.*, **1968**, 1103.

15) M. G. Jones and J. L. Coke, *J. Am. Chem. Soc.*, **91**, 4284 (1969).

16) J. B. Lambert, H. Wayne, and E. S. Magyar, *J. Am. Chem. Soc.*, **99**, 3059 (1977).

17) S. Saito, T. Yabuki, T. Moriwake, and K. Okamoto, *Bull. Chem. Soc. Jpn.*, **46**, 1795 (1973).

18) S. Saito, T. Yabuki, T. Moriwake, and K. Okamoto, *Bull. Chem. Soc. Jpn.*, **51**, 529 (1978).

19) S. Saito, T. Moriwake, K. Takeuchi, and K. Okamoto, *Bull. Chem. Soc. Jpn.*, **51**, 2634 (1978).
20) S. Saito, K. Doihara, T. Moriwake, and K. Okamoto, *Bull. Chem. Soc. Jpn.*, **52**, 1487 (1979).
21) R. A. Sneen, J. V. Carter, and P. S. Kay, *J. Am. Chem. Soc.*, **88**, 2594 (1966).
22) a) J. M. Harris, J. F. Fagan, F. A. Walden, and D. C. Clark, *Tetrahedron Lett.*, **1972**, 3023; b) J. M. Harris, A. Becker, D. C. Clark, J. F. Fagan, F. A. Walden, and S. L. Kennan, *ibid.*, **1973**, 3813; c) J. M. Harris, D. C. Clark, A. Becker, and J. F. Fagan, *J. Am. Chem. Soc.*, **96**, 4478 (1974); d) J. M. Harris, A. Becker, J. F. Fagan, and F. A. Walden, *ibid.*, **96**, 4484 (1974); e) K. Okamoto and T. Kinoshita, *Chem. Lett.*, **1974**, 1037; f) A. Pross, *Tetrahedron Lett.*, **1975**, 637; g) A. Pross and R. Koren, *ibid.*, **1975**, 3613; h) H. Aronovitch and A. Pross, *J. Chem. Soc., Perkin Trans. 2*, **1978**, 540; i) Y. Karton and A. Pross, *ibid.*, **1978**, 595; j) D. J. Raber, J. M. Harris, R. E. Hall, and P. v. R. Schleyer, *J. Am. Chem. Soc.*, **93**, 4821 (1971); k) A. Pross in "Advances in Physical Organic Chemistry," ed by V. Gold and D. Bethell, Academic Press, New York, N. Y. (1977), Vol. 14, pp. 69—132; l) V. B. Griese, *Angew. Chem.*, **89**, 162 (1977); see also Refs. 9 and 10.
23) I. Tabushi, Z. Yoshida, and F. Imashiro, *J. Am. Chem. Soc.*, **98**, 5709 (1976).

Effect of Complexation by Crown Ethers on Anisochrony of Diastereotopic Groups in NMR Spectra

Nobuharu ANDO, Yukio YAMAMOTO, Jun'ichi ODA, and Yuzo INOUYE*

Institute for Chemical Research, Kyoto University, Uji, Kyoto 611

(Received November 20, 1978)

Anisochrony of geminal methyls in alkylamines bearing a chiral center in the molecule is affected by complexation with crown ethers, which amplify the chemical shift non-equivalence in NMR. The resolved signal of *gem*-methyls in valine methyl ester were unequivocally assigned to *pro-R* and *pro-S* methyl groups respectively.

In principle, different NMR chemical shifts are to be expected for diastereotopic groups, since they experience different molecular environments. However, these groups, particularly in acyclic compounds, are often accidentally isochronous because of the practically close similarity of individual surroundings. This situation can often be circumvented by such techniques as to ensure improvement of resolving ability or a change in magnetic environments, probably resulting in manifestation of the latent anisochrony. For example, the application of a higher magnetic field,[1] a change in the solvent medium, and use of NMR shift reagents[2] have generally been employed for this purpose.

Crown ethers have recently been introduced to organic chemistry and proved to be versatile from the viewpoint of both synthetic and mechanistic utilities.[3] Complexation with primary ammonium salt is one of the most important properties of crown ethers.

We now describe the notable effect of crown ethers on anisochrony of diastereotopic groups in amino compounds owing to complexation. Crown ethers were found to realize the potential anisochrony and amplify the chemical shift non-equivalence of paired ligands in alkylamines.

In alkylamines **1** and **2**, the signals for *gem*-methyls were unresolved in the form of free amine, but non-equivalence was observed in the hydrochloride; the chemical shift difference, 0.01 ppm for **1** and 0.02 ppm for **2**. Complexation by 18-crown-6 enhanced the difference up to 0.06 ppm, which probably arised from decrease in conformational mobility and/or the shielding effect of the crown ether. In complexes with dibenzo-18-crown-6, the $\Delta\delta$ value varied in a characteristic way depending on the length of the methylene chain, which may be ascribed to the benzene ring-currents. The chemical shift differences between *gem*-methyls were no longer observed for **3** at any state.

Amino acid esters were also of our great concern from the viewpoint of anisochrony of diastereotopic groups. In contrast to alkylamines, methyl doublets of valine methyl ester (**4**) were unresolved in the hydrochloride, whereas those of the free amine were resolved with $\Delta\delta$ of 0.07 ppm. Here again, a significant difference was caused by complexation with 18-crown-6; 0.14 ppm. The chemical shift difference was furthermore magnified in the case of dibenzo-18-crown-6, 0.22 ppm.

Non-equivalence was not observed in the spectra of leucine methyl ester in any form except for the dibenzo-18-crown-6 complex, for which a significant but rather small $\Delta\delta$ of 0.04 ppm was observed. In ^{13}C-NMR measurements, chemical shift differences of leucine methyl ester were enhanced in the order of the hydrochloride, the free amine, and the complex with 18-crown-6; 0.5, 1.2, and 1.4 ppm, respectively, which was also the case in ^{1}H-NMR of **4**.

In order to assign the resolved signals of *gem*-methyls in **4** ^{1}H-NMR spectra were investigated in every form of isoleucine (**5**) and alloisoleucine (**6**) methyl esters, whose configurations were unambiguously established. For the hydrochloride, the spectral feature of **5** and **6** very much resembled each other, and both of them can not be distinguished by ^{1}H-NMR. Liberation from the hydrochloric salt caused a slight variation in spectra and the complexes with the crown ether showed quite a remarkable difference over the methyl region between the two isomeric amino acid esters. The chemical shift differences of the methyl groups of **5** and **6**, corresponding to R^2 and R^1 respectively, were enhanced as one

Table 1. Chemical shifts,[a,b] δ of methyl doublets in alkylamine

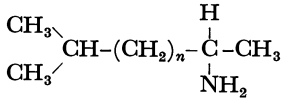

Compound	n	Free amine	Hydrochloride	18-Crown-6 complex[c]	Dibenzo-18-crown-6 complex[c]
1[d]	0	0.89(0.00)	$\begin{matrix}0.98\\0.97\end{matrix}$(0.01)	$\begin{matrix}1.01\\0.95\end{matrix}$(0.06)	$\begin{matrix}0.63\\0.59\end{matrix}$(0.04)
2	1	0.88(0.00)	$\begin{matrix}0.92\\0.90\end{matrix}$(0.02)	$\begin{matrix}0.97\\0.91\end{matrix}$(0.06)	$\begin{matrix}0.70\\0.56\end{matrix}$(0.14)
3	2	0.89(0.00)	0.88(0.00)	0.89(0.00)	0.80(0.00)

a) The coupling constant has a value of about 6—7 Hz.
b) The value in parentheses represents the chemical shift difference ($\Delta\delta$, ppm).
c) The ratio of substrate/crown ether in $CDCl_3$ is 1.0 ± 0.1 (except for **3**; 4.0).
d) For "hydrochloride in $CDCl_3$," the chemical shift difference was 0.01 ppm.

Table 2. Chemical shifts,[a,b] δ, of methyl doublets in amino acid ester

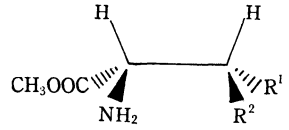

Compound	R^1	R^2	Free amine	Hydrochloride	18-Crown-6 complex[c]	Dibenzo-18-crown-6 complex[c]
4	CH_3	CH_3	0.97 0.90(0.07)	1.04(0.00)	1.11 0.97(0.14)	0.77 0.55(0.22)
5	C_2H_5	CH_3	0.94 0.82(0.12)	1.00 0.98(0.02)	0.95 1.09(0.14)	0.56 0.78(0.22)
6[d]	CH_3	C_2H_5				
7	OCH_3	CH_3	1.23 1.12(0.11)	1.32 1.26(0.06)	1.29 1.33(0.04)	—
8	CH_3	OCH_3				—
Leucine methyl ester			0.94(0.00)	0.96(0.00)	0.98(0.00)	0.63 0.59(0.04)
			[23.0 21.8(1.2)	24.1 23.6(0.5)	22.8 21.4(1.4)][e]	

a) The coupling constant has a value of about 6—7 Hz (except for leucine methyl ester, about 5—6 Hz).
b) The value in parentheses represents the chemical shift difference ($\Delta\delta$, ppm).
c) The ratio of substrate/crown ether in $CDCl_3$ is 1.0 ± 0.1.
d) For simplification's sake, the configuration is depicted here for L-alloisoleucine methyl ester, although the actual experiment was carried out on the enantiomer.
e) ^{13}C chemical shifts (δ_C, ppm from TMS).

traversed from the hydrochloride (0.02 ppm), the free amine (0.12 ppm), the 18-crown-6 complex (0.14 ppm) to the dibenzo-18-crown-6 complex (0.22 ppm), which was also in keeping with the the order found for **4**.

Since the chemical shift difference of *gem*-methyls in **4** corresponds correctly to that between methyl doublets in **5** and **6** at any state, it can be safely concluded that the substitution of ethyl for methyl groups did not make any noticeable change in the magnetic environment or the conformation.

In the spectra of free amino acid esters, the methyl doublet of **6** was located in the magnetic field higher than that of **5**. The situation was reversed in the spectra of the complexes with crown ethers. Consequently, in the presence of chirality as depicted in Table 2, R^2-methyl group was shielded more than R^1-methyl in the complexes with crown ethers. It then follows that, in the case of **4**, the methyl doublets in the higher field in the free amines and in the crown ether complexes can be safely ascribed to the *pro-S* methyl (R^1) and the *pro-R* methyl (R^2), respectively.

In order to simplify ^1H-NMR spectra in the methyl region and to ascertain the above conclusion, *O*-methylthreonine (**7**) and *O*-methylallothreonine (**8**) methyl esters were subjected to the same ^1H-NMR tests. In this case, the trend of augmentation in the chemical shift differences between R^1 and R^2 was different from that found for valine series; the 18-crown-6 complex (0.04 ppm), the hydrochloride (0.06 ppm), and the free amine (0.11 ppm). However, the same situation as in the valine series prevailed for the relative positions of signals; the methyl doublet of **8** appears at a field higher than that of **7** for the free amino esters and the reverse for 18-crown-6 complexes.

The causes of the amplified anisochrony observed for diastereotopic groups in crown ether complexes are still obscure. Since dibenzo-18-crown-6 has a well-defined shielding effect, the relative spatial position can

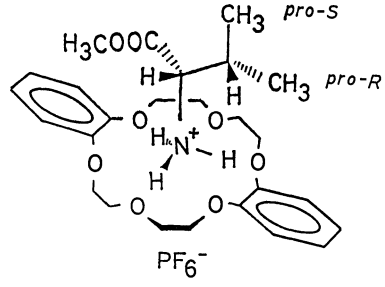

Fig. 1. The relative spatial disposition of *pro-S* and *pro-R* methyls in the valine methyl ester–dibenzo-18-crown-6 complex.

be safely allotted to the methyl groups. That is, *pro-R* methyl of valine methyl ester appearing in a higher magnetic field is disposed closer to the phenyl nuclei than the *pro-S* counterpart, as depicted in Fig. 1, which is consistent with the coupling constant of C_α–H; 4 Hz.

Enhancement of anisochrony of diastereotopic groups by complexation with crown ethers may possibly be applicable for the establishment of stereochemistry, especially of the *erythro-threo* isomerism, and may substitute partially for shift reagents in resolution of complicated spectra.

Experimental

Melting points were measured on hot plate and uncorrected. NMR chemical shifts were given as δ (ppm from TMS) in deuterochloroform (except for hydrochlorides, from DSS, in deuterium oxide) and were determined at 23 °C on a Varian EM-360 (60.00 MHz, with an error of 0.02 ppm) and/or a JEOL JNM-FX 100 (99.55 MHz for ^1H-NMR, 25.00 MHz for ^{13}C-NMR; 5 mm tube; FT conditions: acquisition time 4.1 s for ^1H-NMR, 0.68 s for ^{13}C-NMR; pulse width 38 μs (90°) for ^1H-NMR, 12 μs (90°) for ^{13}C-NMR; spectral width 1000 Hz for ^1H-NMR, 5000 Hz for ^{13}C-NMR; pulse repetition time 6.0 s for ^1H-NMR, 2.5 s for ^{13}C-NMR; number of data points 8192; number of transients 4 or 8 for ^1H-NMR,

20000 for ^{13}C-NMR; and with an error of 0.003 ppm for ^{1}H-NMR, 0.05 ppm for ^{13}C-NMR).

Material. Valine, isoleucine, alloisoleucine, and leucine methyl ester were supplied from commercial source. Esterification of amino acid was carried out according to Fischer's method. *O*-Methylallothreonine methyl ester (**8**) was prepared by the method of West[4] from crotonic acid. All the compounds were purified in the state of hydrochloride by recrystallization from ethanol–ether and the relevant data were listed in Table 3. The amines were liberated with 2 M aq sodium hydroxide just before use. All products gave satisfactory microanalyses (C=±0.80%, H=±0.27%, N=±0.33%).

Typical Procedure for Preparations of Alkylamines. 2-Amino-4-methylpentane (2): 4-Methyl-2-pentanone (20 g, 0.20 mol), sodium acetate (19.7 g, 0.24 mol) and hydroxylamine (16.7 g, 0.24 mol) were dissolved in ethanol (200 ml). After heating under reflux for 5 h, the mixture was filtered and the filtrate was evaporated and the residue was extracted with chloroform. The chloroform layer was washed with sat. aq sodium carbonate and dried over sodium sulfate. Distillation gave the oxime (bp 85—87 °C/19 Torr, 19.6 g, 85%). The oxime (19.0 g) dissolved in dry ether (50 ml) was added dropwise into lithium aluminum hydride (9.7 g) in dry ether (150 ml) and the mixture was heated under reflux for 13 h. The mixture was treated by dropwise addition of water (9.7 ml), 15% sodium hydroxide (9.7 ml), and water (29 ml) successively. The mixture was filtered and dried over sodium sulfate. The filtrate was distilled to give (**2**) (bp 112—114 °C, 6.8 g, 37%).

O-Methylthreonine Methyl Ester (7).[5] Methyl *erythro*-2-bromo-3-methoxybutyrate[4] (1.25 g, 6 mmol, bp 84—85 °C) prepared from methyl crotonate, sodium azide (0.79 g, 20 mmol), and (2,2,1)-cryptand (50 mg) were dissolved in acetonitrile (10 ml). After heating for 42 h under reflux, the mixture was filtered and the filtrate was evaporated. The residue was hydrogenated over 5% Pd–C (100 mg) in methanol (10 ml). The mixture was filtered, evaporated and then purified by passing through IR 120 B resin (2×50 cm column; About 500 ml of distilled water was passed through the column followed by effluence with 3% aqueous ammonia). The product was esterified by Fischer's method to give an amorphous solid (220 mg, 20%).

Table 3. Physical constants of amino compounds

Compound	Bp(°C)	Mp of hydrochloride (°C)
1	83—84	213
2	112—114	143
3	135—136	117—118.5
4	—	112—113
5	—	95—96.5
6	—	126
7	—	—[a]
8	—	164—165(dec)
Leucine methyl ester	—	154—154.5

a) Amorphous solid.

Method of Complexation with Crown Ether.[6] The mixture of crown ether (0.063 mmol) in deuterochloroform (0.35 ml), hydrochloride of amino compound (0.373 mmol) in deuterium oxide (0.40 ml), and lithium hexafluorophosphate (0.373 mmol) was shaken in ice bath for 5 min. After standing for about 30 min, the deuterochloroform layer was separated for spectral measurement at 60 and/or 100 MHz.

References

1) J. Reisse, R. Ottinger, P. Bickart, and K. Mislow, *J. Am. Chem. Soc.*, **100**, 911 (1978).
2) G. P. Schiemenz and H. Rast, *Tetrahedron Lett.*, **1971**, 4685; H. Kakisawa and K. Imaye, *Nippon Kagaku Kaishi*, **1973**, 1238.
3) G. W. Gokel and H. D. Durst, *Synthesis*, **1976**, 168.
4) H. D. West, G. S. Krummel, and H. E. Carter, *J. Biol. Chem.*, **122**, 605 (1937—1938).
5) Y. Nakajima, J. Oda, and Y. Inouye, *Tetrahedron Lett.*, **1978**, 3107.
6) W. D. Curtis, D. A. Laider, J. F. Stoddart, and G. H. Jones, *J. Chem. Soc., Perkin Trans. 1*, **1977**, 1756.

The Transformations of Terpene Ketones by Oxygen. II. The Base-catalyzed Autoxidation of Pulegone and Fukinone and Their Dihydro Compounds

Akio HORINAKA, Eiyu YO, Otoji MORI, and Keizo NAYA*

Department of Chemistry, Faculty of Science, Kwansei Gakuin University, Uegahara, Nishinomiya, Hyogo 662

(Received November 21, 1978)

Upon autoxidation in alkaline media, pulegone and fukinone (**2**) gave pairs of hydroxy ketones respectively as the major products; also, hydroxyeremophilone was isolated as its acetate from **2**. On the other hand, their dihydro compounds afforded hydroxy ketones, diosphenols, and acids.

It is well known that enolizable ketones are oxidized rapidly in strongly basic media. This type of autoxidation has been widely applied to the transformations of the naturally occurring terpene ketones and has produced interesting types of substances related to the biosynthesis.[1] It has been pointed out that oxygen attacks at the site of enolization—for example, 3-keto 5β- and the 5α-steroids[2] gave the oxygenation products at the C-4 and C-2 positions respectively.

Since pulegone (**1**) and fukinone (**2**),[3] together with their dihydro derivatives, (**3** and **4**), could be regarded as the logical precursors of the further oxygenated congeners, the autoxidation has been attempted in order to clarify the nature of the products thoroughly.

The autoxidation of **2** and **3** (a mixture of menthone and neomenthone) would be expected to furnish hydroxyeremophilone (**5**)[4] and buccocamphor (**7**),[5] which are found in the oil of *Eremophila mitcelli* and in the essential oils of various *Barosma* or *Mentha* species respectively. In fact, **5** was isolated, but in a poor yield, as the acetate (**6**) from the oxidation mixture. We wish now to report the base-catalyzed autoxidation of the titled compounds and the structural assignments of the products.

The oxidation was carried out under the following three conditions: a) potassium *t*-butoxide/*t*-butyl alcohol; b) potassium *t*-butoxide/*N*,*N*-dimethylformamide, and c) sodium *t*-butoxide/*t*-butyl alcohol, *N*,*N*-dimethylformamide, and tetrahydrofuran in the presence of triethyl phosphite as a reducing reagent.[6] Under the above conditions, **1** and **2** gave pairs of diastereomeric hydroxy ketones, (**8a** and **8b**) and (**9a** and **9b**) respectively. The dihydro analogues, **3** and **4**, gave also pairs of hydroxy ketones, (**10a** and **10b**) and (**11b** and **12**), besides diosphenols (**14** and (**16** and **17**)), and acids (**18** and **19**), respectively. The oxidation products are shown in Table 1, along with their yields based on the consumed starting materials. The acidic products were isolated as the methyl esters.

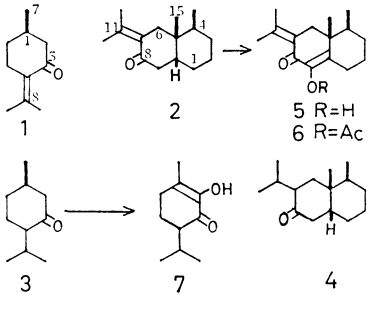

Hydroxy ketones, **8a**, **8b**, **9a**, and **9b**, were prepared independently from pulegone α- and β-epoxide,[7] and fukinone α- and β-epoxide,[8] respectively by treatment with *p*-toluenesulfonic acid in benzene.[9] They were also found as the minor products among the photosensitized oxygenation products of **1**[10] and **2**.[11] The absolute configuration of **9b** was established by X-ray analysis.[12] The saturated hydroxy ketones, **10a**, **10b**, and **11b**, were obtained by the hydrogenation of the respective hydroxy ketones, **8a**, **8b**, and **9b**. The spectral data of **10a** and **10b** were in good agreement with those given in the literature.[13] It is obvious that a hydroxy ketone, **12**, is the rearranged product from **11b** by the stereospecific acyloin rearrangement[14] in an alkaline medium, though **11b** seems to resist the rearrangement in the aprotic solvent, as in the b) condition. The **12** structure was ascertained by its conversion to the ketone (**13**), which was identical with the authentic sample prepared from **4**.[3] On the other hand, the isomeric hydroxy ketone (**11a**) appears to undergo further oxidation without the subsequent rearrangement.

The diosphenol, **14**, was positive to a ferric chloride test (black color), exhibiting an UV maximum at 275 nm and a broad IR band at 1670 cm^{-1} characteristic

TABLE 1. YIELDS OF OXIDATION PRODUCTS DEPENDING ON THE REACTION CONDITIONS

Condition	Compounds											
	Pulegone (**1**)		Fukinone (**2**)		Dihydropulegone (**3**)				Dihydrofukinone (**4**)			
	Products											
	8a+**8b**	**8a**/**8b**	**9a**+**9b**	**9a**/**9b**	**10a**+**10b**	**10a**/**10b**	**14**	**22**	**11b**	**12**	**16**+**17**	**23**
a	11%	4.2	15%	1	14%	4.5	0%	8%	0%	11%	0%	15%
b	21	3.6	18	0	18	5.6	2	9	7	0	0	6
c	17	1.1	10	0	28	12.8	0	a)	(26)		5	a)

a) Identification could not be done because of the small amount.

of diosphenol. Upon acetylation with acetic anhydride–pyridine, **14** readily afforded its acetate (**15**), whose configuration at C-4 remains to be determined. From **4** we obtained an inseparable mixture of the epimeric diosphenols, **16** and **17**, while the acetate was separated into **20** and **21** by preparative TLC. However, the amount of **21** was too minute for further purification. Upon autoxidation, **11a** gave a diosphenol, **16**, whose acetate was identical with the **20** obtained by the autoxidation of **4**. Accordingly, the configurational assignments to **20** and **21** were established.

The acidic products, **18** and **19**, were isolated as methyl esters (**22** and **23**), after esterification with diazomethane; their structures were confirmed by their preparations from **3** and **4** respectively by the following reaction sequences of Baeyer-Villiger oxidation, alkaline hydrolysis, methylation, and oxidation with chromium trioxide.[15,16] The acidic products are derived from the starting ketone *via* α-hydroperoxy ketones, involving the cleavage of the bond adjacent to the carbonyl group.[17]

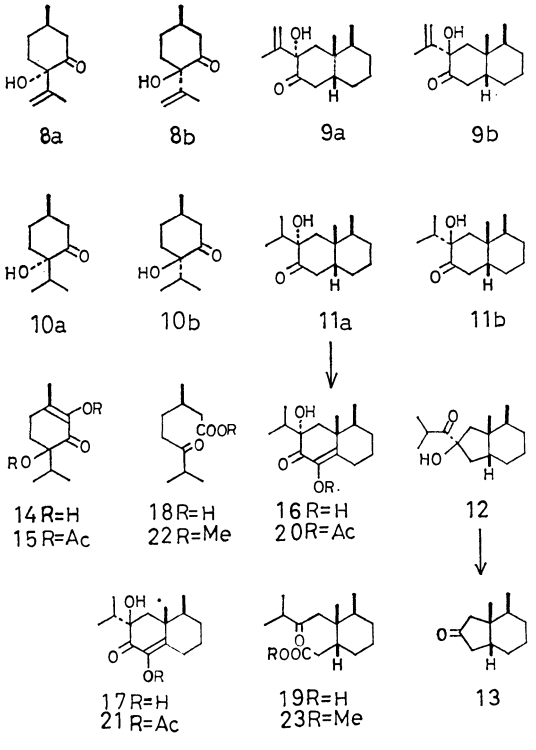

Hydroxyeremophilone (**5**) was subjected to considerable decomposition when left standing in the air, and it was carefully isolated as the acetate (**6**) by chromatography on deactivated silica gel. **6** was synthesized from **2** as follows. 9-Acetoxyfukinone (**24**) was obtained by the treatment of **2** with mercury(II) acetate in acetic acid.[18] The PMR spectrum of **24** showed the signal at δ 5.38 (d, J=12 Hz) attributable to the hydrogen attached to the carbon bearing an acetoxyl group. From an examination of the dihedral angle between 9-H and 10β-H, the coupling constant (12 Hz) can be accounted for by the relative orientation of the α-axial 9-H and β-equatorial 9-acetoxyl groups in a steroidal conformation. The treatment of **24** with DDQ in the presence of hydrogen chloride[19] furnished **6** in a poor yield (10%, based on the consumed **24**). Next, the mild alkaline hydrolysis of **24** and the subsequent oxidation of the product (**25**) with bismuth oxide in acetic acid, as shown previously in the oxidation of 2-hydroxypulegone,[19] gave **5**, which was then immediately acetylated with acetic anhydride–pyridine to yield **6**. These two acetates, prepared independently, showed the same R_f value, 0.75 (silica gel; benzene–ethyl acetate, 10: 1), IR, and PMR spectra. Their characteristic IR bands, UV absorption maxima, and specific rotation agree with those given in the literature.[4] There was no sign of the existence of the monoterpene analogue of **5** in the autoxidation products of **1**. The base-catalyzed autoxidation of the terpene ketones under investigation resulted in poor yields of the products, suggesting that the products tend to collapse readily into undesired compounds under the reaction conditions. In spite of the many visualized spots on TLC, attempts to separate the esters derived from the acidic products in the autoxidation of the conjugated ketones, **1** and **2**, were unsuccessful.

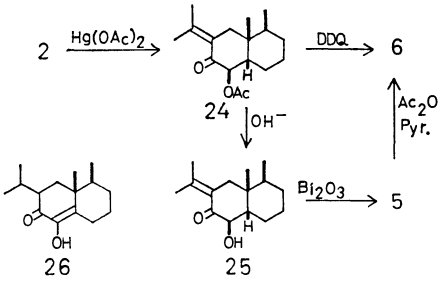

The product oxidized only at the 9-methylene position, namely, buccocamphor, **7**, and its sesquiterpene analogue (**26**) could not be detected in the reaction mixture of the saturated ketones, **3** and **4**. On the other hand, only **11a** among the hydroxy ketones was found to afford a diosphenol, **16**, in a low yield by autoxidation under the b) reaction conditions, but **11a** could not be found in the autoxidation mixture of **4**. No conclusive proof, therefore, could be obtained as to whether diosphenols, **14**, **16**, and **17**, can be produced *via* hydroxy ketones, **10a,b** and **11a,b** or *via* **7** and **26**. The intermediates presumably suffered rapid oxidation to give the diosphenols.

Finally, it should be noted that the relative ratio of the epimeric 4- or 7-hydroxy ketones is markedly affected by the reaction conditions (Table 1). This may reflect the dependence of the preferential conformation of the enolate anions on the reaction conditions.

Experimental

The IR, UV, and mass spectra were taken with Hitachi EPI-G_3, Shimadzu Spectronic 505, and Hitachi RMU-6 spectrophotometers respectively. The PMR spectra were recorded with a Hitachi R-20B (60 MHz) spectrometer, and the chemical shifts are reported in δ-values, with TMS as the internal reference. The optical rotations were measured with a Perkin-Elmer 141 polarimeter. Analytical and preparative GLC were performed with a Shimadzu GC-1C apparatus on a stainless steel column (ϕ=3 mm). The TLC were run on

silica gel (Merck Kieselgel G). All the melting and boiling points are uncorrected.

General Procedure of Autoxidation. *a) Oxidation Catalyzed by Potassium* t-*Butoxide in* t-*Butyl Alcohol*: A ketone (600—800 mg) was dissolved in a solution of 0.5 M potassium *t*-butoxide in *t*-butyl alcohol (20—30 ml). The mixture was stirred vigorously under the bubbling of oxygen at room temperature for 20—40 min, until 1 mol of oxygen has been consumed, and was then diluted with water, acidified with 10% aqueous sulfuric acid, and extracted with ether. The extract was shaken with a saturated sodium hydrogencarbonate solution. The extract was washed with water and dried over sodium sulfate. The removal of the solvent gave an oil, which was subsequently chromatographed on silica gel. Elution with light petroleum–ether (50: 1) or benzene afforded non-acidic products. The sodium hydrogencarbonate solution was acidified with 10% aqueous sulfuric acid and extracted with ether. The extract was treated with diazomethane–etherate. The removal of the solvent gave an oil which was chromatographed on silica gel. Elution with light petroleum–ether (50: 1) gave a methyl ester of the acidic product.

b) Oxidation Catalyzed by Potassium t-*Butoxide in* N,N-*Dimethylformamide*: To a solution of potassium *t*-butoxide (*ca.* 9 mmol) in *N,N*-dimethylformamide (15 ml) we added a ketone (600—800 mg). The solution was stirred vigorously under an oxygen atmosphere at −20——10 °C for 4—40 min, until 1 mol of oxygen had been consumed, and was then worked-up in essentially the same manner as Procedure *a*).

c) Oxidation Catalyzed by Sodium t-*Butoxide in* t-*Butyl Alcohol*, N,N-*Dimethylformamide, and Tetrahydrofuran in the Presence of Triethyl Phosphite*: Sodium hydride (300 mg, 50%) was dissolved in *t*-butyl alcohol (2 ml) and *N,N*-dimethylformamide (3 ml). To this solution we added triethyl phosphite (1 ml) in *N,N*-dimethylformamide (3 ml) and then a ketone (0.8—1.0 g) in tetrahydrofuran (7 ml). Oxygen was passed for 1 h into the cooled mixture at −30——20 °C. After the addition of a solution of sodium hydroxide (0.5 g) in methanol–water (2: 1, 15 ml) the reaction mixture was stirred at room temperature for 20 min and then acidified with acetic acid. After the removal of the solvent *in vacuo* and dilution with water, the mixture was extracted with ether. Subsequently, the extract was worked up in a manner similar to that described above.

*Autoxidation Products of Pulegone (**1**) and Dihydropulegone (**3**).* **8a** and **8b** were found to be identical with authentic samples[9] by a comparison of the IR and GLC (EGA, 2.6 m; column temperature, 140 °C; H_2-flow rate, 60 ml/min; retention time, **8a**: 9.8 min, **8b**: 13.6 min).

The saturated hydroxy ketones (**10a** and **10b**) were found to be identical with the hydrogenation products of **8a** and **8b** respectively by a comparison of the IR and GLC (EGA, 2.6 m; column temperature, 140 °C; retention time, **10a**: 7.5 min, **10b**: 9.4 min); also, their spectral data were in agreement with those given in the literature.[13]

*Diosphenol (**14**)*: A colorless oil; UV: λ_{max}^{MeOH} 275 nm (ε, 4300); IR(film): 3420, 1705, 1670, 1635 cm^{-1}; PMR(CCl_4): 1.82 (t, J=1.0 Hz, 7-Me), 0.94 and 0.69 (each d, J=6.0 Hz, 9- or 10-Me). **14** (28 mg) was acetylated with acetic anhydride–pyridine in the usual manner to give **15** (15 mg).

*Acetate (**15**)*: A colorless oil; UV: λ_{max}^{MeOH} 242 nm (ε, 8100); IR (film): 3450, 1750, 1670, 1640, 1200 cm^{-1}; PMR(CCl_4): 3.24 (br s, OH), 2.15 (s, OAc), 1.78 (s, 7-Me), 0.94 and 0.68 (each d, J=6.0 Hz, 9- or 10-Me).

*Keto Ester (**22**)*: A colorless oil; bp 125—129 °C (bath temperature)/16.5 mmHg†; $[\alpha]_D^{22}$ +9.7° (*c*, 0.51, MeOH); MS: *m/e* 200, M^+, *m/e* 125, base peak; IR(film): 1730, 1710, 1250, 1200, 1160 cm^{-1}; PMR(CCl_4): 3.59 (s, OMe), 1.03 (d, J=7.0 Hz, 9- and 10-Me), 0.89 (d, J=5.0 Hz, 7-Me). **22** was found to be identical with the authentic sample prepared from **3** by a comparison of the IR and GLC (PEG 20M, 2.6 m; column temperature, 146 °C; H_2-flow rate, 58 ml/min; retention time, 24 min) (see below).

*Autoxidation Products of Fukinone (**2**) and Dihydrofukinone (**4**).*

*Hydroxy Ketone (**9a**)*: Mp 47—53 °C, colorless needles (from pentane); MS: *m/e* 236 M^+, *m/e* 109 base peak; IR(CCl_4): 3480, 3060, 1710, 1635, 902 cm^{-1}; PMR(CCl_4): 4.82 (slightly split s) and 4.65 (s) (12-C=CH_2), 3.27 (s, OH), 1.78 (s, 13-Me), 1.03 (s, 15-Me), 0.87 (d, J=6.0 Hz, 14-Me). **9a** was contaminated by a slight amount of **9b**, but **9a** showed the same physical properties as the authentic sample prepared from fukinone α-epoxide in a comparison of the TLC, IR, and PMR. The preparation of **9a** will be described later.

*Hydroxy Ketone (**9b**)*: Mp 73.5—74.0 °C, colorless prisms (from pentane); $[\alpha]_D^{23}$ −80° (*c*, 0.99, $CHCl_3$); MS: *m/e* 236 M^+, *m/e* 109 base peak; IR(CCl_4): 3460, 3060, 1705, 1635, 900 cm^{-1}; PMR(CCl_4): 4.85 (slightly split s) and 4.58 (s) (12-C=CH_2), 3.55 (s, OH), 1.84 (d, J=1.0 Hz, 13-Me), 0.89 (s, 15-Me), 0.87 (d, J=6.0 Hz, 14-Me).

Found: C, 76.10; H, 10.10%. Calcd for $C_{15}H_{24}O_2$: C, 76.22; H, 10.24%. **9b** was found to be identical with the authentic sample prepared from fukinone β-epoxide by a comparison of the IR, PMR, and TLC and by a mixed-melting-point determination.

*Hydroxy Ketone (**11b**)*: Mp 40.0—41.0 °C, colorless prisms (from pentane); $[\alpha]_D^{23}$ −69° (*c*, 1.0, $CHCl_3$); MS: *m/e* 238 M^+, *m/e* 109 base peak; IR(CCl_4): 3450, 1705 cm^{-1}; PMR (CCl_4): 3.47 (s, OH), 0.99 and 0.64 (each d, J=6.5 Hz, 12- or 13-Me), 0.92 (d, J=6.5 Hz, 14-Me), 0.87 (s, 15-Me).

Found: C, 75.42; H, 10.89%. Calcd for $C_{15}H_{26}O_2$: C, 75.58; H, 11.00%. **11b** was found to be identical with the hydrogenation product of **9b** by a comparison of the TLC, IR, and PMR and by a mixed-melting-point determination. The preparation of **9b** and **11b** will be described later.

*Hydroxy Ketone (**12**)*: A colorless oil; $[\alpha]_D^{23}$ +33.7° (*c*, 1.03, $CHCl_3$); MS: *m/e* 238 M^+, *m/e* 109 base peak; IR(CCl_4): 3450, 1693 cm^{-1}; PMR(CCl_4): 3.43 (s, OH), 1.08 (d, J=6.0 Hz, $CHMe_2$), 1.00 (s, 15-Me), 0.81 (d, J=6.0 Hz, 14-Me).

Found: C, 75.41; H, 10.94%. Calcd for $C_{15}H_{26}O_2$: C, 75.58; H, 11.00%. **12** was found to be identical with the rearranged product of **11b** by a comparison of the IR, PMR, and GLC (SF 96, 35 cm; column temperature, 100 °C; H_2-flow rate, 115 ml/min; retention time, 9.5 min). The rearrangement of **11b** will be described later.

*A Mixture of Diosphenols (**16** and **17**)*: A colorless oil; bp 116—135 °C (bath temperature)/0.04 mmHg; UV: λ_{max}^{MeOH} 282 nm (ε, 10000); IR(film): 3430, 1660, 1630 cm^{-1}. This mixture (104 mg) was acetylated with acetic anhydride–pyridine in the usual manner. The mixture was then separated into (**20**) and (**21**) by repeated column chromatography on silica gel, with benzene as an eluent, and by subsequent preparative TLC (benzene–ethyl acetate, 10: 1).

*Acetate (**20**)*: R_f: 0.68, benzene–ethyl acetate, 10: 1; mp 99.5—100.0 °C, colorless prisms (from light petroleum); $[\alpha]_D^{22}$ −80° (*c*, 0.52, $CHCl_3$); IR(KBr): 3450, 1760, 1685, 1635, 1210 cm^{-1}; PMR(CCl_4): 3.11 (br s, OH), 2.18 (s, OAc), 1.27 (s, 15-Me), 0.96 and 0.68 (each d, J=6.0 Hz, 12- or 13-Me), 0.91 (d, J=5.5 Hz, 14-Me).

Found: C, 69.39; H, 8.89%. Calcd for $C_{17}H_{26}O_4$: C, 69.36; H, 8.90%.

*Acetate (**21**)*: R_f, 0.73; a colorless oil; $[\alpha]_D^{25}$ +20° (*c*, 0.26, MeOH); UV: λ_{max}^{MeOH} 249 nm (ε, 8200); IR(film): 3450, 1750, 1675, 1635, 1200 cm^{-1}.

*Keto Ester (**23**)*: Bp 120—122 °C (bath temperature)/0.02

† mmHg=133.322 Pa

mmHg; a colorless oil; $[\alpha]_D^{22}$ +41° (*c*, 0.85, MeOH); MS: *m/e* 237 M^+-31, *m/e* 109 base peak; IR(film): 1735, 1710 cm^{-1}; PMR(CCl_4): 3.56 (s, OMe), 1.01 (s, 15-Me), 0.98 (d, J=6.5 Hz, $CHMe_2$), 0.86 (d, J=7.0 Hz, 14-Me).

Found: C, 71.40; H, 10.56%. Calcd for $C_{16}H_{28}O_3$: C, 71.60; H, 10.52%. **23** was found to be identical with an authentic sample prepared from **4** by a comparison of the IR and GLC (PEG 20M, 2.6 m; column temperature, 195 °C; retention time, 14.9 min). The preparation of **23** will be described later.

*Preparation of the Autoxidation Products. Preparation of Hydroxy Ketones (**9a**, **9b**, **11a**, and **11b**).* A solution of fukinone α-epoxide (1.015 g) and *p*-toluenesulfonic acid (250 mg) in dry benzene (270 ml) was stirred at 40 °C for 7 h. Working-up in the usual manner gave a brown oil, which was subsequently chromatographed on silica gel (30 g, Grade II). Elution with light petroleum–ether (50: 1) gave (**9a**) in a 49% yield as the major product. **9b** was obtained in a similar manner from fukinone β-epoxide.

The catalytic hydrogenation of **9a** and **9b** with 10% palladium charcoal gave the saturated hydroxy ketones (**11a** and **11b**) respectively, in quantitative yields.

*Hydroxy Ketone (**9a**)*: Mp 61.5—62.0 °C; colorless needles (from pentane); $[\alpha]_D^{28}$ +91° (*c*, 1.02, $CHCl_3$).

Found: C, 76.26; H, 10.27%. Calcd for $C_{15}H_{24}O_2$: C, 76.22; H, 10.24%.

*Hydroxy Ketone (**9b**)*: Mp 73.5—74.0 °C; colorless prisms (from pentane); $[\alpha]_D^{23}$ −80° (*c*, 0.99, $CHCl_3$). The further details of **9a** and **9b** will be reported in the succeeding paper on the acid-catalyzed reaction of fukinone epoxides.

*Hydroxy Ketone (**11a**)*: Mp 47—48 °C; colorless prisms (from pentane); $[\alpha]_D^{28}$ +112° (*c*, 1.02, $CHCl_3$); MS: *m/e* 238 M^+, *m/e* 109 base peak; IR(CCl_4): 3480, 1703 cm^{-1}; PMR(CCl_4): 2.89 (s, OH), 0.93 (s, 15-Me), 0.81 (d, J=6.0 Hz, 14-Me), 0.91 and 0.70 (each d, J=6.0 Hz, 12- or 13-Me).

Found: C, 75.31; H, 10.95%. Calcd for $C_{15}H_{26}O_2$: C, 75.58; H, 11.00%. For the data of **11b**, see the above description.

*Rearrangement of Hydroxy Ketone (**11b**) with Potassium* t-*Butoxide in* t-*Butyl Alcohol.* The hydroxy ketone (**11b**) (22.8 mg) was dissolved in 0.5 M potassium *t*-butoxide–*t*-butyl alcohol and then left at room temperature for 5 min. The reaction mixture was diluted with water, acidified with 10% aqueous sulfuric acid, and extracted with ether. The extract was washed with water and dried over anhydrous sodium sulfate. The subsequent removal of the solvent gave an oil which was chromatographed on silica gel (0.5 g). Elution with light petroleum–ether (100: 1) gave a hydroxy ketone (**12**) (19 mg in an 83% yield).

*Reaction of Hydroxy Ketone (**12**) with Periodic Acid.* The hydroxy ketone (**12**) (60 mg) in ethanol (6 ml) was added to a solution of potassium periodate (150 mg) in 1 M aqueous sulfuric acid (7 ml), and the resulting solution was kept at 45 °C for 9.5 h. The reaction mixture was then diluted with water and extracted with ether. The extract was washed with a saturated sodium hydrogencarbonate solution and then water. The dried extract was evaporated to give an oil, which was subsequently chromatographed on silica gel (1 g). Elution with light petroleum–ether (200: 1) gave a ketone (**13**) (17 mg), which was identical with the authentic sample[3] by a comparison of the IR and GLC (SPE, 2.6 m; column temperature, 150 °C; H_2-flow rate, 32 ml/min; retention time, 17.7 min).

*Autoxidation of Hydroxy Ketone (**11a**).* The hydroxy ketone (**11a**) (280 mg) was stirred into a solution of potassium *t*-butoxide (*ca.* 30 mmol) in *N,N*-dimethylformamide (15 ml). After vigorous stirring in the air for 20 min, the mixture was worked-up in the usual manner gave a yellow oil which was subsequently chromatographed on silica gel (2.5 g). Elution with light petroleum–ether (30: 1) afforded diosphenol (**16**) (20 mg); mp 134.0—135.0 °C, colorless prisms (from light petroleum), $[\alpha]_D^{23}$ +150° (*c*, 1.05, $CHCl_3$); MS: *m/e* 252 M^+, *m/e* 41 base peak; UV: λ_{max}^{MeOH} 282 nm (ε, 11400); IR(KBr): 3480, 3400, 1660, 1630, 1000, 990 cm^{-1}; PMR(CCl_4): 1.21 (s, 15-Me), 0.98 and 0.90 (each d, J=6.0 Hz, 12- or 13-Me), 0.71 (d, J=7.0 Hz, 14-Me). The acetylation of (**16**) in the usual manner gave an acetate (**20**) which was found to be identical with the authentic acetate prepared from dihydrofukinone (**4**) mentioned above by a comparison of the IR and PMR spectra and by a mixed-melting-point determination.

*Preparation of Keto Ester (**22**) from Dihydropulegone (**3**).* A solution of dihydropulegone (**3**) (232 mg) in chloroform (1 ml) was added, at 0 °C, to a solution of perbenzoic acid (3 mmol equivalent) in chloroform (12.5 ml) in the presence of a catalytic amount of concentrated sulfuric acid. The mixture was then allowed to stand in a refrigerator for 3 days. The reaction mixture was subsequently concentrated, diluted with water, and extracted with ether. The extract was washed successively with a saturated aqueous sodium hydrogencarbonate solution, a saturated aqueous ferrous sulfate solution, and water. The dried extract was evaporated to give an oil which was chromatographed on silica gel (4 g). Elution with benzene gave a lactone as an oil (156 mg, 61%); IR(film): 1710, 1280, 1225 cm^{-1}; PMR(CCl_4): 4.00 (m, CH–O–), 2.45 (d, J=10 Hz, CO–CH_2–), 0.98 (d, J=6.0 Hz, 7-Me), 0.93 (d, J=6.0 Hz, $CHMe_2$).

A solution of the lactone (103 mg) and potassium hydroxide (1 pellet) in methanol (5 ml) was refluxed for 5 h, and then methyl iodide (1.5 ml) was added. After refluxing for a further 3 h, the resulting mixture was concentrated, acidified with 10% aqueous sulfuric acid, and extracted with ether. The dried extract was evaporated to give an oil which was chromatographed on silica gel (2 g) by elution with benzene to furnish a hydroxy ester (76 mg, 62%); IR(film): 3400, 1720 cm^{-1}. The hydroxy ester (36 mg) in pyridine (0.5 ml) was stirred, drop by drop, into a slurry mixture of chromium trioxide (100 mg) in pyridine (1 ml) under cooling, after which the mixture was kept overnight at room temperature under stirring. Subsequent working-up in the usual manner gave a keto ester (**22**) (17 mg, 48%).

*Preparation of Keto Ester (**23**) from Dihydrofukinone (**4**).* A hydroxy ester (**23**)[15] was prepared from dihydrofukinone (**4**) by essentially the same method described above; the subsequent Jones' oxidation gave a keto ester (**23**) in a 58% yield.

*Isolation of Hydroxyeremophilone Acetate (**6**).* Fukinone (**2**) (1.239 g, 5.62 mmol) was dissolved in 0.5 M potassium *t*-butoxide–*t*-butyl alcohol (40 ml), and the mixture was stirred vigorously in the air at room temperature for 3.5 h. Working-up in the usual manner gave a brown oil (1.226 g), which was then chromatographed on deactivated silica gel (Grade II, 24 g). Elution with light petroleum–ether (50: 1) gave a mixture of hydroxyeremophilone (**5**) and (**2**) (327 mg). Subsequent elution with light petroleum–ether (20: 1) afforded a mixture of two epimeric hydroxy ketones (**9a** and **9b**) (77 mg). The mixture of **5** and **2** was immediately treated with acetic anhydride–pyridine. Working-up in the usual manner gave a yellow oil, which was chromatographed on silica gel (Grade II, 5 g). Elution with light petroleum–ether (50: 1) gave **2** (220 mg) and then hydroxyeremophilone acetate (**6**) (35 mg; 5.6% yield based on the **2** consumed), which was recrystallized from light petroleum; mp 53.5—54.0 °C; colorless prisms; $[\alpha]_D^{25}$ +143° (*c*, 1.02, $CHCl_3$); MS: *m/e* 276 M^+, *m/e* 43 base peak; UV: λ_{max}^{MeOH} 285 nm (ε, 7100), 255 nm (ε,

9300); IR(CCl_4): 1760, 1665, 1635, 1203 cm^{-1}; PMR(CCl_4): 2.17 (s, OAc), 2.06 and 1.84 (each s, 12- or 13-Me), 1.01 (s, 15-Me), 0.99 (d, J=6.0 Hz, 14-Me).

Found: C, 73.69; H, 8.41%. Calcd for $C_{17}H_{24}O_3$: C, 73.88; H, 8.75%.

*Preparation of 9β-Acetoxyfukinone (**24**).* A mixture of fukinone (**2**) (3.446 g, 15.6 mmol) and mercuric acetate (8.45 g, 26.5 mmol) in glacial acetic acid (30 ml) was refluxed for 3.5 h. The resulting dark mixture was decanted to remove the mercury into water and then extracted with ether. The ethereal extract was washed with water and dried over anhydrous sodium sulfate. The removal of the solvent gave a dark viscous oil (3.515 g), which was subsequently chromatographed on silica gel (80 g). Elution with light petroleum–ether (50: 1) afforded the recovered fukinone (**2**) (0.93 g) and 9β-acetoxyfukinone (**24**) (1.357 g, 31%), which was distilled at 130—140 °C (bath temperature)/0.02 mmHg and then crystallized from light petroleum as colorless leaflets; mp 67—68 °C, $[\alpha]_D^{23}$ +160° (c, 1.23, $CHCl_3$); MS: m/e 278 M^+, m/e 28 base peak; UV: λ_{max}^{MeOH} 253 nm (ε, 5800); IR(CCl_4): 1755, 1740, 1707, 1640, 1233 cm^{-1}; PMR(CCl_4): 5.38 (d, J=12 Hz, 9-CH), 2.10 (s, OAc), 1.80 (t, J=1.5 Hz, 12- and 13-Me), 1.00 (s, 15-Me), 0.84 (d, J=6.5 Hz, 14-Me).

Found: C, 73.59; H, 9.38%. Calcd for $C_{17}H_{26}O_3$: C, 73.34; H, 9.41%. Before crystallization it showed a PMR signal at 5.26 (d, J=5.0 Hz) besides that at 5.38, indicating the existence of a small amount of the 9α-acetoxyl isomer.

*Preparation of Hydroxyeremophilone Acetate (**6**).* a) Into a solution of 9β-acetoxyfukinone (**24**) (303 mg, 1.08 mmol) and DDQ (270 mg, 1.19 mmol) in dry dioxane (20 ml) we bubbled anhydrous hydrogen chloride with stirring for 1 min; the stirring was then continued at room temperature for 4 h. After subsequent filtration and evaporation of the solvent, the residue was taken up in ether, washed with a 1% aqueous sodium hydroxide solution, and water. The evaporation of the solvent gave a viscous light brown oil (211 mg), which was chromatographed on silica gel (Grade II, 6 g). Elution with light petroleum–ether (30: 1) gave the recovered **24** (196 mg) and then hydroxyeremophilone acetate (**6**) (20 mg, 10% based on the **24** consumed).

b) An aqueous potassium hydroxide solution (*ca.* 1.8%) was added, over a period of 2 weeks under a nitrogen atmosphere, to a solution of **24** (281 mg, 1.01 mmol) in methanol (10 ml), in the presence of 1 drop of 1% phenolphtalein in ethanol, at such a rate that the solution was kept faintly alkaline. The reaction mixture was then diluted with water and extracted with ether. The extract was worked-up in the usual manner to give a pale yellow oil (165 mg), which was subsequently chromatographed on silica gel (Grade II, 7 g). Elution with benzene gave 9β-hydroxyfukinone (**25**) (144 mg, 61%); a colorless oil; $[\alpha]_D^{23}$ +122° (c, 0.68, $CHCl_3$); UV: λ_{max}^{MeOH} 252 nm (ε, 4500); IR(CCl_4): 3460, 1760 (sh), 1708 (sh), 1692, 1640 cm^{-1}; PMR(CCl_4): 4.17 (d, J=11 Hz, 9α-H), 3.50 (s, OH), 1.87 (d, J=1.5 Hz) and 1.81 (d, J=1.0 Hz) (12- and 13-Me), 0.95 (s, 15-Me), 0.83 (d, J=6.0 Hz, 14-Me).

A mixture of **25** (109 mg, 0.46 mmol) and bismuth oxide (111 mg, 0.24 mmol) in glacial acetic acid (2 ml) was stirred at 120 °C for 10 min. The solution was decanted to remove the bismuth metal into water (20 ml) and then extracted with ether. The subsequent working-up as usual gave a brown oil, which was subjected to preparative TLC to afford **5** (64 mg, 59%). Its acetate (**6**) was obtained in the usual manner.

The authors wish to thank the staff of the Research Laboratory, Toyo Jozo, Co., Ltd., for the microanalysis and MS measurements, and the Institute of Food Chemistry for the measurement of the MS spectra.

References

1) D. H. R. Barton, E. J. Bailey, and J. Elks, *Proc. Chem. Soc.*, **1960**, 214; D. H. R. Barton, S. K. Pradham, S. Sternhell, and J. F. Templeton, *J. Chem. Soc.*, **1961**, 255.

2) B. Camarino, B. Patelli, and R. Sciaky, *Tetrahedron Lett.*, **1961**, 554.

3) K. Naya, I. Takagi, Y. Kawaguchi, Y. Asada, Y. Hirose, and N. Shinoda, *Tetrahedron*, **24**, 5871 (1968).

4) C. Djerassi, R. Mauli, and L. H. Zalkow, *J. Am. Chem. Soc.*, **81**, 3424 (1959).

5) "Rodd's Chemistry of Carbon Compounds," 2nd ed, Elsevier Publishing Co., Amsterdam (1968), Vol. IIB, p. 202.

6) J. N. Gardner, F. E. Carlon, and O. Gnoj, *J. Org. Chem.*, **33**, 3294 (1968).

7) W. Reusch and P. Mattison, *Tetrahedron*, **23**, 1953 (1967); G. W. K. Cavil and C. D. Hall, *Tetrahedron*, **23**, 1119 (1967).

8) K. Kobayashi, Y. Yamamoto, H. Miyanaga, and K. Naya, 23th National Meeting of the Chemical Society of Japan, Tokyo, April 1970, Abstr. No. 18337.

9) W. Reusch, D. F. Andersen, and C. K. Johnson, *J. Am. Chem. Soc.*, **90**, 4988 (1968).

10) K. H. Schulte-Elte, M. Gadola, and B. L. Muller, *Helv. Chim. Acta*, **54**, 1870 (1971).

11) K. Naya and J. Yamamoto, 14th Symposium on the Chemistry of Terpenes, Essential Oils, and Aromatics, Symposium Paper (1970), p. 114.

12) An account will soon be published elsewhere.

13) T. Suga, T. Shishibori, and T. Matsuura, *J. Org. Chem.*, **32**, 965 (1967).

14) "Molecular Rearrangement," ed by P. de Mayo, Interscience Publishers, New York (1963), pp. 18, 801, 1114.

15) M. Kawai and K. Naya, *Chem. Lett.*, **1972**, 389.

16) R. Schollinger and W. Treibs, *Chem. Ber.*, **94**, 2978 (1961).

17) W. von E. Doering and R. M. Haines, *J. Am. Chem. Soc.*, **76**, 482 (1954); T. J. Wallace, H. Pobiner, and A. Schriesheim, *J. Org. Chem.*, **30**, 3768 (1965).

18) R. H. Reitsema, *J. Am. Chem. Soc.*, **79**, 4465 (1957).

19) H. J. Ringold and A. Turner, *Chem. Ind. (London)*, **1962**, 211.

Alkylation of Benzene with Optically Active 3-Chloro-1-butanol, 3-Chlorobutanoic Acid, and Their Esters

Tadashi NAKAJIMA, Shinji MASUDA,[1a] Satoru NAKASHIMA,[1b] Takayuki KONDO,[1c] Yoshiaki NAKAMOTO, and Sohei SUGA*

Department of Industrial Chemistry, Faculty of Technology, Kanazawa University, Kodatsuno, Kanazawa 920

(Received December 14, 1978)

The alkylations of benzene with optically active 3-chloro-1-butanol, 3-chlorobutanoic acid and their esters in the presence of aluminium chloride gave the corresponding 3-phenyl substituted derivatives in good optical yield. All these reactions were found to proceed with inversion of configuration at the attacking carbon atom. The products were not racemized under the conditions used, while the starting materials were racemized to a considerable extent during the reaction. Taking into account of the optical purity of the starting material recovered before the completion of reaction, net stereospecificity of each reaction was calculated to be about 90% except for the case of 3-chloro-1-butanol and its acetic ester. The high degree of stereospecificity of the reaction can be interpreted by the mechanism involving cyclic intermediate formed from the alkylating reagent and aluminium chloride.

Compared to extensive studies on the Friedel-Crafts alkylation of aromatic hydrocarbons with alkyl halide or alcohol, the stereochemistry of these reactions received relatively little attentions.[2] Generally, Friedel-Crafts type alkylation has long been pointed out to proceed with almost complete recemization when an optically active alkylating reagent was used.[3] Some examples of the stereospecific reaction were recently reported, *e.g.* the alkylation of benzene with (+)-γ-valerolactone and (+)-2-methyltetrahydrofuran in the presence of aluminium chloride proceeded with 47% and 35% net inversion of configuration at the attacking carbon, respectively.[4,5] We also observed complete inversion in the reaction of benzene with (+)-propylene oxide[6] and (+)-1,2-epoxybutane[7] by Lewis acid catalysts. The stereospecificity in these reactions has been explained on the basis of the cyclic nature of the alkylating reagents or the enforced proximity of ion pairs produced by the ring opening reaction. Furthermore, (−)-2-chloro-1-phenylpropane reacted with benzene in the presence of aluminium chloride or iron(III) chloride to give (−)-1,2-diphenylpropane with 70—95% retention of configuration.[8] This result was interpreted by the participation of the neighboring phenyl group to the reaction center.

In connection with these observations, it is interesting to investigate the stereochemistry of Friedel-Crafts reaction with acyclic alkylating reagents such as 3-chloro-1-butanol, 3-chlorobutanoic acid and their esters. Little is known about Friedel-Crafts reactions with halogenated alcohol, halogenated carboxylic acid and their ester.[9] In a communication we demonstrated that the alkylation of benzene with optically active 3-chloro-1-butanol (Ia) and 3-chlorobutanoic acid (Ib) by aluminium chloride catalyst proceeded with inversion of configuration to give 3-phenyl-1-butanol (IIa) and 3-phenylbutanoic acid (IIb), respectively.[10] In the present paper, we have extended our previous work on Ia and Ib to their esters, ethyl 3-chlorobutanoate (Ic), 3-chlorobutyl benzoate (Id), and 3-chlorobutyl acetate (Ie) with a view to obtaining more information on the stereochemistry of the Friedel-Crafts alkylation. Furthermore, the net stereospecificity of reaction was determined by taking into account of the remaining optical activity of the starting materials recovered.

Results and Discussion

At first, the reaction was run in usual manner in order to know a general tendency on the stereochemistry of the reaction. The alkylating reagent was gradually added to a stirred mixture of aromatic hydrocarbon and Lewis acid at such a rate that the temperature of the reaction mixture does not rise higher (see the method A in Experimental). Optically active Ia, Ib, Ic, Id, and Ie reacted with benzene in the presence of 1.2 equivalents of aluminium chloride at −5—50 °C to give the corresponding 3-phenyl substituted derivatives, 3-phenyl-1-butanol (IIa), 3-phenylbutanoic acid (IIb), ethyl 3-phenylbutanoate (IIc), 3-phenylbutyl benzoate (IId), and 3-phenylbutyl acetate (IIe), respectively, in optically active form. The results are described in Table 1.

In these reactions, by-products such as haloalkylated and haloacylated compounds and rearrengement products were not obtained under the conditions used. However, the esters (Ic, Id, and Ie), when treated under higher temperature (over 40 °C), gave considerable amounts of the hydrolyzed products (IIb from Ic, and IIa from Id or Ie) along with the normal products. Furthermore, diphenylbutane was also obtained in the case of Id and Ie. These by-products seem to arise from the primary products. This was confirmed by the experimental result that IIc and IId (or IIe) reacted with aluminium chloride in benzene to yield IIb and IIa, respectively.

The absolute configurations of the dextrorotatory chlorides (Ia, Ib, and Ic) and the levorotatory products (IIa, IIb, and IIc) have been established to be *S*[11] and *R*,[12-14] respectively, whereas those of Id, Ie, IId, and IIe are not known yet. The configurations of (+)-Id and (+)-Ie were correlated with that of (+)-Ia (see Experimental) and assigned to be *S*. In the same way, (−)-IId and (−)-IIe were correlated to *R*-(−)-IIa. Consequently, it is apparent that all these reactions proceeded with inversion of configuration at the attacking carbon atom. The optical yield of each reaction was calculated by the use of maximum rotations in Table 2.

TABLE 1. ALKYLATION OF BENZENE WITH OPTICALLY ACTIVE $CH_3CH(Cl)CH_2Y$ BY ALUMINIUM CHLORIDE CATALYST (BY METHOD A)[a]

Compd	$CH_3CH(Cl)CH_2Y$ Y=	$[\alpha]_D$[b] °	Temp °C	Time h	Alkylated product $CH_3CH(Ph)CH_2Y$ Compd	Yield[c] %	$[\alpha]_D$[b] °	Optical yield[d] %
Ia	CH_2OH	−13.8	20	3.5	IIa	83	+1.97	14.1
		−13.8	10	3.5		88	+2.49	17.8
		+23.2	−10	4.5		77	−4.81	20.0
Ib	COOH[e]	+22.5[e]	30	4.0	IIb	81	−13.4	44.5
		−21.2[e]	20	4.0		84	+13.7	48.5
		+27.5[e]	5	4.0		46	−15.8	43.2
Ic	$COOC_2H_5$	+4.86	50	3.5	IIc	57	−0.8	19.7
					IIb	20	−1.5	16.5
		+3.66	40	3.5	IIc	48	−1.4	35.3
					IIb	35	−1.9	29.0
		+4.86	30	3.5	IIc	20	−3.0	53.7
Id	CH_2OCOPh	−41.2[f]	10	1.0	IId	75	+17.2[f]	28.2
		−41.2[f]	0	1.0		80	+18.8[f]	30.8
		−41.2[f]	−5	1.0		78	+20.1[f]	33.0
Ie	CH_2OCOCH_3	−38.4[f]	20	1.0	IIe	70	+11.0[f]	23.5
		−38.4[f]	10	1.0		77	+11.7[f]	23.9
		−38.4[f]	0	1.0		72	+10.2[f]	20.8

a) Molar ratio; $CH_3CH(Cl)CH_2Y$: $AlCl_3$: C_6H_6=1: 1.2: 30—50 CS_2 was added in the reaction below 5 °C. b) Rotations were measured in neat, unless otherwise noted. c) Based on the starting material used. d) Calculated from the maximum rotations of the starting material and the alkylating product as shown in Table 2. e) Measured in toluene (*c* 10.0). f) Measured in chloroform (*c* 5.0).

TABLE 2. MAXIMUM ROTATION OF STARTING MATERIALS AND PRODUCTS

Compd	$[\alpha]_D$/°	Compd	$[\alpha]_D$/°
S-Ia	+48.6 (neat)[a]	*R*-IIa	−45.3 (neat)[e]
S-Ib	−46.6 (toluene)[c]	*R*-IIb	−62.0 (neat)[f]
S-Ic	+31.2 (neat)[c]	*R*-IIc	−38.1 (neat)[g]
R-Id	−41.2 ($CHCl_3$)[d]	*S*-IId	+61.6 ($CHCl_3$)[h]
R-Ie	−38.4 ($CHCl_3$)[d]	*S*-IIe	+49.4 ($CHCl_3$)[i]

a) Calculated based on+23.5°of(+)-Ia obtained by reduction of (+)-Ib (optical purity 48.3%) with $LiAlH_4$. b) See Ref. 20. c) Calculated based on +8.84° of (+)-Ic obtained by esterification of (+)-Ib (optical purity 28.4%). d) This value seems to be of optically pure material because the precursor of this compound, ethyl 3-hydroxybutanoate, was obtained by biological method. See Ref. 21. e) See Ref. 13. f) See Ref. 13. g) See Ref. 22. h) Calculated based on +19.7° ($CHCl_3$) of IId obtained by esterification of(+)-IIa(optical purity 32%)with benzoyl chloride. i) Calculated based on +15.8° ($CHCl_3$) of IIe obtained by esterification of (+)-IIa (optical purity 32%) with acetyl chloride.

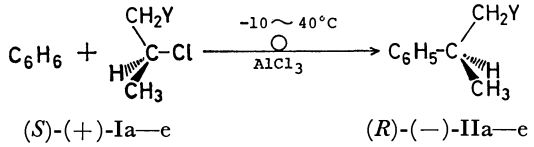

(*S*)-(+)-Ia—e (*R*)-(−)-IIa—e

Ia, IIa: Y=CH_2OH Id, IId: Y=$CH_2OCOC_6H_5$
Ib, IIb: Y=COOH Ie, IIe: Y=CH_2OCOCH_3
Ic, IIc: Y=$COOC_2H_5$

These reactions were so sensitive both to the moisture and to the activity of aluminium chloride used that it was diffcult to control the extent of the stereospecificity with sufficient reproducibility. The observed stereospecificity was found to be 20—30% for the reaction with alcohol (Ia) and its ester (Id and Ie), and 40—50% for that with chloroalkanoic acid (Ib) and its ethyl ester (Ic). The stereospecificity decreased slightly with an increase in reaction temperature. When these reactions were carried out in the presence of aluminium chloride equimolar to the alkylating reagent, the alkylation of benzene did not take place and the starting material was recovered without racemization.

In order to estimate the net stereospecificity of these reactions, one must know whether the starting chloride or the product is racemized in the course of reaction.

TABLE 3. TREATMENT OF THE ALKYLATED PRODUCT WITH ALUMINIUM CHLORIDE IN BENZENE[a]

Alkylated products	Temp °C	Time h	Specific rotation[b]/° Before reaction	Specific rotation[b]/° After reaction
IIa	30	3	−4.80	−4.78
IIb	30	4	−15.8	−15.8
IIc	30	3	−2.22	−2.20
IId	10	1	+20.2[c]	+19.8[c]
IIe	10	1	+7.3[c]	+7.3[c]

a) Molar ratio; II: $AlCl_3$: C_6H_6=1: 1.2: 30.
b) Measured in neat liquid, unless otherwise noted.
c) Measured in chloroform (*c* 5.0).

Table 4. The net stereospecificity in the alkylation of benzene with optically active $CH_3CH(Cl)CH_2Y$ by aluminium chloride catalyst (by method B)[a]

$CH_3CH(Cl)CH_2Y$				Recovered $CH_3CH(Cl)CH_2Y$			Product				
Compd	$[\alpha]_D$[b] °	Temp °C	Time min	Recovered %	$[\alpha]_D$[b] °	Remaining optical activity/%	Compd	$[\alpha]_D$[b] °	Optical yield %[c]	k_1/k_2[d]	Net stereospecificity %[e]
Ia	+19.8[f]	0	90	32	+4.88[f]	25	IIa	−6.36[f]	46	1.31	75
	+19.8[f]	10	90	7		9[i]		−2.29[f]	17	0.91	30
Ib	−11.9[g]	10	60	79	−10.23[g]	86	IIb	+12.7[f]	84	0.64	90
	−11.9[g]	10	90	76	−9.95[g]	84		+12.1[f]	80	0.64	87
Ic	−2.28[h]	30	60	66	−0.70[h]	31	IIc	+1.56[h]	59	2.82	97
	−2.28[h]	30	120	37	−0.17[h]	7		+1.10[h]	42	2.62	98
Id	−35.7	−5	10	61	−13.2	37	IId	+32.4	62	2.01	92
	−35.7	−5	20	34	−5.07	14		+28.5	47	1.82	91
Ie	−38.4	10	20	48	−8.0	21	IIe	+15.1	31	2.12	56
	−38.4	10	30	38	−7.3	19		+13.2	27	1.72	50

a) Molar ratio; $CH_3CH(Cl)\ CH_2Y$: $AlCl_3$: C_6H_6 = 1: 1.2: 30—40. CS_2 was added in the reaction below 5 °C. b) Rotation was measured in $CHCl_3$ (c 5.0), unless otherwise noted. c) See Table 1, footnote c. d) See the text. e) See the description in the text (Eq. 3). f) Measured in benzene (c 5.0). g) Measured in toluene (c 10). h) Neat liquid. i) By the ^1H NMR method using tris[trifluoroacetyl-(+)-camphorato]europium (III) as shift reagent.

At first, to examine the possibility of racemization of the product during the reaction, optically active IIa, IIb, IIc, IId, and IIe were treated with aluminium chloride in benzene under the same conditions as those of the alkylation. The specific rotation of these compounds remained almost unchanged before and after the treatment (Table 3). Thus, it turns out that the lesser stereospecificity in alkylation is not attributed to the successive racemization of the product. Next, we examined the possibility of simultaneous racemization of the starting chloride by observing the optical activity of that recovered before the completion of reaction; the reaction was quenched at about 30—70% conversion of the starting material after all reactants were mixed rapidely at lower temperature (see the method B in Experimental). The results are tabulated in Table 4. The starting chloride was racemized to a considerable extent as the reaction proceeds, and the optical yield of product decreased with the progress of reaction. Thus, these alkylation were found to be accompanied with simultaneous racemization of the starting material.

We have attempted to evaluate the extent of stereospecificity in the alkylation. The net stereospecificity of each reaction can be estimated from the extent of alkylation and the remaining optical activity of the starting material both observed at the same reaction time, by considering a kinetic model as shown in Scheme 1. I_0, I, and II indicate the starting material, the complex with aluminium chloride, and the alkylated product, respectively, and the asterisk indicates optically pure species. For convenience in the analysis we

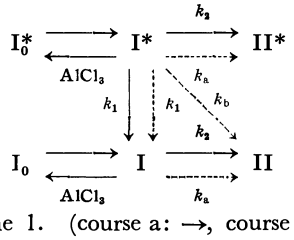

Scheme 1. (course a: →, course b: ⇢)

assumed this reaction model in terms of optically pure and racemic species, although use of the enantiomers would be correct. The concentration of the complex (I* or I) would be equal to that of the starting material (I_0* or I_0) since the reaction from I_0* (or I_0) to I* (or I) is considered to be very rapid. In the conversion of I* into II* and II, two reaction courses are considered as shown in Scheme 1. The course a involves the reaction of I* to II* and the consecutive reaction of I* to II through I. The course b involves the direct conversion of I* into II in addition to the course a. Assuming that the racemization and disappearance of the starting material are pseudo-first-order in I* (or I), the reaction rates, k_1 and k_2, can be deduced from the fraction of the remaining optical activity in the starting material and that of the remaining starting material observed at the same time.[15] Thus, the optical yield of the product in the course a should be represented by Eq. 1.[16]

$$\left(\frac{[II^*]}{[II]+[II^*]}\right)_{\text{course a}} = \frac{k_2}{k_1+k_2}\,\frac{(1-e^{-(k_1+k_2)t})}{(1-e^{-k_1t})} \qquad (1)$$

In the course b, k_a and k_b represent the psendo-first-order rate constants for the formation of II* from I* (or of II from I) and that for the direct conversion of I* into II, respectively. Here,

$$k_a + k_b = k_2.$$

Thus, the optical yield of the product in the course b can be represented by Eq. 2, and corresponds to the observed optical yield.

$$\left(\frac{[II^*]}{[II]+[II^*]}\right)_{\text{course b}} = \frac{k_a}{k_1+k_2}\,\frac{(1-e^{-(k_1+k_2)t})}{(1-e^{-k_1t})} \qquad (2)$$

Consequently, the net stereospecificity $(k_a/(k_a+k_b))$ should be given by Eq. 3.[17]

$$\left(\frac{[II^*]}{[II]+[II^*]}\right)_{\text{course b}} \Big/ \left(\frac{[II^*]}{[II]+[II^*]}\right)_{\text{course a}} = \frac{k_1+k_2}{k_2}\,\frac{(1-e^{-k_1t})}{(1-e^{-(k_1+k_2)t})} \times (\text{observed optical yield \%}) \qquad (3)$$

For example, in the alkylation with (−)-Ib at 10 °C (90 min), (+)-IIb was obtained in 24% yield and in 80% optical yield, and the optical activity of the starting material was depressed to 84% of the initial value. The k_1 and k_2 values were calculated to be $1.94\times10^{-3}\,min^{-1}$ and $3.05\times10^{-3}\,min^{-1}$ based on ln[fraction of remaining optical activity (0.84)] and ln[fraction of remaining chloride (0.76)], respectively. Therefore, the "true stereochemical consequence (net stereospecificity)" of this reaction was calculated to be 87%. Furthermore, the k_1/k_2 value (0.64) suggests that the rate of the alkylation is appreciably faster than that of the racemization of the starting material. The calculated values of the net stereospecificity and k_1/k_2 are given in the 11th and 12th column of Table 4, respectively.

Such high stereospecificities have not been reported in the Friedel-Crafts alkylation with acyclic alkylating reagent. In this case, the polar group (OH, COOH, and COOR) being a part of the alkylating reagent would be responsible for the high stereospecificity of the reaction. The predominance of inversion in the alkylation is reasonably interpreted by considering the formation of cyclic intermediates as follows.

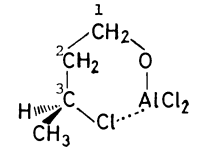

(Ia′)

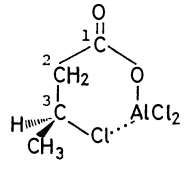

(Ib′)

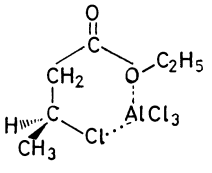

(Ic′)

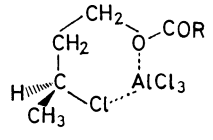

(Id′: R=C_6H_5)
(Ie′: R=CH_3)

In the initial stage of the reaction with Ia and Ib, we observed the evolution of appreciable amounts of hydrogen chloride. This suggests that Ia (or Ib) reacted with aluminium chloride to form the salt evolving hydrogen chloride. The aluminium atom in the salt would coordinate with the chlorine atom at C_3 to form six-membered quasi-ring structure (Ia′ and Ib′), and the C_3–Cl bond would be polarized appreciably. Then, benzene would attack the C_3 atom from the back-side of the leaving chlorine atom. Even if the abstraction of the chlorine atom took place initially to give the carbonium ion (C_3^+), the interaction between the cation and the leaving chloride anion would prevent the rotation about the C_2–C_3 bond. Thus, the stereospecificity of the reaction may be interpreted in terms of the stability of the ring structure and the tightness of this ion pair. The increased tightness of the ion pair would increase the stability of the quasi-ring structure and thus the stereospecificity of the reaction. The higher stereospecificity of the reaction with Ib compared to Ia may be attributed to the enforced tightness of the ion pair by the electron withdrawing effect of the carbonyl group.

In the case of esters, Ic, Id, and Ie, the ether oxygen of ester group coordinates with aluminium chloride to form similar quasi-ring structures (Ic′, Id′, and Ie′). The high stereospecificity in the alkylation may also be interpreted in terms of the tightness of the ion pair as mentioned above. However, the large difference in the stereospecificity between the reaction with Id and Ie remained unexplainable.

The k_1/k_2 value for the reaction with Ia or Ib was found to be 0.6—1.3 while that for the reaction with esters was over 2. The lower value of k_1/k_2 in the former case may be attributed to lesser amounts of aluminium chloride remaining in the reaction mixture, because most of aluminium chloride were consumed for the salt-formation with Ia (or Ib).

Experimental

The optical rotations were taken on a JASCO DIP-SL polarimeter with use of 0.05 and 0.1 dm tubes at 25—30 °C. The NMR spectra were recorded on a JEOL JNM PS-100 spectrometer. Chemical shifts are given in ppm downfield from internal TMS. The IR spectra were determined on a JASCO DS-301 spectrometer. GLPC analyses were carried out on a 3 m column of 10% Carbowax 20 M on Diasolid L for IIa, IIb, and IIc, and on a 2 m column of 10% High Vacuum Silicon grease on Diasolid L for IId and IIe, with a Shimadzu GC-3A instrument.

Commercial grade aluminium chloride was purified by sublimation under nitrogen gas stream. Benzene was washed with concentrated sulfuric acid and water, and distilled after drying on sodium ribbon. Other solvents were dried by the most efficient ways reported in the literature[18] and distilled before use.

(+)-3-Chlorobutanoic Acid (Ib). Racemic Ib was prepared by addition of hydrogen chloride to crotonic acid[19] and resolved by the use of quinine[20] or (+)-ephedrine. When quinine was used as a resolving agent, (+)-Ib was obtained in about 50% optical purity, $[\alpha]_D$ +25.0° (*c* 10, $C_6H_5CH_3$), lit,[19] $[\alpha]_D$ +46.6° (*c* 10, $C_6H_5CH_3$). When (+)-ephedrine was used, (+)-Ib was obtained in lower optical purity, $[\alpha]_D$ +7.82° (neat). In both cases, (−)-Ib was recovered from the mother liquors.

(+)-3-Chloro-1-butanol (Ia). (+)-Ib ($[\alpha]_D$ +22.5°) was reduced with lithium aluminium hydride according to the procedure of Searles[22] to give (+)-Ia, bp 68 °C/20 mmHg, $[\alpha]_D$ +23.5° (neat), optical purity 48.3%.

(+)-Ethyl 3-Chlorobutanoate (Ic). (+)-Ib was esterificated with anhydrous ethanol in the presence of boron trifluoride to give (+)-Ic, bp 62—63 °C/20 mmHg, $[\alpha]_D$ +4.80° (neat). Optically pure (+)-Ic was prepared from thionyl chloride and (+)-ethyl 3-hydroxybutanoate obtained by the yeast reduction of ethyl acetoacetate as follows:[21] ethyl acetoacetate (100 g, 0.77 mol) was treated with baking yeast (1 kg) and sugar (1 kg) in water (10 liter) at 35 °C. After 24 h, (+)-ethyl 3-hydroxybutanoate was isolated by the repeated extraction with ether, bp 75—77 °C/15 mmHg, $[\alpha]_D$ +28.3° (*c* 5.0, $CHCl_3$), yield 56%. The hydroxybutanoate was converted with thionyl chloride in pyridine to (+)-Ic, yield 67%, $[\alpha]_D$ +18.8° (*c* 5.0, $CHCl_3$).

(−)-3-Chlorobutyl Benzoate (Id) was prepared by the esterification of (−)-Ia ($[\alpha]_D$ −46.6° (*c* 5.0, $CHCl_3$) with benzoyl chloride in pyridine at 100 °C, bp 101—102 °C/0.7 mmHg, $[\alpha]_D$ −41.2° (*c* 5.0, $CHCl_3$), yield 81%.

(−)-3-Chlorobutyl Acetate (Ie) was prepared from (−)-Ia ($[\alpha]_D$ −46.6°) and acetyl chloride in pyridine, bp 76—77 °C/17 mmHg, $[\alpha]_D$ −38.4° (*c* 5.0, $CHCl_3$), yield 60%.

Reaction Procedures and Product Identification. Method A: To a stirred mixture of dry benzene (20 ml) and aluminium chloride (9.8 mmol) was added a solution of the starting chloride (Ia, Ib, Ic, Id, or Ie) (8.3 mmol) in benzene (20 ml) at a rate sufficient to maintain the temperature shown in Table 1. The reaction mixture was stirred at that temperature until the starting chloride was almost consumed, and then was poured onto a mixture of crashed ice and 20 ml of concentrated hydrochloric acid. In the case of the reaction with Ia, Id, and Ie, the resulting mixture was treated as follows. The benzene layer was separated and the aqueous layer was extracted three times with 30 ml portions of ether. The combined organic layers were washed with water and dried over anhydrous sodium sulfate. After the removal of solvent, the residue was distilled *in vacuo* to give the corresponding 3-phenyl derivatives (IIa, IId or IIe). The results were summarized in Table 1.

In the case of the reaction with Ib and Ic, the reaction mixture was treated as follows. The benzene layer was separated and extracted five times with 30 ml portions of 5% sodium hydrogencarbonate solution and dried over anhydrous sodium sulfate. After the removal of benzene, the residue was distilled *in vacuo* to give IIc. The hydrogencarbonate solution was acidified with 6 M hydrochloric acid and extracted five times with 30 ml portions of ether and dried over anhydrous sodium sulfate. After the removal of the ether, the residue was distilled *in vacuo* to give IIb.

Method B: In order to estimate the net stereospecificity of the reaction, the experiment was carried out as follows.

To a cooled (−10 °C) suspension of aluminium chloride (5.6 mmol) in dry benzene (6 ml) was added, all at once, a solution of the chloride (4.7 mmol) in benzene (6 ml), and the reaction mixture was stirred at the prescribed temperature for the prescribed period (see Table 4). The resulting mixture was worked up as mentioned above. The unreacted starting material and the product were separated by fractionated distillation *in vacuo*. The results were summarized in Table 4.

(+)-3-Phenyl-1-butanol (IIa): IR(neat); 3340 (νOH), 1600 (skeletal vibration of phenyl ring), 1050 (νC–OH), 760, and 700 cm^{-1} (δCH, monosubstituted phenyl). NMR ($CDCl_3$, 7%); δ 1.26 (d, J=7.0 Hz, 3H, $-CH_3$), 1.70 (s, 1H, –OH), 1.72—1.96 (m, 2H, $-CH_2-$), 2.68—3.07 (m, 1H, –CH=), 3.54 (t, J=6.9 Hz, 2H, $-CH_2O-$), and 7.09—7.39 ppm (m, 5H, phenyl). The GLPC retention time was identical with that of the authentic sample.

(+)-3-Phenylbutanoic Acid (IIb): Bp 106 °C/2.0 mmHg, $[\alpha]_D$ +15.8° (neat), IR(neat); 3000 (νOH, dimeric carboxylic acid), 1710 (νC=O), 1605 (skeletal vibration of phenyl ring), 1300 (νC–O), 760, and 700 cm^{-1} (δCH, monosubstituted phenyl). NMR($CDCl_3$, 7%); δ 1.30 (d, J=7.2 Hz, 3H, $-CH_3$), 2.46—2.63 (m, 2H, $-CH_2-$), 3.03—3.42 (m, 1H, –CH=), 7.21 (s, 5H, phenyl), and 10.30 ppm (s, 1H, –COOH).

(−)-Ethyl 3-Phenylbutanoate (IIc): Bp 118—119 °C/17 mmHg, $[\alpha]_D$ −3.04° (neat). IR (neat); 1740 (νC=O), 1604 (skeletal vibration of phenyl ring), 1170 (νC–O–C), 760, and 700 cm^{-1} (δCH, monosubstituted phenyl). NMR ($CDCl_3$, 7%); δ 0.89 (t, J=7.5 Hz, 3H, $-CH_2C\underline{H}_3$), 1.18 (d, J=6.9 Hz, =CHC$\underline{H}_3$), 2.10—2.77 (m, 2H, $-OC\underline{H}_2CH=$), 3.11—3.48 (m, 1H –CH=), 3.91 (q, J=7.5 Hz, 2H, $-C\underline{H}_2CH_3$), and 7.04—7.38 ppm (m, 5H, phenyl).

(+)-3-Phenylbutyl Benzoate (IId): Bp 140—141 °C/0.5 mmHg, $[\alpha]_D$ +18.8° (*c* 5.0, $CHCl_3$). IR (neat); 1724 (νC=O), 1604 (skeletal vibration of phenyl ring), 1280 (νC–O–C), 758, and 710 cm^{-1} (δ CH, monosubstituted phenyl). NMR ($CDCl_3$, 5%); δ 1.36 (d, J=7.3 Hz, 3H, $-CH_3$), 1.96—2.20 (m, 2H, $-CH_2-$) 2.76—3.15 (m, 1H, –CH=), 4.00—4.42 (m, 2H $-CH_2O-$), 7.24 (s, 5H, =CH–$C_6\underline{H}_5$), 7.14—8.20 ppm (m, 5H, $-OC-C_6H_5$).

(+)-3-Phenyl Butyl Acetate (IIe): Bp 130 °C/14 mmHg, $[\alpha]_D$+15.8° (*c* 5.0, $CHCl_3$). IR (neat); 1745 (νC=O), 1604 (sketetal vibration of phenyl ring), 1245 (νC–O–C), 765, and 700 cm^{-1} (δCH, monosubstituted phenyl). NMR ($CDCl_3$, 7%); δ 1.26 (d, J=7.2 Hz, 3H, $-CH_3$), 1.73—2.05 (m, 2H, =CHC$\underline{H}_2-$), 1.96 (s, 3H, $-COCH_3$), 2.64—3.00 (m, 1H, =CH–), 3.96 (t, J=6.9 Hz, 2H, $-OCH_2O-$), and 7.18—7.37 (m, 5H, phenyl).

The GLPC retention time of the recovered chloride (Ia, Ib, Ic, Id, and Ie) was identical with that of the corresponding starting material, respectively.

Reaction of Optically Active IIa, IIb, IIc, IId, and IIe with Aluminium Chloride. To a stirred mixture of benzene (20 ml) containing aluminium chloride (5.6 mmol) was added a solution of optically active IIa IIb, IIc, IId, or IIe (4.7 mmol) in benzene (5 ml) at the prescribed temperature for 2—3 h. The reaction mixture was worked up as mentioned above. The data of specific rotation of II before and after the reaction were presented in Table 3.

References

1) Present adresses: a) Ashikaga Institule of Technolog, Omaecho, 268-1, Ashikaga; b) Tanabe Seiyaku Co., Ltd., Doshomachi 3-21, Higashiku, Osaka; c) Nihon Iyakuhin Kogyo Co., Ltd., Hariwara-nakamachi 350-1, Toyama.

2) H. Hart, "Friedel-Crafts and Related Reactions," ed by G. A. Olah, Interscience Publisher, New York (1963), Vol. 1, p. 999.

3) C. K. Ingold, "Structure and Mechanism in Organic Chemistry," Cornell University Press, Ithaca, New York (1953), p. 386; C. C. Price and M. Lund, *J. Am. Chem. Soc.*, **62**, 3105 (1940); R. L. Burwell, Jr., and S. Archer, *ibid.*, **64**, 1032 (1942); R. L. Burwell, Jr., L. M. Elkin, and A. D. Schields, *ibid.*, **74**, 4567 (1952).

4) J. I. Brauman and A. J. Pandel, *ibid.*, **89**, 5421 (1967).

5) J. I. Brauman and A. Slladie-Cavallo, *Chem. Commun.*, **1968**, 1124.

6) T. Nakajima, S. Suga, T. Sugita, and K. Ichikawa, *Tetrahedron*, **25**, 1807 (1969).

7) T. Nakajima, Y. Nakamoto, and S. Suga, *Bull. Chem. Soc. Jpn.*, **48**, 960 (1974).

8) S. Masuda, T. Nakajima, and S. Suga, *J. Chem. Soc., Chem. Commun.*, **1974**, 954.

9) G. A. Olah, "Friedel-Crafts Chemistry," John Wiley and Sons, New York (1973), p. 421; K. Sato, Yau-Shin Lin, and T. Amakusa, *Bull. Chem. Soc. Jpn.*, **42**, 2600 (1969); R. A. Banes and A. C. Neto, *J. Org. Chem.*, **35**, 4259 (1970).

10) S. Suga, T. Nakajima, Y. Nakamoto, and K. Matsumoto, *Tetrahedron Lett.*, **1969**, 3283.

11) K. Freudenberg and W. Lwowski, *Ann. Chem.*, **597**, 141 (1955).

12) K. Imano and S. Mitsui, *Nippon Kagaku Zasshi*, **85**, 497 (1964).

13) V. Prelog and H. Scherrer, *Helv. Chem. Acta*, **42**, 2227 (1959).

14) D. J. Cram, *J. Am. Chem. Soc.*, **74**, 2137 (1952).

15) Strictly speaking, rate constant should be estimated for homogeneous reaction. As pointed out by Brauman *et al.*,[4] however, it will be possible to estimate the rate constant with appreciable accuracy by assuming that the complex formation is relatively fast compared to the other steps, and that only dissolved complex takes part in the reaction. In our case,

aluminium chloride was gradually dissolved as the reaction proceeds although the reaction was heterogeneous in the initial stage.

16) For the analysis of complex reaction, see, for example, A. A. Frost and R. G. Pearson, "Kinetic and Mechanism," 2nd ed, John Wiley and Sons, Inc., New York (1953), p. 166.

17) The net stereospecificity in the alkylation of benzene with (+)-γ-valerolactone was calculated using the value of k_1/k_2 obtained in the initial stage of reaction and that of the observed inversion % obtained after the completion of reaction.[4] The stereospecificity calculated in such a manner corresponds to that at $t=\infty$ in our Eq. 3.

18) J. A. Riddick and E. E. Toops, Jr., "Organic Solvents," 2nd ed, Interscience Publishers, Inc., New York (1955).

19) H. Scheibler, *Ber.*, **48**, 1443 (1915).

20) H. Scheibler and J. Magasanic, *Ber.*, **48**, 1810 (1915).

21) D. D. Ridley and M. Stralow, *J. Chem. Soc., Chem. Commun.*, **1975**, 400.

22) S. Searles, Jr., *J. Am. Chem. Soc.*, **79**, 955 (1957).

Preparation of Chlorophyll-a and Chlorophyll-b by Column Chromatography with Sephasorb HP Ultrafine

Masahiko YOSHIURA, Keiji IRIYAMA,* Masaru SHIRAKI, and Akira OKADA

Research Institute for Polymers and Textiles, Sawatari 4-1, Kanagawa-ku, Yokohama 221

(Received December 21, 1978)

A method for the preparation of chlorophyll-a (Chl-a) and chlorophyll-b (Chl-b) by column chromatography with Sephasorb HP Ultrafine has been developed. The partially purified chlorophyll preparation containing Chl-a, Chl-b and nonsorbed carotenes was applied to a Sephasorb HP Ultrafine column and good separation of Chl-a and Chl-b achieved with a solvent program of (I), a diethyl ether/hexane mixture (1 : 9, volume ratio) followed by 0.2 and 0.5 vol % isopropyl alcohol in (I). 13.1 mg of Chl-a and 7.6 mg of Chl-b were obtained from 24.7 mg of the partially purified chlorophyll using the above method.

One of the methods for separation and isolation of chlorophyll in quantities of 0.01—1 g is column chromatography with powdered sugar. Recently, a method has been developed for the partial purification of chlorophyll-a (Chl-a) and chlorophyll-b (Chl-b) extracted from spinach leaves using dioxane[1] and subsequent washing with 80 vol % aqueous methanol[2] prior to chromatographic separation and isolation. Chl-a and Chl-b in the partially purified chlorophyll preparation were subsequently separated and isolated by passage through a powdered sugar column.[3] Special care is, however, required to prepare a powdered sugar column of good quality with good reproducibility, as powdered sugar has a strong tendency to adsorb moisture from the air and the presence of any trace water affects the separation of the pigments. Angapindu *et al.*[4] reported that cellulose was superior to powdered sugar as an adsorbent since passage through the cellulose columns was faster and the carrying capacity greater. Strain and Sato[5] found that the pigment bands were better defined on sugar rather than on cellulose columns. Shimizu[6] reported that the separation between Chl-a and Chl-b zones could not be performed by column chromatography with Sephadex LH-20 eluted with chloroform, although the mobility of Chl-a was greater than that of Chl-b. Sephadex LH-20 is a hydroxypropyl derivative of cross-linked dextran. Sephasorb HP Ultrafine is similar in structure to Sephadex LH-20, but has a higher matrix density making it suitable for the adsorption of a wide range of compounds soluble in organic solvents. The authors have found that the pigment bands are better defined on Sephasorb HP Ultrafine columns than on powdered sugar or cellulose.

Experimental

Materials. All solvents were of reagent grade further purified, by the methods described.[7] Sephasorb HP Ultrafine was purchased from Seikagaku Kogyo Co.

Preparation of Partially Purified Chl-a and Chl-b. The partially purified chlorophyll preparation was obtained according to the method of Iriyama *et al.*[1,2] All procedures for the preparation were conducted at 5 °C in total darkness or under dim green light. Spinach leaves (100 g fresh weight) were homogenized for 3 min in a Waring blender with chilled acetone (500 ml). The dark green extract obtained was filtered through a paper towel to remove the coarse material and the filtrate centrifuged at 10000×g for 5 min to remove the insoluble materials. The deep-green supernatant solution was employed in the partial purification of chlorophyll by the dioxane method.[1] The chlorophyll preparation, twice precipitated from acetone–dioxane solution by the drop-wise addition of water, was dissolved in methanol (500 ml) containing petroleum ether (125 ml, bp 20—40 °C) and then distilled water (250 ml) was added to the solution. The upper petroleum ether layer was washed with 80 vol % aqueous methanol several times to eliminate the remaining photosynthetic yellow pigments from the solution.[2] The solution was evaporated and dried in a vacuum desiccator to give dark-green microcrystals. Thin-layer chromatographic analysis according to the method of Shiraki *et al.*[8] revealed that the dark-green microcrystals (Ppt III) thus obtained contained Chl-a, Chl-b and nonsorbed carotenes. Ppt III was dissolved in a minimum volume of mixed solvent (diethyl ether: petroleum ether=1 : 9, volume ratio) and the solution (developing solution I) applied to the Sephasorb HP Ultrafine column.

Identification and Determination of Chl-a and Chl-b. The pigments were characterized by comparison of the visible absorption spectra with the literature values. The molar extinction coefficients of Comar and Zscheile[9] were used to determine the purity of the Chl-a and Chl-b preparations as standard values. In addition, the purity and chemical stability of Chl-a and Chl-b were examined by chromatography, since it has been recognized by Strain and Svec[10] that spectroscopic observations need to be supplemented by chromatographic tests to demonstrate that the chlorophyll molecules had not been altered. The purity and chemical stability of the pigments were examined by thin-layer chromatography[8] since the technique was simple and rapid. Where necessary, the thin-layer chromatographic observations were supplemented by high-performance liquid chromatographic tests according to the methods described.[11,12] High-performance liquid chromatography[11,12] is relatively complicated, but has the advantage of greater sensitivity. Qualitatively it was possible to detect the pigments in the order of 10^{-8} g and 10^{-10} g using thin-layer chromatography[8] and high-performance liquid chromatography,[11,12] respectively.

Preparation of a Sephasorb HP Ultrafine Column. A wet column was employed using a Pharmacia R25 chromatographic tube (2.5×45 cm) connected, through the UV monitor (JASCO UVIDEC-100), to a fraction collector. The bed volume (cm^3/g dry Sephasorb HP Ultrafine) in petroleum ether was 1.3. 97 g of Sephasorb HP Ultrafine suspended in petroleum ether. The suspension was poured into the chromatographic tube, providing a 26 cm column. The column thus prepared had a capacity of approximately 30 mg of Chl-a+Chl-b without being overloaded. The column was washed with petroleum ether (1000 ml) before use to eliminate the soluble materials from the Sephasorb HP Ultrafine.

Sephasorb HP Ultrafine Column Chromatography. Percolation of the pigment solution and the developing solvents were accelerated by the application of pressure from a rotary pump (SJ-1210, Mitsumi; flow speed: approximately 21.4 ml h^{-1} cm^{-2}) connected to the top of the chromatographic tube by way of a Teflon tube. Chromatograms were monitored by a monochromatic light of 380 nm and each of the pigment fractions collected by a fraction collector.

Results

All experiments were conducted at 20 °C in total darkness or under a dim green light unless otherwise stated.

The developing solution I containing Chl-a, Chl-b and nonsorbed carotenes was added to the top of the Sephasorb HP Ultrafine column and the column washed with the developing solvent system I (diethyl ether: hexane=1: 9, volume ratio) to adsorb the pigments at the top of the column and to elute the nonsorbed carotenes from the column. Subsequently the column was washed with 0.2 vol % isopropyl alcohol in the solvent system I to elute Chl-a from the column. After most of the Chl-a had been eluted, the column was washed with 0.5 vol % isopropyl alcohol in the solvent system I to accelerate the elution of Chl-b. The elution pattern is presented in Fig. 1, where the void volume of the column used here was about 59 ml. The chromatogram shows complete separation between Chl-a, Chl-b and nonsorbed carotenes. The Chl-a and Chl-b preparation thus obtained were evaporated and dried in a vacuum desiccator.

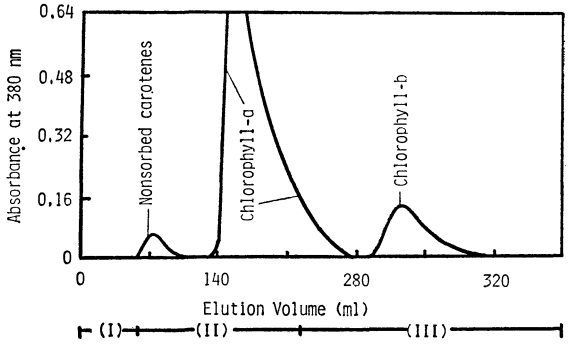

Fig. 1. Chromatogram for Ppt III.[a] Solvent systems for I, II, and III are a diethyl ether/hexane mixture (1: 9, volume ratio), 0.2 vol % isopropyl alcohol in I, and 0.5 vol % isopropyl alcohol in I.
a) For the explanation, see the text.

Thin-layer chromatographic examination of the Chl-a and Chl-b preparations on commercial silica gel sheets showed single spots, respectively. The purity of the Chl-a and Chl-b preparations were further examined by high-performance liquid chromatography[11,12] which supplemented the thin-layer chromatographic observations. The absorption spectra of the Chl-a and Chl-b preparations dissolved in diethyl ether did not show any significant differences in comparison with the literature within experimental error. The ratio of absorbance of the Soret peak at 427.0±1.0 nm to the red peak at 660.0±0.5 nm was 1.30±0.1 for the Chl-a preparation and the ratio of absorbance of the Soret peak at 452.8± 0.3 nm to the red peak at 642.3±0.3 nm was 2.83±0.1 for the Chl-b preparation. The purity of the Chl-a and Chl-b preparations obtained here was greater than 99% on a dry weight basis. 13.1 mg of Chl-a and 7.6 mg of Chl-b were obtained from 24.7 mg of Ppt III using the method developed here. 3.4 mg of nonsorbed carotenes were also isolated. Recovery of the chlorophylls in the column chromatography with Sephasorb HP Ultrafine was about 97%.

The chlorophyll preparations, when isolated in the solid state and stored in evacuated and sealed ampules in total darkness at −20 °C, could be preserved for at least three months without change or alteration. In a few cases, however, the chlorophyll molecules were degraded. For example, Chl-a was converted to chlorophyll-a′ (Chl-a′) and pheophytin-a. Chl-a and Chl-a′ are spectroscopically very similar as well as interconvertible[13] and subsequently spectroscopic observations provide no indication that Chl-a molecules had not altered. It should be noted that the purity of the chlorophyll preparations should be checked by thin-layer or high-performance liquid chromatography before use.

Table 1. Spectral properties of chlorophyll-a and chlorophyll-b with values reported by some authors[a]

	Red peak (nm)	Blue peak (nm)	Absorbance ratio (blue peak/red peak)	Authors
Chlorophyll-a	660.0	429.0	1.32	Comar and Zscheile[b]
	662.0	430.0	1.31	Smith and Benitez[c]
	660.5	428.5	1.30	Strain *et al.*[d]
	660.0 (±0.5)	427.0 (±1.0)	1.30 (±0.1)	This authors
Chlorophyll-b	642.5	453.0	2.82	Comar and Zscheile[b]
	644.0	455.0	2.82	Smith and Benitez[c]
	642.0	452.0	2.84	Strain *et al.*[d]
	642.3 (±0.3)	452.8 (±0.3)	2.83 (±0.1)	This authors

a) Solvent, diethyl ether; temperature, 25 °C.
b) C. L. Comar and F. P. Zscheile, *Plant Physiol.*, **17**, 198 (1942).
c) J. H. C. Smith and A. Benitez, "Modern Methods of Plant Analysis," ed by K. Paeck and M. V. Tracey, Springer-Verlag, Berlin (1955), p. 142.
d) H. H. Strain, M. R. Thomas, and J. J. Katz, *Biochim. Biophys. Acta*, **75**, 306 (1963).

Discussion

The spectral properties of Chl-a and Chl-b in diethyl ether with values reported by some authors are listed in Table 1. The extinction coefficients for Chl-a and Chl-b were not established due to the volatility of diethyl ether at room temperature (20 °C±5). In addition, as diethyl ether has a strong tendency to adsorb moisture from the air and the migration of trace water into chlorophyll solutions in diethyl ether influences the peak positions of Chl-a and Chl-b, the peak positions were shifted to the blue or red regions depending on the water content in solution. Nevertheless, the absorption spectra of the Chl-a and Chl-b preparations dissolved in diethyl ether did not show any significant differences in comparison with the literature values within experimental error as is shown in Table 1. The molar extinction coefficients of Comar and Zscheile,[9] which have been widely used, were used to determine the purity of the Chl-a and Chl-b preparations in this study. The values for the purity of the Chl-a and Chl-b preparations were greater than 99%. Subsequently, the presence of colorless substances as possible contaminants was examined. According to the method of Strain and Svec[10] the preparations were subjected to the test. The purity of the chlorophyll preparations, however, was not higher. In addition, it was found that the Chl-a and Chl-b molecules were degraded during the course of the chlorophyll purification. Thus, the procedure for the elimination of colorless substances from the chlorophyll preparations was not suitable in this case.

There have been no reports on the column chromatographic separation and isolation of chlorophylls with Sephasorb HP Ultrafine and Sephadex LH-20. Sephasorb HP Ultrafine was stable in the solvent systems used in this study as developing solvents. The bed volume obtained on swelling 1 g of dry Sephasorb HP Ultrafine in the solvent systems were relatively small (approximately 1.3 cm^3/g dry gel). No detectable and undesirable substances extracted from Sephasorb HP Ultrafine with the developing solvents used were found. The preparation of Sephasorb HP Ultrafine columns was relatively simple and the column could be used repeatedly for the separation of chlorophylls. In addition, good separation between Chl-a, Chl-b, and nonsorbed carotenes was achieved and Sephasorb HP Ultrafine did not react with chlorophyll molecules to form degradation products of the pigment molecules. For these reasons, Sephasorb HP Ultrafine may be one of the best adsorbents for separating chlorophylls.

The method developed here is suitable for the preparation of Chl-a and Chl-b from Ppt III, which was prepared from spinach leaves according to the method of Iriyama *et al.*[1,2]

References

1) K. Iriyama, N. Ogura, and A. Takamiya, *J. Biochem.*, **76**, 901 (1974).
2) K. Iriyama, M. Shiraki, and M. Yoshiura, *Chem. Lett.*, **1977**, 787.
3) K. Iriyama, M. Shiraki, and M. Yoshiura, *J. Liquid Chromatogr.*, **2**, 255 (1979).
4) A. Angapindu, H. Silberman, P. Tantivatana, and I. R. Kaplan, *Arch. Biochem. Biophys.*, **75**, 56 (1958).
5) H. H. Strain and T. R. Sato, *U.S. Atomic Energy Commision*, **TID 7633**, p. 175 (1956).
6) S. Shimizu, *J. Chromatogr.*, **59**, 440 (1971).
7) J. A. Riddick and W. B. Bunger, "Techniques of Chemistry," 3rd ed, ed by A. Weissberger, Wiley-Interscience, New York (1970), Vol II.
8) M. Shiraki, M. Yoshiura, and K. Iriyama, *Chem. Lett.*, **1978**, 103.
9) C. L. Comar and F. P. Zscheile, *Plant Physiol.*, **17**, 198 (1942).
10) H. H. Strain and W. A. Svec, "The Chlorophylls," ed by L. P. Vernon and G. R. Seely, Academic Press, New York (1966), p. 21.
11) M. Yoshiura, K. Iriyama, and M. Shiraki, *Chem. Lett.*, **1978**, 281.
12) K. Iriyama, M. Yoshiura, and M. Shiraki, *J. Chromatogr.*, **154**, 302 (1978).
13) P. Hynninen, *Acta Chem. Scand.*, **27**, 1478 (1973).

Acetoxymethylation of Coumarins by Manganese(III) Acetate

Kazu KUROSAWA* and Hironobu HARADA

Department of Chemistry, Faculty of Science, Kumamoto University, Kumamoto 860

(Received December 27, 1978)

The reactions of 4-methoxy-, 7-methoxy-, 6,7-dimethoxy-, and 7,8-dimethoxycoumarins with manganese(III) acetate in boiling acetic acid containing acetic anhydride gave 3-(acetoxymethyl)coumarins as the major product. The reactions of coumarin, and 6-methoxy- and 8-methoxycoumarins with manganese(III) acetate yielded a mixture of 3-(diacetoxymethyl)- and nuclear acetoxymethylated coumarins. The reaction of 7-methoxycoumarin with lead(IV) acetate gave 7-methoxy-3-methylcoumarin.

In a previous publication[1] we have reported the oxidation of 2-hydroxybenzophenones with manganese(III) acetate, that gave 9-xanthenones and acetoxymethylated 9-xanthenones. The reactions of aromatic hydrocarbons,[2,3] aromatic ethers,[4] and benzofuran,[5] with manganese(III) acetate have been reported to give acetoxymethylated products. The reaction mechanisms were discussed by Heiba *et al.*[2] However, these papers were primarily concerned with the product analyses and the reaction mechanisms, and the synthetic utility was not investigated in detail. In this paper we will describe the reaction of methoxy-substituted coumarins with manganese(III) acetate, that gave 3-(acetoxymethyl)-, 3-(diacetoxymethyl)-, and di(acetoxymethyl)-coumarins. We have also carried out the reaction of 7-methoxycoumarin with lead(IV) acetate, which yielded mainly 7-methoxy-3-methylcoumarin.

The coumarins studied were coumarin (**1a**), 4-methoxycoumarin (**1b**), 6-methoxycoumarin (**1c**), 7-methoxycoumarin (**1d**), 8-methoxycoumarin (**1e**), 6,7-dimethoxycoumarin (**1f**), and 7,8-dimethoxycoumarin (**1g**). The reactions were carried out in boiling acetic acid containing acetic anhydride, and in boiling acetic anhydride, using 6—12 equivalents of manganese(III) acetate dihydrate for 1 equivalent of the substrate. The reactions were continued until the color of manganese(III) acetate disappeared.

The reaction of **1d** in acetic acid containing acetic anhydride in the substrate/oxidant ratio of 1 : 6 gave an acetate (**2d**) (entry 4). The NMR spectrum indicated the presence of an acetoxymethyl group {δ 2.24 (3H, singlet) and δ 5.03 (2H, doublet, J=1.0 Hz)}. The acetoxymethyl group can be located at 3-position, since the methylene protons at δ 5.03 couple with a lower field proton which appeared at δ 7.69 (1H, broad singlet) as was confirmed by a decoupling experiment. An ABX pattern of three aromatic protons was found in the spectrum {δ 6.75—6.90 (2H, multiplet) and 7.48 (1H, m)}. The yield of **2d** increased with increase of the molar ratio of manganese(III) acetate and the maximum yield was attained for the substrate/oxidant ratio of 1 : 10 (entry 6). When the reaction was conducted for this molar ratio, another product (**4d**) was isolated from the reaction mixture, the structure of which was elucidated as before by the NMR spectrum. It showed the presence of two acetoxyl group at δ 2.15 and a doublet proton at δ 7.66 (J=1.0 Hz), indicating that a diacetoxymethyl group is present in the molecule. The presence of an ABX pattern of three aromatic protons and a lower field proton (δ 7.80, broad s) suggested that the diacetoxymethyl group can be located at 3-position (Fig. 1). When the reaction of **1d** with manganese(III) acetate was conducted in acetic anhydride, a complex mixture of products was obtained. In acetic acid, on the other hand, the reaction did not take place. **1b**, **1f**, and **1g** gave the corresponding 3-(acetoxymethyl)coumarin, **2b**, **2f**, and **2g** in the reaction, respectively (entries 2, 13, and 14). In the case of **1g**, 3,6-di(acetoxymethyl)-7,8-dimethoxycoumarin (**5g**) was obtained in a low yield.

In contrast to the coumarins described above, the reactions of **1a**, **1c**, and **1e** with manganese(III) acetate showed a very different product distribution. In the case of **1a**, 3-(diacetoxymethyl)coumarin (**4a**) was the major product and a small amount of impure 3-(acetoxymethyl)coumarin (**2a**) was isolated (entry 1). **1c** gave 3-(diacetoxymethyl)-6-methoxycoumarin (**4c**) and a mixture of 5- and 7-(acetoxymethyl)coumarins (**3c** and **3c'**). The reaction of **1e** with manganese(III) acetate gave three products: **3e**, **4e**, and **6e** (entry 12). The structure of **3e** was elucidated by the NMR analysis: the chemical shifts of an AB system due to the protons at 6- and 5-positions (δ_A=7.00 and δ_B=7.21, J_{AB}=9.0 Hz) are characteristic of the 7,8-disubstituted

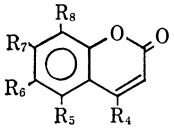

1a—g

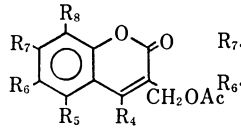

2a, b, d, f, g

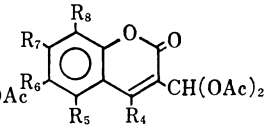

4a, c, d, e

1, 2, and 4 **a**: $R_4=R_5=R_6=R_7=R_8=H$
b: $R_5=R_6=R_7=R_8=H$, $R_4=OCH_3$
c: $R_4=R_5=R_7=R_8=H$, $R_6=OCH_3$
d: $R_4=R_5=R_6=R_8=H$, $R_7=OCH_3$
e: $R_4=R_5=R_6=R_7=H$, $R_8=OCH_3$
f: $R_4=R_5=R_8=H$, $R_6=R_7=OCH_3$
g: $R_4=R_5=R_6=H$, $R_7=R_8=OCH_3$

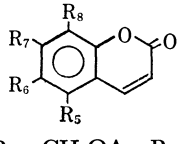

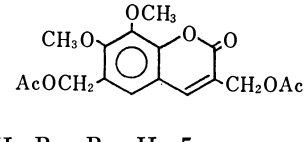

3c : $R_5=CH_2OAc$, $R_6=OCH_3$, $R_7=R_8=H$ **5g**
3c': $R_5=R_8=H$, $R_6=OCH_3$, $R_7=CH_2OAc$
3e : $R_5=R_6=H$, $R_7=CH_2OAc$, $R_8=OCH_3$

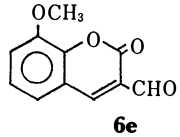

6e

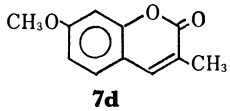

7d

Table 1. The reactions of coumarins with manganese(III) acetate and lead(IV) acetate

Entry	Substrate	Reaction conditions[a]				Product (yield[b]/%)			
		Oxidant	Molar ratio of **1**: oxidant	Solvent	Time / min	Monoacetate	Diacetate	Aldehyde	3-Methyl-coumarin
1	**1a**	$Mn(OAc)_3$	1:10	AcOH, Ac_2O	60	**2a**(5)	**4a**(19)		
2	**1b**	$Mn(OAc)_3$	1:10	AcOH, Ac_2O	120	**2b**(39)			
3	**1c**	$Mn(OAc)_3$	1:10	AcOH, Ac_2O	50	**3c**(4.5[c]), **3c'**(2.5[c])	**4c**(4)		
4	**1d**	$Mn(OAc)_3$	1:6	AcOH, Ac_2O	140	**2d**(24)			
5	**1d**	$Mn(OAc)_3$	1:8	AcOH, Ac_2O	110	**2d**(70)			
6	**1d**	$Mn(OAc)_3$	1:10	AcOH, Ac_2O	200	**2d**(87)	**4d**(7)		
7	**1d**	$Mn(OAc)_3$	1:12	AcOH, Ac_2O	170	**2d**(46)	**4d**(19)		
8	**1d**	$Mn(OAc)_3$	1:12	Ac_2O	90	intractable			
9	**1d**	$Pb(OAc)_4$	1:5	AcOH	30	**2d**(6)			**7d**(5)
10	**1d**	$Pb(OAc)_4$	1:5	Ac_2O	10	**2d**(4)	**4d**(2)		**7d**(5)
11	**1d**	$Pb(OAc)_4$	1:5	C_6H_6	6480				**7d**(23)
12	**1e**	$Mn(OAc)_3$	1:8	AcOH, Ac_2O	105	**3e**(9)	**4e**(9)	**6e**(4)	
13	**1f**	$Mn(OAc)_3$	1:10	AcOH, Ac_2O	80	**2f**(54)			
14	**1g**	$Mn(OAc)_3$	1:10	AcOH, Ac_2O	90	**2g**(55)	**5g**(3)		

a) The reactions were carried out at reflux temperature.
b) Yields are based on the amount of coumarin consumed.
c) The values were estimated from the NMR spectrum.

coumarin (**1g**), in which the corresponding protons appeared at δ 6.91 and 7.23.

The results described above showed that coumarins bearing a methoxyl group at 4- or 7-position react with the carboxymethyl radical,[2] which is formed from the decomposition of manganese(III) acetate, predominantly at the 3-position, where the electron density is much greater than in the other positions owing to the resonance effect of the methoxyl groups. In coumarins bearing no methoxyl group in either position, the competitive reactions occur at the 3-position and at *ortho*-positions to the methoxyl group on the aromatic nucleus. Diacetoxymethylation takes place in the case when a substrate has no sufficient activating group at 4- or 7-position (entries 1, 3, and 12) or when the oxidant is used in large excess (entry 7). On the contrary, the reaction of **1d** with lead(IV) acetate gave 7-methoxy-3-methylcoumarin (**7d**), when treated with 5 equivalents of lead(IV) acetate in boiling benzene. The methylation of aromatic compounds by lead(IV) acetate has precedence.[1,6] The reaction of **1d** with lead(IV) acetate in acetic acid yielded **2d** and **7d** and in acetic anhydride **2d**, **4d**, and **7d**, but they have no synthetic values.

It is thus concluded that the reaction of coumarins bearing a methoxyl group at 4- or 7-position with manganese(III) acetate can give the corresponding 3-(acetoxymethyl)coumarin in moderately good yields.

Experimental

All ^1H chemical shifts (δ) were recorded for the deuteriochloroform solution with a Hitachi R 24 NMR spectrometer with TMS as an internal standard. The IR spectra were recorded for the chloroform solution with a JASCO IRA-1 grating spectrometer. The mass spectrum was recorded with a JEOL JMS-01 SG-2 mass spectrometer. Melting points were determined on a Yanagimoto hot-stage and are uncorrected. The compounds were recrystallized from ethanol, unless otherwise stated, and the yields are summarized in Table 1.

Coumarins. Coumarin (**1a**) was commercially available. 4-Methoxycoumarin (**1b**) was obtained from commercial 4-hydroxycoumarin by methylation.[7] 6-Methoxycoumarin (**1c**) was obtained from coumarin (**1a**) by potassium peroxodisulfate oxidation followed by methylation.[8] 7-Methoxycoumarin (**1d**) was prepared by the Pechmann reaction[9] of resorcinol and malic acid, followed by methylation. 8-Methoxycoumarin (**1e**) was obtained by the reaction of *o*-vaniline and acetic anhydride.[10] 6,7-Dimethoxycoumarin (**1f**) and 7,8-dimethoxycoumarin (**1g**) were prepared by the Pechmann reaction of the corresponding phenols and malic acid.

*Oxidations of Coumarins (**1a—g**) with Manganese(III) Acetate.* A typical oxidation of coumarin was as follows. A mixture of a coumarin (2 mmol), manganese(III) acetate dihydrate[3] (12—24 mmol), and a solvent (50 ml) (if acetic acid was used as the solvent, acetic anhydride (24—48 mmol) was added) was heated under reflux for the time shown in Table 1. After the removal of the solvent *in vacuo*, the resulting mixture was extracted with chloroform. The chloroform solution was evaporated and chromatogrammed on TLC using chloroform as the developing solvent.

1a yielded 3-(acetoxymethyl)coumarin (**2a**). Mp: 106.5—107.5 °C; IR 1740 cm^{-1}; NMR 2.15 (3H, s, OAc), 5.07 (2H, d, J=1.0 Hz, $-CH_2-$), 7.1—7.7 (4H, m, aromatic), and 7.74 (1H, t, J=1.0 Hz, $H_{(4)}$); 3-(diacetoxymethyl)coumarin (**4a**): Mp 139—140 °C; IR 1750 and 1780 cm^{-1}; NMR 2.18 (6H, s, 2×OAc), 7.1—7.7 (4H, m, aromatic), 7.75 (1H, d, J=1.0 Hz, >CH–), and 7.92 (1H, broad s, $H_{(4)}$); MS *m/e* 276 (M^+), 233, 216, 191, 176, 175, 174, 173, 149, and 146 (Found: C, 60.99; H, 4.41%. Calcd for $C_{14}H_{12}O_6$: C, 60.87; H, 4.38%).

1b gave 3-(acetoxymethyl)-4-methoxycoumarin (**2b**). Mp: 114—115 °C; IR: 1740 cm^{-1}; NMR: 2.10 (3H, s, OAc), 4.16 (3H, s, OCH_3), 5.18 (2H, s, $-CH_2-$), 7.15—7.90 (4H, m, aromatic) (Found: C, 63.00; H, 4.92%. Calcd for $C_{13}H_{12}O_5$: C, 62.90; H, 4.87%).

1c yielded a mixture of 5-(acetoxymethyl)- and 7-(acetoxymethyl)-6-methoxycoumarins (**3c** and **3c'**). Mp: 119—123 °C.

(Found: C, 63.22; H, 4.90%. Calcd for $C_{13}H_{12}O_5$: C, 62.90; H, 4.87%); 3-(diacetoxymethyl)-6-methoxycoumarin (**4c**). Mp: 175—177 °C; IR: 1745 and 1778 cm^{-1}; NMR: 2.15 (6H, s, 2×OAc), 3.85 (3H, s, OCH_3), 6.9—7.4 (3H, m, aromatic), 7.70 (1H, d, J=1.0 Hz, >CH–), and 7.83 (1H, broad s, $H_{(4)}$) (Found: C, 58.62; H, 4.62%. Calcd for $C_{15}H_{14}O_7$: C, 58.82; H, 4.61%).

1d gave 3-(acetoxymethyl)-7-methoxycoumarin (**2d**). Mp: 118—119 °C; IR: 1725 and 1755 cm^{-1}; NMR: 2.24 (3H, s, OAc), 3.86 (3H, s, OCH_3), 5.03 (2H, d, J=1.0 Hz, $-CH_2-$), 6.75—6.90 (2H, m, $H_{(6)}$ and $H_{(8)}$), 7.48 (1H, m, $H_{(5)}$), and 7.69 (1H, broad s, $H_{(4)}$) (Found: C, 62.72; H, 4.93%. Calcd for $C_{13}H_{12}O_5$: C, 62.90: H, 4.87%); 3-(diacetoxymethyl)-7-methoxycoumarin (**4d**). Mp: 147—149 °C; IR: 1745 and 1775 cm^{-1}; NMR: 2.15 (6H, s, 2×OAc), 3.89 (3H, s, OCH_3), 6.79—6.95 (2H, m, $H_{(6)}$ and $H_{(8)}$), 7.40 (1H, d, J=9.5 Hz, $H_{(5)}$), 7.66 (1H, d, J=1.0 Hz, >CH–), and 7.80 (1H, broad s, $H_{(4)}$) (Found: C, 58.72; H, 4.69%. Calcd for $C_{15}H_{14}O_7$: C, 58.82; H, 4.61%).

1e yielded 7-(acetoxymethyl)-8-methoxycoumarin (**3e**). Mp: 121—122 °C; IR: 1750 cm^{-1}; NMR: 2.05 (3H, s, OAc), 3.92 (3H, s, OCH_3), 5.21 (2H, s, $-CH_2-$), 6.48 (1H, d, J=10.0 Hz, $H_{(3)}$), 7.00 (1H, d, J=9.0 Hz, $H_{(6)}$), 7.21 (1H, d, J=9.0 Hz, $H_{(5)}$), and 7.90 (1H, d, J=10.0 Hz, $H_{(4)}$) (Found: C, 62.73; H, 5.18%. Calcd for $C_{13}H_{12}O_5$: C, 62.90; H, 4.87%); 3-(diacetoxymethyl)-8-methoxycoumarin (**4e**). Mp: 130—131 °C (CCl_4); IR: 1752 and 1775 cm^{-1}; NMR: 2.15 (6H, s, 2×OAc), 3.96 (3H, s, OCH_3), 6.8—7.4 (3H, m, aromatic), 7.70 (1H, d, J=1.0 Hz, >CH–), 7.85 (1H, broad s, $H_{(4)}$) (Found: C, 58.90; H, 4.72%. Calcd for $C_{15}H_{14}O_7$: C, 58.82; H, 4.61%); 3-formyl-8-methoxycoumarin (**6e**). Mp: 166—168 °C; IR: 1724 and 1750 cm^{-1}; NMR: 3.97 (3H, s, OCH_3), 7.24 (3H, s, aromatic), 8.36 (1H, s, $H_{(4)}$), and 10.17 (1H, s, CHO) (Found: C, 64.70; H, 3.89%. Calcd for $C_{11}H_8O_4$: C, 64.70; H, 3.95%).

1f gave 3-(acetoxymethyl)-6,7-dimethoxycoumarin (**2f**). Mp: 140—141 °C; IR: 1730 and 1740 cm^{-1}; NMR: 2.14 (3H, s, OAc), 3.91 (3H, s, OCH_3), 3.94 (3H, s, OCH_3), 5.06 (2H, d, J=1.0 Hz, $-CH_2-$), 6.85 (1H, s, $H_{(5)}$ or $H_{(8)}$), 6.91 (1H, s, $H_{(5)}$ or $H_{(8)}$), and 7.70 (1H, broad s, $H_{(4)}$). Found: C, 60.30; H, 5.15%. Calcd for $C_{14}H_{14}O_6$: C, 60.43; H, 5.07%.

1g yielded 3-(acetoxymethyl)-7,8-dimethoxycoumarin (**2g**). Mp: 140 °C; IR: 1750 cm^{-1}; NMR: 2.14 (3H, s, OAc), 3.95 (6H, s, 2×OCH_3), 5.00 (2H, d, J=1.0 Hz, $-CH_2-$), 6.92 (1H, d, J=9.0 Hz, $H_{(6)}$), 7.22 (1H, d, J=9.0 Hz, $H_{(5)}$), and 7.69 (1H, t, J=1.0 Hz, $H_{(4)}$) (Found: C, 60.32; H, 5.02%. Calcd for $C_{14}H_{14}O_6$: C, 60.43; H, 5.07%); 3,6-di(acetoxymethyl)-7,8-dimethoxycoumarin (**5g**). Mp: 159—160 °C; IR: 1750 cm^{-1}; NMR: 2.09 (3H, s, OAc), 2.14 (3H, s, OAc), 3.96 (6H, s, 2×OCH_3), 5.00 (2H, d, J=1.0 Hz, $-CH_2-$), 5.23 (2H, s, $-CH_2-$), 6.91 (1H, s, $H_{(5)}$), and 7.87 (1H, t, J=1.0 Hz, $H_{(4)}$) (Found: C, 58.59; H, 5.25%. Calcd for $C_{17}H_{18}O_8$: C, 58.28; H, 5.18%).

Oxidation of ***1d*** *with Lead(IV) Acetate.* A mixture of **1d** (2 mmol), lead(IV) acetate[11] (10 mmol), and a solvent (50 ml) was heated under reflux for the time shown in Table 1. After the removal of the solvent *in vacuo*, the resulting mixture was extracted with chloroform. The chloroform solution was evaporated and then chromatogrammed on TLC, giving **2d**. Mp: 118—119 °C. **4d**. Mp: 147—149 °C. 7-Methoxy-3-methylcoumarin (**7d**). Mp: 144 °C (lit,[12] mp 144 °C); IR: 1725 cm^{-1}; NMR: 2.17 (3H, d, J=1.5 Hz, CH_3), 3.85 (3H, s, OCH_3), 6.65—6.90 (2H, m, $H_{(6)}$ and $H_{(8)}$), 7.39 (1H, m, $H_{(5)}$), and 7.44 (1H, q, J=1.5 Hz, $H_{(4)}$).

References

1) S. Ueda and K. Kurosawa, *Bull. Chem. Soc. Jpn.*, **50**, 193 (1977).
2) E. I. Heiba, R. M. Dessau, and W. J. Koehl, Jr., *J. Am. Chem. Soc.*, **91**, 138 (1969).
3) P. J. Andrulis, Jr., M. J. S. Dewar, R. Dietz, and L. Hunt, *J. Am. Chem. Soc.*, **88**, 5473 (1966).
4) T. Aratani and M. J. S. Dewar, *J. Am. Chem. Soc.*, **88**, 5479 (1966).
5) A. Kasahara, T. Izumi, A. Suzuki, and T. Takeda, *Bull. Chem. Soc. Jpn.*, **49**, 3711 (1976).
6) R. Criegee, "Oxidation in Organic Chemistry," ed by K. S. Wiberg, Academic Press, New York and London (1965), Part A, p. 227.
7) I. M. Heilbron and D. W. Hill, *J. Chem. Soc.*, **1927**, 1707.
8) N. di G. Bargellini and L. Monti, *Gazz. Chim. Ital.*, **45**, I, 96 (1915).
9) H. V. Pechmann, *Ber.*, **17**, 929 (1884).
10) F. Nauthner, *J. Prakt. Chem., Ser. 2*, **152**, 23 (1939).
11) L. F. Audrieth, *Inorg. Synth.*, **3**, 47 (1950).
12) E. Cingolani, A. Schiavello, and C. Sebastiani, *Gazz. Chim. Ital.*, **83**, 647 (1953).

A Simple Synthesis of α-Ylidene γ-Lactones from γ-Trimethylsiloxy Nitriles

Isamu MATSUDA,* Shizuaki MURATA, and Yusuke IZUMI

Department of Synthetic Chemistry, Faculty of Engineering, Nagoya University, Chikusa-ku, Nagoya 464

(Received January 5, 1979)

α-Cyano carbanions which are generated from γ-trimethylsiloxy nitriles have been found to react with aldehydes to give α-(1-hydroxyalkyl)-γ-trimethylsiloxy nitriles (**6**). α-Ylidene γ-lactones (**5**) are derived from **6** in two steps; hydrolytic lactonization to α-(1-hydroxyalkyl) γ-lactones and dehydration. The stereochemistry of the lactones **5** with one exception have been found to be of the *E* form on the basis of the NMR spectra.

α-Methylene-γ-butyrolactones have recently been the subject of extensive research since several sesquiterpenes possess cytotoxic and/or antitumor properties, largely attributed to this system.[1,2] A variety of methods have been developed for the synthesis of this moiety,[3,4] most of the procedures involving the introduction of the α-methylene group into a preformed lactone *via* the enolate anion.[5,6]

In a previous paper,[7] it was shown that the trimethylsilylacetonitrile (TMSAN) anion reacts readily and selectively with epoxides to produce γ-trimethylsiloxy nitriles **3** which are a possible synthetic equivalent of γ-lactones. This paper will report a method for the facile introduction of the α-methylene or alkylidene equivalent group into γ-lactones by the reaction of α-cyano carbanions **2** with aldehydes as a demonstration of the synthetic versatility of γ-trimethylsiloxy nitriles **3**.

Results and Discussion

The dianion character of TMSAN has been suggested in the stepwise ring opening of two equivalents of epoxide.[7] This unusual character is brought about by the intermediate **2** which is generated as a result of the migration of the trimethylsilyl group from the carbon atom to the oxy anion in **1** as shown in Scheme 1. The intermediate **2** has been confirmed by the stepwise addition of different types of epoxide. Substitution of aldehydes in place of epoxides in the reaction of the anion **2** would be expected to give the α-(1-hydroxyalkyl)-γ-trimethylsiloxy nitriles as products which lead to α-alkylidene γ-lactones by additional two steps.

An equivalent of benzaldehyde was added to a solution of **2b** (R^1=Me, R^2=H) formed from the TMSAN anion and propylene oxide in 1,2-dimethoxyethane (DME) and quenched with water, which produced an unexpected product, α-benzylidene γ-lactone **5b** (7%) in addition to other products. Lactone **5c** (6%) was obtained by a similar reaction of benzaldehyde with **2c** [R^1, R^2=$-(CH_2)_4-$]. Lactones **5b** and **5c** were given after purification of the reaction mixture by column chromatography on silica gel. Despite the low yield of **5** under optimum conditions, the result is noteworthy since this one pot reaction provides a general synthetic method for **5**. The reactivity of the anion **2** to aldehydes may decrease since it takes several hours to complete the formation of **2**. Therefore, alternative anions **2** from γ-trimethylsiloxy nitriles **3** have been used in order to enhance the selectivity of nucleophilic attack on the aldehydes. An efficient preparative method for γ-trimethylsiloxy nitriles **3** has been exploited on a large scale.[8] The outline of the procedure is summarized in Scheme 2.

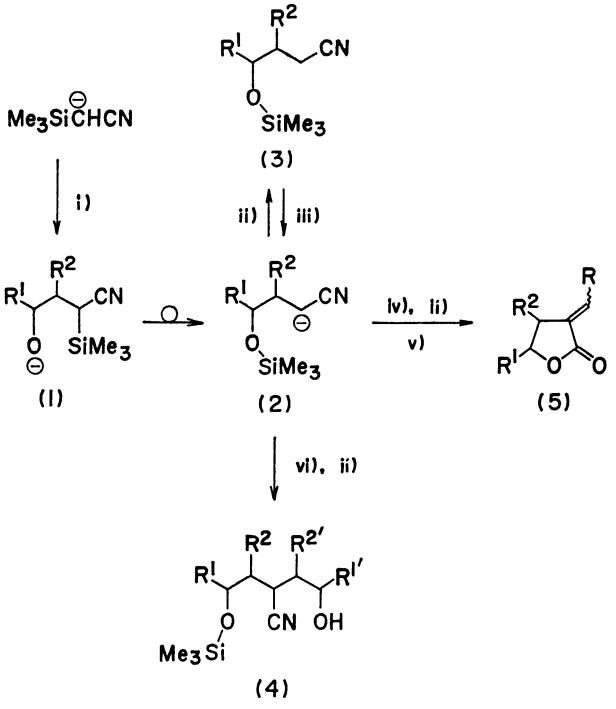

Scheme 1. i) $R^1CH(O)CHR^2$, ii) aq NH_4Cl, iii) LDA, iv) RCHO, v) Silica gel, vi) $R^1CH(O)CHR^2$.

α-Cyano carbanions **2** are generated smoothly by the interaction of nitriles **3** with an equivalent of butyl-

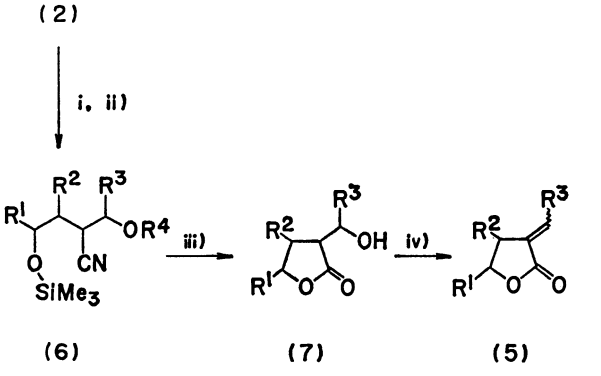

Scheme 2. i) R^3CHO, ii) aq NH_4Cl or Me_3SiCl, iii) 1.5 M. HCl, iv) $MeSO_2Cl$/pyridine, reflux.

TABLE 1. YIELDS OF PRODUCTS AND STEREOISOMERS OF **5**

	R^1	R^2	R^3	R^4	**6** Yield/%	**7** Yield/%	**5** Yield/%	**5** Stereoisomers
a	H	H	Ph	H	63	77	87	*E*
b	Me	H	Ph	H	82	73	63	*E*
c	$-(CH_2)_4-$		Ph	H	84	48	45	*Z*
d	H	H	Me	Me_3Si	65	63	66	*E*
e	Me	H	Me	Me_3Si	69	70	82	*E*
f	$-(CH_2)_4-$		Me	H	64	69	39	*E*
g	Me	H	H	H	59	63	21	—
h	$-(CH_2)_4-$		H	H	77	85	47	—

lithium or lithium diisopropylamide (LDA) in tetrahydrofuran (THF) at −78 °C and react with aldehydes at ambient temperature. After quenching the reaction mixture with either aqueous ammonium chloride (a, b, c, f, g, and h) or chlorotrimethylsilane (d and e), α-(1-hydroxyalkyl)- or (1-trimethylsiloxyalkyl)-γ-trimethylsiloxy nitriles **6** are given. Compounds **6** hydrolyzed with 1.3 M hydrochloric acid in aqueous methanol spontaneously give α-(1-hydroxyalkyl)-γ-lactones **7**. The elimination of water from **7** is achieved by the use of methanesulfonyl chloride in pyridine giving α-alkylidene γ-lactones **5**, the results of which are summarized in the Table.

The structure of **5**, **6**, and **7** have been elucidated on the basis of IR, NMR, and elemental analyses. The IR spectra of **6** is analogous to **4**. The splitting of the trimethylsilyl group in the NMR spectra of **6** reflects the discrimination of diastereomers caused by asymmetric carbon atoms.[7] For example, two separate signals of the trimethylsilyl group at 0.16 and 0.20 ppm are observed and the terminal methyl group is clearly distinguished at 1.28 and 1.40 ppm in the case of **6f**.

The NMR spectra of **7** are more complicated due to the increase in rigidity of the conformations with the formation of lactone rings. The ring methyl group of **7e** appears as a double doublet (J=6.45 and 2.1 Hz) including long range coupling at 1.18 ppm while a pair of doublet at 1.37 and 1.43 ppm (J=6.3 Hz) has been assigned to the terminal methyl of the 1-hydroxyethyl group.

From the NMR spectra and an inspection of the CPK models it was possible to establish the stereochemistry around the olefinic part of the obtained α-alkylidene γ-lactones **5**. The chemical shift of the olefinic proton (6.81 and 6.36 ppm for *E* and *Z* isomers, respectively) is the most remarkable diagnostic point to discriminate between the geometrical isomers of α-ethylidene-γ-butyrolactone **5d**.[9] The observed values of the olefinic proton, 6.77, 6.64, and 6.51 ppm in a series of α-ethylidene γ-lactones (**5d**, **5e**, and **5f**) enabled the *E* isomers to be differentiated. This was coupled with the knowledge that the vinyl proton located in the cis position to the carbonyl group shows significant down field shift (0.6—0.9 ppm) compared with the trans proton in the cases of α-methylene cycloalkanones[10] and α-methylene γ-lactones **5g** and **5h**.

With respect to the α-benzylidene γ-lactones **5a**, **5b**, and **5c**, the olefinic protons show peaks at 7.54, 7.3, and 6.53 ppm, respectively. Relatively sharp peaks at 7.45 and 7.30 ppm have been observed for the phenyl protons of **5a** and **5b**. The multiplet pattern of the phenyl protons divided in two groups with a 3:2 intensity ratio at 7.3 and 7.7 ppm for **5c**, reflecting the different susceptibility among the phenyl protons towards the magnetic anisotropy effect by the carbonyl group. Therefore, it has been concluded that lactones **5a**[11] and **5b** are the *E* isomers whereas **5c** is the *Z* isomer based on the above data. The other isomer is not detectable from the NMR spectra. The selective formation of the isomer **5a**—**5f** shows that the elimination step (**7** to **5**) is a thermodynamically controlled reaction *via* a carbocation intermediate under the above conditions. The formation of the *Z* isomer in **5c** is consistent according to a comparison of both isomers by the CPK models. The *Z* isomer of **5c** is sterically less hindered than the *E* isomer.

The ring juncture in the bicyclo system **5c**, **5f**, and **5g** has been designated trans based on the following. The starting material **3c** has been prepared by the ring opening of cyclohexene oxide with the acetonitrile anion, which arranges the trans relationship between the two substituents.[12] The coupling pattern of the junctional proton in close proximity to the oxygen atom in **5c**, **5f**, and **5g** shows a typical doublet of triplet composed of six peaks (see Experimental). The coupling constants of this pattern reflect the presence of two axial and an equatorial vicinal protons, which suggests a trans juncture in **5**.

The synthesis is attractive as one of the preparative methods of versatile α-ylidene γ-lactones since the preparation involves no specific reagent.

Experimental

The IR spectra were recorded on JASCO IR-403G and IR-S instruments. A JEOL C-60 HL instrument was used to record the ^1H NMR spectra using tetramethylsilane as the internal standard. Trimethylsilylacetonitrile[7] and γ-trimethylsiloxy nitriles[8] were prepared according to the literature. Formaldehyde was generated by the cracking of dried paraformaldehyde. Acetaldehyde was distilled prior to use. Purification of the products was conducted by column chromatography on silica gel using a mixed solvent as eluent (benzene: hexane: ethanol=1: 1: 1/20—1/40).

Synthesis of 5. *α-Benzylidene-γ-valerolactone (5b)*: To a DME (25 ml) solution of the TMSAN anion prepared from TMSAN (1.70 g, 15.0 mmol) and an equivalent of LDA was added a DME (3 ml) solution of propylene oxide (0.87 g, 14.9 mmol) at −78 °C. After stirring for 5 h at −30 °C—

−20 °C, the reaction mixture was cooled to −78 °C and a DME (5 ml) solution of benzaldehyde (1.59 g, 15.0 mmol) added at the same temperature. After the addition, the mixture was stirred for 1 h at −30 °C and for 14 h at ambient temperature and quenched with saturated aqueous NH_4Cl (25 ml). The organic layer was extracted with dichloromethane (20 ml×5). The combined extracts were washed with saturated brine and dried over anhydrous $MgSO_4$. The solvent was evaporated under reduced pressure. Column chromatography of the residue gave 1.20 g (47%) of **3b** and 0.614 g of a yellow oily product ($\nu_{C=O}$ 1750 cm^{-1}). The oily product gave the pure lactone **5b** (0.196 g, 7%) as a yellow oil after purification, which crystallized on standing, mp 54—54.5 °C. Found: C, 76.65; H, 6.73%. Calcd for $C_{12}H_{12}O_2$: C, 76.57; H, 6.43%. IR (KBr disk) 1741 ($\nu_{C=O}$) and 1652 cm^{-1} ($\nu_{C=C}$). ^1H NMR (CCl_4) δ 1.42 (d, J=6.3 Hz, 3H, C<u>H</u>$_3$), 2.63 (d of double d, J=17.3, 5.7, and 3.3 Hz, 1H, C<u>H</u>$_2$), 3.28 (d of double d, J=17.3, 7.8, and 3.1 Hz, 1H, C<u>H</u>$_2$), 4.59 (dd of quartet, J=7.8, 5.7, and 6.3 Hz, 1H, C<u>H</u>–O), and 7.30 ppm (m, 6H, Ph and C=C(H)Ph).

trans-9-Benzylidene-7-oxabicyclo[4.3.0]nonan-8-one (5c): Similarly, from a DME (25 ml) solution of the TMSAN anion (8.05 mmol), cyclohexene oxide (0.793 g, 8.08 mmol), and benzaldehyde (1.02 g, 9.59 mmol), pure **5c** (0.11 g, 6%) was obtained as colorless needles in addition to **3c** (0.989 g, 58%), mp 146—147.5 °C. Found: C, 78.93; H, 7.37%. Calcd for $C_{15}H_{16}O_2$: C, 78.92; H, 7.07%. IR (KBr disk) 1740 ($\nu_{C=O}$) and 1652 cm^{-1} ($\nu_{C=C}$). NMR ($CDCl_3$) δ 1.2—1.7 (m, 9H, cyclohexyl ring protons), 3.75 (d of t, J=3.9 and 10.7 Hz, 1H, C<u>H</u>–O), 6.35 (d, J=3.0 Hz, 1H, C=C(H)), 7.3 (m, 3H, Ph), and 7.7 ppm (m, 2H, Ph).

Synthesis of α-(1-Hydroxyalkyl)-γ-trimethylsiloxy Nitriles (6).

2-Cyano-1-phenyl-4-trimethylsiloxy-1-butanol (6a): To a THF solution of LDA (10.5 mmol) was added a THF (5 ml) solution of **3a** (1.57 g, 9.99 mmol) at −78 °C. The mixture was stirred for 1 h at the same temperature to complete the formation of the anion **2a**. A THF (5 ml) solution of benzaldehyde (0.536 g, 5.05 mmol) was added to the anion solution at −78 °C. The mixture was stirred for 30 min at −78 °C and for 15 h at ambient temperature and the reaction mixture quenched with saturated aq NH_4Cl (30 ml). The organic layer was decanted and the water layer extracted with dichloromethane (20 ml×5). The organic layer and the extracts were collected, washed with saturated brine, and dried over $MgSO_4$. The residue obtained after evaporation of the solvent under reduced pressure was chromatographed to give 1.65 g (63%) of a pale yellow oil, **6a**. Found: C, 63.72; H, 8.13; N, 5.41%. Calcd for $C_{14}H_{21}NO_2Si$: C, 63.84; H, 8.04; N, 5.32%. IR (CCl_4) 3620, 3440, (ν_{O-H}), 2270 ($\nu_{C\equiv N}$), and 1250 cm^{-1} ($\delta_{s,Si-C_3}$). NMR (CCl_4) δ 0.12 (s, 9H, Si–C<u>H</u>$_3$), 1.6—2.0 (broad m, 2H, C<u>H</u>$_2$CCN), 3.12 (q, J=6.0 Hz, 1H, C<u>H</u>–CN), 3.80 (t, J=6.0 Hz, 2H, C<u>H</u>$_2$–O–Si), 4.2 (broad, 1H, O<u>H</u>), 4.9 (broad, 1H, C<u>H</u>–Ph), and 7.50 ppm (s, 5H, Ph).

2-Cyano-1-phenyl-4-trimethylsiloxy-1-pentanol (6b): The analogous treatment of **3b** (0.957 g, 5.59 mmol) with butyllithium (5.1 mmol) and benzaldehyde (0.536 g, 5.05 mmol) in THF (25 ml) gave pure **6b** as a yellow oil (1.14 g, 82%). Found: C, 64.71; H, 8.57; N, 5.13%. Calcd for $C_{15}H_{23}NO_2Si$: C, 64.94; H, 8.34; N, 5.05%. IR (CCl_4) 3620, 3430 (ν_{O-H}), 2260 ($\nu_{C\equiv N}$), and 1249 cm^{-1} ($\delta_{s,Si-C_3}$). NMR (CCl_4) δ 0.10 (s, 9H, Si–C<u>H</u>$_3$), 1.12 (d, J=6.0 Hz, 3H, C<u>H</u>$_3$), 1.55 (m, 2H, C<u>H</u>$_2$), 2.78 (m, 1H, C<u>H</u>–CN), 3.9 (broad m, 2H, O–<u>H</u> and SiO–C<u>H</u>), 4.57 (broad, 1H, Ph–C<u>H</u>–O), and 7.23 ppm (s, 5H, Ph).

3-Hydroxy-3-phenyl-2-(trans-2-trimethylsiloxycyclohexyl)propionitrile (6c): The analogous treatment of **3c** (1.50 g, 7.09 mmol) with LDA (7.40 mmol) and benzaldehyde (0.781 g, 7.40 mmol) in THF (25 ml) gave **6c** as a yellow oil (1.88 g, 84%). Found: C, 68.13; H, 8.62; N, 4.48%. Calcd for $C_{18}H_{27}NO_2Si$: C, 68.09; H, 8.57; N, 4.41%. IR (CCl_4) 3640, 3430 (ν_{O-H}), 2265 ($\nu_{C\equiv N}$), and 1249 cm^{-1} ($\delta_{s,Si-C_3}$). NMR (CCl_4) δ 0.10 (s, 9H, Si–C<u>H</u>$_3$), 1.0—2.1 (broad m, 9H), 2.96 (broad s, 1H, O<u>H</u>), 3.26 (double d, J=9.2 and 2.9 Hz, 1H, C<u>H</u>–CN), 3.4 (broad m, 1H, C<u>H</u>–OSi), 4.68 (d, J=9.2 Hz, 1H, Ph–C<u>H</u>–O), and 7.34 ppm (m, 5H, Ph).

3-Cyano-1,4-bis(trimethylsiloxy)pentane (6d): LDA (10.4 mmol), **3a** (1.55 g, 10.1 mmol), and acetaldehyde (0.6 ml, 10.7 mmol) were mixed in a similar manner in THF (30 ml) and quenched with Me_3SiCl (1.56 g, 14.4 mmol). After evaporation of the solvent, the residue was diluted with Et_2O (30 ml) and the solution filtered. Pure **6d** (1.77 g, 65%) was obtained as a yellow liquid. Found: C, 52.43; H, 9.75; N, 5.40%. Calcd for $C_{12}H_{27}NO_2Si_2$: C, 52.69; H, 9.95; N, 5.12%. IR (CCl_4) 2280 ($\nu_{C\equiv N}$) and 1248 cm^{-1} ($\delta_{s,Si-C_3}$). NMR (CCl_4) δ 0.14, 0.16 (each s, 18H, Si–C<u>H</u>$_3$), 1.29 (d, J=6.3 Hz, 3H, C<u>H</u>$_3$), 1.74 (q, J=6.3 Hz, 2H, C<u>H</u>$_2$CCN), 2.2—2.9 (m, 1H, C<u>H</u>–CN), 3.74 (t, J=6.3 Hz, 2H, C<u>H</u>$_2$–O), and 3.93 ppm (q, J=6.3 Hz, 1H, C<u>H</u>–O).

3-Cyano-2,5-bis(trimethylsiloxy)hexane (6e): The analogous treatment of **3b** (1.38 g, 8.03 mmol) with acetaldehyde (0.5 ml, 8.9 mmol) and Me_3SiCl (1.31 g, 12.1 mmol) gave pure **6e** (1.59 g, 69%) as a pale yellow liquid. Found: C, 54.54; H, 10.02; N, 4.91%. Calcd for $C_{13}H_{29}NO_2Si_2$: C, 54.30; H, 10.17; N, 4.87%. IR (CCl_4) 2265 ($\nu_{C\equiv N}$) and 1249 cm^{-1} ($\delta_{s,Si-C_3}$). NMR (CCl_4) δ 0.12, 0.14 (each s, 18H, Si–C<u>H</u>$_3$), 1.18 (d, J=6.9 Hz, 3H, O–C–C<u>H</u>$_3$), 1.25 (d, J=7.2 Hz, 3H, O–C–C<u>H</u>$_3$), 1.65 (t, J=6.9 Hz, 2H, C<u>H</u>$_2$), 2.43 (m, 1H, C<u>H</u>–CN), and 3.89 ppm (m, 2H, 2×C<u>H</u>–O).

3-Hydroxy-2-(trans-2-trimethylsiloxycyclohexyl)butyronitrile (6f): The analogous treatment of **3c** (3.85 g, 18.2 mmol) with LDA (18.7 mmol) and acetaldehyde (1.1 ml, 19 mmol) in THF (60 ml) gave a colorless oil of pure **6f** (2.96 g, 64%). Found: C, 61.10; H, 9.80; N, 5.44%. Calcd for $C_{13}H_{25}NO_2Si$: C, 61.13; H, 9.87; N, 5.48%. IR (CCl_4) 3660, 3390 (ν_{O-H}), 2275 ($\nu_{C\equiv N}$), and 1250 cm^{-1} ($\delta_{s,Si-C_3}$). NMR (CCl_4) δ 0.16, 0.20 (each s, 9H, Si–C<u>H</u>$_3$), 1.28, 1.40 (each d, J=6.0 Hz, 3H, C<u>H</u>$_3$), 1.1—2.1 (m, 9H, ring protons), 2.4—2.9 (m, 1H, C<u>H</u>–CN), and 3.2—4.1 ppm (m, 3H, O–H and 2×C<u>H</u>–O).

2-Hydroxymethyl-4-(trimethylsiloxy)pentanenitrile (6g): Into a solution of **2b** formed from LDA (10.5 mmol) and **3b** (1.71 g, 9.99 mmol) was bubbled gaseous formaldehyde (0.61 g, 20.4 mmol) in a stream of nitrogen at −78 °C in THF (40 ml). After a work up of the mixture similar to that described above, pure **6g** (1.18 g, 59%) was obtained as a colorless oil. Found: C, 53.45; H, 9.74; N, 7.05%. Calcd for $C_9H_{19}NO_2Si$: C, 53.69; H, 9.51; N, 6.96%. IR (CCl_4) 3650, 3460 (ν_{O-H}), 2270 ($\nu_{C\equiv N}$), and 1246 cm^{-1} ($\delta_{s,Si-C_3}$). NMR (CCl_4) δ 0.13, 0.15 (each s, 9H, Si–C<u>H</u>$_3$), 1.20 (d, J=6.0 Hz, C<u>H</u>$_3$), 1.45—1.93 (m, 2H, C<u>H</u>$_2$–C–O), 2.7 (m, 1H, C<u>H</u>–CN), 3.72 (d, J=6.0 Hz, 2H, C<u>H</u>$_2$–O), 3.7 (broad, 1H, O–<u>H</u>), and 3.93 ppm (quint, J=6.0 Hz, C<u>H</u>–O).

3-Hydroxy-2-(trans-2-trimethylsiloxycyclohexyl)propionitrile (6h): The analogous treatment of **3c** (2.55 g, 12.0 mmol) with LDA (12.5 mmol) and formaldehyde (30 mmol) gave pure **6h** as a colorless oil (2.22 g, 77%). Found: C, 59.93; H, 9.88; N, 6.16%. Calcd for $C_{12}H_{23}NO_2Si$: C, 59.71; H, 9.60; N, 5.80%. IR (CCl_4) 3660, 3440 (ν_{O-H}), 2270 ($\nu_{C\equiv N}$), and 1249 cm^{-1} ($\delta_{s,Si-C_3}$). NMR (CCl_4) δ 0.15 (s, 9H, Si–C<u>H</u>$_3$), 1.1—2.0 (broad, 9H, ring protons), 2.93 (broad s, 1H, O–<u>H</u>), 3.0—3.6

(m, 2H, CH–CN and CH–O), and 3.6—3.85 ppm (m, 2H, CH_2–O).

Synthesis of α-(1-Hydroxyalkyl) γ-Lactones (7). *α-(α-Hydroxybenzyl)-γ-butyrolactone (7a)*: A solution of **6a** (1.27 g, 4.71 mmol) in concd HCl (3 ml) and MeOH (22 ml) was refluxed for 4 h. The mixture was poured into H_2O (100 ml), neutralized with aq $NaHCO_3$, and extracted with dichloromethane (20 ml×5). The extracts were combined, washed with water, and dried over $MgSO_4$. The crude product obtained after evaporation of the solvent was purified by chromatography to give pure **7a** (0.697 g, 77%) as colorless needles, mp 107—109 °C. Found: C, 68.81; H, 6.29%. Calcd for $C_{11}H_{12}O_3$: C, 68.73; H, 6.29%. IR (KBr disk) 3420 (ν_{O-H}) and 1744 cm^{-1} ($\nu_{C=O}$). NMR ($CDCl_3$) δ 1.75—2.7 (m, 2H, CH–CH_2), 2.75—3.1 (m, 2H, CH–C=O and O–H), 3.9—4.4 (m, 2H, CH_2–O), 4.81, 4.84 (each d, J=8.7 Hz), 5.38, 5.39 (each d, J=5.0 Hz, 1H for 4 peaks, CH–O), and 7.30 ppm (s, 5H, Ph).

α-(α-Hydroxybenzyl)-γ-valerolactone (7b): The treatment of **6b** (2.06 g, 7.43 mmol) with concd HCl (4 ml) in MeOH (25 ml) gave pure **7b** (1.17 g, 73%) as a yellow oil. Found: C, 69.80; H, 7.14%. Calcd for $C_{12}H_{14}O_3$: C, 69.88; H, 6.84%. IR (CCl_4) 3630, 3460 (ν_{O-H}), and 1765 cm^{-1} ($\nu_{C=O}$). NMR (CCl_4) δ 1.22 (d, J=6.4 Hz), 1.32 (d, J=5.5 Hz, 3H for two signals, CH_3), 1.5—2.5 (m, 2H, CH_2), 2.6—3.0 (m, 1H, CH–C=O), 4.0 (broad, 1H, O–H), 4.1—5.2 (m, 2H, 2×CH–O), and 7.20 ppm (m, 5H, Ph).

trans-*9-(α-Hydroxybenzyl)-7-oxabicyclo[4.3.0]nonan-8-one (7c)*: **6c** was treated (1.53 g, 4.83 mmol) with concd HCl (3 ml) in DME (30 ml) and pure **7c** (0.571 g, 48%) was obtained as pale yellow needles, mp 180—183 °C. Found: C, 73.42; H, 7.67%. Calcd for $C_{15}H_{18}O_3$: C, 73.14; H, 7.37%. IR (KBr disk) 3450 (ν_{O-H}) and 1755 cm^{-1} ($\nu_{C=O}$). NMR ($CDCl_3$) δ 1.0—2.3 (m, 9H, ring protons), 2.73 (double d, J=12.0 and 3.0 Hz, 1H, CH–C=O), 2.93 (broad, 1H, O–H), 3.64 (m, 1H, CH–O), 5.38 (broad d, J=3 Hz, 1H, Ph–CH–O), and 7.32 ppm (m, 5H, Ph).

α-(1-Hydroxyethyl)-γ-butyrolactone (7d): Treatment of **6d** (1.33 g, 4.87 mmol) with concd HCl (4 ml) in MeOH (30 ml) gave **7d** (0.397 g, 63%) as a pale yellow liquid. Found: C, 55.18; H, 7.96%. Calcd for $C_6H_{10}O_3$: C, 55.37; H, 7.75%. IR ($CHCl_3$) 3620, 3480 (ν_{O-H}), and 1764 cm^{-1} ($\nu_{C=O}$). NMR (CCl_4) δ 1.30 (d, J=6.2 Hz, 3H, CH_3), 1.8—2.6 (m, 3H, CH–C=O and CH_2–CH), and 3.3—4.5 ppm (m, 4H, O–H, CH–OH, and CH_2–O).

α-(1-Hydroxyethyl)-γ-valerolactone (7e): Treatment of **6e** 0.68 g, 2.36 mmol) with concd HCl (2 ml) in MeOH (15 ml) gave **7e** (0.237 g, 70%) as a yellow liquid. Found: C, 58.05; H, 8.55%. Calcd for $C_7H_{17}O_3$: C, 58.31; H, 8.39%. IR ($CHCl_3$) 3480 (ν_{O-H}) and 1755 cm^{-1} ($\nu_{C=O}$). NMR (CCl_4) δ 1.18 (double d, J=6.45 and 2.1 Hz, 3H, CH_3–CH), 1.37 (d, J=6.3 Hz), 1.43 (d, J=6.3 Hz, 3H for two signals, CH_3–C–O), 1.9—2.7 (m, 3H, CH_2 and CH–C=O), 3.7—4.0 (m, 2H, O–H and CH–O–C=O), and 4.3—4.8 ppm (m, 1H, CH–O).

trans-*9-(1-Hydroxyethyl)-7-oxabicyclo[4.3.0]nonan-8-one (7f)*: Treatment of **6f** (1.75 g, 6.84 mmol) with concd HCl (4 ml) in DME (25 ml) gave pure **7f** (0.865 g, 69%) as colorless needles, mp 99—105 °C. Found: C, 65.10; H, 8.98%. Calcd for $C_{10}H_{16}O_3$: C, 65.19; H, 8.75%. IR (KBr disk) 3430 (ν_{O-H}), 1764 and 1749 cm^{-1} ($\nu_{C=O}$). NMR ($CDCl_3$) δ 1.42 (d, J=6.2 Hz, 3H, CH_3), 1.2—2.5 (m, 10H), and 4.2 ppm (broad, 3H, O–H and 2×CH–O).

α-Hydroxymethyl-γ-valerolactone (7g): Treatment of **6g** (1.08 g, 15.36 mmol) with concd HCl (3 ml) in MeOH (25 ml) gave pure **7g** (0.445 g, 63%) as a colorless liquid. Found: C, 55.55; H, 7.99%. Calcd for $C_6H_{10}O_3$: C, 55.37; H, 7.75%. IR ($CHCl_3$) 3400 (ν_{O-H}) and 1759 cm^{-1} ($\nu_{C=O}$). NMR (CCl_4) δ 1.25—1.50 (m, 3H, CH_3), 1.9—2.9 (m, 2H, CH_2), and 3.5—4.9 ppm (m, 4H, O–H, CH–O, and CH_2–O).

trans-*9-Hydroxymethyl-7-oxabicyclo[4.3.0]nonan-8-one (7h)*: Treatment of **6h** (0.490 g, 2.03 mmol) with concd HCl (2 ml) in DME (15 ml) gave pure **7h** (0.293 g, 85%) as a colorless solid, mp 55—56 °C. Found: C, 63.54; H, 8.43%. Calcd for $C_9H_{14}O_3$: C, 63.51; H, 8.29%. IR (KBr disk) 3415 (ν_{O-H}) and 1756 cm^{-1} ($\nu_{C=O}$). NMR ($CDCl_3$) δ 1.2—2.8 (m, 11H, ring protons, CH–C=O, and O–H), and 3.7—4.3 ppm (m, 3H, CH_2–O and CH–O).

Synthesis of α-Alkylidene γ-Lactones (5). *α-Benzylidene-γ-butyrolactone (5a)*: A mixture of **7a** (0.305 g, 1.48 mmol) and methanesulfonyl chloride (0.14 ml) in pyridine (5 ml) was refluxed for 3 h. The reaction mixture was poured into ice (50 g) and concd HCl (15 ml) and the organic materials extracted with dichloromethane (20 ml×5). The extracts were combined and washed with 1 M HCl, water, and 5% aq $NaHCO_3$. After drying over $MgSO_4$, the solvent was evaporated under reduced pressure. The residue was chromatographed to give **5a** (0.153 g, 87%) as colorless needles, mp 115—115.5 °C. Found: C, 75.75; H, 5.75%. Calcd for $C_{11}H_{10}O_2$: C, 75.84; H, 5.79%. IR (KBr disk) 1739 ($\nu_{C=O}$) and 1650 cm^{-1} ($\nu_{C=C}$). NMR ($CDCl_3$) δ 3.20 (doublet of t, J=2.7 and 7.1 Hz, 2H, CH_2–C–C=O), 4.45 (t, J=7.1 Hz, 2H, CH_2–O), 7.45 (s, 5H, Ph), and 7.54 ppm (t, J=2.7 Hz, 1H, C=C(H)).

α-Benzylidene-γ-valerolactone (5b): Similarly, from **7b** (0.305 g, 1.48 mmol), pure **5b** (0.174 g, 63%) was obtained as a yellow oil which solidified in storage.

trans-*9-Benzylidene-7-oxabicyclo[4.3.0]nonan-8-one (5c)*: Similarly, from **7c** (0.607 g, 2.46 mmol), pure **5c** (0.253 g, 45%) was obtained as colorless needles.

α-Ethylidene-γ-butyrolactone (5d): **7d** (0.397 g, 3.07 mmol) gave **5d** (0.228 g, 66%) as a pale yellow liquid by a similar treatment to that described above. Found: C, 64.01; H, 7.45%. Calcd for $C_6H_8O_2$: C, 64.27; H, 7.19%. IR (CCl_4) 1768 ($\nu_{C=O}$) and 1685 cm^{-1} ($\nu_{C=C}$). NMR (CCl_4) δ 1.91 (t of doublet, J=2.0 and 7.4 Hz, 3H, CH_3), 2.88 (m, 2H, CH_2–C=C), 4.41 (t, J=7.2 Hz, 2H, CH_2–O), and 6.77 ppm (t of quartet, J=3.0 and 7.4 Hz, 1H, vinyl proton).

α-Ethylidene-γ-valerolactone (5e): **7e** (0.237 g, 1.64 mmol) gave **5e** (0.170 g, 82%) as a yellow liquid by a similar treatment. Found: C, 66.35; H, 8.29%. Calcd for $C_7H_{10}O_2$: C, 66.65; H, 7.99%. IR (CCl_4) 1767 ($\nu_{C=O}$) and 1683 cm^{-1} ($\nu_{C=C}$). NMR (CCl_4) δ 1.41 (d, J=6.5 Hz, 3H, CH_3–CH), 1.83 (t of d, J=2.2 and 7.4 Hz, 3H, CH_3–C=C), 2.35 (t of double d, J=3.4, 6.1, and 17.0 Hz, 1H, CH_2–C=C), 3.03 (t of double d, J=3.4, 7.7, and 17.0 Hz, 1H, CH_2–C=C), 4.60 (double d of quartet, J=7.7, 6.1, and 6.5 Hz, 1H, CH–O), and 6.64 ppm (t of quart, J=3.4 and 7.4 Hz, 1H, vinyl proton).

trans-*9-Ethylidene-7-oxabicyclo[4.3.0]nonan-8-one (5f)*: **7f** (0.917 g, 4.96 mmol) gave **5f** (0.318 g, 39%) as a yellow oil by a similar treatment. Found: C, 72.21; H, 8.72%. Calcd for $C_{10}H_{14}O_2$: C, 72.26; H, 8.49%. IR (CCl_4) 1778 ($\nu_{C=O}$) and 1689 cm^{-1} ($\nu_{C=C}$). NMR (CCl_4) δ 1.3—2.6 (m, 9H, ring protons), 1.86 (double d, J=7.2 and 1.7 Hz, 3H, CH_3), 3.56 (doublet of t, J=3.7 Hz and 9.0 Hz, 1H, CH–O), and 6.51 ppm (d of quart, J=3.0 and 7.5 Hz, 1H, vinyl proton).

α-Methylene-γ-butyrolactone (5g): A benzene solution of **7g** (0.445 g, 3.42 mmol), methanesulfonyl chloride (0.35 ml), and 1,5-diazabicyclo[5.4.0]undec-5-ene (1 ml) was stirred for 1 h

at ambient temperature. The mixture was poured into water (20 ml) and extracted with dichloromethane (10 ml × 7). The extracts were combined, washed with 1 M HCl (20 ml) and water (20 ml), and dried over $MgSO_4$. After evaporation of the solvent under reduced pressure, the residue was chromatographed to give a pale yellow liquid **5g** (0.081 g, 21%). Found: C, 64.05; H, 7.44%. Calcd for $C_6H_8O_2$: C, 64.27; H, 7.19%. IR (CCl_4)[13] 1772 ($\nu_{C=O}$) and 1671 cm^{-1} ($\nu_{C=C}$). NMR (CCl_4)[13] δ 1.39 (d, J=6.1 Hz, 3H, C$\underline{H}_3$), 2.42 (t of double d, J=3.3, 6.6, and 16.7 Hz, 1H, C$\underline{H}_2$), 3.06 (t of double d, J=2.4, 7.2, and 16.7 Hz, 1H, C$\underline{H}_2$), 4.55 (quart of double d, J=6.1, 6.6, and 7.2 Hz, 1H, C$\underline{H}$–O), 5.50 (double d, J= 6.6 and 7.2 Hz, 1H, 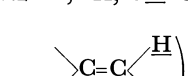), and 6.06 ppm (double d, J=6.6 and 7.2 Hz, 1H, 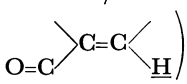).

trans-*9-Methylene-7-oxabicyclo[4.3.0]nonan-8-one (5h)*: In a similar manner, **7h** (0.745 g, 4.38 mmol) gave colorless needles of **5h** (0.315 g, 47%), mp 39—41 °C. (lit,[14] 39—41 °C). Found: C, 71.09; H, 8.03%. Calcd for $C_9H_{12}O_2$: C, 71.02; H, 7.95%. IR (KBr disk)[5] 1758 ($\nu_{C=O}$) and 1673 cm^{-1} ($\nu_{C=C}$). NMR (CCl_4)[6] δ 1.1—2.6 (m, 9H, ring protons), 3.63 (double t, J=3.8 and 10.5 Hz, 1H, C$\underline{H}$–O), 5.32 (d, J=3.0 Hz, 1H, 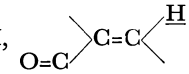), and 5.96 ppm (d, J=3.0 Hz, 1H, 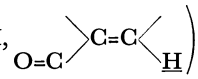).

The authors would like to thank the Ministry of Education, Japan, for a Grant-in-Aid 375469 and Shinetsu Chemical Company for the supply of chlorotrimethylsilane.

References

1) S. M. Kupchan, R. J. Hemingway, D. Werner, and A. Kaim, *J. Org. Chem.*, **34**, 3903, 3908 (1969).
2) K. H. Lee, E. S. Huang, C. Pinatodosi, J. Pagano, and T. A. Geissman, *Cancer Research*, **31**, 1649 (1971).
3) P. A. Grieco, *Synthesis*, **1975**, 67.
4) R. B. Gammill, C. A. Wilson, and T. Bryson, *Synth. Commun.*, **5**, 245 (1975).
5) H. Minato and I. Horibe, *J. Chem. Soc., C*, **1967**, 1575.
6) P. A. Grieco and K. Hiroi, *J. Chem. Soc., Chem. Commun.*, **1972**, 1317.
7) I. Matsuda, S. Murata, and Y. Ishii, *J. Chem. Soc., Perkin Trans. 1*, **1979**, 26.
8) S. Murata and I. Matsuda, *Synthesis*, **1978**, 221, and unpublished results.
9) K. Ohga and T. Matsuo, *Bull. Chem. Soc. Jpn.*, **46**, 2181 (1973); C. P. Casey and W. R. Brunsvold, *J. Organomet. Chem.*, **102**, 175 (1975).
10) L. M. Jackman and S. Sternhell, "Application of Nuclear Magnetic Resonance Spectroscopy in Organic Chemistry," 2nd ed, Pergamon Press, Oxford (1969), p. 192.
11) T. Minami, I. Niki, and T. Agawa, *J. Org. Chem.*, **39**, 3236 (1974).
12) N. G. Gaylord and E. I. Becker, *Chem. Rev.*, **49**, 413 (1951); R. E. Parker and N. S. Isaacs, *Chem. Rev.*, **59**, 737 (1959).
13) J. Haslouin and F. Roussac, *Tetrahedron Lett.*, **1976**, 4651.
14) R. C. Ronald, *Tetrahedron Lett.*, **1973**, 3831; I. Matsuda, *Chem. Lett.*, **1978**, 773.

The Difference in Solvolytic Reactivity between Diastereomers in α-(*trans*-2-Arylcyclopropyl)arylmethyl 3,5-Dinitrobenzoates

Toshimasa TAKATA, Hajime MATSUSAKI, Katsuo OHKATA, and Terukiyo HANAFUSA*

Chemistry Department, Faculty of Science, Hiroshima University, Higashi-senda-cho, Hiroshima 730

(Received January 6, 1979)

Each diastereoisomeric pair of α-(*trans*-2-*p*-tolylcyclopropyl)benzyl and α-(*trans*-2-phenylcyclopropyl)-*p*-tolylmethyl 3,5-dinitrobenzoates (**I-4a, b, II-4a, b**) has been synthesized. The relative solvolytic rates of **I-4b** to **I-4a** and of **II-4b** to **II-4a** in 80% aqueous acetone have been found to be 3.59 and 1.86 respectively at 25 °C. In the presence of 2,6-lutidine, the major products in the solvolysis were homoallylic alcohols.

Although there have been many stereochemical studies in the rate comparisons of rigid cyclic compounds in the solvolysis of cyclopropylmethyl systems,[1-3] no investigations of the difference in reactivity between a diastereoisomeric pair of such systems in which a cyclopropyl group can freely rotate have been reported. One of the reasons for this may be the experimental difficulty in the separation of such diastereomers. It may be of importance, however, to study the conformational situation of a participating cyclopropyl group at the transition state when the free rotation of the group is permitted in the substrate molecule.[4] In connection with our previous researches,[5] we wish now to report such a reactivity difference between diastereoisomers of certain arylcyclopropylmethyl systems.

Each isomer of the titled esters (**I-4a, b** and **II-4a, b**) has been synthesized and successfully isolated by Scheme 1, shown below. The physical properties and spectral and analytical data are summarized in Table 1.

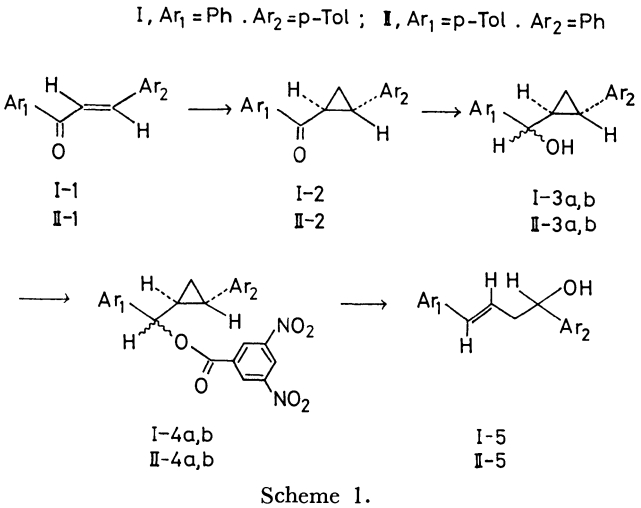

Scheme 1.

The parent alcohols (**I-3a, b** and **II-3a, b**) were mixtures of diastereoisomers, in which one of the diastereoisomers was preferentially produced in the hydride reduction of the ketones (**I-2, II-2**). The chemical shift of the carbinyl proton (a doublet) in the predominant alcohols (**I-3a** and **II-3a**) was slightly higher than that of the other (**I-3b** and **II-3b**). The hydride attack on the carbonyl group generally takes place from the less hindered side of the favorable conformer of the ketones, as is shown in Scheme 2. This reduction results in the preferential formation of

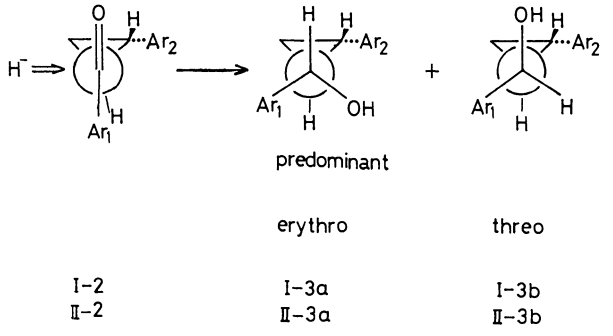

Scheme 2.

the erythro isomer (**I-3a, II-3a**) according to the above scheme. This interpretation accords with the previous result suggested for a similar system by Descotes *et al.*[6] and is consistent with Cram-Prelog rule.[7] If it is assumed that the two most bulky aromatic groups are situated in a *trans* relation in the stable, staggered conformation of the alcohol molecule, the carbinyl proton of *erythro*-isomer (**I-3a** and **II-3a**) may be more highly shielded by the effect of a cyclopropane ring.[8] Thus, the two diastereoisomers in a pair could be distinguished.

The diastereomerically mixed alcohols were converted into 3,5-dinitrobenzoates (**I-4a, b** and **II-4a, b**) by a usual procedure. Separation was made by the fractional recrystallization of the 3,5-dinitrobenzoates. As may be seen from Table 2, all these 3,5-dinitrobenzoates were solvolyzed smoothly in accordance with first-order kinetics. Thus, it was found that the *threo* isomer (**I-4b** or **II-4b**) was more reactive than the *erythro* isomer (**I-4a** or **II-4a**) in the solvolysis of both pairs in 80% aqueous acetone. The order of the difference in reactivity (3.59—1.86) is comparable with that for some rigid polycyclic systems.[3a,d]

When the reaction was interrupted during the course of solvolysis, each starting 3,5-dinitrobenzoate could be recovered in a good yield and neither the homoallylic nor the diastereomeric isomer of the reactant was detected for either series. Thus, it was experimentally confirmed that there was no interconversion between homoallylic and cyclopropylmethyl systems, or between the *erythro* and *threo* isomers, in the present solvolysis.

A product study was carried out in the presence of 2,6-lutidine under solvolytic conditions, since it was preliminarily found that the parent alcohols (**I-3a, b** and **II-3a, b**) and homoallylic alcohols (**I-5, II-5**) were stable under these conditions. The major solvolysis

products after 30 half-lives were homoallylic alcohols, as is shown in Table 3. These alcohols should be produced directly from the 3,5-dinitrobenzoates (**I-4a, b** and **II-4a, b**) under those reaction conditions, since rearranged homoallylic 3,5-dinitrobenzoates could not be solvolyzed under similar conditions.

Starting from the diastereomerically different 3,5-dinitrobenzoates, the same *trans*-homoallylic alcohol was obtained as the sole product, so that it is reasonable to assume the intervention of the common carbocation in the reactions for both diastereomers. In contrast with this finding, a considerable rate difference has been found between *erythro* and *threo* isomers in kinetic studies of the two systems (I and II). Also, the rates are accelerated by the order of 10^4 in comparison with simple secondary arylmethyl systems. This may be attributed to participation by the α-substituted 2-arylcyclopropyl group. In order to attain a transition state which leads to a common carbocation in the present solvolysis, the C_1–C_2 bond of a cyclopropyl group is inevitably antiparallel to the leaving 3,5-dinitrobenzoate group in the *threo* isomers. Then, the aryl group on C_2 of a cyclopropyl group could accommodate the partial positive charge developed at the transition state. In the case of the *erythro* isomers, such

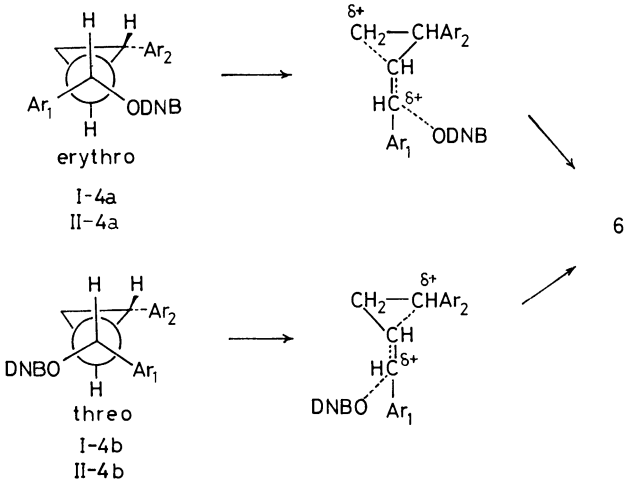

Scheme 3.

concomitant participation from the most stable conformer may result in the formation of a different transition state in which the C_1–C_3 bond is antiparallel to the leaving group. Both transition states are illustrated in Scheme 3. These situations might cause the above rate difference between diastereomeric isomers, although the solvolysis products were the same. Thus, an unsymmetrical participation of a cyclopropyl group has been kinetically demonstrated in systems in which the cyclopropyl group can freely rotate. Regarding with the common intermediate that is a close precursor to the *trans*-homoallylic alcohol, there has been no direct experimental evidence in this study. However, the structure may be illustrated as a homoallylic cation, **6**, which might presumably be stabilized by homoconjugation.

In view of the facts that the secondary benzylic system

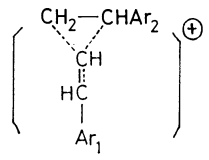

6

is subject to almost no anchimeric assistance, and that the conformational requirement for the transition state in the solvolysis of compounds in which the free rotation of the α-substituted cyclopropyl group is permitted is not so strict as in a rigid polycyclic system, the present results seem to be rather interesting. A related investigation is now in progress.

Experimental

All the melting points are uncorrected. The IR spectra were obtained with a Hitachi 215 grating IR spectrophotometer. The NMR measurements were carried out on a Varian T-60 instrument, using tetramethylsilane as the internal reference. The physical properties of each compound are summarized in Tables 1 and 3.

Phenyl trans-*2*-p-*Tolylcyclopropyl Ketone (I-2) and* p-*Tolyl* trans-*2-Phenylcyclopropyl Ketone (II-2).* The cyclopropyl ketones (**I-2** and **II-2**) were prepared from benzylideneacetophenone derivatives[9] and trimethyloxosulfonium iodide by a previously reported method.[10]

*α-(*trans-*2*-p-*Tolylcyclopropyl)benzyl Alcohol (I-3a, b) and* α-*(*trans-*2-Phenylcyclopropyl)*-p-*tolylmethanol (II-3a, b).* To a stirred suspension of 2 g of $LiAlH_4$ in 200 ml of dry ether were added 13 g (55 mmol) of **I-2** dissolved in 100 ml of dry ether. The mixture was then stirred for 25 h before the excess hydride was carefully decomposed with a minimum amount of water. The mixture was filtered, and the precipitates were washed several times with ether. After the combined ether layer had then been dried, the removal of the solvent gave 10.5 g of **I-3a, b**, a colorless solid. It was found from the NMR spectrum that the solid consists of two diastereoisomers (**I-3a**: **I-3b**=3: 2). When the solid product was recrystallized from petroleum ether, a pure sample of **I-3a** (mp 52—53 °C) was obtained.

Found: C, 85.83; H, 7.59%. Calcd for $C_{17}H_{18}O$: C, 85.67; H, 7.61%.

Another pair of alcohols (**II-3a, b**) was prepared by a similar method in a 89% yield; the recrystallization of the crude product from petroleum ether gave rise to a pure sample of **II-3a** (mp 95—97 °C).

Found: C, 85.55; H, 7.73%. Calcd for $C_{17}H_{18}O$: C, 85.67; H, 7.61%.

*α-(*trans-*2*-p-*Tolylcyclopropyl)benzyl 3,5-Dinitrobenzoate (I-4a, b) and* α-*(*trans-*2-Phenylcyclopropyl)*-p-*tolylmethyl 3,5-Dinitrobenzoate (II-4a, b).* The 3,5-dinitrobenzoate (**I-4a, b**) was prepared by allowing 4.5 g (19 mmol) of **I-3a, b** to react with 5.2 g (22 mmol) of 3,5-dinitrobenzoyl chloride in 75 ml of dry pyridine at room temperature for 30 h. The product was extracted with ether, and the organic layer was successively washed with water, 1M-hydrochloric acid, 5% aqueous sodium hydrogencarbonate, and water. The ether layer was dried over anhydrous sodium sulfate and concentrated under reduced pressure. In the same ratio as the parent alcohols (**I-3a** and **3b**), 3,5-dinitrobenzoate (**I-4a, b**; 6.5 g) was obtained. Recrystallization from benzene and petroleum ether

TABLE 1. PHYSICAL PROPERTIES AND SPECTRAL AND

Compound	Yield %	Mp °C	IR[a] $\tilde{\nu}$/cm^{-1}	NMR δ/ppm Ar$_1$	Ar$_2$	α-H
I-2	68	85—86.5 (lit, 85—87)[b]	1660 1240 810	8.1—7.9 (m, 2H), 7.6—7.5 (m, 3H)	7.07 (s, 4H)	
II-2	93	44.5—46	1680 1610 1240	7.95, 7.30 (ABq, J=8 Hz, 4H)	7.30 (s, 5H)	
I-3[c]	97	oil	3400 1460 1020		7.37(s), 7.00(s)	4.31 (d, J=7 Hz), 4.26 (d, J=7 Hz)
II-3[c]	86	solid	3370 1610 1030		7.4—6.9 (m)	4.38 (d, J=7 Hz), 4.30 (d, J=7 Hz)
I-4a		114—116	1730 1550 1350	7.7—7.2 (m, 5H)	7.03, 6.87 (ABq, J=9Hz, 4H)	5.70 (d, J=8 Hz, 1H)
I-4b	(80)[d]	124—125	1730 1550 1350	7.6—7.2 (m, 5H)	7.07, 6.93 (ABq, J=9 Hz, 4H)	5.80 (d, J=8 Hz, 1H)
II-4a		96.5—98	1730 1550 1350	7.5—7.1 (m, 9H)		5.68 (d, J=8 Hz, 1H)
II-4b	(95)[d]	124—125	1715 1550 1350	7.5—6.9 (m, 9H)		5.80 (d, J=8 Hz, 1H)

a) The infrared spectra of **I-3** was recorded in neat, and the others, in Nujol mulls. b) Ref. 10. c) The data of proton was observed at a higher field in the NMR spectrum was ascribed to the **a**-series, and the other one, to

TABLE 2. KINETIC DATA OF 3,5-DINITROBENZOATES (**I-4a, b** AND **II-4a, b**) IN 80% AQUEOUS ACETONE

Compound	Temp °C[a]	10^4k/s^{-1} [b]	$\Delta H^{\neq}$ kcal/mol[c]	$\Delta S^{\neq}$ eu[c]	k_{rel} at 25°C
I-4a	45.0	1.16±0.07			
	35.0	0.303±0.008			
	25.0	0.0766±0.0032	25.0	−2.62	1.00
I-4b	45.0	3.71±0.19			
	35.0	1.08±0.07			
	25.0	0.275±0.018	23.4	−5.44	3.59
II-4a	45.0	3.99±0.1			
	30.0	0.754±0.001			
	25.0	0.404±0.06	20.7	−13.7	1.00
II-4b	45.0	8.29±0.1			
	30.0	1.57±0.07			
	25.0	0.752±0.05	22.0	−8.14	1.86

a) ±0.03 °C. b) The kinetic plots were linear to a 75% conversion (2 half-lives). c) Calculated from $\Delta H^{\neq}=R\,(T_1T_2/T_2-T_1)\ln(T_1k_2/T_2k_1)$, $\Delta S^{\neq}=R\ln(k_ih/kT_i)+\Delta H^{\neq}/T_i$; T_i, absolute temperature; h, Planck's constant; k, Boltzmann's constant.

gave a pure sample, **I-4b** (mp 124—125 °C). A pure sample of **I-4a** was obtained in a 92% yield by esterification between a pure **I-3a** and 3,5-dinitrobenzoylchloride. By a similar method, another pair of esters (**II-4a, b**) was obtained.

Assignment of the Geometry in 3,5-Dinitrobenzoate. 1) The ratio of the composition of diastereomers for each series was not changed between before and after esterification.

2) The esterification of a pure alcohol (**I-3a**) gave rise

TABLE 3. PHYSICAL PROPERTIES AND SPECTRAL DATA OF

Compound	Mp °C	IR in Nujol mulls $\tilde{\nu}$/cm^{-1}	NMR δ/ppm Aromatic	Vinylic
I-5	78.5—80.0	3350 960	7.4—7.0 (m, 9H)	6.53 (d, J=16 Hz, 1H), 6.12 (dt, J=16, 6 Hz, 2H)
II-5	70—71	3330 960	7.37 (s, 5H), 7.2—7.0 (m, 4H)	6.50 (d, J=16 Hz, 1H), 6.07 (dt, J=16, 6 Hz, 2H)

ANALYTICAL DATA OF **I-2, 3, 4a, b** AND **II-2, 3, 4a, b**

in $CDCl_3$			Found (Calcd)		
Cyclopropyl	Others	(Calcd for)	C, %	H, %	N, %
3.0—2.5 (m, 2H), 2.0—1.3 (m, 2H)	2.30 (s, 3H); Methyl				
3.0—2.5 (m, 2H), 2.0—1.4 (m, 2H)	2.41 (s, 3H); Methyl	($C_{17}H_{16}O$)	86.35 (86.41)	6.90 (6.82)	
2.2—0.8 (m)	2.27 (s); Methyl, 2.00 (s); OH				
2.2—0.8 (m)	2.35 (s); Methyl, 1.95 (s); OH				
2.5—2.1 (m, 1H), 2.1—1.6 (m, 1H), 1.19 (t, J=8 Hz, 2H)	9.15 (s, 4H); Ester, 2.28 (s, 3H); Methyl	($C_{23}H_{21}NO_4$)	66.58 (66.66)	4.68 (4.60)	6.27 (6.48)
2.3—1.6 (m, 2H), 1.3—1.0 (m, 2H)	9.16 (s, 4H); Ester, 2.30 (s, 3H); Methyl	($C_{23}H_{21}NO_4$)	66.10 (66.66)	4.60 (4.60)	6.30 (6.48)
2.6—2.2 (m, 1H), 2.2—1.8 (m, 1H), 1.4—1.1 (m, 2H)	9.16 (s, 4H); Ester, 2.37 (s, 3H); Methyl	($C_{23}H_{21}NO_4$)	66.39 (66.66)	4.65 (4.60)	6.49 (6.48)
2.3—1.6 (m, 2H), 1.6—1.0 (m, 2H)	9.16 (s, 4H); Ester, 2.37 (s, 3H); Methyl	($C_{23}H_{21}NO_4$)	66.65 (66.66)	4.80 (4.60)	6.42 (6.48)

I-3 and **II-3** were obtained with a mixture of two diastereoisomers. The alcohol in which the doublet of the α- the **b**-series. d) Yield from a mixture of two diatereoisomers of alcohol.

to a pure 3,5-dinitrobenzoate (**I-4a**; 92% yield). The geometry of this 3,5-dinitrobenzoate (**I-4a**) should eventually correspond to that of the *erythro* isomer of its parent alcohol (**I-3a**).

3) The chemical shift of the carbinyl proton in **I-4b** is about 0.1 ppm lower than that in **I-4a**. An analogous relation is observed between parent alcohols (**I-3a** and **b**), as has been described before.

Treatment of I-3a, b and II-3a, b with Perchloric Acid. A solution of **I-3a, b** (1.0 g) and 0.2 ml of 70% perchloric acid dissolved in 50 ml of 80% aqueous acetone was stirred at 25 °C for 24 h. After a work-up, 950 mg of a colorless solid were obtained in a 95% yield. Recrystallization from petroleum ether gave rise to a pure sample, *trans*-1-phenyl-4-*p*-tolyl-3-buten-1-ol (**I-5**). Another homoallylic alcohol (II-5) was obtained by a similar method in a 92% yield and was recrystallized from petroleum ether. The spectral data of **I-5** and **II-5** are shown in Table 3.

Preparative Solvolysis of 3,5-Dinitrobenzoate (I-4a, b and II-4a, b). A solution of 388 mg (1 mmol) of **I-4a** and 0.5 ml (*ca.* 4.6 mmol) of 2,6-lutidine in 200 ml of 80% aqueous acetone was heated at 45 °C for 30 half-lives. After the solution had then been concentrated under reduced pressure, 100 ml of water was added and the resulting suspension was extracted with ether. The combined ether extracts were washed with water and dried over anhydrous K_2CO_3. The removal of the solvent under reduced pressure gave 171 mg (71%) of a yellow solid. The other esters (**I-4b** and **II-4a, b**) were solvolyzed in the presence of 2,6-lutidine by a similar method. Each product in solvolysis was identified on the basis of a comparison of its NMR spectra with those of an authentic sample. The product distributions were determined from the ratio of the NMR integral intensities of the α-hydrogen signal for cyclopropyl methanol and the vinylhydrogen signal for homoallyl alcohol. The major products were homoallylic alcohols (**I-5, II-5**), accompanied by a trace of the parent alcohols (**I-3, II-3**).

A mixture containing 110 mg (0.46 mmol) of **I-3a**, 0.3 ml of 2,6-lutidine and 98 mg (0.46 mmol) of 3,5-dinitrobenzoic acid in 100 ml of 80% aqueous acetone was heated at 45 °C for 8 h (*ca.* 5 half-lives). After a usual work-up, 95 mg of a colorless solid were obtained. A comparison of the NMR spectrum before and after heating showed that **I-3a** was stable under these reaction conditions. Also, **II-3b** was not changed into **II-5** under these conditions.

Kinetic Procedures. The acetone was purified by distillation from potassium permanganate, followed by drying (K_2CO_3) and distillation. The water used in the kinetic studies was demineralized and distilled. 80% aqueous acetone (v/v) was prepared at 25 °C by mixing 4 volumes (accurately pipetted) of purified acetone with 1 volume of purified water.

THE HOMOALLYLIC ALCOHOLS (**I-5** and **II-5**)

in $CDCl_3$				Found (Calcd for $C_{17}H_{18}O$: C, 85.67; H, 7.61%)
α	Allylic	Hydroxylic	Methyl	
4.75 (t, J=6 Hz,1H)	2.62 (t, J=6 Hz, 2H)	2.13 (s, 1H)	2.33 (s, 3H)	C, 85.96; H, 7.62%
4.77 (t, J=6 Hz, 1H)	2.63 (t, J=6 Hz, 2H)	1.97 (s, 1H)	2.33 (s, 3H)	C, 85.44; H, 7.65%

For each run, approximately 100 mg (*ca.* 0.25 mmol) of 3,5-dinitrobenzoate (**I-4a, b** or **II-4a, b**) was weighed into a 100 ml volumetric flask and dissolved in 80% aqueous acetone (*ca.* 2×10^{-3} M). Aliquots of the solution (*ca.* 6 ml) were transferred as quickly as possible into glass ampoules, which were in turn sealed and immersed simultaneously into a constant-temperature bath. After approximately 5 min, one ampoule was removed and immediately plunged into an ice–water bath. The rate at each temperature was measured by quenching 5.00 ml aliquots in 25 ml of dry acetone and then immediately titrating with a standard aqueous sodium hydroxide solution (8.357×10^{-3} M), using a Hitachi-Horiba automatic titrator with a glass electrode. The infinite titer was measured after *ca.* 10 half-lives, and 95—103% of 3,5-dinitrobenzoic acid was removed. The rate constants obtained by such procedures were consistent with that obtained by the indicator method using Bromothymol Blue.

A solution of 240 mg of **I-4b** in 200 ml of 80% aqueous acetone was kept in a flask at 35 °C for 1.5 h (*ca.* 1/2 half life). The solution was then poured into a mixture of ether (300 ml) and water (500 ml). The ether layer was washed with water and dried over anhydrous sodium sulfate. The solvent was removed at reduced pressure, the solid residue weighed 230 mg. A comparison of the NMR spectra before and after the reaction indicated that **I-4b** was not isomerized into **I-4a** under the solvolysis conditions. Also, **I-4a** was not converted into the isomeric 3,5-dinitrobenzoate (**I-4b**) under the reaction conditions.

References

1) a) P. R. Story and B. C. Clark, Jr., "Carbonium Ions," ed by G. A. Olah and P. v. R. Schleyer, Interscience, New York, N. Y. (1972), Vol. 3, p. 1007; b) H. G. Richey, Jr., *ibid.*, p. 1201; c) K. B. Wiberg, B. A. Hess, Jr., and A. J. Ashe, *ibid.*, p. 1295; d) M. Hanack and H. J. Schneider, *Angew. Chem., Int. Ed. Engl.*, **6**, 666 (1967); *Fortschr. Chem. Forsch.*, **8**, 554 (1967).

2) a) B. R. Ree and J. C. Martin, *J. Am. Chem. Soc.*, **92**, 1660 (1970); b) V. Buss, R. Gleiter, and P. v. R. Schleyer, *ibid.*, **93**, 3927 (1971); c) G. A. Olah, C. L. Jewell, D. P. Kelly, and R. D. Porter, *ibid.*, **94**, 146 (1972); d) Y. E. Rhodes and V. G. DiFate, *ibid.*, **94**, 7582 (1972), and the references cited in these papers.

3) a) L. Birladeanu, T. Hanafusa, B. Johnson, and S. Winstein, *J. Am. Chem. Soc.*, **88**, 2316 (1966); b) E. C. Friedrich, M. A. Saleh, and S. Winstein, *J. Org. Chem.*, **38**, 860 (1973); c) E. C. Friedrich and M. A. Saleh, *J. Am. Chem. Soc.*, **95**, 2617 (1973); d) P. G. Gassman, R. N. Steppel, and E. A. Armour, *Tetrahedron Lett.*, **1973**, 3287; e) L. A. Paquette, O. Cox, M. Oku, and R. P. Henzel, *J. Am. Chem. Soc.*, **96**, 4892 (1974), and the references cited in these reports.

4) Two reports of studies of the diastereoisomers of phenethyl systems have appeared: S. Winstein, B. K. Morse, E. Grunwald, K. C. Schreiber, and J. Corse, *J. Am. Chem. Soc.*, **74**, 1113 (1952); D. J. Cram, *ibid.*, **74**, 2129 (1952).

5) K. Ohkata, *J. Org. Chem.*, **41**, 2162 (1976); *Bull. Chem. Soc. Jpn.*, **49**, 235 (1976); Y. Ogawa, H. Matsusaki, K. Hanaoka, K. Ohkata, and T. Hanafusa, *J. Org. Chem.*, **43**, 849 (1978).

6) G. Descotes, A. Menet, and F. Collonges, *Tetrahedron*, **29**, 2931 (1973).

7) D. J. Cram and F. A. A. Elhafez, *J. Am. Chem. Soc.*, **74**, 5828, 5851 (1952); D. H. R. Barton, *J. Chem. Soc.*, **1953**, 1027; V. Prelog, *Helv. Chim. Acta*, **36**, 308 (1953).

8) C. D. Poulter, R. S. Boikess, J. I. Brauman, and S. Winstein, *J. Am. Chem. Soc.*, **94**, 2291 (1972), and the references cited therein.

9) D. S. Noyce and M. J. Jorgenson, *J. Am. Chem. Soc.*, **84**, 4312 (1962); J. A. Gautier, M. Miocque, and J. P. Doclos, *Bull. Soc. Chim. Fr.*, **1969**, 4348; V. Hanzlik and A. Bianchi, *Chem. Ber.*, **32**, 2283 (1899); S. T. V. Kostanecki and G. Rossbach, *ibid.*, **29**, 2246 (1896).

10) a) E. J. Corey and M. Chaykovsky, *J. Am. Chem. Soc.*, **87**, 1353 (1965); b) A. Merz and G. Markl, *Angew. Chem., Int. Ed. Engl.*, **12**, 845 (1973).

Mechanism for Reaction of *p*-Nitrotoluene with Sodium Polysulfide to Form *p*-Aminobenzaldehyde

Yoshiro OGATA,* Atsushi KAWASAKI, Yasuhiko SAWAKI, and Yoshiaki NAKAGAWA[1)]

Department of Applied Chemistry, Faculty of Engineering, Nagoya University, Chikusa-ku, Nagoya 464

(Received January 13, 1979)

The conversion of *p*-nitrotoluene to *p*-aminobenzaldehyde was found to be most effectively done by a mixture of Na_2S_4 and *ca.* two equivalents of NaOH to *p*-nitrotoluene. After examination of probable intermediates, toluidine, *p*-nitrobenzaldehyde and *p*-nitrosotoluene were discarded as the intermediate. The reaction of carbanion $ArCO\bar{C}HAr$ with the sulfide and the effect of some nitrobenzenes as an electron accepter were examined. These results suggest a mechanism involving a simultaneous oxidation-reduction in a nitrotoluene molecule.

Sulfur frequently shows a unique ability by which the substrate is oxidized at one site but reduced at another site. A typical example is the conversion of *p*-nitrotoluene to *p*-aminobenzaldehyde. In aqueous ethanolic solution of sodium polysulfide, *p*-nitrotoluene is converted to *p*-aminobenzaldehyde. This reaction is known to be the best route for synthesis of *p*-aminobenzaldehyde. But the reaction mechanism is still obscure and unconvincible.[2,3)] We wish to clarify it by examining the effects of reaction conditions and substrate structure and by isolating intermediates, since the kinetic study was difficult.

Results and Discussion

Effect of Na_2S_x and NaOH. *p*-Nitrotoluene was allowed to react with polysulfide (Na_2S–Na_2S_5). It was found that Na_2S_4 was the best reagent (Table 1) and that elemental sulfur itself was not always essential for this reaction.

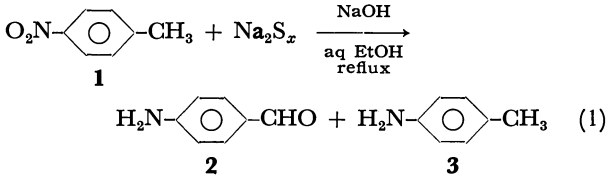

(1)

With 1.9 mol of NaOH for one mol of *p*-nitrotoluene, the highest yield of *p*-aminobenzaldehyde was obtained. If a less amount of NaOH was used, the yield of *p*-toluidine increased, but that of *p*-aminobenzaldehyde decreased remarkably. This may be due to the Eq. 2[4)] which consumes NaOH, decreasing the concentration of benzyl anion (Table 2).

TABLE 1. YIELD OF PRODUCTS IN A REACTION OF *p*-NITROTOLUENE (**1**) WITH Na_2S_x IN AQUEOUS ETHANOL BY REFLUXING FOR 3 h[a)]

Na_2S_x	Yield	
	2 (%)	**3** (%)
$x=1$	6.1	60.1
2	9.3	94.3
3	35.4	21.5
4	43.5	16.4
5	24.4	43.3

a) **1** (0.037 mol), NaOH (0.068 mol).

TABLE 2. EFFECT OF NaOH ON THE YIELDS OF *p*-AMINOBENZALDEHYDE (**2**) AND *p*-TOLUIDINE (**3**) IN THE REACTION OF *p*-NITROTOLUENE (**1**) WITH Na_2S_4 IN 3 h REFLUXING

1 (g)	Na_2S_4 (g)	NaOH (g)	**2** (%)	**3** (%)
5.00	3.40	0	0	101.5
5.00	3.40	0.74	6.8	48.1
5.00	3.40	1.37	24.7	35.3
5.00	3.40	2.74	37.4	16.1
5.00	3.40	4.04	34.0	16.6

$$6NaOH + 1/2S_8 \longrightarrow 2Na_2S + Na_2S_2O_3 + 3H_2O \quad (2)$$

Time Conversion. Figure 1 shows the consumption of *p*-nitrotoluene and the yields of *p*-toluidine and *p*-aminobenzaldehyde. The formation of *p*-toluidine stopped after 30 min.

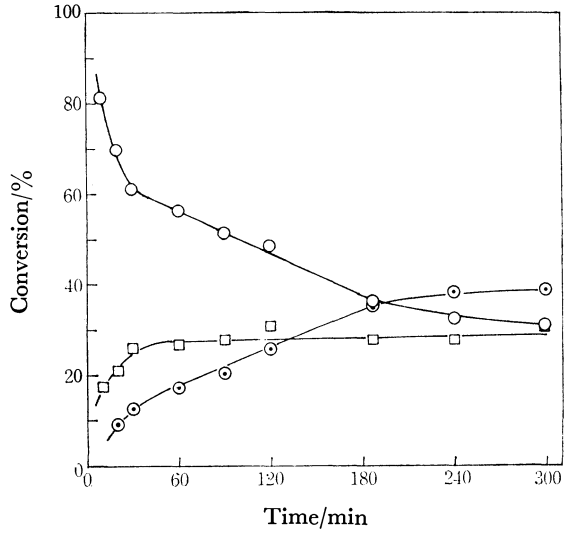

Fig. 1. Reaction of *p*-nitrotoluene with Na_2S_4 in 90% aqueous ethanol at 80 °C. The initial amount of reagents were: *p*-nitrotoluene 0.037 mol; Na_2S_4 3.30 g; NaOH 0.068 mol: (○) *p*-nitrotoluene, (□) *p*-toluidine, (⊙) *p*-aminobenzaldehyde. (*p*-Aminobenzaldehyde was estimated by subtracting the sum of the amount of *p*-nitrotoluene and *p*-toluidine from 0.037 mol.)

Discussion of Mechanisms. Information thus far obtained suggests several mechanisms which will be discussed below.

(I) Mechanism via *Anthranil Nitrone*: Shchukina *et al.*[3)]

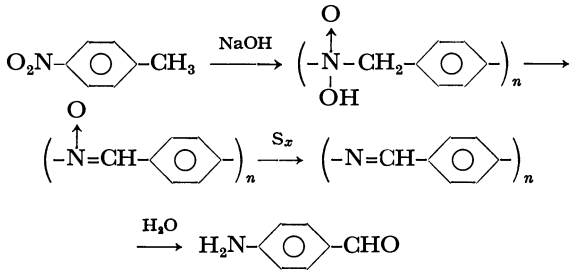

Scheme 1.

proposed a mechanism involving polynitrone formation (Scheme 1). This mechanism employs sulfur as a reducing agent. So that we replaced sulfur with triphenylphosphine which is known to be a strong reductant for nitrone,[5] but no *p*-aminobenzaldehyde was obtained. Hence this mechanism is of doubt.

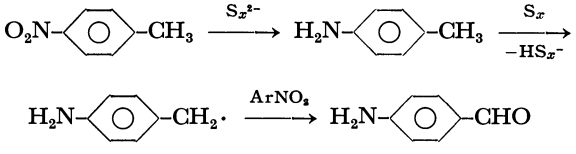

Scheme 2.

(II) Mechanism via p-*Toluidine*: Polysulfenyl radicals are electrophilic,[6] and therefore an amino group would increase the rate of attacks of these radicals on the benzylic position, if the oxidation involved hydrogen abstraction by sulfenyl radicals. But the reaction of *p*-toluidine with Na_2S_x gave no *p*-aminobenzaldehyde even in the presence of a strong electron-accepter such as *m*-dinitrobenzene. Hence, this mechanism can also be eliminated.

(III) Mechanism via p-*Nitrobenzaldehyde*: Hodgson *et al.*[2] proposed a mechanism *via p*-nitrobenzaldehyde. Indeed, substitution of electron-attracting *p*-NO_2 group stabilizes benzyl anion and increases its concentration in a basic solution. The *p*-nitrobenzyl anion may attack

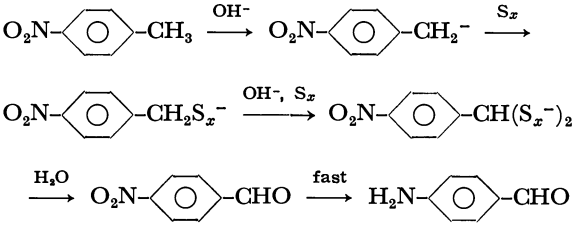

Scheme 3.

the S–S bonds as a nucleophile[7] or it may be converted to a radical by loss of one electron, and then links with polysulfenyl radical to form benzylpolysulfide, which is hydrolyzed to *p*-nitrobenzaldehyde (Scheme 3). The electron-attracting formyl group should accelerate the reduction of nitro group as apparent from our reported Hammett's ρ value of $+3.55$.[8] But our attempt for detection of *p*-nitrobenzaldehyde itself by UV spectrum and trapping *p*-nitrobenzaldehyde by phenylhydrazine were unsuccesful, but in view of its low concentration this mechanism *via p*-nitrobenzaldehyde cannot completely be excluded.

To test the possibility of oxidation of another carbanion with sulfur, *p*-chlorodeoxybenzoin, which loses proton easily with base, was reacted with polysufides but no *p*-chlorobenzil was obtained. Moreover, an attempted reaction of *p*-chlorodeoxybenzoin in the presence of nitrobenzene and Na_2S_x gave virtually no reaction. Hence, a nitro group is necessary for this type of reaction.

(IV) A Probable Mechanism: There are still left two mechanisms as probable candidates. One is the intramolecular direct migration of oxygen and hydrogens, and another is the concurrent oxidation and reduction in a molecule.

The reaction of 4-nitro-*m*-xylene with Na_2S_x gave 3-methyl-4-aminobenzaldehyde (7%) and 4-amino-*m*-xylene (*ca.* 8%), but no 5-methyl-2-aminobenzaldehyde. Therefore, the direct internal migration of oxygen to the nearest ortho position is disfavored. The very low yield of oxidation product (aldehyde) may be due to the electron-releasing methyl group, which lowers the concentration of benzyl anion.

In conclusion, a plausible mechanism which does not contradict with our observations described above may be as shown in Scheme 4.

This tentative mechanism involves conversion of *p*-nitrotoluene to the benzyl anion with hydroxide ion and protonation at the nitro group resulting in the formation of quinonoid isomer of *p*-nitrotoluene. This is a kind of olefin, which may undergo a Michael type addition of polysulfide ion[9] assisted by the electron-attracting *p*-NO_2 group with simultaneous or subsequent elimination of hydroxide ion, giving a hypothetical nitrosobenzyl polysulfide intermediate. Analogous base-catalyzed prototropy would give its quinonoid isomer, whose sulfur atom at the β-position to the benzylic carbon atom would be attacked by polysulfide ion, giving thiobenzaldehyde derivative. The thiolate ion attacks more easily on sulfur atom than on carbon atom, the reaction rate being fast.[10] Further, formation

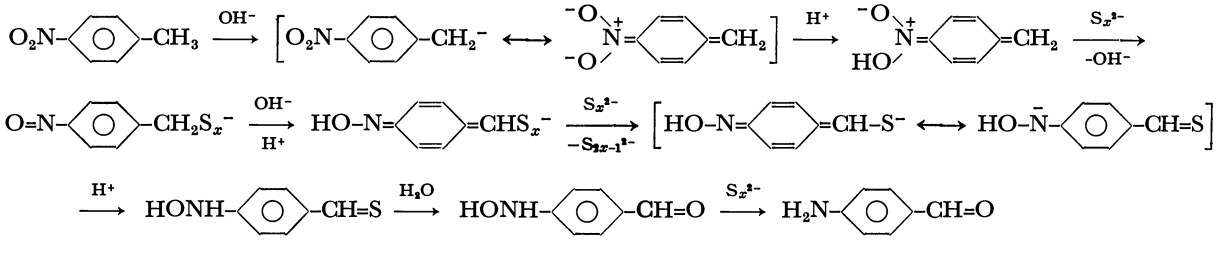

Scheme 4.

of thiocarbonyl as an intermediate of Willgerodt reaction of acetophenone with ammonium polysulfide has been reported.[11] The *p*-hydroxyaminothiobenzaldehyde is easily hydrolyzed[11a] and reduced to *p*-aminobenzaldehyde[12] as apparent from the literature.

Another evidence for supporting this mechanism is that *o*-nitrotoluene can give *o*-aminobenzaldehyde,[13] but *m*-nitrotoluene cannot give *m*-aminobenzaldehyde albeit the simple discussion as an unpublished data.[14] Further, no effect of bubbling air (oxygen) on the conversion of *p*-nitrotoluene was observed, and also neither 4,4′-dinitrobibenzyl nor 4,4′-dinitrostilbene can be detected in the reaction products. Therfore, a mechanism *via* radical, $p\text{-}NO_2\text{–}C_6H_4\text{–}CH_2\cdot$, is less probable.

Experimental

Melting points were measured by a Yanagimoto micro melting point apparatus and were not corrected. IR and NMR spectra were recorded on a Perkin-Elmer 337 spectrophotometer and a Hitachi R-24B NMR spectrometer using Me_4Si as an internal standard. The GLC analysis was performed with a Yanagimoto 550-F gas chromatograph with a flame ionization detecter.

Materials. Sodium polysulfide were prepared by the method of Gabel *et al.*;[15] a yellow hygroscopic solid. Melting points and boiling points of principal reactants were: *p*-nitrotoluene, mp 53—54 °C; *p*-toluidine mp 44—45 °C; 4-nitro-*m*-xylene bp 125—127 °C/15 Torr.

Reaction of p-*Nitrotoluene (1) with* Na_2S_x.[16] A hot aqueous solution (90 ml) of $Na_2S\cdot 9H_2O$ (0.013 mol), S (0.047 g atom), and NaOH (0.067 mol) was poured into a 300 ml round-bottomed flask containing a hot ethanolic solution (30 ml) of **1** (0.036 mol). The mixture was heated under reflux for 3 h and then steam-distilled. The distillate was extracted with ether and the extract was analyzed by GLC. GLC analysis was conducted at 80—250 °C using two sorts of columns (1 m): PEG 20 M, 10% on Chromosorb WAW; Silicon OV 17, 5% on Simalite 201D. The residue was filtered while hot, and then chilled in an ice bath. The crystals of *p*-aminobenzaldehyde (**2**) were collected and washed with ice water. The product was identified by the NMR and IR in comparison with the authentic specimen. The yield of **2** was 52%.

Reaction of **1** *with* Na_2S *to* Na_2S_5. According to the procedure of the reaction of **1** with Na_2S_x, we used Na_2S–Na_2S_5 instead of $Na_2S\cdot 9H_2O$ and S.

Conversion of **1**. A mixture of **1** (0.037 mol), NaOH (0.068 mol), Na_2S_4 (3.3 g), ethanol (90 ml), and water (10 ml) was placed in a 200 ml two-necked flask and refluxed. One ml of sample was pippetted out at appropriate time intervals. Ethanol (5 ml) was added, and the solution was analyzed by GLC (PEG 20 M).

Reaction of p-*Toluidine (3) with* Na_2S_x. According to the procedure of the reaction of **1** with Na_2S_x, a mixture of **3** (0.035 mol), $Na_2S\cdot 9H_2O$ (0.015 mol), S (0.046 g atom), and NaOH (0.071 mol) was allowed to react. The recovery of **3** was 50%. Similarly, a mixture of same reactions as above and *m*-dinitrobenzene (0.036 mol) was allowed to react. The recovery of **3** was 63% and the yield of *p*-nitroaniline was 23%.

Attempted Trap of p-*Nitrobenzaldehyde.* A hot aqueous solution (12 ml) of NaOH (0.013 mol) and Na_2S_4 (0.70 g) was added to a hot ethanolic solution (6 ml) of **1** (7.3×10^{-3} mol) and phenylhydrazine (7.4×10^{-3} mol), refluxed for 1 h and cooled rapidly. The extract with ether was hydrolyzed with 4 N HCl (100 ml), and the ether extract was analyzed by GLC (PEG 20 M).

Reaction of 4-Nitro-m-*xylene (6) with* Na_2S_x. Similar work up for the reaction of **1** with Na_2S_x was applied to **6**; *i.e.*, a mixture of **6** (0.036 mol), $Na_2S\cdot 9H_2O$ (0.014 mol), S (0.055 g atom), and NaOH (0.068 mol) was allowed to react. The yield of 3-methyl-4-aminobenzaldehyde was 70%; mp 104—107 °C (lit,[17] 92 °C); NMR ($CDCl_3$): δ 2.18 (s, 3H, CH_3), 4.19 (s, 2H, NH_2) 6.65 (d, 1H, ArH, J=9 Hz), 7.55 (d, 1H, ArH, J=9 Hz), 7.57 (m, 1H, ArH), 9.70 (s, 1H, CHO).

Reaction of m-*Nitrotoluene (7) with* Na_2S_x. According to the procedure for **1** with Na_2S_x, a mixture of **7** (0.037 mol), $Na_2S\cdot 9H_2O$ (0.013 mol), S (0.050 g atom), and NaOH (0.069 mol) was allowed to react. The recovery of **7** was 30% and the yield of *m*-toluidine was 65%, but no trace of *m*-aminobenzaldehyde was detected with NMR.

Effect of Oxygen on p-*Nitrotoluene Conversion.* A mixture of **1**, NaOH (0.051 mol), Na_2S_4 (3.1 g), ethanol (90 ml), and water (10 ml) was placed in a 200 ml two-necked flask. After the flask had been thermostated at 50±0.5 °C, air was bubbled into the reaction mixture during the run. Two ml of the sample was pippetted out at appropriate time intervals. An ethanolic solution (1 ml) of biphenyl as an internal standard was added, and the solution was analyzed by GLC (PEG 20 M). The similar work up without bubbling of air was also carried out. The conversions (%) at various times were as follows, where figures in parenthesis indicate the conversion without air bubbling; 5 min: 12 (9), 10 min: 30 (24), 15 min: 41 (35), 20 min: 46 (46), 25 min: 47 (47), 30 min: 48 (52).

References

1) Contribution No. 250.
2) H. G. Beard and H. H. Hodgson, *J. Chem. Soc.*, **1944**, 4.
3) M. N. Shchukina and G. S. Predvoditeleva, *Proc. Acad. Soc. U.S.S.R. Chem. Sect. (Eng. transl.)*, **110**, 565 (1956); *Chem. Abstr.*, **51**, 4996b (1957).
4) W. A. Pryor, "Mechanisms of Sulfur Reactions," McGraw-Hill, New York, N. Y. (1962), p. 150.
5) E. Müller, R. Mayer, B. Narr, A. Shick, and K. Scheffler, *Justus Liebigs Ann. Chem.*, **645**, 1 (1961).
6) W. A. Pryor, *J. Am. Chem. Soc.*, **82**, 2715 (1960).
7) Ref. 4, p. 153.
8) M. Hojo, Y. Takagi, and Y. Ogata, *J. Am. Chem. Soc.*, **82**, 2459 (1960).
9) Facile addition of thiolate ion to acrylonitrile has been reported. C. D. Hurd and L. L. Gershheim, *J. Am. Chem. Soc.*, **69**, 2328 (1947).
10) a) A. J. Parker and N. Kharasch, *J. Am. Chem. Soc.*, **82**, 3071 (1960); b) A. Fava, A. Iliceto, and E. Camera, *J. Am. Chem. Soc.*, **79**, 833 (1957).
11) a) J. A. King and F. H. McMillan, *J. Am. Chem. Soc.*, **68**, 632, 1369 (1946); b) J. A. King and F. H. McMillan, *ibid*, **70**, 4143 (1948).
12) R. Willstätter and H. Kubli, *Ber.*, **41**, 1936 (1908).
13) J. R. Geigy and Co., Germ. Patent 86874; *Ber.*, **29**, 530 (1896).
14) Ref. 4, p. 149.
15) Y. O. Gabel and L. P. Speier, *J. Gen. Chem. U.S.S.R.*, **17**, 2277 (1947); *Chem. Abstr.*, **42**, 4976 (1948).
16) E. Campaigne, W. M. Budde, and G. E. Shaefer, *Org. Synth.*, Coll. Vol. IV, p. 31, (1963).
17) J. R. Geigy and Co., Germ. Patent 87255; *Friedlaender Fortschritte der Teerfarbenfabrikation*, **4**, 138 (1896).

Catalytic Hydrolysis of Dinitrophenyl Sulfate by Poly(ethylenimine) Derivatives†

Toyoki KUNITAKE* and Tetsuo SAKAMOTO

Department of Organic Synthesis, Faculty of Engineering, Kyushu University, Fukuoka 812

(Received January 29, 1979)

The catalytic hydrolysis of nitrophenyl sulfates by poly(ethylenimine)(PEI) derivatives was investigated at 30 °C in aqueous buffers. PEI derivatives which were made partly hydrophobic by incorporation of higher alkyl groups include alkylated PEI's, quaternized PEI's, and PEI's with imidazole and hydroxamate functions. Nitrophenyl sulfates could not be cleaved by these polymers. The catalytic hydrolysis of 2-hydroxy-5-nitrophenyl sulfate by an PEI with imidazolylmethyl and dodecyl substituents failed to proceed in spite of the contrary report by Kiefer *et al.* 2,4-Dinitrophenyl sulfate was cleaved fairly readily by PEI derivatives. Simple sulfate transfer was observed in the case of alkylated PEI, but the catalytic hydrolysis proceeded according to the Michaelis-Menten kinetics in the case of quaternized PEI. Partly quaternized PEI's showed highest catalytic efficiencies reported to date for the hydrolysis of dinitrophenyl sulfate.

Poly(ethylenimine) and its derivatives have been used widely as catalysts for hydrolysis[1–5] and decarboxylation.[6,7] Poly(ethylenimine)s with hydrophobic alkyl substituents are particularly interesting because their compact conformations in water provide excellent model enzyme systems.[8] Most of the hydrolytic study have been carried out by using phenyl ester substrates, and some functionalized poly(ethylenimine)s were shown to possess extremely high catalytic activities.

The hydrolysis of sulfate monoesters is usually not markedly accelerated by polymer catalysts. A unique exception is the hydrolysis of 2-hydroxy-5-nitrophenyl sulfate catalyzed by an imidazole-containing poly(ethylenimine). This catalytic hydrolysis was reported to be faster by a factor of more than 10^{12} fold than the imidazole-catalyzed hydrolysis and the catalytic efficiency exceeds that of arylsulfatase A (2-hydroxy-5-nitrophenyl sulfate is the specific substrate for this enzyme).[9]

We have found that some cationic micelles which contain the hydroxamate nucleophile cleave a dinitrophenyl sulfate quite efficiently.[10] Therefore, the functionalized poly(ethylenimine) is also expected to be a good catalyst for the hydrolysis of sulfate esters. In this study, we report the catalytic hydrolysis of nitrophenyl sulfates by various poly(ethylenimine) derivatives. The hydrolysis of a phenyl ester by these polymer catalysts was also examined for comparison. The structures of the polymer catalysts and substrates and their abbreviations are given below:

polymer:

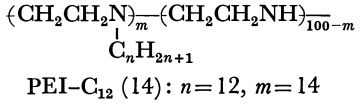

PEI-C_{12} (14): $n=12$, $m=14$

PEI-C_{16} (8) : $n=16$, $m=8$

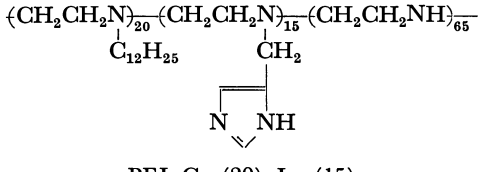

PEI-C_{12} (20)-Im (15)

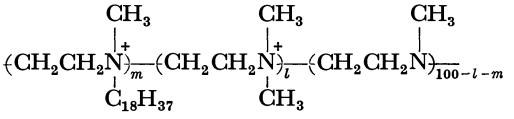

PEI$^+$-C_{18}(9) : $m=9$, $l=0$

PEI$^+$-C_{18}(16): $m=16$, $l=0$

PEI$^+$-C_{18}(12)-C_1(68): $m=12$, $l=68$

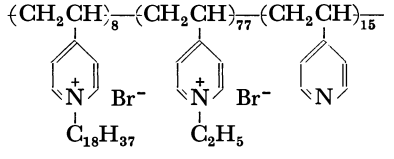

PVP$^+$-C_{18}(8)-C_2(77)

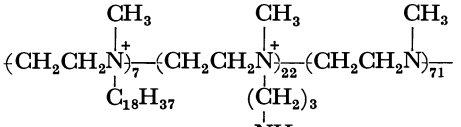

PEI$^+$-C_{18}(7)-NH_2(22)

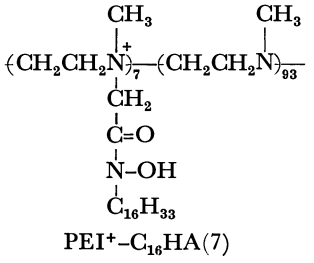

PEI$^+$-C_{16}HA(7)

substrate:

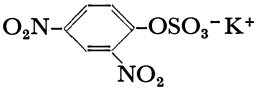

DNPS

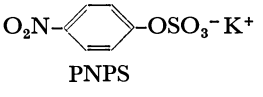

PNPS

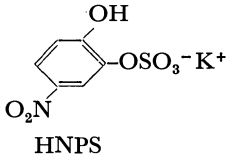

HNPS

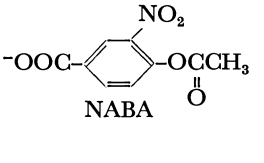

NABA

Experimental

Preparation of Substrates. Potassium 2,4-dinitrophenyl sulfate (DNPS) was prepared according to the procedure of

† Contribution No. 511 from Department of Organic Synthesis.

Sunamoto *et al.*[10,11] Potassium *p*-nitrophenyl sulfate (PNPS) and potassium 2-hydroxy-5-nitrophenyl sulfate (HNPS) were prepared by following the procedures reported by Fendler and Fendler,[12] and Robinson, *et al.*,[13] respectively. The elemental analyses agreed with the calculated values. The preparation of 3-nitro-4-acetoxybenzoic acid (NABA) was reported previously.[14]

Partially Alkylated Poly(ethylenimine). An aqueous solution of commercial poly(ethylenimine) (Tokyo Kasei Co., *MW* 40000—50000, highly branched) was concentrated *in vacuo*, ethanol added to the residue and the solution was again concentrated. This procedure was repeated in order to completely replace water with ethanol. Finally, dry ethanol was added to obtain a 2—5 wt % solution, which was stored over molecular sieve 4A for the later use. The ethanolic solution was concentrated and 10—15 mol % of alkyl iodides (n-$C_{12}H_{25}I$ or n-$C_{16}H_{33}I$) were added. The mixture was heated at 60—70 °C for 24 h under nitrogen, concentrated and poured into excess ether. The yellowish powder was recovered, and washed several times with ether. The polymer was dissolved in water and purified by dialysis. The extent of alkylation was determined by the relative peak area of the main chain methylene proton (at *ca.* 2.7 ppm) and the alkyl proton (at *ca.* 1.3 ppm) in the NMR spectrum (D_2O solution).

Quaternized Poly(ethylenimine).[4] All the primary and secondary amino groups in poly(ethylenimine) were converted to the tertiary amino group by treating with formic acid and formalin. The product polymer was parly quaternized by octadecyl bromide in ethanol. The extent of quaternization was determined by NMR spectroscopy as mentioned above. Further quaternization was performed with methyl bromide in order to obtain PEI^+–C_{18}(16)–C_1(68).

Introduction of Functional Groups. The incorporation of the imidazole group into alkylated poly(ethylenimine) was carried out according to the procedure of Kiefer, *et al.*:[9] PEI–C_{12}(20)–Im(15). The methylated poly(ethylenimine) was allowed to react with *N*-(3-bromopropyl)phthalimide and then with dodecyl bromide and treated with hydrazine hydrate to give PEI^+–C_{18}(7)–NH_2(22).[15] The content of the aminopropyl group was determined from the relative peak area of the aromatic proton prior to the hydrazine treatment and by reaction with 2,4,6-trinitrobenzenesulfonic acid after the hydrazine treatment.[2] The hydroxamate function was introduced by reaction of a polymer with benzyl *N*-hexadecylchloroacetohydroxamate (see below). The hydroxamate content in the polymer was determined from the peak area of the aromatic proton. The benzyl group was removed by treatment with 30% hydrogen bromide in acetic acid. The complete removal was confirmed by NMR spectroscopy. The polymer was purified by reprecipitation after each stage.

Other Materials. The preparation of quaternized poly(vinylpyridine)s was described elsewhere.[16] Commercial hexadecyltrimethylammonium bromide (CTAB) was recrystallized two times from ethanol. For the preparation of benzyl *N*-hexadecylchloroacetohydroxamate, 25.2 g (0.11 mol) of benzyl benzohydroxamate in dry acetone was treated with 12.4 g (0.22 mol) of powdered KOH and 19.5 g (0.055 mol) of hexadecyl iodide. The oily alkylation product was hydrolyzed in a mixture of ethanol and concentrated hydrochloric acid to give *O*-benzyl-*N*-hexadecylhydroxylamine hydrochloride; colorless flakes after two recrystallizations from acetone, yield 16.0 g (75%), mp 77—79 °C. This compound (7.0 g, 0.018 mol) and 4.0 g (0.040 mol) of triethylamine were dissolved in 100 ml of dry ether and 2.1 g (0.018 mol) of chloroacetyl chloride was added dropwise. After the usual work-up, the product was recrystallized from acetone: mp< 30 °C, yield 4.3 g (56%). NMR and IR spectra were consistent with the expected structure.

Polymer Recovery. In connection with the elucidation of the hydrolysis mechanism, the polymer catalyst was recovered after reaction with the substrate under the standard conditions. A polymer catalyst (100 mg, 8—16 unit mM) was mixed with 100—500 mg (3.3—16 mM) of DNPS in 100 ml of 0.01 M borate buffer (pH 9.0) and allowed to stand at 30 °C overnight (1 M = 1 mol dm^{-3}). The mixture was dialyzed for 24 h using a cellophane tube and then concentrated by ultrafiltration (DIAFLO Ultramembrane UM-2, Amicon Co., Exclusion limit 1000). A saturated aqueous solution of KBr was added and the resulting solution was concentrated by ultrafiltration. The ultrafiltration was repeated after addition of water. The concentrate was dried *in vacuo* and its sulfur content was determined.

Kinetic Measurements. The sulfate esters were dissolved in a 3:7 mixture of water and acetonitrile and kept in an ice bath. The substrate solution and an aqueous solution of the polymers were added to buffer solutions (borate or Tris) in a quartz cell which had been maintained at 30 °C. Water was added so that the fraction of acetonitrile became 3 v/v %. The ionic strength was adjusted to 0.01 by KCl. The reaction was followed by using the absorbance increase at 360 nm of 2,4-dinitrophenolate anion ($\varepsilon = 12800\ M^{-1}\ cm^{-1}$) in the case of DNPS substrate. The λ_{max} at 401 nm was used for PNPS. Hitachi UV-visible spectrophotometers (type 124 or 200) equipped with jacketed cell compartments were used. The pH measurement was done by using TOA Electronics MH-10 glass electrodes and the pH change during the hydrolysis was within 0.03. Excess polymers were used relative to substrates and the reaction obeyed the pseudo first-order rate law for more than 80% completion. The overall rate constant of phenol release was corrected for that of the spontaneous release.

Results

Reaction of Sulfate Esters with PEI Derivatives. Nitrophenyl sulfates, PNPS and HNPS, did not react with poly(ethylenimine) derivatives under the reaction conditions employed. For example, a reaction mixture which contain 1.77×10^{-3} M of PEI–C_{12}(20)–Im(15) and 1.0×10^{-4} M of HNPS was allowed to stand for 20 h at 30 °C (pH 8.8, 0.01 M borate buffer and μ= 0.01). No change was detected in the visible spectrum during this period. Nitrocatechol was not detected in the product by thin layer chromatography using the solvent system similar to that of Ref. 9. Therefore, the pseudo first-order rate constant, $k_{1,obsd}$ should be much smaller than $1 \times 10^{-5}\ s^{-1}$ or $k_{2,obsd}$ (apparent second-order rate constant) $\ll 5 \times 10^{-3}\ M^{-1}\ s^{-1}$. This is contrary to the efficient hydrolysis reported by Kiefer *et al.*[9]

On the other hand, DNPS was smoothly cleaved by these polymers. Table 1 summarizes $k_{1,obsd}$ of phenol release from DNPS by various PEI derivatives. In the last column are given $k_{2,obsd}$ values which were derived simply by dividing $k_{1,obsd}$ by the polymer concentration. It is clear from Table 1 that the catalytic groups such as imidazole, hydroxamate or primary amine are not appreciably effective for the sulfate cleavage. However, all of the PEI derivatives are more effective than the conventional cationic micelle (CTAB) or polysoap(PVP^+–C_{18}(8)–C_2(77)). In the subsequent

TABLE 1. CATALYTIC HYDROLYSIS OF DNPS[a)]

Polymer	10^4 [polymer] / M	pH	$10^4\ k_{1,obsd}$ / s^{-1}	$k_{1,obsd}$/[polymer] / $M^{-1}\,s^{-1}$
PEI–C_{12}(14)	20.5	8.86	63.9	3.12
PEI–C_{16}(8)	10.8	9.02	32.0	3.55
PEI–C_{12}(20)–Im(14)	5.19	8.94	31.9	6.14
PEI^+–C_{18}(9)	5.06	8.61	80.6	15.9
PEI^+–C_{18}(16)	5.14	9.52	130	25.3
PEI^+–C_{18}(12)–C_1(68)	1.01	8.88	8.23	8.15
PEI^+–C_{18}(7)–NH_2(22)	1.06	8.82	6.79	6.43
PEI^+–C_{16}HA(7)	9.71	8.43	31.7	3.26
PVP^+–C_{18}(8)–C_2(77)	9.60	9.44	6.4	0.67
CTAB	10.0	8.81	1.90	—

a) [DNPS]$=2.0\times10^{-5}$ M, 3 v/v % EtOH–H_2O, $\mu=$ 0.01 (KCl), 30 °C, 0.01 M borate buffer.

experiments, two types of PEI derivatives, alkylated PEI(PEI–C_{16}(8)) and quaternized PEI(PEI^+–C_{18}(16)) were used for more detailed study.

Product Analysis. Excess amounts of DNPS substrate (3—10 fold excesses) were allowed to react with the above-mentioned two PEI derivatives. The time course of the formation of 2,4-dinitrophenol after correction for the spontaneous release is given in Fig. 1. In the case of alkylated PEI's (Fig. 1a and 1b), the reaction slows down at the release corresponding to *ca.* 0.3 equivalent (in monomer unit) of the polymer. In contrast, the reaction proceeds beyond the concentration of the quaternized polymers (Fig. 1c, 1d, and 1e). These results suggest the presence of different mechanisms of the phenol release for the two types of the polymers.

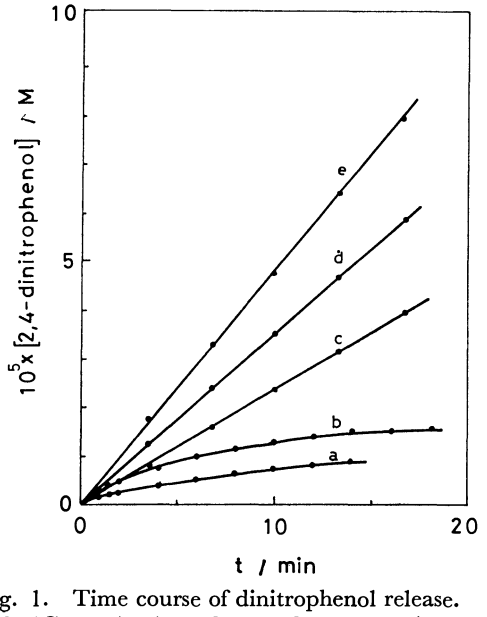

Fig. 1. Time course of dinitrophenol release.
30 °C, 3 v/v % EtOH–H_2O, μ=0.01(KCl), 0.02 M borate, pH 8.4, [DNPS]$=2.4\times10^{-4}$ M. Polymer concentrations: a, [PEI–C_{16}(8)]$=3.95\times10^{-5}$ M; b, [PEI–C_{16}(8)]$=5.92\times10^{-5}$ M; c, [PEI^+–C_{18}(16)]$=2.05\times10^{-5}$ M; d, [PEI^+–C_{18}(16)]$=4.08\times10^{-5}$ M; e, [PEI^+–C_{18}(16)]$=6.16\times10^{-5}$ M.

TABLE 2. SULFUR CONTENT OF PEI CATALYSTS AFTER REACTION WITH DNPS SUBSTRATE

Polymer	Treated with DNPS	Sulfur content /%
PEI–C_{16}(8)	No	—
PEI–C_{16}(8)	Yes	7.06
PEI^+–C_{18}(16)	No	0.00
PEI^+–C_{18}(16)	Yes	0.35

Table 2 summarizes the sulfur content of the polymers before and after the reaction (see Experimental). Apparently, the sulfate group is fixed to the partially alkylated polymer, PEI–C_{16}(8) but not to the quaternized polymer, PEI^+–C_{18}(16). The small sulfur content of the latter polymer is close to the experimental error. The sulfur content of 7% corresponds to the presence of 16 mol % (per monomer unit) of the amidosulfate group according to scheme 1. This value is smaller than the amidosulfate content (30%) estimated from the dinitrophenol release (Eq. 1). Apparently, some of the amidosulfate group was hydrolyzed during the work up of the polymer, as reported by Benkovic and Benkovic in a related system.[17)]

The amino group in the partially alkylated PEI may react with phenyl sulfates *via* sulfate transfer (formation of amidosulfate) or nucleophilic aromatic substitution as shown in Eq. 1. This problem was discussed most recently by Fendler, *et al.*[18)] for the reaction of primary and secondary amines in the micellar system.

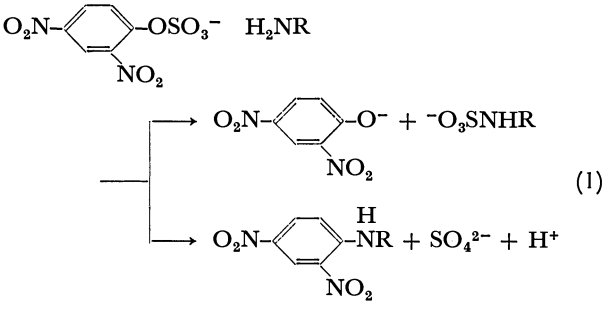

(1)

The occurrence of the nucleophilic aromatic substitution would decrease the sulfur content of the polymer.

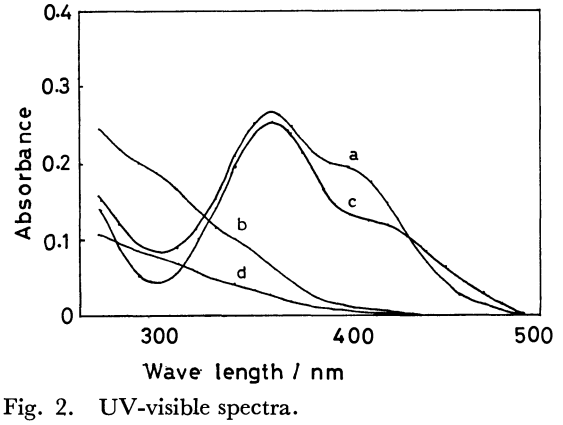

Fig. 2. UV-visible spectra.
a: 1 h after mixing of 1.9×10^{-5} M DNPS and 1.0×10^{-3} unit M PEI–C_{16}(8), pH 8.8, 30 °C. b: The same mixture adjusted to pH 1.6 by hydrochloric acid. c: 1.9×10^{-5} M *N*-methyl-2,4-dinitroaniline, pH 2.1. d: 1.9×10^{-5} M 2,4-dinitrophenol, pH 2.1.

Figure 2 shows a UV-visible spectrum of the reaction mixture after 1 h. (Fig. 2a). Also shown are spectra of the same solution after acidification to pH 1.6 by hydrochloric acid (Fig. 2b) and of *N*-methyl-2,4-dinitroaniline and 2,4-dinitrophenol at pH 2.1 (Fig. 2c and 2d, respectively). The spectrum of the acidified reaction mixture clearly indicates the absence of the dinitroaniline moiety. Therefore, it is concluded that the aromatic substitution path is negligible for alkylated PEI under the present reaction conditions.

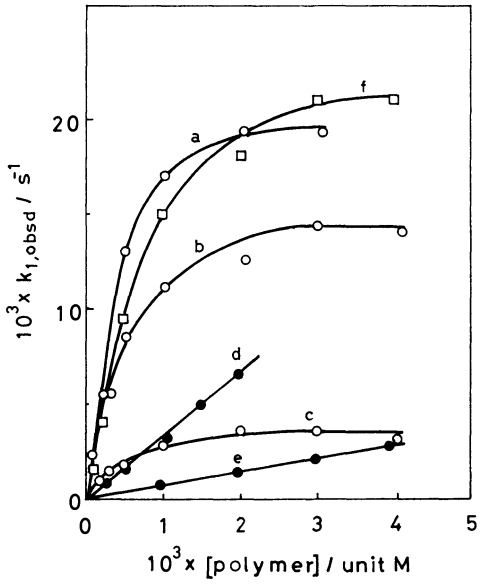

Fig. 3. Dependence of the rate of DNPS cleavage on the concentration of PEI derivatives.
30 °C, 3 v/v % EtOH–H_2O, μ=0.01(KCl), 0.01—0.02 M borate, [DNPS]=2.0×10^{-5} M.
Polymer: PEI$^+$–C_{18}(16)(-○-) a, pH 9.5; b, pH 7.7; c, pH 6.2; PEI–C_{16}(8) (-●-) d, pH 9.0; e, pH 10.1; PEI$^+$–C_{18}(9) (-□-) f, pH 8.5.

Rate Dependence on Polymer Concentration. Figure 3 shows the dependence of $k_{1,obsd}$ of dinitrophenol release on the polymer concentration. In the case of alkylated PEI, $k_{1,obsd}$ increases linearly with the polymer concentration in the range of (1—40)$\times10^{-4}$ M. The results with the quaternized PEI are contrasting in that saturation phenomena are observed. The ease of saturation depends on the pH of the medium.

The saturation kinetics were analyzed according to the Michaelis-Menten kinetics

$$C + S \underset{}{\overset{K_b}{\rightleftharpoons}} CS \xrightarrow{k_{cat}} C + P_1 + P_2 \qquad (2)$$

where C, S, P_1, and P_2 denote polymer, substrate, SO_4^{2-} and 2,4-dinitrophenol, respectively, and CS is the polymer-substrate complex.

Since excess polymer is present ($[C]_0 \gg [S]_0$), the following equations obtain.

$$v = k_{1,obsd}[S]_{total} = k_{cat}[CS] \qquad (3)$$
$$\text{and } [S]_{total} = [S] + [CS]$$

$$K_b \text{ (binding constant)} = \frac{[CS]}{[C][S]} \qquad (4)$$

$$k_{1,obsd} = \frac{k_{cat}\cdot K_b\cdot[C]_0}{K_b[C]_0+1} \qquad (5)$$

Therefore

$$\frac{1}{k_{1,obsd}} = \frac{1}{k_{cat}} + \frac{1}{k_{cat}\cdot K_b\cdot[C]_0} \qquad (6)$$

The data for the PEI$^+$ system in Fig. 3 were plotted using Eq. 6 and linear relations were obtained with satisfactory correlation coefficients. The K_b and k_{cat} thus derived are given in Table 3. As is clear from the data for PEI$^+$, the binding constant K_b decreases with increasing pH but the intra-complex rate constant k_{cat} increases with increasing pH.

Table 3 also contains $k_{2,obsd}$ for PEI–C_{16}(8) determined from the data of Fig. 3. $k_{2,obsd}$ decreases with increasing pH.

pH *Rate Profiles.* Figure 4 illustrates the pH dependence of $k_{1,obsd}$ in the presence of PEI derivatives and a quaternized poly(vinylpyridine). PEI–C_{16}(8) polymer gives a bell-shaped pH dependence with a maximum at *ca.* pH 8. The rate determination was difficult at pH below 7 because of precipitation. A similar pH-rate profile was obtained with an anionic ester substrate NABA (Fig. 5).

On the other hand, when quaternized PEI was used as catalyst, log $k_{1,obsd}$ initially increased linearly with increasing pH and became constant at pH above 8. The log $k_{1,obsd}$ value for NABA (Fig. 5) showed a linear correlation with pH in the pH range studied (pH 7—10). The rate of hydrolysis of NABA by PEI$^+$–C_{18}(16) is 10—100 times slower than that by PEI–C_{16}(8), but the relative effectiveness is reversed in the hydrolysis of DNPS. The reversal suggests that the rate enhancement mechanisms are different between the two systems.

Table 3. Kinetic parameters for the cleavage of DNPS substrate by PEI derivatives[a]

Polymer	pH	Correlation coefficient[b]	$10^3 k_{cat}$ / s^{-1}	K_b / M^{-1}	$k_{cat}\cdot K_b$ or $k_{2,obsd}$ / $M^{-1}\,s^{-1}$
PEI$^+$–C_{18}(16)	9.5	0.991	31.9	761	24.2
	7.7	0.991	22.0	1030	22.7
	6.2	0.997	3.48	2460	8.56
PEI$^+$–C_{18}(9)	8.5	0.997	31.3	745	23.1
PEI–C_{16}(8)	9.0	0.997	—		3.39
	10.1	0.999	—		0.70

a) 30 °C, 0.01—0.02 M borate buffer, μ=0.01(KCl), [DNPS]=2.0×10^{-3} M. b) Correlation coefficients for the plot of Eq. 6 in the case of the Michaelis-Menten kinetics and for the linear relation of Fig. 3, in the case of PEI–C_{16}(8).

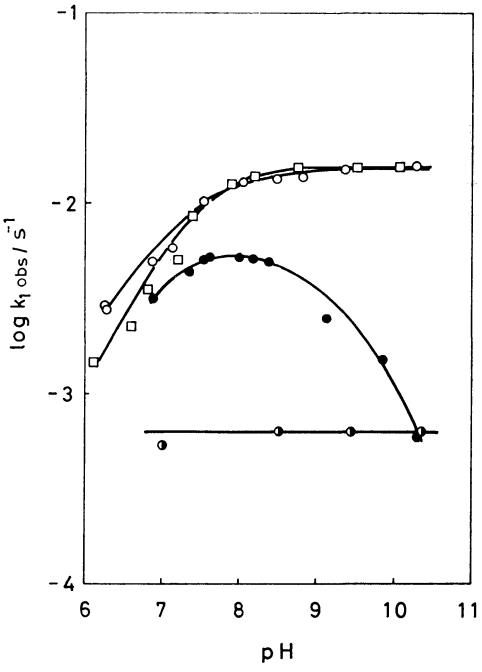

Fig. 4. pH-rate profile for the cleavage of DNPS.
30 °C, 3 v/v % EtOH–H_2O, μ=0.01(KCl), 0.01—0.02 M borate or 0.02 M Tris, [DNPS]=2.2×10^{-5} M, [polymer]=1.0×10^{-3} unit M.
-○-, PEI$^+$–C_{18}(16); -□-, PEI$^+$–C_{18}(9); -●-, PEI–C_{16}(8); -◑-, PVP$^+$–C_{18}(8)–C_2(77).

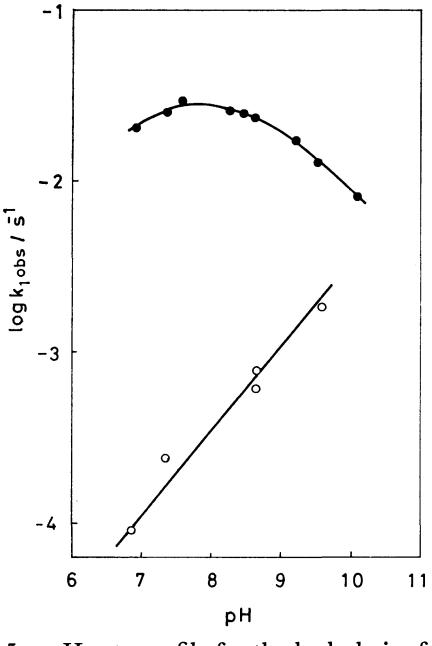

Fig. 5. pH rate profile for the hydrolysis of NABA.
30 °C, 3 v/v % EtOH–H_2O, μ=0.01(KCl), 0.01—0.02 M borate or 0.02 M Tris, [NABA]=2.9×10^{-5} M, [polymer]=1.0×10^{-3} M.
-○-, PEI$^+$–C_{18}(16); -●-, PEI–C_{16}(8).

Discussion

Reaction Scheme. The reaction scheme of alkylated PEI is obviously different from that of quaternized PEI. The most probable mechanisms for these PEI derivatives are shown in Scheme 1. In the case of alkylated PEI, the sulfate group is transfered from DNPS substrate to the nucleophilic amino group. The nucleophilic aromatic substitution was not detected (see above). The amidosulfate group is accumulated with the progress of the reaction, and, as shown in Fig. 1, the remaining amino group becomes less reactive. The zwitterionic adduct, if formed by the nucleophilic attack of tertiary amines toward nitrophenyl sulfates, should be hydrolytically unstable.[19] The accumulation of the amidosulfate group thus indicates the preferential sulfate transfer to the primary and/or secondary amines. This is contrary to the fact that tertiary amines are in general more nucleophilic toward nitrophenyl sulfates than primary and secondary amines.[17,18] The lack of sulfate transfer to the tertiary amino group in PEI may be attributed to severe steric hindrance. The nucleophilic reactivity of sterically-hindered tertiary amines (small molecules) toward sulfate esters is in fact very small.[17] The general-base catalysis by the tertiary amino group, which is sterically less demanding, could not be detected because it is probably less efficient than simple sulfate transfer to the primary and secondary amino groups.

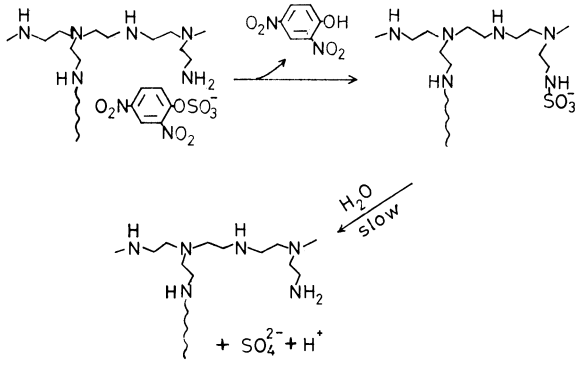

Scheme 1.

The initial rate of sulfate transfer was first order with respect to substrate and polymer. There was found no evidence for substrate binding. However, the bell-shaped pH rate profile of Fig. 4 indicates the cooperative action of substrate attraction by the positively-charged polymer and of the effective neutral nucleophile. Therefore, the imcomplete reaction of the polymer-bound amino group is probably caused by neutralization of the positive charge of alkylated PEI by the negative charge of the amidosulfate group formed. The enhanced catalytic action of partly protonated poly(vinylpyridine) and poly(vinylimidazole) has been known for a long time.[20,21]

On the other hand, the partly quaternized PEI does not contain the primary and secondary amino groups and acts as true catalyst. This is readily seen from the turnover of the polymer catalyst (Fig. 1) and the absence of the intermediate accumulation (Table 2). The catalysis follows the Michaelis-Menten kinetics. The substrate binding is ascribed to both of the hydrophobic and electrostatic attractions between the polymer and substrate. The contribution of the electrostatic interaction is apparent in the fact that K_b decreases with increasing pH.

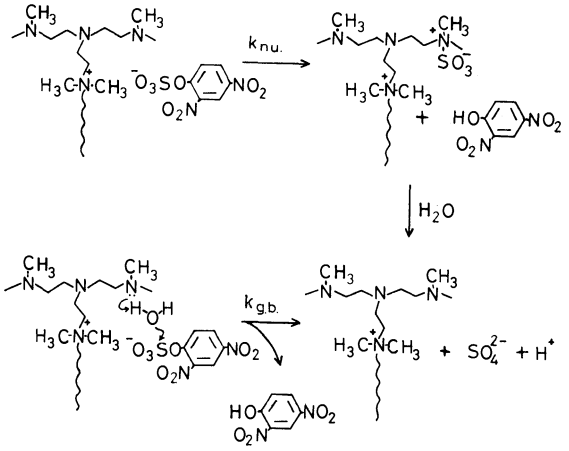

Scheme 2.

The intra-complex catalysis will involve the general-base and/or nucleophilic action of the tertiary amino group (Scheme 2). The turnover could result from the nucleophilic attack of the tertiary amino group which produces the unstable zwitterionic adduct. However, the tertiary amino group in PEI's does not appear to be sufficiently nucleophilic because of steric hindrance, as discussed above. Then, the general-base action may become the preferred pathway. The nucleophilic and general-base mechanisms are usually discriminated by the kinetic solvent isotope effect. However, this technique cannot be applied to the present system, since the side chain aggregation (hence the characteristics of the catalytic domain) would be quite different in H_2O and in D_2O. This effect renders the interpretation of the isotope effect very difficult.

A third possibility is the hydroxide-catalyzed cleavage of the bound substrate. However, this mechanism is not likely, as extensively quaternized PEI, PEI^+–$C_{18}(12)$–$C_1(68)$ is much less effective. The activity of the CTAB micelle and the quaternized poly(vinylpyridine) is also much smaller (Table 1). If the hydroxide-catalyzed hydrolysis is the major catalytic pathway, these systems should be at least equally effective, because of their high densities of the positive charge.

These results are contrasting with those of the NABA hydrolysis. The linear relation of Fig. 5 suggests that the phenyl ester is cleaved by the hydroxide ion which is concentrated in the domain of PEI^+–$C_{18}(16)$. The nucleophilic cleavage of NABA is reflected in a greater efficiency of PEI–$C_{16}(8)$ relative to that of PEI^+–$C_{18}(16)$, as also shown in Fig. 4.

Efficiency of Sulfate Cleavage. Table 4 summarizes the kinetic parameters reported for the cleavage of DNPS in the past. Sulfate esters seem to be less reactive with simple anionic nucleophiles. For instance, either A_1 or general-acid mechanism was suggested to occur for the cyclodextrin-catalyzed hydrolysis.[22] The hydroxamate ion in the cationic micelle is not particularly effective for the sulfate cleavage in spite of its enormous reactivity toward phenyl esters. However, sulfate transfer to the zwitterionic hydroxamate proceeds smoothly in the hydrophobic microenvironment.[10] It appears that basic groups act on sulfate esters particularly effectively (either as nucleophiles or as general bases) when they are fixed at positions close to the quaternary ammonium group in the hydrophobic microenvironment.

A comparison of the rate constants between the piperidine–CTAB system and PEI^+–$C_{18}(16)$ is interesting. Both of the catalytic systems contain the amino group, the dense positive charge and the hydrophobic domain. However, the PEI^+ system is 10^2—10^3 times more efficient in the sulfate transfer than the CTAB system. The difference is even greater when the fact that clean turnover is observed for PEI^+–$C_{18}(16)$ is taken into account. The quaternized PEI is the most effective catalyst and the apparent catalytic rate constant is more than 10^7 times greater than that of the spontaneous hydrolysis.

Finally it is noted that the nitrophenyl sulfates HNPS and PNPS were not cleaved by PEI derivatives under the same condition as used for DNPS hydrolysis: 30 °C, pH 8—10. Therefore $k_{2,obsd}$ should be less than 10^{-3} $M^{-1}\,s^{-1}$. These results are totally different from that reported by Kiefer *et al.*[9] These authors reported the apparent catalytic rate constant of 18 $M^{-1}\,s^{-1}$ which is more than 10^{12} larger than that of imidazole. The discrepancy between the two sets of experiment amount to the order of at least 10^4 in the rate constant. The composition of the imidazole-containing PEI prepared

Table 4. Catalytic efficiencies in the hydrolysis of DNPS

Catalyst or nucleophile	$\frac{k_{cat}\cdot K_b \text{ or } k_2}{M^{-1}\,s^{-1}}$	Remarks	Reference
PEI^+–$C_{18}(16)$	24.2	Saturation kinetics, 30 °C K_b=700—2500 M^{-1}	this study
PEI–$C_{16}(8)$	3.39	30 °C	this study
Piperidine–CTAB	0.098	39.0 °C	23
C_{12}–Im^+–HA[a]–CTAB	11	30 °C	10
β-Cyclodextrin	0.073	Saturation kinetics, 37.3 °C K_b=41.7 M^{-1}	22
Oxime-I[b]	0.67	Saturation kinetics, 40 °C $K_b=6.6\times10^4$ M^{-1}	11
DAP[c]–benzene	0.019	24.5 °C	24
None	1.3×10^{-6}		

a) (1-Dodecylimidazolium)-*N*-benzylacetohydroxamate. b) 10-Hydroxy-11-hydroxyimino[20]paracyclophane. c) Dodecylammonium propionate.

by us, PEI–C_{12}(20)–Im(15) is the same as that of Kiefer *et al.*, except that our polymer contain 20% instead of 10% dodecyl group. In fact, the imidazole-containing PEI showed a rather normal behavior in the cleavage of DNPS (Table 1).

The authors are grateful to Yoshitomi Pharmaceutical Company for kindly performing the sulfur analysis.

References

1) For the articles prior to 1976, see T. Kunitake and Y. Okahata, *Adv. Polym. Sci.*, **20**, 159 (1976).
2) W. J. Spetnagel and I. M. Klotz, *J. Polym. Sci., Polym. Chem. Ed.*, **15**, 621 (1977).
3) W. E. Meyers and G. P. Royer, *J. Am. Chem. Soc.*, **99**, 6141 (1977).
4) Y. Okahata and T. Kunitake, *J. Polym. Sci., Polym. Chem. Ed.*, **16**, 1865 (1978).
5) Y. Okahata and T. Kunitake, *J. Mol. Cat.*, **6**, 163 (1979).
6) J. Suh, I. S. Scarpa, and I. M. Klotz, *J. Am. Chem. Soc.*, **98**, 7060 (1976).
7) W. J. Spetnagel and I. M. Klotz, *J. Am. Chem. Soc.*, **98**, 8199 (1976).
8) I. M. Klotz, G. P. Royer, and A. R. Sloniewsky, *Biochemistry*, **8**, 4752 (1969).
9) H. C. Kiefer, W. I. Congdon, I. S. Scarpa, and I. M. Klotz, *Proc. Nat. Acad. Sci. U.S.A.*, **69**, 2155 (1972).
10) T. Kunitake and T. Sakamoto, *Bull. Chem. Soc. Jpn.*, in press.
11) J. Sunamoto, H. Kondo, H. Okamoto, and K. Taira, *Bioorg. Chem.*, **6**, 951 (1977).
12) E. J. Fendler and J. H. Fendler, *J. Org. Chem.*, **33**, 3852 (1968).
13) D. Robinson, J. N. Smith, B. Spencer, and R. T. Williams, *Biochem. J.*, **51**, 1202 (1952).
14) T. Kunitake, F. Shimada, and C. Aso, *J. Am. Chem. Soc.*, **91**, 2716 (1969).
15) S. Tanamachi, Master Thesis, Faculty of Engineering, Kyushu University, 1978.
16) S. Hirakawa, Master Thesis, Faculty of Engineering, Kyushu University, 1978.
17) S. J. Benkovic and P. A. Benkovic, *J. Am. Chem. Soc.*, **88**, 5504 (1966).
18) E. J. Fendler, R. R. Liechti, and J. H. Fendler, *J. Org. Chem.*, **35**, 1658 (1970).
19) B. E. Fleischfresser and I. Lander, *Aust. J. Chem.*, **15**, 251 (1962).
20) R. L. Letsinger and T. J. Savereide, *J. Am. Chem. Soc.*, **84**, 114, 3122 (1962).
21) C. G. Overberger, T. St. Pierre, N. Vorchheimer, J. Lee, and S. Yaroslavsky, *J. Am. Chem. Soc.*, **87**, 296 (1965).
22) W. I. Congdon and M. L. Bender, *Bioorg. Chem.*, **1**, 424 (1971).
23) J. H. Fendler, E. J. Fendler, and L. W. Smith, *J. Chem. Soc., Perkin Trans. 2*, **1972**, 2097.
24) C. J. O'Connor, E. J. Fendler, and J. H. Fendler, *J. Org. Chem.*, **38**, 3371 (1973).

Reinvestigation of the Mechanism of the Reaction of *N,N*-Dimethylaniline *N*-Oxide with Acetic Anhydride

Shigeru OAE,* Nobuyoshi ASAI, and Ken FUJIMORI

Department of Chemistry, The University of Tsukuba, Sakura-mura, Ibaraki 300-31

(Received February 2, 1979)

The mechanism of the reaction between *N,N*-dimethylaniline *N*-oxide **1** and acetic anhydride to give 2-acetoxy-*N,N*-dimethylaniline **2a** has been reinvestigated by means of our more refined ^{18}O-tracer experiments. Other products of the reaction are 4-acetoxy-*N,N*-dimethylaniline, *N,N*-dimethylaniline **4**, *N*-methylacetanilide, and bis(4-dimethylaminophenyl)methane. The reaction of **1** with ^{18}O-labeled acetic anhydride is considered to involve the initial formation of carbonyl-^{18}O-labeled *N*-acetoxy-*N,N*-dimethylanilinium ion **7a** and the subsequent intramolecular rearrangement of **7a** into **2a** in which the original ^{18}O-label in **7a** is unequally partitioned into two oxygen atoms of **2a** (phenolic oxygen: ethereal oxygen=*ca.* 4: 1). The reaction of **1** with trichloroacetic anhydride gave solely 2-trichloroacetoxy-*N,N*-dimethylaniline but not any **4** which should be formed *via* the free radical mechanism. These observations suggest the occurrence of the two concerted path *via* polarized six-(major) and four-(minor) membered cyclic transition states and rule out the free radical pair mechanism which was proposed ealier by us.[2]

The reaction between *N,N*-dimethylaniline *N*-oxide **1** and acetic anhydride was first investigated in somewhat detail by Huisgen *et al.*[1] Soon after, we also investigated the mechanism by ^{18}O-tracer technique and proposed the radical pair mechanism (**A**) for the formation of 2-acetoxy-*N,N*-dimethylaniline **2a** based on the observation that both carbonyl and ethereal oxygen atom in **2a** was nearly completely equilibrated in the course of the rearrangement from **7a** to **2a**.[2]

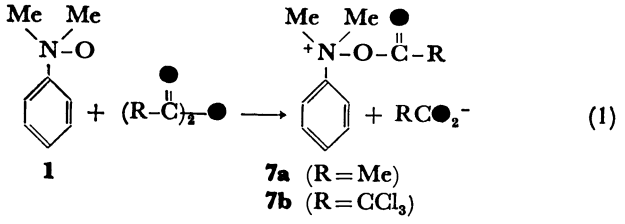

1 **7a** (R=Me) **7b** (R=CCl_3) (1)

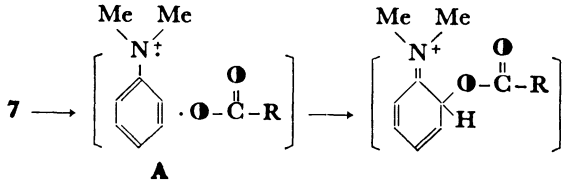

A

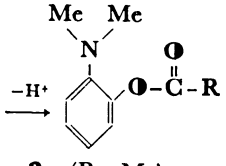

2a (R=Me) **2b** (R=CCl_3) (2)

Later, Iwamura *et al.* observed a CIDNP signal only for *N,N*-dimethylaniline **4** but not for **2a** and *N*-acetyl-*N*-methylaniline **5a**, and the radical mechanism **A** has become quite dubious.[3] In our extensive investigations of the mechanisms of the rearrangement reactions of tertiary amine *N*-oxides with acylating agents by means of ^{18}O-tracer technique, we have seldom encountered the case in which the reaction proceeded solely *via* radical mechanistic path.[4] Thus, the reaction between **1** and acetic anhydride has been reinvestigated by aid of our more sophisticated ^{18}O-tracer technique.

Results and Discussion

The reaction between *N,N*-dimethylaniline *N*-oxide **1** and acetic anhydride was found to give products **2**—**4**, while the distribution of products clearly depends on the solvent as seen in Table 1.

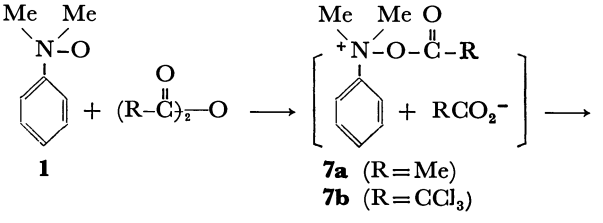

1 **7a** (R=Me) **7b** (R=CCl_3)

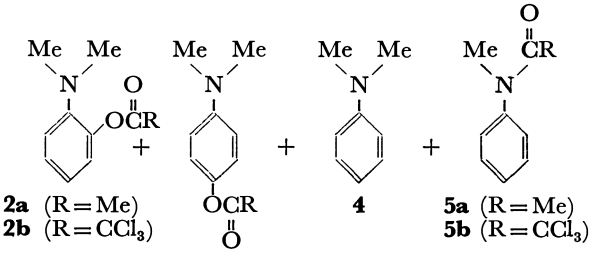

2a (R=Me) **2b** (R=CCl_3) **3a** (R=Me) **4** **5a** (R=Me) **5b** (R=CCl_3)

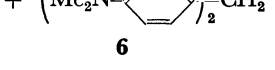

6 (3)

TABLE 1. PRODUCTS OF THE REACTION OF *N,N*-DIMETHYLANILINE *N*-OXIDE **1** WITH ACETIC ANHYDRIDE OR TRICHLOROACETIC ANHYDRIDE

Acid anhydride	Solvent	Yield (%)				
		2	**3**	**4**	**5**	**6**
Acetic anhydride (R=Me)	H_2O[a]	84	—	3	0	0
	50% MeCN–H_2O	66	1	11	2	—
	MeCN	6	0	0.4	48	3
Trichloroacetic anhydride (R=CCl_3)	MeCN	90	0	0	0	0

a) Ref. 1.

In such an aprotic solvent as acetonitrile, demethylation by Polonovski reaction giving **5a** was predominant, however, the rearrangement to afford **2a** was the major course of the reaction in protic media. The first step of the reaction has been believed to be the acetylation of **1** to form *N*-acetoxy-*N*,*N*-dimethylanilinium ion **7** which is then partitioned to go through the different paths (Eq. 1). In acetonitrile, the acetate anion is considered to be a base strong enough to abstract proton from the *N*-methyl group of **7a** to promote the Polonovski reaction eventually to give **5a**; whereas in protic media, the basicity of acetate anion should be markedly reduced by the solvation, and hence the alternative rearrangement reaction becomes predominant.[1,2]

Upon the usual treatment of the *N*-oxide with ^{18}O-labeled acetic anhydride in protic media, **2a** was isolated from the mixture, purified and allowed to react with phenylhydrazine to give crystalline products, *i.e.* 2-hydroxy-*N*,*N*-dimethylaniline and 1-acetoxy-2-phenylhydrazine, which were carefully purified and then subjected to the routine ^{18}O-analysis (Table 2).[5] Meanwhile all the conceivable intermediates and/or transition states of this rearrangement may be illustrated from **A** to **K**.

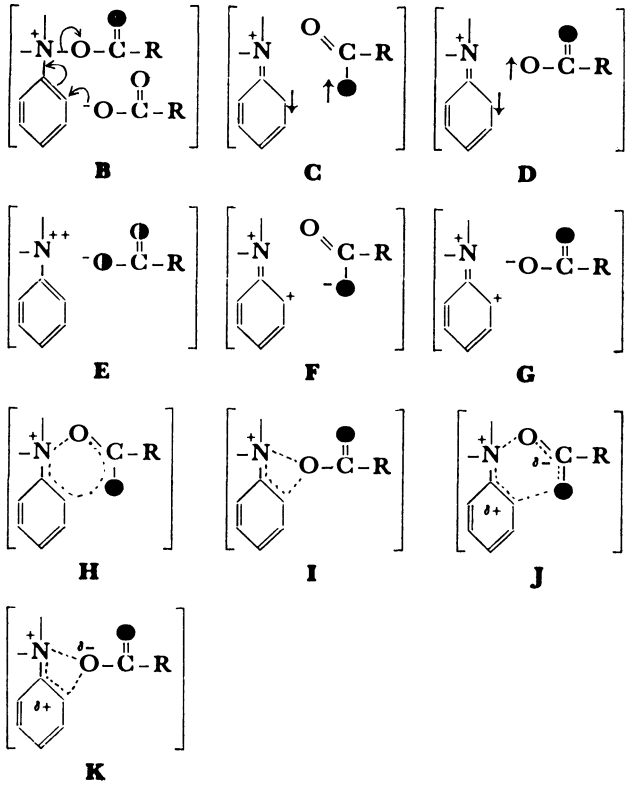

Table 2. ^{18}O-Tracer result of the reaction between **1** and $(MeC)_2{}^{18}O$

Compound	^{18}O-Content of the compd (excess atom %)[a]	
	in 50% MeCN–H_2O	in H_2O
1-Acetyl-2-phenylhydrazine[b]	0.854	0.854
2-Hydroxy-*N*,*N*-dimethylaniline	0.668	0.718
1-Acetyl-2-phenylhydrazine	0.178	0.133

a) ± 0.005 atom %. b) Derived from the starting acetic anhydride.

When the calculated ^{18}O-distributions in **2a** resulted from all these possible mechanistic routes are compared with the observed values in Table 3, the mechanism involving the attack of external acetate anion *via* **B** is obviously ruled out, in keeping with our original argument suggested earlier.[2] Although the observed ^{18}O-data cannot be explained by the radical mechanism **A** (Eq. 2), the possibility of homolytic cleavage of N–O bond of **7a** cannot be rejected completely. Namely, if the radical pair would be a very short lived singlet radical pair such as either **C** or **D**, as suggested by Iwamura *et al.*,[3] the ^{18}O-label may not be completely scrambled in **2a**, since the two oxygens of the acetoxyl radical formed incipiently should be sterically unequal. The formation of **4** which has been confirmed as the radical reaction product by CIDNP study[3] must be produced *via* homolytic cleavage of **7a**. Indeed the reaction of **1** with acetic anhydride initiates the polymerization of styrene.[1,6] These observations seem to imply the involvement of these singlet radical pairs **C** and **D** at least partially.

In order to examine the possible involvement of such a homolytic cleavage, trichloroacetic anhydride was allowed to react with **1**. If the intervention of radical pairs **C** or **D** or both would be responsible for the formation of **2**, the yield of radical reaction product, **4**, should markedly increase in the reaction of **1** with trichloroacetic anhydride (Eq. 4),[7] since the decarboxylation of trichloroacetoxyl radical is well known to be very fast.[8] However, since the reaction of **1** with trichloroacetic anhydride gave only **2b**, but neither any **4** nor hexachloroethane, all the free radical mechanisms **A**, **C**, and **D** cannot be responsible for the major path of the rearrangement.[9]

Thus the ionic mechanisms **E**—**K** still remain. Among these, however, the ion pair mechanisms seem to be highly unlikely, since the ionic cleavage of the N–O bond of **7a** leads to the formation of a highly

Table 3. Theoretical and experimental ^{18}O-distribution in **2a** obtained from **1** and ^{18}O-labeled acetic anhydride[a]

Oxygen	Experimental		Theoretical			
	in 50% MeCN–H_2O	in H_2O	**B**	**A**,**E**	**C**,**F**,**H**,**J**	**D**,**G**,**I**,**K**
Phenolic	79%	84%	100%	50%	100%	0%
Carbonyl	21	16	100	50	0	100

a) Original ^{18}O-content of carbonyl oxygen of **7a** is defined as 100%.

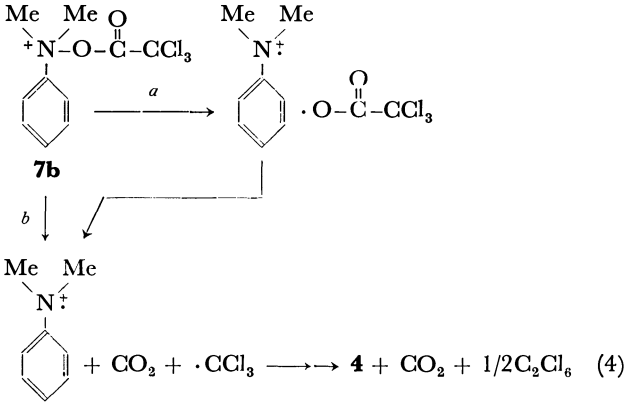

7b

$$+ CO_2 + \cdot CCl_3 \longrightarrow\!\!\rightarrow \mathbf{4} + CO_2 + 1/2C_2Cl_6 \quad (4)$$

energetic double cation species of **4**. Indeed, the ion pair mechanism **E** cannot be accepted since the ^{18}O-distribution in **2a** is uneven and the oxygen scrambling in **2a** decreases with the increase of solvating power of the medium. Only in the case if the ion pair is a very short lived intimate one as illustrated by **F** or **G**, the two oxygen atoms of the acetate anion might not be sterically equal and could give **2a** in which ^{18}O-label is not completely equilibrated. The mechanisms *via* **F** and **G** may also be eliminated in view of the highly unstable *N,N*-dimethylaniline double cation. Meanwhile product ratio **2a** *vs.* the radical product **4** from **7a** was found to increase with the increase of the polar nature of the solvent.[10] Whereas when acetic anhydride was changed to trichloroacetic anhydride, no free radical products were obtained despite the facile homolytic bond cleavage of **7a** by concerted two bond fission to give cation radical of **4**, CO_2, and trichloromethyl radical.[7] All these observations do not seem to be in accordance with the mechanism involving the sigmatropic shift such as **H** or **I**, however, can be best explained in terms of the concurrent heterolytic cleavage of N–O bond of **7a** and a new C–O bond forming *via* such transition states as illustrated by **J** (major path) and **K** (minor path) which are represented as a hybrid of canonical forms, **C**, **F**, and **H** for **J** and that of canonical forms, **D**, **G**, and **I** for **K**. The contribution of each of these canonical forms is considered to depend on the nature of solvent and R group of the acid anhydride used. Similar polarized cyclic transition state has been suggested for the rearrangement of *O*-benzoyl-*N*-(*p*-tolylsulfonyl)-*N*-arylhydroxylamine **8** to 2′-benzoyloxy-*p*-toluenesulfonanilide **9** as shown in Eq. 5.[11]

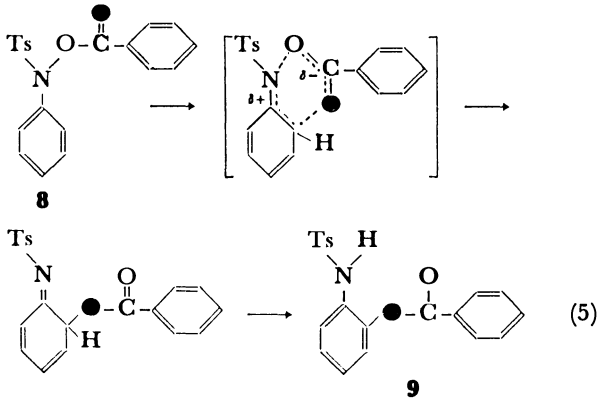

8

9

(5)

Experimental

N,N-Dimethylaniline *N*-oxide **1** was prepared by oxidation of *N,N*-dimethylaniline **4** with hydrogen peroxide in methanol according to the method of Huisgen, Bayerlein, and Hegkamp.[1]

Oxygen-18-labeled acetic anhydride was prepared by the method reported by Oae, Kitao, and Kitaoka;[12] bp 137.5—139 °C. By treatment with phenylhydrazine, a small amount of the acetic anhydride was converted to crystalline 1-phenyl-2-acetylhydrazine which was recrystallized from benzene; mp 129—129.5 °C, and subjected to the ^{18}O-analysis (0.854 excess atom %).

*Reaction between **1** and Acetic Anhydride in 50%(v/v) CH_3CN–H_2O.* Acetic anhydride (1.3 g, 13 mmol) was added dropwise into a solution of **1** (1.0 g, 7.3 mmol) in 14 ml of 50%(v/v) CH_3CN–H_2O with stirring at 0 °C under nitrogen atmosphere. The mixture was stirred for 2 h at 0 °C, then the reaction mixture was treated with an aqueous solution of sodium carbonate under cooling in an ice bath, then extracted with ether and dried. To the solution, 725 mg of 2,4-dichloronitrobenzene was added as the internal standard for the analysis by a GLPC equipped with 2 m stainless steel column packed with 5% PEG-20M on 80 mesh celite. The chromatogram was recorded on Shimadzu GC-6A GLPC instrument.

*Reaction between **1** and Acetic Anhydride in CH_3CN.* The reaction and product analysis were carried out in a same manner described for the reaction in 50%(v/v) CH_3CN–H_2O.

*Reaction between **1** and Trichloroacetic Anhydride.* *N,N*-Dimethylaniline *N*-oxide **1** (100 mg, 0.73 mmol) in 3 ml of dry CH_3CN was treated dropwise with trichloroacetic anhydride (430 mg, 1.4 mmol) at 0 °C under nitrogen atmosphere. The reaction mixture was treated with aqueous solution of sodium carbonate and extracted with ether and dried over sodium sulfate. Into this solution, tetralin (102 mg) was added as the internal standard for GLPC analysis through a stainless steel column packed with 5% SE-30 on 80 mesh celite. The gas chromatogram of the sample solution was recorded on Hitachi 163 GLPC instrument, and only one peak of 2-hydroxy-*N,N*-dimethylaniline was observed.

*Oxygen-18-tracer Experiment of the Reaction between **1** and Acetic Anhydride.* *In 50%(v/v) CH_3CN–H_2O*: The reaction between 1.0 g of **1** and 1.36 g of ^{18}O-labeled acetic anhydride was carried out in a similar manner which was applied for the product analysis. 2-Acetoxy-*N,N*-dimethylaniline **2a** was separated by preparative TLC (Kieselgel G_{254}) at 5 °C with 5% acetone–hexane as an eluent (isolated yield 0.567 g). The product **2a** was treated with 0.377 g of phenylhydrazine and the mixture was allowed to stand overnight at room temperature. A solid mass, separated, was collected and washed with benzene, gave 0.33 g of 1-phenyl-2-acetylhydrazine, which was recrystallized from benzene and subjected to the ^{18}O-analysis; mp 129—129.5 °C. The filtrate was washed with water to remove unreacted phenylhydrazine, dried and solvent was removed. Preparative TLC (Kieselgel GF_{254}) of the residue with 5% acetone–dichloromethane as an eluent gave 0.406 g of 2-hydroxy-*N,N*-dimethylaniline which was distilled under reduced pressure and subjected to the ^{18}O-analysis, mp 44—44.5 °C.

In H_2O: The reaction was carried out in a same manner described above.

Control Experiment on Dilution of ^{18}O-Label in Acetic Anhydride during the Reaction. A solution of 500 mg (4.9 mmol) of ^{18}O-labeled acetic anhydride and 400 mg (0.33 mmol) of **1** in 1 ml of 50%(v/v) CH_3CN–H_2O was stirred for 2 h at 0 °C

under nitrogen atmosphere. Into this solution 520 mg of *N*-methylaniline was added and the solution was stirred for addtional 1 h at room temperature. After the solvent was removed, the residue was washed with benzene to obtain 240 mg of *N*-methylacetanilide which was recrystallized from benzene; mp 102—102.5 °C. Since ^{18}O-content of the *N*-methylacetanilide (0.855 excess atom %) was found to be same to that of 1-acetyl-2-phenylhydrazine (0.854 excess atom %) which was derived from starting ^{18}O-labeled acetic anhydride (Table 2), there is no ^{18}O-dilution of acetic anhydride during the reaction with **1** in the presence of H_2O.

Determination of Oxygen-18 Content. ^{18}O-analysis was carried out by the method developed by Rittenberg-Ponticorbo.[5] Twenty mg of sample was pyrolyzed with 300 mg of purified $HgCl_2$ and $Hg(CN)_2$ respectively, in an evacuated, sealed silica tube at 550 °C for 12 h. Then the tube was broken in a vacuum line and CO_2 formed was purified by distillation and the mass peaks *m/e* 44 and 46 which correspond to $C^{16}O_2$ and $C^{16}O^{18}O$, respectively, were recorded on Hitachi RMU-6MG mass spectrometer. An error of ^{18}O-content was within ± 0.005 atom %. $HgCl_2$ was purified by sublimation under reduced pressure and $Hg(CN)_2$ was purified by recrystallization from absolute ethanol before use.

References

1) R. Huisgen, F. Bayerlein, and W. Hegkamp, *Chem. Ber.*, **92**, 3223 (1959).

2) S. Oae, T. Kitao, and Y. Kitaoka, *J. Am. Chem. Soc.*, **84**, 3366 (1962).

3) H. Iwamura, M. Iwamura, T. Nishida, and I. Miura, *Bull. Chem. Soc. Jpn.*, **43**, 1914 (1970).

4) S. Oae and K. Ogino, *Heterocycles*, **6**, 583 (1977).

5) D. Rittenberg and L. Ponticorvo, *J. Appl. Rad. Isotopes*, **1**, 208 (1956); N. Asai, Ph D. Thesis, The University of Tsukuba, 1978.

6) V. Boekelheide and D. L. Harrington, *Chem. Ind. (London)*, **1955**, 1423.

7) T. Koenig, *J. Am. Chem. Soc.*, **88**, 4045 (1966). Based on the fact that the homolytic decomposition of both *t*-butyl trichloroperacetate and trichloroacetyl peroxide proceeds *via* concerted multi bond cleavage to form trichloromethyl radical, CO_2 and *t*-butoxyl radical, and trichlormethyl radical and CO_2, respectively,[8a,b] the homolytic cleavage of **7b** is expected to be a concerted process as denoted in Eq. 4b.

8) a) P. D. Bartlett and R. R. Hiatt, *J. Am. Chem. Soc.*, **80**, 1398 (1958); b) J. E. Leffler and H. H. Gibson, Jr., *ibid.*, **90**, 4117 (1968).

9) Since the rearrangement product, 2-trichloroacetoxy-*N,N*-dimethylaniline **2b** is very sensitive to moisture and is hydrolyzed very easily to give 2-hydroxy-*N,N*-dimethylaniline and trichloroacetic acid during the treatment of the reaction mixture, ^{18}O-tracer study for the reaction between **1** and trichloroacetic anhydride could not be made.

10) Table 1 of this work and Ref. 1.

11) S. Oae and T. Sakurai, *Tetrahedron*, **32**, 2289 (1976).

12) S. Oae, T. Kitao, and Y. Kitaoka, *J. Am. Chem. Soc.*, **84**, 3359 (1962).

The Nucleophilic Reaction of Electron-deficient Pyridone Derivatives. I. The Ring Transformation of 1-Substituted 3,5-Dinitro-2-pyridones with Sodio β-Keto Esters

Eizo MATSUMURA, Masahiro ARIGA,* and Yasuo TOHDA
Department of Chemistry, Osaka Kyoiku University, Tennoji-ku, Osaka 543

(Received February 9, 1979)

A novel ring transformation is found in a series of reactions of 1-substituted 3,5-dinitro-2-pyridones, electron-deficient substrates, with monosodium salts of β-keto esters. A variety of 1-substituted 3,5-dinitro-2-pyridones are treated with diethyl sodio-3-oxopentanedioate and ethyl sodioacetoacetate to give, in addition to *N*-substituted nitroacetamides (**3**), 2,6-bis(ethoxycarbonyl)-4-nitrophenol (**2**), and 2-ethoxycarbonyl-4-nitrophenol (**4**) respectively. The bicyclic intermediates, 2-azabicyclo[3.3.1]nona-3,7-dienes, can be isolated on the reaction of 3,5-dinitro-1-methyl-2-pyridone at room temperature. The phenol derivatives (**2** and **4**) may consist of the reagent and a C_4–C_5–C_6 moiety of the parent pyridone, while *N*-substituted nitroacetamides, **3**, may result from the other fragment, N–C_2–C_3, of the pyridone. A probable course of the reaction, involving the step-by-step nucleophilic attack of the ambident nucleophiles, sodio β-keto esters, at the ambident electrophilic centers of 2-pyridones to form bicyclic intermediate, is proposed.

In our earlier studies[1] of the nucleophilic substitution reactions of pyridine derivatives, we showed that the reaction of 1-methyl-2-(pyridiniomethyl)pyridinium salt or its homologues with potassium hydroxide solution at a low temperature gave 1-methyl-2-pyridone or its homologues respectively.

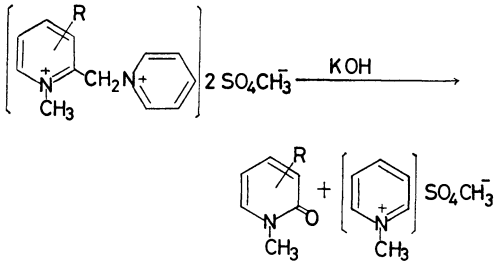

Fig. 1.

In these reactions, the bis(quaternary salts) were converted, without the heterolysis of the N–C_2 bond, to 1-methyl-2-pyridone or its homologues by the easy loss of the pyridiniomethyl group. This reaction has since offered a convenient route for the preparation of 1-methyl-2-pyridone homologues.

On the other hand, the ease of the heterolysis at the N–C_2 bond of the well-known Zincke reaction[2] of 2,4-dinitrophenylpyridinium chloride under similar basic conditions may be ascribed to the presence of a strongly electron-attractive 2,4-dinitrophenyl group on the nitrogen atom.

We have also shown[3] that the reaction of 3-bromo-4-nitropyridine *N*-oxide with one of the monosodium salts of β-keto esters (*i.e.*, ethyl sodioacetoacetate) gave the β-substituted product (*i.e.*, 3-[acetyl(ethoxycarbonyl)-methyl]-4-nitropyridine *N*-oxide), from which 2,3-disubstituted furo[3,2-*c*]pyridine *N*-oxide (*i.e.*, 3-ethoxycarbonyl-2-methylfuro[3,2-*c*]pyridine *N*-oxide) was obtained when it was warmed for a short time in an ethanol solution of sodium ethoxide.

This reaction is an example of a reaction which proceeds step-by-step between an ambident nucleophile and an ambident electrophile.

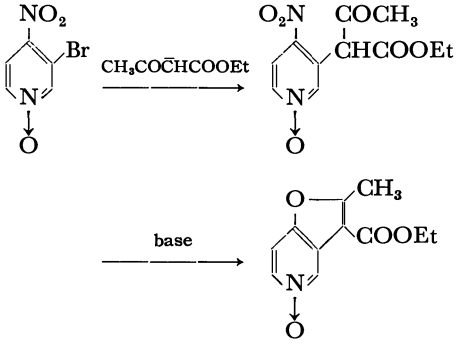

Fig. 2.

The above interesting results prompted us to expand the related reactions in this series to the nucleophilic reaction of 1,3,5-trisubstituted 2-pyridones with monosodium salts of β-keto esters and β-diketones.

Results and Discussion

The reaction of 3,5-dinitro-1-methyl-2-pyridone (**1a**) with 1.5 equimolar amounts of diethyl sodio-3-oxopentanedioate (Na·DOPD) at 50 °C in pyridine gave, after neutralization, 2,6-bis(ethoxycarbonyl)-4-nitrophenol (**2**) and *N*-methyl-α-nitroacetamide (**3a**). The same reaction of **1a** with 3 equimolar amounts of ethyl sodioacetoacetate (Na·EAA) at 70 °C gave 2-ethoxycarbonyl-4-nitrophenol (**4**) and **3a** in good yields. These

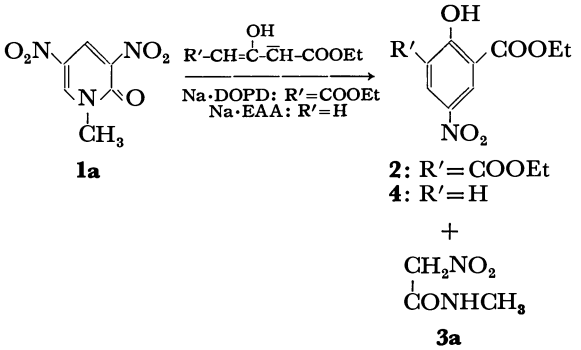

1a

2: R′=COOEt
4: R′=H
+
3a

Fig. 3.

Table 1. Reaction of 3,5-dinitro-1-methyl-2-pyridone (**1a**) with sodium salts of β-keto esters and β-diketones

Substrate	Reagent	Reaction conditions: Solvent	Mole ratio	Temp °C	Time h	Product (Yield/%)	
1a	Na·DOPD	Pyridine	1.5	50	5	**2** (90.4)	**3a** (28.3)
1a	Na·EAA	Pyridine	3.0	70	5	**4** (61.0)	**3a** (16.9)
1a	Na·AA	DMF	3.0	70	5	**5** (53.0)	**3a** (11.5)
1a	Na·EAP	Pyridine	3.0	110	5	**6** (42.0)	**3a** (8.3)

products were identified by their IR, NMR, and results of elemental analysis, and by a mixed-melting-point determination with authentic samples.

The reaction of **1a** with monosodium salts of β-diketones were also carried out. The reaction of **1a** with sodioacetylacetone (Na·AA) gave 2-acetyl-4-nitrophenol (**5**) and **3a**, and a similar reaction of **1a**, at a higher temperature (110 °C), with ethyl sodioacetopyruvate (Na·EAP) gave 2-ethoxyoxalyl-4-nitrophenol (**6**) and **3a**.

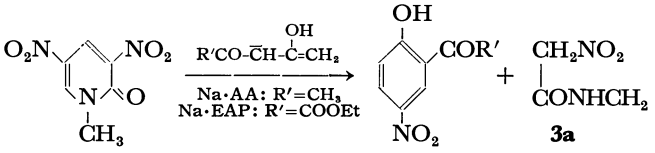

1a **3a**

5: R'=CH_3
6: R'=COOEt

Fig. 4.

It may be considered to be characteristic of these reactions to form a phenol derivative from the active methylene compound used as the ambident nucleophile and the pyridone moiety containing C_4, C_5, and C_6. The formation of the residual moiety of the pyridone would lead to *N*-methyl-α-nitroacetamide (**3a**).

In order to prove the generality of these reactions, various kinds of 1-substituted 3,5-dinitro-2-pyridones, such as 1-(*m*-nitrobenzyl)- (**1b**), 1-(2-pyridylmethyl)- (**1c**), 1-unsubstituted- (**1d**), 1-(2,4-dinitrophenyl)- (**1e**), 1-(2-pyridyl)- (**1f**), 1-(4-methyl-2-pyridyl)- (**1g**), 1-(5-methyl-2-pyridyl)- (**1h**), 1-(6-methyl-2-pyridyl)- (**1i**), 1-hydroxy- (**1j**), 1-methoxy- (**1k**), and 1-(*p*-nitrobenzyloxy)- (**1l**), were prepared and then reacted with either Na·DOPD or Na·EAA.

The reaction of each 1-substituted 3,5-dinitro-2-pyridone with Na·DOPD gave 2,6-bis(ethoxycarbonyl)-4-nitrophenol (**2**) and the corresponding *N*-substituted nitroacetamide (**3**). With each 1-substituted 3,5-dinitro-2-pyridone and Na·EAA, on the other hand, 2-ethoxycarbonyl-4-nitrophenol (**4**) and the corresponding *N*-substituted nitroacetamide (**3**) were obtained.

The results of the above reactions and the spectral data (NMR and IR) of *N*-substituted nitroacetamides are shown in Tables 2 and 3 respectively.

In the case of the reaction of 3,5-dinitro-1-(2-pyridyl)-2-pyridone (**1f**) with Na·DOPD or Na·EAA, the same yellow compound, **7f**, was obtained, together with **3f** and either **2** or **4** respectively. The empirical formula,

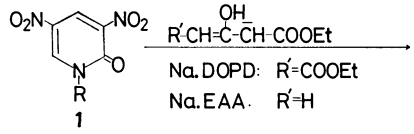

1

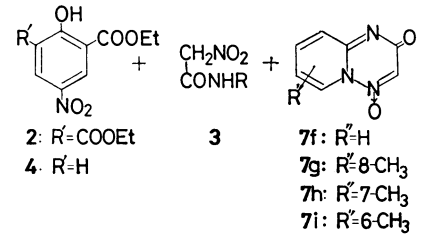

2: R'=COOEt
4: R'=H

3

7f: R''=H
7g: R''=8-CH_3
7h: R''=7-CH_3
7i: R''=6-CH_3

Fig. 5.

$C_7H_5N_3O_2$, of this yellow compound corresponded to the loss of one molecule of water from *N*-(2-pyridyl)-α-nitroacetamide (**3f**). The IR spectra of **7f** showed the presence of an *N*-oxide group (1205 cm^{-1}), a carbonyl group (1730 cm^{-1}), and a C=N double bond (1650 cm^{-1}), while the absorption bands due to the nitro group and the N–H bond which were confirmed in that of **3f** were absent. During the melting-point measurement, **3f** was converted to **7f** by heating it to 120 °C in a capillary. Compound **7f** was also prepared from ethyl nitroacetate and 2-aminopyridine by only heating. The catalytic reduction of **7f** on Raney Nickel in ethanol at 110 °C under 50 atm gave ethyl 2-pyridylcarbamate. From the above observations, 2-oxo-2*H*-pyrido[1,2-*b*]-[1,2,4]triazine 4-oxide was assigned to **7f**, though the C_3 proton was not observed in the NMR spectra of **7f** in trifluoroacetic acid or trifluoroacetic acid-d_1. With **1g**, **1h**, and **1i** all of which correspond to the homologues of **1f**, and Na·DOPD or Na·EAA, **7g**, **7h**, and **7i** were obtained respectively, but on the reaction of **1g**, **7g** was obtained exclusively without any isolation of *N*-(4-methyl-2-pyridyl)-α-nitroacetamide (**3g**). The ease of the cyclization of *N*-(2-pyridyl)-α-nitroacetamide to **7f** in an aqueous solution is likely to be due to the increasing acidic α-amino group which is bonded to the electron-attractive nitroacetyl and 2-pyridyl group, accordingly, the conversion of the resultant *N*-anion with a 1,6-dipole structure to the **7f** compound is favorably oriented for an intramolecular nucleophilic attack on the ω-nitronium ion with a loss of water. Under the same conditions, the fused-ring products (**7h** and **7i**) were also obtained from **3h** and **3i** respectively.

Further information was obtained under milder conditions. From the reaction of **1a** with Na·DOPD

Table 2. Reactions of **1** (**b**—**l**) with sodio β-keto esters

Substrate	Reaction with Na·DOPD at 50 °C Product (Yield/%)			Reaction with Na·EAA at 70 °C Product (Yield/%)		
1b R= 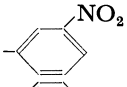	**2** (95.5)	**3b** (77.9)		**4** (60.8)	**3b** (53.4)	
1c R= 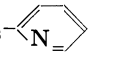	**2** (95.0)	**3c** (42.0)		**4** (51.2)	**3c** (23.2)	
1d R=–H	**2** (42.5)			**4** (21.9)		
1e R= 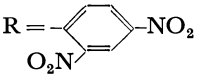	**2** (57.0)	**3e** (43.0)		**4** (50.6)	**3e** (38.7)	
1f R= 	**2** (92.8)	**3f** (84.2)	**7f** (3.8)	**4** (63.5)	**3f** (52.0)	**7f** (3.5)
1g R= 	**2** (77.2)		**7g** (63.2)	**4** (52.0)		**7g** (43.2)
1h R= 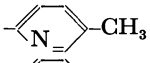	**2** (78.5)	**3h** (59.7)	**7h** (29.9)	**4** (13.4)	**3h** (18.8)	**7h** (1.4)
1i R= 	**2** (82.4)	**3i** (39.5)	**7i** (38.6)	**4** (63.4)	**3i** (17.8)	**7i** (41.5)
1j R=–OH	**2** (96.6)			**4** (83.4)		
1k R=–OCH_3	**2** (98.1)	**3k** (11.1)		**4** (86.5)	**3k** (10.5)	
1l R= 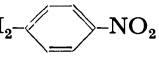	**2** (98.0)	**3l** (38.5)		**4** (88.1)	**3l** (35.2)	

Table 3. *N*-Substituted nitroacetamides

Nitroacetamide O_2NCH_2-CONHR	IR			NMR		
	N–H cm^{-1}	C=O cm^{-1}	NO_2 cm^{-1}	CH_2 δ	NH δ	Solvent
3a	3300	1670	1570, 1340	5.16	7.00	acetone-d_6
3b	3300	1660	1525, 1355	5.38	9.10	acetone-d_6
3c	3170	1690	1565, 1340	5.40	8.20	acetone-d_6
3e	3300	1690	1540, 1340	5.62	11.10	DMSO-d_6
3f	3300	1690	1540, 1340	5.62	9.85	acetone-d_6
3h	3290	1680	1545, 1340	5.52	10.98	acetone-d_6
3i	3300	1690	1530, 1350	5.62	9.95	acetone-d_6
3k	3225	1690	1550, 1330	5.15	11.70	acetone-d_6
3l	3125	1675	1575, 1345	5.18	11.80	acetone-d_6

at room temperature, a colorless crystalline product (**8a**) (mp 155.0—156.0 °C) was obtained in addition to **2** and **3a**. The empirical formula of **8a**, $C_{12}H_{15}N_3O_8$, suggests that it is an adduct of **1a** and diethyl 3-oxopentanedioate. The IR spectra of **8a** showed the presence of a nitro group (1540, 1350 cm^{-1}) and a carbonyl group (1730 cm^{-1}). The NMR spectra of **8a** showed the following: aromatic proton signals of the parent pyridone and the singlet methyl and methylene signals of the reagent disapeared, and the four aliphatic proton signals coupled with each other were observed in the range between 3.9 and 5.4 ppm. Two singlets due to the enol 7-hydroxyl group at 12.64 ppm and due to the strongly hydrogen-bonded 3-hydroxyl group at 18.82 ppm were also observed. On the treatment with only ethanolic sodium ethoxide at 70 °C or with Na·DOPD in pyridine, **8a** was easily converted to **2** and **3a**. On the basis of the above physical and chemical data, 6,8-bis(ethoxycarbonyl)-3,7-dihydroxy-2-methyl-4,9-dinitro-2-azabicyclo[3.3.1]nona-3,7-diene was assigned to **8a**. Similarly, with **1a** and Na·EAA 6-ethoxycarbonyl-3,7-dihydroxy-2-methyl-4,9-dinitro-2-azabicyclo[3.3.1]nona-3,7-diene (**9a**) was obtained.

Meta-bridging bicyclic structures anoalogous to **8a** and **9a** have been described by Strauss *et al.*[4] and Momose *et al.*[5] in connection with the reaction of electron-deficient aromatics (*e.g.*, 1,3,5-trinitrobenzene or 3,5-dinitrobenzene derivatives) with active methylene compounds under basic conditions, but these addition compounds were sodium derivatives.

From the above results, the formation of the intermediate, **8a** or **9a**, may be ascribed to the reaction of an ambident electrophilic end at the 4 and 6-positions of 1,3,5-trisubstituted 2-pyridones with the ambident nucleophilic end of the enolate ion which is obtained from the sodio β-keto esters.

The treatment of ethyl acetoacetate and diethyl 3-oxopentanedioate with 1 mol of sodium ethoxide in ethanol easily gives ethyl sodioacetoacetate and diethyl 3-oxopentanedioate respectively. These ambident

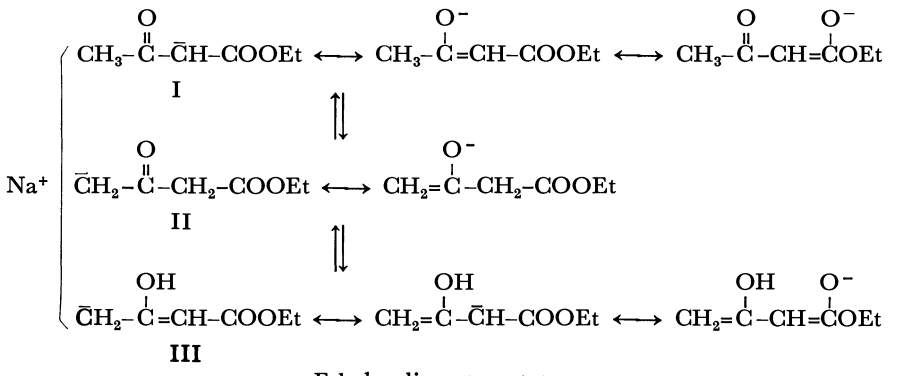

Ethyl sodioacetoacetate

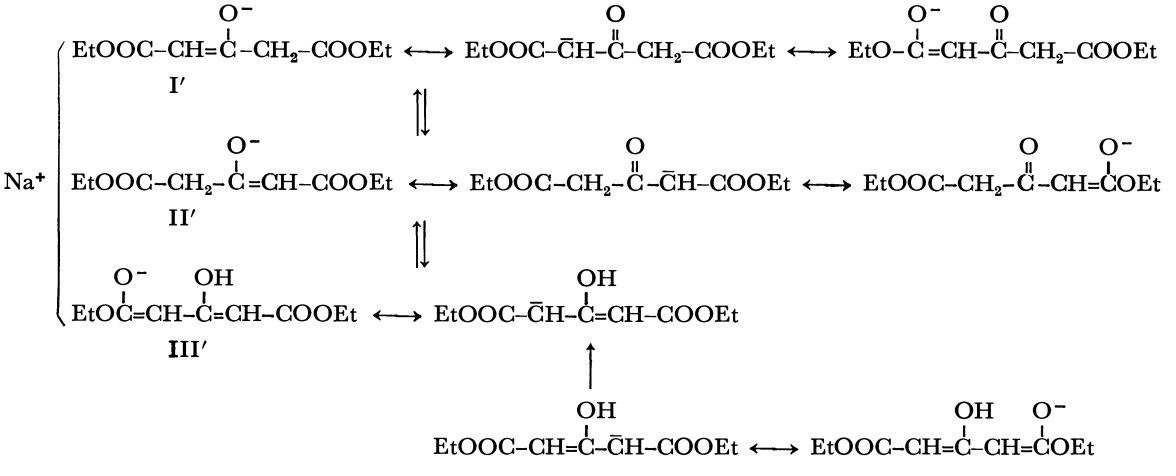

Diethyl sodio-3-oxopentanedioate

anions can be accounted for as shown above:

In the respective ambident tautomers, the enol types of III and III′ are softer uncleophiles than the enolate types of the others. For example, in the case of III with 3,5-dinitro-1-methyl-2-pyridone, the softer C_α-anion would be favorably attacked at the softer C_6-atom of the pyridone nucleus, and another soft C_γ-anion of the resultant adduct (**10**) at the soft C_4-atom, by the step-by-step nucleophilic and intramolecular nucleophilic mechanism leading to **8a** and **9a**.

The ring transformation of **8a** and **9a** which are obtained by the reaction at a low temperature, to **2** and **4** can be carried out by heating under basic conditions. It is proposed that the transformation of the inter-

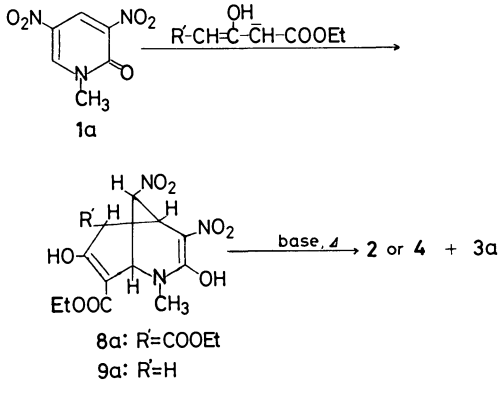

Fig. 6.

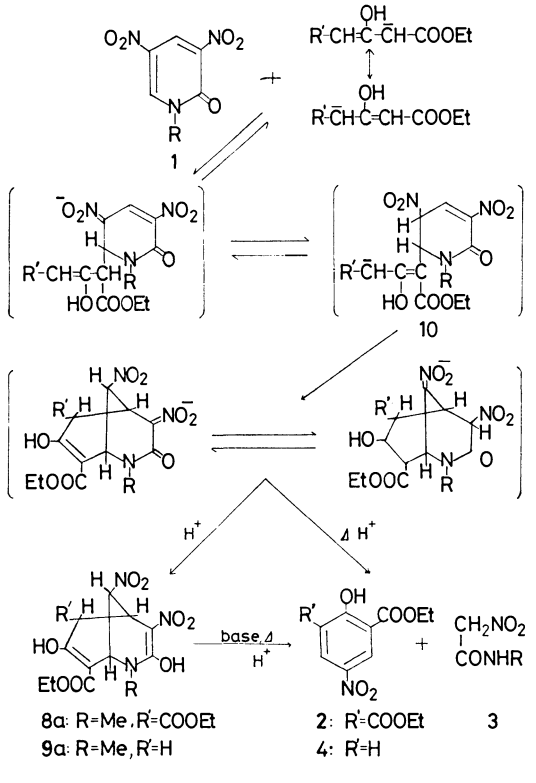

Scheme 1.

mediate **8a** or **9a** into **2** or **4** proceeds by means of the initial nucleophilic attack of the 9-carbanion on the C_5-atom, with the concomitant heterolysis of the C_4–C_5 bond, leaving the electron pair at the C_4-atom. The aromatization of the resultant homolytic moiety, which leads to **2** or **4** can occur with the heterolysis of the C_1–N bond, leaving the electron pair at the N-atom. The residual moiety of the 2-pyridone nucleus yields **3**. In the reaction at a higher temperature, the same products can be obtained without the isolation of the intermediates.

Experimental

All the melting points are uncorrected. The IR spectra were obtained on a Hitachi EPI-S2 as Nujol mulls. The NMR spectra were recorded on a Hitachi R-20B or JEOL FX-100 (unless otherwise noted the former was used), with TMS as the internal standard.

*3,5-Dinitro-1-methyl-2-pyridone (**1a**).* To 30 ml of fuming nitric acid (*d* 1.52) we added 5.0 g of 1-methyl-2-pyridone,[6] then the mixture was heated at 80 °C for 5 h. After almost all the nitric acid has been evaporated under reduced pressure, the mixture was poured onto crushed ice, and the precipitates were recrystallized from water to give 4.7 g (51.4%) of 3,5-dinitro-1-methyl-2-pyridone (**1a**); mp 178.0—179.0 °C (lit, mp 178 °C).[7] IR: 1700 cm^{-1} (C=O), 1530, 1350 (NO_2). NMR (DMSO-d_6): δ 3.65 (3H, s), 8.93 (1H, d), 9.52 (1H, d).

*3,5-Dinitro-1-(m-nitrobenzyl)-2-pyridone (**1b**).* Five grams of 1-(*m*-nitrobenzyl)-2-pyridone[8] were worked-up according to the above method to give 3.1 g (30.0%) of 3,5-dinitro-1-(*m*-nitrobenzyl)-2-pyridone (**1b**); mp 139.0—141.0 °C (recrystallized from aqueous acetic acid). IR: 1690 cm^{-1} (C=O), 1530, 1340 (NO_2). NMR (DMSO-d_6): δ 5.43 (2H, s), 7.62 (1H, d), 7.80 (1H, dt), 8.03 (1H, dt), 8.31 (1H, t), 8.96 (1H, d), 9.84 (1H, d). Found: C, 44.91; H, 2.46; N, 17.71%. Calcd for $C_{12}H_8N_4O_7$: C, 45.01; H, 2.52; N, 17.50%.

*3,5-Dinitro-1-(2-pyridylmethyl)-2-pyridone (**1c**).* Similarly, the nitration of 2-amino-1-(2-pyridylmethyl)-pyridinium chloride, which had been prepared from 2-chloromethylpyridine and 2-aminopyridine by heating, gave 3,5-dinitro-1-(2-pyridylmethyl)-2-pyridone (**1c**) in a 32.0% yield; mp 155.0 °C with dec (water). IR: 1700 cm^{-1} (C=O), 1580, 1340 (NO_2). NMR (DMSO-d_6): δ 5.52 (2H, s), 7.1—7.9 (3H, m), 8.43 (1H, dd), 8.97 (1H, d), 9.49 (1H, d). Found: C, 47.66; H, 2.61; N, 20.16%. Calcd for $C_{11}H_8N_4O_5$: C, 47.85; H, 2.92; N, 20.28%.

*3,5-Dinitro-2-pyridone (**1d**).* This pyridone was obtained by the method of Takahashi *et al.*[9]

*3,5-Dinitro-1-(2,4-dinitrophenyl)-2-pyridone (**1e**).* A mixture of a sodium salt of 2-hydroxypyridine and a 1.1 equimolar amount of 2,4-dinitrochlorobenzene in DMSO was heated at 140 °C for 5 h. The subsequent evaporation of the solvent was followed by extraction with chloroform to give 1-(2,4-dinitrophenyl)-2-pyridone (mp 163.8—164.2 °C) in a 48.0% yield. To a solution of 5.0 g of 1-(2,4-dinitrophenyl)-2-pyridone in 50 ml of fuming sulfuric acid (30% SO_3) we added 9.7 g of potassium nitrate, portion-by-portion, the mixture was then heated at 130 °C for 5 h. The reaction mixture was poured onto crushed ice, the precipitates were recrystallized from aqueous acetic acid to give 3.3 g (49.0%) of 3,5-dinitro-1-(2,4-dinitrophenyl)-2-pyridone (**1e**); mp 165.3—165.5 °C. IR: 1720 cm^{-1} (C=O), 1530, 1350 (NO_2). NMR (DMSO-d_6): δ 7.92 (1H, d), 8.07 (1H, dd), 8.11 (1H, d), 9.18 (1H, d), 9.68 (1H, d). Found: C, 37.84; H, 1.36; N, 20.04%. Calcd for $C_{11}H_5N_5O_9$: C, 37.60; H, 1.44, N, 19.95%.

*3,5-Dinitro-1-(2-pyridyl)-2-pyridone (**1f**).* Three grams of 1-(2-pyridyl)-2-pyridone[10] were treated according to the above method to give 3.05 g (66.7%) of 3,5-dinitro-1-(2-pyridyl)-2-pyridone (**1f**); mp 179.5—180.5 °C (aqueous acetic acid). IR: 1710 cm^{-1} (C=O), 1540, 1350 (NO_2). NMR (DMSO-d_6): δ 7.4—8.1 (3H, m), 8.60 (1H, dd), 9.02 (1H, d), 9.42 (1H, d). Found: C, 45.81; H, 2.31; N, 21.37%. Calcd for $C_{10}H_6N_4O_5$: C, 45.76; H, 2.16; N, 21.67%.

*3,5-Dinitro-1-(4-methyl-2-pyridyl)-2-pyridone (**1g**).* Similarly, the nitration of 1-(4-methyl-2-pyridyl)-2-pyridone[10] gave 3,5-dinitro-1-(4-methyl-2-pyridyl)-2-pyridone (**1g**) in a 63.8% yield; mp 164.0—165.0 °C (aqueous acetic acid). IR: 1720 cm^{-1} (C=O), 1530, 1355 (NO_2). NMR (DMSO-d_6): δ 2.43 (3H, s), 7.41 (1H, dd), 7.30 (1H, d), 8.44 (1H, dd), 9.03 (1H, d), 9.39 (1H, d). Found: C, 48.08; H, 2.73; N, 20.29%. Calcd for $C_{11}H_8N_4O_5$: C, 47.83; H, 2.92; N, 20.29%.

*3,5-Dinitro-1-(5-methyl-2-pyridyl)-2-pyridone (**1h**).* The similar nitration of 1-(5-methyl-2-pyridyl)-2-pyridone[10] gave 3,5-dinitro-1-(5-methyl-2-pyridyl)-2-pyridone (**1h**) in a 53.9% yield; mp 174.0—175.0 °C (aqueous acetic acid). IR: 1720 cm^{-1} (C=O), 1535, 1330 (NO_2). NMR (DMSO-d_6): δ 2.40 (3H, s), 7.8 (2H, m), 8.5 (1H, m), 9.05 (1H, d), 9.40 (1H, d). Found: C, 47.64; H, 2.69; N, 20.01%. Calcd for $C_{11}H_8N_4O_5$: C, 47.83; H, 2.93; N, 20.29%.

*3,5-Dinitro-1-(6-methyl-2-pyridyl)-2-pyridone (**1i**).* Similarly, 3,5-dinitro-1-(6-methyl-2-pyridyl)-2-pyridone (**1i**) was obtained from 1-(6-methyl-2-pyridyl)-2-pyridone[10] in a 58.8% yield; mp 175.5—176.5 °C (aqueous acetic acid). IR: 1710 cm^{-1} (C=O), 1530, 1340 (NO_2). NMR (DMSO-d_6): δ 2.67 (3H, s), 7.4 (1H, m), 7.7 (1H, m), 8.3 (1H, m), 9.02 (1H, d), 9.48 (1H, d). Found: C, 47.96; H, 2.80; N, 20.38%. Calcd for $C_{11}H_8N_4O_5$: C, 47.83; H, 2.93; N, 20.29%.

*3,5-Dinitro-1-hydroxy-2-pyridone (**1j**).* The pyridone was obtained according to the method in the literature[11] in an 80.0% yield; mp 190.0—191.0 °C.

*3,5-Dinitro-1-methoxy-2-pyridone (**1k**).* A mixture of 7.0 g of 1-methoxy-2-pyridone[12] and 70 ml of fuming nitric acid (*d* 1.52) was heated at 80 °C for 10 h. The cold reaction mixture was then poured onto crushed ice, the precipitates were collected by filtration, the filtrate was concentrated, and diluted with water, and the second crop was obtained combined with the above precipitates, and crystallized from water to give 6.5 g (54.0%) of 3,5-dinitro-1-methoxy-2-pyridone (**1k**); mp 158.0—159.0 °C. IR: 1740 cm^{-1} (C=O), 1560, 1330 (NO_2). NMR (DMSO-d_6): δ 3.25 (3H, s), 8.95 (1H, d), 9.82 (1H, d). Found: C, 33.57; H, 2.50; N, 19.50%. Calcd for $C_6H_5N_3O_6$: C, 33.50; H, 2.34; N, 19.54%.

*3,5-Dinitro-1-(p-nitrobenzyloxy)-2-pyridone (**1l**).* 1-(*p*-Nitrobenzyloxy)-2-pyridone[12] was nitrated according to the preceding method to give 3,5-dinitro-1-(*p*-nitrobenzyloxy)-2-pyridone (**11**) in a 70.0% yield; mp 192.0—193.0 °C (water). IR: 1730 cm^{-1} (C=O), 1535, 1330 (NO_2). NMR (DMSO-d_6): δ 5.45 (2H, s), 7.85 (2H, d), 8.25 (2H, d), 9.02 (1H, d), 10.00 (1H, d). Found: C, 42.92; H, 2.28; N, 16.38%. Calcd for $C_{12}H_8N_4O_8$: C, 42.86; H, 2.40; N, 16.67%.

*General Procedure of the Reaction of Pyridones (**1**) with Sodium Salts.* To a solution of pyridone (**1**) in pyridine we added a solution of sodium salt in pyridine with cooling, then the mixture was heated at the required temperature for 5—10 h. The solvent was evaporated under reduced pressure, and the residue was neutralized to pH 3—4 with dil. Hydrochloric acid and then extracted with chloroform. After the extract has been dried over anhydrous sodium sulfate, the chloroform was distilled off, and the residual syrup was column-chromatographed on silica gel (Wakogel C-300). From the benzene elute, phenol derivatives (**2**, **4**, **5**, and **6**)

were obtained, and from the diethyl ether elute, *N*-substituted nitroacetamide (**3**).

*Reaction of 3,5-Dinitro-1-methyl-2-pyridone (**1a**) with Diethyl Sodio-3-oxopentanedioate.* To a solution of 1.0 g of 3,5-dintro-1-methyl-2-pyridone (**1a**) in 100 ml of pyridine we added diethyl sodio-3-oxopentanedioate, prepared from 0.17 g of sodium and 1.7 g of diethyl 3-oxopentanedioate in absolute ethanol, in pyridine with cooling. When the mixture was heated at 50 °C for 5 h and then worked-up according to the general procedure, 1.3 g of (90.4%) of 2,6-bis(ethoxycarbonyl)-4-nitrophenol (**2**)[13] was obtained from the benzene elute and 0.17 g (28.3%) of *N*-methyl-α-nitroacetamide (**3a**),[14] from the diethyl ether elute.

2,6-Bis(ethoxycarbonyl)-4-nitrophenol (**2**); colorless needles (petroleum benzine); mp 58.0—59.0 °C. IR: 3100 cm^{-1} (O–H), 1720 (C=O), 1540, 1340 (NO_2). NMR ($CDCl_3$): δ 1.42 (6H, t), 4.45 (4H, q), 8.81 (2H, s), 12.42 (1H, s). Found: C, 50.94; H, 4.64; N, 4.81%. Calcd for $C_{12}H_{15}NO_7$: C, 50.84; H, 4.63; N, 4.95%.

N-Methyl-α-nitroacetamide (**3a**); colorless needles (diisopropyl ether); mp 75.0—76.0 °C. IR: 3300 cm^{-1} (N–H), 1670 (C=O), 1570, 1340 (NO_2). NMR (acetone-d_6): δ 2.78 (3H, d), 5.16 (2H, s), 7.00 (1H, d). Found: C, 30.32; H, 5.09; N, 23.70%. Calcd for $C_3H_6N_2O_3$: C, 30.51; H, 5.08; N, 23.73%.

*2-Ethoxycarbonyl-4-nitrophenol (**4**).* The treatment of 1.0 g of 3,5-dinitro-1-methyl-2-pyridone (**1a**) with ethyl sodioacetoacetate, prepared from 0.3 g of sodium and 2.2 g of ethyl acetoacetate, at 70 °C for 5 h gave 0.65 g (60.8%) of 2-ethoxycarbonyl-4-nitrophenol (**4**)[15] and 0.05 g (16.9%) of **3a**.

2-Ethoxycarbonyl-4-nitrophenol (**4**); colorless plates (petroleum benzine); mp 97.5—98.0 °C. IR: 3420 cm^{-1} (O–H), 1680 (C=O), 1524, 1335 (NO_2). NMR ($CDCl_3$): δ 1.45 (3H, t), 4.45 (2H, q), 7.03 (1H, d), 8.03 (1H, dd), 8.67 (1H, d), 11.35 (1H, s). Found: C, 51.46; H, 4.24; N, 6.45%. Calcd for $C_9H_9NO_5$: C, 51.19; H, 4.30; N, 6.63%.

*2-Acetyl-4-nitrophenol (**5**).* Colorless needles (petroleum benzine); mp 101.0—102.0 °C (lit, mp 101—102 °C).[16] IR: 3365 cm^{-1} (O–H), 1650 (C=O), 1520, 1350 (NO_2). NMR ($CDCl_3$): δ 2.71 (3H, s), 7.05 (1H, d), 8.26 (1H, dd), 8.62 (1H, d), 12.76 (1H, s). Found: C, 52.98; H, 3.77; N, 7.45%. Calcd for $C_8H_7NO_4$: C, 53.05; H, 3.90; N, 7.73%.

*2-Ethoxyoxalyl-4-nitrophenol (**6**).* Colorless needles (petroleum benzine); mp 57.5—58.5 °C. IR: 3360 cm^{-1} (O–H), 1730 (C=O), 1690 (C=O), 1530, 1340 (NO_2). NMR ($CDCl_3$): δ 1.45 (3H, t), 4.51 (2H, q), 7.11 (1H, d), 8.38 (1H, dd), 8.76 (1H, d), 11.73 (1H, s). Found: C, 50.35; H, 3.66; N, 5.57%. Calcd for $C_{10}H_9NO_6$: C, 50.21; H, 3.77; N, 5.86%.

N-*(m-Nitrobenzyl)-α-nitrocaetamide (**3b**).* Colorless needles (benzene); mp 152.0—153.0 °C. NMR (acetone-d_6): δ 4.47 (2H, d), 5.38 (2H, s), 7.55—8.15 (4H, m), 9.10 (1H, br). Found: C, 45.02; H, 3.53; N, 17.33%. Calcd for $C_9H_9N_3O_5$: C, 45.19; H, 3.79; N, 17.57%.

N-*(2-Pyridylmethyl)-α-nitroacetamide (**3c**).* Colorless needles (diisopropyl ether); mp 83.0—84.0 °C. NMR (acetone-d_6): δ 4.55 (2H, d), 5.40 (2H, s), 7.0—7.9 (3H, m), 8.20 (1H, br), 8.44 (1H, d). Found: C, 49.55; H, 4.29; N, 21.62%. Calcd for $C_8H_9N_3O_3$: C, 49.25; H, 4.65; N, 21.53%.

N-*(2,4-Dinitrophenyl)-α-nitroacetamide (**3e**).* Pale yellow needles (benzene); mp 120.4—121.1 °C. NMR (DMSO-d_6): δ 5.62 (2H, s), 8.5 (2H, m), 8.9 (1H, m), 11.10 (1H, br). Found: C, 35.53; H, 2.08; N, 20.54%. Calcd for $C_8H_6N_4O_7$: C, 35.56; H, 2.24; N, 20.76%.

N-*(2-Pyridyl)-α-nitroacetamide (**3f**).* Colorless needles; dec 120 °C. NMR (acetone-d_6): δ 5.62 (2H, s), 7.1—8.2 (4H, m), 9.85 (1H, br). Found: C, 46.63; H, 3.67; N, 23.26%. Calcd for $C_7H_7N_3O_3$: C, 46.41; H, 3.87; N, 23.20%.

*2-Oxo-2H-pyrido[1,2-b][1,2,4]triazine 4-Oxide (**7f**).* After *N*-(2-pyridyl)-α-nitroacetamide (**3f**) had been obtained, the column was washed with acetone and ethanol to give 0.21—0.24 g (3.5—3.8%) of 2-oxo-2*H*-pyrido[1,2-*b*][1,2,4]-triazine 4-oxide (**7f**); yellow needles (water); dec 210 °C. NMR (CF_3COOD): δ 7.5—7.9 (2H, m), 8.52 (1H, dt), 9.65 (1H, dd). Found: C, 51.35; H, 2.97; N, 25.89%. Calcd for $C_7H_5N_3O_2$: C, 51.54; H, 3.09; N, 25.76%.

*8-Methyl-2-oxo-2H-pyrido[1,2-b][1,2,4]triazine 4-Oxide (**7g**).* Yellow needles (water); dec 210 °C. IR: 1730 cm^{-1} (C=O), 1635 (C=N), 1210 (N→O). NMR (CF_3COOD): δ 3.58 (3H, s), 7.70 (1H, d), 8.35 (1H, dd), 9.38 (1H, d). Found: C, 54.10; H, 3.73; N, 23.60%. Calcd for $C_8H_7N_3O_2$: C, 54.23; H, 3.98; N, 23.72%.

N-*(5-Methyl-2-pyridyl)-α-nitroacetamide (**3h**).* Colorless needles; dec 120 °C. NMR (acetone-d_6): δ 2.43 (3H, s), 5.52 (2H, s), 7.56 (1H, dd), 7.87 (1H, d), 8.11 (1H, s), 10.98 (1H, s). Found: C, 49.38; H, 4.71; N, 21.50%. Calcd for $C_8H_9N_3O_3$: C, 49.23; H, 4.65; N, 21.53%.

*7-Methyl-2-oxo-2H-pyrido[1,2-b][1,2,4]triazine 4-Oxide (**7h**).* Yellow needles (water); dec 248 °C. IR: 1735 cm^{-1} (C=O), 1645 (C=N), 1210 (N→O). NMR (CF_3COOD): δ 2.50 (3H, s), 7.70 (1H, d), 8.37 (1H, dd), 9.37 (1H, d). Found: C, 54.36; H, 3.82; N, 23.68%. Calcd for $C_8H_7N_3O_2$: C, 54.23; H, 3.98; N, 23.72%.

N-*(6-Methyl-2-pyridyl)-α-nitroacetamide (**3i**).* Colorless needles; dec 120 °C. NMR (acetone-d_6): δ 2.36 (3H, s), 5.62 (2H, s), 6.96 (1H, dd), 7.61 (1H, dd), 7.87 (1H, dd), 9.95 (1H, s). Found: C, 49.11; H, 4.55; N, 21.73%. Calcd for $C_8H_7N_3O_3$: C, 49.23; H, 4.65; N, 21.53%.

*6-Methyl-2-oxo-2H-pyrido[1,2-b][1,2,4]triazine 4-Oxide (**7i**).* Yellow needles (water); dec 182 °C. IR: 1730 cm^{-1} (C=O), 1640 (C=N), 1210 (N→O). NMR (CF_3COOD): δ 2.54 (3H, s), 6.5—6.9 (2H, m), 7.5—7.8 (1H, m). Found: C, 54.48; H, 3.81; N, 23.61%. Calcd for $C_8H_7N_3O_2$: 54.23; H, 3.98; N, 23.72%.

*2-Oxo-2H-pyrido[1,2-b][1,2,4]triazine 4-Oxide (**7f**) from N-(2-Pyridyl)-α-nitroacetamide (**3f**).* A mixture of 0.5 g of *N*-(2-pyridyl)-α-nitroacetamide (**3f**) in 10 ml of water was refluxed for 30 min. The mixture was then cooled and the precipitates were collected by filtration to give 0.44 g (98.0%) of 2-oxo-2*H*-pyrido[1,2-*b*][1,2,4]triazine 4-oxide (**7f**). Similarly, **7h** and **7i** were obtained quantitatively from **3h** and **3i** respectively.

*2-Oxo-2H-pyrido[1,2-b][1,2,4]tiazine 4-Oxide (**7f**) (Alternative Method).* A mixture of 2.0 g of 2-aminopyridine and 2.0 g of ethyl nitroacetate[17] was heated slowly then kept at 90 °C for 1 h. When to the reaction mixture we then added a small amount of ethanol, 2.1 g (85.5%) of 2-oxo-2*H*-pyrido[1,2-*b*][1,2,4]triazine 4-oxide (**7f**) were obtained.

*Catalytic Hydrogenation of 2-Oxo-2H-pyrido[1,2-b][1,2,4]-triazine 4-Oxide (**7f**).* A mixture of 0.5 g of 2-oxo-2*H*-pyrido[1,2-*b*][1,2,4]triazine 4-oxide (**7f**), 0.1 g of Raney Nickel, and 50 ml of ethanol in a 100 ml autoclave was heated at 100 °C under 100 atm of hydrogen gas for 5 h. After filtration, the ethanol was distilled off, and the residual syrup was column-chromatographed on silica gel; 0.3 g of ethyl 2-pyridylcarbamate[18] was obtained from the benzene elute, and 0.05 g of 2-aminopyridine, from the diethyl ether elute.

*Reaction of 3,5-Dinitro-1-methyl-2-pyridone (**1a**) with Diethyl Sodio-3-oxopentanedioate at a Low Temperature.* One gram of 3,5-dinitro-1-methyl-2-pyridone (**1a**) was worked-up according to the general procedure at room temperature with diethyl sodio-3-oxopentanedioate, and then before column-

chromatography, diethyl ether was added to the residual syrup. Crystalline precipitates were collected by filtration to give 1.3 g of **8a**, and the filtrate was column-chromatographed with benzene. From the benzene elute 0.13 g of **2**, and from the chloroform elute, and additional 0.3 g of **8a** were obtained.

6,8-Bis(ethoxycarbonyl)-3,7-dihydroxy-2-methyl-4,9-dinitro-2-azabicyclo[3.3.1]nona-3,7-diene (**8a**); colorless plates; mp 155.0—156.0 °C (ethanol). IR: 1740 cm^{-1} (C=O), 1730 (C=O), 1560, 1335 (NO_2). NMR (JEOL FX-100)($CDCl_3$): δ 1.35 (3H, t), 1.42 (3H, t), 3.20 (3H, s), 3.95 (1H, d, J= 2 Hz, H-6), 4.29 (2H, q), 4.40 (2H, q), 4.42 (1H, ddd, J=2, 3, and 4 Hz, H-5), 5.15 (1H, dd, J=4 and 3 Hz, H-1), 5.42 (1H, dd, J=4 and 4 Hz, H-9), 12.64 (1H, s), 18.82 (1H, s). Found: C, 45.31; H, 4.71; N, 10.53%. Calcd for $C_{15}H_{19}N_3O_{10}$: C, 45.26; H, 4.77; N, 10.42%.

*Reaction of 3,5-Dinitro-1-methyl-2-pyridone (**1a**) with Ethyl Sodioacetoacetate at a Low Temperature.* Similarly, the reaction of 1.0 g of 3,5-dinitro-1-methyl-2-pyridone (**1a**) with 3 equimolar amounts of ethyl sodioacetoacetate gave 0.1 g of **4**, 0.05 g of **3a**, and 0.9 g of 8-ethoxycarbonyl-3,7-dihydroxy-2-methyl-4,9-dinitro-2-azabicyclo[3.3.1]nona-3,7-diene (**9a**); colorless needles (ethanol); mp 190.0—191.0 °C. IR: 1730 cm^{-1} (C=O), 1550, 1340 (NO_2). NMR (JEOL FX-100) ($CDCl_3$): δ 1.41 (3H, t), 2.84 (1H, d, J=4 Hz, H-6), 2.99 (1H, d, J=2 Hz, H-6), 3.20 (3H, s), 4.30 (1H, ddt, J=3, 4, and 2 Hz, H-5), 4.37 (2H, q), 4.71 (1H, dd, J=3 and 2 Hz, H-1), 5.30 (1H, t, J=3 Hz, H-9), 12.59 (1H, s), 18.83 (1H, s). Found: C, 43.48; H, 4.31; N, 12.76%. Calcd for $C_{12}H_{15}N_3O_8$: C, 43.79; H, 4.56; N, 12.76%.

*Treatment of 6,8-Bis(ethoxycarbonyl)-3,7-dihydroxy-2-methyl-4,9-dinitro-2-azabicyclo[3.3.1]nona-3,7-diene (**8a**) with Sodium Ethoxide.* A solution of 0.5 g of **8a** and 0.4 g of sodium ethoxide in 50 ml of ethanol was refluxed for 2 h. The solvent was then distilled off, and the residue was neutralized to pH 3.5 with dil. hydrochloric acid and extracted with chloroform. After the extract had then been dried over anhydrous sodium sulfate, the chloroform was evaporated to dryness and the residual syrup was column-chromatographed on silica gel. From the benzene elute 0.1 g of **2**, and from the diethyl ether elute, 0.06 g of **3a** were obtained.

*Treatment of 6,8-Bis(ethoxycarbonyl)-3,7-dihydroxy-2-methyl-4,9-dinitro-2-azabicyclo[3.3.1]nona-3,7-diene (**8a**) with Diethyl Sodio-3-oxopentanedioate.* A mixture of 0.5 g of **8a** and diethyl sodio-3-oxopentanedioate, prepared from 0.03 g of sodium and 0.3 g of diethyl 3-oxopentanedioate, in pyridine was heated at 70 °C for 2 h. The reaction mixture was then worked-up according to the usual procedure to give 0.20 g of **2** and 0.06 g of **3a**.

References

1) E. Matsumura, F. Ishibashi, and T. Nashima, *Bull. Chem. Soc. Jpn.*, **43**, 3540 (1970).
2) T. Zinncke, *Ann.*, **330**, 367 (1904).
3) E. Matsumura and M. Ariga, *Bull. Chem. Soc. Jpn.*, **46**, 3144 (1973); *ibid.*, **50**, 237 (1977).
4) M. I. Foreman, R. Foster, and M. J. Strauss, *J. Chem. Soc., C*, **1969**, 2112; M. J. Strauss, T. Jensen, H. Schran, and K. O'Conner, *J. Org. Chem.*, **35**, 383 (1970); M. J. Strauss, *Acc. Chem. Res.*, **7**, 181 (1974); M. J. Strauss, *Chem. Rev.*, **70**, 667 (1970).
5) K. Kohashi, Y. Ohkura, and T. Momose, *Chem. Pharm. Bull. (Tokyo)*, **18**, 2157 (1970); *ibid.*, **19**, 213, 2065 (1971); *ibid.*, **21**, 118 (1973).
6) E. A. Prill and S. M. McElvain, *Org. Synth.*, Coll. Vol. II, 419 (1951).
7) A. Raczka, A. Swirska, and H. Bojarska Dahlig, *Acta Pol. Pharm.*, **20**, 155 (1063); *cf. Chem. Abstr.*, **62**, 442 (1965).
8) A. H. Barrie, G. T. Newbold, and F. S. Spring, *J. Chem. Soc.*, **1951**, 2590.
9) T. Takahashi and F. Yoneda, *Chem. Pharm. Bull. (Tokyo)*, **6**, 442 (1958).
10) F. Ramirez and P. W. von Ostwalden, *J. Am. Chem. Soc.*, **81**, 156 (1959).
11) M. von Ammers and H. J. den Hertog, *Recl. Trav. Chim. Pays-Bas*, **75**, 1261 (1956).
12) F. T. Dinan and H. Tieckelman, *J. Org. Chem.*, **29**, 1650 (1954).
13) The authentic sample was prepared by the usual esterification from 2-hydroxy-5-nitroisophthalic acid; W. S. Benica and O. Gisvold, *J. Am. Pharm. Assoc.*, **34**, 42 (1945).
14) The authentic methylammonium salt of *N*-methyl-α-nitroacetamide was obtained by the method of F. Ratz, *Monatsh. Chem.*, **26**, 1487 (1905).
15) The authentic sample was obtained by the usual method from commercial 4-nitrosalicylic acid.
16) C. T. Chang, F. C. Chen, T. S. Chen, K. K. Hsu, T. Ueng, and M. Hung, *J. Chem. Soc.*, **1961**, 3414.
17) V. W. Rodinov, I. V. Machinskaya, and V. W. Belikov, *Zh. Obshch. Khim.*, **18**, 917 (1948); *cf. Chem. Abstr.*, **43**, 127 (1949).
18) A. R. Katritzky, *J. Chem. Soc.*, **1956**, 2063.

Electron-organic Chemistry. IV.[1] Structure—Anodic Potential Relationship and Electron-transfer-induced Reactions of [2.2]Para- and -Metaparacyclophanes

Takeo SATO,* Koichi TORIZUKA, Motomu SHIMIZU, Yukio KURIHARA, and Noriko YODA

Department of Chemistry, Tokyo Metropolitan University, Setagaya-ku, Tokyo 158

(Received February 16, 1979)

The anodic peak potentials of [2.2]para- and -metaparacyclophanes were found to be highly dependent on the solvent. A cleavage reaction occured when [2.2]paracyclophane was electrolyzed anodically, using acids or alcohols as nucleophilic solvents, whereas lead tetraacetate oxidation in trifluoroacetic acid–dichloromethane gave nuclear substitution products. The cathodic reduction in hexamethylphosphoric triamide–lithium chloride–acetic acid gave 1,2-di-*p*-tolylethane and its Birch reduction products. On anodic oxidation, [2.2]metaparacyclophane gave a rearrangement reaction product, 4-hydroxy[2.2]metacyclophane. Possible reaction pathways for these reactions were formulated.

The dependence of the half-wave potentials on a molecular geometry and the reaction of the resulting radical ions have aroused considerable current interests.[1-5] Recent findings that cyclophane-radical ions undergo intramolecular reactions,[3-5] such as a transannular reaction, as well as rearrangement and fragmentation reactions led us to investigate the electron-transfer-induced reactions of basic cyclophanes [2.2]-paracyclophane (**1**) and [2.2]metaparacyclophane (**13**).

The anodic half-wave potential of **1**, +1.52 V *vs.* SCE in acetonitrile–tetrabutylammonium perchlorate[4] (+1.47 V in acetonitrile–lithium perchlorate[6]), is anomalously low and is more cathodic by *ca.* 0.5 V[4] than those of [*m*]paracyclophane or 1,2-bis(4-alkylphenyl)ethane. This fact indicates that one of the benzene rings serves as an internal π donor for stabilizing the aryl-cation radical formed. The enhanced π basicity of **1** towards tetracyanoethylene is explainable along the same lines.[7] The anodic peak potential, E_{pa}, for [2.2]metaparacyclophane (**13**) was determined by the cyclic voltammetry at 250 mV/s and was found to be +1.79 V in acetonitrile–tetrabutylammonium perchlorate.[4] It is more cathodic than those of the above model compounds by *ca.* 0.3 V.

The peak potential for these compounds, as determined by the cyclic voltammetry, showed a marked solvent dependence. The results are summarized in Table 1. At the scan rate of 250 mV/s, E_{pa} for **1** varied from +1.57 V in acetonitrile to +1.12 V in trifluoroacetic acid–dichloromethane (1 : 1). A slight cathodic shift was also observed in solutions containing acetic acid, but no peak was recorded in acetic acid–sodium acetate or in acetic acid–ammonium salts.

The controlled potential electrolysis of **1** was carried out in trifluoroacetic acid or trifluoroacetic acid–dichloromethane, using tetrabutylammonium fluoroborate (TBAF) at +1.5—1.7 V, but no product was obtained. When **1** was electrolyzed in acetic acid–TBAF[8] at +1.7—1.9 V, 1,2-bis[4-(acetoxymethyl)-phenyl]ethane (**2**) was obtained in a 24% yield. The structure was confirmed by the ^{1}H NMR and MS spectra and by elemental analyses.

Compound **2** was also formed in a 15% yield when **1** was electrolyzed anodically in acetic acid–sodium acetate.[9] When a similar reaction was carried out in propionic acid–TBAF bispropionate, **3** was obtained.

In order to compare the electrochemical results with these of a chemical method, **1** was treated with lead tetraacetate in acetic acid–dichloromethane.[10] This resulted in the formation of **2** and [2.2]paracyclophan-4-yl acetate (**7**)[11] in 21 and 13% yields respectively. When the oxidation was carried out in trifluoroacetic

Table 1. Anodic peak potentials of [2.2]para- (**1**) and -metaparacyclophanes (**13**) in various solvents, +V *vs.* SCE[a]

Scan rate mV/s	MeCN	TFA–CH_2Cl_2 (1 : 1)	AcOH–CH_2Cl_2 (1 : 4)	AcOH–MeCN (1 : 1)	$PhNO_2$
	[2.2]paracyclophane (**1**)				
50	1.52, 1.75	1.06	1.40 sh	1.28	
100	1.54, 1.77	1.10	1.47 sh	1.32	1.69
250	1.57, 1.80	1.12	1.54 sh	1.36	1.74 sh
500	1.59, 1.82	1.15	1.62 sh	1.43	1.83 sh
	[2.2]metaparacyclophane (**13**)				
50	1.73	1.30, 1.60 sh	—[b]	1.57 sh, 1.73	
100	1.76	1.32, 1.61 sh		1.60 sh, 1.75	
250	1.79	1.34, 1.64 sh		1.65 sh, 1.81 sh	
500	1.82	1.40, 1.71 sh		1.74	

a) Determined in the specified solvent using tetrabutylammonium perchlorate (0.1 M) as the supporting electrolyte. Scan range, 0—+2.2 V. Shoulders are denoted sh. b) No anodic peak was observed up to +2.2 V.

Table 2. The reaction of [2.2]paracyclophane (**1**) with lead tetraacetate[a)]

Compd **1**, mmol	$Pb(OAc)_4$, mmol	Yield/%		
		1	**6**	**8**
3.0	1.5	50	15	trace
3.0	3.0	17	14	12
3.0	7.5	0	0	39

a) The reaction was carried out in trifluoroacetic acid–dichloromethane (1:2) at 0 °C for 12 h.

acid–dichloromethane at 0 °C, however, no cleavage products were obtained.[12)] Instead, 4-hydroxy[2.2]-paracyclophane (**6**)[11)] and *pseudo-para*-dihydroxy[2.2]-paracyclophanes (**8**)[13)] were formed. The results are shown in Table 2. The ready hydrolysis of trifluoro-acetate during handling was noticed.

The formation of **7** is assumed to involve the nucleophilic reaction of acetic acid towards the [2.2]paracyclophane cation radical, **9**, to give **10**, which then undergoes further electron transfer and deprotonation. Oxidation with lead tetraacetate appears to favor this route, especially when trifluoroacetic acid is used as the solvent, for it is known to stabilize aryl-cation radicals.[14)]

On the other hand, the electron abstraction of **1** on a platinum anode gives the cation radical, **11**, which, *via* the acetate radical, **12**, gives diacetate, **2**. The expected side-chain acetoxylation[10)] did not occur, possibly because of an excessive internal strain[15)] present in **1** which was relieved by going into **11**. It is highly probable that electron-transfer and acetoxylation to give (**12**) occur in a concerted manner.

Solvolytic anodic-cleavage reactions occurred in alcoholic solvents, though in low yields. 1,2-Bis[4-(methoxymethyl)phenyl]ethane (**4**) was obtained when **1** was electrolyzed anodically in methanol–TBAF at +1.39 V using a platinum electrode. A similar reaction in ethanol gave a diethoxy compound, **5**.

The anodic electrolysis of **13** in acetic acid–sodium acetate at the controlled potential of +1.80 V gave 4-hydroxy[2.2]metacyclophane (**17**) in a 20% yield, together with the recovered material. The rearranged structure, **17**, was confirmed by comparing the sample with an authentic material prepared from [2.2]meta-cyclophane by treatment with benzoyl peroxide and copper(II) chloride, followed by hydrolysis.[16)] Although [2.2]metacyclophane and derivatives have been shown[4)] to undergo easy transannular dehydrogenation reaction by means of the anodic reaction in acetonitrile, no such reaction was found to occur in acetic acid–sodium acetate. Conversely, no skeletal change occurred when **13** was electrolyzed in a solvent containing acetonitrile.

The possible reaction scheme for the formation of **17** involves the oxygenation of the cation radical, **14**, to give **15**, which is then rearranged to **16**. The deprotonation of **16**, followed by hydrolysis, gives **17**. The addition of water increased the yield of **17**, and it might be possible that water instead of the presumed acetoxylation is responsible for the introduction of the hydroxyl group. That **17** was the initial product of the reaction was shown by gas chromatography of the reaction mixture, which was carefully handled to avoid hydrolysis.

The cathodic reduction of **1** was then carried out under conditions which involved a solvated electron.[17)] To a solution of **1** in hexamethylphosphoric triamide containing lithium chloride, acetic acid was added as a proton source, after which the mixture was electrolyzed cathodically under constant current conditions using a current density of 12 mA/cm². As cathodes, titanium, lead, and platinum were used, while a platinum wire was used as the anode. We thus obtained three cleavage products, **18**—**20**, which were separated by column chromatography on alumina containing silver nitrate. Of the cathode materials, titanium gave the highest yield of cleavage products. When 7.4 F/mol of electricity was passed through, *ca.* 50% of the material was cleaved. The results are summarized in Table 3.

Table 3. The constant-current cathodic reduction of [2.2]paracyclophane (**1**)[a)]

Electrode	Yield/%		
	18	**19**	**20**
Ti	17	21	7.5
Pb	5	trace	trace
Pt	trace	—	—

a) The reaction was carried out in hexamethylphosphoric triamide–lithium chloride–acetic acid at the current density of 12 mA/cm².

A usual Birch reduction using liq ammonia–tetrahydrofuran–ethanol–sodium gave only *dl*-tetrahydro-(**1**),[18)] although a modification of the procedure reported by Marshall *et al.*[19)] gave **18**, but no further reduction products. The cathodic reduction of **18** carried out in the same way as above gave **19** and **20**.

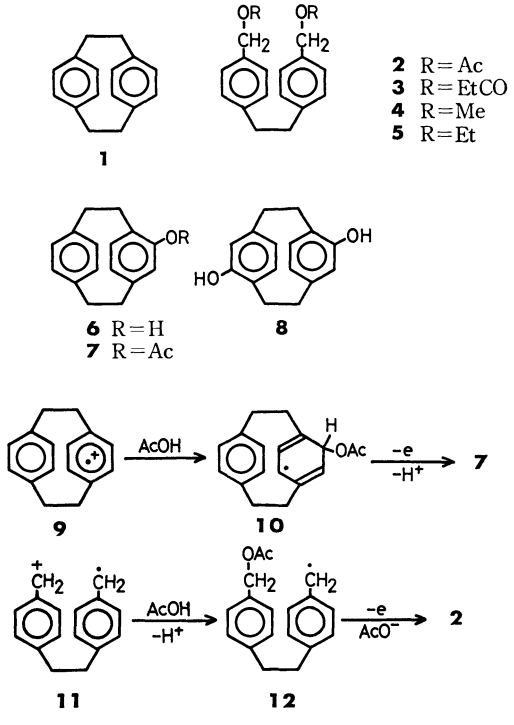

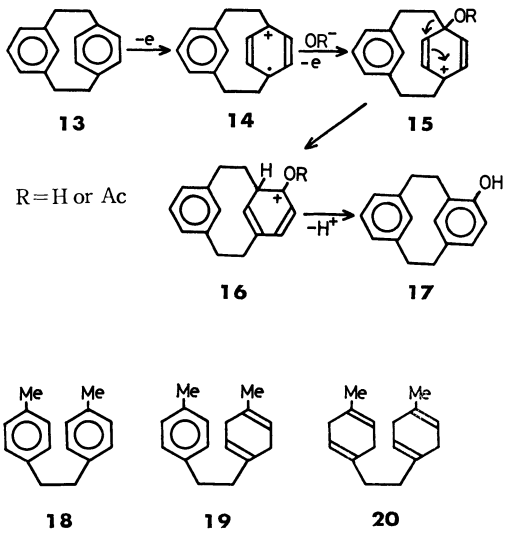

Experimental

Cyclic Voltammetry. Cyclic voltammetry was performed at room temperature using the combination of a generator, Hokuto HB-107A, and a potentiostat, Hokuto HA-101. The H-type cell used consisted of an anode compartment (20 ml) and a cathode compartment separated by a glass frit. A platinum inlay electrode, Beckman No. 39273, was used as the anode, while platinum wire was inserted to serve as the counter electrode. The reference SCE electrode was connected to the side-arm with the aid of two junction bridges, each fitted with a ceramic plug. These were filled with saturated KCl solution and solution containing anolyte.

Controlled-potential and Controlled-current Electrolyses. A Hokuto potentiostat/galvanostat HA-101 (max. output 30 V, 0.1 A) or HA-105 (max. output 200 V, 1 A) was used as the dc source. Coulometry was performed by a Hokuto digital coulometer, HF-102.

A cylindrical cell is equipped with two side arms for connecting the SCE and a nitrogen bubbler. A ceramic thimble was used as the divider. A punched platinum electrode with an area of 40 cm^2 was used as the anode, while a platinum wire was used as the cathode for the anodic experiments. The electrodes used for solvated-electron reduction (Ti, Pb, and Pt) have an area of 8.5 cm^2.

The reference electrode was connected to the side arm through two junction bridges, each fitted with a ceramic plug and each containing a saturated KCl solution and the reaction medium.

1,2-Bis[4-(acetoxymethyl)phenyl]ethane (2). A mixture of **1** (200 mg, 0.91 mmol) in acetic acid (100 ml) containing TBAF (0.1 M) was electrolyzed at the controlled potential of +1.7—1.9 V. When 2F/mol of the electricity had been consumed, the electrolysis was stopped and the resultant reaction mixture was neutralized with aqueous sodium hydrogen carbonate. The ether extracts were evaporated and passed through a Florisil column, using benzene as the eluent. The products were further purified by liquid chromatography on a prepacked silica gel column (Lobar column from Merck). Compound **2** was obtained as colorless crystals (mp 77—78.5 °C (recrystallized from benzene–hexane)) in a 24% yield. The material recovery was 16%. The rest of the material was a colored, tarry matter. ^1H NMR ($CDCl_3$) δ 2.08s (6H), 2.90s (4H), 5.08s (4H), and 7.24s (8H).

Found: C, 73.29; H, 6.75%. Calcd for $C_{20}H_{22}O_4$: C, 73.60; H, 6.79%.

The electrolysis of **1** in acetic acid–sodium acetate also produced **2** in a 15% yield.

1,2-Bis[4-(propionyloxymethyl)phenyl]ethane (3). A mixture of **1** (208 mg, 1.0 mmol) in propionic acid (50 ml) and dichloromethane (150 ml) containing TBAF (0.1 M) was electrolyzed until 1.8 F/mol of electricity had been consumed. Subsequent chromatography on Florisil eluted with benzene–hexane gave **3** as a viscous oil in a 9% yield; this substance solidified on long standing; mp 29—30 °C. The starting material was recovered in a 70% yield. ^1H NMR ($CDCl_3$) δ 1.17t (6H), 2.23q (4H), 5.03s (4H), and 7.20s (8H); MS *m/e* 297 [M^+-57 (COC_2H_5)].

Found: C, 73.76; H, 7.26%. Calcd for $C_{22}H_{26}O_4$: C, 74.55; H, 7.39%.

1,2-Bis[4-(methoxymethyl)phenyl]ethane (4). A mixture of **1** (500 mg, 2.4 mmol) and TBAF (1.1 g, 33 mmol) in methanol (500 ml) was electrolyzed at the constant potential of +1.39 V. A usual work-up, followed by chromatography on silica gel, gave **4** as colorless needles; mp 69—72 °C (recrystallized from hexane); ^1H NMR ($CDCl_3$) δ 2.83s (4H), 3.38s (6H), 4.43s (4H), and 7.16s (8H).

Found: C, 79.98; H, 8.26%. Calcd for $C_{18}H_{22}O_2$: C, 79.96; H, 8.20%.

Cathodic Reduction of 1. The constant-current cathodic reduction of **1** was carried out in hexamethylphosphoric triamide containing lithium chloride (0.3 M), using acetic acid as a proton source, at the current density of 12 mA/cm^2. The results are summarized in Table 3.

The typical reaction was carried out as follows: a mixture of **1** (610 mg, 2.9 mmol), hexamethylphosphoric triamide (75 ml) containing lithium chloride (0.3 M), and acetic acid (2 g) was electrolyzed until 7.4 F/mol of electricity had been consumed, using a titanium cathode and a platinum anode. The voltage between the working and reference electrodes was −2.66——3.2 V. The ether extract was passed through a column packed with Wakogel C-200 containing 20% silver nitrate. The column was then eluted with hexane–benzene.

Compounds **18** (17%), **19** (21%), and **20** (7.5%) were successively eluated. Compound **18** was obtained as colorless needles; mp 80—81.5 °C; ^1H NMR ($CDCl_3$) δ 2.28s (6H), 2.82s (4H), and 7.06s (8H).

Compound **19** was obtained as colorless needles; mp 48—49.5 °C; ^1H NMR δ 1.67s (3H), 2.28s (3H), 2.10—2.40m (4H), 2.57m (4H), 5.40m (2H), and 7.04s (4H); MS *m/e* 212.

Found: C, 89.93; H, 9.39%. Calcd for $C_{16}H_{20}$: C, 90.50; H, 9.50%.

Compound **20** was obtained as colorless needles; mp 57—58 °C; ^1H NMR δ 1.67s (6H), 2.08s (4H), 2.56m (8H), and 5.40m (4H); MS *m/e* 214.

Found: C, 88.54; H, 10.06%. Calcd for $C_{16}H_{22}$: C, 89.65; H, 10.35%.

When **18** was subjected to similar reaction conditions, **19** (13%) and **20** (42%) were obtained.

Anodic Rearrangement of 13. A solution of **13** (52 mg, 0.25 mmol) in acetic acid (50 ml) containing sodium acetate (0.2 M) was electrolyzed at +1.80 V. After 2.8F/mol of electricity had been passed through the reaction mixture was handled as usual and was analyzed by column chromatography on silica gel. In addition to the recovered **13** (36%), 4-hydroxy[2.2]metacyclophane (**17**) (mp 161—164 °C) was obtained in a 20% yield. It was identical with the authentic material prepared according to the literature.[19]

The Reaction of 1 with Lead Tetraacetate. Compound **1** was treated with lead tetraacetate in acetic acid–dichloromethane or in trifluoroacetic acid–dichloromethane.

The reaction in trifluoroacetic acid–dichloromethane is summarized in Table 2. A typical run was carried out as

follows: to a solution of **1** (625 mg, 3.0 mmol) in dichloromethane (80 ml), a solution of lead tetraacetate (670 mg, 1.5 mmol) in TFA (10 ml) was added at 0 °C. After 9 h the reaction mixture was worked-up as usual. Column chromatography on Florisil eluted by benzene gave **1** (50%), **6** (15%) (mp 184—193 °C),[11] and a trace amount of **8**. Compound **8** was obtained in a 39% yield when an excess amount of lead tetraacetate was employed; mp 229—231 °C.[13]

References

1) Part III: T. Sato, K. Torizuka, K. Komaki, and H. Atobe, *J. Chem. Soc., Perkin Trans. 2*, in press.

2) D. Dolphine, *Acc. Chem. Res.*, **7**, 26 (1974).

3) H. O. House, *Acc. Chem. Res.*, **9**, 59 (1976).

4) T. Sato and M. Kamada, *J. Chem. Soc., Perkin Trans. 2*, **1977**, 384; T. Sato and K. Torizuka, *ibid.*, **1978**, 1199.

5) F. Gerson and W. B. Martin, Jr., *J. Am. Chem. Soc.*, **91**, 1883 (1969); Ch. Elshenbroith, F. Gerson, and J. A. Reiss, *ibid.*, **99**, 60 (1977).

6) T. Shono, A. Ikeda, J. Hayashi, and S. Hakozaki, *J. Am. Chem. Soc.*, **97**, 4261 (1975).

7) D. J. Cram and T. H. Bauer, *J. Am. Chem. Soc.*, **81**, 5971 (1959).

8) K. Nyberg, *Chem. Commun.*, **1969**, 774.

9) L. Eberson and K. Nyberg, *J. Am. Chem. Soc.*, **89**, 4669 (1967).

10) D. R. Harvey and R. O. C. Norman, *J. Chem. Soc.*, **1964**, 4880; E. I. Heiba, R. M. Dessau, and W. J. Koehl, Jr., *J. Am. Chem. Soc.*, **90**, 1082 (1968).

11) D. J. Cram and A. C. Day, *J. Org. Chem.*, **31**, 1227 (1966).

12) R. O. C. Norman, C. B. Thomas, and J. S. Willson, *J. Chem. Soc., B*, **1971**, 518; R. O. C. Norman, C. B. Thomas, and J. S. Willson, *ibid., Perkin Trans. 1*, **1973**, 325.

13) H. J. Reich and K. J. Cram, *J. Am. Chem. Soc.*, **91**, 3534 (1969).

14) A. Ronlán, O. Hammerich, and V. D. Parker, *J. Am. Chem. Soc.*, **95**, 7132 (1973).

15) C. Shieh, D. C. McMally, and R. H. Boyd, *Tetrahedron*, **25**, 3653 (1969).

16) K. Nishiyama, K. Hata, and T. Sato, *J. Chem. Soc., Perkin Trans. 2*, **1974**, 577.

17) H. W. Steinber, R. E. Markby, I. Wender, and D. M. Oohilner, *J. Am. Chem. Soc.*, **89**, 186 (1967).

18) J. L. Marshall and B.-H. Song, *J. Org. Chem.*, **39**, 1342 (1974).

19) J. L. Marshall and T. K. Folson, *Tetrahedron Lett.*, **1971**, 757.

Phosphinyl- and Phosphinothioylamino Acids and Peptides. V. Preparation of Dimethylphosphinothioylamino Acids and Solid Phase Peptide Synthesis

Masaaki UEKI,* Toshiyuki INAZU, and Shigeru IKEDA

Department of Chemistry, Science University of Tokyo, 1-3 Kagurazaka, Shinjuku-ku, Tokyo 162

(Received February 19, 1979)

The use of the dimethylphosphinothioyl(Mpt) group for protection of N^{α}-amino functions of amino acids has been studied as the most readily removable group in the phosphinothioyl series. The Mpt-amino acids have been prepared by the alkaline hydrolysis of Mpt-amino acid esters and Schotten-Baumann type reactions of free amino acids. The Mpt group has been removed using a solution of triphenylphosphine dihydrochloride in dichloromethane. L-Leu^5- and D-Ala^2, L-Leu^5-enkephalins have been synthesized by a solid phase method and synthetic L-Leu^5-enkephalin exibited identical activity with an authentic sample.

Recently it has been established that a series of phosphinothioyl groups serve to protect the N^{α}-amino functions of amino acids.[1,2] In a previous paper it was shown that the diphenylphosphinothioyl(Ppt) group was the most useful group since diphenylphosphinothioyl chloride(Ppt–Cl) is readily available from the Friedel-Crafts reaction of benzene and thiophosphoryl chloride and could be used for the preparation of Ppt-amino acids by the Schotten-Baumann type reaction.[3,4] The Ppt group was removed by hydrogen chloride reagents to reproduce the Ppt–Cl. The chloride was relatively inactive to the indole moiety of tryptophan and no other active intermediate was generated during the course of deprotection, and consequently the Ppt-amino acids were successfully utilized for the solid phase synthesis of oligopeptides containing tryptophan.[5] The conditions for removal of the Ppt-group however apper inappropriate for the synthesis of larger peptides on solid supports. In this paper the use of the dimethylphosphinothioyl(Mpt) group has been studied as the most readily removable group in the phosphinothioyl series.

Cleavage of the phosphinothioyl groups is greatly facilitated in the presence of methyl group as substituent on the phosphorus atom.[1] The dimethylphosphinothioyl group was selected in this study since this avoided the introduction of a new asymmetric center on the phosphorus atom. Dimethylphosphinothioyl chloride (**1**) was obtained by chlorinating tetramethyldiphosphine disulfide[6] with sulfuryl chloride.[7]

The Mpt-amino acids were prepared by two methods: the alkaline hydrolysis of Mpt-amino acid esters (Method A) and the direct phosphinothioylation of free amino acids (Method B).

(Method A)

$$(CH_3)_2P(=S)\text{-}Cl + H_2NCHRCO_2R' \xrightarrow{(C_2H_5)_3N} Mpt\text{-}NHCHRCO_2R'$$

1

$$\downarrow \text{1) } OH^- \text{ 2) } H^+$$

(Method B)

$$\mathbf{1} + H_2NCHRCO_2H \xrightarrow[\text{2) } H^+]{\text{1) } OH^-} Mpt\text{-}NHCHRCO_2H$$

The chloride **1** reacted rapidly with the amino acid esters to give the corresponding Mpt-amino acid esters, which were subsequently hydrolysed by aqueous sodium hydroxide to yield Mpt-amino acids. In the case of Mpt-glycine the product was partially extracted by organic solvents from the acidified aqueous reaction mixture saturated with sodium chloride. A small amount of the analytically pure sample of the dicyclohexylamine salt was obtained by laborious extraction, but regeneration of the free acid before use proved impossible. Homologous diethylphosphinothioyl(Ept)-glycine was prepared in a similar manner and substituted for Mpt-glycine in the following peptide synthesis. No difficulty was encounterd in the preparation and isolation of this compound and also in the deprotection of the Ept group as described later. The tyrosine ester reacted with **1** to give a mixture of N^{α}-Mpt and N^{α}-, *O*-bis-Mpt derivatives. Mpt-tyrosine was obtained by alkaline hydrolysis in a similar manner to that for the Ppt-derivatives.[4]

TABLE 1. PREPARATION OF Mpt-L-METHIONINE DCHA SALT

Temperature	Mpt–Cl(eq)	Base	Yield(%)
RT	1.0	1 M NaOH	0
0 °C	1.0	1 M NaOH	58
0 °C	1.0	2 M NaOH	48
0 °C	1.1	1 M NaOH	59
0 °C	1.1(ether solution)	1 M NaOH	68
0 °C	1.2	1 M NaOH	78

In the direct synthesis of Mpt-amino acids by the Schotten-Baumann type reaction several problems were encountered. **1** was rapidly hydrolysed in an alkaline solution, a reaction not found with Ppt–Cl. This problem was solved by conducting the reaction at low temperature with an excess of reagent. The addition of **1** in an ether solution improved the yield as shown in Table 1. The hydrolysis product of **1**, dimethylphosphinothioic acid was not extractable by organic solvents in acidified aqueous solution, and consequently the use of excess reagent did not complicate the purification. The Mpt-amino acids were stored in their dicyclohexylamine(DCHA) or cyclohexylamine(CHA) salts. The physical properties and elemental analysis data are summarized in Table 2.

Removal of the Mpt group was accomplished by hydrogen chloride in organic solvents, in a similar manner to that for the Ppt group, but much more

Table 2. Dimethylphosphinothioyl- and diethylphosphinothioylamino acid salts

Mpt deriv. of	Yield, % (Method)[a]	Mpt–Cl (eq)	Mp (°C)	$[\alpha]_D^{25}$ (deg)[b]	Found (Calcd), % C	H	N
Gly·DCHA	(A)		131—133		55.54 (55.19)	9.62 (9.48)	8.11 (8.04)
Gly·DCHA[c]	78 (A)		181—183		57.12 (57.46)	10.13 (9.83)	7.69 (7.44)
L-Ala·DCHA	57 (B)	1.1	147—148	−10.0	53.66 (53.70)[e]	9.73 (10.22)[e]	7.57 (7.36)[e]
L-Val·DCHA	54 (B)	1.1	148—149	−12.5	58.13 (58.33)	10.49 (10.22)	7.25 (7.15)
L-Leu·DCHA	59 (B)	1.1	146—156	−30.0	59.82 (59.42)	10.66 (10.14)	6.84 (6.93)
L-Ile·CHA	63 (B)	1.1	146—158	−13.8	50.03 (49.43)[f]	9.86 (9.70)[f]	8.55 (8.23)[f]
L-Phe·DCHA	65 (B)	1.1	165—170	−7.5	62.89 (63.02)	9.05 (8.90)	6.49 (6.39)
L-Pro·DCHA	48 (B)	1.1	131—133	−75.0	57.88 (57.45)[g]	9.55 (9.57)[g]	7.14 (7.05)[g]
L-Met·DCHA	78 (B)	1.1	147—149	−10.0	53.34 (52.91)[h]	9.13 (9.27)[h]	6.35 (6.49)[h]
L-Cys(Bzl)·DCHA	67 (B)	3.0	162—164(dec)	+10.0	59.55 (59.51)	8.39 (8.46)	5.43 (5.78)
L-Asp(OBu^t)·DCHA	41 (B)	1.1	154	−20.0	57.38 (57.16)	9.55 (9.30)	5.61 (6.06)
L-Tyr·DCHA	65 (A)		160—161	−10.0	58.04 (58.49)[i]	8.81 (8.80)[i]	6.17 (5.93)[i]
L-Tyr(Bzl)·DCHA	23 (B)	1.1	169—172	−10.0	66.03 (66.19)	8.35 (8.27)	4.81 (5.14)
L-Lys(Z)·DCHA	16 (B)	1.1	123—124	+5.0	60.14 (59.80)[j]	8.67 (8.71)[j]	7.32 (7.47)[j]
L-Trp·DCHA	47 (B)	1.1	180—185(dec)	−12.5[d]	62.48 (62.91)	8.10 (8.38)	8.49 (8.80)
D-Ala·DCHA	41 (B)	2.1	172—173(dec)	+7.5	55.62 (55.63)[k]	10.16 (9.75)[k]	7.89 (7.63)[k]

a) Described in Experimental. b) *c* 1 in EtOH unless otherwise stated. c) Diethylphosphinothioyl derivative. d) *c* 1 in MeOH. e) Calcd for $C_{17}H_{35}N_2O_2PS\cdot H_2O$. f) Calcd for $C_{14}H_{31}N_2O_2PS\cdot H_2O$. g) Calcd for $C_{25}H_{43}N_2O_2PS\cdot 1/2\,H_2O$. h) Calcd for $C_{19}H_{39}N_2O_2PS_2\cdot 1/2\,H_2O$. i) Calcd for $C_{23}H_{39}N_2O_3PS\cdot H_2O$. j) Calcd for $C_{28}H_{48}N_3O_4PS\cdot 1/2\,H_2O$. k) Calcd for $C_{17}H_{35}N_2O_2PS\cdot 1/4\,H_2O$.

rapidly. A solution of triphenylphosphine dihydrochloride in dichloromethane[2,5] effectively increased the rate of removal of the Mpt by a factor of 60 compared to the *t*-butoxycarbonyl(Boc) group;[8] this reagent appears to be very convenient in solid phase synthesis. Deprotection of Mpt-L-phenylalanine resin was completed within 10 min by treatment with 0.5 M (1 M= 1 mol dm^{-3}) hydrogen chloride in dichloromethane containing 0.25 M triphenylphosphine and within 30 min with 0.25 M hydrogen chloride solution.[2]

To demonstrate the synthetic utility of Mpt-amino acids, the solid phase syntheses of L-Leu^5-enkephalin (L-Tyr–Gly–Gly–L-Phe–L-Leu) and the D-Ala^2 analog were attempted. Mpt-L-leucine was esterified with a chloromethyl resin by the caesium salt method.[9] Deprotection of the Mpt group was achieved by treatment with 0.2 M hydrogen chloride solution in dichloromethane containing 0.2 M triphenylphosphine for each 30 min (twice). Coupling of the Mpt- and Ept-amino acids were mediated with the oxidation-reduction condensation method[10] using a 3-fold excess of tris(*p*-methoxyphenyl)phosphine[11] and 2,2′-dithiodipyridine. This enabled tyrosine could be used without protection of the side chain hydroxyl group. Crude peptides were removed from the resin by treatment with hydrogen bromide in trifluoroacetic acid[12] in the presence of anisole. Separation by preparative thin layer

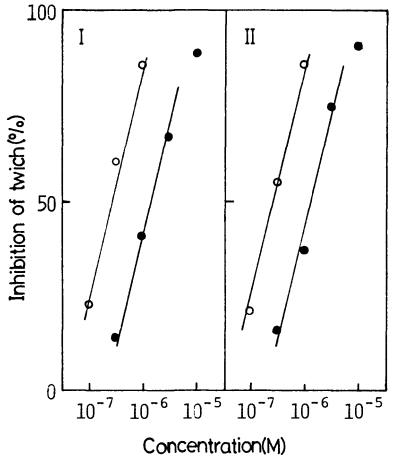

Fig. 1. Dose-response curve of synthetic L-Leu^5-enkephalin (I) and an authentic sample (II). (○: agonist alone, ●: agonist+naloxone 10^{-8} M).

chromatography on silica gel and purification by gel chromatography on Sephadex LH-20 gave the desired compounds in 52 and 40% yields, respectively. The activity of the synthetic L-Leu^5-enkephalin as an opioid agonist in logitudial muscle strips of guinea-pig ileum was identical with that of an authentic sample (Protein Research Foundation, Osaka) as shown in Fig. 1. The activity of D-Ala^2, L-Leu^5-enkephalin is now being studied and the results will be published in due course.

Experimental

Thin layer chromatography (TLC) was performed on silica gel plates (Merck $60F_{254}$) in the following solvent systems: chloroform–methanol–aqueous ammonia (60: 30: 5, R_f^1), 1-butanol–acetic acid–ethyl acetate–water (1: 1: 1: 1, R_f^2) and ethanol–water (7: 3, R_f^3). The peptides were detected on the TLC plates using ultraviolet light, iodine vapor and ninhydrin.

Dimethylphosphinothioyl chloride was prepared according to the literature.[6,7] Distillation of the product was achieved after decomposition of the contaminating dimethylphosphinyl chloride by shaking with water. The chloride **1** solidified on cooling and was stored for several months, without change, in a refrigerator.

N^{α}-Dimethylphosphinothioylamino acids were prepared by the alkaline hydrolysis of N^{α}-dimethylphosphinothioylamino acid esters obtained by the reaction of dimethylphosphinothioyl chloride with amino acid esters(Method A) and the reaction of an ethereal solution of dimethylphosphinothioyl chloride and α-amino acids (or α-amino acids bearing a protected side-chain functional group) in aqueous alkaline solution at controlled pH. The dimethylphosphinothioylamino acids thus prepared were isolated as the dicyclohexylamine(DCHA) or cyclohexylamine(CHA) salts.

Method A. To a suspension of the amino acid ester hydrochloride (5 mmol) in chloroform (10 ml) and triethylamine (10 mmol), Mpt–Cl (5 mmol) in chloroform (5 ml) was added at 0 °C. After stirring at room temperature for 6 h, the solution was washed with water, ice-cold 5% citric acid solution, water, 5% $NaHCO_3$ solution and saturated NaCl solution, dried and evaporated to dryness. The oily residue was dissolved in ethanol (5 ml) and to this solution was added 1 M NaOH solution (5 ml). The reaction mixture was stirred at room temperature for 4 h. After removal of ethanol *in vacuo*, the aqueous solution was extracted twice with ethyl acetate and the ethyl acetate extracts back extracted with 5% $NaHCO_3$ solution. The combined aqueous solutions were acidified at 0 °C to pH 4—5 with solid citric acid, saturated with NaCl and extracted 5 times with ethyl acetate. The ethyl acetate extracts were effectively washed with saturated NaCl solution and dried over anhydrous Na_2SO_4. After removal of the drying reagent, DCHA was added to effect separation of the corresponding salt. On certain occasions the addition of the same volume of ether was necessary to induce precipitation. The product was filtered off and washed with ethyl acetate or ether.

Method B. The amino acid (50 mmol) was dissolved in 1 M NaOH solution (50 ml), and Mpt–Cl (55 mmol) in ether (50 ml) added dropwise at 0 °C. The mixture was vigorously stirred to initiate immediate reaction. 1 M NaOH solution was added at a rate which maintained the pH of the solution at 9.5—10.0. Subsequently the reaction mixture was treated as described in Method A. The product was isolated as the DCHA or CHA salt and purified by recrystallization from ethanol, ethyl acetate or a methanol–ether mixture.

Dichloromethane Solution of Triphenylphosphine Dihydrochloride. Dry hydrogen chloride was passed through a dichloromethane solution of triphenylphosphine and saturated at room temperature. An aliquot of the solution was added to water and titrated with 1 M NaOH solution using phenolphthalein as the indicator to determine the concentration of HCl.

Solid Phase Synthesis of L-Leu^5-enkephalin. Mpt-L-leucine was esterified on resin support by treatment of the caesium salt with a chloromethyl resin prepared by chloromethylating the Bio-Beads S-X1 (Bio-Rad Laboratories) (Leu content; 0.63 mmol/g). The ester resin (1 g) was placed in the reaction vessel of the Beckman model 990 peptide synthesizer using the program described before.[4] Removal of the Mpt group was affected by 0.2 M HCl in dichloromethane solution containing 0.2 M triphenylphosphine (twice for 30 min). After neutralization with 10% triethylamine in dichloromethane, the couplings were mediated with the oxidation-reduction condensation method using tris(*p*-methoxyphenyl)phosphine and 2,2′-dithiodipyridine. Glycine was used as the Ept derivative. The Mpt-L-Leu^5-enkephalin-resin was finally deprotected, washed and dried *in vacuo*. A sample was hydrolysed in 12 M HCl–propionic acid at 130 °C for 2 h[13] to give the amino acid ratios: $Tyr_{0.99}$, $Gly_{1.89}$, $Phe_{1.06}$, $Leu_{0.99}$. The penta-peptide was removed from the resin by bubbling a stream of anhydrous hydrogen bromide through a suspension of the peptide resin in trifluoroacetic acid (10 ml) containing 50 equivalents of anisole for 90 min at room temperature. The filtrate and three trifluoroacetic acid (30 ml) washings were combined and evaporated *in vacuo*. The residue was separated and purified by silica gel preparative layer chromatography using the solvent system 1. The desired band (R_f=0.3—0.4) was eluted with methanol and evaporated *in vacuo* to give a white solid. The solid was dissolved in a small amount of methanol and applied to a Sephadex LH-20 (3×80 cm) column in order to remove the silica gel contaminents. The individual fractions collected (8 ml each) were examined by UV absorbancy at 280 nm. The eluates containing a single component (tube Nos. 27—33) were combined and evaporated to give white crystals; 167 mg (52% from Mpt-L-Leu-resin). An analytical sample was obtained by recrystallization from methanol, mp 158—160 °C (lit,[14] 157—167 °C, lit,[15] 206—208 °C); $[\alpha]_D^{25}$ +27.8° (*c* 0.9, MeOH) (lit,[15] +32.3° (*c* 0.9, MeOH), lit,[16] +20° (*c* 1, MeOH)); R_f^1 0.35 (lit,[17] 0.33), R_f^2 0.73 (lit,[16] 0.85), R_f^3 0.74 (lit,[17] 0.77). Amino acid ratios in hydrolysate by 6 M HCl at 110 °C for 24 h: $Tyr_{0.98}$, $Gly_{2.02}$, $Phe_{0.99}$, $Leu_{1.01}$. Found: C, 59.14; H, 6.95; N, 12.30%. Calcd for $C_{28}H_{38}N_5O_7 \cdot 1/2H_2O$: C, 59.46; H, 6.95; N, 12.38%.

D-Ala^2, L-Leu^5-enkephalin. This peptide was synthesized in a similar manner to above using Mpt-D-alanine at the third acylation step. The desired compound was obtained in 40% yield (from Mpt-L-Leu-resin) as white crystals. An analytical sample was obtained by recrystallization from methanol, mp 182—184 °C; $[\alpha]_D^{25}$ −25.0° (*c* 0.1, MeOH); R_f^1 0.49, R_f^2 0.83, R_f^3 0.71. Amino acid ratios in hydrolysate by 6 M HCl at 110 °C for 24 h: $Tyr_{0.99}$, $Ala_{0.99}$, $Gly_{0.97}$, $Phe_{1.02}$, $Leu_{1.00}$. Found: C, 58.75; H, 7.47; N, 10.94%. Calcd for $C_{29}H_{39}N_5O_7 \cdot 2MeOH$: C, 58.75; H, 7.48; N, 11.05%.

The authors wish to thank Prof. Tetsuo Oka (Tokai University) for the biological activity measurements.

References

1) M. Ueki and S. Ikeda, "Peptide Chemistry 1976,"

ed by T. Nakajima, Protein Research Foundation, Osaka (1977), pp. 1—4.
2) M. Ueki, S. Ikeda, and F. Tonegawa, "Peptides: Proceedings of the 5th American Peptide Symposium," ed by M. Goodman and J. Meienhofer, John Wiley and Sons, Inc., New York (1977), pp. 546—548.
3) M. Ueki and S. Ikeda, *Chem. Lett.*, **1976**, 827.
4) S. Ikeda, F. Tonegawa, E. Shikano, K. Shinozaki, and M. Ueki, *Bull. Chem. Soc. Jpn.*, **52**, 1431 (1979).
5) M. Ueki and S. Ikeda, *Chem. Lett.*, **1977**, 869.
6) G. W. Parshall, *Org. Synth.*, Coll. Vol. V, 1016 (1973).
7) L. Maier, *Chem. Ber.*, **94**, 3051 (1961).
8) F. Tonegawa, M. Ueki, and S. Ikeda, *Bull. Chem. Soc. Jpn.*, to be submitted.
9) B. F. Gisin, *Helv. Chim. Acta*, **56**, 1476 (1973).
10) T. Mukaiyama, R. Matsueda, and M. Suzuki, *Tetrahedron Lett.*, **1970**, 1901.
11) M. Ueki and S. Ikeda, unpublished.
12) E. Schröder, H. S. Petras, and E. Klieger, *Justus Liebigs Ann. Chem.*, **679**, 221 (1964).
13) F. C. Westall, J. Scotchler, and A. B. Robinson, *J. Org. Chem.*, **37**, 3363 (1972).
14) H. H. Büscher, R. C. Hill, D. Romer, F. Cardinaux, A. Closse, D. Hanser, and J. Pless, *Nature*, **261**, 423 (1976).
15) E. Pietrzik, H. Kalbacher, and W. Voelter, *Justus Liebigs Ann. Chem.*, **1977**, 609.
16) D. A. Jones, Jr., *Tetrahedron Lett.*, **1977**, 2853.
17) J. K. Chang and B. T. W. Fong, *Life Sci.*, **1976**, 1473.

NOTES

BULLETIN OF THE CHEMICAL SOCIETY OF JAPAN, VOL. 52 (8), 2428 (1979)

Raman Spectrum of the Complex of Nitrobenzene with Aluminum Chloride

Kunio FUKUSHIMA

Department of Chemistry, Faculty of Science, Shizuoka University, 836 Oya, Shizuoka 422

(Received March 31, 1979)

Synopsis. Raman spectrum of the complex of nitrobenzene with aluminum chloride in a nitrobenzene solution was measured. The shift frequencies and the degree of depolarization of Raman bands of the nitrobenzene in the complex are different from those of nitrobenzene. The differences were discussed based on the prior assignment of Raman bands of nitrobenzene.

Aluminum complex of nitrobenzene is well-known as the acceptor in many charge transfer complexes. Although infrared spectra were reported recently,[1] laser Raman spectral data are not available. In the present study, a laser excited Raman spectrum of the complex of nitrobenzene with aluminum chloride was measured in order to get information of the structure of the complex primarily based on the degree of depolarization.

Experimental

Raman spectrum of the nitrobenzene saturated with anhydrous aluminum chloride at room temperature was measured using 0.1 ml Raman cell. The spectrum was recorded on a Japan Spectroscopic Co., Ltd. Model R-800T Raman Spectrophotometer, being excited with a Spectra Physics argon ion laser (model 165) using 514.5 nm line (300 mW). The Raman shift frequencies, the intensities, and the degree of depolarization are shown in Table 1.

Results and Discussion

The observed Raman bands are classified into two groups. One consists of the Raman bands of the complex, whose shift frequencies are almost the same as those of nitrobenzene and are overlapped by nitrobenzene bands, while the other consists of those marked with C in Table 1. The Raman bands of the latter group except for those having the shift frequencies, 1470 and 1182 cm^{-1}, are due to the nitro group. All the Raman bands of both groups have the values of degree of depolarization smaller than 0.75, showing that the complex has neither symmetry axes nor symmetry planes. Especially, the degree of depolarization ($\rho=0.67<0.75$) of the Raman band (shift frequency, 180 cm^{-1}), which corresponds to an out-of-plane bending vibration (b_1 symmetry species), suggests that the plane including the benzene ring and the nitro group no longer exists in the complex or the plane is no longer symmetry plane, even if it existed. Remarkable changes of the shift frequencies of the nitro group in the complex formation show the coordination of aluminum atom to oxygen atom. The shift frequency, 398 cm^{-1}, of the Raman band of aluminum chloride in the complex is different from those of corresponding bands (a_1 symmetry species; 350 cm^{-1} for acetonitrile solutions;[3] 371 cm^{-1} for the vapor state[4]), but is almost the same as that of monomeric aluminum chloride in argon matrix.[5] Therefore, the almost planar structure similar to that of aluminum chloride in argon matrix,[5] persists even in the complex.

Table 1. Observed shift frequencies (in cm^{-1}), intensities (I) and degree of deaolarization (ρ) of the Raman bands of the nitrobenzene saturated with aluminum chloride at room temperature

Shift frequency	I	ρ		Corresponding bands of the components of the complex[2,5]
1595	17	0.49		$C_6H_5NO_2$ a_1(CC str.)
1546	12	0.35	C	
1533	sh	?		$C_6H_5NO_2$ b_2(NO_2 asym. str.)
1485	2	≈0.40		$C_6H_5NO_2$ a_1(CC str.)
1470	5	0.35	C	
1351	100	0.17		$C_6H_5NO_2$ a_1(NO_2 asym. str.)
1270	14	0.48	C	
1182	4	0.55	C	
1166	sh	?		$C_6H_5NO_2$ b_2(CH bend.)
1110	18	0.16		$C_6H_5NO_2$ a_1
1024	12	0.11		$C_6H_5NO_2$ a_1(CH bend.)
1007	57	0.07		$C_6H_5NO_2$ a_1(ring)
856	27	0.08		$C_6H_5NO_2$ a_1(NO_2 bend.)
850	sh	?	C	
797	1	?		$C_6H_5NO_2$ b_1(CH bend.)
713	<1	?		$C_6H_5NO_2$ b_1(NO_2 wag.)
685	2	0.18		$C_6H_5NO_2$ a_1
615	7	0.60		$C_6H_5NO_2$ b_2(CCC bend.)
610	sh	?		$AlCl_3$ E′
530	<1	?		$C_6H_5NO_2$ b_2(NO_2 rock.)
465	1	≈0	C	
398	9	0.08		$C_6H_5NO_2$ a_1, $AlCl_3$ a_1
250	2	0.50		$C_6H_5NO_2$ b_2
180	4	0.67		$C_6H_5NO_2$ b_1
175	sh	?		$AlCl_3$ E′

References

1) V. P. Basov, Y. P. Lobanov, and A. P. Shut'ko, *Zh. Prikl. Spektrosk.*, **25**, 1114 (1976).

2) J. H. S. Green and D. J. Harrison, *Spectrochim. Acta, Part A*, **26**, 1925 (1970); *V. C. Farmer, ibid.*, **23**, 728 (1967); S. Dähne and H. Stanko, *ibid.*, **18**, 561 (1962); S. Pinchas, D. Samuel, and B. L. Silver, *ibid.*, **20**, 179 (1964); A. Kuwai and K. Machida, *ibid.*, **35**, 27 (1979).

3) B. Izdebska and M. N. Buslayeva, *Rocz. Chem.*, **51**, 1005 (1977); present study.

4) I. R. Beattie and J. R. Horder, *J. Chem. Soc., A*, **1969**, 2655.

5) I. R. Beattie, H. E. Blayden, S. M. Hall, S. N. Jenny, and J. S. Ogden, *J. Chem. Soc., Dalton Trans.*, **1976**, 666; V. H. Schnöckel, *J. Anorg. Allg. Chem.*, **424**, 203 (1976); J. S. Shirk and A. F. Shirk, *J. Chem. Phys.*, **64**, 910 (1976).

BULLETIN OF THE CHEMICAL SOCIETY OF JAPAN, VOL. 52 (8), 2429—2430 (1979)

The Contraction of Water in the Hydration Shell

Kiyoshi SHIMIZU

Department of Applied Chemistry, Faculty of Engineering, Doshisha University, Karasuma Imadegawa, Kamigyo-ku, Kyoto 602

(Received October 4, 1978)

Synopsis. In the aqueous solutions of some sulfates, the contraction of water molecules in a hydration shell and the hydration number were estimated by using the data of the limiting equivalent conductance of the ion and the partial molal volume of electrolytes at an infinite dilution.

In a previous paper,[1] we estimated the partial molal volumes of the ion pairs of some sulfates in aqueous solutions by using the data obtained from the molar conductances obtained under high pressures and discussed the tendency of the metal ion to form an outer-sphere ion pair with the sulfate ion. The partial molal volumes of the electrolytes and the volume changes of the dissociation of the ion pairs in the aqueous solutions at an infinite dilution were always negative. This may be mainly ascribed to the contraction of water molecules in the hydration shell with ions so that the density of water in the neighborhood of an ion may be higher than that of the bulk water.

From the conductance data, the volume of the hydration shell of an ion or electrolyte and the hydration number can be found by applying the Stokes law and the Robinson and Stokes method[2] as follows:

$$r_s = \frac{0.820|z|}{\lambda^\circ \cdot \eta}, \tag{1}$$

where λ° is the limiting equivalent conductance of an ion with the Stokes radius of r_s and an absolute charge, $|z|$, and where η is the viscosity of pure water. r_s is corrected to the effective radius, r_e, by means of the Robinson-Stokes correction factor, f,

$$r_e = r_s \cdot f. \tag{2}$$

Then, the volume of the hydration shell in the neighborhood of the ion, V_H, can be represented by this equation

$$V_H = \frac{4}{3}\pi L(r_e^3 - r_c^3), \tag{3}$$

where L is Avogadro's number, and r_c, the crystallographic radius of the ion. The hydration number, h, is given by this equation

$$h = \frac{V_H}{V_E}, \tag{4}$$

where V_E is the molar volume of water in the hydration shell in the neighborhood of the ion. In most cases, V_E was assumed to be equal to the molar volume of the bulk water, V_B,[2,3] so the hydration number may be underestimated.

As has been mentioned above, the contraction of water molecules surrounding an ion may occur upon a change in the states of the water molecules from the bulk to the hydration during the dissolution and dissociation of electrolyte. It has been shown by Padova[4] that the average theoretical contraction due to the electrostriction per mole of water is $\Delta V = -2.1$ cm^3/mol. Millero *et al.*[5] have determined $\Delta V = V_E - V_B = -3.0$ cm^3/mol from the isothermal compressibility data of aqueous solutions of various salts. Recently, Millero *et al.*[6] have determined the amount of water lost in the ion-pairing process of an aqueous $CaSO_4$ solution by using the value of $V_E - V_B = -3.8$ cm^3/mol.

The partial molal volume of an electrolyte at an infinite dilution, $\bar{V}^\circ(M^{2+}) + \bar{V}^\circ(SO_4^{2-})$, may be represented by the sum of the two major components resulting from the simple model for hydration[7]

$$\bar{V}^\circ(M^{2+}) + \bar{V}^\circ(SO_4^{2-}) = \bar{V}^\circ(\text{int}) + \bar{V}^\circ(\text{elect}), \tag{5}$$

and

$$\bar{V}^\circ(\text{int}) = \frac{4}{3}\pi L[r_c(M^{2+})^3 + r_c(SO_4^{2-})^3], \tag{6}$$

where $\bar{V}^\circ$(int) is the intrinsic partial molal volume of the electrolyte, and $\bar{V}^\circ$(elect), the electrostriction partial molal volume. Then, the electrostriction partial molal volume of the electrolyte can be estimated by using the partial molal volume of the electrolyte at an infinite dilution and related to the hydration number of the electrolyte, n_H, by this equation

$$\bar{V}^\circ(\text{elect}) = n_H(V_E - V_B).^{4,7,8} \tag{7}$$

We assume that n_H in Eq. 7 is equal to the sum of $h(M^{2+})$ and $h(SO_4^{2-})$ in Eq. 4 as a first approximation, though the hydration numbers obtained by the various methods do not always coincide with each other. From Eqs. 4 and 7, we obtain this equation,

$$\frac{V_H(M^{2+}) + V_H(SO_4^{2-})}{V_E} = \frac{V_H(M^{2+}) + V_H(SO_4^{2-})}{V_B + (V_E - V_B)} = \frac{\bar{V}^\circ(\text{elect})}{V_E - V_B}. \tag{8}$$

$V_E - V_B$ for each electrolyte was estimated by means of Eq. 8 with the values of $V_H(M^{2+}) + V_H(SO_4^{2-})$ and $\bar{V}^\circ$(elect) in Tables 1 and 2, and with $V_B = 18.05$ cm^3/mol at 25 °C. These results are also shown in Table 2. The mean value of $V_E - V_B$ is found to be

TABLE 1. LIMITING EQUIVALENT CONDUCTANCE, STOKES, EFFECTIVE, AND CRYSTALLOGRAPHIC RADII, HYDRATION VOLUME, AND HYDRATION NUMBER AT 25 °C

Ion	λ°	r_s / nm	r_e / nm	r_c[9] / nm	V_H / cm^3 mol^{-1}	h
Mg^{2+}	53.1	0.345	0.431	0.065	201.2	13.6
Mn^{2+}	53.2	0.345	0.431	0.080	200.6	13.6
Co^{2+}	55.7	0.330	0.426	0.072	194.0	13.1
Ni^{2+}	54.4	0.337	0.426	0.070	194.1	13.1
Cu^{2+}	54.3	0.338	0.427	0.072	195.4	13.2
Zn^{2+}	53.4	0.344	0.430	0.074	199.5	13.5
SO_4^{2-}	80.0	0.229	0.366	0.273[10]	72.3	4.9

Table 2. Partial molal volumes, hydration number of electrolyte, and contraction volume of water at 25 °C

Electrolyte	$\bar{V}^\circ(M^{2+})+\bar{V}^\circ(SO_4^{2-})$ / cm³ mol⁻¹	$\bar{V}^\circ$(elect) / cm³ mol⁻¹	n_H	V_E-V_B / cm³ mol⁻¹
$MgSO_4$	−7.2[7]	−59.2	17.9	−3.2
$MnSO_4$	−3.7	−56.3	17.1	−3.1
$CoSO_4$	−9.5	−61.7	18.7	−3.4
$NiSO_4$	−10.0[7]	−62.2	18.8	−3.4
$CuSO_4$	−8.1	−60.3	18.3	−3.3
$ZnSO_4$	−8.0	−60.3	18.3	−3.3

−3.3 cm³/mol. This value is in good agreement with those estimated by Padova[4] and Millero *et al.*[5,6] V_E is about 14.8 cm³/mol, and the density of the water in the hydration shell in the neighborhood of the ions is estimated to be about 1.22 g/cm³, comparable to the densities of ice III and/or V under high pressures. The hydration number of the ion, h, is also shown in Table 1. These values are in reasonable agreement with those estimated by Padova[4] and suggest that, especially in a metal ion, the hydration shell may contain the water molecules not only in the first layer, but also in the second and the outer layers.

References

1) K. Shimizu, N. Tsuchihashi, and Y. Kondo, *Rev. Phys. Chem. Jpn.*, **47**, 80 (1977).
2) R. A. Robinson and R. H. Stokes, "Electrolyte Solutions," Butterworths Scientific Publications (1965).
3) J. O'M. Bockris, *Quart. Rev. (London)*, **3**, 173 (1949).
4) J. Padova, *J. Chem. Phys.*, **39**, 1552 (1963); **40**, 691 (1964).
5) F. J. Millero, G. K. Ward, F. K. Lepple, and E. V. Hoff, *J. Phys. Chem.*, **78**, 1636 (1974).
6) F. J. Millero, F. Gombar, and J. Oster, *J. Soln. Chem.*, **6**, 269 (1977).
7) F. J. Millero, *Chem. Rev.*, **71**, 147 (1971); "Water and Aqueous Solutions," ed by R. A. Horne, Wiley-Interscience, N. Y. (1972).
8) F. J. Millero and W. L. Masterton, *J. Phys. Chem.*, **78**, 1287 (1974).
9) L. Pauling, "Nature of the Chemical Bond," Cornell University Press, 2nd ed, Ithaca, N. Y. (1948).
10) O. K. Rice, "Electronic Structure and Chemical Binding," McGraw-Hill Book Company, N. Y. (1940).

BULLETIN OF THE CHEMICAL SOCIETY OF JAPAN, VOL. 52 (8), 2431—2432 (1979)

A Study of Catalysis by Metal Phosphates. V.[1] The Alkylation of Toluene with Methanol over Metal Phosphate Catalysts

Toshiaki SODESAWA,* Isao KIMURA, and Fumio NOZAKI

Department of Industrial Chemistry, Faculty of Engineering, Chiba University, Yayoi-cho, Chiba 260

(Received January 10, 1979)

Synopsis. The side chain alkylation of toluene with methanol over the catalyst of $Ca_3(PO_4)_2$ or K_3PO_4 supported on active carbon gave more ethylbenzene than that over MgO. It was found that there are correlations between the catalytic activities and acid-base properties.

In a previous paper a report was given on the alkylation of phenol with methanol over metal phosphate catalysts.[1] It is well-known that metal phosphates have acid properties. However, it was found that $Ca_3(PO_4)_2$ and K_3PO_4 have not only acidic but also basic sites.[2,3] In this paper, the correlation between the catalytic activity of metal phosphates and their acid-base properties are discussed. The activity sequence and catalytic behavior of metal phosphates are compared with those of other solid acid-base catalysts.

Experimental

The metal phosphates, MgO, and CaO catalysts were prepared according to the method reported.[1] Commercial chemicals of guaranteed grade were used: H-Zeolon, SiO_2–Al_2O_3, $Al_2(SO_4)_3$, Al_2O_3, Na_2WO_4. The catalysts of Na_3PO_4 and K_3PO_4 supported on active carbon (Tsurumicoal Kogyo Co.) were prepared by the impregnating method, the concentration being made about 15 wt %. All the catalysts were activated by calcination in a stream of nitrogen gas at 500 °C for 1 h prior to each test.

The acidity of catalysts was measured by Benesi's method,[4] using the following Hammett indicators: Neutral Red (pK_a = +6.8), Methyl Red (+4.8), Dimethyl Yellow (+3.3), 4-phenylazodiphenylamine (+1.5), dicinnamylideneacetone (−3.0), benzylideneacetophenone (−5.6), anthraquinone (−8.2). As a titration reagent *n*-buthylamine of 0.1 mol/l in benzene solution was added to a known amount of catalysts calcined at 500 °C for 4 h. Hammett indicators were then added and the resulting with coloration was compared visually. Titration with benzoic acid of 0.1 mol/l using Bromothymol Blue (pK_a=7.1), phenolphthalein (9.3), 2,4-dinitroaniline (15.0), and 4-chloro-2-nitroaniline (17.2) as indicators was carried out in order to measure the basicity of catalysts. The procedure was almost the same as in the acidity measurements.

The apparatus and procedure were almost the same as described previously. The reaction products were trapped with ice and analyzed by gas chromatography on a 3 m column of Benton 34(5%)+DNP(5%), hydrogen being passed through as a carrier gas.

Results and Discussion

In the case of alkylation of phenol with methanol over $Ca_3(PO_4)_2$ catalyst, the main products are *o*-cresol and 2,4-xylenol which are produced by the ortho-position alkylation of benzene ring. Results of alkylation of toluene with methanol over various catalysts are given in Table 1. We see that the alkylation of toluene does not occur readily as compared with that of phenol. The methylation of benzene ring over BPO_4 and $Zr_3(PO_4)_2$ gave selectively as much xylenes as that over SiO_2–Al_2O_3 and H-Zeolon catalysts. The BPO_4 catalyst showed the highest activity of all the metal phosphates and produced much *o*-xylene in all xylenes, while $Ca_3(PO_4)_2$ and K_3PO_4 gave only ethylbenzene by the alkylation of side chain. The results differ from those in the case of the base catalyst such as MgO which produced both ethylbenzene and styrene. The Na_3PO_4 catalyst supported on active carbon gave both xylenes and ethylbenzene. The active carbon gave only benzene and no alkylated products. This seems to be in line with other reported results.[5,6] The activity of K_3PO_4 catalyst for the side chain alkylation was not higher than that of MgO–TiO_2[7,8] and Zeolite catalysts exchanged K cation.[9] Improvement in the preparation

TABLE 1. ACTIVITIES OF CATALYSTS FOR ALKYLATION OF TOLUENE

Conditions: reaction temperature t=500 °C (except for SiO_2–Al_2O_3 and H-Zeolon catalysts, in which t was 400 °C), W/F=14.8 g h/mol, feed molar ratio of methanol/toluene/N_2=1/2/5.3.

Catalyst	Conversion of toluene (%)	Yield (%)					
		Ethylbenzene	Styrene	*o*-Xylene	*m*-Xylene	*p*-Xylene	Benzene
BPO_4	9.6	0	0	4.6	3.2	1.8	0
$Zr_3(PO_4)_4$	0.7	0	0	0.3	0.2	0.2	0
$Ca_3(PO_4)_2$	0.3	0.3	0	0	0	0	0
Na_3PO_4–AC[a]	2.3	0.7	0	0.3	0.2	0.1	1.0
K_3PO_4–AC[a]	1.8	1.8	0	0	0	0	0
SiO_2–Al_2O_3	21.7	0	0	9.0	7.0	5.7	0
H-Zeolon	32.6	0	0	9.0	16.0	7.6	7.6
MgO	1.0	0.3	0.7	0	0	0	0

a) AC denotes activated carbon used as a carrier. Na_3PO_4 or K_3PO_4 was supported to make the concentration about 15 wt %.

Table 2. Acid-base properties of catalysts

Catalyst[a]	pK_a							
	−8.2	−5.6	−3.0	+3.3	+4.8	+6.8	+7.1	+9.3
BPO_4	−	+	0.160[b]	+	+	+	−	
$Zr_3(PO_4)_4$	−	+	0.063[b]	+	+	+	−	
$Ca_3(PO_4)_2$				−	+	+	+	0.001[c]
Na_3PO_4					−	+	+	0.006[c]
K_3PO_4						−	+	0.010[c]
SiO_2–Al_2O_3	+	+	0.471[b]	+	+	+	−	
H-Zeolon	+	+	0.513[b]	+	+	+	−	
MgO					−	+	+	0.007[c]
CaO					−	+	+	0.011[c]

a) Calcined at 500 °C. + and − denote positive and negative, respectively. b) Acidity (mmol/g) measured at $H_0 \leqq -3.0$. c) Basicity (mmol/g) measured at $H_0 \geqq 9.3$.

of these catalysts might afford higher activity. The alkylation of ethylbenzene with methanol over K_3PO_4 and Na_3PO_4 supported on active carbon gave a greater amount of cumene than over MgO or CaO. The alkylation over the metal phosphates is essentially different in the reaction route from that of solid base catalysts such as MgO.

The acidity and basicity of various catalyst surfaces were measured (Table 2). It is obvious that the BPO_4 and $Zr_3(PO_4)_4$ catalysts, being as active as SiO_2–Al_2O_3 and H-Zeolon for xylene production in toluene alkylation, have acid sites at $H_0 \leqq -3.0$, while the $Ca_3(PO_4)_2$ and K_3PO_4 being as effective as MgO for ethylbenzene formation have basic sites at $H_0 \geqq 9.3$. The catalytic activities in each case seem to be strongly related to acid or base amounts of each catalyst. However, the route of side chain alkylation over $Ca_3(PO_4)_2$ or K_3PO_4 seems to differ from that over MgO which gives both ethylbenzene and styrene.

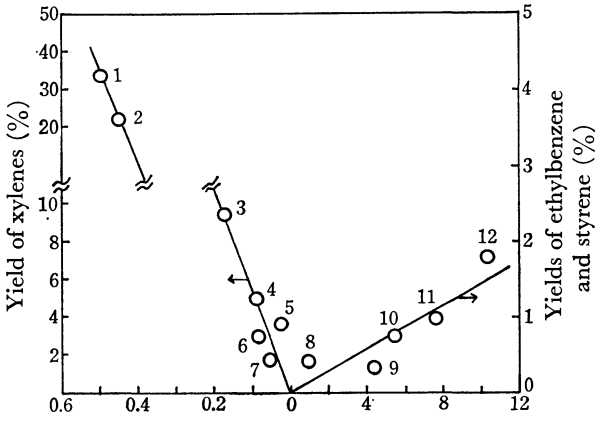

Fig. 1. Correlation between the catalytic activity and the acidity or basicity of various catalysts in the alkylation of toluene with methanol (acidity; $H_0 \leqq -3.0$, basicity; $H_0 \geqq 9.3$)
1: H-Zeolon, 2: SiO_2–Al_2O_3, 3: BPO_4, 4: $Al_2(SO_4)_3$, 5: Al_2O_3, 6: $CrPO_4$, 7: $Ti_3(PO_4)_4$, 8: $Ca_3(PO_4)_2$, 9: Na_2WO_4, 10: Na_3PO_4–AC, 11: MgO, 12: K_3PO_4–AC.

The correlations between the acid-base properties and the activities of various solid catalysts in the alkylation of toluene are shown in Fi . 1. There are correlations between the yields of xylenes and the acidity at $H_0 \leqq -3.0$ or the yields of ethylbenzene and styrene and the basicity at $H_0 \geqq 9.3$. The correlation between the acid-base property and the catalytic activity of $Ca_3(PO_4)_2$ calcined at various temperatures in the alkylation of phenol was reported.[1] It was found that the catalytic activities can be classified into three types of linear relationships, (a) highly dependent on acidity, (b) strongly dependent on basicity, (c) dependent on both acidity and basicity as indicated over $Ca_3(PO_4)_2$ catalyst. In the case of toluene (Fig. 1), it seems that the alkylation is highly related to acidity or basicity of catalysts. The alkylation of toluene over $Ca_3(PO_4)_2$ or K_3PO_4 supported on the active carbon is strongly related to base amounts of the catalyst.

References

1) Part IV of this series: F. Nozaki and I. Kimura, *Bull. Chem. Soc. Jpn.*, **50**, 614 (1977).
2) T. Imanaka, Y. Okamoto, and S. Teranishi, *Bull. Chem. Soc. Jpn.*, **45**, 1353 (1972).
3) A. Tada, *Bull. Chem. Soc. Jpn.*, **48**, 1391 (1975).
4) H. A. Benesi, *J. Phys. Chem.*, **61**, 970 (1975).
5) H. Pines and L. Shaap, *Adv. Catal.*, **12**, 117 (1960).
6) T. Yashima, H. Ahmad, K. Yamazaki, M. Katsuta, and N. Hara, *J. Catal.*, **16**, 273 (1972).
7) O. Takahashi, H. Hattori, and K. Tanabe, Abstr. No. 3E07, 39th Meeting of the Catalysis Society of Japan, Sapporo, August 1976.
8) K. Tanabe, O. Takahashi, and H. Hattori, *React. Kinet. Catal. Lett.*, **7**, 347 (1977).
9) Y. Murakami and H. Ito, 41st Meeting of the Catalysis Society of Japan, Toyama, October 1977, Abstr. No. C-3.

BULLETIN OF THE CHEMICAL SOCIETY OF JAPAN, VOL. 52 (8), 2433—2434 (1979)

Analysis of Glass Films Prepared from Alkoxides on Glass Substrates

Akira Iino and Atsushi Mizuike*

Faculty of Engineering, Nagoya University, Chikusa-ku, Nagoya 464

(Received January 30, 1979)

Synopsis. Sodium in 50 nm thick ZrO_2–SiO_2 glass films has been determined by secondary ion mass spectrometry. A remarkable sodium contamination from the Pyrex glass substrate has been confirmed.

The coating of glass surfaces with glass films of different kinds, prepared *in situ* by hydrolyzing mixtures of alkoxides, offers a new technique to improve the chemical and optical properties of glass surfaces.[1] By this technique, thin homogeneous glass films of various kinds, not obtainable by conventional techniques, may be prepared easily near the transition temperature of the glass.[2] To improve the chemical resistance of Pyrex glass ware, the present authors coated the glass surfaces with ultrathin films of 22 ZrO_2–78 SiO_2 mol% glass prepared from silicon tetraethoxide and zirconium tetrapropoxide. Contamination of sodium from the substrate during the preparation may occur and deteriorate the film. No information on this phenomenon is available to date and consequently the sodium in the films has been determined by secondary ion mass spectrometry (SIMS), which is the most suitable technique at present for the quantitative analysis of ultrathin films.

The glass films were transparent, homogeneous, and 50 ± 5 nm thick. Under the scanning electron microscope (2000X and 10000X), the surfaces of the films were found to be smooth and without pinholes and cracks. The films were not damaged by abrasive action with the fingers. Figure 1 shows the SIMS spectra of 22 ZrO_2–78 SiO_2 mol% glass films and Pyrex and silica glass substrates. In the film on the Pyrex glass substrate, sodium was found, but boron, aluminum, and potassium were found to be absent. The SIMS spectrum of the film on the silica glass substrate was identical with that of 22 ZrO_2–78 SiO_2 mol% glass flakes. The secondary ions originate from the region 10 nm from the surface.[3] The films were ion-etched only about 15 and 10 nm before and during the SIMS measurements, respectively, and therefore, the pure spectra of the films were obtained without interference from the substrate by this technique.

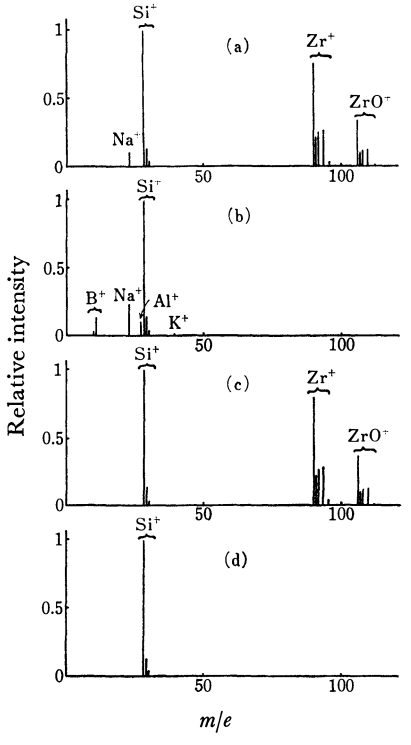

Fig. 1. SIMS spectra.
(a): ZrO_2–SiO_2 glass film on Pyrex glass, (b): Pyrex glass substrate, (c): ZrO_2–SiO_2 glass film on silica glass, (d): silica glass substrate.

Table 1. Sodium concentrations (Na_2O, mol %)

In glass flakes[a)]	In glass films[b)]	(Substrates)
0.0	1.4	(Pyrex)
0.0	0.0	(Silica)
0.29	0.31	(Silica)
2.5	2.5	(Silica)
5.2	5.5	(Silica)

a) Determined by flame photometry (maximum relative error ± 3%). b) Determined by SIMS (maximum relative error ± 10%).

In Table 1, the concentrations of sodium in the coating films have been compared with those in the corresponding glass flakes. Only the Pyrex glass substrate interacts with the glass film. The sodium concentrations in the films were constant between 20 and 35 nm from the surfaces. Additional heating at 450 °C for 5 h did not increase the sodium concentration. Therefore, the sodium contamination from the Pyrex substrate probably resulted from the presence of water in the film[2] between 200 and 400 °C during the preparation of the film.

Experimental

Preparation of Mixed Alkoxide Solutions. Into a 100 ml round-bottomed flask, silicon tetraethoxide (4 ml) (Nakarai Chemicals), zirconium tetrapropoxide (3 ml) (Ventron Corp.), sodium methoxide (0 to 0.6 ml) (Wako Pure Chemical Industries), and 1-butanol (13 ml) (dehydrated with Molecular Sieve 4A) were placed. A reflux condenser was attached to the flask, and the contents were well mixed with a magnetic stirrer for 3 h at 85 ± 5 °C in a stream of nitrogen (10 cm^3 min^{-1}, dried with calcium chloride). The mixture was cooled and stored in a glass stoppered bottle in a desiccator.

Coating. An 8×5 mm Pyrex or silica glass piece, 1 or 1.5 mm thick, was immersed in a 1 : 1 mixture of concentrated

nitric and sulfuric acids for 24 h, rinsed thoroughly with water, and dried over silica gel. The piece was immersed in a mixed alkoxide solution (100-ml beaker), and withdrawn vertically at a speed of 4 mm min^{-1} by a motor to form a film of uniform thickness. Hydrolysis was effected by placing the piece in a desiccator containing a saturated potassium sulfate solution (relative humidity 95%) at 50 °C for 60 min. The piece was heated at 150 °C for 60 min in an electric muffle furnace. Then the temperature was raised at a rate of 10 °C min^{-1}, kept at 550 °C for 30 min, and lowered to 350 °C at a rate of 1 to 2 °C min^{-1}. The piece was then cooled to room temperature.

Preparation and Analysis of Glass Flakes. A mixed alkoxide solution (1 ml) was placed in a 50 ml silica beaker, and allowed to stand for 24 h at ambient temperature (20—25 °C; relative humidity, 40—50%) to effect evaporation of the solvent and hydrolysis. The resulting flakes (*ca.* 3 mm × 3 mm × 50 μm) were heat-treated and annealed as described in the last paragraph, except that the heating time at 150 °C was increased to 2 h. The transparent glass flakes were used as standards in the SIMS determination of sodium in glass films on glass substrates. For standardization, the flakes were decomposed with hydrofluoric and hydrochloric acids, and sodium and zirconium were determined by flame photometry at 589.3 nm and inductively coupled plasma-optical emission spectrometry at 339.2 nm.

SIMS and Other Measurements. A Hitachi IMA-2 ion microanalyzer was operated under the following conditions: primary ions, argon; primary ion accelerating voltage, 5 kV; primary ion current, 0.1 μA; beam diameter, 250 μm; sample chamber pressure, 3×10^{-5} Pa; secondary ion accelerating voltage, 1.5 kV; electron-multiplier voltage; 2 kV. The electric charges accumulated on the glass surfaces were eliminated by the electron spray method. The SIMS spectra were recorded after ion etching 15 nm from the surface by rastering the primary beam (total number of scanning lines, 500; line frequency, 100 Hz) over a square area of 0.8 mm around the spot to be measured. For the determination of sodium in glass films, peak ratios of $^{23}Na^+$ to $^{28}Si^+$ were measured, and the sodium concentrations were obtained from a calibration curve. The curve (peak ratio *vs.* atom % Na) was prepared using glass flake standards [(22—21)ZrO_2–(78—74)SiO_2–(0—5)Na_2O mol % glasses] and was a straight line through the origin. The thickness of the glass films was measured with a Mizojiri Kogaku model II multiple beam interferometer (Hg 546.1 nm, magnification 40X), with a maximum error of ±3 nm.

References

1) H. Dislich, *Glastechn. Ber.*, **44**, 1 (1971).
2) M. Nogami and Y. Moriya, *Yogyo Kyokai Shi*, **85**, 59, 448 (1977).
3) G. Carter and W. A. Grant, *Phys. Chem. Glasses*, **7**, 94 (1966).

BULLETIN OF THE CHEMICAL SOCIETY OF JAPAN, VOL. 52 (8), 2435—2436 (1979)

The Stability of Bis(8-quinolinolato)copper(II)

Hideo AKAIWA* and Hiroshi KAWAMOTO

Department of Applied Chemistry, Faculty of Technology, Gunma University, Kiryu 376

(Received February 5, 1979)

Synopsis. The IR spectra of the titled and related compounds have been measured, and the stabilities of the chelates characterized by the relative strengths of the metal-nitrogen bonds. An explanation has been made by comparing the extraction behavior of Cu(II) and Fe(III) chelates.

The stability constants for several metal complexes of 8-quinolinol and related substances have been determined by Irving and Rossotti, and the contribution of the metal-nitrogen bonds to the stability of the copper-(II) complex of 8-quinolinol demonstrated although no experimental evidence was presented.[1)]

In the work described below, the stability of the metal chelate has been characterized through the effect of the methyl group of the 8-quinolinol skeleton on the metal-nitrogen bonds.

Experimental

Reagents and Apparatus. 8-Quinolinol was obtained from Wako Pure Chemicals. The methyl derivatives of 8-quinolinol were prepared as described by Phillips and Merritt,[2)] and the purity confirmed through melting point measurements, elemental analysis, IR, and NMR spectra.

The IR spectra were measured by a Nippon Bunko IR-F type spectrophotometer. Samples were in the form of Nujol mulls between polyethylene sheets.

Determination of Acid Exponents for the Reagents. The distribution ratios of 8-quinolinol and the methyl derivatives between chloroform and the aqueous phase of $\mu=0.2$ ($NaClO_4$) were measured at 20 °C as a function of pH, and the distribution data analysed according to Dyrssen.[3)]

Synthesis of Copper(II) Complexes. An ethanolic solution of 8-quinolinol and an aqueous solution of copper(II) acetate were mixed in a molar ratio of 2 to 1, and the mixture allowed to stand for two days. The resulting precipitate was filtered, washed with ethanol and dried over a steam bath. The anhydrous copper(II) complexes of the methyl-substituted 8-quinolinols were obtained according to the above procedure.

Extraction Curves. An aqueous solution ($\mu=1.0$: $NaClO_4$) of copper(II) or iron(III) was equilibrated with an equal volume of chloroform containing the reagent (5.0×10^{-3} mol dm^{-3}), the pH of the aqueous phase and the absorbance of the organic phase being measured after separation.

Results and Discussion

The values of the partition coefficients D_R, acid exponents pK_{OH} and pK_{NH} for 8-quinolinol and the methyl-derivatives are given in Table 1, the data of which are in good agreement with the literature values.[4)] The pK_{HO} values for the methyl derivatives are similar whereas the pK_{NH} values increase in the order; 8-quinolinol <5-methyl-8-quinolinol <4-methyl-8-quinolinol. The inductive and resonance effects due to the methyl-group are reflected in the above trend, and thus the stability of a metal complex can be predicted by choosing an appropriate derivative.

Table 1. Equilibrium constants for 8-quinolinol and its derivatives

Reagent	log D_R	pK_{OH}	pK_{NH}
8-Quinolinol	2.37±0.02	9.77±0.10	4.67±0.14
4-Methyl-8-quinolinol	2.65±0.05	10.28±0.19	5.23±0.17
5-Methyl-8-quinolinol	2.83±0.02	10.10±0.21	5.05±0.09

Table 2. Most important IR absorption bands for copper(II) complexes

Ligand	$\bar{\nu}$/cm^{-1} Cu–O	$\bar{\nu}$/cm^{-1} Cu–N
8-Quinolinol	325	290
4-Methyl-8-quinolinol	326	310
5-Methyl-8-quinolinol	321	300

The assignments of the $\bar{\nu}$(Cu–O) and $\bar{\nu}$(Cu–N) frequencies were conducted according to the work of Ohkaku and Nakamoto,[5)] and the results are summarized in Table 2. It should be noted that the bis(8-quinolinolato)copper(II) obtained by the above procedure was of the β-type, which is known to be a dimer having bridged oxygen atoms. As seen from Table 2, the effect of substitution is negligible on the $\bar{\nu}$(Cu–O) frequency indicating that the stability of bis(8-quinolinolato)copper(II) may depend on the strength of the metal-nitrogen bonds. The increasing order of the pK_{NH} values supports the increasing order of the $\bar{\nu}$(Cu–N), strongly suggesting that the stability for the copper(II) complex is mainly due to the metal-nitrogen bonds.

In order to examine the stability of the copper(II) complex in solution, solvent extraction studies were conducted and the extraction behavior of copper(II) compared with that of iron(III) which is a harder acid than copper(II). The extraction curves for iron(III) obtained by using 8-quinolinol and the methyl derivatives were almost identical, which were shown by a single curve having a $pH_{1/2}$ of 1.54±0.05. A notable effect of the substituent on the extraction of copper(II) was however, observed, and $pH_{1/2}$ values decreased in the following order; 8-quinolinol ($pH_{1/2}=2.0$)>5-methyl-8-quinolinol(1.90)>4-methyl-8-quinolinol(1.76).

The above differences in extraction behavior of the metals may be caused by a difference in the acid strength between the ions. The metal-oxygen bonds in tris(8-quinolinolato)iron(III) play an important role in stabilizing the complex. In contrast, the stability for the copper(II) complex depends mainly upon the metal-nitrogen bonds, as is shown by the present IR studies.

This work was supported in part by a Grant-in-Aid for Scientific Research from the Ministry of Education, No. 147033.

References

1) H. Irving and H. S. Rossotti, *J. Chem. Soc.*, **1954**, 2910.
2) J. P. Phillips and L. L. Merritt, Jr., *J. Am. Chem. Soc.*, **71**, 3984 (1949).
3) D. Dyrssen, *Svensk Kem. Tidskr.*, **64**, 213 (1952).
4) Y. Marcus and A. S. Kertes, "Ion Exchange and Solvent Extraction of Metal Complexes," Wiley-Interscience, New York (1969), p. 514.
5) N. Ohkaku and K. Nakamoto, *Inorg. Chem.*, **10**, 798 (1971).

BULLETIN OF THE CHEMICAL SOCIETY OF JAPAN, VOL. 52 (8), 2437—2438 (1979)

Phenanthro[4,5-*bcd*]furan Derivatives. V. The Cyclization of (Dibenzofuran-1-yl)acetic Acid Derivatives

Takaaki HORAGUCHI* and Teishiro ABE†

Department of Chemistry, Faculty of Science, Niigata University, Ikarashi, Niigata 950-21
†*Department of General Education, Niigata University, Ikarashi, Niigata 950-21*

(Received October 16, 1978)

Synopsis. The cyclization of (6-methoxy-1,2,3,4-tetrahydrodibenzofuran-1-yl)acetic acid (**3b**) and (6-methoxy-1,2,3,4,4a,9b-hexahydrodibenzofuran-1-yl)acetic acid (**5**) to the corresponding phenanthro[4,5-*bcd*]furans have been examined. The cyclization of **3b** was difficult, while that of **5** was easy. The difficult cyclization of **3b** has been attributed to strains in the reaction intermediate.

Dendy *et al.*[1] attempted to cyclize the (1,2,3,4-tetrahydrodibenzofuran-1-yl)acetic acids (**3a** and **3b**) to the corresponding phenanthro[4,5-*bcd*]furans (**4a** and **4b**) for the purpose of synthesizing morphenol. All attempts to cyclize **3a** were, however, unsuccessful. **4b** was obtained from Friedel-Crafts reaction of the acid chloride of **3b** but the yield was very low. Dendy *et al.* attributed the failure to ring strain in the products (**4a** and **4b**). 3-(8-Methoxy-4,5-dihydro-3*H*-naphtho-[1,8-*bc*]furan-3-yl)propionic acid (**1**) was readily cyclized by polyphosphoric acid (PPA) to the corresponding phenanthro[4,5-*bcd*]furan (**2**) which has a similar ring skeleton to **4b** in good yield.[2] Therefore, it is improbable that there is great strain in the **4b** molecule. It has previously been reported that the difficult cyclization of **3b** to **4b** may be due to strain in the reaction intermediate (**10**) rather than that of the product (**4b**).[3] Hydrogenation of the carbon-carbon double bond in the furan ring of **3b** would facilitate ready cyclization since the acetic acid side chain would closely approach the benzene ring in molecular terms. Thus, the saturated dibenzofuran derivative (**5**) could be readily cyclized. Consequently the cyclization of **5** to phenanthro[4,5-*bcd*]furan (**6**) has been attempted.

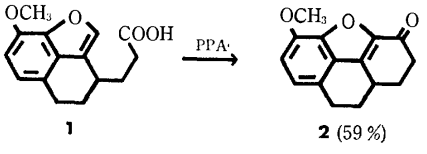

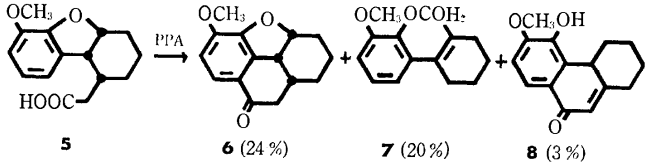

Fig. 1.

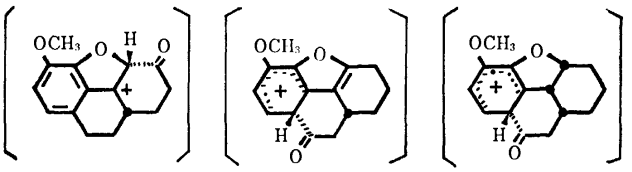

Fig. 2.

The ester (**13**) has been obtained by the Reformatsky reaction of the ketone (**12**). The formation of the ester (**14**) has been reported by Dendy *et al.*,[1] but the IR and NMR spectra of the product here were compatible with the structure of **13**. **13** was hydrogenated in the presence of palladium on charcoal and subsequently hydrolyzed to give **5**. It appears that the configuration of **5** is *cis-syn* as shown, since the furan ring is preferentially hydrogenated from the less hindered face after reduction of the exo-double bond. **5** was heated at 45 °C with PPA, and the desired phenanthro[4,5-*bcd*]-furan (**6**; 24%) was obtained together with a lactone (**7**; 20%) and a hydroxyl ketone (**8**; 3%). Cleavage of the furan ring before the formation of a carbonyl compound yields **7**. Cyclization and subsequent cleavage of the furan ring yields **8**. **5** was heated at 80 °C with PPA and the only product was **8** (40% yield). Under the same conditions (45 and 80 °C), **3b** did not give **4b**, the starting material being recovered. Thus, **5** was cyclized with greater facility than **3b**, as predicted.

These observations suggest that the conformation of the intermediate (**10**) is cup-shaped and possesses a large strain, whereas **11**, the intermediate in the cycliza-

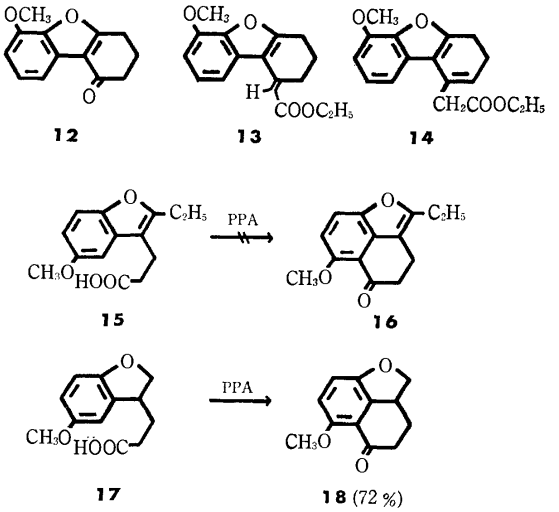

Fig. 3.

tion of **5** to **6**, possesses little strain owing to the saturated furan ring. The strain in the intermediate (**9**) is not large strain as the flexible propionic acid rest of **1** is attached very favorably for the cyclization reaction of **1** to **2**. Support for the above explanation is found in the facts that the cyclization of **15** to **16** is difficult but that of **17** to **18** is easy.[4]

Experimental

*The Cyclization of **5** with Polyphosphoric Acids.* A mixture of **5** (2.0 g) and 20% polyphosphoric acid (160 g) was heated with stirring at 45 °C for 7 h. The mixture was worked up in the usual manner. The resulting oil was chromatographed (benzene–ether 95: 5) on silica gel to give three products.

*Loctone (**7**).* 370 mg (20% yield). Colorless prisms from benzene–hexane; mp 81—82 °C. IR (KBr): ν_{max} 1765 (COO–Ar) cm^{-1}. NMR ($CDCl_3$): δ 1.66—1.81 (4H, m), 2.35 (4H, broad s), 2.89 (2H, s), 3.87 (3H, s), 6.82—7.33 (3H, m).

Found: C, 73.52; H, 6.67%. Calcd for $C_{15}H_{16}O_3$: C, 73.75; H, 6.60%.

*5-Hydroxy-6-methoxy-1,2,3,4,4a,9-hexahydrophenanthrene-9-one (**8**).* 60 mg (3% yield). Colorless plates from acetone–benzene; mp 144—145 °C. IR (KBr): ν_{max} 1665 (C=O), 3200, 3440 (OH) cm^{-1}. NMR (CD_3COCD_3): δ 1.28—1.79 (4H, m), 1.83—2.17 (2H, m), 2.39 (1H, dd, J=3 and 12 Hz), 2.83 (1H, dd, J=5 and 12 Hz), 3.12—3.31 (1H, m), 3.92 (3H, s), 6.20 (1H, s), 7.09 (1H, d, J=8 Hz), 7.62 (1H, d, J=8 Hz), 7.73 (1H, s).

Found: C, 73.51; H, 6.48%. Calcd for $C_{15}H_{16}O_3$: C, 73.75; H, 6.60%.

*5-Methoxy-1,2,3,3a,8,9,9a,9b-octahydrophenanthro[4,5-bcd]furan-8-one (**6**).* 440 mg (24% yield). Colorless needles from benzene–hexane; mp 101—102 °C. IR (KBr): ν_{max} 1690 (C=O) cm^{-1}. NMR ($CDCl_3$): δ 1.02—1.30 (3H, m), 1.53—1.70 (2H, m), 1.95—2.18 (1H, m), 2.40—2.75 (1H, m), 2.50 (1H, dd, J=2 and 17 Hz), 2.79 (1H, dd, J=5 and 17 Hz), 3.81 (1H, t, J=7 Hz), 3.94 (3H, s), 5.10 (1H, q, J=8 Hz), 6.83 (1H, d, J=9 Hz), 7.41 (1H, d, J=9 Hz).

Found: C, 73.58; H, 6.77%. Calcd for $C_{15}H_{16}O_3$: C, 73.75; H, 6.60%.

*Ethyl (6-Methoxy-1,2,3,4-tetrahydrodibenzofuran-1-ylidene)-acetate (**13**).* **13** was prepared by Dendy's method.[1] Colorless needles from ethanol; mp 96—97 °C. (**14**, prepared by Dendy *et al.*;[1] mp 97 °C). IR (KBr): ν_{max} 1695 ($COOC_2H_5$). NMR ($CDCl_3$): δ 1.32 (3H, t, J=7 Hz), 1.90—2.15 (2H, m), 2.90 (2H, t, J=6 Hz), 3.21 (2H, dt, J=1 and 6 Hz), 3.98 (3H, s), 4.21 (2H, q, J=7 Hz), 6.30 (1H, t, J=1 Hz), 6.78 (1H, d, J=7 Hz), 7.18 (1H, t, J=7 Hz), 7.38 (1H, d, J=7 Hz).

*(6-Methoxy-1,2,3,4,4a,9b-hexahydrodibenzofuran-1-yl)acetic Acid (**5**).* Ester **13** (3 g) in ethanol (50 ml) was hydrogenated in the presence of 10% palladium on charcoal (3 g) for 15 h at 7 atm and 60 °C. The resulting ester was purified by chromatography (benzene–ether 95: 5) on silica gel and hydrolyzed to give 1.6 g (59%) of **5**. Colorless needles from benzene–hexane; mp 79—80 °C. IR (KBr): ν_{max} 1710 (COOH) cm^{-1}. NMR ($CDCl_3$): δ 1.10—2.10 (6H, m), 2.25—2.53 (1H, m), 2.43 (2H, broad s), 3.60 (1H, dd, J=3 and 8 Hz), 3.86 (3H, s), 4.86—5.03 (1H, m), 6.72—6.90 (3H, m).

Found: C, 68.58; H, 6.71%. Calcd for $C_{15}H_{18}O_4$: C, 68.68; H, 6.92%.

The authors wish to express their thanks to Mr. Yoshiaki Takahashi for the elemental analyses and Mr. Takao Oono for the nuclear magnetic resonance analyses.

References

1) A. V. Dendy, J. H. P. Tyman, and W. B. Whalley, *J. Chem. Soc.*, **1963**, 4040.

2) T. Horaguchi and T. Shimizu, *Bull. Chem. Soc. Jpn.*, **47**, 485 (1974).

3) T. Horaguchi, *Bull. Chem. Soc. Jpn.*, **50**, 3329 (1977).

4) T. Horaguchi, T. Shimizu, and T. Abe, *Bull. Chem. Soc. Jpn.*, **49**, 737 (1976).

BULLETIN OF THE CHEMICAL SOCIETY OF JAPAN, VOL. 52 (8), 2439—2440 (1979)

Sesquiterpenoids. LIV.[1] Absolute Configuration of Eudesma-4(14),7(11)-dien-8-one

Katsuya ENDO and Hiroshi HIKINO*

Pharmaceutical Institute, Tohoku University, Aoba-yama, Sendai 980

(Received December 26, 1978)

Synopsis. (+)-Eudesma-4(14),7(11)-dien-8-one (**1**) isolated from *Atractylodes* rhizomes has been degraded with basic alumina to the trisnor ketone (**3**). From the CD spectra of **1** and **3**, the absolute configuration of **1** has been established to be 5*S*, 10*R*, which has so far been allocated to the (−)-enantiomer.

During the course of our study on the physiologically active constituents of Oriental medicines, it was found that a methanol extract of *Atractylodes japonica* rhizomes showed a significant antiinflammatory activity. Fractionation of the extract monitored by a pharmacological assay afforded active fractions from which an oily substance was isolated. The mass spectrum of the substance ($[\alpha]_D$+92.6°) showed it to be a sesquiterpenoid having the composition of $C_{15}H_{22}O$. The spectral data, in particular a UV absorption maximum at 246 nm and IR bands at 1676 and 1620 cm^{-1} demonstrated the presence of a conjugated enone system in a six- or larger-membered ring. In the IR and ^1H NMR spectra, peaks compatible with one tertiary methyl (δ 0.73), two vinyl methyls (δ 1.78 and 1.90) and an exo-methylene (1640 and 882 cm^{-1}, δ 4.56 and 4.80) were observed. These structural characteristics indicated that this compound was (+)-eudesma-4(14),7(11)-dien-8-one (**1**) obtained recently from the same plant.[2] The conclusion was substantiated by direct comparison with an authentic specimen.

The substance (**1**) is very unstable when subjected to alumina chromatography. A ketonic compound (**3**) was isolated from the decomposition products in varying yields. The compound (**3**) exhibited in its mass spectrum the molecular ion peak at *m/e* 178 corresponding to the composition $C_{12}H_{18}O$. The presence of a saturated carbonyl (1710 cm^{-1}), a tertiary methyl (δ 0.70) and an exo-methylene (1643 and 886 cm^{-1}, δ 4.48 and 4.77) was observed. The structure of the ketone (**3**) was assigned to 1-methyl-7-methylenebicyclo[4.4.0]decan-3-one, the structure being confirmed by direct comparison with an authentic specimen.[3]

Eudesma-4(14),7(11)-dien-8-one was first isolated in the laevorotatory form ($[\alpha]_D$−55.6°) from *Asarum caulescens*, and was assigned to the stereochemistry **1** although no evidence for it was described.[4] The laevorotatory enantiomer ($[\alpha]_D$−87.4°) was also recently isolated from *Peteravenia schultzii* and assigned to the same stereochemistry (**1**),[5] where specific rotations at 589, 578, 546, and 436 nm were recorded, but no evidence for the assignment was given.

When (+)-eudesma-4(14),7(11)-dien-8-one was isolated from *Atractylodes japonica*, the enantiomeric stereostructure (**2**) was first allocated for it,[6] since its CD curve was found to be enantiomeric with that of the (−)-isomer from *Asarum caulescens* which had been reported to possess the stereostructure **1**. The proposed stereochemistry of the (+)-isomer from *A. japonica* was later altered to **1**, no evidence being reported.[2]

As a result, the same stereostructure **1** is now attributed to both of the (+)- and (−)-isomers with no evidence for the stereochemistry.

The substance (**1**) with the dextrorotatory activity isolated from *A. japonica* exhibited a negative Cotton effect for the n-π^* transition in the ORD and CD curves. The A/B ring fusion of the substance (**1**) was considered to be *trans* by the transformation of germacrone to the *trans*-fused selinane,[4,7] and is now substantiated by the transformation of the substance (**1**) into the trisnor ketone (**3**) having the *trans* ring fusion. The observed negative Cotton effect indicated that the chiral situation of the cisoid enone system is anticlockwise, identical with that of cholest-4-en-6-one (**4**)[8] and enantiomeric with that of cholest-5-en-4-one (**5**).[8] Furthermore, the ketone (**3**) showed a negative Cotton effect at 290 nm for the n-π^* transition in the CD curve. Inspection of the octant diagram demonstrated the absolute configuration of the ketone (**3**) to be 5*S*, 10*R*, identical with the decalone (**6**)[9] and enantiomeric with cholestan-2-one (**7**).[8] These observations led to the conclusion that the absolute configuration of the (+)-enantiomer corresponds to **1**, and consequently that of the (−)-enantiomer to **2**.

Although the reasons for the previous assignments for the absolute stereochemistry are unknown, the ORD curve of the (−)-isomer from *P. schultzii* measured in the range 589—436 nm might be considered as part of a negative Cotton curve but is in fact composed of a positive Cotton curve on a negative plane curve.

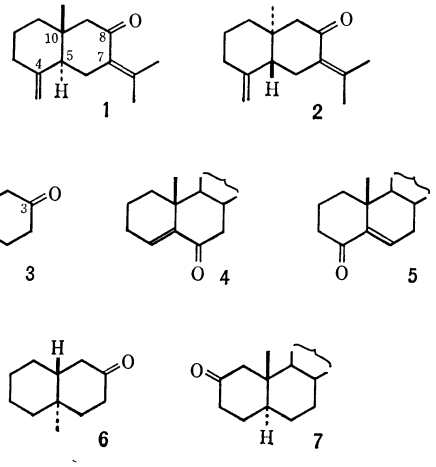

Experimental

The homogeneity of each compound was ascertained dy

silica gel thin layer chromatography (Merck Kieselgel GF_{254} with various solvent systems, the spots being visualized by heating with dil. sulfuric acid), and by gas-liquid chromatography with 10% Silicone SE-30 on Chromosorb-W (Φ 3 mm × 1 m glass column). In the ^1H NMR spectra, chemical shifts (δ) are expressed in ppm downfield from internal TMS. Abbreviations: s=singlet, br=broad.

Isolation of (+)-Eudesma-4(14),7(11)-dien-8-one from Atractylodes japonica *Rhizomes.* The crude drug (435 g), the dried rhizomes of *Atractylodes japonica*, was extracted 6 times with refluxing MeOH (1 liter) for 5 h (each extraction). The MeOH solutions were combined and concentrated to dryness to afford an extract (118 g). The MeOH extract (104 g) was diluted with water and extracted with light petroleum, yielding a petroleum soluble portion (27 g) and a water soluble portion (77 g). The former was applied to a column of silica gel (300 g) and eluted with benzene to give an antiinflammatory active fraction (2.7 g) which was again chromatographed over silica gel (100 g). An eluate (1.0 g) with AcOEt–hexane (1: 49) was purified by repeated silica gel chromatography to give (+)-eudesma-4(14),7(11)-dien-8-one (**1**) as a colorless oil: $[\alpha]_D^{20}$ +92.6° (*c* 0.034, MeOH); ORD (*c* 0.0113, MeOH) $[\alpha]_D^{20}$ +90.8° (589), +110° (546), +181° (436), +187° (414), +57.2° (356) (trough), +3420° (300) (peak), and +4240° (290 nm); CD (*c* 0.0004, MeOH) $[\theta]^{24}$ -3.56×10^3 (320 nm) (negative maximum); MS *m/e* 218 (M^+); UV_{max} (hexane) 246 nm (log ε 3.90); IR (liquid) 1676 (conj. C=O), 1640 (C=C), and 882 ($C=CH_2$); ^1H NMR (100 MHz, CCl_4) δ 0.73 (3H, s, CH_3), 1.78 (3H, s, CH_3), 1.90 (3H, s, CH_3), 4.56 and 4.80 ppm (1H each, br s, $C=CH_2$). These spectral data are in line with those reported.[2,4] The substance showed identical behavior on thin layer chromatography and gas-liquid chromatography with that of an authentic **1**.

*Alumina Treatment of (+)-Eudesma-4(14),7(11)-dien-8-one to (−)-*trans*-1-Methyl-7-methylenebicyclo[4.4.0]decan-3-one.* The compound **1** (1.0 g) was applied to a column of basic alumina (300 g). Elution with AcOEt–hexane (3: 97) (300 ml) afforded the unchanged **1** (0.4 g). Further elution with AcOEt–hexane (1: 1) (130 ml) afforded an oily product (449 mg), which was purified by repeated chromatography over silica gel to furnish (−)-*trans*-1-methyl-7-methylenebicyclo[4.4.0]decan-3-one (**3**) as a colorless oil: $[\alpha]_D^{20}$ −6.6° (*c* 0.0085, MeOH); CD (*c* 0.001, MeOH) $[\theta]^{24}$ -6.74×10^3 (290 nm) (negative maximum); MS *m/e* 178 (M^+); IR (CCl_4) 1710 (C=O), 1643 (C=C), and 886 cm^{-1} ($C=CH_2$); ^1H NMR (60 MHz, CCl_4) δ 0.70 (3H, s, CH_3), 4.48 and 4.77 ppm (1H each, br s, $C=CH_2$). The IR spectrum was superimposable with that of a synthetic (±)-**3**.

We are indebted to Drs. Yoichi Nishikawa and Ichiro Yasuda, Tokyo Metropolitan Research Laboratory of Public Health, and Dr. Ken'ichi Takeda, Shionogi Research Laboratory, for identification of the compounds.

References

1) Part LIII: H. Hikino, *Chem. Ber.*, **111**, 2726 (1978).
2) Y. Nishikawa, I. Yasuda, Y. Watanabe, and T. Seto, *Shoyakugaku Zasshi*, **30**, 132 (1976).
3) H. Minato and T. Nagasaki, *Chem. Commun.*, **1965**, 377.
4) J. Endo and M. Nagasawa, *Yakugaku Zasshi*, **94**, 1574 (1974).
5) F. Bohlmann and A. Suwita, *Phytochemistry*, **17**, 567 (1978).
6) Y. Nishikawa, Y. Watanabe, T. Seto, and I. Yasuda, The 21st Annual Meeting of the Japanese Society of Pharmacognosy, Chiba, October 1975, Abstr. No. 11-9-2.
7) G. D. Joshi, S. K. Paknikar, S. N. Kulkarni, and S. C. Bhattacharyya, *Tetrahedron*, **22**, 1651 (1966).
8) C. Djerassi, R. Riniker, and B. Riniker, *J. Am. Chem. Soc.*, **78**, 6362 (1956).
9) C. Djerassi, W. Closson, and A. E. Lippman, *J. Am. Chem. Soc.*, **78**, 3163 (1956).

BULLETIN OF THE CHEMICAL SOCIETY OF JAPAN, VOL. 52 (8), 2441—2442 (1979)

A Convenient Method for the Preparation of 4-(3-Halogenatedphenyl)- and 4-(3,5-Dihalogenatedphenyl)-4-oxobutyric Acids

Teruomi JOJIMA, Hideo TAKESHIBA,* and Takao KINOTO

Agricultural Chemicals Research Laboratories, Sankyo Co., Ltd., Shinagawa-ku, Tokyo 140

(Received January 12, 1979)

Synopsis. Various 4-(3-halogenatedphenyl)- and 4-(3,5-dihalogenatedphenyl)-4-oxobutyric acids were synthesized by the nuclear halogenation of the corresponding 4-aryl-4-oxobutyric acids in the presence of an excess of aluminum chloride. In most of these reactions, consecutive succinoylation and halogenation of the aromatic compounds were carried out in one pot operation.

When aromatic aldehydes and ketones are halogenated in the presence of a sufficient amount of aluminum chloride to complex completely the carbonyl groups, halogenation takes place in the benzene rings rather than in the side chains[1] (swamping catalyst method). Krausz *et al.*[2] prepared 4-(3-chloro-4-isopropylphenyl)-, 4-(3-chloro-4-*t*-butylphenyl)-, and 4-(3-chloro-4-cyclohexylphenyl)-4-oxobutyric acids from the corresponding 4-aryl-4-oxobutyric acids by this method. However, halogenation of other 4-aryl-4-oxobutyric acids and the usage of halogenating agents other than chlorine have not been reported.

In connection with the synthesis of fungicidal 6-aryl-3(2*H*)pyridazinones, it became necessary for us to prepare various 4-aryl-4-oxobutyric acids bearing halogens on their 3′- and(or) 5′-positions.[3] These acids are required as starting materials for the synthesis of the heterocycles mentioned above.[4]

It is reported that the Friedel-Crafts reaction of *o*-chlorotoluene with succinic anhydride gave rise to 4-(4-chloro-3-methylphenyl)-4-oxobutyric acid (**4**) owing to a *p*-directing effect of the chlorine atom.[5] In our experiment, this result was also confirmed and the reaction of 2,6-dichlorotoluene with succinic anhydride under the same conditions produced only 4-(2,4-dichloro-3-methylphenyl)-4-oxobutyric acid (**5**). Accordingly, the swamping catalyst method would be very helpful to obtain the 3′- and(or) 5′-halogenated products.

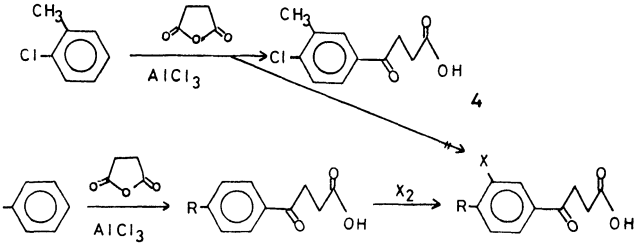

1a: R=CH_3 **2a**: R=CH_3 **3a**: R=CH_3, X=Cl
b: R=H **b**: R=H **b**: R=CH_3, X=Br
c: R=Br **c**: R=Br **c**: R=H, X=Cl
d: R=Cl **d**: R=Cl **d**: R=H, X=Br
e: R=F **e**: R=F **e**: R=Br X=Cl
f: R=Cl, X=Br
g: R=F, X=Cl
h: R=F, X=Br

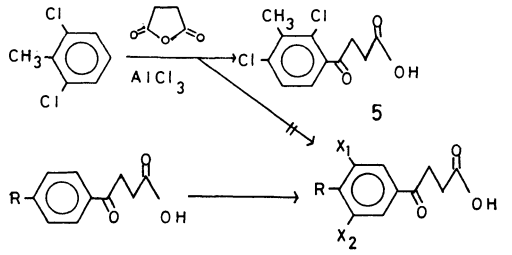

2a: R=CH_3 **6a**: R=CH_3, $X_1=X_2=Cl$
f: R=C_2H_5 **b**: R=CH_3, $X_1=X_2=Br$
g: R=*i*-C_3H_7 **c**: R=CH_3, $X_1=Cl$, $X_2=Br$
h: R=*n*-C_4H_9 **d**: R=C_2H_5, $X_1=X_2=Cl$
i: R=OCH_3 **e**: R=*i*-C_3H_7, $X_1=X_2=Cl$
f: R=*n*-C_4H_9, $X_1=X_2=Cl$
g: R=OH, $X_1=X_2=Cl$

At first, several 4-aryl-4-oxobutyric acids (**2**) were monohalogenated in 1,2-dichloroethane (DCE). The halogenating agents used were chlorine, bromine, and sulfonyl chloride. The molar ratios of the reagents are

TABLE 1. NUCLEAR HALOGENATION OF 4-ARYL-4-OXOBUTYRIC ACIDS (**2**)

Starting material (Method[a])	Halogenating agent	Molar ratio: $AlCl_3$/**1**(or **2**)	Molar ratio: Halogen/**1**(or **2**)	Conditions: Temp °C	Conditions: Time h	Product[b] (Yield[c] %)	Mp °C
1a (B)	Cl_2	2.4	1.7	30—40	15	**3a** (72)	150—156[d]
2a (A)	SO_2Cl_2	2.4	2.2	40—50	8	**3a** (83)	
2a (A)	Br_2	2.4	2.2	20—30	24	**3b**[e] (64)	163—171[f]
1a (B)	Br_2	2.4	1.7	25—30	6	**3b** (75)	
1b (B)	Cl_2	3.0	1.7	20—30	7	**3c**[g] (48)	107—113[d]
1b (B)	Br_2	2.5	2.2	45	11.5	**3d**[h] (70)	119—122[d]
1c (B)	Cl_2	3.0	2.2	20—30	18	**3e**[i] (81)	175—178[f]
1d (B)	Br_2	3.0	2.2	20—30	24	**3f**[j] (89)	160—163[f]
1e (B)	Cl_2	3.0	10.0	20—25	49	**3g**[k] (70)	121—123[d]
1e (B)	Br_2	4.0	5.6	20—25 40	16 17	**3h**[l] (70)	121—124[m]
2a (A)	Cl_2	2.4	2.6	40—45	2	**6a**[n] (31)	183—188[f]
1a (B)	Cl_2	3.0	2.9	3—7	21.5	**6a** (52)	
2a (A)	Br_2	3.0	2.1	20—30 30—35	1 7.5	**6b**[o] (67)	188—191[d]
1a (B)	1) Cl_2 2) Br_2	3.0	1.9 1.1	5—10 30—35	24 19.5	**6c**[p] (50)	183—185[q]
2f (A)	Cl_2	3.0	7.3	0—10	18	**6d**[r] (51)	137—138[f]
2g (A)	Cl_2	3.0	2.8	0—10	16	s)	
2h (A)	Cl_2	3.0	2.8	0—10	16	**6f**[t] (16)	120—122[f]
2i (A)	Cl_2	2.4	3.0	35—40	4.5	**6g**[u] (72)	180—183[f]

a) A: Halogenation of 4-aryl-4-oxobutyric acids (**2**). B: Consecutive succinoylation and halogenation of aromatic compounds (**1**). b) Satisfactory elemental analyses were obtained for all compounds. c) Isolated yield (purity ≥95%, estimated by HPLC). d) Recrystd from benzene. e) NMR (DMSO-d_6): δ 2.41 (s, 3H), 2.60 (t, 2H), 3.23 (t, 2H), 4.90 (s, 1H), 7.47 (d, 1H), 7.89 (dd, 1H), 8.08 (d, 1H). f) Recrystd from CH_3CN. g) NMR (DMSO-d_6): δ 2.79 (t, 2H), 3.30 (t, 2H), 7.2—8.3 (m, 4H), 11.10 (s, 1H). h) NMR (DMSO-d_6): δ 2.79 (t, 2H), 3.29 (t, 2H), 7.2—8.3 (m, 4H), 10.98 (s, 1H). i) NMR (DMSO-d_6): δ 2.59 (t, 2H), 3.24 (t, 2H), 7.9—8.2 (m, 3H). j) NMR (DMSO-d_6): δ 2.57 (t, 2H), 3.28 (t, 2H), 7.78 (d, 1H), 8.03 (dd, 1H), 8.30 (d, 1H). k) NMR (DMSO-d_6): δ 2.60 (t, 2H), 3.30 (t, 2H), 7.53 (dd, 1H), 8.05 (dq, 1H), 8.17 (dd, 1H). l) NMR (DMSO-d_6): δ 2.60 (t, 2H), 3.28 (t, 2H), 7.53 (dd, 1H), 8.09 (dq, 1H), 8.29 (dd, 1H). m) Recrystd from hexane-AcOEt. n) NMR (DMSO-d_6): δ 2.48 (s, 3H), 2.65 (t, 2H), 3.27 (t, 2H), 7.59 (s, 2H), 11.68 (s, 1H). o) NMR (DMSO-d_6): δ 2.57 (s, 3H), 2.58 (t, 2H), 3.25 (t, 2H), 8.10 (s, 2H). p) NMR (DMSO-d_6): δ 2.50 (s, 3H), 2.58 (t, 2H), 3.23 (t, 2H), 7.98 (d, 1H), 8.08 (d, 1H), 11.91 (s, 1H). q) Recrystd from toluene. r) NMR (DMSO-d_6): δ 1.13 (t, 3H), 2.57 (t, 2H), 2.95 (q, 2H), 3.25 (t, 2H), 7.93 (s, 2H). s) Inseparable mixture. t) NMR (DMSO-d_6): δ 0.95 (t, 3H), 1.2—1.7 (m, 4H), 2.6—3.3 (m, 6H), 7.85 (s, 2H). u) NMR (DMSO-d_6): δ 2.57 (t, 2H), 3.24 (t, 2H), 7.99 (s, 2H), 10.33 (s, 1H).

shown along with the reaction conditions in Table 1. Mostly the starting acids (**2**) were prepared *in situ* from the corresponding aromatic compounds and succinic anhydride under the usual Friedel-Crafts conditions.[6] The reaction courses were monitored by high-pressure liquid chromatography (HPLC) in every case. The monohalogenation proceeded smoothly for every halogenating agent used, and the acids halogenated at 3′-position were obtained in good yields.

Next, certain 4-aryl-4-oxobutyric acids were dihalogenated on the 3′- and 5′-positions using more than two molar equivalents of halogenating agents. The dichlorination of the *para*-methyl analog (**2a**) at low temperatures gave higher yield of the product (**6a**) than at elevated temperatures. The nuclear dibromination of **2a** as well as its consecutive chlorination and bromination gave the desired acids (**6a** and **6b**) in good yields. In the case of 4′-isopropyl analog (**2g**), a mixture of variously chlorinated products was obtained, and the desired product (**6c**) could not be isolated.

The dichlorination of 4-(4-methoxyphenyl)-4-oxobutyric acid (**2i**) gave 4-(3,5-dichloro-4-hydroxyphenyl)-4-oxobutyric acid (**6g**) in a good yield. The HPLC indicated that the dichlorination and demethylation took place almost simultaneously in this case. The reaction of 2,6-dichloroanisole with succinic anhydride under the usual Friedel-Crafts conditions produced only tarry materials which could not be purified.

The above experiments have shown that certain 4-aryl-4-oxobutyric acids with halogens on their 3′- and(or) 5′-positions can be conveniently obtained by one pot operation starting from benzene or substituted benzenes.

Experimental

All melting points are not corrected. IR and NMR spectra were recorded on a JASCO IRA-2 spectrophotometer and Varian A-60 nuclear magnetic resonance spectrometer, respectively. HPLC apparatus used was a Hitachi Model 635-T high-pressure liquid chromatograph. Column used was 5×50 cm glass, packed with Hitachi gel 3010. Elution system was MeOH–H_2O–AcOH (94: 5: 1), and wave length was 248 nm through the experiments of monohalogenation and 236 nm through dihalogenation.

Materials. The 4-aryl-4-oxobutyric acids, **2a**,[7] **2f**,[8] **2g**,[9] and **2i**[10] were prepared by the methods described in the literature. 4-(4-*n*-Butylphenyl)-4-oxobutyric acid (**2h**, mp 101 °C) was prepared by a similar method.

Preparation of 4-(3-Halogenatedphenyl)-4-oxobutyric Acids (3) and 4-(3,5-Dihalogenatedphenyl)-4-oxobutyric Acids (6). As a typical run, consecutive succinoylation and chlorination of **1a** are described here. To a mixture of aluminum chloride (32 g, 0.24 mol) and DCE (120 ml) was added portionwise powdered succinic anhydride (11 g, 0.11 mol) with stirring at room temperature. Stirring was continued for further 10 min. Then, toluene (9.2 g, 0.1 mol) was added dropwise in 30 min at 10 °C. After stirring for 1.5 h at 10—15 °C, the reaction mixture was warmed to 30 °C. Chlorine gas (8 ml, 0.17 mol), trapped in a Dry Ice acetone bath was introduced into the reaction mixture in 1 h at 30—40 °C. Stirring was continued thereafter, until the peak due to the monochloro derivative (**3a**) became a maximum on HPLC (relative peak height, *ca.* 95%). Then, the reaction mixture was poured into a mixture of ice (500 g) and concentrated HCl (60 ml), and the resulting oily solid was extracted with ethyl acetate (1 l). The organic solution was repeatedly washed with water, and dried over Na_2SO_4. The filtered ethyl acetate was evaporated *in vacuo*, and the crude product was recrystallized from benzene–hexane (1: 1, 200 ml) to give 16.3 g of 4-(3-chloro-4-methylphenyl)-4-oxobutyric acid (**3a**), as colorless leaflets; mp 150—156 °C. IR (Nujol): 2500—2800 (COOH) and 1700 cm^{-1} (broad, CO). NMR (DMSO-d_6): δ 2.40 (3H, s, CH_3), 2.58 (2H, t, J=6 Hz, $-CH_2-$), 3.25 (2H, t, J=6 Hz, $-CH_2-$), 7.48 (1H, d, J=8 Hz, H-5′), 7.85 (1H, dd, J=8 and 2 Hz, H-6′), and 7.92 (1H, broad s, H-2′). Found: C, 58.80; H, 4.88; Cl, 15.67%. Calcd for $C_{11}H_{11}ClO_3$: C, 58.29; H, 4.89; Cl, 15.64%.

The halogenation of other 4-aryl-4-oxobutyric acids were conducted basically as above. The conditions and results are summarized in Table 1.

Reaction of 2,6-Dichlorotoluene with Succinic Anhydride. To a mixture of aluminum chloride (40 g, 0.3 mol) and DCE (100 ml) was added portionwise powdered succinic anhydride (10 g, 0.1 mol) with stirring. The resulting deep red solution was refluxed for 1 h. The reaction mixture was treated as above to give a crude oily solid (32 g). Recrystallization of this from benzene–hexane (1: 2, 300 ml) gave 7.8 g (30%) of 4-(2,4-dichloro-3-methylphenyl)-4-oxobutyric acid (**5**) as colorless needles; mp 92—94 °C. IR (Nujol): 2500—2800 (COOH), 1700 cm^{-1} (CO); NMR (DMSO-d_6): δ 2.50 (3H, s, CH_3), 2.82 (2H, t, J=6 Hz, $-CH_2-$), 3.14 (2H, t, J=6 Hz, $-CH_2-$), 7.35 (2H, AB-d, aromatic), 9.45 (1H, broad s, OH). Found: C, 50.29; H, 3.77; Cl, 26.95%. Calcd for $C_{11}H_{10}Cl_2O_3$: C, 50.60; H, 3.86; Cl, 27.16%.

The authors are grateful to Dr. Kazuo Tomita and Dr. Takashi Matsui for valuable discussions. They are also thankful to Mr. Toshiaki Yanai, Mr. Tadashi Murakami, Mr. Sohji Sugai, and Mr. Junzo Tobitsuka for technical assistances.

References

1) D. E. Pearson, H. W. Pope, W. W. Hargrove, and W. E. Stamper, *J. Org. Chem.*, **23**, 1412 (1958).
2) F. Krausz, H. Demarne, J. Vaillant, M. Brunaud, and J. Navarro, *Arzneim.-Forsch.*, **24**, 1360 (1974).
3) A prime denotes a substitution on benzene ring.
4) A. Lespagnol and J. Deprey, *Bull. Soc. Chim. Fr.*, **1962**, 1117; E. A. Stech, *J. Am. Chem. Soc.*, **75**, 1117 (1953).
5) L. F. Fieser, E. Berliner, F. J. Bondhus, W. G. Dauben, M. G. Ettinger, G. Faqaz, M. Fields, C. Heiderberger, H. Heymann, W. R. Vaughan, A. G. Wilson, E. W. Wilson, and M. Wu, *J. Am. Chem. Soc.*, **70**, 3174 (1948).
6) "Organic Reactions," ed by R. Adams, John Willey and Sons, Inc., New York (1957), Vol. 5, Chap. 5.
7) F. Muhr, *Chem. Ber.*, **28**, 3215 (1895).
8) F. G. Buddar and F. L. Warren, *J. Chem. Soc.*, **1939**, 944.
9) E. D. Aarnett and F. G. Sanders, *J. Chem. Soc.*, **1933**, 434.
10) L. F. Fieser and V. Desreux, *J. Am. Chem. Soc.*, **60**, 2255 (1938).

BULLETIN OF THE CHEMICAL SOCIETY OF JAPAN, VOL. 52 (8), 2443—2444 (1979)

Oxidation-Reduction Equilibrium between Cation Radicals. An Approach to Determine Ionization Potentials of Electron Donor Molecules

Yôichi IIDA* and Akihiko YAMAGISHI

Department of Chemistry, Faculty of Science, Hokkaido University, Sapporo 060

(Received February 15, 1979)

Synopsis. For several electron donor molecules, the adiabatic ionization potential and the oxidation-reduction potential in the formation of cation radical from its parent molecule were estimated by using the equilibrium constant of a preferred electron transfer reaction from neutral donor molecule to another cation radical molecule in solution.

Earlier, we presented a method for determining electron affinity values of electron acceptor molecules by using preferred electron transfer (*i.e.*, oxidation-reduction) reaction between anion radicals in solution.[1] In this method, we measured the equilibrium constant of such reaction spectrophotometrically, so that we could estimate the difference of the oxidation-reduction potential and the electron affinity between two acceptor molecules.

In a similar way, if we observe chemical equilibrium of preferred electron transfer reaction from neutral electron donor molecule to another cation radical molecule in solution, we can obtain some knowledge regarding the ionization potentials of donor molecules as well as the oxidation-reduction potentials in the formation of their cation radicals. In the present paper, we apply this approach to several donor molecules with low ionization potentials such as *N,N,N',N'*-tetramethyl-*p*-phenylenediamine (TMPD), *N,N*-dimethyl-*p*-phenylenediamine (DMPD), *N,N,N',N'*-tetramethylbenzidine (TMB) and phenothiazine (PT).

In previous papers,[2] we examined the chemical equilibria of such preferred electron transfer reactions in various solvents. First, we shall derive oxidation-reduction potentials for those donor molecules. Hereafter, $E_1(M^{+\cdot}, M)$, $E_2(M^{+\cdot}, M)$, and $E_3(M^{+\cdot}, M)$, (M= TMPD, DMPD, TMB, or PT), are denoted as reversible one-electron reduction potentials of $M^{+\cdot}+e \rightleftarrows M$ in (1 : 3) ethanol–water solution, in aqueous solution and in acetonitrile solution, respectively.

The reaction between neutral phenothiazine and *N,N,N',N'*-tetramethyl-*p*-phenylenediamine cation radical was examined in (1 : 3) ethanol–water solvent. The oxidation-reduction equilibrium is expressed by

$$PT + TMPD^{+\cdot} \rightleftharpoons PT^{+\cdot} + TMPD. \quad (1)$$

If we neglect the effect of counter anions and assume that the activity coefficients of the solutes are unity, the equilibrium constant of this reaction is simply given by

$$K = \frac{[PT^{+\cdot}][TMPD]}{[PT][TMPD^{+\cdot}]}. \quad (2)$$

The equilibrium constant, K, was determined spectrophotometrically to be 0.96×10^{-6} at 10 °C. Using Nernst equation, we obtain a relation of reduction potentials, $E_1(PT^{+\cdot}, PT)=E_1(TMPD^{+\cdot}, TMPD)+0.34$V.

In a similar way, we examined the following reactions and obtained the relations of reduction potentials. In the reaction between neutral phenothiazine and *N,N*-dimethyl-*p*-phenylenediamine cation radical in (1 : 3) ethanol–water solution, $PT+DMPD^{+\cdot} \rightleftharpoons PT^{+\cdot}+DMPD$, $K=[PT^{+\cdot}][DMPD]/[PT][DMPD^{+\cdot}]=(3\pm1)\times10^{-5}$ at 10 °C, and $E_1(PT^{+\cdot}, PT)=E_1(DMPD^{+\cdot}, DMPD)+0.26$ V. From the relation between $E_1(PT^{+\cdot}, PT)$ and $E_1(TMPD^{+\cdot}, TMPD)$, we can estimate the relation, $E_1(DMPD^{+\cdot}, DMPD)=E_1(TMPD^{+\cdot}, TMPD)+0.08$ V. The reaction of $DMPD+TMPD^{+\cdot} \rightleftharpoons DMPD^{+\cdot}+TMPD$ was examined in two different solvents. In aqueous solution, $K=[DMPD^{+\cdot}][TMPD]/[DMPD][TMPD^{+\cdot}]=(2.8\pm0.6)\times10^{-2}$ at 10 °C and $E_2(DMPD^{+\cdot}, DMPD)=E_2(TMPD^{+\cdot}, TMPD)+0.087$ V, while in acetonitrile solution $K=(3.8\pm1.5)\times10^{-2}$ at 10 °C and $E_3(DMPD^{+\cdot}, DMPD)=E_3(TMPD^{+\cdot}, TMPD)+0.078$ V. For the reaction of $DMPD+TMB^{+\cdot} \rightleftharpoons DMPD^{+\cdot}+TMB$ in acetonitrile solution, $K=[DMPD^{+\cdot}][TMB]/[DMPD][TMB^{+\cdot}]=(3\pm1)\times10^{3}$ at 10 °C and $E_3(TMB^{+\cdot}, TMB)=E_3(DMPD^{+\cdot}, DMPD)+0.20$ V. From the relation between $E_3(DMPD^{+\cdot}, DMPD)$ and $E_3(TMPD^{+\cdot}, TMPD)$, we can further obtain $E_3(TMB^{+\cdot}, TMB)=E_3(TMPD^{+\cdot}, TMPD)+0.28$V.

Although we obtained the reduction potentials of TMPD, DMPD, TMB and PT, the used solvents are different from each other. The reason for this is that we have to observe chemical equilibrium between cation radicals and that the stability of the cation radicals greatly depends on the solvents. Rigorously speaking, we cannot compare the values of the reduction potentials in different solvents, and only the comparison of the values in the common solvents is meaningful. However, as was shown above, the dependence of the $E_i(TMPD^{+\cdot}, TMPD)-E_i(DMPD^{+\cdot}, DMPD)$ value, (i=1, 2, or 3), on the solvents used appears to be within ±0.005 V.

Next, we consider the ionization potentials of TMPD, DMPD, TMB and PT on the basis of the above discussion. In a reversible one-electron addition to cation radical molecule, $D^{+\cdot}$, to form neutral molecule, D, in solution, $D^{+\cdot}+e \rightleftharpoons D$, the free energy change in the presence of mercury electrode is given by

$$\Delta G^{\circ}(D) = -I_p(D) + \Delta\Delta G^{\circ}_{solv}(D, D^{+\cdot}) + \chi_{Hg}, \quad (3)$$

where $I_p(D)$ is the ionization potential of the molecule, D, in gas phase, $\Delta\Delta G^{\circ}_{solv}(D, D^{+\cdot})$ is the difference in free energy of solvation between D and $D^{+\cdot}$, and χ_{Hg} is the electron work function of the mercury surface. Note that $I_p(D)$ corresponds to an adiabatic ionization potential, because the reaction involves thermodynamical equilibrium. In the case of oxidation-reduction equilibrium between D_1 and $D_2^{+\cdot}$ in solution, $D_1+D_2^{+\cdot} \rightleftharpoons D_1^{+\cdot}+D_2$, the observed equilibrium constant,

K, is related with ΔG°'s,

$$-RT\ln K = \Delta G^{\circ}(D_2) - \Delta G^{\circ}(D_1) = I_p(D_1) - I_p(D_2) + \Delta\Delta G^{\circ}_{solv}(D_2, D_2^{+\cdot}) - \Delta\Delta G^{\circ}_{solv}(D_1, D_1^{+\cdot}). \quad (4)$$

Therefore, if one assumes that the solvation energy, $\Delta\Delta G^{\circ}_{solv}(D_2, D_2^{+\cdot})$, is almost equal to $\Delta\Delta G^{\circ}_{solv}(D_1, D_1^{+\cdot})$, one can determine from Eq. 4 the difference of the ionization potentials between the D_1 and D_2 molecules. At the present time, although we have not enough knowledge regarding the solvation energy of neutral donor molecule and its cation radical, for neutral acceptor molecule, A, and its anion radical, $A^{-\cdot}$, the magnitude of $\Delta\Delta G^{\circ}_{solv}(A^{-\cdot}, A)$ is found to be hardly influenced by the species of the acceptor molecules, as long as the molecular sizes and the shapes are similar to one another.[1]

Assuming $\Delta\Delta G^{\circ}_{solv}(D_1, D_1^{+\cdot}) \approx \Delta\Delta G^{\circ}_{solv}(D_2, D_2^{+\cdot})$, we will discuss the ionization potentials of TMPD, DMPD, TMB and PT in the following. So far, the ionization potential of TMPD has been studied in most detail.[3,4] Therefore, if the value is one given for I_p(TMPD), the absolute values of I_p(DMPD), I_p(TMB), and I_p(PT) will be determined from Eq. 4 and the observed equilibrium constants. Photoionization of TMPD in gas phase was measured by Batley and Lyons and later by Nakato *et al.*[3,4] The energy for onset of photoionization curve was assumed to correspond to the adiabatic ionization energy, but the onset was rather gradual in the case of TMPD. Batley and Lyons estimated the upper limit of the adiabatic ionization potential as I_p(TMPD)$\leq$6.25 eV, while Nakato *et al.*, I_p(TMPD)$\leq$6.20 eV. In the present paper, referring to Nakato's value, we take I_p(TMPD)=6.20 eV as a standard. Then, by the use of the observed equilibrium constants of oxidation-reduction reactions, together with Eq. 4, the adiabatic ionization potentials of DMPD, TMB, and PT were estimated to be 6.28 eV, 6.48 eV, and 6.54 eV, respectively.

On the other hand, in Table 1, we compare the data with those measured by photoionization method. As has been mentioned, because of gradual onset of photoionization, it is rather difficult to determine exactly the adiabatic ionization energies by photoionization method, where only the upper limits of the ionization energies were estimated. In particular, the onset of ionization of phenothiazine is more gradual than the other diamine compounds. For each of the compounds, however, a fairly good agreement of the adiabatic ionization energies was obtained between the oxidation-reduction equilibrium method and the photoionization method. The order of the adiabatic ionization potentials was estimated as I_p(TMPD)$<I_p$(DMPD)$<I_p$(TMB)$<I_p$(PT) by our method, while in photoionization it appears that I_p(TMPD)$<I_p$(TMB)$\lesssim I_p$(DMPD)$<I_p$(PT). As for the magnitudes of I_p(DMPD) and I_p(TMB) in photoionization, the former value was measured by Nakato *et al.*,[4] while the latter, by Batley and Lyons.[3] Therefore, we consider that systematic determination of the I_p(DMPD) and I_p(TMB) values in photoionization is desirable to compare those values with ours.[6]

Table 1. Adiabatic and vertical ionization potentials (eV) of electron donor molecules

Compound	Adiabatic ionization potential	Vertical ionization potential	Reference
N,N,N',N'-Tetramethyl-*p*-phenylenediamine	$\leq$6.20	6.75	Ref. 4
	$\leq$6.25	6.47	Ref. 3
N,N-Dimethyl-*p*-phenylenediamine	$\leq$6.46	6.97	Ref. 4
	6.28		This work
N,N,N',N'-Tetramethyl-benzidine	$\leq$6.40	6.55	Ref. 3
	6.48		This work
Phenothiazine	$<$7.0	7.38	Ref. 3
		7.26	Ref. 5
	6.54		This work

In Table 1, the data on vertical ionization energies are also given for purposes of comparison. Usually, vertical energies exceed adiabatic energies because of a change of shape of the molecule upon ionization. The difference between the adiabatic and vertical energies is considerable in DMPD and PT, where it amounts up to 0.7 eV. This implies a considerable structural change upon ionization in those molecules. For example, the molecular structure of neutral PT is of bent form, while its cation radical may become planar.[7,8]

So far, photoionization method in gas phase has been widely used to determine vertical ionization potentials of a number of organic molecules, but has some difficulties in obtaining adiabatic ionization potentials. Alternatively, the present approach of oxidation-reduction equilibrium is a useful method to determine adiabatic ionization potentials of such molecules. One of the difficulties of this method lies in the assumption of $\Delta\Delta G^{\circ}_{solv}(D_1, D_1^{+\cdot}) \approx \Delta\Delta G^{\circ}_{solv}(D_2, D_2^{+\cdot})$ in Eq. 4. The problem of the solvation energies of neutral molecule and its cation radical should be solved in order to obtain more exact adiabatic ionization potentials of a number of electron donor molecules.

References

1) Y. Iida and H. Akamatu, *Bull. Chem. Soc. Jpn.*, **40**, 231 (1967); Y. Iida, *Bull. Chem. Soc. Jpn.*, **44**, 1430 (1971); **49**, 3691 (1976); **52**, 1875 (1979).

2) A. Yamagishi, *Bull. Chem. Soc. Jpn.*, **48**, 3475 (1975); A. Yamagishi, *Chem. Lett.*, **1975**, 595.

3) M. Batley and L. E. Lyons, *Mol. Cryst.*, **3**, 357 (1968).

4) Y. Nakato, M. Ozaki, A. Egawa, and H. Tsubomura, *Chem. Phys. Lett.*, **9**, 615 (1971).

5) L. N. Domelsmith, L. L. Munchausen, and K. N. Houk, *J. Am. Chem. Soc.*, **99**, 6506 (1977).

6) In oxidation-reduction equilibrium method, we assume a constant value of $\Delta\Delta G^{\circ}_{solv}(D, D^{+\cdot})$, and the assumption will be justified as long as the sizes and shapes of molecules are similar. However, the size of TMB molecule is rather bigger than those of TMPD and DMPD molecules, and the $\Delta\Delta G^{\circ}_{solv}$(TMB, TMB$^{+\cdot}$) value may be different from the $\Delta\Delta G^{\circ}_{solv}$(TMPD, TMPD$^{+\cdot}$) or $\Delta\Delta G^{\circ}_{solv}$(DMPD, DMPD$^{+\cdot}$) value. This may be a reason why the I_p(TMB) value derived from our method is somewhat greater than the value obtained from photoionization method.

7) Y. Matsunaga and K. Shono, *Bull. Chem. Soc. Jpn.*, **43**, 2007 (1970).

8) J. D. Bell, J. F. Blount, O. V. Briscoe, and H. C. Freeman, *Chem. Commun.*, **1968**, 1656; J. M. Lhoste and F. Tonnard, *J. Chim. Phys.*, **63**, 678 (1966).

BULLETIN OF THE CHEMICAL SOCIETY OF JAPAN, VOL. 52 (8), 2445—2446 (1979)

Synthesis and Absorption Spectra of 1,4-Diazaanthraquinone Derivatives

Hiroyuki NAKAZUMI,* Testuro AGAWA, and Teijiro KITAO

Department of Applied Chemistry, College of Engineering, University of Osaka Prefecture, Sakai 591

(Received February 20, 1979)

Synopsis. A new 5-amino-1,4-diazaanthraquinone and related compounds were prepared from 2,3-dichloro-1,4-naphthoquinone by two different methods. The transition energies and electron densities of 5-amino-1,4-diazaanthraquinone and 1-aminoanthraquinone were calculated by a variable β,γ-modification of the PPP method.

Anthraquinone dyes are of great value as synthetic coloring matter. We have attempted to prepare new azaanthraquinone derivatives for dyes. Although a few styryl derivatives of diazaanthraquinone dyes have been reported,[1] the preparation and absorption spectra of other diazaanthraquinone derivatives for dyes are little known.

In this paper, we wish to report the syntheses and absorption spectra of new 5-amino-1,4-diazaanthraquinone **4** and related compounds which were prepared from 2,3-dichloro-1,4-naphthoquinone by two different methods (Scheme 1). Compound **4** was prepared as follows: Method A. Reduction of 5-nitro-1,4-diazaanthraquinone **3** prepared by the nitration of 1,4-diazaanthraquinone (DAQ) **2**,[2] with sodium sulfide for 2 h gave **4** in 34% yield. Method B. Condensation of 2,3,5-triamino-1,4-naphthoquinone **6**[3] prepared from 2,3-dichloro-1,4-naphthoquinone **1** *via* several steps (**1**→**5**→**6**), with 40% aqueous glyoxal at 90 °C for 3 h gave **4** in 92% yield. Method B is favorable as regards yield. No diazaanthraquinone derivative (**2**, X=CH_3) could be obtained by the Friedel-Crafts reaction of pyrazinedicarboxylic anhydride with toluene. Compounds **3** and **4** were confirmed by the appearance of peaks at 255 and 225, respectively, in the mass spectra. Since the purification of compound **4** was difficult, it was converted into acetylamino (**7**) and benzoylamino derivatives (**8**). These compounds gave satisfactory results of microanalysis. Bromination of **4** gave a mono bromo derivative **9**. The dye properties of these compounds are under investigation.

The absorption spectra of new 1,4-diazaanthraquinones in EtOH are as follows: 5-NH_2-DAQ **4**: λ_{max} 500 nm (ε 5.7×10^3), 5-$NHCOCH_3$-DAQ **7**: λ_{max} 414 nm (ε 4.5×10^3), 5-$NHCOC_6H_5$-DAQ **8**: λ_{max} 424 nm (ε 5.5×10^3), 5-NH_2-6(or 8)-Br-DAQ **9**: λ_{max} 490 nm (ε 6.2×10^3). The absorption maxima of diazaanthraquinone derivatives **4** and **7** were found at longer wavelength (10—20 nm) than those of their carbon analogues, *e.g.*, 1-aminoanthraquinone **10**: λ_{max} 478 nm, 1-acetylaminoanthraquinone **11**: λ_{max} 400 nm. In the benzene solution, the absorption maxima of **4** and **10** lie at 476 and 465 nm, respectively. The solvent-induced wavelength shift for **4** is larger than that for **10**. Calculation of the first excited energy by the variable β,γ-modification of the PPP method for **10** and **4** predicts a small bathochromic shift for the latter compound (**10**: 2.95 eV (f=0.246), **4**: 2.93 eV (f=0.226)). As shown in Fig. 1 the migration of π-electron accompanying the first electron exitation for **4** is from the donor amino group and substituted ring to two carbonyl groups and the pyrazine ring, as well as for carbon analogue **10**. From the result, it is expected that the characterization of the absorption properties of diazaanthraquinone derivatives is similar to that of anthraquinones.

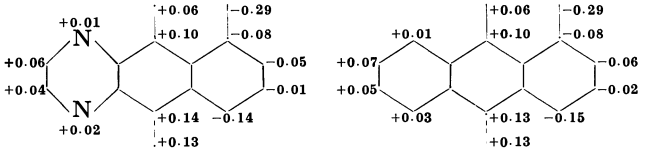

4 **10**

Fig. 1. Change in π-electron density accompanying electronic excitation to the first excited state for 5-amino-1,4-diazaanthraquinone **4** and 1-aminoanthraquinone **10**. A positive sign indicates an increase and a negative sign a decrease in π-electron density.

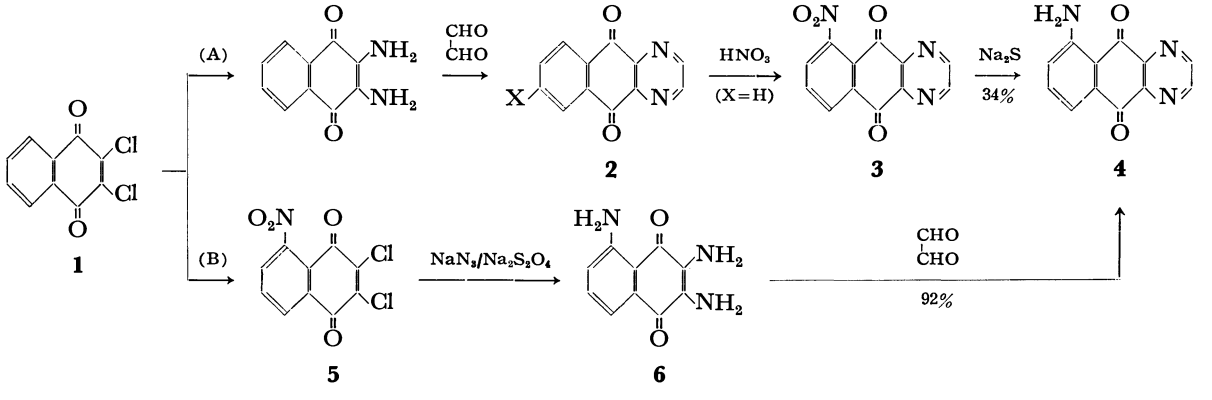

1 **2** **3** **4** **5** **6**

Scheme 1.

Experimental

Infrared spectra were recorded on a Hitachi ESI-S2 spectrophotometer using KBr pellets, UV spectra on a Hitachi EPS-3T spectrophotometer, and mass spectra on a Hitachi RMU-6E mass spectrometer operating at 80 eV. Elemental analyses were recorded on a Yanaco CHN recorder MT-2.

5-Nitro-1,4-diazaanthraquinone **3**. 1,4-Diazaanthraquinone[1] (3.8 g, 0.018 mol) was dissolved in concd H_2SO_4 (10 g), and a mixture of concd H_2SO_4 (15 g) and fuming HNO_3 (d=1.52, 2.1 g) was added dropwise to this solution at 75—80 °C. The mixture was stirred at 75—80 °C for 5 h. After cooling, the mixture was poured into cold water. The resulting solid was separated and washed with water. Recrystallization from benzene gave **3** (1.0 g); yield 22%, mp 275—278 °C, Found: C, 57.64; H, 2.19; N, 15.67%; ν_{CO} 1690 cm^{-1}, NMR (DMSO-d_6) δ=9.10 (2H, s) and 7.50—8.50 (3H, m), MS (80 eV), *m/e* (rel intensity), 255 (M, 100), 225 (85), and 209 (54).

5-Amino-1,4-diazaanthraquinone **4**. Method A. Compound **3** (1.0 g, 0.0039 mol) was added to an aqueous solution (100 ml) of sodium sulfide (1.14 g) and sulfur (0.15 g). The mixture was stirred under reflux for 2 h, and the resulting solid was separated. Recrystallization from water and/or pyridine gave **4** (0.3 g). Method B. To a suspension of 2,3,5-triamino-1,4-naphthoquinone (7.7 g, 0.038 mol) in water (230 ml) was added 40% aqueous glyoxal (7.7 g) at 90 °C. The mixture was stirred at 90 °C for 3 h. After cooling, the resulting solid was separated. Recrystallization from water and/or pyridine gave **4** (7.9 g). Microanalysis of compound **4** gave unsatisfactory results as follows. Found: C, 62.98; H, 3.05; N, 18.34%. Calcd for $C_{12}H_7N_3O_2$: C, 64.00; H, 3.11; N, 18.67%, ν_{CO} 1680 and 1650 cm^{-1}, MS (80 eV), *m/e* (rel intensity) 225 (M, 100), 197 (39), 169 (33), and 143 (18).

5-Acetylamino-1,4-diazaanthraquinone **7**. A solution of **4** (0.5 g) in acetic anhydride (25 ml) was stirred under reflux for 2 h. After cooling, the resulting solid was separated and washed with water. Recrystallization from xylene gave **7** in 67% yield: ν_{CO} 1700 and 1665 cm^{-1}, MS (80 eV), *m/e* (rel intensity), 267 (M, 17), 225 (100), 210 (19), and 197 (39). Found: C, 63.09; H, 3.30; N, 16.11%. Calcd for $C_{14}H_9N_3O_3$: C, 62.92; H, 3.37; N, 15.73%.

5-Benzoylamino-1,4-diazaanthraquinone **8**. Benzoyl chloride (2.6 g) was added dropwise to a solution of **4** (1.4 g) in nitrobenzene (45 ml) at 125 °C for 1.5 h. The mixture was then heated for 1.5 h at the same temperature. After cooling, the resulting solid was separated and washed with ligroin and methanol. Recrystallization from acetonitrile gave **8** (1.3 g) in 64% yield: ν_{CO} 1700 and 1665 cm^{-1}. Found: C, 69.21; H, 3.24; N, 12.93%. Calcd for $C_{19}H_{11}O_3N_3$: C, 69.30; H, 3.34; N, 12.77%.

5-Amino-6(or 8)-bromo-1,4-diazaanthraquinone **9**. Bromine (5.3 g) was added dropwise to a solution of **4** (3.0 g) in *o*-dichlorobenzene (100 ml) at 165—170 °C for 1 h. The mixture was stirred under reflux for 7 h. After cooling, the resulting solid was separated and washed with benzene, methanol, and water. Recrystallization from EtOH gave **9** in 45% yield: ν_{CO} 1700 and 1665 cm^{-1}. Found: C, 46.44; H, 2.08; N, 14.20%. Calcd for $C_{12}H_6N_3BrO_2$: C, 47.38; H, 1.97; N, 13.82%, MS (80 eV), *m/e* (rel intensity), 305 (100), 303 (99), 225 (90), 197 (44), and 169 (48).

Method of SCF-MO Calculation. The calculation was carried out by the Pariser-Parr-Pople method with variable β,γ-approximation. The resonance integrals, β_{rs}'s, were adjusted at each iteration of the SCF calculations by means of the following equations.[4]

$$\beta_{CC} = -1.84 - 0.51P_{CC}$$
$$\beta_{CN} = -2.02 - 0.53P_{CN}$$
$$\beta_{CO} = -2.20 - 0.56P_{CO}$$

where P_{rs} is a bond order between the r and s atoms. The two center repulsion integrals γ_{rs}'s were calculated by the Nishimoto-Mataga equation[5] using the following R_{rs}:

$$R_{CC} = 1.517 - 0.18P_{CC}$$
$$R_{CN} = 1.451 - 0.18P_{CN}$$
$$R_{CO} = 1.410 - 0.18P_{CO}$$

The ionization potentials, $I_{p(r)}$'s, and one-center repulsion integrals, γ_{rr}'s, for carbon, nitrogen, and oxygen atoms were chosen as:

I_p(C)	= 11.16 eV	γ_{rr} = 11.13 eV
I_p(N)	= 14.12 eV	= 12.34 eV
I_p(NH$_2$)	= 26.7 eV	= 17.44 eV
I_p(O)	= 17.7 eV	= 15.23 eV

The authors would like to thank Mr. Y. Kogo, Nippon Kayaku Co., Ltd., for assistance in the molecular orbital calculations.

References

1) G. A. Efimova and L. S. Efros, *Zh. Org. Khim.*, **3**, 388 (1967); *Chem. Abstr.*, **67**, 3068 (1967).
2) G. A. Efimova and L. S. Efros, *Zh. Org. Khim.*, **2**, 531 (1966); *Chem. Abstr.*, **65**, 8910 (1966).
3) M. L. Mosby and M. L. Silva, *J. Chem. Soc.*, **1964**, 3990.
4) K. Nishimoto and L. S. Forster, *Theor. Chim. Acta*, **4**, 155 (1966).
5) K. Nishimoto and L. S. Forster, *Theor. Chim. Acta*, **3**, 407 (1965).

BULLETIN OF THE CHEMICAL SOCIETY OF JAPAN, VOL. 52 (8), 2447—2448 (1979)

Reactions of 2-Tosyloxy- and 2-Chlorotropones with Hydrazine, Methylhydrazine, and Phenylhydrazine

Kimiaki IMAFUKU,* Katsuya KAMACHI,† Yasunori MATSUDA,†† and Hisashi MATSUMURA

Department of Chemistry, Faculty of Science, Kumamoto University, Kurokami, Kumamoto 860

(Received February 22, 1979)

Synopsis. The reactions of 2-tosyloxytropones or 2-chlorotropones with hydrazine, methylhydrazine, and phenylhydrazine gave 2-hydrazinotropones, 2-(α-methylhydrazino)-tropones, and 2-(β-phenylhydrazino)tropones, respectively. All the reactions are normal substitution at C-2 position of the tropone ring. No ciné reaction was observed. The reactivity of hydrazines decreases in the order: $NH_2NH_2 > CH_3NHNH_2 \gg PhNHNH_2$.

In troponoids, ciné substitution very often occurs besides normal substitution, especially when the leaving group is a tosyloxy or halogen group, rather than a methoxyl group.[1] The reactions of tropolone methyl ethers with hydrazine afford 2-hydrazinotropones, which are useful as synthetic intermediates, by normal substitution at the C-2 atom. However, little is known about the reaction of 2-tosyloxytropones or 2-chlorotropones with hydrazine. We wish to report on the reactions of these reactive troponoids with hydrazine, methylhydrazine, and phenylhydrazine.

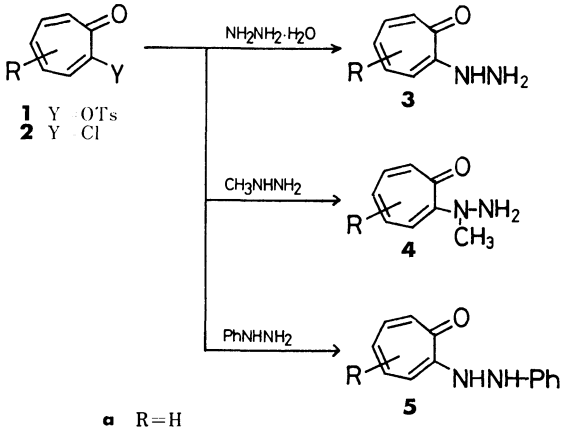

1 Y OTs
2 Y Cl

3, **4**, **5**

a R=H
b R=4-CH_3
c R=6-CH_3

Scheme 1.

Results and Discussion

Reactions with Hydrazine. 2-Tosyloxytropone (**1a**) was refluxed with hydrazine hydrate in methanol for 30 min to afford 2-hydrazinotropone (**3a**)[2] in 48% yield. 4- (**1b**) and 6-methyl-2-tosyloxytropone (**1c**) also gave the corresponding 4- (**3b**)[3] and 6-methyl-2-hydrazinotropone (**3c**)[3] in 31 and 41% yields, respectively.

In a similar manner, the reactions of 2-chlorotropones (**2a**—**c**) with hydrazine hydrate gave 2-hydrazinotropones (**3a**—**c**) in 92, 89, and 91% yields, respectively, all the reactions being normal substitution at the 2-position of tropones.

Reactions with Methylhydrazine. The reactions of 2-tosyloxytropones (**1a**—**c**) with methylhydrazine under reflux in methanol gave 2-(α-methylhydrazino)tropones (**4a**—**c**) in 31, 38, and 34% yields, respectively. The NMR spectrum of **4a** shows peaks at δ 3.29 (s, 3H) for CH_3 and δ 4.29 (br, 2H) for NH_2, indicating the presence of an α-methylhydrazino group. The spectra of **4b** and **4c** also show the presence of the α-methylhydrazino group (Table 1). The position of the *C*-methyl substituent in **4b** and **4c** were confirmed by alkaline hydrolysis to 4-methyltropolone.[4]

Table 1. Characteristics of the products

Compd	Mp °C	$\nu_{max}^{CHCl_3}$ cm^{-1}	λ_{max}^{MeOH} nm (log ε)	δ^{CDCl_3} ppm	Found (Calcd) %
4a	66—67	3320(NH)	259(4.17)	3.29(s, 3H, CH_3)	C 63.73(63.98)
		1610(C=O)	362(3.95)	4.29(br, 2H, NH_2)	H 6.82(6.71)
			418(3.85)	6.4—7.4(m, 5H)	N 18.83(18.66)
4b	89—91	3320(NH)	265(4.22)	2.37(s, 3H, *C*-CH_3)	C 65.57(65.83)
		1585(C=O)	363(3.93)	3.21(s, 3H, *N*-CH_3)	H 7.25(7.37)
			412(3.83)	4.62(br, 2H, NH_2)	N 16.89(17.06)
				6.4—7.3(m, 4H)	
4c	102.5—103	3300(NH)	260(4.24)	2.30(s, 3H, *C*-CH_3)	C 65.68(65.83)
		1615(C=O)	363(3.94)	3.25(s, 3H, *N*-CH_3)	H 7.40(7.37)
			411(3.86)	4.64(br, 2H, NH_2)	N 17.07(17.06)
5a	163—165	3290(NH)	249(4.48)	5.82(br, 1H, NH-Ph)	C 73.63(73.56)
		1600(C=O)	338(4.01)	6.7—7.35(m, 10H)	H 5.64(5.64)
			404(4.07)	8.25(br, 1H, NH-tropone)	N 12.90(13.20)
5b	193—196	3285(NH)	254(4.54)	2.34(s, 3H, CH_3)	C 74.53(74.32)
		1600(C=O)	341(4.03)	5.77(br, 1H, NH-Ph)	H 6.40(6.24)
			403(4.08)	6.5—7.3(m, 9H)	N 12.09(12.38)
				8.25(br, 1H, NH-tropone)	
5c	184—186	3290(NH)	252(4.55)	2.38(s, 3H, CH_3)	C 74.12(74.32)
		1600(C=O)	341(4.01)	5.81(br, 1H, NH-Ph)	H 6.36(6.24)
			401(4.05)	6.2—7.4(m, 9H)	N 12.27(12.38)
				8.20(br, 1H, NH-tropone)	

Heating of 2-chlorotropone (**2a**—**c**) with methylhydrazine afforded the same products (**4a**—**c**) in 69, 72, and 64% yields, respectively. Thus, all the reactions with methylhydrazine are normal substitution reactions, giving no abnormal substitution products.

Reactions with Phenylhydrazine. Heating of 2-tosyloxytropone (**1a**) with phenylhydrazine in methanol under reflux for 30 min gave no product in isolable amount. Prolonged reaction (8 h) afforded 2-(β-phenylhydrazino)tropone[5,6] (**5a**) in only 18% yield. Similarly, both the reactions of 4- (**1b**) and 6-methyl-2-tosyloxytropone (**1c**) gave the corresponding 2-(β-phenylhydrazino)tropones (**5b** and **5c**) in 24 and 14% yields, respectively. Presence of the β-phenylhydrazino group was confirmed by the NMR spectra which show two peaks at δ 5.7—5.8 (br, 1H) for N**H**–Ph and δ 8.2—8.25 (br, 1H) for N**H**–tropone. Palladium-catalyzed hydrogenolysis of **5b** and **5c** yielded 4-[7] and 6-methyl-substituted 2-aminotropones,[3] respectively.

† Present address: Eiken Chemical Co., Ltd., Bunkyo-ku, Tokyo 113.

†† Present address: Yoshitomi Pharmaceutical Industries Ltd., Bunkyo-ku, Tokyo 113.

This indicates that the reactions of **1b** and **1c** with phenylhydrazine are normal substitutions.

Furthermore, the reactions of 2-chlorotropones (**2a**—**c**) with phenylhydrazine gave normally-substituted 2-(β-phenylhydrazino)tropones (**5a**—**c**) in 10, 16, and 16% yields, respectively.

Reactivity of Hydrazines. The reactivity of hydrazines based on the product yields decreases in the following order:

$$NH_2NH_2 \gtrsim CH_3NHNH_2 \gg PhNHNH_2$$

In methylhydrazine, the reactivity enhancement by the +I effect of the methyl group is overcome by its steric effect. Thus, its reactivity might be comparable to that of hydrazine.

On the other hand, the reactivity of phenylhydrazine is considerably decreased by both the −I and steric effects of the phenyl group. The reactivity order is in line with the order of basicity (pK_a) of hydrazines:

$$NH_2NH_2\ (8.07)^{8)} > CH_3NHNH_2\ (7.87)^{8)} \gg PhNHNH_2\ (5.27)^{9)}$$

Experimental

Measurements. Melting points were determined with a Yanagimoto micro-melting point apparatus and are uncorrected. IR spectra were taken on a JASCO IRA-1 spectrophotometer, and UV spectra on a Hitachi EPS-3T spectrophotometer. NMR spectra were recorded on a Hitachi R-24 spectrometer (60 MHz).

Materials. All the known compounds were prepared according to the methods described: **1a**, mp 155.5—156.5 °C (lit,[10] 159—159.5 °C); **1b**, mp 114—118 °C (lit,[11] 117—118 °C); **1c**, mp 165—167 °C (lit,[11] 168—169 °C); **2a**, mp 66—67 °C (lit,[12] 66—67 °C).

4- (2b) and 6-Methyl-2-chlorotropone (2c). 4- (**2b**) and 6-methyl-2-chlorotropone (**2c**) were prepared by the reaction of the corresponding tosylates (**1b** and **1c**) with concentrated hydrochloric acid in dioxane according to the most advantageous method reported.[13,14] **2b**, mp 49—50 °C (lit,[7] 49—51 °C); **2c**, mp 59—60 °C (lit,[7] 60—61 °C).

Reactions with Hydrazine. A mixture of **1** or **2** (1 mmol) and 80% hydrazine hydrate (3 mmol, 185 mg) in methanol (5 ml) was refluxed for 30 min on a water-bath. The reaction mixture was diluted with water and extracted with chloroform. The extract was chromatographed on a Wakogel B-10 plate (30×30 cm²) with ethyl acetate to afford the corresponding 2-hydrazinotropone (**3**) (from benzene–hexane). **3a**, mp 91—93 °C (lit,[2] 95—96 °C); **3b**, mp 120—123 °C (lit,[3] 124 °C); **3c**, mp 122—124 °C (lit,[3] 134—135 °C).

Reactions with Methylhydrazine. The active troponoid (**1** or **2**) (1 mmol) reacted with methylhydrazine (3 mmol, 138 mg) in methanol (5 ml) to give the corresponding 2-(α-methylhydrazino)tropone (**4**) (from benzene–cyclohexane). Characteristic data are given in Table 1.

Alkaline Hydrolysis of 4- (4b) and 6-Methyl-2-(α-methylhydrazino)tropone (4c). *a*) **4b** (15 mg) was heated on a water-bath for 2 h with 10% potassium hydroxide/ethanol–water (1: 1) (4 ml). The reaction mixture was neutralized with 2 M hydrochloric acid and extracted with chloroform. The extract was dried over sodium sulfate, giving pale yellow crystals (11 mg, 88%) by evaporation of chloroform. The crystals were recrystallized from petroleum ether to afford 4-methyltropolone. Mp 73—76 °C (lit,[4] 76—77 °C). *b*) Alkaline hydrolysis of **4c** (210 mg) also gave 4-methyltropolone. Yield 120 mg (69%).

Reactions with Phenylhydrazine. A mixture of **1** or **2** (1 mmol) and phenylhydrazine (3 mmol, 324 mg) in methanol (5 ml) was refluxed for 8 h and worked up to afford the corresponding 2-(β-phenylhydrazino)tropone (**5**) (from ethyl acetate) (Table 1). Compound (**5a**) has been reported (mp 175 °C[5] and 163 °C[6]).

Hydrogenolysis of 4- (5b) and 6-Methyl-2-(β-phenylhydrazino)-tropone (5c). *a*) **5b** (0.5 mmol, 113 mg) in acetic acid (100 ml) was stirred for an hour under hydrogen atomosphere in the presence of 5% palladium–charcoal (100 mg). After removal of the catalyst, the reaction mixture was diluted with water, neutralized with solid sodium carbonate, and extracted with chloroform. The chloroform solution was washed with water, dried over sodium sulfate, and chromatographed on a Wakogel B-10 plate (20×20 cm²) with chloroform to give 2-amino-4-methyltropone. Yield 27 mg (40%); mp 120—121 °C (lit,[7] 122—123 °C). *b*) In a similar manner, hydrogenolysis of **5c** (0.5 mmol, 113 mg) gave 2-amino-6-methyltropone. Yield 32 mg (47%); mp 110—112 °C (lit,[3] 111—112 °C).

We wish to thank Dr. Tetsuo Nozoe, Professor Emeritus of Tohoku University, for his helpful discussion and encouragement. We are also grateful for the supply of methylcyclopentadiene dimer from Hitachi Chemical Co., Ltd.

References

1) a) T. Nozoe, "Nonbenzenoid Aromatic Compounds," ed by D. Ginsburg, Interscience Publishers, Inc., New York (1959), p. 339; b) T. Nozoe, K. Takase, and H. Matsumura, "Dai Yuki Kagaku," Asakura Publishing Co., Tokyo (1960), Vol. 13, p. 343; c) T. Nozoe, *Pure Appl. Chem.*, **28**, 239 (1971); d) F. Pietra, *Chem. Rev.*, **73**, 293 (1973).

2) T. Nozoe, S. Seto, H. Takeda, S. Morosawa, and K. Matsumoto, *Sci. Repts. Tohoku Univ., I*, **36**, 126 (1952).

3) a) P. Akroyd, R. D. Haworth, and J. D. Hobson, *J. Chem. Soc.*, **1951**, 3427; b) P. Akroyd, R. D. Haworth, and P. R. Jefferies, *J. Chem. Soc.*, **1954**, 286.

4) R. D. Haworth, P. B. Moor, and P. L. Pauson, *J. Chem. Soc.*, **1948**, 1045.

5) N. Soma, J. Nakazawa, T. Watanabe, Y. Sato, and G. Sunagawa, *Chem. Pharm. Bull.*, **13**, 457 (1965).

6) H. Sato, M. Yasunami, M. Ando, K. Takase, and T. Nozoe, 37th National Meeting of the Chemical Society of Japan, Yokohama, April, 1978, No. 2D32.

7) T. Sato, *Nippon Kagaku Zasshi*, **80**, 1167 (1959).

8) R. L. Hinman, *J. Org. Chem.*, **23**, 1587 (1958).

9) H.-H. Stroh and G. Westphal, *Chem. Ber.*, **96**, 184 (1963).

10) W. von E. Doering and C. F. Hiskey, *J. Am. Chem. Soc.*, **74**, 5688 (1952).

11) T. Sato, *Bull. Chem. Res. Inst. Non-aqueous Solns. Tohoku Univ.*, **8**, 47 (1959).

12) W. von E. Doering and L. H. Knox, *J. Am. Chem. Soc.*, **74**, 5683 (1952).

13) H. Matsumura, *Nippon Kagaku Zasshi*, **82**, 623 (1961).

14) T. Nozoe and T. Someya, *Bull. Chem. Soc. Jpn.*, **51**, 3316 (1978).

BULLETIN OF THE CHEMICAL SOCIETY OF JAPAN, VOL. 52 (8), 2449—2450 (1979)

The Polymerization of β-Propiolactone by Calcined Synthetic Hydrotalcite

Takuo NAKATSUKA,* Hitoshi KAWASAKI, Shinzo YAMASHITA,** and Shinzo KOHJIYA**

Industrial Technology Center of Okayama Prefecture, Ifuku-cho 4 chome, Okayama 700
***Department of Chemistry, Kyoto Institute of Technology, Matsugasaki, Kyoto 606*

(Received August 7, 1978)

Synopsis. The calcination of synthetic hydrotalcites of different compositions gave aluminium magnesium double oxides with strong basic sites and a high catalytic activity towards the polymerization of β-propiolactone. The strong basic sites were determined and compared with the apparent polymerization rates, suggesting that the strong basic sites are active sites towards the reaction.

Many catalytic reactions precipitated by either aluminium oxide or magnesium oxide have appeared in the literature; however, only a few works have been found regarding aluminium magnesium double oxide catalyses: the polymerization of formaldehyde,[1] the methylation of 3,5-xylenol,[2] and the depolymerization of paraldehyde.[3] In the last work, the correlation between the reactivity and the acid strength of the catalysts was mentioned. These catalysts were prepared by the calcination of hydroxides, nitrates, or carbonates.

Fukuda *et al.*[4] calcined synthetic hydrotalcites[5] with various molar ratios of the two metals in order to prepare aluminium magnesium double oxides, and studied their catalytic activity towards the decomposition of 4-hydroxy-4-methyl-2-pentanone and the methylation of phenol with methanol. The polymerization of propylene oxide was also found to be catalyzed by the oxide.[6] In this paper, these double oxides will be shown to catalyze the polymerization of β-propiolactone, and the active sites for the reaction will be discussed.

Experimental

Reagents. The hydrotalcites were supplied by the Kyowa Chemical Co., Ltd. The β-propiolactone was obtained commercially, dried over anhydrous sodium sulfate, and distilled under 10 Torr. The toluene was dried over calcium hydride and distilled under nitrogen. The acetone, ethanol, and chloroform used were of a reagent grade.

Calcination of Hydrotalcite. About 0.5 g of air-dried hydrotalcite was placed in a 20 ml test tube, calcined in air at elevated temperatures up to 450 °C, and kept at this temperature for 1 h. Then, the calcined hydrotalcite was cooled to 300 °C in air and subsequently to room temperature over anhydrous calcium chloride. After the determination of the calcination loss of hydrotalcite, the air in the tube was replaced with nitrogen and the tube was sealed with a stop cock.

Polymerization Procedure. To the oxide in the tube, 3 ml of toluene, 3 ml of β-propiolactone, and a magnetic stirring bar were added and the tube was sealed off. The reaction was carried out under stirring at a constant temperature for the necessary period of time. Then the reaction mixture was poured into ethanol, and the resulting precipitate was filtered and dried *in vacuo*. The polymer was extracted from the polymer-oxide composite with hot acetone for 10 h, using a Soxhlet extraction apparatus. The viscosity of the extracted polymer was measured at 30 °C in chloroform (0.5 g/dl).

Results and Discussion

The calcination of synthetic hydrotalcite at 450 °C for 1 h caused an almost complete decomposition, evolving carbon dioxide and water; consequently, aluminium magnesium double oxide was formed. The results of the chemical analysis and the measurement of the surface area are summarized in Table 1. A colour change in the indicator adsorbed on the oxide surface was observed for methyl red ($pK_a=4.8$), but not for phenylazonaphthylamine ($pK_a=4.0$). Therefore, the most acidic sites had acid strengths of $4.8 \geqslant H_0 \geqslant 4.0$. In the same manner, the most base strength of the oxides was determined to be $18.0 \geqslant H_- \geqslant 17.2$.

Table 1. Characterization of aluminium magnesium double oxides

Oxide	**1**	**2**	**3**	**4**	**5**
Calcination loss (wt %)	42.5	42.1	41.2	42.9	42.3
Chemical analysis					
MgO (wt %)	47.3	56.7	62.5	72.7	79.4
Al_2O_3 (wt %)	48.0	37.7	30.2	19.7	11.4
MgO/Al_2O_3 (molar ratio)	2.49	3.80	5.23	9.33	17.6
Amount of acid[a] (mmol/g)	0.41	0.32	0.21	0.06	0
Amount of base[b] (mmol/g)	0.63	0.54	0.73	0.85	0.94
Surface area[c] (m^2/g)	216	133	137	187	209

a) This was measured by the titration of butylamine (0.1 mol dm^{-3}) in benzene, using methyl red ($pK_a=4.8$) as an indicator. b) The value was obtained by the titration of benzoic acid (0.1 mol dm^{-3}) in benzene, using 2,4-dinitroaniline ($pK_a=15.0$) as an indicator. c) The surface area was measured by the BET method.

In order to examine the effects of these strong basic sites on the polymerization, the basic sites which have the base strength of $H_- \geqslant 15.0$ were determined (Table 1). The amount of the base was shown to increase with an increase in the molar ratio of magnesium oxide to aluminium oxide, except for the oxides **1** and **2**. This might be due to the increase in the surface area. The amount of the acid ($H_0 \leqslant 4.8$) correlates reversely with the magnesium oxide content. By X-ray analysis, the oxides showed only magnesium oxide diffraction patterns and no hydrotalcite patterns. The aluminium oxide moiety was likely to make a non-crystalline structure.

The results of the polymerization of β-propiolactone

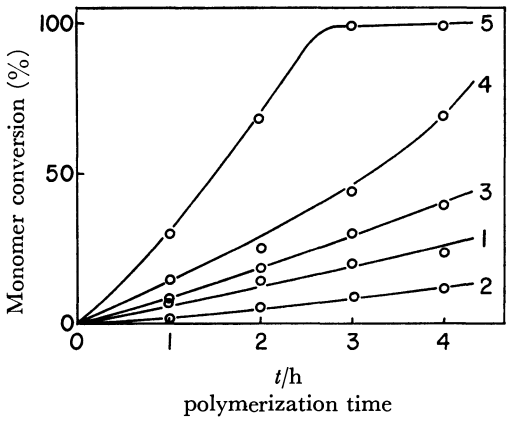

Fig. 1. Time-conversion curves for the polymerization of β-propiolactone catalyzed by the oxides listed in Table 1. β-propiolactone 3 ml, toluene 50 vol % solution, at 50 °C. Oxides **1** to **5** were prepared by the calcination of 0.5 g of corresponding hydrotalcites.

using the oxides in Table 1 as catalysts are summarized in Fig. 1. Since the reproducibility of the reaction was poor, *e.g.*, the variation coefficient of the monomer conversion (oxide **3**; 50 °C; 3 h) over 10 runs was 13%, the calcination and polymerization for hydrotalcites in a experiment were carried out at the same time. From the reaction products (reaction time 3 h; *cf.* Fig. 1), polymers were extracted with acetone. The polymers exhibited ester bands at 1730 and 1170 cm^{-1} in the ir spectra. The values of the weight per centage of the extracted polymer to the polymer-oxide compositions were 31, 36, 34, 25, and 8 for oxides **1** to **5** respectively. The values of the intrinsic viscosity were found to be 0.21, 0.11, 0.25, 0.36, and 0.26, showing that the polymers obtained did not have large molecular weights.[7]

A comparison of the amounts of the bases ($H_- \geqslant 15.0$) of the oxides in Table 1 with the overall initial polymerization rates in Fig. 1 implies that the reaction was initiated by a strong base. On the addition of a small amount of water, the oxides lost their polymerization activity. A carbon dioxide atmosphere also deactivated them. Such variations in the reaction conditions were found to diminish the amount of the strong base. Therefore, the active sites seem to correlate with the basic sites. However, the calcination of hydrotalcites at a reduced pressure (*ca.* 3 Torr) was also found to give oxides with a poor catalytic activity. This finding will be discussed elsewhere.

According to Malinowski's report,[8] magnesium oxide may have two kinds of basic sites on the surface: a strong basic site, O^{2-}, and a weak basic site, OH^-. The probable active site might be attributed to the strong basic surface oxygen. The role of aluminium oxide in the reaction is not yet clear; however, it contributed to the appearance of the strong basic sites ($H_- \geqslant 15.0$) on the double oxide. Magnesium oxide alone, prepared by the calcination of magnesium carbonate, did not exhibit such a strong basicity nor any polymerization activity.

The authors wish to thank Mr. Teruhiko Kumura for the generous gift of hydrotalcites and for the measurement of the surface area.

References

1) Teijin, Jpn. Patent 11391 (1965).
2) N. Isogami and T. Takeda, Jpn. Kohkai Patent 10032 (1973).
3) S. P. Walvekar and A. B. Halgeri, *J. Indian Chem. Soc.*, **50**, 387 (1973).
4) Y. Fukuda, T. Nishizaki, and K. Tanabe, *Nippon Kagaku Kaishi*, **1972**, 1754.
5) S. Miyata, T. Kumura, H. Hattori, and K. Tanabe, *Nippon Kagaku Zasshi*, **92**, 514 (1971).
6) S. Kohjiya, K. Kawabata, and S. Yamashita, Presented at 26th Annual Meeting of Soc. Polym. Sci., Japan, Kyoto, May 1977.
7) T. Kagiya, T. Sano, and K. Fukui, *Kogyo Kagaku Zasshi*, **67**, 951 (1964).
8) St. Malinowski, S. Szczepanska, and J. Sloczynski, *J. Catal.*, **7**, 67 (1967).

The Structure of the Cyclodextrin Complex. VIII. Crystal Structures of α-Cyclodextrin Complexes with 2-Pyrrolidone and *N,N*-Dimethylformamide

Kazuaki HARATA

Research Institute for Polymers and Textiles, Sawatari 4, Kanagawa-ku, Yokohama 221†

(Received October 2, 1978)

Crystal structures of α-cyclodextrin complexes with *N,N*-dimethylformamide and 2-pyrrolidone were determined by the X-ray method. The pentahydrated crystals of both complexes are orthorhombic, and the space group is $P2_12_12_1$ with $Z=4$. The cell dimensions are $a=13.750(1)$, $b=15.318(1)$, and $c=24.544(2)$ Å for the *N,N*-dimethylformamide complex, and $a=13.852(1)$, $b=15.373(1)$, and $c=24.353(2)$ Å for the 2-pyrrolidone complex. The structures were determined by assuming the same α-cyclodextrin packing in the crystal as that found in the isomorphous *p*-nitrophenol complex, and refined by the block-diagonal least-squares method to the final *R*-values of 0.054 for the *N,N*-dimethylformamide complex (5151 reflections) and 0.051 for the 2-pyrrolidone complex (5165 reflections). In both complexes, the guest molecules are included in the α-cyclodextrin cavity. The *N,N*-dimethylformamide molecule is in van der Waals contact with the host α-cyclodextrin molecule, while the 2-pyrrolidone molecule forms a weak N–H···O hydrogen bond with a glycosidic oxygen atom of α-cyclodextrin. The carbonyl oxygen atom of *N,N*-dimethylformamide and 2-pyrrolidone is hydrogen-bonded to water molecules of hydration located at the primary hydroxyl side of α-cyclodextrin. The tilt-angle of the glucose residue against the plane through six glycosidic oxygen atoms indicates clearly that the macro-cyclic conformation of α-cyclodextrin is affected by the packing as well as the size and shape of the guest molecule. The α-cyclodextrin molecules in the crystal are arranged parallel to the ac plane to form molecular layers. Three water molecules are located near the guest molecule, while the other two water molecules fill the intermolecular space.

Crystal structures of several α-cyclodextrin (α-CDx) complexes with benzene derivatives have already been determined by the X-ray method,[1–6] and it has been shown that the benzene ring can be included in the α-CDx cavity. On the other hand, the circular dichroism studies have shown that cyclodextrins form complexes with non-aromatic ring compounds, such as substituted cyclohexanones.[7] In this paper, we deal with the crystal structure of the α-CDx–2-pyrrolidone (1:1) complex to investigate the geometry of inclusion of a non-aromatic compound.

α-CDx dissolves in organic solvents such as DMSO and *N,N*-dimethylformamide (DMF). The X-ray study of α-CDx crystals obtained from a DMSO–methanol solution has shown that the α-CDx molecule includes DMSO and methanol molecules simultaneously.[8] The crystal structure of α-CDx crystallized from DMF–water solution was also determined to investigate the α-CDx–DMF interaction.

Experimental

Crystals of the α-CDx complex with 2-pyrrolidone (PRD) were obtained by cooling an aqueous solution containing α-CDx and PRD in 1:1 molar ratio. The α-CDx–DMF (1:1) complex was crystallized from a DMF–water (1:1) solution. Lattice parameters and reflection intensities were measured on a Rigaku automatic four-circle diffractometer with graphite-monochromatized Cu $K\alpha$ radiation. Intensity data were collected up to 150° in 2θ by using the θ-2θ scan technique. For the DMF complex, 5465 independent reflections were obtained, but 314 reflections with $|F_o|<3\sigma(F)$ were treated as unobserved. The same treatment was done for 245 reflections of the 5410 observed ones for the PRD complex. No corrections were made for absorption and extinction.

Crystal Data: α-CDx–MDF pentahydrate, $C_{36}H_{60}O_{30}\cdot C_3H_7ON\cdot 5H_2O$: *F.W.*=1136.0, orthorhombic, space group $P2_12_12_1$, $Z=4$, $a=13.750(1)$, $b=15.318(1)$, $c=24.544(2)$ Å, $V=5169.5(2)$ Å^3, $D_x=1.460$, $D_m=1.454$ g·cm^{-3}.

α-CDx–PRD pentahydrate, $C_{36}H_{60}O_{30}\cdot C_4H_7ON\cdot 5H_2O$: *F.W.*=1148.0, orthorhombic, space group $P2_12_12_1$, $Z=4$, $a=13.852(1)$, $b=15.373(1)$, $c=24.353(2)$ Å, $V=5186.2$ Å^3, $D_x=1.470$, $D_m=1.461$ g·cm^{-3}.

Determination and Refinement of the Structure

Crystals of the α-CDx complexes with DMF and PRD are isomorphous with the crystals of di-substituted benzene complexes.[1,2,5] A set of coordinates of α-CDx found in the *p*-nitrophenol complex[5] was used to determine initial phases for these complexes. The guest and water molecules were found on Fourier and difference-Fourier maps. Seventy hydrogen atoms in the DMF complex and sixtyfive ones in the PRD complex were found on the difference-Fourier maps. A primary hydroxyl group (O(6,G4)) and two water molecules (W4 and W5) were revealed to be statistically disordered in both complexes. Their occupancies were estimated from an electrondensity map, but they were not refined. The refinement of atomic parameters was carried out by the block-diagonal least-squares method, the quantity minimized being $\Sigma w(|F_o|-|F_c|)^2$, with $w=1.0$ for all the reflections used. Temperature factors of hydrogen atoms were not refined, but fixed as equal to the isotropic ones of heavier atoms to which the hydrogen atoms are bonded. The final *R*-values were 0.054 and 0.051 for the DMF and PRD complexes, respectively. The atomic parameters are listed in Tables 1 and 2.*

† New address: 1-1-4 Yatabe-Higashi, Tsukuba, Ibaraki 300-01.

* The tables of observed and calculated structure factors of both complexes and those of bond distances, bond angles, and conformation angles are kept at the Office of the Chemical Society of Japan (Document No. 7927).

TABLE 1. FINAL ATOMIC PARAMETERS ($\times 10^4$) FOR THE NON-HYDROGEN ATOMS

The anisotropic temperature factors are of the form: $\exp[-(B_{11}h^2+B_{22}k^2+B_{33}l^2+B_{12}hk+B_{23}kl+B_{31}lh)]$. OC indicates the occupancy factor for the disordered atom.

α-Cyclodextrin-N,N-dimethylformamide complex

	x	y	z	B_{11}	B_{22}	B_{33}	B_{12}	B_{23}	B_{31}	OC
C(1,G1)	1565(4)	-501(3)	6915(2)	38(3)	31(2)	10(1)	0(4)	4(2)	0(2)	
C(2,G1)	1278(4)	-1243(3)	6531(2)	47(3)	32(2)	9(1)	-20(4)	5(2)	1(2)	
C(3,G1)	1855(4)	-1165(3)	6007(2)	45(3)	21(2)	10(1)	-2(4)	1(2)	-2(3)	
C(4,G1)	1738(3)	-264(3)	5764(2)	39(3)	25(2)	9(1)	-2(4)	1(2)	5(2)	
C(5,G1)	2018(4)	440(3)	6179(2)	59(3)	22(2)	9(1)	3(4)	-1(2)	2(3)	
C(6,G1)	1844(5)	1362(3)	5971(2)	99(5)	25(2)	15(1)	12(6)	3(3)	-3(4)	
O(2,G1)	1489(3)	-2053(2)	6802(1)	85(3)	30(2)	12(1)	-46(4)	10(2)	-13(2)	
O(3,G1)	1498(3)	-1813(2)	5632(1)	67(3)	21(1)	10(1)	-16(3)	-2(2)	-4(2)	
O(4,G1)	2409(2)	-228(2)	5314(1)	31(2)	32(1)	8(1)	4(3)	7(1)	2(2)	
O(5,G1)	1428(3)	319(2)	6659(1)	54(2)	27(1)	10(1)	25(3)	1(2)	1(2)	
O(6,G1)	871(4)	1487(3)	5785(2)	101(4)	46(2)	18(1)	53(5)	13(2)	0(3)	
C(1,G2)	2072(3)	41(3)	4795(2)	31(2)	31(2)	10(1)	2(4)	8(2)	0(2)	
C(2,G2)	2299(3)	-684(3)	4389(2)	37(3)	25(2)	11(1)	-3(4)	4(2)	-1(2)	
C(3,G2)	3381(3)	-834(3)	4369(2)	36(2)	23(2)	10(1)	-2(4)	2(2)	5(2)	
C(4,G2)	3869(3)	19(3)	4251(2)	28(2)	21(2)	10(1)	6(3)	2(2)	0(2)	
C(5,G2)	3586(3)	750(3)	4634(2)	30(2)	21(2)	13(1)	5(4)	-2(2)	5(2)	
C(6,G2)	3983(4)	1632(3)	4466(3)	48(3)	23(2)	23(1)	-5(4)	-2(3)	9(3)	
O(2,G2)	1833(3)	-1483(2)	4552(1)	43(2)	34(2)	12(1)	-27(3)	4(2)	-2(2)	
O(3,G2)	3643(3)	-1437(2)	3944(1)	55(2)	20(1)	14(1)	1(3)	-7(2)	10(2)	
O(4,G2)	4911(2)	-153(2)	4334(1)	27(2)	26(1)	9(1)	9(3)	7(1)	3(2)	
O(5,G2)	2539(2)	820(2)	4635(1)	32(2)	22(1)	12(1)	11(3)	8(1)	7(2)	
O(6,G2)	3831(3)	1785(3)	3897(2)	64(3)	37(2)	27(1)	18(4)	33(2)	20(3)	
C(1,G3)	5587(3)	72(3)	3921(2)	33(2)	27(2)	7(1)	0(4)	3(2)	4(2)	
C(2,G3)	6216(3)	-727(3)	3826(2)	35(2)	25(2)	8(1)	0(4)	1(2)	-1(2)	
C(3,G3)	6720(3)	-971(3)	4352(2)	29(2)	19(2)	10(1)	6(3)	1(2)	2(2)	
C(4,G3)	7269(3)	-195(3)	4587(2)	33(2)	23(2)	7(1)	3(3)	2(2)	-1(2)	
C(5,G3)	6655(3)	644(3)	4600(2)	40(3)	20(2)	9(1)	1(4)	3(2)	-1(2)	
C(6,G3)	7256(4)	1460(3)	4707(2)	53(3)	21(2)	16(1)	-11(4)	1(2)	-4(3)	
O(2,G3)	5634(2)	-1442(2)	3627(1)	34(2)	27(1)	9(1)	4(3)	-11(2)	-3(2)	
O(3,G3)	7411(2)	-1654(2)	4269(1)	37(2)	21(1)	16(1)	17(3)	-3(2)	-2(2)	
O(4,G3)	7519(2)	-438(2)	5133(1)	30(2)	27(1)	7(1)	-3(3)	3(1)	-2(2)	
O(5,G3)	6182(2)	776(2)	4082(1)	33(2)	22(1)	9(1)	-1(3)	7(1)	-1(2)	
O(6,G3)	8122(3)	1498(3)	4389(2)	48(2)	40(2)	20(1)	-32(4)	12(2)	2(2)	
C(1,G4)	8474(3)	-254(3)	5318(2)	32(2)	25(2)	9(1)	-3(4)	-6(2)	3(2)	
C(2,G4)	8824(4)	-1061(3)	5619(2)	40(3)	27(2)	9(1)	10(4)	-6(2)	-2(2)	
C(3,G4)	8256(4)	-1196(3)	6146(2)	43(3)	17(2)	10(1)	6(4)	-3(2)	-3(2)	
C(4,G4)	8270(3)	-367(3)	6483(2)	38(3)	20(2)	8(1)	-1(4)	-2(2)	4(2)	
C(5,G4)	7876(4)	394(3)	6146(2)	45(3)	17(2)	9(1)	6(4)	-3(2)	3(2)	
C(6,G4)	7939(5)	1259(3)	6441(2)	77(4)	20(2)	12(1)	6(5)	-4(2)	0(3)	
O(2,G4)	8747(3)	-1810(2)	5271(1)	53(2)	33(2)	11(1)	28(3)	-15(2)	-6(2)	
O(3,G4)	8705(3)	-1889(2)	6446(1)	79(3)	22(1)	10(1)	29(3)	6(2)	5(2)	
O(4,G4)	7634(2)	-534(2)	6940(1)	35(2)	28(1)	6(1)	-7(3)	-2(1)	-2(2)	
O(5,G4)	8486(2)	485(2)	5670(1)	42(2)	20(1)	9(1)	-16(3)	-1(1)	3(2)	
O(6A,G4)	9093(15)	1450(11)	6539(7)	79(4)	23(7)	12(3)	-39(17)	-13(8)	8(11)	0.2
O(6B,G4)	7475(4)	1917(3)	6099(2)	73(3)	22(2)	16(1)	26(4)	-2(2)	2(3)	0.8
C(1,G5)	7982(3)	-335(3)	7473(2)	36(3)	29(2)	9(1)	-4(4)	-5(2)	-5(2)	
C(2,G5)	7812(4)	-1125(3)	7833(2)	41(3)	26(2)	9(1)	5(4)	-3(2)	-3(2)	
C(3,G5)	6732(4)	-1319(3)	7892(2)	41(3)	23(2)	10(1)	-6(4)	2(2)	-1(2)	
C(4,G5)	6160(3)	-501(3)	8042(2)	27(2)	28(2)	13(1)	-7(4)	-5(2)	-1(2)	
C(5,G5)	6433(3)	296(3)	7698(2)	34(3)	27(2)	11(1)	-1(4)	0(2)	-2(2)	
C(6,G5)	6029(4)	1152(3)	7901(2)	49(3)	27(2)	18(1)	9(5)	-3(3)	4(3)	
O(2,G5)	8310(3)	-1855(2)	7601(1)	58(2)	31(2)	13(1)	26(3)	2(2)	1(2)	
O(3,G5)	6633(3)	-1972(2)	8306(2)	67(3)	32(2)	17(1)	2(4)	16(2)	14(3)	
O(4,G5)	5156(2)	-705(2)	7943(1)	27(2)	39(2)	13(1)	-10(3)	-15(2)	0(2)	
O(5,G5)	7481(2)	396(2)	7692(1)	34(2)	24(1)	10(1)	-5(3)	-7(1)	0(2)	
O(6,G5)	6180(3)	1266(3)	8480(2)	50(2)	50(2)	18(1)	-4(4)	-29(2)	2(2)	
C(1,G6)	4448(4)	-527(3)	8339(2)	34(3)	33(2)	11(1)	2(4)	5(2)	2(3)	
C(2,G6)	3725(4)	-1266(4)	8365(2)	42(3)	38(2)	21(1)	-8(5)	28(3)	-17(3)	
C(3,G6)	3293(4)	-1397(3)	7791(2)	39(3)	24(2)	18(1)	-8(4)	13(2)	-2(3)	
C(4,G6)	2809(4)	-556(3)	7628(2)	40(3)	26(2)	7(1)	-3(4)	3(2)	-1(2)	
C(5,G6)	3461(4)	242(3)	7687(2)	49(3)	27(2)	9(1)	-8(4)	0(2)	-7(3)	
C(6,G6)	2891(5)	1095(3)	7644(2)	68(4)	29(2)	17(1)	3(5)	4(3)	-16(3)	
O(2,G6)	4159(4)	-2040(3)	8573(2)	78(3)	44(2)	41(1)	-14(4)	38(3)	-54(4)	
O(3,G6)	2590(3)	-2086(2)	7809(2)	54(3)	29(2)	25(1)	-35(4)	21(2)	-20(3)	
O(4,G6)	2544(2)	-630(2)	7066(1)	36(2)	30(1)	8(1)	5(3)	-1(1)	1(2)	
O(5,G6)	3926(3)	248(2)	8222(1)	47(2)	32(2)	8(1)	11(3)	-4(2)	-8(2)	
O(6,G6)	1983(3)	1078(3)	7924(2)	75(3)	55(2)	17(1)	51(5)	-7(2)	8(3)	
C(1,DF)	5343(10)	-1878(9)	6526(4)	233(15)	155(10)	22(2)	-139(21)	51(7)	-41(9)	
C(2,DF)	5072(11)	-1420(9)	5587(3)	292(17)	156(10)	13(1)	105(24)	-9(6)	4(9)	
C(3,DF)	4976(10)	-358(12)	6385(7)	123(11)	231(17)	83(6)	-81(26)	4(18)	11(14)	
N(DF)	5096(5)	-1157(4)	6131(2)	88(4)	59(3)	23(1)	-33(7)	-20(3)	12(4)	
O(DF)	4855(7)	212(6)	6121(5)	162(8)	104(6)	128(5)	-30(13)	-1(10)	-1(12)	
O(W1)	5055(3)	1203(3)	9388(2)	53(3)	89(3)	16(1)	-8(5)	1(3)	-6(3)	
O(W2)	42(4)	1059(4)	7520(2)	87(3)	83(3)	19(1)	-37(6)	-18(3)	28(3)	
O(W3)	106(4)	1565(4)	4664(2)	78(4)	92(4)	24(1)	24(6)	-1(3)	-3(3)	
O(W4A)	247(4)	2387(4)	6734(2)	62(4)	58(3)	23(1)	6(6)	4(3)	-20(4)	0.8
O(W4B)	-165(14)	3321(17)	7104(8)	34(11)	91(16)	17(4)	-49(23)	14(13)	5(11)	0.2
O(W5A)	-341(6)	3236(5)	3151(3)	84(5)	58(4)	29(2)	-11(8)	33(4)	-9(5)	0.7
O(W5B)	661(15)	3137(14)	4247(8)	105(16)	99(13)	34(5)	-37(25)	4(14)	-37(15)	0.3

TABLE 1. (Continued)

α-Cyclodextrin-2-pyrrolidone complex

	x	y	z	B_{11}	B_{22}	B_{33}	B_{12}	B_{23}	B_{31}	OC
C(1,G1)	1549(3)	-499(3)	6896(2)	39(2)	32(2)	10(1)	-1(4)	4(2)	5(2)	
C(2,G1)	1255(4)	-1222(3)	6507(2)	44(3)	37(2)	9(1)	-20(4)	5(2)	-5(2)	
C(3,G1)	1836(3)	-1154(3)	5979(2)	42(3)	22(2)	11(1)	-7(4)	2(2)	-4(2)	
C(4,G1)	1725(3)	-250(3)	5733(2)	35(2)	27(2)	9(1)	-5(4)	3(2)	5(2)	
C(5,G1)	1981(4)	449(3)	6156(2)	57(3)	22(2)	12(1)	7(4)	3(2)	4(3)	
C(6,G1)	1818(5)	1367(3)	5951(2)	106(5)	26(2)	15(1)	20(6)	2(2)	-4(4)	
O(2,G1)	1454(3)	-2031(2)	6780(1)	82(3)	28(2)	12(1)	-45(4)	10(2)	-15(2)	
O(3,G1)	1484(3)	-1801(2)	5604(1)	60(2)	22(1)	11(1)	-15(3)	0(1)	-5(2)	
O(4,G1)	2405(2)	-209(2)	5289(1)	27(1)	31(1)	8(1)	4(3)	5(1)	1(1)	
O(5,G1)	1402(3)	320(2)	6639(2)	57(2)	29(2)	11(1)	28(3)	1(2)	6(2)	
O(6,G1)	837(4)	1481(3)	5767(2)	114(4)	52(2)	19(1)	81(5)	18(2)	17(3)	
C(1,G2)	2076(3)	47(3)	4764(2)	29(2)	29(2)	10(1)	1(4)	8(2)	1(2)	
C(2,G2)	2309(3)	-681(3)	4360(2)	33(2)	27(2)	10(1)	-6(4)	3(2)	1(2)	
C(3,G2)	3391(3)	-832(3)	4353(2)	32(2)	25(2)	11(1)	-1(4)	-1(2)	1(2)	
C(4,G2)	3901(3)	16(3)	4228(2)	26(2)	20(2)	11(1)	6(3)	2(2)	1(2)	
C(5,G2)	3578(3)	759(3)	4598(2)	28(2)	22(2)	14(1)	4(3)	-1(2)	2(2)	
C(6,G2)	3973(4)	1636(3)	4409(2)	47(3)	20(2)	25(1)	-5(4)	3(3)	11(3)	
O(2,G2)	1843(2)	-1473(2)	4518(1)	39(2)	32(2)	12(1)	-24(3)	4(2)	-3(2)	
O(3,G2)	3659(2)	-1453(2)	3939(1)	47(2)	21(1)	14(1)	2(3)	-7(2)	6(2)	
O(4,G2)	4909(2)	-142(2)	4317(1)	26(1)	23(1)	9(1)	8(2)	5(1)	3(1)	
O(5,G2)	2545(2)	828(2)	4597(1)	29(2)	23(1)	13(1)	11(3)	6(1)	6(2)	
O(6,G2)	3816(3)	1754(3)	3833(2)	62(3)	36(2)	29(1)	14(4)	35(2)	20(3)	
C(1,G3)	5580(3)	57(3)	3894(2)	32(2)	26(2)	8(1)	0(4)	4(2)	4(2)	
C(2,G3)	6193(3)	-748(3)	3810(2)	31(2)	24(2)	8(1)	-1(4)	-2(2)	2(2)	
C(3,G3)	6708(3)	-970(3)	4347(2)	28(2)	19(2)	11(1)	2(3)	-1(2)	1(2)	
C(4,G3)	7267(3)	-187(3)	4559(2)	30(2)	22(2)	8(1)	-3(3)	1(2)	-1(2)	
C(5,G3)	6658(3)	650(3)	4565(2)	40(2)	20(2)	10(1)	-4(4)	4(2)	-5(2)	
C(6,G3)	7269(4)	1463(3)	4660(2)	56(3)	20(2)	16(1)	-19(4)	3(2)	-3(3)	
O(2,G3)	5608(2)	-1460(2)	3621(2)	33(2)	27(1)	9(1)	3(3)	-8(1)	-3(2)	
O(3,G3)	7386(2)	-1657(2)	4265(1)	35(2)	20(1)	16(1)	13(3)	-1(1)	-5(2)	
O(4,G3)	7530(2)	-406(2)	5109(1)	28(1)	27(1)	8(1)	-4(3)	4(1)	-2(1)	
O(5,G3)	6175(2)	765(2)	4043(1)	34(2)	20(1)	11(1)	-3(3)	8(1)	-3(2)	
O(6,G3)	8118(3)	1483(2)	4328(2)	51(2)	41(2)	22(1)	-36(4)	13(2)	2(2)	
C(1,G4)	8483(3)	-218(3)	5288(2)	30(2)	28(2)	10(1)	-5(4)	-3(2)	0(2)	
C(2,G4)	8847(3)	-1023(3)	5580(2)	33(2)	25(2)	10(1)	8(4)	-6(2)	-1(2)	
C(3,G4)	8290(3)	-1175(3)	6107(2)	38(2)	18(2)	10(1)	2(4)	-1(2)	-5(2)	
C(4,G4)	8293(3)	-359(3)	6454(2)	34(2)	21(2)	10(1)	-4(4)	-2(2)	2(2)	
C(5,G4)	7896(3)	408(3)	6123(2)	47(3)	17(2)	10(1)	6(4)	-4(2)	1(2)	
C(6,G4)	7967(5)	1273(3)	6428(2)	82(4)	18(2)	15(1)	2(5)	-6(2)	2(3)	
O(2,G4)	8789(2)	-1765(2)	5224(1)	42(2)	34(2)	12(1)	24(3)	-15(2)	-8(2)	
O(3,G4)	8732(3)	-1860(2)	6416(1)	71(2)	20(1)	11(1)	24(3)	-1(1)	-2(2)	
O(4,G4)	7657(2)	-532(2)	6912(1)	33(2)	26(1)	8(1)	-12(3)	-1(1)	0(1)	
O(5,G4)	8500(2)	511(2)	5642(1)	43(2)	22(1)	10(1)	-16(3)	-1(1)	-2(2)	
O(6A,G4)	9103(11)	1465(8)	6530(5)	95(11)	27(5)	21(3)	-37(10)	-18(7)	8(9)	0.3
O(6B,G4)	7485(4)	1934(3)	6098(2)	75(4)	16(2)	16(1)	5(4)	2(2)	-5(3)	0.7
C(1,G5)	7975(3)	-345(3)	7449(2)	34(2)	24(2)	10(1)	-4(4)	-4(2)	-6(2)	
C(2,G5)	7788(3)	-1150(2)	7801(2)	41(3)	27(2)	9(1)	11(4)	-2(2)	-3(2)	
C(3,G5)	6707(4)	-1331(3)	7840(2)	43(3)	25(2)	11(1)	-2(4)	1(2)	2(2)	
C(4,G5)	6154(3)	-509(2)	7994(2)	28(2)	24(2)	13(1)	-6(4)	-6(2)	-3(2)	
C(5,G5)	6450(3)	284(3)	7658(2)	34(2)	29(2)	11(1)	-2(4)	-4(2)	3(2)	
C(6,G5)	6044(4)	1141(3)	7873(2)	44(3)	26(2)	22(1)	9(4)	-1(3)	7(3)	
O(2,G5)	8300(3)	-1883(2)	7586(1)	56(2)	30(2)	13(1)	29(3)	1(2)	4(2)	
O(3,G5)	6546(3)	-2001(2)	8233(2)	82(3)	28(2)	18(1)	0(4)	10(2)	23(3)	
O(4,G5)	5155(2)	-697(2)	7884(1)	28(2)	37(2)	12(1)	-12(3)	-12(2)	1(2)	
O(5,G5)	7484(2)	375(2)	7670(1)	32(2)	22(1)	11(1)	-10(3)	-7(1)	1(2)	
O(6,G5)	6190(3)	1250(3)	8445(2)	47(2)	49(2)	22(1)	-4(4)	-36(2)	3(2)	
C(1,G6)	4453(3)	-559(3)	8299(2)	37(2)	34(2)	10(1)	-1(4)	5(2)	4(2)	
C(2,G6)	3770(4)	-1346(4)	8298(2)	43(3)	44(3)	21(1)	-24(5)	33(3)	-18(3)	
C(3,G6)	3290(3)	-1422(3)	7739(2)	36(2)	23(2)	16(1)	-7(4)	9(2)	-2(2)	
C(4,G6)	2799(3)	-560(3)	7602(2)	36(2)	24(2)	8(1)	2(4)	2(2)	2(2)	
C(5,G6)	3450(4)	225(3)	7666(2)	47(3)	23(2)	10(1)	-8(4)	1(2)	-6(2)	
C(6,G6)	2896(4)	1084(3)	7629(2)	63(3)	29(2)	17(1)	0(5)	-2(3)	-7(3)	
O(2,G6)	4304(4)	-2111(3)	8411(3)	111(4)	40(2)	77(2)	-48(5)	69(4)	-134(6)	
O(3,G6)	2596(3)	-2104(2)	7766(2)	48(2)	27(2)	23(1)	-32(3)	21(2)	-16(2)	
O(4,G6)	2519(2)	-620(2)	7035(1)	34(2)	28(1)	8(1)	-3(3)	-1(1)	2(2)	
O(5,G6)	3914(2)	201(2)	8200(1)	44(2)	33(2)	9(1)	6(3)	-1(1)	-4(2)	
O(6,G6)	2000(3)	1061(3)	7923(2)	75(3)	53(2)	18(1)	61(4)	-6(2)	8(3)	
C(1,P)	4952(6)	-373(5)	6188(5)	80(5)	51(4)	94(5)	-14(8)	-69(7)	43(9)	
C(2,P)	5073(7)	-701(5)	5632(3)	154(8)	47(3)	30(2)	-4(10)	7(4)	4(7)	
C(3,P)	5171(8)	-1669(5)	5699(3)	211(11)	44(3)	25(2)	22(11)	3(4)	-15(8)	
C(4,P)	5241(9)	-1845(5)	6318(3)	220(12)	53(4)	25(2)	-22(12)	-2(4)	-3(8)	
N(P)	5065(7)	-1008(5)	6587(3)	136(7)	51(3)	25(2)	-32(9)	-3(4)	3(6)	
O(P)	4828(7)	419(4)	6311(4)	209(9)	58(3)	112(4)	18(10)	-37(7)	92(11)	
O(W1)	5024(3)	1147(3)	9344(2)	47(2)	62(2)	18(1)	-4(4)	2(2)	-6(2)	
O(W2)	77(4)	1020(3)	7534(2)	88(3)	73(3)	18(1)	-30(5)	-13(3)	23(3)	
O(W3)	41(4)	1623(4)	4675(2)	88(4)	101(4)	26(1)	-1(7)	12(4)	-8(4)	
O(W4A)	239(4)	2364(4)	6749(2)	60(4)	43(3)	19(1)	6(5)	3(3)	-14(3)	0.7
O(W4B)	-114(12)	3259(16)	7189(8)	66(11)	162(18)	33(4)	-21(26)	31(16)	18(12)	0.3
O(W5A)	-322(10)	3213(8)	3088(5)	94(9)	68(7)	28(3)	11(14)	36(8)	10(9)	0.4
O(W5B)	622(7)	3241(6)	4253(4)	109(7)	81(6)	41(3)	-66(11)	19(7)	-39(8)	0.6

TABLE 2. FRACTIONAL COORDINATES ($\times 10^3$) AND ISOTROPIC TEMPERATURE FACTORS (B/Å^2) FOR HYDROGEN ATOMS

α-Cyclodextrin-DMF complex

	x	y	z	B		x	y	z	B
H(C1,G1)	109(4)	-47(4)	730(2)	2.6	H(C6BA,G4)	873(6)	143(5)	649(3)	3.0
H(C2,G1)	50(4)	-123(4)	643(2)	2.8	H(C6BB,G4)	754(6)	119(5)	682(3)	3.0
H(C3,G1)	266(4)	-131(4)	608(2)	2.3	H(O2,G4)	801(4)	-182(4)	492(2)	2.8
H(C4,G1)	95(4)	-18(4)	562(2)	2.3	H(O3,G4)	830(4)	-200(4)	680(2)	2.9
H(C5,G1)	281(4)	36(4)	629(2)	2.8	H(O6B,G4)	701(6)	225(5)	631(3)	3.3
H(C6A,G1)	233(5)	149(4)	563(3)	4.2	H(C1,G5)	876(4)	-12(4)	746(2)	2.3
H(C6B,G1)	200(5)	185(4)	629(3)	4.2	H(C2,G5)	811(4)	-99(4)	823(2)	2.4
H(O2,G1)	110(5)	-250(4)	667(3)	3.4	H(C3,G5)	646(4)	-157(4)	752(2)	2.4
H(O3,G1)	171(4)	-171(4)	524(2)	2.9	H(C4,G5)	626(4)	-35(4)	847(2)	2.4
H(O6,G1)	31(5)	100(5)	571(3)	4.9	H(C5,G5)	615(4)	20(4)	728(2)	2.5
H(C1,G2)	129(4)	22(4)	483(2)	2.4	H(C6A,G5)	634(5)	170(4)	766(2)	3.4
H(C2,G2)	206(4)	-50(4)	397(2)	2.3	H(C6B,G5)	524(5)	115(4)	782(2)	3.4
H(C3,G2)	362(4)	-109(4)	475(2)	2.1	H(O2,G5)	836(5)	-218(4)	779(2)	2.9
H(C4,G2)	376(4)	23(4)	382(2)	1.9	H(O3,G5)	604(5)	-198(4)	820(3)	3.6
H(C5,G2)	387(4)	60(4)	506(2)	2.3	H(O6,G5)	670(5)	168(4)	850(3)	4.0
H(C6A,G2)	475(5)	165(4)	454(2)	3.5	H(C1,G6)	486(4)	-40(4)	873(2)	2.5
H(C6B,G2)	357(5)	217(4)	470(2)	3.5	H(C2,G6)	313(5)	-110(4)	868(2)	3.4
H(O2,G2)	102(4)	-130(4)	449(2)	2.9	H(C3,G6)	383(4)	-157(4)	749(2)	2.9
H(O3,G2)	367(4)	-200(4)	418(2)	2.9	H(C4,G6)	214(4)	-46(4)	788(2)	2.3
H(O6,G2)	326(5)	222(4)	382(3)	4.1	H(C5,G6)	402(4)	23(4)	737(2)	2.5
H(C1,G3)	519(4)	32(4)	358(2)	2.3	H(C6A,G6)	334(5)	167(4)	781(2)	3.6
H(C2,G3)	677(4)	-61(4)	352(2)	2.1	H(C6B,G6)	277(5)	122(4)	719(2)	3.6
H(C3,G3)	622(4)	-119(4)	465(2)	2.3	H(O2,G6)	462(6)	-221(5)	819(3)	5.4
H(C3,G3)	794(4)	-9(4)	435(2)	2.0	H(O3,G6)	233(5)	-221(4)	750(2)	3.8
H(C5,G3)	609(4)	60(4)	493(2)	2.1	H(O6,G6)	173(5)	118(4)	830(3)	4.5
H(C6A,G3)	745(4)	148(4)	513(2)	2.9	H(1,W1)	516(5)	117(4)	902(3)	4.8
H(C6B,G3)	682(4)	206(4)	464(2)	2.9	H(2,W1)	541(5)	116(5)	963(3)	4.8
H(O2,G5)	502(4)	-149(4)	372(2)	2.2	H(1,W2)	74(6)	116(5)	770(3)	5.7
H(O3,G3)	699(4)	-220(4)	428(2)	2.6	H(2,W2)	-31(5)	116(5)	782(3)	5.7
H(O6,G3)	802(5)	177(4)	403(3)	3.8	H(1,W3)	6(6)	144(5)	499(3)	6.1
H(C1,G4)	895(4)	-7(4)	496(2)	2.1	H(2,W3)	-29(6)	200(5)	476(3)	6.1
H(C2,G4)	961(4)	-96(4)	573(2)	2.3	H(1,W4A)	104(6)	261(6)	683(3)	4.4
H(C3,G4)	746(4)	-136(4)	606(2)	2.1	H(2,W4A)	-67(6)	247(6)	672(3)	4.4
H(C4,G4)	903(4)	-18(4)	663(2)	2.0	H(1,W5A)	-34(8)	370(7)	349(4)	5.3
H(C5,G4)	709(4)	25(4)	605(2)	2.1	H(2,W5A)	36(8)	300(7)	319(4)	5.3

α-Cyclodextrin-2-pyrrolidone complex

	x	y	z	B		x	y	z	B
H(C1,G1)	110(4)	-45(4)	725(2)	2.6	H(C4,G4)	903(4)	-21(3)	660(2)	1.9
H(C2,G1)	44(4)	-116(4)	643(2)	2.7	H(C5,G4)	719(4)	25(3)	600(2)	2.1
H(C3,G1)	260(4)	-113(4)	608(2)	2.4	H(C6A,G4)	730(6)	122(5)	680(3)	3.4
H(C4,G1)	97(4)	-12(3)	556(2)	2.4	H(C6B,G4)	870(6)	149(6)	651(3)	3.4
H(C5,G1)	276(4)	39(4)	629(2)	3.0	H(O2,G4)	832(4)	-180(4)	503(2)	2.7
H(C6A,G1)	229(5)	150(4)	559(2)	4.2	H(O3,G4)	866(4)	-226(4)	621(2)	2.7
H(C6B,G1)	206(5)	179(4)	628(2)	4.2	H(C1,G5)	874(4)	-12(3)	741(2)	2.1
H(O2,G1)	126(4)	-247(4)	667(2)	3.1	H(C2,G5)	807(4)	-105(3)	822(2)	2.1
H(O3,G1)	173(4)	-169(4)	523(2)	3.0	H(C3,G5)	642(4)	-154(4)	743(2)	2.5
H(O6,G1)	60(5)	165(4)	602(3)	4.9	H(C4,G5)	625(4)	-36(4)	844(2)	2.3
H(C1,G2)	129(4)	19(4)	478(2)	2.9	H(C5,G5)	626(4)	19(4)	721(2)	2.5
H(C2,G2)	209(4)	-48(3)	394(2)	2.3	H(C6A,G5)	632(4)	167(4)	762(2)	3.5
H(C3,G2)	360(4)	-109(3)	476(2)	2.2	H(C6B,G5)	534(4)	118(4)	777(2)	3.5
H(C4,G2)	376(4)	16(3)	380(2)	1.9	H(O2,G5)	830(4)	-183(4)	719(2)	2.9
H(C5,G2)	380(4)	60(4)	504(2)	2.4	H(O3,G5)	665(4)	-182(4)	846(2)	3.6
H(C6A,G2)	479(4)	166(4)	450(2)	3.5	H(O6,G5)	669(5)	152(4)	864(2)	4.0
H(C6B,G2)	356(4)	214(4)	465(2)	3.5	H(C1,G6)	481(4)	-44(4)	869(2)	2.5
H(O2,G2)	133(4)	-128(4)	432(2)	2.8	H(C2,G6)	320(4)	-125(4)	863(2)	3.3
H(O3,G2)	330(4)	-131(4)	352(2)	2.7	H(C3,G6)	382(4)	-156(4)	741(2)	2.8
H(O6,G2)	299(5)	201(4)	372(3)	4.5	H(C4,G6)	221(4)	-50(3)	787(2)	2.2
H(C1,G3)	517(4)	26(3)	356(2)	2.1	H(C5,G6)	395(4)	19(4)	731(2)	2.5
H(C2,G3)	673(4)	-62(3)	352(2)	2.1	H(C6A,G6)	331(5)	163(4)	779(2)	3.6
H(C3,G3)	620(4)	-121(3)	466(2)	2.0	H(C6B,G6)	278(4)	123(4)	718(2)	3.6
H(C4,G3)	789(4)	-9(3)	430(2)	1.8	H(O2,G6)	406(6)	-276(5)	847(3)	7.9
H(C5,G3)	610(4)	65(3)	491(2)	2.0	H(O3,G6)	235(4)	-214(4)	734(2)	3.5
H(C6A,G3)	745(4)	148(4)	507(2)	2.7	H(O6,G6)	231(5)	83(4)	833(3)	4.7
H(C6B,G3)	681(4)	205(4)	458(2)	2.7	H(1,W1)	536(5)	116(4)	901(2)	4.3
H(O2,G3)	528(4)	-153(3)	395(2)	2.1	H(2,W1)	537(5)	151(4)	968(3)	4.3
H(O3,G3)	705(4)	-218(4)	430(2)	2.6	H(1,W2)	-31(5)	128(5)	779(3)	5.8
H(O6,G3)	802(4)	168(4)	402(2)	3.7	H(2,W2)	-28(5)	129(5)	718(3)	5.8
H(C1,G4)	892(4)	1(3)	496(2)	2.1	H(1,W3)	7(5)	167(5)	502(3)	6.4
H(C2,G4)	960(4)	-96(3)	567(2)	2.4	H(1,W4)	36(7)	279(6)	677(4)	4.2
H(C3,G4)	753(4)	-133(3)	603(2)	2.2					

Description and Discussion of the Structure

The atom numbering for α-CDx in both complexes (Figs. 1 and 2) is the same as that used in other complexes with the isomorphous structure.

Structure of α-CDx. Average bond distances and bond angles over six glucose residues in the α-CDx moiety are shown in Fig. 3. The corresponding distances and angles in the both complexes are in good agreement. No significant differences were observed when they were compared with those found in the α-CDx complexes with *p*-nitrophenol and *p*-hydroxybenzoic acid.[5] The primary hydroxyl group in the G4 residue is statistically disordered (Figs. 1 and 2), and shows *gauche-gauche* and *gauche-trans* conformations, while other primary hydroxyl groups are in the *gauche-*

gauche conformation. A similar disordered conformation of the primary hydroxyl group has been found in other α-CDx complexes[1,2,5] isomorphous to these complexes, although the shape and size of the guest molecule are quite different. The C(6,G4)–O(6B,G4) bond is oriented to the inside of the α-CDx ring, but shows no short contact with the included guest molecule. Therefore, the disorder of the G4 hydroxyl group may not be caused by the inclusion of the guest molecule, but by the packing requirement.

The geometry of the α-CDx ring is given in Tables 3—5. The O(4)···O(4) distances between adjacent glucose residues indicate that the deformation of the pyranose ring is slightly smaller than that found in the complexes with *p*-nitrophenol (4.016—4.493 Å) and *p*-hydroxybenzoic acid (4.053—4.509 Å).[5] The torsion-angle indices[9] (see Table 3) also show a similar tendency: they are 111.4—148.1° in the *p*-nitrophenol complex and 108.9—145.9° in the *p*-hydroxybenzoic acid complex. Between the O(4)···O(4) distances and

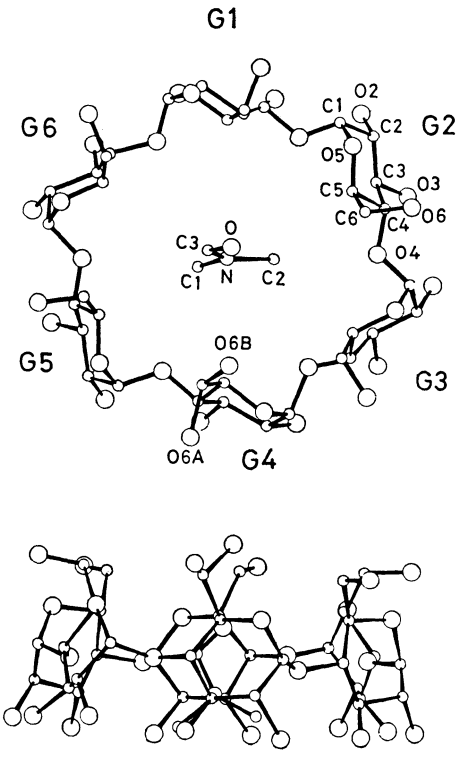

Fig. 1. Structure and numbering scheme of the α-cyclodextrin–*N*,*N*-dimethylformamide complex. O6A and O6B indicate the disordered hydroxyl oxygen atom.

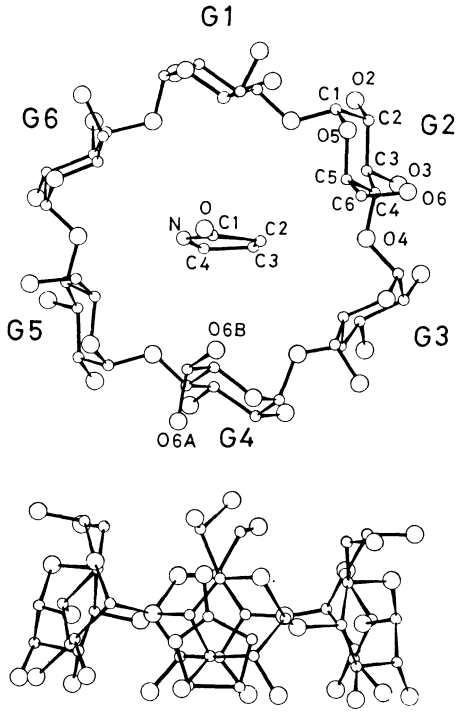

Fig. 2. Structure and numbering scheme of the α-cyclodextrin–2-pyrrolidone complex. O6A and O6B indicate the disordered hydroxyl oxygen atom.

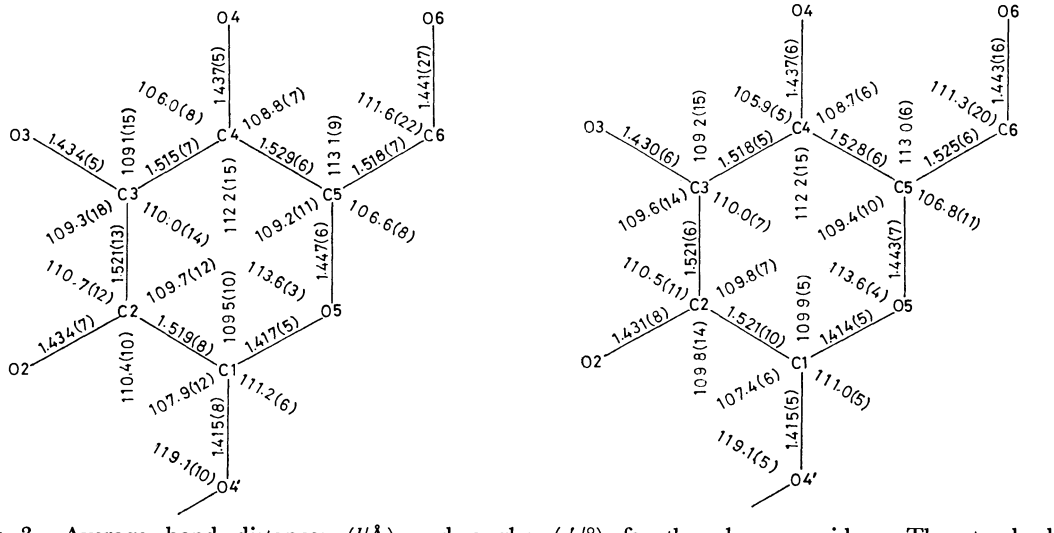

Fig. 3. Average bond distances (l/Å) and angles (ϕ/°) for the glucose residue. The standard deviations were estimated according to the equation $\sigma=[\sum_{i=1}^{6}(x_i-\bar{x})^2/5]^{1/2}$, Where x_i referes to the bond distances or angles in the i-th residue and $\bar{x}$ is the average value.

the torsion-angle index there existed a linear correlation, which was also found in other α-CDx complexes having the isomorphous structure.

The diagonal distances between glycosidic oxygen atoms (8.231—8.906 Å in the DMF complex and 8.294—8.735 Å in the PRD complex) show the distorsion of the α-CDx ring from a regular hexagonal symmetry. The longest diagonal is found along the molecular plane of the guest molecule. The deformation of the α-CDx ring in both complexes is less than that observed in the *p*-nitrophenol and *p*-hydroxybenzoic acid complexes because of the smaller size of the guest molecule. The macro-cyclic conformation of α-CDx ring has usually been described in terms of the conformation angle involving the glycosidic oxygen atoms. Owing to the ring structure of α-CDx, however, the conformation angle is found in a relatively restricted region, and does not seem to be sensitive to the conformational change. The deformation of the α-CDx ring apparently has a much greater effect on the tilt of the glucose residue against the α-CDx molecular plane. Since the planarity of the plane defined by six O(4) atoms is fairly good, in spite of the deformation of the α-CDx ring (Table 4), the tilt angle between the O(4) plane and the plane through O(4′), C(1), C(4), and O(4) for each glucose residue was calculated. These tilt-angles (Table 5) show that the G1 residue is almost perpendicular to the O(4) plane while the G5 residue is most tilted. The standard deviation for the average tilt-angle of the G6 residue is about twice as large as the standard deviation of other residues, indicating that the tilt of the G6 residue is most affected by the guest molecule.

Table 3. Selected geometrical data for α-cyclodextrin

I. Distances between glycosidic oxygen atom (l/Å)[a]	DMF complex	PRD complex
i) O(4)···O(4) distances between adjacent glucose residues		
O(4,G1)···O(4,G6)	4.347	4.300
O(4,G1)···O(4,G2)	4.201	4.201
O(4,G2)···O(4,G3)	4.110	4.131
O(4,G3)···O(4,G4)	4.439	4.399
O(4,G4)···O(4,G5)	4.212	4.205
O(4,G5)···O(4,G6)	4.190	4.199
ii) Diagonal O(4)···O(4) distances		
O(4,G1)···O(4,G4)	8.231	8.294
O(4,G2)···O(4,G5)	8.906	8.735
O(4,G3)···O(4,G6)	8.329	8.384

II. Torsion-angle index (ϕ/°)[b] Residue	DMF complex	PRD complex
G1	121.1	124.7
G2	131.6	132.3
G3	141.9	138.9
G4	112.6	115.6
G5	134.6	133.6
G6	144.7	135.0

a) Estimated standard deviations are in the range from 0.004 to 0.006 Å. b) The torsion-angle index is defined as follows: $|\phi(C(1)\text{-}C(2))| + |\phi(C(2)\text{-}C(3))| + |\phi(C(5)\text{-}O(5))| + |\phi(O(5)\text{-}C(1))| - |\phi(C(3)\text{-}C(4))| - |\phi(C(4)\text{-}C(5))|$, when the conformation angle of C(1)-C(2)-C(3)-C(4) is expressed as ϕ(C(2)-C(3)).

α-CDx - Guest Interaction. Figure 4 shows bond distances and angles in DMF and PRD, and intermolecular atomic contacts between α-CDx and these guests. The bond distances and angles in PRD are in good agreement with those found in (*S*)-5-iodomethyl-2-pyrrolidone and (*S*)-5-oxo-2-pyrrolidinecarboxamide.[10] On the other hand, a rather short C(3)–O distance (1.10 Å) and large C(3)–N–C(2) angle (133°) are found in DMF. This may be due to the large thermal motion of the DMF molecule. A similar effect has

Table 4. Least-squares planes and deviations of atoms from the plane (l/Å)
An asterisk indicates the atom not included in the plane.

I. α-Cyclodextrin-DMF complex

i) The plane through the DMF molecule.
$0.979X+0.178Y-0.097Z=5.119$

C(1,DF)	0.020	N(DF)	−0.023
C(2,DF)	0.003	O(DF)	0.027
C(3,DF)	−0.027		

ii) The plane through six O(4) atoms.
$0.017X+0.996Y+0.091Z=0.811$

O(4,G1)	0.091	O(4,G4)	0.115
O(4,G2)	0.046	O(4,G5)	0.020
O(4,G3)	−0.148	O(4,G6)	−0.125

iii) Deviations of atoms from the plane through C(2), C(3), C(5), and O(5).

Residue	C(1)*	C(2)	C(3)	C(4)*	C(5)	O(5)
G1	−0.666	−0.015	0.015	0.675	−0.016	0.016
G2	−0.688	−0.003	0.003	0.624	−0.003	0.003
G3	−0.704	−0.001	0.001	0.586	−0.001	0.001
G4	−0.640	−0.026	0.025	0.696	−0.027	0.028
G5	−0.697	−0.026	0.024	0.584	−0.025	0.027
G6	−0.736	−0.027	0.025	0.606	−0.027	0.029

II. α-Cyclodextrin-PRD complex

i) The plane through the PRD molecule.
$0.988X+0.153Y+0.015Z=6.936$

C(1,P)	−0.024	C(4,P)	0.030
C(2,P)	0.045	N(P)	−0.003
C(3,P)	−0.046	O(P)	−0.002

ii) The plane through six O(4) atoms.
$0.017X+0.995Y+0.096Z=0.876$

O(4,G1)	0.097	O(4,G4)	0.103
O(4,G2)	0.030	O(4,G5)	0.020
O(4,G3)	−0.129	O(4,G6)	−0.122

iii) Deviations of atoms from the plane through C(2), C(3), C(5), and O(5).

Residue	C(1)*	C(2)	C(3)	C(4)*	C(5)	O(5)
G1	−0.669	−0.010	0.010	0.665	−0.010	0.011
G2	−0.695	−0.002	0.002	0.618	−0.002	0.002
G3	−0.696	−0.001	0.001	0.599	−0.001	0.001
G4	−0.645	−0.026	0.025	0.692	−0.027	0.028
G5	−0.678	−0.025	0.024	0.591	−0.025	0.027
G6	−0.701	−0.005	0.005	0.606	−0.006	0.006

Table 5. Angles (ϕ/°) made between the plane through six O(4) atoms and the plane through O(4'), C(1), C(4), and O(4)
Figures in parentheses are standard deviations.

Residue	*p*-IAN[a]	*p*-IPH[b]	*p*-NPH[c]	*p*-HBA[d]	DMF	PRD	Average
G1	2.1	3.9	3.8	3.9	5.7	5.5	4.2(12)
G2	9.7	11.2	10.1	11.3	12.1	13.5	11.3(14)
G3	10.3	11.8	11.3	11.0	11.7	9.7	11.0(8)
G4	12.1	12.1	14.4	12.1	12.4	14.4	12.9(12)
G5	15.6	15.9	17.0	16.1	15.4	18.1	16.4(10)
G6	15.1	10.9	10.7	7.5	14.2	12.2	11.7(27)

a) *p*-Iodoaniline.[1] b) *p*-Iodophenol.[2] c) *p*-Nitrophenol.[5] d) *p*-Hydroxybenzoic acid.[5]

been observed in the α-CDx complexes with a small guest molecule.[11-13] DMF and PRD show good planarity: the maximum deviation from the plane is 0.046 Å in PRD and 0.027 Å in DMF.

In the α-CDx cavity, the DMF and PRD molecules are located nearly parallel to the O(4,G2)···O(4,G5) diagonal line. In the DMF complex, two methyl groups are located at the O(2), O(3) side, while the C(3) atom is nearly on the O(4) plane. The shortest intermolecular distance between DMF and α-CDx is 3.76 Å, found between O(4,G6) and C(3,DF), indicating that the DMF molecule is in van der Waals contact with the host α-CDx molecule. In the PRD complex, the C(3)–C(4) bond is nearly on the plane composed of twelve secondary hydroxyl groups, and the carbonyl oxygen atom is located at a similar position to that of the oxygen atom found in the DMF complex. Some relatively short contacts are found in the PRD complex: O(4, G2)···C(2,P) of 3.32 Å and O(4,G5)···N(P) of 3.20 Å. The O(4)···N distance indicates the formation of a weak O(4)···H–N hydrogen bond between α-CDx and PRD, since the N–H bond is oriented to the O(4,G5) atom. Thus, the PRD complex shows that the non-aromatic ring compound can be included in the α-CDx cavity.

Molecular Packing and Hydrogen Bonds. Three types of crystal structures have already been found in α-CDx complexes. The "channel-type" structure is built up by a linear stack of α-CDx molecules to form endless channels.[3,4,6,11,14] In the "cage-type"

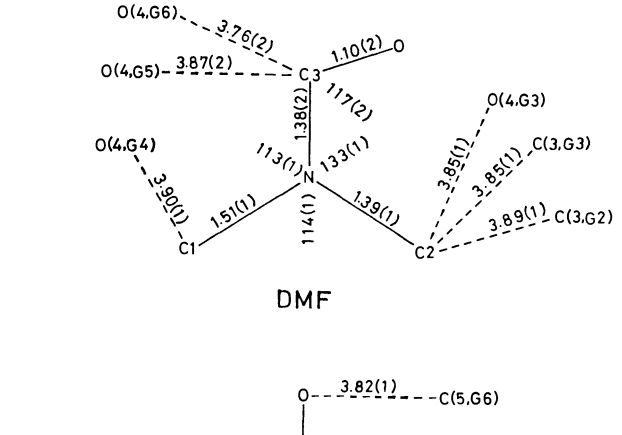

Fig. 4. Bond distances (l/Å) and angles (ϕ/°) in *N*,*N*-dimethylformamide and 2-pyrrolidone. Broken lines indicate contacts with the host α-cyclodextrin.

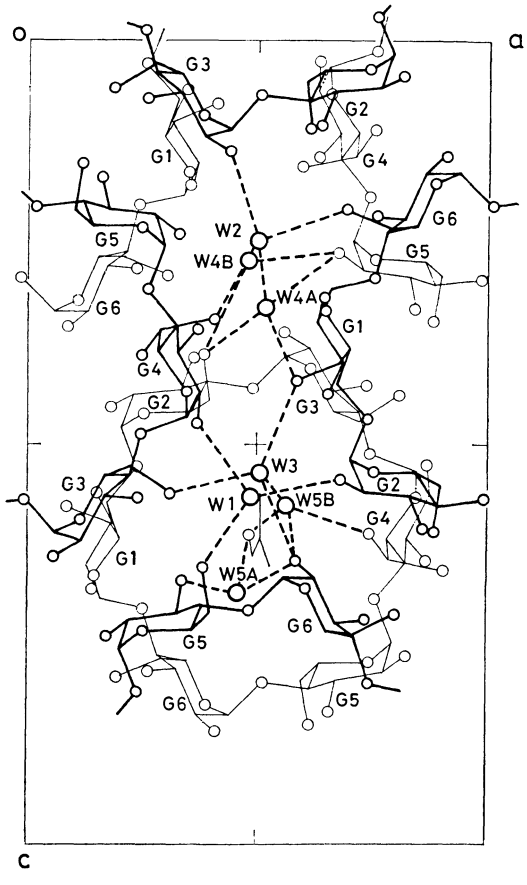

Fig. 5. A schematic drawing of the hydrogen-bond network involving water molecules in the α-cyclodextrin–*N*,*N*-dimethylformamide complex. Small circles indicate hydroxyl groups of α-cyclodextrin. Water molecules are shown by large circles.

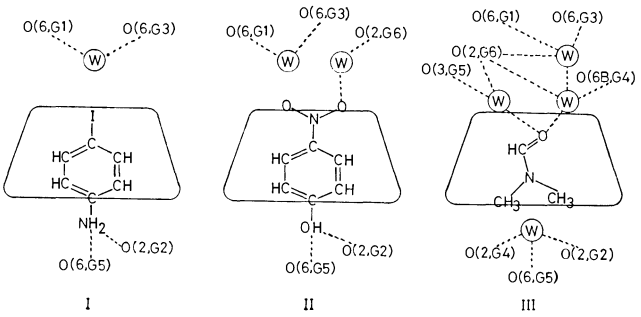

Fig. 6. A schematic drawing of the environment of the guest molecule in the α-cyclodextrin complexes with *p*-iodoaniline (I), *p*-nitrophenol (II), and *N*,*N*-dimethylformamide (III).

structure, α-CDx molecules are arranged in a fish-bone-like fashion, producing an isolated cavity to accommodate a guest molecule.[12,13,15–17] The DMF and PRD complexes have the "layer" structure, in which α-CDx molecules are arranged to form molecular layers in the crystal (Fig. 5).[1,2,5,8]

Hydrogen-bond distances and angles are given in Table 6, and the hydrogen-bonding network involving water molecules is shown in Fig. 5. Several differences are found in the hydrogen-bonding contacts compared with other complexes having the "layer" structure. In the DMF and PRD complexes, five intramolecular O(2)···O(3) hydrogen bonds are observed, but unlike the complexes with *p*-nitrophenol and *p*-hydroxybenzoic acid,[5] the G5 residue forms no hydrogen bond with the G6. These residues seem to be linked by the O(2)···water···O(3) hydrogen bond. Significantly short intermolecular distances are found in the contacts of O(2,G6)···W5, 2.371 Å (O(W5B)) in the DMF complex and 2.340 Å (O(W5A)) in the PRD complex. These may be due to errors caused at the stage of the structure refinement, owing to the low population of the disordered water and the relatively large thermal motion of O(2,G6) (5.4 Å^2 in the DMF complex and 7.9 Å^2 in the PRD complex) compared with the other secondary hydroxyl oxygen atoms (2.1—3.8 Å^2). A similar short contact has been also found in the α-CDx–*p*-nitrophenol complex.[5]

In a layer composed of α-CDx molecules, hydrogen bonds are found between G2 and G6, and G3 and G5. No hydrogen bond was found between G1 and G4, although they face each other (Fig. 5). The adjacent layers are also linked by G1···G3 and G2···G4 hydrogen bonds. The DMF and PRD complexes have different hydrogen-bonding directions. The O(3,G2)–H···O(3,G4)–H···O(2,G5) linkage in the DMF complex is changed to the O(3,G2)···H–O(3,G4)···H–O(2,G5) linkage in the PRD complex.

In the α-CDx complexes with *p*-iodoaniline,[1] *p*-iodophenol,[2] *p*-nitrophenol, and *p*-hydroxybenzoic

Table 6. Hydrogen-bond distances (l/Å), angles (ϕ/°), and intermolecular oxygen–oxygen contacts (l/Å) less than 3.0 Å[a]

α-CDx DMF complex			Distance O-H	Distance H···O	Distance O···O	Angle O-H···O
O(2,G1)-H	O(2,G3)	(h)	0.93	1.89	2.795	165
O(3,G1)-H	O(2,G2)		1.01	1.74	2.738	169
O(2,G2)-H	O(W1)	(c)	1.16	1.51	2.663	172
O(3,G2)-H	O(3,G4)	(h)	1.04	2.29	2.739	104
O(6,G2)-H	O(6B,G4)	(g)	1.04	1.72	2.727	160
O(2,G3)-H	O(3,G2)		0.88	1.97	2.845	173
O(3,G3)-H	O(3,G1)	(i)	1.01	1.68	2.674	168
O(6,G3)-H	O(3,G5)	(d)	0.98	1.87	2.776	152
O(2,G4)-H	O(3,G3)		1.33	1.82	3.080	157
O(3,G4)-H	O(2,G5)		1.04	1.89	2.887	159
O(6B,G4)-H	O(W5B)	(f)	0.97	2.38	2.636	95
O(6B,G4)-H	O(2,G6)	(j)	0.97	1.96	2.873	156
O(2,G5)-H	O(W4B)	(k)	0.69	2.61	2.664	87
O(3,G5)-H	O(W5A)	(b)	0.85	2.16	2.656	117
O(6,G5)-H	O(3,G3)	(e)	0.96	2.24	2.802	116
O(2,G6)-H	O(W5A)	(b)	1.16	1.86	2.659	121
O(3,G6)-H	O(2,G1)		0.87	2.07	2.899	159
O(6,G6)-H	O(3,G2)	(b)	1.01	1.70	2.704	177
O(W1)-H(1)	O(6,G5)		0.91	1.94	2.715	142
O(W1)-H(2)	O(2,G4)	(e)	1.94	2.00	2.877	155
O(W2)-H(1)	O(6,G6)		1.06	1.80	2.846	166
O(W2)-H(2)	O(2,G3)	(b)	0.89	2.09	2.930	159
O(W3)-H(1)	O(6,G1)		0.82	2.25	2.949	143
O(W3)-H(2)	O(W5B)		0.89	2.52	2.725	94
O(W3)-H(2)	O(6,G3)	(a)	0.89	2.49	2.813	102
O(W4A)-H(1)	O(6,G2)	(g)	1.17	2.02	2.791	114
O(W4A)-H(1)	O(2,G5)	(j)	1.17	1.86	2.821	136
O(W5A)-H(1)	O(DF)	(g)	1.10	1.93	2.984	159
O(6,G2)	O(W4B)	(f)			2.823	
O(6,G2)	O(6A,G4)	(g)			2.931	
O(2,G6)	O(W5B)	(b)			2.371	
O(2,G6)	O(W3)	(b)			2.953	
O(W2)	O(W4A)				2.818	
O(W2)	O(6A,G4)	(a)			2.803	
O(W4A)	O(6,G1)				2.838	
O(W5B)	O(DF)	(g)			2.905	

α-CDx-2-pyrrolidone complex			Distance O-H	Distance H···O	Distance O···O	Angle O-H···O
O(2,G1)-H	O(2,G3)	(h)	0.78	2.00	2.775	172
O(3,G1)-H	O(2,G2)		0.99	1.77	2.739	165
O(6,G1)-H	O(W4A)		0.75	2.14	2.870	164
O(2,G2)-H	O(W1)	(c)	0.91	1.88	2.668	143
O(6,G2)-H	O(6B,G4)	(g)	1.24	1.81	2.738	127
O(2,G3)-H	O(3,G2)		0.94	2.24	2.810	118
O(3,G3)-H	O(3,G1)	(i)	0.94	1.76	2.699	175
O(2,G4)-H	O(3,G3)		0.80	2.29	3.042	158
O(3,G4)-H	O(3,G2)	(i)	0.79	2.02	2.736	151
O(2,G5)-H	O(3,G4)		0.98	1.97	2.910	161
O(6,G5)-H	O(3,G3)	(e)	0.94	1.99	2.877	160
O(2,G6)-H	O(W5B)	(b)	1.07	2.08	2.686	113
O(2,G6)-H	O(W5A)	(b)	1.07	2.09	2.340	89
O(3,G6)-H	O(2,G1)		1.07	1.87	2.878	157
O(6,G6)-H	O(3,G2)	(b)	1.14	2.22	2.706	103
O(W1)-H(1)	O(6,G5)		0.93	1.80	2.727	170
O(W1)-H(2)	O(2,G4)	(e)	1.10	1.81	2.862	159
O(W2)-H(1)	O(2,G3)	(b)	0.92	2.07	2.893	147
O(W2)-H(2)	O(6A,G4)	(a)	1.09	1.81	2.876	166
O(W2)-H(2)	O(W4A)		1.09	2.08	2.828	124
O(W3)-H(1)	O(6,G1)		0.83	2.14	2.888	149
O(W4A)-H(1)	O(2,G5)	(j)	0.69	2.48	2.841	112
O(W4A)-H(1)	O(6,G2)	(g)	0.69	2.68	2.781	91
O(6,G2)	O(W4B)	(f)			2.792	
O(6,G2)	O(6A,G4)	(g)			2.904	
O(6B,G4)	O(W5B)	(f)			2.679	
O(2,G5)	O(W4B)	(k)			2.611	
O(3,G5)	O(W5A)	(b)			2.543	
O(6,G6)	O(W2)				2.828	
O(W3)	O(W5B)				2.825	
O(W3)	O(6,G3)	(a)			2.802	
O(W5A)	O(P)	(g)			2.571	
O(W5B)	O(P)	(g)			2.733	

Code	Symmetry operator	Code	Symmetry operator
None	x, y, z	c	1/2−x, −y, −1/2+z
a	−1+x, y, z	d	3/2−x, −y, −1/2+z
b	1/2−x, −y, z	e	3/2−x, −y, 1/2+z

Code	Symmetry operator	Code	Symmetry operator
f	1/2+x, 1/2−y, 1−z	i	1/2+x, −1/2−y, 1−z
g	−1/2+x, 1/2−y, 1−z	j	1−x, 1/2+y, 3/2−z
h	−1/2+x, −1/2−y, 1−z	k	1−x, −1/2+y, 3/2−z

a) The hydrogen bond is doubtful if the H···O distance is longer than 2.5Å or the O–H···O angle is less than 90°.

acid,[5] the guest molecules are so bulky that a part of the guest molecule protrudes from the secondary hydroxyl side of the α-CDx cavity. The environment of the guest molecule is schematically shown in Fig. 6. In the DMF complex, the open end of the primary hydroxyl side of α-CDx is blocked by two water molecules. One (W3) is located near the position found in the *p*-iodoaniline or *p*-nitrophenol complex, but the other (W5) is not found in the complexes with the aromatic guest. W3 is linked to the adjacent three α-CDx molecules. The DMF molecule is so small that the vacant space is filled by W5, which is statistically disordered and occupies two sites. W1 blocks the secondary hydroxyl side of the α-CDx cavity, but it is replaced by the amino or hydroxyl group of the guest molecule in the complexes with *p*-iodoaniline and *p*-nitrophenol. W2, W4A, and W4B are found at the same position as those found in other α-CDx complexes with the "layer" structure. They are arranged in the space elongated along the two-fold screw axis perpendicular to the α-CDx molecular plane (Fig. 5).

So far, it has been considered that the "layer" structure is formed when the guest molecule is too bulky to be enclosed in the α-CDx cavity. But, the DMF and PRD complexes show that a complex with a small guest molecule can also form the "layer" structure. α-CDx crystallized from an ethanol–water solution may also have a layer structure, since the lattice dimensions are almost the same as those of the complexes with the "layer" structure; $a=13.39$, $b=15.49$, $c=24.06$ Å, and the space group $P2_12_12_1$.[18] The α-CDx crystal obtained from a methanol–water or 1-propanol–water solution gives the "cage-type" structure.[15,17] It is very interesting to speculate why the ethanol complex does not form the "cage-type" structure.

The author wishes to thank Dr. Hisashi Uedaira for supporting this study and for helpful discussions. The computaion was done on a HITAC M-160II computer at this institute. Programs used were written in the author's laboratory.

References

1) K. Harata, *Bull. Chem. Soc. Jpn.*, **48**, 2409 (1975).
2) K. Harata, *Carbohydr. Res.*, **48**, 265 (1976).
3) K. Harata, *Bull. Chem. Soc. Jpn.*, **49**, 1493 (1976).
4) K. Harata, *Bull. Chem. Soc. Jpn.*, **49**, 2066 (1976).
5) K. Harata, *Bull. Chem. Soc. Jpn.*, **50**, 1416 (1977).
6) K. Harata, H. Uedaira, and J. Tanaka, *Bull. Chem. Soc. Jpn.*, **51**, 1627 (1978).
7) M. Otagiri, K. Ikeda, K. Uekama, O. Ito, and M. Hatano, *Chem. Lett.*, **1974**, 679.
8) K. Harata, *Bull. Chem. Soc. Jpn.*, **51**, 1644 (1978).
9) A. D. French and V. G. Murphy, *Carbohydr. Res.*, **27**, 391 (1973).
10) J. A. Molin-Case, E. Fleischer, and D. W. Urry, *J. Am. Chem. Soc.*, **92**, 4728 (1970).
11) K. Harata, *Bull. Chem. Soc. Jpn.*, **50**, 1259 (1977).
12) W. Saenger, R. K. McMullan, J. Fayos, and D. Mootz, *Acta Crystallogr., Sect. B*, **30**, 2019 (1974).
13) B. Hingerty and W. Saenger, *J. Am. Chem. Soc.*, **98**, 3357 (1976).
14) A. Hybl, R. E. Rundle, and D. E. Williams, *J. Am. Chem. Soc.*, **87**, 2779 (1965).
15) R. K. McMullan, W. Saenger, J. Fayos, and D. Mootz, *Carbohydr. Res.*, **31**, 211 (1973).
16) P. C. Manor and W. Saenger, *J. Am. Chem. Soc.*, **96**, 3630 (1974).
17) W. Saenger and M. Noltemeyer, *Chem. Ber.*, **109**, 503 (1976).
18) D. French and R. E. Rundle, *J. Am. Chem. Soc.*, **64**, 1651 (1942).

Rayleigh Ratio for Benzene and Its Temperature Dependence

Toshio KAMATA* and Hisae NAKAHARA

National Chemical Laboratory for Industry, Honmachi, Shibuya-ku, Tokyo 151†

(Received October 9, 1978)

The temperature dependence of the Rayleigh ratio for benzene was studied for the purpose of comparing various reported values obtained at different temperatures with each other. The following relationship was obtained for a wavelength of incident light of $\lambda_0=435.8$ nm:

$$R_{90}=(0.1377t+43.06)\times10^{-6}\ \mathrm{cm}^{-1}$$

where t is temperature (°C). Light-scattering photometers were calibrated with benzene purified by a preparative gas chromatograph by using a value of the Rayleigh ratio for benzene of $R_{90}=46.5\times10^{-6}$ cm^{-1} (25 °C, $\lambda_0=435.8$ nm). In order to verify the validity of the calibrations, molecular weight determinations were run on three standard substances: egg white lysozyme, raffinose, and sucrose. The temperature of benzene was directly measured by inserting the sensor of a thermistor thermometer into the benzene within the cell.

Various methods have been proposed for calibrating light scattering photometers. The validity of such calibrations is often examined by comparing the observed values of the Rayleigh ratio, R_{90}, for benzene with the literature data or by determining the molecular weights of proteins or low molecular-weight compounds whose molecular weights are known. However, the most probable value of R_{90} for benzene has been the subject of controversies for many years among investigators, because there were considerable discrepancies among the observed values. In 1962, Kratohvil *et al.*[1] in their critical survey on the calibration of light-scattering photometers criticized most of the published values of the Rayleigh ratio for benzene for being somewhat too high, and suggested a value of $R_{90}\leq 46.5\times10^{-6}$ cm^{-1} as the most probable one at 20 °C for a wavelength of incident light of 435.8 nm. Most later reports[2–6] published since the critical survey of Kratohvil *et al.* support the credibility of this so-called "low value," and now the controversies about the correct R_{90} value for benzene appear to have subsided.

However, since somewhat different temperatures were employed for measurements by different authors, a correct knowledge of the temperature dependence of Rayleigh ratios is essential for comparing literature values with each other. A temperature coefficient of the Rayleigh ratio for benzene determined precisely would also be convenient, in that it would help readily check the adequacy of any value of the Rayleigh ratio for benzene determined at any temperature.

The temperature dependence of the Rayleigh ratio for benzene has been reported by Schmidt,[7] Ehl *et al.*,[8] and Cohen and Eisenberg.[9] The temperature coefficient reported by Schmidt ($\lambda_0=435.8$ nm) and that of Ehl *et al.* ($\lambda_0=546.1$ nm) differ too widely from each other, even if the difference in the wavelength at which measurements were made is taken into account. Cohen and Eisenberg[9] studied the temperature dependence of the Rayleigh ratios for benzene and water at both 435.8 and 546.1 nm. Unfortunately, however, the lack of description for the numerical values of R_{90} at various temperatures or for the temperature coefficient of Rayleigh ratio in their paper makes it difficult to compare their results with those of Schmidt and of Ehl *et al.* Judging from the figures given by them, the temperature coefficient does not depend on the wavelength at which measurements were made.

Such considerable discrepancies among the values obtained by different authors for the temperature coefficient of the Rayleigh ratio for benzene might have partly been caused by the fact that there has always been some kind of uncertainty in measuring the temperature of the benzene on which the Rayleigh ratio measurements are being made. When a heating medium is recirculated to regulate temperature, a difference in temperature between the heating medium and the benzene within the cell develops and increases with increasing temperature. Schmidt[7] measured the temperature of the heating medium and took it as the temperature of benzene. Such a method does not measure the correct temperature of benzene.

In the present study, therefore, the temperature of benzene was directly measured by inserting the sensor of a thermistor thermometer into benzene within the cell as the determination of the Rayleigh ratio was being made.

Prior to determining the temperature dependence of the Rayleigh ratio for benzene, we tried to determine a reference value of the Rayleigh ratio by using standard substances with known molecular weights. Since the use of a single standard substance might lead to an accidental coincidence of the molecular weight found experimentally with that calculated from the molecular formula, three different standard substances, *i.e.*, sucrose, raffinose, and lysozyme, which have different molecular weights and specific refractive index increments, dn/dc, were used to avoid such an accidental coincidence.

The value of the Rayleigh ratio for benzene considered as the most probable since the critical survey by Kratohvil *et al.*,[1] $R_{90}=46.5\times10^{-6}$ cm^{-1} (25 °C, $\lambda_0=435.8$ nm), was adopted for calibrating the light-scattering photometer. Light-scattering measurement were then made on the three standard substances mentioned above and the molecular weights found by experiments and those calculated from the molecular formulas were compared.

Benzene used for calibrating the light-scattering photometer and for determining the temperature dependence of the Rayleigh ratio was a guaranteed reagent further purified by a preparative gas chromatograph.

The temperature dependence of the Rayleigh ratio

† New address: Yatabe, Ibaraki 300-21.

for benzene obtained in this manner was compared with the literature values. At the same time, the literature values of the Rayleigh ratio for benzene were compared with each other by taking into account the effect of temperature on this quantity.

Experimental

Materials. Benzene used was a special grade reagent supplied by Wako Jun'yaku Kogyo Co., purified by a preparative gas chromatograph and freshly distilled prior to light-scattering measurements.

Egg white lysozyme used was a seven-times recrystallized sample supplied by Seikagaku Kogyo Co. Its high purity was confirmed by elementary analysis, sedimentation patterns from the ultracentrifuge technique, chromatograms, and amino acid composition as well as N-end group assay.

Sucrose used was a GR reagent supplied by Kokusan Kagaku Co., twice recrystallized from the system water–ethanol.

As raffinose, a GR reagent from Tokyo Kasei Kogyo Co. was used.

Light Scattering. *Apparatus and Calibration*: Since it is difficult to measure scattered light from solutions of low molecular-weight compounds and to determine their depolarizations correctly using only one light-scattering photometer, two of them were employed to determine Rayleigh factors and depolarizations. For the Rayleigh factor determinations, use was made of a Shimadzu PG-21 light-scattering photometer equipped with a Hamamatsu TV Co's R-105 UH high sensitive photomultiplier tube (anode sensitivity: 1530 μA/μlm). Depolarizations were determined by using a Shimadzu DL-10 model with minor modifications.[10] All light-scattering measurements were made by using a mercury spectral line with the *in vacuo* wavelength of 435.8 nm. First the Rayleigh factor was measured with the PG-21 photometer, and then the light-scattering cell was transferred to the DL-10 apparatus for depolarization measurements, the isotropic part being calculated by using the Cabannes factor.[11]

The photometers were calibrated with respect to the Rayleigh ratio of benzene, for which the previously mentioned value of $R_{90}=46.5\times10^{-6}$ cm^{-1} (25 °C, $\lambda_0=435.8$ nm) was employed.

In order to examine the temperature dependence of the Rayleigh ratio of benzene, a cell jacket was used; through this, thermostated water was recirculated. The temperature of benzene was measured by dipping the tip of a thermistor sensor (glass tube, 3 mm o.d.) attached to a Takara thermistor thermometer STM-005-15 (divided to 0.05 °C) into the benzene within the cell. Readings were taken to the last 0.01 °C. The sensor was thoroughly washed with clean benzene and was so located as not to interfere with the scattered light. The liquid in the cell was gently agitated with a teflon-covered spin bar, 2 mm o.d. and 15 mm long, driven by a magnetic stirrer to prevent any temperature gradient development.

Optical Clarification: A lysozyme solution (in an acetate buffer) was centrifuged for 1 h at 10 °C at 360000 g max. by using a Spinco L_4 preparative ultracentrifuge, and then directly filtered into the light-scattering cell through a Corning ultrafine glass filter. The aqueous solutions of raffinose and sucrose were centrifuged for 1 h at 20 °C at 360000 g max. and then directly filtered into the light-scattering cell through a Millipore filter VS (pore size : 25±3 nm). Benzene, freshly distilled, was filtered through a Corning glass filter into the light-scattering cell for measurements.

Concentration of Solution: Since the concentration of solutions may change during the ultracentrifuge and filtering operations, the solutions in the cell were analyzed for their concentrations. The lysozyme concentration was calculated from the N content by the Kjeldahl method.

Refractive Index Increment: Refractive index increments were measured with a Shimadzu differential refractometer. The values of dn/dc at 20 °C for the wavelength of 435.8 nm for a lysozyme–acetate buffer solution (pH 3.6), an aqueous raffinose solution, and an aqueous sucrose solution were 0.1941, 0.1512, and 0.1484 cm^3/g, respectively.

Refractive Index: The refractive index of benzene at 20 °C for wavelength of 435.8 nm was calculated by substituting the reference value listed in the International Critical Tables into Cauchy's dispersion formula:

$$n = A + B/\lambda^2 + C/\lambda^4. \quad (1)$$

The refractive indices, n, at 435.8 nm of benzene for various temperatures were calculated from the following equation:

$$n = 1.52317 - 0.000665(t-20.00), \quad (2)$$

where t is temperature (°C). As the temperature coefficient of refractive index, that of Coumou[12] was adopted.

Results and Discussion

Effect of Purity on the Rayleigh Ratio of Benzene. In order to know the extent of purification required for benzene to be used as a standard substance, light-scattering measurements were run on special grade benzene further purified by gas chromatography. The results are shown in Table 1.

As seen from the table, the chromatographically purified benzene did not show much difference from the starting special grade reagent. On the contrary, there was a definite difference between the freshly distilled and undistilled samples. Consequently, it was concluded that a purification of the special grade benzene by distillation just before use would be sufficient, and no further purification by preparative gas chromatograph was required. If the special grade benzene is used without any distillation, it may get contaminated by organic substances or sometimes by polymeric as well as fluorescent materials that can not be removed by ultracentrifuging nor by filtration and could seriously affect light-scattering measurements.

Determination of Molecular Weights of Standard Substances. The molecular weights of egg white lysozyme, raffinose, and sucrose were determined with the same light-

Table 1. Rayleigh ratio for benzene purified by various methods

Original sample	Purification	$R_{90}\times10^6$(cm^{-1})
Special grade benzene	Purified by preparative gas chromatography and distilled before light scattering measurement	46.50
Special grade benzene	Distilled before light scattering measurement	46.52
Special grade benzene	——	48.09

scattering photometer that had been calibrated by using the Rayleigh ratio for benzene of $R_{90}=46.5\times10^{-6}$ cm^{-1} (25 °C, 435.8 nm). Egg white lysozyme is regarded as a suitable standard sample, because its molecular weight can be calculated from the knowledge of its higher-order structure determined by amino acid composition as well as by X-ray structural analysis, and because high-purity samples of it can readily be obtained. However, since the possibility of molecular association exists for egg white lysozyme in a certain pH region, it is necessary to find the pH range where no such association will take place before molecular weight measurements are undertaken. Figure 1 shows the molecular weights of lysozyme determined at various pH's. The data of the present work show a slight inconsistency with those of Sophianopoulos and Van Holde[13] obtained by the sedimentation equilibrium method, but in either case, substantially no association was found to occur within a pH range of 3 to 5. Therefore, light-scattering measurements were carried out in this pH region of 3 to 5. Figure 2 shows the light-scattering data for egg white lysozyme in an acetate buffer (pH 3.6). Figures 3 and 4 show the light-scattering plots for raffinose and sucrose, respectively.

The molecular weight was calculated from the following equation:

$$Kc/R_{90} = 1/(M_w P(90°)) + 2A_2c. \quad (3)$$

The isotropic excess light scattering in the 90° direction, R_{90}, was calculated from the Rayleigh factor

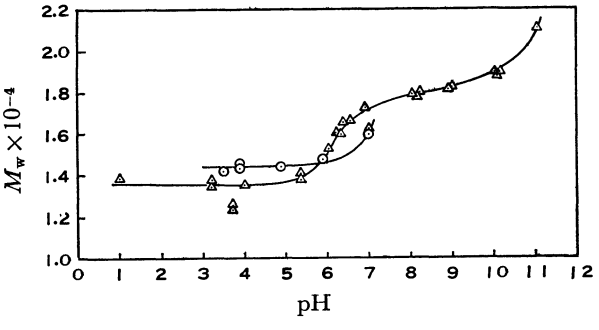

Fig. 1. pH dependence of the molecular weight of egg white lysozyme.
⊙: Present work, ▲: Sophianopoulos and Van Holde.[13]

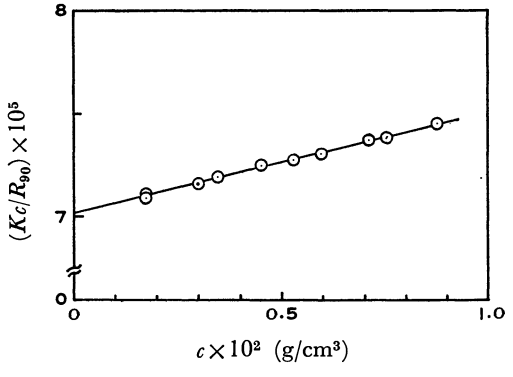

Fig. 2. Plot of Kc/R_{90} *versus* c for egg white lysozyme in acetate buffer (0.15 M NaCl, pH 3.6).
λ_0=435.8 nm.

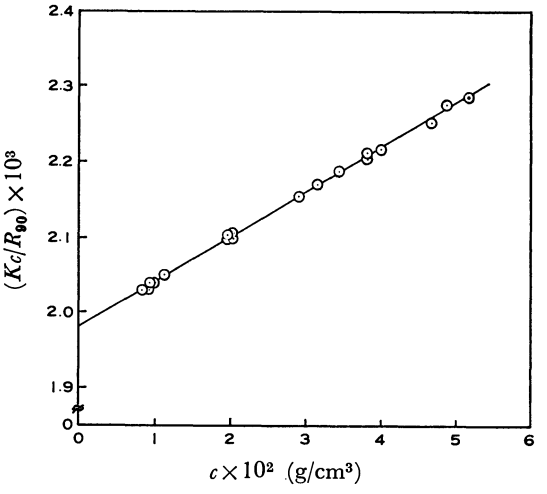

Fig. 3. Plot of Kc/R_{90} *versus* c for raffinose in water.
λ_0=435.8 nm.

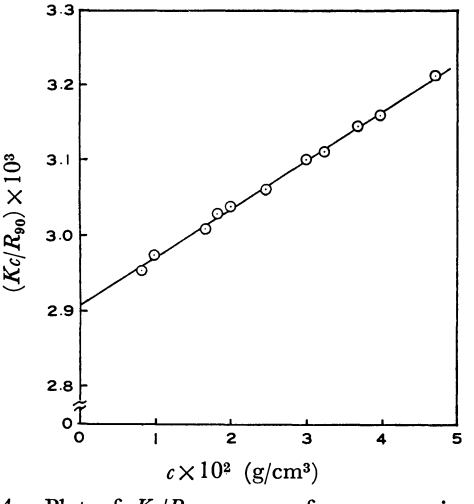

Fig. 4. Plot of Kc/R_{90} *versus* c for sucrose in water.
λ_0=435.8 nm.

determined in unpolarized light, $(R_{90})_u$, using the Cabannes factor, $f_u(90°)$, as follows:

$$R_{90} = (R_{90})_u/f_u(90°), \quad (4)$$

$$f_u(90°) = (6+6\rho_u)/(6-7\rho_u), \quad (5)$$

where ρ_u is the degree of depolarization.

The value of $P(90°)$ was calculated from the dimensions of a lysozyme molecule determined by X-ray structural analysis. Actually, however, since this value (0.9994) was found to be very close to unity, the molecular weight of lysozyme was calculated by assuming $P(90°)=1$.

Likewise, since the raffinose and sucrose molecules are very small compared to the wavelength of incident light, calculation was made by assuming $P(90°)=1$.

The deviation, ΔM, from the true molecular weight, M, of the apparent molecular weight, M_{app}, obtained by approximating the light scattering due to fluctuation of fluid density by that due to fluctuation of the density of pure solvent, was also calculated by the use of the Bullough's approximation.[14] For further details, reference should be made to the literature.[10]

The results of the molecular weight determinations

Table 2. Results for standard substances

Substances	Solvent	dn/dc (cm³/g)	$(Kc/R_{90})_{c\to 0}$	M_{app}	ΔM	M	M(formula)	δ_{app} (%)	δ (%)
Sucrose	Water	0.1484	2.906×10^{-3}	344	3	341	342.3	+0.5	−0.4
Raffinose	Water	0.1512	1.982×10^{-3}	505	3	502	504.2	+0.2	−0.4
Lysozyme	Acetate buffer 0.15 M NaCl (pH 3.6)	0.1941	7.02×10^{-5}	14250	2	14248	14307	−0.4	−0.4

$\delta_{app}=(M_{app}/M(\text{formula})-1)\times100$, $\delta=(M/M(\text{formula})-1)\times100$.

are listed in Table 2. Since the effect of the deviations, ΔM, caused by density fluctuations on the observed values of molecular weight was small, as shown in Table 2, ΔM was neglected in comparing the apparent molecular weight, M_{app}, with that calculated from the molecular formula. Such a comparison resulted in a good agreement, within ±1% in either case. This suggests that the calibration of the light-scattering photometer, using the value of the Rayleigh ratio for benzene of $R_{90}=46.5\times10^{-6}$ cm^{-1} (25 °C, $\lambda_0=435.8$ nm), was reasonable. If the small deviations of molecular weights caused by density fluctuations were considered, the molecular weights observed for egg white lysozyme, raffinose, and sucrose became slightly lower than those calculated from the molecular formulas, the mean deviation being −0.4%. To attribute such discrepancies to the particular value of the Rayleigh ratio for benzene that was adopted for calibrating the light-scattering photometer, however, remains open to question. There is a great difference between the refractive index for benzene and that for the water used as a solvent in light-scattering measurements of three standard substances. It is thus difficult to exclude some uncertainty, however small, that may accompany the operation of converting the apparatus constant, ϕ_{90}, determined by the use of the Rayleigh ratio for benzene to the other, ϕ'_{90}, for water as the solvent. Therefore, our effort to estimate the Rayleigh ratio for benzene by means of standard substances was abandoned. Instead, we confined ourselves to reconfirming the likeliness of the value of $R_{90}=46.5\times10^{-6}$ cm^{-1} (25 °C, $\lambda_0=435.8$ nm), known to be the most probable so far.

Temperature Dependence of Rayleigh Ratio for Benzene. The temperature dependence of the Rayleigh ratio for benzene was studied by assuming the most probable value at 25 °C to be $R_{90}=46.5\times10^{-6}$ cm^{-1}. The results are summarized in Table 3. Also, the variation of the Rayleigh ratios for benzene with temperature is plotted in Fig. 5.

As seen from the plots in Fig. 5, a linear relationship exists between R_{90} and temperature, t, correlated by the following equation:

$$R_{90} = (0.1377t+43.06)\times10^{-6}\ \text{cm}^{-1}. \quad (6)$$

Ehl *et al.*[8] studied the temperature dependence of Rayleigh ratios at a wavelength of 546.1 nm, and reported that it could be expressed as follows by taking the value of R_{90} at 25 °C as a reference:

$$(R_{90})_t = (R_{90})_{25}[1+\alpha(t-25)], \quad (7)$$

where the temperature coefficient was found to be $\alpha=0.368\times10^{-2}$.

Equation 7 yields $\alpha=0.306\times10^{-2}$ from our data and $\alpha=0.220\times10^{-2}$ from those of Schmidt,[7] both at the same wavelength ($\lambda_0=435.8$ nm); there is very poor agreement between the two observations. One of the possible causes for this can be the difference

Table 3. Rayleigh ratio for benzene at various temperatures

Temperature (°C)	n_0	$R_{90}\times10^6$ (cm^{-1})
20.15	1.52307	45.88
20.20	1.52304	45.79
20.70	1.52270	45.86
24.62	1.52010	46.50
25.00	1.51985	46.50
25.11	1.51977	46.56
25.75	1.51935	46.62
28.96	1.51721	47.11
30.11	1.51645	47.19
30.20	1.51639	47.19
30.28	1.51633	47.25
34.91	1.51325	47.77
35.02	1.51318	47.98
35.03	1.51318	47.82
40.16	1.50976	48.63
40.18	1.50975	48.52
44.97	1.50656	49.30
45.11	1.50647	49.25
50.55	1.50285	50.03
51.28	1.50237	50.11
57.51	1.49823	51.00

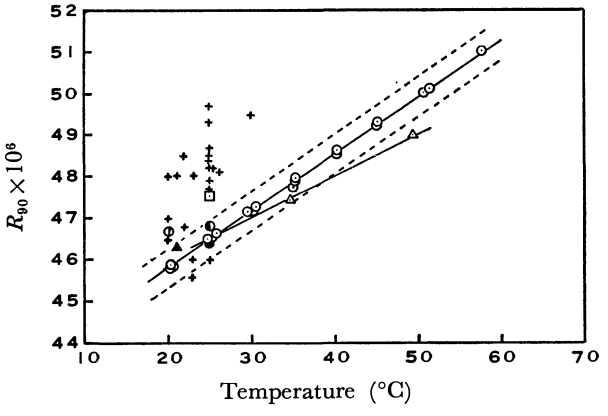

Fig. 5. Temperature dependence of Rayleigh ratio for benzene. ⊙: Present work, ●: Claesson and Ohman,[2] ▲: Huisman,[3] ◫: Bello and Guzman,[4] ◐: Deželić,[5] ⊡: Parfitt and Wood,[6] ◭: Schmidt,[7] +: Reference values listed on critical survey of Kratohvil *et al.*[1] Dashed lines show the experimental error range of ±1%.

in temperatures at which measurements were made. While the present authors inserted the sensor of a thermistor thermometer into the fluid and directly measured the temperature of benzene, Schmidt measured the temperature of the recirculated water and took it as that of the benzene. The temperature of the fluid within a light scattering cell usually shows some deviations from that of the recirculated water, and such deviations tend to become more significant at higher temperatures. The somewhat lower value of Schmidt as compared with ours could have been caused by such a deviation in temperature. Our value of α was a little lower than that of Ehl *et al.*, although both figures were obtained at different wavelengths. Cohen and Eisenberg[9] determined the temperature dependence of Rayleigh ratios at both 435.8 and 546.1 nm, but the lack of the numerical values of R_{90} at various temperatures in their paper inhibits calculation of α values by means of Eq. 7. However, the figures of the temperature dependence of the Rayleigh ratio given in their paper permits us to estimate a temperature coefficient which is closer to ours than to the value of Ehl *et al.*

A number of literature values of the Rayleigh ratio for benzene so far reported (corresponding to $\lambda_0=$ 435.8 nm) are compared in Fig. 5 by considering the temperature effect. As seen from this figure, all literature data[2-6] reported since the critical survey[1] of Kratohvil *et al.* agree within $\pm 2\%$ with the value taken as the most probable one. Particularly, the reported values of Deželič,[5] Huisman,[3] and Claesson and Ohman[2] showed an agreement within $\pm 1\%$. On the other hand, the literature values published before the critical survey mentioned above, except for some which showed agreements within $\pm 2\%$, generally deviated widely even if the temperature dependence was considered.

The author's acknowledgements are due to Dr. S. Nishi, who kindly purified the benzene by preparative gas chromatography, and to Dr. Y. Morita, who conducted the nitrogen analysis.

References

1) J. P. Kratohvil, G. Deželič, M. Kerker, and E. Matijevic, *J. Polym. Sci.*, **57**, 59 (1962).
2) S. Claesson and J. Ohman, *Arkiv Kemi*, **23**, 69 (1964).
3) H. F. Huisman, *Proc. Kon. Ned. Akad. Wet. B*, **67**, 367 (1964).
4) A. Bello and G. M. Guzman, *Eur. Polym. J.*, **2**, 79 (1966).
5) G. Deželič, *J. Chem. Phys.*, **45**, 185 (1966).
6) G. D. Parfitt and J. A. Wood, *Trans. Faraday Soc.*, **64**, 805 (1968).
7) R. L. Schmidt, *J. Colloid Interface Sci.*, **27**, 516 (1968).
8) J. Ehl, C. Loucheux, C. Reiss, and H. Benoit, *Makromol. Chem.*, **75**, 35 (1964).
9) G. Cohen and H. Eisenberg, *J. Chem. Pyhs.*, **43**, 3881 (1965).
10) T. Kamata, H. Nakahara, and S. Hattori, *Bull. Chem. Soc. Jpn.*, **50**, 2558 (1977).
11) J. Cabannes, "La Diffusion Moléculaire de la Lumière," Les Presses Universitaires de France, Paris (1929), Chap. 10.
12) D. J. Coumou, *J. Colloid Sci.*, **15**, 408 (1960).
13) A. J. Sophianopoulos and K. E. Van Holde, *J. Biol. Chem.*, **239**, 2516 (1964).
14) R. K. Bullough, *Proc. R. Soc. London, Ser. A*, **275**, 271 (1963).

Structural Interconversions of Dichlorobis(triphenylphosphine)-nickel(II) in Various Solvents

Hajime KATÔ,* Kazuko YORITA, and Yoshifumi KATO

Department of Chemistry, Faculty of Science, Kobe University, Kobe 657

(Received November 15, 1978)

Structural interconversions, ligand exchange, the temperature- and concentration-dependent equilibrium of configurational isomers, and the solvolysis of $NiCl_2(Ph_3P)_2$ in various solvents have been studied. The MCD and absorption spectra were employed, together with the calculation based on ligand-field theory and the NMR spectra. Paramagnetic tetrahedral $NiCl_2(Ph_3P)_2$ and the solvated paramagnetic octahedral $NiCl_2(Ph_3P)_2(dmso)_2$ are in equilibrium in the coordinating solvent DMSO. The ratio of the former to the latter increases with the rise of concentration and temperature. Configurational isomers of $NiCl_2(Ph_3P)_2$, a paramagnetic tetrahedral one and a diamagnetic square-planar one, are found in a non-coordinating solvent $CHCl_3$. The former species decreases gradually and a yellow precipitate is formed. The same two species, and two other solvated paramagnetic tetrahedral and octahedral species, $NiCl_2(CH_3CN)_2$ and $NiCl_2(CH_3CN)_4$, are found to be in equilibrium in CH_3CN.

Dihalogenonickel(II) tertiary phosphine complexes have been used as a catalyst for a number of synthetic reactions. The solvent and the temperature are often important factors for the catalytic activity. A number of studies[1–5] have been reported on the dynamic interconversion between the paramagnetic tetrahedral form and the diamagnetic square-planar form of these complexes in non-coordinative solvents. By measuring the absorption spectra and the magnetic susceptibility of $NiCl_2(Ph_3P)_2$ in a solution of inert solvents (for example, $CHCl_3$ and benzene), it has been shown that there is a small amount of the trans-square-planar diamagnetic species in equilibrium with the tetrahedral paramagnetic species.[2,3] However, few investigations on the molecular conformation and the dynamic behavior in coordinative solvents are reported.

The molecular structure of $NiCl_2(Ph_3P)_2$ in crystal form is known[6] to be: Ni–Cl=2.27 Å, Ni–P=2.28 Å, ∠Cl–Ni–Cl=123°, ∠P–Ni–P=117°. Its polarized single-crystal electronic spectrum was assigned by taking the effective site-symmetry as C_{2v}.[7] When the molecule is dissolved in various solvents, it may take a tetrahedral, a square-planar, or an octahedral form, and will show a characteristic electronic spectrum depending on each configuration. In addition, the magnetic circular dichroism (MCD) spectrum has the sign as well as the magnitude characteristic of each electronic transition,[8,9] and can be a very powerful means for clarifying the complexity of the absorption spectra, providing further information with which to understand the molecular state.

The absorption and MCD spectra indicate simply the sum of spectra arising from each species in the equilibrium mixture. On the other hand, NMR spectra can be used in another way: if the frequency separation between resonance lines of species in equilibrium is smaller than the frequency of the interconversion or the ligand exchange, only a single line at the average frequency is observed. NMR spectra will thus provide the evidence for the degree of molecular lability and the rate of ligand exchange.

We have therefore studied the structural interconversions of $NiCl_2(Ph_3P)_2$ in various solvents, such as dimethyl sulfoxide (DMSO), *N,N*-dimethylformamide (DMF), acetonitrile (CH_3CN), *etc.*, by the MCD and absorption spectra, the calculations based on ligand-field theory, and the NMR spectra.

Experimental

The following compounds used in this study were prepared and recrystallized according to previously reported procedures; $NiCl_2(Ph_3P)_2$,[1] $Ni(SCN)_2(Ph_3P)_2$,[1] $(Et_4N)_2NiCl_4$,[10] $[Ni(dmf)_6](ClO_4)_2$,[11] $[Ni(dmso)_6](ClO_4)_2$.[12] All solvents were obtained commercially (Guaranteed Reagent of Nakarai Chemical Co.). Acetonitrile was dried and purified by fractional distillation with anhydrous calcium chloride.

Absorption spectra in the range 10000 to 13000 cm^{-1} were measured by a JASCO J-40 spectrophotometer, to which an electro-magnet of field strength 8.9 kG is attached. The spectra in the other ranges were measured with the apparatus previously described.[13,14] NMR spectra were obtained by using a JEOL JNM-PS-100 instrument equipped with a variable-temperature probe. All of the spectra were measured just after preparing the solution, unless otherwise specified.

Results and Discussion

MCD and Absorption Spectra. The MCD spectra of the charge-transfer bands in tetrachloro nickel(II) ions have been studied,[15] but the MCD spectra of the d-d transitions have not yet been reported. The spectrum in solution shows a great change depending on the solvent. The MCD and the absorption spectra of a solution of $(Et_4N)_2NiCl_4$ in CH_3CN are shown in Fig. 1. The absorption spectrum is very similar to the spectrum of Ni(II) ion in tetrahedral sites in the crystal of Cs_2ZnCl_4,[16] and it does not show any significant change when the excess tetramethylammonium chloride (Et_4NCl) is added to the solution. Therefore we may consider that the spectrum arises from a tetrahedral $NiCl_4^{2-}$ ion. The absorption band in the range 13000—17000 cm^{-1} has been assigned as a transition $^3T_1(F)\rightarrow{}^3T_1(P)$.[17] The MCD spectrum in this absorption region shows a dispersion with positive sign in the lower energy region and negative sign in the higher energy region (let us call this "*positive dispersion*").

The MCD spectra of d-d transitions in some octahedral nickel(II) complexes have been studied extensively.[18,19] In octahedral nickel(II) complexes, there are three spin-allowed d-d transitions: $^3A_2\rightarrow{}^3T_2$, $^3T_1(F)$,

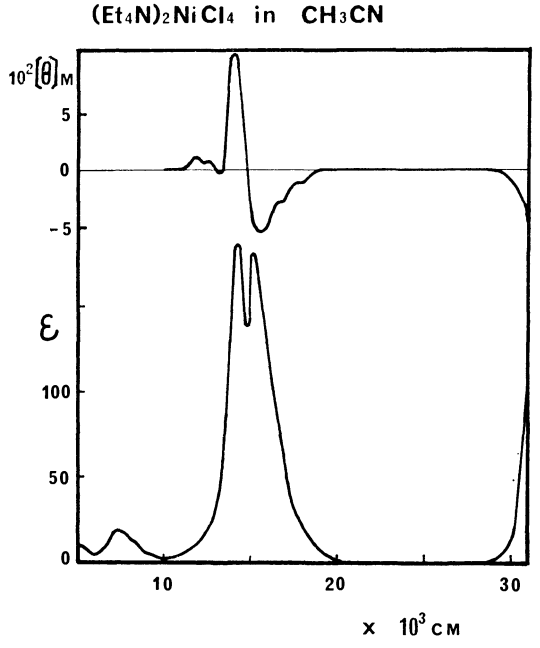

Fig. 1. MCD and absorption spectra of $(Et_4N)_2NiCl_4$ in CH_3CN at room tempepature. $[\theta]_M$ is the molar ellipticity per unit magnetic field. ε is molar extinction coefficient.

and $^3T_1(P)$, in the region from near-infrared to visible. The molar extinction coefficients of these d-d transitions are smaller than those in the tetrahedral complexes, because in the latter complexes there is no center of inversion symmetry and there is greater d-p mixing. The MCD and absorption spectra of a solution of $[Ni(dmf)_6](ClO_4)_2$ in DMF and a solution of $[Ni(dmso)_6](ClO_4)_2$ in DMSO are shown in Figs. 2 and 3 respectively. The MCD spectrum of the band in the 12000—16000 cm^{-1} region is mainly negative and shows a small positive value in the higher energy region (let us call this "*negative dispersion*"). The sign of the dispersion is opposite to that of the tetrahedral complex observed in the 13000—17000 cm^{-1} region. This characteristic difference is very useful in distinguishing whether the complex in solution is in octahedral or in tetrahedral symmetry.

The compounds NiX_2L_2 (L=tertiary phosphines, X=Cl, Br, I, and SCN) have been studied in a series of papers.[1-3] Some of them were found to be in equilibrium of the paramagentic tetrahedral form and the diamagnetic square-planar form in inert solvents. The thiocyanato-complex, $Ni(SCN)_2(Ph_3P)_2$, has been found to be diamagnetic and trans-square planar.[3] The MCD and absorption spectra are shown in Fig. 4. The absorption spectrum shows bands only at energy regions higher than 15000 cm^{-1} and the high-intensity absorption bands at about 24000 and 31000 cm^{-1} are generally referred to as charge-transfer bands. The magnitude of the MCD in comparison with that of the absorption, which may be indicated by the magnitude of $[\theta]_M/\varepsilon$, in the diamagnetic square planar nickel(II) complex is less than 10% of those found in the paramagnetic tetrahedral and the paramagnetic octahedral nickel(II) complexes. This characteristic difference can be useful in finding whether the complex in solution is paramagnetic or diamagnetic.

The MCD and absorption spectra of dichlorobis(triphenylphosphine)nickel(II), $NiCl_2(Ph_3P)_2$, were found to change greatly depending on the solvent, the concentration of the solution, and the temperature. The dependence on the concentration in DMSO is shown in Fig. 3. It shows a drastic change in a narrow range of the concentration. The spectrum of 0.25 M solution shows a strong absorption band in the range 14000—18000 cm^{-1}, and the MCD of the band shows a positive dispersion, which is characteristic of the paramagnetic tetrahedral species. However, as the concentration is reduced to 0.05 M, the intensity of the band in this range decreases and the intensities of the bands at about 7500, 12500, and 23000 cm^{-1} increase. This fact indicates that the paramagnetic tetrahedral species and the paramagnetic octahedral

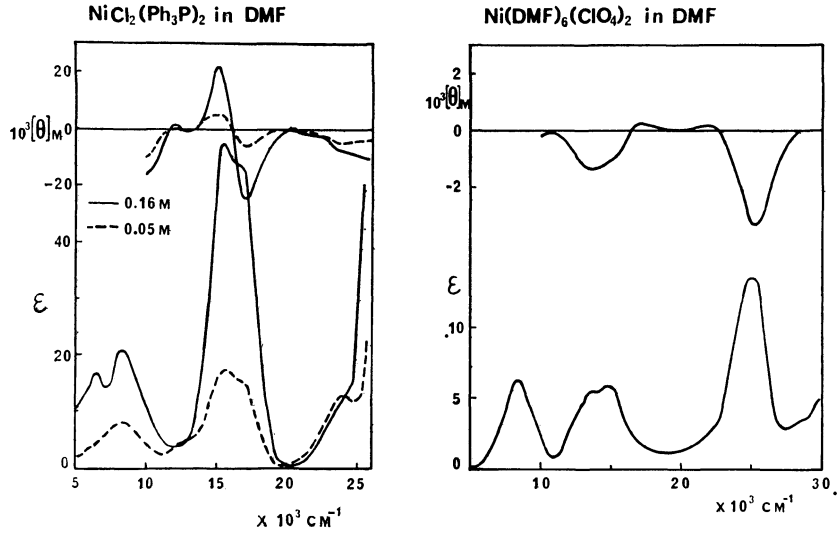

Fig. 2. MCD and absorption spectra of $Ni(dmf)_6(ClO_4)_2$ and the concentration dependence of the spectra of $NiCl_2(Ph_3P)_2$ in DMF at room temperature.

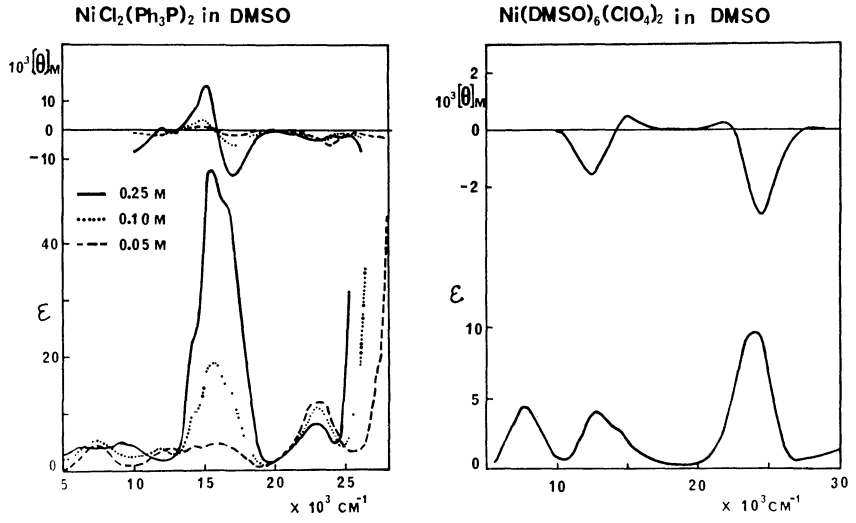

Fig. 3. MCD and absorption spectra of $Ni(dmso)_6(ClO_4)_2$ and the concentration dependence of the spectra of $NiCl_2(Ph_3P)_2$ in DMSO at room temperature.

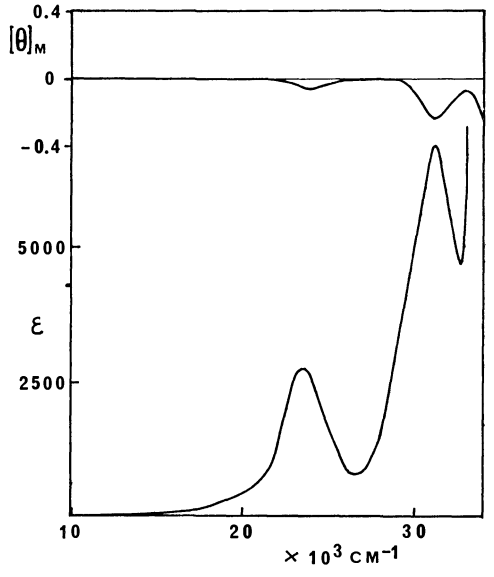

Fig. 4. MCD and absorption spectra of 0.02 M solution of $Ni(SCN)_2(Ph_3P)_2$ in benzene at room temperature.

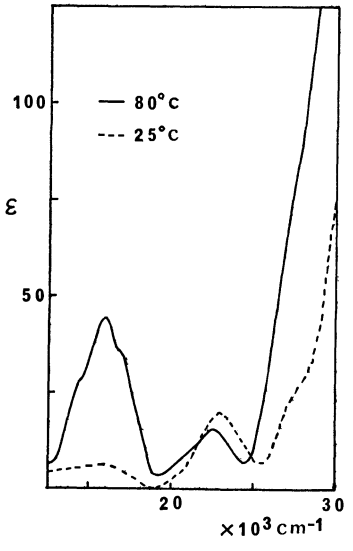

Fig. 5. Temperature dependence of the absorption spectrum of 0.05 M solution of $NiCl_2(Ph_3P)_2$ in DMSO.

species are in equilibrium in the solution and the ratio of the former to the latter decreases as the concentration decreases.

When the temperature of the 0.05 M solution is raised (see Fig. 5), the absorption spectrum becomes very similar to the one observed in the solution of higher concentration at room temperature. When this solution is cooled to room temperature again, the spectrum returns to the one measured before heating. This fact indicates that the octahedral complex in 0.05 M solution at room temperature is $NiCl_2(Ph_3P)_2(dmso)_2$, and as the temperature is raised it tends to become tetrahedral $NiCl_2(Ph_3P)_2$ by expelling the coordinated solvent molecules.

The spectrum is found to change slowly in the course of time (see Fig. 6), and the crystal of triphenylphosphine (Ph_3P) is found to grow in a couple of days after preparing the solution. The spectrum, which is measured after several days, is identified to that of a paramagnetic octahedral species, but it is not identical with the spectrum of $Ni(dmso)_6^{2+}$. It appears therefore that the coordinated Ph_3P tends to be removed gradually and thus the solvated compound $NiCl_2(dmso)_4$ is produced.

In 0.25 M solution, the intensities of absorption bands due to the terahedral species are much greater than those due to the octahedral species. However the molar concentrations of the tetrahedral species and the octahedral species would be almost the same, since the molar extinction coefficients of the bands due to the tetrahedral species are much greater than those due to the octahedral ones.

The spectral behavior observed in DMF solution is similar to that observed in DMSO solution. If we compare the spectrum of 0.05 M $NiCl_2(Ph_3P)_2$ solution in DMF with that in DMSO at room temperature

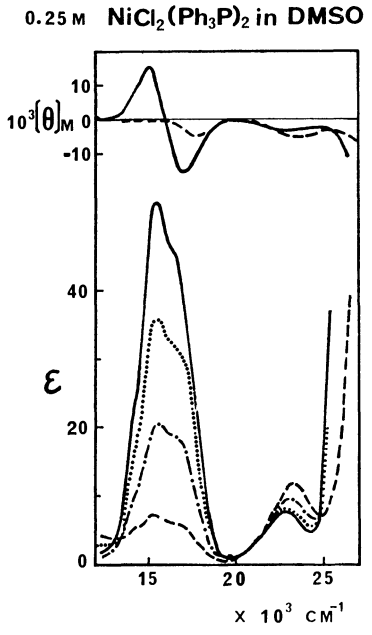

Fig. 6. Change of MCD and absorption spectra of 0.25 M $NiCl_2(Ph_3P)_2$ solution in DMSO at room temperature as a function of time. Measured immediately after preparing the solution (——), after 24 h (----), after 72 h (·—·—), after one week (— —). The sample was kept in dark place at 25 °C.

(Figs. 2 and 3), it is understood that the tetrahedral form of $NiCl_2(Ph_3P)_2$ is slightly more stable in DMF than in DMSO.

The spectrum of $NiCl_2(Ph_3P)_2$ in CH_3CN (Fig. 7) shows that the paramagnetic tetrahedral form of this complex is more stable in CH_3CN than in DMSO or in DMF. The absorption band in the range 14000—18000 cm^{-1} is assigned as a transition $^3T_1(F) \rightarrow {}^3T_1(P)$ of a tetrahedral species, because of the magnitude of the extinction coefficient and because of the MCD spectrum, whose sign and magnitude are very similar to those of $NiCl_4^{2-}$ ion (see Fig. 1). The extinction coefficient of this band in 0.01 M solution is as large as those observed in the more concentrated solutions in DMSO and in DMF (0.25 M in the former and 0.16 M in the latter. See Figs. 2 and 3). If the observed absorption bands were due to a fairly large amount of octahedral species, the apparent molar extinction coefficient should be much smaller. Therefore the complex will be mostly tetrahedral in 0.01 M solution in CH_3CN.

The extinction coefficient of the shoulder-like absorption band at about 24000 cm^{-1} in Fig. 7 is greater than that of the transition $^3A_2 \rightarrow {}^3T_1(P)$ of an octahedral species. The ratio $[\theta]_M/\varepsilon$ is smaller than that of the paramagnetic species, and it is close to the value of $[\theta]_M/\varepsilon$ observed in $Ni(SCN)_2(Ph_3P)_2$ solution in benzene (see Fig. 4), the complex in the solution is known to be diamagnetic square plane.[3] Since the molar extinction coefficient of the diamagnetic species is much greater than that of the paramagnetic species, even a small amount of diamagnetic species causes a strong absorption. Thus the band at about 24000 cm^{-1} may be identified as the absorption due to a small amount of diamagnetic square-plane species in CH_3CN solution.

Absorption bands in the energy region higher than about 27000 cm^{-1} will be mainly attributed to the charge transfer bands of the paramagnetic tetrahedral species, since the sign and magnitude of the MCD and the ratio $[\theta]_M/\varepsilon$ are in good agreement with those observed in charge transfer bands of tetrahalogenonickel(II) complexes.[15]

The spectra of $NiCl_2(Ph_3P)_2$ in non-coordinating solvents, such as chloroform, dichloromethane, and benzene, are different from those in coordinating solvents. The spectrum of 0.05 M solution in $CHCl_3$ is shown in Fig. 8. The absorption spectrum in the

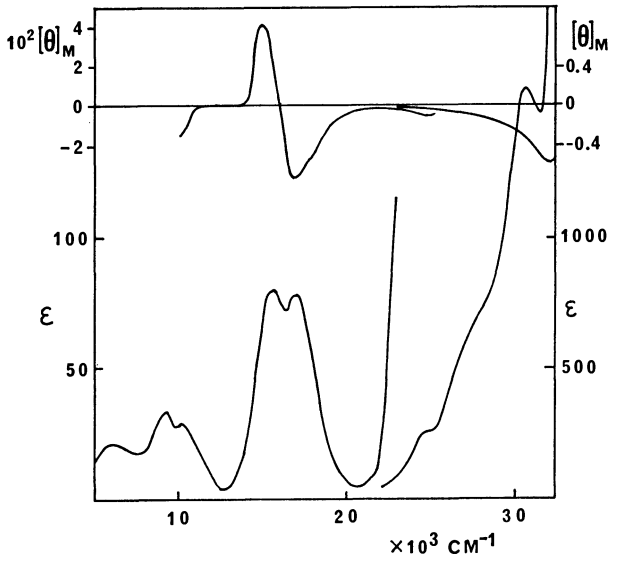

Fig. 7. MCD and absorption spectra of 0.01 M solution of $NiCl_2(Ph_3P)_2$ in CH_3CN at room temperature.

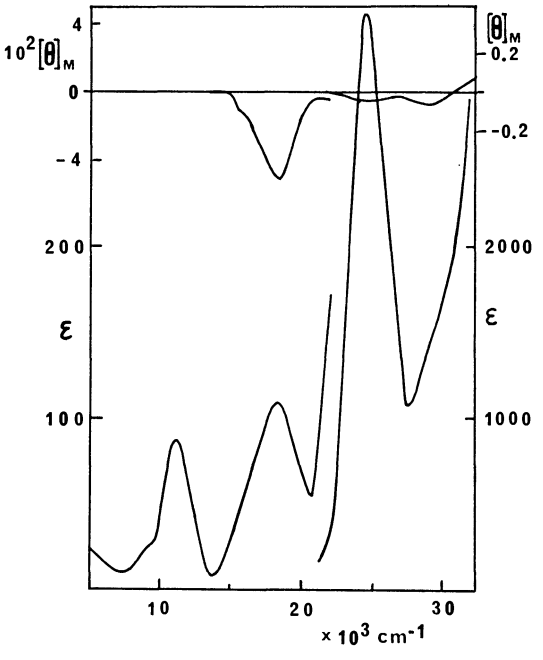

Fig. 8. MCD and absorption spectra of 0.05 M solution of $NiCl_2(Ph_3P)_2$ in $CHCl_3$ at room temperature.

range 5000—20000 cm^{-1} is similar to the crystal absorption spectra of $NiCl_2(Ph_3P)_2$, in which the nickel(II) ion is reported to be in "effective" C_{2v} point-group symmetry.[7] This presumably means that the molecule, which shows a similar absorption spectrum to that in crystal, retains the distorted tetrahedral configulation in non-coordinating solvents. It should be noted that the MCD spectrum of the band in the region of 15000—20000 cm^{-1} is simply negative and that it is different from those observed in coordinating solvents.

The absorption bands in the energy region higher than 22000 cm^{-1} will be of the diamagnetic square-plane species, since the ratios $[\theta]_M/\varepsilon$ of the bands are very close to the one observed in $Ni(SCN)_2(Ph_3P)_2$ solution in benzene. The high extinction coefficient and the small value of $[\theta]_M/\varepsilon$ for the absorption band at about 25000 cm^{-1} are characteristic of diamagnetic square-plane nickel(II) complexes. The intensity of the band is stronger in $CHCl_3$ than in CH_3CN. It appears therefore that the proportion of the diamagnetic species is greater in $CHCl_3$ than in CH_3CN.

Calculations Based on Ligand-field Theory. Energy levels of $NiCl_2(Ph_3P)_2$ and $NiCl_2(Ph_3P)_2(dmso)_2$ are calculated by the following approximation. The magnitude of ligand field parameters D_q of $NiCl_4^{2-}$, $Ni(Ph_3P)_4^{2+}$ in T_d symmetry and $Ni(dmso)_6^{2+}$ in O_h symmetry are estimated to be 350, 550, and 850 cm^{-1} respectively. The ligands, Cl, Ph_3P, and DMSO, are approximated by point charges and the magnitudes of the point charges $-Ze$ are evaluated by using the relation: $D_q=2Ze^2\langle r^4\rangle/27a^5$ in T_d symmetry and $D_q=Ze^2\langle r^4\rangle/6a^5$ in O_h symmetry, where $-Ze$ is the point charge and a is the distance between the nickel atom and the point charge. From the data of X-ray analysis,[17] we assumed the distances between the point charges and nickel atom to be Ni–Cl=2.27 Å and Ni–P=2.28 Å in tetrahedral form, and Ni–Cl=2.38 Å, Ni–P=2.39 Å, and Ni–O=2.10 Å in octahedral form. The values of $\langle r^2\rangle$ and $\langle r^4\rangle$ were calculated by using an analytical SCF function for nickel atoms obtained by Clementi:[20] $\langle r^4\rangle_{Ni(3d)}=3.997a_0^4$ and $\langle r^2\rangle_{Ni(3d)}=1.220a_0^2$, where a_0 is the Bohr radius. The point charges of $NiCl_2(Ph_3P)_2$ are put in the direction of the regular tetrahedron. This may not be an accurate structure since the crystal-structure determination shows that the Cl–Ni–Cl and P–Ni–P bond angles are 123° and 117°, respectively, which are greater than the tetrahedral 109°28′. The effect of lower symmetry C_{2v} is reflected in the magnitude of point charges and distances from the metal. The point charges of $NiCl_2(Ph_3P)_2(dmso)_2$ are put in the direction of regular octahedron so that the same ligands are in trans positions. All the possible configurations of d^8 electrons are considered, and the effect of the spin-orbit interaction is included completely. The spin-orbit coupling constant ζ is assumed to be that of free nickel(II) ion: $\zeta=649$ cm^{-1}. The results of energy level calculations are shown schematically in Figs. 9 and 10.

The energy levels of $NiCl_2(Ph_3P)_2(dmso)_2$ are similar to those of $Ni(dmso)_6^{2+}$. The MCD of the paramagnetic octahedral nickel(II) complexes has been found to arise from the MCD C-term,[18,19] which originates in the population difference among the levels of the ground state $^3A_2$ split by the Zeeman effect. Since the ground state of $NiCl_2(Ph_3P)_2(dmso)_2$ has the same spin de-

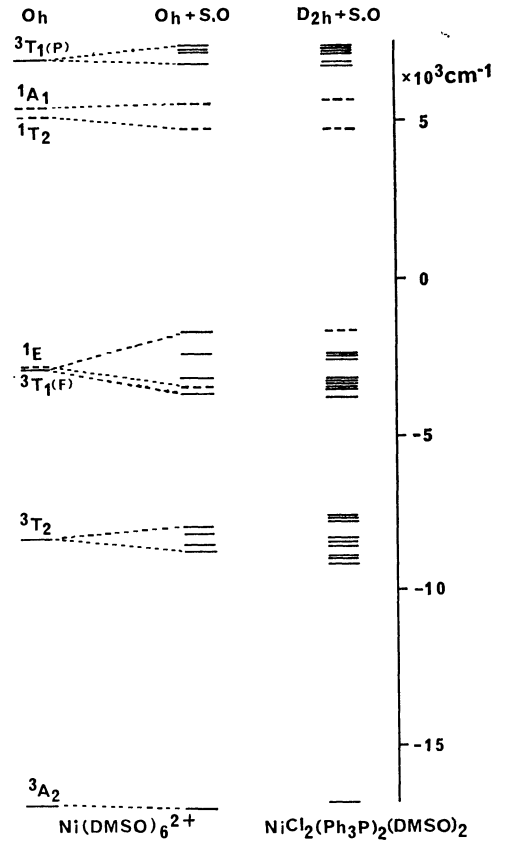

Fig. 9. Calculated energy levels of $Ni(dmso)_6^{2+}$ and $NiCl_2(Ph_3P)_2(dmso)_2$.

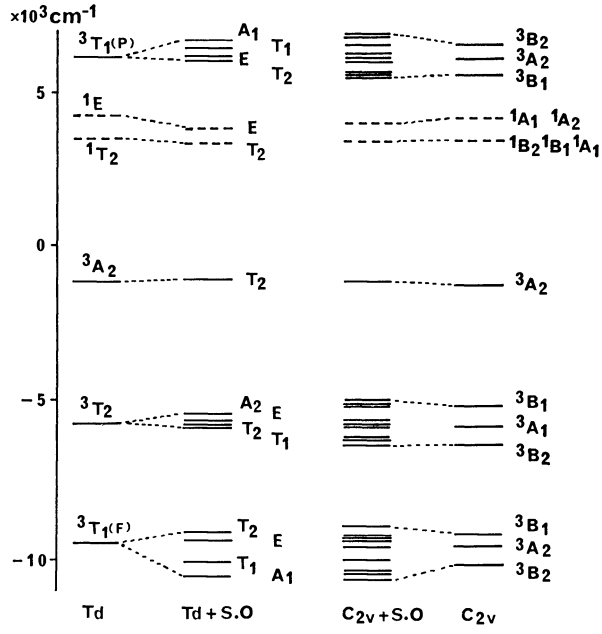

Fig. 10. Calculated energy levels of $NiCl_2(Ph_3P)_2$. The energy levels in rigorously tetrahedral field and in the lower symmetry field are denoted as T_d and C_{2v}, respectively. The inclusion of spin-orbit coupling is shown by adding +S.O.

generacy as that of $Ni(dmso)_6^{2+}$ and their MCD spectra are similar to each other, the MCD spectrum of $NiCl_2(Ph_3P)_2(dmso)_2$ may arise from the MCD C-term.

It has been shown that the major contribution to the MCD of charge-transfer bands of tetrahalogenonickel(II) complexes comes from the C-term, because of the variation of the MCD spectrum with temperature.[15] The analysis of the MCD spectra of the paramagnetic tetrahedral complex $NiCl_2(Ph_3P)_2$ was done for the following two cases. *Case A)* The energy levels are calculated by the above approximation. The calculated energy levels are shown in Fig. 10 as C_{2v}+S.O. *Case B)* The ligand field is assumed to be rigorously tetrahedral and the effect of spin-orbit coupling is included. The magnitude of ligand field parameter D_q is assumed to be 450 cm^{-1}, which is a simple numerical average of the D_q's of $NiCl_4^{2-}$ and $Ni(Ph_3P)_4^{2+}$. The calculated energy levels are shown in Fig. 10 as T_d+S.O.

By using the eigen-functions in *case B)*, we have calculated the levels of MCD parameters A and C for all the allowed transitions among the levels split by spin-orbit interaction in the $^3T_1(F)\rightarrow{}^3T_1(P)$ absorption band; the results are given in Table 1. In the calculation of the MCD parameter B the mixing of the charge transfer states will be significant, but it is hard to evaluate it correctly. Therefore we neglected B. The calculated value of A for the transition $A_1\rightarrow T_2$ is negative, and it leads to a positive dispersion of the MCD spectrum. We shall use the dipole strength D defined in Ref. 9. The calculated value of A/D for the transition $A_1\rightarrow T_2$ is in good agreement with the experimental value -8.4β, which is obtained by assuming that the MCD of 0.01 M solution of $NiCl_2(Ph_3P)_2$ in CH_3CN in the range 14000—18000 cm^{-1} is dominated by the A-term. The magnitudes of the A- and C-terms are dependent, furthermore, on the frequency (ν), the width at half-maximum height of the absorption line (Γ), and temperature (T).[8,9] If we assume $\Gamma h/2\pi\approx 4000$ cm^{-1} and $kT\approx 200$ cm^{-1}, where h is Planck's constant and k is the Boltzmann constant, the A-term for the transition $A_1\rightarrow T_2$ is almost the same order of magnitude as the C-term for the transitions $T_1\rightarrow T_1$, E, and T_2. The A-term is dominant for the transition $A_1\rightarrow T_2$ and the C-term is dominant for the transitions $T_1\rightarrow T_1$, E, and T_2. The C-terms of the latter compose a positive dispersion of the MCD spectrum. Therefore, a positive dispersion of the observed MCD spectrum can be interpreted as the overlap of line shapes due to the A-term of the transition $A_1\rightarrow T_2$ and the C-terms of the transitions $T_1\rightarrow T_1$, E, and T_2.

Table 1. Calculated values of MCD and absorption parameters[a] for the transitions from each level split from $^3T_1(F)$ to each level split from $^3T_1(P)$

Transition	Excitation energy (cm^{-1})	A[b]	C[b]	D[c]	A/D
$A_1\rightarrow T_2$	16400	−79.4	0	95.3	-8.3β
$T_1\rightarrow T_1$	16380	−6.3	3.0	7.2	-8.8β
$\rightarrow E$	16150	−0.5	1.1	2.5	-0.2β
$\rightarrow T_2$	16010	−0.7	−2.7	6.4	-1.1β
$E\rightarrow T_1$	15690	0.3	0.0	0.8	0.4β
$\rightarrow T_2$	15320	0.0	0.0	0.0	0.0
$T_2\rightarrow A_1$	15690	0.0	0.0	0.1	0.0
$\rightarrow T_1$	15460	0.0	0.0	0.0	0.0
$\rightarrow E$	15230	0.0	0.0	0.0	0.0
$\rightarrow T_2$	15090	0.0	0.0	0.0	0.0

a) All values of parameters A, C, and D include the Boltzmann distribution factor of the initial state at room temperature. b) In units of $10^4\beta p^2$, where β is the Bohr magneton and $p=\langle t_2\|er\|e\rangle$. c) In units of 10^3p^2.

In *case A)*, the effects of lower symmetry field and the spin-orbit coupling are comparable. Both the spin and the orbital degeneracies are removed. However, since the eigen-functions are not real, the MCD parameters A, B, and C are nonzero. We have estimated the B-term with the following approximation. As the states to be mixed into one of the states split from $^3T_1(F)$ by the external magnetic field, we have considered only the rest of the states split from $^3T_1(F)$. In the same way, we have considered only the rest of the split states as the states to be mixed into one of the states split from $^3T_1(P)$. By using the eigen-functions in *case A)*, we have calculated the values of MCD parameters A, B, and C. Contrary to our expectation, all of these parameters are found to be smaller than about 1% of the values obtained in *case B)*. Therefore, in this case we cannot explain the observed magnitude of $[\theta]_M$. The main cause of such small valuse seems to be the fact that we estimated the effect of the lower symmetry field and the spin-orbit coupling to be of the same order of magnitude. In fact, the effective field operating in $NiCl_2(Ph_3P)_2$ in solution might be very close to that of tetrahedral symmetry. More extensive study would be necessary with respect to this point.

Proton Nuclear Magnetic Resonance Studies. Proton NMR spectra of dihalogenobis(tertiary phosphine)-nickel(II) complexes have been investigated extensively.[21-26] The signals of the phenyl ring protons of the paramagnetic tetrahedral species are usually substantially displaced from the resonance positions of the diamagnetic species. The shift is upfield for the ortho and para protons and downfield for meta protons; it is interpreted as arising from a contact interaction with unpaired electrons which have been partially delocalized from a nickel atom to the π-orbital of the ligand.[21,22] The kinetics of ligand exchange in the tetrahedral complexes and the thermodynamics and kinetics of the diamagnetic planar↔paramagnetic tetrahedral interconversion have been studied,[23-26] but these studies were done only on the solutions in inert solvents. As we have shown in the studies of the MCD and absorption spectra, the complex $NiCl_2(Ph_3P)_2$ in coordinating solvents can be in equilibrium between a paramagnetic tetrahedral form and a paramagnetic octahedral form.

The proton NMR spectra of $NiCl_2(Ph_3P)_2$ in DMSO at various concentrations are shown in Fig. 11. As the concentration increases, the splitting of the ortho,

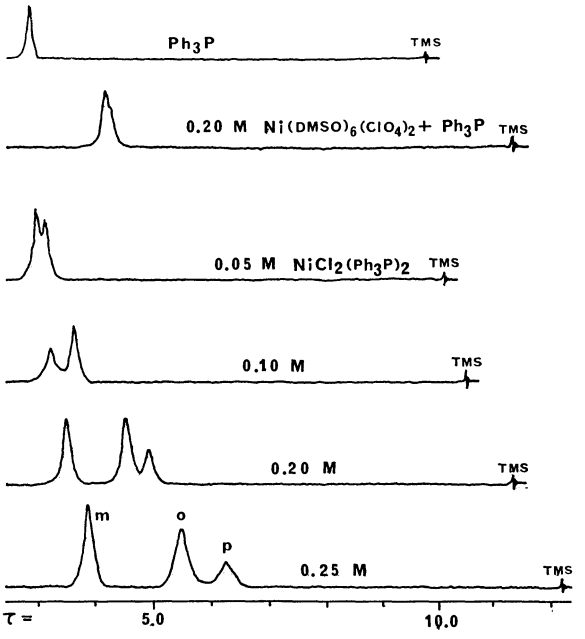

Fig. 11. Proton NMR spectra at several concentrations of the solution of $NiCl_2(Ph_3P)_2$ in DMSO at room temperature. Proton shifts are shown relative to the protons of tetramethylsilane (TMS) in CCl_4 ($\tau=10.0$) as an external standard. The signal of TMS as an internal standard shifts depending on the concentration of nickel(II) ions, and the position is shown as TMS in each spectrum. The spectrum of triphenylphosphine which is added to 0.20 M solution of $Ni(dmso)_6(ClO_4)_2$ in DMSO and the spectrum of triphenylphosphine dissolved in DMSO are shown for comparison.

meta and para protons increases and the signals of phenyl ring protons generally shift upfield. When some excess Ph_3P is added to the 0.2 M solution of $NiCl_2(Ph_3P)_2$, the splitting of the phenyl ring protons decreases and all the signals approach the resonance position of the Ph_3P which is added to the 0.2 M solution of $Ni(dmso)_6(ClO_4)_2$ in DMSO. The signal of the TMS added to a 0.2 M solution of $Ni(dmso)_6(ClO_4)_2$ in DMSO and that of Ph_3P added to the same solution both shifted by 1.5 ppm from the respective signals in the absence of the nickel complex. The signal of TMS in 0.2 M solution of $NiCl_2(Ph_3P)_2$ in DMSO also shifted by the same magnitude. Thus there are nearly the same amount of paramagnetic nickel(II) ions in both 0.2 M $NiCl_2(Ph_3P)_2$ in DMSO and 0.2 M $Ni(dmso)_6(ClO_4)_2$ in DMSO. With respect to the signal of non-coordinating Ph_3P, the ortho and para protons are shifted upfield and the meta protons are shifted downfield. The characteristic shifts are interpreted as arising from the contact shift originating in the paramagnetic tetrahedral form. The configurational equilibrium is significantly dependent on the concentration, and the increase of concentration is favorable for the tetrahedral form in DMSO. The rate of ligand exchange or structual interconversion is fast, since no new peaks and only averaged resonances are observed, showing that it is faster than 10^2 s^{-1}. The splitting of the phenyl ring protons decreases

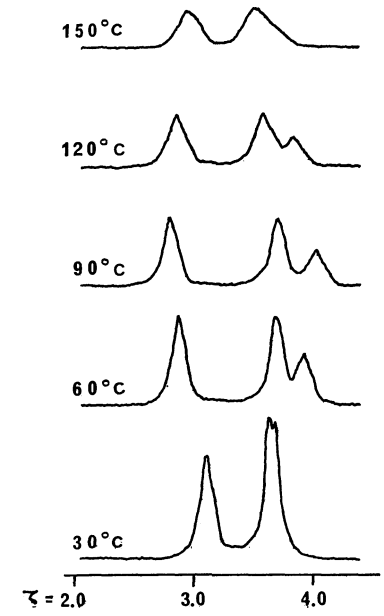

Fig. 12. Proton NMR spectra of 0.1 M solution of $NiCl_2(Ph_3P)_2$ in DMSO in the temperature range 30 to 150 °C.

gradually, within the time scale shown in Fig. 6, and the signals approach the position of the non-coordinating Ph_3P.

The proton NMR spectrum of 0.1 M solution of $NiCl_2(Ph_3P)_2$ in DMSO in the temperature range 30 to 150 °C is shown in Fig. 12. An increase of the contact shift, which reveals the increase of the paramagnetic tetrahedral complex, is observed as the temperature is raised up to 90 °C. As the temperature is raised further, the contact shift begins to decrease and the line broadening is observed. The temperature dependent behaviour may be interpreted as showing that the solvated octahedral molecule $NiCl_2(Ph_3P)_2$-$(dmso)_2$ tends to become tetrahedral $NiCl_2(Ph_3P)_2$ by expelling the coordinated solvent as the temperature is raised; then the rate of ligand exchange increases and the effect becomes predominant at temperatures higher than 100 °C. However, such a change of the proton NMR spectrum is not observed in the

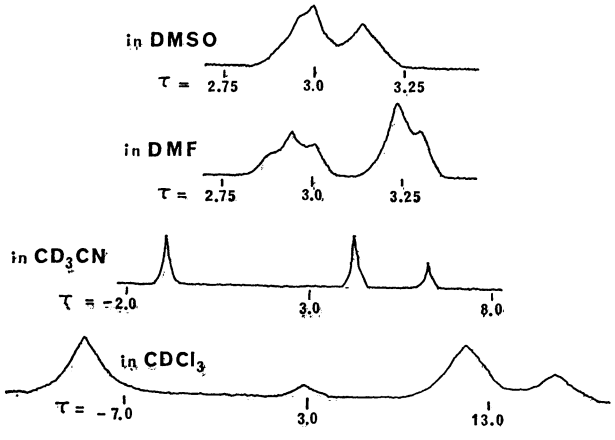

Fig. 13. Proton NMR spectra of $NiCl_2(Ph_3P)_2$ in various solvents at the same concentration; 0.05 M.

solutions in either CH_3CN or $CHCl_3$. The contact shift increases as the temperature is cooled down to -50 °C in both CH_3CN and $CHCl_3$.

The proton NMR spectra of $NiCl_2(Ph_3P)_2$ in various solvents at the same concentration, 0.05 M, are shown in Fig. 13. The ratio of the paramagnetic tetrahedral form of $NiCl_2(Ph_3P)_2$ increases in the solutions in the order DMSO<DMF<CH_3CN<$CHCl_3$. When excess Ph_3P is added to these solutions, all the signals are found to approach the position of the signal of non-coordinating Ph_3P. Therefore the rate of ligand exchange of Ph_3P is faster than 10^2 s^{-1} in all these solutions. It should therefore be noted that the weak signal at about $\tau=3$ in $CDCl_3$ solution is not a signal of the non-coordinating Ph_3P.

Conclusions

The MCD, absorption, and proton NMR spectra thus exhibit consistently the structural interconversions of $NiCl_2(Ph_3P)_2$ in various solvents. Generally, the paramagnetic tetrahedral form of this compound is more stable at high concentrations in both coordinating and non-coordinating solvents. In coordinating solvents, such as DMSO and DMF, the solvent-coordinated paramagnetic octahedral species $NiCl_2(Ph_3P)_2$(solvent molecule)$_2$ are found to increase as the concentration of $NiCl_2(Ph_3P)_2$ is decreased and also as time goes on after making the solution. Further, it is found that the coordinated Ph_3P tends to leave gradually and the solvated complex $NiCl_2$(solvent molecule)$_4$ is formed. However, these solvent molecules will not be so strongly coordinative in comparison with Ph_3P, since it is found that the ratio of the paramagnetic tetrahedral species $NiCl_2(Ph_3P)_2$ increases as the temperature of the solution containing the solvated species is raised.

In non-coordinating solvent $CHCl_3$, no solvated octahedral compound is observed. Configurational isomers of a paramagnetic tetrahedral and a diamagnetic square-planar $NiCl_2(Ph_3P)_2$ are observed. The molecule of the former isomer will retain the distorted tetrahedral configuration which it has in the crystal. The magnitude of the proton NMR signal at $\tau=3$ grows gradually and coincidently all the other signals, which are due to the paramagnetic tetrahedral species, are reduced in intensity without changing their positions. At the same time, the absorption spectra of the solution change to show the bands only in the energy region higher than 25000 cm^{-1}; these bands have a strong resemblance to those of $Ni(SCN)_2(Ph_3P)_2$ (Fig. 4) and may be identified as those of a diamagnetic square-planar species. The rate of interconversion between the paramagnetic tetrahedral form and the diamagnetic square-planar form is sufficiently slow on the NMR time scale, *i.e.* less than 10^2 s^{-1}. It seems to be almost one-way from the paramagnetic tetrahedral form to the diamagnetic square-planar form and irreversible. As the former form decreases gradually, a yellow precipitate is observed to grow. The ratio of the former form to the latter one is greater at high concentrations, and the yellow precipitate grows faster at low concentrations. When the filtrate of the yellow precipitate is dried, only Ph_3P remained. We identified this yellow precipitate to be $NiCl_2$ by measuring the magnetic susceptibility and the melting point. It appears therefore that the paramagnetic tetrahedral $NiCl_2(Ph_3P)_2$ decomposes gradually to $NiCl_2$ and $2Ph_3P$, and since the solvent does not coordinate, $NiCl_2$ precipitates as Ph_3P leaves.

The paramagnetic octahedral species, the paramagnetic tetrahedral species, and the diamagnetic square-planar species seem to coexist in the solution of $NiCl_2(Ph_3P)_2$ in CH_3CN. Some nickel(II)–acetonitrile complexes, $Ni(CH_3CN)_6(BF_4)_2$, $NiCl_2(CH_3CN)_4$, and $NiCl_2(CH_3CN)_2$, have been reported. A chloride ion is well known to be a stronger coordinating ligand than CH_3CN.[27] The MCD and absorption spectra show that the proportion of the diamagnetic species is smaller in the solution in CH_3CN than in $CHCl_3$. The proton NMR spectra show a greater contact shift in $CHCl_3$ than in CH_3CN. This will be due to the liability of ligand exchange between Ph_3P and CH_3CN. Most of the absorption in the range 14000 to 19000 cm^{-1} in Fig. 7 will be due to the tetrahedral $NiCl_2(Ph_3P)_2$, since the tetrahedral complex $NiCl_2(CH_3CN)_2$ will show an absorption band with the peak at about 13000 cm^{-1}. As the time goes on after dissolving $NiCl_2(Ph_3P)_2$ in CH_3CN, a pale yellow precipitate is observed to grow, but it is not so much as in the solution in $CHCl_3$ and the proton NMR signal at about $\tau=3$ is found to grow gradually. The absorption spectrum does not change drastically as in the case of $CHCl_3$ solution; it changes only slightly, suggesting the coexistence of a small amount of a tetrahedral $NiCl_2(CH_3CN)_2$ and an octahedral $NiCl_2(CH_3CN)_4$.

References

1) L. M. Venanzi, *J. Chem. Soc.*, **1958**, 719.
2) C. R. C. Coussmaker, M. H. Hutchinson, J. R. Mellor, L. E. Sutton, and L. M. Venanzi, *J. Chem. Soc.*, **1961**, 2705.
3) M. C. Browning, R. F. B. Davies, D. J. Morgan, L. E. Sutton, and L. M. Venanzi, *J. Chem. Soc.*, **1961**, 4816.
4) R. G. Hayter and F. S. Humiec, *J. Am. Chem. Soc.*, **84**, 2004 (1962).
5) F. A. Cotton, O. D. Faut, and D. M. L. Goodgame, *J. Am. Chem. Soc.*, **83**, 344 (1961).
6) G. Garton, D. E. Henn, H. M. Powell, and L. M. Venanzi, *J. Chem. Soc.*, **1963**, 3625.
7) R. J. Fereday, B. J. Hathaway, and R. J. Dudley, *J. Chem. Soc., A*, **1970**, 571.
8) A. D. Buckingham and P. J. Stephens, *Annu. Rev. Phys. Chem.*, **17**, 399 (1966).
9) P. N. Schatz and A. J. McCaffery, *Quart. Rev. (London)*, **23**, 552 (1969).
10) N. S. Gill and R. S. Nyholm, *J. Chem. Soc.*, **1959**, 3997.
11) R. S. Drago, D. W. Meek, M. D. Joesten, and L. LaRoche, *Inorg. Chem.*, **2**, 124 (1963).
12) F. A. Cotton and R. Francis, *J. Am. Chem. Soc.*, **82**, 2986 (1960).
13) H. Katô, *J. Chem. Phys.*, **59**, 1732 (1973).
14) H. Katô and K. Akimoto, *J. Am. Chem. Soc.*, **96**, 1351 (1974).
15) B. D. Bird, B. Briat, P. Day, and J. C. Rivoal, *Symp. Faraday Soc.*, No. **3**, 70 (1969).

16) H. A. Weakliem, *J. Chem. Phys.*, **36**, 2117 (1962).
17) L. Sacconi "Transition Metal Chemistry," ed by R. L. Carlin, Marcel Dekker Inc., New York (1968), Vol. 4, pp. 199—298.
18) M. J. Harding, S. F. Mason, D. J. Robbins, and A. J. Thomson, *J. Chem. Soc., A*, **1971**, 3047.
19) M. J. Harding, S. F. Mason, D. J. Robbins, and A. J. Thomson, *J. Chem. Soc., A*, **1971**, 3058.
20) E. Clementi, *J. Chem. Phys.*, **41**, 295 (1964).
21) E. A. Lalancette and D. R. Eaton, *J. Am. Chem. Soc.*, **86**, 5145 (1964).
22) G. N. LaMar, W. D. Horrocks, Jr., and L. C. Allen, *J. Chem. Phys.*, **41**, 2126 (1964).
23) L. H. Pignolet and W. D. Horrocks, Jr., *J. Am. Chem. Soc.*, **90**, 922 (1968).
24) L. H. Pignolet and W. D. Horrocks, Jr., *J. Am. Chem. Soc.*, **91**, 3976 (1969).
25) L. H. Pignolet, W. D. Horrocks, Jr., and R. H. Holm, *J. Am. Chem. Soc.*, **92**, 1855 (1970).
26) L. Que, Jr., and L. H. Pignolet, *Inorg. Chem.*, **12**, 156 (1973).
27) B. J. Hathaway and D. G. Holah, *J. Chem. Soc.*, **1964**, 2400.

A Theoretical Consideration of the ^{13}C NMR Chemical Shift of Protonated Systems. I. The Acetone–Sulfuric Acid System

Isao ANDO, Masahiro KONDO, Atsuo NISHIOKA, and Shosuke WATANABE

Department of Polymer Chemistry, Tokyo Institute of Technology, Ookayama, Meguro-ku, Tokyo 152

(Received December 14, 1978)

A quantum-chemical method has been developed using a point-charge model to calculate the ^{13}C chemical shift for protonation in an acidic solution. This method has been applied to the acetone–sulfuric acid system; the gross tendencies between the observed and calculated results agree.

The NMR parameter, the chemical shift, is closely associated with the electronic structure of a molecule. In solution, the electronic structure of the molecule is affected by the surrounding molecules; thus, the chemical shift is solvent-dependent. The nature of the solvent effects may be mainly classified into the following two categories:

(i) The molecule considered forms a loose bonding with a solvent, such as hydrogen bonding or protonation.

(ii) Without such a bonding, the molecule is affected by intermolecular interaction with the surrounding molecules.

For Case (ii), we have successfully interpreted the observation of the solvent effect of the ^{13}C chemical shift[1,2] and the long-range chemical shift by magnetic anisotropy[3] in some organic compounds, acetone, acetonitrile and other compounds, by the application of Klopman's solvaton model[4] to the MINDO/2[5] and CNDO/2 methods.[6] It is the purpose of this work to treat quantum-chemically the protonation in Case (i) and use it in interpreting the behavior of the ^{13}C chemical shift of the protonated acetone molecule which occurs in a strongly acidic solution such as a sulfuric acid solution.

A study of the effect of protonation on the ^{13}C chemical shift of acetone was first done by de Jue[7] using the average-excitation-energy approximation. However, this approximation is too gross to enable us to discuss exactly the nature of the ^{13}C chemical shifts of the molecule being considered. We will, therefore, discuss the behavior of the ^{13}C chemical shifts of the protonated acetone using our proposed model for protonation without the average-excitation-energy approximation.

Theoretical

As a model of protonation we assume that a positive point charge approaches and loosely bonds to the oxygen atom in the carbonyl group of acetone. In order to formulate this model generally, we consider a molecular system with M electrons and N nuclei, adding a point charge. On the basis of this model, the Hamiltonian, H, of the specified molecular system consists of the inherent term, H_{inh}, and the protonation term, H_{prot}, and is given as (in atomic units)

$$H = H_{\mathrm{inh}} + H_{\mathrm{prot}}, \tag{1}$$

$$H_{\mathrm{inh}} = \sum_{i=1}^{M}\left[\left(-\frac{1}{2}\nabla_i^2 - \sum_{n=1}^{N}\frac{Z_n}{r_n}\right) + \frac{1}{2}\sum_{j=1}^{M}\frac{1}{r_{ij}}\right] + \frac{1}{2}\sum_{m=1}^{N}\sum_{n=1}^{N}\frac{Z_m Z_n}{r_{mn}}, \tag{2}$$

$$H_{\mathrm{prot}} = -\sum_{i=1}^{M}\frac{Q_{\mathrm{a}}}{r_{\mathrm{a}i}} + \sum_{n=1}^{N}\frac{Q_{\mathrm{a}}Z_n}{r_{\mathrm{a}n}}, \tag{3}$$

where Q_{a} is the magnitude of the point charge, $r_{\mathrm{a}i}$ and $r_{\mathrm{a}n}$ are the point charge-electron and the point charge-nucleus distances respectively, and Z_n is the charge on the nucleus, n. In these calculations, two additional assumptions were made for Eq. 3; (1) if the electron and the point charge are associated with the same atomic center, the point charge-electron distance, $r_{\mathrm{a}i}$, is taken to be the van der Waals radius of the oxygen atom, and (ii) if the electron and the point charge are associated with different atomic centers, the point charge is assumed to be centered on the atomic center associated with Q_{a}, and then the point charge-electron distance, $r_{\mathrm{a}i}$, is evaluated as the distance between their atomic centers.

Using the Roothaan's matrix notation, the total energy, E_{T}, of the system is given as

$$E_{\mathrm{T}} = 2\sum_{i}^{\mathrm{occ}}\boldsymbol{C}_i^*\boldsymbol{H}\boldsymbol{C}_i + \sum_{i}^{\mathrm{occ}}\sum_{j}^{\mathrm{occ}}\boldsymbol{C}_i^*(2\boldsymbol{J}_j - \boldsymbol{K}_j)\boldsymbol{C}_i + \frac{1}{2}\sum_{m}^{N}\sum_{n}^{N}\frac{Z_m Z_n}{r_{mn}} + \left[2\sum_{i}^{\mathrm{occ}}\boldsymbol{C}_i^*\boldsymbol{D}\boldsymbol{C}_i + \sum_{n}^{N}\frac{Q_{\mathrm{a}}Z_n}{r_{\mathrm{a}n}}\right]. \tag{4}$$

The fourth term is due to the contribution of the protonation, where the elements of D are given as

$$D_{ij} = \int \phi_i^*(1)\left(-\frac{Q_{\mathrm{a}}}{r_{\mathrm{a}1}}\right)\phi_j(1)\mathrm{d}\tau(1) \tag{5}$$

D_{ij} are estimated according to similar procedures developed by Germer.[8]

The integral:

$$D_{\mathrm{ss}} = D_{\mathrm{A}} \tag{6}$$

is calculated for each atomic center, A, using the S orbitals of the atom. The $D_{\mu\nu}$ is approximated as

$$D_{\mu\nu} = \frac{1}{2}S_{\mu\nu}(D_{\mathrm{A}} + D_{\mathrm{B}}), \tag{7}$$

where $S_{\nu\mu}$ is the overlap integral, μ and ν being valence orbitals on the A and B atoms respectively. This approximation was incorporated into the MINDO/2 MO method.

As the effective van der Waals radius of the oxygen atom, 1.4 Å is used.[9]

According to Pople, the ^{13}C chemical shift, σ^{T}, is estimated by the sum of the diamagnetic and paramagnetic contributions. These contributions were calculated according to Pople's GIAO-MO theory[10] without the average-excitation-energy approximation.

The bond lengths and bond angles used are standard values proposed by Pople and Gordon.[11] All the calculation were carried out with the HITAC-8800

computer of the Computer Center of the University of Tokyo.

Experimental

High-resolution pulsed FT ^{13}C NMR spectra were obtained at 25.15 MHz using a JEOL PS-100 spectrometer equipped with a PFT-100 Fourier transform system, a JEC-6 spectrum computer, a ^{2}D field-frequency lock, and a noise-modulated proton-decoupling system. The observed free induction decay after a 90° pulse was sampled at 8192 data points. A deuteron signal of benzene-d_6 sealed in a capillary inserted into an 8 mm o.d. tube was employed for the lock signal, where ^{13}C-enriched tetramethylsilane(20%) dissolved in benzene-d_6 was used as the reference. The ^{13}C chemical shift was corrected for bulk magnetic susceptibility.[12] The bulk magnetic susceptibility for a solution, χ_{soln}, is given as

$$\chi_{soln} = \sum_{i}^{n} \phi_i \chi_i, \quad (8)$$

where χ_i and ϕ_i are the bulk magnetic susceptibility and the volume fraction of the i-th component molecule in solution respectively.

In a strongly acidic solution, the protonation of the acetone molecule may occur. The concentration of acetone is 2 mol % in various sulfuric acid–water concentration ratios. The sulfuric acid concentration varies from 0 to 25 mol % in the total solution.

Results and Discussion

In Fig.1 the ^{13}C chemical shifts of the carbonyl and methyl carbons are shown for 2 mol % acetone in various sulfuric acid–water concentration ratios. The carbonyl carbon chemical shift moves to a much lower field with an increase in the concentration of sulfuric acid. On the other hand, the methyl carbon chemical shift moves to an appreciably lower field upon protonation. These trends agree with de Jue's results,[7] although the concentrations of acetone are different in the two cases.

Let us analyze this behavior upon protonation on the basis of our calculations. The values of the excess charges on the carbon and oxygen atoms in acetone molecules are plotted against the magnitude of the charge, Q_a, associated with the oxygen atom in the carbonyl group in Fig. 2. The electron densities on the oxygen and carbon atoms in the carbonyl group increase with an increase in Q_a, while, on the other hand, that on the methyl carbon decreases. In this molecule, the electrons are drawn to the oxygen atom and the distribution of electrons is polarized by an inductive $-I^-$ type effect, $O^-{=}C^+{-}C^-$. However, its effect decreases by the association with the charge, Q_a. The electron densities on the carbonyl oxygen and carbon atoms increase, and that on the methyl carbon atom decreases, with an increase in Q_a. Then, the charge on the methyl carbon atom becomes positive.

The charges of this distribution of the electron density with an increase in the Q_a in this system cannot explain the observed results. For example, the increase in the electron density on carbonyl carbon with an increase in the Q_a cannot explain the observed low-field shift with an increase in the concentration of sulfuric acid. This suggests that the change in the excitation energy may play an important role in the observation of the chemical shift. Some typical examples of the calculated diamagnetic, ρ^d, paramagnetic, ρ^p, and total chemical shifts are shown against the value of Q_a in Table 1. The calculated chemical shifts are also plotted in Fig. 2. The major part of the Q_a dependence of the chemical shift arises from variations in σ^p. The chemical shifts of the carbonyl and methyl carbons shift to a lower field with an increase in the value of Q_a, and the change in the former is larger than that in the latter. These tendencies agree with the observed ones, but the change in the methyl carbon is too large.

The observed chemical shift of carbonyl carbon

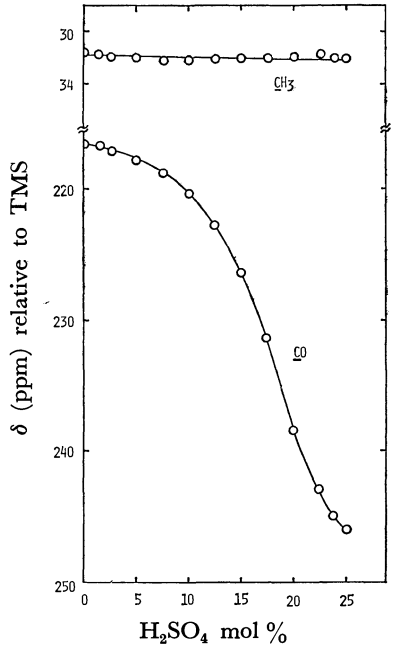

Fig. 1. Observed ^{13}C chemical shifts for 2 mol % acetone in various concentration ratios of sulfuric acid-water.

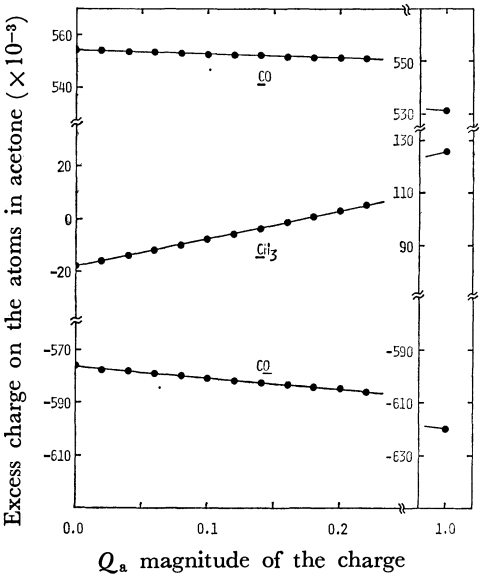

Fig. 2. Dependence of excess charge on carbon and oxygen atoms in acetone upon the magnitude of the charge Q.

Table 1. Dependence of the calculated chemical shifts of methyl and carbonyl carbons in acetone upon the magnitude of the charge, Q_a

Q_a		Calculated chemical shift (ppm)		
		Diamagnetic contribution σ^d	Paramagnetic contribution σ^p	Total contribution σ^T
0.0	CH_3	57.99	−211.55	−153.56
	CO	52.81	−352.58	−299.76
0.01	CH_3	57.99	−212.26	−154.27
	CO	52.81	−354.41	−301.59
0.02	CH_3	57.98	−212.98	−154.99
	CO	52.82	−356.25	−303.43
0.05	CH_3	57.96	−215.14	−157.19
	CO	52.82	−361.94	−309.12
0.10	CH_3	57.91	−218.86	−160.95
	CO	52.83	−371.90	−319.08
0.20	CH_3	57.83	−226.62	−168.79
	CO	52.84	−393.96	−341.11
0.50	CH_3	57.52	−253.95	−196.44
	CO	52.91	−479.29	−426.38
1.00	CH_3	56.30	−320.44	−263.64
	CO	53.04	−738.67	−685.63

moves to a lower field by about 30 ppm for the concentration variation of sulfuric acid from 0 to 25 mol %. This value corresponds to the one calculated when the value of Q_a is about 0.15. When the value of Q_a is 1.0, the calculated value shifts to considerably a lower field. According to these results, if the protonation is complete, dose such a low-field shift arise? This may be interesting problem.

Reviewing our results from the viewpoint of the exchange between free and protonated molecules, the finding that the value of Q_a is about 0.15, considerably smaller than 1, is not surprising. Although, in this work, we have chosen a simple system in applying our developed procedure to the protonation, we should apply a more complicated system to ascertain the applicability of our model.

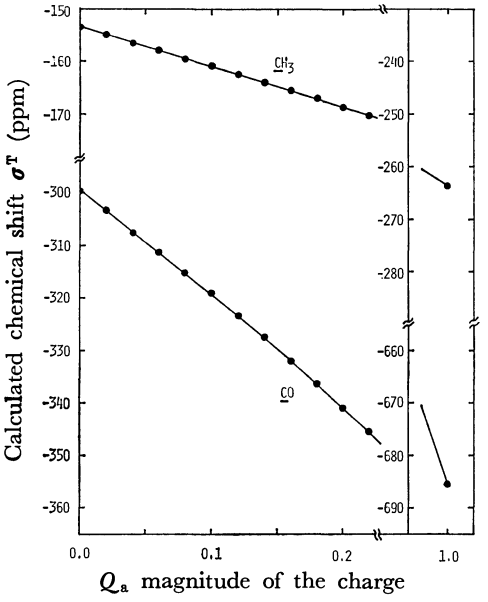

Fig. 3. Dependence of calculated ^{13}C chemical shifts of methyl and carbonyl carbons in acetone upon the magnitude of the charge Q.

References

1) I. Ando, A. Nishioka, and S. Watanabe, *J. Magn. Reson.*, **21**, 429 (1976).
2) I. Ando, Y. Kato, M. Kondo, and A. Nishioka, *Makromol. Chem.*, **178**, 803 (1977).
3) I. Ando and H. S. Gutowsky, *J. Magn. Reson.*, **31**, 387 (1978).
4) a) G. Klopman, *Chem. Phys. Lett.*, **1**, 200 (1967); b) G. Klopman, *J. Am. Chem. Soc.*, **90**, 233 (1968).
5) M. J. S. Dewar and E. Haselbach, *J. Am. Chem. Soc.*, **92**, 590 (1970).
6) J. A. Pople and G. A. Segal, *J. Chem. Phys.*, **44**, 3289 (1966).
7) W. H. de Jue, *J. Phys. Chem.*, **74**, 822 (1970).
8) H. A. Germer, Jr., *Theor. Chem. Acta*, **34**, 145 (1974); **35**, 273 (1974).
9) L. Pauling, "The Nature of the Chemical Bond," 3rd ed, Cornell University Press, Ithaca, N. Y. (1960), p. 260.
10) J. A. Pople, *J. Chem. Phys.*, **37**, 53 (1962).
11) J. A. Pople and M. Gordon, *J. Am. Chem. Soc.*, **89**, 4253 (1967).
12) J. W. Emsley, J. Feeney, and L. H. Sutcliffe, "High Resolution Nuclear Magnetic Resonance Spectroscopy," Pergamon Press, Oxford (1965), Vol. 1.

Topological Ligand Design. I. Definition and Derivation of Simple Ligand Graph*

Susumu TAKAMOTO

Department of Chemistry, Faculty of Sciences, Gakushuin University, Mejiro, Toshima-ku, Tokyo 171

(Received December 18, 1978)

A simple ligand graph and a pattern graph are defined topologically in order to design the patterns of the chelating ligands. This ligand graph, which comprises m donor atoms and n carbon chains capable of forming medium-sized chelate rings, is an irregular graph containing neither multiple lines nor self-loops. All the ligand graphs with $m \leqq 8$ can be systematically obtained from fifty pattern graphs. These are derived from fifteen basic pattern graphs, which are cubic general graphs containing some multiple lines and self-loops. A pattern code and a set of series indices are tabulated for each ligand graph with $m \leqq 8$. For the ligand graphs with $m \leqq 6$, all the geometric isomers of their octahedral chelates are also illustrated.

The chemistry of metal chelates has been remarkably developed and is widely applied. The properties and the reactions of the metal chelates are closely related to their structure. When one seeks the most suitable new chelating reagents for a certain purpose, it would be of great use to look over all the patterns of ligand structures. In their reviews on the ligand design, Goodwin[1] and Black and Hartshorn[2] were chiefly concerned with the systematic outline and classification of the chelate agents already prepared, but their topological diagrams were mathematically incomplete. Thus, purely geometrical investigations are not available for the sysematic derivation of ligand patterns or for the design of new ligands. The graph theory and computer studies have been successfully applied to the numeration and the documentation of the chemical isomers or the homologs for some special kinds of organic compounds.[3] In order to cover all the ligands, one has to treat all the organic compounds, since every compound containing some oxygen- or nitrogen-group elements has more or less ability to coordinate to a metal ion. This designing work is limited to those practical ligands which can form five- or six-membered chelate rings with a metal ion.

Theory and Results

A ligand can be considered as a set of some donor atoms joined by several carbon chains capable of forming medium-sized chelate rings. Then a simple ligand graph L(m, n) can be defined for each ligand, where m is the number of points which correspond to the donor atoms, and n is the number of lines which correspond to the carbon chains. The ligand graph must meet the following requirements: (1) The graph is connected. (2) It is planar. (3) The degree of each point is one, two, or three (The degree of a point is the number of lines incident with it). The first condition is self-evident. A planar graph can be drawn on a plane so that no two lines cross each other. According to the graph theory such a graph is identical to a spherical graph. To be spherical is needed for two carbon chains not to cross each other on a coordination sphere, because these chains are too short to detour. Three would be the maximum degree of a point in any kind of donor atom. Then, for instance, ethylenediamine, 1,3-propylenediamine, 2,3-butenediamine, N,N,N',N'-tetramethylethylenediamine, 1,2-phenylenediamine, and 1,2-cyclohexenediamine are represented by the same ligand graph L(2, 1), since these ligands contain two donor atoms and only one carbon chain which can form a chelate ring. The graph L(2, 1) is unique, but it should be noted that a graph L(m, n) is not generally determined only by a set of m and n.

A graph in the narrow sense of the word does not include multiple lines; that is, two points may be joined by only one line. Molecules such 1,4-diazacycloheptane, for example, can form metal chelates, so some double lines may be included in the ligand graph. But relatively few such ligands form stable chelates because of the steric hindrance and the bond strains. Moreover, this limited number of double lines can be easily derived by joining a pair of adjacent points of degree one or two in a simple ligand graph. Therefore, no multiple lines are included in this simple ligand graph. Also, no self-loop is needed in this graph, since it forms no chelate ring. Thus the simple ligand graph is a normal irregular graph.

Some new terms should be defined. When all the points of degree two in a ligand graph are neglected, the remainder is named a pattern graph P(p, q), and each line in the pattern graph is called a series. Although an isolated circle without a point may not be generally accepted as a graph, in this study it is by exception admitted as a pattern graph. The degree of every point in the pattern graph is one (end point) or three (branch point). A pattern graph may contain some triple and double lines and some self-loops. This value of p is always an even number because the degree of every point is odd.

When all side-chains are removed from a pattern graph, the remainder is called a basic pattern graph B(r,s). All basic pattern graphs but the isolated circle B(0,1) and an isolated line B(2,1) are cubic general graphs; that is, all their points have the same degree of three, and they also may have multiple lines and self-loops. Examples of each graph are shown in Fig. 1.

All the cubic general graphs for $m \leqq 8$ can be constructed from the two simplest cubic graphs B(2,3)

* A preliminary report of this work was presented at the 28th Symposium on Coordination Chemisrty, Matsuyama, October 1978.

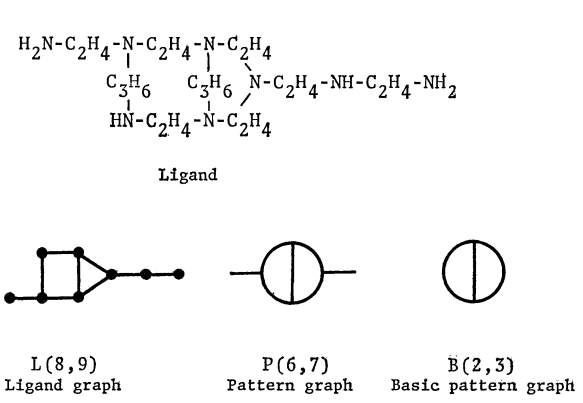

Fig. 1. Reduction of a ligand structure into the basic pattern graph.

by adding new branch lines one by one avoiding the duplication of patterns, up the maximum values of r:

$$r \leqq m - d - 2t - 2l - 3c \tag{1}$$

where d, t, l, and c are the numbers of double lines, triple lines, self-loops, and isolated circes. This restriction is needed to exclude all the multiple lines and self-loops from the ligand graphs which are derived from the pattern graphs. Naturally r is even number.

All the basic pattern graphs for $m \leqq 8$ are shown in Fig. 2. The values of t and c are only applicable in the case of (2-1) and (1-1) in Fig. 2 respectively. Then, for example, (4-2) and (4-4) are not the basic pattern graphs for $m \leqq 7$, because d of (4-2) is 2, and l of (4-4) is 1.

The sum of the degree of the points of a graph $G(x, y)$ is twice the number of lines, and the number of independent cycle i is equal to $y-x+1$. Then in any cubic graph $B(r, s)$ the following relationships are obtained:

$$s = 3r/2, \tag{2}$$

$$i = 1 + r/2. \tag{3}$$

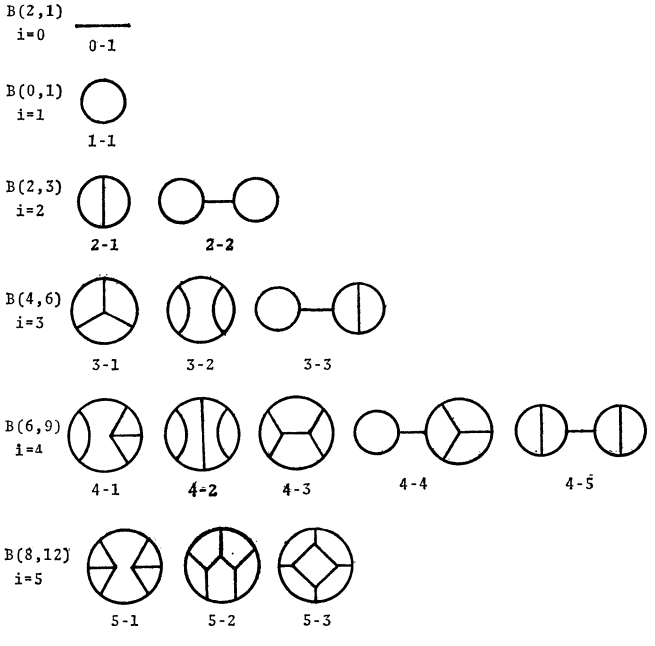

Fig. 2. Basic pattern graphs ($m \leqq 8$).

The pattern graphs are systematically derived from the basic pattern graphs by adding some side-chains one by one, while basic pattern graphs themselves belong to the set of pattern graphs. The maximum valuse of p is also restricted by the right hand side of Eq. 1, although p is not less than r of the original basic pattern graph. Fifty pattern graphs thus obtained for $m \leqq 8$ are illustrated in Fig. 3. As the numbers of points and lines are incresed by the same integer by adding a side-chain to a graph, $q-p$ is always equal to $s-r$ of its original basic pattern graph. However, the number of independent circles i is unchanged by any addition of side-chains.

Similarly, all the ligand graphs are derivable by allotting a definite number of points of degree two to each series of the pattern graph. Ligand graphs thus derived from the same pattern graph are topologically homeomorphic to one another. In this study a pattern graph is simply denoted by a pattern code classified by the basic pattern groups, and alphabetical labels ***a*** to ***h*** are assigned to each series of the pattern graphs, as shown in Fig. 3. Then all the simple ligand graphs can be characterized by a pattern code and a set of eight series indices, which express the number of the points of degree two allotted to each labeled series of the pattern graph. These allotted numbers are properly restricted so that the numerating repetition which is caused by the symmetry of the ligand graph may be avoided, and so that every cycle in ligand graphs may contain at least three points, which are needed to exclude any multiple lines and self-loops. In the case of Fig. 1, two points of degree two are allotted for series ***a*** and ***h*** of the pattern graph (24), because series ***a*** has the highest priority among the four equivalent series ***a***, ***b***, ***c***, and ***d*** in order to avoid the repetition. All the ligand graphs with $m \leqq 8$ and their pattern codes and series indices are listed in Table 1. The numbers of the simple ligand graphs thus designed and of their double-line derivatives are summarized in Table 2.

Each ligand may form some configurationally isomeric chelates with a metal ion in a certain coordination structure. As an example, all the geometric configurations in the octahedral coordination for every simple ligand graph with $m \leqq 6$ are illustrated in Table 3. They were confirmed by use of molecular models.

Discussion

In this study double lines are not included in the simple ligand graph, but double-line derivatives have been derived from the simple ligand graph. All of them, as well as the simple ligand graphs, can directly be derived from the pattern graphs if the restriction 1 is moderated as follows:

$$r \leqq p \leqq m - t - l - 2c. \tag{4}$$

Then the numbers of the pattern graphs and the basic pattern graphs are increased from 50 and 15 to 112 and 34 respectively. There is little merit in complicating the pattern graphs so much, since the number of such less important ligands is limited.

Mechanical derivations of compounds often have

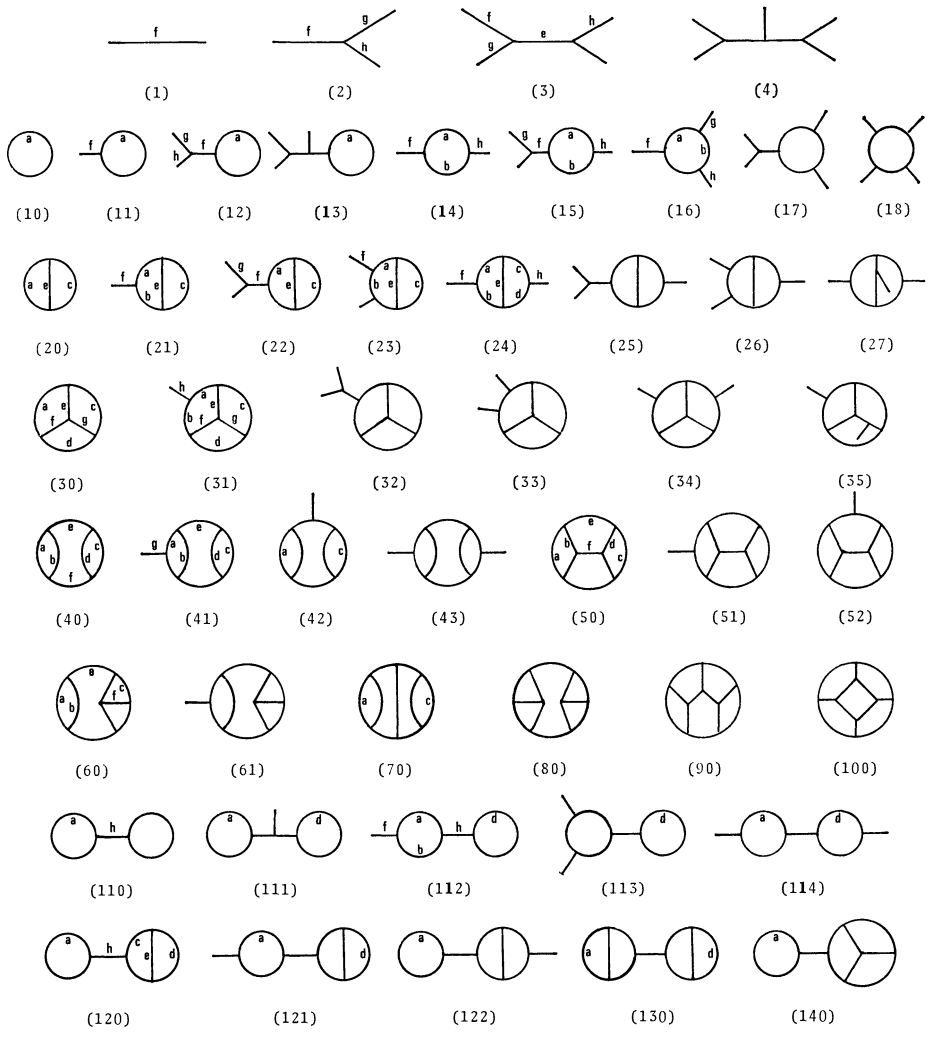

Fig. 3. Pattern graphs and labeling of series ($m \leqq 8$).

a tendency to introduce some useless ligands which may offer some difficulties for coordinating. The present manner of deriving the ligand graphs is sufficiently systematic that it produces no such worthless ligands.

Every ligand graph with $m=5$ can cover all the trigonalbipyramidally or square-pyramidally disposed positions. Every planar graph with $m=6$ can also cover all the octahedral points, but not all the points of a trigonal prism. The planar m-polygonal corners can be covered with only two ligand graphs of order m which have a linear or a circular shape.

Since any donor atoms of nitrogen or oxygen group elements may be held at any points of a ligand graph, ligands of mixed donor atoms may also be expressed by the same ligand graphs. Then, for example, most of the simple cryptands belong to No. 8-055, and edta or its analogs to No. 6-04 in Table 1. The lines in a simple ligand graph might represent not only a carbon chain but also boron-, silicon-, or any other chains.

Previously, the author[4] reported that 1,4,7-triazacyclononane (a type of No. 3-02) forms the most stable metal chelates in all the triamines, and that 1,2-di(1,4,7-triazacyclononan-1-yl)ethane, which is composed of two such triazacycloalkanes connected by a ethylene group (a type of No. 6-28) is also a good chelating agent.[5] Since cyclam (a type of No.4-03) is well known for the extreme stability of its chelates, a ligand of type No. 6-26, which is composed of two triazacycloalkanes and one tetraazacycloalkane, should form the most stable chelates.

Ligands of type No.4-06 or No.6-27 have a basketlike structure. All the lone-pair electrons of their donor atoms are directed to the center of the polyhedron, so no metal ion might enter inside or be coordinated. But if these ligands could be synthesized around a metal ion by some means, the metal atom should be confined completely within their network, and a hydrophobic spherical cation would be produced.

It may be seen from the above lists that only a few types of ligands have ever been prepared; many types with interesting structures still remain unknown. For example, most studies on sexidentate ligands were focused upon only five types of No.6-01 to No.6-05 among the twenty eight ligand graphs with $m \leqq 6$; therefore a number of new ligands with various patterns can be synthesized and investigated in the near future. Showing their possibilities is the most important aim and the successful fruit of this work.

Table 1. Catalog of ligand graphs ($m \leqq 8$)

Graph No.	Pattern code	Series indices, adcdefgh	Graph No.	Pattern code	Series indices, abcdefgh	Graph No.	Pattern code	Series indices, abcdefgh	Graph No.	Pattern code	Series indices, abcdefgh
2-01	1	-----0--	7-01	1	-----5--	8-001	1	-----6--	8-064	21	103-00--
			7-02	2	-----300	8-002	2	-----400	8-065	21	102-10--
			7-03	2	-----210	8-003	2	-----310	8-066	21	102-01--
			7-04	2	-----111	8-004	2	-----220	8-067	21	101-11--
3-01	1	-----1--	7-05	3	----1000	8-005	2	-----211	8-068	21	101-02--
3-02	10	3-------	7-06	3	----0100	8-006	3	----2000	8-069	21	004-00--
			7-07	10	7-------	8-007	3	----1100	8-070	21	003-10--
			7-08	11	5----0--	8-008	3	----0200	8-071	21	003-01--
			7-09	11	4----1--	8-009	3	----0110	8-072	21	002-20--
4-01	1	-----2--	7-10	11	3----2--	8-010	3	----0101	8-073	21	002-11--
4-02	2	-----000	7-11	11	2----3--	8-011	4	--------	8-074	21	002-02--
4-03	10	4-------	7-12	12	3----000	8-012	10	8-------	8-075	21	001-12--
4-04	11	2----0--	7-13	12	2----100	8-013	11	6----0--	8-076	21	001-03--
4-05	20	1-1-0---	7-14	12	2----010	8-014	11	5----1--	8-077	22	1-1-000-
4-06	30	0-00000-	7-15	14	30---0-0	8-015	11	4----2--	8-078	22	0-2-000-
			7-16	14	21---0-0	8-016	11	3----3--	8-079	22	0-1-100-
			7-17	14	20---1-0	8-017	11	2----4--	8-080	22	0-1-010-
			7-18	14	11---1-0	8-018	12	4----000	8-081	22	0-1-001-
5-01	1	-----3--	7-19	14	10---2-0	8-019	12	3----100	8-082	23	101-00--
5-02	2	-----100	7-20	14	10---1-1	8-020	12	3----010	8-083	23	011-00--
5-03	10	5-------	7-21	15	10---000	8-021	12	2----200	8-084	23	002-00--
5-04	11	3----0--	7-22	16	10---000	8-022	12	2----110	8-085	23	001-10--
5-05	11	2----1--	7-23	16	0----100	8-023	12	2----020	8-086	23	001-01--
5-06	14	10---0-0	7-24	20	4-1-0---	8-024	12	2----011	8-087	24	200000-0
5-07	20	2-1-0---	7-25	20	3-2-0---	8-025	13	2-------	8-088	24	110000-0
5-08	20	1-1-1---	7-26	20	3-1-1---	8-026	14	40---0-0	8-089	24	101000-0
5-09	21	001-00--	7-27	20	2-2-1---	8-027	14	31---0-0	8-090	24	100100-0
5-10	30	1-00000-	7-28	21	201-00--	8-028	14	30---1-0	8-091	24	100010-0
			7-29	21	111-00--	8-029	14	22---0-0	8-092	24	100001-0
			7-30	21	102-00--	8-030	14	21---1-0	8-093	24	100000-1
			7-31	21	101-10--	8-031	14	20---2-0	8-094	24	000020-0
6-01	1	-----4--	7-32	21	101-01--	8-032	14	20---1-1	8-095	24	000011-0
6-02	2	-----200	7-33	21	003-00--	8-033	14	11---2-0	8-096	24	000002-0
6-03	2	-----110	7-34	21	002-10--	8-034	14	11---1-1	8-097	24	000001-1
6-04	3	-----000	7-35	21	002-01--	8-035	14	20---3-0	8-098	25	--------
6-05	10	6-------	7-36	21	001-11--	8-036	14	10---2-1	8-099	26	--------
6-06	11	4----0--	7-37	12	000-12--	8-037	15	20---000	8-100	27	--------
6-07	11	3----1--	7-38	22	0-1-000-	8-038	15	11---000	8-101	30	4-00000-
6-08	11	2----2--	7-39	23	001-00--	8-039	15	10---100	8-102	30	3-10000-
6-09	12	2----000	7-40	24	100000-0	8-040	15	10---010	8-103	30	3-00001-
6-10	14	20---0-0	7-41	24	000010-0	8-041	16	10---001	8-104	30	2-20000-
6-11	14	11---0-0	7-42	24	000001-0	8-042	16	20---000	8-105	30	2-11000-
6-12	14	10---1-0	7-43	30	3-00000-	8-043	16	11---000	8-106	30	2-10100-
6-13	16	00---000	7-44	30	2-10000-	8-044	16	10---100	8-107	30	2-10010-
6-14	20	3-1-0---	7-45	30	2-00001-	8-045	16	10---001	8-108	30	2-10001-
6-15	20	2-2-0---	7-46	30	1-11000-	8-046	16	00---200	8-109	30	2-00002-
6-16	20	2-1-1---	7-47	30	1-10100-	8-047	16	00---110	8-110	30	1-11100-
6-17	21	1-1-00--	7-48	30	1-10010-	8-048	17	--------	8-111	30	1-10011-
6-18	21	002-00--	7-49	31	10000000	8-049	18	--------	8-112	31	20000000
6-19	21	001-10--	7-50	31	00100000	8-050	20	5-1-0---	8-113	31	11000000
6-20	21	001-01--	7-51	31	00000010	8-051	20	4-2-0---	8-114	31	10100000
6-21	24	000000-0	7-52	31	00000001	8-052	20	4-1-1---	8-115	31	10010000
6-22	30	2-00000-	7-53	40	201000--	8-053	20	3-3-0---	8-116	31	10000010
6-23	30	1-10000-	7-54	40	111000--	8-054	20	3-2-1---	8-117	31	10000001
6-24	30	1-00001-	7-55	40	110010--	8-055	20	2-2-2---	8-118	31	00200000
6-25	31	00000000	7-56	41	00100-00	8-056	21	301-00--	8-119	31	00110000
6-26	40	101000--	7-57	50	100000--	8-057	21	211-00--	8-120	31	00101000
6-27	50	000000--	7-58	50	000010--	8-058	21	202-00--	8-121	31	00100100
6-28	110	2--2---0	7-59	60	100-00--	8-059	21	201-10--	8-122	31	00100010
			7-60	110	3--2---0	8-060	21	201-01--	8-123	31	00100001
			7-61	110	2--2---1	8-061	21	112-00--	8-124	31	00000020
			7-62	112	10-2-0-0	8-062	21	111-10--	8-125	31	00000011
			7-63	120	2-010--0	8-063	21	111-01--	8-126	31	00000002

Table 1. (Continued)

Graph No.	Pattern code	Series indices, abcdefgh	Graph No.	Pattern code	Series indices, abcdefgh	Graph No.	Pattern code	Series indices, abcdefgh	Graph No.	Pattern code	Series indices, abcdefgh
8-127	28	--------	8-143	41	00110-0-	8-159	60	101-00--	8-175	112	10-2-1-0
8-128	34	--------	8-144	41	00101-0-	8-160	60	100-10--	8-176	112	10-2-0-1
8-129	34	--------	8-145	41	00100-0-	8-161	60	100-01--	8-177	113	---2----
8-130	35	--------	8-146	42	1-1-----	8-162	61	--------	8-178	114	1--1----
8-131	40	301000--	8-147	43	--------	8-163	70	1-1-----	8-179	120	3-010--0
8-132	40	211000--	8-148	50	200000--	8-164	80	--------	8-180	120	2-110--0
8-133	40	202000--	8-149	50	110000--	8-165	90	--------	8-181	120	2-020--0
8-134	40	201100--	8-150	50	101000--	8-166	100	--------	8-182	120	2-011--0
8-135	40	201010--	8-151	50	100100--	8-167	110	4--2---0	8-183	120	2-010--1
8-136	40	111100--	8-152	50	100010--	8-168	110	3--3---0	8-184	121	1--1----
8-137	40	111010--	8-153	50	100001--	8-169	110	3--2---1	8-185	122	2-------
8-138	40	101020--	8-154	50	000020--	8-170	110	2--2---2	8-186	130	1--1----
8-139	40	101011--	8-155	50	000011--	8-171	111	2--2----	8-187	140	2-------
8-140	41	10100-0-	8-156	51	--------	8-172	112	20-2-0-0			
8-141	41	01100-0-	8-157	52	--------	8-173	112	11-2-0-0			
8-142	41	00200-0-	8-158	60	110-00--	8-174	112	10-3-0-0			

Table 2. Number of ligand graphs ($m \leqq 8$)

Donor atoms	2	3	4	5	6	7	8
Basic pattern graphs	1	2	4	4	7	9	15
Pattern graphs	1	2	6	8	16	24	50
Ligand graphs	1	2	6	10	28	63	187
Double-line derivatives	1	2	6	12	37	102	318

Table 3. Octahedral configurations ($m \leqq 6$)

Graph number	Configurations	Graph number	Configurations	Graph number	Configurations	Graph number	Configurations	Graph number	Configurations
2-01		5-01	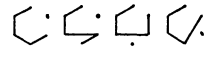	6-01	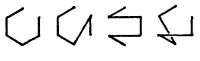	6-11		6-21	
3-01	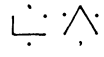	5-02		6-02	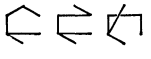	6-12	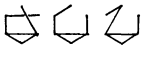	6-22	
3-02		5-03		6-03	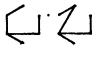	6-13		6-23	
4-01	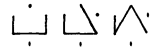	5-04		6-04		6-14		6-24	
4-02		5-05	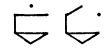	6-05		6-15		6-25	
4-03	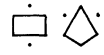	5-06	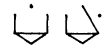	6-06		6-16		6-26	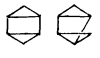
4-04		5-07	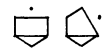	6-07		6-17		6-27	
4-05		5-08		6-08	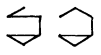	6-18		6-28	
4-06		5-09		6-09		6-19			
		5-10		6-10		6-20			

A ligand containing some special branched carbon atoms, where the branches might form several chelate rings, cannot be represented by a simple ligand graph, for a line of a graph can branch only at the point representing a donor atom. In order to express such complicated ligands the definition of the ligand graph must further be extended. These studies will be reported in a later paper.

The author wishes to express his thanks to Prof. Takeshi Iizuka of Gunma University for valuable suggestions. The present work was partially sup-

ported by a Grant-in-Aid for Scientific Research from the Ministry of Education.

References

1) H. A. Goodwin, "Chelating Agents and Metal Chelates," ed by F. P. Dwyer and D. P. Mellor, Academic Press, New York (1964), pp. 143—181.
2) D. St. C. Black and A. J. Hartshorn, *Coord. Chem. Rev.*, **9**, 219 (1973).
3) "Chemical Applications of Graph Theory," ed by A. T. Balaban, Academic Press, London (1976).
4) T. Arishima, K. Hamada, and S. Takamoto, *Nippon Kagaku Kaishi*, **1973**, 1119.
5) N. Tanaka, Y. Kobayashi, and S. Takamoto, *Chem. Lett.*, **1977**, 101.

A Note on the Nature of Ionic Hydrations and Hydrophobic Interactions in Aqueous Solutions

Kiyoshi ARAKAWA,* Kazuo TOKIWANO,** Norio OHTOMO,** and Hisashi UEDAIRA***

Research Institute of Applied Electricity, Hokkaido University, Kita-ku, Sapporo 060

***Faculty of Engineering, Hokkaido University, Kita-ku, Sapporo 060*

****Research Institute for Polymers and Textiles, Kanagawa-ku, Yokohama 221*

(Received January 16, 1979)

A theoretical consideration on the nature of solute-water and solute-solute interactions in aqueous solutions has been performed. Thermodynamic functions for the creation of cavities accommodating solute molecules were calculated by the use of the scaled particle theory, and the "negative hydration" effect of univalent ions such as Rb^+, Cs^+, Cl^-, I^- *etc.*, which was proposed first by Samoilov, Krestov and others, was interpreted and discussed. The nature of solute-water and solute-solute interactions in aqueous solutions of inert gases and hydrocarbons was elucidated in comparison with the interactions in nonaqueous solutions of those solutes.

Since the presentation of Frank and Evans' work,[1] the anomalously large and negative entropy of solution of nonpolar gases and liquids in water as well as the enormous partial molal heat capacity of those has generally been interpreted as the evidence that the solute molecules cause an increase of "ordering" around themselves within water, that is, the formation of "icebergs." Then, the cause of hydrophobic interactions between nonpolar groups or radicals in aqueous systems was ascribed to the disappearance of "icebergs" at the overlapped co-sphere region about those having direct contacts with each other.[2,3] The problems of the formation of "icebergs" and of the nature of hydrophobic interactions have become an object of increasing amount of debates since then.[4,5]

On the other hand, concerning the nature of ionic hydrations, Samoilov, Krestov and others proposed a dynamic model of ionic hydration and introduced the concept of "negative hydration" for univalent ions such as Cl^-, I^-, Cs^+ *et al.* from the consideration of diffusional behaviors of those within water.[6] The Samoilov model is a kind of the dynamical representation of ion-water interactions at the nearest neighbor of ions, while the Frank-Wen model[7] is a kind of the statical representation of those around ions.[5]

The formation of "icebergs" and the presence of "negative hydration" effect for comparatively large univalent ions are both closely related to the liquid structure of water, and many discussions have been made though no decisive conclusions are obtained at present.

The purpose of the present work is to give an explanation of those effects on the basis of a more sound theoretical ground.

While a number of new statistical mechanical approaches to treat fluids and fluid mixtures have been given for these two decades, the scaled particle theory[8] proposed by Reiss, Frisch, Lebowitz *et al.* has turned out to be one of the most useful approaches.[9] For hard-sphere fluids the theory gives an identical equation of state with that derived from the Percus-Yevick equation, and at the same time it is intuitive like a usual model theory. It gives a simple and useful method to calculate thermodynamic functions for the creation of cavities in fluids.[10] Then, the authors have applied the theory to aqueous solutions of ions as well as to those of nonpolar molecules such as inert gases and hydrocarbons *etc.*

With respect to the nature of the "negative hydration" an explanation of the effect has been given from theoretical viewpoint in the present paper. Concerning the hydrophobic interactions in aqueous systems a great deal of efforts have been devoted to the elucidation of the interactions until now, though many ambiguities are present among the results of those studies.[3–5,11] In the present paper the experimental data from various sources have been examined by the use of the scaled particle theory, and some detailed discussions have been given in combination with those results including the results of computer experiments.[12]

Calculation of Thermodynamic Functions for the Creation of Cavities

The Scaled Particle Theory. The theory is based on the consideration of the properties of a new distribution function $G(r)$ for a fluid composed of spherical molecules, where "$\rho G(r)$ is defined as the local concentration of molecular centers adjacent to a spherical cavity of radius r from which all molecular centers are excluded."[8] ρ is the number density of the fluid. The key relation of the theory is expressed as

$$G(a) = g(a), \tag{1}$$

where $g(r)$ is the ordinary radial distribution function at a separation r and a is a hard-sphere diameter of molecules. Noting that Eq. 1 is an exact relation for a hard-sphere fluid, Reiss *et al.* derived an approximate analytical expression for $G(r)$, and gave an equation of state for a hard-sphere fluid, which has turned out to be identical with the equation as an analytical solution of the Percus-Yevick equation for the fluid.[8]

The dissolution process of a solute molecule into a solvent can be regarded as consisting of two steps: the first step is "the creation of a cavity in the solvent of a suitable size to accommodate the solute molecule" and the second step is "the introduction into the cavity of a solute molecule which interacts with the solvent," as Pierotti stated.[13] According to the scaled particle theory, the reversible work $W \equiv \overline{G}_c$ for the creation of cavities suitable for the accommodation of solute molecules of a diameter a_2 within a fluid composed of N molecules (diameter a_1) at temperature T and

pressure p becomes

$$\overline{G}_c(a_{12}) \equiv W(a_{12}) = K_0 + K_1 a_{12} + K_2 a_{12}^2 + K_3 a_{12}^3, \quad (2)$$

$$K_0 = NkT\left[-\ln(1-\xi)+\frac{9}{2}\left(\frac{\xi}{1-\xi}\right)^2\right]-\frac{\pi}{6}Na_1^3 p,$$

$$K_1 = -\frac{NkT}{a_1}\left[\frac{6\xi}{1-\xi}+18\left(\frac{\xi}{1-\xi}\right)^2\right]+\pi N a_1^2 p,$$

$$K_2 = \frac{NkT}{a_1^2}\left[\frac{12\xi}{1-\xi}+18\left(\frac{\xi}{1-\xi}\right)^2\right]-2\pi N a_1 p,$$

$$K_3 = \frac{NkT}{a_1^2}\frac{4}{3}\pi N p,$$

where k is the Boltzmann constant, $\xi=\pi a_1^3\rho/6$ the packing fraction in the fluid and $a_{12}=(a_1+a_2)/2$.[14]

The enthalpy $\overline{H}_c(a_{12})$ for the creation of the cavities of the diameter a_2 becomes

$$\overline{H}_c = \alpha NkT^2\{\xi/(1-\xi)\}[\{6/(1-\xi)\}\{2(a_{12}/a_1)^2-(a_{12}/a_1)\} + \{36\xi/(1-\xi)^2\}\{(a_{12}/a_1)^2-(a_{12}/a_1)+1/4\}+1], \quad (3)$$

where α is the thermal expansion coefficient.

From Eqs. 2 and 3 we obtain the entropy for the creation of the cavities as

$$\overline{S}_c = (\overline{H}_c-\overline{G}_c)/T. \quad (4)$$

Equations 3 and 4 show that the magnitudes of $\overline{H}_c$ and $\overline{S}_c$ are determined by the parameters a_1, ξ, and α for the fluid as well as by the size a_2 of the cavities, and also show that the attractive molecular interactions in the fluid exert upon $\overline{H}_c$ and $\overline{S}_c$ through α and ξ implicitly.

Calculation of $\overline{H}_c$ and $\overline{S}_c$ for the Creation of Cavities in Water. As the basis for the discussions about the behaviors of solute molecules in water we have calculated $\overline{H}_c$ and $\overline{S}_c$ according to Eqs. 2—4 using the observed values for α and ρ. In Fig. 1 the values of $\overline{S}_c$ for the creation of a cavity are plotted against the diameter of the cavity a for several temperatures from 0 to 70 °C. In the application of the scaled particle theory the determination of molecular parameters, especially diameters of molecules, is important.

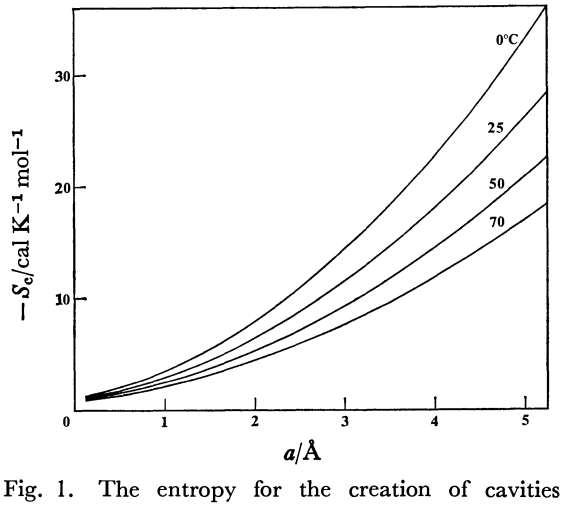

Fig. 1. The entropy for the creation of cavities in water. a: The diameter of the cavities.

The values given in Fig. 1 are those for $a_1=2.82$ Å, where a_1 is the effective hard-core diameter of water molecules.[15] We have calculated those values for another assignment of $a_1=2.75$ Å for comparison, which are given in the tables in later sections. Some deviations are seen, though the deviations have turned out to bring no important influence upon the conclusions in the present paper. The values of $\overline{H}_c$ are also shown in the tables in later sections.

The Nature of Ionic Hydrations: A Consideration from the Entropy of Hydration of Ions

A great deal of efforts have been devoted to make clear the nature of ionic hydrations. However, the results are greatly diversified, as clearly seen in a comprehensive review by Hinton and Amis (1971),[16] many problems being left unsolved for further studies.

Samoilov, Krestov and others proposed a kind of the dynamic model on ionic hydrations,[5,6,17] where the concept of the negative hydration was introduced. However, from the view-point of the statistical theory of fluids no clear explanation of the concept has been given until today. Then, we have attempted here to give an explanation in this section.

The entropy of hydration ΔS_h of ions for the transfer from hypothetical 1 atm in the gas phase to hypothetical 1 M in the aqueous phase is expressed as

$$\Delta S_h = \Delta S_{ideal} + \overline{S}_c + \delta S. \quad (5)$$

In Eq. 5 $\Delta S_{ideal}=R\ln(\overline{V}_2/V_g)$ is the contribution of ions to the entropy of transfer from the state V_g at 1 atm to the state $\overline{V}_2$, where V_g is the molar volume of an ideal gas at the temperature T and $\overline{V}_2$ the volume of the aqueous solution containing 1 mol of ions. $\overline{V}_2$ is 1 dm^3 in this case. $\delta S=\Delta S_h-(\Delta S_{ideal}+\overline{S}_c)$ is an excess entropy, which have been obtained by subtracting the calculated values of $(\Delta S_{ideal}+\overline{S}_c)$ from the experimental values of ΔS_h. δS is ascribed to the contribution caused by the direct ion-water interactions.

The values of ΔS_h, ΔS_{ideal}, $\overline{S}_c$, and δS are given in Table 1. Those determined for $a_{H_2O}=2.75$ Å are given together in the table for comparison, and a certain appreciable differences are seen between the values for $a_{H_2O}=2.82$ Å and those for $a_{H_2O}=2.75$ Å though it does not exert any influences upon the conclusions of the following discussions.

As clearly seen in the table the values of δS for alkali ions larger than K^+ and those for halide ions (Cl^-, Br^-, and I^-) are positive. This supports the idea that these ions exert a structure-breaking action upon the liquid structure of water[5,15] on the whole, which is the so-called "negative hydration" effect of these ions. For alkali ions smaller than K^+ as well as for bivalent and trivalent ions the values of δS become minus, which corresponds to the usual "positive hydration" effect.

In the case of K^+ the values of δS becomes small

Table 1. The entropy of hydration of ions at 25 °C (cal K^{-1} mol^{-1})

	Radius[a] (Å)	ΔS_h[b]	ΔS_{ideal}	$a_{H_2O}=2.82$Å		$a_{H_2O}=2.75$Å	
				$\overline{S_c}$	δS	$\overline{S_c}$	δS
Li^+	0.59	−33.7	−6.4	−3.4	−23.9	−3.1	−24.2
Na^+	1.02	−26.2	−6.4	−6.5	−13.3	−5.9	−13.9
K^+	1.38	−17.7	−6.4	−10.0	−1.3	−9.0	−2.3
Rb^+	1.49	−14.8	−6.4	−11.3	2.9	−10.1	1.7
Cs^+	1.69	−14.1	−6.4	−13.7	6.0	−12.3	4.6
Cl^-	1.81	−18.2	−6.4	−15.3	3.5	−13.7	1.9
Br^-	1.96	−14.5	−6.4	−17.4	9.3	−15.6	7.5
I^-	2.20	−9.0	−6.4	−21.0	18.4	−18.9	16.3
Mg^{2+}	0.72	−74.3	−6.4	−4.2	−63.7	−3.8	−64.1
Ca^{2+}	1.00	−60.8	−6.4	−6.3	−48.1	−5.7	−48.7
Al^{3+}	0.53	−126.6	−6.4	−3.0	−117.2	−2.7	−117.5

a) R. D. Shannon and C. T. Prewitt, *Acta Crystallogr., Sect. B*, **25**, 925 (1969); L. H. Ahrens, *Geochim. Cosmochim, Acta*, **2**, 155 (1952). The ionic radii of polyvalent ions are those determined by taking the value of 6 for their solvation numbers. b) H. L. Friedman and C. V. Krishnan, "Water," ed by F. Franks, Plenum, New York (1973), Vol. 3, Chap. 1, Table V.

and minus, while Samoilov and others proposed that it behaves as a structure breaker (at 25 °C).[6] This contradiction can not be explained successfully at present. At any rate $|\delta S|$ for K^+ is clearly small. As seen in the table, the transition from the positive to negative hydration behavior for univalent ions occurs at about 1.4 Å of ionic radius, which is nearly identical with the effective hard-sphere radius for water molecules, while Samoilov and others proposed it to occur at about 1.1 Å.[6] The presence of negative hydration effect for univalent ions at room temperature is explained here by the application of the scaled particle theory to the calculation of the entropy for the creation of cavities, with the exception of the case of K^+ which is left to further investigations.

A Consideration on Hydrophobic Interactions in Aqueous Solutions

Solubilities of Nonpolar Gases. Determination of Molecular Parameters: The determination of molecular diameters for nonpolar gases has been performed according to the procedures proposed by Bienkowski and Chao by the application of the Percus-Yevick equation in combination with critical data for those.[18]

The diameter a is calculated from the following equation,

$$\frac{a}{\left(\frac{6}{\pi}\frac{\tilde{V}_c}{\tilde{N}}\right)^{1/3}} = 0.544046 - 0.010218T_r, \quad (6)$$

where $\tilde{V}_c$ is the critical molar volume and T_r the reduced temperature. This equation was derived by applying the Percus-Yevick (PY) equation. The formula derived from Carnahan-Starling (CS) equation also was used by Bienkowski and Chao. The values determined by the use of the PY equation as well as those by the CS equation are given together in Table 2. The differences between these two are clearly small. Then we have used the values of the second column (PY), because the CS equation is essentially a conventional one.

Table 2. Effective hard-sphere diameters (Å)

	a (PY)	a (CS)
CH_4	3.59	3.62
C_2H_6	4.15	4.18
C_3H_8	4.63	4.67
n-C_4H_{10}	5.00	5.04
C_2H_4	3.94	3.99
C_2H_2	3.79	3.83
Ne	2.42	2.43
Ar	3.24	3.26
Kr	3.50	3.53
Xe	3.85	3.88
N_2	3.42	3.44
O_2	3.23	3.25
CO	3.47	3.49

A Consideration on Solute-Water Interactions in Comparison with Solute-CCl_4 Interactions: An investigation on the behaviors of nonpolar solute molecules (Table 3) in aqueous environments has been performed by the examination of solubility data from various sources.

The molar entropy and enthalpy of transfer of a solute species from an ideal gas phase at 1 atm to an aqueous solution at an equilibrium concentration x_2, $\overline{S}_2(x_2)-S_2^g$, and ΔH_s, are expressed as

$$\overline{S}_2(x_2)-S_2^g = \Delta S_{ideal} + S_c + \delta S, \quad (7)$$

and

$$\Delta H_s = \overline{H}_c + \delta H + (\alpha RT^2 - RT), \quad (8)^{9)}$$

respectively. ΔS_{ideal} is determined according to the similar procedure to the case of ionic solutions in the preceding section, where the magnitude of $\overline{V}_2(x_2)$, the molar volume of the solution containing 1 mole of solute species at an equilibrium concentration x_2, becomes a function of x_2 in this case, and its magnitude varies in different species being in contrast to the case of ionic hydration as in Table 1. The experimental

values of $\bar{S}_2(x_2)$, ΔH_s, and x_2 have been taken from various sources cited in the footnote of Table 3. The calculated values of the enthalpy and entropy of the creation of cavities, $\bar{H}_c$ and $\bar{S}_c$, are shown in the seventh and ninth columns of the table, respectively, and the excess enthalpy $\delta H=\Delta H_s-(\bar{H}_c+\alpha RT^2-RT)$ and the excess entropy $\delta S=(\bar{S}_2(x_2)-S_2{}^g)-(\Delta S_{ideal}+\bar{S}_c)$ are given in the eighth and tenth colums. In the table the values of $\Delta C_{p,c}$ which are determined from the temperature dependence of $\bar{H}_c$ are given in the eleventh column.

For the purpose of comparing the values of various thermodynamic functions given in Table 3 with those for a nonpolar solvent we have carried out a calculation for the CCl_4 solutions of the same species according to the quite identical procedures described above. The results are given in Table 4.

The features on the whole, which are seen in Tables 3 and 4, are summarized in Table 5 and the temperature dependence of the thermodynamic functions for the creation of cavities is shown in Table 6.

In CCl_4 solutions the negligibly small values of $\bar{S}_c$ suggest that no appreciable perturbation on the liquid structure occurs by the creation of cavities. The enthalpic terms are supposed to be dominant in the solute-solvent interactions in CCl_4 solutions of nonpolar gases. On the contrary the dominant features in aqueous solutions are large minus values of $\bar{S}_c$ and small positive values of $\bar{H}_c$. The greater part of large minus values of $(\bar{S}_2(x_2)-S_2{}^g)_{obsd}$ is attributed to $\bar{S}_c$, and further the small values of $\bar{H}_c$ in sharp contrast to those in CCl_4 solutions are the cause of large minus values of ΔH_s observed. As clearly seen in Table 3, the small values of $\bar{H}_c$ in aqueous solutions comes from

Table 3. The enthalpy (cal mol^{-1}) and entropy (cal K^{-1} mol^{-1}) of transfer of nonpolar solutes from an ideal gas phase at 1 atm to water (25 °C)

	a (Å)	ΔH_s	$\bar{S}_2(x_2)-S_2{}^g$	10^5x_2	$\bar{G}_c$	$\bar{H}_c$	δH	$\bar{S}_c$	δS	$\Delta C_{p,c}$
CH_4	3.59	−3050[a]	−10.5[b]	2.48[b]	5390	900	−3400	−15.1	−2.1	38
C_2H_6	4.15	−3980[a]	−13.4[b]	3.10[b]	6840	1150	−4580	−19.1	−0.6	49
C_3H_8	4.63	−5700[a]	−19.1[a]	2.73[b]	8220	1400	−6550	−22.9	−2.8	60
n-C_4H_{10}	5.00	−6000[a]	−20.3[b]	2.17[b]	9380	1610	−7060	−26.1	−1.2	69
C_2H_4	3.94	−3790[c]	−12.7[d]	8.74[b]	6270	1050	−4290	−17.5	0.6	45
C_2H_2	3.79	−3360[c]	−11.2[d]	75.3[e]	5890	980	−3790	−16.4	5.2	42
Ne	2.42	−1090[f]	−3.6[f]	0.82[f]	2930	460	−1000	−8.3	−4.2	20
Ar	3.24	−2730[g]	−9.1[b]	2.54[b]	4570	750	−2930	−12.8	−3.0	32
Kr	3.50	−3470[f]	−11.6[f]	4.28[f]	5170	860	−3780	−14.5	−2.7	37
Xe	3.85	−4360[f]	−14.6[f]	7.83[f]	6040	1010	−4820	−16.9	−2.1	43
N_2	3.42	−2590[h]	−8.7[h]	1.18[h]	4980	820	−2860	−14.0	−2.9	35
O_2	3.23	−2830[h]	−9.5[h]	2.30[h]	4550	750	−3030	−14.8	−3.6	32

a) W. F. Claussen and M. F. Polglase, *J. Am. Chem. Soc.*, **74**, 4817 (1952). b) K. W. Miller and J. H. Hildebrand, *J. Am. Chem. Soc.*, **90**, 3001 (1969), Table 1. c) See Table IV in Ref. 1. Frank and Evans obtained these values from the data of J. A. V. Butler, *Trans. Faraday Soc.*, **33**, 229 (1937), Table VI. d) See footnote c. The standard state of Frank and Evans is $x_2=1$ for the solution, and we have subtsrcted the term of $R\ln x_2$ from their values. e) Calculated from the values given in Table 2 of W. Hayduk and H. Laudie, *AIChE J.*, **19**, 1233 (1973). f) T. J. Morrison and N. B. Johnstone, *J. Chem. Soc.*, **1954**, 3441. g) See Table IV in Ref. 1. Frank and Evans obtained these values from the data of D. D. Eley, *Trans. Faraday Soc.*, **35**, 1281 (1939). h) E. Douglas, *J. Phys. Chem.*, **68**, 169 (1964); T. J. Morrison and F. Billett, *J. Chem. Soc.*, **1952**, 3819.

Table 4. The enthalpy (cal mol^{-1}) and entropy (cal K^{-1} mol^{-1}) of transfer of nonpolar solutes from an ideal gas phase at 1 atm to CCl_4 (25 °C)

	a (Å)	ΔH_s[a]	$\bar{S}_2(x_2)-S_2{}^g$[b]	10^3x_2[b]	$\bar{G}_c$	$\bar{H}_c$	δH	$\bar{S}_c$	δS	$\Delta C_{p,c}$
CH_4	3.59	−700	−2.4	2.84	3780	3710	−4030	−0.2	−2.9	13
C_2H_6	4.15	−2620[b]	−8.8	20.8	4680	4710	−6050	0.1	−5.6	15
C_2H_4	3·94	−2340	−7.7	14.5	4330	4320	−6280	0.0	−5.1	14
C_2H_2	3.79	−2330	−7.8	11.5	4090	4050	−6000	−0.1	−5.1	14
Ar	3.24	−140[c]	−0.5[c]	1.35[c]	3260	3150	−2910	−0.4	−2.2	11
N_2	3.42	+590	2.1	0.64	3520	3430	−2460	−0.3	−1.2	12
O_2	3.23	+10	0.0	1.20	3250	3130	−2740	−0.4	−2.0	11
CO	3.47	+340	1.0	0.86	3600	3510	−2790	−0.3	−1.8	12

a) See Ref. 1. Frank and Evans obtained these values from the data of J. Horiuti, *Sientific Papers Inst. Phys. Chem. Res.*, Tokyo, **17**, 125 (1931). b) J. E. Jolley and J. H. Hildebrand, *J. Am. Chem. Soc.*, **80**, 1050 (1958), Table II. These authors obtained their values from the data of J. Horiuti (footnote a). c) L. W. Reeves and J. H. Hildebrand, *J. Am. Chem. Soc.*, **79**, 1313 (1957).

Table 5. $\overline{S}_c$, $\overline{H}_c$, and $\Delta C_{p,c}$ for water and CCl_4

Solvent	$\overline{S}_c$	$\overline{H}_c$	$\Delta C_{p,c}$	
CCl_4	0	large plus	small	$\lvert\Delta H_s\rvert < \overline{H}_c$
Water	large minus	small plus	large	$\overline{H}_c \ll \lvert\Delta H_s\rvert \sim \lvert\delta H\rvert$

Table 6. Temperature dependence of thermodynamic functions for the creation of cavities

Solvent	T (°C)	CH_4				Ar			
		$\overline{G}_c$ (cal mol^{-1})	$\overline{H}_c$ (cal mol^{-1})	$\overline{S}_c$ (cal K^{-1} mol^{-1})	$\Delta C_{p,c}$ (cal K^{-1} mol^{-1})	$\overline{G}_c$ (cal mol^{-1})	$\overline{H}_c$ (cal mol^{-1})	$\overline{S}_c$ (cal K^{-1} mol^{-1})	$\Delta C_{p,c}$ (cal K^{-1} mol^{-1})
H_2O	0	4970	−200	−18.9	50	4210	−170	−16.0	42
	25	5390	900	−15.1	38	4570	750	−12.8	32
	50	5730	1820	−12.1	36	4860	1530	−10.3	30
	70	5950	2540	−9.9	36	5050	2130	−8.5	30
CCl_4	25	3780	3710	−0.2	13	3260	3150	−0.4	11
	35	3770	3830	0.2	13	3260	3250	0.0	11

the small values of α for water, which is the direct evidence of the presence of some "bulky structure" decreasing with temperature. This is supposed to be closely related to the behavior of $(\partial U/\partial V)_T$ for water in comparison with that for carbon tetrachloride, which is calculated using the following thermodynamical formula

$$\left(\frac{\partial U}{\partial V}\right)_T = \frac{\alpha T}{\beta} - p, \tag{9}$$

where U is the internal energy. The magnitude of $(\partial U/\partial V)_T$ for water at 25 °C is 1500 atm which is smaller than a half of that for CCl_4.

The magnitudes of $\Delta C_{p,c}$ for water are about three times larger than those for CCl_4, and contribute to the greater part of the enormous partial molal heat capacity for aqueous solutions of nonpolar solutes. Then, it may be said that the cause of icebergs formation proposed first by Frank and Evans is attributed to the effect of the large minus $\bar{S}_c$ and the small positive $\overline{H}_c$ for the creation of cavities in water.

The Nature of Hydrophobic Interactions. The hydrophobic interaction is stated as the "tendency of nonpolar groups of proteins to adhere to one another in aqueous environments" according to Kauzmann,[2] and for the case of two methane molecules in water Ben-Naim made an assertion that the quantity $\delta A_M^{HI} = \Delta\mu_E^\circ - 2\Delta\mu_M^\circ$ serves as a useful measure for the hydrophobic interaction in aqueous media where $\Delta\mu_E^\circ$ and $\Delta\mu_M^\circ$ are the standard free energy of solution of ethane and methane, respectively.[11] Recently, Dashevsky and Sarkisov have carried out a Monte-Carlo calculation in order to examine the nature of the hydrophobic interactions of nonpolar molecules in water.[12]

A Measure for Hydrophobic Interactions: Ben-Naim stated that the magnitude of δA_M^{HI} became about −2.15 kcal mol^{-1} at 25 °C when observed values were used for $\Delta\mu_E^\circ$ and $\Delta\mu_M^\circ$. It is certainly stabilized to the amount of about 0.6 kcal mol^{-1} in comparison with that in alcoholic solutions, and then, he asserted that the quantity δA_M^{HI} might serve as a useful index for measuring hydrophobic interactions in water.[11] Further, the recent remarkable results of Monte-Carlo calculations by Dashevsky and Sarkisov have shown that the free energy of hydrophobic attractions between two methane molecules in 62 water molecules becomes about −2 kcal mol^{-1},[12] and this supports the idea of Ben-Naim that $\delta A_M^{HI} = \Delta\mu_E^\circ - 2\Delta\mu_M^\circ$ is useful as a relative measure for hydrophobic interactions between two methane molecules in aqueous environments. However, it is not exact to assert directly, as Ben-Naim stated, that "the excess attraction, in water, helps the two particles to approach each other in spite of the thermal energy,"[11] since in aqueous solutions of methane under ordinary conditions the dimerization of two methane molecules does not occur. The reason for that will be explained in the next section.

As a result of the present calculation, the free energy for hydrophobic interactions between two methane molecules in aqueous environments, ΔG^{HI}, is expressed as a sum of three terms, except the effect of the mixing entropy term which will be introduced later.

$$\Delta G^{HI} = \Delta\overline{G}_c^{HI} + \Delta(\delta H)^{HI} + \overline{U}_{CH_4-CH_4}, \tag{10}$$

where $\Delta\overline{G}_c^{HI}$ is the contribution from the cavity effect, $\Delta(\delta H)^{HI}$ that from solute-water interactions, and $U_{CH_4-CH_4}$ the direct solute-solute interactions. $\Delta\overline{G}_c^{HI} = \Delta\overline{H}_c^{HI} - T\Delta\bar{S}_c^{HI}$, where $\Delta\bar{S}_c^{HI}$ and $\Delta\overline{H}_c^{HI}$ are expressed as $\Delta\bar{S}_c^{HI} = \bar{S}_{c,C_2H_6} - 2\bar{S}_{c,CH_4}$ and $\Delta\overline{H}_c^{HI} = \overline{H}_{c,C_2H_6} - 2\overline{H}_{c,CH_4}$, respectively. The valuse of $\Delta\bar{S}_c^{HI}$ and $\Delta\overline{H}_c^{HI}$ are 11.1 cal K^{-1} mol^{-1} and −650 cal mol^{-1}, respectively. Then, $\Delta\overline{G}_c^{HI}$ becomes −3960 cal mol^{-1}. The magnitude of $\Delta(\delta H)^{HI} = \delta H_{C_2H_6} - 2\delta H_{CH_4}$ becomes 2220 cal mol^{-1} using the values given in Table 3. The values of $\overline{U}_{CH_4-CH_4}$ is about 300 cal mol^{-1} according to the calculation by Dashevsky and Sarkisov.[12] Thus, the magnitude of ΔG^{HI} at 25 °C becomes about −2 kcal mol^{-1}. This agrees to the estimation by Dashevsky and Sarkisov using the Monte-Carlo method as well as to that by Ben-Naim. It is noticeable that the largest minus contribution to ΔG^{HI} comes from $\Delta\overline{G}_c^{HI}$ and, further, essencially from $\Delta\bar{S}_c^{HI}$.

The Effect of the Change of Mixing Entropy by Hydrophobic Association: According to the result of the Monte-

Carlo calculation by Dashevsky and Sarkisov two methane molecules in 62 water molecules have a trend to associate and the free energy of the methane-methane pair in water becomes about -2 kcal mol^{-1}. Then, the association occurs actually in their simulation. However, in the aqueous solutions of methane being in equilibrium with methane gas at 1 atm no association of solute molecules occurs. The different behavior of methane molecules in these two cases is ascribed to the difference in the concentration of solute particles: in the former case the mole fraction of methane x is about 3×10^{-2} and in the latter x is of the order of 10^{-5}. In order to estimate the effect of concentration thermodynamically we must consider the mixing entropy.

The entropy of mixing for an ideal solution is expressed as

$$\Delta S_{\mathrm{mix}}(x) = -R\{x\ln x+(1-x)\ln(1-x)\}. \quad (11)$$

When all solute molecules are present as dimers, $\Delta S_{\mathrm{mix}}(x)$ varies to $\Delta S_{\mathrm{mix}}(x/2)$, and then the difference $\delta(\Delta S_{\mathrm{mix}})$ becomes

$$\begin{aligned}\delta(\Delta S_{\mathrm{mix}}) &= \Delta S_{\mathrm{mix}}(x/2) - \Delta S_{\mathrm{mix}}(x)\\ &= R\{(x/2)\ln(2x)+(1-x)\ln(1-x)\\ &\quad -(1-x/2)\ln(1-x/2)\}. \quad (12)\end{aligned}$$

In the case of $x\ll1$, $\delta(\Delta S_{\mathrm{mix}})$ becomes, to the order of x^2,

$$\delta(\Delta S_{\mathrm{mix}}) = R\left\{\frac{x}{2}(\ln(2x)-1)+\frac{3}{8}x^2\right\}. \quad (14)$$

For nonpolar molecules such as those tabulated in Table 3 the magnitudes of x are very small and of the order of 10^{-5}, and the change of the mixing entropy per mole of solute molecules by dimerization is safely expressed as $\delta(\Delta S_{\mathrm{mix}})/x=1.15\log x-0.15$ according to Eq.14. For methane x is 2.48×10^{-5} and the value becomes -10.9 cal K^{-1} mol^{-1}. That is, if a dimerization $2(CH_4)\rightarrow(CH_4)_2$ would occur in aqueous solutions of methane at equilibrium with methane gas (1 atm), the change of the mixing entropy per mole of solute species amounts to -10.9 cal K^{-1} mol^{-1}. This contributes to the free energy for the formation of methane-methane pairs in water to about $+3$ kcal mol^{-1} at 25 °C and its total amount becomes positive, and thus, the dimerization can not occur. In the case of Dashevsky and Sarkisov's simulation, x is about 3×10^{-2} and the magnitude becomes -3.8 cal K^{-1} mol^{-1}, and the contribution to free energy is about 1.1 kcal mol^{-1}. Thus, the total amount of free energy remains negative and the dimerization occurs.

As a result of the consideration described above, we can say conclusively as follows:

a) methane molecules (or methyl groups) certainly have a tendency to adhere to one another in aqueous environments, its magnitude being expressed by ΔG^{HI} (authors) or δA^{HI} (Ben-Naim),

b) the largest minus contribution to ΔG^{HI} comes from the cavity effect $\Delta\bar{S}_c^{\mathrm{HI}}$,

c) in the aqueous solutions of methane at ordinary conditions the association of solute molecules does not occur, because the decrease of the mixing entropy fully cancels out the entropy ascribed to the cavity effect,

d) in more concentrated solutions ($x\gtrsim0.01$), for example, in the aqueous solutions of proteins where the local concentration of hydrophobic groups becomes larger to the order of $x\simeq0.01$ or more, the decrease of the mixing entropy becomes smaller in magnitude than the entropy from the cavity effect, and then the tendency to adhere to one another appears actually. This may be also the case for the formation of micelles.

References

1) H. S. Frank and M. W. Evans, *J. Chem. Phys.*, **13**, 507 (1945).
2) W. Kauzmann, *Adv. Protein Chem.*, **14**, 1 (1959).
3) G. Némethy and H. A. Scheraga, *J. Phys. Chem.*, **66**, 1773 (1962).
4) K. Shinoda, *Kagaku To Kogyo*, **21**, 1400 (1968); *J. Phys. Chem.*, **81**, 1300 (1977).
5) K. Arakawa, *Kagaku Sosetsu*, **11**, 13 (1976).
6) O. Ya. Samoilov, "Water and Aqueous Solution," ed by R. A. Horne, Wiley, New York (1972), Chap. 14; G. A. Krestov, *Zh. Strukt. Khim.*, **3**, 137 (1962).
7) H. S. Frank and W-Y. Wen, *Discuss. Faraday Soc.*, **44**, 133 (1957).
8) H. Reiss, *Adv. Chem. Phys.*, **9**, 1 (1965).
9) R. A. Pierotti, *Chem. Rev.*, **76**, 717 (1976).
10) F. Hirata and K. Arakawa, *Bull. Chem. Soc. Jpn.*, **48**, 2139 (1975).
11) A. Ben-Naim, *J. Chem. Phys.*, **54**, 1387 (1971); "Water and Aqueous Solutions," Plenum Press, New York (1974).
12) G. Dashevsky and N. Sarkisov, *Mol. Phys.*, **27**, 1271 (1974).
13) R. A. Pierotti, *J. Phys. Chem.*, **67**, 1840 (1963); **69**, 281 (1965).
14) The "radius of cavity" r in the conditional distribution function $G(r)$ defined in the beginning of this section corresponds to this a_{12}.
15) K. Arakawa, K. Tokiwano, and K. Kojima, *Bull. Chem. Soc. Jpn.*, **50**, 65 (1977).
16) J. F. Hinton and E. S. Amis, *Chem. Rev.*, **71**, 627 (1971).
17) E. R. Nightingale, Jr., "Chemical Physics of Ionic Solutions," ed by B. E. Conway and R. G. Baradas, Wiley, New York (1966), p. 87.
18) P. R. Bienkowski and K. C. Chao, *J. Chem. Phys.*, **62**, 615 (1975); A. P. Kudchadker, G. H. Alani, and B. J. Zwolinski, *Chem. Rev.*, **68**, 659 (1968); J. F. Mathews, *ibid.*, **72**, 71 (1972).

Calculations of the Rate Constants for the HX+NO ⇌ HNO+X Reactions (X=H, F, Cl, Br, and I)

Tetsuo HIGASHIHARA

Department of Chemistry, Faculty of Science, Hiroshima University, Higashisenda-machi, Hiroshima 730

(Received February 9, 1979)

The rate constants for these hydrogen-transfer reactions:

$$HX+NO \rightleftharpoons HNO+X \quad (X=H, F, Cl, Br, \text{and } I)$$

have been calculated by means of the transition-state theory combined with the BEBO method over the temperature range of 250—4000 K. The calculated rate constants were then compared with the experimental kinetic data.

There have been many attempts to estimate the rate constants theoretically for bimolecular reactions; these attempts have been, for example, collision theories, the transition-state theory combined with the BEBO or LEPS method, trajectory calculation, and so on. Although the bond energy-bond order (BEBO) method is an empirical one, this method has many advantages: calculations are easy, there are no parameters which need to be adjusted for each reaction, and the predicted activation energies are generally in good agreement with the experimental kinetic data.

In this study, in order to clarify the effect of the difference in X on the rate constants for these reactions:

$$HX + NO \rightleftharpoons HNO + X \quad (X=H, F, Cl, Br, \text{and } I),$$

the rate constants for these reactions were calculated by using the transition-state theory combined with the BEBO method. The rate constants for these reactions:

$$H_2 + NO \longrightarrow HNO + H \quad (1)$$

$$HCl + NO \longrightarrow HNO + Cl \quad (3)$$

$$HBr + NO \longrightarrow HNO + Br \quad (4)$$

$$HI + NO \longrightarrow HNO + I \quad (5)$$

have been determined by Ando and Asaba[1] for Reaction 1 in shock waves, by Higashihara *et al.*[2,3] for Reactions 3 and 4 in shock waves, and by Holmes[4] for Reaction 5 in a static system. The rate constant of Reaction −1:

$$H + HNO \longrightarrow H_2 + NO \quad (-1)$$

has also been determined by several groups[5] by using various experimental methods over a wide temperature range. Although many kinetic data have thus been accumulated, there have been no theoretical studies for these reactions. Therefore, it is also interesting to try to explain these kinetic data consistently with a theory.

Calculations

The following linear three-atom model was used for the calculations of the BEBO potential energy curve:

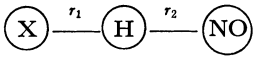

The detailed procedures of calculations were summarized by Johnston (Ref. 6b, p. 339). It should, however, be noted that the following two points were modified in this calculation. First, the new Pauling constant, 0.28, which was evaluated by Gillion,[7] was used instead of 0.26 in Eq. I:

$$r = r_s - 0.28 \ln m \text{ (or } n), \quad \text{(I)}$$

where the subscript s denotes the length of a single bond and where m (or n) is the bond order of H–N (or X–H). Second, the new f value, 0.45,[7] in the Sato anti-Morse function (Eq. II) was used instead of 0.25:

$$V_{tr} = f\{D_e(1+e^{-\beta(r-r_s)})^2 - 1\}, \quad \text{(II)}$$

where β is the Morse parameter. All the molecular parameters necessary for the calculations are sum-

Table 1. Molecular parameters

	D_0 / kcal mol^{-1}	ν / cm^{-1}	D_e / kcal mol^{-1}	r_s / Å	g	I / 10^{40} g cm	F / 10^8 N Å^{-1}	p	β / Å^{-1}
H-H	103.27	4405.3	109.4	0.74	1	0.46	5.74	1.069	—
H-F	134.6	4138	140.5	0.92	1	1.335	9.59	1.034	—
H-Cl	102.1	2989	106.4	1.27	1	2.64	5.16	0.948	—
H-Br	86.7	2649	90.5	1.42	1	3.316	4.12	0.897	—
H-I	70.6	2309	73.9	1.61	1	4.284	3.12	0.800	—
N-O	—	1903.6	—	—	2, 2	16.55	—	—	—
H-NO	48.6	3596	53.74	1.063	1	643.3[a]	7.1	0.984	1.794
F-NO	54.94	766	56.03	1.52	—	—	2.79	—	1.891
Cl-NO	37.15	605	38.01	1.95	—	—	1.92	—	2.024
Br-NO	27.8	542	28.57	2.14	—	—	2.06	—	2.278
I-NO	19.53	440	20.16	2.3	—	—	1.44	—	2.265

a) 10^{120} (g cm)^3.

marized in Table 1. The bond-order index (p or q) was calculated from this equation:

$$p(\text{or } q)=0.28 \ln (D_e/D_x)/(r_x-r_s), \quad \text{(III)}$$

where D_x and r_x are the bond strength and the length of the corresponding noble gas molecule respectively. The BEBO properties of the activated complexes calculated by using this model are summarized in Table 2. In the case of the HI–NO reaction, the maximum value of the potential energy did not exist. In this case, the distance of H–I in the activated complex was assumed to be the same as the He–Kr Lennard-Johnes internuclear distance, and from this distance the bond orders, m and n, were calculated.

The vibrational frequencies of the activated complexes were calculated according to the method of the ***GF*** matrix by using the following model:

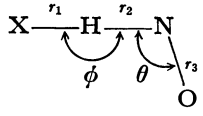

As is shown in Table 2, the bond order of H–N (m) in the activated complex is nearly unity in all cases. This means that the bond angle of H–N–O and the bond length of N–O in the complex may be nearly the same as those of the HNO molecule. Then, $\theta=108.5°$ and $r_3=1.211$ Å, values which are the same as those of the HNO molecule, were assumed. The **G** matrix was constructed according to this model from Table, 7-4 of Ref. 8 (p. 135). The force constants used for each activated complex are listed in Table 3. The values of F_{33} and F_θ in this table are the same as those used by Brown and Pimentel[9] in the calculations of the vibrational frequencies of the HNO molecule.[10] The values of F_{11}, F_{22}, F_{12}, and F_ϕ were calculated by means of the three-atom BEBO method according to the procedures of Ref. 6b. The rest of the interaction force constants were assumed to be 0. The calculated vibrational frequencies are listed in Table 3 for each activated complex. In this table, the moments of inertia, I, of the activated complex and the activation energies, E_0 of the forward and backward reactions are also listed for each activated complex. Though the bending-force constant of H–N–O in the activated complex was assumed to be the same as that of the HNO molecule, this force constant might be appreciably affected by X. Therefore, the vibrational analysis was also carried out using a value one-half the normal F_θ value. The results of the calculations shown in the parentheses of Table 3 indicate that the change in the value of F_θ does not affect the vibrational frequencies very much.

Table 2. Properties of activated complexes calculated from the three-atom BEBO model

	n	m	r_1 / Å	r_2 / Å	V^{*} a) / kcal mol^{-1}
H-H-NO	0.028	0.972	1.741	1.071	56.89
F-H-NO	0.019	0.981	2.030	1.068	88.1
Cl-H-NO	0.008	0.992	2.622	1.065	53.01
Br-H-NO	0.002	0.998	3.160	1.064	36.77
I-H-NO	0.0004	0.9996	3.8	1.063	20.16

a) V^* is the maximum value of the potential energy.

The rate constants were calculated according to this familiar expression from the transition-state theory:

$$k=(kT/h)(Q^*/Q_{\text{react.}}) \exp(-E_0/RT), \quad \text{(IV)}$$

where Q^* and $Q_{\text{react.}}$ are the partition functions of the activated complex and the reactants respectively and where E_0 is the theoretical activation energy.

Furthermore, the rate constants of Reactions 1, 2, 3, 4, and 5 were calculated by using the simple collision theory to check the reliability of the observed kinetic data. The molecular diameters of the reactants

Table 3. Properties of activated complexes

	H-H-N-O	F-H-N-O	Cl-H-N-O	Br-H-N-O	I-H-N-O
F_{11} a)	−0.0194	−0.0738	−0.0202	−0.0021	0.0010
F_{22} a)	6.9516	7.0304	7.0726	7.0726	7.100
F_{12} a)	0.0201	0.1377	0.0572	0.0142	0.0028
F_ϕ a)	0.0853	0.1068	0.0339	0.0083	0.0017
F_{33} a)	10.54	10.54	10.54	10.54	10.54
F_θ a)	0.52 (0.26)	0.52	0.52 (0.26)	0.52	0.52
ν_1(N-H)$_s$ b)	3523.8 (3523.6)	3506.0	3566.5 (3566.4)	3595.3	3604.2
ν_2(N-O)$_s$ b)	1598.3 (1588.4)	1530.4	1532.7 (1520.9)	1533.6	1536.0
ν_3(H-N-O)$_b$ b)	1098.3 (883.1)	942.3	988.8 (737.1)	949.9	945.5
ν_4(X-H-N)$_b$ b)	245.6 (216.8)	607.4	89.6 (84.9)	58.2	21.2
ν_5 b)	167.0i (196.9i)	103.1i	27.5i (27.8i)	18.9i	2.4
ν_6(X-H-N)$_b$ b)	620.6 (620.6)	619.2	322.5 (322.5)	152.0	66.0
I_A c)	8.528	13.859	14.50	18.91	15.18
I_B c)	27.688	222.49	423.91	729.57	985.52
I_C c)	36.22	236.36	438.413	748.58	1000.7
E_{of} d)	58.0	89.8	55.5	39.25	22.96
E_{ob} d)	2.4	2.68	0.88	0.04	0.0

a) 10^8 N Å^{-1}. b) cm^{-1}. c) 10^{40} g cm. d) kcal mol^{-1}.

Table 4. Rate constants calculated from the simple collision theory

	M.D.[a] / Å	Rate expression[b] / $cm^3\ mol^{-1}\ s^{-1}$	Steric factor
1) H_2+NO	2.93	$k=2.1\times10^{13}\ T^{1/2}\exp(-54.6\ kcal/RT)$	2.6×10^{-2}
2) HF+NO	3.0	$k=8.4\times10^{12}\ T^{1/2}\exp(-86.0\ kcal/RT)$	(7.1×10^{-3})
3) HCl+NO	3.36	$k=8.0\times10^{12}\ T^{1/2}\exp(-53.5\ kcal/RT)$	6.4×10^{-2}
4) HBr+NO	3.41	$k=7.0\times10^{12}\ T^{1/2}\exp(-38.1\ kcal/RT)$	9.1×10^{-2}
5) HI+NO	4.12	$k=8.1\times10^{12}\ T^{1/2}\exp(-22.0\ kcal/RT)$	1.6×10^{-3}

a) Molecular diameter of HX. The molecular diameter of NO was assumed to be 3.5 Å. b) The activation energy was assumed to be the same as the standard enthalpy change of the reaction.

and the calculated rate constants are listed in Table 4. The last column of this table shows the steric factor which was obtained from a comparison of the calculated rate constant with the experimental one at the middle temperature of each experiment. The steric factor of Reaction 2 was determined by comparison with the calculated value by using the transition-state theory combined with the BEBO method, since there are no rate data for this reaction. In general, the steric factors for abstraction reactions lie in the 0.01—0.1 range. As is shown in Table 4, the steric factors for these reactions (except for that for Reaction 5) lie in this range; this fact indicates that the observed rate constants are reasonable.

Discussion

As is shown in Table 2, in all the activated complexes the bond order of H–N (m) is very large compared with that of X–H (n). This trend is always observed in the cases of large endothermic or exthothermic reactions, it can be ascribed to the large contribution of the bonding term compared with that of the repulsive one. The bond order, n, gradually decreased as X changed from F to I because of the decrease in the triplet repulsion energy.

Figure 1 compares the calculated rate constants with the experimental ones for Reaction 3. The rate constants were calculated by using two different values of F_θ, since one can not precisely estimate the effect of the X–H bond in the activated complex on the value of F_θ. The solid and dash-dot lines in Fig. 1 show the rate constants calculated by using values of $F_\theta=0.52\times10^{-8}$ and $F_\theta=0.26\times10^{-8}$ N/Å respectively. Thus, the calculated rate constants were not sensitive to the values of F_θ. The circles in this figure are the rate constants determined by Higashihara *et al.*[2] and are compatible with the theoretical values.

Figure 2 compares the experimental rate constants (broken lines) with the theoretical ones (solid lines) for Reactions 1, 4, and 5. The experimental con-

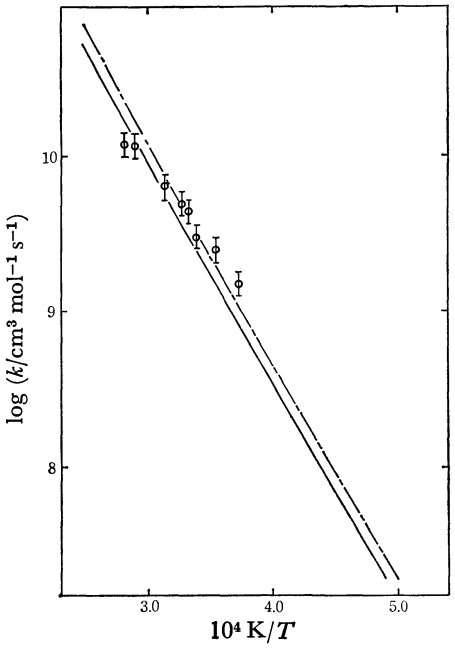

Fig. 1. Comparisons of the calculated and experimental rate constants for the reaction HCl+NO→HNO+Cl. Solid and dash-dot lines represent the calculated rate constants by using $F_\theta=0.52\times10^{-8}$ and $F_\theta=0.26\times10^{-8}$ N/Å, respectively. Circles are the experimental rate constants determined by Higashihara *et al.*[2] The error bars represent ±25% maximum uncertainty.

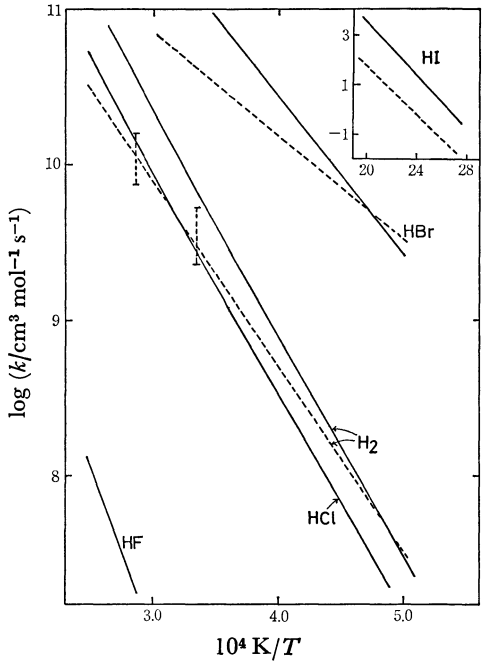

Fig. 2. Comparisons of the calculated rate constants (solid lines) with the experimental ones (broken lines) for the reactions HX+NO→HNO+X. Experimental rate constants are summarized in Table 5.

TABLE 5. KINETIC DATA OBTAINED EXPERIMENTALLY FOR THE HX+NO⇌HNO+X REACTIONS

		Rate constant / $cm^3\ mol^{-1}\ s^{-1}$	Temperature range/K	Method	Reference
1)	H_2+NO	$k=10^{13.5}\exp(-55.2\ kcal/RT)$	2000—3500	Shock Tube	1) Ando and Asaba
3)	HCl+NO	$k=10^{13.2}\exp(-50.2\ kcal/RT)$	2650—3850	Shock Tube	2) Higashihara *et al.*
4)	HBr+NO	$k=10^{12.8}\exp(-30\ kcal/RT)$	2000—3300	Shock Tube	3) Higashihara *et al.*
5)	HI+NO	$k=10^{11.43}\exp(-22\ kcal/RT)$	368— 523	Static Sys.[a]	4) Holmes
−1)	H+HNO	$k\geqq 3\times10^{10}$	226— 294	Disch. Flow[b]	5a) Clyne and Thrush
		$k=(6\pm3)\times10^{12}$	1600—2000	Flame	5b) Bulewicz and Sugden
		$k\leqq(2.7\pm0.6)\times10^{10}$	296	Disch. Flow[b]	5c) Lambert
		$k=6\times10^{10}-6\times10^{11}$	300	Static Sys.[a]	5d) Kohout and Lampe
		$k=(4.8\pm1.2)\times10^{12}$	2000	Flame	5e) Halstead *et al.*
		$k=(2.3\pm1.1)\times10^{12}$	2177	Flame	5f) Smith
		$k\geqq 9.63\times10^{11}$	298	Disch. Flow[b]	5g) Washida *et al.*
		$k=3.0\times10^{11}\ T^{1/2}\exp(-2.4\ kcal/RT)$	—	Estimated	5h) Nicolet
		$k=1.4\times10^{11}\ T^{1/2}$	—	Estimated	5i) Lordi *et al.*
		$k=7\times10^{13}\exp(-3.0\ kcal/RT)$	—	Estimated	5j) Wilde *et al.*

a) Static system. b) Discharge flow system.

ditions and techniques for the data cited in this figure are summarized in Table 5. Unfortunately, there are no rate data for Reaction 2: HF+NO→HNO+F. For Reactions 1 and 4, the agreement between the experiment and theory seems to be reasonable in the temperature ranges within which experiments were carried out. The calculated rate constant for Reaction 5 is greater by about two orders in magnitude than that observed. This is the only example of a large difference between the experimental and theoretical rate constants.

As is listed in Table 5, there are many data for Reaction −1 obtained over the wide temperature range from room temperature to 2177 K by using various experimental techniques. Therefore, this reaction is very suitable for use in testing the application of the BEBO method to the group of reactions considered here. Baulch *et al.*[12] recommended in their data book a value of $k=4.8\times10^{12}\ cm^3\ mol^{-1}\ s^{-1}$ at 2000 K based on the data of Halstead and Jenkin.[5e] At room temperature they suggested that a value of $k\geqq3\times10^{10}\ cm^3\ mol^{-1}\ s^{-1}$ determined by Clyne and Thrush[5a] was likely. Recently, Ando and Asaba[1] determined the rate constant for the $H_2+NO\rightarrow HNO+H$ reaction at 3000 and 3500 K by using a shock-tube method. By combining their value of the rate constant with the equilibrium constant, the rate constant of Reaction −1 can be calculated. The value thus obtained is about one order larger than that recommended by Baulch *et al.* More recently, Washida *et al.*[5g] determined the lower limit for this reaction at room temperature as $k\geqq9.63\times10^{11}\ cm^3\ mol^{-1}\ s^{-1}$ by a method combining a photoionization mass spectrometer with a dischargeflow system. This value is also larger (by more than one order) than that of Clyne and Thrush. Thus, recent studies suggest that this reaction is very fast. Figure 3 shows a comparison of the experimental rate constants (broken lines and circles) with the theoretical ones (solid and dash-dot lines). It may be found from Fig. 3 that the theoretical rate constants are consistent with the recent rate data.

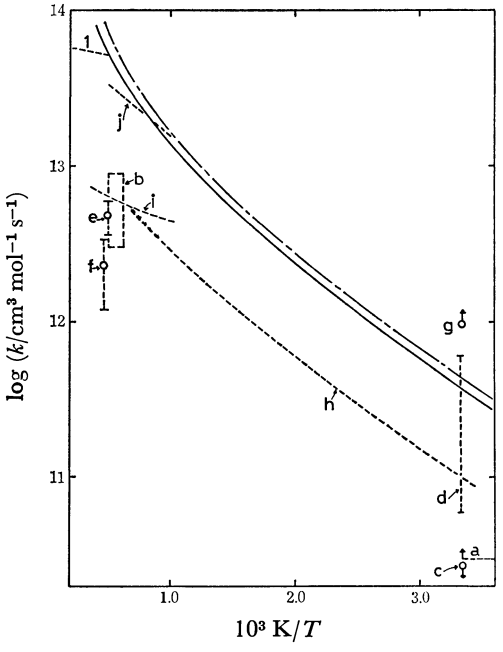

Fig. 3. Comparisons of the calculated rate constants (solid ($F_\theta=0.25\times10^{-8}$ N/Å) and dash-dot ($F_\theta=0.26\times10^{-8}$ N/Å) lines) with the experimental ones for the reaction $H+HNO\rightarrow H_2+NO$. The letters a—j and the number 1 represent the referencies indicated in Table 5.

There is a possibility of tunneling in the cases of hydrogen-transfer reactions at temperatures lower than 1000 K. Therefore, tunneling correction was considered for this reaction. If $u^*\leqq\pi$, where $u^*=h\nu_i/KT$, and $\pi V^*/h\nu_i>1$, where V^* is the maximum value of the potential energy, an approximate tunneling correction[6b] (this is generally known as a high-temperature approximation) is sufficient and the correction factor is given by

$$\Gamma^*_{\text{tt}}=0.5u^*/\sin(0.5u^*).$$

The value of Γ^*_{tt} for this reaction was calculated

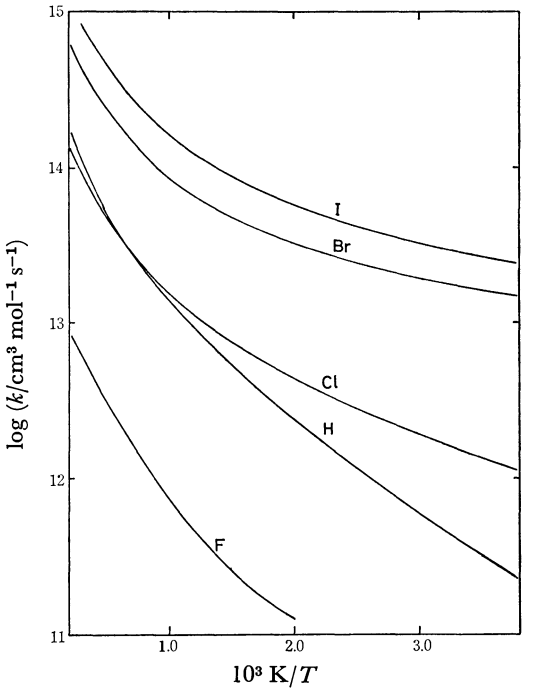

Fig. 4. Calculated rate constants for the reactions X+HNO→HX+NO.

to be 1.04 at 250 K. Thus, this effect was negligibly small and was not taken into account thereafter. Figure 4 shows the calculated rate constants for Reactions −1, −2, −3, −4, and −5. There are no rate data for any of these reactions except Reaction −1.

As is shown in Figs. 2 and 4, the rate constants for both the forward (Reactions 1, 2, 3, 4, and 5) and backward (Reactions −1, −2, −3, −4, and −5) reactions become larger as X changes from F to I. For the forward reactions, this trend may be attributed to two reasons. First, the activation energy becomes smaller as X changes from F to I. Second, as is shown in Table 3, the partition functions of the activated complexes, especially those of the rotation and X–H–N bending modes, become much larger as X changes from F to I, but those for the reactants do not change so much. On the other hand, for the backward reactions the activation energies do not differ very much. Therefore, the trend is mainly a result of the difference in the partition functions of the activated complexes, and is the reverse of that for the $X+H_2 \rightarrow HX+H$ reactions,[6a] in which the rate constant becomes smaller as X changes from F to I, mainly because of the difference in the activation energy.

Conclusion

1. The rate constants determined experimentally for the HX+NO⇄HNO+X reactions were in fair agreement with those predicted by the transition-state theory combined with the BEBO method. Thus, the rate constants for analogous reactions may reasonably be calculated by this method.

2. For the temperature dependence, some difference between the experiment and theory exist. Apparently, more experimental data over a wide temperature range are necessary for all the reactions.

The author wishes to thank Assistant Professor Ichiro Murakami and Dr. Ko Saito for their helpful discussions and guidance throughout this work. He also acknowledges the helpful discussions of Mr. Keijiro Taga and Miss Michiko Miura with respect to the vibrational analysis.

References

1) H. Ando and T. Asaba, *Int. J. Chem. Kinet.*, **8**, 259 (1976).
2) T. Higashihara, K. Saito, and I. Murakami, *Bull. Chem. Soc. Jpn.*, **51**, 3426 (1978).
3) T. Higashihara, K. Saito, and I. Murakami, *Bull. Chem. Soc. Jpn.*, **51**, 3430 (1978).
4) J. L. Holmes, *Proc. Chem. Soc.*, **1962**, 75.
5) a) M. A. A. Clyne and B. A. Thrush, *Discuss. Faraday Soc.*, **33**, 139 (1962); b) E. M. Bulewicz and T. M. Sugden, *Proc. R. Soc. London, Ser. A*, **277**, 143 (1964); c) R. M. Lambert, *Chem. Commun.*, **1966**, 850; d) F. C. Kohout and F. W. Lampe, *J. Chem. Phys.*, **46**, 4075 (1967); e) C. J. Halstead and D. R. Jenkins, *Chem. Phys. Lett.*, **2**, 281 (1968); f) N. Y. Smith, *Combust. Flame*, **18**, 293 (1972); g) N. Washida, H. Akimoto, and M. Okuda, *J. Phys. Chem.*, **82**, 2293 (1978); h) N. Nicolet, *J. Geophys. Res.*, **70**, 679 (1965); i) J. A. Lordi and R. E. Mates, National Aeronautics and Space Administration, NASA CR-393 (1966); j) K. A. Wilde, *Combust. Flame*, **13**, 173 (1969).
6) a) H. S. Johnston and C. Parr, *J. Am. Chem. Soc.*, **83**, 2544 (1963); b) H. S. Johnston, "Gas Phase Reaction Rate Theory," Ronald, New York (1966).
7) R. D. Gillion, *J. Chem. Phys.*, **65**, 5027 (1976).
8) S. Mizushima and T. Shimanouchi, "Infrared Absorption and Ramman Effect," Kyoritsu Shuppan, Tokyo (1958).
9) H. W. Brown and G. C. Pimentel, *J. Chem. Phys.*, **29**, 883 (1958).
10) Although Brown and Pimentel did not give the value of F_{N-H}, the vibrational frequencies of the HNO molecule could be calculated by using F_{33}, F_θ, and F_{N-H} (7.1×10^{-8} N/Å) as 3590 (N–H stretching), 1558 (N–O stretching), and 978 cm^{-1} (H–N–O bending). These calculated frequencies are in good agreement with the observed frequencies (3596, 1562, and 1110 cm^{-1}).[11]
11) G. Herzberg, "Molecular Spectra and Molecular Structure," D. Van Nostrand Co., Prinston, N. J. (1967), Vol. III.
12) D. L. Baulch, D. D. Drysdale, D. G. Horne, and A. C. Lloyd, "Evaluated Kinetic Data for High Temperature Reactions," Butterworths (1973), Vol. 2. In this book, all the rate data for Reaction −1 are summarized except for the data of Washida *et al.*

Electrical Properties and Constitution of Several Low-resistivity Iodine Complexes

Susumu Doi, Akiyoshi Fujita, Shigeo Ikeura, Tamotsu Inabe, and Yoshio Matsunaga*

Department of Chemistry, Faculty of Science, Hokkaido University, Sapporo 060

(Received February 13, 1979)

The electrical resistivity and Seebeck coefficient of the iodine complexes with eight aromatic compounds were examined as functions of the composition and the temperature. The formation of complexes is indicated by maxima or shoulders in the resistivity-composition isotherms at the following compositions: (anthanthrene)$_2$I$_9$, (6,12-dioxoanthanthrene)I$_2$, (6,12-dioxoanthanthrene)I$_3$, (pyranthrene)I$_3$, (violanthrene)$_2$I$_7$, (phthalocyanine)I$_2$, (phthalocyanine)I$_5$, (phenoxazine)$_2$I$_3$, (pyridazine)$_5$I$_9$, and (*N*,*N*′-diphenyl-*p*-phenylenediamine)$_5$I$_{13}$. Furthermore, some sharp resistivity minima are considered as evidence of the complex formation: *e.g.*, (6,12)-dioxoanthanthrene)$_2$I$_3$ and (phthalocyanine)$_2$I$_3$. On the basis of these compositions, a nonintegral formal oxidation state for the organic molecules and the presence of iodine as triiodide or higher polyiodide ions are established for most of the complexes.

In an earlier report from this laboratory, it was demonstrated that the careful examination of the electrical properties as functions of the composition is a powerful tool for elucidating the constitution of semiconducting thiazine–iodine complexes.[1] For example, the resistivity-composition isotherm of the phenothiazine–iodine system shows a shoulder as high as 800 Ω cm at a composition of two molecules of the thiazine to five atoms of iodine and also a minimum as low as 20 Ω cm at a composition of one molecule to three atoms. Moreover, a decrease in the activation energy for semiconduction by a factor of a half and a change in the sign of the Seebeck coefficient from negative to positive can be observed at the former composition. The similarity in vibrational spectrum between the iodine complex and the complex cation radical bromide of the 2 : 1 type, together with the above-mentioned electrical features, led us to propose the formation of a complex cation radical pentaiodide, $(C_{12}H_9NS)_2^+I_5^-$. The complex deposited from solutions is of a mole ratio of 2:3 and deviates as much as a half mole of iodine from this composition. There is no doubt that this amount of extra iodine plays an important role in the occurrence of the unusually low electrical resistivity. In the present paper, we wish to summarize the results of analogous studies on the iodine complexes with the following eight aromatic compounds: anthanthrene (dibenzo[*def*, *mno*]chrysene), 6,12-dioxoanthanthrene, pyranthrene, violanthrene, 29*H*,31*H*-phthalocyanine, phenoxazine, pyridazine, and *N*,*N*′-diphenyl-*p*-phenylenediamine (see the structural formulas given in Fig. 1). The composition ranges examined here were limited mostly by the thermodynamic instability of the iodine-rich complexes. Nevertheless, we believe that our study could cover the low-resistivity complexes in which we were interested.

Before presenting the results, we wish to review briefly the electrical behavior of mixtures. If two coexisting phases are strictly stoichiometric and mechanically mixed without interaction, the logarithmic mixing rule may apply for the resistivity. The composition of a distinct complex may correspond to a minimum in the resistivity-composition isotherm if its resistivity is lower than those of the neighboring

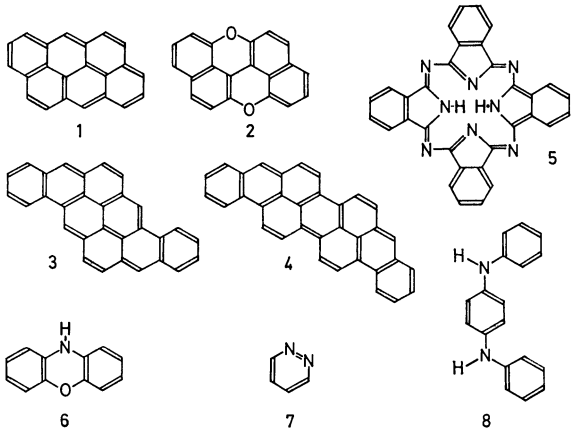

Fig. 1. Structural formulas of the organic component compounds; 1) anthanthrene, 2) 6,12-dixoanthanthrene, 3) pyranthrene, 4) violanthrene, 5) 29*H*,31*H*-phthalocyanine, 6) phenoxazine, 7) pyridazine, and 8) *N*,*N*′-diphenyl-*p*-phenylenediamine.

complexes, or a maximum if its resistivity is higher. On the other hand, the behavior may depend quite differently upon the composition, when the incorporation of a marked stoichiometric imbalance is conceivable for a given phase. As additional carriers are introduced by the imbalance, the stoichiometric composition of a low-resistivity complex may be indicated by a sharp maximum rather than a minimum in the isotherm. In such a case, the nearby minima may be considered to be indicative of the lower and upper limits of the deviation from stoichiometry. When the maximum is too low to be detected, the appearance of a rather broad minimum covering the stoichiometric composition may be expected. Therefore, the formation of complexes can be undoubtedly established by maxima appearing in the resistivity-composition isotherm but not necessarily by minima.

Experimental

Materials. The anthanthrene obtained commercially was reduced to the hydrocarbon by the zinc-dust fusion method.[2] Anthanthrene thus prepared was purified by repeated sublimation in a vacuum. 6,12-Dioxoanthanthrene was synthesized starting from 2,2′-binaphthol, as described

by Pummerer *et al.*[3] Pyranthrene was obtained by the reduction of commercial pyranthrone with zinc dust, pyridine, and acetic acid.[4] By vacuum sublimation through a thin layer of activated alumina the hydrocarbon became orange colored. The violanthrene, supplied some twenty years ago by Prof. Junji Aoki, now of Toho University, was purified by sublimation in a vacuum. Phthalocyanine, pyridazine, and *N,N'*-diphenyl-*p*-phenylenediamine employed in the present work were commercial products. The diamine was recrystallized from ethanol. Phenoxazine was prepared by the condensation of *o*-aminophenol in the presence of iodine.[5] All the iodine complexes, unless otherwise stated, were obtained by careful grinding of the weighed organic compound or complex of a known composition and iodine in an agate mortar in the presence of a small amount of benzene. The phthalocyanine complexes were made by boiling a benzene solution of iodine with powdered phthalocyanine. The iodine contents were determined by microanalysis.

Measurements. The electrical resistivities and Seebeck coefficients of polycrystalline compactions were recorded as functions of the temperature.[1]

Results and Discussion

Anthanthrene–Iodine. As early as 1939, Brass and Clar reported the isolation of the triiodide from a benzene solution;[6] however, no attention has been paid to the electrical properties. In Fig. 2, the electrical resistivity values at 20 °C are plotted against the number of iodine atoms per anthanthrene molecule, *n*. The shaded circles indicate that the samples were treated with a boiling benzene solution of iodine. They might therefore be more homogeneous than those indicated by open circles. There are a maximum of about 20 Ω cm at $n=4.5$ and minima of about 7 Ω cm near $n=4$ and 5 in the resistivity-composition isotherm. This behavior appears to be indicative of the nonstoichiometric nature of the complex. The formation of $(\text{anthanthrene})_2{}^+\text{I}_9{}^-$ may be deduced from the location of the maximum. The incorporation of an excess of either the hydrocarbon or iodine of as much as a half mole into this complex appreciably decreases the resistivity. It must be added that no anomalous features were noted at the composition reported by Brass and Clar, namely $n=3$. The temperature dependence of the resistivity, ρ, follows the typical semiconductor behavior: $\rho=\rho_0\exp(E/kT)$. The values of the activation energy for semiconduction, E, near room temperature are mostly in the range from 0.05 and 0.07 eV. No abrupt change could be detected even at the composition of the resistivity maximum.

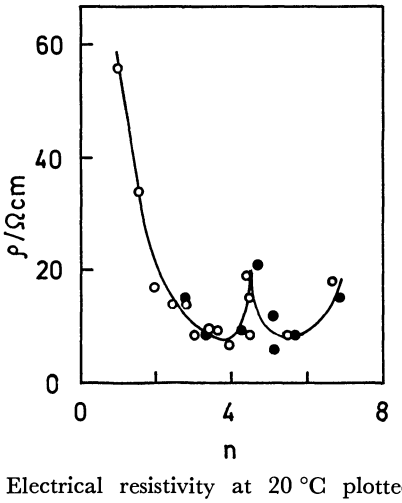

Fig. 2. Electrical resistivity at 20 °C plotted against the iodine content in the anthanthrene-iodine system. The shaded circles indicate that these samples were treated with a boiling benzene solution of iodine.

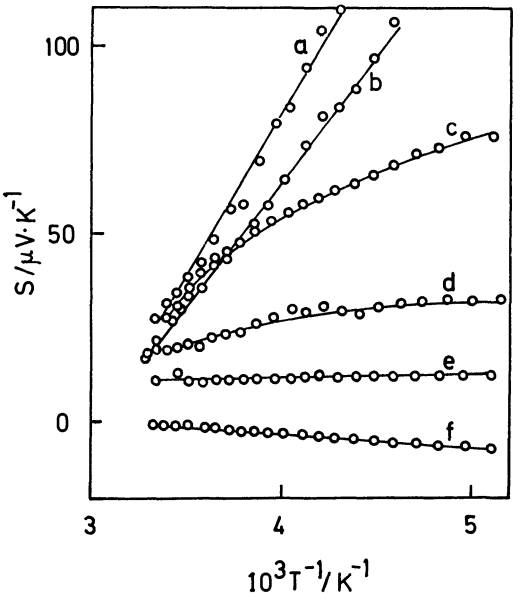

Fig. 3. Seebeck coefficient of the anthanthrene-iodine complexes; a) $n=1.51$, b) 3.70, c) 4.23, d) 4.41, e) 5.07, and f) 6.68.

The variation of the Seebeck coefficient, S, with the reciprocal temperature for six representative samples is illustrated in Fig. 3. Among them, samples b, c, and e are those indicated by shaded circles in Fig. 2. The variation depends markedly upon the composition. At $n=1.5$, a linear relationship with the reciprocal temperature is observed over the whole range (see Curve a). The positive slope may indicate that the contribution of holes to the conduction is larger than that of electrons. By the incorporation of additional iodine the slope in the low-temperature range becomes more gentle. As is shown by Curves c and d, such a tendency is especially large when the composition is close to the above-mentioned complex. The coefficient becomes essentially independent of the temperature near $n=5$ and then changes not only its sign but also the sign of the slope (see Curves e and f). These observations may imply that the ratio of the electron mobility to the hole mobility is nearly unity in the phase of $(\text{anthanthrene})_2\text{I}_9$. The Seebeck coefficient at −23 °C is plotted against n in Fig. 4. The values are rather scattered; nevertheless, it is evident that the coefficient decreases almost linearly with n and becomes zero near $n=6$. As is readily understood from Fig. 3, this slope and the composition where the coefficient changes its sign is not independent of the temperature.

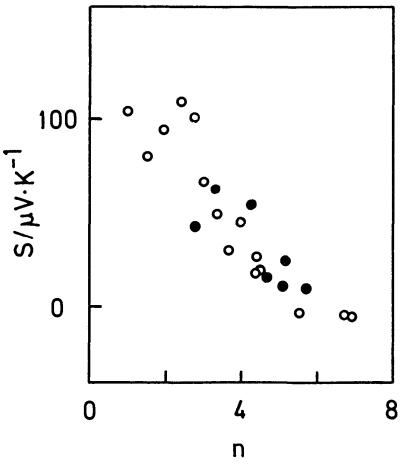

Fig. 4. Seebeck coefficient at −23 °C plotted against the iodine content in the anthanthrene–iodine system. As to the shaded circles, see the caption of Fig. 2.

6,12-Dioxoanthanthrene–Iodine. This compound has the same framework as anthanthrene and has been reported to form a monoiodide by Brass and Clar.[6] The introduction of two oxygen atoms into the framework gives rise to significant localization of the electrons in the highest occupied level, as revealed by a decrease in the total span of the ESR spectrum.[7] In view of these facts, it seemed to be of interest to compare the formation of iodine complexes of these two component compounds.

As is shown in Fig. 5, the resistivity is far more sensitive to the composition than that in the anthanthrene–iodine system. Note that the scale on the ordinate is logarithmic. One maximum with a resistivity of about 60 Ω cm, is located at $n=2$ and the other one at $n=3$. The latter is about tenfold higher than the former. As the ionization potential is known to be close to that of anthanthrene,[7] the formation of cation radical salts is more likely than the formation of molecular adducts. Therefore, the products corresponding to these n values may be (6,12-dioxoanthanthrene)$_3^{2+}(I_3^-)_2$ and (6,12-dioxoanthanthrene)$^+I_3^-$. Thus, the compound differs considerably from anthanthrene in the behavior of iodine complex formation. It is not clear to what extent the former compound is nonstoichiometric. The sharp minima located at $n=1.5$ and 2.5 might be an indication of the formation of (6,12-dioxoanthanthrene)$_2^+I_3^-$ and (6,12-dioxoanthanthrene)$_2^+I_5^-$. The minimum appearing a little above $n=3$ may be due to the nonstoichiometry of the phase at $n=3$. The effect of an excess of the component on the resistivity is so pronounced that the ratio of the value at $n=3$ to that at the last minimum is more than ten. The activation energy for semiconduction in the range from $n=1$ to 3 is 0.08—0.12 eV. At higher iodine contents, a gradual increase is found, reaching almost 0.2 eV by $n=4$.

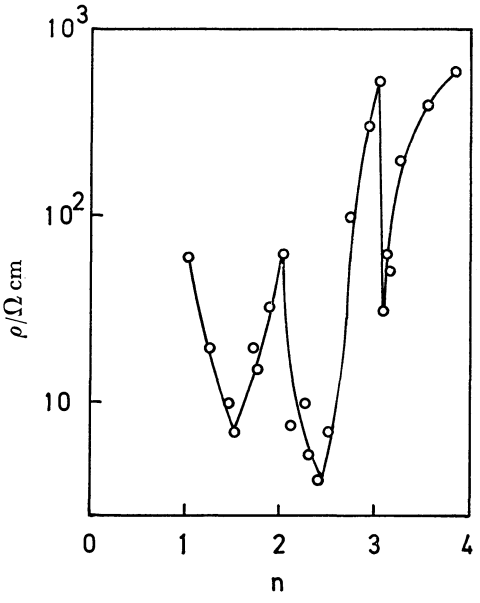

Fih. 5. Electrical resistivity at 20 °C plotted against the iodine content in the 6,12-dioxoanthanthrene–iodine system.

The Seebeck coefficient of this system is independent of the temperature up to $n=2$. The coefficient is as much as +220 μV K^{-1} at $n=1$ and is reduced by a factor of a half by $n=1.5$ and further by the same factor by $n=2$. Above this composition, a positive slope is noted in the plot of S against the reciprocal temperature. The slope becomes steeper as n increases; therefore, the room temperature value changes its sign near $n=3.5$ and is −40 μV K^{-1} at $n=4.9$, which is the highest iodine content examined. In this system, holes appear to be the major carriers in the whole composition range.

Pyranthrene–Iodine. This hydrocarbon is known to form black complexes with bromine and iodine.[8,9] The ESR absorption and the electrical resistivity of the iodine complex were reported for a composition of $n=4$.[9,10] The resistivity-composition isotherm at room temperature is presented in Fig. 6. The presence of a maximum of 35 Ω cm at $n=3$ and minima at $n=2.5$ and 3.5 is clearly noted; therefore, the formation of a simple cation radical triiodide, (pyranthrene)$^+I_3^-$, is feasible. We failed to obtain samples with $n>4$. The activation energy for semiconduction is about 0.06 eV throughout the examined composition range.

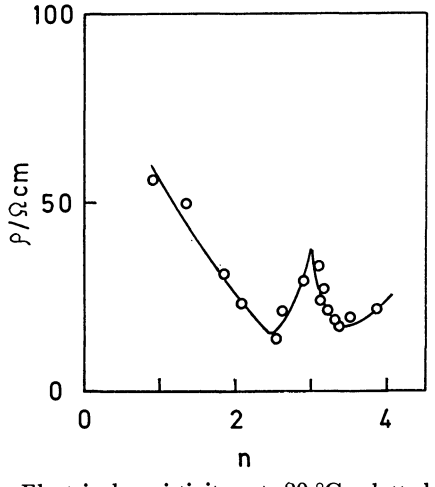

Fig. 6. Electrical resistivity at 20 °C plotted against the iodine content in the pyranthrene–iodine system.

The Seebeck coefficients at room temperature are scattered in a narrow range of +5 to +10 $\mu V\ K^{-1}$ and decrease linearly with the reciprocal temperature at all the compositions. Although the slope tends to be steeper and negative values are observed at low temperatures when n is small, the dependence on the composition is not large enough to find out the correlation between S and n at any temperature.

Violanthrene–Iodine. The formation of the bromine and iodine complexes was described in 1955.[11] The latter is very stable and is one of the halogen complexes most extensively studied in those days. The diamagnetic susceptibility of the violanthrene–iodine system was shown to vary linearly with the halogen content, but the value was found to be markedly less than the one estimated by the application of the additivity rule. The deviation reaches its maximum at $n=4$.[11] The ESR study made later revealed the presence of just enough unpaired electrons to account for the observed deviation.[9] The resistivity-composition isotherm published in 1956 has a broad minimum around $n=4$, the value at this composition being 40 Ω cm.[8] The complex was concluded to be nonstoichiometric on the basis of the equilibrium concentration of iodine in carbon tetrachloride, examined as a function of the composition of the solid complex.[12] No sharp peak was observed in the X-ray diffraction pattern of the samples with $n\simeq4$, suggesting that they are amorphous.[12]

Figure 7 presents the newly-determined resistivity-composition isotherm at room temperature. The shaded circles indicate that these samples were prepared by the treatment of the powdered hydrocarbon with a boiling benzene solution of iodine. This is the method in the previous work for the preparation of a complex.[8,11,12] Contrary to the diagram reported earlier, a maximum can be located at $n=3.5$ and minima around $n=3$ and 4. The observed feature is consistent with the reported nonstoichiometry; the idealized composition may be expressed by the formula (violanthrene)$_2^+I_7^-$. The upper limit of the homogeneity range of this complex is probably near $n=4$. The

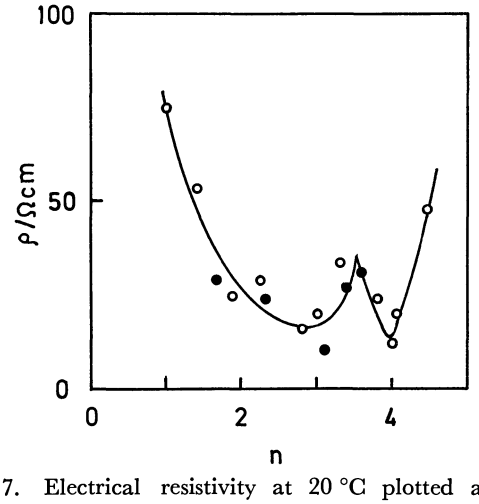

Fig. 7. Electrical resistivity at 20 °C plotted against the iodine content in the violanthrene–iodine system. The shaded circles indicate that these samples were prepared in a boiling benzene solution of iodine.

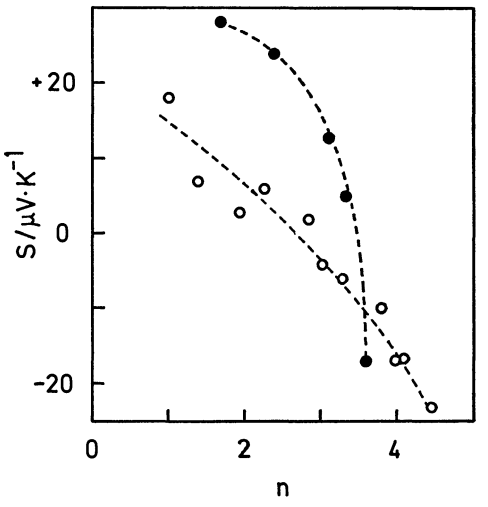

Fig. 8. Seebeck coefficient at 20 °C plotted against the iodine content in the violanthrene–iodine system. As to the shaded circles, see the caption of Fig. 7.

activation energies for semiconduction were scattered in a range from 0.08 to 0.12 eV and the correlation with the composition could not be established.

As is shown in Fig. 8, the room-temperature value of the Seebeck coefficient is positive at $n=1$ and decreases as the iodine content increases. In contrast to the electrical resistivity, the Seebeck coefficient of this system is significantly affected by the method of sample preparation. The open circles and shaded circles are clearly on different curves. The change of the sign occurs below $n=3$ for the samples indicated by open circles, while almost at $n=3.5$ for the samples indicated by shaded circles. When the coefficient is plotted against the reciprocal temperature, the slope in the high-temperature region is negative throughout the examined composition range and becomes more gentle as the iodine content increases. The value tends to saturate at low temperatures. This tendency is observed at higher temperatures when the complex contains more iodine.

Contrary to an earlier observation that the specific volume of the complex with $n<4$ is larger than the sum of the specific volumes of the constituents,[12] no deviation from the additivity could be detected with our polycrystalline compactions.

29H,31H-Phthalocyanine–Iodine. The resistivity of phthalocyanine has been shown by Aoyagi *et al.* to be considerably lowered by the addition of a small amount of iodine.[13] The dark solids obtained by the oxidation of a number of metal phthalocyanines by iodine have been reported to exhibit resistivities of the order of 0.1 to 1 Ω cm by Petersen *et al.*[14] The exact composition of their iodine complexes has been noted to depend on the preparation conditions.

The resistivity-composition isotherm of the phthalocyanine–iodine system presented in Fig. 9 shows a maximum at $n=2$, a shoulder at $n=5$, and minima, at $n=1.5$ and about 6. On the basis of these findings the presence of phases expressed by (phthalocyanine)$_3^{2+}(I_3^-)_2$ and (phthalocyanine)$^+I_5^-$ seems to be certain. The activation energy for semiconduction

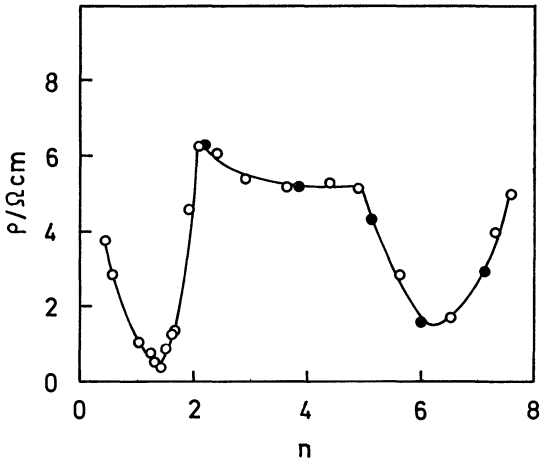

Fig. 9. Electrical resistivity at −23 °C plotted against the iodine content in the phthalocyanine-iodine system. The shaded circles indicate that these samples were made by the addition of iodine to those shown by open circles.

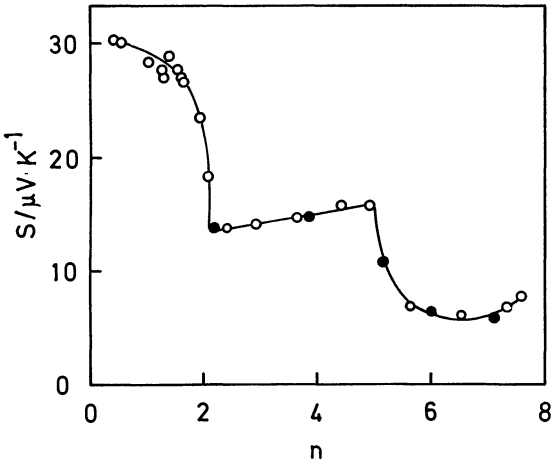

Fig. 10. Seebeck coefficient at −23 °C plotted against the iodine content in the phthalocyanine-iodine system. As to the shaded circles, see the caption of Fig. 9.

is as small as 0.015 eV up to $n=1.5$ and then sharply increases to 0.05 eV by $n=2$. Therefore, the compound, $(\text{phthalocyanine})_2{}^+I_3{}^-$, may be formed in this system. Between $n=2$ and 5 the activation energy stays around 0.04 eV and then around 0.03 eV.

The Seebeck coefficient is positive for all the samples prepared and over the temperature range examined. The slope is mostly negative when plotted against the reciprocal temperature. As is shown in Fig. 10, the values at −23 °C ($10^3/T=5$) are between +27 and +30 μV K^{-1} up to $n=1.5$ and then sharply decrease by a factor of a half by $n=2$. Between $n=2$ and 5 the values remain around +15 μV K^{-1}. Above $n=5$, the coefficient decreases again by a factor of a half. In the last iodine-content range, the Seebeck coefficient shows an increase at low temperatures.

Phenoxazine–Iodine. The organic constituent is structurally related to phenothiazine studied in our previous work[1] and is known to form an iodine complex, the composition of which is the same as that of the sulfur analog; that is, $n=3$.[15] Nevertheless,

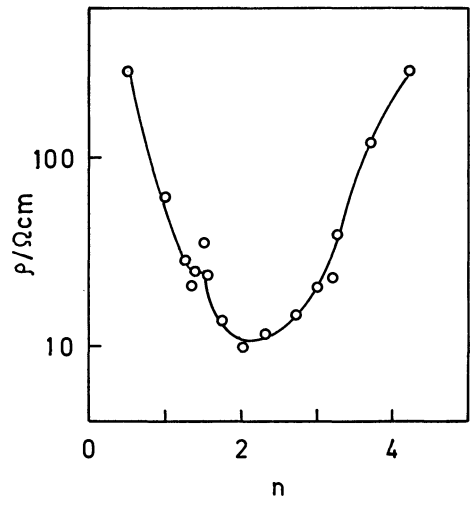

Fig. 11. Electrical resistivity at 20 °C plotted against the iodine content in the phenoxazine-iodine system.

the resistivity-composition isotherm presented in Fig. 11 is distinctly different from that of the phenothiazine-iodine system. A shoulder is located at $n=1.5$ instead of $n=2.5$. Furthermore, the minimum is found at $n=2$ instead of $n=3$. No anomalous feature is observed at $n=3$, which is the composition of the complex crystallized from a benzene solution. The overall appearance is less dramatic; that is, the resistivity at the shoulder is only about threefold larger than that at the minimum. On the other hand, the corresponding ratio in the sulfur analog–iodine system is as much as forty. The activation energy for semiconduction is about 0.13 eV throughout the examined composition range.

The Seebeck coefficient at 20 °C was reported to be slightly positive at $n=3$ and to decrease drastically by lowering the temperature. The coefficient in the composition range of $n=1$—1.5 is about −10 μV K^{-1} and independent of the temperature. When n is increased to 1.5, the room-temperature value is unchanged but the slope is slightly negative against the reciprocal temperature. Above $n=1.5$, the slope becomes increasingly negative. As the dependence on the composition near room temperature is rather small, the coefficient at 70 °C is plotted against n in Fig. 12. The sign changes from negative to positive near $n=1.5$.

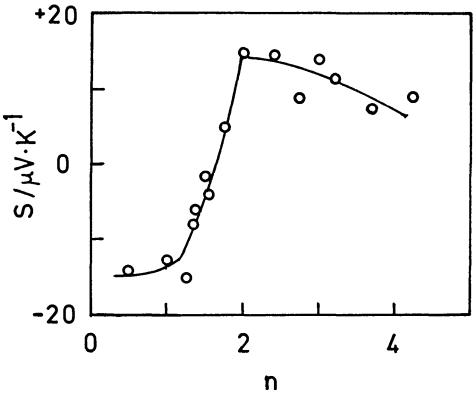

Fig. 12. Seebeck coefficient at 70 °C plotted against the iodine content in the phenoxazine-iodine system.

Of course, the behavior depends markedly upon the temperature selected. If one chooses a low temperature, say −70 °C, the sign is negative over the whole range of n; however, an abrupt change of magnitude may be found above $n=1.5$. The results described above clearly indicate the formation of a complex at $n=1.5$, while no support for the existence of a complex at $n=3$ could be obtained by the present method.

Although the vibrational spectrum could not be examined with the complex crystallized from a benzene solution because of the difficulty of pulverization,[15] samples prepared for this work are composed of fine powders and allow such measurements. As is known for this kind of materials, the spectrum in the rock-salt region is dominated by the electronic absorption. At $n=1.75$, the observed vibrational bands are broad and give a pattern very different from that of the parent organic compound. When a large amount of iodine is added to this sample, say $n>5$, a pattern consisting of sharp bands is recorded. By analogy with the case of the phenothiazine–iodine, the latter spectrum may be assigned to the monopositive ion of phenoxazine. The complex formed at $n=1.5$ is perhaps a complex cation radical salt which can be expressed by (phenoxazine)$_2^+I_3^-$.

Pyridazine–Iodine. Hoare and Pratt have reported that a pyridazine molecule combines with 2—2.8 atoms of iodine to form a black solid and that the resistivities measured using two-probe technique fall in the range of 1—50 Ω cm at room temperature.[16] This organic compound has the lowest molecular weight among the compounds known to form low-resistivity iodine complexes.

There are a peak at $n=1.8$ and minima at about $n=1.6$ and 2 in the resistivity-composition isotherm shown in Fig. 13. The activation energy for semiconduction shows also a discontinuous change at $n=1.8$; namely, the value up to this composition is about 0.035 eV and then suddenly drops to about 0.02 eV. These observations unambiguously establish the idealized composition of a complex in this system, (pyridazine)$_5I_9$. Though the present work provides no evidence for the nature of the iodine, it is likely that the iodine is in the form of a triiodide ion. If so, the above-mentioned product may be expressed by (pyridazine)$_5^{3+}(I_3^-)_3$. The resistivity observed near $n=2$, which may be the upper limit of the homogeneity range including the maximum or may be in an entirely different phase, is as low as 0.4 Ω cm. The Seebeck coefficient is essentially unchanged by the temperature and is scattered in a narrow range of +3 to +10 μV K^{-1}.

N,N′-*Diphenyl*-p-*phenylenediamine–Iodine.* This is one of the iodine complexes of oligoanilinic derivatives extensively studied by Honzl *et al.*[17] The crystal structure of this complex with $n=2.4$ has been analysed by Huml.[18] The diamine molecules are arranged one below the other in layers spaced 3.77 Å apart and the iodine atoms are arranged in chains almost perpendicular to the layers. On the basis of the distribution of distances of iodine atoms, the chains are considered to consist of triiodide ions. Hádek *et al.* have reported the electrical and magnetic properties of the complex with the above-mentioned composition.[19–21] According to their work, the activation energy for semiconduction observed with polycrystalline compactions is 0.07 eV in the temperature range of −50 to +50 °C and 0.21 eV below this range. The Seebeck coefficient is negative near room temperature and changes sign below −70 °C. In addition, the measurements on a complex with $n=2$ are available due to the of work of Sano *et al.*[22] They have concluded that the conductivity due to electrons is larger, but only slightly, than that due to holes; however, the work described below indicates that the behavior may not be so simple as they supposed.

As is illustrated in Fig. 14, the room-temperature resistivity gradually decreases by the increase of iodine content up to $n=2$ and then increases by a factor of ten between $n=2.4$ and 2.6. The value in the range of $n=1.8$ to 2.4 is 4—5 Ω cm. There is a shoulder at $n=2.6$. The activation energy for semiconduction near room temperature is about 0.07 eV over the range

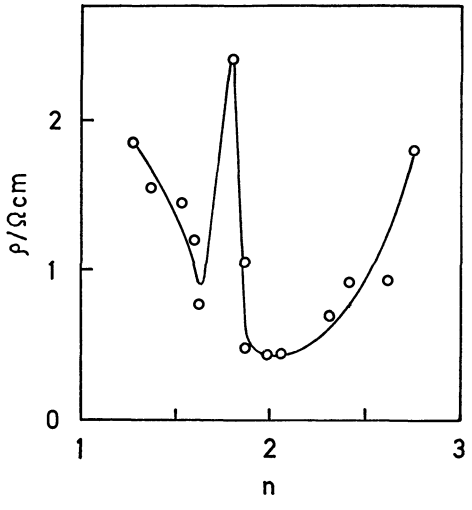

Fig. 13. Electrical resistivity at 20 °C plotted against the iodine content in the pyridazine–iodine system.

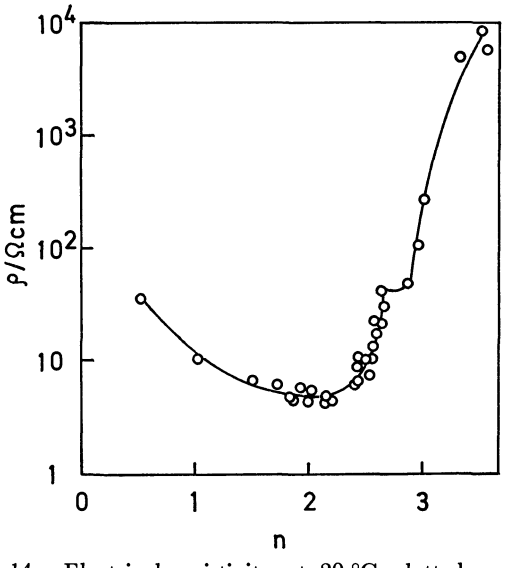

Fig. 14. Electrical resistivity at 20 °C plotted against the iodine content in the *N,N′*-diphenyl-*p*-phenylenediamine-iodine system.

of $n=0.5$—2.4, in accordance with the work by Hádek, and about 0.13 eV in the range of $n=2.5$—2.6. The change of the activation energy by lowering the temperature to about 0.22 eV in both the composition ranges was found around −20 °C, which is displaced by 30° above the temperature reported by Hádek.[19]

Although the Seebeck coefficient at room temperature is negative regardless of the wide variation in composition, the whole range can be divided into three sections according to the magnitude and the temperature dependence: namely, $n<2.4$, $n=2.4$—2.9, and $n>3$. In the first range, the value is −20—−30 $\mu V\ K^{-1}$ at room temperature and shows a minimum of about −60 $\mu V\ K^{-1}$ near −70 °C. The change of the sign occurs at a lower temperature, the value at −130 °C (the lowest temperature examined) being about +90 $\mu V\ K^{-1}$. Thus, the relative contribution of electrons and holes to the conductivity seems to vary with the temperature. The second range cannot be distinguished from the first by the room-temperature value alone but the minimum is more negative and the value is about −50 $\mu V\ K^{-1}$ even at −130 °C. The room-temperature value in the third range is significantly more negative, for example, about −200 $\mu V\ K^{-1}$ at $n=3.30$. The low-temperature value is negative but vanishingly small, passing through a minimum of about −350 $\mu V\ K^{-1}$ located around −20 °C. Thus, the compound appearing in the second composition range seems to be nonstoichiometric to some extent and its composition may be represented by $(N,N'$-diphenyl-p-phenylenediamine$)_5I_{13}$. Because of the relatively small change in resistivity around $n=2$, the resistivity-composition isotherm method fails to establish the ideal composition of the low-resistivity complex studied by Hádek *et al.* and also by Sano *et al.*

The present work was partly supported by the Grant-in-Aid for Scientific Research No.234028 from the Ministry of Education, Science, and Culture.

References

1) S. Doi, T. Inabe, and Y. Matsunaga, *Bull. Chem. Soc. Jpn.*, **50**, 837 (1977).
2) E. Clar, *Ber.*, **72**, 1645 (1939).
3) R. Pummerer, E. Prell, and A. Rieche, *Ber.*, **59**, 2159 (1926).
4) E. Clar, *Chem. Ber.*, **81**, 68 (1948).
5) P. Müller, N. P. Buu-Hoi, and R. Rips, *J. Org. Chem.*, **24**, 37 (1959).
6) K. Brass and E. Clar, *Ber.*, **72**, 1882 (1939).
7) K. Ikegami, Y. Matsunaga, K. Osafune, and E. Osawa, *Bull. Chem. Soc. Jpn.*, **48**, 341 (1975).
8) H. Akamatu, H. Inokuchi, and Y. Matsunaga, *Bull. Chem. Soc. Jpn.*, **29**, 213 (1956).
9) Y. Matsunaga, *J. Chem. Phys.*, **30**, 855 (1959).
10) T. Uchida and H. Akamatu, *Bull. Chem. Soc. Jpn.*, **34**, 1015 (1961).
11) Y. Matsunaga, *Bull. Chem. Soc. Jpn.*, **28**, 475 (1955).
12) H. Akamatu, Y. Matsunaga, and H. Kuroda, *Bull. Chem. Soc. Jpn.*, **30**, 618 (1957).
13) Y. Aoyagi, K. Masuda, and S. Namba, *J. Phys. Soc. Jpn.*, **31**, 524 (1971).
14) J. L. Petersen, C. S. Schramm, D. R. Stojakovic, B. M. Hoffman, and T. J. Marks, *J. Am. Chem. Soc.*, **99**, 286 (1977).
15) Y. Matsunaga and Y. Suzuki, *Bull. Chem. Soc. Jpn.*, **45**, 3375 (1972).
16) R. J. Hoare and J. M. Pratt, *Chem. Commun.*, **1969**, 1320.
17) J. Honzl, K. Ulbert, V. Hádek, and M. Tlusťáková, *Chem. Commun.*, **1965**, 440.
18) K. Huml, *Acta Crystallogr.*, **22**, 29 (1967).
19) V. Hádek, *J. Chem. Phys.*, **49**, 5202 (1968).
20) V. Hádek and K. Ulbert, *Collect. Czech. Chem. Commun.*, **32**, 1118 (1967).
21) V. Hádek, P. Zach, K. Ulbert, and J. Honzl, *Collect. Czech. Chem. Commun.*, **34**, 3139 (1969).
22) M. Sano, K. Ohno, and H. Akamatu, *Bull. Chem. Soc. Jpn.*, **44**, 3269 (1971).

The Solvent Extraction of Uni- and Bivalent Metal Picrates by Dibenzo-24-crown-8

Yasuyuki TAKEDA

Department of Chemistry, Faculty of Science, Chiba University, Yayoi-chō, Chiba 260

(Received February 23, 1979)

The overall extraction equilibrium constants (K_{ex}) for the 1:1:1 and 1:1:2 complexes of dibenzo-24-crown-8 (DB24C8) with several uni- and bivalent metal picrates between benzene and water have been determined at 25 °C. The K_{ex} sequences of the uni- and bivalent metal ions with DB24C8 are $Tl^+ > Cs^+ > Ag^+ > Rb^+ > K^+ > Na^+ \gg Li^+$ and $Ba^{2+} \gg Pb^{2+} \gg Sr^{2+} > Ca^{2+}$, respectively. DB24C8 shows the highest selectivity for Ba^{2+} among all the alkali and alkaline earth metal ions, but no selectivity for the alkali metal ions. The extractability of DB24C8 for the alkali metal ions is not sensitive to the ratio of the ionic size to the cavity size of DB24C8. The plots of log K_{ex} values *vs.* reciprocal crystal ionic radii of the alkali and alkaline earth metals give straight lines, indicating that these straight lines are related to Born's formula of solvation free energy.

Dibenzo-24-crown-8 (DB24C8) forms stoichiometric complexes with alkali metal ions; the alkali metal ion in the complex is trapped in the cavity of the DB24C8 ring by ion-dipole forces.[1] Since DB24C8 is a flexible crown ether and has a large cavity size (>4.0 Å[2]) compared to the alkali metal ionic size, in its complex with the alkali metal ion it is partially wrapped around the alkali metal ion.[1a] Accordingly, when the complex reaction between DB24C8 and metal ions occurs, the metal ion may be expected to require almost complete desolvation, as found in the NMR studies of nonactin.[3] Dicyclohexyl-18-crown-6 (DC18C6) and dibenzo-18-crown-6 (DB18C6), which are rigid crown ethers, show pronounced cation selectivities,[1b,4] while DB24C8 does not.[1b,4a] Some solvent extraction studies of alkali metal ions with DC18C6 and DB18C6 have been reported and these data show that the extractability of the metal ion is very sensitive to the ratio of the ionic size to the cavity size of the crown ether.[5] However, there is only one paper about the solvent extraction study of DB24C8 up to date and in this paper the extraction equilibria have not been discussed in detail.[2] Therefore, the present study was undertaken to determine the extraction constant values of the DB24C8-uni- and bivalent metal picrates and to compare these extraction constant values with those of DB18C6, in order to clarify the role of DB24C8 in the extraction process. Since a large anion is easily extracted into nonpolar solvents, the picrate anion was used as the counter ion. Benzene was used as the solvent because of its nonpolarity.

Experimental

Materials. DB24C8 was obtained from Nisso Co., Ltd. It was dissolved in hexane, and filtered while hot. Then it was recrystallized from hexane and, before use, dried at 50 °C in a vacuum oven. Analytical-grade benzene, HNO_3, $LiOH \cdot H_2O$, NaOH, KOH, $Ca(NO_3)_2 \cdot 4H_2O$, $Sr(NO_3)_2$, $Ba(NO_3)_2$, $Pb(NO_3)_2$, and reagent-grade $TlNO_3$ were purchased from Wako-Pure Chemicals Ltd. $AgNO_3$ and picric acid were analytical grade from Koso Chemical Co., Ltd. Reagent-grade RbOH and CsOH were obtained from Mitsuwa Pure Chemicals Ltd. and Kanto Chemical Co., Inc., respectively. The purities of $TlNO_3$ and the bivalent metal nitrates were determined by means of EDTA titration, and the concentrations of $AgNO_3$, the picric acid, and the alkali metal hydroxide solutions were determined by means of KCl, basic, and acid ones, respectively. Benzene was washed twice with distilled water.

Apparatus and Procedures. The organic phase of DB24C8 (9.2×10^{-5}—2.1×10^{-2} M) and the aqueous phase of the univalent metal hydroxide or nitrate (9.9×10^{-4}—2.9×10^{-2} M), or the bivalent metal nitrate (2.0×10^{-3}—1.1×10^{-1} M) and the picric acid (8.8×10^{-4}—2.7×10^{-2} M) were placed in a stoppered glass tube (volume 30 ml), shaken in a thermostated water bath for about 30 min at 25±0.2 °C, and separated by centrifugation. The initial volume of each phase was 10 ml in all cases. A portion of the aqueous phase about 8 ml was transferred to a 10 ml beaker and the hydrogen ion concentration was determined by a Hitachi-Horiba F-5 pH meter. In the cases of the univalent metal hydroxide, the univalent metal nitrate, and the bivalent metal nitrate, the extractions were carried out at pH 10.0—12.1, 2.3—2.6, and 1.6—2.7, respectively. For the systems of Ag, Tl, and the bivalent metals, the metal in the organic phase was back-extracted into 8 ml of 1 M nitric acid aqueous solution. The Ba concentration of this aqueous phase was determined by flame photometry and the others by atomic absorption spectroscopy using a Seiko SAS-725 atomic absorption spectrophotometer. For the systems of the alkali metals, the picrate in the organic phase was back-extracted into 8 ml of 0.01 M NaOH aqueous solution and the picrate concentration was determined at 356 nm by a Shimadzu UV-200 spectrophotometer ($\varepsilon = 1.45 \times 10^4$ cm^{-1} M^{-1}). In blank experiments, for the alkali metals no detectable extraction was found in the absence of DB24C8, and for Ag and Tl a little detectable extraction was found in the absence of either DB24C8 or picric acid. It was impossible to extract any Mg and Hg into the organic phase.

The Distribution Coefficient of DB24C8. A 100 ml portion of a benzene solution containing DB24C8 and an equal volume of distilled water were placed in a 300 ml separatory funnel and shaken under the same conditions as given above. The concentration range of DB24C8 was from 5.0×10^{-3}—1.0×10^{-2} M. After centrifugation, DB24C8 in the aqueous phase was extracted into chloroform (90 ml). A 80 ml portion of the organic phase was transferred to a 200 ml beaker and left until evaporation was complete. The residue in the beaker was dissolved by chloroform (10 ml) and the DB24C8 concentration was determined spectrophotometricall at 277 nm ($\varepsilon = 5.25 \times 10^3$ cm^{-1} M^{-1}). The average value of the distribution coefficient determined in this way is 1.1×10^3.

Results

When equilibrium takes place between an aqueous solution of a metal ion, M^{m+}, and a picrate ion, A^-,

and a benzene solution of a crown ether, L, the equilibrium constants may be defined by the following equations:

$$K_{ex} = [MLA_m]_o[H^+]^m/[M^{m+}][L]_o[HA]_o^m \quad (1)$$

$$K_{D,L} = [L]_o/[L] \quad (2)$$

$$K_{ex}(HA) = [HA]_o/[H^+][A^-] \quad (3)$$

$$K_{ML} = [ML^{m+}]/[M^{m+}][L] \quad (4)$$

$$K_{ex'} = [MLA_m]_o/[ML^{m+}][A^-]^m \quad (5)$$

where the subscript "o" and the lack of a subscript designates the organic and the aqueous phase, respectively; square brackets indicate the molar concentrations. The distribution ratio of the metal may be represented by

$$D_M = [MLA_m]_o/([M^{m+}] + [ML^{m+}]) \quad (6)$$

In the case of $[M^{m+}] \gg [ML^{m+}]$, Eq. 6 may be transformed into

$$D_M = K_{ex}K_{ex}(HA)^m[L]_o[A^-]^m \quad (7)$$

For the univalent metal ion system the $\log(D_M/[A^-])$ *vs.* $\log[L]_o$ plot in Fig. 1 shows a straight line with a slope of 1 in every case, indicating that DB24C8 forms the 1:1 complex with the univalent metal ion. For the bivalent metal ion system the $\log(D_M/[A^-]^2)$ *vs.* $\log[L]_o$ plot in Fig. 2 and the $\log(D_M/[L]_o)$ *vs.* $\log[A^-]$ plot in Fig. 3 always show lines with slopes of 1 and 2, respectively, indicating that DB24C8 forms the 1:1:2 complex with the bivalent metal ion and the picrate ion. The values of $[L]_o$ and $[A^-]$ in Eq. 7 were calculated from Eqs. 8 and 9 respectively.

$$[L]_o = [L]_t - [MLA_m]_o \quad (8)$$

$$[A^-] = ([HA]_t - m[MLA_m]_o)/\{1 + (K_{HA} + K_{ex}(HA))[H^+]\} \quad (9)$$

where the subscript "t" denotes the total concentration. The value of $K_{ex}(HA)$ was spectrophotometrically determined to be 247 by using the association constant of picric acid ($K_{HA} = 1.9_5$[6]). The equilibrium constants obtained from these data are summarized in Table 1, together with those from the literature.

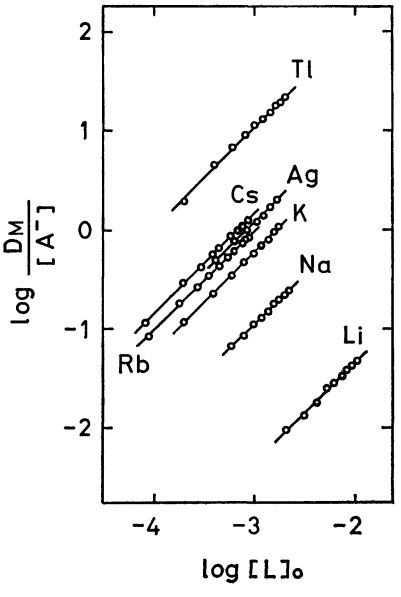

Fig. 1. Plots of $\log(D_M/[A^-])$ *vs.* $\log[L]_o$ for the univalent metals-DB24C8 system at 25 °C.

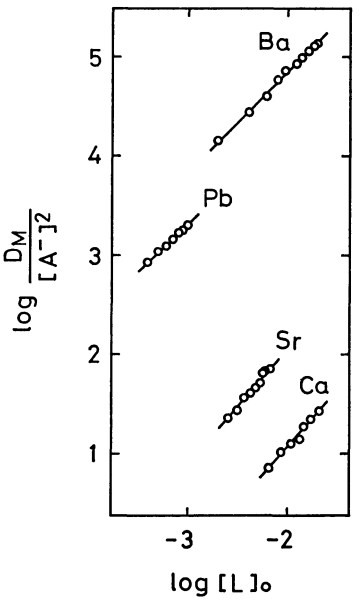

Fig. 2. Plots of $\log(D_M/[A^-]^2)$ *vs.* $\log[L]_o$ for the bivalent metals-DB24C8 system at 25 °C.

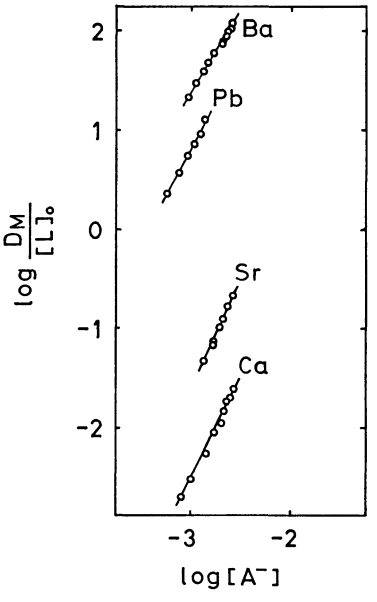

Fig. 3. Plots of $\log(D_M/[L]_o)$ *vs.* $\log[A^-]$ for the bivalent metals-DB24C8 system at 25 °C.

Discussion

The plots of log K_{ex} value *vs.* crystal ionic radius for the DB24C8 and the DB18C6 systems are given in Fig. 4. Table 1 shows that the log K_{ex} value sequences for the alkali metal and the alkaline earth metal ions with DB24C8 are $Cs^+ > Rb^+ > K^+ > Na^+ \gg Li^+$ and $Ba^{2+} \gg Sr^{2+} > Ca^{2+}$ respectively, indicating that in both cases the nearer the crystal radius of the metal ion approaches to the cavity radius of DB24C8 (>2.0 Å[2]), the more extractable the metal ion is, as can

Table 1. Equilibrium constants at 25 °C

Crown ether	$K_{D,L}$	Cation	log K_{ex}
DB24C8	1.1×10^3	Li^+	−1.72
		Na^+	−0.34
		K^+	0.40
		Rb^+	0.61
		Cs^+	0.76
		Ag^+	0.70
		Tl^+	1.67
		Ca^{2+}	−1.72
		Sr^{2+}	−0.80
		Ba^{2+}	2.07
		Pb^{2+}	1.53
DB18C6	8×10^2 [5c]	Na^+	−0.18[5c]
		K^+	2.26[5c]
		Rb^+	1.36[5c]
		Cs^+	0.68[5c]

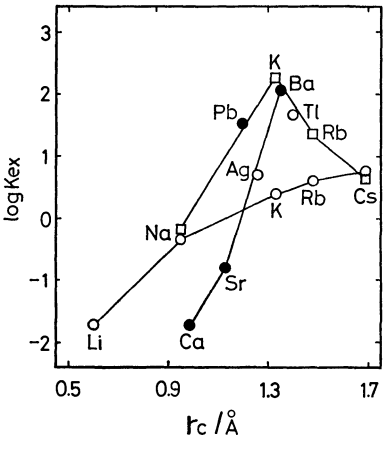

Fig. 4. Plots of log K_{ex} *vs.* crystal ionic radii, r_c, of uni- and bivalent metals for the DB24C8 and DB18C6 systems. ○: DB24C8-univalent metal, ●: DB24C8-bivalent metal, □: DB18C6-univalent metal.

be seen in Fig. 4. DB18C6, which is a rigid ligand,[1b] shows the highest selectivity for K^+ of all the alkali metal ions, and the extractability of DB18C6 for the alkali metal ions is very sensitive to the ratio of the crystal ionic radius to the cavity radius (1.3—1.6 Å[4a]). On the other hand, DB24C8, which is a flexible ligand,[1b] displays no peak selectivity for any alkali metal ion. The extractability of DB24C8 for the alkali metal ions is not sensitive to the ratio of the crystal ionic radius to the cavity radius (Fig. 4), and in the case of DB24C8 the difference in the log K_{ex} values of the neighboring alkali metal ions decreases gradually with an increase in the ionic size (Table 1). It may be noted from Fig. 4 that DB24C8 reveals the highest selectivity for Ba^{2+} among all the alkali and alkaline earth metal ions. It is very noticeable that the difference in the log K_{ex} values of Ba^{2+} and Sr^{2+} with DB24C8 (2.87) is markedly larger than those with 15-crown-5 (−0.50[9]) and 18-crown-6 (0.00[9]). This fact suggests that DB24C8 will be an useful reagent for separating a small amount of Ba from large amounts of Sr by a solvent extraction method.

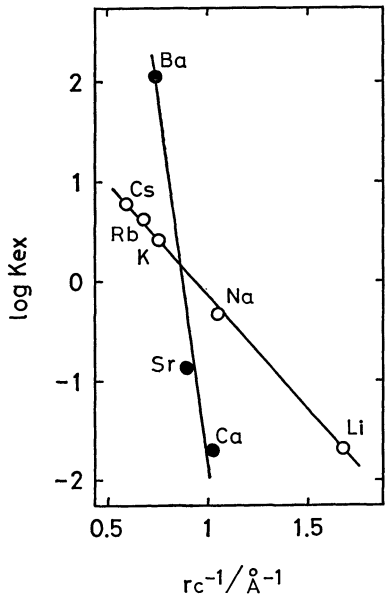

Fig. 5. Plots of log K_{ex} *vs.* reciprocal crystal ionic radii of alkali and alkaline earth metals for the DB24C8 system.

As can be seen from Fig. 4, the crystal radii of Ag^+ (1.26 Å[7]) and Tl^+ (1.40 Å[7]) are nearly equal to that of K^+ (1.33 Å[7]) and those of K^+ and Rb^+ (1.48 Å[7]) respectively. However, the log K_{ex} value of DB24C8 for Ag^+ is larger than that for K^+ and that for Tl^+ is much larger than those for K^+ and Rb^+. The log K_{ex} value of DB24C8 for Pb^{2+}, whose crystal radius (1.20 Å[8]) is nearly identical with that of Sr^{2+} (1.13 Å[7]), is much larger than that for Sr^{2+} (Fig. 4). The extractability of DB24C8 for Tl^+, whose ionic size is nearer to the cavity size of DB24C8 than is that of Ag^+, is much greater than that for Ag^+ (Fig. 4). The crystal radii of Ba^{2+} (1.35 Å[7]) and K^+ are nearly equal and the log K_{ex} value of DB24C8 for Ba^{2+} is much larger than that for K^+, while Ca^{2+} (0.99 Å[7]) and Na^+ (0.95 Å[7]) have nearly identical crystal radii and the log K_{ex} value of DB24C8 for Ca^{2+} is much smaller than that for Na^+ (Fig. 4).

The plot of log K_{ex} value *vs.* the reciprocal crystal ionic radius for the DB24C8 system is given in Fig. 5. The larger the crystal radii of the alkali and alkaline earth metal ions are, the more extractable these ions are. The plots of log K_{ex} values *vs.* the reciprocal crystal ionic radii of the alkali and alkaline earth metals give straight lines with slopes of −2.3 and −13.9 respectively, and the slope of the alkaline earth metal ions is about 6 times steeper than that of the alkali metal ions. Thus, it seems that these straight lines in Fig. 5 are related to Born's formula of solvation free energy.

The author thanks Mr. Hiroshi Gotō and Mr. Fujio Takahashi of this laboratory for their experimental assistance.

References

1) a) N. S. Poonia, *J. Am. Chem. Soc.*, **96**, 1012 (1974);

b) R. M. Izatt, R. E. Terry, D. P. Nelson, Y. Chan, D. J. Eatough, J. S. Bradshaw, L. D. Hansen, and J. J. Christensen, *ibid.*, **98**, 7626 (1976).

2) C. J. Pedersen, *Fed. Proc., Fed. Am. Soc. Exp. Biol.*, **27**, 1305 (1968).

3) J. H. Prestegard and S. I. Chan, *Biochemistry*, **8**, 3921 (1969).

4) a) H. K. Frensdorff, *J. Am. Chem. Soc.*, **93**, 600 (1971); b) E. Shchori, N. Nae, and J. Jagur-Grodzinski, *J. Chem. Soc., Dalton Trans.*, **1975**, 2381; c) N. Matsuura, K. Umemoto, Y. Takeda, and A. Sasaki., *Bull. Chem. Soc. Jpn.*, **49**, 1246 (1976); d) R. M. Izatt, R. E. Terry, B. L. Haymore, L. D. Hansen, N. K. Dalley, A. G. Avondet, and J. J. Christensen, *J. Am. Chem. Soc.*, **98**, 7620 (1976).

5) a) H. K. Frensdorff, *J. Am. Chem. Soc.*, **93**, 4684 (1971); b) P. R. Danesi, H. Meider-Gorican, R. Chiarizia, and G. Scibona, *J. Inorg. Nucl. Chem.*, **37**, 1479 (1975); c) A. Sadakane, T. Iwachido, and K. Tōei, *Bull. Chem. Soc., Jpn.*, **48**, 60 (1975).

6) "Dissociation Constants of Organic Acids in Aqueous Solution," ed by G. Kortün, W. Vogel, and K. Andrussov, Butterworths, London (1961).

7) L. Pauling, "The Nature of the Chemical Bond," 3rd ed, Cornell Univ. Press (1960).

8) R. C. Weast, "Handbook of Chemistry and Physics," 58th ed, CRC Press (1977—1978).

9) Y. Takeda and H. Katō, *Bull. Chem. Soc. Jpn.*, in press.

Measurement and Analysis of the ν_3 Band of CF_4

Tetsuo SUZUKI, Hiroshi OKADA, and Tsunetake FUJIYAMA*

Department of Chemistry, Faculty of Science, Tokyo Metropolitan University, Setagaya-ku, Tokyo 158

(Received March 2, 1979)

The ν_3 fundamental of carbon tetrafluoride has been measured with a tunable diode laser-source spectrometer. The following molecular constants were obtained: $\nu_0-2(B\zeta_3)_{eff}=1283.4067$ cm^{-1}, $B_{eff}^{PR}+B_0-2(B\zeta_3)_{eff}=7.210\times10^{-2}$ cm^{-1}, $B_{eff}^{PR}-B_0=-5.290\times10^{-4}$ cm^{-1}, and $\delta_3=6.153\times10^{-4}$ cm^{-1}. Using the r_g-structure obtained from the gas-electron diffraction study, the above molecular constants were reduced to be: $\nu_0=1283.7181$ cm^{-1}, $B_{eff}^{PR}=0.1915$ cm^{-1}, $B_0=0.1920$ cm^{-1}, and $(B\zeta_3)_{eff}=0.1557$ cm^{-1}. From the $(B\zeta_3)_{eff}$ value, the Coriolis coupling constant for the ν_3 was estimated to be $\zeta_3=0.811$.

Although carbon tetrafluoride is one of the most simple and basic molecules belonging to the point group T_d, very few studies of its rotation-vibration spectra have been reported. This has been largely due to the deficiency in the resolving power of the spectrometers. Edgell *et al.* have observed the ν_3 and ν_4 fundamentals with a rather low-resolution spectrometer and estimated the Coriolis coupling constants, ζ_3 and ζ_4, by analyzing the band contours.[1] The rotation-vibration spectra have been observed for the ν_4 fundamental by Maki *et al.* with a resolution of 0.06 cm^{-1}. From the *J*-structure analysis, the molecular constants, ν_0, $B(1-\zeta_4)$, and B_4-B_0, were determined.[2] The ν_4 fundamental of three isotope species, ^{12}C, ^{13}C, and ^{14}C, were observed with a resolution of 0.06 cm^{-1} by Jones *et al.*[3] The observed spectra were well resolved into *J*-structures, and the molecular constants for the three isotope species were determined.

In the case of the ν_3 fundamental, however, the spacing of the rotational structure is so narrow that the conventional spectrometer cannot resolve its fine structures. The present report will concern itself with the measurement of the rotation-vibration spectra for the ν_3 fundamental of carbon tetrafluoride by the use of a tunable diode laser-source spectrometer and with the analysis of the rotation-vibration spectra.

Experimental

The sample used in this study was a commercial product and was used without further purification. The survey spectrum of the ν_3 band of carbon tetrafluoride was recorded from 1270 to 1290 cm^{-1} using a Nicolet 7199 Fourier transform infrared spectrometer at a 0.06-cm^{-1} resolution. The observation was made at room temperature using a 10-cm gas cell. The sample pressure was about 0.5 Torr.

The high-resolution spectrum was recorded from 1281.28 to 1282.92 cm^{-1} by the use of a tunable diode laser-source spectrometer, (Laser Analytics model LS series). The observation was made at room temperature using a 15-cm gas cell. The pressure was 0.1—0.2 Torr. The resolution of the instrument was 10^{-4}—10^{-3} cm^{-1}; therefore, the line width of the observed spectrum was governed by the Doppler broadening. The line frequencies were calibrated by the use of the (100-000) and (11^10-01^10) transition frequencies of the N_2O vapor[4,5] and the interference fringes arising from a germanium etalon whose free spectral range was 0.04841 cm^{-1} at 1282 cm^{-1}. The precision of the frequency measurement was believed to be 0.002 cm^{-1}, while the accuracy of the frequency measurement was restricted by the ambiguity to be expected in the determination of the band origin of the standard lines. It was, however, believed to be better than 0.005 cm^{-1}.[4,5]

Observed Spectra

The spectra of the ν_3 band recorded by the Fourier transform spectrometer is shown in Fig. 1. There appear an R branch centered around 1285—1286 cm^{-1}, a strong Q branch at 1283 cm^{-1}, and a broad P branch. Overlapped with the P branch, there appear a relatively strong absorption maximum at 1281 cm^{-1} and a weak absorption maximum at 1279 cm^{-1}. Probably the two absorption maxima arise from hot bands. As is shown in Fig. 1, the P and R branches are resolved into fine structures. However, these fine structures cannot easily be identified as *J*-components because their intensities and spacings do not show any apparent regularities.

The intensities of the Q branch at 1283 cm^{-1} and the Q branch of the hot band at 1281 cm^{-1} were carefully measured at various sample pressures. The observed intensity ratio was 1 : 0.231. As the intensity ratio of the Q branch of the ν_3 fundamental and that of the $\nu_3+\nu_2-\nu_2$ hot band is 1 : 0.238, the relatively strong absorption maximum observed at 1281 cm^{-1} is identified as the Q branch of the $\nu_3+\nu_2-\nu_2$ hot band.

The high-resolution spectrum observed by the use of the diode laser-source spectrometer is shown in Fig. 2. In the region from 1281.80 to 1282.72 cm^{-1}, a series of *J*-components of the P branch can be seen clearly, and each *J*-component is further resolved into sub-structure components. The spectrum in the 1282.72—1282.92 cm^{-1} region is quite complex because it is overlapped with the strong Q branch. As the frequency decreases, the spacing of the sub-structure components becomes larger relative to the spacing of the *J*-components. Therefore, it becomes difficult to identify a *J*-component as a definite line group.

It seems that most of the sub-structure components are not completely resolved, because their line-widths are much broader than the Doppler width. The Doppler width is estimated to be about 0.002 cm^{-1} under these experimental conditions.

Analysis of the Observed Band

Rotational Energy Levels of the Ground and Excited Vibrational States. The present analysis is based on the theoretical work reported by Herranz.[6]

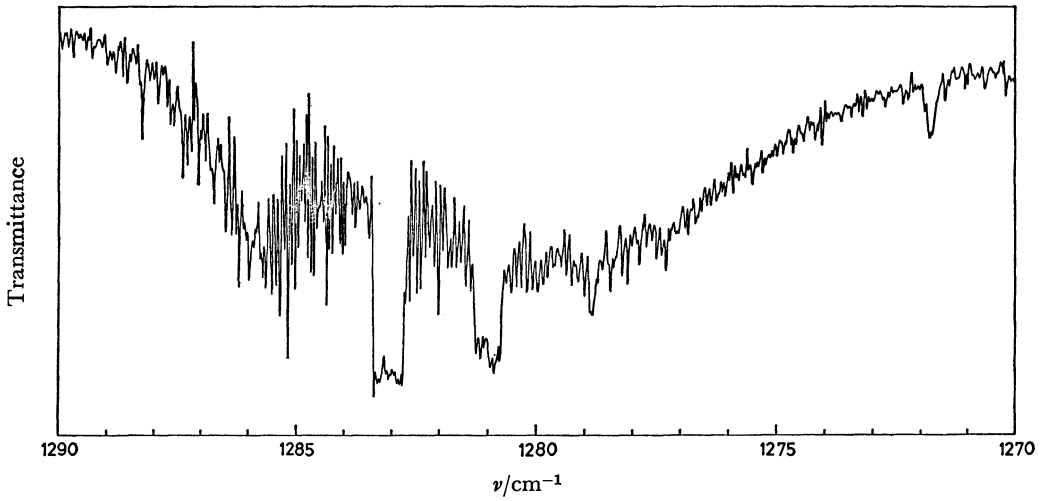

Fig. 1. The spectrum of the ν_3 band recorded by the Fourier transform spectrometer.

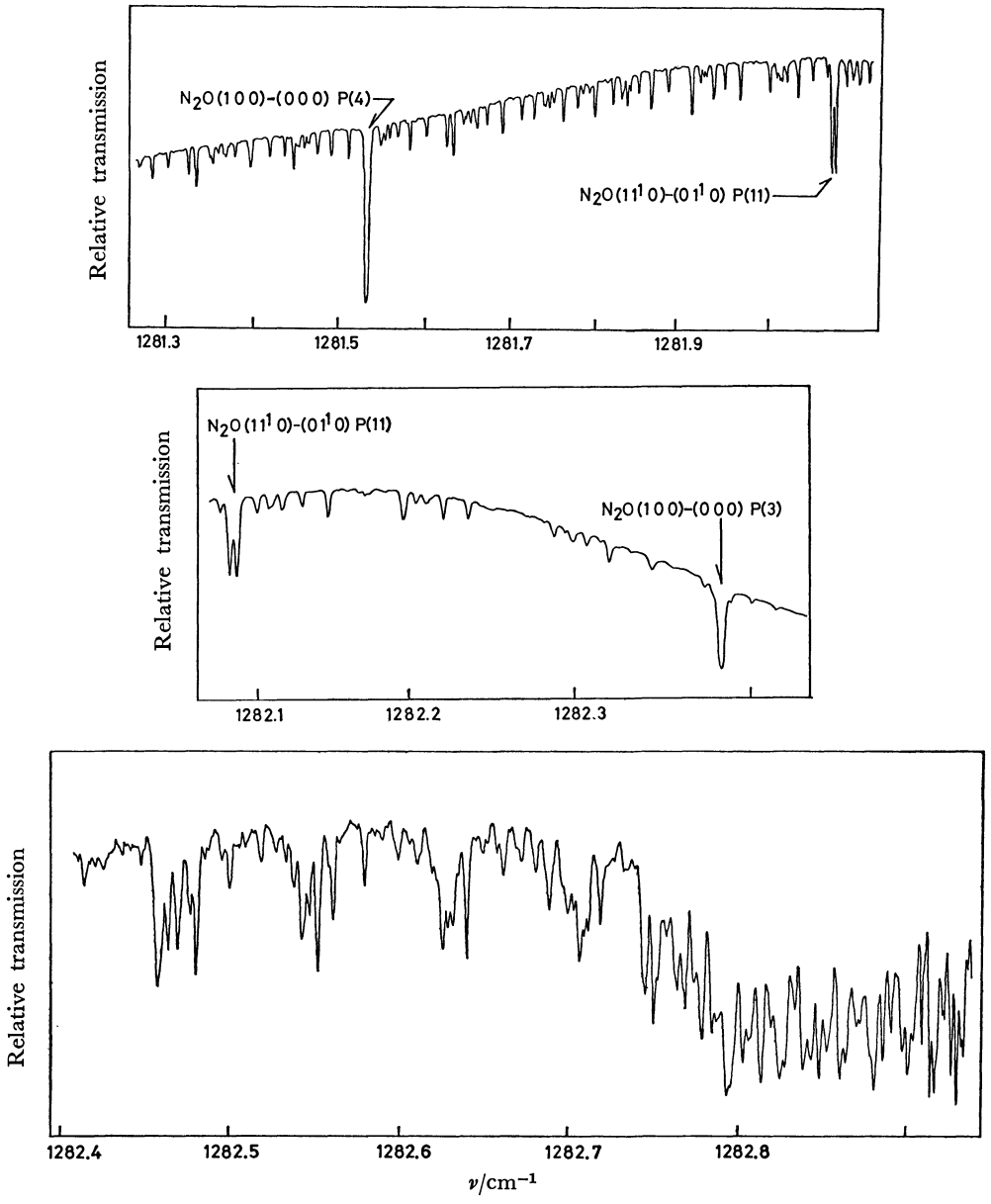

Fig. 2. The high resolution spectrum of the ν_3 band observed by the use of the tunable diode laser source spectrometer.

The term values for the rotational levels of the ground state of an XY_4-type spherical-top molecule can be written as:

$$F_0(J,\tau) = B_0J(J+1) - D_0^JJ^2(J+1)^2 - D^{J\tau}S_{J,\tau}, \quad (1)$$

where B_0 and $D_0{}^J$ are the rotational constant and the centrifugal distortion constant for the ground state respectively. The last term of Eq. 1 represents the splitting of the rotational levels into their sublevels as a consequence of centrifugal distortion. There are $2J+1$ sublevels for each J value including degeneracy; these sublevels are designated by an index, τ. $S_{J,\tau}$ is the eigenvalue of the angular momentum operator:

$$S = P_x^4 + P_y^4 + P_z^4 - (3/5)P^4 + (1/5)P^2, \quad (2)$$

where:

$$P^2 = P_x^2 + P_y^2 + P_z^2, \text{ and } P^4 = (P_x^2+P_y^2+P_z^2)^2.$$

When the wavefunctions of an axially symmetric rotor are chosen as a basis set, the nonvanishing matrix elements for S are:

$$(J,K|S|J,K) = (3/20)(J^2+J)(J^2+J-2-10K^2) + (1/4)K^2(7K^2+5) \quad (3a)$$

and:

$$(J,K|S|J,K\pm4) = (1/8)\{(J\mp K)(J\mp K-1)\times(J\mp K-2)(J\mp K-3)(J\pm K+1)\times(J\pm K+2)(J\pm K+3)(J\pm K+4)\}^{1/2} \quad (3b)$$

when the triply degenerate vibrational mode is excited, the interaction of rotation and vibration removes the degeneracy; therefore, each J level splits into three levels. They are designated by (+), (0), and (−). Each of these levels is further split into sublevels. These sublevels are designated by the same index, τ, as in the ground state. For each J value the number of sublevels is $2J+3$ for the (+), $2J+1$ for the (0), and $2J-1$ for the (−) levels.

The term values for the rotational levels of the excited vibrational state are given by:

$$F^{(+)}(J,\tau) = B_{eff}^{PR}J(J+1) + 2(B\zeta_3)_{eff}J - D_1^JJ^2(J+1)^2 + \frac{S_{J+1,\tau}}{2J^2+3J+1}\{\delta_3 - D^{J\tau}(2J^2-5J+3)\} \quad (4a)$$

$$F^{(0)}(J,\tau) = B_{eff}^{Q}J(J+1) - 2(B\zeta_3)_{eff} - D_1^JJ^2(J+1)^2 - \frac{S_{J,\tau}}{J^2+J}\{\delta_3 + D^{J\tau}(J^2+J-10)\} \quad (4b)$$

$$F^{(-)}(J,\tau) = B_{eff}^{PR}J(J+1) - 2(B\zeta_3)_{eff}(J+1) - D_1^JJ^2(J+1)^2 + \frac{S_{J-1,\tau}}{2J^2+J}\{\delta_3 - D^{J\tau}(2J^2+9J+10)\} \quad (4c)$$

where B_{eff}^{PR} is the effective rotational constant for the (+) and (−) levels, while B_{eff}^{Q} is that for the (0) level. The δ_3 parameter represents the splitting of the J level resulting from the instantaneous breakdown of symmetry which is produced by the vibrational mode. The explicit expression for δ_3 is given in Ref. 6. In order to further specify the characteristics of the sublevels, the τ index is replaced by a double index, nT. The symbol T specifies the type of degeneracy of the sublevel; that is, $T=A$, $T=E$, and $T=F$ refer to nondegenerate, doubly degenerate, and triply degenerate sublevels respectively. The symbol n differentiates the sublevels belonging to the same J and T; that is, $n=1$ refers to the sublevel of the largest $S_{J,\tau}$, $n=2$ refers to the sublevel of the second largest $S_{J,\tau}$, and so on.

The selection rules for electric dipole transitions are:

$$\Delta\tau = 0 \text{ and } \Delta J = -1 \text{ for } F^{(+)}\leftrightarrow F_0$$
$$\Delta J = 0 \text{ for } F^{(0)}\leftrightarrow F_0$$
$$\Delta J = 1 \text{ for } F^{(-)}\leftrightarrow F_0.$$

Taking account of these selection rules, the line frequencies of the fundamental band are expressed as: for the P branch:

$$\nu^P(J,\tau) = \nu_0 - 2(B\zeta_3)_{eff} - \{B_{eff}^{PR}+B_0-2(B\zeta_3)_{eff}\}J + \{(B_{eff}^{PR}-B_0)-(D_1^J-D_0^J)\}J^2 + 2(D_1^J+D_0^J)J^3 - (D_1^J-D_0^J)J^4 + \frac{S_{J,\tau}}{2J^2-J}\{\delta_3+(8J-10)D^{J\tau}\} \quad (5a)$$

for the Q branch:

$$\nu^Q(J,\tau) = \nu_0 - 2(B\zeta_3)_{eff} + (B_{eff}^{Q}-B_0)J(J+1) - (D_1^J-D_0^J)J^2(J+1)^2 - \frac{S_{J,\tau}}{J^2+J}(\delta_3-10D^{J\tau}) \quad (5b)$$

and for the R branch:

$$\nu^R(J,\tau) = \nu_0 - 2(B\zeta_3)_{eff} + \{B_{eff}^{PR}+B_0-2(B\zeta_3)_{eff}\}(J+1) + \{(B_{eff}^{PR}-B_0)-(D_1^J-D_0^J)\}(J+1)^2 - 2(D_1^J-D_0^J)(J+1)^3 - (D_1^J-D_0^J)(J+1)^4 + \frac{S_{J,\tau}}{2J^2+5J+3}\{\delta_3-(8J+18)D^{J\tau}\}. \quad (5c)$$

J takes the values 1, 2,⋯; 1, 2,⋯, and 0, 1, 2,⋯ for the P, Q, and R branches respectively.

The relative intensities of the lines are given by:

$$I_P(J,\tau) = g_T(2J-1)\nu^P(J,\tau)\exp\left\{-\frac{hcF_0(J,\tau)}{kT}\right\}\times\left[1-\exp\left\{-\frac{hc\nu^P(J,\tau)}{kT}\right\}\right]$$

$$I_Q(J,\tau) = g_T(2J+1)\nu^Q(J,\tau)\exp\left\{-\frac{hcF_0(J,\tau)}{kT}\right\}\times\left[1-\exp\left\{-\frac{hc\nu^Q(J,\tau)}{kT}\right\}\right]$$

$$I_R(J,\tau) = g_T(2J+3)\nu^R(J,\tau)\exp\left\{-\frac{hcF_0(J,\tau)}{kT}\right\}\times\left[1-\exp\left\{-\frac{hc\nu^R(J,\tau)}{kT}\right\}\right] \quad (6)$$

where g_T is the nuclear spin statistical weight factor; T, the temperature; h, the Planck constant; c, the light velocity, and k, the Boltzmann constant. As the spin value of a fluorine atom is 1/2, the g_T values are given by:

$$g_A = 5,\ g_E = 2, \text{ and } g_F = 3. \quad (7)$$

Assignment. First our attention was focused on the high-resolution spectrum from 1282.00 to 1282.72 cm^{-1}, because a clear series of J-components appears. These lines certainly belong to a P-branch-line series of $J>7$. The definite assignment of each line can

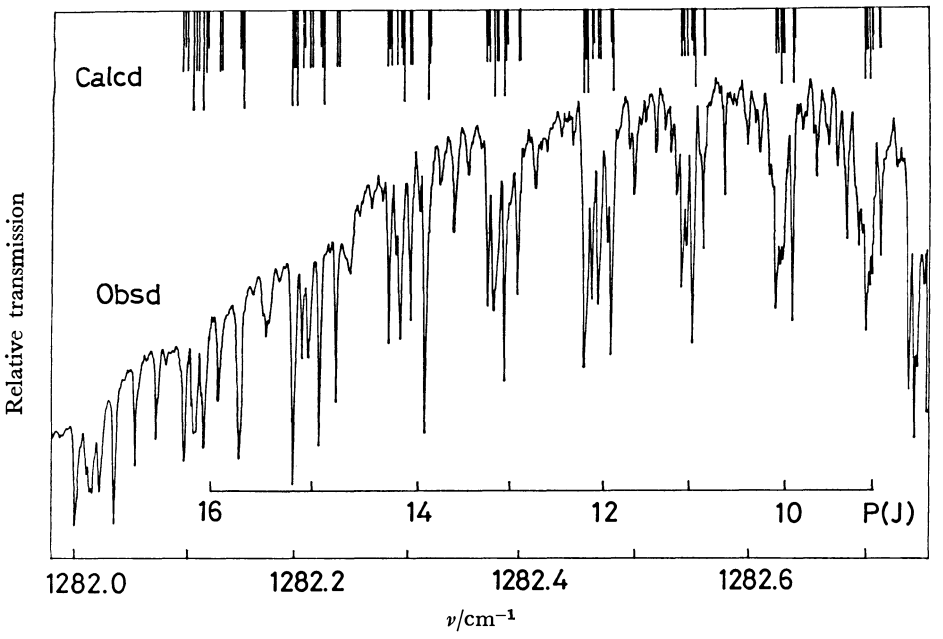

Fig. 3. The observed and calculated spectra in the frequency region of 1282.0—1282.7 cm^{-1}.

be made by calculating the theoretical relative intensities and the relative spacings of the sub-structure components. In Fig. 3, the spectrum calculated from Eqs. 5a, 6, and 7 is compared with the observed spectrum. It can be seen from the figure that some of the observed lines are not completely resolved into the sub-structure components. The Doppler width is sometimes larger than the spacing of the sub-structure components. It is not possible at present to resolve the spectrum of this band into the sub-structures completely by the use of an ordinary spectroscopic method. Therefore, we defined the hypothetical observed frequency for the unresolved lines as:

$$\nu_{max} = \frac{\sum \nu(J,\tau) I(J,\tau)}{\sum I(J,\tau)}. \qquad (8)$$

By doing so, the frequency at the intensity maximum of an unresolved line can be used as an observed frequency. The molecular constants, $\nu_0 - 2(B\zeta_3)_{eff}$, $B_{eff}^{PR} + B_0 - 2(B\zeta_3)_{eff}$, and δ_3 were tentatively determined from the P-branch lines of $9 \leq J \leq 16$ by the least-squares method. Smaller weights were given for the lines which were not fully resolved. Then, the final assignment of all the observed lines from 1281.3 to 1282.72 cm^{-1} was made by the use of the approximate frequencies of the transition lines calculated from these tentatively determined molecular constants and the theoretical relative intensities. The P-branch lines of $J \leq 8$ cannot be found, because they are buried in the strong Q branch.

The observed spectral features of the Q branch were so complex that its analysis was abandoned.

Determination of the Molecular Constants. The molecular constants were determined from the P-branch lines of $9 \leq J \leq 24$ by the least-squares method. The lines which were not fully resolved were given smaller weights. As the number of the observed lines is not enough, the following assumptions were made in the present analysis: $D_1^J = D_0^J$ and the value of D_0^J was fixed at 2.5×10^{-7} cm^{-1}, which has been obtained from the analysis of the ν_4 fundamental.[3] In addition, as the value of $D^{J\tau}$ is theoretically estimated to be 4×10^{-8} cm^{-1} by using the rotational constant[7] and the harmonic force field,[8] the effect of this constant can be regarded as negligible on analyzing the absorption lines of $J \leq 24$. Therefore, we put $D^{J\tau} = 0$ in the least-squares fitting.[9]

The molecular constants which were obtained from the least-squares fitting are listed in Table 1. The observed and calculated frequencies are summarized in Table 2. The standard deviation of the fit is 0.0023 cm^{-1}. For the P(15) lines, the differences between the observed and calculated frequencies are about two times as large as those for the other lines; the reason for this is not yet clear.[10]

Table 1. The molecular constants obtained from ν_3 band of CF_4 (in cm^{-1})

$\nu_0 - 2(B\zeta_3)_{eff}$	1283.4067±0.0044
$B_{eff}^{PR} + B_0 - 2(B\zeta_3)_{eff}$	(7.210±0.054) $\times 10^{-2}$
$B_{eff}^{PR} - B_0$	− (5.290±0.160) $\times 10^{-4}$
δ_3	(6.153±0.110) $\times 10^{-4}$

The uncertainties are twice the standard deviations.

Discussion. The molecular constants, ν_0, $(B\zeta_3)_{eff}$, B_{eff}^{PR}, and B_0, cannot be determined independently from the analysis of the P branch of the ν_3 band alone. However, these constants can be independently determined if we use the r_g-structure obtained from the gas-electron-diffraction study. The rotational constant in the ground state can be calculated following the idea of Morino *et al.*[11]

The nuclear-distance parameter, r_α, is expressed as:

$$r_\alpha = r_g - \frac{\{\langle(\Delta x)^2\rangle + \langle(\Delta y)^2\rangle\}}{2r_e} - \delta_r \qquad (9)$$

where $\langle(\Delta x)^2\rangle$ and $\langle(\Delta y)^2\rangle$ are the mean-square

Table 2. Observed and calculated frequencies of ν_3 band

Assignment J	Assignment τ	Observed frequency (cm^{-1})	Calculated frequency (cm^{-1})	Δ[a] (cm^{-1})
P(9)	1*F*, 2*F*	1282.7195	1282.7230	0.0035
	1*E*, 3*F*	1282.7123	1282.7153	0.0030
	1*A*	1282.7098	1282.7127	0.0029
	4*F*, 5*F*, 2*A*	1282.7074	1282.7095	0.0021
P(10)	1*E*, 1*F*, 1*A*	1282.6412	1282.6431	0.0019
	2*F*, 3*F*	1282.6327	1282.6339	0.0012
	2*A*	1282.6298	1282.6305	0.0007
	4*F*, 2*E*, 5*F*	1282.6266	1282.6269	0.0003
P(11)	1*F*, 2*F*	1282.5615	1282.5625	0.0010
	1*A*, 3*F*, 1*E*	1282.5526	1282.5524	−0.0002
	4*F*	1282.5476	1282.5472	−0.0004
	5*F*, 2*E*, 6*F*	1282.5430	1282.5425	−0.0005
P(12)	1*A*, 1*F*, 1*E*	1282.4811	1282.4812	0.0001
	2*F*, 3*F*	1282.4705	1282.4695	−0.0010
	2*E*, 4*F*	1282.4648	1282.4630	−0.0018
	2*A*, 5*F*, 6*F*, 3*A*	1282.4584	1282.4570	−0.0014
P(13)	1*F*, 2*F*	1282.3992	1282.3991	−0.0001
	1*E*, 3*F*, 1*A*	1282.3870	1282.3859	−0.0011
	4*F*, 5*F*, 2*A*	1282.3773	1282.3768	−0.0005
	6*F*, 2*E*, 7*F*	1282.3722	1282.3702	−0.0020
P(14)	1*A*, 1*F*, 1*E*	1282.3167	1282.3162	−0.0005
	2*F*, 3*F*	1282.3033	1282.3021	−0.0012
	2*A*, 4*F*, 2*E*	1282.2958	1282.2934	−0.0024
	5*F*	1282.2912	1282.2886	−0.0026
	6*F*, 2*E*, 7*F*	1282.2848	1282.2823	−0.0025
P(15)	1*F*, 2*F*	1282.2371	1282.2328	−0.0043
	1*A*, 3*F*, 1*E*	1282.2236	1282.2175	−0.0061
	4*F*, 5*F*	1282.2133	1282.2069	−0.0064
	2*E*, 6*F*	1282.2075	1282.2011	−0.0064
	2*A*, 7*F*, 8*F*, 3*A*	1282.1998	1282.1935	−0.0063
P(16)	1*A*, 1*F*, 1*E*	1282.1507	1282.1485	−0.0022
	2*F*, 3*F*	1282.1340	1282.1318	−0.0022
	2*E*, 4*F*	1282.1233	1282.1205	−0.0028
	2*A*	1282.1215	1282.1187	−0.0028
	5*F*, 6*F*	1282.1151	1282.1128	−0.0023
	3*A*	1282.1126	1282.1103	−0.0023
	7*F*, 3*E*, 8*F*	1282.1052	1282.1033	−0.0019
P(17)	1*F*, 2*F*	1282.0639	1282.0635	−0.0004
	1*E*, 3*F*, 1*A*	1282.0462	1282.0455	−0.0007
	4*F*, 5*F*	1282.0335	1282.0328	−0.0007
	2*A*	1282.0272	1282.0265	−0.0007
	6*F*, 2*E*	1282.0245	1282.0237	−0.0008
	7*F*	1282.0213	1282.0204	−0.0009
	8*F*, 3*E*, 9*F*	1282.0122	1282.0120	−0.0002
P(18)	1*E*, 1*F*, 1*A*	1281.9764	1281.9778	0.0014
	2*F*, 3*F*	1281.9569	1281.9586	0.0017
	2*A*, 4*F*, 2*E*	1282.9433	1281.9449	0.0016
	5*F*	1282.9347	1281.9364	0.0017
	6*F*	1282.9320	1281.9334	0.0014
	3*E*, 7*F*	1282.9279	1281.9294	0.0015
	3*A*, 8*F*, 9*F*, 4*A*	1282.9180	1281.9197	0.0017
P(19)	1*F*, 2*F*	1281.8890	1281.8914	0.0024
	1*A*, 3*F*, 1*E*	1281.8686	1281.8711	0.0025
	4*F*, 5*F*	1281.8536	1281.8558	0.0022
	2*E*, 6*F*	1281.8436	1281.8457	0.0021
	2*A*	1281.8405	1281.8424	0.0019
	7*F*	1281.8359	1281.8386	0.0027
	8*F*, 3*A*	1281.8341	1281.8362	0.0021
	9*F*, 3*E*, 10*F*	1281.8237	1281.8262	0.0025
P(20)	1*A*, 1*F*, 1*E*	1281.8019	1281.8043	0.0024
	2*F*, 3*F*	1281.7811	1281.7827	0.0016
	2*E*, 4*F*, 2*A*	1281.7639	1281.7661	0.0022
	5*F*, 6*F*	1281.7525	1281.7545	0.0020
	3*A*	1281.7467	1281.7493	0.0026
	7*F*, 3*E*	1281.7426	1281.7452	0.0026
	8*F*	1281.7399	1281.7424	0.0025
	9*F*, 4*E*, 10*F*	1281.7294	1281.7316	0.0022
P(21)	1*F*, 2*F*	1281.7149	1281.7165	0.0016
	1*E*, 3*F*, 1*A*	1281.6923	1281.6937	0.0014
	4*E*, 5*F*	1281.6741	1281.6760	0.0019
	2*A*, 6*F*, 2*E*	1281.6624	1281.6636	0.0012
	7*F*	1281.6542	1281.6560	0.0018
	8*F*	1281.6492	1281.6514	0.0022
	3*E*, 9*F*	1281.6460	1281.6482	0.0022
	3*A*, 10*F*, 11*F*, 4*A*	1281.6329	1281.6360	0.0031
P(22)	1*E*, 1*F*, 1*A*	1281.6261	1281.6280	0.0019
	2*F*, 3*F*	1281.6025	1281.6039	0.0014
	2*A*, 4*F*, 2*E*	1281.5840	1281.5851	0.0011
	5*F*, 6*F*	1281.5717	1281.5709	−0.0008
	3*E*, 7*F*	1281.5608	1281.5618	0.0010
	3*A*	1281.5554	1281.5565	0.0011
	8*F*	1281.5527	1281.5538	0.0011
	9*F*, 4*A*	1281.5500	1281.5516	0.0016
	10*F*	b)		
	4*E*	b)		
	11*F*	b)		
P(23)	1*F*	b)		
	2*F*	b)		
	1*A*, 3*F*, 1*E*	1281.5137	1281.5136	−0.0001
	4*F*, 5*F*	1281.4938	1281.4935	−0.0003
	2*E*, 6*F*, 2*A*	1281.4779	1281.4777	−0.0002
	7*F*	1281.4684	1281.4682	−0.0002
	8*F*	1281.4666	1281.4663	−0.0003
	3*A*	1281.4629	1281.4628	−0.0001
	9*F*, 3*E*	1281.4575	1281.4571	−0.0004
	10*F*	1281.4552	1281.4548	−0.0004
	11*F*, 4*E*, 12*F*	1281.4412	1281.4413	0.0001
P(24)	1*A*, 1*F*, 1*E*	1281.4516	1281.4490	−0.0026
	2*F*, 3*F*	1281.4249	1281.4225	−0.0024
	2*E*, 4*F*, 2*A*	1281.4040	1281.4011	−0.0029
	5*F*, 6*F*	1281.3877	1281.3846	−0.0031
	3*A*	1281.3777	1281.3745	−0.0032
	7*F*, 3*E*	1281.3755	1281.3721	−0.0034
	8*F*	1281.3691	1281.3662	−0.0029
	9*F*	c)		
	4*E*, 10*F*	1281.3605	1281.3572	−0.0033
	4*A*, 11*F*, 12*F*, 5*A*	1281.3456	1281.3423	−0.0033

a) Δ = (calculated frequency) − (observed frequency). b) Not observed because of overlapping with N_2O lines.
c) Not observed because of overlapping with other lines.

amplitudes of the harmonic vibrations perpendicular to the internuclear axis, r_g is the internuclear distance which is directly observed by the gas-electron-diffraction method, and δ_r is the small correction for the centrifugal distortion. On the other hand, a moment of inertia in the ground state, I_{zero}, is expressed as:

$$I_{zero} = I_0\left(1-\sum_s \frac{g_s}{2B_0}\alpha^{harm.}\right) \quad (10)$$

where I_0 is effective moment of inertia obtained from spectroscopy, $\alpha^{harm.}$, the harmonic part of the vibration-rotation constant, and g_s, the degree of vibrational degeneracy. The relation between the nuclear-distance parameter, r_z, which is derived from I_{zero}, and the nuclear distance parameter, r_α, of Eq. 9 is:

$$\lim_{T\to 0} r_\alpha \equiv r^0 = r_z. \quad (11)$$

Therefore, r_α can be regarded as r_z if the normal frequencies are much larger than kT/hc. In the case of carbon tetrafluoride, therefore, we get:

$$r_z(\text{C-F}) = (1.3172\pm0.0004)\times10^{-8}\,\text{cm}, \quad \text{and}$$
$$B_0 = 0.1920\pm0.0001\,\text{cm}^{-1},$$

using $r_g(\text{C-F})=(1.3197+0.0004)\times10^{-8}$ cm, which was determined by Fink *et al.*,[7] and the harmonic force field of Ref. 8. The values of the molecular constants which were calculated from the B_0 value and the molecular constants of Table 1 are summarized in Table 3.

Table 3. The molecular constants (in cm^{-1}) determined by using the r_g-structure and the present results

ν_0	1283.7181±0.0044
B_{eff}^{PR}	0.1915±0.0001
B_0	0.1920±0.0001
$(B\zeta_3)_{eff}$	0.1557±0.0003

It is of some interest to estimate the Coriolis coupling constant from the observed $(B\zeta_3)_{eff}$ value. $(B\zeta_3)_{eff}$ is written as:[6]

$$(B\zeta_3)_{eff} = B_e\zeta_3 + (3/4)\beta_3 \quad (12)$$

where;

$$\beta_3 = (1/3)(B_{eff}^{Q}-B_{eff}^{PR}). \quad (13)$$

From these equations, ζ_3 is given by:

$$\zeta_3 = \frac{(B\zeta_3)_{eff}-(1/4)(B_{eff}^{Q}-B_{eff}^{PR})}{B_e}. \quad (14)$$

In order to determine the ζ_3 value, the as-yet-undetermined B_{eff}^{Q} and B_e values are necessary. If we assume that these relations hold:

$$|B_{eff}^{Q}-B_{eff}^{PR}| \lesssim |B_{eff}^{PR}-B_0|$$

and:

$$|B_0-B_e| \lesssim |B_{eff}^{PR}-B_0|,$$

then ζ_3 is approximately expressed as:

$$\zeta_3 \simeq (B\zeta_3)_{eff}/B_0. \quad (15)$$

The error expected in the ζ_3 value thus calculated is of the order of $(2|B_{eff}^{PR}-B_0|)/B_0$. Thus, we obtained $\zeta_3=0.811\pm0.006$. Edgell *et al.* determined the Coriolis conpling constant for the ν_3 band, $\zeta_3=0.84$, by an analysis of the P-R-branch separation of the ν_3 envelope.[1] The present result is significantly smaller than their result. The Coriolis coupling constant for the ν_4 band was obtained by Jones *et al.*[3] Their result, $\zeta_4=-0.366$, predicts that the ζ_3 value will be about 0.866, because of the Corilois sum rule, $\zeta_3+\zeta_4=0.5$. The present estimation is much smaller than their prediction. The reason for this disagreement is not yet clear and must be left for future study.

Incidentally, we wish to add a few lines on a future problem in high-resolution spectroscopy using a tunable diode laser-source spectrometer. In this study, detailed molecular constants could not be obtained, although the spectra have been recorded by the use of a tunable diode laser-source spectrometer whose instrumental resolution was 10^{-4}—10^{-3} cm^{-1}. The reason for this are thought to be:

1) The precision and accuracy of the frequency measurement is not satisfactory enough, although the instrumental resolution surprisingly high.

2) It is difficult to tune a diode laser in the required frequency region and over a wide frequency range.

3) Since an observed linewidth is governed by the Doppler broadening, an effective spectral resolution is not essentially improved very much.

The authors wish to express their thanks to Dr. Shigeo Kondou, of the National Chemical Laboratory for Industry, for obtaining the spectrum recorded by the Fourier transform spectrometer. The authors also would like to thank professor Eizi Hirota, of the Institute for Molecular Science, for giving them the opportunity to use the tunable diode laser-source spectrometer.

References

1) W. F. Edgell and R. E. Moynihan, *J. Chem. Phys.*, **27**, 155 (1957).
2) A. Maki, E. K. Plyler, and R. Thibault, *J. Chem. Phys.*, **37**, 1899 (1962).
3) L. H. Jones, B. J. Krohn, and W. C. Kennedy, *J. Mol. Spectrosc.*, **70**, 288 (1978).
4) R. P. Grosso and T. K. McCubbin, Jr., *J. Mol. Spectrosc.*, **13**, 240 (1964).
5) J. Dupre-Maquaire and P. Pinson, *J. Mol. Spectrosc.*, **58**, 239 (1975).
6) J. Herranz, *J. Mol. Spectrosc.*, **6**, 343 (1961).
7) M. Fink, C. W. Schmiedekamp, and D. Gregory, *J. Chem. Phys.*, to be published.
8) T. Shimanouchi, I. Nakagawa, J. Hiraishi, and M. Ishii, *J. Mol. Spectrosc.*, **19**, 78 (1966).

9) We tried to determine the molecular constants, including the centrifugal distortion constants, with the assumption that $D_0^J=D_1^J$. The following molecular constants were obtained by the least-squares method:

$$\nu_0-2(B\zeta_3)_{eff} = 1283.2978\pm0.0092\,\text{cm}^{-1}$$
$$B_{eff}^{PR}+B_0-2(B\zeta_3)_{eff} = (5.050\pm0.178)\times10^{-2}\,\text{cm}^{-1}$$
$$B_{eff}^{PR}-B_0 = -(1.876\pm0.110)\times10^{-4}\,\text{cm}^{-1}$$

$D_0^J = (6.93 \pm 0.56) \times 10^{-6}\ cm^{-1}$

$\delta_3 = (6.123 \pm 0.054) \times 10^{-4}\ cm^{-1}$

However, these results seem to be unreasonable. The transition frequency of the R-branch line which is calculated from these molecular constants takes a maximum value at $J=11$ and then decreases $J>11$ as the J value increases. This is not consistent with the observed band profile of the R branch (see Fig. 1).

10) Even if we give zero weight to the P(15) lines in the least-squares fitting, the resultant molecular constants are very close to those in Table 1.

11) Y. Morino, K. Kuchitsu, and T. Oka, *J. Chem. Phys.*, **36**, 1108 (1962).

Vibration Spectra and Rotational Isomerism of Chain Molecules. VIII.[1] 1-Chloro-, 1-Bromo-, and 1-Iodopentanes, and 1,4-Dichloro- and 1,4-Dibromobutanes

Hiroatsu MATSUURA,*,† Shuji IMAZEKI, Yoshiki OGAWA, Masaaki SAKAKIBARA,††
Issei HARADA, and Takehiko SHIMANOUCHI†††

Department of Chemistry, Faculty of Science, University of Tokyo, Hongo, Bunkyo-ku, Tokyo 113

(Received March 26, 1979)

The Raman and infrared spectra of 1-chloro-, 1-bromo-, and 1-iodopentanes $CH_3(CH_2)_4X$ (X=Cl, Br, and I), and 1,4-dichloro- and 1,4-dibromobutanes $X(CH_2)_4X$ (X=Cl and Br) were measured for the gaseous, liquid, glassy, and crystalline states. The normal coordinates were calculated for these molecules by the use of a consistent set of force constants. The rotational isomerism was studied by analyzing the spectra with reference to the results of the calculation. The study clarified the isomers present not only in the crystalline state but also in other states of aggregation. In the crystal, 1-chloro-, 1-bromo-, and 1-iodopentanes take the *trans-trans-trans* form and 1,4-dichloro- and 1,4-dibromobutanes take the *gauche-trans-gauche'* form.

Many studies have been made of the rotational isomerism of 1-halogenopentanes[2–7] and 1,4-dihalogenobutanes[8–11] by means of Raman, infrared, and NMR measurements. As a result, the conformer in the crystalline state has been made clear for each of these molecules. However, the rotational isomers existing in other states such as liquid and glass have not yet been fully explored.

In the preceding paper of this series,[1] we reported the vibration spectra and the rotational isomerism of 1-halogenopropanes and 1-halogenobutanes, and obtained information on the conformational stabilities of these molecules. In the present work, we extended our studies to longer halogenoalkanes: 1-halogenopentanes $CH_3(CH_2)_4X$ (X=Cl, Br, and I) and 1,4-dihalogenobutanes $X(CH_2)_4X$ (X=Cl and Br). The rotational isomerism was studied by analyzing the Raman and infrared spectra with reference to the results of the normal coordinate calculation.

Experimental

All the samples used in this study were purchased from Tokyo Kasei Kogyo Co., Ltd. and were distilled prior to the spectroscopic measurements. The Raman and infrared spectra were measured for the gaseous (only for 1-chloropentane), liquid, glassy, and crystalline states by the method reported previously.[12,13] The glassy state for Raman measurements was obtained by immersing the liquid sample enclosed in an ampoule in liquid nitrogen for rapid cooling, and the glassy state for infrared measurements by depositing the gaseous sample onto a cooled plate of KBr or KRS-5. The glassy state of 1,4-dichloro- and 1,4-dibromobutanes for Raman measurements and that of 1,4-dibromobutane for infrared measurements could not be obtained because of rapid crystallization.

Normal Coordinate Treatment

The normal coordinate calculations were carried out with a computer program NCTB2[14] and a HITAC 8800/8700 computer system at the Computer Center of the University of Tokyo. The detailed procedure of the calculations on unbranched halogenoalkanes has been described in the previous paper.[1] The observed frequencies for the molecules treated in this study together with those of the shorter molecules (1-halogenopropanes, 1-halogenobutanes, and 1,3-dihalogenopropanes) were used in the refinement of the force constants.

In the analyses of the observed spectra, the calculation of the normal coordinates plays an important role, since the assignments of the bands to individual conformers rely largely on the calculated frequency values. Therefore, the accuracy of the calculated frequencies has to be high enough to allow the spectral analyses. The high accuracy is particularly required for large molecules, such as those studied in this work, which give many bands in the spectra.

The force constants used in this study have been obtained by the least-squares procedure from about 340 observed frequencies for chloroalkanes, 400 for bromoalkanes, and 400 for iodoalkanes,[15] with root-mean-square deviations of 5.6, 6.1, and 6.5 cm^{-1}, respectively, between the observed and calculated frequencies. These accuracies of the calculations, we believe, are high enough to analyze the spectra of 1-halogenopentanes and 1,4-dihalogenobutanes in this study.

Results

Figures 1—10 show the observed spectra of the 1-halogenopentane and 1,4-dihalogenobutane molecules in various states of aggregation in comparison with the calculated frequencies.[17]

1-Halogenopentane molecules have, as given in Table 1 of Part I of this series,[12] fourteen possible rotational isomers, TTT, TTG, TGT, GTT, TGG, GTG, GGT, TGG', GTG', GG'T, GGG, GGG', GG'G, and GG'G', where the first conformation symbol in each isomer designation is that for the CH_3CH_2–CH_2CH_2 axis and the last for the CH_2CH_2–CH_2X axis. Of these, the isomers with a sequence of the GG' conformation, *i.e.* TGG', GG'T, GGG', GG'G, and GG'G' are unlikely to exist because of the strong

† Present address: Department of Chemistry, Faculty of Science, Hiroshima University, Higashisenda-machi, Hiroshima 730.

†† Present address: Faculty of General Education, Tottori University, Koyama-cho, Tottori 680.

††† Present address: Institute of Information Sciences, University of Tsukuba, Sakura-mura, Ibaraki 300-31.

Table 1. Rotational isomers of 1-halogenopentanes and 1,4-dihalogenobutanes

Molecule	Gas	Liquid	Glass	Crystal
$CH_3(CH_2)_4F$[a]	—[b]	TTG TTT TGT GTT	—[b]	TTG
$CH_3(CH_2)_4Cl$	TTT TTG TGT TGG GTG GTG′	TTT TTG TGT TGG GTG GTG′	TTT TTG TGT TGG GTG GTG′	TTT
$CH_3(CH_2)_4Br$	—[b]	TTT TTG TGT GTT TGG GTG GTG′ GGG	TTT TTG TGT TGG GTG GTG′	TTT TTG[c]
$CH_3(CH_2)_4I$	—[b]	TTT TTG TGT GTT TGG GTG GTG′ GGG	TTT TTG TGT GTT TGG GTG GTG′	TTT
$Cl(CH_2)_4Cl$	—[b]	GTG′ TTT TTG TGG GTG GGG	GTG′ TTT TTG GTG GGG	GTG′
$Br(CH_2)_4Br$	—[b]	GTG′ TTT TTG TGT TGG GTG GGG	—[b]	GTG′

a) Ref. 6. b) Spectral measurements were not made. c) Two crystal modifications have been obtained. For the TTG form, see Ref. 20.

steric hindrance. In fact, existence of the GG′ form of pentane[18] or of 1-halogenobutanes[1] has not been identified in any state of aggregation. 1,4-Dihalogenobutane molecules have ten possible rotational isomers, TTT, TTG, TGT, TGG, GTG, TGG′, GTG′, GGG, GGG′, and GG′G. Of these, the TGG′, GGG′, and GG′G forms are again unlikely to exist.

In the following subsections, the rotational isomerism of the individual molecules is described. For the spectral analyses, the bands due to the skeletal deformation, skeletal stretching, and CH_2 rocking vibrations were primarily used to identify the existing rotational isomers.

1-Chloropentane (See Figs. 1 and 2). The crystalline-state spectra are explained by the existence of the TTT form, since the Raman bands at 263, 347, 448, 714, 737, 759, 835, 892, (and 900), and 955 cm^{-1} are all assigned consistently to this form. The calculated frequencies are 256, 354, 462, 727, 729, 754, 833, 901, and 956 cm^{-1}, respectively.

In the liquid and glassy states, the spectra exhibit many bands to be assigned to various rotational isomers. It is evidently shown that the TTT and TTG forms exist in these states. The relative intensities of the Raman bands at 400, 455, 653, 788, 838, 908, and 923 cm^{-1}, together with those of the bands which have been assigned to the TTT form, increase in going from the liquid state at room temperature to the glassy state at liquid nitrogen temperature. All of these bands correspond to the calculated frequencies for the TTG form: 401, 456, 656, 791, 838, 916, and 929 cm^{-1}.

The liquid- and glassy-state spectra have further additional bands. Spectral observations indicate that these bands lose their intensities largely, when temperature is lowered, as compared with the bands which have been assigned to the TTT and TTG forms. According to the results of the normal coordinate treatment, the bands at 375 and 822 cm^{-1} are assigned to the GTG form (the calculated frequencies: 369 and 823 cm^{-1}), those at 387 and 878 cm^{-1} to the TGG form (384 and 886 cm^{-1}), those at 712, 764, and 855 cm^{-1} to the TGT form (714, 761, and 856 cm^{-1}), and that at 933 cm^{-1} to the GTG′ form (938 cm^{-1}).

Existence of the GTT form is uncertain, since all of the calculated frequencies of this form are almost coincident with those of the other forms mentioned above. For the GGG and GGT forms, no positive evidence of their existence was obtained. According to the calculation, the former form is expected to exhibit bands around 325 and 410 cm^{-1} and the latter at 475 cm^{-1}, but no recognizable bands are actually observed in these frequency regions. Therefore, the GGG and GGT forms do not seem to exist in the liquid or glassy state.

The gaseous-state Raman spectrum is essentially the same as the liquid-state Raman spectrum but relative intensities of several bands are different between them. This suggests that the gaseous and liquid molecules have the same kinds of rotational isomers with different distributions.

The temperature dependence of the liquid-state Raman spectra shows that the TTT and TTG forms have much higher stabilities than the other forms in this state. These two forms are also dominant conformers in the glassy state at liquid nitrogen temperature. These observations are consistent with the result obtained for 1-chlorobutane that the TT and TG forms are more stable than the other forms.[1]

1-Bromopentane (See Figs. 3 and 4). The spectra of the crystalline state is explained by the existence of the TTT form, since the Raman bands at 216, 334, 433, 638 (and 644), 731, 753, 828, 894 (and 899), and 944 cm^{-1} are assigned consistently only to this form. The calculated frequencies are 215, 341, 446, 642, 729, 751, 825, 899, and 943 cm^{-1}, respectively.

In the liquid and glassy states, the existence of the TTT and TTG forms is clear, similarly to the case of 1-chloropentane. In going from the liquid state to

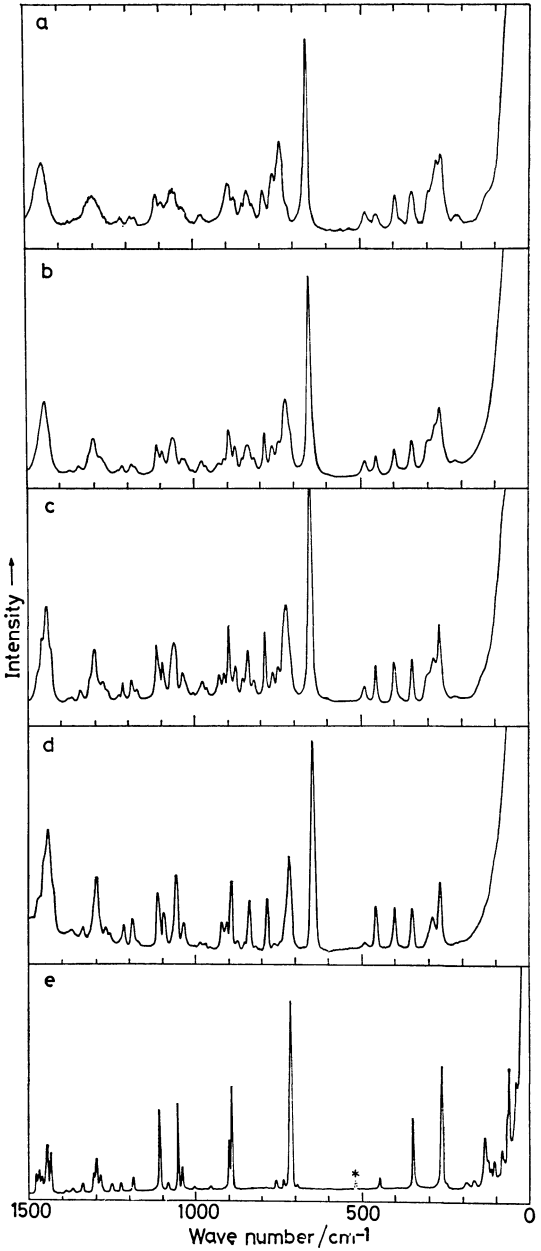

Fig. 1. Raman spectra of 1-chloropentane. a: Gas (23 °C), b: liquid (23 °C), c: liquid (−90 °C), d: glass (liquid nitrogen temperature), e: crystal (liquid nitrogen temperature). The following symbols are used in Figs. 1—10. *: Emission line of Ar^+ laser, △: origin unknown.

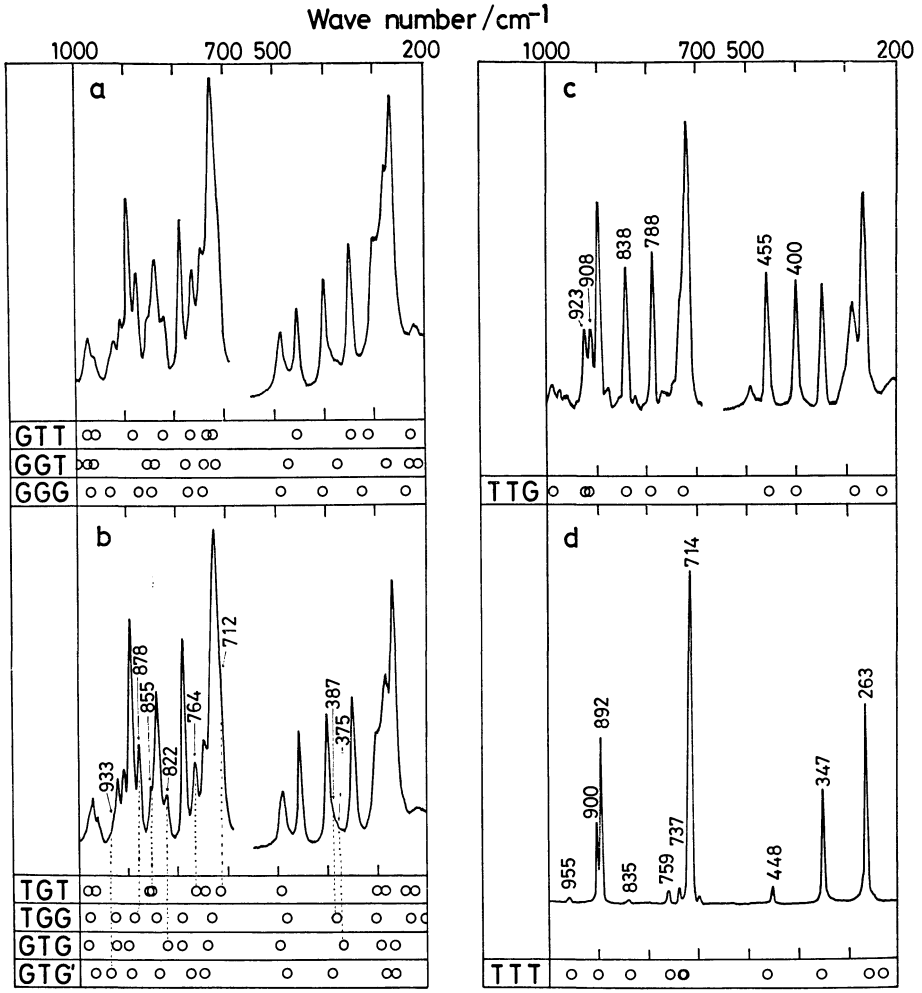

Fig. 2. Comparison between the Raman spectra and the calculated freqencies of 1-chloropentane. a: Liquid (23 °C), b: liquid (−90 °C), c: glass (liquid nitrogen temperature), d: crystal (liquid nitrogen temperature).

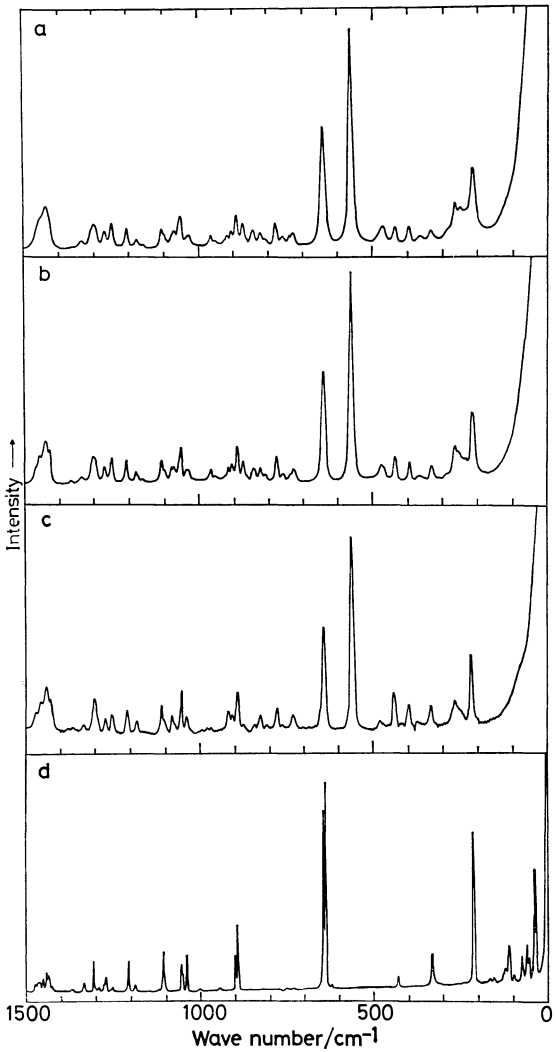

Fig. 3. Raman spectra of 1-bromopentane. a: Liquid (23 °C), b: liquid (−85 °C), c: glass (liquid nitrogen temperature), d: crystal (liquid nitrogen temperature).

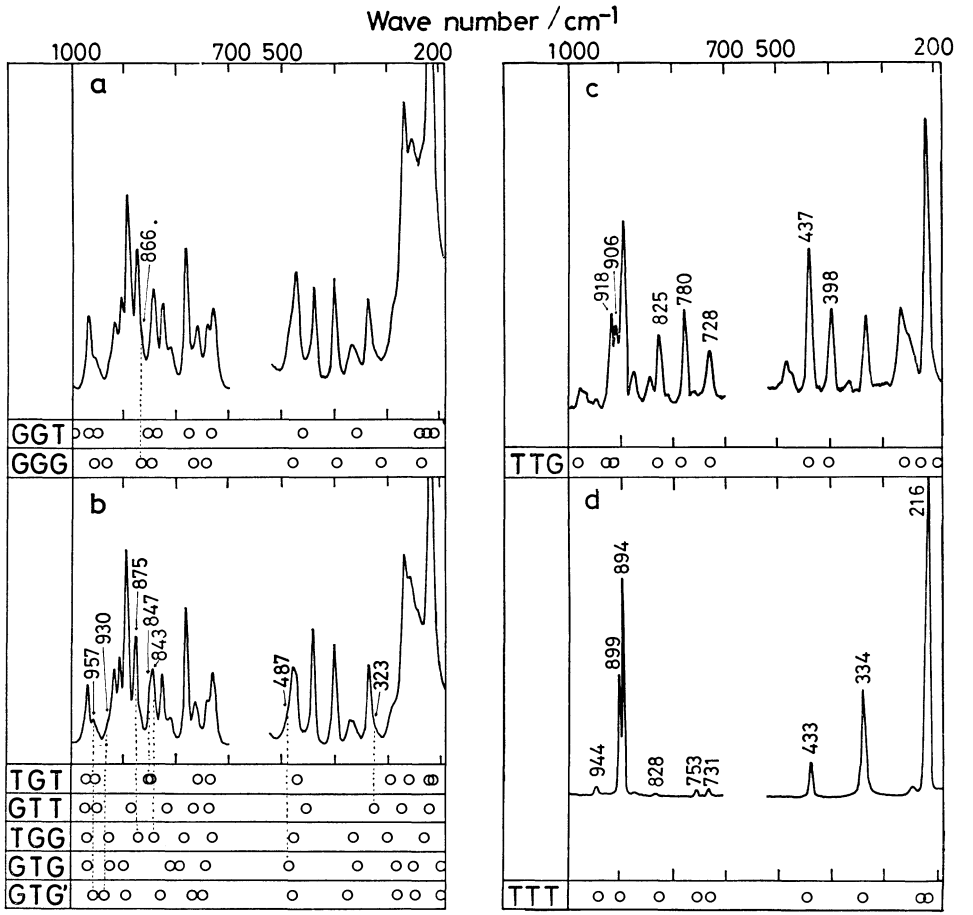

Fig. 4. Comparison between the Raman spectra and the calculated frequencies of 1-bromopentane. a: Liquid (23 °C), b: liquid (−85 °C), c: glass (liquid nitrogen temperature), d: crystal (liquid nitrogen temperature).

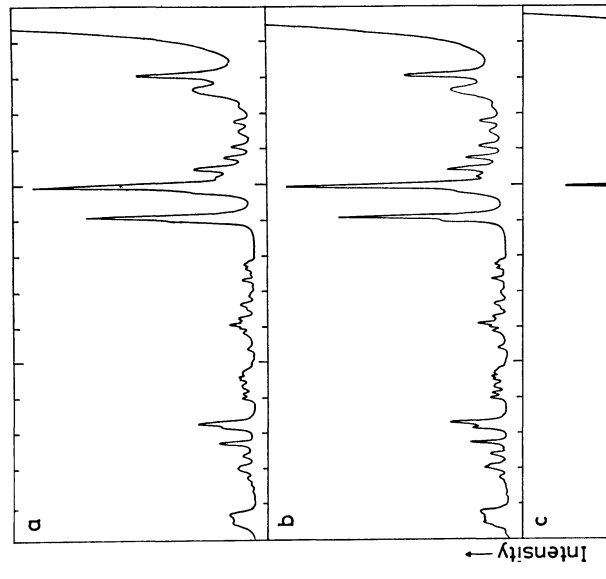

Fig. 5. Raman spectra of 1-iodopentane. a: Liquid (23 °C), b: liquid (−80 °C), c: glass (liquid nitrogen temperature), d: crystal (liquid nitrogen temperature).

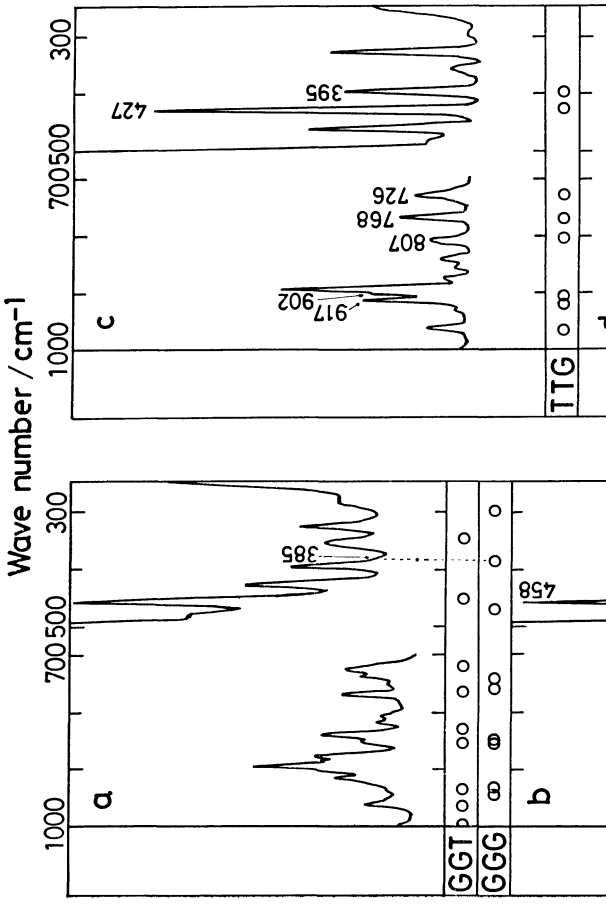

Fig. 6. Comparison between the Raman spectra and the calculated frequencies of 1-iodopentane. a: Liquid (23 °C), b: liquid (−80 °C), c: glass (liquid nitrogen temperature), d: crystal (liquid nitrogen temperature).

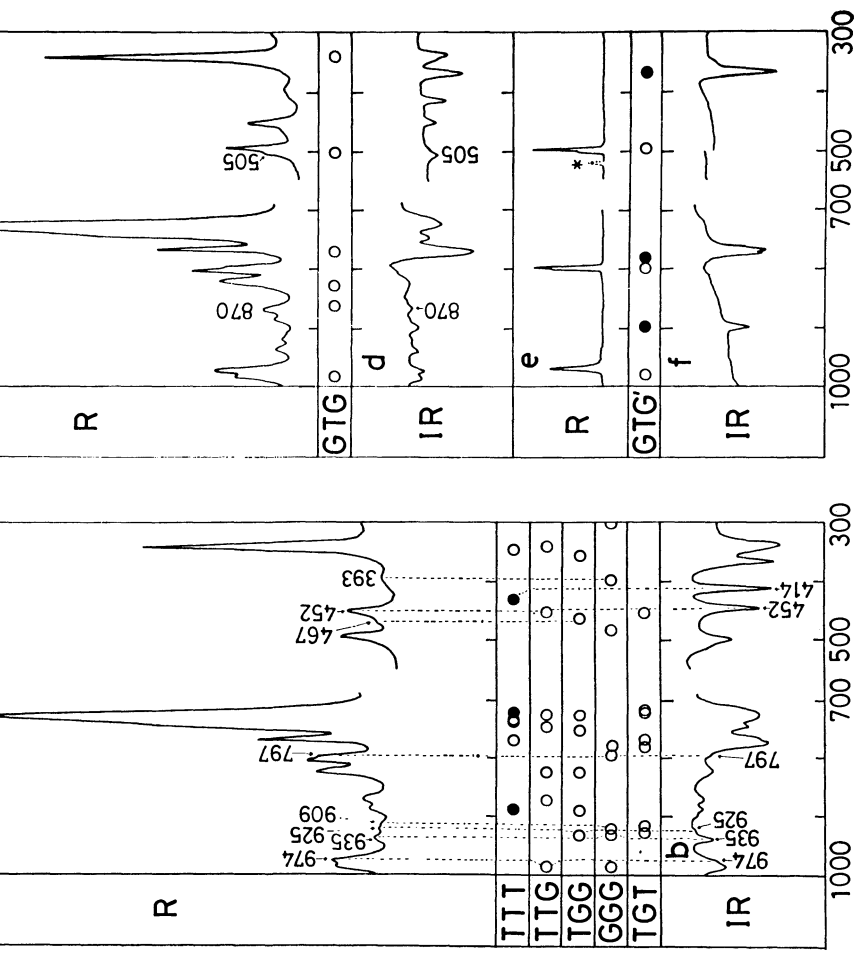

Fig. 8. Comparison between the observed spectra and the calculated frequncies of 1,4-dichlorobutane. a: Liquid (Raman, 23 °C), b: liquid (infrared, room temperature), c: liquid (Raman, −35 °C), d: glass (infrared), e: crystal (Raman, liquid nitrogen temperature), f: crystal (infrared). For the TTT and GTG′ forms, the open and filled circles indicate Raman- and infrared-active vibrations, respectively.

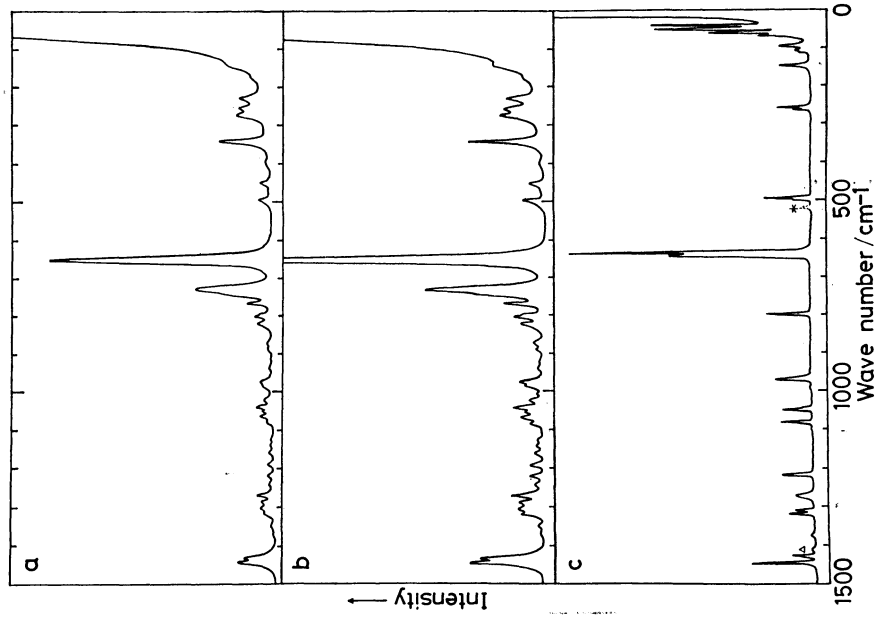

Fig. 7. Raman spectra of 1,4-dichlorobutane. a: Liquid (23 °C), b: liquid (−35 °C), c: crystal (liquid nitrogen temperature).

the glassy state, the relative intensities of the Raman bands at 398, 437, 562, 728, 780, 825, 906, and 918 cm^{-1} of the TTG form increase together with those of the TTT form. The calculated frequencies of the TTG form are 400, 438, 563, 731, 784, 827, 912, and 926 cm^{-1}, respectively.

In addition to the Raman bands of the TTT and TTG forms, the liquid- and glassy-state spectra exhibit many other bands. On the basis of the results of the normal coordinate treatment, the band at 323 cm^{-1} is assigned to the GTT form (the calculated frequency: 326 cm^{-1}), that at 487 cm^{-1} to the GTG form (485 cm^{-1}), those at 843 and 875 cm^{-1} to the TGG form (844 and 874 cm^{-1}), that at 847 cm^{-1} to the TGT form (847 and 850 cm^{-1}), and those at 930 and 957 cm^{-1} to the GTG′ form (936 and 955 cm^{-1}). It is likely that the GGG form is also present in the liquid state, since a very weak Raman band is observed as a shoulder at 866 cm^{-1}, which corresponds to the calculated frequency 867 cm^{-1} of this form.

Existence of the GGT form in the liquid and glassy states is uncertain, as all of the calculated frequencies of this form are almost coincident with those of the other forms mentioned above. Also, the GTT and GGG forms are not confirmed to exist in the glassy state, because their characteristic bands are too weak to identify them in this state.

The TTT and TTG forms are far more stable than the other forms in the liquid state as shown from the temperature dependence of the Raman intensities, and are also predominating isomers in the glassy state. These findings are similar to those for 1-chloropentane.

1-Iodopentane (See Figs. 5 and 6). The molecule takes the TTT form in the crystalline state, since the observed Raman bands at 205, 329, 432, 593, 715, 745, 813, and 898 cm^{-1} are assigned consistently to this form which gives calculated frequencies 191, 331, 438, 590, 721, 736, 811, and 898 cm^{-1}.

The existence of the TTT and TTG forms in the liquid and glassy states is clearly shown from the spectral observation that the bands whose intensities increase at lower temperature are assigned to these forms. The Raman bands of the TTG form are those at 395, 427, 506, 726, 768, 807, 902, and 917 cm^{-1} which are compared with the calculated frequencies 399, 426, 506, 731, 769, 808, 908, and 922 cm^{-1}, respectively.

In addition to the TTT and TTG forms, the existence of other forms in the liquid and glassy states is confirmed by the spectral observations incorporated with the normal coordinate treatment. Of the Raman bands which have not been assigned to the TTT or TTG form, the bands at 458 and 525 cm^{-1} are interpreted to be due to the TGG form (the calculated frequencies: 463 and 516 cm^{-1}), those at 602 and 837 cm^{-1} to the TGT form (598 and 837 cm^{-1}), those at 782 and 799 cm^{-1} to the GTG form (784 and 791 cm^{-1}), that at 817 cm^{-1} to the GTG′ form (814 cm^{-1}), and that at 875 cm^{-1} to the GTT form (883 cm^{-1}).

It is likely that the GGG form exists in the liquid state, since a very weak Raman band is observed at 385 cm^{-1} at room temperature, which is in agreement with the calculated frequency 387 cm^{-1} of this form. However, in the glassy-state spectrum, this band is too weak to confirm existence of this form. Therefore, it is not certain whether the GGG form is present in this state. Existence of the GGT form in the liquid and glassy states is also uncertain, since all of the calculated frequencies are almost coincident with those of the other forms.

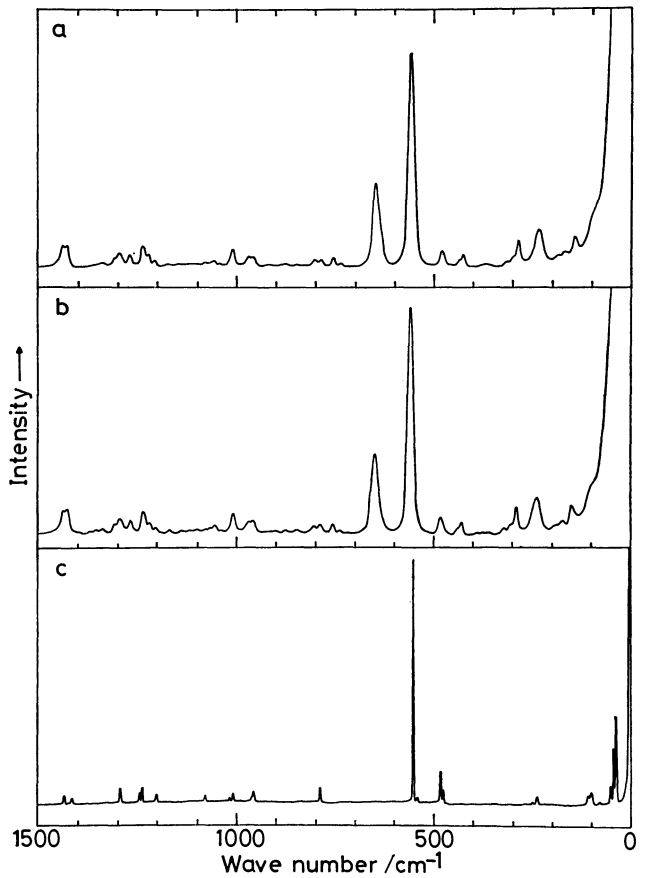

Fig. 9. Raman spectra of 1,4-dibromobutane. a: Liquid (23 °C), b: liquid (−20 °C), c: crystal (liquid nitrogen temperature).

The glassy-state spectra and the temperature dependence of the liquid-state spectra show that the conformational stabilities of the TTT and TTG forms are higher than those of the other forms.

The spectra of the liquid and glassy states exhibit in the C–I stretching region four Raman bands at 506, 525, 592, and 602 cm^{-1} and the corresponding infrared bands at 506, 522, 593, and 603 cm^{-1}. According to the normal coordinate calculation, the TTG, GTG, and GTG′ forms (having the *trans-gauche* conformation about the CC–C–CI axes) give the C–I stretching frequencies of about 505 cm^{-1}, the TGG and GGG forms (having the *gauche-gauche* conformation) about 515 cm^{-1}, the TTT and GTT forms (having the *trans-trans* conformation) about 590 cm^{-1}, and the TGT and GGT forms (having the *gauche-trans* conformation) about 600 cm^{-1}. The observed bands are reasonably assigned to these four groups of conformers. This spectral observation indicates that the C–I stretching frequency can be used to examine the conformation not only about the CC–CI axis but also about the adjacent CC–CCI axis.

1,4-Dichlorobutane (See Figs. 7 and 8). In the crystalline state, the Raman and infrared spectra are quite different from each other and the mutual exclusion in the Raman and infrared activities is clearly observed. Of the two conformers TTT and GTG′ having a center of symmetry, the observed C–Cl stretching frequencies of about 640 cm^{-1} are consistent only with the latter form. The observed frequencies of other bands are also explained by this form. Thus, the molecule in the crystal is found to take the centrosymmetrical GTG′ form.

The observed spectra in the liquid state are explained by the coexistence of the GTG′, TTT, TTG, GTG, GGG, and TGG forms. The bands which are characteristic of the individual conformers are: 175, 452, and 974 cm^{-1} of the TTG form (the calculated frequencies: 181, 456, and 988 cm^{-1}); 230 (Raman) and 414 cm^{-1} (infrared) of the TTT form (213 and 428 cm^{-1}); 393, 797, 909, and 935 cm^{-1} of the GGG form (400, 798, 923, and 933 cm^{-1}); 467 and 925 cm^{-1} of the TGG form (465 and 932 cm^{-1}); and 505 and 870 cm^{-1} of the GTG form (504 and 864 cm^{-1}). In the glassy-state infrared spectrum, most of the liquid-state bands persist but the bands assignable to the TGG form are not observed definitely. Accordingly, the conformers mentioned above for the liquid state but the TGG form are confirmed to be present in the glassy state as well. Existence of the TGT form is not certain in the liquid and glassy states, since all of their frequencies are almost coincident with those of the other forms.

The spectral change with temperature variation in the liquid state shows that the Raman bands at 494, 505, 803, 870, and 974 cm^{-1} are enhanced at lower temperature. This indicates that the GTG′ and GTG forms, to which these bands are assigned, are more stable than the other forms coexisting in the liquid state.

1,4-Dibromobutane (See Figs. 9 and 10). In the crystalline state, the Raman and infrared spectra show the mutual exclusion activities, similarly to the case of 1,4-dichlorobutane. The observed frequencies and the Raman and infrared activities of the individual vibrations agree with those for the GTG′ form, indicating the existence of this form in the crystalline state.

Analyses of the liquid-state Raman and infrared spectra show that all of the seven possible conformers, GTG′, TTT, TTG, GTG, GGG, TGG, and TGT, are present in this state. The following bands give evidences for the existence of these conformers: 148 (Raman), 325 (Raman), 354 (infrared), and 743 cm^{-1} (infrared) of the TTT form (the calculated frequencies: 142, 331, 366, and 735 cm^{-1}); 190, 368, 474, and 787 cm^{-1} of the GGG form (200, 371, 464, and 787 cm^{-1}); 303, 484, and 817 cm^{-1} of the GTG form (305, 481, and 819 cm^{-1}); 318, 443, and 873 cm^{-1} of the TGG form (321, 435, and 878 cm^{-1}); 387 cm^{-1} of the TGT form (399 cm^{-1}); and 428 and 289 cm^{-1} of the TTG form (432 and 289 cm^{-1}).

In the liquid-state Raman spectra, the intensities of the bands at 481, 787, and 959 cm^{-1} are enhanced at lower temperature as compared with those of other bands. The GTG′ form, giving these bands, is thus found to have higher stability than others in the liquid state.

Rotational Isomerism in Comparison with Previous Results. In Table 1, the rotational isomerism of the five molecules studied in this work is summarized. The result of 1-fluoropentane $CH_3(CH_2)_4F$ is also included in this table.

Many studies have been made of the rotational isomerism of 1-halogenopentanes[2–7] and 1,4-dihalogenobutanes.[8–11] Brown and Sheppard[2,9] studied the infrared spectra of many halogenoalkane molecules in the liquid and crystalline states. They concluded that the crystalline-state isomer of 1-bromopentane has a planar conformation of the carbon and bromine atoms. For 1,4-dichloro- and 1,4-dibromobutanes, they showed that these molecules take in the crystalline state the GTG′ conformation with a center of symmetry.

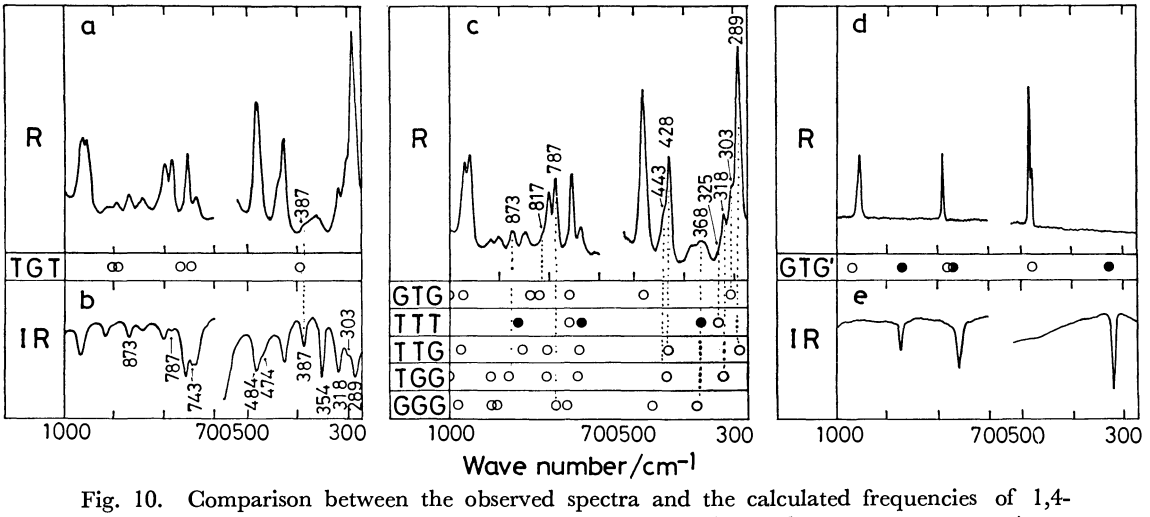

Fig. 10. Comparison between the observed spectra and the calculated frequencies of 1,4-dibromobutane. a: Liquid (Raman, 23 °C), b: liquid (infrared, room temperature), c: liquid (Raman, −20 °C), d: crystal (Raman, liquid nitrogen temperature), e: crystal (infrared). For the TTT and GTG′ forms, the open and filled circles indicate Raman- and infrared-active vibrations, respectively.

Snyder and Schachtschneider[5] measured the infrared spectra of $CH_3(CH_2)_nCl$ (n=1—5) in the crystalline and glassy states. For 1-chloropentane, they concluded on the basis of the normal coordinate analysis that the spectrum of the former state could be explained by the existence of the TTT form and that of the latter state by the coexistence of the TTT and TTG forms.

Crowder and coworkers, on the other hand, interpreted the infrared spectra of 1-iodopentane[7] and 1-fluoropentane[6] in the liquid, glassy, and crystalline states, taking account of only two among various isomers, the TTT and TTG forms. Their observed data for 1-fluoropentane were analyzed in the light of our normal coordinate calculation,[1,14] and it is now shown that the TGT and GTT forms, in addition to the TTT and TTG forms they mentioned, are confirmed to exist in the liquid state. Crowder and Ali[11] also measured the spectra of 1,4-diiodobutane.

The present results of the rotational isomerism in the crystalline state agree with the previous results mentioned above. This study further clarified the rotational isomers present in the liquid and glassy states as well on the basis of the careful spectral observations and the systematic normal coordinate calculation.

Discussion

In our previous study,[1] it was demonstrated that the skeletal deformation vibrations were important for studying the rotational isomerism of halogenoalkanes. In the present study on the longer molecules, the bands in the skeletal deformation region were efficiently used in analyzing the spectra and identifying the rotational isomers present in various states of aggregation. The bands due to the skeletal stretching and the CH_2 rocking vibrations were also found to be useful for studying the rotational isomers.

From the results in this and previous[1] studies on $CH_3(CH_2)_nX$ (n=2—4; X=Cl, Br, and I) and $X(CH_2)_4X$ (X=Cl and Br), it has become clear that the *gauche* conformation about the CC–CX axis is more stable than or as stable as the *trans* conformation in the liquid state. However, in the crystalline state, the accessible conformation about this axis is likely to depend on the subtle balance between the intramolecular forces favoring the *gauche* conformation rather than the *trans* and the intermolecular forces favoring the *trans* conformation. For $X(CH_2)_3X$ (X=Cl, Br, and I)[9,19] and $X(CH_2)_4X$ (X=Cl and Br), the non-planar GG and GTG′ forms exist in the crystalline state. On the other hand, for $CH_3(CH_2)_nX$ (n=2—4; X=Cl, Br, and I), the all-*trans* form exists in the crystalline state. A crystal consisting of the TTG form of $CH_3(CH_2)_4Br$ has also been obtained.[20] It is thus probable that the balance of the intra- and intermolecular forces mentioned above is responsible, at least in part, for the thermodynamic properties of these molecular crystals.

Through this series of studies on the vibration spectra and the rotational isomerism of chain molecules, a reliable and consistent set of force constants has been obtained, which has been satisfactorily utilized for predicting vibrational frequencies of various molecules. The present method of analyzing the spectra in conjunction with the use of the refined force field encourages us to make further studies on the rotational isomerism of large molecules.

The present series of studies has also provided us with various important information for making more advanced investigations in the field of structural chemistry. The conformational polymorphism of halogenoalkane molecules[20] has been in fact investigated in close relation to our fundamental studies in this series.

References

1) Part VII: Y. Ogawa, S. Imazeki, H. Yamaguchi, H. Matsuura, I. Harada, and T. Shimanouchi, *Bull. Chem. Soc. Jpn.*, **51**, 748 (1978).
2) J. K. Brown and N. Sheppard, *Trans. Faraday Soc.*, **50**, 535 (1954).
3) T. Yoshino and H. J. Bernstein, *Can. J. Chem.*, **35**, 339 (1957).
4) P. N. Gates, E. F. Mooney, and H. A. Willis, *Spectrochim. Acta, Part A*, **23**, 2043 (1967).
5) R. G. Snyder and J. H. Schachtschneider, *J. Mol. Spectrosc.*, **30**, 290 (1969).
6) G. A. Crowder and H. -K. Mao, *J. Mol. Struct.*, **23**, 161 (1974).
7) G. A. Crowder and M. Jalilian, *J. Mol. Struct.*, **33**, 127 (1976).
8) J. Goubeau and H. Pajenkamp, *Acta Phys. Austriaca*, **3**, 283 (1949).
9) J. K. Brown and N. Sheppard, *Discuss. Faraday Soc.*, **9**, 144 (1950); *Proc. R. Soc. London, Ser.A*, **231**, 555 (1955).
10) D. W. Aksnes, *Acta Chem. Scand.*, **26**, 164, 1883 (1972).
11) G. A. Crowder and S. Ali, *J. Mol. Struct.*, **27**, 43 (1975).
12) Part I: T. Shimanouchi, Y. Ogawa, M. Ohta, H. Matsuura, and I. Harada, *Bull. Chem. Soc. Jpn.*, **49**, 2999 (1976).
13) Part IV: M. Ohta, Y. Ogawa, H. Matsuura, I. Harada, and T. Shimanouchi, *Bull. Chem. Soc. Jpn.*, **50**, 380 (1977).
14) T. Shimanouchi, H. Matsuura, Y. Ogawa, and I. Harada, *J. Phys. Chem. Ref. Data*, **7**, 1323 (1978).
15) The number of the observed frequencies for iodoalkanes has been increased, from 242 reported previously,[1] with the data for 1,4-diiodobutane included.[16]
16) M. Sakakibara, H. Matsuura, and H. Murata, *J. Mol. Struct.*, **55**, 21 (1979).
17) Detailed tables of the observed frequencies and the vibrational assignments are available on request from the authors.
18) Part II: I. Harada, H. Takeuchi, M. Sakakibara, H. Matsuura, and T. Shimanouchi, *Bull. Chem. Soc. Jpn.*, **50**, 102 (1977).
19) J. Thorbjørnsrud, O. H. Ellestad, P. Klaboe, and T. Torgrimsen, *J. Mol. Struct.*, **15**, 61 (1973).
20) Y. Ogawa and M. Tasumi, *Chem. Lett.*, **1978**, 947.

An MO Study of Organic Sulfur Compounds. Comparison with the Corresponding Oxygen Compounds

Toshio MATSUSHITA, Yoshihiro OSAMURA, Nobuaki MISAWA, Kichisuke NISHIMOTO,* and Yuuho TSUNO†

Department of Chemistry, Faculty of Science, Osaka City University, Sumiyoshi-ku, Osaka 558

†*Department of Chemistry, Faculty of Science, Kyushu University, Hakozaki, Higashi-ku, Fukuoka 812*

(Received March 31, 1979)

The contribution of 3d orbitals of sulfur atom to the electronic structures of the sulfur compounds, H_2CS, CH_3SH, C_6H_5SH, and $C_6H_5SCH_3$ have been studied by means of *ab initio* MO method. The results have been compared with those of the corresponding oxygen compounds in order to clarify the peculiar properties of the sulfur compounds. The global molecular properties are scarcely affected by the 3d orbitals of sulfur atom since they are energetically highly located. However, the local characters such as charge distributions and LUMO are largely varied by the participation of 3d orbitals.

Sulfur forms not only organic sulfur compounds analogous to oxygen compounds but also various stable hypervalent compounds. It is well known that the nucleophilicity of the lone pair of sulfur atom is larger than that of oxygen. However, the basicity of sulfur atom is smaller than that of oxygen, reversely. In this manner, sulfur has some different chemical properties from those of oxygen. Thus it is of interest to investigate the electronic structures of sulfur compounds and consider the origin of peculiar properties theoretically.

We have investigated the effect of 3d orbitals of sulfur atom on the electronic structures of sulfur compounds. 3d orbitals of sulfur are thought to participate in the chemical bonding. The SCF calculation of α-thiocarbanion[1] and the GVB calculation of SF_6[2] showed that the effects of 3d orbitals on the stability and the reactivity are small. The contribution of vacant 3d orbitals to the global molecular properties may be small since they are energetically highly located.

However, in order to explain the NMR chemical shifts of substituted thiophenes in view of charge distribution, the contribution of 3d orbitals can not be neglected.[3] Furthermore, as Inagaki *et al.*[4] pointed out, vacant 3d orbital participation is important in determining the stereochemical courses of reactions where sulfur compounds undergo the attack of nucleophilic reagents.

In the present study, an *ab initio* MO calculation has been carried out for thioformaldehyde, methanthiol, thiophenol, thioanisole, phenol, and anisole in order to clarify the nature of electronic structures of organic sulfur compounds, especially the differences in the role of sulfur and oxygen atoms on the electronic structures of molecules. We have also calculated the rotational barriers of substituted benzenes and consider the steric effect. On the basis of the calculated results, the vacant 3d orbital participation to some molecular properties, such as reactivity, polarity, *etc.* is discussed.

Calculation

Ab initio MO calculation is carried out using a minimal STO-3G basis set with the POLYATOM version 2[5] and GAUSSIAN 70[6] program packages. For sulfur atom, the five 3d functions are added to the minimal basis set. The orbital exponent ζ of 3d functions is obtained by optimizing the total energy of H_2S. The optimized value is found to be 1.77. Boer and Lipscomb[7] reported $\zeta=1.71$, obtained by means of the basis set of Slater type AO's. The orbital exponent of 3d functions optimized for CH_3SH also gives $\zeta=1.77$. This value is used for all the other molecules in the present calculation.[8]

Figure 1 shows the geometric parameters of H_2S, H_2CS, CH_3OH, and CH_3SH used in the present MO calculation. These geometries are taken from experimental data.[9] We assume C_{3v} symmetry for a methyl group. C–S double bond length (1.61 Å) and C–S single one (1.82 Å) are about 0.4 Å longer than the corresponding C–O bond lengths.

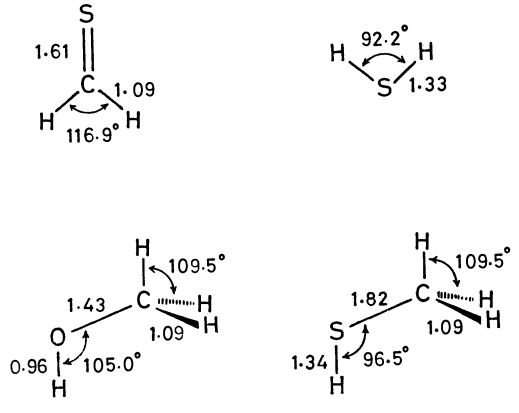

Fig. 1. Geometries of H_2S, H_2CS, CH_3OH, and CH_3SH used in this calculation. Units are shown in Å and degree.

The geometric parameters of C_6H_5OH, C_6H_5SH, $C_6H_5OCH_3$, and $C_6H_5SCH_3$ are given in Fig. 2(a). For phenyl and methyl groups, the geometries of benzene and methanol are used respectively, a staggered conformation being used for $C_6H_5OCH_3$ and $C_6H_5SCH_3$. The numbering of atoms of substituted benzenes is shown in Fig. 2(b).

Results and Discussion

Molecular Orbitals. In order to discuss the difference between the electronic structures of oxygen and

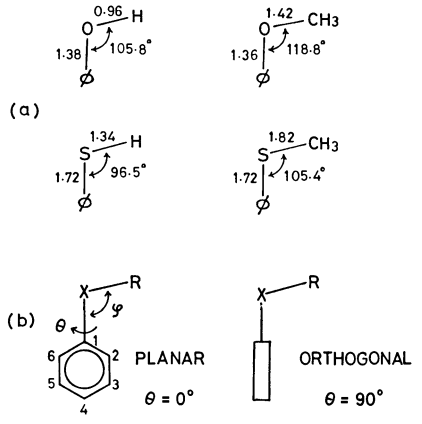

Fig. 2. (a) Geometries of benzene derivatives. Units are shown in Å and degree.
(b) The definition of angle θ and ϕ and the numbering of atoms.

sulfur compounds, we have used a composite molecular model in which the molecular orbitals of whole molecules are represented in terms of the molecular orbitals of the composite subsystems. Using this model, the effects of substituted groups and 3d orbitals on the parent molecules would be clarified in view of the orbital interaction.

The thiocarbonyl group undergoes nucleophilic attacks at the sulfur atom in contrast to the corresponding oxygen compounds.[10] Inagaki *et al.*[4] interpreted this in terms of the orbital interaction based on semi-empirical MO method. The vacant 3d orbitals of sulfur play a significant role in determining the stereochemical courses of the nucleophilic reactions of sulfur compounds. We have investigated the 3d participation by means of *ab initio* MO method.

The modes of orbital interaction between the π orbitals of benzene and π-type orbitals of OH, SH, and SCH_3 groups are shown in Figs. 3—5, the numbering of π orbitals of benzene being given in the left hand side of Fig. 3.

Since the energy of 2p-π of OH group lies lower than that of HOMO's (π_2 and π_3) of benzene, the main component of HOMO of phenol is the π_3 orbital

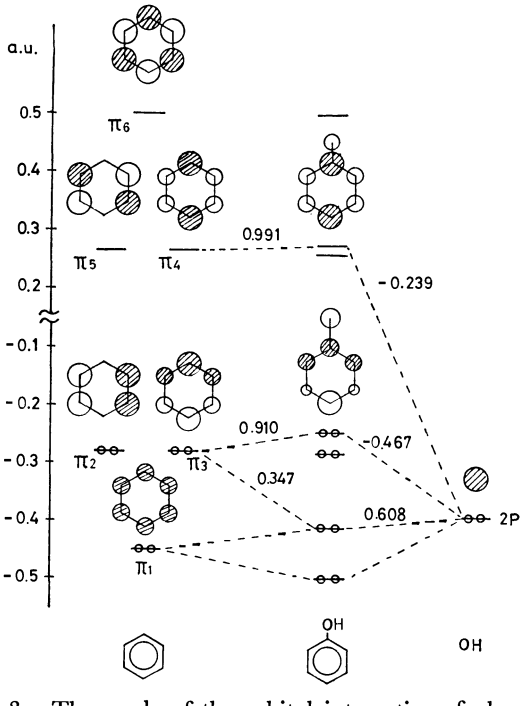

Fig. 3. The mode of the orbital interaction of phenol.

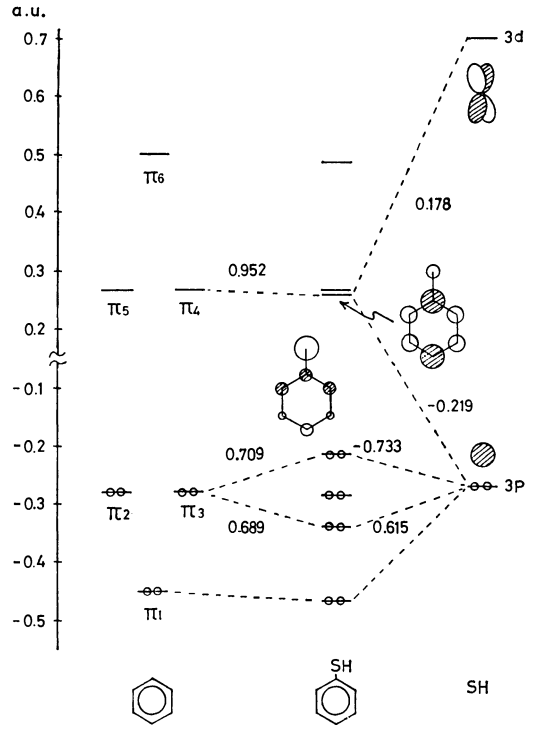

Fig. 4. The mode of the orbital interaction of thiophenol.

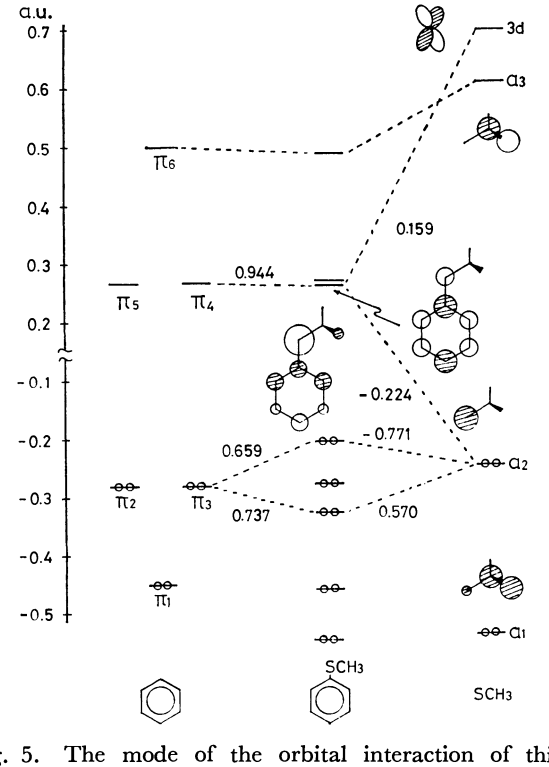

Fig. 5. The mode of the orbital interaction of thioanisole.

of benzene (Fig. 3). The interaction between the π-type orbital of a substituent and π_2 (or π_5) of benzene is symmetry forbidden. In C_6H_5SH (or $C_6H_5SCH_3$), 3p-π of SH group (or a_2 orbital of SCH_3 group) and π_3 orbital mix with each other in nearly equal weight, since the orbital energy of 3p-π of SH group (or a_2 orbital of SCH_3 group) is very close to the π_3 orbital of benzene (Fig. 4 or 5). Consequently the HOMO's of C_6H_5SH and $C_6H_5SCH_3$ have large amplitude at the sulfur atom in contrast to the cases of phenol and anisole. On the other hand, the contribution of the vacant 3d orbitals to *occupied* MO's is small and can be neglected.

The chemical reactivity of a given molecule can be explained qualitatively in terms of the frontier orbitals.[11]

HOMO plays the most important role for the electrophilic reaction. For thiophenol and thioanisole, 3p-π of the sulfur atom has the largest amplitude at HOMO. There are some experimental data showing that an electrophilic reagent attacks the sulfur atom first.[12]

Let us consider LUMO's of molecules, which are responsible for the nucleophilic reaction.

LUMO of C_6H_5SH (or $C_6H_5SCH_3$) has a π_4 character (Fig. 4 or 5) for the following reasons. π_4 is mixed by out of phase combination with 3p-π of the SH group (or a_2 orbital of the SCH_3 group), which gives rise to some increase in orbital energy. However, π_4 interacts strongly with the vacant 3d orbitals. As a result, the π_4 orbital energy is decreased. π_5 orbital also interacts with 3d orbital which is antisymmetric on the molecular axis, but this interaction is very small.

The orbital mixing of π_4 and 2p-π of OH group in phenol should be out of phase so that the orbital energy is increased, but π_5 orbital interacts hardly with oxygen 2p-π (Fig. 3). Thus, the main component of LUMO of phenol is π_5 orbital of benzene.

The LUMO's of benzene are scarcely influenced by the CH_3 group of OCH_3 and SCH_3, since the perturbation of their a_3 orbitals localized mainly in the CH_3 group is very small. It is concluded that the reversal of π_4 and π_5 in thiophenol and thioanisole is clearly due to the contribution of 3d orbitals.

Charge Distribution. Let us consider the effect of 3d orbitals on the charge distribution of the molecules.

Figure 6 shows the net charges of CH_3SH and H_2CS calculated without and with 3d orbitals. In the corresponding oxygen compounds, the electronegative oxygen atom pulls the bonding electrons, so that the neighboring atom has the positive net charge. It should be noted that when the heteroatom is sulfur, the neighboring carbon atom has negative charge (Fig. 6). This tendency is encountered also in other molecules (C_6H_5SH and $C_6H_5SCH_3$). In both cases, CH_3SH and H_2CS, the positive net charges on sulfur atoms are decreased by including the 3d orbitals. This effect is larger in the compound containing C–S double bond (H_2CS) than that with C–S single bond (CH_3SH).

The calculated total electron populations of substituted benzenes are summarized in Table 1. From a comparison of the charge distributions on the phenyl group, it is found that the polarization of the phenyl group in phenol or anisole is larger than that in the corresponding sulfur compounds. Thus, phenol and anisole should show stronger orth-, para-orientation than thiophenol and thioanisole.

The charge density has a linear relationship with NMR chemical shift.[13] The ^{13}C NMR chemical shifts for these molecules are also given in Table 1.[14] The NMR result shows that the polarization of the phenyl

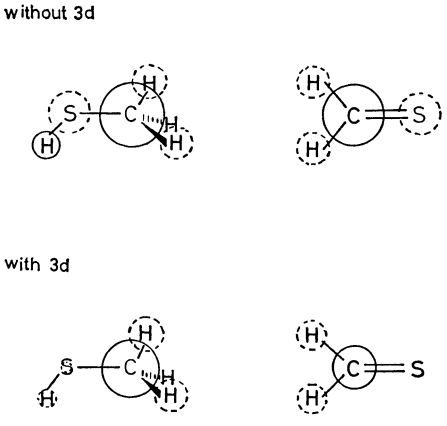

Fig. 6. The net charges of CH_3SH and H_2CS. The circle of the full lines means negative charge and the circle of the dotted lines means positive charge.

Table 1. Calculated total electron populations and carbon-13 NMR chemical shifts for thiophenol, thioanisole, phenol, and anisole

		C-1	C-2	C-3	C-4	C-5	C-6	X[d]
C_6H_5SH	a)	6.018	6.073	6.057	6.072	6.056	6.078	15.982
	b)	(6.098)	(6.075)	(6.055)	(6.073)	(6.055)	(6.074)	(15.841)
	c)	130.7	129.2	128.9	125.4			
$C_6H_5SCH_3$	a)	6.023	6.078	6.057	6.073	6.055	6.077	15.944
	b)	(6.101)	(6.083)	(6.056)	(6.074)	(6.055)	(6.074)	(15.815)
	c)	138.4	126.5	128.6	124.8			
C_6H_5OH		5.870	6.100	6.051	6.076	6.051	6.084	8.295
	c)	154.9	115.4	129.7	121.0			
$C_6H_5OCH_3$		5.862	6.101	6.053	6.078	6.052	6.084	8.255
	c)	160.2	114.1	129.5	120.7			

a) With 3d orbitals. b) Without 3d orbitals. c) ^{13}C NMR chemical shifts (in ppm), Ref. 14. d) X indicates a heteroatom.

group in phenol derivatives is very large and that in thiophenol derivatives is rather small. Thus the calculated electron populations are in good accord with experimental data.

It should be noted that the calculated charge densities of C-1 in C_6H_5SH and $C_6H_5SCH_3$ without 3d orbitals can not explain the ^{13}C NMR data. The calculation without 3d orbitals gives too large a negative charge on C-1, but chemical shifts shows that the charge of this carbon is less negative than that of other ones. On the other hand, the inclusion of 3d orbitals reduces the negative net charges on C-1 in C_6H_5SH (−0.018) and in $C_6H_5SCH_3$ (−0.023) which are smaller than those of all other positions. Therefore, these results show that the effect of 3d orbitals is important for the charge distribution of sulfur compounds.

It is interesting to analyze the electron distribution in a substituted benzene in terms of the intramolecular charge transfer between phenyl group (Ph) and the substituent {XR, (X=O, S and R=H, CH_3)}. This analysis clarifies the difference between oxygen and sulfur compounds for the π (or σ) type donor-acceptor interaction. Figure 7 shows the movements of π and σ electrons. The value of π electron movement gives a measure of the π donating ability of the substituent.

When the substituent has an oxygen atom, it acts as π-donor and σ-acceptor for the phenyl group {Fig. 7(a)}, whereas when the substituent has a sulfur atom, it acts as π-donor and σ-donor for the phenyl group {Fig. 7(c)}. In the cases of both phenol and anisole, the OH and OCH_3 groups always behave as a better π donor than the SH and SCH_3 groups, while the magnitude of charge transfer is almost the same.

The calculation of thioanisole without 3d orbitals shows larger π electron donating ability of the SCH_3 group than that of the OCH_3 group {Fig. 7(b)}. However, since the ^{13}C NMR chemical shift in para-position gives a measure of the π donating ability of the substituent, NMR data indicate that the OCH_3 group is a better π-donor than the SCH_3 group to the phenyl group. Thus the calculation of thioanisole without 3d orbitals is inconsistent with the ^{13}C NMR result. Whereas, the inclusion of 3d orbitals on sulfur atom reduces the magnitude of the charge transfer (0.05) Thus the effect of 3d orbitals seems to be important in view of the π electron donating ability of substituent to the phenyl group.

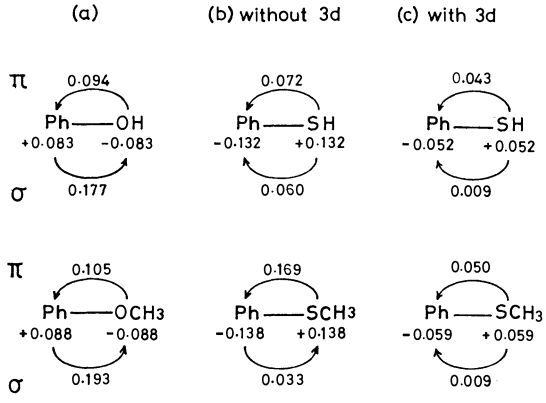

Fig. 7. The net charges and the charge movements of σ and π electrons due to the interaction between phenyl group and substituents.

Rotational Barrier. Let us consider not only the electronic effect but also the steric one. Both effects determine the most stable conformations of C_6H_5SH, $C_6H_5OCH_3$, and $C_6H_5SCH_3$ and the barriers of internal rotation. Our particular interest lies in the 3d orbital contribution of sulfur atom to the rotational barrier and conformation. As mentioned above, it is shown that the effect of 3d orbitals on the charge distribution is important. Let us see whether the participation of 3d orbitals to the rotational barrier is important or not.

Energy variation with the rotation of the SH group in C_6H_5SH is shown in Fig. 8. The bond angle $<$CSH, ϕ, {see Fig. 2(b)} is fixed at 96.5° for this molecule.[15] The planar structure is the most stable, and the calculated rotational barriers without and with 3d are 3.99 and 3.65 kcal·mol^{-1}, respectively. There are no significant changes in both the rotational barrier and the shape of the energy curve caused by including 3d orbitals. The experimental value of rotational barrier of C_6H_5SH is smaller than 0.8 kcal·mol^{-1}.[16] Since the present calculation uses the small basis set, the rotational barrier of C_6H_5SH may be overestimated. Rigorous calculation using a more extended basis set would give a lower rotational barrier.

The energy curve of $C_6H_5SCH_3$ calculated without 3d orbitals is shown in Fig. 9. The change of angle ϕ in $C_6H_5SCH_3$ is very important because of steric hindrance. Thus the rotational energy curve of this molecule is obtained by optimization with respect to angle ϕ. In this molecule, the planar conformations is probably most stable but the energy curve is very flat. (The energy difference between the planar and orthogonal conformations is to be 0.317 kcal·mol^{-1}.) Thus, it seems that the SCH_3 group of $C_6H_5SCH_3$

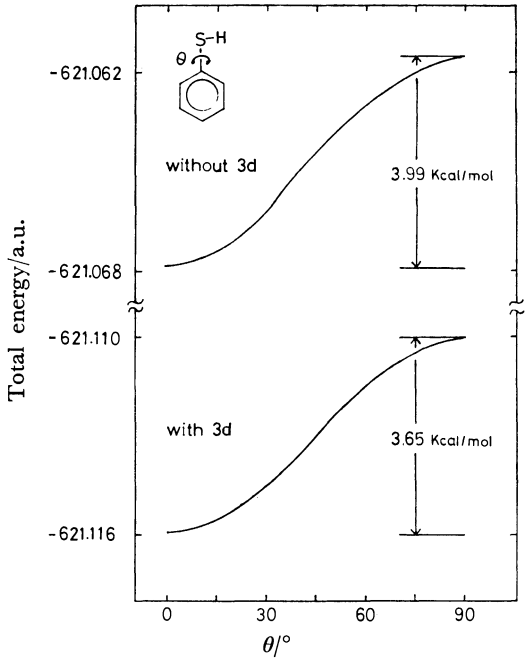

Fig. 8. The energy curve of C_6H_5SH as a function of rotation angle θ.

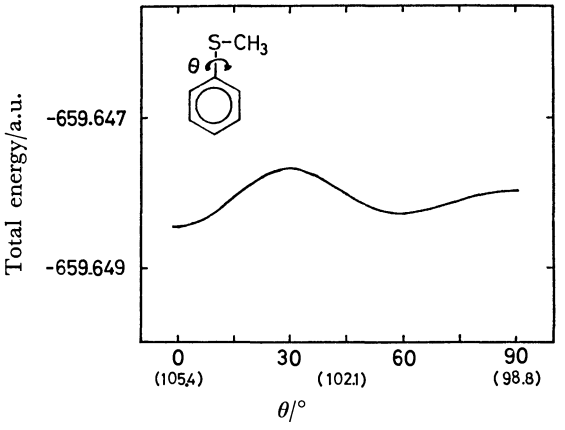

Fig. 9. The energy curve of $C_6H_5SCH_3$ as a function of rotation angle θ. The optimized angle ϕ at each angle θ (0°, 45°, and 90°) is also given in parentheses.

rotates almost freely.

It will be necessary to know the effect of 3d orbitals on the rotational barrier in $C_6H_5SCH_3$. So, we carried out MO calculation including 3d orbitals for planar and orthogonal conformations of this molecule. The geometry of $C_6H_5SCH_3$ optimized with respect to the angle ϕ by a basis set without 3d orbitals is used for the calculation with 3d orbitals. The energy difference is to be 0.237 kcal·mol^{-1}, which is almost the same as the result without 3d orbitals. Therefore, we might conclude that there is very small effect of 3d orbitals on the stable conformations and the rotational barriers in C_6H_5SH and $C_6H_5SCH_3$.

Let us compare oxygen (C_6H_5OH and $C_6H_5OCH_3$) and sulfur compounds (C_6H_5SH and $C_6H_5SCH_3$). The rotational barrier of C_6H_5SH is smaller than that of C_6H_5OH (5.2 kcal·mol^{-1}).[17] The energy curve of $C_6H_5OCH_3$ shown in Fig. 10 is somewhat complicated. The potential curve has two minima at $\theta=0°$ and $\theta=90°$, there are maximum at about $\theta=30°$—$40°$ and $\theta=140°$—$150°$. The stabilization at $\theta=90°$ is probably caused by releasing the steric hindrance between the phenyl and OCH_3 groups, and that at $\theta=0°$ is brought forth by the strong conjugation between these groups. Whereas, $C_6H_5SCH_3$ gives a very flat energy curve because of the cancellation between the conjugation and steric hindrance between the phenyl and SCH_3 groups.

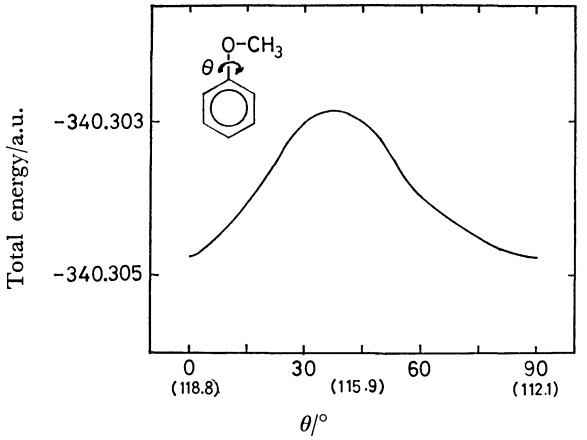

Fig. 10. The energy curve of $C_6H_5OCH_3$ as a function of rotation angle θ. The optimized angle ϕ at each angle θ (0°, 45°, and 90°) is also given in parentheses.

Conclusion

We have discussed the effect of 3d orbitals of sulfur on the electronic structures of molecules and the difference of the electronic structures between the oxygen and sulfur compounds. The calculated results suggest that the contribution of 3d orbitals to the charge distribution is important, but that to the stable conformation and rotational barrier is very small. Since the orbital energies of 3p AO of sulfur atom are almost the same as the 2p AO of carbon atom and the 3p orbitals of sulfur atom are rather diffuse, the molecular properties of sulfur compounds differ somewhat from the corresponding oxygen compounds. The shape and energy of LUMO are particularly sensitive to the participation of 3d orbitals.

The authors would like to express their gratitude to the staff of the Data Processing Center, Kyoto University, for use of the FACOM M190 computer. They thank Dr. Shinichi Yamabe, Nara University of Education, for use of the Gaussian 70 program. This study was partly supported by a Scientific Research Grant (No. 254165) from the Ministry of Education of Japan.

References

1) F. Bernardi, I. G. Csizmadia, A. Mangini, H. B. Schlegel, M. H. Whangbo, and S. Wolfe, *J. Am. Chem. Soc.*, **97**, 2209 (1975).
2) P. J. Hay, *J. Am. Chem. Soc.*, **99**, 1003 (1977).
3) Y. Osamura, O. Sayanagi, and K. Nishimoto, *Bull. Chem. Soc. Jpn.*, **49**, 845 (1976).
4) S. Inagaki, H. Fujimoto, and K. Fukui, *J. Am. Chem. Soc.*, **98**, 4054 (1976).
5) D. B. Neumann, H. Basch, R. L. Kornegay, and L. C. Snyder, POLYATOM (version 2), Program No.238, Quantum Chemistry Program Exchange, Indiana University, Bloomington, Indiana.
6) W. J. Hehre, W. A. Lathan, R. Ditchfield, M. D. Newton, and J. A. Pople, GAUSSIAN 70, Program No.216, Quantum Chemistry Program Exchange, Indiana University, Bloomington, Indiana.
7) F. P. Boer and W. N. Lipscomb, *J. Chem. Phys.*, **50**, 989 (1969).
8) For H_2CS, the optimization of ζ gives 1.69. But the energy difference between $\zeta=1.77$ and 1.69 is very small (4.93×10^{-4} a.u.). Thus we also use $\zeta=1.77$ for H_2CS.
9) a) E. Sutton, "Table of Interatomic Distances and Configuration in Molecules and Ions, Supplement (1956—1959)," The Chemical Society, London (1965); b) D. R. Johnson, F. X. Powell, and W. H. Kirchhoff, *J. Mol. Spectrosc.*, **39**, 136 (1971).
10) a) P. Beak and J. W. Worley, *J. Am. Chem. Soc.*, **92**, 4142 (1970); b) P. Beak and J. W. Worley, *J. Am. Chem. Soc.*, **94**, 597 (1972); c) P. Beak, J. Yamamoto, and C. J. Upton, *J. Org. Chem.*, **40**, 3052 (1975); d) M. Dagonneau, J. F. Hemidy, D. Cornet, and J. Vialle, *Tetrahedron Lett.*, **1975**, 3003.

11) K. Fukui, "Theory of Orientation and Stereoselection," Springer-Verlag, New York (1975).
12) S. Oae, "Yuki-iou Kagobutsu No Kagaku," Kagaku-dojin, Kyoto (1968).
13) "Topics in Carbon-13 NMR Spectroscopy," ed by G. C. Levy, John wiley & Sons, New York (1974), Vol. 1.
14) L. F. Johson and W. C. Jankowski, "Carbon-13 NMR Spectra," John Wiley & Sons, New York (1972).
15) In the orthogonal conformation of thiophenol, angle ϕ is further opimized. The value of ϕ is to be 96.1°. Since the energy difference is less than 10^{-5} a.u., the change of angle ϕ can be neglected.
16) a) D. W. Scott, J. P. McCullough, W. N. Hubbard, J. F. Messerly, I. A. Hossenlopp, F. R. Frow, and G. Waddington, *J. Am. Chem. Soc.*, **78**, 5463 (1967); b) K. O. Simpson and E. T. Beynon, *J. Phys. Chem.*, **71**, 2796 (1967).
17) W. J. Hehre, L. Radom, and J. A. Pople, *J. Am. Chem. Soc.*, **94**, 1496 (1972).

Kinetic Studies of the Proton-transfer of the Bivalent Anions of *ortho*-Hydroxy Azo Compounds in Dioxane–Water Media†

Noboru YOSHIDA and Masatoshi FUJIMOTO*

Department of Chemistry, Faculty of Science, Hokkaido University, Sapporo 060

(Received November 13, 1978)

Kinetics of the proton-transfer reactions in dioxane–water media between hydroxide ion and the bivalent anions of 4-(2,4-dihydroxyphenylazo)benzenesulfonic acid (TPO) and 7-hydroxy-8-phenylazo-1,3-naphthalenedisulfonic acid (HPN) were studied by means of the temperature-jump method. For the change in the mole fraction of dioxane from 0 to 0.174, the acid-dissociation constant, $K_a^c(s)$, was found to decrease from 1.07×10^{-11} to 5.25×10^{-14} mol dm^{-3} for HPN and from 1.32×10^{-12} to 7.08×10^{-15} mol dm^{-3} for TPO.

One of the most pronounced and general features in the chemical effects caused by the change in the solvent composition in binary mixed solvents is the change in the degree of ionic dissociation of weak electrolytes. Dependence of the acid-dissociation constants on the solvent composition is explained in terms of both the dielectric constant of the medium and the solute-solvent interactions.[1]

In dioxane–water media the decrease in the acid-dissociation constants of the bivalent anions of *o*-hydroxy azo compounds such as HPN and TPO is mainly due to the decrease in the dielectric constant of the medium.

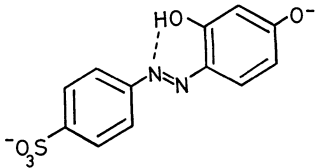

TPO

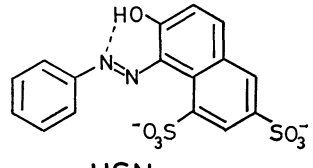

HSN

In the present study we have found that the recombination rate constant, k_f, for the proton-transfer reaction

$$HA^{2-} + OH^- \underset{k_r}{\overset{k_f}{\rightleftharpoons}} A^{3-} + H_2O$$

between hydroxide ion and HPN and TPO decreases with decrease in the dielectric constant of the medium, while the backward rate constant, k_r', is influenced only a little by the change in dielectric constant. Based on the kinetic and the equilibrium data in dioxane–water media, the authors aimed to elucidate the solvent effects on the proton-transfer reaction of HPN and TPO.

Experimental

Water was deionized and distilled. Dioxane was distilled over sodium and used without further purification.[2] HPN and TPO (Wako) were recrystallized from an ethanol–water solution.

Kinetic measurements were carried out at 25 °C; I=0.1 mol dm^{-3} (KNO_3) with a Union Giken co-axial cable temperature-jump apparatus Model RA-105 under compressed nitrogen gas at *ca.* 2 atm to avoid cavitation upon very fast temperature rise. A Hitachi EPS-3T recording spectrophotometer was used in the equilibrium measurements.

The measurements of pH in the mixed solvent were reported in the previous paper.[3] The apparent ionic product K_w^c=[H]·[OH] of the water in dioxane–water was obtained with a Hitachi-Horiba pH-meter F-7ss equipped with a glass electrode 1026A and Ag–AgCl reference electrode type 2010-05T. The values of pK_w^c are summarized in Table 1. The function log U_H is defined as log U_H=pC_H−pH*, where C_H denotes the analytical concentration of proton, and pH* pH-meter readings.

Table 1. Values of log U_H and pK_w^c at various dioxane contents, 25 °C and I=0.1 mol dm^{-3} (KNO_3)

x_{dlox}	log U_H[a]	$pK_w^c=-\log(K_w^c/\text{mol}^2\,\text{dm}^{-6})$
0.000	−0.07	13.73, 13.78[b]
0.023	−0.06	14.05
0.050	−0.09	14.27
0.083	−0.11	14.54
0.128	−0.13	14.97
0.174	−0.13	15.31, 15.38[c]

a) log U=pC_H−pH*, where pH* denotes the pH-meter reading. b) See Ref. 8. c) See Ref. 9.

Results and Discussion

The final step of the acid-dissociation of HPN and TPO can be expressed by

$$HA^{2-} \underset{}{\overset{K_a^c}{\rightleftharpoons}} A^{3-} + H^+. \qquad (1)$$

The acid-dissociation constant, K_a^c, is expressed in terms of the absorbance and the equilibrium concentration of proton, $\bar{C}_H$,

$$C/\Delta A = 1/\Delta\varepsilon + \bar{C}_H/(\Delta\varepsilon\cdot K_a^c) \qquad (2)$$

where $\Delta A=A-A'$, $\Delta\varepsilon=\varepsilon_A-\varepsilon_{HA}$, and $A'=\varepsilon_{HA}C$, ε is the molar absorption coefficient, A the absorbance at the wavelength of the base form of HPN or TPO, and C the total concentration of the Brønsted acid. The plot of $C/\Delta A$ against $\bar{C}_H$ gives straight lines for each solvent composition, yielding $\Delta\varepsilon$ and $K_a^c(s)$ from the intercept and the slope, respectively. In Fig. 1 the acid-dissociation constants determined spectrophotometrically are plotted against the mole fraction of dioxane, x_{dlox}. Increase in the dioxane content in the medium, *viz.*, the decrease in the dielectric constant of the medium leads to a decrease in the dissociation constant of HA^{2-}. Such dependency of $K_a^c(s)$ on the solvent composition has also been observed in the case

† Presented in part at the 26th Annual Meeting on Coordination Chemistry, Sapporo, August 30, 1976, Abstract p. 252 and at the 27th Annual Meeting on Coordination Chemistry, Matsumoto, September 28, 1977, Abstract, p. 233.

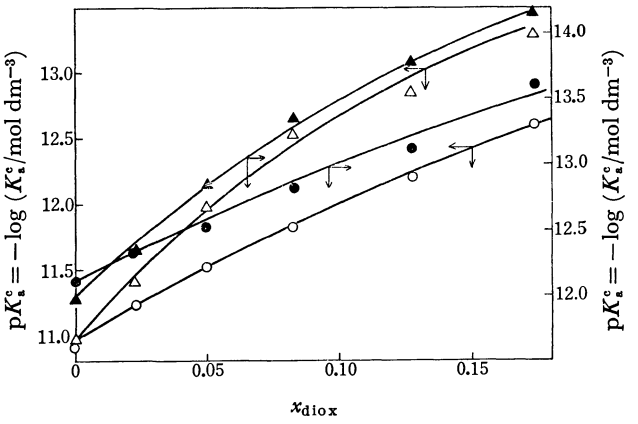

Fig. 1. Dependence of the pK_a^c(s) and pK_a^c(k) on the mole fraction of dioxane at 25 °C and I=0.1 mol dm^{-3} (KNO_3). (1) HSN: ○ the plot of pK_a^c(k) *vs.* x_{dlox}; △ the plot of pK_a^c(s) *vs.* x_{dlox}. (2) TPO: ● the plot of pK_a^c(k) *vs.* x_{dlox}; ▲ the plot of pK (s) *vs.* x_{dlox}.

of the univalent anion of 4-(*p*-nitrophenylazo)-resorcinol.[3]

The proton-transfer reaction between hydroxide ion and the bivalent Brønsted acids, HA^{2-}, is expressed by

$$HA^{2-} + OH^- \underset{k_r}{\overset{k_f}{\rightleftharpoons}} A^{3-} + H_2O \qquad (3)$$

with the equilibrium constant $K_b^c = k_f/k_r' = \bar{C}_A/(\bar{C}_{HA} \cdot \bar{C}_{OH})$, where $k_r' = k_r(H_2O)$. The relaxation time, τ, for Reaction 3 is related to the rate constants as follows.

$$\tau^{-1} = k_f(\bar{C}_{HA} + \bar{C}_{OH}) + k_r'. \qquad (4)$$

If the equilibrium concentration of hydroxide ion is much larger than that of the bivalent anion, Eq. 4 is approximated to $\tau^{-1} = k_f\bar{C}_{OH} + k_r'$ (Fig. 2). The rate constants and equilibrium constants at each solvent composition are summarized in Tables 2 and 3. In

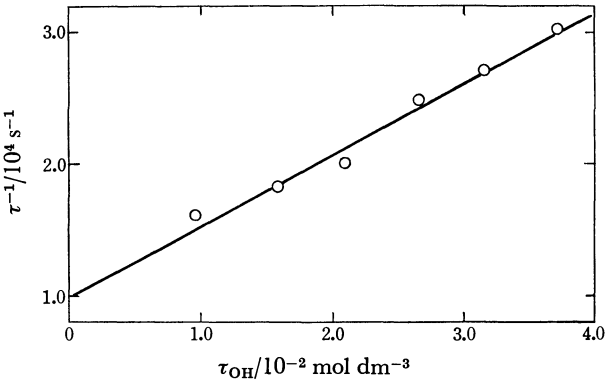

Fig. 2. Plot of the reciprocal relaxation time *vs.* the equilibrium hydroxide ion concentration at x_{dlox}= 0.083 (TPO), 25 °C, and I=0.1 mol dm^{-3} (KNO_3).

Table 2. Rate constants for the proton-transfer reaction of HSN, $HA^{2-} + OH^- \underset{k_r}{\overset{k_f}{\rightleftharpoons}} A^{3-} + H_2O$, at 25 °C and I = 0.1 mol dm^{-3} (KNO_3)

x_{dlox}	pK_a^c(s)	k_f / 10^6 mol^{-1} dm^3 s^{-1}	k_r' / 10^3 s^{-1}	K_b^c / mol^{-1} dm^3	pK_a^c(k)
0.000	10.97	6.3	8.5	741	10.9
0.023	11.40	5.8	8.5	682	11.2
0.050	11.98	5.4	8.5	635	11.5
0.083	12.52	4.9	8.0	613	11.8
0.128	12.82	4.7	8.5	553	12.2
0.174	13.28	4.2	8.5	494	12.6

Table 3. Rate constants for the proton-transfer reaction of TPO, $HA^{2-} + OH^- \underset{k_r}{\overset{k_f}{\rightleftharpoons}} A^{3-} + H_2O$, at I = 0.1 mol dm^{-3} (KNO_3)

x_{dlox}	pK_a^c(s)[a]	k_f / 10^5 mol^{-1} dm^3 s^{-1}	k_r' / 10^3 s^{-1}	K_b^c / mol^{-1} dm^3	pK_a^c(k)	T / K	Ref.
0.000	11.88 (12.20)	6.9	16	43	12.1	298	This work
	—	3.6	8	45	—	285	5
	12.00	8.8	6.5	135	—	288	6
	12.01[b]	8.6	—	—	—	298	7
0.023	12.34 (12.24)	6.4	12	53	12.3	298	This work
0.050	12.85 (12.77)	5.5	8.8	63	12.5	298	This work
0.083	13.33 (13.15)	5.3	10	53	12.8	298	This work
0.128	13.77 (13.56)	4.7	6.0	78	13.1	298	This work
0.174	14.15 (14.25)	3.2	5.8	55	13.6	298	2

a) The values of pK_a^c in parentheses are obtained from the relationship, $pK_a^c = pC_H + \log[(D_B - D)/(D - D_A)]$, where D is the absorbance, subscripts A and B are for the acid and the base form of TPO, respectively. b) $K_a = a_{H^+} \cdot C_A/C_{HA}$, where a_{H^+} is the activity of the proton.

the case of HPN, the value of k_f slightly decreases with increase in the mole fraction of dioxane, x_{dlox}, and that of k_r increases from 1.5×10^2 mol^{-1} dm^3 s^{-1} at $x_{dlox}=0$ to 3.1×10^2 mol^{-1} dm^3 s^{-1} at $x_{dlox}=0.174$ with increase in x_{dlox}. The value of k_f for TPO also gradually decrease with increase in x_{dlox}. The value of k_r' for TPO changes quite a little.

The detailed mechanism of the proton-transfer reaction may be written as follows.[2,3]

$$HA^{2-} \underset{k_{21}}{\overset{k_{12}}{\rightleftharpoons}} HA^{*2-}, \quad (5a)$$

$$HA^{*2-} + OH^- \underset{k_{32}}{\overset{k_{23}}{\rightleftharpoons}} HA^{*2-}\cdots(H_2O)_n\cdots OH^- \quad (5b)$$

$$HA^{*2-}\cdots(H_2O)_n\cdots OH^- \underset{k_{43}}{\overset{k_{34}}{\rightleftharpoons}} A^{3-} + H_2O, \quad (5c)$$

where HA^{2-} stands for the bivalent anion having an intramolecular hydrogen-bond and HA^{*2-} an intermediate species without an intramolecular hydrogen-bond. Assuming the steady state for HA^{*2-} and $HA^{*2-}\cdots(H_2O)_n\cdots OH^-$ and the relationships $k_{21}\gg k_{23}\bar{C}_{OH}$ and $k_{34}\gg k_{32}$, the observed rate constants in Eq. 3 are expressed as follows.

$$k_f = K_{12}k_{23} = (k_{12}/k_{21})k_{23} \quad (6)$$

and

$$k_r = k_{32}/K_{34} = k_{32}/(k_{34}/k_{43}). \quad (7)$$

As shown in Fig. 3 the value of k_f decreases with the decrease in the dielectric constant of the solution, while the value of $k_r'=k_r$ (H_2O) varies little with change in the solvent composition particularly in the case of HPN. The decrease in k_f would be mainly due to the dependence of k_{23} on the dielectric constant provided that the change in the value of K_{12} for the intramolecular process is small.[3] By neglecting the ionic-atmosphere term in Brønsted-Christiansen-Scatchard equation,[4] we obtain

$$\mathrm{d}\log(k_f/\mathrm{mol^{-1}\,dm^3\,s^{-1}})/\mathrm{d}\,D^{-1} = \mathrm{d}\log(k_{23}/\mathrm{mol^{-1}\,dm^3\,s^{-1}})/\mathrm{d}\,D^{-1} \quad (8)$$

and

$$\mathrm{d}\log(k_{23}/\mathrm{mol^{-1}\,dm^3\,s^{-1}})/\mathrm{d}\,D^{-1} = -(z_iz_je^2)/(kTr^*), \quad (9)$$

where z_i and z_j represent the charge of the reactants, D is the dielectric constant of the medium, k Boltzmann's constant, T absolute temperature, r^* the phenomenological reaction distance, and e elementary charge. From the slope in Fig. 3 the value of r^* for TPO is obtained to be 23 Å and that for HPN 26 Å from the plot in lower dioxane content and 66 Å from that in higher dioxane content, respectively. Actually, however, the phenomenological reaction distance r^* should be calculated by considering the ionic strength term, leading to a smaller value for r^*. From the value of r^* there would be intervening water molecules in the encounter complex, $HA^{*2-}\cdots(H_2O)_n\cdots OH^-$.

The kinetic $pK_a^c(k)$ was derived from the following relation.

$$K_a^c(k) = K_b^c(k)\cdot K_w^c(s). \quad (10)$$

In the case of the bivalent anion of a water-soluble Brønsted acid the difference between $pK_a^c(s)$ and $pK_a^c(k)$ (Fig. 1) is large, particularly in the higher dioxane content. On the other hand, in the case of the univalent anion of the sparingly water-soluble Brønsted acid such as 4-(*p*-nitrophenylazo)resorcinol (MAG) the difference is small.[3] Such difference in $pK_a^c(k)$ and $pK_a^c(s)$ would be ascribed to that in the microscopic environment around the solute such as TPO, HPN, and MAG.

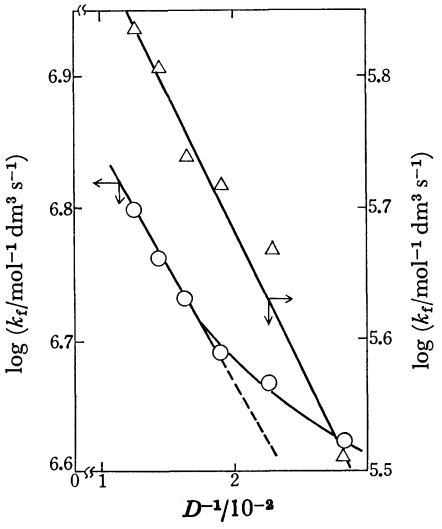

Fig. 3. Dependence of log k_f on the inverse dielectric constant of the medium. ○ The plot for HSN; △ the plot for TPO.

The linear relationship between log (k_f/mol^{-1} dm^3 s^{-1}) and pK_a^c for HPN is as follows (Fig. 4).

$$\log k_f = -1.1\times10^{-1}\,pK_a^c(k) + 8.0 \quad (11)$$

and

$$\log k_f = -7.5\times10^{-2}\,pK_a^c(s) + 7.6 \quad (12)$$

On the other hand, the relationship between pK_w^c and pK_a^c for HSN is expressed by

$$pK_a^c = -\log k_f + \log k_r' + pK_w^c. \quad (13)$$

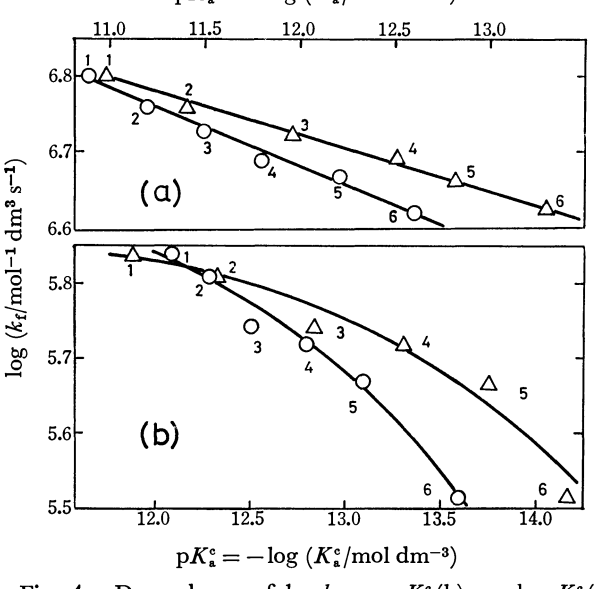

Fig. 4. Dependence of log k_f *vs.* $pK_a^c(k)$ and $pK_a^c(s)$ for HSN (a) and TPO (b): ○, log k_f *vs.* $pK_a^c(K)$. △, log k_f *vs.* $pK_a^c(s)$. x_{dlox}: (1) 0.000, (2) 0.023 (3) 0.050, (4) 0.083, (5) 0.128, and (6) 0.178.

From the plot of pK_w^c against pK_a^c for HPN, the following empirical equations are obtained.

$$pK_w^c = 0.95\, pK_a^c(k) + 3.38 \quad (14)$$

$$pK_w^c = 0.64\, pK_a^c(s) + 6.72 \quad (15)$$

Equations 11 and 13 gives the relationship $pK_w^c = 0.89\, pK_a^c(k) + 8.0 - \log k_r'$ which agrees with Eq. 14, since the value of $\log k_r'$ is evaluated to be 3.93 (Table 2). Equations 12 and 13 give the relationship $pK_w^c = 0.93\, pK_a^c(s) + 7.6 - \log k_r'$ which does not agree with Eq. 15. In the case of TPO, no linear relationships are observed (Fig. 4). The linear relationship between $\log k_f$ and pK_a^c observed for HPN is explained by the constancy of the values of k_r' with variation in solvent composition.

References

1) Ohtaki also pointed out the variation in the ionic product of solvent. See H. Ohtaki, *Pure Appl. Chem.* **34**, 185 (1972).

2) N. Yoshida and M. Fujimoto, *Bull. Chem. Soc. Jpn.*, **49**, 1557 (1976).

3) N. Yoshida and M. Fujimoto, *Bull. Chem. Soc. Jpn.*, **50**, 1328 (1977).

4) G. Scatchard, *Chem. Rev.*, **10**, 229 (1932); J. A. Christiansen, *Z. Phys. Chem.*, **113**, 35 (1924).

5) M. Eigen and W. Kruse, *Z. Naturforsch., Teil B*, **18**, 857 (1963).

6) M. C. Rose and J. Stuehr, *J. Am. Chem. Soc.*, **93**, 4350 (1971).

7) J. L. Haslam and E. M. Eyring, *J. Phys. Chem.*, **71**, 4470 (1967).

8) At $I=0.1$ mol dm^{-3} ($NaClO_4$) and 25 °C. G. K. Pagenkopf and D. W. Margerum, *J. Am. Chem. Soc.*, **90**, 6963 (1968).

9) S. Takamoto, Q. Fernando, and H. Freiser, *Anal. Chem.*, **37**, 1249 (1965).

Preparations and Characterization of Cyclopalladated Complexes of 1-Ethyl-2-phenylimidazole

Katsuma HIRAKI,* Yoshio FUCHITA,* Hiroshi NAKAYA, and Shinji TAKAKURA

Department of Industrial Chemistry, Faculty of Engineering, Nagasaki University, Bunkyo-machi, Nagasaki 852

(Received November 25, 1978)

Reactions of 1-ethyl-2-phenylimidazole (Hepim) with lithium tetrachloropalladate(II) and palladium(II) acetate give dichlorobis(1-ethyl-2-phenylimidazole, 3-*N*)palladium(II) and a new cyclopalladated binuclear complex, di-μ-acetato-bis[2-(1′-ethyl-2′-imidazolyl)phenyl, 1-*C*, 3′-*N*]dipalladium(II), respectively. The latter complex is readily converted by a metathetical reaction with sodium chloride into a chloro-bridged analogue, [{PdCl(epim)}$_2$]. The chloro-bridged complex reacts with 4-picoline, tertiary phosphines, thallium(I) acetylacetonate, sodium diethyldithiocarbamate, and 2,2′-bipyridyl to give the corresponding mononuclear cyclopalladated complexes. All the complexes prepared in this study are characterized by means of IR, ^{1}H-NMR, and mass spectroscopies.

Cyclometallation reactions have recently received considerable attention in view of the formation of stable transition metal-carbon σ-bonds[1–3] and availabilities for the organic syntheses.[3] With respect to the cyclometallation reactions involving aryl-substituted five-membered heterocycles, several works have been reported concerning 1-phenylpyrazole,[4–6] 2,4-diphenyloxazole,[4] and 2-phenyl-3*H*-indole.[7]

It is interesting to investigate the susceptibility to the cyclometallation reactions of aryl-substituted heterocycles. In this paper, we report the cyclopalladation reaction of 1-ethyl-2-phenylimidazole (Hepim) resulting in the formation of an acetato-bridged binuclear complex, a metathetical reaction of the acetato complex into a chloro-bridged one, and the bridge-splitting reactions of the latter complex with 4-picoline (pic), tertiary phosphines, thallium(I) acetylacetonate [Tl(acac)], sodium diethyldithiocarbamate [Na(dedc)], and 2,2′-bipyridyl (bpy).

Experimental

Materials and General Procedures. All the experiments were carried out in an atmosphere of dry dinitrogen. Solvents were dried by usual methods and distilled. 1-Ethyl-2-phenylimidazole,[8] diphenyl-*p*-tolylphosphine,[9] Tl(acac),[10] and thallium(I) cyclopentadienide[11] were prepared according to the published procedures.

IR spectra were measured on a Hitachi model 285 and a Shimadzu IR 450 spectrophotometers. ^{1}H- and ^{13}C-NMR spectra were recorded on JEOL JNM-MH-100 and PFT-100 spectrometers, respectively, using tetramethylsilane as an internal standard. Conductivity measurement was carried out for 1.0×10^{-3} M acetonitrile solution at 25 °C on a Toa Electronics CM-6A conductance meter. Melting points were determined with a Yanaco micro melting point apparatus and are uncorrected. Mass spectra were obtained with a Nichiden-Varian TE-600 gas chromatograph-mass spectrometer.

*Preparation of [PdCl$_2$(Hepim)$_2$] **1**.* 1-Ethyl-2-phenylimidazole (6.56 mmol) in 30 ml of methanol was added to a solution of lithium tetrachloropalladate(II) (3.28 mmol) in 30 ml of methanol. A yellow precipitate formed immediately, which was filtered after standing for 20 h at room temperature and washed with methanol several times. Recrystallization from boiling toluene gave 0.75 g of **1** as yellow needles; yield 44%, mp 242—244 °C (dec).

*Preparation of [{Pd(O$_2$CCH$_3$)(epim)}$_2$] **2**.* To a solution of palladium(II) acetate (17.8 mmol) in 50 ml of acetic acid was added Hepim (21.1 mmol) in 30 ml of acetic acid at room temperature. After refluxing for 30 min, the resulting black mixture was diluted with water and extracted with eight 50 ml portions of dichloromethane. The combined brownish-yellow extracts were concentrated and chromatographed on silica gel. A yellow band eluted by dichloromethane/ethanol (4/1) was collected and the solvent was evaporated. Recrystallization from boiling benzene gave 2.5 g of **2** as yellow crystals; yield 42%, mp 180—219 °C(dec).

*Preparation of [{PdCl(epim)}$_2$] **3**.* Sodium chloride (7.4 mmol) in 60 ml of water was added to a solution of **2** (3.7 mmol) in 200 ml of acetone. A pale yellow precipitate formed immediately, which was filtered after stirring for 20 h at room temperature and washed with water and diethyl ether. Yield 2.0 g, 86%; mp 274—278 °C(dec).

*Reaction of **3** with pic.* 4-Picoline (5.11 mmol) was added to a suspension of **3** (0.64 mmol) in 10 ml of dichloromethane. A clear solution formed immediately, which was concentrated after stirring for 5 h at room temperature. Addition of pentane gave 0.35 g of [PdCl(epim)(pic)] **4** as off white crystals, yield 67%, mp 161—162 °C(dec).

*Reactions of **3** with Triphenylphosphine and Diphenyl-p-tolylphosphine.* These reactions were carried out in the same way as described for **4**, and off white crystals, [PdCl(epim)(PPh$_3$)] **5** and [PdCl(epim)(PPh$_2$–C$_6$H$_4$–CH$_3$-*p*)] **6** were produced: **5**, yield 86%, mp 232—235 °C(dec); **6**, yield 57%, mp 232—234 °C(dec).

*Reaction of **6** with Lithium Bromide.* An acetone suspension containing **6** (0.40 mmol) and lithium bromide monohydrate (2.00 mmol) was refluxed for 10 h. The mixture was filtered and the filter residue was washed with water and diethyl ether. Recrystallization from dichloromethane and pentane gave 0.16 g of [PdBr(epim)(PPh$_2$–C$_6$H$_4$–CH$_3$-*p*)] **7** as pale yellow crystals; yield 74%, mp 229—231 °C(dec).

*Reaction of **3** with Tl(acac).* Thallium(I) acetylacetonate (1.54 mmol) was added to a suspension of **3** (0.64 mmol) in 10 ml of dichloromethane, and the mixture was stirred for 20 h at room temperature. The mixture was filtered and subsequent evaporation of the solvent gave a pale yellow oil. The oil was purified by passing through a short silica gel columm with dichloromethane, and 0.3 g of [Pd(acac)(epim)] **8** was obtained as pale yellow crystals: yield 63%; mp 187—190 °C(dec); Found: M$^+$, 376. Calcd for C$_{16}$H$_{18}$N$_2$O$_2$Pd: M$^+$, 376.

*Reaction of **3** with Na(dedc).* An ethanol suspension containing Na(dedc) (1.92 mmol) and **3** (0.80 mmol) was stirred for 20 h at room temperature. The mixture was evaporated to dryness and the resulting solid was extracted

with dichloromethane. Addition of hexane to the extract afforded pale yellow crystals, [Pd(dedc)(epim)] **9**: yield 78%; mp 178—181 °C(dec); Found: M^+, 425. Calcd for $C_{16}H_{21}N_3S_2Pd$: M^+, 425.

Reaction of ***3*** *with bpy.* 2,2′-Bipyridyl (1.76 mmol) was added to a suspension of **3** (0.80 mmol) in 20 ml of methanol. A yellow clear solution immediately formed. After stirring for 4 h at room temperature, the solution was treated with sodium perchlorate monohydrate (1.60 mmol) to give 1.13 g of [Pd(epim)(bpy)]ClO_4 **10** as yellow crystals; yield 90%, mp 276—277 °C(dec).

Results and Discussion

Elemental analyses and ^{1}H-NMR spectra of all the new complexes prepared in this study are summarized in Table 1.

The reaction of Hepim with lithium tetrachloropalladate(II) in methanol at room temperature afforded dichlorobis(1-ethyl-2-phenylimidazole, 3-*N*)palladium-(II) **1** as yellow needles. In the ^{1}H-NMR spectrum of **1**, the phenyl protons of Hepim appeared as two multiplets at δ 7.4—7.7 (6H) and 7.75—8.0 (4H), similar to the signals of uncoordinated Hepim {two multiplets at δ 7.3—7.5 (3H) and 7.5—7.65 (2H)}. This indicates the presence of unsubstituted phenyl group. Judging from the results of elemental analysis and the ^{1}H-NMR spectrum, **1** contained two moles of Hepim as ligands coordinated only with a nitrogen donor site, but not a cyclopalladated moiety.

$$Li_2[PdCl_4] + 2Hepim \xrightarrow[r.t.]{methanol} [PdCl_2(Hepim)_2]\ \mathbf{1} + 2LiCl$$

1-Ethyl-2-phenylimidazole also reacted with palladium(II) acetate in refluxing acetic acid to produce a new complex **2**, whose IR spectrum exhibited two strong absorption bands due to bridging acetato ligand at 1570 and 1410 cm^{-1}.[13] On the basis of elemental analysis and the characterization of the derivatives from **2** as stated later, **2** was assigned to a binuclear cyclopalladated complex, di-μ-acetato-bis[2-(1′-ethyl-2′-imidazolyl)phenyl, 1-*C*, 3′-*N*]dipalladium(II). It is noteworthy that Hepim reacted with tetrachloropalladate(II) ion to give only the addition product **1** and with palladium(II) acetate to afford the cyclopalladated complex **2**, similar to the case of *N*-benzylideneaniline.[13] As for the ^{1}H-NMR spectrum of **2**, the methyl resonance of bridging acetato ligand showed a sharp singlet at δ 2.20 together with two weak resonances at δ 2.12 and 2.29. These resonances were

$$2[Pd(O_2CCH_3)_2] + 2Hepim \xrightarrow[reflux]{acetic\ acid} [\{Pd(O_2CCH_3)(epim)\}_2]\ \mathbf{2} + 2CH_3CO_2H$$

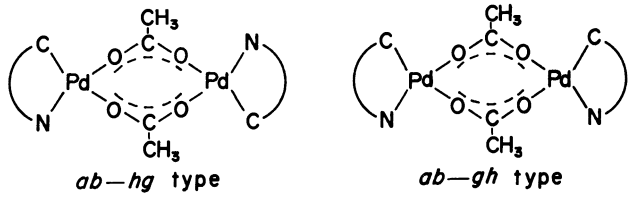

Fig. 1. Structural isomers of **2**.
$\left(\begin{matrix}C\\N\end{matrix}\right)$=(epim,1-*C*,3′-*N*).

Table 1. Elemental analyses and ^{1}H-NMR spectra of the palladium complexes

	Elemental analyses[a] (%)			^{1}H-NMR spectra (δ-value from TMS)[b]					
				epim ring[c]		epim ethyl[d]		Other ligand	
	C	H	N	4′-H	5′-H	$-CH_2-$	$-CH_3$	$-CH_3$	Others
1	50.52 (50.64)	4.59 (4.64)	10.67 (10.74)	7.16(d)	7.00(d)	3.84(q)	1.25(t)	—	—
2	46.86 (46.38)	4.25 (4.19)	7.94 (8.32)	6.39(d)	6.23(d)	3.85(q)	1.25(t)	2.20(s)[e]	—
3	42.24 (42.20)	3.45 (3.54)	8.79 (8.95)	—	—	—	—	—	—
4	49.83 (50.27)	4.40 (4.47)	10.20 (10.34)	7.36(d)	6.84(d)	4.28(q)	1.48(t)	2.40(s)	8.72(dd)[f] (pic-H_α)
5	60.86 (60.54)	4.64 (4.55)	4.49 (4.87)	—[g]	6.81(d)	4.30(q)	1.54(t)	—	—
6	60.93 (61.14)	4.94 (4.79)	4.77 (4.75)	—[g]	6.81(d)	4.30(q)	1.54(t)	2.34(s)	—
7	56.32 (56.85)	4.37 (4.45)	4.33 (4.42)	—[g]	6.81(d)	4.30(q)	1.54(t)	2.34(s)	—
8	50.66 (51.01)	4.84 (4.82)	7.21 (7.44)	7.08(d)	6.75(d)	4.26(q)	1.51(t)	2.02(s) 2.08(s)	5.73(s) (≡CH)
9	45.48 (45.12)	5.10 (4.97)	9.81 (9.87)	6.87(d)	6.76(d)	4.28(q)	1.48(t)	1.28(t)[h] 1.32(t)[h]	3.841(q)[h] ($-CH_2-$)
10	47.59 (47.30)	3.54 (3.59)	10.38 (10.51)	—	—	—	—	—	—

a) Calculated values in parentheses. b) In $CDCl_3$ except for **1** and **4** (CD_2Cl_2); see the text about the aromatic protons of **4**, **8**, and **9**. s=singlet, d=doublet, t=triplet, q=quartet. c) $J_{4',5'}=1.5$ Hz. d) $J=8.0$ Hz. e) See the text. f) $J_{\alpha,\beta}=5.0$ Hz, $J_{\alpha,\beta'}=1.5$ Hz. See Ref. 12. g) Not distinguished owing to overlapping with the aromatic protons. h) $J=7.0$ Hz.

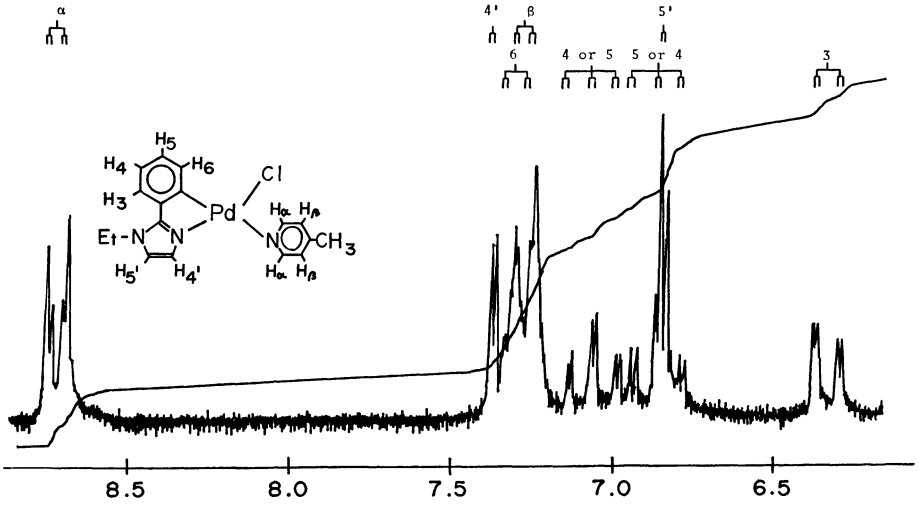

Fig. 2. ^{1}H-NMR spectrum of **4** in CD_2Cl_2 solution (δ-value from TMS).

ascribed to two structural isomers as shown in Fig. 1;[14] the former was to two magnetically equivalent methyl protons in an *ab-hg* type and the latters were to non-equivalent methyl ones in an *ab-gh* type (the isomer ratio *ab-hg* : *ab-gh*=5 : 1, approximately).

Complex **2** was readily converted by metathetical reaction with sodium chloride in acetone into the chloro-bridged analogue, [{PdCl(epim)}$_2$] **3**. The

$$[\{Pd(O_2CCH_3)(epim)\}_2] + 2NaCl \xrightarrow[\text{r.t.}]{\text{acetone}} [\{PdCl(epim)\}_2]\ \mathbf{3} + 2CH_3CO_2Na$$

^{1}H-NMR spectrum of **3** could not be measured owing to its insolubility in usual organic solvents. However, **3** underwent typical bridge-splitting reactions with various reagents as shown in Scheme 1. Reactions of **3** with unidentate ligands, pic, triphenylphosphine, and diphenyl-*p*-tolylphosphine gave neutral mononuclear complexes **4**, **5**, and **6**, respectively.

The ^{1}H-NMR spectrum of **4** (Fig. 2) showed a typical ABCD system characteristic of the *o*-phenylene protons in the 2-(1′-ethyl-2′-imidazolyl)phenyl moiety, differing from the aromatic region of Hepim or **1**. The 6-H of *o*-phenylene group appeared at δ *ca.* 7.3, overlapping with two H_β protons of the picoline ligand (total intensity 3H). The 4- or 5-H was observed at δ 7.06 (1H) or 6.86 (1H) as a double triplet due to coupling with other ring protons. The 3-H appeared at δ 6.33 (1H) as a double doublet due to coupling with 4- and 5-H. The coupling constants were $^3J_{HH}$=7.5 Hz and $^4J_{HH}$=1.5 Hz. These results indicate unambiguously that **4** has the cyclopalladated structure of epim.

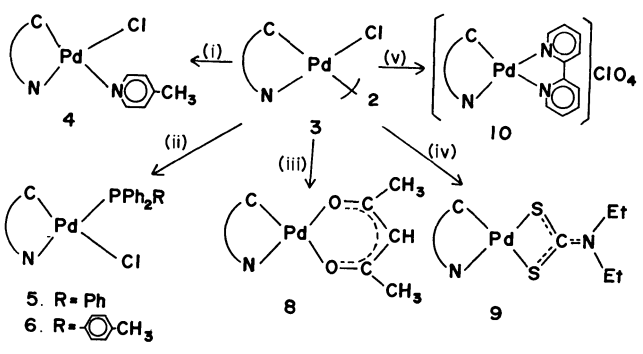

Scheme 1. Bridge-splitting reactions of **3**. Reagents; (i) pic, (ii) PPh_2Ph(for **5**) or PPh_2–C_6H_4–CH_3-*p*(for **6**), (iii) Tl(acac), (iv) Na(dedc), (v) bpy, $NaClO_4$.
$\binom{C}{N}$ = (epim,1-*C*,3′-*N*).

In the far-IR spectrum of **6**, a band at 304 cm^{-1} was assigned to ν(Pd–Cl) frequency in comparison with the corresponding bromo derivative **7**. On the other hand, **4** showed two bands at 316 and 266 cm^{-1} in the range of 350—250 cm^{-1}. The former was assigned to ν(Pd–Cl) frequency and the latter to the palladium-nitrogen stretching one.[15] As for the configuration of **4**, **5**, or **6**, there are two possible isomers as shown in Fig. 3. Crociani *et al.* reported that the ν(Pd–Cl) frequencies trans to an aromatic nitrogen atom and an aryl-carbon one fell in the range of 353—321 and 299—280 cm^{-1}, respectively.[15] Moreover, ^{1}H-decoupled ^{13}C-NMR spectrum of **5** in $CDCl_3$ exhibited a doublet at δ 151.9, which was due to coupling with ^{31}P nucleus ($^2J_{CP}$=27.6 Hz) and assignable to palladium-substituted *o*-phenylene carbon (1-C). This small coupling constant reveals that triphenylphosphine ligand is located at cis position to the 1-C.[16] On the basis of both far-IR and ^{13}C-NMR data, **5** and **6** were ascribed to configuration B. However, **4** could not be assigned whether it had the configuration A or B only from a far-IR spectrum datum.

In the ^{1}H-decoupled ^{13}C-NMR spectrum of **5**, the 2′-, 4′-, and 5′-C's of imidazole ring were observed

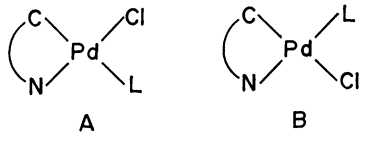

Fig. 3. Possible configurations of **4**, **5**, and **6**.
$\binom{C}{N}$ = (epim,1-*C*,3′-*N*).

at δ 127.2 (doublet, $^3J_{CP}$=4.9 Hz), 139.6 (doublet; $^3J_{CP}$=12.2 Hz, $^1J_{CH}$=146 Hz), and 132.2 (singlet),[17] respectively. A singlet at δ 137.7 was ascribed to imidazole-substituted *o*-phenylene carbon (2-C), and other four carbons (3-, 4-, 5-, and 6-C) upon the phenylene group appeared as four singlets at δ 119.2, 121.7, 123.9, or 126.5. These six kinds of the *o*-phenylene carbons also confirm that **5** contains the cyclopalladated epim structure.

Thallium(I) acetylacetonate and Na(dedc) reacted with **3** to produce neutral complexes **8** and **9**, respectively. The ^{1}H-NMR spectrum of **8** afforded two multiplets; one(1H) at δ 7.57—7.70, assignable to 6-H, the other (4H) at δ 6.99—7.26, which corresponded to 3-, 4-, and 5-H's and overlapped with 4'-H of the imidazole ring. The ^{1}H-NMR spectrum of **9** exhibited a complicated pattern due to the *o*-phenylene protons (4H) in the region of δ 6.95—7.36. The mass spectrometry gave peaks at *m/e* 376 (parent ion corresponding to ^{106}Pd) and 277 (loss of acac) for **8**, and at *m/e* 425 (parent ion corresponding to ^{106}Pd) and 277 (loss of dedc) for **9**. These results confirm the presence of the cyclopalladated structure of epim in both **8** and **9**.

As for the ^{1}H-NMR spectrum of **9**, two methyl protons of diethyldithiocarbamato ligand were unequivalent, indicating that a carbon-nitrogen double bond character is present in this ligand.[18] On the other hand, the methylene protons were observed as one quartet, which was considered to arise from an accidental magnetic degeneracy.

Complex **3** also reacted with bpy in the presence of sodium perchlorate to form a complex **10**. The IR spectrum of **10** showed a strong ν(Cl–O) band at 1080 cm^{-1}, characteristic of perchlorate anion. Molar conductivity (Λ_M=140 Ω^{-1} cm^2 mol^{-1}) in acetonitrile solution indicates that **10** is a uni-univalent electrolyte. The product from the reaction of **3** with thallium(I) cyclopentadienide was too unstable to be isolated in a pure state.

We wish to express our gratitude to Professor Keinosuke Hamada and Mr. Hirofumi Morishita of Nagasaki University for the far-IR measurements, and to Dr. Hideomi Koinuma, the University of Tokyo, for the ^{13}C-NMR measurements, and also to Mrs. Hisako Mazume and Miss Yumi Kojima of Nagasaki University for their technical assistances.

References

1) M. Nonoyama, *Kagaku No Ryoiki*, **28**, 674 (1974).
2) J. Dehand and M. Pfeffer, *Coord. Chem. Rev.*, **18**, 327 (1976).
3) M. I. Bruce, *Angew. Chem. Int. Ed. Engl.*, **16**, 73 (1977).
4) M. I. Bruce, B. L. Goodall, and I. Matsuda, *Aust. J. Chem.*, **28**, 1259 (1975).
5) M. Nonoyama, *J. Organomet. Chem.*, **86**, 263 (1975).
6) S. Trofimenko, *Inorg. Chem.*, **12**, 1215 (1973).
7) Y. A. Ustynyuk, V. A. Chertor, and I. V. Barinov, *J. Organomet. Chem.*, **19**, C53 (1971).
8) H. J. J. Loozen, J. J. M. Drouen, and O. Piepers, *J. Org. Chem.*, **40**, 3279 (1975).
9) J. J. Monagle, J. V. Mangehauer, and D. A. Jones, Jr., *J. Org. Chem.*, **32**, 2477 (1967).
10) W. H. Nelson, W. J. Randall, and D. F. Martin, *Inorg. Syn.*, **9**, 53 (1971).
11) H. Meister, *Angew. Chem.*, **69**, 533 (1957).
12) T. J. Batterham, "NMR Spectra of Simple Heterocycles," ed by E. C. Taylor and A. Weissberger, John Wiley & Sons, New York (1973), Chap. 10.
13) H. Onoue and I. Moritani, *J. Organomet. Chem.*, **43**, 431 (1972).
14) A. J. Deeming and I. P. Rothwell, *J. Chem. Soc., Chem. Commun.*, **1978**, 344.
15) B. Crociani, T. Boschi, R. Pietropaolo, and U. Belluco, *J. Chem. Soc., A*, **1970**, 531.
16) D. J. Cardin, B. Cetinkaya, E. Cetinkaya, and M. F. Lappert, *J. Chem. Soc., Dalton Trans.*, **1973**, 1982.
17) $^1J_{CH}$ of 5'-*C* was not detected owing to overlapping with the phenyl protons of PPh_3.
18) M. C. Cornock and T. A. Stephenson, *J. Chem. Soc., Dalton Trans.*, **1977**, 501.

Kinetics of the Reduction Reaction of Tetranitromethane by Thiosulfate Ion in the Absence and Presence of Copper(II) Ion in Aqueous Mixtures of Methanol and Ethanol

Masaru KIMURA* and Makiko SHUKUTANI

Department of Chemistry, Faculty of Science, Nara Women's University, Nara 630

(Received December 4, 1978)

The kinetics of the reduction reaction of tetranitromethane by the thiosulfate ion in the absence and presence of the copper(II) ion have been investigated in aqueous solution and aqueous mixtures of methanol and ethanol. The mechanism of reaction has been thought to be the following:

$$C(NO_2)_4 + S_2O_3^{2-} \xrightarrow{k_1} C(NO_2)_3^- + NO_2 + S_2O_3^-$$

$$Cu(II) + S_2O_3^{2-} \xrightarrow{k_2} Cu(I) + S_2O_3^-$$

$$C(NO_2)_4 + Cu(I) \xrightarrow{k_3} C(NO_2)_3^- + NO_2 + Cu(II)$$

$$2S_2O_3^- \xrightarrow{\text{rapid}} S_4O_6^{2-}$$

The rate constants k_1 and k_2 have been determined under several conditions. The value of k_1 was hardly affected by ionic strength, permittivity, and acetate ion concentration in the reaction solution, whereas k_2 was markedly increased with decreasing ionic strength (μ), permittivity (D), and acetate ion concentration. For k_2, plots of $\log k_2$ *vs.* $\mu^{1/2}/(1+\mu^{1/2})$ and $\log k_2$ *vs.* $1/D$ gave linear relationships. Under the specified conditions the k_2-term in the reaction mechanism accounts for up to 90% of the reaction, the reaction being composed of a copper(II) catalyzed-chain reaction.

Tetranitromethane (TNM) is reduced by solvated electrons and other reducing radicals such as $H^{\cdot}$, $O_2^{\cdot-}$, $CO_2^{\cdot-}$, $\dot{C}H_2OH$, and so forth,[1–7] becoming the nitroform anion (NF^-) which has a strong absorption peak at 350 nm. Most studies on the TNM reduction reaction have been made by pulse radiolysis techniques, and thus the reducing substances have been restricted to the radical species. The reduction reaction of TNM by reducing agents such as thiosulfate has received little investigation.

Recently, Sellers and Simic[2] and Asmus *et al.*[7] reported that tetranitromethane is easily reduced to the nitroform anion by the copper(I) ion. It is known that the copper(II) ion undergoes facile reduction to the copper(I) ion by the thiosulfate ion in aqueous solution. Thus, it is assumed that tetranitromethane would be reduced by the copper(I) ion which is produced by the reaction between the copper(II) ion and thiosulfate ion. The present paper reports the TNM reduction reaction induced by the reaction between the copper(II) ion and the thiosulfate ion. The large molar absorptivity of the nitroform ion permits low concentrations of the reactants to be used, thus reducing or eliminating problems from the limited solubility of the tetranitromethane and complexing side reactions related to the thiosulfate reaction. The concentrations used were 1×10^{-5}—3×10^{-4} mol dm^{-3} in TNM, 5×10^{-4}—5×10^{-3} mol dm^{-3} in sodium thiosulfate, and 0—2×10^{-4} mol dm^{-3} in copper(II) sulfate.

Experimental

Chemicals. Sodium perchlorate used for adjusting the ionic strength was recrystallized twice from aqueous solution. Methanol and ethanol were distilled in a glass still. Deionized water was further distilled through permanganate solution in a glass still. All other chemicals used were of analytical reagent grade.

Procedure and Apparatus. Unless otherwise stated the reaction of tetranitromethane with thiosulfate ion in the presence of the copper(II) ion was initiated by the addition of thiosulfate solution into the mixture of tetranitromethane and copper(II) under the conditions given. The nitroform anion which is the reduction product of tetranitromethane has an extremely large absorptivity $\varepsilon=1.5\times10^4$ dm^3 mol^{-1} cm^{-1} at 350 nm,[8] and the other species in the reaction solution are transparent under the given concentrations. Consequently the absorbance of the nitroform anion (NF^-) formed was measured at appropriate time of reaction using a Hitachi Model 100-40 spectrophotometer. The cell housing was thermostatted at constant temperature, and in the dark except for the time measuring absorbance.

Results and Discussion

In the Absence of Copper(II). Tetranitromethane was slowly reduced by thiosulfate ion. The reduction rate may be described by Eq. 1.

$$-d[TNM]/dt = d[NF^-]/dt = k_1[TNM][S_2O_3^{2-}] \quad (1)$$

With excess thiosulfate, Eq. 2 is deduced:

$$\ln(A_\infty - A_t)/A_\infty = -k_{obsd}t \quad (2)$$

where $k_{obsd}=k_1[S_2O_3^{2-}]$; A_∞ and A_t indicate the absorbance of NF^- formed at infinity and time t, respectively. A plot of the left-hand side of Eq. 2 against time gave a linear relationship over three half-lives, and the value of A_∞ was proportional to the amount of tetranitromethane added initially. An example of the plots according to Eq. 2 is given in Fig. 1. All the rate constants k_1 obtained are tabulated in Tables 1 and 2, and given in Figs. 4 and 5 together with the rate constant k_2 in the presence of copper(II) (*vide infra*).

Reaction in the Presence of Copper(II). The reduction rate of tetranitromethane by thiosulfate ion was greatly accelerated by the addition of small amounts of copper(II) ion. The rate did not obey Eq. 2. The plots of A_t against reaction time showed a linear

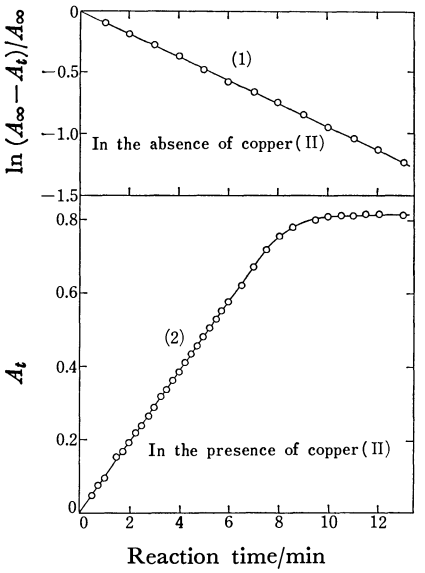

Fig. 1. Examples of the kinetic run in the absence and presence of copper(II) ion. 4.0×10^{-3} mol dm^{-3} in sodium thiosulfate and 5.4×10^{-5} mol dm^{-3} tetranitromethane for line 1; 1.0×10^{-3} mol dm^{-3} in sodium thiosulfate, 5.4×10^{-5} mol dm^{-3} tetranitromethane, and 5.0×10^{-5} mol dm^{-3} in copper(II) sulfate for curve 2; 25 °C; the other conditions as in Table 2.

relationship over half-life time of reaction, indicating the reaction to be of zero order with respect to the TNM concentration. An example of the kinetic behavior is illustrated in Fig. 1 together with the plot according to Eq. 2 in the absence of copper(II) ion. The initial rate of the reaction in the presence of copper(II) ion $V_i=\mathrm{d[NF^-]}/\mathrm{d}t$, was evaluated from the initial slope of the plot of A_t *vs.* t.

Dependence of the Reaction Rate on TNM Concentration. The dependence of the reaction rate on the tetranitromethane concentration was examined at zero, 5.0×10^{-5}, and 2.0×10^{-4} mol dm^{-3} in copper(II) sulfate and is illustrated in Fig. 2. With a concentration of [TNM]≥[Cu(II)], the slopes in the plots became equal to each other irrespective of the copper(II) ion concentrations, and the values of the intercept extrapolated to zero TNM increased with increasing copper(II) concentration.

Dependence of the Reaction Rate on Concentration of Copper(II) and Thiosulfate. Plots of V_i against copper(II) concentration showed linear relationships, and both the intercepts and slopes were found directly proportional to the thiosulfate concentration. Some examples of the plots are given in Fig. 3. The rate constant k_2 was evaluated from the slope of the plot of V_i *vs.* [Cu(II)].

Reaction Mechanism. All the results obtained are accounted for by Reactions 3—6, and the rate law (7).

$$C(NO_2)_4 + S_2O_3^{2-} \xrightarrow{k_1} C(NO_2)_3^- + NO_2 + S_2O_3^- \quad (3)$$

$$Cu(II) + S_2O_3^{2-} \xrightarrow{k_2} Cu(I) + S_2O_3^- \quad (4)$$

$$C(NO_2)_4 + Cu(I) \xrightarrow{k_3} C(NO_2)_3^- + Cu(II) + NO_2 \quad (5)$$

$$2S_2O_3^- \xrightarrow{\text{rapid}} S_4O_6^{2-} \quad (6)$$

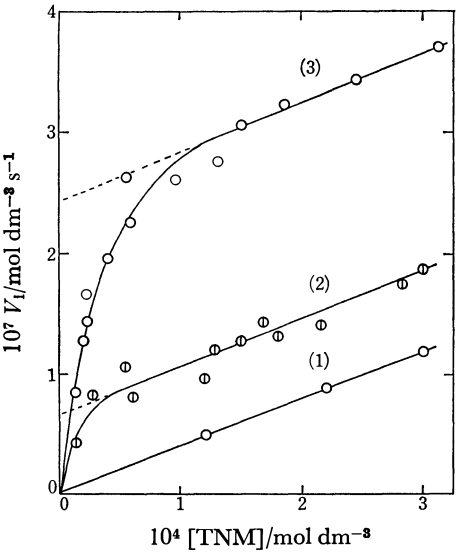

Fig. 2. Dependence of initial rate on the tetranitromethane concentration. Zero, 5.0×10^{-5}, and2.0×10^{-4} mol dm^{-3} in copper(II) sulfate for curves 1, 2, and 3, respectively; varied concentrations of tetranitromethane; 25 °C; the other conditions as in Table 2.

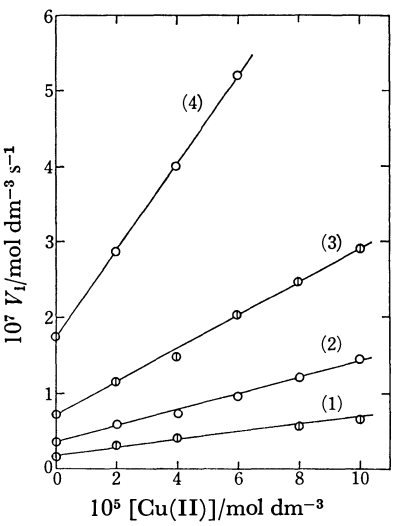

Fig. 3. Dependence of initial rate on concentrations of copper(II) and thiosulfate ions. 5.0×10^{-4}, 1.0×10^{-3}, 2.0×10^{-3}, and 5.0×10^{-3} mol dm^{-3} in sodium thiosulfate for lines 1, 2, 3, and 4, respectively; 20 °C; varied concentrations of copper(II) sulfate; the other conditions as in Table 2.

Under the conditions of $k_3[C(NO_2)_4][Cu(I)] \gg k_2[Cu(II)][S_2O_3^{2-}]$, the rate of formation of the nitroform anion is described by Eq. 7.

$$V_i = \mathrm{d[NF^-]}/\mathrm{d}t = k_1[TNM][S_2O_3^{2-}] + k_2[Cu(II)][S_2O_3^{2-}] \quad (7)$$

Under the condition of the k_2-term in Eq. 7 being much larger than the k_1-term, the rate shows zero-order with respect to the TNM concentration. Reactions 4 and 5 as alternative mechanisms could be also represented by Reactions 4′ and 5′.

$$Cu(II) + S_2O_3^{2-} \underset{k_{-2}}{\overset{k_2}{\rightleftharpoons}} Cu(II)\cdot S_2O_3^{2-} \quad (4')$$

$$C(NO_2)_4 + Cu(II)\cdot S_2O_3^{2-} \xrightarrow{k_3} C(NO_2)_3^- + Cu(II) + S_2O_3^- + NO_2 \quad (5')$$

Assuming the steady concentration for $Cu(II)\cdot S_2O_3^{2-}$ under the conditions of $k_3[TNM] \gg k_{-2}$, an equation identical to Eq. 7 is formed.

Ionic Strength Dependence on k_1 and k_2. Although the values of k_1 were independent of the ionic strength of the reacting solution, the values of k_2 decreased with increasing the ionic strength. Plots of the extended Debye-Hückel equation are given in Fig. 4. The value of the slope of log k_2 *vs.* $\mu^{1/2}/(1+\mu^{1/2})$ was -1.53 a value somewhat smaller than the absolute value predicted for the reaction between divalent ions.

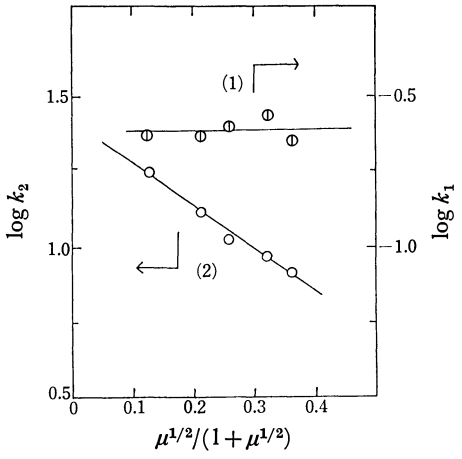

Fig. 4. Ionic strength effects on the rate constants. 0.01 mol dm^{-3} in perchloric acid ; 0.02 mol dm^{-3} in sodium acetate; 20 °C; varied ionic strengths ($NaClO_4$); the other condtions as in Table 1.

This may indicate that the copper(II) ion exists as acetato complexes so that the effective charges reveal smaller values than the divalent ion. Using the data, $K_1=1\times10^2$ dm^3 mol^{-1} and $\beta_2=1\times10^3$ dm^6 mol^{-2} for the formation constants of acetato- and diacetato-copper(II) complexes, respectively,[9] in a solution of 1×10^{-4} mol dm^{-3} copper(II) and 0.01 mol dm^{-3} acetate ion the copper(II) exists as 4.8×10^{-5} mol dm^{-3} Cu_{aq}^{2+} + 4.8×10^{-5} mol dm^{-3} $CuOAc^+$ + 4×10^{-6} mol dm^{-3} $Cu(OAc)_2$ in aqueous solution. Therefore, approximately 50% of copper(II) exists as $CuOAc^+$ species.

Permittivity Dependence of k_1 and k_2. The addition of methanol and ethanol to the reaction solution remarkably accelerated the rate of reaction between tetranitromethane and thiosulfate ion in the presence of the copper(II) ion. Plots of log k_1 *vs.* $1/D$ and log k_2 *vs.* $1/D$ are given in Fig. 5.

Assuming $Z_aZ_b=-4$ for the k_2 reaction, the distance of the closest approach of the reactants in the transition state has been calculated to be 3×10^{-8} cm. The dependence of k_1 on the permittivity was much smaller than for k_2. The dependence of k_1 may indicate that the tetranitromethane molecule is polarized in the transition state, and that side reactions may occur with increasing alcohol concentration.

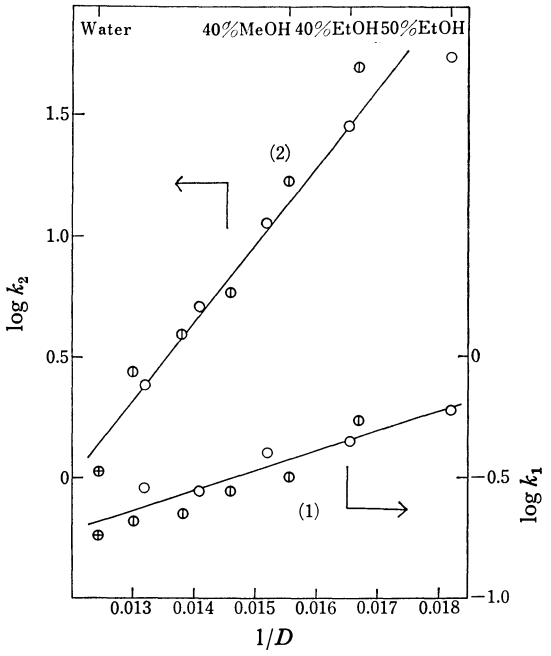

Fig. 5. Permittivity dependence on the rate constants. Plots ⊕, ⊕, and ○ indicate the data in aqueous solution, those in aqueous mixtures with methanol, and those in aqueous mixtures with ethanol, respectively. Varied concentrations 0, 5.0×10^{-6}, 1.0×10^{-5}, 2.0×10^{-5}, 3.0×10^{-5}, 4.0×10^{-5}, and 5.0×10^{-5} mol dm^{-3} in copper(II) sulfate for the aqueous mixtures with methanol and ethanol; 0, 2.0×10^{-5}, 5.0×10^{-5}, 1.0×10^{-4}, and 1.5×10^{-4} mol dm^{-3} in copper(II) sulfate for the aqueous solution; 20 °C; the other conditions as in Table 2. Values of permittivity were cited from a literature by Åkerlöf.[14]

Effect of Acetate Ion. The rate constant k_1 was not affected by the acetate ion concentration, whereas k_2 remarkably decreased with increasing acetate ion concentration. This strong retardation may be due to complex formation of the copper(II) ion with the acetate ion. Assuming that the aquated copper(II) ion is the main reacting species, k_2 should be described by Eq. 8.

$$k_2 = k_2^\circ/(1+K_1[OAc^-] + \beta_2[OAc^-]^2) \quad (8)$$

where k_2° indicates k_2 in the absence of acetate ion. Using values of $k_2^\circ=20$ dm^3 mol^{-1} s^{-1}, $K_1=1\times10^2$ dm^3 mol^{-1}, and $\beta_2=1\times10^3$ dm^6 mol^{-2}, k_2 has been calculated to be 20, 9.5, 5.9, 3.0, 1.9, and 1.0 dm^3 mol^{-1} s^{-1} for zero, 0.01, 0.02, 0.04, 0.06, and 0.10 mol dm^{-3} concentrations of OAc^-, respectively. The values calculated are in good agreement with those obtained experimentally. The rate constants k_1 and k_2 obtained are tabulated in Table 1.

Temperature Dependence. The values of k_1 and k_2 were determined in aqueous solution at an ionic strength of 0.2 mol dm^{-3} containing 0.1 mol dm^{-3} acetate ion at 15, 20, 25, 30, and 35 °C the results of which are listed in Table 2. The values of k_1 and k_2 are described by:

$$k_1 = 1.4\times10^9 \exp[-54000\,\text{J mol}^{-1}/RT]\ \text{dm}^3\ \text{mol}^{-1}\ \text{s}^{-1}$$

and

TABLE 1. ACETATE ION EFFECT ON THE k_1 AND k_2[a)]

$[CH_3COO^-]$/mol dm^{-3}	k_1/dm^3 mol^{-1} s^{-1}	k_2/dm^3 mol^{-1} s^{-1}
0[b)]	0.239[b)]	20.0[b)]
0.01	0.266	9.53
0.02	0.266	8.62
0.04	0.256	5.59
0.06	0.202	1.61
0.10	0.187	1.06

a) 1.5×10^{-4} mol dm^{-3} tetranitromethane; 1.0×10^{-3} mol dm^{-3} sodium thiosulfate; 0, 2.0×10^{-5}, 5.0×10^{-5}, 1.0×10^{-4}, and 1.5×10^{-4} mol dm^{-3} in copper(II) sulfate; varied concentrations of sodium acetate and perchloric acid maintaining the ratio 2 : 1 and pH 4.7 at 20 °C; ionic strength 0.2 mol dm^{-3} ($NaClO_4$). b) pH 5.0 at the unbuffered solution; other conditions as in a).

TABLE 2. TEMPERATURE DEPENDENCE ON THE RATE CONSTANTS[a)]

Temp/°C	k_1/dm^3 mol^{-1} s^{-1}	k_2/dm^3 mol^{-1} s^{-1}
15	0.158	0.82
20	0.187	1.06
25	0.394	1.23
30	0.556	1.66
35	0.680	2.00

a) Conditions as in Table 1; except 0.1 mol dm^{-3} in perchloric acid and 0.2 mol dm^{-3} in sodium acetate, and varied temperatures.

$$k_2 = 1.1\times10^6 \exp[-33000\ \mathrm{J\ mol^{-1}}/RT]\ \mathrm{dm^3\ mol^{-1}\ s^{-1}},$$

respectively.

Mixing Order of Reactants. The addition of the copper(II) ion to the thiosulfate solution before the addition of tetranitromethane results in the formation of copper(I) in solution and the concentration of the copper(I) increases with standing of the copper(II)–thiosulfate mixture. The addition of tetranitromethane to the mixture after a certain time of standing resulted in the tetranitromethane reacting rapidly with all the copper(I) produced during the standing time resulting in the nitroform ion. After the rapid formation of nitroform ion, the nitroform ion concentration increased with time. An example of the behavior is given in Fig. 6.

The values extrapolated to zero time in Fig. 6 correspond to the concentrations of copper(I) formed during the standing time. The extrapolated values, plotted against the standing time of the copper(II)–thiosulfate mixture are given in Fig. 7 together with the results obtained under different conditions.

The slopes in Fig. 7 at zero to about ten min correspond to the rate of reaction between copper(II) and thiosulfate, and increases with decreasing acetate ion concentration. This trend is the same as seen in the values of k_2 in Table 1. From the initial slopes in Fig. 7 k_2 has been evaluated approximately as 4 to 6 dm^3 mol^{-1} s^{-1} and 1 dm^3 mol^{-1} s^{-1} in 0.01 and 0.1 mol dm^{-3} acetate ion, respectively. It is seen from Fig. 7 that the amount of nitroform formed is not related to the molecular oxygen dissolved in solution. Fouda *et al.*[10,11] reported that at temperatures up to 50 °C and

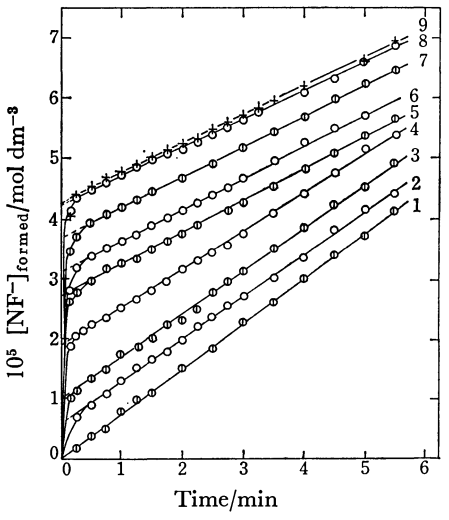

Fig. 6. An example for the kinetic behavior in the addition of tetranitromethane to the copper(II)–thiosulfate mixture after a certain time of standing. The standing time of the mixture is 0, 1, 2, 5, 10, 20, 30, 60, and 120 min for curves 1, 2, 3, 4, 5, 6, 7, 8, and 9, respectively. 1.0×10^{-4} mol dm^{-3} tetranitromethane; 1.0×10^{-4} mol dm^{-3} in copper(II) sulfate; 20 °C; the other conditions are the same as in Table 2.

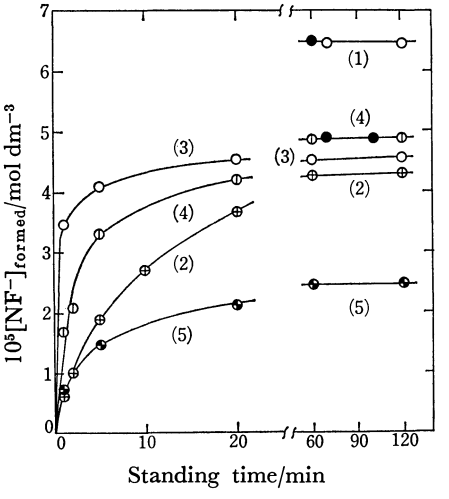

Fig. 7. The values extrapolated to time-zero in the plots of $[NF^-]_{formed}$ *vs.* t were plotted against time of standing. Conditions are 1.0×10^{-4} mol dm^{-3} tetranitromethane, ionic strength 0.2 mol dm^{-3}, 20 °C, and pH 4.7 with 0.2 mol dm^{-3} sodium acetate–0.1 mol dm^{-3} perchloric acid for curves 1 and 2, and with 0.02 mol dm^{-3} sodium acetate–0.01 mol dm^{-3} perchloric acid for curves 3, 4, and 5. Other conditions are 1.0×10^{-3} mol dm^{-3} thiosulfate and 2.0×10^{-4} mol dm^{-3} copper(II) for curve 1; 1.0×10^{-3} mol dm^{-3} thiosulfate and 1.0×10^{-4} mol dm^{-3} copper(II) for curves 2 and 3; 5.0×10^{-4} mol dm^{-3} thiosulfate and 1.0×10^{-4} mol dm^{-3} copper(II) for curve 4; 1.0×10^{-3} mol dm^{-3} thiosulfate and 5.0×10^{-5} mol dm^{-3} copper(II) for curve 5. Plots of ● indicate the data in the absence of oxygen, by bubbling nitrogen gas through the copper(II)–thiosulfate mixture during time of standing.

atmospheric pressure, the copper(I)–thiosulfate species resulting from the reduction of the copper(II) ion in aqueous solution by excess thiosulfate are stable with respect to reoxidation by molecular oxygen to copper(II). Ryabchikov and Sil'nichinko[12] reported that thiosulfate in excess over copper(II) (thiosulfate: copper(II)>3 : 1) results in the reaction:

$$2CuSO_4 + 6Na_2S_2O_3 \longrightarrow 2Na_3[Cu(S_2O_3)_2] + Na_2S_4O_6 + 2Na_2SO_4.$$

The $S_4O_6^{2-}$ ion forms no complexes with the copper(I) ion. Thiosulfate concentrations in the present investigation were 2.5 to 25 times in excess of the copper(II) concentration, and so the conditions are similar to those used by Fouda *et al.*[10,11] and Ryabchikov and Sil'nichinko.[12]

Byerley *et al.*[13] reported that complicated reactions occur in the reaction between the copper(II) ion and thiosulfate ion. It appears however that such complicated reactions do not occur under the present conditions which are designed for extremely low concentrations of copper(II) and thiosulfate ions.

References

1) D. W. Johnson and G. A. Salmon, *J. Chem. Soc., Faraday Trans., 1*, **73**, 256 (1977).
2) R. M. Sellers and M. G. Simic, *J. Chem. Soc., Chem. Commun*, **1975**, 401; *J. Am. Chem. Soc.*, **98**, 6145 (1976).
3) S. A. Chaudhri and K.-D. Asmus, *J. Chem. Soc., Faraday Trans., 1*, **68**, 385 (1972).
4) J. Rabani, W. A. Mulac, and M. S. Matheson, *J. Phys. Chem.*, **69**, 53 (1965).
5) K.-D. Asmus, S. A. Chaudhri, N. B. Nazhat, and W. F. Schmidt, *Trans. Faraday Soc.*, **67**, 2607 (1971).
6) A. Fojtik, G. Czapski, and Henglein, *J. Phys. Chem.*, **74**, 3204 (1970).
7) K.-D. Asmus, A. Henglein, M. Ebert, and J. P. Keene, *Ber. Bunsenges. Phys. Chem.*, **68**, 657 (1964).
8) R. W. Miller and C. T. Kerr, *J. Biol. Chem.*, **241**, 5597 (1966).
9) "Stability Constants of Metal-Ion Complexes," ed by L. G. Sillén and E. Martell, Chem. Soc. Special Publication No. 25, 1971, p. 251.
10) J. J. Byerley, S. A. Fouda, and G. L. Rempel, *J. Chem. Soc., Dalton Trans.*, **1975**, 1329.
11) S. A. Fouda, *M. A. Sc. Thesis, University of Waterloo*, 1972; cited in Ref. 10.
12) D. I. Ryabchikov and V. G. Sil'nichenko, *Bull. Acad. Sci. USSR, Classe Sci. Chim.*, **1947,** 19 ; *Chem. Abstr.*, **42**, 4477 (1948).
13) J. J. Byerley, S. A. Fouda, and G. L. Rempel, *J. Chem. Soc., Dalton Trans.*, **1973,** 889.
14) G. Åkerlöf, *J. Am. Chem. Soc.*, **54**, 4125 (1932).

Preparation and Properties of "β_1 and β_2"-Isomers of the Salicylato(triethylenetetramine)cobalt(III) Complex

Yoshihisa YAMAMOTO* and Eiko TOYOTA

Faculty of Pharmaceutical Science, Higashi Nippon Gakuen University, Ishikari-Tobetsu, Hokkaido 061-02

(Received January 12, 1979)

β-Salicylato(triethylenetetramine)cobalt(III) chloride monohydrate has been obtained from salicylic acid and β-dichloro(triethylenetetramine)cobalt(III) chloride at pH 10—11. The separation of "β_1 and β_2" isomers was attempted by using ion exchange. The IR spectra of the "β_1 and β_2" complexes showed four strong absorption peaks in the 990—1100 cm^{-1} region. This indicates that the complexes assume the β-form. The ^{1}H-NMR spectrum of ammine protons of coordinated triethylenetetramine of the β_1 complex showed six signals with an intensity ratio of 1:1:1:1:1:1, while that of the β_2 complex showed five signals with an intensity ratio of 1:1:1:1:2, in 1.8 mol dm^{-3} D_2SO_4. The order of the chemical shifts in ppm is $N(2)H<N(3)H<N(4)H_2<N(1)H_2$. Thus, the protons of the secondary N(3)H of coordinated triethylenetetramine absorb at lower fields than the terminal $N(1)H_2$ protons. The ^{13}C-NMR spectra of the "β_1 and β_2" complexes in heavy water showed six signals for trien-ligand carbons and seven signals for salicylato-ligand carbons. The spectra of these complexes have shown two different configurations of the "β_1 and β_2" complexes.

The preparation[1–3] and some properties[3–6] of salicylato- or cresotinato(tetraammine)cobalt(III) chloride monohydrate and aslicylato- or cresotinatobis(ethylenediamine)cobalt(III) chloride dihydrate with the formula of 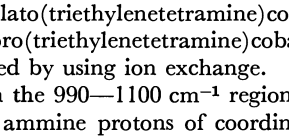 (L: NH_3, L_2: en, R: H, CH_3) have already been reported. The present paper deals with the isolation of β_1 and β_2 isomers of salicylato(triethylenetetramine)cobalt(III) chloride monohydrate[7] and their properties.

As far as the present authors know, no report has appeared on the configuration of a cobalt(trien) complex which is chelated by two oxygen atoms as in the present example, although studies of the stereochemistry of the $[Co(trien)(amino\text{-}acidato)]^{2+}$ complex (trien=triethylenetetramine, amino-acidato=glycinato, sarcosinato···) have been reported by some authors.[8,9]

Results and Discussion

Complexes. Three isomeric forms are possible for the salicylato(triethylenetetramine)cobalt(III) complex, as is shown in Fig. 1. A mixture of β_1 and β_2-salicylato(triethylenetetramine)cobalt(III) chloride monohydrate was obtained from salicylic acid and β-dichloro(triethylenetetramine)cobalt(III) chloride at pH 10—11. The separation of the isomers was achieved by the use of ion-exchange resin. Attempts to obtain the α-form using α-dichloro(triethylenetetramine)cobalt(III) chloride invariably resulted in the isolation of a mixture of the β_1 and β_2-forms at pH 2—8. The α-form may, then, be thermodynamically unstable.[10] The α-glycinato(triethylenetetramine)-cobalt(III) chloride can not be prepared at pH 7—8,[10,11] but it can be prepared at pH 3[11] from glycine and α-dichloro(triethylenetetramine)cobalt(III) chloride.

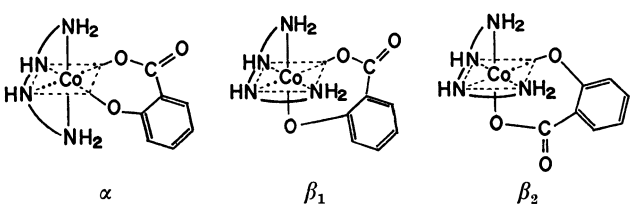

α β_1 β_2

Fig. 1. The α, β_1, and β_2 configurations of $[Co(trien)sal]Cl\cdot H_2O$.

The β_1 and β_2-salicylato(triethylenetetramine)-cobalt(III) picrate complexes have been prepared

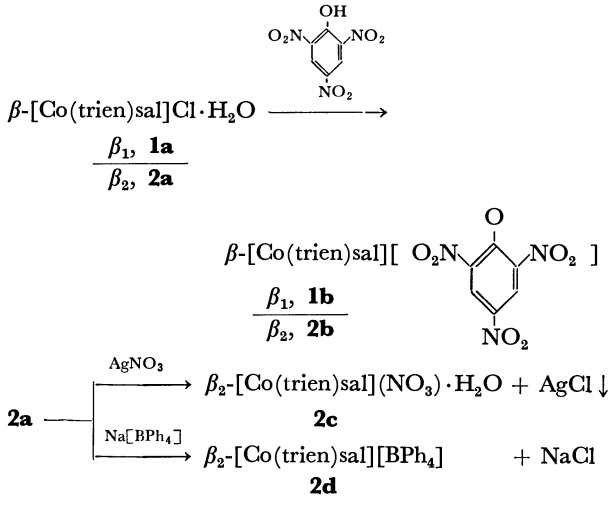

from picric acid and the corresponding chloride monohydrate. The β_1 and β_2 chloride monohydrate complexes (hereafter denoted as **1a** and **2a** respectively) are russet, while the corresponding picrates (denoted by **1b** and **2b** respectively) are orange. They are insoluble in most organic solvents, but the **1a** and **2a** complexes are soluble in water, methyl alcohol, and dimethyl sulfoxide. Salicylato(triethylenetetramine)cobalt(III) nitrate monohydrate (**2c**) has been prepared from silver nitrate and the corresponding chloride monohydrate (**2a**). It is russet and soluble in water. The corresponding tetraphenyl borate (**2d**) has been prepared from sodium tetraphenyl borate and the **2a** complex. It is pink and soluble in acetone and dimethyl sulfoxide. When the **1a** and **2a** complexes are treated with 60% nitric acid, very deep green solutions are formed. They should contain complexes[3–6] similar to $[CoL_4 5\text{-}NO_2sal]^{2+}$ (L: NH_3, L_2:

en). The **1a** and **2a** complexes are diamagnetic and should be a cobalt(III) complex of the low-spin type. The absorption spectra of the **1a**, **1b**, **2a**, **2b**, **2c**, and **2d** complexes are collected in Table 1.

IR Spectra. Buckingham *et al.*, who studied the IR spectra of α, β_1, and β_2-[Co(trien)gly]$^{2+}$,[9,10] reported that the IR spectra of (trien)cobalt(III) complexes showed at least two strong absorption bands for α-complexes and at least four strong absorption bands for β-complexes in the 990—1100 cm^{-1} region. They also reported that the IR spectra of α-complexes showed three absorption bands, while those of β-complexes showed more complicated and usually four strong (and, in some cases, five) absorption bands, in the 3000—3300 cm^{-1} region.[12] The IR spectra of the **1a** and **2a** complexes have four strong peaks in the 990—1100 cm^{-1} region (Table 1) and four peaks in the 3000—3300 cm^{-1} region; *i.e.*, the IR spectrum of the **1a** complex has peaks at 2950, 3075, 3150, 3220, and 3275(sh), and that of the **2a** complex has peaks at 2875, 2950, 3050, 3150(sh), 3200, and 3275(sh), which is the shift on deuteration[12] to 2250—2450 cm^{-1}. This indicates that the complexes assume the β-form. The IR spectral data of the **1a**, **1b**, **2a**, **2b**, **2c**, and **2d** complexes are collected in Table 1.

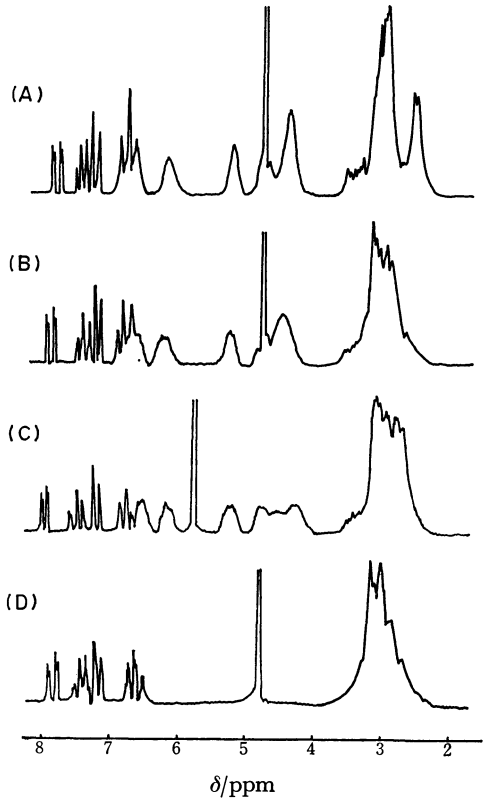

Fig. 2. The ^{1}H-NMR spectra of **1a** and **2a** complexes.
(A): β_2-[Co(trien)sal]Cl·H_2O in 0.1mol dm^{-3} D_2SO_4.
(B): β_1-[Co(trien)sal]Cl·H_2O in 0.1mol dm^{-3} D_2SO_4.
(C): β_1-[Co(trien)sal]Cl·H_2O in 1.8 mol dm^{-3} D_2SO_4.
(D): β_1-[Co(trien)sal]Cl·H_2O in heavy water containing NaOH. Standard: internal DSS.

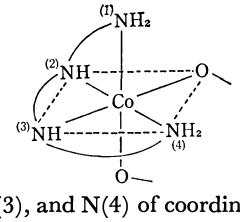

N(1), N(2), N(3), and N(4) of coordinated trien ligand.

NMR Spectra. The ^{1}H-NMR spectra of the **1a** and **2a** complexes were measured in 0.1 mol dm^{-3} DCl, 0.1 mol dm^{-3} D_2SO_4, and 1.8 mol dm^{-3} D_2SO_4. In Fig. 2, the signals (2.3—3.8 ppm, 12H) at the highest field are assigned to the methylene protons of the coordinated trien. The signals of 4.0—6.7 ppm are assigned to the protons of the NH and NH_2 group. The multiplet (6.5—8.2 ppm) at the lowest field is assigned to the protons of the salicylato ligand. The signal of the methylene protons of the coordinated trien of the **1a** complex showed one peak, and that of **2a** showed two peaks in the 2.3—3.8 ppm region, as is shown in Fig. 2 and Table 1. The protons of both the NH and NH_2 groups of the coordinated trien of the **1a** and **2a** complexes showed five signals in the intensity ratio of 1 : 1 : 1 : 1 : 2 in 0.1 mol dm^{-3} D_2SO_4 or in 0.1 mol dm^{-3} DCl. They disappeared in heavy water containing NaOH. Buckingham *et al.* reported that the order of chemical shifts in ppm is $NHR_1R_2 < NH_2R < NH_3$.[11,13] Thus, in β_1 and β_2 also, the proton of the secondary NH of coordinated trien is considered to absorb at lower fields than the terminal NH_2 protons. Marzilli and Buckingham[10] also found that, in the spectra of the β_2-[Co(trien)sar]$^{2+}$ ion, the NH_2 protons in a position *trans* to the coordinated carboxyl oxygen of the sarcosinato ligand absorb at a higher field than those in a position *cis* to the coordinated carboxyl oxygen. If the same relation holds in our β_1 and β_2 complexes, the N(1)H_2 protons of coordinated trien is thought to absorb at a higher field than the N(4)H_2 protons, while the N(3)H proton probably absorbs at a higher field than the N(2)H proton, because N(1) and N(3) are at positions *trans* to the coordinated carboxyl oxygen or phenoxy oxygen.[6] Thus, the order of the ^{1}H chemical shifts in ppm should be: N(2)H<N(3)H<N(4)H_2<N(1)H_2. Now, in the [Co(NH_3)$_4$sal]$^+$ ion[6] it has been found that the NH_3 protons in a position *trans* to the coordinated carboxyl

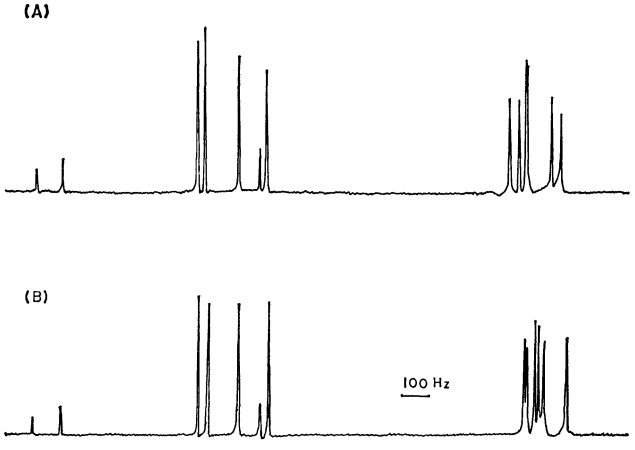

Fig. 3. The ^{13}C-NMR spectra of **1a** and **2a** complexes in D_2O. (A): β_1-[Co(trien)sal]Cl·H_2O. (B): β_2-[Co(trien)sal]Cl·H_2O.

TABLE 1. ^{1}H-, ^{13}C-NMR SPECTRA AND SOME PROPERTIES

Complex	^{1}H-NMR spectra of $NH_2CH_2CH_2NHCH_2CH_2NHCH_2CH_2NH_2$				
	CH_2 δ/ppm	$N(1)H_2$ δ/ppm	$N(4)H_2$ δ/ppm		$N(3)H$ δ/ppm
1a	2.35—3.72 (12H)	4.43 (2H)	a)	5.24 (1H)	6.25 (1H)
	2.39—3.89 (12H)	4.50 (2H)	a)	5.29 (1H)	6.29 (1H)
	2.39—3.76 (12H)	4.34 (1H) 4.57 (1H)	4.81 (1H)	5.23 (1H)	6.20 (1H)
	2.30—3.83 (12H)				
1b	2.31—3.85 (12H)	4.40 (2H)	4.80 (1H)	a)	6.15 (1H)
2a	2.31—2.78 (3H) 2.78—3.68 (9H)	4.31 (2H)	a)	5.23 (1H)	6.18 (1H)
	2.30—2.76 (3H) 2.76—3.80 (9H)	4.40 (2H)	a)	5.25 (1H)	6.19 (1H)
	2.38—2.80 (3H) 2.80—3.80 (9H)	4.34 (2H)	4.76 (1H)	5.21 (1H)	6.07 (1H)
	2.35—2.79 (3H) 2.79—3.73 (9H)				
2b	2.33—2.74 (3H) 2.74—3.81 (9H)	4.32 (2H)	4.77 (1H)	a)	6.08 (1H)
2c	2.28—2.85 (3H) 2.85—3.76 (9H)	4.36 (2H)	4.71 (1H)	5.18 (1H)	6.03 (1H)
2d					
3					

	^{13}C-NMR spectra of $NH_2CH_2CH_2NHCH_2CH_2NHCH_2CH_2NH_2$						OOC–C_6H_4–O (C-1 C-2 C-3 C-4 C-5 C-6 C-7)						
							C-1	C-2	C-3	C-4	C-5	C-6	C-7
1a	46.6	45.8	51.9	52.1	53.9	56.9	118.6	167.8	117.4	134.3	124.2	132.4	174.6[8]
2a	42.0	47.5	48.3	49.7	52.1	52.7	118.1	168.2	117.1	134.5	124.3	132.3	174.1[8]
2c	42.0	47.4	48.3	49.8	52.1	52.6	117.0	168.3	118.4	134.5	124.3	132.3	174.1[8]
3							117.5	167.5	117.5	134.6	124.1	132.7	174.1[9]

oxygen of the salicylato ligand absorb at the highest field. As for the **1a** and **2a** complexes in a 0.1 mol dm^{-3} D_2SO_4 solution, the chemical shift (4.40 ppm) of the proton signal of the $N(1)H_2$ group of the **2a** complex is at a higher field than that (4.50 ppm) of the **1a** complex, as is shown in Fig. 2 and Table 1. Therefore, the $N(1)H_2$ group of the **2a** complex is considered to be at a position *trans* to the carboxyl oxygen of the salicylato ligand, which is more electronegative than the phenoxy oxygen.[6] Thus, the **2a** and **1a** complexes can be assigned to β_2 and β_1 respectively.

In the 1.8 mol dm^{-3} D_2SO_4 solution, the spectrum of the **1a** complex showed six peaks with an intensity ratio of 1 : 1 : 1 : 1 : 1 : 1, while that of the **2a** complex showed five peaks with an intensity ratio of 1 : 1 : 1 : 1 : 2. The signal at 4.50 ppm of the highest field, based on the $N(1)H_2$-group protons of the coordinated trien of the **1a** complex, split into two signals at 4.34 and 4.57 ppm. This seems to be a result of the formation of hydrogen bonding[14] between the carbonyl oxygen of the salicylato ligand and protons of sulfuric acid. The carbonyl oxygen of the coordinated salicylato of the **1a** complex is near to the $N(1)H_2$ protons in a position *trans* to the coordinated phenoxy oxygen of that complex. This is also in harmony with the assignment of the **1a** complex assuming it to have the β_1 form.

In the ^{13}C-NMR spectra of the **1a** and **2a** complexes in heavy water, there have been observed six signals for the trien ligand and seven signals for the salicylato ligand. The chemical shifts of the salicylato ligands of the **1a** and **2a** complexes agreed with each other, but those of the trien ligand were different, as is shown in Fig. 3 and Table 1. The chemical shifts of the salicylato ligand are assigned on the basis of the chemical shift of the salicylato(tetraammine)cobalt(III) chloride monohydrate.[6] Those of the trien ligand are difficult to assign to the individual carbon atom. They have shown the two different configurations of the β_1 and β_2 complexes. The NMR spectral data of the **1a**—**1b** and **2a**—**2c** complexes are collected in Table 1.

OF **1a**, **1b**, **2a**, **2b**, **2c**, AND **2d** COMPLEXES

[N(2)H+salicylato] δ/ppm		(picrate) δ/ppm	IR spectra		Absorption bands		Electric conductivity of aqueous solution
N(2)H δ/ppm	(salicylato) δ/ppm		990—1100 cm^{-1}	$\rho_r(NH_{(2)})_r$ cm^{-1}	nm	ε	S cm^2 eq^{-1}
	[6.49—7.95 (5H)] [1]		999, 1030	835	331	2960[6]	93
	[6.56—7.99 (5H)] [2]		1060 (vs), 1080 (s)		530	270	
6.51 (1H)	6.66—8.00 (4H) [3]						
	6.75—7.90 (4H) [4]						
	[6.48—7.99 (5H)] [5]	9.20 (2H)	1000, 1028	838	520	275[6]	
			1060 (vs), 1075 (vs) [b]				
	[6.51—7.94 (5H)] [1]		990, 1030	835	333	3050[6]	124
	[6.50—7.94 (5H)] [2]		1060 (s), 1075 (vs)		520	270	
	[6.49—7.97 (5H)] [3]						
	6.62—7.93 (4H) [4]						
	[6.50—7.92 (5H)] [5]	9.22 (2H)	1005, 1030	838	510	290[6]	
			1060 (s), 1075 (vs)				
	[6.48—7.99 (5H)] [3]		990, 1030	835	333	2970[6]	
			1050 (s), 1075 (vs)		511	273	
			990, 1030	845	333	2600[7]	
			1048 (s), 1068 (vs)		522	274	
				840	330	2900[6]	
					533	160	

Solvent: 1) 0.1 mol dm^{-3} DCl, 2) 0.1 mol dm^{-3} D_2SO_4, 3) 1.8 mol dm^{-3} D_2SO_4, 4) 0.1 mol dm^{-3} NaOH and D_2O, 5) 0.9 mol dm^{-3} D_2SO_4, 6) H_2O, 7) Acetone, 8, 9) D_2O.
Standard: 1)—5) internal DSS, 8) internal dioxane ($\delta=67.4$), 9) intermal MeOH ($\delta=49.8$ ppm).
Complex 3: 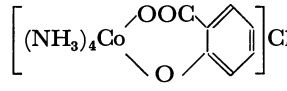 $Cl\cdot H_2O$, Ref. 6.

a) This signal overlapped with each solvent. b) This signal overlapped with picric acid.

Experimental

Measurements. The NMR spectra were recorded with a FX-60 apparatus (JEOL) for ^{13}C-NMR and an R-40 apparatus (Hitachi) for ^1H-NMR. The IR spectra were recorded in potassium bromide disks with a IR-27G apparatus (Shimadzu). The visible absorption spectra were recorded with a Shimadzu MPS-5000 recording spectrophotometer. The magnetic susceptibilities were measured by the Gouy method using a magnetic balance (Shimadzu) at room temperature. The pH was measured with a Toa Electronics pH-meter HM-5B. The electric conductivity of an aqueous solution were determined by the use of a conductometer, CM-30 (Shimadzu), at room temperature.

Preparation of Complexes. β-Salicylato(trien)cobalt(III) Chloride Monohydrate: This complex was prepared from β-dichloro(trien)cobalt(III) chloride[15] (46 g, 148 mmol dm^{-3}) and salicylic acid (20.5 g, 148 mmol dm^{-3}) at pH 10—11 by Morgan's method[2] and was then recrystallized from water. Yield: 40.46 g (69.3%).

*Separation of β_1-Salicylato(trien)cobalt(III) Chloride Monohydrate (**1a**) and β_2-Salicylato(trien)cobalt(III) Chloride Monohydrate (**2a**)*: Five-tenths of a gram of β-[Co(trien)sal]$Cl\cdot H_2O$ was dissolved in 1.5 ml of water, and the solution was passed through a large column of cation-exchange resin (2.5×50 cm, Dowex 50W-X2). Two red bands separated on elution with a 0.3 mol dm^{-3} NaCl solution. The solution of the first band (**1a**) and that of the second band (**2a**) were concentrated in a rotary evaporator, and the NaCl was removed by filtration. The **1a** and **2a** complexes were both recrystallized from water. Yields: 0.022 g (4.4%) for **1a**; 0.42 g (84%) for **2a**; Found **1a**: C, 39.47; H, 6.07; N, 14.45; Cl, 8.76%. **1b**: C, 39.68; H, 6.14; N, 14.39; Cl, 9.00%. Calcd for $CoC_{13}H_{24}N_4O_4Cl$: (*MW* 394.75) C, 39.56; H, 6.13; N, 14.19; Cl, 8.98%.

*β_1-Salicylato(trien)cobalt(III) Picrate (**1b**) and β_2-Salicylato(trien)cobalt(III) Picrate (**2b**)*: An aqueous solution of the **1a** or **2a** complex (0.5 g, 1.27 mmol dm^{-3}) was added to a solution of picric acid (0.29 g, 1.27 mmol dm^{-3}), the mixture was stirred, and the separated orange complex was filtered and recrystallized from water. Yields: 0.36 g (50%) for **1b**; 0.42 g (58.2%) for **2b**; Found **1b**: C, 39.99; H, 4.63; N, 16.96%. **2b**: C, 40.24; H, 4.46; N, 17.06%. Calcd for $CoC_{19}H_{24}N_7O_{10}$: (*MW* 569.37) C, 40.08; H, 4.25; N, 17.22%.

*β_2-Salicylato(trien)cobalt(III) Nitrate Monohydrate (**2c**)*: An aqueous solution of silver nitrate (0.45 g, 2.65 mmol dm^{-3}) was added to an aqueous solution of **2a** (1.0 g, 2.53 mmol dm^{-3}), the mixture was stirred, and the precipitated silver chloride was filtered. The filtrate was concentrated and recrystallized from water as russet crystals. Yield: 0.65 g (60.9%); Found: C, 37.29; N, 5.67; N, 16.56%. Calcd for $CoC_{13}H_{23}N_5O_7$: (*MW* 421.30) C, 37.06; H, 5.74; N, 16.62%.

*β_2-Salicylato(trien)cobalt(III) Tetraphenylborate (**2d**)*: An aqueous solution of the **2a** complex (1.0 g, 2.53 mmol dm^{-3}) was added to a solution (0.95 g, 2.78 mmol dm^{-3}) of sodium tetraphenylborate, the mixture was stirred, and the precipitated pink complex was filtered off and washed with water, and ethanol and dried *in vacuo*. Yield: 1.45 g (86.7%); dec 216 °C, Found: C, 67.12; H, 6.60; N, 8.58%. Calcd for $CoC_{37}H_{42}N_4O_3B$: (*MW* 660.51) C, 67.28; H, 6.41; N, 8.48%.

The authors wish to express their gratitude to Professor Masayasu Mori of Osaka City University for his discussions.

References

1) G. T. Morgan and J. D. M. Smith, *J. Chem. Soc.*, **1922**, 1956.
2) G. T. Morgan and J. D. M. Smith, *J. Chem. Soc.*, **1924**, 1924.
3) Y. Yamamoto, M. Mori, H. Yoneda, S. Misumi, and K. Ito, *Bull. Chem. Soc. Jpn.*, **42**, 984 (1969).
4) Y. Yamamoto, K. Ito, H. Yoneda, and M. Mori, *Bull. Chem. Soc. Jpn.*, **40**, 2580 (1967).
5) Y. Yamamoto, *Bull. Chem. Soc. Jpn.*, **42**, 999 (1969).
6) Y. Yamamoto, *Bull. Chem. Soc. Jpn.*, **51**, 2894 (1978).
7) Y. Yamamoto and E. Toyota, *Chem. Pharm. Bull. (Tokyo)*, **26**, 2275 (1978).
8) D. A. Buckingham, P. J. Cresswell, R. J. Dellaca, M. Dwyer, G. J. Gainsford, L. G. Marzilli, I. E. Maxwell, Ward T. Robinson, A. M. Sargeson, and K. R. Turnbull, *J. Am. Chem. Soc.*, **96**, 1713 (1974).
9) D. A. Buckingham, M. Dwyer, G. J. Gainsford, V. Janson Ho, L. G. Marzilli, Ward T. Robinson, A. M. Sargeson, and K. R. Turnbull, *Inorg. Chem.*, **14**, 1739 (1975).
10) L. G. Marzilli and D. A. Buckingham, *Inorg. Chem.*, **6**, 1042 (1967).
11) B. F. Anderson, J. D. Bell, D. A. Buckingham, P. J. Cresswell, G. J. Gainsford, L. G. Marzilli, G. B. Robertson, and A. M. Sargeson, *Inorg. Chem.*, **16**, 3233 (1977).
12) D. A. Buckingham and D. Jones, *Inorg. Chem.*, **4**, 1387 (1965).
13) D. A. Buckingham, L. Durham, and A. M. Sargeson, *Aust. J. Chem.*, **20**, 257 (1967).
14) M. Senou and T. Arai, "Solvent Effects," Sangyo Tosho Co., Tokyo (1970), Chap. 12.4.
15) A. M. Sargeson and G. H. Searle, *Inorg. Chem.*, **6**, 787 (1967).

X-Ray Diffraction Studies on the Structures of Diammine- and Aquasilver(I) Complexes in Aqueous Solution

Masunobu MAEDA,** Yoshiteru MAEGAWA, Toshio YAMAGUCHI, and Hitoshi OHTAKI*

Department of Electronic Chemistry, Tokyo Institute of Technology at Nagatsuta, Nagatsuta, Midori-ku, Yokohama 227

(Received January 12, 1979)

X-Ray diffraction studies were carried out for aqueous diamminesilver(I) nitrate, silver(I) perchlorate and nitrate solutions. The radial distribution curve of the diamminesilver(I) nitrate solution showed that the length of the Ag–NH_3 bond is (2.22±0.02) Å. In the aqueous silver(I) perchlorate solution, a silver(I) ion is combined with two water molecules at a distance of (2.41±0.02) Å, the result being in good agreement with that obtained for the nitrate solution.

It is well known that silver(I) ion forms the stable diammine complex and the diamminesilver(I) ion is believed to have a linear structure. X-Ray structure analysis[1] showed that in crystals of diamminesilver dinitritoargentate, $[Ag(NH_3)_2]Ag(ONO)_2$, the diamminesilver(I) cation has a linear structure, the Ag–NH_3 bond length being 2.11 Å. However, no X-ray diffraction study of the diamminesilver(I) complex in aqueous solution has been carried out. Miles *et al.*[2] and Geddes and Bottger[3] measured infrared and Raman spectra of various diammine silver salts in crystals and solutions, suggesting a linear structure of the complex.

Most authors reported 2 for the hydration number of silver ion in aqueous solution with various methods.[4–7] On the other hand, an NMR method[8] gave a smaller value (0.7) and conductivity[9] and compressibility[10] measurements gave values of 3—4. The X-ray diffraction study on the aquasilver(I) ion has been carried out neither in the crystalline state nor in aqueous solution, because no crystal containing aquated silver(I) ion has been found and aqua silver(I) ion is readily reduced by X-ray irradiation.

In the present work, we aimed at determining the structures of the diammine- and aquasilver(I) complexes in aqueous nitrate and perchlorate solutions by the X-ray diffraction method with a special precaution for reduction of silver by X-rays.

Experimental

Preparation and Analysis of Sample Solutions. A diamminesilver(I) nitrate solution was prepared by dissolving the required amount of recrystallized silver(I) nitrate in a concentrated ammonia solution. The mole ratio of NH_3/Ag in the solution was adjusted to about 2.5 in which each silver(I) ion should be coordinated with two ammonia molecules according to the stability constant of the complex[11,12] The concentration of the silver(I) ion was determined both by gravimetry as AgCl and by electrogravimetry as Ag. The results obtained by the two independent methods were consistent with each other within 0.2%. The ammonia content of the sample solution was determined by the Kjeldahl method. The concentration of the nitrate ion was determined by the stoichiometry of the silver(I) nitrate.

A silver(I) perchlorate solution was prepared by adding silver(I) carbonate crystals to a boiling $HClO_4$ solution, the crystals having been precipitated by adding a sodium carbonate solution to a solution of silver(I) nitrate and then decanted repeatedly with water until no sodium ion was detected by the flame test.

A silver(I) nitrate solution was prepared by dissolving recrystallized silver(I) nitrate in distilled water.

The concentration of the anion in each solution was determined as previously mentioned.[13] The density of the solutions was measured with pycnometers. The compositions of the sample solutions are given in Table 1.

TABLE 1. COMPOSITIONS (g-atoms/dm³) AND THE STOICHIOMETRIC VOLUMES V PER Ag ATOM OF THE SAMPLE SOLUTIONS

	(A) $Ag(NH_3)_2NO_3$	(B) $AgClO_4$	(C) $AgNO_3$
Ag	3.967	4.235	3.453
Cl	—	4.336	—
N	14.08	—	3.453
O	45.58	61.50	59.44
H	97.69	88.42	98.16
V/Å³	418.6	392.1	480.9
ρ/g cm^{-3}	1.453	1.684	1.471

X-Ray Scatterings. X-Ray measurements were carried out at (25±1) °C with a JEOL θ-θ diffractometer using a Philips Mo X-ray tube (λ=0.7107 Å) over the s range from 0.6 to 16 Å^{-1} ($s=4\pi\sin\theta/\lambda$), where 2θ is the scattering angle. The details of the diffractometer, measurements and data treatments are reported elsewhere.[13–15] Preliminary X-ray measurements revealed that precipitates of silver metal reduced by X-rays appeared on the surface of a solution within a few days. Therefore, prior to measurements, the change of scattered intensities was examined with the elapse of time at two fixed scattering angles of 12° and 60°. In the case of the diamminesilver(I) nitrate solution, the change of scattered intensities was found to be less than 1.5% within two days of X-ray irradiation. The silver(I) perchlorate and nitrate solutions showed a change of less than 2% within one day. Thus, an irradiated sample was replaced by a new one during the experiments every two days for the diamminesilver(I) nitrate solution and every day for the silver(I) perchlorate and nitrate solutions.

Intensities of X-rays scattered were corrected for background, absorption in the sample,[16] polarization[16] and incoherent scatterings,[13] and then scaled to electron units by the conventional methods.[13,17,18] The values of coherent, incoherent and anomalous scatterings of all atoms were quoted from the literature.[19] In the case of the silver(I)

** Present address: Department of Applied Chemistry, Nagoya Institute of Technology, Gokiso, Showa-ku, Nagoya 466.

perchlorate and nitrate solutions the molecular form factor for H_2O[20] was used when we calculated the interaction among water molecules in the systems. Reduced intensities $i(s)$ obtained by subtraction of independent scatterings of each atom and water molecules from the scaled intensities were Fourier transformed into the radial distribution function $D(r)$ after smoothing correction.[21] The modification function used was $\{(f_{Ag}(0)+\Delta f'_{Ag})^2+(\Delta f''_{Ag})^2\}/\{(f_{Ag}(s)+\Delta f'_{Ag})^2+(\Delta f''_{Ag})^2\}\exp(-0.01s^2)$ where f_{Ag}, $\Delta f'_{Ag}$, and $\Delta f''_{Ag}$ are the scattering factor, the real and the imaginary parts of anomalous dispersion of Ag atom, respectively. Spurious ripples found in the hard-core region of the $D(r)$ curves were removed by the previous manner.[13] Experimental scaled intensities, reduced intensities multiplied by s, the $D(r)$ and $D(r)-4\pi r^2\rho_0$ curves for the solutions investigated are shown in Figs. 1—4. Theoretical reduced intensities $i(s)_{calcd}$ of given atom pairs were calculated by Eq. 1 and they were transformed into the theoretical radial distribution curves by Fourier inversion.

$$i(s)_{calcd} = \sum_{i}\sum_{j\neq i} n_{ij}\{(f_i+\Delta f_i')(f_j+\Delta f_j')+(\Delta f_i'')(\Delta f_j'')\} \times \frac{\sin(sr_{ij})}{sr_{ij}} \exp(-b_{ij}s^2) \quad (1)$$

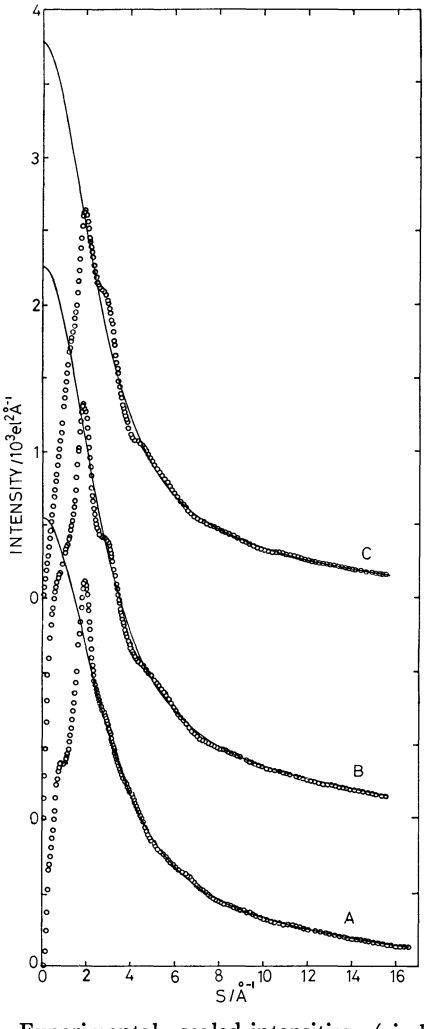

Fig. 1. Experimental scaled-intensities (circles) and calculated intensities (solid lines) of independent scatterings for solutions: A. $Ag(NH_3)_2NO_3$; B. $AgClO_4$; C. $AgNO_3$.

The values of the averaged distance r_{ij} between atoms i and j, the temperature factor $b_{ij}=1/2\langle\Delta r^2\rangle$ ($\langle\Delta r^2\rangle$ is the mean square amplitude of the molecular vibration) and the frequency factor n_{ij} were refined by the least squares method where the following function U was minimized.

$$U = \sum_{s_{min}}^{s_{max}} s^2(i(s)_{obsd}-i(s)_{calcd})^2 \quad (2)$$

Here s_{max} and s_{min} are the upper and lower limits of selected s regions. All calculations were performed with the aid of the M 180 computer by the KURVLR[22] and NLPLSQ[14] programs.

Results

Diamminesilver(I) Nitrate Solution. In the $D(r)$ and $D(r)-4\pi r^2\rho_0$ curves of solution A, three peaks appeared at 1.2, 2.2, and 3—5 Å. The first peak around 1.2 Å corresponds to the N–O bond within NO_3^- ion.[23,24] The O–H and N–H bonds within H_2O and NH_3 molecules also contribute in part to this peak. The second and rather distinct peak appeared at 2.2 Å, which can be ascribed to the distance between Ag and NH_3 molecules. The O–O interaction within the planar NO_3^- ion partly contributes to the peak ($1.26\text{ Å}\times\sqrt{3}=2.18$ Å). The structure of the diamminesilver(I) complex ion was determined by analyzing

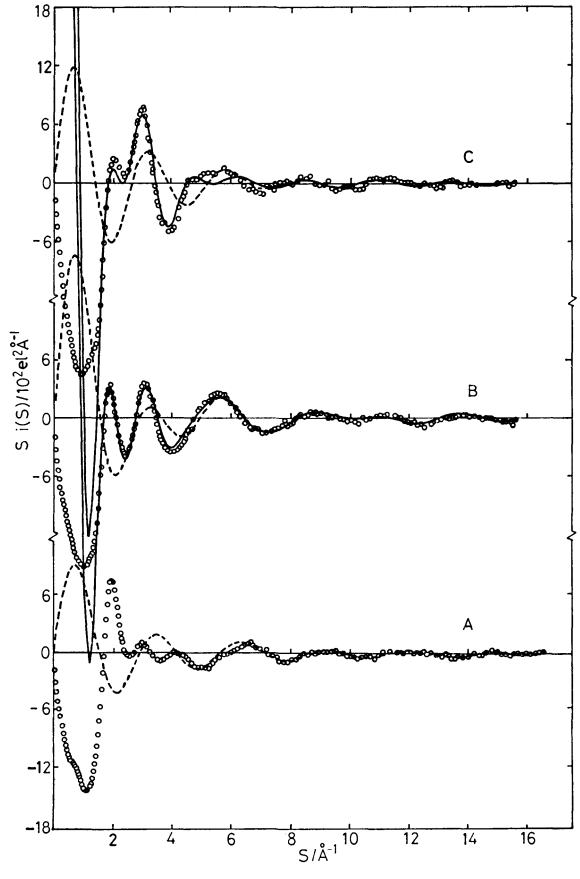

Fig. 2. Observed $s\cdot i(s)$ values (circles) for solutions A, B and C. Dashed and solid lines show the calculated $s\cdot i(s)$ values for the short- and (short+long)-range interactions, respectively, with parameter values listed in Table 3.

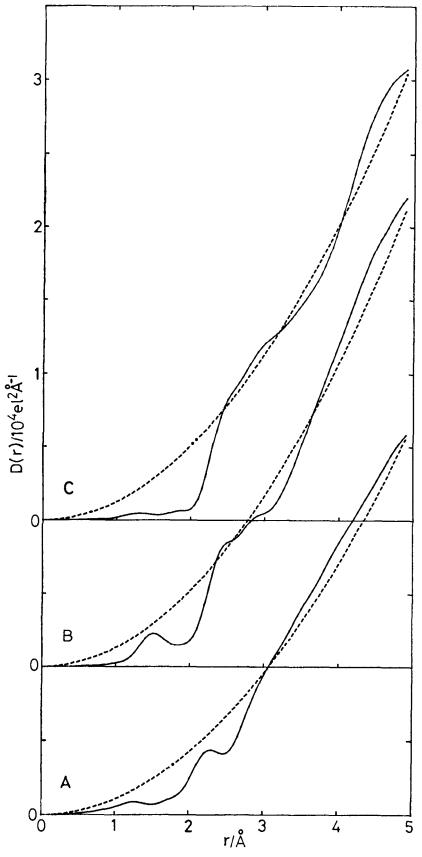

Fig. 3. Radial distribution functions $D(r)$ (solid lines) and $4\pi r^2\rho_0$ (dashed lines) for solutions A, B, and C.

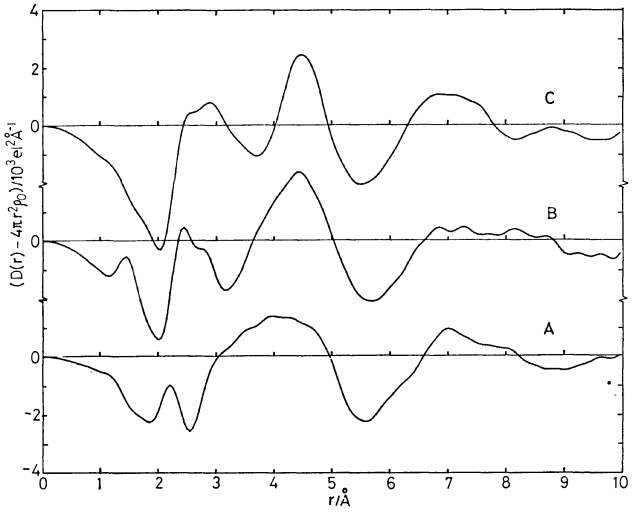

Fig. 4. The $D(r)-4\pi r^2\rho_0$ curves for solutions A, B, and C.

the second peak after subtraction of the peaks due to the N–O and O–O pairs within NO_3^- ion from the $D(r)$ curves. The average distances of the atom pairs used in the calculation were those given in the literature[24] and the temperature factors were calculated from spectroscopic data[25] by the Cyvin method,[26] the values being listed in Table 3.

The chain lines in Fig. 5 (a and b) show the residual

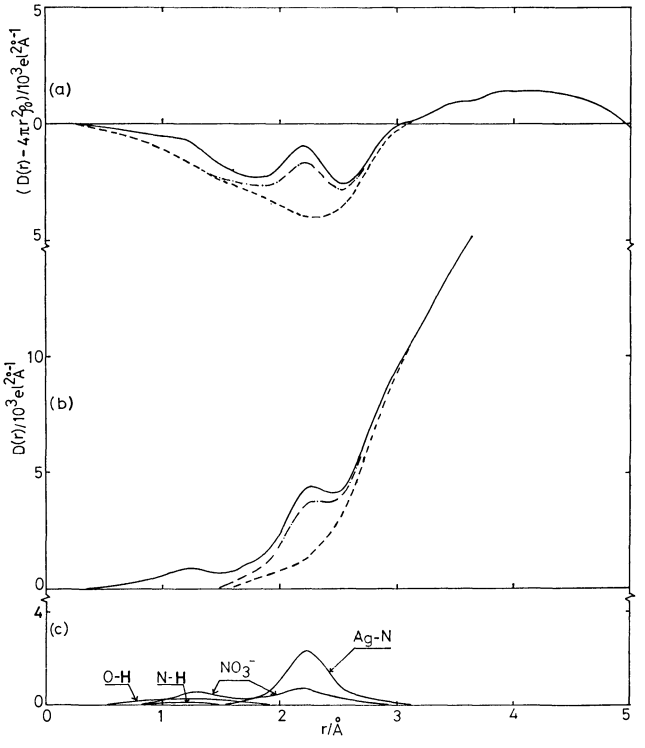

Fig. 5. (a) The $D(r)-4\pi r^2\rho_0$ curve for diamminesilver(I) nitrate solution. The chain line shows the residual curve after subtraction of the theoretical peaks from original curve (solid line), the peaks being those for the O–H and N–H bonds within H_2O and NH_3, respectively, and the N–O and O–O pairs within NO_3^- ion. The dashed line gives the difference between the original curve and the sum of the whole theoretical peaks shown in (c). (b) The corresponding $D(r)$ curve. (c) The theoretical peak shapes of each atom pair.

curves obtained by subtraction of the theoretical curves of the O–H bond within H_2O, the N–H bond within NH_3, the N–O, and O–O contacts within NO_3^- ion from the original curves (solid lines). The length of the Ag–NH_3 bond and the coordination number of the silver ion were determined from the residual curve by the trial-and-error method. The Ag–NH_3 bond length finally determined was (2.22±0.02) Å. The number of ammonia molecules coordinated to a silver(I) ion was estimated to be about 2 from the peak area. The temperature factor for the Ag–NH_3 bond was determined to be 0.002—0.003 Å^2, which was in good agreement with the value of 0.0018 Å^2 calculated by using spectroscopic data.[27] Further subtraction of the theoretical peak due to two Ag–NH_3 bonds from the residual curve gave a smooth background curve (dashed line), which shows no more appreciable intramolecular interaction left within 3 Å, except for a broad peak around 2.8 Å due to the bulk structure.[28]

The theoretical $s\cdot i(s)$ curve of the diamminesilver(I) nitrate solution was calculated on the basis of the proposed models for the complex, nitrate ion, ammonia, and water molecules. The theoretical values (dashed line in Fig. 2, curve A) of $s\cdot i(s)$ thus evaluated were compared with the experimental ones (circles). Over the range of 4 Å^{-1} $<s<$ 15 Å^{-1} satisfactory agreement

was found between them. Discrepancy in the calculated and experimental values at $s<4$ Å^{-1} is due to neglect of long-range interactions in the theoretical calculations.

Silver(I) Perchlorate and Nitrate Solutions. In Fig. 3, we see a peak around 1.5 Å in the $D(r)$ curve obtained for the perchlorate solution (curve B), which is due to the Cl–O bond within the perchlorate ion. A peak around 1.2 Å found in the nitrate system (curve C) is ascribed to the N–O bond within the nitrate ion. Peaks around 2.5, 2.8, and 4.3 Å are seen in the $D(r)$ and $D(r)-4\pi r^2\rho_0$ curves for both the solutions (see Figs. 3 and 4). The second peak around 2.5 Å can be attributed to the Ag–OH_2 bond within the hydrated silver(I) ion, which is expected from the sum of the radius of Ag^+ (1.26 Å[29]) and the size of a water molecule (1.40 Å[30]). The O–O contacts within the anions also contribute to the peak (1.5 Å$\times\sqrt{8/3}$=2.4 Å for tetrahedral ClO_4^- and 1.2 Å$\times\sqrt{3}$= 2.1 Å for planar NO_3^-). The peak around 2.8 Å is due to the hydrogen-bonded H_2O–H_2O interaction in the bulk water structure. Since the peaks at about 2.5 Å and 2.8 Å are overlapped, analysis of the structure of the aquasilver(I) ion from the peak shape at 2.5 Å was not possible without taking into account the contribution of the H_2O–H_2O interaction in the bulk. The wing of the peak due to long-range interactions which appeared at 4.3 Å may partly contribute to the peak at 2.5 Å. The 4.3 Å peak also influences the shape of the 2.8 Å peak. Therefore, in order to analyze the peak shape at 2.5 Å, interactions included in the peaks at 2.8 Å and 4.3 Å must be taken into consideration. The long-range interactions may be estimated on the basis of appropriate models of molecular interactions. The peak at 4.3 Å might include the interaction between silver ion and water molecules in the second hydration sphere.[31] Interactions between the central atoms of the perchlorate and nitrate ions and water molecules hydrated with the anions may also contribute to the broad peak. According to X-ray diffraction studies on concentrated HNO_3[23] and NH_4NO_3[24] aqueous solutions, the N(within NO_3^-)–O(within H_2O in the hydration sphere) interaction should appear at about 3.4 Å. For the perchlorate system, on the other hand, the corresponding Cl–O interaction is expected to appear around 3.6 Å, which is seen as a hump in curve B of Fig. 4. Such a hump has been observed in concentrated $Fe(ClO_4)_3$ aqueous solutions.[32]

Short-range intramolecular interactions mainly contribute to the high angle part of the $s\cdot i(s)$ function, whereas long-range intermolecular interactions largely contribute to the low angle part of the function and rapidly diminish with increasing s values. We have seen in the silver nitrate–ammonia system (Fig. 2, curve A) that the short-range interactions for the diamminesilver(I) nitrate solution are responsible for the $s\cdot i(s)$ values at $s>4$ Å^{-1}. Therefore, at a first step of approach in estimating the parameter values of the short-range interactions in the silver(I) perchlorate

TABLE 2. PARAMETER VALUES OF THE INTRAMOLECULAR INTERACTIONS OBTAINED BY THE LEAST SQUARES REFINEMENTS WITH VARIOUS s RANGES FOR THE SILVER(I) PERCHLORATE SOLUTIONS

The values in parentheses are their standard deviations.

Atom pair	5 Å$^{-1}\leq s\leq$15 Å^{-1}	6 Å$^{-1}\leq s\leq$15 Å^{-1}	7 Å$^{-1}\leq s\leq$15 Å^{-1}	8 Å$^{-1}\leq s\leq$15 Å^{-1}
r_{Ag-OH_2}/Å	2.427 (5)	2.410 (4)	2.406 (4)	2.405 (5)
b_{Ag-OH_2}/Å	0.0040 (3)	0.0040 (2)	0.0040 (2)	0.0039 (2)
n_{Ag-OH_2}	1.98 (3)	1.99 (3)	1.99 (3)	2.00 (4)
r_{Cl-O}/Å	1.474 (3)	1.473 (2)	1.471 (2)	1.472 (2)

TABLE 3. FINAL PARAMETER VALUES AND STANDARD DEVIATIONS (IN PARENTHESES) FOR THE SHORT- AND LONG-RANGE INTERACTIONS OBTAINED BY THE LEAST SQUARES REFINEMENTS FOR THE SILVER(I) PERCHLORATE AND NITRATE SOLUTIONS

System	Atom pair	r_{ij}/Å	b_{ij}/Å	n_{ij}
$Ag(NH_3)_2NO_3$	Ag–NH_3 (within $Ag(NH_3)_2^+$)	2.22 (2)	0.0018[a]	2.0 (5)
	N–O (within NO_3^-)	1.26[b]	0.00086[a]	3.0[c]
$AgClO_4$	Ag–OH_2 (within $Ag(OH_2)_2^+$)	2.410 (4)	0.0040 (2)	1.99 (3)
	Cl–O (within ClO_4^-)	1.473 (2)	0.00076[a]	4.0[c]
	H_2O–H_2O (in the bulk)	2.83 (3)	0.014[d]	4.4[d]
	Cl (within ClO_4^-)–H_2O	3.57 (4)	0.128 (7)	25.6 (8)
	Ag–$(H_2O)_{II}$	4.44 (6)	0.105 (5)	9.5 (3)
$AgNO_3$	Ag–OH_2 (within $Ag(OH_2)_2^+$)	2.450 (8)	0.004 (2)	2.45 (7)
	N–O (within NO_3^-)	1.24 (2)	0.00086[a]	3.0[c]
	H_2O–H_2O (in the bulk)	2.91 (7)	0.014[d]	4.4[d]
	N (within NO_3^-)–H_2O	3.17 (7)	0.036 (8)	43 (2)
	Ag–$(H_2O)_{II}$	4.29 (6)	0.019 (7)	17.3 (6)

a) Calculated values from spectroscopic data (Refs. 25, 27, and 33). b) Ref. 24. c) Fixed on the basis of the structure model. d) Ref. 30.

and nitrate solutions, the least squares method was applied to the $s \cdot i(s)$ values of variable subsets covering various s ranges ($5\,\text{Å}^{-1} \leq s \leq 15\,\text{Å}^{-1}$). Then, long-range interactions were taken into consideration for explaining the data of almost whole angle range of the $s \cdot i(s)$ values.

Short-range Interactions: The structures of hydrated $Ag(OH_2)_n^+$ and the anion (ClO_4^- or NO_3^-) were taken into consideration in calculation of $s \cdot i(s)$ values over the range of $5\,\text{Å}^{-1} \leq s \leq 15\,\text{Å}^{-1}$ with variable s_{min}, the minimum value of the s range. In the calculation, the Ag–OH_2 distance, the temperature factor, and the number of the bond (n) were independently varied. For the tetrahedral ClO_4^- or planar NO_3^- ion, the only Cl–O or N–O distance was independently refined. The temperature factors of the perchlorate and nitrate ions were kept constant at the values calculated from spectroscopic data: 0.00076 Å^2 (Cl–O) and 0.0012 Å^2 (O–O) for ClO_4^-;[33] 0.00086 Å^2 (N–O) and 0.0010 Å^2 (O–O) for NO_3^-.[25]

Table 2 gives the parameter values thus obtained for the short-range intramolecular interactions of the siver(I) perchlorate solution with varying s ranges. As is seen from Table 2, the results were practically independent of selection of the s_{min} values. The values of the parameters determined in the range of $6\,\text{Å}^{-1} \leq s \leq 15\,\text{Å}^{-1}$ are taken as the best ones for both the perchlorate and the nitrate solutions. Calculated $s \cdot i(s)$ curves by using the parameter values thus obtained are shown by dashed lines in Fig. 2 (curves B and C).

Long-range Interactions: Interactions between silver(I) ion and water molecules in the second hydration sphere (abbreviated as Ag–$(H_2O)_{II}$) and the Cl–H_2O or N–H_2O interaction due to the hydration of perchlorate or nitrate ion were taken into account in calculation of $s \cdot i(s)$ values over much wider s ranges. The H_2O–H_2O interaction in the bulk phase was so approximated that "free" water molecules formed tetrahedral frameworks, the parameter values of the tetrahedral pentamer moiety of water, $(H_2O)_5$, being quoted from the work by Narten.[30]

When we took into account the long-range interactions in addition to the short-range intramolecular interactions previously discussed, satisfactory agreements were obtained between the experimental and theoretical $s \cdot i(s)$ values in both the perchlorate and nitrate systems over the whole range of s except $s < 1.5\,\text{Å}^{-1}$, where much longer-range intermolecular interactions and the scattering from the "holes" in an uniform medium[22] contribute to the $s \cdot i(s)$ values. The distance between silver(I) ion and water molecules in the second coordination sphere was estimated to be 4.3—4.4 Å. The Cl(within ClO_4^-)–H_2O and N(within NO_3^-)–H_2O distances were converged to 3.57 Å and 3.17 Å, respectively. The final results are summarized in Table 3, together with the values for the diamminesilver(I) nitrate solution given in the previous section. A small deviation of the theoretical $s \cdot i(s)$ curve from the experimental one was observed in the range of $5\,\text{Å}^{-1} < s < 6\,\text{Å}^{-1}$ in the silver(I) nitrate system. However, no further refinement was possible with any other models of the system. Figure

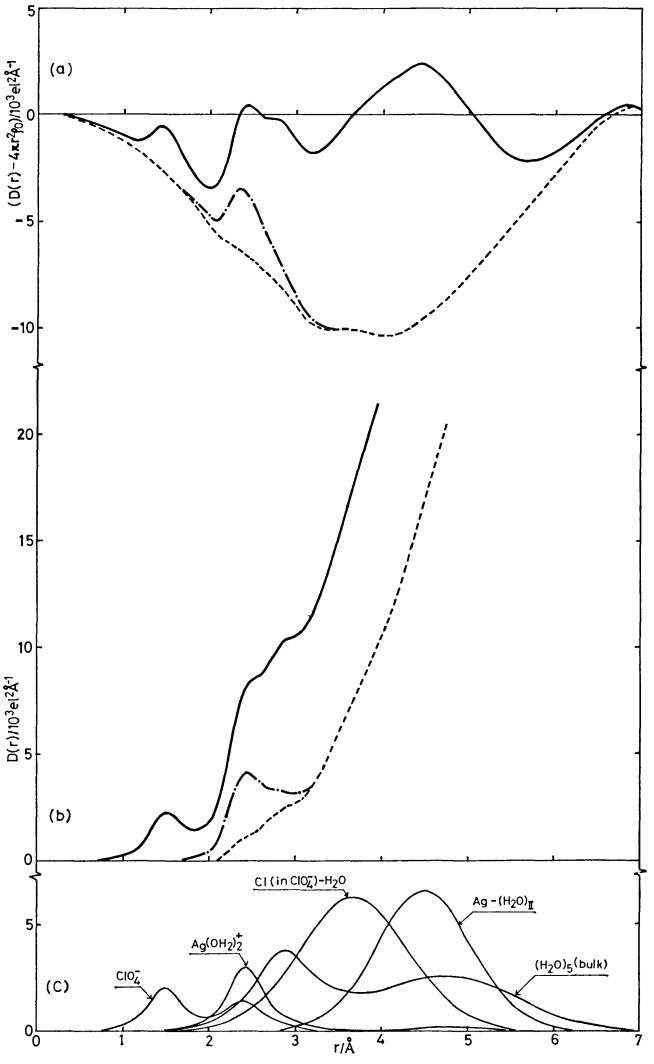

Fig. 6. (a) The $D(r) - 4\pi r^2 \rho_0$ curve for silver(I) perchlorate solution. The chain line shows the residual curve after subtraction of the theoretical peak shapes shown in (c) except for the peak due to the Ag–OH_2 bond from the original curve (solid line). The dashed line indicates the difference between the original curve and the sum of theoretical peak shapes shown in (c). (b) The corresponding $D(r)$ curve. (c) The theoretical peak shapes for each atom pair.

6(c) shows the radial distribution curve of each interaction in the silver perchlorate system estimated from the analysis of the $s \cdot i(s)$ curve described above. The peaks due to the Ag–OH_2 bond are clearly seen at 2.4 Å, shown by chain lines in Fig. 6 (a and b), when the theoretical peaks due to the intra- and intermolecular interactions except for the Ag–OH_2 bond were subtracted from the original curves shown by solid lines in Fig. 6 (a and b). Further subtraction of the peak due to the Ag–OH_2 bond from the residual curves gave smooth background curves, which indicated no other intra- and intermolecular interactions shorter than 6 Å.

Discussion

X-Ray diffraction data revealed that an Ag(I) ion

is coordinated with two ammonia molecules at a distance of 2.22 Å in aqueous solution and no water molecule combines with the diamminesilver(I) complex. The Ag–NH_3 bond in the $Ag(NH_3)_2^+$ complex in solution is longer than that in crystal.[1] In the present X-ray analysis we could not draw a definite conclusion that the complex has a linear structure because non-bonded NH_3–NH_3 distance was not determined. According to the preceeding work,[1] $Ag(NH_3)_2^+$ complex in $[Ag(NH_3)_2]Ag(NO_2)_2$ crystals has a linear structure. Therefore, we would like to say that the diamminesilver (I) ion has a linear structure in solution as well as in crystals. The aquasilver(I) ion may also have a linear structure. The values of the distance between a silver(I) ion and a water molecule r_{Ag-OH_2} and the coordination number of the silver(I) ion n_{Ag-OH_2} in the nitrate system are slighly different from those of the perchlorate system (Table 3). However, the difference is not significant.

It should be noted that the Ag–NH_3 distance is much smaller than the Ag–OH_2 distance observed in the present work, the fact suggesting the formation of strong coordination bonds between silver ion and ammonia molecules compared with that between silver ion and water molecules.

The present work has been partially supported by a Grant-in-Aid for Scientific Research from the Ministry of Education.

References

1) H. M. Maurer and A. Weiss, *Z. Kristallogr.*, **146**, 227 (1977).
2) M. G. Miles, J. H. Patterson, C. W. Hobbs, M. J. Hopper, J. Overend, and R. S. Tobias, *Inorg. Chem.*, **7**, 1721 (1968).
3) A. L. Geddes and G. L. Bottger, *Inorg. Chem.*, **8**, 802 (1969).
4) H. Taube, *J. Phys. Chem.*, **58**, 523 (1954).
5) Ya. I. Tur'yan, *Zh. Fiz. Knim.*, **38**, 1960 (1964).
6) E. N. Gapon, *Z. Anorg. Allg. Chem.*, **168**, 125 (1927).
7) V. Jedináková and J. Celeda, *Collect. Czech. Chem. Commun.*, **36**, 3071 (1971).
8) J. W. Akitt, *J. Chem. Soc., Dalton Trans.*, **1974**, 175.
9) N. I. Gusev, *Russ. J. Phys. Chem.*, **47**, 1309 (1973).
10) D. S. Allam and W. H. Lee, *J. Chem. Soc.*, **1966**, 5.
11) L. G. Sillén and A. E. Martell, "Stability Constants," Spec. Publ. No. 17 and Supplement No. 1, Spec. Publ. No. 25, The Chemical Soc., London (1964) and (1971).
12) M. Maeda, R. Arnek, and G. Biedermann, *J. Inorg. Nucl. Chem.*, **41**, 343 (1979).
13) H. Ohtaki, M. Maeda, and S. Ito, *Bull. Chem. Soc. Jpn.*, **47**, 2217 (1974).
14) H. Ohtaki, T. Yamaguchi, and M. Maeda, *Bull. Chem. Soc. Jpn.*, **49**, 701 (1976).
15) T. Yamaguchi and H. Ohtaki, *Bull. Chem. Soc. Jpn.*, **51**, 3227 (1978).
16) H. A. Levy, M. D. Danford, and A. H. Narten, ORNL-3960 (1966).
17) N. Norman, *Acta Crystallogr.*, **10**, 370 (1957).
18) J. Krogh-Moe, *Acta Crystallogr.*, **9**, 951 (1956).
19) "International Tables for X-Ray Crystallography," Kynoch Press, Birmingham (1974), Vol. IV.
20) F. Hajdu, *Acta Crystallogr., Part A*, **28**, 250 (1972).
21) K. Ichida, F. Yoshimoto, and T. Kiyono, *Joho Shori*, **15**, 414, 477 (1974).
22) G. Johansson and M. Sandström, *Chem. Scripta*, **4**, 195 (1973).
23) K. Michelsen, *Acta Chem. Scand.*, **6**, 801 (1952).
24) R. Caminiti, G. Licheri, G. Piccaluga, and G. Pinna, *J. Chem. Phys.*, **68**, 1967 (1978).
25) Fundamental frequencies (1050, 1415, and 724 cm^{-1}) measured for the sample solution were used for the calculation for NO_3^- ion. The *F* matrices were calculated on the assumption of the modified Urey-Bradley force field.
26) S. J. Cyvin, "Molecular Vibrations and Mean Square Amplitudes," Universitetsforlaget, Oslo (1968).
27) The value of 342 cm^{-1} measured for solution A was used for ν_1 frequency. The ν_3 value of 470 cm^{-1} used was the reported one in Ref. 3.
28) A. H. Narten, *J. Chem. Phys.*, **49**, 1692 (1968).
29) L. Pauling, "The Nature of the Chemical Bond," Cornell University Press, (1960).
30) A. H. Narten, ORNL-3997 (1966) and ORNL-4578 (1970).
31) R. M. Lawrence and R. F. Kruh, *J. Chem. Phys.*, **47**, 4758 (1967).
32) M. Magini, *J. Inorg. Nucl. Chem.*, **40**, 43 (1978).
33) Fundamental frequencies (931, 460, 1100, and 625 cm^{-1}) measured for solution B were used for the calculation for ClO_4^- ion. The *F* matrices were calculated using the modified Urey-Bradley force field.

Oxidation and Reduction of MoO_2–MoO_3 Studied by Infrared Emission Spectroscopy

Akifumi UENO* and Carroll O. BENNETT†

National Chemical Laboratory for Industry, 2-19-19, Mita, Meguro-ku, Tokyo 153

† *Department of Chemical Engineering, University of Connecticut, Storrs, Connecticut 06268*

(Received January 27, 1979)

A sample preparation technique was developed for the study of infrared emission spectroscopy. The emission spectrum of MoO_3 showed peaks at 987 and 925 cm^{-1} in the temperature range of 185 through 505 °C. Peak intensities were proportional to the sample weight. The background intensity in the emission spectrum was measured at 1050 cm^{-1} and it was also proportional to the sample weight. In order to apply emission spectroscopy to the study of reaction kinetics, the reduction of MoO_3 by H_2 and the oxidation of MoO_2 by O_2 were chosen as model reactions. These reactions were studied at 425 to 485 °C and the activation energy for the reduction of MoO_3 was 43 kcal/mol and that for the oxidation of MoO_2 was 38 kcal/mol. The activation energy for the formation of the terminal Mo=O bond was, however, 71.2 kcal/mol.

Oxides of molybdenum are important as oxidation catalysts. In connection with a recent study[1] of the partial oxdation of methanol on MoO_3–Fe_2O_3, attempts were made to investigate the state of the surface of the catalyst by infrared spectroscopy. As a first step it seemed logical to work with pure MoO_3, but we found that it was not possible to prepare a suitable disk of this material for study by the usual scattered transmission tehnique. Although the catalytic behavior of some noble metals such as platinum seem little affected by supports, such is not the case for most transition metals, and *a fortiori* for metal oxides. Thus we have searched for a means of studying unsupported MoO_3. Previous infrared work[2,3] on molybdenum oxides has been done on supported catalysts or by the Nujol method. Vanadium oxides have been studied in KBr disks.[4] These methods are obviously not suited to the observation of the catalyst during catalysis, our ultimate goal.

Although it seems attractive to use emission spectroscopy to observe catalysts at reaction temperatures, typically 200—500 °C, few papers have been published on this subject. Eischens and Pliskin[5] observed the spectrum of a thin layer of oleic acid on an aluminum rod at 200 °C. Low and Inoue[6] used an aluminum plate as the sample substrate. In an ideal arrangement only the sample would be heated, but radiation from the polished heated aluminum is small. Koga *et al.*[7] have used an infrared beam to heat their sample, so that the rest of the cell remained cooler, and interfering radiation was minimized. They observed the emission spectrum of formate ions on the surface of Al_2O_3. Dewing[8] deposited bismuth molybdate on a heated gold foil and observed the emission spectrum of the solid. Cavallini *et al.*[9] showed the utility of infrared emission spectroscopy as applied to the study of the oxidation of metal surfaces.

The experimental arrangement which we have used to obtain the infrared spectrum of CO_2 adsorbed on unsupported NiO[10] is readily adapted to the emission mode. If the temperature is higher than about 200 °C, the source can be turned off and emission spectra obtained. As pointed out by Dewing,[8] a thin layer (about 1 mg/cm^2) of solid must be used so that the black-body radiation of the solid does not overwhelm the emission peaks. For the study of MoO_3, we have evaporated on a stainless-steel mirror a suspension of finely divided ($\approx$5 μm particles) oxide. This sample gives a good emission spectrum of MoO_3 or, after reduction, MoO_2. However, its surface area is so small that there is not enough adsorbed CH_3OH, for example, on the solid to give a spectrum of adsorbed species. In future work it should be possible to use highly divided oxide (100—200 Å) prepared in a flame reactor[11] to permit the observation of adsorbed species. Such solids were not available to us at the time of the work reported here.

Infrared spectroscopy can be used to study the kinetics of changes of solids and species adsorbed on solids by the use of the transient method.[9,12,13] In the work reported here we have applied this method to the reduction and oxidation of the system MoO_3–MoO_2.

Experimental

Sample Preparation. MoO_3 was obtained by the decomposition of ammonium molybdate at 340 °C in air. It was ground to less than 200 mesh. These finely divided particles were suspended in water, and some of the finest part of the suspension was pipetted onto a well polished stainless steel mirror (1.0 cm^2) and then dried at 110 °C. The mean particle size of the sample was about 5 μm, measured by optical microscopy. After weighing, the mirror coated with catalyst was placed in the reaction cell and heated at 485 °C for 16 h with oxygen flow.

Reaction Cell and Optics of Spectrometer. The reaction cell used is the same as the one used in the previous work,[3] except that it was fitted with a BaF_2 window instead of an IRTRAN 6(CdTe) window; the BaF_2 window allows us to use higher temperatures than 300 °C. The window was glued into a stainless steel holder with Vacseal, although this adhesive was prone to leak after some exposure to temperatures above 400 °C. The cell was always used under positive pressure.

The optics of the infrared spectrometer is also the same as previously used,[10] except that the infrared radiation source was turned off to obtain the emission spectrum. The slits were not programmed in the present work and were set at 4.0 mm for all experiments.

In the present experiments, not only the emission from the sample but also that from the stainless steel mirror were recorded. Therefore, a correction was always made by the

subtraction of the emittance due to the mirror from that recorded due to the mirror with its sample. The emission spectrum of the mirror was not sensitive to its degree of polish for all those tested.

The intensities of the emission spectra were expressed in terms of μV on the lock-in amplifier (P.A.R. Model 128).

Chemicals. The gases used in the present experiments were obtained from Matheson. A cooling trap at −50 °C was used for H_2 and O_2 to remove water, and for Ar a Hydrox purifier was used to eliminate water and oxygen. These gases were introduced into the reaction cell with a flow rate of 3.0 ml/s, which corresponds to about 1 s of residence time in the reaction cell.

Procedure for Measurement of Reaction Rates. In order to obtain the reduction rate of MoO_3 by H_2 and the oxidation rate of MoO_2 by O_2, the wave numbers of the emission spectrum were fixed at 1050, 987, and 925 cm^{-1}, and the changes in the emission intensities were recorded separately for each experimental run. The emission spectrum of MoO_3 has peaks at 987 and 925 cm^{-1}, and they represent the termical Mo=O bond and the Mo–O–Mo net plane vibration.[3,9] For the experimental convenience, the increase in the background intensity at 1050 cm^{-1} is chosen to represent the change of bulk MoO_3 to MoO_2 and *vice versa*. The background intensity was sensitive to the oxidation states of molybdenum oxides at the higher wave numbers, and at the lower wave numbers around 825 cm^{-1} it became less sensitive (see Fig. 5). Therefore, the peak heights at 987 and 925 cm^{-1} were calculated by linear interpolation as follows every 1.0 min for the reduction of MoO_3 or every 5.0 s for the oxidation of MoO_2.

$$I_{987}(t) - \left(\frac{987-825}{1050-825}\right)I_{1050}(t) = P_{987}(t) \quad (1)$$

$$I_{925}(t) - \left(\frac{925-825}{1050-825}\right)I_{1050}(t) = P_{925}(t) \quad (2)$$

where $I_{987}(t)$ represents the intensity emitted from the sample at time t after the addition of H_2 (or O_2) at 987 cm^{-1}, and $I_{1050}(t)$, $I_{925}(t)$ also represent the emission at 1050 and 925 cm^{-1} respectively. From $P_{987}(t)$ and $P_{925}(t)$, the rates of reduction or oxidation could be obtained.

X-Ray Diffraction. The identification of MoO_2 and the Mo metal was obtained by X-ray powder diffraction by using Mo or Cu tubes with 40 kV and 20 mA. When the sample was studied by X-ray diffraction, it was exposed to air at room temperature. We confirmed that the sample was not oxidized by air at room temperature as follows: MoO_3 set in the reaction cell was reduced by the addition of H_2 at 485 °C, but the reduction stopped when H_2 was switched to Ar, as determined by the emission spectrum. Then the temperature was decreased to room temperature, keeping the sample in Ar, and its infrared transmission spectrum was observed. This spectrum did not change at all even when exposed to pure O_2 for several days at room

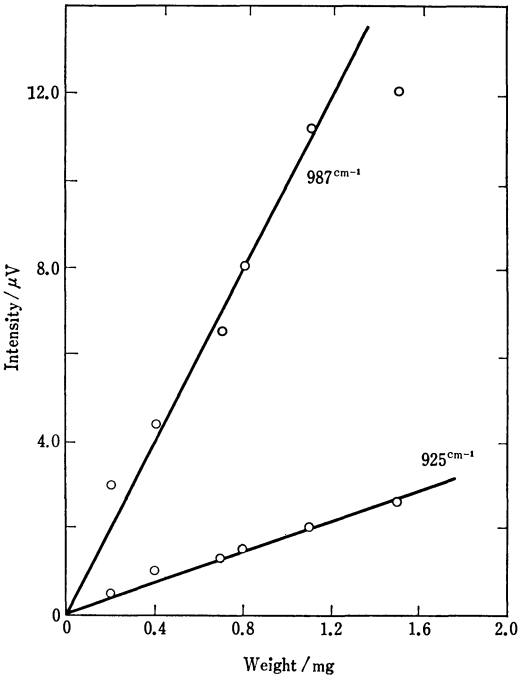

Fig. 2. Relation of emission intensities to sample weight at 485 °C.

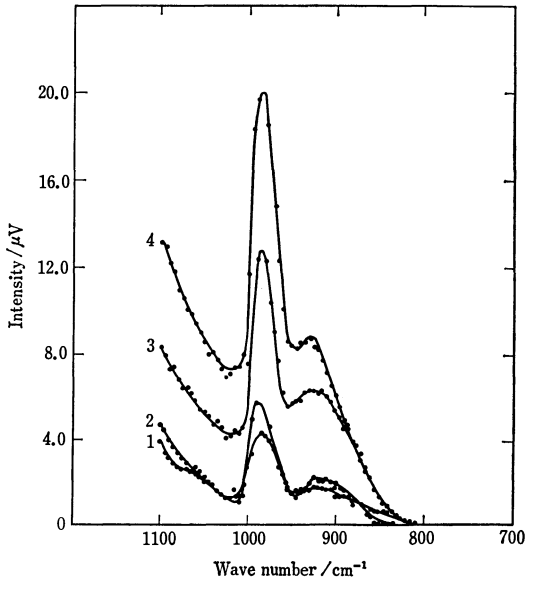

Fig. 1. Emission spectra of MoO_3 at 485 °C.
Sample weights: 1: 0.2 mg, 2: 0.4 mg, 3: 0.8 mg, 4: 1.1 mg.

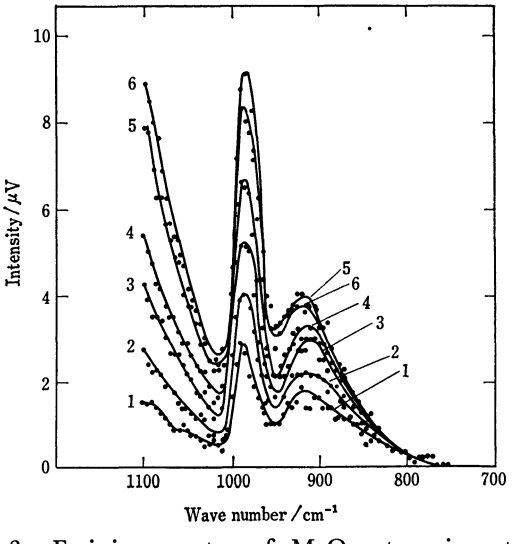

Fig. 3. Emission spectra of MoO_3 at various temperatures for 0.7 mg of sample.
1: 185 °C, 2: 245 °C, 3: 335 °C, 4: 365 °C, 5: 425 °C, 6: 485 °C.

temperature.

Results

Emission Spectra. Figure 1 shows the emission spectra at 485 °C for various sample weights deposited on the mirror. The intensities, corrected for radiation from the mirror, are plotted in Fig. 2 as a function of sample weight. Up to 0.8 mg/cm² a linear relation is obtained; such curves facilitate the comparison of spectra obtained from different samples. Higher sample loadings may show some effect of the submergence on the individual bands by black body radiation for thick samples. This effect is often mentioned, for example by Dewing.[8]

The effect of temperature on the emission spectra is shown in Fig. 3, and the intensities of the various bands vary with temperature as shown in Fig. 4. The surprising linearity of these relations is not in disagreement with the fourth-power law of radiation, as illustrated by the following analysis.

A simple balance of radiant energy at the detector equates the energy received from the sample at T to that lost to the surroundings at ambient temperature T_0:

$$K_1(T^4 - T_d^4) = K_2(T_d^4 - T_0^4) \quad (3)$$

were T_d is the temperature of the detector. The signal depends on T_d, given by

$$T_d = \left(\frac{K_1T^4 + K_2T_0^4}{K_1 + K_2}\right)^{1/4} \quad (4)$$

K_1 and K_2 depend on view factors and emissivities in a complicated fashion, but to a first approximation

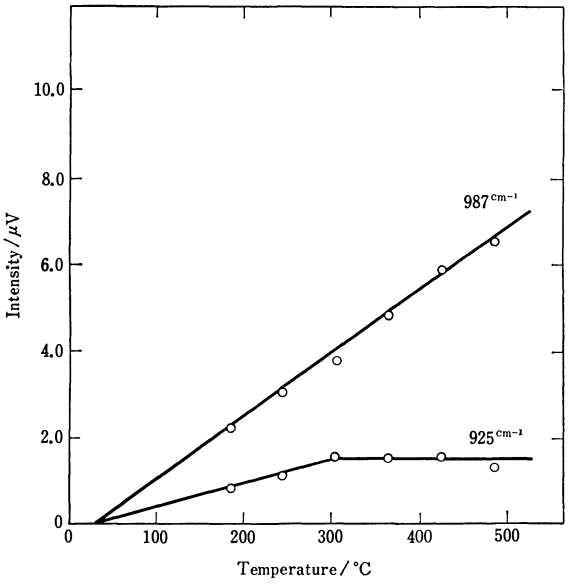

Fig. 4. Effect of temperature on emission intensity.

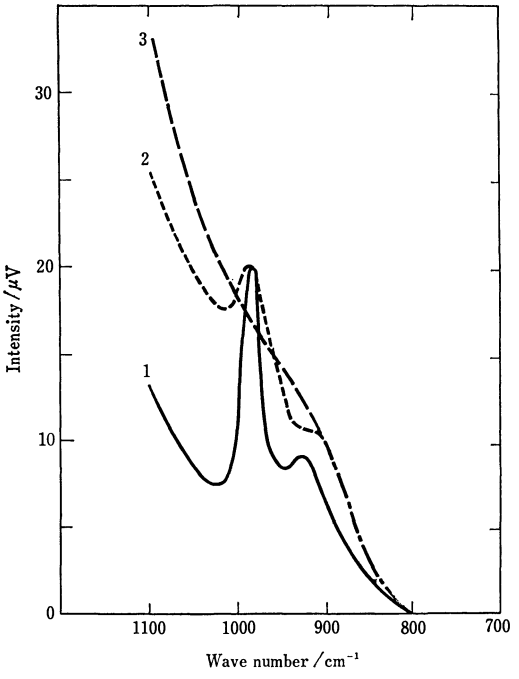

Fig. 5. Changes in emission spectrum of MoO_3 caused by addition of H_2 at 485 °C and 1 atm.
1: In O_2 (1 atm), 2: in H_2 for 2 min, 3: in H_2 for 10 min.

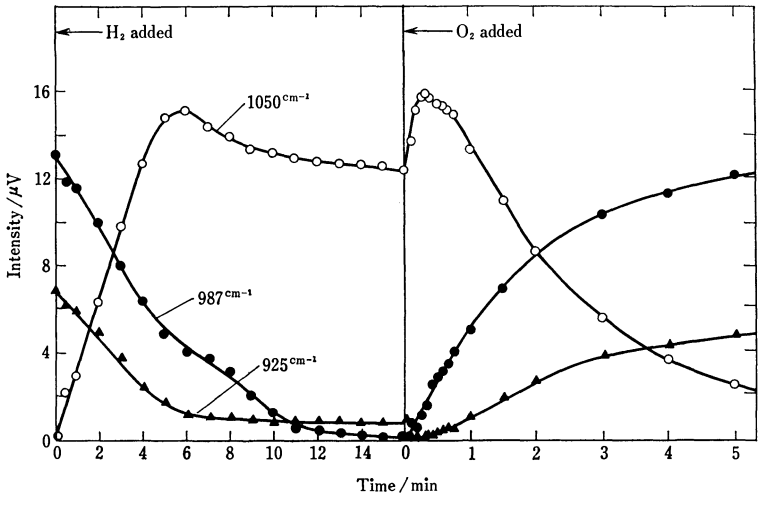

Fig. 6. Variation of emission intensities during reduction and oxidation at 485 °C.
Reduction past MoO_2 toward Mo.

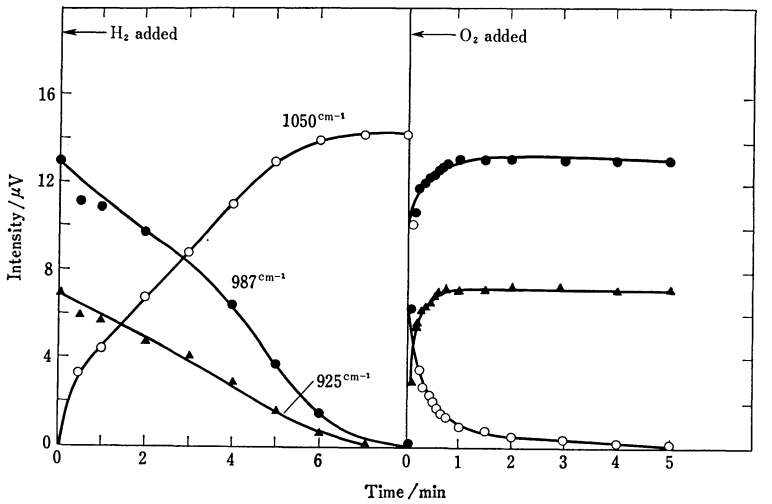

Fig. 7. Variation of emission intensities during reduction of MoO_3 to MoO_2 and during oxidation of MoO_2 to MoO_3, at 485 °C.

they are equal. We then have

$$T_d = \left(\frac{T^4 + T_0^4}{2}\right)^{1/4} \quad (5)$$

For T_0=300 K and T varying from 450 K to 750 K, the relation between T_d and T is almost linear. When T equals T_0, T also equals T_d, and there is no signal. No explanation is offered for the break in the curve for 925 cm^{-1} in Fig. 4.

Application to Kinetics. The MoO_3 sample was exposed to CO over the temperature range 25—485 °C but no adsorption bands nor reduction of the catalyst was observed. CO_2, CH_3OH, HCOOH, and HCHO also had no effect. However, exposure to hydrogen reduced the catalyst to MoO_2 and eventually partly to Mo. The emission spectra changed as shown in Fig. 5; the Mo=O (987 cm^{-1}) and Mo–O–Mo (925 cm^{-1}) bands are removed as the sample is reduced. Flow rates of all these gases were about 3 ml/s.

A quantitative study of the kinetics of reduction by hydrogen (≈1 atm) and oxidation by oxygen (≈1 atm) was made. The intensities at 987 cm^{-1} and 925 cm^{-1} were calculated from Eqs. 1 and 2, and the displacement of the background at 1050 cm^{-1} was measured, taking MoO_3 as zero. These intensities were measured as a function of time during reduction and oxidation at various temperatures. A typical result at 485 °C is shown in Figs. 6 and 7. At various times the sample was "frozen" by switching to argon and cooling as already described. The X-ray diffraction peaks obtained are shown in Fig. 8. We interpret the maximum in the background (1050 cm^{-1}) to be the point where the MoO_3 is exhausted and where Mo metal starts to appear, reducing the emissivity of the sample. We decided to limit our quantitative studies to the interconversion of MoO_3 and MoO_2 only, as shown in Fig. 7. The reduction is stopped when the intensity at 1050 cm^{-1} reaches its maximum.

The experiments described above were repeated at 425, 445, 465, 485, and 505 °C. From the initial slopes of curves such those of Fig. 7 the initial rate

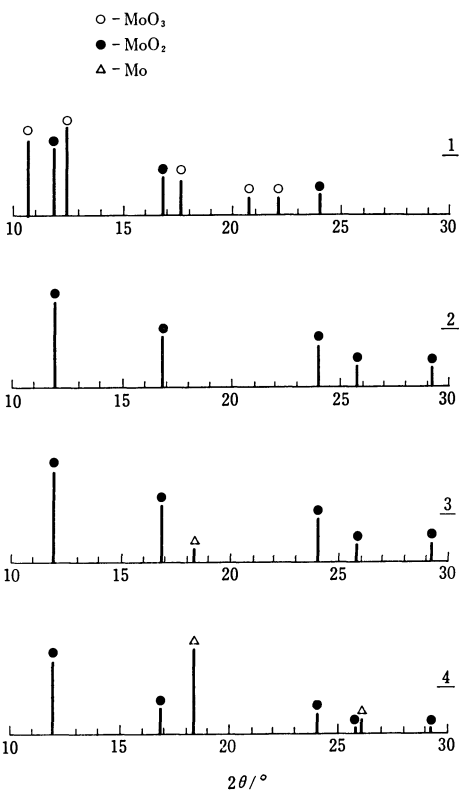

Fig. 8. X-Ray diffraction results during reduction of MoO_3 at 485 °C in H_2 for various times of exposure. 1: 3 min, 2: 6 min, 3: 8 min, 4: 20 min.

can be calculated in arbitrary units such as μV/s. These rates at various temperatures are used to construct the Arrhenius-type diagrams of Figs. 9 and 10. For the reduction of MoO_3 all three lines give an activation energy of 43 kcal/mol (179.7 kJ/mol). For the initial rate of oxidation of MoO_2, the activation energies are different for the three bands: 38.3 kcal/mol for 1050 cm^{-1}; 37.6 kcal/mol for 925 cm^{-1}; and 71.2 kcal/mol for 987 cm^{-1}. The rate of oxidation is so fast that these results are probably less precise than

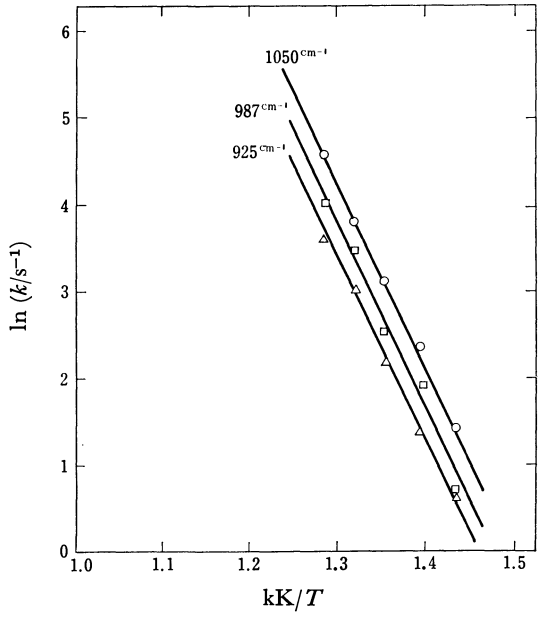

Fig. 9. Reduction rates of MoO_3.

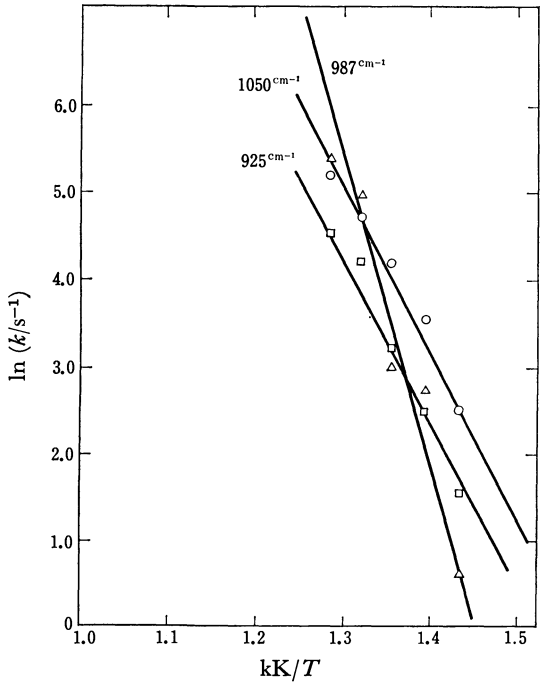

Fig. 10. Oxidation rates of MoO_3.

those for the reduction.

Earlier studies[14,15] of the reduction of MoO_3 by H_2 reported activation energies of 46—48 kcal/mol for the temperature range 365—445 °C, similar to our result of 43 kcal/mol. For the oxidation of MoO_2, Ramodorai *et al.*[15] report $E=40\pm2$ kcal/mol at about 465 °C, in qualitative agreement with our results based on the rate of change at 1050 cm^{-1} or 925 cm^{-1}. Possibly the formation of Mo=O starts only after most of the bulk is oxidized, so that our initial rates based on 987 cm^{-1} are too low. Recent studies[16–18] show that the system is quite complicated.

Summary

Emission spectroscopy can be used to study the structure and kinetics of reduction and oxidation of unsupported MoO_3–MoO_2, a system which has been difficult to study *in situ* by infrared techniques. In accord with Dewing,[8] we find that a sample loading of about 1 mg/cm^2 or less is suitable for the emission work. Infrared spectroscopy can now be used for kinetic measurements in catalysis.[2,3] For the MoO_3–MoO_2 system it furnishes a convenient method of measuring rates of reduction and oxidation.

References

1) Edwards, James, J. Nicolaidis, M. B. Cutlip, and C. O. Bennett, *J. Catal.*, **50**, 24 (1977).
2) T. Fransen, O. Van der Meer, and P. Mars, *J. Phys. Chem.*, **80**, 2103 (1976).
3) C. G. Barraclough, J. Lewis, and R. S. Nyholm, *J. Chem. Soc.*, **1959**, 3552.
4) Y. Kera and K. Hirota, *J. Phys. Chem.*, **73**, 3973 (1969).
5) R. P. Eischens and W. A. Pliskin, *Adv. Catal.*, **10**, 51 (1958).
6) M. J. D. Low and H. Inoue, *Anal. Chem.*, **36**, 2397 (1964).
7) O. Koga, T. Onishi, and K. Tamaru, *J. Chem. Soc., Chem. Commun.*, **1974**, 464.
8) J. Dewing, "Chemisorption and Catalysis," ed by P. Hepple, Inst. of Petroleum (1970), p. 173.
9) L. M. Gratton, S. Paglia, F. Scattaglia, and M. Cavallini, *Appl. Spectrosc.*, **32**, 310 (1978).
10) A. Ueno, J. K. Hochmuth, and C. O. Bennett, *J. Catal.*, **49**, 225 (1977).
11) M. Fromenti, F. Juillet, P. Mériaudeau, S. J. Teichner, and P. Vergnon, *J. Colloid Interfacial Sci.*, **39**, 79 (1972).
12) A. Ueno, T. Onishi, and K. Tamaru, *Trans. Faraday Soc.*, **66**, 756 (1970).
13) C. O. Bennett, *Catal. Rev. Sci. Eng.*, **13**, 121 (1976).
14) J. M. Dunoyer, *J. Chem. Phys.*, **47**, 290 (1959).
15) J. M. Dunoyer, *Ann. Chem.*, **6**, 165 (1951).
16) G. Ramadorai, M. E. Wadsworth, and C. K. Hansen, *Metall. Trans.*, 6B, **4**, 579 (1975).
17) N. Sotani, *Bull. Chem. Soc. Jpn.*, **48**, 1820 (1975).
18) V. P. Panichkina and L. V. Strashinskaya, *Poroshk. Metall.*, **6**, 5 (1975).

Spectrophotometric Determination of Copper Separated by Means of Adsorption of Its Pyrrolidinedithiocarbamate on Naphthalene

Taitiro FUJINAGA, Yasuhiro TAKAGI,† and Masatada SATAKE*,††

Faculty of Science, Kyoto University, Sakyo-ku, Kyoto 606

† *Fukui Prefectural Institute of Public Health, Harame-cho, Fukui 910*

†† *Faculty of Engineering, Fukui University, Bunkyo, Fukui 910*

(Received February 5, 1979)

The copper chelate of APDC was adsorbed on microcrystalline naphthalene to determine trace amounts of copper. The optimum pH range for the adsorption is 1.5—10.5. The chelate in dimethylformamide has an absorption maximum at 435 nm. Beer's law holds in the range 2.5—48 μg of copper in 10 ml of dimethylformamide. The molar absorptivity is 1.3×10^4 l·mol^{-1}·cm^{-1} and the sandell sensitivity 4.8×10^{-3} μg of copper per cm^2. Other factors such as amounts of reagent and naphthalene, shaking time, standing time and diverse ions were studied. The method can be applied to the determination of copper in Bovine Liver and human hair.

Ammonium pyrrolidinedithiocarbamate(APDC) is useful for solvent extraction and atomic absorption spectrophotometric determination of various metal ions. It was used for the extraction and spectrophotometric determination of copper by Looyenga and Boltz.[1]

We have developed a new method involving solid-liquid separation after liquid-liquid extraction, and have applied it to the determination of copper, bismuth and cobalt with APDC as a chelating agent by the naphthalene extraction method.[2] The method is based on the formation of metal chelate which is extractable quantitatively with molten naphthalene. The extract is separated from the aqueous solution and dissolved in a suitable organic solvent, the trace amounts of metal being determined spectrophotometrically.

Most metal chelates in aqueous solution can be easily adsorbed with microcrystalline naphthalene by vigorous shaking for 1 min at room temperature. The method was applied to the spectrophotometric determination of trace metals.[3,4] In the present study, APDC was used as a chelating agent for the determination of trace copper. Satisfactory adsorption of copper chelate on naphthalene is discussed in detail.

Experimental

Reagents. Standard copper solution, 5 ppm. Prepared by diluting 5 ml of standard copper solution (1000 ppm, Wako Pure Chemical Co.) to 1000 ml with water.

APDC solution, 0.2%. Prepared by dissolving 0.2 g of APDC in 100 ml of water.

Buffer Solutions. Prepared from 1 M acetic acid and 1 M ammonium acetate for pH 3—6, and from 1 M aqueous ammonia and 1 M ammonium acetate for pH 8—11.

Naphthalene solution, 20%. Prepared by dissolving 20 g of naphthalene in 100 ml of acetone.

Naphthalene, acetone, dimethylformamide, and all other reagents of analytical grade were used without further purification.

Apparatus. Absorption measurements were made with matching 10 mm glass cells on a Hitachi Model 200-20 spectrophotometer.

pH measurements were made with a Toa-Dempa HM-5A pH meter.

Naphthalene was dried with a Tabai Model K-2 drier (Tabai Mfg. Co., Ltd.).

Samples were ashed with an International Plasma Corp. low-temperature asher, IPC-1000 AN TM1640.

Procedure. Transfer 1—10 ml of 5 ppm standard copper solution to a 100-ml stoppered Erlenmeyer flask, and dilute with water to *ca.* 40 ml. Add 1.5 ml of 0.2% APDC solution and adjust pH to 5.0 with 2.0 ml of buffer solution. Mix the solution well, let stand for 10 min, add 2.0 ml of 20% naphthalene solution and shake vigorously for 1 min. Filter off on a filter paper (*e.g.*, No. 5C, Toyo Roshi Co.) placed flat on a filter plate in a funnel. Wash with water, and dry at 50—60 °C when necessary. Dissolve the crystals with dimethylformamide, dilute to 10 ml and measure the absorbance in a 10-mm cell at 435 nm against the reagent blank prepared similarly.

Results and Discussion

Absorption Spectra. Absorption spectra of the reagent blank and the copper chelate in naphthalene–dimethylformamide solution are shown in Fig. 1. The copper chelate has an absorption maximum at 435 nm where there is practically no absorption due to the reagent blank. Thus, 435 nm was chosen as

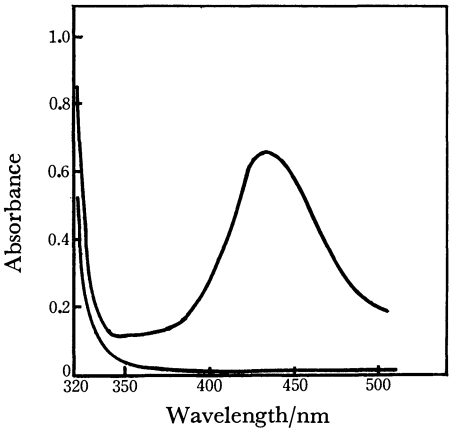

Fig. 1. Absorption spectra of APDC and copper complex in naphthalene–DMF solution.
Cu: 25 μg; 0.2% APDC: 1.5 ml; pH: 5.3; digestion time: 10 min; 20% naphthalene: 2.0 ml; shaking time: 1 min; reference: water; (1) reagent blank, (2) copper complex.

the most suitable wavelength.

Effect of pH. After the pH of sample solutions containing 25 μg of copper and 1.5 ml of 0.2% APDC solution had been controlled to desired values with different buffer solutions or hydrochloric acid, adsorption of the chelate was carried out. The result is shown in Fig. 2. The adsorption of the chelate starts from 2 mol dm^{-3} hydrochloric acid solution, reaches a maximum at pH 1.5, and thereafter remains constant over the range 1.5—10.5. Thus, the pH of the solution was adjusted to 5.3 for adsorption of the chelate.

Effect of Reagent Concentration. Various amounts of 0.2% APDC solution were added to the sample solution containing 25 μg of copper and 2.0 ml of the buffer solution(pH 5.3), the following procedure being the same as above. Figure 3 shows the variation in absorbance with the reagent concentration. The absorbance increases sharply with increase in the amount of reagent up to 0.1 ml of 0.2% APDC solution, becoming almost constant over the range 0.1—5.0 ml. Thus, 1.5 ml of 0.2% APDC solution was used for adsorption of the chelate.

Effect of Buffer Solution. The effect of buffer solution on the absorbance was examined. Addition of 0.5—5.0 ml of the acetate buffer solution caused practically no variation in absorbance. Thus, 2.0 ml of the buffer solution was added for adsorption of the chelate.

Effect of Digestion Time. A solution containing 25 μg of copper, 2.0 ml of the buffer solution(pH 5.3) and 1.5 ml of 0.2% APDC solution was digested at room temperature, the following procedure being the same as above. The absorbance increases with increase in digestion time up to 2 min, remaining almost constant for 2—30 min of digestion time. Thus, 10 min of digestion time was chosen for adsorption of the chelate.

Effect of Naphthalene Concentration. Adsorption of the chelate was carried out by changing the volume of 20% naphthalene–acetone solution added to the solution containing copper chelate. Figure 4 shows the effect of naphthalene concentration on the absorbance. The absorbance increases with increase in the amount of naphthalene up to 0.3 ml of 20% naphthalene solution, becoming almost constant for 0.3—5.0 ml. Thus, 2.0 ml of 20% naphthalene solution was used for adsorption of the chelate.

Effect of Shaking Time. Two ml of 20% naphthalene solution was added to the solution containing the copper chelate, and the mixed solution was shaken vigorously for 100 s. The chelate was completely collected on naphthalene by vigorous shaking for a few seconds. Shaking for 1 min was found to be satisfactory for complete adsorption.

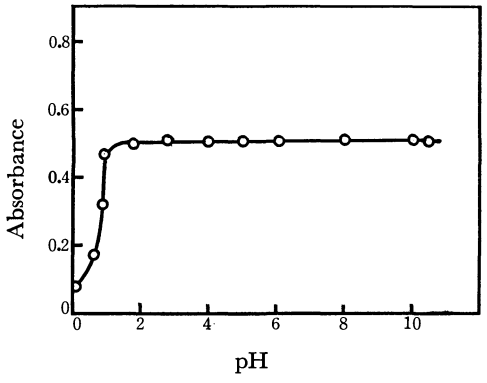

Fig. 2. Effect of pH.
Cu: 25 μg; wavelength: 435 nm; 0.2% APDC: 1.5 ml; digestion time: 10 min; 20% naphthalene: 2.0 ml; shaking time: 1 min, reference: reagent blank.

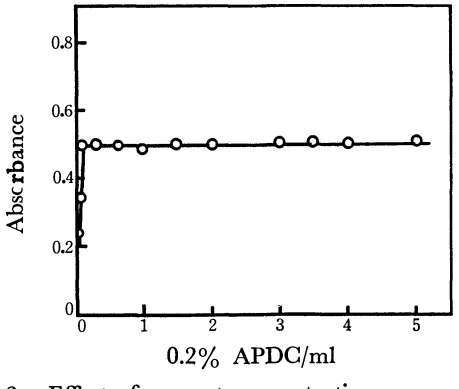

Fig. 3. Effect of reagent concentration.
Cu: 25 μg; pH: 5.3; 0.2% APDC: 1.5 ml; wavelength: 435 nm; digestion time: 10 min; 20% naphthalene: 2.0 ml, reference: reagent blank.

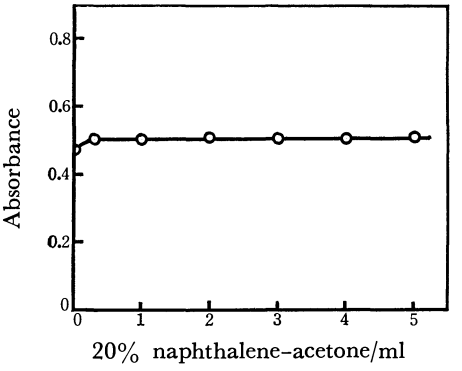

Fig. 4. Effect of naphthalene concentration.
Cu: 25 μg; wavelength: 435 nm; pH: 5.3; 0.2% APDC: 1.5 ml; digestion time: 10 min, reference: reagent blank.

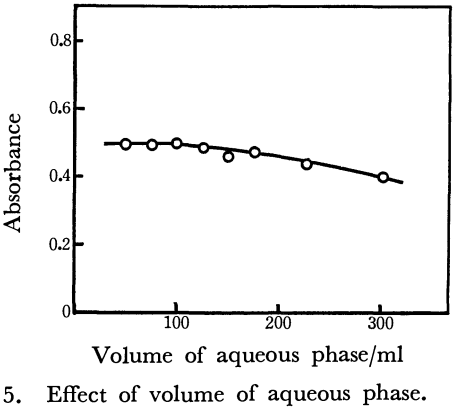

Fig. 5. Effect of volume of aqueous phase.
Cu: 25 μg; wavelength: 435 nm; pH: 5.3; 0.2% APDC: 5.0 ml; 20% naphthalene: 3.0 ml; shaking time: 5 min; reference: reagent blank.

Effect of Volume of Aqueous Phase. The volume of aqueous phase was varied between 50 and 300 ml while other factors were kept constant. Figure 5 shows the effect of volume of aqueous phase on the absorbance. The absorbance was almost constant up to about 100 ml, but decreasing gradually with increase in the volume of aqueous phase. For volumes exceeding 80 ml, the adsorption of the chelate on naphthalene was carried out by using a larger volume of the reagent solution, shaking for a long time and digesting at 40—50 °C. In this series of tests, 5.0 ml of the reagent solution was taken ; the mixed solutions were shaken for 10 min and digested for 20 min, 3.0 ml of 20% naphthalene solution being used.

Table 1. Effect of diverse alkali salts

Alkali metal salt	Amount added (mg)	Absorbance (435 nm)
—	—	0.500
Na_2SO_4	100	0.495
Na_2SO_4	500	0.500
NaCl	100	0.496
NaCl	500	0.498
NH_4Cl	100	0.495
NH_4Cl	500	0.498
$Na_2C_2O_4$	100	0.511
$Na_2C_2O_4$	300	0.518
$Na_2C_2O_4$	500	0.512
$NaH_2PO_4 \cdot 2H_2O$	100	0.501
$NaH_2PO_4 \cdot 2H_2O$	500	0.506
$Na_2HPO_4 \cdot 12H_2O$	100	0.515
$Na_2HPO_4 \cdot 12H_2O$	500	0.521
Na_2CO_3	100	0.500
Na_2CO_3	300	0.501
Na_2CO_3	500	0.493
KNO_3	100	0.509
KNO_3	500	0.513
Na_2SO_3	100	0.507
Na_2SO_3	500	0.526
CH_3COONa	100	0.505
CH_3COONa	500	0.502
KBr	100	0.519
KBr	500	0.520
Sodium tartrate	100	0.515
Sodium tartrate	200	0.518
Sodium tartrate	300	0.520
Sodium tartrate	500	0.522
Sodium citrate	100	0.509
Sodium citrate	500	0.503
KCN (pH 5.0)	100	0.498
KCN (pH 5.0)	200	0.510
KCN (pH 5.0)	300	0.495
KCN (pH 9.0)	0.04	0.000
Disodium EDTA (pH 5.0)	100	0.495
Disodium EDTA (pH 5.0)	200	0.497
Disodium EDTA (pH 5.0)	300	0.500
Disodium EDTA (pH 9.0)	0.04	0.020
Disodium EDTA (pH 9.0)	0.08	0.000

Cu: 25.0 μg; pH: 5.3.

Effect of Standing Time. A mixture of copper chelate and naphthalene was dissolved in dimethylformamide, and the effect of standing time on the absorbance was studied. The color of the chelate in naphthalene–dimethylformamide solution remained unchanged even after 10 h.

Calibration Curve. The absorbances for varying concentration of copper were measured at 435 nm against the reagent blank under the optimum conditions described above. The absorbance shows a linear relationship to the concentration of copper in the range 2.5—48 μg in 10 ml of dimethylformamide. The molar absorptivity is 1.3×10^4 $l \cdot mol^{-1} \cdot cm^{-1}$, the sensitivity being 4.8×10^{-3} μg per cm^2 for an absorbance of 0.001. Ten replicate determinations of the sample solution containing 25 μg of copper give a mean absorbance of 0.500 with a relative standard deviation of 0.89%.

Choice of Solvent. Tests were made with various organic solvents in order to dissolve the mixture of the chelate and naphthalene. The chelate is soluble in organic solvents such as benzene, toluene, xylene, chlorobenzene, *o*-dichlorobenzene, dichloroethane, chloroform, nitrobenzene, acetone, acetonitrile, propylene carbonate, dimethylformamide at room tem-

Table 2. Effect of diverse metal ions

Metal ion	Added as	Ion added (μg)	Absorbance (435 nm)
—	—	—	0.500
Pb^{2+}	Nitrate	10	0.505
Pb^{2+}	Nitrate	50	0.510
Pb^{2+}	Nitrate	100	0.503
Bi^{3+}	Nitrate	10	0.510
Bi^{2+}	Nitrate	50	0.508
Bi^{2+}	Nitrate	100	0.517
Mg^{2+}	Chloride	10	0.506
Mg^{2+}	Chloride	50	0.509
Mg^{2+}	Chloride	100	0.504
Ca^{2+}	Chloride	50	0.498
Ca^{2+}	Chloride	100	0.501
Zn^{2+}	Nitrate	10	0.507
Zn^{2+}	Nitrate	50	0.499
Zn^{2+}	Nitrate	100	0.509
Fe^{3+}	Chloride	10	0.530
Fe^{2+}	Chloride	50	0.821
Ni^{2+}	Chloride	10	0.529
Ni^{2+}	Chloride	50	0.553
Ni^{2+}	Chloride	100	0.589
Co^{2+}	Chloride	10	0.568
Co^{2+}	Chloride	50	0.758
Cd^{2+}	Chloride	10	0.504
Cd^{2+}	Chloride	50	0.498
Cd^{2+}	Chloride	100	0.500
Cr^{6+}	Dichlomate	10	0.494
Cr^{6+}	Dichlomate	50	0.499
Cr^{6+}	Dichlomate	100	0.495
Hg^{2+}	Chloride	10	0.507
Hg^{2+}	Chloride	50	0.499
Hg^{2+}	Chloride	100	0.504

perature. It undergoes decolorization in dioxane and MIBK.

Effect of Diverse Ions. Sample solutions containing 25 μg of copper and various amounts of diverse alkali metal salts or metal ions were prepared, the effect of diverse interfering salts and metal ions on copper determination being studied. The pH of solution was adjusted to 5.3. The results are given in Tables 1 and 2. The following species gave no interference: Na_2SO_4, NaCl, NH_4Cl, $Na_2C_2O_4$, $NaH_2PO_4 \cdot 2H_2O$, $Na_2HPO_4 \cdot 12H_2O$, Na_2CO_3, KNO_3, Na_2SO_3, CH_3COONa, KBr, sodium tartrate, sodium citrate, KCN, EDTA, Cd^{2+}, Pb^{2+}, Bi^{3+}, Mg^{2+}, Ca^{2+}, Zn^{2+}, Cr^{6+}, Hg^{2+}. Fe^{3+}, Ni^{2+}, and Co^{2+} gave interference.

From the results we see that the present method gives the same molar absorptivity, sensitivity, precision and selectivity as those by the chloroform method.[1] The pH range for the adsorption being wider.

Analysis of Copper in Biological Sample. The method was applied to the analysis of copper in Bovine Liver(N. B. S., SRM-1577) and human hair by using spectrophotometry and atomic absorption spectrophotometry. Low-temperature ashed samples were dissolved in concentrated nitric acid on a hot plate and evaporated to dryness. The residue was dissolved with 10 ml of redistilled water. An aliquot of this sample was taken for analysis. Iron(III) was masked with triethanolamine at pH 9.0. The results of Bovine Liver and human hair for copper by the two methods are satisfactory (Tables 3 and 4).

Table 3. Analysis of Bovine Liver for copper

Sample	Certified value (μg/g)	Spectrophotometric value (μg/g)	A.A.S (direct method) value (μg/g)
N.B.S SRM Bovine Liver 1577	193±10	190	191
		193	192
		192	191
		193	190
		194	193

pH: 9.0; Naphthalene: 0.4 g; 10% triethanolamine: 1.5 ml.

Table 4. Result of analysis of human hair for copper

Sample	Spectrophotometric value (μg/g)	A.A.S (direct method) value (μg/g)
Human hair A	8.7	9.8
Human hair B	12.4	11.8
Human hair C	24.0	23.4
Human hair D	27.5	27.8
Human hair E	12.0	12.4

pH: 9.0; Naphthalene: 0.4 g; 10% triethanolamine: 1.5 ml.

References

1) R. W. Loogenga and D. F. Boltz, *Talanta*, **19**, 82 (1972).
2) M. Satake and Y. Takagi, *Bunseki Kagaku*, **26**, 386 (1977).
3) M. Satake, Y. Matsumura, T. Fujinaga, and Y. Takagi, *Bunseki Kagaku*, **27**, 486 (1978).
4) M. Satake, Y. Matsumura, and T. Fujinaga, *Talanta*, **25**, 718 (1978).

Ylide–Metal Complexes. III. Preparation and Properties of Gold(I) Complexes of Alkylidenetriphenylphosphoranes and -arsoranes[1]

Yoshihisa YAMAMOTO* and Zenjiro KANDA

Faculty of Pharmaceutical Science, Higashi Nippon Gakuen University, Ishikari-Tobetsu, Hokkaido 061-02

(Received February 9, 1979)

Ylide-gold complexes of the type triphenylphosphine(triphenylphosphonium alkylide)gold(I) chloride, $[Ph_3\overset{R}{\overset{|}{P}}CH\text{-}Au\text{-}PPh_3]Cl$, and bis(triphenylphosphonium alkylide)gold(I) chloride, $[Ph_3\overset{R}{\overset{|}{P}}CH\text{-}Au\text{-}\overset{R}{\overset{|}{C}}HPPh_3]Cl$, have been obtained from alkylidene triphenylphosphoranes, $Ph_3P{=}CH\text{-}R$ (R: H, CH_3, $CH(CH_3)_2$), and (triphenylphosphine)gold(I) chloride, Ph_3PAuCl. Bis(triphenylarsonium methylide)gold(I) chloride, $[Ph_3AsCH_2\text{-}Au\text{-}CH_2AsPh_3]Cl$, has been synthesized from methylenetriphenylarsorane and Ph_3PAuCl. In these organogold complexes, the ylides are attached to the gold atom through the carbanionic donor atom. The ^{1}H-NMR spectra of $[Ph_3PCH_2\text{-}Au\text{-}PPh_3]Cl$ indicates an intermolecular exchange process in the temperature range $+25$——-50 °C.

The chemistry of ylide complexes of the transition metals has been actively investigated in recent years,[2] in particular, the complexes of methylenetrimethylphosphorane, $(CH_3)_3P{=}CH_2$.[3] The alkylidenetriphenylphosphoranes, $Ph_3P{=}CH\text{-}R$ have, however, been the subject of little research. Previous papers have been concerned with the preparation and physical properties of stable 2/1 complexes[4] of type $[Ph_3\overset{R}{\overset{|}{P}}CH\text{-}M\text{-}\overset{R}{\overset{|}{C}}HPPh_3]Cl$ and stable 1/1 complexes[5] of type $[Ph_3\overset{R}{\overset{|}{P}}CH\text{-}MCl]_n$ (M: Cu, Ag; R: H, CH_3, $CH(CH_3)_2$). 2/1 complexes[6] of $[Ph_3AsCH_2\text{-}Cu\text{-}CH_2AsPh_3]Cl$ and 1/1 complexes[6] of $[Ph_3AsCH_2\text{-}AgCl]_n$ have also been reported. The present paper deals with the preparation and ^{1}H- and ^{13}C-NMR measurements of triphenylphosphine(triphenylphosphonium alkylide)gold(I) chloride $[Ph_3\overset{R}{\overset{|}{P}}CH\text{-}Au\text{-}PPh_3]Cl$, bis(triphenylphosphonium alkylide)gold(I) chloride $[Ph_3\overset{R}{\overset{|}{P}}\text{-}\overset{R}{\overset{|}{C}}H\text{-}Au\text{-}\overset{R}{\overset{|}{C}}HPPh_3]Cl$ and bis(triphenylarsonium methylide)gold(I) chloride $[Ph_3AsCH_2\text{-}Au\text{-}CH_2AsPh_3]Cl$.

Results and Discussion

Ylides. Alkylidenetriphenylphosphoranes, $Ph_3P{=}CH\text{-}R$ (**La**, R=H[7]; **Lb**, R=CH_3[8]; **Lc**, R=$CH(CH_3)_2$[4]), were prepared by the reaction of the corresponding phosphonium bromide with sodium amide in dry THF(tetrahydrofuran). Methylenetriphenylarsorane, **Ld** ($Ph_3As{=}CH_2$), was obtained from methyltriphenylarsonium bromide and sodium amide as reported in the literature.[6,9]

^{13}C-NMR data of the phosphonium ylides(**La**—**Lc**) are given in Table 1, the ^{13}C-NMR spectra of **Lb** and **Lc** being reported for the first time. The coupling constants ($^1J_{CP}$) of those are larger than that of the ylide **La**. This effect should be attributed to both electronic and structural effects.[10]

1/1 Ylide–Gold Complexes. Triphenylphosphine(triphenylphosphonium alkylide)gold(I) chlorides, $[Ph_3\overset{R}{\overset{|}{P}}CH\text{-}Au\text{-}PPh_3]Cl$, have been obtained from ylide $Ph_3P{=}CH\text{-}R$, (triphenylphosphine)gold(I) chloride Ph_3PAuCl, and triphenylphosphine in a solvent at -45 °C (Eq. 1). Attempts to obtain these complexes at room temperature (r.t.) invariably resulted in the isolation of a mixture of 2/1 complexes of the type bis(triphenylphosphonium alkylide)gold(I) chloride and unreacted starting materials, Ph_3PAuCl and PPh_3 as shown in Eq. 2.

$$Ph_3P{=}CH\text{-}R + Ph_3PAuCl \xrightarrow[\text{THF, } PPh_3]{-45\,^\circ C} [Ph_3\overset{R}{\overset{|}{P}}CH\text{-}Au\text{-}PPh_3]Cl \quad (1)$$

R	H	CH_3	$CH(CH_3)_2$
	1a	**1b**	**1c**

$$\xrightarrow[\text{or r. t., } C_6H_6]{\text{r. t., THF}} 1/2[Ph_3\overset{R}{\overset{|}{P}}CH\text{-}Au\text{-}\overset{R}{\overset{|}{C}}HPPh_3]Cl + 1/2PPh_3 + 1/2Ph_3PAuCl \quad (2)$$

All complexes except **1c** are soluble and stable in dichloromethane. The isolation of **1a** requires an excess of triphenylphosphine as a supporting ligand, and the selection of a suitable reaction temperature and solvent is very important. For example, **1a** was not obtained at room temperature or in benzene (Eq. 2). This result differs as in the case of trimethylphosphine(trimethylphosphonium methylide)gold(I) chloride,[11] $[(CH_3)_3PCH_2\text{-}Au\text{-}P(CH_3)_3]Cl$, **2**, which could be isolated from benzene at room temperature. Also, for the preparation of **2** no excess of trimethylphosphine was necessary. This result may depend on the reduced coordination capacity of triphenylphosphine as compared with that of trimethylphosphine. Steric factors[12] seem not to be dominating for metals of coordination number 2.

The ^{1}H-NMR data of **1a** and **1b** are given in Table 1. The ^{1}H-spectrum of **1a** at -50 °C in CD_2Cl_2 showed a double-doublet signal of the methylene protons at 2.31 ppm. This signal broadened at -30 °C, and became a sharp doublet at -10 °C (Fig. 1). The process is reversible. This temperature dependence indicates an intermolecular exchange process in solution (Eq. 3). The chemical shift of the methylene group at -10 °C corresponds to the weighted average for

TABLE 1. ^1H- AND ^{13}C-NMR DATA OF COMPLEXES AND YLIDES

^1H	R CH-P(As) δ/ppm	$^2J_{HCP}$/Hz	$^3J_{HCAuP}$/Hz	CH_3 δ/ppm	$^3J_{HCCP}$/Hz	$^3J_{HCCH}$/Hz	C_6H_5 δ/ppm	Solvent and standard	Temp
1a	2.31 dd	12.9	7.5	—	—	—	7.6 m	CD_2Cl_2, int-TMS	−50 °C
	2.32 d	12.9	—	—	—	—	7.6 m	CD_2Cl_2, int-TMS	−10 °C
1b	2.5 m	—	—	1.49 dd	22.5	6.8	7.6 m	CD_2Cl_2, int-TMS	−50 °C
3a	1.70 d	13.0	—	—	—	—	7.5 m	$CDCl_3$, ext-TMS	r. t.
3b	2.30 m	—	—	1.48 dd	22.2	7.4	7.6 m	$CDCl_3$, ext-TMS	r. t.
4a	1.99 s	—	—	—	—	—	7.5 m	$CDCl_3$, ext-TMS	r. t.

^{13}C	R CH-P(As) δ/ppm	$^1J_{CP}$/Hz	CH-**C**H$_3$ [CH-**C**H] δ/ppm	$^2J_{CCP}$/Hz	CH-**C**H$_3$ δ/ppm	$^3J_{CCCP}$/Hz	C_6H_5 δ/ppm C-1	*o*	*m*	*p*	Solvent and standard
La	−4.3 d	98.6	—	—	—	—	a	a	a	a	C_6D_6, int-TMS
Lb	3.3 d	118.2	11.1 d	4.9	—	—	a	a	a	a	C_6D_6, int-TMS
Lc	21.7 d	116.2	[27.3] d	6.8	30.0 d	9.8	a	a	a	a	C_6D_6, int-TMS
3a	9.5 d	39.1	—	—	—	—	125.9	132.5	129.4	133.4	$CDCl_3$
							(85.4)	(9.8)	(12.2)	(—)	
3b	16.8 d	32.2	13.7 d	2.9	—	—	124.5	133.3	129.5	133.6	$CDCl_3$
							(84.0)	(8.8)	(11.7)	(—)	
4a	14.4 s	—	—	—	—	—	b	131.9	130.1	132.9	$CDCl_3$

Standard: Internal and external TMS ($\delta=0$); $CDCl_3$-d_1 (77.1 ppm).
a) This signal overlapped with deuterobenzene signals. b) This signal was not observed. s: singlet, d: doublet, dd: double doublet, m: multiplet.

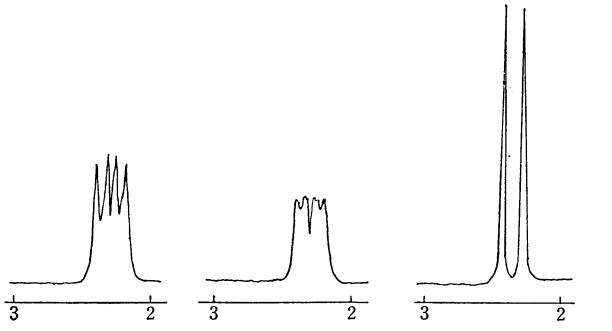

Fig. 1. ^1H-NMR spectra of complex **1a**, $[Ph_3PCH_2$–Au–$PPh_3]Cl$, at three different temperatures.

two species in Eq. 3. The small variation of chemical shifts with temperature suggest a small degree of dissociation:[13]

$$[Ph_3PCH_2\text{-Au-}PPh_3]Cl \rightleftarrows [Ph_3PCH_2\text{-Au}]Cl + PPh_3 \quad (3)$$

2/1 Ylide–Gold Complexes. Bis(triphenylphosphonium alkylide)gold(I) chlorides, $[Ph_3\overset{R}{\overset{|}{P}}CH\text{–Au–}\overset{R}{\overset{|}{C}}HPPh_3]Cl$, (R=H, **3a**; R=$CH_3$, **3b**; R=$CH(CH_3)_2$, **3c**), were prepared by the reaction of ylides Ph_3P=CH–R, with (triphenylphosphine)gold(I) chloride in dry THF at room temperature. **3a** is stable in dichloromethane at room temperature, whereas the corresponding complexes of copper and silver decompose in dichloromethane at room temperature and are stable only at −40 °C and −60 °C, respectively.

The ^1H- and ^{13}C-NMR data of **3a** and **3b** are summarized in Table 1. The data for **3c** is absent due to decomposition in the solvent.

Bis(triphenylarsonium methylide)gold(I) chloride, $[Ph_3AsCH_2\text{–Au–}CH_2AsPh_3]Cl$, **4a**, was obtained from methylene–triphenylarsorane Ph_3As=CH_2 and Ph_3AuCl in dry THF at room temperature.

The ^1H- and ^{13}C-NMR data of **4a** are shown in Table 1. The ^1H-NMR spectrum of **4a** showed a singlet for the methylene group at 1.99 ppm and a multiplet for the phenyl groups at 7.5 ppm in a ratio of 2 : 15.

Experimental

Measurements. The NMR spectra were measured with an FX-60 spectrometer (JEOL) for ^{13}C-NMR, a JNM-PMX-60 (JEOL) and a R-40 (Hitachi) for ^1H-NMR.

Starting Materials. Methylene-,[7] ethylidene-,[8] isobutylidene-[4] triphenylphosphonium ylides were prepared from the corresponding phosphonium bromides by the sodium amide method. Methylenetriphenylarsorane was prepared from methyltriphenylarsonium bromide and sodium amide.[6,9] (Triphenylphosphine)gold(I) chloride was synthesized by the method of Kowala and Swan.[14]

*Preparation of 1/1 Complexes. Triphenylphosphine(triphenylphosphonium methylide)gold(I) Chloride (**1a**):* (Triphenylphosphine)gold(I) chloride (0.24 g, 0.485 mmol dm^{-3}), methylenetriphenylphosphorane (0.115 g, 0.416 mmol dm^{-3}), and triphenylphosphine (0.14 g, 0.534 mmol dm^{-3}) were suspended in dry THF (15 ml) at −60 °C and stirred for approximately 1 h at −45 °C under nitrogen. The color of the ylide changed from yellow to colorless. The white complex precipitated was filtered at −70 °C, washed with

dry pentane and dried under vacuum. Yield 0.28 g (87.3%), mp 139—141 °C, Found: C, 57.40; H, 4.34%. Calcd for $C_{37}H_{32}AuClP_2$; (*MW* 771.03) C, 57.64; H, 4.18%.

*Triphenylphosphine(triphenylphosphonium ethylide)gold(I) Chloride (**1b**)*: (Triphenylphosphine)gold(I) chloride (0.71 g, 1.44 mmol dm^{-3}), ethylidenetriphenylphosphorane (0.42 g, 1.45 mmol dm^{-3}), and triphenylphosphine (0.52 g, 1.98 mmol dm^{-3}) were stirred in THF (25 ml) at −60 °C for 50 min under nitrogen. The color of the ylide changed from orange to colorless. The white precipitate was filtered at −70 °C, washed with dry pentane and dried under vacuum. Yield 0.90 g (79.6%), mp 94—96 °C. Found: C, 57.24; H, 4.43%. Calcd for $C_{38}H_{34}AuClP_2$: (*MW* 785.05) C, 58.14; H, 4.37%.

*Triphenylphosphine(triphenylphosphonium isobutylide)gold(I) Chloride (**1c**)*: (Triphenylphosphine)gold(I) chloride (0.55 g, 1.11 mmol dm^{-3}), isobutylidenetriphenylphosphorane (0.36 g, 1.13 mmol dm^{-3}), and triphenylphosphine (0.39 g, 1.49 mmol dm^{-3}) were stirred in THF (20 ml) at −60 °C for 50 min under nitrogen. The color of the ylide changed from red to colorless. The white complex precipitate was filtered at −70 °C, washed with dry pentane and dried. Yield 0.85 g (94.2%), mp 92—93 °C. Found: C, 58.32; H, 4.96%. Calcd for $C_{40}H_{38}AuClP_2$: (*MW* 813.11) C, 59.09; H, 4.71%. This complex was unstable.

*Preparation of 2/1 Complexes. Bis(triphenylphosphonium methylide)gold(I) Chloride (**3a**)*: (Triphenylphosphine)gold(I) chloride (0.41 g, 0.829 mmol dm^{-3}) was added to a dry THF (20 ml) solution of methylenetriphenylphosphorane (0.54 g, 1.95 mmol dm^{-3}) at −60 °C under nitrogen. The mixture was stirred for 2 h at room temperature and the white precipitate filtered off, washed with dry pentane and dried under vacuum. Yield 0.58 g (89.1%), dec 174 °C. Found: C, 57.66; H, 4.36%. Calcd for $C_{38}H_{34}AuClP_2$: (*MW* 785.05) C, 58.14; H, 4.37%.

*Bis(triphenylphosphonium ethylide)gold(I) Chloride (**3b**) and Bis(triphenylphosphonium isobutylide)gold(I) Chloride (**3c**)*: Complex **3b** was prepared from (triphenylphosphine)gold(I) chloride (0.34 g, 0.69 mmol dm^{-3}) and ethylidenetriphenylphosphorane (0.42 g, 1.45 mmol dm^{-3}) according to the procedure for **3a**. Complex **3c** was prepared from (triphenylphosphine)gold(I) chloride (0.43 g, 0.87 mmol dm^{-3}) and isobutylidenetriphenylphosphorane (0.60 g, 1.88 mmol dm^{-3}) according to the procedure for complex **3a**. Yield 0.48 g (85.6%) for **3b** and 0.67 g (88.6%) for **3c**. Dec 154 °C **3b**, 153 °C for **3c**. Found **3b**: C, 59.33; H, 4.90%. **3c**: C, 60.95; H, 5.83%. Calcd for **3b** $C_{40}H_{38}AuClP_2$: (*MW* 813.11) C, 59.09; H, 4.71%. **3c** $C_{44}H_{46}AuClP_2$: (*MW* 869.21) C, 60.80; H, 5.33%.

*Bis(triphenylarsonium methylide)gold(I) Chloride (**4a**)*: (Triphenylphosphine)gold(I) chloride (0.11 g, 0.222 mmol dm^{-3}) was added to a THF (15 ml) solution of methylenetriphenylarsorane (0.153 g, 0.478 mmol dm^{-3}) at −70 °C under nitrogen. The mixture was stirred for several minutes at −40 °C, and then for 1 h at room temperature. The precipitated white complex was filtered, washed with pentane and dried under vacuum. Yield 0.10 g (51.6%), dec 141 °C. Found: C, 51.80; H, 4.16%. Calcd for $C_{38}H_{34}AuClAs_2$: (*MW* 872.95) C, 52.28; H, 3.93%.

The authors wish to express their thanks to Professor Hubert Schmidbaur of the Technical University of Munich, Germany for his helpful discussions. The present work was partially supported by a Grant-in-Aid for Scientific Research from the Ministry of Education.

References

1) Presented at the 37th National Meeting of the Chemical Society of Japan, Yokohama, April 1978.

2) K. Itoh, M. Fukui, and Y. Ishii, *J. Organomet. Chem.*, **129**, 259 (1977); L. Knoll, *ibid.*, **148**, C25 (1978); H. Schmidbaur, H. P. Scherm, and U. Schubert, *Chem. Ber.*, **111**, 764 (1978).

3) H. Schmidbaur, *Acc. Chem. Res.*, **8**, 62 (1975).

4) Y. Yamamoto and H. Schmidbaur, *J. Organomet. Chem.*, **96**, 133 (1975).

5) Y. Yamamoto and H. Schmidbaur, *J. Organomet. Chem.*, **97**, 479 (1975).

6) W. Richter, Y. Yamamoto, and H. Schmidbaur, *Chem. Ber.*, **110**, 1312 (1977).

7) H. Schmidbaur, H. Stühler, and W. Vornberger, *Chem. Ber.*, **105**, 1084 (1972); R. Köster, D. Simic, and M. A. Grassberger, *Liebigs Ann. Chem.*, **739**, 211 (1970).

8) H. Bock and H. Tom Dieck, *Z. Naturforsch., Teil. B.*, **21**, 739 (1966).

9) Y. Yamamoto and H. Schmidbaur, *J. Chem. Soc., Chem. Commun.*, **1975**, 668.

10) H. Schmidbaur, W. Richter, W. Wolf, and F. H. Köhler, *Chem. Ber.*, **108**, 2649 (1975); H. Schmidbaur, J. Eberlein, and W. Richter, *Chem. Ber.*, **110**, 677 (1977).

11) H. Schmidbaur and R. Franke, *Chem. Ber.*, **108**, 1321 (1975).

12) J. Emsley and D. Hall, "The Chemistry of Phosphorus," Harper and Row, (1976), Chap. 5.

13) L. M. Jackman and F. A. Cotton, "Dynamic Nuclear Magnetic Resonance Spectroscopy," Academic Press (1975), Chap. 8.

14) C. Kowala and J. M. Swan, *Aust. J. Chem.*, **19**, 547 (1966).

The Extraction of the Chromium(III) Ion from Trichloroacetate Solutions to Inert Solvents Containing Trioctylphosphine Oxide

Hisanori IMURA,*,** Toshiyasu KIBA, and Takaharu HONJO

Department of Chemistry, Faculty of Science, Kanazawa University, 1-1 Marunouchi, Kanazawa 920

(Received February 16, 1979)

Chromium(III) has been extracted with 0.1 mol dm^{-3} trioctylphosphine oxide(TOPO) in various inert solvents from a 0.1 mol dm^{-3} trichloroacetate(TCA^-) buffer solution of pH 3.5 to 6.0. As diluents of TOPO, hexane and cyclohexane are most effective, while chloroform is quite ineffective. The extraction mechanism has been clarified by analyzing separately the distribution of water, trichloroacetic acid(HTCA), and the Cr(III) ion between the aqueous and organic phases. Water and HTCA are present in the cyclohexane phase as $H_2O\cdot$TOPO and HTCA·TOPO respectively. Chromium(III) is extracted with TOPO into cyclohexane as an ion-association complex like $Cr(H_2O)_6^{3+}(TCA^-)_3\cdot 3TOPO$, and the extraction constant is $10^{7.68}$. It is concluded that the hexahydrated Cr(III) ion is solvated by three molecules of TOPO, forming an ion pair with three trichloroacetate anions. The extractability of Cr(III) in the present system depends most effectively on the concentration of HTCA-free TOPO in the organic phase.

In a previous report,[1] the present authors found that many metal ions, such as Th(IV), Bi(III), Tm(III), Fe(III), Cr(III), Al(III), Hg(II), Co(II), Mn(II), Ba(II), Ca(II), and Cs(I), could be extracted from trichloroacetate(TCA^-) buffer solutions into polar solvents involving a donor oxygen atom, but not into inert solvents. Additionally, chromiun(III) could be quantitatively extracted with not only polar organic solvents such as isopentyl alcohol, but also with benzene containing trioctylphosphine oxide(TOPO). From the similarity of the visible absorption spectra and the paper electrophoretic behavior of the extracted metals to those of the corresponding metal ions in the aqueous solution, an extraction mechanism of metal ions involving the formation of ion pairs of hydrated metal ions with trichloroacetate anions and solvation by polar solvents has previously been proposed.[1] On the other hand, recently several authors have reported that trichloroacetic acid(HTCA) forms extractable mixed-ligand complexes[2,3] or ion-pair complexes with positively charged chelates.[4]

The extraction of Cr(III) from trichloroacetate buffer solutions with inert solvents containing TOPO is very interesting as a means of clarifying the extraction mechanism in the ion-association system. In the present system, water, trichloroacetate, and TOPO all participate in the extraction process of Cr(III); their effects have been analyzed separately.

Experimental

Reagents. The trichloroacetic acid was purchased from the Kishida Chemical Co. and was dissolved in re-distilled water. A series of buffer solutions (pH 0—10) was prepared by mixing a HTCA solution (10^{-3}—0.2 mol dm^{-3}) and a sodium hydroxide solution of the same concentration as the HTCA solution used. Hereafter, a series of buffer solutions, for instance, prepared by mixing 0.2 mol dm^{-3} HTCA and 0.2 mol dm^{-3} NaOH, will be noted as the 0.1 mol dm^{-3} trichloroacetate buffer solution.

The trioctylphosphine oxide was obtained from the Dojindo Co.

The chromium(III) solution was prepared by dissolving its high-purity metal in 2 mol dm^{-3} hydrochloric acid. The radioisotope, ^{51}Cr, used as a tracer was purchased from the New England Nuclear Co. (U.S.A.).

The organic solvents, such as cyclohexane, benzene, carbon tetrachloride, and chloroform, were purified by the usual methods. The other reagents were of a guaranteed reagent grade and were used without further purification.

Apparatus. The electronic absorption spectra were measured with a Hitachi Model 323 recording spectrophotometer.

The pH value of an aqueous phase was measured with Hitachi-Horiba pH meters, M-5 and M-7.

A Kobe Kogyo Co., Model STL-200(NaI(Tl) crystal), well-type scintillation counter was used for the γ-counting.

An Iwaki KM-Shaker was used for the agitation of an aqueous and an organic phase at 340 strokes per min.

The water content of an organic phase was determined by using a Karl Fisher-Titrator E 452 Metrom.

Extraction and Back-extraction Procedure. In a 50-cm^3 centrifuge tube with a ground-glass stopper, 10 cm^3 of an inert organic solvent containing from 10^{-3} to 10^{-1} mol dm^{-3} TOPO was placed, then 10 cm^3 of a trichloroacetate buffer solution, adjusted to the desired pH value, containing from 10^{-4} to 10^{-1} mol dm^{-3} of the Cr(III) ion, and its radioactive tracer were added. Then the contents were vigorously shaken by using a shaker for 1 to 20 min at room temperature (20—25 °C). After centrifugation, a 3-cm^3 portion was pipeted out from each phase, then the radioactivity was counted by the use of a scintillation counter, and the percentage of extraction($\%E$) of Cr(III) was calculated from the ratio of the counting rate of the two phases: $\%E=D/(1+D)\times 100$, where D is the distribution ratio of Cr(III). The pH value of the aqueous phase was measured after the extraction equilibrium had been established in all cases.

In the back-extraction procedure, 5 cm^3 of the organic phase, prepared by the extraction procedure described above, was shaken with 5 cm^3 of a trichloroacetate buffer solution adjusted to the desired pH value for from 1 to 20 min. The percentage of back-extraction($\%E_b$) was determined in the same manner as in the extraction procedure.

Determination of Trichloroacetic Acid. The method described in the literature[5] was somewhat modified for the determination of the trichloroacetate ion in the present investigation: the concentration of the trichloroacetate buffer solution used in this investigation was too high to be determined by Fujiwara's pyridine-alkali reaction; therefore, after

** Present address: Department of Chemistry, Faculty of Science, Tohoku University, Sendai 980.

the extraction, 5 cm^3 of the aqueous phase was taken out and diluted with water to form about a 10^{-4} mol dm^{-3} trichloroacetate solution. Thus, a test solution was prepared. In a 20-cm^3 centrifuge tube, a 1-cm^3 portion of the test solution was placed together with 5 cm^3 of pyridine. Ten cm^3 of a 10 mol dm^{-3} sodium hydroxide solution was then added, and the content were vigorously shaken for 1 to 2 min. The tube was kept at 92±2 °C for just 3 min in a thermostat. After dipping the tube in water to cool it for 3 min, it was allowed to stand at room temperature for 30 to 60 min. Immediately after centrifugation, the absorbance of the pyridine layer was measured at 520 nm against the reagent blank.

Determination of Water Content of Organic Phase. In order to determine the water content of the cyclohexane phase after the extraction, an aliquot of the organic phase was submitted to Karl Fisher titration by the amperometric method. The potencies of the Karl Fisher reagent used were 1.9 to 2.6 mg H_2O/cm^3.

Results and Discussion

We tried to use various solvents as diluents of TOPO for the extraction of Cr(III) from a 0.1 mol dm^{-3} trichloroacetate buffer solution. The results are shown in Fig. 1, where the extraction decreases in this order: hexane, cyclohexane>toluene>benzene>nitrobenzene, carbon tetrachloride>chloroform. This order agrees with that observed in the extraction of europium nitrate with tributylphosphate in various diluents.[6] In the present extraction system, the effect of diluents may be ascribable to the differences in the interaction between TOPO and each diluent molecule, *e.g.*, dispersion forces, dipole-dipole interactions, or hydrogen bonds. In Fig. 1 the lowering of the distribution ratio of Cr(III) in the range of pH values higher than 5 is ascribed to the precipitation of the hydrated Cr(III) oxide in this pH range.

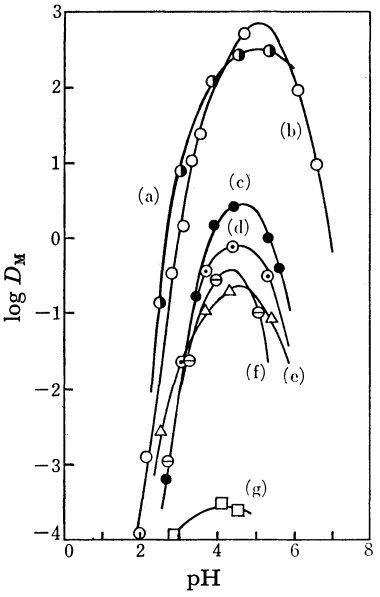

Fig. 1. Extraction of Cr(III) from 0.1 mol dm^{-3} TCA^- buffer solution into various organic solvents containing TOPO in 0.1 mol dm^{-3}. Hexane(a), cyclohexane(b), toluene(c), benzene(d), nitrobenzene(e), carbon tetrachloride(f), chloroform(g).

Chromium(III) could also be extracted from perchlorate solutions into cyclohexane containing 0.1 mol dm^{-3} TOPO, but the percentages of extraction from 0.1 mol dm^{-3} and 0.5 mol dm^{-3} perchlorate solutions at a pH value of 4.0 were only 22% and 85% respectively. In view of this fact, in place of perchlorate sodium chloride was used in order to keep the ionic strength of the aqueous phase constant (0.1). The concentrations of TOPO in cyclohexane and of trichloroacetate in the aqueous phase were kept as low as below 0.1 mol dm^{-3} in order to minimize the difference between the molar concentration and the thermodynamic activity.

Extraction of Water with TOPO. The extraction equilibrium of water by TOPO in cyclohexane can be given as follows:

$$H_2O + qTOPO_{(org)} \rightleftharpoons H_2O \cdot qTOPO_{(org)}, \quad (1)$$

where (org) designates the organic phase. Since the concentration of water in dilute solutions is considered constant, the extraction constant of water is written as

$$K_{H_2O} = \frac{[H_2O \cdot qTOPO]_{org}}{[TOPO]^q_{org}}. \quad (2)$$

Taking logarithms,

$$\log [H_2O \cdot qTOPO]_{org} = q\log [TOPO]_{org} + \log K_{H_2O}, \quad (3)$$

where $[TOPO]_{org}$ means the equilibrium concentration of the free TOPO. The amount of free TOPO remaining in the organic phase was calculated by deducting the amount of TOPO combined with water in the organic phase from that of the TOPO initially taken.

The plot of $\log[H_2O]_{org}$ *vs.* $\log[TOPO]_{org}$ gave a straight line with a slope of unity. From this slope, the species in cyclohexane was determined to be $H_2O \cdot TOPO$, which was just compatible with the $H_2O \cdot TOPO$ in carbon tetrachloride reported by Conocchioli *et al.*[7]

Extraction of Trichloroacetic Acid with TOPO. The extraction equilibrium may be written as

$$HTCA + iTOPO_{(org)} \rightleftharpoons HTCA \cdot iTOPO_{(org)}. \quad (4)$$

Therefore, the extraction constant of trichloroacetic acid is

$$K_{HTCA} = \frac{[HTCA \cdot iTOPO]_{org}}{[HTCA][TOPO]^i_{org}}. \quad (5)$$

In the above equation, water is put aside out of consideration. As will be described later, the water molecule present as $H_2O \cdot TOPO$ in the organic phase may be readily exchanged with trichloroacetic acid. Therefore, it can be assumed that the formation of the water complex of TOPO has no influence on the extraction of trichloroacetic acid. Then, the dissociation equilibrium of trichloroacetic acid in the aqueous phase is also given:

$$HTCA \rightleftharpoons TCA^- + H^+. \quad (6)$$

The acid dissociation constant of HTCA is

$$K_a = \frac{[TCA^-][H^+]}{[HTCA]}. \quad (7)$$

Equation 5 is rewritten by putting Eq. 7 in it,

$$K_{HTCA} = \frac{K_a[HTCA \cdot iTOPO]_{org}}{[TCA^-][H^+][TOPO]^i_{org}} = \frac{D_{HTCA}K_a}{[H^+][TOPO]^i_{org}}, \quad (8)$$

where D_{HTCA} is the distribution ratio of trichloroacetic acid. Taking logarithms of Eq. 8,

$$\log D_{HTCA} = i\log[TOPO]_{org} - pH - \log K_a + \log K_{HTCA}. \quad (9)$$

D_{HTCA} was determined at varying pH values of the aqueous phase for the equilibrium with various concentrations of TOPO as has been described above. Some of the results obtained are shown in Fig. 2, which indicates that the concentration of trichloroacetic acid in the organic phase decreases with the increase in the pH. This suggests that the concentration of TOPO free from trichloroacetic acid increases with the increase in the pH and that almost all of the TOPO becomes free from acid above pH 5.0.

On the other hand, the equilibrium concentration of water in the organic phase after the extraction of trichloroacetic acid is shown against the pH value of the aqueous phase in Fig. 3(a). Water is found to be released from cyclohexane with a lowering of the pH value until pH 2, and then the water concentration nearly reaches solubility in pure cyclohexane. Superposing this Fig. 3(a) on Fig. 2, it can be seen that TOPO tends to combine more strongly with trichloroacetic acid than with water, because the concentration of trichloroacetic acid in the organic phase shows a reverse trend to that of water.

Since TOPO molecules combined with water are readily available for the extraction of trichloroacetic acid, the complex formation of TOPO with water may be negligible in this acid-extraction equilibrium. Therefore, in Eq.9 the equilibrium concentration of TOPO was calculated by deducting the amount of

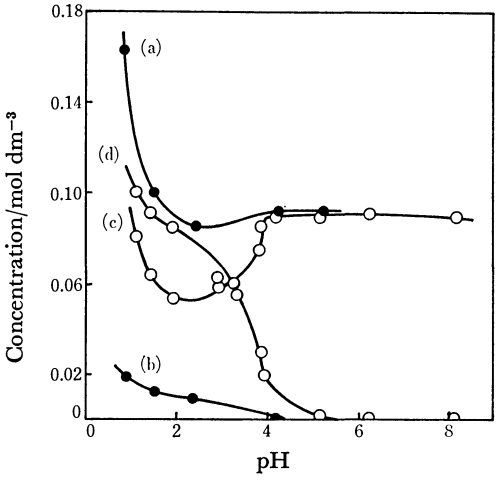

Fig. 2. Concentration of trichloroacetic acid in the organic and the aqueous phase after the extraction from 0.1 mol dm^{-3} TCA$^-$ buffer solution of various pH values. (a) and (c): HTCA in the aqueous phase, (b) and (d): HTCA in the organic phase, (a) and (b): the concentration of TOPO in cyclohexane is 0.01 mol dm^{-3}. (c) and (d): The concentration of TOPO in cyclohexane is 0.1 mol dm^{-3}.

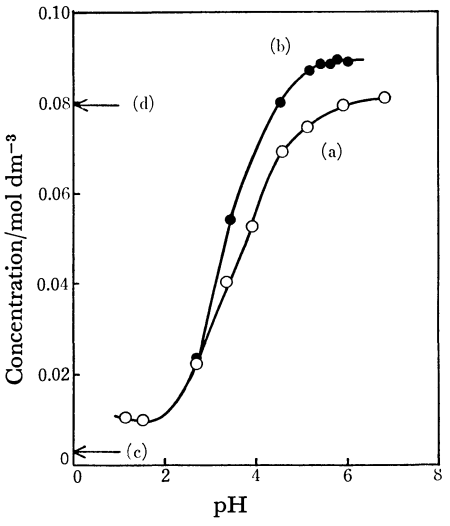

Fig. 3. Water content in the organic phase after the extraction at various pH values. (a): 0.1 mol dm^{-3} TOPO in cyclohexane—0.1 mol dm^{-3} TCA$^-$ buffer solution system, (b): in the presence of 1.9×10^{-3} mol dm^{-3} Cr(III), (c): water content in pure cyclohexane, (d): water content in cyclohexane containing TOPO in 0.1 mol dm^{-3}.

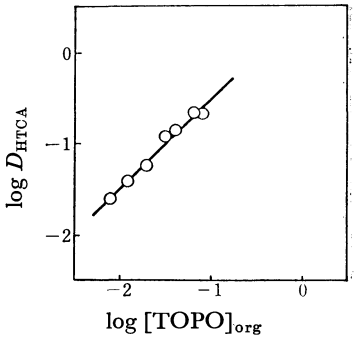

Fig. 4. Plot of log D_{HTCA} *vs.* log[TOPO]$_{org}$ at pH 4.0. Aqueous phase: 0.1 mol dm^{-3} TCA$^-$ buffer solution.

TOPO combined with trichloroacetic acid in the organic phase from that of TOPO initially taken, that is, [TOPO]$_{org}$ (acid extraction)=[TOPO](initial) $-i$[HTCA·iTOPO]. From Fig. 2, the concentration of TOPO combined with trichloroacetic acid was obtained directly from the concentration of trichloroacetic acid in the organic phase. The log-log plot of D_{HTCA} *vs.* the equilibrium concentration of TOPO obtained by calculating as $i=1$ is shown in Fig. 4, in which the log-log plot has a slope of unity. When the D_{HTCA} was plotted against the equilibrium concentration of TOPO obtained by assuming $i=2$ or $i=3$, no slope consistent with the assumed value of i was obtained. Consequently, the species of trichloroacetic acid extracted in cyclohexane was identified as HTCA·TOPO, and the extraction constant of trichloroacetic acid, $K_{HTCA}=10^{3.8}$ was obtained by putting known numerical values in Eq. 9. Compared with the extraction of other acids with TOPO,[8] the extraction constant of trichloroacetic acid is larger than those of such other acid as perchloric and thiocyanic acid. This may be attributed to the larger molar

volume of trichloroacetic acid.

Extraction of Cr(III) with TOPO. Compared with the two simple cases above, the equilibria of the whole extraction process of Cr(III) from trichloroacetate buffer solutions into cyclohexane containing TOPO may be more complicated. The present authors tried first the extraction and the back-extraction of Cr(III). In Fig. 5 the results are shown, together with the extraction conditions. The extraction and the back-extraction curves are symmetrical with each other; therefore, the whole extraction process may be reversible under the given conditions, and the attainment of the equilibria may be as quick as 1 min. In addition, the extraction of Cr(III) in varying amounts was carried out under the same conditions as in the foregoing experiment; the results are shown in Fig.6. When the initial concentration of Cr(III) was less than 2×10^{-3} mol dm^{-3}, the distribution ratio of Cr(III) was constant at a pH value of 3.5. The polymerized or dissociated species of Cr(III) in the organic phase can be left out of consideration. From these results,

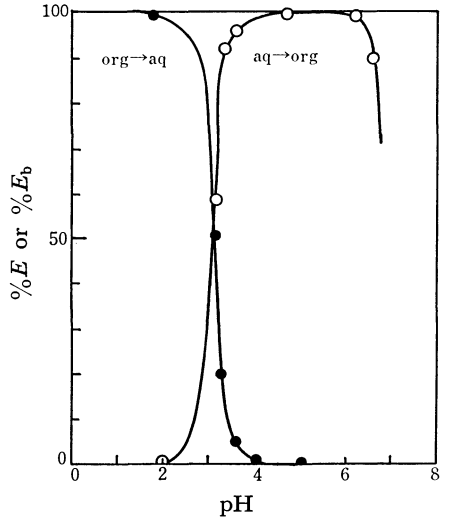

Fig. 5. Extraction and back-extraction of Cr(III) in 0.1 mol dm^{-3} TOPO - cyclohexane - 0.1 mol dm^{-3} TCA$^-$ buffer system. Concentration of Cr(III): 2×10^{-4} mol dm^{-3}, shaking time: 5 min.

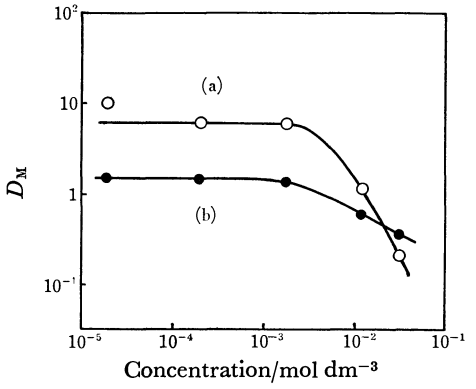

Fig. 6. Effect of the concentration of Cr(III) on the extraction from 0.1 mol dm^{-3} TCA$^-$ buffer solution of pH 3.5. (a): 0.1 mol dm^{-3} TOPO in cyclohexane, (b): 0.2 mol dm^{-3} TOPO in benzene.

the present authors obtain the following equation:

$$Cr(H_2O)_6^{3+} + mTCA^- + nTOPO_{(org)} \rightleftharpoons Cr(H_2O)_p^{3+}(TCA^-)_m\cdot nTOPO_{(org)} + (6-p)H_2O \quad (10)$$

$$K_M = \frac{[Cr(H_2O)_p^{3+}(TCA^-)_m\cdot nTOPO]_{org}}{[Cr(H_2O)_6^{3+}][TCA^-]^m[TOPO]_{org}^n} = \frac{D_M}{[TCA^-]^m[TOPO]_{org}^n}, \quad (11)$$

where K_M is the extraction constant of Cr(III), and D_M, the distribution ratio. Taking logarithms of Eq. 11,

$$\log D_M = m\log[TCA^-] + n\log[TOPO]_{org} + \log K_M. \quad (12)$$

Equation 12 is rewritten by putting Eq. 9 in it:

$$\log D_M = m\log[TCA^-] + n\,pH + \log K_M - n\log K_{HTCA} + n\log D_{HTCA} + n\log K_a. \quad (13)$$

Then the number of trichloroacetate ions participating in the extraction equilibrium of Cr(III) was estimated. The equilibrium concentration of trichloroacetate in the aqueous phase was obtained directly from Fig.2 without any corrections for the trichloroacetate extracted together with Cr(III), since the concentration of Cr(III) was as low as 2×10^{-4} mol dm^{-3}. The plot of log D_M *vs.* log[TCA$^-$] at a constant pH value has a slope of $m=3$, as is shown in Fig. 7. This suggests that the electrically neutral species, $Cr(H_2O)_p^{3+}(TCA^-)_3$, is formed in the aqueous phase and is extracted with TOPO into the organic phase.

The ratio of Cr(III) to TOPO in the extracted species was determined by plotting log D_M against log $[TOPO]_{org}$ at a constant TCA$^-$ concentration. The equilibrium concentration of TOPO was calculated in the same manner as in the acid extraction described above. As is shown in Fig. 8, the log-log plot has a slope of $n=3$, so the chromium(III) ion seemed to be solvated with three TOPO molecules.

The difference in the water concentration, as is shown in Fig. 3(a,b), shows that the additional water is extracted with Cr(III). The relationship between the concentration of Cr(III) extracted in the cyclohexane phase and the increment of water caused by

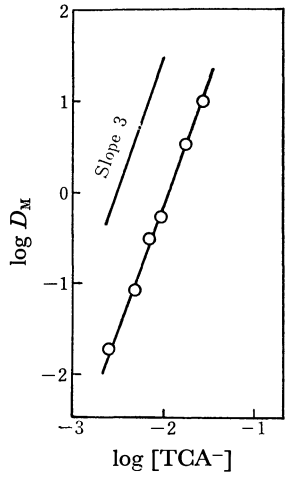

Fig. 7. Dependence of the distribution ratio of Cr(III) on the concentration of trichloroacetate in the aqueous phase at a constant pH value of 3.5.

Table 1. Relationship between the concentration of Cr(III) and the increment of water in cyclohexane after the extraction of Cr(III) with TOPO

pH of buffer solution	$[Cr]_{org}$ / 10^{-2} mol dm^{-3}	$[H_2O]_{org}$ / 10^{-2} mol dm^{-3}	$[H_2O]_{org}/[Cr]_{org}$
3.00[a]	0.067	0.45	6.7
3.20[a]	0.14	0.90	6.4
3.33[a]	0.17	1.1	6.5
4.50[a]	0.19	1.2	6.3
5.00[a]	0.19	1.2	6.3
5.50[a]	0.19	1.1	5.8
6.00[a]	0.19	1.0	5.3
3.51[b]	1.20	7.5	6.3
			mean value = 6.2±0.3

Extraction conditions: organic phase: 10 cm^3 of 0.1 mol dm^{-3} TOPO in cyclohexane, aqueous phase: 10 cm^3 of a 0.1 mol dm^{-3} TCA^- buffer solution. a) The initial concentration of Cr(III) in the aqueous phase was 0.19×10^{-2} mol dm^{-3}. b) The initial concentration of Cr(III) in the aqueous phase was 3.1×10^{-2} mol dm^{-3}.

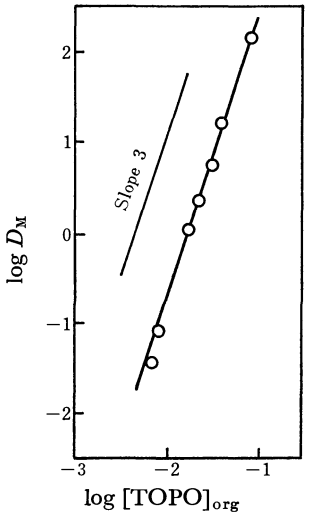

Fig. 8. Dependence of the distribution ratio of Cr(III) on the concentration of free TOPO in the organic phase at pH 4.0.

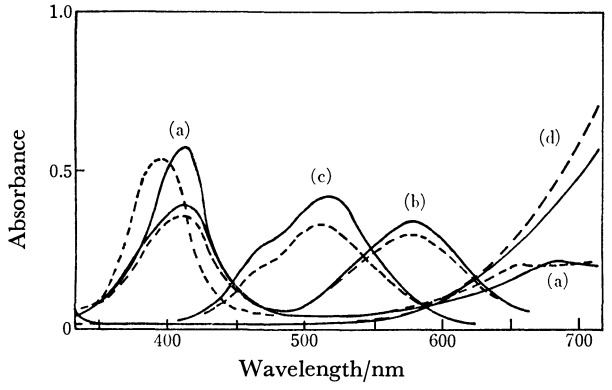

Fig. 9. Absorption spectra of the organic phase(——) after the extraction with 0.1 mol dm^{-3} TOPO and the aqueous phase(----) before the extraction. (a): Ni(II), (b): Cr(III), (c): Co(II), (d): Cu(II). Extraction conditions; organic phase: 0.1 mol dm^{-3} TOPO in cyclohexane, aqueous phase: 0.1—0.5 mol dm^{-3} TCA^- buffer solution of pH 4—5.

the extraction of Cr(III) is summarized in Table 1. The amount of water co-extracted with the Cr(III)–TCA^-–TOPO complex is about 6.2 times that of the Cr(III) extracted. This suggests that a common species of Cr(III) in the aqueous solution, $Cr(H_2O)_6^{3+}$, may be extracted into the organic phase as it is.

This is confirmed by the fact that the absorption spectrum of the extracted Cr(III) species in the organic phase is similar to that of hexaaquachromium(III) in the aqueous solution(Fig. 9(b)). In Fig. 9 the spectra of Co(II), Ni(II), and Cu(II) before and after their extraction in the present system are compared with those of Cr(III). The absorption bands of Co(II), Ni(II), and Cu(II) extracted with TOPO were all shifted to longer wave lengths than those of aqua complexes in the aqueous phase. This suggests that the TOPO molecule acts on the inner solvation sphere of all the metals except Cr(III). On the other hand, a previous report[1] has shown that the inner solvation sphere of any metal does not alter upon its extraction into isopentyl alcohol. These differences may be accounted for by the strong basicity of TOPO and the fast substitution rates of water molecules in the inner coordination sphere of metals other than Cr(III). The absorption bands of Cr(III) were gradually shifted to longer wave lengths when the extract was allowed to stand in the presence of an excess of TOPO. Moreover, the back-extraction curve shown in Fig. 5 was also shifted to a lower pH region; *i.e.*, the shift of $pH_{1/2}$, the pH at the half-extraction, was 0.5 when the extract was allowed to stand for about 48 h at room temperature. These facts suggest that the water molecules in the inner solvation sphere of the Cr(III) extracted are very slowly replaced by TOPO molecules in the organic phase.

On the basis of the above results, it may be stated that the predominant species of Cr(III) extracted from the trichloroacetate buffer solution into cyclohexane containing TOPO is the ion-association complex, $Cr(H_2O)_6^{3+}(TCA^-)_3\cdot3TOPO$, and that the extraction constant of this complex is $10^{7.68}$. In this complex, six molecules of water seem to be present in the inner

solvation sphere of Cr(III), while three molecules of the trichloroacetate ion as well as three molecules of TOPO seem to be present in the outer solvation sphere. The extractability of the Cr(III) ion in the present extraction system depends most on the concentration of TOPO free from trichloroacetic acid in the organic phase and, consequently, on the pH value of the aqueous phase.

References

1) T. Kiba, H. Imura, and T. Honjo, *Chem. Lett.*, **1977**, 805.
2) V. P. R. Rao and V. V. Sarma, *J. Inorg. Nucl. Chem.*, **38**, 1179 (1976).
3) J. Hala, *Collect. Czech. Chem. Commun.*, **39**, 3475 (1974).
4) O. M. Petrukhin, Yu. A. Zolotov, and L. A. Izosenkova, *Radiokhimiya*, **11**, 139 (1969).
5) T. A. Seto and M. O. Schultze, *Anal. Chem.*, **28**, 1625 (1956).
6) S. Siekierski, *J. Inorg. Nucl. Chem.*, **24**, 205 (1962).
7) T. J. Conocchioli, M. I. Tocher, and R. M. Diamond, *J. Phys. Chem.*, **69**, 1106 (1965).
8) M. Niitsu and T. Sekine, *Bull. Chem. Soc. Jpn.*, **50**, 1015 (1977).

Preparation and Solid-phase Thermal *cis-trans* Isomerization of the Mixed Bis(diamine)chromium(III) Complexes of the Type $[CrX_2(aa)(bb)]X \cdot nH_2O$[1)]

Samiran MITRA, Tadatsugu YOSHIKUNI, Akira UEHARA, and Ryokichi TSUCHIYA*

Department of Chemistry, Faculty of Science, Kanazawa University, Kanazawa 920

(Received February 22, 1979)

The mixed bis(diamine)chromium(III) complexes *trans*- and *cis*-$[CrX_2(aa)(bb)]X \cdot nH_2O$ were prepared and characterized where X is chloride or bromide ion; aa and bb are different diamines selected from ethylenediamine (en), propylenediamine (pn) and trimethylenediamine (tn); and *n* is a number of 0 to 2. The *cis-trans* isomerization of the above complexes was investigated non-isothermally (derivatographically) and isothermally in the solid-phase. The isomerization was found to be one-way (*trans*-to-*cis*) and exothermic. The activation energies were estimated for dehydration or dehydration plus dehydrohalogenation (E_d) and isomerization (E_i). The intermediates *mer*-$[CrBr_3(en)(pn)] \cdot 2H_2O$ and *mer*-$[CrBr_3(pn)(tn)] \cdot 2H_2O$ were isolated during the isomerization of *trans*-$[CrBr_2(en)(pn)]Br \cdot 2H_2O$ and *trans*-$[CrBr_2(pn)(tn)](H_5O_2)Br_2$, respectively. Bond rupture was proposed to be operative in the pathway of the isomerization.

We have already studied on the solid-phase *cis-trans* isomerizations of the bis(diamine)dihalogenochromium(III) complexes $[CrX_2(aa)_2]X$,[2-6)] where X is chloride or bromide ion; aa is one of diamines such as ethylenediamine (en), propylenediamine (pn), 2,3-butanediamine (bn) and trimethylenediamine (tn). In the course of our studies, an interesting fact was noticed that the direction of isomerization (whether *trans*-to-*cis* or *cis*-to-*trans*) largely depends upon diamines contained in the complexes. Actually, *trans*-to-*cis* isomerization was recognized in the complexes containing en, pn or bn which is capable of forming five-membered chelate ring with chromium(III) ion, whereas *cis*-to-*trans* isomerization was found in the complexes containing tn which forms six-membered chelate ring. It is, therefore, of much interest to know the details of the isomerization of the complexes having a general formula $[CrX_2(aa)(bb)]X$ where X is the same as described above; aa and bb denote different diamines selected from en, pn, and tn. Among them, the complexes having the combination of five- and six-membered chelate rings are particularly interesting.

As for the chromium(III) complexes containing two different diamines, Pfeiffer *et al.* first reported the mixed tris(diamine) complexes $[Cr(en)_2(pn)]X_3$ (X_3= Cl_3, $(SCN)_3$, I_3, $[Cr(ox)_3]$, or $[Cr(CN)_6]$).[7)] Recently, several mixed bis(diamine) complexes $[CrX_2(aa)(bb)]^+$ (X_2=Cl_2, F_2, $F(H_2O)$, and others) have been characterized and investigated from the viewpoint of hydrolysis kinetics.[8-12)] In general, owing to large solubilities in common solvents, many troublesome steps are required to isolate the mixed bis(diamine) complexes as compared with the simple bis(diamine) complexes $[CrX_2(aa)_2]^+$.[13)] The situation is rather severe for *cis* complexes than for *trans* complexes.

The present study was, therefore, undertaken (1) to prepare *trans*- and *cis*-mixed bis(diamine) complexes $[CrX_2(aa)(bb)]X$, and (2) to investigate the details of thermal *cis-trans* isomerization of the complexes in the solid-phase.

Experimental

Preparation of Complexes. trans-*[CrCl$_2$(en)(pn)]Cl·0.75H$_2$O (I)*, trans-*[CrCl$_2$(pn)(tn)]Cl·H$_2$O (II)*, trans-*[CrCl$_2$(en)(tn)](H$_5$O$_2$)Cl$_2$ (III)*, trans-*[CrBr$_2$(en)(pn)]Br·2H$_2$O (IV)*, trans-*[CrBr$_2$(pn)(tn)](H$_5$O$_2$)Br$_2$ (V)* and trans-*[CrBr$_2$(en)(tn)](H$_5$O$_2$)Br$_2$ (VI)*: For the preparation of these complexes, the starting material *trans*-$[CrF_2(aa)(bb)]Br$ was first prepared by modifying the methods described earlier.[10,11)] One gram of the material was dissolved in 10 ml of concentrated hydrochloric or hydrobromic acid and allowed to stand in a vacuum desiccator containing concentrated sulfuric acid as a desiccant, the desiccator being saturated with hydrogen chloride or hydrogen bromide by placing concentrated hydrochloric or hydrobromic acid in it. After a few days green crystals were separated. They were filtered, washed with ether and dried in a desiccator containing calcium chloride and *in vacuo* over KOH pellets for 2 h. The yields of the chloro complexes and the bromo complexes were about 60% and 65% based on the amounts of the starting materials used, respectively.

cis-*[CrCl$_2$(en)(pn)]Cl (VII)*, cis-*[CrCl$_2$(en)(tn)]Cl (VIII)*, cis-*[CrBr$_2$(en)(pn)]Br·2H$_2$O (IX)* and cis-*[CrBr$_2$(pn)(tn)]Br·H$_2$O (X)*. The *cis* complexes were prepared by using thermal isomerization of the corresponding *trans* complexes in the solid-phase.

First of all, one gram of the corresponding *trans* complexes was triturated thoroughly in a mortar, spread thinly on watch glass and heated in an air-bath at given temperature for a given time. The optimum heating conditions (temperatures and heating times) for obtaining the *cis* complexes were determined non-isothermally (derivatographically) and isothermally. They were 60 min at 140 °C for complex VII, 30 min at 210 °C for complex VIII, 30 min at 125 °C for complex IX, and 70 min at 160 °C for complex X. The products thus obtained were allowed to cool to room temperature, dissolved in *N*,*N*-dimethylformamide (DMF) and filtered (if any insoluble materials remained). To the filtrate appropriate amounts of ether were added drop by drop with stirring, violet crystals being separated. They were filtered, washed with ether and air-dried. The yields of the *cis* complexes were about 40% based on the amounts of the starting *trans* complexes.

As mentioned in the later section, *trans*-$[CrCl_2(pn)(tn)]Cl \cdot H_2O$ (II) decomposed during isomerization at about 220 °C and *trans*-$[CrBr_2(en)(tn)](H_5O_2)Br_2$ (VI) decomposed at 170 °C without isomerization, and so attempts to get the corresponding *cis* complexes failed.

Isolation of Intermediates during Isomerization. *[CrBr$_3$(en)(pn)]·2H$_2$O (XI)* and *[CrBr$_3$(pn)(tn)]·2H$_2$O (XII)*. They were isolated during isomerization of complexes IV and V. Each one gram of these complexes was spread in

TABLE 1. RESULTS OF ELEMENTAL ANALYSES

Complexes	C%		H%		N%	
	Found	Calcd	Found	Calcd	Found	Calcd
I	20.00	19.62	6.49	6.59	18.58	18.30
II	21.92	22.20	6.62	6.68	17.04	17.26
III	16.68	16.45	6.38	6.35	14.99	15.35
IV	12.23	12.98	4.27	4.70	11.46	12.11
V	12.58	12.99	4.36	4.49	9.81	10.07
VI	11.38	11.04	4.39	4.23	9.58	10.31
VII	20.54	20.53	6.19	6.20	19.13	19.15
VIII	20.25	20.53	6.37	6.20	19.14	19.15
IX	13.06	12.98	4.76	4.75	10.91	11.91
X	15.65	15.71	4.43	4.80	11.30	12.20
XI	12.20	12.98	4.41	4.76	11.53	12.11
XII	14.52	15.11	4.48	5.03	11.85	11.75

thin layer on watch glasses and heated for 25 min at 112 °C and 20 min at 150 °C, respectively. The products thus obtained were repeatedly washed with DMF until the washings became colorless. They were then washed with ether and air-dried. Bluish products were obtained with the yields of about 30%. The lattice waters in the crystals probably came from trace amounts of water present in the solvents employed in the procedures. Table 1 summarizes the results of elemental analyses.

Non-isothermal Measurements. Non-isothermal measurements were carried out with a Derivatograph Typ-OD-102 and the enthalpy changes, ΔH, for dehydration and isomerization were evaluated as previously described.[14]

Isothermal Measurements. The rates of dehydration or dehydration plus dehydrohalogenation of complexes I through VI were determined at different temperatures with a CHYO 1001 thermobalance.

The rates of isomerization were followed by measuring the changes in absorbancies for the samples heated in an Abderhalden apparatus or an Ikemoto Rika Kogyo air-bath at various temperatures. Electronic spectra were monitored on a Hitachi Recording Spectrophotometer. The solvent used is DMF, dimethyl sulfoxide (DMSO), or 0.1 mol dm^{-1} HCl, HBr, or $HClO_4$ solution. The isomerization ratios were calculated by using the following simultaneous equations:

$$\left.\begin{aligned} 34.6x + 76.1y &= D_{400} \\ 10.0x + 74.1y &= D_{530} \end{aligned}\right\} \text{ for complexes I and VII}$$

$$\left.\begin{aligned} 38.2x + 60.3y &= D_{400} \\ 5.8x + 63.4y &= D_{520} \end{aligned}\right\} \text{ for complexes III and VIII}$$

$$\left.\begin{aligned} 53.8x + 12.0y &= D_{540} \\ 39.8x + 29.3y &= D_{390} \end{aligned}\right\} \text{ for complexes IV and IX}$$

$$\left.\begin{aligned} 33.9x + 6.9y &= D_{520} \\ 22.7x + 33.9y &= D_{440} \end{aligned}\right\} \text{ for complexes V and X}$$

where x and y are the molar concentrations of *cis*- and *trans*-isomers, the numerical factors are the molar extinction coefficients of pure *cis*- and *trans*-isomers, and D's represent the observed absorbancies at the wavelengths specified by the subscripts. Figure 1 shows, as an example, the electronic spectra of complexes I and VII.

Thin Layer Chromatography (TLC). TLC was employed to distinguish the mixed bis(diamine) complexes *trans*-$[CrX_2(aa)(bb)]X$ from the simple bis(diamine) complexes *trans*-$[CrX_2(aa)_2]X$ and *trans*-$[CrX_2(bb)_2]X$.[10,15] TLC plates used were those of silica gel 60F-254 made by Merck Ltd. Table 2 lists up the results of complexes I through VI together with those of the simple bis(diamine) complexes.

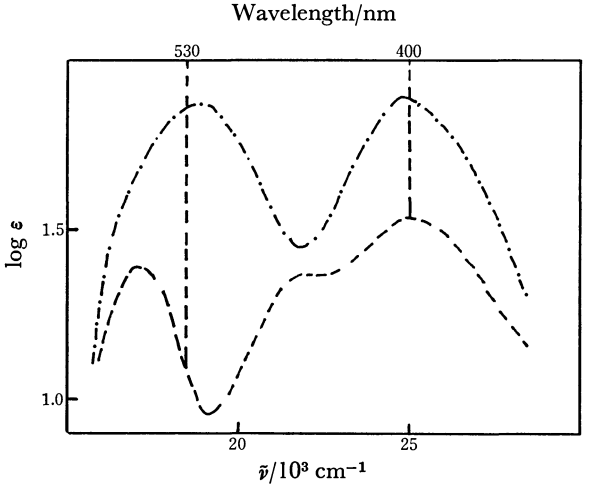

Fig. 1. Electronic spectra of complex I (----) and complex VII (—·—).

TABLE 2. RESULTS OF THIN LAYER CHROMATOGRAPHY FOR *trans*-$[CrX_2(aa)_2]X$, *trans*-$[CrX_2(aa)(bb)]X$, AND *trans*-$[CrX_2(bb)_2]X$[a]

	$[CrCl_2en_2](H_5O_2)Cl_2$	$[CrCl_2(en)(pn)]Cl\cdot 0.75H_2O$	$[CrCl_2pn_2]Cl\cdot 1.5H_2O$
R_f	0.31	0.37	0.43
	$[CrCl_2pn_2]Cl\cdot 1.5H_2O$	$[CrCl_2(pn)(tn)]Cl\cdot H_2O$	$[CrCl_2tn_2]Cl\cdot 0.5H_2O$
R_f	0.57	0.54	0.50
	$[CrCl_2tn_2]Cl\cdot 0.5H_2O$	$[CrCl_2(en)(tn)](H_5O_2)Cl_2$	$[CrCl_2en_2](H_5O_2)Cl_2$
R_f	0.55	0.48	0.43
	$[CrBr_2en_2]Br\cdot H_2O$	$[CrBr_2(en)(pn)]Br\cdot 2H_2O$	$[CrBr_2pn_2]Br\cdot H_2O$
R_f	0.69	0.74	0.86
	$[CrBr_2pn_2]Br\cdot H_2O$	$[CrBr_2(pn)(tn)](H_5O_2)Br_2$	$[CrBr_2tn_2]Br\cdot 2H_2O$
R_f	0.86	0.84	0.82
	$[CrBr_2tn_2]Br\cdot 2H_2O$	$[CrBr_2(en)(tn)](H_5O_2)Br_2$	$[CrBr_2en_2]Br\cdot H_2O$
R_f	0.82	0.76	0.69

a) The mixture of acetic acid and methanol (9 : 1) was used as the eluent. For the chloro complexes, single plate is employed in each run (as given in each row), whereas for the bromo complexes two plates are used: one is for the simple bis(diamine) complexes and the other for the mixed bis(diamine) complexes.

Comparison of the R_f values in the table reveals that the values for *trans*-$[CrX_2(aa)(bb)]X$ are just in between those for *trans*-$[CrX_2(aa)_2]X$ and *trans*-$[CrX_2(bb)_2]X$, indicating that all the mixed bis(diamine) complexes are pure.

Results and Discussion

Derivatography. Dehydration or Dehydration plus Dehydrohalogenation: Figure 2 shows the derivatograms of the chloro complexes I, II, and III, and Fig. 3, those of the bromo complexes IV, V, and VI. Complexes I and II are dehydrated at 70—160 °C and 40—120 °C, respectively. Complex IV evolves 2 mol of water at two separate stages (40—103 °C and 125—158 °C). Complexes III, V, and VI lose 2 mol of water and 1 mol of hydrogen halide (dehydration plus dehydrohalogenation) at temperatures below 140 °C. The enthalpy changes, ΔH, for dehydration or dehydration plus dehydrohalogenation for complexes I to VI were determined to be 17, 42, 55, 43, 49, and 57 kJ mol^{-1}, respectively.

Isomerization. Complexes I, II, III, and V give small but clear exothermic DTA peaks at 200, 220, 235, and 195 °C respectively, and they change in color from green to violet. This indicates that the isomerization takes place. Complex II partially decomposed during the isomerization, and therefore isolation of the corresponding *cis* complex was not possible. Prominent peak only due to mere isomerization can not be seen in the DTA curve of complex IV because the isomerization stage (90—130 °C) overlaps with the first dehydration stage (40—103 °C). Complex VI, after dehydration plus dehydrohalogenation (38—135 °C), remained unchanged up to about 170 °C, after that it melted and decomposed rapidly without isomerization.

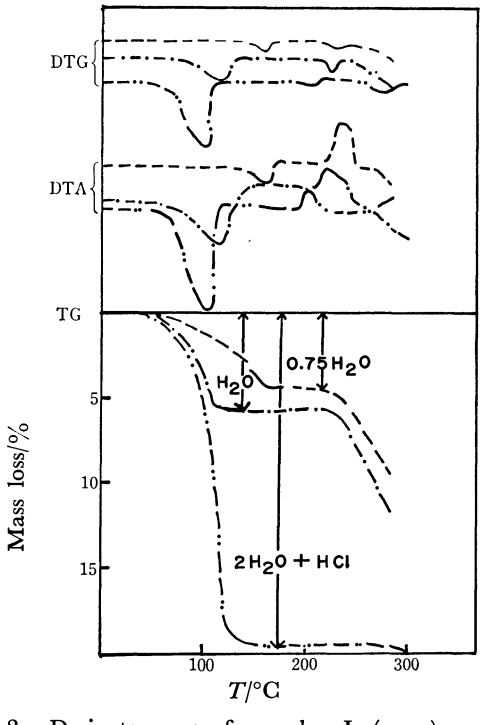

Fig. 2. Derivatograms of complex I (----), complex II (—·—) and complex III (—··—).

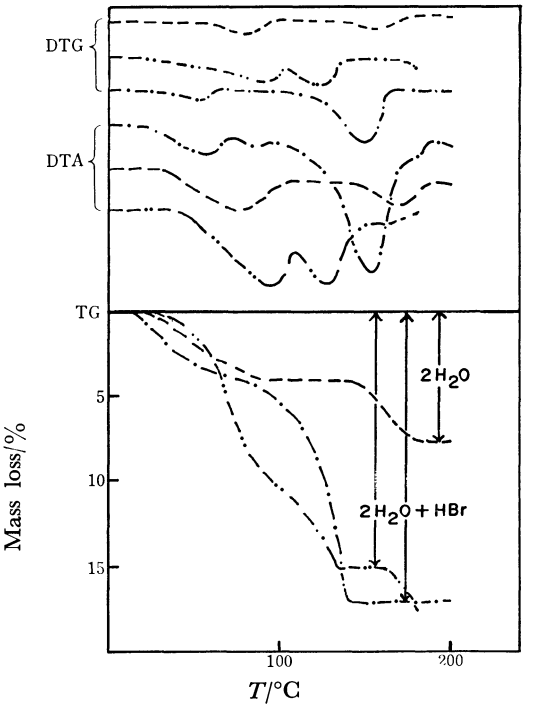

Fig. 3. Derivatograms of complex IV (----), complex V (—·—) and complex VI (—··—).

It must be noted that the *cis* complexes in the present study did not isomerize upon heating. We expected at the beginning of this study that the mixed bis(diamine) complexes having the composition of $[CrX_2(en)(or\ pn)(tn)]X$ might undergo both *trans*-to-*cis* and *cis*-to-*trans* isomerization. The expectation is based on the fact that *trans*-to-*cis* isomerization was recognized in the case of the simple bis(diamine) complexes $[CrX_2en_2(or\ pn_2,\ bn_2)]X$ where en, pn, or bn forms five-membered chelate ring,[2-4] whereas only *cis*-to-*trans* isomerization was detected in the complexes $[CrX_2tn_2]X$ in which tn forms six-membered chelate ring.[5,6] However, as mentioned above, the isomerization in the present case was found to be one-way (*trans*-to-*cis*).

Rate of Dehydration or Dehydration plus Dehydrohalogenation. If the rate of dehydration or dehydration plus dehydrohalogenation at each temperature obeys the first order law, the following equation should hold:

$$2.303 \log a/(a-x) = k_d t$$

where a is the initial amount of the starting complex, x is the amount of dehydrated or dehydrated plus dehydrohalogenated product formed during time t, and k_d is rate constant. Table 3 contains k_d and the rate constants of isomerization (k_1). Linear relationships were obtained when $\log a/(a-x)$ were plotted against time t. From the Arrhenius plots, the activation energies for dehydration of complexes I and II were obtained as 67 and 76 kJ mol^{-1}. For complex IV, the activation energies for the first and second dehydration steps were 46 and 103 kJ mol^{-1} respectively. The dehydration plus dehydrohalogenation stages of complexes III, V, and VI had the activation energies of 55, 112, and 30 kJ mol^{-1} respectively.

Rate of Isomerization. The isomerization of complexes I, III, IV, and V was traced spectrophotom-

Table 3. Rate constants of dehydration or dehydration plus dehydrohalogenation (k_d) and isomerization (k_i) at various temperatures

Complex I													
t/°C	100	109	120	130	138	153	159	172					
$k_d \times 10^4$/s^{-1}	4.27	7.48	12.7	21.7									
$k_i \times 10^4$/s^{-1}					0.24	1.22	2.22	7.70					
Complex II													
t/°C	73	86	94	103	113								
$k_d \times 10^4$/s^{-1}	1.92	4.99	9.21	13.3	26.9								
Complex III													
t/°C	80	87	99	108	205	214	222	238					
$k_d \times 10^4$/s^{-1}	6.73	9.60	17.6	25.6									
$k_i \times 10^4$/s^{-1}					0.81	1.95	3.95	15.3					
Complex IV													
t°/C	70	78	89	100	130	138	146	153	100	108	111	116.5	125
$k_d \times 10^4$/s^{-1}	2.56	4.67	5.76	9.12	8.47	13.9	26.6	44.1					
$k_i \times 10^4$/s^{-1}									0.96	1.66	2.88	4.80	10.4
Complex V													
t/°C	110	115	120	126	133	138	151	156	161	168			
$k_d \times 10^4$/s^{-1}	0.55	0.84	1.42	2.24	3.99								
$k_i \times 10^4$/s^{-1}						0.56	1.41	2.52	4.08	7.20			
Complex VI													
t°/C	80	89	100	110	118								
$k_d \times 10^4$/s^{-1}	3.22	4.32	5.28	6.97	9.90								

Table 4. Temperature (t_d and t_i) and activation energies (E_d and E_i)[a)]

Complex	Dehydration or dehydration plus dehydrohalogenation		Isomerization	
	t_d / °C	E_d / kJ mol^{-1}	t_i / °C	E_i / kJ mol^{-1}
I	102	67	167	155
II	86	76	—	—
III	76	55	224	181
IV	83	46103	117	114
V	136	112	163	123
VI	95	30	—	—

a) t_d and t_i stand for dehydration (or dehydration plus dehydrohalogenation) temperatures and isomerization temperatures where k_d and k_i show a constant value (5×10^4 s^{-1}). The constant value was taken for the convenience of comparison. E_d and E_i designate activation energies for dehydration (or dehydration plus dehydrohalogenation) and isomerization.

etrically. In a manner similar to that of dehydration, the value of $\log b/(b-y)$ were plotted against time t, where b is the initial amount of the *trans* complex, and y is the amount of the corresponding *cis* complex formed by isomerization. Linear relationships were obtained, and only in the case of complex IV the value of $\log b/(b-y)$ converged about 0.1, indicating that 20% of isomerization takes place during dehydration plus dehydrobromination and the remaining in the anhydrous state. Rate constants of isomerization (k_i) are given in Table 3. The activation energies of isomerization were estimated to be 155, 181, 114, and 123 kJ mol^{-1} for complexes I, III, IV, and V, respectively. Table 4 summarizes t_d and E_d (temperature and activation energy for dehydration or dehydration plus dehydrohalogenation), and t_i and E_i (temperature and activation energy for isomerization). Comparison of these values between the chloro complexes (I, II, and III) and the bromo complexes (IV, V, and VI) discloses that the bromo complexes are in general more easily dehydrated and dehydrohalogenated than the corresponding chloro complexes; the same tendency may also be true for isomerization.

Mechanism of Isomerization. Several studies have been reported on the mechanism of solid-phase racemization of metal complexes; *e.g.*, twist mechanism was preferably accepted in the solid-phase racemization of tris(oxalato)metallate,[16,17] and LeMay and Bailar reported that the solid-phase racemization of *l-cis*-$[CrCl_2en_2]Cl \cdot H_2O$ proceeds *via* aquation-anation mechanism.[18] The study on the isotopic exchange of anhydrous *cis*- and *trans*-$[CoCl_2en_2]Cl$* showed that the Cl ion in inner-sphere is exchanged by the Cl* ion in outer-sphere in the solid-phase,[19] implying that a bond rupture process may be included in the exchange.

We have noticed that the solid-phase *cis-trans* isomerization of the simple bis(diamine)chromium(III) complexes do not necessarily require the participation of lattice water unlike the corresponding cobalt(III) complexes,[20,21] and the reaction is, in most cases, accompanied by a small but clear exothermic DTA peak.[2-6] We tentatively speculated that a bond rupture may be involved in the isomerization.[3] In this study, we succeeded in isolating the intermediates XI and XII during the isomerizations of complexes

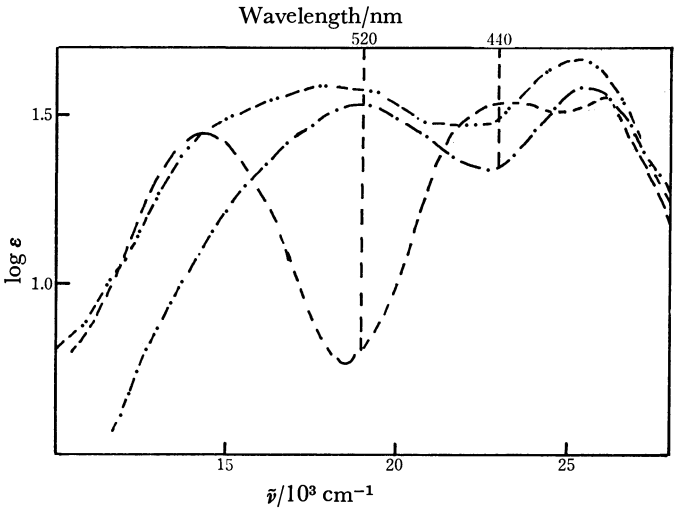

Fig. 4. Electronic spectra of complex V (----), complex X (—·—) and intermediate XII (—··—).

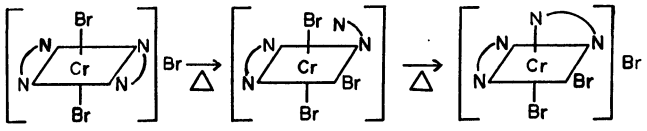

Fig. 5. Possible isomerization pathway.

IV and V as mentioned in the experimental section. Figure 4, as an example, shows the electronic spectra of complex V (*trans*-$[CrBr_2(pn)(tn)](H_5O_2)Br_2$), complex X (*cis*-$[CrBr_2(pn)(tn)]Br \cdot H_2O$) and the intermediate XII ($[CrBr_3(pn)(tn)] \cdot 2H_2O$). As seen from the figure, the *trans* complex V has, as expected, three absorption bands in the range of d-d transition [14.2×10^3 cm^{-1} (log ε=1.44), 23.0×10^3 cm^{-1} (log ε=1.53) and 25.5×10^3 cm^{-1} (log ε=1.51)] and the *cis* complex X has two bands at 19.0×10^3 cm^{-1} (log ε=1.53) and 25.6×10^3 cm^{-1} (log ε=1.58). On the other hand, the intermediate XII has two bands at 18.0×10^3 cm^{-1} (log ε=1.59) and 24.6×10^3 cm^{-1} (log ε=1.66), but the first band is accompanied by two shoulders at $\approx 14.0 \times 10^3$ cm^{-1} (log $\varepsilon \approx 1.42$) and $\approx 21.0 \times 10^3$ cm^{-1} (log $\varepsilon \approx 1.48$). The occurrence of these shoulders in the first band, as has been reported in the studies on [(Cr or Co)Cl_3dien][22] and $[CoCl_3(NH_3)_3]$,[23] supports that three bromide ions in the intermediate XII are arranged in *mer* position. The situation is also true for the intermediate XI (the spectral data were omitted because they were closely similar to those of the intermediate XII). From the above results, it is reasonable to consider that the isomerization of these complexes proceeds through a bond rupture pathway as represented in Fig. 5. It seems that the same mechanism is operative in the simple and mixed bis(diamine)chromium(III) complexes which isomerize with similar exothermic DTA peaks.

The authors wish to express their gratitude to Japan Society for the Promotion of Science for the financial support granted to this research.

References

1) Presented in part at the 35th National Meeting of the Chemical Society of Japan, Osaka, April 1977.
2) R. Tsuchiya, T. Ohki, A. Uehara, and E. Kyuno, *Thermochim. Acta*, **12**, 413 (1975).
3) R. Tsuchiya, T. Yoshikuni, S. Nakagawa, A. Uehara, and E. Kyuno, *Chem. Lett.*, **1977**, 339.
4) T. Yoshikuni, R. Tsuchiya, A. Uehara, and E. Kyuno, *Bull. Chem. Soc. Jpn.*, **50**, 883 (1977).
5) T. Yoshikuni, R. Tsuchiya, A. Uehara, and E. Kyuno, *Bull. Chem. Soc. Jpn.*, **51**, 113 (1978).
6) S. Mitra, A. Uehara, and R. Tsuchiya, *Thermochim. Acta*, accepted and will be published in 1980.
7) P. Pfeiffer, T. Gassman, and H. Pietch, *Z. Anorg. Allg. Chem.*, **57**, 312 (1908).
8) M. C. Couldwell and D. A. House, *Inorg. Chem.*, **11**, 2024 (1972).
9) M. C. Couldwell, D. A. House, and H. K. J. Powell, *Inorg. Chem.*, **12**, 627 (1973).
10) J. W. Vaughn and J. Marzowski, *Inorg. Chem.*, **12**, 2346 (1973).
11) J. W. Vaughn and G. J. Seiler, *Inorg. Chem.*, **13**, 598 (1974).
12) J. W. Vaughn and A. M. Yeoman, *Inorg. Chem.*, **15**, 2320 (1976).
13) Throughout this paper, the terms "simple bis(diamine) complexes" and "mixed bis(diamine) complexes" were employed to express the bis(diamine)dihalogenochromium(III) complexes containing two same diamines ($[CrX_2(aa)_2]X$ and $[CrX_2(bb)_2]X$) and those containing two different diamines ($[CrX_2(aa)(bb)]X$) respectively.
14) R. Tsuchiya, Y. Kaji, A. Uehara, and E. Kyuno, *Bull. Chem. Soc. Jpn.*, **42**, 1881 (1969).
15) J. L. Swain and J. L. Sudmeier, *Anal. Chem.*, **40**, 418 (1968).
16) C. D. Schmulbach, J. Brady, and F. Dachile, *Inorg. Chem.*, **7**, 287 (1968).
17) C. Kutal and J. C. Bailar, Jr., *J. Phy. Chem.*, **76**, 119 (1972).
18) H. E. LeMay, Jr. and J. C. Bailar, Jr., *J. Am. Chem. Soc.*, **90**, 1729 (1968).
19) G. B. Schmidt and K. Rössler, *Radiochim. Acta*, **5**, 123 (1966).
20) R. Tsuchiya, K. Murai, A. Uehara, and E. Kyuno, *Bull. Chem. Soc. Jpn.*, **43**, 1383 (1970).
21) R. Tsuchiya, Y. Natsume, A. Uehara, and E. Kyuno, *Thermochim. Acta*, **12**, 413 (1975).
22) D. A. House, *Inorg. Nucl. Chem. Lett.*, **3**, 67 (1967).
23) H. Siebert, *Z. Anorg. Allg. Chem.*, **389**, 22 (1972).

Enrichment of a Trace Amount of Manganese by the Mixed Resin Prepared from Finely Divided Anion and Cation Exchangers in the Presence of 4-(2-Pyridylazo)resorcinol

Masutaro ABE, Noriko TAKEI, Kunio OHZEKI, and Tomihito KAMBARA*

Department of Chemistry, Faculty of Science, Hokkaido University, Sapporo 060

(Received February 28, 1979)

The enrichment of a trace amount of manganese(II) from sample water was carried out by the combined use of a mixture of finely divided cation and anion exchangers and 4-(2-pyridylazo)resorcinol (PAR). Manganese–PAR complex was effectively collected onto the mixed resin by batch method in the pH range 9.1—10.2. The manganese on the mixed resin was eluted into hydrochloric acid solution, extracted with 4-benzoyl-3-methyl-1-phenyl-2-pyrazolin-5-one (BMPP) into MIBK and determined by atomic absorption spectrometry. The recovery of 3 μg of manganese from the synthetic sample solution (100—500 ml) was in the range 95—97%.

Recently we reported an analytical utilization of a resin mixture of finely divided anion and cation exchangers, the diameter being smaller than 30 μm.[1] A trace amount of copper(II) in a sample water was concentrated on the mixed resin as the complex with 8-hydroxy-5-quinolinesulfonate and determined by atomic absorption spectrometry. This paper describes some preliminary results with the enrichment of manganese(II) by the combined use of the mixed resins with PAR. The compounds BMPP and 4-cinnamoyl-3-methyl-1-phenyl-2-pyrazolin-5-one (CMPP) were examined as the reagents for the solvent extraction-atomic absorption spectrometric determination of manganese.

Experimental

Reagents. Stock solution of manganese(II) (1.0 g l^{-1}, pH=1) was prepared by dissolving the chloride into hydrochloric acid solution and its factor was determined by titration with EDTA. The Dotite PAR (Dojindo Co.) was used without further purification. Fifty milligrams of the reagent were dissolved into 3 ml of 0.1% sodium hydroxide solution and diluted to 100 ml. The reagents BMPP and CMPP were synthesized from 3-methyl-1-phenyl-5-pyrazolone and benzoyl chloride or cinnamoyl chloride (Wako Chemicals Co.) according to the method of Jensen.[2] The former BMPP was recrystallized twice from methanol. The results of elemental analysis were: Found: C, 73.1; H, 5.0; N, 10.1; O, 11.8%. Calcd for $C_{17}H_{14}N_2O_2$: C, 73.4; H, 5.0; N, 10.1; O, 11.5%. The latter CMPP was recrystallized twice from acetone. The results of elemental analysis were: Found: C, 75.0; H, 5.2; N, 9.1; O, 10.7%. Calcd for $C_{19}H_{16}N_2O_2$: C, 75.0; H, 5.3; N, 9.2; O, 10.5%. Solutions of 5×10^{-2} M (mol dm^{-3}) BMPP and CMPP were prepared by dissolving each acid in alkaline solution, the final solution being neutral.

The resin mixture was prepared by mixing suspension of cation exchanger (CRS) with that of anion exchanger (ARS) in the volume ratio of 1 to 1.6. The exchange capacities were 0.031 meq ml^{-1} for CRS and 0.030 meq ml^{-1} for ARS as reported previously.[1]

Apparatus. A Hitachi 508 atomic absorption spectrometer with a Fe–Co–Ni–Cu–Cr–Mn multielement hollow cathode lamp was used for the determination of manganese in MIBK extract under the following conditions: wavelength 279.5 nm, lamp current 10 mA, slit width 0.18 mm, acetylene flow rate 1.5 l min^{-1} and air flow rate 13 l min^{-1}. A Toyo KG 25 filter holder (Toyo Roshi Co.) was used.

General Procedure. An aliquot of sample solution (40—500 ml) containing 3 μg of manganese(II) is taken into a separatory funnel, 1.0 ml of 0.05% PAR solution being added. The solution pH was adjusted to *ca.* 9.6 with the addition of 2 M ammonia–ammonium chloride buffer solution. A 1.0-ml portion of CRS and 1.6 ml of ARS are then added to the sample solution. After shaking for 10 min the mixture is allowed to stand for several minutes until the coagulated resin settles. The mixed resin is separated by filtration with suction from the solution onto a filter paper (Toyo Roshi No. 1). The manganese species on the resin are then eluted with 20 ml of 0.5 M hydrochloric acid into another separatory funnel. The pH of the solution being adjusted to *ca.* 7.3 with 10 ml of 1 M potassium phosphate, 2.5 ml of 0.05 M BMPP are added. The resulting manganese–BMPP complex is extracted into 5.0 ml of MIBK and the organic extract is then subjected to atomic absorption spectrometry. The absorption is corrected from the blank value observed throughout the whole procedure.

Results and Discussion

Effect of PAR. Manganese(II) reacts with PAR to form a water soluble red complex in alkaline solution.[3] The negative logarithms of acid dissociation constants of the pyridine nitrogen, *p*-hydroxyl, and *o*-hydroxyl groups in the PAR molecule are reported to be 2.3, 12.4, and 6.9, respectively.[4] In the alkaline solution, the manganese complex is expected to be present as mono- or divalent anionic species, which is fixed onto the cationic site in the mixed resin.

The effect of PAR on the recovery of manganese was studied in the presence of varying amounts of calcium and chloride ions which are most commonly present in natural water. The optimal pH range was found to be 9.1—10.2 (Fig. 1), which is comparable to the result observed in the spectrophotometric determination of manganese with PAR.[5]

In the presence of 2.3 μmol of PAR, 3 μg of manganese was effectively collected from 40 ml of a calcium chloride solution containing even 50 mg of calcium ion (Fig. 2). In the absence of PAR, the amount of non-fixed manganese increased when the amount of calcium ion increased beyond the exchange capacity of cation exchanger in the mixed resin.

Manganese on the resin was quantitatively eluted with 20 ml of 0.5 M hydrochloric acid.

Extraction of Manganese with BMPP and CMPP. Determination of manganese in the eluate was carried out by using solvent extraction followed by atomic

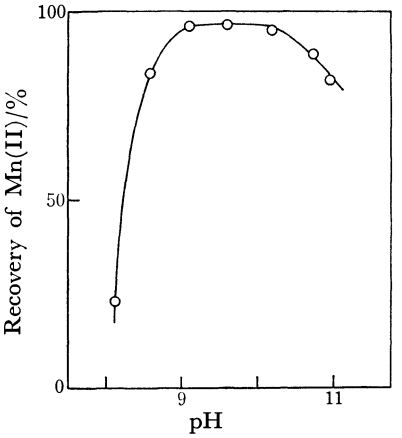

Fig. 1. Effect of pH on the recovery of 3.0 μg of manganese(II) from 40 ml of solutions containing 20 mg of calcium ion and 2.3 μmol of PAR onto the coagulated resin prepared from 1.0 ml of CRS and 1.6 ml of ARS. Buffer solution: NH_3–NH_4Cl, ionic strength: 0.1 (NaCl).

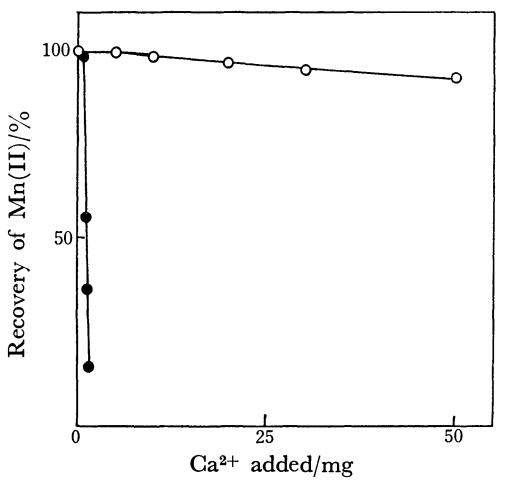

Fig. 2. Recovery of 3.0 μg of manganese(II) from 40 ml of solutions containing varying amounts of calcium chloride in the presence (○) and absence (●) of 2.3 μmol of PAR. ●: Unbuffered, ○: pH 9.6 (ammonia buffer), ionic strength 0.1 (NaCl).

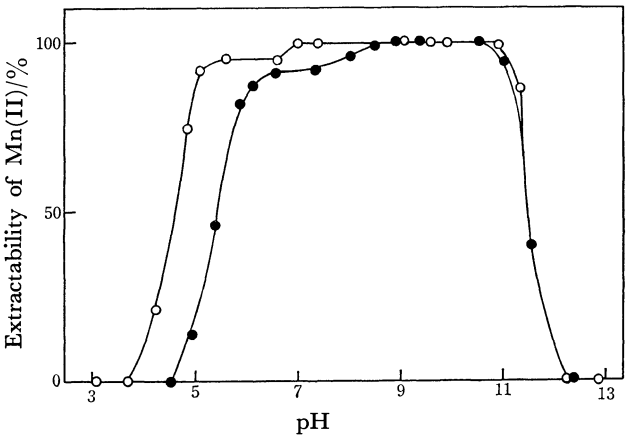

Fig. 3. Effect of pH on the extractability of manganese complex with BMPP (○) and CMPP (●) into MIBK. Solution pH is adjusted with Britton-Robinson buffer solution. Mn 3 μg, ionic strength 0.16 (NaCl), aqueous volume 50 ml, MIBK 5 ml.

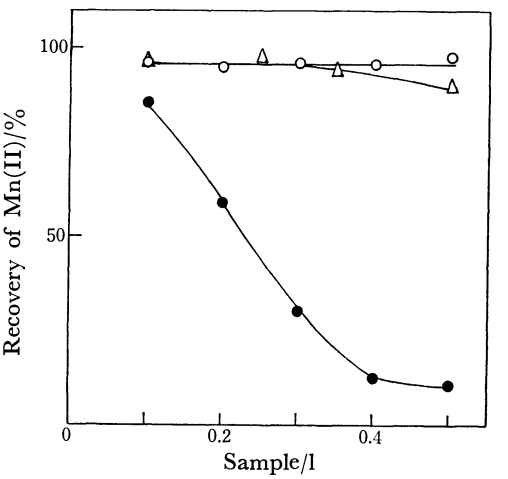

Fig. 4. Recovery of 3 μg of manganese(II) from varying amounts of synthetic sample solution (the composition is found in the text). ●: CRS 1.0 ml, ARS 1.6 ml, PAR 2.3 μmol; △: CRS 2.5 ml, ARS 4.0 ml, PAR 11.5 μmol; ○: CRS 2.5 ml, ARS 4.0 ml, PAR 46 μmol.

absorption spectrometry. The sensitivity of the AAS determination of manganese is enhanced when the organic extract is subjected to analysis.[6,7] In the preliminary tests, the methods employing ammonium 1-pyrrolidinecarbodithioate[8,9] and 8-quinolinolate[7] was examined. In the dithiocarbamate method, the back ground absorption increased with increasing amount of the reagent. On the other hand, the extraction pH higher than 10 was required in the oxinate method.

The use of BMPP and CMPP was studied. In spite of the interest in BMPP,[10] only a little information is available on the extraction of manganese complex into MIBK. The extractability of manganese BMPP complex was constant over the pH range 7.0—11.0 (Fig. 3). Manganese–CMPP complex was quantitatively extracted in the pH range 8.5—10.5. A small step was observed on the extractability-pH curves in both cases. The extraction method with BMPP was tested with the solution containing 20 ml of 0.5 M hydrochloric acid and 2.3 μmol of PAR. The solution composition is almost the same as that of the eluate from the mixed resin. The pH was adjusted by the addition of 1 M potassium phosphate. In the presence of PAR the optimal pH range became narrower in the alkaline region (pH 7.0—8.3), even larger amounts of BMPP up to 125 μmol being added. At the optimum conditions the extraction equilibrium was attained within a few minutes. The organic extract was stable at least within 30 min.

Enrichment of Manganese from Synthetic Sample Solution. The composition of the synthetic sample solution was: Na^+ 32.6, K^+ 7.8, Ca^{2+} 40.0, Mg^{2+} 12.0, Zn^{2+} 0.2, Pb^{2+} 0.005, Fe^{3+} 0.1, Cu^{2+} 0.01, Cl^- 142.22, SO_4^{2-} 58.3, SiO_2 7.5, HCO_3^- 35.4, NO_3^- 0.013, NH_4^+ 0.032 mg l^{-1}. The composition is referred to the ordinary river waters,[11] in which the concentrations of main components are fairly high. With

increasing amounts of PAR and the mixed resin, the recovery of manganese was improved (Fig. 4). By combined use of 2.5 ml of CRS, 4 ml of ARS and 46 μmol of PAR, a 3-μg portion of manganese was effectively recovered from 100—500 ml of the sample solution.

References

1) M. Abe, K. Ohzeki, and T. Kambara, *Bull. Chem. Soc. Jpn.*, **51**, 1090 (1978).
2) B. S. Jensen, *Acta Chem. Scand.*, **13**, 1668 (1959).
3) R. G. Anderson and G. Nickless, *Analyst*, **92**, 207 (1967).
4) A. Corsini, I. Mai-Ling Yih, Q. Fernando, and H. Freiser, *Anal. Chem.*, **34**, 1090 (1962).
5) T. Yotsuyanagi, K. Goto, M. Nagayama, and K. Aomura, *Bunseki Kagaku*, **18**, 477 (1969).
6) F. J. Feldman, R. E. Bosshart, and G. D. Christian, *Anal. Chem.*, **39**, 1175 (1967).
7) H. T. Delves, G. Shepherd, and P. Vinter, *Analyst*, **96**, 260 (1971).
8) R. E. Mansell, *Atomic Absorption Newslett.*, **4**, 276 (1965).
9) R. E. Mansell and H. W. Emmel, *Atomic Absorption Newslett.*, **4**, 365 (1965).
10) Yu. A. Zolotov, "Extraction of Chelate Compounds," translated by J. Schmorak, Ann Arbor-Humphrey Science Publishers, London (1970), p. 91.
11) T. Hanya, "Suisitu Chosaho," (in Japanese), Maruzen, Tokyo (1960), p. 51.

Adsorption Behavior of Phosphate Ion on the Iron(III) Complex of a Chelating Resin

Ryoichi TAKESHITA, Isao YOSHIDA,* and Keihei UENO**

Department of Industrial Chemistry, Kumamoto Institute of Technology, Ikeda 4-22-1, Kumamoto 860

***Department of Organic Synthesis, Faculty of Engineering, Kyushu University, Hakozaki, Higashi-ku, Fukuoka 812*

(Received March 5, 1979)

Phosphate ion in 0.1 M (1 M=1 mol dm^{-3}) sodium chloride solution was adsorbed selectively on the iron(III) complex of a chelating resin. Coordination unsaturated sites of the resin-bound iron(III) ion were considered to be the adsorption sites for phosphate ion, predominating species being dihydrogenphosphate ion ($H_2PO_4^-$). Adsorption capacity of the resin increased with the increasing amount of iron(III) ion loaded on the chelating resin, while the molar ratio of the adsorbed phosphate ion to the resin-bound iron(III) ion became less than unity, indicating that only a fraction of the resin-bound iron(III) ion acts as the adsorption site at higher iron content. The steric and electrostatic interactions among the phosphate ions in the resin matrix may interfere with the stoichiometric adsorption of phosphate ion on the resin-bound iron at higher iron content.

In a previous paper,[1] a report was given on the selective adsorption of arsenite and arsenate ions on the iron(III) complex of a chelating resin, with possible application to the removal of trace of arsenic from waste water of geothermal power plants.

Since the selective adsorption on such a resin is based on the coordination of anionic ligands to the coordination unsaturated sites of the resin-bound metal ion, adsorption of phosphate ion can also be expected on the iron(III) complex of the chelating resin. Such a process may be useful in the tertiary treatment of urban sewage for the effective removal of phosphate ion. This paper describes the nature of the iron(III) complex of chelating resin (Uniselec UR 10) as an adsorbent for phosphate ion.

Experimental

Materials. Uniselec UR 10 chelating resin (Unitika Ltd. Osaka) of 20—50 mesh size was used. Iron(III) complex of chelating resin was prepared by the following procedure. An iron(III) ion solution prepared by dissolving 0.4—5.4 g of iron(III) chloride hexahydrate in 200 ml of 0.3 M sodium acetate–acetic acid buffer (pH 3.0) was mixed with 10 g of sodium form chelating resin which had been conditioned by successive washings with 2 M hydrochloric acid and sodium hydroxide solutions. The resulting iron(III) complex resin was washed with deionized water until the washings became free from iron(III) ion, sucked off, and stored in a sealed bottle in a refrigerator.

The iron content in the resin was measured on the acid eluate by EDTA titration, and expressed in terms of F (mmol/g of dry iron(III) resin). The iron contents ranged from 0.12 to 1.34. The water content was also determined on each grade of the iron(III) resin by measuring the weight loss after drying to constant weight at 110 °C. A stock solution of phosphate ion was prepared from potassium dihydrogenphosphate. All other reagents were of analytical grade.

Procedure for Adsorption Study. Adsorption equilibria were investigated by batchwise operation. A weighed amount of the iron(III) resin, *ca.* 0.5 g, was shaken with 50 ml of a buffered solution containing phosphate ion at a constant temperature for 24 h, which is sufficient to attain approximate equilibrium. For determination of partition ratio and adsorption isotherms, respectively 1.3×10^{-3} M and (6.4×10^{-4}—3.3×10^{-2}) M of phosphate solution were used. The ionic strength of the solution was adjusted to 0.1—0.2 with sodium chloride.

After equilibration, the phosphate ion concentrations were determined by molybdenum blue photometry on solution and resin phases, the latter being analyzed on the 2 M hydrochloric acid eluate.

The partition ratio, K_{ad}, of phosphate ion between aqueous and resin phases can be expressed by

$$K_{ad} = Q/C$$

where C and Q are the phosphate ion concentration in solution (M) and in iron(III) resin(mmol/g of dry iron(III) resin), respectively. Although wet resin was used throughout the experiment, the corrections were made for dry resin by estimating the water content of the wet resin.

Instruments. A Toa model HM-5A pH meter and Shimadzu MPS-50L spectrophotometer were used.

Results and Discussion

Nature of the Iron(III) Chelating Resin. Uniselec UR 10 chelating resin used in the experiment has a three-dimensional network structure containing an *N*-(*o*-hydroxybenzyl)iminodiacetic acid moiety as a chelating group. Since the chelating site has phenolic oxygen in addition to the iminodiacetic acid group which is often found in the conventional chelating resin such as Dowex A-1, the coordination site of the Uniselec resin behaves as a quadridentate ligand to iron(III) ion, resulting in a more stable chelate than that by the Dowex A-1 type resins. As a result, iron(III) ion is so tightly bound to the resin that it is not easily released from the resin even in the presence of a large excess of alkali and alkaline earth cations above pH 3.

Iron(III) ion which is coordinatively hexavalent is bound to the Uniselec resin under so called "coordination unsaturated" conditions, leaving two coordination sites aquated. The sites are expected to act as adsorption sites for the coordinating anions as suggested by Helfferich.[2] A report appeared on the selective adsorption of arsenite and arsenate ions by the iron(III) chelating resin.[1]

pH *Dependence of the Partition Ratio,* K_{ad}. Figure

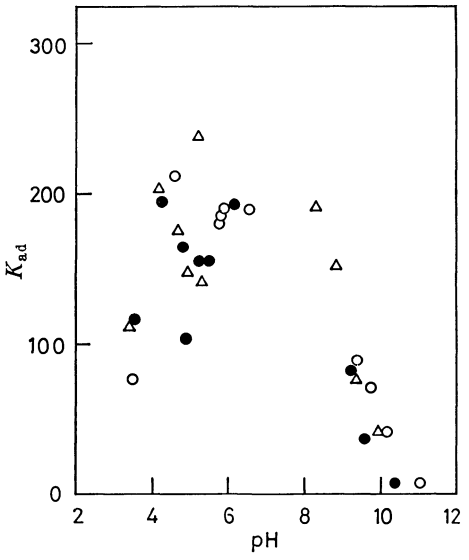

Fig. 1. pH profile of partition ratio, K_{ad}, of the iron(III) resin (F=1.25) at 35 °C. In acidic region, buffered with 0.1 M acetate buffer. In alkaline region, buffered with 0.1 M ammonia–ammonium chloride (○) or with 0.1 M ammonia–ammonium nitrate either in the presence (△) or absence (●) of 0.1 M sodium chloride.

1 shows the pH dependency of the partition ratio, K_{ad}, of phosphate ion at 35 °C. The pH of the aqueous phase was buffered with 0.1 M acetic acid–sodium acetate in the acidic region, and with 0.1 M ammonia–ammonium chloride (○) or 0.1 M ammonia–ammonium nitrate (●, △) in the alkaline region. The symbol (△) shows the partition ratio in the presence of 0.1 M sodium chloride. Though the points are scattered, the adsorption of phosphate seems to be most favorable in the pH region 4—7. The K_{ad} value decreases rapidly with variation in pH on either side of the optimum region. If we consider the acid dissociation constants of phosphoric acid (pK_a; 2.06, 7.03, 12.1), such a pH profile suggests the univalent dihydrogenphosphate ion to be responsible for adsorption. Since the presence of chloride ion gives no adverse effect on K_{ad} value, the adsorption is not due to the ion-exchange reaction.

The nature of the iron(III) resin changes with variation in pH. When pH<1, iron(III) ion may be displaced from the resin with proton, resulting in the loss of adsorption capacity. With increase in pH, the proton dissociation of coordinated water on the resin bound iron(III) ion might occur, forming monohydroxo- and dihydroxo species.

This has been discussed by Harris *et al.*[3] on the iron(III) chelate of monomeric *N*-(*o*-hydroxybenzyl)-iminodiacetic acid in aqueous solution, where the proton dissociation constants of diaquated iron(III) chelate were found to be:

$$FeL(OH_2)_2 \rightleftharpoons FeL(OH_2)(OH)^- + H^+ \qquad \log K = -5.71$$

$$FeL(OH_2)(OH)^- \rightleftharpoons FeL(OH)_2^{2-} + H^+ \qquad \log K = -9.1$$

where H_3L denotes the free ligand. If we assume a similar proton dissociation scheme on the resin bound diaquated iron(III) ion, it may behave as a dibasic

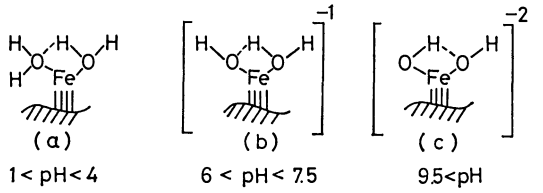

Fig. 2. Possible states of the resin bound iron(III) ion.

acid (Fig. 2). Species (a), (b), and (c) may predominate in the pH regions <4, 6—7.5, and >9.5, respectively. The electrostatic repulsion between the resin bound iron(III) ion and phosphate ion becomes larger in the order (a)<(b)<(c). At the same time, the resistance to the ligand exchange reaction between phosphate ion and the hydrolyzed species would become larger in the order (a)<(b)<(c). Thus, of the three states of the iron(III) resin, the most favorable one for the adsorption of phosphate ion seems to be (a), showing the optimum K_{ad} value in a weakly acidic region.

Adsorption Isotherms with the Iron(III) Resin. The effect of temperature on the adsorption isotherms of phosphate ion with the iron(III) resin is shown in Fig. 3, where the resin of F=1.34 was used at pH 6.0 with ionic strength *ca.* 0.2. The effect of iron(III) ion content on the adsorption isotherms under similar experimental conditions at 35 °C is shown in Fig. 4. The phosphate uptake by the resin, Q, increases with rise in temperature and increase in the iron(III) ion content. It also increases with increase in phosphate ion concentration in the aqueous phase, C, approaching saturation at higher phosphate ion concentration. The results suggest that the adsorption of phosphate is a chemical reaction and that the adsorption sites are the resin bound iron(III) ions.

The adsorption of phosphate ion can be considered to be the ligand exchange reaction between the coordinated water and the phosphate ion. If we assume that the reacting species of the resin bound iron(III) ion is mainly in the state (a), the reaction can be schematically written as follows.

$$RFe(OH_2)_2 + H_2PO_4^- \overset{K_{eq}}{\rightleftharpoons} RFe(H_2PO_4)^- + 2H_2O \qquad (1)$$

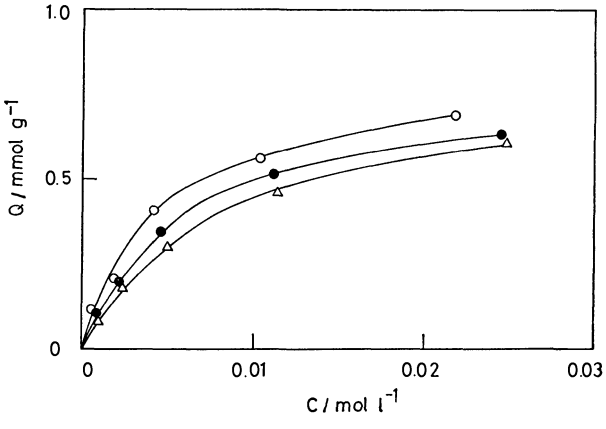

Fig. 3. Adsorption isotherms of the iron(III) resin (F=1.34) at different temperatures (pH=6.0, $\mu \approx 0.2$). —○— 35 °C, —●— 25 °C, —△— 8 °C.

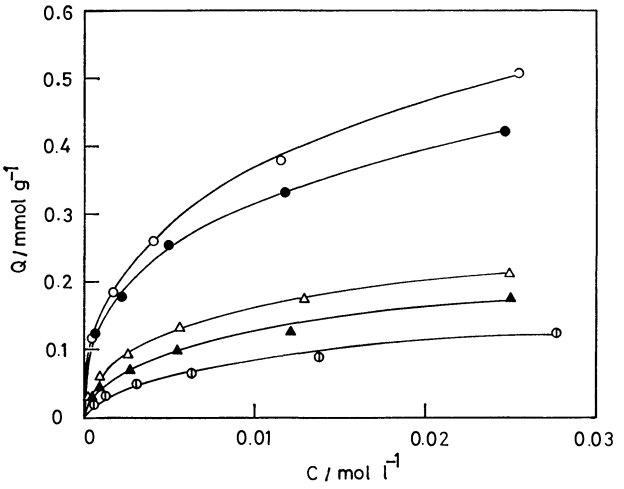

Fig. 4. Adsorption isotherms of the iron(III) resin of various iron contents at 35 °C (pH=6.0, $\mu\approx0.2$). —○— F=0.88, —●— 0.64, —△— 0.31, —▲— 0.23, —⏀— 0.12.

where $RFe(OH_2)_2$ denotes the resin bound iron(III) ion. The equilibrium constant of this reaction can be given by

$$K_{eq} = \frac{X_{RFe(H_2PO_4)^-}}{X_{RFe(OH_2)_2}} \cdot \frac{1}{C} \tag{2}$$

where the mole fractions of unadsorbed and adsorbed sites in the resin, and the molar concentration of phosphate ion in the aqueous phase are expressed as $X_{RFe(OH_2)_2}$, $X_{RFe(H_2PO_4)^-}$, and C, respectively.

The mole fraction of adsorbed site can be written as

$$X_{RFe(H_2PO_4)^-} = \frac{A}{WQ_\infty} = \frac{Q}{Q_\infty} \tag{3}$$

where A is the amount of phosphate adsorbed (mmol) on W g of the iron(III) resin ($Q=A/W$), and Q_∞ is the saturated adsorption capacity of the resin.

By means of the relation

$$X_{RFe(OH_2)_2} + X_{RFe(H_2PO_4)^-} = 1, \tag{4}$$

Eq. 2 can be written as

$$C = -\frac{1}{K_{eq}} + Q_\infty\left(\frac{C}{Q}\right). \tag{5}$$

Thus, the plots of C against C/Q should give a straight line, from which $-1/K_{eq}$ and Q_∞ can be obtained from the intercept and slope, respectively.

The isotherms of the resins of various iron(III) ion contents at various temperatures were treated by means of Eq. 5 where the phosphate ion concentrations of the aqueous phase were in the range (3.2×10^{-4}—2.9×10^{-2}) M after equilibration. The results are shown in Figs. 5 and 6, respectively. The values for K_{eq} and Q_∞, obtained from the intercept and slope of each line drawn by the method of least squares, are summarized in Table 1.

Equilibrium constant, K_{eq}, increased with increase in temperature, indicating that the adsorption is a

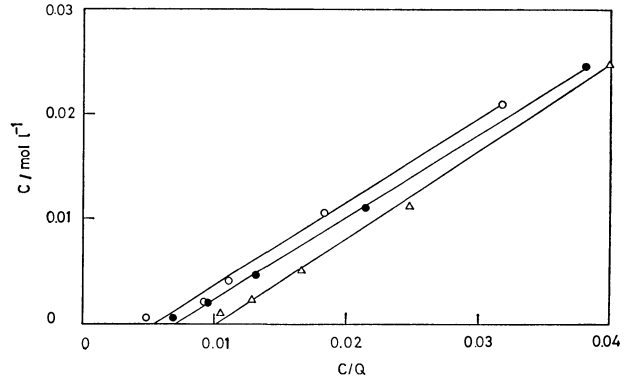

Fig. 5. C *vs.* C/Q plots at different temperatures. —○— 35 °C, —●— 25 °C, —△— 8 °C.

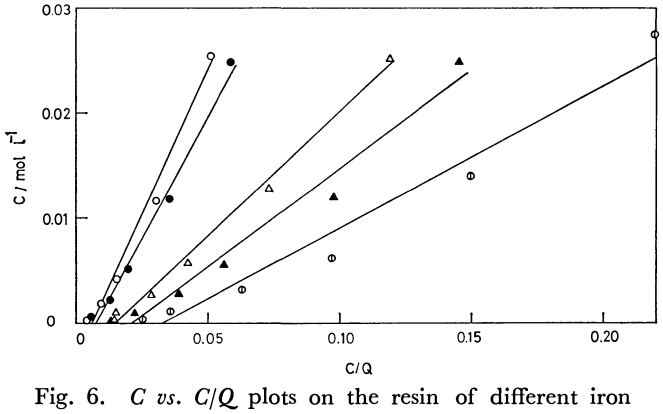

Fig. 6. C *vs.* C/Q plots on the resin of different iron contents. —○— F=0.88, —●— 0.64, —△— 0.31, —▲— 0.23, —⏀— 0.12.

Table 1. Parameters for the adsorption on phosphate ion by iron(III) complex of cherating resin (pH=6.0, μ=0.2)

Resin			Parameters for Eq. 5		
Iron content F/mmol g^{-1}	Water content %	Temp °C	Q_∞ mmol g^{-1}	$K_{eq}\times10^{-2}$ l mol^{-1}	Q_∞/F
0.12	110.0	35	0.13±0.02	2.2±1.1	1.08±0.17
0.23	90.1	35	0.19±0.02	2.7±0.9	0.83±0.09
0.31	89.1	35	0.23±0.02	3.0±0.8	0.74±0.06
0.64	84.9	35	0.46±0.05	3.2±1.6	0.72±0.08
0.88	79.9	35	0.54±0.06	3.0±1.6	0.61±0.07
1.34	72.5	35	0.82±0.07	2.7±0.6	0.61±0.05
1.34	72.5	25	0.77±0.02	2.0±0.2	0.57±0.01
1.34	72.5	8	0.82±0.03	1.2±0.1	0.61±0.02

chemical process as shown by Eq. 1. Saturated capacity, Q_∞, does not change with temperature. It increases with increase in iron(III) ion content in the resin, indicating that the resin bound iron(III) ions act as the adsorption sites for phosphate ion.

We could expect a 1:1 binding ratio for phosphate ion: the resin bound iron(III) ion, since we found a 1:1 complex formation in the spectrophotometric study on the interaction of phosphate ion with the iron(III) chelate of *N*-(*o*-hydroxybenzyl)iminodiacetic acid in aqueous solution at pH 6.0.[4] However, as shown in Table 1, the stoichiometric ratio, Q_∞/F, indicates that only one half of the resin bound iron(III) ions act as adsorption sites at higher iron(III) ion content, the value approaching unity with the decreasing iron(III) ion content. This suggests that, at higher iron(III) ion content, the electrostatic and steric repulsions among the phosphate ions in the resin matrix may interfere with the stoichiometric adsorption of phosphate to the resin–bound iron(III) ion, while at lower iron(III) ion content, the adsorption becomes more stoichiometric due to the smaller interaction among adsorbed phosphate ions.

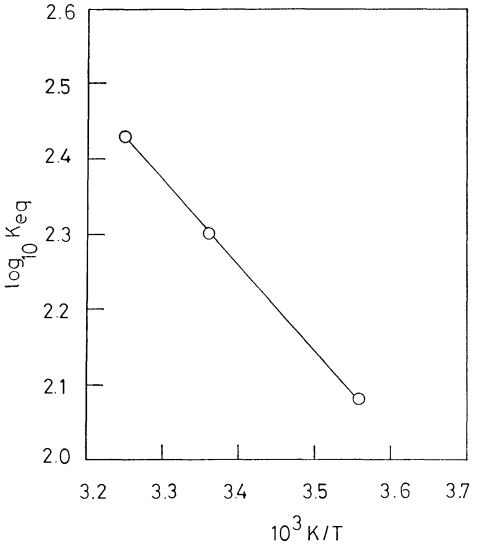

Fig. 7. Arrhenius plots for the standard heat of adsorption. Data from Table 1.

The equilibrium constant, K_{eq}, increases with increase in temperature. Thus we can estimate the apparent standard heat of adsorption from the Arrhenius plots (Fig. 7). The value $\Delta H = 21.8$ kJ mol^{-1} is reasonable for the complex formation.

The authors are grateful to Unitika Ltd. for the supply of Uniselec chelating resin.

References

1) I. Yoshida, K. Ueno, and H. Kobayashi, *Sep. Sci. Technol.*, **13**, 183 (1978).
2) F. Helfferich, "Ion Exchange," McGraw-Hill Inc., New York (1962).
3) W. R. Harris, R. J. Motokaitis, and A. E. Martell, *Inorg. Chem.*, **14**, 974 (1975).
4) I. Yoshida and K. Ueno, unpublished result.

The Determination of Berberine by Ion-pair Extraction-Titration, with Tetrabromophenolphthalein Ethyl Ester as the Indicator

Masahiro TSUBOUCHI

Laboratory of Chemistry, Kochi Medical School, Oko, Nankoku, Kochi 781-51

(Received March 8, 1979)

A method has been developed for the determination of berberine as a quinolizinium medicine. The method is based on the solvent extraction-titration of an ion pair. Sodium tetraphenylborate is used as the titrant, with tetrabromophenolphthalein ethyl ester as the indicator in the presence of chloroform. In the two-phase titration, the proposed procedure gives sharp end points as the organic phase changes from blue to yellow. The aqueous phase is colorless throughout the titration. From a p(berberine)-pH diagram, a theoretical titration curve is constructed. The titration curve at pH 6.5 is not too far from the ideal case.

Various reports have appeared regarding the ion-pair extraction-titration (two-phase titration) method. Methylene Blue,[1] Methyl Orange,[2] Azure A,[2] Bromophenol Blue,[3] and Neutral Red[4] have been used as indicators for the determination of anionic surfactants of quaternary ammonium salts. The ion-pair extraction-titration techniques would be convenient for use in the laboratory because, with them, there is no need for sophisticated instrumentation. End-point detection in two-phase titration is based on the movement of a dye as an indicator from one phase to the other. In general, though, it is difficult to detect the end point because a dye color in an aqueous phase or an organic phase will be reflected in the other layer.[1,2]

This paper will deal with the determination of berberine as a quinolizinium medicine. Nonaqueous titrimetric,[5] gravimetric,[6] and spectrophotometric[7–10] methods were investigated for the determination of berberine. In the two-phase titration proposed here, sodium tetraphenylborate is used as the titrant, with tetrabromophenolphthalein ethyl ester (In) as the indicator in the presence of chloroform. This procedure gives sharp end points as the organic layer changes from blue to yellow, and there is less likelihood of error. A singly charged In anion forms a 1:1 ion pair with berberine in the organic solvent.[8] The aqueous layer is colorless throughout the titration. This is because the indicator itself is not soluble in water, but gives a yellow color in chloroform. When the berberine (Bb) is titrated with a sodium tetraphenylborate (TPB) solution, the $[Bb^+ \cdot TPB^-]$ ion pair is formed in the organic phase and the reaction followed at the end point is:

$$\underset{\text{blue}}{[Bb^+ \cdot In^-]_{org}} + H^+ + [TPB^-]_{aq} \longrightarrow [Bb^+ \cdot TPB^-]_{org} + \underset{\text{yellow}}{[In]_{org}}$$

Experimental

Reagents. Tetrabromophenolphthalein ethyl ester potassium salt was dissolved in ethanol to make the solution 0.1%. A proper quantity of berberine chloride was dissolved in the distilled water. Standardization was done spectrophotometrically with a potassium dichromate solution.[7] The phosphate buffer solution (pH 6.5) was prepared from a 0.3 M disodium hydrogenphosphate solution with several drops of dilute sulfuric acid.

Procedure. The berberine solution (1—10 ml of 0.001 M), 5 ml of the phosphate buffer solution, 10 ml of chloroform, and 2—3 drops of a tetrabromophenolphthalein ethyl ester solution were placed in a 200-ml Erlenmeyer flask. The mixture was titrated with a 0.002 M sodium tetraphenylborate solution, with intermittent shaking by hand, to ensure an equilibrium between the organic solvent and the aqueous phase. The organic phase changes from greenish blue to yellow at the end point.

Results and Discussion

When the mixture of the berberine solution, the buffer solution, chloroform, and the indicator solution is shaken as has been described above, the aqueous phase is colorless and the organic phase is greenish blue. Figure 1 shows the visible absorption spectra of the indicator in chloroform. Near the end point of the titration, the organic phase starts to turn green. When one drop excess of the tetraphenylborate solution is added, the organic phase acquires a distinct yellow color, while the aqueous phase is still colorless. This is due to the fact that the indicator forms an organophilic ion pair with berberine. Therefore, some reflection of the color in the aqueous phase does not interfere with the end-point detection.

The effect of the pH on the proposed method was studied by titrating a series of berberine solutions buffered at various pH values. The results are summarized in Fig. 2. When the berberine solution is titrated with sodium dodecylbenzenesulfonate solution, quan-

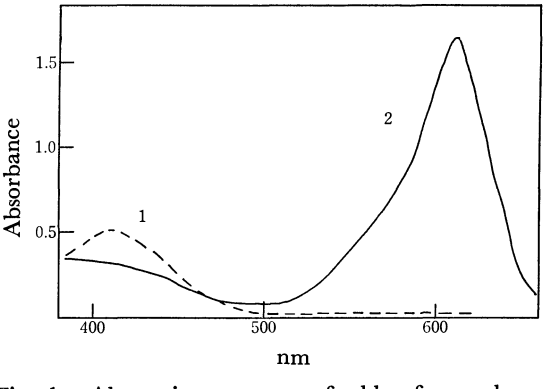

Fig. 1. Absorption spectra of chloroform phase. 1: Extract with 2×10^{-5} M indicator, 2: extract with 2×10^{-5} M indicator and 2×10^{-5} M berberine. Reference: water.

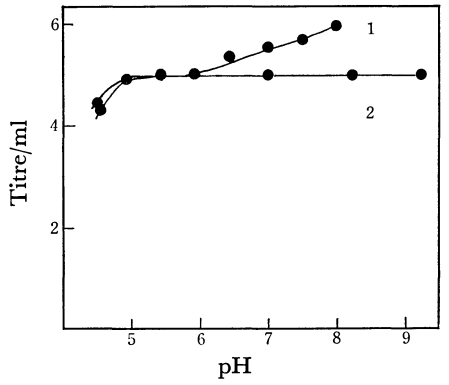

Fig. 2. Effect of pH on titration. 1: Titration with 0.002 M laurylbenzenesulfonate, 2: titration with 0.002 M tetraphenylborate, berberine, 10 ml of 0.001 M.

titative titrations are obtained in the pH range of 5—6. Larger amounts of buffer solution had no influence on the titration, but when less than 1 ml was added, the phase separation was poor.

As in the pH titration of acids and bases or in the pM titration of the metal ion and ethylenediaminetetraacetic acid,[11] berberine titration by the extraction may be generally represented by p(berberine) titration curves. The basic equilibria are given by:

$$(Bb)_w + (TPB)_w \rightleftharpoons (Bb\cdot TPB)_o$$

$$(Bb)_w + (In)_o \rightleftharpoons (Bb\cdot In)_o$$

For simplicity, the charges are omitted. The symbols are: Bb, berberinium ion; TPB, tetraphenylborate ion; In, indicator; o, in the organic phase; w, in the aqueous phase. The corresponding equilibrium constants are:

$$K_{Bb\cdot TPB} = [Bb\cdot TPB]_o/([Bb]_w \times [TPB]_w)$$

$$K_{Bb\cdot In} = [Bb\cdot In]_o/([Bb]_w \times [In]_o)$$

The effective stability constants (12—17 °C) were obtained from absorption measurements with berberine-tetraphenylborate extracts and berberine-indicator extracts at 440 nm[7] and 610 nm[8] respectively. A simple pBb-pH diagram is given in Fig. 3 for the titration. When 50% of TPB is present in free-ion form and 50% in Bb–TPB ion-pair form, the pBb is equal to the logarithm of the effective stability constant (K') of the Bb–TPB ion pair:

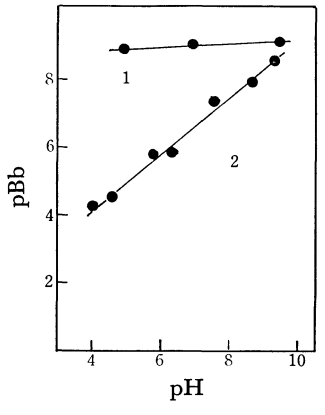

Fig. 3. p(berberine)-pH diagram. 1: $\log K'_{Bb\cdot TPB}$, 2: $\log K'_{Bb\cdot In}$.

$$\log K'_{Bb\cdot TPB} = \log 1/[Bb]_w = pBb$$

Line 2 in Fig. 3 corresponds to the pBb value at which 50% of In is present in free-dye form and 50% in Bb–In ion-pair form:

$$\log K'_{Bb\cdot In} = \log 1/[Bb]_w = pBb$$

From the pBb-pH diagram, a theoretical titration curve is constructed for the 0.002 M TPB titration of 10 ml of 0.001 M Bb at the pH value of 6.5 as is shown in Fig. 4. The pBb at the 50%-color-change point, C, is equal to the logarithm of the effective stability constant of the Bb–In ion pair. A maximum color change is obtained by a minimum increment titrant at this point. The fractional color change from 0.1 to 0.9 covers about 2 pBb units. The shaded areas indicate the region of the color change of the indicator. The titration curve at pH 6.5 is not too far from the ideal one.

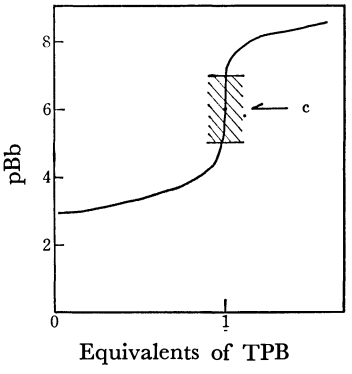

Fig. 4. Titration curve at pH 6.5. 10 ml of 0.001 M berberine is titrated with 0.002 M tetraphenylborate.

Ten identical samples, each with 10 ml of a 0.001 M berberine solution, were titrated with a 0.002 M tetraphenylborate solution according to the procedure. The mean titre was 5.00 ml, with a standard deviation of 0.04 ml.

Various water-immiscible solvents, such as nitrobenzene, isopentyl methyl ketone, butyl acetate, isoamyl alcohol, toluene, 1,2-dichloroethane, chloroform, benzene, carbon tetrachloride, and hexane, were tested. Of these, chloroform was the best solvent for the titration of berberine. The initial volume fluctuations of the aqueous phase (5—20 ml) and the organic phase (7—15 ml) did not have any measurable effect on the determination of the end point.

The effects of other ions on the titration process were studied for 10 ml of the 0.001 M berberine solution. The following ions did not interfere at the 0.01 M level: Na^+, Ca^{2+}, Mg^{2+}, K^+, NH_4^+, NO_3^-, SO_4^{2-}, Br^-, Cl^-, I^-, acetate, carbonate, citrate, and tannate. Amines such as thiamine, papaverine, and diphenhydramine caused positive errors; the maximum permissible amount was the 10^{-4} M level. Dodecyl sulfate, quaternary ammonium, and mercury(II) ions interfered.

Sample of medicine containing berberine chloride (40 mg), tannic acid (40 mg), aluminium 2-hydroxy-3-naphthoate (100 mg), pectin (50 mg), and silicon powder (5 mg) were dissolved in water. The solutions

were filtered and analyzed according to the proposed method and a spectrophotometric method.[7] The mean result of six samples was 39.0 mg of berberine chloride, with a standard deviation of 0.3 mg, while the result was 38.2 mg of berberine chloride by the spectrophotometric method. The proposed indicator has proved applicable to the two-phase titration of anionic surfactants with quaternary ammonium salts.

The author wishes to thank Professor Yuroku Yamamoto of Hiroshima University for his valuable advice.

References

1) A. S. Weatherburn, *J. Am. Oil Chem. Soc.*, **28**, 233 (1951); M. E. Turney and D. W. Cannell, *J. Am. Oil Chem. Soc.*, **42**, 544 (1965).
2) L. K. Wang and P. J. Panzardi, *Anal. Chem.*, **47**, 1472 (1975).
3) J. T. Gross, *Analyst*, **90**, 315 (1965).
4) T. Uno and K. Miyajima, *Chem. Pharm. Bull.*, **10**, 467 (1962).
5) T. Kaito, I. Tomioka, K. Sagara, and Y. Ito, *Bunseki Kagaku*, **22**, 1175 (1973).
6) "The Japanese Pharmacopoeia," Hirokawa Publishing Co., Tokyo (1976), VIII-1, C-506.
7) "The Japanese Pharmacopoeia," IX (1976), C-311.
8) T. Sakai, *Bunseki Kagaku*, **24**, 135 (1975).
9) T. Sakai, I. Hara, and M. Tsubouchi, *Chem. Pharm. Bull.*, **25**, 2451 (1977).
10) T. Sakai, *Bunseki Kagaku*, **27**, 444 (1978).
11) C. N. Reiley and R. W. Schmid, *Anal. Chem.*, **31**, 887 (1959).

ESR Study of ^{63}Cu(II) Doped in Single Crystals of Bis(alkyl 3-alkylidenedithiocarbazato)nickel(II) and -zinc(II). II. Proton Hyperfine Structure and Tetrahedral Distortion

Takayuki Oniki

Pre-dental Course, Kyushu Dental College, Manazuru, Kokurakita-ku, Kitakyushu 803

(Received December 11, 1978)

The ESR spectra of ^{63}Cu(II) diluted in several single crystals of the title Ni(II) and Zn(II) complexes are reported. In the substituted benzylidene groups, hyperfine structure(hfs) due to the magnetically equivalent two protons have been observed. The hfs were resolvable only in a limited magnetic direction due to the small anisotropic coupling constants. The coordination around Cu(II) ion has been found to be *cis* in all the Zn(II) complexes and the ESR parameters are more anisotropic than in the Ni(II) complexes. The relationship between the tetrahedral distortion and the ESR parameters has been interpreted using the d-orbital coefficients in the ground state.

There have been a number of theoretical studies on tetrahedral distortion around copper(II) centers and extensive ESR studies on the solid state system.[1—9] The tendency for $g_{\parallel}$ to increase and $|A_{\parallel}|$ to decrease with increasing tetrahedral distortion has been reported for well-characterized complexes of copper(II) with *N*-salicylidenealkylamine,[10,11] bis(pyrazolyl)gallates,[12] and dipyrromethenates.[13] Yokoi and Addision[14] reported the ESR measurements of several bis(*N*-substituted 2-pyrrolylmethyleneaminato)copper(II) complexes in toluene and concluded that the small value of $|A_0|$ is due to the large positive value of $A_{\perp}$ by tetrahedral distortion. Bates explained the small hf coupling constants on the basis of $3d^84p$ mixing in the $3d^9$ configuration.[4]

The ESR parameters of the Cu(II) site which is tetrahedrally distorted from *cis*-CuN_2S_2 planar symmetry has been discussed in a previous report.[15] The Schiff bases derived from alkyl dithiocarbazate were found to form a series of ligands,[16—19] whose properties were greatly modified by the introduction of organic substituents into the ligand thereby inducing different stereochemistry in the resultant metal complexes. The relationship between the ESR parameters and tetrahedral distortion around the Cu(II) ion site have been investigated by measuring the ESR spectra for ^{63}Cu(II) diluted with Zn(II) complexes in place of the Ni(II) complexes which have a *S*-methyl group, and with the Ni(II) complexes which possess a *S*-benzyl group. In either case the tetrahedral distortion is expected to be larger than in Ni(II) complexes with a *S*-methyl group.

In the first report the ESR spectra of Cu(II)/Ni(bdc)$_2$ exhibited additional hfs. The additional hfs are assignable to two azomethine protons or to noncoordinated nitrogen, in order to establish which was the case the ESR spectra of ^{63}Cu(II) diluted in Zn(II) and in Ni(II) complexes with Schiff bases which have azomethine protons were measured. Figure 1 shows the structures of the host complexes used. The alkyl and alkylidene groups denote methyl and 1-phenylethylidene, methyl and 1-(*p*-tolyl)ethylidene, methyl and *o*-tolylidene, methyl and *m*-tolylidene, methyl and *o*-chlorobenzylidene, benzyl and 1-(2-naphthyl)ethylidene, benzyl and 1-(*p*-tolyl)ethylidene, and benzyl and 1-phenylethylidene, and the corresponding ligands have been abbreviated as pedcH, tedcH, omdcH, mmdcH, ocdcH, bndcH, btdcH, and bpdcH respectively.

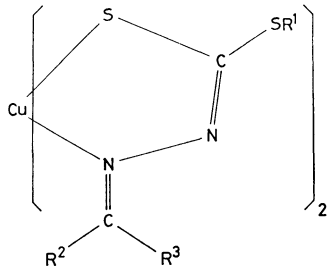

R^1	R^2	R^3	*cis*	*trans*
methyl	—H	*o*-tolyl	Zn(omdc)$_2$	Ni(omdc)$_2$
methyl	—H	*m*-tolyl		Ni(mmdc)$_2$
methyl	—H	*o*-chlorophenyl	Ni(ocdc)$_2$	
methyl	methyl	phenyl	Zn(pedc)$_2$	
methyl	methyl	*p*-tolyl	Zn(tedc)$_2$	
benzyl	methyl	2-naphthyl	Ni(bndc)$_2$	
benzyl	methyl	*p*-tolyl	Ni(btdc)$_2$	
benzyl	methyl	phenyl	Ni(bpdc)$_2$	

Fig. 1. The structures of the host complexes used; bis(alkyl 3-alkylidenedithiocarbazato)nickel(II) or -zinc(II), and abbreviations which are classified into *cis* or *trans* form around copper(II) ion site.

Experimental

The complexes were prepared according to the methods of cited in the literature.[16,17] The ESR spectra were recorded every 5° or 10° around three mutually perpendicular rotational axes. The most elongated axis was defined as the 2-axis, and the broadest crystal face was defined as the 12-plane. The room temperature ESR spectra were taken on a JEOL ME 1X spectrometer at the X band. A frequency counter, Mn(II) diluted with MgO, and DPPH were used as the *g* marker. The second order effects of the ESR spectra were calculated by the method of Iwasaki.[20] The forbidden transitions could not be obtained, so that no attempt was made to determine the quadrupole coupling parameters. The calculations were performed on an Olivetti P 652 computer.

Results and Discussion

Proton Hyperfine Structures. The four complexes with the ligands which have azometihne protons were

Table 1. The ESR parameters for Cu(II) complexes containing azomethine protons. The principal elements of $A(^{63}Cu)$ and A^N are in units of 10^{-4} cm^{-1}

Host	Principal values	Direction cosines 1	2	3
Ni(omdc)$_2$ (*trans*)	$g_x=2.021$ (1)	0.82	±0.16	−0.56
	$g_y=2.044$ (1)	0.13	∓0.99	−0.09
	$g_z=2.129$ (1)	0.56	±0.01	0.83
	$A_x=26$ (3)	0.82	±0.13	−0.56
	$A_y=37$ (3)	0.12	∓0.99	−0.06
	$A_z=175$ (1)	0.57	±0.02	0.83
	$A^N{}_x=19.6$ (5)	0.82	0.08	−0.56
	$A^N{}_y=A^N{}_z=15.6$ (8)			
	$A^H{}_{max}=3$ G			
Ni(mmdc)$_2$ (*trans*)	$g_x=2.024$ (1)	−0.13	0.99	0
	$g_y=2.045$ (1)	0.02	−0.11	0.99
	$g_z=2.139$ (1)	0.99	0.13	−0.01
	$A_x=22$ (3)	−0.13	0.99	0
	$A_y=32$ (3)	0	0	1
	$A_z=176$ (1)	0.99	0.13	0
	$A^N{}_x=18.9$ (5)	−0.09	0.99	0.12
	$A^N{}_y=A^N{}_z=15.0$ (8)			
	$A^H{}_{max}=3$ G			
Zn(omdc)$_2$ (*cis*)	$g_x=2.030$ (1)	0.97	0.02	0.26
		−0.39	−0.10	−0.92
	$g_y=2.150$ (1)	−0.24	−0.31	0.92
		0.88	0.25	−0.40
	$g_z=2.037$ (1)	−0.10	0.95	0.30
		0.27	−0.96	−0.01
	$A_x=17$ (5)	0.91	0.34	0.24
		−0.23	−0.40	−0.89
	$A_y=137$ (1)	−0.15	−0.27	0.95
		0.93	0.20	−0.33
	$A_z=32$ (5)	−0.39	0.90	0.19
		0.30	−0.90	0.33
	$A^N=7$—9			
	$A^H{}_{max}=6$ G			
Ni(ocdc)$_2$ (*cis*)	$g_x=2.027$ (1)	0.91	0.32	0.26
	$g_y=2.125$ (1)	−0.34	0.94	0.04
	$g_z=2.031$ (1)	−0.23	−0.13	0.96
	$A_x=28$ (4)	0.93	0.28	0.22
	$A_y=167$ (1)	−0.29	0.96	0.03
	$A_z=35$ (4)	−0.20	−0.09	0.97
	$A^N=9.5$—11.6			
	$A^H{}_{max}=4$ G			

obtained. Table 1 shows the obtained ESR parameters and direction cosines against 1, 2, and 3 axes. In all the complexes, additional hfs were observed. Figure 2 shows well resolved extra hfs which consist of three lines with an intensity ratio of 1:2:1. It was concluded, that the extra hfs are due to two azomethine protons. The proton hfs were anisotropic and small, and well resolved only in the limited magnetic direction. Table 1 shows, therefore, only the maximum coupling constants(G). The proton hfs were observed in the cases of bis(salicylideneaminato)copper(II),[21] *N,N*-bis(2-pyrrolylmethylene)ethylenediaminatocopper(II),[22] Cu(II) doped in L-alanine,[23] and measured in great

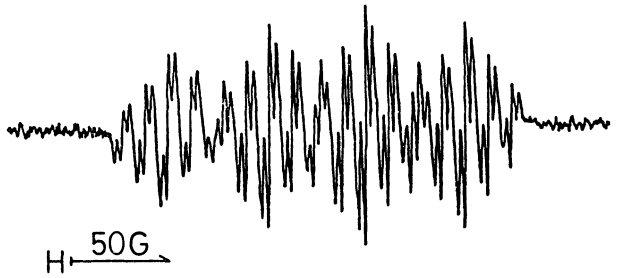

Fig. 2. The well resolved single crystal ESR spectra of ^{63}Cu(II)/Ni(ocdc)$_2$. The proton hfs is well resolved at high field with the intensity ratio of 1:2:1, $(\theta, \varphi)=(15°,0°)$, where θ and φ is the angles in the spherical 123 coordinate.

detail by ENDOR in the case of bis(salicylaldehyde oximato)copper(II).[24] In the present work the proton hfs are observable even if the proton is binded to a carbon atom which is not in the chelate ring.

A methanolic solution of omdcH and copper acetate is deep-green at low temperature, but in a short time, the solution changes in color from deep-green to reddish-brown. Only reddish-brown crystals of Cu(omdc)$_2$ were obtained and readily doped in Ni(omdc)$_2$. Cu(omdc)$_2$, synthesized in the presence of zinc acetate at low temperature, enables the deep-green Cu(omdc)$_2$ to be doped in Zn(omdc)$_2$. In a series of copper(II) complexes, the color is deep-green in the *cis* coordination and reddish-brown in the *trans* coordination. The ESR spectra of deep-green ^{63}Cu(II)/Zn(omdc)$_2$ shows the presence of two magnetically non-equivalent nitrogen hfs in the limited magnetic direction, and small nitrogen hf coupling constants. These results suggest that the coordination around the Cu(II) ion in Zn(omdc)$_2$ is of a *cis* configuration.[15] Cu(bdc)$_2$ and Cu(mmdc)$_2$ are also deep-green in the preparation at low temperature, but the deep-green Cu(II) doped Zn(II) complexes were not obtained due to the inability of achieving single crystals of the Zn(II) complexes at low temperature.

Tetrahedral Distortion. Table 2 shows the ESR parameters of ^{63}Cu(II) in Zn(II) complexes and in the Ni(II) complexes with *S*-benzyl groups. In all the complexes of Table 2, the coordination around the Cu(II) ion was found to be of a *cis* configuration from the same reasoning as described in the case of ^{63}Cu(II)/Zn(omdc)$_2$. The nitrogen hf coupling constants could not be determined accurately for the *cis* coordination since the magnetically non-equivalent nitrogen hfs were well resolved only in the limited magnetic direction along one of the Cu–N axes.

The ESR parameters are more rhombic in the *cis* complexes than in the *S*-methyl containing Ni(II) complexes.[15] The anisotropies of the ESR parameters are probably due to the tetrahedral distortion of the host complexes.

Calculation of d-Orbital Mixing. The electronic spectra of the Cu(II) complexes consist of very strong charge transfer bands, the single d-d transition band being detected in the region 500—650 nm. This band has been tentatively assigned to the $d_{zx}\rightarrow d_{z^2}$ or $d_{zx}\rightarrow d_{x^2-y^2}$ transition for *cis* complexes. The ESR param-

Table 2. The ESR parameters for Cu(II) complexes which do not contain azomethine protons

Host	Principal values	Direction cosines 1	2	3
$Ni(bpdc)_2$ (*cis*)	$g_x=2.032(1)$	0.92	0.34	−0.17
	$g_y=2.148(1)$	0.18	0.01	0.98
	$g_z=2.033(1)$	−0.34	0.94	0.05
	$A_x=21(4)$	0.79	0.58	−0.20
	$A_y=152(1)$	0.25	0.01	0.97
	$A_z=27(4)$	−0.56	0.82	0.15
	$A^N=9.3$—11.8			
$Ni(btdc)_2$ (*cis*)	$g_x=2.030(1)$	0.21	0.93	−0.30
	$g_y=2.141(1)$	0.01	0.31	0.95
	$g_z=2.032(1)$	0.98	−0.20	0.06
	$A_x=24(4)$	0.23	0.89	−0.39
	$A_y=143(1)$	0.01	0.41	0.91
	$A_z=25(4)$	0.97	−0.21	0.10
	$A^N=7.0$—9.1			
$Ni(bndc)_2$ (*cis*)	$g_x=2.029(1)$	−0.25	−0.01	0.97
	$g_y=2.140(1)$	0.96	0.13	0.25
	$g_z=2.032(1)$	−0.13	0.99	−0.03
	$A_x=23(4)$	−0.28	−0.19	0.94
	$A_y=159(1)$	0.95	0.10	0.31
	$A_z=31(4)$	−0.16	0.98	0.15
	$A^N=9.5$—11.7			
$Zn(tedc)_2$ (*cis*)	$g_x=2.031(1)$	0.91	−0.31	−0.29
		0.70	0.30	−0.65
	$g_y=2.153(1)$	0.25	−0.15	0.96
		−0.71	0.17	0.68
	$g_z=2.037(1)$	0.34	0.94	0.06
		0.09	−0.94	−0.34
	$A_x=19(4)$	0.92	−0.16	−0.36
		0.62	0.66	−0.41
	$A_y=140(1)$	0.35	−0.12	0.93
		−0.64	0.13	−0.75
	$A_z=26(4)$	0.19	0.98	0.06
		0.45	−0.74	−0.51
	$A^N=7.7$—9.8			
$Zn(pedc)_2$ (*cis*)	$g_x=2.032(1)$	0.74	0.38	0.55
		−0.72	−0.46	0.52
	$g_y=2.154(1)$	0.54	0.14	−0.83
		0.66	−0.19	0.73
	$g_z=2.037(1)$	−0.40	0.91	−0.10
		0.24	−0.87	−0.44
	$A_x=17(4)$	0.52	0.68	0.51
		−0.66	−0.45	0.60
	$A_y=138(1)$	0.63	0.10	−0.77
		0.73	−0.16	0.67
	$A_z=24(4)$	−0.58	0.72	−0.38
		0.21	−0.88	−0.44
	$A^N=7.8$—9.8			

eters could not be completely determined from only this band. The d-orbital coefficients of the ground-state were then determined from the observed ESR parameters.[25] The ground state function for *trans* coordination is given by,[15]

$$\Phi^\alpha = a|x^2-y^2>^\alpha + b|z^2>^\alpha + ic|xy>^\alpha - id|yz>^\beta + e|zx>^\beta, \quad (1)$$

and for *cis* coordination by,

$$\Phi^\alpha = a|zx>^\alpha + ib|yz>^\alpha + c|z^2>^\beta - d|x^2-y^2>^\beta - ie|xy>^\beta. \quad (2)$$

Table 3 shows the coefficients obtained from Eqs. 1 or 2. Changing the x and z directions produces a larger value of d than c. It is uncertain from only the ESR data whether the axis should be assigned as x or z.

The copper hf coupling constants for the *trans* coordination have the same sign which are in reasonable agreement with the ESR spectra of chloroform solutions (83—86 G). The situation around the Cu(II) ion in chloroform solution is not the same as in the Zn(II) complexes. The ESR spectra of chloroform solutions supports the finding that the copper hf coupling constants are the same sign in *cis* Ni(II) complexes (64—72 G). It is reasonable to assume that the copper hf coupling constants are also the same sign in the Zn(II) complexes.

Figure 3 shows the variations of copper hf coupling constants against the values of c/d. The d-orbital coefficients satisfy the observed g values in all regions of c/d values. The acceptable region which satisfies the copper hf coupling constants is in the narrow range of c/d values. McGregor and Hatfield[26] measured the ESR spectra of bis(2,2′-bipyridyl)thioureacopper(II) perchlorate and determined the d-orbital coefficients only from the g values. The copper hf coupling constants could not be obtained from the single crystal. The method of Swalen *et al.*[25] cannot be applied when the copper hf coupling constants are not obtained, if there is no strong evidence for a relationship between the d-orbital coefficients.

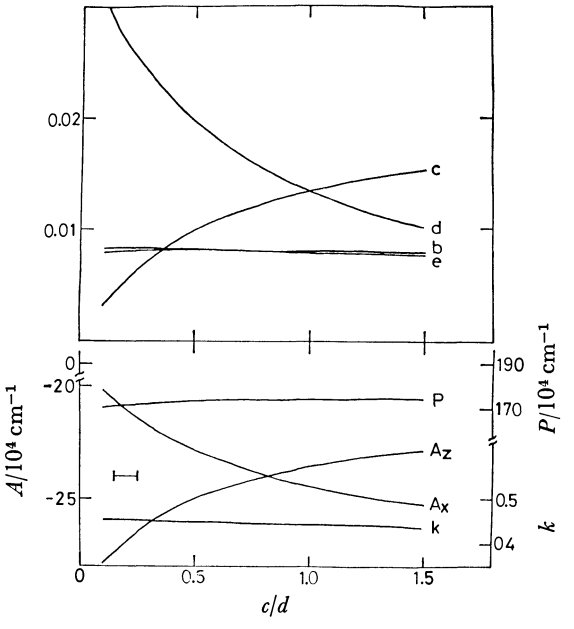

Fig. 3. The example of calculations for $^{63}Cu(II)/Ni(bpdc)_2$; the coefficients of the Kramers doublet (top) and the hf parameters(bottom) *vs.* c/d; the value of A_y is fixed to -152×10^{-4} cm^{-1}, and the value of a is almost constant at 0.99975 in all the c/d values; the acceptable regions are indicated.

Table 3. The best values for the d-orbital coefficients and calculated hyperfine coupling constants (10^{-4} cm^{-1})

Host		a	b	c	d	e	k	P	A_x	A_y	A_z
$Ni(omdc)_2$	(*trans*)	0.9991	−0.0379	0.0159	0.0055	0.0099	0.471	194	−26	−37	−175
$Ni(mmdc)_2$	(*trans*)	0.9990	−0.0391	0.0173	0.0061	0.0104	0.445	204	−22	−32	−176
$Zn(omdc)_2$	(*cis*)	0.9992	0.0095	0.0010	0.0362	0.0087	0.450	160	−17	−137	−26
$Ni(ocdc)_2$	(*cis*)	0.9996	0.0076	0.0026	0.0263	0.0071	0.482	182	−28	−167	−35
$Ni(bpdc)_2$	(*cis*)	0.9996	0.0079	0.0072	0.0241	0.0082	0.447	177	−21	−152	−27
$Ni(btdc)_2$	(*cis*)	0.9998	0.0077	0.0125	0.0132	0.0074	0.462	162	−24	−143	−25
$Ni(bndc)_2$	(*cis*)	0.9995	0.0079	0.0029	0.0295	0.0078	0.461	181	−23	−159	−31
$Zn(tedc)_2$	(*cis*)	0.9994	0.0093	0.0032	0.0324	0.0086	0.454	163	−19	−140	−26
$Ni(tedc)_2$[a]	(*cis*)	0.9997	0.0081	0.0097	0.0162	0.0076	0.505	163	−32	−155	−33
$Zn(pedc)_2$	(*cis*)	0.9995	0.0091	0.0045	0.0303	0.0086	0.439	164	−17	−138	−24
$Ni(pedc)_2$[a]	(*cis*)	0.9998	0.0081	0.0096	0.0160	0.0078	0.507	167	−33	−159	−34

a) From Ref. 15.

Table 4. The bonding parameters obtained from Eqs. 3 and 4 and P values (10^{-4} cm^{-1})

Host		$N\alpha_1^2$	$N\alpha_2^2$	$N\alpha_4^2$ or $N\alpha_3^2$	P
$Ni(omdc)_2$	(*trans*)	0.061	0.157	0.306	194
$Ni(mmdc)_2$	(*trans*)	0.059	0.153	0.310	204
$Zn(omdc)_2$	(*cis*)	0.028	0.078	0.672	150
$Ni(ocdc)_2$	(*cis*)	0.037	0.082	0.678	182
$Ni(bpdc)_2$	(*cis*)	0.037	0.098	0.680	177
$Ni(btdc)_2$	(*cis*)	0.028	0.082	0.684	162
$Ni(bndc)_2$	(*cis*)	0.037	0.086	0.687	181
$Zn(tedc)_2$	(*cis*)	0.030	0.082	0.681	163
$Zn(pedc)_2$	(*cis*)	0.031	0.078	0.671	164

In the *cis*-CuN_2S_2 planar symmetry, the d_{zx} orbital is in the ground state, and the coefficient b is a function of the spin orbital coupling and pure $d_{zx}\rightarrow d_{yz}$ energy separation.

In the case of a small tetrahedral distortion, a mixture of the d_{zx} and d_{yz} orbitals become the ground state, and the excited d_{xy}, $d_{x^2-y^2}$, and d_{z^2} orbitals are mixed in the same manner. A spin orbit interaction also occurs between the d_{yz} and other d orbitals, and the ESR parameters cannot be determined solely from one d-d transition. Assuming the $d_{zx}\rightarrow d_{yz}$ energy separation does not vary from complex to complex, the value of $(b/a)^2$ gives a measure of the degree of tetrahedral distortion since the value of $|b|$ increases with increasing tetrahedral distortion. The increase of $|b|$ values is observed in the case of Zn(II) complexes as may be seen from Table 3.

The copper hf coupling constants in Zn(II) complexes are smaller than in other complexes a result in agreement with that found by Yokoi and Addison.[14] The values of A_x and A_z, however, are negative since the distortion is not so large.

The molecular orbital of an unpaired electron in the *cis* coordination is given by,

$$|zx\rangle = N^{1/2}[d_{zx}-(\alpha_1/\sqrt{2})(s^1-s^2)-(\alpha_2/2) \times(-p_x^1-p_x^2-p_z^1+p_z^2)-(\alpha_3/\sqrt{2}) \times(-s^3+s^4)-(\alpha_4/2)(p_x^3+p_x^4-p_z^3+p_z^4)], \quad (3)$$

and in the *trans* coordination by,

$$|A_{1g}\rangle = N^{1/2}[d_{x^2-y^2}+(b/a)d_{z^2}-(\alpha_1/\sqrt{2})(s^1+s^2) -(\alpha_2/\sqrt{2})(-p_x^1+p_x^2)-(\alpha_3/\sqrt{2})(p_y^3-p_y^4)]. \quad (4)$$

The bonding parameters of $N\alpha_1^2$, $N\alpha_2^2$, and $N\alpha_4^2$ in Eq. 3, and of $N\alpha_1^2$, $N\alpha_2^2$, and $N\alpha_3^2$ in Eq. 4 were obtained as in the first report and are shown in Table 4. The normalization constants N have been assumed to be 0.7 in either case. The small A^N values and large $N\alpha_4^2$ values in the *cis* coordination are explainable as follows. In *cis* coordination, the Cu–N bond length is longer than in *trans* coordination because of steric repulsion by the large phenyl group. The Cu–S bond length on the other hand is shorter than in a *trans* coordination since there is no such repulsion. A similar situation occurs in the case of bis(thiosemicarbazide)nickel sulfate.[27]

The author is grateful to Dr. Kazunori Sakata of Kyushu Technical College for kindly allowing him to take ESR measurements.

References

1) L. L. Lohr and W. N. Lipscomb, *Inorg. Chem.*, **2**, 911 (1963).
2) J. Ferguson, *J. Chem. Phys.*, **40**, 3406 (1964).
3) C. A. Bates, *Proc. Phys. Soc., London*, **83**, 465 (1964).
4) C. A. Bates, W. S. Moore, K. J. Standley, and K. W. H. Stevens, *Proc. Phys. Soc., London*, **79**, 73 (1962).
5) M. Sharnoff, *J. Chem. Phys.*, **42**, 3383 (1965).
6) G. F. Kokoszka, C. W. Reimann, and H. C. Allen, Jr., *J. Phys. Chem.*, **71**, 121 (1967).
7) B. J. Dudley, B. J. Hathaway, and P. G. Hodgson, *J. Chem. Soc., Dalton Trans.*, **1972**, 882.
8) J. Ferguson, *J. Chem. Phys.*, **35**, 1612 (1961).
9) V. G. Krishnan, *J. Chem. Phys.*, **68**, 660 (1978).
10) H. Yokoi, *Bull. Chem. Soc. Jpn.*, **47**, 3037 (1974).
11) R. C. Rosenberg, C. A. Root, P. K. Bernstein, and H. B. Gray, *J. Am. Chem. Soc.*, **97**, 2029 (1975).
12) F. G. Herring, D. J. Patmore, and A. Storr, *J. Chem. Soc., Dalton Trans.*, **1975**, 711.
13) Y. Murakami, Y. Matsuda, and K. Sakata, *Inorg. Chem.*, **10**, 1734 (1971).
14) H. Yokoi and A. W. Addison, *Inorg. Chem.*, **16**, 1341 (1976).
15) T. Oniki, *Bull. Chem. Soc. Jpn.*, **51**, 2551 (1978).
16) M. A. Ali, S. E. Livingstone, and D. J. Phillips, *Inorg.*

Chim. Acta, **5**, 493 (1971).
17) M. A. Ali and M. T. H. Tarafdar, *J. Inorg. Nucl. Chem.*, **39**, 1785 (1977).
18) M. A. Ali, S. E. Livingstone, and D. J. Phillips, *Inorg. Chim. Acta*, **7**, 531 (1973).
19) M. A. Ali and S. G. Teoh, *J. Inorg. Nucl. Chem.*, **40**, 451 (1978).
20) M. Iwasaki, *J. Magn. Reson.*, **16**, 417 (1974).
21) A. H. Maki and B. R. McGarvey, *J. Chem. Phys.*, **29**, 35 (1958).
22) R. L. Lancione, H. C. Allen, and J. R. Buntaine, *J. Coord. Chem.*, **6**, 7 (1976).
23) M. Fujimoto and J. Janecka, *J. Chem. Phys.*, **55**, 1152 (1971).
24) A. Schweiger and Hs. Günthard, *Chem. Phys.*, **32**, 35 (1978).
25) J. D. Swalen, B. Johnson, and H. M. Gladney, *J. Chem. Phys.*, **52**, 4078 (1970).
26) K. T. McGregor and W. E. Hatfield, *J. Chem. Soc., Dalton Trans.*, **1974**, 2448.
27) a) R. Gronbaek, *Acta Crystallogr.*, **16**, 65 (1963); b) R. Gronbaek, *ibid.*, **22**, 2171 (1968).

Circular Dichroism Spectra of Some Transition Metal Complexes with (1*R*,2*R*)-1,2-Cyclopentanediamine

Masafumi GOTO,*Michihiro TAKESHITA, and Tomoya SAKAI

Faculty of Pharmaceutical Sciences, Nagoya City University, Mizuho-ku, Nagoya 467

(Received March 1, 1979)

Bischelates, three isomers of dicyanocobalt(III), *trans*-dichlorocobalt(III), and copper(II), and a monochelate, tetracyanoferrate(II), of the title diamine were prepared, and their CD spectra were reported. Major positive components were found for I_a bands, as was to be expected for the preferred λ conformation, but minor positive components were observed for the I_b band with the *trans*-dianionocobalt(III) complexes. The configurational and the vicinal effects, as calculated from the CD spectra of the *cis*-dicyanocobalt(III) complexes, are shown to be different from those of (1*R*,2*R*)-1,2-cyclohexanediamine. The CD spectra of the Fe(II) and Cu(II) complexes are consistent with the conformational effect of the title diamine.

The optical activity of transition metal complexes has been studied with a variety of ligands. Among them, 1,2-diamines are most widely employed, and the results have been recognized as well established. However, the results have been obtained mostly with en, pn, and chxn as 1,2-diamines.[1,2] The CD spectra of metal chelates with these diamines are almost identical with their corresponding structures, and the proposed empirical rules of the optical activity are based on these results. However, two exceptions are known. Phenyl-substituted diamines, stien[3] and phenen,[4] yield cobalt(III) complexes which have CD spectra different from those of the other diamines mentioned above. Another is the tris cobalt(III) complexes of cptn. An earlier study of the complexes of cptn has been reported by Jaeger and Blumendal.[5] Saito *et al.* have reported that the CD spectrum of Λ-[Co(*S*-cptn)$_3$]Cl$_3$ is anomalous, even though the structure has been confirmed by X-ray crystallography to be similar to that of other corresponding tris(diamine)-cobalt(III) complexes.[6] The CD spectra of Δ- and Λ-[Co(*R*-cptn)$_3$]$^{3+}$ have been reported by Toftlund and Pedersen.[7] The diamine, cptn, may be expected, because of its fused five-membered cyclopentane ring, to form a chelate with a rigid structure on coordination to a metal ion.

Tetragonal complexes, *trans*-dianionobis(diamine)-cobalt(III), exhibit CD spectra which are free from any configurational contribution. The sector rule predicts that the signs of CD components corresponding to the $^1A_{1g}\rightarrow{}^1E_g{}^a$ and $^1A_{1g}{}^a\rightarrow{}^1A_{2g}$ transitions (D_{4h}) are positive and negative respectively with 1,2-diamines which form chelate rings of the λ conformation upon coordination.[2] Anomalous CD spectra can be expected for the tetragonal complexes with resolved cptn if the vicinal effect of this diamine differs from those of other 1,2-diamines.

This paper will deal with the syntheses and CD spectra of *trans*-dichloro and three isomers of dicyanocobalt(III) complexes, the tetracyanoferrate(II) complex, and the biscopper(II) complex with *R*-cptn as the diamine.

Experimental

Materials. The cyclopentanone (Merck, Synthetic Grade) was used without further purification. The pyridine,[8] methanol,[9] and sulfolane[10] were purified according to the known methods. The other chemicals were used as purchased.

*Preparation of (1*R*,2*R*)-1,2-Cyclopentanediamine. 1,2-Cyclopentanedione*: This was prepared by a modification of the method for preparing 1,2-cyclohexanedione.[11] A 3-dm^3 round-bottomed flask containing 1.5 dm^3 of cyclopentanone and fitted with a stirrer and a dropping funnel was placed in a water bath. The contents were warmed to 30 °C, and then a solution containing 361 g (3.25 mol) of selenium dioxide, 420 cm^3 of dioxane, and 155 cm^3 of water was added dropwise into the cyclopentanone over a period of 24 h with stirring. Stirring was continued for further 18 h at 35 °C. The red selenium thus separated was filtered off on a Buchner funnel. The selenium was returned to the reaction flask and extracted with 500 cm^3 of boiling ethanol for 3 h. The solution obtained by filtration was combined with the above filtrate. The combined filtrate was distilled using a 60-cm Vigreau column at 2700 Pa, and the lower-boiling portion (35—90 °C) was removed. The remaining portion was distilled at 1300 Pa until a thick brown residue formed in the distilling flask, thus preventing further distillation. The higher-boiling fraction was redistilled at 2100 Pa, and a fraction which distilled at 86—88 °C was collected. Yield, 74 g (23% based on SeO_2).

The 1,2-cyclopentanedione dioxime and *trans*-1,2-cyclopentanediamine were prepared successively from 1,2-cyclopentanedione according to the method of Jaeger and Blumendal.[5] The optical resolution of the diamine was carried out according to the method of Toftlund and Pedersen[7] to isolate the (1*R*,2*R*)-isomer using (+)-tartaric acid as the resolving agent. The (1*S*,2*S*)-isomer was obtained by employing (−)-tartaric acid as the resolving agent after the recovery of the free base from the remainder of the (1*R*,2*R*)-isomer.

Preparation of Metal Complexes. trans-[*CoCl*$_2$(R-*cptn*)$_2$]-*Cl·0.5H$_2$O*: To 100 cm^3 of an aqueous solution of $CoCl_2\cdot 6H_2O$ (4.76 g, 0.02 mol), *R*-cptn (3.00 g, 0.03 mol) was added, after which, the mixture was aerated for 3 h. To the resultant brown solution, 30 cm^3 of concentrated hydrochloric acid was added. The mixture was then concentrated on a steam bath to near dryness. The separated crystals were collected on a filter and washed thoroughly with acetone until the filtrate showed no blue color. The crystals were then added to 40 cm^3 of methanol. The mixture was refluxed for 2 h and filtered. The filtrate was allowed to stand in a refrigerator overnight; the green crystals thus separated were collected on a filter and washed thoroughly with acetone. Yield, 1.7 g (23%).

Perchlorates: To the filtrate, a large excess of lithium perchlorate was added. The green crystals thus separated were

Table 1. Analytical data of complexes prepared

Complex	Found, %			Calcd, %		
	C	H	N	C	H	N
trans-$[CoCl_2(R\text{-cptn})_2]ClO_4$	28.02	5.36	13.44	27.96	5.63	13.04
trans-$[CoCl_2(R\text{-cptn})_2]Cl\cdot 0.5H_2O$	32.17	6.68	15.19	31.31	6.83	14.60
trans-$[Co(CN)_2(S\text{-cptn})_2]ClO_4\cdot H_2O$	33.61	6.11	19.60	33.93	6.12	19.30
cis-*Λ*-$[Co(CN)_2(S\text{-cptn})_2]ClO_4\cdot 0.5NaClO_4$	30.62	5.03	17.66	30.47	5.12	17.77
cis-*Λ*-$[Co(CN)_2(S\text{-cptn})_2]ClO_4\cdot 0.5H_2O$	34.31	5.48	19.89	34.33	6.00	20.02
$Na_2[Fe(CN)_4(R\text{-cptn})]0.5NaClO_4\cdot 0.5H_2O$	28.87	3.97	21.86	28.65	3.46	22.27
$[Cu(S\text{-cptn})_2]SO_4\cdot 0.5H_2O$	32.79	6.54	15.21	32.55	6.82	15.19

collected on a filter and washed with ethanol and ether. The analytical data are listed in Table 1, along with those for other complexes.

Preparation and Isolation of the Isomers of Dicyanobis(S-cptn)-cobalt(III) Perchlorates: Potassium cyanide (460 mg) was dissolved in 80 cm³ of dimethyl sulfoxide (DMSO) at 60 °C. Into this solution was added 940 mg of *trans*-$[CoCl_2(S\text{-cptn})_2]Cl\cdot 0.5H_2O$ in portions with stirring. The color of the solution turned from green to orange. The solution was allowed to stand at 60 °C for 30 min, cooled to room temperature, and then poured into a column (10 cm × 3 cm) packed with an SP-Sephadex C-25 ion exchanger. The absorbed resin was washed with water to remove the DMSO and mounted on the top of another SP-Sephadex C-25 exchanger (120 cm × 3 cm). When the absorbed band was eluted with a 0.05 mol dm^{-3} aqueous sodium perchlorate at a rate of 500 cm³ d^{-1}, one orange and then two light yellow bands were separated. The first, orange elute was evaporated to dryness at 40 °C with a rotatory evaporator under reduced pressure. Twenty cm³ of acetone was added to remove the sodium perchlorate, leaving an orange residue, which was subsequently dissolved in a minimum amount of hot water and then filtered. The filtrate was allowed to stand in a refrigerator overnight to obtain orange plates. Yield, 100 mg (9%).

The second and the third, light yellow elutes were evaporated at 40 °C with rotatory evaporators to dryness. Ethanol was added to extract light yellow precipitates, and the ethanol solutions were evaporated again to dryness. The residues were dissolved in minimum amounts of hot water, and the solutions were cooled in refrigerators. Separated crystals were collected on filters. Yields, 23 mg and 57 mg for the second and the third fractions respectively.

$Na_2[Fe(CN)_4$(R-cptn)$]0.5NaClO_4\cdot 0.5H_2O$: In a 200-cm³ three-necked round-bottomed flask equipped with a mechanical stirrer and a dropping funnel, iron(II) perchlorate hexahydrate (6.55 g, 18.2 mmol) was placed under nitrogen, and then a 40-cm³ portion of methanol flushed with nitrogen was added through a serum cap with a syringe. The flask was immersed in an ice–water bath. With stirring, a solution of *R*-cptn (3.63 g, 36 mmol) in 25 cm³ of methanol was then added in small portions. White precipitates were formed. To the mixture, a solution of sodium cyanide (3.56 g, 72 mmol) in 8 cm³ of water was added from the dropping funnel with vigorous stirring. The mixture turned into a dark brown solution and was concentrated with a rotatory evaporator, yielding a viscous liquid. Ethanol (200 cm³) was added, and the mixture was allowed to stand in a refrigerator overnight. The yellow precipitates thus separated were collected on a filter and washed with ethanol and then with ether.

The crude product was dissolved in 12 cm³ of water, while the undissolved materials were removed by centrifugation. A methanol solution of sodium perchlorate (16 g/100 cm³) was added to the supernatant liquid, and then 200 cm³ of ethanol. The mixture was allowed to stand in a refrigerator overnight. Separated yellow crystals were collected on a filter and were washed with ethanol and ether subsequently. Yield, 1.6 g (23%).

$[Cu(S\text{-cptn})_2]SO_4\cdot 0.5H_2O$: To a solution of copper(II) sulfate pentahydrate (500 mg) in 30 cm³ of water, *S*-cptn (0.4 g) was added. The solution turned blue. The solution was warmed, and ethanol (40 cm³) was added. The hot mixture was filtered, and the filtrate was allowed to stand in a refrigerator. Separated blue needles were collected on a filter and washed with ethanol. Yield, 250 mg.

Physical Measurements. The electronic spectra were recorded with a Shimadzu UV-200 spectrophotometer. The CD spectra were measured with a JASCO J-40 recording polarimeter using aqueous solutions, unless otherwise stated. The infrared spectra were measured with a JASCO IRA-2 spectrophotometer using KBr disks. The ^{1}H-NMR spectra were measured with a JEOL JNM-MH-100 spectrometer using D_2O solutions and with sodium 2,2-dimethyl-2-silapentane-5-sulfonate (DSS) as the internal standard.

Results and Discussion

The synthesis of *R*-cptn was carried out with cyclopentanone as the starting material. Generally, the yields of 1,2-diketones from ketones with selenium dioxide are affected by the structures of the ketones, and the yield of cyclopentanedione has been reported to be low.[12] The use of cyclopentanone as a solvent improved the yield to 23% based on the SeO_2 but the yield is still low compared to the yield of 60% for 1,2-cyclohexanedione from cyclohexanone. The successive reactions and optical resolution were carried out according to the known methods.[5,7]

The origins of the optical activities of metal chelates have been classified as: (i) configurational, (ii) conformational, and (iii) vicinal effects. The latter two effects correlate with the absolute configuration of a coordinated diamine. The absolute configuration of (−)-cptn was determined by Saito *et al.* as (1*R*,2*R*)-.[6] The absorption and CD spectra of solutions of cobalt(III) complexes of *R*-pn, *R*-bn, and *R*-chxn are similar to each other for the corresponding structures because of their preferred *λ* conformation, in which alkyl group (s) adopt an equatorial position in a five-membered chelate ring.[6] The diamines, *R*-cptn and *R*-chxn, have the same absolute configuration and are expected to coordinate to metal ions exclusively in a *λ* conformation by virtue of their fused ring structures. Therefore,

the electronic and CD spectra of complexes of *R*-cptn are compared with those of *R*-chxn in this report.

trans-*Dichlorocobalt(III) Complex.* Aeration of a mixture of cobalt(II) chloride and *R*-cptn, followed by the addition of concentrated hydrochloric acid, afforded *trans*-dichlorobis((1*R*,2*R*)-1,2-cyclopentanediamine)cobalt(III) chloride. The electronic and CD spectra of this chelate in methanol are shown in Fig. 1, along with the CD spectrum of *trans*-$[CoCl_2(R\text{-chxn})_2]^+$; the latter has been reported by Treptow.[13] The numerical data are listed in Table 2 and compared with those of other complexes. The absorption maximum of the I_a band of the *R*-cptn complex appears at the same energy as the corresponding maximum of the *R*-chxn complex. However, the absorption maximum of the I_b band moved to an energy lower by 1600 cm^{-1} for the *R*-cptn complex. In the CD spectra, the I_a components are almost the same for both complexes. However, the CD spectra for the I_b components are different. A positive component is observed for the *R*-cptn complex. The CD spectra of *trans*-$[CoCl_2(R\text{-cptn})_2]Cl$ were measured in three solvents—pyridine, methanol, and sulfolane. The magnitudes of the major positive CD bands were little affected, but the magnitudes of the minor CD components were changed as follows in $\Delta\varepsilon$:
pyridine, +0.67; methanol, +0.24; sulfolane, +0.19.

*Dicyanobis(*R*-cptn)cobalt(III) Isomers.* Three isomers of $[Co(CN)_2(S\text{-cptn})_2]^+$ were isolated from a reaction mixture of the *trans*-dichloro complex with KCN, followed by column chromatography with SP-Sephadex C-25 resin. The fraction eluted first with a 0.05 mol dm^{-3} $NaClO_4$ was orange in color and exhibited a large splitting in the first absorption band. This was assigned to the *trans*-isomer. The second and third fractions were yellow in color, had similar

Table 2. Comparison of electronic and CD spectra of *R*-cptn and *R*-chxn complexes

Complex	*R*-cptn				*R*-chxn			
	ν_{max} [a]	(ε_{max})	ν^{CD}_{max} [a]	($\Delta\varepsilon_{max}$)	ν_{max} [a]	(ε_{max})	ν^{CD}_{max} [a]	($\Delta\varepsilon_{max}$)
trans-$[CoCl_2L_2]^+$	16.2	(42.5)	16.2	(+1.32)	16.3	(39.2) [b]	16.4	(+0.93) [b]
	20.3	(27.0)	20.3	(+0.29)	21.9	(31.6)	21.4	(−0.10)
	24.9	(77.6)	24.5	(−0.16)	25.6	(53.7)	23.7	(−0.05)
							27.3	(+0.21)
	31.0	(2040)	29.9	(+1.78)	32.4	(1530)	30.5	(+1.12)
			32.7	(−0.12)			35.0	(−3.90)
	39.2	(26600)	37.7	(+9.94)	39.8	(29000)	40.0	(+12)
			43	(+2.5)				
trans-$[Co(CN)_2L_2]^+$	20.6	(sh)	20.0	(+0.20)	22	(sh) [c]	20.9	(−0.28) [c]
	23.7	(75.4)	23.7	(+1.97)	24.4	(67.6)	24.5	(+2.28)
			29.0	(−0.02)	32.0	(69.2)	30.6	(−0.36)
	37.0	(sh, 3760)	37.8	(+9.80)				
	44.0	(19000)	42.7	(+15.2)	46.1	(13800)	44.0	(+16.5)
	47.2	(22500)	47.8	(−7.3)			50.0	(−3.6)
cis-*Δ*-$[Co(CN)_2L_2]^+$	23.2	(86)	25.4	(+1.88)	24.8	(93.3) [c]	25.5	(+2.24) [c]
	24.8	(91.6)						
	31.0	(sh, 100)	31.9	(−0.15)	32.3	(100)	32.4	(−0.20)
	38.0	(sh, 6000)	37.7	(+9.30)			39.8	(+2.10)
			42.6	(−34.9)			44.4	(−24.1)
	45.9	(21200)	48.0	(+45.5)			49.5	(+41.2)
cis-*Λ*-$[Co(CN)_2L_2]^+$	23.2	(83)	23.1	(+1.72)	24.9	(100) [c]	21.6	(−0.38) [c]
	25.0	(88)	27.8	(−0.23)			24.3	(+1.06)
							28.6	(−0.14)
	31.0	(sh, 120)	32.0	(+0.22)	32.3	(98)	32.6	(+0.06)
	38.0	(sh, 4800)	42.6	(+60.8)			44.2	(+48.6)
	46.2	(19100)	48.5	(−45.9)			49.5	(−37.1)
$[Fe(CN)_4L]^{2-}$	25.3	(438)	25.2	(+0.69)	25.5	(407) [d]	22.2	(−0.18) [d]
							26.0	(+0.51)
	31.8	(410)	30.1	(−0.36)	32.0	(457)	30.3	(−0.16)
	36.0	(sh, 1200)	37.0	(sh, +1.00)			37.0	(+0.6)
	42.9	(10500)	41.9	(+2.55)	44.8	(9770)	42.0	(+2.8)
	45.0	(10000)						
$[CuL_2]^{2+}$	17.2	(70)	17.8	(+0.38)	18.5	(83)	16.0	(+0.055)
							19.6	(+0.37)
	35.6	(1800)	35.6	(+3.25)				
	42.9	(6200)	42.6	(+2.70)	41.8	(8300)	41.0	(+3.8)

a) In 10^3 cm^{-1}. b) From Ref. 13. c) From Ref. 14. d) From Ref. 16.

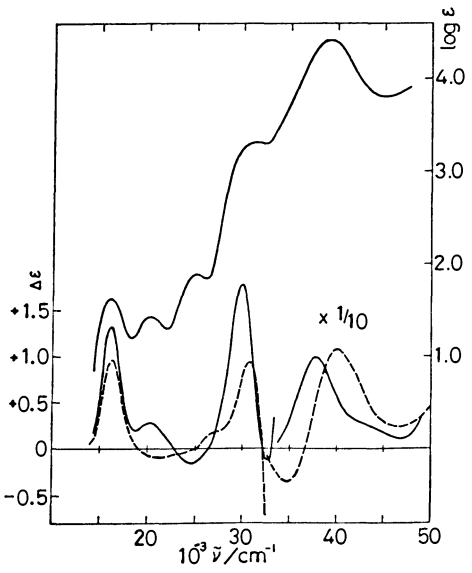

Fig. 1. Electronic and CD spectra of *trans*-$[CoCl_2(diamine)_2]ClO_4$ in methanol. Diamine: *R*-cptn, ——; *R*-chxn, — — —.

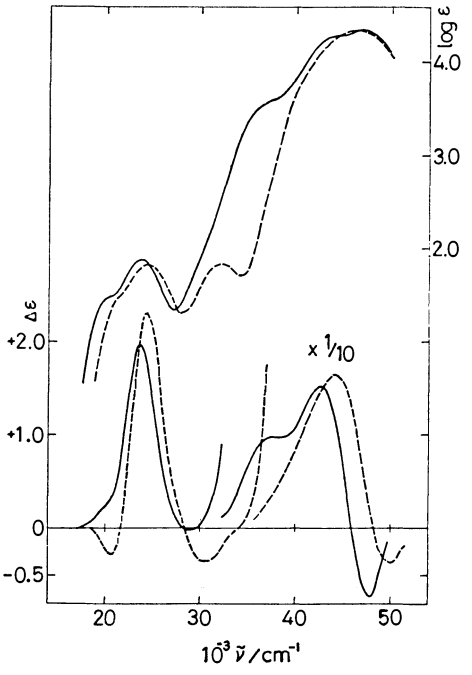

Fig. 2. Electronic and CD spectra of *trans*-$[Co(CN)_2(diamine)_2]^+$ in water. Diamine: *R*-cptn, ——; *R*-chxn, — — —. Data of *R*-chxn are reproduced from Ref. 16.

absorption spectra, and were assigned to *cis*-isomers.

The second fraction was assigned to *cis*-*Λ*-$[Co(CN)_2(S\text{-cptn})_2]^+$, and the third, to *cis*-*Λ*-$[Co(CN)_2(S\text{-cptn})_2]^+$, by comparing the CD spectra in the region between 40000 and 50000 cm^{-1} with those of the corresponding *R*-chxn complexes.[14] The yield of the *cis*-*Δ*-isomer was about one half of that of the *cis*-*Λ*-isomer. The C≡N stretching appeared at 2122 and 2128 for the *trans*-, at 2127 for the *cis*-*Δ*-, and at 2118 cm^{-1} for the *cis*-*Λ*-isomer. The two *cis*-isomers have very similar infrared spectra except for the N–H stretching region. The *cis*-*Δ*-isomer has three absorptions, at 3400, 3200, and 3080 cm^{-1}, while the *cis*-*Λ*-isomer has six absorptions in this region.

The following discussion will be argued, for the sake of brevity, using three complexes, *trans*-$[Co(CN)_2(R\text{-cptn})_2]^+$, *cis*-*Λ*-$[Co(CN)_2(R\text{-cptn})_2]^+$, and *cis*-*Δ*-$[Co(CN)_2(S\text{-cptn})_2]^+$, which should have CD spectra with signs the reverse of those of the enantiomers, *trans*-$[Co(CN)_2(S\text{-cptn})_2]^+$, *cis*-*Δ*-$[Co(CN)_2(S\text{-cptn})_2]^+$, and *cis*-*Λ*-$[Co(CN)_2(S\text{-cptn})_2]^+$ respectively.

The electronic and CD spectra of *trans*-$[Co(CN)_2(R\text{-cptn})_2]^+$ are shown in Fig. 2. The data for the isomers of the *R*-chxn complexes were provided by Kashiwabara.[14] The first absorption band appears at an energy lower by 700 cm^{-1} for the *R*-cptn complex than that for the *R*-chxn complex. The second absorption band of the *R*-chxn complex appears clearly, but that of the *R*-cptn complex is obscured by intense charge-transfer absorptions. In the CD spectra, the first absorption band contains two CD bands of opposite signs for the *R*-chxn complex, while the CD spectrum of the *R*-cptn complex shows two positive components. Another feature of the CD spectrum of the *R*-cptn complex is a positive CD component which appears at 37800 cm^{-1}. The positive CD component, which has a maximum at 42700 cm^{-1} for the *R*-chxn complex, is not symmetric, but has tails on the longer-wavelength side.

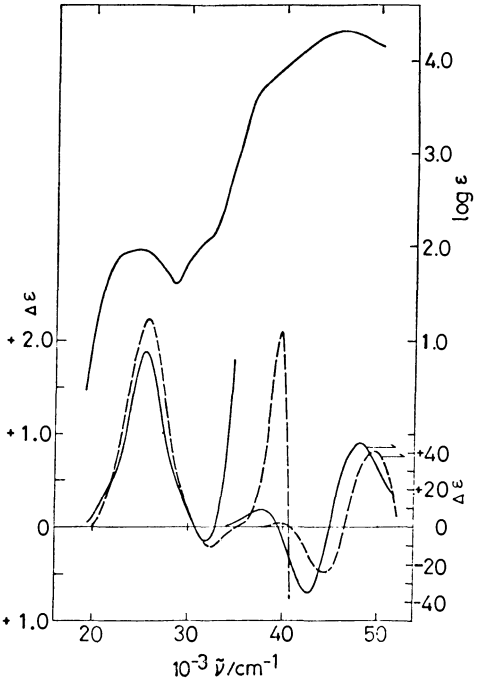

Fig. 3. Electronic and CD spectra of *cis*-*Λ*-$[Co(CN)_2(diamine)_2]^+$ in water. Diamine: *R*-cptn, ——; *R*-chxn, — — —. Data of *R*-chxn are reproduced from Ref. 16.

The electronic and CD spectra of the *cis*-*Λ*- and *cis*-*Δ*-$[Co(CN)_2(R\text{-cptn})_2]^+$ isomers are shown in Figs. 3 and 4 respectively, along with those of the corresponding isomers of the *R*-chxn complexes. For the *R*-cptn complexes, the first absorption bands are not symmetric, and the second absorption bands are obscured

by a partial superposition of intense charge-transfer bands. Their absolute configurations are determined from the CD components between 40000 and 50000 cm^{-1}, which closely resemble those of the *R*-chxn complexes. The absolute configurations of the chxn complexes have been determined[14] from the signs of these components on the basis of the empirical rule presented by Ogino *et al.*[15] In the first absorption bands, both *R*-cptn and *R*-chxn complexes show a positive CD band at 25500 cm^{-1} for *cis*-*Λ*-isomers, but the *R*-chxn complex exhibits a negative CD component at 21600 cm^{-1} in addition to the two components, which are found as a positive component and a negative component in the CD spectra of both complexes for *cis*-*Λ*-isomers.

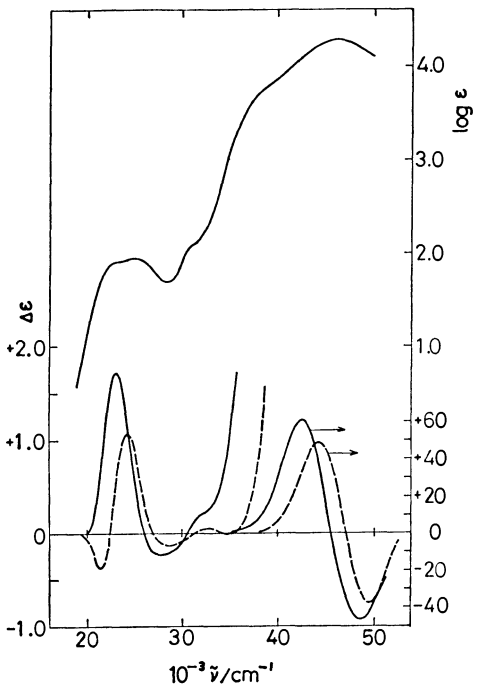

Fig. 4. Electronic and CD spectra of *cis*-*Λ*-$[Co(CN)_2(diamine)_2]^+$ in water. Diamine: *R*-cptn, ——; *R*-chxn, — — —. Data of *R*-chxn are reproduced from Ref. 16.

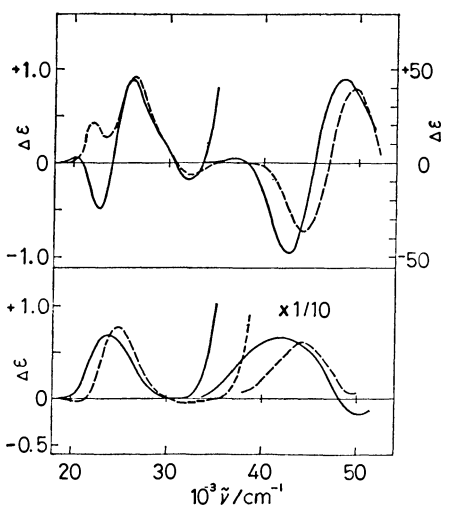

Fig. 5. Calculated configurational (upper, *Λ*) and conformational (bottom, *R*) curves of *cis*-$[Co(CN)_2(diamine)_2]^+$. Diamine: *R*-cptn, ——; *R*-chxn, — — —. Calcd by $\Delta\varepsilon(\Lambda)=1/2[\Delta\varepsilon(\Lambda_{2R})-\Delta\varepsilon(\Delta_{2R})]$ and $\Delta\varepsilon(R)=1/4[\Delta\varepsilon(\Lambda_{2R})+\Delta\varepsilon(\Delta_{2R})]$. Data of *R*-chxn are reproduced from Ref. 16.

The configurational and vicinal curves of *cis*-$[Co(CN)_2(R\text{-cptn})_2]^+$ are shown in Fig. 5, together with those of *cis*-$[Co(CN)_2(R\text{-chxn})_2]^+$.[14] They were derived from the observed curves by the use of the following relations;

$$\Delta\varepsilon(R) = 1/4\{\Delta\varepsilon(\Lambda_{2R}) + \Delta\varepsilon(\Delta_{2R})\}$$
$$\Delta\varepsilon(\Lambda) = 1/2\{\Delta\varepsilon(\Lambda_{2R}) - \Delta\varepsilon(\Delta_{2R})\}$$

where $\Delta\varepsilon(\Lambda_{2R})$ and $\Delta\varepsilon(\Delta_{2R})$ are the observed CD for the *Λ* and *Δ* diastereoisomers of the *cis*-$[Co(CN)_2(diamine)_2]^+$ complexes respectively, and where $\Delta\varepsilon(\Lambda)$ and $\Delta\varepsilon(R)$ are the configurational and the vicinal CD for the complexes.

*Tetracyano(*R*-cptn)ferrate(II) Complex.* Diamagnetic sodium tetracyano(*R*-cptn)ferrate(II) was prepared according to a method similar to that used earlier for preparing this class of compounds.[16] The complex showed absorptions which were almost the same as those of $[Fe(CN)_4(R\text{-chxn})]^{2-}$, as is shown in Table 2. The infrared spectrum showed intense C≡N stretching at 2030 cm^{-1}. The ^{1}H-NMR spectrum showed four types of protons, which resonate at 1.22(2), 1.70(2), 1.86(2), and 2.86(2) ppm, the relative integrated signal areas are indicated in parentheses. The protons corresponding to the signal at 2.86 ppm are the axial protons of methine. The corresponding protons in $[Fe(CN)_4(R\text{-chxn})]^{2-}$ appear at 2.05 ppm.[16] This down-field shift of the axial protons of cyclopentane ring occurs partly because of a decrease in anisotropy from the C–C bond due to the flatness of the cyclopentane ring.

The CD spectra of $[Fe(CN)_4(R\text{-cptn})]^{2-}$ and $[Fe(CN)_4(R\text{-chxn})]^{2-}$ are shown in Fig. 6. The CD spectra differ in the first absorption region. The signs of CD components for the same electronic transitions have been shown not to change in the d^6 diamagnetic isoelectronic and isostructural complexes on the basis of a comparison of the CD spectrum of $[Fe(CN)_4(R\text{-chxn})]^{2-}$ with that of $[Co(CN)_4(R\text{-chxn})]^-$.[16] The CD components of $[Fe(CN)_4(R\text{-pn})]^{2-}$ and $[Fe(CN)_4(R\text{-chxn})]^{2-}$ appear as two components with opposite signs in the first absorption region and are attributed to the conformational effects of *R*-pn and *R*-chxn.[16] The CD spectrum of $[Fe(CN)_4(R\text{-cptn})]^{2-}$ shows a

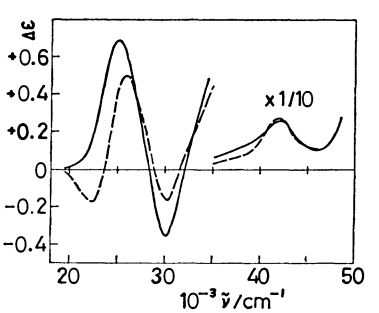

Fig. 6. CD spectra of $[Fe(CN)_4(diamine)]^{2-}$. Diamine: *R*-cptn, ——; *R*-chxn, — — —.

positive component in this region. We attempted to isolate the corresponding tetracyanocobaltate(III) complex, but did not succeed in doing so; however, the difference in the CD spectra between the *R*-cptn and the *R*-chxn complexes is attributable to the difference in the conformational effects of the diamines.

CD Spectra of d^6 Metal Complexes with R-*cptn.* The CD spectra of *trans*-$[CoX_2(R\text{-diamine})_2]^+$ have two components in the region of the first absorption band. The component corresponding to $^1A_{1g}\rightarrow{}^1E_{1g}{}^a$ has a positive sign with a large magnitude and changes in energy depending on the order in the spectrochemical series of the aniono group. The CD components of *trans*-$[CoX_2(R\text{-cptn})_2]^+$ have positive signs as expected for 1,2-diamines of *R*-configurations,[2] and the magnitudes are almost the same as those of the *R*-chxn complexes, as are shown in Figs. 1 and 2. A close relationship holds between the preferred conformation of the coordinated diamines and the sign of this CD component. The other component, corresponding to $^1A_{1g}\rightarrow{}^1A_{2g}$, remains approximately the same in energy as the parent $^1A_{1g}\rightarrow{}^1T_{1g}$ band of $CoN_6{}^{3+}$ ions and has an indefinite sign of a smaller magnitude which depends on the structure of the *R*-diamine and on the solvent. In methanol, the signs of these components of *trans*-dichloro complexes of *R*-pn,[17] *R*-bn,[18] and *R*-chxn[13,18] are negative, while those of phenen[4] and stien[3] are positive, but the signs of these components as well as their magnitudes change as the solvent is varied.[8,18] A good relationship has been found between the donor-power order of the solvent and the change in the CD spectrum for this region.[8] These components of *trans*-$[CoX_2(R\text{-cptn})_2]^+$ were small and positive. The CD component of *trans*-$[CoCl_2(R\text{-cptn})_2]^+$ increased in magnitude in pyridine and decreased in sulfolane, but did not change in sign in the latter solvent. The sign and the magnitude of this CD band suggest that the effect of *R*-cptn on the $^1A_{2g}$ band lies between those of phenyl-substituted diamines and of other alkyl-substituted diamines.

The vicinal curve of the *R*-cptn complexes calculated from *cis*-$[Co(CN)_2(R\text{-cptn})_2]^+$ isomers has positive components and lacks the negative component which appears in the vicinal curve for the *R*-chxn complexes, as is shown in Fig. 5. The vicinal curves of both complexes have features similar to those in the CD spectra of the corresponding *trans*-dicyano complexes in the first absorption region: the *R*-cptn complex exhibits only positive component, while the *R*-chxn complex shows a minor negative and a major positive component.

The CD spectra of $[Fe(CN)_4(R\text{-cptn})]^{2-}$ and $[Fe(CN)_4(R\text{-chxn})]^{2-}$ differ in the first absorption region, as is shown in Fig. 6. The latter CD spectrum shows a minor negative and a major positive component at 22200 and 26000 cm^{-1} respectively, those components are recognized as arising from the $^1A_{2g}$ and $^1E_{1g}{}^a$ transitions of D_{4h} symmetry, *i.e.*, the conformational effect of *R*-chxn.[16] An analogous interpretation is applicable to the positive CD component of $[Fe(CN)_4(R\text{-cptn})]^{2-}$, which lacks a negative component in the first absorption region: the conformational effect intrinsic to the *R*-cptn gives positive CD components in the first absorption band.

The tris complex, Λ-$[Co(S\text{-cptn})_3]Cl_3\cdot 4H_2O$, has shown a significantly different CD spectrum in an aqueous solution from those of Λ-$[Co(en)_3]^{3+}$, Λ-$[Co(S\text{-pn})_3]^{3+}$, and Λ-$[Co(S\text{-chxn})_3]^{3+}$.[6,7] The CD spectrum has a large negative component at 21100 cm^{-1} which is assigned to the $^1A_{1g}\rightarrow{}^1A_{2g}$ component on measurement with a single crystal.[7,19] Therefore, the signs of the D_3 components are the same among these tris complexes. The ratio of the rotatory strength of A_2 to that of the E bands exceeds unity for the cptn complex, but the ratios for the other complexes have values below 0.3.[6]

The calculated configurational curve for the Λ-configuration of *cis*-$[Co(CN)_2(R\text{-cptn})_2]^+$ is composed of two components with opposite signs. The corresponding curve of *cis*-$[Co(CN)_2(R\text{-chxn})_2]^+$ and the CD spectrum of $(+)_D$-$[Co(CN)_2(en)_2]^+$, the absolute configuration of which has been determined to be Λ by Matsumoto *et al.*,[20] are composed of components with the same sign, although the intensity of the component at 26200 cm^{-1} is stronger in the *R*-chxn complex than in the en complex.[14,21] McCaffery *et al.* have assigned the low- and high-energy portions under effective C_2 symmetry to a composite of E_g and A_2 transitions and to a E_g transition under D_3 symmetry respectively, and have stated that two positive CD components appear in this region for $(+)_D$-*cis*-$[Co(CN)_2(en)_2]^+$, since the rotational strength of E_g is greater than that of A_2.[21] The reversal of sign for the CD component at 22600 cm^{-1} for the Λ-configurational curve of the *R*-cptn complexes indicates that the ratio of the rotational strength of A_2 to that of E exceeds unity. This reversed ratio agrees with the ratio for the solution spectrum of Λ-$[Co(S\text{-cptn})_3]^{3+}$. The exceptional CD spectrum of the tris complex arises from the configurational effect intrinsic to cptn as well as from the conformational effect. The solution spectra of Λ- and Δ-$[Co(R\text{-cptn})_3]^{3+}$ also indicate

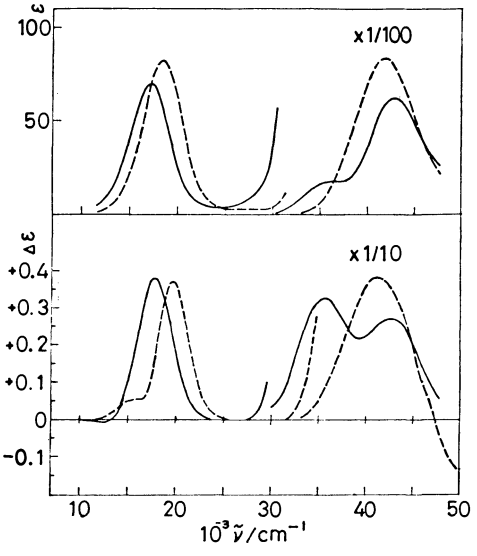

Fig. 7. Electronic and CD spectra of $[Cu(diamine)_2]^{2+}$ in water. Diamine: *R*-cptn, ——; *R*-chxn, — — —.

that the configurational effect for the *Λ*-configuration causes a marked enhancement of the negative CD component[7] and is almost opposite in sign to the configurational effect calculated from the pairs of the tris cobalt(III) complexes of en, *R*-pn, and *R*-chxn.[2]

*Bis(*R*-cptn)copper(II).* The CD and electronic spectra of $[Cu(R\text{-cptn})_2]SO_4\cdot 0.5H_2O$ are shown in Fig. 7, along with those of $[Cu(R\text{-chxn})_2]SO_4\cdot 3.5H_2O$. The d-d transitions of a Cu(II) complex of tetragonal symmetry may be expected to appear as three absorptions in the visible region. These are $^2B_{1g}\rightarrow{}^2A_{1g}$ ($d_{z^2}\rightarrow d_{x^2-y^2}$), $\rightarrow{}^2B_{2g}$ ($d_{xy}\rightarrow d_{x^2-y^2}$), and $\rightarrow{}^2E_g$ ($d_{xz},d_{yz}\rightarrow d_{x^2-y^2}$), where single-electron excitations are shown in parentheses. Hathaway assigned these to: (i) 12200—16800, (ii) 16200—18000, and (iii) 17900—20300 cm^{-1} absorptions respectively.[22] If the sign of the CD component corresponding to each single-electron excitation does not change with an alteration in the electronic configuration from d^6 to d^9, two positive CD components may be expected for $[Cu(R\text{-cptn})_2]^{2+}$, while one negative and one positive components may be expected for $[Cu(R\text{-chxn})_2]^{2+}$ in the region between 16200 and 20300 cm^{-1}. The CD spectrum of $[Cu(R\text{-pn})_2]^{2+}$ has been reported by Gillard and resembles that of $[Cu(R\text{-chxn})_2]^{2+}$.[23] Both have shoulders at 16000 cm^{-1} with intensities of +0.05 in $\Delta\varepsilon$. These CD spectra have been discussed by Kida and Nishida.[24] They resolved the absorption spectra into three absorptions by means of Gaussian curves. Three CD components corresponding to the resolved absorptions are estimated to have a small positive, a small negative, and a large positive signs at 15600, 17500, and 19800 cm^{-1} respectively. The single-electron transfer for these three components are assigned to $d_{z^2}\rightarrow$, $d_{xy}\rightarrow$, and d_{xz}, $d_{yz}\rightarrow d_{x^2-y^2}$ respectively. The sign of each component does not change in Cu(II) complexes from that of the *trans*-dichlorocobalt(III) complexes of these diamines.

The CD spectrum of $[Cu(R\text{-cptn})_2]^{2+}$ in water showed a single positive CD component with a maximum at 17800 cm^{-1}. It shifted to an energy lower by 1800 cm^{-1} from the positive CD component of $[Cu(R\text{-chxn})_2]^{2+}$. In the region between 16000 and 20000 cm^{-1}, two transitions may be expected for $[Cu(R\text{-cptn})_2]^{2+}$, and the observed CD spectrum seems to arise from two positive components spaced with a small energy difference. A very small negative component is found at *ca.* 12500 cm^{-1} and is assigned to the transition of $d_{z^2}\rightarrow d_{x^2-y^2}$.

Circular Dichroism in Charge-transfer Region. The CD components of *cis*-isomers of $[Co(CN)_2(R\text{-cptn})_2]^+$ resembled those of the corresponding isomers of $[Co(CN)_2(R\text{-chxn})_2]^+$ with a decrease in the wave numbers by 1600 cm^{-1} and so were used to identify the absolute configurations. The empirical rule for assigning absolute configurations from these components holds for the cptn complexes. A further characteristic of the *R*-cptn complexes is a moderately strong positive CD component which appears at 37800 and 35600 cm^{-1} for the *trans*-dicyanocobalt(III) and copper(II) complexes respectively. This positive component seems also to be present in the vicinal curve shown in Fig. 5. The origins of this enhancement are, however, ambiguous for the present.

The authors wish to express their thanks to Dr. Kazuo Kashiwabara of Nagoya University for kindly supplying the CD data on the isomers of dicyanobis-(*R*-chxn)cobalt(III) perchlorates.

References

1) Throughout this paper, the following abbreviations are used for diamines: en, ethylenediamine; *R*-pn, (*R*)-1,2-propanediamine; *R*-bn, (2*R*,3*R*)-2,3-butanediamine; *R*-cptn, (1*R*,2*R*)-1,2-cyclopentanediamine; *R*-chxn, (1*R*,2*R*)-1,2-cyclohexanediamine: *R*-phenen, (*R*)-1-phenyl-1,2-ethanediamine; *R*-stien, (1*R*,2*R*)-1,2-diphenyl-1,2-ethanediamine.

2) S. F. Mason, "Fundamental Aspects and Recent Developments in Optical Rotatory Dispersion and Circular Dichroism," ed by F. Ciardelli and P. S. Salvadori, Heyden, London (1973), Chap. 3, 6.

3) P. L. Fereday and S. F. Mason, *J. Chem. Soc. Chem. Commun.*, **1971**, 1314.

4) S. Yano, M. Saburi, S. Yoshikawa, and J. Fujita, *Bull. Chem. Soc. Jpn.*, **49**, 101 (1976).

5) F. M. Jaeger and H. B. Blumendal, *Z. Anorg. Allg. Chem.*, **175**, 161 (1928).

6) M. Ito, F. Marumo, and Y. Saito, *Acta Crystallogr., Sect. B*, **27**, 2178 (1971); Y. Saito, F. Marumo, and M. Ito, *Proc. Jpn. Acad.*, **47**, 495 (1971).

7) H. Toftlund and E. Pedersen, *Acta Chem. Scand.*, **26**, 4019 (1972).

8) C. J. Hawkins, G. A. Lawrance, and R. M. Peachey, *Aust. J. Chem.*, **30**, 2115 (1977).

9) H. Lund and J. Bjerrum, *Ber. Dtsch. Chem. Ges.*, **64**, 210 (1931).

10) E. M. Arnett and C. F. Douty, *J. Am. Chem. Soc.*, **86**, 409 (1964).

11) C. C. Hach, C. V. Banks, and H. Diehl, *Org. Synth.*, Coll. Vol. IV, 229 (1963).

12) L. Long, Jr., and L. F. Fieser, *J. Am. Chem. Soc.*, **62**, 2670 (1940).

13) R. S. Treptow, *Inorg. Chem.*, **5**, 1593 (1966).

14) K. Kashiwabara, T. Yamanaka, K. Saito, N. Komatsu, N. Hamada, H. Nishikawa, and M. Shibata, *Bull. Chem. Soc. Jpn.*, **48**, 3631 (1975).

15) K. Ogino, K. Murano, and J. Fujita, *Inorg. Nucl. Chem. Lett.*, **4**, 351 (1968).

16) M. Goto, M. Takeshita, and T. Sakai, *Inorg. Chem.*, **17**, 314 (1978).

17) R. A. D. Wentworth and T. S. Piper, *Inorg. Chem.*, **4**, 202 (1965).

18) B. Bosnich and J. MacB. Harrowfield, *J. Am. Chem. Soc.*, **94**, 3425 (1972).

19) R. Kuroda and Y. Saito, *Bull. Chem. Soc. Jpn.*, **49**, 433 (1976).

20) K. Matsumoto, S. Ooi, and H. Kuroda, *Bull. Chem. Soc. Jpn.*, **44**, 2721 (1971).

21) A. J. McCaffery, S. F. Mason, and B. J. Norman, *J. Chem. Soc.*, **1965**, 5094.

22) B. J. Hathaway and D. E. Billing, *Coord. Chem. Rev.*, **5**, 143 (1970).

23) R. D. Gillard, *J. Inorg. Nucl. Chem.*, **26**, 1455 (1964).

24) Y. Nishida and S. Kida, Paper presented at the 21st Symposium on Coordination Chemistry, Nagoya, 1971.

The Synthesis of 3′-Methoxy-2′,4,4′,6′- and 2′-Methoxy-3′,4,4′,6′-tetrahydroxychalcone and Some Quinochalcones and a Comparison of Them with Carthamin[1)]

Heitaro OBARA,* Jun-ichi ONODERA, and Satoshi ABE

Department of Applied Chemistry, Faculty of Engineering, Yamagata University, Yonezawa 992

(Received November 16, 1978)

3′-Methoxy-2′,4,4′,6′- and 2′-methoxy-3′,4,4′,6′-tetrahydroxychalcone, 2′,4,4′-trihydroxy-, 2′,4-dihydroxy-4′-methoxy-, and 2′-hydroxy-4,4′-dimethoxy-3′,6′-quinochalcone have been synthesized, and their properties have been compared with those of carthamin.

In 1930, Kuroda[2)] proposed Structure **1** for carthamin, the red coloring matter of the flowers of the Safflower (*Carthamus tinctorius* L.); she also reported a yellow unstable tautomeric form, isocarthamin (**2**), which is very liable to be converted into the stable carthamin. On the other hand, Seshadri *et al.*[3)] reported that the yellow hydroxychalcone (**3**), which is the main component of the flowers, should be called carthamin, while they gave the red pigment which was conventionally called "carthamin" by Kuroda, the constitution of the quinochalcone, carthamone (**4**); they also reported that **4** was obtained by the oxidation of **3** in the presence of peroxidase.

In connection with the synthetic studies of carthamin, we have reported the synthesis of 2′,3′,4,4′,6′-pentahydroxychalcone (**14**),[4)] corresponding to the aglycon of **2** or **3**, and its isomerization into 4′,5,6,7- and 4′,5,7,8-tetrahydroxyflavanone (carthamidin and isocarthamidin).[5)] In this paper, the syntheses of some analogs of **2**, **3**, and **4**, *i.e.*, 3′-methoxy-2′,4,4′,6′- and 2′-methoxy-3′,4,4′,6′-tetrahydroxychalcone (**7** and **11**), 2′,4,4′-trihydroxy-, 2′,4-dihydroxy-4′-methoxy-, and 2′-hydroxy-4,4′-dimethoxy-3′,6′-quinochalcone (**17**, **21**, and **23**), and a comparison of their properties with those of carthamin will be described.

The condensation of 3-methoxy-2,4,6-tris(methoxymethoxy)acetophenone (**5**) with *p*-(methoxymethoxy)-benzaldehyde afforded 3′-methoxy-2′,4,4′,6′-tetrakis-(methoxymethoxy)chalcone (**6**), which was then hydrolyzed with dilute hydrochloric acid in methanol to give **7** as yellow crystals. Similarly, 2′-methoxy-3′,4,4′,6′-tetrahydroxychalcone (**11**) was obtained by the hydrolysis of 2′-methoxy-3′,4,4′,6′-tetrakis(methoxymethoxy)chalcone (**10**), prepared by the methylation of the condensation product (**9**) of 2-hydroxy-3,4,6-tris(methoxymethoxy)acetophenone (**8**) with *p*-(methoxymethoxy)benzaldehyde. The structures of these chalcones were identified by elemental analyses and by studies of their UV, IR, and PMR spectra. The structure of **11** was further confirmed by its conversion

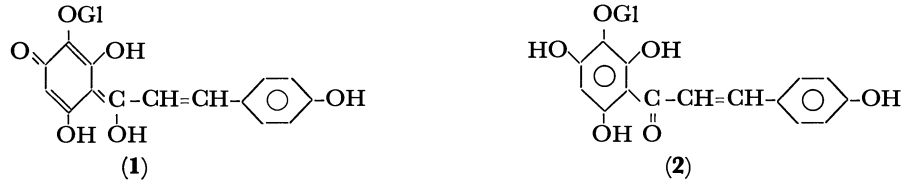

(**1**)

(**2**)

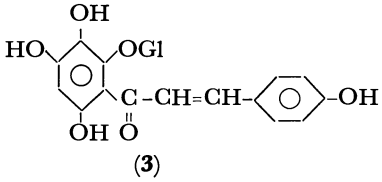

(**3**)

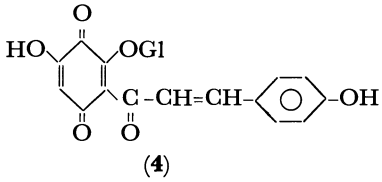

(**4**)

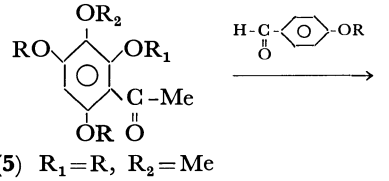

(**5**) R_1=R, R_2=Me
(**8**) R_1=H, R_2=R

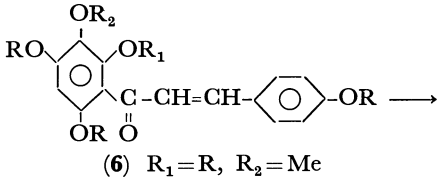

(**6**) R_1=R, R_2=Me
(**9**) R_1=H, R_2=R
(**10**) R_1=Me, R_2=R

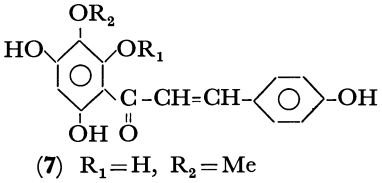

(**7**) R_1=H, R_2=Me
(**11**) R_1=Me, R_2=H

11 ⟶

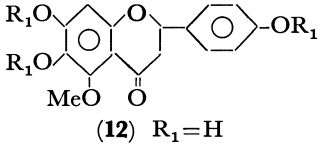

(**12**) R_1=H
(**13**) R_1=Me

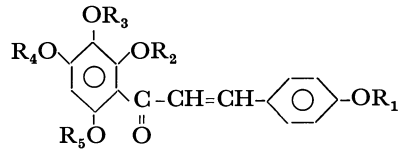

(**14**) $R_1=R_2=R_3=R_4=R_5=H$
(**15**) $R_1=R_2=R_3=R_4=R_5=CH_2OMe$
(**18**) $R_1=CH_2OMe$, $R_2=R_3=R_4=R_5=Me$
(**19**) $R_1=R_2=R_3=R_4=R_5=Me$
(**22**) $R_1=H$, $R_2=R_3=R_4=R_5=Me$

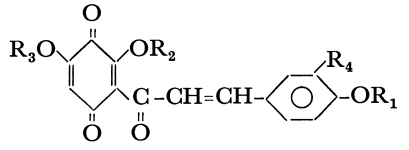

(**16**) $R_1=R_3=CH_2OMe$, $R_2=R_4=H$
(**17**) $R_1=R_2=R_3=R_4=H$
(**20**) $R_1=CH_2OMe$, $R_2=R_4=H$, $R_3=Me$
(**21**) $R_1=R_2=R_4=H$, $R_3=Me$
(**23**) $R_1=R_3=Me$, $R_2=R_4=H$
(**24**) $R_1=R_2=H$, $R_3=Me$, $R_4=NO_2$

($R=CH_2OMe$)

into 5-methoxy-4′,6,7-trihydroxyflavanone (**12**) with acid. The trimethyl ether (**13**) of **12** was completely indentical with an authentic sample of 4′,5,6,7-tetramethoxyflavanone.[6]

2′,4,4′-Trihydroxy-3′,6′-quinochalcone (**17**) was obtained by the oxidation of **14**[4] with silver oxide in ether, or by the demethoxymethylation of 2′-hydroxy-4,4′-bis(methoxymethoxy)-3′,6′-quinochalcone (**16**), prepared by the nitric acid oxidation of 2′,3′,4,4′,6′-pentakis(methoxymethoxy)chalcone (**15**)[4] in acetic acid containing 6 M hydrochloric acid. Since this chalcone (**17**) was unstable in solution, and since we failed in our attempt at methylation in a usual way, its mono and dimethyl ethers were prepared by the following method. 2′,4-Dihydroxy-4′-methoxy-3′,6′-quinochalcone (**21**) was obtained by the demethoxymethylation of 2′-hydroxy-4′-methoxy-4-methoxymethoxy-3′,6′-quinochalcone (**20**), prepared by the nitric acid oxidation of 4-methoxymethoxy-2′,3′,4′,6′-tetramethoxychalcone (**18**), which had itself been obtained by the condensation of 2,3,4,6-tetramethoxyacetophenone[4] with *p*-(methoxymethoxy)benzaldehyde. Similarly, 2′-hydroxy-4,4′-dimethoxy-3′,6′-quinochalcone (**23**) was obtained by the oxidation of 2′,3′,4,4′,6′-pentamethoxychalcone (**19**)[4] with nitric acid in acetic acid. On the other hand, the direct nitric acid oxidation of 2′,3′,4′,6′-tetramethoxy-4-hydroxychalcone (**22**), itself prepared by the demethoxymethylation of **18**, gave nitroquinochalcone, 2′,4-dihydroxy-4′-methoxy-3-nitro-3′,6′-quinochalcone (**24**). The structures of these quinochalcones were determined by studies of their UV, IR, and PMR spectra and by elemental analyses.

The electronic spectra of these synthetic analogs (**7**, **11**, and **17**) and carthamin are shown in Fig. 1. Since a tautomerism was expected between carthamin (**1**) and isocarthamin (**2**), as was described at the beginning, the absorption spectrum of **7** was expected to be similar to that of carthamin, in fact, however, these two spectra did not resemble each other at all. Actually, the **7** chalcone is a stable compound and does not show any unstable behavior such as carthamin does. Further, carthamin showed a characteristic absorption band at 520 nm in its electronic spectrum, but the synthetic quinochalcones do not exhibit absorption maxima in such a long-wavelength region. From these results, it is thought that the structures of the red pigment proposed by Kuroda or Seshadri are not reasonable and that carthamin must have a longer conjugated system.

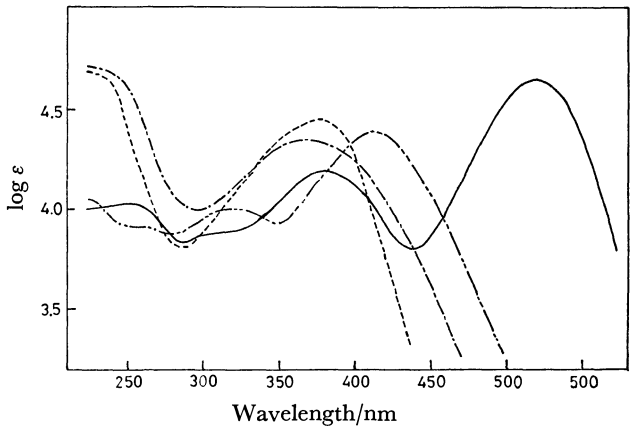

Fig. 1. The electronic spectra of **7** (----), **11** (——–), **17** (————), and carthamin (——) in ethanol.

Experimental

All the melting points are uncorrected. The UV and IR spectra were recorded with a Hitachi 135 spectrophotometer and a Hitachi EPI-S2 spectrophotometer respectively. The PMR spectra were measured with a Hitachi R-22 spectrometer (90 MHz), using tetramethylsilane as the internal standard.

3-Methoxy-2,4,6-tris(methoxymethoxy)acetophenone (**5**). Into a solution of 3-methoxy-2,4,6-trihydroxyacetophenone[7] (2.0 g, mp 169—170 °C, lit,[7] mp 168 °C) in 37 ml of absolute ethanol we vigorously stirred a one-fourth volume of a solution of sodium (3.3 g) in 53 ml of absolute ethanol under a nitrogen atmosphere and under cooling with ice-cold water. After 30 s, a one-fourth volume of chloromethyl methyl ether (11.5 g) was stirred into the above solution over a 5-min interval at 40 °C; this operation was repeated three times under the same conditions. After the addition had been completed, the reaction mixture was evaporated *in vacuo* and the residue was poured into water and extracted with ether. The ether layer was washed with a 5% aqueous $NaHCO_3$ solution and water. The ether was evaporated to give an oily residue, which was then chromatographed over silica gel. Elution with benzene–ethyl acetate (4:1) afforded **5** (1.1 g, 33%) as a light yellow viscous oil, which was used immediately in the subsequent reaction.

3′-Methoxy-2′,4,4′,6′-tetrakis(methoxymethoxy)chalcone (**6**). Into a mixed solution of **5** (0.5 g) and *p*-(methoxymethoxy)-benzaldehyde (0.4 g) in 11 ml of methanol we stirred a 50% aqueous sodium hydroxide solution (5.5 ml) at room temperature. After it had stood overnight, the mixture was poured into cold water and extracted with ether, and then

the ether layer was washed with water. The evaporation of the solvent gave an oily residue, which was then chromatographed over silica gel. Elution with benzene–ethyl acetate (4:1) afforded **6** (0.6 g, 83%). UV (EtOH) λ_{max} 328 nm (log ε=4.38); IR ($CHCl_3$) 1630 cm^{-1} (C=O); PMR ($CDCl_3$) δ 3.41, 3.43, 3.50, and 3.58 (each 2H, s, $-CH_2-\times 4$), 3.89 (3H, s, -OMe), 5.12, 5.17, 5.24, and 5.29 (each 3H, s, $-CH_3\times 4$), 6.87 (1H, s, $C_{5'}$–H), 7.10 (2H, d, J=8.5 Hz, $C_{3,5}$–H), 7.56 (2H, d, J=8.5 Hz, $C_{2,6}$–H), 6.98 (1H, d, J=16.0 Hz, C_α–H), 7.45 (1H, d, J=16.0 Hz, C_β–H), Found: C, 59.87; H, 6.44%. Calcd for $C_{24}H_{30}O_{10}$: C, 60.24; H, 6.32%.

*3'-Methoxy-2',4,4',6'-tetrahydroxychalcone (**7**).* A mixture of **6** (0.4 g), 6 M hydrochloric acid, and methanol (17 ml) was refluxed for 30 s. After cooling, the reaction mixture was poured into 30 ml of cold brine and extracted with ether. The ether layer was dried over anhydrous Na_2SO_4 and concentrated to about 10 ml *in vacuo*. A small quantity of petroleum ether was added to the concentrated solution to give crude **7**, which was then chromatographed over silica gel. Elution with CCl_4–ether–acetic acid (20:10:1) afforded **7** (70 mg, 28%) as yellow crystals; mp 169—171 °C. UV (EtOH) λ_{max} 377 nm (log ε=4.47); IR (KBr) 1620 cm^{-1} (C=O); PMR (acetone-d_6) δ 3.78 (3H, s, -OMe), 6.00 (1H, s, $C_{5'}$–H), 6.92 (2H, d, J=8.5 Hz, $C_{3,5}$–H), 7.57 (2H, d, J=8.5 Hz $C_{2,6}$–H), 7.76 (1H, d, J=16.0 Hz, C_α–H), 8.13 (1H, d, J=16.0 Hz, C_β–H), 8.93, 9.24, 11.10, and 12.18 (each 1H, s, $-OH\times 4$). Found: C, 63.15; H, 4.72%. Calcd for $C_{16}H_{14}O_6$: C, 63.57; H, 4.64%.

*2-Hydroxy-3,4,6-tris(methoxymethoxy)acetophenone (**8**).* To a solution of 2,3,4,6-tetrahydroxyacetophenone[4] (6.0 g) in 150 ml of absolute ethanol, we vigorously stirred a one-fourth volume of a solution of sodium (8.8 g) in 140 ml of absolute ethanol under a nitrogen atmosphere, and under cooling with ice-cold water. After 30 s, a one-fourth volume of chloromethyl methyl ether (31 g) was stirred into the above solution over a 5-min interval at 40 °C; this operation was repeated three times under the same conditions. After the addition had been completed, the reaction mixture was worked up in a manner similar to that used in the preparation of 3-methoxy-2,4,6-tris(methoxymethoxy)acetophenone (**5**) described above. Elution with benzene–ethyl acetate (4:1) afforded **8** (1.34 g, 13%) as a yellow oil. IR ($CHCl_3$) 1620 cm^{-1} (C=O); PMR ($CDCl_3$) δ 2.68 (3H, s, -Ac), 3.55 (6H, s, $-CH_3\times 2$), 3.66 (3H, s, $-CH_3$), 5.13 (2H, s, $-CH_2-$), 5.29 (4H, s, $-CH_2-\times 2$), 6.51 (1H, s, C_5–H), 13.80 (1H, s, -OH). Found: C, 53.46; H, 6.44%. Calcd for $C_{14}H_{20}O_8$: C, 53.16; H, 6.33%.

*2'-Methoxy-3',4,4',6'-tetrahydroxychalcone (**11**).* Into a mixed solution of **8** (1.5 g) and *p*-(methoxymethoxy)benzaldehyde (1.2 g) in methanol (8 ml) we stirred a 50% aqueous sodium hydroxide solution (4 ml) at room temperature. After standing overnight, the reaction mixture was poured into cold 10% acetic acid and extracted with ether. The evaporation of the solvent gave an oily residue, which was then chromatographed over silica gel. Elution with benzene–ethyl acetate (3:1) afforded 2'-hydroxy-3',4,4',6'-tetrakis(methoxymethoxy)chalcone (**9**) (1.66 g, 76%) as yellow crystals; mp 74—76 °C. UV (EtOH) λ_{max} 367 nm (log ε=4.42); IR (KBr) 1622 cm^{-1} (C=O); PMR ($CDCl_3$) δ 3.56 and 3.73 (each 3H, s, $-CH_3\times 2$), 3.60 (6H, s, $-CH_3\times 2$), 5.22 and 5.30 (each 2H, s, $-CH_2-\times 2$), 5.36 (4H, s, $-CH_2-\times 2$), 6.56 (1H, s, $C_{5'}$–H), 7.16 (2H, d, J=8.5 Hz, $C_{3,5}$–H), 7.65 (2H, d, J=8.5 Hz, $C_{2,6}$–H), 7.89 (2H, s, $C_{\alpha,\beta}$–H), 13.80 (1H, s, -OH). This chalcone, **9**, was methylated with dimethyl sulfate–potassium carbonate in acetone, and the resulting oily product was chromatographed over silica gel. Elution with benzene–ethyl acetate (4:1) afforded 2'-methoxy-3',4,4',6'-tetrakis(methoxymethoxy)chalcone (**10**) (74%) as an unstable oil, which was used immediately in the subsequent reaction.

A mixture of the above chalcone, **10** (640 mg), and 6 M hydrochloric acid (4.5 ml) in 11 ml of methanol was refluxed for 1.5 min. After cooling, the reaction mixture was poured into 60 ml of cold brine and extracted with ether. The solvent was evaporated *in vacuo*, and the residue was recrystallized from dilute methanol to give **11** (280 mg, 69%) as bright yellow needles; mp 190—192 °C. UV (EtOH) λ_{max} 368 nm (log ε=4.36); IR (KBr) 1620 cm^{-1} (C=O); PMR (DMSO-d_6) δ 3.76 (3H, s, -OMe), 6.15 (1H, s, $C_{5'}$–H), 6.86 (2H, d, J=8.7 Hz, $C_{3,5}$–H), 7.57 (2H, d, J=8.7 Hz, $C_{2,6}$–H), 7.62 (2H, s, $C_{\alpha,\beta}$–H), 8.23, 10.00, 10.40, and 12.80 (each 1H, s, $-OH\times 4$). Found: C, 63.16; H, 4.65%. Calcd for $C_{16}H_{14}O_6$: C, 63.57; H, 4.64%.

*5-Methoxy-4',6,7-trihydroxyflavanone (**12**).* A mixture of **11** (60 mg) and 6 M hydrochloric acid (1.5 ml) in 8 ml of methanol was refluxed for 8 h. The reaction mixture was then evaporated *in vacuo*, and the residue was extracted with ethyl acetate. The evaporation of the solvent gave a crude product, which was subsequently chromatographed over silica gel. Elution with benzene–ethyl acetate–acetic acid (30:10:1) afforded **12** (26 mg, 43%) as light yellow crystals; mp 232—234 °C. UV (EtOH) λ_{max} 287 nm (log ε=4.16) and 350 nm (log ε=3.67); IR (KBr) 1650 cm^{-1} (C=O); PMR (DMSO-d_6) δ 2.54 (1H, q, J=17.0 and 2.5 Hz, C_3–H), 2.94 (1H, q, J=17.0 and 13.3 Hz, C_3–H), 5.29 (1H, q, J=13.3 and 2.5 Hz, C_2–H), 3.76 (3H, s, -OMe), 6.22 (1H, s, C_8–H), 6.85 (2H, d, J=8.5 Hz, $C_{3',5'}$–H), 7.32 (2H, d, J=8.5 Hz, $C_{2',6'}$–H), 8.25, 9.41, and 10.07 (each 1H, s, $-OH\times 3$). Found: C, 63.46; H, 4.65%. Calcd for $C_{16}H_{14}O_6$: C, 63.57; H, 4.64%. The methylation of this compound with dimethyl sulfate–potassium carbonate in acetone afforded 4',5,6,7-tetramethoxyflavanone (**13**), which was completely identical with an authentic sample.[6]

*2',4,4'-Trihydroxy-3',6'-quinochalcone (**17**).* A mixture of **14**[4] (100 mg), silver oxide (200 mg), and magnesium sulfate (200 mg) in 5 ml of dry ether was stirred for 4 h at room temperature. The reaction mixture was then filtered, and the filtrate was evaporated. The residue was chromatographed over silica gel with toluene–ethyl formate–formic acid (5:2:1) to give crude products. Recrystallization from acetic acid gave **17** (3 mg) as orange needles; mp 234—236 °C. UV (EtOH) λ_{max} 260 nm (log ε=3.90), 310 nm (log ε=3.97), and 412 nm (log ε=4.41); IR (KBr) 1690, 1635, and 1605 cm^{-1} (C=O). Found: C, 62.20; H, 3.80%; M^+, 286. Calcd for $C_{15}H_{10}O_6$: C, 62.94; H, 3.52%; M, 286.

*2'-Hydroxy-4,4'-bis(methoxymethoxy)-3',6'-quinochalcone (**16**).* Into a mixed solution of 2',3',4,4',6'-pentakis(methoxymethoxy)chalcone (**15**)[4] (1.0 g), acetic acid (4 ml), and ether (4 ml) we added 1 ml of nitric acid (d=1.38) under cooling with ice-cold water; the reaction mixture was then kept at 0—5 °C for 10 h. The resulting crystals were filtered and recrystallized from acetic acid–ether to afford **16** (230 mg, 30%); mp 142—143 °C. UV (EtOH) λ_{max} 266, 294, and 406 nm; IR (KBr) 1700, 1630, and 1600 cm^{-1} (C=O); PMR ($CDCl_3$) δ 3.74 (6H, s, $-CH_3\times 2$), 5.23 and 5.26 (each 2H, s, $-CH_2-\times 2$), 6.40 (1H, s, $C_{5'}$–H), 7.08 (2H, d, J=8.5 Hz, $C_{3,5}$–H), 7.66 (2H, d, J=8.5 Hz, $C_{2,6}$–H), 8.05 (1H, d, J=16.0 Hz, C_α–H), 8.28 (1H, d, J=16.0 Hz, C_β–H), 17.76 (1H, s, -OH). Found: C, 60.67; H, 5.02%. Calcd for $C_{19}H_{18}O_8$: C, 60.96; H, 4.85%.

The demethoxymethylation of **16** by warming at 50—60 °C in acetic acid containing 6 M hydrochloric acid af-

forded a small amount of **17**.

*4-Methoxymethoxy-2′,3′,4′,6′-tetramethoxychalcone (**18**).* Into a mixture of 2,3,4,6-tetramethoxyacetophenone[4] (480 mg) and *p*-(methoxymethoxy)benzaldehyde (400 mg) in 5 ml of methanol we added 5 ml of a 50% aqueous sodium hydroxide solution; the reaction mixture was then left to stand over 2 nights at room temperature. The reaction mixture was subsequently worked-up in a manner similar to that of **9**. The resulting products were chromatographed over silica gel with benzene–ethyl acetate (4:1) to give **18** as a light yellow oil (760 mg, 98%). Found: C, 64.36; H, 6.44%; M^+, 388. Calcd for $C_{21}H_{24}O_7$: C, 64.93; H, 6.23%; M, 388.

*2′-Hydroxy-4-methoxymethoxy-4′-methoxy-3′,6′-quinochalcone (**20**).* To a mixture of **18** (200 mg) and acetic acid (1.5 ml) in 1.5 ml of ether we added 0.2 ml of nitric acid (d=1.38), after which the reaction mixture was left to stand overnight in a refrigerator. The resulting product was recrystallized from acetic acid–ether to afford **20** (45 mg, 25%); mp 155—156 °C. IR (KBr) 1702, 1665, and 1620 cm^{-1} (C=O). Found: C, 62.36; H, 4.88%. Calcd for $C_{18}H_{16}O_7$: C, 62.79; H, 6.48%.

*2′,4-Dihydroxy-4′-methoxy-3′,6′-quinochalcone (**21**).* To a solution of **20** (100 mg) in 3 ml of acetic acid we added 0.5 ml of 6 M hydrochloric acid, after which the mixture was warmed at 40—50 °C for 3 min. After cooling, the resulting crude product was recrystallized from acetic acid to afford **21** (55 mg, 63%); mp 252—254 °C. UV (EtOH) λ_{max} 264, 300, and 414 nm; IR (KBr) 1706, 1630, and 1600 cm^{-1} (C=O); PMR (DMSO-d_6) δ 3.82 (3H, s, –OMe), 6.18 (1H, s, $C_{5'}$–H), 6.84 (2H, d, J=8.5 Hz, $C_{3,5}$–H), 7.58 (2H, d, J=8.5 Hz, $C_{2,6}$–H), 7.92 (2H, s, $C_{\alpha,\beta}$–H), 10.30 (bs, –OH). Found: C, 63.60; H, 4.19%. Calcd for $C_{16}H_{12}O_6$: C, 64.00; H, 4.03%.

*2′-Hydroxy-4,4′-dimethoxy-3′,6′-quinochalcone (**23**).* To a solution of 2′,3′,4,4′,6′-pentamethoxychalcone (**19**)[4] (150 mg) in 1.5 ml of acetic acid we added 0.15 ml of nitric acid (d=1.42); the reaction mixture was then left to stand overnight in a refrigerator. The resulting product was filtered and recrystallized from acetic acid to afford **23** (55 mg, 42%); mp 188—189 °C. UV ($CHCl_3$) λ_{max} 261, 297, and 412 nm; IR (KBr) 1714, 1658, and 1630 cm^{-1} (C=O); PMR (DMSO-d_6) δ 3.83 (6H, s, –OMe×2), 6.26 (1H, s, $C_{5'}$–H), 7.08 (2H, d, J=8.5 Hz, $C_{3,5}$–H), 7.71 (2H, d, J=8.5 Hz, $C_{2,6}$–H), 8.00 (2H, s, $C_{\alpha,\beta}$–H). Found: C, 64.96; H, 4.46%. Calcd for $C_{17}H_{14}O_6$: C, 64.82; H, 4.49%.

*2′,4-Dihydroxy-4′-methoxy-3-nitro-3′,6′-quinochalcone (**24**).* This chalcone was obtained by the oxidation of 4-hydroxy-2′,3′,4′,6′-tetramethoxychalcone (**22**) (mp 120—121 °C), which had been prepared by the demethoxymethylation of **18** in a manner similar to that described above. Orange plates from acetic acid; mp 202—204 °C (39%). UV ($CHCl_3$) λ_{max} 277 nm ($\log\varepsilon$=4.32) and 382 nm ($\log\varepsilon$=4.54); PMR (DMSO-d_6) δ 3.84 (3H, s, –OMe), 6.19 (1H, s, $C_{5'}$–H), 7.15 (1H, d, J=8.5 Hz, C_5–H), 7.90 (1H, q, J=8.5 and 2.0 Hz, C_6–H), 7.88 (2H, s, $C_{\alpha,\beta}$–H), 8.20 (1H, d, J=2.0 Hz, C_2–H). Found: C, 55.35; H, 3.26; N, 4.31%. Calcd for $C_{16}H_{11}O_8N$: C, 55.66; H, 3.21; N, 4.06%.

The present work was partly supported by a Grant-in-Aid for Scientific Research from the Ministry of Education.

References

1) Preliminary communications: H. Obara, J. Onodera, and S. Abe, *Chem. Lett.*, **1974**, 335; H. Obara and J. Onodera, *ibid.*, **1974**, 1357.

2) C. Kuroda, *Nippon Kagaku Zasshi*, **51**, 237 (1930); C. Kuroda, *J. Chem. Soc.*, **1930**, 752.

3) T. R. Seshadri and R. S. Thakur, *Curr. Sci.*, **29**, 54 (1960).

4) H. Obara, J. Onodera, and Y. Kurihara, *Bull. Chem. Soc. Jpn.*, **44**, 289 (1971); H. Obara *et al.*, *ibid.*, **51**, 3627 (1978).

5) H. Obara, J. Onodera, and F. Yamamoto, *Chem. Lett.*, **1973**, 915; H. Obara *et al.*, *Bull. Chem. Soc. Jpn.*, **51**, 3627 (1978).

6) M. G. Stout, H. Reich, and M. N. Huffman, *J. Pharm. Sci.*, **53**, 192 (1964).

7) P. S. Phadke, A. V. Rama Rao, and K. Venkataraman, *Indian J. Chem.*, **5**, 131 (1967); *Chem. Abstr.*, **67**, 116792_x (1967).

Coenzyme Models. 18. Metal Catalysis of NADH Model Reduction in Aqueous Systems

Seiji SHINKAI,* Hisatake HAMADA, Yumiko KUSANO, and OSAMU MANABE

Department of Industrial Chemistry, Faculty of Engineering, Nagasaki University, Nagasaki 852

(Received November 17, 1978)

Metal ions (Ni^{2+} and Zn^{2+}) affected the NADH model reduction of 2-pyridinecarbaldehyde and Schiff bases in aqueous systems. In particular, the rate of the dihydroquinoline reduction of *N*-(2-pyridylmethylene)-2-pyridylmethylamine was augmented by more than 200-fold, compared with that in the absence of metal ions. On the other hand, the reduction of benzil, ethyl benzoylformate, and trifluoroacetophenone was not subject to the metal catalysis. The enhanced reactivity is accounted for by the affinity of Schiff bases toward metal ions. The efficiency of the metal catalysis was compared with that of the proton catalysis. This is the first example of the systematic examination of the metal catalysis in aqueous systems.

It is known that some alcohol dehydrogenases contain NAD^+ and Zn^{2+} ion at the active sites and catalyze the interconversion of aldehydes and alcohols coupled to the oxidation-reduction of NAD^+ coenzyme.[1] The role of Zn^{2+} ion, as well as that of NAD^+, has long been a subject of investigation and debate. Recent model studies have established that metal ion not only activates substrates and/or NADH analogues but also helps retaining stereoselective hydrogen transfer from NADH analogues to substrates.[2-6] These successful demonstration in the model system may provide the information relevant to biological NADH dependent oxidation-reduction, but the metal catalysis has been confined strictly to aprotic solvents (*e.g.*, acetonitrile). In fact, it has often been mentioned that metal ion does not act as catalyst in aqueous NADH model reduction.[5,6]

It is proposed that the transition state of NADH reduction is analogous to that pictured for S_N2-type nucleophilic reaction,[7,8] although the detailed mechanism is still a matter of some controversy.[9-12] As for the S_N2-type nucleophilic reaction, Buckingham[13,14] and others[15-17] have reported many examples of metal catalysis in aqueous solutions. For example, metal ions such as Cu^{2+}, Co^{2+}, Ni^{2+}, and Zn^{2+} are good catalysts for the ester hydrolysis of α-amino acids, the rate augmentation amounting to 10^3—10^6 fold. The marked rate acceleration is explained by such that the metal ion can bind to the nitrogen and at the same time remain close to the ester carbonyl group. One would thus anticipate that the metal coordinated substrate may be considerably electrophilic and may serve as a good hydride (or its equivalent) acceptor. The object of the present investigation has been to search for the metal-catalyzed NADH model reduction of the C=O and C=N double bonds by an acid-stable NADH analogue, 1-benzyl-1,4-dihydro-3-quinolinecarboxamide (BzlQH).[18] We thus found that the reduction of Schiff base is remarkably facilitated by added metal ions (Ni^{2+} and Zn^{2+}).

BzlQH;

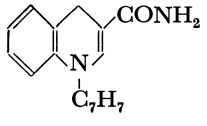

Experimental

Materials. The preparation of BzlQH has been described elsewhere.[19] 2-Pyridylmethylamine dihydrochloride was prepared by Dr. M. Ohnishi (Nagasaki University). Other reagents (trifluoroacetophenone, ethyl benzoylformate, 2-pyridinecarbaldehyde, and benzil) were purified by distillation or recrystallization before use.

Kinetics. Kinetic measurements were carried out at 50±0.1 °C in a 2.2%(v/v) aqueous acetonitrile solution with an ionic strength of 0.2(KCl). The progress of the reaction was followed spectrophotometrically by monitoring the decrease of BzlQH at λ_{max} (343 nm). The details of the method were described in a previous paper of this series.[19] Since excess substrate was present in all the cases, the pseudo first-order behavior was observed for up to 3-half-lives. In the case where the reaction rate was extremely slow, the rate constans were estimated from the initial slope of the reaction. Here, the overall first-order rate constants (k_{obsd}) is expressed by Eq. 1,

$$k_{obsd} = k_d + k_r \quad (1)$$

where k_d is the acid-catalyzed (spontaneous) decomposition of BzlQH and k_r is the pseudo first-order rate constants for the reduction reaction. The k_d value was determined separately from the disapperance of the absorption of BzlQH in the absence of substrate, and the k_r value was determined from Eq. 1. Since the k_r value is linearly correlated to substrate concentrations ([substrate]$=(1—5)\times10^{-3}$ M, [Zn^{2+}]$=(0—5)\times10^{-3}$M), the apparent second-order rate constants (k_2') are given by $k_2'=k_r/$[substrate].

Results and Discussion

Suppressed Catalytic Activity of Metal Ions in Aqueous Systems. Dihydronicotinamides in dry acetonitrile interact strongly with Mg^{2+} ion.[20,21] The interaction is substantiated by bathochromic shifts of the absorption maxima. The absorption maximum of BzlQH in acetonitrile (335 nm, $\varepsilon_{max}=11900\ M^{-1}\ cm^{-1}$) also shifted to longer wavelength on the addition of Mg^{2+} ion (346 nm, $\varepsilon_{max}=14700\ M^{-1}\ cm^{-1}$, [$Mg(ClO_4)_2$]$=1.0\times10^{-2}$ M). On the other hand, the spectrum of BzlQH in an aqueous system (λ_{max} 343 nm, $\varepsilon_{max}=13100\ M^{-1}\ cm^{-1}$) was hardly affected by added metal ions ([Ni^{2+}]$=$[Zn^{2+}]$=(2.5—5.0)\times10^{-3}$ M at pH 4—9). The contrasting results indicate that the metal ion in aqueous solutions is deactivated due to strong solvation.

Benzil, ethyl benzylformate, and trifluoroacetophenone are slowly reduced by BzlQH in an acidic aqueous solution (pH 4.0). The dihydronicotinamide reduction of these substrates in aprotic solvents is efficiently catalyzed by Mg^{2+} ion,[2,4,25,26] whereas the aqueous BzlQH reduction was uncatalyzed by added metal ion ([metal ion (Ni^{2+} or Zn^{2+})]=*ca.* 5×10^{-3} M, pH 4—9). It is presumed that neither BzlQH nor substrate interacts with metal ions during the reduction process. Supposedly, one should employ more coordinative substrates to substantiate the metal catalysis in an aqueous solution.

Reduction of 2-Pyridinecarbaldehyde(2-PyCHO). 2-Acylpyridines are frequently employed in the model reduction in aprotic solvents.[4,27] This is probably due to the high coordination ability of 2-acylpyridines. 2-Acylpyridines are presumed to form the relatively stable complexes with metal ions in an aqueous system,[15] so that it would meet the requirement of the present study. Tagaki and coworkers[28] previously reported the reaction of 1,4-dihydronicotinamide with 2-PyCHO. They found, contrary to their expectation, that the isolated is a covalent adduct which is formed by a nucleophilic attack of 5-position of 1,4-dihydronicotinamide on the carbonyl carbon of 2-PyCHO. BzlQH has within the molecule the basic structure of 1,4-dihydronicotinamide, but the adduct-forming 5-position is involved in the fused ring. Thus, the formation of the adduct is almost unconceivable. Spectral examination of the reaction mixture([2-PyCHO]=1.0×10^{-4} M, [BzlQH]=5.0×10^{-5} M, [Zn^{2+}]=(0—1)$\times10^{-2}$ M, pH 4.7) established that the decrease of the absorption band of BzlQH (343 nm) is accompanied by the appearance of products with 215 and 250 nm which may be compared with the spectrum of a mixture of $BzlQ^+$ and 2-(hydroxymethyl)pyridine (209 and 244 nm). In fact, we have found that 2-PyCHO is reduced by BzlQH in 58—65% yield to corresponding alcohol.[29]

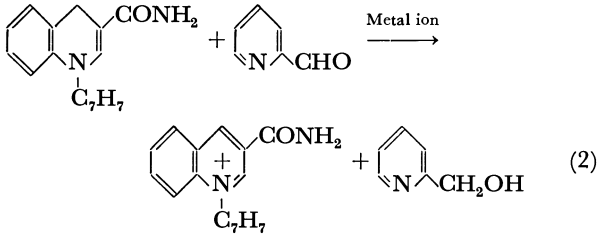

(2)

The apparent second-order rate constants (k_2') for BzlQH reduction of 2-PyCHO are plotted against metal concentrations (Fig. 1). In the alkaline pH region (pH 8.7), the rate constants could not be determined due to the ready precipitation of metal ions. The precipitation was not observed in the acidic pH region (pH 4.7), but the reaction was rather retarded by added metal ions. According to Pocker and Meany,[30] divalent metal ions such as Zn^{2+} and Co^{2+} exhibits a dramatic catalytic effect on the hydration of 2-PyCHO. It is expected, therefore, that the rate suppression may be rationalized in terms of the decrease in the fraction of free ketone. Since the hydration causes the diminution of the absorbancy of 2-PyCHO at around 260 nm,[30] the optical density(OD) was

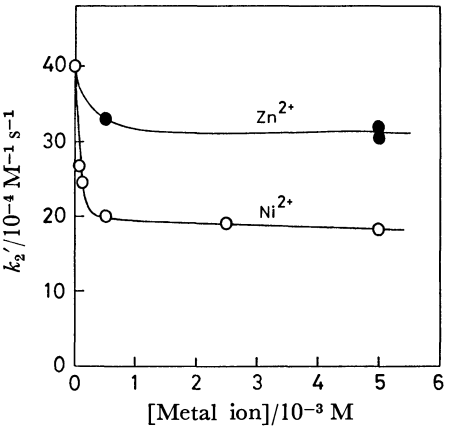

Fig. 1. Metal ion catalysis of the BzlQH reduction of 2-pyridinecarbaldehyde. [2-PyCHO]=5.00×10^{-3} M, [BzlQH]=5.0×10^{-5} M. The pH of the reaction media was maintained with 0.02 M acetate (pH 4.7).

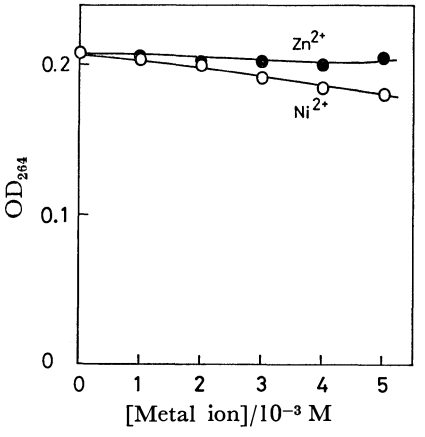

Fig. 2. Hydration equilibrium of 2-pyridinecarbaldehyde: optical density at 264 nm plotted against the concentration of metal ions. pH 4.7 with 0.02 M acetate buffer, [2-PyCHO]=5.0×10^{-5} M.

measured as a function of metal ion concentrations. As shown in Fig. 2, however, the absorption band is affected to a small extent (less than 10%) by added metal ions, indicating that the fraction of free ketone is maintained almost constant. Thus, the rate retardation cannot be attributed wholly to the hydration of 2-PyCHO.

As mentioned above, 2-PyCHO(pK_a 3.8)[31] in acetate buffer is reducible by BzlQH in good yields. If *N*-protonated 2-PyCHO which is presumed to be the active species in the acidic pH region exhibits the reactivity greater than metal-coordinated 2-PyCHO (*i.e.*, $k_H>k_M\gg k_0$ in Eq. 3), added metal ions would suppress the observed reduction rates.

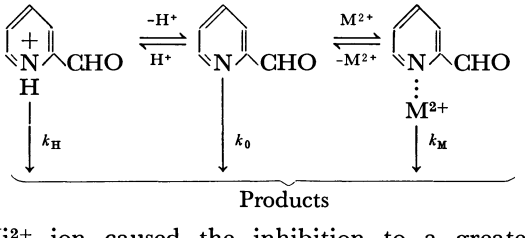

(3)

Ni^{2+} ion caused the inhibition to a greater extent

than Zn^{2+} ion. The trend is compatible with the general order of the stability constants.[17,32] Thus, the above explanation seems most likely at present.

Here, one may notice a dilemma occurring in the metal catalysis in aqueous systems. As mentioned above, stability constants of carbonyl substrates such as ethyl benzoylformate and benzil are extremely small.[32] Although 2-PyCHO in which a nitrogen base is closely fixed near the carbonyl group captures the metal ion to a significant extent, *N*-protonation is more effective than metal coordination.

The above summary suggests that the metal ion catalysis would become effective only for the substrate the C=X double bond of which is able to bind metal ions strongly. Schiff base is the case.[32]

Reduction of Schiff Bases of 2-PyCHO. NADH model reduction of Schiff bases in organic solvents was reported earlier by Pandit *et al.*[33] and Shinkai *et al.*,[8] but there is no precedent for the reduction in an aqueous system.

The spectroscopic measurements indicated that the addition of butylamine ($BuNH_2$) to the basic solution of PyCHO (pH 8.9) enhances the absorption band near 350 nm which is characteristic of the Schiff base.[34]

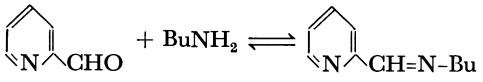

(4)

For example, the OD increase of 0.082 was recorded when butylamine (1.0×10^{-2} M) was added to the solution of 2-PyCHO (5.0×10^{-3} M) at pH 8.9. On the other hand, the formation of the Schiff base was hardly detected in an acetate buffer solution (pH 4.7). In Fig. 3, the OD value at 350 nm was plotted against the concentration of metal ions. The OD value was enhanced gradually with increasing metal ion concentrations and finally reached a plateau. In case 2-pyridylmethylamine ($PyCH_2NH_2$) was employed as an amine counterpart the absorption band was enhanced

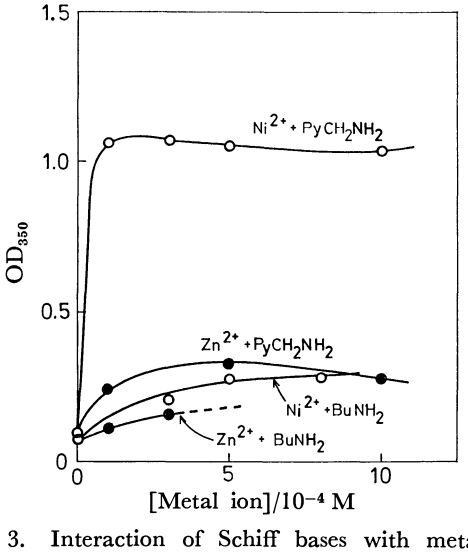

Fig. 3. Interaction of Schiff bases with metal ions: optical density at 350 nm plotted against the concentration of metal ions. pH 8.9 with 0.02 M borate buffer, [2-PyCHO] = 5.00×10^{-3} M, [$BuNH_2$] = [$PyCH_2NH_2$] = 1.00×10^{-2} M. The dotted line indicates the precipitation.

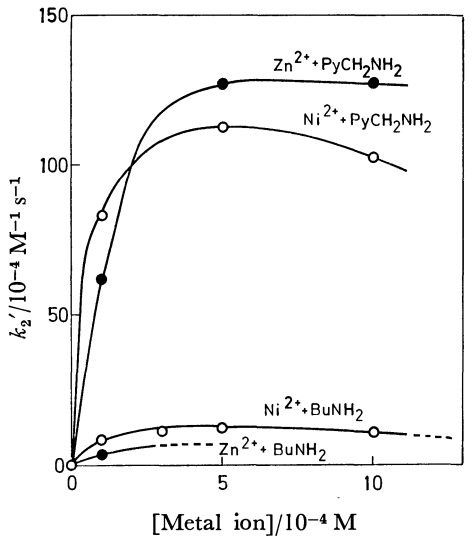

Fig. 4. Metal ion catalysis of the BzlQH reduction of Schiff bases. pH 8.9 with 0.02 M borate buffer, [2-PyCHO] = 5.00×10^{-5} M, [$BuNH_2$] = [$PyCH_2NH_2$] = 1.00×10^{-2} M. The dotted line indicates the precipitation.

at the very low concentration of metal ions, and the solution containing Ni^{2+} ion became yellow (or orange at the higher concentrations). The result endorses that the Schiff base (particularly, *N*-(2-pyridylmethylene)-2-pyridylmethylamine) efficiently interacts with metal ions in an aqueous solution.

The metal-catalyzed reduction was carried out in basic pH region (pH 8.9). The resultant second-order rate constants (k_2') are plotted as a functions of metal ion concentrations (Fig. 4). The BzlQH reduction was undetectable in the absence of metal ions, indicating that the Schiff base itself is insensitive to the BzlQH reduction. As seen in Fig. 4, metal ions efficiently catalyzed the BzlQH reduction. The plots showed rapid increase at low metal concentrations (1×10^{-4} M) followed by a gradual rate saturation. In particular, the reduction of *N*-(2-pyridylmethylene)-2-pyridylmethylamine, the Schiff base from 2-pyridinecarbaldehyde and 2-pyridylmethylamine, was remarkably accelerated. Since the rate constant in no metal system is estimated to be less than 5×10^{-5} M^{-1} s^{-1}, the rate augmentation of more than 200-fold is achieved. The marked rate acceleration is rationalized in terms of efficient binding of metal ions and efficient metal-induced polarization of the C=N double bond. Probably, the curvature in Fig. 4 reflects the progressive increase in the fraction of metal-bound species of the Schiff base, because the OD_{350} in Fig. 3 shows the dependence similar to that in Fig. 4. Thus, the reaction may be written as Eq. 5.

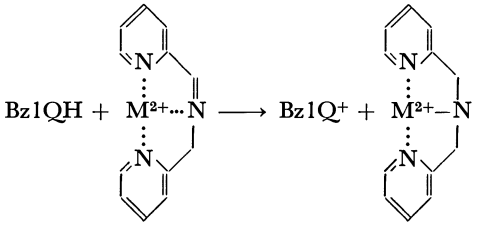

(5)

Figure 3 shows that Ni^{2+} ion forms the complex more efficiently than Zn^{2+} ion. On the other hand, the catalytic efficiency of Zn^{2+} ion is comparable with that of Ni^{2+} ion (Fig. 4). This endorses that, provided the rate constants are calculated based on the complexed substrate concentration, Zn^{2+} ion would give the greater rate constants than Ni^{2+} ion.

4-Pyridinecarbaldehyde(4-PyCHO) and butylamine also formed the corresponding Schiff base in a borate buffer solution (pH 8.9), the OD_{350} value (0.066) being comparable with that from 2-pyridinecarbaldehyde and butylamine. However, the BzlQH reduction was not catalyzed by added metal ions at all (Table 1). The low reactivity is solely ascribable to the difference in the affinity toward metal ions.

We previously reported the dihydronicotinamide reduction of Schiff bases in refluxing methanol.[8] Although the Schiff bases are totally unreactive toward dihydronicotinamide, the reduction reaction was surprisingly facilitated by the addition of small amounts of acid speices. It is summarized, therefore, that the Schiff base can be reduced with the aid of proton catalysis in the acidic pH region and with the aid of metal catalysis in the basic pH region.

Some Characteristics of NADH Model Reduction in Aqueous Systems. Recently, the mechanistic role of metal ions in non-enzymatic dihydronicotinamide reduction has been dissected in aprotic solvents.[2-6] The catalytic behavior may be roughly summarized as follows: (1) activation of substrate and/or dihydronicotinamide at the initial state and (2) facilitation of hydrogen transfer by "bridge" effect of metal ions at the transition state. In aqueous systems, the interaction of metal ions with dihydronicotinamide itself is hardly expected due to the solvation of metal ions. Although there is an effort to synthesize a NADH model system which has within a molecule both dihydronicotinamide and metal-binding site,[35] the catalytic efficiency seems still equivocal. At present, it seems most expeditious to employ the metal-binding substrates to substantiate the aqueous metal catalysis.

Table 1. Apparent second-order rate constants(k_2') for the BzlQH reduction[a]

Substrate[b]	Metal ion / mM	$k_2' \times 10^4/M^{-1}\,s^{-1}$ at pH 4.7	at pH 8.9
2-PyCHO		40.3	ppt[c]
2-PyCHO	Ni^{2+} (5.0)	19.1	ppt[c]
2-PyCHO	Zn^{2+} (5.0)	32.2	ppt[c]
2-PyCHO+$BuNH_2$		39.3	nd[d]
2-PyCHO+$BuNH_2$	Ni^{2+} (0.5)	20.2	12.2
2-PyCHO+$BuNH_2$	Zn^{2+} (0.1)	28.9	3.7
4-PyCHO+$BuNH_2$			nd[d]
4-PyCHO+$BuNH_2$	Ni^{2+} (0.1)		nd[d]
4-PyCHO+$BuNH_2$	Zn^{2+} (0.1)		nd[d]
2-PyCHO+$PyCH_2NH_2$			nd[d]
2-PyCHO+$PyCH_2NH_2$	Ni^{2+} (0.5)		113
2-PyCHO+$PyCH_2NH_2$	Zn^{2+} (0.5)		126

a) 50 °C, μ=0.2 with KCl, 2.2%(v/v) acetonitrile. b) Abbreviations employed are: 2-PyCHO, 2-pyridinecarbaldehyde; 4-PyCHO, 4-pyridinecarbaldehyde; $BuNH_2$, butylamine; $PyCH_2NH_2$ 2-pyridylmethylamine. c) Precipitation was formed. d) The rate was not detected($k_2' < 5 \times 10^{-5}\,M^{-1}\,s^{-1}$).

The present study established that the reduction of C=O and C=N double bonds with adjacent nitrogen base(s) is subject to the metal-catalysis in aqueous systems. We noticed, however, that the proton catalysis is unexpectedly effective.

Another conclusion obtained in the present study is that the Schiff bases serve as good substrates for the metal-assisted BzlQH reduction in aqueous systems. The rate augmentation of two orders of magnitude is remarkable. It seems, therefore, that the interaction with NADH is not a prerequisite for the facile reduction, as proposed by Dunn and coworkers[36,37] in enzymatic systems. It is conceivable, however, that in the hydrophobic pocket of enzymes metal ions may be relatively desolvated and may act more "acidic" catalysts like metal ions in aprotic solvents. The influence of hydrophobic environments on the metal catalysis is now investigated.

References

1) B. Vennesland and F. H. Westheimer, "The Mechanism of Enzyme Action," ed by W. D. McElroy and B. Glass, John Hopkins, Baltimore (1954), p. 357.
2) Y. Ohnishi, M. Kagami, and A. Ohno, *J. Am. Chem. Soc.*, **97**, 4766 (1975).
3) A. Ohno, T. Kimura, A. G. Kim, H. Yamamoto, S. Oka, and Y. Ohnishi, *Bioorg. Chem.*, **6**, 21 (1977).
4) R. A. Gase, G. Boxhoorn, and U. K. Pandit, *Tetrahedron Lett.*, **1976**, 2889.
5) D. J. Greighton, J. Hajdu, G. Mooser, and D. S. Sigman, *J. Am. Chem. Soc.*, **95**, 6855 (1973).
6) D. J. Creighton, J. Hajdu, and D. S. Sigman, *J. Am. Chem. Soc.*, **98**, 4619 (1976).
7) L. C. Kurz and C. Frieden, *J. Am. Chem. Soc.*, **97**, 677 (1975).
8) S. Shinkai, S. Shiraishi, and T. Kunitake, *Bull. Chem. Soc. Jpn.*, **49**, 3656 (1976).
9) A. Ohno and N. Kito, *Chem. Lett.*, **1972**, 369.
10) T. Okamoto, A. Ohno, and S. Oka, *J. Chem. Soc., Chem. Commun.*, **1977**, 181.
11) P. van Eikeren and D. L. Grier, *J. Am. Chem. Soc.*, **99**, 8057 (1977).
12) R. A. Hood, R. H. Prince, and K. A. Rubinson, *J. Chem. Soc., Chem. Commun.*, **1978**, 300.
13) D. A. Buckingham, D. M. Foster, and A. M. Sargeson, *J. Am. Chem. Soc.*, **92**, 6151 (1970).
14) D. A. Buckingham, C. E. Davis, and D. M. Foster, *J. Am. Chem. Soc.*, **92**, 5571 (1970).
15) H. L. Conley and R. B. Martin, *J. Phys. Chem.*, **69**, 2914 (1965).
16) M. L. Bender and B. W. Turnquest, *J. Am. Chem. Soc.*, **79**, 1889 (1957).
17) For a comprehensive review see E. Kimura, *Yuki Gosei Kagaku*, **29**, 1096 (1971).
18) S. Shinkai, H. Hamada, T. Ide, and O. Manabe. *Chem. Lett.*, **1978**, 685.
19) S. Shinkai, H. Hamada, Y. Kusano, and O. Manabe, *J. Chem. Soc., Perkin Trans. 2*, **1979**, 699.
20) A. Ohno, H. Yamamoto, T. Okamoto, S. Oka, and Y. Ohnishi, *Bull. Chem. Soc. Jpn.*, **50**, 2385 (1977).
21) A. Kitani, N. Hashimoto, and K. Sasaki, *Nippon*

Kagaku Kaishi, **1977**, 1103.
22) S. Shinkai, K. Tanaka, T. Ide, and O. Manabe, *J. Polym. Sci., Ploym. Chem. Ed.*, in press.
23) J. J. Steffens and D. M. Chipman, *J. Am. Chem. Soc.*, **93**, 6694 (1971).
24) P. van Eikeren and D. L. Grier, *J. Am. Chem. Soc.*, **98**, 4655 (1976).
25) Y. Ohnishi, T. Numakunai, and A. Ohno, *Tetrahedron Lett.*, **1975**, 3813.
26) Y. Ohnishi, M. Kagami, and A. Ohno, *Tetrahedron Lett.*, **1975**, 2437.
27) Y. Ohnishi, T. Numakunai, and A. Ohno, *Tetrahedron Lett.*, **1976**, 2700.
28) W. Tagaki, H. Sakai, Y. Yano, K. Ozeki, and Y. Shimizu, *Tetrahedron Lett.*, **1976**, 2541.
29) 50 °C for 48 h in ethanol containing 2 M of acetic acid. [BzlQH]=0.033 M, [2-PyCHO]=0.033 M.
30) Y. Pocker and J. E. Meany, *J. Am. Chem. Soc.*, **89**, 631 (1967).
31) W. P. Jencks, "Handbook of Biochemistry and Molecular Biology," ed by G. D. Fasman, CRC Press, Ohio, (1976).
32) A. E. Martell and M. Calvin, "Chemistry of the Metal Chelate Compounds," New York, N. Y., Prentice-Hall (1952).
33) U. K. Pandit, H. van Dam, and J. B. Steevens, *Tetrahedron Lett.*, **1977**, 913.
34) K. Nakamoto and A. E. Martell, *J. Am. Chem. Soc.*, **81**, 5857 (1959); J. Llor and M. Cortijo, *J. Chem. Soc., Perkin Trans. 2*, **1977**, 1111.
35) E. Gabby, Ph. D. Thesis, Columbia University, 1965; T. J. van Bergen and R. M. Kellogg, *J. Am. Chem. Soc.*, **99**, 3882 (1977).
36) S. E. Pattison and M. F. Dunn, *Biochemistry*, **15**, 3696 (1976).
37) C. T. Angelis, M. F. Dunn, D. C. Muchmore, and R. M. Wing, *Biochemistry*, **16**, 2922 (1977).

Catalytic Asymmetric Hydroformylation by the Use of Rhodium-complexes of Chiral Bidentate Phosphorus Ligands Bearing Saturated Ring Skeletons

Teruyuki HAYASHI,* Masato TANAKA, Yoshikazu IKEDA, and Ikuei OGATA
National Chemical Laboratory for Industry, Honmachi, Shibuyaku, Tokyo 151

(Received December 27, 1978)

(1*S*,2*S*)-1,2-Bis(diphenylphosphinoxy)cyclohexane, (1*S*,2*S*)-1,2-bis(phosphinomethyl)cyclohexanes, (2*R*,3*R*)-2,3-*O*-isopropylidene-2,3-dihydroxy-1,4-bis(phosphino)butanes, and (1*R*,2*R*)-1,2-bis(phosphinomethyl)cyclobutanes, whose phosphino groups were diphenylphosphino or 5*H*-dibenzophosphol-5-yl groups where the rotation of phenyl–P bonds is impossible, were used as chiral ligands in rhodium-catalyzed asymmetric hydroformylation. The highest stereoselectivity was attained by the use of (1*R*,2*R*)-1,2-bis(5*H*-dibenzophosphol-5-ylmethyl)cyclobutane or (2*R*,3*R*)-2,3-*O*-isopropylidene-2,3-dihydroxy-1,4-bis(5*H*-dibenzophosphol-5-yl)butane.

The asymmetric hydroformylation reaction[1-4] of olefins by the use of chiral rhodium-complex catalysts is a promising method for synthesizing optically active aldehydes which allow numerous transformations to the final products. However, when compared with the hydrogenation of olefinic double bonds or the hydrosilylation of ketones,[5] the optical yields obtained so far in hydroformylation are relatively low and far from having any practical meaning. The difficulty lies in the fact that the reaction is effected at a higher temperature and consists of more steps, such as carbon monoxide insertion, than hydrogenation or hydrosilylation. In addition, a reactant carbon monoxide of a strong coordination power may compete with the chiral ligands in coordinating with rhodium; this complicates the situation as well.

In order to overcome these difficulties, although there is no doubt that the development of more active catalyst systems[6] which would allow the reaction to be carried out at a lower temperature is of primary importance, the breakthrough may come in the use of a chiral bidentate ligand,[3,4,7] which can be expected to chelate the central rhodium atom to make a more rigid and, therefore, more reliable asymmetric catalyst than a monodentate ligand.

In this paper, several kinds of bidentate chiral ligands, (1*S*,2*S*)-1,2-bis(diphenylphosphinoxy)cyclohexane (I),[8] (1*S*,2*S*)-1,2-bis(diphenylphosphinomethyl)-cyclohexane (IIa),[9,10] (1*S*,2*S*)-1,2-bis(5*H*-dibenzophosphol-5-ylmethyl)cyclohexane (IIb),[10] (2*R*,3*R*)-2,3-*O*-isopropylidene-2,3-dihydroxy-1,4-bis(diphenylphosphino)butane (IIIa),[11] (2*R*,3*R*)-2,3-*O*-isopropylidene-2,3-dihydroxy-1,4-bis(5*H*-dibenzophosphol-5-yl)butane (IIIb),[7] (1*R*,2*R*)-1,2-bis(diphenylphosphinomethyl)-cyclobutane (IVa),[12,13] and (1*R*,2*R*)-1,2-bis(5*H*-dibenzophosphol-5-ylmethyl)cyclobutane (IVb),[13] were prepared and used for the rhodium-catalyzed hydroformylation of four typical kinds of olefins. The results were then compared with those of asymmetric hydrogenation.

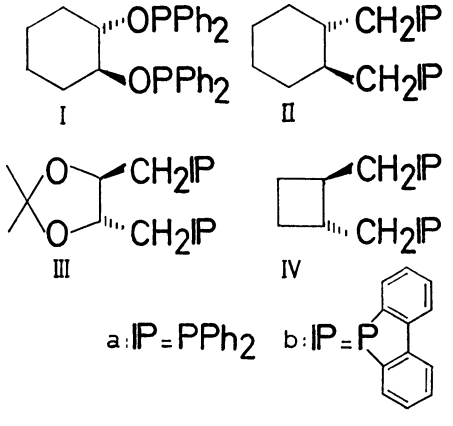

Experimental

All the manipulations of organophosphorus compounds were carried out under a pure nitrogen atmosphere. I (85.5% optical purity),[8] (+)-(1*S*,2*S*)-1,2-bis(hydroxymethyl)cyclohexane ditosylate,[14,15] (+)-(1*R*,2*R*)-1,2-bis(hydroxymethyl)cyclobutane ditosylate,[12] (−)-Diop (IIIa),[11] 2-phenyl-1-butene,[16] and α-acetamidocinnamic acid[17] were prepared as has been described in the literature.

Chiral Bisphosphines. Method A (IIa): Eighty mmol of Na and 20 mmol of Ph_2PCl in 20 ml of dioxane were stirred for 6 h at 110 °C. To the cooled solution, THF (15 ml) was added, and then the ditosylate ($[\alpha]_D$+25.5° (benzene, *c* 3.16), lit,[14] +25.0° (benzene, *c* 5)) (6.7 mmol) in THF (12 ml) was added over 10 min at room temperature. Then the solution was refluxed for 2 h and cooled. After filtration, the filtrate was concentrated, water (10 ml) was added, and the product was extracted with benzene. The organic layer was washed and concentrated, and the residue was subjected to molecular distillation.

Method B (IIb, IIIb, IVa, and IVb): Seven mmol of a phenylphosphine (5-phenyl-5*H*-dibenzophosphole or triphenylphosphine) and 16 mmol of Li wire in 16 ml of THF were stirred for 2 h at room temperature and then refluxed for 10 min. After the excess Li wire had been removed, a 7 mmol portion of *t*-butyl chloride was added and the solution was refluxed for 15 min. To the solution, a THF (8 ml) solution of a ditosylate (3.5 mmol) was added over 7 min at room temperature, after which the mixture was stirred for an additional 2 h, refluxed, and worked up as above (liquid) or finally recrystallized (solid).

The properties of the chiral bisphosphines are listed in Table 1.

Catalytic Hydroformylation Procedure. A rhodium complex (1.35×10^{-2} mmol-Rh), a bisphosphine or diphosphinite (2.7×10^{-2} mmol or 5.4×10^{-2} mmol), a solvent (6 ml), and a substrate (3 ml) were placed in a 50-ml Schlenk-type autoclave (SUS 316) under a pure N_2 atmosphere, and 50 kgw/cm² (at 0 °C) of CO and then the same amount of H_2 were pressurized. The sealed reactor was immersed in a temperature-controlled oil bath, and the reaction solution was magnetically stirred.

TABLE 1. PROPERTIES OF THE CHIRAL BISPHOSPHINE USED

Bisphosphine	Purification	Yield/%	$[\alpha]_D$/°	Found (Calcd), %
IIa	Molecular distillation bp 200—210 °C (bath) ($2—4\times10^{-4}$ mmHg)	80	+50.0[a] (toluene, *c* 2.58)	C 79.52 (79.98) H 7.06 (7.13)
IIb	Recrystallization from toluene-MeOH mp 163.9—165.0 °C	21	−30.4 (toluene, *c* 2.54)	C 80.60 (80.65) H 6.54 (6.35)
IIIa			−12.6[b] (benzene, *c* 1.48)	
IIIb	Recrystallization from benzene-EtOH mp 188.0—189.2 °C	69	−63.2[c] (benzene, *c* 1.05)	
IVa	Recrystallization from EtOH mp 106.2—107.2 °C[d]	73	−15.7[d] (benzene, *c* 1.22)	C 79.23 (79.63) H 6.63 (6.68)
IVb	Molecular distillation bp 215—220 °C (bath) (1.0×10^{-3} mmHg)	49	−5.9 (benzene, *c* 1.21)	C 80.28 (80.34) H 5.99 (5.84)

a) Ref. 12 +52.7° (*c* 1.0, benzene). b) Ref. 11 −12.3° (*c* 4.57, benzene). c) Ref. 21 −65.5° (*c* 2, benzene), mp 188—190 °C. d) Ref. 12 −18.6° (*c* 1.0, benzene), mp 107 °C.

TABLE 2. OPTICAL PURITIES[a] (AND PREVAILING CONFIGURATIONS) OF PRODUCTS IN ASYMMETRIC HYDROFORMYLATION AND HYDROGENATION

Chiral ligand	Hydroformylation[b]				Hydrogenation	
	Styrene[e]	1-Butene	*cis*-2-Butene	2-Phenylpropene	α-Acetamidocinnamic acid[c]	2-Phenyl-1-butene[d]
	Temp 80 °C	90 °C	120 °C	150 °C	25 °C	50 °C
I	0.8(*S*)[f]	2.2(*S*)[g]	0 (*R*)[g]	0.3(*R*)	51.2(*S*)	28.3(*R*)
IIa	15.1(*S*)[h] 12.1(*S*)	9.4(*S*)[g] 11.5(*S*)	3.9(*R*)[g] 3.1(*R*)	0.1(*S*)	24.5(*S*)	4.0(*R*)
IIb	0.6(*R*)	4.8(*S*)	10.7(*R*)	2.7(*R*)	25.7(*R*)	3.2(*S*)
IIIa	18.3(*R*)	6.8(*R*)	9.5(*S*)	1.7(*R*)	77.8(*R*)	24.5(*S*)
IIIb	37.0(*S*)	16.2(*S*)	16.6(*R*)	1.6(*R*)	23.2(*S*)	1.1(*S*)
IVa[i]	4.2(*R*)	1.5(*R*)	8.0(*S*)	0.5(*S*)	52.7(*R*)	22.2(*S*)
IVb[i]	40.3(*S*)	16.2(*S*)	16.8(*R*)	2.5(*R*)	25.5(*S*)	0.1(*R*)

a) The optical purities were calculated on the following bases: *N*-acetyl-(*R*)-phenylalanine: $[\alpha]_D$ −51.8 (*c* 1, EtOH),[25] (*S*)-2-phenylbutane: $[\alpha]_D$ +27.31° (neat),[26] (*S*)-2-phenylpropanal: $[\alpha]_D$ +160° (neat)[23] (Pino, *et al.* claim +238°,[27] (*S*)-2-methylbutanal: $[\alpha]_D$ +31.2° (neat),[28] (*R*)-3-phenylbutanal: $[\alpha]_D$ −31.3° (neat).[29] b) Rh: $[RhCl(CO)_2]_2$, P/Rh=8 (atom ratio), solvent: benzene for styrene and 2-phenylpropene, or ethylbenzene for butenes. c) Substrate: 0.5 g, solvent: EtOH+benzene (1:1) 3.5 ml. d) Sudstrate: 1 ml, solvent: benzene 3 ml. e) P/Rh=4. f) At 110 °C. g) At 130 °C. h) At 90 °C. i) Rh: $[Rh(CO)_3]_4$.

Catalytic Hydrogenation Procedure. [RhCl(1,5-hexadiene)]$_2$ (1.9×10^{-2} mmol), a bisphosphine or diphosphinite (4.0×10^{-2} mmol), a solvent, and a substrate were placed in a 25-ml Schlenk-type autoclave (SUS 316) under a pure N_2 atmosphere, and then the reactor was immersed in a bath of a designated temperature. H_2 was pressurized up to 50 kgw/cm^2 at that temperature, and the reaction solution was magnetically stirred.

Product Analysis. An aliquot of the reaction solution was analyzed by GLC (DEGS), and the remainder was distilled to afford an optically active product whose $[\alpha]_D$ was measured on a JASCO DIP-180 digital polarimeter. In the case of the hydrogenation of α-acetamidocinnamic acid, the reaction solution was worked up according to the literature.[11]

Results and Discussion

The optical purities were calculated through the optical rotation of isolated products; they are listed in Table 2.

A diphosphinite, I, although it resulted in fairly high optical yields in asymmetric hydrogenation,[8] caused a low asymmetric induction in the hydroformylation of any kind of olefins applied. The methylene-bridged analogue of I, a bisphosphine IIa, whose molecular structure is similar to that of I, brought about a much higher stereoselectivity than I.

On the other hand, IIa, with a saturated six-membered ring, was compared with Diop (IIIa), which has a five-membered dioxolane ring and with the IVa of a cyclobutane ring.[13,18] IIIa showed a certain asymmetric induction ability for each of the four olefins, while those of IIa or IVa depended on the structures of the olefins. That is, the ability decreased in the order of IIIa>IIa>IVa for styrene, in that of IIa>IIIa>IVa for 1-butene, and in that of IIIa>IVa>IIa for *cis*-2-butene. In the reaction of styrene or butenes, IIa of the configuration opposite to that of IIIa or IVa gave the antipode opposite to those given by IIIa and IVa; *i.e.*, the prevailing absolute configurations of the products from styrene or butenes were independent of the skeletal ring sizes of the bisphosphines, IIa—IVa.

The bidentate ligands mentioned above have Ph_2P

Table 3. Relative rates[a] (and product linearities (%)[b]) in catalytic hydroformylation[c]

Chiral bisphosphine	Styrene	1-Butene	*cis*-2-Butene	2-Phenylpropene
Temp	80 °C	90 °C	120 °C	150 °C
IIa	0.16 (17)	0.31 (72)	0.21 (0)	0.23 (85)
IIb	0.70 (9)	0.90 (60)	0.50 (1)	0.71 (72)
IIIa	0.47 (35)	2.8 (89)	0.65 (2)	1.3 (86)
IIIb	1.9 (10)	3.5 (68)	0.77 (5)	1.6 (79)
IVa[d]	8.2 (29)	6.4 (90)	0.76 (2)	2.3 (78)
IVb[d]	14 (14)	12 (72)	3.9 (6)	20 (76)

a) Maximum pressure drop, kgw/cm² in 1 h. b) Linear aldehyde/(linear aldehyde + branched aldehyde) × 100. c) Rh: $[RhCl(CO)_2]_2$. d) Rh: $[Rh(CO)_3]_4$.

groups. Upon chelating coordination, the four phenyl groups may protrude toward the coordination sites for a substrate and others, and they are considered to be responsible for the steric regulation. The phenyl group will take various conformations. In contrast to this, in the case of bisphosphines with 5*H*-dibenzophosphol-5-yl (DBP) groups which correspond to the planar Ph_2P groups whose phenyl groups are linked together at the *ortho*-positions, the influence of the rotation of the phenyl group can be excluded.

From this point of view, IIa, IIIa, and IVa, all with Ph_2P groups, were compared with IIb, IIIb, IVb, which have DBP ones. The substitution of DBP groups for Ph_2P ones always brought about a rate enhancement,[19] as is shown in Table 3. Moreover, Table 2 shows that the optical yields in the hydroformylation of styrene and butenes increased in the cases of III and IV upon DBP substitution. The orders of the asymmetric induction abilities among IIb≈IVb were IVb>IIIb>IIb for styrene and IVb—IIIb>IIb for butenes. Thus, IIIb and IVb were the most effective among the bidentate chiral ligands prepared in this study; this is in remarkable contrast to their lower stereoselectivity than IIIa and IVa in asymmetric hydrogenation. On the other hand, the prevailing configuration of the hydrogenation product from α-acetamidocinnamic acid was reversed through the substitution of DBP groups for Ph_2P ones, as is shown in Table 2.[20] In the hydroformylation of styrene and butenes also, IIIb or IVb prefered the opposite antipode to that IIIa or IVa prefered, respectively.

However, by the use of the II of a cyclohexane-ring skeleton, DBP-substitution for Ph_2P groups decreased the optical yields in the hydroformylation of styrene and 1-butene. In addition, the prevailing absolute configuration of the products was not reversed for all the olefins. Thus, the results with II were different from those with III or IV, which has a five- or four-membered ring skeleton, respectively. Furthermore, in the hydroformylation of styrene by the use of IIb, as the reaction temperature rose, the prevailing enantiomer was reversed at around 100 °C, and the optical purity of the product increased with an increase in the temperature up to about 160 °C, as is shown in Fig. 1.[22] This is in contrast with the behavior of IIIb or IVb, which invariably gave prevailing enantiomer

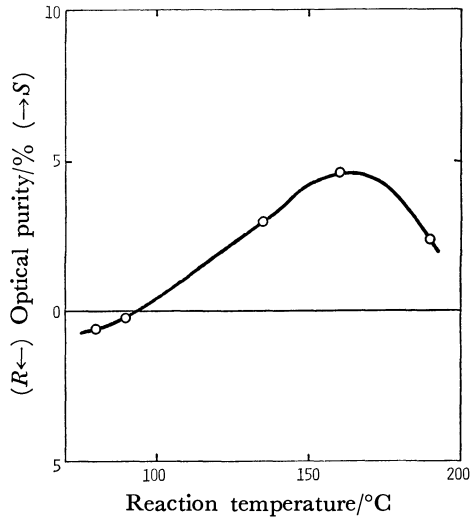

Fig. 1. Effect of reaction temperature on the optical purity of 2-phenylpropanal produced in the hydroformylation of styrene catalyzed by Rh-IIb system. (Other conditions are the same as in Table 2).

with a decrease in the stereoselectivity when the reaction temperature was raised in this range.

The present authors previously reported that the asymmetric induction abilities of IIIb and IVb were fairly high to a vinylidene-type olefin, 2-phenylpropene (V), in hydroesterification.[24] However, it is noteworthy that the abilities of I—IV remained low in the hydroformylation of V (Table 2). This is partly because the low reactivity of V requires a high reaction temperature (150 °C).

References

1) M. Tanaka, Y. Watanabe, T. Mitsudo, K. Yamamoto, and Y. Takegami, *Chem. Lett.*, **1972**, 483.
2) I. Ogata and Y. Ikeda, *Chem. Lett.*, **1972**, 487.
3) G. Consiglio, C. Botteghi, C. Salomon, and P. Pino, *Angew. Chem. Int. Ed. Engl.*, **12**, 669 (1973), and the preceeding papers.
4) R. Stern, A. Hirschauer, and L. Sajus, *Tetrahedron Lett.*, **1973**, 3247.
5) D. Valentine, Jr. and J. W. Scott, *Synthesis*, **1978**, 329.
6) Y. Kawabata, T. Hayashi, and I. Ogata, *J. Chem. Soc., Chem. Commun.*, in press.
7) M. Tanaka, Y. Ikeda, and I. Ogata, *Chem. Lett.*, **1975**, 1115.
8) M. Tanaka and I. Ogata, *J. Chem. Soc., Chem. Commun.*, **1975**, 735.
9) M. Tanaka and I. Ogata, 32nd National Meeting of the Chemical Society of Japan, 3C04, Tokyo, April 1975; R. Glaser, S. Geresh, J. Blumenfeld, and M. Twaik, *Tetrahedron*, **34**, 2405 (1978).
10) M. Tanaka, Y. Ikeda, T. Hayashi, and I. Ogata, 23rd Symposium of Organometallic Chemistry Japan, 204A, Tokyo, October, 1975.
11) H. B. Kagan and T. -P. Dang, *J. Am. Chem. Soc.*, **94**, 6429 (1972).
12) Rhone Poulenc S. A., Japan Kokai, 50-52049 (1975); R. Glaser, J. Blumenfeld, and M. Twaik, *Tetrahedron Lett.*, **1977**, 4639.
13) M. Tanaka, T. Hayashi, and I. Ogata, 36th National

Meeting of the Chemical Society of Japan, 3E41, Osaka, April 1977.
14) D. E. Applequist and N. D. Werner, *J. Org. Chem.*, **28**, 48 (1963).
15) G. A. Haggis and L. N. Owen, *J. Chem. Soc.*, **1953**, 389.
16) S. Sabetay, *Bull. Soc. Chim. Fr.*, **47**, 614 (1930).
17) R. M. Herbst and D. Shemin, *Org. Synth.*, Coll. Vol. II, 1 (1943).
18) R. Glaser, M. Twaik, S. Geresh, and J. Blumenfeld, *Tetrahedron Lett.*, **1977**, 4635.
19) The present authors reported the rate-enhancement effect of DBP-substitution for Ph_2P groups in ligands generally observed in catalytic hydroformylation; see T. Hayashi, M. Tanaka, and I. Ogata, *J. Mol. Catal.*, **6**, 1 (1979).
20) IIIb has been established as giving the antipode of *N*-acetylphenylalanine opposite to that obtained by the use of IIIa.[21]
21) T. -P. Dang, J. -Poulin, and H. B. Kagan, *J. Organomet. Chem.*, **91**, 105 (1975).
22) A similar phenomenon was also observed by the use of neomenthyldiphenylphosphine.[23]
23) M. Tanaka, Y. Watanabe, T. Mitsudo, and Y. Takegami, *Bull. Chem. Soc. Jpn.*, **47**, 1698 (1974).
24) Up to a 69% optical yield has been attained; see T. Hayashi, M. Tanaka, and I. Ogata, *Tetrahedron Lett.*, **1978**, 3925.
25) F. Knoop and J. G. Blanco, *Z. Phys. Chem.*, **146**, 272 (1925).
26) P. W. B. Harrison, J. Kenyon, and J. R. Shepherd, *J. Chem. Soc.*, **1926**, 658.
27) C. Botteghi, G. Consiglio, and P. Pino, *Justus Liebigs Ann. Chem.*, **1974**, 864.
28) E. J. Badin and E. Pacsu, *J. Am. Chem. Soc.*, **67**, 1352 (1945).
29) Determined through the reduction to 3-phenyl-1-butanol. M. Tanaka, unpublished result.

Reaction of Diazonium Salts with Transition Metals. II. Palladium-catalyzed Arylation of Ethylene with Arenediazonium Salts

Kiyoshi KIKUKAWA,* Kazuhiko NAGIRA, Nobuyuki TERAO, Fumio WADA, and Tsutomu MATSUDA

Department of Organic Synthesis, Faculty of Engineering, Kyushu University, Hakozaki, Higashi-ku, Fukuoka 812

(Received January 6, 1979)

Arylation of ethylene (7 atm) was carried out with various arenediazonium tetrafluoroborates (25 mmol) in the presence of bis(dibenzylideneacetone)palladium (0.5 mmol) and sodium acetate (75 mmol). Substituted styrenes were obtained in good yields (61—78%) under mild reaction conditions (1 h, room temperature) in a 1:1 mixture of acetone and dichloromethane, with some exceptions. Phenylbutenes, main by-products in dichloromethane, were presumed to form by the reaction of styrene with ethylene under catalysis of hydridopalladium species.

Previous work[1] has shown that arenediazonium salts are good arylating reagents of olefins in the presence of palladium(0) catalyst. The reaction not only proceeds under much milder conditions than those for the related palladium-catalyzed arylations,[2-4] but also was found to be applicable to unactivated olefins as compared to the copper salt catalyzed arylation (Meerwein arylation[5]). The direct synthesis of 4′-vinylbenzocrown[6] from ethylene and 4′-aminobenzocrown is an example to show synthetic utility of the present arylation, especially to one or more substituted aryl olefins. This paper describes a continuation of our studies on the arylation of ethylene with a variety of monosubstituted benzenediazonium salts to improve yield and to gain a scope of the reaction (reaction 1). A related arylation of ethylene using bromobenzene derivatives has been recently reported.[7]

$$X\text{-}C_6H_4\text{-}N_2^+BF_4^- \xrightarrow[Pd(dba)_2,\ NaOAc]{CH_2=CH_2} X\text{-}C_6H_4\text{-}CH=CH_2 + N_2 \quad (1)$$

X = CH_3, CH_3O, CO_2Et, Cl, Br, and NO_2

Results and Discussion

Reaction of Ethylene with Monosubstituted Benzenediazonium Salts. Although the reaction can be conducted either in aqueous or in non-aqueous media, this study was carried out in the latter system (acetone, dichloromethane or their mixture) by considering increased solubility of ethylene, and tetrafluoroborates (25 mmol) were reacted in the presence of bis(dibenzylideneacetone)palladium(0) [$Pd(dba)_2$] as the catalyst (0.5 mmol). Preliminary experiments with benzenediazonium salt revealed that the formation of stilbene, one of the possible by-products,[7] was very little (below 1%) under the pressure of ethylene of 6—8 atm in both solvents. However, in dichloromethane a considerable amount (30—40% of the product) of higher boiling product was produced (*vide infra*). The by-product did not form in acetone, but the total yield rather decreased (Table 1). Use of a mixture of the solvents(1:1 v/v) was found to give good yield, preventing the formation of the higher boiling product. The amount of the solvent influenced the formation of tarry material which had to be removed from the reaction mixture by chromatography on silica gel, and 150 ml of the solvent to 25 mmol of the diazonium salt was found enough to eliminate the treatment. Thus, the product (styrene and substituted styrenes) could be isolated by simple distillation of the reaction mixture in the presence of a small amount of *t*-butylcatechol. The results were summarized in Table 2. In most cases, substituted styrenes were obtained in good yields in 1 h and at room temperature (20—25 °C). The low yield of vinylmesitylene can be explained by steric effect of the two ortho substituents to suppress the formation of an arenepalladium species, a plausible active intermediate[1], in view of a good result obtained with *o*-methyl counterpart. Nitrobenzenediazonium salts are known to be good substrates in Meerwein arylation, which is generally considered

Table 1. Effects of conditions in the reaction of benzenediazonium salt

Temp °C	Time min	Solvent/ml $(CH_3)_2CO$	Solvent/ml CH_2Cl_2	Yield/%[a] Styrene	Yield/%[a] By-product
0	120	0	100	20	15
0	120	100	0	20	0
r. t.	60	0	100	40	17
r. t.	60	100	0	40	0
r. t.	60	50	50	51	0

a) Analyzed by GLC for the product solution being passed through a silica-gel column. Internal standard; decane. The yield of the by-product was calculated as phenylbutene.

Table 2. Yields of substituted styrenes[a]

Substituent	Yield/%	Substituent	Yield/%
o-CH_3	75	2,4,6-(CH_3)	3[b]
m-CH_3	30	*p*-OCH_3	62
p-CH_3	61	*p*-CO_2CH_3	62
o-Cl	75	*p*-Br	14[c]
m-Cl	78	*p*-NO_2	3[d]
p-Cl	63	*o*-NO_2	—[d]

a) See experimental section for the reaction conditions. b) Mesitylene was produced (18%). c) Ten mg of 4,4′-dibromostilbene was isolated. d) The main product was nitrobenzene (28—32%).

to proceed by a radical process, but in the present reaction reduction to nitrobenzene was the principal course, though 11% of substitution product had been obtained in the reaction with cyclopentene.[1] Purity or stability of a diazonium salt seems to be one of the factors influencing the product yield in this procedure. Thus, *m*-methylbenzenediazonium tetrafluoroborate, which is much more sensitive to decomposition than the other isomers, gave a lower yield. Under the similar conditions naphthalene-2-diazonium salt gave 72% yield of 2-vinylnaphthalene, mp 64—66 °C (lit,[8] mp 65—66 °C).

Structure and Its Possible Route of Formation of the Higher-boiling Product. As mentioned above, a considerable amount of higher-boiling product consisted of at least three components was produced in the arylation with benzenediazonium salt in dichloromethane. Hydrogenation of the fraction over Raney nickel gave a mixture containing *s*-butylbenzene and *n*-butylbenzene in a ratio of 11 to 1. The main component of the by-product by preparative GLC was proved to be *trans*-2-phenylbut-2-ene by comparison with an authentic sample (GLC and NMR), but the remainders, probably a combination of 1-phenylbutenes and the other 2-phenylbutenes, could not be isolated in pure form to allow their structural confirmations. In order to obtain some informations suggesting a likely route to the phenylbutene, the reaction of ethylene was carried out in the presence of styrene (30 mmol) under the conditions used in the above reaction except for the use of a reduced amount of benzenediazonium salt (2 mmol). The amount of the salt is only two equivalents of the palladium catalyst (1 mmol), and was selected with the object of generating hydridopalladium species. No phenylbutenes was produced in acetone, while in dichloromethane there was obtained 32% yield of the higher-boiling product and neither stilbene nor any dimers of styrene were detected. The yield was based on styrene added and much over 100% based on the diazonium salt. On hydrogenation the product afforded an 8 : 1 mixture of *s*-butylbenzene and *n*-butylbenzene. The results show that the phenyl butenes produced by the reaction of styrene and ethylene under the catalysis of the hydridopalladium species. The difference between the behavior of the two solvents may be rationalized by the lability of the catalyst to collapse to palladium(0) under the present reaction conditions. In this connection, it is noted that 1-phenylbutenes were the principal products in the related palladium-catalyzed codimerization reported previously.[9,10]

Experimental

Materials. $Pd(dba)_2$ was prepared by the published method.[11] Substituted anilines were commercial origin and used as received. Most of the arylamines were diazotized in aqueous 1:1 mixture of HBF_4 (42%) with aq $NaNO_2$ at 0 °C. White crystals precipitated were washed with cold 5% HBF_4, cold methanol, and cold ether. The tetrafluoroborate was dried under vacuum and stored in a refrigerator until to be used. Diazotization of those with nitro and ethoxycarbonyl groups was performed in aq H_2SO_4, and the precipitates obtained by addition of HBF_4 (42%) to the mixture at 0 °C were treated as above. Authentic 1-phenylbut-1-ene and *trans*-2-phenylbut-2-ene were prepared by dehydration of 1-phenylbutan-1-ol and 2-phenylbutan-2-ol, respectively. The solvents were distilled and used without further purification.

General Procedure for the Arylation of Ethylene. A mixture of $Pd(dba)_2$ (0.29 g, 0.05 mmol), NaOAc(6.15 g, 75 mmol), and 150 ml of a mixed solvent (acetone and dichloromethane, 1:1) in a glass autoclave(300 ml) was cooled in a Dry Ice–acetone bath, and arenediazonium tetrafluoroborare (25 mmol) was added (addition at a higher temperature caused a reaction of the diazonium salt with the catalyst). After the air in the vessel was displaced with ethylene, the mixture was allowed to warm to room temperature. Ethylene was introduced to a pressure of 6—8 atm and the mixture was stirred for 1 h at room temperature. The reaction mixture was neutralized with aq sat $NaHCO_3$ soln and washed with aq sat NaCl soln, and dried ($MgSO_4$). The solution was placed in a distilling flask containing a small amount of *t*-butylcatechol and the solvent was removed. The residue was distilled under vacuum to give the product. After purity of the distillate was checked by GLC, its structure was confirmed by IR and NMR analyses ($\nu_{C=C}$; 1620—1640 cm^{-1}, δ_{C-H}; 900—910 cm^{-1}, and ABX pattern due to $-CH=CH_2$). Formation of stilbene was examined for the distillation residue by recrystallization or column chromatography (silica gel).

References

1) K. Kikukawa and T. Matsuda, *Chem. Lett.*, **1977**, 159.
2) R. F. Heck, *J. Am. Chem. Soc.*, **93**, 6896 (1971); H. A. Dieck and R. F. Heck, *ibid.*, **96**, 1133 (1974).
3) J. B. Melpolder and R. F. Heck, *J. Org. Chem.*, **41**, 265 (1976).
4) A. J. Chalk and S. A. Magennis, *J. Org. Chem.*, **41**, 273 (1976).
5) C. S. Rondestvedt, Jr., "Organic Reactions," John Wiley & Sons, New York, Vol. 11, (1960), p. 189 and Vol. 24, (1976), p. 225.
6) K. Kikukawa, K. Nagira, and T. Matsuda, *Bull. Chem. Soc. Jpn.*, **50**, 2207 (1977).
7) J. E. Plevyak and R. F. Heck, *J. Org. Chem.*, **43**, 2454 (1978).
8) D. T. Mowry, M. Renoll, and W. F. Huber, *J. Am. Chem. Soc.*, **68**, 1105 (1946).
9) K. Kawamoto, T. Imanaka, and S. Teranishi, *Bull. Chem. Soc. Jpn.*, **43**, 2512 (1970).
10) M. G. Barlow, M. J. Bryant, R. N. Haszeldine, and A. G. Mackie, *J. Organomet. Chem.*, **21**, 215 (1970).
11) T. Ukai, H. Kawazura, Y. Ishii, J. J. Bonnet, and J. A. Ibers, *J. Organomet. Chem.*, **65**, 253 (1974).

Synthesis of Coleon U 12-Methyl Ether

Takashi MATSUMOTO* and Shoji TAKEDA

Department of Chemistry, Faculty of Science, Hiroshima University, Higashisenda-machi, Hiroshima 730

(Received January 16, 1979)

Reduction of 11-benzoyloxy-12-methoxyabieta-8,11,13-trien-7-one with sodium borohydride, followed by dehydration of the resulting alcohols with *p*-toluenesulfonic acid, afforded the corresponding 6,8,11,13-tetraene derivative. This was converted into 11-benzoyloxy-12-methoxyabieta-8,11,13-trien-6-one (**8**) *via* an epoxide. The 6-oxo compound (**8**) was reduced with lithium aluminium hydride. Subsequent oxidation of the resulting alcohol with *m*-chloroperbenzoic acid afforded 6*β*-hydroxy-12-methoxyabieta-8,12-diene-11,14-dione. This compound was further transformed into 11,14-diacetoxy-12-methoxyabieta-8,11,13-trien-6-one (**13**) by a series of reactions: Jones oxidation, reduction with a mixture of zinc powder and hydrochloric acid, and acetylation. The diacetate (**13**) was then oxidized with Jones reagent and the 6,7-dioxo product was immediately converted into 11-acetoxy-6,14-dihydroxy-12-methoxyabieta-5,8,11,13-tetraene (**15**) by repeated column chromatography on silica gel. The tetraene (**15**) was finally hydrolyzed with hydrobromic acid to give coleon U 12-methyl ether.

The isolation and structural elucidation have been reported for many naturally-occurring highly-oxygenated tricyclic diterpenes with a fully substituted aromatic C ring. Some of these also possess the oxygen functions at both the C-6 and C-7 positions in ring B, as depicted in coleon U (**1**) and coleon V (**2**), which were isolated as pigments from leaf-glands of *Plectranthus myrianthus* Briq. (*Labiatae*) by Eugster *et al.*[1] As a part of our synthetic studies on the naturally-occurring diterpenes we attempted to devise an efficient synthetic route for these highly-oxygenated tricyclic diterpenes. This paper will describe a successful synthesis of coleon U 12-methyl ether (**3**), starting from the optically active 11-benzoyloxy-12-methoxyabieta-8,11,13-trien-7-one (**4**) which was previously synthesized[2] from (+)-ferruginol (**5**). Since the total synthesis of (+)-**5** has recently been accomplished in our laboratory,[3] the present work can be regarded as a total synthesis of **3**.

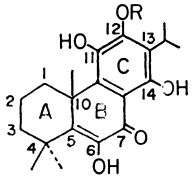

1 R=H
3 R=Me

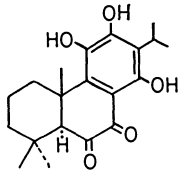

2

Reduction of the carbonyl group in **4** with sodium borohydride in methanol afforded a mixture of the corresponding epimeric alcohols (**6**), which was immediately dehydrated with *p*-toluenesulfonic acid in refluxing toluene to give 11-benzoyloxy-12-methoxyabieta-6,8,11,13-tetraene (**7**) in nearly quantitative yield. The tetraene (**7**) was then subjected to epoxidation at 0—5 °C with *m*-chloroperbenzoic acid in dichloromethane. The resulting epoxide, without purification, was refluxed with hydrochloric acid in ethanol to produce 11-benzoyloxy-12-methoxyabieta-8,11,13-trien-6-one (**8**), whose IR spectrum showed an absorption band of a newly formed carbonyl group at 1718 cm^{-1}. Treatment of **8** with lithium aluminium hydride in refluxing ether afforded an alcohol (**9**). The *β*-configuration of the hydroxyl group at the C-6 position was supported by its NMR spectrum, which showed a signal at δ 4.51 ppm with a half-height width of 9 Hz, suggesting the presence of an equatorial α hydrogen. To introduce an oxygen function at the C-14 position, **9** was oxidized at room temperature with *m*-chloroperbenzoic acid in dichloromethane; the desired 6*β*-

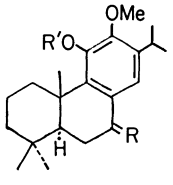

4 R=O, R'=COPh
6 R=H, OH; R'=COPh

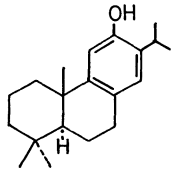

5

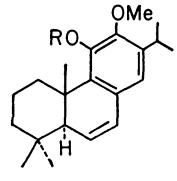

7 R=COPh

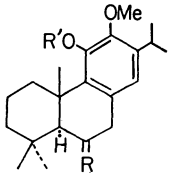

8 R=O, R'=COPh
9 R=α-H, β-OH; R'=H

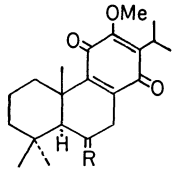

10 R=α-H, β-OH
11 R=O

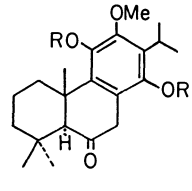

12 R=H
13 R=Ac

hydroxy-12-methoxyabieta-8,12-diene-11,14-dione (**10**) was obtained in 55% yield. The C-14 aromatic proton singlet (δ 6.32 ppm) in **9** disappeared in the NMR spectrum of **10**, while its IR spectrum showed *p*-quinone bands at 1655, 1640, and 1605 cm^{-1}. Oxidation of **10** with Jones reagent at 0—5 °C gave 12-methoxyabieta-8,12-diene-6,11,14-trione (**11**) which, without purification, was used in the next reaction. For the protection of the unstable C ring, the trione (**11**) was reduced with a mixture of zinc powder and dilute hydrochloric acid in refluxing benzene. The resulting crude phenol (**12**) was further acetylated at 75—80 °C with acetic anhydride in pyridine to give 11,14-diacetoxy-12-methoxyabieta-8,11,13-trien-6-one (**13**: 53% yield from **10**). Subsequently, oxidation of the C-7 position in **13** was carried out with Jones reagent at room temperature. The resulting crude 6,7-dioxo compound (**14**) was immediately subjected to repeated column chromatography on silica gel to afford a diosphenol derivative, 11-acetoxy-6,14-dihydroxy-12-methoxyabieta-5,8,11,13-tetraen-7-one (**15**), whose NMR spectrum showed signals due to an acetoxyl group at δ 2.35 ppm, a C-6 hydroxyl group at δ 6.92 ppm, and a hydrogen-bonded C-14 hydroxyl group at δ 13.00 ppm. The acetate (**15**) was finally hydrolyzed at 95—100 °C with hydrobromic acid in acetic acid under a nitrogen atmosphere to afford a phenol (**3**), mp 174—176 °C, $[\alpha]_D$ −12.4° ($CHCl_3$), which was shown to be identical with the authentic coleon U 12-methyl ether by mixed melting point determination and by IR and NMR spectral comparisons.

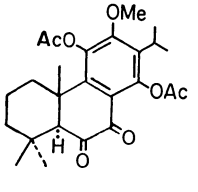

14

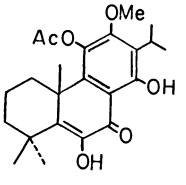

15

Experimental

All melting points are uncorrected. The IR spectra were taken in chloroform, and the NMR spectra in carbon tetrachloride at 60 MHz, with tetramethylsilane as an internal standard, unless otherwise stated. The chemical shifts are presented in terms of δ values; s: singlet, bs: broad singlet, d: doublet, bd: broad doublet, dd: double doublet, m, multiplet. The optical rotations were measured in chloroform using a Yanaco OR-50D. Column chromatography was performed using Merck silica gel (0.063 mm).

*11-Benzoyloxy-12-methoxyabieta-6,8,11,13-tetraene (**7**).* Sodium borohydride (650 mg) was added at 15—20 °C to a stirred solution of 11-benzoyloxy-12-methoxyabieta-8,11,13-trien-7-one (**4**)[2] (1.870 g) in methanol (250 ml). The mixture was stirred at this temperature for 4 h, acidified with dilute hydrochloric acid, and concentrated *in vacuo*. The residue was extracted with ether and the ether extract was washed with brine, dried over sodium sulfate, and then evaporated to afford a mixture of the corresponding 7α- and 7β-alcohol (**6**) which, without purification, was used in the next reaction.

The above mixture (**6**) was refluxed for 2 h with *p*-toluenesulfonic acid (250 mg) in dry toluene (12 ml), cooled, and then diluted with ether. The ether solution was washed with aqueous sodium hydrogencarbonate and water, dried over sodium sulfate, and evaporated *in vacuo*. The crude product was purified by column chromatography on silica gel (100 g) using benzene as the eluent to give a tetraene (**7**) (1.760 g: 97.7%), which was recrystallized from acetone-methanol; mp 151.5—152.5 °C, $[\alpha]_D$ −67.8°; IR: 1734 cm^{-1}; NMR: 0.97 and 1.02 (each 3H and s, $-\underset{|}{C}(CH_3)_2$), 1.14 and 1.20 (each 3H, d, and J=6.5 Hz, $-CH(C\underline{H}_3)_2$), 1.30 (3H, s, $C_{10}-CH_3$), 3.60 (3H, s, $-OCH_3$), 5.87 (1H, dd, J=3 and 9.5 Hz, C_6–H), 6.43 (1H, dd, J=3 and 9.5 Hz, C_7–H), 6.73 (1H, s, C_{14}–H), 7.3—7.7 (3H, m) and 8.0—8.3 (2H, m) (aromatic protons). Found: C, 80.48; H, 8.16%. Calcd for $C_{28}H_{34}O_3$: C, 80.34; H, 8.19%.

*11-Benzoyloxy-12-methoxyabieta-8,11,13-trien-6-one (**8**).* A solution of **7** (1.760 g) and *m*-chloroperbenzoic acid (70%: 1.14 g) in dichloromethane (20 ml) was allowed to stand at 0—5 °C for 45 min. The solution was diluted with ether and then washed successively with aqueous potassium iodide, aqueous sodium thiosulfate, aqueous sodium hydrogencarbonate, and water. After drying over sodium sulfate, the solution was evaporated *in vacuo* to give a crude epoxide which was immediately subjected to the next reaction.

A solution of the above epoxide and concentrated hydrochloric acid (2.0 ml) in ethanol (40 ml) was refluxed for 1.5 h. After the solution had been concentrated *in vacuo*, the residue was extracted with ether. The ether extract was washed with aqueous sodium hydrogencarbonate and brine, dried over sodium sulfate, and then evaporated *in vacuo*. The crude product was recrystallized from ethanol to give a ketone (**8**) (580 mg: 31.8%); mp 182—184 °C; $[\alpha]_D$ +105°; IR: 1735; 1718 cm^{-1}; NMR: 1.05 and 1.31 (each 3H and s, $-\underset{|}{C}(CH_3)_2$), 1.25 (6H, bd, J=7 Hz, $-CH(C\underline{H}_3)_2$), 1.31 (3H, bs, $C_{10}-CH_3$), 2.50 and 2.68 (each *ca.* 0.5H and bs, C_5–H),[4] 3.57 and 3.65 (each *ca.* 2.5H and bs, $-COCH_2-$ and $-OCH_3$),[4] 6.79 (1H, s, C_{14}–H), 7.45—7.7 (3H, m) and 8.05—8.35 (2H, m) (aromatic protons). Found: C, 77.29; H, 7.87%. Calcd for $C_{28}H_{34}O_4$: C, 77.39; H, 7.89%.

The mother liquor of the above crystallization was evaporated *in vacuo* and the residue was chromatographed on silica gel (80 g) using ether–benzene (1 : 99) as the eluent to give additional **8** (485 mg: 26.6%).

*12-Methoxyabieta-8,11,13,-triene-6β,11-diol (**9**).* A mixture of **8** (1.460 g), lithium aluminium hydride (380 mg), and dry ether (50 ml) was refluxed for 1.5 h. The mixture was poured into a mixture of ice and aqueous ammonium chloride, and extracted with ether. The ether extract was washed with brine, dried over sodium sulfate, and evaporated *in vacuo*. The residue was purified by column chromatography on silica gel (20 g), using ether–benzene (3:97) as the eluent, to give an alcohol (**9**) (908 mg: 80.8%), which was recrystallized from hexane; mp 157.5—158.5 °C; $[\alpha]_D$ +34.8°; IR: 3520, 3410 cm^{-1}; NMR: 1.03 and 1.27 (each 3H and s, $-\underset{|}{C}(CH_3)_2$), 1.19 and 1.21 (each 3H, d, and J=7 Hz, $-CH(C\underline{H}_3)_2$), 1.65 (3H, s, $C_{10}-CH_3$), 3.72 (3H, s, $-OCH_3$), 4.51 (1H, m, $W_{1/2}$=9 Hz, C_6–H), 5.92 (1H, s, C_{11}–OH), 6.32 (1H, s, C_{14}–H). Found: C, 75.84; H, 9.73%. Calcd for $C_{21}H_{32}O_3$: C, 75.86; H, 9.70%.

*6β-Hydroxy-12-methoxyabieta-8,12-diene-11,14-dione (**10**).* A solution of **9** (386 mg) and *m*-chloroperbenzoic acid (80%: 429 mg) in dichloromethane (10 ml) was allowed to stand at room temperature for 30 h, and then diluted with ether. The solution was washed successively with aqueous potassium iodide, aqueous sodium thiosulfate, aqueous sodium hydrogencarbonate, and brine. After drying over

sodium sulfate, the solution was evaporated *in vacuo* and the crude product was purified by column chromatography on silica gel (40 g), using ether–benzene (2:98) as the eluent, to give the recovered **9** (64 mg: 16.6%) and a quinone compound (**10**) (222 mg: 55.2%) which was recrystallized from methanol; mp 212—214 °C; $[\alpha]_D$ −51.9°; IR 3625, 3525, 1655, 1640, 1605 cm^{-1}; NMR ($CDCl_3$): 1.02 and 1.26 (each 3H and s, $-\dot{C}(CH_3)_2$), 1.21 (6H, d, J=7 Hz, $-CH(C\underline{H}_3)_2$), 1.69 (3H, s, $C_{10}-CH_3$), 3.90 (3H, s, $-OCH_3$), 4.67 (1H, m, $W_{1/2}$=9 Hz, C_6–H). Found: C, 72.81; H, 8.75%. Calcd for $C_{21}H_{30}O_4$: C, 72.80; H, 8.73%.

*11,14-Diacetoxy-12-methoxyabieta-8,11,13-trien-6-one (**13**).* A solution of **10** (495 mg) in acetone (20 ml) was oxidized with Jones reagent (2.67 mol dm^{-3}: 0.75 ml) at 0—5 °C for 5 min and then diluted with ether. The solution was washed with brine, dried over sodium sulfate, and evaporated *in vacuo* to give a crude 6-oxo compound (**11**); IR: 1720, 1655, 1640, 1605 cm^{-1}.

The above crude compound (**11**) was dissolved in benzene (12 ml) and the solution was stirred and refluxed for 10 min with a mixture of zinc powder (1.2 g) and dilute hydrochloric acid (10%: 12 ml). After cooling, the mixture was extracted with ether and the extract was washed with brine, dried over sodium sulfate, and evaporated *in vacuo* to give a crude phenol (**12**).

The crude phenol (**12**) was immediately acetylated at 75—80 °C for 1.5 h with acetic anhydride (1.0 ml) and pyridine (2.0 ml). After the usual work-up, the product was purified by column chromatography on silica gel (30 g), using ether–benzene (5:95) as the eluent, to give a diacetate (**13**) (327 mg: 53%) which was recrystallized from methanol; mp 183.5—185 °C; $[\alpha]_D$ +130°; IR: 1765, 1720 cm^{-1}; NMR ($CDCl_3$): 1.02 and 1.22 (each 3H and s, $-\dot{C}(CH_3)_2$), 1.29 (6H, d, J=7 Hz, $-CH(C\underline{H}_3)_2$), 1.36 (3H, s, $C_{10}-CH_3$), 2.34 (6H, s, 2-$OCOCH_3$), 2.65 (1H, bs, C_5–H), 3.25(2H, bs, $-COCH_2-$), 3.74 (3H, s, $-OCH_3$). Found: C, 69.79; H, 8.06%. Calcd for $C_{25}H_{34}O_6$: C, 69.74; H, 7.96%.

*11-Acetoxy-6,14-dihydroxy-12-methoxyabieta-5,8,11,13-tetraen-7-one (**15**).* A solution of **13** (372 mg) in acetone (6.0 ml) was oxidized with Jones reagent (2.67 mol dm^{-3}: 0.6 ml) at room temperature for 2 h. After the same work-up as described for the preparation of **11**, the crude 6,7-dioxo compound (**14**) was purified by repeated column chromatography (3 times) on silica gel, using hexane–chloroform (3:7) as the eluent, to give a diosphenol derivative (**15**) (129 mg: 37.2%) which was recrystallized from methanol; mp 145—146 °C; $[\alpha]_D$ +17.9°; IR: 3410, 3160, 1765, 1640, 1615, 1595 cm^{-1}; NMR ($CDCl_3$): 1.44 (9H, s, $-\dot{C}(CH_3)_2$ and $C_{10}-CH_3$), 1.38 (6H, bd, J=7 Hz, $-CH(C\underline{H}_3)_2$), 2.35 (3H, s, $-OCOCH_3$), 3.73 (3H, s, $-OCH_3$), 6.92 (1H, s, C_6–OH), 13.00 (1H, s, C_{14}–OH). Found: C, 68.66; H, 7.61%. Calcd for $C_{23}H_{30}O_6$: C, 68.63; H, 7.51%. Further elution gave the recovered **13** (176 mg: 47.4%).

*Coleon U 12-Methyl Ether (6,11,14-Trihydroxy-12-methoxyabieta-5.8,11,13-tetraen-7-one) (**3**).* A mixture of **15** (157 mg), 47% hydrobromic acid (0.5 ml), and acetic acid (4.0 ml) was heated at 95—100 °C for 1 h in a stream of nitrogen. The reaction mixture was cooled, diluted with ether, and then washed successively with water, aqueous sodium hydrogencarbonate, and brine. The dried solution was evaporated *in vacuo* and the residue was purified by column chromatography on silica gel (15 g) using hexane–chloroform (1 : 1) to give coleon U 12-methyl ether (**3**) (40 mg: 28.3%), which was recrystallized from hexane; mp 174—176 °C dec; $[\alpha]_D$ −12.4°; IR: 3520, 3410, 1642, 1617, 1598 cm^{-1}; NMR ($CDCl_3$); 1.40 and 1.42 (each 3H, d, and J=7 Hz, $-CH(C\underline{H}_3)_2$) 1.44 (6H, s, $-\dot{C}(CH_3)_2$), 1.65 (3H, s, $C_{10}-CH_3$), 3.79 (3H, s, $-OCH_3$), 5.74 (1H, s, C_{11}–OH), 6.93 (1H, s, C_6–OH), 12.57 (1H, s, C_{14}–OH). Found: C, 70.04; H, 7.94%. Calcd for $C_{21}H_{28}O_5$: C, 69.97; H, 7.83%. The identity of the synthetic sample (**3**) with natural coleon U 12-methyl ether was confirmed by mixed melting point determination and by IR and NMR spectral comparisons.

Further elution gave the recovered **15** (62 mg: 39.4%).

The authors are grateful to Arakawa Chemical Co. Ltd. for a generous gift of rosin. Thanks are also due to Professor C. H. Eugster for kindly supplying the natural sample.

References

1) T. Miyase, P. Ruedi, and C. H. Eugster, *Helv. Chim. Acta*, **60**, 2770 (1977).

2) T. Matsumoto and S. Harada, *Chem. Lett.*, **1976**, 1311, *Bull. Chem. Soc. Jpn.*, **52**, 1459 (1979).

3) T. Matsumoto and S. Usui, *Bull. Chem. Soc. Jpn.*, **52**, 212 (1979).

4) These signals arose from rotational isomers due to a methoxyl group, whose free rotation was restricted by two bulky ortho substituents: benzoyloxyl and isopropyl groups.

Asymmetric Cyclization of Propylene Chlorohydrins Catalyzed by an Optically Active Cobalt(salen) Type Complex

Tsutomu TAKEICHI, Michihiro ISHIMORI,* and Teiji TSURUTA

Department of Synthetic Chemistry, Faculty of Engineering, University of Tokyo, Bunkyo-ku, Tokyo 113

(Received January 26, 1979)

By using an optically active cobalt complex, *N,N'*-disalicylidene-(1*R*,2*R*)-1,2-cyclohexanediaminatocobalt(II), as a catalyst, optically active methyloxirane was synthesized by the asymmetric elimination of hydrogen chloride with a base from racemic propylene chlorohydrins. The highest optical purity of methyloxirane so far obtained was 35%, observed when 2-chloro-1-propanol and potassium carbonate were used as substrate and base, respectively. The optical rotations of the products and of the unchanged substrates indicate that (*S*)-1-chloro-2-propanol reacted selectively to produce (*S*)-methyloxirane, whereas in the case of 2-chloro-1-propanol, the (*R*)-isomer was preferentially cyclized to give (*S*)-methyloxirane with inversion of the asymmetric carbon. The physicochemical data of the circular dichroism and absorption spectra indicated a complexation of the optically active cobalt(II) species with potassium carbonate, either the (*R*)- or (*S*)-substrate interacting selectively with the Co*/K_2CO_3 complex formed, followed by cyclization of the substrate.

There has been considerable interest in the reactivities of the square-planar, tetradentate Schiff base complexes of cobalt, such as cobaloxime and Co(salen) in connection with coenzyme B_{12}.[1,2] The reactions of low-spin complexes of cobalt(I) and cobalt(II) with organic halides are of some biochemical importance and constitute a versatile preparative method for organocobalt compounds. Schrauzer has presented evidence indicating that the reaction of vitamin B_{12s} with alkyl halide follows an S_N2 mechanism,[3] involving powerfully nucleophilic cobalt(I) species. On the other hand, Halpern *et al.* reported that the cobalt(II) complexes such as pentacyanocobaltate(II) and cobaloxime(II) react with organic halides by a free radical mechanism.[4]

We recently reported the synthesis of an optically active cobalt complex, *N,N'*-disalicylidene-(1*R*,2*R*)-1,2-cyclohexanediaminatocobalt(II), Co(II)(sal)$_2$(*R*-CHXDA), and asymmetric reactions using the Co^I complexes, reduced derivatives of Co(II)(sal)$_2$(*R*-CHXDA).[5] In continuation of our studies,[6–8] we report here the synthesis of optically active methyloxirane by asymmetric cyclization of propylene chlorohydrins in the presence of the Co(II)(sal)$_2$(*R*-CHXDA) complex, a reaction which presumably involves an interaction between the cobalt species and C–Cl bond of the substrate prior to cyclization.

Experimental

Measurements. Absorption spectra were measured with a Shimadzu automatic recording spectrophotometer Model MPS-50L, and CD spectra with a JASCO Model J-20 spectrometer. Optical rotations were observed with a Perkin-Elmer Polarimeter Model 241. GLC analyses were carried out with a Hitachi Model K-53 Gas Chromatograph equipped with a column containing PEG. Thermogravimetry (TG) and differential thermal analyses(DTA) were made using a Rigaku-denki Model TG-DTA instrument.

Preparation of Co(II)(sal)$_2$(R-CHXDA). Reagents were purified by standard methods.[9] The Co(II)(sal)$_2$(*R*-CHXDA) complex was prepared by a method described previously. *N,N'*-Disalicylidene-(1*R*,2*R*)-1,2-cyclohexanediamine, prepared by the reaction of (1*R*,2*R*)-1,2-cyclohexanediamine and two molar equivalents of salicylaldehyde, was allowed to react with anhydrous cobalt acetate in 1-propanol at 60 °C for 1 h with stirring to give Co(II)(sal)$_2$(*R*-CHXDA) as an orange-red powder.[5]

Preparation of Propylene Chlorohydrin. 1-Chloro-2-propanol was prepared by modifying the procedure of Stewart and Vanderwerf.[10] Into a 2-L flask fitted with reflux condenser, stirrer, and dropping funnel was added 1L of dry ether and 50 g(1.28 mol) of $LiAlH_4$. After the mixture was cooled, 330 g(3.6 mol) of chloroacetone was added over a period of 6 h with stirring. The reaction mixture was stirred for 1 h before decomposition of the excess hydride with water. The ether layer was dried over magnesium sulfate, and 1-chloro-2-propanol was obtained by fractional distillation; bp 50.5 °C/30 mmHg, yield 55%. 2-Chloro-1-propanol was prepared by an analogous procedure involving the reduction of α-chloropropionic acid with $LiAlH_4$; bp 53 °C/29 mmHg, yield 35%.

Thermal Analyses of Potassium Carbonate and Co(II)(sal)$_2$(R-CHXDA). The TG and DTA curves of commercial potassium carbonate, Co(II)(sal)$_2$(*R*-CHXDA), and a mixture of the carbonate and Co^{II} complex are shown in Fig. 1. The results indicate that reagent grade potassium carbonate contains a small amount of water and that it can be completely dried by heating at 130—150 °C. The Co(II)(sal)$_2$(*R*-CHXDA) complex does not decompose on heating with carbonate up to 200 °C, as was also confirmed by infrared studies.

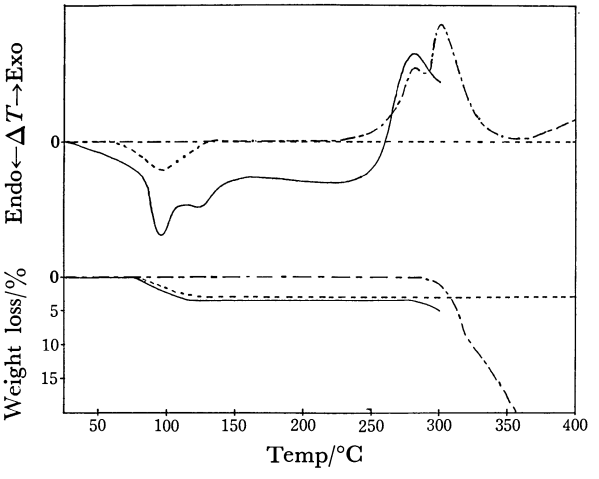

Fig. 1. TG and DTA curves for the systems of Co*(II)/K_2CO_3 (——), K_2CO_3 (----), and Co*(II) (———).

Asymmetric Cyclization of Propylene Chlorohydrins. Into a 50 ml-flask was charged 0.1895 g(0.5 mmol) of Co(II)-(sal)$_2$(*R*-CHXDA) and 8.292 g(60 mmol) of potassium carbonate. The mixture was dried at 130—150 °C for 3 h *in vacuo*. The experiment with hydrous K_2CO_3 did not require this period of heating. After cooling, 40 ml of solvent was added under dry nitrogen. A 120 mmol of 1-chloro-2-propanol or 2-chloro-1-propanol was added to the suspended solution and the reaction mixture was stirred at 25 °C. After an appropriate reaction time, the methyloxirane formed and the unconverted substrate were analyzed by gas chromatography. The optical rotations of the methyloxirane and propylene chlorohydrins recovered by fractional distillation were measured.

The optical purities (*e.e.*) of methyloxirane were evaluated from the optically pure methyloxirane, $[\alpha_o]_D=+12.53°$ (neat).[11] The expected optical purities ($e.e._{calcd}$) of methyloxirane in Tables 1 and 2 were evaluated from the optical purities of the recovered substrates; $e.e._{calcd}=[\alpha]/[\alpha_o]\{(100-\text{conv.})/\text{conv.}\}\times 100$. $[\alpha_o]_D=-19.19°$ (*c* 5.17 $CHCl_3$)[12] and $[\alpha_o]_D=-6.544°$ (neat) (calculated by, $[\alpha_o](\text{neat})=[\alpha_o](CHCl_3)\cdot[\alpha](\text{neat})/[\alpha](CHCl_3)$) for pure (*R*)-1-chloro-2-propanol. $[\alpha_o]_D=+17.39°$(neat)[13] for pure (*S*)-2-chloro-1-propanol.

Results and Discussion

The complex, *N*,*N*′-disalicylidene-(1*R*,2*R*)-1,2-cyclohexanediaminatocobalt(II), has been established as

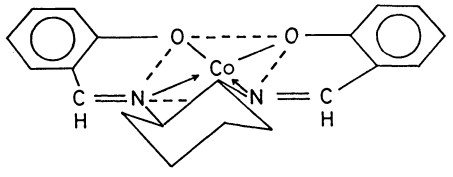

low-spin square-planar complex (μ_{eff} 2.41 B.M.) having a λ-conformation of the central chelate ring.[5] By using the Co(II)(sal)$_2$(*R*-CHXDA) complex as a catalyst, asymmetric cyclization of 1-chloro-2-propanol or of 2-chloro-1-propanol was examined, according to the following principle. Namely, optically active methyloxirane may be obtained when either (*R*)- or (*S*)-substrate selectively interacts with the optically

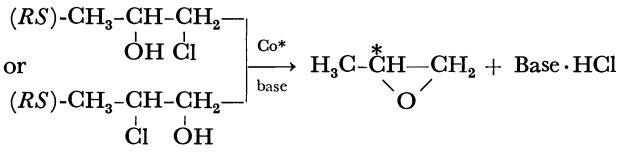

active cobalt species, followed by the elimination of hydrogen chloride from the selected substrate with a base. The results with [Co(III)(sal)$_2$(*R*-CHXDA)]$^+$I$^-$ reported previously,[8] and subsequent experiments using a variety of bases, revealed that the combination of Co(II)(sal)$_2$(*R*-CHXDA) with potassium carbonate was most effective for this asymmetric reaction.

Asymmetric Cyclization. The reactions of 1-chloro-2-propanol and of 2-chloro-1-propanol with potassium carbonate were carried out in the presence of catalytic amounts of Co(II)(sal)$_2$(*R*-CHXDA) in several solvents. To make comparison with these reactions, analogous experiments without the Co^{II} complex were performed under similar conditions. Potassium carbonate is hygroscopic, and thus a small amount of H_2O (or OH^-) contained in it may affect the asymmetric reaction by functioning as a solvating agent for K_2CO_3 and/or axial base for the Co^{II} complex. Thermal analyses (see Experimental) showed that commercial

Table 1. Synthesis of methyloxirane (Me-oxir) by the asymmetric cyclization of 1-chloro-2-propanol (1-Cl-PrOH)

Base	Solvent[a]	Co*(II)[b]	Time / day	Conv.[c] / %	Me-oxir[d] / 1-Cl-2-PrOH / %	Me-oxir $[\alpha]_D^{20}$[e] / °	Me-oxir *e.e.*[f] / %	1-Cl-2-PrOH $[\alpha]_D^{20}$[g] / °	1-Cl-2-PrOH $e.e._{calcd}$[h] / %
Hydrous K_2CO_3	Diox	yes	5	17.2	69	−3.05	24.3	−0.26	19.2
	Diox	—	5	6.7	23	—	—	—	—
	Diox/H_2O	yes	5	11.1	47	−2.96	23.6	−0.18	—
	PrOH	yes	5	47.8	80	−1.68	13.4	−0.98	16.3
	PrOH	—	5	47.0	77	—	—	—	—
	DCE	yes	5	42.5	86	−2.70	21.5	−1.26	25.9
	DCE	—	5	18.4	82	—	—	—	—
	CH_2Cl_2	yes	5	47.7	87	−1.14[i]	18.3	−1.15	19.3
	CH_2Cl_2	—	5	23.1	88	—	—	—	—
	PhCl	yes	5	43.1	85	−2.22	17.7	−2.85[j]	—
Dry K_2CO_3	Diox	yes	5	16.4	82	−2.83	22.6	−0.33	25.9
	PrOH	yes	5	28.2	96	−0.90	7.2	−0.25	9.7
	DCE	yes	5	47.7	87	−0.79	6.3	−1.11	18.5

a) Diox: dioxane, PrOH: 1-propanol, DCE: 1,2-dichloroethane, PhCl: chlorobenzene, Diox/H_2O: 40/1(v/v). b) Co(II)(sal)$_2$(*R*-CHXDA). c) Conversion of 1-Cl-2-PrOH. d) Me-oxir formed/1-Cl-2-PrOH converted (mol/mol) $\times 100$. e) Specific rotation of Me-oxir formed. f) Optical purity of Me-oxir formed; $[\alpha]_D=+12.53°$ (Ref. 11) for pure (*R*)-Me-oxir. g) Specific rotation of non-reacted 1-Cl-2-PrOH recovered. h) Optical purity of Me-oxir, evaluated from the optical purity of non-reacted 1-Cl-2-PrOH; $e.e._{calcd}=[\alpha]/[\alpha_o]\{(100-\text{conv.})/\text{conv.}\}\times 100$; $[\alpha_o]_D=-19.19°$ (*c* 5.17 $CHCl_3$) (Ref. 12), −6.544° (neat) [calcd, $[\alpha_0](\text{neat})=[\alpha_o](CHCl_3)\cdot[\alpha](\text{neat})/[\alpha](CHCl_3)$] or pure (*R*)-1-Cl-2-PrOH. i) Measured in CH_2Cl_2 soln. j) Measured in PhCl/*m*-xylene soln.

Table 2. Synthesis of methyloxirane (Me-oxir) by the asymmetric cyclization of 2-chloro-1-propanol (2-Cl-1-PrOH)

Base	Solvent[a]	Co*(II)[b]	Time day	Conv.[c] %	Me-oxir[d]/2-Cl-1-PrOH %	Me-oxir $[\alpha]_D^{20}$[e] °	Me-oxir *e.e.*[f] %	2-Cl-1-PrOH $[\alpha]_D^{20}$[g] °	2-Cl-1-PrOH *e.e.*$_{calcd}$[h] %
Hydrous K_2CO_3	Diox	yes	15	9.9	62	−4.44	35.4	+0.27[i]	—
	Diox	—	6	2.6	66	—	—	—	—
	PrOH	yes	5	39.7	83	−0.26	2.1	+0.22	1.9
	PrOH	—	5	33.9	87	—	—	—	—
	DCE	yes	4	20.3	77	−1.23	9.8	+0.75	16.7
	DCE	—	4	43.4	25	—	—	—	—
Dry K_2CO_3	Diox	yes	4	8.8	84	−4.39	35.0	+0.64	38.3
	Diox	—	4	trace	—	—	—	—	—
	PrOH	yes	5	41.9	87	−1.92	15.3	+1.71	13.6
	PrOH	—	5	35.5	75	—	—	—	—
	DCE	yes	5	40.3	88	−3.34	26.7	+3.25	27.7
	DCE	—	5	17.8	82	—	—	—	—

a)—h) As in Table 1. $[\alpha]_D^{25}=17.39°$ (neat) (Ref. 13) for pure (*S*)-2-Cl-1-PrOH. i) Measured in Diox/*m*-xylene soln.

potassium carbonate contained about 2.7% water (*i.e.*, 0.213 mol of H_2O per mol of K_2CO_3) and that the carbonate was completely dried by heating at 130—150 °C *in vacuo*. We used both dry potassium carbonate (dry K_2CO_3) and commercial carbonate (hydrous K_2CO_3) as bases for the cyclization reactions.

The results with 1-chloro-2-propanol and 2-chloro-1-propanol are summarized in Tables 1 and 2, respectively. All the asymmetric reactions gave (*S*)(−)-methyloxirane. The highest optical purity was 35.4% ($[\alpha]_D=-4.44°$), when the cyclization of 2-chloro-1-propanol was carried out in a dioxane solution. The highest *e.e.* value from 1-chloro-2-propanol was 24.3%, which was observed in the reaction with hydrous K_2CO_3 in dioxane as well. The unchanged 1-chloro-2-propanol recovered showed (−) optical rotation, while the unchanged 2-chloro-1-propanol gave (+) rotation. These facts suggest that (*S*)-L-(+)-1-chloro-2-propanol is selectively bound to the optically active cobalt complex and converted to (*S*)-L-(−)-methyloxirane where no reaction is involved at the asymmetric center. They also suggest that the cyclization reaction of (*R*)-D-(−)-2-chloro-1-propanol to (*S*)-L-(−)-methyloxirane involves an inversion of configuration at the asymmetric carbon. The stereochemistry of the oxirane formation from halohydrin can be explained

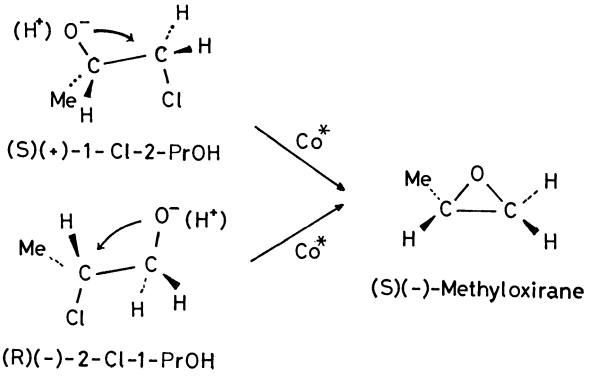

by assuming a mechanism in which cyclization takes place by a backside attack of the alcoholate anion formed initially by the action of a base, at the carbon atom bearing the leaving halogen atom.[14] This S_N2 ring-formation is considered to hold mainly for the above kinetic resolution reactions.

All the reactions using dry K_2CO_3 resulted in higher conversions of the reacted substrates to methyloxirane, as compared to the corresponding reactions with hydrous K_2CO_3. The ratios of methyloxirane formed to reacted 1-chloro-2-propanol or 2-chloro-1-propanol in Tables 1 and 2 are higher than 80%, implying that side reactions such as polymerization are considerably suppressed. This behavior is also demonstrated by the data in dioxane in Table 1; the ratios are 82, 69, and 47% for dry K_2CO_3 (Diox), hydrous K_2CO_3 (Diox), and hydrous K_2CO_3(Diox–H_2O), respectively. On the other hand, there is a tendency that, in regard to asymmetric selectivity, use of dry K_2CO_3, instead of hydrous K_2CO_3, causes decrease in selectivity in the reactions with 1-chloro-2-propanol, while methyloxirane having higher optical activities is obtained from 2-chloro-1-propanol.

The solvent effects were found to be complicated, as might be expected, since the solvents used have functional groups and heterogeneity of the reaction system is changeable according to the nature of solvent. The reaction in dioxane resulted in the best asymmetric selectivity, although the conversion was poor. In 1-propanol, a satisfactory yield of methyloxirane was obtained but the selectivity was disappointing. The results in 1,2-dichloroethane solvents are of interest; especially in the reaction of 2-chloro-1-propanol with dry K_2CO_3, a fairly high selectivity (*e.e.* 26.7%) was observed in spite of a high conversion (40.3% based on initial substrate and 80.6% on K_2CO_3). A similar result was obtained for the 1-chloro-2-propanol/hydrous K_2CO_3 system.

It is considered that, as for cyclization in the presence of Co(II)(sal)$_2$(*R*-CHXDA), the reaction proceeds by

two parallel pathways, with respective cobalt*-catalyzed and non-Co*-catalyzed mechanisms, as given by Eqs. 1 and 2.

$$\text{substrate} + K_2CO_3 \xrightarrow{Co^*} \text{methyloxirane}^* \quad (1)$$

$$\text{substrate} + K_2CO_3 \longrightarrow \text{methyloxirane} \quad (2)$$

The data with dry K_2CO_3 in Table 2, which were the most reproducible, indicated that the highly asymmetric selectivity was achieved in dioxane because the Co*-catalyzed reaction (Eq. 1) took place almost exclusively. The reaction in 1-propanol, a highly polar solvent, involved to a considerable extent the non-Co*-catalyzed pathway (Eq. 2) in addition to Eq. 1, producing methyloxirane with low optical purity. The *e.e.* values of methyloxirane formed in the three solvents decrease in this order: dioxane>1,2-dichloroethane>1-propanol; this is consistent with the presumed order of the extents of Eq. 1 involved in the asymmetric reactions.

Mechanism of Asymmetric Cyclization. In order to obtain insight into the mechanism of the asymmetric cyclization of propylene chlorohydrins, the reaction systems were investigated by absorption and circular dichroism (CD) spectroscopy. The absorption spectrum of the Co(II)(sal)$_2$(*R*-CHXDA) complex itself and that of a binary system of Co(II)(sal)$_2$(*R*-CHXDA) and dry K_2CO_3 are shown in Fig. 2. The spectrum of the latter is very similar to that of the Co^{II} complex itself and is completely different from those of such Co^{I} complexes as $Li^+[Co(I)(sal)_2(R\text{-CHXDA})]^-$ [5] and $Na^+[Co(I)(salen)]^-$.[15] This indicates that the cobalt species in the Co(II)(sal)$_2$(*R*-CHXDA)/K_2CO_3 system is not reduced to Co^{I}, but remains as the Co^{II} state.

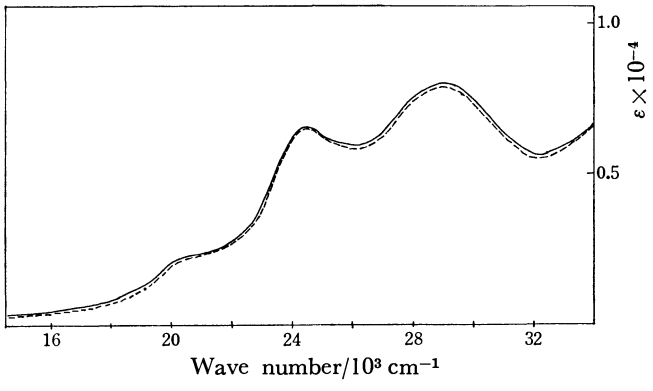

Fig. 2. The absorption spectra of Co*(II) (——) and of Co*(II)/K_2CO_3 (----) in dioxane.

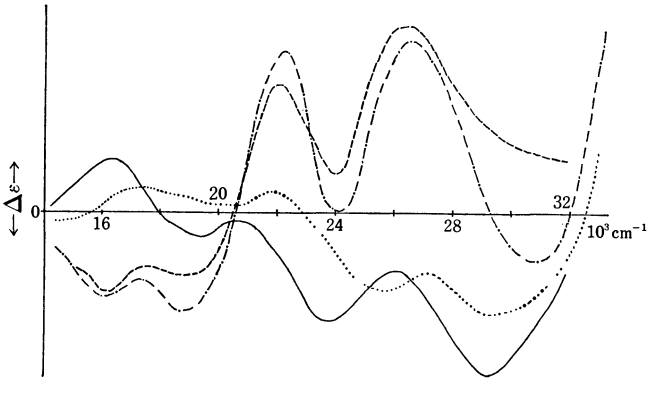

Fig. 3. The CD spectra for the systems of Co*(II)(——), Co*(II)/K_2CO_3 (----), Co*(II)/K_2CO_3/1-Cl-2-PrOH (—·—·), and Co*(II)/K_2CO_3/2-Cl-1-PrOH (·····). Measured as dioxane solutions saturated with the Co* species.

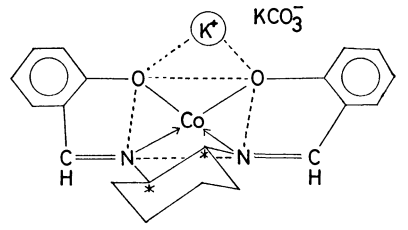

Fig. 4. A possible structure of Co*(II)/K_2CO_3 complex.

The CD spectra of Co(II)(sal)$_2$(*R*-CHXDA) itself and systems of Co^{II}/K_2CO_3, Co^{II}/K_2CO_3/1-chloro-2-propanol, and Co^{II}/K_2CO_3/2-chloro-1-propanol are depicted in Fig. 3. A marked spectral difference is observed between the Co^{II}/K_2CO_3 system and the Co^{II} complex itself, which indicates the formation of a complex between the Co(II)(sal)$_2$(*R*-CHXDA) and K_2CO_3 by combination of a potassium atom of K_2CO_3 with the two phenolic oxygens (Fig. 4), as suggested by related systems.[16]

Little change occurred in the CD spectrum when 1-chloro-2-propanol was added to the Co^{II}/K_2CO_3 system, whereas a drastic change was observed in the case of 2-chloro-1-propanol, as shown in Fig. 3. The CD spectral data for the Co^{II}/K_2CO_3/propylene chlorohydrin systems suggest the formation of new chiral complexes such as (A) and/or (B).[4]

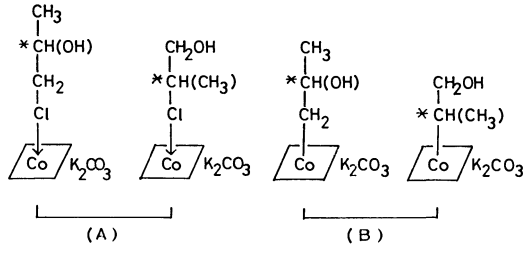

The large CD spectral change for the system of 2-chloro-1-propanol can be interpreted in terms of large chiral and steric effects of the asymmetric moiety, $ClC^*H(CH_3)CH_2OH$ or $-C^*H(CH_3)CH_2OH$, on the chiral circumstance around the central cobalt atom, compared with the case of 1-chloro-2-propanol system. The complexes of type (B) are considered to be rearranged to ketone or aldehyde under basic conditions; the formation of methyloxirane from the (B)-complexes seems unlikely.[5,17]

On the basis of the results so far obtained, this kinetic resolution type reaction which gives rise to optically active methyloxirane from 1-chloro-2-propanol or 2-chloro-1-propanol is considered to proceed by the mechanism depicted in Scheme 1; the selection of (*R*)- or (*S*)-substrate would take place at the stage of coordination of the substrate onto the chiral cobalt complex.

Further investigations are now in progress.

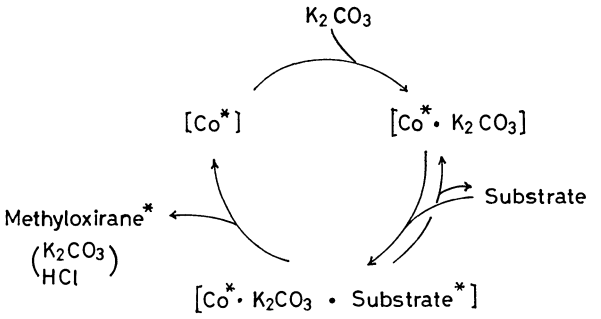

Scheme 1.

References

1) G. N. Schrauzer, *Acc. Chem. Res.*, **1**, 97 (1968); R. H. Abeles and D. Dolphin, *ibid.*, **9**, 114 (1976).

2) G. N. Schrauzer, R. J. Holland, and J. A. Seck, *J. Am. Chem. Soc.*, **93**, 1503 (1971); G. Costa, G. Mestroni, and G. Pellizer, *J. Organomet. Chem.*, **22**, 473 (1970); C. Floriani, M. Puppis, and F. Calderazzo, *ibid.*, **12**, 209 (1968).

3) G. N. Schrauzer and E. Deutsch, *J. Am. Chem. Soc.*, **91**, 3341 (1969).

4) P. W. Schneider, P. F. Phelan, and J. Halpern, *J. Am. Chem. Soc.*, **91**, 77 (1969); L. G. Marzilli, P. A. Marzilli, and J. Halpern, *ibid.*, **93**, 1374 (1971).

5) H. Aoi, M. Ishimori, S. Yoshikawa, and T. Tsuruta, *J. Organomet. Chem.*, **85**, 241 (1975); H. Aoi, M. Ishimori, and T. Tsuruta, *Bull. Chem. Soc. Jpn.*, **48**, 1897 (1975).

6) M. Ishimori, *Catalyst (Jpn.)*, **19**, 419 (1977).

7) M. Ishimori, H. Aoi, Y. Tezuka, and T. Tsuruta, *Bull. Chem. Soc. Jpn.*, **50**, 769 (1977).

8) M. Ishimori, H. Aoi, T. Takeichi, and T. Tsuruta, *Chem. Lett.*, **1976**, 645.

9) J. A. Riddick and W. B. Bunger, "Technique of Organic Chemistry," ed by A. Weissberger, Wiley-Intersci., New York (1970), Vol. II.

10) C. A. Stewart and C. A. Vanderwerf, *J. Am. Chem. Soc.*, **76**, 1259 (1954).

11) Y. Kumata, J. Furukawa, and T. Fueno, *Bull. Chem. Soc. Jpn.*, **43**, 3920 (1970); B. T. Golding, D. R. Hall, and S. Sakrikar, *J. Chem. Soc., Perkin Trans. 1*, **1973**, 1214; N. Spassky, P. Dumas, M. Sepulchre, and P. Sigwalt, *J. Polym. Sci.*: Symposium, **52**, 327 (1975).

12) T. Nakajima, S. Suga, T. Sugita, and K. Ichikawa, *Bull. Chem. Soc. Jpn.*, **40**, 2980 (1967).

13) W. Fickett, H. K. Garner, and H. J. Lucas, *J. Am. Chem. Soc.*, **73**, 5063 (1951).

14) J. D. Bartlett, *J. Am. Chem. Soc.*, **57**, 224 (1935); S. Winstein and H. J. Lucas, *ibid.*, **61**, 1576 (1939).

15) F. Calderazzo and C. Floriani, *Chem. Commun.*, **1967**, 139.

16) M. D. Hobday and T. D. Smith, *J. Chem. Soc., Dalton Trans.* **1972**, 2287; L. F. Lindoy and W. E. Moody, *J. Am. Chem. Soc.*, **99**, 5863 (1977).

17) G. N. Schrauzer and R. J. Windgassen, *J. Am. Chem. Soc.*, **89**, 143 (1967); G. N. Schrauzer and J. W. Sibert, *ibid.*, **92**, 1022 (1970); G. N. Schrauzer, R. J. Holland, and J. A. Seck, *ibid.*, **93**, 1503 (1971).

A New Peptide Synthesis Using 2-Fluoro-1,3,5-trinitrobenzene. Syntheses of Thyrotropin Releasing Hormone and Leucine-Enkephalin

Hideki KINOSHITA,* Katsuhiko INOMATA, Osamu MIYANO, and Hiroshi KOTAKE

Department of Chemistry, Faculty of Science, Kanazawa University, Kanazawa 920

(Received January 29, 1979)

2-Fluoro-1,3,5-trinitrobenzene has been found to be a useful new condensing reagent for peptide synthesis. A variety of dipeptides have been prepared from the corresponding amino acids with the reagent. The Young test under certain conditions did not cause racemization during the procedures. Subsequent application of this reagent enabled the syntheses of thyrotropin releasing hormone and leucine-enkephalin in good yields.

It has been reported[1,2] that the readily available 2-fluoro-1,3,5-trinitrobenzene(FTNB) is a useful new condensing reagent for the preparation of amides, esters, and thiocarboxylic *S*-esters. In this paper, the syntheses of various dipeptides and biologically active peptides, thyrotropin releasing hormone(TRH) and leucine-enkephalin are described.

As a preliminary, several *N*-benzyloxycarbonyl(Z) dipeptide esters were prepared by the reaction of *N*-benzyloxycarbonyl amino acids with amino acid esters using FTNB as a condensing reagent, as shown in Table 1. To an equimolar solution of *N*-benzyloxycarbonyl amino acid and FTNB in acetonitrile was added an acetonitrile solution of pyridine(one equivalent) at 0 °C under a nitrogen atmosphere. After stirring for 3 h at 0 °C, the amino acid ester(one equivalent) was added to the reaction mixture, followed by the addition of a solution of pyridine(one equivalent) in acetonitrile. The solution was stirred for several hours and then worked up to give the desired dipeptide **1a**—**g** in good yield (Table 1).

In a similar manner, the *N*-*t*-butoxycarbonyl(Boc) dipeptide esters(**2a**—**e**) were obtained in excellent yields, the results of which are given in Table 2.

Compound **1g** was obtained in good yield with no side reactions such as *O*-acyl derivatives[3] without protection of the hydroxyl group of *N*-(benzyloxycarbonyl)serine. The condensation reaction of amino acids containing bulky substituents (**2b**,**c**) also proceeded smoothly giving the desired products in good yields. FTNB is then an excellent condensing reagent for peptide synthesis.

The reaction appears to proceed *via* a mechanism similar to the formation of amides[1] and esters[2] as illustrated in the following scheme: First, the anionic sigma complex **3** is formed by the reaction of the amino acid with FTNB in the presence of pyridine followed by the elimination of the picrate to produce an intermediate acyl fluoride **4**, which then reacts with amino acid esters to give the corresponding dipeptide **5**.

Fragment condensation is frequently used to synthesize the more complex peptides, however, the problem of racemization of the acyl peptide exists. Consequently the Young test[4] was applied to determine the applicability of the FTNB method to fragment condensation. The results of which are given in Table 3. The

TABLE 1. PREPARATION OF BENZYLOXYCARBONYL DIPEPTIDE ESTERS

FTNB + Z-A.A.-OH + Py $\xrightarrow[\text{in } CH_3CN]{0\,^\circ C,\ 3\,h}$ $\xrightarrow[0\,^\circ C,\ r.t.,\ 3\,h]{\text{H-A.A.-OR, Py}}$ Z-dipeptide-OR

	Product	Yield/%	Mp/°C (lit)	$[\alpha]_D$/° (lit)	Ref.
1a	Z-Ile-Gly-OEt	85	155—156 (155—156)	−25.9 (0.65, EtOH) (−25.6)	13
1b	Z-Gly-Gly-OEt	85	80—81 (80)		14
1c	Z-Ala-Gly-OEt	85	99—100 (99—100)	−22.3 (3.65, EtOH) (−22.2)	13
1d	Z-Val-Gly-OEt	85	163—164 (162—164)	−27.2 (0.77, EtOH) (−27.0)	13
1e	Z-Met-Gly-OEt	82	96—97 (94—96)	−19.7 (3.50, EtOH) (−19.8)	15
1f	Z-Cys(Bzl)-Gly-OEt	80	97—98 (97—99)	−28.9 (5.86, AcOEt) (−27.0)	15
1g	Z-Ser-Thr-OMe	76	128—130 (126—127)	+7.1 (1.98, DMF) (+6.9)	16

TABLE 2. PREPARATION OF *t*-BUTOXYCARBONYL DIPEPTIDE ESTERS

FTNB $\xrightarrow[0\,^\circ C,\ 1.5\,h,\ \text{in } CH_3CN]{\text{Boc-A.A.-OH, Py}}$ $\xrightarrow[0\,^\circ C,\ r.t.,\ 3\,h]{\text{H-A.A.-OMe, Py}}$ Boc-dipeptide-OMe

	Product	Yield/%	Mp/°C (lit)	$[\alpha]_D$/° (lit)	Ref.
2a	Boc-Phe-Val-OMe	85	117—118 (118—119)	−11.0 (1.89, DMF) (−11.6)	17
2b	Boc-Leu-Leu-OMe	81	141—142 (141—142)	−50.0 (0.39, MeOH) (−50.4)	18
2c	Boc-Ile-Ile-OMe	81	157—158 (158—159)	−36.5 (0.51, MeOH) (−33.3)	19
2d	Boc-Ala-Ala-OMe	76	105—106 (105—108)	−63.6 (0.66, MeOH) (−63.8)	17
2e	Boc-Ala-Val-OMe[a]	83	63—64	−49.5 (0.31, MeOH)	

a) **2e** exhibited NMR spectral data and elemental analysis in accordance with assigned structure.

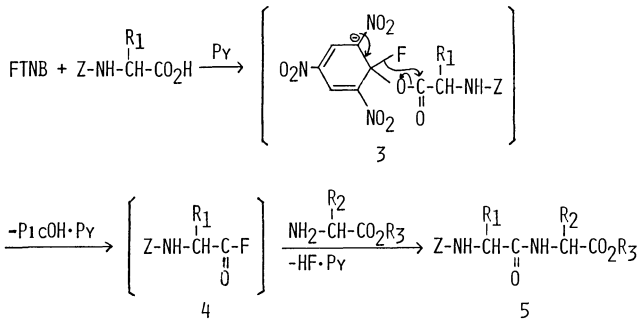

product obtained from the same procedures as described in the preparation of the dipeptides using only FTNB was perfectly optically inactive, regardless of solvent(Entry 1, 2). Accordingly, the reaction conditions which did not induce racemization were investigated; this difficulty was satisfactorily overcome by employing the Eintopf method reported by Wünsch *et al.*[5] As may be seen from the Table, the coexistence of additives such as *N*-hydroxysuccinimide(HONSu) and *N*-hydroxy-5-norbornene-2,3-dicarboximide (HONB) effectively suppressed racemization, twomolar amounts of additive being required. Furthermore, dichloromethane proved to be the best solvent among the solvents investigated. With respect to base, collidine was especially effective. The reaction conditions making use of collidine as a base in the presence of two molar amounts of HONSu in dichloromethane gave optimum results with 98% optical purity(Entry 10).

The results may be explained as follows. In the absence of additive, the intermediary amino acid fluoride is rapidly converted into the oxazolone regarded as an intermediate for racemization.[6,7] In the presence of an additive, the amino acid fluoride reacts more rapidly with HONSu to give the so-called "active ester" of HONSu,[8] which then reacts with the amine component to give the optically pure product.

The optimum conditions for suppression of racemization were utilized to synthesize the biologically active peptides, TRH and leucine-enkephalin uisng the FTNB method.

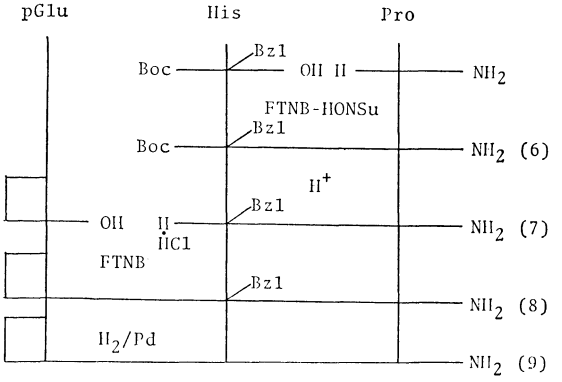

Scheme 1. Synthesis of thyrotropin releasing hormone.

The synthesis of TRH was conducted as illustrated in Scheme 1. α-*t*-Butoxycarbonyl(Boc)-N^{im}-benzyl (Bzl)histidine was condensed with prolinamide in the presence of two molar amounts of HONSu using the FTNB method to give the dipeptide **6** (81% yield after purification by column chromatography). Cleavage of the *t*-butoxycarbonyl group of the protected dipeptide **6** with 5 M-hydrogen chloride in ethyl acetate gave the deprotected product **7** (nearly quantitative yield), which was condensed with pyroglutamic acid using the FTNB method to give the desired protected tripeptide **8** (56% yield after purification by ion-exchange resin column chromatography followed by preparative TLC). Finally, debenzylation of the protected tripeptide **8** by catalytic hydrogenation over palladium black followed by purification of the reaction mixture by preparative TLC gave the desired product, pyroglutamyl-histidyl-prolinamide (**9**) in 75% yield. The specific rotation was in accordance with the literature.[9]

The synthesis of leucine-enkephalin with opiate-

Table 3. The results of the Young Test

FTNB + Bz-Leu-OH (I) + Additive (II) —Base, Solvent, Time/h→ —H-Gly-OEt→ Bz-Leu-Gly-OEt

Entry	Additive	Molar ratio II/I	Reaction conditions: Base	Reaction conditions: Time/h	Solvent[a]	Yield %	Optical purity/%[b]
1	none		Py	2	CH_3CN	60.0	0
2	none		Py	2	CH_3Cl_2	68.8	0
3	HONSu	1	Py	3	CH_3CN	45.6	39.5
4	HONSu	1	Py	3	THF	61.2	34.1
5	HONSu	1	Py	3	$CHCl_3$	65.0	59.6
6	HONSu	1	Py	2	CH_2Cl_2[c]	60.0	76.5
7	HONSu	2	Py	2	CH_2Cl_2[c]	60.0	95.0
8	HONSu	2	2,4-Lutidine	3	CH_2Cl_2[c]	58.0	72.6
9	HONSu	2	2,6-Lutidine	3	CH_2Cl_2[c]	59.3	89.4
10	HONSu	2	Collidine	3	CH_2Cl_2[c]	63.7	98.3
11	HONB	1	Py	2	CH_2Cl_2[c]	50.0	89.0
12	HONB	2	Py	2	CH_2Cl_2[c]	45.0	94.5

a) 5—6 ml of solvent was used. b) Based on $[\alpha]_D^{20}$ −34.0° (3.1, EtOH) reported by M. W. Williams and G. T. Young.[4] c) 1 ml of CH_3CN was added in addition to the solvent to dissolve the additive.

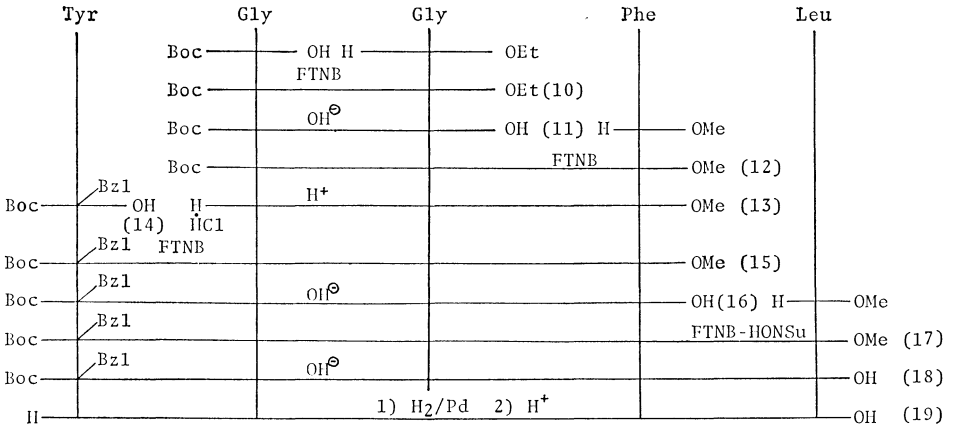

Scheme 2. Synthesis of leucine-enkephalin.

agonist activity was conducted according to Scheme 2. Saponification of the dipeptide **10**, derived from the coupling of *N*-(*t*-butoxycarbonyl)glycine with ethyl glycinate using the FTNB method, gave the dipeptide **11** which was condensed with methyl phenylalaninate using the FTNB method to give the protected ester **12** in 76% yield. Treatment of **12** with 5 M-hydrogen chloride in ethyl acetate gave the desired deprotected tripeptide ester hydrochloride **13** in 81% yield. The melting point and specific rotation were however in disagreement with the values reported by Voelter *et al.*[10] In order to clarify the discrepancy, **12** was prepared by two other methods, the azide and DCC-HONSu methods, and subsequent deprotection of the *t*-butoxycarbonyl group of compound **12** was conducted under the same conditions as described for the FTNB method. It was found that the physical constants of the products obtained from the two methods were consistent with the values obtained from the FTNB method. α-*t*-Butoxycarbonyl-*O*-benzyltyrosine (**14**) was condensed with the tripeptide **13** to give the tetrapeptide ester **15** in 81% yield, which was saponified to give the deprotected tetrapeptide **16** in 86% yield. The desired pentapeptide ester **17** was obtained from the coupling of **16** with methyl leucinate in the presence of two molar amounts of HONSu thereby avoiding racemization (71% yield). Saponification of **17** gave the pentapeptide **18** in 81% yield, which was hydrogenated over 10%-palladium on charcoal followed by cleavage of the *t*-butoxycarbonyl group to give the desired product, leucine-enkephalin (**19**) in 44% yield after treatment with ion-exchange resin column chromatography. The melting point and specific rotation of the product were in accordance with the reported values.[11]

Experimental

All melting points are uncorrected. The NMR spectra were recorded on a JEOL/MH-60. The chemical shifts are reported on the δ scale relative to TMS as an internal standard. The IR spectra were measured with a JASCO IRA-1 diffraction grating infrared spectrometer. The optical rotation values were measured with a JASCO DIP-SL polarimeter.

Materials. All solvents were distilled according to the usual methods and stored over a drying agent. Thin-layer chromatography (TLC) and column chromatography were performed on Merck's Silica gel 60 PF_{254} (Type 7749), on Alumina Woelm (Act. 1), and on Merck's Aluminium oxide 90 (Type 1077).

*Z-Ile-Gly-OEt (**1a**).* To a solution of FTNB (116 mg, 0.5 mmol) and Z-Ile-OH (113 mg, 0.5 mmol) in CH_3CN (5 ml) was added a solution of pyridine(Py) (40 mg, 0.5 mmol) in CH_3CN (1 ml) dropwise at 0 °C under a nitrogen atmosphere. After stirring for 3 h at 0 °C, H-Gly-OEt·HCl (70 mg, 0.5 mmol) was added to the reaction mixture, followed by the addition of a solution of Py (79 mg, 1 mmol) in CH_3CN (1 ml). The solution was stirred at 0 °C for 1.5 h and for additional hours at room temperature. The reaction mixture was evaporated to dryness under reduced pressure and the residue partitioned between AcOEt and water. The AcOEt layer was washed successively with 1M-HCl, 10%-$NaHCO_3$, and a saturated solution of NaCl, dried over Na_2SO_4 and evaporated to dryness *in vacuo*. The residue was subjected to neutral alumina column chromatography using benzene–AcOEt (1:1 v/v) as solvent to give a crystalline product. Recrystallization from benzene–hexane gave the desired product **1a** in 85% yield (149 mg).

In a similar manner, the dipeptides **1b—g** were obtained as shown in Table 1.

*Boc-Phe-Val-OMe (**2a**).* To a solution of FTNB (116 mg, 0.5 mmol) in CH_3CN (5 ml) was added slowly a mixed solution of Boc-Phe-OH (113 mg, 0.5 mmol) and Py (40 mg, 0.5 mmol) in CH_3CN (5 ml) at 0 °C. After stirring for 1.5 h at 0 °C, H-Val-OMe·HCl (84 mg, 0.5 mmol) was added to the solution followed by the addition of a solution of Py (79 mg, 1 mmol) in CH_3CN (0.5 ml). The reaction mixture was stirred for 3 h at room temperature and worked up as described for **1a**. The residue was subjected to neutral alumina column chromatography using benzene–AcOEt (1:1 v/v) as solvent, followed by preparative TLC using benzene–AcOEt (3:2 v/v) as solvent to afford the desired product. Recrystallization from benzene–hexane gave pure **2a** in 85% yield.

By a similar procedure, the dipeptides **2b—e** were obtained as shown in Table 2. The physical constants of **2e** were in disagreement with the reported values,[17] but the structure was confirmed by elemental analysis and NMR data as shown below: NMR ($CDCl_3$) δ 0.93 (d, 6H, J=7 Hz), 1.35 (d, 3H, J=6 Hz), 1.44 (s, 9H), 1.80—2.40 (m, 1H), 3.70 (s, 3H), 4.00—4.67 (m, 2H), 4.95—5.30 (bd, 1H, J=8 Hz), 6.45—6.90 (bd, 1H, J=8 Hz). Found: C, 55.59; H, 8.70; N, 9.27%. Calcd for $C_{14}H_{26}N_2O_5$: C, 55.61; H, 8.67; N, 9.27%.

Young Test (Bz-Leu-Gly-OEt). *Entry 1*: To a solu-

tion of FTNB (116 mg, 0.5 mmol) and Bz–Leu–OH (118 mg, 0.5 mmol) in CH_3CN (5 ml) was added dropwise a solution of Py (40 mg, 0.5 mmol) in CH_3CN (1 ml) at 0 °C under a nitrogen atmosphere. After stirring for 3 h at 0 °C, a solution of H–Gly–OEt (52 mg, 0.5 mmol) in CH_3CN (2 ml) was added to the solution at 0 °C, followed by the addition of a solution of Py (40 mg, 0.5 mmol) in CH_3CN (1 ml). The reaction mixture was allowed to stand overnight at room temperature and evaporated to dryness. The residue was dissolved in AcOEt and the solution washed successively with 10%-$NaHCO_3$, 1M-HCl, and a saturated solution of NaCl and dried over Na_2SO_4. After evaporation of the solvent, the residue was subjected to neutral alumina column chromatography using benzene–AcOEt (1:1 v/v) as solvent followed by preparative TLC using benzene–AcOEt (3:2 v/v) as solvent to afford the product in 60% yield (96 mg): mp 146—147 °C; $[\alpha]_D^{20}$ 0° (2.98, EtOH). *Entry 10*: To a solution of Bz–Leu–OH (118 mg, 0.5 mmol), FTNB (116 mg, 0.5 mmol), and HONSu (115 mg, 1 mmol) in CH_3CN (1 ml) was added CH_2Cl_2 (5 ml) at 0 °C, followed by the addition of a solution of collidine (112 mg, 1 mmol) in CH_2Cl_2 (1 ml). After stirring for 3 h at 0 °C, a solution of H–Gly–OEt (52 mg, 0.5 mmol) in CH_2Cl_2 (2 ml) was added at 0 °C to the solution. The reaction mixture was allowed to stand overnight and worked up as described for Entry 1. Yield, 108 mg (64%): mp 153—154 °C; $[\alpha]_D^{29}$ −33.4° (2.15, EtOH).

*Boc–His(Bzl)–Pro–NH_2 (**6**).* To a solution of FTNB (116 mg, 0.5 mmol) and HONSu (115 mg, 1 mmol) in CH_3CN (1 ml) was added CH_2Cl_2 (5 ml). To the resulting clear solution was added dropwise a solution of Boc–His(Bzl)–OH (173 mg, 0.5 mmol) and triethylamine(TEA) (101 mg, 1 mmol) in CH_2Cl_2 (2 ml) at 0 °C. After stirring for 3 h at 0 °C, H–Pro–NH_2·HCl (76 mg, 0.5 mmol) was added to the solution followed by the addition of a solution of TEA (51 mg, 0.5 mmol) in CH_2Cl_2 (1 ml). The reaction mixture was allowed to stand overnight at room temperature. After evaporation of the solvent, the residue was subjected to ion-exchange resin chromatography (Amberlite IRA-410) using MeOH as solvent and basic alumina column chromatography using benzene–EtOH (8:1 v/v) as solvent to give a solid material. This was separated by preparative TLC using chloroform–MeOH (10:1 v/v) as solvent to give the desired product in 81% yield (179 mg); $[\alpha]_D^{28.5}$ −23.4° (0.64, MeOH); NMR (CD_3OD) δ 1.37 (s, 9H), 1.70—2.20 (m, 4H), 2.70—3.00 (m, 2H), 3.10—3.50 (m, 2H), 4.20—4.60 (m, 1H), 5.06 (s, 2H), 6.90 (s, 1H), 7.20 (s, 5H), 7.53 (s, 1H).

*H–His(Bzl)–Pro–NH_2·2HCl (**7**).* A solution of **6** in AcOEt (2 ml) was treated with 6M-HCl (6 ml) in AcOEt, and the solution allowed to stand at room temperature for 30 min. To the reaction mixture was added dry ether (30 ml). The supernatant liquid was decanted, and the residue washed with dry ether (4×30 ml) to give the salt **7** which was dried *in vacuo* in the presence of solid potassium hydroxide and phosphorous pentoxide, yield, 164 mg. The product was used without further purification in the subsequent reaction.

*pGlu–His(Bzl)–Pro–NH_2 (**8**).* A solution of FTNB (70 mg, 0.3 mmol) in CH_2Cl_2 (1 ml) was cooled at 0 °C and to the solution was added dropwise a mixed solution of pGlu–OH (39 mg, 0.3 mmol) and TEA (31 mg, 0.3 mmol) in CH_2Cl_2 (2 ml). After stirring for 2 h at 0 °C, **7** (120 mg, 0.3 mmol) was added to the reaction mixture followed by the addition of a solution of TEA (91 mg, 0.9 mmol) in CH_2Cl_2 (1 ml). The reaction mixture was allowed to stand overnight at room temperature. The solvent was evaporated *in vacuo*, and the residual oil purified by ion-exchange resin chromatography using MeOH as solvent followed by preparative TLC using chloroform–MeOH (3:1 v/v) as solvent to afford the product in 56% yield (59 mg).

*pGlu–His–Pro–NH_2 (**9**).* The protected tripeptide **8** (57 mg, 0.13 mmol) was dissolved in EtOH (25 ml) and hydrogenated for 12 h over palladium black (20 mg) at room temperature under atmospheric pressure. The catalyst was filtered off followed by evaporation of the filtrate. The crude product was subjected to preparative TLC using chloroform–MeOH (3:1 v/v) to afford the desired TRH (**9**) in 75% yield (35 mg): $[\alpha]_D^{28.5}$ −40.7° (1.00, MeOH) [lit,[8] −42.4° (1.00, MeOH)]. The product gave a positive Paulitest and showed a single spot on TLC in several solvent systems.

*Boc–Gly–Gly–OEt (**10**).* To an CH_3CN solution (6 ml) of FTNB (232 mg, 1 mmol) cooled at −30 °C, was added a solution of Boc–Gly–OH (175 mg, 1 mmol) and TEA (101 mg, 1 mmol) in CH_3CN (5 ml). After stirring for 2 h at 0 °C, H–Gly–OEt·HCl (140 mg, 1 mmol) and then a solution of TEA (202 mg, 2 mmol) in CH_3CN (1 ml) were added to the reaction mixture. The solution was allowed to stand overnight at room temperature and worked up as described for **1a**. After evaporation of the solvent, the residue was subjected to basic alumina column chromatography using benzene–EtOH (1:2 v/v) as solvent and to preparative TLC using benzene–EtOH (8:1 v/v) as solvent to give the desired product as an oil in 82% yield (212 mg).

*Boc–Gly–Gly–OH (**11**).* To a solution of **10** (1.30 g, 5 mmol) in MeOH–H_2O (5 ml) (4:1 v/v), was added 1M-NaOH (5 ml) at 0 °C and the reaction mixture maintained at 0 °C for 2 h and then allowed to stand overnight. The MeOH was removed *in vacuo* and water (5 ml) added to the solution. The resulting aqueous solution was washed with AcOEt and neutralized with 1M-HCl (5 ml). The separated oil was extracted with AcOEt after salting-out, and the organic layer dried over Na_2SO_4 and evaporated to dryness *in vacuo* to give a crystalline product. Recrystallization from AcOEt gave an 87% yield (1.01 g): mp 133—134 °C; Found: C, 46.70; H, 7.02; N, 12.18%. Calcd for $C_9H_{16}N_2O_5$: C, 46.54; H, 6.94; N, 12.06%.

*Boc–Gly–Gly–Phe–OMe (**12**).* To a solution of FTNB (232 mg, 1 mmol) in CH_3CN (2 ml) was added slowly a solution of **11** (232 mg, 1 mmol) and TEA (101 mg, 1 mmol) in CH_3CN (3 ml) at 0 °C. After stirring for 2 h at 0 °C, H–Phe–OMe·HCl (215 mg, 1 mmol) was added to the solution followed by the addition of a solution of TEA (202 mg, 2 mmol) in CH_3CN (1 ml). The reaction mixture was allowed to stand overnight and worked up as described in the preparation of **1a**. The desired product was separated from the residue by basic alumina column chromatography using benzene–EtOH (1:1 v/v) as solvent followed by preparative TLC using benzene–EtOH (8:1 v/v) as solvent; 76% yield as an oil (297 mg): NMR ($CDCl_3$) δ 1.43 (s, 9H), 3.05 (d, 2H, J=6.0 Hz), 3.65 (s, 3H), 3.75 (d, 2H, J=6.3 Hz), 3.87 (d, 2H, J=6.3 Hz), 4.84 (t, 1H, J=6.0 Hz), 5.38—5.65 (m, 1H), 6.85—7.16 (bs, 2H), 7.00—7.43 (m, 5H).

*H–Gly–Gly–Phe–OMe·HCl (**13**).* *Method A*: The product **12** obtained from the FTNB method was dissolved in AcOEt, and 5M-HCl (5 ml) in AcOEt added to the solution at room temperature. After 3 h, the solvent was evaporated to dryness *in vacuo* to give a crude product which was recrystallized from 1-propanol in 81% yield (202 mg): mp 179—180 °C; $[\alpha]_D^{21.5}$ +31.4° (1.05, AcOH). Found: C, 50.81; H, 6.15; N, 12.96%. Calcd for $C_{14}H_{20}N_3O_4Cl$: C, 50.98; H, 6.06; N, 12.74%.

Method B: Boc–Gly–Gly–NH–NH_2 derived from the reac-

tion of **10** with hydrazine was condensed with H–Phe–OMe using the azide method to give the desired tripeptide **12** in 66% yield. **12** was deprotected with hydrogen chloride according to method A. Recrystallization from 1-propanol gave the product **13** in 81% yield: mp 178—179 °C; $[\alpha]_D^{21.5}$ +31.4° (1.05, AcOH).

Method C: **12** was obtained from the reaction of **11** with H–Phe–OMe using the DCC–HONSu method in 89% yield, which was treated according to Method A. Recrystallization from 1-propanol gave the product **13** in 76% yield; mp 178—179 °C; $[\alpha]_D^{22}$ +30.4° (0.99, AcOH).

*Boc–Tyr(Bzl)–Gly–Gly–Phe–OMe (**15**).* To a solution of FTNB (232 mg, 1 mmol) in CH_3CN (4 ml) was added slowly a mixed solution of Boc–Tyr(Bzl)–OH (**14**) (371 mg, 1 mmol) and TEA (101 mg, 1 mmol) in CH_3CN (2 ml) at 0 °C. After stirring at 0 °C for 2 h, **13** (330 mg, 1 mmol) was added to the solution followed by the addition of a solution of TEA (202 mg, 2 mmol) in CH_3CN (2 ml). The reaction mixture was allowed to stand at room temperature, and worked up as described for **1a**. After evaporation of the solvent, the crude product was purified by gradient elution on basic alumina using benzene–EtOH (8:1 v/v to 1:1 v/v). Recrystallization from AcOEt–hexane gave the pure product in 81% yield: mp 112—113 °C; $[\alpha]_D^{32.5}$ +13.8° (1.23, MeOH). Found: C, 64.69; H, 6.64; N, 8.70%. Calcd for $C_{19}H_{27}N_3O_6$: C, 65.00; H, 6.55; N, 8.70%.

*Boc–Tyr(Bzl)–Gly–Gly–Phe–OH (**16**).* To a solution of **15** (406 mg, 0.63 mmol) in MeOH–H_2O (5 ml) (4:1 v/v) was added with stirring 1M-NaOH (0.8 ml) at 0 °C and worked up as described in the preparation of **11**. Recrystallization from chloroform–hexane gave the desired product in 84% yield (341 mg): mp 83—84 °C; $[\alpha]_D^{21}$ +17.3° (1.38, MeOH). Found: C, 63.56; H, 6.59; N, 8.89%. Calcd for $C_{34}H_{40}N_4O_8 \cdot 1/2H_2O$: C, 63.65; H, 6.39; N, 8.74%.

*Boc–Tyr(Bzl)–Gly–Gly–Phe–Leu–OMe (**17**).* To a mixed solution of **16** (327 mg, 0.51 mmol), FTNB (120 mg, 0.52 mmol), and HONSu (120 mg, 1.04 mmol) in CH_3CN (1 ml) was added CH_2Cl_2 (5 ml) at 0 °C followed by the addition of a solution of collidine (126 mg, 1.04 mmol) in CH_2Cl_2 (2 ml). After stirring at 0 °C for 3 h, H–Leu–OMe·HCl (95 mg, 0.52 mmol) was added followed by the addition of a solution of TEA (53 mg, 0.52 mmol) in CH_2Cl_2 (1 ml). The reaction mixture was allowed to stand overnight at room temperature, and then worked up as described for **12**. Recrystallization from chloroform–hexane gave the pure product in 72% yield (280 mg): mp 153—154 °C; $[\alpha]_D^{22}$ −11.4° (1.74, MeOH). Found: C, 64.55; H, 7.08; N, 9.26%. Calcd for $C_{41}H_{53}N_5O_9$: C, 64.80; H, 7.03; N, 9.22%.

*Boc–Tyr(Bzl)-Gly–Gly–Phe–Leu–OH (**18**).* To a solution of **17** (400 mg, 0.53 mmol) in MeOH–H_2O (5 ml) (4:1 v/v) was added with stirring 1M-NaOH (0.6 ml) at 0 °C and worked up as described in the preparation of **11**. Recrystallization from AcOEt gave the desired product in 81% yield (321 mg): mp 149—150 °C; $[\alpha]_D^{28}$ +1.6° (1.26, MeOH). Found: C, 64.53; H, 6.95; N, 9.43%. Calcd for $C_{40}H_{51}N_5O_9$: C, 64.51; H, 6.89; N, 9.39%.

*H–Tyr–Gly–Gly–Phe–Leu–OH (**19**).* The protected pentapeptide **18** (90 mg, 0.12 mmol) was dissolved in MeOH (15 ml), and hydrogenated over 10% palladium on charcoal (250 mg) for 2 h at room temperature under atmospheric pressure. The catalyst was filtered off and the filtrate evaporated to dryness *in vacuo* to give the debenzylated product which was dissolved in 5M-HCl (1 ml) in dioxane. The reaction mixture was allowed to stand for 6 h at room temperature. Evaporation of the solvent gave a residue which was washed with dry ether. The residual product was dissolved in a small amount of water and the aqueous solution passed through an ion-exchange resin column (Amberlite IR-120B) using 5%-NH_4OH as solvent. The eluate was evaporated to dryness *in vacuo* to give the desired leucine-enkephalin (**19**) in 44% yield (30 mg): mp 208—210 °C (dec); $[\alpha]_D^{25}$ −24.0° (1.0, DMF) [lit,[11] mp 206 (dec), $[\alpha]_D^{23}$ −23.4° (1.0, DMF)]. Amino acid analysis (after acidic hydrolysis) showed the presence of tyrosine, glycine, phenylalanine, and leucine in the ratio 1.00:2.15:1.26:0.98.

References

1) H. Kotake, K. Inomata, H. Kinoshita, K. Tanabe, and O. Miyano, *Chem. Lett.*, **1977**, 647.

2) K. Inomata, H. Kinoshita, H. Fukuda, K. Tanabe, and H. Kotake, *Bull. Chem. Soc. Jpn.*, **51**, 1866 (1978).

3) M. Bodanszky and M. A. Ondetti, *Chem. Ind. (London)*, **1966**, 26.

4) M. W. Williams and G. T. Young, *J. Chem. Soc.*, **1963**, 881.

5) F. Weygand, D. Hoffman, and E. Wünsch, *Z. Naturforsch., Teil B*, **21**, 426 (1966).

6) M. Bergmann and L. Zervas, *Biochem. Z.*, **203**, 280 (1928).

7) M. W. Williams and G. T. Young, *J. Chem. Soc.*, **1964**, 3701.

8) J. E. Zimmerman and G. W. Anderson, *J. Am. Chem. Soc.*, **89**, 7152 (1967).

9) J. K. Chang, H. Sievertssen, B. Currie, K. Falkers, and C. Bowers, *J. Med. Chem.*, **14**, 484 (1971).

10) W. Voelter, E. Pietrzik, and H. Kalbacher, *Tetrahedron Lett.*, **1976**, 2119.

11) J. D. Bower, K. P. Guest, and B. A. Morgan, *J. Chem. Soc.*, **1976**, 2488.

12) The abbreviations used for the amino acids in this work are those recommended by the IUPAC-IUB commission on Biochemical Nomenclature, as published in *J. Biol. Chem.*, **247**, 977 (1972).

13) M. Miyoshi and H. Tamura, "Proceedings of the 8th Symposium on Peptide Chemistry," ed by T. Kaneko, Protein Research Foundation, Osaka (1970), p. 36.

14) N. Yamazaki, F. Higashi, and M. Niwano, "Proceedings of the 11th Symposium on Peptide Chemistry," ed by H. Kotake, Protein Research Foundation, Osaka (1973), p. 1.

15) T. Mukaiyama, M. Ueki, R. Matsueda, H. Maruyama, and K. Goto, "Proceedings of the 7th Symposium on Peptide Chemistry," ed by S. Akabori, Protein Research Foundation, Osaka (1969), p. 25.

16) T. Fujii and K. Okawa, *Bull. Chem. Soc. Jpn.*, **39**, 1598 (1966).

17) J. E. Shieds, S. T. McDowell, J. Pavlos, and G. R. Gray, *J. Am. Chem. Soc.*, **90**, 3549 (1968).

18) D. E. Nitecki, B. Halpern, and J. W. Westley, *J. Org. Chem.*, **33**, 864 (1968).

19) C. Toniolo, *Biopolymers*, **10**, 1707 (1971).

Nucleophilic Ion Pairs. 8. Facile Nucleophilic Cleavage of Dinitrophenyl Sulfate in the Presence of Micellar Zwitterionic Hydroxamates†

Toyoki KUNITAKE* and Tetsuo SAKAMOTO

Department of Organic Synthesis, Faculty of Engineering, Kyushu University, Fukuoka 812

(Received January 29, 1979)

The sulfate transfer reaction from dinitrophenyl sulfate to hydroxamate nucleophiles was studied in the presence of several types of aqueous micelles at 30 °C, pH 8—9. The zwitterionic hydroxamate was a nucleophile much better than the anionic hydroxamate in the CTAB micelle. The kinetic behavior of the zwitterionic hydroxamate nucleophile was not straightforward and the reactivity of the nucleophile increased with the increase in the relative concentration of the nucleophile and surfactant. These results in the CTAB micelle was analyzed in terms of the two phase model and the rate enhancement relative to the nonmicellar reaction was attributed to substrate binding in the micellar phase and the micellar activation of the hydroxamate nucleophile. The cleavage of dinitrophenyl sulfate by the micellar zwitterionic nucleophile was faster than that by the nonmicellar hydroxamate and the water cleavage by factors of *ca.* 10^4 and more than 10^7, respectively: the fastest cleavage ever observed at the ambient condition.

The hydrolysis of sulfate monoesters has been studied increasingly well in recent years, due to realization of the importance of sulfate group transfer *in vivo*.[1] In general, sulfate monoesters are difficult to be cleaved in the neutral pH region and detailed mechanistic studies have been rarely made, apart from acid and alkali hydrolyses.[2]

In relation to the enzymatic catalysis, the sulfate transfer reaction has been investigated in the presence of cyclodextrins,[3] macrocyclic compounds[4] and micelles.[5,6] The rate accelerations in these systems, however, are not large. In the hydrolysis of phenyl esters, the micellar hydroxamate and imidazole anions show extremely high nucleophilicities.[7] These reagents, however, are not effective for negatively-charged sulfate esters.

In order to circumvent this disadvantage, a zwitterionic nucleophile, *N*-benzyl-α-(1-dodecyl-3-imidazolio)acetohydroxamate (C_{12}-Im$^+$-HA, **1**), was used in the present study for the sulfate transfer reaction (Eq. 1) in the presence of aqueous micelles of representative surfactants.

The reaction with simpler nucleophiles, *N*-dodecylbenzohydroxamate(LBHA, **2**) and *N*-benzylbenzohydroxamate(BBHA, **3**) was also performed for the comparison purpose.

nucleophile:

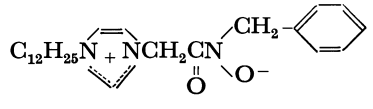

1 C_{12}-Im$^+$-HA

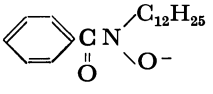

2 LBHA

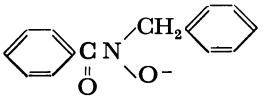

3 BBHA

surfactant:

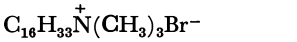

4 CTAB

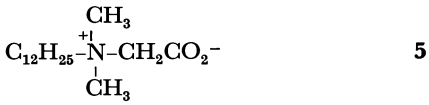

5 $C_{12}\overset{+}{N}2C_1CO_2^-$

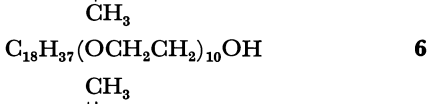

6 POOA

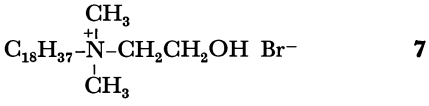

7 $C_{18}\overset{+}{N}2C_1C_2OH$

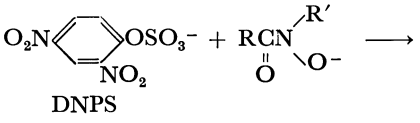

DNPS

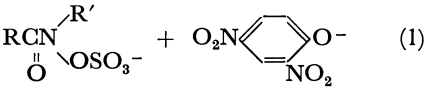

(1)

Experimental

Materials. The zwitterionic nucleophile, C_{12}-Im$^+$-HA, was prepared by the reaction of *N*-dodecylimidazole with benzyl *N*-benzylchloroacetohydroxamate accompanied by hydrogenolysis over Pd/$SrCO_3$,[8] mp 157—158 °C. It was identified by elemental analysis and by NMR and IR spectroscopies. Potassium 2,4-dinitrophenyl sulfate (DNPS) was prepared according to the procedure of Sunamoto *et al.*[4] Its purity was 95% as determined by UV spectroscopy: the impurity was 2,4-dinitrophenol. Hexadecyltrimethylammonium bromide (CTAB) was recrystallized two times from ethanol. Poly(oxyethylene)oleyl alcohol (n=10)(α-(9-octadecenyl)-ω-hydroxydeca(oxyethylene)), POOA was used without further purification. (Carboxymethyl)dodecyldimethylammonium chloride, $C_{12}N^+2C_1CO_2$ was obtained by reaction of *N,N*-dimethyldodecylamine and chloroacetic acid and recrystallized from ethyl acetate:[8] mp 158—160 °C. (2-Hydroxyethyl)dimethyloctadecylammonium bromide, $C_{18}N^+2C_1C_2OH$, was prepared by refluxing an ethanol solution of 10.0 g (0.03 mol) of octadecyl bromide and 3.5 g (0.04 mol) of 2-(dimethylamino)ethanol for 10 h. After solvent removal, the solid residue was recrystallized two times from acetone; colorless needles, mp 209—211 °C (dec), yield 9.3 g (73%). Found: C, 62.43; H, 11.42; N, 3.31%. Calcd for $C_{22}H_{48}NOBr$: C, 62.54; H, 11.45; N, 3.32%.

Rate Measurement. The hydroxamates and surfactants were dissolved in ethanol and water, respectively. DNPS was dissolved in a 3:7 mixture of water and acetonitrile and kept with ice cooling. These solutions were added to

† Contribution No. 537 from Department of Organic Synthesis.

buffer solutions in a UV cell which had been maintained at 30 °C. Water was added so that the fraction of organic solvents (acetonitrile and ethanol) became 3 v/v %. The reaction rate was determined by following the absorbance increase of 2,4-dinitrophenolate anion at 360 nm (ε_{360}= 12800 M^{-1} cm^{-1}), using a Hitachi UV-visible spectrophotometer (type 124 and 200).

Results

Sulfate Transfer to Anionic Hydroxamates. The time course of DNPS hydrolysis in the LBHA–CTAB system obeyed pseudo first-order kinetics: [DNPS]= 1.9×10^{-5} M, [CTAB]=4.50×10^{-3} M. However, the pseudo first-order rate constant $k_{1,obsd}$ did not vary with the concentration change ($(2—6)\times10^{-4}$ M) of LBHA. Furthermore, the logarithm of the apparent second-order rate constant, log $k_{2,obsd}$, increased linearly with pH at pH 8—10. This pH-rate profile is not consistent with the pK_a value(8.41) of LBHA in the CTAB micelle. Because of the complex kinetic behavior and a relatively small reactivity (*ca.* 10% of C_{12}-Im^+-HA under comparable conditions), LBHA was not used in the subsequent experiment.

The sulfate transfer reaction with a non-micellar hydroxamate, *N*-benzylbenzohydroxamic acid(BBHA), [9] was also studied under the following conditions: pH 9.23, 0.01 M borate buffer, μ=0.01(KCl), 30 v/v %EtOH–H_2O, [BBHA]=2.5×10^{-2} M and [DNPS] =2.0×10^{-5} M. $k_{1,obsd}$ obtained from the Guggenheim plot was only slightly larger than that obtained without the hydroxamate under otherwise the same conditions: 9.8×10^{-5} s^{-1} *vs.* 7.3×10^{-5} s^{-1}. Therefore, $k_{2,obsd}$ is estimated to be smaller than 1×10^{-3} M^{-1} s^{-1}.

Sulfate Transfer to Micellar Zwitterionic Hydroxamates. In the presence of excess DNPS, the nucleophilic attack of C_{12}-Im^+-HA obeyed the pseudo first-order kinetics for more than 80% consumption of the nucleophile: [DNPS]=$(0.52—4.6)\times10^{-4}$ M, [C_{12}-Im^+-HA]=0.13×10^{-4} M, [CTAB]=1.0×10^{-3} M, pH 9.2, 30 °C. The spontaneous hydrolysis was similarly carried out in the absence of the nucleophile and its rate constant, k_{spont}, was subtracted from the overall first-order rate constant, $k_{1,obsd}$. In reality, k_{spont} was approximately 1.0×10^{-4} s^{-1} without regard to the pH change, and much smaller than $k_{1,obsd}$ which was $(2—4)\times10^{-3}$ s^{-1}. Therefore, the correction was not necessary at pH 9.

The pseudo first-order rate constant was proportional to the substrate concentration: correlation coefficient= 0.993. Therefore, the reaction was first order with respect to nucleophile and substrate, and the second-order rate constant ($k_{2,obsd}$) was calculated to be 20.8 M^{-1} s^{-1}. Precipitates were formed when the substrate concentration was increased beyond 5×10^{-4} M.

The pseudo first-order kinetics were similarly observed when excess nucleophile was employed: [DNPS]= 1.7×10^{-5} M, [C_{12}-Im^+-HA]=$(0.51—2.6)\times10^{-4}$ M, [CTAB]=4.0×10^{-3} M, pH 9.0, 30 °C. However, the pseudo first-order rate constant was not a linear function of the nucleophile concentration beyond 1.5×10^{-4} M, as shown in Fig. 1. $k_{2,obsd}$ estimated from the linear portion of Fig. 1 is 2.45 M^{-1} s^{-1}.

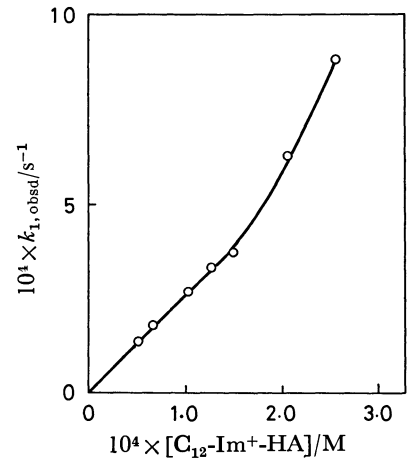

Fig. 1. Rate dependence on nucleophile concentration. pH 9.00±0.1, 30 °C, 3 v/v % EtOH–H_2O, 0.02 M borate buffer, μ=0.01(KCl), [DNPS]=1.72×10^{-5} M, [CTAB]=4.00×10^{-3} M.

This value is only 12% of the rate constant obtained by varying substrate concentrations. Since the pseudo first-order kinetics were always observed for a given run, the discrepancy must arise from the change in the relative concentration of nucleophile, substrate and/or surfactant.

Rate Dependence on Surfactant Concentration. The zwitterionic nucleophile C_{12}-Im^+-HA may form micelles by itself. The property of the mixed micelle of C_{12}-Im^+-HA and CTAB will be affected by their relative concentration, hence the reactivity change of C_{12}-Im^+-HA. Figure 2 shows the variation of the apparent second-order rate constant $k_{2,obsd}$ (pseudo first-order rate constant divided by the nucleophile concentration) with the surfactant concentration at fixed concentrations of DNPS and C_{12}-Im^+-HA. After abrupt increases $k_{2,obsd}$ decreases with increasing surfactant concentrations, irrespective of the type of the surfactant used. The same trend was observed for the hydrolysis of an anionic phenyl ester, 4-acetoxy-3-nitrobenzoic acid (NABA) catalyzed by C_{12}-Im^+-HA in the nonionic micelle.

On the other hand, $k_{1,obsd}$ exhibits a saturation tendency with the simultaneous increase in the concentrations of C_{12}-Im^+-HA and CTAB(the relative concentration of C_{12}-Im^+-HA and CTAB is fixed at 0.26): see Fig. 3. Therefore $k_{2,obsd}$ ($k_{1,obsd}$ divided by the hydroxamate concentration) decreases with the CTAB concentration as also shown in Fig. 3. This tendency corresponds to those in Fig. 2.

pH-*Rate Profile.* The pH-rate profile of the nucleophilic and spontaneous cleavages was studied in the presence of the CTAB and POOA micelles (Fig. 4). log $k_{2,obsd}$ in the presence of the CTAB micelle increases initially with pH but levels off at *ca.* pH 8. This profile appears to reflect the dissociation of the hydroxamic acid. In fact, a linear relation(r=0.997) was obtained when $k_{2,obsd}$ was plotted against α_{HA} (degree of dissociation) which was calculated from Eq. 2 assuming pK_{app}=7.70.

$$\alpha_{HA}=\frac{1}{1+10^{(pK_{app}-pH)}} \quad (2)$$

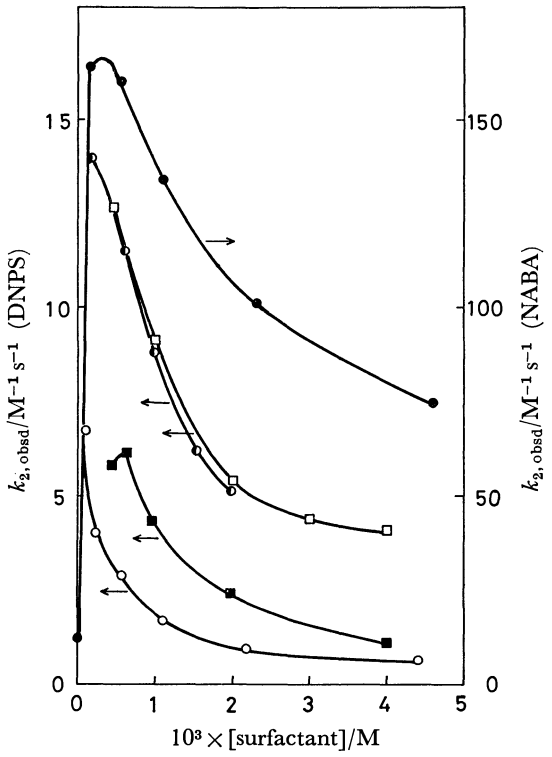

Fig. 2. Rate dependence on surfactant concentration. pH 8.5±0.1, 30 °C, 3 v/v % EtOH-H_2O, 0.02 M borate buffer, μ=0.01(KCl). a) [DNPS]=2.98×10^{-5} M, [C_{12}-Im^+-HA]=3.91×10^{-4} M. b) [NABA]=4.26×10^{-5} M, [C_{12}-Im^+-HA]=3.43×10^{-4} M. —●—, POOA(NABA); —□—, CTAB; —◐—, C_{18}-N^+-$2C_1C_2OH$; —■—, $C_{12}N^+2C_1CO_2^-$; —○—, POOA.

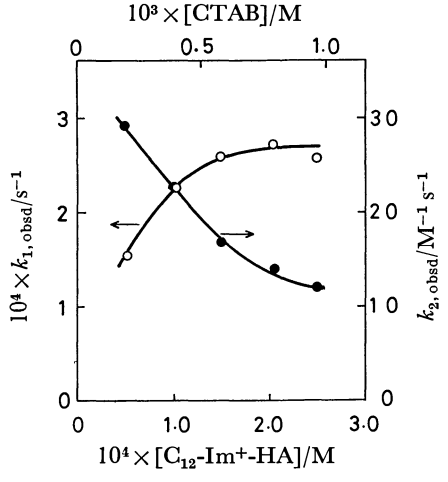

Fig. 3. Rate dependence on concentrations of nucleophile and surfactant at a fixed relative concentration. pH 9.0±0.1, 30 °C, 3 v/v % EtOH-H_2O, 0.02 M borate buffer, μ=0.01(KCl), [DNPS]=1.72×10^{-5} M, [C_{12}-Im^+-HA]/[CTAB]=0.26.

This pK_{app} value agrees with pK_{app} (7.78) obtained in the hydrolysis of *p*-nitrophenyl acetate in the CTAB micelle.[8]

In the POOA system, the pH-rate profile is bell-shaped with the maximum at pH 8.4. This behavior is quite different from what is observed with *p*-nitrophenyl acetate as substrate. In the latter case, a typical saturation profile was found with pK_{app}=8.18. The

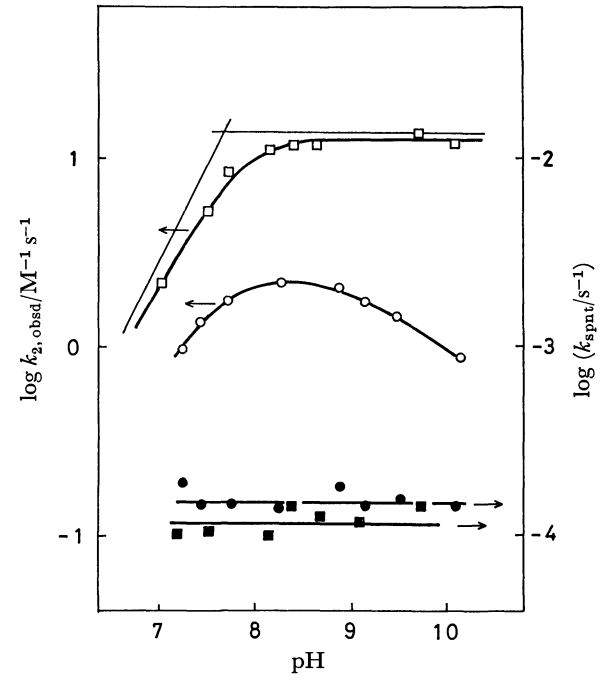

Fig. 4. pH-rate profile. 30 °C, 3 v/v % EtOH-H_2O, 0.01 or 0.02 M borate buffer, μ=0.01(KCl), [DNPS]=(3.2—3.5)$\times10^{-5}$ M, [C_{12}-Im^+-HA]=(2.7—3.0)$\times10^{-4}$ M, [CTAB]=5.13×10^{-4} M, [POOA]=1.00×10^{-3} M. —□—, —■—; CTAB. —○—, —●—; POOA.

interaction of anionic DNPS substrate with C_{12}-Im^+-HA in the nonionic micelle is not so straightforward as that in the cationic micelle.

Figure 4 also contains pH-rate profiles of the spontaneous hydrolysis in the presence of POOA and CTAB. The rate of the spontaneous hydrolysis($\approx10^{-4}$ s^{-1}) does not depend on pH, in consistence with the result of Fendler's.[2]

Discussion

Reaction Scheme. The nucleophilic reaction toward dinitrophenyl sulfate has been studied by several groups of the investigator. For instance, Fendler *et al.* noted that hydrolysis and aminolysis competed in the reaction with a variety of amines.[6]

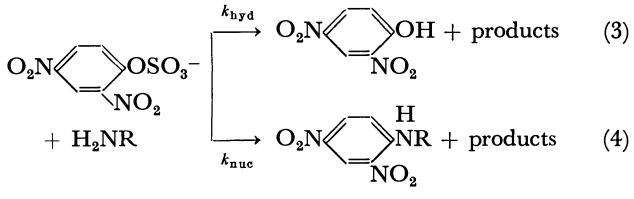

Definite results on the reaction of DNPS with anionic nucleophiles have not been published, probably with the exception of the paper by Sunamoto *et al.*[4] They concluded that the reaction of DNPS with a paracyclophanone oxime involved sulfate transfer to the oximate anion. We do not have direct evidence for the formation of the sulfohydroxamate intermediate; however, the hydroxamate anion would be expected to behave in the same way as the oximate. In our system, the substrate, if decomposed, was completely

converted to dinitrophenol as confirmed spectrally. Therefore, the reaction would proceed by the following equation.

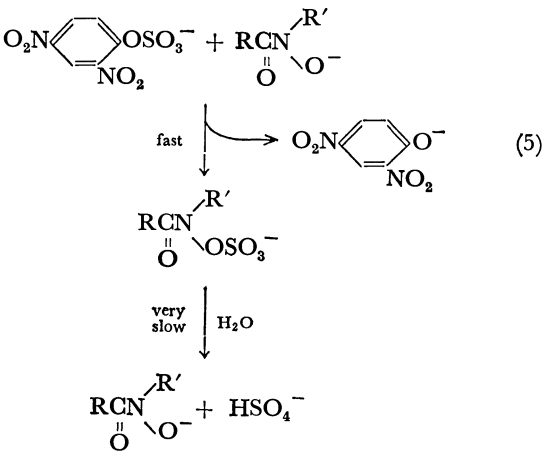

(5)

The stoichiometric reaction of DNPS and C_{12}-Im$^+$-HA was observed in the presence of excess DNPS; thus turnover of the hydroxamate nucleophile was excluded.

The undissociated hydroxamic acid is not involved in the reaction, because the sulfate transfer is observed only in the alkaline region.

Catalytic Efficiency. Some of the rate constants of the DNPS cleavage are collected in Table 1. The uncatalyzed hydrolysis of DNPS in the neutral to alkaline aqueous media is quite slow and barely detectable: $k_{1,obsd}=2.7\times10^{-5}$ s^{-1} at 25 °C, pH 8.0(or 4.9×10^{-7} M^{-1} s^{-1} when divided by 55.5 M). Some rate enhancements are observed in the presence of β-cyclodextrin and a paracyclophanone oxime; however these enhancements are mostly attributed to substrate binding and, in fact, the rate constant of the intracavity sulfate transfer is not necessarily large relative to that of simple alkaline hydrolysis under similar reaction conditions.[4] Micellar CTAB also shows rate acceleration of at most several fold. Larger rate enhancements are found for functional micelles such as CTAB–piperidine[6] and for a reversed micelle (dodecylammonium propionate in benzene).[10] The micellar hydroxamates possess much greater nucleophilicity. However, the coulombic repulsion of the nucleopile and the substrate renders the kinetic behavior rather complex, as observed for the LBHA–CTAB system. The use of the zwitterionic hydroxamate is advantageous in this respect and produces larger reaction rates. $k_{2,obsd}$ for C_{12}-Im$^+$-HA in the CTAB micelle is larger than that for CTAB–piperidine by at least 100 fold and is *ca.* 2×10^7 times larger than that of the water hydrolysis. The different behavior of the anionic and zwitterionic nucleophiles (LBHA and C_{12}-Im$^+$-HA) is observed only in the sulfate cleavage. They possessed similar reactivities in the cleavage of phenyl esters in the CTAB micelle.[8] The enhanced reactivity of a nucleophilic group bound to an ammonium group was also detected in the sulfate cleavage by a partly quaternized poly(ethylenimine).[11]

Kinetic Analysis of Micellar Catalysis. The kinetic behavior of the DNPS cleavage by the micellar hydroxamate is quite complex.

Several cases related to this behavior have been observed in the micellar catalysis. Gitler *et al.*[12] and Tonellato[13] proposed in the hydrolysis of hydrophobic phenyl esters that the saturation kinetics are explicable by assuming active and inactive binding sites in the micelle. However, this interpretation is difficult to accept, since the conventional micellar phase is quite mobile. In fact, the two phase model in which the micellar phase is assumed to be homogeneous has been successfully applied to micellar reactions by Berezin *et al.*[14] and more recently by other workers.[15,16]

This model may be applied to the present system. The kinetic derivation is given in the Appendix. Figure 5 gives plots of $1/k_{2,obsd}$ against the surfactant concentration for the data of Fig. 2. Linear relations are obtained for all cases. According to Eq. 17, the

Table 1. Nucleophilic reactivities in the DNPS cleavage

Catalyst or nucleophile	$k_{1,obsd}$/s^{-1}	$k_{2,obsd}$/M^{-1} s^{-1}	Conditions	Ref.
None	2.7×10^{-5}	4.9×10^{-7} a)	25 °C, pH 8.0	5
β-Cyclodextrin	1.75×10^{-3} b) ($K_S=2.4\times10^{-2}$ M)		37.3 °C, pH 9.98	3
Paracyclophanone oxime c)	4.4×10^{-4} b) ($K_S=1.5\times10^{-4}$ M)		40 °C, 0.1 M NaOH	4
CTAB	1.15×10^{-4} d) (at 1.0×10^{-3} M CTAB)		30 °C, pH 8—10	this study
DAP e)-benzene		0.0187	24.5 °C	9
Piperidine in CTAB		0.098	39 °C	6
BBHA f)		<0.001	30 °C, pH 9.23	this study
LBHA in CTAB	2×10^{-4} d) (at 2×10^{-4} M LBHA)		30 °C, pH 8.5—9.0	this study
C_{12}-Im$^+$-HA				
in DMOG		6.1	30 °C, pH 8.5—9.0	this study
in POOA		6.8		
in CTAB		11		

a) $k_{1,obsd}$/55.5 M. b) Michaelis-Menten kinetics are observed and the maximum values of $k_{1,obsd}$ is given. K_S is the substrate dissociation constant. c) 10-Hydroxy-11-hydroxyimino[20]paracyclophane. d) The kinetics are not straightforward and $k_{1,obsd}$ at the designated nucleophile concentration is given. e) Dodecylammonium propionate. f) *N*-benzylbenzohydroxamic acid; 30 vol/vol % EtOH–H_2O.

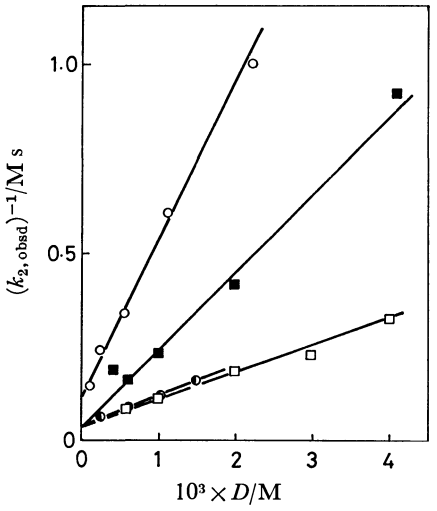

Fig. 5. Relation of $1/k_{2,obsd}$ and surfactant concentration. The data of Fig. 2 are used. —□—, CTAB; —◐—, $C_{18}N^+2C_1C_2OH$; —■—, $C_{12}N^+2C_1CO_2^-$; —○—, POOA.

TABLE 2. KINETIC CONSTANTS IN VARIOUS MICELLES[a]

Micelle	$10^3 \times \bar{k}_M$/s^{-1}	K_b/M^{-1}
CTAB	14.6	1600
$C_{18}N^+2C_1C_2OH$	13.6	1600
POOA	2.38	1400
$C_{12}N^+2C_1CO_2^-$	7.06	3300

a) See Fig. 2 for the reaction condition.

reciprocal of the slope corresponds to the first-order rate constant in the micellar phase ($\bar{k}_M$): see Table 2. The "micellar" rate constant increases in the order: CTAB $\simeq$ $C_{18}N^+2C_1C_2OH$ > $C_{12}N^+2C_1CO_2^-$ > POOA. The same order of the micellar effectiveness was observed in the hydrolysis of *p*-nitrophenyl acetate by several zwitterionic hydroxamates.[8]

The K_b value can be calculated from the intercept of Fig. 5 and is in the range of 1400—3300 M^{-1} as given in Table 2. These values are in reasonable agreement with those of Fendler *et al.*(1300—3100 M^{-1}) which were given as K/N in the hydrolysis of DNPS in the presence of the CTAB micelle.[2]

These results suggest that the kinetic analysis based on the two phase model is essentially valid if the micellar phase is not greatly perturbed. Since dependencies of $k_{2,obsd}$ on the surfactant concentration are alike for an anionic phenyl ester(NABA) and for a sulfate ester(DNPS), the above-mentioned kinetic behavior is never specific to the sulfate ester. A very similar rate dependence was reported for the electron transfer between negatively-charged metal chelates in the presence of the CTAB micelle.[16]

On the other hand, the simple two phase model fails when the micellar microenvironment is significantly altered by the varying nucleophile concentration. $k_{1,obsd}$ shows upward curvature in Fig. 1 beyond the nucleophile concentration of 1.5×10^{-4} M. $k_{2,obsd}$ obtained from the data of Fig. 2 does not agree with that estimated in Fig. 3. These anomalies appear to arise mainly from the change in the microenvironment of micelles which contain different amounts of the nucleophile molecule. The presence of a maximum in the pH-rate profile of the POOA system in Fig. 4 may be explained in the same context.

Appendix

The two phase model is used in the following kinetic analysis. Assuming that catalyst C forms comicelles with surfactants and that substrate S is distributed in the micellar and bulk phases,

$$[C]_{total} = [C]_M DV, \tag{6}$$

$$[S]_{total} = [S]_M DV + [S]_W(1-DV), \tag{7}$$

where D is the surfactant concentration and V is the molar volume of the surfactant. Suffix M and W indicate micellar and bulk (water) phases, respectively.

If the reaction proceeds only in the micellar phase, the overall reaction rate is given by

$$v = v_M DV = k_{2,obsd}[C]_{total}[S]_{total} \tag{8}$$

and

$$v_M = k_M[C]_M[S]_M, \tag{9}$$

where k_M is the second-order rate constant in the micellar phase. The partition coefficient of the substrate is given by

$$P_S = \frac{[S]_M}{[S]_W}. \tag{10}$$

The binding constant of the substrate K_b is expressed in terms of P_S as follows.

$$K_b = \frac{[S]_{total}-[S]_W}{[S]_W \cdot D} = \frac{1}{D} \cdot \frac{[S]_M DV - [S]_W DV}{[S]_W} = (P_S - 1)V. \tag{11}$$

When the substrate stays predominantly in the micellar phase ($P_S \gg 1$)

$$K_b = P_S V. \tag{12}$$

From Eqs. 6, 7, and 8,

$$k_M[C]_M \cdot [S]_M DV = k_{2,obsd}[C]_{total} \cdot [S]_{total}. \tag{13}$$

Therefore,

$$k_M P_S = k_{2,obsd}\{1+(P_S+1)DV\} \tag{14}$$

$$k_{2,obsd} = \frac{\bar{k}_M \cdot K_b}{1+K_b D}, \tag{15}$$

$$\text{where } \bar{k}_M = k_M/V. \tag{16}$$

The reciprocal relation of Eq. 15 is

$$\frac{1}{k_{2,obsd}} = \frac{1}{\bar{k}_M \cdot K_b} + \frac{D}{\bar{k}_M}. \tag{17}$$

$\bar{k}_M$ and K_b are determined from the slope and intercept, respectively, of the relation of Eq. 17.

References

1) A. B. Roy, "The Enzymes," ed by P. D. Boyer, 3rd ed, Academic Press, New York (1971), Vol. 5, p. 1.
2) E. J. Fendler and J. H. Fendler, *J. Org. Chem.*, **33**, 3852 (1968).
3) W. I. Congdon and M. L. Bender, *Bioorg. Chem.*, **1**, 424 (1971).
4) J. Sunamoto, H. Kondo, H. Okamoto, and K. Taira, *Bioorg. Chem.*, **6**, 95 (1977).

5) E. J. Fendler, R. R. Liechti, and J. H. Fendler, *J. Org. Chem.*, **35**, 1658 (1970).
6) J. H. Fendler, E. J. Fendler, and L. W. Smith, *J. Chem. Soc., Perkin Trans. 2*, **1972**, 2097.
7) Eg., T. Kunitake, Y. Okahata, and T. Sakamoto, *J. Am. Chem. Soc.*, **98**, 7799 (1976) and references cited therein.
8) T. Kunitake, Y. Okahata, and T. Tahara, *Bioorg. Chem.*, **5**, 155 (1976).
10) C. J. O'Connor, E. J. Fendler, and J. H. Fendler, *J. Org. Chem.*, **38**, 3371 (1973).
11) T. Kunitake and T. Sakamoto, *Bull. Chem. Soc. Jpn.*, **52**, 2402 (1979).
12) C. Gitler and A. Ochoa-Solano, *J. Am. Chem. Soc.*, **90**, 5004 (1968).
13) U. Tonellato, *J. Chem. Soc. Perkin Trans. 2*, **1976**, 771.
14) I. V. Berezin, K. Martinek, and A. K. Yatsimirski, *Russ. Chem. Rev.*, **42**, 787 (1973).
15) L. K. J. Tong and M. C. Glesmann, *J. Am. Chem. Soc.*, **99**, 6991 (1977).
16) A. A. Bhaleker and J. B. F. U. Engberts, *J. Am. Chem. Soc.*, **100**, 5914 (1978).

Branched-chain Sugars. XVII. Stereoselectivity in the Oxidation of Several Methyl 4,6-*O*-Benzylidene-2-*C*- or -3-*C*-methylene-α- and -β-D-hexopyranosides with *m*-Chloroperbenzoic Acid[1]

Juji YOSHIMURA,* Ken-ichi SATO, and Masuo FUNABASHI

Laboratory of Chemistry for Natural Products, Faculty of Science, Tokyo Institute of Technology, Nagatsuta, Midoriku, Yokohama 227

(Received January 31, 1979)

Stereoselectivity in the peroxy acid oxidation of methyl 4,6-*O*-benzylidene-3-*O*-methyl-2-*C*-methylene-α-D-*ribo*-hexopyranoside (**1b**), its 3-epimer (**2b**), β-anomer of **1b** and **2b**, methyl 4,6-*O*-benzylidene-2-*O*-methyl-3-*C*-methylene-α-D-*arabino*-hexopyranoside and its 2-epimer was examined. The results were compared with those of rigid methylenecyclohexane systems.

In previous papers reports were given on the stereoselectivity examined in the reaction of methyl 4,6-*O*-benzylidene-α- and -β-D-hexopyranosid-2-uloses and -3-uloses with nucleophiles.[2–5] It was found that in the reaction of diazomethane stereoselectivity is mainly controlled by the electrostatic attractive interaction between neighboring axial oxygens and diazomethyl cation in the zwitterionic intermediates.[4,5] The interaction sometimes resulted in a complemental stereoselectivity of diazomethane reaction to that of usual nucleophiles such as hydride anions and carbanions, valuable for a stereospecific synthesis of a proper branched-chain sugar.[6] However, the diazomethane reaction of uloses is sometimes accompanied by ring-expansion reaction, even when the stereoselectivity is the desired one.[7–9] For such cases, it was found that the peroxy acid oxidation of the corresponding methylene derivative provides a reliable pathway to obtain the spiro epoxide which is also afforded by the diazomethane reaction of the ulose.[10,11]

We have examined the stereoselectivity in the peroxy acid oxidation of several 2- or 3-methylen-α- and β-D-hexopyranosides in comparison with that of the diazomethane reaction of the corresponding uloses.

Results and Discussion

As the substrates, methyl 4,6-*O*-benzylidene-3-*O*-methyl-2-*C*-methylene-α-D-*ribo*-hexopyranoside (**1b**), its 3-epimer (**2b**), β-anomer of **1b**(**3b**) and **2b**(**4b**), methyl 4,6-*O*-benzylidene-2-*O*-methyl-3-*C*-methylene-α-D-*arabino*- (**5b**) -β-D-*ribo*-hexopyranosides (**6b**) were synthesized from the corresponding uloses[12] and methyltriphenylphosphonium bromide by the usual method. In the case of **3b**, the corresponding ulose (**3a**)[13] was synthesized by the dimethyl sulfoxide–trifluoroacetic anhydride oxidation[12] of methyl 4,6-*O*-benzylidene-3-*O*-methyl-β-D-altropyranoside (**7**) obtained by the preferential ring-opening of the corresponding 2,3-epoxide of D-*manno* configuration with methanol. The 2,3-epoxide was synthesized by an improved method.[14]

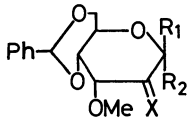

(**1**) R_1=H, R_2=OMe
(**3**) R_1=OMe, R_2=H

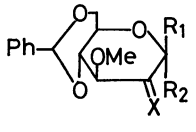

(**2**) R_1=H, R_2=OMe
(**4**) R_1=OMe, R_2=H

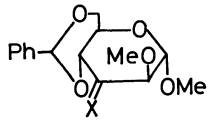

(**5**)

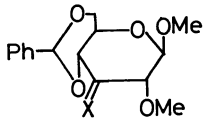

(**6**)

a: X=O
b: X=CH_2

m-Chloroperbenzoic acid oxidation of methylene derivatives was carried out in dry 1,2-dichloroethane at 60 °C, until the starting material disappeared on TLC.

Oxidation of **1b** exclusively gave methyl 2,2′-anhydro-4,6-*O*-benzylidene-2-*C*-hydroxymethyl-3-*O*-methyl-α-D-altropyranoside (**8**) in 82% yield, the product being identical with that obtained by the diazomethane reaction of the corresponding ulose (**1a**).[5] Similarly, oxidation of **2b** exclusively gave the corresponding spiro epoxide (**9**) of D-*manno* configuration in 86% yield, the main product in the reaction of diazomethane with **2a**.[5] Oxidation of **3b** gave an epimeric mixture of the corresponding spiro epoxides (**10**) and (**11**) in 79% yield. Separation of the mixture on preparative TLC gave pure **10** and **11** in the ratio 2:1. In order to determine the configuration of these epimers, they were reduced with lithium aluminum hydride to give the corresponding 2-*C*-methyl derivatives (**12** and **13**), subsequent acetolysis afforded the corresponding tetra-*O*-acetates (**14** and **15**), respectively. By comparison of these α,β-acetates with those obtained from methyl 4,6-*O*-benzylidene-2-*C*-methyl-3-*O*-methyl-α-D-altro- and -allopyranoside,[5] the configuration of the main products (**10**, **12**, and **14**) was determined to be D-*altro* (H_1 protons of **14** appeared at δ 6.41 and 6.22), and that of the minor product D-*allo* (**15**; δ 6.37 and 5.86).

Oxidation of **4b** also gave an epimeric mixture of the corresponding spiro epoxides (**16** and **17**) in 84% yield in the ratio 1.2:1. The configuration of the main product was determined to be D-*gluco* by comparison with that obtained by the diazomethane reaction of **4a**.[5] Similarly the oxidation of **5b** and **6b** gave an epimeric mixture of the corresponding spiro epoxides (**18** and **19**, and **20** and **21**), respectively. The configurations of these compounds were also determined by comparison with those obtained by the diazomethane reaction of **5a** and **6a**.[4] The results are summarized

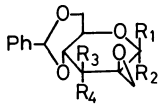

	R_1	R_2	R_3	R_4
(**8**)	H	OMe	H	OMe
(**9**)	H	OMe	OMe	H
(**10**)	OMe	H	H	OMe
(**17**)	OMe	H	OMe	H

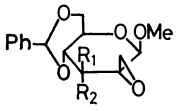

	R_1	R_2
(**11**)	H	OMe
(**16**)	OMe	H

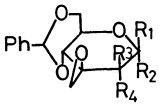

	R_1	R_2	R_3	R_4
(**18**)	H	OMe	OMe	H
(**20**)	OMe	H	H	OMe

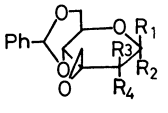

	R_1	R_2	R_3	R_4
(**19**)	H	OMe	OMe	H
(**21**)	OMe	H	H	OMe

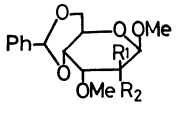

	R_1	R_2
(**7**)	OH	H
(**12**)	OH	Me
(**13**)	Me	OH

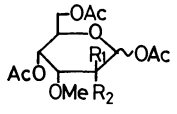

	R_1	R_2
(**14**)	OAc	Me
(**15**)	Me	OAc

Table 1. Comparison of stereoselectivity in the peroxy acid oxidation of methyl 4,6-*O*-benzylidene-2- or -3-methylene-α- and -β-D-hexopyranosides and in the diazomethane reaction of the corresponding uloses

Substrates		Yields (%) of spiro epoxides in the reaction of uloses with diazomethane[a] (a series) and that of methylene derivatives with *m*-chloroperbenzoic acid (b series)	
		Axial attack product	Equatorial attack product
1	a		83.5 (**8**)
	b	82.0 (**8**)	
2	a	31.1	63.7 (**9**)
	b	86.0 (**9**)	
3	a	21.8 (**11**)	65.3 (**10**)
	b	52.7 (**10**)	26.3 (**11**)
4	a	92.5 (**16**)	
	b	38.2 (**17**)	45.2 (**16**)
5	a		41.0 (**19**)[b]
	b	39.5 (**19**)	47.5 (**18**)
6	a	17.6 (**20**)	76.5 (**21**)
	b	42.0 (**21**)	30.0 (**20**)

a) The results are cited from Refs. 4 and 5, except those of **3a**. b) The ring-expansion product of **19** was obtained in 36.9% yield.

in Table 1.

The reaction of **3a** and diazomethane in ethanol was carried out in order to confirm our hypothesis on stereoselectivity. Separation of the products (87% yield) on preparative TLC gave **10** and **11** in the ratio 3:1. Since **4a** exclusively gave an axial attack product in the diazomethane reaction,[4] the predominant equatorial attack also supports our hypothesis, in which the electrostatic attractive force of axial oxygen at C-3 position is stronger than that of lone pair electron of ring oxygen at β-position of the carbonyl group.

By considering both steric (non-bonded interactions) and electrostatic (attractive or repulsive) factors (Table 1), the stereoselectivity in the diazomethane reaction of uloses could be explained by the electrostatic attractive interaction between neighboring axial oxygen atom and diazomethyl cation in the transition state.

Peroxy acid oxidation is known to involve an electrophilic attack of the reagent from the less hindered side of the alkene to give the less hindered epoxide, through a highly ordered transition state.[15,16]

In the *m*-chloroperbenzoic acid oxidation of rigid methylenecyclohexane systems, Carlson and Behn showed that the axial attack percentage[17] is 59—69% due to stronger steric hindrance of axial hydrogen on α-carbon than that of β-carbon in the transition state.[18] From the results obtained here, the axial attack percentage in the case of **4b** (46%) and **6b** (58%) can be considerd as standards for 2-methylene and 3-methylene pyranosides, respectively, since they have no axial substiuents. The lower percentage of axial attack in the case of **4b** than that of cyclohexane systems suggests "the product development control"[18] of C_2–O dipole bisecting C_1–O_1 and C_1–O_5 torsional angle in axial attack epoxide formation of β-anomers. The higher percentage in the case of **3b** (68%) than that of **4b** is estimated as the steric factor of the axial 3-methoxyl group. The predominant axial attack in the case of α-anomer of 2-methylene derivatives (**1b** and **2b**) is attributed to the strong steric factor of the axial methoxyl group at C-1 position, as is known in the reduction of 2-uloses with hydride anions.[5,19]

The lower percentage in the case of **5b** (45%) than that of **6b** should be attributed to the balance of steric factors between axial 1- and 2-methoxyl groups. However, the hindrance of the former seems to be larger than the latter, since the percentage of methyl 4,6-*O*-benzylidene-2-deoxy-3-methylene-α-D-*erythro*-hexopyranoside having no 2-methoxyl group is 25%.[11]

Experimental

General Methods. All melting points were determined on a Yanagimoto micro melting point apparatus and are uncorrected. Solvents were evaporated under reduced pressure at a bath temperature not exceeding 50 °C. Optical rotations were measured in a 0.2 dm tube with a Carl Zeiss LEP-Al polarimeter in chloroform unless otherwise stated. IR spectra were recorded with a Hitachi Model EPI-G2 spectrometer, and NMR spectra with a JNM-PS-100 spectrometer in deuteriochloroform containing tetramethylsilane as an internal standard. Chemical shifts and coupling constants were recorded in δ and Hz units, and IR frequencies in cm^{-1}.

*Methyl-4,6-O-benzylidene-3-O-methyl-β-D-ribo-hexopyranosid-2-ulose (**3a**).* Mesylation of methyl 4,6-*O*-benzylidene-3-*O*-benzoyl-β-D-glucopyranoside in pyridine with methanesulfonyl chloride gave the conceponding 2-*O*-mesylate in 82% yield, which was recrystallized from ethanol–hexane. Mp 194—197 °C; $[\alpha]_D^{22}$ −81.5° (*c* 1.1). IR: 1735 (ester); NMR: 8.20—8.00 and 7.60—7.20 (Ph: m), 5.65 (H_3: t, $J_{2,3}=J_{3,4}=9.0$), 4.80—4.50 (H_2 and H_1: m), 4.38 (H_6: q, $J_{5,6}=4.4$, $J_{6,6'}=10.2$), 3.93—3.44 (H_4, H_5, and $H_{6'}$: m), 3.57 (OMe), 2.99 (OMs).

Found: C, 56.75; H, 5.19; S, 6.26%. Calcd for $C_{22}H_{24}O_9S$: C, 56.89; H, 5.21; S, 6.90%.

A solution of the above mesylate (1 g, 2.2 mmol) and sodium (60.7 mg, 2.6 mmol) in absolute methanol (50 ml) was refluxed for 1 h until the starting material and its de-*O*-benzoylated product disappeared on TLC. The reaction mixture was poured into water, and then extracted with chloroform. The usual work-up of the extract gave methyl 4,6-*O*-benzylidene-2,3-anhydro-β-D-mannopyranoside, which was recrystallized from ethanol–hexane in 83% yield. Mp 181—183 °C; $[\alpha]_D^{22}$ −30.2° (*c* 0.7), [lit,[13] mp 182 °C; $[\alpha]_D^{22}$ −30.4° (*c* 0.82)].

Found: C, 63.91; H, 6.22%. Calcd for $C_{14}H_{16}O_5$: C, 63.62; H, 6.10%.

A solution of the above 2,3-anhydro-mannopyranoside (500 mg) and sodium methoxide (700 mg sodium) in methanol (20 ml) was refluxed for 24 h, poured into water, and then extracted with chloroform. The chloroform layer was evaporated to give a mixture of crystals which were separated on preparative TLC (ether–hexane=1:1, Merck type 60 Kieselgel). Lower R_f product was methyl 4,6-*O*-benzylidene-2-*O*-methyl-β-D-glucopyranoside. Yield, 38%; mp 172—175 °C (ethanol–hexane); $[\alpha]_D^{22}$ −69.6° (*c* 1.5), [lit,[20] mp 175—176 °C; $[\alpha]_D^{14}$ −67.3° (*c* 1.6)].

Found: C, 60.86; H, 7.02%. Calcd for $C_{15}H_{20}O_6$: C, 60.80; H, 6.80%.

Higher R_f product was methyl 4,6-*O*-benzylidene-3-*O*-methyl-β-D-altropyranoside (**7**). Yield, 41%, mp 94—96 °C (ethanol–hexane); $[\alpha]_D^{22}$ −63.0° (*c* 1.2). IR: 3536 (OH); NMR: 7.60—7.30 (Ph: m), 5.57 (PhCH: s), 4.77 (H_1: d, $J_{1,2}=1.2$), 4.38 (H_6: q, $J_{5,6}=4.0$, $J_{6,6'}=7.0$), 4.15—3.67 (H_2, H_3, H_4, H_5, and $H_{6'}$: m), 3.60 (2×OMe), 2.66 (OH: d, $J_{2,OH}=2.0$).

Found: C, 61.10; H, 6.85%. Calcd for $C_{15}H_{20}O_6$: C, 60.80; H, 6.80%. Coupling constants ($J_{1,2}=1.6$, $J_{2,3}=3.6$) in the NMR spectrum of the corresponding 2-acetate support the structure.

Oxidation of the above β-D-altropyranoside with dimethyl sulfoxide–trifluoroacetic anhydride, under similar conditions to those reported,[12] afforded **3a** in 87% yield, which was recrystallized from ethanol–water. Hydrate of **3a**: Mp 85—90 °C; $[\alpha]_D^{22}$ −56.8° (*c* 0.8). IR: 3500 and 3380 (OH); NMR 7.60—7.25 (Ph: m), 5.50 (PhCH: s), 4.52 (H_1: s), 4.37 (H_6: q, $J_{5,6}=3.0$, $J_{5,6'}=7.8$), 4.15—3.50 (H_4, H_5, and OH: m), 3.86 ($H_{6'}$: t, $J_{6,6'}=7.8$), 3.70 (H_3: d, $J_{3,4}=2.0$), 3.67 and 3.63 (2×OMe).

Found: C, 57.76; H, 6.60%. Calcd for $C_{15}H_{18}O_6\cdot H_2O$: C, 57.68; H, 6.46%.

*Wittig Reaction of Uloses (**1a**—**6a**).* A solution of butyllithium (10%; 2.9 ml, 4.5 mmol) in hexane was added dropwise with stirring to a suspension of methyltriphenylphosphonium bromide (2.9 g, 5.6 mmol) in dry tetrahydrofuran (7 ml) cooled in an ice–water bath. A solution of methyl 4,6-*O*-benzylidene-3-*O*-methyl-α-D-*ribo*-hexopyranosid-2-ulose (**1a**)[5] (1 g, 3.4 mmol) in tetrahydrofuran (30 ml) was then rapidly added with vigorous stirring to the resulting yellowish orange suspension. The reaction mixture was kept at room temperature for 30 min until **1a** disappeared on TLC. After addition of ether (70 ml) to the mixture, the precipitate was collected by filtration. The filtrate was evaporated, and the residue was placed on a silica-gel column (Wako-gel C-200: 30 g) followed by elution with benzene to give white crystals (437 mg, 44%), methyl 4,6-*O*-benzylidene-3-*O*-methyl-2-*C*-methylene-α-D-*ribo*-hexopyranoside (**1b**) which were recrystallized from ether–hexane. Mp 82—84 °C; $[\alpha]_D^{22}$ +40.3° (*c* 0.6). NMR: 7.64—7.20 (Ph: m), 5.51 (PhCH: s), 5.30 and 5.25 (exo-CH_2: each s), 4.38 (H_5: m), 4.34 (H_6: q, $J_{5,6}=4.8$), 4.07 (H_3: d, $J_{3,4}=3.2$), 3.66 ($H_{6'}$: t, $J_{5,6'}=J_{6,6'}=11.0$), 3.65 (H_4: q, $J_{4,5}=8.0$), 3.40 and 3.35 (2×OMe).

Found: C, 65.82; H, 6.83%. Calcd for $C_{16}H_{20}O_5$: C, 65.74; H, 6.90%.

A similar reaction of methyl 4,6-*O*-benzylidene-3-*O*-methyl-α-D-*arabino*-hexopyranosid-2-ulose (**2a**) gave the corresponding 2-*C*-methylene derivative (**2b**) in 52% yield, which was recrystallized from ether–hexane. Mp 149—151 °C; $[\alpha]_D^{22}$ +55.4° (*c* 0.9). NMR: 7.60—7.20 (Ph:m), 5.54 (H_1: s), 5.35 and 5.17 (exo-CH_2: each q, $J_{4,CH_2}=1.0$, $J_{gem}=2.0$), 4.23 (H_5: sex), 4.26 (H_4: t, $J_{3,4}=J_{4,5}=9.2$), 3.97 (H_6: q, $J_{5,6}=4.0$), 3.73 ($H_{6'}$: t, $J_{5,6'}=J_{6,6'}=9.4$), 3.58 (H_3: dd), 3.58 and 3.38 (2×OMe).

Found: C, 65.77; H, 6.90%. Calcd for $C_{16}H_{20}O_5$: C, 65.74; H, 6.90%.

A similar reaction of **3a** gave methyl 4,6-*O*-benzylidene-3-*O*-methyl-2-*C*-methylene-β-D-*ribo*-hexopyranoside (**3b**) in 57% yield, which was recrystallized from ethanol. Mp 95—97 °C; $[\alpha]_D^{22}$ −95.5° (*c* 2.8). NMR: 7.60—7.20 (Ph: m), 5.52 (PhCH and H_1: superimposed s), 5.18 and 5.01 (exo-CH_2: each broad s), 4.37 (H_6: q, $J_{5,6}=5.0$, $J_{6,6'}=9.8$), 4.13 (H_5: m), 4.12 (H_3: d, $J_{3,4}=3.0$), 3.73 ($H_{6'}$: t, $J_{5,6'}=9.8$), 3.67 (H_4:q, $J_{4,5}=9.0$), 3.60 and 3.36 (2×OMe).

Found: C, 65.66; H, 7.03%. Cacld for $C_{16}H_{20}O_5$: C, 65.74; H, 6.90%.

A similar reaction of methyl 4,6-*O*-benzylidene-3-*O*-methyl-β-D-*arabino*-hexopyranosid-2-ulose (**4a**)[5] gave the corresponding 2-*C*-methylene derivative (**4b**) in 67% yield, which was recrystallized from ethanol. Mp 156—157 °C; $[\alpha]_D^{22}$ −71.2° (*c* 1.2). NMR: 7.60—7.25 (Ph: m), 5.56 (PhCH: s), 5.50 and 5.42 (exo-CH_2: each broad s), 4.80 (H_1: s), 4.35 (H_6: q, $J_{5,6}=4.0$, $J_{6,6'}=10.0$), 4.00—3.45 (H_3, H_4, and H_5: m), 3.80 ($H_{6'}$:t, $J_{6,6'}=J_{5,6'}=10.0$), 3.62 and 3.60 (2×OMe).

Found: C, 65.49; H, 6.99%. Calcd for $C_{16}H_{20}O_5$: C, 65.74; H, 6.90%.

A similar reaction of methyl 4,6-*O*-benzylidene-2-*O*-methyl-α-D-*arabino*-hexopyranosid-3-ulose (**5a**)[4] gave the corresponding 3-*C*-methylene derivative (**5b**) in 72% yield, which was recrystallized from ethanol. Mp 88—90 °C; $[\alpha]_D^{22}$ +108.7° (*c* 1.1). NMR: 7.70—7.20 (Ph: m), 5.60 (PhCH: s), 5.38 and 5.14 (exo-CH_2: each t, $J_{gem}=J_{4,CH_2}=1.6$), 4.73 (H_1: d, $J_{1,2}=1.2$), 4.40—4.05 (H_5 and H_6: m), 4.00—3.70 (H_4 and $H_{6'}$:m), 3.75 (H_2: d), 3.40 and 3.32 (2×OMe).

Found: C, 66.15; H, 6.86%. Calcd for $C_{16}H_{20}O_5$: C, 65.74; H, 6.90%.

A similar reaction of methyl 4,6-*O*-benzylidene-2-*O*-methyl-β-D-*ribo*-hexopyranosid-3-ulose (**6a**)[4] gave the corresponding 3-*C*-methylene derivative (**6b**) in 60% yield, which was recrystallized from ethanol. Mp 160—161 °C; $[\alpha]_D^{22}$ −61.9° (*c* 1.0). NMR: 7.60—7.20 (Ph: m), 5.60 (PhCH: s), 5.27 (exo-CH_2: t, $J_{4,CH_2}=J_{gem}=2.0$), 4.34 (H_6: q, $J_{5,6}=5.0$), 4.23 (H_1: d, $J_{1,2}=7.6$), 3.94 (H_4: broad d, $J_{4,5}=9.0$), 3.78 ($H_{6'}$: t, $J_{5,6'}=J_{6,6'}=10.0$), 3.58 and 3.57 (2×OMe), *ca.* 3.57 (H_2: d), 3.30 (H_5: sex).

Found: C, 65.70; H, 7.00%. Calcd for $C_{16}H_{20}O_5$: C, 65.74; H, 6.90%.

Oxidation of exo-*Methylene Compounds* (***1b*—*6b***) *with* m-*Chloroperbenzoic Acid.* A solution of **1b** (300 mg, 1.0 mmol) and *m*-chloroperoxybenzoic acid (85% purity, 406 mg, 2.0 mmol) dissolved in 1,2-dichloroethane (15 ml) was heated at 60 °C overnight. The mixture was washed with 0.1 M sodium hydroxide and water, and dried with magnesium sulfate. The organic layer was evaporated to give crystalline methyl 2,2′-anhydro-4,6-*O*-benzylidene-2-*C*-hydroxymethyl-3-*O*-methyl-α-D-altropyranoside (**8**) in 82% yield which was recrystallized from ethanol–hexane. Mp 108—109 °C; $[\alpha]_D^{22}$ +85.0° (*c* 0.7). NMR spectrum was identical with that of the authentic sample.[5]

A similar reaction of **2b** gave methyl 2,2′-anhydro-4,6-*O*-benzylidene-2-*C*-hydroxymethyl-3-*O*-methyl-α-D-mannopyranoside (**9**) in 86% yield which was recrystallized from ethanol–hexane. All the physical constants were identical with those of the authentic sample derived from the reaction of **2a** and diazomethane. Mp 140—141 °C; $[\alpha]_D^{22}$ +76.5° (*c* 0.8).

A similar reaction of **3b** and separation of two products on preparative TLC (ether–hexane 1:1) gave the epimeric pair of spiro epoxides, methyl 2,2′-anhydro-4,6-*O*-benzylidene-2-*C*-hydroxymethyl-3-*O*-methyl-β-D-altropyranoside (**10**) and the corresponding β-D-allopyranoside (**11**), in 52.7 and 26.3% yields, respectively, which were recrystallized from ethanol–hexane.

10: Mp 114—115 °C; $[\alpha]_D^{22}$ −81.6° (*c* 0.8). NMR: 7.60—7.25 (Ph: m), 5.54 (PhCH: s), 5.00 (H_1: s), 4.40 (H_6: q, $J_{5,6}$=4.0), 4.10 (H_5: m), 3.95 (H_4: q, $J_{4,5}$=8.6), 3.83 ($H_{6'}$: t, $J_{5,6'}=J_{6,6'}$=9.0), 3.30 (H_3: d, $J_{3,4}$=2.4), 3.56 and 3.52 (2×OMe), 3.11 and 2.78 (epoxy CH_2: ABq, J=5.3).

Found: C, 61.89; H, 6.65%. Calcd for $C_{16}H_{20}O_6$: C, 62.32; H, 6.54%.

11: Mp 150—151 °C; $[\alpha]_D^{22}$ −61.2° (*c* 0.7). NMR: 7.60—7.25 (Ph: m), 5.50 (PhCH: s), 5.30 (H_1: s), 4.37 (H_6: q, $J_{5,6}$=5.0), 4.16 (H_5: sex), 3.76 ($H_{6'}$: t, $J_{5,6'}=J_{6,6'}$=10.0), 3.76 (H_4: q, $J_{3,4}$=2.2, $J_{4,5}$=9.0), 3.45 (H_3: d), 3.62 and 3.53 (2×OMe), 3.23 and 2.57 (epoxy CH_2: ABq, J=5.4).

Found: C, 62.21; H, 6.57%. Calcd for $C_{16}H_{20}O_6$: C, 62.32; H, 6.54%. Configutations of **10** and **11** were determined by conversions into **14** and **15**, respectively.

A similar reaction of **4b** gave the epimeric pair of spiro epoxide, methyl 2,2′-anhydro-4,6-*O*-benzylidene-2-*C*-hydroxymethyl-3-*O*-methyl-β-D-glucopyranoside (**16**) and the corresponding β-D-mannopyranoside (**17**). Separation of the mixture on preparative TLC (ether–hexane 1:1) gave pure **16** in 45.2% yield, which is identical with the authentic sample obtained by the diazomethane reaction of **4a**.[5] However, pure **17** could not be obtained in a pure state due to its instability on TLC plate. The yield and structure of **17** were estimated form the NMR spectrum of the mixture.

17: NMR 7.60—7.25 (Ph: m), 5.63 (PhCH: s), 4.75 (H_1: s), 4.40 (H_6: q), 3.60 and 3.52 (2×OMe), 3.06 and 2.99 (epoxy CH_2: ABq, J=5.8), H_3, H_4, H_5, and $H_{6'}$, could not be analyzed.

A similar reaction of **5b** and separation of two products on preparative TLC (ether–hexane 1:1) gave the epimeric pair of spiro epoxides, methyl 3,3′-anhydro-4,6-*O*-benzylidene-3-*C*-hydroxymethyl-2-*O*-methyl-α-D-mannopyranoside (**18**) and the corresponding α-D-altropyranoside (**19**) in 47.5 and 39.5% yields, respectively.

18: Sirup; $[\alpha]_D^{22}$ +62.0° (*c* 1.9). NMR: 7.55—7.20 (Ph: m) 5.56 (PhCH: s), 4.76 (H_1: d, $J_{1,2}$=1.8), 4.47—3.75 (H_4, H_5, H_6, and $H_{6'}$: m), 3.11 (H_2: d), 3.54 and 3.37 (2×OMe), 3.17 and 2.70 (epoxy CH_2: ABq, J=6.0).

Found: C, 62.21; H, 6.50%. Calcd for $C_{16}H_{20}O_6$: C, 62.32; H. 6.54%.

19: Mp 141—143 °C (from ether–hexane); $[\alpha]_D^{22}$ +75.3° (*c* 1.3). NMR and IR spectra were identical with those of the authentic sample[4] obtained by the diazomethane reaction of **5a**.

Oxidation of **6b** and separation of two products on preparative TLC (ether–hexane 1:1) gave the epimeric pair of methyl-**3,3′-a**nhydro-4,6-*O*-benzylidene-3-*C*-hydroxymethyl-2-*O*-me**thyl-β**-D-glucopyranoside (**20**) and the corresponding β-D-allopyranoside (**21**) in 30.0% and 42.0% yields, respectively, which were recrystallized from ethanol–hexane.

20: Mp 150—151 °C; $[\alpha]_D^{22}$ −74.2° (*c* 0.8).

21: Mp 156—157 °C; $[\alpha]_D^{22}$ −62.9° (*c* 0.9).

NMR and IR spectra of both **20** and **21** were identical with those of the authentic samples[4] obtained by the diazomethane reaction of **6a**.

Reduction of ***10*** *and* ***11*** *with Lithium Aluminium Hydride.* Lithium aluminium hydride (50 mg) was added to a solution of **10** (150 mg, 0.52 mmol) in tetrahydrofurane (5 ml) and the mixture was then stirred at room temperature for 1 h. The excess hydride was carefully decomposed with water and then filtered. The filtrate was extracted with chloroform. The extract was washed with water, dried with anhydrous magnesium sulfate, and evaporated to give crystalline methyl 4,6-*O*-benzylidene-2-*C*-methyl-3-*O*-methyl-β-D-altropyranoside (**12**) in 91% yield which was recrystallized from ethanol–hexane. Mp 113—114 °C; $[\alpha]_D^{22}$ −64.4° (*c* 1.0). IR: 3520 (OH); NMR: 7.60—7.20 (Ph: m), 5.47 (PhCH: s), 4.44 (H_1: s), 4.34 (H_6: q, $J_{5,6}$=4.0, $J_{6,6'}$=9.0), 4.14 (H_4: q, $J_{3,4}$=2.0, $J_{4,5}$=10.0), 3.94 (H_5: sex), 3.77 ($H_{6'}$: t, $J_{5,6'}$=9.0), 3.47 (H_3: d), 3.56 and 3.47 (2×OMe), 2.70 (OH: broad s), 1.27 (CMe).

Found: C, 61.90; H, 7.30%. Calcd for $C_{16}H_{22}O_6$: C, 61.92; H, 7.15%.

A similar reduction of **11** (150 mg) in THF (5 ml) afforded methyl 4,6-*O*-benzylidene-2-*C*-methyl-3-*O*-methyl-β-D-allopyranoside (**13**) in 89% yield wihch was recrystallized from ethanol–hexane. Mp 118—119 °C; $[\alpha]_D^{22}$ −68.0° (*c* 1.1). NMR: 7.60—7.20 (Ph: m), 5.44 (PhCH: s), 4.43 (H_1: s), 4.35 (H_6: q, $J_{5,6}$=4.0, $J_{6,6'}$=10.4), 4.00—3.48 (H_3, H_4, H_5, and $H_{6'}$: m) 3.60 and 3.48 (2×OMe), 3.30 (OH: broad s), 1.27 (CMe).

Found: C, 61.82; H, 7.41%. Calcd for $C_{16}H_{22}O_6$: C, 61.92; H, 7.15%.

Determination of the Configuration of ***12*** *and* ***13***. A solution of **12** (100 mg) in acetic anhydride (3 ml) containing a drop of 60% perchloric acid was heated at 60 °C for 6 h. Since acetolysis was incomplete, the reaction was repeated at room temperature for 18 h, using *p*-toluenesulfonic acid as a catalyst. The reaction mixture was then poured into cold sodium hydrogencarbonate solution and the resulting solution was extracted with chloroform.

The extracts were washed with water, dried, and evaporated to give a mixture of sirupy 1,2,4,6-tetra-*O*-acetyl-2-*C*,3-*O*-dimethyl-α- and -β-D-altropyranoses (**14**). The configutation was determined without isolation of anomers by direct comparison of the R_f value and NMR spectrum with those of the authentic sample prepared by acetolysis of methyl 4,6-*O*-benzylidene-2-*C*,3-*O*-dimethyl-α-D-altropyranoside.[5]

Compound **13** was also converted into a mixture of sirupy 1,2,4,6-tetra-*O*-acetyl-2-*C*,3-*O*-dimethyl-α- and -β-D-*allo*-pyranoses (**15**), which was identical with that obtained by the acetolysis of methyl 4,6-*O*-benzylidene-2-*C*,3-*O*-dimethyl-α-D-allopyranoside.[5]

14: R_f values, 0.41 and 0.36 (on DC Fertigplatten Kieselgel 60, Merck AG; benzene–acetone 8:1). NMR: 6.37 and 5.86 (H_1:each s), 3.57 (2×OMe), 2.15—2.05 (8×OAc), 1.60 and 1.54 (CMe).

15: R_f values, 0.36 and 0.31 (under the same conditions as above). NMR: 6.41 and 6.22 (H_1: each s), 3.50 and 3.40 (OMe), 2.15—2.05 (8×OAc), 1.68 and 1.56 (CMe).

*Reaction of **3a** with Diazomethane.* To a solution of **3a** (294 mg, 1.0 mmol) in ethanol (30 ml) was added dropwise a solution of diazomethane (2.0 mmol) in ether (10 ml) at 0 °C. After the mixture had been left at room temperature for 12 h, the solution was evaporated to give a sirup. Separation of two products on preparative TLC (ether: hexane= 1:1) gave **10** and **11** in 65.3% and 21.8% yields, respectively. Both were respectively identical with authentic samples obtained *via* the peroxy acid oxidation of (**3b**).

The present work was supported by a Grant-in-Aid for Scientific Research from the Ministry of Education.

Refereneces

1) Part XVI: M. Funabashi, K. Kobayashi, and J. Yoshimura, *J. Org. Chem.*, **44**, 1618 (1979).
2) J. Yoshimura, K. Sato, K. Kobayashi, and C. Shin, *Bull. Chem. Soc. Jpn.*, **46**, 1515 (1973).
3) J. Yoshimura, K. Mikami, K. Sato, and C. Shin, *Bull. Chem. Soc. Jpn.*, **49**, 1686 (1976).
4) K. Sato and J. Yoshimura, *Bull. Chem. Soc. Jpn.*, **51**, 2116 (1978).
5) K. Sato and J. Yoshimura, accepted by *Carbohydr. Res.*
6) W. G. Overend and N. R. Williams, *J. Chem. Soc.*, **1965**, 3446.
7) R. D. King, W. G. Overend, J. Wells, and N R. Williams, *Chem. Commun.*, **1969**, 726.
8) B. Flaherty, S. Nahar, and N. R. Williams, *J. Chem. Soc., Perkin Tarns. 1*, **1973**, 632.
9) J. Yoshimura, K. Kobayashi, K. Sato, and M. Funabashi, *Bull. Chem. Soc. Jpn.*, **45**, 1806 (1972).
10) M. Funabashi, H. Sato, and J. Yoshimura, *Bull. Chem. Soc. Jpn.*, **49**, 788 (1976).
11) M. Funabashi, N.-G. Hong, H. Kodama, and J. Yoshimura, *Carbohydr. Res.*, **67**, 139 (1978).
12) J. Yoshimura, K. Sato, and H. Hashimoto, *Chem. Lett.*, **1977**, 1327.
13) **3a** was also obtained by the same oxidation of methyl 4,6-*O*-benzylidene-3-*O*-methyl-β-D-allopyranoside which was obtained from 1,2,5,6-di-*O*-isopropylidene-3-*O*-methyl-α-D-allofuranose through a four step conversion. Private communication by Dr. Toshio Nakagawa, Yokohama City University.
14) The epoxide was prepared from methyl 4,6-*O*-benzylidene-2-*O*-mesyl-β-D-glucopyranoside obtained by the direct partial mesylation in 6—17 % yield by Guthrie *et al.* (*J. Chem. Soc., C*, **1970**, 1961). To cover the poor stereoselectivity of the partial 2-*O*-mesylation, we carried out the partial 3-*O*-benzoylation according to the method of Collins *et al.* (*J. Chem. Soc., Perkin Trans. 1*, **1972**, 2596), followed by 2-*O*-mesylation.
15) J. B. Lee and B. C. Uff, *Quart. Rev.*, **21**, 429 (1967).
16) D. Swern, "Organic Peroxides," ed by D. Swern, Wiley Interscience, New York (1971), Vol. 11, p. 355.
17) The percentage refers to that of the axial attack product in both axial and equatorial attack products.
18) R. C. Carlson and N. S. Behn, *J. Org. Chem.*, **32**, 1363 (1967).
19) M. Milikovic, M. Gligorijevic, and D. Milikovic, *J. Org. Chem.*, **39**, 2118 (1974).
20) Y. Kondo, *Agric. Biol. Chem.*, **39**, 1879 (1975).

Diazotization of Aromatic Primary Amines of Weak Basicity. II.[1] Reduction of Arenediazonium Salts with Alkylbenzene Derivatives

Ikuo TAKAGISHI, Yoji HASHIDA, and Kohji MATSUI*

Department of Chemistry, Faculty of Engineering, Gunma University, Kiryu, Gunma 376

(Received February 3, 1979)

The diazonio group of arenediazonium salts derived from weakly basic amines were efficiently substituted by hydrogen with alkylbenzenes in sulfuric acid. Several types of evidence, including kinetic results and experiments to trap an intermediate, indicated that the reduction occurs *via* an aryl radical intermediate. In the reduction with toluene, analyses of by-products suggested a radical chain mechanism, which would involve a propagation cycle caused by electron transfer from the benzyl radical to the diazonio group.

The diazonio group of arenediazonium salts is known to be replaced by hydrogen with various reducing agents. These include alcohols,[2] alcohols in combination with metals or metal oxides,[3] ethers,[4] formaldehyde,[5] formic acid and its esters and amides:[6] the ordinary reducing agents of the organic type. However, there has been no report on the reduction of arenediazonium salts by aromatic hydrocarbons.

During the course of our studies on the reaction of arenediazonium salts derived from weakly basic amines, we found that the diazonio group was effectively replaced by hydrogen with alkylbenzene derivatives in sulfuric acid. This paper reports this novel reduction of arenediazonium salts with alkylbenzenes.

Results and Discussion

Reaction of 2-Bromo-4,6-dinitrobenzenediazonium Salt with Alkylbenzenes and Their Derivarives. In this paper, 2-bromo-4,6-dinitrobenzenediazonium salt was chosen as typical of those derived from weakly basic amines. The diazotization was carried out in nitrosylsulfuric acid, which was prepared by adding an 20% excess of sodium nitrite into sulfuric acid. When benzene, halobenzene, or phenol was added to the diazonium solution, the corresponding 2-bromo-4,6-dinitrobiphenyl derivatives resulting from an arylation (acidic Gomberg reaction)[7] of the aromatic substrates with the diazonium compound were obtained, along with a tarry substance.

On the contrary, in the presence of toluene, 1-bromo-3,5-dinitrobenzene was obtained as the main product, showing that the diazonio group was replaced by hydrogen. Similarly, other alkylbenzenes such as ethylbenzene, cumene, and *p*-xylene reduced the diazonium salt effectively. Derivatives of toluene are also able to reduce the diazonium salt very quickly. The results are summarized in Table 1.

As can be seen, there is no observable correlation between *m*- and *p*-substituents and product yields. But the introduction of *o*-substituents into toluene decreases their reducing ability; *e.g.* the reaction with 2,4-dinitrotoluene gave only a tarry substance and unchanged 2,4-dinitrotoluene was recovered quantitatively. In the reaction with *p*-nitrotoluene, *p*-nitrobenzaldehyde was obtained in 51% yield along with 1-bromo-3,5-dinitrobenzene (80%). This observation and the fact that no reduction took place in the presence of benzene indicate that alkyl groups are responsible for the reduction.

TABLE 1. REDUCTION OF 2-BROMO-4,6-DINITROBENZENEDIAZONIUM SALT WITH ALKYLBENZENES

Alkylbenzene[a]				Yield (%) of 1-bromo-3,5-dinitrobenzene
R_1	R_2	R_3	R_4	
CH_3	H	H	CH_3	76
CH_3	H	H	H	70
CH_2CH_3	H	H	H	52
$CH(CH_3)_2$	H	H	H	30
CH_3	H	H	SO_3H	81
CH_3	H	H	NO_2	80
CH_3	H	H	OCH_3	70
CH_3	H	Br	H	82
CH_3	OCH_3	H	NO_2	60
CH_3	Cl	H	NO_2	27
CH_3	NO_2	H	NO_2	0

a) Alkylbenzene: 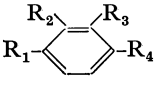

TABLE 2. REDUCTION OF 2-BROMO-4,6-DINITROBENZENEDIAZONIUM SALT WITH BENZENE DERIVATIVES

Reducing agent	Yield (%) of 1-bromo-3,5-dinitrobenzene
Tetralin	44
$C_6H_5CH_2OH$	16
C_6H_5CHO	18
$C_6H_5OCH_3$	11
$C_6H_5C(CH_3)_3$	37

Therefore, to answer the question whether the reducing ability is really limited to alkyl groups, several benzene derivatives containing side chains other than an alkyl group were examined (Table 2).

Table 2 shows that, even though the reducing ability is not high, side chains such as hydroxymethyl-, formyl-, and methoxyl groups are also able to reduce the diazonium compound, as was expected. Since aldehyde[5] and ethers[4] have been known to reduce diazonium compounds, a hydroxymethyl compound would be an intermediate on the course of reduction from methyl compound to aldehyde.

Reactions of 2-Bromo-4,6-dinitrobenzenediazonium Salt with Aliphatic Compounds. From the results described above, it has become apparent that an alkyl group attached to an aromatic nucleus is effective for the reduction. However, it is questionable whether the

Table 3. Reduction of 2-bromo-4,6-dinitrobenzenediazonium salt with alcohols and nitro compound

Reducing agent	Yield (%) of 1-bromo-3,5-dinitrobenzene
CH_3OH	77
CH_3CH_2OH	66
$(CH_3)_2CHOH$	52
$(CH_3)_3COH$	trace
$(CH_3)_2CHNO_2$	62

presence of the aromatic nucleus is really necessary for the reducing ability. To answer this question and to get an insight into the reduction mechanism, the reducing ability of some aliphatic compounds was examined (Table 3).

In accord with our expectation, aliphatic alcohols reduced the diazonium salt. It is noteworthy that the reactions with alcohols gave only the 1-bromo-3,5-dinitrobenzene, suggesting that the reaction proceeded by a radical mechanism, *via* an aryl radical intermediate.[8] Furthermore, diazonium salt could be reduced with an aliphatic nitro compound, resulting in the formation of 1-bromo-3,5-dinitrobenzene. This observation also suggests a radical process for the reaction, because arenediazonium salts are known to decompose in nitroalkanes to give phenols by a heterolytic process.[9]

Reactions of Some Arenediazonium Salts with p-*Toluenesulfonic Acid.* No detailed study has been reported on the reduction of an diazonio group with alkylbenzene.[10] Therefore, to make clear the relation between the chemical constitution of a diazonium salt and its susceptibility to reduction by alkylbenzene, reactions of several arenediazonium salts derived from weakly basic amines with *p*-toluenesulfonic acid were investigated (Table 4).

From Table 4 it is evident that for the effective reduction by *p*-toluenesulfonic acid, a diazonium salt should fulfil the following conditions: 1) The presence of at least two strong electron-withdrawing groups.

Table 4. Reduction of arenediazonium salt with *p*-toluenesulfonic acid

Diazonium salt[a] X	Y	Z	Yield (%) of 1-bromo-3,5-dinitrobenzene
NO_2	NO_2	Br	81
NO_2	NO_2	Cl	77
NO_2	NO_2	NO_2	67
NO_2	Br	NO_2	80
NO_2	H	NO_2	45
NO_2	NO_2	H	trace
Br	NO_2	Br	2
Cl	NO_2	Cl	4
Br	Br	NO_2	6
H	NO_2	H	0

a) Diazonium salt:

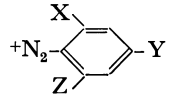

2) The presence of a bulky group at the 2 and 6 positions to the diazonio group; 2,6-dinitrobenzenediazonium salt yielded the reduced product in 45% yield, while in the case of 2,4-dinitrobenzenediazonium salt no reduced product was obtained.[11]

Effects of Sodium Nitrite. In the previous paper[1] we reported that 2-bromo-4,6-dinitrobenzenediazonium salt reacted with sodium nitrite to effect a replacement of the diazonio group by the nitro group. However, in the presence of alkylbenzenes, sodium nitrite was found to act in a different manner. When 2-bromo-4,6-dinitrobenzenediazonium salt was allowed to react with *p*-toluenesulfonic acid in nitrosylsulfuric acid containing an equivalent amount of sodium nitrite, the yield of the reduced product was very poor (≈2%). But when nitrosylsulfuric acid containing 20% excess of sodium nitrite was used, the reduced product was obtained in 81% yield. Figure 1 shows the effect of the amount of sodium nitrite on the decomposition rate of 2-bromo-4,6-dinitrobenzenediazonium salt in sulfuric acid; in the absence of an excess of sodium nitrite, most of the diazonium salt remained unchanged even after 200 min.

These results suggest that an excess of sodium nitrite plays an important role in the decomposition of the diazonium salt to yield the reduced product. It is known that the nitrite ion promotes the homolytic decomposition of a diazonium ion in water[12] and in DMSO;[13] the function of a nitrite ion for the decomposition of a diazonium ion has been explained by suggesting that it combines with the diazonium ion to form a covalent azo compound which decomposes homolytically.[12-15] A similar radical process may be expected in our system. This assumption may be supported by the fact that, when 2,2-diphenyl-1-picrylhydrazyl radical was employed instead of an excess of sodium nitrite, the diazonium salt easily decomposed to give the reduced product in 60% yield. Furthermore, when *p*-iodobenzenesulfonic acid was added to the reaction mixture as a scavenger for the aryl radical[16] in place of *p*-toluenesulfonic acid, 1-

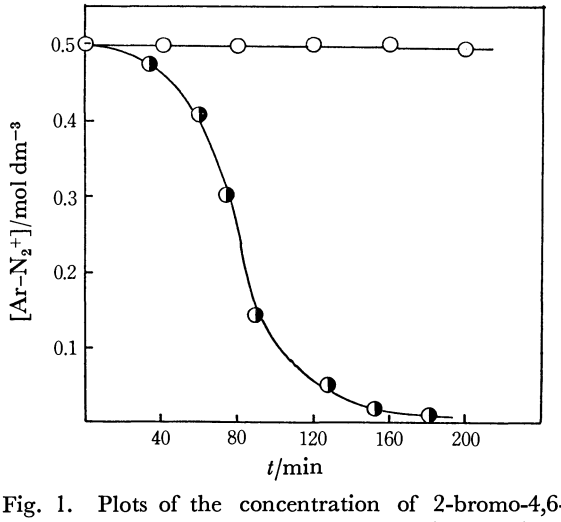

Fig. 1. Plots of the concentration of 2-bromo-4,6-dinitrobenzenediazonium ion as a function of time in sulfuric acid at 52 °C. ○: $NaNO_2/ArNH_2$ (molar ratio) = 1.00, ◑: $NaNO_2/ArNH_2$ (molar ratio) = 1.24.

bromo-2-iodo-3,5-dinitrobenzene was obtained. This result supports the assumption that an intermediary aryl radical abstracts an iodo atom from *p*-iodobenzenesulfonic acid.

By-products of the Reaction of 2-Bromo-4,6-dinitrobenzenediazonium Salt with Toluene. It seemed worthwhile to check the by-products in this reduction from a mechanical point of view.

When toluene was employed as the reducing reagent, phenyltolylmethane was obtained in 10% yield together with the reduced product. Phenyltolylmethane was a mixture of two isomers: one of the isomers was found to be phenyl-*p*-tolylmethane by a comparison with an authentic sample, while the other isomer is still unidentified because of the difficulty in purification.

On the other hand, when a mixture of toluene and chlorobenzene was added to the diazonium solution, a mixture of chlorodiphenylmethanes was obtained, together with phenyltolylmethanes (Table 5).

Chlorodiphenylmethanes were found to consist of a mixture of 60% *o*- and 40% *p*-chlorodiphenylmethane; no *m*-derivative could be detected, suggesting that an electrophilic attack by the benzyl cation upon chlorobenzene took place.[17] In addition, competitive benzylations of mixtures of benzene and chlorobenzene with diazonium salt gave a ratio of chlorodiphenylmethanes (*o*- and *p*-isomer)/diphenylmethane of 0.29, which is close to that of the Friedel-Crafts benzylation in

Table 5. Minor products in the decomposition of 2-bromo-4,6-dinitrobenzenediazonium ion in the presence of an aromatic substrate

No.	Reducing agent	Substrate	By-product	Isomer ratio (%)			k_X/k_H[a)]
				o-	*m*-	*p*-	
1	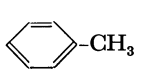		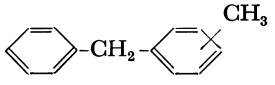	—	—	—	—
2	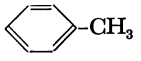	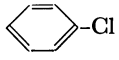	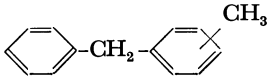	—	—	—	—
			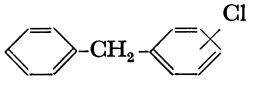	60	0	40	—
3	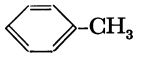	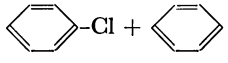	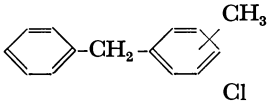	—	—	—	—
			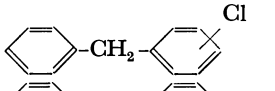	60	0	40	0.29
			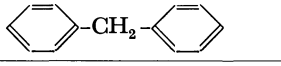				1.00

a) Relative rate for benzylation.

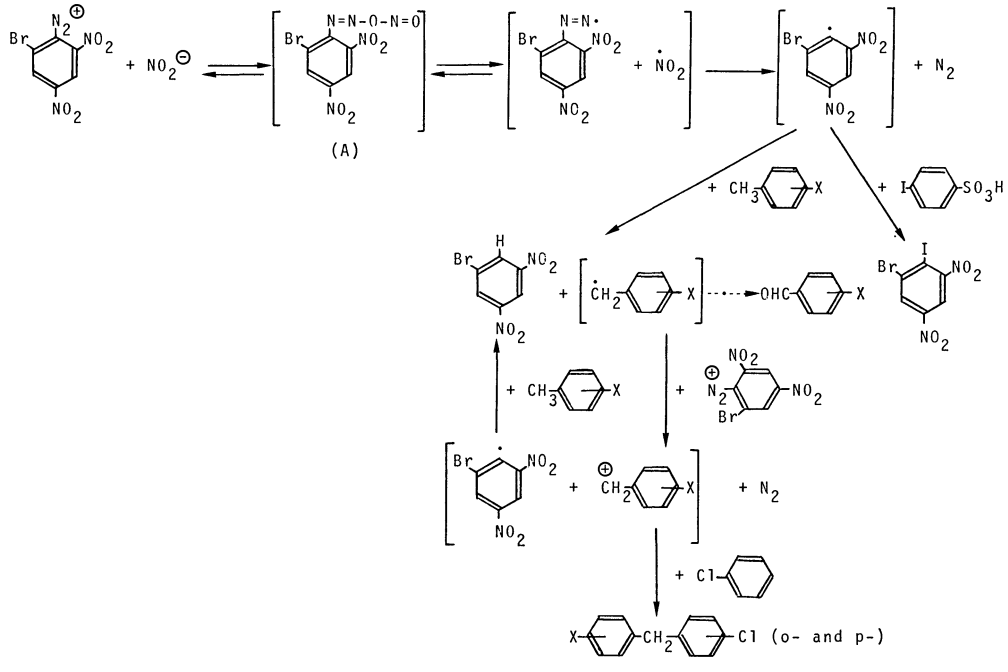

Scheme 1.

nitromethane (0.24).[17] Moreover, when oxygen was bubbled into the reaction mixture as a radical scavenger, the yield of diphenylmethane derivatives decreased to a great extent.[18] These results clearly suggest that the reduction process involves a radical intermediate, but the benzylation of aromatic substrate was performed by the benzyl cation, not by the benzyl radical.

Reduction Process of Arenediazonium Salts with Alkylbenzenes. From the results and considerations described above, the process of reduction of arenediazonium ions may be reasonably explained by Scheme 1.

In a benzenediazonium salt containing several strong electron-withdrawing groups, the electrophilicity of the diazonio group is undoubtedly large. Thus, it can combine with a nitrite ion even in sulfuric acid to give an intermediate (**A**), which easily decomposes, resulting in the formation of an aryl radical. The bulky groups at 2- and 6-positions would accelerate the decomposition of the intermediate (**A**), because the resulting aryl radical is more free from steric strain than the intermediate (**A**). The resulting aryl radical abstracts a hydrogen from toluene to give benzyl radical and reduced product. A subsequent electron transfer from benzyl radical to diazonium ion results in the formation of benzyl cation and aryl radical, which enters the propagation cycle as indicated in Scheme 1. This interpretation is consistent with the observation that slight excess of sodium nitrite is enough to decompose the diazonium ion in our system.

Experimental

Materials. 2,6-Dinitroaniline,[20] 2,6-dibromo-4-nitroaniline,[21] 4-bromo-2,6-dinitroaniline,[22] 2,4-dibromo-6-nitroaniline,[23] and *p*-iodobenzenesulfonic acid[24] were prepared according to the procedures described in the literature. Other reagents, solvents, and starting materials were purchased from standard sources and purified according to literature procedures.

General Procedure for Reduction: Summarized in Tables 1 and 4. Let us take as an example the reaction of 2-bromo-4,6-dinitrobenzenediazonium salt with *p*-nitrotoluene. To nitrosylsulfuric acid, which was prepared from sulfuric acid (20 ml) and sodium nitrite (1.65 g, 0.024 mol), was added in portions 2-bromo-4,6-dinitroaniline (5.20 g, 0.020 mol) at room temperature. The mixture was warmed up to 50 °C and stirred for 3 h to complete the diazotization. Then, with mechanical stirring, *p*-nitrotoluene (2.74 g, 0.02 mol) was added into the diazonium solution and stirring was continued for 3 h at 50 °C. The mixture was then poured into a mixture of ice and water and was extracted with chloroform. The extract was dried with sodium sulfate and concentrated by distillation. The residue was subjected to column chromatography on silica gel eluting with benzene–petroleum ether (1:1 v/v) to yield 1-bromo-3,5-dinitrobenzene (3.87 g, 78%) and *p*-nitrobenzaldehyde (1.38 g, 51%). The products obtained were identified by their NMR, IR, and MS spectra and by a mixed-melting point test with an authentic sample.

The reactions of diazonium salt with substituted benzenes (Table 2) and alcohols (Table 3) were carried out in the same way.

Thermolysis of 2-bromo-4,6-dinitrobenzenediazonium salt (0.02 mol) in the presence of *p*-iodobenzenesulfonic acid (0.06 mol) was carried out in the same way to yield 1-bromo-2-iodo-3,5-dinitrobenzene (1.34 g, 18%), which was identified by a mixed-melting point test with an authentic sample.[1]

Kinetic Measurements. In a volumetric flask, a solution of *ca.* 0.5 mol/dm^3 of diazonium salt containing *p*-toluenesulfonic acid (0.5 mol/dm^3) was prepared at thermostat temperature as described previously. An aliquot of this diazonium solution was taken at a recorded time and was added to an alkaline R-salt (2-naphthol-3,6-disulfonic acid) solution to quench the remaining diazonium salt. After the diazo-coupling, the solution was diluted to a fixed volume and its optical density was measured at the maximum wavelength of absorbance of the dye formed (497 nm).

Analyses of By-products from 2-Bromo-4,6-dinitrobenzenediazonium Salt: Summarized in Table 5. 2-Bromo-4,6-dinitrobenzenediazonium salt (5.20 g, 0.02 mol) was allowed to decompose completely in the presence of toluene (1.84 g, 0.02 mol) and worked up as previously described. Chromatography on silica gel with petroleum ether as the eluent yielded the reduced product (3.52 g, 71.1%) and crude phenyltolylmethane (0.36 g, 10%). The phenyltolylmethane was further fractionated by preparative GLC, and one of the components was identified as phenyl-*p*-tolylmethane by comparison of its NMR spectrum and retention time of GLC to those of an authentic sample.[25] The benzylation in the presence of a mixture of toluene (0.04 mol), benzene (0.04 mol), and chlorobenzene (0.04 mol) was performed as previously described. The isomer ratio and the relative reactivity for the benzylation of chlorobenzene were determined by GLC (10% Carbowax 20M–Diasolide, He; 20 ml/min, 170 °C, 4 mm×4 m) using biphenyl as the internal standard. 2-Chloro- and 4-chlorodiphenylmethane employed as reference compounds for GLC were prepared as described in the literature.[26]

References

1) Part I: E. Ohtubo, T. Kuroda, Y. Hashida, S. Sekiguchi, and K. Matsui, *Nippon Kagaku Kaishi*, 2178 (1975).
2) P. Griess, *Justus Liebigs Ann. Chem.*, **113**, 210 (1860); **117**, 63 (1861).
3) P. Ruggli and E. Peyer, *Helv. Chim. Acta*, **9**, 950 (1926); P. Ruggli, F. Knapp, E. Merz, and A. Zimmermann, *Helv. Chim. Acta*, **12**, 1043 (1929); P. Ruggli and M. Welge, *Helv. Chim. Acta*, **15**, 586 (1932).
4) H. Meerwein, H. Allendörfer, P. Beekmann, F. R. Kunert, H. Morschel, F. Pawellek, and K. L. Wunderlich, *Angew. Chem.*, **70**, 211 (1958).
5) R. G. Brewster and J. A. Poje, *J. Am. Chem. Soc.*, **61**, 2418 (1939).
6) W. Zerweck, M. Schubert, and R. Fleischauer, *Chem. Zentr.*, **1954**, 9141.
7) M. G. Bartle, P. K. Mackie, and J. M. Tedder, *J. Chem. Soc., Chem. Commun.*, **1974**, 271; M. G. Bartle, S. T. Gore, R. K. Mackie, S. Mhatre, and J. M. Tedder, *J. Chem. Soc., Perkin Trans. 1*, **1978**, 401.
8) In the thermolysis of arenediazonium salts in methanol, a replacement of diazonio group by methoxyl group occurs by a ionic mechanism, *via* an aryl cation intermediate, whereas a replacement by hydrogen occurs by a radical mechanism. a) D. F. DeTar and T. Kosuge, *J. Am. Chem. Soc.*, **80**, 6072 (1958); b) T. J. Broxton, J. F. Bunnett, and C. H. Paik, *J. Org. Chem.*, **42**, 643 (1977).
9) Thermolyses of *p*-nitrobenzenediazonium fluoroborate in nitromethane and in 2-nitropropane at 80 °C yield *p*-nitrophenol in 53 and 67% yields, along with a fluorinated compound. But the thermolyses in the presence of pyridine inducing homolytic decomposition yields only the reduction

product. (Y. Hashida, Y. Takeda, and K. Matsui, to be published.)

10) *E.g.* thermolysis of benzenediazonium salt in the presence of toluene in 2,2,2-trifluoroethanol gives normal arylation products [P. Burri and H. Zollinger, *Helv. Chim. Acta*, **50**, 2204 (1973)].

11) In this case, substantial decomposition of diazonium salt did not occur under the given conditions, *e.g.* stirring for 3 h at 50 °C.

12) H. J. Opgenorth and Ch. Rüchardt, *Justus Liebigs Ann. Chem.*, **1974**, 1333.

13) M. Kobayashi, H. Minato, N. Kobori, and E. Yamada, *Bull. Chem. Soc. Jpn.*, **43**, 1131 (1970).

14) H. Zollinger, *Acc. Chem. Res.*, **6**, 335 (1973).

15) H. Zollinger, *Angew. Chem. Int. Ed. Engl.*, **17**, 141 (1978).

16) J. F. Bunnett and C. C. Wasmer, *J. Am. Chem. Soc.*, **88**, 5334 (1966).

17) Friedel-Crafts benzylation of chlorobenzene with benzyl chloride in the presence of $AlCl_3$ in nitromethane give 33% *o*-, 0.6% *m*-, and 66.4% *p*-isomer [G. A. Olah, S. J. Kuhn, and S. H. Flood, *J. Am. Chem. Soc.*, **84**, 1688; 1695 (1962)]. For more detailed data on the isomer ratio, see O. Tsuge and M. Tashiro, *Bull. Chem. Soc. Jpn.*, **40**, 119 (1967).

18) The yield of diphenylmethane was reduced to one-third.

19) See the reference cited in Ref. 8b.

20) F. Ullmann, G. Engi, N. Wosnessensky, E. Kuhn, and E. Herre, *Justus Liebigs Ann. Chem.*, **366**, 79 (1909).

21) S. M. Rosanitsch, *Ber.*, **15**, 471 (1882).

22) P. T. Austen, *Ber.*, **9**, 918 (1876).

23) C. Jackson, *Am. Chem. J.*, **35**, 149 (1906).

24) W. Lenz, *Ber.*, **10**, 1135 (1877).

25) W. H. C. Rueggeberg, M. L. Cushing, and W. A. Cook, *J. Am. Chem. Soc.*, **68**, 191 (1946).

26) A. J. Birch and J. Grimshaw, *J. Chem. Soc.*, **1961**, 1405.

Functionalization of *trans*-Decalin. III. A Stereospecific Preparation of Vicinal *cis* Two Methyl Groups of Eremophilane Skeleton, Leading to *dl*-Dehydrofukinone

Sigeru TORII,* Tsutomu INOKUCHI, and Tetsuo YAMAFUJI

Department of Industrial Chemistry, School of Engineering, Okayama University, Tsushima, Okayama 700

(Received February 10, 1979)

A procedure for the preparation of *dl*-dehydrofukinone (**1**), an eremophilane type sesquiterpene, from the diene adducts (**3**), prepared from the reaction of 4-methyl-3-methoxycarbonyl-2-cyclohexen-1-one with butadiene, is described. Acetalization-reduction ($LiAlH_4$) of **3** followed by treatment of the corresponding mesylate with base provided 5,6-*cis*-5-methyltricyclo[4.4.1.$0^{1,6}$]undec-8-en-2-one (**7**) in 69% overall yields. Reductive cleavage of **7** with lithium metal afforded *trans*-4β,4aβ-dimethyl-$\Delta^{6,7}$-octalin-1-one (**8**), bearing a set of vicinal *cis* two methyl groups on the C-4 and C-4a carbons in an 83% yield. Functionalization of the double bond of **8** involves (1) reduction of carbonyl group and following tetrahydropyranylation, (2) epoxidation followed by regiospecific reduction of the oxirane ring at the C-6 position, and (3) subsequent oxidation of the hydroxyl group, giving *trans*-4aβ,5β-dimethyl-8β-tetrahydropyranyloxydecalin-2-one (**14b**) in good yields. The conversion of **14b** into the desired **1** was achieved smoothly by (1) hydrolysis of tetrahydropyranyl ether, (2) pyrolysis of its mesylate, and (3) subsequent aldol reaction with acetone followed with dehydration and isomerization of the double bond.

As a part of our studies aimed to develop the stereocontrolled construction of a set of vicinal *cis* two methyl groups at the C-4a and C-5 carbons on eremophilane skeleton,[1] we investigated a different approach for the preparation of *dl*-dehydrofukinone (**1**), isolated from the leaves of Gobō (*Arctium lappa* L.).[2] Reported

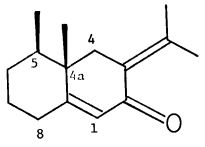

1

synthetic procedures to eremophilanes involve Robinson annelation reaction,[3] being associated with the inevitable epimerization at the C-4a carbon. With respect to stereochemical control of A, B ring junction, the *endo* rule of Diels-Alder reaction[4] is considered to be promising for the present requirement. In this paper, we record Diels-Alder reaction of 4-methyl-3-methoxycarbonyl-2-cyclohexen-1-one (**2b**) with butadiene as well as the transformation of the adducts (**3**) into *dl*-dehydrofukinone (**1**).

The diene addition of **2b**, prepared from methyl 6-methyl-1-cyclohexene-1-carboxylate (**2a**), with butadiene did take place at 150—160 °C in a sealed tube to give the adducts **3a** (11%) and **3b** (45%). Treatment of **3a** with base led to **3b** in a quantitative yield. The cis configuration of the C-4 methyl and C-4a ester groups of the adduct **3b** can be assigned based on their NMR data. The tentative assignment of

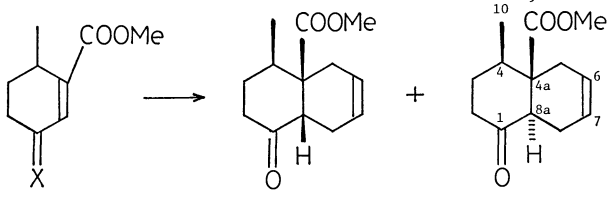

2a: X = H_2
2b: X = O

3a **3b**

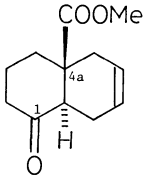

4

the C-4 methyl group of **3b** was carried out by comparison of ^{13}C NMR results of **3b** with methyl *trans*-1-oxo-$\Delta^{6,7}$-octalin-4a-carboxylate (**4**),[5] which lacks the C-4 methyl group. The chemical shift values of the C-2 (δ 40.0) and C-8a (δ 50.5) carbons (Table 1) of **3b** are close to the C-2 (δ 40.0) and C-8a (δ 50.9) of **4**, suggesting absence of the γ-effect[6] between the C-4 methyl and the C-2 and C-8a carbons of **3b**, due to the equatorial conformation of the C-4 methyl group. On the other hand, the steric compression shift of the C-9 carbon (δ 173.1) of **3b** appears at 2.0 ppm higher field than the value (δ 175.1) of **4**.

The conversion of the ester group of **3b** into the corresponding methyl group was explored. By the reported procedure for the preparation of methyl group from ester function by (1) reduction of COOR with $LiAlH_4$, (2) following oxidation of CH_2OH to CHO, and (3) subsequent Wolf-Kishner reduction,[7] we have examined the conversion of **3b** into **8**. But, difficulties were encountered in the attempted reduction of the hindered formyl group of **5d**. Instead, in the preceding paper[1] we described a preparative procedure of the vicinal *cis* two methyl groups *via* methylation of the enolate anion generated by the reduction of cyclopropyl ketone. The promising procedure prompted us to examine reduction of the cyclopropane ring fused on the C-1, C-6 carbon of **7**, prepared by treatment of the mesylate **6** with base[1,8] (Scheme 1). Thus, reduction of **5a**, after acetalization of **3b**,[9] with $LiAlH_4$ provided **5b** in 86% yield (from **3b**). Mesylation of **5b**, giving the corresponding mesylate **5c**, followed with hydrolysis with $HClO_4$ afforded the mesylated ketone **6** in 95% yield (from **5b**). Cyclization of **6** with sodium methoxide in methanol resulted in the

Table 1. The ^{13}C chemical shifts[a] of substituted decalin derivatives

Compound[b]	Carbon No.														
	1	2	3	4	4a	5	6	7	8	8a	9	10	OMe	$-(OCH_2)_2-$	
3a	210.5	36.0	30.1	33.6	52.7	30.1	125.5*	123.3*	22.8	45.7	174.8	15.7	51.9		
3b	208.7	40.0	30.9	40.2	53.8	34.6	125.6*	124.6*	23.2	50.6	173.1	16.0	51.6		
4	208.5	40.4	22.2	36.1	50.6	36.2	126.8*	124.4*	23.2	50.9	175.1		52.0		
8	212.0	41.5	31.2	42.2	39.8	39.5	124.9*	124.3*	21.7	53.1	11.9	14.6			
10	110.0	35.7	28.3	42.8	36.1	41.3	125.7*	124.6*	21.4	47.8	11.9	15.0		64.0	65.4
11	110.0	35.9	19.5	40.7	33.6	43.4	126.1*	124.7*	21.4	47.0	18.2			64.0	65.5
12	70.5	35.0	25.5	43.3	35.0	41.5	125.7*	125.5*	25.5	44.2	13.5	15.3			
13a	70.5	35.3	24.4	43.2	34.0	39.9	53.0*	51.6*	25.4	39.2	14.7	15.3			

a) The chemical shifts are shown in δ values (ppm) relative to internal Me_4Si. b) For the numbering systems, see numbers on the structures. * Theses pairs of shifts may be interchanged since the assignments are ambiguous.

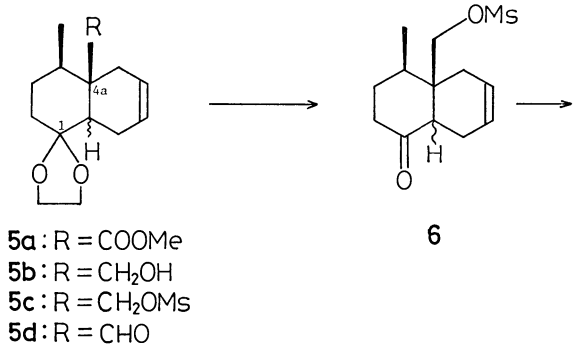

5a: R = COOMe
5b: R = CH_2OH
5c: R = CH_2OMs
5d: R = CHO

6

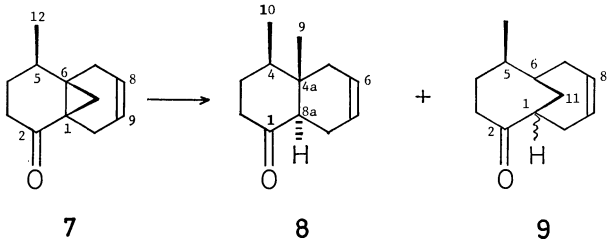

7 **8** **9**

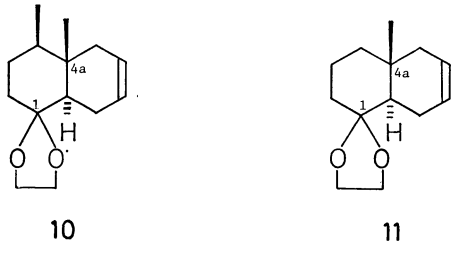

10 **11**

Scheme 1.

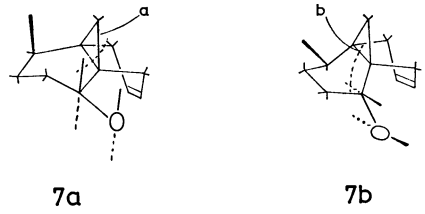

7a **7b**

Scheme 2.

desired **7** in 84% yield.

Reductive cleavage of the cyclopropane ring of **7** with lithium metal in liquid ammonia gave a mixture of **8**[10] (83%) and **9** (10%). The product distribution of the reduction would depend on preferential conformations of the transition states **7a** and **7b** (Scheme 2). Either bond **a** or **b** of the cyclopropane ring of **7** being close to the carbonyl π-electron would be opened by electron transfer from metal lithium.[11] As the result, it appears that the present reduction does preferentially take place through the conformation **7a**. The marked upfield shift in ^{13}C NMR spectra of the C-9 methyl signal of **10** at δ 11.9, contrasting to that of **11**[12] at δ 18.2, can rationally interpret the assigned stereochemistry of **10**, compatible with the calculated values of Crews's substituents increment parameter.[13]

In pursuing the approach from **8** to the important intermediate **14b**, we examined the functionalization of the double bond of **8** by epoxidation followed with regiospecific reduction at the C-6 position and subsequent oxidation of hydroxyl group. Reduction of **8** with $LiAlH_4$ afforded the 1β-alcohol **12** in 90% yield. The structure of **12** can be interpreted on the basis of 1,3-diaxial downfield shift of ^1H NMR signal due to the C-4a methyl group of **12** (δ 0.88), comparing to the value of δ 0.63 of **8**. Epoxidation of **12** with *m*-chloroperbenzoic acid (*m*-CPBA) at 0—10 °C gave the 6α,7α-epoxide **13a** preferentially by attack of the bulky reagent from the less hindered α-face.[14] Assignment of the epoxy ring of **13a** can be made by analysis of the ^{13}C NMR spectra of the C-4a and C-8a carbons, appearing at 1.0 and 5.0 ppm higher fields than those of **12** (Table 1), due to the presence of the γ-effect[6] between either the C-4a or C-8a carbon and the ring of the 6α,7α-epoxide. After protection of the hydroxyl group of **13a** as a tetrahydropyranyl ether, **13b** was treated with lithium metal in liquid ammonia to give the alcohol **14a** (65% yield based on **12**). The reductive cleavage of the carbon–oxygen bond of **13b** can be expected to occur at the C-6 position based on the axial ring opening rule,[15] giving **14a** as a sole product. The structure of **14a** can be confirmed by further elaboration into the enone **16a**. Oxidation of **14a** with pyridinium chlorochromate[16] gave the desired ketone **14b** in 95% yield. The conversion of **14b** into **16a**[17] *via* **15a** and **15b** was carried out in 54% overall yields by hydrolysis of **14b** with pyridinium *p*-toluenesulfonate[18] at 60—63 °C in ethanol and subsequent pyrolysis of the mesylate **15b** at

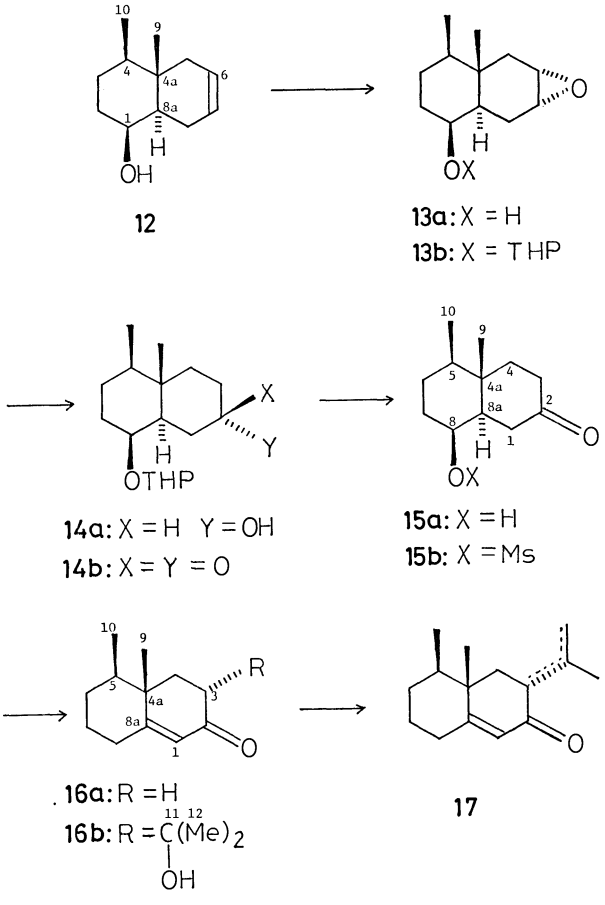

Scheme 3.

130—140 °C in DMSO.

Kinetically controlled aldol reaction[1] of **16a** with acetone in the presence of zinc chloride was allowed to lead to **16b** in 79% yield. The compound **16b** was dehydrated by warming the mesylate of **16b** at 40—50 °C in pyridine and the resulting *exo* and *endo* double bond isomers **17** were converted into the desired *dl*-dehydrofukinone (**1**) either by passing an activated alumina column or by treatment with $RhCl_3 \cdot 2H_2O$ (72% yield). The desired product **1** was shown to be identical by IR and ^1H NMR spectral comparison with those of authentic specimen.[19]

Experimental

The melting points and boiling points are uncorrected. IR spectra were determined with a JASCO IRA-1 grating spectrometer. ^1H NMR spectra were determined at 60 MHz with a Hitachi R-24 instrument and at 100 MHz with a JEOL MH-100 spectrometer. ^{13}C NMR spectra were determined at 25.05 MHz with a JEOL pulsed Fourier transform spectrometer, Model FX-100. Samples were dissolved in $CDCl_3$ and the chemical shift values were expressed in δ values (ppm) relative to Me_4Si as an internal standard Elemental analyses were performed in our laboratory.

*Methyl 6-Methyl-1-cyclohexene-1-carboxylate (**2a**).* A solution of 6-methyl-1-cyclohexene-1-carboxylic acid[20] (18.1 g, 129 mmol) in MeOH (40 ml, 989 mmol) and 1,2-dichloroethane (300 ml) containing concd H_2SO_4 (10 ml) was refluxed for 24 h and worked up in the usual manner to give 18.5 g (93%) of **2a**: bp 85.0—90.0 °C/25 Torr; IR (neat) 1712 (ester C=O), 1641 cm^{-1} (C=C); ^1H NMR (60 MHz) δ 1.05 (d, 3, J=6.5 Hz, CH_3), 1.44—2.73 (m, 4, CH_2), 1.98—2.32 (m, 2, CH_2), 2.42—2.91 (m, 1, CH), 3.66 (s, 3, OCH_3), 6.83 (t, 1, J=4 Hz, HC=C). Found: C, 70.22; H, 9.31%. Calcd for $C_9H_{14}O_2$: C, 70.10; H, 9.15%.

*4-Methyl-3-methoxycarbonyl-2-cyclohexen-1-one (**2b**).* A mixture of **2a** (1.79 g, 12 mmol) and SeO_2 (1.92 g, 17 mmol) in dioxane (10 ml) was heated at 85 °C for 20 h and at reflux for 3 h. The precipitate was filtered and washed with benzene. The combined filtrates were concentrated and the residue was dissolved in CH_2Cl_2 (20 ml). To this solution was added dropwise a chromium trioxide solution[21] with vigorous stirring for 30 min under N_2 at 0 °C. The mixture was worked up in the usual manner and the crude product was chromatographed (SiO_2, hexane–ether 2:1) to give 928 mg (46%) of **2b** as an oil: bp 132.0—133.0 °C/9 Torr; IR (neat) 1722 (ester C=O), 1683 (C=O), 1620 cm^{-1} (C=C); ^1H NMR (60 MHz) δ 1.23 (d, 3, J=7 Hz, CH_3), 1.63—2.27 (m, 2, CH_2), 2.35 (t, 2, J=2 Hz, $COCH_2$), 2.65—3.20 (m, 1, CH), 3.76 (s, 3, OCH_3), 6.42 (s, 1, HC=C); ^{13}C NMR δ 18.0 (q, C_4–Me), 28.8 (d, C-4), 29.1 (t, C-5), 33.4 (t, C-6), 52.4 (q, OMe), 131.8 (d, C-2), 153.2 (s, C-3), 166.7 (s, ester C=O), 199.6 (s, C-1). Found: C, 64.13; H, 7.35%. Calcd for $C_9H_{12}O_3$: C, 64.27; H, 7.19%.

*Methyl cis-4β-Methyl-1-oxo-Δ^{6,7}-octalin-4a-carboxylate (**3a**) and Methyl trans-4β-Methyl-1-oxo-Δ^{6,7}-octalin-4a-carboxylate (**3b**).* A mixture of **2b** (2.95 g, 17.5 mmol), 1,3-butadiene (2.3 g, 41.0 mmol) and 2,5-di-*t*-butylhydroquinone (50 mg) in benzene (10 ml) was heated at 150—160 °C for 3 days in a sealed tube and extracted with hot MeOH. The extract was filtered and the filtrate was concentrated. Distillation at 80—90 °C/3 Torr afforded an unchanged **2b** (1.14 g) and the residue in the flask was chromatographed (SiO_2, hexane–AcOEt 2:1) to give 263 mg (11% based on recovered **2b**, R_f 0.75, hexane–AcOEt 2:1) of **3a** and 1.08 g (45%, R_f 0.68) of **3b**. The physical constants together with elemental analyses of **3a** and **3b** are as follows: **3a**, mp 84.0—85.0 °C (hexane); IR (Nujol) 3027, 1720 (ester C=O), 1714 (C=O), 1653 cm^{-1} (C=C); ^1H NMR (60 MHz) δ 1.12 (d, 3, J=7 Hz, CH_3), 1.70—2.60 (m, 9, CH_2, CH), 3.00—3.40 (m, 1, COCH), 3.69 (s, 3, OCH_3), 5.55 (m, 2, HC=C). Found: C, 70.38; H, 8.32%. Calcd for $C_{13}H_{18}O_3$: C, 70.24; H, 8.16%. **3b**: mp 88.0—89.0 °C (hexane); IR (Nujol) 3018, 1721 (ester C=O), 1698 (C=O), 1655 cm^{-1} (C=C); ^1H NMR (60 MHz) δ 0.94 (d, 3, J=6.5 Hz, CH_3), 1.68—2.50 (m, 9, CH_2, CH), 2.69—3.10 (m, 1, COCH), 3.59 (s, 3, OCH_3), 5.60 (m, 2, HC=C). Found: C, 70.36; H, 8.32%. Calcd for $C_{13}H_{18}O_3$: C, 70.24; H, 8.16%.

*Conversion of **3a** into **3b**.* A mixture of **3a** (32 mg, 0.14 mmol) and MeONa (10 mg, 0.19 mmol) in MeOH (0.5 ml) was stirred for 24 h at room temperature and worked up in the usual manner to give 32 mg (100%) of **3b** as a solid.

*Methyl 1,1-Ethylenedioxy-4β-methyl-Δ^{6,7}-octalin-4a-carboxylate (**5a**).* A mixture of **3b** (420 mg, 1.89), ethylene glycol (2.3 g, 37.0 mmol), and *p*-toluenesulfonic acid (50 mg) in benzene (40 ml) was refluxed for 24 h in a Dean-Stark apparatus and worked up in the usual manner to give 466 mg (92%) of **5a** as an oil: bp 61.0—63.0 °C/0.01 Torr (Kugelrohr); IR (neat) 3022, 1727 (ester C=O), 1664 cm^{-1} (C=C); ^1H NMR (60 MHz) δ 0.92—1.05 (m, 3, CH_3), 1.35—2.85 (m, 10, CH_2, CH), 3.62—3.80 (m, 3, OCH_3), 3.95 (br s, 4, CH_2O), 5.49—5.88 (m, 2, HC=C). Found: C, 67.57; H, 8.49%. Calcd for $C_{15}H_{22}O_4$: C, 67.65; H, 8.33%.

*4aβ-Hydroxymethyl-4β-methyl-Δ^{6,7}-octalin-1-one Ethylene Acetal (**5b**).* To a suspension of $LiAlH_4$ (50 mg, 1.32 mmol)

in THF (2 ml) was added a solution of **5a** (115 mg, 0.43 mmol) in THF (2 ml) at 0 °C. The mixture was stirred for 10 h at room temperature, quenched with AcOEt (1 ml) and 5% aqueous $NaHCO_3$, and worked up in the usual manner to give 95 mg (93%) of **5b** as an oil: bp 57.0—59.5 °C/0.005 Torr (Kugelrohr); IR (neat) 3450 (OH), 3021, 1660 cm^{-1} (C=C); ^1H NMR (60 MHz) δ 0.79—1.09 (m, 3, CH_3), 1.18—2.64 (m, 10, CH_2, CH), 3.59 (br s, 1, OH), 3.00—3.70 (m, 2, CH_2O), 3.78—4.10 (m, 4, CH_2O), 5.60 (br s, 2, HC=C). Found: C, 70.68; H, 9.41%. Calcd for $C_{14}H_{22}O_3$: C, 70.56; H, 9.30%.

*4β-Methyl-4aβ-methylsulfonyloxymethyl-Δ^{6,7}-octalin-1-one Ethylene Acetal (**5c**).* A mixture of **5b** (386 mg, 1.62 mmol), $MeSO_2Cl$ (592 mg, 5.2 mmol), and pyridine (2.5 ml) was stirred for 2 h at 0 °C and for 3 h at room temperature, quenched with cold aqueous 5% $NaHCO_3$, and worked up in the usual manner to give 500 mg (97%) of **5c** as an oil: IR (neat) 3028, 1671 (C=C), 1175 cm^{-1} (SO_2); ^1H NMR (60 MHz) δ 0.92 (d, 3, J=7 Hz, CH_3), 1.40—2.59 (m, 10, CH_2, CH), 3.01 (s, 3, SO_2CH_3), 3.93 (s, 4, CH_2O), 4.29 (AB_q, 2, J=8 Hz, CH_2O), 5.63 (br s, 2, HC=C). Found: C, 57.11; H, 7.79%. Calcd for $C_{15}H_{24}O_5S$: C, 56.95; H, 7.65%.

*1,1-Ethylenedioxy-4β-methyl-Δ^{6,7}-octalin-4aβ-carbaldehyde (**5d**).* To a suspension of pyridinium chlorochromate (117 mg, 0.44 mmol) and AcONa (42 mg, 0.51 mmol) in CH_2Cl_2 (3 ml) was added a solution of **5b** (35 mg, 0.15 mmol) in CH_2Cl_2 (1 ml) at 0 °C. The mixture was stirred for 30 min at 0—5 °C and for 3 h at room temperature, diluted with ether, and passed through short silica gel column eluting with ether. The elute was concentrated and the residue was chromatographed (SiO_2, hexane–AcOEt 3:1) to give 29 mg (84%) of **5d** as an oil: bp 88.5—90.0 °C/0.015 Torr (Kugelrohr); IR (neat) 3015, 2750, 2680, 1712 (C=O), 1662 cm^{-1} (C=C); ^1H NMR (60 MHz) δ 0.83—1.08 (m, 3, CH_3), 1.27—2.81 (m, 10, CH_2, CH), 3.85—4.01 (m, 4, CH_2O), 9.50, 10.02 (s, 1, CHO). Found: C, 71.31; H, 8.76%. Calcd for $C_{14}H_{20}O_3$: C, 71.16; H, 8.53%.

*4β-Methyl-4aβ-methylsulfonyloxymethyl-Δ^{6,7}-octalin-1-one (**6**).* A solution of **5c** (90 mg, 0.28 mmol) and 70% $HClO_4$ (90 mg) in THF (3 ml) and water (1.5 ml) was stirred for 1 h at 0 °C and for 10 h at room temperature and worked up in the usual manner to give 76 mg (98%) of **6**: IR (neat) 3033, 1710 (C=O), 1656 (C=C), 1177 cm^{-1} (SO_2); ^1H NMR (60 MHz) δ 0.92—1.34 (m, 3, CH_3), 1.57—2.78 (m, 10, CH_2, CH), 2.93, 3.02 (s, 3, SO_2CH_3), 4.18 (s, 2, CH_2O), 5.64 (m, 2, HC=C). Found: C, 57.30; H, 7.66%. Calcd for $C_{13}H_{20}O_4S$: C, 57.34; H, 7.40%.

*5,6-cis-5-Methyltricyclo[4.4.1.0^{1,6}]undec-8-en-2-one (**7**).* To a solution of **6** (257 mg, 0.95 mmol) in MeOH (2 ml) was added a solution of MeONa (254 mg, 4.7 mmol) in MeOH (2.5 ml). The mixture was stirred for 24 h at room temperature and worked up in the usual manner to give 139 mg (84%) of **7** as an oil: bp 40.5—42.0 °C/0.02 Torr (Kugelrohr); IR (neat) 3079, 3030, 1680 cm^{-1} (C=O); ^1H NMR (60 MHz) δ 0.76—2.83 (m, 11, CH_2, CH), 1.05 (d, 3, J=6 Hz, CH_3), 5.49—5.33 (m, 2, HC=C); ^{13}C NMR δ 14.4 (t, C-11), 18.4 (q, C-12), 25.1 (t, C-10), 26.7 (t, C-4), 29.4 (t, C-7), 31.6 (s, C-6), 32.9 (d, C-5), 34.2 (s, C-1), 36.4 (t, C-3), 122.2, 123.6 (d, C-9, C-8), 210.1 (s, C-2). Found: C, 81.84; H, 9.03%. Calcd for $C_{12}H_{16}O$: C, 81.77; H, 9.15%.

trans-*4β,4aβ-Dimethyl-Δ^{6,7}-octalin-1-one (**8**) and 5,6-cis-5-Methylbicyclo[4.4.1]undec-8-en-2-one (**9**).* To a blue solution of lithium (84 mg, 12.1 mmol) in liquid NH_3 (*ca.* 30 ml) was added a solution of **7** (245 mg, 1.39 mmol) and *t*-BuOH (104 mg, 1.39 mmol) in DME (4 ml). After being stirred for 1.5 h at −78 °C, the blue solution was quenched with NH_4Cl (500 mg), allowed to stand at room temperature until liquid NH_3 had evaporated, and worked up in the usual manner. The crude product was chromatographed (SiO_2, hexane–AcOEt 4:1) to give 202 mg (83%) of **8** (R_f 0.8, hexane–AcOEt 2:1) and 24 mg (10%) of **9** (R_f 0.5). Physical constants together with elemental analyses of **8** and **9** are as follows: **8**, bp 38.0—39.5 °C/0.02 Torr (Kugelrohr); IR (neat) 3025, 1711 (C=O), 1658 cm^{-1} (C=C); ^1H NMR (60 MHz) δ 0.63 (s, 3, CH_3), 0.91 (d, 3, J=6 Hz, CH_3), 1.53—2.56 (m, 10, CH_2, CH), 5.63 (m, 2, HC=C). Found: C, 80.94; H, 10.27%. Calcd for $C_{12}H_{18}O$: C, 80.85; H, 10.18%. **9**: mp 91.0—95.0 °C; IR (Nujol) 3019, 1698 (C=O), 1656 cm^{-1} (C=C); ^1H NMR (60 MHz) δ 0.93 (m, 3, CH_3), 1.05—2.56 (m, 13, CH_2, CH), 5.65 (m, 2, HC=C). Found: C, 80.94; H, 9.94%. Calcd for $C_{12}H_{18}O$: C, 80.85; H, 10.18%.

trans-*4β,4aβ-Dimethyl-Δ^{6,7}-octalin-1-one Ethylene Acetal (**10**).* A mixture of **8** (131 mg, 0.73 mmol), ethylene glycol (700 mg, 11.3 mmol), and *p*-toluenesulfonic acid (40 mg) in benzene (30 ml) was refluxed for 24 h in a Dean-Stark apparatus and worked up in the usual manner to give 158 mg (97%) of **10** as an oil: bp 73.0—75.0 °C/0.03 Torr (Kugelrohr); IR (neat) 3020, 1559 (C=C), 1159, 1092, 1040, 985, 897 cm^{-1}; ^1H NMR (100 MHz) δ 0.81 (s, 3, CH_3), 0.84 (d, 3, J=6 Hz, CH_3), 1.10—2.44 (m, 10, CH_2, CH), 3.72—4.04 (m, 4, CH_2O), 5.61 (br s, 2, HC=C). Found: C, 75.64; H, 10.03%. Calcd for $C_{14}H_{22}O_2$: C, 75.63; H, 9.97%.

trans-*4β,4aβ-Dimethyl-Δ^{6,7}-octalin-1β-ol (**12**).* To a suspension of $LiAlH_4$ (64 mg, 1.69 mmol) in THF (2 ml) was added a solution of **8** (100 mg, 0.56 mmol) in THF (2 ml) at 0 °C. The mixture was stirred for 1 h at 0—5 °C and for 9 h at room temperature, and worked up in the usual manner to give 91 mg (90%) of **12** as white crystals: mp 52.5—53.5 °C; IR (Nujol) 3330 (OH), 3012, 1658 cm^{-1} (C=C); ^1H NMR (60 MHz) δ 0.86 (complex d, 3, J=5 Hz, CH_3), 0.88 (s, 3, CH_3), 1.07—2.65 (m, 10, CH_2, CH), 1.64 (s, 1, OH), 3.76 (m, 1, CHO), 5.55 (m, 2, HC=C). Found: C, 79.68; H, 10.99%. Calcd for $C_{12}H_{20}O$: C, 79.94; H, 11.18%.

trans-*6α,7α-Epoxy-4β,4aβ-dimethyldecalin-1β-ol (**13a**).* To a solution of *m*-CPBA (208 mg, 1.21 mmol) in CH_2Cl_2 (3 ml) was added a solution of **12** (128 mg, 0.71 mmol) in CH_2Cl_2 (1 ml) at 0 °C. The mixture was stirred for 1 h at 0 °C and for 20 h at 5 °C, washed with aqueous 10% $Na_2S_2O_3$ (3 ml), aqueous 5% NaOH, and brine, dried (Na_2SO_4), and concentrated. The crude product was chromatographed (SiO_2, hexane–AcOEt 2:1) to give 127 mg (91%) of **13a** as an oil: bp 37.0—38.0 °C/0.0075 Torr (Kugelrohr); IR (neat) 3444 (OH), 3020, 1258, 1227, 1150, 1043, 1013 cm^{-1}; ^1H NMR (60 MHz) δ 0.82 (unresolved m, 3, CH_3), 0.88 (s, 3, CH_3), 1.07—2.26 (m, 11, CH_2, CH, OH), 2.98—3.36 (m, 2, CHO), 3.70 (br s, 1, CHO). Found: C, 73.59; H, 10.45%. Calcd for $C_{12}H_{20}O_2$: C, 73.43; H, 10.27%.

trans-*6α,7α-Epoxy-4β,4aβ-dimethyldecalin-1β-ol Tetrahydropyranyl Ether (**13b**).* A mixture of **13a** (123 mg, 0.63 mmol), 2,3-dihydropyran (1.01 g, 11.9 mmol), and pyridinium *p*-toluenesulfonate[18] (79 mg, 0.31 mmol) in CH_2Cl_2 was stirred for 20 h at room temperature, diluted with ether (5 ml), and worked up in the usual manner. The crude product was chromatographed (SiO_2, hexane–AcOEt 4:1) to give 136 mg (77%) of **13b** as an oil: bp 63.0—66.0 °C/0.004 Torr (Kugelrohr); IR (neat) 1439, 1352, 1202, 1129, 1072, 1031, 1022 cm^{-1}; ^1H NMR (60 MHz) δ 0.70—0.99 (m, 3, CH_3), 0.88 (s, 3, CH_3), 1.06—2.41 (m, 16, CH_2, CH), 2.97—3.33 (m, 2, CHO), 3.33—4.18 (m, 3, CH_2O, CHO),

4.43—5.54 (m, 1, CHO). Found: C, 72.59; H, 10.09%. Calcd for $C_{17}H_{28}O_3$: C, 72.82; H, 10.06%.

trans-*7α-Hydroxy-4β,4aβ-dimethyldecalin-1β-ol Tetrahydropyranyl Ether (**14a**).* To a blue solution of lithium (84 mg, 12.1 mmol) in liquid NH_3 (*ca.* 25 ml) was added a solution of **13b** (136 mg, 0.48 mmol) in DME (4 ml). The mixture was stirred for 1 h at −78 °C and for 1.5 h at −33 °C, quenched with NH_4Cl (500 mg), and worked up in the usual manner. The crude product was chromatographed (SiO_2, hexane–AcOEt 2:1) to give 116 mg (85%) of **14a** as an oil: bp 123.0—126.0 °C/0.005 Torr (Kugelrohr); IR (neat) 3370 (OH), 1255, 1200, 1132, 1110, 1077, 1056, 1022, 1000 cm^{-1}; ^1H NMR (60 MHz) δ 0.80 (unresolved d, 3, J=6 Hz, CH_3), 0.87 (s, 3, CH_3), 1.08—2.17 (m, 19, CH_2, CH, OH), 3.26—4.00 (m, 3, CH_2O, CHO), 4.12 (m, 1, CHO), 4.45—4.73 (m, 1, CHO). Found: C, 72.16; H, 10.78%. Calcd for $C_{17}H_{30}O_3$: C, 72.30; H, 10.71%.

trans-*8β-Tetrahydropyranyloxy-4aβ,5β-dimethyldecalin-2-one (**14b**).* To a suspension of pyridinium chlorochromate (299 mg, 1.12 mmol) and AcONa (183 mg, 2.23 mmol) in CH_2Cl_2 (3 ml) was added a solution of **14a** (105 mg, 0.37 mmol) in CH_2Cl_2 (2 ml) at 0 °C. After being stirred for 0.5 h at 0—5 °C and for 3 h at room temperature, the mixture was diluted with ether (3 ml) and passed through a short silica gel column eluting with ether. The elute was concentrated and the residue was chromatographed (SiO_2, hexane–AcOEt 2:1) to give 97 mg (93%) of **14b** as an oil: bp 96.0—99.0 °C/0.01 Torr (Kugelrohr); IR (neat) 1710 cm^{-1} (C=O); ^1H NMR (60 MHz) δ 0.91 (d, 3, J=5 Hz, CH_3), 1.09 (s, 3, CH_3), 1.28—2.99 (m, 18, CH_2, CH), 3.27 (m, 3, CH_2O, CHO), 4.41—4.74 (m, 1, CHO). Found: C, 72.91; H, 10.15%. Calcd for $C_{17}H_{28}O_3$: C, 72.82; H, 10.06%.

trans-*8β-Hydroxy-4aβ,5β-dimethyldecalin-2-one (**15a**).* A solution of **14b** (96 mg, 0.34 mmol) and pyridinium *p*-toluenesulfonate (20 mg, 0.08 mmol) in EtOH (3 ml) was stirred for 20 h at 60—63 °C. The mixture was concentrated and the residue was chromatographed (SiO_2, hexane–AcOEt 2:1) to give 64 mg (95%) of **15a** as a white solid: mp 87.0—88.5 °C; IR (Nujol) 3405 (OH), 1695 cm^{-1} (C=O); ^1H NMR (100 MHz) δ 0.91 (d, 3, J=6 Hz, CH_3), 1.13 (s, 3, CH_3), 1.25—2.09 (m, 8, CH_2, CH), 2.00 (s, 1, OH), 2.13—2.99 (m, 4, CH_2CO), 3.76 (br s, 1, CHO); ^{13}C NMR δ 13.2 (q, C-9), 15.6 (q, C-10), 25.3 (t, C-6), 34.2 (t, C-7), 35.9 (s, C-4a), 38.2 (t, C-3), 39.6 (t, C-4), 42.1 (d, C-8a), 42.1 (t, C-1), 42.7 (d, C-5), 70.7 (d, C-8), 213.3 (s, C-2). Found: C, 73.26; H, 9.99%. Calcd for $C_{12}H_{20}O_2$: C, 73.43; H, 10.27%.

trans-*4aβ,5β-Dimethyl-8β-methylsulfonyloxydecalin-2-one (**15b**).* A mixture of **15a** (60 mg, 0.31 mmol), $MeSO_2Cl$ (178 mg, 1.55 mmol), and pyridine (1.5 ml) was stirred for 1 h at 0 °C and for 2 h at room temperature, quenched with cold water and worked up in the usual manner to give 73 mg (88%) of **15b**; IR (neat) 1710 (C=O), 1378, 1178 cm^{-1} (SO_2); ^1H NMR (100 MHz) δ 0.94 (d, 3, J=6 Hz, CH_3), 1.08 (s, 3, CH_3), 1.17—2.87 (m, 12, CH_2, CH), 3.00 (s, 3, SO_2CH_3), 4.72 (m, 1, CHO). Found: C, 57.06; H, 8.28%. Calcd for $C_{13}H_{22}O_4S$: C, 56.92; H, 8.08%.

*4aβ,5β-Dimethyl-$\Delta^{1,8a}$-octalin-2-one (**16a**).* A mixture of **15b** (73 mg, 0.266 mmol) and DMSO (2 ml) was heated at 130—140 °C for 2 h, and worked up in the usual manner. The crude product was chromatographed (SiO_2, hexane–AcOEt 3 : 1) to give 33 mg (64%) of **16a** as an oil: bp 72.5—75.0 °C/0.02 Torr (Kugelrohr) (lit,[17] 96.0—99.0 °C/0.2 Torr); IR (neat) 1675 (C=O), 1615 (C=C), 1235, 1188, 1030, 955, 877 cm^{-1}; ^1H NMR (60 MHz) δ 0.93 (unresolved d, 3, J=6 Hz, CH_3), 1.10 (s, 3, CH_3), 1.10—2.53 (m, 11, CH_2, CH), 5.69 (br s, 1, HC=C); ^{13}C NMR δ 15.3 (q, C-10), 16.0 (q, C-9), 26.5 (t, C-7), 30.5 (t, C-8), 33.3 (t, C-6), 34.0 (t, C-3), 35.5 (t, C-4), 39.0 (s, C-4a), 43.2 (d, C-5), 124.0 (d, C-1), 171.4 (s, C-8a), 199.7 (s, C-2).

*3α-(1-Hydroxy-1-methylethyl)-4aβ,5β-dimethyl-$\Delta^{1,8a}$-octalin-2-one (**16b**).* To a stirred solution of *i*-Pr_2NLi (103 mg, 0.96 mmol) in THF (1.5 ml) was added a solution of **16a** (19 mg, 0.11 mmol) in THF (0.5 ml). After being stirred for 40 min at −78 °C, a solution of $ZnCl_2$ (14 mg, 0.11 mmol) in ether (0.5 ml) was added and to this mixture acetone (62 mg, 1.1 mmol) was added. The mixture was stirred for 10 min, quenched with cold aqueous 5% tartaric acid, and extracted with ether–benzene. The extract was washed with brine, dried (Na_2SO_4), and concentrated. The residue was chromatographed (SiO_2, hexane–AcOEt 4:1) to give 20 mg (79%) of **16b**; IR (neat) 3440 (OH), 3027, 1650 (C=O), 1626 cm^{-1} (C=C); ^1H NMR (100 MHz) δ 0.93 (unresolved d, 3, J=6 Hz, CH_3), 1.14 (s, 3, CH_3), 1.23 (s, 6, CH_3), 1.29—2.62 (m, 10, CH_2, CH), 4.72 (br s, 1, OH), 5.70 (s, 1, HC=C); ^{13}C NMR δ 15.1 (q, C-10), 15.9 (q, C-9), 24.6 (q, C-12), 26.2 (t, C-7), 28.3 (q, C-13), 30.4 (t, C-8), 32.9 (t, C-6), 38.6 (t, C-4), 39.6 (s, C-4a), 43.6 (d, C-5), 51.2 (d, C-3), 72.4(s, C-11), 124.6 (d, C-1), 172.0 (s, C-8a), 203.3 (s, C-2), Found: C, 76.33; H. 10.37%. Calcd for $C_{15}H_{24}O_2$: C, 76.32; H, 10.24%.

dl-*Dehydrofukinone (**1**).* To a solution of **16b** (18 mg, 0.076 mmol) in pyridine (0.5 ml) was added $MeSO_2Cl$ (74 mg, 0.65 mmol) at 0 °C. The mixture was stirred for 2 h at room temperature and for 2 h at 40—45 °C, quenched with cold water, and worked up in the usual manner. The crude product was chromatographed (SiO_2, hexane–AcOEt 4:1) to give 12 mg (72%) of a mixture of double bond isomers **17** (3-isopropenyl:3-isopropylidene *ca.* 5:1 based on ^1H NMR): bp 47.0—52.0 °C/0.01 Torr (Kugelrohr); IR (neat) 1674 (C=O), 1624 (C=C), 883 cm^{-1}; ^1H NMR (60 MHz) δ 4.83, 4.98 (br s, HC=C). Without further separation of the double bond isomers, **17** was passed through an activated alumina 300 (Nakarai Chemicals) column (10 g) with hexane–AcOEt (10:1) to give **1** in a quantitative yield: bp 48.0—53.0 °C/0.01 Torr (Kugelrohr); IR (neat) 1663 (C=O), 1629 (C=C), 1459, 1439, 1373, 1294, 1221, 1196, 1101, 1035, 884, 846 cm^{-1}; ^1H NMR (100 MHz) δ 0.92 (unresolved m, 3, CH_3), 0.97 (s, 3, CH_3), 1.16—1.66 (m, 5, CH_2, CH), 1.85, 2.09 (s, 3, $C=C(CH_3)_2$), 2.16—2.40 (m, 5, CH_2), 2.88 (d, 1, J= 14 Hz, COCH), 5.76 (s, 1, HC=C); ^{13}C NMR δ 15.4 (q, C-10), 16.0 (q, C-9), 22.0 (q, C-12), 22.5 (q, C-13), 26.5 (t, C-7), 30.5 (t, C-8), 32.5 (t, C-6), 41.0 (t, C-4), 41.9 (s, C-4a), 42.5 (d, C-5), 126.1 (d, C-1), 128.1 (s, C-3), 142.1(s, C-11), 168.6 (s, C-8a), 192.2 (s, C-2).

*Conversion of **17** into **1** with $RhCl_3 \cdot 2H_2O$.* A solution of **17** (26 mg, 0.12 mmol) and $RhCl_3 \cdot 2H_2O$ (2 mg, 0.008 mmol) in EtOH (2.5 ml) was heated at 95—100 °C for 6 h in a sealed tube. The mixture was concentrated and the residue was chromatographed (SiO_2, hexane–AcOEt 4:1) to give 18 mg (86%) of **1**.

References

1) S. Torii, T. Inokuchi, and K. Kawai, *Bull. Chem. Soc. Jpn.*, **52**, 861 (1979).

2) Isolation: a) K. Naya, K. Tsuji, and U. Haku, *Chem. Lett.*, **1972**, 235; Synthesis: b) M. Ohashi, *Chem. Commun.*, **1969**, 893.

3) a) M. E. Jung, *Tetrahedron*, **32**, 3 (1976); b) R. E. Gawley, *Synthesis*, **1976**, 777; c) C. Berger, M. Franck-Neumann, and G. Ourisson, *Tetrahedron Lett.*, **1968**, 3451; d) R. M. Coates and J. E. Shaw, *Chem. Commun.*, **1968**, 47;

e) J. A. Marshall and T. M. Warne, Jr., *J. Org. Chem.*, **36**, 178 (1971); f) A. K. Torrence and A. R. Pinder, *Tetrahedron Lett.*, **1971**, 745.

4) a) J. Sauer, *Angew. Chem., Int. Ed. Engl.*, **6**, 16 (1967); b) L. J. Dolby, S. Esfandiari, C. A. Elliger, and K. S. Marshall, *J. Org. Chem.*, **36**, 1277 (1971); c) K. P. Dastur, *J. Am. Chem. Soc.*, **96**, 2605 (1974); d) J. N. Marx and L. R. Norman, *J. Org. Chem.*, **40**, 1602 (1975).

5) S. Torii, T. Kunitomi, and T. Okamoto, *Bull. Chem. Soc. Jpn.*, **47**, 2349 (1974).

6) D. K. Dalling and D. M. Grant, *J. Am. Chem. Soc.*, **94**, 5318 (1972).

7) a) Ref. 3e; b) Y. Kitagawa, A. Itoh, S. Hashimoto, H. Yamamoto, and H. Nozaki, *J. Am. Chem. Soc.*, **99**, 3864 (1977).

8) T. Nakano and A. K. Banerjee, *J. Chem. Soc., Perkin Trans. 1*, **1977**, 2581.

9) An epimeric mixture of the acetal **5a** at C-8a carbon was obtained and the product **5a** was used without further purification.

10) E. Piers and T.-W. Hall, *J. Chem. Soc., Chem. Commun.*, **1977**, 880.

11) W. G. Dauben and E. J. Deviny, *J. Org. Chem.*, **31**, 3794 (1966).

12) The compound **11** was prepared from **4** in a similar manner as described for the preparation of **10**. Physical properties and elemental analysis of **11** are as follows: bp 69.0—71.5 °C/0.01 Torr (Kugelrohr); IR (neat) 3020, 1655 cm^{-1} (C=C); ^1H NMR (100 MHz) δ 0.90—2.08 (m, 11, CH_2, CH), 0.95 (s, 3, CH_3), 3.72—4.03 (m, 4, CH_2O), 5.43—5.74 (m, 2, HC=C). Found: C, 74.95; H, 9.81%. Calcd for $C_{13}H_{20}O_2$: C, 74.96; H, 9.68%.

13) P. Crews and E. Kho-Wiseman, *Tetrahedron Lett.*, **1978**, 2483.

14) J. Schweng and E. Zbiral, *Justus Liebigs Ann. Chem.*, **1978**, 1089.

15) A. S. Hallsworth and H. B. Henbest, *J. Chem. Soc.*, **1957**, 4604.

16) E. J. Corey and J. W. Suggs, *Tetrahedron Lett.*, **1975**, 2647.

17) E. Piers, R. W. Britton, and W. de Wall, *Can. J. Chem.*, **47**, 4307 (1969).

18) M. Miyashita, A. Yoshikoshi, and P. A. Grieco, *J. Org. Chem.*, **42**, 3772 (1977).

19) We are grateful to Professor K. Naya, Kwansei Gakuin University, for providing ^1H NMR and IR spectra of natural dehydrofukinone (**1**).

20) W. S. Rapson and R. G. Shuttleworth, *J. Chem. Soc., Part 1*, **1940**, 636.

21) H. C. Brown, C. P. Garg, and K.-T. Liu, *J. Org. Chem.*, **36**, 387 (1971).

Synthesis of α-Trialkylsilyl Ketones[1,2]

Michio OBAYASHI, Kiitiro UTIMOTO,* and Hitosi NOZAKI
Department of Industrial Chemistry, Kyoto University, Yoshida, Kyoto 606

(Received February 19, 1979)

The isomerization of 2-trimethylsilyl-2,3-dialkyloxiranes occurs in the presence of MgI_2 to give α-trimethylsilyl ketones only, if one starts from (2*S**,3*S**)-isomers. In contrast, however, the reaction of (2*S**,3*R**)-oxiranes produces enol silyl ethers in addition to α-trimethylsilyl ketones. The reaction proceeds *via* the Mg salts of regio- and stereoselectively produced β-iodo-β-trimethylsilyl alcohols, each diastereomer of which behaves differently. Remarkably, Li salts of both iodohydrins [(2*S**,3*S**)- and (2*S**,3*R**)-isomers] give α-trimethylsilyl ketones exclusively. This provides efficient procedures for preparing α-trimethylsilyl ketones from a mixture of diastereomeric silyloxiranes.

Organosilicon chemistry has contributed much to the development of modern methodology of organic synthesis.[3] Particularly, α-trialkylsilyl ketones (IV) have attracted considerable attention as precursors for olefins with predictable geometry.[4,5] The preparation of IV usually involves acylation of α-trimethylsilyl Grignard compounds[6] or oxidation of the β-trimethylsilyl alcohols,[4] as direct silylation of the corresponding ketones gives none of the expected products.[7] This article describes a synthetic route to IV including the rearrangement of silyloxiranes (II and VI) as a key step.

The rearrangement of II and VI proceeds in the presence of MgI_2.[1a,8] The required oxiranes are readily accessible from internal olefins silylated on sp^2 carbon (I and V).[9]

For example, oxidation of (*E*)-5-trimethylsilyl-4-decene (Ic)[9g] with *m*-chloroperbenzoic acid gave IIc in 86% yield. Treatment of IIc with MgI_2 (10 equiv.) in ether at reflux afforded 5-trimethylsilyl-4-decenone (IVc) in 72% yield (Scheme 1 and Table 1).

Table 1. Reaction of silyloxiranes with MgI_2

Oxirane	Isomeric purity %	Products	
		IV (%)	VIII (%)
IIa	>99	93 (quant.)[a]	0
VIa	91	48	9
IIb	>99	74	0
VIb	96	40	18
IIc	>99	72	0

a) The yield in parentheses is that before purification.

In contrast with II the corresponding diastereomer VI gave a mixture of IV and trimethylsilyl enolate VIII (Scheme 2).

Regioselective formation of IV should be ascribed to the oxirane cleavage at the silylated carbon to oxygen bond followed by the hydride shift to that carbon. Furthermore, oxirane cleavage accompanied by R migration and the 1,3 shift of Me_3Si group from carbon to oxygen should explain the formation

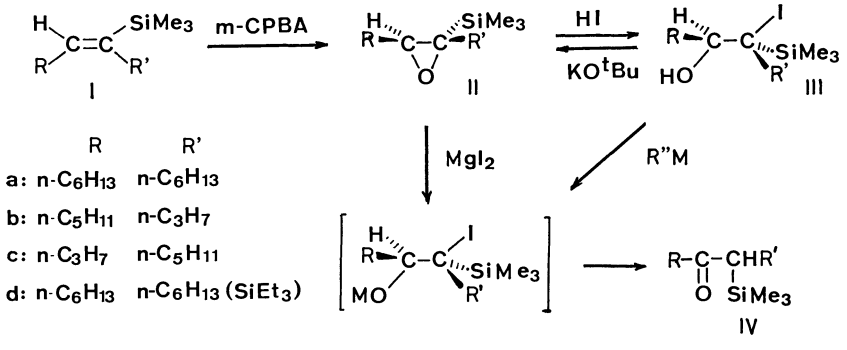

Scheme 1.

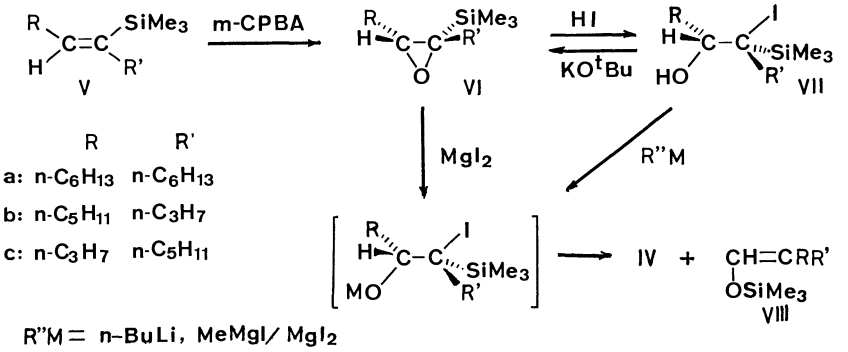

Scheme 2.

of VIII. Reasonable accounts for the observed reactivity difference between II and IV have stemmed from the following investigations.

As known already, the reaction of trimethylsilyloxiranes with $MgBr_2$ or HBr gives β-bromo-β-trimethylsilylalkanols, regio- and stereoselectively.[8,10e-g] We have found that treatment of IIa with aq HI gives iodohydrin IIIa in a quantitative yield.[13] Silyloxiranes VIa and VIc were transformed analogously into iodohydrins VIIa and VIIc, respectively. Furthermore, Scheme 3 shows that IX gives X, with the preferential cleavage of O–$CHSiMe_3$ bond.[14]

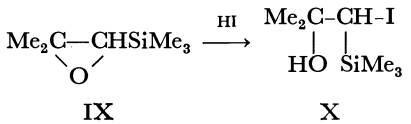

Scheme 3.

This is in contrast to the general belief that silicon stabilizes β-carbocation instead of the plus charge on the carbon directly attached to silicon.[3] The stereochemistry of the iodohydrins was established by regeneration of the starting silyloxiranes by the action of KO^tBu. All observations indicate that iodide ion is attached regio- and stereoselectively to the silylated carbon upon iodohydrin formation.

The iodohydrins III and VII thus obtained were treated with an organometallic reagent R″M. For example, reaction of IIIa with *n*-BuLi (1 equiv.) in ether gave IVa in a quantitative yield (Table 2).[15] Unexpectedly analogous treatment of the diastereomer VIIa afforded the same product IVa in 90% yield. It is remarkable that both diastereomeric iodohydrins give the same α-trimethylsilyl ketone in excellent yields.[16] α-Triethylsilyl ketone (IVd) could also be obtained from IIId. These and other results are listed in Table 2.

The silylated olefins (I and V) are prepared by the alkylation of C≡CSi moiety.[9a-d,9g] Furthermore, the silylated ketones (IV) are transformed into trisubstituted ethylenes by the published procedure stereoselectively.[5] The present study, therefore, links two synthetic sequences to afford a means of preparing trisubstituted ethylenes of any desired stereochemistry starting from silylacetylenes.

Remarkably, treatment of IIIa with MeLi in THF gave predominantly the starting silyloxirane (IIa) instead of α-silyl ketone (IVa) obtained above. Solvent effect must play an important role in the reaction of Li salt of iodohydrin. The O–Li should have become more nucleophilic in THF than in ether.

Furthermore, Mg salts of diastereomeric iodohydrins behaved differently from Li salts. Treatment of IIIa with MeMgI (1 equiv.) and MgI_2 (10 equiv.) at reflux gave IVa[17] in 92% yield. The diastereomeric iodohydrin (VIIa), however, was transformed into a mixture of IVa (29%) and trimethylsilyl enolate VIIIa (43%).

The rearrangement of silyloxiranes in the presence of MgI_2 showed similar product distributions depending on the sorts of the starting diastereomers. Furthermore, treatment of IIa with MgI_2 at room temperature provided IIIa (28%) along with IVa (30%). These observations indicate that the Mg salt of iodohydrin should be an intermediate[18,19] in the MgI_2 reaction giving IV or VIII in the subsequent step.

The relative orientations of the C–Si and the C–O bonds deviate markedly from the coplanar alignment which favors the β-carbocation stabilized by the C–Si bond.[3] The preference for oxirane cleavage at the silylated carbon with inversion in the iodohydrin formation suggests that the silyl group actually facilitates bimolecular nucleophilic displacements at the carbon attached to silicon.[20,21] Penta-coordinated silicon intermediate explains the observations,[22] as shown in Scheme 4.

Rearrangement of iodohydrin to α-trialkylsilyl ketone is ascribed to MI-elimination under 1,2-hydrogen

Table 2. Conversion of silyloxiranes to IV and VIII *via* iodohydrins III and VII

Oxirane	Isomeric purity %	Iodohydrin %	Reagent (R″M)	Products	
				IV (%)	VIII (%)
IIa	>99	IIIa, quant.	*n*-BuLi	(quant.)[a]	0
VIa	91	VIIa, 94	*n*-BuLi	90 (99)[a]	0
IIb	>99	IIIb, (92)[a]	*n*-BuLi	(quant.)[a]	0
IId	>99	IIId, (quant.)[a]	*n*-BuLi	87	0
VIc	97	VIIc, (92)[a]	*n*-BuLi	(quant.)[a]	0
IIa	>99	IIIa, quant.	$MeMgI/MgI_2$	92	0
VIa	91	VIIa, 94	$MeMgI/MgI_2$	29	43

a) Yields in parentheses are those before purification. The crude products were almost pure on GLPC, TLC, and NMR analysis.

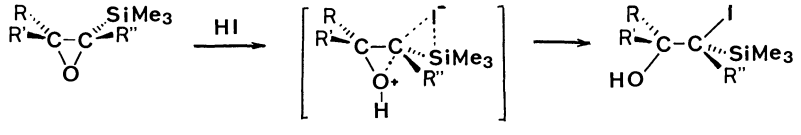

(One of R, R', and R" is H)

Scheme 4.

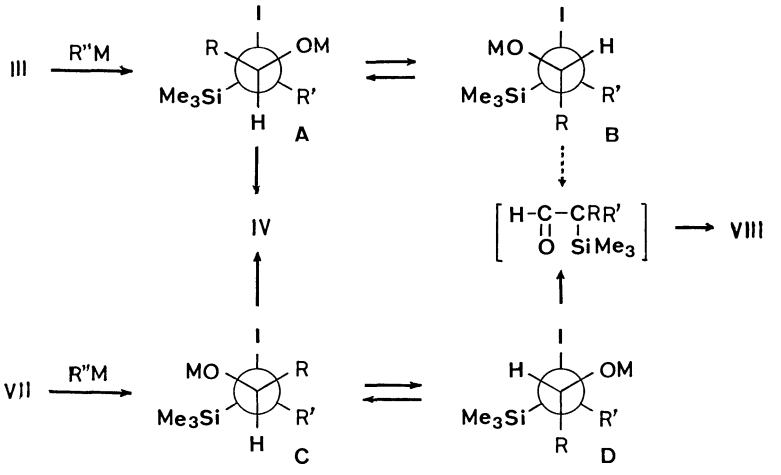

Scheme 5.

migration, while the one affording IV is accounted for by assuming MI elimination under 1,2-migration of R and the subsequent 1,3-migration of Me_3Si group (Scheme 5). The observed selectivity is explained on the following assumption: (i) migratory aptitude H> R; (ii) anti conformation of the migrating group and iodine;[23] (iii) Me_3Si>R, I in effective size; (iv) if M=Li, **A** (→IV)>**B** (→VIII) and **C** (→IV)>**D** (→VIII) in populations as R>OLi>H in effective size; (v) if M=MgI, **A**>**B** but **C**<**D** as OMgI and Me_3Si should be in anti positions each other because of the larger effective size of OMgI group. Possibly $\Delta F^{\ddagger}$ (**D**→VIII) is comparable with $\Delta F^{\ddagger}$ (**D**→**C**→IV).

Finally, other methods for obtaining α-trialkylsilyl ketones have been studied.

The procedure *via* β-trimethylsilyl alcohols XII (Scheme 6) reported by Hudrlik[4] was reinvestigated and applied to the synthesis of α-triethylsilyl ketones. Furthermore, T. H. Chan and his coworkers have reported that the reaction of α-silylalkyllithium with acid chlorides afforded, after hydrolysis with dilute hydrochloric acid, the desilylated ketones in moderate yield.[24] This reaction must proceed *via* α-silyl ketone, which is easily desilylated in acidic conditions. It was expected that careful work-up should afford α-silyl ketones. Indeed, 1-trimethylsilylhexyllithium (XI) was prepared by the addition of *n*-BuLi to $Me_3SiCH{=}CH_2$ and treated with butyryl chloride to give IVc in 45% yield (Scheme 6). Analogously 1-trimethylsilylhexylcopper obtained from XI and one equivalent of CuI afforded IVc in 71% yield. Reaction of XI with acetyl chloride gave 3-trimethylsilyl-2-octanone in 17% yield. On the other hand reaction of 1-triethylsilylhexyllithium prepared from *n*-BuLi and

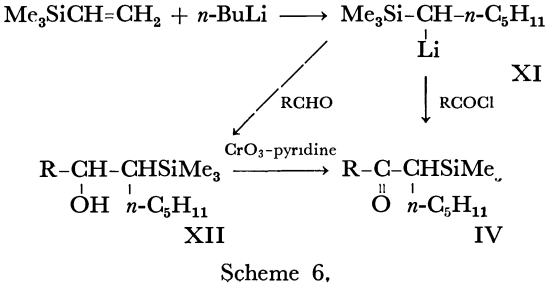

Scheme 6.

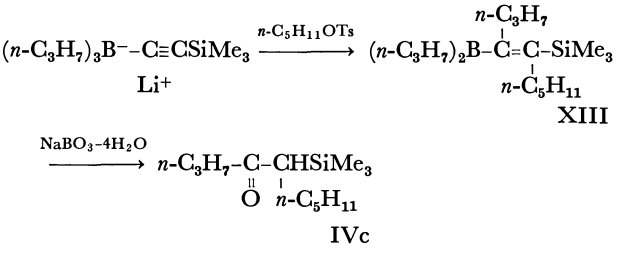

Scheme 7.

$Et_3SiCH{=}CH_2$ with butyryl chloride gave no desired product.

α-Trimethylsilyl ketone (IVc) has alternatively been obtained by the mild oxidation of 4-dipropylboryl-5-trimethylsilyl-4-decene (XIII)[25] with $NaBO_3$–$4H_2O$ in 57% overall yield (Scheme 7).

Experimental

Gas chromatography was performed on Shimadzu GC-4BPT with 3 m×3 mm glass column packed with 20% polyethylene glycol and 20% HVSG on Chromosorb W-AW (80—100 mesh). Mass spectra were obtained on Hitachi RMU-6L with 70V chamber voltage, NMR were measured on Varian EM-360, JEOL JNM-PMX 60, and Varian EM-390 with Me_4Si as internal standard and CCl_4 as solvent. ^{13}C-NMR on Varian CFT-20 with Me_4Si as internal standard and $CDCl_3$ as solvent. IR on Shimadzu IR-27G spectrometer. Elemental microanalyses were performed by Elemental Analyses Center of Kyoto University. All the reactions were carried out under an atmosphere of dry argon. All mass spectra were those of the samples after gas chromatographic separation.

Silylated Olefins I and V. (E)-7-Trimethylsilyl-7-tetradecene (Ia, R=R'=n-C_6H_{13}): The chloroplatinic acid-catalyzed reaction of trichlorosilane and 7-tetradecyne and the following treatment with MeMgI gave Ia in 70% yield (E>99%).[26,27] Bp 120 °C/0.07 mmHg; IR (neat) 1611, 1200, 830, 747, 685 cm^{-1}; MS *m/e* (rel. %), 268 (M^+, 0.4), 253 (8), 194 (13), 96 (13), 73 (100), 59 (21); NMR (CCl_4) δ=0.00 (9H, s), 0.67—1.07 (6H, m), 1.07—1.70 (16H, m), 1.70—2.30 (4H, m), 5.58 (1H, br-t, J=7 Hz).

Found: C, 76.20; H, 13.46%. Calcd for $C_{17}H_{36}Si$: C, 76.03; H, 13.51%.

(E)-7-Triethylsilyl-7-tetradecene (Id, $R=R'=$n-C_6H_{13}): Yield, 77%; $E>99\%$; IR (neat) 1610, 1232, 1010, 722 cm^{-1}; NMR (CCl_4) δ=0.30—1.70 (37H, m), 1.70—2.35 (4H, m), 5.62 (1H, t, J=6 Hz).

Found: C, 77.39; H, 13.39%. Calcd for $C_{20}H_{42}Si$: C, 77.33; H, 13.63%.

Silylated Olefins I ($R\neq R'$). These materials were prepared by the double alkylation of $HC\equiv CSiMe_3$.[9g]

Silylated Olefins V ($R=R'$ and $R\neq R'$). These compounds were prepared by the reductive alkylation of the corresponding $RC\equiv CSiMe_3$ according to the reported procedure.[9c,d]

(Z)-7-Trimethylsilyl-7-tetradecene (Va, $R=R'=$n-C_6H_{13}):[9d] Yield, 95%; E/Z=9/91; bp 120 °C/0.07 mmHg.

(Z)-4-Trimethylsilyl-4-decene (Vb, R=n-C_5H_{11}, R'=n-C_3H_7): Yield, 79%; E/Z=4/96; bp 100 °C/10 mmHg; IR (neat) 1611, 1240, 830, 750, 682 cm^{-1}; MS *m/e* (rel. %), 212 (M^+, 2), 197 (24), 169 (3), 156 (4), 155 (4), 138 (20), 127 (8), 113 (8), 99 (10), 73 (100), 59 (30); NMR (CCl_4) δ=0.08 (9H, s), 0.67—1.05 (6H, m), 1.05—1.67 (8H, m), 1.70—2.30 (4H, m), 5.85 (1H, br-t, J=7 Hz).

Found: C, 73.68; H, 13.54%. Calcd for $C_{13}H_{28}Si$: C, 73.50; H, 13.28%.

(Z)-5-Trimethylsilyl-4-decene (Vc, R=n-C_3H_7, R'=n-C_5H_{11}): Yield, 72%; E/Z=3/97; bp 118—122 °C/20 mmHg; IR (neat) 1610, 1240, 837, 758, 690 cm^{-1}; MS *m/e* (rel. %), 212 (M^+, 0.2), 197 (11), 169 (3), 155 (2), 138 (14), 127 (7), 113 (6), 101 (3), 99 (8), 95 (7), 82 (9), 74 (10), 73 (100), 59 (28), 45 (12), 43 (7), 41 (5); NMR (CCl_4) δ=0.10 (9H, s), 0.90 (6H, t, J=6 Hz), 1.10—1.60 (8H, m), 1.80—2.25 (4H, m), 5.85 (1H, br-t, J=7 Hz).

Found: C, 73.45; H, 13.00%. Calcd for $C_{13}H_{28}Si$: C, 73.50; H, 13.28%.

1-Trimethylsilyl-1-alkynes. These precursors of silylated olefins V[9c,d] were obtained by the usual trimethylsilylation of the corresponding alkynyl Grignard compounds. 1-Trimethylsilyl-1-pentyne was, however, prepared by the following procedure. To a solution of $Me_3SiC\equiv CSiMe_3$ (3.3 g, 19 mmol) in 15 ml of THF and 13 ml of HMPA was added MeLi (21 mmol, 14 ml of 1.48 M ethereal solution) at −78 °C. The mixture was warmed up to 0 °C and stirred for 1 h at 0 °C. The resulting mixture was treated with *n*-PrBr (2.0 ml, 22 mmol), stirred for 3 h at a room-temperature, and poured into aq NH_4Cl overlaid with hexane. The hexane layer was washed (aq NH_4Cl, sat. NaCl), dried ($MgSO_4$), and concentrated, affording 1.5 g (56%) of *n*-$C_3H_7C\equiv CSiMe_3$.

2-Trialkylsilyl-2,3-dialkyloxiranes II and VI. These oxiranes were prepared by *m*-CPBA oxidation of the corresponding silylated olefins.

(2S,3S*)-2-Trimethylsilyl-2-pentyl-3-propyloxirane (IIc, R=n-C_3H_7, R'=C_5H_{11})*: To a solution of *m*-chloroperbenzoic acid (85% purity, 1.2 g, 6.0 mmol) in CH_2Cl_2 was added (*E*)-5-trimethylsilyl-4-decene (Ic, 1.0 g, 4.9 mmol) at 0 °C. The mixture was poured into aq K_2CO_3 overlaid with ether. The ether layer was washed (aq K_2CO_3, sat. NaCl) and dried ($MgSO_4$). Chromatography of the concentrate on silica-gel column (benzene) afforded IIc (0.96 g). Yield, 86%; >99% purity; bp 72—77 °C/3 mmHg; IR (neat) 1243, 839, 752, 693 cm^{-1}; MS *m/e* (rel. %), 228 (M^+, 0.5), 213 (2), 199 (13), 185 (3), 171 (5), 143 (4), 130 (11), 113 (4), 75 (29), 73 (100), 59 (15), 43 (9); NMR (CCl_4) δ=0.00 (9H, s), 0.67—1.10 (6H, m), 1.10—1.70 (12H, m), 2.45—2.70 (1H, m).

Found: C, 68.60; H, 12.62%. Calcd for $C_{13}H_{28}OSi$: C, 68.35; H, 12.35%.

(2S,3S*)-2-Trimethylsilyl-2,3-dihexyloxirane (IIa, R=R'=n-C_6H_{13})*: Yield, 68%; >99% purity; oil; IR (neat) 1241, 834, 747 cm^{-1}; MS *m/e* (rel. %), 284 (M^+, 1), 269 (2), 227 (6), 213 (23), 199 (4), 185 (4), 155 (7), 143 (17), 130 (14), 129 (9), 113 (5), 95 (5), 75 (28), 73 (100), 59 (13), 43 (14); NMR (CCl_4) δ=0.00 (9H, s), 0.67—1.05 (6H, m), 1.05—1.65 (20H, m), 2.40—2.70 (1H, m); ^{13}C-NMR ($CDCl_3$) δ=−2.94, 14.06, 22.64, 26.34, 27.03, 28.20, 29.37, 30.08, 30.87, 31.77, 31.89, 57.16, 60.59.

Found: C, 71.91; H, 12.93%. Calcd for $C_{17}H_{36}OSi$: C, 71.76; H, 12.75%.

(2S,3S*)-2-Trimethylsilyl-2-propyl-3-pentyloxirane (IIb, R=n-C_5H_{11}, R'=n-C_3H_7)*: Yield, 86%; >99% purity; bp 70—75 °C/3 mmHg; IR (neat) 1239, 830, 746 cm^{-1}; MS *m/e* (rel. %), 228 (M^+, 0.4), 213 (2), 199 (1), 185 (1), 171 (29), 143 (8), 130 (7), 113 (15), 75 (28), 73 (100), 59 (13), 43 (9); NMR (CCl_4) δ=0.00 (9H, s), 0.65—1.13 (6H, m), 1.13—1.65 (12H, m), 2.45—2.73 (1H, m).

Found: C, 68.37; H, 12.61%. Calcd for $C_{13}H_{28}OSi$: C, 68.37; H, 12.61%.

(2S,3S*)-2-Triethylsilyl-2,3-dihexyloxirane (IId, R=R'=n-C_6H_{13})*: Yield, 98%; 99% purity; oil; IR (neat) 1230, 1005, 720 cm^{-1}; NMR (CCl_4) δ=0.40—1.70 (41H, m), 2.50—2.70 (1H, m).

Found: C, 73.81; H, 13.18%. Calcd for $C_{20}H_{42}OSi$ C, 73.54; H, 12.96%.

(2S,3R*)-2-Trimethylsilyl-2,3-dihexyloxirane (VIa, R=R'=n-C_6H_{13})*: Yield, 93%; 91% purity; oil; IR (neat) 1249, 842, 757 cm^{-1}; MS *m/e* (rel. %), 284 (M^+, 1), 269 (2), 227 (5), 213 (20), 199 (6), 185 (6), 155 (9), 143 (16), 130 (12), 129 (11), 113 (6), 95 (6), 75 (33), 73 (100), 59 (15), 43 (13); NMR (CCl_4) δ=0.08 (9H, s), 0.65—1.05 (6H, m), 1.05—1.70 (20H, m), 2.37—2.67 (1H, m); ^{13}C NMR ($CDCl_3$) δ=−1.08, 14.08, 22.67, 26.05, 27.25, 29.33, 29.74, 30.47, 31.93, 37.93, 57.14, 64.04.

Found: C, 71.71; H, 12.93%. Calcd for $C_{17}H_{36}OSi$: C, 71.76; H, 12.75%.

(2S,3R*)-2-Trimethylsilyl-2-propyl-3-pentyloxirane (VIb, R=n-C_5H_{11}, R'=n-C_3H_7)*: Yield, 93%; 96% purity; oil; IR (neat) 1243, 840, 756, 693 cm^{-1}; MS *m/e* (rel. %), 228 (M^+, 1), 213 (2), 199 (2), 185 (2), 171 (27), 157 (3), 143 (10), 130 (7), 113 (20), 75 (32), 73 (100), 59 (15), 43 (10); NMR (CCl_4) δ=0.08 (9H, s), 0.70—1.10 (6H, m), 1.10—1.80 (12H, m), 2.40—2.67 (1H, m).

Found: C, 68.23; H, 12.47%. Calcd for $C_{13}H_{28}OSi$: C, 68.35; H, 12.35%.

(2S,3R*)-2-Trimethylsilyl-2-pentyl-3-propyloxirane (VIc, R=n-C_3H_7, R'=n-C_5H_{11})*: Yield, 68%; 97% purity; oil; IR (neat) 1240, 840, 755, 690 cm^{-1}; MS *m/e* (rel. %), 228 (M^+, 0.3), 213 (1), 199 (12), 185 (3), 171 (7), 157 (2), 143 (4), 141 (11), 130 (10), 129 (7), 115 (5), 113 (5), 99 (7), 85 (5), 81 (5), 75 (31), 74 (10), 73 (100), 59 (18), 45 (12); NMR (CCl_4) δ=0.10 (9H, s), 0.90 (3H, t, J=6 Hz), 0.98 (3H, t, J=6 Hz), 1.13—1.70 (12H, m), 2.46—2.62 (1H, m).

Found: C, 68.64; H, 12.55%. Calcd for $C_{13}H_{28}OSi$: C, 68.35; H, 12.35%.

Isomerization of 2-Trimethylsilyl-2,3-dialkyloxiranes II and VI in the Presence of MgI_2. *5-Trimethylsilyl-4-decanone (IVc, R=n-C_3H_7, R'=n-C_5H_{11})*: To a solution of MgI_2 (10 mmol) in 10 ml of ether was added trimethylsilyloxirane IIc (R=C_3H_7, R'=C_5H_{11}, 0.23 g, 1 mmol dissolved in 5 ml of ether). The resulting mixture was stirred at reflux for 2 h and then treated with 6 ml of 1,4-dioxane at 0 °C overnight. The solution was freed from solids by filtration. The solids were washed with hexane several times and the combined organic layer was washed (sat. $NaHCO_3$, sat. NaCl) and dried ($MgSO_4$). Chromatography of the concentrate on silica-gel column (benzene) afforded 0.16 g (72%) of IVc. Bp 110—

120 °C/23 mmHg; IR (neat) 1686, 1249, 837, 750, 690 cm^{-1}; NMR (CCl_4) δ=0.00 (9H, s), 0.87 (6H, t, J=6 Hz), 1.00—1.90 (10H, m), 1.90—2.33 (3H, m).

Found: C, 68.85; H, 12.11%. Calcd for $C_{13}H_{28}OSi$: C, 68.35; H, 12.35%.

Attempted purification of IVc by GLPC resulted in 1,3-migration of Me_3Si group affording the respective silyl enol ether; IR (neat), 1671, 1243, 838, 749 cm^{-1}; MS *m/e* (rel. %), 228 (M^+, 5), 213 (8), 185 (7), 171 (59), 158 (10), 143 (12), 130 (35), 75 (31), 73 (100), 43 (10).

*8-Trimethylsilyl-7-tetradecanone (IVa, R=R'=*n*-C_6H_{13})*: Yield, 93% based on IIa; oil; IR (neat) 1686, 1240, 833, 747 cm^{-1}; NMR (CCl_4) δ=0.00 (9H, s), 0.60—1.03 (6H, m), 1.03—1.80 (18H, m), 1.80—2.45 (3H, m).

Found: C, 69.37; H, 12.97%.[28] Calcd for $C_{17}H_{36}OSi$: C, 71.76; H, 12.75%.

Purification of IVa by GLPC afforded the silyl enol ether; IR (neat) 1670, 1242, 836, 747 cm^{-1}; MS *m/e* (rel. %), 284 (M^+, 10), 269 (13), 255 (2), 241 (4), 227 (83), 213 (100), 200 (20), 185 (14), 157 (13), 143 (53), 140 (70), 75 (23), 73 (81); NMR (CCl_4) δ=0.13 (9H, s), 0.67—1.05 (6H, m), 1.05—1.67 (16H, m), 1.67—2.30 (4H, m), 4.15—4.65 (1H, m).

*4-Trimethylsilyl-5-decanone (IVb, R=*n*-C_5H_{11}, R'=*n*-C_3H_7)*: Yield, 74% based on IIb; bp 120—130 °C/16 mmHg; IR (neat) 1686, 1245, 840, 754, 694 cm^{-1}; NMR (CCl_4) δ=0.00 (9H, s), 0.65—1.03 (6H, m), 1.03—1.80 (10H, m), 2.00—2.45 (3H, m).

Found: C, 68.30; H, 12.65%. Calcd for $C_{13}H_{28}OSi$: C, 68.35; H, 12.35%.

Purification of IVb by GLPC gave the enol silyl ether; MS *m/e* (rel. %), 228 (M^+, 13), 213 (8), 199 (47), 185 (48), 171 (8), 157 (5), 143 (16), 130 (72), 75 (28), 73 (100), 45 (10), 43 (4).

*Isomerization of Trimethylsilyloxirane Va to α-Trimethylsilyl Ketone IVa and 1-Trimethylsilyloxy-2-hexyl-1-octene (VIIIa, R=R'=*n*-C_6H_{13})*: The mixture containing 48% of IVa and 9% of VIIIa was separated by chromatography on silica-gel column (hexane and benzene). VIIIa: Oil; IR (neat) 1661, 1251, 1190, 1156, 1100, 881, 845, 757 cm^{-1}; MS *m/e* (rel. %), 284 (M^+, 10), 269 (3), 255 (1), 227 (1), 213 (38), 199 (5), 157 (9), 143 (79), 81 (16), 75 (20), 73 (100), 67 (15), 55 (16), 43 (20); NMR (CCl_4) δ=0.13 (9H, s), 0.60—1.05 (6H, m), 1.05—1.65 (16H, m), 1.65—2.30 (4H, m), 5.90 (1H, br-s).

Found: C, 72.06; H, 13.04%. Calcd for $C_{17}H_{36}OSi$: C, 71.76; H, 12.75%.

*Isomerization of Trimethylsilyloxirane Vb to α-Trimethylsilyl Ketone IVb and 1-Trimethylsiloxy-2-propyl-1-heptene (VIIIb, R=*n*-C_5H_{11} R'=*n*-C_3H_7)*: The products contained 40% of IVb and 18% of VIIIb. VIIIb: Oil; IR (neat) 1664, 1245, 1154, 1092, 874, 838, 748 cm^{-1}; MS *m/e* (rel. %), 228 (M^+, 10), 213 (4), 171 (50), 157 (8), 143 (35), 129 (5), 75 (20), 73 (100), 45 (13), 43 (7); NMR (CCl_4) δ=0.13 (9H, s), 0.65—1.07 (6H, m), 1.07—1.63 (8H, m), 1.63—2.30 (4H, m), 5.93 (1H, br-s).

Found: C, 68.49; H, 12.48%. Calcd for $C_{13}H_{28}OSi$: C, 68.35; H, 12.35%.

β-Iodo-β-trialkylsilyl Alcohols III and VII. (7S,8S*)-8-Iodo-8-trimethylsilyl-7-tetradecanol (IIIa, R=R'=*n*-C_6H_{13})*: To a solution of trimethylsilyloxirane IIa (0.28 g, 1 mmol) in 5 ml of ether was added 1 ml of 57% HI at 0 °C. After stirring for 1 h, the mixture was poured into sat. $NaHCO_3$ overlaid with ether. The ether layer was washed (10% $Na_2S_2O_3$, sat. $NaHCO_3$, sat. NaCl) and dried ($MgSO_4$). Chromatography of the concentrate on silica-gel column (benzene) gave 0.41 g (quantitative yield) of IIIa. Oil; IR (neat) 3475, 1240, 840, 756, 690 cm^{-1}; NMR (CCl_4) δ=0.23 (9H, s), 0.90 (6H, t, J=6 Hz), 1.07—1.80 (20H, m), 1.50 (1H, d, J=6.6 Hz, CH-OH), 3.44 (1H, m, CH-OH). Hydroxyl proton was checked by D_2O-added NMR as well as double resonance irradiated at 3.44 which induced singlet at 1.50.

Found: C, 49.40; H, 9.23%. Calcd for $C_{17}H_{37}OSiI$: C, 49.50; H, 9.04%.

(7S,8S*)-8-Iodo-8-triethylsilyl-7-tetradecanol (IIId, R=R'=*n*-C_6H_{13})*: Quant. yield based on IId; oil; IR (neat) 3475, 1230, 1003, 725 cm^{-1}; NMR (CCl_4) δ=0.40—1.15 (21H, m), 1.15—2.15 (20H, m), 1.52 (1H, d, J=6.8 Hz), 3.45 (1H, m). IIId was used for the successive reaction without purification.

(7R,8S*)-8-Iodo-8-trimethylsilyl-7-tetradecanol (VIIa, R=R'=*n*-C_6H_{13})*: Yield, 94% based on VIa; oil; IR (neat) 3500, 1367, 1240, 840, 758, 690 cm^{-1}; NMR (CCl_4) δ=0.23 (9H, s), 0.90 (6H, t, J=6 Hz), 1.10—1.87 (18H, m), 1.37 (1H, d, J=8.3 Hz), 1.87—2.20 (2H, m), 3.00 (1H, m).

Found: C, 49.27; H, 8.83%. Calcd for $C_{17}H_{37}OSiI$: C, 49.50; H, 9.04%.

(4R,5S*)-5-Iodo-5-trimethylsilyl-4-decanol (VIIc, R=*n*-C_3H_7, R'=*n*-C_5H_{11})*: Crude yield, 92% based on VIc; oil; IR (neat) 3500, 1369, 1240, 840, 755, 690 cm^{-1}; NMR (CCl_4) δ=0.23 (9H, s), 0.76—1.13 (6H, m), 1.13—1.87 (10H, m), 1.38 (1H, d, J=9 Hz), 1.87—2.30 (2H, m), 3.05 (1H, m). VIIc was used for the successive reaction without purification.

Reaction of (4R,5S*)-5-Iodo-5-trimethylsilyl-4-decanol (VIIc) with KO^{t}Bu.* To a solution of KO^{t}Bu (1.0 g, 9 mmol) in 5 ml of THF was added VIIc (0.16 g, 0.92 mmol) in 5 ml of THF at 0 °C. The resulting mixture was warmed up to a room-temperature, stirred for 1 h, and poured into aq NH_4Cl overlaid with ether. The ether layer was washed (aq NH_4Cl, sat. NaCl) and dried ($MgSO_4$), affording 97 mg (92%) of (2*S**,3*R**)-2-trimethylsilyl-2-pentyl-3-propyloxirane (VIc, 96% purity) after chromatography of the concentrate on silica-gel column (benzene).

Reaction of β-Iodo-β-trialkylsilyl Alcohols III and VII with n*-BuLi. 8-Trimethylsilyl-7-tetradecanone (IVa)*: To a solution of (7*S**,8*S**)-8-iodo-8-trimethylsilyl-7-tetradecanol (IIIa, 0.35 g, 0.85 mmol) in 5 ml of ether was added *n*-BuLi (0.85 mmol, 1.12 ml of 0.76 M hexane solution) at −20 °C. The reaction mixture was warmed up to a room-temperature, stirred for 1.5 h, and poured into aq NH_4Cl overlaid with ether. The ether layer was washed (aq NH_4Cl, sat. NaCl) and dried ($MgSO_4$), yielding 0.24 g (quantitative) of IVa.

*8-Triethylsilyl-7-tetradecanone (IVd, R=R'=*n*-C_6H_{13})*: Yield, 87% based on IIId; oil; IR (neat) 1687, 1230, 1130, 1002, 725 cm^{-1}; NMR (CCl_4) δ=0.40—1.10 (21H, m), 1.10—1.90 (18H, m), 2.00—2.45 (3H, m).

Found: C, 73.77; H, 12.77%. Calcd for $C_{20}H_{42}OSi$: C, 73.54; H, 12.96%.

Purification of IVd by GLPC gave the enol silyl ether; MS *m/e* (rel. %), 326 (M^+, 10), 297 (16), 269 (44), 255 (48), 241 (10), 227 (11), 213 (18), 185 (33), 157 (42), 143 (25), 116 (15), 115 (90), 104 (12), 103 (100), 87 (75), 75 (40), 59 (42), 43 (17), 41 (17), 29 (29).

Reaction of 8-Iodo-8-trimethylsilyl-7-tetradecanol (IIIa and VIIa) with MeMgI/MgI_2. To a solution of (7*S**,8*S**)-8-iodo-8-trimethylsilyl-7-tetradecanol (IIIa, 0.40 g, 0.96 mmol) in 4 ml of ether was added MeMgI (1 mmol, 0.79 ml of 1.27 M ethereal solution) at −20 °C. The reaction mixture was warmed to a room-temperature and treated with MgI_2 (10 mmol) in 10 ml of ether. The resulting mixture was stirred at reflux for 2 h and then treated with 6 ml of 1,4-dioxane at 0 °C followed by stirring at a room-temperature

overnight. The solution was freed from solids by filtration. The solids were washed with hexane several times and the combined organic layer was washed (sat. $NaHCO_3$, sat. NaCl) and dried ($MgSO_4$). Chromatography of the concentrate on silica-gel column (benzene) gave 0.25 g (92%) of 8-trimethylsilyl-7-tetradecanone (IVa). The same treatment of (7*R**,8*S**)-isomer (VIIa) afforded 1-trimethylsilyloxy-2-hexyl-1-octene (VIIIa, 43%) along with IVa (29%) after chromatography on silica-gel column (hexane and benzene).

Further Methods for Obtaining α-Trialkylsilyl Ketones.

Preparation of 5-Trimethylsilyl-4-decanone (IVc) via *5-Trimethylsilyl-4-decanol (XIIc)*: To a solution of $Me_3SiCH{=}CH_2$ (2.0 g, 2.9 ml, 20 mmol) in 60 ml of THF was added *n*-BuLi (26 mmol, 20 ml of 1.28 M hexane solution) at −78 °C and the reaction mixture was stirred for 1 h at a room-temperature.[29] The resulting mixture was treated with butyraldehyde (1.6 g, 1.8 ml, 22 mmol) at −78 °C and overnight at a room-temperature. The whole mixture was worked up with aq NH_4Cl, washed (aq NH_4Cl, sat. NaCl), and dried (Na_2SO_4). Chromatography of the concentrate on silica-gel column (hexane/THF=10/1) gave 4.0 g of 5-trimethylsilyl-4-decanol (yield, 87%; bp 89—91 °C/1 mmHg). To a mixture of CrO_3 (15 g, 150 mmol) and pyridine (24 ml, 300 mmol) in 300 ml of CH_2Cl_2 was added the above alcohol (4.0 g) in 16 ml of CH_2Cl_2 and the resulting mixture was stirred at a room-temperature for 15 min. After filtration, the filtrate was washed (aq NH_4Cl, 1M-HCl, sat. $NaHCO_3$, sat. NaCl) and dried (Na_2SO_4). Chromatography of the concentrate on silica-gel column (benzene) gave 3.1 g (77%) of IVc.

Preparation of 3-Trimethylsilyl-2-octanone via *3-Trimethylsilyl-2-octanol*: Yield, 36% based on $Me_3SiCH{=}CH_2$; bp 102 °C/20 mmHg; NMR (CCl_4) δ=0.06 (9H, s), 0.70—1.80 (11H, m), 1.80—2.45 (1H, m), 1.99 (3H, s).

Found: C, 65.87; H, 12.07%. Calcd for $C_{11}H_{24}OSi$: C, 65.93; H, 12.07%.

Purification by GLPC gave the enol silyl ether; MS *m/e* (rel. %), 200 (M^+, 8), 185 (6), 171 (11), 157 (5), 144 (12), 143 (75), 130 (7), 115 (8), 75 (30), 73 (100), 45 (14).

Preparation of 5-Triethylsilyl-4-decanone via *5-Triethylsilyl-4-decanol*: A solution of 1-triethylsilylhexyllithium prepared from $Et_3SiCH{=}CH_2$ (2.8 g, 20 mmol) and *n*-BuLi (26 mmol) in 30 ml of THF, was treated with butyraldehyde (1.8 ml, 22 mmol) at −78 °C and then at a room-temperature for 3 days. The same treatment as described above gave 4.2 g (77%) of 5-triethylsilyl-4-decanol.[30] The oxidation of this alcohol (3.5 g, 13 mmol) with CrO_3–pyridine afforded 3.0 g (86%) of 5-triethylsilyl-4-decanone. Oil; IR (neat) 1687, 1235, 1137, 1004, 723 cm^{-1}; NMR (CCl_4) δ=0.25—2.00 (31H, m), 2.00—2.57 (3H, m).

Found: C, 71.29; H, 12.59%. Calcd for $C_{16}H_{34}OSi$: C, 71.04; H, 12.67%.

Purification by GLPC gave the enol silyl ether; IR (neat) 1670, 1230, 1170, 998, 730 cm^{-1}; MS *m/e* (rel. %), 270 (M^+, 3), 255 (2), 241 (5), 227 (5), 213 (30), 185 (10), 171 (9), 157 (19), 115 (35), 103 (37), 87 (30), 75 (27), 59 (25), 55 (14), 40 (100).

Preparation of 5-Trimethylsilyl-4-decanone (IVc) by the Acylation of 1-Trimethylsilylhexyllithium (XI): To a solution of butyryl chloride (0.55 ml, 5.0 mmol) in 5 ml of THF was added XI, prepared from $Me_3SiCH{=}CH_2$ (5.0 mmol) and *n*-BuLi (6.5 mmol) in 30 ml of THF, at −78 °C. The reaction mixture was stirred at a room-temperature overnight, washed (aq NH_4Cl, sat. $NaHCO_3$, sat. NaCl), and dried over Na_2SO_4. Chromatography of the concentrate on silica-gel column (benzene) gave 0.51 g (45%) of IVc.

Preparation of 5-Trimethylsilyl-4-decanone (IVc) by the Acylation of 1-Trimethylsilylhexylcopper: To a suspension of CuI (2.1 g, 11 mmol) in 10 ml of THF was added XI prepared from $Me_3SiCH{=}CH_2$ (10 mmol) and *n*-BuLi (13 mmol), at −30—−40 °C. The mixture was gradually warmed up to −20 °C and stirred for 0.5 h at −20 °C. The resulting mixture was treated with butyryl chloride (10 mmol, 1.1 ml) at −78 °C and overnight at a room-temperature. The whole was poured into aq NH_4Cl overlaid with ether. The ether layer was washed (aq NH_4Cl, sat. $NaHCO_3$, sat. NaCl) and dried ($MgSO_4$). Chromatography of the concentrate on silica-gel column (benzene) gave 1.6 g (71%) of IVc.

Preparation of 5-Trimethylsilyl-4-decanone (IVc) by the Oxidation of 4-Dipropylboryl-5-trimethylsilyl-4-decene (XIII): To a solution of $LiC{\equiv}CSiMe_3$, prepared from $HC{\equiv}CSiMe_3$ (0.54 ml) and *n*-BuLi (3.3 mmol, 4.2 ml of 0.78 M hexane solution) in 10 ml of THF, was added n-Pr_3B (0.66 ml, 3.3 mmol) at 0 °C. The mixture was stirred at a room-temperature for 1 h and at reflux for 16 h. The resulting mixture was treated with $NaBO_3$–$4H_2O$ (2.0 g, 13 mmol) at a room-temperature for 5 h and poured into aq NH_4Cl overlaid with ether. The ether layer was washed (aq NH_4Cl, sat. NaCl) and dried ($MgSO_4$). Distillation of the concentrate afforded 0.30 g (57%) of IVc.

The authors wish to thank the Ministry of Education, Science and Culture, Japan, for the Grant-in-Aid (911506, 011010, 110309, 203014, 303023).

References

1) Preliminary reports dealing with certain aspects of this work have appeared: (a) M. Obayashi, K. Utimoto, and H. Nozaki, *Tetrahedron Lett.*, **1977**, 1807; (b) M. Obayashi, K. Utimoto, and H. Nozaki, *ibid.*, **1978**, 1383.

2) α-Trialkylsilyl ketone means α-trialkylsilyl-substituted ketone in this paper.

3) For recent reviews, see (a) I. Fleming, *Chem. Ind. (London)*, **1976**, 449; (b) P. F. Hudrlik, "New Application of Organometallic Reagents in Organic Synthesis," ed by D. Seyferth, J. Organomet. Chem. Library, Elsevier, Amsterdam (1976), Vol. 1, p. 127; (c) E. W. Colvin, *Chem. Soc. Rev.*, **7**, 15 (1978).

4) (a) P. F. Hudrlik and D. Peterson, *Tetrahedron Lett.*, **1974**, 1133; *J. Am. Chem. Soc.*, **97**, 1464 (1975).

5) K. Utimoto, M. Obayashi, and H. Nozaki, *J. Org. Chem.*, **41**, 2940 (1976).

6) C. R. Hauser and C. R. Hance, *J. Am. Chem. Soc.*, **74**, 5091 (1952).

7) Generally trimethylsilyl enolates were obtained. See (a) G. Stork and P. F. Hudrlik, *J. Am. Chem. Soc.*, **90**, 4462, 4464 (1968); (b) H. O. House, M. Gall, and H. C. Olmstead, *J. Org. Chem.*, **34**, 2324 (1969), **36**, 2361 (1971) and references cited therein.

8) Recently it has been reported that silyloxiranes undergo $MgBr_2$-catalyzed ring cleavage producing α-silyl ketones in some cases. See P. F. Hudrlik, R. N. Misra, G. P. Withers, A. M. Hudrlik, R. J. Rona, and J. P. Arcoleo, *Tetrahedron Lett.*, **1976**, 1453.

9) (a) J. J. Eisch and G. A. Damasevitz, *J. Org. Chem.*, **41**, 2214 (1976); (b) K. Uchida, K. Utimoto, and H. Nozaki, *ibid.*, **41**, 2215 (1976); (c) *ibid.*, **41**, 2941 (1976); (d) K. Uchida, K. Utimoto, and H. Nozaki, *Tetrahedron*, **33**, 2987 (1977); (e) T. H. Chan, W. Michajlowskij, B. S. Ong, and D. N. Harpp, *J. Organomet. Chem.*, **107**, Cl (1976); (f) W. Michajlowskij and T. H. Chan, *Tetrahedron Lett.*, **1976**, 4439; (g) M. Obayashi, K. Utimoto, and H. Nozaki, *ibid.*, **1977**, 1805.

10) (a) J. J. Eisch and J. T. Trainer, *J. Org. Chem.*, **28**,

2870 (1963); (b) A. G. Brook, D. M. MacRae, and A. R. Bassindale, *J. Organomet. Chem.*, **86**, 185 (1975); (c) P. F. Hudrlik, D. Peterson, and R. J. Rona, *J. Org. Chem.*, **40**, 2263 (1975); (d) J. J. Eisch and J. E. Galle, *ibid.*, **41**, 2615 (1976); (e) C. M. Robbins and G. H. Whitham, *J. Chem. Soc., Chem. Commun.*, **1976**, 697; (f) P. F. Hudrlik, J. P. Arcoleo, R. H. Schwartz, R. N. Misra, and R. J. Rona, *Tetrahedron Lett.*, **1977**, 591; (g) P. F. Hudrlik, A. M. Hudrlik, R. J. Rona, R. J. Misra, and G. P. Withers, *J. Am. Chem. Soc.*, **99**, 1993 (1977). For an application see P. Magnus and G. Roy, *J. Chem. Soc., Chem. Commun.*, **1978**, 297.

11) Silyloxiranes as carbonyl precursors: (a) G. Stork and E. Colvin, *J. Am. Chem. Soc.*, **93**, 2080 (1971); (b) G. Stork and M, E. Jung, *ibid.*, **96**, 3682 (1974).

12) Products resulting from both cleavage at silylated carbon and cleavage at β carbon were formed in the reactions of triphenylsilylethylene oxide with HCl, with $MgBr_2$, and with amines.[10d]

13) The structure of iodohydrins was determined by NMR.

14) Yield of X, 61% based on 2-trimethylsilyl-3,3-dimethyloxirane (IX); NMR (CCl_4) δ=0.23 (9H, s), 1.39 (3H, s), 1.41 (3H, s), 1.60—1.80 (1H, m), 3.42 (1H, s). The structure of X was determined by selective formation of 1-iodo-2-methylpropene (yield 77%) by the action of BF_3–etherate.[10g] NMR (CCl_4) δ=1.83 (3H, s), 1.92 (3H, s), 5.83 (1H, br-s).

15) Direct treatment of VIa with LiI in ether gave no rearranged product. This fact excludes another path through the starting silyloxirane VIa.

16) No product resulting from the reaction of IVa with *n*-BuLi[5] was observed. This fact means the rearrangement of iodohydrin is sufficiently slower than the addition of *n*-BuLi to α-silyl ketones.

17) Reaction of IVa with *i*-Bu_2AlH in hexane,[4] after acidic work-up, gave 7-tetradecene in 70% yield based on IIa.

18) The following scheme seems unprobable.

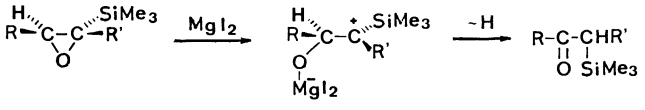

According to this scheme, 1-trimethylsilylcyclohexene oxide would afford 2-trimethylsilylcyclohexanone. Such a product, however, was not formed but trimethylsiloxymethylenecyclopentane was obtained in 12% yield. NMR (CCl_4) δ= 6.06 (1H, br-s).[8]

19) I. Kuwajima and his coworkers published another type of α-trimethylsilyl ketone synthesis by the rearrangement of silyl-substituted chlorohydrin; T. Sato, T. Abe, and I. Kuwajima, *Tetrahedron Lett.*, **1978**, 259.

20) C. Eaborn and J. E. Jeffrey, *J. Chem. Soc.*, **1954**, 4266.

21) ^{13}C NMR data of oxiranes shown below gave no correlation between the chemical shift (δ ppm, $CDCl_3$) in the ground state and the oxirane cleavage at the silylated carbon.

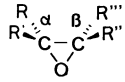

R	R′	R″	R‴	α-C	β-C
H	*n*-Hex	*n*-Hex	$SiMe_3$	57.16	60.59
n-Hex	H	*n*-Hex	$SiMe_3$	57.14	64.04
Me	Me	H	$SiMe_3$	58.55	58.20
Et	H	*n*-Hex	*n*-Pr	63.18	64.66

22) Analogous penta-coordinated silicon intermediates were suggested: M. T. Reetz and N. Greif, *Angew. Chem. Int. Ed. Engl.*, **16**, 712 (1977).

23) B. Rickborn and R. M. Gerkin, *J. Am. Chem. Soc.*, **93**, 1693 (1971).

24) T. H. Chan, E. Chang, and E. Vinokur, *Tetrahedron Lett.*, **1970**, 1137.

25) K. Utimoto, M. Kitai, M. Naruse, and H. Nozaki, *Tetrahedron Lett.*, **1975**, 4233.

26) R. A. Benkeser, M. L. Nelson, and J. V. Swisher, *J. Am. Chem. Soc.*, **83**, 4385 (1961).

27) K. Utimoto, M. Kitai, and H. Nozaki, *Tetrahedron Lett.*, **1975**, 2825.

28) This α-silyl ketone could not be obtained in a pure form.

29) At −30 °C the addition was incomplete.[4]

30) The reaction of 1-triethylsilylhexyllithium with acetaldehyde gave no addition product.

31) Reaction of (*2S*,3R**)-2-trimethylsilyl-2-propyl-3-pentyloxirane (VIb, 96% purity) with $KSiMe_3$ gave predominantly (*Z*)-4-trimethylsilyl-4-decene (Vb, *E*/*Z*=17/83).[32]

32) P. B. Dervan and M. A. Shippey, *J. Am. Chem. Soc.*, **98**, 1265 (1976).

Syntheses of Steroidal π-Allyl Palladium Chloride Complexes†

J. Yasuo SATOH and C. Akira HORIUCHI*

Department of Chemistry, Rikkyo (St. Paul's) University, Nishi-Ikebukuro, Toshima-ku, Tokyo 171

(Received February 24, 1979)

The reaction of the following steroidal olefins with palladium(II) chloride in the presence of potassium acetate in acetic acid afforded the corresponding steroidal π-allyl palladium chloride complexes: 5α-cholest-1-, -2-, and -3-ene; cholest-4- and -5-ene; 3-methyl- and 3-phenyl-5α-cholest-2-ene; 3β-chloro- and 3β-acetoxycholest-5-ene; and 5β-cholest-1-, -2-, and -3-ene.

There has been a considerable amount of work done on the syntheses of π-allyl palladium complexes in the area of the chain compound.[1] Also, in the case of monocyclic π-allyl palladium complexes, their syntheses have been reported for 1-*p*-menthen-3-ol,[2] 3-halocycloalkene,[3] β-pinene,[4] cycloalkene,[5] and alkylidenecycloalkanes.[5] On the other hand, with respect to steroids there have been no reports of syntheses except for the case of π-allyl palladium complexes of Δ^4-3-oxo steroids,[6] and of 5α-cholest-3-ene,[7] cholest-4-ene,[7] cholest-5-ene,[7] 5α-cholest-6-ene,[7] ergosterol,[8] and 3-methoxy-*cis*-19-norpregna-1,3,5(10),17(20)-tetraene.[10] These syntheses have mainly depended on methods using sodium tetrachloropalladate(II) or bis(benzonitrile)dichloropalladium(II). In addition, the preparations of π-allyl palladium complexes of chain compounds[11] using palladium(II) chloride and sodium acetate have also been described.

There is one report which does make some reference to a π-allyl palladium complex: F. J. McQuillin and D. G. Parker[12] reported that the reaction of (+)-3,7-dimethyl-1,6-octadiene with palladium(II) chloride and potassium acetate in acetic acid gave α-terpinyl acetate as the main product and π-allyl palladium complex as a minor product. However, there has been no report concerning the synthesis of cycloalkenyl π-allyl palladium complexes using palladium(II) chloride and potassium acetate. Hence, we attempted the syntheses of some steroidal π-allyl palladium complexes according to the procedures described by McQuillin and Parker. Not only did we want to demonstrate such syntheses, but we are planning a research project to investigate the stereospecificity of nucleophilic substitutions for the steroidal π-allyl palladium complexes.

In the present paper, we would like to report that the reaction of the following steroidal olefins readily yielded the corresponding steroidal π-allyl palladium chloride complexes: 5α-cholest-1- (**1**), -2- (**2**), and -3-ene (**3**); cholest-4- (**4**) and -5-ene (**5**); 3-methyl- (**6**) and 3-phenyl-5α-cholest-2-ene (**7**); 3β-chloro- (**8**) and 3β-acetoxycholest-5-ene (**9**), with a functional group at the C_3-position; and 5β-cholest-1- (**10**), -2- (**11**), and -3-ene (**12**).

Results and Discussion

The reactions of 5α-cholest-1- (**1**) and -2-ene (**2**) with palladium(II) chloride both yielded yellowish crystals (**19**); mp 154—159 °C. When **1** was used as the starting material, **2** was given in a 25% yield. It is considered that **1** was isomerized to the more stable 2-ene compound (**2**) by a 1:3 shift of a hydrogen from the allylic position to a double-bond carbon in the presence of palladium(II) chloride in acetic acid.[13] The NMR spectrum of **19** showed a multiplet at δ 4.9—5.6 ppm due to three protons. From this spectrum, however, it could not be determined whether the structure of **19** was of the 1-3η- or 2-4η-type; and so the following procedure was carried out: the 2α-bromo-5α-cholestan-3-one (**13**) was reduced with sodium borodeuteride to give the 3-deuteriobromohydrin (**14**). This bromohydrin was then converted to 3-deuterio-5α-cholest-2-ene (**15**). By treating **15** with palladium(II) chloride according to the method mentioned above, yellowish crystals (**19'**) were obtained. The NMR spectrum of **19'** showed AB-type signals, doublets (J=6.8 Hz) at δ 5.45 and 5.05 ppm. From this fact, complex **19** was confirmed to be a 1-3η-type complex, namely, di-μ-chloro-bis[(1-3η-5α-cholesten-2α-yl)palladium(II)], in which the palladium is coordinated at the α-face of the steroid, not showing the C-19 methyl signal in the low field.[7-9]

Similarly, 5α-cholest-3-ene (**3**) gave the α-3-5η-complex (**20**).[7] In the case of cholest-4-ene (**4**), a yellowish crystalline material was also obtained, and on chromatography two π-allyl complexes were yielded, which were confirmed to be α-3-5η- (**20**)[7] and β-3-5η-type complexes (**21**);[7] on the other hand, with cholest-5-ene (**5**) the two complexes which were obtained were crystals (**22**, mp 105—109 °C and **23**, mp 151—155 °C) which had α-5-7η- (**22**)[7] and α-4-6η-type (**23**)[7] structures.

The reaction of 3-methyl-5α-cholest-2-ene (**6**) gave complex (**24**); mp 161—165 °C. This product was presumed to be an α-1-3η-type complex from the AB-type signals due to the C_1–H and the C_2–H in its NMR spectrum. In the case of 3-phenyl-5α-cholest-2-ene (**7**), two compounds, **25** and **26**, were given. Compound **25** showed doublets due to the C_1- and C_2-protons at δ 4.80 and 5.30 ppm respectively in the NMR spectrum, while compound **26** showed two multiplets due to the C_2- and C_4-protons at δ 4.6—5.2 and 5.5—5.8 ppm respectively in the NMR spectrum. From these data, the two complexes were confirmed to be α-1-3η- (**25**) and α-2-4η-type complexes (**26**). These results suggest that the reaction of a 2-ene derivative possessing a methyl group at the C_3 position gives a product which has a greater regioselectivity than in the case of the phenyl group.

Similarly, the reaction of 3β-chloro- (**8**) and of 3β-acetoxycholest-5-ene (**9**) with palladium(II) chlo-

† A preliminary report on this work was presented at the 34 th National Meeting of the Chemical Society of Japan, Hiratsuka, April 1976.

Table 1. Yields and physical data of steroidal π-allyl palladium chloride complexes (**19**—**29′**)

Materials	Products	Isolated yield/%	Mp(dec) °C	NMR ($CDCl_3$, δ/ppm)	Elemental analysis(%)
1	**19**	51	154—159	0.92 (s, 3H) 4.9—5.6 (m, 3H)	Found (Calcd for $C_{54}H_{90}Pd_2Cl_2$) C H 64.61 8.77 (63.40) (8.86)
2	**19**	61			
15	**19′**		157—160	0.92 (s, 3H) 5.05 (d, J=6.8 Hz, 1H) 5.45 (d, J=6.8 Hz, 1H)	
3	**20**[7]	48	165—168	0.90 (s, 3H) 4.81 (m, 1H) 5.12 (d, J=6.5 Hz, 1H)	63.42 8.90 (63.40) (8.86)
4	**20**[7]	30			
	21[7]	4	165—170	1.42 (s, 3H) 4.85 (m, 1H) 5.28 (d, J=6.5 Hz, 1H)	63.81 8.80 (63.40) (8.86)
5	**22**[7]	18	105—109	0.98 (s, 3H) 4.55 (dd, J=7.0 and 1.0 Hz, 1H) 5.14 (d, J=7.0 Hz, 1H)	63.86 8.95 (63.40) (8.86)
	23[7]	2	151—155	1.12 (s, 3H) 3.76 (m, 2H)	63.91 8.96 (63.40) (8.86)
6	**24**	65	161—165	0.92 (s, 3H) 4.79 (d, J=6.8 Hz, 1H) 5.27 (d, J=6.8 Hz, 1H)	Found (Calcd for $C_{56}H_{94}Pd_2Cl_2$) C H 63.90 8.86 (63.99) (9.01)
7	**25**	34	178—181	0.94 (s, 3H) 4.97 (d, J=7.1 Hz, 1H) 5.75 (d, J=7.1 Hz, 1H)	Found (Calcd for $C_{66}H_{98}Pd_2Cl_2$) C H 68.59 8.43 (67.45) (8.41)
	26	20	173—178	0.93 (s, 3H) 5.50—5.80 (m, 2H)	68.18 8.51 (67.45) (8.41)
8	**27**	60	123—126	1.03 (s, 3H) 4.45—5.00 (m, 1H) 4.71 (d, J=7.5 Hz, 1H) 5.21 (d, J=7.5 Hz, 1H)	Found (Calcd for $C_{54}H_{88}Pd_2Cl_4$) C H 59.96 8.24 (59.40) (8.12)
9	**28**	54	122—126	1.04 (s, 3H) 2.11 (s, 3H) 4.25 (d, J=7.5 Hz, 1H) 4.73 (d, J=7.5 Hz, 1H) 5.05—5.70 (m, 1H)	Found (Calcd for $C_{58}H_{94}O_4Pd_2Cl_2$) C H 61.06 8.39 (61.16) (8.32)
10	**29**	63	170—173	1.27 (s, 3H) 4.70—5.18 (m, 2H) 5.18—5.55 (m, 1H)	Found (Calcd for $C_{54}H_{90}Pd_2Cl_2$) C H 63.14 8.95 (63.40) (8.86)
11	**29**	76			
18	**29′**		157—160	1.28 (s, 3H) 5.05 (d, J=6.8 Hz, 1H) 5.45 (d, J=6.8 Hz, 1H)	
12	**21**[7]	58	165—170		

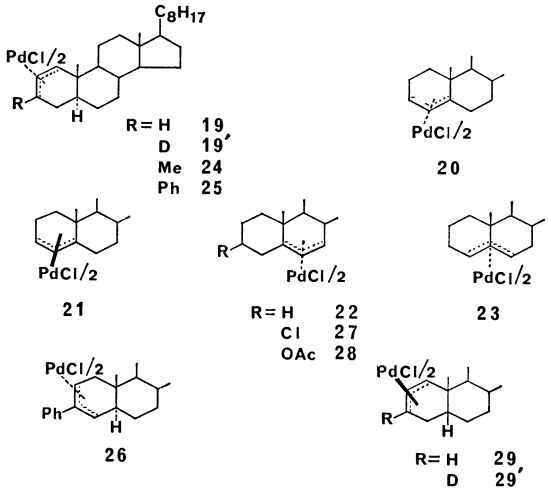

ride yielded 3β-chloro-α-5-7η- (**27**) and 3β-acetoxy-α-5-7η-type complexes (**28**) respectively. These structures were determined from the NMR spectra, which showed the doublets due to the C_6- and C_7-positions.

5β-Cholest-1- (**10**) and -2-ene (**11**) gave the same product (**29**). The NMR spectrum showed two multiplets at δ 5.18—5.55 ppm (1H) and at δ 4.70—5.18 ppm (2H). From the NMR spectrum, however, it could not be determined whether the structure of **29** was of the 1-3η- or 2-4η-type; therefore, the following procedure was carried out: the deuteride derivative, namely, 3-deuterio-5β-cholest-2-ene (**18**), was prepared from 2β-bromo-5β-cholestan-2-one (**16**) according to the procedure described for **15**. This structure was determined from the fact that no signal due to the C_3–H appeared in the NMR spectrum. The reaction of **18** with palladium(II) chloride gave a yellowish compound (**29'**). The NMR spectrum of **29'** showed doublets at δ 4.96 and 5.40 ppm and showed the C-19 methyl signal at δ 1.27 ppm.[7-9] From these data, compound **29'** was determined to be di-μ-chloro-bis[(1-3η-5β-cholesten-2β-yl)palladium(II)]. The reaction of 5β-cholest-3-ene (**12**) with palladium(II) chloride yielded a compound which was identical with the compound, **21**, obtained in the case of cholest-4-ene.

Thus, on the basis of all of the foregoing results, it can be concluded that the reagent used in this work [palladium(II) chloride containing potassium acetate in acetic acid] is applicable to the steroidal olefins. In the reaction of 5α- and 5β-steroidal olefins with this reagent, the former products were α-π-allyl palladium complexes, in which palladium coordinated at the α-face, while the latter products were β-π-allyl palladium complexes in which palladium coordinated at the β-face. These results are also in agreement with the facts that the α-face of 5α-steroidal olefins is less hindered than the β-face, and that the β-face of 5β-steroidal olefins is less hindered than the α-face.[14] This method showed more regioselectivity than the method using bis(benzonitrile)palladium chloride reported by Knox *et al.*[7]

Experimental

All the melting points are uncorrected. The IR and NMR spectra were measured using a Hitachi model 215 grating infrared spectrometer and a nuclear magnetic resonance spectrometer, Hitachi-Perkin Elmer R-20A, in carbon tetrachloride and deuteriochloroform, with TMS as the internal standard.

General Procedure. A mixture of steroidal olefin (1.30×10^{-3} mol), palladium(II) chloride (2.60×10^{-3} mol), potassium acetate (2.60×10^{-3} mol), and acetic acid (15 ml) was stirred at 55—60 °C. After 20—25 h, the reaction mixture turned to brownish yellow; and then it was filtered to remove the unchanged palladium(II) chloride. The filtrate was taken up in ether, and the ether extracts were washed with a sodium hydrogen carbonate solution and with water, and then dried and evaporated. The resultant oil was chromatographed on neutral aluminum oxide. Elution with benzene gave yellowish or greenish crystals from acetone.

Materials. The following compounds were synthesized by the methods described in literature: 5α-cholest-1-[15] (**1**), -2-[15] (**2**), and -3-ene[16] (**3**); cholest-4-[17] (**4**) and -5-ene[18] (**5**); 3-methyl-[19] (**6**) and 3-phenyl-5α-cholest-2-ene[20] (**7**); 3β-chloro-[18] (**8**) and 3β-acetoxycholest-5-ene[21] (**9**); and 5β-cholest-1-[22] (**10**), -2-[22] (**11**), and -3-ene[23] (**12**).

*Synthesis of 3-Deuterio-5α- (**15**) and 3-Deuterio-5β-cholest-2-ene (**18**).* A mixture of 2α-bromo-5α-cholestan-3-one (**13**) (100 mg) and methanol-d_1 was treated with sodium borodeuteride (80 mg) with at room temperature. After 1 h, water was added and the mixture was extracted with ether. The ethereal solution was washed with water, dried, and evaporated under reduced pressure. The resultant oil, on crystallization from methanol, gave needles of 3-deuteriobromohydrin (**14**) (53 mg); mp 103—105 °C, IR (KBr): 3400 cm^{-1}, NMR (CCl_4): δ=4.05 (1H, q, J=12 and 4.5 Hz). A mixture of **14** (50 mg) and zinc powder in acetic acid was stirred under refluxing conditions. After the usual work-up, the resultant oil, on crystallization from acetone, gave needles of **15** (33 mg); mp 73—74 °C, IR (KBr): 1640 cm^{-1}; NMR (CCl_4): δ=5.50 (1H, m, $W/2$= 7.5 Hz). The reduction of 2β-bromo-5β-cholestan-3-one (**16**) (233 mg) was done in accordance with the procedure described for **14**. Attempts to crystallize the resultant oil (**17**) were unsuccessful, and so the products were used in the next step without purification [IR (NaCl): 3384 cm^{-1}]. A mixture of the 3-deuteriobromohydrin (**17**) (200 mg), zinc powder, and acetic acid was stirred under refluxing conditions. After the usual work-up, the resultant oil, on crystallization from acetone, gave needles of **18** (108 mg); mp 46.5—47.5 °C, IR (KBr): 3025, 2250, and 1647 cm^{-1}; NMR (CCl_4): δ=5.45 (1H, m, $W/2$=10.5 Hz).

The authors are indebted to Professor Masayoshi Nakahara and Associate Professor Eiichi Miki for their valuable suggestions and to Messrs. Kohei Nakamichi, Ryusuke Misago, and Masami Sawayama for their collaboration in the experimental work. This research was supported in part by a Matsunaga Research Grant from the Matsunaga Science Foundation.

References

1) M. Herberhold, "Metal π-Complexes," Elsevier Publishing Company, Amsterdam (1972), Vol. 2, pp. 147—150.

2) G. A. Gray, W. R. Jackson, and J. J. Rooney, *J.*

Chem. Soc., **1970**, 1788.
3) H. A. Quinn, W. R. Jackson, and J. J. Rooney, *J. Chem. Soc.*, **1972**, 180.
4) K. Dunne and F. J. McQuillin, *J. Chem. Soc.*, **1970**, 2200.
5) B. M. Trost and P. E. Strege, *Tetrahedron Lett.*, **1974**, 2603.
6) R. W. Howsam and F. J. McQuillin, *Tetrahedron Lett.*, **1968**, 3667.
7) D. M. Jones and J. D. Knox, *J. Chem. Soc., Chem. Commun.*, **1975**, 165.
8) D. H. R. Barton and H. Patin, *J. Chem. Soc., Chem. Commun.*, **1977**, 799.
9) K. Henderson and F. J. McQuillin, *J. Chem. Soc., Chem. Commun.*, **1978**, 15.
10) B. M. Trost and T. R. Verhoeven, *J. Am. Chem. Soc.*, **100**, 3455 (1978).
11) J. Lukas, S. Coren, and J. E. Blom, *Chem. Commun.*, **1969**, 1303.
12) F. J. McQuillin and D. G. Parker, *J. Chem. Soc.*, **1974**, 809.
13) R. F. Heck, "Organotransition Metal Chemistry," Academic Press, New York and London (1974), p. 80.
14) K. Abe, Ph. D. Thesis, Rikkyo University, 1976.
15) T. Nakano, M. Hasegawa, and C. Djerassi, *Chem. Pharm. Bull.*, **11**, 465 (1963).
16) J. Mckenna, J. K. Norymberski, and R. D. Stubbs, *J. Chem. Soc.*, **1959**, 2502.
17) A. S. Hallaworth, H. B. Henbest, and T. I. Wrigley, *J. Chem. Soc.*, **1957**, 1969.
18) R. B. Turner, W. R. Meador, and R. E. Winkler, *J. Am. Chem. Soc.*, **79**, 4122 (1957).
19) H. Aebli, C. A. Grob, and E. Schumacher, *Helv. Chim. Acta*, **41**, 774 (1958).
20) J. A. Zderic, M. E. C. Rivera, and D. C. Limon, *J. Am. Chem. Soc.*, **82**, 6373 (1960).
21) A. H. Blatt, *Org. Synth.*, Coll. Vol. II, 191 (1950).
22) K. Abe and J. Y. Satoh, *Bull. Chem. Soc. Jpn.*, **51**, 941 (1978).
23) B. R. Davis and P. D. Woodgate, *J. Chem. Soc.*, **1966**, 2006.

ortho-Disubstituted *F*-Benzenes. II.[1] One-pot Syntheses of (*F*-Benzo)heterocyclic Compounds

Yoshinari INUKAI,† Takaaki SONODA, and Hiroshi KOBAYASHI*

Research Institute of Industrial Science, Kyushu University 86, Hakozaki, Fukuoka 812

† *Department of Organic Synthesis, Faculty of Engineering, Kyushu University 36, Hakozaki, Fukuoka 812*

(Received February 26, 1979)

Convenient one-pot methods of converting *F*-benzene into substituted (*F*-benzo)furans, (*F*-benz)oxazole, -imidazolines, and -thiazoline are described. Ambident nucleophiles are generated *in situ* from ketone, amide, urea, thiourea, and their derivatives in the presence of sodium hydride. Enolate-anion nucleophiles are also generated *in situ* from silyl enol ethers in the presence of potassium fluoride in anhydrous DMF.

Research in our laboratories has been directed at the *ortho*-difunctionalization of simple, commercially available *F*-benzene.[2] This has led to the preparation of related (*F*-benzo)heterocyclic compounds, which were in most cases synthesized through laborious reaction sequences.[3] In a previous paper[1] we described the intramolecular cyclization of *ω*-functionalized *F*-anilide into some (*F*-benz)azacyclic compounds. Here we wish to report a convenient one-pot method for converting *F*-benzene into substituted (*F*-benzo)-furans, (*F*-benz)oxazole, -imidazolines, and -thiazoline by the use of such ambident nucleophiles as ketone, amide, urea, and their derivatives. Several preceding works with similar schemes have appeared in the literature.[4]

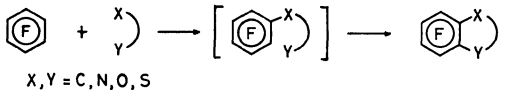

Scheme 1.

Results and Discussion

A range of (*F*-benzo)furans (**1**) were obtained by the reaction of *F*-benzene with the corresponding ketones (**2**). The reactions were carried out by adding the ketone to a mixture of *F*-benzene and two equivalents of sodium hydride in DMF.

The presence of four unequivalent fluorines in (**1a**) and (**1e**), based upon their ^{19}F-NMR spectra, and the regio-isomerism between (**1b**) and (**1c**) indicate the compounds (**1**) to have a benzofuran skeleton, which is compatible with their characteristic UV bands.

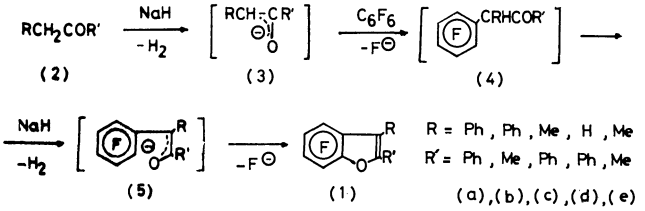

Scheme 2.

The reaction presumably proceeds in two steps *via* an intermediary (*F*-phenyl) ketone (**4**), as shown in Scheme 2. The presence of a phenyl group seems to give a higher yield than does a methyl group. One reason for this might be the resonance stabilization of the enolate anion forms, (**3**) and (**5**), resulting from the *α*- and *β*-phenyl groups, promoting the nucleophilic substitution of fluorine on the aromatic nucleus. Also, the steric bulkiness of a phenyl group, especially that adjacent to the ketone carbonyl, favors the intramolecular cyclization by hindering intermolecular aromatic substitution or aldol condensation. This presumption is compatible with the observation that the inverse addition of *F*-benzene to a mixture of ketone and sodium hydride afforded yields of less than 5% of the expected products (**1**) except for the 49% yield from phenyl benzyl ketone (**2a**). Sterically less hindered ketones would promote the aldol condensation or intermolecular aromatic substitution in basic media, thus consuming the starting ketones or intermediary (*F*-phenyl) ketones (**4**) prior to the intramolecular cyclization.

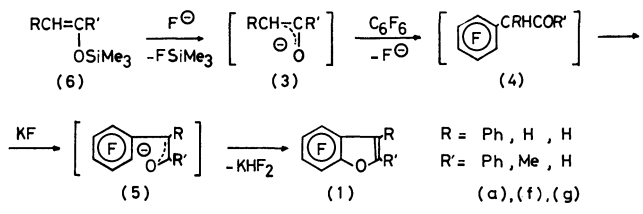

Scheme 3.

The generation of an enolate anion in neutral media can be achieved by the Si–O bond cleavage of silyl enol ethers in the presence of fluoride ions.[5] Also, one may expect that the protection of a ketone in the form of silyl enol ether suppresses the condensation reactions with the enolate. However, no satisfactory results have far been obtained except in the case of trimethylsilyl 1,2-diphenylvinyl ether (**6a**). The reactions using the trimethylsilyl enol ethers, (**6f**)[6] and (**6g**),[7] which were derived from acetone and tetrahydrofuran respectively, afforded none of the expected products (**1**), in which the intermolecular condensation or aromatic substitution of intermediary (*F*-phenyl) ketones (**4**) seemed to be preferred.

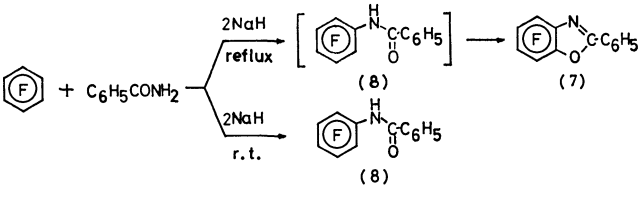

Scheme 4.

2-Phenyl-*F*-benzoxazole (**7**) was previously synthesized from *F*-aniline by way of benz-*F*-anilide (**8**).[1] The preparation of this compound was much simplified by the present one-pot reaction of *F*-benzene and benzamide under reflux. The reaction proceeds step-by-step *via* benz-*F*-anilide (**8**), and the intramolecular cyclization of the intermediary anilide required a higher temperature,[1] since the anilide (**8**) was isolated in an 80% yield when the reaction was carried out at room temperature.

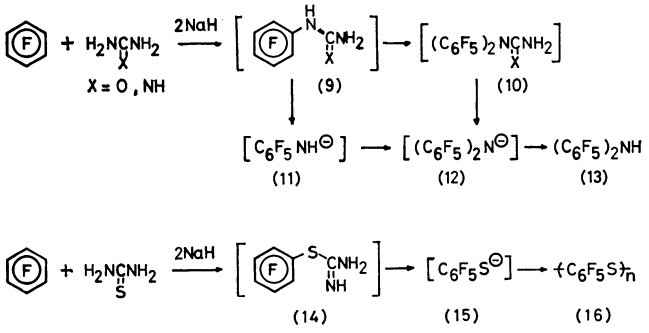

Scheme 5.

Urea, guanidine, and thiourea were also regarded as possible polyfunctional nucleophiles. The reactions with these nucleophiles, however, afforded no heterocyclic products; instead, di(*F*-phenyl)amine (**13**) was obtained from the former two and poly(thio-*F*-*p*-phenylene) (**16**) from the last one. The occurence of the above products indicates that the intermediary *F*-phenyl derivatives (**9**) and (**14**) cleave at the α–β bond prior to the intramolecular cyclization, thus liberating *F*-anilide anion (**11**) and *F*-benzothiolate anion (**15**) respectively, in the presence of an excess of hydride ions. The anions (**11**) and (**15**) afford the amine (**13**) and sulfide (**16**) respectively upon subsequent aromatic substitution. The intermediary *N*-carbamoyl-*F*-aniline (**9**), though not isolated, would be deprotonated at the α-amide in preference to the γ-amide. Such an α-amide anion favors the intermolecular nucleophilic aromatic substitution rather than the intramolecular cyclization, and in the presence of *F*-benzene it forms *N*,*N*-di(*F*-phenyl)urea (**10**), which then liberates the di(*F*-phenyl)amide anion (**12**) in the presence of an excess of sodium hydride. This may provide another possible route to di(*F*-phenyl)-amine.

The reaction with *N*,*N*′-dimethylurea gave 1,3-dimethyl(*F*-benz)imidazolin-2-one (**17**), where the active α-amide hydrogen of the intermediary *N*-carbamoyl-*F*-aniline is replaced with a methyl group; the only dissociable hydrogen of the intermediate is that of the γ-amide, and the α,β-bond cleavage seems to be suppressed. Increased steric hindrance by the methyl group would also favor the intramolecular cyclization.

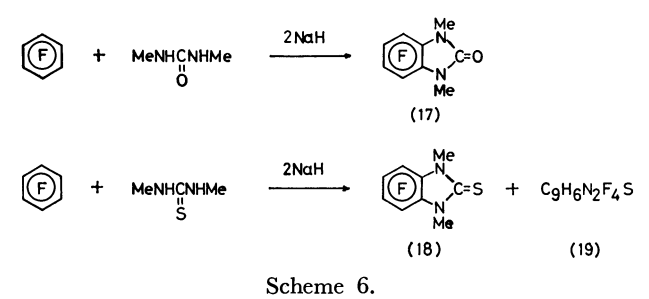

Scheme 6.

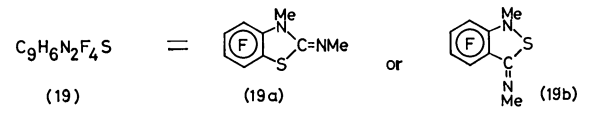

Scheme 7.

The reaction with the *N*,*N*′-dimethylthiourea similarly afforded 1,3-dimethyl(*F*-benz)imidazoline-2-thione (**18**) and a comparable amount of poly(thio-*F*-*p*-phenylene) in addition to an isomeric product, $C_9H_6N_2F_4S$ (**19**). The ^{19}F-NMR and ^{1}H-NMR of the last product indicate the presence of four unequivalent aromatic fluorines and two unequivalent methyl groups on hetero atoms respectively, suggesting that the heterocyclic moiety has either thiazoline (**19a**) or isothiazoline (**19b**) structure. The rearrangement into the isothiazolidine structure seems less probable under the present reaction conditions. The results indicate that, in the reaction with *N*,*N*′-dimethylthiourea, the nucleophilic attacks by the amide and thiolate anions proceed competitively at the stage of the first aromatic substitution and/or the subsequent intramolecular cyclization.

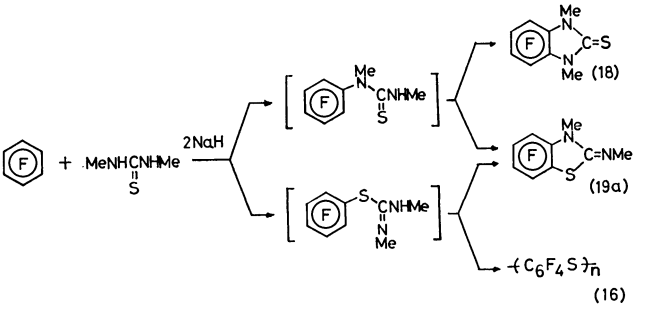

Scheme 8.

Experimental

The melting points are uncorrected. The IR and UV spectra were obtained with JASCO IR A-1 and Hitachi 220 spectrophotometers respectively. The ^{1}H-NMR and ^{13}C-NMR chemical shifts were recorded on Hitachi R-24 and JEOL JNM FX 100 instruments respectively, against the internal TMS reference. The ^{19}F-NMR chemical shifts were recorded on Varian EM 390 and JEOL PS-100 instruments as positive values downfield from the internal *F*-benzene reference. The mass spectra were obtained with JEOL JMS-07 and Hitachi RMS-4 spectrometers.

*Preparation of (F-Benzo)furan Derivatives (**1a**—**e**).* *General Procedure Using Sodium Hydride*: A solution of a ketone (**2**) (10 mmol) in anhydrous DMF (5 ml) was added dropwise into a stirred mixture of *F*-benzene (10 mmol), sodium hydride (20 mmol), and anhydrous DMF (10 ml) over a 30-min period at room temperature and under a dry nitrogen atmosphere. The mixture was stirred at 80 °C for an additional 5 h and then poured into ether. The ethereal solution was washed with water, dried over sodium sulfate, and evaporated. The residue was fractionated by chromatography on a neutral

alumina column. The fraction eluted with hexane gave a (*F*-benzo)furan derivative (**1**), which was further purified by sublimation.

2,3-Diphenyl-F-*benzofuran* (***1a***); Yield: 50%. White needles, mp 163.5—164.5 °C. ^{1}H-NMR ($CDCl_3$): 7.2—7.6 ppm (m, arom.). ^{19}F-NMR ($CHCl_3$): −1.8 (1F), 0.0 (1F), 1.2 (1F), 14.2 ppm (1F).[8] UV: λ_{max} (cyclohexane); 232 (log ε 4.34), 297 nm (4.40).[9] Found: C, 70.12; H, 2.83%; M$^+$, 342. Calcd for $C_{12}H_{10}F_4O$: C, 70.18; H, 2.95%, M, 342.

2-Methyl-3-phenyl-F-*benzofuran* (***1b***); Yield: 29%. White needles, mp 86—87 °C. ^{1}H-NMR ($CDCl_3$): 2.45 (s, 3H, CH_3), 7.4—7.9 ppm (m, 5H, arom.). ^{19}F-NMR ($CHCl_3$): −2.1 (1F), −0.5 (2F), 15.2 ppm (1F).[8] UV: λ_{max} (cyclohexane); 246 nm (log ε 4.19).[9] Found: C, 64.47; H, 3.03%; M$^+$, 280. Calcd for $C_{15}H_8F_4O$: C, 64.29; H, 2.88%; M, 280.

2-Phenyl-3-methyl-F-*benzofuran* (***1c***); Yield: 27%. White needles, mp 109.5—110.5 °C. ^{1}H-NMR ($CDCl_3$): 1.6 (s, 3H, CH_3), 7.3—7.5 ppm (m, 5H, arom.). ^{19}F-NMR ($CHCl_3$): −2.6 (1F), 0.5 (2F), 9.5 ppm (1F).[8] UV: λ_{max} (cyclohexane); 285 nm (log ε 4.40).[9] Found: C, 64.06; H, 3.10%; M$^+$, 280. Calcd for $C_{15}H_8F_4O$: C, 64.29; H, 2.88%; M, 280.

*2-Phenyl-(*F-*benzo)furan* (***1d***); Yield: 49%. White needles, mp 112—114 °C (lit,[10] 114.5—115.5 °C). Found: C, 62.93; H, 2.23%; M$^+$, 266.

2,3-Dimethyl-F-*benzofuran* (***1e***); Yield: 2.3%. White needles, mp 37.5—38.5 °C. ^{1}H-NMR ($CDCl_3$): 2.25 (s, 3H, CH_3), 2.35 ppm (s, 3H, CH_3). ^{19}F-NMR ($CHCl_3$): −3.5 (1F), −1.3 (1F), −0.5 (1F), 8.7 ppm (1F).[8] UV: λ_{max} (cyclohexane); 247 nm (log ε 4.11).[9] Found: C, 54.89; H, 2.76%; M$^+$, 218. Calcd for $C_{10}H_6F_4O$: C, 54.89; H, 2.77%; M, 218.

General Procedure Using Trimethylsilyl Enol Ethers (***6***).[6,7] A solution of a trimethylsilyl enol ether (**6**) (2.5 mmol) in anhydrous DMF (10 ml) was added, dropwise into a stirred mixture of *F*-benzene (2.5 mmol), anhydrous potassium fluoride (5 mmol), and anhydrous DMF (10 ml) over a 30-min period at room temperature and under a dry nitrogen atmosphere. The mixture was stirred at 80 °C for an additional 8 h and subsequently worked-up in a manner similar to that described above. **1a**; Yield: 49%. The reactions using trimethylsilyl isopropenyl ether (**6f**) and trimethylsilyl vinyl ether (**6g**), which had been prepared according to the literature,[6,7] afforded neither the expected (*F*-benzo)-furan (**1g**) nor 2-methyl derivative (**1f**).

Reactions of F-*Benzene with Benzamide. 2-Phenyl*-F-*benzoxazole* (***7***): A solution of benzamide (1.21 g, 10 mmol) in anhydrous DMF (20 ml) was added dropwise into a stirred mixture of *F*-benzene (1.86 g, 10 mmol), sodium hydride (20 mmol) and anhydrous DMF (2.5 ml) over a 15-min period at room temperature and under a dry nitrogen atmosphere. The mixture was stirred at 80 °C for an additional 2 h, subsequently refluxed for an additional 3 h, and then poured into ether. The ethereal solution was washed with water, dried over sodium sulfate, and evaporated off. The residue was chromatographed on a silica gel column. The fraction eluted with hexane gave 2-phenyl-*F*-benzoxazole (**7**) (0.85 g, 32%). The product was indentified by comparison with an authentic specimen.[1]

Benz-F-*anilide* (***8***): A solution of benzamide (2.42 g, 20 mmol) in anhydrous DMF (10 ml) was added dropwise into a stirred mixture of *F*-benzene (3.72 g, 20 mmol), sodium hydride (40 mmol), and anhydrous DMF (10 ml) over a 30-min period at room temperature and under a dry nitrogen atmosphere. The mixture was then stirred at room temperature for an additional 24 h and subsequently worked-up in a manner similar to that described above. The residue obtained after evaporation was recrystallized from benzene to give benz-*F*-anilide (**8**) (4.59 g, 80%). The product was identified by comparison with an authentic specimen.[1]

Reactions of F-*Benzene with Urea and Its Derivatives.*

Reaction with Urea: A solution of urea (0.50 g, 7.5 mmol) in anhydrous DMF (15 ml) was added dropwise into a stirred mixture of *F*-benzene (1.40 g, 7.5 mmol), sodium hydride (15 mmol), and anhydrous DMF (15 ml) over a 30-min period at room temperature and under a dry nitrogen atmosphere. The mixture was stirred at 80 °C for an additional 3 h and poured into ether. The ethereal solution was washed with water, dried over sodium surfate, and evaporated off. The residue was chromatographed on a silica gel column. The fraction eluted with hexane gave di(*F*-phenyl)amine (**13**) (0.73 g, 56%). The product was identified by comparison with an authentic specimen.[11]

Reaction with Guanidine: Di(*F*-phenyl)amine (**13**) was obtained in an 8% yield according to the above procedure by using guanidine in place of urea.

Reaction with Thiourea: A solution of thiourea (0.57 g, 7.5 mmol) in anhydrous DMF (15 ml) was added dropwise into a stirred mixture of *F*-benzene (1.40 g, 7.5 mmol), sodium hydride (15 mmol), and anhydrous DMF (15 ml) over a 30-min period at room temperature and under a dry nitrogen atmosphere. The mixture was stirred at 80 °C for an additional 3 h and then poured into a mixture of ether and water. The resulting precipitates were filtered off and washed with water and ether successively. Drying in a desiccator resulted in poly(thio-*F*-*p*-phenylene) (**16**) (1.21 g) as a pale yellow powder; mp>290 °C. The sulfur test using sodium tetracyanonitrosylferrate(III) was positive. The product was assigned by means of IR spectral comparison.[12]

Reaction with N,N′-*Dimethylurea.* A solution of *N,N′*-dimethylurea (1.93 g, 23 mmol) in anhydrous DMF (20 ml) was added dropwise into a stirred mixture of *F*-benzene (3.72 g, 20 mmol), sodium hydride (46 mmol), and anhydrous DMF (40 ml) over a 30-min period at room temperature and under a dry nitrogen atmosphere. The mixture was stirred at 80 °C for an additional 2 h and then poured into ether. The ethereal solution was washed with water, dried over sodium sulfate, and evaporated off. The residue was chromatographed on a neutral alumina column. The fraction eluted with hexane gave 1,3-dimethyl(*F*-benz)imidazolin-2-one (**17**) (0.86 g, 19%). Recrystallization from aqueous methanol afforded white needles; mp 104.5—105.5 °C. IR(KBr): 1710 cm^{-1} (C=O). ^{1}H-NMR ($CDCl_3$): 3.55 ppm (s). ^{19}F-NMR ($CHCl_3$): −6.6 (2F), −5.1 ppm(2F). ^{13}C-NMR ($CDCl_3$): 29.60 (CH_3), 154.23 ppm (C=O). UV: λ_{max} (EtOH); 209.5 (log ε 4.23), 224 (3.94), 277 nm (3.49). Found: C, 46.25; H, 2.59; N, 12.00; F, 29.7%; M$^+$, 234. Calcd for $C_9H_6N_2F_4O$: C, 46.17; H, 2.58; N, 11.96; F, 32.5%; M, 234.

Reaction with N,N′-*Dimethylthiourea.* A solution of *N,N′*-dimethylthiourea (1.04 g, 10 mmol) in anhydrous DMF (15 ml) was added dropwise into a stirred mixture of *F*-benzene (1.86 g, 10 mmol), sodium hydride (20 mmol), and anhydrous DMF (40 ml) over a 25-min period at room temperature and under a dry nitrogen atmosphere. The mixture was stirred at 80 °C for an additional 2 h, subsequently refluxed for an additional 3 h, and then poured into a mixture of ether and water. The resulting precipitates, poly(thio-*F*-*p*-phenylene) (**16**) (1.71 g), were filtered out, and the filtrate was extracted with ether. The ethereal extract was washed with water, dried over sodium sulfate, and evaporated off. The residue was separated into two components by elution chromatography using hexane on a

silica-gel column.

An earlier fraction gave 1,3-dimethyl(*F*-benz)imidazoline-2-thione (**18**) (19%).[13] Recrystallization from ethanol afforded white needles; mp 123.5—124.5 °C. IR(KBr): 1160 cm^{-1} (C=S). ^{1}H-NMR ($CDCl_3$) 3.90 ppm (s). ^{19}F-NMR ($CDCl_3$): −2.2 (2F), −0.1 ppm (2F). ^{13}C-NMR ($CDCl_3$): 33.86 (CH_3), 172.90 ppm (C=S). UV: λ_{max} (EtOH); 218 (log ε 4.08), 248 (4.24), 302 nm (4.35). Found: C, 43.53; H, 2.53; N, 11.22; F, 30.7%; M^+, 250. Calcd for $C_9H_6N_2F_4S$: C, 43.20; H, 2.42; N, 11.20; F, 30.4%; M, 250. The sulfur test using sodium tetracyanonitrosylferrate(III) was positive.

A later fraction gave the isomeric product (**19**) (7%).[13] Sublimation afforded white needles; mp 80—81 °C. IR (KBr): 1670 cm^{-1} (C=N). ^{1}H-NMR ($CDCl_3$): 3.10 (s, 3H, CH_3), 3.60 ppm (d, J=3Hz, 3H, CH_3). ^{19}F-NMR ($CHCl_3$): −5.8 (1F), 0.3 (1F), 2.7 (1F), 20.5 ppm (1F). ^{13}C-NMR ($CDCl_3$): 32.53 (d, J=0.34 Hz, CH_3), 40.93 (CH_3), 154.91 ppm (C=N). UV: λ_{max} (EtOH); 220 (log ε 4.41), 263 (3.80), 290 nm (3.44). Found: C, 42.94; H, 2.48; N, 11.12; F, 30.1%; M^+, 250. Calcd for $C_9H_6N_2F_4S$: C, 43.20; H, 2.42; N, 11.20; F, 30.4%; M, 250. The sulfur test using sodium tetracyanonitrosylferrate(III) was positive. The combined fractions eluted with hexane amounted to a total of 0.64 g.

We wish to thank Professor Nobuo Ishikawa and Mr. Kiyoshi Tanaka of the Tokyo Institute of Technology and Messrs. Akira Kito and Atsushi Iyoda of the Government Industrial Research Institute at Osaka for their measurements of the ^{19}F-NMR spectra. Financial support from the Ministry of Education under a Grant-in-Aid for Co-operative (A) Research (Project No. 335041) is also gratefully acknowledged.

References

1) Part I: Y. Inukai, Y. Oono, T. Sonoda, and H. Kobayashi, *Bull. Chem. Soc. Jpn.*, **52**, 516 (1979).

2) According to the revised nomenclature of highly fluorinated organic compounds by J. A. Young, *J. Chem. Document*, **14**, 98 (1974); *J. Fluorine Chem.*, **6**, 571 (1975).

3) G. G. Yakobson, T. D. Petrova, and L. S. Kobrina, "Fluorine Chemistry Reviews," ed by P. Tarrant, Marcel Dekker, New York (1974), Vol. 7, Chap. 2.

4) For example: a) J. Burdon, V. A. Damodaran, and J. C. Tatlow, *J. Chem. Soc.*, **1964**, 763; b) F. I. Abezgauz and S. V. Sokolov, *J. Gen. Chem., USSR*, **37**, 759 (1967); c) C. Wakselman and J. C. Blazejewski, *J. Chem. Soc., Chem. Commun.*, **1977**, 341.

5) I. Kuwajima, *Yuki Gosei Kagaku Kyokai Shi*, **34**, 964 (1976).

6) The trimethylsilyl enol ethers (**6**), except for trimethylsilyl vinyl ether (**6g**), were prepared according to the method reported by H. O. House, L. J. Czube, M. Gall, and H. D. Olmsted, *J. Org. Chem.*, **34**, 2324 (1969).

7) The trimethylsilyl vinyl ether (**6g**) was prepared according to the method reported by M. E. Jung and R. B. Blum, *Tetrahedron Lett.*, **1977**, 3791.

8) The chemical shifts were measured against the internal fluorobenzene reference; the values are given here after having been converted against an *F*-benzene reference, where the diference between the former reference and the latter one is regarded as 49.7 ppm.

9) An aryl substituent on the 2-position of the benzofuran structure[14] causes a bathochromic shift by 40—50 nm in the characteristic band of unsubstituted or 2-alkylbenzofuran near the 240-nm region.[15] A substituent at the 3-position, though, hardly affects the UV band.[16] Similarly the fluorine substituents on the fused aromatic ring in the present cases has little effect on their UV spectra.

10) G. M. Brooke, W. K. R. Musgrave, and T. R. Thomas, *J. Chem. Soc., C*, **1971**, 3596.

11) G. Baum and C. Tamborski, *Chem. Ind. (London)*, **1964**, 1949.

12) M. E. Peach, *Can. J. Chem.*, **46**, 2699 (1968).

13) The yield was estimated from the ^{1}H-NMR peak area ratio.

14) A. S. Angeloni, F. Delmoro, and M. Tramontini, *Ann. Chim. (Roma)*, **53**, 1751 (1963).

15) a) J. I. Jones and A. S. Lindsey, *J. Chem. Soc.*, **1950**, 1836; b) R. Andrisano, *Ricerca Sci.*, **30**, 131 (1960); *Chem. Abstr.*, **55**, 17206e (1961).

16) a) G. Cardillo, R. Cricchio, and L. Merlini, *Tetrahedron*, **27**, 1875 (1971); b) T. Sonoda, S. Kobayashi, and H. Taniguchi, *Bull. Chem. Soc. Jpn.*, **49**, 2596 (1976).

The Conformation of a Diastereoisomeric Pair of 2,2-Dimethyl-4-phenyl-3-pentanols[1)]

Yoshio KODAMA, Ken NISHIHATA, Shoji ZUSHI, Motohiro NISHIO,*
Jun UZAWA,† Kazuhiko SAKAMOTO,††,2) and Hiizu IWAMURA††,3)

Central Research Laboratories, Meiji Seika Kaisha, Ltd., Morooka, Kohoku, Yokohama 222

†*The Institute of Physical and Chemical Research, Wako 351*

††*Research Centre for Spectrochemistry, Faculty of Science, The University of Tokyo, Tokyo 113*

(Received March 7, 1979)

The conformations of a diastereoisomeric pair of 2,2-dimethyl-4-phenyl-3-pentanols were studied by means of ^{1}H-NMR, ^{13}C-NMR, IR, GC, and MS analyses. All of the results point to an unambiguous conclusion that these molecules are present dominantly in conformers where the *t*-butyl and the phenyl group lie close to each other. The generality of the phenomenon (favored *gauche* interaction) as well as the nature of the interactions involved were discussed in light of the conformational problems of the structurally related molecules. The presence of an attractive interaction (CH/π interaction) is suggested between an alkyl and a phenyl group, the possible importance of which in some dynamic phenomena (*e.g.*, selectivities in certain reactions) has then been discussed on this basis.

Evidence has been accumulated that an alkyl group orients itself close to a phenyl group in some molecular environments. The *t*-butyl group in (*SR*/*RS*)[4)] (**1**) and (*SS*/*RR*)-1-phenylethyl *t*-butyl sulfoxides (**2**) as well as in the corresponding sulfide (**3**) and sulfone (**4**), for example, has been shown to be oriented *gauche* with respect to the phenyl group (Fig. 1). Thus,

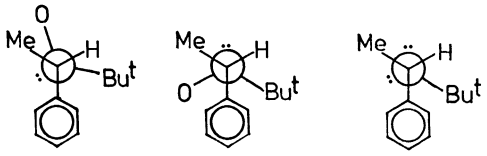

1 X=SO **2** X=SO **3** X=S

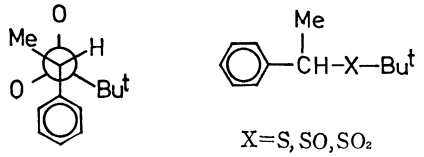

4 X=SO_2 X=S, SO, SO_2

Fig. 1.

X-ray crystallographic works on these sulfoxides (*p*-Br derivatives) have demonstrated that the dihedral angle defined by C(Bu^t)–S–C–C(Ph) is *ca.* 84° and 65° in **1** and **2**[5)] respectively. Conclusions regarding the conformations of **3** and **4** have been drawn from indirect evidence (for **3**)[6)] and an unpublished X-ray work (for **4**).[7)] The above findings led us to NMR,[5,8)] ORD/CD[5)] and dipole-moment studies[9)] of the diastereoisomeric sulfoxides; the conformations adopted by **1** and **2** in the crystal fields have been shown to be maintained in solutions. In an attempt to explore the generality of the phenomenon, we also extended this work to a conformational study of some structurally related alcohols, (*RS*/*SR*)- and (*SS*/*RR*)-2,2-dimethyl-4-phenyl-3-pentanols.

Experimental

Preparation of Alcohols. The treatment of 2-phenylpropionaldehyde with *t*-butylmagnesium chloride gave 2,2-dimethyl-4-phenyl-3-pentanol, with an (*RS*/*SR*) configuration (**5**, Fig. 2).[4,10)] The reaction mixture was shown to be almost diastereoisomerically pure.[11)] The oxidation of **5** to a ketone, followed by $LiAlH_4$ reduction, gave (*SS*/*RR*)-alcohol (**6**).

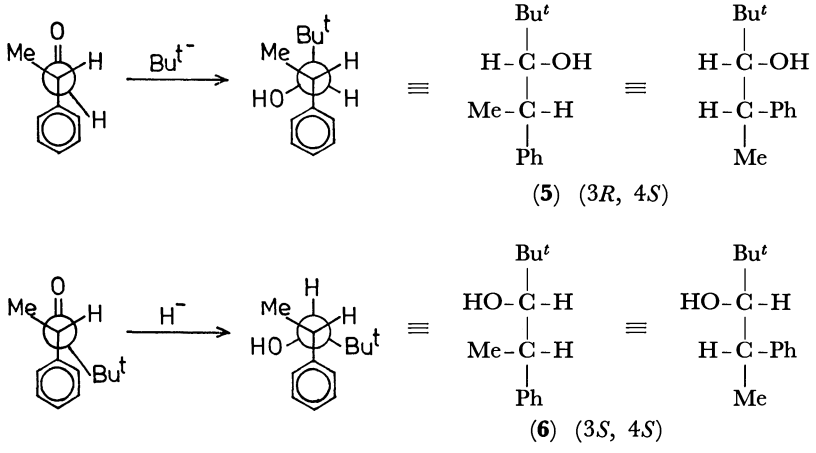

(**5**) (3*R*, 4*S*)

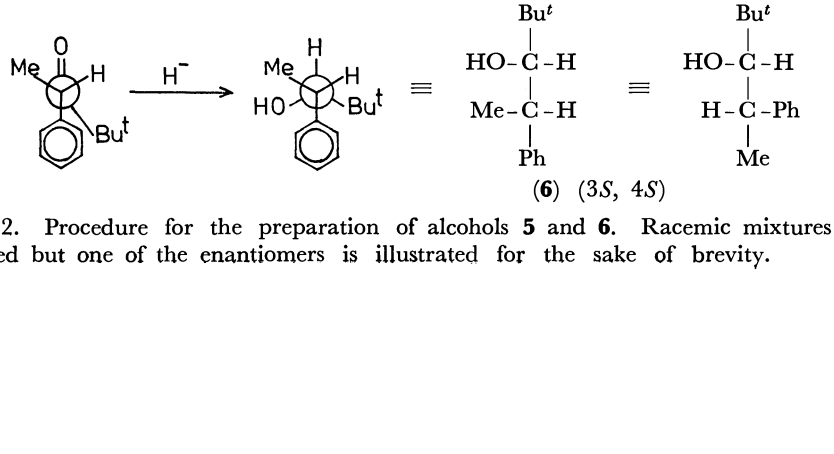

(**6**) (3*S*, 4*S*)

Fig. 2. Procedure for the preparation of alcohols **5** and **6**. Racemic mixtures were used but one of the enantiomers is illustrated for the sake of brevity.

This was again shown to be produced with an almost total exclusion of the other isomer.[10,11] The samples prepared as above and purified chromatographically gave correct analytical data (see Tables 1, 2, and 4 for the spectral data). The configuration assignment of the alcohols has been made by Felkin and his group;[10-12] it is consistent with our own conclusion.

NMR Measurements. The NMR spectra were determined for 0.2 mol/l solutions on a JEOL MH-100 spectrometer (for ^1H) and a JEOL FX-100 spectrometer (for ^{13}C). The chemical shifts are given relative to tetramethylsilane as the internal reference and are accurate to ± 0.01 ppm for the ^1H data and ± 0.04 ppm for the ^{13}C data. The coupling constants are accurate to ± 0.02 Hz. The assignments of the ^{13}C resonances were made by the use of the gated decoupling technique.

IR Measurements. The infrared spectra were obtained at 20 °C for dilute solutions (5.6—8.0 mmol/l) in carbon tetrachloride with a Perkin-Elmer model 112G or a JASCO DS-402G spectrometer. The error in the measurements is estimated to be less than 2.5 cm^{-1}.

GC. A Hewlett-Packard 5830A gas chromatograph equipped with a 6-foot column was packed with Diasolid ZS. The temperature was maintained at 150 °C. The flow rate of the He carrier gas was 35 ml/min. The retention times were 1.61 and 1.46 min respectively for **5** and **6**.

MS. A Hitachi RMU-6MG mass spectrometer was used. The samples were introduced gas-chromatographically. The temperature at the ion source, the ionizing potential, and the accelerating voltage were 230 °C, 20 eV, and 3.2 kV respectively.

Results

NMR Results. Tables 1 and 2 list the proton and carbon magnetic resonance parameters respectively for **5** and **6**.

Vicinal H/H Coupling: An inspection of the Newman projections in which the "bulkiest" groups (Bu^t and Ph) are arranged *anti* (Fig. 3) would lead us to a prediction that the vicinal coupling constant, $^3J_{HH}$, is larger in the (*SS*/*RR*) isomer (**6**) than in the (*RS*/*SR*) alcohol (**5**). This stems from a simple consideration of the Karplus relationship,[13] in which $^3J_{HH}$ is largest (*ca.* 10—12 Hz) when the relevant protons are oriented *anti* or eclipsed. The experimental values, however, were found to be smaller than 4 Hz for both compounds. This promptly rules out the conformation depicted in Fig. 3 for **6**; a much larger $^3J_{HH}$ value is expected for this conformation (H/H *anti*). Possible valence angle deformations involving the respective atoms could render the vicinal coupling constant a poor guide with regard to the conformational problem. In this

TABLE 1. PROTON NMR PARAMETERS FOR (*RS*/*SR*)- AND (*SS*/*RR*)-2,2-DIMETHYL-4-PHENYL-3-PENTANOL

	Bu^t	Me	H_a	H_x	H_o	H_m	OH
			(*RS*/*SR*) (**5**)				
δ[a]	0.90	1.25	2.94	3.33	7.17	7.17	1.48
LIS(obsd)[b]	0.33	0.44	0.48	1.00	0.25	0.03	
(calcd)	0.33	0.44	0.53	1.00	0.19	0.07	
ASIS[c]	+0.04	0.00	+0.07	+0.07	—	—	
J_{HaHx}		3.7 Hz (CCl_4), 3.7 Hz (benzene)					
			(*SS*/*RR*) (**6**)				
δ	0.79	1.32	2.95	3.28	7.22	7.22	(1.3)[d]
LIS(obsd)	0.31	0.37	0.37	1.00	0.38	0.08	
(calcd)	0.28	0.43	0.42	1.00	0.38	0.05	
ASIS	+0.02	+0.05	+0.11	+0.07			
J_{HaHx}		3.9 Hz (CCl_4), 3.7 Hz (benzene)					

a) Ppm downfield from internal TMS in CCl_4. b) Relative chemical shifts induced by the addition of $Eu(fod)_3$ in CCl_4 solutions. c) δ(benzene) $-\delta(CCl_4)$. d) Not observable, but suggested to be present about here by decoupling experiments (see text).

TABLE 2. CARBON NMR PARAMETERS FOR (*RS*/*SR*)- AND (*SS*/*RR*)-2,2-DIMETHYL-4-PHENYL-3-PENTANOL

(*RS*/*SR*) (**5**)									
	1	2, 6	3, 5	4	7	8	9	10	11
δ[a]	147.99	127.36	128.34	125.88	41.13	82.92	36.06	26.82	16.53
$^1J_{CH}$/Hz	—	154.3	159.2	162.1	125.0	140.6	—	125.0	127.0
(*SS*/*RR*) (**6**)									
δ	144.12	128.84	128.22	126.31	41.71	83.35	35.87	26.70	22.42
$^1J_{CH}$	—	156.2	159.2	159.2	126.0	139.6	—	125.0	127.0
Δ[b]	+3.87	−1.48	+0.12	−0.43	−0.58	−0.43	+0.19	+0.12	−5.89

a) Ppm downfield from internal TMS in $CDCl_3$ (20% w/v). b) $\Delta = \delta(RS/SR) - \delta(SS/RR)$.

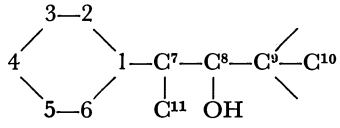

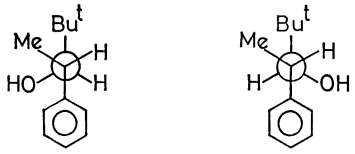

(**5**) (**6**)

Fig. 3.

regard, it should be noted that the one-bond coupling constants, $^1J_{CH}$, are quite normal for relevant sp^3-hybridized linkages[14] (for C^7–H and C^8–H, see Table 2). It follows, therefore, that there are no appreciable distortions about the bond angles and bond lengths involving these nuclei. It was also noted that there was little effect in $^3J_{HH}$ with the change in the solvent or the addition of a lanthanoide-shift reagent (LSR). This demonstrates that the conformational equilibria of these alcohols are not much perturbed by the change in the solvent polarity or by complexation.

Lanthanoide Shift Reagent-induced Shift (LIS): One of the most remarkable features to be seen in Table 1 is that the LIS for H_a is appreciably larger in **5** than in **6**, whereas the reverse is true for the *ortho* and *meta*-protons on the phenyl ring. To explain this, we must consider that the hydroxyl oxygen (the substrate-LSR complexation site) is closer to H_a and remoter from the phenyl group in **5** than in **6**. This, along with the coupling data, rules out the possibility that the conformations of these alcohols are like those shown in Fig. 3 (Bu^t/Ph *anti*). To be consistent with the LIS data, we must presume that such conformations as illustrated in Fig. 4 are predominant in these solutions. Note that in both conformations the *t*-butyl group orients itself *gauche* to the phenyl group. For the (*RS*/*SR*)-isomer (**5**), however, a completely staggered conformation is incompatible with the coupling data.

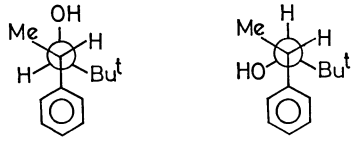

(**5**) (**6**)

Fig. 4.

We, therefore, carried out computer simulations of the LIS for these compounds. Thus, a program was written in which the LIS for each proton could be calculated[8] according to the McConnell and Robertson equation.[15] The necessary parameters were assumed as usual, and the LIS data listed in Table 1 were used. For the protons of Me, Bu^t, H_o, and H_m, the contributions of various rotational forms were averaged. The lanthanoide(Ln)–O–C angle was taken to be 130°. The procedure is illustrated in Fig. 5. A Gaussian weight factor (w) for the rotamer population was defined as in Eq. 1,[16] where A is the distribution coefficient and θ is a torsional angle for the rotation of Ln around the C–O bond. For steric reasons,

$$w(\theta) = \frac{A}{\sqrt{\pi}} \exp\left[-A^2(\theta-\theta_0)^2\right] \quad (1)$$

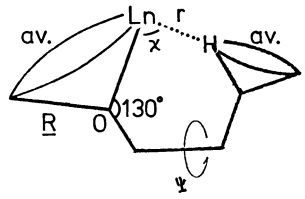

$$\Delta\nu_i = K(3\cos^2\chi_i - 1)/r_i^3$$

Fig. 5. Procedure for calculating the pseudocontact shifts.

θ_0 was taken so that the position of LSR was farthest from the center of the phenyl ring. The agreement factor (AF) was defined as in Eq. 2:

$$AF(\%) = 100(\sum_i |\mathrm{LIS}_{\mathrm{obsd},i} - \mathrm{LIS}_{\mathrm{calcd},i}|)/\sum_i \mathrm{LIS}_{\mathrm{obsd},i} \quad (2)$$

while the Ln–O distance (R) and the O–C–C–C(Ph) dihedral angle (ψ) were allowed to vary in order to enable us to obtain the best fit with the experimental values.

The AF values of 5 and 6% were the best fits where R=0.30 nm, ψ=210°, and A=0.2 for **5** and R=0.30 nm, ψ=285°, and A=0.6 for **6**. From these data, the H_a–C–C–H_x dihedral angles were estimated to be around 150° and 45° for **5** and **6** respectively.

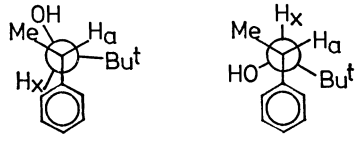

(**5**) (**6**)

Fig. 6. Computer-simulated conformations for **5** and **6**.

This is illustrated in Fig. 6. On the basis of the Karplus relationship (Eq. 3):

$$^3J_{HH} = 8.5\cos^2\theta - 0.28 \quad (0°—90°)$$
$$= 9.5\cos^2\theta - 0.28 \quad (90°—180°) \quad (3)$$

the H_a/H_x dihedral angles, 45°, 50°, 150°, and 135°, give $^3J_{HH}$ values of *ca.* 4.0, 3.2, 6.8, and 4.5 Hz respectively. The computational results are, therefore, not so incompatible with the coupling data in view of the fact that they merely reflect the weighted mean of the possible rotamers. This conclusion is consistent with the solvent effect induced by benzene (ASIS) as well; a larger ASIS was observed for H_a in **6** than in **5** (Table 1). This is expected since H_a in **6** is oriented more apart from the hydroxyl oxygen than in **5**. The trend observed for the LSR distribution index (A) is also reasonable in view of steric considerations. On the basis of the simulated conformations (Fig. 6), the phenyl group in **6** can be said to hinder more effectively the approach of LSR and, hence, give rise to a larger A (0.6 *vs.* 0.2). Also noteworthy are the differences observed in the shielding constants for the *t*-butyl and hydroxyl protons of the isomers. The signals appropriate to the *t*-butyl and OH protons in **6** are appreciably shifted toward the high-field region compared to those in **5** (0.79 *vs.* 0.90 ppm and

1.3 *vs.* 1.48 ppm in CCl_4 respectively). This can be ascribed to the anisotropic shielding effect of the phenyl group. According to the suggested conformations, the *t*-butyl and the hydroxyl group in **6** lie closer to the phenyl ring than do those in **5**; therefore, they suffer from a more profound ring-current effect.

^{13}C-Chemical Shift: In Table 2 are included the differences $[\Delta=\delta(RS/SR)-\delta(SS/RR)]$ in the carbon resonances between these isomers. Table 3 lists the corresponding data for some structurally related sulfoxide diastereoisomers, **1** and **2**. The most remarkable differences are those (Δ) observed for the quaternary ring carbon (C^1) and for the methyl carbon (C^{11}) shifts. The peak assignable to C^1 appears at a magnetic field lower by 3.9 ppm for **5** than for **6**. The methyl carbon of **5**, in contrast, gives rise to a signal which is 5.9 ppm higher than that of **6**. Similar trends are also noted for the sulfoxide pairs.

The above results can be explained in terms of the γ-effect or the so-called steric compression shift.[17] On the basis of the suggested conformations (Fig. 6), the hydroxyl group in **5** lies closer to the methyl group than in **6**. It is, therefore, reasonable to expect a more pronounced γ-effect for the methyl carbon in **5**. For the quaternary ring carbon C^1, on the other hand, it is anticipated that such an effect is more profound in the (*SS/RR*) alcohol (**6**) than in the (*RS/SR*) one (**5**). Thus, both OH and Bu^t lie closer to the aromatic carbon in **6** than in **5**. The same trend observed for the sulfoxide pairs (Δ=2.7 and −1.8 ppm respectively for C^1 and C^{11}, where R=H; see Table 3) can be understood on a similar basis. The S–O oxygen atom has been established to be closer to the methyl group in **1** than in **2**.[5] The reverse is true for the spatial relationships of O and Bu^t with respect to the phenyl group. The chemical-shift differences between isomers (Δ) are somewhat smaller for sulfoxides than for the case of alcohol. This is also reasonable in view of the longer bond lengths (S–C *vs.* C–C and S–O *vs.* C–O) for sulfoxides relative to alcohols. The interatomic distances of the respective nuclei are longer for the sulfur compounds; hence, the γ-effects are smaller.

Intramolecular OH/π Interaction. IR Spectra: The above findings led us to an expectation that, whereas an intramolecular OH/π bonding can be operative in the (*SS/RR*)-isomer (OH/Ph *gauche*), this interaction will be absent for the (*RS/SR*)-isomer (**5**), which has a hydroxyl group apart from the phenyl ring. In order to clarify this point, we have examined the IR spectra of these compounds, together with the lower homologues in which the *t*-butyl group is replaced by the methyl, ethyl, and isopropyl groups.[10] Table 4 summarizes the results.

As is shown by a typical example of the IR traces of **5** and **6** in Fig. 7, these alcohols possess characteristic doublet O–H stretching bands, one at 3630—3645 cm^{-1} and the other at 3600—3610 cm^{-1}. It goes without saying that the former is to be assigned to the free OH group.[18] The trend for the position of the high-frequency band to move still to the higher-frequency side as the substituents go from the methyl through ethyl to isopropyl and *t*-butyl seems to demonstrate the effect of steric congestion by the alkyl groups.[18,19] Thus, the conformation in which the torsion angle between the OH and alkyl groups is small ($\leq 60°$) is suggested for the free OH species.

In the *threo* (see footnote a in Table 4 for these

Table 3. Carbon NMR parameters for (*SR/RS*)- and (*SS/RR*)-1-phenylethyl *t*-butyl sulfoxides $p(R)C_6H_4CHMeSOC_4H_9$

	1[a]	2,6	3,5	4	7	8	9	10	11
(*SR/RS*) (**1**)									
R=H	140.0[b]	128.1	129.0	127.8	56.9		55.1	23.7	17.8
R=Br	139.2	132.2	129.8	121.7	56.1		55.4	23.7	17.5
(*SS/RR*) (**2**)									
R=H	137.3	129.1	128.4	127.9	54.8		55.1	23.6	19.6
R=Br	136.4	131.6	130.8	122.2	54.4		55.1	23.6	19.5
Δ[c]									
R=H	+2.7	−1.0	+0.6	−0.1	+2.1		0.0	+0.1	−1.8
R=Br	+2.8	+0.6	−1.0	−0.5	+1.7		+0.3	+0.1	−2.0

a) For numbering of the carbon atoms, see Table 2. b) Ppm downfield from internal TMS in $CDCl_3$. c) $\Delta=\delta(SR/RS)-\delta(SS/RR)$.

Table 4. IR spectral data for the diastereoisomeric pairs of alcohols RCHOHCHPhMe

	Me	Et	Pr^i	Bu^t
erythro[a]	3611.8[b] (0.8$_6$)[c]	3609.5 (1.8$_5$)	3614.4 (2.4$_8$)	3612 (1.0)
	3637.0 (1)	3640.2 (1)	3645.8 (1)	3645 (1)
threo[d]	3595.4 (11)	3601.0 (4.8)	3606.6 (5.5)	3600 (1.9)
	3629.0 (1)	3637.0 (1)	3648.2 (1)	3646 (1)

a) (*RS/SR*) for R=Bu^t, but (*SS/RR*) for R=Pr^i, Et, or Me. According to the sequence rule, the configurationally related alcohols do not necessarily have the same symbols (Bu^t>CHMePh; but Pr^i, Et, Me<CHMePh). b) Wave number in cm^{-1}. c) Relative intensity. d) (*SS/RR*) for R=Bu^t, (*RS/SR*) for the lower homologues.

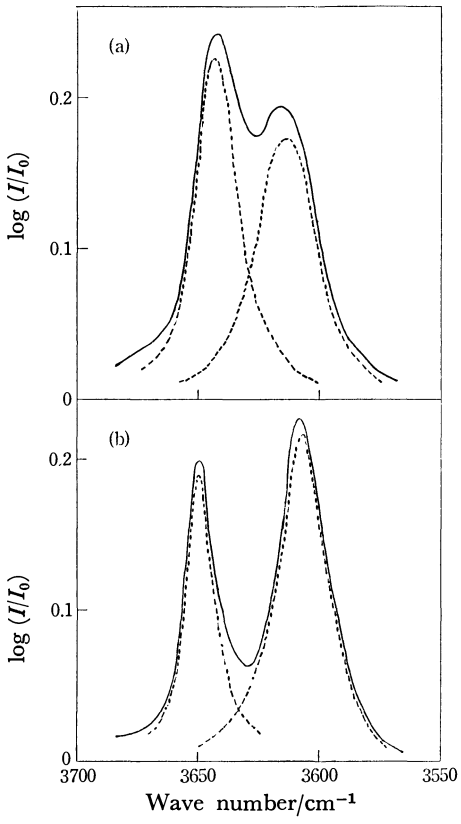

Fig. 7. Parts of the IR-traces for (a) (*RS*/*SR*)-(**5**) and (b) (*SS*/*RR*)-2,2-dimethyl-4-phenyl-3-pentanol (**6**). The dissection of the doublet bands was made by assuming the Lorentzian curve.

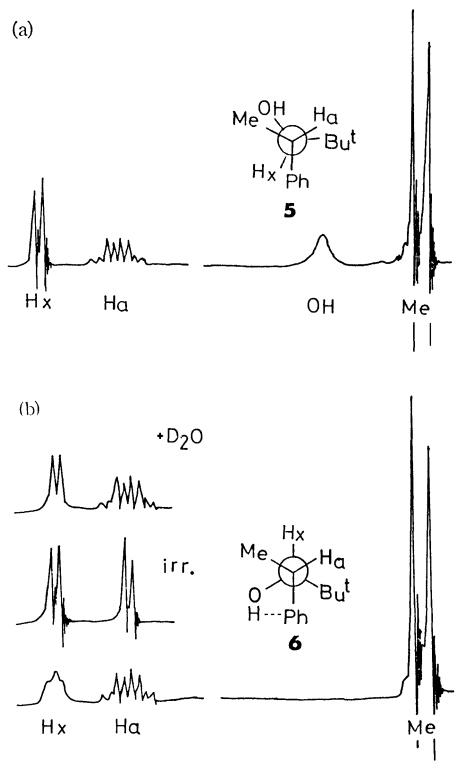

Fig. 8. Proton NMR spectra of **5** and **6** obtained for CCl_4 solutions. See text for inserts.

notations) series, the lower-frequency band is always stronger than the higher-frequency band.[11] It is also suggested by the wave number, as well as by the intensity of the lower-wave-number bands, that the OH/π bonding is strongest in the methyl and gets weaker as the substituent goes to the ethyl and isopropyl.[20] In other words, the OH and the phenyl groups come closer as Group R becomes smaller.

In the *erythro* series, the low-frequency bands are at *ca.* 3610 cm^{-1}. There are two possibilities for the origin of these bands: a weak OH/π bonding, or just a second free OH due to the presence of a OH rotamer in which the hydrogen atom bisects the hydrogen and carbon atoms. If the former is the case, we have to assume the contribution of a conformer with Bu^t/Ph *trans* (see Fig. 3) for **5**. We must reserve our conclusion on this matter until the effects of ring substituents on these low-frequency bands have been studied by performing a standard operational test for the OH/π interaction.[21] (The ν_{O-H} absorptions of these alcohols has already been reported by Sicher *et al.*[11] The present work conforms mostly to their method, but differs in some details because of differences in the resolution of the spectra and the method of the dissection of the doublet bands.)

NMR, GC, and MS Analyses: It has been shown by the above results that a major portion of the hydroxyl group in **6** interacts with the phenyl group, whereas in **5** it is almost free from intramolecular OH/π interaction. This conclusion is supported by an inspection of the NMR spectra. Parts of the proton NMR spectra are given in Fig. 8. The signal appropriate to H_x in **6** appears as a broad peak in both the solvents examined. In contrast, H_x in **5** gives rise to a sharp doublet (spin-coupled only with H_a). This is ascribed to the presence of a further coupling with the hydroxyl proton by H_x in **6**. The broad H_x signal collapsed to a doublet on decoupling (irradiation at *ca.* 130 Hz from TMS, where the broad signal of OH proton was assumed to be present under these conditions) or when the solution was treated with deuterium oxide. Also, the alcoholic hydrogen of **6** could hardly be observed because of the line broadening, while OH in **5** gives rise to a singlet. In the (*RS*/*SR*) isomer the non-bonded alcoholic hydrogen rapidly (at the NMR time scale) exchanges with that in the other molecules, thus giving rise to an observable peak. In the (*SS*/*RR*)-alcohol, on the other hand, the exchange rate is slowed down by the complexation of the hydroxyl group with the π-system, thus resulting in the disappearance of the OH signal.

Further support for the contribution of the intramolecular OH/π interaction in **6** (and its absence in the case of **5**) comes from comparisons of the chromatographic behavior[11] and the mass-fragmentation patterns.[12] Thus, the gas-chromatographic retention time is appreciably shorter for **6** than for **5**.[11] The relative intensity of the molecular ion peak *vs.* the dehydrated ion peak (M^+/M^+-H_2O) is larger for **6** (2.0) than for **5** (0.6). These results can be explained[12] in terms of the presence of OH/π bonding for **6**.

In summary, all of the results point to an unequivocal conclusion that, in the molecules presently studied,

the *t*-butyl group lies *gauche* to the phenyl group.

Discussion

Generality of the gauche *Conformation.* The conformations of **5** and **6** are indeed the consequences of the balance of a number of effects. The interactions involving the hydroxyl group, among others, should be taken into consideration. This seems to be of relatively minor importance in this particular case, however, since, in the (*RS*/*SR*) isomer (**5**), the conformer which lacks the OH/π interaction is found to be preferred. We wish here to emphasize that, in the cases studied thus far (**1**—**6**), the *t*-butyl group is always found to be close to the phenyl group, irrespective of the nature of the X group in the following general structure (Fig. 9) and irrespective of the conditions studied. Moreover, our preliminary data suggest that the above situation (alkyl/Ph *gauche*) holds also in the lower alkyl homologues.[6,22] It, therefore, follows that, in these compounds, an alkyl group has a general tendency to be closer to the phenyl group (or apart from Me) if these groups are present in the molecule.

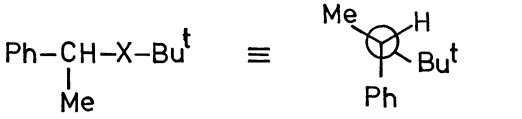

	1	2	3	4	5	6
X =	SO	SO	S	SO_2	CHOH	CHOH

Fig. 9.

The conformations of molecules have frequently been interpreted in terms of the repulsive forces arising from interaction between nonbonded groups.[23] Such approaches assume that bringing "bulky" groups into proximity leads to unfavorable interactions; the nature of which is generally ascribed to the van der Waals repulsion. However, evidence has been accumulated that this approach does not apply in a number of cases. Thus, the two large groups in a rotamer are very often found to be *gauche* or to eclipse one another, not only in sp^3-sp^3 single-bond systems, but also in most sp^2-sp^3 as well as in certain double-bond systems. To cite only a few cases, it is established that 1,2-difluoroethane and propyl halides prefer a *gauche* rather than an *anti* conformation. Propionaldehyde is known to exist dominantly in the conformation where the methyl group is eclipsed with the C=O double bond. Enthalpy differences in favor of a *cis* over a *trans* isomer are well documented for 1-halopropenes, 1,2-difluoroethylenes, *etc.*[24]

The most impressive of all, however, are probably the cases where such groups as *t*-butyl or trimethylsilyl groups are involved. The examples include *meso*-3,4-dichloro-2,2,5,5-tetramethylhexane (**7**),[25] tetra-*t*-butyldiphosphine (**8**),[26] 1,1,2,2-tetra-*t*-butylethane (**9**),[27] 1,1,2,2-tetrakis(trimethylsilyl)ethane (**10**),[27] and 1,3,5-trineopentylbenzene (**11**)[28] systems (Fig. 10). In all these cases, the bulkiest groups are found to be close to each other in the preferred conformations. It seems, therefore, that this situation (favored *gauche* interaction) is a rule rather than an exception.

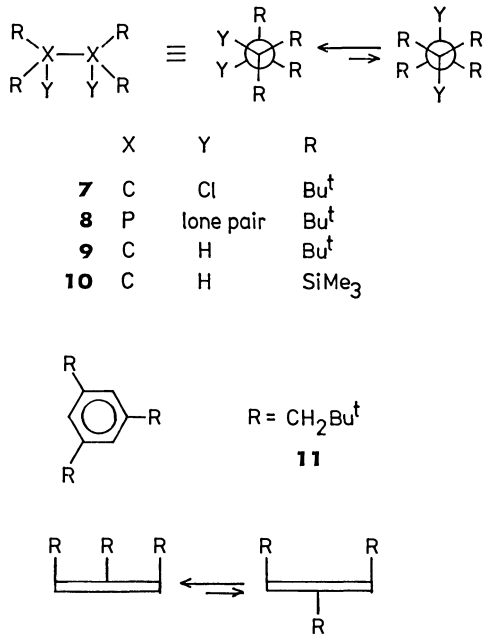

	X	Y	R
7	C	Cl	Bu^t
8	P	lone pair	Bu^t
9	C	H	Bu^t
10	C	H	$SiMe_3$

Fig. 10.

A number of approaches have been made to account for these "anomalies." The importance of attractive forces between nonbonded groups or atoms was suggested recently, while other workers favor interpretations in terms of repulsive steric effects or a conjugative stabilization (or destabilization) transmitted through bonds.[29] In particular, Carter and his group[28] advanced a concept of attractive steric effects on the basis of their findings regarding the conformational preference of the neopentyl groups in symmetrically substituted trineopentylbenzene systems (**11**). Their suggestion finds support in molecular mechanics calculations,[30] where the origin of the attractive forces is ascribed to London dispersion forces.

In the present case, where the interactions of an alkyl group with a phenyl group are concerned, the same approach will probably not apply, however. In the framework of the traditional approach, *i.e.*, the bulk-repulsive concept, the present result might be explained by regarding the "size" of a phenyl group as effectively smaller than that of a methyl group. A phenyl group is, of course, nonspherical and is capable of relieving the "steric constraint" which might occur in the interaction with the *t*-butyl group by a rotation about the C–C(Ph) bond. This possibility was argued in our earlier papers.[5,6] However, we found recently[31] that benzyl *t*-butyl sulfoxide (**12**) also adopts a conformation (in solution) similar to those established for **1**—**6**. This conclusion is based on NMR (LIS-simulation) evidence. Moreover, the stereospecificity and the stereoselectivities in the diastereotopos-differentiating reactions of **12** can be understood only on the basis of the *gauche* conformation.[32] In short, the preferred rotamer of **12** in solution again suggests that the *t*-butyl group is *gauche* with respect to the phenyl group. Note that in **12** the methyl group is absent. It follows that an interaction other than repulsive Me/Bu^t interaction should also be taken

into consideration.

Possibility of Attractive Alkyl···π-System Interaction; CH/π Interaction Hypothesis. A reexamination of the X-ray data on (*SR*/*RS*) (**1**) and (*SS*/*RR*)-1-(*p*-bromophenyl)ethyl *t*-butyl sulfoxide (**2**) (Fig. 1, X=SO) has revealed that a methyl group on Bu^t is oriented so as to be in close proximity to the phenyl ring, the C(Me^1)–C^1 distance being *ca.* 0.33 nm in both compounds (Fig. 11).[33] This is much shorter than the sum of the so-called van der Waals radii of the relevant groups (0.37 nm: 0.20 for a methyl and 0.17 nm for the half-thickness of a benzene molecule). To account for these findings, we recently suggested the importance of an attractive force involving an alkyl and an unsaturated group, namely, CH/π interaction.[31,32] A complexation of the benzene π-system has been known to occur with the acidic hydrogen atom of chloroform[35] or phenylacetylene.[36] For the non-acidic hydrogens of simple alkyl moieties in aliphatic molecules, however, the importance of such an interaction has not yet been suggested.[37]

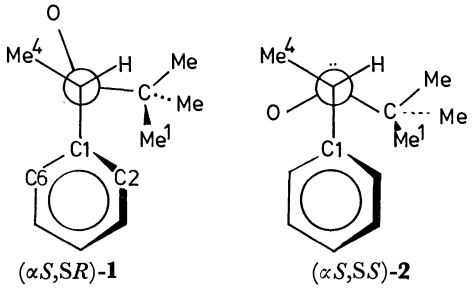

(α*S*,S*R*)-**1** (α*S*,S*S*)-**2**

Fig. 11. Newman projections for the X-ray crystallographic structures of **1** and **2** (*p*-Br derivatives).

The presence of such a weak interaction has been supported by a semi-empirical MO calculation of a methane/benzene model system.[31] Thus, attractive potential curves were obtained by the CNDO/2 method, where the stabilization energy was estimated to be *ca.* 3.5 kJ/mol at the maximum,[38] the approximate distance between a methane hydrogen (carbon) at this position and the benzene plane being 0.20 nm (0.31 nm: 0.20+0.11). This compares well with the X-ray data cited above.

The magnitude of the interaction energy is very small for a single CH/π bonding. However, a CH group does not generally exist in an isolated state. They are present, more frequently, as parts of an atomic cluster, such as a methyl, ethyl or isopropyl group. It seems, therefore, to be reasonable, in some molecular environments, to expect a simultaneous action of multiple interactions. It might well be that the total interaction energy becomes significant.[39]

The recognition of the above fact would be of help in explaining certain well-known but poorly understood phenomena, especially in the dynamic interaction of reacting molecules. To mention briefly a few examples, it has long been recognized that the extent of asymmetric synthesis is uniformly higher for the phenyl keto esters (R=Ph) than for the methyl keto esters (R=Me) in the Prelog reaction system (Fig. 12).[40a] We suggest that the free-energy level at the competing diastereomeric transition states can be

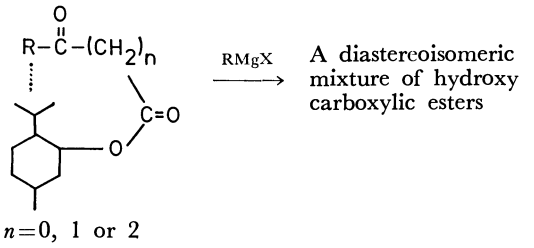

Fig. 12.

affected by an intervention of CH/π complexation. In the case of benzoylformate (R=Ph, n=0), the difference in the activation free energy, $\Delta\Delta G^{\ddagger}$, can be amplified by the interaction of Ph with the chiral aliphatic alcohol moiety (menthol group). Such an effect is absent in the case of pyruvate (R=Me, n=0), where we have a non-π system as R. Similar relationships hold also for the β-keto (n=1) and γ-keto ester (n=2) series.

A similar argument likely applies to the asymmetric reduction of ketones with optically active Grignard reagents (Fig. 13). The data listed in Table 5 are extracted from the works of Mosher and his group.[40b] A significant increase in the optical yield (%e.e.) has been reported when a phenyl group is incorporated in both the substrate and the chiral-reagent part (compare Tables 5a and 5b). In terms of the traditional

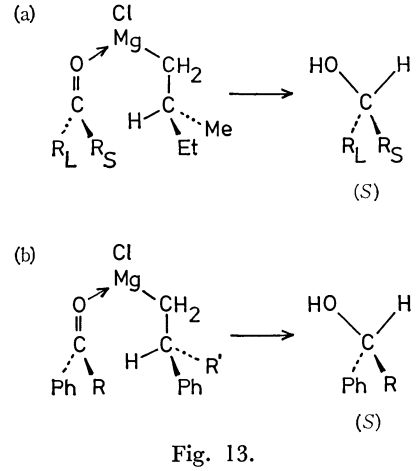

Fig. 13.

bulk-repulsive concept, the optical yield would be anticipated to decrease as the "bulk" of the substituent increases. Quite an inverse trend is observed for all cases, however, where we have a phenyl group in either side of the reacting species (Table 5b and column 3 in Table 5a). The results are comprehensible if one assumes the intervention of an attractive alkyl/phenyl interaction.[32,41] An interaction of this type could well be expected to increase with the number of CH groups in the aliphatic moieties, R and/or R′.

In this respect, the most interesting is probably the recent finding of Endo and his group.[42] In the course of an effort to find the factors controlling chemical reactions, they arrived at a model reaction system. This is composed of the oxidative coupling of a pair of thiols (D-SH and A-SH, Fig. 14) to disulfides. The ratio of the unsymmetrical disulfide over a symmetrical one (r=DSSA/DSSD) reflects the probability of the

TABLE 5. ASYMMETRIC REDUCTIONS WITH OPTICALLY ACTIVE GRIGNARD REAGENTS[a)]

(a)

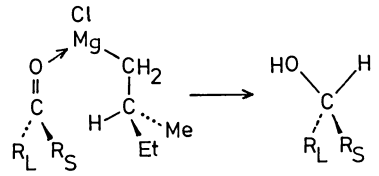

(S)

$R_S \backslash R_L$	Bu^t	$c\text{-}C_6H_{11}$	Ph[b)]
Me	13	4	4% e.e.
Et	11	9	6
Pr^n	11	9	6
Pr^i	0	2	24

(b)

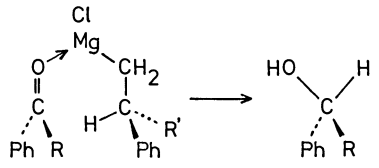

(S)

R \ R′	Me	Et	Pr^i
Me	38	47	—
Et	38	52	66
Bu^i	—	53	—
Pr^i	59	82	80

a) (*S*)-alcohols obtained in excess. *Cf.* Tables 5.6 and 5.7 in Ref. 40. b) See also G. P. Giacomelli, R. Menicagli, and L. Lardicci, *Tetrahedron Lett.*, **1971**, 4135; R. Kretchmer, *J. Org. Chem.*, **37**, 801 (1972).

molecular recognition between the interacting species. The recognition has been found to be most selective when an isopentyl group is introduced as the alkyl substituent (R) in the A-SH molecule (r=21.2, but it gradually decreases on going from $i\text{-}C_5H_{11}$ to $i\text{-}C_6H_{13}$ and then to $i\text{-}C_7H_{15}$ group). Such a remarkable dependence of the selectivity on the structure was not observed for A-SH where a series of straight-chain alkyl groups were used as R. An inspection of the CPK molecular models suggests that the complexes of the reacting species may well be stabilized by the CH/π type interaction; with the aromatic part of the D-SH molecule (dimethylaminophenyl group), the interaction is possible if we have an alkyl group as R in A-SH. This might be expected to be most selective when the R is a branched one and has an appropriate length (Fig. 14b).

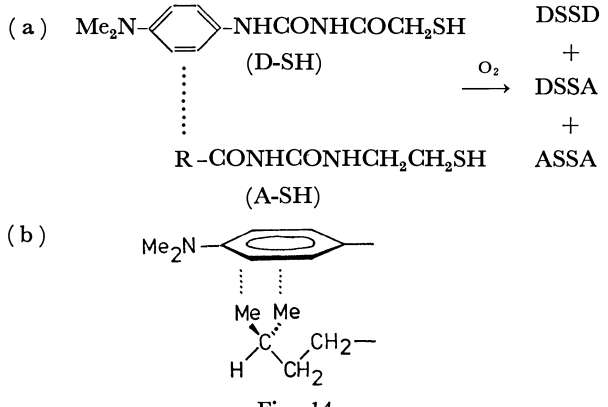

Fig. 14.

We wish to take this opportunity to point out the possibility that a weak interaction of such a kind plays an important role in determining the 3-D structure and the specificity of some globular proteins. These include enzymes, hemoglobins, or immunoglobulins.[43)] As has been emphasized by Watson,[46)] the secondary forces involved in the specific biopolymer interactions should never be too strong. Instead, they should be moderately weak, thus making it possible to assume a rapid recombination of biochemically important molecules (and therefore to be compatible with the cellular existence). Our knowledge about the weak chemical interactions is, however, still very incomplete.[46)] To be a candidate for these forces an interaction must be weak and also have the proper steric requirements. In addition to this, the groups involved in a weak secondary force used in biological devices must be widely distributed in nature. All of the prerequisites are fulfilled by the CH/π interaction—it is weak enough and orientation-dependent. Simple aliphatic groups are so abundant that we can find these moieties in virtually all components of natural sources. As to the abundancy of the groups, we will cite here the case of amino acid: both the aliphatic residues (Ala, Val, Leu, Ile, Met) and the aromatic ones (Phe, Tyr, Trp, His) are commonly found in proteins.

We wish to thank Drs. Tadashi Endo (Aoyama Gakuin Univ.), Naoya Nakagawa (Univ, of Electro-Communications), and Minoru Hirota (Yokohama National Univ.) for their valuable discussions and comments.

References

1) Presented in part at the 26th IUPAC Congress, Tokyo 1977, Abstr., p. 35, 1041 and the 8th International Symposium on Organic Sulfur Chemistry, Portoroz 1978, Abstr., p. 176.

2) Present address: Faculty of Engineering, University of Saitama, Shimo-okubo, Urawa 338.

3) Present address: Institute for Molecular Science, Myodaiji, Okazaki 444.

4) The correct sequence rule symbols for these configurations are (α*S*,S*R*/α*R*,S*S*), (α*S*,S*S*/α*R*,S*R*), (3*R*,4*S*/3*S*,4*R*), and (3*S*,4*S*/3*R*,4*R*) respectively for **1**, **2**, **5**, and **6**. Abbreviated notations are used in the text for the sake of brevity.

5) Y. Iitaka, Y. Kodama, K. Nishihata, and M. Nishio, *J. Chem. Soc., Chem. Commun.*, **1974**, 389; *J. Chem. Soc., Perkin Trans. 2*, **1976**, 1490.

6) K. Nishihata and M. Nishio, *Tetrahedron Lett.*, **1977**, 1041.

7) Y. Kodama, K. Nishihata, Y. Iitaka, and M. Nishio, to be published.

8) Y. Kodama, K. Nishihata, and M. Nishio, *J. Chem. Res. (S)*, **1977**, 102.

9) M. Hirota, Y. Takahashi, M. Nishio, and K. Nishihata, *Bull. Chem. Soc. Jpn.*, **51**, 2358 (1978).

10) M. Cherest, H. Felkin, and N. Prudent, *Tetrahedron Lett.*, **1968**, 2201; see also C. A. Kingsbury and W. B. Thornton, *J. Org. Chem.*, **31**, 1000 (1966); D. J. Cram and F. A. Abd Elhafez, *J. Am. Chem. Soc.*, **74**, 5828 (1952).
11) J. Sicher, M. Cherest, Y. Gault, and H. Felkin, *Collect. Czech. Chem. Commun.*, **28**, 72 (1963); Y. Gault and H. Felkin, *Bull. Soc. Chim. Fr.*, **1965**, 742.
12) H. E. Audier, H. Felkin, M. Fetizon, and W. Vetter, *Bull. Soc. Chim. Fr.*, **1965**, 3236.
13) M. Karplus, *J. Chem. Phys.*, **30**, 11 (1959); *J. Am. Chem. Soc.*, **85**, 2870 (1963).
14) M. Nakamura, N. Nakamura, and M. Ōki, *Chem. Lett.*, **1977**, 17; *Bull. Chem. Soc. Jpn.*, **50**, 2986 (1977).
15) H. M. McConnell and R. E. Robertson, *J. Chem. Phys.*, **29**, 1361 (1958).
16) I. M. Armitage, L. D. Hall, A. G. Marshall, and L. G. Werbelow, *J. Am. Chem. Soc.*, **95**, 1437 (1973).
17) D. M. Grant and B. V. Cheney, *J. Am. Chem. Soc.*, **89**, 5315 (1967); J. D. Roberts, F. J. Weigert, J. I. Kroschwitz, and H. J. Reich, *ibid.*, **92**, 1338 (1970).
18) H. Iwamura and M. Ōki, *Bull. Chem. Soc. Jpn.*, **32**, 950 (1959).
19) K. U. Ingold and D. R. Taylor, *Can. J. Chem.*, **39**, 481 (1961).
20) H. Iwamura and K. Hanaya, *Bull. Chem. Soc. Jpn.*, **43**, 3901 (1970).
21) M. Ōki and H. Iwamura, *Bull. Chem. Soc. Jpn.*, **32**, 955, 1135 (1959); **34**, 1395 (1961).
22) J. Uzawa, Y. Kodama, S. Zushi, Y. Fukuda, K. Nishihata, and M. Nishio, to be published.
23) D. H. R. Barton, *Science*, **169**, 539 (1970).
24) For reviews, see E. L. Eliel, N. L. Allinger, S. J. Angyal, and G. A. Morrison, "Conformational Analysis," Interscience, N. Y. (1965), and G. J. Karabatsos and D. J. Fenoglio, *Top. Stereochem.*, **5**, 167 (1970).
25) D. C. Best, G. Underwood, and C. A. Kingsbury, *Chem. Commun.*, **1969**, 627.
26) S. Aime, R. K. Harris, and M. E. McVicker, *J. Chem. Soc., Chem. Commun.*, **1974**, 426; **1975**, 886; H. C. E. McFarlane and W. McFarlane, *ibid.*, **1975**, 582.
27) S. Brownstein, J. Dunohues, D. Lindsay, and K. U. Ingold, *J. Am. Chem. Soc.*, **99**, 2073 (1977).
28) R. E. Carter, B. Nilsson, and K. Olsson, *J. Am. Chem. Soc.*, **97**, 6155 (1975).
29) For recent papers, see, *e.g.*, S. Wolfe, *Acc. Chem. Res.*, **5**, 102 (1972); N. D. Epiotis, R. L. Yetes, and F. Bernardi, *J. Am. Chem. Soc.*, **97**, 5961 (1975); J. E. Eliers and A. Liberles, *ibid.*, **97**, 4183 (1975); R. Bingham, *ibid.*, **98**, 535 (1976).
30) R. E. Carter and P. Stilbs, *J. Am. Chem. Soc.*, **98**, 7515 (1976).
31) Y. Kodama, K. Nishihata, M. Nishio, and N. Nakagawa, *Tetrahedron Lett.*, **1977**, 2105.
32) M. Nishio, *Kagaku No Ryoiki*, **31**, 834, 998 (1977). An X-ray study of *p*-Br-**12** demonstrated the *anti* conformation to be preferred (Y. Kodama, unpublished results) in a solid, but we feel that this is a consequence of the intermolecular interactions involved in the crystal field. A quantitative estimate of the dipole moment[9] and the NOE experiment (J. Uzawa, unpublished results) gave data in favor of the *anti*-conformation for **12**, but do not exclude the possibility of the *gauche* conformation.
33) Short interatomic contacts were also observed for the C(Me[4])/O distance: 0.30 and 0.32 nm in **1** and **2** respectively, suggesting a possible intervention of the CH_3/O hydrogen bond.[34]
34) M. Nishio, *Kagaku No Ryoiki*, **33**, 422 (1979).
35) G. C. Pimentel and A. L. McClellan, "The Hydrogen Bond," W. H. Freeman, San Francisco (1960), p. 202.
36) N. Nakagawa and S. Fujiwara, *Bull. Chem. Soc. Jpn.*, **33**, 1534 (1961).
37) See, however, N. Nakagawa, *Nippon Kagaku Zasshi*, **82**, 141 (1961). See also D. J. Sutor, *J. Chem. Soc.*, **1963**, 1105 for the case of CH_3/O.
38) The datum was erroneously reported to be 4.8 kJ in Ref. 31. For a CH_4/C_2H_2 system, the stabilization energy has been estimated to be *ca.* 4.8 kJ/mol (N. Nakagawa, personal communication). These data probably represent the maximum values, since the energies are frequently overestimated by this approximation.
39) It might be that this type of interaction (CH_3/π and CH_3/X, X=O or N) is entropically advantageous in that the chance for the interaction increases upon a clustering of CH groups into certain arrangements. We wish to refer this concept (a multiple as well as a chance effect) to the "isopropyl effect," the implications of which will be discussed elsewhere (M. Nishio and T. Endo, to be published; *cf.* Ref. 34).
40) J. D. Morrison and H. S. Mosher, "Asymmetric Organic Reactions," Prentice-Hall, N. J. (1971), (a) Chap. 2, (b) Chap. 5.
41) M. Nishio, 6th Symposium on Biomimetic Chemistry, Tokyo, 1978, Abstr. 55.
42) T. Endo, A. Kuwahara, H. Tasai, T. Murata, M. Hashimoto, and T. Ishigami, *Nature*, **268**, 74 (1977).
43) The possible importance of the CH/π interaction in chemical as well as biochemical systems has been discussed in Refs. 32, 34, 44, and 45.
44) M. Nishio, "Stereochemistry of Molecular Interactions—An Essay on Biological Stereochemistry," J. Japan. Chem. Monograph Series 16, Nankodo, Tokyo (1978), Chap. 6.
45) M. Nishio, 29th Symposium on Protein Structure, Osaka, 1978, Abstr. 161.
46) J. D. Watson, "Molecular Biology of the Gene," W. A. Benjamin, Menlo Park, Calif. (1965), Chap. 4.

Enantioface-differentiating (Asymmetric) Hydrogenation of Keto Ester with Modified Nickel Catalyst. XXXII. Structural Requirements of Modifying Reagent and Substrate

Shinji Okamoto, Tadao Harada, and Akira Tai*

Division of Organic Chemistry, Institute for Protein Research, Osaka University, Suita, Osaka 565

(Received March 29, 1979)

The enantioface-differentiating hydrogenation of α-, β-, γ-, and δ-keto esters over α-, β-, and γ-amino acid-MRNi has been conducted. The optimum enantio-differentiating power of α-amino acid-MRNi has been found in the hydrogenation of the β-keto ester and that of β-amino acid-MRNi found in the hydrogenation of the γ-keto ester. The results have been explained in terms of the intermolecular recognition between substrate and modifying reagent through the functional groups.

Asymmetrically modified nickel catalysts (MNi) provide attractive catalysts for the enantioface-differentiating hydrogenation of prochiral unsaturated compounds because of their simplicity and wide applicability.

The modifying reagents which have high enantio-differentiating power with one type of substrate do not necessarily do so with another substrates.[1] Therefore, the choice of modifying reagent suited to each type of substrate is the most important criteria for preparing an effective catalyst. In general, α-amino acid- or α-hydroxy acid-MRNi show good enantio-differentiating power with β-keto esters but not with α- and γ-keto esters. In a preceding paper which dealt with the hydrogenation of β-keto esters with tartaric acid-MNi, it was shown that the intermolecular hydrogen bond between substrate and the modifying reagent were one of the most important factors governing the optical yield of the reaction.[2] On this basis, the effect of the structural relation between the modifying reagent and the substrate on the enantio-differentiating power of the modified catalyst has been investigated by monitoring the optical yields of the hydrogenations of α-, β-, γ-, and δ-keto esters over α-, β-, and γ-amino acid-MRNi.

Results and Discussion

The substrates and the modifying reagents used in this study are as follows;

Modifying reagents

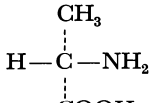

(*S*)-alanine

(I)

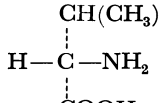

(*S*)-valine

(II)

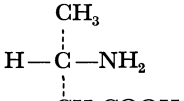

(*S*)-3-aminobutyric acid

(III)

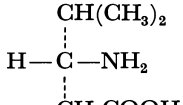

(*S*)-3-amino-4-methylpentanoic acid

(IV)

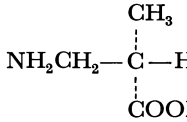

(*S*)-3-amino-2-methylpropionic acid

(V)

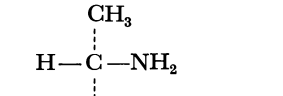

(*S*)-4-aminopentanoic acid

(VI)

Substrates

$CH_3CO(CH_2)_nCOOCH_3$

- $n=0$ methyl pyruvate (**1**)
- $n=1$ methyl acetoacetate (**2**)
- $n=2$ methyl 4-oxopentanoate (**3**)
- $n=3$ methyl 5-oxohexanoate (**4**)

The modification of Raney nickel was conducted as previously reported.[3]

The hydrogenation of each substrate was performed in an autoclave at 100 kg/cm² of initial hydrogen pressure at 60 °C. The optical yields of the reactions are summarized in Table 1.

In the hydrogenation of various keto esters over α-amino acid-MRNi the maximum optical yield was obtained with methyl acetoacetate as shown in Fig. 1. Methyl 4-oxopentanoate gave the optimum optical yield on hydrogenation with a β-amino acid-MRNi (Fig 2). In the β-amino acid-MRNi, III and IV, in which the chiral center is at the β-position of the carboxyl group and V in which the chiral center is at the α-position of the carboxyl group, the same trend in enantio-differentiating power with change in substrate was observed.

From a geometrical point of view, it is thought that the positions of the $-NH_2$ and $-COOH$ groups in the modifying reagent and those of the $-CO-$ and $-COOCH_3$ groups in the substrate are the most important factors in the optical yield of hydrogenation, *i.e.*, a reasonable optical yield is only attained when the substrate can make a stabilized complex with the modifying reagent involving more than two pairs of interaction through functional groups as indicated above.

As shown in Fig. 2, with a structural fit between the substrate and the modifying reagent, the optical yield is not influenced by the position of the chiral center.

In the case of the γ-amino acid-MRNi, no significant enantio-differentiating power was observed in all substrates examined ($n=0$ to 3). The low optical

Table 1. Hydrogenation of keto esters with Raney nickel catalyst modified with α-, β-, and γ-amino acid

Substrate $CH_3(CH_2)_nCO_2CH_3$	Optical yield(%) and configuration of enantiomer produced in excess modifying reagent					
	α-amino acid		β-amino acid			γ-amino acid
	I	II	III	IV	V	VI
1 (n=0)	0	0.3(*S*)	0.6(*R*)	0.4(*R*)	0.2(*S*)	0.9(*R*)
2 (n=1)	1.6(*R*)	8.9(*R*)	1.1(*R*)	3.8(*R*)	2.4(*R*)	0.1(*S*)
3 (n=2)	0.4(*R*)	2.8(*R*)	7.4(*S*)	7.5(*S*)	4.8(*S*)	0
4 (n=3)	0.1(*R*)	0	0.4(*R*)	0.1(*R*)	0.2(*R*)	0.1(*S*)

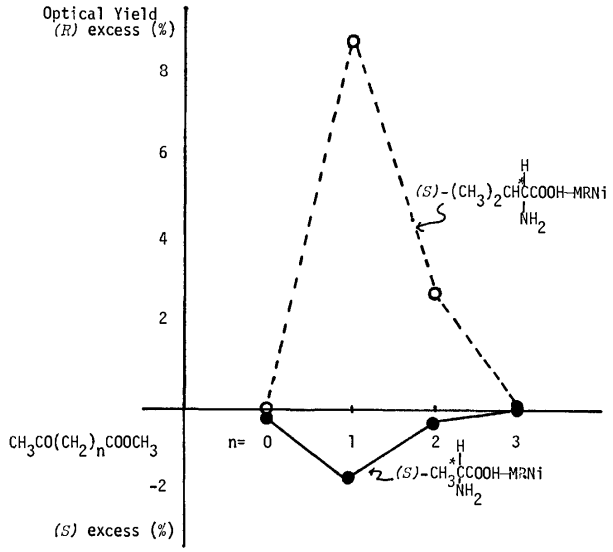

Fig. 1. Optical yield of the hydrogenation of $CH_3C(=O)-(CH_2)_n-COOCH_3$ (n=0—3) with α-amino acid–MRNi.

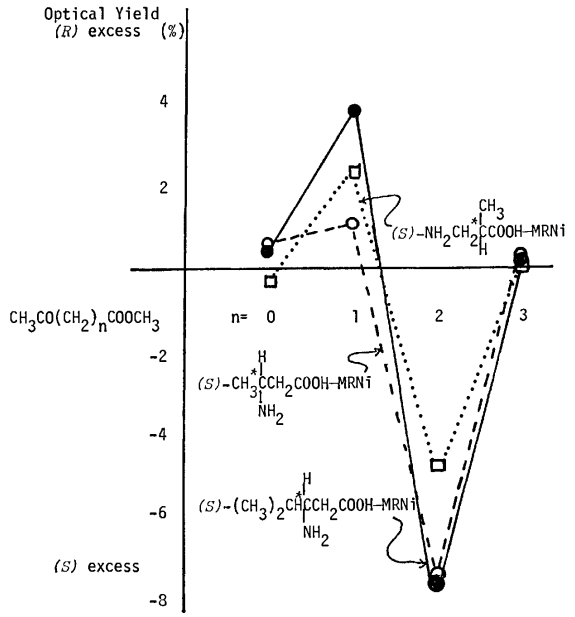

Fig. 2. Optical yield of the hydrogenation of $CH_3C(=O)-(CH_2)_n-COOCH_3$ (n=0—3) with β-amino acid–MRNi.

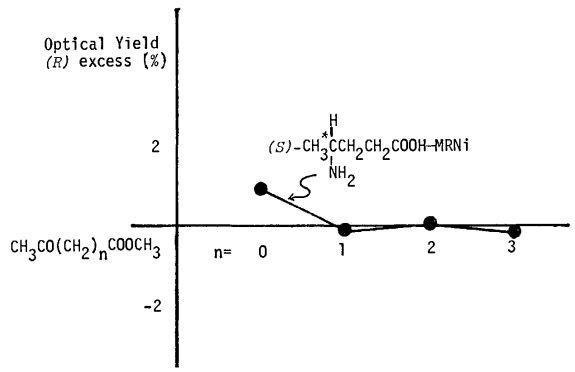

Fig. 3. Optical yield of the hydrogenation of $CH_3C(=O)-(CH_2)_n-COOCH_3$ (n=0—3) with γ-amino acid–MRNi.

yields in the reactions with the γ-amino acid–MRNi, even in the case of the δ-keto ester, may be ascribed to the lack of rigid intermolecular interaction due to the flexible nature of the molecules. Thus, the formation of rigid interaction between the substrate and the modifying reagent is the most important factor in obtaining a reasonable optical yield in this reaction system.

No special models demonstrating the mode of differentiation between the direction of enantioface-differentiation and absolute configuration of the modifying reagent, were derive from the present data. The structural requirement between the substrate and the modifying reagent provides, however, useful information as to the design of effective catalysts for enantio-differentiating reactions.

Experimental

Gas chromatographic analysis was conducted with a Shimadzu GC-4APF apparatus using a 300×0.5 cm glass column packed with neopentyl glycol succinate (5%) on Chromosorb W. Optical rotation was measured with a Perkin Elmer 241 polarimeter at 589 nm. NMR and IR spectra were measured on Hitachi R-24 and Shimadzu IR-27G spectrometers respectively.

Modified Raney Nickel Catalyst. The Raney nickel

catalyst was prepared as reported before.[3] A portion of the Raney nickel (0.1 g) was added to a 1% aqueous solution of the modifying reagent (20 ml). The mixture was allowed to stand with occasional shaking at 0 °C for 15 min. After decantation, the catalyst was washed with a portion of water (1 ml) and three portions of methanol (3×10 ml).

Hydrogenation and Optical Yield. Into a 10 ml flask equiped with a small gas inlet tube, was introduced the modified catalyst (0.1 g) suspended in the substrate (0.028 mol). The flask was placed in an autoclave and the hydrogenation conducted under hydrogen (90 kg/cm²) at 60 °C until no more consumption of hydrogen was observed. After filtration of the catalyst, the filtrate was distilled under reduced pressure. GLC analysis of each distillate indicated that the hydrogenation was complete.

Methyl lactate, bp 60—61 °C/35 mmHg† and methyl 3-hydroxybutyrate bp 61—62 °C/12 mmHg were obtained almost quantitatively from methyl pyruvate and methyl acetoacetate respectively.

A mixture of methyl 4-hydroxypentanoate and 4-pentanolide, and a mixture of methyl 5-hydroxyhexanoate and 5-hexanolide were obtained from methyl 5-oxopentanoate and methyl 5-oxohexanoate respectively. The optical yields of the hydrogenations of methyl pyruvate and methyl acetoacetate were calculated from the optical rotation of the products based on the values of $[\alpha]_D^{20}$ −8.25° (neat) for methyl (*S*)-lactate[4] and $[\alpha]_D^{20}$ −22.95° (neat) for methyl (*R*)-3-hydroxybutyrate.[5] The hydrogenation product of methyl 5-oxopentanoate was refluxed with Amberlyst 15 in benzene for 3 h to give 4-pentanolide bp 88—84 °C/13 mmHg.

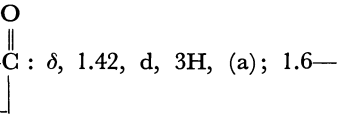

NMR for $CH_3C(a)-CH_2(b)-CH_2(b)-C(=O)O(a)$: δ, 1.42, d, 3H, (a); 1.6—2.6, m, 4H, (b); 4.68, m, 1H, (c). The optical yield of the hydrogenation was indirectly evaluated from the optical rotation of 4-pentanolide derived from the hydrogenation product based on the value of $[\alpha]_D^{22}$ −35.1±1° (*c* 4.018, dioxane) for (*S*)-5-pentanolide.[6]

The hydrogenation product of methyl 5-oxohexanoate was also converted to 5-hexanolide (bp 97—99 °C/12 mmHg)

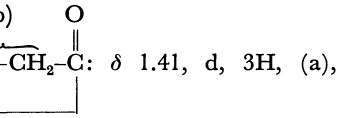

NMR for $CH_3C(a)-CH_2(c)-CH_2(b)-CH_2(b)-C(=O)O(a)$: δ 1.41, d, 3H, (a), 1.6—2.8, m, 4H, (b), 2.5, m, 2H, (c), 4.5, m, 1H, (d), by the same method as above. The optical yield of the hydrogenation was indirectly determined from the optical rotation of 5-hexanolide thus obtained based on $[\alpha]_D^{20}$ −51.4° (*c*=4, ethanol) for (*S*)-5-hexanolide.[7]

Modifying Reagents. *(S)-3-Aminobutyric Acid (III)*: This compound was obtained by the optical resolution of ethyl (*RS*)-3-aminobutyrate with (*R,R*)-tartaric acid in methanol and saponification of the resolved ester. From ethyl (*RS*)-3-aminobutyrate (131 g), optically pure (+)-(*S*)-III (7.5 g) was obtained. $[\alpha]_D^{25}$ +37.0° (*c* 0.5, H_2O) (lit, $[\alpha]_D^{19}$ 38.8° (*c* 0.8, H_2O)).[8] Mp 221 °C. Found: C, 46.69; H, 8.99; N, 13.60%. Calcd for $C_4H_9O_2N$: C, 46.59; H, 8.80; N, 13.58%.

(S)-3-Amino-4-methylpentanoic Acid (IV): (*S*)-Valine was converted to (+)-methyl (*S*)-3-phthalimido-4-methylpentanoate (VII) by the reported method.[9] To a solution of hydrazine hydrate (90%, 13 g) in a mixture of water (100 ml) and methanol (200 ml), VII (32 g) was added and the mixture maintained at room temperature for one week. After removal of the methanol from the reaction mixture and acidification of the residue with hydrochloric acid to pH 4, the precipitate was removed. Condensation of the filtrate to dryness gave crude 3-amino-4-methylpentanoic acid hydrazide as an oil. The oil was refluxed with 2M†† hydrochloric acid (300 ml) for 4 h and the resulting solution concentrated to dryness to give 3-amino-4-methylpentanoic acid hydrochloride. The crude amino acid hydrochloride was charged on to a column of IR 120B (H^+ type) and eluted with 0.2 M aqueous ammonia. Evaporation of water from the eluate gave crude crystals of IV. Recrystallization from a mixture of methanol and ether yielded (*S*)-(+)-IV (6 g). Mp 212 °C, $[\alpha]_D^{23}$ +52.3° (*c* 0.6, H_2O), (lit, $[\alpha]_D^{24}$ −39.2° (*c* 0.51, H_2O) for (*R*)-(−)-IV.[11]) Found: C, 54.66; H, 10.09; N, 10.49%. Calcd for $C_6H_{13}O_2N$: C, 54.94; H, 9.99; N, 10.68%.

(S)-3-Amino-2-methylpropionic Acid (V): This compound was obtained by the Hoffman degradation of (*S*)-3-carbamoyl-2-methylpropionic acid (VIII) ($[\alpha]_D^{23}$ −22° (*c* 2, ethanol)) which was prepared from (*E*)-3-carbamoylmethacrylic acid.[10] To a solution of KOBr prepared from bromine (12 g) and 10% aqueous potassium hydroxide (400 ml), VIII was added (9.8 g). The mixture was maintained at 55 °C for 1 h and then cooled to 0 °C. The solution was acidified to pH 2 with hydrochloric acid and concentrated to dryness. The residue was extracted with three portions of ethanol (3× 30 ml) and the combined extracts condensed to dryness to give crude crystals of 3-amino-2-methylpropionic acid hydrochloride. The hydrochloride was dissolved in water (200 ml) and passed through a column of Dowex-50. The amino acid loaded on the resin was eluted with 0.2 M aqueous ammonia. Evaporation of water from the eluate gave crystals of V. Recrystallization from a mixture of methanol and ethanol gave (*S*)-(+)-V (5.3 g), mp 194—5 °C, $[\alpha]_D^{21}$ +15.4° (*c* 5, H_2O), (lit, (*R*)-(−)-V, $[\alpha]_D^{26}$ −15.4° (*c* 1, H_2O).[11]) Found: C, 46.06; H, 9.10; N, 13.31%. Calcd for $C_4H_9NO_2$: C, 46.59; H, 8.80; N, 13.58%.

(S)-(+)-4-Aminopentanoic Acid (VI): This compound was obtained by the optical resolution of 4-(benzoylamino)-pentanoic acid with quinine and saponification of the resolved acylamino acid.[12] 4-(Benzoylamino)pentanoic acid (65 g) gave (*S*)-(+)-VI (2.7 g) as crystals, mp 205 °C, $[\alpha]_D^{23}$ +12.1° (*c* 10, H_2O) (lit, $[\alpha]_D^{20}$ +12.0° (*c* 10, H_2O)).[8] Found: C, 50.88; H, 9.69; N, 11.57%. Calcd for $C_5H_{11}NO_2$: C, 51.26; H, 9.46; N, 11.96%.

*Substrate. Methyl Pyruvate (**1**)*: This was obtained from silver pyruvate (190 g) and methyl iodide (164 g) by a conventional procedure (yield 70%), bp 61—63 °C/13 mmHg. GLC (80 °C) showed a single peak. The IR spectrum (neat) was identical with that from an authentic sample.

*Methyl Acetoacetate (**2**)*: The commercial product (Nihongosei Co.) was used without further purification.

*Methyl 4-Oxopentanoate (**3**)*: This compound was obtained by the esterification of 4-oxopentanoic acid with methanol in the presence of Amberlyst 15 (yield 90%). GLC (130 °C) showed 98% purity. H^1 NMR (CCl_4) and IR spectra were consistent with the structure of **3**. Elementary analysis was conducted as the 2,4-dinitrophenylhydrazone of **3**. Found: C, 48.19; H, 4.97; N, 17.30%. Calcd for $C_{13}H_{16}O_6N_4$; C, 48.15; H, 4.97; N, 17.28%.

*Methyl 5-Oxohexanoate (**4**)*: 5-Oxohexanoic acid was obtained from methyl acetoacetate and methyl acrylate (yield 68%).[13] The esterification of the acid with methanol

† 1 mmHg=133.3 Pa.

†† 1 M=1 mol dm^{-3}.

in the presence of Amberlyst 15 gave **4** (yield 90%). Bp 96 °C/15 mmHg. GLC analysis (130 °C) showed a single peak. Elemental analysis was conducted as the 2,4-dinitrophenylhydrazone of **4**. Found: C, 48.19; H, 4.97; N, 17.30%. Calcd for $C_{13}H_{16}O_6N_4$: C, 48.15; H, 4.97; N, 17.28%.

The authors would like to thank Professor Yoshiharu Izumi for his helpful suggestions and discussions. Thanks are also due to Mrs A. Kobatake for the elemental analyses. The present work was partly supported by a Grant-in-Aid for Scientific Research from the Ministry of Education.

References

1) Y. Izumi, M. Imaida, T. Harada, T. Tanabe, S. Yajima, and T. Ninomiya, *Bull. Chem. Soc. Jpn.*, **42**, 241 (1969); Y. Izumi, *Angew. Chem. Int. Ed. Engl.*, **10**, 871 (1971).
2) A. Tai, H. Watanabe, and T. Harada, *Bull. Chem. Soc. Jpn.*, **52**, 1468 (1979).
3) H. Ozaki, A. Tai, S. Kobatake, H. Watanabe, and Y. Izumi, *Bull. Chem. Soc. Jpn.*, **51**, 3559 (1978).
4) T. Purdie and J. C. Irvine, *J. Chem. Soc.*, **75**, 484 (1899).
5) T. Harada and Y. Izumi, *Chem. Lett.*, **1978**, 1195.
6) H. Minato, *Chem. Pharm. Bull.*, **9**, 625 (1961).
7) R. Kuhn and D. Jerchel, *Ber.*, **76**, 413 (1943).
8) K. Balenovic, D. Cerar, and Z. Funks, *J. Chem. Soc.*, **1952**, 3316.
9) K. Balenovic and D. Dvornik, *J. Chem. Soc.*, **1962**, 1386.
10) R. Adams and D. Fles, *J. Am. Chem. Soc.*, **81**, 4946 (1959).
11) Y. Kakimoto and M. D. Armstrong, *J. Biol. Chem.*, **236**, 3283 (1961).
12) E. Fischer and R. Groh, *Ann. Chem.*, **383**, 363 (1911).
13) N. F. Albertson, *J. Am. Chem. Soc.*, **70**, 669 (1948).

One-electron Reduction of 1-Benzyl-3-carbamoylpyridinium as a NAD$^+$ Model

Yutaka OHNISHI* and Miyoko KITAMI

Sagami Chemical Research Center, Nishi-Ohnuma, Sagamihara, Kanagawa 229

(Received April 2, 1979)

The pyridyl radical generated chemically or electrochemically by the 1e-reduction of 1-benzyl-3-carbamoylpyridinium undergoes dimerization to give mainly four dimers, diastereomers of 4,4′- and 4,6′-linked dimers. Isomerization between the dimers proceeds readily.

A pyridyl redical NAD· is recognized as a significant intermediate[1] in biological interconversion between NAD$^+$ and NADH, this being supported by results from oxidation and transhydrogenation in model systems.[2] Pyridyl radicals having carbamoyl group on C_3 can be readily generated by chemical,[3] photochemical,[4] electrochemical,[5–7] or radiochemical[8,9] one-electron reduction of the corresponding cations. The transient radicals react with each other to give dimerized products. However, there seems to be confusion concerning the products, particularly in the structures of the dimers.[3–7,10] Recently, Moracci *et al.* reported that 1e-reduction of 1-benzyl-3-carbamoylpyridinium (BzNA$^+$) gives a diastereomeric pair of 4,4′-linked dimer.[7] Formation of 4,6′- and 6,6′-dimers has also been postulated by other investigaters. Furthermore, Kosower *et al.* predicted the formation of a dihydronicotinamide by the dispropotionation of the 3-substituted pyridyl radical.[11] The formation of a dihydronicotinamide was also demonstrated in the electrolysis of the corresponding 1-alkyl-3-carbamoylpyridinium at a potential on the polarographic first wave.[12]

We have studied biomimetic conversion from a pyridinium into the corresponding dihydropyridine and found that a pyridyl radical, BzNA·, arising in the 1e-reduction of BzNA$^+$, gives none of 1-benzyldihydronicotinamides (BzNAH); it mainly gives two pairs of 4,4′- and 4,6′-linked dimers in analogy with the dimerization of 1-methyl-3-cyanopyridyl radical.[13] Isomerization between the dimers of BzNA· was also observed. In this article we wish to describe the details.

Results and Disscusion

Chemical 1e-reduction of the chloride of BzNA$^+$ was carried out using zinc powder–copper sulfate in methanol–aqueous ammonia.[3,4] Electrochemical 1e-reduction was performed with an Hg-pool electrode at

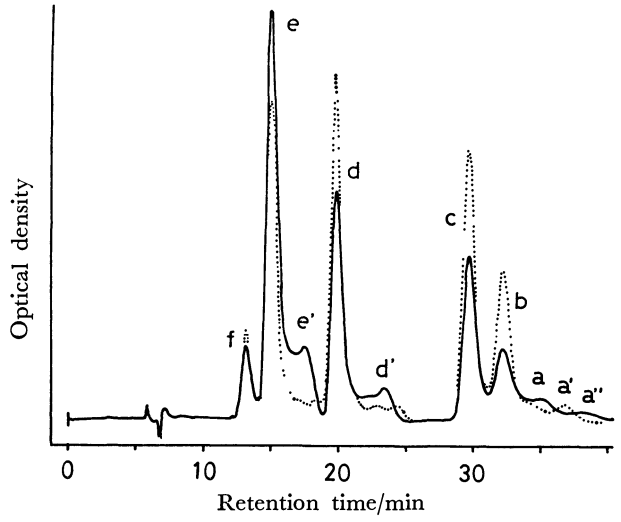

Fig. 1. HPLC trace of the reaction mixtures of one-electron reduction of BzNA$^+$ chemically (——) and electrochemically (·····).

−1.30 V, where the reversible 1e-reduction occurs[14] at pH 7.4 with McIlvaine's buffer. As shown in Fig. 1, many products were found in both chemical and electrochemical reaction mixtures by means of high pressure liquid chromatography (HPLC). We have confirmed the formation of 1,2-, 1,4-, or 1,6-BzNAH with HPLC. However, none of the products was found in the reaction mixtures. This result shows that disproportionation of BzNA·'s did not take place.[11,12] We have attempted the isolation and identification of four major products, **b**, **c**, **d**, and **e**. They could be isolated and purified by careful fractional recrystallization and column chromatography. In order to obtain unequivocal information on coupling positions of the dimers, the reduction of BzNA$^+$ deuterated on the C_4 of the nicotinamide ring was also carried out chemically.

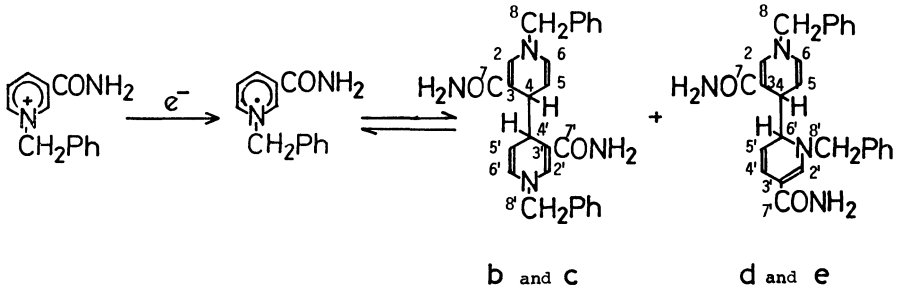

Scheme.

Table 1. ^{1}H NMR data for dimers[a)]

	b	c	d	e
H_4	3.34(d, J_{45}=4.2)	3.22(d, J_{45}=3.8)	3.20(dq, J_{45}=4.4, $J_{46'}$=3.6)	3.80(dq, J_{45}=5.0, $J_{46'}$=4.2)
H_5	4.48(q, J_{45}=4.2, J_{56}=8.0)	4.35(q, J_{45}=3.8, J_{56}=7.8)	4.70(q, J_{45}=4.4, J_{56}=8.0)	4.63(q, J_{45}=5.0, J_{56}=8.0)
H_6	5.92(d, J_{56}=8.0)	6.04(d, J_{56}=7.8)	6.20(d, J_{56}=8.0)	6.18(d, J_{56}=8.0)
H_2	7.28(s)	7.24(s)	7.24(d, J=2.0)	7.26(d, J=2.0)
$H_{4'}$			6.37(d, $J_{4'5'}$=10.0)	6.39(d, $J_{4'5'}$=9.6)
$H_{5'}$			4.80(q, $J_{5'6'}$=5.2, $J_{4'5'}$=10.0)	4.72(q, $J_{4'5'}$=9.6, $J_{5'6'}$=4.8)
$H_{6'}$			4.03(bq, $J_{5'6'}$=5.2, $J_{46'}$=3.6)	4.04(bp, $J_{5'6'}$=4.8, $J_{46'}$=4.2)
$H_{2'}$			7.32(d, J=2.0)	7.34(d, J=1.0)
Amide	6.40(ds)	6.96(bs)	6.30(bs)	6.33(bs)
Amide			6.70(bs)	6.64(bs)
H_8	4.31(s)	4.36(s)	4.43(s)	4.38(s)
$H_{8'}$			4.42(ABq, J_{AB}=*ca.* 13, $\nu_0\delta_{AB}$=*ca.* 0)	4.38(ABq, J_{AB}=*ca.* 12 $\nu_0\delta_{AB}$=*ca.* 0)
Aromatic	7.3(m)	7.33(m)	7.40(m)	7.37(m)

a) The numbers represent chemical shifts, δ with ppm, from TMS in $(CD_3)_2SO$. Coupling constants, J with Hz, are shown in parentheses.

Table 2. ^{13}C NMR data for dimers[a)]

	d	e	1,4-BzNAH[b)]	1,6-BzNAH[b)]
C_7	169.5	169.3	169.0	167.5
C_2	138.0	138.5	137.8	144.9
C_6	130.7	131.0	129.5	47.0
C_5	101.4	100.9	101.8	109.1
C_3	100.2	100.1 or 100.2	100.3	99.2
C_8	56.2	55.9 or 56.1	55.9	58.5
C_4	41.4	37.5	22.3	122.5
$C_{7'}$	167.3	167.4		
$C_{2'}$	145.5	144.5		
$C_{6'}$	60.6	60.1		
$C_{5'}$	110.7	109.6		
$C_{3'}$	103.7	100.2 or 100.1		
$C_{8'}$	58.3	56.1 or 55.9		
$C_{4'}$	122.7	123.3		

a) The numbers present chemical shifts, δ with ppm, from TMS in $(CD_3)_2SO$. b) Moracci's data.[7)]

^{1}H and ^{13}C NMR data of these compounds are summarized in Tables 1 and 2. Spectra of both **b** and **c** provide reasonable evidence for a symmetric structure. The tracer experiment established the coupling positions in the dimers. ^{1}H NMR spectra of **b** and **c** derived from BzNA$^+$-4d_1 showed no methine signal at δ 3.34 and 3.22, respectively, indicating that they have only 4-substituted 1,4-dihydronicotinamide structure; namely **b** and **c** can be identified as 4,4'-dimers of BzNA· and are a diastereomeric pair with respect to the C_4–$C_{4'}$ stereochemistry.[15)]

The complexity of ^{1}H and ^{13}C NMR spectra of **d** where two types of amide-signals are present suggest unsymmetric structure. The ^{1}H NMR signals at δ 3.20 and 6.37, not present in the spectrum of **d** obtained in the tracer experiment, should be due to the methine proton on C_4 of the 4-substituted 1,4-dihydropyridine structure and the vinyl proton of the 1,2- or 1,6-dihydro structure, respectively. However, the signal at δ 4.80, which is assigned to the proton on C_5, has a large coupling constant, J=5.2 Hz. This excludes the 1,2-dihydropyridine structure for the dimer **d**.[17)] The ^{13}C NMR spectrum of **d** is composed of that of 1,4- and 1,6-BzNAH expect that signals for methylene carbons appear as signals for methine carbons. Since a similar agreement between ^{13}C NMR spectra of 1,4-BzNAH and **b** or **c** is recognized, this observation and ^{13}C NMR spectrum with the off-resonance proton decoupling technique in the dimer **d** strongly indicate the presence of 4-substituted 1,4-dihydro and 6-substituted 1,6-dihydronicotinamide structures. The ^{1}H and ^{13}C NMR spectral data are in line with the structure of 4,6'-linked dimer.[18)] The complex signals could be assigned as shown in Tables 1 and 2. By similar analyses of ^{1}H and ^{13}C NMR spectra of **e** and the corresponding deuterated one, it can be concluded that **e** is the other diastereomer of 4,6'-dimer **d**.

Thus, the structures of four products isolated in the 1e-reduction of BzNA$^+$ can be established as two pairs of diastereomeric isomers of 4,4'- and 4,6'-linked dimers. The ratios of the yields of compounds **b**, **c**, **d**, and **e** from the chemical reduction are 1.0 : 1.4 : 3.0 : 4.5 at 4 °C and 1.0 : 2.6 : 2.3 : 3.3 at 60 °C, respectively. The ratio in the electrolysis at ambient temperature is 1.0 : 1.8 : 1.7 : 1.4. Although the ratios are labile, the total yield of four major products is larger than 95% in all cases. We assume that the residue should contain 2,2'-, 2,4'-, 2,6'- and 6,6'-dimers.

Statistically dimerization of BzNA· may give 12 dimers; six pairs of diastereomeric isomers. However, taking into account the far larger spin densities on

C_4 and C_6 of pyridyl radicals than C_2,[19] three pairs, 4,4′-, 4,6′- and 6,6′-dimers, may predominate. Actually, it was proved that the dimers obtained mainly have 4,4′- or 4,6′-bonding, the formation of other dimers not being appreciable. A small or negligible amount, if any, of 6,6′-dimers results from steric hindrance for dimerization. Furthermore, it should be taken into account that pyridyl radical in our reaction systems was generated on and participated by a metal surface, Zn or Hg. The difference of the metal might contribute to the dissimilarity between chemical and electrochemical reductions with respect to the ratios of the yields of four major dimers.

We have found isomerization between dimerization products. Even upon being left to stand overnight at room temperature in the dark with exclusion of air, a solution of 4,6′-dimer **d** gave 4,4′-dimer **c** mainly together with minor amounts of **a**, **b**, **d**, **d′**, **e**, and **e′**. **e** in methanol kept at 82 °C for 2 h also isomerized into a mixture of **a**, **a′**, **b**, **c**, **d**, **d′**, **e**, and **e′**; **c** was predominant. A solution of the most stable dimer **c** gave a mixture of **a**, **a′**, **b**, and **c** by heating at 82 °C for 15 h. In this mixture, small amounts of **a″**, **e**, and **d** were also detected. It was observed that the rate of the isomerization of **d** is accelerated by exposing the solution to scattered light. The isomerization indicates that the 4,4′-dimers are thermally more stable than the 4,6′-dimers and that the C–C bond coupling two pyridyl moieties is so weak that the dimer dissociates reversibly into two BzNA·'s.[20] The latter seems reasonable because of steric crowd of the dimers and of the resonance-stabilized structure of the radical.

Experimental

^1H and ^{13}C NMR spectra were taken on a Varian XL-100-15A. HPLC was effected with a Toyo Soda HLC-803 instrument and 30 cm LS-410K column under the following conditions. For BzNAHs, mobile phase, methanol–water (5:4 v/v); flow rate, 0.30 ml/min; detecter, UV-photometer at 350 nm; for the dimers, methanol–water (2:1 v/v); 0.54 ml/min, UV-photometer at 360 nm, respectively. Polarogram was recorded with a Yanaco Type P8-D Polarograph, macro scale electrolysis being performed with a potentiostat (Hokuto Denko Ltd.).

Reduction in Zinc Powder/Copper Sulfate System. To zinc powder (1.4 g) in 10 ml of water was added 0.5 g of copper sulfate pentahydrate in 20 ml of water under vigorous magnetic stirring, a mixture of 28% aqueous ammonia (10 ml) and methanol (50 ml) then being added. A solution of 0.1 g of $BzNA^+Cl^-$ in 20 ml of water was added to the above mixture at a definite temperature. After 20 min, the mixture was analyzed by HPLC (Fig. 1).

In preparative experiments, zinc powder (0.6 g)/H_2O (10 ml), $CuSO_4 \cdot 6H_2O$ (2.5 g)/H_2O (20 ml), 28% aqueous ammonia (10 ml)/methanol (50 ml) and 5.0 g of $BzNA^+Cl^-$/H_2O (20 ml) or 6.0 g of $BzNA^+$-$4d_1$ ClO_4^- in a mixture of H_2O (15 ml) and methanol (15 ml) were used, the reaction being carried out precipitate and inorganic materials were collected by filtration and were washed with 70 ml of hot methanol. Crystals of **c** obtained by cooling the methanol solution were separated by filtration. The filtrate was concentrated partially and cooled to give crystals of **d**. Further concentration and filtration gave crude crystals of **e** and the filtrate containing **b** predominantly. The filtrate was concentrated and chromatographed on a basic alumina eluting with a mixture of methanol and hexane (3:7 v/v). Several fractions containing only **b** were collected. Elimination of the solvents gave crystals of **b**. On the other hand, when the first aqueous filtrate was left to stand at room temperature for some time, yellow solids of **d** and **e** and orange viscous oil containing **b**, **d**, **e**, and **f** separated. After removal of the yellow solids and the oil by filtration and decantation, the solution was cooled in an ice bath to give crystals of **e** which were recrystallized from an aqueous methanol: mp (dec) 155 °C. Found: C, 72.99; H, 6.13; N, 13.19%. Calcd for $C_{26}H_{26}N_4O_2$: C, 73.22; H, 6.14; N, 13.14%. The yellow solids and the oil were treated similarly by fractional recrystallization to give pure dimers.

Absorption maxima of **b**, **c**, **d**, and **e** were observed at 355, 355, 359, and 359 nm, respectively, with a spectrometer (Shimadzu SPD-1) equipped with the HPCL instrument. In the treatments described above, HPLC was used effectively to estimate the composition of mixture and purity of isolated product.

Electrochemical Reduction. Electrolysis was carried out in a three-compartment cell, the cathode being a mercury pool (area, 12.6 cm^2), the anode a coil of Pt wire, and the reference electrode a saturated calomel electrode. The cathode was isolated from the anolyte with a glass filter and agar gel. Argon was blown continuously through the catholite before and during electrolysis. After preelectrolyzing the McIlvaine's buffer (pH 7.4, 30 ml), 102.5 mg of $BzNA^+Cl^-$ was added. Electrolysis was carried out at −1.30 V and stopped coulometrically at 25% conversion because of coating on the mercury surface with solid products. Dimethyl sulfoxide was then poured into the cathodic cell. After the mixture had been stirred until the mercury became clear, the solution was analyzed by HPLC.

We thank Dr. Y. Kikuchi for his help in the electrochemistry and Mr. K. Sato for measuring NMR spectra.

References

1) E. M. Kosower, "Free Radicals in Biology," ed by W. A. Pryor, Academic Press, New York, N. Y. (1976), Vol. II, Chap. 1.

2) a) J. J. Steffens and D. M. Chipman, *J. Am. Chem. Soc.*, **93**, 6694 (1971); b) A. Ohno and N. Kito, *Chem. Lett.*, **1972**, 369; c) D. J. Creighton, J. Hadju, C. Mooser, and D. S. Sigman, *J. Am. Chem. Soc.*, **95**, 6855 (1973); d) J. Hadju and D. S. Sigman, *ibid.*, **98**, 6060 (1976); e) P. van Eikeren and D. L. Grier, *ibid.*, **99**, 8057 (1977).

3) K. Wallenfels and M. Gellrich, *Chem. Ber.*, **92**, 1406 (1959).

4) K. Kano and T. Matsuo, *Bull. Chem. Soc. Jpn.*, **49**, 3269 (1976).

5) a) A. L. Underwood and R. W. Burnett, "Electroanalytical Chemistry," ed by A. D. Bard, Marcel Dekker, New York, N. Y. (1972), Vol. 6, p. 26; b) P. J. Elving, "Topics in Bioelectrochemistry and Bioenergetics," ed by G. Milazzo, Miley, New York, N. Y. (1976), Vol. 1, p. 179.

6) C. O. Schmakel, K. S. V. Santhanam, and P. J. Elving, *J. Electrochem. Soc.*, **121**, 1033 (1974) and *J. Am. Chem. Soc.*, **97**, 5083 (1975).

7) F. M. Moracci, F. Liberatore, A. Arnone, I. Garelli, and M. E. Cardinali, *J. Org. Chem.*, **43**, 3420 (1978).

8) E. J. Land and A. J. Swallow, *Biochem. Biophys. Acta*, **162**, 327 (1968).

9) S. S. Chan, T. M. Nordlund, H. Frauenfelder, J. E. Harrison, and I. C. Gunsalus, *J. Biol. Chem.*, **250**, 716 (1975).

10) E. M. Burnett and A. L. Underwood, *Biochemistry*, **7**, 3328 (1968).
11) E. M. Kosower, A. Teuerstein, H. D. Burrows, and A. J. Swallow, *J. Am. Chem. Soc.*, **100**, 5185 (1978).
12) Y. Paiss and G. Stein, *J. Chem. Soc.*, **1958**, 2905.
13) I. Carelli, M. E. Cardinali, A. Casini, and A. Arnone, *J. Org. Chem.*, **41**, 3967 (1976).
14) $BzNA^+$ has the first wave of polarography at -1.00 V (*vs.* SCE) in pH 7.4 with McIlvaine's buffer.
15) Comparision of ^1H NMR data showed that Morraci's dimers **2** and **3** are identical to **c** and **b**, respectively,[7] and Wallenfels's dimer which had been assigned to 6,6′-dimer is identical to **c**.[3,16]
16) H. Diekman, G. Englert, and K. Wallenfels, *Tetrahedron*, **20**, 281 (1964).
17) ^1H NMR signal from methylene protons of C_2 of 1-phenyl-*N*,*N*-dimethyl-1,2-dihydronicotinamide is split into doublet by the proton on C_6 with 1.0 Hz of the coupling constant: Y. Ohnishi and M. Kitami, unpublished data.
18) It should be noted that 4,6′-dimer reported by Kano and Matsuo[4] is identical to **d** on the basis of ^1H NMR data.
19) J. K. Dohrmann and R. Becker, *J. Magn. Reson.*, **27**, 371 (1977).
20) a) F. T. McNamara, J. W. Nieft, J. F. Ambrose, and E. S. Huyser, *J. Org. Chem.*, **42**, 988 (1977); b) B. Schroeder, W. P. Neumanm, J. Hooaender, and H.-P. Becker, *Angew. Chem. Int. Ed. Engl.*, **11**, 850 (1972).

Induced Circular Dichroism of β-Cyclodextrin Complexes with Substituted Benzenes

Hiroshi SHIMIZU, Akira KAITO, and Masahiro HATANO*

Chemical Research Institute of Non-aqueous Solutions, Tohoku University, Katahira, Sendai 980

(Received November 7, 1978)

The induced circular dichroism (ICD) of β-Cyclodextrin(β-CDx)-substituted benzene complexes was investigated. We observed the ICD on the absorption bands of achiral substituted benzene molecules, which is considered to be induced by the dissymmetric field of the chiral β-CDx host molecule. The electronic transitions which are polarized along the long axis of the substituted benzenes showed positive ICD, while the sings of the ICD of short-axis polarized transitions are negative. The rotational strengths of these inclusion complexes were calculated by the Kirkwood-Tinoco expression. From the comparison between the experimental and calculated results, it is concluded that these β-CDx complexes favor the axial inclusion in which the long axis of the substituted benzenes is parallel to the axis of the β-CDx cavity.

The cyclodextrins (CDxs) are a series of oligosaccharides produced by the action of *Bacillus macerans* amylase on starch.[1] CDxs are cyclic oligosaccharides composed of D(+)-glucopyranose units which are connected with each other by the α-(1,4)-glucoside bond. The number of glucose units of CDx is designated by a Greek letter: α- for 6, β- for 7, γ- for 8, and so on.

CDx has a hydrophobic cavity in the center of a CDx molecule. And it is known that CDx includes aromatic compounds, alkyl halides, gases, *etc.* as guest molecules in the CDx cavity, resulting in the formation of inclusion complexes.[2] These inclusion phenomena of CDx have been employed as one approach to the enzyme model, since CDx exhibited the steric specificity in a way similar to the formation of enzyme–substrate complexes.[3]

Inclusion complex formation is associated with a favorable enthalpy change and an unfavorable or slightly favorable entropy change. Several proposals[4] for the driving force of the complex formation have been made to interpret this favorable enthalpy change:

a) van der Waals interactions between the guest and host molecules

b) hydrogen bonding between the guest molecule and the hydroxyl groups of CDx

c) release of high energy water molecules in complex formation

d) decrease in strain energy in the ring frame of CDx.

From the results of the X-ray crystallography of the α-cyclodextrin–potassium acetate complex, Hybl *et al.*[5] revealed that α-CDx has a doughnut-shape with all the glucose units in substantially undistorted chair conformations. In addition, many investigations on the structure of inclusion complexes have been made by means of various physicochemical methods, *e.g.*, X-ray analysis,[6] NMR,[7] ESR,[8] UV,[9] CD,[10–12] *etc.*

Since CDxs are composed of chiral glucose units, the circular dichroism (CD) is expected to be induced on the absorption bands of the achiral guest molecules which are included in the cavity of chiral β-CDx. We thus investigated ICD spectra of β-CDx inclusion complexes with substituted benzenes in aqueous solution, and calculated the rotational strength on the basis of the Kirkwood-Tinoco equation,[13] with the goal of predicting the orientation of the guest molecules in these inclusion complexes.

Experimental

β-CDx and substituted benzenes were commercial products. β-CDx, benzoic acid, and *p*-nitrophenol were recrystallized from aqueous solutions. Aniline, phenol, and nitrobenzene were distilled under reduced pressure. *p*-Nitroaniline and *p*-hydroxybenzoic acid were recrystallized from methanol and ether, respectively. An inclusion complex was prepared by mixing β-CDx and the corresponding substituted benzene in an aqueous solution or in 0.1 M aqueous HCl.

The circular dichroism and absorption spectra were measured at room temperature using a JASCO J-20A spectropolarimeter and a Hitachi EPS-3T spectrophotometer, respectively.

Formation constants, K, and the difference in the molar extinction coefficients for right and left circularly polarized light in liter mol^{-1} cm^{-1}, $\Delta\varepsilon$, of inclusion complexes were determined by means of Benesi-Hildebrand method.[14]

On the other hand, the composition ratio of inclusion complexes was defined by Job's continuous variation method.[15]

The dipole strengths, D, of substituted benzenes were estimated from the absorption spectra as accurately as possible by use of the following approximate expression:

$$D = 0.92 \times 10^{-38}\sqrt{\pi}\cdot\varepsilon_{max}\cdot\frac{\Delta}{\lambda_{max}} \quad (1)$$

where ε_{max} is the maximum value for the molar extinction coefficient, λ_{max} is the wavelength at absorption maximum, and Δ is the half-band width at 1/e of maximum absorption. Similarly, the experimental rotational strengths, R, were obtained by the expression of Moscowitz:[16]

$$R = 0.696 \times 10^{-42}\sqrt{\pi}\cdot[\theta]_{max}\cdot\frac{\Delta}{\lambda_{max}} \quad (2)$$

where $[\theta]_{max}$ is the maximum value for the molar ellipticity and Δ is the half-band width at 1/e of maximum ellipticity.

Theoretical

The theoretical rotational strength of the transition from the ground state, 0, to the excited state, a, in benzene derivative, R_{i0a}, was calculated by the following expression developed by Kirkwood and Tinoco:

$$R_{i0a} = \pi\tilde{\nu}_{ai}\mu_{i0a}^2\sum_j\frac{\tilde{\nu}_{bj}^2(\alpha_{33}-\alpha_{11})_j(GF)_{ij}}{\tilde{\nu}_{bj}^2-\tilde{\nu}_{ai}^2} \quad (3)$$

$$(GF)_{ij} = \frac{1}{r_{ij}^3}\left[\hat{e}_i\cdot\hat{e}_j-\frac{3(\hat{e}_i\cdot\vec{r}_{ij})(\hat{e}_j\cdot\vec{r}_{ij})}{r_{ij}^2}\right]\hat{e}_i\times\hat{e}_j\cdot\vec{r}_{ij} \quad (4)$$

Table 1. The averaged wave number of the electronic transitions ($\tilde{\nu}_{bj}$) and polarizability (α) of the bonds in a glucose residue

Bond	$(\alpha_{33}-\alpha_{11})\times10^{24}$ / cm^3	$\tilde{\nu}_{bj}\times10^{-3}$ a) / cm^{-1}
C-C	0.71 b)	70.85 e,f)
C-OC	0.43 c)	67.53 g,h)
O-H	0.45 d)	80.78 g,h)

a) $\tilde{\nu}_{bj}$ is approximated by a wave number midway between the first absorption band and its ionization potential. b) C. G. LeFevre and J. W. LeFevre, *J. Chem. Soc.*, **1956**, 3549. c) R. J. W. LeFevre *et al.*, *J. Chem. Soc.*, **1963**, 479. d) C. G. LeFevre *et al.*, *J. Chem. Soc.*, **1960**, 123. e) L. W. Pickett *et al.*, *J. Chem. Soc.*, **73**, 4862 (1951). f) R. F. Pottie *et al.*, *J. Am. Chem. Soc.*, **83**, 3204 (1961). g) A. J. Harrison *et al.*, *J. Chem. Phys.*, **30**, 355 (1959). h) K. Watanabe, *J. Chem. Phys.*, **26**, 542 (1957).

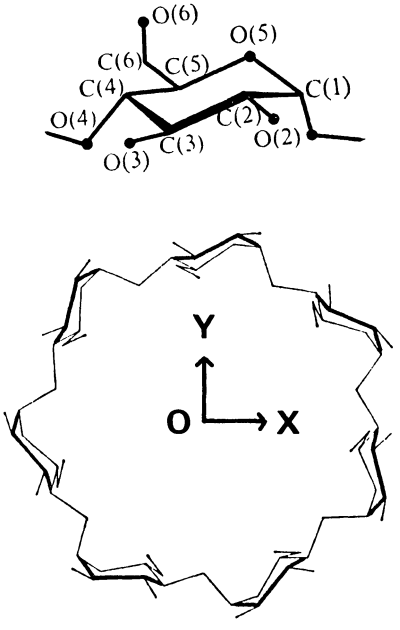

Fig. 1. A glucose residue and the assumed structure of β-CDx.

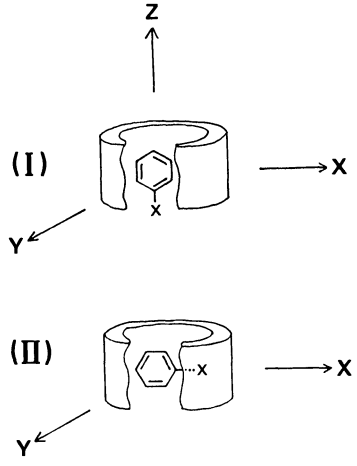

Fig. 2. The two models of the complex. (I); Axial inclusion, (II); equatorial inclusion.

Here $\hat{e}_j$ is the unit vector in the direction of the symmetry axis of the bond in β-CDx; $\hat{e}_i$ is the unit vector in the direction of the electric dipole moment, $\vec{\mu}_{i0a}$, of the transition from the ground state, 0, to the excited state, a, in the benzene derivative, and $\tilde{\nu}_{ai}$ is its wave number; α_{33} and α_{11} are bond polarizabilities at zero frequency parallel and perpendicular, respectively, to the symmetry axis of the bond in β-CDx; $\vec{r}_{ij}$ is the vector pointing from the center of benzene derivatives to each bond in β-CDx; and $\tilde{\nu}_{bj}$ is the averaged wave

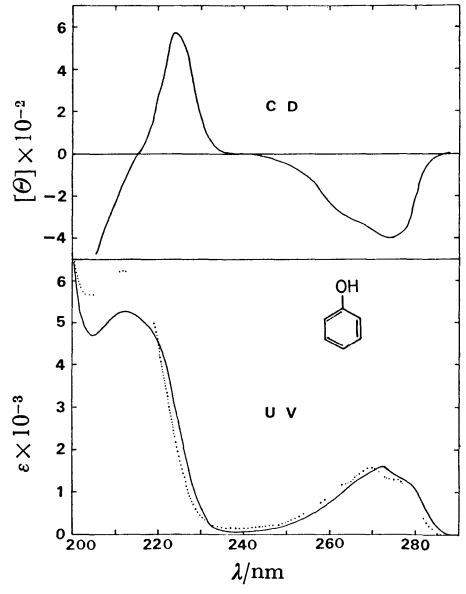

Fig. 3. CD (upper) and UV absorption (lower) spectra of β-CDx complex with phenol in aqueous solution at room temperature. Dotted line; in the absence of β-CDx, solid line; β-CDx (1.35×10^{-2} M)+phenol (2.09×10^{-4} M).

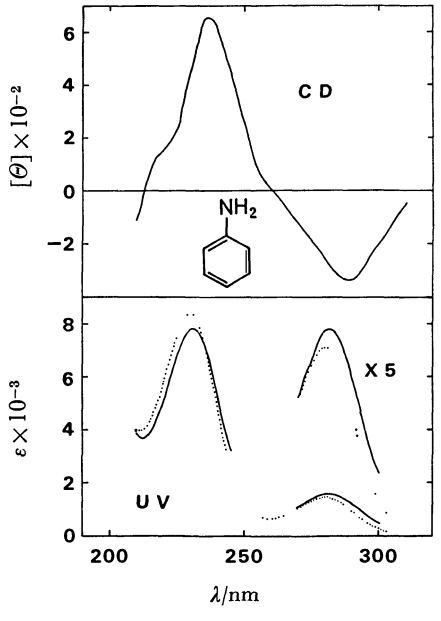

Fig. 4. CD (upper) and UV absorption (lower) spectra of β-CDx complex with aniline in aqueous solution at room temperature. Dotted line; in the absence of β-CDx, solid line; β-CDx (1.46×10^{-2} M)+aniline (1.56×10^{-4} M).

Table 2. Observed and calculated energy and dipole strength (D) of the electronic transitions of benzene derivatives

Benzene derivative	Experiment		Calculation		Assignment and Φ
	$\tilde{\nu}\times10^{-3}$ / cm^{-1}	D / Debye^2	$\tilde{\nu}\times10^{-3}$ / cm^{-1}	D / Debye^2	
Phenol[c]	37.0[a]	1.37	37.0	0.98	B_2
	47.4	6.26	46.3	4.5	A_1
			54.2	14.1	B_2
			54.8	19.0	A_1
Aniline[c]	35.6[a]	1.15	35.1	1.3	B_2
	43.5	8.00	43.2	9.6	A_1
			52.0	8.1	B_2
			53.8	15.7	A_1
Nitrobenzene[c]	—[a]	—	35.8	0.48	B_2
			39.7	10.7	A_1(CT)
			47.9	1.2	B_2
			50.2	1.9	B_2
			52.2	7.1	A_1
p-Nitrophenol	31.6[b]	20.23	26.7	15.3	A_1(CT)
			29.4	0.06	B_2(CT)
			39.9	0.13	B_2
			43.9	0.38	A_1(CT)
	44.1	8.15	44.7	3.8	B_2
			48.0	3.0	A_1
p-Nitroaniline[d]	26.3[a]	27.51	32.6	18.9	A_1(CT)
			34.7	0.24	B_2
	44.1	14.52	43.1	4.1	B_2(CT)
			48.7	0.15	A_1
Benzoic acid[c]	36.5[b]	0.70	37.7	0.23	A′(131.3°)
	43.4	10.27	44.1	11.8	A′(9.8°)
			50.8	1.1	A′(−32.4°)
			52.9	10.4	A′(82.8°)
			53.4	13.4	A′(5.5°)
p-Hydroxy-benzoic acid			36.5	0.21	A′(−12.6°)
	39.1[b]	19.34	39.4	19.6	A′(3.3°)
			45.7	2.0	A′(86.7°)
	48.5	14.44	48.6	9.4	A′(97.8°)

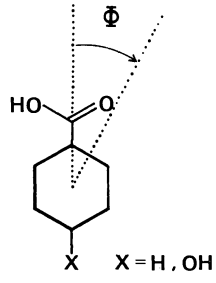

a) In aqueous solution. b) In 0.1 M aqueous HCl. c) A. Kaito, A. Tajiri, and M. Hatano, *J. Am. Chem. Soc.*, **98**, 384 (1976). d) A. Kaito, A. Tajiri, and M. Hatano, *Bull. Chem. Soc. Jpn.*, **49**, 2207 (1976).

number of the electronic transitions of the bond in β-CDx.

In this paper, $\tilde{\nu}_{bj}$ is approximated by a wavenumber midway between the first absorption band in the bond of β-CDx and its ionization potential. The values of $(\alpha_{33}-\alpha_{11})$ and $\tilde{\nu}_{bj}$ for each bond are listed in Table 1.

Table 2 shows the observed and calculated wave number, $\tilde{\nu}$, and dipole strength, D, of the electronic transitions of benzene derivatives, along with the assignment of each electronic transition.[17] The calculated values in this table were obtained by the Pariser-Parr-Pople (PPP) method. The experimental values in Table 2 were used for the calculation except in the case of nitrobenzene. The experimental value of nitrobenzene could not be estimated because of its insolubility in water.

As shown in Fig. 1, the origin of the coordinates was chosen in the center of a ring of β-CDx which was assumed to have a seven-fold symmetry axis, The

coordinates of a glucose residue were determined so as to fit the distance of O(4)–O(4′) with X-ray data (4.23 Å).[18] In the determination of the coordinates of β-CDx, hydroxyl groups of O(2)–H and O(3)–H were assumed to form hydrogen bonding with the hydroxyl group of the neighboring glucose unit. The effect of all the C–H bonds was neglected, since these bonds may have isotropic polarizability.

In the present calculation, we considered two models for the inclusion complexes, as shown in Fig. 2: *i.e.*, the axial inclusion (I) in which the long axis of benzene derivatives is parallel to the axis of β-CDx cavity (z-axis) and the equatorial inclusion (II) in which the short axis is parallel to the z-axis.

Finally, the calculation of the rotational strengths of these complexes were carried out by putting the electric dipole moment at the origin.

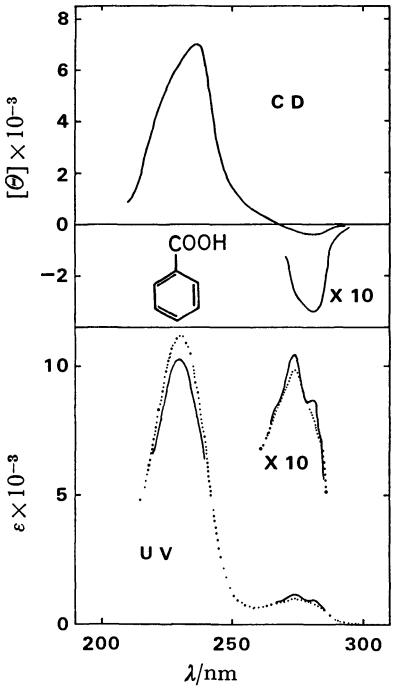

Fig. 5. CD (upper) and UV absorption (lower) spectra of β-CDx complex with benzoic acid in 0.1 M aqueous HCl at room temperature. Dotted line; in the absence of β-CDx, solid line; β-CDx (1.46×10^{-2} M) +benzoic acid (1.29×10^{-4} M).

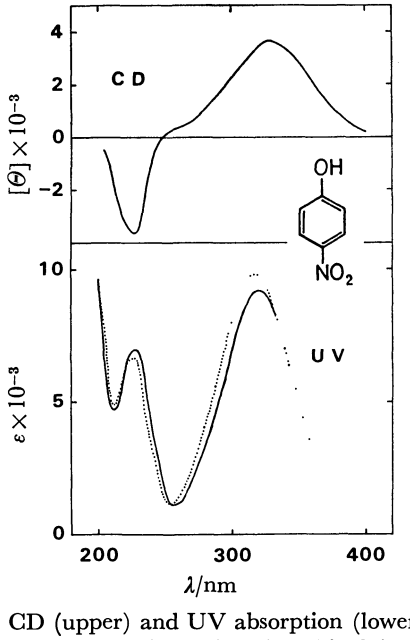

Fig. 6. CD (upper) and UV absorption (lower) spectra of β-CDx complex with *p*-nitrophenol in 0.1 M aqueous HCl at room temperature. Dotted line; in the absence of β-CDx, solid line; β-CDx (1.37×10^{-2} M) +*p*-nitrophenol (1.33×10^{-4} M).

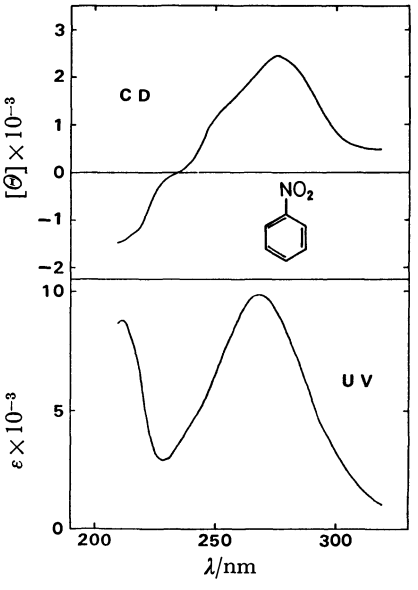

Fig. 7. CD (upper) and UV absorption (lower) spectra of β-CDx complex with nitrobenzene in aqueous solution at room temperature; β-CDx (1.63×10^{-2} M)+ nitrobenzene (1.20×10^{-4} M).

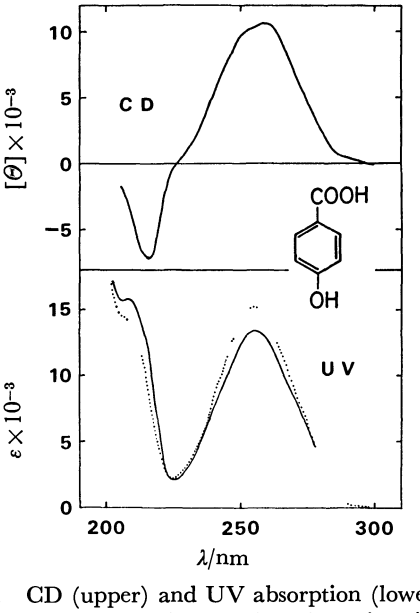

Fig. 8. CD (upper) and UV absorption (lower) spectra of β-CDx complex with *p*-hydroxybenzoic acid in 0.1 M aqueous HCl at room temperature. Dotted line; in the absence of β-CDx, solid line; β-CDx (1.21×10^{-2} M)+*p*-hydroxybenzoic acid (8.17×10^{-5} M).

Results and Discussion

Figures 3—10 show the CD (upper) and UV (lower) spectra of β-CDx complexes with various substituted benzenes. The β-CDx complex with phenol (in Fig. 3) showed positive and negative ICD bands at 224 and at 275 nm, respectively. These ICD bands were assigned to the $^1A_1 \leftarrow {}^1A_1$ and $^1B_2 \leftarrow {}^1A_1$ transitions, respectively, from the results calculated by use of the PPP method in Table 2. The β-CDx–aniline complex (Fig. 4) and the β-CDx–benzoic acid complex (Fig. 5) exhibited ICD bands similar to the bands of the β-CDx–phenol complex.

On the other hand, as shown in Fig. 6, the β-CDx complex with *p*-nitrophenol showed negative and positive ICD bands at 227 and at 329 nm. These bands were attributed to the $^1B_2 \leftarrow {}^1A_1$ and $^1A_1 \leftarrow {}^1A_1$ transitions, respectively. Each sign of the ICD spectra of β-CDx with nitrobenzene (Fig. 7) and *p*-hydroxybenzoic acid (Fig. 8) is the same as that of the β-CDx–*p*-nitrophenol complex.

Two negative ICD bands of β-CDx–*p*-nitroaniline complex observed at 230 and 296 nm were assigned to the $^1B_2 \leftarrow {}^1A_1$ transitions, and the lowest positive ICD band was attributed to the $^1A_1 \leftarrow {}^1A_1$ transition (Fig. 9).

As seen from each figure, the ICD bands of these inclusion complexes were observed at the absorption of benzene derivatives. In addition, from the assignment based on the SCF-MO calculation by the PPP method, it was found that the electronic transitions which are polarized along the long axis of substituted benzenes showed positive ICD, while the sign of the ICD of short-axis polarized transitions are negative.

In Table 3, formation constants, *K*, and UV and CD spectral data of β-CDx inclusion complexes are summarized.

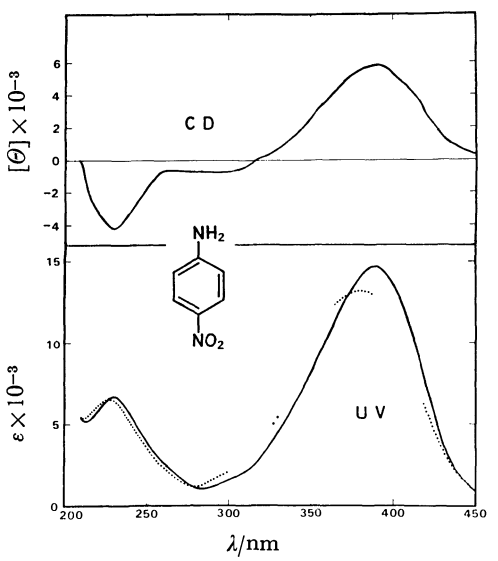

Fig. 9. CD (upper) and UV absorption (lower) spectra of β-CDx complex with *p*-nitroaniline in aqueous solution at room temperature. Dotted line; in the absence of β-CDx, solid line; β-CDx (1.47×10^{-2} M) + *p*-nitroaniline (8.41×10^{-5} M).

Figure 10 illustrates Job's continuous variation plots for β-CDx and benzoic acid systems. From this figure, it can be seen that the composition ratio of β-CDx to benzoic acid is 1:1.

The observed and calculated rotational strengths of β-CDx complexes with benzene derivatives are compared in Table 4. It is seen from Table 4 that the values calculated by assuming the axial inclusion (I) are in fairly good agreement with the experimental values. On the contrary, the signs of the calculated rotational strengths for equatorial inclusion (II) disagree with the experimental results. Therefore, the orientation of the guest molecule which is included in the β-CDx cavity can be regarded as the axial inclusion (I).

Finally, the effects of the translation and rotation of the guest molecules in the β-CDx cavity on the signs and magnitudes of the calculated rotational

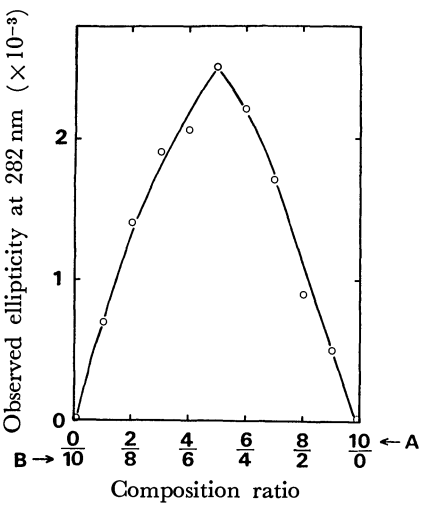

Fig. 10 Job's continuous variation plots for β-CDx (A)–benzoic acid (B) system in 0.1 M aqueous HCl. A; β-CDx (1.646×10^{-2} M), B; benzoic acid (1.646×10^{-2} M).

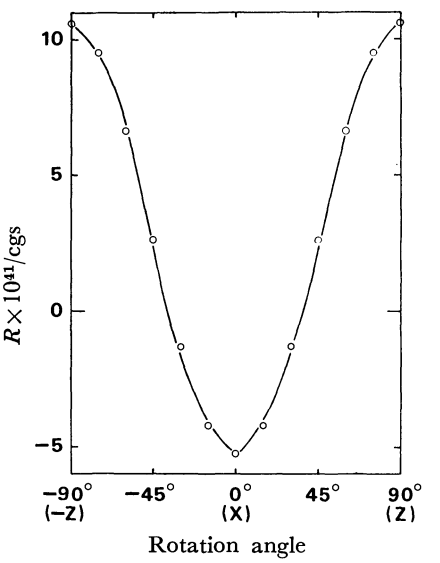

Fig. 11. Dependence of calculated rotational strength of the $^1B_2 \leftarrow {}^1A_1$ transition of phenol on the rotation of the electric transition moment in the x-z plane.

Table 3. The formation constants (K), UV absorption bands, and induced CD bands of β-cyclodextrin complexes with benzene derivatives in aqueous solution

Benzene derivative	K / M^{-1}	UV λ_{max} / nm	UV $\varepsilon \times 10^{-3}$ / $(M \cdot cm)^{-1}$	CD λ_{max} / nm	CD $\Delta\varepsilon \times 10^{-2}$ / $(M \cdot cm)^{-1}$
Phenol	99	212.5	5.28	224	0.17
		271.5	1.62	275	−0.18
Aniline	184	231.5	7.82	238	0.26
		282	1.55	288	−0.10
Nitrobenzene	—	268.5	9.82	275	0.75[b]
p-Nitrophenol[a]	244	229	7.02	227	−1.57
		321	9.24	329	1.42
p-Nitroaniline	312	230	6.71	230	−1.58
				296	−0.22
		389	14.66	390	2.24
Benzoic acid[a]	604	230.5	10.35	238	2.28
		274	1.05	282	−0.13
		281	0.87		
p-Hydroxybenzoic acid[a]	158	208.5	15.96	216	−2.41
		256	13.44	259	3.61

a) In 0.1 M aqueous HCl. b) $\Delta\varepsilon$ of β-CDx complex with nitrobenzene was estimated by assuming that all the molecules of nitrobenzene in the solution form complexes because of the insolubility of nitrobenzene itself in water.

Table 4. Comparison of the observed and calculated rotational strength (R) of β-cyclodextrin complexes with benzene derivatives

Benzene derivative	Assignment	λ_{max} / nm	$R \times 10^{40}$/cgs Experiment	$R \times 10^{40}$/cgs Calculation (I) Axial	$R \times 10^{40}$/cgs Calculation (II) Equatorial
Phenol	B_2	275	−0.34	−0.53	1.06
	A_1	224	0.16	7.92	−3.96
Aniline	B_2	288	−0.24	−0.42	0.83
	A_1	238	0.55	8.33	−4.16
Nitrobenzene	B_2			−0.17	0.34
	A_1	275	2.97	9.51	−4.75
	B_2			−0.13	0.25
	B_2		−(large)	−2.30	4.61
p-Nitrophenol	A_1	329	7.50	12.28	−6.14
	B_2	227	−3.83	−4.37	8.73
p-Nitroaniline	A_1	390	9.14	13.05	−6.52
	B_2	296	−0.52	−0.08	0.17
	B_2	230	−5.37	−7.78	15.55
	A_1			0.20	−0.10
Benzoic acid	A′	282	−0.15	0.08	0.18
	A′	238	5.69	10.18	−4.86
p-Hydroxy-benzoic acid	A′	259	11.17	16.34	−8.13
	A′	216	−3.08	−9.16	18.85

strengths were investigated. The sign of the calculated rotational strength was unchanged by the translations of the guest molecules along the x-, y-, and z-axes, while their magnitudes were affected by the translation and became maxima when the center of the guest molecule was placed on the point about 2 Å away from the origin along the z-axis. The rotation of the guest molecule in the x-y plane had no influence on the calculated rotational strengths. On the other hand, the calculated rotational strengths were very sensitive to the rotation of the guest molecules in the x-z plane, as demonstrated in Fig. 11.

In conclusion, when the direction of the electric dipole moment is known, we can estimate the orientation of the chromophore which is included in the cavity of β-CDx.

Finally, it is stated that the measurements of ICD spectra in combination with the theoretical calculation

of rotational strengths are quite useful for the investigations of the structure of these inclusion complexes.

References

1) F. Schardinger, *Zentr. Bakt. Parasitenk.*, II, **29**, 188 (1911).

2) F. Cramer, W. Saenger, and H-Ch. Spatz, *J. Am. Chem. Soc.*, **89**, 14 (1967); W. Saenger, K. Beyer, and P. C. Manor, *Acta Crystallogr., Sect. B*, **32**, 120 (1976).

3) F. Cramer and W. Kampe, *J. Am. Chem. Soc.*, **87**, 1175 (1965); D. W. Griffiths and M. L. Bender, *Adv. Catal.*, **23**, 209 (1973).

4) M. L. Bender and M. Komiyama, "Cyclodextrin Chemistry," Springer-Verlag, Berlin (1978), p. 23.

5) A. Hybl, R. E. Rundle, and D. E. Williams, *J. Am. Chem. Soc.*, **87**, 2779 (1965).

6) P. C. Manor and W. Saenger, *Nature*, **237**, 392 (1972); B. Hingertz and W. Saenger, *ibid.*, **255**, 396 (1975).

7) P. V. Demarco and A. L. Thakkar, *Chem. Commun.*, **1970**, 2; D. D. MacNicol, *Tetrahedron Lett.*, **38**, 3325 (1975).

8) K. Flohr, R. M. Paton, and E. T. Kaiser, *J. Am. Chem. Soc.*, **97**, 1209 (1975); J. Martinie, J. Michon, and A. Rassat, *ibid.*, **97**, 1818 (1975).

9) J. L. Hoffman and R. M. Bock, *Biochemistry*, **9**, 3542 (1970); K. Mochida, A. Kagita, Y. Matsui, and Y. Date, *Bull. Chem. Soc. Jpn.*, **46**, 3703 (1973).

10) D. A. Rees, *J. Chem. Soc., B*, **1970**, 877.

11) S. Takenaka, N. Matsuura, and N. Tokura, *Tetrahedron Lett.*, **26**, 2325 (1974).

12) K. Harata and H. Uedaira, *Bull. Chem. Soc. Jpn.*, **48**, 375 (1975).

13) I. Tinoco, Jr., *Adv. Chem. Phys.*, **4**, 113 (1962).

14) H. A. Benesi and J. H. Hildebrand, *J. Am. Chem. Soc.*, **71**, 2703 (1949).

15) P. Job, *Ann. Chim. Phys.*, **9**, 113 (1928).

16) "Optical Rotatory Dispersion," ed by C. Djerassi, McGraw-Hill Book Co. Inc., New York, N. Y. (1960).

17) A. Kaito, A. Tajiri, and M. Hatano, *J. Am. Chem. Soc.*, **98**, 384 (1976); A. Kaito, A. Tajiri, and M. Hatano, *Bull. Chem. Soc. Jpn.*, **49**, 2207 (1976).

18) B. Hingertz and W. Saenger, *J. Am. Chem. Soc.*, **98**, 3357 (1976).

Zeeman Absorption Spectra of 2,3-Dichloro-9,10-anthraquinone Crystals

Mizuka SANO,* Takatoshi NARISAWA, Kohji IZAWA, and Yasumasa J. I'HAYA

Department of Materials Science, The University of Electro-Communications, Chofu 182

(Received March 26, 1979)

Polarized $T \leftarrow S_0$ absorption spectra were measured for 2,3-dichloro-9,10-anthraquinone melt-grown single crystals in a magnetic field of 50 kOe. From the analysis of the Zeeman absorption patterns, the lowest triplet state of 2,3-dichloro-9,10-anthraquinone in the crystalline state has been assigned to $^3A_1(\pi\pi^*)$. The c-polarized first absorption peak at 21734.7 cm^{-1} has been interpreted as gaining intensity mainly from an x-polarized transition from the ground state to a $B_1(n\pi^*)$ perturbing singlet state, which is directly spin-orbit-coupled with the y spin-sublevel of the $^3A_1$ state. The a- and b-polarized first peaks, at 21733.9 and 21733.6 cm^{-1}, respectively, have been interpreted as gaining intensity through the configurational mixing of the $^3A_1(\pi\pi^*)$ state with a nearby $^3B_1(n\pi^*)$ state.

Recently, we have studied the triplet states of 9,10-anthraquinone (abbreviated to AQ) crystals by Zeeman absorption spectroscopy,[1] and assigned the origin peak of the lowest triplet state at 22154.0 cm^{-1} to $^3B_{1g}$ ($n\pi^*$). The phosphorescence spectrum of an AQ crystal was also indicative of an $n\pi^*$ emitting state, the strongest peak being located 1680 cm^{-1} from the origin peak of the phosphorescence. We have extended our study to 2,3-dichloro-9,10-anthraquinone (abbreviated to 2,3-DCAQ) in order to determine whether the compound, a substituted AQ, also possesses the lowest triplet state of $n\pi^*$ character.

We chose 2,3-DCAQ because it crystallizes in such a manner that its molecular x, y, and z axes are nearly parallel to the crystallographic c, b, and a axes, respectively.[2] This kind of molecular alignment in a crystal is favorable for determining the direction of the electronic transition moment. We will present an assignment of the triplet-state electronic configuration of 2,3-DCAQ crystals, based on experimental proof obtained by means of Zeeman spectroscopy.

Experimental

2,3-DCAQ was prepared by cyclocondensation of *o*-(3,4-dichlorobenzoyl)benzoic acid obtained by the Friedel-Crafts reaction between *o*-dichlorobenzene and phthalic anhydride.[3] Crude 2,3-DCAQ was purified by recrystallization twice from benzene, sublimation *in vacuo*, and then by zone-refining carried out for 150 passes, three successive refinings of 50 passes each. A single crystal was melt-grown in a Bridgman furnace. Crystal samples of suitable size, *ca.* 5×5 mm^2 in area and 2—5 mm in thickness, were cut from the crystal, and their faces identified by the X-ray diffraction method.

Absorption spectra were analyzed with an NLM-E2M spectrometer equipped with an Echelles grating in a Czerny-Turner mount. The reciprocal dispersion of the spectrometer was 0.055 nm mm^{-1} at 460 nm in the 12 th order of the grating. The incident light from an Osram 450 W regulated xenon-arc-lamp was chopped at 720 Hz, the light passing through the sample being detected by a combination of an HTV R376 photomultiplier tube and an NF LI-572 lock-in amplifier.

Two types of optical cryostats including superconducting magnets, an Oxford 55 and a Sinkukiko 60, were used for Zeeman spectroscopy. The incident light propagates along the magnetic field in the former and passes through the sample perpendicular to the magnetic field in the latter. The magnetic field could be controlled to any required value up to *ca.* 55 kOe†. Phosphoresence of a crystal immersed in pumped liquid helium was excited by 365 nm radiation filtered from an ORC 1 kW superhigh-pressure mercury arc through Toshiba UV-D1C and IRQ-80 filters.

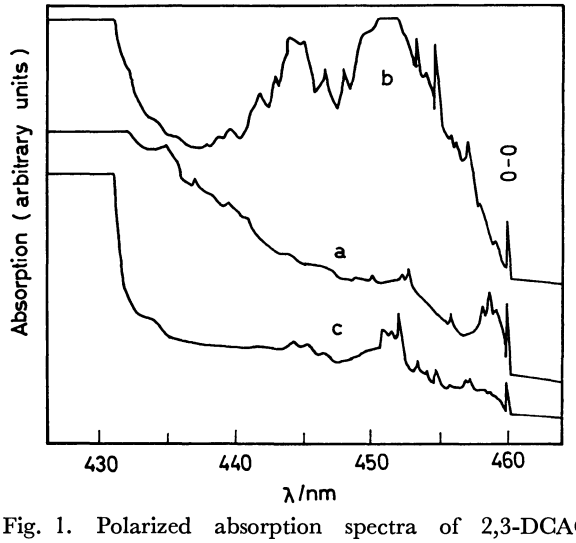

Fig. 1. Polarized absorption spectra of 2,3-DCAQ crystals at 1.7 K. (a) E//a, (b) E//b, (c) E//c.

Results and Discussion

Figure 1 shows the polarized absorption spectra of 2,3-DCAQ crystals at 1.7 K. The recordings of spectra (a) and (b) refer to a 3.8 mm thick crystal with light incident on the ab plane; the recording of (c) refers to a 2.3 mm crystal with light incident on the ac plane. The first peak, moderately intense and sharp (*ca.* 1.5 cm^{-1} in width) was observed at approximately 460 nm. Several successive intense peaks were observed in the spectral region 460—440 nm. All the peaks were found to split into sublines upon the application of a magnetic field, which indicates that they could be ascribed to the $T \leftarrow S_0$ transitions.

The high-resolution spectrometer revealed that the a- and the b-polarized first peaks were located at 21733.9 and 21733.6 cm^{-1} (A=0.87 for a 3.8 mm thick crystal), respectively, and the c-polarized first peak at 21734.7 cm^{-1}. The wave-number difference of *ca.* 1 cm^{-1} observed between the c-polarized peak and the a- or b-polarized peak is understood as an indication of the triplet factor group splitting.

† $Oe = 1000/4\pi$ A m^{-1}.

The phosphorescence spectrum observed for a 2,3-DCAQ crystal at 1.7 K shows sharp and intense peaks at 460.4 nm (21712 cm^{-1}) and 499.0 nm (20033 cm^{-1}) (Fig. 2), the former located *ca.* 22 cm^{-1} below the first peak in the absorption spectrum, and the latter 1679 cm^{-1} from the former peak. The wave-number difference corresponds to the C=O stretching mode frequency of 1676 cm^{-1} observed for AQ in the IR spectrum.[4] A moderately intense peak was observed at 543.5 nm (18393 cm^{-1}), which could be assigned to the overtone frequency of the C=O stretching mode.

The phosphorescence spectrum of 2,3-DCAQ in heptane (Shpol'skii matrix) at 1.7 K, on the other hand, shows a weak peak at 457.6 nm (21844 cm^{-1}) and a sharp, strongest peak at 495.9 nm (20157 cm^{-1}), located 1687 cm^{-1} from the weak peak (Fig. 3). Each peak is accompanied by two other peaks at intervals of 66 and 29 cm^{-1}. The peaks seem to arise from molecules in different sites in the matrix. A similar multiple structure has been reported for AQ in heptane.[5]

From the results, the first peaks in the absorption spectra are considered to arise from the origin for the lowest $T_1 \leftarrow S_0$ transition of 2,3-DCAQ.

The crystal structure of 2,3-DCAQ corresponds to a space group symmetry of D_2 with four molecules per unit cell. The molecules can be regarded as planar in the crystal, belonging to the C_{2v} point group.[2] The z axis is taken along the molecular twofold axis, and the z,y-plane as the plane of the molecule. Table 1 gives the squared direction cosines of the molecular axes with respect to the crystallographic axes. The x, y, and z molecular axes are nearly parallel to the c, b, and a crystallographic axes, respectively.

Figure 4 shows the Zeeman patterns for the first absorption peaks observed with polarized light, E, in the presence of a magnetic field, *H*, of 50 kOe, directed along the a, b, and c crystallographic axes of the 2,3-DCAQ single crystal. A single peak was found to split into sublines in the magnetic field. The transition to a triplet state from the ground state acquires the polarization of the transition to a perturbing singlet state, and assumes a spin-orbit interaction between the perturbing singlet state and the triplet state in the first-order approximation. The intensities of the individual Zeeman sublines depend on the polarization of the transition to the perturbing singlet state, p, and the route effective in the spin-orbit interaction, u.

The relative intensities of the Zeeman sublines for

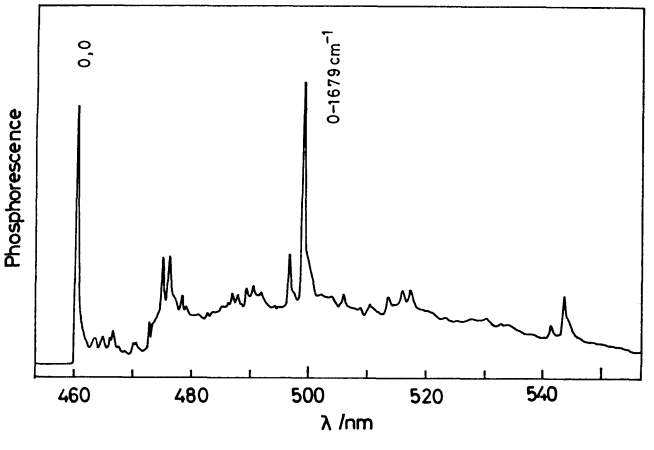

Fig. 2. Phosphorescence spectrum of a 2,3-DCAQ crystal at 1.7 K.

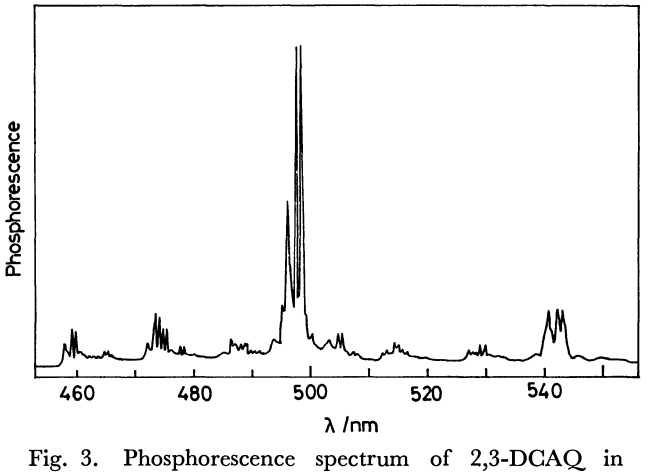

Fig. 3. Phosphorescence spectrum of 2,3-DCAQ in heptane at 1.7 K.

Table 1. Squared direction cosines for a 2,3-DCAO crystal

	x	y	z
a	0.082	0.001	0.917
b	0.075	0.923	0.002
c	0.843	0.077	0.080

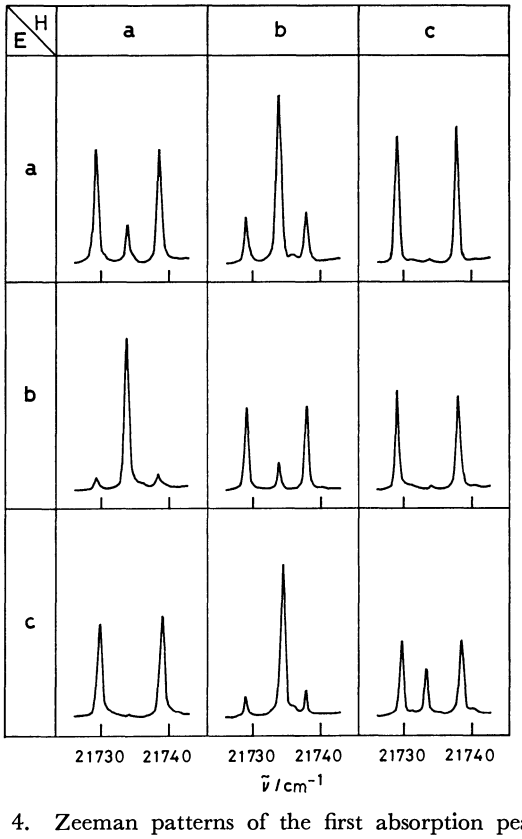

Fig. 4. Zeeman patterns of the first absorption peaks for 2,3-DCAQ crystals at 50 kOe.

Table 2. Relative intensities of the Zeeman sublines for a triplet factor group of D_2 symmetry

H	E	A		B_1		B_2		B_3	
		I_0	$I_{\pm1}$	I_0	$I_{\pm1}$	I_0	$I_{\pm1}$	I_0	$I_{\pm1}$
a	a	$2l_u^2l_p^2$					$n_u^2l_p^2$		$m_u^2l_p^2$
	b		$m_u^2m_p^2$		$n_u^2m_p^2$			$2l_u^2m_p^2$	
	c		$n_u^2n_p^2$		$m_u^2n_p^2$	$2l_u^2n_p^2$			
b	a		$l_u^2l_p^2$				$n_u^2l_p^2$	$2m_u^2l_p^2$	
	b	$2m_u^2m_p^2$			$n_u^2m_p^2$				$l_u^2m_p^2$
	c		$n_u^2n_p^2$	$2m_u^2n_p^2$			$l_u^2n_p^2$		
c	a		$l_u^2l_p^2$			$2n_u^2l_p^2$			$m_u^2l_p^2$
	b		$m_u^2m_p^2$	$2n_u^2m_p^2$					$l_u^2m_p^2$
	c	$2n_u^2n_p^2$			$m_u^2n_p^2$		$l_u^2n_p^2$		

Table 3. Intensity ratios, $I_0/I_{\pm1}$, calculated for x-, y-, and z-routes in the spin-orbit interaction for 2,3-DCAO

H	u		
	x	y	z
a	0.18	0.00	22.2
b	0.16	23.9	0.01
c	10.8	0.17	0.17

a triplet factor group of D_2 symmetry, obtained on the assumption that only one of the spin-orbit-coupling routes is effective,[6] are summarized in Table 2, where l_p, m_p, and n_p (also l_u, m_u, and n_u) represent the direction cosines of the axes a, b, and c with respect to the molecular axis p (also u), respectively, and I_0 and $I_{\pm1}$ represent the relative intensity of the central Zeeman line and that of the wing lines, respectively.

In the absence of a magnetic field, the absorption intensities observed with the a-, b-, and c-polarized lights, I_a, I_b, and I_c, are given as $2l_p^2$, $2m_p^2$, and $2n_p^2$, respectively, which are seen to be independent of the effective route in the spin-orbit interaction. The intensity ratios, $I_a : I_b : I_c$, are calculated to be 0.1 : 0.09 : 1 for an x-polarized transition in the molecular framework, showing that such a transition provides its intensity predominantly to the c-polarized absorption. The ratios are similarly calculated to be 0 : 1 : 0.08 for a y-polarized transition, and 1 : 0 : 0.09 for a z-polarized transition. However, the absorptions for the 2,3-DCAQ crystal were observed along all three crystallographic axes, and the ratios, $I_0 : I_b : I_c$, were found to be 1 : 0.6 : 0.4. This indicates that not only a z-polarized transition but also y- and x-polarized transitions are included in the absorption.

Table 2 gives the intensity ratio, $I_0/I_{\pm1}$, for each direction of a magnetic field. The ratios are equal to $2l_u^2/(1-l_u^2)$, $2m_u^2/(1-m_u^2)$, and $2n_u^2/(1-n_u^2)$ for a magnetic field directed along the a-, b-, and c-axes, respectively, which are seen to be independent of the polarization of the transition in the molecule. Ratios calculated for x-, y-, and z-routes in the spin-orbit interaction are given in Table 3.

As shown in Fig. 4, the Zeeman pattern such that the central line is stronger than the wing lines is observed only in a b-directed magnetic field for the c-polarized peak, in an a-directed field for the b-polarized peak, and in a b-directed field for the a-polarized peak. This indicates that each peak gains intensity through only one route in the spin-orbit interaction. The Zeeman pattern with a strong central line appears in a b-directed magnetic field for the y route, and in an a-directed field for the z route (Table 3).

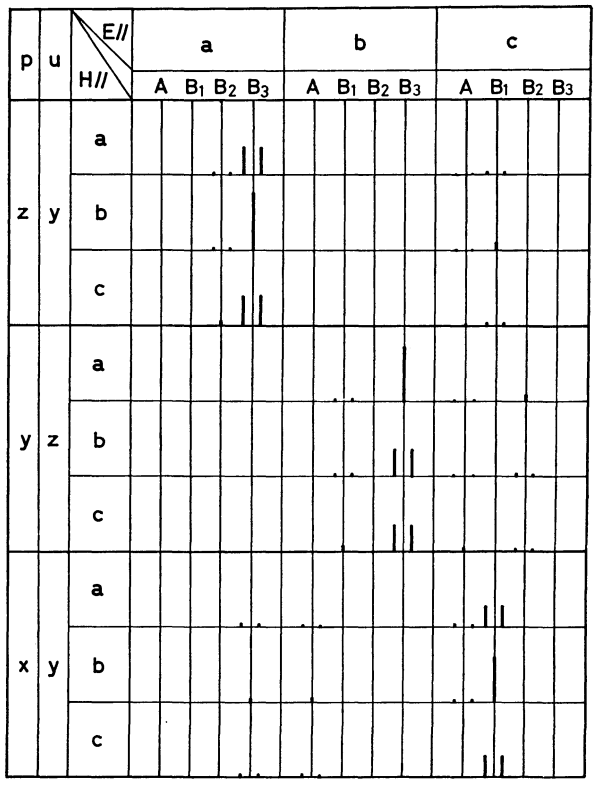

Fig. 5. Calculated relative intensities of the Zeeman sublines for a 2,3-DCAQ crystal.

The c-polarized peak, which arises mainly from an x-polarized transition in the molecular framework, shows the Zeeman pattern with a strong central line in a b-directed magnetic field. Thus an x-polarized transition to a perturbing singlet state is considered to provide intensity through the y route to the transition to the triplet state of A_1 species. Similarly, the Zeeman patterns for the b- and a-polarized peaks show that y- and z-polarized transitions also provide intensity to the absorption to the lowest triplet state through

the z and y routes, respectively.

The intensities of the Zeeman sublines, I_0 and $I_{\pm 1}$, for each triplet factor group state of a 2,3-DCAQ crystal are calculated from Tables 1 and 2 for these three combinations of polarization, p, and spin-orbit-coupling route, u. Figure 5 shows the relative values of the intensities in thick bars. It is seen that the a- and b-polarized absorptions arise mainly from the transition to the B_3 factor group state, and the c-polarized absorption mainly from the transition to the B_1 state. This seems to explain the wave-number difference of *ca.* 1 cm^{-1} observed between the c- and the a- or b-polarized first absorption peaks, *i.e.*, the triplet factor group splitting.

A simple molecular-orbital description of 2,3-DCAQ leads to the prediction that the low-energy $\pi\pi^*$ state is of species A_1 or B_2, and the $n\pi^*$ state is of species A_2 or B_1. In general, the transition to an $n\pi^*$ triplet state is much stronger, 10^2—10^3 times, than that to a $\pi\pi^*$ triplet state. Thus if the $\pi\pi^*$ triplet state is mixed more than 10% with the triplet state of $n\pi^*$ character, the general appearance of the spectrum and the polarization characteristics are expected to resemble those of pure $^3n\pi^*$ state.[7]

The absorption to the lowest triplet state of the 2,3-DCAQ crystal was found to have a mixed character of the $^3\pi\pi^*$ and $^3n\pi^*$ states, as shown by the direction of its polarization. It is therefore concluded that the lowest triplet state belongs to $^3A_1(\pi\pi^*)$, gaining $n\pi^*$ character from a nearby-located $n\pi^*$ triplet state. The location of the $n\pi^*$ state could not be determined precisely, but a broad and intense b-polarized absorption arising mainly from the y-polarized transition in the molecular framework was observed at approximately 452 nm, though the maximum absorption was off-scale. The lowest $n\pi^*$ triplet state may be located in this spectral region, *ca.* 400 cm^{-1} above the lowest $\pi\pi^*$ triplet state.

For the 0—0 transition to the $^3A_1(\pi\pi^*)$ state, the possible mechanisms[8] for gaining the major part of the intensity are (i) direct spin-orbit coupling between the $^3A_1$ state and an $n\pi^*$ perturbing singlet state, (ii) configurational mixing between the $^3A_1$ state and a nearby $n\pi^*$ triplet state,[7] and (iii) mixing of the $^3A_1$ state with a nearby $n\pi^*$ triplet state through spin-orbit interaction.[9] The observed c-polarized $T_1 \leftarrow S_0$ absorption can be explained in terms of mechanism (i): The transition to the $^3A_1(\pi\pi^*)$ state gains its intensity from an x-polarized transition to a $B_1(n\pi^*)$ perturbing singlet state through the y route in the spin orbit interaction.

We must further explain the contribution of the y route associated with the z polarization and that of the z route associated with the y polarization to the $T_1 \leftarrow S_0$ absorption. Mechanism (ii) can explain these contributions: The y and z spin-sublevels of the $^3A_1(\pi\pi^*)$ state are mixed electrostatically with the y and z spin-sublevels of a nearby $^3B_1(n\pi^*)$ state, respectively, which are in turn spin-orbit-coupled to $A_1(\pi\pi^*)$ and $B_2(\pi\pi^*)$ perturbing singlet states, respectively. The transitions from the ground state to these singlet states are expected to be z- and y-polarized, respectively. This is what we have observed for the 2,3-DCAQ crystal. Mechanism (iii) can not explain the observed z-polarized absorption from a group-theoretical point of view.

The $^3A_1(\pi\pi^*)$ state can be mixed with the other $n\pi^*$ triplet state, *i.e.*, $^3A_2(n\pi^*)$ by mechanisms (ii) and (iii). However, this scheme can not explain the observed polarization characteristics.

For a 2,3-DCAQ crystal, the absorption to the lowest triplet state of $A_1(\pi\pi^*)$ species can be explained by a mechanism in which direct spin-orbit coupling with a perturbing $^1B_1(n\pi^*)$ state and electrostatic mixing with a nearby $^3B_1(n\pi^*)$ state operate for the $^3A_1(\pi\pi^*)$ state simultaneously.

The phosphorescence spectrum of 2,3-DCAQ in heptane showed a weak origin peak and a strongest peak corresponding to the C=O stretching mode. The same features were observed in the phosphorescence spectra of 1-chloro-AQ and 2-chloro-AQ in heptane at 1.7 K. The spectra are indicative of an $n\pi^*$ emitting state. If the emitting state is regarded as the T_1 state for 2,3-DCAQ in heptane, a comparison between the heptane-solution spectrum and the crystal spectrum shows that a low-lying $^3\pi\pi^*$ state is lowered in energy below the $^3n\pi^*$ state by changing the environment from heptane to 2,3-DCAQ. The phosphorescence spectra of aromatic carbonyl compounds, where the $n\pi^*$ and $\pi\pi^*$ triplet states are very close to each other, have been reported to be strikingly dependent on the nature of the environment.[10–13]

References

1) T. Narisawa, M. Sano, and Y. J. I'Haya, *Chem. Lett.*, **1975**, 1289.
2) S. G. Il'in, L. A. Chetkina, and G. A. Gol'der, *Kristallografya*, **20**, 1051 (1975).
3) M. Tanaka and N. Tanaka, *Bull. Chem. Soc. Jpn.*, **3**, 286 (1928).
4) C. Pecile and B. Lunelli, *J. Chem. Phys.*, **46**, 2109 (1967).
5) O. S. Khalil and L. Goodman, *J. Phys. Chem.*, **80**, 2170 (1976).
6) R. M. Hochstrasser and T. S. Lin, *J. Chem. Phys.*, **49**, 4929 (1968).
7) T. H. Cheng and N. Hirota, *Mol. Phys.*, **27**, 281 (1974).
8) Since the absorption peak under consideration is of pure electronic origin, we exclude the vibronic-coupling mechanism from this discussion: E. C. Lim and J. M. H. Yu, *J. Chem. Phys.*, **47**, 3270 (1967).
9) H. Hayashi and S. Nagakura, *Mol. Phys.*, **24**, 801 (1972).
10) Y. H. Li and E. C. Lim, *Chem. Phys. Lett.*, **7**, 15 (1970).
11) W. A. Case and D. R. Kearns, *J. Chem. Phys.*, **52**, 2175 (1970).
12) L. Goodman and M. Koyanagi, *Mol. Photochem.*, **4**, 369 (1972).
13) A. M. Nishimura and D. S. Tinti, *Chem. Phys. Lett.*, **13**, 278 (1972).

The Liquid-phase Oxidation of Hydrocarbons with Molecular Oxygen. II.[1] A Highly Selective Formation of α-Tetralone by the Metal-catalyzed Oxidation of Tetralin in the Presence of *N,N*-Dialkylamides

Fujio MIZUKAMI, Yutaka HORIGUCHI, Masaki TAJIMA, and Juichi IMAMURA*

National Chemical Laboratory for Industry, Honmachi, Shibuya-ku, Tokyo 151

(Received February 20, 1979)

The metal-ion catalyzed oxidation of tetralin was carried out in different solvents in which metal salts tend to be soluble. It was found that, for the production of α-tetralone, a chromium salt is the best catalyst among the first-transition-metal salts employed, while *N,N*-dialkylamides are the best solvents or the best additives. For example, in the tris(acetylacetonato)chromium(III)-catalyzed oxidation of tetralin in the presence of *N,N*-dimethylacetamide, α-tetralone was obtained in a 93.0% yield at a 27.2% tetralin conversion. The decomposition of α-tetralyl hydroperoxide (THP) with different first-transition-metal catalysts was also carried out in *N,N*-dimethylformamide in order to elucidate the formation mechanism for α-tetralone in the oxidation of tetralin in the presence of *N,N*-dialkylamides. It was concluded that the product distribution in the oxidation mainly depends on the decomposition mechanism of THP, and that *N,N*-dialkylamides seem to promote the reaction of the α-tetralylperoxyl radical with low valent metal ions, $ROO\cdot + M^{n+} \longrightarrow \alpha\text{-tetralone} + OH^- + M^{(n+1)+}$.

The dehydrogenation of α-tetralone is a commercial process for the production of α-naphthol.[2–4] α-Tetralone can be easily obtained by the liquid-phase autoxidation of tetralin, but in this oxidation α-tetralol is also produced in a large amount. α-Tetralol tends to undergo dehydration rather than dehydrogenation[5–7] and is unsuitable as a raw material for the production of α-naphthol. What is worse, the boiling point of α-tetralol is very close to that of α-tetralone. For these reasons, many investigations[6–12] have been undertaken in search of a method for the highly selective formation of α-tetralone in the autoxidation of tetralin. However, no satisfactory process for the production of α-tetralone has so far been found. In order to seek a better method of producing α-tetralone, we first studied the oxidation of tetralin in both the presence and absence of additives in acetic acid, using first-transition-metal salts as a catalyst. Chromium salts showed the highest ratio of α-tetralone/α-tetralol (ON/OL), while cobalt salts showed the highest activity in this tetralin oxidation. On the basis of this result, we further studied the effects of solvents and additives on the oxidation of tetralin; we thus found a satisfactory process for the production of α-tetralone by the liquid-phase oxidation of tetralin with molecular oxygen. This new process will now be reported in the present paper.

Experimental

Materials. The tetralin, metal salts, additives, and solvents employed were all of a reagent grade and were used without further purification. The α-tetralyl hydroperoxide (THP) was synthesized according to the procedure of Knight and Swern.[13] This peroxide was 97% pure, as confirmed by iodometric titration.

Oxidation of Tetralin. The oxidation of tetralin was performed in closed systems at higher pressures (a SUS-316 autoclave equipped with a magnetic stirrer, a thermocouple, and a pressure controller) and at atmospheric pressures (a 200 cm³ three-necked flask equipped with a thermometer, a reflux condenser, an oxygen inlet, and a Teflon stirring bar).

A mixture of tetralin and a solvent or an additive containing a catalyst was placed in a reaction vessel and warmed to the desired temperature. Oxygen was then introduced into the vessel. However, in the oxidation under atmospheric pressure, the air in the vessel was quickly expelled by 600 cm³ of oxgen in order to increase oxygen content in the reaction mixture when the temperature of the mixture had reached the desired temperature.

The oxidation was terminated by stopping the oxygen feed and by quickly cooling the vessel in an ice-cold bath.

Decomposition of THP. A four-necked flask (200 cm³, round-bottomed) equipped with a thermometer, a reflux condenser, a dropping funnel, and a nitrogen inlet was filled with nitrogen gas. Into the flask, were placed a Teflon stirring bar and a 50 cm³ solution of *N,N*-dimethylformamide (DMF) containing a catalyst. A stream of nitrogen was gently bubbled through the solution. The solution was then stirred and warmed to the desired temperature. To the vigorously stirred solution, was added a 25 cm³ solution of DMF containing 2.5 g of THP.

Analysis. The peroxide concentration was determined by the usual method.[14] The α-tetralone, α-tetralol, and tetralin in the reaction mixture were identified and their amounts were determined using gas chromatography with a Shimadzu GC-4CPT chromatograph (2 m × 3 mm column packed with 10% Carbowax 4000 on Chromosorb AW; programming, 5 °C/min from 120 to 173 °C, He 40 cm³/min). *o*-Bromoanisole was used as the internal standard. Before GLC analysis, the remaining peroxide was reduced with an excess of triphenylphosphine.[15] The "net α-tetralol" is the difference between the total amount of α-tetralol after reduction and the amount of peroxide before reduction.

Results

The best conditions for producing α-tetralone in the liquid-phase oxidation of tetralin were examined using cobalt and chromium salts as catalysts.

The Selection of Solvents. The $Co(C_6H_5COO)_2$-catalyzed oxidation of tetralin under an atmospheric pressure at 51 °C was carried out in different solvents in which metal salts tend to be soluble. The results are shown in Table 1. Tetralin was almost not oxidized at all in either dimethyl sulfoxide or tetrahydrothiophene 1,1-dioxide for 3 h. Although DMF brought a very high yield of peroxide, DMF gave by far the highest ON/OL ratio and the lowest α-tetralol yield among the solvents listed in Table 1.

The Determination of the Catalyst Concentration and Reac-

Table 1. Product distribution for the cobalt-catalyze oxidation of tetralin in different solvents under atmospheric pressure

Run No.	Solvent	Tetralin conversion %	Yield[a]/mol% α-Tetralone	α-Tetralol	Peroxide	Total	ON/OL	Reaction time min
1	Acetic acid	19.4	27.0	37.2	14.5	78.7	0.73	126
2	Propionic acid	25.6	32.4	37.1	16.8	86.3	0.87	207
3	Acetonitrile	27.3	39.7	12.3	44.7	96.7	3.2	164
4	Propionitrile	25.3	32.4	9.1	41.6	83.1	3.6	237
5	Ethyl acetate	20.7	28.7	12.7	48.9	90.3	2.3	287
6	Acetic anhydride	31.8	33.7	28.3	0.3	62.3	1.2	245
7	Dioxane	22.3	24.0	2.8	63.1	89.9	8.6	250
8	DMF	21.9	32.7	1.4	56.1	90.2	23	175
9	Dimethyl sulfoxide	≃0.0	—	—	—	—	—	180
10	Tetrahydrothiophene 1,1-dioxide	≃0.0	—	—	—	—	—	180

Reaction conditions: $[Co(C_6H_5COO)_2]=2.8\times10^{-3}$ M, $[tetralin]_{initial}=3.88$ M, the reaction temperature was 51±1 °C. a) Based on the amount of tetralin consumed.

Table 2. Product distribution for the tris(acetylacetonato)chromium(III)-catalyzed oxidation of tetralin in DMF

Run No.	Catalyst [Cr(acac)$_3$] M	Initial [tetralin] M	Reaction temperature °C	Tetralin conversion %	Yield[a]/mol% α-Tetralone	α-Tetralol	Peoxide	Total	Reaction time min
11	0.0266	3.85	140—218	33.9	54.2	16.6	3.0	73.8	2.5
12	0.0266	3.85	120—128	34.5	77.1	9.4	3.0	89.5	30
13	0.0266	3.85	100±1	32.2	80.5	7.8	2.0	90.3	150
14	0.0060	3.90	90±1	23.5	79.5	5.7	5.4	90.6	140
15	0.0238	7.25	130±1	43.8	70.9	8.5	8.3	87.7	30
16	0.0010	7.25	100±2	38.4	65.4	−1.2	26.1	90.3	90
17	0.0030	6.12	72±1	18.5	90.7	2.1	4.7	97.5	450
18	0.0053	5.76	100±1	39.6	83.5	3.5	3.7	90.7	150
19	0.0106	5.76	100±2	39.2	83.9	4.8	3.4	92.1	100
20	0.0265	5.74	100±2	34.7	86.5	7.6	3.5	97.6	66

Reaction conditions: the O_2 pressure was 20 kg/cm^2 G. a) Based on the amount of tetralin consumed.

Table 3. Product distribution for the oxidation of tetralin catalyzed by different chromium salts in the presence of DMF

Run No.	Catalyst	Reaction temperature °C	Tetralin conversition %	Yield[a]/mol% α-Tetralone	α-Tetralol	Peroxide	Total	Reaction time min
21	$Cr(acac)_3$	110±1	30.1	79.1	6.5	5.3	90.9	51
22	$Cr(OAc)_3$	109±2	28.9	80.8	5.8	4.9	91.5	70
23	$Cr(NO_3)\cdot9H_2O$	110±2	30.1	81.3	4.9	4.3	90.5	120
24	$CrCl_3\cdot6H_2O$	100—120	29.3	76.5	7.2	5.9	89.6	22
25	$CrF_3\cdot3H_2O$	110±1	29.8	74.1	3.3	13.6	91.0	130
26	$Cr(OH)_3$	110±1	29.3	80.4	4.6	5.3	90.3	105
27	$Cr_2(SO_4)_3\cdot xH_2O$	110±1	31.3	76.2	2.7	9.7	88.6	115
28	3% Cr-naphthenate	110±2	29.3	75.7	9.7	4.8	90.2	48
29	Cr_2O_3	110±1	29.9	61.5	2.4	26.9	90.8	320

Reaction conditions: $[Cr]=6.0\times10^{-3}$ M, $[tetralin]_{initial}=4.90$ M; the O_2 pressure was 20 kg/cm^2 G. a) Based on the amount of tetralin consumed.

Table 4. Product distribution for the bis(acetylacetonato)cobalt(II)-catalyzed oxidation of tetralin in the presence of additives in DMF

Run No.	Additive	Reaction temperature °C	Tetralin conversion %	Yield[a]/mol% α-Tetralone	α-Tetralol	Peroxide	Total	Reaction time min
30	—	72.5±1	23.1	73.5	14.6	5.6	93.7	60
31	KSCN	72.5±1	32.1	72.4	16.2	3.2	91.8	100
32	$NaNO_2$	71—75	21.1	76.7	13.3	5.0	95.0	120
33	LiBr	72.5±1	23.3	72.6	15.0	3.8	91.4	60

Reaction conditions; $[Co(acac)_2]=[additive]=1.06\times10^{-2}$ M; the O_2 pressure was 20 kg/cm² G, $[tetralin]_{initial}=3.85$ M. a) Based on the amount of tetralin consumed.

Table 5. Product distribution for the oxidation of tetralin catalyzed by different transition-metal salts in DMF

Run No.	Catalyst Metal salts	Concn 10^3 M	Initial [tetralin] M	React. temp °C	Tetralin conv. %	Yield[a]/mol% α-Tetralone	α-Tetralol	Peroxide	Total	ON/OL	Reaction time min	Maximum rate of O_2 absorption 10^3 mol min^{-1}
34	$Cr(acac)_2$	6.0	3.90	90±1	23.5	79.5	5.7	5.4	90.6	14	143	2.5
35	$CrCl_3\cdot6H_2O$	6.0	3.92	90±2	18.5	71.4	9.9	6.8	88.1	7.2	240	1.0
36	$Cr(OAc)_3$	6.0	3.91	90±1	28.1	78.6	4.6	5.9	89.1	17	111	3.3
37	$Mn(OAc)_2\cdot4H_2O$	6.0	3.92	90±2	18.2	56.0	21.7	3.4	81.1	2.6	240	2.3
38	$FeCl_3$	6.0	3.93	90±1	26.2	63.5	7.3	15.6	86.4	8.7	223	1.2
39	$Co(OAc)_2\cdot4H_2O$	6.0	3.92	90±2	21.6	68.5	18.0	≃0.0	86.5	3.8	240[b]	14
40	$Ni(OAc)_2\cdot4H_2O$	6.0	3.89	90±1	24.6	53.4	≃0.0	37.8	91.2	—	240[b]	4.5
41	$Cu(OAc)_2\cdot H_2O$	6.0	3.90	90±2	7.3	70.3	19.0	0.9	90.2	3.7	240[b]	4.3
42	$Cr(acac)_3$	6.0	6.10	90±1	26.0	84.9	5.1	3.5	93.5	17	105	4.0
43	$Ni(OAc)_2\cdot4H_2O$	6.0	6.13	90±1	25.0	72.4	3.0	18.4	93.8	24	180	5.3
44	$Co(OAc)_2\cdot4H_2O$	6.0	3.91	65±1	28.5	72.6	14.7	6.9	94.2	4.9	73	3.8
45	$Co(OAc)_2\cdot4H_2O$	3.0	3.90	90±2	27.4	74.4	18.8	≃0.0	93.2	4.0	40	13
46	$Co(OAc)_2\cdot4H_2O$	3.0	3.91	65±1	28.0	53.8	2.8	37.2	93.8	19	80	2.8

Reaction conditions: the O_2 pressure was 20 kg/cm² G. a) Based on the amount of tetralin consumed. b) The O_2 absorption rate fell suddenly about 20 min after the introduction of oxygen.

tion Temperature. Table 2 shows the effects of the catalyst concentration and the reaction temperature on the product distribution in the $Cr(acac)_3$-catalyzed oxidation of tetralin in DMF. The α-tetralone yield decreased with an increase in the reaction temperature (Runs 11—13). At reaction temperatures above 120 °C, it was also difficult to carry out the oxidation of tetralin at an approximately constant temperature. Accordingly, the optimum reaction temperatures for producing α-tetralone in the $Cr(acac)_3$-catalyzed oxidation of tetralin in the presence of DMF seem to be below 120 °C.

It was seen from Runs 18—20 that, at catalyst concentrations above 5×10^{-3} M**, the product distribution in the oxidation of tetralin is almost not at all dependent on the catalyst concentration, and all the α-tetralone yields obtained in these three runs are above 83%. A high α-tetralone yield was also obtained in the oxidation at the 3×10^{-3} M $Cr(acac)_3$ concentration, although the oxidation rate was very slow (Run 17). However, in the oxidation at the 1×10^{-3} M $Cr(acac)_3$ concentration, the peroxide yield was relatively high and the α-tetralone yield was relatively low (compare Run 15 with Run 16). Therefore, the best region of catalyst concentrations for the selective formation of α-tetralone appears to be 10^{-3} M$<$[Cr]$\leqq10^{-2}$ M in the $Cr(acac)_3$-catalyzed oxidation of tetralin in the presence of DMF.

The Effects of Ligands and Additives. Table 3 shows the oxidation of tetralin with nine kinds of chromium catalysts in DMF. Chromium(III) oxide, which is insoluble in a mixed solution of DMF and tetralin, showed a low α-tetralone yield and a very high peroxide yield in comparison with the other Cr catalysts. However, all the other Cr catalysts which are more or less soluble in the reaction mixture gave high α-tetralone yields (above 74%) and showed similar product distributions, although their oxidation activities were considerably different from each other. Such a phenomenon was also observed for the $Co(acac)_2$-catalyzed oxidation of tetralin in DMF in both the presence and absence of an additive, as is shown in Table 4. The four product distributions were very similar to each other (Runs 30—33). It was thus found that, for the tetralin oxidation in the presence of the appropriate amount of DMF, the counter anions and additives employed have much influence on the oxidation rate, but almost none on the product distribution. This fact seems to indicate that the counter anions and additives do not alter the oxidation mech-

** 1 M=1 mol dm^{-3}.

Table 6. Product distribution for the tris(acetylacetonato)chromium(III)-catalyzed oxidation of tetralin in the presence of *N,N*-dialkylamides

Run No.	Additive	Tetralin conversion / %	Yield[a] /mol%				Reaction time / min	Maximum rate of O_2 absorption / 10^3 mol min^{-1}
			α-Tetralone	α-Tetralol	Peroxide	Total		
47	DMF	28.1	84.7	2.0	4.0	91.6	285	1.4
48	DMA	29.5	85.5	5.8	2.8	94.1	88	15
49	DMP	30.0	88.4	1.2	3.2	92.8	198	2.8
50	DEF	28.1	82.1	5.2	5.2	92.5	240	2.8
51	DEA	29.9	89.0	1.4	3.9	94.3	183	5.3

Reaction conditions: $[Cr(acac)_3]=2.0\times10^{-3}$ M; $[tetralin]_{initial}=6.12$ M; the reaction temperature was 80±1 °C; the O_2 pressure was 20 kg/cm² G. DMA: $(CH_3)_2NCOCH_3$, DMP: $(CH_3)_2NCOC_2H_5$, DEF: $(C_2H_5)_2NCOH$, DEA: $(C_2H_5)_2NCOCH_3$. a) Based on the amount of tetralin consumed.

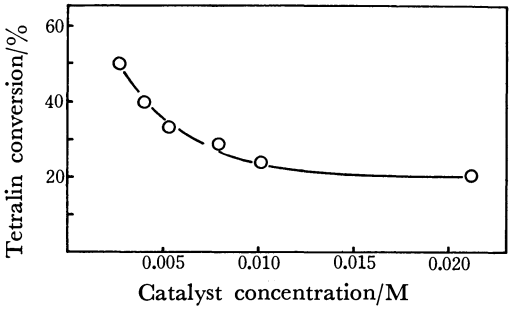

Fig. 1. Relationship between the catalyst concentration and the tetralin conversion in the $Co(acac)_2$-catalyzed oxidation of tetralin in DMF at 72±2 °C. Reaction conditions: $[tetralin]_{initial}=3.85$ M, the O_2 pressure was 20 kg/cm² G.

anism of tetralin, but the solubilities of metal (Co or Cr) catalysts and the ligand-replacement rates of active metal complexes in the reaction solution.

The Effects of Metal Ions. The effects of different first-transition-metal ions on the oxidation of tetralin in DMF are shown in Table 5. Chromium catalysts showed the highest α-tetralone yields among the catalysts employed and showed relatively high ON/OL ratios. Iron and Ni catalysts also showed high ON/OL ratios, but they also gave quite high peroxide yields. On the other hand, Mn, Co, and Cu catalysts were more favorable for producing α-tetralol than Cr, Ni, and Fe. Therefore, chromium salts are the best catalysts for producing α-tetralone in the oxidation of tetralin.

As can be seen from Runs 39—41 in Table 5, Co showed the highest activity, and Ni and Cu showed quite high activities, but these activities fell suddenly twenty minutes after the introduction of oxygen. This phenomenon was examined in detail for the oxidation of tetralin with Co catalysts, and it was observed that the tetralin conversion decreases with an increase in the Co concentration or the reaction temperature (Fig. 1 or Runs 39 and 44 in Table 5). This is thought to be due to the action of autoxidation inhibitors generated in consecutive oxidations, because the primary oxidation products of tetralin are easily oxidized with an increase in the Co concentration and in the reaction temperature. Actually, Martan *et al.*[16] have isolated α-naphthol and 1,4-dihydroxynaphthalene, both inhibitors, as higher products in the oxidation of tetralin

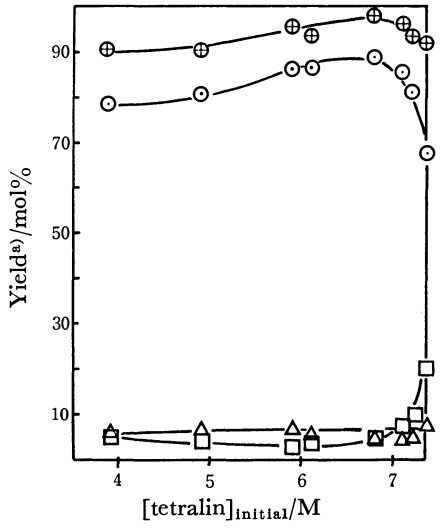

Fig. 2. The $Cr(acac)_3$-catalyzed oxidation of tetralin in DMF at 90±2 °C. Reaction conditions: $[Cr(acac)_3]=6.0\times10^{-3}$ M, the O_2 pressure was 20 kg/cm²G, the tetralin conversion was 26.0±2.5%. ⊙: Tetralone, △: α-tetralol, □: peroxide, ⊕: total. a) Based on the amount of tetralin consumed.

catalyzed by $Co(OAc)_2$.

The Effects of the Initial Tetralin Concentration. Figure 2 shows the dependence of the product distributions on the initial substrate concentration in the oxidation of tetralin catalyzed by $Cr(acac)_3$ in the presence of DMF at 90 °C. The right end of the abscissa in Fig. 2 indicates a neat tetralin solution without DMF. At initial tetralin concentrations above 7 M, the α-tetralone yield decreased suddenly and the peroxide yield increased rapidly with an increase in the tetralin concentration, although the α-tetralol yield was almost independent of the initial substrate concentration. At initial tetralin concentrations below 6.8 M, the α-tetralone yield decreased slowly upon a decrease in the tetralin concentration. From these facts and the solubility of $Cr(acac)_3$, the optimum region of initial tetralin concentration for producing α-tetralone seems to be 5.5—6.5 M in the oxidation of tetralin catalyzed by $Cr(acac)_3$ in the presence of DMF.

The Oxidation of Tetralin in the Presence of Different Amides and Oxygen Pressure. Table 6 shows the oxidation of tetralin catalyzed by $Cr(acac)_3$ in the presence of five kinds of *N,N*-dialkylamides at 80 °C,

Table 7. Effect of oxygen pressure on the tris(acetylacetonato)chromium(III)-catalyzed oxidation of tetralin in the presence of DMA

Run No.	O_2 pressure / kg cm^{-2} G^{-1}	Catalyst concentration / 10^3 M	Reaction temperature / °C	Tetralin conversion / %	Yield[a]/mol% α-Tetralone	α-Tetlalol	Peroxide	Total	Reaction time / min	Maximum rate of O_2 absorption / 10^3 mol min^{-1}
52	20	3.0	80±3	28.9	84.2	6.2	2.8	93.2	87	16
53	10	3.0	80±1	41.7	88.3	≃0.0	4.5	92.8	260	4.7
54	2.5	3.0	80±1	27.2	93.0	0.5	1.6	95.1	270	2.0
55	20	2.0	80±1	29.5	85.5	5.8	2.8	94.1	88	15
56	6	2.0	80±2	31.2	89.3	1.7	3.3	94.3	147	5.8

Reaction conditions: $[\text{tetralin}]_{\text{initial}}=6.12$ M. a) Based on the amount of tetrain consumed.

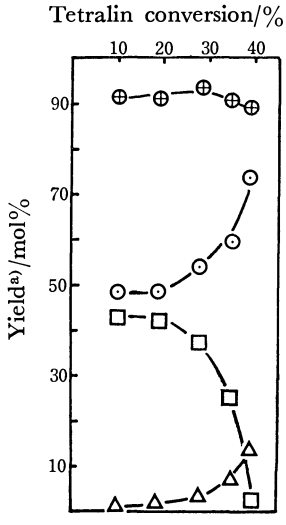

Fig. 3. The $Co(OAc)_2 \cdot 4H_2O$-catalyzed oxidation of tetralin in DMF at 65±2 °C. Reaction conditions: $[Co(OAc)_2 \cdot 4H_2O]=3.0\times10^{-3}$ M, $[\text{tetralin}]_{\text{initial}}=$ 3.91 M, the O_2 pressure was 20 kg/cm² G. ⊙: α-Tetralone, △: α-tetralol, □: peroxide, ⊕: total. a) Based on the amount of tetralin consumed.

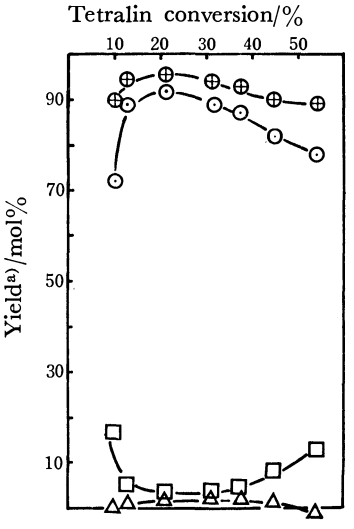

Fig. 4. The $Cr(acac)_3$-catalyzed oxidation of tetralin in the presence of DMA at 80±2 °C. Reaction conditions: $[Cr(acac)_3]=2.0\times10^{-3}$ M, $[\text{tetralin}]_{\text{initial}}=$ 6.12 M, the O_2 pressure was 6 kg/cm² G. ⊙: α-Tetralone, △: α-tetralol, □: peroxide, ⊕: total. a) Based on the amount of tetralin consumed.

All these amides brought about high α-tetralone yields and product distributions very similar to one another; that is, we could observe almost no substituent effect of these amides on the product distribution, although these amides had much influence on the oxidation rate of tetralin. Table 7 shows the effect of the oxygen pressure on the oxidation of tetralin in the presence of *N,N*-dimethylacetamide (DMA), which gave the highest oxidation rate among the amides employed. The oxidation rate of tetralin fell with a decrease in the oxygen pressure. This indicates that, at oxygen pressures below 20 kg/cm² G, the oxidation rate depends on the concentration of molecular oxygen in a mixed solution of DMA and tetralin. Accordingly, the differences between the oxygen absorption rates listed on Table 6 appear to be attributable mainly to the differences between the solubilities of oxygen in mixed solutions of different amides and tetralin. For the tetralin oxidation in the presence of *N,N*-dialkylamides (Runs 47—56), the recoveries of these amides ranged from 93 to 98%. Tetralin was also oxidized with molecular oxygen in the presence of acetamide at 95 °C under atmospheric pressure ($[\text{tetralin}]_{\text{initial}}=$ 6.12 M). This oxidation stopped at about a 10% tetralin conversion (the α-tetralone, α-tetralol, and peroxide yields are 47.3, 2.0 and 7.0% respectively), and the recovery of acetamide in this run was very low. This acetamide reactivity seems to come from the property[17–19] that primary and secondary amides can easily liberate their amino protons.

The Time-course of the Product Distributions. The product formation for different tetralin conversions was examined in the oxidation of tetralin catalyzed by $Co(OAc)_2 \cdot 4H_2O$ in DMF at 65 °C (Fig. 3). The yields of both α-tetralone and α-tetralol increased with an increase in the tetralin conversion; on the contrary, the peroxide yield decreased as the tetralin conversion increased. The total amount of the increment in the α-tetralone yield and that in the α-tetralol yield was nearly equal to the decrement in the peroxide yield. The increment in the α-tetralone yield was appreciably more than that in the α-tetralol yield. Accordingly, THP seems to be preferentially converted into α-tetralone, although THP decomposes to both α-tetralone and α-tetralol.

The product formation for various tetralin conversions was also examined in the $Cr(acac)_3$-catalyzed oxidation of tetralin in the presence of DMA at 80 °C

Table 8. Product distribution for the metal-catalyzed decomposition of THP in DMF in a nitrogen atomosphere

Run No.	Metal salt	THP conversion %	Yield[a]/mol% α-Tetralone	Yield[a]/mol% α-Tetralol	ON/OL	Reaction time min
57	$Cr(OAc)_3$	87.9	85.3	6.2	14	210
58	$Mn(OAc)_2 \cdot 4H_2O$	97.6	54.7	27.0	2.0	50
59	$FeCl_3$	99.2	79.2	15.0	5.3	15
60	$Co(acac)_2$	96.7	69.9	21.7	3.2	20
61	$Ni(OAc)_2 \cdot 4H_2O$	96.6	93.0	$\simeq$0.0	—	15
62	$Cu(OAc)_2 \cdot H_2O$	98.5	81.6	9.5	8.6	15

Reaction conditions: [metal salt] $=6.0\times10^{-3}$ M; $[THP]_{initial}=0.20$ M; the reaction temperature was 71—75 °C.
a) Based on the amount of THP converted.

(Fig. 4). For tetralin conversions below 25%, the percentage of the decrease in the peroxide yield was nearly equal to that of the increase in the α-tetralone yield, and α-tetralol was only produced in a very low yield below 2%. This seems to show that the THP generated by the tetralin oxidation is converted almost exclusively into α-tetralone. On the other hand, for tetralin conversions above 25%, the α-tetralone yield decreased and the peroxide yield increased as the tetralin conversion was increased. The α-tetralol yield also had a minus sign for tetralin conversions above 50%. These facts suggest that the α-tetralone produced in the oxidation is further oxidized into a peroxide different from THP during the prolonged reaction time. Accordingly, in order to obtain α-tetralone in a high purity and a high yield, the $Cr(acac)_3$-catalyzed oxidation of tetralin in the presence of DMA should be stopped at 20—30% tetralin conversions.

The Decomposition of THP. The decomposition of THP with six kinds of first-transition-metal catalysts was carried out in DMF 71—75 °C in a nitrogen atmosphere. The ON/OL ratios decreased in this order: Ni>Cr>Cu>Fe>Co>Mn, as is shown in Table 8. This order is fully consistent with that of the decreasing reduction potentials[20-22] for these low-valent metal ions. In the oxidation of tetralin shown in Table 5, the ON/OL ratios decreased in this order: Ni>Cr>Fe>Co$\simeq$Cu>Mn. This order is inconsistent with that in the THP decomposition. However, except for the Cu catalyst, which gave too low a tetralin conversion in the oxidation (Run 41 in Table 5), the decreasing order of ON/OL ratios in the oxidation is in fair agreement with that in the THP decomposition. In addition, the product distributions in the decomposition of THP with six kinds of transition-metal catalysts are similar to those in the corresponding oxidation of tetralin. Accordingly, the product distribution in the tetralin oxidation is thought to depend mainly on the decomposition mechanism of the THP produced in the oxidation.

Discussion

The liquid-phase oxidation of tetralin has been widely studied, and the following elementary reactions (Eqs. 1—7) have been proposed in previous reports.[1,16,23-30] Equations 1—3 are elementary reactions involving metal ions. From Eqs. 1—3, two kinds of regeneration mechanisms of metal ions can be derived; one (the A-mechanism) is composed of Reactions 1 and 2, and the other (the B-mechanism), of Reactions 1 and 3.[31] The A-mechanism is the so-called Haber-Weiss mechanism[32-35] and is much more common as a regeneration mechanism of metal ions than the B-mechanism.

If metal ions catalyze both the tetralin oxidation and the THP decomposition by only the A-mechanism, α-tetralol will be produced in a higher yield than α-tetralone, as can be seen from Reactions 4—7, which follow Reactions 1 and 2. For most runs in the present work, however, the α-tetralol yields were lower than the α-tetralone yields. Although α-tetralol resulting from the tetralin oxidation can be converted into α-tetralone according to Reaction 8, Reaction 8 con-

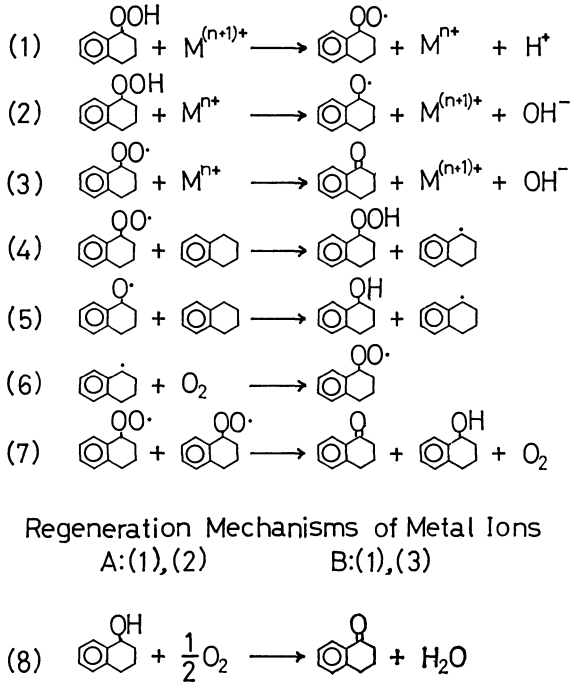

tributes almost nothing to the formation of α-tetralone in the oxidation of tetralin in the presence of *N,N*-dialkylamides, as can be seen from Figs. 3 and 4. Also, α-tetralone was always the main product in the decomposition of THP with six kinds of first-transition-metal catalysts in DMF under a nitrogen atmosphere. This fact cannot be explained by only the A-mechanism. On the other hand, if the B-mechanism contributes

only to the regeneration of metal ions, the main products in both the tetralin oxidation and the THP decomposition will be α-tetralone. However, for the oxidation of tetralin in aliphatic acids, the α-tetralol yields were higher than the α-tetralone yields, as is shown in Table 1. Accordingly, it seems reasonable to assume that the regeneration of metal ions actually proceeds by both mechanisms, A and B, with A or B predominating according to the reaction conditions.

As is shown in Tables 1 and 6, DMF brought about relatively a very high ON/OL ratio and in the presence of *N,N*-dialkylamides α-tetralone was produced in a very high yield. These facts suggest that, in the presence of *N,N*-dialkylamides, the B-mechanism rather than the A-mechanism performs the regeneration of metal ions. The predominance of the B-mechanism is further strengthened by the simultaneous use of highly reductive metal catalysts and *N,N*-dialkylamides, as can be seen from Tables 5 and 8. However, the actions of *N,N*-dialkylamides for the selective formation of α-tetralone cannot be interpreted explicitly at present. If *N,N*-dialkylamides promote Reaction 1 and suppress Reaction 2, Reaction 3 will be remarkably accelerated by highly reductive metal ions such as Cr^{2+}, and such metal catalysts will give high ON/OL ratios and high α-tetralone yields. It has been reported that *N,N*-dialkylamides have high hydrogen-bonding abilities[36] and DMF forms electron-donor-acceptor complexes[37] with halo hydrocarbons with acceptor properties. It was also observed in the present work that, when THP is dissolved in a solution of *N,N*-dialkylamides, the solution turns pale pink. Accordingly, the association between THP and *N,N*-dialkylamides may promote Reaction 1 and may inhibit Reaction 2. Furthermore, the absorption spectra of the DMF complexes of Cr(III)[38] show that DMF has a ligand-field strength comparable to that of the SCN^- ligand, which occupies a higher position in the spectrochemical series[39,40] than the H_2O, RCO_2^-, ROOH ligands. Compared with ligands such as aliphatic acids, anhydrides, ethers and water, therefore, *N,N*-dialkylamides stabilize t_{2g} orbitals and unstabilize e_g orbitals in octahedral transition-metal complexes. This suggests that Cr^{2+} ($(t_{2g})^3(e_g)^1$ electron configuration) and Co^{2+} ($(t_{2g})^5(e_g)^2$) ions are labilized by *N,N*-dialkylamides ligands, while on the contrary, Cr^{3+} ($(t_{2g})^3(e_g)^0$) and Co^{3+} ($(t_{2g})^6(e_g)^0$) are stabilized by them; *i.e.*, the reducing power of both Cr^{2+} and Co^{2+} ions is increased by the coordination of *N,N*-dialkylamides. Accordingly, it may be concluded that, in the presence of *N,N*-dialkylamides, Reaction 3 proceeds relatively smoothly and that α-tetralone is produced in a very high yield.

References

1) F. Mizukami and J. Imamura, *Bull. Chem. Soc. Jpn.*, **51**, 1404 (1978).
2) U. S. Patent 2 503 641 (1950).
3) U. S. Patent 3 378 591 (1968).
4) British Patent 1 426 542 (1976).
5) J. Orlowski, L. Cieslakowa, and Z. Krol, *Przem. Chem.*, **47**, 266 (1968); *Chem. Abstr.*, **70**, 3611f (1969).
6) Japan Kokai 50—112 347 (1975).
7) Japan Kokai 52—10 248 (1977).
8) U. S. Patent 3 310 586 (1967).
9) U. S. Patent 3 404 185 (1968).
10) U. S. Patent 3 422 147 (1969).
11) Japan Kokai 50—58 044 (1975).
12) Japan Kokai 51—48 643 (1976).
13) H. B. Knight and D. Swern, *Org. Synth.*, **34**, 90 (1954).
14) W. O. Lundberg, "Autoxidation and Antioxidants," Interscience Publication, New York (1961), Vol. 1, p. 375.
15) L. Horner and W. Jurgeleit, *Justus Liebigs Ann. Chem.*, **591**, 138 (1955).
16) M. Martan, J. Manassen, and D. Vofsi, *Tetrahedron*, **26**, 3815 (1970).
17) J. Zabicky, "The Chemistry of Amides," Interscience Publication, London (1970).
18) R. J. Balahura, *Can. J. Chem.*, **52**, 1762 (1974).
19) M. Nonoyama and K. Nonoyama, *Kagaku No Ryoiki*, **31**, 136 (1977).
20) W. M. Latimer, "The Oxidation States of the Elements and Their Potentials in Aqueous Solutions," 2nd ed, Prentice-Hall, New York (1952).
21) C. F. Bell and K. A. K. Lott, "Modern Approach to Inorganic Chemistry," Butterworth and Co., Ltd., London (1963).
22) "Kagaku-Binran," ed by The Chemical Society of Japan, Maruzen, Tokyo (1966), Kiso-hen II, p. 1061.
23) A. Robertson and W. A. Waters, *J. Chem. Soc.*, **1948**, 1574.
24) A. E. Woodward and R. B. Mesrobian, *J. Am. Chem. Soc.*, **75**, 6189 (1953).
25) Y. Kamiya, B. Beaton, A. Lafortune, and K. U. Ingold, *Can. J. Chem.*, **41**, 2020 (1963).
26) Y. Kamiya and K. U. Ingold, *Can. J. Chem.*, **42**, 2424 (1964).
27) A. Mukherjee and W. F. Graydon, *J. Phys. Chem.*, **71**, 4232 (1967).
28) A. S. Hay and H. S. Blanchard, *Can. J. Chem.*, **43**, 1306 (1965).
29) A. I. Kamneva, V. I. Zakharova, L. N. Piterskii, V. A. Selenznev, and A. V. Artemov, *Neftekhimiya*, **15**, 403 (1975).
30) Y. Kamiya and K. U. Ingold, *Can. J. Chem.*, **42**, 1027 (1964).
31) D. A. S. Ravens, *Trans. Faraday Soc.*, **55**, 1768 (1959).
32) F. Haber and J. Weiss, *Proc. R. Soc. London, Ser. A*, **147**, 332 (1934).
33) J. Weiss, *Trans. Faraday Soc.*, **31**, 1547 (1935).
34) J. Weiss, *J. Phys. Chem.*, **41**, 1107 (1937).
35) A. Robertson and W. A. Waters, *Trans. Faraday Soc.*, **42**, 201 (1946).
36) J. D. Crowley, G. S. Teague, Jr., and J. W. Lowe, Jr., *J. Paint Tech.*, **38**, 269 (1966), **39**, 19 (1967).
37) V. M. Luk'yanets, R. G. Makitra, and Ya. M. Tsikanchuk, *Zh. Obshch. Khim.*, **47**, 506 (1977); *J. General Chem., USSR*, **47**, Part 1, 463 (1977).
38) S. T. D. Lo and T. W. Swaddle, *Inorg. Chem.*, **15**, 1881 (1976).
39) F. Basolo and R. G. Pearson, "Mechanism of Inorganic Reactions," John Wiley & Sons, New York (1967), p. 67.
40) F. A. Cotton and G. Wilkinson, "Advanced Inorganic Chemistry," A Comprehensive Text, 2nd ed, John wiley & Sons, New York (1966).

Studies on Inorganic Precipitate Membranes: Membrane Potential and Bi-ionic Potential

M. Nasim Beg,* Fasih A. Siddiqi,† Surendra P. Singh,
(Miss) Veena Gupta, and Poorna Prakash
Physical Chemistry Division, Department of Chemistry, Aligarh Muslim University, Aligarh, U.P., India
(Received August 19, 1978)

Electrical potentials arising across barium(II) phosphate, mercury(II) iodide and cobalt(II) chromate membranes using various 1:1 electrolytes are reported. Thermodynamically effective fixed charge density, which is an important parameter governing the membrane phenomena, has been evaluated by the theory of Toyoshima and Nozaki. Using the values of effective fixed charge density determined, the theory of bi-ionic potentials developed by Toyoshima and Nozaki based on the principles of the irreversible thermodynamics has been examined. Theoretical predictions were borne out quite satisfactorily by our experimental results.

In recent years we have studied a large number of parchment supported inorganic precipitate and polymeric composite membranes.[1-6] Various transport parameters such as ion migration, self diffusion coefficient, hydrodynamic permeability *etc.* occuring across the membranes have been evaluated in the light of the theory described by Speigler[7] and by the use of the generalized Stefan-Maxwell equations. The theory of absolute reaction rates,[8] Eisenman-Sherry theory of membrane selectivity[9] and the theory of irreversible thermodynamics developed by Kedem and Katchalsky,[10] Smit and Staverman,[11] Bearman and Krikwood,[12] and Kobatake and coworkers[13-16] have been applied to evaluate apparent fixed charge density as well as to examine the various aspects of membranes.

In this communication a series of membrane potentials and bi-ionic potentials observed across parchment supported barium(II) phosphate, mercury(II) iodide and cobalt(II) chromate membranes using various 1:1 electrolytes are presented. Thermodynamically effective fixed charge density, which is an important parameter governing the membrane phenomena has been evaluated by the recently developed theory of Toyoshima and Nozaki based on the principles of irreversible thermodynamics.[17] An effort has been made to examine the validity of the theory of Toyoshima and Nozaki[17] for bi-ionic potential.

Experimental

Preparation of Membranes. Parchment supported barium(II) phosphate, mercury(II) iodide and cobalt(II) chromate membranes were prepared by the method of interaction suggested by Siddiqi, Beg, and coworkers.[1-6] To precipitate barium(II) phosphate in the interstices of parchment paper, a 0.2 M solution of barium(II) chloride was placed inside a glass tube, to one end of which was tied the parchment paper (supplied by M/s- Baired and Tatlock London Ltd.). The tube was suspended for 72 h in a 0.2 M solution of potassium dihydrogenphosphate. The two solutions were interchanged later and kept for another 72 h. The membrane was taken out and washed with deionized water to remove free electrolyte. Similar procedure was adopted for the preparation of mercury(II) iodide and cobalt(II) chromate membranes by taking 0.2 M solutions of mercury(II) chloride and potassium iodide, cobalt(II) chloride and potassium chromate, respectively.

Measurements of Membrane Potential and Bi-ionic Potential. Membrane potential E_m were obtained by constructing a cell of the following type taking different concentrations C'_N and C''_N of an electrolyte such that $C''_N/C'_N=10$

SCE	Solution C'_N	Membrane	Solution C''_N	SCE

and the bi-ionic potentials (BIP) were determined by setting up another cell of the type

SCE	Solution AP	Membrane	Solution BP	SCE

and keeping the same concentration of both the electrolytes AP and BP. The various salt solution (chlorides of Li^+, Na^+, K^+) were prepared from analytical grade reagents and deionized water. All measurements were carried out using a water thermostate maintained at 25±0.1 °C. The solutions on either sides of the membrane were vigorously stirred by a pair of magnetic stirrer.

Results and Discussion

When two electrolyte solutions of different concentrations are separated by a membrane, the mobile species penetrate the membrane and various transport phenomena are induced in the system. The fixed charge theory of Teorell-Meyer-Seivers (TMS) for charged membranes is a pertinent starting point for the investigation of the actual mechanisms of the ionic or molecular processes which occur in the membrane phase. Based on the fixed charge concept various mathematically rigorous equations for membrane potential and bi-ionic potential have in recent years been derived.[17-22] Most recently Toyoshima and Nozaki[17] have derived equations for membrane potential and bi-ionic potential using the principles of non-equilibrium thermodynamics and by utilizing appropriate assumptions for the mobilities and activity coefficients of small ions in the membrane phase.[17] The effect of ionic interaction, mass flow and osmotic effect were neglected. For a negatively charged membrane separating two 1:1 electrolytes (common co-ions) of the same concentration, these authors derived following expression for bi-ionic potential, E_{BIP},

$$E_{BIP} = (F/RT)[2\ln K_A/K_B + \ln(JV_A + 1/JV_B + 1)]. \quad (1)$$

Knowing the values of parameters K_A, K_B, V_A, V_B, and the flux J, the values of theoretical E_{BIP} can be

† Present address: Department of Biophysics, Michigan State University, East Lansing, Michigan 48824, (U.S.A.).

Table 1. The values of membrane potentials, E_m (mV) observed across parchment supported barium(II) phosphate, mercury(II) iodide and cobalt(II) chromate membranes at 25±0.1 °C

Membrane concentration (M)	Barium(II) phosphate			Mercury(II) iodide			Cobalt(II) chromate		
	KCl	NaCl	LiCl	KCl	NaCl	LiCl	KCl	NaCl	LiCl
1/0.1	1.51	−4.39	−4.98	6.68	−1.35	−13.40	−5.30	−7.90	−14.32
0.5/0.05	2.90	−3.89	−4.01	10.03	2.24	−8.27	−3.20	−5.50	−11.50
0.1/0.01	9.82	2.10	1.96	31.11	23.59	14.77	4.50	−1.23	−5.50
0.05/0.005	16.34	7.95	2.50	39.58	34.35	25.22	8.80	2.63	−1.00
0.01/0.001	33.78	22.05	20.15	49.86	46.32	40.63	21.20	16.83	13.80

Dilute solution side taken as positive.

Table 2. The values of the membrane parameters V_N and $(\overline{X}/K_N)$ derived from the Toyoshima and Nozaki theory for parchment supported membrane

Membrane parameters	Mercury(II) iodide		Barium(II) phosphate		Cobalt(II) chromate	
	V_N	$\overline{X}/K_N$	V_N	$\overline{X}/K_N$	V_N	$\overline{X}/K_N$
KCl	2.05	0.438	2.00	0.092	1.75	0.012
NaCl	1.73	0.474	1.88	0.066	1.75	0.013
LiCl	1.53	0.490	1.86	0.026	1.55	0.010

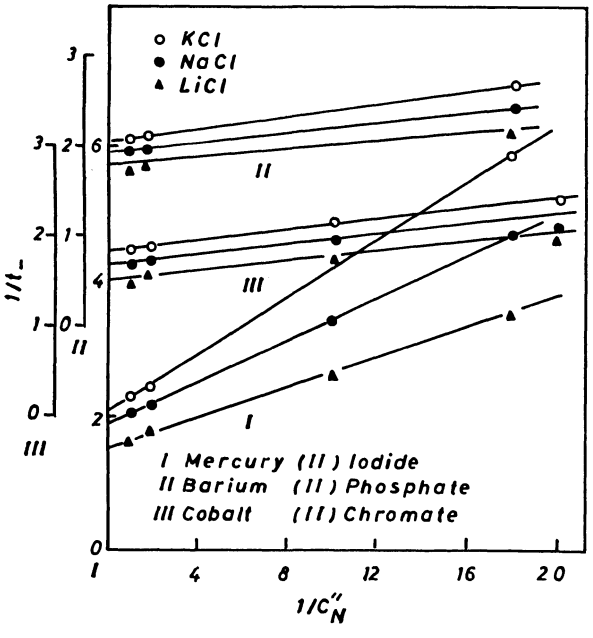

Fig. 1. Plots of $1/t$ against $1/C$ for various electrolytes across (i) mercury(II) iodide, (ii) barium(II) phosphate and (iii) cobalt(II) chromate membranes.

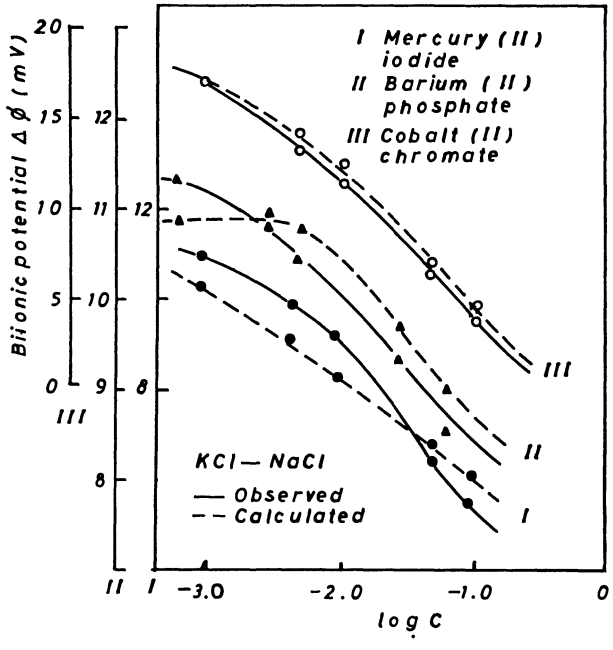

Fig. 2. Plots of bi-ionic potentials against log C for KCl–NaCl pair of electrolytes across (i) mercury(II) iodide, (ii) barium(II) phosphate and (iii) cobalt(II) chromate membranes.

calculated using Eq. 1. For the evaluation of these parameters, following equations have been forwarded[17]

$$(2J+1)\ln(g_A+2J/g_B+2J) - \ln(JV_A+1/JV_B+1) - \ln(g_A/g_B) = 0 \quad (2)$$

where

$$V_N = 1 + V_N^\circ/V_P^\circ \quad (N=A, B) \quad (3a)$$

and

$$g_N = 1 + [1+(2K_NC/\overline{X})^2]^{1/2} \quad (N=A, B) \quad (3b)$$

In Eq. 3a, V_N° and V_P° are the mobilities of cation N and anion P, respectively in bulk solution. In Eq. 3b, $\overline{X}$ is the effective charge density of the membrane and K_N is defined by

$$1/K_N = \exp[(\mu_N^{\circ m} - \mu_N^{\circ b} + \mu_P^{\circ m} - \mu_P^{\circ b})/2RT] \quad (3c)$$

where $\mu_N^{\circ m}$ is the standard chemical potential of cation N ion in the membrane phase and $\mu_N^{\circ b}$ is that in bulk solution and $\mu_P^{\circ m}$ and $\mu_P^{\circ b}$ are the corresponding values of anion P. In order to derive the values of the parameters V_N and $\overline{X}$ occuring in Eq. 3a and 3b Toyoshima and Nozaki[17] derived another equation for membrane potential E_m arising across a membrane when it is used to separate two solutions of an electrolyte at

different concentrations C'_N and C''_N

$$(F/RT)E_m = -\ln\gamma - (1-2/V_N)X \ln\frac{\sqrt{1+(2C''_N K_N/\overline{X})^2}+(1-2/V_N)}{\sqrt{1+(2C'_N K_N/\overline{X})^2}+(1-2/V_N)} + \ln\frac{\sqrt{1+(2C''_N K_N/\overline{X})^2}+1}{\sqrt{1+(2C'_N K_N/\overline{X})^2}+1} \quad (4)$$

where $\gamma = C''_N/C'_N$.

Equation 4 on expansion in powers of concentration ratio=10 being kept constant yield

$$(F/RT)E_m = -(1-2/V_N)\ln\gamma - 2(1-1/V_N)X (1/V_N)(1-1/\gamma)(\overline{X}/K_N)(1/C''_N) + \cdots \quad (5)$$

The apparent transference number t_- for co-ion was defined by the Nernst equation

$$-(F/RT)E_m = (1-2t_-)\ln\gamma. \quad (6)$$

Combining Eqs. 5 and 6 and expanding $1/t_-$ as a power of series of $1/C''_N$, following expression was obtained

$$1/t_- = V_N + (V_N-1)\left[\frac{\gamma-1}{\gamma\ln\gamma}\right]\left(\frac{\overline{X}}{K_N}\right)\left(\frac{1}{C''_N}\right) + \cdots \quad (7)$$

Equation 7 predicts a linear relationship between $1/t_-$ and $1/C''_N$. The values of V_N and $(\overline{X}/K_N)$ can be determined from the ordinate intercept and initial slope of a plot for $1/t_-$ against $1/C''_N$. The apparent transference number t_- was calculated from membrane potential data (Table 1) using Eq. 6. The values of V_N and $\overline{X}/K_N$ thus derived for the membrane and various 1:1 electrolyte systems using Fig. 1 are given in Table 2. The values of V_N and $(\overline{X}/K_N)$ were then used to calculate J and g_N using Eqs. 2 and 3. Once the membrane parameters V_N, g_N, J and $(\overline{X}/K_N)$ are known for the membrane electrolyte systems, one can calculate theoretical bi-ionic potential using Eq. 1. The bi-ionic potential thus obtained were plotted as a function of log C in Fig. 2 (shown by dotted lines). In order to compare theoretical bi-ionic potential values, the observed bi-ionic potentials were also plotted in the same graph (shown by solid lines). Figure 2 demonstrates that the theoretical predictions are borne out quite satisfactorily by our experimental results on parchment supported membranes. However, a slight deviation in the values may be accounted due to various reasons, most notably due to the various degree of interaction of ions with the membranes of low fixed charge site.

The authors are grateful to Professor Wasiur Rahman, Head, Department of Chemistry for providing research facilities and to C.S.I.R. (India) for the award of fellowship to SPS, VG, and PP.

References

1) F. A. Siddiqi, M. N. Beg, S. P. Singh, and A. Haque, *Bull. Chem. Soc. Jpn.*, **49**, 2854, 2864 (1976); *Electrochim. Acta*, **22**, 631, 638 (1977).
2) F. A. Siddiqi, M. N. Beg, P. Prakash, and S. P. Singh, *Indian J. Chem.*, **16A**, 7 (1978).
3) F. A. Siddiqi, M. N. Beg, and P. Prakash, *J. Electroanal. Chem.*, **80**, 223 (1977); *J. Polym. Sci.*, in press; *J. Electroanal. Chem.*, in press.
4) N. Lakshminarayanaiah and F. A. Siddiqi, *J. Polym. Sci.*, **8**, 2849 (1970); *Biophys. J.*, **11**, 603, 617 (1971); **12**, 150 (1972); *Z. Phys. Chem. (Fr.)*, **78**, 150 (1972).
5) M. N. Beg, F. A. Siddiqi, and R. Shyam, *Can. J. Chem.*, **55**, 1680 (1977).
6) M. N. Beg, F. A. Siddiqi, R. Shyam, and M. Arshad, *J. Membrane Sci.*, **2**, 365 (1977).
7) K. S. Speigler, *Trans. Faraday Soc.*, **54**, 1408 (1958); K. S. Speigler, R. L. Yoest, and M. R. J. Wyllie, *Discuss. Faraday Soc.*, **21**, 174 (1956).
8) B. J. Zwolinsky, H. Eyring, and C. E. Reese, *J. Phys. Chem.*, **53**, 1426 (1949).
9) G. Eisenman, *Biophys. J.*, **2**, 259 (1962); "In Membrane Transport and Metabolism," ed by A. Kleinzellers and A. Kotyk, Acad. Press, New York (1961); H. Sherry, "Ion Exchange, Vol. 72," ed by J. A. Marinsky, Dekker, New York (1968).
10) O. Kedem and A. Katchalsky, *Trans. Faraday Soc.*, **59**, 1918, 1931, 1941 (1963); *Biochem. Biophys. Acta*, **27**, 229 (1958).
11) J. A. M. Smit and A. J. Staverman, *J. Phys. Chem.*, **74**, 966 (1970).
12) R. J. Bearman and J. W. Kirkwood, *J. Chem. Phys.*, **28**, 136 (1958).
13) Y. Kobatake, N. Takeguchi, Y. Toyoshima, and H. Fujita, *J. Phys. Chem.*, **69**, 3981 (1965).
14) Y. Toyoshima, M. Yuasa, Y. Kobatake, and H. Fujita, *J. Phys. Chem.*, **72**, 2871 (1968); *Trans. Faraday Soc.*, **63**, 2803, 2814 (1967).
15) N. Kamo, Y. Toyoshima, H. Nozaki, and Y. Kobatake, *Kolloid-Z. Z. Polym.*, **248**, 914 (1971); **249**, 1061 (1971).
16) N. Kamo, M. Ookawa, and Y. Kobatake, *J. Phys. Chem.*, **77**, 92, 299 (1973).
17) Y. Toyoshima and H. Nozaki, *J. Phys. Chem.*, **74**, 2704 (1970).
18) C. E. Mrarshall, *J. Phys. Chem.*, **52**, 1284 (1948).
19) K. Sollner, *J. Phys. Chem.*, **53**, 1211 (1952); *ibid.* **53**, 1226 (1949).
20) M. R. J. Wyllie, *J. Phys. Chem.*, **58**, 67 (1954).
21) R. P. Buck, "CRC Critical Reviews in Analytical Chemistry," (1976), p. 323.
22) F. Helfferich, "Ion Exchange," McGraw Hill, New York (1962).

Vibrational Spectra and Assignments for the Fundamental Vibrations of Imidazolidine-2-thione and -2-selenone

K. DWARAKANATH and D. N. SATHYANARAYANA*

Department of Inorganic and Physical Chemistry, Indian Institute of Science, Bangalore 560012, India

(Received November 18, 1978)

Infrared spectra of imidazolidine-2-thione (*N,N'*-ethylenethiourea, ETU) and its *N,N'*-deuterated (ETU-d_2) and *S*-methylthiouronium iodides have been recorded from 4000 to 30 cm^{-1}. Normal coordinate analyses of ETU and ETU-d_2 have been made for all the fundamental frequencies, employing a Urey-Bradley potential function supplemented with valence type constants for the out of plane modes of the planar skeleton. Raman frequencies of ETU from literature have been utilised. The results of the vibrational analyses are discussed in relation to the group frequencies in structurally related molecules and frequency shifts on deuteration and *S*-methylation. The normal coordinate treatment is also performed for the planar vibrations of imidazolidine-2-selenone (*N,N'*-ethyleneselenourea, ESU) to propose assignments for ESU and so also to support the assignments of ETU.

Imidazolidine-2-thione, commonly referred to as *N,N'*-ethylenethiourea (ETU), is of considerable importance as a ligand in transition metal chemistry. ETU is an interesting molecule as a simple symmetrically disubstituted cyclic thiourea, NH–CH_2–CH_2–NH–C=S, which has a –NHCSNH– group constrained in a *cis-cis* position. It may be expected to exhibit vibrations characteristic of this grouping and a comparison of the vibrations of ETU with those of sym. *N,N'*-dimethylthiourea[1] may be of interest. Very recently, the normal coordinate calculations on *N,N'*-ethyleneurea (imidazolidin-2-one) have been published[2] and its extension to the analogous sulfur and selenium compounds is desirable. On these accounts, a knowledge of the normal coordinates of ETU and its seleno analo ue would be valuable.

Previous assignments of the principal bands of ETU were based upon empirical criteria.[3–5] An approximate normal coordinate analysis of only the in-plane vibrations of ETU treating methylene groups as point masses has also been reported.[6] However, the vibrational assignments are not complete and many of the fundamentals are uncertain or unassigned. In order to obtain as complete a vibrational assignment of the fundamentals as possible, the infrared spectra of ETU as well as its *N,N'*-deuterated (ETU-d_2) and the *S*-methyl derivatives are studied. The Raman data from literature[4,7] are also made use of. The assignments are supported by accomplishing normal coordinate analyses of ETU and ETU-d_2 for all the fundamental vibrations. The coordinate treatment is also extended to the in-plane vibrations of imidazolidine-2-selenone (*N,N'*-ethyleneselenourea, ESU) with which it can profitably be compared since only the sulfur-involving frequencies of ETU are expected to vary principally in ESU.

Experimental

ETU was prepared and purified according to Allen *et al.*[8] mp 197—198 °C. The *N,N'*-deuterated compound (ETU-d_2) was obtained by repeated exchange reaction with heavy water. The *S*-methyl derivative of ETU was prepared by a standard procedure.[9]

Spectra. Infrared spectra of the solid samples were measured on a Carl-Zeiss UR10 spectrophotometer from 4000 to 400 cm^{-1} in Nujol mull and KBr pellet. The observed frequencies were calibrated with standard frequencies of polystyrene. Infrared spectra between 400 to 30 cm^{-1} were recorded on a Polytec FIR 30 Fourier transform spectrometer. The instrument was calibrated by means of water vapor frequencies. The Raman frequencies[7] of ETU and the infrared bands[5] of ESU are quoted from published spectra. The infrared spectra of ETU-d_0 and ETU-d_2 between 300 to 50 cm^{-1} are given in Fig. 1.

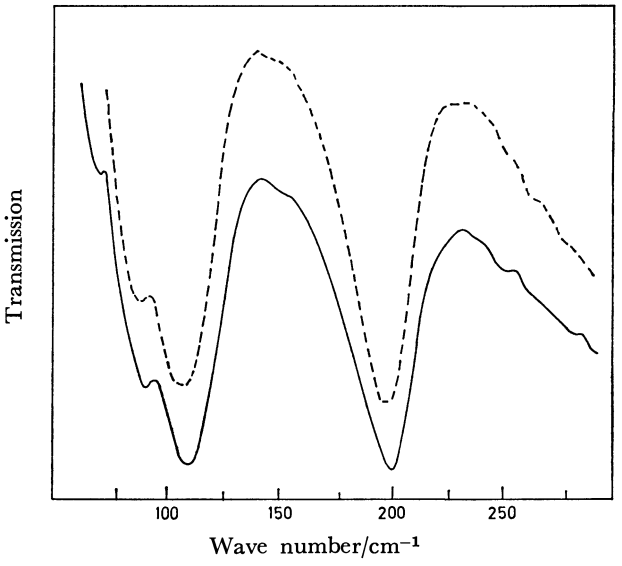

Fig. 1. Infrared spectra of ETU-d_0 (—) and ETU-d_2 (----).

Normal Coordinate Analysis

It is known by the X-ray crystal structure determination[10] that ETU has a C_{2v} symmetry. The 30 normal vibrations of ETU and ESU in the C_{2v} symmetry are classified into 19 in-plane ($10A_1$ and $9B_2$) and 11 out-of-plane ($5A_2$ and $6B_1$) modes of which the vibrations belonging to A_1, B_1, and B_2 species are infrared active and all are Raman active. The internal coordinates are depicted in Fig. 2. The out of plane vibrations of the planar ring are described in terms of the out of plane bending of the C–S and N–H groups and the torsional coordinates of the CN and C'N bonds.

TABLE 1. FORCE CONSTANTS OF IMIDAZOLIDINE-2-THIONE AND -2-SELENONE

Urey-Bradley constants[a] (mdyn/Å)								
	ETU	ESU		ETU	ESU		ETU	ESU
K(CX)	3.40	2.80	H(XCN)	0.09	0.08	F(XCN)	1.10	0.80
K(CN)	5.90	6.05	H(CNC)	0.40	0.36	F(CNC)	0.30	0.30
K(CN′)	3.10	3.00	H(NCN)	0.48	0.25	F(NCN)	0.68	0.72
K(CC)	2.95	2.95	H(NCC)	0.28	0.32	F(NCC)	0.45	0.45
K(CH)	4.40	4.40	H(HCH)	0.41	0.41	F(HCH)	0.06	0.06
K(NH)	5.30	5.30	H(HCC)	0.15	0.15	F(HCC)	0.50	0.50
			H(NC′H)	0.26	0.26	F(NC′H)	0.55	0.55
$k(CH_2)$	−0.016	−0.016	H(CNH)	0.28	0.27	F(CNH)	0.45	0.40
(mdyn·Å/rad²)			H(C′NH)	0.12	0.12	F(C′NH)	0.55	0.55

Valence constants (mdyn·Å/rad²)					
B_1	$f(\pi CS)$	0.080	A_2	$f(\pi NH)$	0.192
Species	$f(\pi NH)$	0.145	Species	$f(\tau$ ring)	0.144
	$f(\tau$ ring)	0.062			
	$f(\pi CS, \pi NH)$	−0.030			
	$f(\pi CS, \tau$ ring)	−0.020			

a) X=S or Se.

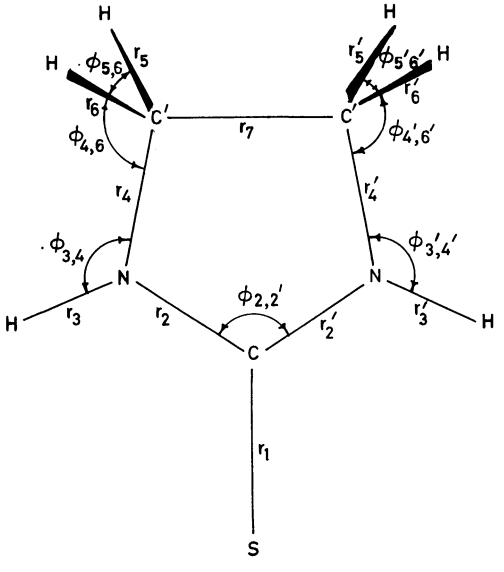

Fig. 2. Structure and internal coordinates of *N,N′*-ethylenethiourea.
Torsional coordinates are formed from the bond numbers.

The molecular parameters were taken from the X-ray structure data[10]—r(N–H) 0.99, r(C–H) 0.90, r(C–C) 1.536, r(C–N) 1.322, r(C′–N) 1.471 and r(C–S) 1.708 Å; ∠SCN 125.0°, ∠CNC 112.6°, ∠NCC 102.4°, ∠CNH 123.7°, ∠NC′H 104.07°, ∠CCH 109.6°, and ∠HCH 126.5°. For ESU, C=Se distance was assumed to be 1.86 Å and the rest of the structural parameters were the same as those of ETU. The symmetry coordinates used were constructed by standard procedures[11,12] and are not reported here for the sake of briefness.

The Wilson's GF matrix method[13] was employed. The numerical computations were performed with an IBM 360/44 Computer using programs similar to those of Shimanouchi.[14] Infrared frequencies were used for the calculations. Since the Urey-Bradley force (UBF) function has been successful in satisfactorily explaining the vibrational spectra of thioamides[15–18] and thioureas,[19,20] it was employed presently. For the out of plane A_2 and B_1 fundamentals, the Urey-Bradley force constants for the CH_2 groups, and the valence force constants for the out of plane deformations and torsional modes were used. The initial UBF constants were taken from succinonitrile[21] for the $-CH_2-CH_2-$ part and from *N*-methyl thioacetamide[15,16] (NMTA) for the –NHCSNH– part. The zeroth order calculated frequencies were close to the observed ones lending confidence to the assignments obtained. For the out-of-plane vibrations of the molecular skeleton, valence force constants were used and the initial values were taken from *N*-methylthiourea.[22] The force constants were refined by an iterative procedure and the final values of the force constants of ETU are presented in Table 1. The force constants of ETU were then transferred to ESU. In accord with the concept of selenation,[23] minimum modifications were effected in the force constants of ETU, particularly for those connected with the thioureide group to obtain a desired agreement between the calculated and observed frequencies for the in-plane fundamentals of ESU. The final values of the force constants of ESU are also given in Table 1.

Results and Discussion

Force Field. The agreement between the observed and calculated frequencies for both ETU and ETU-d_2 is good. The final values of the force constants of ETU seem appropriate and they are comparable with the corresponding ones in NMTA[15,16] and thioacetamide[15,17] (TAM) for the –NHCSNH– part and those from succinonitrile[21] for the $-CH_2-CH_2-$ part. These demonstrate the transferability of the UBF constants. For example, the C=S stretching constant of ETU (3.40 mdyn/Å) is similar to that of TAM[17] and NMTA[16] (3.40 and 3.45 mdyn/Å, respectively). Similarly, the C–N stretching constant of ETU (5.90

mdyn/Å) is also comparable with that of TAM and NMTA (5.70 mdyn/Å).

The agreement between the calculated and observed frequencies of ESU is good and the final values of the force constants of ESU differ very little from the transferred force constants of ETU. The C=Se stretching constant (2.80 mdyn/Å) is lower than the C=S stretching force constant of ETU (3.40 mdyn/Å), and the C–N constant of ESU (6.05 mdyn/Å) is slightly higher than that of ETU (5.90 mdyn/Å). A similar trend is noticed in the C–S and C–N force constants for thiourea and selenourea.[19] This indicates the increased contribution of the cannonical form $S^{-}-\overset{|}{C}=N^{+}<$ over the other structure, $S=\overset{|}{C}-N<$ in the selenium compound compared to the analogous sulfur compound.

Vibrational Assignments. Imidazolidine-2-thione: The observed and calculated fundamentals of ETU and ETU-d_2 are presented in Table 2 along with the assignments as derived from the potential energy distributions among the symmetry coordinates.

In-plane Vibrations: *Vibrations of the Methylene Groups*: *CH_2 Stretching and Bending.* There are two CH_2 stretching vibrations of ETU one each belonging to A_1 and B_2 species. A medium broad band at 2900 cm^{-1} has been attributed to both these modes. The CH_2 bending modes (ν_4 and ν_{14}) are assigned to the bands at 1470 and 1480 cm^{-1} (respectively). These are compatible with those of *N,N'*-ethyleneurea.[2]

CH_2 Wagging. The symmetric CH_2 wagging (A_1) is found as a mixed vibration contributing almost equally to the bands at 1286 and 1212 cm^{-1} whereas the asymmetric CH_2 wagging (B_2) may be assigned at 1312 cm^{-1}. The assignment of CH_2 wagging vibrations is similar to the corresponding modes in *N,N'*-ethyleneurea[2] at 1274 and 1207 cm^{-1}, in ethylene trithiocarbonate[24] at 1279 and 1248 cm^{-1}, and in thiazolidine[25] around 1320 and 1260 cm^{-1}.

Vibrations of the Thioureide Group: *NH Group Vibrations.* The symmetric and antisymmetric NH stretching modes (ν_1 and ν_{11}) are easily assigned to the broad bands centered at 3275 and 3250 cm^{-1}, which on deuteration are replaced by new bands at 2435 and 2400 cm^{-1}, respectively. In *N,N'*-ethyleneurea[2] both NH stretching vibrations are observed as a single strong band at 3285 cm^{-1}.

The symmetric NH bending (A_1) is found to be a mixed vibration contributing equally to the bands at 1528 and 1212 cm^{-1}. This assignment qualitatively agrees with the earlier ones of Klaboe,[4] and Mecke *et al.*[3] However, in *N,N'*-ethyleneurea, the corresponding mode is observed as a pure vibration at 1385 cm^{-1}. The asymmetric NH bending (B_2) is however found as a pure vibration at 1376 cm^{-1} and this assignment is similar to that of *N,N'*-ethyleneurea for a medium band at 1423 cm^{-1}. In ETU-d_2, the ND bending contributes to the bands at 860 and 892 cm^{-1} in the A_1 symmetry species whereas in the B_1 type the 927 cm^{-1} band originates from ND bending.

C–N and C=S Group Vibrations. The symmetric C–N stretching (A_1) coupled with NH bending is associated with the 1528 cm^{-1} band, whereas the asymmetric C–N stretching (B_2) is pure and is assigned at 1508 cm^{-1}. The CN stretching frequency (B_2) of ETU is about 50 cm^{-1} higher than the corresponding mode in *N,N'*-ethyleneurea as expected due to the increased C–N bond order. The infrared bands at 1508 and 1528 cm^{-1} show a pronounced shift towards higher frequencies and are observed at 1557 and 1570 cm^{-1} in the *S*-methylated ETU, the shift being explained by the increased double bond character of the CN bond following the methylation of the sulfur atom.

The nature of the C=S stretching mode of ETU is interesting. The C=S stretching coordinate is distributed principally among two vibrations giving rise to the strong bands in the infrared at 516 and 925 cm^{-1}, a major proportion of 42% for the 516 cm^{-1} and a lesser proportion of 26% for the 925 cm^{-1} band. In support of this assignment, very strong bands are observed in the Raman[4,7] at 927 and 513 cm^{-1}. The assignment of the 516 cm^{-1} band qualitatively agrees with the recent one of Verani[5] but differs from that of Klaboe,[4] and Mecke *et al.*,[7] who have assigned the C=S stretching frequency around 1200 cm^{-1}.

The attribution of the 516 cm^{-1} band to the C=S stretching mode is further supported from the infrared spectra of ESU and the *S*-methyl derivative of ETU. On *S*-methylation, which diminishes the double bond character of the C=S bond, the 516 cm^{-1} band of ETU shows a pronounced red shift and is found in the spectrum of the *S*-methyl derivative at 477 cm^{-1}. The 516 cm^{-1} band of ETU is replaced in the spectrum of ESU by a band at a much lower wave number, 357 cm^{-1}, thus confirming its assignment. In the metal complexes of ETU, increase in the C–N stretching band and decrease in the C–S stretching band (at 516 cm^{-1}), similar to that on *S*-methylation but of smaller magnitude, are observed.[25,26]

The C=S bending may be assigned at 343 cm^{-1}. This frequency is in between the corresponding frequency in NMTA[15,16] at 370 cm^{-1} and in thiazolidine-2-thione[28] at 292 cm^{-1}. In support of this assignment, the 345 cm^{-1} band of ETU is replaced in ESU by a new band at a lower frequency, 280 cm^{-1}.

Ring Vibrations. There are two ring deformation vibrations. The ring deformation belonging to the A_1 species is coupled and contributes chiefly to the bands at 925 and 516 cm^{-1}. The ring deformation belonging to the B_2 representation, on the other hand, is associated with the 678 cm^{-1} band. The latter assignment differs from that of Klaboe,[4] and Devillanova and Verani[5] who have assigned it to an NH out-of-plane bending. The assignment of the 678 cm^{-1} band to a ring deformation mode is comparable with the 703 cm^{-1} band of *N,N'*-ethyleneurea[2] and with similar assignments made for other five membered heterocyclic compounds. For instance, a ring deformation mode has been assigned in 2,5-pyrrolidinedithione[29] at 649 cm^{-1} and in thiazolidines[25,28] near 675 cm^{-1}. It is interesting to note that the 678 cm^{-1} band of ETU almost completely vanishes on *N*-deuteration. However, there is a new weak band at 645 cm^{-1} in the infrared spectrum of ETU-d_2 corresponding to the 678 cm^{-1} absorption of ETU as expected from the computed frequencies of ETU-d_2 and confirming its assignment to a ring deformation mode.

TABLE 2. OBSERVED AND CALCULATED FUNDAMENTALS (in cm^{-1}) AND ASSIGNMENTS FOR IMIDAZOLIDINE-2-THIONE

ETU-d_2		ETU-d_0			
		Obsd		Calcd	Assignment[a] (PED[b]/%)
Obsd	Calcd	Raman	IR		
A_1 species					
2435	2390	3293	3275	3268	νNH(100)
2880	2896	2900	2900	2896	νCH_2(99)
1465	1476	1520	1528	1528	νCN(37), δNH(36)
1445	1458	1473	1470	1463	δCH_2(89)
1280	1274	1286	1286	1282	$w CH_2$(40), νCC(20)
860	861	1213	1212	1225	$w CH_2$(49), δNH(35)
1200	1146	1106	1120	1118	νCC(42), νCN(17)
1022	1031	1000	1008	1008	νC'N(66), νCC(18)
1004		973			
892	894	927	925	899	ring def(37), νCS(26), νCN(20)
507	506	513	516	512	νCS(42), ring def(37)
B_2 species					
2400	2384	3250	3250	3266	νNH(100)
2925	2909	2900	2900	2911	νCH_2(99)
1492	1500	1520	1508	1509	νCN(75)
1445	1434	1480	1480	1475	δCH_2(81)
927	931	1380	1376	1379	δNH(79)
1315	1339	1310	1312	1313	$w CH_2$(59), νC'N(16)
1140	1144	1045	1050	1057	νC'N(72)
645	662	660	678	670	ring def(89)
326	333	333	343	344	δCS(91)
B_1 species					
2965	2996	2986	2986	2996	νCH_2(100)
1298	1300	1310	1312	1300	$t CH_2$(94)
920	904	927	925	905	$r CH_2$(85)
450	465	592	598	579	πNH(97)
200	200	205	200	205	πCS(70), τ ring(28)
107	90	80	109	99	τ ring(83)
			90		
A_2 species					
2930	2984	2936		2984	νCH_2(100)
1286	1277	1286	1286	1277	$t CH_2$(96)
	1080	1106	1108	1081	$r CH_2$(88)
512	532	660	678	666	πNH(97)
87	86	80	90	91	τ ring(99)

a) The frequencies of ETU-d_2 are so arranged as to approximately correspond to the assignments and the PEDs given for ETU-d_0; ν=stretching, δ=bending, r=rocking, w=wagging, t=twisting, π=out-of-plane bending and τ=torsion. b) PED=Potential energy distributions ($100 L_{ik}^2 F_{ii}/\lambda_k$); those less than 15% are omitted.

Out-of-plane Vibrations: B_1 *Vibrations.* The out-of-plane CH_2 stretching is assigned to a weak band at 2967 cm^{-1} comparable with the very weak Raman band of *N,N'*-ethyleneurea[2] at 2980 cm^{-1}. The CH_2 twisting of ETU at 1312 cm^{-1} is slightly higher than that in thiazolidines[25,28] and succinimides[30] assigned around 1230 to 1270 cm^{-1}. According to the normal coordinate treatment, the band at 925 cm^{-1} could also be assigned to CH_2 rocking and this is compatible with CH_2 rocking in ethylene trithiocarbonate[24] and thiazolidines[25,28] assigned between 935 to 950 cm^{-1}.

There are three skeletal modes belonging to B_1 species. The NH out-of-plane bending is assigned at 598 cm^{-1} and its origin from an NH group is confirmed by deuteration studies. On deuteration a new strong broad band at 450 cm^{-1} is observed in agreement with the calculated frequency at 465 cm^{-1}. If, on the other hand, the 678 cm^{-1} band is assigned to NH out-of-plane bending and the 598 cm^{-1} band to ring deformation, then the calculated frequencies for ETU-d_2 are not consistent with observed ones. The strong 598 cm^{-1} absorption of ETU is rather broad and typical of NH bands due to out-of-plane bending. The 678 cm^{-1} band may however be assigned to an NH bending of A_2 symmetry overlapping with the B_2 fundamental due to ring deformation.

The infrared and Raman spectra of ETU exhibit a strong band near 110 cm^{-1} (which is rather broad

Table 3. Observed and calculated fundamentals and assignments for imidazolidine-2-selenone

Frequency/cm^{-1} Obsd	Calcd	Assignment[a] (PED[b]/%)
A_1 species		
3520	3268	νNH(100)
n. a.	2896	νCH_2(99)
1500	1492	νCN(41), δNH(36)
1450	1461	δCH_2(87)
1275	1262	$w CH_2$(61)
1190	1211	δNH(45), $w CH_2$(20)
1080	1098	νCC(43), νCN(17)
988	981	νC'N(67), νCC(22)
		νCSe(58), ring def(47)
357	371	νCSe(58), ring def(28)
B_2 species		
3250	3266	νNH(100)
n. a.	2911	νCH_2(99)
1515	1514	νCN(79)
1475	1476	δCH_2(83)
1350	1357	δNH(58), $w CH_2$(31)
1300	1300	$w CH_2$(45), δNH(32)
1026	1038	νC'N(74)
664	660	ring def(89)
276	280	δCSe(92)

n. a.=not available. a), b): as in Table 2.

in the infrared with a shoulder band at 90 cm^{-1}). This band has been assigned to ring torsion of species B_1. Such features have been observed in related five-membered ring systems,[24,31-34] such as ethylene trithio-[24] and -triselenocarbonate[34] (at ≈90 and 70 cm^{-1}, respectively) and other cyclic carbonates[33] (≈95 cm^{-1}), *etc.* Lattice modes are assigned at still lower frequencies. The calculations for ETU indicate that the other ring puckering mode (of A_2 species) could be assigned in the same region. Since it was not possible to record the far infrared spectra of ETU in solution a doubt can arise that the band around 110 cm^{-1} could be due to lattice modes. An alternate choice for ring torsions may then be the strong band at 200 cm^{-1}, compatible with the assignment in ethylene carbonate[35] (at 215, 230 cm^{-1}) and *N,N'*-ethyleneurea[2] (near 250 cm^{-1}). In such a case, the assignment of C=S out of plane bending presents a difficulty. The former assignment is therefore preferred. Since the out of plane vibrations are fairly independent of each other, even if the latter assignment is preferred, it does not affect the overall results.

A_2 Vibrations. The vibrations belonging to A_2 species, according to the selection rules, are infrared inactive but Raman active for the molecular symmetry C_{2v}. These modes may be observed in the infrared if the molecule is not exactly of C_{2v} symmetry or if the site symmetry is lower. The X-ray structure data[10] of ETU indicate some deviations from C_{2v} symmetry.

The infrared and Raman bands observed corresponding to the calculated vibrations of the A_2 species of ETU and ETU-d_2 are also shown in Table 2. This seems to indicate the overlapping of the fundamentals. No new Raman band without a corresponding infrared band was observed. This shows that the effective molecular symmetry of ETU in the solid state may be slightly lower than C_{2v}.

Imidazolidine-2-selenone: The normal coordinate calculations for ETU is extended to the in-plane vibrations of ESU in an attempt to assign the planar frequencies of ESU and also to confirm some of the assignments made for ETU themselves. The frequency data together with their potential energy distributions derived from the calculations are shown in Table 3. The experimental frequencies are quoted from a published spectrum.[5]

As observed from Tables 2 and 3, the nature of the bands of ESU are very similar to the corresponding ones of ETU and only the bands at 925 and 516 cm^{-1} in the A_1 symmetry species and 343 cm^{-1} in the B_2 species of ETU are significantly shifted to lower frequencies suggesting the higher contribution from the C–S group vibrations to these bands. The assignments of ESU are thus straightforward.

Of particular interest in the spectrum of ESU are the C=Se stretching and bending vibrations. Notably, the potential energy distributions indicate that the observed band at 357 cm^{-1} may be assigned to C=Se stretching and it has considerable contribution from ring deformations. The C=Se stretching also contributes significantly (27%) to the (calculated) higher frequency band at 828 cm^{-1}. The present assignment of the 357 cm^{-1} band qualitatively agrees with Devillanova and Verani[5] who have attributed it to a coupled mode consisting of C=Se stretching, NCSe and NCN bending. The 357 and 828 cm^{-1} bands of ESU correspond approximately to the 516 and 925 cm^{-1} bands of ETU and thus represent a large decrease of over 100 to 140 cm^{-1} from sulfur to the corresponding selenium-involving vibration. The C=Se bending mode is found at 280 cm^{-1} thus producing a decrease of over 60 cm^{-1} from the C=S bending of ETU at 343 cm^{-1}.

References

1) R. K. Ritchie, H. Speeding, and D. Steele, *Spectrochim. Acta, Part A*, **27**, 1597 (1971).
2) Y. Saito and K. Machida, *Bull. Chem. Soc. Jpn.*, **50**, 359 (1977).
3) R. Mecke, R. Mecke, and A. Luttringhaus, *Chem. Ber.*, **90**, 975 (1957).
4) P. Klaboe, *Acta Chem. Scand.*, **22**, 1532 (1968).
5) F. A. Devillanova and G. Verani, *J. Chem. Soc., Perkin Trans. 2*, **1977**, 1529.
6) U. Agarwala and P. B. Rao, *Indian J. Pure Appl. Phys.*, **7**, 229 (1969).
7) "Raman/IR-Atlas," ed by B. Schrader and W. Meiler, Verlag Chemie GmBH, Weinhein/Bergstr. (1974).
8) C. F. H. Allen, C. O. Edens, and J. V. Allan, *Org. Synth.*, **3**, 394 (1955).
9) E. Brand and F. C. Brand, *Org. Synth.*, **3**, 440 (1955).
10) P. J. Wheatley, *Acta Crystallogr.*, **6**, 369 (1953).
11) T. Onishi and T. Shimanouchi, *Spectrochim. Acta*, **20**, 325 (1964).
12) T. Miyazawa and K. Fukushima, *J. Mol. Spectrosc.*, **3**, 308 (1965).

13) E. B. Wilson, Jr., *J. Chem. Phys.*, **7**, 1047 (1939); **9**, 76 (1941).
14) T. Shimanouchi, "Computer Programs for Normal Coordinate Treatment of Polyatomic Molecules," University of Tokyo (1968).
15) I. Suzuki, *Bull. Chem. Soc. Jpn.*, **35**, 1286, 1449, 1456 (1962).
16) C. N. R. Rao and G. C. Chaturvedi, *Spectrochim. Acta, Part A*, **27**, 520 (1971).
17) W. Walter and P. Staglich, *Spectrochim. Acta, Part A*, **30**, 1739 (1974); and the references given there.
18) A. Ray and D. N. Sathyanarayana, *Bull. Chem. Soc. Jpn.*, **46**, 1969 (1973).
19) D. Hadzi, J. Kidric, Z. V. Knezevic, and B. Barlic, *Spectrochim. Acta, Part A*, **32**, 693 (1976).
20) R. K. Gosavi, U. Agarwala, and C. N. R. Rao, *J. Am. Chem. Soc.*, **89**, 235 (1967).
21) T. Fujiyama, K. Tokumaru, and T. Shimanouchi, *Spectrochim. Acta*, **20**, 415 (1964).
22) K. Dwarakanath and D. N. Sathyanarayana, *Bull. Chem. Soc. Jpn.*, **52**, 2084 (1979).
23) K. A. Jensen, *Ann. New York Acad. Sci.*, **192**, 115 (1972).
24) G. Borch, L. Henriksen, P. H. Nielsen, and P. Klaboe, *Spectrochim. Acta, Part A*, **29**, 1109 (1973).
25) M. Guiliano, G. Davidovica, J. Chouteau, J. L. Larice, and J. P. Roggero, *J. Mol. Struct.*, **25**, 339 (1975).
26) S. L. Holt, Jr., and R. L. Carlin, *J. Am. Chem. Soc.*, **86**, 3017 (1964).
27) F. A. Devillanova and G. Verani, *Transition Met. Chem.*, **2**, 9 (1977).
28) K. Geetharani and D. N. Sathyanarayana, *Indian J. Chem.*, **14A**, 170 (1976).
29) K. Geetharani and D. N. Sathyanarayana, *Indian J. Pure Appl. Phys.*, **15**, 21 (1977).
30) T. Woldbaeck, P. Klaboe, and D. H. Christensen, *Acta Chem. Scand.*, **30A**, 531, 547 (1976).
31) C. S. Blackwell and R. C. Lord, in "Vibrational Spectra and Structure," ed by J. R. Durig, Marcel Dekker, New York (1972), Vol. 1, p. 20.
32) K. R. Gayathri Devi, D. N. Sathyanarayana, F. A. Devillanova, and G. Verani, *Spectrochim. Acta*, in press (1979).
33) R. A. Pethrick and A. D. Wilson, *Spectrochim. Acta, Part A*, **30**, 1073 (1974).
34) L. Henriksen, P. H. Nielsen, G. Borch, and P. Klaboe, *Spectrochim. Acta, Part A*, **31**, 191 (1975).
35) B. Fortunato, P. Mirone, and G. Fini, *Spectrochim. Acta, Part A*, **27**, 1917 (1971).

An ESR Study of the Photolysis of *N*-Nitrosodialkylamines

A. John ELLIOT† and Jeffrey K. S. WAN*

Department of Chemistry, Queen's University, Kingston, Ontario, Canada K7L 3N6

(Received November 20, 1978)

The nitroxide radicals which are formed when acidic, neutral, and alkaline solutions containing *N*-nitrosodialkylamines are photolysed, have been characterized by electron spin resonance spectroscopy. Nitrosamines are found to be photolytically active only in acidic solutions. In neutral and alkaline solutions nitrosamines only participate in secondary reactions involving the alcohol derived radicals. Some possible reaction pathways have been postulated.

As a class of compounds, *N*-nitrosodialkylamines when photolysed in neutral solutions, are effectively stable towards UV irradiation.[1-3] However in dilute acid solutions, nitrosamines undergo a large variety of photoinitiated free radical reactions, many of which are of interest in synthetic organic chemistry.[1-4] The primary photochemical event have been established to be an acid catalysed breaking of the nitrogen-nitrogen bond to produce an aminium radical and nitrogen monoxide. A generalized reaction scheme is given below: (for more detailed information the reader is directed to the review article by Chow[3] and references therin).

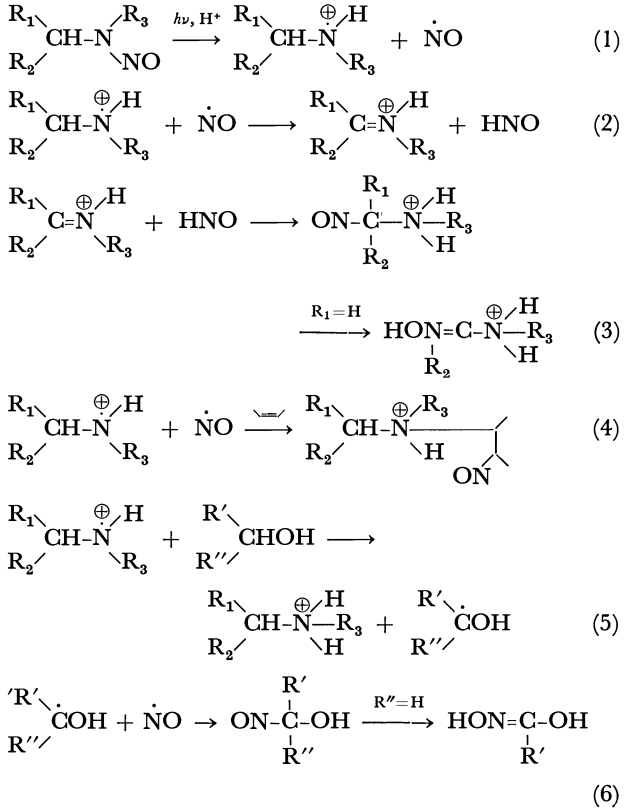

To the best of our knowledge, the only photochemical ESR investigations of the photolysis of nitrosamines are two communications from this laboratory[5,6] which supported the N–N cleavage as the primary chemical event. As can be seen from the above scheme, any ESR study to characterize the free radical intermediates will be bedevilled by a host of nitroxide radicals formed from the various *C*-nitroso compounds by spin trapping,[7]

or by secondary photolysis.[3,7]

Many of these problems can be minimized by photolysing flowing solutions and in this report we will describe the radicals obtained when solutions containing either *N*-nitrosodimethylamine, *N*-nitrosodicyclohexylamine or 1-nitrosopyrollidine were photolysed.

Experimental

The chemicals were purchased from Aldrich (*N*-nitrosodicyclohexylamine, 1-nitrosopyrollidine, acetone oxime, cyclopentanone oxime, maleic acid), K and K (*N*-nitrosodimethylamine), Baker (triethylamine), BDH (propionic acid), McArthur Chemicals (acetic acid). The solvents were obtained from a number of commercial sources. All chemicals were used as supplied except triethylamine which was distilled before use.

The concentrations of the nitrosamines in the solutions were 0.03—0.1 mol dm^{-3} and when di-*t*-butyl peroxide was added, its concentration was 1—2 vol %. All solutions were deoxygenated by purging with gaseous nitrogen. The flowing solutions were photolysed directly in the cavity of a Varian E-3 spectrometer with light from a 1000 W high pressure mercury lamp. The flow rate was varied (0—4 ml min^{-1}) to optimize the spectrum under study. For most samples this flow was 0.5 to $\approx$1.0 ml/min. The sample temperature in the cavity was regulated by flowing thermostated nitrogen gas by the spectrosil flow tube. The ESR simulations were performed on a Nicolet 1180 computer.

Results

Photolysis of Acidic Solutions. *(a)*N-*Nitrosodimethylamine (NDMA)*: No radicals were detected on photolysis of flowing solutions of NDMA in acetic acid, or 10 vol % acetic acid : benzene, however, if an alcohol was added to this solution an ESR spectrum was observed. In general the spectrum arose from two radicals, one of which, a nitroxide with $a^N \approx$ 1.45 mT, was formed through secondary processes as its intensity increased markedly relative to the second radical on decreasing the flow rate. This secondary radical was not studied in detail. With the other radical (I), the number of interacting nuclei varied depending on the alcohol added. With 2-propanol and 2-butanol, splittings from two nitrogens and two protons were observed from I (see Fig. 1 and Table 1)

† Present address: Department of Chemistry, University of Calgary, Calgary, Canada T2N 1N4.

Table 1. The hyperfine coupling constants (mT) for radical I

Solvent	a^H	a^H	a^H	a^N	a^N
10 vol% acetic acid : 2-propanol	0.87	0.83	—	0.29	1.40
8 vol% acetic acid : 30 vol% water : 2-propanol	0.94	0.94	—	0.29	1.39
10 vol% acetic acid : 10 vol% 2-propanol : benzene	0.78	0.78	—	0.38	1.34
4 vol% 2-propanol : acetic acid	0.86	0.86	—	0.34	1.38
10 vol% acetic acid : 2-butanol	0.94	0.77	—	0.31	1.38
10 vol% acetic acid : 1-propanol	0.98	0.66	0.62	0.34	1.34
10 vol% acetic : ethanol	0.91	0.76	0.71	0.31	1.35

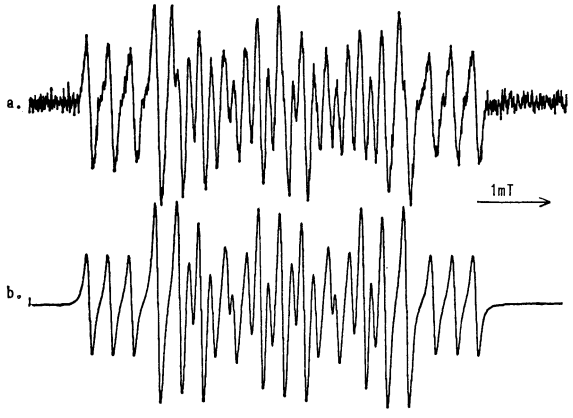

Fig. 1. (a) The ESR spectrum recorded when a NDMA: 8 vol % acetic acid: 30 vol % H_2O: 1% di-*t*-butyl peroxide: 2-propanol solution was photolysed at 22 °C. (b) The simulated ESR spectrum of radical I.

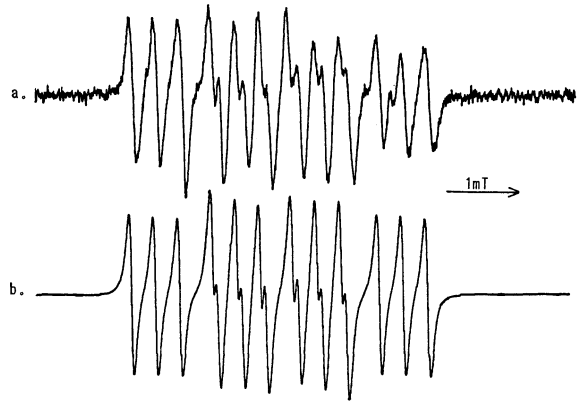

Fig. 2. (a) The ESR spectrum recorded when a NDCHA: 10 vol% acetic acid: ethanol solution was photolysed at 8 °C. (b) The simulated ESR spectrum of radical II.

but when the alcohol was ethanol or 1-propanol, an additional proton splitting was found (Table 1). When di-*t*-butyl peroxide was added to the solution, the spectral intensity of I increased about five fold. Although the hyperfine coupling constants showed little variation with temperature (−30 °C to +35 °C), they did vary slightly with solvent (Table 1). Linewidth effects associated with the coupling of the ***g***- and ***A***-tensors as the radical tumbled slowly could be observed as temperature was lowered in the alcoholic solvents.

For a DMNA:2-propanol solution (with and without di-*t*-butyl peroxide), the same spectrum was observed

Table 2. The coupling constants (mT) for radical II

Solvent	a^H	a^N	a^N
10 vol% acetic acid : 2-propanol	1.20	0.33	1.11
10 vol% HCl (concd) : 2-propanol	1.21	0.40	1.13
10 vol% acetic acid : ethanol	1.20	0.33	1.10
10 vol% acetic acid : 20 vol% H_2O : 2-propanol	1.25	0.36	1.15
acetic acid	1.22	0.39	1.16

regardless of whether the acid was acetic or propionic but if maleic acid (0.2 mol dm^{-3}) or concentrated hydrochloric acid (2—10 vol %) was added, no spectrum was observed. Addition of 10 vol % cyclohexene to a DMNA : 10 vol % acetic acid : 2-propanol solution (8 °C) only slightly reduced the yield of I. However, if the flow was stopped, the solution photolysed for a few minutes, and then the spectrum recorded with the light blocked, the spectrum of a persistent nitroxide radical (a^N=1.55 mT, a^H=0.18 mT, linewidth≈0.2 mT) was recorded. In the absence of cyclohexene, no spectrum was observed after this sequence as both I and the other nitroxide decay within seconds.

(b) N-*Nitrosodicyclohexylamine (NDCHA)*: In contrast to DMNA, when DCHNA was photolysed in acetic acid, 2-propanol containing 10 vol % acetic acid or 10 vol % hydrochloric acid, ethanol containing 10 vol % acetic acid or 0.2 mol dm^{-3} maleic acid, the same radical (II) was always observed. A representative spectrum is shown in Fig. 2 and the coupling constants (for two nitrogens and a proton) are given in Table 2. As with NDMA solutions, a second nitroxide radical spectrum was also observed but its intensity relative to II decreased on increasing the flow rate and it is considered to arise from secondary processes. When di-*t*-butyl peroxide was added to any of the NDCHA solutions studied the intensity of II remained unaltered. Addition of cyclohexene to the solutions did not affect the intensity either.

(c) 1-Nitrosopyrollidine (NP): A limited number of experiments were undertaken with NP. On photolysing a NP:10 vol % acetic acid : 2-propanol solution, radicall III was observed (in addition, a secondary nitroxide was also observed). The coupling constants for III in the solution were a^N=1.36 mT and a^N=a^H= 0.28 mT. The intensity of III increased on the addition of di-*t*-butyl peroxide to the solution. When the 2-propanol was replaced by either ethanol or 1-propanol, the spectrum of radical III (which was weak) appeared to have an extra proton coupling(a^H ≈0.58 mT) in

Table 3. Coupling constants (mT) of radicals formed in neutral solutions from NDCHA

Alcohol	a^N	a^N a)	a^H a)	Assignment
Ethanol	1.44	0.07 (2)	0.03 (6)	$\left(\mathrm{HO-\overset{CH_3}{\overset{\vert}{C}}-\overset{H}{\overset{\vert}{}}}\right)_2\mathrm{NO}$
	1.41	0.51 (2)	0.03 (2)	?
2-Propanol	1.54	—	—	$\left(\mathrm{HO-\overset{CH_3}{\overset{\vert}{C}}-\overset{CH_3}{\overset{\vert}{}}}\right)_2\mathrm{NO}$
	1.32	1.23	—	$\mathrm{HO-\overset{CH_3}{\overset{\vert}{C}}-\overset{CH_3}{\overset{\vert}{}}-HNO}$
1-Propanol b)	1.40	0.49 (2)	—	$\left(\mathrm{HO-\overset{CH_2CH_3}{\overset{\vert}{C}}-\overset{H}{\overset{\vert}{}}}\right)_2\mathrm{NO}$
2-Butanol	1.51	0.27	—	?

a) The number of equivalent nuclei are given in parentheses if different from one. b) Other radicals also present but spectrum too complicated to analysed (see Fig. 4).

addition to the above.

It should be noted that while radicals I, II, and III had half lives of about a second at 10—20 °C, their spectral intensities were not excessively large. When a 10 vol % acetic acid : 2-propanol solution containing either NDMA or NDCHA was photolysed, the respective radicals, I or II, were still observed (although at reduced intensity) when a filter (which blocked light $\lambda<320$ nm) was inserted in the light beam.

Photolysis of Neutral and Basic Solutions. Photolysis of DCHNA in static alcohol solutions will, after a few minutes, produce strong spectra of nitroxide radicals but if the solutions were flowed no radicals could be detected. However, if di-*t*-butyl peroxide was added to the flowing solutions nitroxide radicals were observed. The effect of adding di-*t*-butyl peroxide was to generate alcohol-derived radicals.

$$t\text{-BuOOtBu} \xrightarrow{h\nu} 2t\text{-BuO}\cdot \quad (8)$$

$$t\text{-BuO}\cdot + \mathrm{R'R''CHOH} \longrightarrow t\text{-BuOH} + \mathrm{R'R''\dot{C}OH} \quad (9)$$

The results are summarized for NDCHA in Table 3. The spectra obtained for the alcohols, ethanol and 1-propanol, with NDCHA are shown in Figs. 3 and 4. Only ethanol and 2-propanol were studied for DMNA and, although the spectral intensity was greatly reduced in ethanol, the radicals were the same as in DCHNA.

When a NDCHA : ethanol solution (with or without di-*t*-butyl peroxide) has 10 vol % triethylamine added, only the diethyl nitroxide radical was observed ($a^N=$ 1.58 mT, $a^H=1.08$ mT (4 protons)). Photolysis of a blank solution containing no NDCHA produced no detectable radicals. If the base pyridine was added to a NDCHA : ethanol solution, no radicals were detected on photolysis, whereas on addition of di-*t*-butyl peroxide, the spectrum was the same as when the pyridine was absent.

Fig. 3. (a) The ESR spectrum recorded when a NDCHA: ethanol solution containing di-*t*-butyl peroxide was photolysed at −10 °C. (b) The centre portion of the spectrum expanded. (c) The simulated ESR spectrum of (b) using the coupling constants in Table 3.

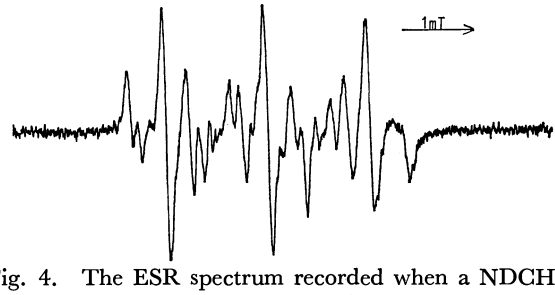

Fig. 4. The ESR spectrum recorded when a NDCHA: 1-propanol solution containing di-*t*-butyl peroxide was photolysed at 10 °C.

Photolysis of Acetone Oxime (AO) and Cyclopentanone Oxime (CPO). As oximes are generated in the photolysis of nitrosamines (Reaction 3), alcohol (2-propanol or ethanol) solutions containing di-*t*-butyl peroxide and AO or CPO were photolysed to see if the oximes would act as spin traps for the alcohol derived radicals (Reaction 9). Only the alcohol radical was observed on photolysis.

If AO or CPO were photolysed in a 25 vol % 2-propanol (or ethanol): acetic acid solution, a nitroxide radical $a^N=a^H=1.40$ mT was observed. When di-*t*-butyl peroxide was added to the solution, the alcohol derived radical was also observed. Obviously the oximes do not act as efficient spin trapping agents for those alcohol derived radicals.

Discussion

Identification of the Radicals. The likely structures for radicals I, II and III, are given below:

$$\mathrm{CH_3-NH-CH_2-\underset{\underset{O}{\vert}}{N}-\overset{\overset{R'}{\vert}}{\underset{\underset{R''}{\vert}}{C}}-OH}$$

I

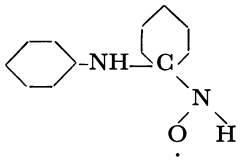

II

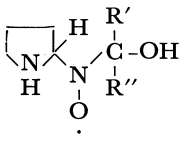

III

R′ and R″ are the substituents on the alcohol (see Reaction 9). The secondary amine nitrogen may also be protonated in these acidic solutions. The large nitrogen coupling constants (1.1—1.4 mT) observed for all radicals are consistent with nitroxide radicals.[7–14] For radicals I and III, the observation of an extra proton splitting (≈0.6 mT) when ethanol or 1-propanol was present is indicative of spin trapping of the alcohol radical[7,8] whereas for II, the a^{H}—a^{N}_{NO} is characteristic of a –NHO fragment.[12] From the magnitude of the smaller nitrogen coupling constant (≈0.3 mT) in all three radicals, it is possible to assign this nitrogen as being directly bonded to the nitroxide nitrogen[9–11] or to a carbon adjacent to this nitrogen.[11,12] However since proton splittings consistent with a CH_2 fragment (a^{H}≈0.8 mT) in I and CH (a^{H}≈0.3 mT) in III were always present and, together with the close similarity between the coupling constants for I, II, and III and those observed for radicals of the form[12]

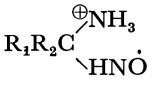

all suggest our assignment for I, II, and III are correct.

All the nitroxide radicals observed when neutral solutions containing di-*t*-butyl peroxide and NDCHA (or NDMA) were photolysed had a^{N}_{NO}≈1.3 to 1.6 mT. This indicates that the radicals are not alkoxy-substituted nitroxides (a ≈2.8 mT)[7,8] formed from *t*-BuO. Some tentative assignments are given in Table 3. In ethanol solutions, where the linewidths were small enough to resolve splittings of about 0.03 mT (Fig. 3), only one of the two radicals could be assigned. The small splittings in both radicals are consistent with protons bound to a β-carbon.[13–14]

Possible Reaction Pathways. As I, II, and III were relatively long lived ($t_{1/2}$≈second) and their steady state concentrations were relatively low, this implies that these radicals are formed by minor pathways. Although I, II, and III are structurally similar it is obvious that II is formed from a mechanism different to I and III as alcohol derived radicals (Reaction 9 and/or 5) are involved in the generation of I and III but not II.

Since the alcohol-derived radicals appear not to be trapped by oximes, it is likely that they are trapped by the *C*-nitroso intermediate[7,8] formed in Reaction 3 to generate I and III

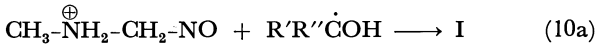

(10a)

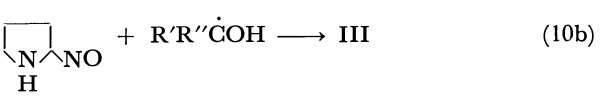

(10b)

The lifetime of the *C*-nitroso compound before it isomerizes to the oxime should be sufficiently long for Eq. 10 to occur as *C*-nitrosomethane and -ethane *etc.* can be isolated and characterized.[15] The increase in yield of I and III on addition of di-*t*-butyl peroxide reflects the additional formation of alcohol radicals through Eq. 9 over the original reaction (Eq. 5).

While II is formed through an alternative mechanism to I and III, the photoproducts from NDCHA are also different from *N*-nitrosodi-*n*-alkylamines and *N*-nitrosocyclicamines (*e.g.* 1-nitrosopiperidine) in that no oxime can be formed (although the *C*-nitroso intermediate might be). The principal product for NDCHA is the imine

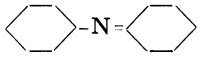

formed *via* Reaction 2, whereas oximes are principal products for the other two classes of nitrosamines.[1,2] The isotopic labelling experiments of Axenrod and Milne[16] have demonstrated that the reactants in Eq. 2 are not necessarily those formed in the original photochemical cage in Eq. 1. Hence the aminyl radical and NO must have a reasonable lifetime in solution (although they were not detected). It is not unreasonable to suggest that some of the dicyclohexylaminyl radicals might rearrange to a carbon centre radical

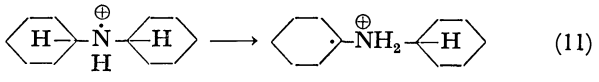

(11)

which then could react with HNO formed in Reaction 2.

(12)

Circumstantial evidence supporting this mechanism is the observation of II but not I when hydrochloric acid was used instead of acetic acid in the photolyses. In NDMA solution, the presence of the stronger acid may increase the rate of nitroso-oxime isomerization and hence minimize the spin trapping reaction (Eq. 10). In the mechanism proposed above for II, there is no equivalent step to be interfered with by the hydrochloric acid.

The absence of I when maleic acid was present is evidence for the facile photoaddition of NDMA to double bonds[17] Eq. 4 whereas with NDCHA, which does not undergo photoaddition[18], radical II was still observed. Apparently photoaddition of NDMA to cyclohexene is not as efficient as to maleic acid since I was still observed with 10 vol % cyclohexene present. However some photoaddition did occur as evidenced by the persistent nitroxide radical (a^{N}_{NO}=1.55 mT, a^{H}=0.18 mT) observed after a static solution was photolysed. This radical is consistent with what would be expected from spin trapping by the photoaddition product in an acetic acid: 2-propanol solution.

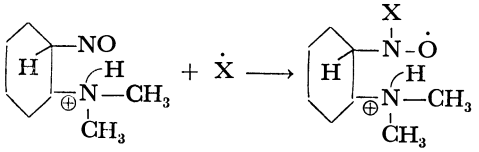

(13)

Although positive identification was not possible of all the nitroxide radicals generated when neutral alcohol and alkaline solutions of DCHNA containing

di-*t*-butyl peroxide were photolysed, these experiments do indicate that nitrosamines are susceptible to reaction with alcohol radicals. The absence of a nitrogen splitting extra to that of the nitroxide nitrogen suggests the pathway, in part, might be Reactions 8 and 9 followed by

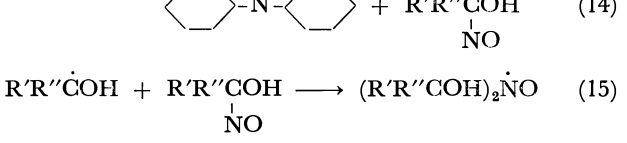

(14)

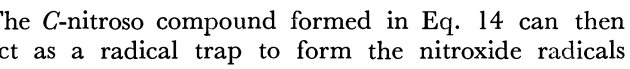

(15)

The *C*-nitroso compound formed in Eq. 14 can then act as a radical trap to form the nitroxide radicals observed in Eq. 15. When the alcohol is 2-propanol apparently a minor reaction is

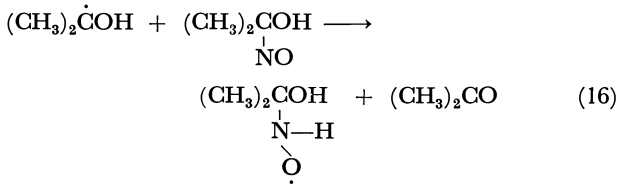

(16)

Reaction 14 may not occur in acid solutions due to protonation of NDCHA.[3] Furthermore, we have no explanation for the results observed when triethylamine was present. However, these results in neutral and alkaline solution support the product analyses[1–4] which conclude that nitrosamines are photolytically active only in acid solutions. In neutral solutions they are only involved in secondary reactions initiated photochemically.

This research was supported by the National Research Council of Canada. The authors thank Dr. K. S. Chen for some helpful discussions.

References

1) Y. L. Chow, *Tetrahedron Lett.*, **1964**, 2333; *Can. J. Chem.*, **45**, 54 (1967).
2) E. M. Burgess and J. M. Lavanish, *Tetrahedron Lett.*, **1964**, 1227.
3) Y. L. Chow, *Acc. Chem. Res.*, **6**, 354 (1973).
4) Y. L. Chow, M. P. Lau, R. A. Perry, and J. N. S. Tam, *Can. J. Chem.*, **50**, 1077 (1972).
5) E. Jakubowski and J. K. S. Wan, *Mol. Photochem.*, **5**, 439 (1973).
6) B. B. Adeleke and J. K. S. Wan, *Mol. Photochem.*, **6**, 329 (1974).
7) E. G. Janzen, *Acc. Chem. Res.*, **4**, 31 (1971).
8) F. P. Sargent and E. M. Gardy, *Can. J. Chem.*, **52**, 3645 (1974).
9) E. G. Janzen, C. A. Evans, and J. I. Liu, *J. Mag. Res.*, **9**, 513 (1973).
10) C. Lagercrantz, *J. Am. Chem. Soc.*, **95**, 220 (1973).
11) G. R. Chalfont, M. J. Perkins, and A. Horsfield, *J. Chem. Soc., B*, **1970**, 401.
12) D. J. Edge and R. O. C. Norman, *J. Chem. Soc., B*, **1969**, 182.
13) H. Lemaire, R. Ramasseul, and A. Rassat, *Mol. Phys.*, **8**, 557 (1964).
14) E. T. Strom and A. L. Bluhm, *Chem. Commun.*, **1966**, 115.
15) H. T. J. Chilton and B. G. Gowenlock, *J. Chem. Soc.*, **1954**, 3174.
16) T. Axenrod and G. W. A. Milne, *Tetrahedron*, **24**, 5775 (1968).
17) Y. L. Chow, *Can. J. Chem.*, **43**, 2711 (1965).
18) Y. L. Chow, C. Colon, and S. C. Chen, *J. Org. Chem.*, **32**, 2109 (1967).

Kinetics and Mechanism of Formation of Pentaammine(glycine)rhodium(III) Ion from Pentaammineaquarhodium(III) Ion and Glycine in Weakly Acidic Media

C. CHATTERJEE* and A. K. BASAK†

Department of Chemistry, Indian Institute of Technology, Powai, Bombay 400076, India

† *Department of Chemistry, University College of Science, Calcutta 700009, India*

(Received July 25, 1978)

The rates of formation of pentaammine(glycine)rhodium(III) ion from pentaammineaquarhodium(III) ion and glycine in weakly acidic media have been studied spectrophotometrically at different glycine and acid concentrations in the temperature range of 60—80 °C. The rate has been found to be insensitive towards the change in ionic strength from μ=0.5 to 2.0 M of the medium. The activation parameters, ΔH^* and ΔS^* values are 22.2±1.0 kcal mol^{-1} and −9.2 e.u. respectively. The results are in accord with a mechanism involving a fast 1:1 outer-sphere association between the pentaammineaquarhodium(III) ion and glycine in zwitter ionic form followed by its transformation into the product by a process where the incoming ligand is appreciably bonded to the metal ion in the transition state.

Kinetics and mechanism of the substitution reactions involving replacement of coordinated water in pentaammineaquacobalt(III), ($3d^6$) ion by various nucleophiles including neutral and anionic in nature have been the subject of several investigations. However, there has been increasing interest in recent years on rhodium(III), ($4d^6$) complexes, which furnish further data for a comparative analysis of the reactivity of related octahedral structures. Though the rates of reactions have been generally found dependent upon the entering ligand concentration, they actually proceed by different mechanisms due to bond formation by the incoming nucleophile which is more significant in the transition state in the case of rhodium(III) than in cobalt(III) as is evident from the water exchange and anation reactions of the complexes of the type $M(NH_3)_5OH_2^{3+}$, where M=Co(III)[1,3a-c] and Rh(III).[2,4,5] In order to test further the generality of nucleophilic attack of the entering group on the substrate Rh(III) complex, it appeared worthwhile to extent the work to uncharged ligands, and with this end in view the kinetics of reactions of pentaammineaquarhodium(III) ion with glycine in weakly acidic media (pH=*ca.* 2—4) forming pentaammine(glycine)rhodium(III) ion $[Rh(NH_3)_5glyH]^{3+}$ has been studied in detail. In order to study the kinetics of such reaction the hitherto unknown $Rh(NH_3)_5glyH^{3+}$ in the form of perchlorate salt has been isolated. The results presented here show indeed a difference in mechanistic behaviour between cobalt(III) and rhodium(III) ions in conformity with the investigations reported earlier.

Experimental

Materials. The pentaammineaquarhodium(III) perchlorate was prepared from pentaamminechlororhodium(III) complex as described in the literature.[6] The purity of the complex was checked by elemental and spectral analyses.[7]

The pentaammine(glycine)rhodium(III) perchlorate was prepared for the first time by refluxing an aqueous solution (50 ml) of pentaammineaquarhodium(III) perchlorate (0.0005 mol) and an excess of glycine(0.005 mol) for few hours at 90 °C. The solution was then concentrated to one third of its original volume and kept in a refrigerator. The resulting crystals were filtered and washed with a water–ethanol(1:1) mixture. The complex was recrystallized from a cold aqueous solution by the addition of 30% perchloric acid. The recrystallized product was washed first with a water–ethanol mixture and finally with absolute ethanol. The purity of the complex was ascertained by the elemental analysis: Calcd for $[Rh(NH_3)_5glyH](ClO_4)_3$: C, 4.28; N, 14.96; H, 3.56%. Found: C, 4.45; N, 14.85; H, 3.58%.

Glycine used were of reagent grade (G. R., E. Merck). All other chemicals used were either of reagent grade purity or prepared in the pure state by suitable methods.

Besides elemental analysis, spectral measurements of glycine complex of rhodium(III) furnish further evidence regarding the mode of bonding of amino acid in the complex. It is well known that an amino acid usually coordinates to a metal ion with its amino and carboxyl groups. In some complexes of cobalt(III),[8,9] however, glycine has been observed to act as an unidentate ligand although no such complexes of rhodium(III) have been isolated before. The analytical results of pentaammine complex clearly indicate the unidentate nature of coordinated glycine molecule. Since the complex was obtained from an acidic solution, the amino acid retains an acidic proton and is coordinated as a neutral ligand in agreement with the elemental analysis. Glycine may be bound with the rhodium(III) ion as an unidentate ligand either with an oxygen atom of the carboxyl group or with the nitrogen atom of the amino group. The results of the absorption measurements for the present complex, however, suggest that the coordination of glycine correspond to the former. The position and intensities of the first and second bands of the glycine complex (λ_{max}; 322 nm, ε_M=144.0, λ_{max}; 266 nm, ε_M=111.0) corresponding to $^1A_{1g}\rightarrow{}^1T_{1g}$ and $^1A_{1g}\rightarrow{}^1T_{2g}$ transitions, match very well with those of the pentaammine carboxylatorhodium(III) ion[7] in which the ligand undoubtedly coordinates to rhodium(III) ion with its carboxyl group. In accord with the postulate of the oxygen-bonded amino acid, IR spectrum of the complex shows a close similarity to that of the corresponding Co(III) complex, with a strong band at about 1630 cm^{-1} assignable to C–O stretching band of the coordinated carboxyl group and the deformation band of $-NH_3^+$ group at about 1490 cm^{-1}.

Apparatus and Procedure. The kinetic measurements were performed employing a Carl-Zeiss(VSU-2P) spectrophotometer with a quartz cell of suitable light path. The pH measurements were made using a radiometer pH meter with a glass electrode and a reference calomel electrode connected to the experimental solution through 1 M NaCl–1 M $NaClO_4$ salt bridges connected in series. The course

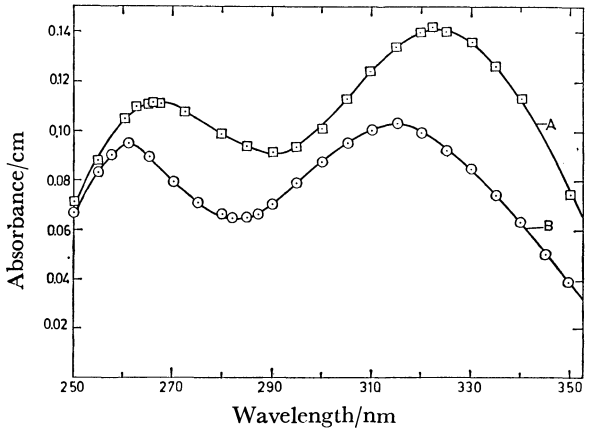

Fig. 1. Absorption spectra.
A: $[Rh(NH_3)_5glyH](ClO_4)_3$, 0.001 M; B: $[Rh(NH_3)_5OH_2](ClO_4)_3$, 0.001 M.

of the anation reactions of pentaammineaquarhodium(III) ion with glycine in weakly acidic media was followed by observing the increase in absorbance at 322 nm where the molar extinction coefficients of the reacting complex and the product differ appreciably (Fig. 1). A sample quenching technique was used. Ionic strength of the solutions was kept constant with sodium perchlorate. The absorbances of the solutions at the end of the reactions were found to be in close agreement with those of the solution containing isolated complex, indicating that under the experimental conditions there was no interference due to reverse aquation of the glycine complex. The concentrations of the reactants were such that the pseudo first order rate law was applicable and the pseudo first order anation rate, k_{obsd}, was evaluated graphically for each experiment by plotting $\log (A_\infty - A_0)/(A_\infty - A_t)$ *versus* time (t), where A denotes measured absorbance and subscripts denote time as usual. A_∞ is the calculated value for complete transformation of the aqua complex to the pentaammine(glycine)rhodium(III) complex.

Results and Discussion

The pseudo first order rate constant, k_{obsd}, was evaluated under different sets of experimental conditions (*viz.* glycine concentration, acid concentration, temperature and ionic strength). It has been observed that at constant pH, (*i.e.*, keeping T_G/T_A constant, where T_G and T_A are the concentrations of total glycine and perchloric acid respectively in the experimental solution) the rate shows first order dependence on total glycine concentration (Fig. 2), and at a fixed glycine concentration the rate decreases with increase in acid concentration (Fig. 3). The experimental conditions were so chosen that the reacting complex present in the aqua form and the results are consistent with the sequence of changes as delineated below:

$$GH + H^+ \rightleftharpoons GH_2^+ \quad (1)$$

$$R^{3+}\text{-}OH_2 + GH \rightleftharpoons R^{3+}\text{-}OH_2\cdots GH \quad \text{(outer sphere association)} \quad (2)$$

$$\downarrow k' \text{ slow}$$

$$R^{3+}\text{-}GH + H_2O \quad (3)$$

where $R^{3+}=Rh(NH_3)_5^{3+}$.
According to the above scheme,

$$k_{obsd} = K_{o.s.} \cdot k'[GH] \quad (4)$$

where $K_{o.s.}$ is the outer sphere association constant.

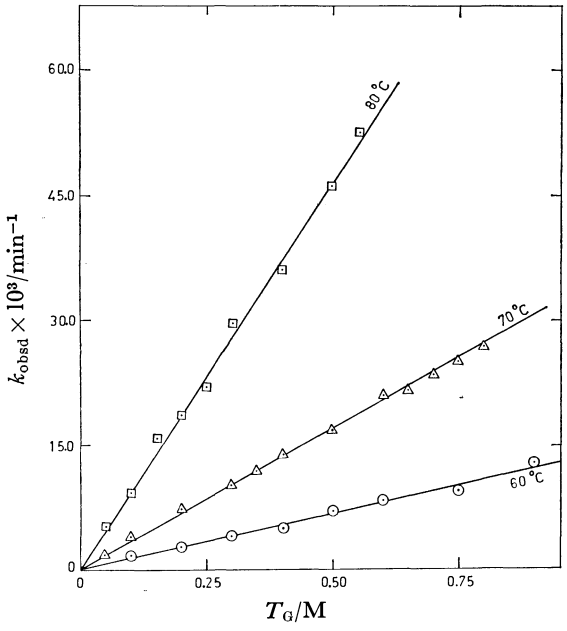

Fig. 2. Dependence of k_{obsd} on total glycine concentration (T_G). $[Rh(NH_3)_5OH_2^{3+}]$, 0.001 M; $T_G/T_A=20.0$; $T_A=[HClO_4]$; $\mu(HClO_4+NaClO_4)$, 1.0.

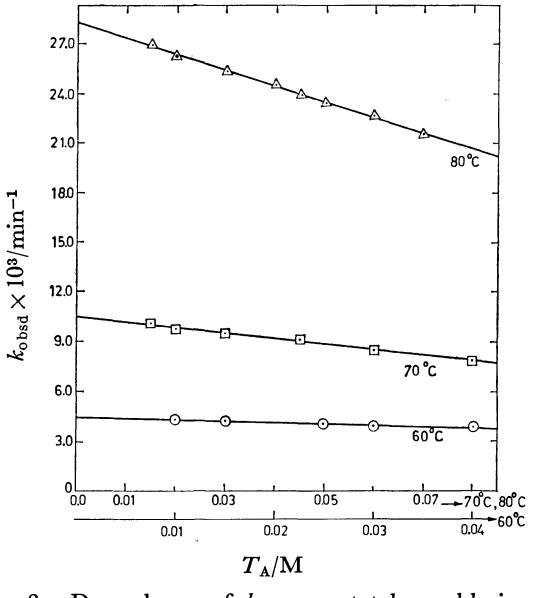

Fig. 3. Dependence of k_{obsd} on total perchloric acid concentration (T_A) at constant glycine concentration. $[Rh(NH_3)_5OH_2^{3+}]$, 0.001 M; $T_G=0.3$ M; $\mu(HClO_4+NaClO_4)$, 1.0.

From the protonation equilibrium of glycine (Eq. 1), the value of GH in terms of T_G and T_A can be expressed in the following manner:

$$T_G = [GH] + [GH_2^+],$$

$$T_A = [GH_2^+] + [H^+],$$

$$K_H = T_A - [H^+]/(T_G - T_A + [H^+])[H^+]. \quad (5)$$

On simplifying Eq. 5 and neglecting insignificant $[H^+]^2$ term we have $[H^+]=T_A/K_H T_G - K_H T_A + 1$.
Substituting the value of $[H^+]$

$$[GH] = T_G(1 + T_G K_H - T_A K_H)/(1 + T_G K_H). \quad (6)$$

Hence Eq. 4 can be written as

TABLE 1. VALUES OF THE RATE CONSTANTS AND ACTIVATION PARAMETERS ($\mu=1.0$)

Temp °C	$k/10^2$ M^{-1} min^{-1} I[a]	II[b]	III[c]	Average
60	1.35	1.47	1.38	1.40
70	3.42	3.50	3.38	3.43
80	9.36	9.40	9.45	9.40

ΔH^*, 22.2±1.0 kcal mol^{-1}. ΔS^*, −9.2 e.u.
a) From k_{obsd} *vs.* T_G plot at fixed value of T_G/T_A. b) From intercept of k_{obsd} *vs.* T_A plot at fixed value of T_G. c) From slope of k_{obsd} *vs.* T_A plot at fixed value of T_G.

TABLE 2. ACTIVATION PARAMETERS FOR THE REACTIONS OF $M(NH_3)_5OH_2^{3+}$ IONS (M=Co or Rh)

System	ΔH^* kcal mol^{-1}	ΔS^* e.u.	Ref.
$Co(NH_3)_5OH_2^{3+}/O^{18}H_2$	26.6±0.3	6.7	1
$Co(NH_3)_5OH_2^{3+}$/glyH	27.6	5.2	11
	29.0	—	12
$Rh(NH_3)_5OH_2^{3+}/O^{18}H_2$	23.9±0.3	−3.0	2
$Rh(NH_3)_5OH_2^{3+}$/glyH	22.2±1.0	−9.2	Present work

$$k_{obsd} = kT_G - kT_AT_GK_H/(1+T_GK_H) \quad (7)$$

where $k=k'\cdot K_{o.s.}$ and K_H=equilibrium constant for the protonation of glycine (Eq. 1). Under the experimental conditions the value[10] of K_H is *ca.* 200 and hence $T_GK_H \gg 1$. Consequently Eq. 7 may be written as

$$k_{obsd} \approx k(T_G - T_A) \quad (8)$$

$$\approx k(1-T_A/T_G)T_G. \quad (9)$$

The observed dependence of rate on T_A and T_G mentioned above are in conformity with the Eqs. 8 and 9 respectively. The value of k for any particular temperature could be evaluated independently from (i) the slope of k_{obsd} *vs.* T_G plot (Fig. 2) and also from (ii) the slope and intersept of k_{obsd} *vs.* T_A plot (Fig. 3). The values thus obtained are in good agreement with each other and are listed in Table 1. In case of anation of amino acid complex, $K_{o.s.}$ represents the outer sphere complex formation constant between $[Rh(NH_3)_5OH_2]^{3+}$ and the amino acid zwitter ion. Although the net charge of amino acid is zero, the zwitter ion has a separated negative charge on the carboxylate part and can undergo ion pair formation with multivalent cation. Since the net charge of glycine zwitter ion is zero, the $K_{o.s.}$ value should be smaller than those for anionic ligands. The influence of ionic strength on the anation reaction has been studied and the value of rate constant at fixed T_G/T_A has been found to be almost independent of the variation of ionic strength from μ=0.5 to 2.0 M of the medium. This lack of dependence of rate on ionic strength clearly excludes the participation of either G^- or GH_2^+ ion as a reactive species in the anation process. Hence, the overall reaction is best accounted for as an ion pair equilibrium followed by the slow interchange of the bound water and the entering ligand in the ion pair. The ΔH^* and ΔS^* values for the reactions were evaluated in the usual way by making use of Eyring equation from the k values at different temperatures (Table 1). The activation parameters for the water exchange and formation of glycine complex of similar octahedral cobalt(III) and rhodium(III) complexes are collected in Table 2 for the sake of comparison. A perusal of the results reveals that ΔH^* values for the water exchange[2] and for the present system of rhodium(III) complex are fairly close and much smaller than those of the corresponding cobalt(III) systems.[1,11,12] On the basis of the values of the activation parameters, the water exchange of $[Co(NH_3)_5OH_2]^{3+}$ and replacement of aqua ligand by glycine have been proposed to take place by dissociative mechanism. However, if the same type of mechanism is operative for the present system, owing to the greater loss of crystal field energy one would expect a higher enthalpy of activation for the rhodium(III) complex compared to analogous and isoelectronic (d^6) cobalt(III) substrates. Thus the experimental results cannot be explained by above mechanism, but suggest significant bond formation by the reagent in the transition state in the transformation of the outer sphere associated species. Moreover, a decrease of ΔS^* towards a negative value, going from cobalt(III) to rhodium(III) system is also in keeping with a mechanism involving a more pronounced participation of the incoming ligand in the transition state for the latter. Hence, on the basis of ΔH^* and ΔS^* values it may be concluded that the transformation of outer sphere complex into the product occurs by a sort of associative process in which the bond making and bond breaking in the transition state proceed synchronously.

The authors thank Professor K. Saito of Tohoku University, Japan, for the sample of $RhCl_3\cdot 3H_2O$ used in the preparation of the title compounds. Helpful discussions with Professor D. Banerjea are gratefully acknowledged.

References

1) H. R. Hunt and H. Taube, *J. Am. Chem. Soc.*, **80**, 2642 (1958).
2) F. Monacelli and E. Viel, *Inorg. Chim. Acta*, **1**, 467 (1967).
3) a) C. H. Langford and W. R. Muir, *J. Am. Chem. Soc.*, **89**, 3141 (1967); b) J. O. Edwards, F. Monacelli, and G. Ortaggi, *Inorg. Chim. Acta*, **11**, 47 (1974), and references cited therein; c) D. A. House, *Coord. Chem. Rev.*, **23**, 246 (1977).
4) F. Monacelli, *Inorg. Chim. Acta*, **2**, 263 (1968).
5) C. Chatterjee and P. Chaudhuri, *Indian J. Chem.*, **11**, 777 (1973).
6) G. W. Bushnell, G. C. Lalor, and E. A. Moelwyn-Hughes, *J. Chem. Soc., A*, **1966**, 719.
7) H. H. Schmidtke, *Z. Phys. Chem.*, **45**, 307 (1965).
8) J. Fujita, T. Yasui, and Y. Shimura, *Bull. Chem. Soc. Jpn.*, **38**, 654 (1965).
9) G. Brubaker and P. D. Schaffer, *Inorg. Chem.*, **10**, 811 (1971).
10) L. G. Sillén and A. E. Martell, "Stability Constants for Metal-ion Complexes," The Chemical Society London, (1964), Special Publication No. 17, Table No. 130; p. 337.
11) D. Banerjea and J. Roy, *Z. Anorg. Allg. Chem.*, **400**, 89 (1973).
12) T. Murakami, K. Ogino, H. Kobayashi, and K. Saito, *Bull. Chem. Soc. Jpn.*, **44**, 129 (1971).

Studies on Uranyl Complexes. II. Unidentate Carboxylate Coordination in Uranyl Complexes of α-, β-, and γ-Amino Acids: A Polarographic Study††

V. V. RAMANUJAM,* K. RENGARAJ,† and B. SIVASANKAR

Department of Inorganic Chemistry, University of Madras, A.C. College of Technology Campus, Madras 600025, India

†*Department of Chemical Engineering, A.C. College of Technology, Madras 600025, India*

(Received September 7, 1978)

Polarographic investigation of uranyl complexes with potentially bidentate α-, β-, and γ-amino acids have been carried out. The polarographic behaviour of these complexes as a function of pH and ligand concentration has revealed the nature of binding to be unidentate carboxylate coordination in the complexes. The amino group is not involved in coordination. The relative stabilities of α-, β-, and γ-amino acid complexes are discussed.

While the chelates formed by amino acids with 3d metal ions have been fairly well characterized, the amino acid complexes of *f* block metal ions have received relatively much less attention. Even among the few investigations carried out on uranyl–amino acid complexes reports are conflicting regarding the chelating ability of the amino acids towards this ion, and the effect of ring size and substituents of the complexes. Cefola *et al.*,[1] Farooq *et al.*,[2] and Tewari *et al.*[3] have postulated chelation involving the carboxyl oxygen and the amino nitrogen in uranyl complexes with glycine, α-alanine, asparagine and glutamine, while Li *et al.*[4] and Feldman *et al.*[5] have suggested that the amino nitrogen is not involved in coordination in uranyl complexes of glycine, serine, aspartic acid and glutamic acid.

The present investigation is oriented primarily towards establishing the nature of binding in uranyl complexes with simple amino acids, *i.e.* to find whether complexation occurs through the amino nitrogen and carboxyl oxygen leading to chelation or whether the ligand is bound only through the carboxyl oxygen. When a complex is reduced under polarographic conditions, the magnitude of the shift in $E_{1/2}$ relative to the simple aqua ion is a measure of the stability of the complex. A chelate complex shows, because of its higher stability, a much larger shift in $E_{1/2}$ than a non-chelate one. Further the amino acid ligand (anion) on liberation from the complex undergoing polarographic reduction gets protonated depending on pH conditions. A study of the polarographic behaviour under varying pH conditions yields useful information on the way in which the ligand is bound as an anion or as a zwitter ion and so on, from which the nature of binding can be inferred.[6,7] Stability constants obtained from polarographic measurements of the complexes are reported.

Experimental

The effect of varying pH on the $E_{1/2}$ of uranyl complexes at constant concentration of ligand and the effect of varying ligand concentration on $E_{1/2}$ at constant pH were investigated by measuring the $E_{1/2}$ values for solutions containing 8×10^{-4} M (M=mol dm^{-3}) $UO_2(ClO_4)_2$ maintained at a constant ionic strength of 0.1 M with respect to $NaClO_4$ and at a temperature of 30.0±0.1 °C. The polarograms were recorded with an automatic Metrimpex type OH 105 Universal Polarograph with a three-electrode set up. Some of the complexes were studied with a manual set up consisting of the polarographic bridge of Physics Instruments Co., in conjunction with a Multiflex galvanometer for measuring diffusion currents and a Leeds Northrup K 3 Universal Potentiometer for measuring the applied potentials. The electrode characteristics were: $h=40.0\pm0.5$ cm, $t=3.85$ s, and $m^{2/3}t^{1/6}=4.25$ mg$^{2/3}$ s$^{-1/2}$. The $E_{1/2}$ values were measured to an accuracy of ±0.5 mV and were reproducible to ±2 mV. The reversibility of each system studied was checked by logarithmic analysis or by measuring the difference in $E_{1/4}-E_{3/4}$ values. The reduction of UO_2^{2+} ion was found to be a reversible one electron process with an $E_{1/2}$ of −0.175 V (*vs.* SCE).

Conductometric titrations of the sodium salts of the ligands against uranyl perchlorate were performed for determining the maximum number of ligand molecules coordinated to the uranyl ion. A direct-reading conductance meter (Toshniwal Conductivity Analyser type L 01.06) provided with a cell of cell constant 0.738 was used. All pH measurements were made with an Elico pH meter (Model L I.10T). The dissociation constants of the amino acids were determined potentiometrically. All the chemicals used were of BDH or Fluka puriss grade.

Results and Discussion

The ligands chosen were glycine, DL-α-alanine, DL-2-aminobutyric acid, β-alanine, 4-aminobutyric acid and isobutyric acid, all except the last one potentially bidentate ligands capable of forming five-, six-, or seven- membered rings. Isobutyric acid was chosen as a reference ligand having only unidentate function through its carboxyl group. A comparison of the shift in $E_{1/2}$ for polarographic reduction of the amino acid complexes with that for the isobutyrate complex would show whether chelation occurs or not, and if it occured, yield information correlating ring size and stability of the complex.

Effect of pH *on the* $E_{1/2}$ *of the Complexes.* The manner in which $E_{1/2}$ depends on pH often provides useful information regarding the electrode reactions and the different species existing under different pH conditions and thus the mode of binding in the complex.

The coordinating(donor) atom exists in the protonat-

†† Abstracted in part from the Ph. D. Thesis submitted by K. Rengaraj to the University of Madras, 1978.

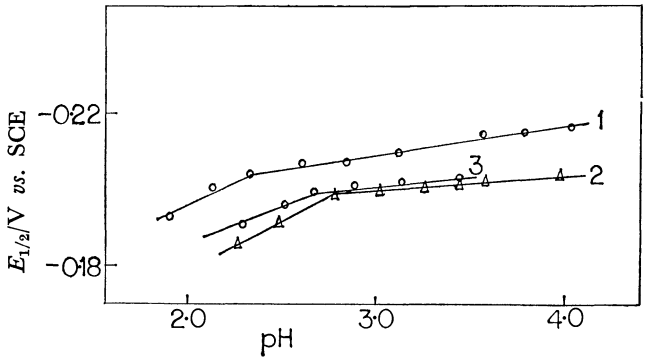

Fig. 1. Uranyl-α-amino acid complexes: plot of pH *vs.* $E_{1/2}$. 1: Glycinate, 2: α-alaninate and 3: DL-2-aminobutyrate. Concentrations: $[UO_2^{2+}]=0.0008$ M, [glycine]=0.1067 M, [α-Alanine]=0.09114 M, [2-aminobutyric acid]=0.1063 M.

Table 1. Stability constants of uranyl complexes of α-, β- and γ-amino acids

Complex	Dissociation constants of ligands		pH range	$\log \beta UO_2(HL)_2^{2+}$
	pK_{COOH}	$pK_{NH_3^+}$		
Glycinate	2.45	9.69	2.5—4.0	2.14
α-Alaninate	2.48	9.67	2.7—4.0	2.15
2-Aminobutyrate	2.36	9.60	2.7—4.0	2.12
β-Alaninate	3.60	10.07	3.5—4.3	3.49
4-Aminobutyrate	4.04	10.26	3.00—4.10 and 4.1—5.4	4.44
Isobutyrate	4.76	—	3.00—4.8	5.66[a]

a) $\log \beta_{ML_2}$

ed form over a range of pH, and complexation takes place with deprotonation. On polarographic reduction of the complex, the liberated ligand will recombine with protons if pH conditions suit such protonation. In solutions of pH greater than the pK of the coordinating group, protonation would not occur. If, however, the solution pH is below the pK of the coordinating group, the released ligand will get protonated. A plot of the variation of the measured $E_{1/2}$ with pH would show breaks corresponding to the pK values of the coordinating groups present in the ligand.

For the potentially bidentate amino acid with amino and carboxyl groups as possible coordinating groups the following relationships between $E_{1/2}$ and pH are valid.

1. At $pH<pK_{COOH}<pK_{NH_3^+}$:

$$E_{1/2} = E^\circ_s - \frac{0.0591}{n}\log \beta_{ML_p} - p\frac{0.0591}{n}\log K_1K_2[L^-] - 2Z\frac{0.0591}{n}pH.$$

2. At $pH=pK_{COOH}<pH<pK_{NH_3^+}$:

$$E_{1/2} = E^\circ_s - \frac{0.0591}{n}\log \beta_{ML_p} - p\frac{0.0591}{n}\log K_2[L^-] - Z\frac{0.0591}{n}pH.$$

3. At $pH>pK_{NH_3^+}>pK_{COOH}$:

$$E_{1/2} = E^\circ_s - \frac{0.0591}{n}\log \beta_{ML_p} - p\frac{0.0591}{n}\log [L^-].$$

Here K_1 and K_2 correspond to pK_{COOH} and $pK_{NH_3^+}$ respectively. $E_{1/2}$ is the half-wave potential of the complex and E°_s is the standard reduction potential of the cation $\simeq E_{1/2}$ of the uncomplexed aqua ion; β_{ML_p} is the overal stability constant of the complex ML_p, and Z is the number of protons involved in the electrode reaction.

The slope $d(E_{1/2})/d(pH)$ of each region of the $E_{1/2}$ *vs.* pH diagram is equal to $0.0591/n$ Z, where Z is the number of protons involved in the electrode reactions which will be 2, 1, and 0 at $pH<pK_{COOH}$, $pK_{COOH}<pH<pK_{NH_3^+}$, and $pH>pK_{NH_3^+}>pK_{COOH}$, respectively.

Uranyl-α-Amino Acid Complexes. The variation of $E_{1/2}$ as a function of pH was investigated between pH 1.80 and 4.0 with all the three α-amino acid complexes. The $E_{1/2}$ *vs.* pH diagrams (Fig. 1) show breaks at pH values 2.35 for glycinate, 2.70 for α-alaninate, and 2-aminobutyrate complexes. The pK_{COOH} values of these acids are presented in Table 1. Below pH 1.80 the $E_{1/2}$ values were found to be independent of pH with a constant value of −0.175 V (*vs.* SCE). Since this is the $E_{1/2}$ of the uncomplexed aqua uranyl cation, the inference is that no complexation occurs. Beyond pH 4.0 the polarograms were distorted possibly due to hydrolysis. In the region of $pH>pK_{COOH}$, the $E_{1/2}$ values were very nearly independent of pH upto about pH 4 in all the cases. With the experimental pH below the $pK_{NH_3^+}$ of the acids concerned, the amino group, if involved in coordination, would get protonated at the electrode surface on liberation when the complex undergoes polarographic reduction. No such protonation was indicated from the experimental studies. The inference is that the amino group is not involved in coordination. In other words, no chelate ring is formed.

The effect of the ligand concentration was investigated at pH 3.15±0.1 for glycinate, 3.25±0.1 for α-alaninate, and at pH 3.5±0.1 for 2-aminobutyrate complex. The plots of $E_{1/2}$ *vs.* $\log HL$[10] for all the three complexes gave a $(p\text{-}q)$ (where p and q are the number of ligands attached to the metal in the oxidised and reduced forms respectively) value of two in the ligand concentration range of 0.17—0.6 M. Since polarographic reduction of the complexed $(UO)_2^{2+}$ ion occurs only to the lower oxidation state (UO_2^+) and not to the metallic state, the variation of $E_{1/2}$ with ligand concentration will indicate only the difference in the number of ligands coordinated to the higher and lower oxidation states and thus only the ratio of stability constants of the complex between the oxidized and reduced forms can be determined.[8] However, if the absolute value of 'p' or 'q' is known, it is possible to calculate the individual stability constants.[9] The value of 'p' was found to be two from conductometric titrations. Figure 3 gives the conductemetric titration of the sodium salt of α-alaninate against uranyl perchlorate. The break at 5 ml of uranyl perchlorate corresponds to the formation of the complex species with the metal: ligand ratio of

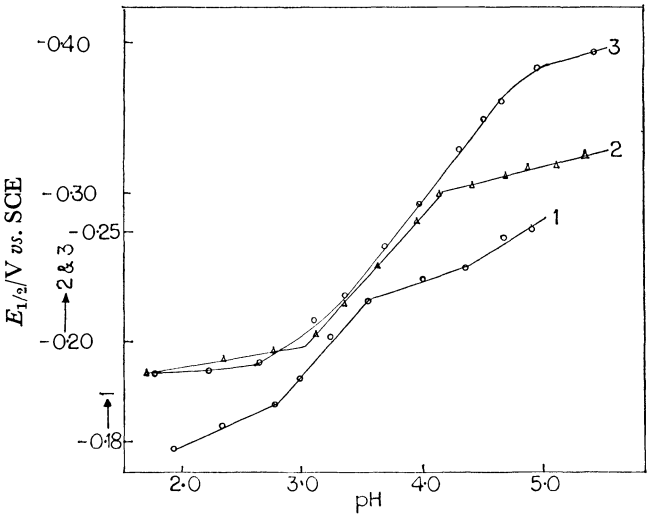

Fig. 2. Variation of $E_{1/2}$ with pH for uranyl complexes. 1: β-Alaninate, 2: 4-aminobutyrate and 3: isobutyrate. Concentrations: $[UO_2^{2+}]=0.0008$ M, [β-alanine]= 0.1007 M, [4-aminobutyric acid]=0.1008 M, [isobutyric acid]=0.100 M.

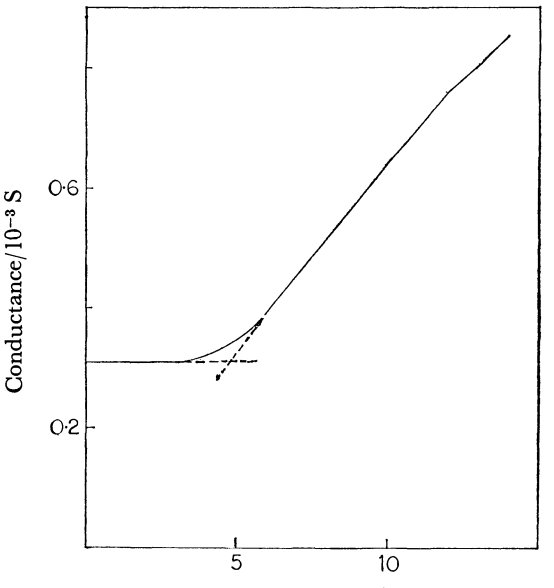

Fig. 3. Concudctometric Titration of sodium salt of α-alanine *vs.* uranyl perchlorate. 10 ml of ligand (0.08072 M)+100 ml water titrated against uranyl perchlorate (0.0801 M).

1:2. The value of '*p*', the maximum number of ligands coordinated to the metal is thus 2. Since (*p-q*) values determined polarographically are also found to be equal to two, it is evident that '*q*' is zero and that UO_2^+ ion does not form a complex. The stability constants of the complexes calculated using Lingane equation[10] give the $\log \beta_{M(HL)_2^{2+}}$ values presented in Table 1.

The similarity in the nature of binding in these complexes is evident from (a) the identical nature of the $E_{1/2}$ *vs.* pH curves, (b) the similar $\Delta E_{1/2}$ values for similar concentrations of the ligands under similar conditions of pH and (c) the close similarity in the $\log \beta_{M(HL)_2^{2+}}$ values. The low $\log \beta_{M(HL)_2^{2+}}$ values are indicative of the absence of chelation. The electrode reaction for all the three complexes may be expressed in the general form (at $pH > pK_{COOH}$)

$$UO_2(HL)_2^{2+} + e^- \rightleftharpoons UO_2^+ + 2HL,$$

HL being the zwitter ion of the type $H_3N^+-CH_2-COO^-$.

Uranyl–β-Alaninate Complex. The variation of $E_{1/2}$ with pH investigated in the pH region of 1.90—4.90 indicated that below pH 1.90 complexation did not occur and beyond pH 4.90 the polarograms were distorted. The $E_{1/2}$ *vs.* pH diagram (Fig. 2) showed a break at pH 3.5 corresponding to pK_{COOH} of β-alanine (*cf.* Table 1). In the pH region between 2.75 and 3.5 the $d(E_{1/2})/d(pH)$ slope has a value of 0.055 corresponding to the involvement one proton per metal atom in the reduction process. The variation of $E_{1/2}$ with ligand concentration indicated the (*p-q*) value to be one. However, conductometric titrations of the sodium salt of β-alanine with uranyl perchlorate indicated the value of '*p*' to be two. It is evident that one ligand molecule is coordinated to the UO_2^+ ion. The electrode process may be formulated as (at $pH < pK_{COOH}$)

$$UO_2(HL)_2^{2+} + H^+ + e^- \rightleftharpoons UO_2(HL)^+ + H_2L^+$$

H_2L^+ being the species $H_3N^+-(CH_2)-COOH$.

In the pH region beyond pK_{COOH}, the $E_{1/2}$ values were very nearly independent of pH upto about pH 4.30, beyond which once again the $E_{1/2}$ values became pH dependent possibly due to hydrolytic reactions and formation of hydroxo species. The fact that protons are not involved in the reduction process in the pH region between 3.5 and 4.3 leads to the inference that the amino nitrogen is not coordinated to the metal atom. The plot of $E_{1/2}$ *vs.* log HL indicated the value of (*p-q*) to be two in the ligand concentration range of 0.1 to 0.7 M. Since the value of '*p*' determined conductometrically was also equal to two, '*q*' was taken to be zero meaning that UO_2^+ ion was not complexed. The electrode reaction in this region is expressed by the following equation at $pK_{COOH} < pH < pK_{NH_3^+}$,

$$UO_2(HL)_2^{2+} + e^- \rightleftharpoons UO_2^+ + 2HL.$$

The stability constant was calculated using Lingane equation, and the $\log \beta_{M(HL)_2^{2+}}$ value was found to be 3.49 ± 0.05.

Uranyl–4-Aminobutyrate Complex. The variation of $E_{1/2}$ with pH (Fig. 2) indicated that below pH 1.70, UO_2^{2+} ion was not complexed and beyond pH 5.4, precipitation occurred for a metal concentration of 8×10^{-4} M and ligand concentration of 0.1 M. The break corresponding to pK_{COOH} (4.04) was observed at pH 4.10. In the pH region 3—4.1 the number of protons involved in the reduction was found to be two. The $E_{1/2}$ values were independent of pH at $pH > pK_{COOH}$, clearly indicating the absence of coordination by the amino nitrogen. The variation of $E_{1/2}$ with ligand concentration investigated at pH 4.9 indicated the value of (*p-q*) to be two, and the value of '*p*' was found to be two from conductometric titrations. The electrode processes between pH 3.00 and

4.10 ($pH < pK_{COOH}$)

$$UO_2(HL)_2^{2+} + 2H^+ + e^- \rightleftharpoons UO_2^+ + 2H_2L^+,$$

and at pH 4.9 ($pH > pK_{COOH}$)

$$UO_2(HL)_2^{2+} + e^- \rightleftharpoons UO_2^+ + 2HL.$$

The $\log \beta_{M(HL)_2^{2+}}$ calculated using the Lingane equation was found to be 4.44±0.05.

Uranyl–Isobutyrate Complex. Below pH 2.0 complexation of uranyl was not observed and above pH 5.7 the metal precipitated. The break in the $E_{1/2}$ *vs.* pH relationship (Fig. 2), was observed at 4.8, the pK_{COOH} of the ligand being 4.76. In the pH region below pK_{COOH} the $d(E_{1/2})/d(pH)$ has a value of 0.11 corresponding to the involvement of two protons in the reduction process. The effect of ligand concentration on $E_{1/2}$ was investigated at pH 3.05. The plot of $E_{1/2}$ *vs.* $\log L^-$ gave a value of two for $(p\text{-}q)$ and the value of 'p' was found to be two from conductometric titrations. The stability constant ($\log \beta_{ML_2}$) was found to be 5.66±0.10. The electrode process may be formulated as ($pH < pK_{COOH}$)

$$UO_2L_2 + 2H^+ + e^- \rightleftharpoons UO_2^+ + 2HL.$$

Conclusions. The $\Delta E_{1/2}$ values for the typical amino acid complexes of uranyl reported here are lower than that for the unidentate complex formed by isobutyric acid. So are the $\log \beta_{M(HL)_2^{2+}}$ values. The results clearly indicate that the amino acids do not form chelate complexes with uranyl ion. Furthermore, the carboxyl group itself is rendered a poorer complexing site because its basicity is lowered by the proximity of the more basic amino group in the same molecule. It may be seen from the figures that $\Delta E_1/_2$ for uranyl ion in the presence of α-, β-, and γ-amino acids are all lower than the value in the presence of isobutyric acid for similar conditions of pH and ligand concentration. If chelate rings had been formed, the $\Delta E_{1/2}$ values would have been larger.

The range of pH in which the complexes undergo reduction reversibly before hydrolysis sets in is also indicative of the relative stabilities of the complexes. For α-amino acid systems the maximum pH upto which hydrolysis can be neglected is 4.0, 4.9 for β-alaninate, 5.4 for 4-aminobutyrate, and 5.7 for isobutyrate complexes.

The order of stability of uranyl complexes in the present investigation turns out to be isobutyrate>4-aminobutyrate>β-alaninate>glycinate = α-alaninate = 2-aminobutyrate. This order clearly points to the absence of chelation in uranyl amino acid complexes.

References

1) M. Cefola, R. C. Taylor, P. S. Gentile, and A. V. Celiano *J. Phys. Chem.*, **66**, 790 (1962).
2) Omar Farooq, A. V. Malik, N. Ahmed, and S. M. F. Rahman, *J. Electroanal. Chem.*, **24**, 464 (1970).
3) R. C. Tewari and M. N. Srivastava, *Talanta*, **20**, 360 (1973).
4) N. C. Li, E. Doody, and J. M. White, *J. Am. Chem. Soc.*, **80**, 5901 (1958).
5) I. Feldman and L. Koval, *Inorg. Chem.*, **2**, 145 (1963).
6) I. M. Kolthoff and C. Auerbach, *J. Am. Chem. Soc.*, **74**, 1452 (1952).
7) R. L. Pecsok, *Anal. Chem.*, **25**, 561 (1953).
8) D. R. Crow, "Polarography of Metal Complexes," Academic Press, London (1969), p. 75.
9) J. Hala, *Cell. Czech. Chem. Commun.*, **29**, 905 (1964).
10) J. J. Lingane, *Chem. Rev.*, **29**, 1 (1941).

NOTES

BULLETIN OF THE CHEMICAL SOCIETY OF JAPAN, VOL. 52 (9), 2717—2718 (1979)

Flat-band Potential of p-Type GaP in Acetonitrile Solutions

Kiyoshi SATOH, Hiroshi YONEYAMA,* and Hideo TAMURA*

Department of Applied Chemistry, Faculty of Engineering, Osaka University, Yamadakami, Suita, Osaka 565

(Received February 20, 1979)

Synopsis. An interaction of quinone compounds such as tetrachloro-*p*-benzoquinone and *p*-benzoquinone with surface hydroxyl groups of a p-type GaP electrode seems to play an important role in determining the magnitude of photovoltage in acetonitrile solutions. The same holds for p-type InP and Si.

The maximum photovoltage at an illuminated semiconductor electrode in a redox electrolyte is equal to the potential difference between the flat-band potential of the electrode E_{fb} and the redox potential of the electrolyte.[1] In aqueous solutions, E_{fb} is in many cases a function of the solution pH, not being influenced by the redox species. Thus, a theoretical maximum photovoltage can be estimated easily by using E_{fb} measured in a base electrolyte into which a redox species is added. However, this may not be true in nonaqueous electrolytes,[2] although the invariance of E_{fb} has sometimes been assumed.[3-5] This note reports on the finding that the interaction of an organic redox species with hydroxyl groups of the electrode surface changes E_{fb} to a large extent.

Experimental

p-Type GaP, InP, and Si were used. Etching of GaP and InP was carried out with HCl, and that of Si with CP-4A.[6] Immediately after chemical etching, the electrodes were washed with de-ionized water for 15 min, followed by rinsing with acetonitrile (AN), and finally dried under evacuated conditions. An Ag wire immersed in AN containing 0.01 mol dm^{-3} $AgNO_3$ was used as a reference electrode. The potential given in this paper refers to this electrode.

Acetonitrile was purified according to the procedure reported.[7] Tetraethylammonium perchlorate (TEAP) as a supporting electrolyte was prepared in this laboratory. Its concentration was usually 0.1 mol dm^{-3}. Tetrachloro-*p*-benzoquinone (Chloranil CA) and *p*-benzoquinone (BQ) used as redox species were of reagent grade. The redox electrolytes of CA/CA$^{\cdot-}$ and BQ/BQ$^{\cdot-}$ were prepared by electrolyzing CA and BQ in TEAP/AN at -0.45 and -0.95 V, respectively, where CA$^{\cdot-}$ and BQ$^{\cdot-}$ denote the anion radicals of CA and BQ. A 500 W xenon lamp was used as a light source.

Results and Discussion

BQ and CA were found to be reduced almost reversibly to give BQ$^{\cdot-}$ and CA$^{\cdot-}$, respectively, making it possible to estimate the formal potential E^0 of BQ/BQ$^{\cdot-}$ and CA/CA$^{\cdot-}$ from the halfwave potentials of the reduction reaction,[8,9] the estimated E^0 being -0.81 and -0.31 V, respectively. The value of E_{fb} of p-type Si reported[4] is *ca.* -0.4 V; that of p-type GaP would be *ca.* 0.8 V, as judged from the reported value for n-type GaP.[2] The value of E_{fb} of p-type InP determined in TEAP/AN is *ca.* 1.2 V. Although the reproducibility is poor, it is not a serious problem. If the redox species has no significant influence on E_{fb}, the maximum photovoltage values given in Table 1 would be expected. In the case of InP the potential difference between E_{fb} and the redox potential exceeds the bandgap of InP, so that no electrochemical equilibrium can be established.

The open circuit potentials of the semiconductor electrodes in the dark were almost equal to the redox potentials of the electrolytes. When illumination of 1.8 W/cm^2 was made, the electrode potential shifted anodically by the amount of the photovoltage (Table 1). The photovoltage increased by 60—80 mV with increasing illumination intensity from 0.18 to 1.8 W/cm^2, gradually tending to saturation. This suggests that the maximum photovoltage cannot be achieved even under imaginary intense illumination conditions. In addition it should be noted that (1) the photovoltage appeared in the system where it was not expected (Si–CA/CA$^{\cdot-}$), and (2) almost the same photovoltage was obtained at the same electrode independent of the kind of the redox electrolyte. These results suggest that E_{fb} is variable in such a manner that the more negative the redox potential of a chemical species added to TEAP/AN, the larger the negative shift of E_{fb}. This was investigated in detail for p-type GaP.

Values of E_{fb} of a p-type GaP electrode in a variety of electrolytes, obtained by Schottky-Mott plots of the electrode capacitance, are given in Table 2. The capacitance was measured at 0.5, 1.0, and 5 kHz, the same E_{fb} being obtained. However, E_{fb} was scattered to about ± 0.2 V when pretreatment of the electrode was repeated in each run. The scatter was large enough to shadow a small change in E_{fb} which

TABLE 1. THE MAXIMUM PHOTOVOLTAGE PREDICTED AND VALUES EXPERIMENTALLY OBTAINED WITH ILLUMINATION OF 1.8 W/cm^2

Electrode	Redox species[a)]	ΔE_{max}/V	ΔE_{expt}/V
p-Si	BQ/BQ$^{\cdot-}$	0.4	0.23
p-Si	CA/CA$^{\cdot-}$	0	0.21
p-GaP	BQ/BQ$^{\cdot-}$	1.6	0.40
p-GaP	CA/CA$^{\cdot-}$	1.1	0.42
p-InP	BQ/BQ$^{\cdot-}$	—	0.41
p-InP	CA/CA$^{\cdot-}$	—	0.42

a) The concentration was 9.1×10^{-3} mol dm^{-3} CA/7.1×10^{-4} mol dm^{-3} CA$^{\cdot-}$, and 8.5×10^{-3} mol dm^{-3} BQ/6.6×10^{-4} mol dm^{-3} BQ$^{\cdot-}$.

Table 2. Flat-band potential of a p-type GaP in a variety of acetonitrile solutions

	Solution[a)]	E_{fb}/V
1	0.1 M TEAP/AN	0.75
2	0.01 M CA	0.3
3	0.01 M BQ	−0.3
4	1.0×10^{-4} M CA	0.6
	1.0×10^{-3} M CA	0.5
	1.0×10^{-2} M CA	0.4
5	4.6×10^{-3} M HCl	0.72
	4.6×10^{-2} M HCl	0.78
	4.1×10^{-1} M HCl	0.84
6	5.6×10^{-2} M HCl+1.0×10^{-4} M CA	0.80
	5.6×10^{-2} M HCl+1.0×10^{-3} M CA	0.80
	5.6×10^{-2} M HCl+1.0×10^{-2} M CA	0.80

a) M = mol dm^{-3}.

should have been brought about by changing the electrolyte from one kind to another. Thus, the pretreatment of the electrode was made only at the beginning of a series of runs. In this way, a small change was noticeable.

The following results were obtained. (1) Addition of CA and BQ to the base electrolyte of TEAP/AN greatly shifts E_{fb} towards negative potentials. The shifts is higher for BQ than for CA. (2) E_{fb} shifts cathodically with an increase in the concentration of CA, but a reverse tendency was obtained in the case of HCl. (3) When HCl and CA coexist, E_{fb} is primarily determined by HCl. The results were obtained in the electrolytes containing 150—500 ppm water. The water content increased steadily during the course of measurements, and it was not possible to clarify the effect of water on E_{fb}. A trial was made to decrease the water content to 34 ppm in the initial stage of the measurments, but no appreciable difference was observed.

The results (1)—(3) show that a dissociative equilibrium of surface hydroxyl groups of the electrode with the electrolyte should be a principal factor in determining E_{fb}. The positive shift of E_{fb} by addition of HCl should be related to

$$-GaOH + H^+ \rightleftharpoons Ga^+ + H_2O \quad (1)$$

as in the cases of aqueous solutions.[10] On the other hand, the negative shift by addition of the quinone compounds indicates that negatively charged sites become abundant at the electrode surface by the addition. A tentative model for explanation is

$$-GaOH + Q \rightleftharpoons GaO^- + QH^+ \quad (2)$$

where Q denotes the quinone molecule. The magnitude of the change in E_{fb} caused by the addition of a quinone compound to the base solution of TEAP/AN would be high for a molecule having a large effective electron density of the quinone ring, which is in agreement with the results. BQ/BQ^- has a more negative E^0 value than CA/CA^-. A large photovoltage is expected for the former redox electrolyte than the latter if E_{fb} does not differ a great deal. However, the larger negative shift of E_{fb} in the former cancels the advantage of E^0, so that almost the same photovoltage is obtained.

Equation 2 gives a tentative explanation of the observed phenomena. Any model is applicable if the formation of negative sites by addition of quinone compounds is reasonably explained. The interaction of organic species with the electrode surface was postulated in the case of GaAs in AN solutions,[11] but its mechanism has not been clarified.

According to the present results, the invariance of E_{fb} may be expected when complete elimination of hydroxyl groups on the electrode surface is achieved. In order to prepare such an electrode, anodic polarization of the electrode in an electrolyte free of water may be useful. However, the preparation of such an electrolyte is practically difficult at least for AN,[12] so that E_{fb} will be varied more or less by adding an organic redox species to AN solutions.

References

1) H. Gerischer, *J. Electroanal. Chem.*, **58**, 263 (1975).
2) K. Nakatani and H. Tsubomura, *Bull. Chem. Soc. Jpn.*, **50**, 783 (1977).
3) S. N. Frank and A. J. Bard, *J. Am. Chem. Soc.*, **97**, 7427 (1975).
4) D. Laser and A. J. Bard, *J. Phys. Chem.*, **80**, 459 (1976).
5) P. A. Kohl and A. J. Bard, *J. Am. Chem. Soc.*, **99**, 7531 (1977).
6) P. J. Holmes, "The Electrochemistry of Semiconductors," Academic Press, New York (1962), p. 368.
7) E. T. Seo and R. F. Nelson, *J. Am. Chem. Soc.*, **88**, 3498 (1966).
8) J. D. Davis, *Trans Faraday Soc.*, **60**, 3195 (1964).
9) M. E. Poever, *Nature*, **191**, 702 (1961).
10) G. Horowitz, *J. Appl. Phys.*, **49**, 3571 (1978).
11) P. A. Kohl and A. J. Bard, *J. Electrochem. Soc.*, **126**, 59 (1979).
12) M. Walter and L. Ramaley, *Anal. Chem.*, **45**, 165 (1973).

BULLETIN OF THE CHEMICAL SOCIETY OF JAPAN, VOL. 52 (9), 2719—2720 (1979)

Infrared Emission Spectra of CO_2 in the Explosion Reaction of CO and O_2 Using a Rapid-Scan Spectrometer

Masako TANAKA,* Shigeo NAGASAKA, Sadao SAWAMURA, and Meiseki KATAYAMA

Department of Atomic Science and Nuclear Engineering, Faculty of Engineering, Hokkaido University, Sapporo 060

(Received October 9, 1978)

Synopsis. The infrared emission spectra of CO_2 were observed by means of a rapid-scan infrared spectrometer during the explosion of CO–O_2 in a cylindrical vessel. The R-branch band heads of 001-000 and 011-010 were detected. The time dependences of the emission intensities of these band heads, $\nu_1+\nu_3$, and $2\nu_2+\nu_3$, were studied.

It is well known that infrared emissions due to CO_2 are observed in a CO–air flame; past studies have been reviewed by Gaydon.[1] However, there have been very few studies of the CO_2 emission spectra in the explosion of a CO–O_2 mixture by means of a rapid-scan spectrometer other than those by Bullock *et al.*[2,3] As previously reported,[4] we constructed a new rapid-scan spectrometer which had a better resolving power than that of Bullock. This paper will be concerned with the detailed spectra and the time dependence of each band after the explosion.

The rapid-scan infrared spectrometer was constructed by modifying a Shimadzu IRG-27 apparatus which is equipped with an oscillating mirror and a PbSe detector. The details of the optics and electronic circuits for synchronization have been described elsewhere.[4] The scan time was 10 ms. The scan rate was 125 cm^{-1}/ms at 3000 cm^{-1} and 12 cm^{-1}/ms at 500 cm^{-1}. The time interval of the repetition was 20 ms. The observed resolving power was 15 cm^{-1} at 3000 cm^{-1}, with the slit width of 700 μm.

The explosion was provoked by a spark discharge. A pyrex cylindrical vessel of 70 mmϕ and 40 cm long was used for the reaction. The vessel had electrodes at one end and an optical window 12 cm away from the electrodes. The CO and O_2 were passed through a liquid nitrogen trap before they were used. The total pressure was 225—350 mmHg. All the spectra were recorded at the slit width of 500 μm.

Some typical emission spectra after the explosion are shown in Figs. 1(a) and (b). In Fig. 1(a), well-resolved R-branch band heads due to the 001-000 and 011-010 transitions are observed at 2401 and 2389 cm^{-1} respectively. The bands in the band-head region are very similar to those in the spectrum obtained in the stationary flames of CO and O_2 by Benedict.[5] Two absorption bands are observed. One is the self absorption of CO_2 at around 2350 cm^{-1}, while the other is the absorption due to unreacted CO at around 2150 cm^{-1}. The band shape of CO seems very broad because the linearity of the sweeping time with the wave number is not established beyond 7.5 ms, as has been described in a previous report.[4] The emission band maximum of the CO_2 fundamental seems to be at around 2280 cm^{-1} immediately after the explosion. The rise and decay of this band maximum was more rapid compared with the other bands.

As is shown in Fig. 1(b), broad emission bands at 3480 cm^{-1} and a shoulder at 3700 cm^{-1} are observed. The weak, fine structures observed of these bands are considered to be due to the absorption of the H_2O in the optical path. The 3480 cm^{-1} and 3700 cm^{-1} bands were assigned to the 021-000 and 101-000 transitions respectively. When 5 mmHg of H_2O are added, the explosion proceeds vigorously, as is well known. The emission spectra are shown in Figs. 2(a) and (b). Again, bands similar to those seen in Fig. 1 appeared, but the emission intensity of each band, especially that at 2280 cm^{-1}, were very much higher than in a dry mixture at the initial stage.

The time dependences of the combination bands and the fundamental band heads are plotted in Figs. 3 and 4. In the explosion shown in Fig. 3, the time for the flame fromt to run across the optical window was estimated to be less than 10 ms. The rise time of the emission to the peak intensity in Fig. 3 is 70—80 ms, which is much longer than the value given above, and CO was found to decrease during the emission rise. These facts suggest that the emission-rising process is caused by the combustion occurring after the flame front has passed and that the emission-decay

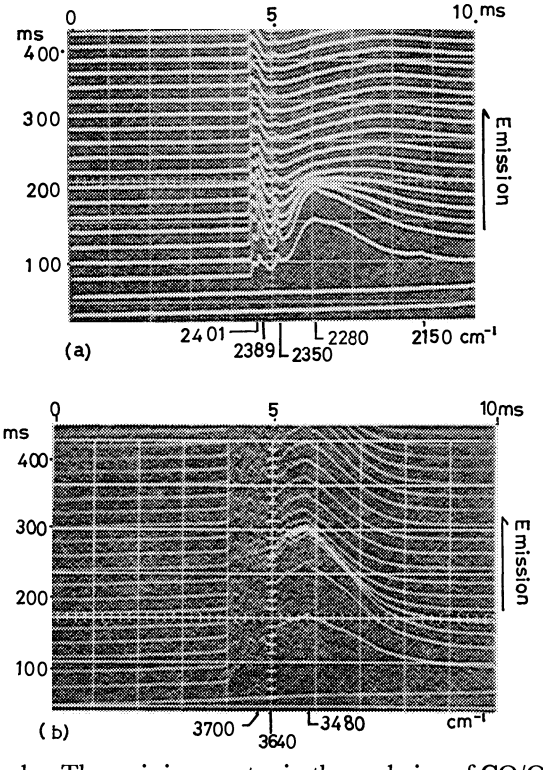

Fig. 1. The emission spectra in the explosion of CO/O_2. CO 150 and O_2 75 mmHg. 5 mV/div and 1 ms/div. Center wave number is 2350 cm^{-1} in (a) and 3640 cm^{-1} in (b). The spectra were recorded with the slit width of 300 μm in (a).

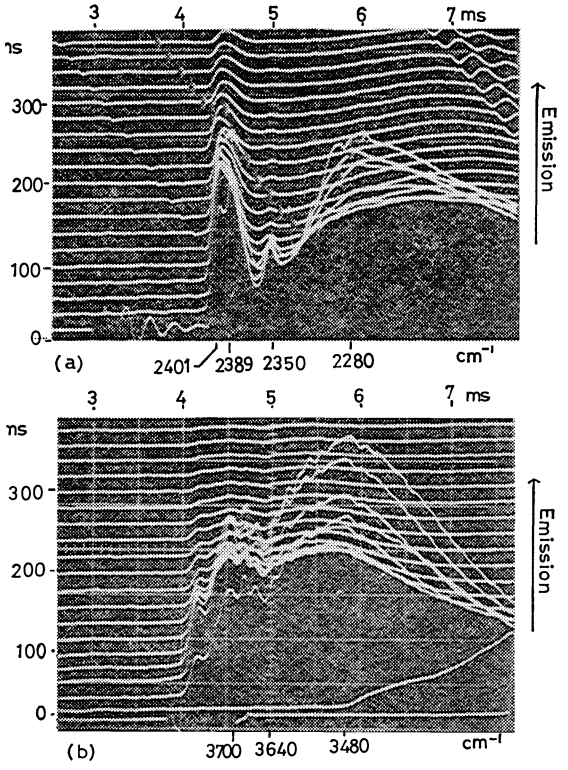

Fig. 2. The emission spectra in the explosion of $CO/O_2/H_2O$. CO 150, O_2 75 and H_2O 5 mmHg. 5 mV/div and 0.5 ms/div. The center wave number are the same as in Fig. 1.

process is the cooling process. It may be seen in Fig. 3(a) that the rises and decays of the two combination bands are similar. On the other hand, in the band-head region, as is shown in Fig. 3(b), the rise times of the 001 band and the 011 band are about the same, but the decay of the 011 band is faster than that of the 001 band. Then the intensities of the two bands are reversed after 300 ms. In H_2O-added mixtures, the rise and the decay of the emission bands are considerably increased. In this case, the reversing of the intensities in the band-head region occurred early, at 60 ms, as is shown in Fig. 2(a). "Afterglows" appeared during the emission-decay process, as is shown in Fig. 3. Bullock had already observed the "afterglows," but only in the self-absorption region. However, in this experiment they were observed in the combination bands and band heads, and not in the region of the absorption or on the low-frequency side of the emission. Figure 4 indicates that the combination band decayed faster than the fundamental band head. Such differences in the decay rate were observed also when excess O_2 or N_2 was added to CO–O_2 stoichiometric mixtures. In the O_2-rich mixtures, the decay rates of the combination bands and the two band heads increased to about an equal extent, but when 20 mmHg of N_2 was added, only those of the band heads increased. It should be pointed out that different time dependences were observed between the two band heads and between the band heads and the combination bands in the cooling process, although

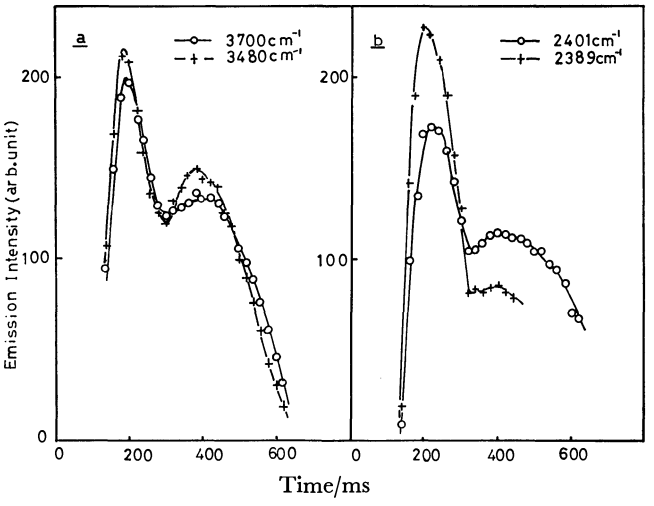

Fig. 3. Time dependence of the emission intensity in the explosion of CO/O_2.

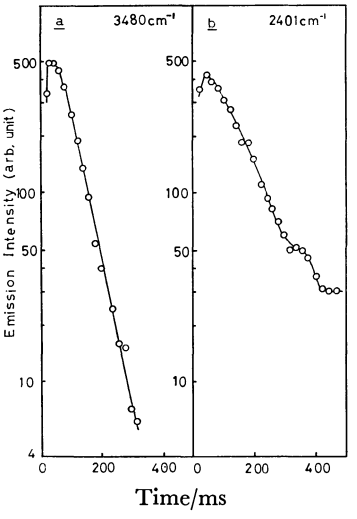

Fig. 4. Time dependence of the emission intensity in the explosion of $CO/O_2/H_2O$.

the reason for this is not clear.

We are greatly indebted to Mr. Yuji Matsui of Shimadzu Seisakusho, Ltd., for the design and construction of the optics of the intrument. We also wish to thank Messers Ikuo Murai and Masatoshi Kitaichi for their help in making the spark-discharge circuits.

References

1) A. G. Gaydon, "The Spectroscopy of Flames," Chapman and Hall, London (1974), p. 221.
2) B. W. Bullock and S. Silverman, *J. Opt. Soc. Am.*, **40**, 608 (1950).
3) B. W. Bullock, G. A. Hornbeck, and S. Silverman, *J. Chem. Phys.*, **18**, 1114 (1950).
4) M. Tanaka, S. Nagasaka, S. Sawamura, and M. Katayama, *Nippon Kagaku Kaishi*, **1978**, 1322.
5) W. S. Benedict, R. C. Herman, and S. Silverman, *J. Chem. Phys.*, **19**, 1352 (1952).

BULLETIN OF THE CHEMICAL SOCIETY OF JAPAN, VOL. 52 (9), 2721—2722 (1979)

Dissociation Constants of Several Protonated Amines in Propylene Carbonate

Kosuke IZUTSU,* Toshio NAKAMURA, and Izumi IIJIMA

Department of Chemistry, Faculty of Science, Shinshu University, Asahi, Matsumoto 390

(Received November 6, 1978)

Synopsis. The dissociation constants pK(BH$^+$) of five protonated monoamines in propylene carbonate have been determined potentiometrically using a glass electrode which was calibrated in a picric acid-picrate buffer solution. The pK(BH$^+$) values found at 25 °C were 10.1 for aniline, 11.9 for pyridine, 15.9 for ammonia, 17.0 for 1,3-diphenylguanidine, and 17.9 for triethylamine.

The dissociation and homoconjugation constants of several acids (HA) have been determined in propylene carbonate,[1] the results of which showed that propylene carbonate is a somewhat stronger base than acetonitrile, being of the same order of strength as acetone. In the present paper, the dissociation constants, pK(BH$^+$), of five protonated monoamines (BH$^+$) in propylene carbonate are presented. The pK(BH$^+$) values were obtained potentiometrically using a glass electrode which had been shown to respond with a Nernstian slope to paH in propylene carbonate. In each measurement, the electrode was calibrated in a picric acid–tetraethylammonium picrate buffer solution, the paH of which was calculated from the pK(HA) of picric acid of 9.30.[1]

Experimental

Materials. Propylene carbonate was a synthetic grade Merck product and purified as described in a previous report.[1] The water content of the purified solvent was less than 0.005%. Aniline, pyridine, 1,3-diphenylguanidine, and triethylamine were analytical reagent grade products (Wako Chemicals Co.), and purified by the method of Coetzee and Padmanabhan.[2] Pyridine was distilled from potassium hydroxide and then from barium oxide.[3] Ammonia was drawn into the propylene carbonate and the concentration of the resulting solution was determined by titration with perchloric acid.

The perchlorates of aniline, pyridine, 1,3-diphenylguanidine, triethylamine, and ammonia were prepared by neutralizing the bases with 70% perchloric acid, followed by recrystallization and careful drying *in vacuo*.[2] In the neutralization of triethylamine and the recrystallizations of the perchlorates of pyridine, 1,3-diphenylguanidine, and triethylamine, ethanol was used as the solvent.

Potentiometric Measurements. Potentiometric measurements were conducted at 25.0±0.5 °C as previously reported.[1] In the paH measurement of mixtures of a base and its perchlorate, 50 ml of the perchlorate solution was placed in the cell and appropriate volumes of the stock solution of the base were titrated to change the value of $\log(C_{BH^+}/C_B)$ from +1.0 to −1.0. Before and after each titration, the glass electrode was checked in the standard buffer solution (4×10^{-3} mol dm^{-3} picric acid and 4×10^{-3} mol dm^{-3} tetraethylammonium picrate) of paH 9.3_3. The potentials obtained in the standard buffer solution before and after each titration agreed within ±1 mV.

Results and Discussion

Typical results of the potentiometric measurements are shown in Table 1. In this case, 50 ml of 3.0×10^{-3} mol dm^{-3} pyridinium perchlorate in propylene carbonate was titrated with 3.0 mol dm^{-3} pyridine in the same solvent. The pK(BH$^+$) value was calculated according to Eq. 1,

$$pK(BH^+) = paH + \log\frac{C_{BH^+}f_{BH^+}}{C_B} \quad (1)$$

where $\log f_{BH^+} = -0.69C_{BH^+}^{1/2}$.[1] In Table 1, the p$K$(BH$^+$) values for $\log(C_{BH^+}/C_B)$ between +1.0 and −1.0 are constant within ±0.02. The titrations were conducted three or four times for each of the five protonated monoamines. In all cases, the values of pK(BH$^+$) in each titration were nearly constant (the largest standard deviation, 0.06). This indicates that under the experimental conditions the reaction BH$^+$= B+H$^+$ predominates in solution.

In Table 2, the pK(BH$^+$) values obtained are summarized. The standard deviations of the pK(BH$^+$) values in Table 2 are equal to or less than 0.1. But since the Nernstian response of the glass electrode was verified only at the paH range between 5 and 10,[1] it seems better to consider that the uncertainties of the pK(BH$^+$) values are about ±0.15 pK units.[4]

The values of pK(BH$^+$) in propylene carbonate are smaller than those in acetonitrile by approximately 0.5 pK units (except in the case of 1,3-diphenylguanidine where the difference is 0.9 pK units). As reported,[1] propylene carbonate is a 10 to 40 times stronger

Table 1. Potentiometric determination of pK(BH$^+$) of the pyridinium ion in propylene carbonate[a]

$\log(C_{BH^+}/C_B)$	E/mV	paH[b]	pK(BH$^+$)
+1.00	$-334._0$	11.03	11.99
+0.70	$-351._5$	11.32	11.98
+0.40	$-368._5$	11.61	11.97
+0.22	$-378._5$	11.78	11.96
+0.10	$-386._0$	11.91	11.97
0.00	$-391._0$	11.99	11.95
−0.30	$-407._0$	12.26	11.92
−0.60	$-426._0$	12.58	11.94
−0.78	$-437._0$	12.77	11.95
−0.90	$-445._5$	12.91	11.97
−1.00	$-453._0$	13.04	12.00
			Av 11.96±0.02

a) 50 ml of 3.0×10^{-3} mol dm^{-3} pyridinium perchlorate in propylene carbonate was titrated with up to 0.50 ml of 3.0 mol dm^{-3} pyridine in propylene carbonate.
b) paH was obtained by paH=9.33−(E+233.5)/59.2.

Table 2. $pK(BH^+)$ of protonated monoamines in propylene carbonate and acetonitrile

Monoamine	$pK(BH^+)$ in PC[a)]	$pK(BH^+)$ in AN[a,b)]	ΔpK
Aniline	10.09±0.10	10.56	0.47
Pyridine	11.92±0.07	12.33	0.41
Ammonia	15.90±0.04	16.46	0.56
1,3-Diphenyl-guanidine	16.98±0.04	17.90	0.92
Triethylamine	17.94±0.06	18.46	0.52

a) PC=propylene carbonate, and AN=acetonitrile.
b) Values from Ref. 2.

base towards protons than acetonitrile. The solvation of protonated amines would also be stronger in propylene carbonate than in acetonitrile, though the difference between the two solvents appears to be smaller than in the case of the proton. On the basis of these considerations, the above differences in $pK(BH^+)$ values between the two solvents are reasonable.[5)]

References

1) K. Izutsu, I. M. Kolthoff, T. Fujinaga, M. Hattori, and M. K. Chantooni, Jr., *Anal. Chem.*, **49**, 503 (1977).
2) J. F. Coetzee and G. R. Padmanabhan, *J. Am. Chem. Soc.*, **87**, 5005 (1965).
3) E. K. Ralph and W. A. Gilkerson, *J. Am. Chem. Soc.*, **86**, 4783 (1964).
4) The approximate values of $\{dpK(BH^+)/dT\}/K$ at 25 °C, as determined from the measurement of the heat of the reaction of $BH^+=B+H^+$, are -0.01_2 for aniline, -0.01_3 for pyridine, -0.02_5 for 1,3-diphenylguanidine, and -0.03_3 for triethylamine. K. Izutsu, T. Nakamura, and T. Hizawa, unpublished results.
5) Talarmin *et al.* reported $pK(HA)$ of 11.3 for picric acid, $pK(BH^+)$ of 12.4 for aniline and 19.4 for 1,3-diphenylguanidine. These values were determined using both hydrogen and glass electrodes, which were standardized in a solution of trifluoromethanesulfonic acid ($pK(HA)=2.2$), and by assuming the Nernstian response of these electrodes. The large discrepancies in pK values between the results of Talarmin *et al.* and this study require further study. J. Talarmin, M. L'Her, and J. Courtot-Coupez, *C. R. Hebd. Seances Acad. Sci., Ser. C*, **287**, 105 (1978).

BULLETIN OF THE CHEMICAL SOCIETY OF JAPAN, VOL. 52 (9), 2723—2724 (1979)

Thermochromism of Metal Chelates with Triphenylmethane Complexons in Aqueous Solutions. II. Inhibitive Effects of the Protolysis of Aqua Cu^{2+} Ion on the Thermochromism of Cu(II)–Xylenol Orange Chelate

Shoji NAKADA, Mutsuo YAMADA, Tasuku ITO,† and Masatoshi FUJIMOTO*

Department of Chemistry, Faculty of Science, Hokkaido University, Sapporo 060

(Received January 18, 1979)

Synopsis. Temperature-dependent protolytic equilibrium, $Cu(OH_2)_n^{2+} \underset{k_{-1}}{\overset{k_1}{\rightleftharpoons}} Cu(OH)(OH_2)_{n-1}^{+}+H^+$, was found to inhibit thermochromic changes of Cu(II)–Xylenol Orange (XO) chelate in unbuffered weakly acid aqueous solutions. The rate constants, k_1 and k_{-1}, at 25 °C and I=0.1 mol dm^{-3} were evaluated to be 10^3—10^4 s^{-1} and *ca.* 2×10^9 mol^{-1} dm^3 s^{-1}, respectively.

In previous papers we reported the thermochromism of the metal chelates of triphenylmethane complexons in aqueous solutions.[1] For the Cu(II)–XO complex the observed thermochromism was primarily ascribed to the temperature-dependent acid-dissociation equilibria between two 2 : 1 Cu(II)–XO chelates, AH and A: AH⇌A+H, where AH denotes a complex species having an uncoordinated free phenolic hydroxyl group and A a complex species having a coordinated phenolate group,[1] the charges being omitted. In unbuffered weakly acid aqueous solutions containing a large excess of Cu(II) ion the thermochromic change was not observed. In the present communication we aim to solve the problems on this phenomenon based on the spectrophotometric and the temperature-jump measurements.

Figure 1 shows the absorption spectra at various temperatures of an unbuffered aqueous solution containing 500-fold excess of Cu(II) ion over XO (2×10^{-5} mol dm^{-3}). With the rise of temperature from 15 to 60 °C the absorbance at 574 nm increases only by 7% and the thermochromic change was not observed.** The pH of the solution varies from 4.86 at 15 °C to 4.46 at 60 °C. On the basis of the values of ΔH and ΔS determined for the equilibrium AH⇌A+H,[1] only a negligibly small change in pH should be expected. The large decrease in pH observed above strongly suggests the possibility of a contribution of the temperature-dependent protolysis of a large excess of Cu^{2+} ion. This possibility was proved based on the temperature-jump data for aqueous solutions of Cu(II) ion containing uncomplexing acid-base indicators, Bromocresol Green (BCG), Bromocresol Purple (BCP), and Bromophenol Blue (BPB).

The pH of unbuffered solution containing 2×10^{-5} mol dm^{-3} BCG and 1×10^{-2} mol dm^{-3} $Cu(ClO_4)_2$ varied from 5.40 at 14 °C to 5.10 at 60 °C, and the absorbance at 628 nm, the λ_{max} of BCG, markedly decreased with the rise of temperature.

Figures 2(a) and 2(b) show the typical relaxation signals observed for the unbuffered systems, Cu(II)–XO and Cu(II)–BCG, respectively. In the Cu(II)–XO system, a fast relaxation signal of an increasing absorbance at 574 nm was observed in 5 μs region,

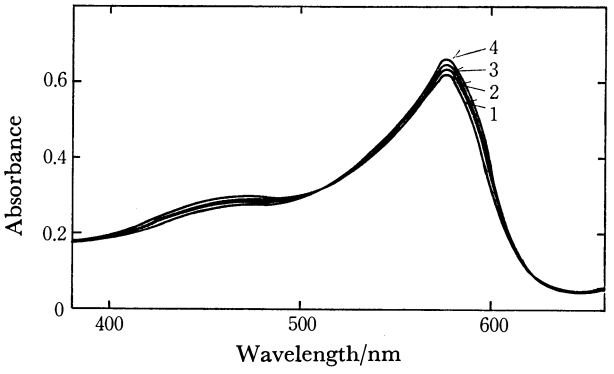

Fig. 1. Absorption spectra of an aqueous solution of Cu(II)–XO. At 15 (1), 25 (2), 44 (3), and 60 °C (4). $[Cu]_0=1.0\times10^{-2}$ and $[XO]_0=2\times10^{-5}$ mol dm^{-3} ($[\ ]_0$ denotes the total concentration). I= 0.1 mol dm^{-3} ($NaClO_4$). The pH of the solution varied from 4.86 (15 °C) to 4.46 (60 °C).

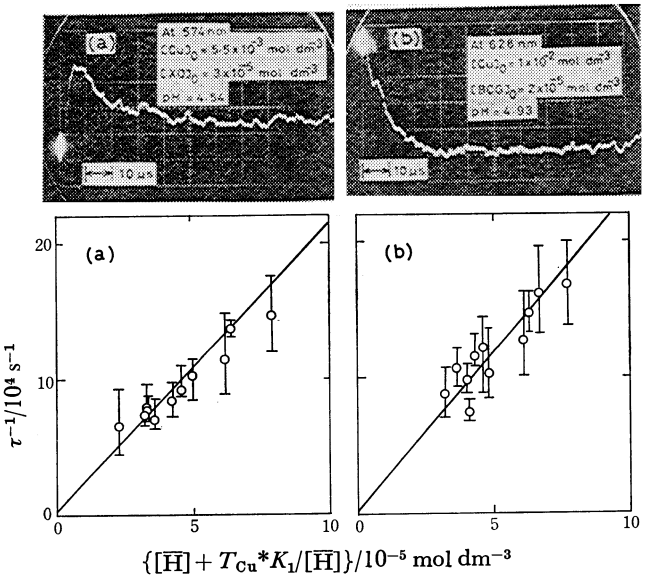

Fig. 2. Temperature-jump signals and the plots of τ^{-1} *vs.* $([\overline{H}]+T_{Cu}{}^*K_1/[\overline{H}])$ at 25 °C and I=0.1 mol dm^{-3} ($NaClO_4$) for Cu(II)-XO (a) and Cu(II)-BCG (b).

† Present address: Institute for Molecular Science, Okazaki 444.

** In the case of a solution of the same pH containing only a small excess of Cu(II) ion over XO the absorbance at 574 nm increased so markedly as *ca.* 30% even in unbuffered systems.[1]

Table 1. The rate constants, k_1 and k_{-1}, for the protolytic reaction, $Cu(OH_2)_n^{2+} \underset{k_{-1}}{\overset{k_1}{\rightleftharpoons}} Cu(OH)(OH_2)_{n-1}^{+} + H^+$ (I=0.1 mol dm^{-3} ($NaClO_4$))

X	$k_1/10^4$ s^{-1}	$k_{-1}/10^9$ mol^{-1} dm^3 s^{-1}	T/K
XO	1.4±1.0	1.8±0.3	298
BCG	1.0±0.9	1.3±0.5	290
	2.4±2.0	2.0±0.4	298

prior to a slower signal in 10 μs region indicating a decrease in the absorbance (Fig. 2(a)). The signal in the 5 μs region corresponds to the fast protonation-deprotonation AH⇌A+H.[1] The slower relaxation signal is ascribed to the protolysis of Cu^{2+} ion coupled with the fast thermochromic change of the Cu(II)–XO system. In the Cu(II)–GCB system, however, the fast relaxation signal in the region of 5 μs was not observed, only the slower signal was invariably observed in the 10 μs region (Fig. 2(b)). The slower signals observed in both systems are interpreted as a process involving the protolysis of the excess of Cu^{2+} ion.[2]

Assuming pre-equilibria for the thermochromic changes of the Cu(II)–XO system and also for the protonation-deprotonation process of the indicator, and regarding the protolysis of the Cu^{2+} ion in the unbuffered aqueous solution as a rate-determining step, we describe the given coupled reactions by the following two-step mechanism:

$$HX \underset{}{\overset{K_x}{\rightleftharpoons}} H + X \qquad (1)$$

and

$$Cu(OH_2)_n^{2+} \underset{k_{-1}}{\overset{k_1}{\rightleftharpoons}} Cu(OH)(OH_2)_{n-1}^{+} + H^+, \qquad (2)$$

where X denotes the base form of the chelate, A, or that of the acid-base indicator, In, and $K_x=K_a$ or K_{In}. In Eq. 1 the charges are omitted. With appropriate assumptions on the experimental conditions the relaxation time τ observed in the 10 μs region can be expressed as Eq. 4:

$$\tau^{-1} = k_1 + k_{-1}\left\{[\overline{H}] + [\overline{CuOH}]\cdot\frac{[\overline{H}]+K_x}{[\overline{X}]+[\overline{H}]+K_x}\right\} \qquad (3)$$

$$\simeq k_1 + k_{-1}\left\{[\overline{H}] + \frac{T_{Cu}{}^*K_1}{[\overline{H}]}\right\}, \qquad (4)$$

where T_{Cu} denotes the total concentration of Cu(II), and $^*K_1=[\overline{CuOH}][\overline{H}]/[\overline{Cu}]=10^{-7.34}$.[3] [¯] denotes the equilibrium concentration. CuOH indicates the deprotonated species, $Cu(OH)(OH_2)_{n-1}^{+}$.

The plots of τ^{-1} against $[\overline{H}]+T_{Cu}{}^*K_1/[\overline{H}]$ give fairly good straight lines for both systems, Cu(II)–XO and Cu(II)–BCG (Figs. 2(a) snd 2(b)). Table 1 shows the values of the rate constants, k_1 and k_{-1}, for the protolytic reaction (2) estimated from the intercepts and the slopes of the straight lines. The estimated value of k_{-1} ($\simeq 2\times10^9$ mol^{-1} dm^3 s^{-1}) lies nearly in the order of magnitude of the rate constant for the recombination of $CuOH^+$ and H^+ reported by Eigen *et al.* based on the sound absorption measurements ($k_{-1}\simeq 1\times10^{10}$ mol^{-1} dm^3 s^{-1}).[4] The value of $^*K_1$ derived from the ratio k_1/k_{-1}, however, varies in the range 10^{-5} —10^{-7} mol dm^{-3} owing to the large errors inherent in the estimation of the intercepts.

The system Cu(II)–BCP gave a slower relaxation signal in the 10 μs region only in the pH-region 5.2—5.9. In this system no linear relationship was obtained, presumably due to the contribution of the dimer formation in the Cu(II) species above pH 5.5.

As regards the Cu(II)–BCG system we estimated the activation enthalpies for k_1 and k_{-1} to be $\Delta H^{\ddagger}=19$ kcal mol^{-1} and $\Delta H^{\ddagger}=9$ kcal mol^{-1}, respectively. The difference in the values, 10 kcal mol^{-1}, agrees well with the value of ΔH for the protolytic equilibrium (2), 10—12 kcal mol^{-1}.[3]

On the basis of the results mentioned above we ascribe the observed inhibition of the thermochromism of Cu(II)–XO chelate in the presence of a large excess of Cu(II) ion in unbuffered aqueous solutions to the protolysis of the excess of aqua Cu^{2+} ion.

Experimental

A highly purified specimen of 3,3′-bis[*N*,*N*-bis(carboxymethyl) aminomethyl]-*o*-cresolsulfonaphthalein (Xylenol Orange) was used throughout the present work.[5] Reagent grade acid-base indicators, BCG, BCP, and BPB (Wako), were used. The pH values of the unbuffered solutions were adjusted with $HClO_4$ and NaOH (0.1 mol dm^{-3}) in the ranges 4.0—5.2, 4.4—5.2, and 4.3—5.9 for Cu(II)–BCG, –BPB, and –BCP systems, respectively. In the case of buffered systems, acetate, citrate, and phthalate buffers were used. The details on the measurements using a co-axialcable temperature-jump apparatus were described in a previous paper.[6]

References

1) S. Nakada, M. Yamada, T. Ito, and M. Fujimoto, *Chem. Lett.*, **1977**, 1243; *Bull. Chem. Soc. Jpn.*, **52**, 766 (1979).

2) The change in absorbance of the Cu(II)–BPB system was too small to evaluate the exact value of τ.

3) R. Arnek and C. C. Patel, *Acta Chem. Scand.*, **22**, 1097 (1968).

4) M. Eigen, W. Kruse, G. Maass, and L. De Maeyer, "Progress in Reaction Kinetics," Pergamon, Oxford (1964), Vol. 2, p. 286; L. P. Holmes, D. L. Cole, and E. M. Eyring, *J. Phys. Chem.*, **72**, 301 (1968).

5) S. Nakada, M. Yamada, T. Ito, and M. Fujimoto, *Bull. Chem. Soc. Jpn.*, **50**, 1887 (1977).

6) N. Yoshida and M. Fujimoto, *Bull. Chem. Soc. Jpn.*, **50**, 1328 (1977).

BULLETIN OF THE CHEMICAL SOCIETY OF JAPAN, VOL. 52 (9), 2725—2726 (1979)

Isomerism of the Metal Complexes Containing Multidentate Ligands. VIII. Chromatographic Behavior of $[CoN_6]^{3+}$-type Complexes on an SP-Sephadex Column[1)]

Katsumi SAKAKIBARA, Yuzo YOSHIKAWA,* and Hideo YAMATERA
Department of Chemistry, Faculty of Science, Nagoya University, Chikusa-ku, Nagoya 464

(Received March 26, 1979)

Synopsis. An empirical rule is presented for the elution order of $[CoN_6]^{3+}$-type complexes in chromatography on SP-Sephadex columns. The relative elution rates have been correlated with the number and the kind of the octahedral faces of the complex on which ion association with a phosphate ion occurs.

The application of ion-exchange Sephadex to the column-chromatographic separation of isomers of a metal complex was first described by Yoshikawa and Yamasaki, who successfully resolved the optical isomers[2)] of $[Co(en)_3]^{3+}$ and separated the three geometrical isomers[3)] of $[Co(dien)_2]^{3+}$. Subsequently the technique has been widely used to separate and resolve the isomers of many complexes. It is still difficult, however, to predict the elution order for a given mixture of isomers.

This note is concerned with a working hypothesis, which correlates the elution order with the structure of geometrical isomers of the $[CoN_6]^{3+}$-type complexes. The predictions from the hypothesis have been compared with the experimental results of isomer separation on several complexes with five-membered chelate rings.

Experimental

Materials. All Complexes,** $[Co(NH_3)_6]^{3+}$, $[Co(NH_3)_4(en)]^{3+}$, $[Co(NH_3)_2(en)_2]^{3+}$, $[Co(en)_3]^{3+}$, $[Co(dien)_2]^{3+}$,[3)] $[Co(en)(trien)]^{3+}$,[4,5)] $[Co(linpen)]^{3+}$,[6)] $[Co(hexaen)]^{3+}$,[7)] and $[Co(pn)_3]^{3+}$,[8)] were prepared according to the literature. For each complex in which geometrical isomerism occurs, an equimolar mixture of the geometrical isomers was prepared with the isomers isolated in advance.

Chromatography. The mixture of $[Co(dien)_2]^{3+}$ isomers was adsorbed at the top of an SP-Sephadex C-25 column (ϕ 1.4×*ca.* 130 cm) and eluted with 0.1 M Na_3PO_4. The elution curve was drawn by measuring the absorbance of each fraction of the eluate. Similar experiments were also made on the same column with 0.15 M Na_2SO_4, 0.15 M $Na_2\{(+)\text{-}C_4H_4O_6\}$(sodium tartrate), 0.3 M NaCl, and 0.3 M $NaClO_4$ as eluents. The isomer contained in each band was identified by the IR spectra, the results of which are shown in Fig. 1, where the vertical lines indicate the peak positions (in elution volume) in each curve.

The mixtures of the isomers of $[Co(NH_3)_2(en)_2]^{3+}$, $[Co(dien)_2]^{3+}$, $[Co(en)(trien)]^{3+}$, $[Co(linpen)]^{3+}$, $[Co(hexaen)]^{3+}$, and $[Co(NH_3)_4(en)]^{3+}$ were examined for elution order on another column (ϕ 2.7×127 cm) with 0.1 M Na_3PO_4 as the eluent. In each experiment either $[Co(en)_3]^{3+}$ or $[Co(NH_3)_6]^{3+}$ was added as a reference, of which the peak position in each elution curve is shown by a dashed vertical line (Fig. 2). The separation of $[Co(pn)_3]^{3+}$ isomers was also made in a similar manner.

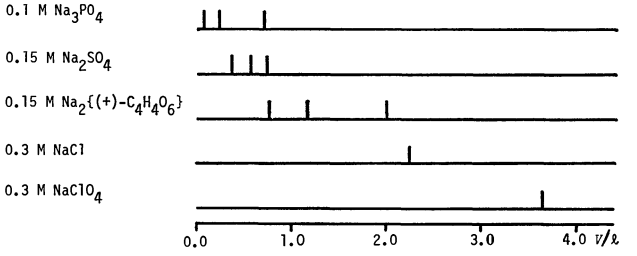

Fig. 1. Separation of the isomers of $[Co(dien)_2]^{3+}$ with different eluents. Column size: ϕ1.4×*ca.* 130 cm (SP-Sephadex C-25).

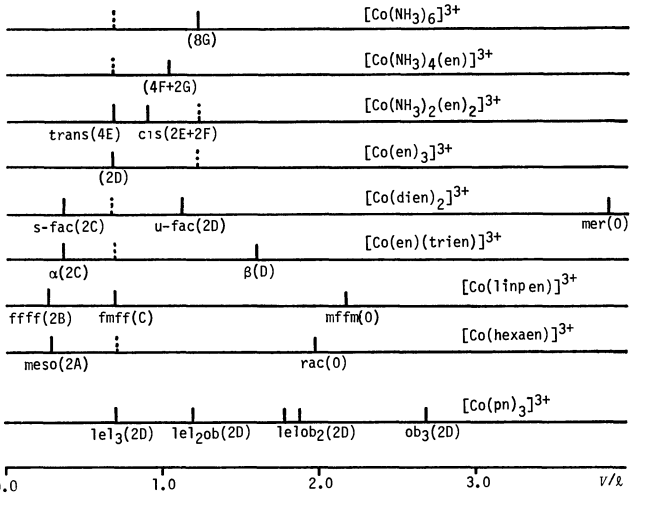

Fig. 2. The elution order of $[CoN_6]^{3+}$-type complexes. Column size: ϕ2.7×127 cm (SP-Sephadex C-25). Eluent: 0.1 M Na_3PO_4.

Results and Discussion

The factors influencing the relative rates of elution of geometrical isomers of cationic Co(III) complexes on an SP-Sephadex column are probably two: the interaction between SP-Sephadex and the complex cation, and the interaction between the complex cation and the eluent anion. Different eluents were used to separate the isomers of $[Co(dien)_2]^{3+}$ (Fig. 1). The same elution order (*s-fac*, *u-fac*, and *mer*) was shown by 0.1 M Na_3PO_4, 0.15 M Na_2SO_4, and 0.15 M $Na_2\{(+)\text{-}C_4H_4O_6\}$ eluents, whereas 0.3 M NaCl and 0.3 M $NaClO_4$ resulted in no clear separation. These results indicate that the interaction of the complex cation with the eluent anion, not with SP-Sephadex, is the dominant factor in the separation of geometrical

** The following abbreviations are used in this note: en, ethylenediamine; dien, diethylenetriamine; trien, triethylenetetramine; linpen, linear pentaethylenehexamine; hexaen, hexaethylenehexamine; pn, propylenediamine.

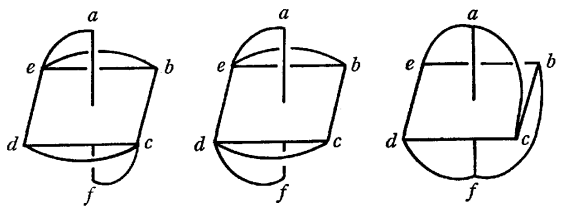

Fig. 3. Three geometrical isomers of $[Co(dien)_2]^{3+}$.

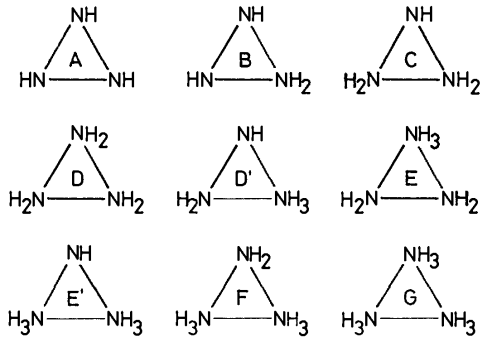

Fig. 4. Classification of the octahedral faces available for ion-pairing.

isomers.[9]

The structure of each geometrical isomer may or may not favor ion association. Experimental results so far reported on $[Co(en)_3]^{3+}$–oxo anion systems have indicated that three hydrogen bonds can be formed between a trigonal-pyramidal or tetrahedral oxo anion and a set of three N–H bonds extending along a direction perpendicular to an octahedral face of the complex. Two faces of the $[Co(en)_3]^{3+}$ octahedron are suitable for such ion association, whereas chelate rings will sterically interfere with ion association on the six other faces of the octahedron.[10]

In the three geometrical isomers of $[Co(dien)_2]^{3+}$ (Fig. 3), ion association will occur on the two faces, *abc* and *def*, in the *s-fac* isomer and on the two faces, *abc* and *bcf*, in the *u-fac* isomer. Each octahedral face of the *mer* isomer, however, is hindered from ion association by the chelate ring, which is consistent with the experimental results that the *mer* isomer was the final one to be eluted.

The elution behavior of the *s-fac* and *u-fac* isomers will be discussed in connection with the tendency for hydrogen bonding of the N–H protons with an oxo anion. That tendency will be in the order: secondary amine>primary amine>ammonia.[9] Consequently the octahedral faces may be classified according to the types of amine groups on the faces, in effect, according to the number of hydrogen atoms attached to the nitrogen atoms; the face containing three secondary amine groups is designated A, the face containing two secondary and one primary amine groups is designated B, *etc.* (Fig. 4). In this way a letter of the alphabet is affixed to each face in the order of increasing number of total hydrogen atoms attached to the nitrogen atoms on the face. This serves as an index. In the situation that two types of faces exist with an equal number of attached hydrogen atoms, the designation is D and D′ for example. A face carrying a prior alphabetical name will have a greater tendency to ion-pair formation. The *s-fac* isomer of $[Co(dien)_2]^{3+}$ has two C faces, and the *u-fac* isomer has two D faces. Consequently the tendency to associate with eluent anions will be in the order: *s-fac*>*u-fac*>*mer*. This order agrees with the order found experimentally.

Based on the preceding discussion, the elution order for $[CoN_6]^{3+}$-type complexes can be predicted and explained. Figure 2 gives the experimental results, where the position of the peak is shown for each isomer together with the number and type of octahedral face on which ion association with a phosphate ion occurs. The experimental elution results agreed completely with the prediction for the isomers of each complex investigated. There are however some cases where comparison is not straight-forward, *e.g.*, *trans*-$[Co(NH_3)_2(en)_2]^{3+}$ (4E), $[Co(en)_3]^{3+}$(2D), and *fmff*-$[Co(linpen)]^{3+}$ (C) were eluted at similar positions, a fact attributed to the counterbalance of the effect of decreasing number of faces available for ion-pairing and that of the increasing tendency of the faces to ion-pairing. Elution was slower for *u-fac*-$[Co(dien)_2]^{3+}$(2D) than for $[Co(en)_3]^{3+}$(2D), which has been attributed to the fact that the two D faces of the former complex cannot simultaneously have suitable N–H orientations for hydrogen bonding with the eluent anion.

$[Co(pn)_3]^{3+}$(2D) represents an example of a special case where the conformational effect is important; in this complex, the conformation of the chelate rings are not as flexible as in other complexes. Combination of the asymmetries at the ligands and the central cobalt gives rise to four enantiomeric pairs of isomers, in which the flexibility of the chelate rings is restricted by steric interaction of the bulky methyl group of pn. The N–H bonds at the both ends of a *lel* chelate ring are suitably oriented for hydrogen bonding, while those of the *ob* chelate ring are not.[8] The experimental result for $[Co(pn)_3]^{3+}$ indicates that the N–H orientation greatly affects the rate of elution.

References

1) K. Sakakibara, Y. Yoshikawa, and H. Yamatera, Presented at the 27th Symposium on Coordination Chemistry of the Chemical Society of Japan, September 1977.

2) Y. Yoshikawa and K. Yamasaki, *Inorg. Nucl. Chem. Lett.*, **6**, 523 (1970).

3) Y. Yoshikawa and K. Yamasaki, *Bull. Chem. Soc. Jpn.*, **45**, 179 (1972).

4) D. P. Schaefer and G. R. Brubaker, *Inorg. Chem.*, **8**, 1794 (1969).

5) K. Sakakibara, K. Kobayashi, Y. Yoshikawa, and H. Yamatera, Presented at the 36th National Meeting of the Chemical Society of Japan, April 1977.

6) Y. Yoshikawa and K. Yamasaki, *Bull. Chem. Soc. Jpn.*, **46**, 3448 (1973).

7) Y. Yoshikawa, *Chem. Lett.*, **1978**, 109.

8) S. E. Harnung, S. Kallesøe, A. M. Sargeson, and C. E. Schäffer, *Acta Chem. Scand.*, *A*, **28**, 385 (1974).

9) G. H. Searle, *Aust. J. Chem.*, **30**, 2625 (1977).

10) S. F. Mason and B. J. Norman, *J. Chem. Soc.*, *A*, **1966**, 301; F. R. Keene and G. H. Searle, *Inorg. Chem.*, **13**, 2173 (1974); M. Fujita and H. Yamatera, *Bull. Chem. Soc. Jpn.*, **49**, 1301 (1976).

BULLETIN OF THE CHEMICAL SOCIETY OF JAPAN, VOL. 52 (9), 2727—2728 (1979)

Preparation of Fortamine and 6-*epi*-Purpurosamine B from Fortimicin B

Hiroshi SANO,* Tomoko SAKAGUCHI, and Yasuki MORI

Tokyo Research Laboratory, Kyowa Hakko Kogyo Co., Ltd., 3-6-6 Asahimachi, Machida 194

(Received September 13, 1978)

Synopsis. Benzyl alcoholysis and hydrolysis of tetrakis-*N*-(benzyloxycarbonyl)fortimicin B and further transformation of the solvolysis products are described. Several derivatives of 6-*epi*-purpurosamine B and fortamine potentially useful for the synthesis of fortimicin analogs are presented.

Fortimicins A and B were found by Nara and his coworkers in the culture broth of *micromonospora* sp. MK-70.[1] It was also found that fortimicin B is obtained by hydrolysis of fortimicin A.[2] Both antibiotics belong to a class of pseudodisaccharide composed of 6-*epi*-purpurosamine B and fortamine which is a novel diaminocyclitol. In the course of the synthetic studies of fortimicins and their analogs through coupling reaction of these two components, it will be useful to obtain them from the natural products as their suitable protected derivatives. The present paper reports the preparation of fortamine and 6-*epi*-purpurosamine B by solvolysis of protected fortimicin B and their derivatives.

Fortimicin B was benzyloxycarbonylated to 1,4,2′,6′-tetrakis-*N*-(benzyloxycarbonyl)fortimicin B (**1**). Upon benzyl alcoholysis, **1** afforded α- and β-benzyl glycosides of 2,6-bis-*N*-(benzyloxycarbonyl)-6-*epi*-purpurosamine B (**2** and **3**) and 1,4-bis-*N*-(benzyloxycarbonyl)fortamine (**4**) after separation by silica gel chromatography. Each structure was confirmed by the PMR spectra.

When **2** was hydrogenolyzed with a palladium catalyst α-benzyl glycoside (**5**) was obtained. It should be noted that the 1-*O*-benzyl group resisted even to prolonged hydrogenolysis.

Upon hydrolysis of **1** with 2 M hydrochloric acid, 2,6-bis-*N*-(benzyloxycarbonyl)-6-*epi*-purpurosamine B (**6**) and **4** were obtained. Hydrogenolysis of **6** and hydrolysis of **4** afforded 6-*epi*-purpurosamine B (**7**) and fortamine (**8**) respectively as their hydrochloride.

Acetylation of **6** gave crystalline product of acetate (**9**) and when it was hydrogenolyzed 1-*O*-acetyl-6-*epi*-α-purpurosamine B (**10**) was obtained. **4** and **10** are important intermediates for fortimicin analog syntheses.

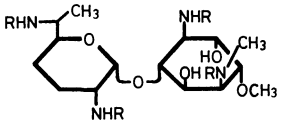

Fortimicin B R = H

1 R = Z

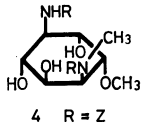

4 R = Z

8 R = H

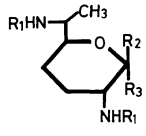

2 R_1 = Z R_2 = H R_3 = OCH_2Ph

3 R_1 = Z R_2 = OCH_2Ph R_3 = H

5 R_1 = H R_2 = H R_3 = OCH_2Ph

6 R_1 = Z R_2,R_3 = H,OH

7 R_1 = H R_2,R_3 = H,OH

9 R_1 = Z R_2 = H R_3 = OAc

10 R_1 = H R_2 = H R_3 = OAc

Z = CO_2CH_2Ph

Experimental

TLC was carried out on 7.5×2.5 cm slides coated with silica gel (Wakogel B-5, Wako Pure Chemicals Co., Ltd., Osaka) for protected compounds and 20×5 cm plates of cellulose (Avicel SF, Funakoshi Pharmaceutical Co., Ltd., Tokyo) for free compounds. Silica-gel column chromatography was performed with Kiesel gel 60 (E. Merck, Darmstadt, Germany). Melting point was not corrected.

*1,4,2′,6′-Tetrakis-*N*-(benzyloxycarbonyl)fortimicin B (**1**).* To an ice-cooled suspension of fortimicin B (10.0 g) and anhydrous sodium carbonate (8.79 g) in aqueous acetone (1:1, 250 ml), benzyloxycarbonyl chloride (25.1 ml) was added and the mixture was stirred for 1 h in the ice bath and then for 2 h at room temperature. The reaction mixture was evaporated to remove acetone and extracted with chloroform. The chloroform solution was dried over anhydrous magnesium sulfate and evaporated to give a pale yellow sirup, which was washed with hexane to give a colorless powder, 24.8 g (96.6%); $[\alpha]_D^{26}$ +42°(*c* 1, MeOH); R_f 0.41 (benzene:ethanol=9:1); PMR (in CD_3OD): δ 2.96 (3H, s, NCH_3), 3.31 (3H, s, OCH_3).

Found: C, 63.68; H, 6.38; N, 6.06%. Calcd for $C_{47}H_{56}N_4O_{13}$: C, 63.78; H, 6.38; N, 6.33%.

*Benzyl Alcoholysis of **1**.* A solution of **1** (1.20 g) in 1 M hydrogen chloride–benzyl alcohol (60 ml) was heated at 50 °C for 4 h. Basic lead carbonate (7.45 g) was added and the mixture was stirred for several hours to render pH about 5. The mixture was centrifuged and the clear supernatant was evaporated under reduced pressure to give a yellow sirup, which was washed with hexane and chromatographed on a silica-gel column with benzene:ethyl methyl ketone (EMK)(25 : 1—4 : 1, gradually changed). Evaporation of the fractions in turn gave benzyl 2,6-bis-*N*-(benzyloxycarbonyl)-α-6-*epi*-purpurosaminide B (**2**), benzyl 2,6-bis-*N*-(benzyloxycarbonyl)-β-6-*epi*-purpurosaminide B (**3**) and 1,4-bis-*N*-(benzyloxycarbonyl)fortamine (**4**), respectively (cited in the order of elution).

*Benzyl 2,6-Bis-*N*-(benzyloxycarbonyl)-α-6-*epi*-purpurosaminide B (**2**).* Crystals (from ethanol), 397 mg (56%); mp 131.5—134.5 °C; $[\alpha]_D^{26}$ +78° (*c* 1, MeOH); R_f 0.49 (benzene:EMK=15:1); PMR (in $CDCl_3$): δ 1.16 (3H, d, *J*=6 Hz, 6-CH_3), 4.55 (2H, ABq, *J*=12 Hz, 1-O-$C\underline{H}_2Ph$), 4.83 (1H, d, *J*=3 Hz, H-1), 5.07, 5.10 (each 2H, s, CO·O$C\underline{H}_2Ph$).

Found: C, 69.48; H, 6.61; N, 5.40%. Calcd for $C_{30}H_{34}N_2O_6$: C, 69.41; H, 6.74; N, 5.30%.

*Benzyl 2,6-Bis-*N*-(benzyloxycarbonyl)-β-6-*epi*-purpurosaminide B (**3**).* Crystals (from ethanol), 61 mg (9%); mp 180.5—183.5 °C; $[\alpha]_D^{27}$ −77° (*c* 0.6, $CHCl_3$); R_f 0.29 (benzene : EMK=15:1); PMR (in $CDCl_3$): δ 1.21 (3H, d, *J*=6 Hz, 6-CH_3), 4.27 (1H, d, *J*=8 Hz, H-1), 4.70 (2H, ABq, *J*=12 Hz, 1-O-$C\underline{H}_2Ph$), 5.11 (4H s, CO·O$C\underline{H}_2Ph$).

Found: C, 69.28; H, 6.86; N, 5.28%.

*1,4-Bis-*N*-(benzyloxycarbonyl)fortamine (**4**).* Crystals (from ether), 340 mg (53%); mp 161—166 °C; $[\alpha]_D^{27}$ +47° (*c* 1, MeOH); R_f 0.41 (chloroform:methanol=24:1); PMR (in $CDCl_3$): δ 3.05 (3H, s, NCH_3), 3.29 (3H, s, OCH_3), 5.10, 5.16 (each 2H, s, CO·O$C\underline{H}_2Ph$).

Found: C, 60.75; H, 6.37; N, 5.90%. Calcd for $C_{24}H_{30}$-

N_2O_8: C, 60.43; H, 6.17; N, 5.89%.

Benzyl α-6-epi-Purpurosaminide B Dihydrochloride (5). A solution of **2** (871 mg) in dioxane (23 ml) was hydrogenolyzed in the presence of 10% palladium on carbon for 24 h under 50 psi hydrogen atmosphere. After filtration the filtrate was neutralized with 2 M hydrochloric acid, and then evaporated under reduced pressure to give a solid, 351 mg (90%), $[\alpha]_D^{26}$ +78°→+80° (*c* 1, H_2O); R_f 0.23 (1-butanol : pyridine : water : acetic acid=6 : 4 : 3 : 1); PMR (in D_2O): δ 1.16 (3H, d, *J*=7 Hz, 6-CH_3), 4.62 (2H, s, 1-O-C<u>H</u>$_2$Ph), 5.10 (1H, d, *J*=4 Hz, H-1), 7.37 (5H, s, C_6H_5).

Hydrolysis of 1. To a solution of **1** (1.00 g) in dioxane (30 ml), 4 M hydrochloric acid (30 ml) was added and the mixture was heated at 90 °C for 2 h. The solution was evaporated to 20 ml. Water (200 ml) was added and precipitates were filtered to give a solid, which was chromatographed on a silica-gel column with toluene: EMK(6 : 1—4 : 1, gradually changed). Evaporation of the fractions in turn gave, 2,6-bis-*N*-(benzyloxycarbonyl)-6-*epi*-purpurosamine B (**6**) (70 mg, 15%) and 1,4-bis-*N*-(benzyloxycarbonyl)-fortamine (**4**) (140 mg, 27%) in the order of elution.

2,6-Bis-N-(benzyloxycarbonyl)-6-epi-purpurosamine B (6). A solid; $[\alpha]_D^{26}$ +11° (*c* 1, MeOH); R_f 0.60 (toluene: EMK=3:2); PMR (in $CDCl_3$): δ 1.13 (d, *J*=6 Hz), 1.22 (d, *J*=6 Hz) (3H in total, 6-CH_3), 5.11 (4H, s, C<u>H</u>$_2$Ph), 7.37 (10H, s, C_6H_5).

Found: C, 64.40; H, 6.60; N, 6.34%. Calcd for $C_{23}H_{28}N_2O_6$: C, 64.47; H, 6.59; N, 6.54%.

Fortamine Dihydrochloride (8). A suspension of **4** (100 mg) in 6 M hydrochloric acid (25 ml) was heated to reflux for 2 h. The resulting clear solution was evaporated to give a solid, which was dissolved in water and washed with ether. The aqueous layer separated was evaporated to give a residue, which was crystallized from ethanol to give needles, 54 mg (91%); mp 230—240 °C (dec); $[\alpha]_D^{25}$+4° (*c* 0.8, H_2O); R_f 0.27 (1-butanol : pyridine : water : acetic acid=6 : 4 : 3 : 1); PMR (in D_2O): δ 2.87 (3H, s, NCH_3), 3.53 (3H, s, OCH_3), 3.54 (1H, H-1), 3.77 (1H, q, H-4), 3.91 (1H, t, H-6), 4.03 (1H, q, H-3), 4.25 (1H, q, H-5), 4.26 (1H, q, H-2). $J_{1,2}$=8 Hz, $J_{2,3}$=3 Hz, $J_{3,4}$=6 Hz, $J_{5,6}$=8 Hz, $J_{1,6}$=8 Hz. Free base (in D_2O): δ 2.38 (3H, s, NCH_3), 2.83 (1H, t, H-1), 3.13 (1H, q, H-4), 3.37 (1H, t, H-6), 3.45 (3H, s, OCH_3), 3.64 (1H, q, H-2), 3.81 (1H, q, H-5). $J_{1,2}$=10 Hz, $J_{2,3}$=3 Hz, $J_{3,4}$=3 Hz, $J_{4,5}$=5 Hz, $J_{5,6}$=10 Hz, $J_{1,6}$=10 Hz.

Found: C, 34.42; H, 7.22; N, 10.04%. Calcd for $C_8H_{18}N_2O_4 \cdot 2HCl$: C, 34.53; H, 7.39; N, 9.72%.

6-epi-Purpurosamine B Dihydrochloride (7). To a solution of **6** (5.10 g) in dioxane (250 ml), 2 M hydrochloric acid (11.7 ml) was added and hydrogen was bubbled through the solution in the presence of palladium–carbon. After 2 h water (100 ml) was added and the reaction was continued for further 1 h. The solution was filtered and evaporated to give a solid, 2.60 g (93%), which was crystallized from ethanol–ether to give colorless crystals, mp 186—191 °C (dec), $[\alpha]_D^{24}$ +6°→+23° (*c* 0.6, water), R_f 0.26 (1-butanol: pyridine : water : acetic acid=6 : 4 : 3 : 1), PMR (in D_2O): δ 1.29 (d, *J*=7 Hz), 1.30 (d, *J*=7Hz) (total 3H, 6-CH_3), 4.80 (more intense, d, *J*=8.5 Hz), 5.38 (d, 3Hz) (total 3H, H-1).

Found: C, 36.43; H, 7.29; N, 11.65%. Calcd for $C_7H_{16}N_2O_2 \cdot 2HCl$: C, 35.72; H, 6.85; N, 11.42%.

1-O-Acetyl-2,6-bis-N-(benzyloxycarbonyl)-α-6-epi-purpurosamine B (9). To a solution of **6** (2.0 g) in pyridine (55 ml), acetic anhydride (1.5 ml) was added and the solution was allowed to stand at room temperature overnight. After a drop of water was added, the solution was evaporated and the residue was dissolved in chloroform. The solution was washed with water and evaporated to give a solid, which was crystallized from toluene to give needles of **9**, 1.81 g (79%), mp 153.5—156.5 °C, $[\alpha]_D^{26}$ +41° (*c* 1, MeOH), R_f 0.52 (toluene : EMK=3 : 1), PMR (in $CDCl_3$): δ 1.12 (3H, d, *J*=7Hz, 6-CH_3), 2.10 (3H, s, Ac), 5.09 (4H, s, C<u>H</u>$_2$Ph), 6.08 (1H, d, *J*=3Hz, H-1), 7.33 (10H, s, C_6H_5).

Found: C, 63.95; H, 6.45; N, 5.85%. Calcd for $C_{25}H_{30}N_2O_7$: C, 63.82; H, 6.43; N, 5.95%.

1-O-Acetyl-α-6-epi-purpurosamine B Dihydrochloride (10). Hydrogen was bubbled through a solution of **9** (600 mg) in dioxane (26 ml) in the presence of palladium–carbon. During the course of the reaction pH was maintained at 3—4 with 2 M hydrochloric acid, and water (0.2 ml×3) was added at 30 min intervals. The solution was filtered and evaporated to give a solid, 357 mg (99%), $[\alpha]_D^{24}$ +40° (*c* 1, MeOH), R_f 0.25 (1-butanol : pyridine : water : acetic acid=6 : 4 : 3 : 1), IR: 1730 (ester) cm^{-1}, PMR (in CD_3OD): δ 1.32 (3H, d, *J*=6Hz, 6-CH_3), 2.25 (3H, s, Ac), 6.30 (1H, bs, H-1).

Found: C, 32.87; H, 7.78; N, 8.22%. Calcd for $C_9H_{18}N_2O_3 \cdot 2HCl \cdot 3H_2O$: C, 32.83; H, 7.96; N, 8.50%.

References

1) T. Nara, M. Yamamoto, I. Kawamoto, K. Takayama, R. Okachi, S. Takasawa, T. Sato, and S. Sato, *J. Antibiot.*, **30**, 533 (1977); R. Okachi, S. Takasawa, T. Sato, M. Yamamoto, I. Kawamoto, and T. Nara, *J. Antibiot.*, **30**, 541 (1977).

2) R. S. Egan, R. S. Stanaszek, M. Cirovic, S. L. Mueller, J. Tadanier, J. R. Martin, P. Collum, A. W. Goldstein, R. L. Devault, A. C. Sinclair, E. E. Fager, and L. M. Mitscher, *J. Antibiot.*, **30**, 552 (1977).

BULLETIN OF THE CHEMICAL SOCIETY OF JAPAN, VOL. 52 (9), 2729—2730 (1979)

A Synthetic Route to 5-Aryl-2-oxazolidinone Derivatives

Yuji TSUJIMOTO,* Atsushi KOSAKA, Mitsunori HAYASHI,
Takuji MIYAMOTO, and Yoshinobu ODAIRA

Department of Petroleum Chemistry, Faculty of Engineering, Osaka University, Suita, Osaka 565

(Received September 20, 1978)

Synopsis. 5-Aryl-2-oxazolidinones have been synthesized readily by the elimination of dimethylamine from the corresponding (2-hydroxyethyl)ureas. The ureas are obtainable by the photoreaction of tetramethylurea with *para*-substituted benzaldehydes (Method A) or with *para*-substituted methyl benzoates (Method B). The electronic character of the substituent on the benzene ring determines which method is suitable for the preparation of (2-hydroxyethyl)ureas.

2-Oxazolidinones (*e.g.*, Furazolidone[1a] and Methoxadone[1b]) are of pharmaceutical importance,[2] and research has been devoted to establishing convenient synthetic routes for 2-oxazolidinones.[3-5] Most of the reported methods, however, consist of tedious multiple steps.[6]

As part of the studies on the application of *N,N*-dimethylcarbamoyl compounds to synthetic chemistry,[5,7-10] a convenient synthetic route to 5-aryl-2-oxazolidinones (**7**) by the photoreaction of tetramethylurea with aromatic compounds such as benzaldehyde and methyl benzoate, followed by the thermal cyclization has been found.

It may be reasonable to consider that the exploitation of convenient synthetic route to **3** is essential, because the desired ones (**7**) are accessible from a series of (2-hydroxyethyl)ureas (**3**) in satisfactory yields as described later. Consequently one-step preparation for **3**, through photochemical hydrogen abstraction of the *para*-substituted benzaldehydes (**1**) from tetramethylurea (**2**) was designed.

Irradiation of an acetonitrile solution of **1** and **2** gives the desired ureas (**3**) in one-step, although the yields are low as shown in Table 1, together with pinacols derived from the photoreduction of the corresponding **1** (20—40%) and dimeric urea (**4**). In some cases, **7** was also found, for example, **1c** gave **7c** (11% yield).

The ureidomethylation (Method A) is apparently induced by hydrogen abstraction by the excited n-π^* triplet state of **1** from **2**. The formation of **3** was heavily suppressed in the case of **1d** and **1e** which has an electron withdrawing group substituent in the benzene ring because of the low efficiency for hydrogen abstraction.[11]

To overcome this defect in Method A, the photoreaction of *para*-substituted methyl benzoates (**5**) with **2** (Method B) was designed, based on the result that the photoreaction of aromatic esters such as **5d** or **5e** in an appropriate hydrogen donating solvent readily affords some alcohol derivatives derived from reduction

TABLE 1. YIELDS AND SPECTRAL DATA OF **3**

Compound[a]	Yield/%[b]	IR ν/cm^{-1}	NMR(in $CDCl_3$) δ/ppm
3a	29 (0.4)[c]	1600 820	2.8 (s, 6H), 2.83 (s, 3H), 3.0, 3.6 (ABX octet, 2H), 3.8(s, 3H), 4.9(ABX q, 1H), 5.9 (br s, 1H)[d], 6.3—7.4 (A_2B_2, 4H)
3b	28	1600 830	2.3 (s, 3H), 2.8(s, 9H), 3.0, 3.6 (ABX octet, 2H), 4.9 (ABX q, 1H), 5.8(br s, 1H), 7.0—7.4 (m, 4H)
3c	26 (11)[c]	e)	e)
3d	5 (2)[c] 53[f]	1715 1600 820	2.8 (s, 9H), 3.1, 3.6 (ABX octet, 2H), 3.9 (s, 3H), 5.0 (ABX q, 1H), 6.4 (d, 1H)[d], 7.0—8.0 (A_2B_2, 4H)
3e	7 11[f]	2200 1600 825	2.8 (s, 6H), 3.1 (s, 3H), 3.2 (ABX octet, 2H), 5.0 (ABX q, 1H), 6.0 (br s, 1H), 7.2—7.6 (m, 4H)

a) Satisfactory elemental analyses were obtained for all new compounds (**3**). b) Based on the consumed aldehydes (**1**) or esters (**5**), c) Yield of 2-oxazolidinones (**7**). d) D_2O exchangeable. e) Ref. 7. f) Method B.

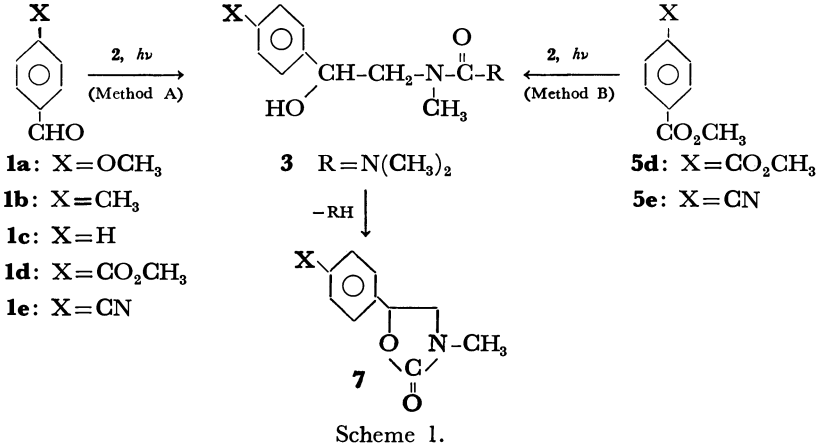

Scheme 1.

Table 2. Yields and spectral data of **7**

Compound[a]	Yield/%[b]	IR ν/cm^{-1}	NMR (in $CDCl_3$) δ/ppm
7a	69	1740	2.9 (s, 3H), 3.4, 3.8 (ABX sextet, 2H), 3.8 (s, 3H), 5.4 (ABX t, 1H), 6.8—7.4 (m, 4H)
7b	72	1730 825	2.3 (s, 3H), 2.9 (s, 3H), 3.4, 3.9 (ABX sextet, 2H), 5.4 (ABX t, 1H), 7.2—7.4 (m, 4H)
7c	79	1730 750 690	2.9 (s, 3H), 3.4, 3.9 (ABX sextet, 2H), 5.4 (ABX t, 1H), 7.2—7.4 (m, 5H)
7d	73	1730 1715 820	2.9 (s, 3H), 3.4, 3.9 (ABX sextet, 2H), 3.8 (s, 3H), 5.5 (ABX t, 1H), 7.3—8.0 (A_2B_2, 4H)
7e	77	2200 1740	2.9 (s, 3H), 3.4, 4.0 (ABX sextet, 2H), 5.5 (ABX t, 1H), 7.4—7.8 (A_2B_2, 4H)

a) Satisfactory elemental analyses were obtained for all new compounds (**7**). b) Based on the consumed ureas (**3**).

of the ester group and subsequent coupling of the resulting radicals.[12] Irradiation of **5d** with **2** in acetonitrile through a quartz filter led to the formation of **3d** in 53% yield. In the case of **5e**, photoureidomethylation of the aromatic ring described previously in aromatic nitriles[8] proceeded to give benzylurea (**6e**) (15% yield), and **3e** (11% yield).

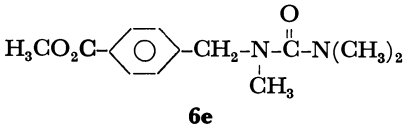

6e

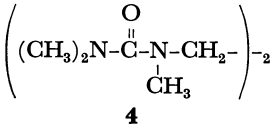

4

(2-Hydroxyethyl)ureas (**3**), prepared by Method A or B, were subsequently subjected to thermal reaction. A solution of **3** (0.05 M) in xylene was refluxed for 10 h, enabling the cyclization to proceed smoothly to give the 5-aryl-2-oxazolidinone derivatives (**7**) in good yields (Table 2).

Experimental

Materials. Methyl terephthalaldehydate (**1d**) was obtained by the Sommelet reaction.[12] *p*-Cyanobenzaldehyde (**1e**) was prepared according to the procedure of Lieberman *et al.*[13] Methyl *p*-cyanobenzoate (**5e**) was prepared by the esterification of the corresponding acid. All other aldehydes, dimethyl terephthalate (**5d**) and tetramethylurea (**2**) were commercially available.

General Procedure for Preparation of (2-Hydroxyethyl)ureas (3). *Method A*: The aldehydes (**1**) and a three molar excess of tetramethylurea (**2**) were dissolved in acetonitrile. After nitrogen was bubbled through the solution for 15 min, the solution was irradiated with a 500 W high pressure mercury arc through a Pyrex filter for 10 h at room temperature. After evaporation of the solvent, the unreacted **2** was recovered *in vacuo* and the residue chromatographed on silica gel. The products (**3**) were eluted with a mixture of benzene–ether.

Method B: A solution of **5d** or **5e** and a ten molar excess of **2** in the same solvent was similarly irradiated through a quartz filter for 20 h. After irradiation, a similar procedure was conducted. From the volatile components, methanol was detected by GLC (20% PEG, 20 M on Celite 545). Benzylurea (**6e**) was confirmed by a comparison with an authentic sample alternatively prepared.

Alternate Synthesis of 1-(p-Methoxycarbonylbenzyl)-1,3,3-trimethylurea (6e). **6e** was prepared from *p*-methoxycarbonylbenzyl bromide and an excess of trimethylurea in the presence of potassium amide in liquid ammonia according to the method by Bryant *et al.*[14] Bp 120 °C (0.6 Torr); IR (neat) 1700, 1600 cm^{-1}; NMR ($CDCl_3$) δ 2.5 (s, 3H), 2.6 (s, 6H), 3.8 (s, 3H), 4.4 (s, 2H), 7.2—8.0 (A_2B_2, 4H). Found: C, 62.22; H, 7.39; N, 10.90%. Calcd for $C_{13}H_{18}N_2O_3$: C, 62.38; H, 7.25; N, 11.19%.

General Procedure for Synthesis of 5-Aryl-2-oxazolidinones (7). A solution of **3** (0.35—0.45 mmol) in xylene (8 ml) was heated under reflux for 10 h. After removal of the solvent, the residue was chromatographed on silica gel. Elution with benzene–ether gave **7**.

References

1) a) 3-(5-Nitrofurfurylideneamino)-2-oxazolidinone; b) 5-(*o*-Methoxyphenoxymethyl)-2-oxazolidinone.
2) M. E. Dyen and D. Swern, *Chem. Rev.*, **67**, 197 (1967), and references cited therein.
3) S. S. Simons, Jr., *J. Org. Chem.*, **38**, 414 (1973).
4) S. G. Cristol, R. P. Evans, and K. L. Lockwood, *J. Org. Chem.*, **42**, 2378 (1977).
5) Y. Tsujimoto, A. Nakahara, Y. Nishimura, T. Miyamoto, and Y. Odaira, *Bull. Chem. Soc. Jpn.*, **49**, 3705 (1976).
6) R. Baltzly and J. S. Buck, *J. Am. Chem. Soc.*, **62**, 164 (1940), as an example.
7) Y. Katsuhara, R. Tsujii, K. Hara, Y. Shigemitsu, and Y. Odaira, *Tetrahedron Lett.*, **1974**, 453.
8) Y. Tsujimoto, M. Hayashi, Y. Nishimura, T. Miyamoto, and Y. Odaira, *Chem. Lett.*, **1977**, 677.
9) T. Miyamoto, Y. Tsujimoto, T. Tsuchinaga, Y. Nishimura, and Y. Odaira, *Tetrahedron Lett.*, **1978**, 2155.
10) Y. Tsujimoto, Y. Nishimura, A. Kosaka, H. Kiriyama, T. Miyamoto, and Y. Odaira, *Tetrahedron Lett.*, **1979**, 373.
11) N. J. Turro, "Molecular Photochemistry," W. A. Benjamin, New York (1967), p. 144.
12) K. Fukui, K. Senda, Y. Shigemitsu, and Y. Odaira, *J. Org. Chem.*, **37**, 3176 (1972).
13) R. C. Fuson and H. G. Cooke, Jr., *J. Am. Chem. Soc.*, **62**, 1180 (1940).
14) S. V. Lieberman and R. Connor, *Org. Synth.*, Coll. Vol. II, 441 (1966).
15) D. R. Bryant, S. D. Work, and C. R. Hauser, *J. Org. Chem.*, **29**, 235 (1964).

BULLETIN OF THE CHEMICAL SOCIETY OF JAPAN, VOL. 52 (9), 2731—2732 (1979)

A Stereoselective Total Synthesis of Methyl α-DL-Daunosaminide

Isao IWATAKI, Yasuo NAKAMURA, Koji TAKAHASHI, and Takeshi MATSUMOTO*

Department of Chemistry, Faculty of Science, Hokkaido University, Sapporo 060

(Received December 4, 1978)

Synopsis. Starting from crotonoyl chloride, methyl α-DL-daunosaminide was synthesized through the *cis* hydroxylation of a key intermediate, 1,1-ethylenedioxy-4-hexen-3-one, followed by oxymation, catalytic hydrogenation (Pt, AcOH), and treatment with MeOH/HCl.

Daunosamine (**1**) is the amino sugar moiety of the two antibiotics daunomycin[1] and adriamycin.[2] Both of these antibiotics, but adriamycin in particular, have attracted attention as promising anticancer agents. A number of syntheses of daunosamine have previously been described.[3–7] However, all these syntheses were carried out, starting from naturally occurring hexoses, through rather lengthy routes. In previous papers[8] we reported the synthesis of some deoxyhexoses from unnatural compounds through 2-ethoxy-6-methyl-3,4-2*H*-dihydropyran as a key intermediate. We wish to report here a new route to daunosamine as racemic methyl glycoside hydrochloride, starting from crotonoyl chloride and vinyl chloride.[9] The success of the present synthesis suggests the possibility of extending the new route as a general synthetic method for 2,6-dideoxyhexoses.

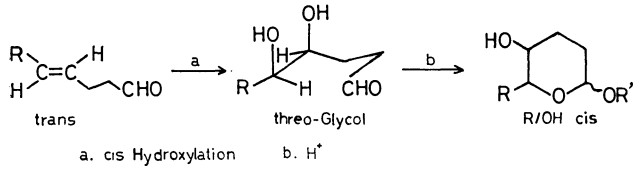

First, crotonoyl chloride was converted, by means of the Friedel-Crafts reaction with vinyl chloride, to 1-chloro-1,4-hexadien-3-one (**2**). α-Keto acetal, **3**, was obtained by the reaction of **2** with 1,2-ethanediol in the presence of potassium carbonate at −10 °C. The *cis* hydroxylation ($KMnO_4$, acetone, −40 °C) of **3** afforded dihydroxy derivative, **4**, which was transformed to the oxime, **5**, and was then hydrogenated over a Pt catalyst under acidic conditions (AcOH), according to the Roth method.[10] The amino diol, **6**, thus obtained was treated with methanolic hydrogen chloride to give methyl pyranoside, **7**. The 3-epimer of **7** was not isolated. The following NMR data (pyridine-d_5) indicate the **7** stereostructure. The signals around δ 2.45 ppm (q, 2H, J=9 and 3 Hz) are attributable to the C_2 protons. They are practically magnetically equivalent (the AA′ part of the AA′XY system) and couple to the anomeric proton H_1 (δ 4.78, t) with J=3 Hz. This establishes the equatorial configuration of H_1, therefore, **7** is the α-anomer. The coupling constant $(J_{2a,3a}+J_{2e,3a})/2$=9 Hz[11] was confirmed by the double-resonance technique, showing the presence of the axial proton at C_3. The broad triplet (1H, J=3 Hz) at δ 4.43 indicates the equatorial configuration of H_4, and $J_{4,5}$=3 Hz was acertained by the spin decoupling. Since the C_4–C_5 moiety has the *threo* configuration, the methyl group at C_5 is equatorial.

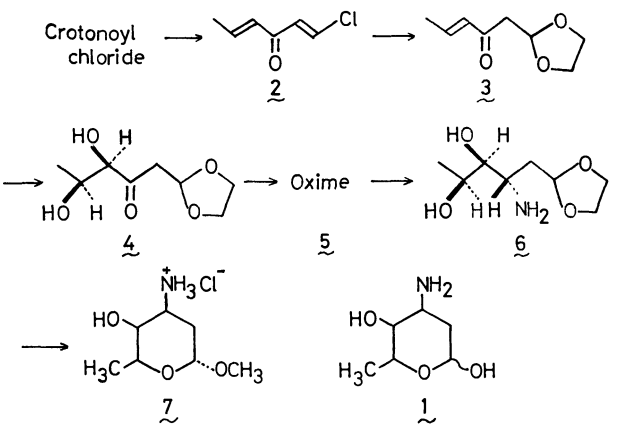

Experimental

All the melting points and boiling points are uncorrected. The IR spectra were recorded on a JASCO IR-S spectrophotometer. The NMR spectra were measured on a Varian A-60 instrument. For column chromatography, Merck silica gel (0.08 mm) was used, while for TLC, Wakogel B-5 was utilized. The starting material, 1-chloro-1,4-hexadien-3-one (**2**), was prepared by a modification of the Kochetkov method,[12] using vinyl chloride instead of acetylene, in a yield of 53%.

*1,1-Ethylenedioxy-4-hexen-3-one (**3**).* Into a suspension of potassium carbonate (65 g, 0.47 mol) in a mixture of water (20 cm³) and 1,2-ethanediol (100 cm³, 1.8 mol), a solution of **2** (50 g, 0.38 mol) in tetrahydrofuran (50 cm³) was stirred at −10 °C. The mixture was stirred for a further 3 h at this temperature and then for 24 h at room temperature. The reaction mixture was poured into water and extracted with petroleum ether, and the extract was dried (Na_2SO_4). The subsequent evaporation of the solvent and distillation (78—82 °C/2 mmHg**) of the residue gave **3** as a colorless liquid (8.5 g, 14%); 2,4-dinitrophenylhydrazone mp 121 °C. Found: C, 61.42; H, 7.71%. Calcd for $C_8H_{12}O_3$: C, 61.53; H, 7.69%.

*1,1-Ethylenedioxy-4,5-dihydroxyhexan-3-one (**4**).* The acetal **3** (10 g, 0.064 mol) in acetone (100 cm³) was cooled to −40 °C, and then, to the solution a cold solution of potassium permanganate (12 g, 0.075 mol) in water (400 cm³) and acetone (200 cm³) was added. After the manganese dioxide formed had been filtered off, the solvent was distilled off, the residue was poured into water and extracted with ethyl acetate, and the organic phase was dried. The removal of the solvent *in vacuo* gave a colorless oil, which was subsequently purified by column chromatography on silica gel (150 g), with ethyl acetate–benzene (1 : 1) as an eluent, to give **4** (4.3 g, 35%). Found: C, 50.52; H, 7.38%. Calcd for $C_8H_{14}O_5$: C, 50.50; H, 7.73%. NMR ($CDCl_3$) δ=1.2 (3H, d, J=7 Hz), 3.2 (2H, d, J=5 Hz), 3.6 (4H, m), 4.2—4.44 (2H, m),

** 1 mmHg≈133.322 Pa.

5.4 (1H, t, J=5 Hz) and 5.9 ppm (2H, s); IR (neat) 3440 (OH) and 1718 cm^{-1} (C=O).

*1,1-Ethylenedioxy-3-hydroxyimino-4,5-hexanediol (**5**).* To a mixture of sodium ethoxide (0.5 g, 0.0073 mol) and hydroxylamine hydrochloride (0.7 g, 0.01 mol) in 50 cm^3 of ethanol, **4** (2.3 g, 0.012 mol) was added at room temperature, after which the soln was stirred for 24 h. After the solvent had been removed *in vacuo*, the oxime, **5**, was extracted with ether and the solvent was evaporated to give a colorless oil (1.4 g, 56%). This was used in the subsequent reaction without purification. IR (neat) 3120 and 1030 cm^{-1} (N–OH).

*1,1-Erhylenedioxy-3-amino-4,5-hexanediol (**6**).* The oxime, **5** (2 g, 0.0098 mol), was hydrogenated over the Adams catalyst (0.2 g of PtO_2) in 30 cm^3 of acetic acid at atmospheric pressure for 12 h at room temperature.[9] Then the catalyst was filtered off, and the solvent was removed *in vacuo*. The residue was dissolved in a mixed solvent of water (1.2 dm^3) and methanol (400 cm^3), and the solution was passed through Amberlite IR-400 to remove the residual acetic acid. The subsequent evaporation of the solvent under reduced pressure left 1.5 g (81%) of crystalline **6**, which was recrystallized from 1-propanol–ether as colorless crystals. Mp 111—112 °C. Found: C, 50.06; H, 8.75; N, 7.63%. Calcd for $C_8H_{17}NO_4$: C, 50.25; H, 8.96; N, 7.35%. IR (Nujol) 1705 (NH) and 1135 cm^{-1} (acetal).

*Methyl α-DL-Daunosaminide Hydrochloride (**7**).* The amine, **6** (0.3 g, 0.016 mol), was dissolved in 2%-methanolic hydrogen chloride (9 cm^3), after which the soln was stirred for 24 h at 40 °C under a N_2 stream. The reaction mixture was then cooled, and the excess hydrochloric acid was neutralized with sodium hydrogen carbonate. After the evaporation of the filtered solution *in vacuo*, the residue was extracted with ethanol. The solvent was distilled off, and the residual solid was recrystallized from 1-propanol to afford 0.28 g (84%) of colorless crystals. Mp 161—163 °C. Found: C, 42.80; N, 7.84; N, 7.14%. Calcd for $C_7H_{16}NO_3Cl$: C, 42.53; H, 8.10; N, 7.09%. NMR (pyridine-d_5) δ=4.78 (1H, t, J=3 Hz), 4.43 (1H, br s), 4.32 (1H, m), 3.87 (1H, dq, J=1.5 and 6 Hz), 3.20 (3H, s), 2.45 (2H, q, J=9 and 3 Hz) and 1.39 (3H, d, J=6 Hz); IR (Nujol) 3300 (OH), 1620, 1580, 1510 (NH_3^+), 1200, 1130, 1080, 1060, and 980 cm^{-1}.

References

1) E. Arcamone, G. Cassinelli, P. Orezzi, G. Franceschi, and R. Mondelli, *J. Am. Chem. Soc.*, **86**, 5335 (1964).

2) F. Arcamone, G. Franceschi, S. Penco, and A. Selva, *Tetrahedron Lett.*, **1969**, 1007.

3) A. C. Richardson, *Carbohydr. Res.*, **4**, 422 (1967); *J. Chem. Soc., Chem. Commun.*, **1965**, 627.

4) H. H. Baer, K. Capek, and M. C. Cook, *Can. J. Chem.*, **47**, 89 (1969).

5) J. P. Marsh, C. W. Mosher, E. M. Acton, and L. Goodman, *Chem. Commun.*, **1967**, 973.

6) D. Horton and W. Weckerie, *Carbohydr. Res.*, **44**, 227 (1975).

7) T. E. Walker and R. Baker, *Carbohydr. Res.*, **64**, 266 (1978).

8) S. Yasuda, T. Ogasawara, S. Kawabata, I. Iwataki, and T. Matsumoto, *Tetrahedron*, **29**, 4087 (1973).

9) A similar principle of synthesis was applied to the total synthesis of the mushroom toxin muscarine: T. Matsumoto, A Ichihara, and N. Ito, *Tetrahedron*, **25**, 5889 (1969). A 6-step total synthesis of a DL-daunosamine derivative from 3-buten-2-ol has recently been reported: I. Dyong and R. Wiemann, *Angew. Chem.*, **90**, 682 (1978).

10) W. Roth, W. Pigman, and I. Danishefsky, *Tetrahedron*, **20**, 1675 (1964).

11) $J_{2a,e}$=13 Hz and $J_{2e,3}$=5 Hz are shown for a compound related to daunosamine. See Ref. 6. Practically identical NMR data (100 MHz, pyridine-d_5) have been reported for **7**: F. Arcamone, G. Cassenelli, G. Franceschi, R. Mondelli, P. Orezzi, and S. Penco, *Gazz. Chim. Ital.*, **100**, 949 (1970).

12) N. K. Kochetkov, A. Ya. Khorlin, B. P. Gottikh, and A. N. Nesmeyanov, *Izv. Akad. Nauk SSSR Otdel. Khim. Nauk*, **1956**, 1053.

BULLETIN OF THE CHEMICAL SOCIETY OF JAPAN, VOL. 52 (9), 2733—2734 (1979)

Preparation of Anhydrous *N,N'*-Dicyclohexylalloxan and Its Use in Dehydration

Takeshi ENDO and Makoto OKAWARA*

Research Laboratory of Resources Utilization, Tokyo Institute of Technology, Nagatsuta-cho, Midori-ku, Yokohama 227

(Received December 15, 1978)

Synopsis. Anhydrous *N,N'*-dicyclohexylalloxan has been prepared and used as a dehydrating agent for carboxylic acids in the esterification of carboxylic acids with alcohols.

Alloxan(A), a vicinal carbonyl compound (reducton), is known to play an important role in biological oxidation-reduction systems in the same way as ascorbic acid. The central carbonyl, activated by the two adjacent carbonyl groups, is reactive such that it readily combines with one mole of water to form the hydrate (A-hydrate).[1] The photochemical reactions of the A-hydrate have been reported.[2,3]

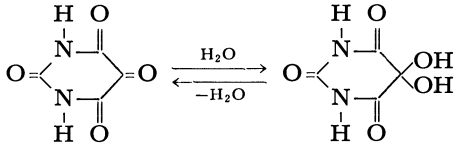

(A) (A-hydrate)

The study of alloxan has been extended especially in the redox system mediated by the alloxan radical produced photochemically or chemically from the A-hydrate.[4,5]

This paper describes the synthesis of anhydrous *N,N'*-dicyclohexylalloxan and the use of the hydrate in the esterification of carboxylic acids with alcohols.

A and A-hydrate are soluble in water and alcohols, but insoluble in common organic solvents. The preparation of *N,N'*-dialkylalloxan was directed to achieving soluble alloxan in general organic solvents. Alloxans may be prepared by oxidation of the corresponding barbituric acids, which are obtained from diethyl malonate and ureas, using chromium trioxide.[6] *N,N'*-Dicyclohexyl barbituric acid(**1**) was prepared by the reaction of malonic acid and dicyclohexylcarbodiimide (DCC).[7] *N,N'*-Dicyclohexylalloxan (**2**) as the hydrate was obtained by the oxidation of **1** with chromium trioxide at room temperature in a mixture of acetic acid and water, and identified by IR and elemental analyses.

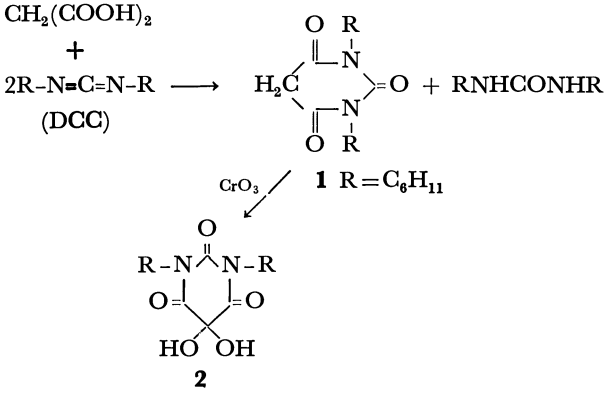

2

Anhydrous alloxan was prepared by heating alloxan hydrate *in vacuo* (4 mmHg†) at 150 °C.[8] Anhydrous *N,N'*-dicyclohexylalloxan was prepared by 1) heating the hydrate at reduced pressure (170—180 °C/1 mmHg), 2) treatment with acetic anhydride at 80 °C or 3) treatment with DCC at room temperature. Synthetically method 1 is the most convenient, since for methods 2 and 3 a process is needed to separate **3** from the reaction mixture. In the IR spectrum of **3** the OH group absorption (3450 cm^{-1}) disappeared completely and was accompanied by the appearance of a new absorption band of the C–O group at 1760 cm^{-1}.

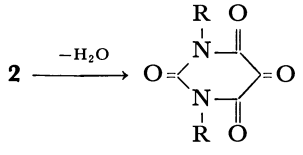

3

Compound **3** thus obtained was examined in terms of its suitability as a dehydrating agent. Anhydrous alloxan (A) is not suitable as a dehydrating agent because of possible side reactions. Acetic acid was treated with equimolar quantities of **3** in tetrahydrofuran (THF) at room temperature to give quantitatively acetic anhydride together with **2**. The esterification of carboxylic acids with alcohols using **3** was conducted in THF at room temperature. The corresponding esters were obtained in reasonable yields as shown in Table 1. In the condensation of carboxylic acids and amines the same method is impossible to use since **3** reacts preferentially with amines.[9] The reaction may proceed *via* an activated intermediate of the carboxylic acid as shown below:

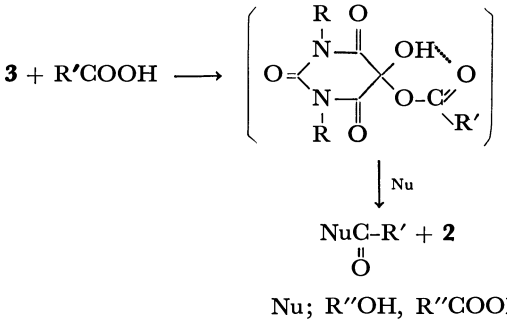

Nu; R″OH, R″COOH

Several anhydrous inorganic salts (*e.g.* Na_2SO_4, $MgSO_4$) have been used as dehydrants. **3** is novel example of a dehydrating agent for ester formation which can be reproduced by heating **2** and can be used repeatedly.

† 1 mmHg=133.322 Pa.

Table 1. Esterification of carboxylic acids with alcohols by anhydrous *N,N*-dicyclohexylloxan (**3**)

Carboxylic acid (R′)	Alcohol (R″)	Yield of isolated ester (%)
CH_3	CH_3CH_2	55
CH_3	$CH_2C_6H_5$	60
CH_3	$C_{12}H_{25}$	53
C_6H_5	CH_3CH_2	40

Experimental

The synthesis of *N,N′*-dicyclohexylbarbituric acid(**1**) (mp 207—208 °C) was prepared from DCC and malonic acid.[7]

Preparation of N,N′-*Dicyclohexylalloxan (**2**).* To a solution of chromium trioxide (15 mmol) in a mixture of water–acetic acid (15 ml) (1/4, v/v) was added a solution of **1** (10 mmol) at 30 °C. After stirring for 2 h at 25—30 °C, the reaction mixture was poured into water and then the precipitate filtered and dried under vacuum. The alloxan was recrystallized from carbon tetrachloride. Yield; 90%, mp 212—214 °C. IR (KBr, cm^{-1}): 3370 (ν_{OH}); 1690 (ν_{CO}). Found: C, 59.20; H, 7.47; N, 8.62%. Calcd for $C_{16}H_{24}O_5N_2$: C, 59.24; H, 7.46; N, 8.64%.

Preparation of Anhydrous N,N′-*Dicyclohexylalloxan (**3**).* **3** was synthesized by three methods: 1) **3** was sublimated by heating **2** at 170—180 °C/1 mmHg for 15 h (97% yield). 2) A solution of **2** (10 mmol) in acetic anhydride (30 ml) was heated at 80 °C for 5 h. After the excess acetic anhydride was removed under vacuum, the residue was recrystallized from carbon tetrachloride to give **3** (90% yield). 3) To a solution of **2** (10 mmol) in THF (30 ml), DCC (10 mmol) was added at room temperature and the reaction mixture stirred at 40 °C for 7 h. The *N,N′*-dicyclohexylurea was filtered and the THF evaporated under vacuum. The residue was recrystallized from carbon tetrachloride to give **3′** (85 yield). Mp 229—231 °C. IR (KBr, cm^{-1}): 1760, 1710, 1690 (ν_{CO}). UV (THF, nm): 420, 257 (λ_{max}). Found: C, 62.70; H, 7.59; N, 9.45%. Calcd for $C_{16}H_{22}O_4N_2$: C, 62.75; H, 7.52; N, 9.48%.

*Reaction of **3** with Acetic Acid.* To a solution of **3** (30 mmol) in THF (30 ml) was added acetic acid (33 mmol) at room temperature and the reaction mixture was stirred at room temperature for 7 h. The THF was removed and the residue was distilled to give acetic anhydride quantitatively and **2** was recovered from the residue.

*Esterification of Carboxylic Acids with Alcohols by the Use of **3**.* To a solution of **3** (10 mmol) in THF (30 ml) was added the carboxylic acid at room temperature; alcohol (11 mmol) was then added to the reaction mixture. After the mixture was stirred at room temperature for 10 h, the THF was evaporated. The obtained residue was distilled to give the corresponding ester as shown in Table 1, and **2** was obtained quantitatively from the residue after distillation.

References

1) M. B. Rubin, *Chem. Rev.*, **75**, 155 (1975).
2) T. Matsuura, R. Sugae, R. Nagashima, and K. Omura, *Tetrahedron*, **24**, 6149 (1968).
3) Y. Otsuji, S. Wake, and E. Imoto, *Tetrahedron*, **26**, 4139 (1970).
4) T. Endo and M. Okawara, *Chem. Lett.*, **1977**, 1487.
5) T. Endo, E. Fujiwara, and M. Okawara, *J. Polym. Sci. Polym. Lett. Ed.*, **16**, 211 (1978).
6) A. V. Homgren and W. Wenner, *Org. Synth.*, Coll. Vol. IV, 23 (1963).
7) A. K. Bose and S. Garrett, *J. Am. Chem. Soc.*, **84**, 1310 (1962).
8) R. Moubasher and A. M. Othman, *J. Am. Chem. Soc.*, **72**, 2666 (1950).
9) J. W. Clark-Lewis and J. A. Edgar, *J. Chem. Soc.*, **1965**, 5551.

BULLETIN OF THE CHEMICAL SOCIETY OF JAPAN, VOL. 52 (9), 2735—2736 (1979)

The Asymmetric Hydroformylation of Vinyl Acetate

Yoshihisa WATANABE,* Take-aki MITSUDO, Yukio YASUNORI,
Junichi KIKUCHI, and Yoshinobu TAKEGAMI

Department of Hydrocarbon Chemistry, Faculty of Engineering, Kyoto University, Sakyo-ku, Kyoto 606

(Received January 16, 1979)

Synopsis. Vinyl acetate gives selectively (*S*)-2-acetoxypropanal in 10—24% optical yields by the asymmetric hydroformylation with μ,μ'-dichlorotetracarbonyldirhodium-(—)-DIOP. (*R*)-Benzylmethylphenylphosphine and neomenthyldiphenylphosphine give low optical yields. The reaction depends essentially on the DIOP/rhodium ratio. Just 2 mol or more of (—)-DIOP per g-atm of rhodium is required for the asymmetric reaction. Other reaction variables (temperatures and pressures of hydrogen and carbon monoxide) have minor effects.

More recently, a chiral phosphine–rhodium complex system has been shown to be effective for the asymmetric hydroformylation of olefins.[1] These studies have been mainly concentrated on styrene and butenes. Styrene gives 2-phenylpropanal as the major product in moderately high optical yields up to 44%[1b] but such 1-alkenes as 1-butene and 1-octene give branched chain-aldehydes with optically active carbons as minor products in only low optical yields. Little attention, however, has been paid to the asymmetric hydroformylation of *O*- and *N*-vinyl compounds, which are selectively formylated on the inner carbon adjacent to the oxygen and nitrogen to produce aldehydes with an optically active carbon.[2] Thus, vinyl acetate gives 2-acetoxypropanal in an excellent yield. Compared with simple olefins, *O*- and *N*-vinyl compounds appear to be more suitable for the asymmetric hydroformylation.

The present study will deal with the asymmetric hydroformylation of vinyl acetate using a chiral phosphine–rhodium complex, and the effects of several reaction variables (ligands, temperatures, and pressures of hydrogen and carbon monoxide) will be described in some detail.

Experimental

All the ^{1}H NMR spectra were recorded on a JEOL JNM-PM-60 spectrometer, using Me_4Si as the internal standard. The optical rotations were measured on a JASCO model DIP-180 automatic polarimeter using samples as a neat liquid. The GPC analysis was carried out on a Shimadzu model GC-3B apparatus equipped with a column (3 mmϕ, 3 m) packed with diethylene glycol adipate polyester on Chromosorb.

Materials. The vinyl acetate was refluxed over active calcium sulfate for one or two days, distilled, and stored in a refrigerator. Neomenthyldiphenylphosphine(abbreviated as nmdpp),[3] (*R*)-benzylmethylphenylphosphine(bmpp),[4] 2,2-dimethyl-4,5-bis(diphenylphosphino)-1,3-dioxolane ((—)-DIOP),[5] and μ,μ'-dichlorotetracarbonyldirhodium[6] were prepared according to the methods in the literature.

Reaction Procedure. The reaction was carried out in a manner similar to that described in a previous paper.[1a] The 2-acetoxypropanal was separated by vacuum distillation (bp, 65—68 °C/30 Torr), and then the optical rotation was measured. The 2- and 3-acetoxypropanal were identified by GPC and ^{1}H NMR analysis. 2-Acetoxypropanal, ^{1}H NMR ($CDCl_3$): δ (ppm) 1.35 (d, 3H, J=7.5 Hz, CH_3), 2.15 (s, 3H, CH_3), 4.95 (q, 1H, J=7.5 Hz, CH), 9.94 (s, 1H, CHO). 3-Acetoxypropanal, ^{1}H NMR ($CDCl_3$): δ (ppm) 2.03 (s, 3H, CH_3), 2.83 (t, d, 2H, J_t=6, J_d=1 Hz, CH_2), 9.98 (t, 1H, J=1 Hz, CHO).

Reduction of 2-Acetoxypropanal. Optically active 2-acetoxypropanal, whose configuration and maximum rotation are unknown, was reduced to a known compound, (*S*)-1,2-propanediol ($[\alpha]_{D\ max}$=+16.28°[7]): To a suspension of lithium aluminum hydride (3 g) in tetrahydrofuran (20 ml) was added, drop by drop, a 2-acetoxypropanal (5 ml, $[\alpha]_D$=—11.26°) solution in tetrahydrofuran (20 ml), and then the mixture was refluxed for 4 h. The resultant solution was hydrolyzed with 1M HCl (30 ml), and the precipitates thus formed were filtered off. The filtrate was dried with disodium sulfate, concentrated, and analyzed by GPC. $[\alpha]_D$=+2.35°; optical yield, 14.4%.

Results and Discussion

Under the typical oxo reaction conditions (120 °C and CO/H_2=50/50 atm) using a rhodium catalyst such as $[RhCl(CO)_2]_2$, vinyl acetate is readily hydroformylated to give 2-acetoxypropanal selectively. The reaction is completed in less than 1 h. A chiral phosphine–$[RhCl(CO)_2]_2$ system is effective for the asymmetric hydroformylation. The reaction was examined in some detail by changing several reaction variables, using (—)-DIOP, (*R*)-bmpp, and nmdpp as chiral phosphines. Some typical results are summarized in Table 1.

$$AcOCH{=}CH_2 \xrightarrow[[RhL^*]]{CO,\ H_2} AcOC^*(CHO)-CH_3 + AcOCH_2CH_2CHO$$

A tertiary phosphine–rhodium catalyst requires a much longer reaction time for completion than does $[RhCl(CO)_2]_2$; even at the DIOP/Rh ratio of 1.0, the product yields amounted to only 25% even after 18 h (Run 1). Such a retardation effect appears to come from the coordination of the phosphine to the rhodium, showing that the active catalyst species are $HRh(CO)_{3-n}L_n$ (n=1, 2, L=ligand) in place of $HRh(CO)_3$. The retardation effect appears to be largest with bmpp, followed by (—)-DIOP and nmdpp. The stereochemical control, however, is largest with (—)-DIOP. (*R*)-Bmpp and nmdpp are much less effective (Runs 13 and 14).

With (—)-DIOP, the (—)-DIOP/Rh ratio has a great effect on the stereoselectivity (see Runs 1—3), while the other reaction conditions are fixed. At the ratios of 1.0 and 1.5, the stereochemical control was not effective, giving only low optical yields, 0.8 and

Table 1. Asymmetric hydroformylation of vinyl acetate with $[RhCl(CO)_2]_2$-(−)-DIOP

Run	Reaction conditions				Product yield[a] %	2-Acetoxypropanal		
	Molar ratio (−)-diop/Rh	CO/H_2 atm/atm	Temp °C	Time h		Selectivity %	$[\alpha]_D$ °	Optical yield[b] %
1	1.0	50/50	120	18	25	100	−0.60	0.8
2	1.5	50/50	120	16	45	100	−1.29	1.7
3	2.0	50/50	120	15	61	100	−11.26	15
4	4.0	50/50	120	18	50	100	−11.72	15
5	2.0	50/50	70	42	13	92	−18.4	23
6	2.0	50/50	80	17	12	89	−17.32	22
7	2.0	50/50	100	20	56	87	−12.60	16
8	2.0	50/50	140	3	45	100	−9.25	12
9	2.0	20/50	120	2	59	100	−11.54	15
10	2.0	65/50	120	6	61	100	−9.18	12
11	2.0	50/20	120	6	45	100	−10.40	13
12	2.0	50/70	120	8	43	100	−8.55	11
13[c]	4.0	50/50	120	21	25	100	−1.63	2.1
14[d]	8.0	50/50	120	1	73	100	−0.36	0.5

a) Isolated yields of 2- and 3-acetoxypropanal. b) Calcd from the $[\alpha]_D$ values of 1,2-propanediol derived from 2-acetoxypropanal. c) (*R*)-Benzylmethylphenylphophine was used. d) Neomenthyldiphenylphophine was used.

1.7% respectively. A small increase in the ratio to 2.0, however, resulted in a larger stereoselectivity, an optical yield of up to 15%. Additional increases in the ratio, to 3.0, 4.0, and 8.0, however, showed no additional increase in the stereoselectivity. Thus, the (−)-DIOP/Rh ratio clearly has a critical point at 2.0 in the reaction. The efficiency of the DIOP ligand in some asymmetric reactions has been considered to come from its chelating ability as a bidentate,[8] and some metal complexes chelated by DIOP are known.[9] The results obtained here, however, appear to throw doubt on the idea that (−)-DIOP acts as a bidentate ligand in this reaction.

The active catalyst species for the asymmetric hydroformylation has normally been considered to be $HRh(CO)L_2$* rather than $HRh(CO)_2L$*, where L* is a chiral ligand.[1] Even at the (−)-DIOP/Rh ratio of 1.0, a retardation in the reaction rate was observed, showing that the rhodium catalyst is changed into the $HRh(CO)_2P\frown P$ species (DIOP is presented as P⌒P), still with no effect on the stereochemical control. Just one additional mole of (−)-DIOP per g-atm of rhodium seems to change the rhodium catalyst into another species, $HRh(CO)(P\frown P)_2$, with a conformational rigidity; this species is really active in the asymmetric reaction. Thus, the fact described above could be explained by considering that the DIOP acts as a monodentate ligand. A similar doubt has been suggested in the asymmetric hydrocarboxylation catalyzed by (−)-DIOP–palladium chloride.[10]

Among other reaction variables, such as the reaction temperatures and partial pressures of carbon monoxide and hydrogen, the reaction temperature has the largest effect on the stereoselectivity (see Runs 3, 5—8). Under fixed conditions, a (−)-DIOP/Rh ratio of 2.0 and an initial partial pressure of 50 atm of either carbon monoxide or hydrogen, a lower reaction temperature (70—140 °C) gave a higher stereoselectivity. At 70 °C the highest optical yield of 23% was achieved, but the reaction rate became remarkably slow. At lower temperatures (70—100 °C), 3-acetoxypropanal was produced as a by-product. Lowering the reaction temperature exhibits the same tendency as with styrene.[1]

The stereoselectivity of this reaction, however, was not significantly affected by changing the initial pressures of carbon monoxide and hydrogen. Under the fixed conditions, a (−)-DIOP/Rh ratio of 2.0 and at 120 °C, the effects of the pressures on the stereoselectivity were examined. When the pressure of hydrogen was fixed at 50 atm, the stereoselectivity was almost unchanged, giving 15% optical yields at 20—50 atm of carbon monoxide, but it decreased to 12% at 65 atm (Runs 3, 9, and 10). When the pressure of carbon monoxide was fixed at 50 atm, the stereoselectivity was the largest (15% optical yield) at 50 atm of hydrogen, but decreased to 13 and 11% at higher (70 atm) and lower (20 atm) pressures of hydrogen respectively (Runs 3, 11, and 12). Accordingly, the pressures have a minor effect on the reaction of vinyl acetate.

In the present study, vinyl acetate shows a larger stereoselectivity than any other olefins except styrene. The largest stereoselectivity with styrene has been considered to arise from the conformational rigidity concerned with the phenyl group,[1a] though the mechanism of the asymmetric induction is not clear. With vinyl acetate, the acetoxyl group seems to play some role in the asymmetric induction.

The present work was partially supported by a grant-in-Aid for Development Scientific Research and for Scientific Research from the Ministry of Education.

References

1) See, for example: a) M. Tanaka, Y. Watanabe, T. Mitsudo, and Y. Takegami, *Bull. Chem. Soc. Jpn.*, **47**, 1698 (1974), and the references cited therein; b) M. Tanaka, Y. Ikeda, and I. Ogata, *Chem. Lett.*, **1975**, 1115; c) A. Stefani and D. Tatone, *Helv. Chim. Acta*, **60**, 518 (1977), and the references cited therein.

2) Ajinomoto Co., Inc., France Patent 1,361,797; *Chem. Abstr.*, **61**, 11894 (1964); Y. Watanabe, T. Mitsudo, M. Tanaka, and Y. Takegami, *Yukagaku*, **23**, 304 (1974).

3) J. D. Morrison, R. E. Burnett, A. M. Aquiar, C. J. Morrow, and C. Phillips, *J. Am. Chem. Soc.*, **93**, 1301 (1971).

4) K. Nauman, G. Zon, and K. Mislow, *J. Am. Chem. Soc.*, **91**, 7012 (1969).

5) H. B. Kagan and T. P. Dang, *J. Am. Chem. Soc.*, **94**, 6429 (1972).

6) J. A. McCleverty and G. Wilkinson, *Inorg. Synth.*, **8**, 211 (1966).

7) B. T. Golding, D. R. Hall, and S. Sakrikar, *J. Chem. Soc., Perkin Trans. 1*, **1978**, 1214.

8) R. Glaser, *Tetrahedron Lett.*, **1975**, 2127.

9) S. Brunie, J. Mazan, N. Langlois, and H. B. Kagan, *J. Organomet. Chem.*, **114**, 225 (1976).

10) G. Consiglio, *J. Organomet. Chem.*, **132**, C26 (1977).

BULLETIN OF THE CHEMICAL SOCIETY OF JAPAN, VOL. 52 (9), 2737—2738 (1979)

Studies on the Syntheses of Sesquiterpene Lactones. III. Improved Synthesis of Vulgarin

Masayoshi ANDO,* Kiyoshi TAJIMA, and Kahei TAKASE

Department of Chemistry, Faculty of Science, Tohoku University, Aramaki-aza-Aoba, Sendai 980

(Received January 18, 1979)

Synopsis. An improved synthesis of vulgarin is described. Epoxidation of 1-oxo-5α*H*,6β,11β*H*-eudesm-3-en-6,13-olide and successive treatment of the resulting epoxide with silica gel gave vulgarin. Oxidation of 1-oxo-5α*H*,6β,11β*H*-eudesm-3-en-6,13-olide with air or oxygen gas gave 4α-hydroperoxy-1-oxo-5α*H*,6β,11β*H*-eudesm-2-en-6,13-olide and 4β-hydroperoxy-1-oxo-5α*H*,6β,11β*H*-eudesm-2-en-6,13-olide, which were transformed into vulgarin and C_4-epivulgarin, respectively.

Many compounds with a γ-hydroxy α,β-unsaturated carbonyl moiety fused on various skeletons have been found in natural products. Since some of them have considerable biological activities as shown in abscisic acid and ecdysone, the synthesis of γ-hydroxy α,β-unsaturated carbonyl moiety has drawn much attention, several efficient methods for preparing this functional group being reported.[1] Vulgarin (**5**) is a typical example of the sesquiterpenes possessing a γ-hydroxy α,β-unsaturated carbonyl group.[2] Reports have been given on the synthesis of vulgarin[3,5] and its α-methylene γ-lactone derivative, arglanine.[4,5] In connection with the general synthesis of γ-hydroxy α,β-unsaturated carbonyl moiety we have examined a more efficient synthesis of vulgarin.

The starting material is a β,γ-unsaturated acetal (**1**) prepared from the corresponding α,β-unsaturated ketone.[5] Treatment of **1** with boiling 50% aqueous acetic acid gave the desired β,γ-unsaturated ketone (**2**)[2,4] in a quantitative yield. Methods for the preparation of γ-hydroxy α,β-unsaturated ketones *via* the corresponding β,γ-unsaturated ketones are limited[1] probably because of difficulty in the preparation of the intermediates.[6] Since the β,γ-unsaturated ketone (**2**) was obtained in an excellent yield, the synthesis of vulgarin *via* intermediate (**2**) was examined in two procedures.

Epoxidation of **2** with *m*-chloroperbenzoic acid gave an epoxy ketone (**4**) in a quantitative yield. The stereochemical assignment of the epoxide ring of **4** is based on the consideration that the epoxidation proceeds from the less hindered α-side. **4** was transformed into vulgarin in 90% yield by treatment with silica gel TLC for 1 h.

During the course of attempted purification of **2** by TLC of silica gel we observed that this compound gradually turned into two kinds of more polar substances at the surface of silica gel. In order to examine the transformation, **2** was allowed to stand on the surface of silica gel in TLC on exposure to air for 12 days to give 4α-hydroperoxide (**7**) in a 46% yield and 4β-hydroperoxide (**8**) in a 13% yield accompanied by vulgarin in a 9% yield. The structure of **7** and **8** were deduced from the analyses of their NMR spectra. The assigned stereochemistry at C_4 in **7** and **8** was unambiguously demonstrated by their conversion into vulgarin and C_4-epivulgarin (**6**) in quantitative yields by treatment with KI in aqueous acetic acid.

The oxidation reaction of **2** by molecular oxygen in solution was also investigated. Since the γ-lactone moiety was considered to be sensitive in autoxidation in strong basic conditions, we chose neutral or slightly acidic[7] conditions. The β,γ-unsaturated ketone (**2**) gave vulgarin by bubbling oxygen gas into 50% aqueous acetic acid solution at refluxing temperature. This reaction was very slow at room temperature but proceeded in a moderate rate by addition of active charcoal[8] into the reaction mixture. In this case the major product was not vulgarin but the corresponding hydroperoxide (**7**). In MeOH and DMF solutions, the oxidation reaction of **2** by molecular oxygen in the presence of active charcoal proceeded in the same manner as in 50% aqueous acetic acid solution. The results are summarized in Table 1. The resulting hydroperoxides (**7**) and (**8**) were transformed into vulgarin and C_4-epivulgarin, respectively, in quantitative yields.

The acetal (**1**) also gave vulgarin (**5**) in a 50% yield by bubbling oxygen gas in boiling 50% aqueous acetic acid solution. Yamakawa *et al.* reported a similar reaction in an acetal (**3**), but did not mention the reaction path.[4] These reactions probably proceeded through autoxidation of the corresponding β,γ-unsaturated ketones formed under the reaction conditions and successive decomposition of the resulting hydroperoxides to the corresponding alcohols.

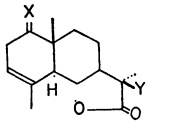

(**1**) X=O,O], Y=H
(**2**) X=O, Y=H
(**3**) X=O,O], Y=SeC_6H_5

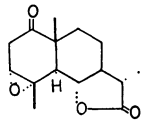

(**4**)

(**5**) X=OH, Y=CH_3
(**6**) X=CH_3, Y=OH
(**7**) X=O_2H, Y=CH_3
(**8**) X=CH_3, Y=O_2H

Experimental

All the melting points were uncorrected. IR spectra were determined on Shimadzu IRG-1 and Nihonbunko IRA-2 spectrometers. NMR spectra were recorded on a Hitachi R-24 spectrometer in $CDCl_3$ containing TMS as an internal standard.

1-Oxo-5αH,6β,11βH-eudesm-3-en-6,13-olide (2) from 1,1-Ethylenedioxy-5αH,6β,11βH-eudesm-3-en-6,13-olide (1). A solution of **1** (800 mg, 2.74 mmol) in 50% AcOH aq (76 ml) was refluxed for 1 h and 15 min under N_2, cooled and poured into satd. NaCl aq soln. The mixture was worked up as usual to give 677 mg (100%) of **2**, (mp 139 °C).

Table 1. Oxidation of **2** with molecular oxygen

Run	Reaction conditions				Isolated yield/%			
	Solvent	Catalyst	Temperature	Time/h[a)]	**7**	**8**	**5**	**6**
i	50% AcOH aq	None	Room temp	24	(Recovered starting material)			
ii	50% AcOH aq	None	Reflux	2.5	0	0	24	0
iii	50% AcOH aq	C[b)]	Reflux	1	0	0	38	9
iv	50% AcOH aq	C[b)]	Room temp	70	49	13	19	0
v	MeOH	C[b)]	Room temp	87	71	16	12	0
vi	DMF	C[b)]	Room temp	76	62	9	12	0

a) The reactions were stopped at the time when **2** disappeared in the reaction mixture by TLC analysis except in the case of run i. b) Active charcoal (powder).

*3α,4α-Epoxy-1-oxo-5αH,6β,11βH-eudesman-6,13-olide (**4**).* A mixture of **2** (47 mg, 0.19 mmol) and *m*-chloroperbenzoic acid (33 mg, 0.19 mmol) in CH_2Cl_2 (3 ml) was allowed to stand at room temperature for 75 h. The mixture was worked up as usual to give 50 mg (100%) of spectroscopically pure **4** as a crystalline material, which was recrystallized from ether to give prisms, mp 151 °C. IR (KBr): 1770 and 1712 cm^{-1}. NMR: δ 1.24 (3H, d, J=6.4 Hz, C_{11}–Me), 1.27 (3H, s, C_{10}–Me), 1.59 (3H, s, C_4–Me), 2.05 (1H, d, J=11.5 Hz, C_5–H), 2.79 (1H, d, J=1.6 Hz, C_2–H), 2.83 (1H, d, J=4.0 Hz, C_2–H), 3.25 (1H, dd, J=1.6 and 4.0 Hz, C_3–H), 4.06 (1H, broad t, J=11.5 Hz, C_6–H). Found: C, 67.82; H, 7.71%. Calcd for $C_{15}H_{20}O_4$: C, 68.16; H, 7.63%.

*Vulgarin from **4**.* The $CHCl_3$ solution of **4** (50 mg, 0.19 mmol) was impregnated into TLC of silica gel (Merck GF_{254}, thickness 0.25 mm, 20 cm×20 cm sheet), which was developed by dipping in AcOEt–$CHCl_3$ (1:1) for 1 h. The most polar band was collected and extracted with acetone to give 45 mg (90%) of vulgarin.

*Air Oxidation of **2** at the Surfaces of Silica Gel TLC.* The $CHCl_3$ solution of **2** (21 mg, 0.08 mmol) was impregnated into TLC of silica gel (Merck GF_{254}, thickness 0.25 mm, 20 cm×10 cm sheet), which was developed by dipping in AcOEt–$CHCl_3$ (1:1). The TLC plate was dried and allowed to stand at room temperature exposed to air for 12 days. The black band monitored by an UV lamp was collected from TLC and extracted with acetone to give 22 mg of oil, which was shown to be a 10:3 mixture of **7** and **8** from the analysis of the NMR spectrum. This was purified by preparative TLC [Merck silica gel GF_{254}, thickness 0.25 mm, EtOAc:$CHCl_3$ (1:1)]. The first band (R_f 0.50) gave 3 mg (13%) of **8**, which was recrystallized from ether to give colorless prisms; mp 178 °C. IR (KBr): 3360, 3300, 1765, 1745, and 1682 cm^{-1}. NMR: δ 1.21 (3H, d, J=6.8 Hz, C_{11}–Me), 1.32 (3H, s, C_{10}–Me), 1.67 (3H, s, C_4–Me), 2.14 (1H, d, J=11.6 Hz, C_5–H), 4.24 (1H, m, C_6–H), 5.98 (1H, d, J=10.2 Hz, C_2–H), and 6.76 (1H, d, J=10.2 Hz, C_3–H). The second band (R_f 0.40) gave 11 mg (46%) of **7**, which was recrystallized from ether to give colorless prisms; mp 175 °C. IR (KBr): 3320, 1770, 1748, 1677, and 1660 cm^{-1}. NMR: δ 1.22 (3H, d, J=6.4 Hz, C_{11}–Me), 1.25 (3H, s, C_{10}–Me), 1.48 (3H, s, C_4–Me) 2.85 (1H, d, J=11.6 Hz, C_5–H), 4.13 (1H, dd, J=8.0 and 11.6 Hz, C_6–H), 6.02 (1H, d, J=10.6 Hz, C_2–H), 6.72 (1H, d, J=10.6 Hz, C_3–H). Found: C, 63.86; H, 7.41%. Calcd for $C_{15}H_{20}O_5$: C, 64.27; H, 7.19%.

*Oxidation of **2** by Molecular Oxygen in MeOH in the Presence of Active Charcoal.* Oxygen gas was bubbled into a solution of **2** (20 mg, 0.08 mmol) in MeOH (3 ml) in the presence of active charcoal (20 mg) at room temperature for 87 h. The mixture was worked up as usual to give 22 mg of oil, which was separated by TLC (Merck silica gel GF_{254}, thickness 0.25 mm, EtOAc:$CHCl_3$=1:1) to give 16 mg (71%) of **7**, 3.5 mg (16%) of **8**, and 2.5 mg (12%) of vulgarin.

*Vulgarin from **7**.* A mixture of **7** (9 mg, 0.032 mmol), KI aq soln (KI 30 mg, H_2O 1.5 ml), AcOH (0.1 ml), and $CHCl_3$ (0.5 ml) was stirred for 2 h at room temperature. The mixture was worked up as usual to give 8.5 mg (100%) of vulgarin.

*C_4-Epivulgarin from **8**.* **8** (9 mg, 0.032 mmol) was treated as mentioned above to give 8.5 mg (100%) of C_4-epivulgarin.

*Oxidation of **1** by Molecular Oxygen in Boiling 50% AcOH Aq Soln.* Oxygen gas was bubbled into a solution of **1** (30 mg, 0.10 mmol) in 50% AcOH aq soln (3 ml) under refluxing for 3 h, cooled and poured into satd. NaCl aq soln. The mixture was worked up as usual to give an oily crude product, which was chromatographed over silica gel (Merck, <230 mesh, 1.5 g) and eluted with $CHCl_3$ to give 13.5 mg (50%) of vulgarin.

References

1) a) Rearrangement of 1,4-*endo*-peroxides: R. J. Conca and W. Bergmann, *J. Org. Chem.*, **18**, 1104 (1953); b) Oxidation of α,β-unsaturated ketones with selenium dioxide: A. Zürcher, H. Heusser, O. Jeger, and P. Geistlich, *Helv. Chim. Acta*, **37**, 1562 (1954); c) Oxidation of dienol acetates with monoperoxyphthalic acid: L. F. Fieser and W. -Y. Haung, *J. Am. Chem. Soc.*, **75**, 5356 (1953); d) Photosensitized oxidation of β,γ-unsaturated ketones: N. Furutachi, Y. Nakadaira, and K. Nakanishi, *Chem. Commun.*, **1968**, 1625; e) Autoxidation of β,γ-unsaturated ketones: L. F. Fieser, T. W. Greene, F. Bischoff, G. Lopez, J. J. Rupp, *J. Am. Chem. Soc.*, **77**, 3928 (1955); f) Rearragement of β,γ-epoxy ketones: J. Grigor, W. Laird, D. Mclean, G. T. Newbold, and F. S. Spring, *J. Chem. Soc.*, **1954**, 2333.

2) K. S. Rybalko and L. Dolejš, *Collect. Czech. Chem. Commun.*, **26**, 2909 (1961); T. A. Geissman and G. A. Ellestad, *J. Org. Chem.*, **27**, 1855 (1962).

3) V. K. Honwad, E. Siscovic, and A. S. Rao, *Tetrahedron*, **23**, 1273 (1967).

4) K. Yamakawa, T. Tominaga, and K. Nishitani, *Tetrahedron Lett.*, **1975**, 4137.

5) M. Ando, A. Akahane, and K. Takase, *Bull. Chem. Soc. Jpn.*, **51**, 283 (1978).

6) H. J. Ringold and S. K. Malhotra, *Tetrahedron Lett.*, **1962**, 669; J. H. Babler, N. C. Malek, and M. J. Caghlam, *J. Org. Chem.*, **43**, 1821 (1978).

7) 50% AcOH aq soln was employed since **2** was not epimerized to the corresponding conjugated enone in this solvent even at refluxing temperature.

8) Recently the carbon catalyzed autoxidation of fluorene in alkali solution was reported: K. Yang and M. A. Johnson, *J. Org. Chem.*, **42**, 3754 (1977).

BULLETIN OF THE CHEMICAL SOCIETY OF JAPAN, VOL. 52 (9), 2739—2740 (1979)

Phase Transfer Catalyzed Reaction of Organic Thiocyanates with Hydroxide Ion

Yumihiko YANO, Akira KURASHIMA, and Waichiro TAGAKI*

Department of Chemistry, Faculty of Engineering, Gunma University, Kiryu, Gunma 376

(Received February 26, 1979)

Synopsis. The reactions of 9-fluorenyl, phenacyl, benzhydryl, and benzyl thiocyanates (or the corresponding bromides with sodium thiocyanate) with hydroxide ion under phase transfer conditions afforded 9,9′-bifluorenylidene, 2,3-dibenzoylthiirane, thiobenzophenone and dibenzyl disulfide, respectively.

It is well known that carbanion-forming reactions are accelerated by cationic micelles.[1] Favored formation of carbanion is also known for phase transfer catalyzed reactions,[2] including our own works.[3–5] Recently, we have demonstrated that the mechanism of hydrolysis for esters bearing α-hydrogen changes from addition-elimination to elimination-addition mechanism under micellar conditions.[6] This finding has led us to check the reaction in the title.

In this paper, we describe the reactions of organic thiocyanates with hydroxide ion in the two-phase system, together with the reactions of the corresponding organic bromides with hydroxide ion in the presence of sodium thiocyanate, in the hope of finding a convenient method for the preparation of thiocarbonyl compounds.

Results and Discussion

Thiocarbonyl compounds are usually prepared by the reaction of the corresponding carbonyl compounds or acetals with hydrogen sulfide in the presence of H^+ or by HCN elimination from organic thiocyanates with base.[7] In these reactions anhydrous conditions are usually required. The present reaction was carried out by stirring two phases of organic thiocyanates dissolved in CH_2Cl_2 or benzene and aqueous sodium hydroxide in the presence of hexadecyltrimethylammonium bromide (CTABr) as the phase transfer catalyst. Other catalysts, such as methyltrioctylammonium chloride and benzyltriethylammonium bromide, did not make much difference in the yields of products. The reactions could also be performed by using organic bromides and sodium thiocyanate to give the corresponding organic thiocyanates *in situ* during the reaction. The results are summarized in the Table.

The run 1 indicates the formation of 9,9′-bifluorenylidene in more than 90% yield. The same result was obtained by using 9-bromofluorene and sodium thiocyanate. Although 9-bromofluorene is known to give 9,9′-bifluorenylidene with base,[8] the present reaction was found to be much slower in the absence of sodium thiocyanate than in its presence. Thus, the reaction of 9-bromofluorene is considered to proceed through the formation of 9-thiocyanofluorene.

The episulfide obtained in the reaction of benzoylmethyl thiocyanate (run 2) is presumably the *trans*-isomer since *trans*-1,2-dibenzoylethylene was obtained on treatment of the episulfide with triphenylphosphine. In the case of benzhydryl thiocyanate (run 3) thiobenzophenone was obtained in a quantitative yield. Finally, dibenzyl thiocyanate gave disulfide (run 4).

These results may be tentatively accounted for by the following reaction scheme where **A**, **B**, **C**, and **D** stand for the products of runs 1—4, respectively.

TABLE 1. $R_1R_2CHSCN \xrightarrow[\text{CTABr, under } N_2]{\text{aq NaOH/}CH_2Cl_2 \text{ or benzene}}$ Products

Run	R_1	R_2	Conditions [NaOH]	Conditions Temp	Conditions Time	Products (yield)	
1	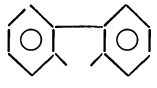		5 M[a]	r.t	2—3 h	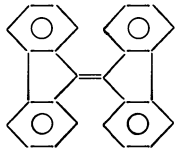	(90—96%)
2	C_6H_5CO	H	5 M[a]	r.t	18 h	$C_6H_5COCH(S)CHCOC_6H_5$	(37—45%)
						Unidentified[c]	
3	C_6H_5	C_6H_5	15 M[b]	60—70 °C	2—3 days	$(C_6H_5)_2C{=}S$ [d]	(90%)
4	C_6H_5	H	15 M[a]	60—70 °C	24 h	$(C_6H_5CH_2S)_2$ [e]	(30%)

a) With CH_2Cl_2. b) With benzene. c) This was found in the aqueous layer and precipitated by acidifying the solution. d) The absorption spectrum (λ_{max} 595 nm, ε=167 in *i*-PrOH)[10] indicated a quantitative yield. e) Starting material was recovered (65%).

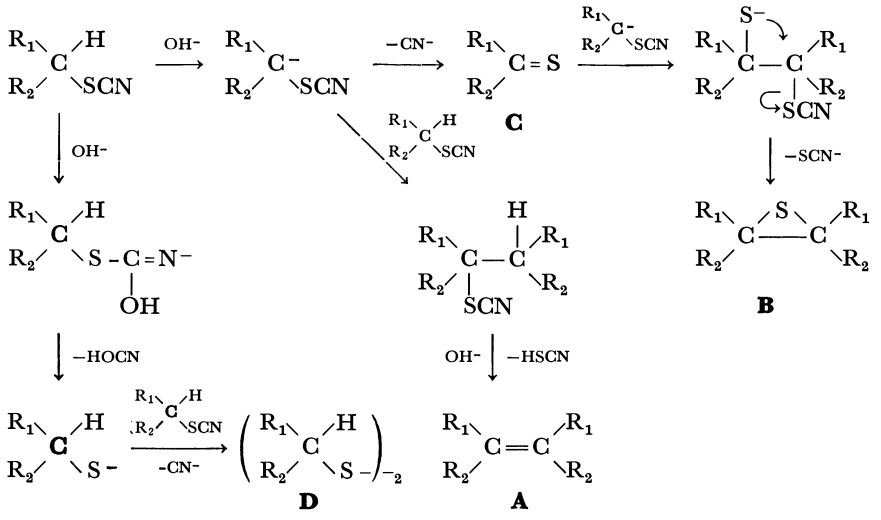

Scheme 1.

Carbene coupling can be conceivable for the formation of **A**.[9] However, no carbene adduct was obtained in the presence of cyclohexene or styrene. Episulfide (**B**) might be formed by the addition-elimination of SCN^- to **A**. However, 1,2-dibenzoylethylene (**A**) did not give the episulfide of run 2 in the presence of NaSCN under the present reaction conditions. In the case of run 4 to form **D**, the benzyl methylene may not be active enough to form carbanion under the present phase transfer conditions.

The above reaction is highly dependent on the structure of substrate and does not appear to be generally useful for synthetic purposes except for the run 3. In the run 3, benzhydryl bromide or thiocyanate can be readily converted to the thioketone in a quantitative yield, and this method may be generally applicable to the synthesis of diaryl thioketone.

Experimental

All melting points are uncorrected. The thiocyanates were prepared from the corresponding bromides and sodium thiocyanate in dry acetone.[10]

Phenacyl thiocyanate, mp 75 °C (from ether) (lit,[11] mp 75—76 °C), 70%.

9-Fluorenyl thiocyanate, mp 118—119 °C (from benzene), 78%.

Benzhydryl thiocyanate, mp 35 °C (from ether) (lit,[12] mp 35—36 °C), 93%. The other reagents were purchased from Tokyo Kasei Co.

Reaction of Thiocyanates with Hydroxide Ion under Phase Transfer Conditions. A mixture of the organic thiocyanate (10 mmol), CTABr (0.1 mmol) in CH_2Cl_2 (6 ml) and aqueous sodium hydroxide (2 ml) was stirred under N_2 atmosphere. The CH_2Cl_2 layer was separated and dried over Na_2SO_4. After CH_2Cl_2 was evaporated, the products were isolated by column chromatography (silica gel; benzene) for phenacyl and benzyl thiocyanates. 9,9′-Bifluorenylidene and 2,3-dibenzoylthiirane were isolated by recrystallization.

9,9′-Bifluorenylidene, mp 189—190 °C ($CHCl_3$–EtOH) (lit,[13] mp 188 °C).

2,3-Dibenzoylthiirane, mp 77—77.5 °C (CH_2Cl_2–EtOH); NMR ($CDCl_3$) δ 4.00 (2H, s), 7.3—8.1 (10H). Found: C, 71.30; H, 5.00; S, 11.80%. Calcd for $C_{16}H_{12}O_2S$: C, 71.64; H, 4.47; S, 11.95%.

Reaction of the Bromides with a Mixture of Sodium Thiocyanate and Sodium Hydroxide under Phase Transfer Conditions. A mixture of the bromides (5 mmol), CTABr (0.1 mmol) in benzene (5 ml) and an aqueous solution containing equal amount of sodium thiocyanate and sodium hydroxide was stirred at a given temperature. The product isolation was performed with the same procedure as in the above reaction of thiocyanates.

Desulfurization of 2,3-Dibenzoylthiirane by Triphenylphosphine. A mixture of 2,3-dibenzoylthiirane 0.32 g (1.2 mmol) and triphenylphosphine 0.5 g (1.9 mmol) in 10 ml of xylene was refluxed overnight. Xylene was evaporated and the residue was subjected to column chromatography (silica gel; benzene). *trans*-1,2-Dibenzoylethylene was obtained (0.24 g, 85%), mp 109 °C (lit,[14] mp 109—110 °C).

References

1) J. H. Fendler and E. J. Fendler, "Catalysis in Micellar and Macromolecular Systems," Academic Press, New York (1975); C. A. Bunton, "Application of Biochemical Systems in Organic Chemistry," ed by J. B. Jones, C. J. Sih, and D. Perlman, John Wiley, New York (1976), Part 2, p. 731.

2) W. P. Weber and G. W. Gokel, "Phase Transfer Catalysis in Organic Synthesis," Springer-Verlag KG (1977).

3) W. Tagaki and H. Hara, *Chem. Commun.*, **1973**, 891.

4) Y. Yano, T. Okonogi, M. Sunaga, and W. Tagaki, *Chem. Commun.*, **1973**, 527.

5) W. Tagaki, I. Inoue, Y. Yano, and T. Okonogi, *Tetrahedron Lett.*, **1974**, 2587.

6) W. Tagaki, S. Kobayashi, K. Kurihara, A. Kurashima, Y. Yoshida, and Y. Yano, *J. Chem. Soc., Chem. Commun.*, **1976**, 843.

7) A. Ohno, "Organic Chemistry of Sulfur," ed by S. Oae, Plenum Press, New York (1977), Chap. 5.

8) D. Bethell, *J. Chem. Soc.*, **1963**, 666.

9) C. K. Ingold and J. A. Jessop, *J. Chem. Soc.*, **1929**, 2357; V. Franzen, *Chem. Ber.*, **93**, 557 (1960).

10) A. Ceccon, U. Miotti, U. Tonellato, and M. Padovan, *J. Chem. Soc., B*, **1969**, 1084.

11) L. Szekeres, *Magy. Kem Foly.*, **59**, 228 (1953), *Chem. Abstr.*, **48**, 11347 (1954).

12) A. Iliceto, A. Fava, U. Mazzcato, and P. Radici, *Gazz. Chim. Ital.*, **90**, 919 (1960).

13) E. Campaigne and W. B. Reid, Jr., *J. Am. Chem. Soc.*, **68**, 769 (1946).

14) R. E. Lutz, *Org. Synth.*, Coll. Vol. III, 248 (1955).

BULLETIN OF THE CHEMICAL SOCIETY OF JAPAN, VOL. 52 (9), 2741—2742 (1979)

Kinetics of Reaction of 4-Substituted ω-Bromo-1-acetonaphthones with Aniline in Methanol

P. ANANTHAKRISHNA NADAR* and C. GNANASEKARAN
Postgraduate Department of Chemistry, V.H.N.S.N. College, Virudhunagar 626002, India

(Received September 25, 1978)

Synopsis. Rate constants have been measured for the reactions of 4-substituted ω-bromo-1-acetonaphthones with aniline in methanol at three temperatures. Arrhenius parameters, the enthalpies and the entropies of activation have been evaluated. The Hammett ρ value of 0.90 obtained at 40 °C indicates that a triangular transition state is more likely in this reaction.

In a previous paper[1] we reported a study of the reaction of 4-substituted ω-bromo-1-acetonaphthones with benzoate ion. The reaction between 4-substituted ω-bromo-1-acetonaphthones and aniline is now investigated with a view to examine the applicability of the Hammett equation.

Experimental

Materials. All the 4-substituted ω-bromo-1-acetonaphthones were prepared from the corresponding acetonaphthones by treatment with bromine. Their purities were ascertained by microanalysis and TLC.[2]

Methanol was dried and purified by the method of Lund and Bjerrum.[3]

Rate Measurement. The kinetic procedure was similar to that employed previously[4] and the rate constants were calculated using the suitable second-order rate equation when two moles of aniline are consumed per mole of the ω-bromoacetonaphthones.

Products. Standard solutions of the appropriate ω-bromo-1-acetonaphthone and aniline in methanol were mixed in the molar ratio 1:4 and maintained at the kinetic temperature until completion. After concentration of the solution to small volume under reduced pressure, the products precipitated were collected, and recrystallized. In all cases only the ω-anilinoacetonaphthone was formed. No other product was detected. Table 1 lists the compounds isolated, their mp and elemental analyses.

Results and Discussion

The reaction is found to be first order in each of the reactants. This was established by usual procedure with ω-bromo-1-acetonaphthone. Hence we assume that the reaction follows a two-stage mechanism, with the bimolecular rate-determining first stage.

$$RCOCH_2Br + PhNH_2 = RCOCH_2NHPh + HBr \quad (1)$$

$$HBr + PhNH_2 = PhNH_3^+Br^- \quad (2)$$

where R is 4-substituted 1-naphthyl group.

The kinetic data are presented in Table 2. The entropies of activation are found to be negative as expected for bimolecular reactions.[5] But they are more negative than those observed in reactions with benzoate ion.[4] This may be due to the fact that charge is dispersed in the transition state in the case of reactions with benzoate ion, while in the present case the charge is newly produced in the transition state.

A linear relationship between the enthalpies and the entropies of activation has been realised. As explained by Exner,[6,7] the isokinetic relationship has also been examined through a plot of $\log k_1$ *versus* $\log k_2$ where k_1 and k_2 refer to the rate constants at temperatures T_1 and T_2 respectively with $T_1 > T_2$. From the slope (b=0.854) of the linear plot, the isokinetic temperature (β) is calculated to be 508 K, when T_1=323 and T_2=303 K.

The plot of $\log k/k_0$ at 40 °C against σ constants[8] of the 4-substituents in 1-naphthyl system is linear. The ρ value is 0.90 at 40 °C (excluding the result for 4-OCH_3). The correlation coefficient is 0.998 showing excellent Hammett fit.

Depending upon the mode of attack of aniline, one may consider transition states I and II in this reaction.

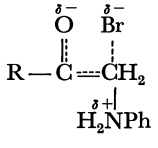

I

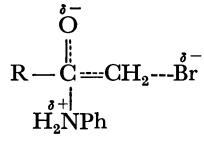

II

The formation of II may require very high ρ value in view of the ρ values of 3.2 and 2.76(2.24) found for the addition reactions of methoxide, and hydroxide ion, respectively, to substituted benzaldehydes.[9,10] The low ρ value observed in the reaction of 6-substituted ω-bromo-2-acetonaphthones[4] with aniline was ascribed to S_N2 attack of aniline at the methylene carbon. The ρ value of 0.90 calculated in the present case is significantly higher than the ρ values obtained in S_N2 displacement of substituted ω-bromoacetonaphtones at methylene carbon by different nucleophiles.[11] This may, therefore, point out that a triangular transition state III which is a hybrid between I and II is more likely in the present case.

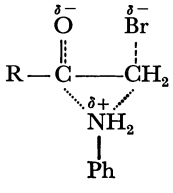

III

The cause for the difference in the nature of the transition state in the present case compared to that in the case of 6-substituted ω-bromo-2-acetonaphthones may possibly be due to the partial inhibition of resonance between >C=O group and the ring as a result of the

Table 1. 4-Substituted ω-anilino-1-acetonaphthones

Substituent	Mp °C	Formula	Calcd, % C	Calcd, % H	Found, % C	Found, % H
H	150—151[a)]	$C_{18}H_{15}NO$	82.8	5.8	82.5	5.9
F	123—124[b)]	$C_{18}H_{14}FNO$	77.4	5.0	77.3	5.1
Cl	139—140[a)]	$C_{18}H_{14}ClNO$	73.1	4.7	73.0	4.6
Br	120—121[a)]	$C_{18}H_{14}BrNO$	63.5	4.1	63.6	3.8
CH_3	100—101[a)]	$C_{19}H_{17}NO$	82.9	6.2	82.6	6.0
OCH_3	144—145[a)]	$C_{18}H_{17}NO_2$	78.3	5.8	78.1	5.4

Compounds crystallized from a) benzene-light petroleum (bp 40—60 °C) and b) light petroleum (bp 40—60 °C).

Table 2. Rate constants and activation parameters for the reaction between 4-substituted ω-bromo-1-acetonaphthones and aniline

Substituent	Rate constant $k/10^{-4}$ l mol^{-1} s^{-1} 30 °C	40 °C	50 °C	E_a kcal mol^{-1}	ΔH^* kcal mol^{-1} (40 °C)	ΔS^* e. u. (40 °C)	log PZ
H	3.77	7.65	15.9	14.8	14.2	−27.6	7.2
F	4.46	8.83	18.2	14.5	13.9	−28·0	7.1
Cl	6.11	12.5	25.3	14.1	13.5	−28.8	7.0
Br	6.24	12.6	25.5	14.1	13.5	−28.9	7.0
CH_3	2.78	5.79	12.2	15.1	14.5	−27.3	7.3
OCH_3	2.38	4.80	10.3	15.2	14.6	−27.2	7.5

ω-bromoacetyl group going out of coplanar configuration in the presence of *peri*-H interaction.[12)] Such inhibition of resonance is absent in the 2-series. The inhibition of resonance helps the carbonyl carbon to acquire more positive charge in 1-series than 2-series. Presumably this may be responsible for the operation of the transition state III in 1-series as compared to its counterpart in 2-series, thereby making the ρ value larger in the former case than in the latter case.[4)]

The authors dedicate this paper to Professor V. Baliah, Vice-Chancellor, Nagarjuna University, India on the occasion of his 60 th birthday and thank the managing board of V.H.N.S.N. College, Virudhunagar for the research facilities.

References

1) P. Ananthakrishna Nadar and C. Gnanasekaran, *Indian J. Chem.*, **16B**, 139 (1978).
2) P. Ananthakrishna Nadar and C. Gnanasekaran, *J. Chem. Soc., Perkin Trans. 2*, **1978**, 277.
3) H. Lund and J. Bjerrum, *Ber.*, **64**, 210 (1931).
4) P. Ananthakrishna Nadar and C. Gnanasekaran, *Indian J. Chem.*, **14B**, 606, (1976).
5) A. Frost and R. G. Pearson, "Kinetics and Mechanism," John Wiley & Sons Inc., New York, N.Y. (1961), p. 144.
6) O. Exner, *Nature*, **210**, 488 (1964); **227**, 336 (1970).
7) O. Exner, *Collect. Czech. Chem. Commun.*, **29**, 1094 (1964).
8) V. Baliah and P. Ananthakrishna Nadar, *Indian J. Chem.*, **9**, 1241 (1971).
9) W. J. Bover and P. Zuman, *J. Chem. Soc., Perkin Trans. 2*, **1973**, 786; *J. Am. Chem. Soc.*, **95**, 2531 (1973).
10) M. R. Crampton, M. A. El Ghariani, and M. J. Willison, *J. Chem. Soc., Perkin Trans. 2*, **1974**, 441.
11) D. J. Pasto, K. Garves, and M. P. Serve, *J. Org. Chem.*, **33**, 774 (1967).
12) P. H. Gore, J. A. Hoskins, C. K. Thadani, R. J. W. Le' Fevre, L. Radom, and G. L. D. Ritchie, *J. Chem. Soc., B*, **1969**, 426.

BULLETIN OF THE CHEMICAL SOCIETY OF JAPAN, VOL. 52 (9), 2743—2744 (1979)

Configuration et Conformation en Solution de Quelques α-Hydroxyiminocetones Cycliques

Jean BERNADOU* et Monique BONNAFOUS

Laboratoire de Pharmacie Chimique, Université Paul Sabatier, 31077 Toulouse Cedex, France

(Manuscrit reçu le 9 Novembre, 1978)

Synopsis. Les dérivés α-hydroxyiminés des cyclanones en C_6 (un isomère), C_8 (deux isomères) et C_{12} (un isomère) ont tous la configuration *anti* ; la conformation est variable selon la taille du cycle: *s-cis* pour le terme en C_6, *s-cis* ou *s-trans* pour les termes en C_8, *s-trans* pour le terme en C_{12}.

Les configurations et les conformations en solution de certaines α-hydroxyiminocétones RC(NOH)COR′ sont encore discutées: ainsi pour la benzile-monoxime Z(R=R′=C_6H_5) Sadler[1] et Armand[2] proposent une conformation *s-cis*, Cherry[3] et Pigenet[4] une conformation *s-trans*; Kataoka[5] attribue à l'hydroxyimino-2 cyclohexanone (R–R′=–$(CH_2)_4$–) la configuration Z et Ferris[6] la configuration E.

Dans le cas des benzile-monoximes Z et E et de leurs dérivés dichlorés en para, nous avons déja démontré une conformation de type *s-trans*.[7]

En série cyclique nous reprenons ici les travaux de Kataoka sur les dérivés α-hydroxyiminés de la cyclohexanone (un seul isomère: **1**), la cyclooctanone (deux isomères: **2** et **3**) et la cyclododécanone (un seul isomère **4**); grâce à une analyse en spectroscopie infra-rouge complétée par l'étude de la complexation avec le Cu^{2+} et des réactions de réarrangement de Beckmann, nous confirmons pour **2** et **4** la configuration E annoncée en précisant leur conformation (*s-trans*) et nous proposons pour **1** et **3** une configuration E et une conformation *s-cis* (Tableau 1).

Spectroscopie Infrarouge. Des solutions de concentrations variées sont analysées (Tableau 2) : l'intensite relative des bandes O–H libre et O–H lié, les premieres augmentant au dépens des secondes par dilution, traduit pour les quatre dérivés étudiés l'existence de liaisons hydrogènes intermoléculaires; celles-ci n'intéressent pas le groupe carbonyle (une seule bande C=O libre) ; elles sont difficilement rompues par dilution pour **1** et **3** et beaucoup plus facilement pour **2** et **4**. Ceci correspond (Tableau 2):

— dans le premier cas à des constantes d'association élevées (K_2=750 pour **1** et 110 pour **3**) que l'on peut rapprocher de celle de l'isonitrosocamphre E (K_2=150) de structure bien définie (*s-cis* E)[8,9] et qui se présente en solution suffisamment concentrée sous forme de dimères fermés A (Tableau 3); ces résultats

Tableau 1. Structures

	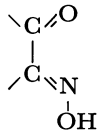	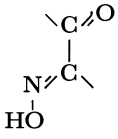
Configuration	*E*	*E*
Conformation	*s-cis*	*s-trans*
Produit	**1** et **3**	**2** et **4**

Tableau 3.

Formes d'association en solution

(A) 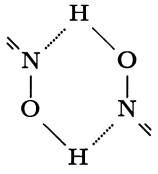

(B) 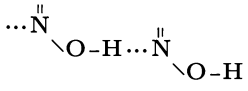

(C) 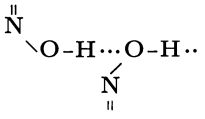

Complexation avec Cu^{2+}

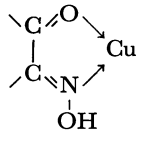

Tableau 2. Résultats expérimentaux

	F °C	Infrarouge: Bandes OH[a] lib. (conc. 0,100M)[b]	Bandes OH[a] lié (conc. 0,100M)[b]	Bandes OH[a] lib. (conc. 0,001M)[c]	Bandes OH[a] lié (conc. 0,001M)[c]	Bandes CO lib.	Conste d'associat. K_2 (d)	Complexat. avec Cu^{2+}
1	60	3560 f	3250 F	3560 m	3250 m	1715	750	+(vert)
2	huile	3610 m	3310 m	3610 F	—	1715	10	−(bleu)
3	99	3580 f	3260 F	3590 F	3280 f	1705	110	+(vert)
4	70	3580 F	3300 m	3580 F	—	1700	9	−(bleu)

a) Intensité relative des bandes: F (fort), m (moyen), f (faible). b) Cuve de 0.5 mm. c) Cuve de 50 mm. d) En solution diluée dans CCl_4, l'autoassociation des molécules étudiées peut être décrite par les équilibres (13): $D_1+D_1 \rightleftarrows D_2$, $D_2+D_1 \rightleftarrows D_3$ et $D_{n-1}+D_1 \rightleftarrows D_n$ avec les constantes d'équilibre: $K_2=x_2/x_1^2$, $K_3=x_3/x_1x_2$ et $K_n=x_n/x_1x_{n-1}$ (dans ces expressions, x_1, x_2,⋯, x_n désignent les fractions molaires des monomolécules D_1, des dimères D_2 et des différents polymères). Pour **1** et **3** no us avons vérifié expérimentalement que $K_n=K_3=0$.

Tableau 4. Réarrangement de Beckmann

Produit	Réactif	Produit final	Référence
1	$C_6H_5SO_2Cl$ + alcali dil.	$NC(CH_2)_4COOH$	6
	PO_4H_3 97%/H_2O	—	5
2	PO_4H_3 97%/H_2O	$NC(CH_2)_6COOH$	5
3	PO_4H_3 97%/H_2O	$NC(CH_2)_6COOH$	5
4	PO_4H_3 97%/H_2O	$NC(CH_2)_{10}COOH$	5

nous permettent de proposer pour **1** et **3** une structure *s-cis E*.

— dans le deuxième cas les constantes d'association sont beaucoup plus faibles (K_2=10 pour **2** et 9 pour **4**), voisines de celle mesurée pour la diacétylmonoxime (K_2=5) qui se présente en solution suffisamment concentrée sous forme de polymères ouverts de type B ou C (Tableau 3) et de structure *s-trans E* bien définie.[9] Ces résultats nous permettent de proposer pour **2** et **4** une structure *s-trans E*.

Complexation avec le Cuivre. Seules les α-hydroxyiminocétones cycliques *s-cis E* peuvent donner avec l'ion cuivrique Cu^{2+} un complexe vert (Tableau 3)[10]; c'est ce que l'on observe pour **1** et **3**; pour **2** et **4**, il n'y a pas de complexation, on observe seulement la coloration bleu pale du réactif et on doit rejeter la structure *s-cis E*.

Réarrangement de Beckmann.[5,6,11] L'obtention d'un nitrile R–CN est caractéristique d'une configuration *E*, celle d'un isonitrile R–NC d'une configuration *Z*. Pour les quatre dérivés étudiés, la réaction de réarrangement de Beckmann (Tableau 4) conduit aux acides nitriles correspondants $HOCO(CH_2)_nCN$, ce qui est en faveur de la configuration *E*.

Ainsi nous confirmons pour **1** la structure *s-cis E* proposée par Ferris. Nous pensons que **2** et **3** sont deux isomères de configuration identique mais de conformation différente (**2**: *s-trans E*; **3**: *s-cis E*); le caractère partiel de double liaison de la liaison centrale du motif α-hydroxyiminocétone confère au cycle une certaine analogie avec celui du cyclooctène pour lequel on connait effectivement les deux isomères *s-cis* et *s-trans*.[12] Enfin pour **4** nous confirmons la configuration *E* attribuée par Kataoka et proposons la conformation *s-trans*.

Partie Experimentale

*Synthese. L'hydroxyimino-2 Cyclohexanone **1** a été Obtenue selon la Technique de Geissman*:[14] Saponification de l'éthoxycarbonyle-2 cyclohexanone (0.05 mol) par de la potasse diluée (0.06 mol) puis traitement par le nitrite de sodium (0.06 mol) en milieu sulfurique ; en même temps que la nitrosation se produit une décarboxylation qui libère **1** avec un bon rendement (90%). Le produit après extraction éthérée peut être purifié par chromatographie sur colonne (silice G, solvant d'élution: butanone–ether de pétrole 6-14). $C_6H_9NO_2$ calculé % C 56,69; H 7,09; N 11,02; O 25,20; trouvé % C 56,47; H 6,99; N 11,07; O 25,40; RMN δ_{TMS}: 1,83 (4H; m), 2,55 ($C\underline{H}_2$-C(NOH); t), 2,75 ($C\underline{H}_2$-CO; t), 12,17 (NO$\underline{H}$; s).

La Nitrosation de la Cyclooctanone a été Conduite selon des Conditions Voisines de celle de Kataoka: La cyclooctanone (0.2 mol) en milieu éthéré chlorhydrique (0.02 mol de HCl) est traitée à 0 °C par du nitrite d'isopropyle (0.24 mol); les produits de la réaction, après neutralisation, sont extraits à l'éther puis sépares par chromatographie sur colonne de gel de silice (solvant cyclohexane–acétate d'éthyle 1–1); en tête sort l'*hydroxyimino-2 cyclooctanone **2*** sous forme d'une huile légèrement jaune; $C_8H_{13}NO_2$ calculé % C 61,93; H 8,39; N 9,03; O 20,65; trouvé % C 61,86; H 8,46; N 8,86; O 20,72; RMN δ_{TMS}: 1,55 (8H; m), 2,40 ($C\underline{H}_2$-C(NOH) et $C\underline{H}_2$-CO; 2t), 10,83 (NO$\underline{H}$; s). *L'hydroxyimino-2 cyclooctanone **3*** qui sort ensuite de la colonne est un produit bien cristallise: F 99 °C; $C_8H_{13}NO_2$ calculé % C 61,93; H 8,39; N 9,03; O 20,65; trouvé % C 61,85; H 8,50; N 9,02; O 20,46. RMN δ_{TMS}: 1,53 (8H; m), 2,57 ($C\underline{H}_2$-C(NOH); t), 2,67 ($C\underline{H}_2$-CO; t), 11,77 (NO$\underline{H}$; s).

La nitrosation de la cyclododécanone, conduite comme pour la cyclooctanone, mène avec un bon rendement (80%) à un seul dérivé bien cristallisé, l'*hydroxyimino-2 cyclododécanone **4***: F 70 °C ; $C_{12}H_{21}NO_2$ calculé % C 68,25; H 9,95; N 6,63; O 15,17; trouvé % C 68,16; H 9,84; N 6,49; O 15,40; RMN δ_{TMS}: 1,22 (16H; m), 2,58 ($C\underline{H}_2$-C(NOH); t), 2,77 ($C\underline{H}_2$-CO; t), 12,48 (NO$\underline{H}$; s).

Spectroscopie Infrarouge. Spectrophotomètre Perkin Elmer 337; cuves de 0,5 et 50 mm avec fenêtres en NaCl; solvant CCl_4. La détermination graphique des constantes d'association a été faite selon la methode de Ossart.[13]

Spectrométrie de Résonnance Magnétique Nucléaire. Spectromètre Varian T 60; Solvant DMSO-d_6; concentration 5%.

Complexes avec Cu^{2+}. Une pincée de produit est mise en solution dans de l'alcool à 95 °C; on rajoute quelques gouttes d'une solution aqueuse saturée d'acétate de cuivre et on note la coloration verte (formation d'un complexe) ou bleu (pas de formation de complexe).

References

1) P. W. Sadler, *J. Chem. Soc.*, **1961**, 2162.
2) J. Armand, et J. P. Guette, *Bull. Soc. Chim. Fr.*, **1969**, 2894.
3) P. C. Cherry, W. R. T. Cottrell, G. D. Meakins, et E. E. Richards, *J. Chem. Soc.*, **1968**, 459.
4) C. Pigenet, J. Armand, et H. Lumbroso, *Bull. Soc. Chim. Fr.*, **1970**, 2124.
5) M. Kataoka et M. Ohno, *Bull. Chem. Soc. Jpn.*, **46**, 3474 (1973).
6) A. F. Ferris, G. S. Johnson, F. E. Gould, et H. K. Latourette, *J. Org. Chem.*, **25**, 492 (1960).
7) J. Bernadou, J. P. Fayet, M. Bonnafous, et P. Mauret, *Communi. Soc. Pharm. Toulouse (France)*, 5 juillet 1978.
8) A. Daniel et A. A. Pavia, *C. R. Acad. Sci.*, **263**, 643 (1966).
9) J. Bernadou, J. P. Fayet, M. Bonnafous, et P. Mauret, *Commun. Journées Chim. Org. d'Orsay (France)*, 7—9 septembre 1977.
10) T. W. J. Taylor, *J. Chem. Soc.*, **1931**, 2018.
11) A. H. Blatt et A. Barnes, *J. Am. Chem. Soc.*, **56**, 1148 (1934).
12) E. L. Eliel, N. L. Allinger, S. J. Angyal, et G. A. Morrison, "Conformational Analysis," Interscience Division, J. Wiley & Sons, New York (1965).
13) A. Ossart, H. Sauvaitre, et P. Pineau, *J. Chim. Phys.*, **64**, 953 (1967).
14) T. A. Geissman et M. J. Schlatter, *J. Org. Chem.*, **11**, 771 (1946).

BULLETIN OF THE CHEMICAL SOCIETY OF JAPAN, VOL. 52 (9), 2745—2746 (1979)

The Relationship of π-Binding Energy with Molecular Connectivity in Hydrocarbons

Satya P. GUPTA* and Prithvi SINGH

Department of Chemistry, Birla Institute of Technology and Science, Pilani-333031, India

(Received September 11, 1978)

Synopsis. Hückel's π-binding energy, E_π, in hydrocarbons is found to be parallel to Kier's molecular connectivity index, χ. In either class of hydrocarbons, alternant or non-alternant, the regression analysis reveals a highly significant linear correlation between E_π and ${}^1\chi^v$ (the first order valence connectivity index).

The molecular connectivity index, χ, signifies the degree of branching or connectivity in a molecule and is derived from the numerical extent of branching or connectivity in the molecular skeleton.[1-3] Kier *et al.* have shown that this index can be correlated with several physicochemical and biological properties of the molecules.[3] The χ has several versions. The simplest as well as extended versions in it (${}^m\chi$) all are calculated from a hydrogen suppressed graph of the molecule. The simplest version designated as ${}^1\chi$ and known as first-order term in χ is computed by[1-3]

$$ {}^1\chi = \sum (\delta_i \delta_j)^{-1/2} \qquad (1) $$

where the sum is over all connections or edges in the hydrogen suppressed graphs, and δ_i and δ_j are numbers assigned to each atom reflecting the number of atoms adjacent or connected to atoms i and j, which are formally bonded. The nature of the atoms is not considered in the calculation.

To account for the nature and unsaturation of the bonds in χ, Kier and Hall[3,4] proposed the valence molecular connectivity (χ^v) where the atom connectivity term, δ^v, is defined as:

$$ \delta_i^v = Z_i^v - h_i \qquad (2) $$

in which Z_i^v represents the number of valence electrons of atom i, and h_i the number of hydrogen atoms attached to it. Thus the use of δ^v permits the calculation of valence χ term of first-order, ${}^1\chi^v$, by the expres sion:

$$ {}^1\chi^v = \sum (\delta_i^v \delta_j^v)^{-1/2}. \qquad (3) $$

The details of calculation of this term and other higher terms in χ can be seen in Ref. 3.

The electronic interaction depends upon the specific orientation of atoms in a molecule, hence it becomes obvious that the binding energy of electrons must be in some way related with χ.

Using Eqs. 2 and 3, the ${}^1\chi^v$ values are calculated for some alternant and non-alternant hydrocarbons and listed in Tables 1 and 2 respectively. Hückel's π-binding energy values, E_π, are taken from the literature.[5] A plot of E_π *versus* ${}^1\chi^v$ is shown, for alternant hydrocarbons, in Fig 1, and for non-alternant hydrocarbons, in Fig 2. A straight line is obtained in both the cases. The level of significance of this linear correlation between E_π and ${}^1\chi^v$ in two cases is shown by Eqs. 4 and 5 respectively.

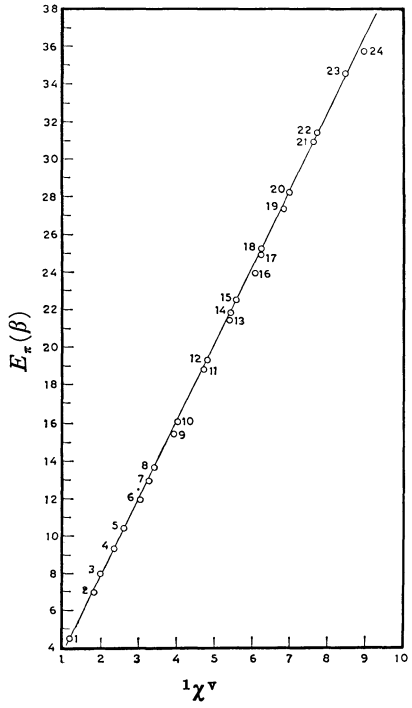

Fig. 1. A plot of E *versus* χ in alternant hydrocarbons. Numbers refer to compounds in Table 1.

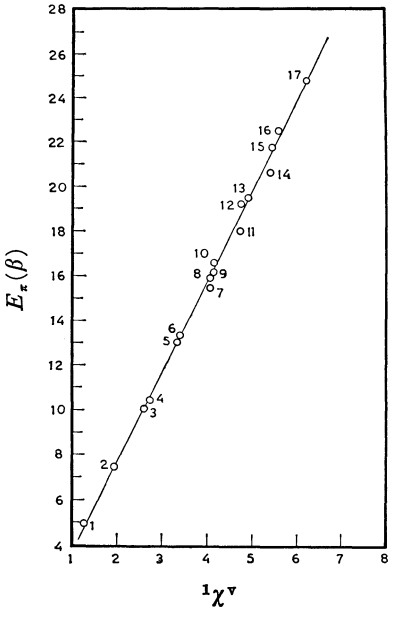

Fig. 2. A plot of E *versus* χ in non-alternant hydrocarbons. Numbers refer to compounds in Table 2. To save space compounds 18 and 19 were not shown.

Table 1. E_π and $^1\chi^v$ values for alternant hydrocarbons

Compd No.	Compound	$^1\chi^v$	E_π (β) Hückel	E_π (β) Calcd from Eq. 4
1	1,3-Butadiene	1.150	4.472	4.378
2	1,3,5-Hexatriene	1.817	6.988	7.093
3	Benzene	2.000	8.000	7.837
4	3,4-Dimethylene-1,5-hexadiene	2.351	9.332	9.266
5	Styrene	2.608	10.422	10.312
6	3,4-Divinyl-1,3,5-hexatriene	3.038	11.925	12.062
7	1-Phenyl-1,3-butadiene	3.274	12.932	13.023
8	Naphthalene	3.405	13.683	13.556
9	1-Phenyl-1,3,5-hexatriene	3.941	15.459	15.737
10	1-Vinylnaphthalene	4.019	16.129	16.055
11	Stilbene	4.732	18.878	18.957
12	Anthracene	4.810	19.314	19.274
13	1,4-Diphenyl-1,3-butadiene	5.399	21.401	21.671
14	9-Vinylanthracene	5.429	21.790	21.793
15	Pyrene	5.560	22.505	22.326
16	1,6-Diphenyl-1,3,5-hexatriene	6.065	23.934	24.382
17	Naphthacene	6.215	24.931	24.992
18	Triphenylene	6.232	25.274	25.061
19	Triphenylethylene	6.810	27.270	27.414
20	Perylene	6.976	28.245	28.089
21	Picene	7.637	30.943	30.780
22	Benzo[*ghi*]perylene	7.720	31.425	31.118
23	Coronene	8.464	34.572	34.146
24	Tetraphenylethylene	8.974	35.719	36.221

$$E_\pi = 4.070\,^1\chi^v - 0.302$$
$$n=24,\ r>0.999,\ s=0.229,\ F_{1,22}>20000 \quad (4)$$
$$E_\pi = 4.068\,^1\chi^v - 0.551$$
$$n=19,\ r=0.999,\ s=0.358,\ F_{1,17}=8483. \quad (5)$$

In these two equations, as obtained by regression analysis, the statistical parameters: n (the number of data points), r (the correlation coefficient), s (the standard deviation), and F (the F ratio between the variances of calculated and observed data) exhibit very high level of significance of the correlations. The E_π values reproduced from Eqs. 4 and 5 are found to be in very good agreement with the Hückel ones (Tables 1 and 2).

Now these correlations can be used to predict the binding energy of any conjugated system. The calculation of χ is utterly simple. These correlations suggest that in biochemical studies χ would be very well able to account for the activity that would depend upon the binding energy of the compounds.

Table 2. E_π and $^1\chi^v$ values for non-alternant hydrocarbons

Compd No.	Compound	$^1\chi^v$	E_π (β) Hückel	E_π (β) Calcd from Eq. 5
1	Methylenecyclopropene	1.264	4.962	4.592
2	Fulvene	1.931	7.466	7.305
3	6-Vinylfulvene	2.608	10.052	10.059
4	Pentalene	2.738	10.456	10.588
5	2-Methylene-2*H*-indene	3.336	13.043	13.021
6	Azulene	3.405	13.363	13.302
7	Fulvadiene	4.065	15.468	15.987
8	Sesquifulvene	4.072	15.931	16.015
9	*s*-Indacene	4.143	16.231	16.304
10	Acenaphthylene	4.149	16.619	16.329
11	Heptafulvalene	4.738	18.005	18.725
12	9-Methylenefluorene	4.758	19.224	18.806
13	Cyclopent[*fg*]-acenaphthylene	4.893	19.476	19.356
14	Heptafulvadiene	5.399	20.608	21.414
15	9-Allylidenefluorene	5.435	21.767	21.561
16	Fluoranthene	5.565	22.500	22.089
17	Benzo[4,5]cyclophepta-[1,2,3-*de*]naphthalene	6.220	24.741	24.754
18	9,9′-Bifluorenylidene	9.060	36.525	36.308
19	1,2-Di(9-fluorenylidene)ethane	9.720	39.073	38.993

The financial assistance provided by CSIR, New Delhi, in the form of a PDF to one of the authors (PS) is thankfully acknowledged.

References

1) M. Randić, *J. Am. Chem. Soc.*, **97**, 6609 (1975).
2) L. B. Kier, L. H. Hall, W. J. Murray, and M. Randić, *J. Pharm. Sci.*, **64**, 1971 (1975).
3) L. B. Kier and L. H. Hall, "Molecular Connectivity in Chemistry and Drug Research," Academic Press, New York (1976).
4) L. B. Kier and L. H. Hall, *J. Pharm. Sci.*, **65**, 1806 (1976).
5) C. A. Coulson and A. Streitwieser Jr., "Dictionary of π-Electron Calculations," W. H. Freeman and Company, San Fransisco (1965).

Molecular Structure of Bromoform as Determined by a Joint Analysis of Electron Diffraction and Microwave Data†

Koichi TAMAGAWA and Masao KIMURA*

Department of Chemistry, Faculty of Science, Hokkaido University, Sapporo 060

(Received August 2, 1978)

The gas phase molecular structure of bromoform has been studied by electron diffraction. By a joint analysis of the diffraction results and the moments of inertia for $CH^{79}Br_3$, $CD^{79}Br_3$, $CH^{81}Br_3$, and $CD^{81}Br_3$ obtained by Williams *et al.*, the bond distances in r_g and the bond angles in φ_{av} have been determined as follows: r_g(C–Br) = 1.924±0.005 Å, r_g(Br···Br) = 3.175±0.003 Å, r_g(C–H) = 1.11_1±0.04_6 Å, φ_{av}(BrCBr) = 111.7±0.4°, and φ_{av}(HCBr) = 107.2±0.5°. The uncertainties represent the estimated limits of error. The anharmonicity parameter of the Morse-type potential, a_3, for the nonbonded Br···Br atom pair has been estimated as -1.3 ± 0.9 Å^{-1}.

In a series of fluoromethanes, $CH_{4-n}F_n$ (n=1—4), the systematic decrease in the C–F distances and the F–C–F bond angles with an increase in the number of F atoms has been observed.[1-4] The results of population analysis for these compounds have supported these trends.[6] According to our recent studies on a series of chloromethanes,[7-9] the C–Cl distances have shown a similar shortening with increasing number of Cl atoms, while the Cl–C–Cl bond angles increase in contrast with the trend observed in fluoromethanes.

In the molecular structures of the bromomethanes, $CH_{4-n}Br_n$ (n=1—4), only the r_e structure of CH_3Br investigated by Duncan[1] and the r_a structure of CH_2Br_2 determined by Beagley *et al.*[5] have been reported. The molecular structure of $CHBr_3$ was studied by Morino *et al.* by means of the visual method of electron diffraction[10] and by Williams *et al.* by means of microwave spectroscopy.[11] The results of structural analysis for $CHBr_3$ are however not precise and accurate enough to be compared critically with those of related molecules. There is no reliable structural data for CBr_4. Thus, in order to investigate the variations in structure with the number of bromine atoms, it is necessary to determine the structures of $CHBr_3$ and CBr_4 and moreover, it is desirable to reinvestigate the structures of CH_2Br_2 and CH_3Br in a series of studies. In the present study the structure of $CHBr_3$ was determined by a joint analysis of the diffraction data newly obtained and the rotational constants determined by Williams *et al.*[11] The structures of carbon tetrabromide,[12] methylene dibromide,[12] and methyl bromide[13] will be reported later.

Experimental

A guaranteed reagent purchased from Nakarai Chemical Co., Ltd. was used after distillation. Diffraction photographs were taken at 19 °C with a diffraction unit equipped with an r^3-sector.[14] The experimental conditions were as follows: camera length: 244.3 and 109.3 mm; sample pressure: about 3 Torr; exposure times: about 120 and 240 s for the long and

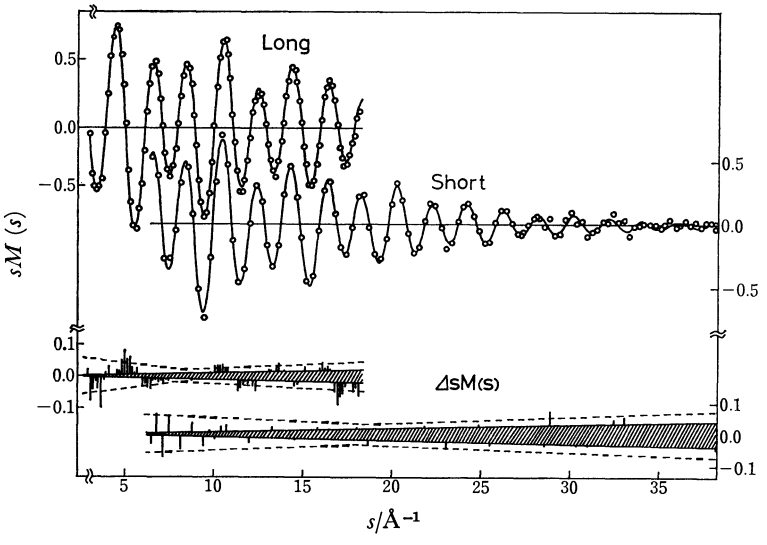

Fig. 1. Experimental (open circles) and theoretical (smooth curve) molecular intensities for $CHBr_3$; $\Delta sM(s) = sM(s)^{obsd} - sM(s)^{calod}$. The indices of resolution are 0.918—0.967 and 0.869—0.928 for the long and short camera lengths, respectively.

† Throughout this paper 1 Å = 100 pm and 1 Torr = 133.322 Pa are used. For the definitions of various distances, see, *e.g.*, K. Kuchitsu and S. J. Cyvin, "Molecular Structures and Vibrations," ed by S. J. Cyvin, Elsevier, Amsterdam (1972) Chap. 12; see also L. S. Bartell, K. Kuchitsu, and H. M. Seip, *Acta Crystallogr., Sect. A*, **32**, 1013 (1976). Notations r_{av} and φ_{av} are used for the values determined by joint analysis.

short camera lengths respectively; accelerating voltage: about 42 kV; beam current: 0.20 μA. The scale factor for the diffraction patterns was determined with reference to the diffraction patterns of carbon disulfide taken under the same experimental conditions.[15]

The data were reduced to the molecular intensities by our usual procedures.[16] Three and four plates from the long and short camera lengths, respectively, were used for analysis. The observed molecular intensities covered the ranges of $3.0 \leqq s \leqq 18.0$ Å^{-1} and $6.5 \leqq s \leqq 38.2$ Å^{-1} for the long and short camera lengths, respectively.

The observed molecular intensities and the theoretical curves calculated using the best-fit parameters are shown in Fig. 1 together with the differences (experimental minus theoretical).[17] The narrow shaded area corresponds to ±2 in the last digit of the digital voltmeter reading, *i.e.*, the limits of detection in photometry. The outer boundaries drawn by the broken lines show the estimated limits of error in the intensity measurements. They indicate the normally expected range of random scattering of differences between experimental and theoretical intensities. Some points exceed the boundaries for accidental reasons. The least-squares refinement with zero-weights for these points showed that the irregularities did not affect the derived parameter values. Figure 2 shows the radial distribution curve corresponding to the molecular intensities from the short camera length shown in Fig. 1.

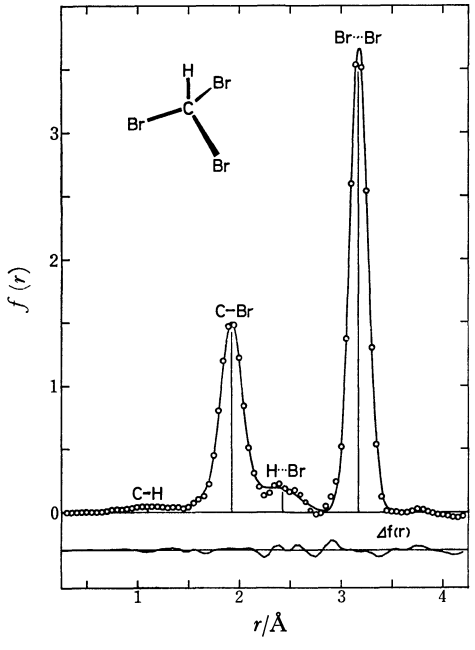

Fig. 2. Experimental (open circles) and theoretical (smooth curve) radial distribution curve for $CHBr_3$: $\Delta f(r) = f(r)^{obsd} - f(r)^{calcd}$. Damping factor, exp[−0.00153 s^2].

Analysis of Electron Diffraction Intensities

The structural parameters were determined by applying the least-squares method to the reduced molecular intensities with a conventional diagonal-weight matrix.[16] The elastic and inelastic scattering factors and the phase shifts between C, H, and Br atoms were taken from the Tables of Schäfer *et al.*[18] C_{3v} symmetry was assumed for the geometry in equilibrium. Five independent parameters were chosen for refinement: the C–Br and Br···Br distances, the mean amplitudes, and the index of resolution. The r_g(C–H) distance was fixed at 1.107 Å, a value determined from methane,[19] and also at values shifted by ±0.050 Å. The mean amplitudes of the C–H and H···Br pairs were fixed at 0.078 and 0.113 Å, which were calculated using the force constants given by Galasso *et al.*[20] The asymmetry constants, $\kappa (= (1/6)a_3(1+8\chi/(1+\chi)^2)l^4)$, for the C–H and C–Br bonds were estimated to be 1.2×10^{-5} and 3.5×10^{-6} Å^3, assuming the anharmonicity parameters, a_3,[21] to be 1.98 and 2.0 Å^{-1}, respectively. The a_3 values for the nonbonded H···Br and Br···Br pairs were assumed to be zero. The results of the least-squares analysis thus obtained are summarized in Table 1. The errors in the scale factor were estimated to be 0.06% and 0.10% for the long and short camera lengths, respectively. The shifts of ±0.050 Å in an assumed r_g(C–H) value brought about changes of ±0.0012 Å in the resulting r_g(C–Br), but caused no significant changes in the other structural parameters as compared with the random errors. The limits of error for the parameter values, except for r_g(C–Br), were estimated from 2.6 times the random standard deviations and the error in the scale factor. For r_g(C–Br), the error due to the uncertainty of the r_g(C–H) distance was further added. Variations in the plausible ranges of mean amplitudes for the nonbonded pairs and κ values for the C–Br, C–H, and H···Br pairs caused no significant changes in the resulting parameter values. Variation in the κ_{BrBr} value associated with variation in a_3(Br···Br) was found to cause only a little change in the r_g(Br···Br) distance, while the a_3(Br···Br) value itself took a significant role in the determination of the r_{av} structure by the joint analysis. The details of this however will be deferred

Table 1. Results of the least-squares analysis of diffraction intensities for bromoform[a] (in Å units)

Parameter	Long	Short	Weighted average	$r_g - r_\alpha^0$[b]	r_α^0
r_g(C–Br)	$1.922_3(5_9)$	$1.925_3(5_8)$	$1.923_8(4_2)$	0.002_8	1.921_0
r_g(Br···Br)	$3.176_7(2_6)$	$3.174_2(3_9)$	$3.175_9(2_2)$	0.001_6	3.174_3
r_g(C–H)	[1.107±0.050]	[1.107±0.050]		[0.014$_4$]	[1.093]
l(C–Br)	$0.062_0(9_1)$	$0.051_0(8_5)$	$0.056_1(6_3)$		
l(Br···Br)	$0.074_6(5_8)$	$0.071_1(2_5)$	$0.071_7(2_4)$		
R[c]	$0.094_3(8_1)$	$0.125_9(13_8)$			

a) Parenthesized values represent the limits of error. The values in brackets were those assumed. b) Vibrational corrections were calculated from the force constants cited in Ref. 20. a_3 for the nonbonded Br···Br pair was assumed to be 0 Å^{-1}. c) $R = \{\sum_i w_i(\Delta sM(s)_i)^2 / \sum_i w_i(sM(s)_i^{obsd})^2\}^{1/2}$ where $\Delta sM(s)_i = sM(s)_i^{obsd} - sM(s)_i^{calcd}$.

until the next section. The structural parameters determined from the data for the long and short camera lengths agree with each other within the limits of error. The most probable parameter values from the diffraction data were determined by taking the weighted average of both results. The observed mean amplitudes for the C–Br and Br···Br pairs agree with the calculated values, 0.0533 and 0.0740 Å, respectively, within the limits of error.

Joint Analysis of Diffraction and Microwave Data

The r_g distances determined by electron diffraction were converted to r_α^0 distances using the equation:[22]

$$r_g - r_\alpha^0 \cong \left(\frac{3}{2}\right) a_3(\langle\Delta z^2\rangle_T - \langle\Delta z^2\rangle_0) + \frac{\langle\Delta x^2\rangle_0 + \langle\Delta y^2\rangle_0}{2r_g} + \delta r_{\text{cent}}$$

The corrections were calculated using the force constants determined by Galasso *et al.*,[20] and the $r_g - r_\alpha^0$ values thus obtained are listed, together with the r_α^0 values in Table 1.

The ground state rotational constants, B_0, for $CH^{79}Br_3$, $CD^{79}Br_3$, $CH^{81}Br_3$, and $CD^{81}Br_3$ have been determined by Williams *et al.* using microwave spectroscopy.[11] The B_0 values were converted to the effective moments of inertia, $I_b^{(\text{eff})}$. The $I_b^{(\text{eff})}$ values thus obtained were reduced to the zero-point average moments of inertia, $I_b^{(z)}$, by correcting for harmonic vibrations by the standard method.[23]

In calculating the corrections, ΔI_b, the contribution from the centrifugal distortion was neglected[24] and the electronic contribution[24] was assumed to be zero because the g tensors were not available for $CHBr_3$. This assumption would not introduce significant errors, since the electronic contribution estimated from the results for formaldehyde[25] and ethylene[26] appears to be less than a few percent of the corrections themselves. A significant part of the corrections derives from terms of the $1/\omega$ type, where ω is the vibrational frequency.[27] The experimental frequencies and the frequencies calculated using the force constants agree within a few percent. Thus in the present study the overall uncertainties included in $\Delta I_b^{(z)}$ were tentatively assumed to be 10% of the correction values themselves. The uncertainties in the moments of inertia, $I_b^{(z)}$, were then estimated from the errors included in the experimental moments of inertia, $I_b^{(\text{eff})}$, and the errors included in the corrections, $\Delta I_b^{(z)}$. Table 2 lists the results.

The isotope effects for the bond distances were estimated using the equation:[28]

$$\delta r_z \cong \left(\frac{3}{2}\right) a_3 \delta\langle\Delta z^2\rangle_0 - \delta(\langle\Delta x^2\rangle_0 + \langle\Delta y^2\rangle_0)/2r_z$$

Assuming the anharmonicity parameters, a_3, to be 2.0 ± 0.5 and 1.98 ± 0.5 Å^{-1} for C–Br and C–H, respectively, the isotopic differences were estimated to be -0.0009 ± 0.0015 Å for δr_z(C–D) (r_z(C–D) minus r_z(C–H)). The secondary isotope effect for r_z(C–H) and the primary and secondary isotope effects for r_z(C–Br) were estimated to be of the order of 1×10^{-6} Å, and consequently were neglected in the analysis. The isotope effect for the Br–C–Br bond angle, $\delta\varphi_z$(BrCBr) (φ_z of the isotopic species minus φ_z of the parent species $CH^{79}Br_3$), was tentatively assumed for all isotopic species to be $0.00\pm0.01°$ because of a lack of an established method of estimation.

Table 3. r_{av} and the final r_g structure for $CHBr_3$[a] (in Å and degree units)

	r_{av} and φ_{av}[b]	r_g[c]
C–Br	$1.921_0(4_2)$	1.924(5)
Br···Br	$3.179_1(1_5)$	3.175(3)
C–H	$1.09_7(4_6)$	$1.11_1(4_6)$
BrCBr	$111.6_3(3_8)$	
HCBr	$107.1_6(4_2)$	

a) Parenthesized values represent the limits of error referred to the last digits. b) Calculated from the r_{av} distances. c) Estimated from the r_{av} distances using a_3(Br···Br) $=-1.3\pm0.9$ Å^{-1}.

Four moments of inertia, $I_b^{(z)}$, are available. Unfortunately however the Br isotopic species provide no independent information, as we have usually experienced for molecules containing heavier atoms. The observed $I_b^{(z)}$ give relations among three parameters (r_z(C–Br), r_z(Br···Br), and r_z(C–H)). The relations from $CH^{79}Br_3$ and $CD^{79}Br_3$ practically coincide however with those from $CH^{81}Br_3$ and $CD^{81}Br_3$, respectively. Therefore, a complete r_z structure cannot be determined by the microwave data alone. The process of joint analysis to determine the complete r_{av} structure is illustrated in Fig. 3, where the r_z(C–Br) $-$ r_z(Br···Br) space is spread out. Assigning r_z(C–H) at a certain value, an approximately linear relation between r_z(C–Br) and r_z(Br···Br) is defined by a given $I_b^{(z)}$

Table 2. Experimental moments of inertia, vibrational corrections and calculated moments of inertia for $CHBr_3$[a]

	$CH^{79}Br_3$	$CD^{79}Br_3$	$CH^{81}Br_3$	$CD^{81}Br_3$
B_0[b]	1247.61(3)	1239.45(3)	1217.30(3)	1209.51(8)
$I_b^{(\text{eff})}$[c]	$405.08_7(2_8)$	$407.75_4(2_8)$	$415.17_4(2_9)$	$417.84_8(2_9)$
ΔI_b	$0.08_8(0_9)$	$0.08_5(0_9)$	$0.08_8(0_9)$	$0.08_5(0_9)$
$I_b^{(z)}$[d]	$405.17_5(3_0)$	$407.83_9(3_0)$	$415.26_2(3_1)$	$417.93_3(3_1)$
$I_b^{(\text{av})}$[e]	405.17_2	407.83_4	415.26_8	417.93_7

a) Units of B_0 are MHz and those of I are amu Å^2. Conversion factor, 505391 amu Å^2 MHz. Parenthesized values are estimated errors. b) Taken from Ref. 11. c) The errors of $I_b^{(\text{eff})}$ were taken to be 3 times the errors of B_0. d) Average moments of inertia ($I_b^{(z)} = I_b^{(\text{eff})} + \Delta I_b$). e) Calculated from the final average structures.

for each of the H- and D-species. The observed $I_b^{(z)}$ for both species and the isotope species, δr_z(C–D) and δr_z(Br···Br) for the D-species possess uncertainties however and the relationships between r_z(C–Br) and r_z(Br···Br) for both species are manifested by two approximately straight belts on the r_z(C–Br)-r_z(Br···Br) space. Thus, a parallelogram, formed by the crossing of the two belts is the range allowed by $I_b^{(z)}$ for the r_z(C–H) value. Two parallelograms, a and b, are depicted in Fig. 3 by broken lines as examples, indicating the allowed ranges for r_z(C–H) values of 1.060 and 1.140 Å, respectively. Setting different values of r_z(C–H) shifts the parallelogram along the two parallel lines M_1 and M_2. The point ED in Fig. 3 represents the r_α^0 structure determined by electron diffraction with a_3(Br···Br) equal to zero, and the elliptical curve indicates the limits of error. The ranges satisfying the electron diffraction data and the moments of inertia from microwave spectroscopy do not overlap. Among the parameter values assumed in the present analysis the most ambiguous and influential one is a_3(Br···Br). The inconsistency between the electron diffraction data and the microwave data is in all probability due to the assumption that a_3(Br···Br) is zero. Variation in the value of a_3(Br···Br) affects the isotopic differences, δr_z(Br···Br), and consequently the range between M_1 and M_2 shifts. This shifts however is small and cannot be depicted in Fig. 3 discriminately. Variation in the value of a_3(Br···Br) causes a small change in the r_g(Br···Br) distance and a relatively large change in the correction value, r_g(Br···Br)$-$ r_α^0(Br···Br). As a result, the point ED and consequentry the elliptical curve (error limits) in Fig. 3 shifts along the Br···Br axis without influencing the other parameter values. As an example, a change in the a_3(Br···Br) value of -1.0 Å^{-1} brings about changes of -0.0011, -0.0047, and 0.0036 Å in r_g(Br···Br), the correction, r_g(Br···Br)$-r_\alpha^0$(Br···Br), and r_α^0(Br···Br) respectively. The two ellipses, ED_1 and ED_2, depicted by the dotted lines are the extreme cases where the results from both electron diffraction and microwave data overlap, corresponding to the a_3(Br···Br) values of -0.4 and -2.2 Å^{-1}, respectively. The shaded area is the range allowed by both the diffraction and the microwave data, assuming the a_3(Br···Br) value takes the range discussed above. On the basis of this, the most probable average distances, r_{av}(Br···Br) and r_{av}(C–Br), and the limits of error were determined from the center, O, and the boundary of the shaded area in Fig. 3. The most probable value for r_{av}(C–H) was taken as the value that brings the center of the parallelogram to the point O, and the limit of error was taken as the range where the parallelogram overlaps with the shaded area. The r_{av} values thus determined are listed in Table 3. The most probable value of a_3 and error limit are -1.3 ± 0.9 Å^{-1} from values corresponding to the extreme cases, ED_1 and ED_2. As may be seen in Table 3 and also in Fig. 3, r_{av}(C–H) cannot be determined precisely. Most of the r_g(C–H) distances reported so far for several molecules are in the range 1.100—1.110 Å, which corresponds to 1.085—1.095 Å in r_{av}(C–H). Even though the range of r_{av}(C–H) in the present molecule is limited to the range mentioned above, the limit of error for the r_{av}(Br···Br) becomes smaller by only 0.0003 Å. The calculated moments of inertia corresponding to the r_{av} structure are compared with the observed moments of inertia in the bottom row of Table 2. The r_g(Br···Br) distance converged

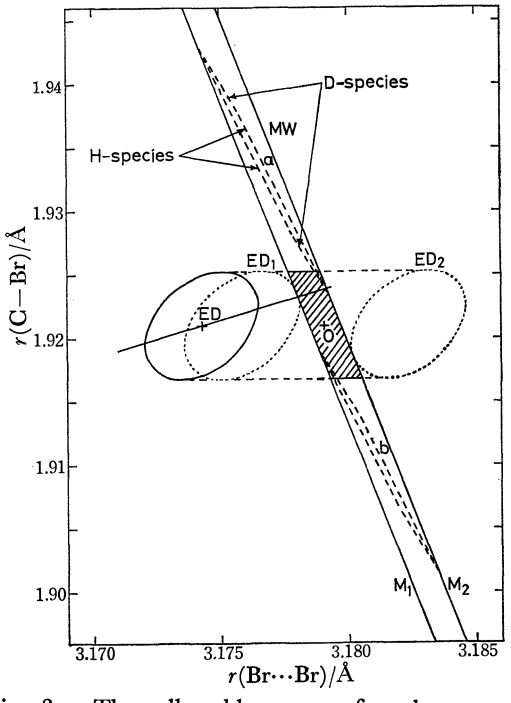

Fig. 3. The allowable range for the parameters, r(C–Br) and r(Br···Br). The values allowed by the four moments of inertia (MW) are shown by the range between the two parallel solid lines, M_1 and M_2. Two parallerograms drawn by the broken lines show the ranges allowed at r_z(C–H) = 1.06 Å (a) and 1.14 Å (b), respectively. The point ED represents the r_α^0 distances determined by electron diffraction with a_3-(Br···Br) equal to 0 Å^{-1}, and the ellipse indicates the limits of error. The ellipses, ED_1 and ED_2, correspond to the a_3(Br···Br) values of -0.4 and -2.2 Å^{-1} respectively (see text). The shaded area shows the probable range of the average structure. The point O is the center of this range. The solid line passing through the point ED shows the direction of change in r(C–Br) and r(Br···Br) when the scale factor used in the electron diffraction analysis is allowed to change.

TABLE 4. C–H DISTANCES AND BOND ANGLES OF BROMOFORM AND RELATED MOLECULES[a] (in Å and degree units)

Molecule	Method		r(C–H)	XCX[b]	Ref.
HCF_3	MW	r_0	1.098	108.80(75)	4
$HCCl_3$	ED+MW	r_g	1.136(35)	110.0(2)	8
$HCBr_3$	ED+MW	r_g	$1.11_1(4_6)$	111.7(4)	c)
HCI_3	ED	r_g	—	112.0(11)	29
HCH_3	ED	r_g	1.107(1)	109.5	19
$HC(CH_3)_3$	MW	r_s	1.108(1)	111.15(10)	30
$HC(NO_2)_3$	ED	r_a	—	110.7(10)	31

a) Numbers in parentheses represent uncertainties quoted in the original papers. b) For $HCCl_3$ and $HCBr_3$, φ_{av}. For the other molecules, except for methane, the angles are in the structures specified in the third column. c) The present study.

at 3.175 Å with analysis of the diffraction data assuming a_3(Br···Br) to be -1.3 Å^{-1}.

Discussion

The Br–C–Br bond angle shown in Table 3 is larger than the tetrahedral angle by about 2°. The XCX bond angles and the C–H distances of related molecules are listed in Table 4. The XCX bond angles for molecules with larger substituents are larger than the tetrahedral angle in all probability due to repulsion. A general trend for the C–H bond lengths cannot be found from the data in Table 4.

In the present study, it has been found that the anharmonicity parameter, a_3, for the nonbonded Br···Br pair must be negative in order that the electron diffraction results and the moments of inertia may be consistent. A recent study on $CHCl_3$[8] has shown that a negative a_3 values is preferable for the nonbonded Cl···Cl pair. No theoretical method for estimating these values is available at the present.

The authors wish to thank Professor Takao Iijima of Gakushuin University and Professor Shigehiro Konaka for their helpful advice and discussion. The computations were performed on an electronic computer FACOM 230-75 of the Computing Center, Hokkaido University.

References

1) J. L. Duncan, *J. Mol. Struct.*, **6**, 447 (1970).
2) E. Hirota, T. Tanaka, A. Sakakibara, Y. Ohashi, and Y. Morino, *J. Mol. Spectrosc.*, **34**, 222 (1970).
3) S. N. Ghosh, R. Trambarulo, and W. Gordy, *J. Chem. Phys.*, **20**, 605 (1952).
4) L. E. Sutton, "Tables of Interatomic Distances and Configurations in Molecules and Ions," Chemical Society, London (1958) and Supplement (1965).
5) B. Beagley, D. P. Brown, and J. M. Freeman, *J. Mol. Struct.*, **20**, 315 (1974).
6) D. P. Brown, Ph. D. Thesis, 1971, University of Manchester Institute of Science and Technology.
7) CH_2Cl_2: H. Kunimi and M. Kimura, Symposium on Molecular Structure, Tokyo, October, 1974.
8) $CHCl_3$: H. Kunimi and M. Kimura, Symposium on Molecular Structure, Nagoya, October, 1973.
9) CH_3Cl, CCl_4: K. Suzuki, Y. Todo, and M. Kimura, 35th National Meeting of the Chemical Society of Japan, Sapporo, August, 1976.
10) Y. Morino, M. Kimura, and M. Hasegawa, *Nippon Kagaku Kaishi*, **67**, 93 (1946).
11) Q. Williams, J. T. Cox, and W. Gordy, *J. Chem. Phys.*, **20**, 1524 (1952).
12) K. Tamagawa and M. Kimura, Symposium on Molecular Structure, Sapporo, August, 1977.
13) K. Tamagawa and M. Kimura, Symposium on Molecular Structure, Hiroshima, October, 1978.
14) Y. Murata, K. Kuchitsu, and M. Kimura, *Jpn. J. Appl. Phys.*, **9**, 591 (1970).
15) For the r_a(C–S) distance, see, K. Tamagawa, T. Iijima, and M. Kimura, *J. Mol. Struct.*, **30**, 243 (1976).
16) S. Konaka and M. Kimura, *Bull. Chem. Soc. Jpn.*, **43**, 1693 (1970).
17) The numerical data of the total intensity, the background, and the elements of the correlation matrix are deposited with the Chemical Society of Japan (Document No. 7928).
18) L. Schäfer, A. C. Yates, and R. A. Bonham, *J. Chem. Phys.*, **55**, 3055 (1971).
19) L. S. Bartell, K. Kuchitsu, and R. J. De Neui, *J. Chem. Phys.*, **35**, 1211 (1961).
20) V. Galasso, G. De Alti, and G. Costa, *Spectrochim. Acta*, **21**, 669 (1965).
21) K. Kuchitsu and Y. Morino, *Bull. Chem. Soc. Jpn.*, **38**, 805 (1965).
22) K. Kuchitsu and S. Konaka, *J. Chem. Phys.*, **45**, 4342 (1966).
23) K. Kuchitsu, "MTP International Review of Science, Physical Chemistry, Series One," ed by G. Allen, Medical and Technical Publishing Co. Ltd., Oxford (1972), Vol. 2, Chap. 6.
24) T. Oka and Y. Morino, *J. Mol. Spectrosc.*, **6**, 472 (1961).
25) T. Oka, *J. Phys. Soc. Jpn.*, **15**, 2274 (1960).
26) J. L. Duncan, *Mol. Phys.*, **28**, 1177 (1974).
27) T. Iijima and S. Tsuchiya, *J. Mol. Spectrosc.*, **44**, 88 (1972).
28) K. Kuchitsu, *J. Chem. Phys.*, **49**, 4456 (1968).
29) H. Sanpei and M. Kimura, preliminary result.
30) D. R. Lide, Jr., *J. Chem. Phys.*, **33**, 1519 (1960).
31) N. I. Sadova, N. I. Popik, L. V. Vilkov, Yu. A. Pankrushev, and V. A. Shlyapochnikov, *Zh. Strukt. Khim.*, **15**, 695 (1974).

Nitrogen 14 Nuclear Quadrupole Resonance Study of Several Condensed Ring Compounds

Yukio HIYAMA, Takuya MARUIZUMI, and Eiji NIKI*

Department of Industrial Chemistry, Faculty of Engineering, The University of Tokyo, Hongo, Tokyo 113

(Received October 3, 1978)

The ^{14}N nuclear quadrupole resonance spectra of 2-mercaptobenzothiazole, isatin(1*H*-indole-2,3-dione), and isatoic anhydride(2*H*-3,1-benzoxazine-2,4(1*H*)-dione) have been observed at room temperature by the nuclear double resonance method. The quadrupole coupling constants and the asymmetry parameters thus obtained were interpreted by the Townes and Dailey theory.

In this paper, we wish to report the first observation of the nuclear quadrupole resonance (NQR) of the ^{14}N in several condensed ring heterocyclic compounds. The parameters thus obtained, *i.e.*, the quadrupole coupling constant (e^2Qq/h) and the asymmetry parameter (η) correspond to the electronic environment around each nitrogen atom. In the case of nitrogen, these parameters are usually dominated almost entirely by the distribution of the valence electrons in each nitrogen atom. The three frequencies[1] of ^{14}N NQR are given by:

$$\nu_{\pm} = 3/4e^2Qq/h(1\pm\eta/3) \quad (1), (2)$$

$$\nu_0 = \nu_+ - \nu_- = 1/2\eta e^2Qq/h \quad (3)$$

where e^2Qq/h and η are the quadrupole coupling constant and the asymmetry parameter respectively.

The frequency, ν_0, is relatively low, almost always below 1000 kHz. In this case, such conventional NQR techniques as using a regenerative spectrometer may not be accessible because of their low sensitivity. Therefore the nuclear double resonance technique[2] in the laboratory frame (^1H–^{14}N cross relaxation) was employed.

Experimental

The double resonance technique will be briefly described. A single cycle in an experiment consists of three stages. In the first, the major nuclei which give strong NMR signals, such as ^1H, are polarized in a high magnetic field ($\simeq$1T) for two or three high-field spin-lattice relaxation times, T_1. Next, the sample demagnetization is performed adiabatically. The minor nuclei (searched for NQR signals) are irradiated with a certain RF field; intensity, H_{1B}, and frequency, ν_B, after the sample has been removed from the magnet to the region of a zero external field for a cerain time period, τ s. In the third stage, the sample is returned to the magnet. A 90° pulse is immediately applied to monitor the remaining magnetization of the major nuclei. The amplitude of the free induction decay (FID) or echo is recorded. If H_{1B} is applied at the frequency of the quadrupole resonance of the minor nuclei, the monitored magnetization, $M(\tau)$, can be expected to vary as;

$$M(\tau) = M(0)\exp[-(1/T_{1d}+1/\tau_{AB})]. \quad (4)$$

Here, T_{1d} is the spin-lattice relaxation time in a zero magnetic field for the major nuclei and τ_{AB} is the cross relaxation time between the major spin and the minor spin, which has a finite value if ν_B is equal to the resonance frequency. The NQR absorption line is recorded as a dip of the magnetization of the major nuclei. If T_1 is 100 s, one scanning of ν_B from 2 MHz to 3 MHz by 10 kHz steps takes 6 h.

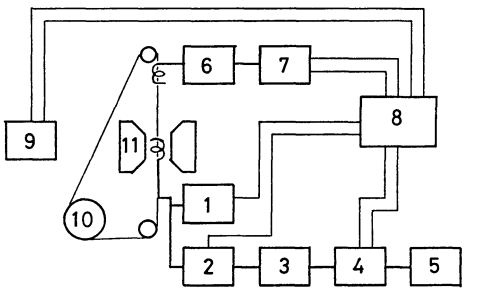

Fig. 1. Nuclear double resonance apparatus.
1) Transmitter, 2) preamplifier, 3) receiver amplifier, 4) gated integrator, 5) chart recorder, 6) wideband power amplifier, 7) PLL synthesizer, 8) pulse generator, 9) motor driver, 10) stepping motor, 11) magnet pole piece.

The double resonance apparatus was built in this laboratory[3] (Fig. 1).

Pulsed NMR. We used a conventional, single-coil, pulsed, proton magnetic resonance spectrometer operating at 26.7 MHz (6.28×10^{-1} T). The transmitter was a modified YAESU FL-101 apparatus operating as a C-class amplifier. The pre-amplifier and receiver amplifier were hand-made. The spectrometer was constructed with care taken to insure stability of sensitivity and a short recovery time.

Gated Integrator. The monitored FID was stored by means of a gated integrator. We used a box-car detector as the gated integrator by inserting a reset circuit. The integrated signal was recorded on a chart recorder as one bar, whose height was proportional to the remaining magnetization $M(\tau)$.

Sample Elevator Mechanism. The sample is moved by a small elevator mechanism driven by a stepping (pulse) motor. The advantage of the stepping motor is that the velocity and the distance can be controlled electronically by means of the pulse frequency and the total number of pulses respectively. The stepping motor is ASTROSYN 34 PM-C004.

Frequency Synthesizer and Wide-band Power Amplifier. The frequency, ν_B, must be fixed during each experimental cycle. The stability required in this experiment is higher than that of a standard signal generator. Also, it is necessary to set the irradiation frequency programmably. Therefore, we employed a PLL (phase-locked loop) frequency synthesizer, whose frequency program can be set automatically. The output of the synthesizer, which is sometimes phase- or pulse- modulated, is fed to an ENI 240L wide-band power amplifier. H_{1B} is applied to the sample within a soleniod coil.

Helmholtz Coil. A small Helmholtz coil is used to cancel any remaining fields to within$\pm10^{-4}$ T over the volume of the sample in the zero-field region. Sometimes, a pure iron magnetic shield is used in order to cancel the fairly high

remaining field ($\simeq 10^{-2}$ T).

Coherent Pulse Generator. The timing of the entire experimental cycle is automatically and programmably controlled by a coherent pulse generator, which was designed and built up in our laboratory. This generator, whose components are almost all TTLs(7400 series), is composed of a quartz time base and programmable dividers.

All experiments were done at room temperature. The sweeping of the minor spin irradiation (H_{1B}) was performed in 10 kHz steps from 400 kHz to 3800 kHz; therefore the total experimental error may amount to about 10 kHz.

Sample. All the samples were polycrystalline guaranteed-grade chemicals obtained from the Tokyo Kasei Kogyo Co., Ltd. Each sample volume was approximately 1 cm^3, packed in a test tube 10 mm in diameter. We tried to detect the ^{14}N NQR spectra of some other condensed ring compounds, but failed. The compounds which did not give resonances were indigo, thionine, luminol, uric acid, *N,N'*-dithiobismorpholine, and thiooxy purine. In these six compounds, the proton spin-lattice relaxation time, T_1, was too short to satisfy the adiabatic condition for the double resonance experiment.

Results

T_1, the Spin-lattice Relaxation Time in a High Magnetic Field. The T_1 of each compound was determined by the 90° pulse-t-90° pulse method. The obtained time constant of each compound is listed in the 2nd column in Table 1. For a compound with the time constant of 50 s, the experimental cycle was set at 120 s.

Table 1. Observed parameters

Compound	Resonance freq./kHz					
	T_1/s	ν_+	ν_-	ν_0	e^2Qq/h	η
2-Mercapto-benzothiazole 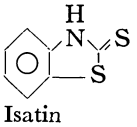	50	2140	1520	620	2440	0.51
Isatin 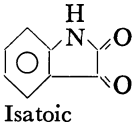	20	2540	2050	490	3060	0.32
Isatoic anhydride 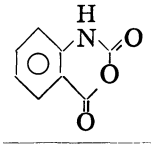	60	2790	—	750	3220	0.47

NQR. The observed frequencies, coupling constants, and asymmetry parameters are given also in Table 1, together with the formula of each molecule.

2-Mercaptobenzothiazole gave two strong signals, which correspond to ν_+ and ν_0 lines, and also a weak signal at 1520 kHz. This corresponds to ν_- line. The crystal and molecular structure[4] shows that there are four molecules per unit cell. However only one set of signals was obtained.

Proton relaxation time of isatin is 20 s at room temperature. For the double resonance experiment, a relaxation time constant of the major spin of about 20 or 30 s may be most favorable because of the stability of the apparatus and the lesser demands on the experimenter's patience. This chemical also gave all three lines, ν_+, ν_-, and ν_0, as is illustrated in Fig. 2. The crystal and molecular structure of isatin was elucidated by Goldschmidt and Llewellyn.[5]

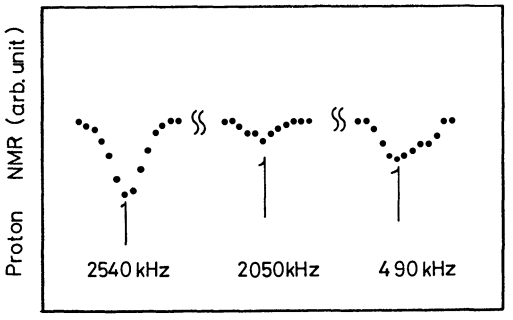

Fig. 2. Chart recorder outputs which show ^{14}N nuclear quadrupole resonance of isatin by proton-nitrogen double resonance method. B spin irradiation (searching irradiation) was performed in 10 kHz steps.

Isatoic Anhydride gave only two resonance lines, which correspond to the ν_+ line and the ν_0 line respectively. No structural data by X-ray diffraction has been reported for this compound.

Discussion

In 2-mercaptobenzothiazole(I), thione-thiol tautomerism is possible, as is illustrated below:

(Ia) (Ib) (I)

The X-ray structural study[4] supports the thione(Ia) form, while it gives no evidence for the thiol(Ib) form.

In isatin(II) and isotoic anhydride(III), lactam-lactim tautomerism can exist, as is shown below:

(IIa) (IIb) (II)

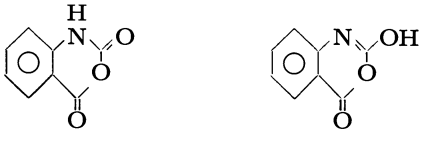

(IIIa) (IIId) (III)

The infrared results[6,7] support the lactam form(a) for both compounds.

In order to interpret the observed NQR results, the Townes and Dailey theory[1] was employed. For all three compounds, the electronic environment around each nitrogen atom may be assumed to be pyrrole-like, considering the other spectroscopic results.[4-7] The pyrrole-type formula[1] is as follows;

$$(e^2Qq/e^2Qq_0)(1+\eta/3) = L-B \quad (5)$$

$$(e^2Qq/e^2Qq_0)\eta = 3/2(A-B)(1-\cot^2\gamma). \quad (6)$$

Here, L is the pi population, A is the the N–H sigma population, B is the averaged N–C sigma population, 2γ is the CNC angle, and q_0 is the electric-field gradient caused by a 2p electron of the nitrogen atom.

For the two compounds whose molecular structures have been determined by the X-ray studies,[4,5] each bond angle, 2γ, was replaced by the corresponding value obtained from the studies. On the other hand, for isatoic anhydride, 2γ was assumed to 120°. In order to calculate the population numbers, L and A, the N–C population, B, and the atomic coupling constant, e^2Qq/h, were assumed to 1.15 and 9.1 MHz[8] respectively. Using the coupling constants and asymmetry parameters obtained at this time, the population numbers, L and A, were calculated by the above formulas [(5), (6)]; they are shown in Table 2. One may easily note that, for all the compounds, the L values are much less than 2.0, around 1.5; this fact may be explained by considering that the pi electrons take part in the conjugation of the heterocyclic ring.

Table 2. The Townes and Dailey analysis by means of a pyrrole-type formula

Compound	A(N–H)	L(pi)	NET $(2.3+A+L)$
2-Mercapto-benzothiazole	1.30	1.46	5.06
Isatin	1.28	1.52	5.10
Isatoic anhydride	1.32	1.56	5.18

e^2Qq_0/h=9.1 MHz. B=1.15.

References

1) E. A. C. Lucken, "Nuclear Quadrupole Coupling Constants," Academic Press, London and New York (1969).
2) R. E. Slusher and E. L. Hahn, *Phys. Rev.*, **166**, 332 (1968).
3) Y. Hiyama, Master's Thesis, University of Tokyo (1976).
4) J. P. Chesiek and J. Donohue, *Acta Crystallogr., Sect. B*, **27**, 1441 (1971).
5) G. H. Goldschmidt and F. J. Llewellyn, *Acta Crystallogr.*, **3**, 294 (1950).
6) D. G. O'Sullivan and P. W. Sadler, *J. Chem. Soc.*, **1956**, 2202.
7) D. G. O'Sullivan and P. W. Sadler, *J. Chem. Soc.*, **1957**, 2916.
8) C. T. O'Konski and T. K. Ha, *J. Chem. Phys.*, **56**, 3169 (1972).

Neutron Diffraction Study of Aqueous Ionic Solutions. I. Aqueous Solutions of Lithium Chloride and Caesium Chloride

Norio OHTOMO† and Kiyoshi ARAKAWA*

Research Institute of Applied Electricity, Hokkaido University, Sapporo 060

†*Faculty of Engineering, Hokkaido University, Sapporo 060*

(Received November 10, 1978)

The structure factors $S_m(Q)$ for aqueous solutions of LiCl and CsCl at room temperature, including those for heavy water, have been determined by means of the time-of-flight (TOF) neutron diffraction method using an electron linear accelerator (LINAC). Analysis of the diffraction data has been carried out for the aqueous ionic solutions as well as for pure heavy water. The following results were obtained with respect to the structure of the nearest hydration shell: (a) the coordination numbers are 4 for Li^+ and 6 for Cl^- in the LiCl solution, and 8 for Cs^+ and 6 for Cl^- in the CsCl solution, (b) the average ion-oxygen distances are 1.90 ± 0.05 Å for Li^+, 2.95 ± 0.10 Å for Cs^+ and 3.10 ± 0.05 Å for Cl^-, and (c) around cations water molecules take the configuration to orient the axis of one of two lone-pair hybrids on a straight line joining an oxygen atom and a cation.

Since the work of Bernal and Fowler in 1933,[1] many X-ray diffraction studies have been carried out for clarification of the liquid structure of ionic solutions. Lawrence and Kruh made a comprehensive X-ray diffraction study on ionic solutions.[2] In the last decade neutron diffraction studies have appeared as a new means for giving basic data such as the number of hydrated water molecules in the first shell (coordination number), the ion-oxygen distances, and the orientational arrangements within the shell. The results obtained so far, such as on the coordination number, were found to be greatly diverse, as pointed out by Hinton and Amis.[3] A more precise determination of these quantities is desirable.

The first application of the neutron diffraction method to aqueous electrolyte (LiCl) solutions was attempted by Narten *et al.*,[4] who analyzed their data of aqueous LiCl solutions on the basis of their "near-neighbor model" for water. Licheri *et al.* carried out studies on aqueous solutions of electrolytes along the same line.[5–11] However, the present authors have shown that the structure model of water of Narten *et al.* used as a basis for their analysis is physically unacceptable.[12] Soper *et al.* in another approach by means of the neutron diffraction method have given an ion-water configuration using their "first-order difference spectroscopy".[13]

Many problems remain unsolved with respect to the hydrated structure within ionic solutions, but the neutron diffraction method is becoming one of the most powerful means for its elucidation. We have carried out studies on aqueous ionic solutions by means of the method for which neutron diffraction data of heavy water are required. Since there are small discrepancies in the structure factor curves for heavy water given by us,[12] by Page and Powles[14] and by Narten,[15] measurement on heavy water (D_2O) was carried out again.

Measurements were carried out for aqueous solutions of LiCl and CsCl, the former for observing the pronounced effects of Li^+ on the configuration of water molecules in the first hydration sphere due to the small size of the ion, and the latter in view of the different behavior of Cs^+ expected in water as compared with Li^+. The results obtained by means of TOF neutron diffraction are reported, together with the new results for heavy water.

Apparatus and Procedures

Details of the apparatus and procedure have been reported.[12,16] The neutron diffraction experiment was performed by means of the TOF diffraction method using pulsed neutrons produced by LINAC. Thin-walled cylindrical vanadium and quartz were used as container of samples. Measurements were made at room temperature and at the scattering angle $2\theta = 45°$.

All the data were smoothed out according to the usual least-square fitting procedure and corrections (multiple scattering, absorption, background counting and Placzek corrections) were made for the smoothed spectrum. Absolute calibration was then performed by comparison of the count rate time-spectrum from the sample with that from a polycrystalline vanadium rod of the same shape and dimension as the sample.[12]

Results and Analysis of Heavy Water

Neutron diffraction data for heavy water are required for analysis of the data of aqueous ionic solutions.

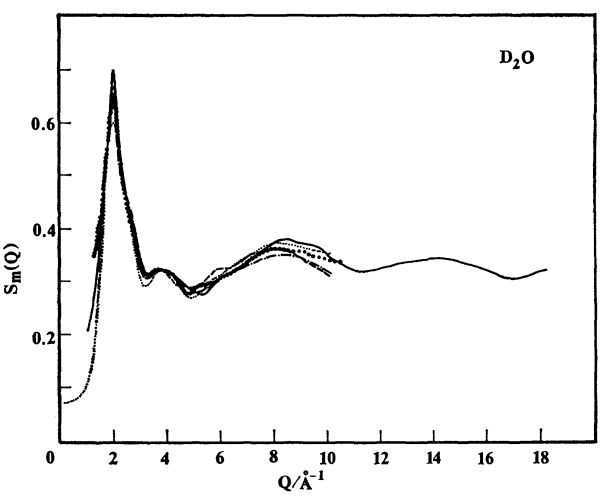

Fig. 1. Observed structure factors for D_2O.
• : $S_m(Q)$ by the authors (14 °C), ——: $S_m(Q)$ by the authors (17 °C),[12] – – –: $S_m(Q)$ by the authors (25 °C), —·—: $S_m(Q)$ by Page and Powles (22 °C), ·····: $S_m(Q)$ by Narten (25 °C).

Measurements for D_2O (99.75% D) were carried out at room temperature (14, 18, and 25 °C).

The absolute structure factors $S_m(Q)$ obtained for liquid heavy water are shown in Fig. 1, together with reported factors for the sake of comparison.[12,14,15] All five curves agree as a whole. The two curves except for the authors' were obtained by the conventional steady-state experiment using reactors as neutron sources. The accuracy of the present TOF experiment using LINAC ($2\theta=45°$) as a neutron source is as follows: the statistical errors are 0.5—0.6% in the Q range 2—5 Å^{-1} and 0.9% at about 8 Å^{-1}.

We proposed the "revised watery model" as a structure model for liquid water and made an analysis by means of the formula[12]

$$S_m(Q) = f_1(Q) + f_{2C}(Q)[(S_C(Q)-1]. \quad (1)$$

A further slight refinement of the model was performed as follows. (a) The rotational angle ξ[17] is taken to be 60°. (b) Concerning the factor $[S_c(Q)-1]$, we used the values obtained according to the procedure of Page and Powles[14] starting from the X-ray data of Narten instead of the direct use of Narten's value of $[S_c(Q)-1]$.[18] (c) The intramolecular contribution $f_1(Q)$ has been taken to be the weighted average value of three varieties of the intramolecular factors, which correspond to the three groups of water molecules in the tetrahedral pentamer according to the manner of hydrogen-bonding (Fig. 5, Ref. 12).[19] This improves the agreement between the calculated and observed curves in the high Q region ($Q \gtrsim 8$ Å^{-1}). The $S_m(Q)$ for the present "revised watery model" is given in Fig. 2 and is compared with the calculated factors for other models, the "uncorrelated orientation model"[14] and the "revised watery model" (free rotation) by the authors.[12] The main features of the three curves are in good agreement with each other except for the bump at about 4 Å^{-1}.

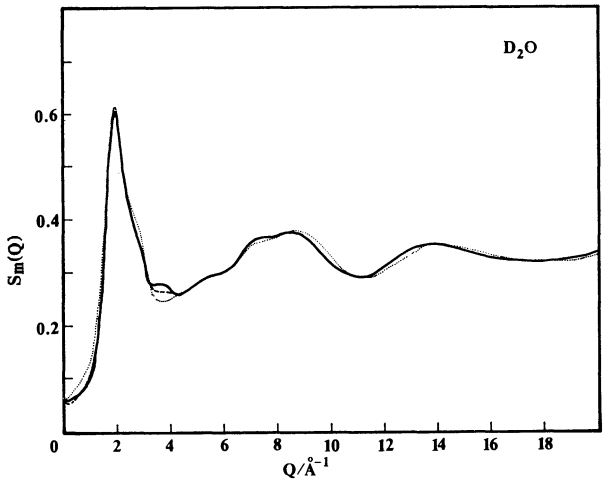

Fig. 2. Comparison between the calculated curves of $S_m(Q)$ for various structure models of liquid water.
——: $S_m(Q)$ for the "revised watery model" ($\xi=60°$),
– – – –: $S_m(Q)$ for the "revised watery model" (free rotation),
……: $S_m(Q)$ for the "uncorrelated orientation model".

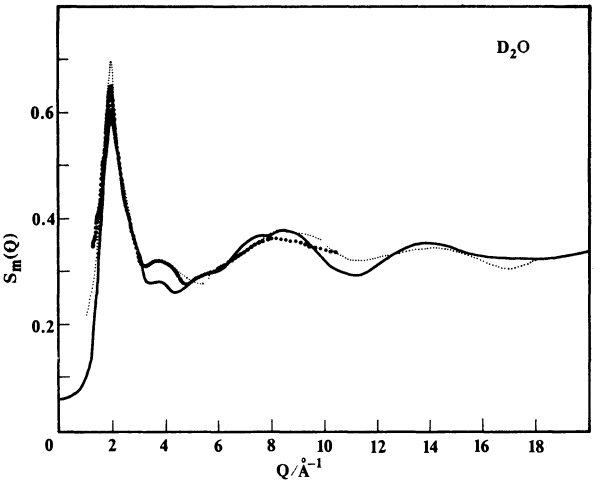

Fig. 3. Comparison between the calculated $S_m(Q)$ values for the present "revised watery model" and the observed ones by the authors.
——: Calculated $S_m(Q)$ for the "revised watery model",
• : observed $S_m(Q)$ in the present study (14 °C),
……: observed $S_m(Q)$ previously.[12]

In Fig. 3, the calculated curve of $S_m(Q)$ for the present "revised watery model" is compared with the observed $S_m(Q)$ curve. From Figs. 2 and 3, we see that the behavior of the curves near 4 Å^{-1} is essential for judging the adequacy of the model proposed.[14] The curves (Fig. 2) show a gradual approach to the observed curve, indicating that the "revised watery model" is the best of all the models for liquid water presented so far in neutron diffraction studies.

Results and Analysis of Aqueous Solutions of LiCl and CsCl

Diffraction Data. Two 1.0 M alkali halide solutions (M: mol dm^{-3}) were prepared by the addition

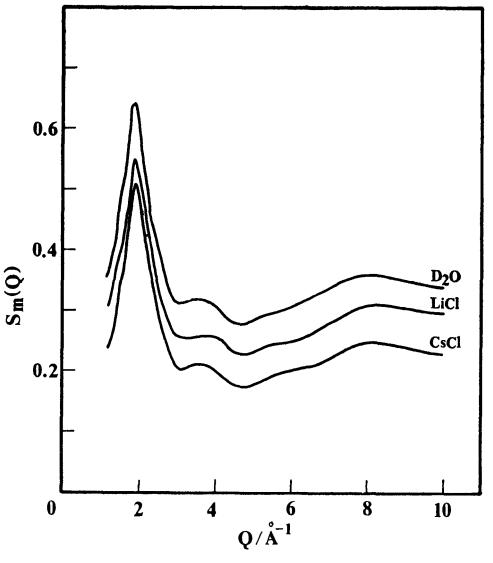

Fig. 4. Observed structure factors for LiCl and CsCl solutions at 1 M, compared with the factor for D_2O (14 °C).

of extra pure anhydrous lithium chloride and caesium chloride to heavy water.[20]

The structure factors are shown in Fig. 4 for LiCl and CsCl solutions including those for pure heavy water.[21] The change of the bump at *ca.* 4 $Å^{-1}$ as well as that of the main peak with a shoulder at 2.8 $Å^{-1}$ indicates the effects of ions on the structure of the first hydration sphere.

Method for Analysis. All the neutron diffraction studies for aqueous ionic solutions have been made so far for concentrated solutions (>1 M).[4,13] We give here the diffraction data for more dilute solutions (1 M). In order to analyze the data of dilute solutions, we have subtracted the structure factor $S_m(Q)_{D_2O}$ of D_2O multiplied by an appropriate fraction from the total structure factor $S_m(Q)_{total}$ of solutions. The remaining factor, $\Delta S_m(Q)$, becomes

$$\Delta S_m(Q) = S_m(Q)_{total} - (1-x)S_m(Q)_{D_2O}, \quad (2)$$

$$x = \frac{c(n_+ + n_-)}{55.3}, \quad (3)$$

where x is the mole fraction of D_2O coordinated in the nearest hydration shell around ions, n_+ and n_- are the coordination number about the cation and the anion, respectively, and c is concentration.

In order to determine the structure of the nearest hydration shell we compare the observed values of $\Delta S_m(Q)$ with those calculated for various structure models assumed.

Procedure for Analysis of LiCl and CsCl Solutions. The structure of the hydration shell is characterized by parameters, coordination number n, ion-oxygen distances, and orientational arrangements of water molecules around ions (Fig. 5).

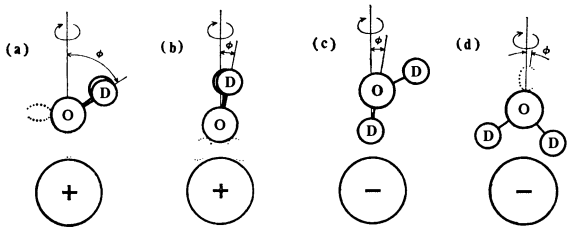

Fig. 5. Orientational arrangements of water molecules around ions.
(a) Linear form for cation, (b) bifurcated form for cation, (c) linear form for anion, (d) bifurcated form for anion.

The coordination number and ion-oxygen distances, so far obtained experimentally, are given in Tables 1 and 2. They are very diversified. As regards configuration of water molecules around ions, two forms, "linear" and "bifurcated," are expected for cations where lone-pair electrons are in the vicinity of the ions (Figs. 5(a) and (b)) and also for anions, where deuterium atoms are located in the vicinity of the ions (Figs. 5(c) and (d)). Very few experimental results have been reported so far concerning the orientation of water molecules around ions.

We have calculated $\Delta S_m(Q)$ for a number of structure models in which the magnitudes of parameters have been varied (Table 3). For each of the LiCl and CsCl solutions, the 24 different structures with respect to the coordination number and the type of orientational configurations are assumed, ion-oxygen distances and the angle ϕ being varied successively at intervals of 0.05 Å and 10°, respectively, for each of the 24 structure models. As a whole, we calculated the $\Delta S_m(Q)$ curves for 264 different models of the structure of the

Table 1. Coordination numbers of Li^+, Cs^+, and Cl^- determined from X-ray (X) and neutron (N) diffraction studies as well as molecular dynamics (MD) and monte calro (MC) calculations

Ion	Coordination number, n	Solute	Concentration/M	Method	Reference
Li^+	4±1	LiCl	<7	X,N	v
	4	LiCl		MC	vii
	4 and 6	LiBr	2.1—5.6	X	ix
	4—6	LiF		MC	x
	5.7±0.2	LiCl	2	MD	xiv
	7.1±0.1	LiI	2.2		
Cs^+	2.0—6.2	CsCl	2.5—10	X	ii
	1.9—6.0	CsBr	2.5, 5		
	2.3—2.7	CsI	2.5		
	7.3±0.7	CsF	2.2	MD	xiv
	8.2±0.8	CsCl			
	7			MD	xv
Cl^-	8—9	LiCl	6	X	i
	5.4—11.0	LiCl	2.5—10	X	ii
	8.2	MgCl		X	iv
	8.9	$MgCl_2$			
	7.9—8.0	$CaCl_2$			
	8.0	$BaCl_2$			
	8.0	$SrCl_2$			
	6±1	LiCl	<7	X,N	v
	7.1—10.2	LiCl	2.15—7.30	X	vi
	5—7			MC	vii
	4	HCl	<7	X	xi
	6	$CaCl_2$	1, 2, 4	X	xii
	6	$[Cr(H_2O)_6]Cl_3$	0.25	X	xiii
	7.4±0.4	LiCl	2	MD	xiv
	6.7±0.3	NaCl	2.2		
	7.9±0.3	CsCl	2.2		
	5.5±0.2	NaCl	5.32	N	xvii
	6	$NiCl_2$	2, 4	X	xviii
	6	$CrCl_2$	1	X	xix

i) E. W. Brady, *J. Chem. Phys.*, **28**, 464 (1958). ii) Ref. 2. iii) G. Licheri, G. Piccaluga, and G. Pinna, *Chem. Phys. Lett.*, **12**, 425 (1971). iv) J. N. Albright, *J. Chem. Phys.*, **56**, 3783 (1972). v) Ref. 4. vi) G. Licheri, G. Piccaluga, and G. Pinna, *J. Appl. Cryst.*, **6**, 392 (1973). vii) H. Kistenmacher, H. Popkie, and E. Clementi, *J. Chem. Phys.*, **61**, 799 (1974). viii) H. Bertagnolli, J. U. Weidner, and H. W. Zimmermann, *Ber. Bunsenges. Phys. Chem.*, **78**, 2 (1974). ix) Ref. 5. x) J. Fromm and E. Clementi, *J. Chem. Phys.*, **62**, 1388 (1975). xi) R. Triolo and A. H. Narten, *J. Chem. Phys.*, **63**, 3624 (1975). xii) Ref. 7. xiii) Ref. 8. xiv) K. Heinzinger and P. C. Vogel, *Z. Naturforsch.*, **31a**, 463 (1976). xv) Ref. 22. xvi) P. Bopp, K. Heinzinger, and G. Jancso, *Z. Naturforsch.*, **32a**, 620 (1977). xvii) Ref. 13. xviii) Ref. 9. xix) Ref. 11.

Table 2. Average ion-oxygen distances of the first hydration shell determined from X-ray (X) and neutron (N) diffraction studies as well as molecular dynamics (MD) and monte calro (MC) calculations

Ion	Distance r/Å	Solute	Concentration/M	Method	Reference
Li^+–O	1.95—2.25	LiCl	<7	X,N	v
	2.1	LiCl	2.15—7.30	X	vi
	2.1	LiBr	2.15—7.30	X	vi
	1.9—2.0			MC	vii
	2.139—2.250	LiBr	2.1—5.6	X	xiv
	2.06	LiCl		MD	xiv
	2.10	LiI		MD	xiv
Cs^+–O	3.15	CsCl	2.5—10	X	ii
	3.15—3.22	CsBr	2.5, 5	X	ii
	3.02—3.15	CsI	2.5	X	ii
	3.14			X	viii
	3.10±0.06	CsCl		MD	xiv
	3.10±0.04	CsF		MD	xiv
	3.32			MD	xv
Cl^-–O	3.15—3.2	LiCl	2.5—10	X	ii
	3.20	HCl	1, 4.3	X	iii
	3.2	$MgCl_2$		X	iv
	3.10—3.193	LiCl	<7	X,N	v
	2.9—3.25	LiCl	2.15—7.30	X	vi
	3.4—3.5			MC	vii
	3.137—3.149	$CaCl_2$	1, 2, 4	X	xii
	3.135	$[Cr(H_2O)_6]Cl_3$	0.25	X	xiii
	2.68	LiCl		MD	xiv
	2.66	CsCl		MD	xiv
	2.66	NaCl		MD	xiv
	3.2	$NiCl_2$	5.32	N	xvii
	3.134—3.145	$NiCl_2$	2, 4	X	xviii
	3.08	$CrCl_3$	1	X	xix

References are the same as those in Table 1.

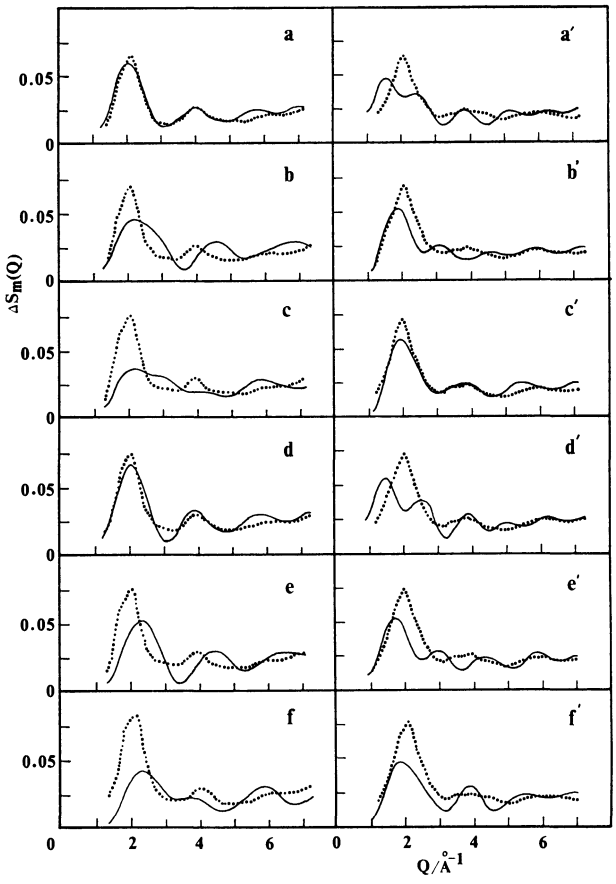

Fig. 6. Changes in the calculated $\Delta S_m(Q)$ with variation of the coordination number for LiCl (a—f) and CsCl (a'—f') solutions.
• : Observed $\Delta S_m(Q)$ (14 °C), (a), (a') $n_+=4$, $n_-=6$, (b), (b') $n_+=6$, $n_-=6$, (c), (c') $n_+=8$, $n_-=6$, (d), (d') $n_+=4$, $n_-=8$, (e), (e') $n_+=6$, $n_-=8$, (f), (f') $n_+=8$, $n_-=8$.

Table 3. Range of parameters for structure models

Ion	Coordination number, n	Ion-oxygen distance, r/Å	Type of configuration around ions (Angle, ϕ/°)
Li^+	4, 6, 8	1.90—2.25	linear (44.75—64.75)
			bifurcated (0.0—20.0)
Cs^+	4, 6, 8	2.85—3.35	linear (44.75—64.75)
			bifurcated (0.0—20.0)
Cl^-	6, 8	3.05—3.20	linear (0.0—20.0)
			bifurcated (0.0—20.0)

Table 4. Coordination numbers, ion-oxygen distances and configurations around ions determined in the present study

Ion	Coordination number, n	Ion-oxygen distance, r/Å	Configuration around ions (Angle, ϕ/°)
Li^+	4	1.90±0.05	linear (54.75)
Cs^+	8	2.95±0.10	linear (54.75)
Cl^-	6	3.10±0.05	undetermined

first hydration shell in the LiCl solution, comparing the calculated curves with those observed, and those for 744 different models in the CsCl solution.

Results of Analysis. We determined the best structure model of the first hydration shell for both solutions. However, it is not possible to show all the curves calculated for the assumed models for comparison (264 and 744 models for LiCl and CsCl solutions, respectively); only typical features of the curves are given.

The calculated $\Delta S_m(Q)$ curves for different sets of coordination numbers are shown for both solutions in Fig. 6; for the LiCl solution, those with various magnitudes of parameter ($r_{Li^+\text{-}O}$, $r_{Cl^-\text{-}O}$, and orientational configurations *etc.*) are shown in Figs. 7(a)—(d) in the case of $n_{Li^+}=4$ and $n_{Cl^-}=6$.

The calculated $\Delta S_m(Q)$ curves of the best mode's thus determined for both solutions are given in Fig. 8 (each curve in Figs. 6(a) and (c') is identical with the best fit curve, respectively). The magnitudes of parameter and orientational configurations for the best structure model of the first hydration shell are given in Table 4.

Concerning the configuration of water molecules within the first hydration shell around cations, the results agree with the conclusion obtained by the

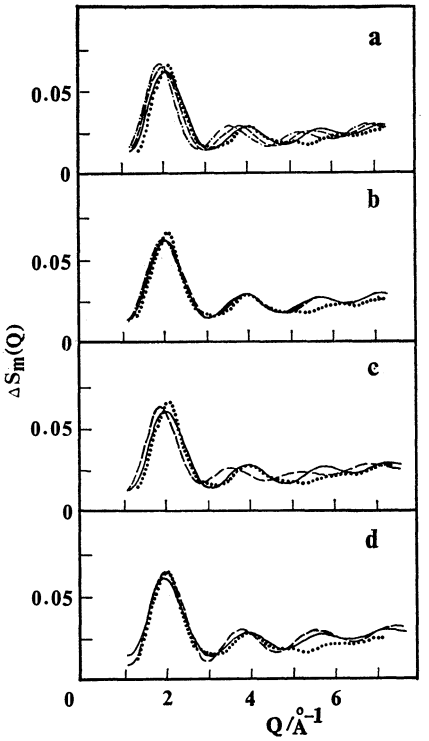

Fig. 7. Changes in the calculated $\Delta S_m(Q)$ with variation of physical parameters for the LiCl solution.
• : Observed $\Delta S_m(Q)$ (14 °C), (a) r_{Li^+-O} (all other parameters are identical with those given in Table 4), ——: 1.90 Å, – – –: 2.00 Å, —•—: 2.10 Å,
(b) r_{Cl^--O} (all other parameters are identical with those given in Table 4), ——: 3.10 Å, – – –: 3.05 Å, —•—: 3.15 Å,
(c) configurations around Li^+ (all other parameters are identical with those given in Table 4), ——: linear, – – –: bifurcated,
(d) configurations around Cl^- (all other parameters are identical with those given in Table 4), ——: linear, – – –: bifurcated.

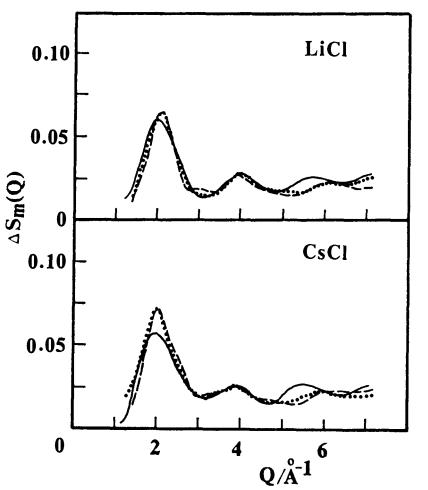

Fig. 8. The best fit curves with the observed $\Delta S_m(Q)$.
• : Observed $\Delta S_m(Q)$ (14 °C), ——: observed $\Delta S_m(Q)$ (18 °C),[21] – – –: calculated $\Delta S_m(Q)$.

molecular dynamics study of Briant and Burton.[22] However, with respect to the configuration around Cl^-, we can not determine which type of configuration, linear or bifurcated, is predominant (Fig. 7(d)).

From the structure analysis where the parameters have been varied systematically (Table 3), we conclude that the structure models shown in Table 4 give the best fit curves with those observed for the LiCl and CsCl solutions at 1 M.

References

1) J. D. Bernal and R. H. Fowler, *J. Chem. Phys.*, **1**, 515 (1933).
2) R. M. Lawrence and R. F. Kruh, *J. Chem. Phys.*, **47**, 4758 (1967).
3) J. F. Hinton and E. S. Amis, *Chem. Rev.*, **71**, 627 (1971).
4) A. H. Narten, F. Vaslow, and H. A. Levy, *J. Chem. Phys.*, **58**, 5017 (1973).
5) G. Licheri, G. Piccaluga, and G. Pinna, *Chem. Phys. Lett.*, **35**, 119 (1975).
6) G. Licheri, G. Piccaluga, and G. Pinna, *J. Chem. Phys.*, **63**, 4412 (1975).
7) G. Licheri, G. Piccaluga, and Pinna, *J. Chem. Phys.*, **64**, 2437 (1976).
8) R. Caminiti, G. Licheri, G. Piccaluga, and G. Pinna, *J. Chem. Phys.*, **65**, 3134 (1976).
9) R. Caminiti, G. Licheri, G. Piccaluga, and G. Pinna, *Faraday Discuss. Chem. Soc.*, **64**, 62 (1977).
10) R. Caminiti, G. Licheri, G. Piccaluga, and G. Pinna, *J. Chem. Phys.*, **68**, 1967 (1978).
11) R. Caminiti, G. Licheri, G. Piccaluga, and G. Pinan, *J. Chem. Phys.*, **69**, 1 (1978).
12) N. Ohtomo and K. Arakawa, *Bull. Chem. Soc. Jpn.*, **51**, 1649 (1978).
13) A. K. Soper, G. W. Neilson, J. E. Enderby, and R. A. Howe, *J. Phys. C, Solid State Phys.*, **10**, 1973 (1977).
14) D. I. Page and J. G. Powles, *Mol. Phys.*, **21**, 901 (1971).
15) A. H. Narten, *J. Chem. Phys.*, **56**, 5681 (1972).
16) T. Matsumoto, N. Ohtomo, and M. Senda, *J. Nucl. Sci. Technol.*, **15**, 863 (1978).
17) For the average rotational angle ξ, related to the average of the intermolecular distance r_{DD}, see Fig. 6 in Ref. 14 and Fig. 5 in Ref. 12.
18) Concerning the factor $[S_C(Q)-1]$, in the preceding paper we used the values of X-ray data of Table II in the paper of Narten and Levy (*J. Chem. Phys.*, **55**, 2263 (1971)).
19) In the former report three forms of hydrogen bonded D_2O molecules (Fig. 5) were taken into consideration in the calculation of $f_{2c}(Q)$. However, in the calculation of $f_1(Q)$, the intramolecular separation and the bond angle of the central molecule (r_{OD}: 1.01 Å, T: 109.5°) were used. In the present analysis the effect of the presence of three forms has fully been taken into consideration in $f_1(Q)$ as well as $f_{2C}(Q)$.
20) Samples composed of naturally occurring elements were used. Values of coherent scattering amplitudes of the elements are as follows: -0.18×10^{-12} cm for Li, 0.49×10^{-12} cm for Cs and 0.99×10^{-12} cm for Cl. (B. Dorner and R. Comes, "Dynamics of Solids and Liquids by Neutron Scattering," ed by S. W. Lovessey and T. Springer, Springer-Verlag, Berlin (1977), Chap. 3, pp. 136—141).
21) For the confirmation of the reproducibility of the observed data we give another $\Delta S_m(Q)$ curve observed at 18 °C The two curves agree well.
22) C. L. Briant and J. J. Burton, *J. Chem. Phys.*, **64**, 2888 (1976).

Oxidation of 3,5-Di-*t*-butylcatechol Catalyzed by Metal Acetylacetonates in Organic Solvents

Hiroyuki SAKAMOTO, Takuzo FUNABIKI,* Satohiro YOSHIDA, and Kimio TARAMA

Department of Hydrocarbon Chemistry, Faculty of Engineering, Kyoto University, Kyoto 606

(Received November 21, 1978)

The oxidation of 3,5-di-*t*-butylcatechol (3,5-DTBC) has been studied in organic solvents in the presence of metal acetylacetonates ($M(acac)_2$). The catalytic activity of $M(acac)_2$ decreased in the order M=Mn>Co> Ni≫Fe, and the product was 3,5-di-*t*-butyl-*o*-benzoquinone (3,5-DTBQ). The kinetic analysis has suggested a mechanism in which the radical chain reactions involving 3,5-di-*t*-butyl-*o*-benzosemiquinone (3,5-DTBSQ·) and hydroperoxyl radical (·OOH) are initiated by the reaction of 3,5-DTBC with the initially formed dioxygen metal complexes. Kinetic parameters for the complexation of molecular oxygen by $Mn(acac)_2$ and $Co(acac)_2$ were estimated: $\Delta H^{\neq}$(kJ mol^{-1})=4.6±0.8 for Mn, 29.7±0.8 for Co; $\Delta S^{\neq}$(J mol^{-1} K^{-1})=−200±2 for Mn, −135±2 for Co.

There has been much interest recently in the study of the oxidation of catechol and the reversible absorption of oxygen by transition metal complexes, because both are related to biological phenomena which involve enzymes and hemoglobin. The oxidation of catechols is accompanied by the aromatic ring cleavage[1–4] or by the dehydrogenation to form *o*-benzoquinones.[3–9] The latter reaction has been catalyzed by enzymes,[5] aqueous bases,[4,6] metal ions in basic media,[4,7] metal oxides such as PbO_2 and Ag_2O,[8] and metal salts such as Ag_2CO_3,[9] but transition metal complexes have rarely been used as catalysts.[10] Recently, the formation of the dioxygen complex of cobalt(II) acetylacetonate, in which the metal-oxygen bond is very weak, has been proposed in the oxidation of cumene,[11] α-methylstyrene,[11] and 1-phenylethanol.[12] Thus, the dioxygen complex is expected to be an active species in the oxidation of catechol. We have studied the oxidation of 3,5-di-*t*-butylcatechol (3,5-DTBC) by metal acetylacetonates ($M(acac)_2$: M=Mn, Fe, Co, Ni, Cu) in order to determine the catalytic activity of these readily available complexes for the oxidation of catechol and to obtain information about the activation of oxygen by coordinating to metal complexes. 3,5-DTBC was used as reactant to avoid the solvolytic attack on the quinonoid nucleus,[4,6,13] and the reactions were performed in the organic solvents without base to avoid the complexity caused by the dissociation of the catechol to catechol anion. The coordination of catechol to the metal complex as mono- or dianion, which was proposed by Grinstead[4] or Martell,[7] will be neglected in the present conditions.

Experimental

Materials. Metal acetylacetonates and 3,5-DTBC were recrystallized from chlorobenzene and heptane, respectively. 3,5-Di-*t*-butyl-*o*-benzoquinone (3,5-DTBQ) was prepared by the method of Grinstead[4] and recrystallized from 2,2,4-trimethylpentane. All the solvents were distilled before use.

Manometric Study. All the reactions were performed at 25 °C in a 50 cm^3 two-necked flask which was attached to an ordinary vacuum line system. The reaction was started by the addition of the 3,5-DTBC solution with an injection syringe through a serum cap to the catalyst solution, which was stirred magnetically in an oxygen atmosphere. The reaction was followed by measuring the oxygen absorption with a gas burette under a constant pressure. The yield of 3,5-DTBQ was determined spectrophotometrically.

Spectroscopic Study. The rate of the reaction (rate of the formation of 3,5-DTBQ) in acetone was measured spectrophotometrically on a JASCO UVIDEC-1 spectrophotometer with a 1 cm quartz cell in air. λ_{max} and ε of 3,5-DTBQ in acetone were 399 nm and 1.85×10^3 mol^{-1} dm^3 cm^{-1}, respectively. The initial concentration of the dissolved oxygen was estimated by the use of the tabulated data.[15] ESR spectra were taken on a JEOL PE-2X spectrometer modified with a JEOL ES-SCXA gunn diode microwave unit.

Results and Discussion

Catalytic Activity. Figure 1 shows the oxygen absorption curves in the oxidation of 3,5-DTBC by $M(acac)_2$ in acetonitrile. Oxygen was absorbed without an induction period by the manganese, cobalt, and nickel complexes, but $Cu(acac)_2$ exhibited a different mode of the oxygen absorption. This suggests that the mechanism for the former three complexes is

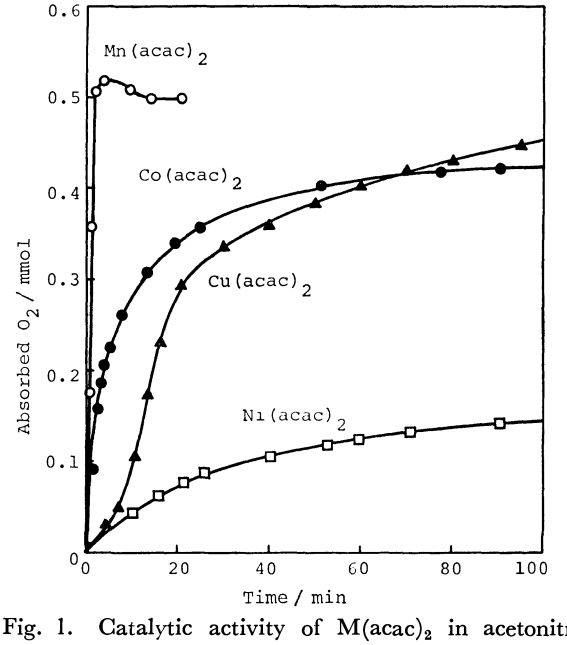

Fig. 1. Catalytic activity of $M(acac)_2$ in acetonitrile solvent at 25 °C under oxygen atmosphere.
$[M(acac)_2]_0$=0.1 mmol; $[3,5\text{-DTBC}]_0$=1.0 mmol; total volume=10 cm^3.

different from that for $Cu(acac)_2$. The catalytic activity evaluated from the maximal rate of the oxygen absorption decreased in the order M=Mn>Co>Cu>Ni≫Fe(no reaction). This order is different from that reported for the oxidation of cumene and α-methylstyrene (Co>Mn>Ni).[11] The inactivity of $Fe(acac)_2$ is due to its ready conversion to an inactive Fe(III) species in the presence of oxygen.[16]

Table 1. Catalytic activity and solvent effect[a]

Catalyst	Solvent	Reaction time (min)	Moles O_2 absorbed per mole 3,5-DTBC	Yield of 3,5-DTBQ (%)
non	Acetonitrile	120	0	0
$Mn(acac)_2$	Acetonitrile	5	0.50	95—100
$Fe(acac)_2$	Acetonitrile	120	0	0
$Co(acac)_2$	Acetonitrile	120	0.42	75—80
$Ni(acac)_2$	Acetonitrile	180	0.23	40—45
$Cu(acac)_2$	Acetonitrile	120	0.48	45—50
$MnCl_2 \cdot 4H_2O$[b]	Acetonitrile	120	0	0
$FeCl_2 \cdot 4H_2O$	Acetonitrile	120	0.07	0
$CoCl_2 \cdot 6H_2O$	Acetonitrile	120	0	0
$NiCl_2 \cdot 6H_2O$	Acetonitrile	120	0	0
$CuCl_2 \cdot 2H_2O$	Acetonitrile	120	0	0
$Mn(OAc)_2 \cdot 4H_2O$	Acetonitrile	20	0.48	75—80
$Co(OAc)_2 \cdot 4H_2O$	Acetonitrile	120	0.45	75—80
$Ni(OAc)_2 \cdot 4H_2O$	Acetonitrile	180	0.24	40—45
$Cu(OAc)_2 \cdot H_2O$	Acetonitrile	70	0.70	95—100
$Mn(acac)_2$	Acetone	5	0.51	95—100
$Mn(acac)_2$	Benzene	7	0.49	95—100
$Mn(acac)_2$	Methanol	10	0.51	95—100

a) $[Catalyst]_0=0.1$ mmol; $[3,5\text{-DTBC}]_0=1.0$ mmol; total volume=10 cm^3 at 25 °C under oxygen atmosphere. b) The solution was somewhat heterogeneous.

The solvent effect was studied with $Mn(acac)_2$. As shown in Table 1, the rate decreased in the order: acetone≳acetonitrile>benzene>methanol, but the solvent effect was not so remarkable. Catalytic activity in organic solvent was also studied with some metal salts. As shown in Table 1, metal halides, which are active in $KHCO_3$ buffered aqueous methanol,[4] were not active. Metal carboxylates were active as metal acetylacetonates, but induction periods were clearly observed in the oxygen absorption curves, as in the case of $Cu(acac)_2$.

The oxidation product, which was isolated by ether extraction, was 3,5-DTBQ, and its yield was >95% in the case of $Mn(acac)_2$. The result that the maximal amount of the absorbed oxygen with $Mn(acac)_2$ was slightly greater than one-half of 3,5-DTBC (see Fig. 1) suggests a two-step reaction (Reactions 1 and 2) rather than the single step 3.

$$3,5\text{-DTBC} + O_2 \longrightarrow 3,5\text{-DTBQ} + H_2O_2 \quad (1)$$

$$H_2O_2 \longrightarrow H_2O + 0.5O_2 \quad (2)$$

$$3,5\text{-DTBC} + 0.5O_2 \longrightarrow 3,5\text{-DTBQ} + H_2O \quad (3)$$

The formation of hydrogen peroxide was confirmed by iodometry and the blue color of potassium ferricyanide.[17] It was also observed that the complex catalyzed the rapid decomposition of hydrogen peroxide (Reaction 2).

Kinetic and Spectroscopic Studies. Kinetic studies were performed with $Mn(acac)_2$ and $Co(acac)_2$ in acetone, which was the most effective solvent for the oxidation. The reaction catalyzed by $Ni(acac)_2$ was too slow to be followed spectrophotometrically. Acetone was stable under the oxidation conditions, for no

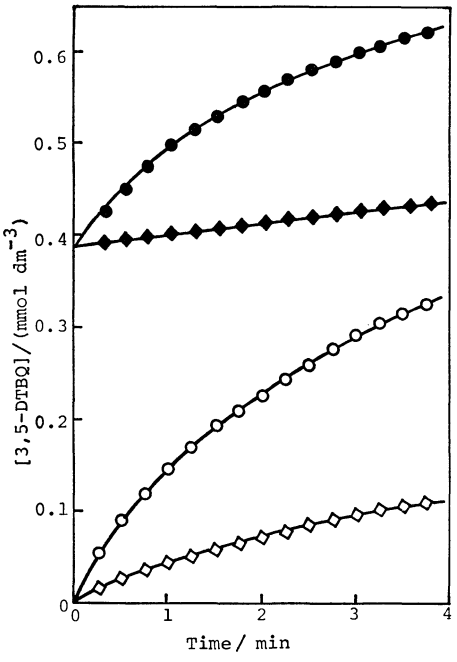

Fig. 2. The oxidation of 3,5-DTBC at 25 °C under air.
(○): $[Mn(acac)_2]_0=3.21\times10^{-5}$ mol dm^{-3} and $[3,5\text{-DTBC}]_0=0.588$ mmol dm^{-3}. $r_0=2.30\times10^{-6}$ mol dm^{-3} s^{-1}.
(◇): $[Co(acac)_2]_0=7.73\times10^{-5}$ mol dm^{-3} and $[3,5\text{-DTBC}]_0=0.531$ mmol dm^{-3}. $r_0=3.11\times10^{-7}$ mol dm^{-3} s^{-1}.
(●): $[Mn(acac)_2]_0=3.21\times10^{-5}$ mol dm^{-3}, $[3,5\text{-DTBC}]_0=0.588$ mmol dm^{-3}, and $[3,5\text{-DTBQ}]_0=0.380$ mmol dm^{-3}. $r_0=1.97\times10^{-6}$ mol dm^{-3} s^{-1}.
(◆): $[Co(acac)_2]_0=7.73\times10^{-5}$ mol dm^{-3}, $[3,5\text{-DTBC}]_0=0.531$ mmol dm^{-3}, and $[3,5\text{-DTBQ}]_0=0.380$ mmol dm^{-3}. $r_0=0.79\times10^{-7}$ mol dm^{-3} s^{-1}.

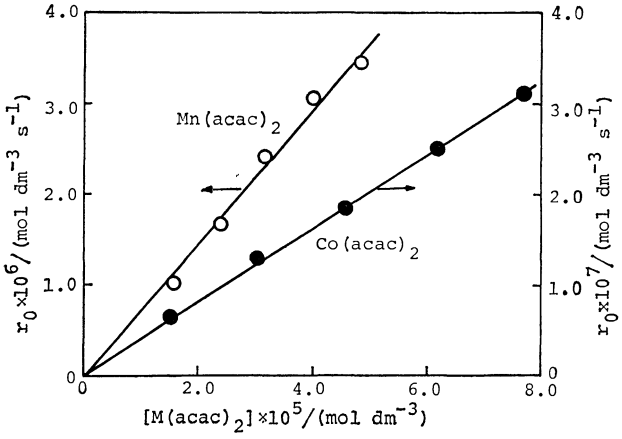

Fig. 3. Dependence of r_0 on the catalyst concentration at 25 °C under air.
(○): $[3,5\text{-DTBC}]_0=0.588$ mmol dm^{-3}.
(●): $[3,5\text{-DTBC}]_0=0.531$ mmol dm^{-3}.

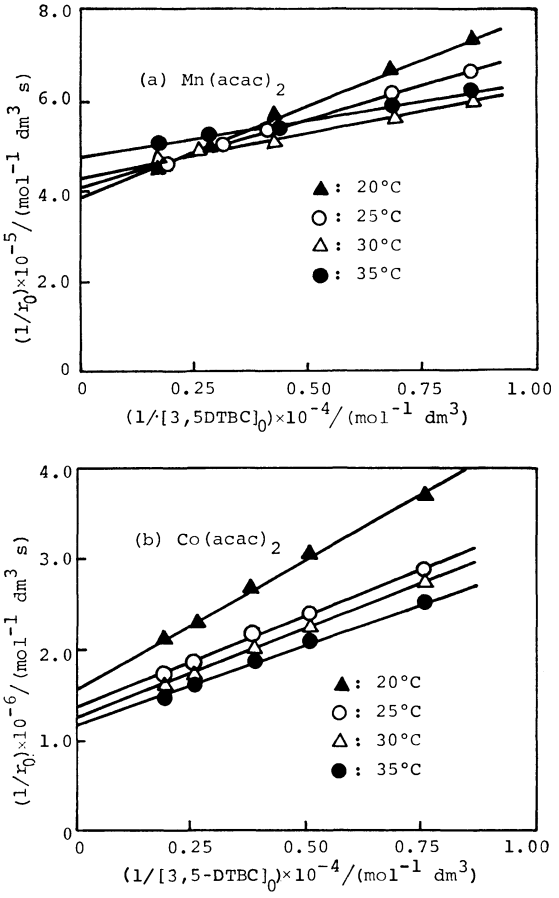

Fig. 4. Plots of $1/r_0$ *vs.* $1/[3,5\text{-DTBC}]_0$.
(a) $[Mn(acac)_2]_0 = 3.21 \times 10^{-5}$ mol dm^{-3}.
(b) $[Co(acac)_2]_0 = 7.71 \times 10^{-5}$ mol dm^{-3}.

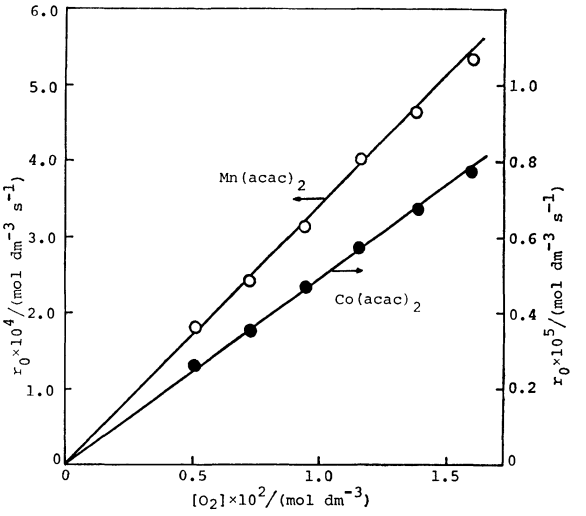

Fig. 5. Dependence of r_0 on the oxygen concentration at 25 °C.
$[3,5\text{-DTBC}]_0 = 0.1$ mol dm^{-3}.
(○): $[Mn(acac)_2]_0 = 1.25$ mmol dm^{-3}.
(●): $[Co(acac)_2]_0 = 2.50$ mmol dm^{-3}.
(The oxygen concentration was estimated by literature.[15])

oxidation product of acetone was detected by GLC in gaseous or liquid phase. A typical example of the oxidation of 3,5-DTBC is shown in Fig. 2. Figures 3 and 4 show the clear linear relations between the initial rate and catalyst concentration and between the reciprocals of the initial rate and of 3,5-DTBC concentration. As shown in Fig. 2, the addition of 3,5-DTBQ decreased the initial rate (r_0). Since Mn(III) and Co(III) species ($\lambda_{max} = 590$ nm (Mn), 595 nm (Co)) were formed by the addition of 3,5-DTBQ, the retardation may be attributed to the formation of these inactive species. Although Vásvari and Gál reported that Co(III) was formed in the initial stage of the oxidation of 1-phenylethanol catalyzed by $Co(acac)_2$,[13] the oxidation of the metal complexes was rather slow in the present condition and was affected by 3,5-DTBQ. Retardation by the addition of water, which was observed in the oxidation of acrylaldehyde[18] and tributylphosphine[19] by $Co(acac)_2 \cdot 2H_2O$, was not observed even in the presence of 5.0×10^{-4} mol dm^{-3} of water. The effect of the oxygen concentration (oxygen pressure) on the initial rate was studied manometrically in the presence of high concentrations of 3,5-DTBC and catalysts; a first order dependence was observed, as shown in Fig. 5. We have tried to detect radical intermediates by the spin trapping method, as previously reported.[20] Double triplets were observed with 5,5-dimethyl-1-pyrroline 1-oxide in the reaction solution catalyzed by $Mn(acac)_2$: $a_N = 14.6$ G (in acetone), 14.2 G (in benzene), $a_{\beta H} = 16.6$ G, $g = 2.0060$. The radical has not been assigned yet, but it may be a radical such as 3,5-di-*t*-butyl-*o*-benzosemiquinone (3,5-DTBSQ·) rather than the hydroxyl radical ($a_N = 14.3$ G, $a_{\beta H} = 11.7$ G, $g = 2.0061$ in H_2O) or the hydroxyl radical ($a_N = 15.3$ G, $a_{\beta H} = 15.3$ G, $g = 2.0060$ in H_2O).[21]

Reaction Mechanism. In the studies of oxidation of catechol catalyzed by metal ions[4] or metal chelates,[7] aqueous methanol was used as a solvent, and the reaction was promoted in the basic media. The proposed mechanisms in these conditions involved the initial coordination of catechol dianion to metal ion (**1**) or of monoanion to metal chelate (***2***, L: 4-nitrocatechol or tetrabromocatechol),[7] followed by the reaction with oxygen. A ternary complex coordinated by oxygen and catechol anion has been proposed as an active complex.[4,7] In our present con-

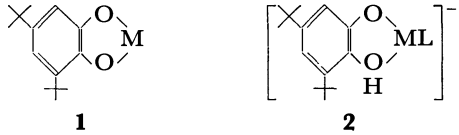

1 **2**

ditions, in organic solvents without base, the coordination of catechol to metal complexes as a mono- or dianion is improbable. This is reflected by the small solvent effect. We can expect that catechol itself coordinates to the metal complexes, but the coordination must be much weaker than that of anions in the basic aqueous media. In addition, the acac ligand initially occupies four coordination sites; this is less desirable for the coordination of catechol than the system by Martell,[7] in which a 1: 1 ratio of metal ion and ligand was used to leave a maximum number of coordination sites open.

On the other hand, Kamiya has studied the oxidation

of hydrocarbons (cumene, α-methylstyrene) by metal acetylacetonates, and proposed that the reaction was initiated by the activated oxygen molecule coordinated to metal acetylacetonates (M=Co(II), Mn(II)).[11]

$$M(acac)_2 + O_2 \rightleftharpoons M(acac)_2^{\delta+}O_2^{\delta-}$$

$$M(acac)_2^{\delta+}O_2^{\delta-} + \diagdown C{=}C \diagup \longrightarrow$$

$$M(acac)_2{-}O_2{-}\overset{|}{C}{-}\overset{|}{C}\cdot \longrightarrow$$

Since the present reaction condition is similar to that suggested by Kamiya rather than those of Grinstead or Martell, it seems likely that the oxidation of 3,5-DTBC is initiated by a process similar to the oxidation of hydrocarbon rather than the processes proposed in the basic aqueous media. We propose here the following reaction sequences as a very probable mechanism; it well explains the kinetic results and the formation of hydrogen peroxide and a radical intermediate.

$$M(acac)_2 + O_2 \underset{k_{-1}}{\overset{k_1}{\rightleftharpoons}} M(acac)_2 \cdots O_2 \quad (4)$$

$$M(acac)_2 \cdots O_2 + 3,5\text{-DTBC} \xrightarrow{k_2} M(acac)_2 + 3,5\text{-DTBSQ}\cdot + \cdot OOH \quad (5)$$

$$3,5\text{-DTBC} + \cdot OOH \xrightarrow{k_3} 3,5\text{-DTBSQ}\cdot + HOOH \quad (6)$$

$$3,5\text{-DTBSQ}\cdot + 3,5\text{-DTBSQ}\cdot \xrightarrow{k_4} 3,5\text{-DTBQ} + 3,5\text{-DTBC} \quad (7)$$

$$3,5\text{-DTBSQ}\cdot + \cdot OOH \xrightarrow{k_5} 3,5\text{-DTBQ} + HOOH \quad (8)$$

$$M(acac)_2 + 3,5\text{-DTBQ} \xrightarrow{k_6} \text{Inactive species} \quad (9)$$

$$M(acac)_2 + HOOH \xrightarrow{k_7} M(acac)_2 + H_2O + 0.5O_2 \quad (10)$$

The high initial rate of oxidation without the induction period can be explained by the activation of oxygen by the formation of a weak metal-oxygen bond, followed by the abstraction of hydrogen from 3,5-DTBC to form 3,5-DTBSQ· and ·OOH. The Reactions 6 and 7 were assumed by reference to the autoxidation of hydrocarbon[22] and the dismutation of 3,5-DTBSQ· anion.[6] The possible termination reactions other than 7 are 8 and 11, but the latter may be neglected for a low concentration of

$$\cdot OOH + \cdot OOH \longrightarrow HOOH + O_2 \quad (11)$$

the ·OOH radical compared with that of 3,5-DTBSQ·. Reactions 9 and 10 explain the retardation effect of 3,5-DTBQ and the decomposition of hydrogen peroxide, respectively.

In the initial period of the reaction, we can neglect Reactions 9 and 10. By applying the steady-state treatment for $M(acac)_2\cdots O_2$, 3,5-DTBSQ·, and ·OOH (Eqs. 12—14), we obtain the rate equation 15 for the formation of 3,5-DTBQ:

$$\frac{d[M(acac)_2\cdots O_2]}{dt} \equiv 0 = k_1[M(acac)_2][O_2] - k_{-1}[M(acac)_2\cdots O_2] - k_2[M(acac)_2\cdots O_2][3,5\text{-DTBC}] \quad (12)$$

$$\frac{d[3,5\text{-DTBSQ}\cdot]}{dt} \equiv 0 = k_2[M(acac)_2\cdots O_2][3,5\text{-DTBC}] + k_3[3,5\text{-DTBC}][\cdot OOH] - 2k_4[3,5\text{-DTBSQ}\cdot]^2 - k_5[3,5\text{-DTBSQ}\cdot][\cdot OOH] \quad (13)$$

$$\frac{d[\cdot OOH]}{dt} \equiv 0 = k_2[M(acac)_2\cdots O_2][3,5\text{-DTBC}] - k_3[3,5\text{-DTBC}][\cdot OOH] - k_5[3,5\text{-DTBSQ}\cdot][\cdot OOH] \quad (14)$$

$$\frac{d[3,5\text{-DTBQ}]}{dt} = k_4[3,5\text{-DTBSQ}\cdot]^2 + k_5[3,5\text{-DTBSQ}\cdot][\cdot OOH] = k_2[M(acac)_2\cdots O_2][3,5\text{-DTBC}] \quad (15)$$

Using the stoichiometric equation 16, we obtain Eq. 17:

$$[M(acac)_2] = [M(acac)_2]_0 - [M(acac)_2\cdots O_2] \quad (16)$$

$$[M(acac)_2\cdots O_2] = \frac{k_1[M(acac)_2]_0[O_2]}{k_1[O_2]+k_{-1}+k_2[3,5\text{-DTBC}]} \quad (17)$$

Assuming $[3,5\text{-DTBC}] \simeq [3,5\text{-DTBC}]_0$ and $[O_2] \simeq [O_2]_0$, we obtain the equation for the initial rate of the formation of 3,5-DTBQ and its linearized form:

$$\left(\frac{d[3,5\text{-DTBQ}]}{dt}\right)_0 = r_0 = \frac{k_1k_2[3,5\text{-DTBC}]_0[O_2]_0[M(acac)_2]_0}{k_1[O_2]_0+k_{-1}+k_2[3,5\text{-DTBC}]_0} \quad (18)$$

$$1/r_0 = \frac{k_1[O_2]_0+k_{-1}}{k_1k_2[M(acac)_2]_0[O_2]_0}\left(\frac{1}{[3,5\text{-DTBC}]_0}\right) + \frac{1}{k_1[M(acac)_2]_0[O_2]_0} \quad (19)$$

Eqs. 18 and 19 are consistent with the results shown in Figs. 3 and 4, respectively. If we ignore the pre-equilibrium (Eq. 4), the reactions of Eqs. 4 and 5 are described by Eq. 20.

$$M(acac)_2 + O_2 + 3,5\text{-DTBC} \xrightarrow{k} M(acac)_2 + 3,5\text{-DTBSQ}\cdot + \cdot OOH \quad (20)$$

In this case, the initial rate equation 21 is obtained by a similar steady-state treatment.

$$r_0 = k[M(acac)_2]_0[O_2]_0[3,5\text{-DTBC}]_0 \quad (21)$$

Eq. 21 is not consistent with the results in Fig. 4, indicating that we can not neglect the pre-equilibrium.

The first order dependence of the rate on the oxygen concentration, as shown in Fig. 5, is consistent with the rate equation 18, because the rate equation 22 is derived by assuming $k_1[O_2]_0+k_{-1} \ll k_2[3,5\text{-DTBC}]_0$. This assumption

$$r_0 = k_1[M(acac)_2]_0[O_2]_0 \quad (22)$$

is not unreasonable in the presence of a high concentration of 3,5-DTBC (about 10^3 greater than the concentrations in the spectroscopic studies). We observed that the rate was independent of the concentration of 3,5-DTBC in the region of 0.1—0.3 mol dm^{-3}; this result supports our assumption.

Reaction 5 is the step of the abstraction of the hydrogen of catechol by the activated oxygen, and may proceed stepwise *via* a ternary complex, but the kinetic results are not enough to discriminate

$$M(acac)_2\cdots O_2 + 3,5\text{-DTBC} \rightleftharpoons M(acac)_2\cdots O_2(3,5\text{-DTBC})$$

$$M(acac)_2\cdots O_2(3,5\text{-DTBC}) \longrightarrow M(acac)_2 + 3,5\text{-DTBSQ}\cdot + \cdot OOH$$

between a one-step and a two-step process. The coordination of 3,5-DTBC to the oxygen complex is not impossible, because acac can coordinate as a monodentate ligand, but the complex seems far less stable than the ternary complexes proposed by Grinstead[4] or Martell.[7] Vásvari and Gál has proposed the splitting of the O–O bond by the following reactions in the oxidation of 1-phenylethanol (ROH) with $Co(acac)_2$,[12] but the process

$$ROH\cdot Co(acac)_2\cdots O_2 + Co(acac)_2 \longrightarrow Co(acac)_2O\cdot + ROH\cdot Co(acac)_2\cdot O$$

$$ROH\cdot Co(acac)_2O\cdot \longrightarrow Co(acac)_2OH(RO\cdot)$$

$$Co(acac)_2O\cdot + ROH \longrightarrow Co(acac)_2OH(RO\cdot)$$

is not consistent with the formation of hydrogen peroxide in the present system.

The reversible formation of a 1:1 dioxygen-transition metal complex and the reaction of the activated oxygen are of current interest. Many examples of a dioxygen cobalt complex have been found,[23] and recently the formation of dioxygen complexes of manganese tetraphenylporphyrin[24] and phthalocyanin[25] have been reported. Thus, the formations of the dioxygen complexes of metal acetylacetonates are probable. The values of k_1 (Reaction 4) were estimated from the intercepts Fig. 4 (Table 2), or from the slopes in Fig. 5 (27.5 and 0.2 $dm^3\ mol^{-1}\ s^{-1}$ for Mn and Co, respectively). The agreement of the values estimated in the different conditions was fairly good for $Mn(acac)_2$, but rather poor for $Co(acac)_2$. The smaller values obtained from Fig. 5 may be ascribed to the fact that the reaction was retarded by 3,5-DTBQ even in the initial stage, especially in the case of $Co(acac)_2$. The activation parameters (ΔH^* and ΔS^*) for this step are given in Table 2, and the values for the cobalt complex are comparable to those of $[Co(Ph_2PCH{=}CHPPh_2)(O_2)]^+$ ($\Delta H^*=14.2$ kJ mol^{-1}, $\Delta S^*=-117$ J $mol^{-1}\ K^{-1}$).[26] The proposed mechanism is consistent with the order of the catalytic activity (Mn>Co>Ni), because it is expected that the low redox potential facilitates the electron transfer from metal to oxygen. The inactivity of $Fe(acac)_2$ may be ascribed to the stabilization of a Fe(III) species rather than $Fe(acac)_2\cdots O_2$ by the extreme electron transfer. We could not find any product formed by the aromatic ring cleavage, and this indicates that the activation of oxygen by coordination to $M(acac)_2$ is not enough, compared with that of superoxide[3] or singlet oxygen.[27]

Table 2. Kinetic parameters of k_1

Catalyst[a]	Temp (°C)	$1/(k_1\times[M(acac)_2]\times[O_2])$[b]	k_1 ($dm^3\ mol^{-1}\ s^{-1}$)	ΔH^* (kJ mol^{-1})	ΔS^* (J $mol^{-1}\ K^{-1}$)
$Mn(acac)_2$	20	3.96×10^5	29.9	4.6 ± 0.8	-200 ± 2
	25	4.09×10^5	31.5		
	30	4.33×10^5	33.0		
	35	4.79×10^5	34.0		
$Co(acac)_2$	20	1.55×10^6	3.17	29.7 ± 0.8	-135 ± 2
	25	1.35×10^6	3.96		
	30	1.20×10^6	4.95		
	35	1.15×10^6	5.98		

a) The concentrations of catalysts were same as those of Fig. 4. b) The concentrations of oxygen at 20, 25, 30, and 35 °C were estimated to be 2.63, 2.42, 2.18, and 1.88 mmol dm^{-3}, respectively.[15]

From the viewpoint of the potential use of the dioxygen metal complex as catalysts for the oxidation of organic substrates, this work has shown that metal acetylacetonates function as an efficient catalyst for the oxidation 3,5-DTBC. Mckillop and Ray[10] have recently shown that $Co(acacene)(O_2)\cdot H_2O$ catalyzes the oxidation of hydroquinones; $Co(acacene)(O_2)\cdot H_2O$ was presumed to be an active species, but no mechanism has been proposed. The mechanism proposed here is a new radical mechanism for the oxidation of 3,5-DTBC which does not involve the redox of metal ion[4] and is different from the ionic mechanism.[7] We have not studied in detail the oxidation catalyzed by $Cu(acac)_2$ and metal carboxylates, which may be explained by the most common pathway for catalysis by transition metal complexes involving the decomposition of peroxides.

References

1) "Molecular Mechanisms of Oxygen Activation," ed by O. Hayaishi, Academic Press, New York (1974).
2) J. Tsuji and H. Takayanagi, *J. Am. Chem. Soc.*, **96**, 7349 (1974); M. M. Rogić and T. R. Demmin, *ibid.*, **100**, 5472 (1978).
3) Y. Moro-oka and C. S. Foote, *J. Am. Chem. Soc.*, **98**, 1510 (1976).
4) R. R. Grinstead, *Biochem.*, **3**, 1308 (1964).
5) J. M. Nelson, *Adv. Enzymol.*, **4**, 99 (1944).
6) C. A. Tyson and A. E. Martell, *J. Phys. Chem.*, **74**, 2601 (1970).
7) C. A. Tyson and A. E. Martell, *J. Am. Chem. Soc.*, **94**, 939 (1972).
8) W. Flaig, T. Ploetz, and H. Biegans, *Ann.*, **597**, 196 (1955).
9) V. Balogh, M. Fetizon, and M. Golfier, *J. Org. Chem.*, **36**, 1339 (1971).
10) A. McKillop and S. J. Ray, *Synthesis*, **1977**, 847.
11) Y. Kamiya, *J. Catal.*, **24**, 69 (1972).
12) G. Vásvari and D. Gál, *J. Chem. Soc., Faraday Trans.* **1**, **73**, 1537 (1977).
13) D. R. Eaton, *Inorg. Chem.*, **3**, 1268 (1964); D. C. Reitz, J. R. Hollahan, F. Dravnicks, and J. E. Wertz, *J. Chem. Phys.*, **34**, 1457 (1961).
14) C. A. Tyson and A. E. Martell, *J. Am. Chem. Soc.*, **90**, 3379 (1968).
15) "Solubilities of Inorganic and Organic Compounds," ed by H. Stephen and T. Stephen, Pergamon, New York (1966), Vol. 1, Part 1, p. 571.
16) D. A. Buckingham, R. C. Gorges, and J. T. Henry, *Aust. J. Chem.*, **20**, 281 (1967).
17) F. Feigl, "Spot Tests in Inorganic Analysis," Elsevier, Lausanne (1954), p. 354.
18) Y. Ohkatsu, T. Osa, and A. Misono, *Bull. Chem. Soc. Jpn.*, **40**, 2116 (1967).

19) R. P. Hanzlik and D. Williamson, *J. Am. Chem. Soc.*, **98**, 6570 (1976).
20) H. Sakamoto, T. Funabiki, and K. Tarama, *J. Catal.*, **48**, 427 (1977).
21) J. R. Harbour, V. Chow, and J. R. Bolton, *Can. J. Chem.*, **52**, 3549 (1974).
22) J. A. Howard and K. U. Ingold, *Can. J. Chem.*, **45**, 785 (1967).
23) F. Basolo, B. M. Hoffman, and J. A. Ibers, *Acc. Chem. Res.*, **8**, 384 (1975).
24) B. Gonzalez, J. Kouba, S. Yee, C. A. Reed, J. F. Kirner, and W. R. Scheidt, *J. Am. Chem. Soc.*, **97**, 3247 (1975).
25) K. Uchida, S. Naito, M. Soma, T. Onishi, and K. Tamaru, *J. Chem. Soc., Chem. Commun.*, **1978**, 217.
26) L. Vaska, L. S. Chen, and W. V. Miller, *J. Am. Chem. Soc.*, **93**, 6671 (1971).

The Oxidation Activity and Acid-Base Properties of Co_3O_4-V_2O_5 and Co_3O_4-MoO_3 Systems

Mamoru Ai

Research Laboratory of Resources Utilization, Tokyo Institute of Technology, 4259 Nagatsuta, Midori-ku, Yokohama 227

(Received November 27, 1978)

The acidity and basicity of Co_3O_4–V_2O_5 and Co_3O_4–MoO_3 systems, with different compositions, were measured by means of the adsorption of NH_3, pyridine, and CO_2. The values of acidity were also confirmed by studying the catalytic activity for acid-catalyzed reactions, such as the dehydration of isopropyl alcohol and the isomerization of 1-butene. With the addition of V_2O_5 or MoO_3, the basicity rapidly decreases and the acidity gradually increases. The catalytic activity for the oxidation of hexane is well correlated with the basicity of the catalysts. With the Co_3O_4-rich catalysts, $V/(Co+V)$ or $Mo/(Co+Mo)<0.4$, butadiene is mainly oxidized to CO_2; the rate is also correlated to the basicity. However, the Co_3O_4-poor catalysts, $V/(Co+V)$ and $Mo/(Co+Mo)>0.6$, show a good selectivity for the maleic anhydride formation. The Co_3O_4-containing catalysts, regardless of the composition, are not effective for the selective oxidation of butene to butadiene. In the oxidation of methanol, the Co_3O_4-rich catalysts give only CO_2. However, with the Co_3O_4-poor catalysts, formaldehyde is almost the sole product. It is concluded that the catalytic behavior is to be interpreted, to a considerable extent, in terms of the acid-base properties of the metal oxides.

Co_3O_4 is a typical metal oxide with an eminent oxidizing power; it is, therefore, employed as a main component of catalysts suitable for the complete combustion of organic compounds. In the preceding paper,[1] we reported on the Co_3O_4-based catalysts modified by controlling the amount of P_2O_5 and K_2O added. It was found that the catalytic activity for the complete oxidation of various types of reactants, such as hexane, butene, phenol, and methanol, was correlated with the basicity of the catalysts.

It is interesting to note that, as a component of mixed-oxide catalysts suitable for certain selective oxidations, Co_3O_4 is also employed.[2] What is the role of Co_3O_4 in the multi-component catalysts?

In this work, Co_3O_4 was combined with an acidic oxide, such as V_2O_5 and MoO_3, which are widely used as the main components of various catalysts suitable for selective oxidation. We attempted to find how the addition of V_2O_5 or MoO_3 to Co_3O_4 modifies the catalytic behavior and to see whether or not the oxidation activity and selectivity for different types of oxidations can be interpreted in terms of the acid-base properties of the composite oxides.

Experimental

The catalysts used in this study were two series of binary oxides, Co_3O_4–V_2O_5 and Co_3O_4–MoO_3, with different compositions. As the starting materials, $Co(NO_3)_2 \cdot 6H_2O$, NH_4VO_3, and $(NH_4)_6Mo_7O_{24} \cdot 4H_2O$ were used. They were prepared by the procedures described in the preceding paper.[1]

The acidity and the basicity of the catalysts were determined by studying the adsorption of basic and acidic molecules, such as NH_3, pyridine, and CO_2, from the gas phase using either the static or pulse method. The technique of the measurements has also been described previously.[1,3-6]

The vapor-phase oxidation of 1-butene, butadiene, hexane, and methanol, the isomerization of 1-butene, and the dehydration of isopropyl alcohol (IPA) were carried out in an ordinary continuous-flow reaction system. The reactor and the experimental procedures were the same as those employed in earlier works.[1,3-7]

Results

Surface Areas. The effect of the V_2O_5 and MoO_3 content on the specific surface area was first checked by the BET method using nitrogen at −196 °C. The results are shown in Table 1. The surface area increases gradually with the addition of V_2O_5 or MoO_3 and reaches a broad maximum when the amount of the second components is about 10 at %.

Table 1. Surface areas of the Co_3O_4–V_2O_5 and Co_3O_4–MoO_3 catalysts used

Composition $V/(Co+V)$	Surface area (m^2/g)	Composition $Mo/(Co+Mo)$	Surface area (m^2/g)
0	4.0	0	4.0
0.01	4.9	0.01	6.3
0.02	5.7	0.02	7.2
0.04	6.3	0.04	8.8
0.07	7.3	0.06	8.7
0.10	9.6	0.08	8.2
0.15	8.3	0.10	10.7
0.20	8.0	0.15	8.8
0.30	7.6	0.20	8.6
0.50	6.6	0.30	8.3
0.70	3.8	0.40	6.3
0.80	4.7	0.50	4.7
0.90	3.7	0.60	3.6
1.00	3.2	0.70	4.0
		0.80	3.2

Acidity. Since pure Co_3O_4 has a fair amount of acidic sites, probably of a weak acid strength compared with those of V_2O_5 and MoO_3, NH_3 was adsorbed on the Co_3O_4-rich catalysts to the same extent as on the V_2O_5- and MoO_3-rich catalysts, even at 175 °C. At higher temperatures, the decomposition of NH_3 was enhanced because of the eminent oxidizing power of Co_3O_4. Therefore, it seems difficult to measure the acidity by means of the NH_3 adsorption.

Therefore, another attempt was made to determine the acidity; that is, the amount of pyridine required to poison the isomerization activity for 1-butene was measured by the pulse method in the same way as in earlier studies.[3–5,7] A difficulty arose in this method, too, especially in the case of the Co_3O_4-rich catalysts, because they exhibit a very low isomerization activity; moreover, they oxidize the adsorbed pyridine at high temperatures. The results are shown in Figs. 1 and 2.

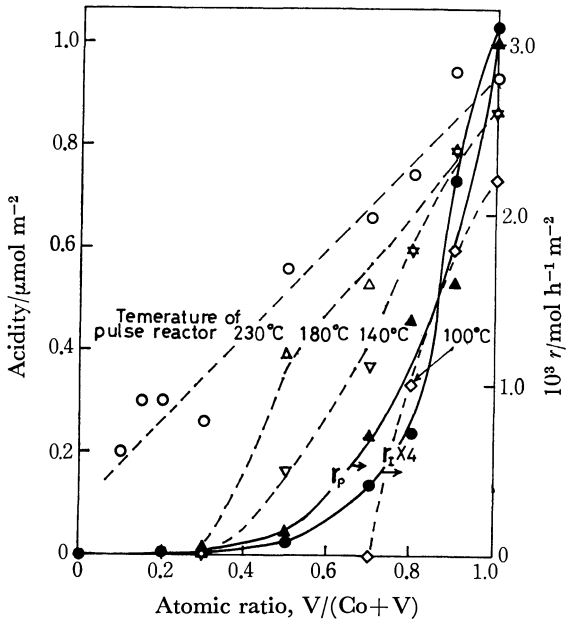

Fig. 1. Acidity of Co_3O_4–V_2O_5 as a function of the V_2O_5 content. Amount of pyridine required to poison the isomerization of 1-butene (pulse method): broken line, dehydration activity for IPA at 187 °C (r_p): ▲, isomerization activity for 1-butene at 260 °C (r_I): ●.

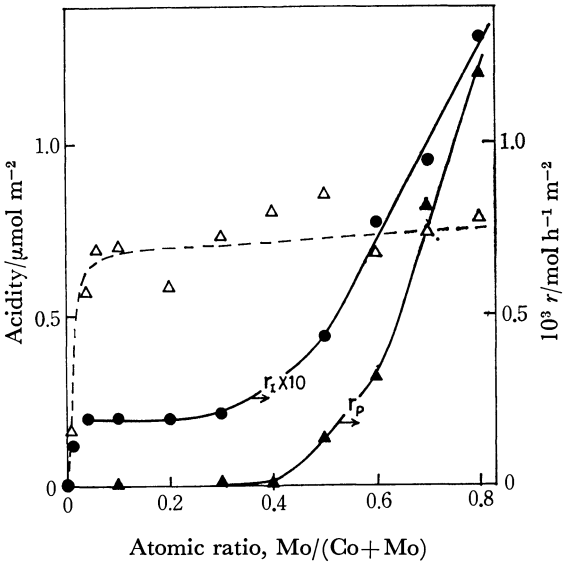

Fig. 2. Acidity of Co_3O_4–MoO_3 as a function of the MoO_3 content. Amount of pyridine required to poison the isomerization of 1-butene at 175 °C (pulse method): △, broken line, dehydration activity for IPA at 187 °C (r_p): ▲, isomerization activity for 1-butene at 272 °C (r_I): ●.

In order to confirm the values of the acidity, the catalytic activity for certain acid-catalyzed reactions was investigated. The dehydration of IPA to propylene and the isomerization of 1-butene to 2-butenes, in the presence of an excess of air, were chosen as the model reactions.[3–5,7] The reactions were carried out at the IPA and butene concentrations of 1.33 and 1.0 mol % in air, and at the total flow rate of 1.0 l/min, by changing the amount of catalyst in the range from 1 to 20 g. The initial rate of IPA dehydration at 187 °C, r_p, and that of butene isomerization at 260 or 272 °C, r_I (mol h^{-1} m^{-2} of catalyst), are plotted together with the values of acidity, in Figs. 1 and 2.

Basicity. The basicity of the Co_3O_4-containing catalysts, as determined by the amounts of CO_2 irreversibly adsorbed at 20 °C, is plotted in Fig. 3.

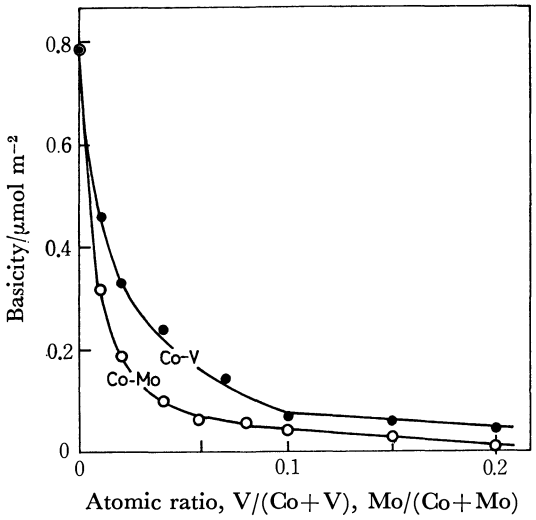

Fig. 3. Basicity of Co_3O_4–V_2O_5 and Co_3O_4–MoO_3 as a function of the V_2O_5 or MoO_3 content. Irreversible adsorption of CO_2 at 20 °C (static method).

Oxidation of Hexane. Alkanes and hydrogen act upon metal-oxide catalysts more or less as electron-donating reagents. However, this tendency might be so weak that the activity for the combustion of these compounds is really governed by the intrinsic oxidation activity rather than by the activation of the reactant molecules.[1,3,8] For convenience in the experimental procedures, combustion of hexane was chosen as a model reaction which reflects the intrinsic oxidation activity of the catalysts.

The reaction was carried out keeping the following conditions constant at T=262 °C; hexane=0.6 mol % in air, and total flow rate=1.0 l/min, while the amounts of the catalysts were varied in the range from 1 to 20 g to achieve a proper conversion. The main product was CO_2. The initial rate of CO_2 formation, r_{CO_2}(mol h^{-1} m^{-2} of catalyst), was measured with each catalyst as an index of the activity. The results are plotted as a function of the basicity of the catalysts in Fig. 4. A fairly good correlation is obtained between the activity and the basicity.

Oxidation of Butadiene. As a model reaction of "acid-formation" reactions, the oxidation of butadiene

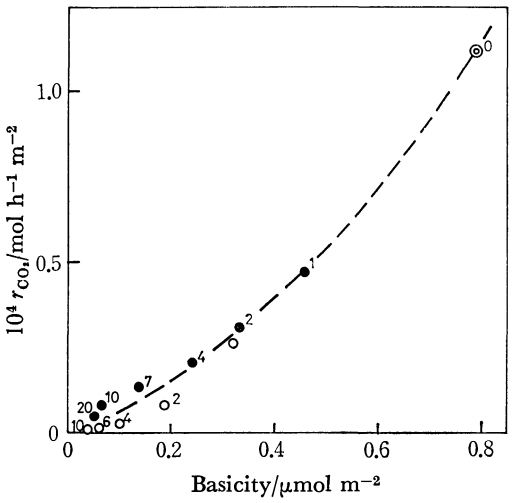

Fig. 4. Relation between the basicity and the oxidation activity for hexane. Co_3O_4–V_2O_5: ●, Co_3O_4–MoO_3: ○. r_{CO_2}: rate of CO_2 formation at T=262 °C and hexane=0.6 mol % in air. Numbers correspond to the content (atomic percent) of V_2O_5 or MoO_3 in the binary oxides.

to maleic anhydride was chosen in the same way as in the previous studies.[3-5,7] The reaction was carried out in the temperature range from 250 to 480 °C, at the butadiene concentration of 1.0 mol % in air, and with a total flow rate of 1.0 l/min, by changing the amounts of the catalysts from 1 to 20 g. The Co_3O_4-rich catalysts, V/(Co+V) and Mo/(Co+Mo)<0.4, were very active. However, the main product was CO_2, and the amount of CO were far lower than those of CO_2. The maleic anhydride, acetic acid, and the other compounds were formed in negligibly small amounts. The initial rates of CO_2 formation at 255 °C for the Co_3O_4–V_2O_5 and at 275 °C for the Co_3O_4–MoO_3, r_{CO_2}(mol/h·m^2 of catalyst), are plotted as a function of the basicity of the catalysts in Fig. 5.

On the other hand, the Co_3O_4-poor catalysts, V(Co+V) and Mo/(Co+Mo)>0.6, were fairly inactive compared with the Co_3O_4-rich catalysts. However, they were selective in forming acidic products. The selectivity to maleic anhydride at a fixed conversion, 50 to 60%, is shown in Fig. 6.

Oxidation of 1-Butene. As a model of the "base-formation" reactions, the oxidation of butene to

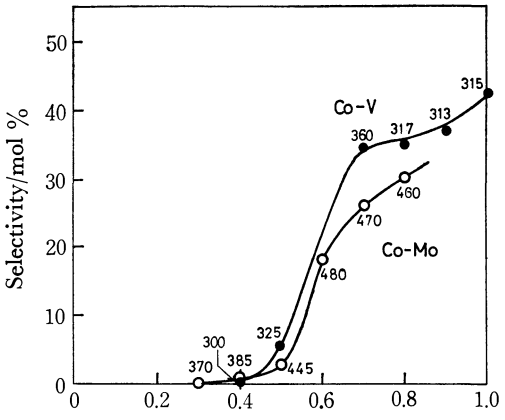

Fig. 6. Selectivity of butadiene to maleic anhydride as a function of the catalyst composition. Co_3O_4–V_2O_5: ●, Co_3O_4–MoO_3: ○. Conversion=50—60%, butadiene=1.0 mol % in air. Numbers correspond to the reaction temperatures (°C).

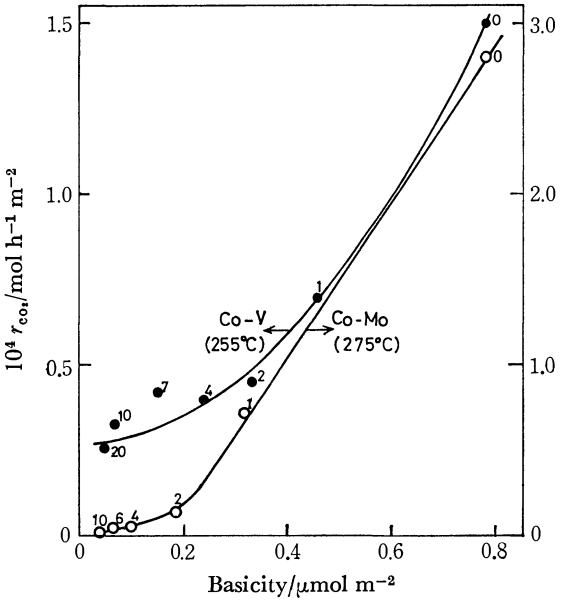

Fig. 5. Relation between the basicity and the activity for the oxidation of butadiene to CO_2. Co_3O_4–V_2O_5 (255 °C): ●, Co_3O_4–MoO_3 (275 °C): ○. Butadiene =1.0 mol% in air. Numbers correspond to the content (atomic percent) of V_2O_5 or MoO_3.

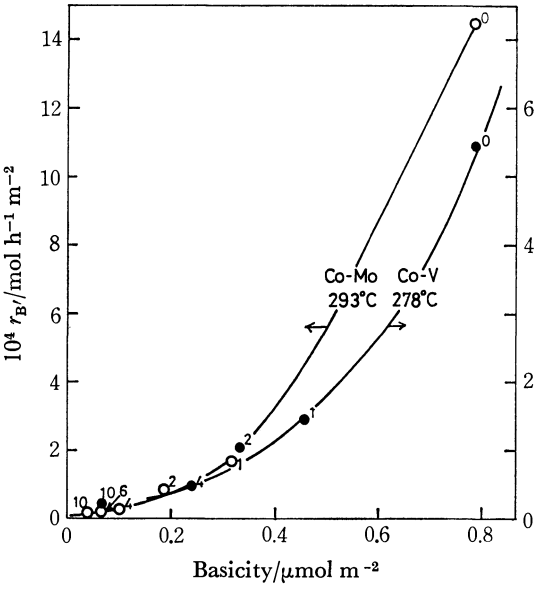

Fig. 7. Relation between the basicity and the activity for the oxidation of 1-butene to butadiene. Co_3O_4–V_2O_5 (278 °C): ●, Co_3O_4–MoO_3 (298 °C): ○. Concentration: 1-butene–oxygen–nitrogen=1.0–1.0–98.0 mol %. Numbers correspond to the content (atomic percent) of V_2O_5 or MoO_3.

butadiene was investigated.[3-5,7] The reaction was carried out in the temperature range from 270 to 420 °C, keeping the conditions constant at the concentrations of 1-butene, oxygen, and nitrogen of 1.0, 1.0, and 98.0 mol % respectively, and at the total flow rate of 1.0 l/min, while the amounts of the catalysts were varied in the range from 1 to 20 g. The main products were butadiene, CO_2, and CO; the amounts of the other products were very small.

The initial rates of butadiene formation at 278 °C for the Co_3O_4–V_2O_5 and at 293 °C for the Co_3O_4–MoO_3, r_β' (mol h^{-1} m^{-2} of catalyst) are plotted as a function of the basicity of the catalysts in Fig. 7. The selectivity to butadiene is shown in Fig. 8.

Oxidation of Methanol. Since it has been found that the catalytic activity and selectivity in the oxidation of methanol can be interpreted in terms of the acid-base properties of the catalysts,[9] the catalytic behavior of the Co_3O_4-containing catalysts for methanol oxidation was investigated.

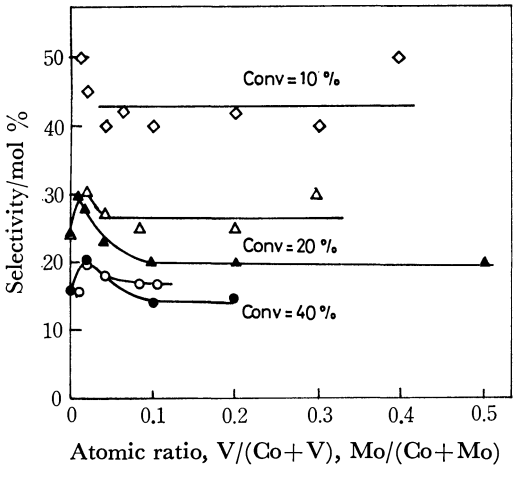

Fig. 8. Selectivity of 1-butene to butadiene as a function of the catalyst composition. Co_3O_4–V_2O_5: ▲ ●, Co_3O_4–MoO_3: ◇ △ ○. T=270—420 °C.

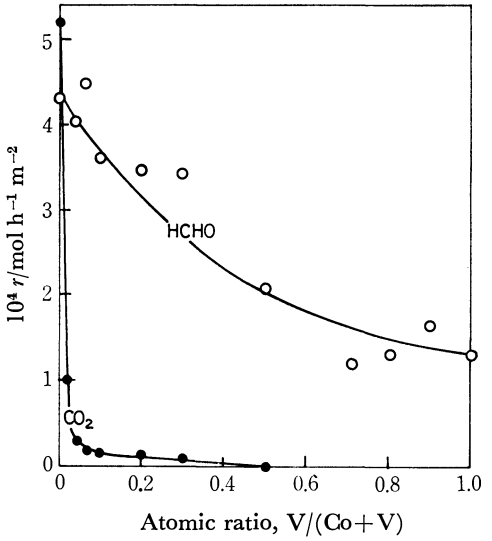

Fig. 9. Activity of Co_3O_4–V_2O_5 for the oxidation of methanol. Formaldehyde: ○, CO_2: ●. T=193 °C, methanol=2.6 mol % in air.

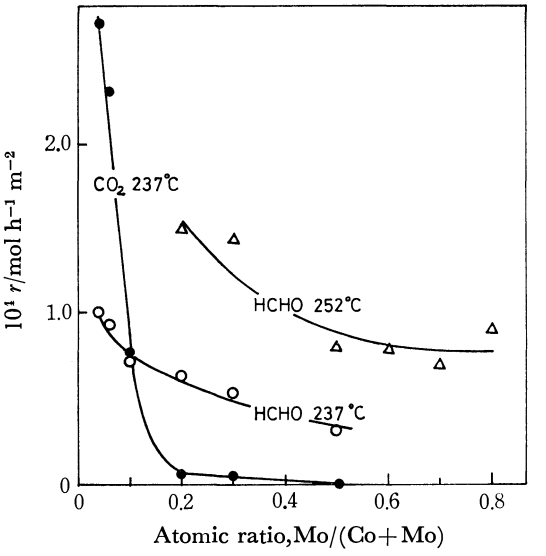

Fig. 10. Activity of Co_3O_4–MoO_3 for the oxidation of methanol. Formaldehyde: ○ △, CO_2: ●. Methanol =2.6 mol % in air.

The reaction was carried out at 193 °C for the Co_3O_4–V_2O_5 and at 237 and 252 °C for the Co_3O_4–MoO_3. The methanol concentration was 2.6 mol % in air, the total flow rate was 1.0 l/min, and the amounts of the catalysts used were from 1 to 20 g. The main products were formaldehyde and CO_2, and the amounts of the other products were very small. The initial rates of formaldehyde and CO_2 formation, r_F and r_{CO_2} (mol h^{-1} m^{-2} of catalyst), were measured following the principle of the differential reactor. The results are shown in Figs. 9 and 10.

Discussion

In the case of the Co_3O_4–V_2O_5 catalysts, the catalytic activities for the two acid-catalyzed reactions varied in the same direction as do the values of acidity (Fig. 1). We would like here to advance the theory that the amounts of pyridine required to poison the isomerization at different temperatures reflect the numbers of acidic sites with different acid-strengths; that is, the activity at a low temperature corresponds to the number of acidic sites of a strong acid-strength. According to the theory, it may be supposed from Fig. 1 that the V_2O_5 or V_2O_5-rich catalysts have stronger acidic sites than do the Co_3O_4-rich catalysts.

In the case of the Co_3O_4–MoO_3 system, however, a large discrepancy in the shape of curves is observed between the acidity and the activities for the acid-catalyzed reactions. Taking into consideration the fact that, because of the low isomerization activity, reliable data cannot be obtained even by the pulse method, especially in the Co_3O_4-rich catalysts, it is believed that the catalytic activities reflect the true acidity better than the amounts of pyridine. That is, the acidity of the Co_3O_4–MoO_3 increases steadily with an increase in the MoO_3, as in the case of the Co_3O_4–V_2O_5 system.

From the results shown in Figs. 1—3 and the above consideration, the following arguments may be put forward. The generation of marked acidic or basic properties is not observed upon the combination of Co_3O_4 with V_2O_5 or MoO_3. As can easily be expected from the acidic nature of V_2O_5 and MoO_3, the basicity of Co_3O_4 is extinguished rapidly with a small amount of these additives. In contrast, the acidity increases steadily with the content of the acidic oxides; in other words, the acidity of the acidic oxides is rapidly extinguished by combination with a basic oxide such as Co_3O_4.

The results shown in Fig. 4 indicate that the activity for hexane oxidation is independent of the acidity of the catalyst and is dependent on the basicity. This finding is in line with the results obtained from the Co_3O_4–P_2O_5 and Co_3O_4–K_2O systems.[1]

The results shown in Figs. 5 and 7 indicate that, even for the oxidation of olefins, the activity of the Co_3O_4-rich catalysts is correlated with the basicity rather than with the acidity of the catalysts. With regard to this finding, we would make the following proposal.

As has been proposed in the previous studies,[1,5,7] the oxidation activity is governed generally by three functions; (i) the activation of olefin by acidic sites; (ii) the activation of gaseous oxygen, which is connected with the basic character, and (iii) the oxidizing power of the surface oxygen species. The Co_3O_4-rich catalysts are poor in the acidic property; consequently, their ability to activate olefin is low, and, moreover, they have an extremely high oxidizing power. Possibly, a sufficient activation of the olefin by acidic sites is not a necessary condition for the oxidation and the reaction is mainly decided by the (ii) function and the (iii) function. This is the reason why the oxidation activity for olefin is correlated with the basicity.

On the other hand, the results in Fig. 6 indicate that the Co_3O_4-poor catalysts are effective for the "acid-formation-type" oxidation. This finding is also in line with the results obtained with other V_2O_5- and MoO_3-based catalysts and supports the proposal that a requirement for an effective catalyst for "acid-formation" reaction is the possession of a sufficient acidic property.[1,3–5,7]

With regard to the oxidation of butene to butadiene, both the Co_3O_4–V_2O_5 and Co_3O_4–MoO_3 are not effective over a full range of compositions. To explain the results, the following consideration is envisaged as a possibility. When the contents of V_2O_5 or MoO_3 are low, the oxidizing power is so strong that the reaction without the activation of butene on acidic sites takes place non-selectively. On the other hand, when the content of V_2O_5 or MoO_3 are high, the oxidizing power is highly suppressed; this is surely one of the necessary conditions for any type of selective-oxidation catalyst. However, another condition is also required for an effective catalyst for the "base-formation-type" oxidation; that is, the possession of a moderate character both in the acid and the base is required for the butadiene formation.[1,3–5] The V_2O_5- and MoO_3-rich catalysts are too acidic to be satisfactory for this type of oxidation.

Actually, the Co_3O_4-containing catalysts are proposed as catalysts suited only for "acid-formation" reactions such as the synthesis of acrylic acid[2,10] and of methacrylic acid.[2]

As for the oxidation of methanol, the activity to form CO_2 (Figs. 9 and 10) varies in the same fashion as does the basicity (Fig. 3). This finding supports the view that the CO_2 formation is catalyzed by the basic sites.[9] However, it seems difficult to explain the activity for formaldehyde formation merely by the acidity, as in the previous study.[9] At any event, it is also true in the case of the Co_3O_4-containing catalysts that formaldehyde is the sole product as long as the catalysts are acidic enough and that the selectivity to formaldehyde decreases, and that of of CO_2 increases, with an increase in the basic properties.[9]

It can be concluded that the acidic and basic properties of the Co_3O_4-containing mixed oxides are modified, as can be expected from the acidic nature of the additives, and that the catalytic behavior in oxidation is to be interpreted, to a considerable extent, in terms of the acid-base properties.

References

1) M. Ai, *J. Catal.*, **54**, 223 (1978).
2) T. Ohara, *Yuki Gosei Kagaku Kyokai Shi*, **29**, 52 (1971); *Shokubai*, **19**, 157 (1977).
3) M. Ai and T. Ikawa, *J. Catal.*, **40**, 203 (1975).
4) M. Ai, *J. Catal.*, **40**, 318 (1975).
5) M. Ai, *Bull. Chem. Soc. Jpn.*, **49**, 1328 (1976).
6) M. Ai, *J. Catal.*, **50**, 291 (1977).
7) M. Ai, *J. Catal.*, **52**, 16 (1978).
8) W. M. H. Sachtler and N. H. de Boer, *Proc. 3rd Intern. Congr. Catal.*, Amsterdam, 1964, **1**, 252 (1965).
9) M. Ai, *J. Catal.*, **54**, 426 (1978).
10) D. J. Hucknall, "Selective Oxidation of Hydrocarbons," Academic Press, London/New York (1974), pp. 47—51.

Photooxygenation Product of Dibenzo[*a,j*]perylene

Takashi KAJIWARA, Shoji FUJISAWA,* Koichi OHNO,** and Yoshiya HARADA**

Department of Chemistry, Faculty of Science, Toho University, Funabashi-shi, Chiba 274

***Department of Chemistry, College of General Education, The University of Tokyo, Komaba, Meguro-ku, Tokyo 153*

(Received November 28, 1978)

The photooxygenation of dibenzo[*a,j*]perylene by visible light irradiation was studied spectroscopically. The structure of unstable photooxygenation product was deduced from spectroscopic data and results of MO calculations to be as 8,12b-endoperoxide of dibenzo[*a,j*]perylene. This endoperoxide released oxygen gradually at room temperature, recovering the original hydrocarbon. The activation energy for this dark reaction was determined to be 21.4±0.5 kcal/mol in benzene and 22.6±0.5 kcal/mol in ethanol.

Reactions of excited aromatic hydrocarbons with molecular oxygen have been extensively studied in relation to the properties of singlet oxygen and quenching of excited singlet or triplet states.[1] However, the mode of reaction is by no means simple and investigations have been concentrated on rather small molecules as anthracene and 9,10-diphenylanthracene. Rubrene may be the only medium size aromatic hydrocarbon which received detailed and sufficiently unambiguous investigations.[2] Helianthrene (dibenzo[*a,o*]perylene) and its derivatives have also attracted the interest of several authors but the structures of their photooxygenation products have yet to be determined by further investigations.[2]

In the course of the syntheses and the study of photoconductive properties of aromatic hydrocarbons,[3] we observed that dibenzo[*a,j*]perylene, a structural isomer of helianthrene, underwent a typical photochemical reaction in organic solvents like benzene and ethanol. This phenomenon had already been reported by Clar[4] and could be interpreted as photooxygenation reaction like those of helianthrene and its derivatives. We have further investigated this reaction and the properties of the rather unstable oxygenation product because Clar's report was not much more than mere observation and also because photooxygenation process might possibly be related to the photoconductive properties of evaporated thin films or crystals of similar aromatic hydrocarbons.

Experimental

Synthesis of Dibenzo[a, j]*perylene.* Dibenzo[*a,j*]perylene was synthesized by almost the same method as Clar's.[4] 1-Chloroanthrone (mp 138 °C) was boiled and stirred with zinc chloride in pyridine at 200 °C for 20 h. Then it was treated with sodium dithionite to give dibenzo[*a, j*]perylene-3,9-dione. The dibenzoperylenequinone was boiled with zinc dust in pyridine, and glacial acetic acid was gradually added to the solution, which was then boiled and stirred for 5 h. From the reaction product, dibenzo[*a, j*]perylene was extracted with benzene and was purified by column chromatography with activated alumina. Further purification was carried out by high vacuum sublimation.

Photooxygenation and Related Measurements. Benzene or ethanol solution of dibenzo[*a, j*]perylene in 1 cm rectangular silica cell was irradiated by a 30 W tungsten lamp through a sharp cut off filter, Toshiba VY-50, transparent only for wavelength longer than 500 nm. The spectral change induced by the irradiation was observed with a Shimadzu UV-210 spectrophotometer.

The rate of thermal detachment of oxygen from the photooxygenation product was also observed by the same spectrophotometer, while the temperature of the sample solution was controlled to within ±0.5 °C by a specially designed bronze cell holder and a thermister temperature controller. Benzene and ethanol were used as solvents and temperature was controlled at several points between 40 °C and 75 °C.

The ESR spectrum of *ca.* 10^{-5} mol/l benzene solution of dibenzoperylene[5] was measured with ESR spectrometer NIHON DENSHI JES-PE-3X, before and after visible light irradiation under air pressure of about 0.1 Pa and 100 kPa.

A preliminary measurement of the overall efficiency of the photooxygenation reaction was also performed as follows. Benzene solution of dibenzo[*a,j*]perylene in a 1 cm rectangular silica cell was irradiated with the 556 nm monochromatic light, and the decrease of the hydrocarbon was monitored by the optical density change at 556 nm. The photon flux of the impinging light was measured making use of potassium tris-(oxalato)ferrate(III) actinometer.

It has also been ascertained that singlet molecular oxygen reacts with dibenzo[*a, j*]perylene in its ground state to give the same oxygenation product as that obtained by photooxygenation. The singlet molecular oxygen was produced by adding NaOCl (*ca.* 5% commercial antiseptic solution PURELOX) onto H_2O_2 (35%, Koso Chemical Ltd.), and was immediately introduced, bubbling, into benzene solution of the hydrocarbon, which had previously been placed upon 30% H_2O_2.[6] The concentration of the benzene solution was about 10^{-5} mol/l and its spectra were measured before and after reaction and compared to each other.

Benzene and ethanol were reagent grade and were used without further purification.

Results and Discussion

Benzene or ethanol solution of dibenzo[*a,j*]perylene had been pink color but it changed to brownish color upon irradiation by room light. When the brownish solution was left in the dark at room temperature for a few days, the original color recovered. This phenomenon, which might be said a kind of photo- and thermo-chromism, could be repeated several times, although some percentage of dibenzo[*a,j*]perylene suffered permanent destruction due to some unknown side-reaction.

The absorption spectra of dibenzo[*a,j*]perylene in benzene are shown in Fig. 1. A strong absorption band with a typical vibrational structure is observed in the region between 450 and 600 nm. The region around 330—430 nm (especially 340—390 nm) seemed to be overlapped by some impurity absorption and

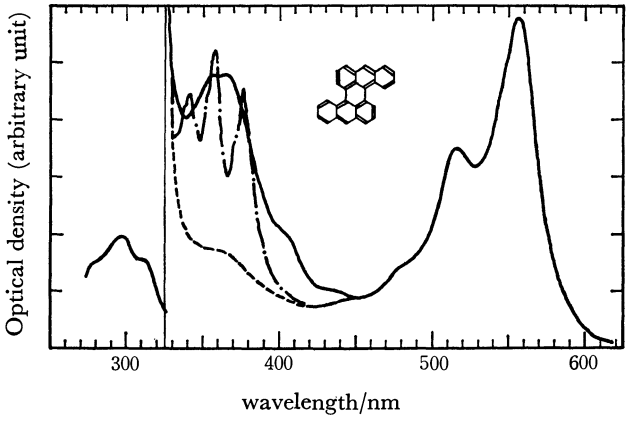

Fig. 1. Absorption spectra of dibenzo[*a*,*j*]perylene in benzene.
—— and -·-·-: Uncorrected spectra of two samples obtained by different purification procedures, ——: corrected spectra.

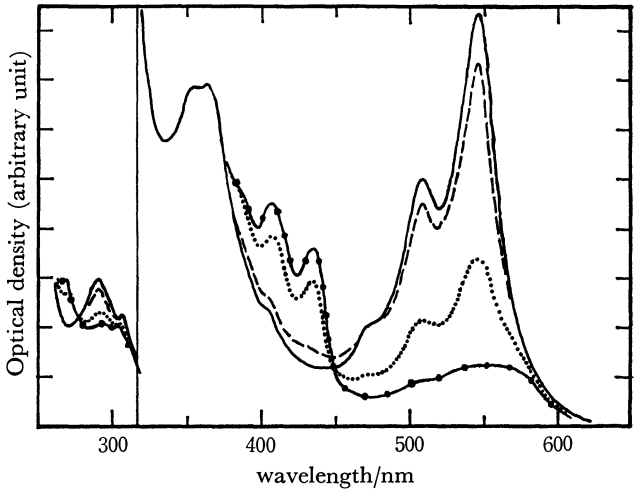

Fig. 2. Change of absorption spectra by visible light irradiation in ethanol.
——: Before irradiation, ·····: after 12 minutes irradiation, ——: after 50 minutes irradiation, -·-·-: left in the dark at room temperature for a day after 50 minutes irradiation.

was different from sample to sample. Repeated purification procedures by column chromatography and high vacuum sublimation could not eliminate completely the impurities responsible to those absorption. The fluorescence excitation spectra of very dilute benzene solution (*ca.* 10^{-7} mol/l) monitored by the fluorescence band shown in Fig. 4 under unaerobic conditions showed a broad and rather weak absorption band around 370 nm. This excitation spectra should resemble to the true absorption spectra. Taking also account of the spectral change during photochemical reaction, which will be described later, we deduced the true spectral shape in this region and showed it in Fig. 1.† Fortunately, there was only little change in this region of spectra during the photooxygenation and thermal deoxygenations. Therefore, we are free from complications due to these impurities in the present study.

When irradiated by a tungsten lamp through a sharp cut off filter, Toshiba VY-50, the spectra of ethanol solution changed as shown in Fig. 2. We could observe an isosbestic point near 455 nm. It is also illustrated in this figure that the solution regained about 85% intensity of original spectra after keeping it about a day in the dark at room temperature. We could observe the same spectral change also for benzene solution. A small deviation of the recovered spectra from the isosbestic point indicates that a small fraction of dibenzo[*a*,*j*]perylene was permanently destroyed. By a careful treatment up to 95% intensity could be recovered both in benzene and ethanol. The spectral change above mentioned did not occur when the solution was evacuated to about 0.1 Pa as was expected.

The following two types of reaction paths can be proposed for this type of photooxygenation reaction.

(1) $A(Ground) + h\nu \longrightarrow A^*(Singlet)$
$A^*(S) \longrightarrow A^*(Triplet)$
$A^*(T) + O_2(G, {}^3\Sigma_g^-) \longrightarrow AO_2$

(2) $A(G) + h\nu \longrightarrow A^*(S)$
$A^*(S) \longrightarrow A^*(T)$
$A^*(T) + O_2(G, {}^3\Sigma_g^-) \longrightarrow A(G) + O_2(S, {}^1\Delta_g)$
$A(G) + O_2(S, {}^1\Delta_g) \xrightarrow{k} AO_2$

We could observe that the rate of photobleaching of dibenzo[*a*,*j*]perylene was much faster in CCl_4 than in benzene. Because it has been reported that the lifetime of $^1\Delta_g O_2$ in CCl_4 is 700 μs, and is much longer than in benzene (lifetime 24 μs),[9] this observation suggests the participation of singlet oxygen. Furthermore, a similar spectral change was observed, when the benzene solution of dibenzo[*a*,*j*]perylene was treated under dark with singlet molecular oxygen as has been described in the experimental section. It should be also mentioned that A (Ground)$+O_2(^1\Delta_g)$ correlates with the ground state of the product AO_2 exothermically and $A^*(T)+O_2$ (G, $^3\Sigma_g$) can only correlate with the excited state of AO_2 endothermically[10] (see Fig. 6). These observations and consideration lead to the conclusion that the type (2) is the appropriate reaction. Also it is reasonable to assign the new band between 370 and 450 nm to some sort of endoperoxide as is usually obtained or assumed in cases of similar reactions of other aromatic hydrocarbons.[2,4] We can assume several possible structures for the endoperoxide as shown in Fig. 3.

† The spectrum of helianthrene reported by Clar (p. 49, Ref. 5) was quite similar to that of our dibenzo[*a*, *j*]perylene, which implied that we synthesized helianthrene instead of dibenzo[*a*, *j*]perylene through some error. Brockmann and Mühlmann have reported different absorption maxima of helianthrene,[7] but they didn't give the whole spectra. We ascertained that our hydrocarbon could not be helianthrene because the intermediate quinone, which we used for dibenzo-[*a*, *j*]perylene synthesis, did not give bisanthene-3,10-dione by photochemical reaction in pyridine under unaerobic condition. Helianthrene quinone, which is an inevitable intermediate for helianthrene synthesis, should give bisanthene-3,10-dione by such a reaction.[8]

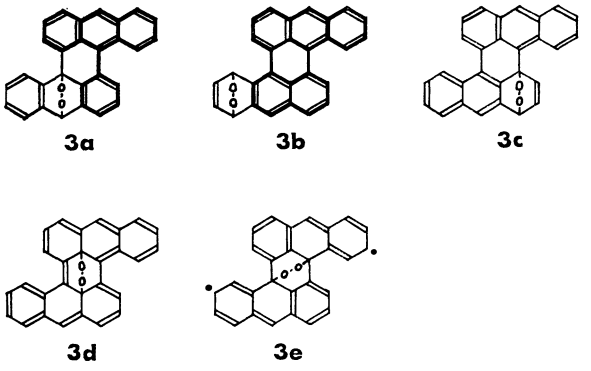

Fig. 3. Possible structures of photooxygenation products of dibenzo[a,j]perylene.
a: 9-Phenylanthracene type structure (8,12b-endoperoxide), **b**: benzo[a]perylene type structure (9,12-endoperoxide).

A biradical form similar to the structure **3e** in Fig. 3 was proposed for the thermochromic form of $\Delta^{10,10'}$-bianthrone by Woodward and Wasserman.[11] We performed ESR measurement as described before but it didn't show any increase of ESR signal that could be attributed to the formation of any kind of biradical endoperoxide. Thus we can disregard the structure **3e**.

In order to select the most probable structure out of **3a**—**3d**, we carried out MO calculations. Table 1 shows the calculated self-polarizabilities for all carbon sites of dibenzo[a,j]perylene.

In view of the structures of similar hydrocarbons, tetrabenzo[*a,cd,j,lm*]perylene[12] and dibenzo[*jk,uv*]-dinaphtho[2,1,8,7-*defg*: 2′,1′,8′,7′-*opqr*]pentacene,[13] dibenzo[a,j]perylene must have a non-planar structure due to the steric hindrances of two pairs of hydrogen atoms, the mean angle between two anthracene skeleton planes being about 30° (see Fig. 6a). However, we assumed a planar structure for the present MO calculations to avoid less important but cumbersome problems. Since the qualitative or semiquantitative features of π-electron systems are not very sensitive to these moderate deviations from planarity. The present calculation based on the planarity approximation seems to be sufficient for our purpose to select the appropriate structure of photooxygenation product. The calculated results indicate that the structure **3a** is the most probable one because the sum of two self-polarizabilities corresponding to this structure is larger than the pair self-polarizabilities corresponding to the other structures. Thus we may be able to disregard **3c**, **3d**, and **3e** from the possible structures of the endoperoxide.

Table 1. Self-polarizabilities (πrr) of dibenzo[a,j]perylene

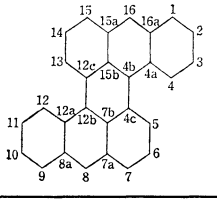

Position	πrr	Fr	Position	πrr	Fr
1, 9	0.461	0.462	4c, 12c	0.355	0.140
2, 10	0.406	0.405	5, 13	0.491	0.473
3, 11	0.421	0.415	6, 14	0.400	0.397
4, 12	0.438	0.446	7, 15	0.509	0.484
4a, 12a	0.355	0.143	7a, 15a	0.330	0.102
4b, 12b	0.395	0.188	8, 16	0.604	0.544
7b, 15b	0.354	0.152	8a, 16a	0.329	0.102

Pair positions	Sum of πrr's	Corresponding endoperoxide in Fig. 3
8+12b(16+4b)	0.999	**3a**
1+4(9+12)	0.899	**3b**
7+4c(15+12c)	0.864	**3c**
7b+15b	0.708	**3d**

It may be of some interest to note that although the sums of self-polarizabilities of para-positions corresponding to the structures **3a**, **3b**, and **3c** (0.999, 0.899, and 0.864, respectively) are similar to the corresponding values of anthracene (1.052 for 9,10-positions and 0.908 for 1,4-positions), the value of the self-polarizability of the 8-(and 16-) position of dibenzo[a,j]perylene, 0.604, is much larger than that for the 9-position of anthracene (0.526) and even larger than the value, 0.601, of the very reactive 6-(and 13-) position of pentacene. This may be the reason why dibenzo[a,j]-perylene is so liable to react with singlet oxygen. The calculated values of free valence, which are given in Table 3, also suggest that 8-(and 16-) position is very reactive.

Thus we presume that the course of the reaction is as follows.

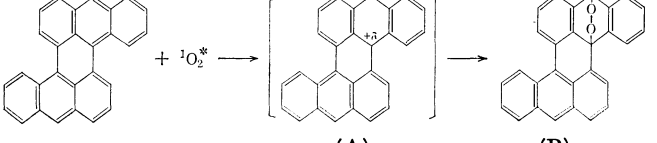

The second step from (A) to (B) should be very fast because of the enhanced density of reacting electron as a result of the first step reaction.

Further, we tried to see if the observed spectra of the photooxygenation product is compatible with this structure. Because of the high sensitivity of dibenzo-[a,j]perylene to light and the instability of its photo-oxygenation product, it was difficult to obtain its correct spectra by a single run of the experiment. Figure 4 shows the spectrum composed of several experimental data.

The spectrum has some ambiguity in two regions. First, we could not completely bleach the region longer than 450 nm because the thermal decomposition of the oxygenation product brought about the reverse reaction and furthermore because the oxygenation product was also gradually decomposed, probably by further photochemical reaction,[7] to give some unknown final product which had a long absorption tail in this region. But it is certain that there is at most only

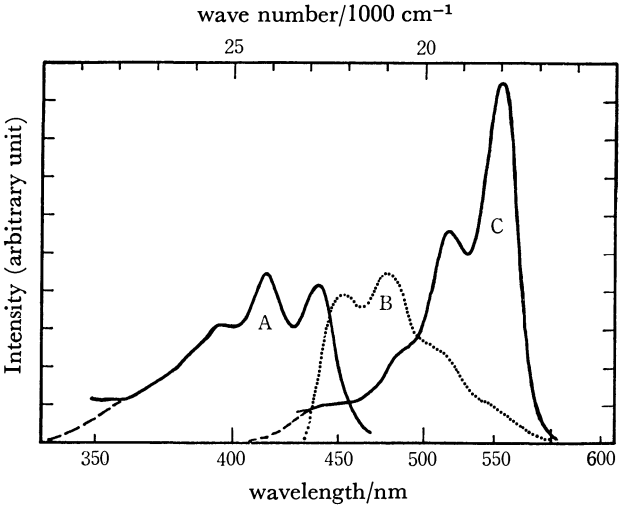

Fig. 4. Absorption and fluorescence spectra of photooxygenation product.
A: Corrected absorption spectra, benzene solution, B: fluorescence spectra, benzene solution, C: absorption spectra of dibenzo[*a*,*j*]perylene, the concentration of which is the same as A.

very weak absorption in this region, which can not be assigned to any allowed transitions. Another evidence to assure that the endoperoxide has no allowed absorption band in the region longer than 450 nm is that a fluorescence spectrum, which shows a good mirror image relation with the new absorption band between 380 and 450 nm, was observed for the partly photobleached benzene solution of dibenzo[*a*,*j*]perylene (Fig. 4).

Since the absorption bands in the long wavelength region of the spectra of such endoperoxides are considered to be due to π-π^* transitions, we calculated the transition energies for the conjugated π-electron systems as dwawn with thick lines in Fig. 3 on the basis of the P-P-P method. From the consideration of self-polarizabilities and free valences, it is sufficient to consider only the two structures, 8,12b-endoperoxide (**3a**) and 1,4-endoperoxide (**3b**).

The results of the calculation are shown in Table 2. The observed transition energies of benzo[*a*]perylene and 9-phenylanthracene, which have similar π-conjugation systems as those of **3a** and **3b**, respectively, are also shown in Table 2 together with the transition energies of related compounds, dibenzo[*a*,*j*]perylene and perylene. It is well-known that there are many factors that prevent a precise comparison between the observed and calculated results. But the overall correspondence is fairly good as is shown in Table 2.

Firstly, we assume that the structure of the photooxygenation product corresponds to **3b**. Both the calculated results and observed spectra of benzo[*a*]perylene predict that 1,4-endoperoxide (**3b**) should show the longest wavelength absorption band (so-called p-band) near 500 nm (20000 cm^{-1}). This value is rather larger than the observed one for the photooxygenation product, 435 nm. Furthermore, the observed oscillator strength for p-band of the photooxygenation product (about 80% of the p-band of

Table 2a. Electronic transitions for structures depicted in Fig. 3 and related compounds
The energies in wave number (cm^{-1}), and oscillator strength (in parenthesis).

	Calcd[a] 9-Phenylanthracene type structure (Fig. 5a)				Obsd 9-Phenylanthracene[d]	Obsd Photooxygenation product[e]
β^*[b]	−2.38	−2.00	−1.50	−1.00	(small, ≈0)	
θ[c]	0	32.8	50.9	65.1	(≈90°)	(≈60°, see text)[f]
p-Band	20999 (1.02)	21485 (0.98)	22208 (0.91)	23032 (0.84)	25900 (0.15)[g]	22750 (0.86)[h]
α-Band	28278 (0.0)	28539 (0.0)	28883 (0.0)	29221 (0.0)		
	34430 (0.07)	34861 (0.06)	35454 (0.05)	36066 (0.03)		
	35009 (0.14)	35401 (0.14)	35950 (0.14)	36541 (0.13)		
β-Band	36629 (1.00)	37054 (1.05)	37631 (1.13)	38219 (1.22)		
	39766 (1.12)	40058 (1.12)	40436 (1.11)	40795 (1.08)		

a) Approximations for the calculations are as follows. i) The P-P-P method using the electron repulsion integral γ by Nishimoto and Mataga. $\beta = -2.38$ eV. ii) CI among 36 one electron excitation configurations. iii) Regular hexagonal structure with the C–C bond length of 1.397 Å. b) The resonance integral between the 9-carbon atom of the anthracene skeleton and the 1′-carbon of the phenyl group. c) The angle between the phenyl and anthracene skeleton planes, calculated from the approximate relation $\beta^* = \beta\cos\theta$. d) I. B. Berlman, "Handbook of fluorescence spectra of aromatic molecules," 2nd ed, Academic Press, New York (1971), p. 363. e) Present observation, see Fig. 4. f) Obtained by the graphic interpolation of the calculated θ- wave number relations. g) Calculated from the spectra reported in Berlman's book sited in d), based on the relation $f = 4.02 \times 10^{-9} \int \varepsilon \, d\bar{\nu}$. See the footnote**) in the text. h) Calculated from the spectra shown in Fig. 4 as is described in the footnote**) in the text. Almost the same value is obtained by the interpolation of the calculated θ-oscillator strength relation.

Table 2b. Electronic transitions for structures depicted in Fig. 3 and related compounds

Benzo[a] perylene		Dibenzo[a,j]perylene		Perylene	
Calcd[a]	Obsd	Calcd[a]	Obsd[c]	Calcd[a]	Obsd[b]
20830 (p-band) (0.96)	19880	18603 (p-band) (1.07)	18320	24553 (p-band) (1.00)	23000
29187 (α-band) (0.0)	29500	28705 (α-band) (0.0)	27000	30842 (α-band) (0.0)	
29697 (0.0)		34500 (0.20)		41920 (β-band) (1.80)	39600
30120 (0.02)		37333 (β-band) (2.03)	34480		
34560 (0.02)					
37193 (0.50)					
39153 (β-band) (1.34)	36230				
40160 (0.36)					

a) The approximations used for calculations are the same as in Table 2a. b) R. S. Becker, *J. Chem. Phys.*, **38**, 2144 (1963). c) This work and E. Clar, "Aromatic hydrocarbons, Academic Press, New York (1964), Vol. 2, p. 43.

dibenzo[a,j]perylene†† is considerably smaller than the calculated value for the p-band of benzo[a]perylene (about 90% of the p-band of dibenzo[a,j]perylene).

On the other hand, as we can see in Table 2, the calculated transition energy and oscillator strength of the 9-phenylanthracene type structure (corresponding to 8,12b-endoperoxide, **3a**), agree fairly well with the observed ones, if its phenyl plane has a proper angle (about 60°) with the plane of anthracene skeleton.

Of course, these agreements should not be taken too seriously since the adopted model of the molecular structure holds only the minimum characteristics of the endoperoxide and neglects all the finer details belonging to the real endoperoxide molecule and also because of the well-known limitations of MO calculations. Nevertheless all the observed data and calculated results seem to lead to the conclusion that the photooxygenation product of dibenzo[a,j]perylene is 8,12b-endoperoxide.†††

As has been already mentioned, the molecular structure of dibenzo[a,j]perylene should be such as depicted in Fig. 5a.

O_2 may attach this hydrocarbon as illustrated in Fig. 5b; the angle between phenyl (A) plane and the anthracene plane should increase owing to the increased

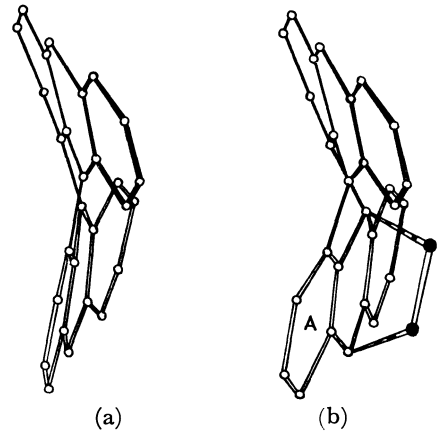

Fig. 5. Possible three dimentional structures of dibenzo-[a,j]perylene and its photooxygenation product (8,12b-endoperoxide). a: Dibenzo[a,j]perylene, b: 8,12b-endoperoxide. ○: Carbon, ●: oxygen.

sp³ nature of the bonds extending from the 8- and 12b-carbon atoms and also owing to the steric hindrance of the H-atoms bonded to the 12- and 13-carbon atoms. Thus we can explain the rather high value of the angle, 60°, that has been predicted from the calculation. This structure also answers the question why a doubly photooxygenated product such as

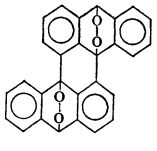

was not obtained, which seems to be quite probable considering the well-known reactivity of 9-phenylanthracene to singlet molecular oxygen. The second molecular oxygen, if attached to the 8,12b-endoperoxide, will introduce intolerable steric hindrance,

†† This value was estimated from the ratio of area under each absorption band shown in Fig. 4, using the following formula

$$f = 4.02 \times 10^{-9} \int \varepsilon d\bar{\nu}$$

where f is the oscillator strength, ε the decadic molar extinction coefficient (l/mol cm), and $\bar{\nu}$ the wave number in cm^{-1}.

††† It is reported that helianthrene is most probably attacked by the singlet oxygen at similar positions.[2]

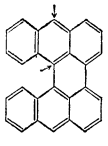

TABLF 3. RATES OF THE OXYGEN DETACHMENT FROM 8,12b-ENDOPEROXIDE OF DIBENZO[*a*,*j*]PERYLENE

T/K	Rate/s^{-1}	
	in benzene	in ethanol
318	3.4×10^{-4}	
323	5.2×10^{-4}	
328	9.0×10^{-4}	
333	1.7×10^{-3}	7.2×10^{-4}
338	2.6×10^{-3}	1.2×10^{-3}
343	4.0×10^{-3}	1.9×10^{-3}
348		3.1×10^{-3}

and the double-photooxygenation product may be unstable and may decompose rapidly.††††

The rate of O_2 detachment from the endoperoxide are shown in Table 3.

The detachment was monitored with the increasing band at 556 nm in benzene (and 546.5 nm in ethanol) of the recovered hydrocarbon and obeyed the first-order reaction scheme fairly well. The rate depends strongly on temperature and its temperature dependence seems to be explained by the existence of an activated transient state. The activation energy was calculated from the data in Table 3 to be 21.4 ± 0.5 kcal/mol in benzene and 22.5 ± 0.5 kcal/mol in ethanol. The frequency factor was also calculated to be 1.9×10^{11} s^{-1} in benzene and 4.9×10^{11} s^{-1} in ethanol, and these values suggest that the O_2-detachment reaction is spin allowed. The activation energy can be explained by the fact that the endoperoxide ground state necessarily correlates endothermically with an excited state of composite system A (Ground State)$+O_2$ ($^1\Delta_g$) owing to spin conservation as is illustrated in Fig. 6. It is interesting that the observed activation energy is almost the same as the energy of the singlet O_2 $^1\Delta_g$ state (22.5 kcal/mol), even if it might be only an accidental coincidence. Thus it may be possible that O_2 is released from the oxygenated hydrocarbon in its $^1\Delta_g$ singlet state,[14] but this must be clarified by further investigation.

Finally, we report a preliminary measurement of the overall efficiency of the present photooxygenation reaction. Though unfortunately, we could not afford to perform detailed measurements of lifetimes of A*(S), A*(T), and $O_2(^1\Delta_g)$ that are necessary to analyse each step of complicated photooxygenation reactions, we measured only the overall quantum efficiency of the photooxygenation upon irradiation of benzene solution by 556 nm under atmospheric pressure. The apparent overall quantum efficiency depended moderately on the concentration of dibenzo[*a*,*j*]perylene. They were *ca.* 1/30 for 7.2×10^{-6} mol/dm^3 and *ca.* 1/45 for 5.6×10^{-6} mol/dm^3. These values were about fifteen times larger than those for rubrene photooxygenation

†††† It has been reported that, similar hydrocarbons, dimethoxyhelianthrene and dibenzoyloxyhelianthrene uptake equimolar molecular oxygen rapidly, but further photooxygenation takes place only very slowly leading to final decomposition products.[7]

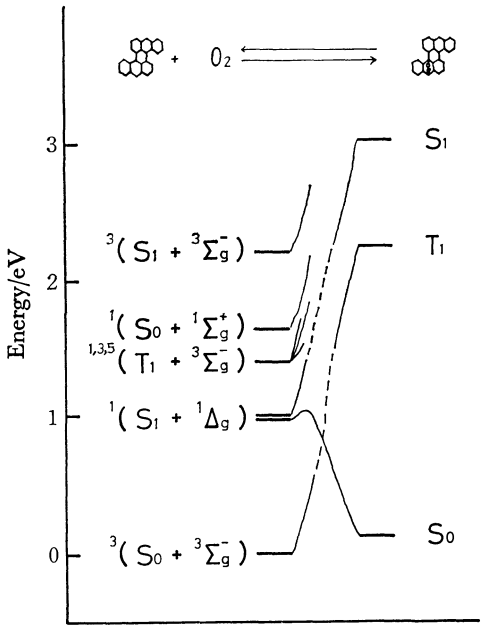

Fig. 6. State correlation diagram depicting the photooxygenation of dibenzo[*a*,*j*]perylene and thermal deoxygenation of the photooxygenation product, 8,12b-endoperoxide. The relative energies of the states were estimated from spectroscopic data and the activation energy for the reaction as is given in the text.

measured under similar conditions, and indicates that sensitized $^1\Delta_gO_2$ production may be quite efficient in this system. Assuming that the efficiency of $^1\Delta_gO_2$ producton by the energy transfer from triplet dibenzo[*a*,*j*]perylene is nearly 100%,[1,2] and using the reported lifetime, 24 μs, of the O_2 $^1\Delta_g$ state in benzene, we obtained 2×10^8 dm^3/mol s^{-1} as a lower limit of k, the rate of the reaction $A(G)+O_2(S, ^1\Delta_g)\longrightarrow AO_2$.

Finally, it might be better to mention that the application of NMR, IR, and X-ray crystallography, which are very powerful methods for structural analysis in many fields of organic chemistry, is presently very difficult for unstable derivatives of large condensed aromatic hydrocarbons.

The authors are grateful to Prof. Ryo Hirasawa of the University of Tokyo for his assistance in ESR measurements and helpful discussion.

References

1) D. R. Kearns, *Chem. Rev.*, **71**, 395 (1971).
2) K. Gollnick, and G. O. Schenck, "1,4-Cycloaddition Reaction," ed by J. Hamer, Academic Press, New York, N. Y. (1967), pp. 255—345; T. Matsuura, "Sanso Sanka Hanno (in Japanese)," Maruzen, Tokyo (1977), pp. 223—280.
3) Y. Kamura, H. Inokuchi, J. Aoki, and S. Fujisawa, *Chem. Phys. Lett.*, **46**, 356 (1977).
4) E. Clar, "Aromatic Hydrocarbons," Academic Press, New York, N. Y. (1964), Vol. 2, pp. 42—45.
5) In this paper, the concentration of dibenzo[*a*,*j*]perylene was estimated from the optical density of the solution. We assumed that the molar extinction coefficient at the absorption maximum (556 nm in benzene and 546 nm in ethanol) was about 10^{-5} l/mol cm, which was estimated from the spectral

shape as shown in Fig. 4 and the calculated oscillator strength as given in Table 2. The corresponding value by Clar is about 3.2×10^{-4} l/mol cm in benzene. The true value may be between these two values.

6) C. S. Foote and Wexler, *J. Am. Chem. Soc.*, **86**, 3879 (1964); T. Kajiwara and D. R. Kearns, *ibid.*, **95**, 5886 (1973).

7) H. Brockmann and R. Muhlmann, *Ber. Bunsenges. Phys. Chem.*, **81**, 467 (1948).

8) H. Brockmann and R. Muhlmann, *Ber. Bunsenges. Phys. Chem.*, **82**, 348 (1948).

9) P. B. Merkel and D. R. Kearns, *J. Am. Chem. Soc.*, **94**, 7244 (1972).

10) A. U. Khan and D. R. Kearns, *J. Chem. Phys.*, **48**, 3272 (1968).

11) R. B. Woodward and E. Wasserman, *J. Am. Chem. Soc.*, **81**, 5007 (1959).

12) Y. Kohno, M. Konno, Y. Saito, and H. Jnokuchi, *Acta Crystallogr., Sect. B*, **31**, 2076 (1975).

13) I. Oonishi, S. Fujisawa, J. Aoki, and T. Danno, *Bull. Chem. Soc. Jpn.*, **51**, 2256 (1978). The conventional name, diphenanthro[5,4,3-*abcd*:5′,4′,3′-*jklm*]perylene, was used in this report. Dibenzo[*ik*,*uv*]dinaphtho[2,1,8,7-*defg*: 2′,1′,8′,7′-*opqr*]-pentacene is the correct IUPAC name of this compound.

14) C. Dufraisse, J. Rigandy, I. I. Basselier, and N. K. Cuong, *C. R. Acad. Sci.*, **260**, 5031 (1965).

The Base-catalyzed Tautomerization of Acetylacetone in Organic Solvents. The Correlation of the Catalytic Coefficient with the Partition Coefficient

Hitoshi WATARAI and Nobuo SUZUKI*

Department of Chemistry, Faculty of Science, Tohoku University, Sendai 980

(Received January 5, 1979)

The keto-enol tautomerization rate of acetylacetone catalyzed by triethylamine or tributylamine was observed in eight organic solvents, and the catalytic coefficient for each process of the ketonization and enolization was obtained. A remarkable solvent effect on the catalysis was discussed following the linear free-energy relationship between the catalytic coefficient and the liquid-liquid partition coefficients of the keto and enol forms. It was concluded that, in the homogeneous base-catalysis, the solvent affects the free-energy change of the transition state more greatly than those of the keto and enol forms. On the contrary, in the heterogeneous catalysis by the silica surface, the free-energy change of the keto and enol forms was suggested to be the main factor governing the kinetic solvent effect.

In the course of our study of the kinetic behavior of acetylacetone, a well-known extractant,[1] in a liquid-liquid partition system, we found that the keto-enol tautomerization rate in an organic phase is very slow and that the addition of a base, such as amine, trialkyl phosphate and trialkylphosphine oxide, which are often used in synergic extractions,[1] remarkably enhances the tautomerization rate in an organic phase. Those catalytic effects strongly depend on the nature of the solvent.

From the standpoint of the transition-state theory,[2] a kinetic solvent effect is thought to be due to the difference in solvent effects on the reactant and on the transition state. Many kinetic studies of the solvent effect, however, have dealt with the solvent effect only on a rate constant, which reflects the free-energy difference between the reactant and the transition state. We think that the experimental resolution of an activation free energy into two parts is more worthwhile than a qualitative and conventional discussion of the relationship between an activation energy and the solvent property. Previously, we reported the utility of a liquid-liquid partition coefficient in evaluating the contribution of the free-energy change of the reactant to the activation free energy.[3,4] In the present study, we will show a further application of the rate-partition approach to the solvent effect on the base-catalyzed tautomerization rate of acetylacetone in organic solvents.

Experimental

Materials. The acetylacetone was used after the distillation of a commercially purchased reagent (Nakarai,G. R.). The triethylamine (TEA) and tributylamine (TBA) used as catalysts were purified by double distillation over sodium and kept in a darkened desiccator. The organic solvents were distilled after drying over sodium or phosphorus pentaoxide. The purity of the amines and the solvents were checked by GLC. Redistilled water was used throughout. The preparation of a nonaqueous solution was carried out in a gloved box desiccated by silica gel.

Kinetic Measurements. Although the keto-enol equilibrium of acetylacetone in an inert solvent is not attained even after one week, the addition of an amine at a concentration of 10^{-3} M (1 M=1 mol dm^{-3}) remarkably accelerates the tautomerization rate. The measurement of the rate of the catalysis has been carried out by means of a Hitachi 356 spectrophotometer at 290 nm for aromatic–solvent systems and at 271 nm, the absorption maximum of acetylacetone, for the other systems. The catalysis was initiated by one of the following two methods, depending on the solvent used: when the enol fraction at equilibrium in a given solvent was below 0.8, the vapor injection method[5] was employed, while in a solvent in which the enol fraction was over 0.8, an alternative method was employed since the vapor injection method does not produce a sufficient absorbance difference between that at the initial time and at equilibrium; *ca.* 1 ml of the pure liquid of acetylacetone was heated for one hour at 100 °C, cooled to room temperature rapidly, and diluted with an organic solvent in a Teflon flask, and then a 50-μl portion of this solution was spiked into 4 ml of the solution of a catalyst in an optical cell which was thermostated with circulating water at 25±0.1 °C. By the heating procedure, the enol fraction of 0.82 at room temperature decreases to 0.66. From the absorbance change, as recorded on a Hitachi 056 recorder, an observed rate constant $k_{obsd}(s^{-1})$ was obtained within an error of ±3%. The rate constants obtained by the two different initiation methods were confirmed to coincide in the benzene system.

It was noted in a preliminary experiment that the surface of the quartz cell acts as an effective catalyst on the tautomerization. The catalytic activity of the surface depends on the solvent and increases in an inert solvent such as hexane. Hence, it was necessary to make the surface inert by treating the cell and all of the volumetric glassware with a 1% benzene solution of dichlorodimethylsilane.[6]

An increase in the TEA concentration up to 0.2 M shows no influence on either the apparent absorption coefficient or on the shape of the spectrum of acetylacetone, so that the amine is confirmed to participate only in a kinetic process as a catalyst in the tautomerization process. The catalytic experiment was carried out in $8—10\times10^{-5}$ M for acetylacetone, in $10^{-5}—10^{-1}$ M for TEA, and in 10^{-5}—0.15 M for TBA.

Equilibrium Measurements. The apparent partition coefficient of acetylacetone (P) between water (10^{-3} M perchloric acid) and heptane, chlorobenzene, or 1,2-dichloroethane was determined spectrophotometrically within a precision of ±3% by the batch method. Similarly, P in the nonaqueous two-phase system of heptane/acetonitrile was determined. Each solvent of heptane and acetonitrile was mutually saturated before the partition experiment, since the mutual solubility is not negligible, it is determined by GLC to be 2.8 wt % acetonitrile in heptane and 10.1 wt % heptane in acetonitrile at 25 °C. The enol fractions of acetylacetone in the organic

solvents were determined within a precision of ±0.01 by the NMR method[7] using a Varian A-60 NMR apparatus at 25 ±1.5 °C.

Results

The Catalytic Coefficients of TEA and TBA. The observed tautomerization rate constant was proportional to the concentration of amine, [B], in all the systems investigated;

$$k_{obsd} = k_B[B] \quad (1)$$

where $k_B(M^{-1}\,s^{-1})$ refers to a catalytic coefficient. Some typical examples of the plot of k_{obsd} *vs.* [B] in heptane and benzene systems are shown in Fig. 1. The slopes of Fig. 1 give the catalytic coefficients. The catalytic coefficients for the eight solvent systems

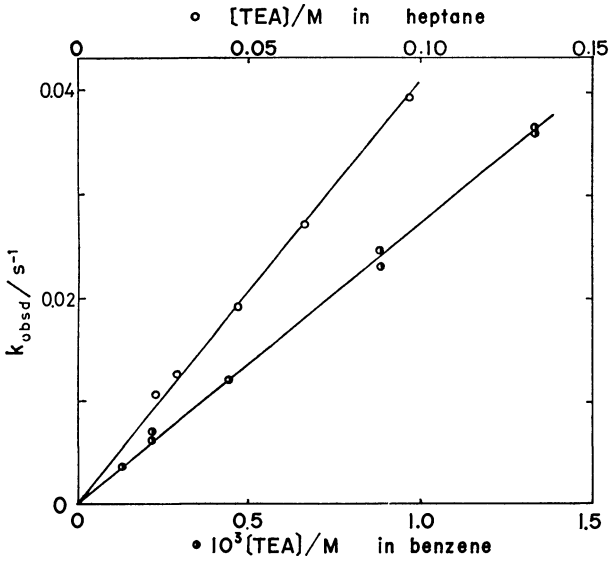

Fig. 1. The effect of TEA on the keto-enol tautomerization rate of acetylacetone in heptane and in benzene.

Table 1. The catalytic coefficients of the amines in relation to the tautomerization rate, the apparent partition coefficients (P) between water and organic solvent, and the enol fraction (f_0) in organic solvents of acetylacetone

No. Solvent	$k_B/M^{-1}\,s^{-1}$ TEA	$k_B/M^{-1}\,s^{-1}$ TBA	P	f_0
1. Heptane	4.17×10^{-1}	2.00×10^{-1}	0.887	0.97
2. Cyclohexane	5.25×10^{-1}	2.37×10^{-1}	1.03[a]	0.95[b]
3. Toluene	2.10×10	3.27	4.57[a]	0.91
4. Benzene	2.73×10	4.22	5.93[a]	0.88
5. Chlorobenzene	8.67×10	1.98×10	5.27	0.91
6. 1,2-Dichloroethane	3.62×10^2	9.83×10	11.5	0.79
7. Dichloromethane	4.42×10^2	1.97×10^2	22.5[a]	0.78
8. Acetonitrile	5.88×10^2	2.02×10^2	7.85[c]	0.60

a) Quoted value; H. Johansson and J. Rydberg, *Acta Chem. Scand.*, **23**, 2797 (1969). b) Quoted value; R. A. Dwek and G. Allen, *J. Chem. Soc., B*, **1966**, 161. c) Estimated value; see text.

are tabulated in Table 1. It appeares that the catalytic coefficient increases with the increase in the dielectric constant of the solvent. TEA is more effective than TBA in every solvent. A linear correlation between the logarithmic values of the catalytic coefficients of TEA and TBA appeared.

The Partition Coefficients and the Enol Fractions. The apparent partition coefficients (P) and the enol fraction (f_0) are listed in Table 1. The partition coefficient in the system of acetonitrile-water was estimated from the results in the systems of heptane/water and heptane/acetonitrile. It appears that the organic solvent with a smaller f_0 shows a larger value of P.

Discussion

Correlation between the Catalytic Coefficient and the Partition Coefficient. The catalytic coefficients for the ketonization ($k_{B,k}$) and the enolization ($k_{B,e}$) were estimated by the following equations, neglecting any spontaneous process:

$$k_{B,k} = (1-f_0)k_B$$
$$k_{B,e} = f_0 k_B \quad (2)$$

The calculated results are listed in Table 2, together with the partition coefficients of the keto (P_K) and enol (P_E) forms of acetylacetone calculated using the values of P, f_0, and the enol fraction in the aqueous phase, f=0.15.[5]

In order to examine the free-energy relationship between the two processes, *i.e.*, the base catalysis in an organic solvent and the transfer of acetylacetone from water to the solvent, log $k_{B,k}$ and log $k_{B,e}$ were plotted against log P_E and log P_K respectively. The results are shown in Figs. 2 and 3. In the catalyses by both TEA and TBA, satisfactory linear correlations are obtained.

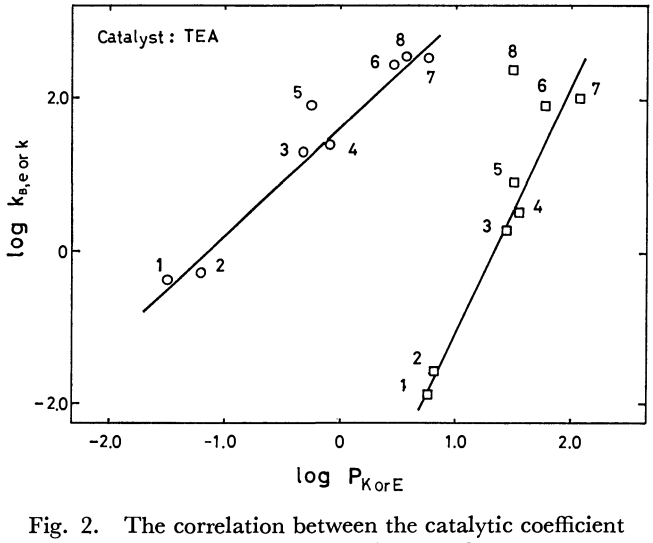

Fig. 2. The correlation between the catalytic coefficient of TEA and the partition coefficient of acetylacetone. The numbers in this figure correspond to those in Table 1.
○: log $k_{B,e}$ *vs.* log P_K, r=0.974; □: log $k_{B,k}$ *vs.* log P_E, r=0.983 except for acetonitrile.

Table 2. The catalytic coefficients in relation to the ketonization ($k_{B,k}$)[a] and enolization ($k_{B,e}$)[a] reactions and the partition coefficients of the keto (P_K) and enol (P_E) forms of acetylacetone at 25 °C

No. Solvent	TEA		TBA		log P_K	log P_E
	log $k_{B,k}$	log $k_{B,e}$	log $k_{B,k}$	log $k_{B,e}$		
1. Heptane	−1.90	−0.39	−2.22	−0.71	−1.51	0.76
2. Cyclohexane	−1.58	−0.30	−1.93	−0.65	−1.21	0.82
3. Toluene	0.28	1.28	−0.53	0.47	−0.32	1.44
4. Benzene	0.52	1.38	−0.30	0.57	−0.08	1.54
5. Chlorobenzene	0.89	1.90	0.25	1.26	−0.25	1.51
6. 1,2-Dichloroethane	1.88	2.46	1.31	1.89	0.46	1.78
7. Dichloromethane	1.99	2.54	1.64	2.19	0.77	2.07
8. Acetonitrile	2.37	2.55	1.91	2.08	0.54	1.47

a) $M^{-1}s^{-1}$.

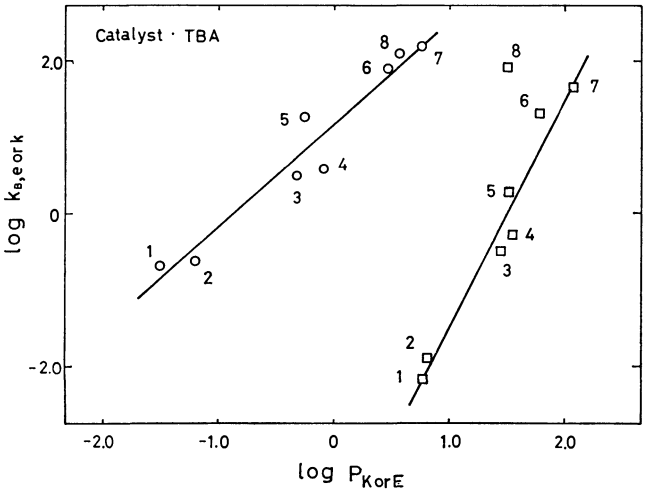

Fig. 3. The correlation between the catalytic coefficient of TBA and the partition coefficient of acetylacetone. The numbers in this figure correspond to those in Table 1.
○: log $k_{B,e}$ *vs.* log P_K, r=0.968; □: log $k_{B,k}$ *vs.* log P_E, r=0.977 except for acetonitrile.

A free-energy consideration of the base catalysis leads to the following equation;

$$\Delta G^{*} - \Delta G^{*\circ} = \delta\Delta G_X - \sum_i \delta\Delta G_i \qquad (3)$$

where ΔG^{*} and $\Delta G^{*\circ}$ are, respectively, the activation free energies in a given solvent and in the hypothetical standard solvent and where $\delta\Delta G_X$ and $\delta\Delta G_i$ are the respective transfer free energies of the transition state and the reactant, i, from the standard solvent to the other solvent. For the ketonization and the enolization reactions, Eq. 3 leads to;

$$\begin{aligned} \Delta G_k^{*} - \Delta G_k^{*\circ} &= \delta\Delta G_X - \delta\Delta G_E - \delta\Delta G_B, \\ \Delta G_e^{*} - \Delta G_e^{*\circ} &= \delta\Delta G_X - \delta\Delta G_K - \delta\Delta G_B, \end{aligned} \qquad (4)$$

where the subscripts X, E, K, and B correspond to the transition state, the enol form, the keto form, and the base catalyst respectively. Equation 4 can be rewritten by introducing the catalytic coefficient and the partition coefficient;

$$\begin{aligned} RT\ln(k_{B,k}/k^{\circ}_{B,k}) &= \delta\Delta G_B - \delta\Delta G_X - RT\ln(P_E/P_E^{\circ}), \\ RT\ln(k_{B,e}/k^{\circ}_{B,e}) &= \delta\Delta G_B - \delta\Delta G_X - RT\ln(P_K/P_K^{\circ}), \end{aligned} \qquad (5)$$

where the superscript ○ denotes the standard solvent. The linear relationships obtained in Figs. 2 and 3 for the seven inert solvents prove that the term of $\delta\Delta G_B - \delta\Delta G_X$ is proportional to both $RT\ln(P_E/P_E^{\circ})$ and $RT\ln(P_K/P_K^{\circ})$.

Now, we may assume the following proportionality:

$$\begin{aligned} \delta\Delta G_B &= a\delta\Delta G_K = a'\delta\Delta G_E, \\ \delta\Delta G_X &= b\delta\Delta G_K = b'\delta\Delta G_E, \end{aligned} \qquad (6)$$

where a, b, a', and b' are proportional constants following the relation of $a'/a = b'/b = c$ (constant). Equation 6 is based on the assumption that the solute-solvent interaction which occurs during the base catalyzed tautomerization process does not include specific interactions, *e.g.*, a strong dipole-dipole interaction and a hydrogen-bonding interaction. The correlation between $\delta\Delta G_K$ and $\delta\Delta G_E$ is shown in Fig. 4, in which the linear correlation between the logarithmic values of the partition coefficients of the keto and enol forms of acetylacetone

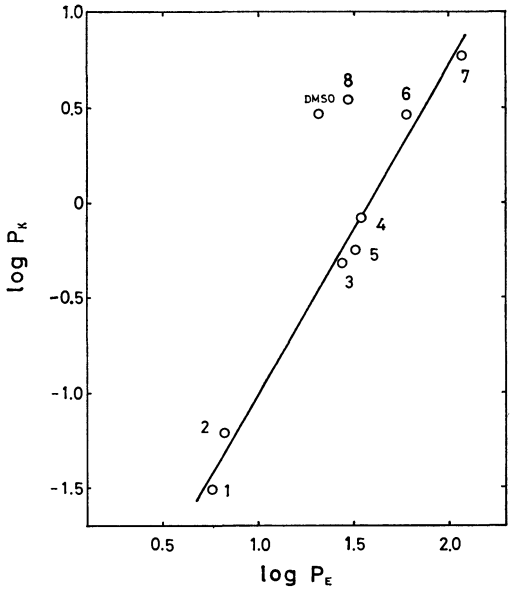

Fig. 4. The correlation between the partition coefficient of the keto (P_K) and the enol (P_E) forms of acetylacetone. The numbers in this figure correspond to those in Table 1.
log P_K=1.71 log P_E+2.73, r=0.993 except for acetonitrole and DMSO[3]

is shown for the seven inert solvents, allowing the estimation of the "c" constant from the slope as 1.71. A linear relationship was observed among the gas solubilities[8] and between the solubilities of bis(acetylacetonato)copper(II) and bis(dipropionylmethanato)-copper(II),[9] also. By the introduction of Eq. 6 into Eq. 5, we obtain the following equations;

$$\begin{aligned} \log k_{B,e} &= (b-a-1)\log P_K \\ &\quad + \{\log k^{\circ}_{B,e} - (b-a-1)\log P_K^{\circ}\}, \\ \log k_{B,k} &= (b'-a'-1)\log P_E \\ &\quad + \{\log k^{\circ}_{B,k} - (b'-a'-1)\log P_E^{\circ}\}. \end{aligned} \tag{7}$$

Consequently, the slopes of Figs. 2 and 3 give the set of the proportional constants of $(b-a)$ and $(b'-a')$ —2.32 and 4.16 for TEA-catalysis and 2.37 and 4.01 for TBA-catalysis. The deviation observed for the acetonitrile system in Figs. 2 and 3 may be attributed to the destabilization in a polar solvent such as acetonitrile of the enol form, which is less polar than the keto form; this is also suggested by the deviation in Fig. 4.

Relationship among $\delta\Delta G_X$, $\delta\Delta G_K$, and $\delta\Delta G_E$. In the above section, the relationship between the catalytic coefficient and the partition coefficient has been proved in terms of the free energy. The result shows that the lowering of the standard free energy of the tautomers causes a descrease in the activation free energy because of the further lowering of the standard free energy of the transition state compared to those of the tautomers. The values of $\delta\Delta G_X$ are more sensitive to the solvent than those of $\delta\Delta G_K$ and $\delta\Delta G_E$. The transition state is expected to be a complex of an ion-pair or charge-transfer type between the amine and acetylacetone. Then, $\delta\Delta G_X$ can be separated into $\delta\Delta G_B$ and $\delta\Delta G_{X,r}$,

$$\delta\Delta G_X = \delta\Delta G_B + \delta\Delta G_{X,r}, \tag{8}$$

where $\delta\Delta G_{X,r}$ is the residual part which is obtained by substracting $\delta\Delta G_B$ from $\delta\Delta G_X$. $\delta\Delta G_{X,r}$ can be expected to be the transfer free energy of a state like an ion-pair of the proton and the enolate anion of acetylacetone. Equations 6 and 8 lead to this relation,

$$\delta\Delta G_{X,r} = (b-a)\delta\Delta G_K = (b'-a')\delta\Delta G_E, \tag{9}$$

or

$$\begin{aligned} \delta\Delta G_{X,r} &= 2.43\delta\Delta G_K = 4.16\delta\Delta G_E \\ &\qquad \text{for TEA-catalysis,} \\ \delta\Delta G_{X,r} &= 2.37\delta\Delta G_K = 4.01\delta\Delta G_E \\ &\qquad \text{for TBA-catalysis.} \end{aligned} \tag{10}$$

Equation 10 shows that $\delta\Delta G_{X,r}$ is most affected by the solvent in the transfer free energies of the three states and that the change in $\delta\Delta G_{X,r}$ is the main factor governing the solvent effect on the rate of the catalysis. The difference in the solvent effect on the three states is probably due to the difference in the electric property; *e.g.*, the expected order of the delocalization of the electron density is the transition state> the keto form> the enol form.

Although the details of the reaction mechanism of the base-catalyzed tautomerization are still obscure, it can reasonably be expected that the proton transfer will occur *via* an intramolecular process assisted by the amine, rather than by an intermolecular process, as proposed by Baba and Takemura[10] for the base-catalysis of anthrone–anthranol interconversion in nonpolar solvents. This interpretation is supported by the fact that, even in inert solvents, TEA and TBA effectively catalyze the tautomerization of acetylacetone.

Free-energy Consideration of the Effect of the Silica Surface. As was mentioned in the Experimental section, the tautomerization rate is extremely enhanced by the contact with the wall of the quartz cell, depending on the solvent used. In considering the solvent effect in this heterogeneous catalysis, we applied the free-energy treatment developed in this study. It was assumed that the transition state is the adsorbed acetylacetone on the silica surface and that the solvation effects on the transition state and on the silica surface are negligible or compensate each other, *i.e.*, $\delta\Delta G_B - \delta\Delta G_X = \text{const}$ in Eq. 5. Then, Eq. 5 degenerates to;

$$\log k_{obsd} = -\log f_0(1-f_0)P + \text{const.} \tag{11}$$

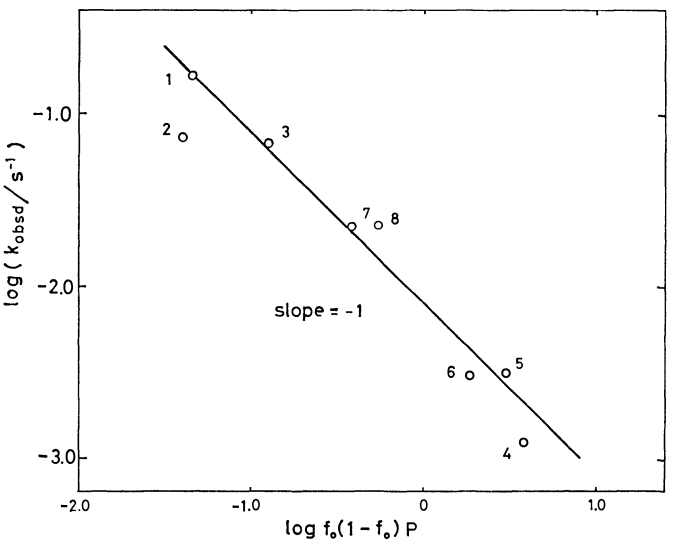

Fig. 5. The solvent effect on the silica surface catalysis. Solvent; 1: hexane, 2: cyclohexane, 3: carbon tetrachloride, 4: dichloromethane, 5: chloroform, 6: 1,2-dichloroethane, 7: benzene, 8: toluene.

According to the above equation, the experimental results are plotted in Fig. 5. A satisfactory linear relationship, with the slope of minus one, was obtained, in agreement with the prediction from Eq. 11. If the assumption of $\delta\Delta G_B - \delta\Delta G_X = \text{const}$ does not hold, the slope will differ from a minus one. Consequently, in this case the states most affected by the solvent are suggested to be the keto and enol forms, contrary to the results of the homogeneous amine catalysis. It is of interest that the solvent effect is in reverse directions in the two systems, *i.e.*, the heterogeneous and homogeneous catalyses. Further investigation employing a variety of solvents will enable us to assess the generality of this conclusion.

References

1) A. K. De, S. M. Khopkar, and R. A. Chalmers, "Solvent Extraction of Metals," Van Nostrand Reinhold Company, London (1970).

2) S. Glasstone, K. J. Laidler, and H. Eyring, "Theory of Rate Processes," McGraw-Hill Book Company, New York (1940).
3) H. Watarai and N. Suzuki, *J. Inorg. Nucl. Chem.*, **38**, 1683 (1976).
4) H. Watarai and N. Suzuki, *Bull. Chem. Soc. Jpn.*, **50**, 757 (1977).
5) H. Watarai and N. Suzuki, *J. Inorg. Nucl. Chem.*, **36**, 1815 (1974).
6) A. M. Del and C. Battle, *J. Chromatogr.*, **28**, 82 (1967).
7) H. Watarai and N. Suzuki, *J. Inorg. Nucl. Chem.*, **38**, 301 (1976).
8) J. E. Jolley and J. H. Hildebrand, *J. Am. Chem. Soc.*, **80**, 1050 (1958).
9) H. Koshimura, *J. Inorg. Nucl. Chem.*, **38**, 1705 (1976).
10) H. Baba and K. Takemura, *Nippon Kagaku Zasshi*, **89**, 629 (1968).

The Kinetics of Oxygen Exchange between Arsenate Ions and Water. III. Catalysis by Periodate Ions

Akiko OKUMURA,* Seiko WATANABE, Miyoko SAKAUE, and Nobukazu OKAZAKI

Department of Chemistry, Nara Women's University, Nara 630

(Received January 9, 1979)

Oxygen exchange between arsenate ions and water is remarkably catalyzed by the addition of a small amount of periodate ions.† The reaction has been studied at 30.0 °C over the pH range of 6.7—11.4. The rate law of the catalytic reaction has been found to be $R_C=k\cdot[H^+][As(V)][I(VII)]$, where R_C is defined as the increase in the rate of oxygen exchange of arsenate ions by the addition of periodate ions. The catalytic process has been interpreted in terms of the reversible condensation of arsenate ions with periodate ions to form the arsenatoperiodate ions, and the rate constant of the condensation reaction between $H_2AsO_4^-$ and $H_4IO_6^-$ has been estimated to be 340 $M^{-1}\,s^{-1}$ at 30.0 °C.

In a previous paper,[1] it has been shown that the oxygen exchange reaction of arsenate ions with water is strongly accelerated by the addition of a small amount of arsenious acid. The catalytic process has been identified with the reversible condensation of arsenate ions with arsenite species to form the arsenatoarsenite ions, and the rate constants of this condensation reaction have been estimated.

The study of an oxygen exchange reaction of an oxoanion in the presence of a catalytic amount of another oxoanion may provide a means of studying the kinetics and equilibriums of the condensation reactions involving the two oxoanions. In this paper a study of the interaction of arsenate ions with periodate ions in solution by means of the oxygen exchange reaction will be reported.

Experimental

Materials. Water enriched in oxygen-18 (2 atom %) was obtained from a fractionating column in this laboratory. It was refluxed with alkaline permanganate, and distilled twice. Normal water was treated in the same way. Disodium hydrogenarsenate heptahydrate(Guaranteed reagent, Merck), sodium periodate (Guaranteed reagent, Merck), and all the other chemicals (Guaranteed reagent, JIS) were used without further purification.

The concentration of the stock solution of sodium periodate (1.63×10^{-2} M) was checked spectrophotometrically each time before use with iron(II)-2,4,6-tri-2-pyridyl-1,3,5-triazine.[2]

Procedure. The procedures were almost the same as those used earlier.[1,3] The exchange reaction was started by mixing an isotopically equilibrated solution of disodium hydrogenarsenate in $H_2{}^{18}O$ with water of normal isotopic composition. A small amount of the stock solution of periodate was added, and the pH of the solution was fixed by the addition of a measured quantity of either a solution of sodium hydroxide or hydrochloric acid. The pH of the solution was measured with a Radiometer PHM type-26 pH meter. All experiments were performed at 30.0 °C. At intervals aliquots of the reacting solution were drawn, and the reaction was quenched by precipitating the arsenate ions as $BaHAsO_4\cdot H_2O$ with barium chloride solution. The precipitate, after being washed three times with absolute ethanol and dried, was converted into carbon dioxide by the guanidinium chloride method.[4] The isotopic analysis of the carbon dioxide was made on a Hitachi RMS-I type mass-spectrometer.

The rate of the oxygen exchange of arsenate ions was calculated by means of the formula:

$$R=-\frac{1}{t}\cdot\frac{[As(V)][H_2O]}{4[As(V)]+[H_2O]}\cdot\ln\left(1-\frac{O_0-O_t}{O_0-O_\infty}\right)$$

where O_0, O_t, and O_∞ are the ^{18}O-contents of the carbon dioxide at times 0, t, and infinity, respectively, and where [As(V)] and $[H_2O]$ are the molar concentrations of the arsenate and water, respectively.

Results and Discussion

pH *Dependence.* In Fig. 1, log R_0 and log R are plotted against pH, where R_0 and R designate the rates of the oxygen exchange reaction between arsenate ions and solvent water without and with the addition of periodate ions, respectively. The concentration of arsenate was 0.07 M, and no inert salt was added. The concentrations of the periodate were 10^{-5} M for series

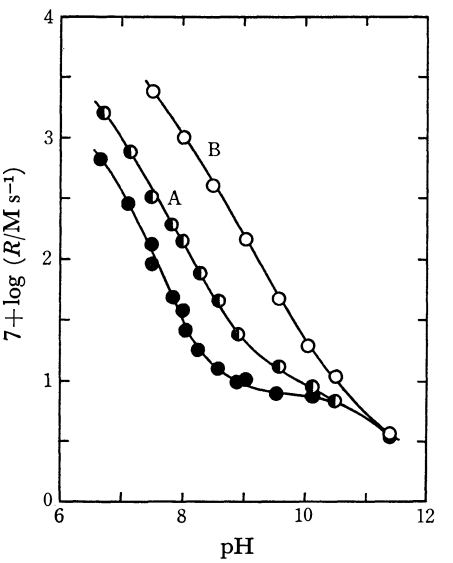

Fig. 1. The rate of oxygen exchange reaction of arsenate ions with water *versus* pH.
([As(V)]=0.07 M, I=0.2 M, 30.0 °C)
●: In the absense of periodate ions.
◐ (A): in the presence of periodate ions, [I(VII)]=8.4×10^{-6} M.
○ (B): in the presence of periodate ions, [I(VII)]=8.2×10^{-5} M.

† In this paper the word "periodate" is used to signify both periodate and orthoperiodate.

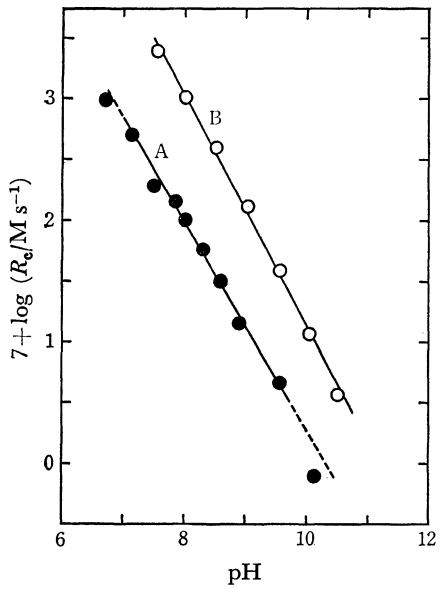

Fig. 2. pH dependence of the catalyzed portion of the exchange rate R_c.
● (A): [I(VII)]=8.4×10^{-6} M.
○ (B): [I(VII)]=8.2×10^{-5} M.

A and 10^{-4} M for series B. The catalytic effect decreases with the increasing pH value and disappears at pH 10.5 for series A and at 11.4 for series B. Even in the low concentration ratio: [I(VII)]/[As(V)]=10^{-4}, the catalytic action of periodate ions is so large as to increase the oxygen exchange rate 3.5 fold at pH 8.5.

Figure 2 shows the dependence of R_c on pH. R_c is defined as $R-R_0$ and corresponds to the catalyzed portion of the exchange reaction. The slopes of the lines passing through the plots are -0.86 ± 0.02 for series A and -0.95 ± 0.03 for series B within the pH regions 7.17—9.57 and 7.52—10.51, respectively. R_c depends upon the first power of the hydrogen ion concentration in both series. It may be inferred from these results that the acidic species of arsenate and periodate ions are more reactive. The role of hydrogen ion in the rate equation is to shift the acid dissociation equilibrium of the oxoanions in favor of the more reactive ionic species.

Dependence of the Catalytic Rate R_c on [I(VII)]. This has been studied at two pH's, 8.0 and 9.2. The concentration of periodate was varied between 3.0×10^{-5} M and 11.6×10^{-5} M (pH 8.0) and between 8.9×10^{-5} M and 44.0×10^{-5} M (pH 9.2). The plots of log R_c against log [I(VII)] are shown in Fig. 3. The slopes of the straight lines obtained by least square fits of the data are 1.03 ± 0.01 and 0.93 ± 0.07 for the pH values of 8.0 and 9.2, respectively. The log R_c: log [I(VII)] plot deviates downwards from the straight line at [I(VII)] $<3.0\times10^{-6}$ M (pH 8.0) (not shown in the figure). This is probably due to the decomposition of the periodate by a trace amount of reducing impurities which are present in the solution.

Dependence of the Catalytic Rate R_c on [As(V)]. This has been studied under the following conditions. A: pH=8.00, [I(VII)]=8.10×10^{-5} M, I(NaCl)=0.55 M, [As(V)]=0.034—0.138 M; B: pH=9.08, [I(VII)]=8.84×10^{-5} M, I(NaCl)=1.00 M, [As(V)]=0.035—0.275 M. The plots of log R_c against log [As(V)] are shown in Fig. 4. The slopes of the straight lines obtained are 0.97 ± 0.07 for A and 1.04 ± 0.11 for B.

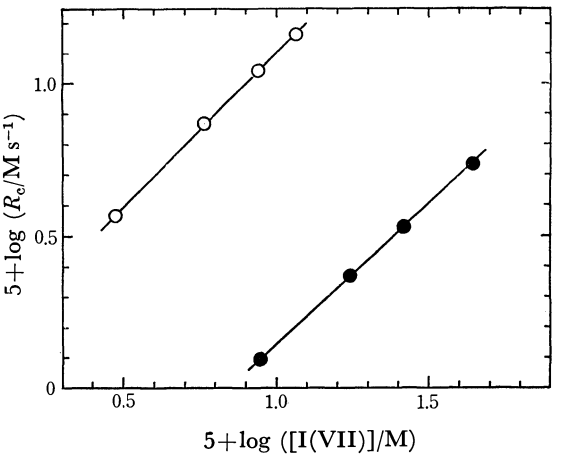

Fig. 3. Dependence of the catalytic rate R_c on [I(VII)] ([As(V)]=0.07 M, I=0.2 M)
○: pH=8.0, [I(VII)]=$(3.0-11.6)\times10^{-5}$ M.
●: pH=9.2, [I(VII)]=$(8.9-44.0)\times10^{-5}$ M.

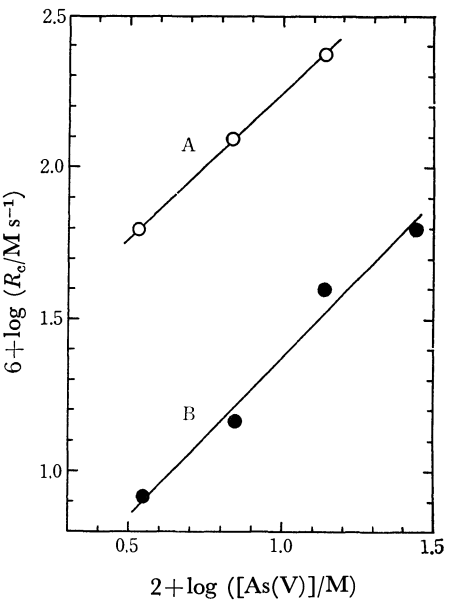

Fig. 4. Dependence of the catalytic rate R_c on [As(V)].
○ (A): pH=8.0, [I(VII)]=8.10×10^{-5} M, I(NaCl) =0.55 M, [As(V)]=0.034—0.138 M.
● (B): pH=9.08, [I(VII)]=8.84×10^{-5} M, I(NaCl) =1.0 M, [As(V)]=0.035—0.275 M

Evaluation of the Rate Constants. The catalytic reaction rate R_c may be expressed generally as the sum of the kinetic terms as follows:

$$R_c = \sum k_{ij}[\mathrm{As(V)}]_i[\mathrm{I(VII)}]_j$$

where $[As(V)]_i$ denotes the various ionic species of the arsenate ions, and $[I(VII)]_j$ those of the periodate ions, and k_{ij} is the rate constant of the reaction between $[As(V)]_i$ and $[I(VII)]_j$. In the pH range 6—11, the dominating ionic species of the arsenate are $H_2AsO_4^-$, $HAsO_4^{2-}$, and AsO_4^{3-}, and those of the periodate are $H_4IO_6^-$, IO_4^-, and $H_3IO_6^{2-}$. The concentrations of

$H_4IO_6^-$ and IO_4^- are mutually related by the relation $K_d = a_{IO_4^-} \cdot a_{H_2O}^2 / a_{H_4IO_6^-} = 40$ [5] and are kinetically equivalent.

The rate law of the catalytic process may now be given as

$$R_c = k_1[H_4IO_6^-][H_2AsO_4^-] + k_2[H_3IO_6^{2-}][H_2AsO_4^-] + k_3[H_4IO_6^-][HAsO_4^{2-}] + k_4[H_3IO_6^{2-}][HAsO_4^{2-}] + k_5[H_4IO_6^-][AsO_4^{3-}] + k_6[H_3IO_6^{2-}][AsO_4^{3-}],$$

where $[H_4IO_6^-]$ is the concentration of the periodate monoanions inclusive of IO_4^-. The value of R_c becomes negligible at the pH values greater than 10.5, where the dominating ionic species are $H_3IO_6^{2-}$, $HAsO_4^{2-}$, and AsO_4^{3-}, the concentration of AsO_4^{3-} increasing with the increase in pH. If the rate constants k_4, k_5, and k_6 had significant values, the k_4-, k_5-, and k_6-terms should contribute appreciably to the catalytic rate R_c. The contributions of the k_4-, k_5-, and k_6-terms may be ignored.

The rate law can be rewritten as:

$$\frac{R_c}{[H_2AsO_4^-][H_4IO_6^-]} = k_1 + \left(k_3 + \frac{K_2'(I)}{K_2(As)} \cdot k_2\right) \frac{K_2(As)}{[H^+]} \quad (1)$$

where $K_2(As)$ and $K_2'(I)$ are the second ionization constant of arsenic acid and the apparent second ionization constant of periodic acid, respectively, under the conditions of the kinetic runs. The concentrations of the ionic species of the periodate were evaluated by means of the apparent ionization constants written in the forms:

$$a_{H^+}(a_{IO_4^-} + a_{H_4IO_6^-})/a_{H_4IO_6^-} = K_1'(I)$$
$$a_{H^+} \cdot a_{H_4IO_6^-}/(a_{H_4IO_6^-} + a_{IO_4^-}) = K_2'(I)$$

The values of the ionization constants necessary to calculate the concentrations of the ionic species of the arsenate and the periodate are indicated in Table 1.

Table 1. Acid dissociation constants of arsenic acid and periodic acid under the condition of the kinetic runs: I=0.2 M, 30 °C.

As(V)	pK_2 [3]	6.56	I(VII)	pK_1'	1.34
	pK_3 [3]	11.33		pK_2'	7.87
				pK_3	11.35

$K_1'(I)$(I=0) at 30.0 °C was obtained by interpolation of the data determined by Crouthamel *et al.*[5] to 30.0 °C, and this value was converted to $K_1'(I)$(I=0.2 M) using Guntelberg's equation. $K_2'(I)$ and $K_3(I)$ were evaluated similarly by using $K_2'(I)$(I=0) and $K_3(I)$(I=0.1 M) determined by Buist and coworkers[6] at various temperatures.

In Fig. 5, the data corresponding to pH 6.7—9.8 in Fig. 1 are replotted according to equation 1. From the intercept of the straight line through the plots, the value of k_1 is determined to be 338±27 M^{-1} s^{-1}. From the slope of the line, the value of $[k_3 + k_2 \cdot K_2'(I)/K_2(As)]$, is obtained as 35.9±0.1 M^{-1} s^{-1}. It is impossible to evaluate the values of k_2 and k_3 separately. Taking 4.8×10^{-2} as the value of $K_2'(I)/K_2(As)$, k_3= 36 M^{-1} s^{-1} and k_2=750 M^{-1} s^{-1} may be obtained as the upper limits of these constants.

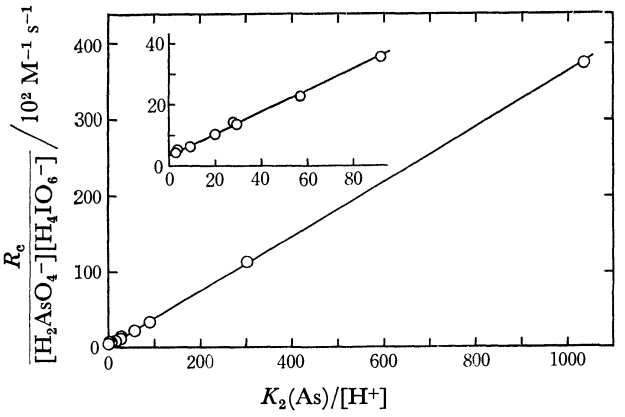

Fig. 5. $R_c/[H_2AsO_4^-][H_4IO_6^-]$ as a function of $K_2(As)/[H^+]$.

By analogy with the case of arsenious acid catalysis of the arsenate oxygen exchange,[1] it is natural to interpret the rate term $k_{ij}[As(V)]_i[I(VII)]_j$ in terms of the reversible condensation of arsenate ions with periodate ions. The possibility of general acid catalysis of the arsenate oxygen exchange by oxoanions has been ruled out in the previous paper.[1] In the present case, general acid catalysis by periodate ions is also ruled out by the fact that the value of k_1 in the rate term $k_1[H_2AsO_4^-][H_4IO_6^-]$ is larger than that of k in the rate term $k[H_2AsO_4^-][H_2AsO_4^-]$, since $H_4IO_6^-$ is weaker acid than $H_2AsO_4^-$. The hydrogen-bond association of arsenate ions with periodate ions would not affect the rate of the oxygen exchange of arsenate ions significantly.

The rate constants of the condensation reactions between anions obtained in this work are listed in Table 2, along with those obtained before.[1,3]

Table 2. The rate constants of the condensation reactions between anions

Reactions	Rate const/M^{-1} s^{-1}	Ref.
$H_2AsO_4^- + H_2AsO_4^-$	0.074	3
$H_2AsO_4^- + HAsO_4^{2-}$	0.0064	3
$H_2AsO_4^- + H_3AsO_3$	6.8	1
$H_2AsO_4^- + H_2AsO_3^-$	<7	1
$HAsO_4^{2-} + H_3AsO_3$	<0.02	1
$H_2AsO_4^- + H_4IO_6^-$	338	This work
$H_2AsO_4^- + H_3IO_6^{2-}$	<750	This work
$HAsO_4^{2-} + H_4IO_6^-$	<36	This work

For the reversible condensation process, two paths are possible. Path a): Periodate acts as the nucleophile, and arsenate as the substrate (an oxygen atom of periodate ion attacking the arsenic atom of the arsenate). Path b): Arsenate acts as the nucleophile, and periodate as the substrate (an oxygen atom of the arsenate ion attacking the iodine atom of the periodate). In both cases an identical dianion, arsenatoperiodate, is formed.

In the periodate oxidation of the organic substances, the periodate ion acts as an electrophile or a nucleophile depending on the nature of the substrate.[7,8]

By the principle of microscopic reversibility, the bond

fission in the reverse reaction must occur at the same position as in the forward reaction. The result that the oxygen exchange reaction of arsenate is catalyzed by periodate ions requires the reaction to proceed *via* Path a). Path b) does not lead to the oxygen exchange of arsenate with water.

If it is assumed that Path a) and Path b) occur simultaneously in a solution containing arsenate and periodate ions, a path in which the condensation proceeds through Path b) and the hydrolysis through Path a) would be an alternative mechanism for the periodate catalysis.

Another possibility is a mechanism which involves the rapid exchange of periodate ions with solvent water[9] and subsequent condensation through Path a) and hydrolysis through Path b).

In order to see whether or not the catalytic action of the periodate ion is observed in the oxygen exchange of other oxoanions, we have studied the oxygen exchange reactions of selenic acid, phosphate ions, and chromate ions with water in the presence of periodate ions. It was found that the periodate ion has a remarkable effect on the oxygen exchange between chromate and water, the effect being greater than that on the arsenate exchange. From the results obtained so far, the rate constant for the reaction: $HCrO_4^- + H_4IO_6^- \rightleftharpoons H_3CrIO_9^{2-} + H_2O$, may be estimated to be $10^4\ M^{-1}\ s^{-1}$ at 0 °C. The effect could not be found with selenic acid and phosphate ions. It is known that the reversible condensation process: $2HCrO_4^- \rightleftharpoons Cr_2O_7^{2-} + H_2O$, plays a dominant role in the oxygen exchange of chromate ion with water,[10] while the oxygen exchange of selenic acid[11] and phosphate ions[12] does not involve the condensation mechanism. It is probable that the condensation process is responsible for the periodate catalysis.

The catalysis of the hydration of carbon dioxide by various anions has been studied by Dennard and Williams.[13] They have found that $H_4IO_6^-$ is a weak catalyst, and $H_2AsO_3^-$ is a far better catalyst than H_3AsO_3, the catalytic constant of $H_2AsO_3^-$ being $1.9 \times 10^3\ M^{-1}\ s^{-1}$ at 0 °C. These results are in contrast with those obtained for the arsenate exchange, for which H_3AsO_3 and $H_4IO_6^-$ are excellent catalysts and H_3AsO_3 is a better catalyst than $H_2AsO_3^-$. The mechanism of the oxoanion catalysis of the hydration of carbon dioxide would be different from that of the oxygen exchange of arsenate ions.

References

1) A. Okumura, N. Yamamoto, and N. Okazaki, *Bull. Chem. Soc. Jpn.*, **46**, 3633 (1973).
2) G. Avigad, *Carbohydr. Res.*, **11**, 119 (1969).
3) A. Okumura and N. Okazaki, *Bull. Chem. Soc. Jpn.*, **46**, 2937 (1973).
4) P. D. Boyer, D. J. Graves, C. H. Suelter, and M. E. Dempsey, *Anal. Chem.*, **33**, 1906 (1961).
5) C. E. Crouthamel, A. M. Hayes, and D. S. Martin, *J. Am. Chem. Soc.*, **73**, 82 (1951).
6) G. J. Buist, W. C. P. Hipperson, and J. D. Lewis, *J. Chem. Soc., A*, **1969**, 307.
7) C. A. Bunton and V. J. Shiner, *J. Chem. Soc.*, **1960**, 1593.
8) G. J. Buist, C. A. Bunton, and J. Lomas, *J. Chem. Soc., B*, **1966**, 1099.
9) I. Pecht and Z. Luz, *J. Am. Chem. Soc.*, **87**, 4068 (1965).
10) R. H. Holyer and H. W. Baldwin, *Can. J. Chem.*, **45**, 413 (1967).
11) A. Okumura and N. Okazaki, *Bull. Chem. Soc. Jpn.*, **46**, 1080 (1973).
12) C. A. Bunton, D. R. Llewellyn, C. A. Vernon, and V. A. Welch, *J. Chem. Soc.*, **1961**, 1636.
13) A. E. Dennard and R. J. P. Williams, *J. Chem. Soc., A*, **1966**, 812.

Ultrasonic Velocity and Compressibility in Aqueous Solutions of Alkali Metal Chlorides

Hisashi UEDAIRA* and Yasuko SUZUKI

Research Institute for Polymers and Textiles, 1-1-4 Yatabe-Higashi, Tsukuba, Ibaraki 300-21

(Received February 8, 1979)

The ultrasonic velocity of aqueous solutions of alkali metal chlorides was measured by the use of the sing-around technique at 0.5 and 1 mol kg^{-1} over the temperature range from 30 to 85 °C; compressibilities of the solutions were also determined. It was found that the ultrasound velocity *versus* temperature curves show a maximum, while the compressibility *versus* temperature ones show a minimum. Both maxima and minima appear at lower temperatures than that observed for pure water. The maximum shifted values were found for Na^+ ion. The results were explained by the dynamic structure of the water around the ions.

One of the abnormal properties of water is the variation of ultrasound velocity with temperature in water. That is, the propagation velocity of ultrasound in normal liquids falls off with increasing temperature; however, for water the ultrasonic velocity attains a maximum value of 1557 m s^{-1} at a temperature of 74 °C, and only above this temperature does the ultrasound velocity diminish. The adiabatic compressibility of water shows a minimum at 64 °C. These phenomenon are due to the peculiar liquid structure of water.

The temperature of maximum sound velocity in water is changed by the presence of ions,[1-3] since the water structure is affected by the ions. Thus, from the effects upon the ultrasound velocity and the compressibility of water by the ions it is possible to obtain some information with regard to the ion–water interactions.

There have been several studies of the ultrasound velocity in aqueous electrolyte solutions. However, only a few systematic investigations[1-3] have been reported so far over a sufficiently wide range of concentration and temperature.

We have, therefore, attempted to measure the ultrasound velocity of aqueous solutions of alkali metal chlorides over a wide range of temperature; the adiabatic compressiblities of these solutions were also determined. The results are discussed on the basis of the dynamic structure of water around cations.

Experimental

Alkali metal chlorides (G. R., E. Merck Co.) were used without further purification.

Sound velocity was measured by the "sing-around" technique, using an apparatus (Choonpa Kogyo Co.) at 5 MHz. Procedures of the measurement of the sound velocity are described elesewhere.[4] Ultrasound velocity in the solutions was determined at 5 °C intervals over a temperature range from 30 to 85 °C and at 1 °C intervals in case of need. The constancy of temperature was ± 0.01 °C.

Adiabatic compressibility κ was calculated by the following relation:

$$\kappa = 1/u^2 d, \tag{1}$$

where u is the velocity of ultrasound and d the density of the solution. Values of the densities at the experimental temperature and concentration were calculated from the following polynomials of the concentration or temperature:

$$d = d_0 + \sum_{i=1}^{5} a_i m^i \tag{2}$$

and

$$d = d_0 + \sum_{i=1}^{5} b_i t^i, \tag{3}$$

where d_0 is the density of pure water, m the molality, and t the temperature (°C). Values of the coefficients a_i and b_i in the polynomials were determined from the densities of solution of alkali metal chlorides,[5] using a HITAC 8400.

Results and Discussion

The temperature dependence of ultrasonic velocities in aqueous solutions of alkali metal chlorides are shown in Figs. 1 and 2 at salt concentrations 0.5 and 1 mol kg^{-1}. Only the ultrasound velocity in CsCl solution is lower than that in water over all the range of temperature at both concentrations. The difference of the sound velocities in the salt solutions and water increases with increasing concentration. The temperature of maximum sound velocity, T_{vm}, varies according to the kinds of salts and their concentrations, and shifts to lower temperatures than 74 °C.

At any temperature the sound velocity in the salt

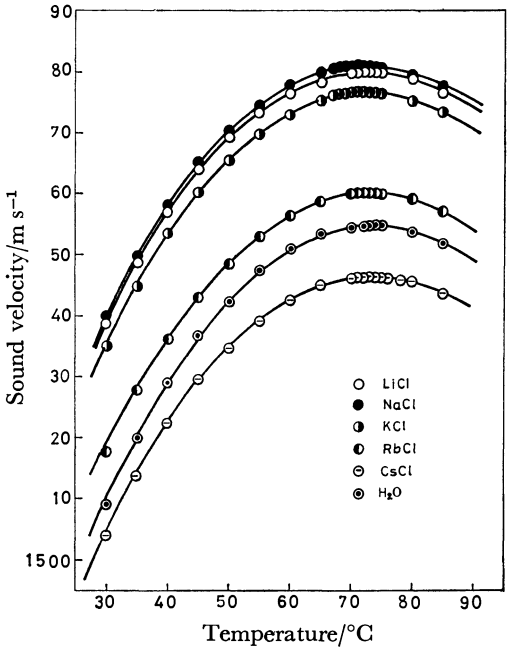

Fig. 1. Variation of ultrasonic velocity with temperature in aqueous solutions of alkali metal chlorides at 0.5 mol kg^{-1}.

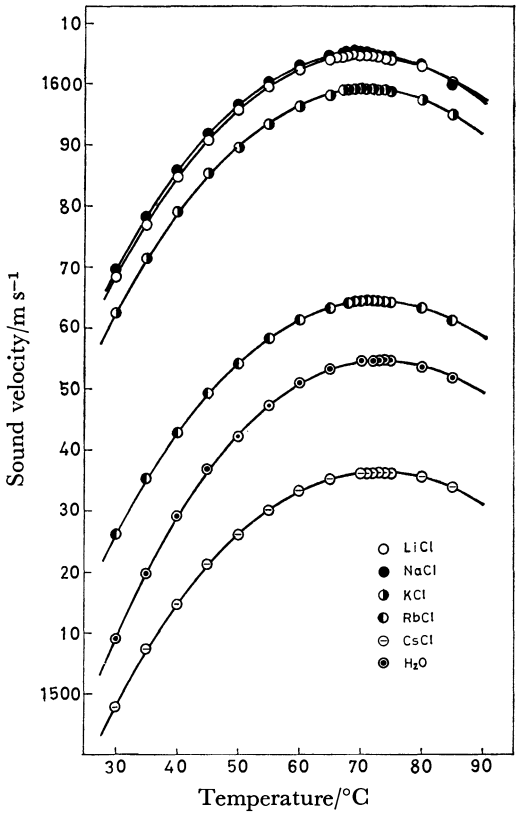

Fig. 2. Variation of ultrasonic velocity with temperature in aqueous solutions of alkali metal chlorides at 1 mol kg^{-1}.

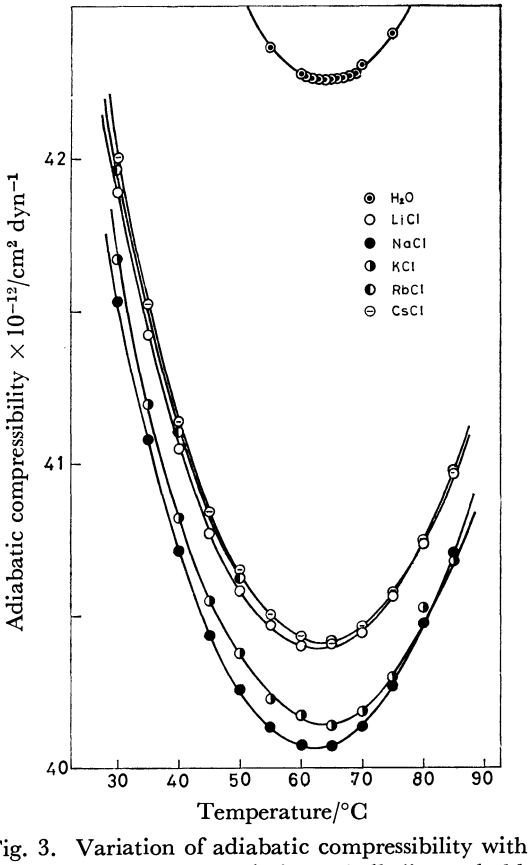

Fig. 3. Variation of adiabatic compressibility with temperature of aqueous solutions of alkali metal chlorides at 0.5 mol kg^{-1}.

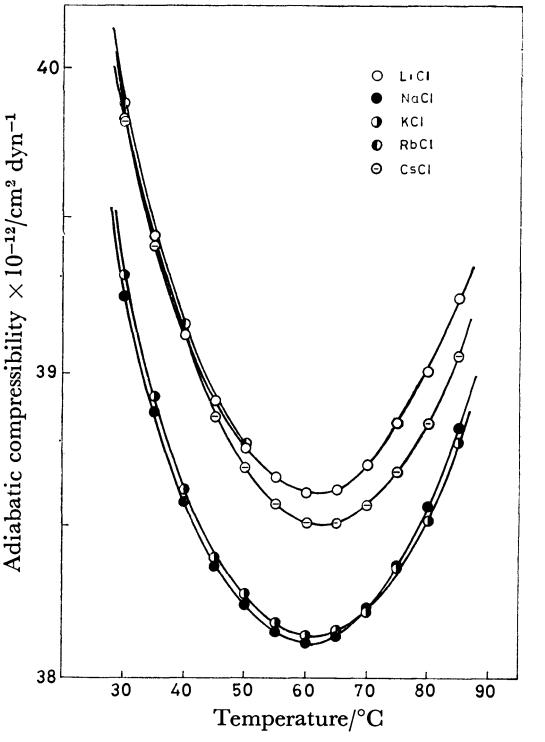

Fig. 4. Variation of adiabatic compressibility with temperature in aqueous solutions of alkali metal chlorides at 1 mol kg^{-1}.

solutions decreases in the order:

$$\text{NaCl} > \text{LiCl} > \text{KCl} > \text{RbCl} > \text{CsCl}$$

but above 70 °C the velocity in the 1 mol kg^{-1} solution of LiCl becomes larger than that in NaCl solution.

The temperature dependence of the compressibilities are shown in Figs. 3 and 4. The compressibilities of RbCl solution at temperature higher than 50 °C could not be calculated, since the values of densities in the temperature range were not found in the literature.

All the values of compressibilities for the salt solutions are smaller than that of water and the order of magnitude differes in different concentrations. Below 70 °C the compressibility of NaCl solution is the lowest at each concentration. Judging from the fact that the values of compressibilities for LiCl, RbCl, and CsCl solutions do not differ markedly from one another, the large density of CsCl solution is thought to account for the fact that the sound velocity in CsCl solution is smaller than that in water. From the above-mentioned results, it seems difficult to connect directly the sound velocity and compressibility with the structure of solutions.

According to Hirata and Arakawa,[6] the compressibility of water is equal to $\kappa_\infty + \kappa_{\text{relax}}$ under our experimental conditions, where κ_∞ and κ_{relax} are the instantaneous and the relaxational parts of the compressibility, respectively.[7] As the temperature rises, κ_∞ increases due to thermal motion but κ_{relax} decreases due to thermal rupture of water structure. The competition between these two opposing tendencies leads to the compressibility minimum at 64 °C and the sound velocity maximum at 74 °C.

An ion affects the thermal motion of the water molecules around it. Thus the temperature of the

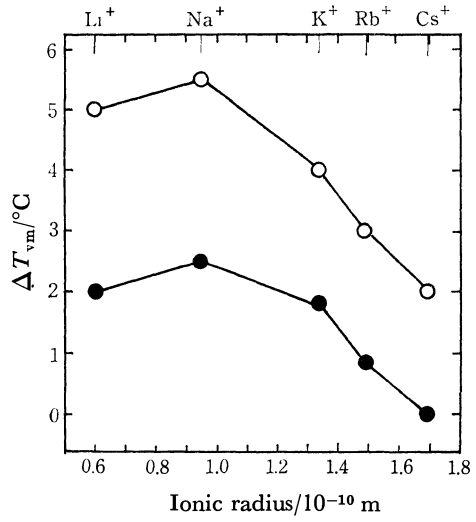

Fig. 5. Relation between ΔT_{vm} and ionic radius.
-●- 0.5 mol kg^{-1}; -○- 1 mol kg^{-1}.

compressibility minimum(T_{cm}) and the sound velocity maximum(T_{vm}) must reflect the change of water structure due to the presence of the ions. Because the chlorine ion is common to all the salts treated in the present study, the relative effects of the cations can be compared.

Figure 5 shows the relation between the ionic radius and $\Delta T_v = T^\circ_{vm} - T_{vm}$, where T°_{vm} is 74 °C. Figure 6 shows the relation between the ionic radius and $\Delta T_{cm} = T^\circ_{cm} - T_{cm}$, where T°_{cm} is 64 °C. These results show a maximum at the Na^+ ion. The curves shift to nearly parallel accordingly to the concentration or the kind of anion.

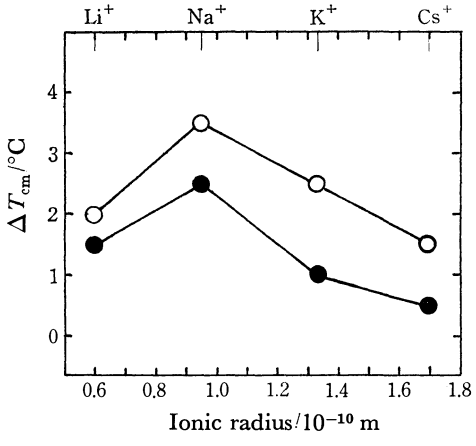

Fig. 6. Relation between ΔT_{cm} and ionic radius.
-●- 0.5 mol kg^{-1}; -○- 1 mol kg^{-1}.

Eigen and Mass[8] measured "the absorption-volume of particle" $Q\cdot\lambda$ in the reaction of alkali metal nitrilotriacetate and alkali metal acetylenediaminetetraacetate complex in aqueous solutions. $Q\cdot\lambda$ is a parameter which characterizes the chemical equilibrium. $Q\cdot\lambda$ *versus* the frequency of the ultrasound curve shows a maximum. The values of $(Q\cdot\lambda)_{max}$ were greatest at Na^+ ion. Hindeman[9] measured the chemical shifts of protons in aqueous solutions of alkali metal halides. The absolute value of the chemical shift for the cations shows a maximum at Na^+ ion.

There are many thermodynamic properties which do exhibit a maximum at Na^+ ion. Desnoyers and Jolicoeur[10] proposed a possible explanation; these maxima may appear because "the strength of ion–solvent interactions decreases with increasing size of the ions, but the coordination number of the ion increases with increasing size." According to X-ray analysis and neutron scattering, the coordination numbers of alkali metal ions are 4 for Li^+, Na^+, and K^+ ions,[11] and 8 for Cs^+ ion.[12] The above suggestion leaves something to be desired. In order to explain the above results, it is necessary to consider the state of the water molecules around the ion more deeply.

The compressibility of the solution will be discussed, since it is a fundamental thermodynamic quantity. Attention will be directed to the concentration range, at which the cospheres of the cation and the anion do not overlap.

The compressibility of an aqueous electrolyte solution is smaller than that of pure water. This is ascribed to two effects:[6] (1) the decrease of compressibility caused by the introduction of incompressible ions, and (2) the change of water structure around the ion. Among the effects, the contribution of effect (1) is larger, and depends more on the concentration rather than on the kind of ions (see Figs. 3 and 4). Recently, Subrahmanyan and Moorthy[13] showed that if these are no interactions between water and solutes, T_{cm} is always lower than T°_{cm}. What they called the dilution effect corresponds to effect (1). Thus, we have the following relation, taking account of effects (1) and (2):

$$T_{cm} = T^{id}_{cm} + T^{ion}_{cm} \quad (4)$$

$$\Delta T_{cm} = T^\circ_{cm} - (T^{id}_{cm} + T^{ion}_{cm}) \quad (5)$$

where T^{id}_{cm} and T^{ion}_{cm} are the contribution by the dilution effect and the ion–water interaction, respectively, and $T^{id}_{cm} > T^{ion}_{cm}$. The value of T^{id}_{cm} is about constant in the case of the alkali metal ions if the concentration is constant, and so ΔT_{cm} depends mainly on T^{ion}_{cm}.

The Na^+ ion is a weak structure-making ion. According to Samoilov,[14] τ_i/τ_o for Na^+ ion is 1.3 at 25 °C, where τ_i and τ_o are the mean residence times of a water molecule in the immediate neighborhood of the ion in the aqueous solution and in the immediate vicinity of a water molecule in pure water, respectively. Since the coordination number of the water molecule around Na^+ ion is 4, the water structure around Na^+ ion is like that of pure water. No disordered water molecules exist outside the reoriented water molecules around an Na^+ ion. Therefore, T^{ion}_{cm} for Na^+ ion is very small and the decrease of the compressibility of the NaCl solution is mainly caused by the dilution effect.

The alkali metal ions do not change the water structure so much. The structure-breaking ion make the thermal motion of water molecules more intense, but the structure-making ions show a contrary effect. Samoilov[14] proved that the surface density of the distribution of water molecule around the ion decreases with increasing the ionic radius. The surface densities

of K^+, Rb^+, and Cs^+ ions are smaller than that of pure water. Therefore, the structure-breaking ion causes the compressibility of the solution to increase in comparison with that of NaCl solution, as seen in Figs. 3 and 4. The value of T_{cm}^{ion} increases and so ΔT_{cm} decreases with increasing size of the ions in the case of K^+, Rb^+, and Cs^+ ions. Nomoto and Endo[3] found that ΔT_{vm} of NH_4I solution is zero up to the concentration of 25 wt%. Both NH_4^+ and I^- ions are the structure-breaking ions. They mentioned that neither ion destroys the water structure markedly and both expand the water lattice.

Water molecules adjacent to Li^+ ion strongly reorient around it; according to Passynski,[15] they should be regarded as incompressible. The disordered water molecules exist outside these reoriented water molecules.[16] The Li^+ ion with immobile water molecules, therefore, behaves like a structure-breaking ion in the case of the acoustic and some thermodynamic phenomena. This model is supported by the fact that the compressibilities of the LiCl, RbCl, and CsCl solutions have values close to each other.

Now we shall call attention to fact that the compressibilities of the solutions are divided into two groups. In the first group, as mentioned above, are the compressibilities of the solutions of LiCl, RbCl, and CsCl. These cations interact strongly with water molecules, though there is a difference in that Li^+ ion is a structure maker but Rb^+ and Cs^+ ions are structure breakers. The second group includes the compressibilities of the solutions of NaCl and KCl. Na^+ and K^+ ions interact weakly with water molecules, and their effects are directly opposite to each other. In the case of the alkali metal–chelate complex, the reactions are divided into two groups in the same way (Ref. 7, Fig. 3).

References

1) G. M. Marks, *J. Acoust. Soc. Am.*, **31**, 936 (1959).
2) P. F. Cholpn, *Soviet Phys. Acoust.*, **12**, 72 (1966).
3) O. Nomoto and H. Endo, *Bull. Chem. Soc. Jpn.*, **44**, 16 (1971).
4) Y. Suzuki and H. Uedaira, *Nippon Kagaku Kaishi*, **1974**, 830.
5) "International Critical Tables," ed by E. W. Washburn, National Research Council, McGraw-Hill Co., New York and London (1928), Vol. 3.
6) F. Hirata and K. Arakawa, *Bull. Chem. Soc. Jpn.*, **45**, 2715 (1972).
7) L. Hall, *Phys. Rev.*, **73**, 775 (1948).
8) M. Eigen and G. Mass, *Z. Phys. Chem. Neue Folge*, **49**, 163 (1966).
9) J. C. Hindeman, *J. Chem. Phys.*, **36**, 1000 (1962).
10) J. E. Desnoyer and C. Jolicoeur, Modern Aspects of Electrochemistry," ed by J. O'M. Bockris and B. E. Conway, Plenum, New York (1969), Vol. 5.
11) H. Ohtaki and M. Maeda, *Kagaku Sosetsu*, **11**, 119 (1976).
12) N. Ohtomo and K. Arakawa, *Bull. Chem. Soc. Jpn.*, in press.
13) S. V. Sabrahmanyam and N. M. Moorthy, *J. Solution Chem.*, **4**, 347 (1975).
14) O. Ya. Samoilov, "Ion No Suiwa," (Translation from Russian by H. Uedaira), Chijin Shokan, Tokyo (1976), Chap. 4.
15) A. G. Pasynskii, *Zh. Fiz. Khim.*, **11**, 606 (1938).
16) H. S. Frank and W.-Y. Wen, *Faraday Discuss. Chem. Soc.*, **24**, 133 (1957).

Charge-transfer Absorption Intensity and Magnetic Property of Solid Ion Radical Salts

Yôichi IIDA

Department of Chemistry, Faculty of Science, Hokkaido University, Sapporo 060

(Received February 9, 1979)

The electronic spectrum of solid ion radical salt is known to be different from the monomer spectrum of the radical ion and to show an intermolecular charge-transfer transition between ion radicals in the low-energy region. The intensity of the charge-transfer absorption was theoretically obtained by applying one-dimensional half-occupied Hubbard model to the segregated stack of ion radicals of solid ion radical salts. The intensity of the charge-transfer absorption was then correlated to the magnetic properties of those solid ion radical salts.

The prominent magnetic, electrical and optical properties of a number of solid ion radical salts have been the subject of many theoretical and experimental investigations over the past fifteen years.[1–15] In such solid ion radical salts, the planar ion radical molecules are known to form, in themselves, a plane-to-plane stacking into infinite one-dimensional columns so as to make a large overlap between their half-occupied molecular orbitals.[5–8] In this case, since any individual radical molecule interacts through charge-transfer most strongly with two other neighboring radicals, the electronic spectrum of the solid salt differs distinctly from the monomer spectrum of the radical ion in solution but shows a charge-transfer transition between ion radicals in the low-energy region. So far, many investigators have observed such charge-transfer absorptions of solid ion radical salts and attempted to explain the electronic state of segregated stack of ion radicals in terms of an isolated cluster model such as a dimer of ion radicals.[3–5] Rigorously speaking, however, the cluster model approximation is not applicable to one-dimensional column composed of infinite stack of ion radical molecules.

In a previous paper,[9] we applied infinite one-dimensional Hubbard model to the columns of ion radical molecules, and investigated the transition energy and the line shape of such charge-transfer absorptions on the basis of Green's function method. In the present paper, we further attempted to explain the intensity of the charge-transfer absorption of solid ion radical salts in terms of the same model. So far, it has been suggested that ion radical salts with strong intensity of the charge-transfer absorption show almost diamagnetic susceptibility and possess strong antiferromagnetic spin exchange interaction between nearest neighbor ion radical molecules, while ion radical salts with weak charge-transfer absorption show almost free paramagnetism obeying Curie law.[2–5,13–15] By using our theoretical approach, we shall give strong theoretical basis to such a close correlation between the intensity of the charge-transfer absorption and the magnetic properties of solid ion radical salts.

Theoretical

For the sake of simplicity, we consider one-dimensional segregated stacks of ion radical molecules in simple solid ion radical salts where each ion radical has one unpaired electron. Hereafter, we take only the half-occupied molecular orbital of the unpaired electron for one site of the ion radical molecule, and assume a model of non-alternant one-dimensional column composed of infinite number of such sites. In this model, each ion radical site has one identical molecular orbital with equal energy level, and there is one electron per each site. Along such one-dimensional column, an unpaired electron transfers from one site to another site, but a strong repulsive force will take place when an electron happens to come onto a site which is already occupied by another electron with opposite spin. Let us denote the intra-site Coulomb repulsive energy as I, and consider a system of electrons described by the following Hamiltonian, which is often called the Hubbard Hamiltonian,[10]

$$\mathcal{H} = \sum_{i,j,\sigma} t_{ij} C_{i\sigma}^{+} C_{j\sigma} + I \sum_{i} n_{i\downarrow} n_{i\uparrow}, \tag{1}$$

where $n_{i\sigma}=C_{i\sigma}^{+}C_{i\sigma}$, and $C_{i\sigma}^{+}$ and $C_{i\sigma}$ are the creation and annihilation operators of an electron with σ-spin at the i-th site, respectively, and where t_{ij} is the transfer matrix element between the i-th and j-th sites, and the repulsive potential, I, appears only when two electrons with up and down spins are at the same site. Since each ion radical site has identical molecular orbital with equal energy level, we put $t_{ii}=0$ without loss of generality. The unperturbed band energy, ε_k, of the system is related to t_{ij} by

$$\varepsilon_k = \sum_{j} t_{ij} e^{i\boldsymbol{k}\cdot(\boldsymbol{R}_i-\boldsymbol{R}_j)}. \tag{2}$$

In the case of non-alternant one-dimensional model, we assume that the transfer matrix elements exist only between nearest neighbor sites. Then, the unperturbed band energy is simply given by

$$\varepsilon_k = 2T\cos ka, \quad \left(-\frac{\pi}{a}\leq k\leq\frac{\pi}{a}\right), \tag{3}$$

where $T(<0)$ is the transfer matrix element between nearest neighbors and a is the lattice separation.

Hereafter, we confine our system within the framework of the one-particle Green's function given by Hubbard in his first paper (it is often referred to as Hubbard I).[10] The Green's function is given by

$$G_{k\sigma}(E) = \frac{1}{2\pi}\left\{\frac{E_{k\sigma}^{U}-I(1-n_{-\sigma})}{E_{k\sigma}^{U}-E_{k\sigma}^{L}}\,\frac{1}{E-E_{k\sigma}^{U}} + \frac{I(1-n_{-\sigma})-E_{k\sigma}^{L}}{E_{k\sigma}^{U}-E_{k\sigma}^{L}}\,\frac{1}{E-E_{k\sigma}^{L}}\right\}, \tag{4}$$

where

$$n_\sigma = \langle n_{i\sigma} \rangle,$$

$$E^U_{k\sigma} = \frac{1}{2}(\varepsilon_k + I + \sqrt{\varepsilon_k^2 + 2(2n_{-\sigma}-1)\varepsilon_k I + I^2}),$$

$$E^L_{k\sigma} = \frac{1}{2}(\varepsilon_k + I - \sqrt{\varepsilon_k^2 + 2(2n_{-\sigma}-1)\varepsilon_k I + I^2}).$$

Here $E^L_{k\sigma}$ is the energy of an electron with σ-spin which moves about avoiding other electrons with $-\sigma$-spin, while $E^U_{k\sigma}$ is the energy of an electron which propagates mainly among sites already occupied with electrons with $-\sigma$-spin. The optical transition from $E^L_{k\sigma}$ to $E^U_{k\sigma}$ corresponds to the intermolecular charge-transfer absorption of the one-dimensional system of solid ion radical salt. The charge-transfer absorption spectrum corresponds to the real part of frequency-dependent conductivity tensor, $\sigma_{\mu\nu}(\omega)$, which is given by[11]

$$\sigma_{\mu\nu}(\omega) \sim \frac{ie^2}{V} \lim_{\delta \to 0_+} \sum_{k,\sigma} \frac{1}{\omega - E^U_{k\sigma} + E^L_{k\sigma} - i\delta} \frac{1}{E^L_{k\sigma} - E^U_{k\sigma}} \times \frac{\partial E^U_{k\sigma}}{\partial k_\mu} \frac{\partial E^L_{k\sigma}}{\partial k_\nu} (f(E^L_{k\sigma}) - f(E^U_{k\sigma})), \quad (5)$$

where ω is the frequency of electromagnetic wave, V is the volume of the system, and $f(E)$ is the Fermi distribution function. If the direction of the one-dimensional column is chosen as x axis, the total intensity of the charge-transfer absorption per unit volume, A, is given by

$$A = \int_0^\infty \mathrm{Re}\, \sigma_{xx}(\omega) \mathrm{d}\omega = -\frac{\pi e^2}{V} \sum_{k,\sigma} \frac{1}{E^L_{k\sigma} - E^U_{k\sigma}} \times \frac{\partial E^U_{k\sigma}}{\partial k_x} \frac{\partial E^L_{k\sigma}}{\partial k_x} (f(E^L_{k\sigma}) - f(E^U_{k\sigma})). \quad (6)$$

We assume a paramagnetic state for simple ion radical salt where each ion radical carries one unpaired electron. This leads to half-occupied Hubbard model with $n_\downarrow = n_\uparrow = 1/2$. In the case when the intra-site Coulomb repulsion energy, I, is much larger than the energy due to the observed temperature, we can well put $f(E^L_{k\sigma}) - f(E^U_{k\sigma}) = 1$. If our system has N one-dimensional chains per unit area perpendicular to the chain axis, we have

$$A = \frac{2\pi N e^2}{L} \sum_{k_x} \frac{1}{(\sqrt{\varepsilon_k^2 + I^2})^3} \frac{1}{4}(\varepsilon_k + \sqrt{\varepsilon_k^2 + I^2}) \times (\sqrt{\varepsilon_k^2 + I^2} - \varepsilon_k) \left(\frac{\partial \varepsilon_k}{\partial k_x}\right)^2, \quad (7)$$

where L is the length of the chain. The summation with k_x in Eq. 7 was carried out by integrating with $(L/2\pi)\int \mathrm{d}k_x$ in the first Brillouin zone. By the use of Eq. 3, we have

$$A = Ne^2 \int_{-\pi/a}^{\pi/a} \frac{1}{4} I^2 \frac{(2Ta)^2 \sin^2 k_x a}{(\sqrt{I^2 + 4T^2 \cos^2 k_x a})^3} \mathrm{d}k_x. \quad (8)$$

By replacing the parameters of $k_x a$ and $2T/I$ into x and t, respectively, we have

$$A = \frac{Ne^2}{4a} I(at)^2 \int_{-\pi}^{\pi} \frac{\sin^2 x}{(\sqrt{1 + t^2 \cos^2 x})^3} \mathrm{d}x. \quad (9)$$

This function can be evaluated only in terms of elliptic integral. However, in the limit of small transfer matrix element region of $|t| = |2T/I| \ll 1$, we have an approximation by expanding

$$1/(\sqrt{1 + t^2 \cos^2 x})^3 = 1 - \frac{3}{2} t^2 \cos^2 x + \frac{3 \cdot 5}{2 \cdot 4} t^4 \cos^4 x + \cdots \quad (10)$$

Therefore, we can obtain

$$A = \frac{Ne^2}{4a} I(at)^2 \int_{-\pi}^{\pi} (\sin^2 x - \frac{3}{2} t^2 \sin^2 x \cos^2 x + \cdots) \mathrm{d}x = \frac{N\pi e^2}{4a} I(at)^2 \left(1 - \frac{3}{8} t^2 + \cdots\right). \quad (11)$$

This is the final expression for the absorption intensity of the charge-transfer transition between ion radicals in non-alternant one-dimensional column of simple solid ion radical salt.

Discussion

In the preceding section, the charge-transfer absorption intensity, A, was expressed as a function of intra-site Coulomb repulsion energy, I, and the nearest neighbor transfer matrix element, T. Obviously, if $T=0$, that is, if no transfer of unpaired electron between ion radical molecules takes place in solid ion radical salt, we have $A=0$ in Eq. 11 and no charge-transfer absorption appears in the solid-state spectrum. On the other hand, for non-zero T value, as long as $2|T| \ll I$, the intensity, A, will be non-zero and will increase progressively with the increase of the $|t| = 2|T|/I$ value, as is given by Eq. 11. In most solid ion radical salts, the I values are known to be of the order of 1 eV, while the magnitudes of $|T|$, to be of the order of 0.1 eV or more.[9,13-15] Therefore, in these solid salts, the magnitude of A is not zero, and this is the reason why a number of solid ion radical salts, such as 7,7,8,8-tetracyanoquinodimethane (TCNQ) anion radical salts, show marked charge-transfer absorptions in their solid-state spectra.[3-5] According to our previous paper,[9] we obtained theoretically the transition energy and the line shape of the charge-transfer absorption of the same system as the present model. The peak energy of the charge-transfer absorption corresponds to $\omega = I$. Thus, from the peak position of the observed charge-transfer absorption, we can estimate the I value experimentally. Therefore, by the use of Eq. 11 together with the estimated I value, we can estimate the T value if the absolute intensity measurements are made with the charge-transfer absorption of solid ion radical salt. This procedure will be the most direct way to estimate the I and T values of our Hubbard model.

Next, we examine how the intensity of the charge-transfer absorption is related to the magnetic properties of solid ion radical salt. In a region of small $|T|$ limit, the system of the present Hubbard model leads to a stabilization of antiferromagnetic state between ion radical molecules.[12] For a pair of nearest neighbor ion radicals, if the direct small exchange interaction is neglected, the energy gap between the parallel and antiparallel spin state is given by $2J = 4T^2/I$. The stabilization of the antiparallel spin state is caused by the intermolecular charge-transfer effect of the unpaired electrons. Therefore, we can well consider our system

of simple solid ion radical salt as one-dimensional Heisenberg antiferromagnetic system with an exchange interaction, J. On the other hand, the charge-transfer absorption intensity, A, in Eq. 11 can be approximated as $A \approx N\pi e^2 I(at)^2/4a = N\pi e^2 a\, T^2/I$ in a region of small $|T|$ limit, where we neglected the terms higher than t^4. In this case, we obtain the relation of $A \approx N\pi e^2 aJ/2$, so that A is nearly proportional to the magnitude of J. The physical meaning of this situation is as follows. Those solid ion radical salts which have very weak charge-transfer absorption intensity will possess very small J values, and thus, show the magnetic properties of almost free paramagnetism obeying Curie law.[14-16] On the other hand, those ion radical salts which have very strong charge-transfer absorptions will possess large J values, and thus, show almost diamagnetic susceptibilities.[2-5,13] So far, these theoretical correlations between the optical and magnetic properties have agreed qualitatively with the experimental observations in a number of solid ion radical salts.[2-5,13-16] Here, we note that, in such ion radical salts, as the I values are of the order of 1 eV and the $|T|$ values are of the order of 0.1 eV, the condition of the small $|T|$ limit approximation is fulfilled. More quantitative measurements of the charge-transfer absorption intensity together with the J values are required to confirm our theoretical relationship $A \propto J$ as well as to determine the magnitudes of the I and $|T|$ values of those solid ion radical salts in more detail.

References

1) L. R. Melby, R. J. Harder, W. R. Hertler, W. Mahler, R. E. Benson, and W. E. Mochel, *J. Am. Chem. Soc.*, **84**, 3374 (1962).

2) W. J. Siemons, P. E. Bierstedt, and R. G. Kepler, *J. Chem. Phys.*, **39**, 3523 (1963); R. G. Kepler, *J. Chem. Phys.*, **39**, 3528 (1963).

3) Y. Iida, *Bull. Chem. Soc. Jpn.*, **42**, 71, 637 (1969); **43**, 2772 (1970); **44**, 663, 1777 (1971); **45**, 105, 624 (1972); Y. Iida and Y. Matsunaga, *Bull. Chem. Soc. Jpn.*, **41**, 2615 (1968).

4) Y. Sato, M. Kinoshita, M. Sano, and H. Akamatu, *Bull. Chem. Soc. Jpn.*, **42**, 3051 (1969); Y. Oohashi and T. Sakata, *Bull. Chem. Soc. Jpn.*, **46**, 3330 (1973).

5) J. Tanaka, M. Tanaka, T. Kawai, T. Takabe, and O. Maki, *Bull. Chem. Soc. Jpn.*, **49**, 2358 (1976).

6) H. Kobayashi, Y. Ohashi, F. Marumo, and Y. Saito, *Acta Crystallogr., Sect. B*, **26**, 459 (1970), and the references cited therein.

7) J. L. deBoer and Aafje Vos, *Acta Crystallogr., Sect. B*, **28**, 835, 839 (1972).

8) M. Konno, H. Kobayashi, F. Marumo, and Y. Saito, *Bull. Chem. Soc. Jpn.*, **46**, 1987 (1973).

9) Y. Iida, *Bull. Chem. Soc. Jpn.*, **50**, 1445 (1977).

10) J. Hubbard, *Proc. R. Soc. London, Ser. A*, **276**, 238 (1963).

11) K. Kubo, *J. Phys. Soc. Jpn.*, **31**, 30 (1971).

12) Z. G. Soos and D. J. Klein, *J. Chem. Phys.*, **55**, 3284 (1971); M. Takahashi, *Prog. Theor. Phys. (Kyoto)*, **42**, 1098 (1969).

13) Y. Iida, *Bull. Chem. Soc. Jpn.*, **51**, 2523, 3637 (1978).

14) Y. Iida, *Bull. Chem. Soc. Jpn.*, **52**, 689 (1979).

15) Y. Iida, *Bull. Chem. Soc. Jpn.*, **52**, 1523 (1979).

16) The theoretical approach in the present paper is applicable not only to solid ion radical salts but also to crystals of neutral free radicals such as 2,2-diphenyl-1-picrylhydrazyl (DPPH). DPPH crystals show antiferromagnetic spin exchange interaction between unpaired electrons of nearest neighbor DPPH molecules but have the exchange interaction parameter as small as $J = 1.55 \times 10^{-5}$ eV. In accordance with this small exchange interaction, the electronic spectrum of solid DPPH is very similar to the spectrum of free DPPH in solution and shows no intermolecular charge-transfer absorption (*i.e.*, $A \approx 0$). See, for example, Z. G. Soos and R. C. Hughes, *J. Chem. Phys.*, **46**, 253 (1967), and H. Inokuchi, Y. Harada, and Y. Maruyama, *Bull. Chem. Soc. Jpn.*, **35**, 1559 (1962).

Electronic Absorption Spectra and Geometry of Radical Ions of Tetraphenylethylene

Hiroshi SUZUKI,* Kinko KOYANO, Tadamasa SHIDA,** and Akira KIRA***

Department of Chemistry, College of General Education, The University of Tokyo, Komaba, Meguro-ku, Tokyo 153

***Department of Chemistry, Faculty of Science, The University of Kyoto, Kitashirakawa-oiwake-cho, Sakyo-ku, Kyoto 606*

****The Institute of Physical and Chemical Research, Wako-shi, Saitama 351*

(Received February 14, 1979)

The geometry of the radical ions of tetraphenylethylene was studied by means of electronic absorption spectroscopy. The spectrum of the anion radical produced by γ-ray irradiation in frozen 2-methyltetrahydrofuran changes markedly on controlled warming. The resultant spectrum resembles the spectra of the anion radical in fluid solutions produced by potassium reduction and by pulse radiolysis. These spectra are distinctly different from the spectra of diphenylmethanide ion and of diphenylmethyl radical. From these facts it is inferred that the relaxed anion radical has a geometry in which the central ethylenic bond is twisted by an angle considerably smaller than 90°, in contrast with the near 90° twist in the dianion, and in which each bond connecting a phenyl group with an ethylenic carbon atom is twisted by a smaller angle than in the molecule. The spectrum of the cation radical produced by γ-ray irradiation in frozen matrices is similar to that of the cation radical produced by pulse radiolysis in fluid solutions and changes only slightly on controlled warming. The geometry of the relaxed cation radical is suggested to be similar to that of the molecule, in contrast with that of the anion radical.

The geometries of the tetraphenylethylene molecule (TPE), anion radical ($TPE^{-\cdot}$), and dianion (TPE^{2-}) are an interesting subject of study because of the possibility of twisting of the central ethylenic bond ("α-α' bond") as well as the bonds connecting a phenyl group with an ethylenic carbon atom ("α-1 bonds").

TPE is considered to have a propeller-like geometry, in which each phenyl group is twisted around an α-1 bond by about 35—42° out of the plane of the α-α' bond.[1]

In order to explain the strong tendency of alkali salts of $TPE^{-\cdot}$ in ethereal solvents to disproportionate to TPE and alkali salts of TPE^{2-},[2-16] Garst *et al.*[6-9,17,18] and Szwarc *et al.*[10-16,19-21] suggested the hypothesis that $TPE^{-\cdot}$ and TPE^{2-} had markedly different geometries. According to their hypothesis, $TPE^{-\cdot}$ has a geometry similar to that of TPE, while TPE^{2-} has a geometry in which two $-CPh_2^-$ groups are perpendicularly twisted around the α-α' bond; owing to the difference in the geometry, $TPE^{-\cdot}$ forms a loose solvent-separated ion pair with an alkali metal ion, while TPE^{2-} forms a tight contact ion aggregate with two metal ions.[10-14,22] This hypothesis also accounts for the relative slowness of the disproportionation.[15,16,23]

The suggested geometry of TPE^{2-} seems to be supported by the similarity of the electronic absorption spectrum of the dianion[24] to those of carbanions of $R-CPh_2^-$ type (*i.e.*, 1,1-diphenyl-1-alkanides), such as 1,1-diphenyl-1-hexanide $[CH_3(CH_2)_4CPh_2^-]$[26] and 1,1,4,4-tetraphenyl-1,4-butanediide $[Ph_2C(CH_2)_2CPh_2^{2-}]$,[31] since this similarity would indicate that the the π-π interaction across the α-α' bond is almost completely absent in TPE^{2-}.

As to the geometry of $TPE^{-\cdot}$, however, no reliable evidence has been presented. In the present work the geometry of this anion radical as well as that of the corresponding cation radical ($TPE^{+\cdot}$) is studied by means of electronic absorption spectroscopy mainly using radiation-chemical techniques, which enable us to study counterion free systems.

Experimental

Spectra of the Radical Ions in Fluid Solutions. The electronic absorption spectrum of $TPE^{-\cdot}$ produced by alkali metal reduction is contaminated to some extent by the concomitantly produced TPE^{2-}. Therefore, the spectrum of $TPE^{-\cdot}$ has been revised several times in the literature.[2-4,6,7,10,15,23,25] In the present work TPE was reduced by potassium in 1,2-dimethoxyethane (DME). Since the disproportionation of alkali salts of $TPE^{-\cdot}$ is endothermic,[2-4,7,10-15] the spectrum ascribable mainly to $TPE^{-\cdot}$ was obtained by measurement at low temperature (about −50 °C) in the presence of a large excessof TPE.

Attempts to produce $TPE^{+\cdot}$ in fluid solution by oxidation with antimony(V) chloride and to measure its spectrum were unsuccessful.

Spectra of the Radical Ions Produced by Pulse Radiolysis of Fluid Solutions at Room Temperature. In order to obtain the spectra of the counterion free radical ions in fluid solutions at room temperature, pulse radiolysis measurements were made. Solutions of TPE were irradiated with 1—2-μs pulses of a 2.5-MeV electron beam with a peak current of 80 mA. Spectra immediately after pulses are assignable to the solute anion if degassed 2-methyltetrahydrofuran (MTHF) or ethanol is used as solvent, and to the solute cation if aerated acetone is used as solvent.[32]

Spectra of the Radical Ions Produced by γ-Ray Irradiation of Frozen Solutions at 77 K. It is known that unambiguous spectra of radical ions can be obtained by γ-ray irradiation of rigid solutions at low temperature.[33-35] The details of experimental procedure have been described in previous papers,[35-38] so only minimum essential information on the experimental conditions will be given here.

TPE was dissolved in MTHF, *s*-butyl chloride (BuCl), or a Freon mixture (FM: an equivolume mixture of trichlorofluoromethane and 1,2-dibromo-1,1,2,2-tetrafluoroethane), to a concentration of 15—60 mol m^{-3}, unless otherwise indicated. The solution was degassed, frozen to a glassy solid at 77 K in liquid nitrogen, and irradiated with γ-rays from ^{60}Co to the dose of $(1—3)\times10^{19}$ eV g^{-1}. The measurement of the spectra was carried out by the use of a Cary 14RI spectrophotometer. The spectrum obtained with the MTHF solution can be

assigned to $TPE^{-\cdot}$ and the spectrum obtained with the BuCl solution, as well as that obtained with the FM solution, to $TPE^{+\cdot}$.[34,35]

The spectra after "illumination (photobleaching)" or after "controlled warming" of γ-irradiated solutions were also measured. Illumination was made by using a tungsten lamp and glass filters. Controlled warming was carried out by taking the γ-irradiated solution out of the liquid nitrogen for a limited time (a few seconds) and then refreezing it at 77 K.

Molecular Orbital Calculation

A semiempirical SCF-MO-CI calculation of π electronic states of the radical ions was made for various geometries by the use of a method developed by Longuet-Higgins and Pople.[39] The details of the calculation procedure are substantially the same as those described in a previous paper.[38]

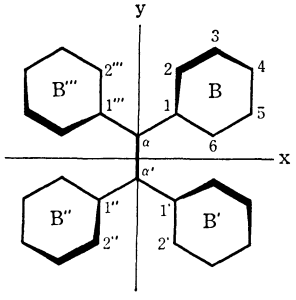

Fig. 1. The carbon skeleton of TPE.

The carbon skeleton of TPE and the numbering of the carbon atoms are illustrated in Fig. 1. All the carbon atoms were assumed to be trigonal. The dihedral angle between the σ-bond planes centered on atoms α and α', for example, is denoted by $\theta_{\alpha\alpha'}$. The calculation was made only for geometries belonging to symmetry group D_2 or D_{2h} with the relation $\theta_{\alpha 1}=\theta_{\alpha' 1'}=\theta_{\alpha' 1''}=\theta_{\alpha 1'''}$. Such a geometry in which $\theta_{\alpha 1}=A°$ and $\theta_{\alpha\alpha'}=B°$ is represented as (A, B).

As a matter of course, the MO calculation based on the π electron approximation becomes less valid as the planarity of the system is lost. However, the calculation is useful as a limited guide for rough characterization of the absorption bands and for qualitative prediction of the relation between the bands and the geometry of the system.

Results and Discussion

Designation of Spectra and of Geometries. For the sake of convenience, the electronic absorption spectra of a radical ion measured under different conditions are designated as follows: The spectrum of a radical ion immediately after its production by γ-ray irradiation in a frozen matrix is designated as F (*frozen*), that after illumination as P (*photobleached*), that after controlled warming as W (*warmed*), and that in a fluid solution as R (*relaxed*). The same designations also apply to the geometries of the radical ion under the respective conditions. In addition, the geometry of the parent neutral molecule is designated as N (*neutral*).

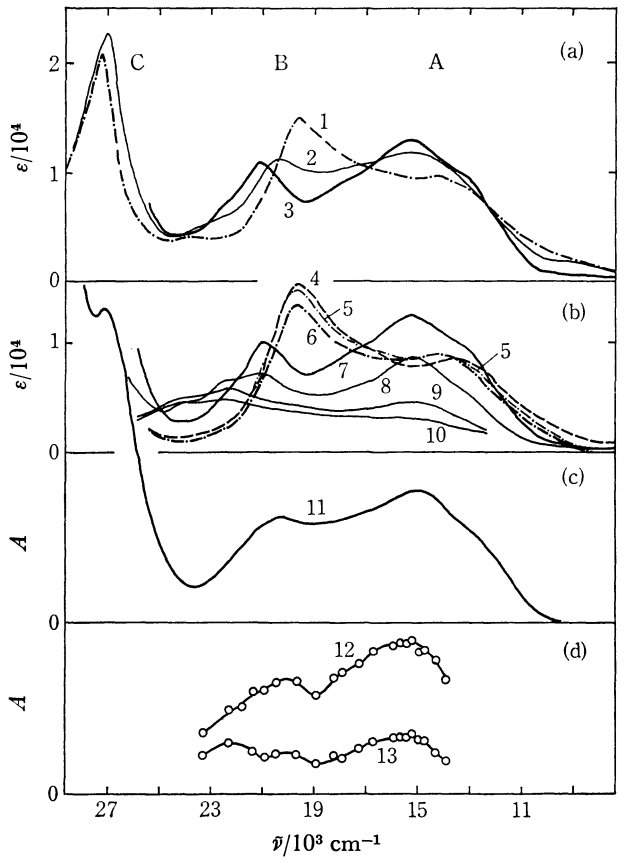

Fig. 2. Electronic absorption spectra of $TPE^{-\cdot}$.
——: Spectrum F, ——: spectrum W or R, -·-·-: spectrum P.
(a) Curve 1: spectrum of a sample obtained by γ-ray irradiation of a dilute solution of TPE in MTHF at 77 K and subsequent illumination with light of $\lambda>700$ nm. Curve 2: spectrum obtained after controlled warming of the sample for curve 1. Curve 3: spectrum of a sample obtained by γ-ray irradiation and subsequent controlled warming. (b) Curve 4: spectrum F. Curve 5: spectrum obtained after illumination of the sample for curve 4 with light of $\lambda>620$ nm. Curve 6: spectrum obtained after subsequent illumination with light of $\lambda>450$ nm. Curve 7: spectrum obtained after controlled warming of the sample for curve 6. Curves 8, 9, and 10: spectra obtained after successive warming of the sample for curve 7. (c) Curve 11: spectrum of $TPE^{-\cdot}$ produced by potassium reduction of TPE in DME at −50 °C. (d) Spectra obtained by radiolysis of a saturated solution of TPE in degassed ethanol at room temperature with a 1-μs electron pulse. Curve 12: spectrum at the end of the pulse. Curve 13: spectrum at 6 μs after the pulse.

The Anion Radical. Assignment of Absorption Bands: Representative spectra of $TPE^{-\cdot}$ measured under various conditions are shown in Fig. 2, and relevant data are shown in Table 1. The values of molar absorption coefficient (ε) for spectra F were determined on the basis of the fact that the yield of the electron from the solvent per unit energy absorbed, $G(e^-)$, is 2.55 for MTHF,[35,37,38] and those for spectra P and W were determined on the assumption that the concentration of the anion radical did not vary on illumination

Table 1. Data on electronic absorption spectra of $TPE^{-\cdot}$

Spectrum Class	No. in Fig. 2	Band C λ_{max}/nm	Band C $\varepsilon/10^4$	Band B λ_{max}/nm	Band B $\varepsilon/10^4$	Band A λ_{max}/nm	Band A $\varepsilon/10^4$
F	4			511	1.54	*ca.* 750	0.85
P	1	368	2.08	512	1.49	*ca.* 700	0.95
P	6			508	1.33	713	0.90
W	2	371	2.27	496	1.13	650	1.19
W	3			476	1.09	652	1.30
R(K/DME)	11	372		498		670	
R(Li/THF)[a]		375	2.35	495	0.85	660	1.13
R(Pulse)	12			*ca.* 500		*ca.* 655	

a) Taken from Ref. 15.

or on controlled warming.

Most of the spectra shown in Fig. 2 cover only the visible region, because the intense absorption by TPE in the near-ultraviolet region obscures the absorption by $TPE^{-\cdot}$ in the same region. By reducing the concentration of TPE in the MTHF solution, part of the electrons produced upon γ-ray irradiation survived scavenging by TPE and became trapped electrons, which exhibited an absorption in the near-infrared region.[37] The absorption, however, could be eliminated by illuminating the γ-irradiated sample with red light. The spectrum of $TPE^{-\cdot}$ which appeared after the illumination extends to the near-ultraviolet region (Curve 1 in Fig. 2). The main bands are designated as A, B, and C, as shown in Fig. 2.

According to the results of the MO calculation, the π bond order of each α-1 bond increases in going from TPE to $TPE^{-\cdot}$. Therefore, the resistance to torsion of the bond will be stronger in $TPE^{-\cdot}$ than in TPE. This, in turn, suggests that the torsion angle of the bond, $\theta_{\alpha 1}$, is possibly smaller in $TPE^{-\cdot}$ than in TPE. Thus, as a tentative model for geometry F of $TPE^{-\cdot}$, geometry (30, 0) was adopted, instead of geometry (35—42, 0) assumed for TPE.[1] The result of the MO calculation for geometry (30, 0) is shown in Table 2, which includes all the transitions having oscillator strength (f) larger than 0.01 and having transition energy (ΔE) smaller than 4.5 eV. By comparison between Fig. 2 and Table 2, bands A, B, and C are ascribed to transitions 2, 7, and 8, respectively.

As is seen in Table 2, transitions 2, 7, and 8 can be well approximated as one-electron excitations. The orbitals involved can be approximately expressed as follows:

$$(b_1)\quad \psi_{13} \approx a\phi_{+1}(E) - b[\phi_{+1}(B) + \phi_{+1}(B') + \phi_{+1}(B'') + \phi_{+1}(B''')]$$

$$(b_3)\quad \psi_{14} \approx a\phi_{-1}(E) + b[\phi_{-1}(B) - \phi_{-1}(B') - \phi_{-1}(B'') + \phi_{-1}(B''')]$$

$$(a)\quad \psi_{15} \approx a[\phi_{-1}(B) - \phi_{-1}(B') + \phi_{-1}(B'') - \phi_{-1}(B''')]$$

$$(b_1)\quad \psi_{21} \approx b\phi_{+1}(E) - a[\phi_{-1}(B) + \phi_{-1}(B') + \phi_{-1}(B'') + \phi_{-1}(B''')]$$

In these expressions, a and b represent coefficients bearing the relation $a>b>0$; $\phi_{+1}(E)$ and $\phi_{-1}(E)$ represent the bonding and the antibonding π orbital of the central ethylenic bond (the $\alpha-\alpha'$ bond), respectively; $\phi_{+1}(B)$ and $\phi_{-1}(B)$, for example, represent the following π orbitals of benzene ring B (see Fig. 1):

$$\phi_{+1}(B) = 12^{-1/2}(2\chi_1+\chi_2-\chi_3-2\chi_4-\chi_5+\chi_6)$$

$$\phi_{-1}(B) = 12^{-1/2}(2\chi_1-\chi_2-\chi_3+2\chi_4-\chi_5-\chi_6)$$

Comparison of Spectra and Inference of Geometries: The spectrum of a DME solution of the potassium salt of $TPE^{-\cdot}$ at -50 °C (Curve 11 in Fig. 2) is very similar to the spectra of tetrahydrofuran (THF) solutions of the lithium and the sodium salt of $TPE^{-\cdot}$ reported by Lundgren *et al.*[15] The latter two spectra are virtually identical, and do not vary with temperature. Furthermore, the enthalpy changes on the dissociation of the ion pairs of $TPE^{-\cdot}$ with the alkali metal cations have small negative values.[15] From these facts the following inferences are drawn: The alkali salts of $TPE^{-\cdot}$ form loose solvent-separated ion pairs in THF and probably in DME also; the spectra of the ion pairs and the spectrum of $TPE^{-\cdot}$ free from the counterion are almost identical, suggesting that the effect of the counterion in the ion pairs on the spectrum of $TPE^{-\cdot}$ is very small and that the geometry of $TPE^{-\cdot}$ in the ion pairs is similar to the geometry of $TPE^{-\cdot}$ free from the counterion in the fluid solutions. Thus, the spectra of ethereal solutions of alkali salts of $TPE^{-\cdot}$ can be considered to directly reflect geometry R of $TPE^{-\cdot}$.

Table 2. Results of the MO calculation for $TPE^{-\cdot}$ of geometry (30, 0)

Transition[a]	ΔE/eV	$\bar{\nu}/10^3$ cm^{-1}	λ/nm	f	P[b]	Character[c]	$\Delta P_{\alpha 1}$[d]	$\Delta P_{\alpha\alpha'}$[e]
2	1.583	12.76	784	0.337	x	0.977(14—15)	−0.061	+0.149
7	2.062	16.62	602	0.168	y	0.970(14—21)	−0.101	+0.177
8	3.025	24.38	410	0.277	y	0.957(13—14)	+0.105	−0.333
11	4.207	33.91	295	0.031	x	0.673(14—23)	−0.029	+0.070
12	4.295	34.62	289	0.057	y	0.659(14—25)	−0.039	+0.068

a) Transitions are numbered in the order of increasing transition energy. b) The polarization of the transition. For the coordinate axes, see Fig. 1. c) The wave function of the excited state of the transition. Only the electron configuration whose coefficient in the wave function is the largest is shown, together with the coefficient. Symbol (i—j) denotes the electron configuration arising from the ground configuration by promotion of an electron from the ith π SCF-MO (ϕ_i) to the jth one (ϕ_j). The orbital index i runs from 1 for the lowest orbital to 26 for the highest one in the order of increasing energy. The coefficient of the ground configuration in the wave function of the ground state is 0.993. d) The change in the π bond order of the α-1 bond ($P_{\alpha 1}$) on the transition. The value of $P_{\alpha 1}$ in the ground state is 0.331. e) The change in the π bond order of the α-α' bond ($P_{\alpha\alpha'}$) on the transition. The value of $P_{\alpha\alpha'}$ in the ground state is 0.659.

Transient spectra of $TPE^{-\cdot}$ produced by pulse radiolysis of a degassed ethanol solution of TPE at room temperature (Curves 12 and 13 in Fig. 2) resemble the spectra of alkali salts of $TPE^{-\cdot}$ in ethereal solutions. Therefore, the geometry of $TPE^{-\cdot}$ produced by pulse radiolysis is probably similar to that of $TPE^{-\cdot}$ produced by alkali metal reduction. It is inferred that $TPE^{-\cdot}$ produced by pulse radiolysis in fluid solution takes the relaxed geometry within the time interval of a pulse width.

The end-of-pulse spectrum of a degassed MTHF solution of TPE closely resembles that of the ethanol solution, except for the appearance of an absorption band at about 500 nm in the former, a band which is ascribed to a relatively long-lived chemical species other than $TPE^{-\cdot}$.

The spectra of γ-irradiated MTHF frozen solutions of TPE (spectra F of $TPE^{-\cdot}$; Curve 4 in Fig. 2) are markedly different from spectra R of $TPE^{-\cdot}$. Controlled warming of the frozen solutions distinctly changed the color of the solutions from purple to dark blue. The spectra after the warming, *i.e.*, spectra W (Curves 3 and 7 in Fig. 2), resemble spectra R. These facts indicate that $TPE^{-\cdot}$ produced in frozen solutions nearly retains the geometry of the neutral TPE (geometry N) owing to the rigidness of the environment, and that during the process of controlled warming the geometry of $TPE^{-\cdot}$ is relaxed to a geometry (geometry W) which is almost identical with geometry R. This means that geometry R of $TPE^{-\cdot}$ is distinctly different from geometry N, in opposition to the aforementioned hypothesis proposed by Garst *et al.* and by Szwarc *et al.* Since the same spectral change from F to W was observed both for solutions of concentration of about 50 mol m^{-3} and for much more dilute solutions, and since spectra W closely resemble spectra R, the spectral change cannot be due to formation of chemical species other than $TPE^{-\cdot}$, such as dimer anions.

Thus, geometry F is inferred to be nearly similar to geometry N, although it may have been partially relaxed towards geometry R, and the spectral change from F to W is interpreted as a result of the geometrical change from F to W. In the spectral change, band A shifts to shorter wavelengths and increases in intensity, band B shifts to shorter wavelengths and decreases in intensity, and band C shifts to longer wavelengths and increases in intensity. This spectral change is in qualitative agreement with what is expected from the result of the MO calculation shown in Tables 3 and 4 if the geometrical change occurs in such a way that $\theta_{\alpha 1}$ becomes smaller and/or $\theta_{\alpha\alpha'}$ becomes larger. Such a geometrical change is conceivable, in view of the result

Table 3. Dependence of transitions in $TPE^{-\cdot}$ on torsion angle $\theta_{\alpha 1}$

Geometry	Transition 8		Transition 7		Transition 2	
	ΔE/eV	f	ΔE/eV	f	ΔE/eV	f
(0, 0)	2.587	0.415	2.234	0.009	1.680	0.276
(15, 0)	2.801	0.346	2.302	0.102	1.723	0.346
(30, 0)	3.025	0.277	2.062	0.168	1.583	0.337
(45, 0)	3.470	0.209	1.654	0.193	1.328	0.301

Table 4. Dependence of transitions in $TPE^{-\cdot}$ on torsion angle $\theta_{\alpha\alpha'}$

Geometry	Transition 8		Transition 7		Transition 2	
	ΔE/eV	f	ΔE/eV	f	ΔE/eV	f
(30, 0)	3.025	0.277	2.062	0.168	1.583	0.337
(30, 15)	2.941	0.299	2.116	0.161	1.626	0.331
(30, 30)	2.616	0.301	2.247	0.152	1.753	0.316
(30, 45)	2.497	0.170	2.171	0.236	1.962	0.279

of the MO calculation that on the change from TPE to $TPE^{-\cdot}$ the π bond orders of the α-1 bond and of the α-α' bond increases and decreases, respectively.[40]

Even in geometry W, $\theta_{\alpha\alpha'}$ cannot be too large. If $\theta_{\alpha\alpha'}$ were so large that the π-π interaction across the α-α' bond were negligibly small, the spectrum of $TPE^{-\cdot}$ would be the superposition of the spectra of a 1,1-diphenyl-1-alkanide ion and of a 1,1-diphenylalkyl radical. Solvent-separated ion aggregates formed of 1,1-diphenyl-1-alkanides and alkali metal cations exhibit an intense absorption band which has its maximum at about 495—501 nm;[26,31] diphenylmethyl radical exhibits a weak band with its maximum at 460 nm and an intense band with its maximum at 335 nm.[41] The observed spectra of $TPE^{-\cdot}$ are definitely different from the superposition of such absorptions.

Angles $\theta_{\alpha 1}$ and $\theta_{\alpha 1'''}$, for example, cannot be simultaneously 0° because of the steric interference of the geminal phenyl groups. Therefore, it is considered that, in going from TPE to the relaxed $TPE^{-\cdot}$, $\theta_{\alpha 1}$'s (*i.e.*, $\theta_{\alpha 1}$, $\theta_{\alpha' 1'}$, $\theta_{\alpha' 1''}$, and $\theta_{\alpha 1'''}$) decrease from about 35—42° not to 0° but to an angle appreciably larger than 0°, while $\theta_{\alpha\alpha'}$ increases from 0° not to 90° as in TPE^{2-} but to an angle considerably smaller than 90°. By consulting the result of the MO calculation (*cf.* Tables 3 and 4), a geometry in which $\theta_{\alpha 1}$'s are about 15—30° and $\theta_{\alpha\alpha'}$ is about 0—30° is proposed as a plausible geometry of the relaxed $TPE^{-\cdot}$. Thus, it is concluded that the geometry of the relaxed $TPE^{-\cdot}$ is different from the geometries of both TPE and TPE^{2-}.

Extensive warming until the rigid MTHF matrix became a viscous fluid brought about a change of the color of the solution to greenish blue and a homogeneous diminution of the absorption by $TPE^{-\cdot}$ with a concomitant appearance of new peaks at 445 and 413 nm (see Curves 9 and 10 in Fig. 2). The new absorption is attributable to 1,1,2,2-tetraphenylethyl radical formed by neutralization of $TPE^{-\cdot}$ with a proton produced upon γ-ray irradiation.[35] Part of the absorption at about 450 nm in the spectrum at 6 μs after the pulse obtained by pulse radiolysis of an ethanol solution of TPE (Curve 13 in Fig. 2) may be attributed to the tetraphenylethyl radical.

Illumination of the γ-irradiated MTHF frozen solution with light of $\lambda > 630$ nm and with light of $\lambda > 420$ nm only slightly changed the spectrum. Thus, the change from spectrum F to spectrum P (Curves 5 and 6 in Fig. 2) is much smaller than the change from F to W. However, the tendencies induced by illumination and by warming are similar. This suggests that illumination may cause a local heating of the matrix to allow the limited relaxation of the radical ions.

Controlled warming of samples exhibiting spectrum P changed the spectrum to spectrum W (Curve 7 in Fig. 2), which was almost identical with that obtained by direct controlled warming of γ-irradiated samples.

The Cation Radical. Assignment of Absorption Bands: Spectra of $TPE^{+\cdot}$, so far unknown in the literature, were measured under various conditions, and representative ones are shown in Fig. 3. Relevant data are given in Table 5. The molar absorption coefficient cannot be precisely evaluated for spectra F of cation radicals.[35] The values of the molar absorption coefficients shown in Fig. 3 and Table 5 were tentatively determined on the assumption that all the positive charges produced in the matrix by γ-ray irradiation were transferred to TPE molecules to produce $TPE^{+\cdot}$. The main bands are designated as A and B, as shown in Fig. 3.

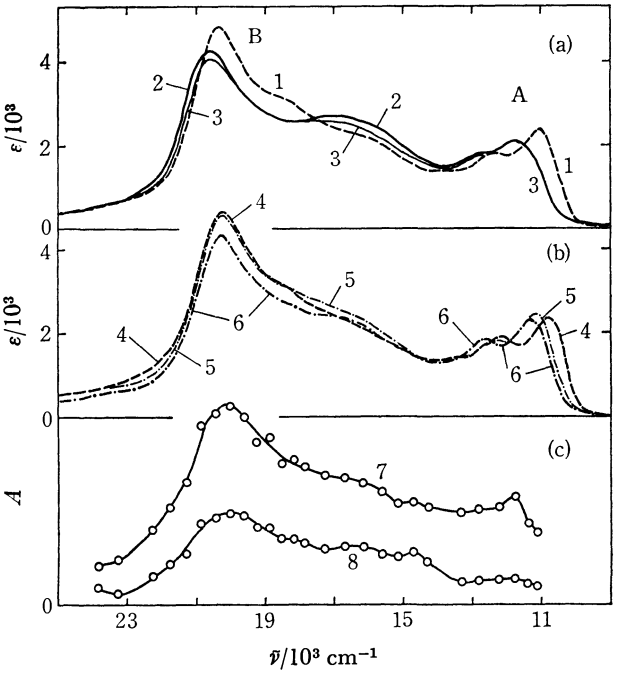

Fig. 3. Electronic absorption spectra of $TPE^{+\cdot}$.
(a) Curve 1: spectrum of a sample obtained by γ-ray irradiation of a solution of TPE in FM at 77 K. Curve 2: spectrum obtained after controlled warming of the sample for curve 1. Curve 3: spectrum obtained after repeated controlled warming of the same sample. (b) Curve 4: spectrum of a sample obtained by γ-ray irradiation of a solution of TPE in BuCl at 77 K. Curve 5: spectrum obtained after illumination of the sample for curve 4 with light of $\lambda>660$ nm. Curve 6: spectrum obtained after illumination of the sample for curve 5 with light of $\lambda>370$ nm. (c) Spectra obtained by pulse radiolysis of a solution of TPE in aerated acetone at room temperature. Curve 7: spectrum at the end of the pulse. Curve 8: spectrum at 5 μs after the pulse.

Table 5. Data on electronic absorption spectra of $TPE^{+\cdot}$

Class	Spectrum No. in Fig. 3	Solvent	Band B λ_{max}/nm	Band B $\varepsilon/10^3$	Band A λ_{max}/nm	Band A $\varepsilon/10^3$
F	4	BuCl	494	4.85	929	2.33
F	1	FM	492	4.85	907	2.41
P	6	BuCl	493	4.28	887	2.26
W	2	FM	484	4.23	853	2.08
R(Pulse)	7,8	Acetone	*ca.* 500		*ca.* 850	

Prolonged γ-ray irradiation for 20—30 min of dilute (2—4 mol m^{-3}) frozen solutions of TPE in FM and in a 5: 1 mixture of 3-methylpentane and BuCl gave spectra of $TPE^{+\cdot}$ which exhibited a band having its maximum at 358 nm (band C). The intensity of band C is comparable to that of band B.

The result of the MO calculation for $TPE^{+\cdot}$ is quite similar to that for $TPE^{-\cdot}$, as should be the case because of the pairing properties of π orbitals of the alternant hydrocarbon. Similarly to the case of $TPE^{-\cdot}$, bands A, B, and C are ascribed to transitions 2, 7, and 8, respectively. As is seen in Table 6, these transitions can be well approximated as one-electron transitions. Of the orbitals involved, ϕ_{13} and ϕ_{14} are similar to the corresponding orbitals of $TPE^{-\cdot}$, and ϕ_6 and ϕ_{12} can be approximately expressed as follows:

$$(b_3)\quad \phi_6 \approx b\phi_{-1}(E) + a[\phi_{+1}(B)-\phi_{+1}(B')-\phi_{+1}(B'')+\phi_{+1}(B''')]$$

$$(b_2)\quad \phi_{12} \approx a[\phi_{+1}(B)+\phi_{+1}(B')-\phi_{+1}(B'')-\phi_{+1}(B''')]$$

The behavior of transitions 2, 7, and 8 with the change in geometry is expected to be quite similar to that of the corresponding transitions in $TPE^{-\cdot}$.

Comparison of Spectra and Inference of Geometries: Spectrum F of $TPE^{+\cdot}$ (Curves 1 and 4 in Fig. 3) is similar as a whole to spectrum F of $TPE^{-\cdot}$ (Curve 4 in Fig. 2). Thus, geometries F of $TPE^{+\cdot}$ and of $TPE^{-\cdot}$ seem to be similar.

In contrast with the case of $TPE^{-\cdot}$, spectrum F of $TPE^{+\cdot}$ changes only slightly both on controlled warming and on illumination [*cf.* Fig. 3, (a) and (b)]. The spectra of $TPE^{+\cdot}$ produced by pulse radiolysis of solutions of TPE in aerated acetone at room temperature (spectrum R; Curves 7 and 8 in Fig. 3) are similar to the spectra of $TPE^{+\cdot}$ in rigid matrices, especially to spectra W (Curves 2 and 3 in Fig. 3). This indicates that geometry R of $TPE^{+\cdot}$ is only slightly different

Table 6. Results of the MO calculation for $TPE^{+\cdot}$ of geometry (30, 0)[a]

Transition	ΔE/eV	$\bar{\nu}/10^3$ cm^{-1}	λ/nm	f	P	Character	ΔP_{a1}	$\Delta P_{aa'}$
2	1.576	12.70	787	0.297	x	0.968(12—13)	−0.061	+0.148
7	2.063	16.63	601	0.141	y	0.959(6—13)	−0.096	+0.167
8	3.015	24.30	412	0.381	y	0.942(13—14)	+0.098	−0.312

a) See footnotes of Table 2. The coefficient of the ground configuration in the wave function of the ground state is 0.993. The values of P_{a1} and $P_{aa'}$ in the ground state are 0.331 and 0.660, respectively.

from geometry F and probably from geometry N.

A detailed comparison of the spectra, however, reveals that there are small, but significant, differences among the spectra of $TPE^{+\cdot}$ measured under different conditions. Especially, in going from spectrum F to spectrum W, both bands A and B shift to shorter wavelengths (*cf.* Table 5), probably indicating that, in going from geometry F to geometry W, $\theta_{\alpha 1}$'s become slightly smaller and/or $\theta_{\alpha\alpha'}$ becomes slightly larger. Both bands A and B are located at slightly shorter wavelengths in spectrum F of the FM solution (Curve 1 in Fig. 3) than in spectrum F of the BuCl solution (Curve 4 in Fig. 3). This fact suggests that the FM glass at 77 K is softer than the BuCl glass at 77 K[35] and that $TPE^{+\cdot}$ in the former is relaxed to some extent immediately after its production, while $TPE^{+\cdot}$ in the latter is almost unrelaxed.

In conclusion, the geometries of relaxed $TPE^{-\cdot}$ and $TPE^{+\cdot}$ are considerably different. This is a rather unexpected finding, because the π bond orders of each bond in the anion and the cation of an alternant hydrocarbon should be equal and hence one would not expect a significant difference for the geometries of the two ions within the framework of π electron approximation. However, a few similar examples are found in the literature: While the geometry of the anion radical of cyclooctatetraene is inferred to be planar,[42,43] the geometry of the corresponding cation radical is suggested to be similar to that of the neutral cyclooctatetraene, a tub form;[35] according to Ishizu *et al.*,[44] the torsion angle of the coannular bond (the 1-1′ bond) of the cation radical of 2,2′,4,4′,6,6′-hexamethylbiphenyl is close to that of the parent neutral molecule (about 70°), while that of the anion radical of 2,2′,6,6′-tetramethylbiphenyl is much smaller (45—50°) (although Sullivan and Fong[45] have cast some doubt on this conclusion). It is of interest that in all these examples, including the present case, the geometry of the cation radical is inferred to be similar to that of the parent neutral molecule while that of the anion radical is considered to be different from that of the molecule.

References

1) H. Suzuki, *Bull. Chem. Soc. Jpn.*, **33**, 389 (1960).
2) A. G. Evans, J. C. Evans, E. D. Owen, and B. J. Tabner, *Proc. Chem. Soc.*, **1962**, 226.
3) J. E. Bennett, A. G. Evans, J. C. Evans, E. D. Owen, and B. J. Tabner, *J. Chem. Soc.*, **1963**, 3954.
4) A. G. Evans and B. J. Tabner, *J. Chem. Soc.*, **1963**, 4613.
5) J. F. Garst and R. S. Cole, *J. Am. Chem. Soc.*, **84**, 4352 (1962).
6) J. F. Garst, E. R. Zabolotny, and R. S. Cole, *J. Am. Chem. Soc.*, **86**, 2257 (1964).
7) J. F. Garst and E. R. Zabolotny, *J. Am. Chem. Soc.*, **87**, 495 (1965).
8) J. F. Garst, J. G. Pacifici, and E. R. Zabolotny, *J. Am. Chem. Soc.*, **88**, 3872 (1966).
9) J. F. Garst, "Free Radicals," ed by J. K. Kochi, John Wiley and Sons, New York (1973), Vol. I, Chap. 9.
10) R. C. Roberts and M. Szwarc, *J. Am. Chem. Soc.*, **87**, 5542 (1965).
11) M. Szwarc, *Prog. Phys. Org. Chem.*, **6**, 323 (1968).
12) M. Szwarc, *Acc. Chem. Res.*, **2**, 87 (1969).
13) A. Cserhegyi, J. Jagur-Grodzinski, and M. Szwarc, *J. Am. Chem. Soc.*, **91**, 1892 (1969).
14) M. Szwarc and J. Jagur-Grodzinski, "Ions and Ion Pairs in Organic Reactions," ed by M. Szwarc, John Wiley and Sons, New York (1974), Vol. 2, Chap. 1.
15) B. Lundgren, G. Levin, S. Claesson, and M. Szwarc, *J. Am. Chem. Soc.*, **97**, 262 (1975).
16) B. DeGroof, G. Levin, and M. Szwarc, *J. Am. Chem. Soc.*, **99**, 474 (1977).
17) E. R. Zabolotny and J. F. Garst, *J. Am. Chem. Soc.*, **86**, 1645 (1964).
18) J. F. Garst, *J. Am. Chem. Soc.*, **93**, 6312 (1971).
19) M. Szwarc, *Proc. R. Soc. London, Ser. A*, **279**, 260 (1964).
20) J. Jagur-Grodzinski, M. Feld, S. L. Yang, and M. Szwarc, *J. Phys. Chem.*, **69**, 628 (1965).
21) G. Levin, B. Lundgren, M. Mohammed, and M. Szwarc, *J. Am. Chem. Soc.*, **98**, 1461 (1976).
22) J. Smid, "Ions and Ion Pairs in Organic Reactions," ed by M. Szwarc, John Wiley and Sons, New York (1972), Vol. 1, Chap. 3.
23) G. Levin, S. Claesson, and M. Szwarc, *J. Am. Chem. Soc.*, **94**, 8672 (1972).
24) The Na salt of TPE^{2-} forms solvent-separated ion aggregates in tetrahydrofuran (THF) at −78 °C, for which the wavelength at the maximum of the main absorption band (λ_{max}) is 510 nm.[10] Li, Na, K, and Ba salts form contact ion aggregates in various solvents at room temperature, for which λ_{max} ranges from 463 nm to 495 nm, depending on the kind of metal cation and of solvent.[2-4,6,10,15,16,21,23,25]
25) A. G. Evans and B. J. Tabner, *J. Chem. Soc.*, **1963**, 5560.
26) The Li salt of the diphenylhexanide forms solvent-separated ion pairs in THF and in 1,2-dimethoxyethane (DME), for which λ_{max} is 495—496 nm.[27-30] It forms contact ion pairs in various solvents such as hexane, benzene, and diethyl ether, for which λ_{max} ranges from 410 nm to 451 nm, depending on the kind of solvent.[28,30]
27) T. E. Hogen-Esch and J. Smid, *J. Am. Chem. Soc.*, **88**, 307 (1966).
28) R. Waack and M. A. Doran, *J. Phys. Chem.*, **67**, 148 (1963).
29) R. Waack and M. A. Doran, *J. Am. Chem. Soc.*, **85**, 1651 (1963).
30) R. Waack, M. A. Doran, and P. E. Stevenson, *J. Am. Chem. Soc.*, **88**, 2109 (1966).
31) Li and Na salts of the tetraphenylbutanediide form solvent-separated ion aggregates in THF at −(50—70) °C, for which λ_{max} is 500—501 nm.[27] Li, Na, and Cs salts form contact ion aggregates in THF at room temperature, for which λ_{max} ranges from 460 nm to 485 nm, depending on the kind of alkali metal cation.[22,27]
32) S. Arai, A. Kira, and M. Imamura, *J. Chem. Phys.*, **54**, 5073 (1971).
33) T. Shida and W. H. Hamill, *J. Chem. Phys.*, **44**, 2375 (1966).
34) T. Shida and W. H. Hamill, *J. Chem. Phys.*, **44**, 4372 (1966).
35) T. Shida and S. Iwata, *J. Am. Chem. Soc.*, **95**, 3473 (1973).
36) W. H. Hamill, "Radical Ions," ed by E. T. Kaiser and L. Kevan, Interscience, New York (1968), Chap. 9.
37) T. Shida, *J. Phys. Chem.*, **73**, 4311 (1969).
38) T. Shida and S. Iwata, *J. Phys. Chem.*, **75**, 2591 (1971).
39) H. C. Longuet-Higgins and J. A. Pople, *Proc. Phys. Soc. London, Sect. A*, **68**, 591 (1955).
40) The partial π bond orders of the α-1 and the α-α′ bond for the half-filled orbital (ψ_{14}) in $TPE^{-\cdot}$ of geometry (30,0) are +0.064 and −0.158, respectively.

41) N. Kanamaru and S. Nagakura, *Bull. Chem. Soc. Jpn.*, **43**, 3443 (1970).
42) T. J. Katz and H. L. Strauss, *J. Chem. Phys.*, **32**, 1873 (1960).
43) R. Chang and C. S. Johnson, Jr., *J. Chem. Phys.*, **46**, 2314 (1967).
44) K. Ishizu, M. Ohuchi, F. Nemoto, and M. Suga, *Bull. Chem. Soc. Jpn.*, **46**, 2932 (1973).
45) P. D. Sullivan and J. Y. Fong, *J. Phys. Chem.*, **81**, 71 (1977).

A Molecular Orbital Study on the Nucleophilicity and the Electrophilicity of Free Radicals in Abstraction Reactions

Hiroyuki SHINOHARA,* Akira IMAMURA,** Takahiro MASUDA,*** and Masaharu KONDO***

Department of Radiology, Fujigaoka Hospital, Showa University, Fujigaoka, Midori-ku, Yokohama 227
***Department of Chemistry, Shiga University of Medical Science, Seta Tsukinowa-cho, Otsu 520-21*
****Department of Chemistry, Faculty of Science, Tokyo Metropolitan University, Fukasawa, Setagaya-ku, Tokyo 158*

(Received February 14, 1979)

The polarities (nucleophilicity and electrophilicity) of free radicals in abstraction reactions were studied by the comparison of the stabilization energies due to delocalization of electrons (SEDE) between a radical and a substrate. The stabilization energies were calculated by the CNDO/2 method for several substrate–radical systems. For the reactions of the methyl radical with chlorinated methanes, the nucleophilicity of the radical was well interpreted by the SEDE from the radical to the substrate. Similarly, the nucleophilicity of the hydrogen atom in chlorine abstraction from chlorinated methanes was indicated by the SEDE from the hydrogen atom to the substrate. In an electrophilic reaction such as hydrogen abstraction by the methyl radical from aliphatic hydrocarbons, the activation energy was found to decrease linearly with an increase in the SEDE from the substrate to the radical. This result is consistent with the electrophilic tendency of the reaction. The SEDE calculated for the reactions of a radical with a series of substrate thus indicates the polarity of the free radical in the abstraction reactions.

The polarity of a free radical has been an interesting subject in organic chemistry ever since a number of observations were published on the polar effect in radical reactions.[1] The Hammett and the Taft equations allow the quantitative study of polar effects in radical reactions as well as ionic reactions. On the basis of ρ values, various kinds of radicals have been found to react as electrophiles in abstraction reactions,[1-8] while a few radicals undergo the nucleophilic reactions.[9-16] The argument about the polarity of the radical, however, was generally empirical and no successful theoretical elucidation of the factors determining the polarity has been given.

The theory of chemical reactivity has succeeded in explaining the relative reactivity of the substrate toward a given radical. The Evans-Polanyi relationship[17] and the delocalizability[18] in the frontier electron theory developed by Fukui and his coworkers are typical theories. In the Evans-Polanyi relationship, the resonance stabilization energy of the formed radical is an important factor in determining the reactivity. On the other hand, the delocalizability is a measure of the stabilization energy due to delocalization of electrons (SEDE) between a substrate and a radical, and is recognized as an excellent reactivity index. Imamura has recently developed a molecular orbital (MO) method which evaluates semiempirically the SEDE from a substrate to a radical or *vice versa*.[19]

In the present work, an attempt was made to explain the polarity of free radicals in terms of the SEDE, which was calculated by the CNDO/2 method for the substrate–radical system. In the nucleophilic reactions, such as hydrogen abstraction by the methyl radical from chlorinated methanes[20] and chlorine abstraction by the hydrogen atom from chlorinated methanes,[21] the SEDE from the radical to the substrate was found to correlate linearly with the activation energy. The SEDE from the substrate to the radical also correlates with the activation energy in electrophilic reactions such as the hydrogen abstraction by the methyl radical from aliphatic hydrocarbons.[21] For several kinds of radicals, the polarity in abstraction reactions is discussed on the basis of both the SEDE and their physical properties.

Method of Calculation

The total energies for the isolated molecule as well as the reacting system were calculated by the UHF method[22] in the CNDO/2 approximation.[23,24] The values of the parameters included in the method are the same as those used in the original papers.[23,24]

Geometries. Geometries used for the calculation are as follows: for CH_4,[25] r(C–H) = 1.09 Å; for CH_3Cl,[26] r(C–H) = 1.103 Å and r(C–Cl) = 1.782 Å; for CH_2Cl_2,[27] r(C–H) = 1.082 Å and r(C–Cl) = 1.772 Å; for $CHCl_3$,[27] r(C–H) = 1.10 Å and r(C–Cl) = 1.758 Å; for CCl_4,[27] r(C–Cl) = 1.755 Å; for aliphatic hydrocarbons, r(C–H) = 1.09 Å and r(C–C) = 1.54 Å. The bond angles for chlorinated methanes and aliphatic hydrocarbons are assumed to be the same as that of methane (109.47°).

Stabilization Energy Analysis. To calculate the SEDE, it was assumed that in a hydrogen abstraction by a radical from a substrate the reaction proceeds through the following steps:

$$RH + X \longrightarrow [R\cdots H\cdots X] \longrightarrow R + HX$$

where RH and X denote a substrate (hydrogen donor) and a radical, respectively. The SEDE (ΔE) is defined by Eq. 1

$$\Delta E = E(R\cdots H \quad X) - E(R\cdots H\cdots X) \qquad (1)$$

where the first term on the right hand side in Eq. 1 denotes the energy of the reacting system in which the delocalization of electrons between RH and X is forbidden. The second term includes the delocalization of electrons. The SEDE is calculated as follows. (i) The total energy of the reacting system [R···H···X] without delocalization of electrons is calculated with the UHF method in the CNDO/2 approximation after dropping all the resonance integrals (I_{rs}) between atomic orbitals (AO's) on the fragment RH and those on the fragment X. Thus we obtain the MO's localized on the fragments RH and X. (ii) By using the MO's obtained in step (i), the modified resonance integrals between AO's (I'_{rs}) are calculated according to Eq. 2

in order to take the delocalization of electrons between particular MO's into account:

$$I'_{rs} = \sum_{(i_1-j_1)} C_{RHi_1,r} C_{Xj_1,s} I_{i_1 j_1}, \quad (2)$$

where $C_{RHi_1,r}$ is the coefficient of AO in the i_1-th MO of substrate RH and $C_{Xj_1,r}$ is for radical X. $\sum_{(i_1-j_1)}$ denotes the summation over a particular orbital set (i_1-j_1). (iii) I'_{rs} is employed to calculate the total energy of the reacting system with the delocalization of electrons, which corresponds to the nucleophilic or the electrophilic nature of the radical in question. (iv) When the vacant MO's of the substrate and the occupied MO's of the radical are chosen for i_1 and j_1, respectively, in Eq. 2, the difference between the two energies obtained in steps (i) and (iii) corresponds to the SEDE from radical to substrate. This energy should be the nucleophilic stabilization energy; it is represented by the symbol N. When the occupied MO's of the substrate and the vacant MO's of the radical are chosen for i_1 and j_1, respectively, the electrophilic stabilization energy E is obtained. Table 1 shows the schematic representation of intermolecular interaction between the MO's of RH and X obtained by dropping the I_{rs} (they interact electrostatically with each other, but the delocalization of electrons is prohibited).

TABLE 1. THE SCHEMATIC REPRESENTATION OF THE ORBITAL INTERACTIONS BETWEEN SUBSTRATE RH AND RADICAL X[a)]

Interaction	α-Spin			β-Spin		
Electrostatic (Zero)	RH	Occ	Vac	RH	Occ	Vac
	X	Occ	Vac	X	Occ	Vac
Nucleophilic-1 (1N)	RH	Occ	Vac	RH	Occ	Vac
	X	Occ	Vac	X	Occ	Vac
Electrophilic-1 (1E)	RH	Occ	Vac	RH	Occ	Vac
	X	Occ	Vac	X	Occ	Vac
Nucleophilic-2 (2N)	RH	Occ	Vac	RH	Occ	Vac
	X	Occ	Vac	X	Occ	Vac
Electrophilic-2 (2E)	RH	Occ	Vac	RH	Occ	Vac
	X	Occ	Vac	X	Occ	Vac
All	RH	Occ	Vac	RH	Occ	Vac
	X	Occ	Vac	X	Occ	Vac

a) The symbols for the orbital interactions used in the text are given in the parentheses. An interaction including the $I_{i_1 j_1}$ is represented by a solid line.

Results

A. Hydrogen Abstraction Reaction by the Methyl Radical. A-1: The Nucleophilicity of the Methyl Radical in Hydrogen Abstractions with Chlorinated Methanes:[20] The coordinate system assumed for the reaction of the methyl radical with methyl chloride is shown in Fig. 1 as an example. Without loss of generality, it is assumed that the methyl radical has four valence electrons with α-spin and three valence electrons with β-spin. The electron distribution shown in Fig. 2 indicates that the delocalization of electrons occurs from the methyl radical to methyl chloride by the interaction $1N$, and from methyl chloride to the methyl radical by $1E$. Thus the stabilization energy represented by N or E corresponds to the

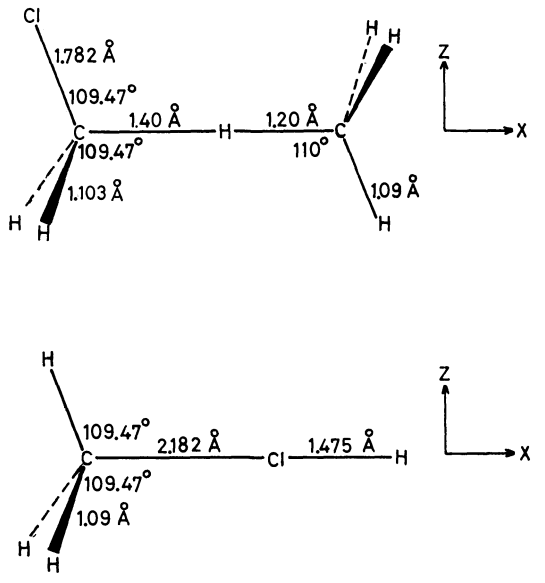

Fig. 1. Interaction models for hydrogen and chlorine abstraction reactions by radicals.

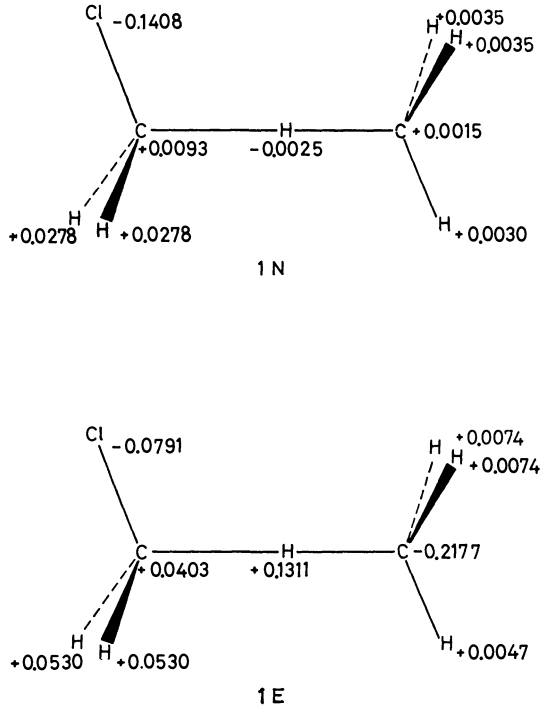

Fig. 2. The electron distribution of CH_3Cl–CH_3 system by the nucleophilic and the electrophilic interactions.

direction of the delocalization of electrons occurring between a substrate and a radical. Figure 3a shows the correlation between the activation energy[20] and the electron density on the hydrogen atom to be abstracted. The activation energy decreases with a decrease in the electron density, and thus the methyl radical reacts as a nucleophile. The nucleophilicity of the methyl radical is explained essentially by the SEDE, as summarized in Table 2. In the reactions with chlorinated methanes the electrophilic stabilization energy $2E$ decreases with the increasing number of chlorine atoms, while the nucleophilic stabilization energy $2N$ increases. As is shown

in Fig. 3b, the reactivities of chlorinated methanes are correlated with the sum of $2N$ and $2E$ calculated by the present procedure. It should be noted that the change of $2N$ from molecule to molecule is much larger than that of $2E$, although $2E$ is larger than $2N$. This suggests that the nucleophilic stabilization energy governs the relative reactivities (Fig. 3c). The conclusion is consistent with the linear relation between the electron density and $2N$, as is shown in Fig. 3d.

The electrophilic stabilization energy depends mainly on the delocalization of electrons with β-spin from the occupied MO's of the substrate to the vacant MO's of the methyl radical, because the stabilization energy for the $2E$ interaction is almost the same as that for the $1E$ interaction, as indicated in Table 2. On the other hand, the nucleophilic stabilization energy depends not only on the delocalization of electrons with α-spin from the occupied MO's of the methyl radical to the vacant MO's of the substrate, but also on the delocalization of

Table 2. The nucleophilicity of the methyl radical in hydrogen abstraction reactions with chloromethanes

Substrate	Orbital[a] interaction	Total[b] energy	Stabilization[b] energy	ET[c]
CH_4 (12.8)[d]	Zero	−18.9882	0	0
	$1N$	−19.0345	0.0463	0.0822
	$1E$	−19.1333	0.1451	−0.2043
	$2N$	−19.0441	0.0559	0.0892
	$2E$	−19.1339	0.1457	−0.2048
	All	−19.2779	0.2897	−0.0276
CH_3Cl (9.4)	Zero	−34.3920	0	0
	$1N$	−34.4449	0.0529	0.0985
	$1E$	−34.5321	0.1401	−0.1982
	$2N$	−34.4555	0.0635	0.1065
	$2E$	−34.5328	0.1408	−0.1987
	All	−34.6894	0.2974	0.0004
CH_2Cl_2 (7.2)	Zero	−49.8072	0	0
	$1N$	−49.8659	0.0587	0.1126
	$1E$	−49.9436	0.1364	−0.1945
	$2N$	−49.8773	0.0701	0.1212
	$2E$	−49.9442	0.1370	−0.1952
	All	−50.1120	0.3048	0.0162
$CHCl_3$ (5.8)	Zero	−65.2482	0	0
	$1N$	−65.3124	0.0642	0.1264
	$1E$	−65.3817	0.1335	−0.1918
	$2N$	−65.3245	0.0763	0.1354
	$2E$	−65.3823	0.1341	−0.1923
	All	−65.5601	0.3119	0.0269

a) See Table 1. b) Atomic units. c) Electron transfer quantity due to delocalization of electrons. Positive values correspond to that from the radical to the substrate and negatives, *vice versa*. d) The values denote the activation energy (kcal/mol). Ref. 20.

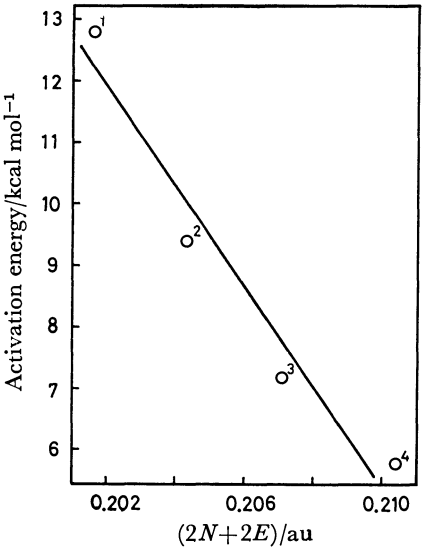

Fig. 3b. The correlation of the activation energy[20] and $(2N+2E)$ for hydrogen abstraction by the methyl radical from chloromethanes. 1—4, see the caption in Fig. 3a.

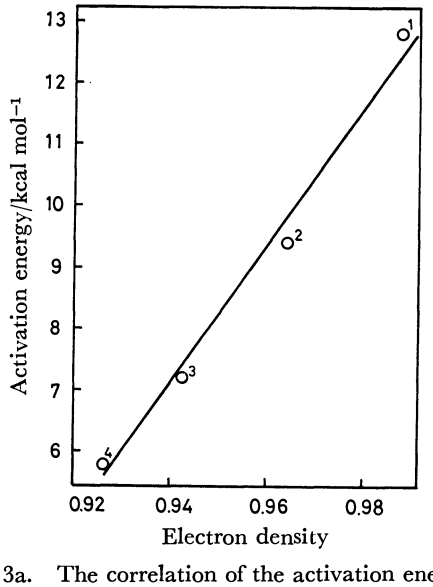

Fig. 3a. The correlation of the activation energy[20] and the electron density for hydrogen abstraction by the methyl radical from chloromethanes. 1: CH_4, 2: CH_3Cl, 3: CH_2Cl_2, 4: $CHCl_3$.

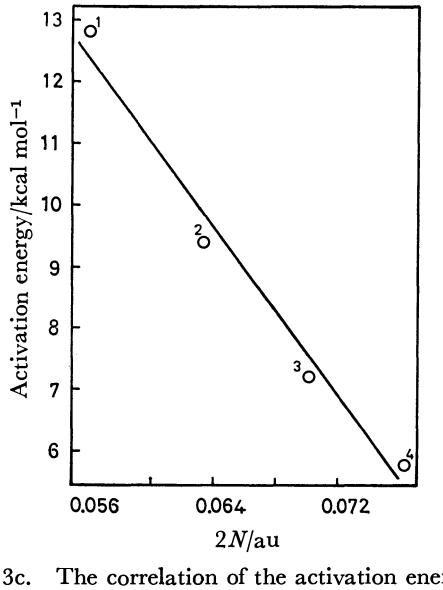

Fig. 3c. The correlation of the activation energy[20] and $2N$ for hydrogen abstraction by the methyl radical from chloromethanes. 1—4, see the caption in Fig. 3a.

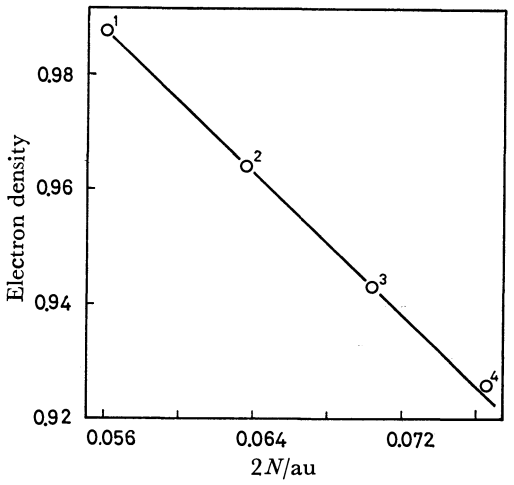

Fig. 3d. The correlation of the electron density and $2N$ for hydrogen abstraction by the methyl radical from chloromethanes. 1—4, see the caption in Fig. 3a.

electrons with β-spin, although the former contribution is larger than the latter. The total stabilization energy including the interaction between the occupied MO's of the substrate and the methyl radical ("All" in Table 2) is larger than that due to the delocalization of electrons, as is shown in Table 2. This energy can be considered to include the redistribution energy in addition to the delocalization energy, which is much larger than the redistribution energy and comes to about 70% of "All". As the ratio of $(2N+2E)$ to "All" is nearly constant for every substrate, a good correlation between the activation energy and "All" is also observed in Table 2.

A-2: The Electrophilicity of the Methyl Radical in Hydrogen Abstraction Reactions with Aliphatic Hydrocarbons:[21] The coordinate system assumed for the reaction is the same as that used in Fig. 1. Figure 4a shows the correlation between the activation energy and the electron density on the hydrogen atom. Contrary to the methyl chloride–methyl radical system, the activation energy decreases with an increase in the electron density and, in this case, the methyl radical reacts as an electrophile. The electrophilic stabilization energy $2E$ was found to correlate linearly with the activation energy, as is shown in Fig. 4a. The results suggest that the electrophilic stabilization energy gives a theoretical basis for the electrophilicity of the methyl radical. A linear relation between the electron density and $2E$ is also shown in Fig. 4b.

On the basis of the results obtained above, the polarity of a free radical can be defined as follows: If the reactivity of the radical toward a series of substrates

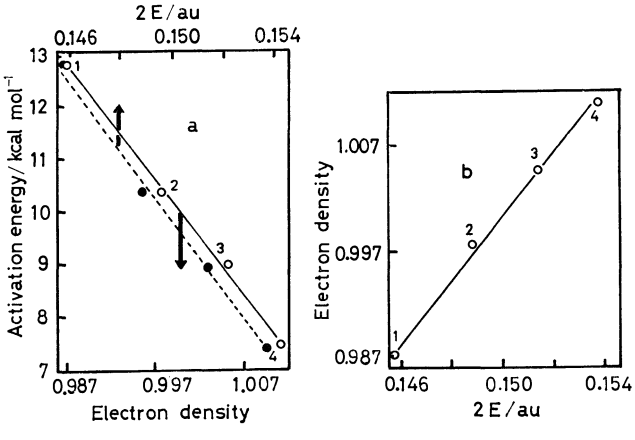

Fig. 4a. The correlation of the activation energy[21] with the electron density and $2E$ for hydrogen abstraction by the methyl radical from aliphatic hydrocarbons. 1: CH_3–H, 2: CH_3CH_2–H, 3: $(CH_3)_2CH$–H, 4: $(CH_3)_3C$–H. For the reaction of the methyl radical with CH_4, 12.8 kcal/mol of the activation energy was used in the present work as the average value in Ref. 12 and 42.

Fig. 4b. The correlation of the electron density with $2E$.

TABLE 3. THE ELECTROPHILICITY OF THE METHYL RADICAL IN HYDROGEN ABSTRACTION REACTIONS WITH ALIPHATIC HYDROCARBONS

Substrate	Orbital[a] interaction	Total[b] energy	Stabilization[b] energy	ET[c]
CH_3CH_3 (10.4)[d]	Zero	−27.6864	0	0
	$2N$	−27.7421	0.0551	0.0902
	$2E$	−27.8353	0.1489	−0.2160
	All	−27.9821	0.2957	−0.0341
$CH_3CH_2CH_3$ (9.0)	Zero	−36.3794	0	0
	$2N$	−36.4350	0.0556	0.0910
	$2E$	−36.5309	0.1515	−0.2246
	All	−36.6806	0.3012	−0.0377
$(CH_3)_3CH$ (7.5)	Zero	−45.0686	0	0
	$2N$	−45.1234	0.0557	0.0920
	$2E$	−45.2224	0.1538	−0.2334
	All	−45.3749	0.3063	−0.0403

a—d) See the notes in Table 2. The activation energy is cited from Ref. 21.

TABLE 4. THE NUCLEOPHILICITY OF THE HYDROGEN ATOM IN CHLORINE ABSTRACTION REACTIONS WITH CHLOROMETHANES

Substrate	Orbital[a] interaction	Total[b] energy	Stabilization[b] energy	ET[c]
CH_3Cl (7.9)[d]	Zero	−25.8786	0	0
	$1N$	−25.9415	0.0629	0.1233
	$1E$	−25.9342	0.0556	−0.0861
	All	−26.0565	0.1779	0.0568
CH_2Cl_2 (6.0)	Zero	−41.2827	0	0
	$1N$	−41.3478	0.0651	0.1302
	$1E$	−41.3375	0.0548	−0.0845
	All	−41.4663	0.1836	0.0593
CH_3Cl (4.3)	Zero	−56.7160	0	0
	$1N$	−56.7828	0.0668	0.1359
	$1E$	−56.7700	0.0540	−0.0834
	All	−56.9052	0.1892	0.0606
CCl_4 (3.5)	Zero	−72.1550	0	0
	$1N$	−72.2232	0.0680	0.1404
	$1E$	−72.2086	0.0536	−0.0828
	All	−72.3487	0.1937	0.0621

a—d) See the notes in Table 2. The activation energy is cited from Ref. 20.

increases with an increase in the nucleophilic stabilization energy, the radical is a nucleophile. Similarly, the radical is an electrophile when the reactivity increases with the increase in the electrophilic stabilization energy.

B: Chlorine Abstraction Reactions by the Hydrogen Atom. Nagai *et al.*[11] reported the nucleophilicity of the triethylsilyl and phenyldimethylsilyl radicals in chlorine abstractions with polychloroalkanes. If the present analysis is applied to the reactions, the information on the theoretical basis of the Taft equation will be obtained from the reactivities of polychloroalkanes toward these radicals. Unfortunately, the molecules and the radicals are too large for the calculation to be carried out. Thus the chlorinated methane–hydrogen atom system[20] was taken as a model case. As will be discussed below, the nucleophilic nature of a radical in hydrogen abstraction depends on the ionization potential of the radical. When the ionization potential is rather low, the nucleophilicity is observed. If the hydrogen atom, which is known to have a high ionization potential (13.6 eV),[28] reacts as a nucleophile in chlorine abstractions with chlorinated methanes, the silyl radical would be expected to react as a nucleophile, because its ionization potential is lower than that of the hydrogen atom. The coordinate system assumed for the reaction is given in Fig. 1. As shown in Fig. 5, the nucleophilic stabilization energy $1N$ correlates with the relative reactivity, so that the hydrogen atom reacts as a nucleophile. The result suggests that the nucleophilicity of the silyl radicals in chlorine abstractions from polychloroalkanes will be interpreted by the SEDE, if the energy is calculated for the reacting system.

C: Hydrogen Abstraction Reactions by Various Kinds of Radicals.[29] For the hydrogen abstractions involving several radicals with hydrocarbons, the activation energy

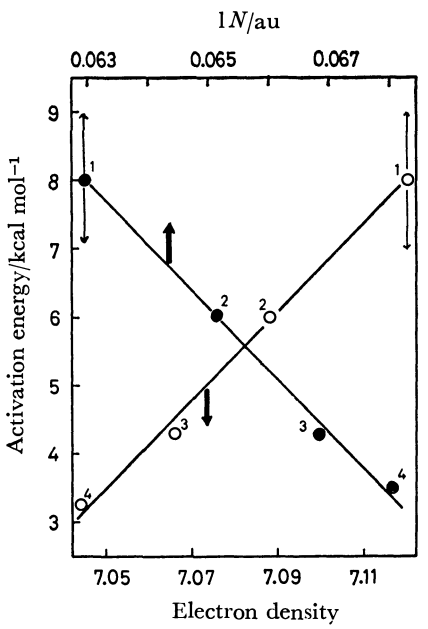

Fig. 5. The correlation of the activation energy[20] with the electron density and $1N$ for chlorine abstraction by the hydrogen atom from chloromethanes. 1: CH_3Cl, 2: CH_2Cl_2, 3: $CHCl_3$, 4: CCl_4.

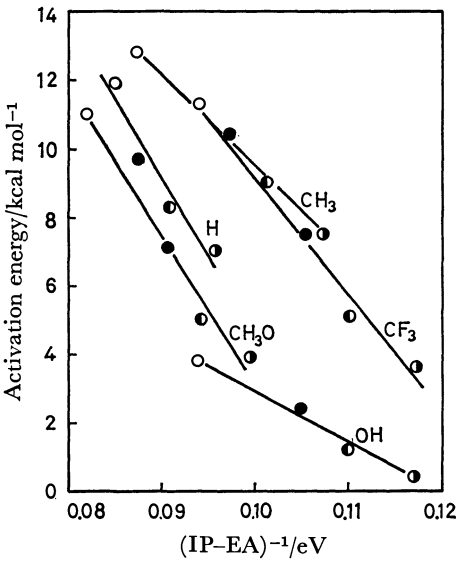

Fig. 6. The correlation between the activation energy[28] and 1/(IP–EA) for hydrogen abstractions by various kinds of radicals from aliphatic hydrocarbons. EA: electron affinity of the radical, IP: ionization potential of the aliphatic hydrocarbon. ○: CH_4, ●: CH_3CH_3, ◐: $CH_3CH_2CH_3$, ◑: $(CH_3)_3CH$.

is plotted against the reciprocal of the difference between the ionization potentials of the hydrocarbons and the electron affinities of the radicals in Fig. 6. The reciprocal of the difference between the ionization potential of hydrocarbon and the electron affinity of the radical is not directly related to the electrophilic stabilization energy, but is qualitatively associated with it. From the linear correlation shown in Fig. 6, it may be inferred that the electrophilic stabilization energy is an important factor in determining the reaction rates for the radicals with low electron affinity (H: 0.80 eV, CH_3O: 0.38 eV)[28] and with high electron affinity (CF_3: 1.85 eV, OH: 1.83 eV).[28] The correlation in Fig. 6 is also consistent with the order of reactivity of the C–H bonds (primary<secondary<tertiary). The result supports the significance of the electrophilic stabilization energy in hydrogen abstractions from aliphatic hydrocarbons, although the important role of the dissociation energy of the C–H bond should also be taken into consideration.[30]

Figure 7 shows the difference in the polarity between the phenyl[31] and the hydroxyl[32] radicals in the reactions with chlorinated methanes. In spite of its high electron affinity (2.20 eV),[28] the phenyl radical reacts as a nucleophile, while the hydroxyl radical and the chlorine atom (3.61 eV)[33] react as electrophiles in the reactions. The difference in behavior is interpreted by the ionization potentials of the radicals (C_6H_5: 9.90 eV,[28] OH: 13.18 eV,[28] Cl: 13.01 eV[34]). The low ionization potential of the phenyl radical is a cause of the nucleophilicity. A radical with a high ionization potential, such as the hydroxyl radical, on the other hand, reacts as an electrophile. Although the stabilization energy analysis was not carried out for these radicals, the correlation between the electron density and the SEDE in Figs. 3d, 4, and 5 indirectly interprets the nucleo-

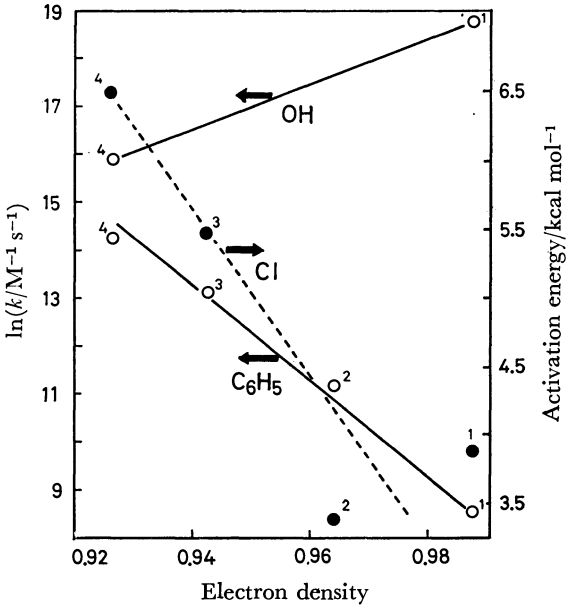

Fig. 7. The nucleophilicity of the phenyl radical and the electrophilicity of the hydroxyl radical or the chlorine atom in hydrogen abstractions with chloromethanes.

philicity of the phenyl radical[35] and the electrophilicity of the hydroxyl radical or the chlorine atom.

Discussion

The polar effect may explain the substituent effect in hydrogen abstraction reactions[1,2,5-7] where an empirical linear energy relation such as the Hammett or the Taft equation holds. In the present work, the electron density on the hydrogen atom was found to correlate with the activation energy. However, for a more fundamental understanding, the polarity of a radical in hydrogen abstraction should be explained by a quantity derived from the reaction system, not one taken from an individual reactant. The stabilization energy due to delocalization of electrons (SEDE), calculated by the CNDO/2 method for the reaction system which consists of a substrate and a radical, is a more essential quantity. As described above, the change of the electrophilic stabilization energy indicates the electrophilic tendency of the radical, and the nucleophilic stabilization energy corresponds to the nucleophilicity.

Since the electron affinity or the ionization potential of a radical can be related with the electrophilic or the nucleophilic stabilization energy,[36] respectively, the Hammett ρ values are expected to correlate with the physicochemical properties of the radical. In fact, Sakurai *et al.*[37] reported a linear relation between the negative ρ values and the electron affinity of the radical for hydrogen abstraction from substituted toluenes. Pryor *et al.*[38] revealed that the isopropyl and the *t*-butyl radicals react as nucleophiles. The positive ρ values increase with the decreasing ionization potentials (IP) of the radicals (CH_3: $\rho=-0.10$,[39] IP=9.86 eV,[28] *i*-C_3H_7: $\rho=0.8$, IP=7.90 eV,[28] *t*-C_4H_9: $\rho=1.0$, IP=7.07 eV[28]). The quantitative correlation may be given by the SEDE, because it is calculated for the reacting system and includes both reactants.

The present analysis is based on the zero differential overlap approximation,[23,24] and thus the quantitative treatment is not sufficient. Furthermore, the SEDE were not calculated for the transition state in the reacting system. The geometries shown in Fig. 1 were tentatively chosen as interaction models, because the reaction path could not be obtained by the CNDO/2 method. However, the essential features of the radical reagent obtained in the present work will probably be valid, because for an argument on the polarity[40] the absolute value of the stabilization energy is not necessarily required but a relative one is sufficient. For a more elaborate approach, the *ab initio* MO method might be adapted to the present analysis. The method of Kitaura and Morokuma,[41] which divides the intermolecular interaction energy into the electrostatic, the polarization, the exchange, and the delocalization energies, will make it possible to apply the *ab initio* method to the present analysis.

We would like to express our gratitude to the Computer Center of Tokyo University for the generous permission to use the HITAC 8700/8800 computer.

References

1) C. Walling, "Free Radicals in Solution," Wiley, New York, N. Y. (1957), pp. 132—140, 365—369, 375—376, 474—491.
2) W. A. Pryor, "Free radicals," McGraw-Hill, New York, N. Y. (1966), p. 170 ff.
3) D. C. Nonhebel and J. C. Walton, "Free-radical Chemistry," Cambridge University Press, London (1974), pp. 178—185.
4) K. U. Ingold and B. P. Roberts, "Free Radical Substitution Reactions," Wiley-Interscience, New York (1971), p. 158.
5) E. S. Huyser, "Free Radical Chain Reactions," Wiley-Interscience, New York (1970), pp. 70, 143, 346, 358.
6) G. A. Russell, "Free Radicals," ed by J. K. Koichi, Wiley, New York (1973), Vol. 1, pp. 293—298.
7) W. A. Pryor, T. H. Lin, J. P. Stanley, and R. W. Henderson, *J. Am. Chem. Soc.*, **95**, 6993 (1973).
8) I. B. Afanas'ev, *Russ. Chem. Rev. (Engl. Transl.)*, **40**, 216 (1971).
9) W. C. Danen and D. G. Saunders, *J. Am. Chem. Soc.*, **91**, 5924 (1969).
10) H. G. Kuivila and E. J. Walsh, Jr, *J. Am. Chem. Soc.*, **88**, 571 (1966).
11) Y. Nagai, K. Yamazaki, I. Shiojima, N. Kobori, and M. Hayashi, *J. Organomet. Chem.*, **9**, 21 (1967).
12) H. Sakurai and K. Mochida, *J. Organomet. Chem.* **42**, 339 (1972).
13) W. A. Pryor, W. H. Davis, Jr., and J. P. Stanley, *J. Am. Chem. Soc.*, **95**, 4754 (1973).
14) W. A. Pryor and W. H. Davis, Jr., *J. Am. Chem. Soc.*, **96**, 7557 (1974).
15) R. W. Henderson and R. D. Ward, Jr., *J. Am. Chem. Soc.*, **96**, 7556 (1974).
16) R. W. Henderson, *J. Am. Chem. Soc.*, **97**, 213 (1975).
17) M. G. Evans and M. Polanyi, *Trans. Faraday Soc.*, **32**, 1340 (1936).
18) K. Fukui, H. Kato, and T. Yonezawa, *Bull. Chem. Soc. Jpn.*, **34**, 1111 (1961).

19) A. Imamura and K. Hirao, *Bull. Chem. Soc. Jpn.*, **52**, 287 (1979). H. Shinohara, A. Imamura, T. Masuda, and M. Kondo, *ibid.*, **51**, 1917 (1978); H. Shinohara, A. Imamura, T. Masuda, and M. Kondo, *ibid.*, **52**, 974 (1979).

20) E. W. R. Steacie, "Atomic and Free Radical Reactions," Reinhold Co., New York (1954), Vol. 11.

21) N. N. Tikhomirova and V. V. Voevodski, *Dokl. Akad. Nauk SSSR*, **79**, 993 (1951).

22) J. A. Pople and R. K. Nesbet, *J. Chem. Phys.*, **33**, 571 (1954).

23) J. A. Pople, D. P. Santry, and G. A. Segal, *J. Chem. Phys.*, **43**, s129 (1965); J. A. Pople and G. A. Segal, *ibid.*, **43**, s136 (1965).

24) J. A. Pople and G. A. Segal, *J. Chem. Phys.*, **44**, 3289 (1966).

25) H. C. Allen, Jr, and E. K. Plyler, *J. Chem. Phys.*, **26**, 972 (1957).

26) W. Gordy, D. F. Smith, and R. F. Trambarulo, "Microwave Spectroscopy," John Wiley and Sons, Inc., New York (1953).

27) "Molecular Structures and Dimensions," ed by O. Kennard and D. G. Watson, A 1, Crystallographic Data Centre Cambridge, International Union of Crystallography, N. V. A. Oosthoek's Uitegevers Mij Utrecht (1972).

28) F. M. Page, "Hand Book of Chemistry and Physics," 53rd ed, 1972—1973, CRC Press.

29) R. R. Baldwin and R. W. Walker, *J. Chem. Soc., Perkin Trans. 2*, **1973**, 361.

30) Bond dissociation energies (kcal/mol) cited from Ref. 8 are as follows: CH_3–H (104), CH_3CH_2–H (98), $(CH_3)_2CH$–H (94), $(CH_3)_3C$–H (91).

31) I. V. Afanas'ev, *Usp. Khim.*, **40**, 385 (1971).

32) M. Anbar, D. Meyerstein, and P. Neta, *J. Chem. Soc., B*, 742 (1966).

33) J. H. Knox, *Trans Faraday Soc.*, **58**, 275 (1962); P. Goldfinger, *J. Chim. Phys.*, **55**, 234 (1958).

34) C. Moore, "Atomic Energy Levels," Circ. No. 467, Vols. I—III, National Bureau of Standards, Washington (1949).

35) The phenyl radical reacts as an electrophile in hydrogen abstraction reactions with substituted toluenes. Ref. 7.

36) The electrophilic (E) and the nucleophilic (N) stabilization energies are approximated by Eqs. 3 and 4, respectively.

$$E = \sum_{i=1}^{m} \sum_{j=p+1}^{q} \frac{(\sum_r \sum_s C_{\mathrm{RH}i,r} C_{\mathrm{X}j,s} I'_{rs})^2}{\varepsilon_j - \varepsilon_i} \tag{3}$$

$$N = \sum_{i=m+1}^{n} \sum_{j=1}^{p} \frac{(\sum_r \sum_s C_{\mathrm{RH}i,r} C_{\mathrm{X}j,s} I'_{rs})^2}{\varepsilon_i - \varepsilon_j} \tag{4}$$

where the occupied MO's of RH are denoted by 1, 2,⋯, m and the vacant MO's by $m+1$, $m+2$,⋯, n, while 1, 2,⋯, p and $p+1$, $p+2$,⋯,q denote the occupied and the vacant MO's of X, respectively. ε_i or ε_j is the i-th or the j-th MO energy.

37) H. Sakurai and K. Tokumaru, *Kagaku No Ryoiki, Zokan*, **81**, 355 (1967).

38) W. H. Davis, Jr., and W. A. Pryor, *J. Am. Chem. Soc.*, **99**, 6365 (1977).

39) W. A. Pryor, U. Tonellato, D. L. Fuller, and S. Jumonville, *J. Org. Chem.*, **34**, 2018 (1969).

40) The stabilization energies were calculated for hydrocarbon-H systems along the reaction path, and the electrophilicity of the H atom determined by the SEDE was not dependent on the reaction path. The nucleophilicity of the Cl_2^- radical was also independent of the assumed geometries. Although the geometries in Fig. 1 are tentatively chosen in the present work, we believe that the result need not be revised when the geometry is changed slightly. *Bull. Chem. Soc. Jpn.*, in press.

41) K. Kitaura and K. Morokuma, *Int. J. Quantum Chem.*, **10**, 325 (1976).

42) A. F. Trotman-Dickenson, *Adv. Free Radical Chem.*, **1**, 1 (1965).

Binding Forces Contributing to the Association of Cyclodextrin with Alcohol in an Aqueous Solution

Yoshihisa MATSUI* and Kazuo MOCHIDA

Department of Agricultural Chemistry, Shimane University, Nishikawazu, Matsue 690

(Received February 16, 1979)

The association constants and thermodynamic parameters were determined for complexes of α- and β-cyclodextrins (CD) with a variety of alcohols (ROH) by the spectrophotometric examination of the inhibitory effect of ROH on the association of CD with azo dyes, and they were analyzed in connection with the partition coefficients of ROH in a diethyl ether–water solvent system in order to elucidate the binding forces contributing to the association of CD with an organic substrate. Hydrophobic and van der Waals interactions were of primary importance in the complexation. Among them, the latter was preferential in α-CD–1-alkanol adducts, while the former, in β-CD–1-alkanol adducts. As the bulkiness of ROH increased, the stability of the α-CD adduct was lowered owing to van der Waals repulsion between ROH and the relatively small α-CD cavity, whereas that of the β-CD adduct was enhanced by the attainment of the close van der Waals contact of ROH with the relatively large β-CD cavity.

Cyclodextrin (CD) is a doughnut-shaped molecule and includes a variety of substrates within the hole of the doughnut.[1–4] The stability of the CD adducts varies markedly either with the size of the CD cavity or with the structure of a substrate. In order to understand the mechanism from which the substrate specificity arises, it is necessary to clarify binding forces contributing to the inclusion process. Hydrogen bonding,[5–8] van der Waals interactions,[8–13] and/or hydrophobic interactions[2,12–17] have been proposed to explain the inclusion phenomena. Among them, hydrophobic interactions have been regarded as especially significant on the basis of the fact that the inclusion phenomena of CD exclusively occur in an aqueous solution.[2] However, a number of thermodynamic parameters determined for the inclusion equilibria indicated that the process is governed by a negative enthalpy change. The entropy term was always negative and contributed unfavorably to the complexation, despite hydrophobic interactions being normally caused by a favorable positive entropy change.[18–19]

Bender *et al.*[2,10] and Bergeron *et al.*[11,20] explained the thermodynamic parameters in terms of the relief of high energy water from the CD cavity. According to them, the water molecules associated with the cavity are enthalpy rich, because they can not have a full complement of hydrogen bonds owing to interference from the glucopyranose rings of CD. The inclusion of a substrate results in the expulsion of these high energy water molecules into bulk water. Another binding force was proposed by Saenger *et al.*,[21–24] who systematically examined the molecular structures of α-CD adducts by means of X-ray crystallography. They found that the macrocycle of α-CD bears an unstrained hexagonal geometry in most of α-CD adducts except for a α-CD–water adduct, in which the macrocyclic conformation of α-CD is unsymmetrically distorted and energetically unstable. The relief of conformational strain energy in the α-CD–water adduct upon substrate inclusion was regarded as the main binding force of complexation. However, Tabushi *et al.*[13] recently showed that the strain relief as well as the relief of high energy water molecules is not major driving force of inclusion, but van der Waals interactions and the breaking of water clusters around an apolar guest molecule are of primary importance in the stabilization of an inclusion complex.

The present study was undertaken to estimate the extent of the contribution of these binding forces to the inclusion process on the basis of the association constants (K_a) and the thermodynamic parameters for the complexation of α- and β-CD with a variety of alcohols (ROH). The observed K_a values were analyzed in connection with the partition coefficients (P_e) of ROH's which are a reasonable measure of hydrophobicity and is often successfully applied to biological structure-activity relationship studies.[25–31] ROH's are well suited for substrates, since they are the simplest organic analogs of water which plays an important role in the inclusion process.

Experimental

Materials. The α- and β-CD were prepared by the method of Lane and Pirt.[32] These substances were separated and purified according to the directions of Cramer and Henglein.[33] Unless otherwise noted, ROH's of reagent grade were used after distillation. 3-Methyl-2-butanol and 3,3-dimethyl-2-butanol were prepared by the reduction of the corresponding 2-butanones with $LiAlH_4$: bp 112.8—113.2 °C (lit,[34] bp 113—114 °C) for the former and bp 120.5—122.2 °C (lit,[34] bp 120—121 °C) for the latter. 2-Methyl-2-pentanol and 2-methyl-2-hexanol were prepared by the reaction of acetone with propyl- and butylmagnesium bromides respectively: bp 52—56 °C/45 mmHg (1 mmHg=133.322 Pa) (lit,[34] bp 122.5—123.5 °C/762 mmHg) for the former and bp 64—67 °C/30 mmHg (lit,[34] bp 141—142 °C/755 mmHg) for the latter. 3-Methyl-3-pentanol and 3-ethyl-3-pentanol were prepared by the reaction of ethylmagnesium bromide with 2-butanone and 3-pentanone respectively: bp 121—123 °C (lit,[34] bp 122.5 °C/758 mmHg) for the former and bp 56—58 °C/33 mmHg (lit,[34] bp 142 °C/764 mmHg) for the latter. 2-Methyl-1-butanol, 2-pentanol, 2-hexanol, 4-methyl-2-pentanol, cyclobutanol, cyclopentanol, cycloheptanol, and cyclooctanol of reagent grade were used without further purification. An azo dye, sodium 4-(4-hydroxy-1-naphthylazo)-1-naphthalenesulfonate (**1**), was prepared and purified as has been described previously.[35] Methyl Orange (**2**) of reagent grade was used without further purification.

Apparatus. Absorption spectra were recorded using a Hitachi Model 124 spectrophotometer. The cells (1.0 cm) were maintained at a constant temperature by means of a

jacket through which water was circulated from a constant-temperature bath. The pH of an aqueous solution was measured by means of an Orion Model 801A digital pH/mV meter. A Hitachi Model 063 gas chromatograph with a FID detector and 2% DEGS columns was used for the quantitative determination of ROH in diethyl ether and in water.

Spectrophotometric Determination of Equilibrium Constants for the Association of α- and β-CD with ROH. The association constant (K_a) for a CD–ROH system was determined by the spectrophotometric examination of the inhibitory effect of the ROH on the association of the CD with a dye. In order to obtain the K_a values in a satisfactory accuracy by this method, it is necessary to choose such a dye as to exhibit a large absorbance change upon the addition of a small amount of CD. If the concentration of CD is high, a large amount of ROH must be added to a CD–dye solution for the sufficient observation of the inhibitory effect of ROH on the association of CD with the dye. However, the addition of a large amount of ROH is undesirable owing either to low solubility in some ROH's or to alteration in solvent composition. In the present study, azo dyes, **2** and **1**, were used for α- and β-CD systems respectively. In 0.10 mol/dm^3 H_2SO_4 containing Na_2SO_4 for the adjustment of the ionic strength (I_c) to be 0.50 mol/dm^3, **2** gave an absorption maximum at 507 nm, the absorbance of which was markedly lowered by the addition of a small amount of α-CD (Fig. 1). Similarly, the addition of β-CD to a solution of **1** in a citrate–phosphate buffer (pH 6.4, I_c=0.05 mol/dm^3, and 25 °C) markedly lowered the absorbance at λ_{max} of 485 nm.[35] Each azo dye forms a 1:1 complex with CD at a CD concentration below 2 mmol/dm^3.[35] Although such experimental conditions as pH and I_c were different between α- and β-CD systems, these may little affect the K_a values since both of CD and ROH are neutral molecules.

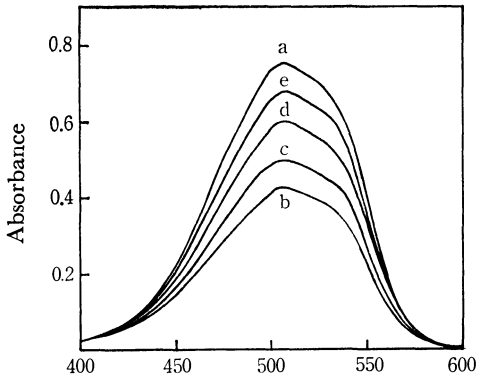

Fig. 1. Effect of α-CD and 1-butanol on the spectrum of **2** in 0.10 mol/dm^3 H_2SO_4 (I_c=0.50 mol/dm^3) at 25 °C.
a) 1.86×10^{-5} mol/dm^3 **2**; b) a+1.01 mmol/dm^3 α-CD; c) b+6.07 mmol/dm^3 1-butanol; d) b+24.3 mmol/dm^3 1-butanol; e) b+70.7 mmol/dm^3 1-butanol.

The addition of ROH to each CD–azo dye system resulted in an increase in absorbance (Fig. 1), indicating that a part of the added ROH is included by CD to expel the complexed azo dye to a bulk solution. Upon an assumption that each ROH also forms a 1:1 inclusion complex with CD, a relation between the absorbance and the concentration of the added ROH was analyzed by the application of the law of mass action and Lambert-Beer's law to the following two chemical equilibria:

$$\mathrm{CD} + \mathrm{AZO} \rightleftharpoons \mathrm{CDAZO} \quad (1)$$

$$\mathrm{CD} + \mathrm{ROH} \rightleftharpoons \mathrm{CDROH} \quad (2)$$

where AZO represents an azo dye, and CDAZO and CDROH, corresponding CD complexes. The initial and equilibrium concentrations were designated by a_0 and a for AZO, b_0 and b for ROH, and c_0 and c for CD respectively. Since CD, ROH, and CDROH are spectrophotometrically transparent in a visible region, the change (ΔA) in absorbance of an azo dye with the addition of CD and ROH is related to the equilibrium concentration (a_0—a) of CDAZO by Eq. 3:

$$a_0 - a = \frac{\Delta A}{\Delta\varepsilon}, \quad (3)$$

where $\Delta\varepsilon$ is the difference in molar absorbance between AZO and CDAZO. Similarly, a is given by

$$a = \frac{(\Delta A_\infty - \Delta A)}{\Delta\varepsilon}, \quad (4)$$

where ΔA_∞ is the difference in absorbance between AZO and CDAZO ($\Delta A_\infty = \Delta\varepsilon \cdot a_0$). The dissociation constant (K_d) for CDAZO is represented by $K_d = c\cdot a/(a_0-a)$, so that the equilibrium concentration of CD is given by

$$c = \frac{K_d(a_0-a)}{a}. \quad (5)$$

On the other hand, the association constant (K_a) for CDROH is represented by

$$K_a = \frac{c_0-c-(a_0-a)}{c[b_0-c_0+c+(a_0-a)]}. \quad (6)$$

Since the value of a_0-a is very small compared with either c_0-c or b_0-c_0+c under the experimental condition of $a_0 \ll b_0$, c_0, Eq. 6 is simplified as Eq. 7:

$$K_a = \frac{c_0-c}{c(b_0-c_0+c)}. \quad (7)$$

The values of K_d and $\Delta\varepsilon$ are easily determined by the Hildebrand-Benesi plot[36] (Table 1). By indroducing these values and the observed ΔA value into Eqs. 3, 4, and 5, we obtain the value of c, which is in turn introduced into Eq. 7 to give the K_a value. Actually, absorption spectra were measured at five or more different concentrations of ROH for each CD–ROH system. The calculated values of log K_a were in good agreement with one another wihin the standard error of ±0.04.

Table 1. The K_d and $\Delta\varepsilon$ values for CD–azo dye inclusion complexes at various temperatures

T/K	K_d/mmol/dm^3	$\Delta\varepsilon\times10^{-4}$/(mmol/dm^3)$^{-1}$ cm^{-1}
	α-CD–**2** system[a]	
283	0.762	3.95
288	0.917	3.93
293	1.08	3.90
298	1.25	3.88
	β-CD–**1** system[b]	
288	0.320	0.773
293	0.360	0.763
298	0.397	0.740
303	0.457	0.723
308	0.491	0.684

a) pH 1.2, I_c=0.50 mol/dm^3, and λ=507 nm.
b) pH 6.4, I_c=0.05 mol/dm^3, and λ=485 nm.

Determination of Thermodynamic Parameters for the Association of CD with ROH. The K_a values were determined at 10, 15, 20, and 25 °C for α-CD–ROH systems and at 15, 20, 25, 30, and 35 °C for β-CD–ROH systems. The method of least squares was applied to the relationship between log K_a and $1/T$. The values of ΔH and ΔS were calculated from the slope and the intercept respectively of the straight line obtained. The values of K_d and $\Delta\varepsilon$ at temperatures used for the determination of K_a are shown in Table 1.

Determination of Partition Coefficient of ROH in a Diethyl Ether–Water System. A proper amount of ROH was added to a mixture of diethyl ether (5 cm³) and water (5 cm³). The resulting mixture was vigorously shaken in a constant-temperature bath at 25 °C for *ca.* 1—2 min and was then allowed to stand in the bath. The aliquots of diethyl ether and aqueous solutions were analyzed by gas chromatography to determine the concentrations of ROH in diethyl ether (c_e) and in water (c_w). The partition coefficient (P_e) of ROH was evaluated as the mean of the values of c_e/c_w determined at five or more different amounts of the added ROH. The standard errors of log P_e were less than 0.04 except for the case of methanol, where it was 0.08.

Results

Table 2 shows the values of log K_a for each CD–ROH system, log P_e for ROH in a diethyl ether–water system, and a few related parameters for each ROH. The number of ROH examined is thirty-four, involving twenty-seven saturated aliphatic ROH's, five alicyclic ROH's, and two aromatic ROH's. Among the saturated aliphatic ROH's, twelve are primary, nine, secondary, and six, tertiary. All the structural isomers are involved among them with regard to saturated aliphatic monofunctional ROH's containing less than five carbon atoms in a molecule. Table 3 shows the thermodynamic parameters determined for the association of several ROH's with CD.

Discussion

Three characteristic relationships were recognized between the structure and log K_a for the examined

Table 2. The values of log K_a, log P_e, log P_o, E_s, and ν (25 °C)

No.	ROH	log K_a		log P_e	log P_o[a]	E_s[b]	ν[c]
		α-CD	β-CD				
1	Methanol	−0.03	−0.49	−1.15	−0.82	0.00	0.52
2	Ethanol	0.75	−0.03	−0.50	−0.32	−0.07	0.56
3	1-Propanol	1.37	0.57	−0.02	0.34	−0.36	0.68
4	2-Propanol	0.69	0.58	−0.18	0.06	−0.47	0.76
5	1-Butanol	1.95	1.22	0.61	0.88	−0.39	0.68
6	2-Methyl-1-propanol	1.44	1.62	0.65	0.83	−0.93	0.98
7	2-Butanol	1.42	1.19	0.41	0.61	−1.13	1.02
8	2-Methyl-2-propanol	0.64	1.68	0.09	0.37	−1.54	1.24
9	1-Pentanol	2.51	1.80	1.20	1.40	−0.40	0.68
10	2-Methyl-1-butanol	2.04	2.08	1.13			1.00
11	3-Methyl-1-butanol	1.87	2.25	1.19	1.16	−0.35	0.68
12	2,2-Dimethyl-1-propanol	1.47	2.76	1.21	1.36	−1.74	1.34
13	2-Pentanol	2.13	1.49	0.89	1.34		
14	3-Pentanol	1.94	1.35	0.96	1.37		
15	3-Methyl-2-butanol	1.27	1.92	0.94			
16	2-Methyl-2-butanol	1.53	1.91	0.64	0.89		
17	1-Hexanol	2.95	2.34	1.80	2.03		0.73
18	2-Hexanol	2.55	1.98	1.58			
19	4-Methyl-2-pentanol	1.72	2.04	1.47			
20	3,3-Dimethyl-2-butanol	1.30	2.75	1.56			
21	2-Methyl-2-pentanol		1.99	1.16			
22	3-Methyl-3-pentanol		2.15	1.10			
23	1-Heptanol	3.36	2.85	2.40	2.41		0.73
24	2-Methyl-2-hexanol		2.33	1.79			
25	3-Ethyl-3-pentanol		2.28	1.63			
26	1-Octanol	3.80	3.17	2.91	3.15	−0.33	0.68
27	2-Octanol	3.15	3.13	2.87			
28	Cyclobutanol	1.59	1.18	0.18		−0.06	
29	Cyclopentanol	1.66	2.08	0.74		−0.51	
30	Cyclohexanol	1.81	2.70	0.95	1.23	−0.79	0.87
31	Cycloheptanol	1.90	3.23	1.22		−1.10	
32	Cyclooctanol	2.25	3.30	1.70			
33	Benzyl alcohol	1.33	1.70	0.96	1.10	−0.38	0.70
34	2-Phenylethanol		2.15	1.18	1.30	−0.38	0.70

a) Ref. 27. b) Ref. 38. c) Ref. 39.

Table 3. Thermodynamic parameters for the association of CD with ROH in an aqueous solution at 25 °C

ROH	α-CD			β-CD		
	ΔG kJ mol^{-1}	ΔH kJ mol^{-1}	ΔS J mol^{-1} K^{-1}	ΔG kJ mol^{-1}	ΔH kJ mol^{-1}	ΔS J mol^{-1} K^{-1}
1-Butanol	−11.1	−12	−2	−7.0	2.9	33
1-Pentanol	−14.3	−16	−5	−10.3	4.6	50
1-Hexanol	−16.8	−19	−8	−13.3	0.4	46
2,2-Dimethyl-1-propanol	−8.4	−12	−12	−15.5	−8.8	21
Cyclohexanol	−10.3	−14	−14	−15.3	−10.0	17

ROH's by a direct comparison of the data in Table 2 with one another.

1) The values of K_a for CD–ROH adducts change with a change in the structure of ROH to a great extent (from −0.03 to 3.80 and from −0.49 to 3.30 for α- and β-CD systems respectively). This fact suggests that neither hydrogen bonding nor the relief of conformational strain energy of CD is of primary importance in stabilizing an inclusion complex between CD and ROH, since these binding forces have been regarded as either weak[2] or virtually constant,[21–24] independent of the structure of a guest molecule, in an aqueous solution.

2) A considerably high positive correlation exists between the observed log K_a and log P_e values. Thus, for α-CD systems;

$$\log K_a = 0.83 \log P_e + 1.00, \quad (8)$$
$$n=29,\ r=0.895,\ \text{and}\ s=0.381,$$

and for β-CD systems;

$$\log K_a = 0.90 \log P_e + 0.98, \quad (9)$$
$$n=34,\ r=0.871,\ \text{and}\ s=0.441,$$

where n, r, and s are the number of data, a correlation coefficient, and the standard deviation of residuals respectively. These observations indicate that hydrophobic interactions play a significantly important role in the complexation.

3) Virtually half of the examined ROH's associate with α-CD more strongly than with β-CD, while the others are reverse. The log K_a values for α-CD complexes with the following ROH's are larger, by 0.5 or more, than those for the corresponding β-CD complexes: Ethanol, 1-propanol, 1-butanol, 1-, 2-, and 3-pentanols, 1- and 2-hexanols, 1-heptanol, and 1-octanol. All of these ROH's contain a straight-chain alkyl group. On the other hand, the following ROH's associate with β-CD more strongly than with α-CD by 0.5 or more in log K_a: 2-Methyl-2-propanol, 2,2-dimethyl-1-propanol, 3-methyl-2-butanol, 3,3-dimethyl-2-butanol, cyclohexanol, cycloheptanol, and cyclooctanol. All of these ROH's contain a bulky alkyl group. It is interesting to compare data for the structural isomers of 1-pentanol and 2,2-dimethyl-1-propanol with each other. The log P_e values for the isomers are 1.20 and 1.21, being virtually equal to each other. Nevertheless, the log K_a value for a α-CD–1-pentanol adduct (2.51) is larger than that for a α-CD–2,2-dimethyl-1-propanol adduct (1.47) by more than unity, whereas the log K_a value for a β-CD–1-pentanol adduct (1.80) is smaller than that for a β-CD–2,2-dimethyl-1-propanol adduct (2.76) by nearly unity. These observations indicate that not only hydrophobic interactions but also the bulkiness of a guest molecule relative to the size of the CD cavity affects on the stability of a CD–ROH adduct. It seems that straight-chain alkanols with rod-like structure are closely fitted to the relatively small α-CD cavity, whereas they are too small in size to be in close contact with the relatively large cavity of β-CD. On the other hand, bulky or globular molecules, such as multi-branched alkanols and cycloalkanols, may be too large in size to be included deeply within the α-CD cavity, while they may be closely fitted to the β-CD cavity. In this connection, it is interesting that the log K_a value for a β-CD–3-ethyl-3-pentanol adduct (2.28) is significantly smaller than that for the corresponding straight-chain isomer (1-heptanol) system (2.85). In this case, the guest molecule is so large in size that it may be difficult even for β-CD to include deeply the guest within the cavity. The above presumptions were substantiated by an examination with the Corey-Pauling-Koltum molecular models, too. Thus, ROH's in α-CD–1-pentanol and β-CD–2,2-dimethyl-1-propanol adducts are readily inserted into the bottom of the corresponding CD cavity to come into close contact with the C-5 hydrogens which locate at the bottom-half of the CD cavity. On the other hand, ROH's in α-CD–2,2-dimethyl-1-propanol and β-CD–3-ethyl-3-pentanol adducts are only able to be inserted into the top-half of the corresponding CD cavity not or hardly to come into contact with the C-5 hydrogens. Taking into account the fact that the CPK models are constructed on the basis of van der Waals radii of atoms, we may say that van der Waals interactions also significantly contribute to the complexation of CD with ROH.

Correlation between log K_a and log P_e. In order to learn the implication of the results in Table 2 more closely, the correlation between log K_a and log P_e was examined either graphically or by regression analysis. The partition coefficient of an organic compound in an apolar solvent–water system is a practical and reasonable index of the hydrophobicity of the compound.[25–31] Although 1-octanol is ordinarily used as an apolar solvent,[27,30] diethyl ether was used in the present study, since a number of ethereal oxygens are aligned within the CD cavity to give an ether-like atmospher.[10] However, it was found that a good linear correlationship exists between the observed P_e and the partition coefficient (P_0) in a 1-octanol–water system for twenty ROH's thus far reported.

$$\log P_e = (1.03\pm0.03)\log P_0 - (0.26\pm0.04), \quad (10)$$
$$n=20,\ r=0.993,\ \text{and}\ s=0.115.$$

A similar equation has been reported by Leo *et al.*[27] for a variety of organic compounds including ROH's:

$$\log P_e = (1.13\pm0.04)\log P_0 - (0.17\pm0.05), \quad (11)$$
$$n=71,\ r=0.988,\ \text{and}\ s=0.186.$$

Accordingly, no difference may arise in conclusion whether $\log P_e$ or $\log P_0$ is used as an index of the hydrophobicity of ROH.

Regression analysis of $\log P_e$ for twenty-seven acyclic alkanols examined showed that the following equation holds for with a very high multiple correlation coefficient:

$$\log P_e = -1.72 + 0.58N - 0.22S - 0.61T, \quad (12)$$
$$n=27,\ r=0.998,\ \text{and}\ s=0.061,$$

where N is the number of carbon atoms contained in ROH, S and T, indicator variables which are equal to zero or unity. If the ROH is primary, $S=T=0$; if secondary, $S=1$ and $T=0$; if tertiary, $S=0$ and $T=1$. Equation 12 indicates that $\log P_e$ of ROH is virtually defined only by the number of carbon atoms in ROH and the class of the ROH.

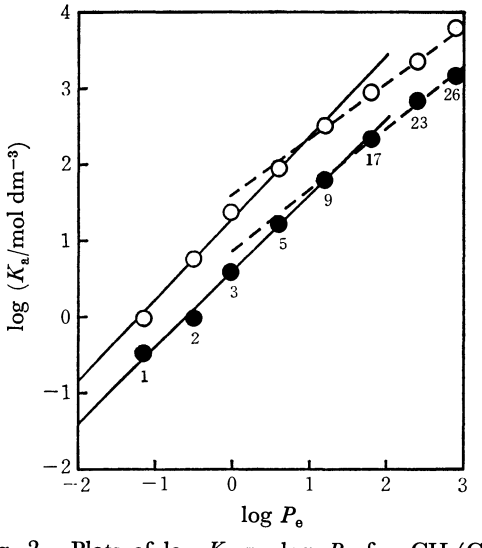

Fig. 2. Plots of $\log K_a$ *vs.* $\log P_e$ for $CH_3(CH_2)_nOH$ (n=0—7).
○: α-CD system; ●: β-CD system.
The solid and dashed lines were obtained by the application of the least squares method to the set of data for n=0—4 and n=4—7 respectively. Numbers shown refer to the numbers in the first column of Table 2.

Figure 2 shows the plot of $\log K_a$ *vs.* $\log P_e$ for CD–1-alkanol systems. Both the plots for α- and β-CD systems gave approximately straight lines with a slope of *ca.* unity. For the α-CD system,

$$\log K_a = 0.92\log P_e + 1.25, \quad (13)$$
$$n=8,\ r=0.994,\ \text{and}\ s=0.153,$$

and for the β-CD system,

$$\log K_a = 0.94\log P_e + 0.58, \quad (14)$$
$$n=8,\ r=0.998,\ \text{and}\ s=0.099.$$

However, it was recognized in each system that a refractive point does exist around the point corresponding to 1-pentanol and the plots for the higher alkanols tend to locate below a straight line drawn through the plots for the lower alkanols. The solid and dashed lines in Fig. 2 were obtained by the application of the least squares method to the sets of data from methanol to 1-pentanol and from 1-pentanol to 1-octanol respectively. Taking into account the depth of the CD cavity (*ca.* 7 Å[2]) together with the mean length of an aliphatic C–C bond (1.537 Å[37]), we can presume that the whole molecule of 1-butanol or even 1-pentanol is completely included within the CD cavity, while a part of the molecule of 1-hexanol or higher alkanols is protruded from the CD cavity to a bulk solution. In the case of the latter, interactions between CD and ROH may be lowered either by the incomplete liberation of iceberg water[18] or water cluster[19] around the apolar alkyl chain of ROH upon inclusion or by the incomplete van der Waals contact of the alkyl group with the CD cavity.

It is also evident from Fig. 2 that each 1-alkanol associates with α-CD more strongly by a factor of 6—7 than with β-CD. Although pH and I_c of solutions used are different between α- and β-CD systems for the sake of experimental convenience (*cf.* Experimental), such difference may have no or little effect on the value of $\log K_a$, since both of CD and ROH are neutral molecules. The difference in $\log K_a$ between α- and β-CD systems might be attributed to the difference either in size or, if any, in hydrophobicity between the α- and β-CD cavities. However, no evidence has ever been offered for a postulate that the hydrophobicity of the α-CD cavity is greater than that of the β-CD cavity. The solubility of α-CD in water is rather 8 times that of β-CD.[1] Thus, it is unlikely that the α-CD cavity is more hydrophobic than the β-CD cavity to cause the difference in $\log K_a$ between α- and β-CD systems. It is much reasonable to consider that α-CD includes 1-alkanol in closer contact with each other than β-CD does. According to Bergeron and Meely,[20] the relief of high-energy water molecules in the inclusion process of CD is substantiated by the fact that a number of organic molecules associate with β-CD more strongly than with α-CD. However, the reverse is true for the present CD–1-alkanol systems, indicating that the basis given by them is not always general.

Figures 3 and 4 show the plots of $\log K_a$ *vs.* $\log P_e$ for branched or cyclic ROH–CD systems. Both of the plots for the α- and β-CD systems showed considerable scatter in contrast to the plots for 1-alkanol systems. However, a remarkable trend was found by comparing both plots with each other. Most of the plots for a α-CD system (Fig. 3) locate below the straight line obtained by the regression analysis of the data for a α-CD–1-alkanol system (Eq. 13), while those for a β-CD system (Fig. 4) locate above the straight line given by Eq. 14. This observation shows that it is general for a bulky ROH to associate with α-CD less strongly and with β-CD more strongly than a rod-like 1-alkanol if the $\log P_e$ values are the same.

An interesting indication is afforded by the plots of $\log K_e$ *vs.* $\log P_e$ for cycloalkanols shown by solid circles

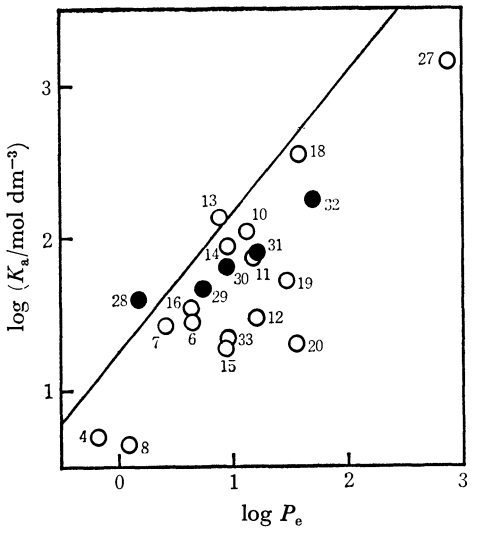

Fig. 3. Plots of log K_a *vs.* log P_e for complexes of α-CD with branched ROH's (○) and cycloalkanols (●). The solid line was given by the plots for a α-CD–1-alkanol system. Numbers shown refer to the numbers in the first column of Table 2.

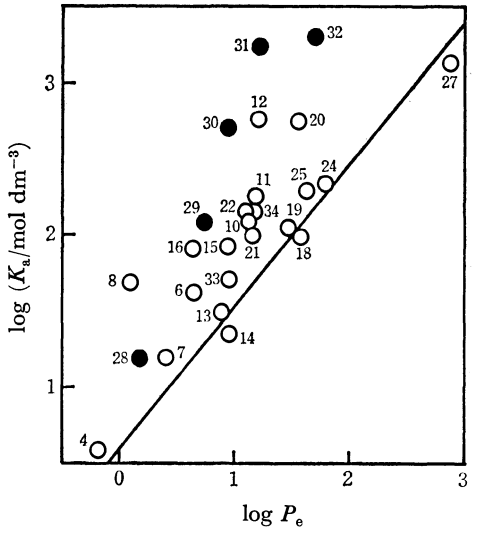

Fig. 4. Plots of log K_a *vs.* log P_e for complexes of β-CD with branched ROH's (○) and cycloalkanols (●). The solid line was given by the plots for a β-CD–1-alkanol system. Numbers shown refer to the numbers in the first column of Table 2.

in Figs. 3 and 4. In the case of a α-CD system, a plot for cyclobutanol locates slightly above the straight line for a 1-alkanol system. As the size of the cycloalkanol ring increases, the plot comes to locate below the line and the difference between them increases. On the other hand, each plot for a β-CD–cycloalkanol system locate above the straight line for 1-alkanols. The difference between them increases with increasing size of the cycloalkanol ring. The maximum difference is attained at the plot for cycloheptanol and the difference for cyclooctanol is significantly smaller than that for cycloheptanol. These results suggest that the α- and β-CD cavities are large in size enough to come into the closest contact with cyclobutanol and cycloheptanol respectively.

Polarizability, molar refraction (MR), Taft's steric substituent constant (E_s),[38] and the ν parameter given by Charton[39] are frequently used for a comparative index of molecular bulkiness in the quantitative study of structure-activity relationship. Among them, the first two were not suitable for the present study, since they vary markedly with a change in the number of carbon atoms in molecule but slightly with a change in structure among isomers. In contrast, the values of E_s and ν for structural isomers are significantly different from one another, so that the possibility is present that either E_s or ν is accessible for the index of molecular bulkiness in the present case. A correlation analysis for ROH's with the known values of E_s and ν (Table 2) gave Eqs. 15—18. For a α-CD system,

$$\log K_a = 0.92 \log P_e + 0.42E_s + 1.24, \quad (15)$$
$$n=17,\ r=0.953,\ \text{and}\ s=0.271,$$
$$\log K_a = 0.95 \log P_e - 0.88\nu + 1.67, \quad (16)$$
$$n=17,\ r=0.968,\ \text{and}\ s=0.269,$$

and for a β-CD system,

$$\log K_a = 0.97 \log P_e - 0.65E_s + 0.60, \quad (17)$$
$$n=18,\ r=0.938,\ \text{and}\ s=0.383,$$
$$\log K_a = 0.91 \log P_e + 1.36\nu - 0.17, \quad (18)$$
$$n=18,\ r=0.962,\ \text{and}\ s=0.296.$$

The results of the F- and t-tests showed that all of Eqs. 15—18 are reliable with a 95% level of confidence, although the values for r and s indicate that ν is somewhat preferred to E_s as an index of molecular bulkiness. In each equation, the dependence of log K_a on log P_e was virtually constant (0.91—0.97) and equal to those for 1-alkanol systems (0.92—0.94, *cf.*, Eqs. 13 and 14). On the other hand, the dependence of log K_a on either E_s or ν was remarkably different between α- and β-CD systems: The coefficient of E_s was positive in sign for a α-CD system and negative for a β-CD system, while the reverse is true for the coefficients of ν. These clear-cut differences in sign between α- and β-CD systems reflect the fact that a bulky ROH is subject to van der Waals repulsion by the α-CD cavity and to van der Waals attraction by the β-CD cavity.

Thermodynamic Parameters for CD–ROH Systems. The above presumptions on the driving forces of inclusion were substantiated by the determination of thermodynamic parameters, ΔH and ΔS, for the association of CD with ROH (Table 3). It is very interesting that both of ΔH and ΔS for β-CD–1-alkanol systems are positive. This fact indicates that the complexation is not governed by enthalpy but by entropy. It has rarely been reported that the inclusion process of CD is accompanied by a positive entropy change. Only a α-CD–1-adamantanecarboxylate system, reported by Komiyama and Bender,[17] falls under this category. Among the binding forces proposed for the inclusion phenomena of CD, only hydrophobic interactions are governed by entropy. Thus, it is obvious that hydrophobic interactions play a primary role in the complexation of β-CD with 1-alkanols.

As the bulkiness of ROH increases, the ΔH term becomes negative and the contribution of ΔS to the binding becomes low even in the case of a β-CD system. Such a change may be attributed to an increase in contribution of van der Waals interactions ($\Delta H<0$, $\Delta S<0$) to the complexation.

On the other hand, both of ΔH and ΔS are negative in the case of α-CD–1-alkanol systems, where it was suggested that the contribution of van der Waals interactions is very large. A decrease in the stability of α-CD–ROH adducts with an increase in bulkiness of ROH is mainly caused by a marked decrease in contribution of the ΔH term to the complexation. Komiyama and Bender[17] have also suggested that the contribution of the ΔH term to complexation is very little compared with that of the ΔS term in the complexation of bulky 1-adamantanecarboxylate with α-CD.

In conclusion, it was shown that hydrophobic and van der Waals interactions are of primary importance in the inclusion process of CD–ROH systems. Among them, the latter is preferential for α-CD–1-alkanol adducts and the former for β-CD–1-alkanol adducts. As the bulkiness of ROH increases, the stability of α-CD adducts decreases owing to van der Waals repulsion, while that of β-CD adducts increases owing to the attainment of the close van der Waals contact of ROH with the β-CD cavity. The present conclusion is very similar to that given by Tabushi *et al.*[13] by means of theoretical calculation.

The authors are indebted to Miss Mutsuko Kanzaki for her help in making some of the measurements.

References

1) D. French, *Adv. Carbohydr. Chem.*, **12**, 189 (1957).
2) D. W. Griffiths and M. L. Bender, *Adv. Catal.*, **23**, 209 (1973).
3) T. Kuge and K. Takeo, *Denpun Kagaku*, **21**, 151 (1974).
4) A. Mifune and A. Shima, *Yuki Gosei Kagaku Kyokai Shi*, **35**, 116 (1977).
5) F. Cramer and W. Kampe, *J. Am. Chem. Soc.*, **87**, 1115 (1965).
6) Y. Matsui, H. Naruse, K. Mochida, and Y. Date, *Bull. Chem. Soc. Jpn.*, **43**, 1909 (1970).
7) J. L. Hoffman and R. M. Bock, *Biochemistry*, **9**, 3542 (1970).
8) C. Van Hooidonk and J. C. A. E. Breebaart-Hansen, *Recl. Trav. Chim. Pays-Bas*, **90**, 680 (1971).
9) B. Casu and L. Rava, *Ric. Sci.*, **36**, 733 (1966).
10) R. L. VanEtten, J. F. Sebastian, G. A. Clowes, and M. L. Bender, *J. Am. Chem. Soc.*, **89**, 3242 (1967).
11) R. J. Bergeron, M. A. Channing, G. J. Gibeily, and D. M. Pillor, *J. Am. Chem. Soc.*, **99**, 5146 (1977).
12) a) K. Harata, *Bull. Chem. Soc. Jpn.*, **49**, 2066 (1976); b) K. Harata, H. Uedaira, and J. Tanaka, *ibid.*, **51**, 1627 (1978).
13) I. Tabushi, Y. Kiyosuke, T. Sugimoto, and K. Yamamura, *J. Am. Chem. Soc.*, **100**, 916 (1978).
14) F. Cramer, W. Saenger, and H.-Ch. Spatz, *J. Am. Chem. Soc.*, **89**, 14 (1967).
15) P. V. Demarco and A. L. Thakkar, *J. Chem. Soc., Chem. Commun.*, 2 (1970).
16) C. Van Hooidonk and J. C. A. E. Breebaart-Hansen, *Recl. Trav. Chim. Pays-Bas*, **91**, 958 (1972).
17) M. Komiyama and M. L. Bender, *J. Am. Chem. Soc.*, **100**, 2259 (1978).
18) W. Kauzmann, *Adv. Protein Chem.*, **14**, 1 (1959).
19) G. Némethy and H. A. Scheraga, *J. Chem. Phys.*, **36**, 3401 (1962).
20) R. J. Bergeron and M. P. Meeley, *Bioorg. Chem.*, **5**, 197 (1976).
21) P. C. Manor and W. Saenger, *J. Am. Chem. Soc.*, **96**, 3630 (1974).
22) W. Saenger, M. Noltemeyer, P. C. Manor, B. Hingerty, and B. Klar, *Bioorg. Chem.*, **5**, 187 (1976).
23) B. Hingerty and W. Saenger, *J. Am. Chem. Soc.*, **98**, 3357 (1976).
24) W. Saenger, R. K. McMullan, J. Fayos, and D. Mootz, *Acta Crystallogr., Sect. B*, **30**, 2019 (1974).
25) K. Kiehs, C. Hansch, and L. Moore, *Biochemistry*, **5**, 2602 (1966).
26) F. Helmer, K. Kiehs, and C. Hansch, *Biochemistry*, **7**, 2858 (1968).
27) A. Leo, C. Hansch, and D. Elkins, *Chem. Rev.*, **71**, 525 (1971).
28) C. Hansch, A. Leo, and D. Nikaitani, *J. Org. Chem.*, **37**, 3090 (1972).
29) C. Hansch, A. Leo, S. H. Unger, K. H. Kim, D. Nikaitani, and E. J. Lien, *J. Med. Chem.*, **16**, 1207 (1973).
30) R. N. Smith, C. Hansch, and M. M. Ames, *J. Pharm. Sci.*, **64**, 599 (1975).
31) C. Silipo and C. Hansch, *J. Am. Chem. Soc.*, **97**, 6849 (1975).
32) A. G. Lane and S. J. Pirt, *J. Appl. Chem. Biotechnol.*, **21**, 330 (1971).
33) F. Cramer and F. M. Henglein, *Chem. Ber.*, **91**, 308 (1958).
34) "Lange's Handbook of Chemistry," ed by J. A. Dean, 11th ed, McGraw-Hill, New York (1973), pp. 7-78—7-244.
35) Y. Matsui and K. Mochida, *Bull. Chem. Soc. Jpn.*, **51**, 673 (1978).
36) J. H. Hildebrand and H. A. Benesi, *J. Am. Chem. Soc.*, **71**, 2703 (1949).
37) A. J. Gordon and R. A. Ford, "The Chemist's Companion," Wiley-Interscience, New York (1972), p. 108.
38) R. W. Taft, Jr., "Steric Effects in Organic Chemistry," ed by M. S. Newman, John Wiley & Sons, New York (1956), p. 556.
39) M. Charton, *J. Am. Chem. Soc.*, **97**, 1552 (1975).

NMR Studies on Zerovalent Metal π-Complexes of Dibenzylideneacetone. II. Structure and Pt-H Coupling in the Binuclear Platinum Complex

Hisao TANAKA and Hiroshi KAWAZURA*

Faculty of Pharmaceutical Sciences, Josai University, Sakado, Saitama 350-02

(Received March 1, 1979)

The NMR analysis on the olefinic protons of the binuclear complex $Pt_2[(C_6H_5CH{=}CH)_2CO]_3$ was conducted on the deuteriated compounds $Pt_2[(C_6D_5CH{=}CH)_2CO]_3$, $Pt_2[(C_6D_5CD{=}CH)_2CO]_3$, and $Pt_2[(C_6D_5CH{=}CD)_2CO]_3$. Examination of the various ^1H NMR parameters revealed the individual characteristics of the six coordinated olefins of three dibenzylideneacetone ligands with respect to the metal-olefin bonding and coordination geometry. The three ligands which triply bridge the two Pt atoms are composed of one *s-cis,cis* ligand which is distant from the Pt atoms and of two *s-cis,trans* ligands which are close to the Pt atoms. Asymmetry in the coordination, which is caused by the gliding of the olefinic double bond to the metal atom, becomes greater as the olefinic moiety approaches the metal atom more closely. The major transmission route of the Pt–olefinic proton coupling is attributable to metal to olefin π-back bonding.

The first introduction of the zerovalent Pd complex of dibenzylideneacetone(dba), $Pd_2(dba)_3$(solvent) (solvent: dba, $CHCl_3$, CH_2Cl_2, and so on) was made by Ishii's group.[1] Maitlis' group[2] prepared its Pt analog $Pt_2(dba)_3$(dba). A novel type of these Pd and Pt complexes, which contains a ligand where only the olefinic portions are involved in the bonding to the metals, has attracted much interest and has been extensively investigated, especially in connection with the reactivity with various compounds.[3–6] For the Pd complex, the X-ray analyses on $Pd_2(dba)_3(CHCl_3)$[6] and $Pd_2(dba)_3(CH_2Cl_2)$[7,8] have been also performed. However, the bonding and structural studies on $Pt_2(dba)_3$ have not been done until now.

In the preceding paper,[9] the ligand conformations of $Pd_2(dba)_3$ in solution have been clarified by the ^1H NMR method and have been compared with those in crystalline state.[6,8] In this study, the treatment established with $Pd_2(dba)_3$ is applied to evaluate the structure of $Pt_2(dba)_3$. Our continuing interest in the relation between NMR parameters and metal-olefin bonding is intensified by a new insight into the coordination geometry of the olefins in the present complex; we now have a suitable model for olefin coordination.

Results and Discussion

The ^1H NMR spectra of the olefinic protons in the deuteriated $Pt_2(dba)_3$ compounds, $Pt_2[(C_6D_5CH{=}CH)_2CO]_3$, $Pt_2[(C_6D_5CD{=}CH)_2CO]_3$, and $Pt_2[(C_6D_5CH{=}CD)_2CO]_3$, are shown in Figs. 1-A, B, and C, respectively. These spectra exhibit some additional absorptions due to the couplings of the olefinic protons with the ^{195}Pt isotope (natural abundance 34%). The chemical shift δ_A of the olefinic proton on the carbonyl side (H_A) and the chemical shift δ_B of the olefinic proton on the phenyl side (H_B) were exactly determined from each main peak in the spectra of Figs. 1-B and C, respectively. Further analysis was conducted by spin decoupling in the spectrum of Fig. 1-A, to find the pairs of H_A and H_B in *trans* position of the olefinic moieties and hence to determine the olefinic coupling constant J_{AB}. Thus the spectrum was found to consist of six AB quartet patterns with attendant ^{195}Pt satellites. The J_{AB}, δ_A, and δ_B values together with the internal shift $\delta_{AB}(=\delta_B-\delta_A)$ and the mean shift $\delta_H[=(\delta_A+\delta_B)/2]$ are summarized in Table 1, where the six olefins **a** to **f** are arranged in the decreased order of $\bar{\delta}_H$ (in the

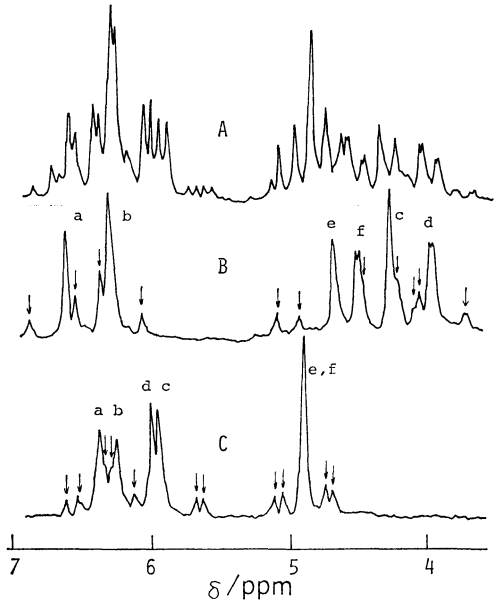

Fig. 1. ^1H NMR spectra of $Pt_2[(C_6D_5CH{=}CH)_2CO]_3$ (A), $Pt_2[(C_6D_5CD{=}CH)_2CO]_3$ (B), and $Pt_2[(C_6D_5CH{=}CD)_2CO]_3$ (C) recorded in $CDCl_3$ at 25 °C. In B and C, **a**—**f** denote the proton signals of the respective olefins and the arrows indicate the satellites due to the ^{195}Pt couplings of the olefinic protons.

TABLE 1. ^1H NMR PARAMETERS OF THE OLEFINIC PROTONS OF dba IN $Pt_2(dba)_3$ IN $CDCl_3$ AT 25 °C

Olefins	J_{AB}/Hz	δ_A/ppm	δ_B/ppm	δ_{AB}/ppm	$\bar{\delta}_H$/ppm
a	12.7	6.666	6.396	−0.270	6.531
b	12.7	6.357	6.278	−0.079	6.318
c	10.9	4.301	5.969	1.668	5.135
d	11.2	4.000	6.023	2.023	5.012
e	10.9	4.704	4.905	0.201	4.805
f	11.1	4.537	4.905	0.368	4.721

δ_A and δ_B: in ppm with tetramethylsilane. $\delta_{AB}=\delta_B-\delta_A$ and $\bar{\delta}_H=(\delta_A+\delta_B)/2$. For free dba (in $CDCl_3$ at 25 °C): J_{AB}, 16.0 Hz; δ_A 7.090; δ_B 7.750; δ_{AB}, 0.660; and $\bar{\delta}_H$, 7.420 ppm.

increased order of the chemical screening).

The ^{195}Pt coupling with H_A (J_{Pt-A}) and that with H_B (J_{Pt-B}) were definitely determined[10] from the separation of the two satellites which are symmetrically disposed on either side of each main signal in the spectra of Figs. 1-B and C, respectively. But for the couplings with H_B's of olefins **e** and **f** a definitive assignment was difficult, because of an identity of the chemical shifts of the respective protons. Table 2 lists the coupling constants J_{Pt-A} and J_{Pt-B}, together with their average $\bar{J}_{Pt-H}[=(J_{Pt-A}+J_{Pt-B})/2]$ and difference $J_{Pt-A,B}(=J_{Pt-A}-J_{Pt-B})$.

TABLE 2. 195 Pt–OLEFINIC PROTON COUPLINGS IN $Pt_2(dba)_3$ IN $CDCl_3$ AT 25 °C

Olefins	J_{Pt-A}/Hz	J_{Pt-B}/Hz	$\bar{J}_{Pt-H}$/Hz	$J_{Pt-A,B}$/Hz
a	53.7	49.3	51.5	4.4
b	48.3	56.6	52.5	−8.3
c	43.9	65.4	54.7	−21.5
d	50.8	63.8	57.3	−13.0
e	84.0	43.0 a) (32.2)	63.5 (58.1)	41.0 (51.8)
f	87.9	32.2 a) (43.0)	60.1 (65.5)	55.7 (44.9)

a) The coupling of H_B's of olefins **e** and **f** were not determined (see text).

Bonding Nature. The chemical shifts $\bar{\delta}_H$'s for all the olefinic portions move to the high field side and the coupling constants J_{AB}'s are reduced as a consequence of direct coordination of the olefinic double bond to the Pt atom. However, the degrees of the up field shift ($\Delta\bar{\delta}_H$) and of the reduction of the coupling (ΔJ_{AB}) from $\bar{\delta}_H$ and J_{AB} of free dba allow us to divide the six olefinic moieties into two groups: the two olefins **a** and **b** have ΔJ_{AB} of 3.3 Hz and $\Delta\bar{\delta}_H$ of about 1.0 ppm, and for the remaining four, **c**—**f**, ΔJ_{AB} and $\Delta\bar{\delta}_H$ lie in the narrow range of 4.8—5.1 Hz and 2.3—2.7 ppm. When we recall[9] that both the parameters directly reflect the strength of metal-olefin π-bonding which is controlled mainly by the distance from each olefin to the metal atom, the above fact leads us to state that olefins **a** and **b** with the smaller ΔJ_{AB} and $\Delta\bar{\delta}_H$, are weaker in the π-bonding and are more distant from the Pt atom than the other four.

The average values of ΔJ_{AB} and $\Delta\bar{\delta}_H$ in the six olefins are 4.4 Hz and 2.00 ppm, respectively. These are small compared with the corresponding values 6.1 Hz and 3.3 ppm in the zerovalent dba complex $Pt(PPh_3)_2(dba)$.[11] This can be understood in terms of the stabilization effect of the electron donative ligand PPh_3, whose the ionization potential is lower than that of olefin.[12,13] The average values of ΔJ_{AB} and $\Delta\bar{\delta}_H$ in $Pt_2(dba)_3$ are larger than those[9] of 2.7 Hz and 1.51 ppm in $Pd_2(dba)_3$. The larger values in $Pt_2(dba)_3$ can be explained from the view of $nd^{10}-nd^9(n+1)s^1$ promotion energies[14,15] of these d^{10} metals. The above facts indicate that in so far as judging from the average bonding strength in all the coordinated olefins, the binuclear complex is ordinary and to be expected. The characteristics of the binuclear complex appear in the remarkably unbalanced distribution of the bonding strength to the chemically equivalent olefins, as appreciated from the $\Delta\delta_H$ spreading from 0.89 ppm, a popular value of the divalent Pt–olefin complexes, to 2.70 ppm, a typical value of the zerovalent Pt–olefin complexes.[16]

Ligand Conformation. The six olefinic moieties of the three dba ligands can also be classified into two distinct groups with respect to the internal shift δ_{AB}: the two olefins **c** and **d** with δ_{AB} larger than 1.6 ppm and the remaining four with δ_{AB} smaller than 0.4 ppm. Referring to the definitive relation[9,17] between the magnitude of δ_{AB} and the conformation of olefinic moiety ($\delta_{AB}\gtrsim 1.0$ ppm for *s-trans* form and $\delta_{AB}\lesssim 0.4$ ppm for *s-cis* form), we can assign the olefins **c** and **d** with the larger δ_{AB} values to be in the *s-trans* form and the olefins **a**, **b**, **e**, and **f** with the smaller δ_{AB} values to be in the *s-cis* form. Another support for the above assignment was obtained from the temperature dependence of δ_{AB} (Fig. 2). Raising the temperature from −60 to 25 °C the δ_{AB} values of olefins **a** and **b** increased by *ca.* 0.1 ppm, while those of olefins **c** and **d** decreased by *ca.* 0.03 ppm and those of olefins **e** and **f** were unchanged. The temperature change of δ_{AB} implies a conformational distortion of the ligand in which the *s-cis* and *s-trans* olefins acquire some *s-trans* and *s-cis* characters, respectively. Then, since the δ_{AB} is a minimum in the *s-cis* form and a maximum in the *s-trans* form,[17] the δ_{AB} values of *s-cis* and *s-trans* olefins should increase and decrease, respectively, with a rise of temperature. Thus, the preceding assignment for olefins **a**—**d** can be established. The constancy[18] of the δ_{AB} in the *s-cis* olefins **e** and **f** may be due to their diminished thermal flexibilities, which are suggested by their stronger π-bonding with the Pt atom than that of the other *s-cis* olefins.

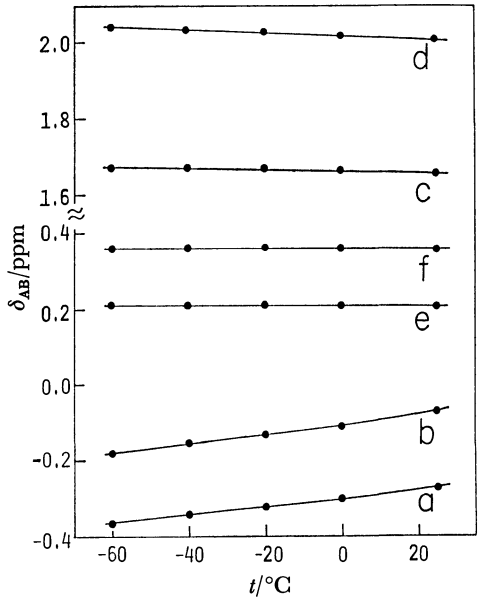

Fig. 2. Temperature dependence of the internal shift δ_{AB} for each olefinic moiety **a** to **f** in $Pt_2(dba)_3$, measured in $CDCl_3$.

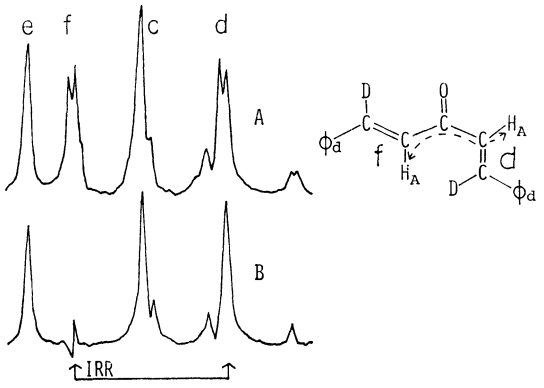

Fig. 3. The high field spectrum of $Pt_2[(C_6D_5CD{=}CH)_2\text{-}CO]_3$ showing the splitting of 1.5 Hz of H_A's in olefins **d** and **f** (A) and the spectrum decoupled by the irradiation of H_A of olefin **f** (B).

A clue to find the pair of the olefinic moieties which constitute one dba ligand was provided by the observation of the fine splitting (1.5 Hz) of the H_A signals in olefins **d** and **f** (Fig. 3-A); decoupling of the H_A signal showed that these splittings came from the long range coupling between the H_A's (Fig. 3-B). This indicates that *s-cis* olefin **f** and *s-trans* olefin **d** are linked to constitute the *s-cis,trans* dba ligand. The remaining three *s-cis* and one *s-trans* olefins inevitably give one *s-cis,trans* and one *s-cis,cis* dba. The most probable pair yielding another *s-cis,trans* conformation would be olefins **c** and **e**, because not only *s-trans* olefins **c** and **d** but also *s-cis* olefins **e** and **f** are closely similar to each other in all the NMR data gathered in Tables 1, 2, and Fig. 2. Thus, third dba ligand with *s-cis,cis* conformation should be composed[19] of olefins **a** and **b**, which also have analogous NMR parameters to justify the combination. This is the first finding of the *s-cis,cis* form fixed as a ligand, though it is a prevailing conformation[17] in the free dba.

Two types of the bonding scheme will be considered from the manner where the two *s-cis,trans* ligands, together with the symmetric *s-cis,cis* ligand, are bridged to the two Pt atoms:

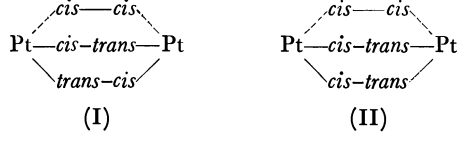

The solid and broken lines denote the strong and weak bonds, respectively in the π-bonding strength as already determined. Scheme I is reasonable if we consider the fact that in a crystal[8] of $Pd_2(dba)_3(CH_2Cl_2)$ the two *s-cis,trans* ligands together with the symmetric *s-trans,trans* ligand are allocated in such a manner as in I. Scheme I with *the same* conformational combination (*cis-cis-trans*) around each metal atom is also rationalized by the fact that *the same* bonding strength is given for each metal atom; it binds the two of the three olefins strongly and the one weakly: this situation is completely complementary with the situation[9] in $Pd_2(dba)_3$, which is obtained by substituting the word *different* instead of *the same* in the above description. It may be reasonable to say that the olefin conformations around the metal can control the geometry about the metal-olefin bonds and hence the bonding strength to the metal. Scheme II is in conflict with the above consideration.

Pt–H Coupling. As shown in Table 2, the Pt couplings with the individual protons ($J_{Pt\text{-}A}$ and $J_{Pt\text{-}B}$) distribute in so much large a range, from 32 to 88 Hz, as to cover the values[16] for various Pt–olefin complexes, but the average value of the twelve couplings falls in 56.6 Hz, a popular value of the Pt–olefinic proton coupling. Interestingly, the mean coupling $\bar{J}_{Pt\text{-}H}$ keeps an approximate correlation with the mean shift $\bar{\delta}_H$; as $\bar{\delta}_H$ decreases with going from olefin **a** to **f**, $\bar{J}_{Pt\text{-}H}$ tends to increase. This means that the Pt–olefinic proton coupling is influenced mainly by the same origin as that in the up field shift, *i.e.* metal to olefin π-back donation. This deduction is easily accepted if one considers[20] that in zerovalent Pt–olefin complexes the π-back bonding plays a major role[25] in the total Pt–olefin bonding. The coupling may be transmitted by a Fermi contact mechanism *via* the σ-π mixing[26] on the olefinic carbon with the strong π-back bonding. Thus, the Pt–H coupling increases with an increase of the π-back donation, closely related to an approach of the olefin to the metal atom.

Another interesting feature appears in the coupling difference $J_{Pt\text{-}A,B}$. The absolute value of $J_{Pt\text{-}A,B}$ also correlates roughly with $J_{Pt\text{-}H}$ and with $\bar{\delta}_H$. The origin of the appearance of $J_{Pt\text{-}A,B}$ must be ascribed to an asymmetric coordination owing to the gliding[27] of the olefinic double bond to the metal atom:

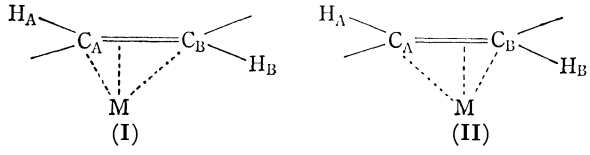

Through the gliding, one of the carbons C_A and C_B approaches the metal while the other departs from the metal. In the first approximation, it could be said that the carbon close to the metal takes the larger π-back donation and so the proton attached to this carbon spin-couples with the metal atom more strongly. Thus, the positive sign of $J_{Pt\text{-}A,B}$ in olefins **a**, **e**, and **f** can be interpreted on the basis of gliding model I, where the metal atom glides toward C_A, whereas the negative sign in olefins **b**, **c**, and **d** can be interpreted on the basis of gliding model II where the metal atom glides toward C_B. The magnitude of $J_{Pt\text{-}A,B}$ can be explained in terms of the extent of coordination asymmetry coming from the gliding such as exemplified by the ratio of the C_A–M and C_B–M distances. The X-ray analysis[8] on the analogous compound $Pd_2(dba)_3$ has clarified the existence of the glidings shown in I and II. Eventually, the correlation between $\bar{J}_{Pt\text{-}H}$ and $J_{Pt\text{-}A,B}$ in $Pt_2(dba)_3$ indicates that the closer the olefinic moiety approaches the metal, the greater becomes the asymmetry in coordination, as expected from the structure where the two olefinic moieties of dba ligand bridge the two metal atoms.

Experimental

Materials. The binuclear Pt complex $Pt_2(dba)_3(dba)$ was synthesized according to the literature.[4] Recrystallization of the complex in $CHCl_3$ gave deep purple solids with the formula $Pt_2(dba)_3(CHCl_3)$, where an involvement of the solvent molecule was found by mass and elemental analyses. $Pt_2[(C_6D_5CH{=}CH)_2CO]_3(CHCl_3)$, $Pt_2[(C_6D_5CD{=}CH)_2CO]_3(CHCl_3)$, and $Pt_2[(C_6D_5CH{=}CD)_2CO]_3(CHCl_3)$ were prepared by the above procedure using the respective deuteriated dba.[17]

^1H NMR Measurements. The ^1H NMR spectra of the deuteriated complexes in $CDCl_3$ were recorded through a number of pattern accumulations by a JEOL PS-PFT/EC 100 pulsed Fourier transform system. This system overcame the low solubility of the binuclear complex. The measuring conditions were the same as those stated in the preceding paper.[9]

References

1) Y. Takahashi, Ts. Ito, and Y. Ishii, *J. Chem. Soc., Chem. Commun.*, **1970**, 1065.

2) K. Moseley and P. M. Maitlis, *J. Chem. Soc., Chem. Commun.*, **1971**, 982.

3) Ts. Ito, S. Hasegawa, Y. Takahashi, and Y. Ishii, *J. Chem. Soc., Chem. Commun.*, **1972**, 629; *J. Organomet. Chem.*, **73**, 401 (1974).

4) K. Moseley and P. M. Maitlis, *J. Chem. Soc., Chem. Commun.*, **1971**, 1604; *J. Chem. Soc., Dalton Trans.*, **1974**, 169.

5) W. J. Cherwinski, B. F. G. Johnson, and J. Lewis, *J. Chem. Soc., Dalton Trans.*, **1974**, 1405.

6) J. Ukai, H. Kawazura, Y. Ishii, J. Bonnet, and J. A. Ibers, *J. Organomet. Chem.*, **65**, 253 (1974).

7) M. C. Mazza and C. G. Pierpont, *J. Chem. Soc., Chem. Commun.*, **1973**, 207.

8) C. G. Pierpont and M. C. Mazza, *Inorg. Chem.*, **13**, 1891 (1974).

9) H. Kawazura, H. Tanaka, K. Yamada, Y. Takahashi, and Y. Ishii, *Bull. Chem. Soc. Jpn.*, **51**, 3466 (1978).

10) For some cases one of the two satellites was observed. In these cases the coupling was estimated from the observed satellite only.

11) $Pt_2(PPh_3)_2(dba)$ ligated by either of the two olefinic moieties of dba was prepared after the procedure of Ref. 5 to give the J_{AB}, δ_A, and δ_B values of the coordinated olefinic moiety 9.9 Hz, 4.04 and 4.15 ppm with tetramethylsilane (in $CDCl_3$ at 25 °C).

12) G. Distefano, G. Inorta, S. Pignataro, and A. Foffani, *J. Organomet. Chem.*, **14**, 165 (1968).

13) K. Watanabe, *J. Chem. Phys.*, **26**, 542 (1967).

14) R. Ugo, *Co-ordination Chem. Rev.*, **3**, 319 (1968).

15) L. Malatesta and S. Cenini, "Zerovalent Compounds of Metals," Academic Press, New York (1974), p. 39.

16) M. Herberhold, "Metal π-Complexes," Elsevier, New York (1974), Vol. 2, pp. 31—57.

17) H. Tanaka, K. Yamada, and H. Kawazura, *J. Chem. Soc., Perkin Trans. 2*, **1978**, 231.

18) This constancy is to be expected if one considers that the δ_{AB} in the *s-trans* olefins **c** and **d**, with the bonding strength similar to that of the *s-cis* olefins **e** and **f**, changes only slightly. The δ_{AB} does not increase so remarkably with a distortion around the *s-cis* form, while it decreases rapidly around the *s-trans* form.[17]

19) Thus, the *s-cis,cis* ligand (olefins **a** and **b**) with the larger separation between the two olefinic double bonds, together with the two *s-cis,trans* ligands with the smaller separation, bridges the two Pt atoms. Then, the *s-cis,cis* ligand should be distorted so as to reduce the C–C(O)–C angle, in contrast to an increase[8] of the angle of the *s-trans, trans* ligand in a crystal of $Pd_2(dba)_3(CH_2Cl_2)$. This seems to be the reason for the abnormal negative sign of δ_{AB} in the *s-cis* olefins **a** and **b**.

20) In divalent Pt–olefin complexes where the σ and π-bonds contribute nearly equally to the total Pt–olefin bond, the σ-bond as well as the π-bond should be important for the coupling transmission. For example, the up field shift ($\Delta\delta_H$) for ethylene in zerovalent $Pt(PPh_3)_2(C_2H_4)$[21] is 3.26 ppm much larger than the value of 1.11 ppm in divalent $[PtCl_3(C_2H_4)]^-$,[22] in contrast to the similar J_{Pt-H} values of 62 and 66.8 Hz in the respective complex. The distance[23] between Pt and C in the zerovalent complex (2.11 Å) is similar to that[24] in the divalent complex (2.14 Å), indicating a similar total bonding (σ and π) strength in both the complexes. These facts lead us to consider that the Pt-H coupling is generally affected both by σ and π-bondings, while the up field shift is only affected by π-bonding.

21) C. D. Cook and G. S. Jauhal, *J. Am. Chem. Soc.*, **90**, 1464 (1971).

22) H. P. Fritz, K. E. Schwarzhans, and D. Sellmann, *J. Organomet. Chem.*, **6**, 551 (1966).

23) P. T. Cheng, C. D. Cook, S. C. Nyburg, and K. Y. Wan, *Inorg. Chem.*, **10**, 2210 (1971).

24) W. C. Hamilton, K. A. Klanderman, and R. Spratley, *Acta Crystallogr., Sect. A*, **25**, 5172 (1969).

25) R. Jones, *Chem. Rev.*, **68**, 551 (1966).

26) S. Cenini, R. Ugo, and G. La. Monica, *J. Chem. Soc., A*, **1971**, 416.

27) For an asymmetrically substituted ethylene, such a gliding coordination is expected in every case. For example, it is significant for the styrene ligand in $[(PhCH{=}CH_2)PdCl_2]_2$ (J. R. Holden and N. C. Benziger, *J. Am. Chem. Soc.*, **77**, 4987 (1955)).

Magnetic Study of *N,N,N′,N′*-Tetramethyl-*p*-phenylenediamine (Wurster's Blue) Tetrafluoroborate Cation Radical

Jun YAMAUCHI,* Hideo FUJITA, and Yasuo DEGUCHI
College of Liberal Arts and Sciences, Kyoto University, Kyoto 606

(Received March 15, 1979)

Wurster's Blue cation radical, which is composed of TMPD cation and BF_4 anion moieties, was prepared and its magnetic properties were examined. The cation radical shows similar magnetic behavior to that of the TMPD–ClO_4 cation radical, but there is a slight perturbation when changing the counteranions from perchlorate to tetrafluoroborate. A phase transition takes place at 190.5 K, which is attributable to a dimerization involving a small molecular displacement in the crystal lattice. These phenomena are discussed using the magnetic susceptibility data, thermal study, and ESR observations due to triplet exciton. The magnetic data are described by comparison with Wurster's Blue perchlorate cation radical.

The phase transition of *N,N,N′,N′*-tetramethyl-*p*-phenylenediamine (TMPD) perchlorate has been studied extensively. The cation radical called Wurster's Blue perchlorate experiences the first-order phase transition at about 190 K, as was ascertained from magnetic susceptibilities,[1–2] heat capacity,[3] electron spin resonance,[4] nuclear magnetic resonance,[5] and crystal structure determinations.[6] The nature of the phase transition was discussed previously.[7] Some of the anion radicals composed of tetracyanoquinodimethane (TCNQ)[8] and several kinds of neutral radicals[9] also exhibit magnetic phase transition; the former undergo first-order transitions and the latter second-order. On the other hand, Wurster's Blue iodide (TMPD-I) is paramagnetic from room temperature till liquid nitrogen temperature and no phase transition has been observed in this temperature range.[10] In the case of donor and acceptor complexes of TMPD, there exist both diamagnetic and paramagnetic species. For instance, the complex compounds of TMPD with chloranil and bromanil are almost diamagnetic, while TMPD–iodanil compound is weakly paramagnetic.[11] TCNQ salt with TMPD, which is also one of the donor and acceptor complexes, shows a weak paramagnetism; there is a thermally accessible triplet state lying above a singlet ground state with an energy separation $\Delta E=0.075$ eV.[12] Thus, the magnetic properties of the cation radical of TMPD vary with counteranions.

Hunig has pointed out a two-step redox system for the stable radical ions of nitrogen-containing aromatic molecules.[13] According to the fundamental work of Michaelis, the three oxidation levels are called "reduced form," "semiquinone," and "oxidized form."[14] Among these oxidation levels "semiquinone" has one unpaired electron in each molecule. Hunig isolated the above-mentioned three types of compounds with a careful choice of counteranions (perchlorate or tetrafluoroborate).[15] Thus, it might be an interesting problem to see the influence of tetrafluoroborate anion moiety upon magnetic interactions between unpaired electrons of TMPD cation moiety. After a successful attempt to prepare Wurster's Blue tetrafluoroborate, its magnetic properties were made clear and discussions on the magnetic phase transition were made in comparison with Wurster's Blue perchlorate.

Experimental

A detailed description of the apparatus and experimental techniques used in this experiment was published previously.[16] Only a brief comment will be given here. The diamagnetic contribution was calculated from Pascal's constants to be -153×10^{-6} emu/mol, on the assumption that diamagnetism of BF_4^- is -32×10^{-6} emu/mol. This contribution is a little larger than that of TMPD–ClO_4 obtained by Michaelis *et al.*,[17] -138×10^{-6} emu/mol, in spite of the minor difference between the presumed diamagnetic susceptibilities of BF_4^- and ClO_4^- anion moieties. As a paramagnetic susceptibility standard, we used the 4-methyl derivative of 4-hydroxy-2,2,6,6-tetramethylpiperidine-1-oxyl (TANOL), which conforms to the Curie law from room temperature down to 1.8 K.[18] The differential scanning calorimeter was a conventional one, Perkin-Elmer DSC-1. We made a temperature calibration using hexane and chloroform.

Samples were prepared following the procedure of Michaelis and Granick,[17] with a slight modification as required. One gram of *N,N,N′,N′*-tetramethyl-*p*-phenylenediamine, prepared by the method of Cox *et al.*,[19] was dissolved in a mixed solution of 18 ml water and 24 ml methanol containing 9 g of sodium tetrafluoroborate. It was cooled to -10 °C, then 32 ml of 0.252 mol kg^{-1} aqueous bromine solution was added dropwise. The crystals were filtered, washed several times with small portions of ice-cold methanol, then abundantly with dry ether. The yield of TMPD–BF_4 melting at 126—127 °C (dec) after recrystallization from methanol was 0.8 g (52%). The crystals have a brownish purple metallic luster. Chemical analysis gave 6.64% (H), 47.85% (C), and 11.12% (N), which is to be compared with calculated values of $C_{10}H_{16}N_2BF_4$: 6.42 % (H), 47.82% (C), and 11.16% (N).

Results

Figure 1 shows the magnetic susceptibility versus temperature curve, in which one can recognize a sharp peak around 190 K. Upon lowering the temperature, the susceptibility drops steeply and then decreases gradually. This behavior is quite similar to that of TMPD–ClO_4 salt. In order to compare the magnetic behavior between Wurster's Blue tetrafluoroborate and perchlorate salts we also carried out a susceptibility measurement on the perchlorate salt as shown in Fig. 2, although many investigations have already been published.[1–2] It should be noted here that some of the differences are found in the maximum value of magnetic

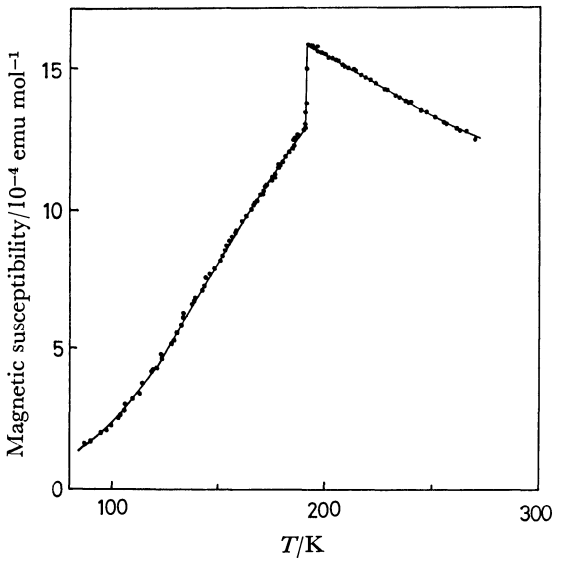

Fig. 1. Magnetic susceptibility *versus* temperature curve of TMPD–BF_4 cation radical.

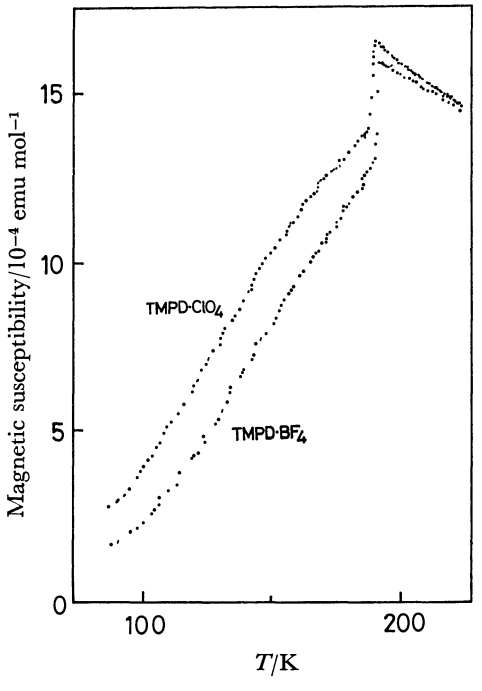

Fig. 2. Magnetic susceptibility *versus* temperature curves of TMPD–BF_4 and –ClO_4 cation radicals below the transition temperatures.

TABLE 1. MAGNETIC SUSCEPTIBILITY RESULTS AND TRANSITION TEMPERATURE

	χ_{max} [a]	T_{max}/K	$\Delta\chi_{tr}$ [a]	χ_{77} [a]	T_{tr}/K	
TMPD–BF_4	16.0	191	3.1	0.82	190.5 [b]	Present work
TMPD–ClO_4	16.8	190	2.8	2.00	190	Present work
	15.8	186	0.8		186	Duffy[1]
	14.5	189	1.4		189	Okumura[2]

a) $\times 10^{-4}$ emu/mol. b) The transition temperature was determined from thermal studies.

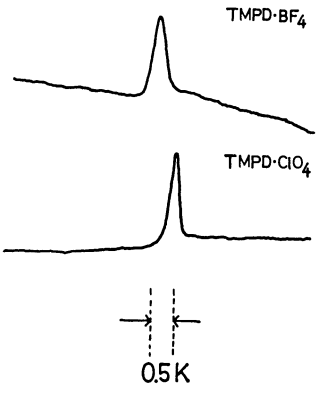

Fig. 3. Differential scanning calorimetry. The temperature was gradually elevated from right to left. The temperature difference was calibrated by the melting points of hexane and chloroform.

susceptibility (χ_{max}), in the temperature where the susceptibility takes its maximum value (T_{max}), and in the temperature dependence of the susceptibility below T_{max}. The former two characteristics are summarized in Table 1 and the latter is depicted in Fig. 2.

According to the thermal study using the differential scanning calorimeter (DSC), endothermic or exthothermic behavior was observed with TMPD–BF_4 at a slightly higher temperature than with TMPD–ClO_4. The temperature difference was found to be 0.5 K, as

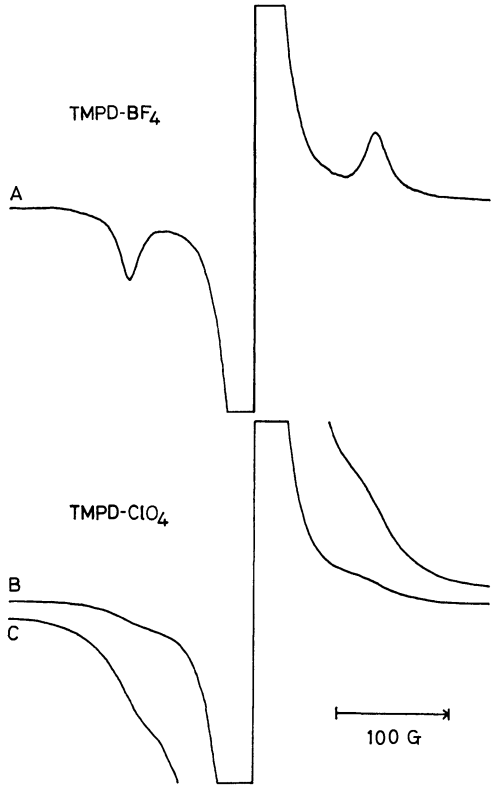

Fig. 4. Polycrystalline ESR spectra at 77 K. The triplet excitons can be clearly observed in TMPD–BF_4 (A), while the fine structure in TMPD–ClO_4 is exchange-narrowed because of the fast motion of triplet excitons (B and C). The field modulation was 1 G in A and B and 10 G in C.

shown in Fig. 3. The abscissa is a temperature scale, but only the difference between the peaks was calibrated using the standard materials described in the experimental section.

Electron spin resonance was observed at room temperature and at liquid nitrogen temperature in order to obtain information on the phase transition. The polycrystalline spectrum at 77 K is given in Fig. 4. This is characteristic of triplet exciton spectrum of polycrystalline samples.[20] A single crystal study of this exciton in TMPD-ClO_4 has been reported elsewhere.[4] The powder pattern of TMPD-ClO_4 at 77 K is also drawn in Fig. 4 for comparison. The ESR data are tabulated in Table 2.

Table 2. ESR results and zero field splitting parameters

	g-value[a]	Linewidth/G[a]	E/G	D/G
TMPD-BF_4	2.00325	2.64	73.0	0
TMPD-ClO_4	2.00325	2.68	75.7[b]	0[b]

a) At room temperature. b) Ref. 4.

Discussion

The magnetic behavior of Wurster's Blue tetrafluoroborate and that of perchlorate salts above the transition temperature are identical, as seen from Tables 1 and 2. The ESR g-values and linewidths at room temperature show the same experimental values. The magnetic susceptibility also shows the same temperature variation, as far as we could determine, although Duffy[1] and Okumura[2] have published smaller values in TMPD-ClO_4. These facts indicate that the crystal structure of TMPD-BF_4 may have the same molecular packing of TMPD cations as that of TMPD-ClO_4 salt along the a-axis.[6]

The magnetic susceptibilities of TMPD-BF_4 and -ClO_4 salts start to deviate from each other in the vicinity of the transition temperature and then exhibit sharp decreases at 191 and 190 K, respectively. The decreases ($\Delta\chi_{tr}$) at these temperatures are steeper than those published previously for TMPD-ClO_4 salt (see Table 1). The discontinuity comes from cooperative phenomena of a first-order nature, as suggested in TMPD-ClO_4, so that the above fact may be concerned with the degree of purification of the crystals. In fact, Okumura reported 81% radical contribution due to a deterioration of the crystal. On the other hand, Duffy observed 94% radical concentration calculated from the Curie constant. However, both their room temperature susceptibilities show nearly the same value, 10.5×10^{-4} emu/mol.

TMPD-BF_4 salt also experiences a magnetic phase transition accompanied by a crystal distortion. The proposed model in TMPD-ClO_4 salt is that there is a strongly alternating antiferromagnet and a regular antiferromagnet in the low and high temperature phases, respectively.[21] This is caused by a dimerization of TMPD cation molecules in the crystal. This may be also true in TMPD-BF_4 and can be ascertained partly from the low temperature ESR study which indicates the presence of triplet excitons.

The transition temperature of TMPD-ClO_4 salt has been reported by many investigators: 186 K (Duffy),[1] 189 K (Okumura),[2] and 189.9 K (Chihara *et al.*).[3] In our study a good agreement with a precise heat capacity measurement by Chihara *et al.* was obtained in TMPD-ClO_4. However, the DSC study gave 0.5 K difference between the transition temperatures of BF_4 and ClO_4 salts, so that we concluded that the transition temperature of TMPD-BF_4 is 190.5 K in spite of the susceptibility maximum at 191 K. This is partly because we believe the experimental errors in the heat capacity and DSC measurements are smaller than those in the susceptibility measurement. The error found in the susceptibility is at most 0.5 K.

The magnetic susceptibilities below the transition temperature are different, as is shown in Fig. 2. This means that, although both of the cation radicals have dimerized structures which form a strongly alternating antiferromagnet, the triplet exciton density in TMPD-BF_4 is much smaller at a given temperature than that of TMPD-ClO_4. This fact suggests that the observation of triplet exciton spectra of TMPD-BF_4 may be possible at a higher temperature region, because one can observe fine-structure due to triplet entities in ESR measurements at a relatively low triplet density.[22] In fact, we were able to observe clearly the fine-structure of triplet excitons in TMPD-BF_4 at 77 K, while in the case of TMPD-ClO_4 the spectrum at 77 K shown in Fig. 4 was an exchange-narrowed one with a feeble indication of triplet excitons around the strong absorption. At 77 K the exchange interactions between triplet excitons are not small enough to be neglected in the case of TMPD-ClO_4 salt. McConnell *et al.*[4] noted that they have seen clear exciton paramagnetic resonance spectra in polycrystalline samples of TMPD-ClO_4 at 50 K. The spectra in Fig. 4 can be accounted for by the spin Hamiltonian:

$$\mathcal{H} = DS_z^2 + E(S_x^2 - S_y^2),$$

where S_x, S_y, and S_z are the components of spins in the direction of the principal fine structure axes, and D and E are zero-field splitting parameters. The spectral analysis implies the vanishing of D as in the case of TMPD-ClO_4 salt.[4] The spectral separation between the two side-absorptions was 219.1 G, leading to $|E|=73.0$ G for TMPD-BF_4, while $|E|=75.7$ G for TMPD-ClO_4. These facts give microscopic evidence for a dimerization of TMPD cations below the transition temperature. In order to obtain the principal coordinates of dipolar interactions, however, more detailed experiments using single crystals must be performed.

A comparison of the ionic radii of BF_4^- and ClO_4^- suggests that tetrafluoroborate anions have a smaller ionic radius. However, the conjecture that both of the crystals have the same structure in the high temperature region is reasonable if we take into account that there are no significant differences in the magnetic properties. On the contrary, in the low temperature phase, the smaller anion moiety makes it easier for the TMPD cations to get nearer. Therefore, the presumption that the molecular displacement of TMPD cations

of BF_4 salt at the transition temperature may be larger explains the larger $\Delta\chi_{tr}$ and smaller susceptibility values, that is, the larger antiferromagnetic interactions at or below T_{tr}. In this context, the triplet interaction parameters, D and E, are also dependent on the distance between the dimerized molecules. Since D and E are inversely proportional to the third power of distance, the shorter the distance between TMPD cations, the larger the D and E values. However, BF_4 salt has a smaller E value, 73.0 G, than that of 75.7 G for ClO_4 salt. This is because the D and E values also depend on the molecular symmetry around the pairing axis. The most perfect vanishing of the D value is also explainable by the molecular conformation.[4)]

In conclusion, the cation radical TMPD–BF_4 experiences a phase transition of the first-order at 190.5 K. This transition may be accompanied by a dimerization of TMPD cation molecules, as proposed in the case of TMPD–ClO_4 salt. The magnetic susceptibility measurements, thermal calorimetry, and ESR observations support these conclusions. Observation of the triplet excitons at the low temperature phase supports the strongly alternating antiferromagnetic interaction. The magnetic properties of the two cation radicals, TMPD–BF_4 and –ClO_4, are almost identical. The few discrepancies might be due to the ionic radii of the anions, BF_4^- and ClO_4^- and this influence should be clarified by X-ray crystal analysis.

References

1) W. Duffy, Jr., *J. Chem. Phys.*, **36**, 490 (1962).
2) K. Okumura, *J. Phys. Soc. Jpn.*, **18**, 69 (1963).
3) H. Chihara, M. Nakamura, and S. Seki, *Bull. Chem. Soc. Jpn.*, **38**, 1776 (1965).
4) D. D. Thomas, H. Keller, and H. M. McConnell, *J. Chem. Phys.*, **39**, 2321 (1963).
5) A. Kawamori and K. Suzuki, *Mol. Phys.*, **8**, 95 (1964); M. Inoue, H. Kuramoto, and D. Nakamura, *Bull. Chem. Soc. Jpn.*, **50**, 2885 (1977).
6) J. L. de Boer and A. Vos, *Acta Crystallogr., Sect. B*, **28**, 835, 839 (1972).
7) G. T. Pott and J. Kommandeur, *J. Chem. Phys.*, **47**, 395 (1967); H. J. Monkhorst, G. T. Pott, and J. Kommandeur, *ibid.*, **47**, 401 (1967); G. T. Pott, C. F. van Bruggen, and J. Kommandeur, *ibid.*, **47**, 408 (1967).
8) R. G. Kepler, *J. Chem. Phys.*, **39**, 3528 (1963).
9) J. Yamauchi, *J. Chem. Phys.*, **67**, 2850 (1977) and references therein.
10) J. L. de Boer and A. Vos, *Acta Crystallogr., Sect. B*, **24**, 542 (1968).
11) H. Kainer and A. Uberle, *Chem. Ber.*, **88**, 1147 (1955).
12) M. Kinoshita and H. Akamatu, *Nature*, **207**, 291 (1965).
13) S. Hunig, *Pure Appl. Chem.*, **15**, 109 (1967).
14) L. Michaelis, *Chem. Rev.*, **16**, 243 (1935).
15) S. Hunig, *Liebigs Ann. Chem.*, **676**, 32 (1964).
16) J. Yamauchi, *Bull. Chem. Soc. Jpn.*, **44**, 2301 (1971).
17) L. Michaelis and S. Granick, *J. Am. Chem. Soc.*, **65**, 1747 (1943).
18) J. Yamauchi, K. Watanabe, H. Nishiguchi, and Y. Deguchi, *Bull. Inst. Chem. Res. (Kyoto Univ.)*, **50**, 483 (1972).
19) J. R. Cox, Jr., and B. D. Smith, *J. Org. Chem.*, **29**, 488 (1964).
20) E. Wasserman, L. C. Snyder, and W. A. Yager, *J. Chem. Phys.*, **41**, 1763 (1964).
21) Z. G. Soos and R. C. Hughes, *J. Chem. Phys.*, **46**, 253 (1967).
22) D. B. Chesnut and W. D. Phillips, *J. Chem. Phys.*, **35**, 1002 (1961); D. B. Chesnut, *ibid.*, **40**, 405 (1964).

An Analysis of the UV, ORD, and CD Bandshapes of the DNA–Acridine Orange Complex by the Linear Response Polarizability Theory

Hirotoshi Ito and Yasumasa J. I'Haya*

Department of Materials Science, The University of Electro-Communications, Chofu-shi, Tokyo 182

(Received March 12, 1979)

The linear response polarizability theory of the spectral bandshapes is applied to the numerical analysis of the UV, ORD, and CD spectra of the DNA–Acridine Orange complex by using various models of conformation. In all calculations, we make use of an infinite orders approximation for the intermonomer electronic interaction, since convergence of the Dyson-type series for the polymer polarizability tensor sometimes becomes seriously slow, in particular in such case that the transition moments of a constituent monomer such as Acridine Orange are quite large. It is found that among the various outside-stacking models, a dimer-pairs repeating sequence model newly proposed leads to reasonable results for the UV, ORD, and CD spectral bandshapes.

The binding of dye molecules to some species of macro-biomolecules exhibits metachromasy, *i.e.*, appreciable change in the UV absorption spectra of the dye molecules. Such formation of molecular complexes often accompanies the extrinsically induced Cotton effect which usually appears in the corresponding UV absorption region of the dye. For instance, the interaction of nucleic acids with acridine dyes is the case for this phenomena. The spectral profiles for the UV, ORD, and CD bands of the DNA–dye and/or RNA–dye complexes remarkably change depending upon the several binding modes of the dyes to the polymers, which have specifically been discussed in terms of the phosphate/dye ($=P/D$) ratio in the literature. It is a hard task to analyze these profiles in detail, since there is a difficulty in properly assuming the definite models of conformation for such complicated molecular complexes. Nevertheless, there have been published several investigations on the bandshapes of biopolymer–dye complexes.[1–7]

In order to elucidate the spectral profiles, there have been mainly two models proposed; one is the outside-stacking model of dyes bound weakly to the phosphate groups corresponding to the case $P/D \approx 1$, and the other is the intercalation model in which monomeric dyes are strongly penetrated between the base-pairs corresponding to the case $P/D \gg 1$. In opposition to this, there is a finding that the latter model is good enough even for the low P/D ratio, for example $P/D=4$.[8] If we can clarify further detail of the bandshapes for these models in terms of Green's function method, some useful information which we might have discarded up to now will be expected to become available for the determination of unknown structures of biopolymer–dye complexes, including the mutual geometries among dyes and the binding sites of dyes. This paper is a mere trial but the first attempt to attain this aim. In our method, dye molecules play a roll as kinds of probes to see the structures of macromolecules in the bandshape analysis. In order to provide a theoretical foundation for analyzing these bandshapes of molecular complexes, we firstly need to prepare such a theoretical tool that is capable of being satisfactorily checked with a model polymer of known structure.

Recently, we have presented the linear response theory of the UV, ORD, and CD bandshapes for homopolymer systems[9–12] which has satisfactorily, to some extent, been applied to polyadenylic acid to which an X-ray analysis datum is available. By applying this theory to various models of the DNA–Acridine Orange (AO) complex, we compute the UV, ORD, and CD bandshapes in order for seeking possibilities of a further detailed analysis for such a complicated system.

Basic Formulas for Computing the UV, ORD, and CD Curves

The basic formulas necessary for the calculations of the UV, ORD, and CD bandshapes are collected below:

$$\boldsymbol{\alpha}_m^{\mathrm{M}}(\bar{\nu}) = \underset{(+)}{-}(hc)^{-1}\sum_{\lambda}\boldsymbol{\mu}_{0\lambda}^{(m)}\boldsymbol{\mu}_{\lambda 0}^{(m)}[(\bar{\nu}-\bar{\nu}_{\lambda 0}^{(m)}+i\eta_{\lambda}^{(m)})^{-1} - (\bar{\nu}+\bar{\nu}_{\lambda 0}^{(m)}-i\eta_{\lambda}^{(m)})^{-1}], \quad (1)$$

$$\boldsymbol{\alpha}_{mn}^{\mathrm{P}}(\bar{\nu}) = \boldsymbol{\alpha}_m^{\mathrm{M}}(\bar{\nu})\delta_{mn} \underset{(+)}{-} \boldsymbol{\alpha}_m^{\mathrm{M}}(\nu)\cdot\mathbf{U}_{mn}\cdot\boldsymbol{\alpha}_n^{\mathrm{M}}(\nu) + \sum_{l}^{\mathrm{N}}\boldsymbol{\alpha}_m^{\mathrm{M}}(\bar{\nu})\cdot\mathbf{U}_{ml}\cdot\boldsymbol{\alpha}_l^{\mathrm{M}}(\bar{\nu})\cdot\mathbf{U}_{ln}\cdot\boldsymbol{\alpha}_n^{\mathrm{M}}(\bar{\nu}) \underset{(+)}{-} \cdots, \quad (2)$$

$$\mathbf{U}_{mn} = \mathbf{I}_{mn}/r_{mn}^3 - 3\mathbf{r}_{mn}\mathbf{r}_{mn}/r_{mn}^5, \quad (3)$$

$$\mathbf{r}_{mn} = \mathbf{r}_n - \mathbf{r}_m = x_{mn}\mathbf{i} + y_{mn}\mathbf{j} + z_{mn}\mathbf{k}, \quad (4)$$

$$\beta(\bar{\nu}) = (1/12)\sum_{m}^{\mathrm{N}}\sum_{n}^{\mathrm{N}}\mathbf{r}_{mn}\cdot(\boldsymbol{\alpha}_{mn}^{\mathrm{P}}(\bar{\nu}):\boldsymbol{\varepsilon}), \quad (5)$$

$$\varepsilon_{xyz} = -\varepsilon_{xzy} = \varepsilon_{zxy} = -\varepsilon_{zyx} = \varepsilon_{yzx} = -\varepsilon_{yxz} = 1, \quad (6)$$

$$\varepsilon(\nu) = \underset{(-)}{+}(8\pi^2 N_{\mathrm{A}}/2302.6)\bar{\nu}[N^{-1}\sum_{m}^{\mathrm{N}}\sum_{n}^{\mathrm{N}}(1/3)\mathrm{Tr}\,\boldsymbol{\alpha}_{mn}^{\mathrm{P}}(\bar{\nu}), \quad (l\ \mathrm{mol}^{-1}\ \mathrm{cm}^{-1}), \quad (7)$$

$$[\Phi(\nu)] = \underset{(-)}{+}288\pi^2 N_{\mathrm{A}}\bar{\nu}^2[N^{-1}\mathrm{Re}\,\beta(\bar{\nu})], \quad (\mathrm{deg\ cm^2/dmol^{-1}}), \quad (8)$$

$$[\Theta(\nu)] = \underset{(-)}{+}288\pi^2 N_{\mathrm{A}}\bar{\nu}^2[N^{-1}\mathrm{Im}\,\beta(\bar{\nu})], \quad (\mathrm{deg\ cm^2/dmol^{-1}}). \quad (9)$$

The notations and units used above are just the same as those of our previous paper.[12] $\boldsymbol{\mu}_{0\lambda}^{(m)}\boldsymbol{\mu}_{\lambda 0}^{(m)}$ is a dyadic product of the transition moment between the λth excited state and the ground state of the mth monomer. To avoid confusion in the formulations which have appeared in the literature on this subject, it seems well to comment upon the sign convention. Depending upon the definition for the monomer polarizability tensor α_m^{M}, that is, either the minus or the plus signs before Eq. 1, the upper or the lower (parenthesized) signs in Eqs. 2, 7, 8, and 9 appear respectively. Although we have chosen the plus sign before Eq. 1 in our previous papers, the

minus sign in Eq. 1 is rather recommended because it is the customarily used definition. Another reason is that if we choose the minus sign in Eq. 1 the plus and the minus signs appear alternately in the expansion formula (Eq. 2) derived perturbatively from the classical electromagnetic theory,[13,14] Note that in the literature we sometimes find the opposite sign convention for $\mathbf{U}_{mn}$[15] which leads to Eq. 2 with all the plus signs even by using the conventional definition (minus) for Eq. 1.

Let us consider a biopolymer–dye complex in which the dyes are regularly arrayed and bound to the biopolymer one way or another. It is now assumed that experimentally and/or theoretically we will be able to know the monomer polarizability tensor $\boldsymbol{\alpha}^{p}_{mn}(\bar{\nu})$ for the mth constituent dye chromophore bound to the biopolymer. Then, we can derive the matrix element of the polarizability tensor $\boldsymbol{\alpha}^{p}_{mn}(\bar{\nu})$ for the biopolymer–dye complex, by using hypothetically a Dyson-type equation (Eq. 2). In Eq. 2, the interactions among the dyes and the macromolecular skeleton are neglected for simplicity. Actually, this means that the macromolecule–dye complex could be approximated as a polymer (N-mer) of aggregated dyes, in so far as we are concerned with the specific wavelength region of our interest.

From Eq. 2, we can calculate the UV absorbance $\varepsilon(\bar{\nu})$ and the optical rotatory parameter $\beta(\bar{\nu})$.[14] Different from our previous paper,[12] let us relate $\beta(\bar{\nu})$ of Eq. 5 with the familiar scalar triple product $\mathbf{r}_{mn}\cdot\boldsymbol{\mu}^{(m)}_{\lambda 0}\times\boldsymbol{\mu}^{(n)}_{\lambda 0}$:

$$\begin{aligned}\beta(\bar{\nu}) &= (1/12)\sum_{m}^{N}\sum_{n}^{N}\sum_{k}(\mathbf{r}_{mn})_k\sum_{t}\sum_{j}\alpha^{\mathrm{P}ij}(\bar{\nu})\varepsilon_{jik}\\ &= -(1/12)\sum_{m}^{N}\sum_{n}^{N}\sum_{i}\sum_{j\neq k}\sum_{k}(\mathbf{r}_{mn})_k(\alpha^{\mathrm{P}ij}_{mn}(\bar{\nu})-\alpha^{\mathrm{P}ji}_{mn}(\bar{\nu}))_k\\ &= -(1/12)\sum_{m}^{N}\sum_{n}^{N}[x_{mn}\vdots y_{mn}\vdots z_{mn}]\begin{bmatrix}\alpha^{\mathrm{P}yz}_{mn}(\bar{\nu})-\alpha^{\mathrm{P}zy}_{mn}(\bar{\nu})\\ \cdots\cdots\cdots\\ \alpha^{\mathrm{P}xz}_{mn}(\bar{\nu})-\alpha^{\mathrm{P}zx}_{mn}(\bar{\nu})\\ \cdots\cdots\cdots\\ \alpha^{\mathrm{P}xy}_{mn}(\bar{\nu})-\alpha^{\mathrm{P}yx}_{mn}(\bar{\nu})\end{bmatrix},\end{aligned}\tag{10}$$

where the symbol $(\ )_k$ denotes the kth component of the vector and $i,j,k=x,y,z$. Equation 10 is a working formula for the evaluation of $\beta(\bar{\nu})$, with simultaneous use of Eq. 2.

On the other hand, if we formally assume the polymer polarizability tensor as

$$\begin{aligned}\alpha^{\mathrm{P}}_{mn}(\bar{\nu}) = \underset{(+)}{-}(hc)^{-1}\sum_{\lambda}\boldsymbol{\mu}^{\mathrm{P}(m)}_{0\lambda}\times\boldsymbol{\mu}^{\mathrm{P}(n)}_{\lambda 0}[(\bar{\nu}-\bar{\nu}^{\mathrm{P}}_{\lambda 0}+i\eta^{\mathrm{P}})^{-1}\\ -(\bar{\nu}+\bar{\nu}^{\mathrm{P}}_{\lambda 0}-i\eta^{\mathrm{P}}_{\lambda})^{-1}],\end{aligned}\tag{11}$$

Eq. 10 leads to the familiar formula for describing optical rotation:

$$\begin{aligned}\beta(\bar{\nu}) = \underset{(+)}{-}(-12hc)^{-1}\sum_{m}^{N}\sum_{n}^{N}\sum_{\lambda}\mathbf{r}_{mn}\cdot\boldsymbol{\mu}^{\mathrm{P}(m)}_{0\lambda}\times\boldsymbol{\mu}^{\mathrm{P}(n)}_{\lambda 0}[(\bar{\nu}-\bar{\nu}^{\mathrm{P}}_{\lambda 0}+i\eta^{\mathrm{P}}_{\lambda})]^{-1}\\ -(\bar{\nu}+\bar{\nu}^{\mathrm{P}}_{\lambda 0}-i\eta^{\mathrm{P}}_{\lambda})^{-1}],\end{aligned}\tag{12}$$

which indicates the conformationally induced exciton-type optical rotation. However, Eq. 12 contains unknown quantities relating to the polymer and can not be practically used for the evaluation of $\beta(\bar{\nu})$. Instead, going back to Eq. 5, we can derive the following equation to a first order approximation with respect to $\mathbf{U}_{mn}$ in Eq. 2:

$$\begin{aligned}\beta(\bar{\nu}) &= (1/12)\sum_{m}^{N}\sum_{n}^{N}\mathbf{r}_{mn}\cdot[\boldsymbol{\alpha}^{\mathrm{M}}_{m}(\bar{\nu})\vdots\boldsymbol{\varepsilon}-(\boldsymbol{\alpha}^{\mathrm{M}}_{m}(\bar{\nu})\cdot\mathbf{U}_{mn}\cdot\boldsymbol{\alpha}^{\mathrm{M}}_{n}(\bar{\nu}))\vdots\boldsymbol{\varepsilon}]\\ &= 0\underset{(+)}{-}(12)^{-1}\sum_{m}^{N}\sum_{n}^{N}\sum_{k}(\mathbf{r}_{mn})_k\sum_{i}\sum_{j}(\alpha^{\mathrm{M}}_{m}(\nu)\cdot\mathbf{U}_{mn}\cdot\alpha^{\mathrm{M}}_{n}(\nu))_{ij}\varepsilon_{jik}\\ &= \underset{(+)}{-(-12)^{-1}}(hc)^{-2}\sum_{m}^{N}\sum_{n}^{N}\sum_{\lambda}\sum_{\lambda'}(\boldsymbol{\mu}^{(m)}_{0\lambda}\cdot\mathbf{U}_{mn}\cdot\boldsymbol{\mu}^{(n)}_{\lambda' 0})\\ &\quad\times(\mathbf{r}_{mn}\cdot\boldsymbol{\mu}^{(m)}_{0\lambda}\times\boldsymbol{\mu}^{(n)}_{\lambda' 0})[(\bar{\nu}-\bar{\nu}^{(m)}_{\lambda 0}+i\eta^{(m)}_{\lambda})^{-1}\\ &\quad-(\bar{\nu}+\bar{\nu}^{(m)}_{\lambda 0}-i\eta^{(m)}_{\lambda})^{-1}][(\bar{\nu}-\bar{\nu}^{(n)}_{\lambda' 0}+i\eta^{(n)}_{\lambda'})^{-1}\\ &\quad-(\bar{\nu}+\bar{\nu}^{(n)}_{\lambda' 0}-i\eta^{(n)}_{\lambda'})^{-1}].\end{aligned}\tag{13}$$

Equation 13 does not contain any unknown polymer parameter and is found to be quite similar to the equations derived by Applequist[14] and Kirkwood *et al.*[16,17] Equations 12 and 13 are exactly the same formulas from a viewpoint of a first order approximation. However, we can preferentially make use of Eq. 13 when we wish to take higher order terms into account. For example, replacing $\mathbf{U}_{mn}$ in Eq. 13 with

$$\begin{aligned}\mathbf{U}_{mn} = \mathbf{U}_{mn} + \sum_{l}\mathbf{U}_{ml}\cdot\boldsymbol{\alpha}^{\mathrm{M}}_{l}\cdot\mathbf{U}_{ln}\\ + \sum_{l}\sum_{s}\mathbf{U}_{ml}\cdot\boldsymbol{\alpha}^{\mathrm{M}}_{l}\cdot\mathbf{U}_{ls}\cdot\boldsymbol{\alpha}^{\mathrm{M}}_{s}\cdot\mathbf{U}_{sn}+\cdots,\end{aligned}\tag{14}$$

we can to infinite order approximation describe $\beta(\bar{\nu})$ in terms of a sum of the product of the scalar triplet product $\mathbf{r}_{mn}\cdot\mu^{(m)}_{0\lambda}\times\mu^{(n)}_{\lambda' 0}$ and the intermonomer interaction $\boldsymbol{\mu}^{(m)}_{0\lambda}\cdot\mathbf{U}_{mn}\cdot\boldsymbol{\mu}^{(n)}_{\lambda' 0}$.

Infinite Orders Approximation for the Polymer Polarizability Tensor

In a previous calculation of the bandshapes of polyadenylic acid,[12] we took into account Eq. 2 up to the second order terms with respect to $\mathbf{U}_{mn}$. However, the expansion series of Eq. 2 very slowly converge in the case that chromophores have large transition moments, so that we must include higher order terms in Eq. 2 for the present calculation of the DNA–AO complex. It may rather be clever to choose the following computational scheme which involves the intermonomer interactions $\mathbf{U}_{mn}$ to infinite orders, since such a calculation in the expanded form of power series becomes time-consuming due to the increase in the number of overlappings of the *DO* loops in a computer program.

If we follow the upper sign convention in Eqs. 1, 2, 7, 8, and 9, Eq. 2 reduces to

$$\begin{aligned}\alpha^{\mathrm{P}} &= (1+\boldsymbol{\alpha}^{\mathrm{M}}\cdot\mathbf{U})^{-1}\boldsymbol{\alpha}^{\mathrm{M}}\\ &= \begin{bmatrix}\mathbf{1} & \boldsymbol{\alpha}^{\mathrm{M}}_{1}\cdot\mathbf{U}_{12}\cdots\boldsymbol{\alpha}^{\mathrm{M}}_{1}\cdot\mathbf{U}_{1\mathrm{N}}\\ \boldsymbol{\alpha}^{\mathrm{M}}_{2}\cdot\mathbf{U}_{21} & \mathbf{1}\quad\cdots\boldsymbol{\alpha}^{\mathrm{M}}_{2}\cdot\mathbf{U}_{2\mathrm{N}}\\ \cdots\cdots & \cdots\cdots\\ \boldsymbol{\alpha}^{\mathrm{M}}_{\mathrm{N}}\cdot\mathbf{U}_{\mathrm{N}1} & \boldsymbol{\alpha}^{\mathrm{M}}_{\mathrm{N}}\cdot\mathbf{U}_{\mathrm{N}2}\cdots\quad\mathbf{1}\end{bmatrix}^{-1}\begin{bmatrix}\boldsymbol{\alpha}^{\mathrm{M}}_{1} & \mathbf{0}\cdots\mathbf{0}\\ \mathbf{0} & \boldsymbol{\alpha}^{\mathrm{M}}_{2}\cdots\mathbf{0}\\ & \cdots\cdots\\ \mathbf{0} & \mathbf{0}\cdots\boldsymbol{\alpha}^{\mathrm{M}}_{\mathrm{N}}\end{bmatrix},\end{aligned}\tag{15}$$

where

$$\mathbf{1}=\begin{bmatrix}1&0&0\\0&1&0\\0&0&1\end{bmatrix},\qquad \mathbf{0}=\begin{bmatrix}0&0&0\\0&0&0\\0&0&0\end{bmatrix}.\tag{16}$$

The tensor components of the 3×3 matrix for $\boldsymbol{\alpha}^{\mathrm{M}}_{m}(\bar{\nu})$ are given as

$$\alpha^{\mathrm{M}ij}_{m}(\bar{\nu}) = \mathrm{Re}\,\alpha^{\mathrm{M}ij}_{m}(\bar{\nu}) + i\mathrm{Im}\,\alpha^{\mathrm{M}ij}_{m}(\bar{\nu}),\quad (i,j=x,y,z),\tag{17}$$

and we finally obtain

$$\mathrm{Re}\,\alpha_m^{Mij}(\bar{\nu}) = -\sum_{\lambda}(hc)^{-1}[\mu_{0\lambda}^{(m)}]_i[\mu_{\lambda 0}^{(m)}]_j\{(\bar{\nu}-\bar{\nu}_{\cdot 0}^{(m)})[(\bar{\nu}-\bar{\nu}_{\lambda 0}^{(m)})^2 + \eta_\lambda^{(m)2}]^{-1} - (\bar{\nu}+\bar{\nu}_{\lambda 0}^{(m)})[(\bar{\nu}+\bar{\nu}_{\lambda 0}^{(m)})^2+\eta_\lambda^{(m)2}]^{-1}\}, \quad (18)$$

$$\mathrm{Im}\,\alpha_m^{Mij}(\nu) = +\sum_{\lambda}(hc)^{-1}[\mu_{0\lambda}^{(m)}]_i[\mu_{\lambda 0}^{(m)}]_j\{\eta_\lambda[(\bar{\nu}-\bar{\nu}_{\lambda 0}^{(m)})^2 + \eta_\lambda^{(m)2}]^{-1} + \eta_\lambda[(\bar{\nu}+\bar{\nu}_{\lambda 0}^{(m)})^2+\eta_\lambda^{(m)2}]^{-1}\}. \quad (19)$$

Being utilized the subroutine to compute the inverse of the $3N\times 3N$ complex matrix, the matrix elements $\alpha_{mn}^{p}(\bar{\nu})$ can easily be obtained, and then the three bandshape functions for the molar absorptivity (Eq. 7), molar rotation (Eq. 8), and molar ellipticity (Eq. 9) are computed by making use of Eqs. 10 and 15.

Specification of Models and Computational Procedures

As shown in Fig. 1, we assume such a regular model that the dyes are helically aggregated on the sites of the polymer skeleton. Here, the Cartesian coordinate is taken along the radial (r), tangential (t), and vertical (z) directions of the first dye monomer site considered. By doing so, we can relate the non-interacting monomer polarizability tensor of the mth site, $\boldsymbol{\alpha}_m^{M}(\bar{\nu})$, with that of the first site, $\boldsymbol{\alpha}_1^{M}(\bar{\nu})$:

$$\boldsymbol{\alpha}_m^{M}(\bar{\nu}) = \mathbf{R}[+(m-1)\phi]\cdot\boldsymbol{\alpha}_1^{M}(\bar{\nu})\cdot\mathbf{R}[-(m-1)\phi] = \mathbf{R}_z[-(m-1)\phi]\cdot\boldsymbol{\alpha}_1^{M}(\bar{\nu})\cdot\mathbf{R}_z[+(m-1)\phi], \quad (20)$$

where

$$\mathbf{R}(\phi) = \mathbf{R}_z(-\phi) = \begin{pmatrix} \cos\phi & -\sin\phi & 0 \\ \sin\phi & \cos\phi & 0 \\ 0 & 0 & 1 \end{pmatrix}. \quad (21)$$

For instance, if we put the first dye on the r',t'-plane determined by the parameters of angles such as $\theta°$, *tilt*°, and *twist*° as depicted in Fig. 1, the components of the transition moment $\boldsymbol{\mu}_{0\lambda}^{(1)}$ in the Cartesian coordinate are given by

$$\begin{bmatrix} [\mu_{0\lambda}^{(1)}]_r \\ [\mu_{0\lambda}^{(1)}]_t \\ [\mu_{0\lambda}^{(1)}]_z \end{bmatrix} = \mathbf{R}_t(+|twist|)\cdot\mathbf{R}_{r'}(-|titl|)\begin{bmatrix} [\mu_{0\lambda}^{(1)}]_{r'} \\ [\mu_{0\lambda}^{(1)}]_{t'} \\ [\mu_{0\lambda}^{(1)}]_{z'} \end{bmatrix}$$

$$= \begin{bmatrix} \cos(+|twist|) & 0 & -\sin(+|twist|) \\ 0 & 1 & 0 \\ \sin(+|twist|) & 0 & \cos(+|twist|) \end{bmatrix} \times \begin{bmatrix} 1 & 0 & 0 \\ 0 & \cos(-|tilt|) & \sin(-|tilt|) \\ 0 & -\sin(-|tilt|) & \cos(-|tilt|) \end{bmatrix}\begin{bmatrix} [\mu_{0\lambda}^{(1)}]_{r'} \\ [\mu_{0\lambda}^{(1)}]_{t'} \\ [\mu_{0\lambda}^{(1)}]_{z'} \end{bmatrix}. \quad (22)$$

By defining the plus sign of the angles counter-clockwise, we can write more generally

$$\begin{bmatrix} [\mu_{0\lambda}^{(1)}]_r \\ [\mu_{0\lambda}^{(1)}]_t \\ [\mu_{0\lambda}^{(1)}]_z \end{bmatrix} = \mathbf{R}_t[-|twist|\cdot\mathrm{sgn}(twist)]\cdot \mathbf{R}_{r'}[-|tilt|\cdot\mathrm{sgn}(tilt)]\begin{bmatrix} [\mu_{0\lambda}^{(1)}]_{r'} \\ [\mu_{0\lambda}^{(1)}]_{t'} \\ [\mu_{0\lambda}^{(1)}]_{z'} \end{bmatrix}. \quad (23)$$

Thus, we can compute the bandshapes by making use of Eqs. 7, 8, and 9 for either the outside-stacking or the intercalation model by changing the parameters (a, ϕ, *pitch*, θ, *tilt*, *twist*) as illustrated in Fig. 1.

With the scope of outside-binding models, we newly propose a dimerpairs repeating sequence model illustrated in Fig. 2. Looking at this model, every dye is

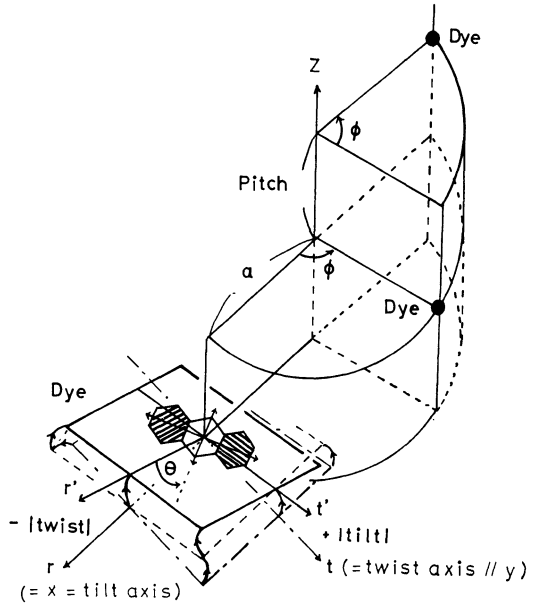

Fig. 1. A model of the Acridine Orange polymer helically stacked on the one-strand of DNA–AO complex and its geometrical parameters.

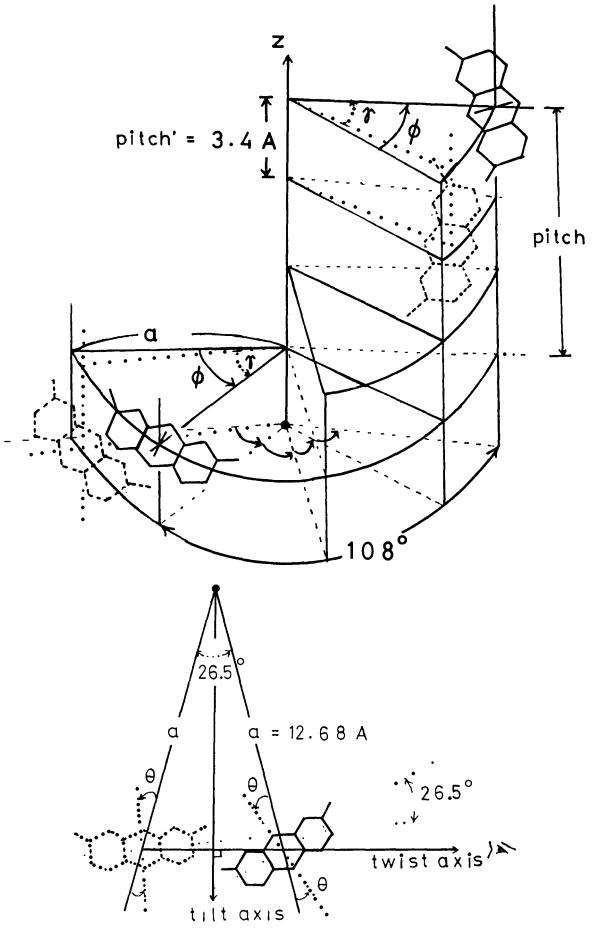

Fig. 2. A dimer-pairs repeating sequence model $[(\mathrm{dye})_2]_N$ for DNA–AO complex and its geometrical parameters.

found to be arrayed on the site of the same strand. However, if we change our views just for the computational convenience, we can readily regard this single-stranded polymer of the dyes as the double-stranded one, *i.e.*, one strand consisting of the dyes shown with the dotted line and another strand building from the dyes drawn with the solid line. This may be the special case of the double-stranded model shown in Fig. 1 of our previous paper.[12] In Table 1, the double-stranded DNA–AO polymer model presented by Tinoco *et al.*[1] is described by the parameters assigned in Fig. 2. Corresponding to Eq. 20 which defines the polarizability tensor of the mth monomer, the polarizability tensor of the m'th monomer can be obtained by a simple rotation from the position m, being assumed the geometry of the double-stranded DNA–AO complex, so as to satisfy

$$\boldsymbol{\alpha}^{M}_{m'}(\bar{\nu}) = \mathbf{R}(\gamma)\cdot\boldsymbol{\alpha}^{M}_{m}(\bar{\nu})\cdot\mathbf{R}(-\gamma), \quad (m' = \text{opposite site of } m), \tag{24}$$

and the position vectors are given by

$$\mathbf{r}_m = a\cos(m\phi)\hat{\mathbf{i}} + a\sin(m\phi)\hat{\mathbf{j}} + n\,\text{pitch}\,\hat{\mathbf{k}}, \tag{25}$$

$$\mathbf{r}_{m'} = a\cos(m\phi+\gamma)\hat{\mathbf{i}} + a\sin(m\phi+\gamma)\hat{\mathbf{j}} + (n\,\text{pitch}+\text{pitch}')\hat{\mathbf{k}}. \tag{26}$$

Results and Discussion

The spectroscopic parameters of the monomer dye, Acridine Orange, necessary for the calculations of the UV, ORD, and CD bandshapes of the polymer complex are experimentally determined as given in Table 1. In Table 2 are listed the various models assumed for the DNA–AO complex and the parameters describing the corresponding models. The results of model calculations are given through Fig. 3 to Fig. 10. In what follows, we are concerned specifically with the visible region of the whole bandshapes obtained. Tentatively, we assume that the dyes helically aggregate as if they were tilted and twisted in their molecular planes (see Fig. 1), with the parameters which are quite similar to the base parameters of the B-DNA geometry; *i.e.* *tilt*=2.1°, *twist*=−4.9°, a (variable in Å). Incidentally, the model presented by Tinoco *et al.*[1] corresponds to *tilt*=0.0°, *twist*=0.0°, a=12.68 Å. The assumption above implies that the molecular planes of the bound dyes are almost vertical to the helical axis of DNA, and in fact this nearly vertical orientation has experimentally been suggested.[19] It was shown in the study of polyadenylic acid[12] that the tilt and twist of the chromophores in the polymer system give rise to a large effect in the spectral bandshapes. We do not enter into the effect of tilting and twisting of the dyes beyond that, since there are some other unknown factors with regard to the parameters describing the DNA–AO complex.

Table 1. Spectroscopic parameters for the Acridine Orange monomer taken from the experimental data[a]

Energy $\frac{hc\bar{\nu}^{(m)}_{\lambda 0}}{\text{eV}}$	Oscillator strength $f_{\lambda 0}$	Damping factor[b] $\frac{\eta_\lambda}{\text{eV}}$	Polarization direction of transition moment
2.504	0.570	0.09540	long-axis
3.806	0.420	0.15475	long-axis
4.166	0.920	0.16297	long-axis
4.563	0.676	0.23062	short-axis

a) From Ref. 20. b) Estimated from Eq. 27 of Ref. 12.

Table 2. Various models for the DNA–AO complex and figure index

Fig. No.	Models	a Å	*tilt* degree	*twist* degree	ϕ degree	*pitch* Å	*pitch'* Å	γ degree	θ degree
3	Single-stranded intercalation[a] 5-mer	4.00	2.1	−4.9	72	6.80			36 40 45
4	Single-stranded outside-stacking N-mer (N=2, 3, 5, 11)	12.68	2.1	−4.9	36	3.40			52
5	5-mer	12.68 13.50 14.50	2.1	−4.9	36	3.40			90
6	Dimer	12.68	2.1	−4.9	36	3.40			40, 50, 60, 90
7	5-mer	12.68	2.1	−4.9	36	3.40			0, 35, 50, 55, 90
8	5-mer	12.68	2.1	−4.9	36	3.40			49, 50, 51, 52, 53, 54, 55
9	Double-stranded outside-stacking[b] 5-mer	12.68	0.0	0.0	36	3.40	2.72	−117.6	90
10	Outside-stacking N-dimer-pairs repeating sequence[c]								
	$(\text{Dye})_2$	12.68	2.1	−4.9	108	10.20	−3.40	−26.5[d]	55, 60
	$[(\text{Dye})_2]$	12.68	2.1	−4.9	108	10.20	−3.40	−26.5[d]	45, 55, 60

a) From Ref. 6. b) From Ref. 1. c) This model may be regarded as a single-stranded polymer of dyes rather than the double-stranded one. d) From the outside-stacking model proposed by Obendorf *et al.* (a=6 Å, ϕ=26.5°, *pitch*=4 Å).[21]

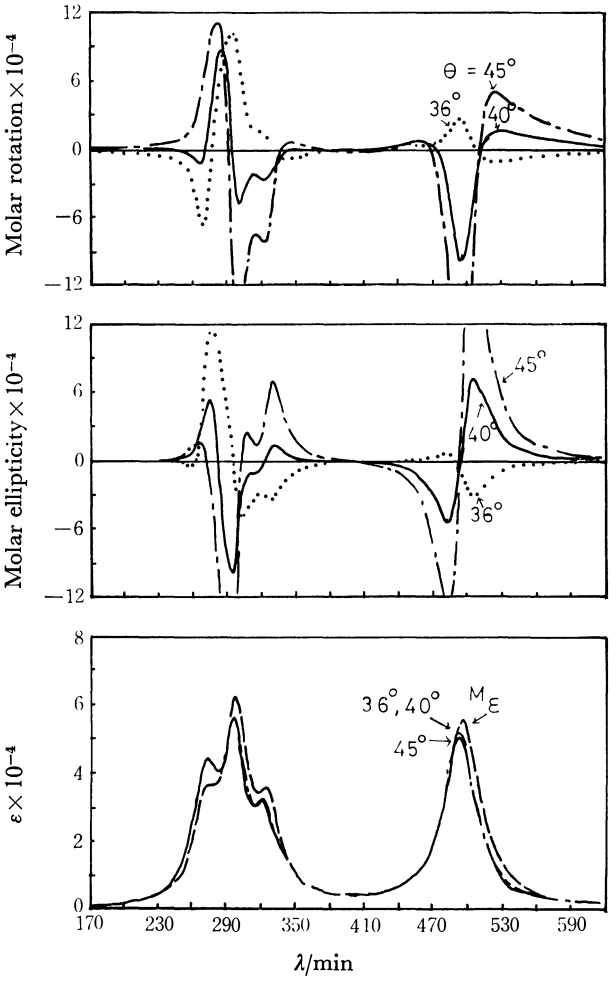

Fig. 3. The ORD (top), CD (middle), and UV (bottom) bandshapes for the intercalation model (see Table 2). $^{M}\varepsilon$ in the bottom shows the UV absorption spectrum of the AO monomer through Fig. 3 to Fig. 10.

Intercalation Model. Let us assume a simple model that the dyes are penetrated between every two base-pairs and constitute the single-stranded pentamer (5-mer) of the dyes as given in Table 2. This corresponds to the intercalation model for $P/D=4$—5. The spectral profiles computed with this model are shown in Fig. 3. In the visible region of the ORD and CD curves computed for the $\theta=40°$ model (see Fig. 1), we obtain the bandshapes having reasonable peaks and troughs in their spectral intensities in comparison with the curves of $P/D=5$ observed by Yamaoka and Resnik.[18] The first (longest wavelength) UV band computed shows only a minor blue shift and a slight decrease of intensity, even if whatever values are given for θ. Since the chain-length effect in the bandshapes is small even if we take N to be larger than 5 for the outside-stacking model (see below), qualitative feature to be obtained for the $N>5$ cases of the intercalation model might not be much different from Fig. 3. In short, in so far as the ORD and CD curves for low P/D ratios are concerned, the adequacy of this model is numerically proved. It seems that the feature of the first UV band observed for $P/D=5$ can qualitatively be reproduced for the specific θ-value ($\theta=40°$), though there still remains dissatisfaction about the intensity of the first UV band.

*Outside-stacking Models. Chain-length (*N*) Effect and Radius (*a*)-Dependence of the ORD, CD, and UV Bandshapes*: In Fig. 4, we investigated the chain-length effect of the bandshapes for the parameter $N=2$, 3, 5, 11 in the single-stranded models, fixing $\theta=52°$, which reproduces appropriately the ORD and CD curves. We found a tendency such that the computed curves for the $N=8$—11 models converge to certain shapes (approximately to that of the $N=5$ model). Therefore, for saving computational time, we carried out the model calculations of the DNA–AO complex only with the $N=2$ and $N=5$ species.

With a fixed θ-value $\theta=90°$, the dependence of the bandshapes for the single-stranded models upon the value of the radius, $a=12.68$, 13.5, and 14.5 Å, was examined as shown in Fig. 5. When we fix the parameters except the position of the binding site ($\vec{a}$), and make the value of $|\vec{a}|$ larger by degrees, the intermonomer interaction $\mathbf{U}_{mn}$ between the dyes becomes small, so that the ORD and CD curves decrease their

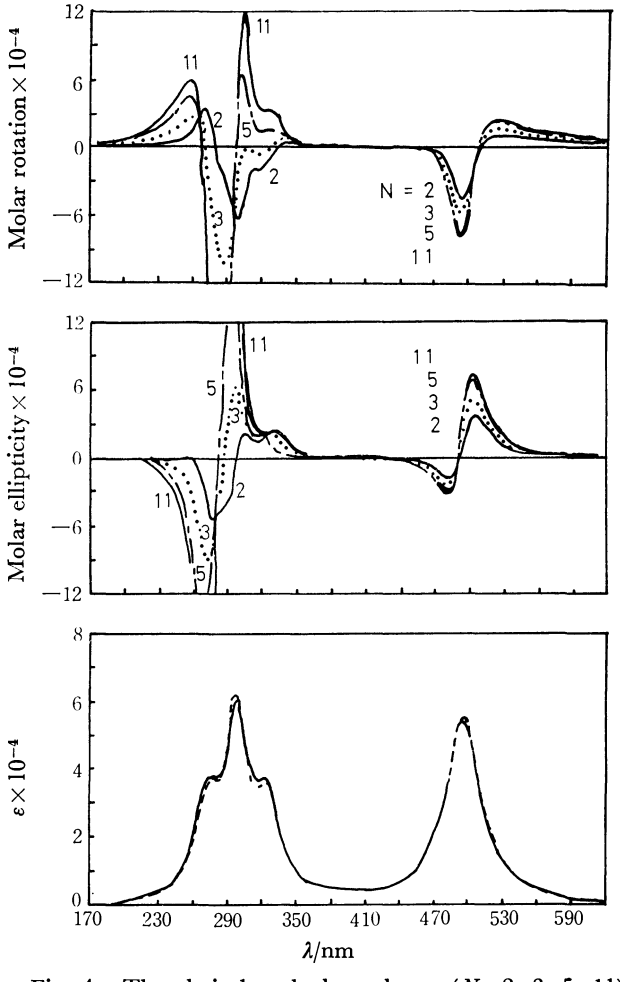

Fig. 4. The chain-length dependence ($N=2$, 3, 5, 11) of the ORD (top), CD (middle), and UV (bottom) bandshapes of the single-stranded outside-stacking N-mer model (see Table 2).

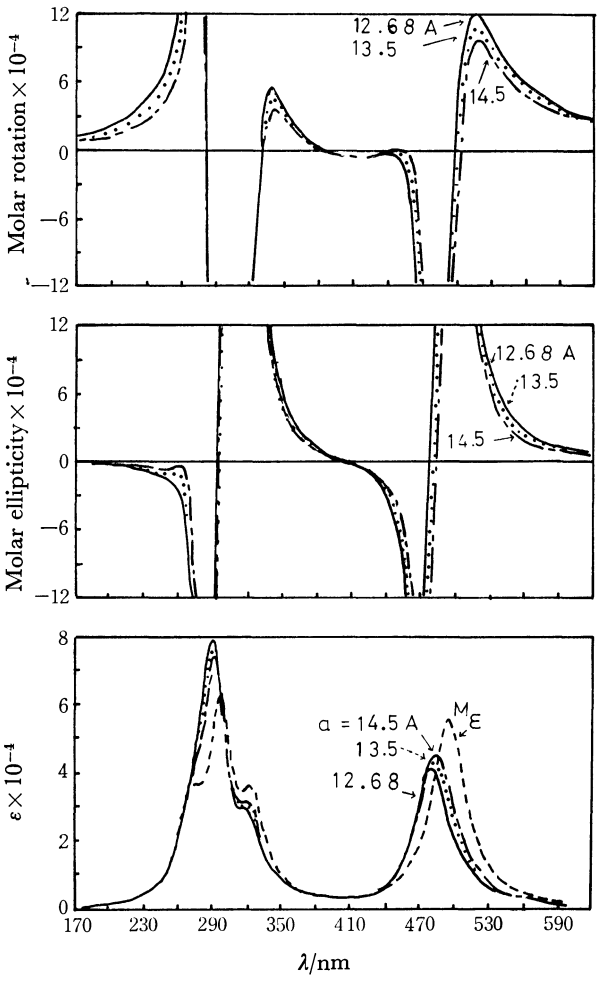

Fig. 5. Dependence of the ORD (top), CD (middle), and UV (bottom) bandshapes of the single-stranded outside-stacking 5-mer model (see Table 2) on the radius (a) of the helix.

intensities with the increase of $|\vec{a}|$ while the first UV band hardly change its peak and intensity. It is thus difficult to consider the possibility that the dyes will bind to the sites inside beyong the limit of 12.68 Å. For instance, in the stacking model presented by Obendorf *et al.*,[21] the binding site was set to be $|\vec{a}|=$ 6 Å and other parameters adopted were quite similar to our values. From Fig. 5, it is predicted that their model is indisputably denied.

Single-Stranded Dimer Model: From comparison of Figs. 4, 6, 7, and 8 it can be concluded that the qualitative feature of the UV, ORD, and CD bandshapes computed for the dimer does not very much change even for the $N>3$ polymers. In other words, the qualitative feature of these bandshapes in the visible region is mainly determined by the nearest neighbor interactions of the dyes with the intermonomer distance nearly equal to 3.4 Å. This suggestion also coincides with the experimental conclusion for the complexes of the low P/D ratios that the main binding species are dimeric molecules bound to the outside sites, while for those of $P/D\gg1$, it is usually accepted that the main binding species are monomeric. From our calculation, we have confidence in suggesting a model such that not the monomeric but the dimeric dyes are sparsely dispersed on the binding sites. If this assumption is correct, such a dimer model flexibly applies to the cases for $P/D\approx1$ as well as $P/D\gg1$. However, if this dimeric model is denied for $P/D\gg1$, we must consider that the optical activity may be induced not only by the local steric interaction between the monomeric dye and the base-pair (*i.e.*, conformationally induced optical activity), but also by the interaction between the dye and the sugar phosphate groups (*i.e.*, the intrinsic optical activity induced by the assymmetric environments). This monomeric binding is certainly the consensus ascertained experimentally for $P/D\gg1$. We do not carry out possible model calculations taking account of such effects, since there is no definite experimental datum in the shorter wavelength region available.

In Fig. 6, the model calculation for $\theta=90°$ gives the reasonable blue shift and intensity descent in the first UV band which are comparable to the bandshapes experimentally observed for $P/D=2$—5.[18] On the other hand, the calculation for $\theta=50°$ gives the reasonable ORD and CD curves for the corresponding experimental curves.[18] We could not find out a proper θ-value so as

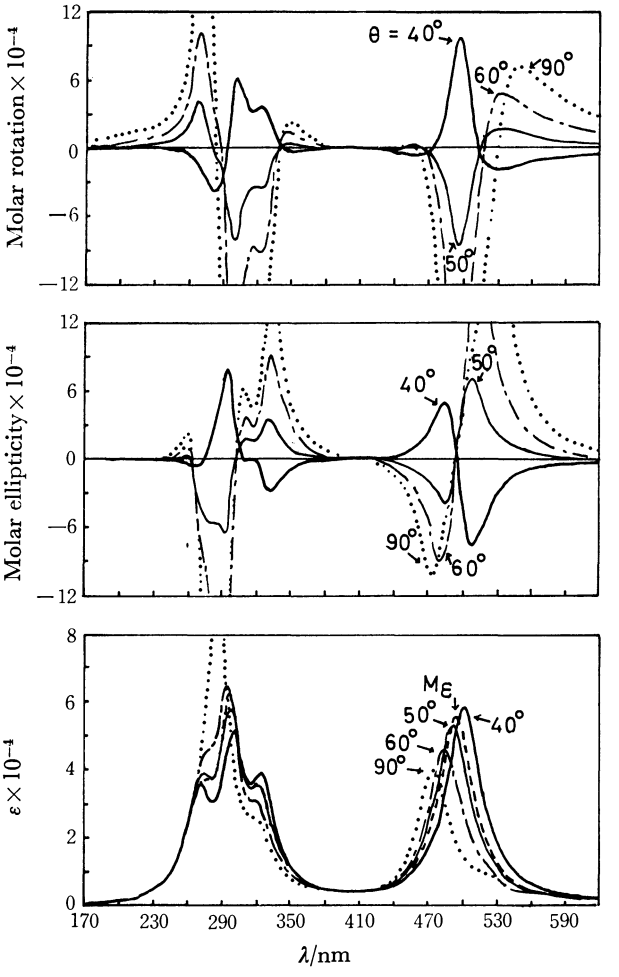

Fig. 6. The ORD (top), CD (middle), and UV (bottom) bandshapes for the outside-stacking dimer model (see Table 2).

to obtain the agreement of the computed UV, ORD, and CD bandshapes with experiments at the same time. It should be noticed that for $0°\leq\theta\leq40°$ the red shift and the intensity ascent are observed in the first UV band and that the reversed Cotton effect and the red shift in the ORD and CD bands come to be large. Such bandshapes computed happen to correspond to the experimental ones for $P/D\gg1$ and may be true if the species of the dimeric dyes are dispersedly bound to DNA. However, we must not forget that depending upon the experimental condition the reversed Cotton effect can be seen even for $P/D\approx1$.[6,22]

Single- and Double-Stranded 5-mer Models: As will be expected from the discussion of the chain-length effect, we obtain almost the same results in Fig. 7 as those in Fig. 6. The model calculation for $\theta=90°$ (the radial orientation of the long axis of the dye molecule) gives the reasonable blue shift and intensity descent which are comparable with the first UV band observed for the low P/D ratios, but the ORD and CD curves computed are too intense in comparison with the experimental ones. Our previous study[20] on the shift of the UV band suggested the radial orientation, but found that although the qualitative feature of the bandshapes is satisfied,[5] the ORD curves computed are extraordinarily strong in their intensites which may be brought about just due to the assumption of a smaller value of $|\vec{a}|=9.1$ Å compared with $|\vec{a}|=12.68$ Å, as is readily understood from the present results. On the other hand, the model calculation for $\theta=0°$ (tangential orientation of the long axis) gives a large red shift and a large reversed Cotton effect.

In Fig. 7, it should be noticed that the single-stranded models for $\theta=50°$—$55°$ give the ORD and CD curves comparable for the experimental ones of the low P/D ratios, while we have only the imperceptible UV intensity descent. When we compute the bandshapes in more detail, particularly for $\theta=49°$—$55°$ using the same model, we obtain the results as shown in Fig. 8. It is interesting to note that drastic changes of the ORD and CD curves occur for small changes in the vicinity of a specific value $\theta=55°$, and that the UV bandshape computed changes a little comparing with the experimental UV band.

By using the model presented by Tinoco *et al.*,[1] we computed the bandshapes for the single- and double-stranded DNA–AO complexes fixing $\theta=90°$, which are shown in Fig. 9. In this calculation, we used the spectral

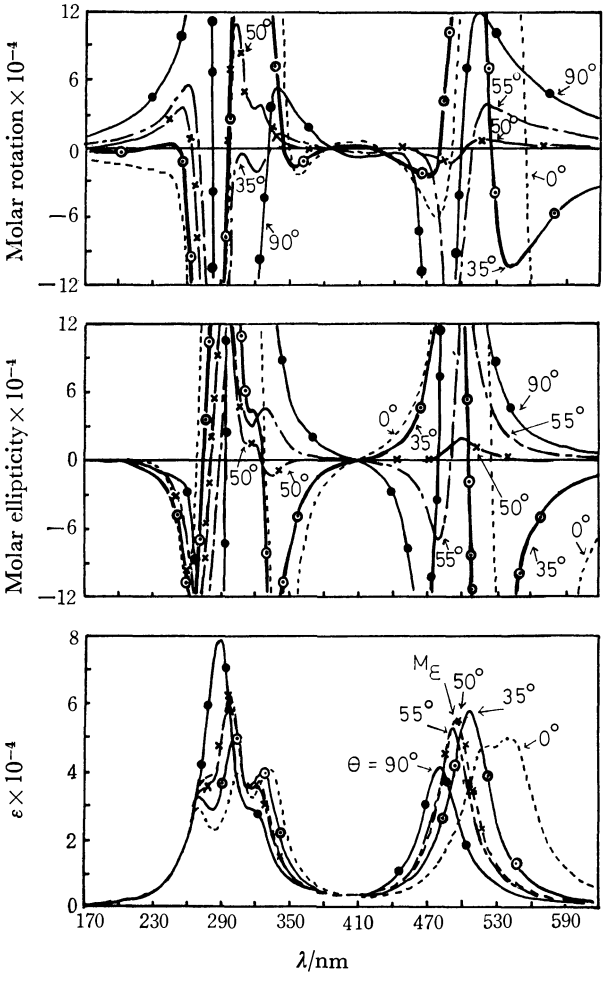

Fig. 7. Dependence of the ORD (top), CD (middle), and UV bottom) bandshapes for the outside-stacking 5-mer model (see Table 2) on the twisting angle (θ) of the short axis of the AO dye from the radial direction of the helix.

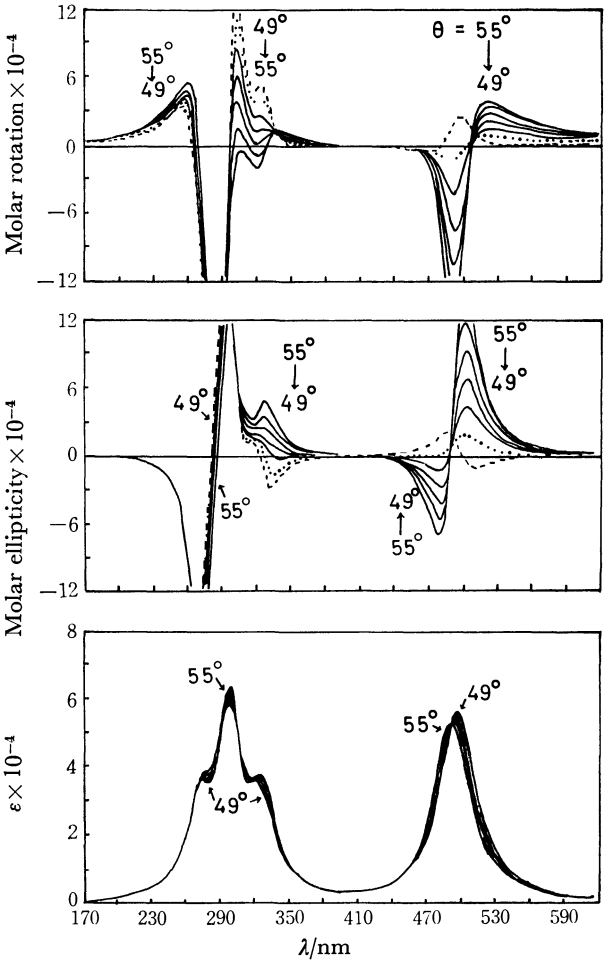

Fig. 8. The selected θ-dependence of the ORD (top), CD (middle), and UV (bottom) bandshapes for the single-stranded outside-stacking 5-mer model (see Table 2).

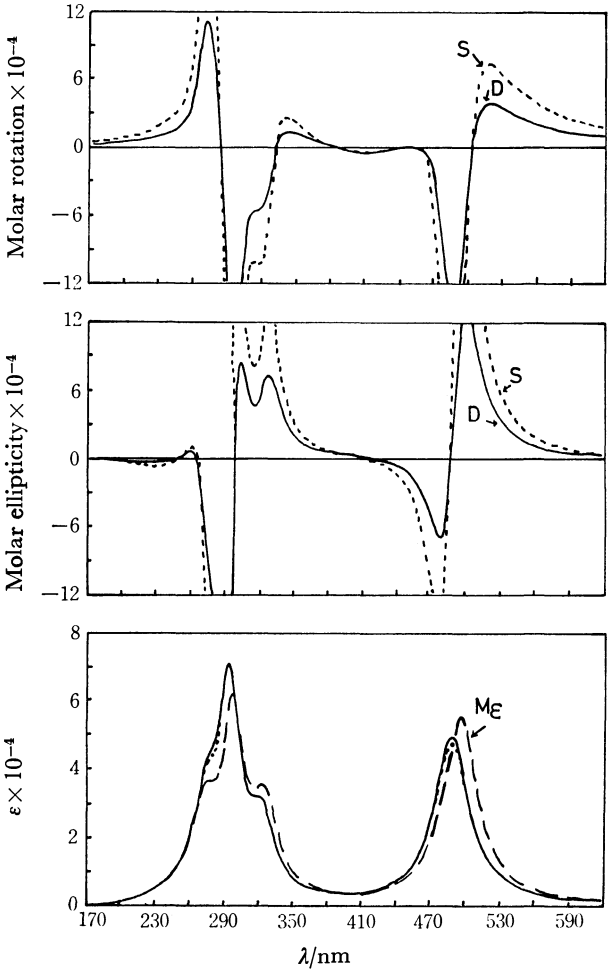

Fig. 9. The ORD top), CD (middle), and UV (bottom) bandshapes for the single-stranded 5-mer model (see Table 2) similar to the Tinoco-Woody-Bradley model. The S and D denote the single- and double-strands, respectively.

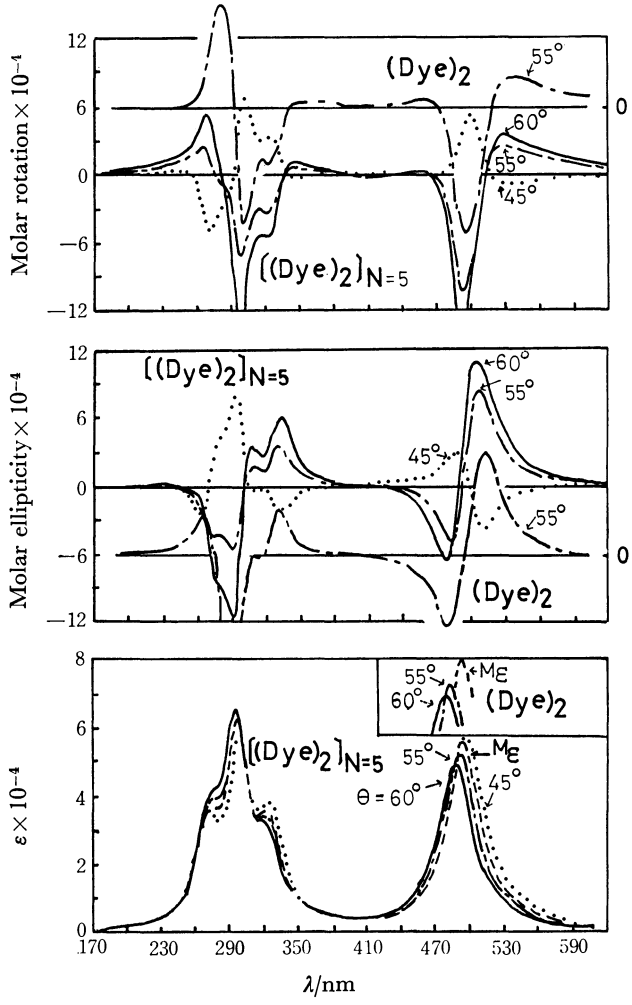

Fig. 10. The ORD (top), CD (middle), and UV (bottm) bandshapes for the one dimer-pair $(Dye)_2$ and/or the five dimer-pairs repeating sequence models $[(Dye)_2]_5$ (see Table 2).

parameters given in Table 1 and the screened potential $\mathbf{U}^{\text{screen}}_{mn}=(1/\varepsilon)\mathbf{U}^{\text{bare}}_{mn}$ with the dielectric constant $\varepsilon=2.0$, instead of the bare interaction $\mathbf{U}_{mn}=\mathbf{U}^{\text{bare}}_{mn}$. If we assume that the radial orientation ($\theta=90°$) of the dyes is experimentally correct, the discrepancy mentioned about Figs. 7 and 8 is found to be overcome in Fig. 9 by the inclusion of the dielectric screening effect and the dye-dye interaction between the double strands. However, ε is simply the parameter assumed tentatively and it may be difficult to choose the value which has a real physical meaning. We notice in Fig. 9 that the qualitative feature of the bandshapes for the single-stranded polymer is not definitely changed by allowing for the dye-dye interaction between the double strands. Concerning this model, there also remains dissatisfaction with regard to the fact that the extent of the blue shift and the intensity descent in the first UV band is small compared with the experimental bandshapes for the low P/D ratios.

Dimer-Pairs Repeating Sequence Model: For the dimer model mentioned in the previous paragraphs, we assume a rather different model as shown in Fig. 2 and in the bottom line of Table 2, which we call a dimer-pairs repeating sequence model. It is necessary to note that the model drawn in Fig. 2 is a kind of visualization of an external association model of dimer dyes, *i.e.*, the polymer of the dimer units which was used by Imae and Ikeda[6] for the calculations of CD curves. As shown in Fig. 10, the $(Dye)_2$- and $[(Dye)_2]_5$-models for $\theta=55°$ and 66° give the similar bandshapes, which are approximately comparable with the UV, ORD, and CD bandshapes observed for the low P/D ratios. For the models within the range $0°\leq\theta\leq45°$, the reversed Cotton effect can be seen in the visible region, and only small intensity increase and red shift in the first UV band are observed.

From the discussions mentioned above, it is found that the outside-stacked *one* dimer-pair model and/or the outside-stacked *five* dimer-pairs repeating sequence model is a good example to be able to well predict the experimental UV, ORD, and CD bandshapes for the low P/D ratios, as far as the models assumed in Table 2 are concerned. We obtain the reasonable bandshapes for the intercalation models of the low P/D ratio ($P/D=5$), but in the present paper we do not consider the possible intercalation models for $P/D\gg1$.

There still remain a lot of problems such as the correct assignment of the transition energies and the polarization directions of the transitions for the monomer dye, the introduction of the bandshape functions involving the vibrational levels, and the suitable determination of the damping factors ($=\Gamma/2$) of the monomer band governing the bandshapes of the polymer. The study on this line is now in progress.

References

1) I. Tinoco, Jr., R. W. Woody, and D. F. Bradley, *J. Chem. Phys.*, **38**, 1317 (1963).
2) D. F. Bradley, I. Tinoco, Jr., and R. W. Woody, *Biopolymers*, **1**, 239 (1963).
3) M. R. Philpott, *J. Chem. Phys.*, **53**, 968 (1970).
4) M. R. Philpott, *J. Chem. Phys.*, **54**, 4223 (1971).
5) Y. J. I'Haya, T. Nakamura, Y. Yagi, T. Sano, and H. Ito, *Int. J. Quantum Chem., Symp.*, **5**, 361 (1971).
6) I. Imae and S. Ikeda, *Polym. J.*, **8**, 531 (1976).
7) T. Imae and S. Ikeda, *Biopolymers*, **15**, 1655 (1976).
8) J. H. Perrin and P. A. Hart, *J. Pharm. Sci.*, **59**, 431 (1970) and references cited therein.
9) H. Ito, T. Eri, and Y. J. I'Haya, *Chem. Phys.*, **8**, 68 (1975), **10**, 497 (1975).
10) H. Ito, T. Eri, and Y. J. I'Haya, *Chem. Phys. Lett.*, **39**, 150 (1976), **45**, 610 (1977).
11) H. Ito and Y. J. I'Haya, 26th IUPAC Congress Abstracts (Tokyo, September 4—10, 1977) Sessions II and III, p. 594.
12) H. Ito, Y. J. I'Haya, and T. Eri, *Bull. Chem. Soc. Jpn.*, **51**, 1341 (1978).
13) C. J. Böttcher (1973), "Theory of Electric Polarizability," p. 208, Elsevier Scientific Publishing Company.
14) J. Applequist, *J. Chem. Phys.*, **58**, 4251 (1973).
15) A. R. Zib and W. Rhodes, *J. Chem. Phys.*, **57**, 5354 (1972).
16) J. G. Kirkwood, *J. Chem. Phys.*, **5**, 479 (1937).
17) W. W. Wood, W. Fickett, and J. G. Kirkwood, *J. Chem. Phys.*, **20**, 561 (1952).
18) K. Yamaoka and R. A. Resnik, *J. Phys. Chem.*, **70**, 4051 (1966).
19) S. F. Mason and A. J. McCaffery, *Nature*, **204**, 468 (1964).
20) H. Ito and Y. J. I'Haya, *Int. J. Quantum Chem.*, **2**, 5 (1968).
21) O. K. Obendorf, J. P. Glusker, P. R. Hansen, H. M. Berman, and H. L. Carrell, *Bioinorg. Chem.*, **6**, 29 (1976).
22) D. M. Neville, Jr., and D. F. Bradley, *Biochim. Biophys. Acta*, **50**, 397 (1961).

The Mass-transfer Rate through the Liquid-Liquid Interface. VII. Diffusion through a Spherical Interface Involving the Adsorption-Desorption Process

Teruya SHIMBASHI

Department of Chemical Engineering, Tokyo Institute of Technology, Meguro-ku, Tokyo 152

(Received March 14, 1979)

A theoretical formula for the transfer rate of a solute through a spherical interface has been proposed, considering the adsorption-desorption process and the variation in the amount of adsorption. Computational results indicate that, in the usual particle-diameter (radius <1 mm), the diffusion coefficient has practically no relation to the transfer rate in the case of a significant interfacial resistance, such as is observed in the transfer of fatty acids. The concentrations of butylamine in the aqueous, continuous phase in a stirred extraction vessel have been predicted.

In the treatment of mass transfer through oil–water interfaces, the adsorption-desorption process on the interface has usually been disregarded in chemical engineering practice; that is, the two concentrations in both phases next to the interface have been assumed to be in equilibrium. The ground of this disregard of the process is supposedly that the transfer rate has not physically, but rather formally been treated in terms of the "mass-transfer coefficient;" also, that the resistance encountered when a solute molecule transfers through an oil–water interface has been generally considered to be negligible.

Some authors have studied and investigated, however, about the magnitudes of the interfacial resistances; their results[1-7] indicate that usually the resistance is fairly significant. A theoretical formula[8] of mass-transfer rates was derived in the case of linear diffusion through the plane interface in a finite composite medium, considering the adsorption-desorption process on the interface and also the variation in the amount of adsorption; the analytical results[7] from the observed transfer rates of propylamine and butylamine through the water–benzene interface using the derived formula showed that the activation free energies of desorption of the solutes from the interface were about 18 kcal†/mol at 50 °C, which agreed with the results[4-6] obtained by other procedures from the transfer rates of fatty acids through oil–water interfaces.

In an actual and effective operation of the technical extraction of substances, the oil–water system is composed of a dispersed phase and a continuous phase in a stirred vessel or in a dropping tower; the role of the interfacial process of transfer may become important as the liquid-drop goes to smaller sizes.

Below we shall treat theoretically, from the above point of view, the mass-transfer rates through a spherical interface involving the adsorption-desorption process and the variation in the amount of adsorption.[9]

Theory

Modified Fick's diffusion equations for a composite spherical system[10] are defined by

$$\partial u_1/\partial t = D_1(\partial^2 u_1/\partial r^2), \quad 0 \leq r < R_1, \quad t > 0; \tag{1}$$

$$\partial u_2/\partial t = D_2(\partial^2 u_2/\partial r^2), \quad R_1 < r < R_2, \quad t > 0, \tag{2}$$

where u_1 and u_2 are related to c_i, $i=1$ or 2, as $u_i \equiv rc_i$; here, c_i is the local concentration of the solute in Phase i; D_1 and D_2 are the diffusion coefficients; r is the distance from the center of the composite (concentric) sphere; t is the time, and R_1 and R_2 are constants.

The boundary conditions are represented by

$$-D_1\{(\partial u_1/\partial r)/r-(u_1/r^2)\} + D_2\{(\partial u_2/\partial r)/r-(u_2/r^2)\} = \Gamma_\infty(\mathrm{d}\theta/\mathrm{d}t), \quad r = R_1, \quad t > 0; \tag{3}$$

$$-D_1\{(\partial u_1/\partial r)/r-(u_1/r^2)\} = k_{a1}(1-\theta)u_1/r - k_{d1}\theta, \quad r = R_1, \quad t > 0; \tag{4}$$

$$D_2\{(\partial u_2/\partial r)/r-(u_2/r^2)\} = k_{a2}(1-\theta)u_2/r - k_{d2}\theta, \quad r = R_1, \quad t > 0; \tag{5}$$

$$u_1 = 0, \quad r = 0, \quad t > 0; \tag{6}$$

$$u_2 = R_2 c_{2\omega}, \quad r = R_2, \quad t > 0, \tag{7}$$

where Γ_∞ is the saturated value of the amount of adsorption per unit of area of the interface; θ is the fraction of the total interface occupied by adsorbed molecules; k_{a1} and k_{a2} are the rate constants of adsorption to the interface from Phase 1 and Phase 2 respectively; k_{d1} and k_{d2} are the rate constants of desorption from the interface to Phase 1 and Phase 2 respectively, and $c_{2\omega}$ is a constant. Equation 3 relates the variation in the amount of adsorption to the fluxes, while Eqs. 4 and 5 give the relation between the adsorption-desorption mechanism and the fluxes.

The initial conditions are assumed to be

$$u_1 = rc_{10}, \quad 0 \leq r < R_1, \quad t = 0; \tag{8}$$

$$u_2 = rc_{2\omega}, \quad R_1 < r \leq R_2, \quad t = 0; \tag{9}$$

$$\theta = \theta_0, \quad t = 0, \tag{10}$$

where c_{10} and θ_0 are constants as well as $c_{2\omega}$.

Equations 1—10 are to be solved by means of the Laplace transformation; in an extreme case, $(R_2-R_1)\to 0$ (then $R_1=R_2=R$), considering a dynamic system such as in a stirred vessel, the solution may be expressed as

$$c_{1,t} = (k_{a1}k_{d2})^{-1}k_{a2}k_{d1}c_{2\omega} + (2/r)\sum_{n=1}^{\infty}\boldsymbol{D}^{-1}\xi_t \sin(r\alpha_n) \times \exp(-D_1\alpha_n^2 t); \tag{11}$$

$$\theta_{,t} = (k_{a2}/k_{d2})c_{2\omega} + 2(\Gamma_\infty R)^{-1}\sum_{n=1}^{\infty}\boldsymbol{D}^{-1}\{\zeta_{1,t}\sin(R\alpha_n) + \zeta_{2,t}\cos(R\alpha_n)\}\exp(-D_1\alpha_n^2 t); \tag{12}$$

$$\boldsymbol{D} \equiv \phi_1 \sin(R\alpha_n) + \phi_2 \cos(R\alpha_n);$$

† 1 kcal=4184 J.

$$\phi_1 \equiv \{D_1R^{-1}(k_{d1}+k_{d2})-k_{a1}k_{d2}\}(\Gamma_\infty D_1 R\alpha_n)^{-1} + \{R^{-1}(D_1R^{-1}-k_{a1}) - \Gamma_\infty^{-1}(k_{d1}+k_{d2})\}\alpha_n + D_1\alpha_n^3;$$

$$\phi_2 \equiv \{k_{a1}k_{d2}-D_1R^{-1}(k_{d1}+k_{d2})\}(\Gamma_\infty D_1)^{-1} - (D_1R^{-1}+k_{a1})\alpha_n^2;$$

$$\xi_i \equiv \{k_{a1}(c_{10}+D_1\alpha_n^2 I_{1,i})-k_{d1}\theta_0\}\alpha_n - \{k_{a1}k_{d2}(c_{10} + D_1\alpha_n^2 I_{1,i})-k_{a2}k_{d1}(c_{2\omega}+D_1\alpha_n^2 I_{2,i})\}(\Gamma_\infty D_1\alpha_n)^{-1};$$

$$\zeta_{1,i} \equiv -(D_1\alpha_n)^{-1}\{D_1R^{-1}[k_{a1}(c_{10}+D_1\alpha_n^2 I_{1,i})-k_{d1}\theta_0] - (k_{a1}-D_1R^{-1})[k_{a2}(c_{2\omega}+D_1\alpha_n^2 I_{2,i})-k_{d2}\theta_0]\};$$

$$i_{2,i} \equiv k_{a1}(c_{10}+D_1\alpha_n^2 I_{1,i}) - k_{d1}\theta_0 + k_{a2}(c_{2\omega}+D_1\alpha_n^2 I_{2,i}) - k_{d2}\theta_0;$$

$$I_{1,i+1} \equiv \frac{1}{2\pi i}\int_{\sigma_1-i\infty}^{\sigma_1+i\infty}\{\bar{c}_{1,i}(\sigma)\}_{r=R}\bar{\theta}_{,i}(-D_1\alpha_n^2-\sigma)d\sigma;$$

$$I_{2,i+1} \equiv \frac{1}{2\pi i}c_{2\omega}\int_{\sigma_1-i\infty}^{\sigma_1+i\infty}\sigma^{-1}\bar{\theta}_{,i}(-D_1\alpha_n^2-\sigma)d\sigma,$$

where the subscript i designates including perturbation[11] to the ith term, provided $I_{1,0}=I_{2,0}=0$; $\bar{c}_1(p)$ and $\bar{\theta}(p)$ are the image functions corresponding to $c_1(t)$ and $\theta(t)$ respectively; here, p is the conversion parameter of the Laplace transformation; $\pm\alpha_n$ are the roots (generally complex) of α in the next equation:

$$a_1\sin(R\alpha) + a_2\cos(R\alpha) = 0; \quad (13)$$

$$a_1 \equiv \{D_1R^{-1}(k_{d1}+k_{d2})-k_{a1}k_{d2}\} \times(\Gamma_\infty\alpha)^{-1}-(D_1R^{-1}-k_{a1})D_1\alpha;$$

$$a_2 \equiv D_1^2\alpha^2 - \Gamma_\infty^{-1}D_1(k_{d1}+k_{d2}).$$

The amount of solute in the sphere of Phase 1 on the condition that $(R_2-R_1)\to 0$ is represented by

$$q = 4\pi\int_0^R c_1^* r^2 dr = (4/3)\pi R^3(k_{a1}k_{d2})^{-1}k_{a2}k_{d1}c_{2\omega} + 8\pi\sum_{n=1}^{\infty}(\alpha_n\boldsymbol{D})^{-1}\xi^* \times\{\alpha_n^{-1}\sin(R\alpha_n)-R\cos(R\alpha_n)\}\exp(-D_1\alpha_n^2 t), \quad (14)$$

where the superscript* indicates the convergence in the progress of the perturbation.

Let us consider a stirred vessel with a certain volume, V, which is filled with Phase 1 (dispersed) and Phase 2 (continuous), with liquids of Phase 1 and Phase 2 constantly flowing in and out at the volumetrical rates of F_1 and F_2 respectively; these liquids (solvents) are immiscible and dissolved a solute in the initial concentrations of c_{10} and c_{20} respectively.

We calculate the concentration, $c_{2\omega}$, of the solute in Phase 2 (continuous) in the steady state; the dispersed particles are taken to be spheres of complete mixing,[12] and the distribution of the particle-diameters as well as the coalescence and fission of particles are disregarded for the sake of simplification.

The transfer rate of the solute from a sphere of Phase 1 to Phase 2 that is continuous (we use Eq. 14) is approximately given as

$$v = -dq/dt = 8\pi D_1\sum_{n=1}^{\infty}\boldsymbol{D}^{-1}\xi^*\{\sin(R\alpha_n)-R\alpha_n\cos(R\alpha_n)\} \times\exp(-D_1\alpha_n^2 t).$$

The probability of the residence of a particle in the vessel (for complete mixing) may be represented as $Z=\exp(-Ft/V)$, where $F=F_1+F_2$; the probability density of the residence time is given by

$$f(t)=d(1-Z)/dt=(F/V)\exp(-Ft/V);$$

so the average rate of transfer may be expressed as

$$\bar{v} = \int_0^\infty vf(t)dt = 8\pi D_1(F/V)\sum_{n=1}^{\infty}\boldsymbol{D}^{-1}\xi^*\{D_1\alpha_n^2+(F/V)\}^{-1} \times\{\sin(R\alpha_n)-R\alpha_n\cos(R\alpha_n)\}.$$

Considering the mass-balance, we obtain this relation: $\bar{v}nV=(c_{2\omega}-c_{20})F_2$, where n is the number of particles per unit volume in the vessel, and after rearranging the relation, we may obtain a representation (for $\theta_0=0$) of the concentration sought as

$$c_{2\omega} = \{c_{20}+6D_1(R^3\gamma)^{-1}\sum_{n=1}^{\infty}[\psi_1(\alpha_n)+D_1\alpha_n^2 I_2^*\psi_2(\alpha_n)]\} \times\{1-6D_1(R^3\gamma)^{-1}\sum_{n=1}^{\infty}\psi_2(\alpha_n)\}^{-1}; \quad (15)$$

$$\psi_1(\alpha_n) \equiv k_{a1}(c_{10}+D_1\alpha_n^2 I_1^*)(\Gamma_\infty D_1\alpha_n^2-k_{d2})\Delta;$$

$$\psi_2(\alpha_n) \equiv k_{a2}k_{d1}\Delta; \quad \gamma \equiv F_2/F_1;$$

$$\Delta \equiv \{\alpha_n^{-1}\sin(R\alpha_n)-R\cos(R\alpha_n)\}\{\boldsymbol{D}[D_1\alpha_n^2+(F/V)]\}^{-1}.$$

Some Computational Results

Figure 1 shows the time-dependences of the amount of solute in a sphere (where q_∞ is the value in a transfer-equilibrium), with hypothetical values given to the parameters in Eq. 14; Curve a, in the case of an insignificant interfacial resistance ($\Delta F^*_{di}\approx 4$ kcal/mol), and Curve b (where $k_1=(5/6)\times10^{-5}$ cm/s; see Appendix), in the case of a significant interfacial resistance ($\Delta F^*_{di}\approx$

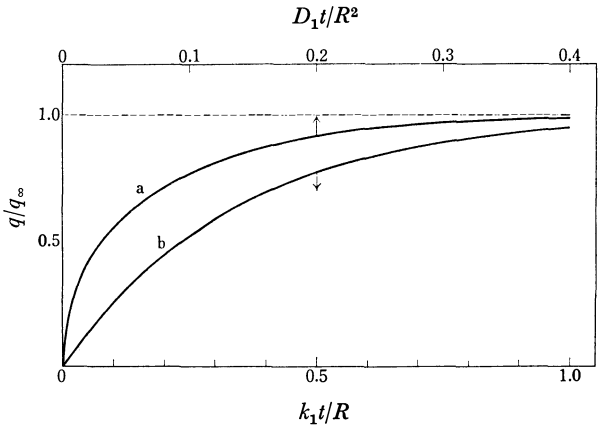

Fig. 1. Change in the amount of solute in a sphere. $D_1=10^{-5}$—10^{-3} cm²/s; $R=1$—0.01 mm.

Curve	a	b[a]
Γ_∞/mol m^{-2}	7×10^{-6}	7×10^{-6}
k_{d1}/mol cm^{-2} s^{-1}	1	1 (5)$\times10^{-9}$
k_{d2}/mol cm^{-2} s^{-1}	1	5 (1)$\times10^{-9}$
k_{a1}/cm s^{-1}	10^1	1 (5)$\times10^{-5}$
k_{a2}/cm s^{-1}	10^1	5 (1)$\times10^{-5}$
$c_{2\omega}$/mol m^{-3}	1	1
c_{10}/mol m^{-3}	0	0
θ_0	0	0

a) The values of k_{d1}, k_{d2}, k_{a1}, and k_{a2} substituted all the figures in the parentheses for ones on the left of the parentheses were also examined.

16 kcal/mol);[5,7] here, $\Delta F^{\ddagger}_{di}$ is the activation free energy of desorption from the interface to the ith phase; the diffusion coefficient, D_1, was changed at intervals from 10^{-5} to 10^{-3} cm^2/s, and the radius of the sphere, R, from 1 to 0.01 mm, in both cases.

The values of the rate constants of adsorption and desorption were given by the following formulas:[1]

$$k_{ai} = \lambda_i(kT/h) \exp(-\Delta F^{\ddagger}_{ai}/RT);$$
$$k_{di} = \Gamma_\infty(kT/h) \exp(-\Delta F^{\ddagger}_{di}/RT);$$

i=1 and 2, where λ_i($\approx$10 Å††) is the length of the adsorption path from the boundary site of Phase i to the interface; $\Delta F^{\ddagger}_{ai}$ is the activation free energy of adsorption from Phase i to the interface; k is the Boltzmann constant; h is the Planck constant; R is the gas constant, and T (=300 K) is the absolute temperature.

The procedure of calculation was as follows. Definite values were assigned to D_1, Γ_∞, R, k_{a1}, k_{d1}, and k_{d2} in Eq. 13, and the roots were found; although the roots, α_m (m=1, 2, ···), were generally complex, they were real[13] in those cases.

The values were assigned to D_1, Γ_∞, R, k_{a1}, k_{a2}, k_{d1}, k_{d2}, c_{10}, $c_{2\omega}$, θ_0, and α_n's ($n \leq 20$ usually suffices for convergence) in Eq. 14, and the amount of solute in the sphere, q, was computed as a function of the time, t. In those cases, $\theta \approx 0.005 \ll 1$, and the q value was computed approximately by the zero perturbation (substitute $c_{1,0}$ and ξ_0 for c_1* and ξ* in Eq. 14 respectively; see also Eqs. 4 and 5).

The computational results fell closely near the curves, a and b, in Fig. 1, in agreement with the values on the curves to the third decimal-digit. This means that, in the above ranges of conditions, the q value may be expressed approximately by the following sublimate relations in the cases of "an insignificant interfacial resistance" and of "a significant interfacial resistance" respectively:

$$q/q_\infty = f_1(D_1t/R^2), \text{ and } q/q_\infty = f_2(t/R),$$

where f_1 and f_2 designate functional relations.

The a curve well fits the next equation[14] of no interfacial resistance:

$$q/q_\infty = 6\pi^{-1/2}(D_1t)^{1/2}/R - 3D_1t/R^2 + \{12(D_1t)^{1/2}/R\} \times \sum_{n=1}^{\infty} \text{ierfc}\{nR/(D_1t)^{1/2}\}. \quad (16)$$

This may be an expression of the functional relation, f_1.

The b curve indicates that the q value in the case of "a significant interfacial resistance" ($\Delta F^{\ddagger}_{di} \approx 16$ kcal/mol) has practically no relation to the diffusion coefficient, D_1. This means that the diffusion process in bulk phases cannot be the rate-determining step under these conditions (see Appendix).

The a, b, and c curves in Fig. 2 predict the changes in the concentration of solute ($c_{2\omega}$) in the continuous phase (aqueous) as functions of F/V, as calculated by means of Eq. 15 (of I_1*=I_2*=0) when a 1 mol/m^3 (c_{20}) aqueous solution of butylamine and a solvent, benzene, was allowed to flow into a stirred vessel in the flow ratio γ=5 (water/benzene) at 50 °C, and the spherical particles of the dispersed phase had radii (R) of exactly 1, 0.1, and 0.01 mm respectively; the other parameters were set as follows: $D_1=3.206\times10^{-5}$ cm^2/s;[15] $\Gamma_\infty=6.83\times10^{-6}$ mol/m^2;[18] $k_{a1}=7.85\times10^3$ cm/s;[7] $k_{a2}=1.089\times10^{-4}$ cm/s;[7] k_{d1}=1 mol/cm^2 s;[7] $k_{d2}=5\times10^{-9}$ mol/cm^2 s;[7] $c_{10}=\theta_0=0$.

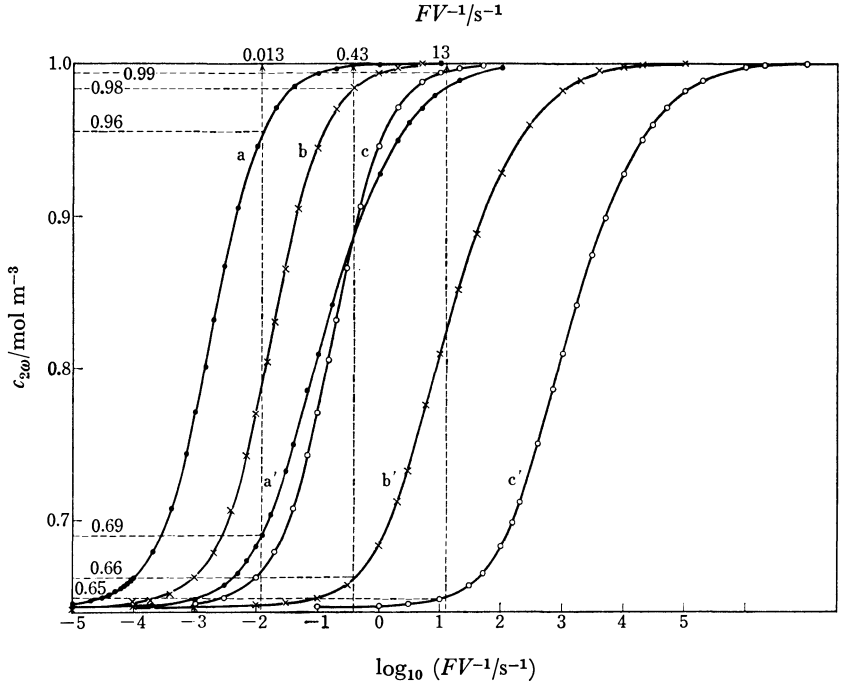

Fig. 2. F/V Dependence of $c_{2\omega}$. Sample: 1 mol/m^3 aqueous solution of butylamine and benzene; γ (water/benzene)=5; temperature=50 °C. a, a′: R=1 mm; b, b′: R=0.1 mm; c, c′: R=0.01 mm.

†† 1 Å=10^{-10} m.

The a′, b′, and c′ curves in Fig. 2 indicate the relation supposing the interfacial resistance was negligible; the two parameters were reset as follows: $k_{a2}=2.178\times10^4$ cm/s and $k_{d2}=1$ mol/cm² s.

An examination of the magnitude of the interfacial resistance may be effectively made under the given conditions provided the F/V ratios are set as 0.013, 0.43, and 13 s^{-1} in experiments with $R=1$, 0.1, and 0.01 mm respectively: If the resistance is significant ($\Delta F^{\neq}_{d2}=18$ kcal/mol), the $c_{2\omega}$ values are determined to be 0.96, 0.98, and 0.99 mol/m³ respectively, while if the resistance be negligible, the $c_{2\omega}$ values are determined to be lower[19] than 0.69, 0.66, and 0.65 mol/m³ respectively.

The author is indebted to Professors Hikoji Inazumi and Tadao Shiba of this Institute for their helpful discussions concerning this subject.

Appendix

When the transfer resistance in the bulk phases is negligible as compared with the interfacial resistance, the next equation may be derived as a specific case of Eq. 14, neglecting also the variation in the amount of adsorption on the interface:[1,3]

$$q = q_\infty - (q_\infty - q_0)\exp(-3k_1 t/R); \quad (17)$$
$$k_1 \equiv k_{a1}\{1+(k_{d1}/k_{d2})\}^{-1},$$

where q_0 is the initial amount of solute in a sphere and k_1 is the effective rate constant for transferring through the interface from Phase 1 to Phase 2. Equation 15 may then be simplified as follows:

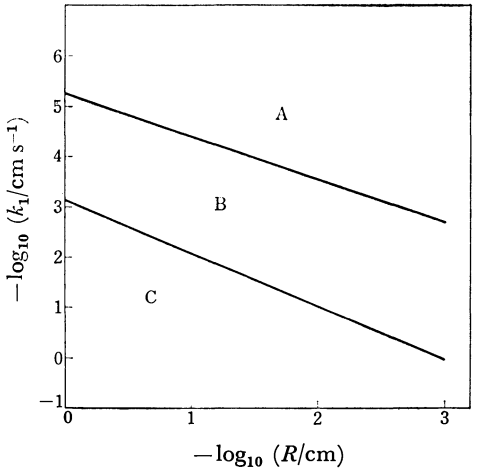

Fig. 3. Limits of application of the specific equations. $D_1=10^{-5}$ cm²/s; $q/q_\infty=0.5$. A: Bulk-diffusional resistance is negligible (Eq. 17 is applicable). B: Neither bulk-diffusional nor interfacial resistance is negligible. C: Interfacial resistance is negligible (Eq. 16 is applicable).

$$c_{2\omega} = (c_{10}+c_{20}H)(K+H)^{-1}; \quad (18)$$
$$H \equiv \gamma\{1+(R/3k_1)(F/V)\};\ K \equiv (k_{a1}k_{d2})^{-1}k_{a2}k_{d1}.$$

The computational values using these formulas also fit well the b curve in Fig. 1 and the a, b, and c curves in Fig. 2.

Figure 3 shows the limits of the application of Eqs. 16 and 17 to pairs of values of k_1 and R at $D_1=10^{-5}$ cm²/s. The lines indicating the limits were drawn on the assumption that every pair of k_1 and R on the lines made the q value computed by means of the specific equations (Eq. 16 or 17) deviate from that computed by means of Eq. 14 exactly 5% at the time of q/q_∞(Eq. 14)$=0.5$;[20] these lines should be considered to give a sort of standard, and the change in the time, t, as well as in the diffusion coefficient, D_1, transfers the position of the 5% lines.

References

1) T. Shimbashi and T. Shiba, *Bull. Chem. Soc. Jpn.*, **38**, 572 (1965).
2) T. Shimbashi and T. Shiba, *Bull. Chem. Soc. Jpn.*, **38**, 581 (1965).
3) T. Shimbashi and T. Shiba, *Bull. Chem. Soc. Jpn.*, **38**, 588 (1965).
4) W. Nitsch, *Chem.-Ing.-Tech.*, **38**, 525 (1966).
5) T. Shimbashi and T. Shiba, *Nippon Kagaku Zasshi*, **92**, 676 (1971).
6) M. Harada, T. Imamura, K. Fujiyoshi, and W. Eguchi, *J. Chem. Eng. Jpn.*, **8**, 233 (1975).
7) T. Shimbashi, *Nippon Kagaku Kaishi*, **1976**, 373.
8) T. Shimbashi, *Bull. Chem. Soc. Jpn.*, **48**, 626 (1975).
9) This treatment is almost the same as the linear diffusion through a plane interface treated before, and so the description will be abbreviated.
10) J. Crank, "The Mathematics of Diffusion," Clarendon Press, Oxford (1956), p. 84.
11) The calculation of $I_{1,i}$ and $I_{2,i}$ is easy, but somewhat lengthy, and so it is omitted here.
12) This means that the time-average of the local concentration of the solute tends to be constant in every part in the vessel because of the random change in the relative positions of the dispersed particles.
13) This is determined, for example, by the means described in Footnote 19 in the literature of Ref. 7.
14) H. S. Carslaw and J. C. Jaeger, "Conduction of Heat in Solids," 2nd ed, Clarendon Press, Oxford (1960), p. 234.
15) This was estimated by Wilke's method[16] from the literature.[17]
16) C. R. Wilke, *Chem. Eng. Progr.*, **45**, 218 (1949).
17) J. T. Davies and J. B. Wiggill, *Proc. R. Soc., London, Ser. A*, **255**, 277 (1960).
18) This is equivalent to the value of $B=24.3\times10^{-16}$ cm²/molecule cited in the literature of Ref. 7.
19) It is considered that the apparent diffusion coefficient is greater than the value estimated because of agitations.
20) Change in the values of the rate constants of adsorption and desorption on condition that $k_1=$const, $k_{a1}/k_{d1}=$const, and $k_{a2}/k_{d2}=$const gives practically constant q's computed by Eq. 14, agreeing to the third decimal-digit.

The Electronic Spectra of Anthraquinone in Shpol'skii Matrices and in Crystals at 4.2 K

Eiji KANEZAKI,† Nobuyuki NISHI, and Minoru KINOSHITA*

The Institute for Solid State Physics, The University of Tokyo, Roppongi, Minato-ku, Tokyo 106

(Received March 28, 1979)

The lower excited singlet and triplet states of 9,10-anthraquinone-d_0 and -d_8 are examined in normal alkanes and in crystals at 4.2 K with the phosphorescence excitation method. The $S\leftarrow S_0$ and $T\leftarrow S_0$ excitation spectra are analyzed by considering environmental effects on and isotopic changes in the vibrational structure. The low energy region of the spectra can be explained without taking the A_u origin in close proximity of the B_{1g} origin into account. The latter origin band in the singlet and triplet spectra in hexane and in crystals, respectively, is weaker by a factor of 10^{-3}—10^{-2} than the strongest vibronic band in the respective regions. No clear evidence has been found about the location of the singlet and triplet A_u states in the excitation spectra.

The investigation of the energy separation between the two low lying n,π^* states of quinones has attracted much interest,[1–8] because its determination measures the magnitude of the electronic interaction of the nonbonding orbitals. In a *p*-quinone molecule, only the through bond interaction is dominant, as in the cases of pyrazine and quinoxaline,[9] in which the two interacting nonbonding orbitals are concluded to have an energy separation of the order of 1 eV ($\simeq$8067 cm^{-1}), in good agreement with the theoretical calculation.[9,10]

Although there is a discrepancy in the assignment of the He-I photoelectron spectrum of *p*-benzoquinone between the two groups,[2,10,11] the energy levels of the two nonbonding orbitals are separated by 0.9[10] or 0.3 eV.[2,11] The Coulomb integrals for the n_+,π^* and n_-,π^* states, J_{n_+,π^*} and J_{n_-,π^*}, may differ from each other and modify the energy separation between the two zero-order n,π^* states. From the absorption experiments on *p*-benzoquinone crystals, the separation has been reported to be about 225 cm^{-1} in the singlet state[3] and 320 cm^{-1} in the triplet state.[6] Recently Goodman and Brus[12] have examined excitation spectra of *p*-benzoquinone in a neon host. They could not observe the broad band, which had been assigned to a different electronic origin, but observed very strong origin bands which they assigned to the ^1A_u and ^3A_u states. Their conclusion is that the two n,π^* states are nearly degenerate in *p*-benzoquinone. Although we do not agree with their conclusion, because they did not consider the possibility of a structural change induced by the host, their results give us very important information about the assignment of the two origins.

The assignment of the lowest triplet state of anthraquinone (AQ) has also attracted much attention from many workers.[13–17] The polarization measurement indicates that the phosphorescence of AQ has the transition dipole moment along the oxygen-oxygen direction(z).[13] Thus, it is concluded that the radiative transition from the lowest triplet state of AQ borrows its activity from the z axis polarized $^1B_{1u}(\pi,\pi^*)\rightarrow{}^1A_g$ transition.

The phosphorescence spectrum of AQ in hexane is known to arise from the $^3B_{1g}(n,\pi^*)\rightarrow{}^1A_g$ transition. The AQ molecules in this matrix seem to retain the inversion symmetry, because the 0,0 band is missing.[17] On the other hand, the spectrum in pentane was analyzed to be a two-site emission. One of the sites produces a strong origin band induced by breakdown of the inversion symmetry.[17]

The $T\leftarrow S_0$ absorption spectrum of crystalline AQ has been obtained and the Zeeman experiment has been performed on the individual bands in the spectrum. From the very weak intensity and the Zeeman patterns of the 0,0 band, the lowest triplet state of AQ is assigned to $^3B_{1g}(n,\pi^*)$, which is located at 22154 cm^{-1} [14] or at 22150 cm^{-1}. [15] The vibronic bands appearing in the spectrum are ascribed to the ungerade-type vibrations, since the inversion symmetry of the molecule is conserved even in the crystal.[18]

The purpose of this work is to analyze the excitation spectra of AQ-d_0 and AQ-d_8 in the above two Shpol'skii matrices and to find evidence for the location of the A_u state. We will also discuss the structure of the $T\leftarrow S_0$ excitation spectra of both isotope crystals.

Experimental

9,10-Anthraquinone (AQ-d_0) and spectrograde hexane were purchased from Tokyo Kasei Co., Ltd. Merck Uvasol pentane was used without further purification. 2,3-Dichloroquinoxaline (DCQ) and 9,10-anthraquinone-d_8 (AQ-d_8) were from Eastman Kodak and Merck Sharp and Dohme Ltd., respectively.

An Ushio UXL-1000DO 1 kW xenon lamp was used as a light source for excitation and absorption experiments. A Molectron DL-200 tunable dye laser equipped with a Molectron UV-1000 1 MW N_2 laser was used to detect the origin bands in the $T\leftarrow S_0$ excitation spectra. Most of the high resolution spectra were observed through a Jobin Yvon HR 1000 monochromator fitted with a 1800 grooves/mm, 120 $\times$ 140 mm^2 grating, and a Spex 1700-III 3/4 m or a Bausch & Lomb 1/2 m monochromator was used to isolate a specific band of emission for excitation studies or microwave experiments.

Results and Discussion

Phosphorescence. The spectra of AQ-d_0 in hexane and pentane showed sharp bands. These spectra were essentially the same as those reported by Khalil and Goodman.[17] The high resolution spectra of AQ-d_8 in these matrices are shown in Fig. 1. We could detect

† Present address: Faculty of Engineering, Tokushima University, Minamijosanjima, Tokushima 770.

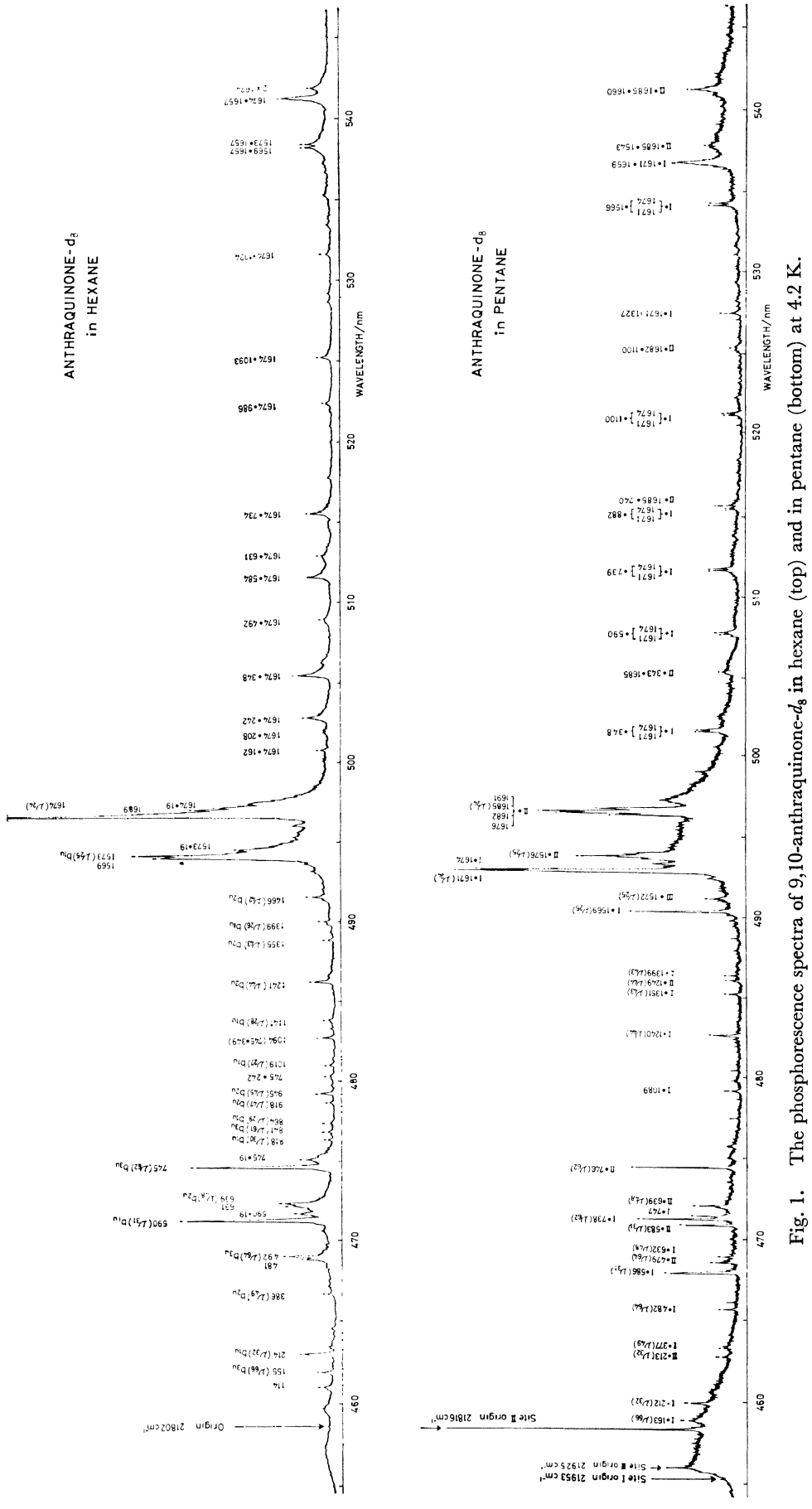

Fig. 1. The phosphorescence spectra of 9,10-anthraquinone-d_8 in hexane (top) and in pentane (bottom) at 4.2 K.

the origin band at 21802 cm^{-1} in hexane, the intensity of which was about 10^{-3} of that of the strongest band assigned as being due to the b_{1u} C=O stretching vibration(ν_{24}). This vibronic band has a single peak and is accompanied with a broad tail towards the low energy side. This feature is also seen in its combination bands with totally symmetric vibrations. The shape of this tail is apparently different from that seen in the band at 0—745 cm^{-1}. The band assigned to ν_{25} shows a doublet structure at 0—1569 and 0—1573 cm^{-1}. Most of the b_{1u} and b_{2u} vibrations, except for the two C–D stretching modes, are found in the spectrum.

Three-site emission is observed in pentane at 4.2 K. Most of the active bands were analyzed to be bands originating from two sites. The emission from site I has a very, very weak origin at 21953 cm^{-1}. The vibrational structure is almost the same as that in hexane. The origin band of the emission from site II reveals the strongest intensity in the spectrum. The energy of this origin band is close to that in hexane. The most intense vibronic band due to ν_{24} splits into two lines for site I and into four or more for site II. The combination bands with a_g vibrations show a similar band shape, which is very helpful for the analysis.

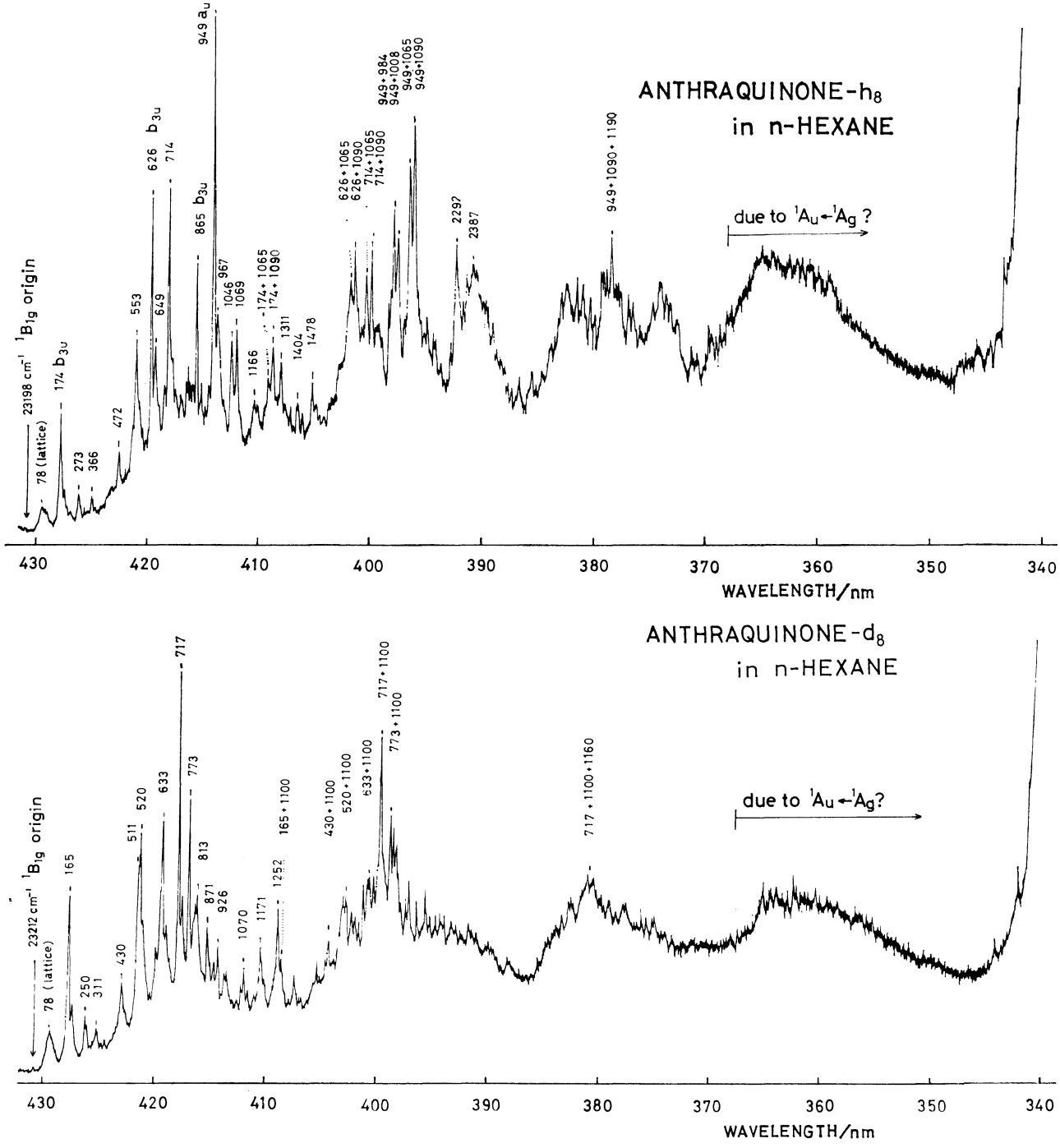

Fig. 2. The S←S_0 excitation spectra of 9,10-anthraquinone-d_0 and -d_8 in hexane at 4.2 K. Detection bandwidth is 4 nm centered at 497 nm.

The band width of the site II origin is about 2 cm^{-1} and those of other bands are generally much narrower in pentane than those in hexane. In spite of the very strong intensity of the origin band of site II, no other a_g fundamental band shows distinguishable activity in the spectrum. This indicates that any distortion of the site II molecules is not very large.

$S(n,\pi^*)\leftarrow S_0$ Excitation. The two n,π^* states in question are $^1B_{1g}$ and ^1A_u in the low energy region of AQ. The transitions from the ground state to both of these n,π^* states are symmetry forbidden processes, and would become allowed by borrowing intensities mainly from $^1B_{1u}(\pi,\pi^*)\leftarrow{}^1A_g$ and $^1B_{2u}(\pi,\pi^*)\leftarrow{}^1A_g$ transitions through u-type out-of-plane vibrations for the transition to the $^1B_{1g}$ state and g-type vibrations for that to the ^1A_u state, or by molecular distortion to a lower symmetry.

Spectra in Hexane: The excitation spectra of AQ-d_0 and -d_8 in hexane are shown in Fig. 2. A very, very weak but distinct band at 23198 cm^{-1} in the spectrum of AQ-d_0 and at 23212 cm^{-1} in that of AQ-d_8 was observed in the hexane matrix. The vibrational structures were analyzed by taking these bands as an electronic origin and the results are given in the figure.

The spectrum of AQ-d_0 has a structure quite similar to that of crystalline *p*-benzoquinone observed by Trommsdorff.[3] The bands in the spectra of AQ-d_0 and *p*-benzoquinone exhibit a good correspondence with each other, except for the strong bands, which have been assigned to the $^1B_{1g}$ and ^1A_u origins of *p*-benzoquinone. The strongest band in the *p*-benzoquinone spectrum is the one at 0+946 cm^{-1}. The corresponding band also appears as the strongest band in the AQ-d_0 spectrum in hexane at 0+949 cm^{-1}. Other bands seen in the *p*-benzoquinone spectrum at 0+141, 0+597, 0+679, 0+836, 0+1044, 0+1069, and 0+1161 cm^{-1} correspond well to the bands at 0+174, 0+553, 0+626, 0+865, 0+1046, 0+1066, and 0+1166 cm^{-1}, respectively, in the spectrum of AQ-d_0. These frequencies are surprisingly closely related to each other. In the case of AQ-d_0, however, there is no strong band in the lower energy region which corresponds to the strong broad band assigned as the ^1A_u origin of *p*-benzoquinone.

The broad band at 0+78 cm^{-1} and the sharp band at 0+174 cm^{-1} of AQ-d_0 correspond well with the first two vibrational bands of AQ-d_8 at 0+78 and 0+165 cm^{-1} in their intensity and frequency. The corresponding bands are also observed in the phosphorescence spectra of AQ-d_0 and -d_8 in hexane (at 0*−76 and 0*−167 cm^{-1} for AQ-d_0, where 0*=21783 cm^{-1}) and assigned to a lattice mode and a b_{3u} out-of-plane vibration, respectively.[17] The vibration of 141 cm^{-1} found in the spectrum of a *p*-benzoquinone crystal was also assigned to a b_{3u} skeletal mode by Trommsdorff.[3] The appearance of the b_{3u} vibration clearly indicates that these bands are associated with the $^1B_{1g}\leftarrow{}^1A_g$ transition.

The spectra of the two isotopes show different structures in the region from 0+500 to 0+1200 cm^{-1} mainly in their intensity relation. The strongest band of AQ-d_0 at 0+949 cm^{-1} shifts to 0+717 cm^{-1} for AQ-d_8. This frequency lowering by about 230 cm^{-1} excludes an assignment of these bands to vibrations belonging to another electronic state. The isotopic ratio of 1.32 (=949/717) indicates that these vibrations are to be assigned to a C–H(D) bending mode. Considering the assignment of the 946 cm^{-1} vibration of *p*-benzoquinone,[3] we also assign the 949 cm^{-1} vibration tentatively to an a_u out-of-plane C–H bending vibration. However, we could not eliminate the possibility of a b_{3u} vibration, because the band observed at 970 cm^{-1}

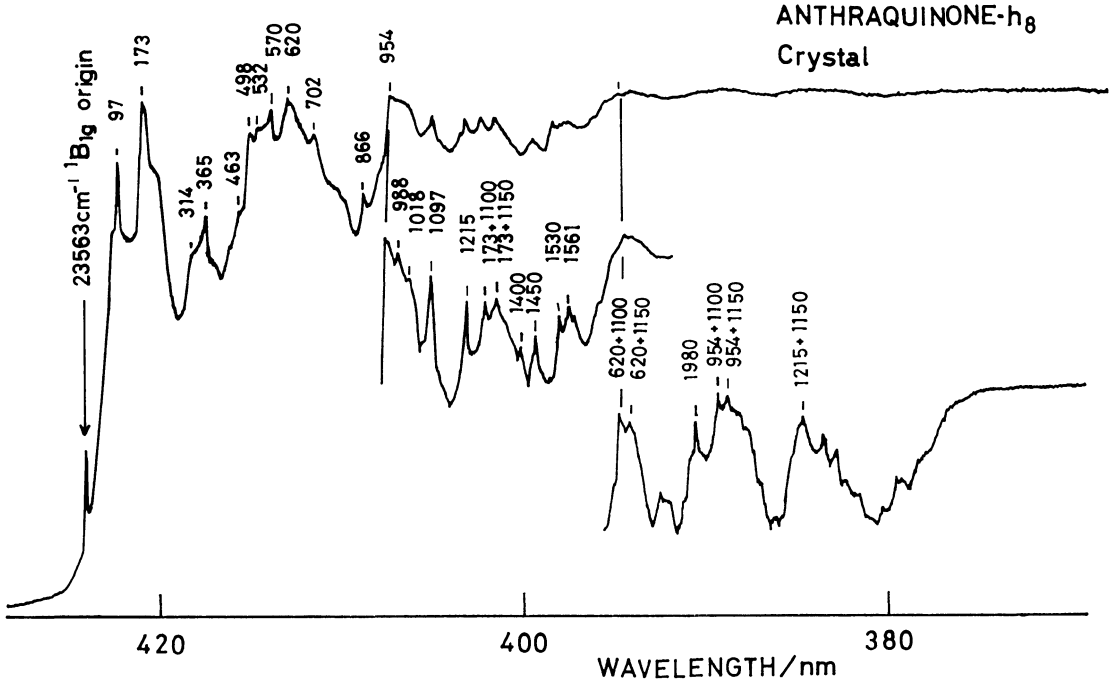

Fig. 3. The $S\leftarrow S_0$ absorption spectrum of crystalline 9,10-anthraquinone-d_0 at 4.2 K.

in the infrared spectrum was assigned to ν_{61}, a b_{3u} C–H bending mode.[18]

Other strong bands of AQ-d_0 at 0+553, 0+626, 0+714, and 0+865 cm^{-1} correspond with those of AQ-d_8 at 0+511, 0+520, 0+633, and 0+813 cm^{-1}, respectively. The combination bands of these strong lines with the 1065 and 1090 cm^{-1} vibrations of AQ-d_0 and the 1100 cm^{-1} vibration of AQ-d_8 are found strongly and this proves that these bands do not belong to a different electronic transition. Such combination bands were also observed in the spectrum of a *p*-benzoquinone crystal by Trommsdorff,[3] who assigned the 1100 cm^{-1} vibration as being due to the totally symmetric C=O stretching vibration.

Spectrum of Neat Crystal: The absorption spectrum of the AQ-d_0 crystal is shown in Fig. 3. The origin band was observed at 23563 cm^{-1}, which is about 360 cm^{-1} higher in energy than the $^1B_{1g}$ origin in hexane. The

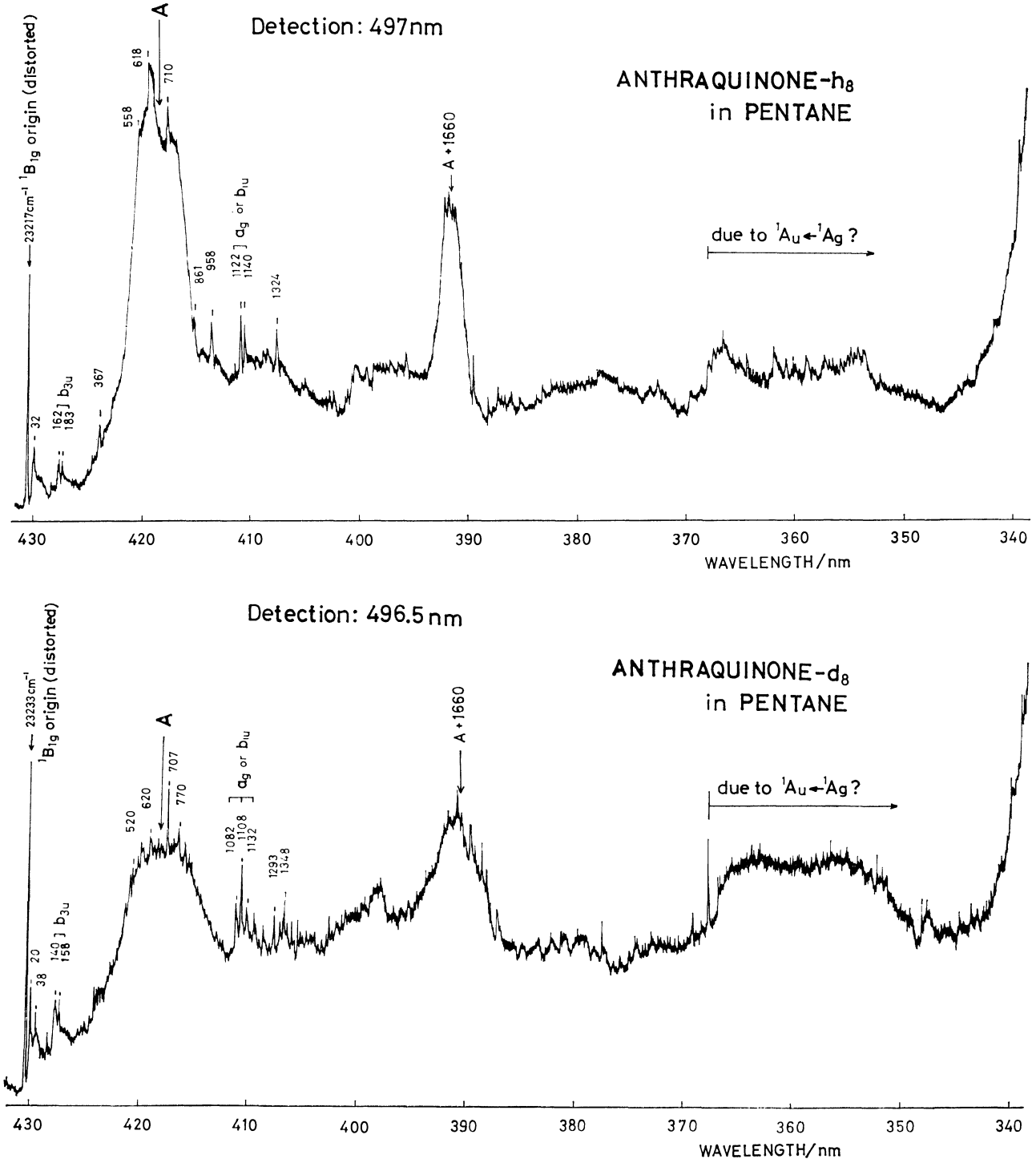

Fig. 4. The S←S_0 excitation spectra of 9,10-anthraquinone-d_0 and -d_8 in pentane at 4.2 K. Detection bandwidth is 5 nm centered at 497 nm.

band at 0+97 cm^{-1} corresponds with a lattice mode. and the band at 0+173 cm^{-1} to the b_{3u} mode found in the hexane system. The vibrational structure of the strong bands in this spectrum coincides quite well with that in hexane. Combination bands with a_g vibrations of 1100 and 1150 cm^{-1} are also active in the crystal.

Spectra in Pentane: The excitation spectra of AQ-d_0 and -d_8 in pentane were observed by monitoring the strong bands around 497 nm of the phosphorescence from site II with a detection bandwidth of 4—5 nm The observed spectra in Fig. 4 show a strong origin band to the higher energy side by about 20 cm^{-1} with respect to the origin band in hexane. The appearance of the strong origin band is consistent with that observed at 21790 cm^{-1} for AQ-d_0 and at 21816 cm^{-1} for AQ-d_8 in the phosphorescence in pentane. Therefore, we are really observing the same species with a distorted structure.

Apart from the intense broad bands around 420 and 390 nm, which will be shown to be due to molecular aggregates, the spectra consist of a number of sharp bands and a hump around 365 nm. The sharp bands in the lower energy region may be classified into two groups. One of the groups consists of the bands which correspond to those found in the hexane system; these bands can be assigned to b_{3u} and a_u vibrations. Since the fundamental frequencies measured from the origin band fit quite well to those observed in hexane, there is no possibility that these bands belong to the $^1A_u \leftarrow {}^1A_g$ transition which could be observed for the distorted species. If the bands belonging to the $^1A_u \leftarrow {}^1A_g$ transition appeared in the same region, the vibrations should be assigned to b_{1g} or b_{2g} symmetry.

The bands in the other group are characteristic of a distorted species, for which a_g and b_{1u} in-plane vibrations may show some activity. The bands appearing around 0+1100 cm^{-1} do not have a corresponding band in the spectrum in hexane. The vibration of about 1100 cm^{-1} is known to form combination bands with b_{3u} and a_u vibrations in hexane and is assigned to the a_g C=O stretching vibration. The b_{1u} C=O stretching vibration is also expected to acquire activity, if the molecular symmetry is reduced by the environment to C_{2v} with the C_2 axis along the C=O bonds.

In pentane, the phosphorescence emission shows strong sharp bands overlapping a very broad background. The broad background was assigned to molecular aggregates.[17] As a matter of fact, the strong broad bands also appear at 420 and 390 nm in the excitation spectra monitored at 497 nm. The position and relative intensity of the broad band around 420 nm were found to change markedly when the wavelength setting of the detecting monochromator was changed; some examples are shown in Fig. 5. The energy shift of the band center seems to be just equivalent to the difference in the wavelength of the monitored light. Furthermore, the intensity of the broad band relative to that of the origin band at 23217 cm^{-1} also changes with cooling condition of the sample and initial guest concentration. The spectra of the two isotopes in Fig. 4 were taken at the concentrations differing by a factor

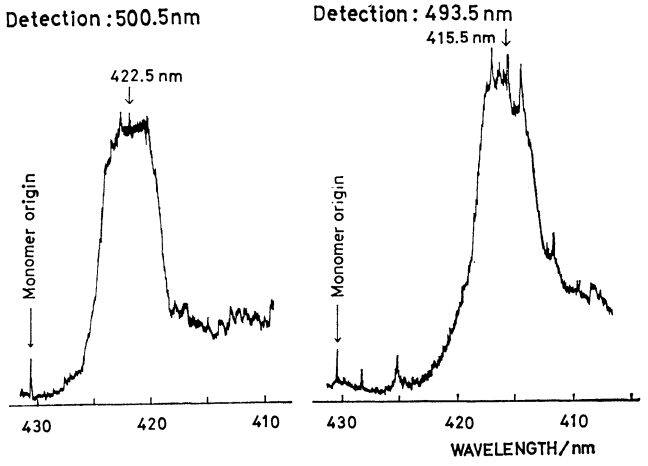

Fig. 5. Variation of the broad band position in the excitation spectrum with detection wavelength of the emission from anthraquinone-d_0 in pentane at 4.2 K.

of three. These results suggest that the broad band around 420 nm arises from molecular aggregates. The broad band around 390 nm (about 1660 cm^{-1} higher in energy) seems to be its combination band, although the bandwidth is about half.

The $^1A_u \leftarrow {}^1A_g$ Transition: It was expected that the forbidden $^1A_u \leftarrow {}^1A_g$ transition would appear in the excitation spectrum in pentane, when the phosphorescence from the distorted species was monitored. For this purpose, we have carefully adjusted the detecting monochromator to a desired wavelength. In this respect, it is of great interest to pay attention to the sharp band appearing at 367.65 nm in the excitation spectrum of AQ-d_8 in pentane. The band lies at 4033 cm^{-1} from the strong origin and could not be assigned to a combination band or an overtone band. Furthermore, the hump with weak but sharp bands is commonly found around 365 nm in all the four spectra in Figs. 2 and 4. As the $^1B_{1g}$ origin lies within 35 cm^{-1} in the four systems, the origin of the $^1A_u \leftarrow {}^1A_g$ transition in these systems is also expected to appear at nearly the same position. The region where the hump is observed clearly satisfies this condition. The sharp band at 367.65 nm in the spectrum of AQ-d_8 is quite within the reasonable bounds of possibility of the ^1A_u origin. A weak similar band is also seen at 367.7 nm in the spectrum of AQ-d_0 in pentane.

$T(n,\pi^*) \leftarrow S_0$ Excitation. A mixed crystal of AQ with 0.1% of 2,3-dichloroquinoxaline (DCQ) emits a strong phosphorescence from the lowest triplet state of DCQ. The vibrational structure of the phosphorescence spectrum is in good agreement with the result reported by Tinti and El-Sayed.[19] The excitation spectrum of crystalline AQ was observed by monitoring this emission. The spectra for the AQ-d_0 and -d_8 crystals are shown in Fig. 6. The excitation spectrum of AQ-d_0 is essentially the same as the absorption spectrum reported by Drabe *et al.*[14] and Narisawa *et al.*,[15] except for minor details. Carefully comparing the spectra of the two isotopes, we could notice a structural difference around 443 nm. AQ-d_8 shows an intensity increment of the broad band around 0+327 cm^{-1}. Another obvious

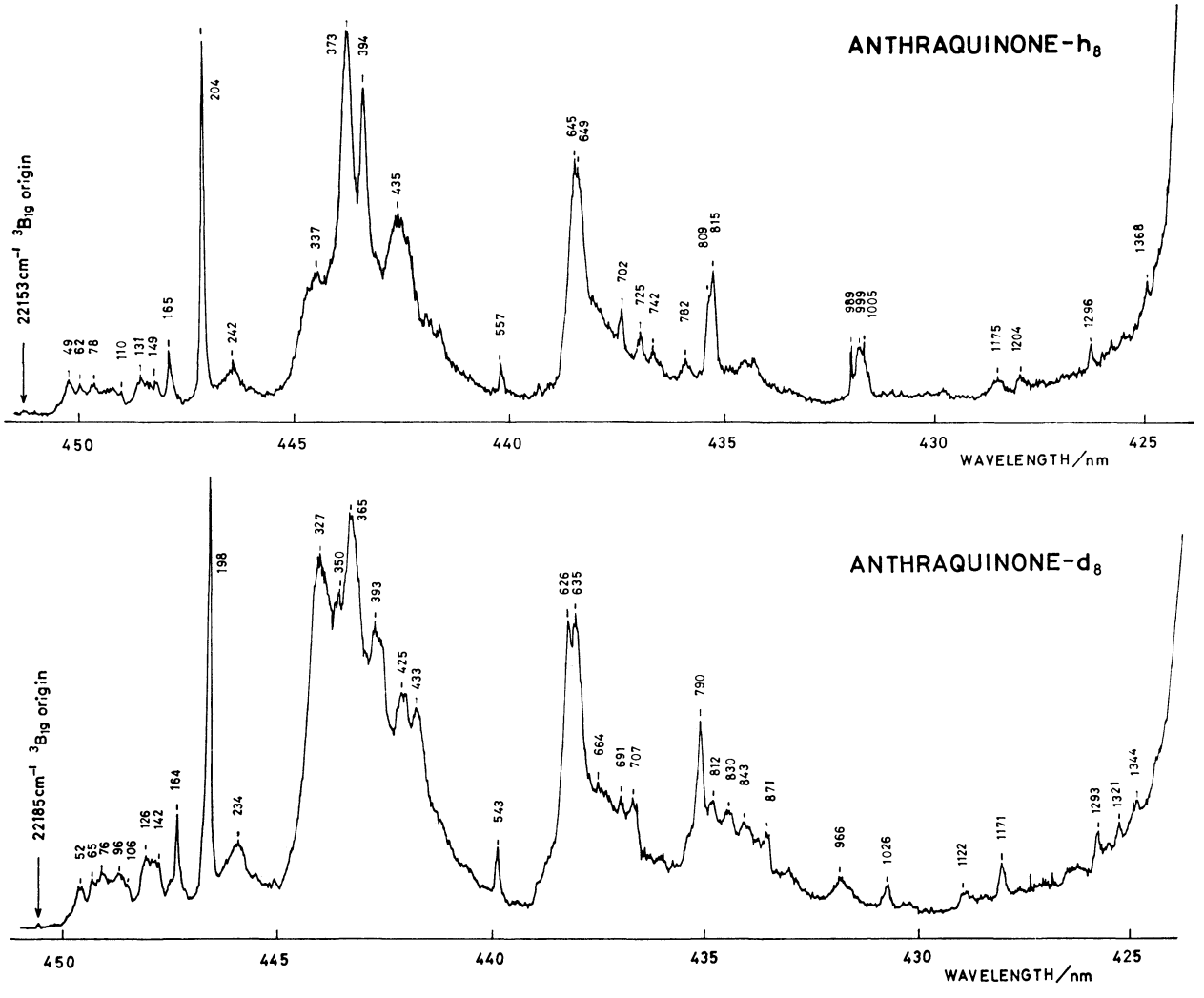

Fig. 6. The T←S_0 excitation spectra of crystalline 9,10-anthraquinone-d_0 (top) and -d_8 (bottom) at 4.2 K. The whole phosphorescence from the doped 2,3-dichloroquinoxaline was monitored.

difference can be found around 0+830 and 0+1000 cm^{-1}. This difference can be attributed to an isotopic frequency shift of vibrations, thereby suggesting some participation of hydrogen bending vibrations in the transition mechanism.

MIDP Excitation Spectra: Since each of the transitions from the ground state to the three spin states in a single vibronic level of an excited triplet state has a different selection rule, depending on the spin-orbit coupling processes involved, microwave induced delayed phosphorescence (MIDP)[20] signals in an isolated molecule reflect the transition probability characteristic of each sublevel excitation. In a mixed crystal, however, the selective populations of the spin states are sometimes not maintained during energy transfer processes, and MIDP signals show a modified spin population depending on the relative orientations of the molecular spin axes between the guest and host and between the host molecules.[20,21]

The short axes(z) of the AQ molecules in a crystal are nearly parallel to each other, but the long axis(y) of an AQ molecule is approximately parallel to the normal axis(x) of the translationally inequivalent molecules.[22] In the mixed crystal of AQ with DCQ, it is reasonably assumed that the guest molecules replace the host molecules substitutionally. Therefore, it is expected that the population of T_z produced in DCQ by direct T←S_0 excitation of the mixed crystal may not be affected very much by energy transfer and trapping processes, whereas the populations of T_y and T_x may or may not mix with each other depending on whether the main energy transfer mechanism is one-dimensional or not. A single band excitation of the AQ-d_0 crystal yielded the steady state population ratios of $N_z: N_y: N_x$ to be approximately 1.9: 2.1: 1 for the 0+165 cm^{-1} band and 5.5: 0.55: 1 for the 0+204 cm^{-1} band. From these results, it was concluded that the mechanism is mainly one-dimensional and that the mixing of the populations of T_y and T_x during the energy transfer has a minor effect on the relative populations in our systems.

The excitation spectrum shown in the upper part of Fig. 7 was taken by sampling the DCQ phosphorescence in the AQ-d_8 crystal for a period of 110 ms just after excitation lasting 30 ms. The repetition rate was 2 Hz. Since the decay times of T_z, T_y, and T_x were observed

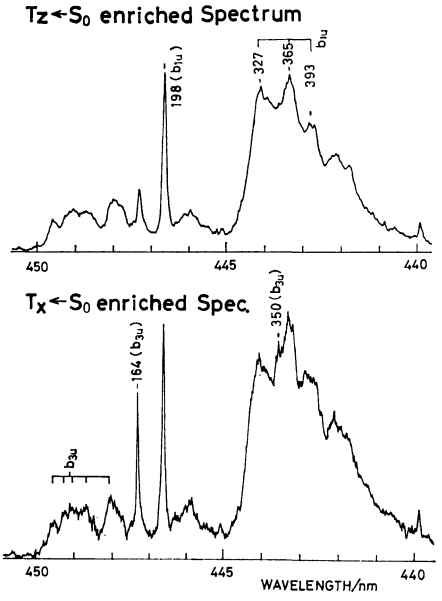

Fig. 7. The $T\leftarrow S_0$ excitation spectra of crystalline 9,10-anthraquinone-d_8 at 1.4 K. The absorption to T_z is enhanced in the upper spectrum by choosing the sampling time, while that to T_x is enhaced in the lower spectrum by using microwave modulation.

to be 150, 260, and 2700 ms, respectively, this spectrum contains an enhanced contribution from the $T_z\leftarrow S_0$ transition of AQ-d_8, by comparison with an excitation spectrum taken under steady state condition.

The lower spectrum of Fig. 7 is an MIDP excitation spectrum taken by sampling only the portion of the MIDP signal on sweeping the microwave frequency through the $T_y\leftrightarrow T_x$ transition of DCQ 950 ms after excitation. The microwave sweep increases the T_y emission in proportion to the population of T_x produced mostly by the $T_x\leftarrow S_0$ transition of the host molecules The assignments of the vibronic bands were performed according to the selection rule that a b_{1u} vibration is actively involved in the excitation to the T_z sublevel in the $^1B_{1g}$ state and a b_{3u} vibration is involved in the excitation to the T_x sublevel. Some of the results are shown in Fig. 7.

The sharp band at $0+164\ cm^{-1}$ is notably enhanced by the $T_y\leftrightarrow T_x$ pumping and assigned to a b_{3u} vibration. The vibration of $165\ cm^{-1}$ has also appeared in the $S\leftarrow S_0$ excitation spectrum of AQ-d_8 in hexane. This was assigned to the $\nu_{66}(b_{3u})$ mode. The intensity of the band at $0+350\ cm^{-1}$ is markedly increased by the $T_y\leftrightarrow T_x$ pumping, and this band can be assigned to a b_{3u} vibration. At first sight, the broad bands at $0+365$ and $0+393\ cm^{-1}$ also seem to be intensified by the microwave transition, but this could be due to their overlapping with the band at $0+350\ cm^{-1}$. The broad low frequency bands which should be considered as being due to lattice modes behave like b_{3u} vibrations. Murao and Azumi[23] also found that the fundamental lattice band is exceedingly active in the emission spectrum from the T_x sublevel of AQ-d_0 in octane.

Except for several broad bands around $0+400\ cm^{-1}$, most of the strong bands in Fig. 6 were assigned on the basis of the relation of the isotopic ratio of the vibrational frequency and the relative intensity found in the phosphorescence spectra of both isotopes in hexane and in octane.[23] The fundamental frequencies obtained are summarized in Table 1, together with those found in the emission[17] and in the infrared absorption spectra.[18] The frequency changes of these vibrations in the $^3B_{1g}$ state are not very large, except for the C–H(D) bending mode(ν_{45}), which shows a frequency reduction of 16—17 per cent.

The antisymmetric C=O stretching mode(ν_{24}) and the out-of-plane C–H bending mode(ν_{63}) are found to be active in the phosphorescence spectrum.[17] However, we are not certain whether these vibrations appear in the $T\leftarrow S_0$ excitation spectrum. If the frequency of ν_{24} is increased for any reason in the $^3B_{1g}$ state or is decreased by less than 16 per cent, then the vibronic band due to ν_{24} would be hidden in the region of $S\leftarrow S_0$ absorption. The symmetric C=O stretching mode(ν_3) of about 1100 cm^{-1} is known to form several combination bands in the $S\leftarrow S_0$ excitation in hexane, as discussed above. Therefore, we may also expect the appearance of its combination bands in the $T\leftarrow S_0$ excitation spectrum. The band appearing at $0+1295\ cm^{-1}$ might be attributed to a combination band with the ν_{32} mode. However, this band seems to be too weak to be assigned to the combination band of ν_3.

Any strong vibronic interaction between the $^3B_{1g}$

Table 1. The vibrational frequencies observed in the $^3B_{1g}\leftarrow{}^1A_g$ excitation spectra of the anthraquinone crystals with the corresponding frequencies found in the phosphorescence spectra in hexane and in the infrared absorption spectra of crystals

Assignment	9,10-Anthraquinone-d_0			9,10-Anthraquinone-d_8		
	T_1(cryst.)	S_0(hexane)[a]	IR(cryst.)[b]	T_1(cryst.)	S_0(hexane)	IR(cryst.)[b]
ν_{66} b_{3u} skel. def.	165 cm^{-1}	167	167	164	155	161
ν_{32} b_{1u} skel. def.	204	228	237	198	214	222
ν_{64} b_{3u} C=O bend.	—	(517)	491	350	492	(398)
ν_{31} b_{1u} skel. def.	645	620	626	626	590	605
ν_{62} b_{3u} skel. def.	815	791	816	790	745	744
ν_{45} b_{2u} C–H bend.	999	1155	1207	812	945	965
ν_{44} b_{2u} ring str.	1204	1339	1335	1122	1241	1246

a) Ref. 17, b) Ref. 18; skel., skeletal; def., deformation; bend., bending; str., stretching.

and ^3A_u states through the ν_{24} mode would have a possibility of causing a frequency shift of this vibration. The strong band at $0+373\ cm^{-1}$ for AQ-d_0 and at $0+365\ cm^{-1}$ for AQ-d_8 might be considered to be due to ν_{24} of reduced frequency, as a result of the pseudo-Jahn-Teller effect. However, the PMDR studies of *p*-benzoquinone[24] and AQ-d_0[23] did not demonstrate any detectable molecular distortion along the b_{1u} coordinate. These results are therefore consistent with the fact that the origin band is vanishingly weak in the excitation spectra of the AQ crystals and in the emission spectra of AQ-d_0 and -d_8 in hexane. The frequency reduction from $1676\ cm^{-1}$ in the ground state to 373 (or 365) cm^{-1} in the $^3B_{1g}$ state would be too large to explain the absence of molecular distortion along the b_{1u} direction. The above discussion suggests that the frequency of the ν_3 vibration and possibly that of the ν_{24} vibration are higher than $1100\ cm^{-1}$ in the $^3B_{1g}$ state.

The Broad Band Cluster: Drabe *et al.* assigned the center of the broad band cluster from 445 to 441 nm (*i.e.*, $22560\pm10\ cm^{-1}$) as the origin of the ^3A_u state.[14] Instead of taking the origin at the center of the cluster, the strongest band position may be a more adequate choice for the origin, that is, $22526\ cm^{-1}$ ($0+373\ cm^{-1}$) for AQ-d_0 and $22550\ cm^{-1}$ ($0+365\ cm^{-1}$) for AQ-d_8. This assignment was proposed mainly from analogy with the absorption spectrum of a *p*-benzoquinone crystal, which exhibited a strong broad absorption at $320\ cm^{-1}$ to the higher energy side from the $^3B_{1g}$ origin. However, this broad band assigned as the ^3A_u origin was not found in the excitation spectrum of the isolated *p*-benzoquinone molecule in a neon matrix.[12] Goodman and Brus concluded that this broad band might be vibronic absorption induced by the environment.[12] Therefore, it seems that the assignment of the cluster is still inconclusive. The cluster may be interpreted in several ways.

In the first place, we examine the possibility that the ^3A_u origin may be in the cluster and the vibronic bands thereafter would belong to the $^3A_u \leftarrow {}^1A_g$ transition. In this case, a vibronic band is expected to have a band shape similar to that of the origin, because the ^3A_u origin band has an allowed character and coupling with a non-totally symmetric phonon is not expected in this transition. The shapes of the clusters are different in the spectra of the two isotopes, although the spectral positions of the clusters are coincident. Therefore, the vibrational bands coupled with the origin band would give rise to a more complex spectrum for AQ-d_8 than for AQ-d_0. The observed spectrum of AQ-d_8, however, does not include such a complicated structure and the difference between the two spectra is thus attributed to the involvement of C–H(D) bending vibrations. This cluster does not seem to behave as an origin in the spectrum.

The second case is that the strongest band in the cluster would be assigned to the ^3A_u origin as before, but the vibronic bands in the cluster are built on the $^3B_{1g} \leftarrow {}^1A_g$ transition and are induced by a strong interaction between the vibronic levels in $^3B_{1g}$ and the ^3A_u origin. In this case, the fact that the intensity of the band at $0+327\ cm^{-1}$ is comparable with that at $0+365\ cm^{-1}$ in the spectrum of AQ-d_8 indicates that the coupling should be very strong in AQ-d_8. However, the intensity of the corresponding band at $0+337\ cm^{-1}$ in the spectrum of AQ-d_0 is less than half of that of the strongest band at $0+373\ cm^{-1}$ and the energy gap between the two bands is nearly the same as that for AQ-d_8. This fact probably eliminates the possibility that the strong interactions exist between the vibrational levels in $^3B_{1g}$ and the ^3A_u origin.

Thirdly, the coupling of a vibronic band with phonon modes may be considered. Vibrational frequencies of 350—450 cm^{-1} correspond to those of in-plane C=O bending vibrations in the ground state. A b_{2u} mode is found at $387\ cm^{-1}$ in the infrared absorption spectrum and assigned to ν_{49}.[18] A Raman band at $485\ cm^{-1}$ was attributed to the b_{3g} C=O bending mode.[25] The former b_{2u} vibration was also found in the phosphorescence spectrum of AQ-d_8 in hexane (Fig. 1) and in that of an isotopically mixed crystal.[14] Since the triplet state is n,π^* in character, frequency reduction of C=O bending vibrations can be expected, although delocalization of the nonbonding orbitals over the whole σ framework probably decreases this effect to some extent. Such a change in the force field around the C=O groups is considered to induce an interaction with local lattice modes. Here, we have to attach importance to the fact that the lattice modes coupled with the very weak $^3B_{1g}$ origin band appear with different relative intensities among the bands in the spectra of the two isotopic crystals. It would then be possible that these b_{2u} and b_{3g} vibrations couple with some lattice modes of b_g and b_u symmetries, respectively, resulting in the same behavior as b_{1u} vibrations. This explains the similarity in frequency and the difference in relative intensity of the peaks in the broad band clusters in the two excitation spectra. This idea is consistent with the interpretation suggested by Goodman and Brus[12] that the broad absorption band of *p*-benzoquinone may be vibronically induced by the environment.

Finally, it is also possible to consider that the Duschinsky effect[26,27] is prominent in the triplet manifold and that the transition intensity shared by ν_{24} is distributed over several bands with b_{1u} symmetry, including the bands coupled with lattice modes. This allows some strong bands to appear in the low frequency region, where the fundamental band of the ν_{24} mode in the ground state coordinate cannot be expected to appear.[28]

As discussed above, the assignment of the ^3A_u origin to the broad band around 443 nm does not explain satisfactorily the intensity relation among the near lying bands. We conclude that no tangible evidence for that assignment has been found in the excitation spectra of the AQ crystals. From analogy with the singlet system, we presently lean towards the possibility that the ^3A_u state in the AQ crystal lies outside the region accessible by the $T \leftarrow S_0$ excitation technique. Further studies are indispensable to draw a final conclusion.

The technical assistance of Noriko Iwasaki in the experiments is gratefully acknowledged. The present

work was partially supported by a Grant-in-Aid for Special Project Research from the Ministry of Education, Science, and Culture (No. 310901).

References

1) R. Hoffman, *Acc. Chem. Res.*, **4**, 1 (1971).
2) G. Lauer, W. Schafer, and A. Schweig, *Chem. Phys. Lett.*, **33**, 312 (1975).
3) H. P. Trommsdorff, *J. Chem. Phys.*, **56**, 5358 (1972).
4) H. Veenvliet and D. A. Wiersma, *Chem. Phys.*, **2**, 69 (1973).
5) R. M. Hochstrasser, L. W. Johnson, and H. P. Trommsdorff, *Chem. Phys. Lett.*, **21**, 251 (1973).
6) T. M. Dunn and A. H. Francis, *J. Mol. Spectrosc.*, **50**, 14 (1974).
7) H. Veenvliet and D. A. Wiersma, *Chem. Phys.*. **8**, 432 (1975).
8) H. P. Trommsdorff and J. P. Galaup, *Chem. Phys.*, **12**, 463 (1976).
9) Y. Miyagi, M. Koyanagi, and Y. Kanda, *Chem. Phys. Lett.*, **40**, 98 (1976).
10) D. O. Cowan, R. Gleiter, J. A. Hashmall, E. Heilbronner, and V. Hornung, *Angew. Chem. Int. Ed. Engl.*, **10**, 401 (1971); T. Kobayashi, *J. Electron Spectrosc. Relat. Phenom.*, **7**, 349 (1975).
11) D. Dougherty and S. P. McGlynn, *J. Am. Chem. Soc.*, **99**, 3234 (1977).
12) J. Goodman and L. E. Brus, *J. Chem. Phys.*, **69**, 1604 (1978).
13) J. W. Sidman, *J. Am. Chem. Soc.*, **20**, 4567 (1956); H. H. Dearman, N. Sundarachri, and D. Ulku, *J. Chem. Phys.*, **45**, 4363 (1966).
14) K. Drabe, H. Veenvliet, and D. A. Wiersma, *Chem. Phys. Lett.*, **35**, 469 (1975).
15) T. Narisawa, M. Sano, and Y. I'Haya, *Chem. Lett.*, **1975**, 1289.
16) J. P. Galaup, J. Megel, and H. P. Trommsdorff, *Chem. Phys. Lett.*, **41**, 397 (1976).
17) O. S. Khalil and L. Goodman, *J. Phys. Chem.*, **80**, 2170 (1976).
18) C. Pecil and B. Lunelli, *J. Chem. Phys.*, **46**, 2109 (1967).
19) D. S. Tinti and M. A. El-Sayed, *J. Chem. Phys.*, **54**, 2529 (1971), and the references therein.
20) N. Nishi and M. Kinoshita, *Bull. Chem. Soc. Jpn.*, **49**, 1221 (1976).
21) N. Nishi, M. Kinoshita, T. Nakashima, R. Shimada, and Y. Kanda, *Mol. Phys.*, **33**, 31 (1977).
22) K. Lonsdale, H. J. Milledge, and K. El-Sayed, *Acta Crystallogr.*, **20**, 1 (1966).
23) T. Murao and T. Azumi, Abstr. No. 1D14, Symp. on Molecular Structure and Electronic States, Hiroshima, Japan, October 1978.
24) B. H. Loo and A. H. Francis, *J. Chem. Phys.*, **58**, 4223 (1970).
25) S. N. Singh and R. Singh, *Spectrochim. Acta, Part A*, **24**, 1591 (1968).
26) F. Duschinsky, *Acta Physicochim.*, **7**, 551 (1937).
27) G. J. Small, *J. Chem. Phys.*, **54**, 3300 (1971).
28) N. Nishi, K. Matsui, M. Kinoshita, and J. Higuchi, *Tech. Report of ISSP, Ser. A*, No. 930 (1978), *Mol. Phys.*, **38**, 1 (1979).

Enthalpies of Dilution of Aqueous Sodium Chondroitin 4-Sulfate and 6-Sulfate

Hideya Tsuge,* Masakatsu Yonese, and Hiroshi Kishimoto

Faculty of Pharmaceutical Sciences, Nagoya City University, Tanabe-dori, Mizuho-ku, Nagoya 467

(Received March 29, 1979)

Enthalpies of dilution of aqueous sodium chondroitin 4- and 6-sulfate were measured by a microcalorimeter from the various initial concentrations $m=0.16$—0.07 monomole kg^{-1} to the final concentration $m'=3.85\times10^{-3}$ monomole kg^{-1} at various temperatures. The concentration and temperature dependencies of measured enthalpies well agreed quantitatively with the theoretical ones calculated by Manning's limiting law, when the distance between the neighboring charges of polyion, b, was assumed to be 4.8 Å, which was obtained from X-ray diffraction measurement.

Chondroitin 4- and 6-sulfate, whose repeating units are composed of *N*-acetyl-D-galactosamine 4- and 6-sulfate together with D-glucuronic acid, respectively, are known to be the important components of mammalian connective tissues and have been investigated from various points of view. In our laboratory, the counter ion binding of chondroitin sulfates was confirmed to exist at low concentrations from the measurements of two thermodynamic properties, molal osmotic coefficients[1] and partial molar volumes.[2] Also, the electrolyte permeability of the gelatin–chondroitin sulfate mixed membrane as a model of connective tissue has been investigated.[3] In this work, the enthalpies of dilution ($\Delta_{dil}H$) of aqueous chondroitin 4- and 6-sulfate were measured by a twin-type microcalorimeter, and the behaviors of chondroitin sulfate at moderate concentrations were discussed by applying Manning's limiting law[4,5] to our results.

Experimental

Materials. Chondroitin 4-sulfate (ChS-A), extracted from whale cartilage as sodium salt, was obtained from Seikagaku Kogyo Co., Ltd. (Tokyo, Japan). It has an average molecular weight of 2.0×10^4 as determined by viscosity measurement.[6,7]

Two kinds of chondroitin 6-sulfate (ChS-C), extracted from shark cartilage as sodium salts, were offered from Kaken Yakukako Co., Ltd. (Tokyo, Japan). Their molecular weights were determined to be 5.7×10^4 and 1.1×10^4, respectively. Distilled and deionized water was used for the preparation of aqueous ChS salt solutions.

Method.[8] The calorimeter used was a twin-type conduction microcalorimeter (CM 204 D1 of Rhesca. Co., Ltd.). A micro volt meter AM-1001 B of Ohkura Electric Co. was used as an output amplifier. Each solution cell (sample side or reference side) of the calorimeter consists of a reaction-vessel and an ampoule. The content of the ampoule can be mixed with that of the reaction-vessel by destroying the ampoule.

Sample Side: Aqueous solution of ChS salt (1—2 ml) in the ampoule. Water (30—50 ml) in the reaction-vessel.

Reference Side: The same amounts of water as the sample side in the ampoule and the reaction-vessel, respectively.

After a steady state had been reached (after about 20 h), ampoules of both sides were destroyed at the same time and the heats arised from mixing were measured. The heats correspond to the dilution enthalpies of ChS salts from the various initial concentrations $m=0.16$—0.07 monomole kg^{-1} to the final concentration $m'=3.85\times10^{-3}$ monomole kg^{-1}, where monomole means the molar amount of the repeating disaccharide unit of ChS. The heats divided by the amount of ChS in monomole give the dilution enthalpies per ChS monomole, $\Delta_{dil}H$.

Results

The exothermic quantities, *i.e.* $-\Delta_{dil}H$, of NaChS-A and NaChS-C at several temperatures were plotted against the initial concentrations m in Figs. 1 and 2, respectively. The value of $-\Delta_{dil}H$ increased monotonously with m.

Of NaChS-C samples having different molecular weights, the higher molecular weight sample showed the greater $-\Delta_{dil}H$ by about 400 J monomole^{-1} at different m and temperatures than the lower one.

Since the plots in Figs. 1 and 2 showed qualitatively the greater $-\Delta_{dil}H$ at the higher temperature, we plotted $-\Delta_{dil}H$ against temperature in Figs. 3 and 4 for the NaChS-A and NaChS-C, which were diluted from 0.1 monomole kg^{-1} to $m'=3.85\times10^{-3}$ monomole kg^{-1}, showing fairly linear relations.

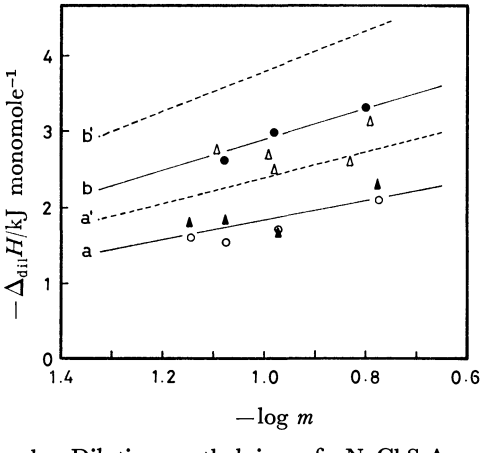

Fig. 1. Dilution enthalpies of NaChS-A *vs.* solute concentration

○: at 292.15 K, ▲: at 298.15 K, △: at 310.15 K, ●: at 323.15 K.

Theoretical values: solid lines in $b=4.8$ Å (a; at 292.15 K, b; at 323.15 K), broken lines in $b=6.3$ Å (a′; at 292.15 K, b′; at 323.15 K).

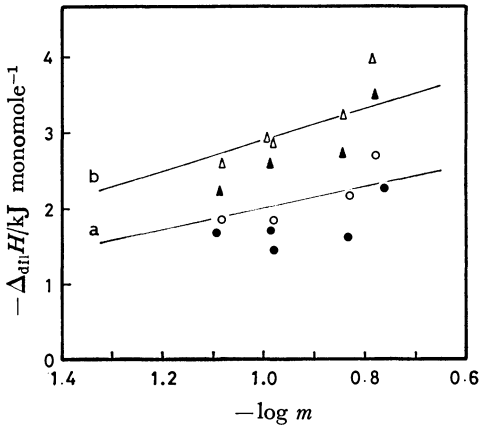

Fig. 2. Dilution enthalpies of NaChS-C *vs.* solute concentration
○: $M.W.=5.7\times10^4$ at 298.15 K, ●: $M.W.=1.1\times10^4$ at 298.15 K, △: $M.W.=5.7\times10^4$ at 323.15 K, ▲: $M.W.=1.1\times10^4$ at 323.15 K.
Theoretical values: a: $b=4.8$ Å at 298.15 K, b: $b=4.8$ Å at 323.15 K.

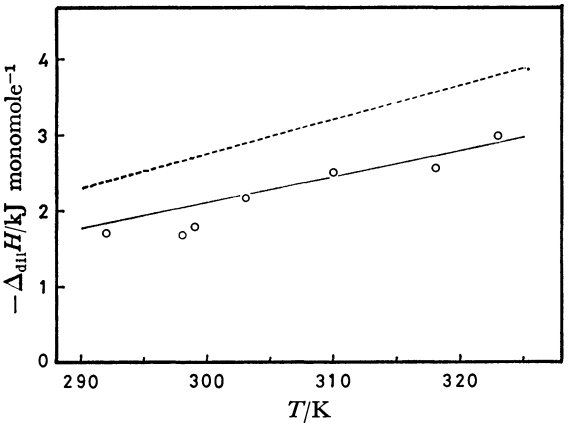

Fig. 3. Effect of temperature on the dilution enthalpies of NaChS-A from 0.1 monomole kg^{-1} to 3.85×10^{-3} monomole kg^{-1}. Solid line: $b=4.8$ Å, broken line: $b=6.3$ Å.

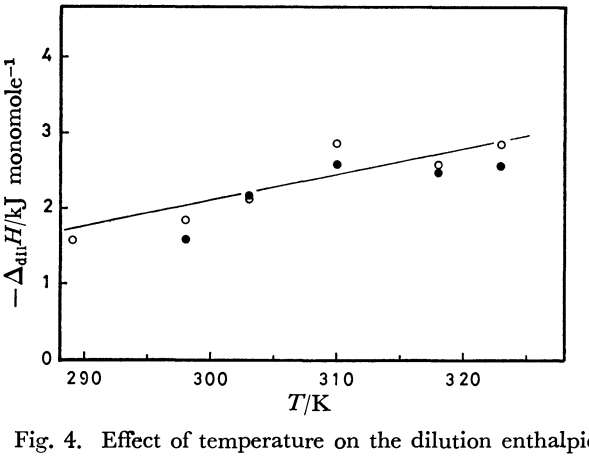

Fig. 4. Effect of temperature on the dilution enthalpies of NaChS-C from 0.1 monomole kg^{-1} to 3.85×10^{-3} monomole kg^{-1}. ○: $M.W.=5.7\times10^4$, ●: $M.W.=1.1\times10^4$.
Solid line: $b=4.8$ Å.

Discussion

To examine to what extent the enthalpies of dilution of aqueous NaChS solutions may be explained by the electrostatic interaction of polyion with counterions, $\Delta_{dil}H$ was divided as follows.[9,10]

$$\Delta_{dil}H = \Delta_{dil}H^\circ + \Delta_{dil}H^{el}, \quad (1)$$

where $\Delta_{dil}H^\circ$ is the enthalpy of dilution of polyelectrolyte solution into a hypothetical reference state, in which all the ions are discharged and $\Delta_{dil}H^{el}$ is the contribution from the electrostatic interaction of polyion with counterion and can be evaluated by various electrostatic theories, *e.g.* Manning's limiting law.[4] Manning's theory replaces a polymer chain with infinitely long line charges and considers the two modes of interaction: Debye-Hückel "ion atmosphere" and condensation of counterions on the line charge. There, polyions are assumed to interact only negligibly with each other. Recently, this theory was applied to the thermodynamic properties of polyelectrolyte solutions, showing that this model is a good representation of the polyelectrolyte solution at low concentration.[11] T. Okubo *et al.* used successfully Manning's theory for the enthalpies of dilution of polyacrylate, carboxymethylcellulose, *etc.*

According to Manning, the electrostatic Helmholtz free energy F^{el} for this model[4] may be shown to be

$$F^{el}/VkT = -\xi n_e \ln \kappa, \quad (2)$$

where V is total volume, k is Boltzmann constant, T is absolute temperature, ξ is charge density parameter, n_e is equivalent polyion concentration (charge/ml), and κ is Debye screening parameter. The value of κ is given by Eq. 3 at a salt-free solution.

$$\kappa^2 = \frac{4\pi e^2}{\varepsilon kT} n_g z_g, \quad (3)$$

where e is a protonic charge, ε is the dielectric constant of solvent and n_g and z_g are the concentration (ion/ml) and valence, respectively, of counterion. The value of ξ is given by

$$\xi = e^2/\varepsilon kTb, \quad (4)$$

where b is the distance between the neighboring charges of a polyion. Different theoretical treatments are given for the case of $\xi\geq1$ and $\xi\leq1$. For the critical value of $\xi=1$, b is equal to 7.1 Å in water at 298.15 K. The ξ value of ChS salt equals to the case of $\xi\geq1$ as can be presumed by its structure. Starting from Eq. 2, $\Delta_{dil}H^{el}$ could be finally expressed as follows.[12]

$$\Delta_{dil}H^{el} = RT/\xi\left(1+\frac{T\mathrm{d}\varepsilon}{\varepsilon \mathrm{d}T}\right)\ln(m/m'), \quad \xi\geq1 \quad (5)$$

There, the choice of ξ value, which is the only adjustable parameter in Manning's theory, of ChS salts is a subject of discussion.

Two theoretical values of b were discussed with experimental $\Delta_{dil}H$ as follows. One was a structural value which obtained from X-ray diffraction measurement.[13,14] It was reported that ChS salts have eight-fold, three-fold and two-fold single stranded helical conformations. Their disaccharide lengths are 9.3—9.8 Å. The value of $b=4.8$ Å, which is a half of 9.6 Å for

disaccharide lengths of three-fold helical molecule of ChS-A and ChS-C salts, gives the structural value. Another was the value of $b=6.3$ Å. We previously measured the molal osmotic coefficients of ChS-A and ChS-C salts by vapor pressure osmometry. If the ξ value was considered as an adjustable parameter, experimental coefficients at infinite dilution ϕ_0 well agreed with the theoretical coefficients calculated from $\phi=(2z_g\xi)^{-1}$ using $b=6.3$ Å.[1)]

Theoretical $-\Delta_{dil}H^{el}$, calculated from Eqs. 4 and 5, are shown by solid lines with $b=4.8$ Å in Figs. 1, 2, 3, and 4 and by broken line with $b=6.3$ Å, for the case of NaChS-A only, in Figs. 1 and 3, respectively. It was confirmed that the theoretical enthalpic values for $b=4.8$ Å well agreed quantitatively with experimental values. In the above-mentioned treatment, the non-electrostatic enthalpies of dilution had been implicitly assumed to be negligible. However, it can be safely stated that the assumption is at least relatively a self-consistent one over the experimental range of temperature and concentration.

As the conclusion, at least tentative, ChS salt in aqueous solution may behave in such a way that the polyion of ChS has a stretched conformation with disaccharide lengths of *ca.* 12.6 Å at infinite dilution and a conformation nearly like solid state at moderate concentration.

References

1) M. Yonese, H. Tsuge, and H. Kishimoto, *Nippon Kagaku Kaishi*, **1978**, 108.
2) H. Tsuge, M. Yonese, and H. Kishimoto, *Nippon Kagaku Kaishi*, **1978**, 609.
3) M. Yonese and M. Nakagaki, *Yakugaku Zasshi*, **95**, 75, 641, 665 (1975).
4) G. S. Manning, *J. Chem. Phys.*, **51**, 924 (1969).
5) G. S. Manning, *Annu. Rev. Phys. Chem.*, **23**, 117 (1972).
6) M. B. Mathews, *Arch. Biochim. Biophys.*, **61**, 367 (1956).
7) M. Nakagaki and K. Ikeda, *Bull. Chem. Soc. Jpn.*, **41**, 555 (1968).
8) H. Kishimoto and K. Sumida, *Chem. Pharm. Bull.*, **22**, 1108 (1974).
9) J. Škerjanc, D. Dolar, and D. Leskovšek, *Z. Phys. Chem. (Frankfurt am Main)*, **56**, 207 (1967).
10) G. E. Boyd and D. P. Wilson, *J. Phys. Chem.*, **80**, 805 (1976).
11) "Polyelectrolyte," ed by E. Selegny, D. Reidel Pub. Co., Dordrecht-Holland (1974).
12) K. Mita and T. Okubo, *J. Chem. Soc., Faraday Trans. 1*, **70**, 1546 (1974).
13) S. Arnott, J. M. Guss, D. W. L. Hukins, and M. B. Mathews, *Science*, **180**, 743 (1973).
14) D. H. Isaac and E. D. T. Atkins, *Nature (London), New Biol.*, **244**, 252 (1973).

Direct Measurement of Interaction Energy between Solids and Gases. IV. Acidic and Catalytic Properties of Amorphous and Crystalline Alumino-silicates

Tatsuo MASUDA,*,† Hitofumi TANIGUCHI, Kazuo TSUTSUMI, and Hiroshi TAKAHASHI
Institute of Industrial Science, The University of Tokyo, 7-22-1 Roppongi, Minato-ku, Tokyo 106
(Received April 3, 1979)

Surface acidities and acid strength distributions of amorphous silica–alumina, Y-type faujasite and mordenite have been examined by measuring the differential heats of adsorption of ammonia. The number of acid sites with adsorption heats higher than 70 kJ/mol increased in the order: $NH_4Y > NH_4M > RENH_4Y >$ silica–alumina. On the other hand, the order of the acid strength was: $NH_4M > RENH_4Y >$ silica–alumina $> NH_4Y$. The high catalytic activities of zeolites for cumene cracking and toluene disproportionation were correlated with acid strength, Brönsted acidity, and electrostatic effect.

Zeolite have been shown to be more active than amorphous silica–alumina catalysts for many reactions. Miale *et al.*[1] compared the relative rates of hexane cracking reaction by a wide variety of zeolite catalysts with those by amorphous silica–alumina catalysts. They showed the superior activity of zeolite catalysts, that is, the relative rate, compared with silica–alumina taken as 1, was more than 10000. Plank *et al.*[2] showed the high activity of zeolite catalysts for gas oil cracking. Venuto and co-workers have shown that zeolites can catalyze a wide range of organic reactions.[3] In a previous paper,[4] the cumene cracking activities were measured for several FCC catalysts and the present authors concluded that the higher activity of zeolite-cracking catalysts could not be explained only by an acidity increase. Tung[5] proposed the time variant Brönsted acidity of zeolite catalysts to explain their high activity compared with that of amorphous silica–alumina. The nature of active centers of zeolite catalysts has been reviewed recently.[6]

In this work, cumene cracking and toluene disproportionation reaction were measured over amorphous silica–alumina, Y-faujasite and mordenite. The results of activity were correlated with acid strength distribution, IR spectra of adsorbed pyridine and electrostatic effects evaluated from nitrogen adsorption.

Experimental

Materials. The solid acids used in this study were shown in Table 1. Silica–alumina (Al_2O_3 contents, 28 wt %), Na-type mordenite and rare-earth(RE)exchanged Y-faujasite supplied by Catalysts and Chemicals Ind. Co. Ltd. NH_4M and $RENH_4Y$ were prepared by a conventional cation exchange procedure with NH_4NO_3 solution and then calcined in air at 600 °C and 400 °C for 3 h, respectively. NH_4Y, prepared by an ion exchange with NH_4Cl solution of NaY-faujasite supplied by Linde Co. was calcined in air at 400 °C for 3 h. The degree of ion-exchange was determined by flame photometry. All the catalysts were used as granule of 28—60 mesh.

Apparatus and Procedure. Experimental procedures and analysis of differential heats of adsorption of ammonia to estimate the acidity and acid strength distribution were carried out as described in a previous paper.[7] The same apparatus was used to measure the heat of adsorption of nitrogen and argon on solid acid catalysts. Each catalysts received a heat treatment at 400 °C under a pressure of 1.3×10^{-3} Pa for 5 h before calorimetric measurements.

The infrared absorption spectra of the adsorbed pyridine on solid acid catalysts were recorded on Hitachi infrared spectrometer model EPI-G3 by use of a conventional *in situ* cell connected to a vacuum line. The catalysts were pressed into a wafer with a thickness of about 10 mg/cm² and heat-treated at 400 °C under a pressure of 1.3×10^{-3} Pa for 4 h. The infrared spectra were measured at 25 °C.

The catalytic reactions were carried out in a pulse reactor system. The apparatus and experimental procedure were described in detail in a previous paper.[4] The catalysts were pretreated at 400 °C for 4 h in a stream of helium gas as a carrier. The helium flow rate during the pretreatment was 30 cm³/min. The catalyst bed used in a cumene cracking reaction consisted of 20 mg catalysts diluted with 130 mg of catalytically inert quartz beads and the reaction was carried out at 300 °C and at a helium flow rate of 60 cm³/min. Toluene disproportionation reaction was carried out at 400 °C and at a helium flow rate of 30 cm³/min over 150 mg of catalysts. The catalytic activity was estimated by means of a conversion rate of cumene and toluene.

Table 1. Surface area, SiO_2/Al_2O_3 molar ratio and the degree of exchange of solid acid catalysts

	SA[a]	NH_4Y	$RENH_4Y$	NH_4M
Surface area ($s/m^2\ g^{-1}$)	511	595	451	430
SiO_2/Al_2O_3 molar ratio	4.3	5.0	4.82	10.9
Ion exchange/%	—	96.0	96.3[b]	98.1

a) Silica–alumina. b) 64.0% rare earth and 32.3% NH_4^+ exchanged.

Results

Catalytic Activity. The cumene cracking and toluene disproportionation activities over mordenite, Y-faujasite and silica–alumina are shown in Table 2. $RENH_4Y$ had higher initial activity for cumene cracking than NH_4Y and NH_4M. A large drop in conversion with an increase in the pulse number was observed over NH_4M, indicating the formation of non-volatile residure which left portions of the active site inaccessible to the reactants. NH_4M showed higher activity for toluene disproportionation and the order of activity was: $NH_4M > RENH_4Y > NH_4Y >$ silica–alumina in agree-

† Present address: Catalysts and Chemicals Ind. Co., Ltd., 2-6-2 Ohtemachi, Chiyoda-ku, Tokyo 100.

Table 2. Cumene cracking[a] and toluene disproportionation[b] activity over silica–alumina, NH_4Y, $RENH_4Y$, and NH_4M

	Cumene conversion/%[c]	Cumene conversion/%[d]	Toluene conversion/%[e]
SA	3.5	0	0
NH_4Y	68.9	48.3	5.5
$RENH_4Y$	83.0	37.1	18.6
NH_4M	71.1	10.5	56.9

a) React. temp: 300 °C, 60 cm³ of He/min. b) React. Temp: 400 °C, 30 cm³ of He/min. c) Conversion of the first pulse (5 μl). d) Conversion of the pulse (5 μl) after 180 μl of the reactant was charged. e) Average conversion of the first 5 pulses (2 μl × 5).

ment with the results of Nakano *et al.*[8] Conversions of cumene or toluene over amorphous silica–alumina were slight or none under these reaction conditions.

Differential Heats of Adsorption of Ammonia. In Fig. 1, the differential heats of adsorption of ammonia on silica–alumina, NH_4Y, $RENH_4Y$, and NH_4M are shown. The nature of differential heat curves of silica–alumina and NH_4Y has been discussed previously.[7] The differential heat curve of $RENH_4Y$ showed the existence of strong acid sites of heats of adsorption higher than 105 kJ/mol compared with that of NH_4Y, but the number of acid sites between adsorption heats of 80—100 kJ/mol decreased markedly. Initial heat of NH_4M was higher than 150 kJ/mol and the differential heat curve was very similar to that of $RENH_4Y$.

The acid strength distributions of these solid acid catalysts are shown in Fig. 2. The maximum distributions were observed at *ca.* 98 kJ/mol for mordenite and Y-faujasites and the other maximum distributions were also observed at 110 kJ/mol and 77, 120 kJ/mol for $RENH_4Y$ and NH_4M, respectively. Silica–alumina possessed a maximum distribution at 105 kJ/mol.

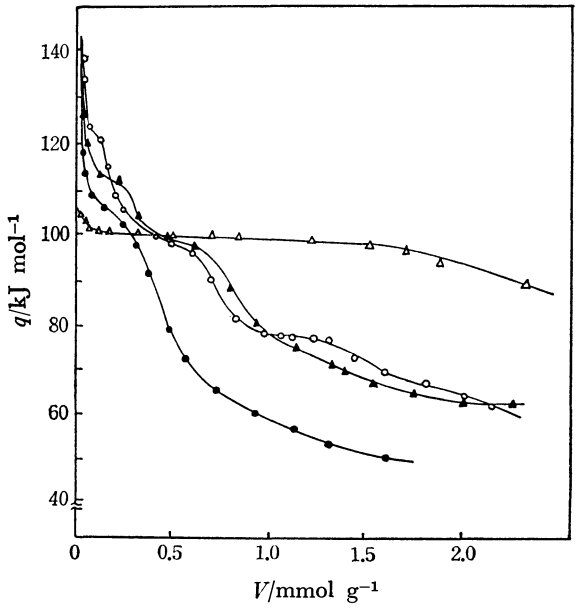

Fig. 1. Heats of adsorption of ammonia on solid acid catalysts at 25 °C.
-△-: NH_4Y, -▲-: $RENH_4Y$, -○-: NH_4M, -●-: SA.

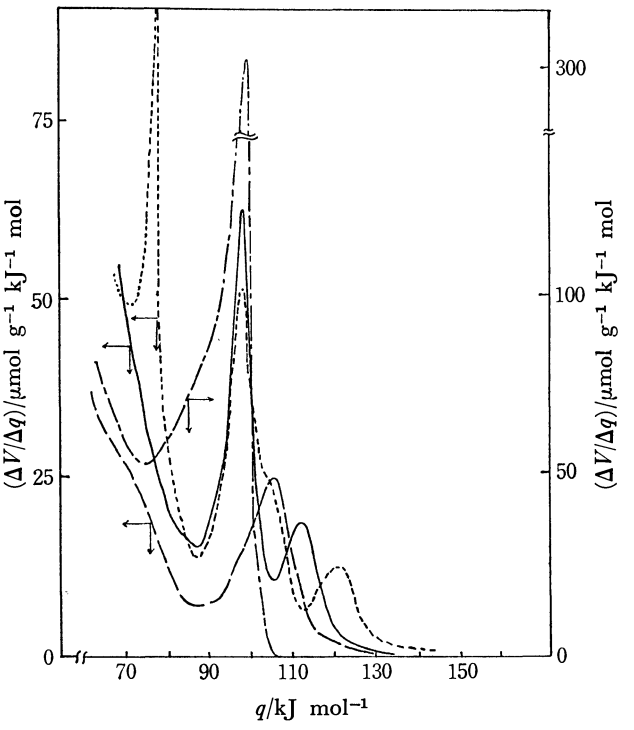

Fig. 2. Acid site distributions of solid catalysts.
----: NH_4M, -·-·: NH_4Y, ——: $RENH_4Y$, ——: SA,

Infrared Spectra of Adsorbed Pyridine. Infrared spectra of pyridine on silica–alumina and zeolites are shown in Fig. 3. The adsorbed pyridine has strong and

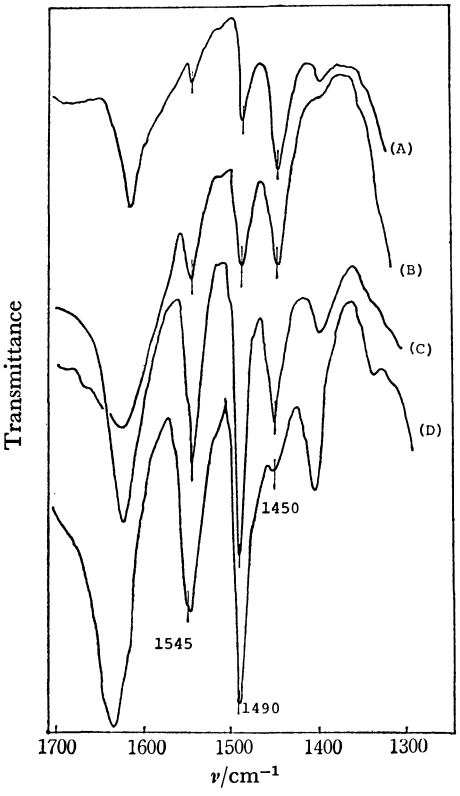

Fig. 3. Spectra of adsorbed pyridine on solid acids after pyridine dosing at 25 °C and evacuating at 150 °C for 1 h, (A) SA; (B) NH_4M; (C) $RENH_4Y$; (D) NH_4Y.

sharp bands characteristic of pyridinum ions (B-Py) at 1545 cm^{-1} and coordinately-bonded pyridine (L-Py) at 1450 cm^{-1}. In these spectra, the hydrogen-bonded species were removed by evacuation at 150 °C for 1 h, which was confirmed by the disappearences of their characteristic absorption bands at 1593 and 1438 cm^{-1}. It is apparent that the fraction of L-Py was higher in silica–alumina than in zeolites. The exchange with rare-earth cations in $RENH_4Y$ results in a formation of Lewis acid sites and enhances the acid strength as shown in Fig. 2. The band near 1443 cm^{-1} due to pyridine interacted with the rare-earth cations could not be observed after the evacuation at 150 °C. Strong adsorption band of L-Py was observed on NH_4M in contrast with the results of Yashima *et al.*[9]

Heats of Adsorption of Nitrogen and Argon. The integrated heats of adsorption of nitrogen and argon on silica–alumina, NH_4Y, $RENH_4Y$, and NH_4M are collected in Table 3. They were taken up to 20—35 μmol/g of the amount adsorbed for zeolites and about 10 μmol/g for silica–alumina. The order of integral heats was: $NH_4M > RENH_4Y > NH_4Y >$ silica–alumina. For zeolites, this order coincides with that of acid strength in Fig. 2. A large difference in adsorption heats between argon and nitrogen was observed over NH_4M.

Table 3. Heat of adsorption of nitrogen and argon on solid acids (q/kJ mol^{-1})

	SA	NH_4Y	$RENH_4Y$	NH_4M
N_2	6	11.8	14.5	23.1
Ar	5	9.0	10.1	16.8

Discussion

A high activity of zeolites has led to suggestions that the active sites such as Brönsted acid sites, Lewis acid sites and electrostatic fields on crystalline alumino-silicates are considerably different from those on amorphous alumino-silicates. Oblad[10] has compared the acidic nature of zeolite cracking catalysts with that of silica–alumina and concluded that the activity of zeolites was related to the intrinsic "protonic acidity" of the alumino-silicate lattice.

The present authors have previously shown that the cumene cracking activity over amorphous silica–alumina had a linear correlation with the number of acid sites higher than 70 kJ/mol of adsorption heats of ammonia.[4] The surface acidities obtained from Fig. 1 are 0.65, 1.32, 1.56, and 3.95 mmol/g for silica–alumina, $RENH_4Y$, NH_4M, and NH_4Y, respectively. An increase in acid strength in $RENH_4Y$ can be explained by inductive effects of rare-earth cation on the acidic hydroxyl groups. These values suggest that the excellent activity of zeolite catalysts for cumene cracking can not be explained only in terms of acidity increase. However, the existence of strong acid sites in NH_4M and $RENH_4Y$ leads to a large aging of cumene cracking activity, *i.e.*, the formation of non-volatile residue.

It is evident that the catalysts such as NH_4M and $RENH_4Y$ which possessed stronger acid sites showed higher conversion for toluene disproportionation, indicating that the reaction was effectively promoted by strong acid sites, *i.e.*, the sites having the heat of adsorption of ammonia higher than *ca.* 100 kJ/mol. However, it is difficult to explain the difference in activities for toluene disproportionation between silica–alumina and NH_4Y in terms of acid strength.

Differential heats in Fig. 1 contain both the interaction of ammonia with Brönsted and with Lewis acid sites, and it is difficult to differentiate these two sites from heat curves. The relatively homogeneous acid sites at 98 kJ/mol in adsorption heats of NH_4Y in Fig. 2, combined with the results of infrared spectra, can probably attributed to protonic acid sites because of the existence of weak band of L-Py in Fig. 3. The apparent ratios of the peak height of L-Py to B-Py, compared with that of silica–alumina taken as 1, were 0.57, 0.19, 0.03 for NH_4M, $RENH_4Y$, and NH_4Y, respectively. If we assume that the number of Brönsted acid sites is equal to that of Lewis acid sites in silica–alumina, the Brönsted acidities of silica–alumina, NH_4M, $RENH_4Y$, and NH_4Y should be 0.32, 0.99, 1.11, and 3.82 mmol/g, respectively. Brönsted and Lewis acid sites concentration of the solid acids were summarized in Table 4. If Brönsted rather than Lewis acid sites are the seats of activity for toluene disproportionation as mentioned by Benesi,[11] the absence of activity over silica–alumina must somewhat be due to its small Brönsted acidity and this is also true for cracking activity. The higher initial activity over $RENH_4Y$ for cumene cracking can be related to its relatively strong acid sites and larger number of Brönsted acid sites.

It has long been believed that the zeolite surfaces were heteropolar. Therefore, molecules occuluded within the zeolite framework are subject to its electrostatic field. Huang *et al.*[12] obtained the isosteric heat of adsorption of krypton from adsorption isotherms and discussed the surface electrostatic effects associated with lattice cations of Y-faujasites. They concluded that the existence of bivalent cations on zeolite surface had no influence on the adsorption of krypton because of its smaller contribution to polarization energy. Meanwhile the use of nitrogen molecules should be suitable for studies of electrostatic effects of solid surfaces because of its large quadrupole moment and relatively large polarizability.

If we can assume that the polarizability of nitrogen is almost the same as that of argon, the difference of

Table 4. Brönsted and Lewis acid sites concentration measured by the infrared spectra of adsorbed pyridine

	Catalysts			
	SA	NH_4M	$RENH_4Y$	NH_4Y
Acidity/mmol g^{-1}	0.65	1.56	1.32	3.95
L-Py/B-Py	1	0.57	0.19	0.03
B-sites[a]/mmol g^{-1}	0.32	0.99	1.11	3.82
L-sites[b]/mmol g^{-1}	0.33	0.57	0.21	0.13

a) The number of Brönsted acid sites. b) The number of Lewis acid sites.

adsorption heats between them is probably due to the quadrupole-electrostatic field gradient interaction. Therefore, the higher adsorption heats of nitrogen on $RENH_4Y$ compared with that on NH_4Y can be ascribed to the contribution of quadrupole interaction of nitrogen with rare-earth cations. It is noteworthy that the order of integral heats of nitrogen coincides with that of activity for toluene disproportionation. These facts indicate that the cages and channels of zeolitic crystalline structure are characterized by the existences of high electrostatic field and its gradient, and therefore they act as strong polarizing agents for hydrocarbon transformation reactions.

It may be concluded from the present work that the acidity of zeolite catalysts appears to be the same kind as silica–alumina but differs in both quantity and quality of acid sites. Acid strength distributions of each solid acids obtained from differential heats of adsorption of ammonia are extensively different depending upon their crystalline structure and the existence of cations. The acid sites having the adsorption heats of ammonia higher than *ca.* 100 kJ/mol are effective for toluene disproportionation at 400 °C and these values are considerably high compared with the effective acid strength for cumene craking. Heats of adsorption of nitrogen indicate the high electrostatic field over zeolite surfaces. The low Brönsted acidity as well as the low electrostatic effects probably correlate with the low activity of amorphous silica–alumina.

This work was partly supported by a Grant-in-Aid for Science Research from the Ministry of Education.

References

1) J. N. Miale, N. Y. Chen, and P. B. Weisz, *J. Catal.*, **6**, 278 (1966).
2) C. J. Plank, E. J. Rosinski, and W. P. Hawthorne, *Ind. Eng. Chem. Prod. Res. Dev.*, **3**, 165 (1964).
3) P. B. Venuto and P. S. Landis, *Adv. Catal.*, **18**, 259 (1968).
4) T. Masuda, H. Taniguchi, K. Tsutsumi, and H. Takahashi, *J. Jpn. Petrol. Inst.*, **22**, 67 (1979).
5) S. E. Tung, *J. Catal.*, **17**, 24 (1970).
6) J. A. Rabo, "Zeolite Chemistry and Catalysis," ACS Monograph No. 171 (1976).
7) T. Masuda, H. Taniguchi, K. Tsutsumi, and H. Takahashi, *Bull. Chem. Soc. Jpn.*, **51**, 1965 (1978).
8) N. Nakano, Y. Nishimura, and H. Takahashi, *Bull. Jpn. Petrol. Inst.*, **13**, 205 (1972).
9) T. Yashima and N. Hara, *J. Catal.*, **27**, 329 (1972).
10) A. G. Oblad, *Oil Gas J.*, **74**, 84 (1972).
11) H. A. Benesi, *J. Catal.*, **8**, 368 (1967).
12) Y. Huang, J. E. Benson, and M. Boudart, *Ind. Eng. Chem. Fundam.*, **8**, 347 (1969).

An Analysis of Impedance in the Kolbe Reaction on Platinum and Gold Anodes in Aqueous Acetate Solutions

Isao SEKINE* and Hideki OHKAWA

Department of Industrial Chemistry, Faculty of Science and Technology, Science University of Tokyo, Noda, Chiba 278

(Received July 31, 1978)

The Kolbe reaction occurring on platinum or gold anodes in aqueous acetate was studied by analyzing the equivalent circuit of the impedance obtained with a phase-sensitive detector. In the case of platinum, the equivalent circuit at the potential for the Kolbe reaction is represented by a parallel combination of the double-layer capacity, C_{dl}, and the charge-transfer resistance, θ, in series with the solution resistance, R_{sol}. The C_{dl} value of 2.00 V obtained by a complex impedance plane plot is nearly identical to that calculated by assuming that the Helmholtz layer is occupied by CH_3COO^-. In the potential range more negative than 2.00 V, the Kolbe reaction occurs. The steep decrease in the differential capacity is considered to be a result of the decrease in the adsorption pseudo-capacity. The θ value of the oxygen evolution increases with an increase in the acetate concentrations. It is shown that the surface coverage of CH_3COO^- may be obtained by "Frumkin's treatment" in conjunction with the high-frequency capacitance, C_{HF}, and the low-frequency capacitance, C_{LF}, from the complex capacitance plane plot (Y/ω plane plot). The Kolbe reaction does not occur at all with gold anodes, and the specific circular arc was not seen in the Y/ω plane plot. Impedance measurements, therefore, confirm that an adsorption pseudo-capacity of CH_3COO^- is not present with gold anodes.

Electrochemical studies of the Kolbe reaction using various techniques have been reported by many investigators.[1-3] The Kolbe reaction was, for example, examined with platinum or gold anodes in acetate or propionate solutions.[4-7] In aqueous acetate solutions the Kolbe reaction proceeds efficiently on platinum at anodic potentials greater than *ca.* 2.00 V, with the release of ethane and carbon dioxide, whereas the reaction does not occur at any potentials on gold anodes.[1] These phenomena result from the difference in anode surface states; ellipsometry[8] shows that the adsorption of a layer of CH_3COO^- or $CH_3COO\cdot$ about 10 Å thick on the platinum at anodic potentials greater than 2.00 V is favorable to the Kolbe reaction, while the oxide (Au_2O_3) more than 30 Å thick formed on gold anodes inhibits the reaction.

According to an analysis of the impedance of the Kolbe reaction by Kunugi *et al.*,[9] the double-layer capacity decreases from 30 to 10 $\mu F/cm^2$ when the anodic reaction changes from the oxygen evolution to the Kolbe reaction. Such behavior can be explained by attributing it to the change from the acetate ion to the methyl radical. However, only this explanation for these phenomena seems not to be sufficient. Furthermore, the equivalent circuit has not appeared in the literature.

In the present study, impedance measurements were made on platinum and gold anodes in aqueous acetate solutions using a phase-sensitive detector (PSD). The equivalent circuits corresponding to the adsorbed layer on the platinum anode or the oxide layer on the gold anode are derived from the impedance analysis. The possibility of the occurrence of the Kolbe reaction is discussed.

Experimental

Apparatus. The impedance was measured with a PSD (Fuso Seisakusho, model 332). The reference signal of the sinusoidal wave in PSD was within 3.5 mV (RMS) over the frequency range of 9 kHz—10 Hz.

Electrodes. A section (0.10 cm in diameter) of platinum or gold wire served as the working electrode. The pretreatment of these anodes was carried out as has been described previously.[4] The counter electrode was a spiral platinum wire. The potential was measured with reference to a saturated calomel electrode (SCE), and the electrode was gradually polarized to the positive potential with 10 mV/s. The parallel capacity and resistance were simultaneously plotted with a two-pen recorder. All the circuits were shielded and grounded.

Solutions. Test solutions were prepared from the reagent-grade chemicals and triply distilled water. Acetic acid was refluxed in the presence of potassium permanganate to oxidize the contaminating aldehydes, and was then redistilled in the presence of fresh diphosphorus pentaoxide to remove the water. Potassium acetate was used without further purification. The aqueous acetate solutions used were 1: 1 mixtures of equimolar solutions of potassium acetate and acetic acid at 0.5, 1, 2, and 5 M respectively. All the experiments were carried out at 25 °C.

Results and Discussion

Platinum Electrode. It has previously been reported that the remarkable decrease at 2.00 V in the differential capacity obtained by an impedance bridge is a necessary condition to promote the Kolbe reaction on a platinum anode in an aqueous acetate solution.[4]

Figure 1 shows the relationship between the parallel capacitance and the potential (C_p—E), as measured by a PSD. Two peaks were observed at around 0.80 and 1.35 V. The capacity at potentials greater than 1.35 V markedly decreases and levels off to a constant value at 2.25 V. It has already been reported that an oxygen evolution reaction and adsorption of CH_3COO^- compete in the potential range where the Kolbe reaction does not occur. Such a competition can be analyzed with the aid of the complex impedance plane plot[10] (Z plane plot) obtained at various acetate concentrations.

Figure 2 shows the results of the Z plane plot observed on a platinum anode at various acetate concentrations.

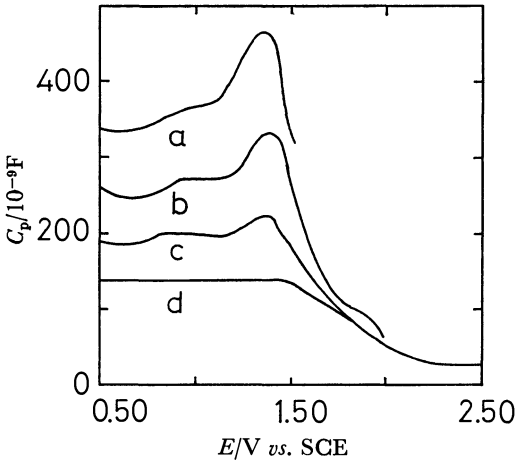

Fig. 1. Parallel capacitance *vs.* potential curves on Pt in 2 M acetate with various frequencies.
sweep rate: 10 mV/s,
a: 15 Hz, b: 60 Hz, c: 3 kHz, d: 8 kHz.

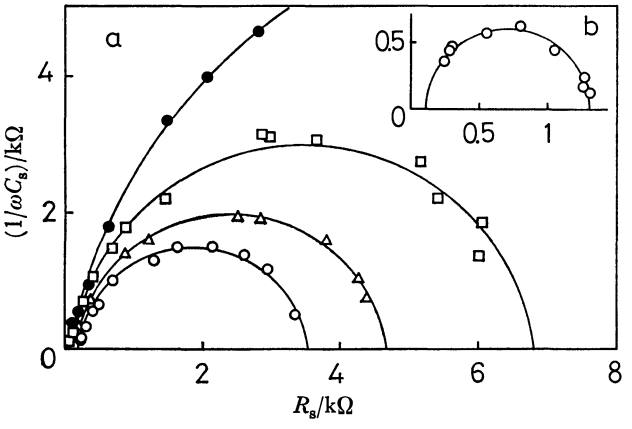

Fig. 2. Complex impedance plane plot of Pt in various acetate concentrations.
a: 1.50 V, -○-: 0.5 M, -△-: 1 M, -□-: 2 M, -●-: 5 M, b: 2.00 V, -○-: 0.5 M.

The diameter of the semicircle in the Z plane shows the charge-transfer resistance, θ. If the value of θ at 1.50 V is determined only by oxygen evolution, it will not be affected by the acetate concentrations. Since θ increases with an increase in the acetate concentration, it may be concluded that an oxygen-evolution reaction is inhibited by the adsorption of CH_3COO^-. Since the loci of the Z plane plot are given only by the semicircle, the rate-determining step of the Kolbe reaction or the oxygen evolution on the platinum is regarded as a charge-transfer process, representing an activation polarization.

The C_{dl} values at each concentration, as calculated from, $\omega_{max}(=1/\theta C_{dl})$, corresponding to the top of the semicircle, are shown in Fig. 3. At more negative potentials than 2.00 V, where the oxygen evolution proceeds, the C_{dl} value of platinum depends on the bulk concentration of the acetate ion and decreases with an increase in the concentration. By contrast, C_{dl} at 2.10 V, where the Kolbe reaction proceeds, is almost independent of the bulk concentration. From the above results, it can be said that, when the electrode

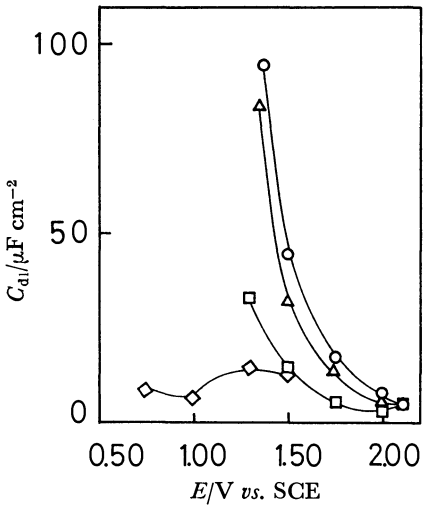

Fig. 3. Double layer capacity *vs.* potential plots.
-○-: Pt-0.5 M, -△-: Pt-2 M, -□-: Pt-5 M, -◇-: Au-5 M.

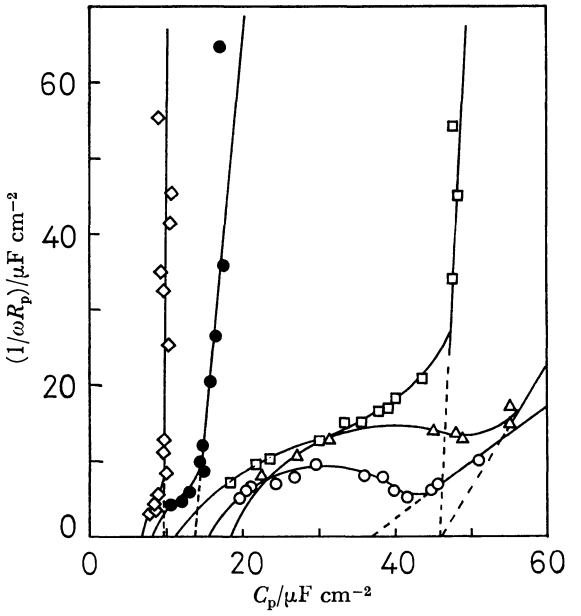

Fig. 4. Complex capacitance plane plot of Pt in 0.5 M acetate.
-○-: 0.75 V, -△-: 1.37$_5$ V, -□-: 1.50 V, -●-: 1.75 V, -◇-: 2.00 V.

reaction changes from the oxygen evolution to the Kolbe reaction, C_{dl} decreases and then remains approximately constant (5—8 μF/cm²). Such behavior in C_{dl} was found to be similar to that observed for C_p in the C_p—E curve described above.

To elucidate further the decrease and then the constancy in C_{dl} at the potential where the Kolbe reaction proceeds, the above results were analyzed on the basis of the complex capacitance-plane plot[11,12] (Y/ω plane plot) (Fig. 4). At the more negative potentials than 2.00 V, the quarter circle was found in the high-frequency region, while the straight line was found in the lower-frequency region.

If the high-frequency capacitance, C_{HF}, is determined by extrapolation to an infinite frequency ($\omega=\infty$) in a

quarter circle, and the low-frequency capacitance, C_{LF}, by linear extrapolation to the C_p axis, the definitions of C_{HF}, C_{LF} and the adsorption pseudo-capacity, ΔC, are as follows:[13]

$$C_{HF} = (\partial q/\partial E)_{\mu,\Gamma} \quad (1)$$

$$C_{LF} = (\partial q/\partial E)_{\mu} = (\partial q/\partial E)_{\mu,\Gamma} + (\partial q/\partial \Gamma)_{\mu,E}(\partial \Gamma/\partial E)_{\mu} \quad (2)$$

$$\Delta C = C_{LF} - C_{HF} = (\partial q/\partial \Gamma)_{\mu,E}(\partial \Gamma/\partial E)_{\mu} \quad (3)$$

where Γ, q, and μ represent surface excess, the surface charge density, and the chemical potential respectively.

The quarter circle was obtained at 0.75 and 1.35 V, where the first and second capacity peaks were obtained respectively in the C_p—E curves. It is known that the first capacity peak is due to an adsorption of oxygen-containing species (OH^-, H_2O, O^{2-}, *etc.*)[4] and that the rate-determining step of adsorption is a diffusion process when the Y/ω plane plot gives a quarter circle.[11,12] As has been described above, the adsorption of oxygen-containing species is diffusion-controlled and the adsorption pseudo-capacity gives a value of 10—20 $\mu F/cm^2$. The second peak is regarded as the adsorption of CH_3COO^- in the potential range of oxygen evolution.[4] In this case, the CH_3COO^- is specifically adsorbed by forming a partly covalent bond with platinum and is perhaps responsible for the pseudo-capacity.[14]

Since the Y/ω plane plot gives a quarter circle at 1.37_5 V, the rate-determining step in the adsorption of CH_3COO^- is a diffusion-controlled process and produces an adsorption pseudo-capacity, ΔC. A ΔC value of 20 $\mu F/cm^2$ is observed at 1.37_5 V. In the C_p—E curve noted above, the C_p value decreased markedly with an increase in the positive potentials to more than 1.30—1.40 V indicated a second capacity peak, and C_{dl} decreased similarly (Figs. 1 and 3). These results can be explained by a diminution of the quarter circle, representing the magnitude of the adsorption pseudo-capacity, ΔC; *i.e.*, if $(\partial \Gamma/\partial E)_{\mu}=0$ in Eq. 3, the ΔC due to the adsorption of CH_3COO^- will vanish. The above conditions are satisfied by the fact that Γ for the adsorption of CH_3COO^- is constant against the potentials. The limiting case in the Y/ω plane plot is at 2.00 V, where the quarter circle almost disappears and a straight line is obtained.

In order to determine the surface coverage of CH_3COO^- from the C_{HF} values, "Frumkin's treatment" was performed. If the electric double layer is constructed by two parallel condensers, one is covered by the adsorbate, while the other is not; the charge on the electrodes is then given as follows:[15]

$$q = q_0(1-\theta_s) + q^*\theta_s$$

where q_0 and q^* correspond to the electrode charges when $\theta_s=0$ and $\theta_s=1$ respectively; and where θ_s is the fractional coverage of the surface $(=\Gamma/\Gamma_{max})$. The C_{LF} value given in Eq. 2 is converted to Eq. 4:

$$C_{LF} = dq/dE = (\partial q/\partial E)_{\theta_s} + (\partial q/\partial \theta_s)(d\theta_s/dE) = \{C_0(1-\theta_s)+C^*\theta_s\} + (q^*-q_0)(d\theta_s/dE) \quad (4)$$

where $C_0=dq_0/dE$ and $C^*=dq^*/dE$. The first two terms of Eq. 4 are replaced by Eq. 1 and:

$$C_{HF} = (\partial q/\partial E)_{\theta_s} = C_0(1-\theta_s) + C^*\theta_s \quad (5)$$

As an example, θ_s of CH_3COO^- was obtained from the platinum anode in a 2 M acetate solution; the values of C_{HF} for C^* and C_0 were 6 and 24 $\mu F/cm^2$, obtained at 2.00 and 0.90 V, respectively. Because the adsorption of CH_3COO^- is negligible at potentials less than 1.30 V, as shown by a previous study,[9] the condition of $\Delta C \fallingdotseq 0$ is satisfied at 2.00 V in Fig. 4. The values of θ_s were calculated from Eq. 5; *e.g.*, when $C_{HF}=20$ $\mu F/cm^2$ at 1.50 V, then $\theta_s=0.2$, and when $C_{HF}=12$ $\mu F/cm^2$ at 1.75 V, $\theta_s=0.7$. The θ_s values obtained by the above method agreed approximately with the surface coverage obtained from the difference between the currents observed in the presence and in the absence of acetate ions in a phosphate solution using the linear-potential-sweep method.

The admittance for a first-order electrode reaction proceeding on the Y/ω plane is characterized by Eq.6.[16] Since only the perpendicular line against the C_p axis is observed, the straight lines obtained at 1.50 and 1.75 V indicate that the oxygen evolution follows a first-order electrode reaction:

$$Y/\omega = jC_{dl} + 1/\omega\theta \quad (6)$$

The intercept at the C_p axis gives both C_{dl} and C_{LF}, according to Eq. 6. Therefore, it may be concluded that the C_{dl} value on the Z plane at the potentials of oxygen evolution contains the adsorption pseudo-capacity, ΔC, of CH_3COO^-. For example, at 1.50 V in a 2 M acetate solution, the C_{dl} obtained on the Z plane corresponding to C_{LF} on the Y/ω plane is 33 $\mu F/cm^2$. Consequently, $\Delta C(=C_{LF}-C_{HF})$ is 13 $\mu F/cm^2$, since C_{HF} is equal to 20 $\mu F/cm^2$. For the above derivation, the adsorption of CH_3COO^- was taken to proceed simultaneously with the oxygen evolution on the Y/ω plane.

As ΔC approximates zero at 2.00 V, where the Kolbe reaction proceeds, the C_{dl} value extrapolated to the C_p axis almost represents that of C_{HF}. Thus, a C_{HF} value of 5—6 $\mu F/cm^2$ was found at 2.00 V in 0.5—2 M acetate solutions. Accordingly, the equivalent circuit of platinum at potentials less than 2.00 V is shown in Fig. 5(a). That the adsorption of CH_3COO^- is the diffusion-controlled process and gives the pseudo-capacity, ΔC, is shown by the elements of C_{HF}, ΔC, and Z_w. This impedance, Z_w, is considered to be equivalent to the Warburg impedance in a diffusion process:

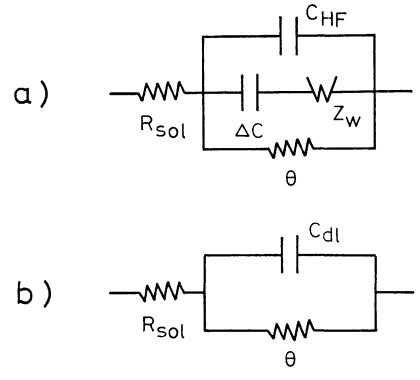

Fig. 5. Electrical equivalent circuit.

$$Z_w = (1-j)(\tau_D/2\omega)^{1/2}\cdot\Delta C^{-1} \quad (7)$$
$$\tau_D = (\partial\Gamma/\partial C_A)_E^2/D$$

τ_D: mean diffusion-controlled relaxation time;
C_A: concn of adsorbate; D: diffusion coefficient.

The coefficient, $(\tau_D/2)^{1/2}\cdot\Delta C^{-1}$, was about 200—400 $\Omega\cdot cm^2\cdot s^{-1/2}$ in the potential range from 0.90 to 1.50 V in the 0.5 M acetate solution. The τ_D was calculated from ω_{max} $(=1/\tau_D)$, corresponding to the top of the quarter circle. The θ, combined with other parallel elements, shows the charge-transfer resistance for the oxygen-evolution reaction. Since ΔC is almost equal to zero at potentials greater than 2.00 V, the equivalent circuit for the Kolbe reaction is simply shown by Fig. 5(b).

The facts that C_p is constant at potentials greater than 2.00 V and that C_{dl} decreases to an almost constant value of 5—8 $\mu F/cm^2$ result from the fact that: the constancy in C_{dl} is explained on the basis of the concept of electric double layer, and the results of ellipsometry.[8] The total capacitance, C_{dl}, is generally considered to be the serial combination of a Helmholtz capacity, C_H; a diffuse double-layer capacity, C_D, and a film capacity, C_{film}, due to the formation of a film on a solid electrode interface:

$$1/C_{dl} = 1/C_{film} + 1/C_H + 1/C_D \quad (8)$$

Since a sufficiently high concentration is employed in this study $1/C_D$ becomes small and:

$$1/C_{dl} = 1/C_{film} + 1/C_H \quad (9)$$

According to Hoare,[17] oxygen evolves from the platinum surface covered by an electronically conducting monolayer of adsorbed oxygen (Pt–O). In addition, ellipsometry confirmed that the thickness of an adsorption layer does not exceed 10 Å, even in the Kolbe reaction region.[8] Therefore, the incorporation of CH_3COO^- into the Pt–O layer seems more reasonably to be expected than that of the adsorption layer of CH_3COO^- onto the oxide film (PtO). Hence, C_{dl}, represented by C_H, is due to the specific adsorption of CH_3COO^- into the Helmholtz layer. This C_H can be explained on the basis of a Helmholtz parallel-plate condenser model:

$$C_{dl} \fallingdotseq C_H = \varepsilon/4\pi d \quad (10)$$

where d is the distance between the condenser plates and ε is the dielectric constant. Using a dielectric constant of acetic acid of 6.2 and a thickness of C_H of the order of 10 Å, C_H can be estimated to be about 6 $\mu F/cm^2$. This C_H value is almost equal to those of C_{dl} and C_{HF} obtained from the Z plane plot and the Y/ω plane plot respectively at 2.00 V.

The Kolbe reaction at the surface covered by CH_3COO^- or $CH_3COO\cdot$ at potentials above 2.00 V is due to:

$$CH_3COO\cdot_{(ad)} + CH_3COO^- \longrightarrow C_2H_6 + 2CO_2 + e$$ [18]

Gold Electrode. The differential capacity on a gold anode in an aqueous acetate solution, as measured with an a.c. bridge in series with a capacitor and a resistor, increased markedly at potentials above 1.50 V.[19]

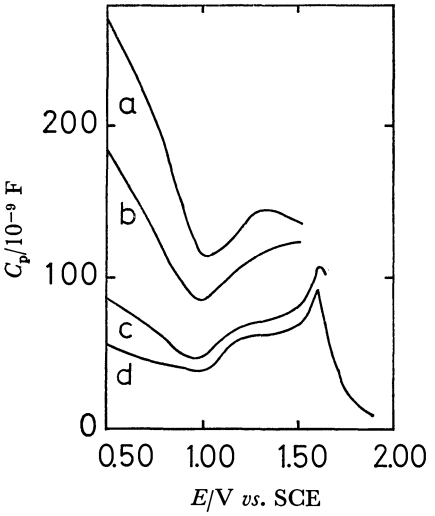

Fig. 6. Parallel capacitance *vs.* potential curves on Au in 2 M acetate with various frequencies.
sweep rate: 10 mV/s,
a: 20 Hz, b: 80 Hz, c: 400 Hz, d: 3 kHz.

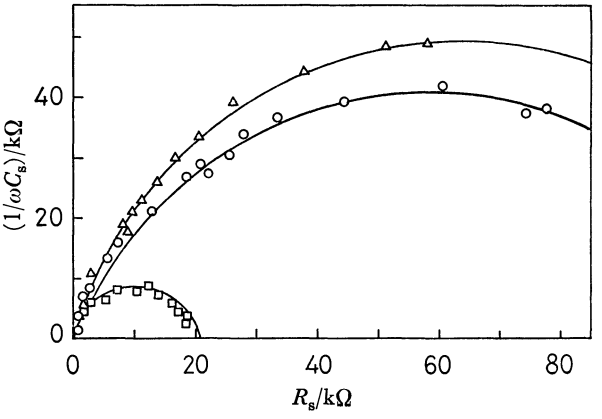

Fig. 7. Complex impedance plane plot of Au in 5 M acetate.
-○-: 1.00 V, -△-: 1.30 V, -□-: 1.50 V.

Figure 6 shows the C_p—E curves of gold anodes measured with the PSD in parallel with a capacitor and resistors. A constant value was reached at potentials above 1.60 V, in contrast to the results of a previous paper.[19] In order to determine the rate-determining step of the oxygen evolution reaction in the presence of CH_3COO^- with gold anodes, the Z plane plot was worked out; the results are shown in Fig. 7. The rate-determining step that occurs at potentials above 1.36 V[20] was found to be a charge-transfer process according to Eq. A, because the only semicircle was observed in the Z plane at 1.50 V.

$$H_2O_{(ad)} \longrightarrow OH_{(ad)} + H^+ + e \quad (A)$$
$$OH_{(ad)} + OH_{(ad)} \rightleftarrows O_{(ad)} + H_2O \quad (B)$$
$$O_{(ad)} + O_{(ad)} \rightleftarrows O_{2(ad)} \rightleftarrows O_2 \quad (C)$$

The C_{dl} value on gold in a 5 M acetate solution is shown in Fig. 3.

The Y/ω plane plot (Fig. 8) was worked out with a gold anode in an acetate solution in order to examine the behavior of CH_3COO^-, since the adsorption of CH_3COO^- on platinum occurs at around 1.30 V, with

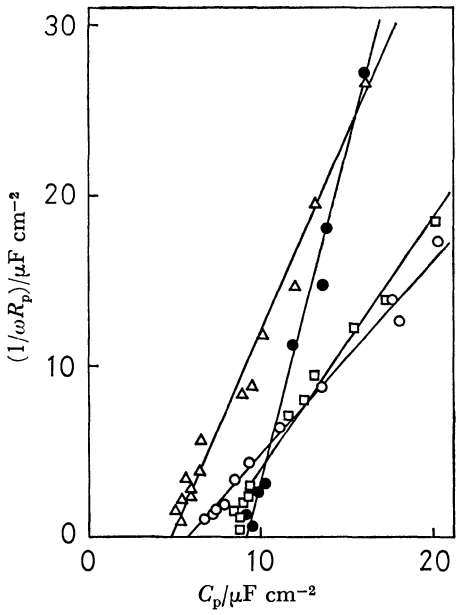

Fig. 8. Complex capacitance plane plot of Au in 2 M acetate.
-○-: 0.75 V, -△-: 1.00 V, -□-: 1.30 V, -●-: 1.50 V.

the evolution of oxygen. The loci of the plot in the potential range of 0.75 to 1.50 V differ from those on platinum anodes; they represent an approximately straight line without a specific circular arc. The C_{dl} value obtained at the intercept of the C_p axis (Eq. 6) is of the order of 6—10 $\mu F/cm^2$ in the potential range from 0.75 to 1.50 V. These potentials are on the Y/ω plane. Since the presence of the semicircle or the quarter circle is quite doubtful, the adsorption of CH_3COO^- on a gold anode is unlikely. In addition, the surface coverage of CH_3COO^- on a gold anode is negligible at concentrations higher than 0.5 M, as has previously been reported.[6]

Since the characteristics of the C_p—E curve at potentials less than 1.50 V shown in Fig. 6 are similar to those of the capacity-potential curve of gold anodes in perchloric acid reported by Schmid and Hackerman,[21] it may be concluded that the present C_p—E curves are not affected by the adsorption of CH_3COO^-. According to Schmid and Hackerman,[21] the capacity hump in the potential range from 0.9 to 1.3 V is due to the adsorption of oxygen-containing species, *i.e.*, OH^-, O^{2-}, *etc.*

Thermodynamically, the formation of oxide on gold anodes at potentials above 0.93 V (*vs.* SCE) in acetate solutions (pH=4.80) is possible *via* Eq. D;

$$2Au + 3H_2O = Au_2O_3 + 6H^+ + 6e^{22)} \qquad (D)$$

$$E^\circ = 1.457 - 0.591pH\ (vs.\ NHE)$$

E°: equilibrium potential

Therefore, the adsorption of oxygen-containing species, *e.g.*, water, on gold seems reasonable.

The specific circular arc with gold anodes, however, was not observed on the Y/ω plane at the potentials where the oxygen-containing species adsorbs. The quarter circle on platinum anodes was obtained on the Y/ω plane in the potential range from 0.75 to 0.90 V, where the first peak of the capacity was observed with the C_p—E curves. In this potential range, the adsorption of oxygen-containing species on platinum anodes is possible.

The difference between the adsorption of oxygen-containing species on platinum and gold anodes is considered to be as follows. Since the adsorption of reacting species can be detected by the specific arc on the Y/ω plane, the adsorption of oxygen-containing species on platinum is verified by the quarter circle. Water adsorbed on a gold anode is immediately changed to the oxide, Au_2O_3, according to Eq. D, and the surface is completely covered with the oxide.

Since the time constant of the adsorption layer differs from that of oxide, the Y/ω plane plot with gold anodes will not show a circular arc indicating the adsorption.

The results presented above support the notion that the Kolbe reaction occurs on surfaces covered with CH_3COO^- or $CH_3COO\cdot$.[3] The equivalent circuit of the oxygen evolution on a gold anode, which does not contain the adsorption pseudo-capacity of CH_3COO^-, is shown in Fig. 5b.

References

1) T. Dickinson and W. F. K. Wynne-Jones, *Trans. Faraday Soc.*, **58**, 382, 388, 400 (1962).
2) K. Sugino, T. Sekine, and N. Sato, *Electrochem. Tech.*, **1**, 112 (1963).
3) A. K. Vijh and B. E. Conway, *Z. Anal. Chem.*, **224**, 160 (1967).
4) I. Sekine and T. Sekine, *J. Electrochem. Soc. Jpn.*, **36**, 201 (1968).
5) I. Sekine, *Denki Kagaku*, **40**, 156 (1972).
6) I. Sekine, *Denki Kagaku*, **41**, 412 (1973).
7) I. Sekine, *Denki Kagaku*, **43**, 313 (1975).
8) I. Sekine, K. Kudo, and G. Okamoto, *J. Res. Inst. Catal., Hokkaido Univ.*, **24**, 44 (1976).
9) A. Kunugi, S. Iseki, K.Ohashi, and S. Nagaura, *Denki Kagaku*, **37**, 41 (1969).
10) J. H. Sluyters, *Recl. Trav. Chim. Pays-Bas*, **79**, 1092 (1960).
11) K. Takahashi, *Electrochim. Acta*, **13**, 1609 (1968).
12) R. D. Armstrong, W.P. Race, and H. R. Thirsk, *J. Electroanal. Chem.*, **16**, 517 (1968).
13) M. Sluyters-Rehbach and J. H. Sluyters, "Electroanalytical Chemistry," ed. by A. J. Bard, Marcel Dekker, Inc., New York (1970), Vol. 4, p. 1.
14) A. P. Tomilov, S. G. Mairanovskii, M. Ya. Fioshin, and V. A. Smirnov, "The Electrochemistry of Organic Compounds," Halsted Press, New York (1972), p. 379.
15) R. Payne, "Techniques of Electrochemistry," ed. by E. Yeager and A. J. Salkind, Wiley-Interscience, New York (1972), Vol. 1, p. 120.
16) R. DE Levie, *Electrochim. Acta*, **10**, 395 (1965).
17) J. P. Hoare, "The Electrochemistry of Oxygen," Interscience, New York (1968), p. 84.
18) B. E. Conway and A. K. Vijh, *Chem. Rev.*, **67**, 623 (1967).
19) I. Sekine and T. Sekine, *Denki Kagaku*, **36**, 286 (1968).
20) See also p. 87 in Ref. 17.
21) G. M. Schmid and N. Hackerman, *J. Electrochem. Soc.*, **109**, 243 (1962).
22) M. Pourbaix, "Atlas of Electrochemical Equilibria in Aqueous Solutions," Pergamon Press, Cebelcor (1966), p. 399.

The Mechanism of Catalyzed Hydrogen-Deuterium Exchange on Gold Deposited over Poly(tetrafluoroethylene)

Itsuo IIDA

Sagami Chemical Research Center, Nishi-Ohnuma, Sagamihara, Kanagawa 229

(Received September 13, 1978)

The H_2–D_2 exchange reaction over Au(0.3%)/PTFE(poly(tetrafluoroethylene)) was studied. The apparent activation energy was found to be 29 kJ mol^{-1}. The dependence of the reaction rate on the total pressure was measured at 518, 432, and 393 K. It was found that the pressure exponent of the exchange reaction decreases with the increase in the total pressure and that in the lower pressure range, the reaction order is as high as 2. The rate equation obtained from the pressure dependence was $R=k\{KP/(1+KP)\}^2$. Accordingly, it was concluded that the H_2–D_2 exchange reaction over gold takes place between molecularly adsorbed hydrogen and deuterium through a dimeric intermediate. The heat of adsorption on the active sites in the gold surface was 5.9 kJ mol^{-1}.

The H_2–D_2 exchange reaction on metal catalysts has been extensively studied as a measure of hydrogen activation.[1,2] Transition metals are known to be effective catalysts for this exchange. By contrast, non-transition metals are notably less efficient than transition metals, due to their smaller ability to interact with hydrogen.

The earliest views on the mechanisms of this exchange were those of Bonhoeffer and Farkas,[3] who suggested the following steps:

$$\left.\begin{aligned} H_2 + 2* &\rightleftarrows 2H* \\ D_2 + 2* &\rightleftarrows 2D* \\ HD + 2* &\rightleftarrows H* + D* \end{aligned}\right\} \quad (1)$$

This mechanism should operate when the adsorption-desorption process is rapid. Certain drawbacks to this mechanism soon, however, became evident. For example, Benton and White[4] showed that the desorption of adsorbed hydrogen from the surface of nickel powder only occurred above 173 K, although the H_2–D_2 exchange reaction proceeded measurably on nickel at about 83 K.

An alternative mechanism was therefore proposed as follows:[5,6]

$$\left.\begin{aligned} H_2 + D* &\rightleftarrows H* + HD \\ D_2 + H* &\rightleftarrows D* + HD \end{aligned}\right\} \quad (2)$$

This is called the Rideal-Eley mechanism.

It has been accepted that the Bonhoeffer-Farkas mechanism operates with transition metals above room temperature, where the adsorption-desorption process is fast. The Rideal-Eley mechanism is likely to apply to low-temperature reactions, where dissociated atoms are irreversibly adsorbed.

There have been many studies on the H_2–D_2 exchange reaction which attempted to distinguish between the Bonhoeffer-Farkas mechanism and the Rideal-Eley mechanism.[1,2]

On the other hand, Schwab and Killman suggested the following reaction mechanism for the exchange reaction over nickel foil, on the basis of the isotope effect of the reaction rate:[7,8]

$$\left.\begin{aligned} H_2 + * &\rightleftarrows H_2* \\ D_2 + * &\rightleftarrows D_2* \\ H_2* + D_2* &\rightleftarrows 2HD* \\ HD + * &\rightleftarrows HD* \end{aligned}\right\} \quad (3)$$

In this case, the isotope exchange takes place between molecularly adsorbed hydrogen and deuterium. However, A. Farkas made the criticism that their treatment on the basis of the isotope effect cannot provide proof for or against any mechanism.[8]

In this paper, we examine the H_2–D_2 exchange reaction on gold supported over poly(tetrafluoroethylene) (PTFE), which has already been proved to be a good support for platinum.[9] Although there are a few works on the H_2–D_2 exchange reaction over gold catalyst,[10,11] the kinetic behaviour of this exchange reaction has not yet been fully studied. In our study, the diagnostic test of a mechanism is based on the pressure dependence of the reaction rate.

Experimental

The rate of the H_2–D_2 exchange reaction was measured in a closed circulation system with a volume of 330 cm^3. Auxiliary equipment consisted of a mercury diffusion pump backed by a mechanical pump and isolated from the reaction apparatus by a liquid nitrogen trap. The pressure of the reaction system was measured with a mercury manometer which was covered with a small amount of silicone oil (Dow Corning 705 Fluid Lot. No. 33) at the top.

The isotope distribution in the gas phase was determined by gas chromatography at 77 K, using a column filled with alumina/5% manganese chloride. Prior to each measurement, the catalyst was subjected to heat-treatment *in vacuo* at 518 K.

Hydrogen of seven nine purity (Nippon Sanso Co., Ltd.,) and deuterium of 99.5% purity (Showa Denko Co., Ltd.,) were passed through a liquid nitrogen trap before use.

Gold (0.3%) supported on PTFE catalyst was prepared as follows: PTFE (914J. Mitsui Fluoro Chemicals Co., Ltd.,) was soaked in an acetone solution of chloroauric acid and the solvent was evaporated; after evacuation at room temperature, the sample was heated to 463 K and evacuation was continued for 30 min at the same temperature, after which hydrogen gas (40 kPa) was circulated over the catalyst at 463 K for 3 h, followed by evacuation overnight at the same temperature. The amount of the catalyst used was 5.06 g.

For the blank test, an equimolar mixture of H_2 and D_2 at the pressure of 46.3 kPa was circulated over 5.26 g of PTFE at 503 K; it was found that no appreciable amount of HD was formed even after 140 min.

Results

The time course of the H_2–D_2 exchange reaction is

described by the first order equation:

$$\ln \frac{\chi_e - \chi_t}{\chi_e - \chi_0} = -k_e t, \quad (4)$$

where χ_0, χ_t, and χ_e are the fractions of hydrogen deuteride present at times zero and t and at equilibrium. The total rate of exchange, R (cm³/min), is given by

$$R = k_e N \quad (5)$$

where N is the total amount of hydrogen gas (H_2, D_2) introduced. We could not calculate the absolute rate (the exchange rate per unit metal surface area) since the surface area of gold was not determined.

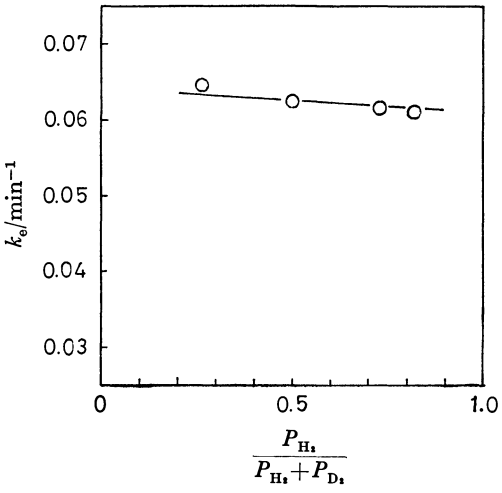

Fig. 1. First order rate constant (k_e) at 518 K against the fraction of hydrogen. Total pressure was kept constant at 24.9 kPa.

The dependence of the first order rate constant, k_e, on the composition of the mixture of H_2 and D_2 under the total pressure of 24.9 kPa was studied. The results (Fig. 1) show that there exists little isotope effect in the H_2–D_2 exchange reaction on Au/PTEE. Therefore, an equimolar mixture of H_2 and D_2 was employed in contact with the catalyst in all later experiments.

The temperature dependence of the first order rate constant, k_e, plotted in Arrhenius form is shown in

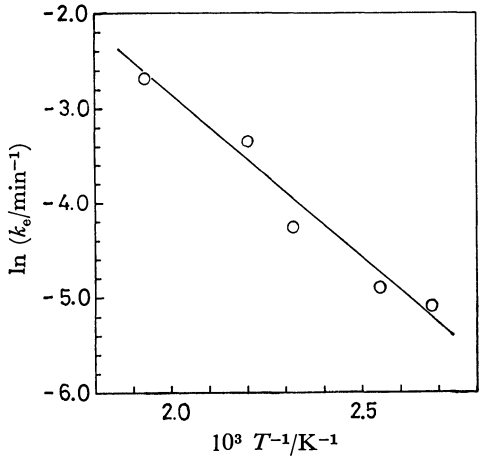

Fig. 2. Arrhenius plots for the H_2–D_2 exchange reaction on Au(0.3%)/PTFE. P=34.7 kPa.

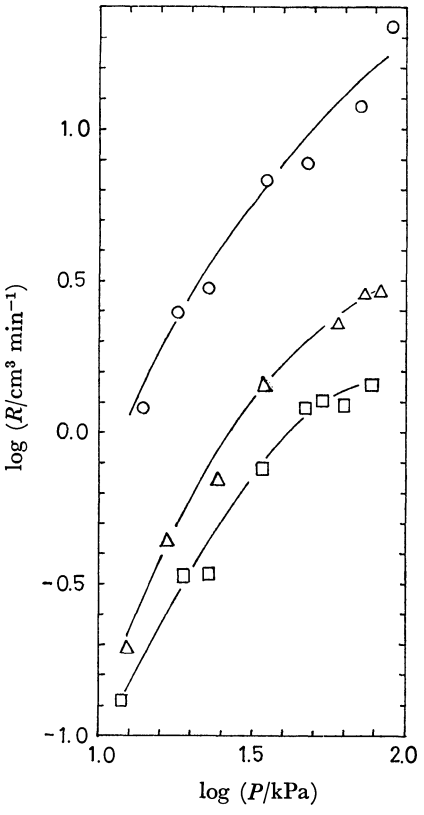

Fig. 3. Dependencies of the H_2–D_2 exchange reaction on the total pressure at 518, 432, and 393 K. -○-; 518 K, -△-; 432 K, -□-; 393 K.

Fig. 2. The apparent activation energy calculated from the slope of the line is 29 kJ mol^{-1}, which is the same as that over gold wire obtained by Avdeenko *et al.*[12]

The logarithms of the total rates of the exchange at 518, 432, and 393 K are plotted against those of the total pressure P of hydrogen in Fig. 3. It is shown in Fig. 3 that the pressure exponent of this exchange reaction decreases with the increase in the total pressure. For example, at 518 K, the pressure exponent decreased from 2 at pressures between 13 and 20 kPa to 1.0 at pressures between 50 and 70 kPa; at 393 K, it decreased from 2 at pressures between 13 and 20 kPa to 0.5 at pressures between 50 and 70 kPa.

It is surprising that the reaction order was found to be 2 in the lower pressure range, because neither the Bonhoeffer-Farkas mechanism nor the Rideal-Eley mechanism can explain such a high reaction order. For the Bonhoeffer-Farkas mechanism, where the exchange reaction proceeds by way of dissociative adsorption and desorption, the reaction order should vary from first at low coverages to zero at high coverages. For the Rideal-Eley mechanism, the order should be first, providing the atomic layer is complete and the molecular species only weakly adsorbed or not at all.

Consequently, we must consider the Schwab mechanism, in which the H_2—D_2 exchange reaction goes through an associative intermediate, as expressed by

$$H_2(a) + D_2(a) \rightleftarrows \begin{matrix} H\cdots H \\ \vdots \quad \vdots \\ D\cdots D \end{matrix} \rightleftarrows 2HD(a). \quad (6)$$

In this case, the reaction velocity is proportional to the square of the coverage of the molecularly adsorbed hydrogen. Using the Langmuir equation, total rate of exchange is given by

$$R = k\left(\frac{KP}{1+KP}\right)^2, \tag{7}$$

where K denotes the adsorption constant.

By rearranging Eq. 7, we get the following equation:

$$\frac{P}{\sqrt{R}} = \frac{1}{\sqrt{k}K} + \frac{P}{\sqrt{k}}. \tag{8}$$

Therefore, it can be expected that when $P/\sqrt{R}$'s are plotted against total pressure, P, a straight line will be obtained.

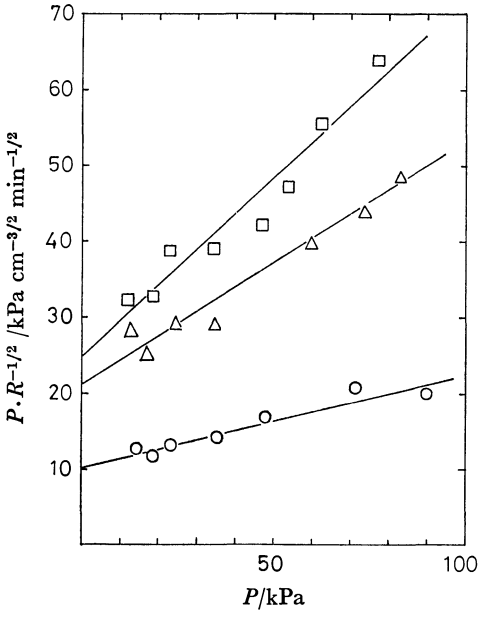

Fig. 4. Relation between the total pressure (P) and $P/\sqrt{R}$. -○-; 518 K, -△-; 432 K, -□-; 393 K.

The graphs of $P/\sqrt{R}$ against P at 518, 432, and 393 K are shown in Fig. 4; they give reasonably good straight lines. Accordingly, we get Eq. 7 as the rate equation for the H_2–D_2 exchange reaction on Au/PTFE.

From the slopes and intercepts of the graphs in Fig. 4, we can calculate the rate constant, k, for the surface exchange and the adsorption constant, K, at 518, 432, and 393 K; these are summarized in Table 1.

TABLE 1. RATE CONSTANT OF THE H_2–D_2 EXCHANGE REACTION AND ADSORPTION CONSTANT OF HYDROGEN MOLECULE ON Au/PTFE

T/K	k/cm^3 min^{-1}	K/kPa^{-1}
518	65.6	0.0122
432	9.66	0.0152
393	4.49	0.0190

In Fig. 5, ln k and ln K are plotted against $1/T$. The heat of hydrogen adsorption on the surface of gold and the activation energy of the surface reaction, given by the slopes of the lines in Fig. 5, are 5.9 kJ mol^{-1} and 37

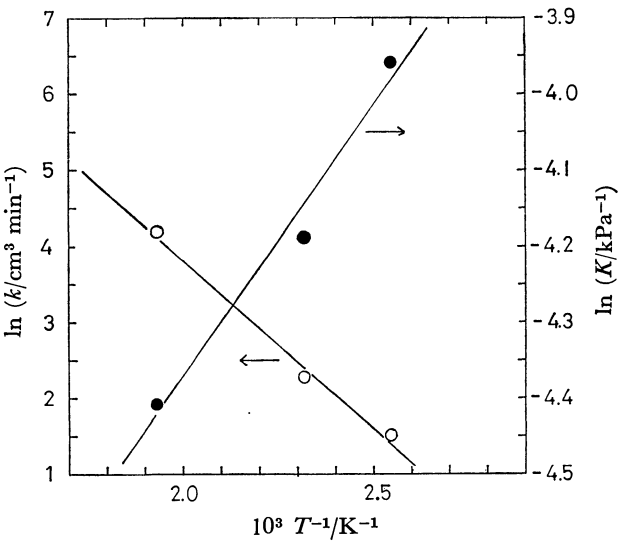

Fig. 5. Temperature dependencies of logarithm of rate constant (k) and that of adsorption constant (K).

kJ mol^{-1}, respectively. Although in the case of the H_2–D_2 exchange reaction on copper catalyst Kiyomiya *et al.* found a marked isotope effect,[13] we found little isotope effect for the reaction on gold. Therefore, the heat of adsorption obtained is not the average of that for hydrogen and deuterium. The heat of adsorption for hydrogen and that for deuterium are the same and are both 5.9 kJ mol^{-1}.

Discussion

Although Trapnell did not find chemisorption of hydrogen on the evaporated film of gold in the temperature range 293 K to 93 K,[14] there are a few reports on the H_2–D_2 exchange reaction on gold which indicate that the adsorption of hydrogen on gold does occur.[10,11] For example, Taylor and his coworkers[11] found the H_2–D_2 exchange reaction to take place on gold foil. They speculated that the hydrogen atoms were chemisorbed on the vacant d-orbital created by a promotion of a d-electron to the top of the s-band, since no d-orbitals are normally available in gold for surface bond formation.

On the other hand, Wise and Sancier found that after treatment of gold foil with hydrogen plasma, the rate of the H_2–D_2 exchange reaction on it became greater and that the activation energy was reduced from 90.0 kJ mol^{-1} over the untreated catalyst to 46 kJ mol^{-1}. Since the high activity of treated gold was reduced by evacuation at 615 K, chemisorbed hydrogen seems to have been formed, giving rise to the enhanced activity and presumably reacting with gaseous hydrogen (Rideal-Eley mechanism). However, they also paid attention to the fact that over gold foil treated with hydrogen plasma, another heterogeneous reaction of higher activation energy takes place which predominates at temperatures in excess of 450 K. They suggested that the reaction may proceed by the Bonhoeffer-Farkas mechanism in the higher temperature range.

In both of the works mentioned above, the pressure dependence of the exchange reaction was not studied

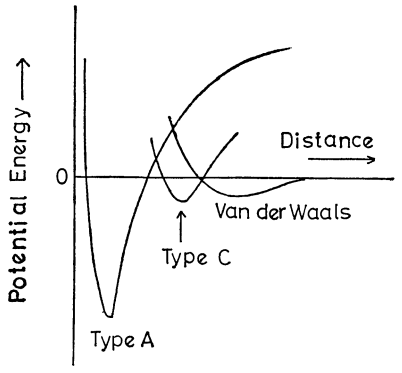

Fig. 6. Potential energy curves for Type A (M–H) and Type C (M···H_2) chemisorbed hydrogen.

and the interpretations are not more than conjectures. It could be said that the results in these works do not exclude the possibility that the reaction goes through an associative intermediate.

As far as we know, we were the first to study the pressure dependencies of the H_2–D_2 exchange reaction on gold catalyst. We found that the pressure exponent of the H_2–D_2 exchange reaction was as high as 2 at the lower pressure range. Usually one cannot decide the mechanism of the H_2–D_2 exchange reaction only by measuring the pressure dependencies. In our case, however, the pressure exponent we obtained precludes mechanisms other than that proposed by Schwab and Killman. Moreover, the rate equation (Eq. 7) which we confirmed at 518, 432, and 393 K strongly supports the mechanism; the exchange reaction takes place between molecularly adsorbed hydrogen and deuterium.

At this stage, we consider the nature of the hydrogen adsorbed. Dowden[15] has pointed out that there is probably an initial state of chemisorption in many cases, named Type C chemisorption (molecular), on the empty atomic d-orbitals; this type is intermediate between physical adsorption and strong chemisorption, as shown in Fig. 6. Concerning this suggestion, Clark[16] commented that the potential energy curves of chemisorption of hydrogen on sp and d metals may be quite similar and that, for transition metals, the Type C potential curve may intersect the curve for strong atomic adsorption in such a way that very little activation energy is required for the hydrogen to transfer to the final atom curve, Type A, whereas in a nontransition metal, the crossing point may be located in a postition that requires a large activation energy for the transfer. Actually, preformed hydrogen atoms can be chemisorbed on Group IB metals,[17] which may indicate that chemisorption of hydrogen atom is limited by a large activation energy and not by the inability of gold to chemisorb.

Our results showed that hydrogen is adsorbed on a gold surface molecularly and that the heat of adsorption is as low as 5.9 kJ mol^{-1}, which seems correspond to Type C chemisorption.

On the other hand, it was shown by Hoffmann,[18] using arguments based on the conservation of orbital symmetry,[19] that in the gas phase reaction, the coplanar path proceeding through a square transition state is thermally forbidden. An approximate energy barrier for the process is that amount of energy necessary to raise two electrons from the bonding σ_g orbital in H_2 up to the non-bonding hydrogen 1s level, or 498 kJ mol^{-1}. In the study of the H_2–D_2 exchange reaction in the gas phase, Bauer and Ossa found that the activation energy was 177 kJ mol^{-1} and the possibility of an atomic exchange mechanism, *i.e.* $H_2 \rightarrow 2H$ followed by $H+D_2 \rightarrow HD+D$ was considered to be ruled out.[20] Various theoretical studies searching for a low-lying four-centre transition state have been, done but none of them has succeeded in explaining the low activation energy observed.[21]

On the other hand, in our study the activation energy for the surface exchange was found to be 37 kJ mol^{-1}. Therefore, a large amount of stabilization of H_4 intermediate does occur on the surface of gold. Although Mango and Schachtschneider pointed out that the reactions which are symmetry forbidden can become allowed by interaction with the d-orbital of a transition metal,[22] the argument cannot proceed in a similar fashion in the case of the reaction on gold for the lack of the vacant d-orbital. Nevertheless, there are various kinds of approaches for two hydrogen molecules to form a H_4 intermediate: *e.g.* an orthogonal approach passing through a tetrahedron, rectangle, and rhombus, and an allowed path suggested by Gimarc[23] passing through Y- and T-shaped transition states. Moreover, various kinds of sites differing in electronic or in geometric structure exist in the metal surface. Therefore, it seems that further theoretical studies will be necessary to understand the transition state of the surface exchange on gold completely.

The author is grateful to Professor Kenzi Tamaru of the University of Tokyo and Professor Atsumu Ozaki of Tokyo Institute of Technology for helpful comments. Acknowledgement is made to Dr. Toshihiko Kondo for helpful discussions.

References

1) G. C. Bond, "Catalysis by Metals," Academic Press, London (1962), p. 149.
2) A. Ozaki, "Isotopic Studies of Heterogeneous Catalysis," Kodansha, Tokyo, Academic Press, New York, San Francisco, and London (1977), p. 9.
3) K. F. Bonhoeffer and A. Farkas, *Z. Phys. Chem. (Leipzig)*, **12B**, 231 (1931).
4) A. F. Benton and T. A. White, *J. Am. Chem. Soc.*, **52**, 2325 (1930).
5) E. K. Rideal, *Proc. Cambridge Phil. Soc.*, **35**, 130 (1939).
6) A. Couper and D. D. Eley, *Discuss. Faraday Soc.*, **8**, 172 (1950).
7) G.-M. Schwab and E. Killman, *Bull. Soc. Chim. Belg.*, **67**, 305 (1958).
8) G.-M. Schwab and E. Killman, Proc. 2nd, Int. Congr. Catalysis, 1047 (1960).
9) I. Iida, J. Kato, and K. Tamaru, *Z. Phys. Chem. Neue Folge*, **107**, 219 (1977).
10) H. Wise and K. M. Sancier, *J. Catal.*, **2**, 149 (1963).
11) R. J. Mikovsky, M. Boudart, and H. S. Taylor, *J. Am. Chem. Soc.*, **76**, 3814 (1954).
12) M. A. Avdeenko, G. K. Boreskov, and M. G. Slin'ko,

"Problem of Kinetics and Catalysis," ed by S. Z. Roginskii, U.S.S.R. Acad. Sci. Press, Moscow, **9**, 61 (1957).
13) M. Kiyomiya, N. Momma, and I. Yasumori, *Bull. Chem. Soc. Jpn.*, **47**, 1852 (1974).
14) B. M. W. Trapnell, *Proc. R. Soc. London, Ser. A*, **218**, 566 (1953).
15) D. A. Dowden, "Chemisorption," ed by W. E. Garner, Butterworth, London and Washington D. C. (1958), p. 5.
16) A. Clark, "The Chemisorptive Bond," Academic Press, New York and London (1974), p. 67.
17) J. Pritchard and F. C. Tompkins, *Trans. Faraday Soc.*, **56**, 540 (1960).
18) R. Hoffmann, *J. Chem. Phys.*, **49**, 3739 (1968).
19) R. B. Woodward and R. Hoffmann, "The Conservation of Orbital Symmetry," Verlag Chemie, Gmbh. Weinheim (1970).
20) S. H. Bauer and E. Ossa, *J. Chem. Phys.*, **45**, 434 (1966).
21) D. M. Silver and R. M. Stevens, *J. Chem. Phys.*, **59**, 3378 (1973) and references therein.
22) F. D. Mango and J. H. Schachtschneider, *J. Am. Chem. Soc.*, **89**, 2484 (1967).
23) B. M. Gimarc, *J. Chem. Phys.*, **53**, 1623 (1970).

Reversible Binding of NO to Fe(II)edta

Yukio HISHINUMA,* Ryuichi KAJI,* Hidetoshi AKIMOTO, Fumito NAKAJIMA, Toshikatsu MORI, Tomoichi KAMO, Yoshijiro ARIKAWA,** and Shigeru NOZAWA**

Hitachi Research Laboratory, Hitachi Ltd., Hitachi, Ibaraki 317

***Babcock-Hitachi Ltd., Kure, Hiroshima 737*

(Received September 27, 1978)

The equilibrium constants, enthalpy, and entropy of the reversible binding of nitrogen oxide to Fe(II)edta in an aqueous solution have been measured in the temperature range 38.5 to 70 °C. Experiments were carried out by absorbing NO under O_2 free conditions. The results show that, in the absorption of NO with Fe(II)edta solution, the value of $\Delta H°$ is -15.8 kcal/mol and $\Delta S°$ is -20.7 e.u.

A number of nitrogen monoxide complexes have been known for many years and have attracted the attention of many chemists because the way that NO interacts with transition metal complexes is similar to the way that CO and O_2 interact with those complexes. And recently, the structure of these complexes, the coordination geometry of the NO ligand,[1-4] ways of synthesizing nitrosyl complexes, and the coordinated NO reaction[5] have been under investigation.

In the course of our attempts to develop a method of removing nitrogen monoxide from a flue gas, we found that many of the peptide and amino acid complexes of iron(II) and cobalt(II) bind NO reversibly in aqueous solutions and, therefore, it became necessary to make a detailed investigation of the conditions under which this binding occurs. But only a few data are available with respect to the thermodynamics of this reaction. The experiments reported in this paper were carried out to determine the thermodynamics of the reversible binding of molecular NO to Fe(II)edta.

Although it has been known that the aqueous solution of Fe(II)edta absorbs NO, it has not been known whether Fe(II)edta binds NO reversibly, and the data have not been reported in its thermodynamics in detail. We found that, under O_2 free conditions, a light yellow aqueous solution of Fe(II)edta turns dark green as it absorbs NO, and it turns light yellow again upon heating, in a vacuum or when purged with nitrogen. We have been able to show that these color changes are caused by the following reversible reaction.

$$Fe^{II}edta + NO(g) \rightleftharpoons Fe^{II}(NO)edta. \quad (1)$$

In this paper, we discuss the thermodynamics of the coordination of molecular NO to Fe(II)edta in an aqueous solution in the temperature range 38.5 to 70 °C.

Experimental

Materials. Reagent grade iron(II) sulfate and EDTA were used without further purification. The nitrogen monoxide gas that was used was an extra pure mixture of NO and N_2 (NIHON SANSO).

Preparation of Fe(II)edta. The aqueous solution of Fe(II)edta was prepared according to the following method. EDTA was first dissolved in distilled water under O_2 free conditions and the pH of the solution was adjusted to *ca.* 9 by adding a dilute NaOH solution. An equivalent amount of $FeSO_4$ was added to the solution and the pH of the solution was adjusted to the desired values by adding a dilute HCl or NaOH solution.

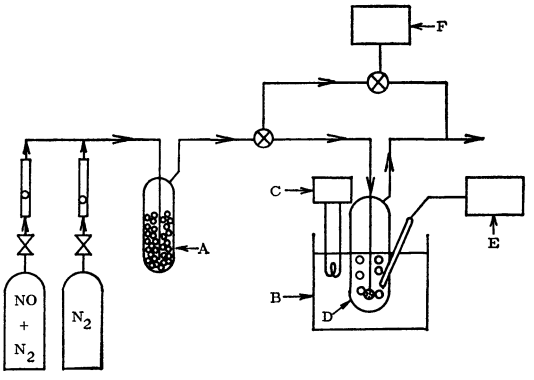

Fig. 1. Schematic diagram of apparatus.
A: gas mixer, B: water bath, C: thermostat
D: absorber, E: pH meter, F: NO_x meter.

The concentration of iron(II) was measured with the usual 1,10-phenanthroline method.[6]

Equilibrium Measurements. Equilibrium constants were determined at 38.5, 55, and 70 °C. A schematic diagram of the apparatus is shown in Fig. 1. The temperature was controlled to within ±1 °C by a thermostat. All experiments were carried out under O_2 free conditions to avoid irreversible oxidation of the Fe(II)edta. A 100 ml quantity of the Fe(II)-edta solution (0.008—0.036 M) was introduced to an absorber. A mixture of NO and N_2 of known NO concentration was bubbled through the solution and the NO concentration in the outlet gas was measured with Beckman Model 951 NO_x meter. The gas flow rate was 0.73 N.T.P. l/min. NO absorption was carried out until equilibrium was reached, *i.e.* until the NO concentration in the outlet gas became equal to that n the inlet gas.

The amount of NO absorbed was determined by graphical integration of the NO concentration in the outlet gas.

Results and Discussion

To confirm the stoichiometry of NO uptake by Fe(II)edta, we first measured the quantitative NO uptake of an aqueous Fe(II)edta solution. The experiments were performed by absorbing pure NO gas obtained from Matheson Co. with a 0.1 M Fe(II)edta solution at pH 6 at room temperature. It was found from these experiments that 1.0 mol of NO was taken up by each mole of Fe(II)edta initially present, and hence that Fe(II)edta binds NO in a molar ratio of unity. The NO uptake by Fe(II)edta was also found by visible spectroscopy measurements to be reversible.

Figure 2 shows the visible absorption spectrum of the

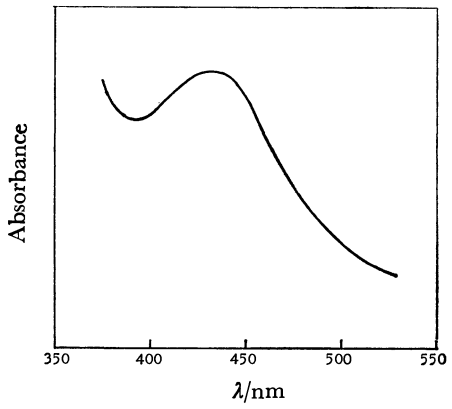

Fig. 2. Spectrum of $Fe^{II}(NO)$ edta at 15 °C.

aqueous Fe(II) (NO)edta solution. The initial light yellow color of the Fe(II)edta solution changes to dark green upon NO absorption and an absorption peak appears at λ=434 nm. When the solution is heated or purged with N_2, it regains its original light yellow color, with the desorption of NO. This indicates that Reaction 1 is completely reversible. Furthermore, the pH of the solution increased from 6.0 to 7.2 after absorbing NO. This increase is probably caused by the displaced carboxylic group since it binds the H^+ in the solution. The expression of the equilibrium constant for Eq. 1 can be written as

$$K_c = \frac{[Fe^{II}(NO)edta]}{[Fe^{II}edta]\cdot[NO]_{aq}} \quad (2)$$

Equation 2 can also be written as

$$K_c = \frac{[Fe^{II}(NO)edta]\cdot H}{\{[Fe^{II}edta]_0 - [Fe^{II}(NO)edta]\}\cdot[NO]_g} \quad (3)$$

where $[Fe^{II}edta]_0$ is the initial molar concentration of Fe(II)edta, $[Fe^{II}(NO)edta]$ is the equilibrium molar concentration of the NO adduct, $[NO]_g$ is the partial pressure of the NO in the gas, and H is the Henry's constant for the solubility of NO in water.

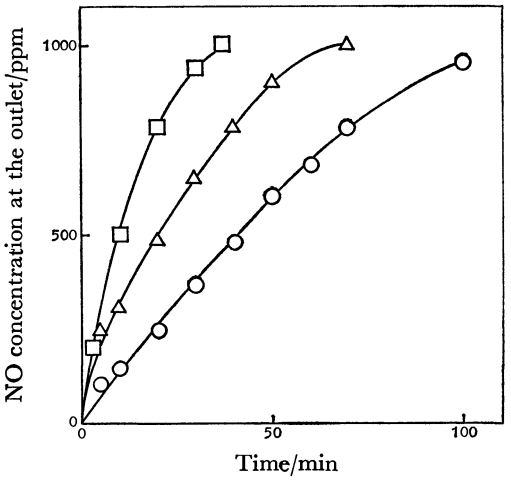

Fig. 3. Graphical illustration of the canges in NO concentration at the absorber outlet.
Inlet gas contents: NO 1000 ppm, N_2 balance, gas flow rate: 730 Nml/min, temperature: 55 °C, pH: 3.0, Fe(II)edta concentration: -□- 0.008 M, -△- 0.016 M, -○- 0.036 M.

Figure 3 shows changes in NO concentration at the absorber outlet for various concentrations of the Fe(II)-edta solution. By graphically integrating the outlet NO concentration curves, the amount of absorbed NO in each solution can be obtained.

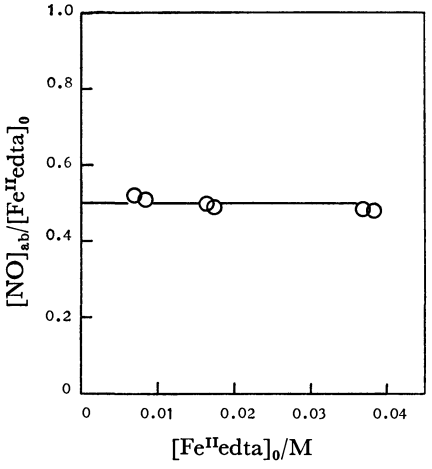

Fig. 4. Effect of $Fe^{II}edta$ concentration on NO absorption.

Figure 4 shows the effect of $[Fe^{II}edta]_0$ on the molar ratio of the absorbed NO to $[Fe^{II}edta]_0$ obtained from Fig. 3. It was found that the ratio was not affected by $[Fe^{II}edta]_0$ of 0.008—0.036 M at pH 3.

The effect of pH on the molar ratio of absorbed NO to total iron(II) ($[Fe^{II}]_0+[Fe^{II}edta]_0$) is shown in Fig. 5. The ratio was not affected by the pH value of the solution in the pH range of 3—6, but this ratio decreased drastically below a pH of 3.

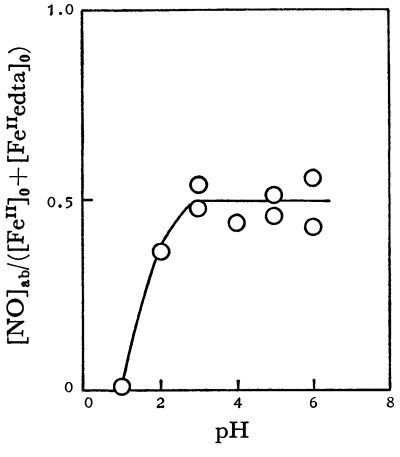

Fig. 5. Effect of pH on NO absorption.
Inlet gas content: NO 1000 ppm, N_2 balance, gas flow rate: 730 Nml/min, temperature: 55 °C, Fe(II): 0.02 M, edta: 0.02 M.

Because Fe(II)edta is very stable and almost 100% of the Fe(II) in the solution exists as Fe(II)edta,[7] in the pH-range 3—6, Eq. 3 can be rewritten as

$$\frac{[Fe^{II}edta]_0}{[NO]_{ab}} = 1 + \frac{H}{[NO]_g\cdot K_c} \quad (4)$$

In this experiment, the NO concentration and tempera-

Table 1. Thermodynamic data for reversible NO coordination to iron complexes

Complex	State	Temperature °C	H/K_c atm	K_c M^{-1}	$\Delta H°$ kcal/mol	$\Delta S°$ e.u.
Fe(II)edta	aqueous solution	38.5	0.18×10^{-3}	3.48×10^{6}		
		55.0	0.850×10^{-3}	0.859×10^{6}	−15.8	−20.7
		70.0	2.38×10^{-3}	0.339×10^{6}		
Fe(II)edta[9]	aqueous solution	60—70	—	—	−14.1	—
Fe(III)Cl(TPP)[10]	solid	25.0	—	$3.45\ atm^{-1}$	−5.26	−15

ture were kept constant and, therefore, $H/[NO]_g$ was constant. This indicates that the equilibrium constant K_c which is defined by Eqs. 2 and 3, is not affected by pH in the range 3—6. But below a pH of 3 the dissociation of Fe(II)edta takes place, which gives rise to a decrease in the NO absorption.

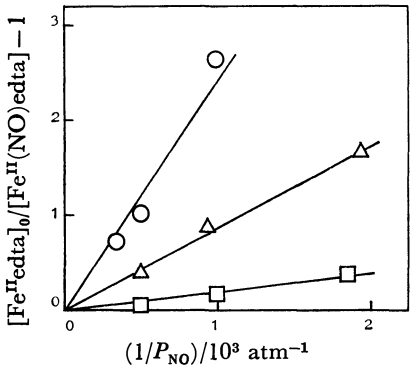

Fig. 6. Plot of $[Fe^{II}\ edta]_0/[Fe^{II}(NO)edta]-1$ *vs.* $1/P_{NO}$
pH: 3.0, temperature: -○- 70 °C, -△- 55 °C, -□- 38.5 °C.

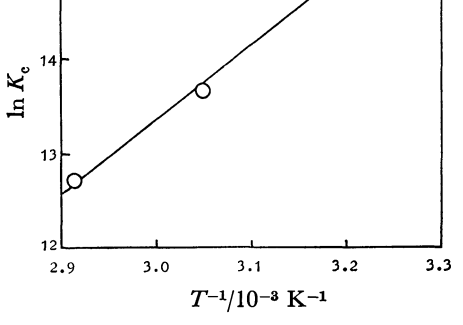

Fig. 7. van't Hoff plot of equilibrium constants for Eq. 1.

Figure 6 shows the relation between $[Fe^{II}edta]_0/[Fe^{II}(NO)edta]-1$ and $1/P_{NO}$ at temperatures of 38.5, 55, and 70 °C. H/K_c can be obtained from the slope of each line for each of these temperatures. Using Henry's constants,[8] the equilibrium constant at each temperature was obtained. These values are summarized in Table 1. Figure 7 shows the van't Hoff plot of these equilibrium constants. The values of thermodynamic quantities obtained from the van't Hoff plot are also given in Table 1. Enthalpy and entropy for Reaction 1 are $\Delta H°=-15.8$ kcal/mol and $\Delta S°=-20.7$ e.u., respectively. Recently Hasui studied the binding of NO to Fe(II)edta in an aqueous solution and measured its equilibrium constants in the temperature range 60—70 °C in the pH range 2.4—8.5.[9] They reported that the enthalpy change for the coordination of NO to Fe(II)edta was $\Delta H°=-14.1$ kcal/mol. This value is approximately same as our data.

The binding of gases with metal complexes is characterized by a small negative change in enthalpy and a relatively large change in entropy to compensate for the enthalpy change. This occurs because a gas loses its translational and rotational degree of freedom by coordination. The stability of such reversible complexes is examined by comparing their $\Delta H°$ values. But to the authors' knowledge, the only available thermodynamic data to date for the reversible binding of NO with iron complexes other than Fe(II)edta are those obtained by Vasca.[10] Their data are shown in Table 1 together with our data. But their data are for NO absorption by Fe(III)Cl (TPP) (TPP=tetraphenyl porphinate)in the solid state. Further extensions of the present work to different solvent systems and ligands will enable us to establish more fully the factors contributing to the stability of reversible NO complexes.

References

1) R. Eisenberg and C. D. Meyer, *Acc. Chem. Res.*, **8** 26 (1975).
2) B. B. Wayland and L. W. Oison, *J. Am. Chem. Soc.*, **96**, 6037 (1974).
3) W. R. Scheidt and M. E. Frisse, *J. Am. Chem. Soc.*, **97**, 17 (1975).
4) B. L. Haymore and J. A. Ibers, *Inorg. Chem.*, **14**, 2610 (1975).
5) S. G. Clarkson and F. Basolo, *Inorg. Chem.*, **12**, 1528 (1973).
6) JIS K1010.
7) Anders Ringbom, "Complexation in Analytical Chemistry," John Wiley and Sons Inc., New York (1963).
8) J. H. Perry, "Chemical Engineers' Handbook," 4th ed, Mcgraw-Hill, New York (1963).
9) H. Hasui, H. Osuo, H. Ohmichi, Y, Fukusyu, H. Tarui, *Nippon Kagaku Kaishi*, **1978**, 447.
10) L. Vaska and H. Nakai, *J. Am. Chem. Soc.*, **95**, 5431 (1973).

Decay of Naphthalene Phosphorescence in the Presence of Some Chlorinated Compounds. An External Heavy Atom Effect

Nozomu EBARA,* Yusuke YAJIMA, and Hiroshi WATANABE

Department of Chemistry, College of General Education, The University of Tokyo, Meguro-ku, Tokyo 153

(Received January 12, 1979)

The decay of the phosphorescence of naphthalene in the mixed solutions of methylcyclohexane and several chlorinated compounds has been analyzed. In many cases the decay was almost exponential and the decay constant was a function of the concentration of chlorinated compounds. In the case of carbon tetrachloride, the decay was distinctly non-exponential. The decay was analyzed by a Laplace transformation method. In this case a complex was formed, in equilibrium with the free naphthalene molecule, and the decay constant of the former increased when the concentration of CCl_4 increased. The external heavy atom effect takes place in two ways: one by complex formation with the molecule containing heavy atoms and another by a long range interaction through a statistical distribution of the latter molecules around the phosphorescing molecule.

The interaction of a molecule with molecules containing heavy atoms may frequently result in an apparent decrease in the triplet lifetime of the former. This external heavy atom effect has been the subject of a number of experimental and theoretical investigations. Quantitative treatment of the effect has led to an elucidation of the mechanism in terms of enhanced spin-orbit interaction through formation of CT complexes in which emitting triplet species may be either a locally excited state of one of the component molecules[1-9] or a CT state.[10-13] Previous investigators have laid stress on a particular route of enhancement, for example,

a) mixing of the triplet state with the locally excited singlet state,[1-3]

or

b) mixing of the triplet state with the CT singlet state.[4,5,13]

The heavy atom effect on the phosphorescence of stable CT complexes has been investigated.[7-12] It has been shown that the rate constants of both $S_1 \rightsquigarrow T_1$ and $T_1 \rightarrow S_0$ transitions are increased. Furthermore, it has also been demonstrated that the $T_1 \rightsquigarrow S_0$ radiationless transition is not much enhanced and the observed reduction in the triplet lifetimes is mainly due to a change in the radiative lifetime.[7]

The decay of benzene phosphoresence in rare gas hosts has been reported.[14-20] It has been found that heavy atoms such as Kr or Xe have a drastic effect on the decay rate. Moreover, the geometrical arrangement of the heavy atoms around the molecule has been found to affect its lifetime. The mechanism has been elucidated by K. C. Lin and S. H. Lin[3] in terms of enhanced spin-orbit coupling in the benzene ring in the presence of a heavy atom perturber. Najbar[17-20] has discussed their experimental results in terms of a mean lifetime averaged over different sites, each occupied by a benzene molecule and a variable number of heavy atoms.

The dependence of the heavy atom effect on the distance between the emitting molecule and the heavy atom has also been investigated. Kavarnos *et al.*[21] have synthesized several bromine-substituted naphthonorbornanes and have measured their radiative as well as non-radiative lifetimes. Giaccino and Kearns[22] have doped naphthalene molecules into crystals of various halogen-containing molecules and have measured the phosphorescence lifetimes. None of them, however, could find any distinct relationship between the lifetime and the halogen–naphthalene distance.

Eisenthal[8] has found that in the presence of tetrachloro- or tetrabromophthalic anhydride or in the presence of propyl iodide the phosphorescence of 2-chloronaphthalene becomes very similar to that of naphthalene. He claimed that the CT singlet state playes an important role in the donor phosphorescence. Similar observations were also reported by other authors.[23]

It has been shown that the lifetime is dependent on the concentration of concomitant heavy atom compounds. If the heavy atom effect manifests itself through formation of a CT complex, the decay of phosphorescence would consist of two exponential components, one for the complex and another for naphthalene itself, and the ratio of their coefficients would be a function of the concentration. In a separate experiment on the phosphorescence of haloalkylnaphthalenes, we have found some evidence for a non-complexed external heavy atom effect. If such is the case, the concentration dependence is a function of the distribution of heavy atom molecules around the phosphorescing molecule.

In the following, we have employed chlorinated compounds because they seemed least liable to form complexes with naphthalene. The decay curve of naphthalene molecule in the presence of chlorinated moleculas was analyzed as a function of the concentration of the latter.

Experimental

Naphthalene-d_0 and naphthalene-d_8 were zone-refined several times. Methylcyclohexane (MCH) and the following liquid samples were purified by column chromatogram or distilled: carbon tetrachloride, dichloromethane, propyl chloride, butyl chloride, cyclohexyl chloride, benzyl chloride, chlorobenzene, *o*-dichlorobenzene, and *m*-dichlorobenzene. Naphthalene was dissolved in a chlorinated compound–MCH mixture in various mole fractions from 0: 1 to 1: 0. The concentration of naphthalene molecule was kept at 5×10^{-3} mol dm^{-3} in every case. Samples were excited at 315 nm at 77 K and the decay of phosphorescence was displayed on a recorder. In the photoselection experiment, the exciting light was passed through a Gran-Thomson prism and the emission was observed through a plastic polarizer.

Results and Discussion

The decay of naphthalene phosphorescence in the presence of the above chlorinated compounds was almost exponential, except for the case of carbon tetrachloride (Figs. 1—3). The decay constants were sometimes very sensitive to the presence of chlorinated molecules and sometimes quite insensitive. There seemed no distinct relation to the extent of CT interaction. Generally, compounds with one chlorine atom were insensitive and compounds with more than one chlorine atom were sensitive. In the latter case, the concentration dependence was remarkable, although the exponential behavior seemed to appear quite clearly. There were two characteristic observations to be noted.

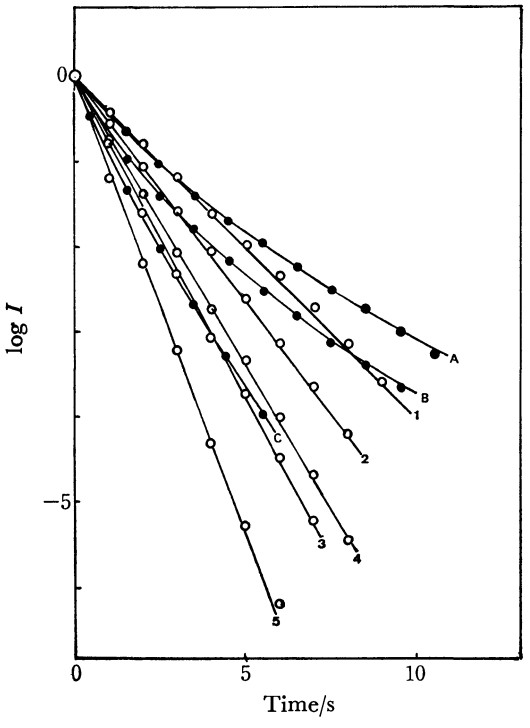

Fig. 1. Phosphorescence decay of naphthalene in MCH in the presence of CH_2Cl_2 or CCl_4 of various mole fractions: CH_2Cl_2, 1) 0.0, 2) 0.02, 3) 0.14, 4) 0.87, 5) 1.00; CCl_4, A) 0.25, B) 0.35, C) 0.60.

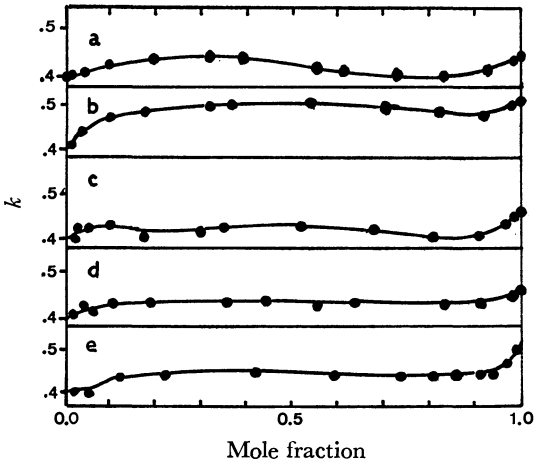

Fig. 2. Phosphorescence decay constant of naphthalene in the mixed solution of MCH and monochloro compounds: a) C_6H_5Cl, b) $C_6H_5CH_2Cl$, c) $C_6H_{11}Cl$, d) C_4H_9Cl, e) C_3H_7Cl.

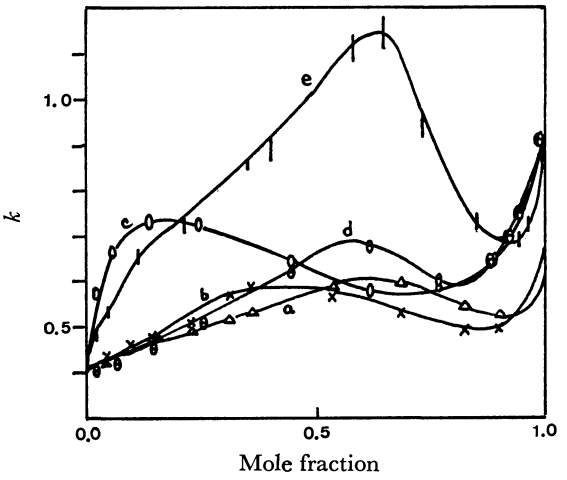

Fig. 3. Phosphorescence decay constant of naphthalene in the mixed solution of MCH and di- or tetrachloro compounds: a) o-$C_6H_4Cl_2$, b) m-$C_6H_4Cl_2$, c) CH_2Cl_2, d) CH_2Cl_2 in EtOH, e) CCl_4.

(1) The decay constant increased when the mole fraction of chlorinated compound increased, until it reached a maximum. After this concentration, the solid solution lost its transparency, indicating that two solid phases separated out.

(2) The decay constant increased again when the mole fraction of chlorinated compound approached 1.0. However, the rate constant in this region was less than the maximal value. As this region was very near to the pure phase of chlorinated compound, it may be reasonable to assume that the sample was again single phase.

Hence, the regions of monotonic increase (from the mole fraction of 0.0 to the maximum of k and from the minimum of k to mole fraction 1.0) seem to be important.

If the concentration dependence is the result of complex formation, the decay should be non-exponential. One may well think that the experimental accuracy had failed to detect its bicomponent character, but then the observed large change in the rate constant should be within this inaccuracy, which is unrealistic. Moreover, the molecule employed seemed quite unsusceptible to complex formation. It can be shown by a model calculation that a decay of a statistical body, of which the distribution of the decay constant has a fairly sharp peak, seems like a true exponential decay. Hence, it may be concluded that the decay is not bicomponent, but is multicomponent and that the decay component distribution has a sharp peak around a point which moves toward larger values with increasing concentration of the chlorinated compound.

We assume that the distribution of chlorinated compound around naphthalene molecules is random but statistically uniform, and that the decay constant of each naphthalene molecule is determined by its environment. As the heavy atom effect is short-range, the decay constant of each naphthalene molecule is mainly determined by the distance to its nearest chlorinanated

molecule. The distribution of the nearest distance is expressed[24] by

$$\rho dr = 4\pi r^2 C \exp(-4\pi r^3 C/3) dr$$

with a peak at

$$r_{max} = (2\pi C)^{-1/3}$$

where C is the concentration of the chlorinated molecule in $Å^{-3}$ and r in Å (Fig. 4). The distribution of k itself can not be estimated, but it is a sharp function of r and would have a sharp peak at the respective value of $k(r_{max})$, which would shift monotonically toward larger values according to the concentration.

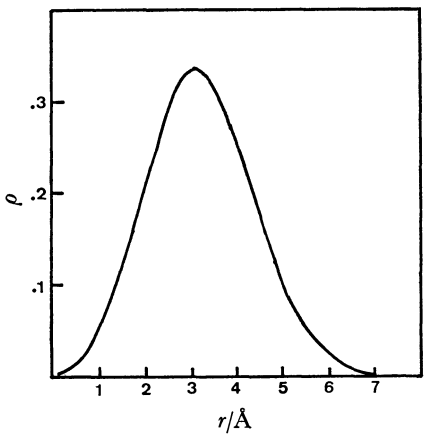

Fig. 4. Distribution of nearest distance $\rho(r)$ at $C=5.3 \times 10^{-3}$ $Å^{-3}$.

It may be asked that the observed effect may be ascribed to a medium-range CT interaction, rather than a heavy atom effect. It can be discarded because the observed effect seemed irrelevant to the extent of the donor character of the chlorinated compounds. It is often suggested that the overlap integrals between orbitals of the heavy atom and those of atoms participating in the triplet state serve as a measure of the heavy atom effect. In our experiment, however, they are somewhat smaller to account for the observed concentration dependence of the heavy atom effect. We assume that the effect is mainly carried by the framework of the surrounding solvent molecules, as can be shown by a CNDO calculation. In addition, the heavy molecule would exert an out-of-plane interaction. In this respect, we have carried out a photoselection measurement of the phosphorescence of naphthalene in the mixture solution of CCl_4 and EPA (Fig. 5). The phosphorescence tended to depolarize when CCl_4 was added, indicating that the phosphorescence has some in-plane character. It follows that the triplet state mixed with π-π^* singlet states by the presence of a perturber. If the interaction of the perturber destroys the planar symmetry of the molecule, one center spin-orbit integral on the heavy atom suffices to effectively mix the π-π^* triplet state with the π-π^* singlet states, thereby remarkably decreasing the radiative lifetime.

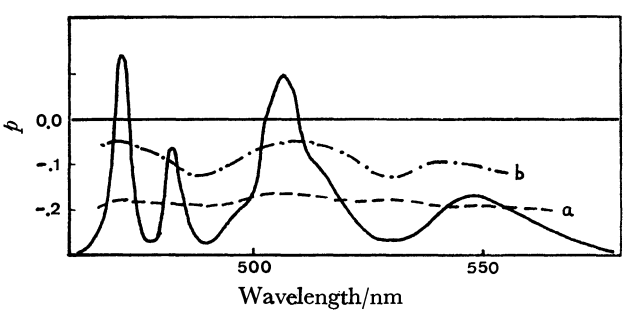

Fig. 5. Polarization of the phosphorescence of naphthalene in a) EPA and b) CH_2Cl_2–EPA (mole fraction 0.23).

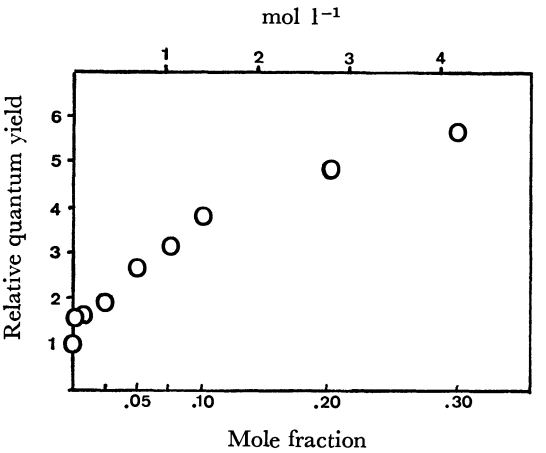

Fig. 6. Apparent quantum yield of $C_{10}D_8$ in EPA in the presence of CCl_4.

We have measured a relative quantum yield of the phosphorescence as a function of the concentration of CCl_4 in the EPA–CCl_4 mixture solution (Fig. 6). If we assume that the radiationless lifetime is not affected and that the lifetime of $C_{10}D_8$ (22 s) is equal to the radiative lifetime of $C_{10}H_8$, then a six time increase of the radiative decay constant leads to a mean total decay constant of 0.59—0.64 s^{-1} at 0.3 mole fraction, according to the extent to which the fluorescence ($q=0.18$) is quenched by an enhanced intersystem crossing. This value of the decay constant can be compared with the observed mean value of 0.78 s^{-1}. Thus the experiment of Eisenthal, in which the phosphorescence spectrum of chloronaphthalene becomes very similar to that of naphthalene in the presence of alkyl bromide or iodide, may also be interpreted by assuming that the totally-symmetric bands acquire large oscillator strengths from π-π^* singlet states.

If the solvent molecules participate in the heavy atom effect, the latter may be sensitive to the kind of solvent. In Fig. 3 the same chlorinated compound CH_2Cl_2 was examined with two different solvents, methylcyclohexane and ethanol. They had quite different profiles, although the decay constant of naphthalene was the same in either solvent when the perturber was absent.

In the case of monochloro compounds (Fig. 2), the heavy atom effect manifested itself only slightly. The decay constant in the presence of the perturber is always very near to that in the absence of the perturber. In contrast, the change was remarkable in the case of

dichloro compounds (Fig. 3). There seemed to be no parallelism between the heavy atom effect and the ability of forming a CT complex. Only a tentative explanation can be given at present. The contraction of MCH when chilled from room temperature to 77 K was measured to be 75%, so that the mean distance between two solvent molecules is 5.4 Å, which we assume to be the same as the mean distance between a naphthalene molecule and a nearest solvent molecule. In a solution of 0.6 mole fraction of chlorobenzene the mean distance from a naphthalene molecule to the nearest chlorobenzene molecule is 6.4 Å, and the mean distance from a naphthalene molecule to the nearest chlorine atom is also 6.4 Å, assuming a free rotation for the chlorobenzene molecule. But in the case of *p*-dichlorobenzene, the mean distance to the nearest chlorine atom is reduced by 1.6 Å, a half of the center-of-molecule chlorine distance. The difference may give rise to a drastic change, as the distance dependence of the heavy atom effect is large.

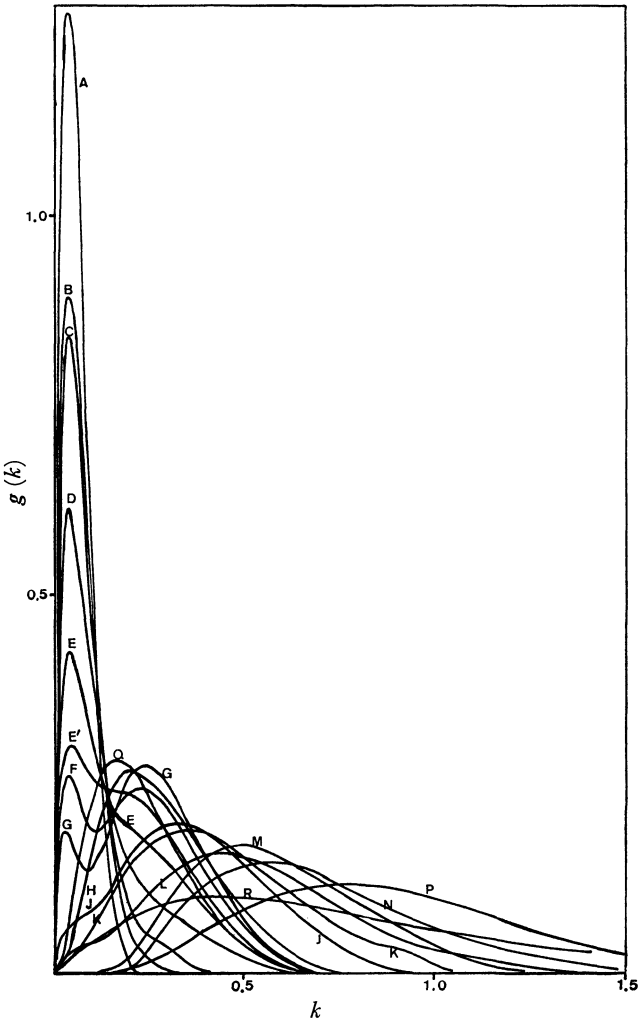

Fig. 7. Distribution function of the decay constant of $C_{10}D_8$ in the mixed solution of CCl_4 and MCH in varying mole fraction of CCl_4: A) 0.00, B) 0.005, C) 0.01, D) 0.025, E) 0.05, F) 0.07, G) 0.10, H) 0.15, J) 0.20, K) 0.25, L) 0.30, M) 0.41, N) 0.51, P) 0.60, Q) 0.99, R) 1.00.

The decay of naphthalene in CCl_4 was non-exponential (Fig. 1). As CCl_4 can form a CT complex with naphthalene, we expected that the decay had two components and the peak of the complex would move in accordance with the advent of statistical heavy atom effect. Very rough estimates of the mean rate constants are illustrated in Fig. 3; these show a similar inflecting profile. The decay curves were analyzed by a method of Laplace transformation developed by one of the authors.[25] The decay function can be expressed as

$$f(t) = \int_{s_0}^{\infty} g(s) \exp(-st) \mathrm{d}s$$

where $g(s)$ is a normalized distribution function of the decay constant. $g(s)$ is approximated by a power series with an exponential function which guarantees the convergence:

$$g(s) = \sum_{i}^{N} A_i (s - s_0)^i \exp(-Bs)$$

where A_i's are the coefficients to be determined and N and B are ajustable parameters. A method of least squares was applied for A_i's to obtain the best fit to the observed decay curve. The results are shown in Fig. 7. The peak of the complex is gradually formed at the expense of that of free naphthalene molecule, and the former moves according to the concentration. Thus the external heavy atom effect takes place in two ways: one by forming a CT complex with a molecule containing heavy atoms, and the other by a statistical approach of heavy molecules to the phosphorescing molecule.

When the mole fraction of the halogenated compound was large, the rate constant became small again, contrary to expectation. It might be supposed that in an incommodious crystal lattice of the halogenated compound the naphthalene molecule is deprived of the solvent molecules which bring the heavy atom effect in a favorable position or that the disposition of the naphthalene molecule itself is unfavorable. The singular nature at high concentration limit is open to future investigation.

This work was partly supported by a Grant-in-Aid for Scientific Research from the Ministry of Education.

References

1) H. Tsubomura and R. S. Mulliken, *J. Am. Chem. Soc.*, **82**, 5966 (1960).
2) G. J. Hoijtink, *Mol. Phys.*, **3**, 67 (1960).
3) K. C. Lin and S. H. Lin, *Mol. Phys.*, **21**, 1105 (1971).
4) J. N. Murrell, *Mol. Phys.*, **3**, 319 (1960).
5) S. P. McGlynn, R. Sunseri, and N. D. Christodouleas, *J. Chem. Phys.*, **37**, 1818 (1962).
6) J. Czekalla and K. J. Mager, *Z. Electrochem.*, **66**, 65 (1962).
7) K. B. Eisenthal and M. A. El-Sayed, *J. Chem. Phys.* **42**, 794 (1965).
8) K. B. Eisenthal, *J. Chem. Phys.*, **45**, 1850 (1966).
9) M. Gronkiewicz, B. Kozankiewicz, and J. Prochorow, *Chem. Phys. Lett.*, **38**, 325 (1976).
10) S. Iwata, J. Tanaka, and S. Nagakura, *J. Chem. Phys.*, **47**, 2203 (1967).
11) T. Kobayashi and S. Nagakura, *Bull. Chem. Soc. Jpn.*, **45**, 987 (1972).

12) S. Matsumoto, S. Nagakura, Y. Shimozato, H. Hayashi, and J. Nakamura, *Bull. Chem. Soc. Jpn.*, **47**, 60 (1974).
13) S. Tamauchi, K. Matsuzaki, and T. Azumi, *J. Lumin.*, **12/13**, 369 (1976).
14) M. R. Wright, R. P. Frosh, and G. W. Robinson, *J. Chem. Phys.*, **33**, 934 (1960).
15) P. M. Johnson and L. Ziegler, *J. Chem. Phys.*, **56**, 2169 (1972).
16) Yei Ping Hsu and P. M. Johnson, *J. Chem. Phys.*, **59**, 136 (1973).
17) J. Najbar *J. Lumin.*, **11**, 207 (1975/1976).
18) J. Najbar and A. Chodkowska, *J. Lumin.*, **11**, 215 (1975/1976).
19) J. Najbar, J. B. Birks, and T. D. S. Hamilton, *Chem. Phys.*, **23**, 281 (1977).
20) J. Najbar and T. D. S. Hamilton, *Chem. Phys. Lett.*, **59**, 226 (1978).
21) G. Kavarnos, T. Cole, P. Scribe, J. C. Dalton, and N. J. Turro, *J. Am. Chem. Soc.*, **92**, 1032 (1971).
22) G. G. Giachino and D. R. Kearns, *J. Chem. Phys.*, **52**, 2964 (1970).
23) L. G. Thompson and S. E. Webber, *J. Phys. Chem.*, **76**, 221 (1972).
24) A. Inoue, H. Chuman, and N. Ebara, *Bull. Chem. Soc. Jpn.*, **51**, 345 (1978).
25) K. Tsuji, H. Watanabe, and K. Yoshioka, *Adv. Mol. Relaxation Processes*, **8**, 49 (1976).

Raman Spectra of a Compound under Inversion Motions: *N,N'*-Dimethylpiperazine

Kunio FUKUSHIMA

Department of Chemistry, Faculty of Science, Shizuoka University, 836, Oya, Shizuoka 422

(Received February 16, 1979)

Raman spectra of methanol and aqueous solutions of *N,N'*-dimethylpiperazine were measured. Forms of stable conformers in various states were studied by comparison of the spectra obtained under various conditions. It was found that hydrogen bonding to nitrogen atoms of *N,N'*-dimethylpiperazine causes a conformational change.

Many proofs of the inversion motion of the molecule have been given by NMR studies.[1-6] In order to study the conformation of molecules subjected to inversion motions, ring inversion and inversion at nitrogen, *N,N'*-dimethylpiperazine was studied by Raman spectroscopy because of its high molecular symmetry. Since suppression of inversion motion at nitrogen by hydrogen bonding was expected, effect of the suppression on molecular conformation was studied by measuring Raman spectra of solutions of the substance.

Experimental

Commercial *N,N'*-dimethylpiperazine (grade GR, Tokyo Kasei Chemical Co., Ltd.) was used without further purification. Raman spectra were measured with a Model R-800T Raman spectrophotometer (Japan Spectroscopic Co., Ltd.) under excitation with a Spectra Physics argon ion laser (model 165) using 514.5 nm line (300 mW). 0.1 ml or 0.3 ml Raman cells were used. Infrared spectra of the liquid were recorded on a Hitachi EPI-G3 spectrophotometer and a Hitachi FIS-3 far infrared spectrometer. The results of the measurements are shown in Table 1 and Fig. 1.

Results and Discussion

Comparison of Raman Spectra of N,N'-*Dimethylpiperazine in Liquid State with Infrared Spectra.* Coincidence of Raman shift frequency with infrared absorption maximum frequency is observed only for 1420 cm^{-1} and 630 cm^{-1} (Table 1). The couples, 1450 cm^{-1} (Raman) and 1455 cm^{-1} (IR), 1020 cm^{-1} (Raman) and 1018 cm^{-1} (IR), are close, both being in the higher frequency region (>1000 cm^{-1}), and the difference in Raman shift frequency and infrared absorption maximum frequency is expected to be intrinsically small. For all the other couples, frequencies of Raman shift and infrared absorption maximum differ a great deal. This suggests that the mutual exclusion rule holds for the Raman spectra and infrared spectra. Thus, conformers in the liquid take molecular forms each having a center of symmetry, diaxial conformer (AA), diequatorial conformer (EE) or some other form. A Raman line and the corresponding infrared band are observed at *ca.* 630 cm^{-1}, their intensity or absorbance being very small. This can be interpreted as due to cis form (AE conformer), as confirmed by dipole moment measurement to exist in mole fraction of 0.103 for a benzene solution.[7]

Raman Spectrum Change Associated with the Change of State, Pure Liquid to Solutions. The Raman lines having shift frequencies (1313 cm^{-1}, 1173 cm^{-1}, 457 cm^{-1}, 277 cm^{-1}) higher than those of the pure liquid (1306 cm^{-1}, 1160 cm^{-1}, 440 cm^{-1}, 251 cm^{-1}) appear in the spectrum of aqueous solution A (Table 1 and Fig. 1), the weaker Raman lines corresponding to the latter coexisting with the former. In the case of aqueous solution B, where the fraction of water is smaller than that of aqueous solution A, shift frequency values of the

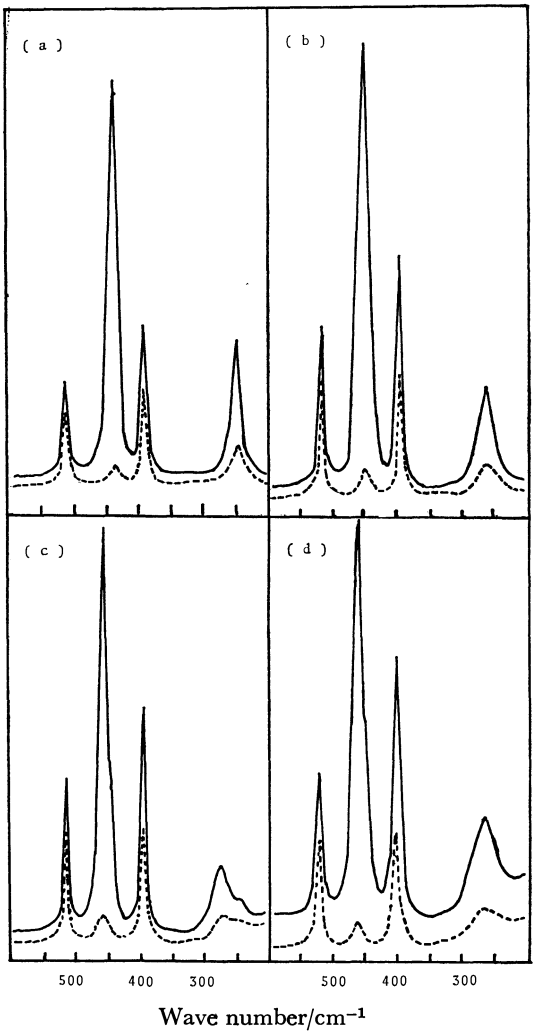

Fig. 1. Raman spectra of *N,N'*-dimethylpiperazine (*N,N'*-dmp) in lower shift frequency region.
(a) Liquid (b) aqueous solution B (mole fraction of *N,N'*-dmp, 0.433) (c) aqueous solution A (mole fraction of *N,N'*-dmp, 0.205) (d) methanol solution (mole fraction of *N,N'*-dmp, 0.197); solid line, $I_{\parallel}$; dotted line, $I_{\perp}$.

Table 1. Raman spectra of *N,N'*-dimethylpiperazine compared with infrared spectra of the pure liquid

IR Liquid ν[a]	Raman					
	Liquid		Aqueous soln A		Methanol soln	
	ν[a]	ρ[b]	ν[a]	ρ[b]	ν[a]	ρ[b]
	1467(32)	0.75	1473(45)	0.75	—[c]	—[c]
1455(s)						
	1450(?)[d]	?[d]	1455(?)[d]	?[d]	—[c]	—[c]
	1440(17)	0.75	1445(19)	0.75	—[c]	—[c]
1420(vw)	1420(12)	0.75	1427(21)	0.75	—[c]	—[c]
	1385(3)	0.75	1390(5)	0.75	1391(9)	0.75
1372(m)						
	1335(3)	0.75	1340(4)	0.75	1341(6)	0.75
			1313(38)	0.49	1314(43)	0.49
	1306(41)	0.47	1306(?)[d]	?[d]	1306(?)[d]	?[d]
1294(s)						
1283(sh)						
	1263(7)	0.75	1257(7)	0.75	1259(8)	0.75
	1196(11)	0.75	1202(16)	0.75	1203(17)	0.75
			1173(14)	0.64	—[c]	—[c]
1171(vs)						
	1160(22)	0.44	1160(?)[d]	?[d]	—[c]	—[c]
	1130(24)	0.75	1130(?)[d]	?[d]	—[c]	—[c]
			1116(31)	0.75	—[c]	—[c]
1122(m)						
1094(m)						
	1075(5)	0.35	1077(7)	0.38	1079(14)	0.42
1058(w)						
	1046(8)	0.75	1043(12)	0.75	—[c]	—[c]
	1020(13)	0.75	1019(10)	0.75	—[c]	—[c]
1018(m)						
977(vw)						
921(w)						
	856(5)	0.75	852(8)	0.75	854(8)	0.75
810(m)						
	780(100)	0.24	773(100)	0.18	774(100)	0.17
718(vvw)						
630(vvw)	630(1)	?[d]	630(1)	?[d]	630(1)	?[d]
	513(19)	0.75	514(27)	0.75	516(25)	0.75
			457(70)	0.06	456(67)	0.05
	440(78)	0.04	440(?)[d]	?[d]	440(?)[d]	?[d]
	393(30)	0.64	394(39)	0.49	396(44)	0.43
365(m)						
324(sh)						
278(w)						
			277(10)	0.34	264(17)	0.33
	251(26)	0.29	250(?)[d]	?[d]	250(?)[d]	?[d]
144(sh)						
	137(?)[d]	?[d]	140(?)[d]	?[d]	—[c]	—[c]
135(w)						

Figures in parentheses represent relative intensities, the maximum value being 100. a) Frequency in cm^{-1}. b) Degree of depolarization. c) Raman lines, the frequency, the intensity and ρ of which could not be determined because of overlapping with the Raman lines of methanol. d) Intensity and ρ could not be determined precisely.

four Raman lines have intermediate values between those for the pure liquid and those for aqueous solution A. For aqueous solution C (mole ratio, solute 1 : water 9.015) the four Raman lines corresponding to those of the pure liquid disappear. For a methanol solution, almost the same spectrum as that of aqueous solutions is observed.

Interpretation of Results. The spectrum change associated with the change of state, pure liquid to solution, is considered to be due to the conformational

Table 2. Calculated normal frequencies (in cm^{-1})

Conformer	Symmetry species	Frequency	Description
EE	A_g	422	C–N(–CH_3)–C skeletal deformation
		369	C–N(–CH_3)–C skeletal deformation+N–C–C deformation
		254	C–N(–CH_3)–C skeletal deformation+N–C–C deformation
	B_g	457	C–N(–CH_3)–C skeletal deformation+N–C–C deformation
		395	C–N(–CH_3)–C skeletal deformation+N–C–C deformation
		186	N–CH_3 torsion
AA	A_g	496	C–N(–CH_3)–C skeletal deformation+N–C–C deformation
		437	C–N(–CH_3)–C skeletal deformation
		173	C–N(–CH_3)–C skeletal deformation+N–C–C deformation+N–CH_3 torsion
	B_g	502	C–N(–CH_3)–C skeletal deformation+N–C–C deformation
		356	C–N(–CH_3)–C skeletal deformation+N–C–C deformation
		183	N–CH_3 torsion

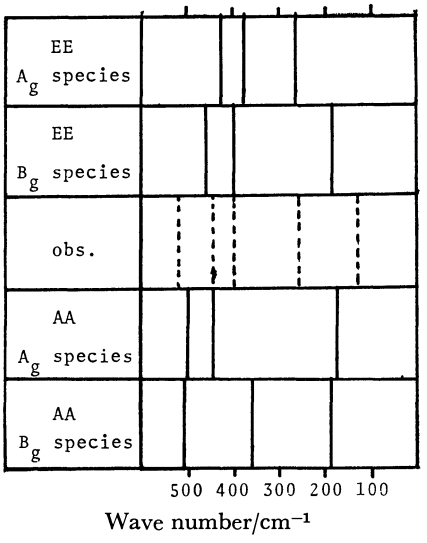

Fig. 2. Calculated frequencies of A_g and B_g species of *N,N'*-dimethylpiperazine compared with observed Raman shift frequencies.

change caused by hydrogen bonding or the change of nature of bonding in *N,N'*-dimethylpiperazine molecule. As the number of Raman lines arising from hydrogen bonded species is the same as that of the liquid, the species is also considered to have a center of symmetry. The molecular shape of species can be deduced as follows.

Normal vibration calculation of conformers (AA conformer and EE conformer belonging to C_{2h} point group) was carried out using force constants of related molecules.[8,9] The calculated frequencies of Raman active skeletal deformation vibrations (Table 2 and Fig. 2) are sensitive to conformational change. They are compared with the observed frequencies of the liquid in the table and the figure. Assigning polarized Raman lines ($0<\rho<0.75$) to calculated frequencies of A_g species and depolarized Raman lines ($\rho=0.75$) to those of B_g species, the calculated frequencies of EE conformer almost fit the observed Raman lines. However, those of AA conformer do not correspond exactly to the observed frequencies. The Raman lines of the pure liquid (440 cm^{-1}, 251 cm^{-1}), whose shift frequencies change with change of state, pure liquid to solution, are assigned to C–N(–CH_3)–C skeletal deformation vibrations.

The change can be interpreted as due to the conformational change arising from the change of valence state of nitrogen atoms. It can not be explained in terms of the conformational change of EE conformer to AA conformer for the following reason. Of the calculated frequencies of A_g species of EE conformer, both 422 cm^{-1} and 369 cm^{-1} increase and 254 cm^{-1} decreases by the conformational change. Thus, the observed frequency of polarized Raman line (251 cm^{-1}) of the pure liquid is expected to decrease if the change is caused by the conformational change. However, the frequency increases to 277 cm^{-1}. Of the calculated frequencies of B_g species of EE conformer, 457 cm^{-1} increases and 186 cm^{-1} does not change its frequency considerably, while 395 cm^{-1} decreases its frequency by the conformational change of EE conformer to AA conformer. Therefore, if the change is due to the conformational change, a depolarized Raman line is expected to appear in the region 300 cm^{-1}—400 cm^{-1}. However, this is not the case. It can thus be concluded that the conformer having a center of symmetry and a molecular shape similar to that of EE conformer exists in pure liquid in abundance and that another conformer, also having a center of symmetry and differing from the above conformer in the molecular conformation around nitrogen atoms, appears in aqueous solutions and in a methanol solution as a results of hydrogen bonding to nitrogen atoms.

Probable Conformers in Solutions and in Pure Liquid. Hydrogen-bonded species. By the formation of hydrogen bonding to nitrogen atoms of *N,N'*-dimethylpiperazine, valence orbitals of the nitrogen atoms may become similar to sp^3 hybrid orbitals, and the molecular conformation having bond angles close to tetrahedral angles would become abundant. Conformers in pure liquid. For trimethylamine, C–N–C angles have been found to be $108.7°\pm1°$, which is almost a tetrahedral angle corresponding to sp^3 hybrid orbitals.[10] Considering resemblace of the skeleton of C–N(–CH_3)–C of *N,N'*-dimethylpiperazine with trimethylamine, the valence orbitals of nitrogen atoms in *N,N'*-dimethylpiperazine are expected to be almost sp^3 orbitals, which do not seem to be affected much by hydrogen bonding to the

nitrogen atoms. However, a remarkable frequency change in the deformation vibrations of C–N(–CH_3)–C skeleton by hydrogen bonding is observed, suggesting the change in the valence state of nitrogen atoms. In pure liquid, therefore, time-averaged orbitals of the nitrogen atoms during inversion motions might be in sp^2 state. In accordance with the assumption, a simple calculation revealed that planar conformation around the nitrogen atoms can be realized by changing the azimuthal angle of N–CH_2–CH_2–N internal rotation axis from 60° to 46°34′ and all the C–N–C angles from at tetrahedral angle to 120° with no changes in all the bond lengths and other bond angles (tetrahedral angles), which require large energy. In the model, CH_2–CH_2 bond length is assumed to be the same as that of CH_2–N bond length on the basis of Rerat's work.[11]

References

1) R. G. Lett, L. Petrakis, A. F. Ellis, and R. K. Jensen, *J. Phys. Chem.*, **74**, 2816 (1970).
2) R. A. Spragg, *J. Chem. Soc., B*, **1968**, 1128.
3) R. K. Harris and R. A. Spragg, *J. Chem. Soc., B*, **1968**, 684.
4) M. Freifelder, R. W. Mattoon, and R. W. Kriese, *J. Org. Chem.*, **31**, 1196 (1966).
5) L. W. Reeves and K. O. Stromme, *J. Chem. Phys.*, **34**, 1711 (1961).
6) J. L. Sudmeier and G. Occupati, *J. Am. Chem. Soc.*, **90**, 154 (1968).
7) N. L. Allinger, J. G. D. Carpenter and F. M. Karkowski, *J. Am. Chem. Soc.*, **87**, 1232 (1965).
8) G. Dellepiane and G. Zerbi, *J. Chem. Phys.*, **48**, 3573 (1968).
9) H. Takahashi, T. Shimanouchi, K. Fukushima, and T. Miyazawa, *J. Mol. Spectrosc.*, **13**, 43 (1964).
10) "Tables of Interatomic Distances and Configuration in Molecules and Ions, Supplement 1956—1959," The Chem. Soc., London (1965).
11) C. Rerat, *Acta Crystallogr.*, **13**, 72 (1960).

Vibrational Spectra and Normal Coordinate Calculations for Methyl-1-propynylmercury(II) and Its Deuterated Analogues†

Yoshika IMAI* and Koyo AIDA

Department of Applied Science, Faculty of Engineering, Tohoku University, Sendai 980

(Received March 31, 1979)

Infrared spectra (4000—80 cm^{-1}) of $CH_3HgC{\equiv}CCH_3$, $CD_3HgC{\equiv}CCH_3$, $CH_3HgC{\equiv}CCD_3$, and $CD_3HgC{\equiv}CCD_3$ have been obtained in carbon tetrachloride, carbon disulfide and benzene solutions, as well as in the solid state at liquid nitrogen temperature. Raman spectra (4000—0 cm^{-1}) have also been recorded on benzene solutions and on solids at room temperature. Assignments for all the fundamentals have been made assuming C_{3v} molecular symmetry. Normal coordinate calculations have been carried out in order to confirm the proposed assignments.

In a previous paper[1] a report was given on the vibrational spectra and normal coordinate calculations for methylethynylmercury(II). The study has now been extended to methyl-1-propynylmercury(II). Although many acetylides of the type $RHgC{\equiv}CR'$ have been prepared,[2] no vibrational study on these compounds except methylethynylmercury(II) seems to have been reported. In the present study, infrared and Raman spectra have been obtained for methyl-1-propynylmercury(II) and its deuterated analogues. Assignments for all the fundamentals are made assuming C_{3v} symmetry. Normal coordinate calculations have been carried out in order to confirm the proposed assignments.

Experimental

Methyl-1-propynylmercury(II) was prepared in the following way.

Methylmercury(II) iodide was dissolved in an aqueous solution of potassium hydroxide. Methylacetylene, generated by the action of 1,2-dibromopropane with potassium hydroxide in ethanol,[3] was passed through the solution. White precipitates were filtered and washed with water and then dried in a desiccator over potassium hydroxide pellets. The crude product was purified by sublimation in a vacuum.

Deuterated compounds were prepared in a similar way using methyl-d_3-mercury(II) bromide and/or methylacetylene-d_4, prepared from methyl-d_3-magnesium bromide and mercury(II) bromide, and by the action of D_2O with magnesium carbide,[4] respectively.

Methyl-1-propynylmercury(II) melts at 80—81 °C (no value was found in literature). The mercury content was determined for the undeuterated compound by the method of Spahr *et al.*[5] Found, 78.0%. Calcd for C_4H_6Hg, 78.8%. The molecular weight was also cryoscopically determined in benzene. Calcd for C_4H_6Hg, 255. Measured, 260.

The infrared spectra in the range 4000—400 cm^{-1} were recorded on a Perkin-Elmer 337 spectrophotometer in annealed solid films at liquid nitrogen temperature. Cooling was necessary to prevent sublimation during the course of the measurements. The spectra were also obtained in carbon tetrachloride and carbon disulfide solutions. The instrument was calibrated in the usual way.[6]

Far-infrared spectra in the range 400—80 cm^{-1} were recorded on a Hitachi FIS-III Far-infrared spectrophotometer which had been evacuated in order to remove atmospheric water vapor. The spectra were measured in annealed solid films at liquid nitrogen temperature in order to prevent sublimation. The spectra in benzene solutions were also obtained using polyethylene bags. The instrument was calibrated with water vapor frequencies.

Raman spectra were recorded in the solid state in capillary tubes on a JEOL JRS-S1 Raman spectrophotometer equipped with a 50 mW NEC GLG 108 He-Ne laser. The instrument was calibrated with the emission lines of Ne. The spectra were also measured in benzene solutions in order to obtain qualitative polarizations.

Results and Vibrational Assignments

The infrared and Raman spectra of the four isotopic methyl-1-propynylmercury(II) are shown in Figs. 1 and 2. The symmetry coordinates are summarized in Table 1 and observed frequencies are given in Tables 2—4.

The CHgC skeleton is linear in many organomercurials.[7] It is thus reasonable to assume the same skeleton for the present compounds. Since the two methyl groups in each compound are separated from each other to a greater extent than those in dimethylmercury(II),[8] where the free rotation of methyl groups is believed to be present, it is likely that the free rotation

TABLE 1. DESCRIPTION OF THE SYMMETRY COORDINATES FOR METHYL-1-PROPYNYLMERCURY(II)

Vibrational mode	Coordinate	
	A_1	E
$CH_3(CD_3)$ st. (Me–CC)	S_1	S_{10}
$CH_3(CD_3)$ st. (Me–Hg)	S_2	S_9
C≡C st.	S_3	
$CH_3(CD_3)$ def. (Me–CC)	S_4	S_{11}
$CH_3(CD_3)$ def. (Me–Hg)	S_5	S_{12}
C–C st.	S_6	
$CH_3(CD_3)$ rock. (Me–CC)		S_{13}
$CH_3(CD_3)$ rock. (Me–Hg)		S_{14}
CH_3–Hg(CD_3–) st.	S_7	
Hg–CC st.	S_8	
CCC def.		S_{15}
CCHg def.		S_{16}
CHgC def.		S_{17}

Abbreviations: st., stretching; def., deformation; rock., rocking.

† A preliminary report of this work was presented at the 37th National Meeting of the Chemical Society of Japan, Yokohama, April 1978.

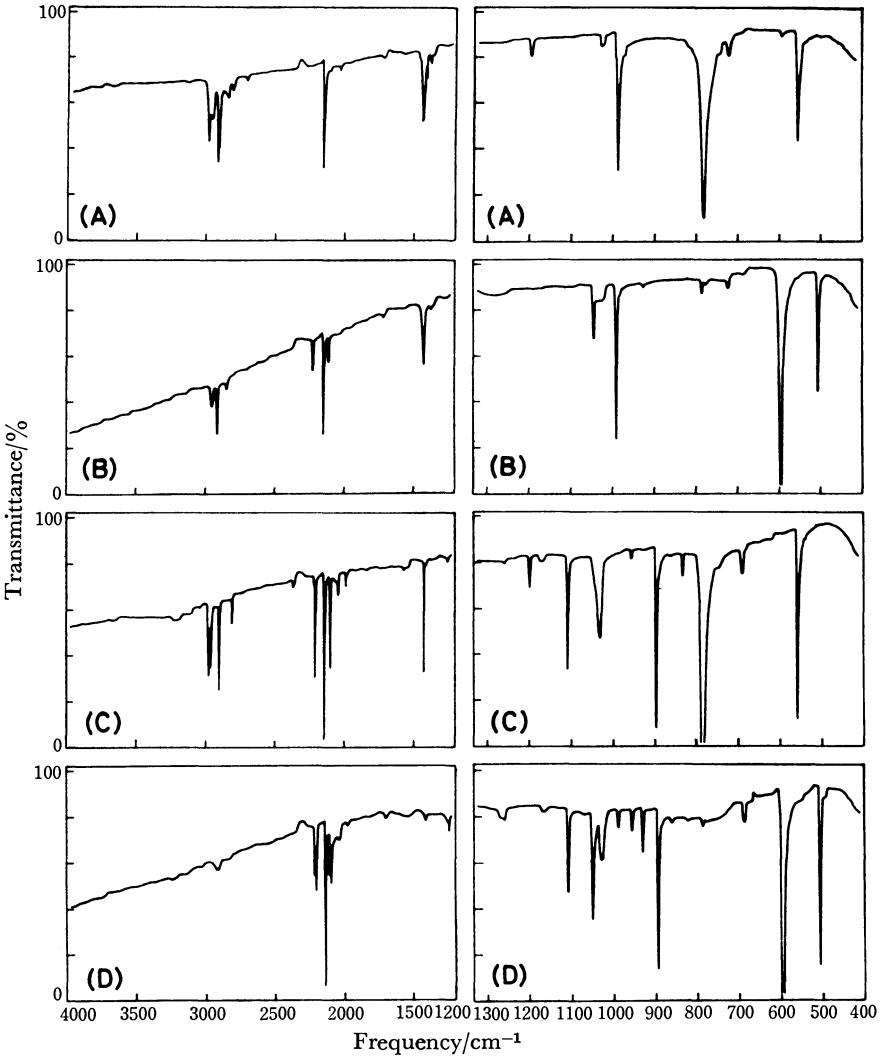

Fig. 1. Infrared spectra of $CH_3HgC{\equiv}CCH_3$ (A), $CD_3HgC{\equiv}CCH_3$ (B), $CH_3HgC{\equiv}CCD_3$ (C), and $CD_3HgC{\equiv}CCD_3$ (D), in the solid state at −196 °C.

Table 2. Observed and calculated frequencies (cm^{-1}) for $CH_3HgC{\equiv}CCH_3$

No.	Infrared		Raman		Calcd	PED		
	solid	soln	solid	soln				
1	2911	2914	2910	2915 p	2920	$100S_1$		
2	2901	2906	2900	2905 p	2904	$98S_2$		
3	2150	2157	2147	2158 p	2152	$85S_3$	$11S_6$	
4	1380	1367	1370	1371	1371	$93S_4$		
5	1197	1200	1196	1202 p	1201	$78S_5$	$17S_2$	
6	990	997			997	$77S_6$	$17S_8$	
7	556	553	555	556 p	558	$91S_7$		
8	336	340	330	340 p	341	$74S_8$	$12S_7$	
9	2980	2977	2980	2980	2981	$100S_9$		
10	2950	2945	2948		2956	$100S_{10}$		
11	1435	1437	1430		1440	$91S_{11}$		
12	1421	1412			1416	$97S_{12}$		
13	1028	1021	1025		1030	$88S_{13}$		
14	782	772	785		780	$97S_{14}$		
15			366	363	365	$74S_{15}$	$25S_{16}$	
16	220	203	219	205	200	$79S_{16}$	$21S_{17}$	
17			73		76	$69S_{17}$	$29S_{16}$	

Abbreviation: p, polarized.

Table 3. Observed and calculated frequencies (cm^{-1}) for $CD_3HgC{\equiv}CCH_3$

No.	Infrared		Raman		Calcd	PED		
	solid	soln	solid	soln				
1	2914	2913	2910	2910 p	2920	$100S_1$		
2	2119	2120	2113	2107 p	2119	$94S_2$		
3	2151	2159	2145	2160 p	2152	$84S_3$	$11S_6$	
4	1375	1370	1368	1372	1372	$93S_4$		
5	929	930	929	932 p	927	$69S_5$	$19S_2$	$10S_7$
6	991	997			999	$73S_6$	$15S_8$	
7	507	504	505	508 p	503	$78S_7$	$12S_5$	
8	337	339	338	340 p	337	$71S_8$	$15S_7$	
9	2230	2228	2220	2220	2222	$99S_9$		
10	2950	2950	2951		2956	$100S_{10}$		
11	1429	1437	1430		1440	$91S_{11}$		
12	1046	1026	1030		1025	$98S_{12}$		
13	1029	1026	1030		1030	$88S_{13}$		
14	596	589			579	$99S_{14}$		
15			364	360	365	$74S_{15}$	$25S_{16}$	
16	212	195	210	196	199	$80S_{16}$	$20S_{17}$	
17			70		69	$70S_{17}$	$28S_{16}$	

Abbreviation: p, polarized.

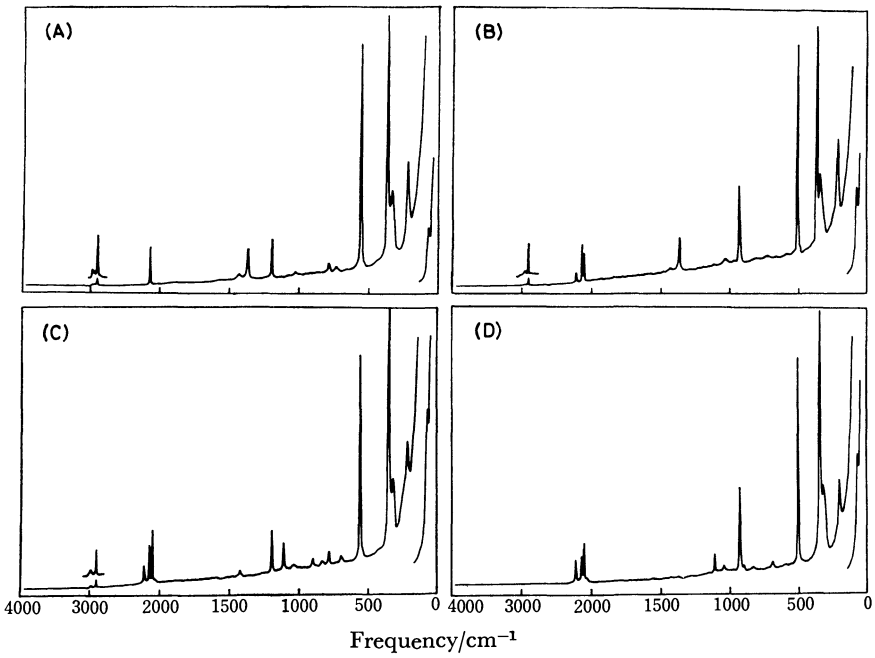

Fig. 2. Raman spectra of $CH_3HgC{\equiv}CCH_3$ (A), $CD_3HgC{\equiv}CCH_3$ (B), $CH_3HgC{\equiv}CCD_3$ (C), and $CD_3HgC{\equiv}CCD_3$ (D), in the solid state at room temperature.

Table 4. Observed and calculated frequencies (cm^{-1}) for $CH_3HgC{\equiv}CCD_3$

No.	Infrared		Raman		Calcd	PED		
	solid	soln	solid	soln				
1	2102	2107	2105	2110 p	2092	$78S_1$	$20S_3$	
2	2902	2903	2905	2908 p	2905	$97S_2$		
3	2149	2156	2152	2150 p	2167	$65S_3$	$20S_1$	$12S_6$
4	1110	1113	1108	1111	1109	$54S_4$	$38S_6$	
5	1200	1200	1190	1201 p	1201	$79S_5$	$17S_2$	
6	899	903	896		902	$39S_6$	$40S_4$	$18S_8$
7	559	556	555	560 p	555	$93S_7$		
8	321	325	313	325 p	326	$72S_8$	$10S_7$	
9	2979	2977	2981		2981	$100S_9$		
10	2217	2209	2221	2220	2204	$98S_{10}$		
11	1032	1038	1039		1033	$94S_{11}$		
12	1425	1412	1425		1416	$97S_{12}$		
13	835	829	830		817	$84S_{13}$	$11S_{15}$	
14	783	774	780		780	$97S_{14}$		
15	345		347	348	343	$68S_{15}$	$28S_{16}$	
16	209	196	209	195	192	$75S_{16}$	$24S_{17}$	
17			72		74	$67S_{17}$	$30S_{16}$	

Abbreviation: p, polarized.

takes place also in methyl-1-propynylmercury(II). However, the observed spectra can satisfactorily be explained on the assumption of C_{3v} symmetry (a staggered form) for these molecules. With this symmetry, the molecule is expected to have $8A_1$, A_2, and 9E vibrational modes, in which the A_2 mode is inactive in both the infrared and Raman spectra, while the A_1 and the E modes are active in both.

Since the vibrational coupling of the two methyl groups in a molecule is expected to be very small, vibrations of one methyl group are hardly influenced by deuteration of the other. Taking their isotopic shifts and polarizations of Raman bands into consideration, together with the data for related compounds,[9,10] assignments for the methyl groups are easily made.

A strong infrared absorption at *ca.* 2150 cm^{-1} in each isotopic species is hardly affected by deuteration and the corresponding Raman band in solution is polarized. This is undoubtedly assigned to the C≡C stretching.

C–C stretching vibrations for $CH_3C{\equiv}N$ and $CH_3C{\equiv}CH$[10] have been observed at *ca.* 900 cm^{-1}. We have assigned the strong infrared bands at *ca.* 990 cm^{-1} for $CH_3HgC{\equiv}CCH_3$ and $CD_3HgC{\equiv}CCH_3$ to this mode. Upon deuteration of the 1-propynyl group, these bands shift to *ca.* 900 cm^{-1} for $CH_3HgC{\equiv}CCD_3$ and $CD_3HgC{\equiv}CCD_3$, suggesting a vibrational coupling between the C–C stretching and the vibrations of the neighbouring methyl group.

The remaining skeletal vibrations are expected to appear below 600 cm^{-1}. In the solution Raman spectrum for $CH_3HgC{\equiv}CCH_3$, the four bands appear at 556, 363, 340, and 205 cm^{-1}, the bands at 556 and 340 cm^{-1} being polarized. Upon deuteration of the methyl group ($CD_3HgC{\equiv}CCH_3$), the 556 cm^{-1} band shifts to 508 cm^{-1}, while the 340 cm^{-1} band remains at the same position. In contrast, the 340 cm^{-1} band shifts to 325 cm^{-1} upon deuteration of the 1-propynyl group ($CH_3HgC{\equiv}CCD_3$). Thus, the 556 cm^{-1} band can be assigned to the CH_3–Hg stretching and the 340 cm^{-1} to the Hg–CC stretching vibrations. The remaining two bands at 363 and 205 cm^{-1} seem to be due to the skeletal deformations. The former band slightly shifts to lower frequency upon deuteration of the 1-propynyl group, while the latter band exhibits a very small isotopic shift upon deuteration of either methyl or 1-propynyl group. The HgCC deformation in $CH_3HgC{\equiv}CH$[1] has been assigned at 272 cm^{-1}, lower than the CCC deformation in $CH_3C{\equiv}CH$[10] at 336 cm^{-1}. From

the results, the 205 cm^{-1} band is assigned to HgCC deformation and the 306 cm^{-1} to CCC deformation.

The assignment of CHgC deformation is fairly difficult, since the mode is expected to appear below 150 cm^{-1} in weak intensity. In this study, the Raman bands at *ca.* 70 cm^{-1} in the solid state were tentatively assigned to this mode. No solution Raman spectra in this range could be observed owing to obscurity in the background.

Normal Coordinate Calculations and Discussion

Normal coordinate calculations were carried out by Wilson's GF-matrix method on an ACOS 77/700 computer at the Computer Center, Tohoku University, using the iterative least-squares procedure in the usual way. For lack of structural data, the molecular parameters were transferred from those of CH_3HgCl,[11] $CH_3HgC{\equiv}N$[12] and $CH_3C{\equiv}CH$;[13] r(C–H) of CH_3CC, 1.11 Å; r(C–H) of CH_3, 1.10 Å; r(C–C), 1.46 Å; r(C≡C), 1.21 Å; r(CH_3–Hg), 2.08 Å; r(Hg–CC), 2.05 Å; ∠HCH of CH_3CC, 108.5°; ∠HCH of CH_3, 110.7°. The least-squares refinement was carried out in terms of the symmetry force constants, which were fitted to the infrared frequencies in solutions, except for the HgCC and CHgC deformations which were taken from the Raman spectra for solutions and solids, respectively, for the four isotopic species simultaneously.

The symmetry force constants, together with uncertainties from the last cycle of the least-squares refinements, are given in Table 6. The average errors are 0.35% and 0.97% for the A_1 and E vibrations, respectively, the sum of the weighted squares of errors $\sum(\lambda_{obsd}-\lambda_{calcd})^2/\lambda_{obsd}$ being 2.39×10^{-3} and 2.54×10^{-3} for the A_1 and E vibrations, respectively. The agreements between the calculated and the observed frequencies are satisfactory for the four isotopic species (Tables 2—5). The potential energy distributions are also given in these tables. A strong vibrational coupling exists between the C–C stretching and the CD_3 symmetric deformations (Tables 4 and 5, mode Nos. 4 and 6).

Table 5. Observed and calculated frequencies (cm^{-1}) for $CD_3HgC{\equiv}CCD_3$

No.	Infrared		Raman		Calcd	PED
	solid	soln	solid	soln		
1	2102	2106	2101	2110 p	2092	$78S_1$ $20S_3$
2	2117	2120	2119	2121 p	2120	$94S_2$
3	2149	2156	2154	2158 p	2168	$66S_3$ $19S_1$ $12S_6$
4	1110	1113	1109	1113	1110	$54S_4$ $38S_6$
5	932	935	929	929 p	935	$64S_5$ $18S_2$ $10S_7$
6	896	905			896	$32S_6$ $30S_4$ $17S_5$ $14S_8$
7	507	504	505	509 p	500	$79S_7$ $12S_5$
8	320	325	322	325 p	323	$70S_8$ $14S_7$
9	2225	2227	2225	2232	2222	$99S_9$
10	2213	2211	2210	2210	2204	$98S_{10}$
11	1051	1035	1040		1033	$94S_{11}$
12	1030	1035	1040		1025	$98S_{12}$
13	822	820	829		817	$84S_{13}$ $11S_{15}$
14	587	589	592		579	$99S_{14}$
15			349	347	343	$68S_{15}$ $28S_{16}$
16	202	190	201	190	191	$77S_{16}$ $22S_{17}$
17			70		68	$69S_{17}$ $29S_{16}$

Abbreviation: p, polarized.

Table 6. Symmetry force constants and their uncertainties for methyl-1-propynylmercury(II)[a]

		σ			σ
F_1	4.890	0.015	F_9	4.721	0.012
F_2	4.630	0.075	F_{10}	4.648	0.012
F_3	14.098	0.070	F_{11}	0.546	0.003
F_4	0.571	0.005	F_{12}	0.513	0.003
F_5	0.534	0.025	F_{13}	0.680	0.007
F_6	5.168	0.122	F_{14}	0.428	0.004
F_7	2.478	0.079	F_{15}	0.533	0.096
F_8	2.992	0.242	F_{16}	0.316	0.019
			F_{17}	0.228	0.030
$F_{2,5}$	−0.548	0.077			
$F_{4,6}$	−0.364	0.020	$F_{15,16}$	0.259	0.060
$F_{5,7}$	−0.096	0.040			
$F_{7,8}$	−0.471	0.225			

a) The stretching force constants are given in mdyn/Å, the deformation force constants in mdyn·Å, the stretching-deformation interaction constants in mdyn.

Table 7. Comparison of force constants (mdyn/Å)

	f(M–CC)	f(M–CH_3)
$CH_3HgC{\equiv}CCH_3$	2.99[a]	2.48[a]
$CH_3HgC{\equiv}CH$	2.83[1]	2.54[1]
CH_3HgCl		2.55[9]
CH_3HgBr		2.48[9]
CH_3HgI		2.38[9]
$SiH_3C{\equiv}CH$	3.30[14]	
$SiH_3C{\equiv}CSiH_3$	3.35[14]	
$SiH_3C{\equiv}CCH_3$	3.30[14]	
SiH_3CH_3		2.97[14]
$Si(CH_3)_4$		2.88[15]
$GeH_3C{\equiv}CH$	3.46[16]	
GeH_3CH_3		2.87[17]
$Ge(CH_3)_4$		2.65[15]

a) This work.

In these calculations, the symmetry force constants F_7 and F_8 turn out the CH_3–Hg and Hg–CC valence stretching force constants. A comparison of force constants is given in Table 7. We see that the force constants for the M–CC bond are always larger than those for the M–CH_3 bond. This is in line with the expectation on the basis of the hybridization of the carbon atom adjacent to the metal atom; the sp hybrid in M–CC and the sp^3 hybrid in M–CH_3, make the former bond stronger than the latter.

One of authors (Y.I.) wishes to express his thanks to Assist. Prof. Fumio Watari for helpful suggestions throughout this work and for the computer programs used in calculations.

References

1) Y. Imai, F. Watari, and K. Aida, *Spectrochim. Acta, Part A*, in press.
2) L. G. Makarova and A. N. Nesmeyanov, "The Organic Compounds of Mercury," North-Holland Co., Amsterdam (1967), Chap. 5.
3) J. R. Johnson and W. L. McEwen, *J. Am. Chem. Soc.*, **48**, 469 (1926).
4) H. Hunziker, W. Good, R. Meyer, and H. H. Günthard, *Helv. Chim. Acta*, **45**, 59 (1962).
5) R. J. Spahr, R. R. Vogt, and J. A. Nieuwland, *J. Am. Chem. Soc.*, **55**, 2465 (1933).
6) R. N. Jones and A. Nadeau, *Spectrochim. Acta, Part A*, **20**, 1175 (1964).
7) D. Grdenić, *Quart. Rev.*, **19**, 303 (1965).
8) I. S. Butler and M. L. Newbury, *Spectrochim. Acta, Part A*, **33**, 669 (1977).
9) P. L. Goggin, G. Kemeny, and J. Mink, *J. Chem. Soc., Faraday Trans. 2*, **72**, 1025 (1976).
10) G. Herzberg, "Infrared and Raman Spectra of Polyatomic Molecules," D. Van Nostrand Co., New York (1964), pp. 333 and 338.
11) W. Gordy and J. Sheridan, *J. Chem. Phys.*, **22**, 92 (1954).
12) J. C. Mills, H. S. Preston, and C. H. L. Kennard, *J. Organomet. Chem.*, **14**, 33 (1968).
13) L. F. Thomas, E. I. Sherrad, and J. Sheridan, *Trans. Faraday Soc.*, **51**, 619 (1955).
14) J. L. Duncan, *Spectrochim. Acta, Part A*, **20**, 1807 (1964).
15) F. Watari, *Spectrochim. Acta, Part A*, **34**, 1239 (1978).
16) J. Parker and J. A. Ladd, *Trans. Faraday Soc.*, **66**, 1907 (1970).
17) E. Clark and A. Weber, *J. Chem. Phys.*, **45**, 1759 (1966).

Studies on the Aqueous Solutions of Guanidinium Salt. XI. Volume Changes of Mixing of Aqueous Solutions of Guanidinium Bromide and Tetraalkylammonium Bromide at 25 °C

Koichiro MIYAJIMA, Hiromitsu YOSHIDA,* and Masayuki NAKAGAKI

Faculty of Pharmaceutical Sciences, Kyoto University, Yoshida-Shimoadachi-cho, Sakyo-ku, Kyoto 606

(Received May 4, 1979)

The volume changes on mixing aqueous solutions of guanidinium bromide with those of tetrabutyl- and tetramethylammonium bromide were measured with a vibration densimeter at 25 °C. The excess volume change of mixing was positive and large for the system of tetrabutylammonium bromide–guanidinium bromide–water. On the basis of the interaction parameters of Friedman's formalism, this result was interpreted in terms of an interaction between guanidinium cation and tetrabutylammonium cation through the change of water structure.

In a previous paper,[1] we reported that the free energy of mixing for the ternary system, guanidinium bromide (GuBr)–tetrabutylammonium bromide (Bu_4NBr)–water was negative and large in magnitude. This result was interpreted in terms of either direct (complex formation) or indirect (through the change of water structure) interaction between the guanidinium cation (Gu^+) and the tetrabutylammonium cation (Bu_4N^+). In other words, $g_{B^+C^+}$, the interaction parameter of the mixed cation pair in Friedman's formalism,[2] was the predominant factor for the mutual salting-in of this system.

In contrast to this result, in the ternary system containing Bu_4NBr and alkali halides, such as KBr or CsBr,[3] the mutual salting-out was observed, in spite of the facts that both K^+ and Cs^+ were structure breaker ions similar to the guanidinium ion.

The volume changes of mixing for the ternary systems KBr–Bu_4NBr–H_2O[4] and NaBr–tetrapropylammonium bromide–H_2O[5] were also determined and large excess volume changes of mixing with positive signs were obtained. The increase of the solution volume by mixing was attributed mainly to the interaction of hydrophobic cations through the change of water structure.

Previously,[6] the authors reported that in organic solutes including ions, the size, shape, and functional groups were the important factors which determine the nature of the solute-water interaction. The structure breaking action of guanidinium ion would thus be different from K^+ and Cs^+, and similar to that of urea with regard to the hydrogen bonding with water molecules.

From these standpoints, it is interesting to investigate the volume change on mixing aqueous solutions of GuBr and Bu_4NBr. In this paper, we reported the volume changes of mixing of the ternary system GuBr–Bu_4NBr–H_2O and GuBr–tetramethylammonium bromide (Me_4NBr)–H_2O up to 2 molalities of total concentration. The data obtained were analyzed by Friedman's formalism and the results are discussed in terms of the interionic interactions and concomitant structural change of water.

Experimental

Materials. GuBr was prepared and purified by the method described elsewhere.[1] Bu_4NBr and Me_4NBr were purchased from Wako Junyaku Co., Ltd. and recrystallized two or more times from the appropriate solvents, as described elsewhere.[7] These compounds were dried *in vacuo* over phosphorous pentoxide before use. The salts were dissolved in redistilled and deionized water.

Method. Stock solutions of total molalities of 2 mol·kg^{-1} with different ionic mole fractions were prepared by weighing and mixing each salt solution. Each stock solution was diluted by weight to the desired molalities before use. About fifteen kinds of sample solutions with different molalities and the same ionic mole fraction were used for the measurement. Solution densities were determined by Seiko SDM 421 and 422 vibration densimeters, which were linked with a quartz oscillator and a digital counter. Pure water and aqueous sodium chloride solution were used as the standards for the calibration of the apparatus. Measurements were done at least twice for every solution and were accurate to $\pm 1 \times 10^{-5}$ g/cm^3. The temperature of the cell chamber was maintained at 25±0.01 °C.

Results and Discussion

Apparent Molal Volumes. The apparent molal volume ϕ_v of the 1 : 1 electrolyte in the solution volume V has been defined in the molality scale:

$$\phi_v = \frac{V - 55.51\bar{V}_A^0}{m} \quad (1)$$

where $\bar{V}_A^0$ is the molal volume of pure water, and m is the solute molality. If we consider a solution in which two electrolytes, B and C having a common ion are dissolved, Eq. 1 can be modified into the following form by using the density and molality and rewriting ϕ_v as $\phi_v(x,m)$,

$$\phi_v(x, m) = \frac{1}{m}\left\{\frac{1000 + m_B M_B + m_C M_C}{d} - \frac{1000}{d_A}\right\}, \quad (2)$$

where d and d_A are the densities of the solution and pure water, respectively, and $m_B(m_C)$ and $M_B(M_C)$ are the molalities and molecular weight of B(C), respectively. In this paper, B denotes GuBr and C denotes tetraalkylammonium bromide. $\phi_v(x,m)$ is the mean apparent molal volume of the mixed electrolyte or the pseudo binary salt at total molality m and ionic mole fraction x, given as

$$m = m_B + m_C, \text{ and } x = m_C/m. \quad (3)$$

For the various x's, the relation between $\phi_v(x,m)$ and m is obtained from the density data, and is shown in Fig. 1 for the GuBr–Bu_4NBr–H_2O system and in Fig. 2

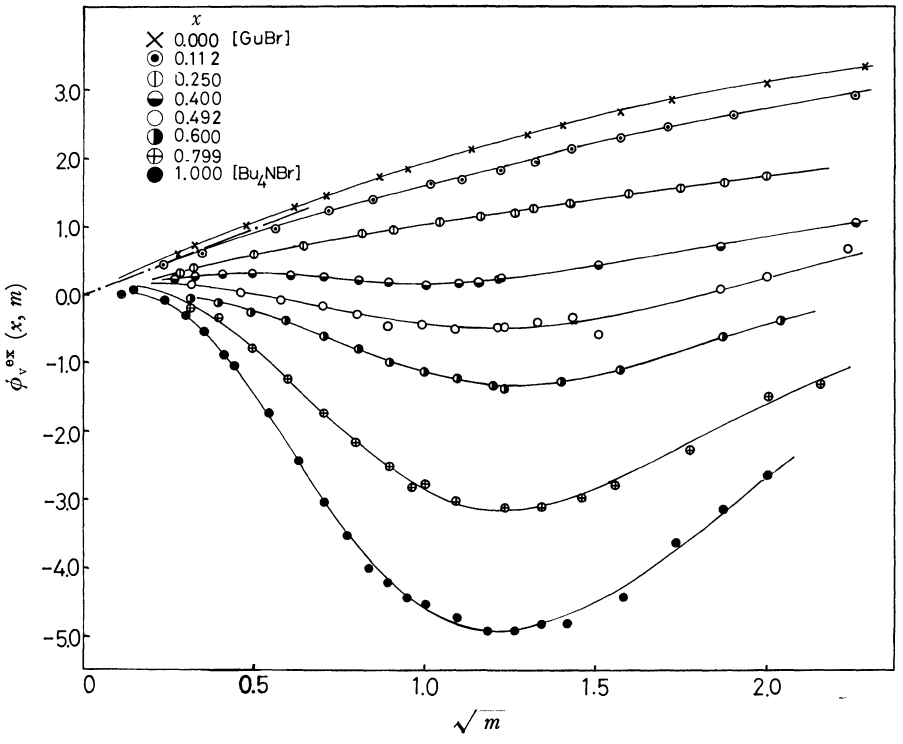

Fig. 1. The concentration dependence of the excess apparent molal volume of H_2O–GuBr–Bu_4NBr system at 25 °C. —— Debye-Hückel line.

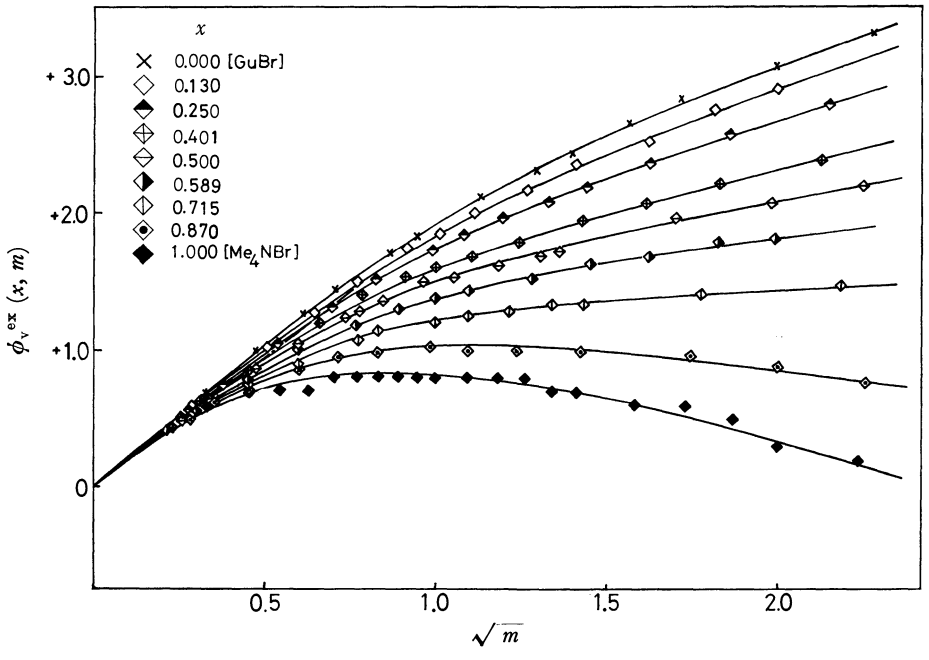

Fig. 2. The concentration dependence of the excess apparent molal volume of H_2O–GuBr–Me_4NBr system at 25 °C. —— Debye-Hückel line.

for the GuBr–Me_4NBr–H_2O system. In both figures the ordinate represents the excess apparent molal volume $\phi_v^{ex}(x,m)$, defined as the deviation from $\phi_v(x,0)$, the mean apparent molal volume at infinite dilution.

$$\phi_v^{ex}(x, m) = \phi_v(x, m) - \phi_v(x, 0). \quad (4)$$

The additivity rule has to hold for $\phi_v(x,0)$ as

$$\phi_v(x, 0) = x\phi_v(1, 0) + (1-x)\phi_v(0, 0), \quad (5)$$

where $\phi_v(0,0)$ and $\phi_v(1,0)$ are the apparent molal volume at infinite dilution for the electrolyte B and C, respectively. As seen in Figs. 1 and 2, the concentration dependence curves of $\phi_v^{ex}(x,m)$ are located between those of binary solutions in both the systems. These curves are expressed in the form of Eq. 6:

$$\phi_v^{ex}(x, m) = \sum_i q_i m^{i/2}, \quad (q_1 = 1.865) \quad (6)$$

and each q_i coefficient is obtained by a least squares

fit with a computer program. These coefficients represent the various intetractions contributing to the solution volumes; they are not useful, however, for interpreting the volume change in terms of ionic interactions, except for calculating ϕ_v at the desired molality.

In the mixing of inorganic electrolytes, the Young's mixture rule[8] is an adequate description of the volume properties of a mixture:

$$\phi_v(x, m) = x\phi_v(1, m) + (1-x)\phi_v(0, m). \quad (7)$$

Equation 7 means that the mixing of two binary solutions at constant total molality produces a ternary solution whose volume is exactly the sum of the volumes of the binary solutions. Combining Eqs. 4, 5, and 7, we have

$$\phi_v^{ex}(x, m) = x\phi_v^{ex}(1, m) + (1-x)\phi_v^{ex}(0, m). \quad (8)$$

This equation may express that the volume changes resulting from the new ionic interaction in the ternary solution are equal to the arithmetic means of the volume changes resulting from the ionic interaction in each binary solution. Most inorganic electrolyte mixtures obey this rule, although slight deviations are obtained.[9] The x-dependence of $\phi_v^{ex}(x,m)$ is shown in Fig. 3 at

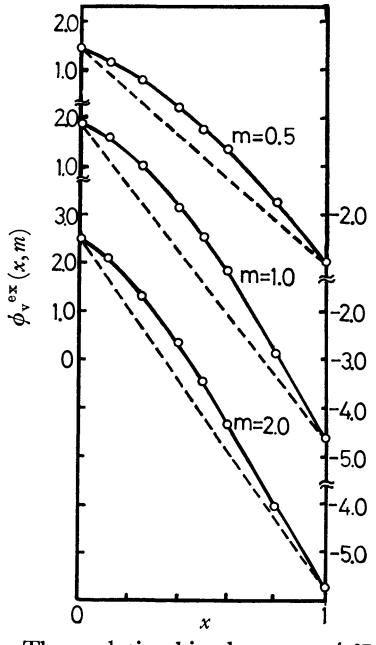

Fig. 3. The relationship between ϕ_v^{ex} and x for H_2O–GuBr–Bu_4NBr system at various m. Dotted line is obtained from Young's rule. Solid line is obtained from experiment.

m=0.5, 1.0, and 2.0 for the GuBr–Bu_4NBr–H_2O system, for which the mixture rule does not hold, and a positive deviation from Eq. 8 is observed. In this case, the addition of term Δ to Eq. 8 is required:

$$\phi_v^{ex}(x, m) = x\phi_v^{ex}(1, m) + (1-x)\phi_v^{ex}(0, m) + \Delta. \quad (9)$$

In the case of the common anion mixing, this deviation may be attributed to the difference in the cation-cation interactions; these are discussed in next section.

Excess Volume Change of Mixing. The excess volumes of the pseudo-binary salt solution may be defined as the product of the total molality and the excess apparent molal volume:

$$V^{ex}(x, m) = m\phi_v^{ex}(x, m). \quad (10)$$

The excess volume change of mixing $\Delta_m V^{ex}$ has been given as the deviation from the linear relationship between V^{ex} and x at constant molality.[4]

$$\Delta_m V^{ex}(x, m) = V^{ex}(x, m) - xV^{ex}(1, m) - (1-x)\phi_v^{ex}(0, m). \quad (11)$$

On substituting Eq. 10 to Eq. 11, we obtain

$$\Delta_m V^{ex}(x, m) = m\{\phi_v^{ex}(x, m) - x\phi_v^{ex}(1, m) - (1-x)\phi_v^{ex}(0, m)\} = m\cdot\Delta. \quad (12)$$

Therefore the Δ in Eq. 9 correspond to $\Delta_m V^{ex}/m$. As shown in Figs. 4 and 5, $\Delta_m V^{ex}$ plotted against x are

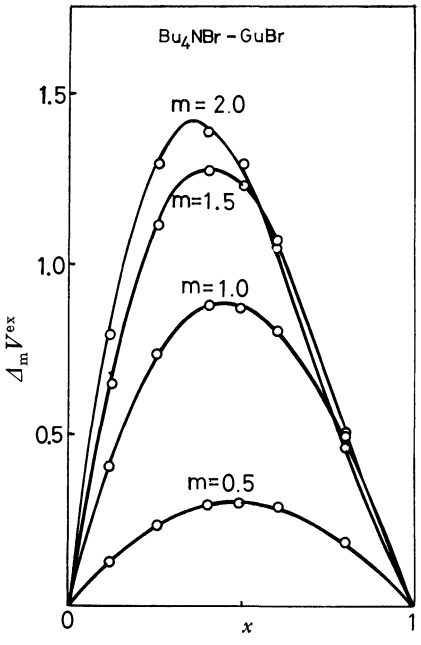

Fig. 4. The relationship between $\Delta_m V^{ex}$ and x at various m of the H_2O–GuBr–Bu_4NBr system.

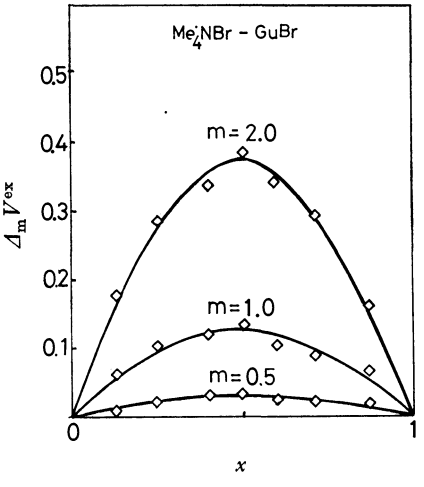

Fig. 5. The relationship between $\Delta_m V^{ex}$ and x at various m of the H_2O–GuBr–Me_4NBr system.

both positive and nearly parabolic. The maximum points for the system GuBr–Bu_4NBr–H_2O are left from the vertical line of $x=0.5$. The $\Delta_m V^{ex}$ values and the degree of the skewness increased with increasing the total molality. The magnitude of $\Delta_m V^{ex}$ for the system containing Bu_4NBr is six or seven times larger than that for the system containing Me_4NBr. From this experimental result, the observed large values of $\Delta_m V^{ex}$ are considered to be due to the change of the hydration of tetraalkylammonium salts as shown in next section, because the mixing of inorganic salts solution is not accompanied by such a large volume change and the hydration cosphere of the Bu_4N^+ is more extensive than that of the Me_4N^+. In the binary tetraalkylammonium salt solutions in the relatively low concentration range, the decrease of the apparent or partial molal volume was considered to take place because of the formation of cage-like structure around the tetraalkylammonium ion[10] and the overlap of the cage by cation-cation interactions.[11] To interpret the $\Delta_m V^{ex}$ dependences on the ionic strength and/or ionic mole fraction in Figs. 4 and 5, one may introduce the following Friedman's treatment:[2,4]

$$\Delta_m V^{ex}(x, m) = x(1-x)\{v_0+v_1(1-2x)+\cdots\} \qquad (13)$$

where v_0 and v_1 are volumetric interaction parameters. To evaluate v_0 and v_1, the quantities $\Delta_m V^{ex}(x,m)/x(1-x)$ are plotted against x. This relation would be linear if the higher terms are negligibly small. As seen in the upper corner of Fig. 6, v_0 and v_1 has been obtained from the intercept and slopes.

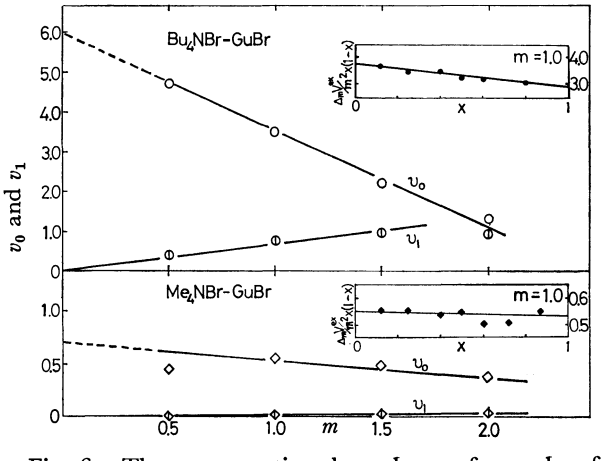

Fig. 6. The concentration dependence of v_0 and v_1 for the ternary systems.

In the common ion mixing, one can easily consider the pairwise and triplet interactions between like-charged ions, which mainly influence the excess function of mixing at relative low concentrations. Applying a treatment similar to the excess free energy of mixing,[1,2] v_0 and v_1 can be described as

$$v_0 = (2v_{B^+C^+}-v_{C^+C^+}-v_{B^+B^+}) + v_0(\text{trip})\cdot m, \qquad (14\text{-a})$$

and

$$v_1 = v_1(\text{trip})\cdot m, \qquad (14\text{-b})$$

where v_{ij} is the concrete interaction parameter of cation i and j, and v_0(trip) and v_1(trip) are the triplet interaction parameters.[1] As predicted from Figs. 4 and 5, the signs and magnitude of $\Delta_m V^{ex}$ are determined mainly by the v_0 values, while the skewness of the curve depends on the v_1 values.

The large excess volume change does not always arise from the volume difference of two kinds of solutes. In the volume changes of mixing of the ternary system KBr–tetrapropylammonium bromide–H_2O and KBr tetrakis(2-hydroxyethyl)ammonium bromide–H_2O, the former system showed large $\Delta_m V^{ex}$, while the latter underwent almost no volume change, although the ion sizes of the two kinds of cations are nearly the same.[4] Based on the above result and the similar properties of Bu_4N^+ and tetrapropylammonium ion($Pr_4(N^+)$), we will discuss the large $\Delta_m V^{ex}$ for the system GuBr–Bu_4NBr–H_2O by focusing on the change of water structure and the structuredness of a hydration cosphere by the interionic interactions.

The curves in Fig. 6 can be expressed by Eq. 13 within experimental error. According to Eq. 13, the contribution of the triplet interaction term(v_0(trip)) become large with increase of total molality, but the pairwise interaction term $(2v_{B^+C^+}-v_{C^+C^+}-v_{B^+B^+})$ contributes more significantly to v_0 in the concentration range studied. Since v_0 decreases almost linearly with m, as seen in Fig. 6, the value of $(2v_{B^+C^+}-v_{C^+C^+}-v_{B^+B^+})$ was obtained by extrapolating Eq. 13 to infinite dilution. Although it is quite difficult to evaluate the v_{ij} from the present approach, the free energy of mixing for the same system will help us in estinating the signs and magnitude of the v_{ij}. Among the three parameters of the pairwise term, $v_{B^+B^+}$ the interaction parameter between Gu^+'s, must be small, because of the weak hydration of the guanidinium cation.[12] Therefore, it is reasonable to neglect the contribution of $v_{B^+B^+}$ to the pairwise term. The $v_{C^+C^+}$ between Bu_4N^+'s has a negative sign, because two cations approach each other at a suitable distance and tend to link up to release water molecules of the cosphere to bulk solution,[11] leading to a small volume. On the other hand, the $v_{B^+C^+}$ between Gu^+ and Bu_4N^+ must be positive, since the hydrophobic hydration originally makes a negative contribution to the solution volume.[10] Indeed the hydration cosphere itself around a hydrophobic ion is more bulky than pure water, but the tight packing based on the formation of cage decreases the void space of liquid water. The latter effect dominate over the former. The guanidinium ion reduces and breaks the cage-like structure around a hydrophobic ion, leading to a large volume. From the consideration above, both parameters, $v_{B^+C^+}$ and $-v_{C^+C^+}$ make positive contributions to the solution volume.

In the free energy of mixing of the system KBr–Pr_4NBr–H_2O,[3] where the mutual salting-out was observed, the formation of like-cation pairs were more favoured than that of mixed cation pairs. On the other hand, the positive value of $\Delta_m V^{ex}$ was obtained from the volume of mixing of the same system and attributed also to the interaction of a like cation pair.

In contrast to the above results, a large mutual salting-in was observed in the free energy of mixing of the system GuBr–Bu_4NBr–H_2O,[1] where the forma-

tion of mixed cation pair was preferred to that of the like cation pairs.

These facts strongly suggest that $v_{B^+C^+}$ parameter should contribute more significantly than $v_{C^+C^+}$ parameter to the large $\Delta_m V^{ex}$ of the system GuBr–Bu_4NBr–H_2O. Consequently, the increase of solution volume observed in the above two systems would depend on the different cation-cation interaction, that is, C^+–C^+ interaction for the system KBr–Pr_4NBr–H_2O and B^+–C^+ interaction for the system GuBr–Bu_4NBr–H_2O. This concept is consistent with the general aspects of dissolution of hydrophobic solute in aqueous guanidinium solution, that is, the guanidinium ion breaks the water structure and weakens the water-structure-enforced association of hydrophobic solute. Since the interaction of hydrophobic solute with K^+ and guanidinium ion take place through the structure of water, the difference in the interaction indicates that the guanidinium ion breaks water structure in a different way from K^+.

Partial Molal Volumes, $\bar{V}_i$. Since $\phi_v(x,m)$ are regarded as the apparent molal volumes of the pseudo-binary salt, the partial moal volume of this salt $\xi(x,m)$ may be defined as[13]

$$\xi(x, m) = \left(\frac{\partial V}{\partial m}\right)_x = \phi_v(x, 0) + \frac{\sqrt{m}}{2}\left(\frac{\partial \phi_v(x, m)}{\partial \sqrt{m}}\right), \quad (15)$$

Using Eq. 6, we obtain

$$\xi(x, m) = \phi_v(x, 0) + \sum q_i\left(1+\frac{i}{2}\right)m^{i/2}. \quad (16)$$

$\xi(x,m)$ are computable. As the solution volume is the sum of the partial molal volumes of the individual components,

$$V(x, m) = 55.51\bar{V}_A + (1-x)m\bar{V}_B + xm\bar{V}_C. \quad (17)$$

Differentiating Eq. 17 with m or x, and applying the Gibbs-Duhem relation to the differentiated equation, we have the partial molal volume of solute B and C,

$$\bar{V}_B = \xi(x, m) - x\left(\frac{\partial \phi_v(x, m)}{\partial x}\right)_m \quad (18\text{-a})$$

$$\bar{V}_C = \xi(x, m) - (1-x)\left(\frac{\partial \phi_v(x, m)}{\partial (1-x)}\right)_m \quad (18\text{-b})$$

$\bar{V}_A$ values did not change appreciably with m and were nearly the same as $\bar{V}_A^0$ in this experimental method. The partial molal volumes of tetrabutylammonium bromide $\bar{V}_C$ are calculated from Eq. 18-b and are shown in Fig. 7 at various x values. With decreasing x, the curves of $\bar{V}_C$ *vs.* $\sqrt{m}$ become flat, accompanying the shift of the minimum values. However, this figure is not suitable for the comparison of the m_C dependence of $\bar{V}_C$ in water and with that in aqueous GuBr solution. To elucidate the volume change of Bu_4NBr in the GuBr solution, $\bar{V}_C$ at constant rational mole fraction, N_C were calculated and replotted against m_C'. N_C and m_C' are defined as[1]

$$N_C = \frac{2m_C}{55.51+2m_C} = \frac{2m_C'}{55.51+2m_C'+2m_B} \quad (19)$$

where m_C' is the molality of Bu_4NBr in ternary solution

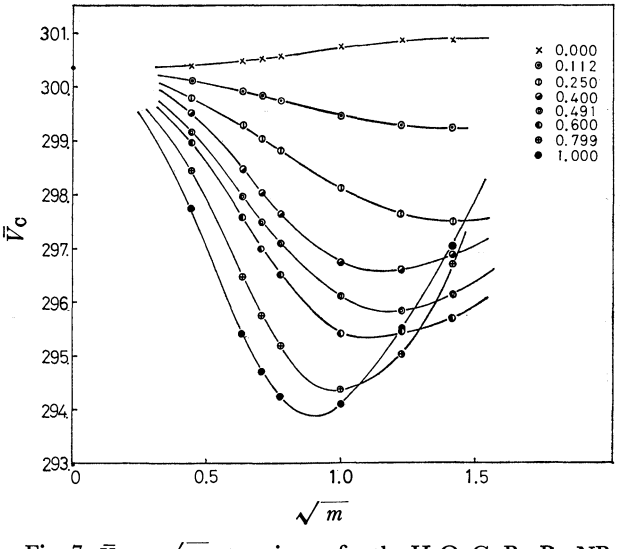

Fig. 7. $\bar{V}_C$ *vs.* $\sqrt{m}$ at various x for the H_2O–GuBr–Bu_4NBr system.

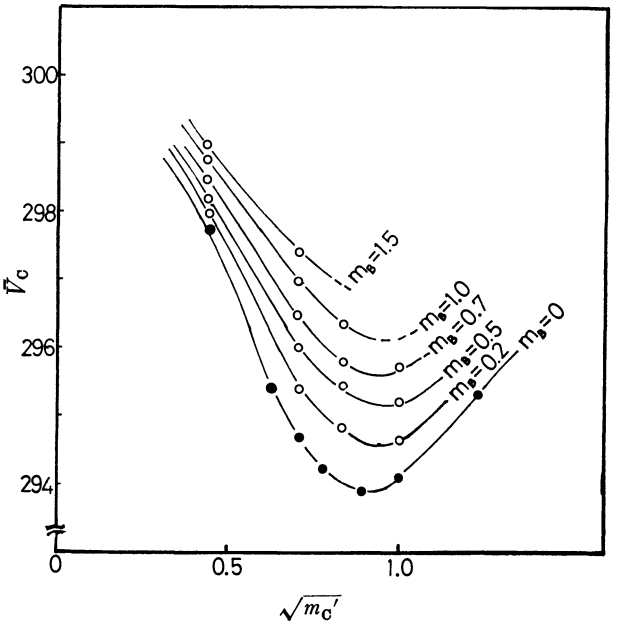

Fig. 8. $\bar{V}_C$ *vs.* $\sqrt{m_C'}$ at various m_B for the H_2O–GuBr–Bu_4NBr system.

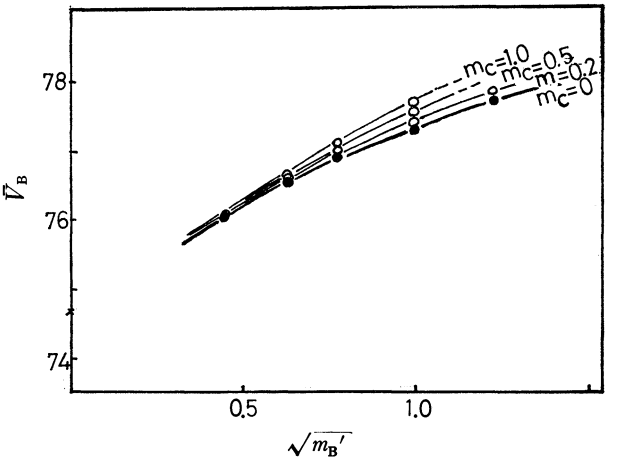

Fig. 9. $\bar{V}_B$ *vs.* $\sqrt{m_B'}$ at various m_C for the H_2O–GuBr–Bu_4NBr system.

having the same N_C in the binary solution. This treatment means that the guanidinium bromide solution is regarded as a solvent. As seen in Fig. 8, the $\bar{V}_C$ *vs.* m_C' curves clearly shift upward with increase of m_B, but the concentrations of Bu_4NBr having the minimum $\bar{V}_C$ value are independent of m_B. $\bar{V}_B$ *vs.* $\sqrt{m_B'}$ curves are shown in Fig. 9. The V_B values change only slightly with increase of m_C. These facts indicate that the large volume change of mixing for this system is due to the change of the hydration of Bu_4N^+ caused by the change of solvent structure.

References

1) K. Miyajima, H. Yoshida, and M. Nakagaki, *Bull. Chem. Soc. Jpn.*, **51**, 2826 (1978).

2) H. L. Friedman, "Ionic Solution Theory," Interscience Pub. New York, N. Y., London (1962), Vol, 3; R. H. Wood and H. L. Anderson, *J. Phys. Chem.*, **70**, 992 (1966).

3) W-Y. Wen, K. Miyajima, and A. Otsuka, *J. Phys. Chem.*, **75**, 2148 (1971).

4) W-Y. Wen and K. Nara, *J. Phys. Chem.*, **71**, 3907 (1967).

5) J. Padava, D. Rosenzweig, and Y. Marcus, *J. Chem. Thermodynamics*, **8**, 431 (1976).

6) K. Miyajima, H. Yoshida, and M. Nakagaki, *Bull. Chem. Soc. Jpn.*, **51**, 2508 (1978).

7) B. E. Conway, R. E. Verrall, and J. E. Desnoyers, *Trans. Faraday Soc.*, **62**, 2738 (1966).

8) T. F. Young and M. B. Smith, *J. Phys. Chem.*, **58**, 716 (1954).

9) F. J. Millero, *Chem. Rev.*, **71** 147 (1971).

10) W-Y. Wen and S. Saito, *J. Phys. Chem.*, **68**, 2639 (1964); F. Frank and H. T. Smith, *Trans. Faraday Soc.*, **63**, 2586 (1967).

11) J. E. Desnoyers, M. Arel, G. Perron, and C. Jolicoeur, *J. Phys. Chem.*, **73**, 3346 (1969).

12) K. Miyajima, K. Inari, S. Hamaguchi, H. Yoshida, and M. Nakagaki, *Nippon Kagaku Kaishi*, **1975**, 1447.

13) J. Padova and I. Lewkowicz, *J. Chem. Phys.*, **65**, 3611 (1976).

Vapor Pressure Osmometry and Conductance Studies of Solutions of Bis(tetraalkylammonium) Electrolytes in Methanol, Ethanol, and 2-Propanol

Ha Chung LEE, Hiroyasu NOMURA,* Yutaka MIYAHARA, and R. E. VERRALL**

Department of Chemical Engineering, Faculty of Engineering, Nagoya University, Chikusa-ku, Nagoya 464

***Department of Chemistry and Chemical Engineeing, University of Saskatchewan, Saskatoon, Saskatchewan, S7N,OWO, Canada*

(Received May 14, 1979)

Vapor-pressure depressions and electric conductivities have been measured for bis(tetraalkylammonium) electrolytes in methanol, ethanol, and 2-propanol. The analysis of the data of vapor pressure osmometry (VPO) of these bolaform salts was carried out taking into account the two-step dissociation equilibrium as follows.

$$M^{2+} + 2X^- \underset{K_d^I}{\rightleftharpoons} MX^+ + X^- \underset{K_d^{II}}{\rightleftharpoons} MX_2$$

In each solvent, the ionic association constants, K_a^I and K_a^{II} ($K_a = 1/K_b$), tend to decrease with increasing ionic size. This tendency is greater in K_a^I than in K_a^{II}. The K_a^I values of bis(tetraalkylammonium) electrolytes show virtually no dependence on the dielectric constant of solvent. On the contrary, the values of K_a^{II} strongly depend on the dielectric constant of solvent. Using the values of K_a^I and K_a^{II} in 2-propanol, the ultrasonic relaxation data were analyzed.

In a recent series of papers,[1-5] vapor pressure lowering data obtained by means of vapor pressure osmometer (VPO) measurements have been reported for a variety of electrolytes in nonaqueous solvents. The concentration dependence of the activities of the salts has been analyzed assuming the existence of a dissociation and/or association equilibrium. Vapor pressure osmometry is particularly useful in studying cases of neutral species where the use of conductance techniques is precluded.[5] As well, in the case where ionic equlibria are being studied, it provides a method of estimating equilibrium constants complementary to conductance studies.

There have been numerous investigations of solution properties of 1:1 electrolytes in nonaqueous solutions. However, because of the low solubility of 2:1 electrolytes in nonaqueous solvents,[6-8] only a few results have been reported for these systems. A series of electrolytes that circumvent this solubility problem in nonaqueous solvents is the bis(tetraalkylammonium) or bolaform type of electrolyte. Their moderately high solubility is due to the rather large portion of hydrocarbon moieties in their elemental composition. These salts had been considered as model systems to examine the contribution of cation-cation ion pairing to the non-ideal behavior of R_4N^+ ions in aqueous solutions. Conductance studies of several of these systems have been reported by Evans *et al.*[9]

In the present paper we report vapor pressure lowering and conductance measurements of some bis(tetraalkylammonium) salts in methanol, ethanol and 2-propanol in order to estimate the degree of ionic dissociation in these solvents. Also, the present results are compared with those previously obtained[10] by means of ultrasonic relaxation studies of these electrolytes in 2-propanol.

Theoretical

A salt, MX_2, dissolved in non-aqueous solvent can exhibit a two-step dissociation equilibrium, as follows:

$$\begin{aligned} M^{2+} + 2X^- &\underset{K_d^I}{\rightleftharpoons} MX^+ + X^- \quad \text{step I} \\ MX^+ + X^- &\underset{K_d^{II}}{\rightleftharpoons} MX_2 \quad \text{step II} \end{aligned} \tag{1}$$

The activity of the solvent is related to the activity coefficients of the undissociated salt and ions by an integrated form of the Gibbs-Duhem equation. For the reactions represented by equation 1 this expression is given as

$$\ln a_1 = -\frac{1}{N_1}\left(m_2 + m_3 + m_4 + m_5 + \int_0^{m_3} m_3 \, d\ln \gamma_3 + \int_0^{m_4} m_4 \, d\ln \gamma_4 + \int_0^{m_5} m_5 \, d\ln \gamma_5\right) \tag{2}$$

where a_1 is the activity of the solvent,
N_1 is the mole number of the solvent ($=1000/M_1$; M_1 is the molecular weight of the solvent),
m is the molal concentration of the added solute,
m_2 is the molality of undissociated salt MX_2,
m_3 is the molality of cation M^{2+},
m_4 is the molality of anion X^-,
m_5 is the molality of cation MX^+,
α is defined as $\alpha = m_5/m$ ($0 < \alpha < 1$),
β is defined as $\beta = m_3/m_5$ ($\beta > 0$),
γ_i is the mean activity coefficients of the ions, suffixes 3, 4, and 5 referring to M^{2+}, X^-, and MX^+, respectively, and γ_2, the activity coefficient of the undissociated salt, is assumed to be unity.

From these definitions it follows that in Eq. 2

$$\begin{aligned} m_2 &= m[1-\alpha(1+\beta)] \\ m_3 &= m\alpha\beta \\ m_4 &= m\alpha(1+2\beta) \\ \text{and } m_5 &= m\alpha \end{aligned} \tag{3}$$

The dissociation equilibrium constants are obtained by curve fitting procedures using Eq. 2. In order to do this, values of the activity coefficients in terms on the

right-hand side of Eq. 2 must be evaluated. We have assumed that the activity coefficients of the ions are represented by the Güntenberg-type equation:[11]

$$\ln \gamma_{\pm} = -\frac{A|z_1 z_2|\sqrt{I}}{1+\sqrt{I}}, \quad A = \frac{1.825\times 10^6}{(\varepsilon T)^{3/2}} \tag{4}$$

Numerical values of the density d_0 and the dielectric constant ε of the solvent used in calculations were obtained from Ref. 12.

As in previous work,[4] a function, h, defined as

$$h = \frac{N_1 \ln a_1}{m} + 1 \tag{5}$$

was used for the analysis of the experimental results.

Experimental

Materials. The bis(tetraalkylammonium) salts, 1,4-bis-(triethylammonio) butane dibromide, 1,5-bis(triethylammonio) pentane dibromide, and 1,10-bis(triethylammonio) decane dibromide, abbreviated hereafter J4, J5, and J10, respectively, were prepared and purified as described eleswhere.[13] Before use, the salts were dried for a period of five days in a vacuum oven at 50 °C over molecular sieves 3A (1/8 in. pellet). Fresh molecular sieves were used each day.

Reagent grade methanol and 2-propanol (Kishida Chemical Co. Ltd.) were further purified by drying with anhydrous calcium sulfate and finally distilled in the presence of molecular sieves in a nitrogen atmosphere. Reagent grade ethanol (Nakarai Chemical Co., Ltd.) was refluxed with magnesium metal and magnesium ethoxide in a dry nitrogen atmosphere for a period of 12 h and then distilled over molecular sieves in a dry nitrogen atmosphere. The water content of the purified solvents was checked by Karl-Fisher analysis and found to be less than 0.0018, 0.028, and 0.009 wt % for methanol, ethanol, and 2-propanol, respectively.

The preparation and handling of the salts and their solutions was carried out in a dry box under a nitrogen atmosphere in order to avoid contact with the moist air.

Vapor Pressure Osmometry and Conductance. The experimental method and equipment have been reported in a previous paper.[4]

Results

Vapor Pressure Osmometry. The proportionality constants K_s of the apparatus were determined using standard substances: benzil for methanol and ethanol and 1-octadecanol for 2-propanol. The values of the constants K_s and K_e ($=BrR/\Delta H$, see Ref. 3 for definition of terms), and their ratios are summarized in Table 1. Vapor pressure depression measurements were carried out at 45.0, 55.1, and 60.0 °C for methanol, ethanol, and 2-propanol, respectively.

Table 1. Proportionality constants of VPO in various solvents

T/°C	K_s/Ω	$K_e(=BrR/\Delta H)/\Omega$	K_s/K_e
	MeOH–Benzil		
45	−42100	−43200	0.974
50	−38000	−37200	1.022
	EtOH–Benzil		
55.1	−27600	−28300	0.973
	i-PrOH–1-Octadecanol		
60	−21800	−23900	0.911
70	−17300	−18200	0.951

Values of h, calculated by introducing the experimental values of activity coefficients a_1 in Eq. 5, are given in Table 2. Plots of h *vs.* the concentration in molality units are shown in Figs. 1—3. The behavior of the values of h ($h \leqq 0$) clearly shows the existence of a dissociation equilibrium.[3]

Attempts to fit the profiles of h *vs.* concentration using the procedures of one-step dissociation equation such as R_4NX in acetone did not give good fitting in this case. In order to estimate the two-step dissociation constants K_d^{I} and K_d^{II} in Eq. 1, the following procedures

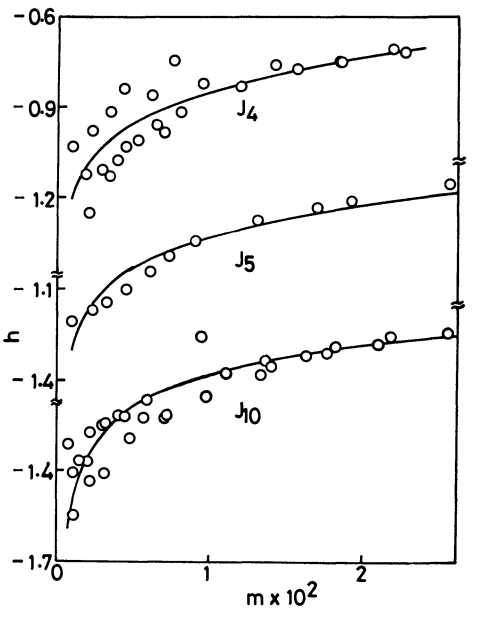

Fig. 1. Relationships between h and concentration for J4, J5, and J10 in methanol at 45 °C.

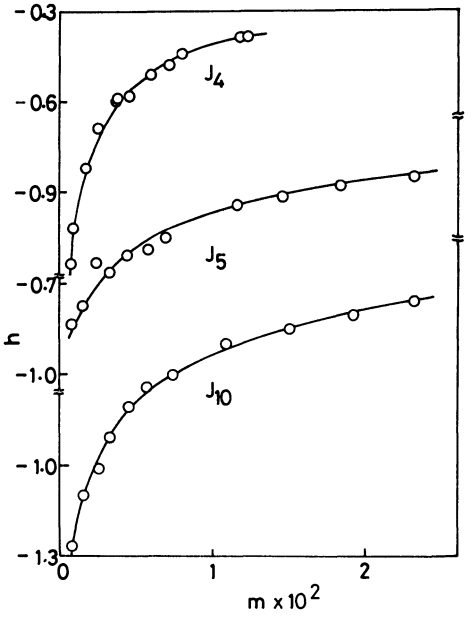

Fig. 2. Relationships between h and concentration for J4, J5, and J10 in ethanol at 55.1 °C.

Table 2. h values of bis-tetraalkylammonium salts in various solvents

$m\times10^2$	h	$m\times10^2$	h	$m\times10^2$	h	$m\times10^2$	h
MeOH-J4 at 45 °C		0.1083	−1.5454	1.2277	−0.3841	0.6614	−0.2234
0.0946	−1.0361	0.1110	−1.4028			0.7964	−0.2173
0.1021	−1.4673	0.1446	−1.3661	EtOH-J5 at 55.1 °C		0.8087	−0.2177
0.1242	−0.6932	0.2035	−1.3666	0.0824	−0.8349	0.8951	−0.1888
0.1855	−1.1250	0.2147	−1.2706	0.1566	−0.7703	1.1360	−0.1504
0.2058	−1.2533	0.2232	−1.4365	0.2421	−0.6328	1.2427	−0.1598
0.2173	−0·9836	0.2943	−1.2504	0.3315	−0.6625	1.2611	−0.1186
0.2882	−1.1181	0.3022	−1.4069	0.4456	−0.6079	1.6673	−0.0934
0.3345	−1.1303	0.3164	−1.2383	0.5831	−0.5879	1.7946	−0.1000
0.3461	−0.9222	0.3939	−1.2114	0.6965	−0.5487	2.0913	−0.0855
0.3895	−1.0805	0.4414	−1.2151	1.1706	−0.4435	2.0914	−0.0673
0.4334	−0.8423	0.4785	−1.2882	1.4653	−0.4187	2.4574	−0.1028
0.4490	−1.0324	0.5634	−1.2271	1.8362	−0.3834	2.4800	−0.0829
0.5147	−1.0150	0.5883	−1.1633	2.3225	−0.3507	2.5151	−0.0799
0.6153	−0.8636	0.6998	−1.2249				
0.6504	−0.9635	0.7158	−1.2126	EtOH-J10 at 55.1 °C		2-PrOH-J10 at 60 °C	
0.6993	−0.9893	0.8713	−1.0982	0.0833	−1.2691	0.1085	−0.5616
0.7616	−0.7487	0.9397	−0.9480	0.1574	−1.1006	0.1178	−0.6590
0.8037	−0.9208	0.9726	−1.1478	0.2548	−1.0086	0.1401	−0.4926
0.9526	−0.8288	1.0999	−1.0728	0.3287	−0.9069	0.2145	−0.5519
1.1904	−0.8382	1.3316	−1.0804	0.4579	−0.8055	0.2307	−0.4426
1.4087	−0.7658	1.3574	−1.0312	0.5746	−0.7404	0.2361	−0.4547
1.5599	−0.7779	1.3933	−1.0522	0.7409	−0.7068	0.3230	−0.4037
1.8301	−0.7542	1.6626	−1.0156	1.0913	−0.6018	0.3475	−0.4016
2.1927	−0.7121	1.7612	−1.0063	1.5030	−0.5559	0.4588	−0.3643
2.2599	−0.7261	1.8205	−0.9864	1.9196	−0.5087	0.4673	−0.3658
1.8366	−0.7521	2.0910	−0.9802	2.3156	−0.4655	0.4893	−0.3416
		2.1659	−0.9562			0.6049	−0.3225
MeOH-J5 at 45 °C		2.5414	−0.9441	2-PrOH-J5 at 60 °C		0.6244	−0.2838
0.0961	−1.2045	2.6814	−0.9238	0.1029	−0.4989	0.6696	−0.2951
0.2293	−1.1707			0.1118	−0.6119	0.8026	−0.2993
0.3236	−1.1469	EtOH-J4 at 55.1 °C		0.1138	−0.5295	0.9293	−0.2535
0.4556	−1.1039	0.0841	−1.1356	0.2001	−0.3353	0.9574	−0.2135
0.6087	−1.0421	0.0868	−1.0143	0.2004	−0.3102	0.9590	−0.2323
0.7265	−0.9942	0.1696	−0.8204	0.2330	−0.4087	1.4045	−0.1609
0.9031	−0.9455	0.2564	−0.6890	0.3121	−0.3207	1.4173	−0.1633
1.3085	−0.8704	0.3624	−0.6033	0.3264	−0.2862	1.7633	−0.1169
1.6969	−0.8282	0.3798	−0.5922	0.4304	−0.2735	1.7825	−0.1160
1.9320	−0.8082	0.4631	−0.5882	0.4427	−0.3105	2.2173	−0.0797
2.5625	−0.7500	0.6028	−0.5152	0.4731	−0.2263	2.2386	−0.0605
		0.7151	−0.4800	0.5553	−0.2647	2.6255	−0.0485
MeOH-J10 at 45 °C		0.7976	−0.4413	0.5646	−0.2547	2.6301	−0.0408
0.0680	−1.3111	1.1804	−0.3861	0.5767	−0.2337	2.6835	−0.0411

were carried out; From Eq. 1, one can write the following equations:

$$K_d^{I} = m\alpha\beta(1+2\beta)\frac{\gamma_{M^{2+}}\gamma_{X^-}}{\gamma_{MX^+}}$$
$$K_d^{II} = \frac{m\alpha^2(1+2\beta)}{1-\alpha(1+\beta)}\frac{\gamma_{MX^+}\gamma_{X^-}}{\gamma_{MX_2}} \quad (6)$$

In the first approximation, to simplify the calculations, assume the values of $(\gamma_{M^{2+}}\gamma_{X^-}/\gamma_{MX^+})$ and $(\gamma_{MX^+}\gamma_{X^-}/\gamma_{MX_2})$ to be unity. The function h can be expressed as

$$h = -\alpha(1+2\beta) \quad (7)$$

By means of the complete grid search techniques, the dissociation constants, K_d^{I} and K_d^{II}, were estimated so that the standard deviation

$$\sigma^2 = \sum\left(\frac{h_{exp}-h_{cal}}{h_{exp}}\right)^2 \quad (8)$$

is minimized.

In the second step, using the values of K_d^{I} and K_d^{II} obtained and Eq. 4 for $\gamma_{\pm}$, the values of α and β in Eq. 6 are corrected, then the computer method used in the first step was repeated, still assuming the γ_{MX^+} and γ_{MX_2} to be unity, because of their very low concentration.

The values of K_d^{I} and K_d^{II} obtained using this method are summarized in Table 3. The solid lines in Figs. 1—3 are the results obtained using these "best fit" values. It can be seen that there is good agreement between experimental and calculated values.

Conductometry.[14] The concentration dependence of the equivalent conductivities of J5 and J10 in 2-

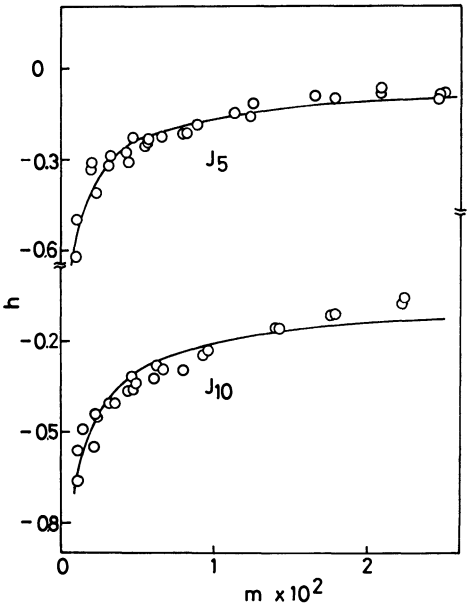

Fig. 3. Relationships between h and concentration for J5, and J10 in 2-propanol at 60 °C.

Table 3. Dissociation constants obtained by VPO and conductometry

Solute	$K_d^I \times 10^4$	$K_d^{II} \times 10^4$	Standard deviation for the function h	$K_d^I \times 10^4$
		MeOH at 45 °C		
J4	3.33 (2.71)	375.9 (305.6)	0.135	
J5	5.84 (4.75)	611.1 (496.8)	0.047	
J10	15.56 (12.2)	1944.4 (1521.7)	0.078	
		EtOH at 55.1 °C		
J4	5.00 (3.32)	20.58(13.7)	0.030	
J5	0.034(—)	40.53(26.9)	0.028	
J10	6.67 (4.11)	77.78(48.0)	0.016	
		i-PrOH at 60 °C		at 25 °C
J5	4.12 (2.30)	2.12(1.18)	0.037	6.25
J10	4.67 (2.33)	3.76(1.88)	0.054	7.23

The values in the brackets show the corrected values at 25 °C.

propanol obtained at 25 °C is shown in Fig. 4. Conductance data have been analyzed by the treatment proposed by Davis[6] and Monk,[7] in which deviations from the limiting Onsager equation are interpreted in terms of ion-association. At concentrations where the extent of association is small, the second step of Eq. 1 can be disregarded and the solution contains three species: M^{2+}, MX^-, and X^-. If α is the fraction of intermediate product, MX^-, defined in Eq. 2 (neglecting the difference between m (mol/kg) and c (mol/l), this α is consistent with that defined in Eq. 2. This assumption can be acceptable in these experimental conditions.), the equivalent conductivity will be given by:

$$\Lambda = (1-\alpha)\Lambda_{M^{2+}} + \frac{1}{2}\Lambda_{MX^-} + \left(1-\frac{\alpha}{2}\right)\Lambda_{X^-}$$
$$\Lambda = (1-\alpha)(\Lambda_{M^{2+}}+\Lambda_{X^-}) + \frac{\alpha}{2}(\Lambda_{MX^-}+\Lambda_{X^-}) \quad (9)$$

In this equation, the solution is regarded as a mixture

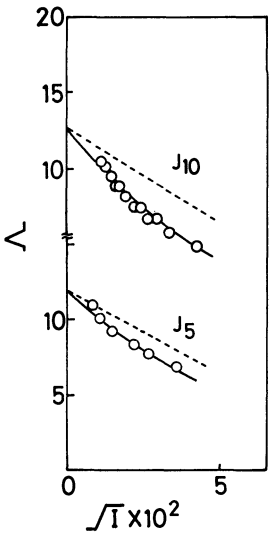

Fig. 4. Relationships between Λ and concentration for J5, and J10 in 2-propanol at 25 °C.

of a completely dissociated uni-bivalent salt of concentration c, where c refers to the molar concentration of the solution (mol/l).

In solving the equation for α, the equivalent conductivity at infinite dilution of the intermediate ion is indespensable. The equivalent conductivity of intermediate product, Λ_{MX^+}, is assumed to be 0.6 times of $\Lambda_{M^{2+}}$, similarly to that of Monk *et al.* Using the values of λ_{Br^-} in the literature,[15] the values of $\lambda^\circ_{M^{2+}}$ were determined by the extrapolating procedure in the plots of Λ *vs.* $I^{1/2}$. Using the limiting Onsager equation, the empirical equations were obtained:

$$\Lambda = 12.0-111.13I^{1/2}-\alpha(6.11-74.07I^{1/2}) \text{ for J5,}$$
$$\Lambda = 15.6-125.23I^{1/2}-\alpha(8.61-86.18I^{1/2}) \text{ for J10} \quad (10)$$

The dissociation constant K_d^I can be obtained *i.e.*

$$K_d^I = \frac{c(2-\alpha)(1-\alpha)}{\alpha}\frac{\gamma_{M^{2+}}\gamma_{X^-}}{\gamma_{MX^+}} \quad (11)$$

By means of the usual computer method, using Eqs. 10 and 11, the dissociation constant K_d^I was determined so that the standard deviation

$$\sigma^2 = \Sigma\left(\frac{\Lambda_{exp}-\Lambda_{cal}}{\Lambda_{exp}}\right)^2 \quad (12)$$

is minimized.

The values obtained for J5 and J10 are summarized in the 5 th column of Table 3; In Fig. 4, solid lines show the best fitting ones. In Fig. 4, the dashed lines show the limiting Onsager's law.

Discussion

The VPO measurements were carried out at different temperatures because of the different optimum experimental conditions for the three solvents. In order to compare the K_d values obtained from the two techniques it was necessary to estimate the K_d^I and K_d^{II} values from VPO measurements for 25 °C. In a previous paper,[10] the apparent activation energy ΔH of ionic association was estimated to be 3.3 and 3.9 kcal/mol for J5 and J10,

respectively, in 2-propanol. As well, the ionic association constants in nonaqueous solvent depend mainly on the dielectric constant and its temperature dependence. Assuming the temperature dependence of K_d^I and K_d^{II} to be equivalent, the activation energies in methanol and ethanol were estimated from the values in 2-propanol, taking into consideration the difference in dielectric constants of the solvents. The estimated values for the VPO method at 25 °C are shown in brackets, in Table 3. It is seen that the agreement between K_d^I values at 25 °C derived from VPO and conductance data is within an order of magnitude. Figures 1—4 also show that there is no apparent evidence of micell formation in these systems.

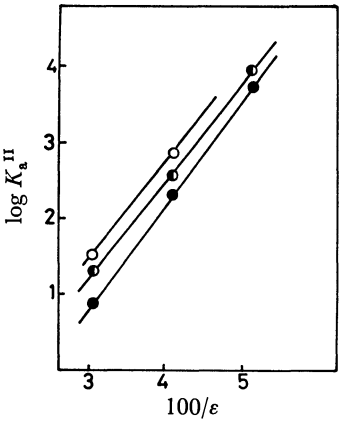

Fig. 5. Relationships between log K_a^{II} and $100/\varepsilon$
○; J4, ◐; J5, ●; J10.

Solvent and Ionic Dependence of Ionic Accosiation Constants. In each solvent, the ionic association constant, K_a^I and K_a^{II}, defined as $K_a=1/K_d$, tends to decrease with increasing ionic size. (As usual, the equilibrium properties of electrolytes in nonaqueous solvents are discussed using the ionic association constant, K_a, rather than K_d. We will talk about K_a instead of K_d.) This tendency is greater in K_a^{II} than in K_a^I. The K_a^I values of bis-(tetraalkylammonium) electrolyte show virtually no dependence on the dielectric constant of solvent. On the contrary, the values of K_a^{II} strongly depend on the dielectric constant of the solvent. The relationship between log K_a^{II} and $100/\varepsilon$, where ε refers to the dielectric constant of solvent, is shown in Fig. 5. As is seen in Fig. 5, log K_a^{II} increases linearly with increasing values of $100/\varepsilon$. This behavior is in good agreement with that of tetraalkylammonium ions in nonaqueous solvents.[15] This result indicates that the ionic association in step II (in Eq. 1) is a solvent-separated type. It looks strange that in 2-propanol, the values of K_a^{II} are greater than that of K_a^I for both J5 and J10. However, as pointed by Evans *et al.*[15] and discussed in our previous paper,[10] the Et_4N^+, Br^- ions and Et_4NBr in 2-propanol are strongly solvated with 2-propanol. It may be considered that J5 and J10 are also strongly solvated with 2-propanol as solvent. At this stage, the solvent effects on the dissociation equilibria of J5 and J10 in 2-propanol can not be explained completely, but it may be roughly considered as follows: The value of K_a^I and K_a^{II} for J10 in 2-propanol are comparable and also of the same order of magnitude as K_a for Et_4NBr in 2-propanol, 8.45×10^{-4} by conductometry[15] and 5.05×10^{-4} by VPO. This fact clearly indicates that in a solvent of low dielectric constant, the ionic sites of $J10^{2+}$ ion act independently because of the long distances between them.

Interpretations for Dynamic Data by Means of Ultrasonic Method: In a previous paper,[10] ultrasonic absorption data obtained over the frequency range 5—95 MHz by the pulse method were reported for tetraethylammonium bromide, J5, and J10 in 2-propanol in the temperature range 0—25 °C. A single relaxation curve was observed under all experimental conditions. However, because of the lack of thermodynamic and conductance data for J5 and J10, a complete kinetic analysis could not be carried out.

The equilibria, Eq. 1, can be symbolized as

$$\mathrm{A} \underset{k_{-1}}{\overset{k_1}{\rightleftharpoons}} \mathrm{B} \underset{k_{-2}}{\overset{k_2}{\rightleftharpoons}} \mathrm{C} \qquad \begin{matrix} & \mathrm{D} & & \mathrm{D} \end{matrix} \tag{13}$$

where A, B, C, and D refer to MX_2, MX^+, M^{2+}, and X^- in Eq. 1 respectively, and the equilibrium concentration of them is shown as $\bar{A}$, $\bar{B}$, $\bar{C}$, and $\bar{D}$, respectively. As shown by the VPO data, this two-step reaction should be closely coupled. Under such conditions, the reciprocal relaxation terms can be expressed as[16,17]

$$\left.\begin{aligned} 2\pi f_{r1} &= \frac{1}{\tau_1} = \frac{a_{11}+a_{22}}{2}[1+(1-b)]^{1/2} \\ 2\pi f_{r2} &= \frac{1}{\tau_2} = \frac{a_{11}+a_{22}}{2}[1-(1-b)]^{1/2} \end{aligned}\right\} \tag{14}$$

and

$$b = \frac{4(a_{11}a_{22}-a_{12}a_{21})}{(a_{11}+a_{22})^2}$$

where

$$\begin{aligned} a_{11} &= k_1 + k_{-1}(\bar{B}+\bar{C}) \\ a_{12} &= -k_1(\bar{B}-\bar{C}) \\ a_{21} &= -(k_2+k_{-2}\bar{C}) \\ a_{22} &= -k_2 + k_{-2}(\bar{C}+\bar{D}) \end{aligned}$$

and the maximum excess absorption per wavelength is in this case represented by

$$\left.\begin{aligned} \mu_{max\,1} &= \frac{\pi(\Delta V_1+X\Delta V_2)^2}{2\beta_0 RT}\left\{\left(\frac{1}{\bar{A}}+\frac{1}{\bar{B}}+\frac{1}{\bar{C}}\right)\right. \\ &\quad \left. + 2X\left(\frac{1}{\bar{D}}-\frac{1}{\bar{B}}\right) + X^2\left(\frac{1}{\bar{B}}+\frac{1}{\bar{C}}+\frac{1}{\bar{D}}\right)\right\}^{-1} \\ \mu_{max\,2} &= \frac{\pi(Y\Delta V_1+\Delta V_2)^2}{2\beta_0 RT}\left\{\left(\frac{1}{\bar{A}}+\frac{1}{\bar{B}}+\frac{1}{\bar{C}}\right)Y^2\right. \\ &\quad \left. + 2Y\left(\frac{1}{\bar{D}}-\frac{1}{\bar{B}}\right) + \left(\frac{1}{\bar{B}}+\frac{1}{\bar{C}}+\frac{1}{\bar{D}}\right)\right\}^{-1} \end{aligned}\right\} \tag{15}$$

where

$$X = \frac{-k_2-k_{-2}\bar{C}}{a_{11}+1/\tau_2}$$

$$Y = \frac{k_{-1}(\bar{D}-\bar{B})}{a_{22}+1/\tau_1}$$

Using the ionic association constants for J5 and J10

reported here, we can estimate the experimental relaxation frequencies. Since the kinetic constants, k_{-1} and k_{-2}, can be considered to represent diffusion control processes, their values are of the order of 10^{-10} $M^{-1}\,s^{-1}$. Assuming the values of k_{-1} and k_{-2} to be 2.35×10^{-10}, which is obtained for Et_4NBr in 2-propanol, the values of k_1 and k_2 can be estimated from the values of K_a^{I} and K_a^{II}.

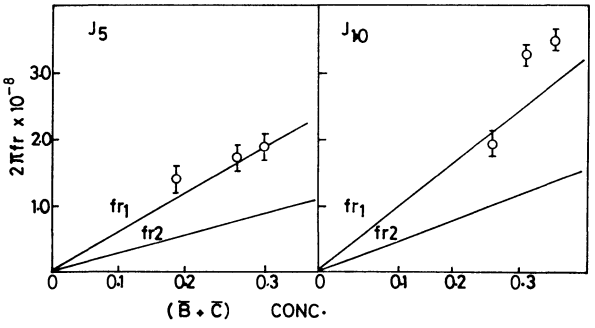

Fig. 6. Relationships between $2f_r$ and $(\bar{B}+\bar{C})$ in Eq. 14 (solid lines show the estimated one) for J5 and J10 in 2-propanol.

Figure 6 shows the relaxation frequencies estimated by the above method for J5 and J10 in 2-propanol at 25 °C. For J5 in 2-propanol, the agreement between the estimated and experimental values of higher relaxation frequencies is good. However, for J10 the agreement is not so good, but still within an order of magnitude. Considering the assumptions used for VPO data analysis and the method of obtaining these estimates, this difference is acceptable.

For the case of J5 in 2-propanol, the maximum excess absorption per wavelength should be expressed by Eq. 15. In Eq. 15, the value of Y is almost zero and from a plot of $\mu_{max\,2}$ against $(1/\bar{B}+1/\bar{C}+1/\bar{D})$. One can estimate the value of ΔV_2 to be 52.9 ml/mol. This value is of a reasonable magnitude and compares with that for malonic acid in aqueous solution, 50.3 ml/mol.[17]

References

1) H. Nomura, M. Ando, and Y. Miyahara, *Nippon Kagaku Zasshi*, **90** 1222 (1969).
2) H. Nomura, M. Ando, and Y. Miyahara, *Nippon Kagaku Zasshi*, **91**, 840 (1970).
3) M. Imura, H. Nomura, F. Kawaizumi, and Y. Miyahara, *Bull. Chem. Soc. Jpn.*, **47**, 2559 (1974).
4) H. C. Lee and Y. Miyahara, *Bull. Chem. Soc. Jpn.*, **51**, 1012 (1978).
5) H. C. Lee and Y. Miyahara, *Bull. Chem. Soc. Jpn.*, **51**, 3140 (1978).
6) E. C. Righellate and C. W. Davis, *Trans. Faraday Soc.*, **26**, 592 (1930).
7) I. L. Jenkins and C. B. Monk, *J. Am. Chem. Soc.*, **72**, 2695 (1950).
8) T. L. Broadwater, T. J. Murphy, and D. F. Evans, *J. Phys. Chem.*, **80**, 753 (1976).
9) J. Thomas and D. F. Evans, *J. Phys. Chem.*, **76**, 3812 (1972); T. L. Broadwater and D. F. Evans, *J. Phys. Chem.*, **73**, 3985 (1969).
10) R. E. Verrall and H. Nomura, *J. Solution Chem.*, **6**, 541 (1977).
11) E. Güntenberg, *Z. Phys. Chem.*, **123**, 199 (1926).
Unfortunately, at this stage, we have no experimental values of ionic radii of bis(tetraalkylammonium) electrolytes in nonaqueous solvents, and so we have used Eq. 4 to calculate values of $\gamma_\pm$. However, as seen in Ref. 12, in the very low concentrations, as in this work, the difference between observed and calculated ones from Eq. 4 can be negligible small.
12) R. A. Robinson and R. H. Stokes, "Electrolyte Solutions," 2nd ed, Butterworth, London (1965).
13) L. A. Burns and R. E. Verrall, *J. Solution Chem.*, **2**, 489 (1973).
14) As seen in Ref. 11, the only reason to use Monk and Davis' method is that it does not need the values of the ionic radii.
15) M. A. Matesich, J. A. Nadas, and D. F. Evans, *J. Phys. Chem.*, **74**, 4568 (1970).
16) L. G. Jackopin and E. Yeager, Technical Report No. 35. ONR Contract No. 1430(04), Project No. 384—305, Western Reserve University, 1969.
17) T. Sano and T. Yasunaga, *J. Phys. Chem.*, **77**, 2031 (1973).

An Application of Neutron Activation Analysis to Biological Materials. III. Natural Abundance of Small and Micro Amounts of Elements and Their Interactions in Human Tissues

Minoru TERAI,* Akiko AKABANE, Michio MATSUMOTO,** and Keisuke HASHIMOTO**

Department of Chemistry, Faculty of Science, Tokyo Metropolitan University, Fukasawa, Setagaya-ku, Tokyo 158

***The Pathological Institute, Juntendo University, School of Medicine, Hongo, Bunkyo-ku Tokyo 113*

(Received January 24, 1979)

The natural abundance of the principal inorganic elements in five human tissues (brain, kidney, lung, liver, and heart) have been determined by neutron activation analysis. Cl, K, and Mn are equally distributed in all tissues. The highest concentration of Sc(0.22 ± 0.044 ppm) is found in the liver. V(0.64 ± 0.51 ppm) and Cr (0.19 ± 0.11 ppm) concentrations in the lung are significantly higher than in other tissues at a 95% confidence level. The lowest concentration of Br(2.7 ± 1.8 ppm) is found in the brain. The highest concentration of Cd (74 ± 11 ppm) appears in the kidney and differs significantly from that in other tissues. Significant correlations appear to exist between many pairs of elements in the kidney and the lung, whereas there are relatively few in the liver. The normal significant correlations between Na, Cl, K, Sc, Zn, Se, Cd, and other elements are given.

There are increasing reports concerning the physiological activity of small or micro amounts of metals contained in the cells or tissues of several organs. For example, micro amounts of Cu in the human body play an important role in hematopoitic activity.[1] Wilson's disease (hepato-lenticular degeneration) is at times characterized by an accumulation of Cu in the liver and brain tissues.[2] Schroeder[3] reported that Cd is related to the hypertension found in man. Hadjimarkos[4,5] suggested that trace amounts of Se appear capable of increasing the susceptibility to dental caries. Se is also reported to offer protection against human cancer.[6,7] Dick[8] has reported the physiological interactions between Cu, Mn, Mo, and sulfate. And Gather *et al.*[9] reported the role of Se in preventing the hazardous action of organic mercury. Sufficient information, however, concerning the effect of trace amounts of heavy metals in human tissues on physiological activities remains scant. Physiological functions in the human body are influenced by the heavy metals and chemical compounds are required further investigation. In this study, an attempt has been made to determine simultaneously the concentration of 15 elements in specified pathological conditions. The organs studied have been the brain, kidneys, lung, liver, and heart. The abundances and interactions of the elements in these tissues have been determined by neutron activation analysis.

Experimental

Collection and Preparation of the Samples. The human tissues analyzed were obtained from 9 autopsy cases examined in the Pathological Institute, Juntendo University, School of Medicine, Tokyo. Tissue samples were taken from minimally affected areas in the above mentioned organs, taking special care to avoid local neoplastic invention. All samples were dried in the desiccator (P_2O_5) for 7 days. The dried tissues (50 mg) were weighed and heat-sealed in clean polyethylene bags. The distribution of age, sex, and the causes of death are shown in Table 1.

Preparation of the Reference Samples. High purity metals, Mg, Cr, Mn, Fe, Co, Cu, Zn, and Cd, and special grade NaCl, KBr, Sc_2O_3, SeO_2, and V_2O_5 were used as standard material. A definite amount of each metal or compound was dissolved in nitric acid or pure water. A reference standard was prepared by pipetting an appropriate volume of the stock solution, impregnating it in a small sheet of filter paper and drying at room temperature. The amounts of Na, Mg, K, Cr, Mn, Fe, Cu, Zn, Se, and Cd in the reference standard were 1 μg, those of Co, Sc, and V were 0.1 μg and those of Cl and Br were 1.54 and 2.04 μg. The sheets of filter paper

TABLE 1. DISTRIBUTION OF AGE, SEX AND THE CAUSES OF DEATH FOR THE SUBJECTS

Age (years)	Sex	The causes of death
7	f	Pyothorax
40	f	Cerebello-pontine-angle tumor
61	f	Olivo-ponto-celebellar atrophy
34	m	3rd degree burn
51	m	Liver cirrhosis
61	m	Liver cirrhosis
62	m	Myocard infarction
63	m	Myocard infarction
70	m	Hodgkin's disease

a) f: female, m: male.

TABLE 2. THE NUCLEAR DATA OF THE NUCLIDES USED IN THIS STUDY

Stable isotope	Natural abundance (%)	Nuclear reaction	Radio isotope	Half life	γ-Ray energy (keV)
^{23}Na	100	n, γ	^{24}Na	15.1 h	1367
^{26}Mg	11.7	n, γ	^{27}Mg	9.45 m	1014
^{37}Cl	24.47	n, γ	^{38}Cl	37.3 m	1642
^{41}K	6.68	n, γ	^{42}K	12.4 h	1525
^{45}Sc	100	n, γ	^{46}Sc	83.4 d	1120
^{51}V	99.75	n, γ	^{52}V	3.57 m	1434
^{50}Cr	4.31	n, γ	^{51}Cr	27.8 d	320
^{55}Mn	100	n, γ	^{56}Mn	2.57 h	1811
^{58}Fe	0.33	n, γ	^{59}Fe	45 d	1099
^{59}Co	100	n, γ	^{60}Co	5.26 y	1173
^{65}Cu	30.91	n, γ	^{66}Cu	5.1 m	1039
^{64}Zn	48.9	n, γ	^{65}Zn	245 d	1115
^{74}Se	0.87	n, γ	^{75}Se	120 d	265
^{79}Br	50.5	n, γ	^{80}Br	17.6 m	617
^{114}Cd	100	n, γ	^{115}Cd	2.69 d	412

Table 3. The mean values and the standard deviations of the elements in the human tissues (ppm)

Elements	Brain M.V.±S.D.	Kidney M.V.±S.D.	Lung M.V.±S.D.	Liver M.V.±S.D.	Heart M.V.±S.D.
Na	1900±720	1000±710	2200±1800	970±670	1400±780
Mg	810±310	510±460	520±290	500±350	400±170
Cl	1000±550	990±570	1700±1200	870±480	1100±540
K	130±43	69±48	140±110	83±36	110±60
Sc	0.0069±0.0029	0.0065±0.0032	0.054±0.040	0.22±0.044	0.0087±0.0040
V	0.11±0.063	0.13±0.11	0.64±0.51	0.17±0.13	0.12±0.087
Cr	0.044±0.023	0.041±0.020	0.19±0.11	0.041±0.017	0.038±0.018
Mn	2.6±1.0	2.9±1.6	3.1±1.7	3.9±2.0	2.3±0.69
Fe	12±7.7	23±12	25±8.1	37±28	13±8.7
Co	0.0088±0.0049	0.034±0.039	0.018±0.0085	0.021±0.013	0.013±0.0076
Cu	37±11	14±10	9.4±5.5	22±14	16±7.2
Zn	87±23	140±45	100±34	140±63	99±23
Se	1.5±0.50	3.7±1.5	0.80±0.29	2.0±0.35	1.6±0.59
Br	2.7±1.8	35±26	44±40	7.7±3.6	19±17
Cd	4.1±3.0	74±11	6.2±3.8	12±8.9	4.7±2.0

a) M.V.: mean value, S.D.: standard deviation.

were then heat-sealed in clean polyethylene bags.

Neutron Activation and Determination of γ-Ray Spectra. Samples and reference standards were irradiated in a rotary specimen rack in a TRIGA MARK II reactor (Rikkyo University) with a thermal neutron flux of 5×10^{11} n·cm^{-2}·s^{-1}. The irradiation period was 3 min for short-lived nuclides, and 24 h(intermittent irradiation of 6 h a day for 4 days) for long-lived nuclides. Irradiated samples and reference sample were removed from the polyethylene bag and transferred to new one before measuring the γ-ray spectra.

The γ-ray spectra were determined on a Ge(Li) γ-ray detector and 4096 channel pulse height analyzer (Type 8100: Camberra Inductries Inc. USA).

The nuclear data of the nuclides used in this study, are shown in Table 2.

Results and Discussion

The data have been analyzed by evaluating the mean values and the standard deviations for 15 elements in each tissue, after rejection of the widely different values according to the method of Smirnoff, the results of which are shown in Table 3. The results of the t-test for the elemnts for every two tissues are shown in Tables 4(1)—(8). In the Tables, the symbol "*" illustrates the significant difference in mean values between two tissues at a 95% confidence level. The coefficient of correlation for every two elements in each tissue are shown in Tables 5(1)—(3). In Table 5, the symbols

Tabel 4. The significant difference in the abundance of the elements in human tissue at 95% confidence level

(1) Na and Mg

Mg \ Na	Bn	Ky	Lg	Lr	Ht
Bn		**	--	**	--
Ky	--		--	--	--
Lg	--	--		--	--
Lr	--	--	--		--
Ht	**	--	--	--	

(2) Cl and K

K \ Cl	Bn	Ky	Lg	Lr	Ht
Bn		--	--	--	--
Ky	--		--	--	--
Lg	--	--		--	--
Lr	--	--	--		--
Ht	--	--	--	--	

(3) Sc and V

V \ Sc	Bn	Ky	Lg	Lr	Ht
Bn		--	**	**	--
Ky	--		**	**	--
Lg	**	**		**	**
Lr	--	--	**		**
Ht	--	--	**	--	

(4) Cr and Mn

Mn \ Cr	Bn	Ky	Lg	Lr	Ht
Bn		--	**	--	--
Ky	--		**	--	--
Lg	--	--		**	**
Lr	--	--	--		--
Ht	--	--	--	--	

(5) Fe and Co

Co \ Fe	Bn	Ky	Lg	Lr	Ht
Bn		**	--	--	--
Ky	--		--	--	--
Lg	**	**		**	**
Lr	--	--	**		**
Ht	--	--	**	--	

(6) Cu and Zn

Zn \ Cu	Bn	Ky	Lg	Lr	Ht
Bn		--	--	--	--
Ky	**		--	--	--
Lg	--	--		--	--
Lr	--	--	--		--
Ht	--	--	--	--	

(7) Se and Br

Br \ Se	Bn	Ky	Lg	Lr	Ht
Bn		**	**	--	--
Ky	**		**	**	**
Lg	**	--		--	--
Lr	**	--	--		--
Ht	**	--	--	--	

(8) Cd

Cd	Bn	Ky	Lg	Lr	Ht
Bn		**	--	--	--
Ky			**	**	**
Lg				--	--
Lr					--
Ht					

**: Significant difference at a 95% confidence level.
--: No difference.
Bn: Brain, Ky: Kidney, Lg: Lung, Lr: Liver, Ht: Heart.

"**" and "*" show the significant correlation at 95% and 99% confidence levels respectively. The symbols "−**" and "−*" show the reverse correlations at the same levels. The symbols "+" and "−" show the tendency of normal and reverse interactions.

The Abundances of the Elements in Human Tissue (Table 3). *Sodium*: The highest concentration of Na is found in the lung, but no significant difference exists in the average value of Na for any pair of tissues. Na and Cl are the main electrolytes in blood serum and therefore, it appears that the high content of Na and Cl in the lung are influenced by the blood volume existing at the time of death. The standard deviation of Na level is small in the brain and the mean value differs significantly from those in the kidney and liver at a 95% confidence level (Table 4 (1)).

Magnesium: The concentration of Mg in the brain is relatively higher than that in other tissues and is significantly different from the smallest level found in the heart at a 95% confidence level. The mean values of Mg were found to be small for all tissues except the brain (Table 4 (1)).

Chlorine: The highest concentration of Cl as well as Na is in the lung. No significant differences were found

TABLE 5-1. THE CORRELATIONS OF THE ELEMENTS IN THE HUMAN TISSUES

Brain

Kidney	Na	Mg	Cl	K	Sc	V	Cr	Mn	Fe	Co	Cu	Zn	Se	Br	Cd
Na		−**	*	+	*	*	−**	+	+	**	−	+	*	+	**
Mg	−		−*	−*	−	−	**	−	−	+	−	+	−	−	−**
Cl	*	+		+	*	+	−*	−	+	+	−	−	**	+	*
K	*	*	*		*	+	−	−	−	−	+	−*	+	−	*
Sc	*	+	+	+		*	−**	−*	+	+	−	−	*	+	*
V	−*	**	−**	−**	−**		−*	−**	−	**	−	−	−	−	**
Cr	+	−	+	+	+	+		+	+	−	**	+	−	−	−*
Mn	**	+	**	*	+	−	−		−**	−	+	−	−	+	−*
Fe	+	*	+	*	−	−	−	*		*	−	*	*	*	+
Co	**	*	+	*	+	**	−	*	*		−	*	*	*	+
Cu	+	+	−	+	−	−	+	+	**	+		−	−	−	−
Zn	**	+	**	**	*	−	**	**	**	+	*		+	*	−
Se	*	**	*	*	+	−	+	*	*	*	**	*		*	+
Br	+	+	**	+	**	+	*	+	−	−	−	+	+		+
Cd	*	+	*	*	+	−	*	+	+	+	+	*	**	*	

*, ** : Significant correlation at a 99% and 95% levels

−*, −** : Reverse significant correlation at a 99% and 95% levels

TABLE 5-2. THE CORRELATIONS OF THE ELEMENTS IN THE HUMAN TISSUES.

Liver

Lung	Na	Mg	Cl	K	Sc	V	Cr	Mn	Fe	Co	Cu	Zn	Se	Br	Cd
Na		+	*	*	−	−	−	−	−	+	*	−	−	+	−
Mg	+		−	+	+	−	−	−	−	**	−	−	−	−	−
Cl	*	+		*	−	−*	+	+	−	+	*	−	+	+	+
K	*	*	*		−	−**	+	−	+	−	*	−	+	−	+
Sc	*	*	*	*		−	−	+	+	+	−	*	+	−	+
V	+	*	+	+	**		−	−	−	−	−	−	−	−	*
Cr	**	*	+	*	*	+		+	*	−**	+	−	+	−	−
Mn	+	−	+	−	+	−	−		+	−	−	+	*	−	*
Fe	**	**	**	*	+	+	+	+		−	−	−	+	−	−
Co	+	+	+	**	+	+	*	−	+		−	**	+	+	+
Cu	+	+	+	+	*	−	*	*	**	+		−	−	−	−
Zn	*	*	*	*	*	**	*	+	+	+	*		**	−	*
Se	8	*	**	*	*	+	−*	+	+	+	*	**		−	*
Br	**	*	*	+	*	*	+	−	−	−	−	*	+		−
Cd	+	*	+	+	*	**	+	*	+	−	*	**	*	**	

TABLE 5-3. THE CORRELATION OF THE ELENTS IN THE HUMAN TISSUES

Heart

	Na	Mg	Cl	K	Sc	V	Cr	Mn	Fe	Co	Cu	Zn	Se	Br	Cd
Na		-	*	*	-*	+	-*	*	+	-	+	+	+	+	+
Mg			-	+	*	+	+	+	-	-	+	-*	+	-	-*
Cl				*	-	+	-*	**	+	-	+	**	+	+	+
K					-	**	-*	**	+	-	+	-	*	-	-
Sc						+	+	-	-	-	-	-*	-	-	-*
V							*	+	-	+	-	+	**	-	-**
Cr								-*	-	*	-*	+	-*	+	-
Mn									+	+	+	+	**	-	-
Fe										-	*	-	+	-**	+
Co											-	**	-	+	+
Cu												-	+	-	+
Zn													-	+	*
Se														-**	-
Br															+
Cd															

between the pairs of tissues analyzed (Table 4 (2)).

Potassium: The distribution of K is similar to that for Na and Cl (Table 4 (2)).

Scandium: Little data on the physiological activities and/or toxicities of Sc in human body exists.[10] Sc is widely distributed in all the organs but the highest concentration of Sc is observed in the liver. The concentrations of Sc decrease in the following order: lung, heart, brain and kidney (Table 4 (3)).

Vanadium: The highest mean value of V is found in the lung, corroborating the data of Tipton and Cook.[11] The average value of V in the lung significantly differs from that found in the other organs at a 95% confidence level, but in the other organs there are no significant differences in the V contents. Schroeder[12] found trace amounts of V in the lungs of sucklings and higher V levels in the adult lungs. In the lung of a 7 year old girl the V concentration was found to be 0.0083 ppm, although the average level in adult lungs is 0.72 ± 0.49 ppm. This suggests that the large amounts of V in the adult lung results from an accumulation of inhaled fly ash (Table 4 (3)).

Chromium: The abundances of Cr are similar to V. As Cr is one of the essential elements in living cells, it is widely distributed in all organs. The higher abundance in the lung may be attributed to the accumulation of fly ash deposition in the pulmonary tissues through inhalation. The Cr concentration gradually enriches in the lung due to ageing[13] (Table 4 (4)).

Manganese: Manganese is widely distributed in all the tissues. No significant differences however were found in any two tissues and the results are slightly higher than that reported by Sumino *et al.*[14] and Tipton *et al.*[11] The weight loss of the tissues after drying for 7 days is *ca.* 80% for the wet weight, and consequently the figures cannot be compared without a calibration (Table 4 (4)).

Iron: The mean value of Fe is slightly lower in the brain and the heart than in other tissues (Table 4 (5)).

Cobalt: The highest value of Co is found in the kidney and the lowest in the brain. The average content of Co is widely distributed in each tissue (Table 4 (5)).

Copper: The highest content of Cu is present in the brain and significant differences exist between some pairs of tissues such as the brain and the kidney, the lung and the heart, the lung and the liver at 95% confidence level. The value of 22 ppm in the liver is lower than the value of 35 ppm reported by Bruckmann and Zondek[15] (Table 4 (6)).

Zinc: Similar abundances of Zn were detected in the kidney and the liver and these results agree with the values of Tipton and Cook.[11] The Zn content in the kidney is significantly higher than in the brain (Table 4 (6)).

Selenium: There are few reports on the Se contents in human tissue.[6,16] The Se concentration in the kidney is significantly higher than in the other tissues. Allaway *et al.*[6] have reported that the Se contents in blood serum inversely correlate with the cancer death rate. Such a trend was not found in the present work (Table 4 (7)).

Bromine: The highest content of Br is found in the lung and the lowest in the brain which amounts to only 6.1% of the lung. One of the authors has reported that the abundance of Br in the optic nerve is smaller than in the other eye organs. Suggesting that Br interferes with the actions of the nervous organs (Table 4 (7)).

Cadmium: An extremely high value of Cd was found in the kidney (74 ± 11 ppm). Several reports[17,18] have suggested that Cd accumulates in the kidney and is not excreted. The Cd content of the standard American has been found to be 30—40 ppm in the kidney and 2—3 ppm in the liver,[19] Whereas in the Japanese it is twice this value.[17] These results therefore are in good agreement[19] (Table 4 (8)).

Interaction of the Elements in Human Tissue. Several interesting facts have emerged from the present study and are shown in the Tables 5 (1)—(3). The principal points are:

Characteristics in the Brain: Several elements have been correlated with other elements, for example, Na normally correlates with Cl, Sc, V, Co, Se, Cd, and inversely with Mg, Cr. Significant inverse correlations were found between (Mg and Na, Cl, K, Cd), (Cr and Na, Cl, Sc, V, Cd) and (Mn and Sc, V, Fe, Cd), and a significantly normal correlation between (Na and Cl, Sc, V, Co, Se, Cd), (Sc and Na, Cl, K, V, Se Cd), (Co and Na, V, Fe, Zn, Se, Br), and (Se and Na, Cl, Sc, Fe, Co, Br). Cu in the brain normally correlates with only Cr and other pairs of elements including Cu have inverse interactions.

Characteristics in the Kidney and the Lung: Similar tendencies of correlation of the elements are found in the kidney and the lung. Normal significant correlations exist for each of the pairs of elements in both tissues, and significant inverse correlations in four pairs in the kidney and one pair in the lung. Inverse interactions between V and other elements except Mg, Cr, Co, and Br at the kidney exist.

Sc significantly correlates with Na, Mg, Cl, K, V, Cr, Cu, Zn, Se, Br, and Cd in the lung. A more characteristic factor is that there is a significant inverse correlation between Cr and Se, and there appears inverse interactions in the lung.

Characteristic in the Liver: Inverse interactions exist although no significant correlations are present in the liver.

Characteristics in the Heart: Significant inverse correlations are found between (Cr and Na, Cl, K, Mn, Cu, Se) and (Sc and Na, Zn, Cd). Normal significant correlations are also found between (Cl and Na, K, Mn, Zn) and (K and Na, V, Mn, Se). Such tendencies as reported above are almost uniformly distributed in the elements in the heart.

References

1) R. B. Rucker, H. E. Parker, and J. C. Rogler, *J. Nutr.*, **98**, 57 (1969).
2) G. E. Cartwright, "Symposium on Copper Metabolism," ed by W. D. McElroy and B. Glass, John Hopkins Press, Baltimore, Maryland (1950), p. 244.
3) E. J. Underwood, "Trace Elements in Human and Animal Nutrition," 3rd ed, (1975), Chap. 10.
4) D. M. Hajimarkos, *Arch. Environ. Health*, **10**, 893 (1965).
5) D. M. Hajimarkos, *Caries Res.*, **3**, 14 (1969).
6) R. J. Shamberger and D. V. Frost, *Can. Med. Ass. J.*, **100**, 682 (1969).
7) W. H. Alloway, J. Kubota, F. L. Loses, and M. Roth *Arch. Environ. Health*, **16**, 342 (1968).
8) A. T. Dick, *Soli Sci.*, **81**, 229 (1956).
9) H. E. Ganther, C. Goudie, M. L. Sunde, M. J. Kopecky, P. Wagner, Sang-Hwan Oh, and W. G. Hoekstra, *Science*, **173**, 1121 (1972).
10) J. N. Hathcock, C. H. Hill, and G. Matrone, *J. Nutr.*, **82**, 106 (1964).
11) I. H. Tipton and M. J. Cook, *Health Phys.*, **9**, 103 (1964).
12) H. A. Schroeder, J. J. Balassa, and I. H. Tipton, *J. Chron. Dis.*, **16**, 1047 (1963).
13) H. A. Schroeder, J. J. Balassa, and I. H. Tipton, *J. Chron. Dis.*, **16**, 941 (1962).
14) K. Sumino, K. Hayakawa, T. Shibata, and S. Kitamura, *Arch. Environ. Health*, **30**, 489 (1975).
15) S. Brukmann and S. G. Zondek, *Nature(London)*, **146**, 3 (1940).
16) R. J. Shamberger and D. V. Frost, *Can Med. Ass. J.*, **100**, 682 (1969).
17) H. M. Perry Jr., I. H. Tipton, H. A. Schroeder, R. L. Steiner, and M. J. Cook, *J. Chronic Dis.*, **14**, (1961).
18) H. A. Schroeder and J. J. Balassa, *J. Chronic Dis.*, **14**, 236 (1961).
19) E. J. Underwood, "Trace Elements in Human and Animal Nutrition," 3rd ed, (1975), Chap. 10.

Trimethylenediamine Complexes. VII.[1] Optically Active Mixed-Ligand Cobalt(III) and Chromium(III) Complexes Containing Trimethylenediamine and the Acetylacetonate Anion

Mamoru NAKANO, Shinichi KAWAGUCHI,* and Hiroshi KAWAGUCHI[2]

Department of Chemistry, Faculty of Science, Osaka City University, Sumiyoshi-ku, Osaka 558

(Received February 16, 1979)

The $[M(acac)(tn)_2]^{2+}$ and $[M(acac)_2(tn)]^+$ complexes (M=Co and Cr) have been prepared and resolved by (*R,R*)-tartratoarsenate(III) and hydrogen-(*R,R*)-di-*O*-benzoyltartrate, respectively. On the basis of the CD-spectral studies in comparison with the corresponding ethylenediamine complexes, the absolute configurations of $(+)_{589}$-$[Co(acac)(tn)_2]^{2+}$, $(-)_{589}$-$[Co(acac)_2(tn)]^+$, $(+)_{589}$-$[Cr(acac)(tn)_2]^{2+}$, and $(-)_{589}$-$[Cr(acac)_2(tn)]^+$ were all assigned to *Λ*. Electronic spectra of these complexes and proton NMR spectra of the cobalt(III) complexes are also reported.

There have been published many papers dealing with the interrelation between the Cotton effect and the absolute configuration of dissymmetric metal complexes.[3] The absolute configurations of $(+)_{589}$-$Co(en)_3^{3+}$ [4] and $(-)_{589}$-$Co(tn)_3^{3+}$ [5] were determined by X-ray analysis both to be *Λ*. By comparison of the CD spectrum with that of *Λ*-$Co(en)_3^{3+}$, absolute configurations of a number of dissymmetric D_3 and D_2 complexes have been assigned. Although the CD-spectral feature in the first d-d band region of *Λ*-$Co(tn)_3^{3+}$ [6] is remarkably different from that of *Λ*-$Co(en)_3^{3+}$,[7] the empirical criterion of McCaffery *et al.*[8] seems to be applicable also to the six-membered chelate compounds.[9] However, the assignment of the E and A_2 components of the CD band in the first absorption region is not unambiguous for $Co(tn)_3^{3+}$,[10] whereas *Δ*-$[Co(R,R\text{-ptn})_3]Cl_3 \cdot 2H_2O$ (ptn=2,4-pentanediamine) was confirmed to have negative E and positive A_2 components in the solid-state CD spectrum[11] in accordance with the informations from the solution spectra.[12]

Thus synthesis and examination of the absolute configuration of still more dissymmetric trimethylenediamine complexes especially of metal ions other than cobalt(III) are desired. The present paper is concerned with the optically active $Cr(acac)_x(tn)_{3-x}$ complexes (x=1 or 2), which are compared with the $Cr(acac)_x(en)_{3-x}$ complexes and also with the corresponding cobalt(III) complexes.

Experimental

Preparation and Resolution of Complexes. The starting compounds, *trans*-$[CoCl_2(tn)_2]Cl$,[13] $Na[Co(NO_2)_2(acac)_2]$,[14] *trans*-$[CrCl_2(tn)_2]Cl$,[15] and *cis*-$[CrCl_2(tn)_2]Cl \cdot H_2O$[15] were prepared according to the literatures. The resolving agents, sodium (*R,R*)-tartratoarsenate(III) and (*R,R*)-di-*O*-benzoyltartaric acid were prepared by the reaction of sodium hydrogen-(*R,R*)-tartrate with arsenic(III) oxide[16] and that of (*R,R*)-tartaric acid with benzoyl chloride,[17] respectively.

$(-)_{589}$-Acetylacetonatobis(trimethylenediamine)cobalt(III) Iodide, $(-)_{589}$-[Co(acac)(tn)$_2$]I_2: Preparation and optical resolution of this compound were performed in a similar way as that for the corresponding ethylenediamine complex.[18] To a 1 M sodium hydroxide solution (60 ml) containing acetylacetone (8 g) was added *trans*-$[CoCl_2(tn)_2]Cl$ (12.5 g), and the solution was heated at about 70 °C until it turned red. The solution was then cooled to room temperature and an excess amount (37.5 g) of potassium iodide was added to the solution kept in ice to deposit a red precipitate, which was filtered, washed with cold water followed by cold methanol, and air-dried. The yield was 20.0 g (89.6%) and recrystallization from hot water gave red prisms. Found: C, 23.54; H, 4.94; N, 9.90%. Calcd for $C_{11}H_{27}O_2N_4I_2Co$: C, 23.59; H, 4.86; N, 10.00%.

A mixture of the racemic complex (8 g) and silver acetate (5 g) was stirred in water (25 ml) for 30 min. Silver iodide and unreacted silver acetate were filtered and washed with water (10 ml). To the filtrate was added slowly a solution (8 ml) of sodium (*R,R*)-tartratoarsenate(III) hydrate (3.75 g) and the mixture was kept in a desiccator to precipitate red orange crystals. The yield was 1.5 g (13.4%). Found: C, 29.10; H, 4.50; N, 7.14%. Calcd for $C_{19}H_{35}O_{16}N_4As_2Co$: C, 29.75; H, 4.39; N, 6.98%.

A mixture of the diastereomer (1.5 g) and potassium iodide (1.0 g) was stirred in an 0.1 M sodium hydroxide solution (10 ml) for 10 min to separate out white and red precipitates. When washed with methanol, the red precipitate was dissolved to leave the white one. A red precipitate was recovered on addition of diethyl ether to the washings. The yield was 0.6 g (56.0%). Found: C, 23.49; H, 4.92; N, 9.60%. In order to assure the optical purity, the resolution process was repeated and the final product showed the following molar rotation in aqueous solution at room temperature: $[M]_{589}=-430°$, $[M]_{546}=-1180°$, $[M]_{436}=+6970°$.

$(-)_{589}$-Bis(acetylacetonato)(trimethylenediamine)cobalt(III) Iodide Hydrate, $(-)_{589}$-[Co(acac)$_2$(tn)]$I \cdot H_2O$: A method of preparation analogous to that for $[Co(acac)_2(en)]ClO_4$[19] was employed. Trimethylenediamine (1.2 g) and active charcoal (1.0 g) were added to a solution (100 ml) of $Na[Co(NO_2)_2(acac)_2]$ (6.2 g). After stirring for 15 min at room temperature, the charcoal was filtered and washed with water (30 ml). The filtrate and washings were combined and concentrated to *ca.* 50 ml by evaporation at 50 °C. The concentrate was then filtered and potassium iodide (30 g) was added to the filtrate to precipitate deep red needles on cooling. The yield was 6.5 g (81.9%), and recrystallization from hot water gave deep red needles. Found: C, 32.99; H, 5.52; N, 5.88%. Calcd for $C_{13}H_{26}O_5N_2ICo$: C, 32.79; H, 5.50; N, 5.88%.

After a mixture of the racemic complex (4.5 g) and silver acetate (4.0 g) was stirred in water (20 ml) for 10 min, silver iodide and remaining silver acetate were separated by filtration and washed with water (10 ml). A solution (50 ml) of sodium hydrogen-(*R,R*)-di-*O*-benzoyltartrate (3.6 g) was added slowly to the filtrate and the solution was kept in a desiccator to deposit a deep violet precipitate. The yield was 1.5 g (23.1%). Found: C, 54.13; H, 5.44; N, 3.95%. Calcd for $C_{31}H_{37}O_{12}N_2Co$: C, 54.07; H, 5.42; N, 4.07%.

A mixture of the diastereomer (1.0 g) and silver acetate (1.0 g) was stirred in methanol (20 ml). A precipitate was

filtered and washed with methanol (20 ml). The washings was combined with the filtrate and the solvent was evaporated to dryness. The residue was dissolved in water (5 ml) and the solution was filtered. Solid potassium iodide was added to the filtrate to separate out a deep red precipitate. The yield was 0.3 g (43.4%). Found: C, 32.80; H, 5.50; N, 5.85 %. The specimen was dissolved in a minimum amount of water and the solution was cooled to deposit a precipitate. After filtration, potassium iodide was added to the filtrate to obtain a precipitate which showed an improved optical activity. This procedure was repeated to attain the following constant molar rotation in aqueous solution at room temperature: $[M]_{589}=-1810°$, $[M]_{546}=+9140°$, $[M]_{436}=-15610°$.

$(+)_{589}$-Acetylacetonatobis(trimethylenediamine)chromium(III) Iodide Hemihydrate, $(+)_{589}$-[Cr(acac)(tn)$_2$]I$_2\cdot 0.5H_2O$: To an aqueous solution (25 ml) of acetylacetone (1.0 g) and sodium hydroxide (0.4 g) was added *cis*-[$CrCl_2(tn)_2$]Cl·H_2O (3.3 g), and the mixture was stirred at 70 °C to become a clear orange solution. After cooling to room temperature, solid potassium iodide (10 g) was dissolved in the solution, which was then kept in an ice bath to separate out an orange precipitate. The crude product was filtered, washed with small portions of water and acetone successively and air-dried. The yield was 2.0 g (35.0%) and recrystallization from hot water gave orange plates. Found: C, 23.61; H, 5.01; N, 9.94; I, 45.09 %. Calcd for $C_{11}H_{28}O_{2.5}N_4I_2Cr$: C, 23.50; H, 5.02; N, 9.96; I, 45.14%.

In a similar manner to the corresponding cobalt(III) complex, the racemic compound (2.0 g) was converted to the acetate and resolved by the (*R,R*)-tartratoarsenate(III). The diastereomer (0.9 g) was then treated with potassium iodide to give $(+)_{589}$-[Cr(acac)(tn)$_2$]I$_2\cdot 0.5H_2O$ (0.3 g). Found: C, 23.58; H, 4.98; N, 9.73%. After repeated resolution the final specimen showed the following molar rotation in aqueous solution at room temperature: $[M]_{589}=+310°$, $[M]_{546}=+630°$, $[M]_{436}=-5020°$.

$(-)_{589}$-Bis(acetylacetonato)(trimethylenediamine)chromium(III) Iodide Hydrate, $(-)_{589}$-[Cr(acac)$_2$(tn)]I·H_2O: To an aqueous solution (50 ml) of acetylacetone (2.0 g) and sodium hydroxide (0.8 g) was added *trans*-[$CrCl_2(tn)_2$]Cl (3.1 g), and the mixture was heated at 70 °C to result in a red solution. After cooling solid potassium iodide (10 g) was added and the solution was kept in ice to form a red precipitate, which was filtered and extracted with acetone. The solvent was evaporated and the residue was recrystallized from hot water to obtain red needles. The yield was 1.5 g (32.2%). Found: C, 33.67; H, 5.59; N, 6.09; I, 27.45%. Calcd for $C_{13}H_{26}O_5N_2ICr$: C, 33.27; H, 5.58; N, 5.97; I, 27.04%.

The racemic iodide (1.5 g) was converted to the acetate and resolved by the (*R,R*)-di-*O*-benzoyltartrate. The diastereomer (2.7 g) was treated in a similar manner as the case of $[Co(acac)_2(tn)]^+$ to obtain $(-)_{589}$-[Cr(acac)$_2$(tn)]I·H_2O (1.4 g). Found: C, 34.18; H, 5.40; N, 5.98%. The resolution procedure was repeated until the following constant molar rotation was observed in aqueous solution at room temperature: $[M]_{589}=-420°$, $[M]_{546}=+5000°$, $[M]_{436}=-5750°$.

Measurements. The electronic absorption spectra were measured by a Hitachi EPS-3T spectrophotometer. The optical rotations were determined with a Yanagimoto OR-50 polarimeter, and the CD spectra with JASCO J-20 recording spectrometer. The proton NMR spectra were recorded on a JEOL-C 60HL spectrometer with TMS as an external reference.

Results and Discussion

The mixed ligand complexes [Co(acac)(en)$_2$]I$_2$·H_2O,[18] [Co(acac)$_2$(en)]I,[20] [Cr(acac)(en)$_2$]Cl$_2$·H_2O,[21] and [Cr(acac)$_2$(en)]Cl·$1.5H_2O$[21] were prepared and resolved by $Na_2[(R,R)As_2(C_4H_2O_6)_2]\cdot 2H_2O$ according to previously reported procedures. The same resolving agent was successfully applied to the acetylacetonatobis(trimethylenediamine) complexes. The enantiomer of $[Co(acac)(tn)_2]^{2+}$ forming a less-soluble diastereomer with the resolving agent shows an opposite CD pattern as compared with that of the corresponding diastereomer of $[Co(acac)(en)_2]^{2+}$ as is seen in Fig. 1. It is worth noting that the solubility criterion for relative configuration does not hold even in this couple of quite similar complexes. In the case of bis(acetylacetonato)(trimethylenediamine) complexes, on the other hand, the tartratoarsenate was not suitable and the di-*O*-benzoyltartrate was used as a resolving agent. Brennan, Igi, and Douglas resolved $[Co(acac)_2(tn)]^+$ as the (*R,R*)-tartrate.[22]

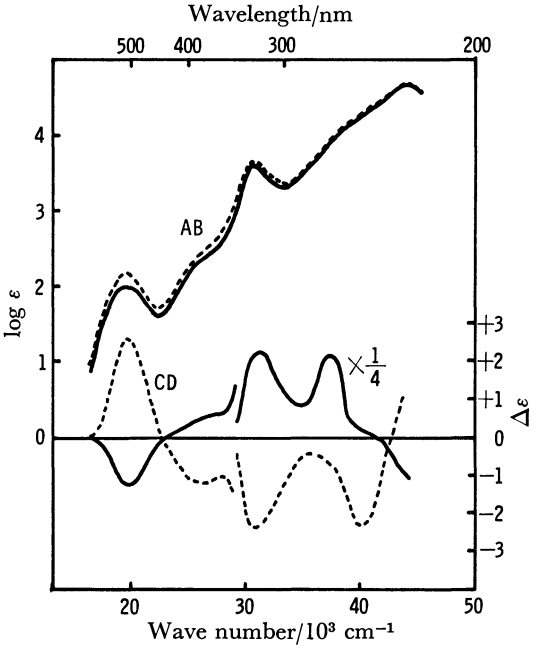

Fig. 1. Absorption (AB) and circular dichroism (CD) spectra of $(-)_{589}$-[Co(acac)(tn)$_2$]I$_2$ (——) and $(+)_{589}$-[Co(acac)(en)$_2$]I$_2$·H_2O (----) in water.

The cobalt(III) complexes $(-)_{589}$-$[Co(acac)(tn)_2]^{2+}$ and $(-)_{589}$-$[Co(acac)_2(tn)]^+$ are quite stable and the aqueous solutions showed no change in the optical rotation at room temperature over one month. On the contrary, the corresponding chromium(III) complexes are not so stable. The optical rotations of $(+)_{589}$-$[Cr(acac)(tn)_2]^{2+}$ and $(-)_{589}$-$[Cr(acac)_2(tn)]^+$ in aqueous solutions diminished gradually on standing at room temperature to one-half after six days. The absorption spectra also changed, indicating that reactions other than racemization proceeded.

Electronic Spectra. The electronic absorption spectra of the complexes obtained are displayed in

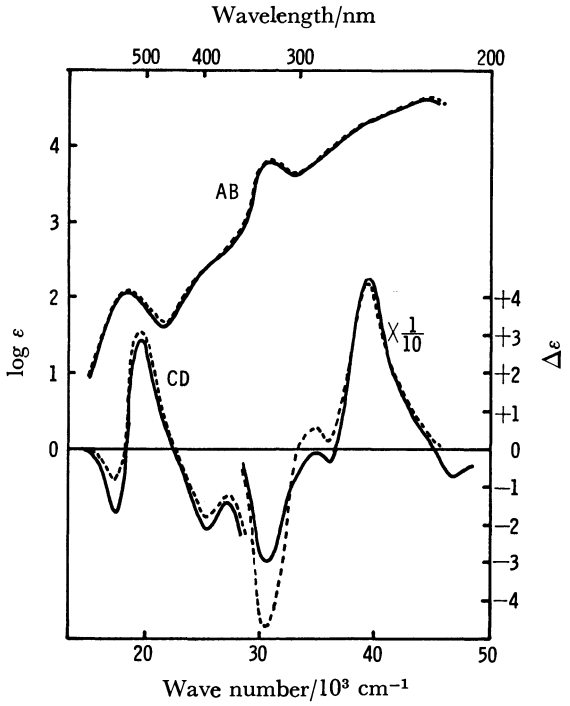

Fig. 2. Absorption (AB) and circular dichroism (CD) spectra of $(-)_{589}$-$[Co(acac)_2(tn)]I \cdot H_2O$ (——) and $(-)_{589}$-$[Co(acac)_2(en)]I$ (– – –) in water.

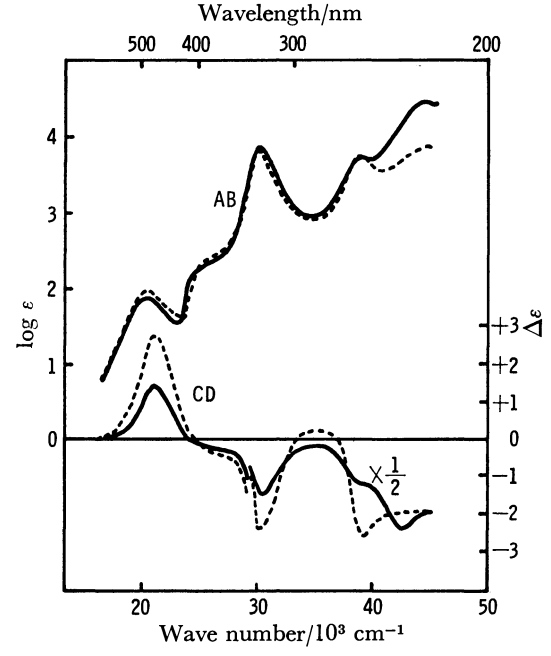

Fig. 3. Absorption (AB) and circular dichroism (CD) spectra of $(+)_{589}$-$[Cr(acac)(tn)_2]I_2 \cdot 0.5H_2O$ (——) and $(+)_{546}$-$[Cr(acac)(en)_2]Cl_2 \cdot H_2O$ (– – –) in water.

Figs. 1—4 together with those of the corresponding ethylenediamine complexes for the sake of comparison. In the earlier papers of this series,[23–25] several dianionobis(trimethylenediamine)cobalt(III) complexes have been reported, of which the first absorption maxima all located in the lower energy region than those of the corresponding ethylenediamine complexes, indicating that the ligand field of trimethylenediamine

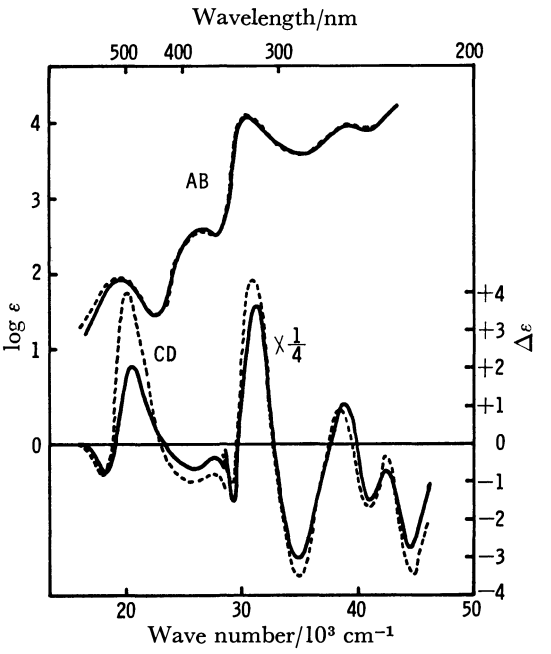

Fig. 4. Absorption (AB) and circular dichroism (CD) spectra of $(-)_{589}$-$[Cr(acac)_2(tn)]I \cdot H_2O$ (——) and $(+)_{546}$-$[Cr(acac)_2(en)]Cl \cdot 1.5H_2O$ (– – –) in water.

is a little weaker than that of ethylenediamine. In the present case, however, the first bands of $[Co(acac)(tn)_2]^{2+}$ (19800 cm^{-1}) and $[Co(acac)_2(tn)]^+$ (18500 cm^{-1}) nearly coincide with the data for $[Co(acac)(en)_2]^{2+}$ (19800 cm^{-1})[26] and $[Co(acac)_2(en)]^+$ (18600 cm^{-1}),[20] respectively, and those of $[Cr(acac)(tn)_2]^{2+}$ (20300 cm^{-1}) and $[Cr(acac)_2(tn)]^+$ (19200 cm^{-1}) are even higher in frequency than $[Cr(acac)(en)_2]^{2+}$ (20200 cm^{-1}) and $[Cr(acac)_2(en)]^+$ (19000 cm^{-1}).[21] In either of cobalt(III) and chromium(III) complexes, participation of acetylacetone as ligand diminishes the frequency of the absorption maximum due to its lower field as compared with ethylenediamine and trimethylenediamine. As to the assignment of the UV absorption bands, Boucher[20] discussed on $[Co(acac)_2(en)]^+$ and Kaizaki *et al.*[21] on $[Cr(acac)_2(en)]^+$.

CD Spectra and Absolute Configuration. Figures 1—4 show the CD spectra of the $[Co(acac)_x(tn)_{3-x}]$ and $[Cr(acac)_x(tn)_{3-x}]$ complexes ($x=1$ or 2) together with those of the corresponding ethylenediamine complexes. The CD pattern of $(-)_{589}$-$[Co(acac)(tn)_2]^{2+}$ in aqueous solution is just opposite in sign as compared with that of $(+)_{589}$-$[Co(acac)(en)_2]^{2+}$ which was reported to have the *Λ* configuration.[26] Thus a *Λ* configuration is assigned to $(-)_{589}$-$[Co(acac)(tn)_2]^{2+}$ and has in fact been confirmed by X-ray analysis.[27] The CD spectra of $(-)_{589}$-$[Co(acac)_2(en)]^+$ and $(-)_{589}$-$[Co(acac)_2(tn)]^+$ show a striking resemblance to each other (Fig. 2). Boucher assigned the *Λ* configuration to the ethylenediamine complex on the basis of the positive sign of the dominant CD band (A_2+B_2) in the first absorption region.[20] Then the *Λ* configuration of $(-)_{589}$-$[Co(acac)_2(tn)]^+$ is quite obvious and the same conclusion was drawn already by Brennan *et al.*[22]

Kaizaki *et al.* prepared and characterized $(+)_{546}$-$[Cr(acac)(en)_2]Cl_2$ and $(+)_{546}$-$[Cr(acac)_2(en)]Cl$ by the

absorption and CD spectra in both the visible and ultraviolet region, assigning the *Λ* configuration to both of the mixed-ligand complexes.[21] As is seen in Figs. 3 and 4, the CD spectra of $(+)_{589}$-$[Cr(acac)(tn)_2]^{2+}$ and $(-)_{589}$-$[Cr(acac)_2(tn)]^{+}$ are quite similar to those of $(+)_{546}$-$[Cr(acac)(en)_2]^{2+}$ and $(+)_{546}$-$[Cr(acac)_2(en)]^{+}$, respectively, except that the rotational strength of each CD band is smaller for the tn complex than for the corresponding en complex. Thus the two (acetylacetonato)(trimethylenediamine)chromium(III) complexes may be concluded to have the *Λ* configuration. The X-ray analysis of a red prism of $(-)_{589}$-$[Cr(acac)_2(tn)]I \cdot H_2O$ now in progress confirms the *Λ* configuration with a tn chelate ring of chair form.[28]

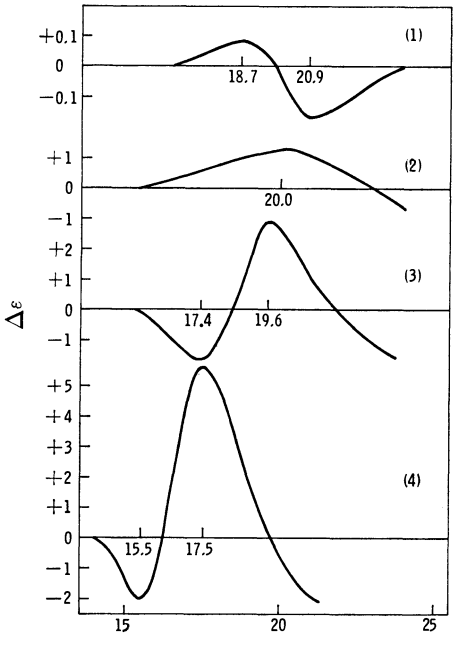

Fig. 5. Circular dichroism spectra in the first d-d absorption region of *Λ*-$[Co(tn)_3]^{3+}$ (1),[6] *Λ*-$[Co(acac)(tn)_2]^{2+}$ (2), and *Λ*-$[Co(acac)_2(tn)]^{+}$ (3) in water and of *Λ*-$[Co(acac)_3]$ (4)[29] in ethanol.

Figure 5 compares the CD patterns of the $[Co(acac)_x(tn)_{3-x}]$ complexes (x=0—3) in the first absorption region. The absolute configuration of $(-)_{546}$-$[Co(acac)_3]$ was determined as *Λ* by X-ray analysis.[29] The predominant positive CD band at 17500 cm^{-1} was assigned to the E component on the basis of the polarized crystal spectrum[30] in accordance with the empirical spectroscopic rule that for the *Λ* isomer the CD component with E symmetry has positive rotational strength.[8] The CD spectral pattern of *Λ*-$[Co(acac)_2(tn)]^{+}$ is quite similar to that of $[Co(acac)_3]$ except that the peak positions are shifted to the higher energy region due to the higher ligand field of tn than that of acac. Thus the positive CD band at 19600 cm^{-1} of *Λ*-$[Co(acac)_2(tn)]^{+}$ may be assigned to the E component.

The positive CD band of $[Co(tn)_3]^{3+}$ was attributed to the E component based on the ion-pairing effect.[31,9] It should be noted that the E component lies at lower energy side of the A_2 component for $[Co(tn)_3]^{3+}$ on the contrary to the $[Co(acac)_3]$ case where the E component lies at higher energy side of the A_2 component. *Λ*-$[Co(acac)(tn)_2]^{2+}$ exhibits a single positive CD band which is drawn as a reverse of the band observed for *Δ*-$[Co(acac)(tn)_2]^{2+}$ (Fig. 1). The E-A_2 split seems small and cancellation of the two components with each other is extensive, leaving residue of the predominant E component.

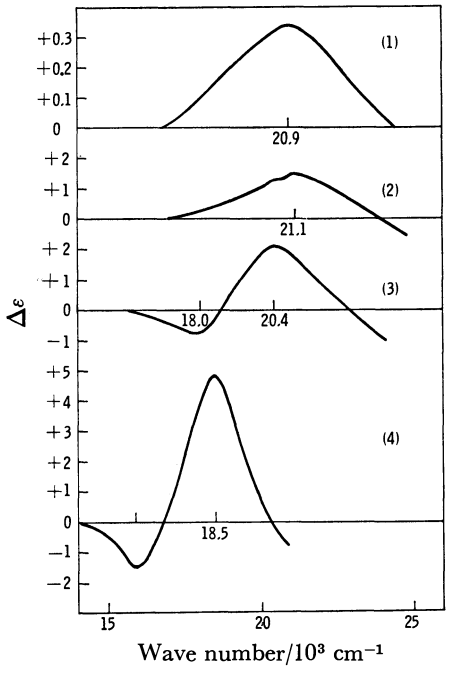

Fig. 6. Circular dichroism spectra in the first d-d absorption region of *Λ*-$[Cr(tn)_3]^{3+}$ (1),[35] *Λ*-$[Cr(acac)(tn)_2]^{2+}$ (2), and *Λ*-$[Cr(acac)_2(tn)]^{+}$ (3) in water and of *Λ*-$[Cr(acac)_3]$ (4)[32] in ethanol.

In a similar fashion Fig. 6 shows the CD spectra of the $[Cr(acac)_x(tn)_{3-x}]$ complexes in the first d-d absorption region. Mason *et al.*[32] prepared optically pure $(-)_{589}$-$[Cr(acac)_3]$ and assigned the absolute configuration to *Δ* based on comparison of the CD spectrum with those of four isomers of tris((+)-3-acetylcamphorato)chromium(III)[33] of which *Λ*(+)-*trans*-$[Cr((+)\text{-atc})_3]$ had been confirmed to be *Λ* by X-ray analysis.[34] The curve (4) in Fig. 6 is drawn as a reverse of the CD spectrum reported by Mason *et al.* for *Δ*-$[Cr(acac)_3]$,[32] showing the CD spectrum of *Λ*-$[Cr(acac)_3]$. Thus the positive major band at 18500 cm^{-1} can be assigned to the E component. The CD spectrum of *Λ*$(-)_{589}$-$[Cr(acac)_2(tn)]^{+}$ is also similar in the pattern to that of *Λ*-$[Cr(acac)_3]$ and the positive major band is assigned to the E component.

The CD spectrum of $(+)_{546}$-$[Cr(tn)_3]^{3+}$ reproduced in Fig. 6 was reported by Kaizaki *et al.*[35] On addition of sodium selenite to the solution, intensity of the positive CD band at 477 nm was diminished and a new negative CD band appeared at 435 nm. Thus the positive band was assigned to the ^4E component and the absolute configuration of $(+)_{546}$-$[Cr(tn)_3]^{3+}$ was concluded to be *Λ*.[35] The CD pattern of $(+)_{589}$-$[Cr(acac)(tn)_2]^{2+}$ (curve 2 in Fig. 6) is similar to that of $(+)_{546}$-$[Cr(tn)_3]^{3+}$

and the positive CD band is considered to be a residue of the predominant ^4E component after cancellation with a negative ^4A component.

The ligand-metal-ligand bond angle θ exceeds 90° in the six-membered chelate ring formed by trimethylenediamine with cobalt(III), whereas θ is generally less than 90° in the five-membered ethylenediamine cobalt(III) chelates. The empirical criterion relating the positive E component of the lowest-energy d-d absorption band to the Λ isomer of the cobalt(III) ethylenediamine chelate[8] has been shown to apply to the cobalt(III) trimethylenediamine complexes in spite of the larger angle θ.[31] In contrast with the N–Co–N angle of 96(1)° in $(-)_{589}$-$[Co(acac)(tn)_2]^{2+}$,[27] the N–Cr–N angle in $(-)_{589}$-$[Cr(acac)_2(tn)]^+$ was found to be 88.8(4)°.[28] The striking resemblance of the CD patterns depicted in Fig. 6 to those in Fig. 5 indicates that the same generalization as established for the cobalt(III) complexes applies to the chromium(III) complexes, too.

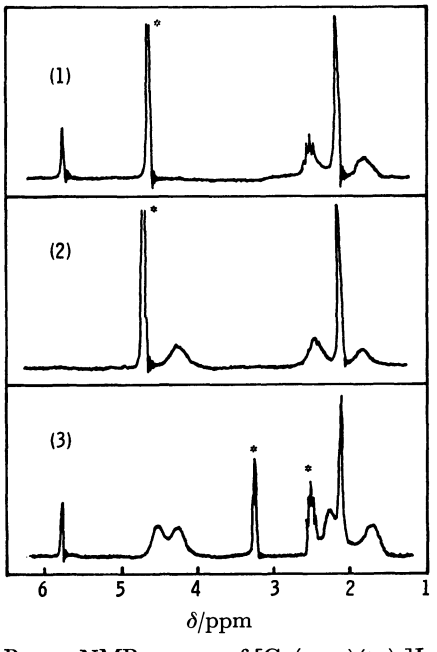

Fig. 7. Proton NMR spectra of $[Co(acac)(tn)_2]I_2$ in D_2O (1), *ca.* 0.1 M DCl–D_2O (2), and dimethylsulfoxide-d_6 (3). The asterisks denote the peaks due to solvent impurities.

Proton NMR Spectra. Figure 7 shows the proton NMR spectra of $[Co(acac)(tn)_2]I_2$ in D_2O, DCl–D_2O and DMSO-d_6. Two sharp signals observed at 5.75 and 2.16 ppm in D_2O with the area ratio of *ca.* 1:6 are assigned to the methine and methyl protons of the acetylacetonate ligand. The methine signal is lost in acidic solution due to the exchange reaction. Three broad signals observed at 4.24, 2.51, and 1.84 ppm in 0.1 M DCl–D_2O solution with the relative intensity of 2:2:1 are assigned to the NH_2, α-CH_2 and β-CH_2 protons of trimethylenediamine, NH_2–$CH_2(\alpha)$–$CH_2(\beta)$–$CH_2(\alpha)$–NH_2. In neutral D_2O the amine protons are deuterated and the methylene signals become sharper.

In DMSO-d_6 solution the methylene protons resonate at a little higher field (2.28 and 1.70 ppm) and the amine protons exhibit two signals at 4.55 and 4.27 ppm with equal intensities. Clifton and Pratt found that the chemical shifts of ammine or amine protons trans to halide or oxygen-donor ligand in $[CoX(NH_3)_5]^{(3-n)+}$ and *cis*-$[CoCl_2(en)_2]^+$ are appreciably smaller than those of the cis amine protons.[36] The same situation is realized in $[Co(acac)(tn)_2]^{2+}$ and the 4.27 ppm signal is assigned to the amine groups trans to the acetylacetonate oxygen and the 4.55 ppm signal to the mutually trans amine groups.

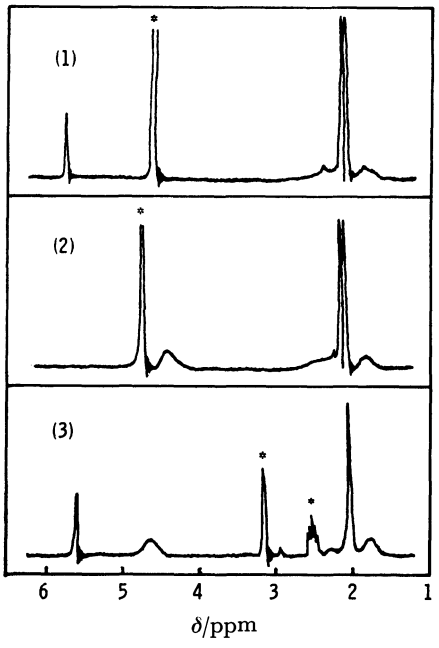

Fig. 8. Proton NMR spectra of $[Co(acac)_2(tn)]I \cdot H_2O$ in D_2O (1), *ca.* 0.1 M DCl–D_2O (2), and dimethylsulfoxide-d_6 (3). The asterisks denote the peaks due to solvent impurities.

As is seen in Fig. 8 the spectrum of $[Co(acac)_2(tn)]^+$ in D_2O shows two methyl signals at 2.11 and 2.15 ppm together with a methine signal at 4.28 ppm in accord with expectations. In DCl–D_2O solution three signals due to trimethylenediamine are observed at 4.47, 2.43, and 1.88 ppm with the relative intensity of 2:2:1 and assigned to the NH_2, α-CH_2 and β-CH_2, respectively. In DMSO-d_6, however, the relative intensities of the two methylene signals are reversed, the higher-field signal at 1.80 ppm being twice as large in area as the lower-field one at 2.27 ppm. It is not conceivable that the α-CH_2 protons resonate at a higher field than the β-CH_2 in this case, but nonequivalence of the geminal α-CH_2 protons may be responsible for this phenomenon. The complex *cis*-$[Co(CN)_2(tn)_2]^+$ shows three methylene signals of equal intensity in D_2O.[25] The two protons in each methylene group of $NH_2CH_2CHXCH_2NH_2$ (X=OH or Cl) coordinated to platinum(II) are not equivalent, the axial proton resonating at higher field than the equatorial one.[37] In the spectrum of $[Co(acac)_2(tn)]^+$, the signal at 2.27 ppm may be attributed to the equatorial protons of the two α-CH_2 groups and the chemical shift of the axial α-CH_2 protons may be

assumed to coincide with that of β-CH_2 by chance. The trimethylenediamine molecule coordinated to cobalt(III) has the chair conformation in crystals of $(-)_{589}$-$[Co(tn)_3]Br \cdot H_2O$,[5] $(+)_{589}$-$[Co(en)_2(tn)]Br_3$,[38] $(-)_{589}$-$[Co(acac)(tn)_2][As\text{-}(+)\text{-}tart]_2 \cdot H_2O$,[27] $(-)_{589}$-*cis*-$[Co(NCS)_2(tn)_2][Sb\text{-}(+)\text{-}tart] \cdot 2H_2O$,[39] *trans*-$[Co(NO_3)_2(tn)_2]NO_3$,[40] and $[Co(CO_3)(tn)_2]ClO_4$.[41] However, the chair conformation of the six-membered chelate ring seems only slightly more stable than the skew-boat conformation,[42] and the CD spectra of $[Co(tn)_3]^{3+}$ ions in solutions were interpreted to indicate the equilibrium between these two conformers.[43] The remarkable difference now observed in the NMR spectra in D_2O and DMSO-d_6 may reflect the change of the equilibrium among conformers with solvent.

The authors wish to thank Mr. J. Gohda for the elemental analyses and Dr. T. Kinoshita for the PMR measurements. This work was supported in part by the Grant-in-Aid administered by the Ministry of Education.

References

1) Part VI: Y. Ito, A. Terada, and S. Kawaguchi, *Bull. Chem. Soc. Jpn.*, **51**, 2898 (1978).
2) Present address: Faculty of Science, Kochi University, Kochi 780.
3) Y. Saito, *Coord. Chem. Rev.*, **13**, 305 (1974); C. J. Hawkins, "Absolute Configuration of Metal Complexes," Wiley-Interscience, New York (1971).
4) Y. Saito, K. Nakatsu, M. Shiro, and H. Kuroya, *Acta Crystallogr.*, **8**, 729 (1955); *Bull. Chem. Soc. Jpn.*, **30**, 795 (1957).
5) Y. Saito, T. Nomura, and F. Marumo, *Bull. Chem. Soc. Jpn.*, **41**, 530 (1968); **42**, 1016 (1969).
6) M. Fujita, Y. Yoshikawa, and H. Yamatera, *J. Chem. Soc., Chem. Commun.*, **1975**, 941.
7) S. F. Mason and B. J. Peart, *J. Chem. Soc., Dalton Trans.*, **1977**, 937.
8) A. J. McCaffery, S. F. Mason, and R. E. Ballard, *J. Chem. Soc.*, **1965**, 2883.
9) M. Kojima, M. Fujita, and J. Fujita, *Bull. Chem. Soc. Jpn.*, **50**, 898 (1977); M. Kojima and J. Fujita, *ibid.*, **50**, 3237 (1977).
10) R. R. Judkins and D. J. Royer, *Inorg. Chem.*, **13**, 945 (1974).
11) R. Kuroda and Y. Saito, *Bull. Chem. Soc. Jpn*,. **49**, 433 (1976).
12) F. Mizukami, H. Ito, J. Fujita, and K. Saito, *Bull. Chem. Soc. Jpn.*, **45**, 2129 (1972); A. Kobayashi, F. Marumo, Y. Saito, J. Fujita, and F. Mizukami, *Inorg. Nucl. Chem. Lett.*, **7**, 777 (1971).
13) A. Werner, *Ann.*, **386**, 265 (1912).
14) L. J. Boucher, *Inorg. Chem.*, **6**, 2162 (1967).
15) E. Pedersen, *Acta Chem. Scand.*, **24**, 3362 (1970).
16) G. G. Henderson, *J. Chem. Soc.*, **1895**, 102.
17) C. L. Butler and L. H. Cretcher, *J. Am. Chem. Soc.*, **55**, 2605 (1933).
18) I. K. Reid and A. M. Sargeson, *Inorg. Synth.*, **9**, 167 (1967).
19) R. D. Archer and B. P. Cotsoradis, *Inorg. Chem.*, **4**, 1584 (1965).
20) L. J. Boucher, *Inorg. Chem.*, **9**, 1202 (1970).
21) S. Kaizaki, J. Hidaka, and Y. Shimura, *Inorg. Chem.*, **12**, 135 (1973).
22) B. J. Brennan, K. Igi, and B. E. Douglas, *J. Coord. Chem.*, **4**, 19 (1974).
23) H. Kawaguchi, N. Yano, and S. Kawaguchi, *Bull. Chem. Soc. Jpn.*, **42**, 136 (1969).
24) H. Kawaguchi and S. Kawaguchi, *Bull. Chem. Soc. Jpn.*, **43**, 2103 (1970).
25) H. Kawaguchi and S. Kawaguchi, *Bull. Chem. Soc. Jpn.*, **46**, 3453 (1973).
26) A. J. McCaffery, S. F. Mason, and B. J. Norman, *J. Chem. Soc.*, **1965**, 5094.
27) K. Katsumoto, H. Kawaguchi, H. Kuroya, and S. Kawaguchi, *Bull. Chem. Soc. Jpn.*, **46**, 2424 (1973).
28) K. Matsumoto, S. Ooi, H. Kuroya, M. Nakano, and S. Kawaguchi, presented at the 28th Symposium on the Coordination Chemistry of the Chemical Society of Japan which was held at Matsuyama in October, 1978.
29) R. B. Von Dreele and R. C. Fay, *J. Am. Chem. Soc.*, **93**, 4936 (1971).
30) T. S. Piper, *J. Chem. Phys.*, **35**, 1240 (1961).
31) P. G. Beddoe and S. F. Mason, *Inorg. Nucl. Chem. Lett.*, **4**, 433 (1968).
32) S. F. Mason, R. D. Peacock, and T. Prosperi, *J. Chem. Soc., Dalton Trans.*, **1977**, 702.
33) G. W. Everett, Jr. and A. Johnson, *Inorg. Chem.*, **13**, 489 (1974).
34) W. DeW. Horrocks, Jr., D. L. Johnston, and D. MacInnes, *J. Am. Chem. Soc.*, **92**, 7620 (1970).
35) S. Kaizaki, J. Hidaka, and Y. Shimura, *Bull. Chem. Soc. Jpn.*, **43**, 1100 (1970).
36) P. Clifton and L. Pratt, *Proc. Chem. Soc.*, **1963**, 339.
37) T. G. Appleton and J. R. Hall, *Inorg. Chem.*, **11**, 117 (1972).
38) H. V. F. Schousboe-Jensen, *Acta Chem. Scand.*, **26**, 3413 (1972).
39) K. Matsumoto, M. Yonezawa, H. Kuroya, H. Kawaguchi, and S. Kawaguchi, *Bull. Chem. Soc. Jpn.*, **43**, 1269 (1970).
40) E. Yasaki, I. Oonishi, H. Kawaguchi, S. Kawaguchi, and Y. Komiyama, *Bull. Chem. Soc. Jpn.*, **43**, 1354 (1970).
41) R. J. Geue and M. R. Snow, *J. Chem. Soc., A*, **1971**, 2981.
42) J. R. Gollogly and C. J. Hawkins, *Inorg. Chem.*, **11**, 156 (1972).
43) P. G. Beddoe, M. J. Harding, S. F. Mason, and B. J. Peart, *Chem. Commun.*, **1971**, 1283.

Potentialities of Field Desorption Mass Spectrometry Using Emitter Current Programmer for Direct Analysis of Multicomponents

Hiroaki SHIRAISHI,* Akira OTSUKI, and Keiichiro FUWA

Department of Chemistry and Physics, National Institute for Environmental Studies, Yatabe, Ibaraki 300-21

(Received February 26, 1979)

The influence of emitter current on field desorption (FD) mass spectra was examined with use of an emitter current programmer (ECP). Reproducibility of FD mass spectra measured by electronic detection is improved with ECP and the integration of stored spectra on the computer. The FD mass spectra of some surfactants are shown as an example of complex mixture. The FD mass spectra of poly(oxyethylene) alkylphenyl ethers show that the distribution pattern of molecular ion peaks depends upon emitter current. The fractional desorption also occurs in the FD mass spectra of α-hydro-ω-(octadecylamino)poly(oxyethylene) measured with a constant emitter current. The emitter current required for desorption of hexadecyltrimethylammonium chloride is greatly affected by coexisting with another ammonium salt. Use of ECP supplies information on the analysis of multicomponents.

Field desorption mass spectrometry (FDMS) has been found to be useful for analysis of thermally labile and non-volatile compounds. However, the formation of ions in FD-MS is affected by various parameters such as electric field strength, emitter temperature, morphology and surface properties of the emitter needles and kind of sample loading.[1,2] Maine *et al.*[3] found that automatic control of the emitter temperature is essential for obtaining reproducible results from successive analysis of the same sample. They suggested that the most important factors are the emitter temperature and the use of an emitter current programmer, which provides precise control of the magnitude and rate of change of current in the emitter wire, for obtaining reproducible FD mass spectra.

Several emitter current control devices[3–5] were reported; they are not yet available commercially. In an attempt to develop a method for identification and analysis of several types of surfactants, an emitter current programmer was constructed with a slight modification of that by Maine *et al.* The possibility for separation and analysis of multicomponents using the ECP has been examined.

Experimental

Apparatus. Mass spectrometry was performed on a JEOL JMS-OlSG double focusing mass spectrometer with a combined field desorption/field ionization/electron impact ion source, connected to JMS-2000 mass data analysis system (Japan Electronic and Optics laboratory). FD-emitter used was 10 μm tungsten wire with carbon needles grown at high temperature.[6] An anode potential of 10 kV and cathode potential of −3 kV were applied. Emitter curent was increased linearly by use of a modified emitter current programmer during the course of repetitive magnet scanning. The emitter was loaded with 0.2—1 μg samples from stock solutions (*ca.* 1 μg/μl) using microsyringe technique.[7]

Figure 1 shows a block diagram of the modified ECP. Operation modes are the same as those described by Maine *et al.* The current programming rate can be set at a desired value in the range 1–100 mA/min. The emitter current is regulated within 0.05 mA at any level between 0 and 60 mA. Initial and final current values can be controlled within this range.

Initial focussing was done on acetone introduced *via* the batch inlet. After measurements of each sample the emitter current was increased to 60 mA in order to clean the emitter.

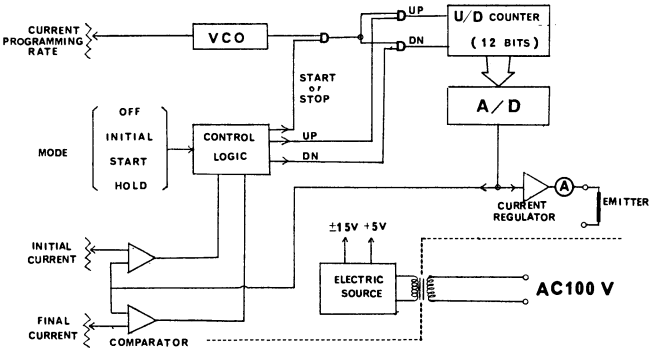

Fig. 1. The block diagram of ECP.

Materials. Poly(oxyethylene) octylphenyl and dodecylphenyl ethers supplied by Gasukuro Kogyo Co., Ltd. and Daiichi Seiyaku Co., Ltd., respectively, and other surfactants from Wako Pure Chemical Industries, Ltd. were used.

Results and Discussion

The FD mass spectrum of sodium dodecylbenzenesulfonate (DBS), a typical anionic surfactant, was measured by repetitive magnet scanning at 11 s intervals, the emitter current increasing linearly at a rate of 3 mA/min. Integration of all the spectra collected on the computer showed *m/e* 719 $(2M+Na)^+$, 371 $(M+Na)^+$, and 348 $(M)^+$ ion peaks (Fig. 2). Each coefficient of variation calculated from seven measurements of the same sample was ±4% for the intensity of the base peak $(M+Na)^+$ to the total intensity of all peaks, ±30% and ±20% for those of M^+ and $(2M+Na)^+$ peaks, respectively. FD mass spectra obtained with a single magnet scan and electric detection gave less reproducible spectra due to the fluctuation of ion current. FD mass spectrum of DBS was considerably affected by emitter current (Fig. 2(b)). In general, $(2M+Na)^+$ ion has a relatively high intensity at lower emitter current, but at higher emitter current the intensity of this cluster ion rapidly decreased whereas $(M)^+$ and $(M+Na)^+$ peaks increased. Emission controlled FD mass spectra of some sulfonates were studied by Schulten and Kummler.[8] They used a vacuum evaporated AgBr plate for photographic detection and found that $(nM+Na)^+$ cluster ion with $n=1$ is mostly prominant, molecular ion having

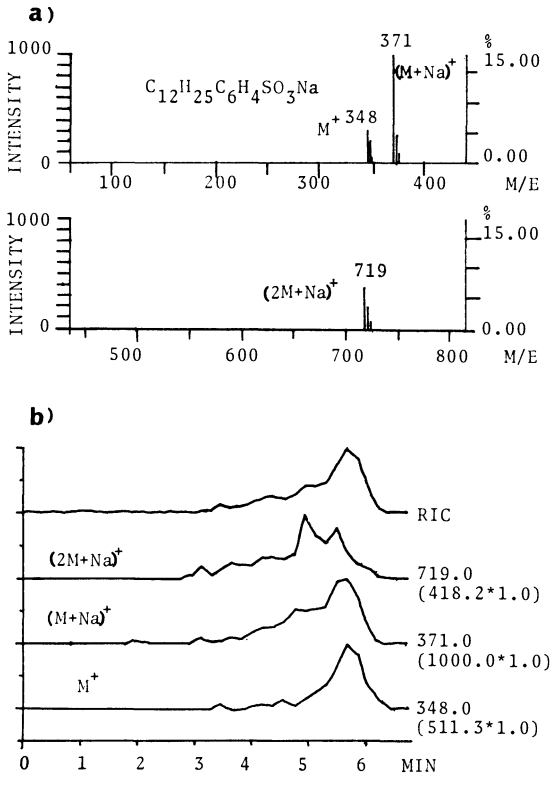

Fig. 2(a). The FD mass spectrum of DBS; initial current 0 mA, current programming rate 3 mA/min, sum of the stored spectra.
(b). Reconstructed mass chromatogram; RIC (reconstructed ion current): sum of ion intensities between *m/e* 50 to 800. ion intensities are plotted on ordinate and full scales are designated in parentheses.

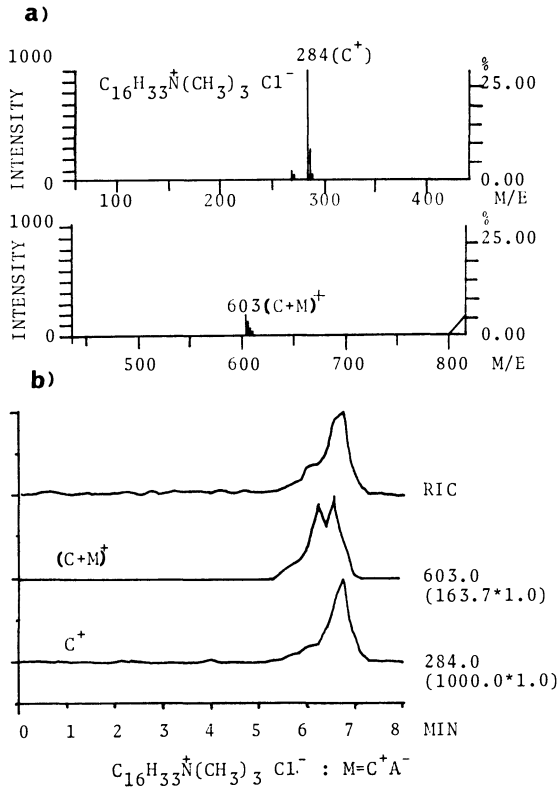

Fig. 3. The FD mass spectrum of CA (a) and reconstructed mass chromatogram (b). Initial current 10 mA, current programming rate 3 mA/min, sum of the stored spectra.

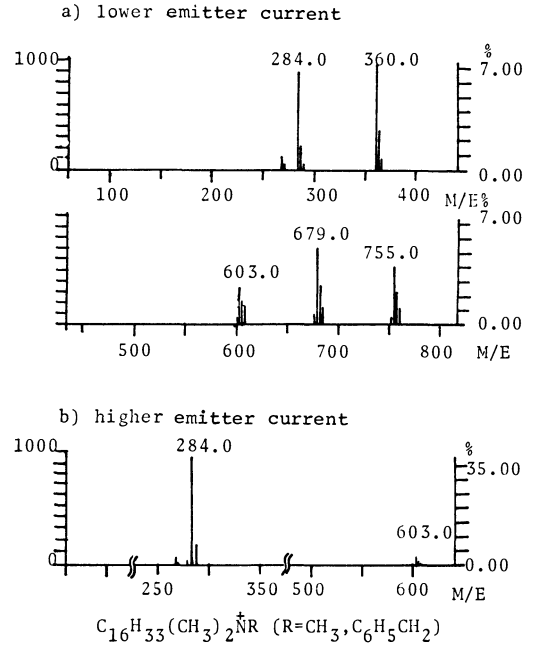

Fig. 4. The FD mass spectra of equimolar mixture of CA and BA. Emitter current: (a) 17 mA, (b) 19 mA.

relatively smaller intensity. The integration of spectra, obtained by electric detection and linear current program, gives reproducible spectra consisting of the spectrum obtained by Schulten and Kummler by potographic detection and emission controlled time/current program.

Figure 3 shows the integrated FD mass spectrum (a) of hexadecyltrimethylammonium chloride (CA), a typical cationic surfactant, and the reconstructed mass chromatogram (b) obtained under the same conditions as those of DBS except for the initial current value. The ion peaks at *m/e* 284, 603, and 269 were assigned to salt cation (molecular ion minus chloride ion), cluster ion of the type, molecular ion plus cation portion, and fragment ion peak $(M-Me)^+$, respectively. The intensities of these ion peaks were also dependent upon emitter current. Reconstructed mass chromatogram (Fig. 3(b)) indicates that the intensity of cluster ion $(M+C)^+$ decreases at higher emitter current, while the intensities of salt cation and fragment ions increase. Disappearance of the cluster ion at the higher emitter current can be attributed to weak binding of the cluster ion that thermally decomposes. Figures 4(a) and (b) show the FD mass spectra of equimolar mixture of hexadecyltrimethylammonium chloride(CA)and benzylhexadecyldimethylammonium chloride (BA). Lower emitter current gave ion peaks of two salt cations (*m/e* 284, 360) and relatively high intensities of three cluster ions (*m/e* 603, 679, 755) of the type $(M+C)^+$. The ion peak at *m/e* 679 demonstrates the production of a mixed cluster ion consisting of both cation portions and chloride ion. A similar phenomenon has been observed by Veith,[9] who used simple ammonium salts. On the

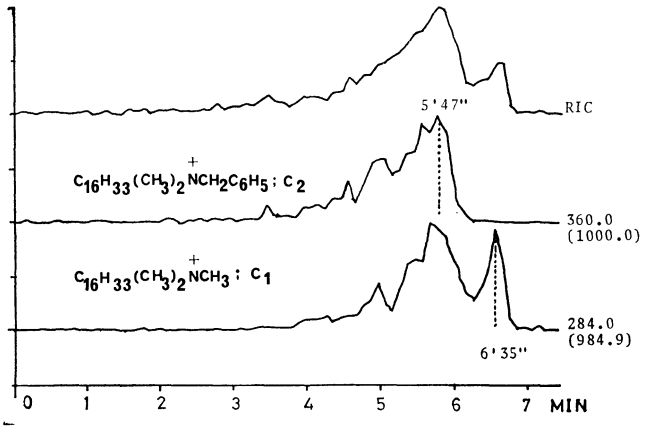

Fig. 5. Reconstructed mass chromatogram of equimolar mixture of CA and BA.
Current programming rate 3 mA/min.

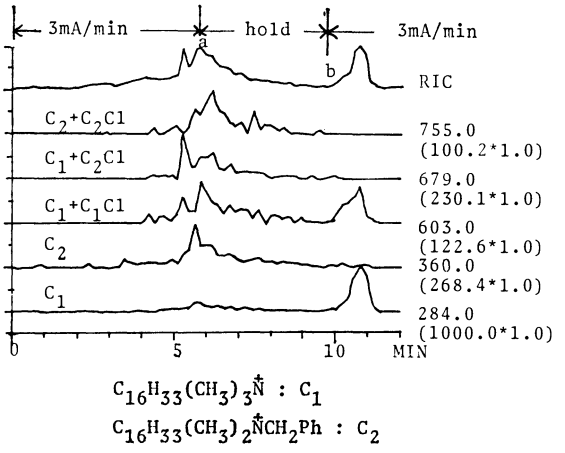

Fig. 6. Reconstructed mass chromatogram of equimolar mixture of CA and BA.

other hand, higher emitter current gave only the spectrum of CA due to the disapperance of BA at lower emitter current. Figure 5 shows the reconstructed mass chromatogram of two salt cations during the course of a linear emitter current programming, suggesting that the part of CA on the emitter wire can be desorped at lower emitter current when BA coexist, compared with that in Fig. 3(b), but further increase in emitter current is required for the desorption of the remaining part of CA after all BA was desorped. The results indicate that emitter current required for desorption of CA is greatly affected by the presence of BA, *viz.*, emitter current required for field desorption changes with not only the properties of individual compounds but also the interaction of each component loaded on emitter wire. When emitter current was increased to 17 mA at a rate of 3 mA/min and kept constant for 4 min, a mixture of CA and BA was found to be separated by fractional desorption (Fig. 6). This suggests that the use of ECP producing programmed thermal gradients makes the separation and analysis of multicomponents in complex mixtures by mass chromatograpy or selected ion monitoring techniques possible.

The FD mass spectra of poly(oxyethylene) alkylphenyl ethers, nonionic surfactants, were measured. The results indicate only molecular ions with different polymerization degree of ethylene oxide unit.[10] Single scan FD mass spectra of poly(oxyethylene) octhylphenyl ethers (PO) obtained during the course of a linear emitter current programming are shown in Fig. 7. The distribution pattern of molecular ion peaks is also dependent upon emitter current, *viz.*, at lower emitter current the distribution pattern of ions is weighted for low mass region, whereas at higher emitter current it is weighted for high mass region, suggesting that fractional desorption occurs. The integrated FD mass spectrum of PO and the reconstructed mass chromatogram of selected ions are shown in Figs. 8(a) and (b). Figure 8(b) shows that the fractional desorption of mixtures occurs by thermal gradient. A similar fractional desorption was observed in the FD mass spectra

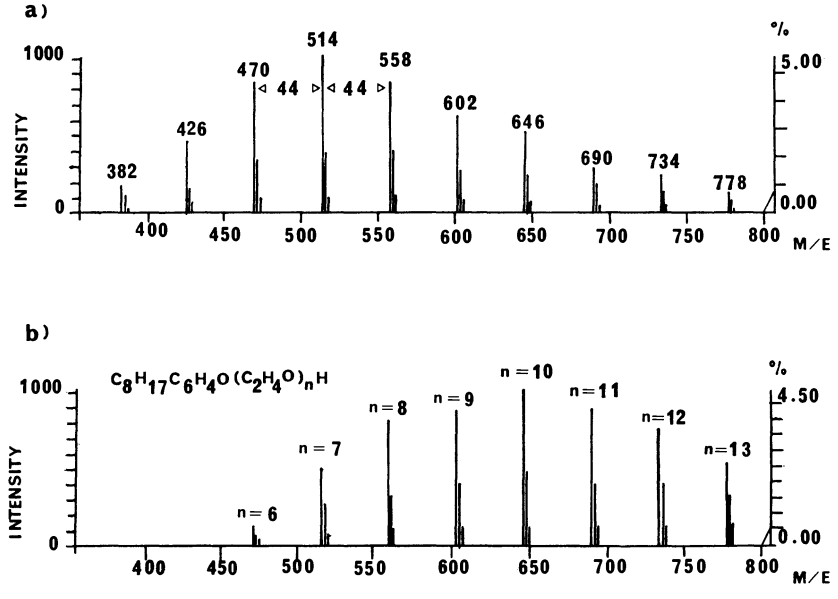

Fig. 7. The FD mass spectra of PO; emitter current (a) 14 mA (b) 16 mA.

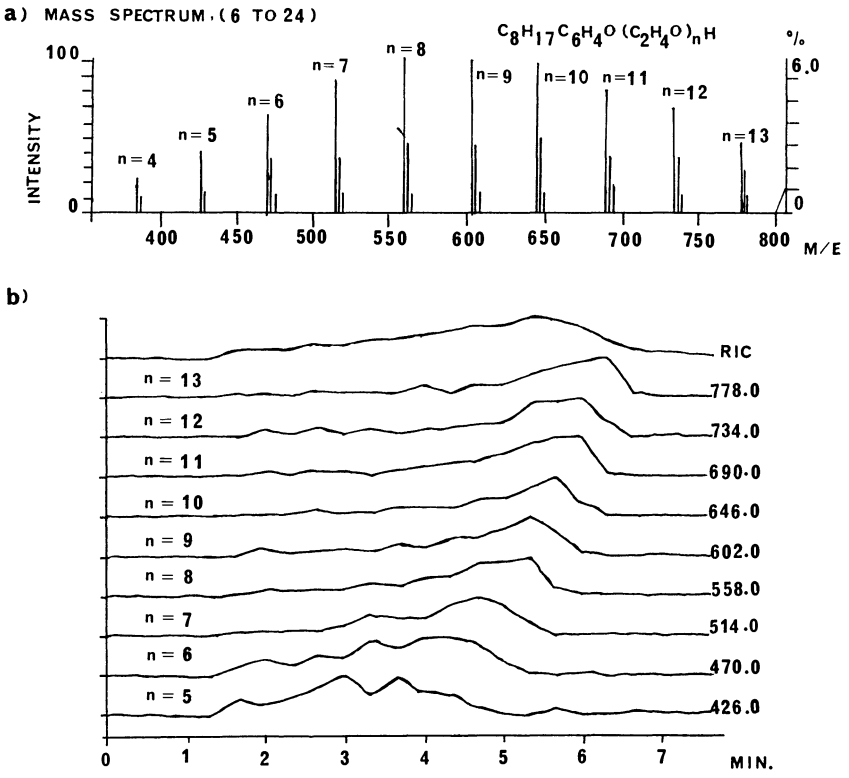

Fig. 8. (a) The FD mass spectrum of PO; sum of the stored spectra, small peaks are neglected. (b) Reconstructed mass chromatogram; current programming rate 3 mA/min.

of poly(oxyethylene) nonylphenyl and dodecylphenyl ethers. The result suggests that the true distribution of multicomponents in the original sample can be estimated at least from an integration of stored spectra during the course of slow increase in emitter current or photographic detection. The series of weak peaks found at *m/e* 14 lower and higher than the major ion peaks exhibit the existence of impurities having different alkyl side chains. The impurities correspond to poly(oxyethylene)nonylphenyl and hexylphenyl ethers. The FD mass spectra of α-hydro-ω-(octadecylamino)poly(oxyethylene) obtained under the following conditions are shown in Figs. 9(a) and (b): initial emitter current was set at 14 mA and kept constant during repetitive magnet scanning at 18 s intervals. Integration of the spectra of first 20 scans (a) and next 30 scans (b) indicates different distribution pattern of protonated molecular ions, suggesting that a similar fractional

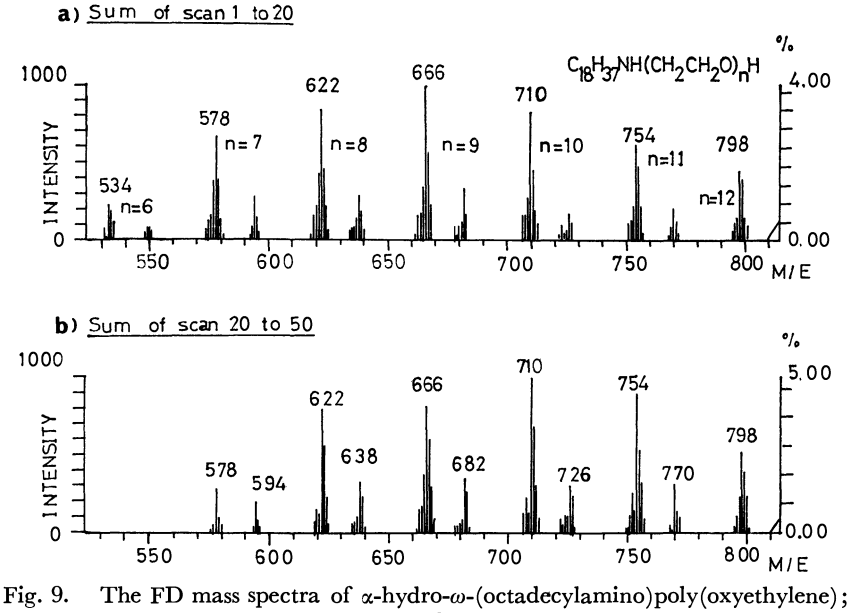

Fig. 9. The FD mass spectra of α-hydro-ω-(octadecylamino)poly(oxyethylene); emitter current 17 mA, (a) sum of the first 20 scans and (b) next 30 scans.

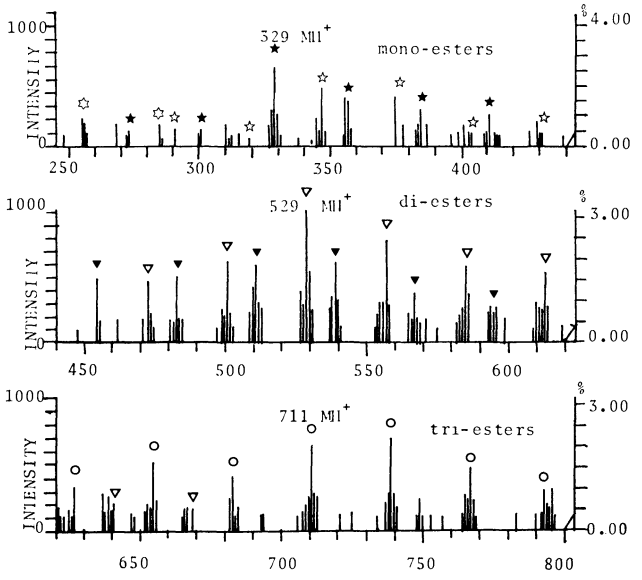

Fig. 10. The FD mass spectrum of "Span 20", Current programming rate 3 mA/min, sum of 20 scans, ☆, ▽ and ○ indicate mono-, di- and tri-esters of sorbitans respectively. ★ and ▲ indicate mono- and di-esters of sorbid respectively, ☆ indicates unreacted fatty acids.

desorption was taking place. The series of minor ion peaks found at 28 mass lower than the protonated molecular ion peaks correspond to the protonated molecular ions of α-hydro-ω-(hexadecylamino)poly-(oxyethylene) contained in the commercial samples as impurities.

The FD mass spectra of a group of nonionic surfactant, called "Span" known as a complex mixture of mono-, di-, tri-, and tetra-esters of 1,5- and 1,4-sorbitans and mono- and di-esters of 1,4: 3,6-sorbid were measured. Figure 9 shows the integrated FD mass spectra of "Span 20" as an example of complex mixtures, showing many protonated molecular ion peaks of the esters and molecular ion peaks of unreacted fatty acids and fragment ions at m/e 183, 211, 239, and 269 $(RCO)^+$ in low mass region. The protonated molecular ions of esters of sorbitan and sorbid observed in the FD mass spectra of various "Span"s are given in Table 1. Since these ions might consist of some isomers, the total carbon number of acyl groups ($l+n$, $l+n+m$) can be calculated. The composition of acyl groups in the samples can be estimated from the distribution of protonated molecular ion peaks of mono-esters. With linear increase in emitter current, desorption of di-esters occurs before that of tri-esters, the esters of sorbid being generally desorped prior to the esters of sorbitans. Because of fractional desorption, an integration of single scan spectra was needed to identify all the components in the mixtures.

The present study and others[11] indicate that there are two types of FD mass spectrum, one obtained from single scanning at near the best anode temperature and the other an integrated FD mass spectrum obtained from repetitive magnet scanning or photoplate detection, the latter being much more reproducible than the former when the cluster and fragment ions are produced.

Table 1. Protonated molecular ions of esters observed in the FD mass spectra of "Span"s

Mono-esters			Di-esters			Tri-esters	
n	A	B	$n+m$	A	B	$l+m+n$	A
8	291	273	20	473	455	28	599
10	319	301	22	501	483	30	627
12	347	329	24	529	511	32	655
14	375	357	26	557	539	34	683
16	403	385	28	585	567	36	711
18	431	413	30	613	595	38	739
$18F_1$	429	411	32	641	623	40	767
			34	669	651	42	795
			36	697	679		

A and B indicate esters of sorbitans and sorbid, respectively. l, m, and n indicate carbon numbers of each fatty acid.

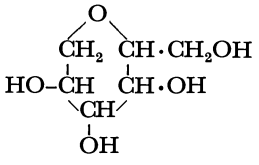

1,5-Sorbitan

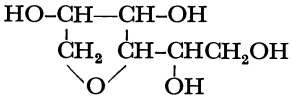

1,4-Sorbitan

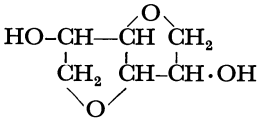

1,4:3,6-Sorbid

The present study also suggests that the compounds, from which cluster and fragment ions will be produced, and a complex mixture sample in which fractional desorption occurs, should be measured with ECP as an integrated FD mass spectrum. It seems that when the integrated FD mass spectrum is taken, the effect of the difference in morphology of emitter needles on the reproducibility of FD mass spectrum can be reduced. In FD-MS, the thermal gradient produced by ECP has become a powerful means for analysis of complex mixtures.

References

1) H. D. Beckey and H.-R. Schulten, *Angew. Chem.*, **87**, 425 (1975); *Angew. Chem. Int. Ed. Engl.*, **14**, 403 (1975).
2) H. D. Beckey, "Principles of Field Ionization and Field Desorption Mass Spectrometry," Pergamon, Oxford (1977).
3) J. W. Maine, B. Soltmann, J. F. Holland, N. D. Young, J. N. Gerber, and C. C. Sweeley, *Anal. Chem.*, **48**, 427 (1976).
4) H.-R. Schulten and N. M. M. Nibbering, *Biomed. Mass Spectrom.*, **4**, 55, (1977).
5) H. U. Winkler, W. Neumann, and H. D. Beckey, *Int. J. Mass Spectrom. Ion Phys.*, **21**, 57 (1976).
6) H. D. Beckey, E. Hilt, and H.-R. Schulten, *J. Phys. E: Sci. Instr.*, **6**, 1043 (1973).
7) H. D. Beckey, A. Heindrichs, and H. U. Winkler, *Int. J. Mass Spectrom. Ion Phys.*, **3**, 9 (1970).
8) H.-R. Schulten and D. Kummler, *Z. Anal. Chem.*, **278**, 13 (1976).
9) H. J. Veith, *Org. Mass Spectrom.*, **11**, 629 (1976).
10) A. Otsuki and K. Fuwa, *Talanta*, **24**, 584, (1977).
11) H. Budzikiewicz and M. Linscheid, *Biomed. Mass Spectrom.*, **4**, 103 (1977).

An X-Ray Photoelectron Spectroscopic Study of 2-Mercaptobenzothiazole Metal Complexes

Tooru YOSHIDA,* Kiyoshi YAMASAKI, and Shigemasa SAWADA
Osaka Prefectural Industrial Research Institute, Enokojima, Nishi-ku, Osaka 550

(Received March 1, 1979)

The X-ray photoelectronic spectra of 2-mercaptobenzothiazole (LH) and its metal complexes have been measured. On the basis of the chemical shifts of the N(1s), S(2p), and Cu($2p_{3/2}$) electron binding energies, the coordination mode of the ligand and the oxidation state of the copper atom have been examined. It is suggested that, in HgL_2, PbL_2, AgL, and CuL_3H_2Cl complexes, the ligand is solely coordinated through the exocyclic sulfur atom, and that, in CuL, CuL_2, PtL_2, PdL_2, NiL_2, and CdL_2 complexes, the ligand is coordinated through both the exocyclic sulfur and nitrogen atoms. In CuL_2 and CuL_3H_2Cl, it was found that the copper was present in a (+1) oxidation state, and that part of the ligand molecules, bis(benzothiazol-2-yl) disulfide, resulted from oxidation of LH by the Cu^{2+} ion on complex formation.

The use of 2-mercaptobenzothiazole as an analytical reagent has been known for a long time,[1-3] and the structures of its complexes with several metal ions have been investigated using a variety of physical techniques.[4-9]

In the copper complex prepared from the reaction of 2-mercaptobenzothiazole with copper(II) chloride, the copper has been reported to be in a (+2) oxidation state, in spite of its diamagnetism.[7,9] Clear evidence for this assignment has however not been given. Furthermore, it is well known that sulfur-containing ligands often reduce the Cu(II) ion to Cu(I) on complex formation.[10]

X-Ray photoelectron spectroscopy (XPS) is sensitive to charge distribution and is suitable for the detection of protonated atoms and the oxidation state.[11]

The purpose of the present study is to confirm the oxidation state of copper in complexes with 2-mercaptobenzothiazole, and to examine the mode of coordination of the ligand in several metal complexes.

Experimental

Chemicals. 2-Mercaptobenzothiazole, the sodium salt, and 2-mercaptobenzimidazole (abbreviated as LH, LNa, and L'H, respectively) were obtained commercially and were of analytical grade. They were used after recrystallization from ethanol. Bis(benzothiazol-2-yl) and bis(benzimidazol-2-yl) disulfides (abbreviated as L–L and L'–L') were obtained by standard methods: the oxidation of LH and L'H in ethanol by H_2O_2 and I_2, respectively. L'H and L'–L' were used as reference compounds. All the copper salts used were analytical reagents. All ligands and metal complexes were analysed elementally.

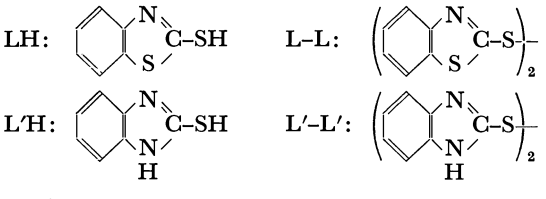

Preparation of the Metal Complexes. *CuL*: Method (a) (according to the literature). An ethanol solution of LH was added to an aqueous solution of copper(I) chloride saturated with KCl[3] which gave an orange yellow precipitate. Found: C, 36.86; H, 1.71; N, 6.09; S, 27.47; Cu, 27.50%. Calcd for CuL: C, 36.60; H, 1.74; N, 6.10; S, 27.89; Cu, 27.67%. Method (b). A solution of LH (4—6 mmol) in ethanol (100 ml) was added to a solution of CuX_2 ($X=CH_3COO$ or NO_3) (2 mmol) in ethanol (50 ml). The orange-yellow and pale yellow compounds precipitated were digested on a water bath for approximately 1 h. The suspension was cooled and filtered on a suction pump through a qualitative filter paper to give a pale yellow crystalline precipitate (L–L). The filtrate, containing a fine orange-yellow precipitate was filtered through a quantitative filter paper and the resulting amorphous precipitate (CuL) washed with hot ethanol. The yields were approximately 90% for CuL and L–L. Found: C, 37.00; H, 1.67; N, 6.11; S, 27.57; Cu, 27.90%.

CuL_2: Method (a). A solution of CuX_2 ($X=Cl$, CH_3COO, NO_3, $1/2(SO_4)$) (2 mmol) in water (50 ml) was substituted for the solution of CuX_2 in ethanol in the above preparation procedure for CuL by method (b). The orange-yellow precipitate was washed with water and ethanol (yield>95%). Found: C, 42.34; H, 2.03; N, 7.08; S, 32.12; Cu, 16.20%. Calcd for CuL_2: C, 42.48; H, 2.02; N, 7.08; S, 32.36; Cu, 16.06%. Method (b). A solution cotaining LH and L–L (2 mmol and 1 mmol, respectively) in a mixture of ethanol (100 ml) and *N,N*-dimethylformamide (DMF) (50 ml) was added to a solution of CuCl (2 mmol) in an aqueous solution saturated with KCl (30 ml). The pale orange-yellow precipitated was digested with stirring on a water bath for approximately 1 h. The suspension was cooled and filtered and the collected precipitate washed with water, an ethanol–DMF mixture (30 ml, 2: 1), and ethanol (yield 80%). Found: C, 42.26; H, 1.99; N, 7.00; S, 32.02; Cu, 16.11%.

CuL_3H_2Cl: A solution of $CuCl_2$ (2 mmol) in ethanol (50 ml), in a procedure similar to method (b) above for CuL, gave a pale yellow complex (yield>95%). Found: C, 42.43; H, 2.17; N, 7.04; S, 31.23; Cl, 5.80; Cu, 10.63%. Calcd for CuL_3H_2Cl: C, 42.07; H, 2.34; N, 7.01; S, 32.05; Cl, 5.93; Cu, 10.60%. In the preparation of CuL_3H_2Cl, more than 5% water produced a mixture of CuL_2 and CuL_3H_2Cl, and greater than 20% gave CuL_2 quantitatively.

Other Metal Complexes: PtL_2, PdL_2, NiL_2, CdL_2, HgL_2, PbL_2, and AgL were prepared according to the literatures.[7,8]

All compounds used were dried in an air oven at 105 °C for a minimum of 2 h.

The structures of the two complexes prepared by methods (a) and (b) in the cases of CuL and CuL_2 were analysed by powder X-ray diffraction analysis.

Physical Measurements. The X-ray photoelectron spectra were measured on an AEI-ES200 spectrometer. Al $K\alpha$ (1486.6 eV) X-ray radiation was used as the excitation source. Samples were ground and dusted onto a double-backed adhesive tape. The measurements taken at room temperature

under vacuum (about 10^{-7} Torr). The binding energy of the C(1 s) peak assigned to the carbon of benzene was used as the energy standard throughout the experiments and taken to be 285.0 eV. The reproducibility was ± 0.1 eV.

The IR spectra of LH and the copper complexes were recorded on an IR spectrometer, model IR-G (Japan Spectroscopic Co., Ltd.). The spectrum of CuL_3H_2Cl was the only one which exhibited a similar N–H band to that of LH in the region 2800—3150 cm^{-1}. Magnetic measurements were conducted at room temperature using the Faraday method on a magnetic balance, model MB-2 (Shimadzu Co., Ltd.). The diamagnetic corrections were estimated by the use of Pascal's Constants[12] and all copper complexes were found to be diamagnetic.

Results

The measured binding energies are given in Table 1.

Free Ligands. The N(1s) electron spectra of L'H and L'–L', and the S(2p) electron spectrum of L'H are shown in Fig. 1. The N(1s) spectrum of L'H showed a single peak with the full-width at a half-maximum height (FWHM) of 1.7 eV. L'–L' showed two peaks with almost equal intensities. The S(2p) spectrum of L'H as well as that of L'–L' showed an unsymmetrical peak with a FWHM of 2.3 eV. Two peaks, p_1 and p_2, indicated by broken lines in the figure, have been attributed to $S(2p_{1/2})$ and $S(2p_{3/2})$ electrons, respectively. The S(2p) spectra of LH, LNa, and the metal complexes were resolved graphically on the basis of the shape L'H containing one type of sulfur atom.

Table 1. Binding energies

Compound	Binding energy/eV		
	N(1s)	$S(2p_{3/2})$	$Cu(2p_{3/2})$
LH	400.6	164.5; 162.3	
LNa	398.9	164.2; 162.2	
L–L	399.0	164.5	
L'H	400.6	162.4	
L'–L'	400.5; 399.1	164.5	
CuL	399.4	164.4; 162.8	933.5
CuL_2	399.4	164.4; 162.8	933.5
CuL_3H_2Cl	400.6; 398.9	164.5; 162.7	933.5
PtL_2	399.8	164.5; 162.9	
PdL_2	399.7	164.5; 162.9	
NiL_2	399.6	164.4; 162.6	
CdL_2	399.4	164.4; 162.6	
HgL_2	399.0	164.2; 163.1	
PbL_2	399.0	164.3; 162.4	
AgL	399.1	164.4; 162.7	
$CuCl_2$			935.8
$Cu(CH_3COO)_2$			935.2

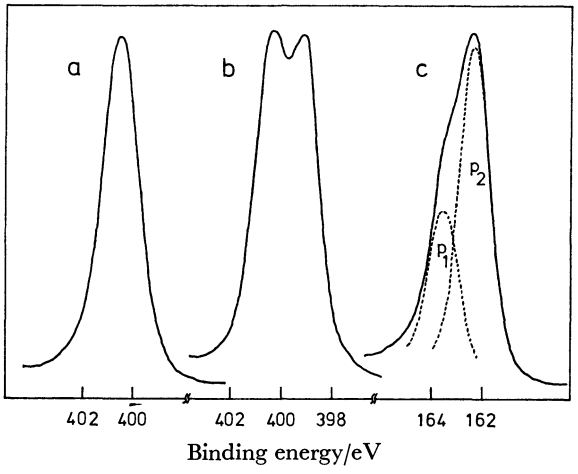

Fig. 1. Electron spectra of the reference compounds.
a: N(1 s) of L'H, b: N(1 s) of L'–L', c: S(2 p) of L'H.

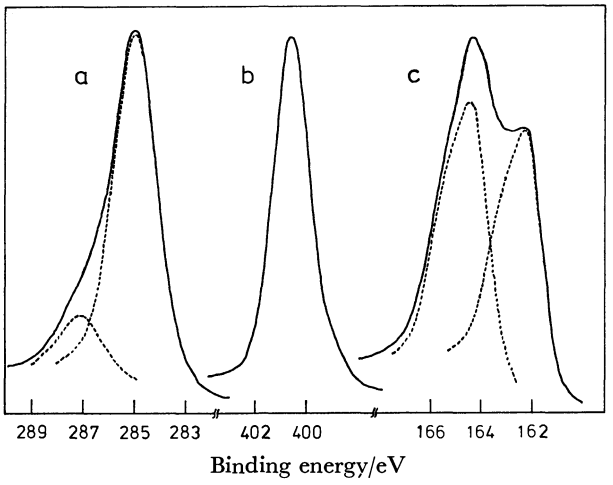

Fig. 2. Electron spectra of LH.
a: C(1 s), b: N(1 s), c: S(2 p).

The C(1s), N(1s), and S(2p) electron spectra of LH are shown in Fig. 2. The C(1s) spectrum showed a main peak and a weak peak on the higher energy side. The former has been assigned to the carbon in the benzene ring and the latter to the thioamide group. The N(1s) spectrum together with the L'H showed a single peak, but the S(2p) spectrum showed a broad peak with a shoulder suggesting two types of sufur atoms. The two peaks indicated by the broken lines which were obtained by a graphical resolving, were almost equal in intensity. The peak with the lower binding energy of the two appeared to weaken with X-ray radiation time. Such X-ray damage in the S(2p)

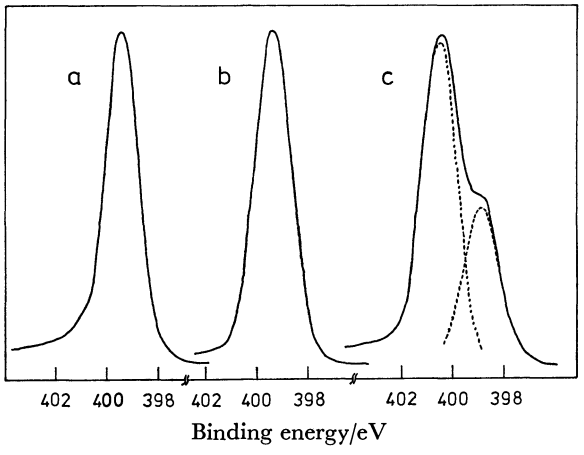

Fig. 3. N(1 s) electron spectra of the copper complexes.
a: CuL, b: CuL_2, c: CuL_3H_2Cl.

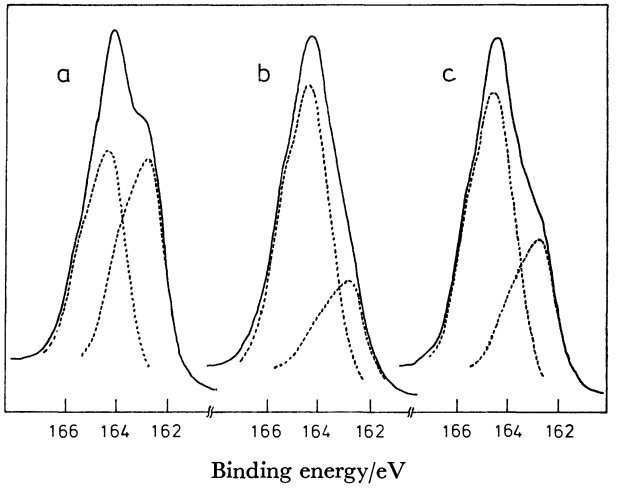

Fig. 4. S(2 p) electron spectra of the copper complexes.
a: CuL, b: CuL_2, c: CuL_3H_2Cl.

spectra was not observed in the other samples. The N(1s) and S(2p) spectra of LNa were similar to those of LH in shape. The S(2p) spectrum of L–L, which contains two types of sulfur atoms, was almost the same as those of L'–L' and L'H in shape.

Complexes. The N(1s) and S(2p) spectra of CuL CuL_2, and CuL_3H_2Cl are shown in Figs. 3 and 4. The N(1s) spectra of CuL and CuL_2 as well as those of the other metal complexes showed a single peak with a FWHM of 1.5—1.7 eV. The N(1s) spectrum of CuL_3H_2Cl showed two peaks with an intensity ratio of approximately 2: 1. The S(2p) spectra of the three copper complexes as well as those of the other metal complexes showed the presence of two types of sulfur atoms. The two peaks, indicated by broken lines in the figures were obtained by graphical resolving. The approximate intensity ratio of the two peaks of CuL as well as the other complexes was 1: 1, however, that of CuL_2 was 3: 1, and that of CuL_3H_2Cl 2: 1.

The $Cu(2p_{3/2})$ electron region spectra of CuL_2, $CuCl_2$, and $Cu(CH_3COO)_2$ are shown in Fig. 5. In the case of CuL_2 as well as CuL_3H_2Cl the broad satellite was not observed in the higher energy region than a main peak as was seen for $CuCl_2$ and $Cu(CH_3COO)_2$.

Discussion

Free Ligands. The peak with the higher binding energy of the two in the N(1s) spectrum of L'–L' may be assigned to the protonated nitrogen atom and the other to the deprotonated atom, considering that the N(1s) binding energy of a protonated nitrogen atom is approximately 1.5 eV higher than that of a deprotonated one.[13]

LH and L'H are able to exist in two tautomeric conformations, the thiol form and the thioketo form. IR, NMR, and X-ray analysis studies[6,8,14] have indicated that the thioketo form dominates in LH and L'H in the solid state. The results in this study indicate that both LH and L'H exist entirely in the thioketo form, since the N(1s) spectra showed a single peak with a binding energy corresponding to the –NH type.

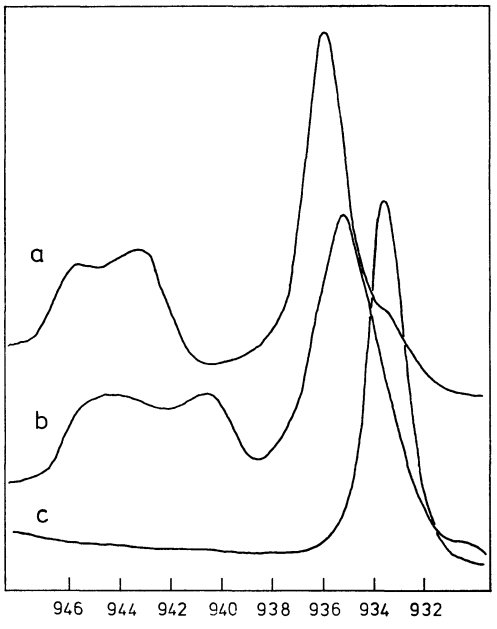

Fig. 5. $Cu(2\ p_{3/2})$ electron region spectra.
a: $CuCl_2$, b: $Cu(CH_3COO)_2$, c: CuL_2.

The peak with the higher binding energy of the two in the S(2p) spectrum of LH can be readily assigned to the endocyclic sulfur atom and the other to the exocyclic, by comparing the binding energies (164.5 and 162.3 eV) with that of L'H, which has only the exocyclic atom. The binding energies of two types of sulfur atoms of LNa, when compared with those of the corresponding sulfur atoms of LH, give a difference of 0.3 eV for the endocyclic sulfur atom and 0.1 eV for the exocyclic atom. Furthermore, the N(1s) binding energy of LNa was only 0.2 eV lower than that of the deprotonated nitrogen of L'–L'. From these results, it is suggested that in LNa, the contribution of $-\overset{-}{N}-\underset{|}{C}=S$ dominates that of $-N=\underset{|}{C}-S^-$, and that an apparent unit negative charge on the nitrogen atom is delocalized by conjugation within the hetero five-membered ring.

Complexes. It has been reported that CuL_2 may be prepared by the reaction of $CuCl_2$ with LH in ethanol.[7,9] Repeated attempts to prepare CuL_2 in this way however failed and a complex with an elemental analysis of CuL_3H_2Cl was obtained. CuL_2 was obtained only in the presence of some amount of water as described above.

CuL_2 involves only one type nitrogen atom, a deprotonated type, whereas CuL_3H_2Cl involves both protonated and deprotonated nitrogen atoms, with a ratio of 2: 1. This result supports the experimental evidence that CuL_2 does not show the N–H band in the IR spectrum, whereas CuL_3H_2Cl does.

The diamagnetism of Cu(II) complexes has been explained by two theories. One is that the paramagnetism is quenched by a strong spin-spin interaction between the two copper(II) ions,[15] and the other is a reduction of the Cu(II) ion to Cu(I) by a ligand on complex formation.[10] The diamagnetism of the complex of the copper(II) salt with LH has been explained by

the former theory.[7,9] This explanation was however found to be completely excluded on the basis of the following evidence obtained.

A Cu(II) complex typically exhibits a satellite on the higher-energy side of the primary peak in the $Cu(2p_{3/2})$ electron region spectrum, as seen for $CuCl_2$ and $Cu(CH_3COO)_2$ in Fig. 5. A Cu(I) complex does not exhibit this.[16] On the basis of the absence of the satellite in the spectra of CuL_2 and CuL_3H_2Cl, it is suggested that CuL_2 and CuL_3H_2Cl are Cu(I) complexes. This agrees with their magnetic moments, *i.e.* both complexes are diamagnetic. Furthermore, the $Cu(2p_{3/2})$ binding energies of CuL_2 and CuL_3H_2Cl, as well as CuL, are about 2 eV lower than those of $CuCl_2$ and $Cu(CH_3COO)_2$. This difference in binding energy is comparable to the difference between CuCl and $CuCl_2$ (1.8 eV).[16]

The inequality of intensities of the two types of peaks in the S(2p) spectra of CuL_2 and CuL_3H_2Cl is thought due to the change in the state of a part of the exocyclic sulfur atoms, *i.e.* the change of a thiocarbonyl group to a disulfide group. This is supported by the following facts; the S(2p) binding energy of the sulfur atom of a disulfide group is close to that of an endocyclic one and L–L was obtained from the reaction of LH with copper(II) salts instead of H_2O_2. CuL_2 could be prepared from the reaction of CuCl with LH and L–L.

It is thought that the Cu(II) ion is reduced to the Cu(I) ion by LH on complexing giving CuL_2 and CuL_3H_2Cl, and that the resulting L–L is coordinated to the Cu(I) ion. Therefore, it is thought that, in the stoichiometric forms of CuL_2 and CuL_3H_2Cl, the half and the one-third of the ligands, respectively, should be replaced by 1/2(L–L).

In general, coordination of a ligand to a metal ion causes a decrease in the electron density on the coordinating atom, giving rise to an increase in the core-electron binding energy of the atom. The N(1s) chemical shifts, which are the differences between the N(1s) binding energies of the complexes and LNa, were 0.5—0.9 eV in CuL, CuL_2, PtL_2, PdL_2, NiL_2, and CdL_2, and very small in HgL_2, PbL_2, and AgL. The N(1s) chemical shift of the deprotonated nitrogen atom of CuL_3H_2Cl was not appreciable, and the N(1s) binding energy of the protonated nitrogen of the complex was the same as that of LH.

From these results, it may be concluded that, in CuL, CuL_2, PtL_2, PdL_2, NiL_2, and CdL_2 an M–N bond is present, and in HgL_2, PbL_2, AgL, and CuL_3HCl_2 it is absent.

The S(2p) binding energies of the two types of sulfur atoms of all the present complexes, when compared with the corresponding ones of LNa, were equal to or larger than those of the latter; the differences were 0—0.3 eV for an endocyclic sulfur atom and 0.2—0.9 eV for an exocyclic one. The S(2p) chemical shfts for an exocyclic sulfur were comparable with the values (0.3—0.9 eV)[17] due to the coordination of thiourea or thiazole through the sulfur atom. Therefore, it may be concluded that the exocyclic sulfur atom-metal ion bond is present in all the complexes.

The small positive chemical shifts of an endocyclic sulfur atom appears to suggest the absence of the sulfur-metal ion bond based on the following. The binding energies of the endocyclic sulfur atoms of all the complexes were equal to or smaller than that of the corresponding sulfur atom of LH. The sulfur atom present in the skeleton of the five-membered ring has very weak coordinating ability, since the lone pairs on the sulfur atom are involved in the resonance structures of the molecule.[18]

These results concerning the mode of coordination of LH largely supports the IR results[6–8] in all the complexes. The IR data however suggested that bonding occurred only through the sulfur atom in CuL,[3] and through both the sulfur and the nitrogen in PbL_2 and AgL.[7] This difference of assignments by XPS and IR can not be explained, but may be due to large uncertainties encountered in assigning C=S, M–N, and M–S vibrations in the ligands containing H–N–C=S and their metal complexes.[19]

The authors wish to thank Mr. Yukihiro Sato for his aid in performing these experiments, and Mr. Taichiro Hirohara for the elemental analysis.

References

1) M. Kuras, *Collect. Czech. Chem. Commun.*, **11**, 367 (1939).
2) A. K. Majumdar and M. M. Chakrabartty, *Anal. Chim. Acta*, **20**, 379 (1959).
3) M. M. Khan and A. U. Malik, *J. Inorg. Nucl. Chem.*, **34**, 1847 (1972).
4) M. Tamura, H. Hada, J. Noguchi, and S. Hayashi, *J. Phys. Chem.*, **66**, 559 (1962).
5) B. C. Bera and M. M. Chakrabartty, *Talanta*, **13**, 1549 (1966).
6) R. F. Wilson and P. Merchant, Jr., *J. Inorg. Nucl. Chem.*, **29**, 1993 (1967).
7) I. P. Khullar and U. Agarwala, *Can. J. Chem.*, **53**, 1165 (1975).
8) J. Dehand and J. Jordanov, *Inorg. Chim. Acta*, **17**, 37 (1976).
9) M. F. El-Shazly, T. Salem, M. A. El-Sayed, and S. Hedewy, *Inorg. Chim. Acta*, **29**, 155 (1978).
10) a) F. Petillon, J. E. Guerchais, and D. M. L. Goodgame, *J. Chem. Soc., Dalton Trans.*, **1973**, 1209; b) D. De Filippo, F. Devillanova, E. F. Trogu, G. Verani, C. Preti, and P. Viglino, *Can. J. Chem.*, **51**, 1172 (1973); c) C. Preti and G. Tosi, *Can. J. Chem.*, **53**, 177 (1975); d) C. Preti and G. Tosi, *Can. J. Chem.*, **54**, 1558 (1976).
11) a) K. Siegbahn, *et al.*, "ESCA Atomic, Molecular and Solid State Structure Studied by Means of Electron Spectroscopy," Almqvist and Wiksells AB, Uppsala (1967); b) K. Siegbahn, *et al.*, "ESCA Applied to Free Molecules," North-Holland Publ. Co., Amsterdam (1969).
12) B. N. Figgis and J. Lewis, "Modern Coordination Chemistry," ed by J. Lewis and R. G. Wilkins, Interscience Publ., Inc., N. Y. (1967) p. 403.
13) L. E. Cox, J. J. Jack, and D. M. Hercules, *J. Am. Chem. Soc.*, **94**, 6575 (1972).
14) a) M. St. C. Flett, *J. Chem. Soc.*, **1953**, 347; b) C. N. R. Rao, R. Venkataraghavan, and T. R. Kasturi, *Can. J. Chem.*, **42**, 36 (1964); c) D. Harrison and J. T. Ralph, *J. Chem. Soc., B*, **1967**, 14; d) G. R. Form, E. S. Raper, and T. C. Downie, *Acta Crystallogr., Sect. B*, **32**, 345 (1976).
15) a) C. M. Harris, B. F. Hoskins, and R. L. Martin,

J. Chem. Soc., **1959**, 3728; b) B. Singh, Lakshmi, and U. Agarwala, *Inorg. Chem.*, **8**, 2341 (1969); c) J. C. Chudy and J. A. W. Dalziel, *J. Inorg. Nucl. Chem.*, **37**, 2459 (1975).

16) D. C. Frost, A. Ishitani, and C. A. Mcdowell, *Mol. Phys.*, **24**, 861 (1972).

17) a) V. Srinivasan and R. A. Walton, *Inorg. Chim. Acta*, **25**, L85 (1977); b) D. A. Edwards, R. Richards, R. E. Myers, and R. A. Walton, *Inorg. Chim. Acta*, **23**, 215 (1977).

18) R. T. Morrison and R. N. Boyd, "Organic Chemistry," Allyn and Bacon Inc., Boston (1963).

19) a) C. N. R. Rao and R. Venkataraghavan, *Spectrochim. Acta*, **18**, 541 (1962); b) B. Singh, Lakshmi, and U. Agarwala, *Inorg. Chem.*, **8**, 2341 (1969); c) D. De Filippo, F. Devillanova, C. Preti, E. F. Trogu, G. Verani, and P. Viglino, *Can. J. Chem.*, **51**, 1172 (1973).

Use of a Programmable Monochromator and a SIT Detector in Flame Atomic Emission Spectrometry

Naoki FURUTA,*,† Cameron W. McLEOD,** Hiroki HARAGUCHI,** and Keiichiro FUWA**

Division of Chemistry and Physics, National Institute for Environmental Studies, Yatabe, Ibaraki 300-21

***Department of Chemistry, Faculty of Science, The University of Tokyo, Bunkyo-ku, Tokyo 113*

(Received March 15, 1979)

A multielement detection system which uses a programmable monochromator and a SIT image detector has been constructed, and evaluated by measuring the flame emission of 22 elements in the nitrous oxide–acetylene flame. The detection limits for the elements under optimized experimental conditions are reported, and are compared with those obtained by a standard photomultiplier tube.

The silicon intensified target tube (SIT) coupled with an optical multichannel analyser (OMA) has been utilized as a detector system in emission,[1–6] absorption[7–9] and fluorescence[10] spectroscopic studies. Attractive analytical features of the SIT detection system, which have been well-documented in the reports from Morrison and his coworkers,[1,4–6] include the simultaneous multielement analysis capability, the facility to correct for spectral and background interference and detection power equivalent to the photomultiplier tube (PMT) in the visible region, although detection performance is relatively poorer in the ultraviolet. As is well known,[11] the standard SIT image detector consists of about 500 light sensitive elements (channels) within an area of approximately 62.5 mm^2 (length 12.5 mm, height 5 mm) so that, when situated in a dispersing instrument, simultaneous detection of atomic lines is possible. The range of wavelengths which are detected simultaneously is determined primarily by the reciprocal linear dispersion (RLD) of the monochromator. In order to take advantage of the SIT–OMA system for simultaneous multielement analysis, relatively low-dispersion monochromators which provide a spectral window generally greater than 20 nm have been preferred. The use of the low-dispersion monochromator, however, may result in severe spectral interference in atomic emission spectroscopy in high temperature media, particularly in inductively coupled plasma (ICP) emission spectroscopy.

In the present study, the SIT–OMA system has been combined with a medium resolution monochromator (focal length, 1 m; RLD, 0.4 nm/mm) to evaluate detectability performance. The use of the medium resolution monochromator reduces the spectral region spatially detected by the SIT–OMA system (5 nm for present instrumentation) and sacrifices to some extent the capability for simultaneous multielement analysis.

Recently, the present authors have developed a programmable monochromator controlled by a minicomputer, where a slew-scan technique was employed as has been reported by other workers.[12–16] The programmable monochromator of the slew scan type is convenient for rapid sequential multielement analysis and has more inherent flexibility for multielement detection than the well-established direct reading system where only fixed wavelengths of the desired elements are available.[17] However, the slew scan technique suffers from the problem of irreproducibility in wavelength setting, precision being limited to $\pm$0.1 nm, as has already been pointed out.[13,16] To avoid the error caused by irreproducible wavelength setting in the slit-based spectrometer, it was decided to adopt the SIT as the spatial detector in the slew scan system. The important capability of simultaneous multielement analysis is still retained provided element lines are within a 5 nm range for the present instrumentation ($\pm$2.5 nm from the central OMA channel).

In this study, the analytical performance of the SIT–OMA-detector is considered when combined with the programmable monochromator system. The nitrous oxide–acetylene flame was selected as the excitation source for initial studies.

Experimental

Instrumentation. The experimental system is shown in Fig. 1. A nitrous oxide†† –acetylene flame was supported on a burner assembly (5 cm slot burner) of a commercially available spectrophotometer (Shimadzu AA 650). The monochromator (Jobin Yvon HR 1000; focal length, 1 m) had dual entrance and exit ports and was equipped with a holographic grating (2400 grooves/mm); the desired optical path

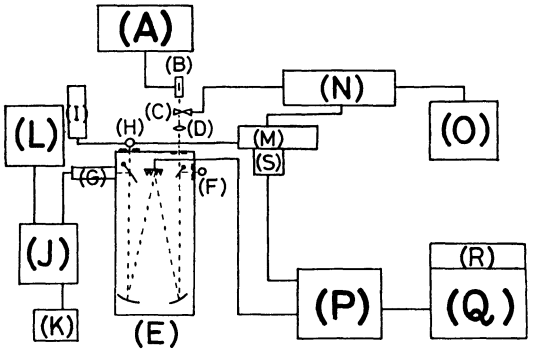

Fig. 1. Schematic diagram of computer-controlled instrumentation for multielement analysis.
(A) Flame gas controlls, (B) burner, (C) chopper, (D) lens, (E) monochromator, (F) Hg lamp, (G) SIT, (H) photomultiplier, (I) power supply, (J) optical multi-channel analyser, (K) oscilloscope, (L) X-Y recorder, (M) pre-amplifier, (N) lock-in-amplifier, (O) recorder, (P) minicomputer, (Q) teletype, (R) tape reader/puncher, (S) interface for peak sensor.

† Present address: Department of Chemistry, The University of Alberta, Edmonton, Alberta, Canada T6G 2G2.

†† N_2O, dinitrogen oxide in IUPAC nomenclature.

was selected by mirrors positioned beside the entrance and exit slits. The entrance slits were used to receive radiation from the flame and a mercury penray lamp, respectively, the latter being used for wavelength calibration of the monochromator scanning system. The flame focused on the entrance slit was imaged down a factor of 2 using a single spherical silica lens (diameter, 60 mm; focal length, 219 mm). The SIT detector tube (Princeton Applied Research Co., SIT 1205D/01) and a standard photomultiplier (Hamamatsu TV Co., R919) sensitive to ultraviolet and visible light were positioned at the exit ports. The slit unit was removed in the former case, and a plate was equipped on the SIT adaptor to obstruct 50% of the incident light to enable dark current correction. The lateral length of the SIT detector was 12.5 mm and for the monochromator RLD of 0.4 nm/mm, a 5 nm spectral window was obtained. The resolution power for the SIT, 0.032 nm, was about 7 times poorer than that by PMT (slit width, 10 μm). The SIT signal after processing in the OMA (Princeton Applied Research Co., OMA 1205A) was displayed on the oscilloscope and/or could be recorded by an external X-Y recorder (Yokogawa Electric Works, Ltd., 3078).

For PMT detection, a pre-amplifier (laboratory constructed), a light chopper and a lock-in-amplifier (Princeton Applied Research Co., 125A and 5203, respectively) were used.

A minicomputer (Hewlett Packard 2108) was employed to control the monochromator wavelength by the slew scanning technique. A mercury penray lamp (Ultra-Violet Co., 11SC-I) was used for initial wavelength calibration.

Procedure. For wavelength calibration, the scanning system was referenced to the mercury lines at 253.65 and 507.30 nm using the Hg lamp. This procedure determined the number of steps/wavelength (nm) to be employed in wavelength selection by the stepping motor, when controlling the grating angle. After calibration, the wavelengths of the desired atomic lines could be set arbitrarily by command from the computer. The details of the slew scanning system will be described elsewhere.[18]

The experimental conditions for the measurement of atomic emission using the nitrous oxide–acetylene flame were optimized in terms of the flame and slit conditions. Once the conditions had been optimized, a standard solution was aspirated and the accumulated spectrum was stored in OMA memory [A]. The procedure was repeated for the blank solution using memory [B]. The subtracted spectrum [A-B] provided the emission line(s) of the element(s). The emission intensity was obtained by noting the peak height (generally for channel 250±2) and subtracting the average reading of the side background for 10 channels around the peak channel. The background noise level ([A-B] spectrum for the channel range 240—260) was obtained when distilled water was aspirated and subtraction of the [A] and [B] memories was performed. The PMT detection system was used for comparison studies. The signal and background noise were measured from the pen deflection on the chart recorder paper.

The detection limits in Tables 1 and 2 are defined as the concentrations which represent a signal equivalent to twice the standard deviation of the background noise level. The values were obtained from the standard calibration curve for each element prepared by the least squares method. The optimized conditions determined are also summarized in Table 1 with the wavelengths of analytical lines. The chemicals used were of analytical reagent grade and deionized and distilled water was used as the blank solution.

Results and Discussion

Flame Background Correction. The atomic emission

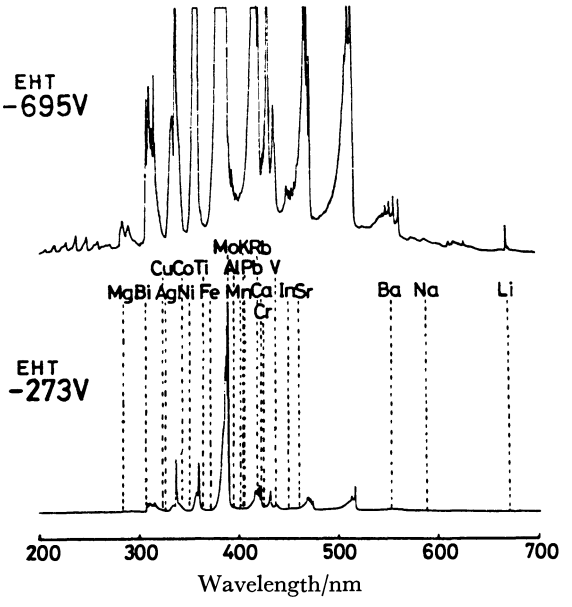

Fig. 2. Emission spectra of nitrous oxide–acetylene flame observed by photomultiplier tube.

of 22 elements in the nitrous oxide–acetylene flame was measured by the SIT–OMA system coupled to the programmable monochromator. Figure 2 shows the N_2O–C_2H_2 flame emission spectra recorded by the PMT when only distilled water was aspirated. The upper curve was recorded at a high EHT (—695 V) to indicate the prominent background constituents of the flame. Background species at approximate wavelengths are NO (200—280 nm), OH (280—330 nm), NH (336 nm), CN (350—442 nm), CH (387—431 nm), and C_2 (437—600 nm). The analytical lines of the elements used in the study are indicated by the dotted lines on the lower spectrum.

Flame emission spectra observed by the SIT–OMA system for a 5 nm spectral window are shown in Figs. 3

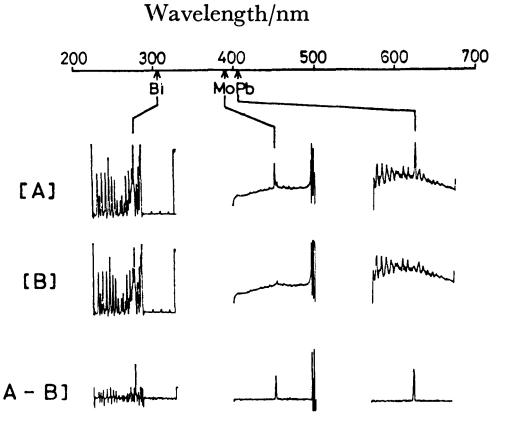

Fig. 3. Emission spectra observed by SIT–OMA system near Bi(306.8 nm), Mo(390.3 nm), and Pb(405.8 nm) lines in nitrous oxide–acetylene flame (Bi 100 μg/ml, Mo 10 μg/ml, Pb 50 μg/ml).
[A]: Spectra for sample solutions, [B]: spectra for blank solution, [A-B]: spectra corrected for flame background.

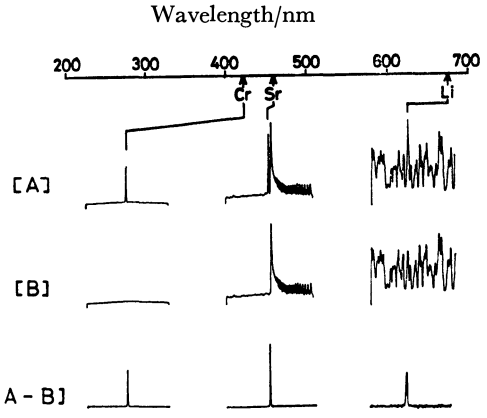

Fig. 4. Emission spectra observed by SIT–OMA system near Cr(425.4 nm), Sr(460.7 nm), and Li(670.8 nm) lines in nitrous oxide–acetylene flame (Cr 1 μg/ml, Sr 0.1 μg/ml, Li 0.005 μg/ml).
[A]: Spectra for sample solutions, [B]: spectra for blank solution, [A-B]: spectra corrected for flame background.

and 4 for Bi, Mo, Pb, and Cr, Sr, and Li, respectively. Since the SIT–OMS system has 2 memories, each memory was used for the emission measurements of the sample solution and the blank solution, respectively. Spectra [A-B] in Figs. 3 and 4 are the corrected spectra calculated from the [A] and [B] memories, and subtraction is automatically performed in the OMA. The background at the Bi wavelength is particularly severe and corresponds to the OH vibrational fine structure. The predominant background species at the Mo wavelength is CH, while at the Pb wavelength CN is predominant. For Sr and Li, the predominant species is C_2, while at the Cr wavelength flame background is negligible.

Detection Limits and Precision. The analytical performance data summarized in Table 1 were obtained by accumulating the signals for 4.1 s. In the SIT–OMA system, the scanning rate of the electron beam over 500 channels was 32.8 ms, and the 4.1 s accumulation time corresponded to 125 times accumulation of the signals at each channel in the SIT detector. The dynamic range of the SIT–OMA system is 10^5 counts and the real-time dynamic range (real-time is a single scan) is about 750 counts for each channel. Therefore, the entrance slit width and slit height were required to be adjusted to obtain the appropriate signal intensities which were within the dynamic range of the SIT–OMA system. Before adjustment of the slit conditions mentioned above, the flame conditions and height above the burner head were optimized for each element using a constant nitrous oxide flow rate of 7.5 l/min. The experimental results obtained through the above procedures are summarized in Table 1, along with the analytical lines and other experimental conditions. The detection limit data are similar to those obtained by Howell and Morrison[6] who used a 0.5 m monochromator–SIT combination. The relative standard deviation (RSD) values for the concentration indicated in parenthesis were generally in the 3% range, although for some elements of low sensitivity, *e.g.* Bi, Pb where concentrations were relatively closer to the respective detection limits, higher RSD values were obtained.

Regarding the flame operating conditions, it can be seen from Table 1 that the elements such as Ti, V, Al, and Mo were atomized effectively in the reducing atmosphere of the C_2H_2-rich flame and in the high temperature region corresponding to a high position above the burner head. These conditions are required to prevent formation of the refractory oxide species. In contrast, optimum sensitivity for Co, Pb, Fe was obtained in the oxygenated atmosphere of the C_2H_2-lean flame and at a low position above the burner. In this way, the optimum conditions in the N_2O–C_2H_2 flame are very different for the elements. This spread in the optimum values constitutes a major problem in utilizing the N_2O–C_2H_2 source for multielement analysis, since fixed flame conditions and flame height would be desirable for rapid analysis. The other major drawback in the N_2O–C_2H_2 excitation source is that elements whose resonance lines are in the UV region are not sufficiently excited to observe atomic emission.[19]

Comparison of SIT and PMT Detection. So far, to evaluate SIT detector performance, the detection limits obtained by the SIT image detector have been compared with those obtained in separate studies by the PMT.[1–10] In the present study, the detection limits of 8 elements were also obtained by a PMT (R919). The experimental conditions for the SIT detector were the same as those shown in Table 1, and the conditions for the PMT were independently determined by optimization procedures for each element.

As is well known,[6] the photon quantum yield of the SIT in the ultraviolet region is worse by 1—2 orders of magnitude when compared to that of the PMT, while it is almost comparable with or better than that of the PMT in the visible region. Although a rigorous comparison of data is ruled out due to fundamental design differences between the SIT and the PMT, for standard measurement conditions, *i.e.* SIT accumulation time of 4.1 s and a PMT time constant of 2 s, a general trend in the results can be pointed out. Poor SIT detector performance is evident in the UV, *e.g.* for Mg and Ag where detection limits are about 20 times poorer than the PMT data. The excellent detection power in the visible region is, however, clearly seen from Table 2.

Conclusions

Use of the SIT detector for slew scan multielement analysis is advantageous in that it allows for a less accurate wavelength setting of the monochromator than otherwise would be required for PMT detection. Rapid analysis may be performed with the present system (*e.g.*, less than 5 min required for 10 elements). The results shown in Tables 1 and 2 and Figs. 3 and 4 demonstrate the following important capabilities of the SIT–OMA system: 1) high detection limits for many elements, 2) multielement detection over a small wavelength range (5 nm), 3) the facility to correct for background interference. However, the relatively poor sensitivity of the SIT in the ultraviolet region and the insufficient excitation efficiency of the N_2O–C_2H_2 flame detract from the

Table 1. The flame emission detection limits of various elements for SIT detection under optimized experimental conditions

Element	Wavelength nm	C_2H_2[a] Flow rate l/min	Flame[b] height mm	Slit width μm	Slit height mm	Detection limit[c] μg/ml	RSD[d] %
Mg	285.21	5.75	7.5	70	3	0.22	3.0(1)
Bi	306.77	6.13	5	30	2.8	21	12.6(100)
Cu	324.75	5.75	4	165	2	0.066	5.6(1)
Ag	328.07	6.0	4	60	1	0.11	2.3(5)
Co	345.35	5.75	9	160	5	0.21	8.4(1)
Ni	352.45	5.75	6	150	3	0.61	2.8(10)
Ti	365.35	7.5	10	250	6	0.15	3.8(5)
Fe	371.99	5.75	8	150	5	0.13	7.2(1)
Mo	390.30	6.5	9	150	1	0.17	15.4(1)
Al	396.15	7.25	8	150	0.3	0.032	7.4(0.5)
Mn	403.08	6	5	100	1	0.017	2.1(1)
K	404.41	5.75	10	250	5	7.5	—
Pb	405.78	5.75	8	170	5	0.95	11.4(10)
Rb	420.19	5.75	6	150	1.4	2.2	5.1(50)
Ca	422.67	6	4.5	40	0.4	0.002	2.8(0.1)
Cr	425.43	6	6	120	1.5	0.0028	2.2(0.1)
V	437.92	7.5	8	125	2	0.018	2.4(0.5)
In	451.13	6	4.5	130	0.9	0.0092	1.6(0.5)
Sr	460.73	6.25	7	120	3	0.0008	1.5(0.05)
Ba	553.56	6.25	4.5	180	1	0.064	3.7(1)
Na	589.00	6	7.5	100	1.5	0.00066	—
Li	670.78	6.25	6	170	2.3	0.00013	2.1(0.005)

a) The flow rate of nitrous oxide was fixed at 7.5 l/min. b) Height above the burner head. c) See text for definition. d) Relative standard deviation calculated from 10 determinations. Value in parenthesis is concentration at which determination was performed.

Table 2. Comparison of detection limits for SIT and PMT

Element	Wavelength nm	SIT μg/ml	PMT μg/ml
Mg	285.21	0.24	0.004
Bi	306.77	24	23
Ag	328.07	0.20	0.060
Mo	390.30	0.39	0.87
Pb	405.78	0.35	0.48
Cr	425.44	0.005	0.018
Sr	460.73	0.0005	0.0007
Li	670.78	0.00028	0.0022

use of the present instrumental system for analytical flame emission spectrometry. Particularly, the flame requires tedious optimization procedures to achieve sufficient sensitivity for each element. The ICP excitation system would overcome to some extent the poor SIT sensitivity in the UV. A further advantage of the ICP source relative to the N_2O–C_2H_2 flame is that near-optimum sensitivity for all elements is provided by one set of ICP operating conditions.[20] The application of the present instrumental system to ICP emission spectrometry is in progress, and will be reported in the near future[21].

The authors express their thanks to Dr. A. Otsuki, National Institute for Environmental Studies, for his helpful discussion and encouragement. C.W.M. is grateful to the Inner London Education Authority (U.K.) for the award of The Robert Blair Fellowship and receipt of a travel grant.

References

1) K. W. Busch, N. G. Howell, and G. H. Morrison, *Anal. Chem.*, **46**, 575, 1231 (1974).
2) F. L. Fricke, O. Rose, Jr., and J. A. Caruso, *Anal. Chem.*, **47**, 2018 (1975).
3) F. L. Fricke, O. Rose, Jr., and J. A. Caruso, *Talanta*, **23**, 317 (1976).
4) N. G. Howell, J. D. Ganjei, and G. H. Morrison, *Anal. Chem.*, **48**, 319 (1976).
5) J. D. Ganjei, N. G. Howell, J. R. Roth, and G. H. Morrison, *Anal. Chem.*, **48**, 505 (1976).
6) N. G. Howell and G. H. Morrison, *Anal. Chem.*, **49**, 106 (1977).
7) D. G. Mitchell, K. W. Jackson, and K. M. Aldous, *Anal. Chem.*, **45**, 1215A (1973).
8) K. W. Jackson, K. M. Aldous, and D. G. Mitchell, *Appl. Spectrosc.*, **28**, 569 (1974).
9) K. M. Aldous, D. G. Mitchell, and K. W. Jackson, *Anal. Chem.*, **41**, 1034 (1975).
10) T. L. Chester, H. Haraguchi, D. O. Knapp, J. D. Messman, and J. D. Winefordner, *Appl. Spectrosc.*, **30**, 410 (1976).
11) Y. Talmi, *Anal. Chem.*, **47**, 658A, 699A (1975).
12) E. Cordos and H. V. Malmstadt, *Anal. Chem.*, **45**, 425 (1973).
13) D. J. Johnson, F. W. Plankey, and J. D. Winefordner, *Anal. Chem.*, **47**, 1739 (1975).
14) R. W. Spillman and H. V. Malmstadt, *Anal. Chem.*, **48**, 303 (1976).

15) P. W. J. M. Boumans, G. H. van Gool, and J. A. J. Jansen, *Analyst*, **101**, 585 (1976).
16) H. Kawaguchi, M. Okada, T. Ito, and A. Mizuike, *Anal. Chim. Acta*, **95**, 145 (1977).
17) V. A. Fassel, *Science*, **202**, 183 (1978).
18) N. Furuta, H. Haraguchi, and K. Fuwa, *Anal. Chem.*, to be submitted.
19) G. D. Christian, and F. J. Feldman, *Appl. Spectrosc.*, **25**, 660 (1971).
20) R. H. Scott, V. A. Fassel, R. N. Kniseley, and D. E. Nixon, *Anal. Chem.*, **46**, 75 (1974).
21) N. Furuta, C. W. McLeod, H. Haraguchi, and K. Fuwa, *Appl. Spectrosc.*, to be submitted.

Phase Transformation of Iron Vanadium Sulfides at High Temperatures

Hiroaki WADA

National Institute for Researches in Inorganic Materials, Namiki 1-1, Sakura-Mura, Niihari-Gun, Ibaraki 300-31

(Received March 27, 1979)

The phase relations of iron vanadium sulfides with the atomic Fe: V ratios 3: 2 and 71: 29 were examined by the high-temperature DTA and X-ray measurements. It was found that the structure of iron vanadium sulfide changes gradually from a less symmetric form to a highly symmetric form with the increase in temperature. Two types of phase transformations by vacancy order-disorder were observed at temperatures above 800 °C. One was due to the intralayer disordering of metal vacancies: V_3S_4-type⟶$Cd(OH)_2$-type (type Ia) or V_3S_4-type+NiAs-type⟶$Cd(OH)_2$-type (type Ib) at T_1. The other was due to the entirely interlayer disordering of metal vacancies: $Cd(OH)_2$-type⟶NiAs-type (type II) at T_2 ($T_2 > T_1$). The tentative phase diagram of iron vanadium sulfides with the atomic Fe: V ratio 3: 2 was constructed on the basis of the DTA results.

The phase equilibrium study of a part of the Fe–V–S system has been made recently by means of thermogravimetry.[1] The phase relations of the Fe–V–S system at high temperatures (500—800 °C) were presented in an earlier publication.[2] From the powder X-ray diffraction patterns of the quenched specimens and the behavior of the composition-equilibrium sulfur pressure relations, it has been shown that the Fe–V–S system has extensive solid solution phases, *i.e*, $(Fe,V)_{1-x}S$, $(Fe,V)_{3\pm x}S_4$, and $(Fe,V)_{5\pm x}S_8$, which have a lattice intermediate between the NiAs-type and the $Cd(OH)_2$-type lattice. These phases exhibited the ordered structures of the metal vacancies due to the removal of metal atoms from every second metal layer in the fundamental NiAs-type structure, in spite of the quenching of specimens from high temperature to room temperature. This fact appears to indicate the non-quenchability of the high-temperature state, because the energy of thermal agitation promotes a state of disorder of metal vacancies with increasing temperature and the disordered phases become stable at high temperatures. Hence, it is desirable to observe the crystal structure of sulfide specimens *in situ* in order to know its real phase relations at high temperatures. However, comparatively few data have been collected on this subject with respect to iron vanadium sulfides.

The vacancy order-disorder transformation of compounds in the V–S system has been reported recently by several investigators. Nakazawa *et al.* studied a V_5S_8 single crystal by means of high-temperature X-ray measurements and found that the V_5S_8 phase has the intralayer order-disorder transformation at about 800 °C.[3] Oka *et al.* called attention to the order-disorder transformation of the metal vacancies and determined the phase diagram of the V–S system in the compositional range from $VS_{1.30}$ to $VS_{1.70}$ by means of high-temperature DTA and X-ray measurements.[4] Also, they explained the order-disorder transformation on the basis of statistical thermodynamic theory.[5] From these reports, it is expected that compounds in the ternary system Fe–V–S have similar phase transformations at high temperatures owing to the disordering of metal vacancies.

The primary aim of this investigation was to observe the structural change of iron vanadium sulfides with temperature and to elucidate the process of its structural phase transformations. The high-temperature DTA and X-ray measurements were employed in this study to obtain direct information on the thermal behavior and structural property of compounds. The author reports in this paper the results of high-temperature experiments of iron vanadium sulfides with the atomic Fe: V ratios 3: 2 and 71: 29.

Experimental

Materials and General Procedure. The sulfide samples were synthesized by heating the mechanical mixtures of reagent grade $VOSO_4 \cdot 3H_2O$ and $FeSO_4 \cdot (NH_4)_2SO_4 \cdot 6H_2O$ in an H_2S atmosphere at 1050 °C for 4 h, and were used as starting materials. The sulfur composition of the sample was adjusted to the desired one by holding it for 5 h at the pre-determined sulfur pressure and temperature and quenching it to room temperature. The general experimental procedures, the apparatus, and the chemical analyses are the same as those described in the previous paper.[1] $Fe_{0.60}V_{0.40}S_x$ and $Fe_{0.71}V_{0.29}S_x$, in the compositional range of $x = 1.20$—1.35, were used chiefly in the high-temperature experiments.

X-Ray Study and DTA Method. The high-temperature X-ray measurements were carried out by the film method. The X-ray powder diffraction patterns of samples were recorded at various temperatures with a precession camera ($R = 100$ mm, Mo $K\alpha$ radiation with Zr filter). A high-power X-ray generator (Rigaku RU-200: 60 kV-200 mA) was employed for rapid measurements at high temperatures. The sulfide sample was sealed in vacuum in a silica-glass capillary (diameter 0.2 mm and thickness 0.01 mm). The capillary was mounted on a usual type of goniometer head and covered by a minifurnace with two small windows along the path of the X-ray beams. Temperature regulation was carried out up to 950 °C within the accuracy of ±5 °C with the P.I.D control system by using a Pt–13%Rh thermocouple. The temperature of the sample was raised and kept at the desired one. The sample was exposed to X-rays for 3 h and powder photographs were taken under the conditions of 50 kV-180 mA.

The DTA measurements were carried out at the heating rate of 20 °C/min up to 1100 °C by using a Rigaku Thermoflex DTA. About 130 mg of the sulfide powder was sealed in vacuum in a micro silica capsule specially designed for the DTA method; pure α-Al_2O_3 was used as the reference substance.

Results and Discussion

The High-temperature X-Ray Study. The high-temperature X-ray studies were carried out in orde-

to clarify the real phase relations and the phase transformation of iron vanadium sulfide which could not be determined directly only from the thermochemical data on its composition-equilibrium sulfur pressure relations.[2] Representative compounds of $Fe_{0.60}V_{0.40}S_{1.31}$, $Fe_{0.60}V_{0.40}S_{1.28}$, and $Fe_{0.71}V_{0.29}S_{1.20}$, were selected for this study. Photographs were taken first at room temperature, and then at various temperatures up to 950 °C during both the heating and cooling processes.

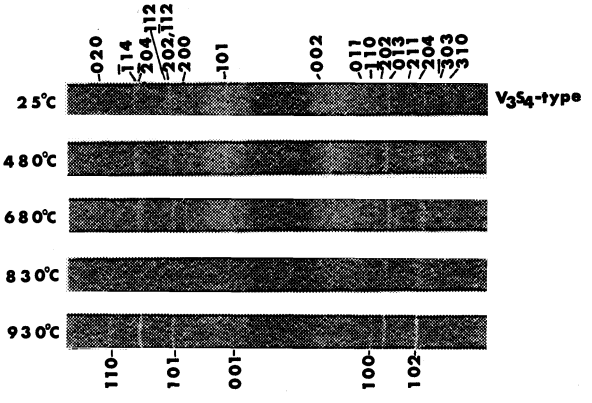

Fig. 1. The X-ray powder photographs of $Fe_{0.60}V_{0.40}S_{1.31}$.

Figure 1 shows a series of diffraction patterns for $Fe_{0.60}V_{0.40}S_{1.31}$, which has the monoclinic V_3S_4-type structure (nonreduced space group I2/m referred to the fundamental NiAs-type cell) at room temperature; its composition corresponds to that of the metal-rich phase boundary of $(Fe,V)_3S_4$ solid solution at 727 °C.[2]

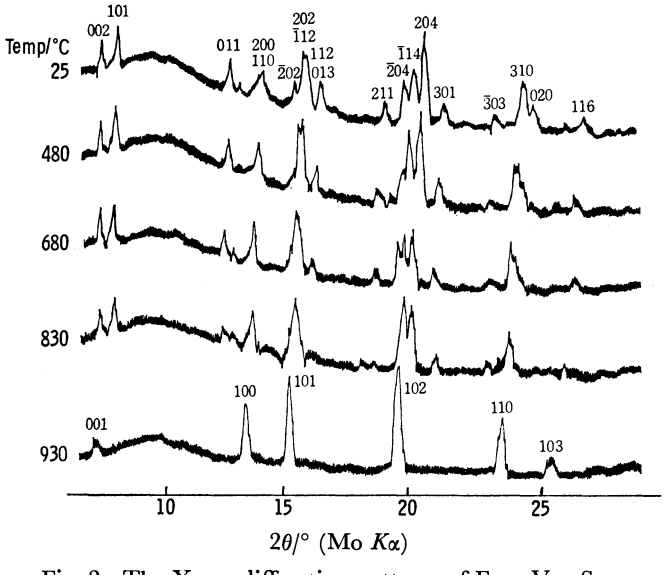

Fig. 2. The X-ray diffraction patterns of $Fe_{0.60}V_{0.40}S_{1.31}$.

Figure 2 gives the X-ray diffraction profiles which were reproduced from Fig. 1 by means of the micro photo-densitometer in order to represent the 2θ-intensity relations of reflections. It can be seen from these figures that the splitting of reflections which would be characteristic of the V_3S_4-type cell decreases gradually with increasing temperature and its peak positions are shifted slightly to the lower side of 2θ values at high temperatures. This result suggests a gradual structural transformation of the monoclinic V_3S_4-type phase from a less symmetric low temperature form to a highly symmetric high temperature form. It should be emphasized that a new phase with the trigonal $Cd(OH)_2$-type structure appears at about 930 °C. However, the high-temperature phase was not quenchable at all. On cooling the sample to room temperature, only the original patterns of V_3S_4-type was observed. This suggests that the phase transformation process of $(Fe,V)_3S_4$ solid solution is reversible.

Table 1. The relation of the unit cell dimensions of $Fe_{0.60}V_{0.40}S_{1.31}$ with temperature

Temp °C	a Å[b]	b Å	c Å	β °	Volume Å^3
25	5.90±1	3.33±1	11.19±2	92.1±1	219±1
480	5.96±2	3.39±1	11.30±2	91.9±1	228±1
680	5.99±2	3.42±1	11.33±4	91.7±1	232±1
830	6.01±2	3.44±1	11.40±4	91.2±2	236±1
930	3.477±6[a]		5.738±9[a]		60.1±2[a]

a) Trigonal phase. The unit cell dimensions are calculated on the basis of a $Cd(OH)_2$-type hexagonal lattice.
b) Å$=10^{-1}$ nm.

Lattice parameters of $Fe_{0.60}V_{0.40}S_{1.31}$ were calculated by the least-squares method[6] from the data which were obtained by the film method. Temperature dependence of the unit cell dimensions is given in Table 1. It is noted that the a-, b-, and c-dimensions and the unit cell volume, V, expand linearly with the increase in temperature. On the contrary, the β-angle decreases gradually from 92.1 to 91.2 at temperatures between 25 and 830 °C. Also, the value of the $c\cdot\sin\beta/2b$ ratio, which corresponds to the c/a ratio in the NiAs-type structure, decreases from 1.68 to 1.65 in the temperature range from 25 to 930 °C. This indicates that the interlayer spacing is reduced relative to the intralayer spacing with increasing temperature, due to the difference of the directional character of the structure in the thermal expansion. In this connection, the relative expansion coefficients ($\alpha_a=1/a_{25°C}\cdot da/dT$ and analogously for α_b and α_c) were calculated from the linear relations of the unit cell dimensions with temperature. It was found that α_a, α_b, and α_c, and the volume expansion coefficient, β, are 24×10^{-6} K^{-1}, 41×10^{-6} K^{-1}, 22×10^{-6} K^{-1}, and 95×10^{-6} K^{-1}, respectively.

A few remarks should be made here regarding the process of the phase transformation of a V_3S_4-type cell. A possible model of the structural transformation process is shown schematically in Fig. 3. The crystal structure of the monoclinic V_3S_4-type is characterized by the ordered arrangement of metal vacancies which are confined to the alternate metal layers in the fundamental NiAs-type structure.[7] This vacancy-ordered phase is stable at lower temperatures. As the temperature is raised, the energy of thermal agitation gradually increases the degree of disorder. The ordered arrangement of vacancies within the metal-deficient layer

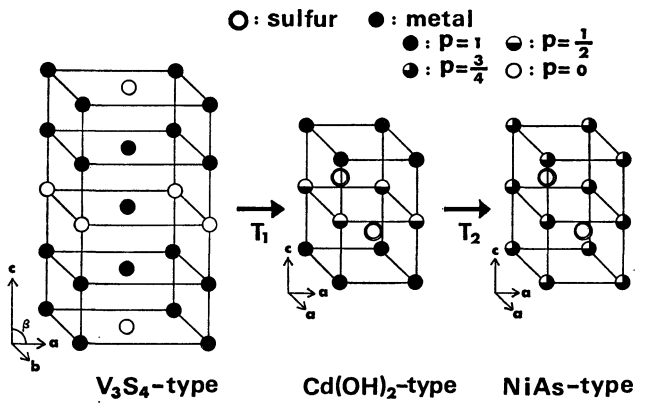

Fig. 3. A schematic model of the structural transformation of the V_3S_4-type phase with $a \approx \sqrt{3} \cdot a_{NiAs}$; $b \approx a_{NiAs}$; $c \approx 2c_{NiAs}$; $\beta \approx 92°$. Hexagonal array of sulfur is omitted in a picture of the V_3S_4-type structure for convenience. Symbol p denotes the occupation probability of a metal atom for each site.

changes to the entirely disordered one of the solid solution at high temperatures. A trigonal $Cd(OH)_2$-type phase with the complete intralayer disordering becomes stable at temperatures above T_1. Further temperature elevation promotes the successive phase transformation from a trigonal $Cd(OH)_2$-type to a hexagonal NiAs-type, based on the complete intra- and inter-layers disordering. A nonstoichiometric NiAs-type phase appears at temperatures above T_2. The schematic model of a disordering process of metal vacancies, however, may need some modifications because both the intra- and inter-layers disordering take place concomitantly with increasing temperature.[3] As shown in Fig. 2, the intensity of the (001) reflection of a trigonal

TABLE 2. VARIATION OF *d*-SPACINGS WITH TEMPERATURE

hkl	d_{obsd}/Å					
	25 °C	500 °C	730 °C	800 °C	850 °C	900 °C
002	5.65	5.69	5.70	5.71	5.74	5.77
101	5.17	5.19	5.26	5.28	5.30	
011	3.20	3.24	3.26	3.28	3.27	
103	3.12	3.15	3.17			
100[a]	3.00	3.04	3.06	3.06	3.05	3.04
200, 110	2.90	2.94	2.97	2.99		
$\bar{2}02$	2.60	2.68	2.70	2.70	2.68	2.69
112	2.58	2.62	2.64	2.65		
013	2.51	2.53	2.55	2.55	2.56	
211	2.15	2.17	2.20	2.20	2.21	
$\bar{2}04$	2.08	2.09	2.09	2.09	2.09	2.09
$\bar{1}14$	2.04	2.06	2.08	2.05	2.06	
204	2.00	2.02	2.04			
301	1.93	1.94	1.96	1.96	1.97	
$\bar{3}03$	1.77	1.78	1.79	1.79		
110[a]	1.73	1.76	1.76	1.76	1.75	1.75
310	1.69	1.71	1.73	1.73	1.73	
020	1.66	1.69	1.71	1.72		
116	1.57	1.58	1.59	1.60	1.62	1.62

a) (100) and (110) reflections are referred to the hexagonal NiAs-type structure.

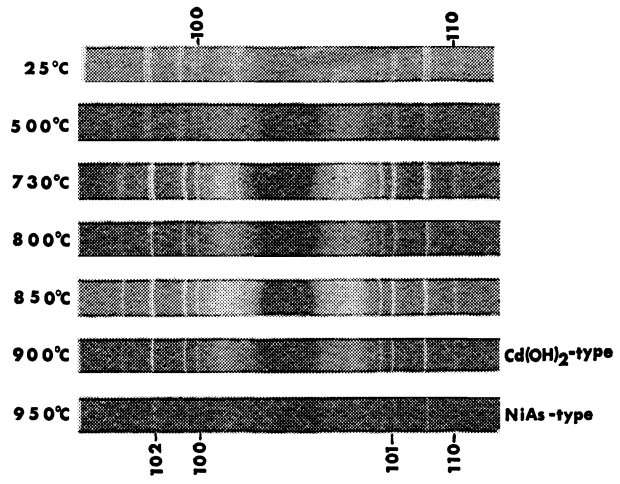

Fig. 4. The X-ray powder photographs of $Fe_{0.60}V_{0.40}S_{1.28}$.

phase is very weak compared with that of the corresponding (002) reflection of the ordered V_3S_4-type phase. This may be indicative of some degree of the interlayer disordering in the process of the phase transformation.

Figure 4 shows a series of the high-temperature X-ray diffraction patterns of $Fe_{0.60}V_{0.40}S_{1.28}$. The temperature dependence of *d*-spacings is listed in Table 2. The X-ray powder photograph taken at room temperature indicates clearly the presence of two phases, which are composed of $(Fe,V)_{1-x}S$ with hexagonal NiAs-type structure and $(Fe,V)_3S_4$ with the monoclinic V_3S_4-type structure. However, both phases show very similar X-ray diffraction patterns, so that some reflections overlap each other. The former could be distinguished from the latter only by the presence of (100) and (110) reflections, referred to the hexagonal structure.

On heating the sample up to 850 °C, the splitting of reflections which are attributed to the V_3S_4-type structure gradually decreases, but the two phases still coexist. However, mutual solubility of both phases increases with increasing temperature. A new solid solution phase is formed due to the reaction of two phases at temperatures above 850 °C. The phase described above has a trigonal $Cd(OH)_2$-type structure with intralayer disordering. Again, on heating the sample up to 950 °C, the trigonal phase transforms perfectly to the high-temperature phase with the hexagonal NiAs-type structure. This phase transformation was reversible. The trigonal phase decomposed to the original two different phases on quenching below 850 °C, owing to the phase separation.

Figure 5 shows the results of the high-temperature X-ray study of $Fe_{0.71}V_{0.29}S_{1.20}$, which is composed of a two-phase mixture of $(Fe,V)_{1-x}S$ and $(Fe,V)_3S_4$ at room

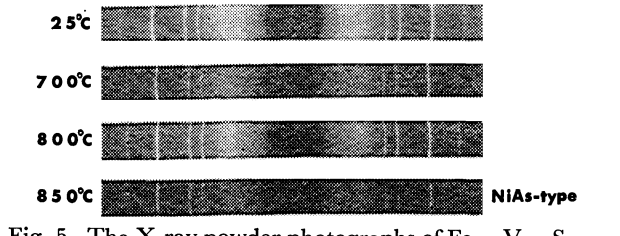

Fig. 5. The X-ray powder photographs of $Fe_{0.71}V_{0.29}S_{1.20}$.

temperature. The intensity of the super-structure reflections derived from the $(Fe,V)_3S_4$ phase decreases gradually with increasing temperature. Finally, a high-temperature phase with the hexagonal NiAs-type structure appears at about 850 °C. However, the trigonal phase with the complete intralayer disordering could not be observed in the process of this phase transformation. This may suggest that the occurrence of the trigonal phase at high temperatures is affected by the bulk concentration of metal vacancies in the original low-temperature phases.

The High-temperature DTA Measurement. In order to determine the temperature of the phase transformation accurately, the DTA measurements were carried out in the temperature range from 25 to 1100 °C. Iron vanadium sulfides with the atomic Fe: V ratios 3: 2 and 71: 29 were used chiefly for the comparison with the results of the high-temperature X-ray experiments.

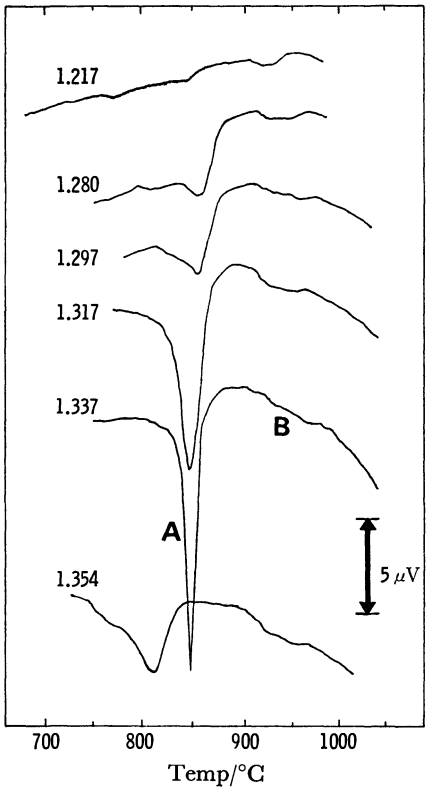

Fig. 6. DTA curves for $Fe_{0.60}V_{0.40}S_x$.

Figure 6 shows representative differential heating curves obtained with the composition $Fe_{0.60}V_{0.40}S_x$, where x lies in the range from 1.217 to 1.354. It is evident that each heating curve has two endothermic peaks in the temperature range from 700 to 1000 °C. As shown in Fig. 6, the lower one, A, is large and rather sharp in shape. On the other hand, the higher one, B, is small and broad. Note that the profile of the endothermic peaks varies clearly with the composition of sulfides. The sharpest and largest peak is observed at 842 °C in the heating curve of the composition $x=1.337$, which is close to the stoichiometric composition, $(Fe_{0.60}V_{0.40})_3S_4$. The A peak for the compositions on the sides more rich in metal than $x=1.333$ becomes broader and smaller with decreasing sulfur content. Also, the heating curve of the composition $x=1.354$ shows the tendency for the A peak to grow broader and to be shifted significantly to the low temperature side with increasing sulfur content that characterizes the thermal behavior of the composition on the side more rich in sulfur than $x=1.333$. On the other hand, the B peaks exhibit essentially similar profiles for all of the composition studied and observed at temperatures above 900 °C.

By the direct comparison with the results of the high-temperature X-ray experiments, it is concluded that: (1) the A peak is related to the phase transformations, such as V_3S_4-type→$Cd(OH)_2$-type (type Ia) and V_3S_4-type+NiAs-type→$Cd(OH)_2$-type (type Ib), at the temperature T_1, and (2) the B peak is related to the phase transformation from $Cd(OH)_2$-type to NiAs-type (type II) at the temperature T_2. The tentative phase diagram of iron vanadium sulfides with the atomic Fe: V ratio 3: 2 is shown in Fig. 7, where the temperatures (T_1 and T_2) at which maxima were observed on the heating curves are plotted against composition. The transformation temperature, T_1, of type Ia is connected smoothly to that of type Ib. The phase boundary curve which was determined by the T_1 values has the maximum temperature of 854 °C at the composition near $x=1.27$. A rapid decrease of the temperature T_1 is observed at the compositions on the sulfur-richer side of $x=1.333$. For example, T_1 is about 813 °C at $x=1.354$. Such a compositional

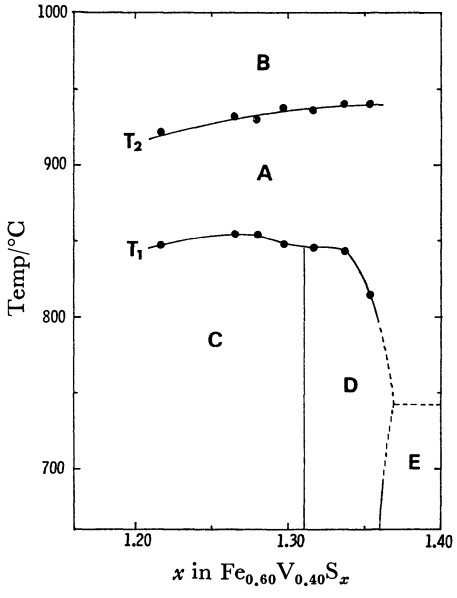

Fig. 7. Tentative phase diagram of a part of the Fe–V–S system at section with atomic Fe: V ratio 3: 2. Phase relations are represented as follows.
A: $(Fe_{0.60}V_{0.40})_{1-x}S$ ($Cd(OH)_2$-type),
B: $(Fe_{0.60}V_{0.40})_{1-x}S$ (NiAs-type),
C: $(Fe,V)_{1-x}S$ (NiAs-type)+$(Fe,V)_{3\pm x}S_4$ (V_3S_4-type),
D: $(Fe_{0.60}V_{0.40})_{3\pm x}S_4$ (V_3S_4-type),
E: $(Fe,V)_{3\pm x}S_4$ (V_3S_4-type)+FeS_2 (pyrite).
The phase boundary between A and E is determined on the basis of the stability limit of pyrite.[8]

dependence of T_1, as mentioned above, is similar to that of the V–S system which has been reported by Oka *et al.*[4] As shown in Fig. 7, the transformation temperature T_2 of the type II increases slightly with increasing sulfur content. The T_2 changes from 920 to 940 °C in the compositional range of x=1.217—1.354. However, the T_2 value is quite ambiguous because of the broadness of the B peak, as shown in Fig. 6.

The profiles on the differential heating curves of $Fe_{0.71}V_{0.29}S_x$ was essentially the same as those of $Fe_{0.60}V_{0.40}S_x$, except that the phase transformation took place at lower temperatures. The T_1 and T_2 of $Fe_{0.71}V_{0.29}S_{1.30}$ are 820 °C and 910 °C, respectively. The T_1 of $Fe_{0.71}V_{0.29}S_{1.20}$ is about 770 °C. These temperatures are relatively lower than those of the corresponding composition of $Fe_{0.60}V_{0.40}S_x$. According to Oka *et al.*, the T_1 of $VS_{1.33}$ is about 1200 °C.[4] This temperature is much higher than that of $Fe_{0.60}V_{0.40}S_{1.337}$ (about 840 °C). From these facts, it can be concluded that the temperature of the phase transformation of iron vanadium sulfides decreases with increasing Fe content, when the S/(Fe+V) ratio is held constant.

The author wishes to express his thanks to Professor Mitsuoki Nakahira of Okayama College of Science for his encouragement and helpful discussion throughout this study. Thanks are also due to Dr. Hiromoto Nakazawa for his invaluable discussion, and to Drs. Akihiko Nukui and Mamoru Watanabe for their technical assistance with the high-temperature X-ray measurements during this work.

References

1) H. Wada, *Bull. Chem. Soc. Jpn.*, **51**, 1368 (1978).
2) H. Wada, *Bull. Chem. Soc. Jpn.*, **52**, 2130 (1979).
3) H. Nakazawa, M. Saeki, and M. Nakahira, *Less Common Metals*, **40**, 57 (1975).
4) Y. Oka, K. Kosuge, and S. Kachi, *J. Solid State Chem.* **23**, 11 (1978).
5) Y. Oka, K. Kosuge, and S. Kachi, *J. Solid State Chem.* **24**, 41 (1978).
6) Computer program written by T. Sakurai, Institute of Physical and Chemical Research, Tokyo.
7) M. Cheverton and A. Sapet, *C. R. Acad. Sci., Paris*, **261**, 928 (1965).
8) G. Kullerud and H. S. Yoder, *Economic Geology*, **54**, 533 (1959).

Sodium Ion Exchange on Crystalline Zirconium Titanium Phosphate

Yutaka YAZAWA, Toru EGUCHI, Kazunori TAKAGUCHI, and Isao TOMITA*,†

Department of Chemistry, Faculty of Science, Tokyo Kyoiku University, Otsuka, Tokyo 112

(Received March 28, 1979)

A new ion exchanger, crystalline zirconium titanium phosphate with variable zirconium to titanium mole ratios has been prepared and the sodium ion exchange behavior studied. In the zirconium-rich exchanger a half-exchanged monosodium phase was produced. This differs from the titanium-rich exchanger where a disodium phase was formed without formation of the intermediate monosodium phase. The pH titration curves were complicated but a trend emerged with variation in the Zr/Ti ratio. On the basis of the X-ray evidence and the shapes of the titration curves it is thought that the synthesized phosphates are solid solutions rather than a mechanical mixture of the two metal phosphates.

Considerable work have been reported on the ion exchange behavior of alkali metal ions on inorganic ion exchangers of the α-zirconium phosphate type.[1] Among the exchangers, α-titanium phosphate, $Ti(HPO_4)_2 \cdot H_2O$ (designated as α-TP) has the same layer structure as α-zirconium phosphate (α-ZP) with approximately the same interlayer distance of 7.56 Å. The ion exchange properties however differ in some respects from that of α-ZP. For example, in H^+–Na^+ ion exchange, both a monosodium phase and a disodium phase exist for α-ZP, which are immiscible with each other when they coexist. In X-ray powder diffractometry of α-TP, the monosodium phase[2] was not observed as was the case of H^+–Li^+ exchange.[3] The ion sieve effect exhibited by exchangers of this type also differs in that in acid media α-ZP can absorb K^+ ions but α-TP cannot.

Synthesis of the crystalline mixed phosphate of zirconium and titanium having variable zirconium to titanium mole ratios has been attempted and the sodium ion-exchange behavior studied.

Experimental

Synthesis of the Exchangers. Hydrochloric acid solutions (2 mol dm^{-3}) of zirconium dichloride oxide and titanium tetrachloride were prepared. The zirconium to titanium mole ratio in the mixed solutions was varied between experiments. The solution was added dropwise, with stirring to H_3PO_4 (2 mol dm^{-3}) kept at 60—70 °C. The resultant colorless gel was allowed to stand overnight, filtered and washed with 2% H_3PO_4 solution until free from chloride ion. The obtained amorphous salt was refluxed at the boiling point in concentrated H_3PO_4 for 48 to 200 h. The product was centrifuged and washed with deionized water until the pH of the supernatant solution exceeded 3. The microcrystalline product was stored over silica gel. The exchanger will be designated as ZTP hereafter.

Analysis of the Exchangers. The zirconium to titanium mole ratio in the exchangers was determined as follows. A weighed amount (100 mg) of the exchanger was dissolved in hot concd H_2SO_4 (20 cm^3). After cooling, the solution was diluted to 200 cm^3, and the ice-cooled 5% cupferron aqueous solution (10 cm^3) added. The precipitate was filtered and washed with 1.2 mol dm^{-3} HCl, ignited and weighed as the sum of ZrO_2 and TiO_2.

In a separate experiment, the exchanger (120 mg) was dissolved in hot concd H_2SO_4 (20 cm^3). After cooling, the solution was added to 1.5% H_2O_2 (200 cm^3). To this was added $NH_4H_2PO_4$ (1.5 g) and the resulting gelatinous precipitate aged on a steam bath at 50—60 °C for 2 h. The precipitate was filtered and washed with 1% NH_4NO_3, ignited and weighed as ZrP_2O_7. The zirconium to titanium mole ratio was estimated from the results of both experiments.**

Ion Exchange. The experiment was conducted by the batch method. Mixed solutions of 0.1 mol dm^{-3} NaCl and 0.1 mol dm^{-3} NaOH at variable mixing ratios were prepared to give solutions of differing values of pH keeping the sodium concentration constant. ZTP (250 mg) was placed in contact with each of the above mentioned solutions (25 cm^3), and shaken for 4 days at 25 °C. The solution was centrifuged, and the supernatant liquid subjected to pH measurement. Analysis for sodium was by flame photometry, and for phosphorus colorimetrically by the phosphomolybdic acid method. X-ray powder diffractometry was conducted on the exchangers obtained at various stages of ion exchange. Thermal analysis (TG and DSC) was performed to determine the number of waters of crystallization per formula weight of the exchanged phase.

Results and Discussion

Synthesized Exchangers. In Table 1, the zirconium to titanium mole ratios in the starting mixture and in the product together with the theoretical exchange capacity of the exchangers are shown. In each exchanger, the Zr/Ti ratio in the product was less than that in the starting mixture.

The X-ray powder patterns of the exchangers resembled that of α-ZP and α-TP, but the interlayer distance (d_{002}) estimated from the first reflection peak

Table 1. Composition of synthesized ion exchanger, $Zr_xTi_{1-x}(HPO_4)_2 \cdot H_2O$

Notation	Mixing mole ratio (Zr/Ti) of starting materials	Mole ratio (Zr/Ti) of products	x	Estimated exchange capacity (meq/g)
ZTP(3.25)	3.38	3.25	0.77	6.87
ZTP(0.93)	1.13	0.93	0.48	7.17
ZTP(0.25)	0.37	0.25	0.20	7.50

† Present address: Tokyo University of Fisheries, Kōnan, Minato-ku, Tokyo 108.

** There is the possibility that a small amount of titanium coprecipitates with the zirconium phosphate. Volumetric determination of titanium after reduction to the +3 state by liquid zinc amalgam gave a somewhat lower Zr/Ti ratio.[4]

at the lowest angle was 7.63 Å in each case. This figure is slightly larger than that for α-ZP and α-TP. Furthermore, a mechanical mixture of α-ZP and α-TP gave a more complicated powder pattern in which a single reflection from the (002) plane existed but several reflections at higher angles appeared separately as shown in Fig. 1.

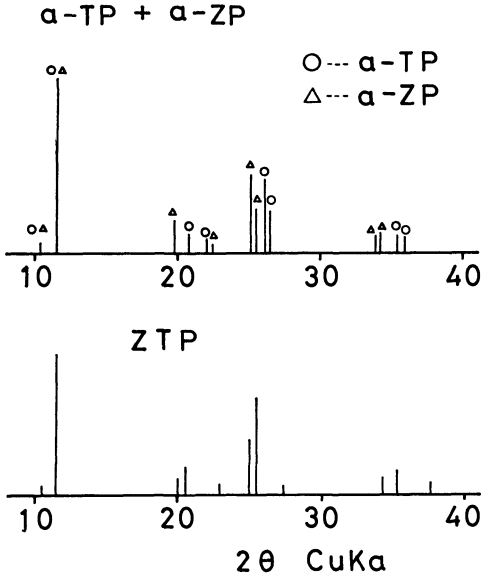

Fig. 1. Comparison of X-ray powder diffraction patterns between α-TP, α-ZP, and ZTP.

The results of thermogravimetric analysis are given in Table 2. The weight loss at 100—250 °C is ascribed to the water of crystallization, and the loss at 400—550 °C to condensation of the phosphate group. These data indicate that ZTP with all Zr/Ti mole ratios is monohydrate. Thus, ZTP is assumed to be isomorphous with α-ZP and α-TP. Analogously with α-ZP, the three oxygen atoms of the phosphate group are bonded to the three metal atoms in a layer. In ZTP, the three metal atoms consist of Zr and/or Ti. Since the crystal ionic radius of Zr^{4+} and Ti^{4+} differs considerably (0.79 and 0.68 Å respectively), the structure of the lattice is assumed to be less ordered than that of α-ZP or α-TP, and the remaining P–O bond of each phosphate group, to which an exchangeable H atom is bonded, may tilt from the perpendicular. This may result in a slight expansion of the interlayer distance and lead to the phosphate groups in ZTP having different values of acidity. The synthesized exchangers will be designated as ZTP(3.25), ZTP(0.93), and ZTP(0.25), depending upon the Zr/Ti ratios. The refluxing time was 200 h for ZTP(0.93) and 48 h for the others but the degree of crystallization did not greatly differ.

TABLE 2. RESULTS OF THERMOGRAVIMETRY

Exchanger	Water of crystallization (mol/mol ZTP)	Dehydration due to condensation of phosphate (mol/mol ZTP)
ZTP(3.25)	1.09	1.05
ZTP(0.93)	1.05	1.00
ZTP(0.25)	1.03	1.04

Ion Exchange. Figure 2 illustrates the pH-titration curves for sodium ion exchange and the phosphate release curves indicate the extent of hydrolysis of the exchanger. The titration curve for ZTP(3.25) has a point of inflection at approximately 3.5 meq Na^+ absorbed/g ZTP corresponding to approximately one half of the calculated exchange capacity of 6.87 meq/g.

In the titration curve for ZTP(0.93), the inflection is observed at approximately 3 meq/g, which is less than one half of the theoretical capacity of 7.2 meq/g. In the

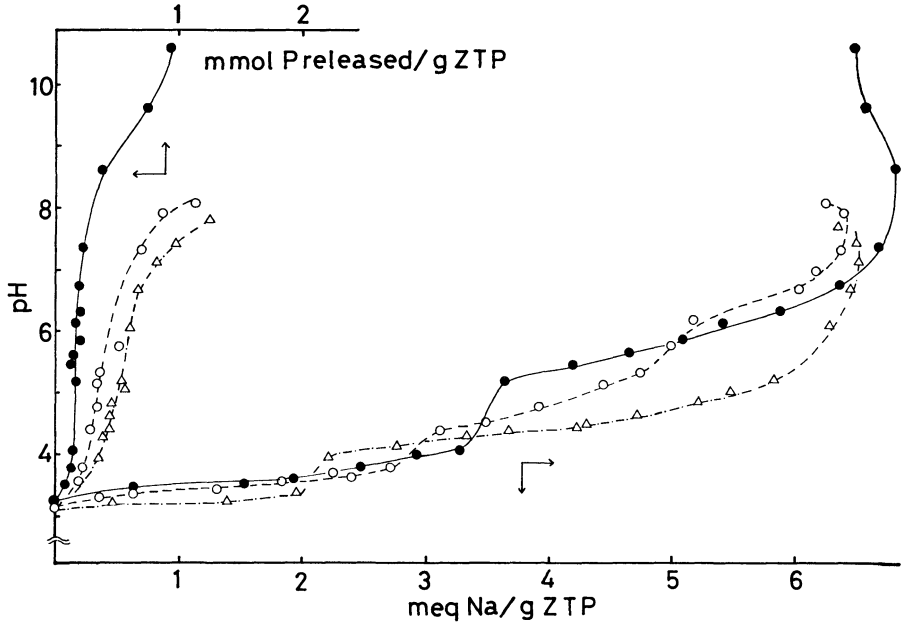

Fig. 2. The pH-titration curves for sodium ion exchange and the phosphate release curves.
-●-: ZTP (3.25), --○--: ZTP (0.93), and -·-△-·-: ZTP (0.25).

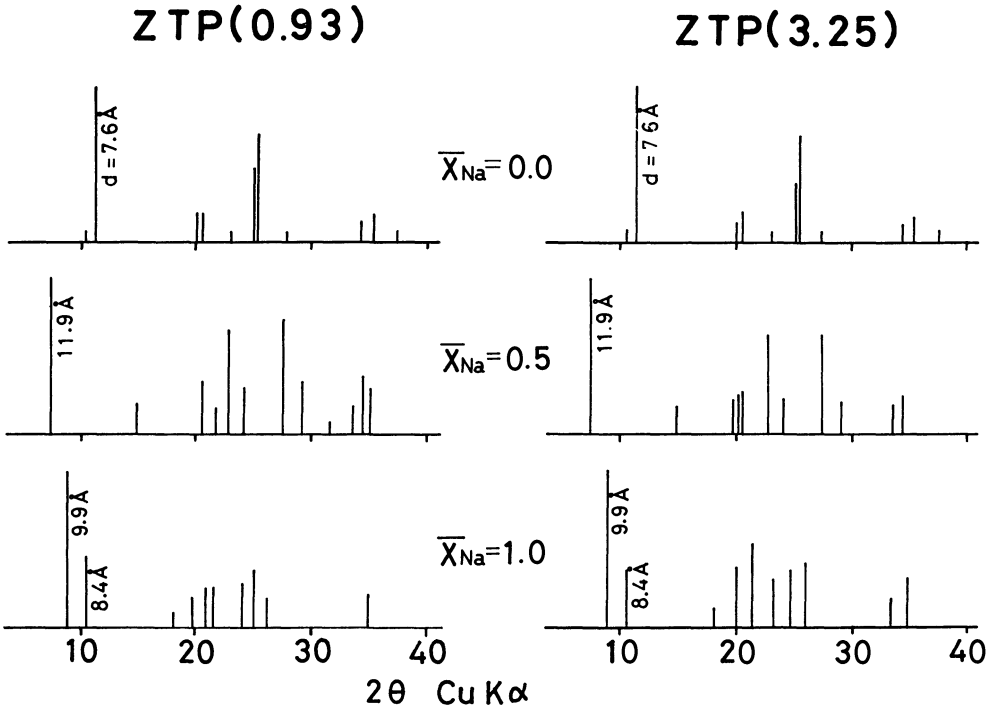

Fig. 3. The X-ray powder diffraction patterns of ZTP (3.25) and ZTP (0.93) at various stages of exchange. $\bar{X}_{Na}$ denotes the ionic fraction of sodium ion in the exchanger.

titration curve for ZTP(0.25), the inflection point is at approximately 2.2 meq/g, a value far less than half of the exchange capacity of 7.50 meq/g. This shift of the inflection has neither been observed in α-ZP nor in α-TP. Furthermore, the rise in pH at the inflection was very small compared to the clear and large pH change in the case of α-ZP. The cause for the "inflection shift" is not clear, but if the exchanger was a mechanical mixture of α-ZP and α-TP, the pH titration curve should be the composite curve for both exchangers. This however was not the case in the present study, and the curves indicate the solid-solution character of ZTP, in which the acidity of the phosphate protons varies depending upon the Zr/Ti mole ratio.

The ease of hydrolysis increased as the titanium mole fraction of the exchanger increased. As a result, the observed exchange capacity did not increase as suggested from the theoretical value.

Figure 3 illustrates the X-ray powder patterns for the exchangers (ZPT(3.25) and ZTP(0.93)) at several stages of exchange. The ionic fraction of sodium in the exchanger phase is denoted by $\bar{X}_{Na}$. In ZTP(3.25) and ZTP(0.93), the trend was very similar, namely, as the exchange of sodium ion proceeded, a new phase having an interlayer distance of 11.9 Å appeared. The diffraction peak intensity increased until, at the mid point of exchange, only this phase was observed.*** Up to $\bar{X}_{Na}$=0.61 for ZTP(3.25) and $\bar{X}_{Na}$=0.54 for ZTP(0.93), two peaks appeared at 9.9 and 8.4 Å. Finally at $\bar{X}_{Na}$=0.95 for ZTP(3.25) and $\bar{X}_{Na}$=0.90 for ZTP(0.93), the peak at 11.9 Å completely disappeared leaving the peaks at 9.9 and 8.4 Å.

For the sodium ion exchange on α-ZP, the point of inflection is found at the point of half exchange. Clearfield *et al.*[5] reported that the monosodium salt having an interlayer distance of 11.8 Å and the disodium salt having an interlayer distance of 9.9 Å exist, where the monosodium salt is a pentahydrate when stored at a relative humidity of 100%. Dried overnight at 35 °C or over diphosphorus pentaoxide this salt is converted to a monohydrate with an interlayer distance of 7.9 Å.

Similar phenomena were observed for ZTP(3.25) and ZTP(0.93). The monosodium form of ZTP(3.25) when stored at a relative humidity of 75%, it contained 4.7 mol of water of crystallization per formula weight. Dehydration of this monosodium form took place in two steps. Dried at 50 °C for 1 h it converted to the monohydrate having an interlayer distance of 7.9 Å (Fig. 4). The disodium salt when dried at 50 °C overnight, lead to the disappearance of the peak at 9.9 Å, the peak at 8.4 Å remained. The results for ZTP(0.93) were essentially the same. The indication is that the two peaks correspond to two types of disodium forms having different waters of crystallization, although the accurate number of the hydration could not be estimated. The monohydrate of the disodium form of α-ZP has an interlayer distance of 8.42 Å and thus the disodium form of ZTP with a spacing of 8.4 Å is most probably a monohydrate. The monohydrates of the monosodium and disodium forms did not regain the interlayer spacings when stored over saturated aqueous sodium chloride solution (relative humidity ≈75%).

In Fig. 5, the X-ray powder patterns for ZTP(0.25) at several stages of exchange together with those of the

*** Under some conditions of drying, the reflection peak appeared at 7.9 Å instead of 11.9 Å. The interlayer distance is relatively sensitive to the water content of the exchanger, and consequently to the drying conditions.[4]

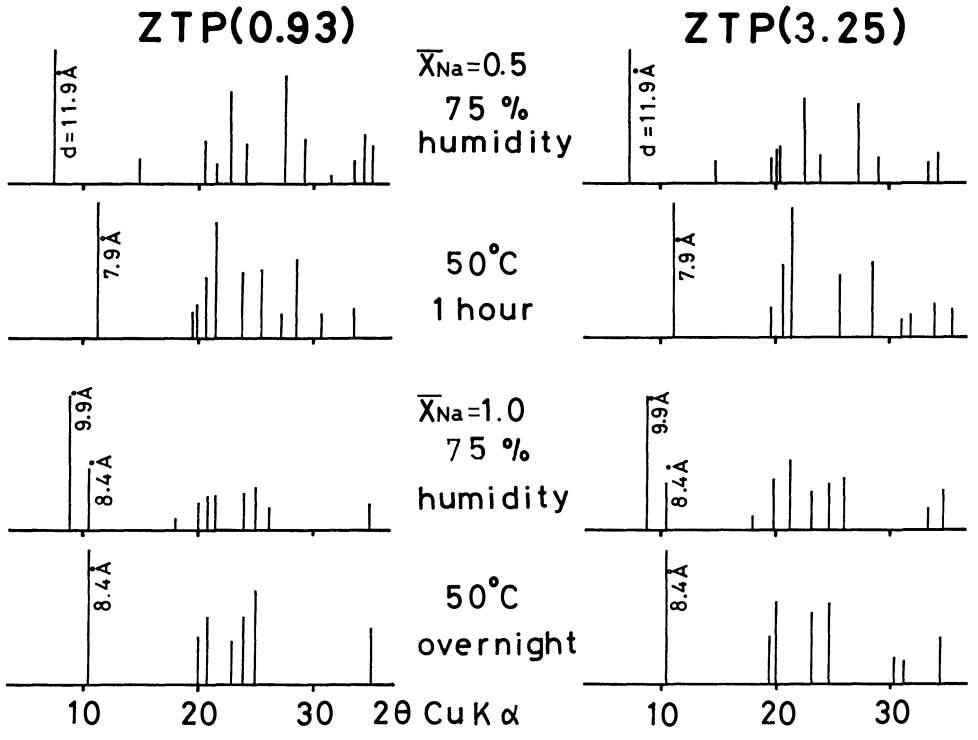

Fig. 4. Change in X-ray powder diffraction patterns of ZTP (3.25) and ZTP (0.93) depending on storage conditions.

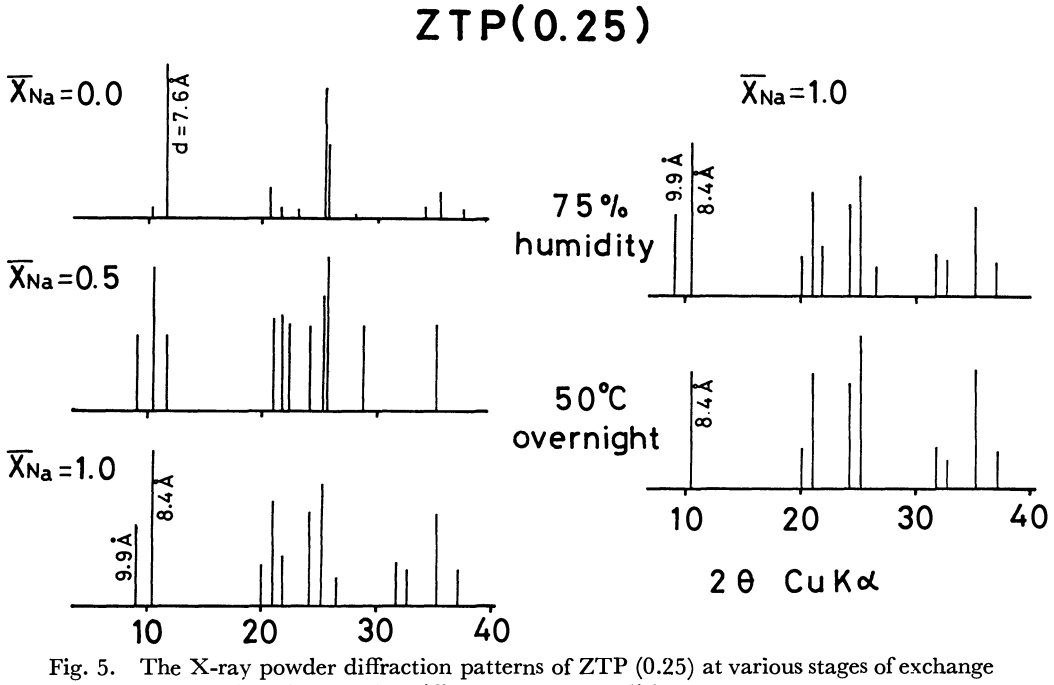

Fig. 5. The X-ray powder diffraction patterns of ZTP (0.25) at various stages of exchange and those of sodium form under different storage conditions.

disodium form under different storage conditions are shown. The X-ray pattern at $\bar{X}_{Na}=1.0$ was the same as for the foregoing two exchangers. The monosodium form however was not observed in this case, *i.e.*, as exchange proceeded, the disodium form phases were formed without the formation of the intermediate. In fact, at $\bar{X}_{Na}=0.5$, two peaks of the disodium form, 9.9 Å and 8.4 Å coexisted with the peak at 7.6 Å, which belongs to the unexchanged hydrogen form. Nevertheless, a small pH jump existed in the titration curve. In this case, the absence of a monosodium form does not correspond to a smooth titration curve without structure.

Further experimentation is continuing on the ion exchange behavior of other alkali metal ions such as lithium and potassium, and will be reported in due course.

Conclusions

A crystalline phosphate ion exchanger containing both zirconium and titanium has been synthesized. The sodium ion exchange behavior on the exchanger is interesting in that the presence or absence of the monosodium phase is dependent upon the Zr/Ti mole ratio in the exchanger. As an ion exchanger, ZTP is preferred to α-TP since it has higher resistance to hydrolysis.

The present work was partially supported by a Grant-in-Aid for Scientific Research from the Ministry of Education.

References

1) A. Clearfield, G. H. Nancollas, and R. H. Blessing, "Ion Exchange and Solvent Extraction," ed by J. A. Marinsky and Y. Marcus, Marcel Dekker, New York (1973), Vol. 5.

2) K. Takaguchi, M. Sc. Thesis, Tokyo Kyoiku University, Tokyo (1977). With regard to the sodium ion exchange on α-TP, the pH titration curves have been given by the following authors: G. Alberti, P. Cardini-Galli, U. Costantino, and E. Torracca, *J. Inorg. Nucl. Chem.*, **29**, 571 (1967). E. Kobayashi, *Bull. Chem. Soc. Jpn.*, **48**, 3114 (1975).

3) K. Takaguchi and I. Tomita, *J. Chromatogr.*, **118**, 263 (1976).

4) K. Iwase and I. Tomita, unpublished data.

5) A. Clearfield, W. L. Duax, A. S. Medina, G. D. Smith, and J. R. Thomas, *J. Phys. Chem.*, **73**, 3423 (1969).

Synthesis of 4-(Glycosyl)isoxazoline *N*-Oxides and Related Substances[1)]

Eisuke KAJI,* Hiromi ICHIKAWA, and Shonosuke ZEN
School of Pharmaceutical Sciences, Kitasato University, Shirokane, Minato-ku, Tokyo 108
(Received February 13, 1979)

4-(Glycosyl)isoxazoline *N*-oxides were synthesized directly from *aldehydo* sugars by one-step cyclization with double mole of methyl nitroacetate in a satisfactory yield. 2,3-*O*-Isopropylidene-D-glyceraldehyde reacted with methyl nitroacetate to give 4-(1,2-*O*-isopropylidene-D-*glycero*-dihydroxyethyl)-3,5-bis(methoxycarbonyl)isoxazoline *N*-oxide. The same treatment of 2,3: 4,5-di-*O*-isopropylidene-*aldehydo*-L-arabinose and penta-*O*-acetyl-*aldehydo*-D-glucose also gave the corresponding homologs. From the corresponding cyclic *aldehydo* sugars, 4-aldofuranosyl-3,5-bis(methoxycarbonyl)isoxazoline *N*-oxides, *e.g.* 4-(2,3-*O*-isopropylidene-β-D-erythrofuranosyl)-, 4-[(4*R*)-3-*O*-benzyl-1,2-*O*-isopropylidene-β-L-threofuranos-4-yl]-, 4-(2,3,5-tri-*O*-benzyl-β-D-ribofuranosyl)-, and 4-(2,3,5-tri-*O*-benzoyl-β-D-ribofuranosyl)-derivatives were synthesized. The latter was converted into 3,5-dicarbamoyl-4-(β-D-ribofuranosyl)isoxazoline by deoxygenation followed by carbamoylation and deprotection.

Recently numerous reports have appeared on the synthesis of *C*-glycosyl heterocycles related to *C*-nucleoside antibiotics and their analogs in the quest of potential chemotherapeutic compounds,[2)] such as polyhydroxyalkyl-[3)] or *C*-glycosyl[4)] isoxazolines and isoxazoles, and their carbocyclic analogs.[5)] The heterocyclic moiety was obtained mostly by 1,3-dipolar cycloaddition of olefinic or acetylenic dipolarophiles to sugar nitrile oxides, or by that of olefinic sugars to some nitrile oxides, affording 3- or 5-(glycosyl)isoxazolines or isoxazoles. However, no 4-(glycosyl)isoxazoline or isoxazole appears to have been prepared. A previous work[6)] on the synthesis of 4-substituted isoxazoline *N*-oxide led us to develop a new route to the above-mentioned *C*-nucleoside. In the present paper we give syntheses of some 4-(polyhydroxyalkyl)- and 4-(glycosyl)isoxazoline *N*-oxides by means of one-step cyclization of *aldehydo* sugars with double mole of methyl nitroacetate.

First we examined the condensation of 2,3-*O*-isopropylidene-D-glyceraldehyde (**1a**) with methyl nitroacetate in order to confirm the reaction conditions. It was found that **1a** reacts with two equivalents of methyl nitroacetate in the presence of one equivalent of diethylamine in *N*,*N*-dimethylacetamide (DMA) to afford 4-(1,2-*O*-isopropylidene-D-*glycero*-dihydroxyethyl)-3,5-bis(methoxycarbonyl)isoxazoline *N*-oxide (**2a**) in 74% yield. The structure of **2a** was confirmed by its IR, UV, and ^{1}H-NMR spectra and elemental analysis. Fractional recrystallization of **2a** from hexane resulted in the isolation of two diastereomers (**2a**$_1$: mp 121.5—124 °C and **2a**$_2$: mp 86.5—87.5 °C) in a *ca.* 3: 2 ratio. The relatively small $J_{4,5}$ value (3.5—4.0 Hz) shows the 4,5-*trans* configuration of **2a**$_1$ and **2a**$_2$.[6,7)] The opposite sign of CD spectra centered at 270 nm might be attributed to a symmetric relationship on the configuration of the isoxazoline ring as shown is Scheme 3. Accordingly (4*R*,5*S*) and (4*S*,5*R*) configuration could fit both isomers. However, we can offer no convincing argument as to the assignment of each isomer.

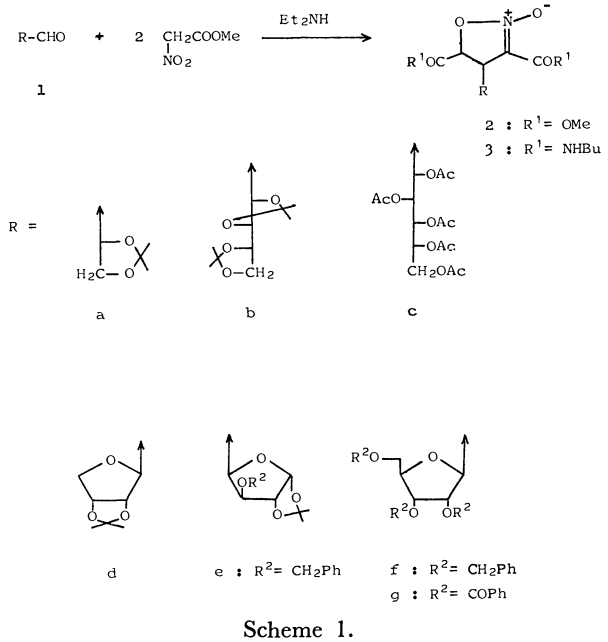

Scheme 1.

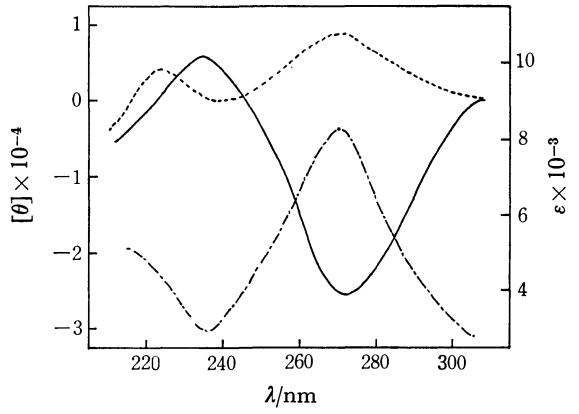

Fig. 1. CD and UV spectra of **2a**$_1$ and **2a**$_2$ in MeOH
——: CD (**2a**$_1$), – – –: CD (**2a**$_2$), —·—: UV (**2a**$_1$ and **2a**$_2$).

The same treatment of 2,3,: 4,5-di-*O*-isopropylidene-*aldehydo*-L-arabinose (**1b**) and penta-*O*-acetyl-*aldehydo*-D-glucose (**1c**) also gave the corresponding homologs (**2b** and **2c**) in 48 and 64% yields, respectively, their diastereomers not being detected. 3,5-Bis(butylcarbamoyl) derivatives (**3a**$_1$ and **3b**) were prepared by treatment of **2a**$_1$ and **2b** with butylamine in methanol. Deisopropylidenation of **2a**$_1$ and **2b** by Dowex 50 W in methanol gave **5a**$_1$ and **5b**, respectively. The latter

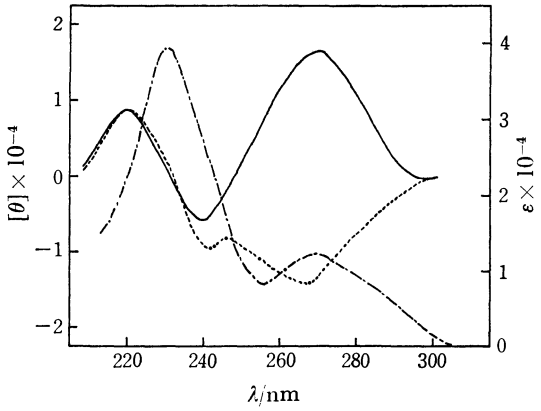

Fig. 2. CD and UV spectra of $\mathbf{2g_1}$ and $\mathbf{2g_2}$ in MeOH. ——: CD ($\mathbf{2g_1}$), ----: CD ($\mathbf{2g_2}$), —·—: UV ($\mathbf{2g_1}$ and $\mathbf{2g_2}$).

seems to have been formed through the 3,4-deprotected intermediate which was isolated. Deacetylation and carbamoylation of **2c** led to a mixture of products which could not be characterized.

It is of interest to explore a route to 4-aldofuranosylisoxazolines, since naturally occurring *C*-nucleosides contain a D-ribofuranosyl moiety. For synthesis of 4-aldofuranosylisoxazolines, 2,5-anhydro-aldoses and 1,4-pentodialdofuranose were employed. 2,5-Anhydro-3,4-*O*-isopropylidene-D-ribose (**1d**), 3-*O*-benzyl-1,2-*O*-isopropylidene-α-D-*xylo*-pentodialdo-1,4-furanose (**1e**), 2,5-anhydro-3,4,6-tri-*O*-benzyl-D-allose (**1f**) and its 3,4,6-tri-*O*-benzoyl analog (**1g**) were condensed with methyl nitroacetate by the above-mentioned procedure, affording the corresponding 4-aldofuranosylisoxazoline *N*-oxides (**2d**—**2g**) in a satisfactory yield except **2e** (6%). *C*-Glycoside **2f** was obtained as a mixture of two diastereomers indicated by two sets of singlet for the methyl of the methoxycarbonyl groups of **2f** in its ^{1}H-NMR spectrum. With regard to compound **2g**, two diastereomers ($\mathbf{2g_1}$: mp 97.5—99 °C and $\mathbf{2g_2}$: mp 68—71 °C) were isolated through column chromatography on silica gel in a *ca.* 1 : 3 ratio. The ^{1}H-NMR

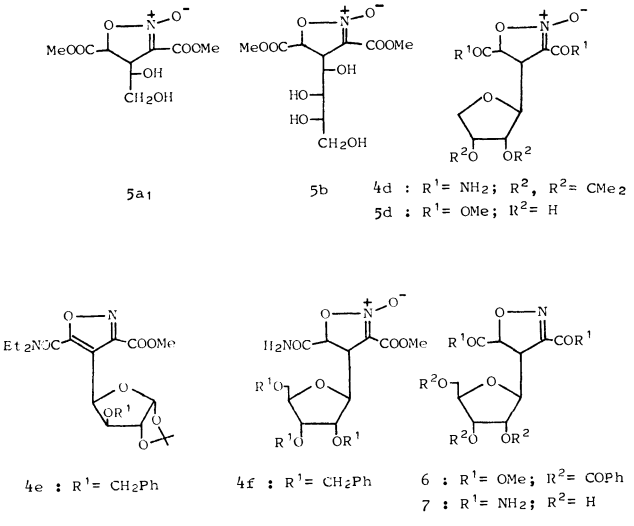

Scheme 2.

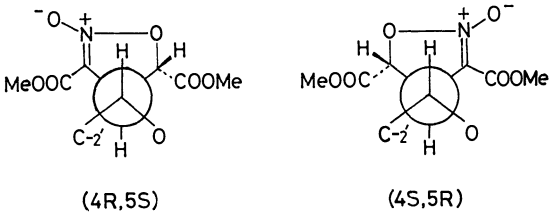

Scheme 3.

and CD spectra (Fig. 2) of $\mathbf{2g_1}$ and $\mathbf{2g_2}$ also indicate that the isomers have either (4*R*,5*S*)- or (4*S*,5*R*)-isoxazoline moiety as described for compound **2a**.

In view of biological activities of several nucleosides possesing carbamoyl groups in the heterocyclic portion, carbamoylation of **2d**—**2f** with methanolic ammonia or butylamine in methanol was carried out, affording mono- or dicarbamoyl derivatives (**3d**, **4d**, and **4f**). On the other hand carbamoylation of **2e** with diethylamine in methanol gave 5-diethylcarbamoyl-3-methoxycarbonylisoxazole (**4e**), the structure of which was confirmed by its spectral and elemental analysis. The formation of **4e** would have resulted from a base catalyzed transformation of isoxazoline *N*-oxide into isoxazole.[6,8] In other cases, however, no isoxazole derivative was observed.

Deisopropylidenation of **2d** was achieved using Dowex 50 W resin in aqueous methanol, giving **5d**. Since direct debenzoylation of $\mathbf{2g_2}$ (major isomer) with saturated methanolic ammonia was unsuccessful because of the lability of $\mathbf{2g_2}$ in such a medium, it was subsequently deoxygenated with triethyl phosphite, leading to an isoxazoline (**6**) in 49% yield. Debenzoylation and carbamoylation of **6** was accomplished with saturated methanolic ammonia, giving **7** in 55% yield, biological assay of which is now in progress.

Experimental

Melting points are uncorrected. ^{1}H-NMR spectra were recorded with a 60 MHz Varian T-60 and a 100 MHz JEOL PS-100 spectrometer with a spin decoupler using tetramethylsilane as an internal standard in chloroform-*d*, acetone-d_6 and methanol-d_4 solution, and sodium 2,2-dimethyl-2-silapentane-5-sulfonate in deuterium oxide. IR, UV, CD, and MS were measured with JASCO IRA-1, Hitachi 340, JASCO J-20, and JMS D-100 spectrometers, respectively. TLC was carried out on Kiesel gel G (Merck), spots being detected with iodine vapor or 10% sulfuric acid on a hot plate. Silica gel (Kanto Kagaku, up to 100 mesh) was used for column chromatography. For preparation of *aldehydo* sugars, reported procedures were applied to 2,3-*O*-isopropylidene-D-glyceraldehyde (**1a**),[9] 2,3:4,5-di-*O*-isopropylidene-*aldehydo*-L-arabinose (**1b**),[10] penta-*O*-acetyl-*aldehydo*-D-glucose (**1c**),[11] 2,5-anhydro-3,4-*O*-isopropylidene-D-ribose (**1d**),[12] 3-*O*-benzyl-1,2-*O*-isopropylidene-α-D-*xylo*-pentodialdo-1,4-furanose (**1e**),[13] 2,5-anhydro-3,4,6-tri-*O*-benzyl-D-allose (**1f**),[14] and 2,5-anhydro-3,4,6-tri-*O*-benzoyl-D-allose (**1g**).[14]

*4-(1,2-O-Isopropylidene-*D-glycero-*dihydroxyethyl)-3,5-bis(methoxycarbonyl)isoxazoline* N-*Oxide (2a) (A Typical Procedure for Condensation).* To a solution of **1a** (0.69 g, 5.3 mmol) in 30 ml of anhydrous DMA were added methyl nitroacetate (1.2 g, 10.6 mmol) and an equivalent of diethylamine (0.52

ml, 5.3 mmol). The mixture was stirred at room temperature for 16 h. After the starting materials had been almost consumed by TLC (silica gel, ethyl acetate–hexane (1:1)) analysis, the mixture was poured into a mixture of benzene (40 ml) and ice–water (80 ml), and the aqueous phase was extracted with benzene (3×40 ml). The combined extract was washed with water (3×80 ml) and dried over anhydrous sodium sulfate. Evaporation gave a yellowish syrup, which was purified by column chromatography on silica gel eluted with ethyl acetate–hexane (1:1), giving 1.2 g (74%) of **2a**. Fractional recrystallization of **2a** from ethyl acetate–hexane resulted in isolation of two diastereomers (**2a**$_1$ and **2a**$_2$) in a ratio of *ca.* 3:2. **2a**$_1$: mp 122.5—123.5 °C; $[\alpha]_D^{20}$ −117° (*c* 2.5, $CHCl_3$); UV_{max} (MeOH) 270 nm (ε 8400); IR (KBr) 1760—1740 (ester C=O), 1630—1620 (C=N), 1380 and 1150 cm^{-1} (CMe_2); ^{1}H-NMR ($CDCl_3$) δ=1.37 and 1.50 (each 3 H, s, CMe_2), 3.87 and 3.90 (each 3 H, s, ester Me), 3.97—4.07 (3H, m, H-1′,2′), 4.57 (1H, dd, $J_{4,1'}$=6 Hz, H-4), 5.08 (1H, d, $J_{4,5}$=3.5 Hz, H-5); CD (MeOH) $[\theta]_{273}$ −26000 (negative maximum).

Found: C, 47.52; H, 5.58; N, 4.59%; M$^+$, 303. Calcd for $C_{12}H_{17}NO_8$: C, 47.52; H, 5.65; N, 4.62%; M, 303.

2a$_2$: mp 86.5—87.5 °C; $[\alpha]_D^{20}$ −23° (*c* 2.5, $CHCl_3$); UV_{max} (MeOH) 270 nm (ε 8300); IR (KBr) 1760—1740 (ester C=O), 1630—1620 (C=N), 1380 and 1150 cm^{-1} (CMe_2); ^{1}H-NMR ($CDCl_3$) δ=1.37 and 1.50 (each 3H, s, CMe_2), 3.90 and 4.07 (each 3H, s, ester Me), 4.65 (1H, m, H-4), 5.21 (1H, d, $J_{4,5}$=4 Hz, H-5); CD (MeOH) $[\theta]_{268}$+8140 (positive maximum).

Found: C, 47.28; H, 5.60; N, 4.48%; M$^+$, 303.

*4-(1,2: 3,4-Di-*O*-isopropylidene-*L*-arabino-tetrahydroxybutyl)-3,5-bis(methoxycarbonyl)isoxazoline* N-*Oxide* (**2b**) *from* **1b**. Reaction time 2.5 h; Yield 48%; mp 86—87 °C (hexane); $[\alpha]_D^{20}$ −36° (*c* 2.6, $CHCl_3$); IR (KBr) 1755 and 1710 (ester C=O), 1635 (C=N), 1380 and 1150 cm^{-1} (CMe_2); ^{1}H-NMR ($CDCl_3$) δ=1.40 (12H, m, CMe_2), 3.87 (6H, s, ester Me), 3.5—4.2 (5H, m, H-4,2′,3′,4′), 4.52 (1H, m, H-1′), 5.05 (1H, d, $J_{4,5}$=2 Hz, H-5).

Found: C, 50.89; H, 6.34; N, 3.49%; M$^+$, 403. Calcd for $C_{17}H_{25}NO_{10}$: C, 50.61; H, 6.25; N, 3.47%; M, 403.

*3,5-Bis(methoxycarbonyl)-4-(*D*-gluco-pentaacetoxypentyl)-isoxazoline* N-*Oxide* (**2c**) *from* **1c**. Yield 64% (yellowish syrup); $[\alpha]_D^{25}$ +6° (*c* 3.4, $CHCl_3$); IR (liq. film) 1750 (ester C=O), 1640 cm^{-1} (C=N); ^{1}H-NMR ($CDCl_3$) δ=2.10—2.16 (15H, m, OAc), 3.83 and 3.95 (each 3H, s, ester Me), 4.0—4.3 (3H, m, H-4,5′), 5.08 (2H, d, $J_{4,5}$=2.5 Hz, H-5,1′), 5.0—5.6 (3H, m, H-2′,3′,4′).

*4-(2,3-*O*-Isopropylidene-β-*D*-erythrofuranosyl)-3,5-bis(methoxycarbonyl)isoxazoline* N-*Oxide* (**2d**) *from* **1d**. Reaction time 3 days. Solvent system for chromatography, ethyl acetate–hexane (1:2); Yield 32% (yellowish syrup); $[\alpha]_D^{20}$ −41° (*c* 1.0, $CHCl_3$); IR (liq. film) 1740 (ester C=O), 1630 (C=N), 1380 and 1160 cm^{-1} (CMe_2); ^{1}H-NMR ($CDCl_3$) δ=1.37 and 1.53 (each 3H, s, CMe_2), 3.88 and 3.92 (each 3H, s, ester Me), 3.65—4.38 (3H, m, H-4,4′), 4.6—5.0 (3H, m, H-1′,2′,3′), 5.11 (1H, d, $J_{4,5}$=1.5 Hz, H-5).

Found: C, 48.28; H, 5.71; N, 3.58%. Calcd for $C_{14}H_{19}NO_9$: C, 48.69; H, 5.55; N, 4.06%.

*4-[(4R)-3-*O*-Benzyl-1,2-*O*-isopropylidene-β-*L*-threofuranos-4-yl]-3,5-bis(methoxycarbonyl)isoxazoline* N-*Oxide* (**2e**) *from* **1e**. Solvent system for chromatography, chloroform–ethyl acetate (5:1); yield 6% (yellowish syrup); $[\alpha]_D^{20}$ −64.9° (*c* 2.0, $CHCl_3$); IR (liq. film) 1760—1735 (ester C=O), 1620 (C=N), 1380 cm^{-1} (CMe_2); ^{1}H-NMR ($CDCl_3$) δ=1.33 and 1.50 (each 3H, s, CMe_2), 3.77 and 3.83 (each 3H, s, ester Me), 3.95—4.8 (4H, m, H-4,2′,3′,4′), 4.53 (2H, broad, CH_2Ph), 5.30 (1H, m, H-5), 5.99 (1H, d, H-1′), 7.37 (5H, s, Ph).

Found: C, 55.71; H, 5.81; N, 2.96%; M$^+$, 451. Calcd for $C_{20}H_{25}NO_{10}$: C, 55.87; H, 5.58; N, 3.10%; M, 451.

*4-(2,3,5-Tri-*O*-benzyl-β-*D*-ribofuranosyl)-3,5-bis-(methoxycarbonyl)isoxazoline* N-*Oxide* (**2f**) *from* **1f**. Solvent system for chromatography, ethyl acetate–hexane (2:1) followed by acetone–hexane (1:3); yield 60% (a syrupy mixture of two diastereomers); $[\alpha]_D^{20}$ −21.3° (*c* 2.1, $CHCl_3$); IR (liq. film) 1760 and 1740 (ester C=O), 1630 cm^{-1} (C=N); ^{1}H-NMR ($CDCl_3$) δ=3.45 (1H, dd, $J_{4,1'}$=4.7 Hz, $J_{1',2'}$=4.3 Hz, H-1′), 3.67, 3.70, 3.78, and 3.80 (6H, s, ester Me), 3.85—4.0 (4H, m, H-3′,4′,5′), 4.14 (1H, dd, $J_{4,5}$=2.5 Hz, $J_{4,1'}$=4.7 Hz, H-4), 4.46—4.58 (7H, m, CH_2Ph, H-2′), 5.30 (1H, d, $J_{4,5}$=2.5 Hz, H-5).

Found: C, 65.19; H, 5.88; N, 2.29%; M$^+$, 604. Calcd for $C_{33}H_{35}NO_{10}$: C, 65.44; H, 5.83; N, 2.31%; M, 604.

*4-(2,3,5-Tri-*O*-benzoyl-β-*D*-ribofuranosyl)-3,5-bis(methoxycarbonyl)isoxazoline* N-*Oxide* (**2g**) *from* **1g**. Reaction time 3 days. By column chromatography on silica gel eluted with ethyl acetate–hexane (1:2), two diastereomers of **2g** (**2g**$_1$: R_f 0.35 and **2g**$_2$: R_f 0.25) were isolated in a *ca.* 1:3 ratio in a combined yield of 67%. **2g**$_1$: mp 97.5—99 °C; $[\alpha]_D^{20}$ +62.9° (*c* 0.45, MeOH); UV_{max} (MeOH) 230 nm (ε 40000), 269 nm (ε 12000); IR (KBr) 1725 (ester C=O), 1640 cm^{-1} (C=N); ^{1}H-NMR ($CDCl_3$) δ=3.65 and 3.71 (each 3H, s, ester Me), 4.18 (1H, dd, $J_{4,5}$=3.0 Hz, $J_{4,1'}$=5.3 Hz, H-4), 4.53—4.77 (4H, m, H-1′,4′,5′), 5.19 (1H, d, $J_{4,5}$=3.0 Hz, H-5), 5.59 (1H, dd, $J_{2',3'}$=5.9 Hz, $J_{3',4'}$=7.7 Hz, H-3′), 5.78 (1H, dd, $J_{1',2'}$=3.5 Hz, $J_{2',3'}$=5.9 Hz, H-2′), 7.5—8.0 (15H, m, Ph); CD (MeOH) $[\theta]_{269}$ +16200 (positive maximum).

Found: C, 61.19; H, 4.54; N, 2.13%; M$^+$, 647. Calcd for $C_{33}H_{29}NO_{13}$: C, 61.20; H, 4.51; N, 2.16%; M, 647.

2g$_2$: mp 68—71 °C; $[\alpha]_D^{20}$ −61.4° (*c* 0.51, MeOH); UV_{max} (MeOH) 230 nm (ε 39000), 270 nm (ε 1100); IR (KBr) 1725 ester C=O), 1640 cm^{-1} (C=N); ^{1}H-NMR ($CDCl_3$) δ=3.68 and 3.73 (each 3H, s, ester Me), 4.27 (1H, dd, $J_{4,5}$=2.3 Hz, $J_{4,1'}$=5.5 Hz, H-4), 4.5—4.7 (3H, m, H-4′,5′), 4.76 (1H, m, H-1′), 5.14 (1H, d, $J_{4,5}$=2.3 Hz, H-5), 5.55—5.70 (2H, m, H-2′,3′), 7.3—8.1 (15H, m, Ph); CD (MeOH) $[\theta]_{266}$ −13000 (negative maximum).

Found: C, 60.99; H, 4.59; N, 2.10%; M$^+$, 647.

*3,5-Bis(butylcarbamoyl)-4-(1,2-*O*-isopropylidene-*D*-glycero-dihydroxyethyl)isoxazoline* N-*Oxide* (**3a**$_1$) *(A Typical Procedure for Butylcarbamoylation)*. A solution of **2a**$_1$ (200 mg, 0.66 mmol) in methanol (5 ml) was refluxed in the presence of excess butylamine (480 mg, 6.6 mmol) for 1 h. After evaporation the residue was chromatographed on silica gel eluted with ethyl acetate–hexane (1:1), giving 85 mg (34%) of **3a**$_1$ as colorless needles: mp 109—110 °C (hexane); $[\alpha]_D^{25}$ +8° (*c* 1.7, $CHCl_3$); IR (KBr) 3300 (NH), 1680 and 1650 (amide I), 1615 (C=N), 1540 (amide II), 1380 and 1160 cm^{-1} (CMe_2); ^{1}H-NMR ($CDCl_3$) δ=1.33 and 1.48 (each 3H, s, CMe_2), 3.93—4.23 (3H, m, H-4, 2′), 4.77 (1H, m, H-1′), 4.98 (1H, d, $J_{4,5}$=3 Hz, H-5), 6.70 and 8.00 (each 1H, broad, NH).

Found: C, 56.09; H, 8.11; N, 10.90%; M$^+$, 385. Calcd for $C_{18}H_{31}N_3O_6$: C, 56.16; H, 8.04; N, 10.88%; M, 385.

*3,5-Bis(butylcarbamoyl)-4-(1,2:3,4-di-*O*-isopropylidene-*L*-arabino-tetrahydroxybutyl)isoxazoline* N-*Oxide* (**3b**) *from* **2b**. Yield 38%; mp 137.5—139 °C (hexane); $[\alpha]_D^{20}$ −2° (*c* 2.5, $CHCl_3$); IR (KBr) 3300 (NH), 1680 and 1650 (amide I), 1610 (C=N), 1530 (amide II), 1380 and 1160 cm^{-1} (CMe_2); ^{1}H-NMR ($CDCl_3$) δ=1.38—1.50 (6H, m, CMe_2), 3.8—4.3 (5H, m, H-4,2′,3′,4′), 4.73 (1H, m, H-1′), 4.92 (1H, d, $J_{4,5}$=3 Hz, H-5), 6.6 and 8.0 (each 1H, broad, NH).

Found: C, 56.91; H, 8.12; N, 8.60%. Calcd for $C_{23}H_{39}N_3O_8$: C, 56.89; H, 8.10; N, 8.65%.

*3,5-Bis(butylcarbamoyl)-4-(2,3-*O*-isopropylidene-β-*D*-erythrofuranosyl)isoxazoline* N-*Oxide* (**3d**) *from* **2d**. Reaction time 20

min. Solvent system for chromatography, ethyl acetate–hexane (1: 3); yield 12%; mp 141.5—142 °C (ethyl acetate–hexane); $[\alpha]_D^{20}$ +0.5° (*c* 0.2, $CHCl_3$); IR (KBr) 3340 and 3300 (NH), 1645 (amide I), 1620 (C=N), 1550 (amide II), 1380 and 1155 cm^{-1} (CMe_2); ^{1}H-NMR ($CDCl_3$) δ=0.93 (6H, t, $CH_2C\underline{H}_3$), 1.32—1.48 (14H, m, CMe_2, CH_2), 3.25—3.38 (4H, m, $NHC\underline{H}_2$), 3.88—4.3 (4H, m, H-4,1′,4′), 4.89—4.98 (2H, m, H-2′,3′), 5.13 (1H, d, $J_{4,5}$=3 Hz, H-5), 6.56 and 7.95 (each 1H, broad, NH).

Found: C, 55.97; H, 7.79; N, 9.80%; M^+, 427. Calcd for $C_{20}H_{33}N_3O_7$: C, 56.19; H, 7.78; N, 9.83%; M, 427.

*3,5-Dicarbamoyl-4-(2,3-O-isopropylidene-β-*D*-erythrofuranosyl)-isoxazoline* N-*Oxide (**4d**).* A solution of **2d** (100 mg, 0.29 mmol) in saturated methanolic ammonia (1 ml) was stored at room temperature for 0.5 h and then evaporated to dryness. The residue was crystallized from ethyl acetate, giving 14 mg (15%) of **4d**: mp 222 °C (dec); $[\alpha]_D^{20}$ −4.3° (*c* 0.47, MeOH); IR (KBr) 3460—3400 (NH), 1685 and 1655 (amide I), 1615 (C=N), 1385 and 1150 cm^{-1} (CMe_2); ^{1}H-NMR (acetone-d_6) δ=1.32 and 1.45 (each 3H, s, CMe_2), 3.81 (1H, dd, J_{gem}=10 Hz, $J_{3,4'a}$=2 Hz, H-4′a), 4.00 (1H, d, $J_{4,1'}$=6 Hz, H-1′), 4.08 (1H, dd, H-4′b), 4.34 (1H, dd, $J_{4,5}$=3 Hz, H-4), 4.84—5.08 (3H, m, H-5,2′,3′), 6.84—7.88 (4H, m, $CONH_2$).

Found: C, 45.71; H, 5.42; N, 13.24%; M^+, 315. Calcd for $C_{12}H_{17}N_3O_7$: C, 45.71; H, 5.44; N, 13.33%; M, 315.

*4-[(4R)-3-O-Benzyl-1,2-O-isopropylidene-β-*L*-threofuranos-4-yl]-5-diethylcarbamoyl-3-methoxycarbonylisoxazole (**4e**).* A solution of **2e** (74 mg, 0.16 mmol) in methanol (5 ml) was kept with diethylamine (0.17 ml, 1.6 mmol) at room temperature for 5 h. After evaporation the residue was crystallized from methanol–diethyl ether to give 26 mg (35%) of **4e**: mp 174—179.5 °C; $[\alpha]_D^{20}$ −189° (*c* 0.32, $CHCl_3$); IR (KBr) 1760 (ester C=O), 1710 cm^{-1} (amide); ^{1}H-NMR ($CDCl_3$) δ=1.19 (6H, t, $CH_2C\underline{H}_3$), 1.32 and 1.50 (each 3H, s, CMe_2), 2.96 (4H, q, $C\underline{H}_2CH_3$), 3.82 (3H, s, ester Me), 4.35 (1H, d, H-3′), 4.46 (2H, d, $C\underline{H}_2Ph$), 4.58 (1H, d, $J_{1',2'}$=4 Hz, $J_{2',3'}$=0 Hz, H-2′), 5.42 (1H, d, $J_{3',4'}$=4 Hz, H-4′), 5.82 (1H, d, $J_{1',2'}$=4 Hz, H-1′), 7.16 (5H, s, Ph).

Found: C, 60.35; H, 6.50; N, 5.69%; M^+, 475. Calcd for $C_{24}H_{30}N_2O_8$: C, 60.75; H, 6.37; N, 5.90%; M, 475.

*4-(2,3,5-Tri-O-benzyl-β-*D*-ribofuranosyl)-5-carbamoyl-3-methoxycarbonylisoxazoline* N-*Oxide (**4f**).* A solution of **2f** (208 mg, 0.34 mmol) in saturated methanolic ammonia (1 ml) was stored at room temperature for 1 h and then evaporated to dryness. The residue was chromatographed on silica gel eluted with ethyl acetate–hexane (3: 2). A fraction of R_f 0.3 was collected and crystallized from ethyl acetate–hexane, giving 44 mg (22%) of **4f**: mp 128.5—129.5 °C; $[\alpha]_D^{20}$ +1.4° (*c* 0.3, $CHCl_3$); IR (KBr) 3415 (NH), 1730 (ester C=O), 1680 (amide), 1615 cm^{-1} (C=N); ^{1}H-NMR ($CDCl_3$) δ=3.3—3.65 (3H, m, H-1′,5′), 3.79 (3H, s, ester Me), 3.85—4.18 (3H, m, H-2′,3′,4′), 4.11 (1H, dd, H-4), 4.4—4.62 (6H, m, $C\underline{H}_2Ph$), 5.14 (1H, d, $J_{4,5}$=3.3 Hz, H-5), 5.60 and 6.45 (each 1H, broad, $CONH_2$), 7.2—7.3 (15H, m, Ph).

Found: C, 65.10; H, 5.79; N, 4.73%; M^+, 590. Calcd for $C_{32}H_{34}N_2O_9$: C, 65.07; H, 5.80; N, 4.74%; M, 590.

*4-(*D*-glycero-Dihydroxyethyl)-3,5-bis(methoxycarbonyl) isoxazoline* N-*Oxide (**5a**$_1$) (A Typical Procedure for Deisopropylidenation)*: A solution of **2a**$_1$ (major isomer, 726 mg, 2.4 mmol) in aqueous methanol (50 ml) was treated with acidic resin (Dowex 50 W-X8, 4 g) under stirring at room temperature for 4 h. After evaporation the residue was crystallized from ethyl acetate–hexane, giving 630 mg (quantitative) of **5a**$_1$: mp 145.5—147 °C; $[\alpha]_D^{20}$ −124° (*c* 0.2, MeOH); IR (KBr) 3430 and 3320 (OH), 1730 (ester C=O), 1615 cm^{-1} (C=N); ^{1}H-NMR (acetone-d_6) δ=3.6—3.7 (3H, m, H-1′,2′), 3.80 (6H, s, ester Me), 4.06 (1H, m, H-4), 5.28 (1H, d, $J_{4,5}$=2 Hz, H-5).

Found: C, 40.91; H, 4.97; N, 5.16%. Calcd for $C_9H_{13}NO_8$: C, 41.07; H, 4.98; N, 5.32%.

*4-(*L*-arabino-Tetrahydroxybutyl)-3,5-bis(methoxycarbonyl)isoxazoline* N-*Oxide (**5b**) from **2b**.* The reaction mixture obtained after stirring for 0.5 h was chromatographed on silica gel eluted with ethyl acetate–chloroform (3: 1), giving 3,4-diol (colorless syrup, R_f 0.4); yield 36%; $[\alpha]_D^{20}$ −93.7° (*c* 2.7, MeOH); IR (liq. film) 3460 (OH), 1760—1735 (ester C=O), 1630 cm^{-1} (C=N); ^{1}H-NMR ($CDCl_3$) δ=1.42 and 1.45 (each 3H, s, CMe_2), 2.4—3.2 (2H, broad, OH), 3.87 and 3.90 (each 3H, s, ester Me), 3.75 (4H, m, H-2′,3′,4′), 4.18 (1H, dd, H-4), 4.58 (1H, dd, H-1′), 5.12 (1H, d, $J_{4,5}$=2.5 Hz, H-5) and 1,2,3,4-tetrol (**5b**, R_f 0.1); yield 17%; mp 66 °C (dec); $[\alpha]_D^{20}$ +39.7° (*c* 3.0, MeOH); IR (KBr) 3360 (OH), 1735 and 1700 (ester C=O), 1630 cm^{-1} (C=N); ^{1}H-NMR (methanol-d_4) δ=3.83 and 3.87 (each 3H, s, ester Me), 3.70—4.03 (5H, m, H-4,2′,3′,4′), 4.37 (1H, m, H-1′), 5.68 (1H, d, $J_{4,5}$=3 Hz, H-5).

Found: C, 40.46; H, 5.08; N, 3.98%. Calcd for $C_{11}H_{17}NO_{10}$: C, 40.87; H, 5.30; N, 4.33%.

*4-(β-*D*-Erythrofuranosyl)-3,5-bis(methoxycarbonyl)isoxazoline* N-*Oxide (**5d**) from **2d**.* Reaction time 10 h. Solvent system for chromatography, ethyl acetate–acetone–benzene (4: 5: 3); yield 29%; mp 167—169.5 °C (ethyl acetate–hexane); $[\alpha]_D^{20}$ +14.7° (*c* 0.2, MeOH); IR (KBr) 3480 (OH), 1765 and 1730 (ester C=O), 1620 cm^{-1} (C=N); ^{1}H-NMR ($CDCl_3$) δ=2.9—3.3 (2H, broad, OH), 3.71 and 3.84 (each 3H, s, ester Me), 5.02 (1H, d, $J_{4,5}$=2 Hz, H-5), 3.8—4.35 (6H, m, other protons).

Found: C, 42.89; H, 4.91; N, 4.33%; M^+ 306. Calcd for $C_{11}H_{15}NO_9$: C, 43.28; H, 4.95; N, 4.59%; M 306.

*4-(2,3,5-Tri-O-benzoyl-β-*D*-ribofuranosyl)-3,5-bis(methoxycarbonyl)isoxazoline (**6**).* A mixture of **2g**$_2$ (major isomer, 970 mg, 1.5 mmol) and triethyl phosphite (300 mg, 1.8 mmol) in anhydrous toluene (4 ml) was refluxed for 5 h under nitrogen atmosphere. The solvent was evaporated and the residue was chromatographed on silica gel eluted with ethyl acetate–hexane (1: 1), giving 632 mg of amorphous solid. Recrystallization from benzene–hexane gave 461 mg (49%) of **6** as colorless prisms: mp 92.5—93.5 °C; $[\alpha]_D^{20}$ −134° (*c* 0.25, $CHCl_3$); UV_{max} (MeOH) 230 nm (ε 42000), 272^{sh} nm (ε 4600); IR (KBr) 1720 (ester C=O), 1630 cm^{-1} (C=N); ^{1}H-NMR ($CDCl_3$) δ=3.60 and 3.68 (each 3H, s, ester Me), 4.36 (1H, dd, $J_{4,5}$=5.0 Hz, $J_{4,1'}$=5.0 Hz, H-4), 4.48—4.66 (3H, m, H-4′,5′), 4.77 (1H, dd, $J_{4,1'}$=5.0 Hz, $J_{1',2'}$=7.8 Hz, H-1′), 5.23 (1H, d, $J_{4,5}$=5.0 Hz, H-5), 5.43 (1H, dd, $J_{1',2'}$=7.8 Hz, $J_{2',3'}$=5.8 Hz, H-2′), 5.65 (1H, dd, $J_{2',3'}$=5.8 Hz, $J_{3',4'}$=3.5 Hz, H-3′).

Found: C, 62.48; H, 4.54; N, 2.15%. Calcd for $C_{33}H_{29}NO_{12}$: C, 62.76; H, 4.63; N, 2.22%.

*3,5-Dicarbamoyl-4-(β-*D*-ribofuranosyl)isoxazoline (**7**).* A solution of **6** (200 mg, 0.32 mmol) in saturated methanolic ammonia (15 ml) was stored at room temperature for 7 h, when TLC (silica gel, ethyl acetate–hexane (1: 1)) showed complete consumption of **6**. The syrupy residue on evaporation was dissolved in methanol and chromatographed on silica gel eluted with methanol–ethyl acetate (1: 3), giving 51 mg (55%) of **7** as colorless prisms: mp 198—198.5 °C; $[\alpha]_D^{20}$ −173° (*c* 0.14, MeOH); UV_{max} (MeOH) 225 nm (ε 5400); IR (KBr) 3400—3280 (NH, OH), 1655 (amide), 1605 cm^{-1} (C=N); ^{1}H-NMR (D_2O) δ=3.5—3.8 (2H, m, H-5′), 3.9—4.1 (3H, m, H-1′,2′,4′), 4.16 (2H, m, H-4,3′), 5.25 (1H, d, $J_{4,5}$=3.7 Hz, H-5).

Found: C, 41.58; H, 5.23; N, 14.32%. Calcd for $C_{10}H_{15}N_3O_7$: C, 41.52; H, 5.23; N, 14.53%.

The authors are indebted to Mr. Chiharu Ichikawa and Miss Yohko Tabuchi for their technical assistance. The present work was supported in part by a Grant-in-Aid for Scientific Research No. 255337 from the Ministry of Education, Science and Culture.

References

1) The Synthetic Reactions of Aliphatic Nitro Compounds. Part XV; Presented at the 10th Congress of Heterocyclic Chemistry, Tsukuba, October, 1977, Abstr. No. 1-17; A part of this work has been published as a preliminary communication: E. Kaji and S. Zen, *Synth. Commun.*, **9**, 165 (1979) (Part XIV of this series).

2) S. Hanessian and A. G. Pernet, *Adv. Carbohydr. Chem. Biochem.*, **33**, 111 (1976); J. M. J. Tronchet, *Biol. Med.* (*Paris*), **4**, 83 (1975).

3) J. M. J. Tronchet, S. J. Thorndahl, L. Faivere, and R. Massard, *Helv. Chim. Acta*, **56**, 1303 (1973), **53**, 1484 (1970), and **52**, 2569 (1969).

4) H. P. Albrecht, D. B. Repke, and J. G. Moffatt, *J. Org. Chem.*, **40**, 2143 (1975); J. M. J. Tronchet and J. Poncet, *Carbohydr. Res.*, **46**, 119 (1976) and their preceding papers.

5) G. Just and B. Chalard-Faure, *Can. J. Chem.*, **54**, 861 (1976).

6) S. Zen and E. Kaji, *Chem. Pharm. Bull.*, **22**, 477 (1974).

7) A. T. Nielsen and T. G. Archibald, *J. Org. Chem.*, **34**, 984 (1969).

8) S. Zen and M. Koyama, *Bull. Chem. Soc. Jpn.*, **44**, 2882 (1971).

9) E. Baer and H. O. L. Fischer, *J. Biol. Chem.*, **128**, 463 (1939); D. Horton, J. B. Highes, and J. K. Thomson, *J. Org. Chem.*, **33**, 728 (1968).

10) J. English, Jr., and P. H. Griswold, Jr., *J. Am. Chem. Soc.*, **67**, 2039 (1945).

11) M. L. Wolfrom, *J. Am. Chem. Soc.*, **51**, 2188 (1929).

12) J. Defaye and T. Reyners, *Bull. Soc. Chim. Biol.*, **50**, 1625 (1968).

13) D. Horton and F. O. Swanson, *Carbohydr. Res.*, **14**, 159 (1970).

14) H. P. Albrecht, D. B. Repke, and J. G. Moffatt, *J. Org. Chem.*, **38**, 1836 (1973).

Studies on Biologically Active Pteridines. II.[1] Synthesis of Some 2-Pyrimidinyl- and 2-Pteridinyl-amino Acids

Takashi SUGIMOTO,* Keiko SHIBATA, Sadao MATSUURA, and Toshiharu NAGATSU**

Department of Chemistry, College of General Education, Nagoya University, Chikusa-ku, Nagoya 464
***Laboratory of Cell Physiology, Department of Life Chemistry, Graduate School at Nagatsuta, Tokyo Institute of Technology, Midori-ku, Yokohama 227*

(Received February 13, 1979)

Synthesis of some pyrimidines and pteridines with an amino acid residue at the 2-position was investigated. 4-Amino-6-hydroxy-2-methylthio-5-nitrosopyrimidine, on heating with amino acids in water, underwent aminolysis at the 2-position to give the corresponding *N*-(4-amino-6-hydroxy-5-nitroso-2-pyrimidinyl)amino acids. These (5-nitroso-2-pyrimidinyl)amino acids, after reduction of the nitroso group to an amino group, condensed with biacetyl or a pentose phenylhydrazone to give *N*-(4-hydroxy-6,7-dimethyl-2-pteridinyl)amino acids and *N*-(4-hydroxy-6-polyhydroxypropyl-2-pteridinyl)amino acids, respectively.

Various 2-amino-4-hydroxypteridines and their 5,6,7,8-tetrahydro derivatives having an alkyl or polyhydroxyalkyl substituent at the 6-position possess distinctive biological activities. For example, biopterin [2-amino-4-hydroxy-6-(L-*erythro*-1,2-dihydroxypropyl)-pteridine] is a growth factor for *Crithidia fasciculate*[2,3] and the 5,6,7,8-tetrahydro derivative is a potent coenzyme for phenylalanine,[4] tyrosine,[5,6] and tryptophan hydroxylases.[7]

The relation between the structure of 6-substituted 5,6,7,8-tetrahydro-2-amino-4-hydroxypteridines and the coenzyme activities for tyrosine hydroxylase has been studied extensively by Nagatsu and his coworkers.[6,8,9] However, the pteridines used in their study vary only in the substituents attached to the pyrazine ring of the compounds except a few cases.[8] It is of interest to investigate how the biological activities of such pteridines will be changed by modification in the pyrimidine rather than the pyrazine moiety. This paper describes the synthesis of 6- or 6,7-disubstituted 2-amino-4-hydroxypteridines possessing a carboxyalkyl group attached to the 2-amino group. The choice to introduce a carboxyalkyl group rather than a simple alkyl group stemmed from an anticipation that such polar group would cause a stronger interaction of the pteridine with the biological systems. In addition, it is expected that further modification of the compounds at the carboxyl group, for example the formation of an amido linkage to polyamines or proteins, would widen the utility of these compounds.

The amino acid residue of the pteridines (**3**, **4**, and **5**) was introduced prior to the formation of the pteridine ring by nucleophilic displacement of the methylthio group of 4-amino-6-hydroxy-2-methylthio-5-nitrosopyrimidine (**1**) by an appropriate amino acid in analogy to the aminolysis of **1** by simple aliphatic amines.[10] When the methylthiopyrimidine was heated with an excess amount of 6-aminohexanoic acid in an aqueous solution, the solution changed the color from blue to dark red and evolved methanethiol. The displacement became complete after refluxing for 1 h and the yield of 6-[(4-amino-6-hydroxy-5-nitroso-2-pyrimidinyl)amino]hexanoic acid (**2a**) was about 70%. The reaction of **1** with 4-aminobutanoic acid and β-alanine took place in a similar manner to give the 4-(2-pyrimidinylamino)butanoic and 3-(2-pyrimidinylamino)propanoic acids (**2b** and **2c**), respectively. However, the displacement reaction of **1** with several α-amino acids proceeded much easier when the sodium salts of the acids in place of the free acids were employed. Thus, heating of **1** with L-alanine in the presence of an equivalent amount of sodium hydroxide yielded *N*-(4-amino-6-hydroxy-5-nitroso-2-pyrimidinyl)-L-alanine (**2d**) in 53% yield; in the absence of sodium hydroxide, the yield was 22%. Under similar conditions, **1** reacted with D-alanine and glycine to give the *N*-(2-pyrimidinyl)-D-alanine (**2e**) and the *N*-(2-pyrimidinyl)glycine (**2f**), respectively.

These *N*-(2-pyrimidinyl)amino acids showed two pK_a values at about 2.4 and 7.9, which were attributed to the ionization of the pyrimidine ring to form a cation (pK_a 2.4) and to form an anion (pK_a 7.9); pK_a values due to the ionization of the carboxyl group could not be determined on a spectroscopic measurement. Thus, all the *N*-(2-pyrimidinyl)amino acids, despite of the different carbon chain between the carboxyl and amino groups, exhibited UV spectra (Table 1) very similar to those of known 4-amino-6-hydroxy-2-methylamino-5-nitrosopyrimidine.[11] These physical data, together with elemental analyses, confirmed the structure of the aminolysis products.

The nitrosopyrimidines (**2a**—**f**) were converted to the corresponding 2-amino-4-hydroxy-6,7-dimethylpteridines (**3a**—**f**) having a carboxyalkyl group attached to the 2-amino group in a conventional way: by reduction of the 5-nitroso group to an amino group by catalytic hydrogenation, followed by condensation with biacetyl. By using glyoxal instead of biacetyl in the above course, **2f** gave *N*-(4-hydroxy-2-pteridinyl)glycine (**4**).

Several pteridines analogous to biopterin or neopterin having a di- or trihydroxypropyl substituent at the 6-position were also synthesized starting from the 5-nitrosopyrimidines (**2a** and **2f**). Condensation of the 5-amino analogue of **2a** or **2f** with L-arabinose phenylhydrazone at pH 2—3, followed by air oxidation at pH 7—8 gave 6-[[4-hydroxy-6-(L-*erythro*-1,2,3-trihydroxypropyl)-2-pteridinyl]amino]hexanoic acid (**5a**) and the lower homologue (**5b**), respectively. Condensation of the 5-amino analogue of **2a** with 5-deoxy-L-arabinose phenylhydrazone in a way similar to that for biopterin[1] afforded 6-[[4-hydroxy-6-(L-*erythro*-1,2-dihydroxypropyl)-2-pteridinyl]amino]hexanoic acid (**5c**).

Table 1. The pK_a values and UV spectra of *N*-(2-pyrimidinyl)amino acids and *N*-(2-pteridinyl)amino acids

Compound	pK_a	pH of buffer[a)]	λ_{max} (log ε)[b)]	Ionic species[c)]
2a	2.49±0.01	0.25	212(3.90), 268(4.06), *310*(*3.96*)	+
	8.10±0.01	5.5	216(3.77), 230(3.89), 258(3.66), 326(4.34)	○
		10.5	214(3.82), 328(4.36)	−
2b	2.46±0.01	0.25	212(3.92), 270(4.10), *310*(*3.81*)	+
	7.87±0.01	5.0	215(3.82), 230(3.93), 257(3.70), 326(4.36)	○
		10.0	213(3.86), 327(4.39)	−
2c	2.41±0.03	0.25	211(3.98), 269(4.16), *310*(*4.03*)	+
	7.91±0.02	5.0	215(3.85), 230(3.98), 257(3.75), 326(4.40)	○
		10.0	213(3.92), 327(4.44)	−
2d	2.31±0.01	0.25	209(3.96), 271(4.13), *310*(*3.99*)	+
	7.86±0.01	5.0	214(3.83), 230(3.93), 261(3.68), 326(4.37)	○
		10.0	213(3.89), 328(4.40)	−
2e	2.30±0.01	0.25	209(3.96), 271(4.13), *310*(*4.00*)	+
	7.86±0.01	5.0	215(3.82), 230(3.93), 261(3.68), 327(4.37)	○
		10.0	214(3.89), 328(4.38)	−
2f	2.31±0.01	0.25	209(3.99), 270(4.17), *310*(*4.03*)	+
	7.98±0.01	5.0	214(3.85), 230(3.98), 260(3.74), 326(4.41)	○
		10.0	211(3.89), 327(4.43)	−
3a	−2.36±0.03	−4.0	220(4.18), 254(4.11), 340(3.94)	2+
	2.60±0.01	0.25	219(4.29), 253(4.06), 324(3.96), 400(3.10)	+
	8.59±0.02	6.0	213(4.23), 279(4.24), 350(3.85)	○
		10.5	260(4.31), 366(3.91)	−
3b	−2.45±0.02	−4.0	219(4.22), 253(4.14), 339(3.98)	2+
	2.40±0.02	0.25	219(4.26), 253(4.05), 293(3.73), 323(3.93), 397(3.26)	+
	8.92±0.05	6.0	223(4.24), 279(4.25), 350(3.86)	○
		11.0	259(4.34), 365(3.94)	−
3c	−2.55±0.02	−4.0	220(4.18), 253(4.10), 338(3.95), 398(3.76)	2+
	2.22±0.02	−0.25	218(4.26), 253(4.05), 290(3.77), 323(3.91), 395(3.42)	+
	8.89±0.02	5.5	224(4.21), 278(4.24), 349(3.86)	○
		11.0	259(4.34), 364(3.93)	−
3d	−2.95±0.05	−4.0	222(4.13), 253(4.11), 286(3.76), 336(3.88), 393(3.53)	2+
	1.46±0.05	−0.75	218(4.09), 261(4.07), 285(4.04), 324(3.66), 389(3.88)	+
	3.2±0.1	2.5	220(4.21), 276(4.18), 344(3.84)	+[d)]
	8.97±0.02	6.0	224(4.20), 279(4.25), 350(3.87)	○
		11.0	259(4.34), 364(3.93)	−
3e	−3.02±0.05	−4.0	221(4.11), 253(4.08), 286(3.72), 336(3.85), 392(3.46)	2+
	1.57±0.05	−0.75	218(4.06), 261(4.03), 285(4.00), 324(3.61), 390(3.84)	+
	3.6±0.1	2.5	221(4.16), 276(4.15), 344(3.80)	+[d)]
	9.02±0.05	6.0	224(4.18), 278(4.23), 350(3.84)	○
		11.0	259(4.32), 364(3.91)	−
3f	−2.91±0.03	−4.0	221(4.12), 252(4.08), 287(3.68), 336(3.87), 391(3.41)	2+
	1.30±0.01	−0.75	219(4.11), 255(4.05), 285(3.98), 323(3.72), 387(3.82)	+
	3.36±0.01	2.5	220(4.20), 275(4.15), 343(3.83)	+[d)]
	8.45±0.01	6.0	222(4.21), 278(4.23), 350(3.86)	○
		10.5	259(4.25), 360(3.89)	−
4	−3.2±0.1	−4.0	209(4.06), 235(4.02), *280*(*3.70*), 318(3.72), 390(3.43)	2+
	0.88±0.02	−1.0	209(4.13), 235(4.08), *280*(*3.73*), 315(3.78), 384(3.44)	+
	3.26+0.02	2.0	214(4.09), 234(4.06), 273(4.12), 342(3.76)	+[d)]
	7.90±0.01	5.5	221(4.07), 275(4.19), 347(3.78)	○
		10.0	261(4.34), 365(3.84)	−
5a	2.10±0.04	0.25	213(4.22), 242(4.26), 324(3.94)	+
	7.96±0.01	5.0	221(4.15), *241*(*4.08*), 281(4.31), 353(3.81)	○
		10.0	216(4.07), 265(4.41), 372(3.90)	−
5b	−1.6±0.1	−4.0	210(4.11), 251(4.09), 285(3.77), 323(3.80), 394(3.46)	2+
	1.01±0.03	−0.5	211(4.14), 239(4.12), 282(4.19), 322(3.74), 389(3.35)	+
	3.10±0.02	2.0	213(4.11), 239(4.08), 277(4.21), 347(3.79)	+[d)]
	7.81±0.01	5.0	225(4.05), 240(4.04), 280(4.29), 352(3.79)	○
		10.0	218(4.00), 266(4.37), 369(3.87)	−

Table 1. (Continued)

Compound	pK_a	pH of buffer[a)]	λ_{max} (log ε)[b)]	Ionic species[c)]
5c	2.13±0.01	0.25	212(4.03), 242(4.23), 325(3.90)	+
	7.95±0.02	5.0	221(4.12), *241(4.06)*, 281(4.29), 353(3.80)	○
		10.5	218(4.05), 265(4.41), 372(3.89)	−
6a	−2.45±0.02	−4.0	220(4.21), 254(4.13), 340(3.97)	2+
	2.59±0.02	0.25	219(4.32), 252(4.09), 324(3.98), 400(3.13)	+
	8.46±0.02	6.0	223(4.26), 279(4.26), 350(3.87)	○
		10.5	260(4.34), 365(3.94)	−
6b	−2.42±0.06	−4.0	220(4.20), 253(3.13), 339(3.97)	2+
	2.51±0.02	0.25	219(4.31), 252(4.09), 324(3.98), 396(3.09)	+
	8.50±0.01	5.5	225(4.22), 279(4.25), 350(3.86)	○
		10.5	260(4.33), 366(3.93)	−

a) Negative figures are H_0 values. b) Wavelength in nm measured in aqueous buffer of given pH; shoulders or inflexions in italics. c) Ionic species shown by 2+ (dication), + (monocation), ○ (neutral molecule), and − (monoanion) are regarded only to the pyrimidine or pteridine chromophore unless otherwise indicated. d) Zwitter ions.

The structures of these *N*-(2-pteridinyl)amino acids (**3**, **4**, and **5**) were confirmed by the elemental analyses and the close similarity of their UV spectra (Table 1) to those of 4-hydroxy-6,7-dimethyl-2-methylaminopteridine[12] or biopterin.[13] The pteridines (**3d—f**, **4**, and **5b**) derived from α-amino acids exhibited four pK_a values at about 8.8, 3.3, 1.0, and −3.0 which were measured by a spectroscopic method.[14] The values at 8.8, 3.3, and −3.0 are attributed to the ionization of the pteridine ring to form anionic species by losing a proton from the ring (pK_a 8.8) and to form cationic species by single or double protonation (pK_a 3.3 and −3.0, respectively). The pK_a value at 1.0 could be attributed to the ionization of the carboxyl group, since no pK_a was detected by a spectroscopic measurement at this range with **3a—c** where the carboxyl group was separated far from the pteridine chromophore by a long carbon chain of two or more carbon atoms. The acidity of the monocations (protonated at the pteridine ring) of **3d—f**, **4**, and **5b** (pK_a about 1.0) was fairly strengthened compared to those of glycine (pK_a 2.22[15]) and alanine (pK_a 2.22[15]) owing to the electron withdrawing pteridinyl group attached to the nitrogen atom.

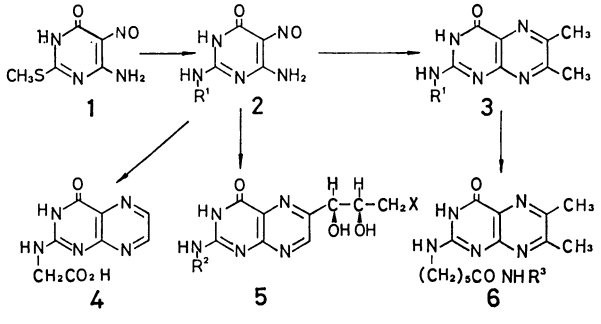

2,3	R¹
a	-(CH₂)₅CO₂H
b	-(CH₂)₃CO₂H
c	-CH₂CH₂CO₂H
d	-C(CH₃)H-CO₂H (L)
e	-C(H)CH₃-CO₂H (D)
f	-CH₂CO₂H

5	R²	X
a	-(CH₂)₅CO₂H	-OH
b	-CH₂CO₂H	-OH
c	-(CH₂)₅CO₂H	-H

6	R³
a	-H
b	-C₄H₉

As a model for making a peptide linkage between the present synthesized *N*-(2-pteridinyl)amino acids and a protein, conversion of the carboxyl group of **3a** into a carbamoyl group was examined. First, the carboxylic acid (**3a**) was treated with hydrogen chloride in methanol to give the methyl ester which on subsequent treatment with ammonia gave 6-[(4-hydroxy-6,7-dimethyl-2-pteridinyl)amino]hexanamide (**6a**). The conversion, however, was found to undergo much easier by employing a mixed anhydride[16] as an intermediate: **3a** was treated with ethyl chloroformate in *N*,*N*-dimethylformamide in the presence of triethylamine to form an anhydride. Without isolation, the anhydride was treated with butylamine to give the *N*-butyl-6-(2-pteridinylamino)hexanamide (**6b**) in a good yield. The latter method involving an anhydride would be applicable for making a peptide linkage between the present synthesized pteridines and a protein.

Experimental

The elemental analyses were conducted at the Analytical Section, Meijo University, Nagoya. The pK_a values were determined spectroscopically,[14] and the UV spectra in an appropriate buffer solution on a Shimadzu UV-300 spectrophotometer.

Synthesis of N-*(4-Amino-6-hydroxy-5-nitroso-2-pyrimidinyl)amino Acids(2a—f).* *Method A*: A mixture of 4-amino-6-hydroxy-2-methylthio-5-nitrosopyrimidine (**1**)[17] (10 g) and 6-aminohexanoic acid (20 g) in water (400 ml) was heated under reflux for 1 h. The resulting solution was adjusted to pH 2—3 with formic acid and chilled. Filtration and washing with water gave an orange powder (8.5 g) of 6-[(4-amino-6-hydroxy-5-nitroso-2-pyrimidinyl)amino]hexanoic acid (**2a**), which was pure enough for further reactions. The analytical sample (orange needles) was prepared by dissolving in hot dilute ammonia then acidifing with formic acid, mp 232.5—233.5 °C, dec (Found: C, 44.53; H, 5.65; N, 25.69%. Calcd for $C_{10}H_{15}N_5O_4$: C, 44.60; H, 5.62; N, 26.01%). A similar treatment of **1** with 4-aminobutanoic acid or β-alanine gave the 4-(2-pyrimidinylamino)butanoic acid(**2b**)[77% yield, mp 240—241 °C, dec (from water)(Found: C, 39.33; H, 4.92;

N, 29.32%. Calcd for $C_8H_{11}N_5O_4$: C, 39.83; H, 4.60; N, 29.04%)] and the 3-(2-pyrimidinylamino)propanoic acid(**2c**) [68% yield, mp >300 °C (Found: C, 37.58; H, 4.11; N, 30.65%. Calcd for $C_7H_9N_5O_4$: C, 37.01; H, 3.99; N, 30.83 %)], respectively.

Method B: A solution of **1** (9.0 g) and L-alanine (8.9 g) in 0.25 M sodium hydroxide (400 ml) was heated under reflux for 2 h. After concentration *in vacuo* to about 200 ml, the solution was adjusted to pH 2—3 with formic acid and chilled. The orange flakes (5.8 g, 53%) of the *N*-(2-pyrimidinyl)-L-alanine (**2d**), purified in the same way as above, darkened without melting above 245 °C (Found: C, 34.42; H, 4.50; N, 28.46%. Calcd for $C_7H_9N_5O_4 \cdot H_2O$: C, 34.29; H, 4.52; N, 28.56%). Similarly, **1** reacted with D-alanine and glycine to give the *N*-(2-pyrimidinyl)-D-alanine(**2e**)[18% yield; darkened above 245 °C without melting (Found: C, 34.38; H, 4.52; N, 28.28%. Calcd for $C_7H_9N_5O_4 \cdot H_2O$: C, 34.29; H, 4.52; N, 28.56%)] and the *N*-(2-pyrimidinyl)-glycine(**2f**)[63% yield; darkened above 280 °C without melting (Found: C, 31.42; H, 3.71; N, 30.33%. Calcd for $C_6H_7N_5O_4 \cdot H_2O$: C, 31.17; H, 3.92; N, 30.30%)], respectively.

Synthesis of N-*(4-Hydroxy-6,7-dimethyl-2-pteridinyl)amino Acids (3a—f)*. A solution of **2a** (4.3 g) in 2 M sodium hydroxide (60 ml) was hydrogenated over palladium on carbon (5%, 2 g) at room temperature and atmospheric pressure till the calculated amount of hydrogen was absorbed. After acidifing with concd hydrochloric acid (20 ml), the catalyst was removed by filtration. The filtrate, after being adjusted to pH 2—3 with ammonia, was heated with biacetyl (3.0 g) under reflux for 1 h. Refrigeration gave a yellow solid, which was crystallized from 50% aqueous methanol to give yellow needles (70 % yield) of 6-[(4-hydroxy-6,7-dimethyl-2-pteridinyl)amino]-hexanoic acid (**3a**), mp 215—219 °C, dec (Found: C, 51.94; H, 6.61; N, 21.30%. Calcd for $C_{14}H_{19}N_5O_3 \cdot H_2O$: C, 52.00; H, 6.55; N, 21.66%).

In an analogous way, its lower homologues (**3b—f**) were synthesized from the corresponding pyrimidines (**2b—f**): the 4-(2-pteridinylamino)butanoic acid (**3b**) [80% yield, mp 238—240 °C, dec (from water) (Found: C, 48.72; H, 5.82; N, 23.40%. Calcd for $C_{12}H_{15}N_5O_3 \cdot H_2O$: C, 48.80; H, 5.80; N, 23.72%)], 3-(2-pteridinylamino)propanoic acid (**3c**) [70% yield, darkened above 275 °C without melting (Found: C, 49.73; H, 4.98; N, 26.44%. Calcd for $C_{11}H_{13}N_5O_3$: C, 50.18; H, 4.98; N, 26.61%)], *N*-(2-pteridinyl)-L-alanine (**3d**) [50% yield, darkened above 180 °C and did not show sharp mp (from water) (Found: C, 46.95; H, 5.40; N, 24.63%. Calcd for $C_{11}H_{13}N_5O_3 \cdot H_2O$: C, 46.97; H, 5.38; N, 24.90%)], *N*-(2-pteridinyl)-D-alanine (**3e**) [45% yield, darkened above 180 °C without showing sharp mp (from water) (Found: C, 46.84; H, 5.14; N, 24.59%. Calcd for $C_{11}H_{13}N_5O_3 \cdot H_2O$: C, 46.97; H, 5.38; N, 24.90%)], *N*-(2-pteridinyl)glycine (**3f**) [87 % yield, mp 206—210 °C, dec (from water) (Found: C, 45.13; H, 4.87; N, 25.95%. Calcd for $C_{10}H_{11}N_5O_4 \cdot H_2O$: C, 44.94; H, 4.90; N, 26.21%)].

N-*(4-Hydroxy-2-pteridinyl)glycine (4)*. A solution of the 5-amino analogue of **2f** (2.0 g) in water (pH 6—7, 80 ml), prepared in the same way as above, was heated with glyoxal sodium hydrogensulfite (3.5 g) under reflux for 1 h. The solution was adjusted to pH 2—3 with hydrochloric acid and chilled to give a solid. Crystallization of the solid from water gave colorless prisms (1.1 g) of **4** which darkened above 250 °C without melting (Found: C, 40.28; H, 3.77; N, 28.94%. Calcd for $C_8H_7N_5O_3 \cdot H_2O$: C, 40.17; H, 3.79; N, 29.28%).

*6-[[4-Hydroxy-6-(*L-erythro-*1,2,3-trihydroxypropyl)-2-pteridinyl]amino]hexanoic Acid (5a) and the Homologue (5b)*. A solution of **2a** (4.0 g) in 2 M sodium hydroxide (100 ml) was hydrogenated and separated from the catalyst as above. The filtrate was adjusted to pH 3—4, diluted with methanol (100 ml), and then heated with L-arabinose phenylhydrazone (3.8 g) under nitrogen and reflux for 2 h. After cooling, the solution was adjusted to pH 8—9 with ammonia and stirred under bubbling air at room temperature for 20 h. The orange solution was evaporated to dryness *in vacuo* and the residue was extracted with 1 M ammonia (200 ml). The extract was adjusted to pH 2—3 with formic acid and chromatographed on a Florisil column[1] (4.5×40 cm) using water as the elution solvent. The eluate was evaporated to dryness and the residue was extracted with hot water (100 ml). The extract, on concentration to about 50 ml and chilling, gave pale yellow prisms (2.0 g) of **5a**, mp 186—190 °C, dec (from water) (Found: C, 46.55; H, 5.84; N, 17.95%. Calcd for $C_{15}H_{21}N_5O_6 \cdot H_2O$: C, 46.75; H, 6.02; N, 18.17%).

By using **2f** in place of **2a** in the foregoing condensation, *N*-[4-hydroxy-6-(L-*erythro*-1,2,3-trihydroxypropyl)-2-pteridinyl]glycine (**5b**) was obtained in 53% yield as colorless needles, mp 177—180 °C, dec (from water) (Found: C, 40.15; H, 4.49; N, 20.98%. Calcd for $C_{11}H_{13}N_5O_6 \cdot H_2O$: C, 40.12; H, 4.59; N, 21.27%).

*6-[[4-Hydroxy-6-(*L-erythro-*1,2-dihydroxypropyl)-2-pteridinyl]-amino]hexanoic Acid (5c)*. The 5-nitrosopyrimidine (**2a**) (4.0 g) was hydrogenated in the same way as above to the 5-amino analogue, which was heated under reflux with 5-deoxy-L-arabinose phenylhydrazone (4.5 g) in 50% aqueous methanol (200 ml) at pH 3—4 and under nitrogen for 20 min. The solution, after cooling in an ice bath, was added to an ice chilled solution of potassium hexacyanoferrate (III) (30 g), potassium iodide (5 g), 35% hydrogen peroxide (10 ml), and formic acid (10 ml) in water (200 ml). The mixture was stirred under bubbling oxygen at 0—5 °C for 2 h and then at 20—25 °C for 10 h. The resulting solution was concentrated *in vacuo* to about 100 ml and chromatographed on a Florisil column as above. The eluate was evaporated to dryness and the residue was extracted with methanol (200 ml). Evaporation of the extract and subsequent crystallization from 90% ethanol gave pale yellow needles (0.47 g) of **5c**, mp 216—218 °C, dec (from 90% ethanol) (Found: C, 48.55; H, 6.25; N, 18.55%. Calcd for $C_{15}H_{21}N_5O_5 \cdot H_2O$: C, 48.77; H, 6.28; N, 18.96%).

Conversion of 3a into the Carboxamides (6a and 6b).

Method A: To a solution of **3a** (300 mg) in anhydrous methanol (30 ml), dry hydrogen chloride was passed till saturation. The solution, after being allowed to stand at 25 °C for 10 h, was evaporated to dryness *in vacuo*. The residue was dissolved in 20% aqueous ammonia (100 ml) and kept at 25 °C for 10 h. Evaporation of the solution gave a solid which was chromatographed on a Florisil column (2× 20 cm), eluted by 0—2% ammonia (500 ml) gradiently. The eluate, on evaporation to dryness and subsequent crystallization from dil formic acid, gave colorless needles (200 mg) of the 6-(2-pteridinylamino)hexanamide (**6a**), mp 212—215 °C dec (from water) (Found: C, 52.07; H, 6.88; N, 26.01%. Calcd for $C_{14}H_{20}N_6O_2 \cdot H_2O$: C, 52.16; H, 6.88; N, 26.07%).

Method B: Ethyl chloroformate (50 mg) was added to a solution of **3a** (125 mg) and triethylamine (100 mg) in *N,N*-dimethylformamide (1 ml) at −5 °C. After stirring for 15 min, butylamine (75 mg) was added to the solution. The mixture was stirred at −5 °C for 30 min and then at 25 °C for 1 h. Evaporation of the solution *in vacuo* gave an oily residue, which was chromatographed on a Florisil column (1×20 cm) eluted by 20% aqueous acetone containing 2% ammonia. The eluate was evaporated to dryness and the residue was extracted with ethanol (50 ml). Concentration of the extract to about 5 ml and chilling gave pale yellow

needles (47 mg) of the *N*-butyl-6-(2-pteridinylamino)hexanamide (**6b**), which decomposed above 150 °C (from 90% ethanol) (Found: C, 57.21; H, 7.53; N, 22.04%. Calcd for $C_{18}H_{28}N_6O_2 \cdot H_2O$: C, 57.11; H, 7.99; N, 22.21%).

The authors would like to thank Mrs. Noriko Nishioka for the measurement of pK_a values and UV spectra.

References

1) Part I: T. Sugimoto and S. Matsuura, *Bull. Chem. Soc. Jpn.*, **52**, 181 (1979).
2) E. L. Patterson, H. P. Broquist, A. M. Albrecht, M. H. von Saltza, and E. L. R. Stokstad, *J. Am. Chem. Soc.*, **77**, 3167 (1955).
3) E. L. Patterson, R. Milstrey, and E. L. R. Stokstad, *J. Am. Chem. Soc.*, **78**, 5868 (1956).
4) S. Kaufmann, *Pharmacol. Rev.*, **18**, 61 (1966).
5) A. R. Brenneman and S. Kaufmann, *Biochem. Biophys. Res. Commun.*, **17**, 177 (1964).
6) Y. Numata, T. Kato, T. Nagatsu, T. Sugimoto, and S. Matsuura, *Biochem. Biophys. Acta*, **480**, 104 (1977).
7) T. Nukiwa, C. Tohyama, C. Okita, T. Takaoka, and A. Ichiyama, *Biochem. Biophys. Res. Commun.*, **60**, 1029 (1974).
8) T. Nagatsu, K. Mizutani, I. Nagatsu, S. Matsuura, and T. Sugimoto, *Biochem. Pharmacol.*, **21**, 1945 (1972).
9) Y. Numata, K. Ikuta, T. Kato, T. Nagatsu, T. Sugimoto, and S. Matsuura, *Biochem. Pharmacol.*, **24**, 1998 (1975).
10) R. M. Cresswell and T. Straus, *J. Org. Chem.*, **28**, 2563 (1963).
11) B. Roth, J. M. Smith, Jr., and M. E. Hultquist, *J. Am. Chem. Soc.*, **73**, 2864 (1951).
12) W. V. Curran and R. B. Angier, *J. Am. Chem. Soc.*, **80**, 6095 (1958).
13) T. Sugimoto and S. Matsuura, *Bull. Chem. Soc. Jpn.*, **48**, 3767 (1975).
14) A. Albert and E. P. Serjeant, "Ionization Constants of Acids and Bases," Methuen, London (1962).
15) A. Albert, *J. Biochem.*, **47**, 531 (1950).
16) B. F. Erlanger, F. Borek, S. M. Beiser, and S. Lieberman, *J. Biol. Chem.*, **228**, 713 (1957) and **234**, 1090 (1959).
17) C. O. Johns and E. J. Baumann, *J. Biol. Chem.*, **14**, 381 (1913).

Asymmetric Transformation of Alanine *via* Optically Labile Imidazolines

Saizo SHIBATA,* Hajime MATSUSHITA, Kunio KATO, Masao NOGUCHI, Masahiko SABURI,** and Sadao YOSHIKAWA**

Central Research Institute, The Japan Tobacco and Salt Public Corporation, 6-2 Umegaoka, Midori-ku, Yokohama, Kanagawa 227

***Department of Synthetic Chemistry, Faculty of Engineering, The University of Tokyo, Hongo, Bunkyo-ku, Tokyo 113*

(Received February 14, 1979)

Hydrolysis of an imidazoline derived from (*S*)-alanine and (*S*)-2-(aminomethyl)pyrrolidine afforded (*R*)-alanine in the optical yield of 93.8% (e.e.). The asymmetric transformation was explained on the basis of preferential crystallization of one epimer followed by epimerization of the other epimer in a solution. It was found that the epimerization was catalyzed by amines. (2*S*)-*N*-isopropyl-2-aminopropylamine was also examined as a diamine component of imidazolines.

In an ideal and complete optical resolution, a racemic compound would be separated into 50% of each enantiomer. On the other hand, an asymmetric transformation is a unique method to obtain optically active compounds because it is possible to convert a racemic compound into one of the isomerides in 100% yield. Optically labile compounds are suitable for the asymmetric transformation and it has been reported by many workers.[1] On the other hand, optically stable compounds are not suitable for the transformation, and conversion of the compounds into the optically labile intermediates is indispensable. From this point of view, amino acids, aldehydes, and ketones have been studied in our laboratories.[2]

We also studied on the asymmetric transformation of carboxylic acids. It was reported by Yonetani *et al.* that imidazoline derivatives of amino acids are racemized easily.[3] The asymmetric transformation of α-substituted carboxylic acids might be possible using the optical lability of the derivatives in an asymmetrical circumstance. The *N*-protected alanine was used as a model of the carboxylic acid. (*S*)-2-(Aminomethyl)-pyrrolidine and (2*S*)-*N*-isopropyl-2-aminopropylamine were used as chiral diamine components to prepare the imidazoline derivatives.

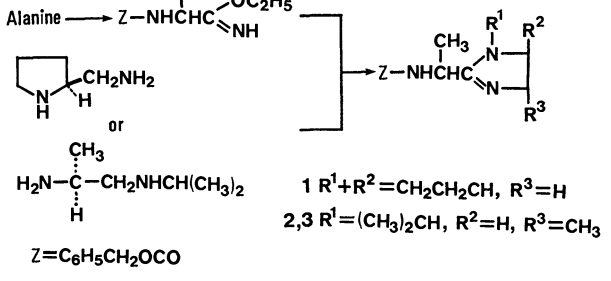

Experimental

Optical activities were determined with a JASCO Digital Automatic Polarimeter Model DIP 4. Nuclear magnetic resonance spectra were obtained with a JNM-PS-100 Spectrometer with tetramethylsilane as an internal standard. Accurate mass determinations were carried out on a Hitachi RMU-7 instrument operated at 70 eV.

(S)-(+)-2-(Aminomethyl)pyrrolidine. This compound was prepared as reported previously:[4] bp 72.5—74 °C/2933 Pa; (lit, bp 65 °C/1466 Pa).

(2S)-(+)-N-Isopropyl-2-aminopropylamine. (*S*)-Alanine (60 g, 0.67 mol) was converted to (*S*)-*N*-phthaloylalanyl chloride by the method described by Job and Bruice:[5] bp 149—154 °C/400 Pa; yield 125.7 g (79%). Isopropylamine (34.3 g, 0.58 mol) and sodium hydrogencarbonate (53.6 g, 0.64 mol) were dissolved in 426 ml of water and the solution was cooled in an ice bath to 10 °C. To this solution, a solution of (*S*)-*N*-phthaloylalanyl chloride (125.7 g, 0.53 mol) in dioxane (193 ml) was added dropwise with vigorous stirring. After the addition had been completed, the white precipitates thus formed were collected by filtration and washed with water. Recrystallization of the crude product from methanol gave *N*-isopropylamide of (*S*)-*N*-phthaloylalanine (55.1 g, 0.21 mol). Removal of the phthaloyl group from *N*-isopropylamine of (*S*)-*N*-phthaloylalanine (55.1 g, 0.21 mol) by equimolar hydrazine hydrate gave (*S*)-*N*-isopropylalaninamide (*ca.* 0.2 mol). (*S*)-*N*-Isopropylalaninamide (*ca.* 0.2 mol) was reduced by lithium aluminium hydride in tetrahydrofuran (reflux 15 h). After the usual treatment, (2*S*)-*N*-isopropyl-2-aminopropylamine was obtained by fractional distillation: bp 144—146 °C (13.5 g, 0.116 mol, 17.3% yield based on (*S*)-alanine); $[\alpha]_D^{20}$ +22.2° (neat); MS *m/e* 116.1296 (M^+, $C_6H_{16}N_2$; calcd 116.1313); IR (Nujol) 1370 and 1380 cm^{-1}($CH(CH_3)_2$);NMR ($CDCl_3$) δ=1.07 (N–C–CH_3, *d*) and 1.07 ppm (N–C–$(CH_3)_2$, *d*).

(−)-Ethyl (S)-2-(Benzyloxycarbonylamino)propioimidate. Preparation of this compound was previously reported:[6] mp 72.5—74 °C; $[\alpha]_D^{25}$ −1.3° (*c* 12.65, 99.5% ethanol); (lit, mp 71.5—73.0 °C; $[\alpha]_D^{24}$ −1.4° (*c* 12.65, anhydrous ethanol)).

(+)-Ethyl (R)-2-(Benzyloxycarbonylamino)propioimidate. This compound was prepared from (*R*)-alanine by the same method described for the preparation of (−)-ethyl (*S*)-2-(benzyloxycarbonylamino)propioimidate:[6] mp 72.5—74 °C; $[\alpha]_D^{23}$ +1.3° (*c* 12.65, 99.5% ethanol); MS *m/e* 250.1306 (M^+, $C_{13}H_{18}N_2O_3$; calcd 250.1316); IR (Nujol) 1645 (C=N) and 1710 cm^{-1} (C=O); NMR ($CDCl_3$) δ=7.27 (phenyl, s), 5.08 (phenyl–CH_2–O, s), 1.35 (N–C–CH_3, d) and 1.29 ppm (O–C–CH_3, t).

Preparation of Imidazolines. Imidazoline derivatives of alanines were prepared by the coupling method described by Hirotsu *et al.*[6]

Imidazoline Derivative (1): The reaction of (*S*)-2-(aminomethyl)pyrrolidine and the (*S*)- or the (*R*)-imidate mentioned above gave the imidazoline derivative (**1**). Preparation from the (*S*)-imidate: Yield 86%; mp 86—87.5 °C; $[\alpha]_D^{23}$ −94.1° (*c* 1.0, methanol); MS *m/e* 287.1634 (M^+, $C_{16}H_{21}N_3O_2$, calcd 287.1633); IR (Nujol) 1620 (C=N) and 1710 cm^{-1} (C=O);

Table 1. Configuration and optical purity of alanine residues of imidazoline derivatives

Diamine component	Config. of starting alanine	Imidazoline	Alanine obtained after hydrolysis[a]		
			Config.	e.e. (%)	Yield (%)
(*S*)-2-(Aminomethyl)pyrrolidine	*S*	**1**	*R*	93.8	89.2[b]
	R	**1**	*R*	93.2	90.1
(2*S*)-*N*-Isopropyl-2-aminopropylamine	*S*	**2**	*S*	91.9	5.6
	R	**3**	*R*	91.8	4.3

a) Configuration, optical purity, and yield were determined according to the DNP-method after hydrolysis of imidazoline derivatives.[3] b) Based on imidazoline.

NMR ($CDCl_3$) $\delta=1.40$ (N=C–C–CH_3, d) and 5.05 ppm (phenyl-CH_2–O, s). Preparation from the (*R*)-imidate: Yield 75%; mp 86—87.5 °C; $[\alpha]_D^{23}$ −94.9° (*c* 1.0, methanol); MS *m/e* 287.1643 (M^+, $C_{16}H_{21}N_3O_2$, calcd 287.1633); IR (Nujol) 1620 (C=N) and 1710 cm^{-1} (C=O); NMR ($CDCl_3$) $\delta=1.40$ (N=C–C–CH_3, d) and 5.05 ppm (phenyl–CH_2–O, s).

Imidazoline Derivative (2): This compound was prepared from (2*S*)-*N*-isopropyl-2-aminopropylamine and the (*S*)-imidate: Yield 57%; mp 71.5—73 °C; $[\alpha]_D^{23}$ −57.9° (*c* 1.0 methanol); MS *m/e* 303.1930 (M^+, $C_{17}H_{25}N_3O_2$, calcd 303.1945); IR (Nujol) 1610 (C=N) and 1710 cm^{-1} (C=O); NMR ($CDCl_3$) $\delta=1.38$ (N=C–C–CH_3, d) and 5.03 ppm (phenyl–CH_2–O, s).

Imidazoline Derivative (3): This compound was prepared from (2*S*)-*N*-isopropyl-2-aminopropylamine and the (*R*)-imidate: Yield 64%; mp 120—122.5 °C; $[\alpha]_D^{23}$ −36.2° (*c* 1.0, methanol); MS *m/e* 303.1955 (M^+, $C_{17}H_{25}N_3O_2$, calcd 303.1945); IR (Nujol) 1600 (C=N) and 1695 cm^{-1} (C=O); NMR ($CDCl_3$) $\delta=1.37$ (N=C–C–CH_3, d) and 5.08 ppm (phenyl–CH_2–O, s).

Determination of the Optical Purity and the Configuration of the Alanine after the Asymmetric Transformation. The configuration and the optical purity of the alanine residues of the imidazoline derivatives were determined as DNP-alanine (DNP; 2,4-dinitrophenyl) prepared after hydrolysis of the derivatives according to the method described by Yonetani *et al.*[3] (hydrolysis conditions: 6 M HCl, 110 °C, 20 h). The specific optical rotation of the prepared DNP-alanine was observed at 546 nm and the concentration of the solution was calculated from the extinction coefficient at 360 nm; authentic DNP-(*S*)-alanine: $[\alpha]_{546}^{32}$ +221° (*c* 0.22, 1% $NaHCO_3$); $\lambda_{max}^{1\%\ NaHCO_3}$ 360 nm ($\varepsilon=1.72\times10^4$).

Results and Discussion

Imidazoline derivatives prepared from (*S*)-2-(aminomethyl)pyrrolidine and the imidates derived from (*S*)-alanine and (*R*)-alanine have the same crystal habit (platelets) and melting point, and showed identical spectral data. The hydrolysis of these imidazoline derivatives gave (*R*)-alanine (Table 1). These facts indicate that the bond between α-carbon and hydrogen is labile enough to epimerize in the course of the preparation. (Hereafter the imidazoline was called **1**).

High optical yield (93.8 or 93.2%) of alanine obtained in the case of **1** was considered to be due to a combination of epimerization and resolution by preferential crystallization of one diastereomer. In order to clarify the resolution process, optical purity of alanine residue of **1** in the reaction mixture was examined. Two batches of a reaction mixture of **1** were examined. After removal of the solvent from the reaction mixture under reduced pressure, the oily residue was directly hydrolyzed in one

Table 2. Configuration and optical purity of alanine obtained by the hydrolysis of the reaction mixture of **1** before and after crystallization

	Alanine obtained after hydrolysis[a]		
	Config.	e.e. (%)	Yield (%)
Oily mixture	*R*	35.1	84.1[b]
Crystallized crude mixture	*R*	63.5	87.0

a) Configuration, optical purity, and yield were determined according to the DNP-method after hydrolysis of imidazoline.[3] b) Based on imidate

experiment. In another experiment, the oily residue was allowed to stand at room temperature for 12 h. The crystallized crude mixture was then subjected to hydrolysis without any purification, and the configuration and the optical yields of the resultant alanine were determined. The results are shown in Table 2. The optical yield (35.1%) of the alanine obtained from the oily mixture was the same as that obtained from the hydrolyzate of the imidazoline derivatives after the mutarotation in methanol (*vide infra*). Since no purification was performed in both cases, the difference between the oily mixture and the crystallized mixture is attributable to the epimerization promoted by the preferential crystallization of one diastereomer out of the liquid phase in which a rapid equilibration is maintained.

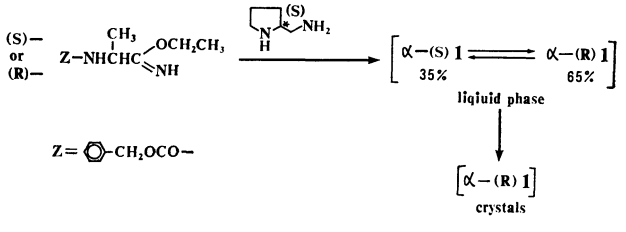

It is required for this mechanism that the rate of epimerization is fast enough. The rates of epimerization of **1** in several solvents (methanol, ethanol, benzene, and dichloromethane) were observed (Fig. 1). It was fast in methanol or ethanol but the epimerization was not detected in the aprotic solvents. A mixture of dichloromethane and ethanol (equimolar quantities with **1**) was examined as a solvent because, in the course of coupling reaction of ethyl (*S*)- or (*R*)-2-(benzyloxycarbonylamino)propioimidate with (*S*)-2-(aminomethyl)pyrrolidine in dichloromethane, ethanol in amounts equimolar to **1** is to be produced. No epimerization

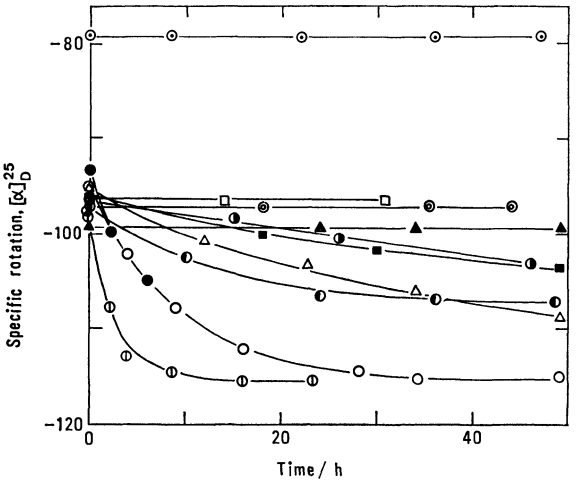

Fig. 1. Mutarotation of **1**.
○: Methanol, △: ethanol, ⊙: benzene, ▲: dichloromethane, □: ethanol (1 molar equivalent) in dichloromethane, ◎: ethanol (5 molar equivalents) and triethylamine (0.5 molar equivalents) in dichloromethane, ●: the reaction mixture of **1**, ◑: pyrrolidine (5.7 molar equivalents) in dichloromethane, ◐: propylamine (5.7 molar equivalents) in dichloromethane, ◑: *N*-methylpyrrolidine (5.7 molar equivalents) in dichloromethane, ■: quinuclidine (5.7 molar equivalents) in dichloromethane.

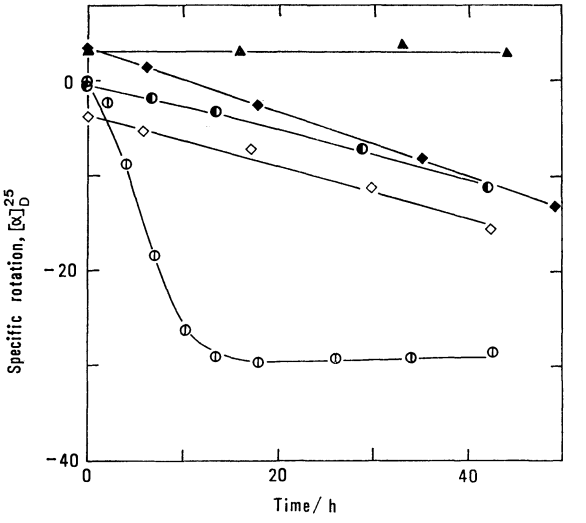

Fig. 2. Mutarotation of **2**.
◐: Propylamine (5.7 molar equivalents) in dichloromethane, ◆: dipropylamine (5.7 molar equivalents) in dichloromethane, ◇: *N*-isopropylethylenediamine (5.7 molar equivalents) in dichloromethane, ◑: pyrrolidine (5.7 molar equivalents) in dichloromethane, ▲: dichloro methane.

could be observed under such circumstance. An increase in the content of ethanol and an addition of some triethylamine in dichloromethane was also examined. As shown in the figure, no epimerization was observed. On the other hand, when the crystalline imidazoline **1** was dissolved in the crude reaction mixture of imidazoline, which contains an excess amount of (*S*)-2-(aminomethyl)pyrrolidine, an appreciable epimerization was observed. The rate was as fast as that in methanol. This suggested that (*S*)-2-(aminomethyl)pyrrolidine catalyzes this epimerization. Accordingly, the rate of epimerization in a dichloromethane solution containing (*S*)-2-(aminomethyl)pyrrolidine was studied, and it is observed that the rate was fairly fast. There are a pyrrolidine ring moiety and a primary amine group in (*S*)-2-(aminomethyl)-pyrrolidine. In order to reveal the effect of the nature of amines on the ability of acceleration of the rate, the rates in dichloromethane solutions each containing propylamine, pyrrolidine, *N*-methylpyrrolidine and quinuclidine are examined. The acceleration of the rate of epimerization was found to be in the order of pyrrolidine (cyclic secondary amine)>propylamine (acyclic primary amine)>*N*-methylpyrrolidine and quinuclidine (tertiary amine). The small effect of tertiary amine on the acceleration of the rate suggests that this catalytic action of amines does not depend only on the basicity of amines.

Imidazoline derivatives **2** and **3** were prepared from (2*S*)-*N*-isopropyl-2-aminopropylamine and the imidates derived from (*S*)-alanine and (*R*)-alanine respectively. The imidazoline derivative **2** was isolated as longitudinal crystals by recrystallization from petroleum ether and **3** was isolated as fine needles by recrystallization from acetone–petroleum ether. The physical data of these imidazoline derivatives were apparently different. Hydrolysis of **2** and **3** gave the starting alanines, (*S*) and (*R*) respectively, both with high optical purity (Table 1). It is considered that the epimerizations of both diastereomers **2** and **3** are rather slow. Epimerization of **2** was examined and the results are shown in Fig. 2. The results indicate that the rate of epimerization promoted by primary or acyclic secondary amine was far slower than pyrrolidine. Since the rate of crystallization of **2** or **3** seemed to be similar to that of **1**, the failure of asymmetric transformation in the case of **2** or **3** may be attributed to the slow epimerization. This fact suggests that the efficient catalytic action of (*S*)-2-(aminomethyl)pyrrolidine was attributed to the pyrrolidine moiety and does not due to the chelate effect of the diamine.

It is explicable that the alanine was obtained in low yield by the hydrolysis of **2** and **3**. The existence of an isopropyl group on nitrogen atom in diamine moiety is common to these imidazolines. The difficulty of the hydrolysis is explained on the basis of the steric hindrance of this isopropyl group. Similar description was given in the case of hydrolysis of proteins containing valine or isoleucine residue.[7]

It was revealed that the epimerization of the imidazoline derivatives were efficiently catalyzed by pyrrolidine. The asymmetric transformation of **2** was attempted using pyrrolidine. The imidazoline **2** (53 mg) was dissolved in the dichloromethane solution containing pyrrolidine (5.7 molar equivalent). After 24 h the solvent was removed under reduced pressure. Because the excess pyrrolidine prevented the crystallization, the residue was dissolved in dichloromethane and washed with water to remove the pyrrolidine. The dichloro-

methane layer was dried and evaporated under reduced pressure, and the residue was recrystallized from acetone–petroleum ether to give 23 mg of crystals in the form of fine needles. The melting point (111—115°) and IR spectrum of the crystals were almost identical with those of **3**. It showed that the asymmetric transformation from **2** to **3** occured by the catalytic action of pyrrolidine. The low yield of **3** based on **2** was considered the removal of the pyrrolidine interrupted the epimerization during crystallization.

References

1) M. M. Harris, "Progress in Stereochemistry," ed by W. Klyne and P. B. D. Mare, Buntterworths Scientific Publications, London (1958), Vol. 2, p. 157.

2) M. Saburi and S. Yoshikawa, *Kagakusosetsu*, **13**, 109 (1976); H. Matsushita, Y. Tsujino, M. Noguchi, and S. Yoshikawa, *Bull. Chem. Soc. Jpn.*, **49**, 3629 (1976); H. Matsushita, Y. Tsujino, M. Noguchi, M. Saburi, and S. Yoshikawa, *Bull. Chem. Soc. Jpn.*, **51**, 862 (1978).

3) K. Yonetani, Y. Hirotsu, and T. Shiba, *Bull. Chem. Soc. Jpn.*, **48**, 3302 (1975).

4) S. Schnell and P. Karrer, *Helv. Chim. Acta*, **38**, 2036 (1955).

5) R. C. Job and T. C. Bruice, *J. Am. Chem. Soc.*, **96**, 809 (1974).

6) Y. Hirotsu, T. Shiba, and T. Kaneko, *Bull. Chem. Soc. Jpn.*, **40**, 2945 (1967).

7) R. Takahashi, "Seikagaku Jikkenkoza," Tokyokagakudojin, Tokyo (1976), Vol. 1, II, p. 30.

An Examination of the Displacement Reactions in Alkyldicyclohexylborane and Alkyldi-exo-norbornylborane

Hiroaki TANIGUCHI*

Richard B. Wetherill Laboratory, Purdue University West Lafayette, Indiana 47907, USA

(Received February 20, 1979)

Displacements involving the reaction of olefins with alkyldicyclohexylborane and alkyldi-*exo*-norbornylborane were studied. In the case of alkyldicyclohexylborane, the 1-ethylbutyl group could be displaced selectively by 1-decene to produce hexenes. However, the hexyl group could not be displaced selectively, the reaction proceeding to produce both 1-hexene and cyclohexene. In contrast, in the case of alkyldi-*exo*-norbornylborane, the norbornyl group bonded so tightly to the boron atom that it was possible to displace both the 1-ethylbutyl and the hexyl groups selectively and completely by 1-decene with no loss of 2-norbornyl–boron bonds. The results suggest the possibility of contrathermodynamic isomerization of olefins by the combination of "isomerization-displacement" with di-*exo*-norbornylborane.

Organoboranes undergo displacement of contained olefins when they are heated in the presence of another olefin.[1-4]

$$(RCH_2CH_2)_3B + 3R'CH{=}CH_2 \rightleftharpoons 3RCH{=}CH_2\uparrow + (R'CH_2CH_2)_3B$$

Detailed studies of this reaction have been published by Brown and his coworkers using homogeneous trialkyl- or dialkylboranes (R_3B or R_2BH).[5,6]

The displacement reaction is a reversible reaction and can be brought to completion by using an excess of olefin or by removing the displaced olefin from the reaction media by distillation.

The rate of the displacement reaction is essentially independent of the concentration of the displacing olefin.

The rate of displacement varies with the type and structure of the olefin bonded to boron atom.

Results and Discussion

In this study, the displacement reaction involving the organoboranes derived from the hydroboration of several types of olefins with dicyclohexylborane and di-*exo*-norbornylborane has been examined. It was thought to be interest to clarify the displacement reaction with organoboranes which have more than one alkyl group in a molecule in order to confirm which alkyl group is more easily displaced. Such a study would establish the conditions under which only one attached alkyl group could be selectively displaced, making it possible to use repeatedly a particular dialkylboryl unit, such as dicyclohexylboryl- or di-*exo*-norbornyl-boryl-group.

In studying the displacement reaction, it was very difficult to follow on a small scale the reaction process quantitatively by determining the amounts of olefin displaced.

An alternative procedure was adopted. Aliquots of the reaction mixture were removed and oxidized and the decreasing or increasing amounts of alcohols determined by glpc analysis were taken as a measure of the displacement reaction. The following standard procedure was utilized.

A three-necked flask fitted with a thermometer and a side arm closed by rubber septum was attached to a microdistillation system. The olefins were hydroborated using dicyclohexylborane or di-*exo*-norbornylborane, which had been prepared from cyclohexene or norbornene in THF solvent and used *in situ*. Hydroboration was carried out in diglyme or triglyme solution. After the completion of the hydroboration, all THF was removed by vacuum evaporation. Then a 100% excess of 1-decene and calculated amount of the internal standard were added to the reaction mixture. The mixture was rapidly heated to the desired temperature. At appropriate intervals of time, aliquots were withdrawn from the reaction flask and oxidized with alkaline hydrogen peroxide. Alcohols thus produced were taken up in ether and the dried ether extract was analyzed by NMR. The ratio of the original alkyl groups displaced from the organoborane was calculated from the decreasing amount of alcohols found in each aliquot.

During the course of reaction, the displaced olefins were removed from the distillation system into a cooled receiver and the distillate was analyzed by GLPC. A static nitrogen atmosphere was maintained throughout the reaction.

Displacements Involving Hexyldicyclohexylboranes. The displacement reaction with hexyldicyclohexylborane was carried out at different temperatures in the hope that only the hexyl group would be displaced by 1-decene so that the dicyclohexylborane moiety could be used repeatedly. However, it was found that the cyclohexyl group was readily eliminated to generate cyclohexene so that it was not practical to remove the hexyl group selectively. The results are given in Table 1. We see that the hexyl moiety of hexyldicyclohexylborane is displaced a little more easily than cyclohexyl moiety. However, the difference in the rate of displacement is too small to displace only the hexyl group. Both the hexyl and the cyclohexyl groups are displaced almost completely under these conditions and analysis of the decanols by GLPC established that there is no significant loss of boron–hydrogen bond in the process.

The purity of displaced hexene is much more selective at higher temperature than at lower temperature. This indicates that at lower temperature the displacement rate of the hexyl group is low. Consequently, some of

* On leave of absence from the Research Center, Maruzen Oil Co., Ltd. Present address: Research Center of Maruzen Oil Co., Ltd., Satte-cho, Kitakatsushika-gun, Saitama 340-01.

Table 1. Displacement reaction with hexyldicyclohexylborane[a)]

Reaction temp	Displaced ratio of original alkyl group			
	160 °C		130 °C	
Reaction time/h	Hexyl %	Cyclohexyl %	Hexyl %	Cyclohexyl %
0	0	0		
0.5	37	14	0	0
1	60	38	0	0
2	76	44	17	0
4	89	62	54	24
6	93	78	63	33
8	97	85	65	33
24	100	99	83	68
48			93	86
72			100	94

	Distilled olefins			
	Hexene %	Cyclohexene %	Hexene %	Cyclohexene %
1-Hexene	94.3	100	73.5	100
trans-2-Hexene	0.7		1.3	
cis-2-Hexene	3.9		22.6	
3-Hexene	1.1		2.6	

a) Initial charge: hexyldicyclohexylborane 10 mmol, 1-decene 60 mmol, solvent (diglyme or triglyme) 10 ml, internal standard (tridecane) 5 mmol.

Table 2. Displacement reaction with 1-ethylbutyldicyclohexylborane[a)]

Reaction temp	Displaced ratio of original alkyl group			
	160 °C		130 °C	
Reaction time/h	1-Ethylbutyl %	Cyclohexyl %	1-Ethylbutyl %	Cyclohexyl %
0	0	0		
0.5	98	24	81	0
1	98	52	94	0
2	98	65	98	11
4	98	85	98	31
6	99	92	98	45
8	99	96	97	49
24	100	99	99	79
48			99	92
72			100	98

	Distilled olefins			
	Hexene %	Cyclohexene %	Hexene %	Cyclohexene %
1-Hexene	0.1	100	0.1	100
cis-2-Hexene	42.8		57.3	
trans-2-Hexene	57.1		42.6	
3-Hexene				

a) Initial charge: 1-ethylbutyldicyclohexylborane 10 mmol, 1-decene 60 mmol, solvent (triglyme) 10 ml, internal standard (tridecane) 4.83, 5.33 mmol

the hexyldicyclohexylborane is isomerized to the isomeric *sec*-hexyldicyclohexylborane and the *sec*-hexyl groups thus formed are much more easily eliminated from the boron atom than the hexyl group. The relationship is illustrated as follows:

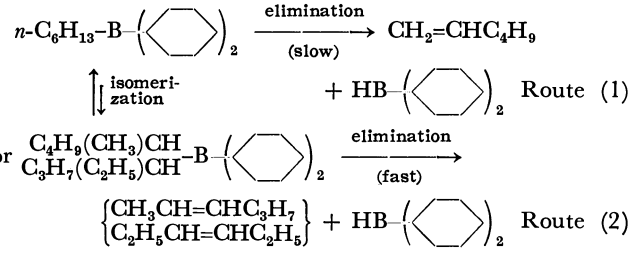

At lower temperature, Route 1 is so slow that Route 2 would play an important role.

$C_3H_7(C_2H_5)CH$–B–(cyclo-$C_6H_{11})_2$: It has been established that the secondary alkyl group is displaced much more easily than the normal alkyl group.[6] The displacement reaction with 1-ethylbutyldicyclohexylborane was undertaken in order to compare the displacement rate of the secondary alkyl group with that of the cyclohexyl group. The results are given in Table 2. We see that it is possible to displace the 1-ethylbutyl group selectively. The best results were obtained under the conditions 130 °C for 1—1.5 h in triglyme solvent, more than 94% of the 1-ethylbutyl group being displaced by 1-decene with negligible loss of the cyclohexyl group.

The concentration of 1-hexene in the displaced olefins was very low although under these conditions some isomerization of 1-ethylbutyldicyclohexylborane to hexyldicyclohexylborane would have been expected. The reason must be that the elimination of 1-ethylbutyl group is relatively fast and the dissociated internal hexenes fail to associate again with the dicyclohexylborane because of the faster reason with 1-decene. This behavior is different from that observed in the case of hexyldicyclohexylborane in which only a little of 2- and 3-hexenes were present in the distilled hexenes.

There is a considerable difference in the distribution of the displaced hexenes at different temperatures.

n-*C_6H_{13}–B–(cyclo-$C_6H_{11})_2$*. *Under Neat Conditions*: The displacement reaction with hexyldicyclohexylborane under neat conditions was carried out in the hope that the rate of elimination of the cyclohexyl group would be much smaller in the absence of etheric solvent so that the selective displacement of the hexyl group would be possible. The results are summarized in Table 3 and compared with those of the displacement reaction in diglyme.

It was unexpected that the absence of the etheric solvent failed to decelerate the rate of the displacement reaction (Table 3). It was impossible to displace only the hexyl group under the conditions of a neat reaction.

Cyclopentyldicyclohexylborane. In order to examine which group, cyclopentyl- or cyclohexyl-, is more easily eliminated from the mixed organoborane, the displacement reaction with cyclopentyldicyclohexylborane was

TABLE 3. EFFECT OF SOLVENT IN THE DISPLACEMENT REACTION WITH HEXYLDICYCLOHEXYLBORANE[a] AT 160 °C

Solvent	Displaced ratio of original alkyl group			
	Neat		Diglyme 10 ml	
Reaction time/h	Hexyl %	Cyclohexyl %	Hexyl %	Cyclohexyl %
0	0	0		
0.5	40	26	37	14
1	55	41	60	38
2	62	43	76	44
4	88	61	89	62
6	95	84	93	78
8	97	91	97	85
24	100	99	100	99

Distilled olefin					
Hexene %		Cyclohexene %	Hexene %		Cyclohexene %
1-Hexene	86.9	100	1-Hexene	94.3	100
trans-2-Hexene	1.1		*trans*-2-Hexene	0.7	
cis-2-Hexene	9.9		*cis*-2-Hexene	3.9	
3-Hexene	2.1		3-Hexene	1.1	

a) Initial charge: hexyldicyclohexylborane 10 mmol, 1-decene 60 mmol, solvent neat or diglyme, internal standard (tridecane) 5.0 mmol.

TABLE 4. DISPLACEMENT REACTION WITH CYCLOPENTYLDICYCLOHEXYLBORANE AT 160 °C

Reaction time/h	Displaced ratio of original alkyl group	
	Cyclopentyl	Cyclohexyl
0	0	0
0.5	62	23
1	87	46
2	97	65
4	99	84
6	99	91
8	100	96
24	100	100

a) Initial charge: cyclopentyldicyclohexylborane 10 mmol, 1-decene 60 mmol, solvent (triglyme) 10 ml, internal standard (dodecane) 5.5 mmol.

undertaken. The cyclopentyl group is displaced at approximately twice the rate of the cyclohexyl group (Table 4).

Displacement Reaction with Alkyldi-exo-*norbornylborane.* The norbornyl group is so tightly bound to a boron atom that is not displaced by 1-decene under the same conditions as at which displacement of other olefins could proceed.[6] Thus, it was anticipated that treatment of hexyldi-*exo*-norbornylborane with 1-decene might result in selective elimination of the hexyl group. Difficulty in testing this procedure is caused by the relative unavailability of pure dinorbornylborane which cannot be synthesized directly from norbornene and BH_3.[7] Thus crude (71%) di-*exo*-norbornylborane, which can be prepared directly from BH_3 and norbornene, was used.

The best conditions for preparing di-*exo*-norbornylborane directly are as follows. A norbornene solution in THF is added to a BH_3–THF solution in the ratio (norbornene/BH_3)=2.0 at 0 °C and the mixture is stirred at 0 °C for 1 h. On completion of the process, the mixture contained 71% di-*exo*-norbornylborane, 13% tri-*exo*-norbornylborane, 16% BH_3, but no mono-*exo*-norbornylborane.

It might be possible to determine the relative elimination rate of the norbornyl group and other alkyl groups from the data obtained by using the crude di-*exo*-norbornylborane.

TABLE 5. DISPLACEMENT REACTION WITH HEXYLDI-*exo*-NORBORNYLBORANE AND 1-ETHYLBUTYLDI-*exo*-NORBORNYLBORANE[a] AT 160 °C

Raw material	Displaced ratio of original alkyl group			
	Hexyldi-*exo*-norbornylborane		1-Ethylbutyldi-*exo*-norbornylborane	
Reaction time/h	Hexyl %	Norbornyl %	1-Ethylbutyl %	Norbonyl %
0	0	0	0	0
0.5	13	0	96	0
1	28	0	96	0
2	47	0	97	0
4	77	0	96	0
6	86	0	97	9
8	90	2.3	98	11
24	98	21	100	21

Distilled olefins					
Hexene %		Norbornene %	Hexene %		Norbornene %
1-Hexene	95.7	100	1-Hexene	0.1	100
2-Hexenes, 3-Hexene	4.3		*cis*-2-Hexene	41.3	
			trans-2-Hexene, 3-Hexene	58.6	

a) Initial charge: raw material 10 mmol, 1-decene 60 mmol, solvent (triglyme) 10 ml, internal standard (tridecane) 5.1 mmol.

Hexyldi-exo-*norbornylborane and 1-Ethylbutyldi*-exo-*norbornylborane.* Displacement reaction with hexyldi-*exo*-norbornylborane and 1-ethylbutyldi-*exo*-norbornylborane were carried out to see whether selective displacement of hexyl group is possible in these derivatives (Table 5). It was confirmed that selective displacement of the hexyl group is possible. For example, 90% of the hexyl group was removed with only 2% loss of the norbornyl group by the displacement reaction with hexyldi-*exo*-norbornylborane at 160 °C for 8 h. Even more favorable conditions would be found for complete selective displacement in hexyldi-*exo*-norbornylborane by working at lower temperatures. The results indicate

Table 6. Displacement reaction with cyclohexyldi-*exo*-norbornylborane[a] at 160 °C

Reaction time/h	Displaced ratio of original alkyl group	
	Cyclohexyl %	Norbornyl %
0	0	0
0.5	28	0
1	47	0
2	63	0
4	85	1.7
6	94	14
8	97	11.5

a) Initial charge: cyclohexyldi-*exo*-norbornylborane 10 mmol, 1-decene 60 mmol, solvent (triglyme) 10 ml, internal standard (tridecane) 5.29 mmol.

that the norbornyl group can be eliminated by 1-decene under severe conditions. It was found by means of GLPC analysis of the distilled olefins after 24 h reaction that norbornene is present in a large amount.

Cyclohexyldi-exo-*norbornylborane*. The displacement reaction with cyclohexyldi-*exo*-norbornylborane was carried out to make clear the relative rate of displacement by 1-decene of the cyclohexyl group and the norbornyl group (Table 6). It is evident that the cyclohexyl group can be displaced selectively by 1-decene from cyclohexyldi-*exo*-norbornylborane.

Di-*exo*-norbornylborane is an excellent agent for the contrathermodynamic isomerization of olefin.[8] The isomerization rate was almost the same as that of dicyclohexylborane, the selectivity of the primary position being a little better. It was found that di-*exo*-norbornylborane is an excellent agent for a selective displacement reaction, much better results being expected by using pure di-*exo*-norbornylborane which could be synthesized by indirect methods.

Di-*exo*-norbornylborane is an excellent agent for achieving the movement of a double bond from the interior of a carbon chain to the terminal position of olefins *via* hydroboration-isomerization displacement.

Experimental

Materials. The solvents, olefins and preparation of the BH_3–THF solution have been described.[6] Norbornene (reagent grade, Aldrich Chemical Co.) was used without further purification and stored under nitrogen as a THF solution in a volumetric flask. 1-Decene (Chem Samples Co.) was distilled from lithium aluminum hydride and stored under nitrogen.

Hydroboration-Displacement Experiments. Alkyldicyclohexylborane: After all systems were dried and flushed with nitrogen, 4 ml (10.8 mmol) of BH_3–THF solution (2.70 M) and 10 ml of solvent (diglyme or triglyme) were placed in a 50 ml three-necked flask fitted with a thermometer, a side arm containing a rubber septum and a distillation system, consisting of a Vigreaux column ($2\phi \times 13$ 1 cm), a distillation head, a Liebig condenser, and a receiver which can be cooled in an ice bath, the top of which is connected to a Hg bubbler to maintain a static pressure of nitrogen gas. 2.10 ml (21 mmol) of cyclohexane was added slowly at 0 °C by means of a hypodermic syringe. After addition, the ice bath was removed and the mixture was stirred at room temperature for 2 h. The dicyclohexylborane thus prepared was used *in situ* in subsequent processes.

The reaction mixture, containing precipitated dicyclohexylborane dimer was cooled in an ice bath and 10 mmol of each olefin (directly or as a THF solution) was added dropwise at 0 °C. Stirring was continued at 0 °C for 3 h. The ice bath was then removed and the reaction mixture was stirred overnight (13—15 h) at room temperature in order to complete the reaction.

The flask was connected to a vacuum system at the top of the receiver and almost all of the THF and unreacted olefins were removed from the mixture by vacuum evaporation (35 °C, 10—13 mmHg, 20 min). 11.4 ml (60 mmol) of 1-decene and a measured amount of internal standard (*n*-dodecane or *n*-tridecane) were then added by means of a hypodermic syringe. The flask was dipped into an oil bath, the temperature of which was controlled with an electric temperature controller. At certain time intervals, 1 ml aliquots were withdrawn with a hypodermic syringe, the samples being oxidized by alkaline hydrogen peroxide in the usual manner. The alcohols formed were extracted with 10 ml of ether and dried on K_2CO_3.

The samples were analyzed by gas chromatography (Carbowax 20 M, 10% on Varaport 100/120, 1/8″ × 12 ft, FID). During the course of displacement reaction, the displaced olefin was collected into an ice-cooled receiver, and the distribution of isomers of displaced olefins was analyzed by gas chromatography. During the entire operation, the system was maintained under a static pressure of nitrogen gas.

Alkyldi-exo-*norbornylborane*: A 4 ml sample of BH_3–THF solution (10.7 mmol) was placed in a 50 ml three-necked flask and cooled in an ice bath. A 6.69 ml (21.4 mmol) of norbornene–THF solution (3.20 M) was added slowly at 0 °C by means of a hypodermic syringe and the mixture was maintained at 0 °C for 1 h. Crude di-*exo*-norbornylborane solution was used *in situ* in subsequent processes. 10 ml of each of the olefins and 10 ml of solvent (diglyme or triglyme) were added slowly at 0 °C to the mixture. The same procedure as that for monoalkyldicyclohexylborane then followed.

The author wishes to express his gratitude to Professor Herbert C. Brown for his guidance and encouragement.

References

1) R. Köster, *Angew. Chem.*, **68**, 3831 (1956).
2) R. Köster, *Justus Liebigs Ann. Chem.*, **618**, 31 (1958).
3) H. C. Brown and B. C. Subba Rao, *J. Org. Chem.*, **22**, 1136 (1957).
4) H. C. Brown and B C. Subba Rao, *J. Am. Chem. Soc.*, **81**, 6434 (1959).
5) H. C. Brown and M. V. Bhatt, *J. Am. Chem. Soc.*, **88**, 1440 (1966).
6) H. C. Brown, M. V. Bhatt, T. Munekata, and G. Zweifel, *J. Am. Chem. Soc.*, **89**, 567 (1967).
7) H. Taniguchi, unpublished results.
8) H. Taniguchi and H. C. Brown, unpublished results.

Distribution of Alkylboranes in the Reaction of Norbornene and Cyclopentene with Borane-THF

Hiroaki TANIGUCHI*

Richard B. Wetherill Laboratory, Purdue University, West Lafayette, Indiana 47902, USA

(Received February 28, 1979)

Systematic studies of the partial alkylation of diborane with norbornene and cyclopentene were carried out in THF and the equilibrium distribution of the borane derivatives was determined. Di-*exo*-norbornylborane was obtained in 71% yield with no mono-*exo*-norbornylborane as a by-product, under the conditions: initial ratio of norbornene to borane 2: 1, temperature 0 °C and reaction time 1 h. Mono-*exo*-norbornylborane was obtained in 72—75% yield under the conditions: initial ratio of norbornene to borane 1: 1, temperature 25 °C, and reaction time 48 h. In the dialkylborane $[R_2BH]_2$, norbornene and cyclopentene exhibit very different behavior during the course of equilibration reaction.

Di-*exo*-norbornylborane is promising as a new agent for the contrathermodynamic isomerization of olefins.[1] It is desirable to find a simple synthetic route for this dialkylborane.

The easiest route to obtain the disubstituted boranes would be the partial alkylation of BH_3, but direct partial alkylation of BH_3 by norbornene does not seem to have been studied. It is possible to obtain a mixture of BH_3, RBH_2, R_2BH, and R_3B from the direct reaction of 2 mol olefin and 1 mol BH_3, but not pure dialkylboranes.[2] However, pure dialkylboranes such as bis(1,2-dimethylpropyl)borane and dicyclohexylborane can be obtained from some special types of hindered olefins.[3] A complete study of the composition or the equilibrium distribution realized in the partial alkylation of diborane with different types of olefins does not seem to have been carried out. I herewith report a systematic study on the partial alkylation of diborane with norbornene, cyclopentene being considered as a comparable raw material.

Results and Discussion

Kinetic Study of Partial Alkylation. (1) Partial Alkylation of Diborane with Norbornene and Cyclopentene in THF at 0 °C: Partial alkylation of BH_3 with norbornene in the ratios 1: 1, 1: 2, and 1: 3 was carried out at 0 °C.

A solution of norbornene in THF was slowly added to a solution of diborane in THF at 0 °C. After 1 h, excess methanol was added and the amounts of methyl borate $[B(OCH_3)_3]$, dimethoxy-*exo*-norbornylborane methoxy-di-*exo*-norbornylborane obtained were determined by titration and NMR analysis. The amounts of tri-*exo*-norbornylborane were calculated from the difference between the theoretical amounts of the borane compounds found and the sum of the amounts of the rest three boron derivatives found. Partial alkylation of BH_3 with cyclopentene under the same conditions was also undertaken to clearify the influence of the particular olefin and to compare results with the data obtained by Brown *et al.*[2] The results are summarized in Table 1.

We see that the derivative of the alkylboranes formed is dialkylborane $[R_2BH]$. Under mild conditions it is possible to obtain R_2BH as the main product of both the 1: 1 and 1: 2 ratio reaction mixtures. This could be accounted for as follows: RBH_2 exists neither as a complex with other alkylboranes nor THF, but exists either free or as a very weak complex reacting much faster than BH_3 which undergoes fairly strong complexation with THF. On the other hand, R_2BH sould form a relatively stable dimer 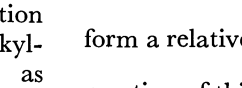 . The rate of reaction of this dimer with olefin should be smaller than that of the corresponding dimer of monoalkylborane.

The difference between norbornene and cyclopentene is not remarkable but appreciable. In the case of norbornene, it is possible to obtain alkylborane products containing no RBH_2. If the reaction is to be used for synthesis, this undesirable by-product should be avoided.

The data differ considerably from those obtained in the earlier study.[2] Cause of this difference might be due to the difference in analytical procedure. The amounts of the alkylborane derivatives were determined by distillation of the methoxyalkylboranes formed after methanolysis of reaction products. It was found that methoxyalkylboranes can easily undergo redistribution at higher temperature.[4] In the present procedure, NMR analysis was carried out for the methanolyzed product, no high temperature treatment being involved.

The conditions for these experiments were too mild to complete the hydroboration of norbornene. Thus in Expt. H-60 (Table 1) large amounts of R_2BH and unreacted norbornene remained in the reaction mixture.

(2) Partial Alkylation of Diborane with Norbornene and Cyclopentene in THF at Room Temperature: Interesting results were obtained in the kinetic study of partial alkylation. Partial alkylation reactions were carried out at 25—28 °C for 24 h. Olefins were added to the BH_3–THF solution at 0 °C, and the reaction mixture was left to stand at room temperature for 24 h with stirring. Excess methanol was added, the same analytical procedure as that given in (1) being applied. The results are summarized in Table 2.

RBH_2 is obtained as the main product in the reaction at the ratio 1: 1, indicating the complex $[(R_2BH)_2]$, which is evidently formed initially, undergoes rearrangement during the course of longer reaction time at higher temperature to produce RBH_2.

* On leave of absence from the Research Center, Maruzen Oil Co., Ltd. Present address: Research Center, Maruzen Oil Co., Ltd., Satte-cho, Kitakatsushika-gun, Saitama, 340-01.

Table 1. Partial alkylation[a] of diborane with cyclopentene and norbornene at 0 °C for 1 h

Expt.	Olefin	$\left(\frac{\text{Olefin}}{BH_3}\right)$ Ratio $\frac{\text{mol}}{\text{mol}}$	H_2 Gas generated by methanolysis $\left(\frac{H_2\ \text{mmol}}{BH_3\ \text{mmol}}\right)$	Yield (per 100 mmol BH_3) BH_3 %	RBH_2 %	R_2BH %	R_3B %
H-56	Norbornene	1.02	1.74	43(52)[b]	2	37	9
H-59	Norbornene	2.04	1.15	16	0	71	13
H-60	Norbornene	3.08	0.42	1	0	46	53
H-57	Cyclopentene	1.04	1.92	39(49)[b]	2	45	4
H-62	Cyclopentene	2.04	1.01	13	2	56	29
c)	Cyclopentene	1		46	6	32	8 (loss 8)
c)	Cyclopentene	2		17	8	30	31 (loss 14)

a) Olefin was added dropwise into BH_3–THF solution at 0 °C over a period of 13 min. b) Correct value calculated from theoretical amounts of olefin. c) H. C. Brown, A. Tsukamoto, and D. B. Bigley, *J. Am. Chem. Soc.*, **82**, 4703 (1960).

Table 2. Partial alkylation[a] of diborane with cyclopentene and norbornene at room temperature for 24 h

Expt.	Olefin	$\left(\frac{\text{Olefin}}{BH_3}\right)$ Ratio $\frac{\text{mol}}{\text{mol}}$	H_2 Gas $\left(\frac{H_2\ \text{mmol}}{BH_3\ \text{mmol}}\right)$	Yield (per 100 mmol BH_3) BH_3 %	RBH_2 %	R_2BH %	R_3B %
H-65-1	Norbornene	1.02	2.02	11(16)[b]	65	19	0
H-64-6	Norbornene	2.04	1.13	3	30	57	15
H-66-4	Norbornene	3.10	0.00	1	0	4	95
H-58	Cyclopentene	1.04[e]	1.93	22	43	33	2
H-70-1	Cyclopentene	1.02[e]	1.79	19	45	31	5
H-67-6	Cyclopentene	2.01	1.04	6	25	48	21
d)	Cyclopentene	1[e]		30	45	2	19 (loss 4)
d)	Cyclopentene	2[e]		11	19	22	37—39
d)	Cyclopentene	2		15	44	10	42—44

a) Olefin was added dropwise into BH_3–THF at 0 °C over a period of 13 min. b) Correct value calculated from theoretical amounts of olefin. c) The same experiments were repeated in order to check the accuracy. d) H. C. Brown, A. Tsukamoto, and D. B. Bigley, *J. Am. Chem. Soc.*, **82**, 4703 (1960). e) BH_3 gas was passed into olefin–THF solution.

$$R_2BH + BH_3 \rightleftharpoons 2RBH_2$$

The most evident difference between norbornene and cyclopentene is the disparity in the (RBH_2/R_2BH) ratio in the 1:1 reaction. The (RBH_2/R_2BH) ratio in norbornene is 3:4 (Expt. H-65). In contrast, the (RBH_2/R_2BH) ratio in cyclopentene is only 1:4—1:5 (Expt. H-58, H-70). This indicates that the stability of the (dicyclopentylborane)$_2$ complex is much higher than that of (di-*exo*-norbornylborane)$_2$ complex. A possible reason could be the difference in the steric hindrance of the two alkyl groups with large steric requirement of norbornyl group in the dimer decreasing the stability of $(R_2BH)_2$. In the 1:3 mixture of BH_3 and norbornene, the reaction proceeds almost completely to form the trialkylborane.

Thermodynamic Study of Partial Alkylation. Equilibration of BH_3–Norbornene and BH_3–Cyclopentene System in THF at Room Temperature: The reaction of BH_3 and norbornene or cyclopentene in THF was studied at room temperature in order to estimate the approximate rate of equilibration and the composition at equilibrium. The equilibration reaction was carried out using two kinds of starting materials in order to confirm that the attained composition was that of true equilibrium mixture: distribution of the kinetic mixture from BH_3 and olefin, redistribution of trialkylborane with borane. It was confirmed that the same equilibrium distribution is attained from both combinations of starting materials.

In the experiments using (BH_3+olefin) as the starting materials, the addition of olefin to BH_3–THF solution was carried out at 0 °C by the usual method, the reaction mixtures being stirred at room temperature. 1/10 aliquots were taken out at appropriate intervals and analyzed.

In the experiments using (R_3B+BH_3) as the starting material, R_3B was synthesized first by the reaction of BH_3 with olefin in 1:3 ratio at room temperature for 1 h and BH_3 was added to the solution of R_3B in THF at 0 °C. The reaction mixtures were allowed to stand at room temperature and the same sampling procedure was carried out. Representative results are shown graphically in Figs. 1—5. Data of the equilibrium

Table 3. Equilibrium distribution of the partial alkylation of diborane with cyclopentene and norbornene at room temperature in THF

Olefin	Olefin: BH_3 Ratio	Starting material	Time to attain equilibrium distribution h	Equilibrium distribution BH_3 %	RBH_2 %	R_2BH %	R_3B %
Norbornene	1.02	Olefin+BH_3 ⟶	48	12—14	72—74	13—16	0—2
		⟵ R_3B+BH_3[a)]	48—72	14—17	72—75	13—12	0—2
	2.04	Olefin+BH_3 ⟶	24	1—3	26—27	56—57	15—18
		⟵ R_3B+BH_3[a)]	24	4—2	26—27	54—60	11—17
Cyclopentene	1.02	Olefin+BH_3 ⟶	48	24—27	46—51	24	0—6
		⟵ R_3B+BH_3[b)]	48	20—24	48—52	27—30	0—2
	2.02	Olefin+BH_3 ⟶	48	3	28—29	52—56	11—17
		⟵ R_3B+BH_3[b)]	48	3—4	25—30	52—55	12—15

a) R=tri-*exo*-norbornyl-. b) R=cyclopentyl-.

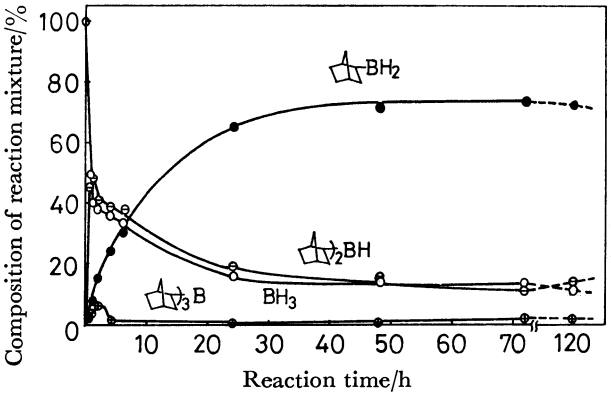

Fig. 1. The equilibration of BH_3+norbornene (1: 1)⟶ in THF solution at R.T.

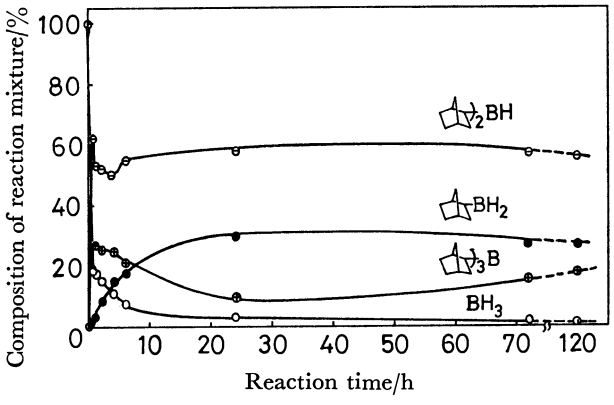

Fig. 2. The equilibration of BH_3+norbornene (1: 2)⟶ in THF solution at R.T.

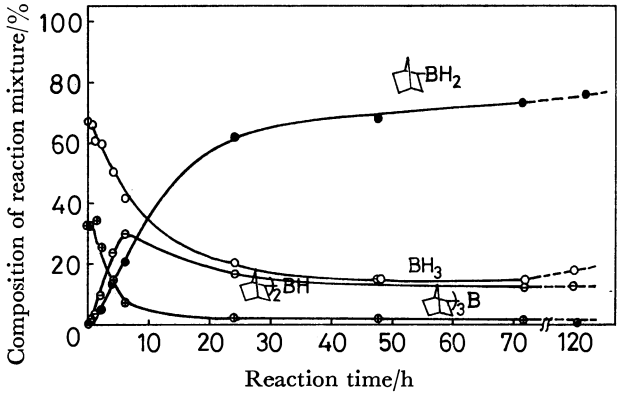

Fig. 3. The equilibration of tri-*exo*-norbornylborane +BH_3 (1: 2)⟶ in THF solution at R. T.

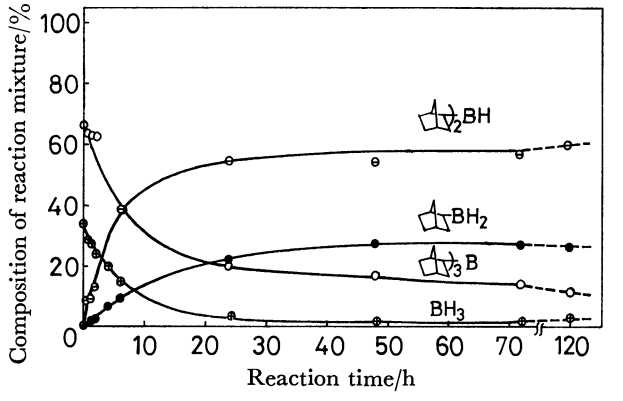

Fig. 4. The equilibration of tri-*exo*-norbornylborane +BH_3 (2: 1)⟶ in THF solution at R. T.

distributions are summerized in Table 3.

We see that the distribution of the borane products from borane and olefin and that from borane and trialkylborane of the same (olefin: BH_3) ratio are almost the same, indicating they are true equilibrium distributions. In the (olefin: BH_3) ratio=2, the composition of the equilibrium is almost the same in both norbornene and cyclopentene. On the other hand, in the (olefin: BH_3) ratio=1, it is quite different, indicating that the stabilities of the $(R_2BH)_2$ complexes of these two olefins differ considerably. The main route to give RBH_2 is postulated to be as follows.

(i) Starting material: Olefin+BH_3

$$BH_3 + 2\text{Olefin} \xrightarrow{\text{fast}} R_2BH$$

$$R_2BH + BH_3 \xrightarrow{\text{slow}} 2RBH_2$$

(ii) Starting material: R_3B+BH_3

(ii-a) $R_3B + BH_3 \rightleftharpoons$ 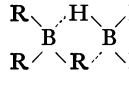

$\longrightarrow R_2BH + RBH_2$

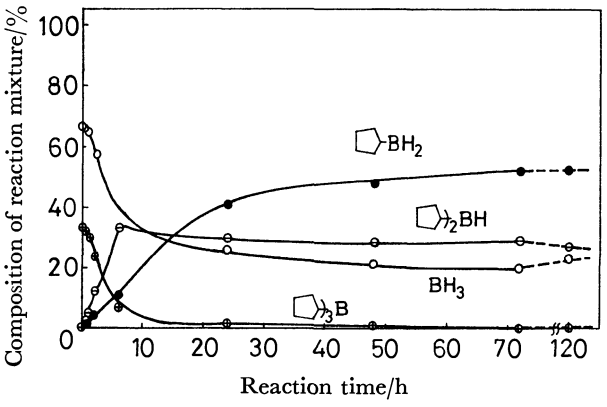

Fig. 5. The equilibration of tricyclopentylborane+BH_3 (1:2)→ in THF solution at R. T.

(ii-b) $R_2BH + BH_3 \rightleftharpoons$ 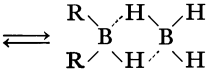 $\rightleftharpoons$ 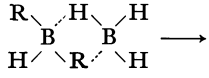 $\longrightarrow 2RBH_2$

In the case of norbornene (Fig. 3), the rate of (ii-b) reaction should be much smaller than that of cyclopentene (Fig. 5).

Mono-*exo*-norbornylborane can be synthesized in 72—75% yield by the reaction of norbornene and BH_3 in 1:1 ratio at room temperature for 40 h.

Experimental

Materials. Norbornene (reagent grade, Aldrich Chemical Co.), mesitylene (Coleman and Bell Co.) for the internal standard of NMR analysis and methanol (Mallinckrodt Chemical Works) for the methanolysis of products were used without further purification. Cyclopentene (Phillips Petroleum Co.) was distilled from lithium aluminum hydride and stored under nitrogen. The other reagents were the same as those used by Brown *et al.*[2]

Partial Alkylation of BH_3 with Olefin at 0 °C. Experiments were carried out with use of a 100-ml 2-necked round-bottom flask fitted with a reflux condenser which was connected with glass stopcock and a bubbling gas outlet at the top and a side arm fitted with a rubber cap to permit the flushing of all systems with nitrogen before the reaction.

A solution of 10 mmol, 20 mmol, or 30 mmol norbornene in THF (2.20 M) was added to a solution of 10 mmol of BH_3 in THF (2.69 M) at 0 °C over a period of 13 min.

The reaction was carried out at 0 °C for 1 h. The ice bath was then removed and methanol (50—100% excess) was added dropwise at room temperature. Stirring was continued for 10 min, and all the hydrogen gas generated during the course of methanolysis was collected into the gas burrette and measured. The solvent (THF), excess MeOH, and methylborate [$B(OCH_3)_3$] were removed by vacuum distillation (30—35 °C, 15—13 mmHg, 20 min) and trapped with a Dry Ice bath. The trapped mixture was analyzed for boric acid by titration with standard sodium hydroxide in the presence of 10 mmol of mannitol.

The residue containing dimethoxy-*exo*-norbornylborane, methoxy-di-*exo*-norbornylborane, and tri-*exo*-norbornylborane was analyzed by NMR. The amounts of mono- and di-*exo*-norbornylborane could be estimated. The amount of tri-*exo*-norbornylborane was calculated as the difference of the sum of the initial borane and the amounts of $B(OCH_3)_3$, $RB(OCH_3)_2$, $R_2B(OCH_3)$ found.

Equilibration of BH_3 and Olefin (1: 1 or 1: 2). 80 mmol of norbornene in 26 ml of THF was added slowly to a stirred solution of 80 mmol (2.69 M) BH_3–THF solution at 0 °C over a period of 13 min. The ice bath was then removed and the reaction mixture was stirred at room temperature.

At certain intervals, 1/10 aliquots were withdrawn with a hypodermic syringe, weighed and put into a 50-ml two-necked flask fitted with a reflux condenser and a side arm for a rubber cap purged with nitrogen, subsequent treatment being the same as described above.

Equilibration of BH_3 and R_3B. 90 mmol of norbornene in 20 ml of THF was added slowly to a stirred solution of 30 mmol BH_3–THF at 0 °C over a period of 13 min. The reaction mixture was kept at room temperature for 1 h to complete the formation of tri-*exo*-norbornylborane. The mixture was then cooled in an ice bath to 0 °C and 15 mmol of BH_3–THF solution was added dropwise to the mixture. The ice bath was removed and the reaction mixture was stirred at room temperature. At certain time intervals, 1/10 aliquots were withdrawn with a syringe, subsequent treatment being the same as described above.

NMR Analysis. The methoxyl protons of $RB(OCH_3)_2$ and $R_2B(OCH_3)$ have a sharp singlet peak. The contents of these compounds in the residue were measured by use of mesitylene as an internal standard. It has a sharp singlet peak of benzene proton at $\delta=6.67$, no absorption at $\delta=3$—4. The experiments were carried out in nitrogen. NMR spectral data are given in Table 4.

Table 4. NMR spectral data

Methoxy borane	δ/ppm
Methoxydi-*exo*-norbornylborane	3.61
Dimethoxy-*exo*-norbornylborane	3.50
Methoxydicyclopentylborane	3.65
Dimethoxycyclopentylborane	3.52

The author wishes to express his sincere thanks to Prof. Herbert C. Brown for his guidance throughout the course of this study.

References

1) H. Taniguchi, *Bull. Chem. Soc. Jpn.*, **52**, 2942 (1979).
2) H. C. Brown, A. Tsukamoto, and D. B. Bigley, *J. Am. Chem. Soc.*, **82**, 4703 (1960).
3) H. C. Brown, "Boranes in Organic Chemistry," Cornell University Press (1972), p. 269.
4) H. C. Brown and S. K. Gupta, *J. Am. Chem. Soc.*, **92**, 6983 (1970).

The Synthesis of 5,2′-Dihydroxy-6,8-dimethoxyflavone and Its Isomers: A Revised Structure of Skullcapflavone I

Tokunaru HORIE,* Masao TSUKAYAMA,** Mitsuo MASUMURA,**
Mitsuru NAKAYAMA,*** and Shûichi HAYASHI***

Technical College, Tokushima University, Minamijosanjima-cho, Tokushima 770
***Department of Applied Chemistry, Faculty of Engineering, Tokushima University, Minamijosanjima-cho, Tokushima 770*
****Department of Chemistry, Faculty of Science, Hiroshima University, Higashisenda-machi, Hiroshima 730*

(Received February 20, 1979)

5,2′-Dihydroxy-6,8-dimethoxyflavone, which had been proposed as the structure of skullcapflavone I isolated from *Scutellaria baicalensis* Georgi, was synthesized from 2-hydroxy-3,5,6-trimethoxyacetophenone. However, the synthetic flavone was not identical with the natural flavone. Thus, two isomeric flavones, 5,2′-dihydroxy-7,8-dimethoxyflavone and 5,2′-dihydroxy-6,7-dimethoxyflavone, were prepared from the corresponding acetophenones; the structure of skullcapflavone I was confirmed to be 5,2′-dihydroxy-7,8-dimethoxyflavone.

Skullcapflavone I has recently been isolated from roots of *Scutellaria baicalensis* Georgi, along with skullcapflavone II; its structure has been proposed as 5,2′-dihydroxy-6,8-dimethoxyflavone (**1**) on the basis of the spectroscopic data and degradative studies.[1] The properties of skullcapflavone I are not, however, consistent with those of 5,2′-dihydroxy-6,8-dimethoxyflavone (**1**) synthesized from 2-hydroxy-3,5,6-trimethoxyacetophenone (**7**). Therefore, two isomers of **1**, 5,2′-dihydroxy-7,8-dimethoxyflavone (**2**) and 5,2′-dihydroxy-6,7-dimethoxyflavone (**3**), were prepared in order to confirm the structure of skullcapflavone I; consequently, the properties of the former were thus found to be identical with those of skullcapflavone I. We wish now to report that the structure of natural skullcapflavone I is 5,2′-dihydroxy-7,8-dimethoxyflavone (**2**).

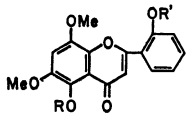

(**1**) R=R′=H
(**9**) R=Me, R′=H
(**10**) R=R′=Ac

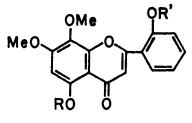

(**2**) R=R′=H
(**12**) R=Me, R′=$C_6H_5CH_2$
(**13**) R=Me, R′=H
(**14**) R=R′=Ac

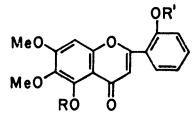

(**3**) R=R′=H
(**16**) R=Me, R′=H
(**17**) R=R′=Ac

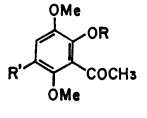

(**4**) R=Me, R′=Ac
(**5**) R=Me, R′=OH
(**6**) R=Me, R′=OMe
(**7**) R=H, R′=OMe

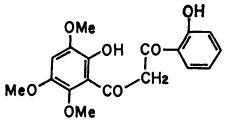

(**8**)

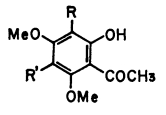

(**11**) R=OMe, R′=H
(**15**) R=H, R′=OMe

1,3-Diacetyl-2,5,6-trimethoxybenzene (**4**)[2] was oxidized with 30% hydrogen peroxide in a mixture of acetic acid and concentrated sulfuric acid; the hydrolysis of the resultant compound gave 3-hydroxy-2,5,6-trimethoxyacetophenone (**5**). The acetophenone **5** was converted into the methyl ether (**6**) and was then demethylated with anhydrous aluminum chloride in ether to give 2-hydroxy-3,5,6-trimethoxyacetophenone (**7**). After the condensation of **7** with 2-benzyloxybenzoyl chloride, the debenzylated diketone (**8**) was obtained by the Baker-Venkataraman rearrangement. The compound **8** was cyclized with anhydrous sodium acetate in acetic acid to yield a 2′-hydroxyflavone derivative (**9**), which was then converted with anhydrous aluminum chloride in acetonitrile into 5,2′-dihydroxy-6,8-dimethoxyflavone (**1**) (mp 246.5—248 °C). The flavone **1** afforded the corresponding diacetate (**10**). The flavone **1** and the diacetate **10** should be consistent with skullcapflavone I and its diacetate respectively, but they were not identical with each other, as is shown in Tables 1 and 2. That is, in the NMR spectra of the acetate of skullcapflavone I and the diacetate **10**, it appears that there is a remarkable difference between the chemical shifts of protons on the A ring of the flavone nucleus, but that other proton signals show very similar chemical shifts. Therefore, it may be assumed that the structure of skullcapflavone I is the isomer of **1**, that is, **2** or **3**.

2′-Hydroxy-5,7,8-trimethoxyflavone (**13**) could not be prepared from the acetophenone (**11**)[3] *via* the corresponding diketone by the method described above. The condensation of the acetophenone **11** with 2-benzyloxybenzaldehyde in the presence of piperidine gave an oily chalcone derivative, which was then converted into a benzyloxyflavone derivative (**12**) by oxidative cyclization with selenium dioxide. The flavone **12** was debenzylated with palladium charcoal to give a hydroxyflavone derivative (**13**) and was then demethylated with anhydrous aluminum chloride in acetonitrile to afford the desired flavone **2** (mp 253—254 °C), which was subsequently converted into the diacetate (**14**). 5,2′-Dihydroxy-6,7-dimethoxyflavone **3** was also synthesized from the acetophenone (**15**)[4] *via* the corresponding chalcone by using the same method as was used in the case of the flavone **2**. The flavone **3** led to the diacetate (**17**).

The physical and spectral data of synthetic flavones and these acetates are listed in Tables 1 and 2. In Tables 1 and 2, the NMR and UV spectral data of skullcapflavone I and its diacetate are shown to be identical with those of the synthetic flavone **2** and the

Table 1. Mp and UV spectra of flavones[a)]

Compound	Mp/°C		λ_{max}/nm (log ε)
Skullcapflavone I[1)]	263—265	(EtOH)	271(4.40), 340(4.05)
	(266—267)[b)]	($EtOH–AlCl_3$)	280(4.34), 342(4.05), 400(3.84)
Acetate[1)]	143—144		
1	246.5—248	(EtOH)	284(4.41), 321(4.10), 339(4.11)
		($EtOH–AlCl_3$)	253(4.03), 287_i(4.29), 301(4.35), 339(4.21), 355_i(4.19)
		(EtOH–AcONa)	285(4.37), 319_i(4.02), 340(4.00), 411(3.77)
10	195—195.5	(EtOH)	269(4.47), 345(3.69)
2	253—254	(EtOH)	273(4.44), 343(4.11)
	(266.5—267.5)[b)]	($EtOH–AlCl_3$)	282(4.39), 294_i(4.34), 345(4.11), 404(3.91)
		(EtOH–AcONa)	271(4.41), 343(4.01), 416(3.81)
14	135—136	(EtOH)	257(4.45), 303(4.13)
3	254—255	(EtOH)	248(4.12), 271(4.36), 339(4.26)
		($EtOH–AlCl_3$)	254(4.09), 278_i(4.35), 285.5(4.44), 354(4.28)
		(EtOH–AcONa)	270.5(4.34), 337(4.15), 415(3.73)
17	145—146	(EtOH)	254(4.31), 301(4.28)

a) i: Inflection point. b) The melting points were measured with a Yanagimoto micro-melting-point apparatus in our laboratory.

Table 2. NMR spectra of flavones

Compound	Solvent	C_3–H	Arom H		OMe	OAc	OH
			A ring	B ring			
Skullcapflavone I[1)]	DMSO	6.55—7.90(6H, m)			3.82(3H, s)	—	10.79
					3.91(3H, s)	—	12.64
Acetate[1)]	$CDCl_3$	6.50(s)	6.69(s)	7.16—7.81(4H, m)	3.82(3H, s)	2.28(3H, s)	—
					3.91(3H, s)	2.40(3H, s)	—
1	DMSO	6.91—7.95(6H, m)			3.85(3H, s)	—	10.93
					3.93(3H, s)	—	12.16
10	$CDCl_3$	6.50(s)	6.90(s)	7.10—7.83(4H, m)	3.88(3H, s)	2.27(3H, s)	—
					3.94(3H, s)	2.43(3H, s)	—
2	DMSO[a)]	7.09(s)	6.54(s)	6.9—7.95(4H, m)	3.78(3H, s)	—	10.99
					3.88(3H, s)	—	12.86
14	$CDCl_3$[a)]	6.44(s)	6.64(s)	7.1—7.85(4H, m)	3.84(3H, s)	2.30(3H, s)	—
					3.92(3H, s)	2.40(3H, s)	—
3	DMSO	7.11(s)	6.90(s)	6.90—7.80(4H, m)	3.71(3H, s)	—	10.95
					3.89(3H, s)	—	12.99
17	$CDCl_3$	6.45(s)	6.80(s)	7.10—7.80(4H, m)	3.83(3H, s)	2.27(3H, s)	—
					3.93(3H, s)	2.46(3H, s)	—

a) The NMR spectra of 2 and 14 could be superimposed on those of the literature.[1)]

diacetate **14** respectively. The melting point of the flavone **2** was not depressed by admixture with the natural flavone, and the UV spectrum of the flavone **2** was also superimposable on that of the natural flavone. On the basis of these results, the structure of skullcapflavone I was confirmed to be 5,2′-dihydroxy-7,8-dimethoxyflavone **2**, which had previously been proposed as the structure of andrographin isolated from *Andrographis paniculata*.[5)] The flavone **2** has also been produced in differentiating tissue cultures of *Andrographis paniculata*.[6)]

Experimental

All the melting points were determined in glass capillaries and are uncorrected. The NMR spectra were measured with a JEOL PS-100 spectrometer (100 MHz), using tetramethylsilane as the internal standard (δ, ppm). The UV spectra were taken on a Hitachi 124 spectrophotometer.

*2,3,5,6-Tetramethoxyacetophenone (**6**).* 1,3-Diacetyl-2,5,6-trimethoxybenzene (**4**)[2)] (10 g) and concd sulfuric acid (5 ml) were dissolved in acetic acid (5 ml) below 10 °C, and to the solution with stirring was then added dropwise a mixture of 30% hydrogen peroxide (7 g) and acetic acid (10 ml) below 10 °C. The resulting mixture was subsequently stirred for 5 h at room temperature. After the addition of water to the reaction mixture, the mixture was extracted with ether, and the ethereal solution was washed with aqueous sodium carbonate and water. The solvent was evaporated from the ethereal solution to give crude 3-acetoxy-2,5,6-trimethoxyacetophenone.[7)] The acetophenone was hydrolyzed with 10% sodium hydroxide in methanol (50 ml) for 10 min; then, a crude phenol derivative (**5**) (6 g) was obtained by a usual treatment. A mixture of **5** (16 g) and dimethyl sulfate (20 g) was refluxed with anhydrous potassium carbonate (40 g) in anhydrous acetone (65 ml) for 5 h. After water had been added to the mixture, the solvent was removed, and then the residue was extracted with ether. The ethereal solution was washed with 10% aqueous sodium hydroxide and water, and dried. The solvent was removed, and the residue was distilled under reduced pressure to give an acetophenon (**6**) (15.5 g); it solidified at room temperature: bp 108 °C/0.25 mmHg; NMR ($CDCl_3$) δ 2.47 (3H, s, CH_3CO), 3.73 and 3.83 (each 6H, s, OCH_3), 6.51 (1H, s, Arom H). Found: C, 60.02; H, 6.78%. Calcd for $C_{12}H_{16}O_5$: C, 59.99; H, 6.71%.

2-Hydroxy-3,5,6-trimethoxyacetophenone (7). A mixture of **6** (5 g) and anhydrous aluminum chloride (5.2 g) in anhydrous ether (40 ml) was stirred for 5 h in an ice bath and then allowed to stand overnight in a refrigerator. The reaction mixture was poured into diluted hydrochloric acid, and the solvent was evaporated to afford a precipitate (**7**), which was subsequently recrystallized from methanol as yellow needles (2.6 g): mp 62—63.5 °C; NMR (DMSO) δ 2.41 (3H, s, CH_3CO), 3.63 (3H, s, OCH_3), 3.76 (6H, s, $OCH_3\times2$), 6.80 (1H, s, Arom H), 9.43 (1H, s, OH). Found: C, 58.48; H, 6.24%. Calcd for $C_{11}H_{14}O_5$: C, 58.40; H, 6.24%.

2-Hydroxy-3,5,6-trimethoxy-ω-(2-hydroxybenzoyl)acetophenone(8). A mixture of **7** (2 g) and 2-benzyloxybenzoyl chloride (3.5 g) was heated in the presence of pyridine (3.5 g) at 100 °C for 5 h, and then the reaction mixture was poured into a mixture of ice and hydrochloric acid. The mixture was extracted with ethyl acetate and treated by a usual method. The solvent was then evaporated, and the residue was dried sufficiently to give a crude ester (3.2 g). The ester was stirred in the presence of freshly powdered potassium hydroxide (3.5 g) in pyridine (10 ml) at 60 °C for 4 h, and then a mixture of ice and hydrochloric acid was added to the mixture. After the mixture had been extracted with ether and treated by a usual method, the ether was evaporated to yield a precipitate (**8**), which was subsequently recrystallized from ethyl acetate as yellow plates (300 mg): mp 140—140.5 °C. Found: C, 62.56; H, 5.35%. Calcd for $C_{18}H_{18}O_7$: C, 62.42; H, 5.24%.

2'-Hydroxy-5,6,8-trimethoxyflavone (9). A mixture of **8** (150 mg) and anhydrous sodium acetate (1 g) in acetic acid (6 ml) was heated for 4 h, and then water was added to the reaction mixture to give a precipitate (**9**), which was subsequently recrystallized from methanol as pale yellow needles (100 mg): mp 231—232 °C; NMR (DMSO) δ 3.66, 3.87, and 3.96 (each 3H, s, OCH_3), 6.9—7.9 (6H, m, Arom H). Found: C, 65.66; H, 4.94%. Calcd for $C_{18}H_{16}O_6$: C, 65.85; H, 4.91%.

5,2'-Dihydroxy-6,8-dimethoxyflavone (1). A mixture of **9** (240 mg) and anhydrous aluminum chloride (0.5 g) in acetonitrile (3 ml) was heated at 80 °C for 4 h, and then 2% aqueous hydrochloric acid was added to the reaction mixture. The mixture was heated on a water bath for 30 min and then allowed to stand at room temperature to give a precipitate (**1**), which was subsequently recrystallized from methanol as yellow needles (200 mg); mp 246.5—248 °C. Found: C, 65.02; H, 4.66%. Calcd for $C_{17}H_{14}O_6$: C, 64.96; H, 4.49%.

The Diacetate (10) of 1. The flavone **1** was converted into a diacetate (**10**) by an acetic anhydride-pyridine method; it was subsequently recrystallized from methanol as colorless prisms; mp 195—196.5 °C. Found: C, 63.41; H, 4.67%. Calcd for $C_{21}H_{18}O_8$: C, 63.31; H, 4.55%.

2'-Benzyloxy-5,7,8-trimethoxyflavone (12). A mixture of 2-hydroxy-3,4,6-trimethoxyacetophenone (**11**)[3] (3.5 g) and 2-benzyloxybenzaldehyde (bp 153—155 °C/1 mmHg) (3.5 g) was refluxed in the presence of piperidine (4.5 g) in ethanol (20 ml) for 7 h; the solvent was then removed under reduced pressure, and the residue was extracted with ethyl acetate. The solution of ethyl acetate was washed with diluted hydrochloric acid and water, and dried. The solvent was evaporated to give a crude chalcone, which was subsequently refluxed in the presence of selenium dioxide (4 g) in 1-pentanol for 22 h. The reaction mixture was filtered out, and the filtrate was condensed sufficiently under reduced pressure. The residue was extracted with ethyl acetate, and the extract was washed with aqueous sodium carbonate solution and diluted hydrochloric acid, and dried. After the removal of the solvent, the residue was solidified in a small amount of ether and the solid was recrystallized from ethyl acetate as yellow prisms of **12** (2.6 g): mp 145.5—146.5 °C. Found: C, 71.52; H, 5.23%. Calcd for $C_{23}H_{22}O_6$: C, 71.76; H, 5.30%.

2'-Hydroxy-5,7,8-trimethoxyflavone (13). The flavone **12** (1.01 g) was hydrogenated over palladium on charcoal (10%; 190 mg) in methanol until the uptake of hydrogen ceased. The solvent was then removed under reduced pressure, and the residue was recrystallized from methanol to give yellow needles (**13**) (744 mg): mp >270 °C. Found: C, 65.82; H, 4.91%. Calcd for $C_{18}H_{16}O_6$: C, 65.85; H, 4.91%.

5,2'-Dihydroxy-7,8-dimethoxyflavone (2). The flavone **13** (147 mg) was heated with anhydrous aluminum chloride (0.4 g) in acetonitrile (1 ml) at 80 °C for 2.5 h. The mixture was then heated with diluted hydrochloric acid (15 ml) for 3 min on a water bath to give a precipitate (**2**), which was subsequently recrystallized from methanol to give yellow needles (118 mg): mp 253—254 °C. Found: C, 64.69; H, 4.43%. Calcd for $C_{17}H_{14}O_6$: C, 64.96; H, 4.49%.

The Diacetate (14) of 2. The flavone **2** was converted into a diacetate (**14**) as colorless needles: mp 135—136 °C. Found: C, 63.08; H, 4.51%. Calcd for $C_{21}H_{18}O_8$: C, 63.31; H, 4.55%.

2'-Hydroxy-5,6,7-trimethoxyflavone (16). A mixture of 2-hydroxy-4,5,6-trimethoxyacetophenone (**15**)[4] (1.1 g) and 2-benzyloxybenzaldehyde (1.15 g) was refluxed in the presence of piperidine (1.2 ml) in ethanol (8 ml) for 7 h, and then the reaction mixture was worked-up in the same manner as in the case of **12** to give an oily chalcone. After the chalcone had been treated with selenium dioxide (1.5 g) in 1-pentanol for 20 h to afford an oily flavone, the oily compound was chromatographed over a polyamide column with methanol. The eluate containing the major product was again chromatographed over a silica-gel column with chloroform to give a yellow oily compound (1 g). This oily compound was treated with palladium on charcoal to give a precipitate (**16**), which was subsequently recrystallized from methanol as colorless prisms (550 mg): mp 241—242 °C. Found: C, 65.69; H, 4.85%. Calcd for $C_{18}H_{16}O_6$: C, 65.85; H, 4.91%.

5,2'-Dihydroxy-6,7-dimethoxyflavone (3). A mixture of **16** (100 mg) and anhydrous aluminum chloride (0.3 g) in acetonitrile (1 ml) was heated at 70 °C for 2 h, and then the reaction mixture was worked-up in the same manner as in the case of **1** to give a precipitate, which was subsequently recrystallized from methanol as pale yellow needles (**3**) (52 mg): mp 254—255 °C. Found: C, 64.99; H, 4.40%. Calcd for $C_{17}H_{14}O_6$: C, 64.96; H, 4.49%.

The Diacetate (17) of 3. The flavone **3** was converted into a diacetate (**17**), which was then recrystallized from aqueous methanol as colorless plates: mp 145—146 °C. Found: C, 63.25; H, 4.46%. Calcd for $C_{21}H_{18}O_8$: C, 63.31; H, 4.55%.

The authors are grateful to professor Michio Takido, Department of Pharmacy, College of Science and Technology, Nihon University, for the sample of natural skullcapflavone I.

References

1) M. Takido, M. Aimi, S. Takahashi, S. Yamanouchi, H. Torii, and S. Dohi, *Yakugaku Zasshi*, **95**, 108 (1975).
2) M. Healey and R. Robinson, *J. Chem. Soc.*, **1934**, 1625.
3) W. Baker, *J. Chem. Soc.*, **1941**, 662.
4) V. D. N. Sastri and T. R. Seshadri, *Proc. Indian Acad. Sci., Sect. A*, **23**, 262 (1946).
5) M. E. Ali, K. M. Biswas, and S. A. Chowdhury, *Chem. Abstr.*, **78**, 43200t (1973).
6) M. A. F. Jalal, K. H. Overton, and D. S. Rycroft, *Phytochemistry*, **18**, 149 (1979).
7) H. H. Lee and C. H. Tan, *J. Chem. Soc.*, **1965**, 2743.

Structural Studies of the Interaction between Indole Derivatives and Biologically Important Aromatic Compounds. IV. The Crystal and Molecular Structure of Tryptamine : Adenin-9-ylacetic Acid (1 : 1) Hemihydrate Complex

Toshimasa ISHIDA,* Masatoshi INOUE,* Susumu SENDA, and Ken-ichi TOMITA**

Osaka College of Pharmacy, Kawai, Matsubara, Osaka 580

***Faculty of Pharmaceutical Sciences, Osaka University, Yamadakami, Suita, Osaka 565*

(Received February 28, 1979)

The crystal structure of tryptamine: adenin-9-ylacetic acid (1 : 1) hemihydrate complex has been determined by the X-ray method. The crystal is monoclinic, space group $P2_1/c$ with unit-cell dimensions: $a=9.164(2)$, $b=6.908(1)$, $c=29.524(4)$ Å and $\beta=110.98(2)°$. The structure was solved by application of MULTAN and refined by the block-diagonal least-squares method to give a final R-value of 0.064. No specific interaction between indole and adenine rings is observed. Both component molecules are held together by three-dimensional frameworks of hydrogen bonds around a twofold screw axis to form an infinite helical array along the b-direction. Two kinds of dimer formation around a center of symmetry are observed between adenin-9-ylacetic acid molecules.

In previous communications, reports were given on the crystal structures of 1-methyl-3-carbamoylpyridinium: indole-3-acetic acid (1 : 1) complex[1] and 7,8-dimethyl-isoalloxazine-10-acetic acid: tryptamine (1 : 1) complex[2] selected as suitable models for indole–NAD^+ and indole–FAD interaction, respectively.

Prominent stacking of indole–pyridinium or indole–isoalloxazine rings by charge-transfer interactions was observed. However, when we compare the spectroscopic data of these model complexes with those of indole–NAD^+ and the indole–FAD complexes, we see that there is a slight difference in the association constant and λ_{max} of charge-transfer band.

We thus synthesized the title complex. The present paper deals with crystal structure analysis of the complex which may provide further insight into intermolecular stacking interaction of indole–adenine rings suggested from spectroscopic studies.[3–12]

Experimental

Potassium adenin-9-ylacetate was synthesized according to the reported procedure.[13] Its aqueous solution was absorbed to the Amberlite-IRA-401 anion-exchange resin (OH-type) column, and eluted with an equimolar aqueous solution of tryptamine hydrochloride. Transparent platelet crystals were obtained by slow evaporation of the elute at room temperature.

The UV spectra and thermal analysis of the crystals indicated a one-to-one stoichiometry of adenin-9-ylacetic acid (AAA) and tryptamine (TPA) with a halfmolar water molecule.

Oscillation and Weissenberg photographs showed the space group to be $P2_1/c$. The density was measured by the floatation method in a benzene–carbon tetrachloride mixture. The cell dimensions were refined by the least-squares method, using 30 reflections measured on a Rigaku-Denki automatic four-circle diffractometer with Ni-filtered Cu $K\alpha$ radiation. The crystal data are given in Table 1.

Intensity data were collected on a diffractometer with the same radiation using $\omega/2\theta$ scanning technique within $\sin\theta/\lambda$ less than 0.55 Å^{-1} with scan speed 4°/min, and background being measured for 5s. A total of 2431 independent reflections were corrected for Lorentz and polarization factors, but not for absorption because of the smallness of the crystal (dimension: 0.3×0.3×0.4 mm). The intensities of three standard reflections, measured every 50 reflections, showed no deterioration during the course of data collection.

TABLE 1. CRYSTAL DATA OF TPA: AAA(1 : 1) COMPLEX

Chemical formula	$C_{17}H_{19}N_7O_2\cdot 1/2H_2O$
Molecular weight	362.39
Crystal system	Monoclinic
Space group	$P2_1/c$
Cell constant	
a/Å	9.164(2)
b/Å	6.908(1)
c/Å	29.524(4)
β/°	110.98(2)
Volume/Å^3	1745.1
Z	4
D_m/g·cm^{-3}	1.375(2)
D_x/g·cm^{-3}	1.379
μ(Cu $K\alpha$)/cm^{-1}	9.38

All the numerical calculations were carried out on an NEAC-2200-700 computer of the Computation Center of Osaka University using "UNICS" program (1973).[14] Atomic scattering factors cited in "International Tables for X-Ray Crystallography"[15] were used.

Determination and Refinement of the Structure

The structure was solved by the direct method with the program MULTAN[16] using 493 reflections with $|E|\geqq 1.20$. An E-map computed with the phase set of the highest figure of merit (1.249) revealed the positions of all non-hydrogen atoms except a water molecule. At the stage $R=0.143$, a difference Fourier synthesis gave two peaks related by a center of symmetry at (0,1/2,0) which could be assigned to the disordered oxygen atoms of the water molecules (occupancy: 1/2 per one peak), and nineteen hydrogen atoms other than those of the water molecule. The final block-diagonal least-squares refinement was computed with the following weighting scheme: $w=0.30$ for $F_o=0.0$, $w=1.0$ for $0<F_o\leqq 21.0$ and $w=1.0/[1.0+0.263(F_o-21.0)]$ for $F_o>21.0$. In the last cycle of refinement, none of the positional parameters shifted more than one-fourth of

Table 3. Atomic coordinates ($\times 10^4$) and their standard deviations of non-hydrogen atoms

Atom	x	y	z	Atom	x	y	z
AN1	1303(3)	11380(4)	432(1)	TN1	6894(3)	293(3)	1882(1)
AC2	948(4)	10219(5)	741(1)	TC2	7413(3)	950(4)	2352(1)
AN3	1592(3)	8534(4)	929(1)	TC3	8184(3)	2663(4)	2388(1)
AC4	2702(3)	8021(4)	754(1)	TC4	8727(3)	4602(4)	1709(1)
AC5	3200(3)	9072(4)	442(1)	TC5	8549(4)	4547(5)	1227(1)
AC6	2458(3)	10850(4)	277(1)	TC6	7760(4)	3031(5)	931(1)
AN6	2860(3)	12029(4)	−18(1)	TC7	7133(3)	1536(5)	1111(1)
AN7	4377(3)	8095(3)	343(1)	TC8	7328(3)	1582(4)	1601(1)
AC8	4546(4)	6494(4)	599(1)	TC9	8131(3)	3091(4)	1909(1)
AN9	3570(3)	6360(3)	849(1)	TC10	8934(3)	3828(4)	2839(1)
AC10	3531(4)	4831(4)	1180(1)	TC11	8092(3)	5697(4)	2866(1)
AC11	4388(3)	5337(3)	1708(1)	TN12	6526(2)	5285(3)	2893(1)
AO12	4438(2)	4005(2)	2002(1)	O(H_2O)	517(7)	5120(8)	−130(2)
AO13	4961(2)	6976(3)	1820(1)				

Table 4. Anisotropic thermal parameters ($\times 10^4$) and their standard deviations of non-hydrogen atoms

The anisotropic temperature factors are expressed in the form $\exp\{-(B_{11}h^2+B_{22}k^2+B_{33}l^2+B_{12}hk+B_{13}hl+B_{23}kl)\}$.

Atom	B_{11}	B_{22}	B_{33}	B_{12}	B_{13}	B_{23}
AN1	135(4)	188(6)	15(0)	49(8)	25(2)	−5(2)
AC2	144(5)	245(8)	16(0)	60(10)	41(3)	−1(3)
AN3	161(4)	237(7)	17(0)	60(9)	49(2)	9(3)
AC4	123(4)	178(7)	10(0)	12(8)	17(2)	−2(3)
AC5	115(4)	158(6)	10(0)	14(8)	19(2)	−3(2)
AC6	124(4)	156(6)	12(0)	25(8)	17(2)	−8(3)
AN6	184(4)	191(6)	19(0)	85(9)	52(2)	47(3)
AN7	140(4)	172(6)	13(0)	42(7)	34(2)	4(2)
AC8	153(5)	173(7)	12(0)	55(9)	26(2)	6(3)
AN9	154(4)	149(5)	11(0)	25(7)	26(2)	12(2)
AC10	190(5)	143(6)	12(0)	−59(9)	25(2)	4(3)
AC11	99(4)	105(5)	11(0)	−8(7)	28(2)	−2(2)
AO12	138(3)	112(4)	12(0)	−19(5)	35(1)	9(2)
AO13	156(3)	114(4)	13(0)	−78(6)	30(2)	−8(2)
TN1	116(4)	145(5)	24(1)	−66(7)	51(2)	−34(3)
TC2	111(4)	139(6)	22(1)	14(8)	60(3)	3(3)
TC3	86(4)	117(5)	16(0)	29(7)	38(2)	−1(3)
TC4	119(4)	158(6)	15(0)	−37(8)	25(2)	1(3)
TC5	151(5)	255(8)	16(1)	17(11)	32(3)	19(3)
TC6	151(5)	310(10)	15(1)	88(12)	30(3)	−9(4)
TC7	112(4)	257(8)	18(1)	48(10)	16(2)	−53(4)
TC8	87(4)	140(6)	18(0)	−14(8)	31(2)	−21(3)
TC9	77(3)	115(5)	15(0)	−4(7)	28(2)	−7(2)
TC10	104(4)	161(6)	14(0)	55(8)	30(2)	−2(3)
TC11	109(4)	127(6)	14(0)	−30(8)	32(2)	−13(3)
TN12	110(3)	113(5)	13(0)	22(6)	34(2)	−5(2)
O(H_2O)	267(11)	252(13)	33(1)	235(21)	80(6)	55(7)

the estimated standard deviations. The final R-value including $F_o=0.0$ is 0.064. The observed and calculated structure factors are given in Table 2.[17] The final positional and thermal parameters with their standard deviations for non-hydrogen atoms are given in Tables 3 and 4, respectively. The coordinates and isotropic thermal parameters for hydrogen atoms except those of the water molecule are given in Table 5.

Results and Discussion

Molecular Structure. The bond distances and angles with their standard deviations for non-hydrogen atoms are shown in Fig. 1, with the atomic numbering used in this work. The least-squares planes of adenine, carboxyl, indole, and aminoethyl moieties are given in Table 6, together with the displacement of atoms from

Table 5. Hydrogen atom coordinates ($\times 10^3$) and isotropic temperature factors with their standard deviations

Atom	x	y	z	B/Å^2
AH2	6(4)	1071(5)	86(1)	3.3(7)
AH6A	373(5)	1186(6)	−11(1)	5.0(9)
AH6B	214(5)	1298(6)	−19(1)	5.0(9)
AH8	534(4)	539(5)	61(1)	3.5(8)
AH10A	405(4)	360(5)	110(1)	3.6(8)
AH10B	239(4)	445(5)	114(1)	4.0(8)
TH1	627(4)	−81(5)	175(1)	3.0(7)
TH2	719(4)	20(5)	264(1)	2 6(7)
TH4	929(3)	570(4)	192(1)	2.1(6)
TH5	905(4)	563(5)	106(1)	4.5(9)
TH6	766(4)	306(5)	55(1)	3.2(7)
TH7	655(4)	36(5)	88(1)	4.0(8)
TH10A	1005(4)	424(5)	287(1)	2.5(7)
TH10B	907(4)	303(5)	316(1)	3.2(7)
TH11A	788(3)	651(4)	255(1)	2.0(6)
TH11B	872(4)	644(5)	318(1)	2.6(7)
TH12A	612(4)	650(5)	295(1)	2.5(7)
TH12B	636(5)	427(6)	309(1)	5.5(10)
TH12C	581(4)	482(5)	257(1)	2.7(7)

the planes. The torsion angles are given in Table 7. The bond lengths and angles of the adenine ring agree with those found in related compounds within their standard deviations.[18] The purine base is planar with a maximum deviation of 0.024 Å for AN3. The bond parameters for the carboxyl group are also within their expected ranges as having no hydrogen atom, the group being almost planar and at approximately right angles to the purine base (dihedral angle=78.0°). The molecular conformation of AAA with the torsion angle, τ and ω, is very similar to one of the same molecule determined by Voet[19] (τ=84.3°, ω=7.7°), both molecules lying in (+)clinal and synperiplanar for τ and ω, respectively.

The bond lengths and angles of the TPA molecule agree with the values found in the crystal structures of the other TPA molecules: TPA,[20] TPA picrate,[21] TPA hydrochloride,[22] TPA phenylacetate,[23] TPA thymine-1-ylacetate,[24] and TPA 7,8-dimethylisoalloxazine-10-acetate.[2] The indole ring is also planar with a maximum shift of 0.025 Å for TC8, the dihedral angle between the indole ring and the aminoethyl group being 74.6°. Three hydrogen atoms (TH12A—TH12C) found in the difference map are tetrahedrally bound to TN12, indicating the amino group to be in a cationic $-NH_3^+$ form. The conformation of the TPA molecule in this crystal is similar to the hitherto analysed TPA molecules except thymine-1-ylacetate. The conformation having the torsion angles, χ and ϕ, in (+)anticlinal and in (−)synclinal regions, respectively, is thought to be the most stable one.[20]

Crystal Structure. The crystal structure projected along the b-axis is shown in Fig. 2. The intermolecular distances and angles for the hydrogen bonds and the

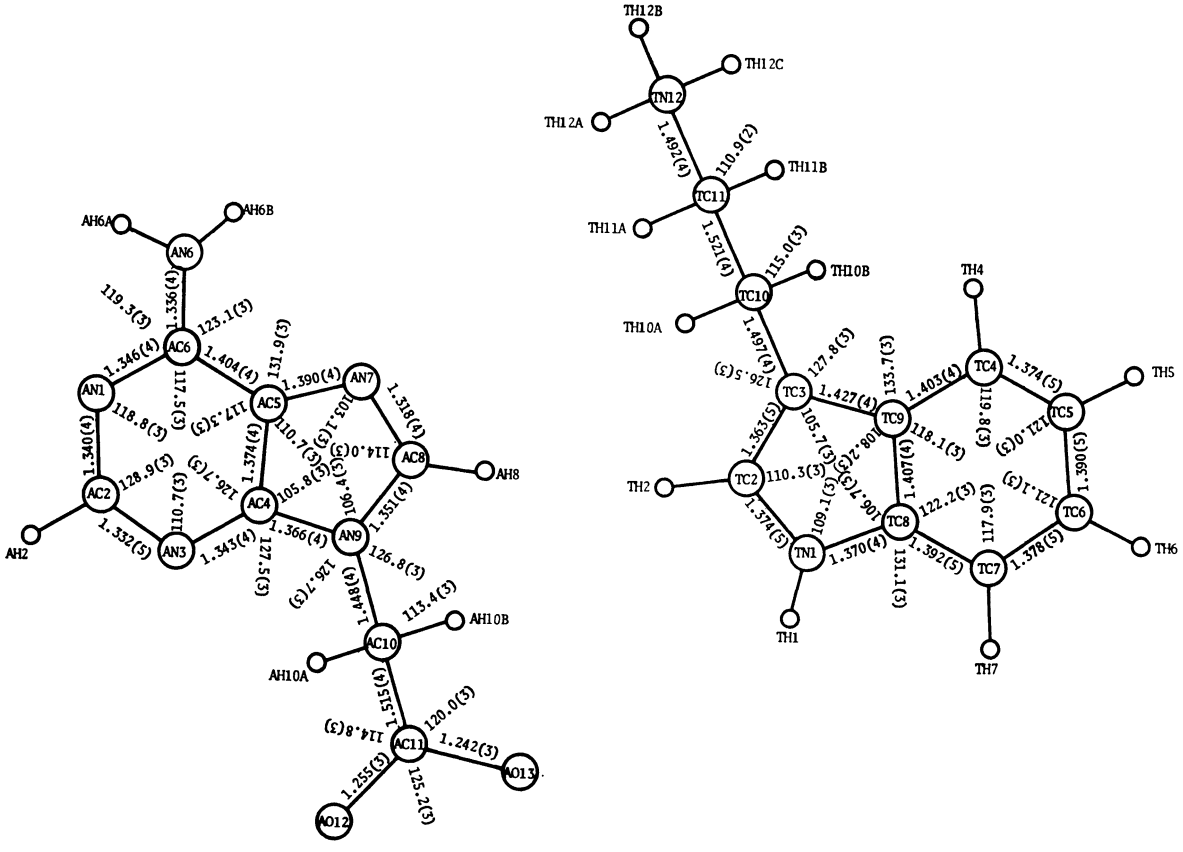

Fig. 1. Bond lengths and angles.

Table 6. Deviations of atoms from the least-squares planes

Equations of the best planes expressed by $m_1X+m_2Y+m_3Z=d$ in an orthogonal space

Plane	m_1	m_2	m_3	d
Purine ring	0.4328	0.4604	0.7750	4.8820
Carboxyl group	0.9435	−0.3247	−0.0658	0.5803
Indole ring	0.8419	−0.4977	0.2086	4.6306
Aminoethyl group	0.0555	−0.0222	0.9982	8.0422

Deviations (/Å) from the best planes:

AAA		TPA	
Purine ring		Indole ring	
AN1*	0.020	TN1*	0.005
AC2*	0.011	TC2*	−0.021
AN3*	−0.024	TC3*	−0.016
AC4*	−0.007	TC4*	0.018
AC5*	−0.014	TC5*	−0.016
AC6*	−0.009	TC6*	−0.021
AN7*	−0.004	TC7*	0.005
AC8*	0.009	TC8*	0.025
AN9*	0.018	TC9*	0.021
AN6	−0.049	TC10	−0.052
AC10	−0.036	TH1	0.062
AH2	0.014	TH2	−0.017
AH8	0.015	TH4	0.029
Carboxyl group		TH5	−0.081
AC10*	0.001	TH6	−0.055
AC11*	−0.004	TH7	−0.019
AO12*	0.001	Aminoethyl group	
AO13*	0.001	TC10*	0.0
AH10A	−0.821	TC11*	0.0
AH10B	0.853	TN12*	0.0
		TH10A	−0.125
Atoms with asterisks define the plane.		TH10B	−0.887
		TH11A	0.871
		TH11B	−0.859
		TH12A	−0.104
		TH12B	−0.536
		TH12C	0.904

Table 7. Torsion angles (/°) of TPA and AAA molecules

AAA	
AC4–AN9–AC10–AC11	−76.5
AC8–AN9–AC10–AC11 ; τ	98.5
AN9–AC10–AC11–AO12	183.2
AN9–AC10–AC11–AO13 ; ω	3.9
TPA	
TC2–TC3–TC10–TC11 ; χ	108.5
TC9–TC3–TC10–TC11	−72.0
TC3–TC10–TC11–TN12 ; ϕ	−65.7

short contacts less than 3.5 Å are given in Table 8.

In the crystal, the complex formation is mainly due to the salt bridge between the amino and carboxyl groups. Both the molecules are linked by the hydrogen bonds of the amino nitrogen atom(TN12) to the carboxyl oxygen atom(AO12 and AO13), which are formed around a twofold screw axis, AO13 participating further

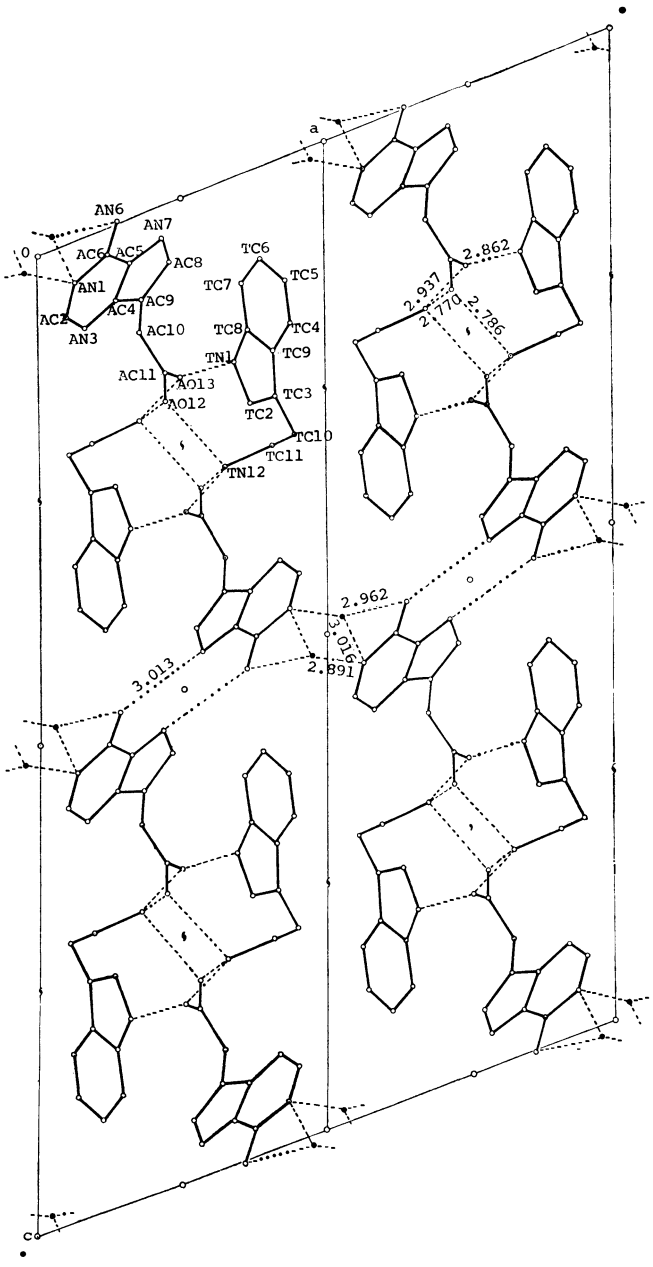

Fig. 2. The crystal structure viewed along the b-axis.

in a hydrogen bond with TN1 of the indole ring, which may strengthen the salt bridge formation. The complex molecules form an infinite helical array with two complex pairs per turn (Fig. 3). The packing mode is found frequently in the crystal structures of the complex formed by a salt bridge between the acid and amine components, such as the 5-methoxytryptamine: 5-methoxyindole-3-acetic acid (1 : 1) complex,[25] 5-methoxytryptamine: indole-3-acetic acid (1 : 1) complex,[25] TPA: phenylacetic acid (1 : 1) complex[23] and TPA: thymine-1-ylacetic acid (1 : 1) complex.[24]

On the other hand, AAA molecule is further linked by two kinds of hydrogen-bonding schemes with the neighboring AAA molecules related by a center of symmetry. One is a linkage by two identical hydrogen bonds of AN6 to AN7. This kind of dimer formation is frequently observed in adenine derivatives.[19,26–29] The

Table 8. Hydrogen bonds and short contacts less than 3.5 Å
Superscribed numbers represent the symmetry operators.

Hydrogen bonds

Donor	Acceptor	Distance/Å		Angle/°
		D···A	H···A	D–H···A
TN12[1)]	AO12[1)]	2.786(3)	1.79(3)	176(3)
TN12[2)]	AO12[1)]	2.770(3)	1.83(3)	170(3)
TN12[1)]	AO13[2)]	2.937(3)	2.07(5)	150(4)
TN1[3)]	AO13[1)]	2.862(4)	2.00(4)	150(3)
O(H_2O)[3)]	AN1[1)]	3.016(7)	—	—
O(H_2O)[1)]	AN1[5)]	2.891(7)	—	—
AN6[4)]	AN7[1)]	3.013(4)	2.07(4)	172(4)
AN6[1)]	O(H_2O)[3)]	2.962(7)	2.15(4)	144(8)

Short contacts

O(H_2O)[1)]–AC4[1)]	3.331(7)	O(H_2O)[1)]–AN9[1)]	3.335(7)
AC11[1)]–TN12[1)]	3.343(4)	AO12[1)]–TC2[1)]	3.307(4)
AO12[1)]–TC3[1)]	3.338(4)	AO13[1)]–TC11[1)]	3.493(4)
AO13[1)]–TN12[1)]	3.194(3)	AO13[1)]–AN9[1)]	2.723(3)
AO12[1)]–TC11[2)]	3.376(4)	TN1[1)]–TN12[2)]	3.429(4)
TC2[1)]–AO12[2)]	3.261(4)	TC2[1)]–TN12[2)]	3.449(4)
TN12[1)]–AN3[2)]	3.498(4)	AN1[1)]–AC10[3)]	3.390(4)
AC6[1)]–O(H_2O)[3)]	3.432(7)	AN1[1)]–AN1[5)]	3.389(5)

Symmetry code

1) x, y, z 2) $1-x, -1/2+y, 1/2-z$ 3) $x, 1+y, z$ 4) $1-x, 2-y, -z$ 5) $-x, 2-y, -z$

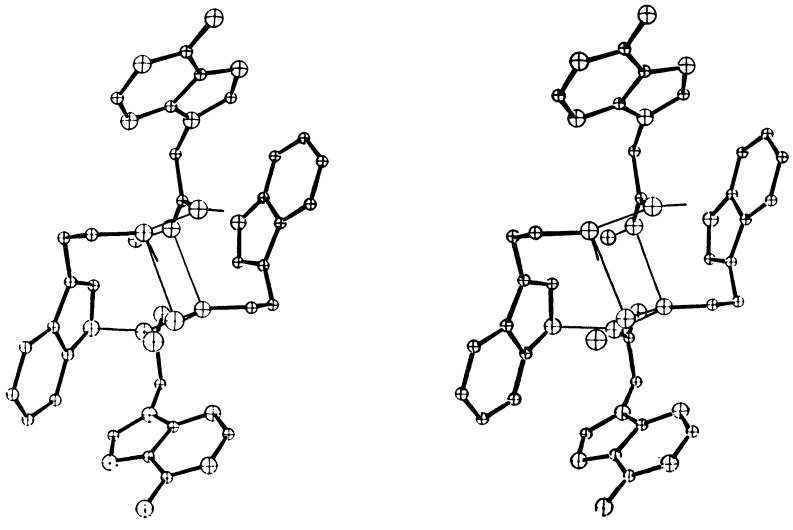

Fig. 3. The stereoscopic view of two complex pairs around a twofold screw axis.

other is the bond to the disordered crystal water (AN1··· O(H_2O)). The water molecule is not located on a center of symmetry, but found at two equally disordered positions separated from a center of symmetry by 0.715 Å. The water molecule is further hydrogen bonded to AN6.

The dihedral angle between the indole and adenine rings is at approximately right angles (72.7°). Neither hydrogen bond nor short contacts less than 3.5 Å exist between both rings. Contrary to our expectation, there is no specific interaction between the indole and adenine rings in this complex, whereas the interaction through the hydrogen bond is observed in the related crystal structures.[30,31] The hydrogen bonds between the carboxyl and amino groups might be preferable to any specific interaction of indole–adenine rings.

References

1) T. Sakaki, M. Inoue, S. Senda, and K. Tomita, *Biochem. Biophys. Res. Commun.*, **83**, 21 (1978).
2) T. Ishida, M. Inoue, T. Fujiwara, and K. Tomita, *J. Chem. Soc., Chem. Commun.*, **1979**, 358.
3) E. J. Gabbay, K. Sanford, C. S. Baxter, and L. Kapicak, *Biochemistry*, **12**, 4021 (1973).
4) R. Lawaczeck and K. G. Wagner, *Biopolymers*, **13**, 2003 (1974).
5) F. Morita, *Biochim. Biophys. Acta*, **343**, 674 (1974).
6) F. Brun, J. J. Toulmé, and C. Héléne, *Biochemistry*, **14**,

558 (1975).
7) H. Sigel and C. F. Naumann, *J. Am. Chem. Soc.*, **98**, 730 (1976).
8) V. Wray and K. G. Wagner, *Z. Naturforsch., Teil C*, **32**, 315 (1977).
9) N. H. Kolodny, A. C. Neville, D. L. Coleman, and P. C. Zamecnik, *Biopolymers*, **16**, 259 (1977).
10) J. Reuben, *FEBS Lett.*, **94**, 20 (1978).
11) J. J. Toulmé, *Bioinorg. Chem.*, **8**, 319 (1978).
12) J. C. Maurizot, G. Boubault, and C. Héléne, *Biochemistry*, **17**, 2096 (1978).
13) K. L. Carraway, P. C. Huang, and T. G. Scott, "Synthetic Procedures in Nucleic Acid Chemistry," ed by W. W. Zorbach and R. S. Tipson, John Wiley and Sons, New York (1968), Vol. 1, p. 3.
14) The Universal Crystallographic Computing System (Library Programs in the Computing Center of Osaka University, 1973), The Crystallographic Society of Japan.
15) "International Tables for X-Ray Crystallography," Kynoch Press, Birmingham (1974), Vol. 4.
16) G. Germain, P. Main, and M. M. Woolfson, *Acta Crystallogr., Sect. A*, **27**, 368 (1971).
17) Table 2 has been deposited at the Chemical Society of Japan (Document No. 7929).
18) D. Voet and A. Rich, "Nucleic Acid Research and Molecular Biology," Academic Press (1970), Vol. 10, pp. 183—265.
19) D. Voet, *J. Am. Chem. Soc.*, **95**, 3763 (1973).
20) M. Inoue, T. Sakaki, A. Wakahara, and K. Tomita, *Biochim. Biophys. Acta*, **543**, 123 (1978).
21) G. L. Gartland, G. R. Freeman, and C. E. Bugg, *Acta Crystallogr., Sect. B*, **30**, 1841 (1974).
22) A. Wakahara, T. Fujiwara, and K. Tomita, *Bull. Chem. Soc. Jpn.*, **46**, 2481 (1973).
23) M. Inoue, T. Sakaki, T. Fujiwara, and K. Tomita, *Bull. Chem. Soc. Jpn.*, **51**, 1123 (1978).
24) T. Ishida, M. Inoue, and K. Tomita, *Acta Crystallogr., Sect. B*, **35**, 1642 (1979).
25) T. Sakaki, A. Sogo, A. Wakahara, T. Kanai, T. Fujiwara, and K. Tomita, *Acta Crystallogr., Sect. B*, **32**, 3235 (1976).
26) S. H. Kim and A. Rich, *Proc. Natl. Acad. Sci. U. S. A.*, **60**, 402 (1968).
27) S. S. Tavale, T. D. Sakore, and H. M. Sobell, *J. Mol. Biol.*, **43**, 375 (1969).
28) J. M. Broomhead, *Acta Crystallogr.*, **1**, 324 (1948).
29) W. Cochran, *Acta Crystallogr.*, **4**, 81 (1951).
30) T. Kaneda and J. Tanaka, *Bull. Chem. Soc. Jpn.*, **49**, 1799 (1976).
31) M. Ohki, A. Takenaka, H. Shimanouchi, and Y. Sasada, *Bull. Chem. Soc. Jpn.*, **50**, 2573 (1977).

New Applications of Crown Ethers. I. Primary Alkylamine-Water-Crown Ether System as a Hydroxide Ion Source in the Reduction with Carbonylhydridoferrate Anion

Fumio WADA,* Ryoji ISHIHARA, Yasufumi KAMOHARA, and Tsutomu MATSUDA

Department of Organic Synthesis, Faculty of Engineering, Kyushu University, Hakozaki, Higashi-ku, Fukuoka 812

(Received March 1, 1979)

Utility of the primary alkylamine–water–crown ether system as an effective source of hydroxide ion was studied by the reduction of benzylideneacetone with carbonylhydridoferrate anion. Excellent conversion and selectivity for the reduction were attained in a two-phase system (benzene–water) in the presence of dicyclohexano-18-crown-6, comparable to those obtained with use of potassium hydroxide in place of the amine. Effects of several alkylamines and crown ethers were presented. IR examination of pentacarbonyliron–butylamine–water in benzene with or without the crown ether showed that the presence of the crown ether markedly alters the route of formation of the reducing agent(s).

The macrocyclic polyethers (crown ethers) form stable complexes with alkali and alkaline earth metal cations as well as primary alkylammonium ions. The chemistry of the ammonium salt complexes was investigated in detail by Cram and his collaborators.[1] They utilized the nature of the complexes as a novel method for optical resolution of amino acids.[2]

Primary alkylamine in water is in equilibrium as shown by Eq. 1. When an alkylammonium hydroxide is brought into formation of a complex (**1**) with a crown ether, the equilibrium would shift to the right, and in a two phase, *e.g.* benzene and water, the resulting complex could be transferred to the organic phase to greater extent. The phenomenon can be considered to be production of an increased concentration of hydroxide ion from an alkylamine and water, especially in the organic phase.

$$RNH_2 + H_2O \rightleftharpoons \overset{+}{R}NH_3\,OH^- \quad (1)$$

$$\overset{+}{R}NH_3\,OH^- + \text{crown ether} \rightleftharpoons [\overset{+}{R}NH_3 \cdot \text{crown ether}]\,OH^- \quad (2)$$

1

The postulate led us to study the use of primary alkylamine–water–crown ether system as a source of hydroxide ion in organic reactions.

Pentacarbonyliron and its polynuclear homologs can be converted into carbonylhydridoferrate anions ($HFe(CO)_4^-$ from $Fe(CO)_5$) by the action of a strong base. The hydrido anions have been used in the selective reduction of activated double bonds.[3] This paper reports on the use of primary alkylamine–water–crown ether combination as an effective alkali in the hydrido anion reduction. Unsaturated esters (acrylates or cinnamates) could be reduced by the reduction system, but side reactions such as transamination and Michael addition as well as hydrolysis are involved, thus affording unreproducible results. Benzylideneacetone was selected as an adequate substrate, although its reduction was also accompanied by Michael addition. The present study was undertaken in order to confirm the possibility of suppression of the side reaction by a technique consisting of phase-transfer effect and enhancement of hydroxide ion activity.

Results and Discussion

Effect of Dicyclohexano-18-crown-6 (DC18C6). Benzylideneacetone (1 mmol) was allowed to react with a reduction system, butylamine(2 mmol)–water(0.5 ml)–$Fe(CO)_5$(4 mmol)–benzene(2 ml), at 25 °C under vigorous stirring for 24 h. GLC analysis of the product in the benzene layer showed a 77% consumption(conversion) of the substrate and 22% formation of 4-phenyl-2-butanone (based on benzylideneacetone reacted; selectivity). The balance represents the extent of side reaction. Two of the by-product A and B were observed in the ratio 9: 1. Treatment of benzylideneacetone with 2 molar excess of butylamine in benzene gave the main by-product which coincided with peak A and was considered to be the Michael adduct. Attempt to isolate the two peaks from the reduction mixture for structural identification by preparative GLC was unsuccessful because of decomposition of the components during the course of separation. The results of the reduction under various conditions are summarized in

TABLE 1. REDUCTION OF BENZALACETONE[a] WITH $Fe(CO)_5$–RNH_2–H_2O–CROWN ETHER–BENZENE SYSTEM

Run	CE[a]	Base[a]	Reaction time/h	Result[b] Conversion %	Result[b] Selectivity %
1	DC18C6	*n*-C_4NH_2	24	100	88
2	DC18C6	*t*-C_4NH_2	24	77	95
3	DC18C6	*n*-C_8NH_2	24	100	65
4	DC18C6	*n*-C_8NH_2	5	84	83
5	DC18C6	KOH	24	93	93
6	—	*n*-C_4NH_2	24	76	22
7	—	*t*-C_4NH_2	24	38	61
8	—	*n*-C_8NH_2	24	84	32
9	—	KOH	24	10	100
10	DC18C6	*n*-C_4NH_2	9	65	86
11	18C6	*n*-C_4NH_2	9	51	29
12	DC18C6	K_2CO_3	24	87	92
13	DC18C6	CH_3CO_2K	24	17	88

a) Reaction conditions: benzalacetone, 1 mmol; crown ether (CE), 1 mmol; base, 2 mmol, at 25 °C. b) Determined by GLC.

Table 1. When an equimolar amount of DC18C6 was added, the reduction of benzylideneacetone proceeded to give 100% conversion and 88% selectivity. The result is nearly comparable to that obtained with $Fe(CO)_5$–KOH–DC18C6 combination (Run 5, Table 1), and evidences pronounced effect of the crown ether addition. The expected phase-transfer effect in the present system is also observed in the $Fe(CO)_5$–KOH combination. Other weak bases, K_2CO_3 and CH_3CO_2K, can also act as a hydroxide ion source in the presence of DC18C6, though less effectively in the latter. Fedoryński *et al.*[4] recently reported that a combination of K_2CO_3 and a crown ether in non-polar solvents can be used effectively for generating carbanions from active methylene compounds in a solid-liquid system.

Effect of Structures of Primary Alkylamines and Crown Ethers. The stability of primary alkylammonium ion–crown ether complexes depends on the structure of the amines, and steric bulk of the alkyl groups is an important factor.[5] The steric effect was examined with the use of *t*-butylamine in the reduction. Its use in place of butylamine gave a low conversion as expected, but selectivity for reduction was considerably high even in the absence of DC18C6. The low conversion could be much improved by the addition of the crown ether, accompanied by increase in selectivity. The high selectivity obtained with the tertiary-amine under both conditions can be interpreted by the decrease in nucleophilic function of the amine due to the bulky *t*-butyl group. Octylamine was more efficient than butylamine for the reduction probably because of an increase of its solubility and the resulting increase of hydroxide ion concentration in the benzene layer even in the absence of the crown ether. However, the increase of solubility of the amine seems to cause an increase of Michael adduct leading to a lower selectivity.

18-Crown-6(18C6) is a more favorable complexing agent to alkylammonium salts than DC18C6. However, it gave no improvement in both conversion and selectivity as compared to the latter. This might be attributed to a larger solubility of 18C6 and its ammonium ion complex in water. Benzocrown ethers, benzo-18-crown-6 and dibenzo-18-crown-6, were less efficient than 18C6. This indicates that conversion and selectivity in the present reduction depend not only on the stability of **1** but also on solubilities of **1** and free amines in the benzene layer.

Routes of the Formation of Reducing Agent. In the present reduction, reducing agents are considered to be $HFe(CO)_4^-$ and $HFe_2(CO)_8^-$ which might be formed from the mononuclear anion under the reaction conditions. Collman *et al.*[3d] reported that $Na^+HFe_2(CO)_8^-$ is more reactive (>26 times) than $Na^+HFe(CO)_4^-$ in the reduction of activated double bonds in THF. A qualitative examination for the presence of the reagents and also for the effect of DC18C6 on their formation was made by IR measurement.[6] When $Fe(CO)_5$ (1 mmol) was allowed to react with a mixture of butylamine (2 mmol) and water (0.5 ml) in benzene (4 ml) at 25 °C under vigorous stirring in the presence of the crown ether, the color of the mixture turned rapidly from yellow to deep-red. A spectrum of the benzene layer taken 2 h after mixing showed the formation of $HFe(CO)_4^-$ (ν_{CO} 1915 cm^{-1} sh), 1880 cm^{-1} (s)) and $HFe(CO)_{11}^-$ (ν_{CO} 2070 cm^{-1} (vw), 1995 cm^{-1}(s), 1978 cm^{-1} (m), 1950 cm^{-1} (sh)), and the presence of a small quantity of unreacted $Fe(CO)_5$ (ν_{CO} 2020 cm^{-1} (s), 1995 cm^{-1} (s)). On the other hand, in the absence of the crown ether the color change to deep-red proceeded slowly, the IR spectrum of the benzene layer indicating a large quantity of $Fe(CO)_5$ remaining unreacted. Hydrido anions observed in the spectrum were small amounts of $HFe_2(CO)_8^-$ (ν_{CO} 1913 cm^{-1}) and $HFe_3(CO)_{11}^-$, the absorption of $HFe(CO)_4^-$ being very weak.

The marked effect of DC18C6 in the formation of $HFe(CO)_4^-$ strongly suggests that there are two major routes for the formation of the anion, the reaction of $Fe(CO)_5$ with free amine and that with hydroxide ion in **1** derived according to Eq. 2. The reaction of $Fe(CO)_5$ with alkylamines, especially with secondary amines, was studed in detail by Edgell *et al.*[7] Application of their results to the present primary amine system gave the following results. A reaction of a primary amine with $Fe(CO)_5$ gives an equilibrium mixture of $R\overset{+}{N}H_2COFe(CO)_4^-$ (**3**) and $[R\overset{+}{N}H_3][RNHCOFe(CO)_4^-]$ (**4**); in the presence of water and excess amine they are hydrolyzed to an equimolar mixture of $[R\overset{+}{N}H_3][HFe(CO)_4^-]$ (**2**) and $[R\overset{+}{N}H_3][RNHCO_2^-]$ (**5**) (Scheme 1). Under the present conditions containing only a small quantity of water (especially in the benzene layer) hydrolysis would be sluggish and far from complete. The lower selectivity for benzylideneacetone in the absence of DC18C6 (Table 1) can be accommodated with the slow formation of the hydrido anions (HFe-

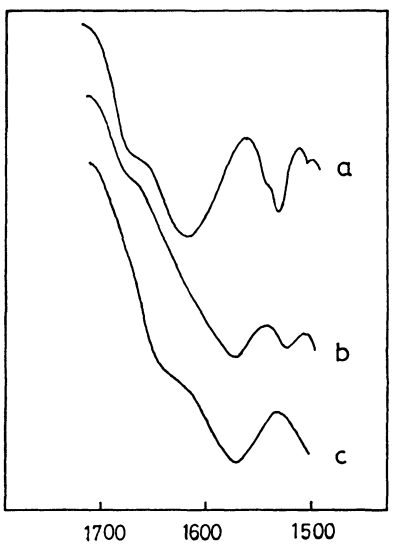

Fig. 1. IR spectra of the reaction mixture of $Fe(CO)_5$ and butylamine, and butylcarbamate solution.
a) $Fe(CO)_5$–*n*-$BuNH_2$–DCl8C6–H_2O–C_6H_6.
b) $Fe(CO)_5$–*n*-$BuNH_2$–H_2O–C_6H_6.
c) $[n\text{-Bu}\overset{+}{N}H_3][n\text{-BuNHCO}_2^-]$–DCl8C6–$C_6H_6$.
The crown ether was added to solubilize the salt in benzene.

$(CO)_4^-$ and $HFe_2(CO)_8^-$). The formation of butylcarbamate salt (**5**) in the reduction mixture was also confirmed by comparison of its IR spectrum with that of an authentic butylcarbamate solution (1570 cm^{-1}) (Fig. 1).

In the absence of a crown ether.

$$RNH_2 + Fe(CO)_5 \rightleftharpoons \underset{\mathbf{3}}{R\overset{+}{N}H_2COFe(CO)_4^-}$$

$$\overset{RNH_2}{\rightleftharpoons} [R\overset{+}{N}H_3][RNHCOFe(CO)_4^-]$$
$$\mathbf{4}$$

$$\mathbf{3} \text{ and } \mathbf{4} \xrightarrow{H_2O,\ RNH_2}$$

$$[R\overset{+}{N}H_3][HFe(CO)_4^-] + [R\overset{+}{N}H_3][RNHCO_2^-]$$
$$\mathbf{2} \qquad\qquad \mathbf{5}$$

Scheme 1.

In the presence of a crown ether (CE).

$$RNH_2 + H_2O \rightleftharpoons R\overset{+}{N}H_3\,OH^-$$

$$R\overset{+}{N}H_3\,OH^- \overset{CE}{\rightleftharpoons} [R\overset{+}{N}H_3 \cdot CE]\,OH^-$$
$$\mathbf{1}$$

$$\mathbf{1} + Fe(CO)_5 \longrightarrow \underset{\mathbf{6}}{[R\overset{+}{N}H_3 \cdot CE][HFe(CO)_4^-]}$$

$$+ \underset{\mathbf{7}}{[R\overset{+}{N}H_3 \cdot CE]\,HCO_3^-}$$

$$\text{and/or } \underset{\mathbf{8}}{[R\overset{+}{N}H_3 \cdot CE]_2CO_3^{2-}}$$

Scheme 2.

Scheme 2 is a modification of the pathway commonly accepted for the formation of carbonylhydridoferrate anions by causic alkalis (so-called base reaction), and could be realized by complexization of the alkylammonium hydroxide with crown ether. Hydroxide ion of **1** would effectively react with $Fe(CO)_5$ to give **6** and **7** (and/or **8**). The rapid formation of $HFe(CO)_4^-$ in a large quantity and the enhanced conversion in the reduction, as high as that observed when KOH was used, could be interpreted by this route, though the extent of the participation of $HFe_2(CO)_8^-$ in the reduction is not clear. IR inspection of the reduction mixture obtained in the presence of DC18C6 indicated the presence of hydrogencarbonate and/or carbonate ions (*ca.* 1620 cm^{-1}) and a marked decrease of the butylcarbamate ion (Fig. 1). It is obvious that the increased formation of **6** (and its polynuclear homologs) as well as **7** and **8** cause a decrease of free alkylamine, especially in the benzene layer, by its conversion into the onium ion complexes. An interpretation for the increase in selectivity in the reduction effected by the addition of DC18C6 is given by Scheme 2.

It is concluded that the primary alkylamine–water–crown ether system can be used as effective hydroxide ion source especially in a two phase system.

Eoperimental

Materials. Benzylideneacetone, DC18C6,[8] and benzocrown ethers[8] were prepared by conventional methods. Commercial 18C6 (Bokusuy Brown Co.) was used. Pentacarbonyliron (Alfa Products), primary amines, water, and benzene were distilled and stored under nitrogen.

General Procedure. All reactions were carried out under nitrogen with a vessel (*ca.* 10 ml) equipped with an outer jacked for circulation of water (thermostated at 25±0.5 °C) and a serum cap for introduction of pentacarbonyliron by means of a syringe. Water (0.5 ml), alkylamine (2 mmol), benzene (2 ml) containing heptadecane as an internal standard, benzylideneacetone (1 mmol) and a crown ether (1 mmol) were placed in the vessel, and then pentacarbonyliron (4 mmol) was added. The mixture was vigorously stirred at 25 °C. After a certain time (24 h or 8 h), the reaction mixture was neutralized by addition of aq HCl, and the aqueous layer was extracted by ether twice. The products in the combined organic layer were analyzed by GLC (PEG 20M 10%-Celite 545, 3 mm×2 m, FID).

References

1) a) D. J. Cram and J. M. Cram, *Science*, **183**, 803 (1974); b) D. J. Cram, R. C. Helgeson, L. R. Sousa, J. M. Timko, N. Newcomb, P. Moreau, F. Dejong, G. W. Gokel, L. A. Domeier, S. O. Peacock, M. Madan, and L. Kaplan, *Pure Appl. Chem.*, **43**, 327 (1975).

2) E. P. Kyba, K. Koga, L. R. Sousa, M. G. Siegel, and D. J. Cram, *J. Am. Chem. Soc.*, **95**, 2692 (1972).

3) a) R. Noyori, I. Umeda, and T. Ishigami, *J. Org. Chem.*, **37**, 1542 (1972); b) H. Alper, *ibid.*, **37**, 3972 (1972); c) F. Wada and T. Matsuda, *Nippon Kagaku Kaishi*, **1973**, 2177 (1973); d) J. P. Collman, R. G. Finke, P. L. Matlock, R. Wahren, R. G. Komoto, and J. I. Brauman, *J. Am. Chem. Soc.*, **100**, 1119 (1978).

4) M. Fedoryńsky, K. Wojciechowski, Z. Matacz, and M. Makosza, *J. Org. Chem.*, **43**, 4682 (1978).

5) D. J. Cram and J. M. Cram, *Acc. Chem. Res.*, **11**, 8 (1978).

6) For characteristic IR absorptions of the carbonylhydridoferrate anions and manipulation for IR measurement, *cf.* F. Wada and T. Matsuda, *J. Organomet. Chem.*, **61**, 365 (1973).

7) W. F. Edgell, M. T. Yang, B. J. Bulkin, R. Bayer, and N. Koizumi, *J. Am. Chem. Soc.*, **87**, 3090 (1965).

8) C. J. Pedersen, *J. Am. Chem. Soc.*, **89**, 2495 (1967).

Sodium Methoxide Catalyzed Isomerization of Dimethyl 1-Oxo-*cis*-3a,7a-dihydroindene-3a,7a-dicarboxylates to Dimethyl 3-Oxo-1,7-indandicarboxylates

Tadao UYEHARA,* Shoichi MIYAKOSHI, and Yoshio KITAHARA†

Department of Chemistry, Faculty of Science, Tohoku University, Aoba, Aramaki, Sendai 980

(Received March 6, 1979)

Treatment of dimethyl 1-oxo-*cis*-3a,7a-dihydroindene-3a,7a-dicarboxylates (**A**) with sodium methoxide in methanol gave particular dimethyl 3-oxo-1,7-indandicarboxylates (**F**). A multistep mechanism for the isomerization was proposed on the basis of the positional correlations between the dihydroindenones **A** and the corresponding isomers **F**. The isomerization seems to be initiated by the addition of a methoxide to the 1 position of the dihydroindenones **A** affording the cyclohexadienide anions (**B**), which cyclize to give dimethyl 1-oxo-*cis*-3a,7a-dihydroindene-3a,4-dicarboxylates (**C**). The dihydroindenones **C** become enolates (**D**), whose methoxycarbonyl group at the 3a position (E_9) shifts to the 1 position of the enolates of **F**, (**E**), with the aid of aromatization. The same treatment of methyl 3-oxo-*cis*-3a,7a-dihydroindene-3a-carboxylates gave key information on the process for the isomerization of **A**.

Dimethyl 1-oxo-*cis*-3a,7a-dihydroindene-3a,7a-dicarboxylate (**1**) is a product of a thermal rearrangement of dimethyl 2-oxobicyclo[3.2.2]nona-3,6,8-triene-6,7-dicarboxylate (dimethyl homobarrelenone-6,7-dicarboxylate).[1] During the course of investigation on the structure of **1**, it was found that the dihydroindenone is sensitive to sodium methoxide in methanol.[2] When a solution of **1** in methanol was added to a solution of sodium methoxide at 0 °C or at room temperature, the mixture immediately turned violet and then rapidly became pale yellow. The product, obtained in 95% yield, was dimethyl 3-oxo-1,7-indandicarboxylate (**2**). Under the same conditions the 7-methoxy derivative of **1**, (**3**), was isomerized to dimethyl 6-methoxy-3-oxo-1,7-indandicarboxylate (**4**).[2] This paper deals with an attempt to clarify the mechanism of isomerization.

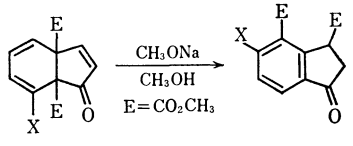

1 X=H **2** X=H
3 X=OCH_3 **4** X=OCH_3

Results and Discussion

Several alkyl derivatives of **3** were prepared and treated with sodium methoxide in methanol to examine the generality and limit of isomerization and the positional correlations between the *cis*-3a,7a-dihydroindenones and the products.

Dimethyl 2-isopropyl-7-methoxy-1-oxo-*cis*-3a,7a-dihydroindene-3a,7a-dicarboxylate (**5**) is the product of a thermal rearrangement of dimethyl 3-isopropyl-1-methoxyhomobarrelenone-6,7-dicarboxylate (**5a**) derived by the regioselective Diels-Alder reaction of 7-isopropyl-2-methoxy-2,4,6-cycloheptatrien-1-one (7-isopropyl-2-methoxytropone, **5b**) with dimethyl acetylenedicarboxylate.[3] Similarly, dimethyl esters of 3-isopropyl- and 5-isopropyl-7-methoxy-1-oxo-*cis*-3a,7a-dihydroindene-3a,7a-dicarboxylic acids (**6** and **7**) were prepared from 6- and 4-isopropyl-2-methoxytropones (**6b** and **7b**) *via* the homobarrelenones (**6a** and **7a**), respectively.[3]

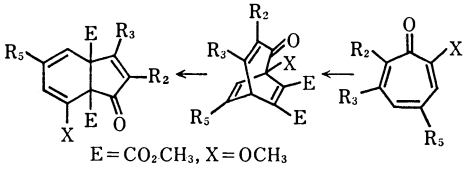

5 R_2=*i*-Pr, R_3=R_5=H **5a** **5b**
6 R_2=R_5=H, R_3=*i*-Pr **6a** **6b**
7 R_2=R_3=H, R_5=*i*-Pr **7a** **7b**

The conditions and results of the reactions of the *cis*-3a,7a-dihydroinden-1-ones with sodium methoxide in methanol are given in Table 1. A solution of **5** was added to a solution of sodium methoxide in methanol at room temperature (Run 5). The mixture soon turned reddish violet and then slowly became pale yellow. After being left to stand for 4 h, the solution was acidified and extracted promptly with three portions of dichloromethane. The product (**8**) is an isomer of **5** whose infrared spectrum shows a typical absorption due to the carbonyl of a 1-indanone, at 1691 cm^{-1}. The ultraviolet spectrum of **8** exhibits an absorption maximum of the electron transfer band at 270 nm, which is 25 nm longer than that of **2**. The difference suggests that **8** is one of the 5-methoxy-1-indanones.[4] The NMR spectrum of **8** indicates that the compound is dimethyl 2-isopropyl-6-methoxy-3-oxo-1,7-indandicarboxylate, showing an AB pattern at δ=7.10 and 7.88 (J=8.6 Hz) for H_5 (R_6) and H_4 (R_5), respectively, a doublet at δ=4.25 (J=3.4 Hz) for H_1 (R_3) and a doublet of doublets at δ=2.81 (J=4.1 and 3.4 Hz) for H_2.

Under the same conditions, **7** was isomerized to dimethyl 4-isopropyl-6-methoxy-3-oxo-1,7-indandicarboxylate (**9**) (Run 6), whose structure was deduced on the basis of its spectra.

3-Isopropyldihydroindenone **6** was inactive to sodium methoxide in methanol at room temperature (Run 7), whereas the isomer (**10**) was obtained when **6** and the base were heated under reflux in methanol (Run 8).

† Deceased February 4, 1976.

Product **10** has a characteristioc absorption maximum at 271 nm, its NMR spectrum showing an AB pattern at δ=7.05 and 7.93 (J=8.7 Hz) for H_5 (R_6) and H_4 (R_5), respectively, and AB pattern at δ=2.67 and 3.08 (J=19.2 Hz) for the *geminal* protons at the 2 position. Thus compound **10** should be dimethyl 1-isopropyl-6-methoxy-3-oxo-1,7-indandicarboxylate. The fact that **6** was isomerized to **10** seems to supply valuable information on the mechanism of the isomerization, but the reaction conditions were different from those for other dihydroindenones.

Table 1. A sodium methoxide catalyzed isomerization of dimethyl 1-oxo-*cis*-3a,7a-dihydroindene-3a,7a-dicarboxylates in methanol

Run	Dihydro-indenone	Conditions (temp, time)	Product	Yield[a] %
1	**1**[b]	0 °C, 5 min	**2**	95
2	**1**	r.t., 5 min	**2**	87
3	**1**	reflux, 10 min	**2**	74.5
4	**3**	r.t., 5 min	**4**	90
5	**5**	r.t., 4 h	**8**	96.5
6	**7**	r.t., 4 h	**9**	98
7	**6**	r.t., 12 h	—	95[c]
8	**6**	reflux, 12 h	**10**	63.4
9	**11**	r.t., 12 h	**13**	77
10	**12**	r.t., 12 h	—	95[c]
11	**12**	reflux, 12 h	**14**	74.5
12	**16**[d]	r.t., 4 h	**17**	70

a) After isolation. b) Ref. 2. c) Recovery. d) Methyl 4-methoxy-3-oxo-*cis*-3a,7a-dihydroindene-3a-carboxylate.

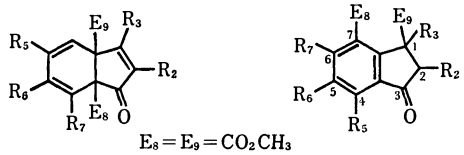

$E_8=E_9=CO_2CH_3$

5	R_2=*i*-Pr, $R_3=R_5=R_6=$H, $R_7=OCH_3$	**8**
6	R_3=*i*-Pr, $R_2=R_5=R_6=$H, $R_7=OCH_3$	**10**
7	R_5=*i*-Pr, $R_2=R_3=R_6=$H, $R_7=OCH_3$	**9**
11	$R_3=CH_3$, $R_2=R_5=R_6=R_7$H	**13**
12	$R_3=CH_3$, $R_2=R_5=R_6=$H, $R_7=OCH_3$, $E_8=CO_2CH_3$, $E_9=$H	**14**
16	$R_2=R_3=R_5=R_6=$H, $R_7=OCH_3$	**17**

In order to know the generality of formation of dimethyl 1-alkyl-3-oxo-1,7-indandicarboxylates from the corresponding dimethyl 3-alkyl-1-oxo-*cis*-3a,7a-dihydroindene-3a,7a-dicarboxylate, we developed a general synthetic method for 3-methyl-2-cyclopenten-1-ones from 2-cyclopenten-1-ones, prepared dimethyl 3-methyl-1-oxo-*cis*-3a,7a-dihydroindene-3a,7a-dicarboxylates (**11** and **12**)[5] and treated them with sodium methoxide.

Isomerization of **11** proceeded at room temperature to give dimethyl 1-methyl-3-oxo-1,7-indandicarboxylate (**13**) (Run 9). The other 3-methyldihydroindenone **12** was not isomerized at room temperature, giving the somer (**14**) in boiling methanol (Runs 10 and 11, respectively). Thus dimethyl 3-alkyl-1-oxo-*cis*-3a,7a-dihydroindene-3a,7a-dicarboxylates in general are isomerized with sodium methoxide to the corresponding dimethyl 1-alkyl-3-oxo-1,7-indandicarboxylates.

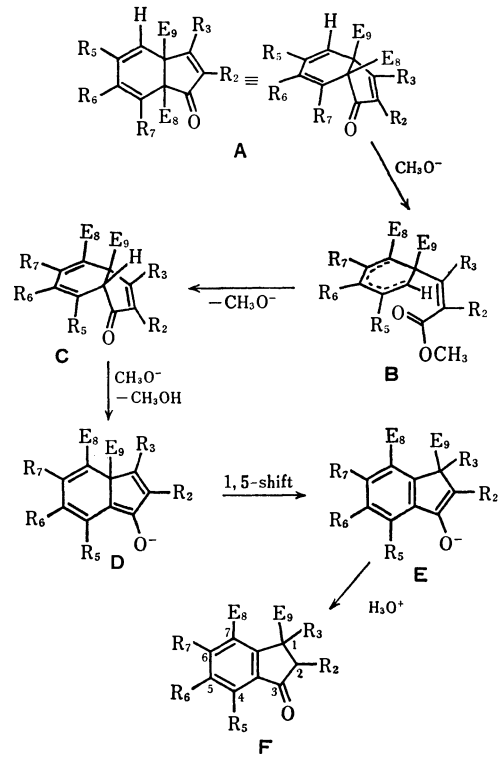

Scheme 1.

From the results we are able to estimate positional correlations between the dihydroindenones and the isomeric indanones. A mechanism for the isomerization is proposed as a working hypothesis which satisfies the positional correlations (Scheme 1). The mechanism shows that sodium methoxide acts as a catalyst in the first and second steps (**A** to **C**). To know the role of sodium methoxide in the reactions, **1** was teated with sodium ethoxide in ethanol. The reaction of **1** at room temperature for 10 min gave diethyl 3-oxo-1,7-indandicarboxylate (**15**) in 64.2% yield. The same reaction for 10 s afforded a mixture of **1** (recovered) and *dimethyl* 3-oxo-1,7-indandicarboxylate **2** in a 81 : 19 ratio. Thus, the alkoxides are shown to be the catalysts for the isomerization.

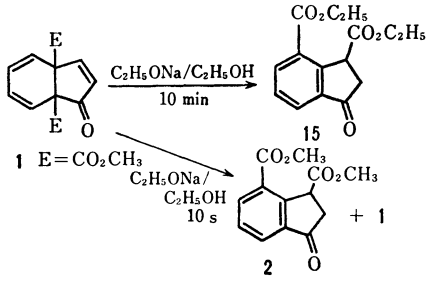

The tentative mechanism shows that E_9 of the dihydroindenones shifts to the 1 position of the indan-3-ones and E_8 of the former corresponds to the methoxycarbonyl group at the 7 position of the latter. For confirmation of the working hypothesis, either methyl ester of 1-oxo-*cis*-3a,7a-dihydroindene-3a- or 7a-carboxylic acid is necessary. We were able to prepare methyl 4-methoxy-3-oxo-*cis*-3a,7a-dihydroindene-3a-carboxylate

(**16**).[3]

When **16** was treated with sodium methoxide in methanol (Run 12), methyl 5-methoxy-1-oxo-4-indancarboxylate (**17**) was obtained in 70% yield. Thus, the methoxycarbonyl group at the 7a position of the dihydroindenones should correspond to that at the 7 position of the products, indan-3-ones.

Formation of the intermediate **B** is supported by the following results. When methyl 4-methoxy-1-methyl-3-oxo-*cis*-3a,7a-dihydroindene-3a-carboxylate (**18**), derived from **16** *via* the pyrazoline (**19**), was treated with sodium methoxide in methanol, 1,2,3-trisubstituted benzene (**20**) was formed selectively. Its absorption spectra show that the compound is not methyl 5-methoxy-3-methyl-1-oxo-4-indancarboxylate. The ultraviolet spectrum does not exhibit the typical absorption maximum of 1-indanones, at *ca.* 300 nm. The infrared spectrum shows no absorption at *ca.* 1700 cm^{-1} due to the carbonyl of 1-indanones. The NMR spectrum of **20** indicates that the compound is methyl 3-(3-methoxy-2-methoxycarbonylphenyl)butanoate: the spectrum exhibits a doublet at δ=1.24 (3H, J=6.8 Hz) for CH_3–(CH), an ABC pattern at δ=6.68 (dd, J=8.0 and 0.9 Hz), 6.78 (dd, J=8.0 and 0.9 Hz) and 7.20 (t, J=8.0 Hz) for the three adjacent protons on the benzene ring, an ABC pattern at δ=2.34 (dd, J=15.0 and 9.0 Hz), 2.59 (dd, J=15.0 and 5.6 Hz) and 3.14 (ddq, J=9.0, 5.6, and 6.8 Hz) for the $-CH_2-CH(CH_3)$ system, and three singlets at δ=3.54 (3H), 3.73 (3H), and 3.81 (3H) for the methyl protons of the ether and the esters.

The process for formation of **20** should be addition of a methoxide to the 3 position of **18** giving the anion (**B'**), which corresponds to the intermediate **B** in Scheme 1, followed by aromatization to the intermediate (**21**).[6]

The reaction of dimethyl 4,7-dimethoxy-1-oxo-*cis*-3a,7a-dihydroindene-3a,7a-dicarboxylate (**22**)[3] and sodium methoxide gave a mixture of several products which could not be separated.

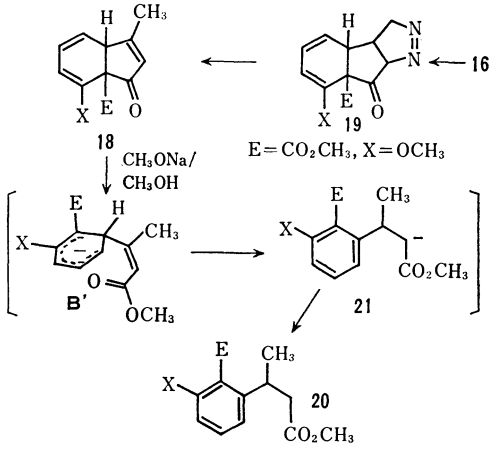

The infrared spectrum of the mixture shows no typical absorption for the carbonyl of 1-indanones. If the working hypothesis is correct, **22**, would not give 1-indanones.

The fourth step of the mechanism (**D** to **E**) is the 1,5-shift of the methoxycarbonyl group and the aromatization. This type of migration of an alkoxycarbonyl group was observed on a cyclopentadiene skeleton.[7]

So far, the mechanism (Scheme 1) seems to be adequate for the isomerization of dimethyl 1-oxo-*cis*-3a,7a-dihydroindene-3a,7a-dicarboxylates to dimethyl 3-oxo-1,7-indandicarboxylates.

Experimental

General. Melting point were determined on a Thomas Hoover MP apparatus, and are uncorrected. Infrared spectra were recorded on Hitachi EPI-3 and Model 215 Spectrophotometers. Ultraviolet spectra were recorded on a Hitachi EPS-2T spectrometer. NMR spectra were obtained on Varian A-60 and HA-100 spectrometers equipped with spin decouplars, using tetramethylsilane as an internal standard. Mass spectral studies were conducted using a Hitachi RMU-6D spectrometer.

*Reaction of Dimethyl 1-Oxo-*cis*-3a,7a-dihydroindene-3a,7a-dicarboxylates with Sodium Methoxide in Methanol at Room Temperature. General Procedure*: To a freshly prepared solution of sodium methoxide in methanol (100 mg of sodium and 10 ml of absolute methanol) was added rapidly a solution of the dihydroindenones (*ca.* 100 mg) in methanol (10 ml) at room temperature (on a water bath), and the mixture was allowed to stand for 5 min to 12 h. The reaction was quenched by 2 M-hydrochloric acid, diluted with water and extracted rapidly with three portions of dichloromethane (20 ml each). The extracts were combined, washed with two portions of water (20 ml each), dried over Na_2SO_4, and concentrated *in vacuo*. Isolation and purification of each product were performed with chromatography on silica gel and/or recrystallization.

*Reaction of Dimethyl 1-Oxo-*cis*-3a,7a-dihydroindene-3a,7a-dicarboxylates with Sodium Methoxide in Boiling Methanol. General Procedure*: A solution of sodium methoxide in methanol, prepared from 100 mg of sodium and 10 ml of methanol, was heated under reflux. To the solution was added a solution of the dihydroindenones (*ca.* 100 mg) in methanol (10 ml). After 10 min or 12 h reflux, the mixture was poured on a mixture of 2 M-hydrochloric acid and ice, and extracted with three portions of dichloromethane (20 ml each). The usual work-up followed by recrystallization or molecular distillation gave the 1-indanones.

Physical Properties of the New Dimethyl 3-Oxo-1,7-indandicarboxylates. Dimethyl trans*-2-Isopropyl-6-methoxy-3-oxo-1,7-indandicarboxylate (**8**)*: Colorless needles (from CH_3OH), mp 105—106 °C; UV_{max} (CH_3OH) 233 (log ε 4.28), 270 (4.16), and 296 nm (3.88); IR (KBr) 1725, 1691, 1581, and 814 cm^{-1}; NMR ($CDCl_3$) δ=0.85 (3H, d, J=7.0 Hz, CH_3), 1.05 (3H, d, J=7.0 Hz, CH_3), 2.37 (1H, doublet of sept, J=4.1 and 7.0 Hz, $CH(CH_3)_2$), 2.81 (1H, dd, J=4.1 and 3.4 Hz), 3.68 (3H, s), 3.90 (3H, s), 3.97 (3H, s), 4.25 (1H, d, J=3.4 Hz, H_1), 7.10 (1H, d, J=8.6 Hz, H_5), and 7.88 (1H, d, J=8.6 Hz, H_4). Found: C, 63.68; H, 6.30%. Calcd for $C_{17}H_{20}O_6$: C, 63.74; H, 6.29%.

*Dimethyl 4-Isopropyl-6-methoxy-3-oxo-1,7-indandicarboxylate (**9**)*: Colorless needles (from ether–CH_3OH), mp 177–178 °C; UV_{max} (CH_3OH) 236 (log ε 4.41), 275 (4.17), and 300 nm (3.69)^{sh}; IR (KBr) 1728, 1698, 1597, and 1461 cm^{-1}; NMR ($CDCl_3$) δ=1.25 (3H, d, J=6.9 Hz, CH_3), 1.27 (3H, d, J=6.9 Hz, CH_3), 2.84 (1H, dd, J=18.2 and 4.2 Hz, H_2-*cis* to C_1-ester), 2.92 (1H, dd, J=18.2 and 7.8 Hz, H_2-*trans* to C_1-ester), 3.67 (3H, s), 3.86 (3H, s), 3.95 (3H, s), 4.24 (1H, sept, J=6.9 Hz, $CH(CH_3)_2$), 4.47 (1H, dd, J=7.8 and 4.2 Hz, H_1), and 6.97 (1H, bs, $W_{1/2}$=1.6 Hz, H_5). Found: C,

63.51; H, 6.41%; M+, 320. Calcd for $C_{17}H_{20}O_6$: C, 63.74; H, 6.29%; M, 320.

*Dimethyl 1-Isopropyl-6-methoxy-3-oxo-1,7-indandicarboxylate (**10**)*: Colorless prisms (molecular distillation, bp 160 °C (bath)/0.2 Torr), mp 150—151 °C; UV_{max} (CH_3OH) 228 (log ε 4.31), 271 (4.20), 285 (4.10)^{sh}, and 294 nm (3.95)^{sh}; IR (KBr) 1735, 1709, 1581, 1470, and 828 cm^{-1}; NMR ($CDCl_3$) δ=0.51 (3H, d, J=6.8 Hz, CH_3), 1.03 (3H, d, J=6.8 Hz, CH_3), 2.67 (1H, d, J=19.2 Hz, H_2), 2.89 (1H, sept, J=6.8 Hz, $CH(CH_3)_2$), 3.08 (1H, d, J=19.2 Hz, H_2), 3.65 (3H, s), 3.93 (6H, s), 7.05 (1H, d, J=6 8 Hz, H_5), and 7.93 (1H, d, J=8.7 Hz, H_4). Found: C, 63.59; H, 6.29%; M+, 320. Calcd for $C_{17}H_{20}O_6$: C, 63.74; H, 6.29%; M, 320.

*Dimethyl 1-Methyl-3-oxo-1,7-indandicarboxylate (**13**)*: Colorless oil; UV_{max} (CH_3OH) 219 (log ε 4.51), 241 (4.01)$^{++}$, 292 (3.39), and 301 nm (3.39); IR (film) 1740, 1722, 1600, 1588, 1479, and 773 cm^{-1}; NMR ($CDCl_3$) δ=1.68 (3H, s, CH_3), 2.72 (1H, d, J=18.8 Hz, H_2), 2.98 (1H, d, J=18.8 Hz, H_2), 3.68 (3H, s), 3.91 (3H, s), 7.57 (1H, t, J=7.4 Hz, H_5), 7.99 (1H, dd, J=7.4 and 1.5 Hz, H_6 or H_4), and 8.35 (1H, dd, J=7.4 and 1.5 Hz, H_4 or H_6). Found: M+, 262 Calcd for $C_{14}H_{14}O_5$: M, 262.

*Dimethyl 6-Methoxy-1-methyl-3-oxo-1,7-indandicarboxylate (**14**)*: Colorless needles (from CH_3OH), mp 118—119 °C; UV_{max} (CH_3OH) 228 (log ε 4.43), 271 (4.33), and 295 nm (4.13); IR (KBr) 1740^{sh}, 1732, 1713, 1706, 1581, and 824 cm^{-1}; NMR ($CDCl_3$) δ=1.60 (3H, s, CH_3), 2.60 (1H, d, J=18.5 Hz, H_2), 3.06 (1H, d, J=18.5 Hz, H_2), 3.67 (3H, s), 3.89 (3H, s), 3.97 (3H, s), 7.07 (1H, d, J=8.5 Hz, H_5), and 7.90 (1H, d, J=8.5 Hz, H_4). Found: C, 61.34; H, 5.49%; M+, 292. Calcd for $C_{15}H_{16}O_6$: C, 61.64; H, 5.52%; M, 292.

*Reactions of Dimethyl 1-Oxo-*cis*-3a,7a-dihydroindene-3a,7a-dicarboxylate (**1**) with Sodium Ethoxide in Ethanol. A)*: To a solution of sodium ethoxide in ethanol, prepared from 100 mg of sodium and 10 ml of absolute ethanol, was added rapidly a solution of 98.8 mg (0.40 mmol) of **1** in 10 ml of ethanol, and the mixture was allowed to stand at room temperature for 10 min. The solution was poured on 2 M-hydrochloric acid (20 ml), diluted with water and extracted with three portions of dichloromethane (20 ml each). The usual work-up afforded 101 mg of red oil, which was chromatographed on silica gel. The product (71 mg, 64.2%) was identical with diethyl 3-oxo-1,7-indandicarboxylate (**15**) which was derived from **2** with sodium ethoxide in ethanol. **15**: Colorless needles (from ethanol), mp 78—80 °C; UV_{max} (CH_3OH) 218 (log ε 4.70), 240 (4.06)^{sh}, 265 (3.28)^{sh}, 290 (3.53), and 299 nm (3.55); IR (KBr) 1729, 1715, 1703, 1588, and 763 cm^{-1}; NMR ($CDCl_3$) δ=1.23 (3H, t, J=7.1 Hz), 1.39 (3H, t, J=7.1 Hz), 2.72 (1H, dd, J=19.2 and 4.4 Hz, H_2-*cis* to C_1-ester), 3.07 (1H, J=19.2 and 8.2 Hz, H_2-*trans* to C_1-ester), 4.19 (2H, q, J=7.1 Hz), 4.38 (2H, q, J=7.1 Hz), 4.71 (1H, dd, J=8.2 and 4.4 Hz, H_1), 7.55 (1H, t, J=7.4 Hz, H_5), 7.95 (1H, dd, J=7.4 and 1.5 Hz, H_6 or H_4), and 8.30 (1H, dd, J=7.4 and 1.5 Hz, H_4 or H_6). Found: C, 64.87; H, 5.74%; M+, 276. Calcd for $C_{15}H_{16}O_5$: C, 65.21; H, 5.84%; M, 276.

B): To a solution of sodium ethoxide in ethanol, prepared from 150 mg of sodium and 10 ml of absolute ethanol, was added a solution of 104 mg of **1** in 10 ml of ethanol in one portion. After 10 s, 10 ml of 2 M-hydrochloric acid was added to the solution which was still violet. The mixture was extracted rapidly with three portions of dichloromethane (20 ml each). The usual work-up gave 108.1 mg of pale red oil, whose chromatography on silica gel gave 81 mg (77.9%) of **1** and 19 mg (18.3%) of dimethyl 3-oxo-1,7-indandicarboxylate **2**.

*Reaction of Methyl 4-Methoxy-3-oxo-*cis*-3a,7a-dihydroindene-3a-carboxylate (**16**) with Sodium Methoxide in Methanol.* To a solution of sodium methoxide in methanol, freshly prepared from 150 mg of sodium and 15 ml of absolute methanol, was added a solution of 101.2 mg of **16** in 10 ml of methanol, and the mixture was allowed to stand at room temperature for 4 h. The usual work-up afforded pale red oil (81.3 mg), which was chromatographed on silica gel giving 71 mg (70 %) of methyl 5-methoxy-1-oxo-4-indancarboxylate (**17**), as colorless oil. **17**: UV_{max} (CH_3OH) 224 (log ε 4.48), 253 (3.92)^{sh}, and 303 nm (3.30); IR (film) 1723, 1692, and 1598 cm^{-1}; NMR ($CDCl_3$) δ=2.72 (2H, m, H_2), 3.12 (2H, m, H_3), 3.90 (3H, s), 4.02 (3H, s), 7.19 (1H, dt, J=8.0 and 0.5 Hz, H_6), and 7.95 (1H, d, J=8.0 Hz, H_7). 2,4-DNP of **17**: mp 221 °C (dec). Found: C, 53.75; H, 4.27; N, 13.90%. Calcd for $C_{18}H_{16}N_4O_7$: C, 54.00; H, 4.03; N, 14.00%.

*Preparation of Methyl 7-Methoxy-3-methyl-1-oxo-*cis*-3a,7a-dihydroindene-3a-carboxylate (**18**).* To a solution of 473 mg (2.15 mmol) of **16** in 10 ml of ether was added an excess of an ethereal solution of diazomethane, and the mixture was allowed to stand overnight at room temperature. After removal of the excess of diazomethane and the solvent, crystallization of the residue gave 379 mg (67.3%) of the pyrazoline (**17**). A solution of 186.4 mg (0.71 mmol) of **17** in 5 ml of xylene was heated under reflux for 1 h. Removal of the solvent *in vacuo* followed by recrystallization from methanol gave 136 mg (0.52 mmol, 73%) of **18**. **17**: Colorless prisms (from CH_3OH), mp 150—151 °C (dec); IR (KBr) 1758, 1742, and 1653 cm^{-1}; Found: C, 59.51; H, 5.31; N, 10.71%. Calcd for $C_{13}H_{14}N_2O_4$: C, 59.54; H, 5.38; N, 10.68%. **18**: Colorless prisms (frm CH_3OH), mp 143—144 °C; IR (KBr) 1723, 1708, 1655, 1638, and 1599 cm^{-1}; NMR ($CDCl_3$) δ= 2.18 (3H, t, J=1.4 Hz, CH_3), 3.64 (3H, s), 3.73 (3H, s), 3.88 (1H, dddd, J=5.2, 2.2, 1.8, and 1.4 Hz, H_{7a}), 5.14 (1H, d, J=6.5 Hz, H_6), 5.51 (1H, dd, J=9.5 and 6.5 Hz, H_5), 5.99 (1H, ddd, J=9.5, 6.5, and 1.8 Hz, H_4), and 6.03 (1H, dq, J=2.2 and 1.4 Hz, H_2). Found: C, 66.51; H, 6.03%. Calcd for $C_{13}H_{14}O_4$: C, 66.66; H, 6.02%.

*Reaction of Methyl 7-Methoxy-3-methyl-1-oxo-*cis*-3a,7a-dihydroindene-3a-carboxylate (**18**) with Sodium Methoxide in Methanol.* To a solution of sodium methoxide in methanol, freshly prepared from 100 mg of sodium and 10 ml of absolute methanol, was added a solution of 135 mg (0.576 mmol) of **18** in 10 ml of methanol at room temperature, and the mixture was allowed to stand for 1 h. The usual work-up gave 149.7 mg (0.562 mmol, 97%) of methyl 3-(3-methoxy-2-methoxycarbonylphenyl)butanoate (**20**), as colorless oil which was purified by molecular distillation: 90—95 °C (bath)/0.06 Torr. **20**: UV_{max} 280 nm (log ε 3.43); IR (film) 1733, 1588, and 802 cm^{-1}. Found: C, 63.24; H, 6.94%; M+, 266. Calcd for $C_{14}H_{18}O_5$: C, 63.14; H, 6.81%; M, 266.

References

1) a) T. H. Kinstle and P. D. Carpenter, *Tetrahedron Lett.*, **1969**, 3943; b) T. Uyehara, M. Funamizu, and Y. Kitahara, *Chem. Ind. (London)*, **1970**, 1500.

2) T. Uyehara, M. Funamizu, S. Miyakoshi, and Y. Kitahara, *Chem. Ind. (London)*, **1972**, 610.

3) T. Uyehara, S. Miyakoshi, and Y. Kitahara, *Bull. Chem. Soc. Jpn.*, **52**, 2023 (1979).

4) A. I. Scott, "Interpretation of the Ultraviolet Spectra of Natural Products," Pergamon Press, London (1964), p. 109.

5) T. Uyehara, S. Miyakoshi, and Y. Kitahara, *Synth. Commun.*, **3**, 365 (1973).

6) We have not investigated the process for the aromatization.

7) P. Schmidt, R. F. Hoffmann, and J. Baekes, *Angew. Chem. Int. Ed. Engl.*, **11**, 513 (1972).

Acyl Cyanide. V. The Synthesis of 1-Cyano-1-alkenyl Esters by the Reaction of Acyl Cyanides with Acid Anhydrides and Isocyanates

Akira Oku,* Shigeru Nakaoji, Toshio Kadono, and Hideki Imai

Department of Chemistry, Kyoto Institute of Technology, Matsugasaki, Sakyo-ku, Kyoto 606

(Received March 9, 1979)

The reactions of enolizable acyl cyanides (acetyl, propionyl, and isobutyryl cyanide) with acid anhydrides (acetic, propionic, butyric, isobutyric, and benzoic anhydride) in the presence of a catalytic amount of tertiary amines (pyridine, lutidines, 4-(dimethylamino)pyridine) produced the corresponding 1-cyano-1-alkenyl carboxylates. In the reactions of propionyl cyanide, (*Z*)-1-cyano-1-propenyl carboxylates were formed predominantly over the (*E*)-isomers (isomer ratios *Z*/*E* were *ca.* 80/20). The reactions of the cyanides with isocyanates also gave the corresponding 1-cyano-1-alkenyl carbamates in moderate yields, and the acid-treatments of 1-cyano-2-methyl-1-propenyl phenylcarbamate induced its annelation into 3-phenyl-1,3-oxazolidine-2,4-dione derivatives.

Only a limited number of methods have been known for the synthesis of 1-cyano-1-alkenyl esters, known as versatile reagents for ring formations[1] and polymerizations,[2] and they are classified into two groups: dehydrohalogenation of 1-cyano-2-haloethyl acetate by tertiary amines,[3] and base-catalyzed addition of hydrogen cyanide to ketene.[4] However, these methods are limited to the preparation of 1-cyanovinyl esters. We therefore have tried to find a more general and convenient method for the synthesis of a variety of unsubstituted and substituted 1-cyano-1-alkenyl esters.

Related to the synthetic method of the cyanoalkenyl esters, it has been reported[5] that when the reaction of aliphatic acyl chloride with metal cyanide (Eq. 1) known as an authodox preparative method[6] of acyl cyanides was carried out in the presence of crown ether, acyl cyanide was not isolated. In addition, our analogous examination in the reaction of acetic anhydride with potassium cyanide in the presence of crown ether proved it unsuccessful in the synthesis of acetyl cyanide. However, 1-cyanovinyl acetate was obtained instead. The formation of the ester seems to be accountable by the base-catalyzed dimerization of acetyl cyanide followed by dehydrocyanation as was proposed by Tate[7] (Eq. 2). If this mechanism is correct, then the maximum yield of the ester, calculated upon the basis of inorganic cyanide consumed, should not exceed 50%. However, the ester was isolated in 52% from the reaction of isobutyric anhydride (two parts) and potassium cyanide (one part) in the presence of 18-crown-6 in 1,2-dimethoxyethane. Evidently, this fact implies that an alternative reaction path must (co)exist to produce the ester. We clarified this is the acylation of acyl cyanide intermediate by acetic anhydride (Eq. 3). We have extended this reaction to a variety of acyl cyanide–acid anhydride combinations and established its versatile characters. Also the carbamoylation of acyl cyanides with isocyanates was investigated to prepare 1-cyano-1-alkenyl carbamates (Eq. 4).

$$R^1R^2CHCOCl + Metal\text{–}CN \longrightarrow R^1R^2CHCOCN \quad (1)$$

$$R^1R^2CHCOCN + CN^- \longrightarrow R^1R^2CH\text{–}C(CN)_2O^-$$

$$\xrightarrow{R^1R^2CHCOCN} R^1R^2CH\text{–}C(CN)_2OCOCHR^1R^2$$

$$\xrightarrow{base} R^1R^2C{=}C(CN)OCOCHR^1R^2 \quad (2)$$

$$R^1R^2CHCOCN + (R^3CO)_2O \longrightarrow R^1R^2C{=}C(CN)OCOR^3 \quad (3)$$

$$R^1R^2CHCOCN + R^4\text{–}NCO \longrightarrow R^1R^2C{=}C(CN)OCONHR^4 \quad (4)$$

Results and Discussion

Both acyl cyanides and acid anhydrides are known as acylating reagents and they stay unchanged when mixed. However, a catalytic amount of tertiary amines, usually pyridine derivatives, induced a condensation reaction between these two reagents affording the corresponding 1-cyano-1-alkenyl esters in good yields.

Reaction of Acetyl Cyanide with Acid Anhydrides. When a mixture of acetyl cyanide and an acid anhydride was treated with a catalytic amount of pyridine in tetrahydrofuran at ambient temperature, the corresponding 1-cyanovinyl carboxylate (**1**—**3**) was obtained. The results are tabulated in Table 1. All the product esters showed $\nu(C{\equiv}N)$ at 2210 cm^{-1} about 50 cm^{-1} lower than that of saturated nitriles, and the terminal methylene protons in NMR around δ 5.7 (J=3 Hz), thus demonstrating the product structures to be the expected ones.

Reaction of Propionyl Cyanide with Acid Anhydrides. As shown in Table 1, the product esters 1-cyano-1-propenyl carboxylates (**5**—**8**) consisted of two geometrical isomers (*Z*- and *E*-isomer). Their NMR assignment was carried out as follows.

First, we noticed that the major isomer shows higher chemical shifts of the terminal methylene protons than the minor one in any isomeric couple. If the Pascual's equation[8] which was proposed for the substituent effects in determining the chemical shifts of olefinic protons is applicable in our cases (Eq. 6), then the calculated chemical

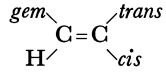

$$\delta(H) = 5.28 + \sigma(gem) + \sigma(cis) + \sigma(trans) \quad (6)$$

shifts δ(H) are 5.90 for *E*-isomer and 5.83 for *Z*-isomer, thus indicating the major isomer should have a *Z*-configuration. Second, the greater deshielding effect of an acetoxyl group than a cyano group on a vicinal *cis* proton in β-substituted styrenes[9] also suggests that

Table 1. Reaction of acyl cyanides with acid anhydrides

$$R^1R^2CH\text{–}CO\text{–}CN + (R^3CO)_2O \xrightarrow{\text{pyridine}} R^1R^2C{=}C(CN)OCOR^3$$

Compd	R^1	R^2	R^3	Solvent	Time h	Yield[b] %	Isomer ratio (Z/E)	PMR chemical shifts/ppm: $\Delta\delta$ between R^1 and R^2	PMR chemical shifts/ppm: $\Delta\delta$ ($\delta_Z-\delta_E$) of Olefin H	PMR chemical shifts/ppm: $\Delta\delta$ ($\delta_Z-\delta_E$) of Allylic Me
1	H	H	CH_3	THF	20	39		0.078		
2	H	H	C_2H_5	THF	24	44		0.080		
3	H	H	C_3H_7	THF	24	37		0.083		
4[c]	H	H	CH_3	THF	23	—[d]				
5	CH_3	H	CH_3	THF	24	65	77/23		−0.03	0.23
6	CH_3	H	C_2H_5	THF	24	80	80/20		−0.03	0.18
7	CH_3	H	iso-C_3H_7	THF	48	75	76/24		−0.03	0.20
8	CH_3	H	C_6H_5	THF	48	43[e]	69/31		−0.06	0.23
9	CH_3	CH_3	CH_3	DME	26	66		0.25		
10	CH_3	CH_3	C_2H_5	DME	22	40		0.26		
11	CH_3	CH_3	C_3H_7	DME	22	39		0.28		
12	CH_3	CH_3	C_6H_5	DME	48	61[f]		0.26		

a) Temperature 25 °C. Reactant ratios were 1:1:0.03 (cyanide/anhydride/pyridine). b) Isolated yields. c) 1.0 mol equiv of pyridine was added. d) 1,1-Dicyanoethyl acetate (**4**) was formed (76%). e) Determined by VPC, **6** was also formed (9%). f) Determined by VPC, 1-cyano-2-methyl-1-propenyl isobutyrate (**13**) was also formed (19%).

the olefinic proton of the *Z*-isomer should appear at higher field than the *E*-isomer. Third, on geometrical analysis of the shielding effect of the cyano group on the chemical shifts of allylic methyl group, it became evident that the methyl protons of the *E*-isomer should appear at a higher field than the *Z*-isomer, and this agreed with the observed results (see Table 1). Therefore, we concluded that the major isomers are (*Z*)-1-cyano-1-propenyl carboxylates. The demonstrated *Z*-configuration of the major product suggested us that this configuration is stabilized by a dipolar interaction rather than by steric factors in the structure determining step.

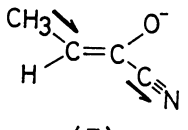

(Z)

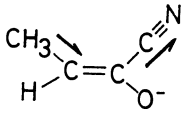

(E)

Reaction of Isobutyryl Cyanide with Acid Anhydrides. In the NMR spectra of the products, the differences in chemical shifts between the two allylic methyl groups ($\Delta\delta$) are analogous to those between *E* and *Z* isomers in the case of 1-cyano-1-propenyl esters (Table 1). The reaction with benzoic anhydride produced 1-cyano-2-methyl-1-propenyl isobutyrate (**13**) as a by-product. (Analogous side reaction was also observed in the reaction of propionyl cyanide with the same anhydride). Despite of the fact that isobutyryl cyanide undergoes dimer formation followed by the elimination of hydrogen cyanide to afford this ester, another reaction channel *via* acyl exchange between cyanide and benzoic anhydride seems also plausible (Eq. 7).

$$(CH_3)_2CHCOCN + (PhCO)_2O \rightleftharpoons (CH_3)_2CHCOOCOPh + PhCOCN \quad (7)$$

Tertiary Amine Catalysts. The presence of tertiary amine catalysts is essential in the present synthesis of cyanoalkenyl esters. Among several tertiary amines examined, pyridine derivatives with moderate basicity were found to be suitable for this purpose, *e.g.*, 4-(dimethylamino)pyridine, pyridine, lutidines, and picolines. Such strong bases as triethylamine and 1,7-diazabicyclo[4.3.0]non-6-ene were inadequate because they induced considerable degradation of the product esters. Solid-phase catalysts such as basic alumina and Amberlite IRA-400 were inactive in this reaction. Calcined anhydrous Hydrotalcite,[10] however,catalyzed the reaction to give the expected ester **5** (17%) in the reaction of propionyl cyanide with acetic anhydride besides 1,1-dicyanopropyl acetate **15** (22%) and 1,1-dicyanopropyl propionate **16** (13%) as by-products.

Reaction of Acyl Cyanides with Isocyanates. The above-mentioned reactions of acyl cyanides seemed to signify that acyl cyanide reacted in its enol (or enolate) form with acid anhydride. This prompted us to examine the reaction of acyl cyanides with isocyanates where the latter reacted as carbamoylating reagents to the former

Table 2. Reaction of acyl cyanides with isocyanates[a]

$$R^1R^2CH\text{–}COCN + R^3NCO \xrightarrow{\text{pyridine}} R^1R^2C{=}C(CN)OCONHR^3$$

17—19

Compd	R^1	R^2	R^3	Solvent	Time h	Yield[a] %
17	CH_3	CH_3	C_6H_5	C_6H_6	20	62
18	CH_3	CH_3	C_2H_5	THF	20	25
19	CH_3	H	C_6H_5	THF	24	53[c]

a) Cyanide/isocyanate/pyridine=1:1:0.25 mole ratio. b) Isolated yields. c) Determined by NMR, not isolated. Isomer ratio *Z*/*E*=7/3.

giving rise to the formation of 1-cyano-1-alkenyl carbamates. Results are shown in Table 2. None of *C*-acylated products anticipated from the result of the reaction of carbamoyl cyanides with isocyanates[11] was detected in the reaction mixture. The rate of carbamate formation was relatively slow in this reaction that the formation of the acyl cyanide dimer became unnegligible, especially in the reactions with aliphatic isocyanate.

As part of structure-determining experiments of the carbamates, the hydrogenation of 1-cyano-2-methyl-1-propenyl phenylcarbamate (**17**) over Pd/carbon catalyst was carried out in acetic acid. The carbamate slowly absorbed one mole of hydrogen to give not the expected acyclic carbamate but a cyclic iminourethane, *i.e.*, 3-phenyl-4-imino-5-isopropyl-1,3-oxazolidin-2-one (**21**). Analogous five-membered heterocyclic compound was obtained when carbamate **17** was hydrolyzed in aqueous sulfuric acid and its structure was attributed to 3-phenyl-5-isopropylidene-1,3-oxazolidine-2,4-dione (**20**).

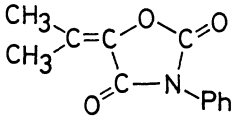

20

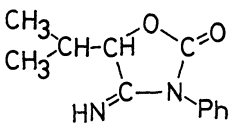

21

Experimental

General. The NMR spectra were measured by Varian T-60A spectrometer in CCl_4 solutions unless otherwise stated and the chemical shifts are given in δ-units. The IR and MS spectra were taken on JASCO IRA-1 and Hitachi RMU-6L spectrometer respectively. Acyl cyanides were prepared from the corresponding carboxylic acids *via* the reaction of acyl bromides with copper(I) cyanide.[6a]

Reaction of Acyl Cyanides with Acid Anhydrides. A General Procedure: The mixture of an acyl cyanide (0.02 mol) and an acid anhydride (0.02 mol) dissolved in 10 ml of solvent (1,2-dimethoxyethane or tetrahydrofuran) was cooled at 0 °C, to which a solution of pyridine (0.001 mol) which was dissolved in 10 ml of the same solvent was added. The reaction mixture then was stirred at 25 °C for a certain period. After removing solvents, the residue was distilled in vacuum to give the corresponding 1-cyano-1-alkenyl carboxylate. For the product yields and reaction conditions, see Table 1. The spectroscopic data are as follows.

*1-Cyanovinyl Acetate (**1**)*: Bp 48—52 °C/9 Torr. IR (liquid) 2220 and 1765 cm^{-1}. NMR 5.74 (2H, a pair of d, J=2.8 Hz), 2.27 (3H, s).

*1-Cyanovinyl Propionate (**2**)*: Bp 34—38 °C/0.5 Torr. IR (liquid) 2240 and 1770 cm^{-1}. NMR 5.77 (2H, a pair of d, J=3 Hz), 2.54 (2H, q, J=7.3), 1.24 (3H, t, J=7.3).

*1-Cyanovinyl Butyrate (**3**)*: Bp 55—58 °C/3 Torr. NMR 5.64 (2H, d, J=2.8 Hz), 2.40 (2H, t, J=6.8), 1.70 (2H, sext, J=7.2 and 6.8), 0.99 (3H, t, J=7.2).

*1-Cyano-1-propenyl Acetate (**5**)*: Bp 95—98 °C/37 Torr. IR (liquid) 2220 and 1765 cm^{-1}. NMR: (*Z*)-isomer 6.15 (1H, q, J=7.3 Hz), 2.20 (3H, s), 1.75 (3H, d, J=7.3); (*E*)-isomer 6.18 (1H, q, J=7.3), 2.15 (3H, s), 1.98 (3H, d, J=7.3). *Z*/*E*=77/23.

*1-Cyano-1-propenyl Propionate (**6**)*: Bp 108—110 °C/29 Torr. IR (liquid) 2220 and 1765 cm^{-1}. NMR: (*Z*)-isomer 6.25 (1H, q, J=7.2), 2.54 (2H, q, J=7.6), 1.75 (3H, d, J=7.2), 1.18 (3H, t, J=7.6); (*E*)-isomer 6.28 (1H, q, J=7.4), 2.55 (2H, q, J=7.6), 1.93 (3H, d, J=7.4), 1.15 (3H, t, J=7.6). *Z*/*E*=8/2.

*1-Cyano-1-propenyl Isobutyrate (**7**)*: Bp 115 °C/26 Torr. IR (liquid) 2220 and 1760 cm^{-1}. NMR: (*Z*)-isomer 6.23 (1H, q, J=7.2), 2.75 (1H, hept. J=7.2), 1.73 (3H, d, J=7.2), 1.24 (6H, d, J=7.2); (*E*)-isomer 6.26 (1H, q, J=7.5), 2.78 (1H, hept. J=7.2), 1.93 (3H, d, J=7.5), 1.20 (6H, d, J=7.2). *Z*/*E*=76/24.

*1-Cyano-1-propenyl Benzoate (**8**)*: Separated by VPC. IR (liquid) 2220 and 1730 cm^{-1}. NMR: (*Z*)-isomer 8.2—7.95 (3H, m), 7.7—7.3 (2H, m), 6.22 (1H, q, J=7.2), 1.80 (3H, d, J=7.2); (*E*)-isomer 6.28 (1H, q, J=7.4), 2.03 (3H, d, J=7.4). *Z*/*E*=69/31.

*1-Cyano-2-methyl-1-propenyl Acetate (**9**)*: Bp 90 °C/25 Torr. IR (liquid) 2210 and 1760 cm^{-1}. NMR 2.17 (3H, s), 2.02 (3H, s), 1.77 (3H, s).

*1-Cyano-2-methyl-1-propenyl Propionate (**10**)*: Bp 125 °C/60 Torr. IR (liquid) 2220 and 1765 cm^{-1}. NMR 2.47 (2H, q, J=7.5), 2.04 (3H, s), 1.77 (3H, s), 1.20 (3H, t, J=7.5).

*1-Cyano-2-methyl-1-propenyl Butyrate (**11**)*: Bp 125—130 °C/45 Torr. IR (liquid) 2200 and 1760 cm^{-1}. NMR 2.43 (2H, t, J=6.5), 1.70 (2H, sext. J=6.5 and 7.0), 1.00 (3H, t, J=7.0), 2.06 (3H, s), 1.77 (3H, s).

*1-Cyano-2-methyl-1-propenyl Benzoate (**12**)*: Separated by VPC. IR (liquid) 2230 and 1750 cm^{-1}. 8.07 (2H, m), 7.6 (3H, m), 2.09 (3H, s), 1.83 (3H, s).

Reaction of Isobutyric Anhydride with KCN in the Presence of 18-Crown-6. A mixture of isobutyric anhydride (7.1 g, 0.04 mol), KCN (1.5 g, 0.02 mol), and 18-crown-6 (0.5 g, 2 mmol) in 30 ml of dimethoxyethane was stirred at 25 °C for 7 h. The mixture was poured into 60 ml of petroleum ether, filtered, and the filtrate was evaporated followed by fractional distillation to give 1-cyano-2-methyl-1-propenyl isobutyrate (**13**) 2.35 g (52%), bp 110—115 °C/20 Torr. IR (liquid) 2210 and 1760 cm^{-1}. NMR 2.60 (1H, hept, J=7.2), 2.01 (3H, bs), 1.75 (3H, bs), 1.25 (6H, d, J=7.2).

Reaction of Propionyl Cyanide with Acetic Anhydride in the Presence of Calcined Hydrotalcite. Propionyl cyanide (2.49 g, 0.03 mol) and acetic anhydride (3.09 g, 0.03 mol) were mixed in 20 ml of THF, to which was added 3.0 g of Hydrotalcite (calcined at 470 °C for 2 h under vacuum) under N_2-atmosphere. The reaction mixture was stirred at ambient temperature for 23 h, filtered, and the solvent was removed. The residue contained three products which were separated preparatively by VPC; 1-cyano-1-propenyl acetate (**5**) 17%, *Z*/*E*=7/3; 1,1-dicyanopropyl acetate (**15**) 22%, NMR 1.32 (3H, t, J=7.2), 2.25 (3H, s), 2.35 (2H, q, J=7.2), IR (nujol) 2260 and 1770 cm^{-1}; 1,1-dicyanopropyl propionate (**16**) 13%, NMR 1.27 (3H, t, J=7), 1.33 (3H, t, J=7), 2.17—2.77 (4H, a mixture of two q).

Reaction of Acyl Cyanide with Isocyanate. A mixture of phenyl isocyanate (6.1 g, 0.05 mol), isobutyryl cyanide (5.0 g, 0.05 mol) and pyridine (1.0 g) in 50 ml of dry benzene was warmed at 33 °C for 20 h. After removing solvent, the residue was washed with petroleum ether and the obtained solid (7.6 g) was then chromatographed (silica gel, chloroform) to give 1-cyano-2-methyl-1-propenyl phenylcarbamate (**17**) 6.9 g (62 %), mp 129 °C (benzene). NMR ($CDCl_3$) 1.83 (3H, s), 2.06 (3H, s), 6.95 (1H, bs), 7.1—7.4 (5H, m). IR (Nujol) 3300, 2240, 1740, and 1550 cm^{-1}. MS (*m*/*e*) 216 (M^+). Found: C, 66.90; H, 5.79; N, 12.70%. Calcd for $C_{12}H_{12}N_2O_2$: C, 66.65; H, 5.59; N, 12.96%.

*1-Cyano-2-methyl-1-propenyl ethylcarbamate (**18**)*: Yield 25%, mp 53.5—54 °C, recrystallized from cyclohexane/benzene=10/2. NMR ($CDCl_3$) 1.20 (3H, t, J=7.5), 1.81 (3H, s), 2.05

(3H, s), 3.23 (2H, quintet, J=7.5 and 6), 5.97 (1H, bt, J=6). MS (*m/e*) 168 (M^+). Found: C, 57.53; H, 7.29; N, 16.43%. Calcd for $C_8H_{12}N_2O_2$: C, 57.23; H, 7.19; N, 16.66%.

*1-Cyano-1-propenyl phenylcarbamate (**19**)*: Yield 53% (by NMR), not isolated. NMR (*Z*)-isomer 7.30 (5H, m), 5.76 (1H, q, J=7.5), 1.78 (3H, d, J=7.5). (*E*)-isomer 7.30 (5H, m), 6.15 (1H, q, J=7.2), 1.72 (3H, d, J=7.2). *Z*/*E*=7/3.

*Hydrolysis of **17** in 25% Sulfuric Acid*: The mixture of **17** (0.945 g, 4.4 mmol, in 5 ml of dioxane) and 5 ml of 50% H_2SO_4 was heated at 100 °C for 17 h. After cooling the solution, water (50 ml) was added to separate colorless solids, which was filtered, dried, and chromatographed (silica gel, chloroform). The fraction eluting faster than the unreacted **17** was collected and recrystallized from cyclohexane to give 3-phenyl-5-isopropylidene-1,3-oxazolidine-2,4-dione **20**, 95 mg (10%), mp 93—94 °C. NMR ($CDCl_3$) 2.03 (3H, s), 2.27 (3H, s), 7.43 (5H, m). IR (Nujol) 1800, 1720, and 1185 cm^{-1}. MS (*m/e*) 217 (M^+). Found: C, 66.51; H, 5.14; N, 6.42%. Calcd for $C_{12}H_{11}O_3N$: C, 66.36; H, 5.07; N, 6.45%.

*Hydrogenation of **17***: A solution of **17** (1 mmol) dissolved in a mixture of acetic acid and methanol (5 ml+30 ml) absorbed *ca.* 25 ml of H_2 (1 mmol) over 5% Pd–carbon (100 mg) during 10 days. Evaporation of solvents separated a half-solidified material, which was then washed with CCl_4 and the residue was chromatographed (silica gel, chloroform) to give colorless solids of 3-phenyl-4-imino-5-isopropyl-1,3-oxazolidin-2-one (**21**), 175 mg (80%), mp 219—220 °C. MS (*m/e*) 218 (M^+). NMR (acetone-d_6) 0.80 (3H, d, J=7 Hz), 1.15 (3H, d, J=7), 2.48 (1H, m, probably a pair of splitted heptets, J=2.2 and 7), 5.02 (1H, d, J=2.2), 7.2—7.55 (3H, m), 7.7—7.9 (2H, m). IR (Nujol) 3250, 3070, 1740, 1625, and 1560 cm^{-1}. Found: C, 65.80; H, 6.41; N, 12.68%. Calcd for $C_{12}H_{14}N_2O_2$: C, 66.04; H, 6.47; N, 12.83%.

The authors wish to express their thanks to Mr. Hiroyuki Ueda for his assistance in this study.

References

1) For examples, a) J. C. Little, *J. Am. Chem. Soc.*, **87**, 4020 (1965); b) W. L. Dilling and J. C. Little, *ibid*, **89**, 2741 (1967); c) P. S. Warton and R. T. Aw, *J. Org. Chem.*, **31**, 3787 (1966); d) A. J. Birch and E. G. Hutchinson, *J. Chem. Soc., Perkin Trans. 1*, **1973**, 1757.

2) For examples, a) J. B. Dickey, U. S. Patent 2472811 (1949), *Chem. Abstr.*, **43**, 6465 (1949); b) J. B. Dickey, U. S. Patent 2611765 (1952), *Chem. Abstr.*, **47**, 917 (1953); c) J. B. Dickey, U. S. Patent 2464120 (1949), *Chem. Abstr.*, **43**, 5636 (1949).

3) J. W. Baker, *J. Chem. Soc.*, **1942**, 520. See also H. Lange and H. Kranz, U. S. Patent 2266771 (1942), *Chem. Abstr.*, **36**, 2353 (1942); and L. H. Lee, U. S. Patent 3306880 (1967), *Chem. Abstr.*, **66**, 95594 (1967).

4) F. Johnston, U. S. Patent 2395930 (1946); H. J. Hagemeyer, Jr., *Ind. Eng. Chem.*, **41**, 770 (1949).

5) K. E. Koenig and W. P. Weber, *Tetrahedron Lett.*, **1974**, 2275.

6) a) V. V. Tschelinzeff and Z. W. Schmidt, *Ber.*, **62**, 2210 (1929); b) D. T. Mowry, *Chem. Rev.*, **42**, 209 (1948); c) T. S. Oakwood and C. A. Weisberger, *Org. Synth.*, Coll. Vol. III, 112 (1955).

7) D. E. Tate, *J. Am. Chem. Soc.*, **78**, 5575 (1956).

8) C. Pascual, J. Meier, and W. Simon, *Helv. Chim. Acta*, **49**, 164 (1966); S. W. Tobey, *J. Org. Chem.*, **34**, 1281 (1969).

9) H. Kasiwagi and J. Niwa, *Bull. Chem. Soc. Jpn.*, **36**, 405 (1963).

10) Before calcination, its composition is expressed by $MgCO_3 \cdot 5Mg(OH)_2 \cdot 2Al(OH)_3 \cdot 4H_2O$.

11) A. Oku, T. Suzuki, H. Koura, and F. Mashio, *Bull. Chem. Soc. Jpn.*, **49**, 3574 (1976).

Reduction of Methylene Blue with L-Ascorbic Acid or L-Cysteine in Micellar Systems

Manabu Senō,* Kouichi Kousaka, and Hideo Kise

Institute of Industrial Science, The University of Tokyo, Roppongi 7-22, Minato-ku, Tokyo 106

(Received April 27, 1979)

The reduction of Methylene Blue (MB) with L-ascorbic acid to the corresponding leuco compound has been studied in aqueous surfactant solutions. The reduction was accelerated in the presence of cationic surfactant hexadecyltrimethylammonium bromide, but tetrabutylammonium bromide, which has no ability of micelle formation, does not show any effects on the reaction rate. The micellar effects are largely affected by pH of the medium, and the rate enhancing effects of the micelles are retarded by KCl. These results could be interpreted by the change in dissociation state of the substrate on the micelle surface and by the binding of the reaction product, leuco MB, to the micelles. The binding site of leuco MB was found to be outer core of the HTAB micelle by NMR. Similar results were obtained in the reduction of MB with L-cysteine, although the reduction did not proceed without the addition of cationic surfactant. The interaction between dissolved oxygen and the substrate in HTAB micellar solutions was also investigated.

Oxidation and reduction are fundamentally important reactions of metabolism in living systems catalyzed by oxidase and reductase. These enzymes are usually composed of two parts, coenzyme and apo-enzyme. Coenzymes are compounds which transfer electrons to substrates, whereas apo-enzymes are spherical proteins which provide the reaction sites. Associates of surfactant molecules are similar to spherical proteins in several respects.[1] (1) The micellar structure has many similar features to spherical proteins; (2) denaturants of proteins also destroy micellar structure; (3) the binding constants of substrates with micelles are in the same order as those with enzymes; (4) kinetics of micellar catalysis obeys the Michaelis-Menten equation which is applied extensively to the enzyme catalysis.

This report describes the results of micellar effects on the reduction of Methylene Blue (MB) with L-ascorbic acid or L-cysteine, and the oxidation of leuco MB with oxygen in the presence of surfactants.

Experimental

Materials. Methylene Blue was recrystallized three times from ethanol. L-Ascorbic acid and L-cysteine of reagent grade were used without further purification. Hexadecyltrimethylammonium bromide (HTAB) and sodium dodecyl sulfate (SDS) were recrystallized three times from ethanol–ether. Poly(oxyethylene) oleyl ether (POOE) was obtained commercially and used without further purification.

Reduction Rate Measurement of Methylene Blue. After mixing an aqueous solution of L-ascorbic acid (1.29×10^{-3} M) with an aqueous solution of MB (1.23×10^{-5} M) containing a certain amount of a surfactant, the decrease in the intensity of absorption peak of MB at 660 nm was followed. The pH of the solution was adjusted with a phosphate buffer, but sometimes sodium hydroxide or hydrochloric acid were used in order to avoid complexity caused by the buffer solution. The pH of reaction mixtures was measured with a Toa HM-5A pH meter. The reactions were carried out in UV cells of 10 or 2 mm path length and the decrease in absorption intensity of MB was recorded with a Union stopped-flow spectrophotometer model RA-1100 with a RA-1085 digital memory unit. For tracing slower reactions, a Union SM-401 spectrophotometer was employed. The reactions of MB with L-cysteine were examined by similar procedures.

Oxidation of Leuco Methylene Blue with Oxygen. Leuco MB was prepared by the electrolytic reduction of MB in 0.01 M hydrochloric acid solution. The solution was diluted with air-saturated water containing a given amount of surfactant. The oxidation rate was determined by measuring the increase in absorbance of MB at 660 nm in a UV cell of 10 mm path length at 25 °C.

Determination of Dynamic Solubilization Site of Leuco Methylene Blue. The ^{1}H NMR spectra were recorded on a Hitachi 60 MHz spectrometer and used for the determination of solubilization site of leuco MB. All spectra were measured on freshly prepared solutions at 35 °C. A 30% solution of tetramethylsilane in deuteriochloroform was used as an external standard.

Results and Discussion

Reduction of Methylene Blue with L-Ascorbic Acid. Under neutral conditions the reduction of MB with L-ascorbic acid is a reversible reaction as shown below and the position of equilibrium lies far to the left.

$$\mathrm{MB} + \mathrm{AsH} \rightleftarrows \mathrm{MBH} + \mathrm{As}$$

In the present investigation an excess amounts of L-ascorbic acid over those of MB were used, and the pseudo first order rate constants k_1 were determined from the relation shown below.

$$-\mathrm{d[MB]}/\mathrm{d}t = k_1[\mathrm{MB}]$$

The effects of the addition of various surfactants on the rate constant k_1 and the apparent equilibrium constant $K=[\mathrm{MBH}]/[\mathrm{MB}]$ were examined.

Figure 1 shows the effects of the addition of surfactants on k_1. The reduction of MB is accelerated by the addition of a cationic surfactant HTAB. The addition of a nonionic surfactant POOE also accelerates the reduction, but the effect is not so large as that of HTAB. On the other hand, an anionic surfactant SDS inhibits the reduction due to the formation of complex salt with MB. Tetrabutylammonium bromide, which is the compound of the same type as HTAB but has no ability of micelle formation, does not show any acceleration effect on the reaction. This indicates that micelle formation is essential for catalytic activity.

The dependence of k_1 on the HTAB concentration near critical micelle concentration (CMC) is shown in Fig. 2. Unlike the ordinary behavior of micellar

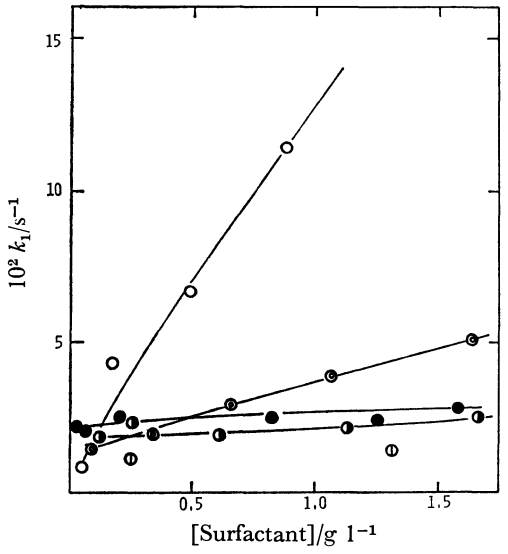

Fig. 1. Rate constant for the reaction of Methylene Blue with L-ascorbic acid as a function of surfactant concentration. Methylene Blue 1.23×10^{-5} M, ascorbic acid 1.29×10^{-3} M, 25 °C, pH 6.80.
○, HTAB; ●, POOE ($n=10$); ◑, POOE ($n=50$); ◎, poly(oxyethylene) *p*-nonylphenyl ether ($n=10$); ⦶, tetrabutylammonium bromide.

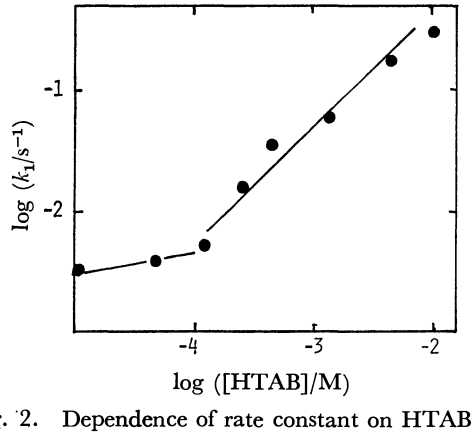

Fig. 2. Dependence of rate constant on HTAB concentration. Methylene Blue 1.23×10^{-5} M, ascorbic acid 1.29×10^{-3} M, 25 °C, pH 6.80.

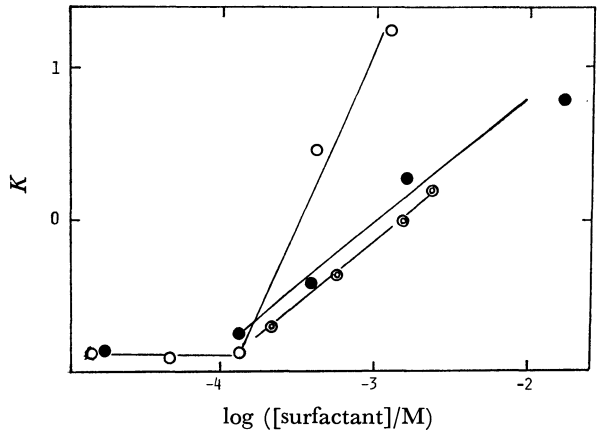

Fig. 3. Dependence of K on surfactant concentration. Methylene Blue 1.23×10^{-5} M, ascorbic acid 1.29×10^{-3} M, 25 °C, pH 6.80.
○, HTAB; ●, POOE ($n=10$); ◑, POOE ($n=50$); ◎, poly(oxyethylene) *p*-nonylphenyl ether ($n=10$).

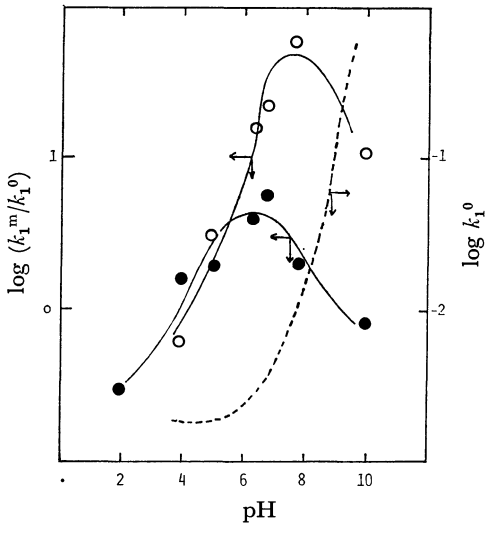

Fig. 4. Relationship between relative rate and pH. k_1^m and k_1^0 are rate constants with and without surfactant, respectively. Methylene Blue 1.23×10^{-5} M, ascorbic acid 1.29×10^{-3} M, 25 °C. ○, HTAB 1.37×10^{-3} M; ●, POOE ($n=10$) 1.97×10^{-3} M.

catalyses,[2] a linear relationship between k_1 and HTAB concentration is observed far above the CMC where the micelle concentration is much higher than those of the substrates. This lack of saturation in the rate profile suggests that the interaction between the cationic micelle and MB is weak, *i.e.* the binding constant is small. This seems reasonable because MB has the same positive charge as HTAB. The association between them is considered to be originated from hydrophobic interaction which competes with electrostatic repulsion between MB and the cationic head groups of the micelle.

Figure 3 shows the effect of surfactants on the apparent equilibrium constant K. HTAB has a large effect on K as well as on k_1, while POOE shows a medium effect on K. As will be discussed later, reduced MB (leuco MB) is most likely solubilized in the HTAB micelle core, and this would reduce the direct contact with oxidizing species leading to the increase in the apparent equilibrium constant.

The dependence of k_1 on pH is shown in Fig. 4. In these experiments, pH of the solutions was adjusted by using dilute aqueous solutions of hydrochloric acid or sodium hydroxide in order to exclude the possible effect of buffer solution.[3] The reduction rate in HTAB or POOE micellar solutions increases with increasing pH as well as in the absence of surfactants over most of the range of pH investigated. This implies that ascorbic acid reacts with MB faster in anionic form than in neutral form. The above observation suggests that the rate acceleration by HTAB is likely to be attributed to the concentration of MB and anionic ascorbic acid on the surface of the micelle where the pH is higher than

bulk water phase.

It should be noted that, as shown in Fig. 4, both HTAB and POOE have inhibitory effects on the reaction below pH 4. Under these acidic conditions ascorbic acid is considered to be neutral and binds easier with the micelles. The separate solubilization of MB and ascorbic acid into the micelles may be the reason for the rate retardation, although it is difficult to draw any definite conclusion from these pH studies.

It was reasonably expected that competitive binding of counter ions on the micellar surface occurs by the addition of inorganic salts, so that the local concentration of anionic substrates on HTAB micelle surface was expected to be reduced. Figure 5 shows the effect of potassium chloride on k_1 in HTAB solutions. The acceleration effect of HTAB is markedly reduced which may be due to the reduction of the binding of the substrate on the micelle surface.

To clarify the origin of nonionic micellar effects on the reduction rate shown above, the effect of solvent polarity was examined. The reactions were carried out in methanol–water mixed solvents. The reaction rate increases with increasing content of methanol (Fig. 6). This implies that less polar media favor the reaction and that the micellar effects of nonionic surfactants arise at least partly from the change of local polarity of the micellar systems.

The Dynamic Solubilization Site of Leuco Methylene Blue. Leuco MB is expected to be solubilized in surfactant micelles for its low solubility in water. NMR studies of surfactant solutions have been carried out in order to determine the dynamic solubilization site of organic compounds.[4] We studied the ^1H NMR of aqueous HTAB solutions in the presence of leuco MB in order to determine the solubilization site of leuco MB. Table 1 summarizes the observed chemical shifts and the results on pyrene reported by Grätzel *et al.*[5] Pyrene has been considered to be solubilized in HTAB micelle core causing higher shifts of resonance band of HTAB

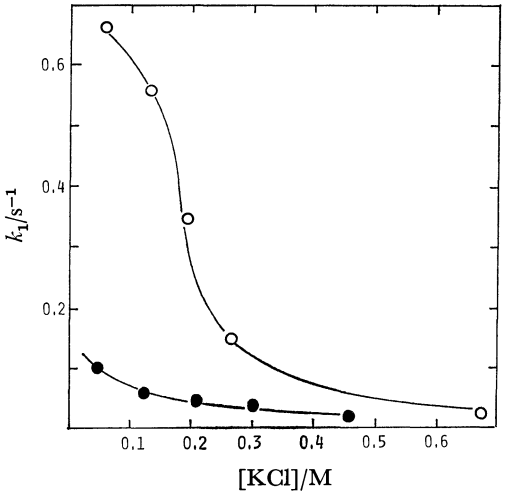

Fig. 5. Effect of KCl on the reduction rate of Methylene Blue with ascorbic acid in surfactant solutions. Methylene Blue 1.23×10^{-5} M, ascorbic acid 1.29×10^{-3} M, 25 °C, pH 6.80. ○, HTAB 8.05×10^{-3} M; ●, POOE ($n=10$) 5.00×10^{-3} M.

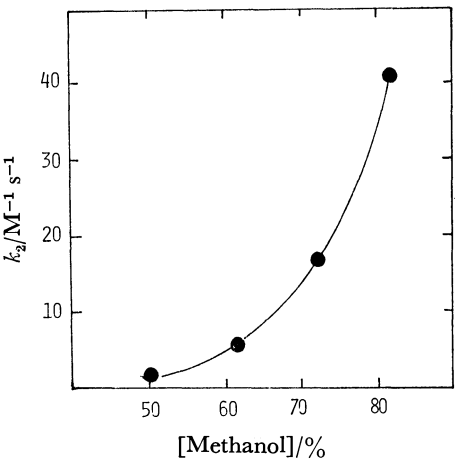

Fig. 6. Effect of methanol content on the reduction rate of Methylene Blue with ascorbic acid at 25 °C. Methylene Blue 8.05×10^{-5} M, ascorbic acid (Na salt) 5.82×10^{-3} M, without buffer.

Table 1. Change in chemical shift of HTAB protons by the addition of solubilizates[a)]

Proton	Δδ			
	MB 5.0×10^{-3} M	Leuco MB 1.3×10^{-4} M	Leuco MB 8.2×10^{-4} M	Pyrene[b)] 1.0×10^{-2} M
$N(CH_3)_3$	0.00	0.027	0.039	0.033
$(CH_2)_n$	0.00	0.005	0.008	0.016

a) Ppm relative to an external TMS standard. [HTAB]= 0.1 M. Δδ=Difference in chemical shifts of HTAB protons with and without solubilizates. MB=Methylene Blue. b) Ref. 5.

protons. As seen in Table 1, the protons of methyl groups attached to nitrogen exhibit upfield shifts by the addition of leuco MB which are comparable to that of pyrene of higher concentration. This seems to suggest that leuco MB is located in the outer core and near surface of the micelle.

Reduction of Methylene Blue with L-*Cysteine.* Similar to the reduction with ascorbic acid, both acceleration by HTAB and inhibition by KCl were observed in the reduction of MB with L-cysteine as shown in Figs. 7

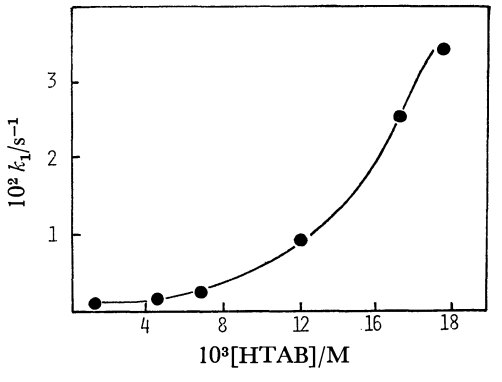

Fig. 7. Effect of HTAB on the reduction rate of Methylene Blue with L-cysteine. Methylene Blue 1.27×10^{-5} M, cysteine 3.12×10^{-3} M, 25 °C, pH 6.80.

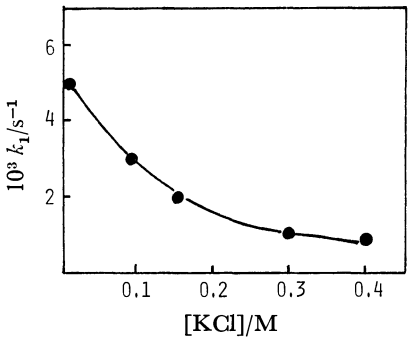

Fig. 8. Effect of KCl on k_1 in aqueous HTAB solutions.
Methylene Blue 1.27×10^{-5} M, cysteine 3.12×10^{-3} M, HTAB 9.41×10^{-3} M, 25 °C, pH 6.80.

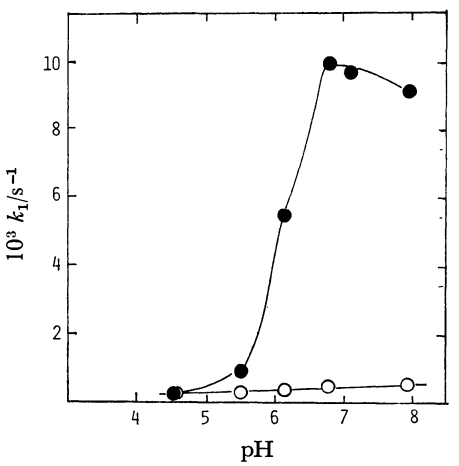

Fig. 9. Effect of pH on the reduction rate of Methylene Blue with L-cysteine at 25 °C. Methylene Blue 1.27×10^{-5} M, cysteine 8.25×10^{-3} M.
○, Without surfactant; ●, HTAB 1.13×10^{-2} M.

and 8. However, quite different results were obtained for the dependence of k_1 on pH as shown in Fig. 9. In HTAB micellar systems k_1 increases with the increase of pH followed by rate saturation above pH 7, whereas k_1 is almost independent of pH in the reaction without surfactants.

In general, there are two distinguished factors govering the micellar effects on organic reactions. One is the local concentration effect of substrates or catalysts at the reaction site, which is caused by electrostatic or hydrophobic interactions between micelles and the substrates. Another is the medium effect on the stability of transition states.[6] Many studies have revealed that the surface of cationic micelles is more basic than bulk water phase. Heitmann[7] suggested that the pK_a value of the SH group of *N*-dodecanoyl-DL-cysteine incorporated in cationic micelles is larger by unity than the value in micelle free solutions.

It is obvious that the results shown in Fig. 9 cannot be explained by pH effect of the cationic micelle surface and other factors must be effective in this case. It should be noted that, contrary to L-cysteine, the solubility of L-cystine in water is very low and in the presence of HTAB micelles it is likely to be solubilized in the micelles. In the present system, a large excess of HTAB micelles would solubilize the reaction products separately for each other, which would suppress the reverse reaction of leuco MB with L-cystine and increase the apparent k_1.

Another factor which should be taken into consideration is the effect of dissolved oxygen. It has been reported that the reduction of MB is inhibited by dissolved oxygen in aqueous solutions.[8] There is a possibility that oxygen participates in the reduction with L-cysteine through the following two processes. One is the inhibition of reduction by L-cysteine, and another is the rapid oxidation of leuco MB. Although we found it difficult to examine the effect of the former process, the latter was examined by the following method. Leuco MB was prepared electrolytically and the effect of HTAB micelle on its oxidation by dissolved oxygen was examined. Since the dissociation state and the micro environment of leuco MB would change by the addition of HTAB as describe above, the oxidation rate by dissolved oxygen was expected to be affected by HTAB. Actually however, the oxidation rate was found to be almost independent of HTAB concentration as seen in Fig. 10. It is interesting to note that different trends for the effect of added KCl on the oxidation rate

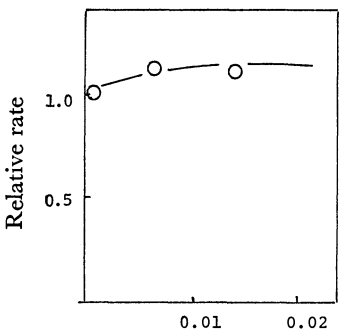

Fig. 10. Effect of HTAB on the relative oxidation rate of leuco Methylene Blue with dissolved oxygen in aqueous solutions.
Leuco Methylene Blue 1.33×10^{-5} M, 25 °C, pH 2.10.

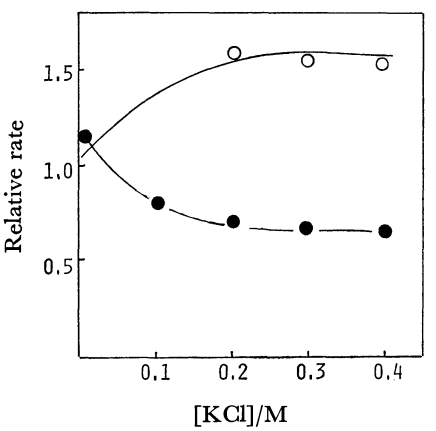

Fig. 11. Effect of KCl on the relative oxidation rate of leuco Methylene Blue with dissolved oxygen in aqueous HTAB solutions.
Leuco Methylene Blue 1.33×10^{-5} M, at 25 °C, pH 6.80. HTAB ○, 5.49×10^{-4} M; ●, 1.42×10^{-2} M.

were observed below and above cmc of HTAB (Fig. 11). The rate is lowered by the addition of KCl above cmc of HTAB, and this implies that cancelling the electric charge on the micelle surface would lead to the inhibition of the oxidation. The above observations tentatively lead to the conclusion that dissolved oxygen has, if any, small effect on the reduction system of MB by L-cysteine.

References

1) H. Schott, *J. Am. Oil Chem. Soc.*, **45**, 823 (1968).
2) C. A. Bunton, L. Robinson, and L. Sepulveda, *J. Org. Chem.*, **35**, 108 (1970).
3) C. A. Bunton and M. J. Minch, *J. Phys. Chem.*, **78**, 1490 (1974).
4) J. H. Fendler and E. J. Fendler, "Catalysis in Micellar and Macromolecular Systems," Academic Press, New York (1975), p. 55.
5) M. Grätzel, K. Kalyanasundaram, and J. K. Thomas, *J. Am. Chem. Soc.*, **96**, 7869 (1974).
6) Ref. 4, Chaps. 4 and 5.
7) P. Heitmann, *Eur. J. Biochem.*, **5**, 305 (1968).
8) Z. I. Vishivevskaya and A. M. Zhabtinski, *Biofizika*, **14**, 228 (1969).

Electronic State of Ethoxycarbonylnitrene Generated by α-Elimination under Two-phase Conditions

Manabu SENŌ,* Tomiyuki NAMBA, and Hideo KISE

Institute of Industrial Science, The University of Tokyo, 7-22 Roppongi, Minato-ku, Tokyo 106

(Received November, 1, 1978)

The base decomposition of ethyl *p*-nitrophenylsulfonyloxycarbamate in organic-aqueous two-phase systems in the presence of *cis*- or *trans*-4-methyl-2-pentene and quaternary ammonium or phosphonium halides afforded both stereospecific and nonstereospecific addition products of ethoxycarbonylnitrene. The electronic state of the nitrene was analyzed on the basis of Skell's hypothesis.

In the previous paper,[1] we reported that ethoxycarbonylnitrene was generated by α-elimination reaction of ethyl *p*-nitrophenylsulfonyloxycarbamate (**1**) and reacted with cyclohexene in organic-aqueous two-phase systems in the presence of phase transfer catalysts. In these reactions the variation of reaction path through singlet or triplet nitrene was shown as the dependence of addition/insertion product ratio on the concentration of cyclohexene.

In the present study the electronic state of ethoxycarbonylnitrene generated under two-phase conditions is examined by analyzing the composition of the reaction products with *cis*- or *trans*-4-methyl-2-pentene on the basis of Skell's hypothesis.[2]

Results and Discussion

Table 1 shows the yield of aziridines and the fraction of nonstereospecific addition (inversion) products in the reaction with *cis*- and *trans*-4-methyl-2-pentene under two-phase conditions (Scheme 1). No significant differences were observed in the catalysis of ammonium chlorides and bromides, but ammonium iodides gave unusual results; that is, the yields of addition product are low and the fractions of nonstereospecific addition product are decreased.

The ethoxycarbonylnitrene generated by α-elimination is supposed to be a singlet nitrene, which adds stereospecifically to olefins with complete retention of configuration.

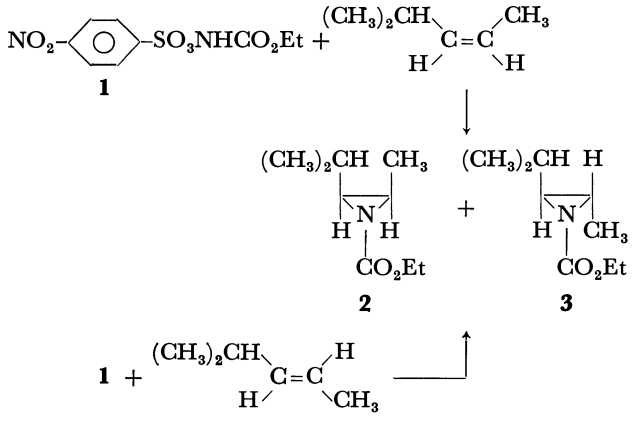

Scheme 1.

Since the ground state of the nitrene is triplet, a part of the singlet nitrene decays to the triplet nitrene, which adds nonstereospecifically to olefins. As a side reaction, ethyl carbamate is formed by hydrogen abstraction reaction from the triplet nitrene. The reaction scheme is summarized in Fig. 1.

When triethylbenzylammonium chloride (TEBACl) was used as a phase transfer catalyst, the relationship between the concentration of *cis*- or *trans*-4-methyl-2-

TABLE 1. REACTION OF ETHYL *p*-NITROPHENYLSULFONYLOXYCARBAMATE (**1**) WITH *cis*- AND *trans*-4-METHYL-2-PENTENES[a]

Catalyst	From *cis*-olefin		From *trans*-olefin	
	% Yield of aziridine	% Fraction of *trans*-product	% Yield of aziridine	% Fraction of *cis*-product
$(CH_3)_4NBr$	0	0	0	0
$(C_2H_5)_4NBr$	11.4	59.3	5.2	17.6
$(n\text{-}C_4H_9)_4NBr$	19.8	41.9	17.8	14.8
$(n\text{-}C_4H_9)_4PBr$	16.6	46.5	13.7	13.9
$(n\text{-}C_4H_9)_4NI$	6.3	15.3	5.3	11.8
$n\text{-}C_8H_{17}N(C_2H_5)_3Br$	25.6	38.0	20.2	20.3
$n\text{-}C_{12}H_{25}N(C_2H_5)_3Br$	27.0	46.0	20.9	14.2
$n\text{-}C_{16}H_{33}N(C_2H_5)_3Br$	29.0	42.4	23.9	18.3
$n\text{-}C_{16}H_{33}N(CH_3)_3Br$	22.2	48.2	16.5	15.5
$(C_6H_5CH_2)N(C_2H_5)_3Cl$	26.7	38.2	24.9	17.3
$(C_6H_5CH_2)N(C_2H_5)_3Br$	34.3	35.3	28.3	19.4
$(C_6H_5CH_2)N(C_2H_5)_3I$	11.3	10.0	4.7	6.4

a) **1** 0.01 mol, olefin 0.02 mol, catalyst 1.0 mmol, CH_2Cl_2 40 ml, $NaHCO_3$ 0.03 mol, H_2O 30 ml, room temperature, 2 h.

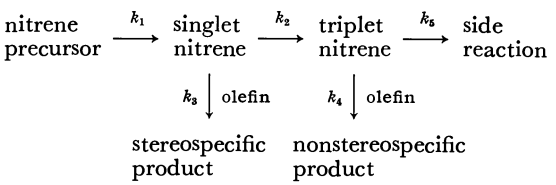

Fig. 1. Reaction scheme.

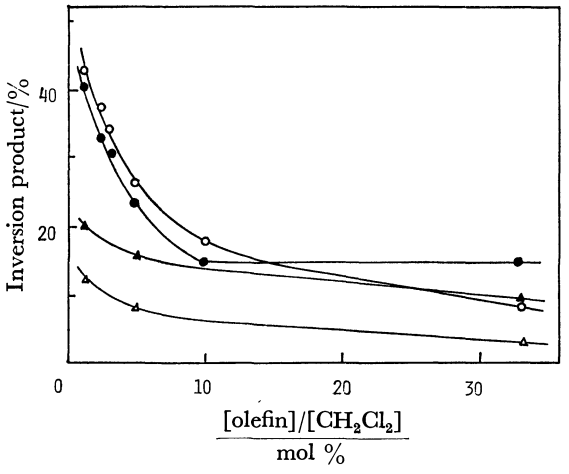

Fig. 2. Addition of ethoxycarbonylnitrene to *cis*- and *trans*-4-methyl-2-pentene under two-phase conditions in the presence of TEBACl.
●; *cis*-4-Methyl-2-pentene under two-phase conditions, ▲; *trans*-4-methyl-2-pentene under two-phase conditions, ○; *cis*-4-methyl-2-pentene in the homogeneous system,[3] △; *trans*-4-methyl-2-pentene in the homogeneous system.[3]

pentene in dichloromethane and the fraction of inversion product is shown in Fig. 2. In comparison with the results for the homogeneous system investigated by Lwowski *et al.*,[3] which are also shown in Fig. 2, the portion of the inversion product of the reaction with *cis*-4-methyl-2-pentene under two-phase conditions is a little low, while that of the reaction with *trans*-4-methyl-2-pentene is a little high, but concerning the dependence on the olefin concentration, the same trend is found for both the homogeneous and the two-phase systems. Thus, the increase in the concentration of olefin leads to a descrease in the inversion product. This can be explained as a consequence of an increasing frequency of the singlet nitrene reaction at higher concentrations of the olefins.

Now we consider the electronic state of the ethoxycarbonylnitrene generated in the present system according to the method proposed by Lwowski *et al.*[3,4] The fraction of the aziridine produced from the triplet nitrene in the total aziridine obtained is designated $[T]$, and the fraction of the "*trans*-aziridine" **3** in the aziridine produced from the triplet nitrene is designated α. If one assumes that the composition of the aziridine mixture produced from the triplet nitrene depends on the position of the equilibrium of the two conformers of open-chain biradical intermediate and not on the nature of the starting olefin, the fraction A of **3** in the aziridine mixture obtained from the *cis*-olefin and the fraction B of the "*cis*-aziridine" **2** in the aziridine mixture obtained from the *trans*-olefin are expressed respectively as;

$$A = [T]\alpha, \quad B = [T](1-\alpha) \tag{1}$$

The following relation is derived from Eq. 1.

$$\alpha = A/(A+B) \tag{2}$$

In order to know the value of A/B from the experimental data, the difference in the reactivity of *cis*- and *trans*-olefins toward the nitrene should be taken into consideration. From the measurements on the homogeneous system by Lwowski *et al.*,[3] the ratio of the reactivity $k_{4,trans}$: $k_{4,cis}$ is determined to be 0.7. This value is affected by the nature of olefin, but not affected by the nature of nitrene. Then, we can adopt this value for the present systems and then we can obtain the value of A/B from the experimental data shown in Fig. 2, by comparing the value of A at a given concentration with the value of B at 1/0.7 of that concentration. The values of A/B thus obtained vary from 1.5 to 2.1 in the concentration range from 33 to 1.5 mol %. The average value of A/B is 1.8, and the value of α is determined to be 0.64 from Eq. 2.

When the fraction of the aziridine produced from the singlet nitrene in the total aziridine is denoted as $[S]$, we get from Eq. 1

$$[T] = 1.56A, \quad [S] = 1 - [T] \tag{3}$$

From the reaction scheme shown in Fig. 1, the following relation is obtained by assuming the stationary state with respect to the triplet nitrene,

$$\frac{[T]}{[S]} = \frac{k_2}{k_3\{[\text{olefin}] + (k_5/k_4)\}} \tag{4}$$

Then, a plot of $[T]/[S]$ *vs.* $1/\{[\text{olefin}]+(k_5/k_4)\}$ should give a strainght line having the slope of k_2/k_3. Various plots were drawn by assuming various values of k_5/k_4 and the value of k_5/k_4 which gives the best straight line was determined. The selected value of k_5/k_4 for the two-phase reaction with TEBACl is 0.005, and then

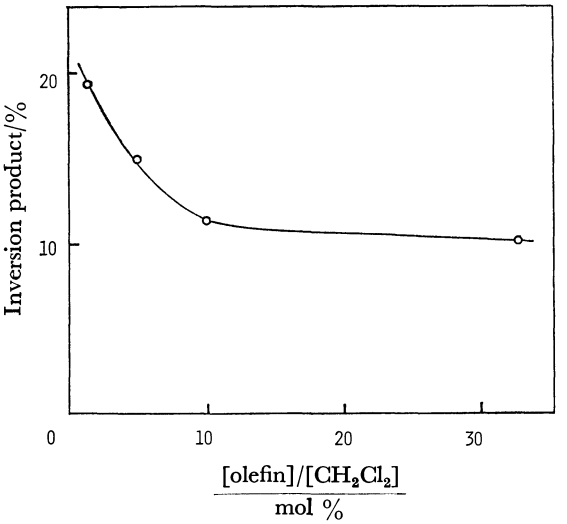

Fig. 3. Addition of ethoxycarbonylnitrene to *cis*-4-methyl-2-pentene under two-phase conditions in the presence of TEBAI.

the value of k_2/k_3 is determined to be 0.033 from the slope of the line.

When triethylbenzylammonium iodide (TEBAI) is used as a phase transfer catalyst, the relationship between the concentration of *cis*-4-methyl-2-pentene in dichloromethane and the inversion product is shown in Fig. 3. According to the same procedure as the case of TEBACl, the values of k_5/k_4 and k_2/k_3 were determined to be 0.07 and 0.033, respectively.

Table 2. Rate constant ratios k_2/k_3 and k_5/k_4 of the reactions of ethoxycarbonylnitrene under various conditions

	Two-phase system		Homogeneous system	
	TEBACl	TEBAI	α-Elimination with triethylamine[a]	Thermolysis of ethyl azidoformate[b]
k_2/k_3	0.033	0.033	0.036	0.10
k_5/k_4	0.005	0.07	0.015	0.03

a) From Ref. 4. b) From Ref. 3.

Table 2 summarizes the values of k_2/k_3 and k_5/k_4. The results of the two-phase reactions using TEBACl or TEBAI as phase transfer catalysts are compared with those of α-elimination reaction by triethylamine in a homogeneous system[3] and the thermolysis of ethyl azidoformate.[4] It is revealed from these results that the singlet nitrenes generated in the two-phase system and in the homogeneous system have the similar reactivity and the addition reaction of the singlet nitrene is about 30 times faster than the decay to the triplet state. However, there is a difference in the reactivity of the triplet nitrene. In the case of TEBACl, the ratio of side reactions such as hydrogen abstraction to form ethyl carbamate is low compared with the case of homogeneous system, while the ratio of side reactions (k_5/k_4) is very high in the case of TEBAI. Iodide ions from the catalyst is considered to enter into the organic phase easier than chloride or bromide ions, and the results imply that triplet nitrene is consumed by iodide ions in some unknown processes.

Experimental

The materials used and the authentic samples of the aziridines are described in the previous paper.[1] The reactions of ethyl *p*-nitrophenylsulfonyloxycarbamate (**1**) with *cis*- or *trans*-4-methyl-2-pentene were carried out in dichloromethane solutions and aqueous sodium hydrogencarbonate solutions in the presence of phase transfer catalysts. The details of the reactions and the analyses of the products are also described in the previous paper.[1]

References

1) M. Senō, T. Namba, and H. Kise, *J. Org. Chem.*, **43**, 3345 (1978).
2) P. S. Skell and R. C. Woodworth, *J. Am. Chem. Soc.*, **78**, 4496 (1956); P. S. Skell and R. C. Woodworth, *ibid.*, **81**, 3383 (1959).
3) J. S. McConaghy, Jr., and W. Lwowski, *J. Am. Chem. Soc.*, **89**, 2257 (1967).
4) J. S. McConaghy, Jr., and W. Lwowski, *J. Am. Chem. Soc.*, **89**, 4450 (1967).

Modifizierte Wichterle-Reaktion. Ein Weg zur Darstellung von 2-Cyclohexenonen und 1,4-Diketonen. Synthese von 4-Estren-3,17-dion und Dihydrojasmon

Makoto KOBAYASHI und Takeshi MATSUMOTO*

Department of Chemistry, Faculty of Science, Hokkaido University, Sapporo 060

(Eingegangen November 20, 1978)

Während die Behandlung von 2-(3-Chlor-2-butenyl)-2-methylcyclohexanon mit konz. H_2SO_4 2,5-Dimethylbicyclo[3.3.1]non-2-en-9-on als Hauptprodukt ergab, wurde beim Erhitzen in HCO_2H in Anwesenheit von $HClO_4$ 4a-Methyl-$\Delta^{1(8a)}$-2-octalon in 70 bis 98%-iger Ausbeute erhalten. Unter diesen Bedingungen reagierten andere α-(Chlorbutenyl)ketone analog und lieferten die entsprechende Annelierungsprodukte in hohen bis mässigen Ausbeuten. Aus α-(2-Haloallyl)ketonen wurden 1,4-Diketone gewonnen. Als Anwendungsbeispiele wurden 4-Estren-3,17-dion und Dihydrojasmon synthetisiert.

Bei Synthesen von Naturstoffen spielen Cyclisierungsreaktionen eine wichtige Rolle. Die Robinson-Annelierung ist eine der wirksamsten Cyclisierungsreaktionen, die bis jetzt entwickelt worden ist.[1] 1947 berichteten Wichterle *et al.* über eine Modifizierung der Robinson-Annelierung,[2] in der 1,3-Dichlor-2-buten (DCB) anstatt Methylvinylketons verwendet wurde: d.h., das durch Alkylierung von Carbonylverbindung mit DCB dargestellte α-(3-Chlor-2-butenyl)keton **1** wurde mit konz. H_2SO_4 behandelt, wobei das entsprechende 2-Cyclohexenon-Derivat **2** entstand (Schema-1a). Wie bereits Prelog sowie andere Autoren gezeigt haben, führt aber die Einwirkung von konz. H_2SO_4 auf α-(Chlorbutenyl)ketone **3** in den meisten Fällen nicht zu bicyclischen Produkten **4**, die für den Aufbau von gewissen Naturstoffen wertvoll sind, sondern zu verbrückten Olefinen von Typ **5**.[3] Marshall *et al.* untersuchten daher die Cyclisierungsbedingungen von **3** näher und es gelang, unter relativ milden Bedingungen das

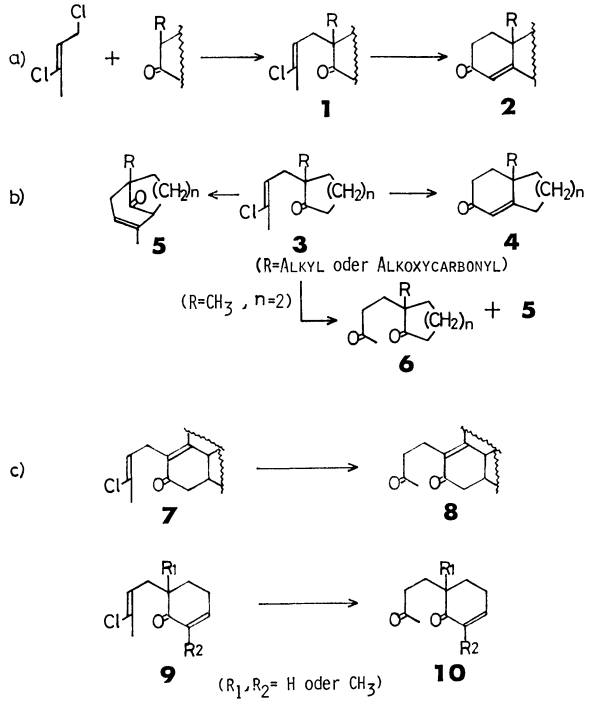

Schema 1. Wichterle-Reaktion unter konventionellen Bedingungen.

1,5-Diketon **6** in mässiger Ausbeute zu isolieren (Schema-1b).[4] Anderseits liefern unter den oben erwähnten konventionellen Bedingungen chlorbutenylierte α,β-Enone **7** sowie **9** die entsprechenden 1,5-Diketone **8** und **10** in guten Ausbeuten, was zur Konstruktion des Steroid-A-Rings angewandt wurde (Schema-1c).[5] Wegen des oben beschriebenen Nachteils, dass oft verbrückte Bicyclene als Hauptprodukt entstehen, wurde die Wichterle-Reaktion zur Synthese von Naturstoff bisher selten verwendet.[6]

Es ist wohlbekannt, dass ein Vinylhalogenid wegen des Doppelbindungscharakters zwischen Halogen- und Kohlenstoffatom im allgemeinen eine geringe Reaktionsfähigkeit besitzt. Ausser der gewöhnlicher Hydrolyse unter stark saueren Bedingungen wurden vor kurzem einige milde Umwandlungen von Vinylhalogeniden zu den entsprechenden Ketonen berichtet, bei welchen Übergangsmetalle verwendet wurden.[7]

Im Zusammenhang mit dem Versuch zur Darstellung eines Zwischenproduktes bei der Totalsynthese eines Diterpens war es erforderlich, die Cyclisierungsbedingungen der Wichterle-Reaktion zu untersuchen. Dabei stellte sich heraus, dass sich α-(Chlorbutenyl)keton beim Erhitzen mit Mineralsäure in saueren Lösungsmitteln wie HCO_2H leicht ins entsprechende 2-Cyclohexenon-Derivat umwandeln lässt. Darüber möchten wir hier zusammen mit den einfachen Anwendungen zur Darstellung von Steroid-Skeletten und Dihydrojasmon berichten.[8]

A. Lösungsmitteleffekt und Reaktionsweg

Unter Verwendung von 2-(3-Chlor-2-butenyl)-2-methylcyclohexanon (**11**) als Modellverbindung wurde der Optimierungsversuch durchgeführt. Der Lösungsmitteleffekt ist in Tabelle-1 zusammengestellt. Daraus ergab sich, dass dieser Ringschluss von **11** zu 4a-Methyl-$\Delta^{1(8a)}$-2-octalon (**12**) in Lösungsmittel wie HCO_2H sowie CH_3NO_2 in Anwesenheit von starker Säure (Nr. 4, 8) und H_2O (Nr. 3) unter Kochen leicht stattfindet. Bei Verwendung von HCO_2H als Lösungsmittel und $HClO_4$ als Säure-Katalysator erhielt man die beste Ausbeute an **12** (Nr. 1).[9] Weder 1,5-Diketon **13** noch verbrücktes Bicyclen **14** wurden isoliert (Schema-2).[4] Besonders bemerkenswert ist

Tabelle 1. Lösungsmitteleffekt in cyclisierung von **11** zu **12**[a]

Nr.	Lösungsmittel	pK_b[b]	Säure	Rückflussdauer	Ausb. an **12**[c]
1	HCO_2H	>20.2	$HClO_4$[d]	1.5 h	98%
2	HCO_2H		HBr[e]	1	90
3	HCO_2H[f]		*p*-TsOH	2.5	77
4	HCO_2H		—	18	0
5	AcOH	20.2	$HClO_4$	2	98
6	AcOH		H_2SO_4[d]	4	90
7	AcOH[g]		*p*-TsOH[h]	3	≈0
8	AcOH		CF_3CO_2H[i]	7	≈0
9	CF_3CO_2H		$HClO_4$	2.5	60
10	Cl_2CHCO_2H		$HClO_4$	0.75[j]	75
11	$CH_3CH_2CO_2H$	20	$HClO_4$	7	50
12	CH_3NO_2	25	$HClO_4$	1[k]	55
13	EtOH	≈16	$HClO_4$	3	0
14	Dioxan	≈17.8	$HClO_4$	5.5	0
15	DMSO		$HClO_4$	3	0

a) Verhältnis von Substrat–Säure–Lösungsmittel=100 mg: 1 ml: 9 ml. b) pK_b-Werte des Gleichgewichtes: Lösungsmittel+H_3O^+ ⟹ Lösungsmittel-H^++H_2O, J. B. Hendrickson, D. J. Cram, und G. S. Hamond, "Organic Chemistry," 3 Auflage, McGraw-Hill Kogakusha Ltd., Tokyo (1970), S. 304—307. c) Ausbeute des isolierten Produktes. d) 60% wässrig. e) 47% wässrig. f) 90% wässrig. g) Eisessig. h) Monohydrat. i) 80% wässrig. j) bei 130 °C. k) bei 75 °C

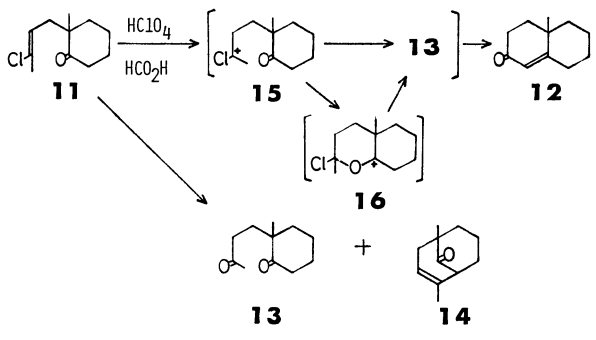

Schema 2. Reaktionsweg der modifizierte Wichterle-Reaktion.

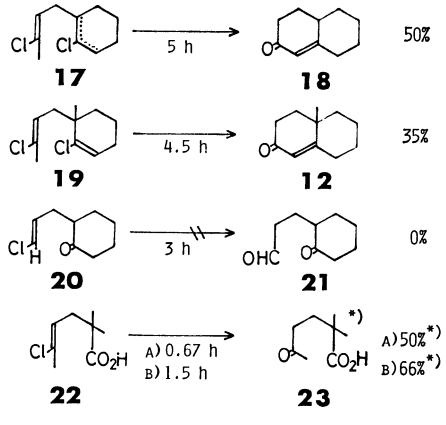

A) $HClO_4$-HCO_2H, Rückfluss. B) HBr-HCO_2H, Rückfluss.
*) als Methylester isoliert.

Schema 3.

die Tatsache, dass diese Cyclisierung sehr stark vom Lösungsmittel abhängig ist. Es scheint, dass eine enge Beziehung zum pK_b-Wert des Lösungsmittels besteht. In den Lösungsmitteln wie HCO_2H (pK_b≈20.2) sowie CH_3NO_2 (pK_b≈25), die schwächer basisch als Olefin (pK_b≈18) sind, sollte die Protonierung an die C=C-Doppelbindung des Chlorbutenyl-Restes viel günstiger sein als in den stärker basischen alkoholischen (pK_b≈16) bzw. ätherischen (pK_b≈17.5) Lösungsmitteln. Das durch Addition des Protons an den Chlorbutenyl-Rest gebildete intermediäre Ion **15** würde über das 1,5-Diketon **13** ins Endeprodukt **12** umgewandelt werden. Dass die Reaktion die Anwesenheit von H_2O erfordert (Nr. 7), ist verständlich, wenn man die intermediäre Bildung des 1,5-Diketons **13** annimmt. Obwohl die Möglichkeit der Carbonylgruppenbeteiligung (**15**→**16**→**13**, Schema-2) nicht ausgeschlossen werden kann, erscheint dieser Verlauf auf Grund der unten beschriebenen Befunde weniger wahrscheinlich.

Um den Reaktionsweg von **11** zu **12** genauer zu untersuchen, wurden Dichlordiolefine **17** und **19** dargestellt und den neuen Cyclisierungsbedingungen der Wichterle-Reaktion unterworfen. Da diese beiden Verbindungen keine Carbonylgruppe enthalten, ist eine Carbonylgruppenbeteiligung beim Hydrolysierungsschritt zum Diketon nicht möglich. Obwohl die Reaktionszeit im Vergleich mit **11** etwas länger dauerte, ergaben diese Dichlordiolefine in mässigen Ausbeuten Octalon-Derivate **18** bzw. **12** (Schema-3).[3a] Dies weist darauf hin, dass die Nachbargruppenbeteiligung (**15**→**16**→**13**→**12**) beim Ringschluss unter diesen neuen Bedingungen nicht so wichtig sein sollte. Um diesen Punkt weiter aufzulkären, wurde die Umwandlung von 2-(3-Chlorallyl)cyclohexanon (**20**) in den entsprechenden Ketoaldehyd **21** versucht. Nicht nur unter den neuen, sondern auch unter den konventionellen (konz· H_2SO_4) Bedingungen wurde **21** nicht erhalten. Des weitern verlief die Hydrolyse von 5-Chlor-2,2-dimethyl-4-hexensäure (**22**) zur Ketocarbonsäure **23** nicht so glatt. Dies deutet darauf hin, dass eine Beschleunigung der Hydrolyse durch einen Nachbargruppeneffekt der Carboxylgruppe nicht stattfindet. Diese Ergebnisse

könnten zeigen, dass bei der Cyclisierung von α-(Chlorbutenyl)ketonen ein intermediäres Carboniumion wie **15** zuerst entsteht und dessen Stabilität sehr wichtig ist, und dass die Methylgruppe des Chlorbutenyl-Restes für die Stabilisierung von **15** eine grosse Rolle spielt. Alle bisher erwähnten Befunde zusammengenommen, könnte der Reaktionsweg der neuen Ringschlussreaktion von **11** über **15** und **13** zu **12** führen (Schema-2).

Sehr interessant ist, dass das verbrückte Bicyclen **14** unter den oben beschriebenen Bedingungen in guter Ausbeute ins Octalon **12** überführt wurde, während in EtOH keine Reaktion eintrat und das Ausgangsmaterial **14** fast quantitativ zurückgewonnen wurde. Die basekatalysierte Retro-Aldolkondensation von **24** zu **12** ist schon bekannt.[10] In diesem Fall würde **14** zuerst zum Ketol **24** hydratisiert, das weiter ins 1,5-Diketon **13** über **25** säurekatalysiert überführt und zum **12** recyclisiert würde (Schema-4).

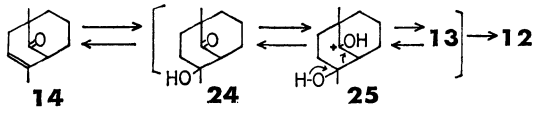

$HClO_4$-HCO_2H, 1 h RÜCKFLUSS, 82%
$HClO_4$-EtOH , 3 h RÜCKFLUSS, 0%

Schema 4.

B. Reaktionsbeispiele[11]

Um den Anwendungsbereich und die Grenze dieser Annelierung zu untersuchen, liessen sich viele α-(Chlorbutenyl)ketone HCO_2H mit $HClO_4$ bzw. HBr umsetzen. Die Resultate sind in Tabelle-2 zusammengefasst. In allen Fällen wurden weder das entsprechende 1,5-Diketon noch verbrückte Bicyclen wie Typ **5** isoliert. Aus 6-Chlor-3,3-dimethyl-5-hepten-2-on (**28**) wurden Trimethylcyclohexenone **29** und **30** im Verhältnis von *ca.* 1 : 2 erhalten.[13] Die Konstitutionen von **29** und **30** folgten aus den charakteristischen NMR-Signalen (2 breite Tripletts bei 2.43 ppm für die Methylenprotonen an C-6 von **29** und bei 2.30 ppm für die Methylprotonen an C-4 von **30**) sowie MS-Fragmentierungen (*m/e* 112 ($M^+-C_2H_2$) von **29** und *m/e* 82 ($M^+-C_4H_8$) von **30**). Ausserdem unterstützt die mechanistische Überlegung auch, dass **30** das Hauptprodukt wird, weil der Weg zu **30** im Übergangszustand die kleinere sterische Hinderung erfährt als derjenige zu **29**.[13] Bei der Umsetzung von **26** und **33a** war im Vergleich mit **11** eine längere Reaktionszeit erforderlich. Es scheint, dass die Reaktionszeit auch von der Menge der zugesetzten Säure abhängt. In den in der Tabelle-1 gezeigten Beispielen wurde 1 ml 60% $HClO_4$ zugegeben, die im Fall des Substrates **11** (100 mg) 18 Äq. entspricht. Setzt man beim grossen Ansatz der Reaktion von **11** zu **12** eine kleinere Menge $HClO_4$ (≈2 Äq.) zu, so wurde eine Abnahme der Reaktionsgeschwindigkeit (≈8 h) und der Ausbeute (≈70%) beobachtet.

2-(3-Chlor-2-butenyl)-3-methyl-2-cyclohexenon (**35**) und 4-(3-Chlor-2-butenyl)-7a-methyl-5,6,7,7a-tetrahydroindan-1,5-dion (**40**) wurden jeweils direkt bis zum α,β: γ,δ-Dienon **36** und -Diendion **41** cyclisiert.[3a,15] Im Genensatz dazu fand im Fall des 6-(3-Chlor-2-butenyl)-6-methyl-2-cyclohexenons (**37**) eine intramolekulare Michael-Reaktion statt und 5-Acetyl-1-methylbicyclo-

TABELLE 2.

Nr.	Substrat	Produkt	Medium	Rückflussdauer (h)	Ausb. (%)
1	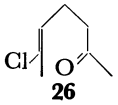 **26**	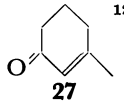 [12] **27**	a)	3	77
2	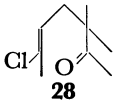 **28**	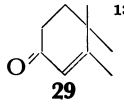 [13a] **29**	a)	0.75	25
		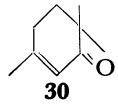 **30**			48
3	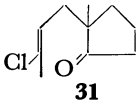 **31**	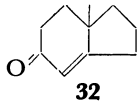 [14] **32**	a)	1	50
4	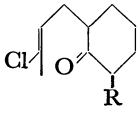 **33a** (R=H)	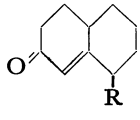 [3,4] **18**	a)	5	75
	33b ($R=CH_3$)	**34**		1	70
5	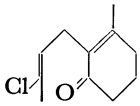 **35**	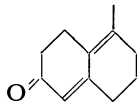 **36**	a)	1.5	70

TABELLE 2. Fortsetzung

Nr.	Substrat	Produkt	Medium	Rückflussdauer (h)	Ausb. (%)
6	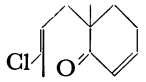 **37**	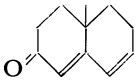 **38**	a)	3	22
		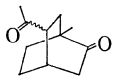 **39**			71
7	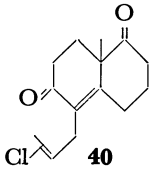 **40**	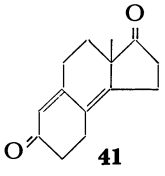 **41**	a)	1	65
8	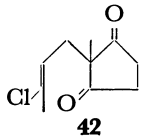 **42**	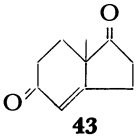 **43**	b)	2.5	40
		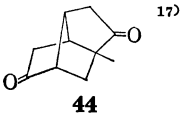 [17] **44**			10
9	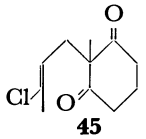 **45**	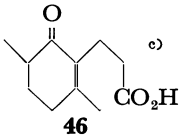 [c] **46**	b)	1.5	58.5[c]
		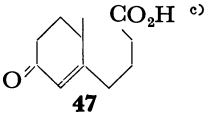 [c] **47**			9.7[c]
10	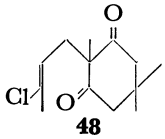 **48**	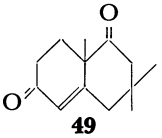 **49**	b)	1.5	32
		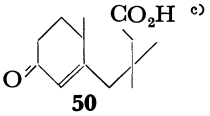 [c] **50**			30[c]
11	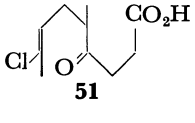 **51**	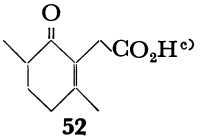 [c] **52**	b)	1.5	50[c]
		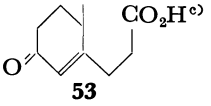 [c] **53**			4[c]
12	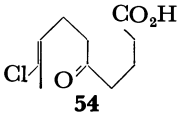 **54**	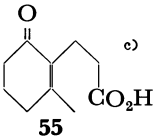 [c] **55**	a)	2	63[c]
		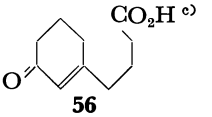 [c] **56**			18.5[c]

a) $HClO_4$–HCO_2H. b) HBr–HCO_2H. c) als Methylester isoliert.

[2.2.2]octan-2-on (**39**) entstand als Hauptprodukt.[4] Das erwartete Annelierungsprodukt **38** wurde als Nebenprodukt nur in 22%-iger Ausbeute erhalten.[4] Ein 1,5-Diketon wie Typ **8** oder **10**, das bei der Behandlung mit konz·H_2SO_4 hauptsächlich entsteht, wurde in keinen Fall isoliert.

Bei Ringschlüssen von 2-(3-Chlor-2-butenyl)-2-methylcycloalkan-1,3-dion konnte man im allgemeinen mit HBr eine bessere Ausbeute erziehen als mit $HClO_4$. Beim Erhitzen in HCO_2H mit HBr wurde aus 2-(3-Chlor-2-butenyl)-2-methylcyclopentan-1,3-dion (**42**)das Annelierungsprodukt **43** in mässiger Ausbeute erhalten,[16] wobei ein Nebenprodukt **44** mit der gleichen Formel ($C_{10}H_{12}O_2$) wie **43** in einer Ausbeute von 10% kristallin isoliert wurde.[17] Bei 2-(3-Chlor-2-butenyl)-2-methylcyclohexan-1,3-dion (**45**) verlief anderseits bei 60 °C eine Ringöffnung zur Chlorketocarbonsäure **57** glatt,[18] die über **58** zu den 2-Cyclohexenon-Derivaten **46** und **47** weiter cyclisiert wurde.[19,20] Das erwünschte Wieland-Miescher-Keton, 8a-Methyl-1,6-dioxo-1,2,3,4,-6,7,8,8a-octahydronaphthalin wurde nicht erhalten. Im Gegensatz dazu wurde aus dem Trimethylkörper **48** das Dioxohydronaphthalin-Derivat **49** neben **50** im Verhältnis von *ca.* 1:1 isoliert. Wegen der sterischen Hinderung zwischen Hydroxygruppe und *gem*-Dimethylgruppe (**59a** und **59b**) sollte sich die Ringspaltung von **48** zu **60** im Vergleich mit **45** ziemlich unterdrücken lassen (Schema-5). Analog wurden aus Chlorketocarbonsäuren **51** und **54** die entsprechenden 2-Cyclohexenon-Derivate **52**[21] und **53** bzw. **55** und **56** dargestellt. Die oben beschriebenen Ketocarbonsäuren wurden alle nach Behandlung mit ether. CH_2N_2 als Methylester isoliert und die Ausbeuten bestimmt.

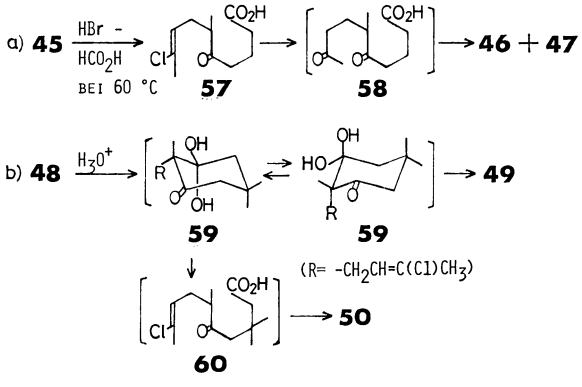

Schema 5.

C. Synthese von 4-Estren-3,17-dion

Als ein weiteres Anwendungsbeispiel wurde die Synthese von 19-Nor-steroid versucht. Es wurde zuerst versucht, ausgehend von **43**[22] und dessen Derivaten **43a**, **b**[2,23] durch die Stork'sche reduktive Alkylierung[6d] oder aus dem von **43** leicht abgeleiteten **40** durch selektive Hydrierung 4-(3-Chlor-2-butenyl)-7a-methylhexahydroindan-1,5-dion (**61**) darzustellen, das in ein wichtiges Zwischenprodukt **64** überführt werden könnte. Alle Versuche waren aber erfolglos. Dan wurde **40** mit konz. H_2SO_4 zum ungsättigten Triketon **62** hydrolysiert, das in AcOH mit 10% Pd–C unter Normaldruck

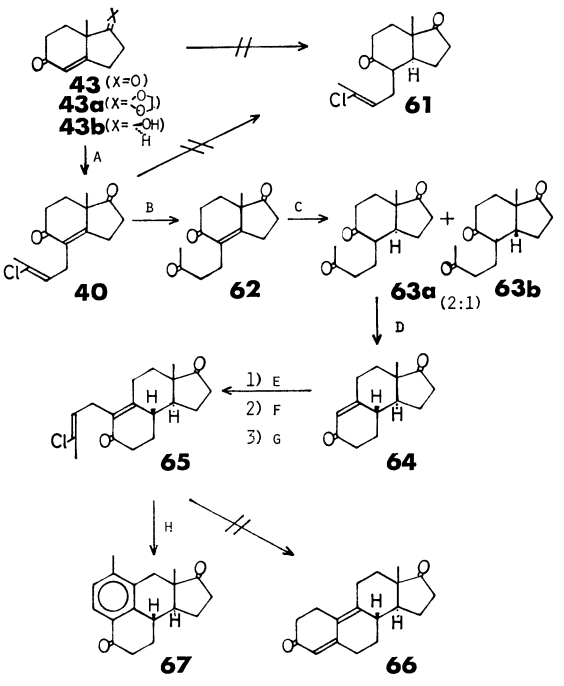

A) DCB-^{t}AmOK. B) H_2SO_4. C) H_2/Pd-C. D) p-TsOH. E) PYRROLIDIN. F) DCB. G) H_2O. H) $HClO_4$-HCO_2H.

Schema 6.

hydriert wurde, wobei man ein Gemisch von **63a** und **63b** im Verhältnis von 2:1 erhielt. Ohne Trennung und Reinigung wurde das rohe Hydriergemisch in AcOH mit *p*-TsOH under Rückfluss weiter zum bekannten tricyclischen Diketon **64** cyclisiert, das nach der Säulenchromatographie an SiO_2 in 40%-iger Ausbeute aus **62** isoliert wurde.[15] **64** wurde dann über Dienamin mit DCB weiter zu **65** alkyliert. Die Cyclisierung von **65** in HCO_2H mit $HClO_4$ ergab aber kein 4,9-Estradien-3,17-dion, sondern ein bekanntes tetracyclisches Diketon **67** (Schema-6).[15] Als nächstes wurde die reduktive Alkylierung von **68** versucht, das aus **64** mit $NaBH_4$ leicht zugänglich ist.[15] Die reduktive Chlorbutenylierung von **68** in flüss·NH_3 mit Li-DCB und die anschliessende Oxydation mit CrO_3 lieferten die gewünschte Verbindung **70** in geringer Ausbeute. Bei der Alkylierung von **69** liess sich die Ausbeute ebenfalls nicht verbessern (≈17%). Deshalb wurden die Bedingungen der Stork'schen reduktiven Alkylierung von **12** sowie **33a** als Testverbindungen untersucht (Tabelle-3). Wenn man 0.8 Äq. ^{t}BuOH zusetzte und

TABELLE 3. TESTEXPERIMENT DER REDUKTIVEN ALKYLIERUNG

Substrat	Medium	Alkylierungsreagenz	Ausb.
33a	NH_3	DCB	20%
33a	NH_3–THF	DCB	15
33a	NH_3–^{t}BuOH–THF	$H_3CC(Cl)=CH-CH_2I$	30
12	NH_3–^{t}BuOH–THF	$H_3CC(Cl)=CH-CH_2I$	23

anstatt DCB 1-Jod-3-chlor-2-buten als Alkylierungsreagenz verwendete,[25] konnte die Ausbeute wenig erhöht werden. Die hier erhaltenen Verbindungen, 1-(3-Chlor-2-butenyl)-2-decalon (**72a**) und 1-(3-Chlor-

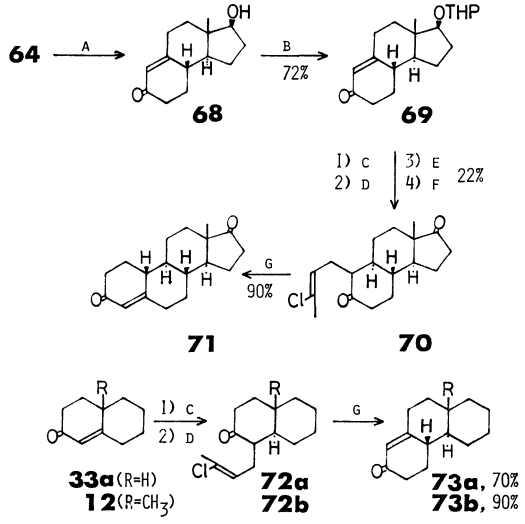

Schema 7.

2-butenyl)-4a-methyl-2-decalon (**72b**) wurden durch Behandlung in HCO_2H mit $HClO_4$ in die entsprechenden Hydrophenanthren-Derivate **73a** bzw. **73b** in guten Ausbeuten überführt.[6d] Analog zum oben erwähnten Testexperiment wurde **69** in flüss·NH_3–THF mit Li und ^{t}BuOH versetzt und dann mit 1-Jod-3-chlor-2-buten reduktiv alkyliert. Das nach üblicher Aufarbeitung erhaltene Rohprodukt wurde zur Abspaltung der Schutzgruppe in MeOH mit H_2SO_4 versetzt und anschliessend mit CrO_3 oxydiert, so dass man nach der chromatographischen Reinigung 10-(3-Chlor-2-butenyl)-des-A-estran-5,17-dion (**70**) in 22%-iger Ausbeute erhielt. Ausserdem wurde Des-A-estran-5,17-dion als Hauptkomponente isoliert und dessen Ausbeute betrug *ca.* 40%. **70** wurde in HCO_2H in Gegenwart von $HClO_4$ erhitzt, wobei das Zielprodukt **71** in einer Ausbeute von 90% entstand (Schema-7). Die IR-, NMR-, und MS-Spektren vom hier synthetisierten **71** sind in Übereinstimmung mit denjenigen in der Literatur und die Konstitution von **71** wurde dadurch ermittelt.[26]

D. Darstellung von 1,4-Diketonen und Synthese von Dihydrojasmon

Wie in Abschnitten A, B, und C beschrieben, wurde festgestellt, dass die modifizierte Wichterle-Reaktion zur Darstellung von 2-Cyclohexenonen geeignet ist. Es wurde dann versucht, sie auf die Umwandlung von α-(2-Haloallyl)keton wie **74** ins 1,4-Diketon wie **77** zu übertragen.[27]

Nienhaus *et al.* haben bereits darüber berichtet, dass die Behandlung von 2-(2-Chlorallyl)cyclohexanon (**74**)

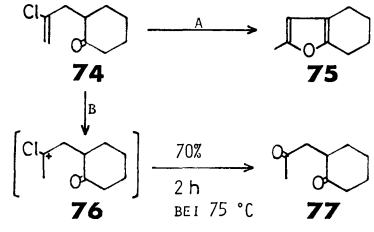

Schema 8.

Tabelle 4.

Nr.	Substrat	Produkt	Reaktionszeit (h)	Ausb. (%)
1	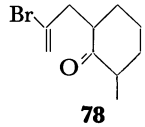 **78**	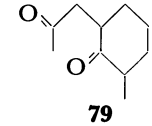 **79**	1.5 bei 70 °C	75
2	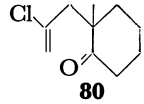 **80**	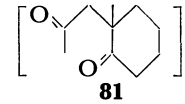 **81**	5 bei 75—80 °C	(Kompliziertes Gemisch)
3	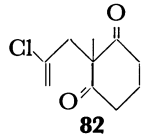 **82**	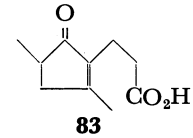 **83**	3.5 Rückfluss	30[b]
4	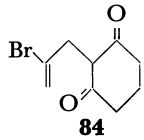 **84**	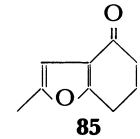 **85**	2.5 bei 80 °C	55[c]
5	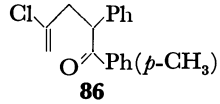 **86**	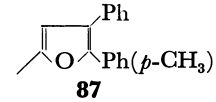 **87**	1 Rückfluss	80

a) In HCO_2H mit $HClO_4$. b) Als Methylester isoliert. c) Die Ausbeute ist auf die reagierte Ausgangsverbindung **84** benzogen. Eine kleine Menge **84** wurde zurückgewonnen.

mit konz·H_2SO_4 2-Methyl-4,5,6,7-tetrahydrobenzofuran (**75**) in guter Ausbeute liefert.[28] Dagegen entstand beim Erhitzen von **74** in HCO_2H in Gegenwart von $HClO_4$ 1,4-Diketon **77** in 70%-iger Ausbeute,[29] vermutlich über das Carboniumion **76**. Im NMR-Spektrum des Rohproduktes war das Furan-Derivat **75** nicht zu erkennen. Die Optimierungesversuche zeigten, dass die Umwandlung von **74** in **77** im Vergleich mit α-Chlorbutenylketon wie Typ **1** bei relativ tieferer Temperatur verläuft und dass beim Kochen weniger 1,4-Diketon **77** entsteht. Es zeigte sich auch, dass durch den Zusatz von fast äquimolarer Menge $HClO_4$ eine bessere Ausbeute resultiert (Schema-8).

In Tabelle-4 sind andere Beispiele zusammengefasst. Während 2-(2-Bromallyl)-6-methylcyclohexanon (**78**) das entsprechende 1,4-Diketon **79**[27c] in 75%-iger Ausbeute ergab, wurde aus 2-(2-Chlorallyl)-2-methylcyclohexanon (**80**) kein erwünschtes Produkt **81**,[29,30] sondern nur ein kompliziertes Gemisch erhalten. Sogar durch die Behandlung mit konz·H_2SO_4 konnte **80** nicht in **81** überführt werden. Wie das Molekülmodell zeigt, könnte der Angriff eines Nucleophils auf das zwischenstufige Carboniumion wegen der sterischen Hinderung in der Umgebung des in α-Stellung zur Carbonylgruppe liegenden quartären Kohlenstoffatoms gestört werden. 2-(2-Chlorallyl)-2-methylcyclohexan-1,3-dion (**82**) ergab analog zu **45** beim Kochen über Ringöffnung und anschliessende Cyclisierung 2-(2-Carboxyethyl)-3,6-dimethyl-2-cyclopentenon (**83**), das nach Veresterung mit CH_2N_2 isoliert und dessen Konstitution spektroskopisch bestätigt wurde. Anderseits wurden aus den leicht enolisierbaren α-(2-Haloallyl)ketonen **84** bzw. **86** die Furan-Derivate **85** bzw. **87** erhalten.[31]

Aufgrund der oben beschriebenen Ergebnisse wurde die Synthese von Dihydrojasmon versucht.[32] Ausgehend von Acetessigsäureethylester wurde **89a** durch γ-Alkylierung mit NaH/*n*-BuLi/*n*-$C_5H_{11}Br$ in THF

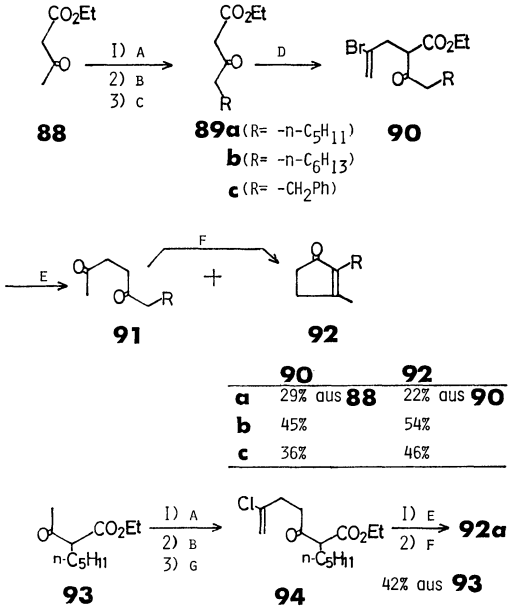

88 **89a** (R= -n-C_5H_{11}) **b** (R= -n-C_6H_{13}) **c** (R= -CH_2Ph) **90** **91** **92**

	90	92
a	29% aus **88**	22% aus **90**
b	45%	54%
c	36%	46%

93 **94** 42% aus **93**

A) NaH. B) n-BuLi. C) R-Br. D) NaH/CH_2=C(Br)CH_2Br. E) $HClO_4$-HCO_2H. F) 0.5n-NaOH. G) CH_2=C(Cl)CH_2Cl.

Schema 9.

dargestellt.[33] Ohne Reinigung wurde **89a** mit NaH/2,3-Dibrompropen zu **90a** alkyliert. Beim Erhitzen von **90a** in HCO_2H mit $HClO_4$ entstand ein Gemisch von Undecan-2,5-dion (**91a**) und Dihydrojasmon **92a** im Verhältnis von 8:3 (NMR), das ohne Trennung anschliessend mit 0.5 M-NaOH umgesetzt wurde.[34] Nach chromatographischer Reinigung wurde Dihydrojasmon **92a** in 22%-iger Ausbeute aus **90a** isoliert. Auf die gleiche Weise wurde aus Acetessigsäureethylester 2-Hexyl-3-methyl-2-cyclopentenon (**92b**) und 2-Benzyl-3-methyl-2-cyclopentenon (**92c**) in 24%-iger bzw. 16.5%-iger Gesamtausbeute synthetisiert (Schema-9a).

Die Totalausbeute an Dihydrojasmon durch den oben erwähnten Syntheseweg ist gering. Ein Grund dazu scheint in der γ-Alkylierungsstufe zu liegen, weil die α-Alkylierung von **89a** mit 2,3-Dibrompropen gut verläuft. Folgenderweise wurde die verbesserte Ausbeute verwirklicht. Der α-pentylierte Ketoester **93**, der nach einer Vorschrift in guter Ausbeute zugänglich ist,[35] wurde in THF mit NaH 1 h bei Raumtemperatur gerührt und nach Abkühlen auf 0 °C mit *n*-BuLi und anschliessend mit 2,3-Dichlorpropen versetzt. Das NMR-Spektrum des Rohproduktes zeigte, dass das γ-Alkylierungsprodukt **94** in 80%-iger Ausbeute entsteht (isolierte Ausb. 60%). Ohne Reinigung wurde das Rohprodukt in HCO_2H mit $HClO_4$ 4 h bei 90 °C erhitzt, wobei Decarboxylierung, Hydrolyse des Vinylchlorides und teilweise Ringschluss stattfanden und eine Mischung von **91a** und **92a** (*ca.* 1:2) erhalten wurde. Die anschliessende Behandlung dieser Mishung mit 0.5 M-NaOH lieferte Dihydrojasmon in 42%-iger Ausbeute aus **93**. Das hier dargestellte Dihydrojasmon wurde durch den Vergleich der spektroskopischen Daten mit denjenigen in der Literatur identifiziert.[32] Die modifizierte Wichterle-Reaktion erwies sich somit als eine Methode zur Darstellung von 2,3-disubstituierten 2-Cyclopentenonen.

Experimenteller Teil

Allgemeine Bemerkungen. Die IR-Spektren wurden mit einem Gerät JASCO.IR-S gemessen und die Lage der Banden in cm^{-1} angegeben. Die MS-Spektren wurden mit einem Gerät Hitachi RMU-6E erhalten. Die NMR-Spektren wurden mit den Geräten Hitachi R-20B bei 60MHz und JEOL.PS-100 bei 100 MHz aufgenommen. Die chemische Verschiebungen sind in ppm (interner Standard; TMS=0 ppm) angegeben. Die Signale wurden durch folgende Abkürzungen charakterisiert; s=Singulett, d=Dublett, t=Triplett, q=Quartett, m=Multiplett und b=breites Band. Die Schmelzpunkte wurden in einer Kapillare bestimmt und sind nicht korrigiert. Es wurden 99—100% HCO_2H und 60% oder 70% $HClO_4$ sowie 47% HBr verwendet. Die Abkürzung RT. bedeutet Raumtemperatur.

Abschnitte A und B.

Darstellung von Ausgangsmaterien.

2-bzw. 6-(3-Chlor-2-butenyl)-1-chlor-cyclohexen (17). Zu einer Lösung von 1 g **33a** in 20 ml CCl_4 fügte man 5 g PCl_5 und erhitzte 4 h unter Rückfluss. Nach Abkühlen auf RT. wurde das Reaktionsgemisch auf 50 ml H_2O gegossen und mit $CHCl_3$ extrahiert. Die $CHCl_3$-Auszüge wurden mit gesätt. $NaHCO_3$-Lösung neutralgewaschen, getrocknet und

eingedampft. Der Rückstand wurde an der 100-fachen Menge SiO_2 mit Hexan chromatographiert. Man erhielt 830 mg (75%) **17** als ein Gemisch von 2- und 6-Alkylisomeren; IR (Film): 1667, 1653 cm^{-1}; NMR (CCl_4): 2.09 (3H, d, J=1.5 Hz), 5.35 (1H, qt, J=1.5, 7 Hz), 5.75 (0.7 H, t, J=3 Hz); MS: 204, 206, 208 (M^+), 169, 171 (M^+-Cl), 115, 117 ($M^+-C_4H_6Cl$).

*1-Chlor-6-(3-chlor-2-butenyl)-6-methylcyclohexen (**19**).* Gleicherweise wurden 125 mg **19** (57%) aus 200 mg **11** und 1 g PCl_5 erhalten; IR (Film): 1668, 1644 cm^{-1}; NMR (CCl_4): 1.14 (3H, s), 2.10 (3H, d, J=1.5 Hz), 5.32 (1H, qt, J=1.5, 7 Hz), 5.74 (1H, t, J=3.5 Hz); MS: 218, 220, 222 (M^+), 183, 185 (M^+-Cl), 129, 131 ($M^+-C_4H_6Cl$).

*2-(3-Chlorallyl) cyclohexanon (**20**).* Eine Lösung von 5 g Pyrrolidinenamin des Cyclohexanons[36] und 5 ml 1,3-Dichlorpropen in 20 ml Dioxan wurde 18 h unter Ar gekocht. Nach Abkühlen auf RT. wurde die Lösung mit 1 ml konz.HCl und 10 ml H_2O versetzt und 4 h weiter unter Rückfluss erhitzt. Nach Entfernung von Dioxan extrahierte man die wässrige Phase mit AcOEt. Die AcOEt-Auszüge wurden mit gesätt. $NaHCO_3$-Lösung neutralgewaschen, getrocknet und eingedampft. Man erhielt 4.5 g (80%) **20**; Kp. 93 °C/3 Torr; IR (Film): 1710, 1630 cm^{-1}; NMR ($CDCl_3$): 5.3—6.2 (2H, m); MS: 172, 174 (M^+), 137 (M^+-Cl); Gef: C, 62.45; H, 7.38; Cl, 20.45%. Ber. für $C_9H_{13}ClO$: C, 62.61; H, 7.54; Cl, 20.58%.

*5-Chlor-2,2-dimethyl-4-hexensäure(**22**).* Das zur Darstellung von **28** verwendete rohe Chloraldehyd (2 g) in 10 ml Aceton wurde bei RT. mit CrO_3 (Jones-Reagenz) versetzt und 48 h bei RT. gerührt. Nach Zugabe von *i*-PrOH wurde die Reaktionsmischung mit H_2O verdünnt und mit AcOH extrahiert. Die AcOEt-Extrakte wurden dann mit 5% NaOH-Lösung ausgeschüttelt. Die alkalische Phase wurde mit 3 M-HCl schwach angesäuert und wieder mit $CHCl_3$ extrahiert. Nach Abdampfen des Lösungsmittels wurde der Rückstand bei 135—140 °C (Öl-Bad)/12 Torr destilliert. Ausb. 1.1 g (50%); IR (Film): 1705, 1670, 1640 cm^{-1}; NMR (CCl_4): 1.24 (6H, s), 2.10 (3H, d, J=1.5 Hz), 5.42 (1H, qt, J=1.5, 7 Hz); Gef: C, 54.48; H, 7.38; Cl, 20.12%. Ber. für $C_8H_{13}ClO_2$: C, 54.39; H, 7.36; Cl, 20.11%.

*6-Chlor-5-hepten-2-on (**26**).* Zu einer Lösung von 13.6 g EtONa in 100 ml EtOH fügte man 25 g Acetessigsäureäthylester und 25 g 1,3-Dichlor-2-buten (DCB) bei 0 °C unter Rühren und N_2. Die Lösung wurde 24 h bei RT. stehengelassen und dann 1 h gekocht. Das ausgefallene NaCl wurde abgesaugt, und das Filtrat zur Trockene eingeengt. Zur Suspension des oben erhaltenen Rückstandes in 320 ml H_2O wurde eine Lösung von 25 g NaOH in 180 ml H_2O unter Rückfluss innerhalb von 2 h tropfenweise gegeben und weiter 4 h gekocht. Nach Abkühlen auf RT. wurde die wässrige Phase mit NaCl gesättigt und mit Ether mehrmals extrahiert. Die organische Phase wurde mit 3 M-HCl, mit gesätt. $NaHCO_3$-Lösung gewaschen, getrocknet und eingedampft. Der Rückstand wurde dann bei 78—80 °C/20 Torr destilliert. Ausb. 15 g (53%); IR (Film): 1720, 1663 cm^{-1}; NMR (CCl_4): 2.06 (6H, bs), 5.42 (1H, qt, J=1.5 Hz); MS: 146, 148 (M^+), 111 (M^+-Cl).

*6-Chlor-3,3-dimethyl-5-hepten-2-on (**28**).* Zur Suspension von 12.4 g NaOH, 1.13 g *n*-Bu_4NBr, 12.4 g H_2O und 17.4 ml Benzol wurde eine Mischung von 25 g Isobutyraldehyd und 32.5 g DCB bei 70 °C unter Rühren langsam zugetropft und weiter 2 h bei der gleichen Temp. gerührt.[37] Nach Abkühlen wurde das Reaktionsgemisch auf H_2O gegossen und mit AcOEt ausgezogen. Nach üblicher Aufarbeitung destillierte man das Rohprodukt bei 75 °C/12 Torr. Zu einer Lösung von 64 mmol CH_3MgI in 30 ml Ether wurde eine Lösung von 8 g (53 mmol) des oben erhaltenen alkylierten Aldehydes in 10 ml Ether bei 0 °C zugegeben und 18 h bei RT. gerührt. Nach Zugabe der gesätt. NH_4Cl-Lösung extrahierte man mit Ether und erhielt 7 g Alkohol, der anschliessend ohne Reinigung oxydiert wurde. Eine Lösung vom rohen Chloralkohol (7 g) in 200 ml Aceton wurde mit CrO_3 (Jones-Reagenz) bei 0 °C versetzt und bei RT. über Nacht gerührt. Nach Entfernung von Aceton wurde der Rückstand in Ether aufgenommen. Die etherische Phase wurde mit 5% NaOH-Lösung, mit H_2O gewaschen, getrocknet und eingedampft. Man erhielt nach Destillation bei 89—90 °C/12 Torr 3 g **28** (14% aus Isobutyraldehyd); IR (Film): 1708, 1663 cm^{-1}; NMR ($CDCl_3$): 1.17 (6H, s), 2.07 (3H, d, J=1.5 Hz), 2.12 (3H, s), 5.33 (1H, qt, J=1.5, 7 Hz); MS: 174, 176 (M^+), 139 (M^+-Cl); Gef: C, 61,91; H, 8.68; Cl, 20.04%. Ber. für $C_9H_{15}ClO$: C, 61, 89; H, 8.68; Cl, 20.34%.

*2-(3-Chlor-2-butenyl)-2-methylcyclopentanon (**31**).* Ein Gemisch von 2-Methylcyclopentanon (5 g) und $NaNH_2$ (2 g) in 30 ml Benzol wurde 5 h unter Rühren und N_2 gekocht. Nach Abkühlen auf RT. wurde die Lösung mit 6 ml DCB in 6 ml Benzol tropfenweise versetzt und 3 h unter Rückfluss erhitzt. Nach üblicher Aufarbeitung wurde das Rohprodukt an der 10-fachen SiO_2 mit Benzol–Hexan (1: 1) chromatographiert und man erhielt 3.2 g (34%) **31**; IR (Film): 1740, 1665 cm^{-1}; NMR (CCl_4): 0.99 (3H, s), 2.05 (3H, d, J=1.5 Hz), 5.35 (1H, qt, J=1.5, 7 Hz); Gef: C, 64.33; H, 8.18; Cl, 18.62%. Ber. für $C_{10}H_{15}ClO$: C, 64.34; H, 8.10; Cl, 18.99%.

*2-(3-Chlor-2-butenyl)cyclohexanon (**33a**).*[38a] Analog zur Darstellung von **20** wurde eine Lösung von Pyrrolidinenamin von Cyclohexanon (16 g) in 55 ml Dioxan mit 16 ml DCB 18 h unter Ar gekocht. Nach der schon beschriebenen Aufarbeitung erhielt man 11 g (58%) **33a** nach Destillation bei 85—100 °C/3 Torr; IR (Film): 1715, 1675 cm^{-1}; NMR (CCl_4): 2.07 (3H, d, J=1.5 Hz), 5.49 (1H, qt, J=1.5, 7 Hz).

*2-(3-Chlor-2-butenyl)-2-methylcyclopentan-1,3-dion (**42**).* 2-Methylcyclopentan-1,3-dion[38] (2.2 g) wurde in 5.6 ml 20% KOH-Lösung gelöst und mit 0.5 g KI und 2.2 ml DCB versetzt. Die Reaktionsmischung wurde *ca.* 1.5 h bei 90 °C gerührt, bis diese gegen Lackmus neutral reagierte. Nach Abkühlen auf RT. und Zugabe von H_2O wurde die Mischung mit Ether extrahiert. Die Ether phase wurde mit gesätt. $NaHCO_3$-Lösung neutralgewaschen, über Na_2SO_4 getrocknet und eingedampft. Das Rohprodukt (3.9 g) wurde an der 15-fachen Menge SiO_2 mit Benzol–AcOEt (9: 1) chromatographiert. Man erhielt 2.7 g (67%) **42**; IR (Film): 1765, 1725, 1660 cm^{-1}; NMR (CCl_4): 1.15 (3H, s), 2.10 (3H, d, J=1.5 Hz), 2.36 (2H, d, J=7 Hz), 2.70 (4H, s), 5.34 (1H, qt, J=1.5, 7 Hz); Gef: C, 59.95; H, 6.45; Cl, 17.43%. Ber. für $C_{10}H_{13}ClO_2$: C, 59.85; H, 6.53; Cl, 17.67%.

Analog wurden **45** als Öl aus 2-Methylcyclohexan-1,3-dion[38] (76%) und **48** als farblose Kristalle aus 2-Methyldimedon[38] (80%) dargestellt.

*2-(3-Chlor-2-butenyl)-2-methylcyclohexan-1,3-dion (**45**):* IR (Film): 1730, 1690, 1665 cm^{-1}; NMR ($CDCl_3$): 1.25 (3H, s), 2.09 (3H, d, J=1.5 Hz), 5.30 (1H, qt, J=1.5, 7 Hz).

*2,5,5-Trimethyl-2-(3-chlor-2-butenyl)cyclohexan-1,3-dion (**48**):* Schmp. 69—70 °C (Hexan); IR (Nujol): 1725, 1690, 1665 cm^{-1}; NMR ($CDCl_3$): 0.90 (3H, s), 1.10 (3H, s), 1.23 (3H, s), 2.09 (3H, d, J=1.5 Hz), 5.32 (1H, qt, J=1.5, 7 Hz); Gef: C, 64.50; H, 7.90; Cl, 14.41%. Ber. für $C_{13}H_{19}ClO_2$: C, 64.33; H, 7.86; Cl, 14.64%.

*8-Chlor-5-methyl-4-oxo-7-nonensäure (**51**).* 1 g **42** in 18 ml H_2O wurde mit 6.3 g $Ba(OH)_2 \cdot 8H_2O$ versetzt und 4 h unter Rückfluss erhitzt.[39] Nach Abkühlen wurde das überschüssige $Ba(OH)_2$ durch Einleitung von CO_2 in die Reaktionsmischung ausgefällt, bis diese gegen Lackmus neutral reagierte. Das ausgefallene $BaCO_3$ wurde abgesaugt, die

Carbonsäure durch Zugabe von 2 M-HCl in Freiheit gesetzt und mit $CHCl_3$ extrahiert. Die $CHCl_3$-Auszüge wurden über Na_2SO_4 getrocknet und eingedampft. Man erhielt 880 mg (81%) **51**, die ohne weitere Reinigung in HCO_2H mit HBr umgesetzt wurde. Zur Analyse wurde **51** mit CH_2N_2 in den Methylester umgewandelt; IR(Film): 1740, 1715 cm^{-1}; NMR ($CDCl_3$): 1.14 (3H, d, J=7 Hz), 2.06 (3H, d, J=1.5 Hz), 3.65 (3H, s), 5.37 (1H, qt, J=1.5, 7 Hz); MS: 232, 234 (M^+); Gef: C, 57.93; H, 7.48; Cl, 13.60%. Ber. für $C_{11}H_{17}ClO_3$: C, 56.77; H, 7.36; Cl, 15.24%.

*9-Chlor-5-oxo-8-decensäure (**54**).* Zu einer Lösung von 1.5 g Cyclohexan-1,3-dion in 3.5 g 20% KOH-Lösung fügte man 1.4 ml DCB und 0.5 g KI und erhitzte 1.5 h bei 85 °C unter Rühren. Nach Abkühlen auf RT. wurde die Reaktionsmischung auf 15 ml 3% NaOH-Lösung gegossen und dreimal mit Ether ausgeschüttelt, um das dialkylierte Produkt zu entfernen. Unter Eiskühlung und Rühren wurde die wässrige Phase mit 6 M-HCl auf pH 4 eingestellt, wobei 2-(3-Chlor-2-butenyl)cyclohexan-1,3-dion (1.2 g, 44%) ausfiel. Dieses monoalkylierte Dion wurde ohne weitere Reinigung mit $Ba(OH)_2$ umgesetzt.

0.5 g vom oben erhaltenen monoalkylierten Dion wurden in 7 ml H_2O mit 1.7 g $Ba(OH)_2 \cdot 8H_2O$ 4 h unter Rückfluss gekocht.[39] Analog zu **51** erhielt man 520 mg (95%) **54**, die auch ohne Reinigung in HCO_2H mit $HClO_4$ umgezetzt wurde. Zur Analyse wurde die Säure mit CH_2N_2 in den Methylester überführt; IR(Film): 1740, 1715, 1670 cm^{-1}; NMR ($CDCl_3$): 2.05 (3H, d, J=1.5 Hz), 3.65 (3H, s), 5.43 (1H, qt, J=1.5, 7 Hz); Gef: C, 56.95; H, 7.44; Cl, 14.90%. Ber. für $C_{11}H_{17}ClO_3$: C, 56.75; H, 7.36; Cl, 15.24%.

Allgemeine Vorschrift der Cyclisierung.

Eine Lösung von α-chlorbutenyliertem Keton in HCO_2H wurde mit einer kleinen Menge $HClO_4$ (60% od. 70% wässrig) oder HBr (47% wässrig) versetzt und unter Rückfluss erhitzt, bis das Ausgangsmaterial dünnschichtchromatographisch nicht nachgewiesen wurde. Danach wurde die Reaktionsmischung i. Vak. eingeengt und in einem organischen Lösungsmittel wie AcOEt, $CHCl_3$ usw. aufgenommen. Die organische Phase wurde dann vorsichtig mit gesätt. $NaHCO_3$-Lösung neutralgewaschen, getrocknet und eingedampft. Der Rückstand wurde danach chromatographisch oder durch Destillation gereinigt. Das Verhältnis von Mineralsäure und HCO_2H zu Substrat kann man gegebenfalls vielfach ändern.

*4a-Methyl-$\Delta^{1(8a)}$-2-octalon (**12**).* a) 100 mg **11** in 9 ml HCO_2H wurden mit 1 ml $HClO_4$(60%) versetzt und 1.5 h gekocht. Nach der oben erwähnten Aufarbeitung wurde das Rohprodukt an der 50-fachen Menge SiO_2 mit AcOEt–Benzol (1: 19) chromatographiert. Ausb. 80 mg (98%).

b) 14 g **11** in 200 ml HCO_2H wurden mit 15 ml $HClO_4$ (60%) 8 h gekocht. Nach Abdampfen von HCO_2H und Aufarbeitung wurde der Rückstand bei 94—96 °C/3 Torr destilliert. Ausb. 8 g (70%); NMR ($CDCl_3$): 1.26 (3H, s), 5.75 (1H, bs); MS: 164 (M^+).

*Behandlung von **17** und **19**.* *a) **18** aus **17**:* 245 mg **17** wurden in 10 ml HCO_2H suspendiert und mit 1 ml $HClO_4$ (70%) 5 h rückfliessend erhitzt. Ausb. 90 mg (50%).

*b) **12** aus **19**:* Analog wurde eine Lösung von 110 mg **19** in 10 ml HCO_2H mit 1 ml $HClO_4$(60%) 4.5 h gekocht. Ausb. 30 mg (35%).

*2,2-Dimethyl-5-oxohexansäure (**23**).* a) mit $HClO_4$. Zu einer Lösung von 465 mg **22** in 10 ml HCO_2H fügte man 1.5 ml $HClO_4$ (70%) und kochte 40 Min. unter Rückfluss. Nach Abkühlen auf RT. wurde das Reaktionsgemisch auf 100 ml H_2O gegossen und mit $CHCl_3$ extrahiert. Die $CHCl_3$-Auszüge wurden mit H_2O gewaschen, getrocknet und eingedampft. Der Rückstand wurde in AcOEt gelöst und mit ether. CH_2N_2 verestert. Man erhielt 225 mg (50%) **23** als Methylester; Kp. 95 °C/12 Torr; IR (Film): 1730, 1725 cm^{-1}; NMR ($CDCl_3$): 1.20 (6H, s), 2.12 (3H, s), 3.65 (3H, s); MS: 172 (M^+), 141 ($M^+ - OCH_3$), 129 ($M^+ - COCH_3$); Gef: C, 62.17; H, 9.45%. Ber. für $C_9H_{16}O_3$: C, 62.76; H, 9.36%.

b) mit HBr. 522 mg **22** in 20 ml HCO_2H wurden mit 3 ml HBr versetzt und 1.5 h gekocht. Nach Veresterung mit CH_2N_2 wurden 336 mg (66%) **23** erhalten.

*Umwandlung von **14** in **12**.* Eine Lösung von 255 mg **13** in 20 ml HCO_2H wurde mit 1 ml $HClO_4$ (70%) versetzt und 1 h unter Rückfluss erhitzt. Nach üblicher Aufarbeitung erhielt man 210 mg (82%) **12**.

*3-Methyl-2-cyclohexenon (**27**).* 19 g **26** wurden in 300 ml HCO_2H mit 30 ml $HClO_4$ (60%) 3 h unter Rückfluss gekocht. Nach Aufarbeitung ergab Destillation bei 79—80 °C/15 Torr 11 g (77%) **27**; IR (Film): 1673, 1635 cm^{-1}; NMR (CCl_4): 1.93 (3H, s), 5.20 (1H, q, J=1 Hz); MS: 110 (M^+), 82 ($M^+ - C_2H_4$).

*3,4,4-Trimethyl-2-cyclohexenon (**29**) und 3,6,6-Trimethyl-2-cyclohexenon (**30**).* Eine Lösung von 500 mg **28** in 25 ml HCO_2H wurde mit 2.5 ml $HClO_4$ (70%) 45 Min. unter Rückfluss erhitzt. Nach Abdampfen von HCO_2H wurde der Rückstand in Ether gelöst und mit gesätt. $NaHCO_3$-Lösung neutralgewaschen, getrocknet und eingedampft. Das Rohprodukt wurde dann dünnschichtchromatographisch(Laufmittel: Hexan–AcOEt 1: 1) abgetrennt. Man erhielt 100 mg (25%) **29** und 193 mg (48%) **30**. **29**; Kp. 106—110 °C (Öl-Bad)/12 Torr; IR (Film): 1666, 1615 cm^{-1}; NMR ($CDCl_3$): 1.20 (6H, s), 1.90 (3H, d, J=1 Hz), 2.43 (2H, bt, J=6 Hz), 5.75 (1H, bs); MS: 138 (M^+), 110 ($M^+ - C_2H_4$ bzw. CO), 96 ($M^+ - C_3H_6$). **30**; Kp. 87—90 °C (Öl-Bad)/12 Torr; IR (Film): 1668, 1640 cm^{-1}; NMR ($CDCl_3$): 1.10(6H, s), 1.80 (2H, bt, J=6 Hz), 1.92 (3H, d, J=1 Hz), 2.30 (2H, bt J=6 Hz), 5.71 (1H, q, J=1 Hz); MS: 138 (M^+), 110 ($M^+ - CO$), 82 ($M^+ - C_4H_8$).

*7a-Methyl-5,6,7,7a-tetrahydro-5-indanon (**32**).* Eine Lösung von 250 mg **31** in 9 ml HCO_2H wurde mit 1 ml $HClO_4$ (60%) versetzt und 1 h rückfliessend gekocht. Nach Aufarbeitung wurde das Rohprodukt säulenchromatographisch gereinigt, wobei 100 mg (50%) **32** mit Benzol–AcOEt (19: 1) eluiert wurden; IR (Film): 1665 cm^{-1}; NMR (CCl_4): 1.17 (3H, s), 5.60 (1H, d, J=1 Hz); MS: 150 (M^+), 112 ($M^+ - C_2H_4$).

*$\Delta^{1(8a)}$-2-Octalon (**18**).* 19 g **33a** wurden in 300 ml HCO_2H mit 30 ml $HClO_4$ (60%) 3 h gekocht. Nach üblicher Aufarbeitung ergab Destillation bei 90—106 °C/3 Torr 11.5 g (75%) **18**; IR (Film): 1670, 1620 cm^{-1}; NMR (CCl_4): 5.79 (1H, s).

*8-Methyl-$\Delta^{1(8a)}$-2-octalon (**34**).* Eine Lösung von 600 mg **33b** in 30 ml HCO_2H wurde mit 3 ml $HClO_4$ (60%) versetzt und 1 h gekocht. 345 mg (70%) **34** wurden säulenchromatographisch abgetrennt; IR (Film): 1670, 1615 cm^{-1}; NMR (CCl_4): 1.10 (3H, d, J=6 Hz), 5.80 (1H, d, J=1 Hz).

*5-Methyl-2-oxo-2,3,4,6,7,8-hexahydronaphthalin (**36**).* 150 mg **35**[38a] wurden in 10 ml HCO_2H mit 1 ml $HClO_4$ (60%) 1 h rückfliessend umgesetzt. Nach chromatographischer Reinigung erhielt man 86 mg (70%) **36**; IR (Film): 1660, 1632, 1585 cm^{-1}; NMR (CCl_4): 1.35 (3H, s), 5.54 (1H, bs).

*4a-Methyl-2-oxo-2,3,4,4a,5,6-hexahydronaphthalin (**38**) und 5-Acetyl-1-methylbicyclo[2.2.2]octan-2-on (**39**).* Eine Lösung von 510 mg **37**[4] in 30 ml HCO_2H wurde mit 3 ml $HClO_4$ (60%) versetzt und 3 h unter Rückfluss umgesetzt. Nach Aufarbeitung wurde der Rückstand an der 50-fachen Menge SiO_2 chromatographiert, wobei 90 mg (22%) **38** und 320 mg (71%) **39** mit Benzol–AcOEt (19: 1) abgetrennt wurden. Die Konstitution von **38** wurde durch den Vergleich der spektroskopischen Daten mit denjenigen in der Literatur[4] ermittelt. **39**; Schmp. 76—77 °C (Isopropylether); IR (Nujol): 1715

cm^{-1}; NMR ($CDCl_3$): 0.92 (3H, s), 2.15 (3H, s); MS: 180 (M^+); Gef: C, 73.33; H, 9.02%. Ber. für $C_{11}H_{16}O_2$: C, 73.30; H, 8.95%.

*Des-A-estra-$\Delta^{9(10),8(14)}$-dien-5,17-dion (**41**).* 370 mg **40**[15] wurden in 15 ml HCO_2H gelöst und mit 1 ml $HClO_4$ (60%) 1 h gekocht. Das Rohprodukt wurde an der 50-fachen Menge SiO_2 mit Benzol–AcOEt (4: 1) chromatographiert. Man erhielt 205 mg (65%) **41**. Die spektroskopischen Daten von **41** sind in Übereinstimmung mit denjenigen in der Literatur[15]; IR (Film): 1745, 1663, 1635, 1585 cm^{-1}; NMR (CCl_4): 1.14 (3H, s), 5.68 (1H, bs).

*7a-Methyl-5,6,7,7a-tetrahydroindan-1,5-dion (**43**) und 1-Methyl-brexan-4,9-dion (**44**).* Eine Lösung von 1.89 g **42** in 100 ml HCO_2H wurde mit 10 ml HBr 1.5 h unter Rückfluss gekocht. Nach Abdampfen von HCO_2H wurde der Rückstand in AcOEt aufgenommen. Die organische Phase wurde mit gesätt. $NaHCO_3$-Lösung neutralgewaschen, getrocknet und eingedampft. Das Rohprodukt wurde dann an der 100-fachen Menge SiO_2 chromatographiert, wobei 150 mg (10%) **44**[17] mit Benzol–AcOEt (4: 1) eluiert wurden, dann folgten 620 mg (40%) **43**. **43**; Schmp. 70—71 °C (Ether); IR (Nujol): 1745, 1675 cm^{-1}; NMR ($CDCl_3$): 1.32 (3H, s), 5.94 (1H, d, J=1.5 Hz); Gef: C, 73.32; H, 7.12%. Ber. für $C_{10}H_{12}O_2$: C, 73.14; H, 7.37%.

*2-(2-Carboxyethyl)-3,6-dimethyl-2-cyclohexenon (**46**) und 3-(3-Carboxypropyl)-4-methyl-2-cyclohexenon (**47**).* Eine Lösung von 240 mg **45**[18] in 18 ml HCO_2H wurde mit 2 ml HBr versetzt und 1 h bei 60 °C erhitzt. HCO_2H wurde abgezogen und der Rückstand in $CHCl_3$ gelöst. Die organische Phase wurde mit H_2O gewaschen, getrocknet und eingedampft. Man erhielt 207 mg (77%) **57**. Zur Analyse wurde **57** mit CH_2N_2 in den Methylester umgewandelt; IR (Film): 1740, 1710, 1675 cm^{-1}; NMR ($CDCl_3$): 1.12 (3H, d, J=6 Hz), 2.09 (3H, d, J=1.5 Hz), 3.65 (3H, s), 5.49 (1H, qt, J=1.5, 7 Hz); Gef: C, 58.66; H, 7.98; Cl, 13.73%. Ber. für $C_{12}H_{19}ClO_3$: C, 58.41; H, 7.76; Cl, 14.37%. 1.38 g von der oben erhaltenen rohen Carbonsäure **57** wurden in 60 ml HCO_2H mit 6.5 ml HBr 1.5 h rückfliessend erhitzt. Nach üblicher Aufarbeitung erhielt man ein Gemisch **46** und **47**, das mit CH_2N_2 verestert und chromatographisch mit Benzol–AcOEt (4: 1) auseinander abgetrennt wurde. Methylester von **46** (940 mg, 58.5% aus **45**); IR (Film): 1740, 1660, 1630 cm^{-1}; NMR ($CDCl_3$): 1.12 (3H, d, J=6 Hz), 1.96 (3H, s), 3.62 (3H, s); Gef: C, 68.56; H, 8.58%. Ber. für $C_{12}H_{18}O_3$: C, 68.54; H, 8.63%. Methylester von **47** (155 mg, 9.7% aus **45**); IR (Film): 1744, 1670, 1625 cm^{-1}; NMR ($CDCl_3$): 1.21 (3H, d, J=6 Hz), 3.65 (3H, s), 5.76 (1H, bs); MS: 210 (M^+); Gef: C, 68.56; H, 8.59%. Ber. für $C_{12}H_{18}O_3$: C, 68.54; H, 8.63%.

*3,3,8a-Trimethyl-1,6-dioxo-1,2,3,4,6,7,8,8a-octahydronaphthalin (**49**) und 4-Methyl-3-(2,2,-dimethyl-3-carboxypropyl)-2-cyclohexenon (**50**).* Eine Lösung von 800 mg **48** in 40 ml HCO_2H wurde mit 4 ml HBr 1.5 h gekocht. Nach Entfernung von HCO_2H wurde der Rückstand auf H_2O gegossen und mit AcOEt extrahiert. Die AcOEt-Auszüge wurden mit 10% NaOH-Lösung geschüttelt, getrocknet und eingedampft. Der erhaltene neutrale Teil wurde dünnschichtchromatographisch gereinigt. Man erhielt 220 mg (32%) **49**; Schmp. 93—94 °C (Ether); IR (Nujol): 1705, 1660, 1615 cm^{-1}; NMR ($CDCl_3$): 0.80 (3H, s), 1.15 (3H, s), 1.42 (3H, s), 5.82 (1H, d, J=2 Hz); MS: 206 (M^+); Gef: C, 75.59; H, 8.74%. Ber. für $C_{13}H_{18}O_2$: C, 75.69; H, 80.8%. Die alkalische Phase wurde unter Eiskühlung mit 6 M-HCl angesäuert und mit $CHCl_3$ extrahiert. Der sauere Teil wurde dann in AcOEt mit CH_2N_2 verestert. Der Methylester wurde dann durch Dünnschichtchromatographie an SiO_2 (Laufmittel: AcOEt–Hexan 1: 1) gereinigt. Man erhielt 240 mg (30%) **50** als Methylester; IR (Film): 1730, 1660, 1615 cm^{-1}; NMR (CCl_4): 1.07 (6H, s), 1.22 (3H, d, J=6 Hz), 3.60 (3H, s), 5.64 (1H, bs); MS: 238 (M^+); Gef: C, 70.01; H, 9.46%. Ber. für $C_{14}H_{22}O_3$: C, 70.55; H, 9.31%.

*2-Carboxymethyl-3,6-dimethyl-2-cyclohexenon (**52**) und 3-(2-Carboxyethyl)-4-methyl-2-cyclohexenon (**53**).* Eine Lösung von 510 mg **51** in 20 ml HCO_2H wurde mit 2.7 ml HBr 1.5 h rückfliessend erhitzt. Nach üblicher Aufarbeitung und Versterung mit CH_2N_2 wurde die Reaktionsmischung dünnschichtchromatographisch an SiO_2(Laufmittel: Benzol–AcOEt 4: 1) gereinigt. Als Methylester erhielt man 230 mg (50%) **52** und 20 mg (4%) **53**. Methylester von **52**; IR (Film): 1740, 1662, 1640 cm^{-1}; NMR (CCl_4): 1.09 (3H, d, J=6 Hz), 1.88 (3H, s), 3.21 (2H, s), 3.57 (3H, s); Gef: C, 67.10; H, 8.16%. Ber. für $C_{11}H_{16}O_3$: C, 67.32; H, 8.22%. Methylester von **53**; IR (Film): 1730, 1665, 1630 cm^{-1}; NMR ($CDCl_3$): 1.24 (3H, d, J=7 Hz), 2.54 (4H, s), 3.68 (3H, s), 5.74 (1H, bs); MS: 196 (M^+); Gef: C, 66.94; H, 8.13%. Ber. für $C_{11}H_{16}O_3$: C, 67.32; H, 8.22%.

*2-(2-Carboxyäthyl)-3-methyl-2-cyclohexenon (**55**) und 3-(3-carboxypropyl)-2-cyclohexenon (**56**).* Eine Lösung von 260 mg **54** in 13 ml HCO_2H wurde mit 2 ml $HClO_4$ (60%) versetzt und 2 h gekocht. Analog wurden die beiden Carbonsäuren **55** (136 mg, 63%) und **56** (40 mg, 18.5%) als Methylester abgetrennt (Laufmittel: AcOEt–Hexan 1: 1). Methylester von **55**; IR (Film): 1745, 1665, 1630 cm^{-1}; NMR ($CDCl_3$): 1.99 (3H, s), 3.65 (3H, s); Gef: C, 67.33; H, 8.14%. Ber. für $C_{11}H_{16}O_3$: C, 67.32; H, 8.22%. Methylester von **56**: IR (Film): 1745, 1670, 1630 cm^{-1}; NMR ($CDCl_3$): 3.65 (3H, s), 5.81 (1H, t, J=1 Hz); MS: 196 (M^+); Gef: C, 66.34; H, 8.38%. Ber. für $C_{11}H_{16}O_3$: C, 67.32; H, 8.22%.

Abschnitt C.

*1-(3-Chlor-2-butenyl)-2-decalon (**72a**).* *a*) Zu einer Lösung von 210 mg (0.03 g-Atom) Li in *ca.* 50 ml NH_3 wurden 1.5 g (0.01 mol) **33a** bei −33 °C hinzugefügt und 1 h bei der gleichen Temp. gerührt. Dazu wurden 4.5 ml DCB bei −33 °C tropfenweise gegeben und die Reaktionslösung weiter 1 h gerührt. Nach Entfernung von NH_3 wurde die Reaktionsmischung mit H_2O verdünnt, mit 6 M-HCl schwach angesäuert und mit AcOEt extrahiert. Die AcOEt-Auszüge wurden mit H_2O gewaschen, getrocknet und eingedampft. Der Rückstand wurde an der 30-fachen Menge SiO_2 chromatographiert, wobei 430 mg (20%) **72a** mit Benzol eluiert wurden; IR (Film): 1710, 1670 cm^{-1}; NMR ($CDCl_3$): 2.05 (3H, bs), 5.51 (1H, bt, J=7 Hz); MS: 240, 242 (M^+), 205 (M^+—Cl); Gef: C, 69.41; H, 8.81; Cl, 14.61%. Ber. für $C_{14}H_{21}ClO$: C, 69.84; H, 8.79; Cl, 14.73%.

b) Zu einer Lösung von 105 mg (15 mg-Atom) Li in 30 ml NH_3 wurde eine Lösung von 750 mg (5 mmol) **33a** und 0.38 ml (4 mmol) *t*BuOH in 20 ml THF bei −33 °C gegeben und 1 h bei der gleichen Temp. gerührt. Dann wurde eine Lösung von 1.6 ml (15 mmol) 1-Jod-3-chlor-2-buten in 3.5 ml THF bei −33 °C zugetropft und die Reaktionslösung 1 h gerührt. Nach der oben erwähnten Aufarbeitung erhielt man 350 mg (30%) **72a**.

*2-Oxo-2,3,4,4a,4b,5,6,7,8,8a,9,10-dodecahydrophenanthren (**73a**).* Eine Lösung von 138 mg **72a** in 6 ml HCO_2H wurde mit 0.5 ml $HClO_4$ (70%) versetzt und 1 h unter Rückfluss gekocht. Nach üblicher Aufarbeitung wurde das Rohprodukt durch präparative Dünnschichtchromatographie an SiO_2 (Laufmittel: Benzol–AcOEt 9: 1) gereinigt. Man erhielt 83 mg (70%) **73a** als farbloses Öl; IR (Film): 1670, 1623 cm^{-1}; NMR ($CDCl_3$): 5.77 (1H, bs); MS: 204 (M^+), 176 (M^+—C_2H_2); Gef: C, 81.00; H, 9.90%. Ber. für $C_{14}H_{20}O$: C, 82.30; H, 9.87%.

*1-(3-Chlor-2-butenyl)-4a-methyl-2-decalon (**72b**).*[6d] Analog

zur Darstellung von **72a** (Vorschrift b) wurden 820 mg **12** reduktiv alkyliert. Man erhielt 300 mg (23%) **72b**; IR (Film): 1708, 1663 cm^{-1}; NMR ($CDCl_3$): 1.11 (3H, s), 2.05 (3H, d, J=1.5 Hz), 5.49 (1H, qt, J=1.5, Hz).

*8a-Methyl-2-oxo-2,3,4,4a,4b,5,6,7,8,8a,9,10-dodecahydrophenanthren (**73b**).* Analog **73a** wurde eine Lösung von 256 mg **72b** in 8 ml HCO_2H mit 0.5 ml $HClO_4$ (70%) versetzt und 0.5 h bei 95 °C erhitzt. 197 mg (90%) **73b** wurden erhalten; Schmp. 125—127 °C (Ether); IR (Nujol): 1660, 1615 cm^{-1}; NMR ($CDCl_3$): 1.00 (3H, s), 5.80 (1H, bs).

*17-Tetrahydropyranyloxy-des-A-estr-9-en-5-on (**69**).* Eine Lösung von 1 g **68**[15] in 20 ml abs. THF wurde bei RT. in Gegenwart von einer katalytischen Menge $POCl_3$ mit 4 ml Dihydropyran versetzt und 1 h stehengelassen. Die Reaktionslösung wurde dann mit H_2O, mit gesätt. $NaHCO_3$-Lösung gewaschen, getrocknet und eingedampft. Der Rückstand wurde dünnschichtchromatographisch an SiO_2 (Laufmittel: AcOEt–Hexan 1:1) gereinigt. Man erhielt 1 g (72%) 69 als farbloses Öl; IR (Film): 1670, 1620 cm^{-1}; NMR ($CDCl_3$): 0.95 (3H, s), 5.85 (1H, bs); MS: 304 (M^+).

*10-(3-Chlor-2-butenyl)-des-A-estran-5,17-dion (**70**).* *a*) Zu einer Lösung von 70 mg Li in 50 ml NH_3 wurde eine Lösung von 1 g **69** und 0.25 ml *t*BuOH in 25 ml THF gegeben. Die blaue Lösung wurde 0.5 h bei −33 °C gerührt, mit 1.3 ml DCB in 5 ml THF tropfenweise versetzt und 1 h bei der gleichen Temp. gerührt. Nach Abdampfen von NH_3 wurde das Reaktionsgemisch auf H_2O gegossen, mit 6 M-HCl schwach angesäuert und mit AcOEt extrahiert. Nach Eindampfen von AcOEt wurde der Rückstand in 15 ml MeOH gelöst, mit einer katalytischen Menge H_2SO_4 versetzt und 24 h bei RT. stehengelassen. Nach Entfernung von MeOH wurde der Rückstand in 50 ml Aceton aufgenommen, mit CrO_3(Jones-Reagenz) versetzt und bei RT. über Nacht gerührt. Nach Abdampfen von Aceton wurde der Rückstand in $CHCl_3$ gelöst. Die organische Phase wurde mit H_2O gewaschen, getrocknet und eingedampft. Das Rohprodukt wurde dann an der 50-fachen Menge SiO_2 mit Benzol–AcOEt (7:3) chromatographiert, wobei 170 mg (17%) **70** eluiert wurden, dann folgten 310 mg (42%) Des-A-estran-5,17-dion.

b) Auf die gleiche Weise wurden 300 mg **69** mit 1-Jod-3-chlor-2-buten reduktiv alkyliert. Die anschliessenden Abspaltung der Schutzgruppe und Oxydation ergaben 65 mg (22%) **70**; IR (Film): 1740, 1710, 1660 cm^{-1}; NMR ($CDCl_3$): 0.98 (3H, s), 2.07 (3H, bs), 5.50 (1H, bt, J=7 Hz); MS: 308, 310 (M^+), 273 (M^+−Cl); Gef: C, 70.18; H, 7.95; Cl, 11.72%. Ber. für $C_{18}H_{25}ClO_2$: C, 70.00; H, 8.16; Cl, 11.48%.

*4-Estren-3,17-dion (**71**).* Eine Lösung von 95 mg **70** in 5 ml HCO_2H wurde mit 0.5 ml $HClO_4$ (70%) versetzt und 0.5 h bei 95 °C erhitzt. Nach üblicher Aufarbeitung wurde das Rohprodukt dünnschichtchromatographisch gereinigt. Man erhielt 75 mg (90%) **71**; Schmp. 152—154 °C (CH_2Cl_2–Isopropyl ether); IR (Nujol): 1738, 1668, 1620 cm^{-1}; NMR ($CDCl_3$): 0.95 (3H, s), 5.82 (1H, bs); MS: 272 (M^+), 244.

Abschnitt D.

Darstellung von α-(2-Haloallyl)ketonen.

*2-(2-Bromallyl)-6-methylcyclohexanon (**78**).* Eine Lösung von 4 g Pyrrolidinenamin des 2-Methylcyclohexanons[36] in 15 ml Dioxan wurde mit 2.6 ml 2,3-Dibrompropen versetzt und 18 h unter Ar rückfliessend gekocht. Danach wurden 1 ml 6 M-HCl und 5 ml H_2O zugegeben und die Reaktionslösung 3 h gekocht. Nach Abkühlen auf RT. wurde das Reaktionsgemisch auf Eis gegossen und mit AcOEt extrahiert. Die organische Phase wurde mit gesätt. $NaHCO_3$-Lösung neutralgewaschen, getrocknet und eingedampft. Der Rückstand wurde an der 20-fachen Menge SiO_2 mit Benzol chromatographiert. Man erhielt 3.5 g (62%) **78** als Öl; IR (Film): 1720, 1630 cm^{-1}; NMR (CCl_4): 0.99 (3H, d, J=6 Hz), 5.40 (1H, t, J=1 Hz), 5.60 (1H, t, J=1 Hz); MS: 230, 232 (M^+): Gef: C, 51.83; H, 6.57; Br, 34.80%. Ber. für $C_{10}H_{15}BrO$: C, 51.96; H, 6.54; Br, 34.57%.

*2-(2-Chlorallyl)-2-methylcyclohexanon (**80**).* Ein Gemisch von 3 g 2-Methylcyclohexanon und 1.3 g $NaNH_2$ in 20 ml Benzol wurde 5 h unter Rückfluss und Ar gerührt. Nach Abkühlen anf RT. wurde eine Lösung von 3.6 ml 2,3-Dichlorpropen in 7 ml Benzol unter Rühren tropfenweise hinzugefügt und die Reaktionslösung 2 h rückfliessend erhitzt. Nach üblicher Aufarbeitung wurde das Rohprodukt an der 20-fachen Menge SiO_2 chromatographiert, wobei 1 g (20%) 6-Methyl-2-(2-chlorallyl)cyclohexanon mit Benzol–Hexan (3:1) eluiert wurde, dann folgten 2.1 g (42%) **80**; IR (Film): 1715, 1635 cm^{-1}; NMR (CCl_4): 1.26 (3H, s), 2.62 (2H, s), 5.09 (1H, t, J=1 Hz), 5.21 (1H, d, J=1.5 Hz); MS: 186, 188 (M^+), 151 (M^+–Cl); Gef: C, 64.46; H, 8.13; Cl, 19.10%. Ber. für $C_{10}H_{15}ClO$: C, 64.34; H, 8.04; Cl, 19.03%.

*2-(2-Chlorallyl)-2-methylcyclohexan-1,3-dion (**82**).* Zu einer Lösung von 1.1 g 2-Methylcyclohexan-1,3-dion und 0.56 g KOH in 2.24 ml H_2O fügte man 1 ml 2,3-Dichlorpropen und 0.3 g KI und rührte 1.5 h bei 90 °C. Nach Abkühlen auf RT. wurde die Reaktionsmischung auf Ether gegossen. Die etherische Phase wurde mit H_2O gewaschen, getrocknet und eingedampft. Der Rückstand wurde an der 30-fachen Menge SiO_2 mit Benzol–AcOEt (4:1) chromatographiert. Man erhielt 1 g (50%) **82** als farbloses Öl; IR (Film): 1730, 1700, 1630 cm^{-1}; NMR ($CDCl_3$): 1.32 (3H, s), 2.90 (2H, s), 5.09 (1H, t, J=1 Hz), 5.12 (1H, d, J=1.5 Hz); MS: 200, 202 (M^+); Gef: C, 59.78; H, 6.61; Cl, 17.74%. Ber. für $C_{10}H_{13}ClO_2$: C, 59.85; H, 6.53; Cl, 17.67%.

*2-(2-Bromallyl)cyclohexan-1,3-dion (**84**).* Zu einer Lösung von MeOK aus 1.6 g K in 14 ml abs. MeOH wurden 4.4 g Cyclohexan-1,3-dion hinzugefügt. Diese Lösung wurde bei 50 °C mit einer Lösung von 4.6 ml 2,3-Dibrompropen versetzt und 10 Min. unter Rückfluss erhitzt. Nach Entfernung von MeOH wurde der Rückstand in 40 ml 3% NaOH-Lösung aufgenommen und mit Ether geschüttelt. Die wässrige Phase wurde unter Eiskühlung mit 6 M-HCl auf pH 4 eingestellt, wobei 3.1 g (33%) **84** ausfielen; Schmp. 119—120 °C (MeOH–Isopropylether–AcOEt); IR (Nujol): 1635, 1565 cm^{-1}; MS: 151 (M^+−Br); Gef: C, 46.82; H, 4.84; Br, 34.58%. Ber. für $C_9H_{11}BrO_2$: C, 46.77; H, 4.80; Br. 34.59%.

*α-(2-Chlorallyl)-4-methoxydeoxybenzoin (**86**).* Ein Gemisch von 1 g 4-Methoxydeoxybenzoin[40] und 276 mg NaH (50% Ölsuspension) in 10 ml Benzol wurde 1 h unter Rühren und Ar gekocht. Nach Abkühlen wurde 0.55 ml 2,3-Dichlorpropen in 10 ml Benzol zugetropft und die Reaktionslösung 1.5 h unter Rückfluss erhitzt. Nach üblicher Aufarbeitung wurde das Rohprodukt an der 30-fachen Menge SiO_2 mit Benzol chromatographiert. Man erhielt 930 mg (70%) **86**; Schmp. 114—115 °C (CH_2Cl_2–Isopropyläther); IR (Nujol): 1665, 1635 1605, 1575 cm^{-1}; NMR ($CDCl_3$): 2.74 (1H, dd, J=7, 14.5 Hz), 3.24 (1H, dd, J=7, 14.5 Hz), 3.75 (3H, s), 4.93 (1H, t, J=7 Hz), 4.98 (1H, d, J=1 Hz), 5.04 (1H, d, J=1 Hz), 7.24 (5H, s), 6.80 (2H, d, J=9 Hz), 7.95 (2H, d, J=9 Hz); MS: 265 (M^+−Cl); Gef: C, 71.76; H, 5.69; Cl, 11.97%. Ber. für $C_{18}H_{17}ClO_2$: C, 71.88; H, 5.66; Cl, 11.81%.

*2-(2-Bromallyl)-3-oxononansäureethylester (**90a**).* γ-Alkylierung von 2.6 g Acetessigsäureethylester mit n-$C_5H_{11}Br$ wurde nach der Vorschrift von Huckin *et al.*[33] durchgeführt. Zu 365 mg NaH (50% Ölsuspension) in 5 ml THF wurden 1.5 g **89a** in 10 ml THF tropfenweise gegeben, 0.5 h bei RT. und dann 10 Min. bei 50 °C unter Ar gerührt. Die so erhaltene Enolatlösung von **89a** wurde mit 0.84 ml 2,3-Dibrompropen in 5 ml THF versetzt und 18 h bei RT. gerührt. Die

Reaktionsmischung wurde auf H_2O gegossen, mit 6 M-HCl schwach angesäuert und mit Benzol extrahiert. Die Benzolauszüge wurden mit gesätt. NaCl-Lösung gewaschen, getrocknet und eingedampft. Der Rückstand wurde an der 10-fachen Menge SiO_2 mit Benzol chromatographiert. Man erhielt 1.7 g (29% aus **88**) **90a**; IR (Film): 1745, 1720, 1630 cm^{-1}; NMR ($CDCl_3$): 0.89 (3H, bt, J=5 Hz), 1.27 (3H, t, J=7 Hz), 2.93 (2H, bd, J=7 Hz), 3.90 (1H, t, J=7 Hz), 4.17 (2H, q, J=7 Hz), 5.39 (1H, d, J=2 Hz), 5.62 (1H, m); MS: 239 (M^+−Br); Gef: C, 52.81; H, 7.41; Br, 25.03%. Ber. für $C_{14}H_{23}BrO_3$: C, 52.67; H, 7.26; Br, 25.03%. Analog wurden **90b** und **c** dargestellt.

2-(2-Bromally)-3-oxodecansäureethylester (90b): IR (Film): 1750, 1725, 1633 cm^{-1}; NMR ($CDCl_3$): 0.88 (3H, bt, J=7 Hz), 1.25 (3H, t, J=7 Hz), 2.95 (2H, bd, J=7 Hz), 3.91 (1H, t, J=7 Hz), 4.18 (2H, q, J=7 Hz), 5.42 (1H, d, J=2 Hz), 5.62 (1H, m); MS: 253 (M^+−Br); Gef: C, 54.19; H, 7.63; Br, 24.52%. Ber. für $C_{15}H_{25}BrO_3$: C, 54.05; H, 7.56; Br, 23.97%.

2-(2-Bromallyl)-3-oxo-5-phenylpentansäureethylester (90c); IR (Film): 1750, 1725, 1633 cm^{-1}; NMR (CCl_4): 1.19 (3H, t, J=7 Hz), 2.82 (4H, s), 2.86 (2H, bd, J=7 Hz), 3.78 (1H, t, J=7 Hz), 4.05 (2H, q, J=7 Hz), 5.31 (1H, d, J=2 Hz), 5.53 (1H, m), 7.08 (5H, s); MS: 259 (M^+−Br); Gef: C, 56.78; H, 5.73; Br, 23.98%. Ber. für $C_{16}H_{19}BrO_3$: C, 56.64; H, 5.64; Br, 23.56%.

6-Chlor-3-oxo-2-pentyl-6-heptensäureethylester (94). **93** wurde nach der Vorschrift von Marvel *et al.*[35] dargestellt (Kp. 120 °C/12 Torr). Zu einer Suspension von 500 mg NaH (55% Ölsuspension) in 25 ml THF wurden 2 g **93** bei 0 °C unter Ar hinzugefügt und 1 h bei RT. gerührt. Dann wurde die Lösung bei 0 °C mit 6.8 ml 15% *n*-BuLi in Hexan versetzt und weiter 10 Min. gerührt. Dazu wurde 1 ml 2,3-Dichlorpropen in 2 ml THF bei 0 °C tropfenweise gegeben und die Reaktionsmischung 0.5 h bei RT. gerührt. Nach Zugabe von 7 ml 3.5 M-HCl und 15 ml Ether unter Eiskühlung wurde die Reaktionsmischung mit Ether ausgezogen. Die Ether auszüge wurden mit H_2O neutralgewaschen, getrocknet und eingedampft. Man erhielt 3 g (80%) vom Rohprodukt **94**, das ohne weitere Reinigung in **92a** umgewandelt wurde. Zur Analyse wurde eine Probe an SiO_2 chromatographiert (isolierte Ausb. 60%); IR (Film): 1745, 1718, 1635 cm^{-1}; NMR ($CDCl_3$): 0.89 (3H, bt, J=6 Hz), 1.28 (3H, t, J=7 Hz), 3.44 (1H, t, J=7 Hz), 4.17 (2H, q, J=7 Hz), 5.12 (2H, bs); Gef: C, 61.49; H, 8.44; Cl, 12.60%. Ber. für $C_{14}H_{23}ClO_3$: C, 61.72; H, 8.44; Cl, 12.90%.

Allgemeine Vorschrift der Hydrolyse.

Eine Lösung von α-(2-Haloallyl)keton in HCO_2H wurde mit einer kleinen Menge $HClO_4$ (60 od. 70% wässrig) versetzt und bei 70—75 °C erhitzt. Nach der in Abschnitten A und B beschriebenen Aufarbeitung wurde das Rohprodukt säulen- oder dünnschichtchromatographisch gereinigt.

2-(2-Oxopropyl)cyclohexanon (77). Eine Lösung von 500 mg **74**[28] in 20 ml HCO_2H wurde mit 0.3 ml $HClO_4$ (70%) versetzt und 2 h bei 75 °C erhitzt. Man erhielt 320 mg (70%) **77**; IR (Film): 1710 cm^{-1}; NMR (CCl_4): 2.10 (3H, s).

6-Methyl-2-(2-oxopropyl)cyclohexanon (79). 410 mg **78** wurden in 10 ml HCO_2H mit 0.2 ml $HClO_4$ (70%) 1.5 h bei 70 °C erhitzt. 224 mg (75%) **79** wurden erhalten; Kp. 77—80 °C (Öl-Bad)/1 Torr; IR (Film): 1710 cm^{-1}; NMR CCl_4): 0.95 (3H, d, J=6 Hz), 2.12 (3H, s); MS: 168(M^+); Gef: C, 70.41; H, 9.34%. Ber. für $C_{10}H_{16}O_2$: C, 71.39; H, 9.59%.

2-(2-Carboxyethyl)-3,5-dimethyl-2-cyclopentenon (83). Zu einer Lösung von 500 mg **82** in 20 ml HCO_2H fügte man 1.5 ml $HClO_4$ (70%) und kochte 3 h unter Rückfluss. Nach Abdampfen von HCO_2H wurde der Rückstand in AcOEt aufgenommen. Die organische Phase wurde mit H_2O gewaschen, eingeengt und mit CH_2N_2 versetzt. Der Methylester wurde dünnschichtchromatographisch an SiO_2 (Laufmittel: Benzol–AcOEt 4: 1) gereinigt. Ausb. 146 mg (30%); IR (Film): 1740, 1695, 1643 cm^{-1}; NMR ($CDCl_3$): 1.14 (3H, d, J=7 Hz), 2.07 (3H, s), 2.47 (4H, s), 3.65 (3H, s); MS: 196 (M^+); Gef: C, 67.47; H, 8.25%. Ber. für $C_{11}H_{16}O_3$: C, 67.32; H, 8.22%.

2-Methyl-4-oxo-4,5,6,7-tetrahydrobenzofuran (85). 1 g **84** wurde in 30 ml HCO_2H mit 3 ml $HClO_4$ (60%) 2.5 h bei 80 °C erhitzt. Nach Aufarbeitung wurde der Rückstand dünnschichtchromatographisch an SiO_2 (Laufmittel: AcOEt–Hexan 1: 1) abgetrennt. Neben dem nicht umgesetzten Ausgangsmaterial **84** (195 mg) erhielt man 290 mg (55%) **85** als Öl; IR (Film): 1675, 1582, 1240 cm^{-1}; NMR ($CDCl_3$): 2.30 (3H, s), 2.88 (2H, t, J=6 Hz), 6.22 (1H, q, J=1 Hz); MS: 150 (M^+); Gef: C, 71.59; H, 6.78%. Ber. für $C_9H_{10}O_2$: C, 71.98; H, 6.71%.

5-Methyl-2-(p-methoxyphenyl)-3-phenylfuran (87). 160 mg **86** wurden in 10 ml HCO_2H mit 1.5 ml $HClO_4$ (60%) 1 h rückfliessend erhitzt. Man erhielt 112 mg (80%) **87** als Öl; IR (Film): 1610, 1580, 1564, 1250 cm^{-1}; NMR (CCl_4): 2.31 (3H, s), 3.67 (3H, s), 5.98 (1H, bs), 6.63 (2H, d, J=8.5 Hz), 7.28 (2H, d, J=8.5 Hz), 7.20 (5H, s); MS: 264 (M^+); Gef: C, 81.61; H, 6.04%. Ber. für $C_{18}H_{16}O_2$: C, 81.79; H, 6.10%.

Dihydrojasmon (92a). *a*) aus **90a**. Eine Lösung von 950 mg **90a** in 33 ml HCO_2H wurde mit 4.5 ml $HClO_4$ (60 %) versetzt, langsam bis auf 80 °C erwärmt und 2 h bei 80—90 °C erhitzt. Nach Abdampfen von HCO_2H wurde der Rückstand auf gesätt. $NaHCO_3$-Lösung gegossen und mit AcOEt extrahiert. Die AcOEt-Auszüge wurden mit gesätt. NaCl-Lösung gewaschen, getrocknet und eingedampft. Der Rückstand wurde 1 ml EtOH gelöst und mit 3 ml 0.5 M-NaOH 2.5 h gekocht. Nach üblicher Aufarbeitung wurde das Rohprodukt chromatographisch an SiO_2 (Laufmittel: AcOEt–Hexan 1: 1) gereinigt. Man erhielt 110 mg (22% aus **90a**) **92a**; IR (Film): 1706, 1648 cm^{-1}; NMR (CCl_4): 0.89 (3H, bt, J=6 Hz), 2.01 (3H, s); MS: 166 (M^+), 151, 110.

b) aus **94**. Eine Lösung von 1 g **94** in 25 ml HCO_2H wurde mit 3 ml $HClO_4$ (70%) und 2 ml H_2O 4 h bei 90 °C erhitzt. Das erhaltene Gemisch (*ca.* 600 mg) von **91** und **92a** wurde in 2 ml EtOH gelöst und mit 6 ml 0.5 M-NaOH 4 h bei 90 °C erhitzt. 233 mg (42% aus **93**) **92a** wurden erhalten.

Analog wurden **92b** und **92c** dargestellt.

2-Hexyl-3-methyl-2-cyclopentenon (**92b**);[41] IR (Film): 1700, 1644 cm^{-1}; NMR (CCl_4): 0.85 (3H, bt, J=6 Hz), 1.97 (3H, s); Gef: C, 79.35; H, 11.33%. Ber. für $C_{12}H_{20}O$: C, 79.94; H, 11.18%.

2-Benzyl-3-methyl-2-cyclopentenon (92c); IR (Film): 1700, 1645, 1605, 1586 cm^{-1}; NMR (CCl_4): 2.02 (3H, s), 3.44 (2H, s), 7.08 (5H, s); MS: 186 (M^+); Gef: C, 83.73; H, 7.67%. Ber. für $C_{13}H_{14}O$: C, 83.83; H, 7.58%.

Herrn Dipl.-Chem. G. Stoll und Herrn G. Burger danken wir für die Korrektur des Deutschen. Herren Y. Shoji und K. Okada danken wir für die experimentelle Mitarbeit.

Literatur und Anmerkung

1) E. D. Bergman, D. Ginsburg, und R. Pappo, *Org. React.* Vol. X, 179, (1959); M. E. Jurg, *Tetrahedron*, **32**, 3 (1976); R. E. Gawley, *Synthesis*, **1976**, 777.

2) O. Wichterle, *Collect. Czech. Chem. Commun.*, **12**, 93 (1947); O. Wichterle und M. Hudliky, *ibid.*, **12**, 101, 129 (1947); O. Wichterle, J. Procházka, und J. Hofman, *ibid.*, **13**, 300 (1948).

3) a) V. Prelog, P. Barman, und M. Zimmermann, *Helv. Chim. Acta*, **32**, 1284 (1949); V. Prelog und M. Zimmermann, *ibid.*, **32**, 2360 (1949). b) S. A. Julia, *Bull. Soc. Chim. Fr.*, **21**, 780 (1954). c) W. G. Dauben und J. W. MacFarland, *J. Am. Chem. Soc.*, **82**, 4245 (1960).

4) J. A. Marshall und D. J. Schaeffer, *J. Org. Chem.*, **30**, 3642 (1965).

5) a) L. Velluz, G. Nominé und J. Mathieu, *Angew. Chem.*, **72**, 725 (1965); L. Velluz, J. Valls und G. Nominé, *Angew. Chem. Int. Ed. Engl*, **4**, 81 (1965). b) S. Danishefsky, L. S. Grawely, D. M. Solomon, und P. Heggs, *J. Am. Chem. Soc.*, **93**, 2356 (1971). c) A. A. Akhrem und Y. A. Titov, "Total Steroid Synthesis," Plenum Press, New York, N. Y. (1970).

6) a) R. Robinson und A. R. Pinder, *J. Chem. Soc.*, **1954**, 1224. b) G. T. Tatevosyan und V. O. Babayan, *J. Gen. Chem. U. S. S. R. (Eng. Transl.)*, **22**, 1465 (1952); S. A. Vardanian, P. A. Zagorets, und G. T. Tatevosyan, *ibid.*, **23**, 867 (1953). c) D. Cain und F. N. Tuller, *J. Org. Chem.*, **34**, 222 (1969). d) G. Stork, P. Rosen, N. L. Goldman, P. V. Coombs, und J. Tsuji, *J. Am. Chem. Soc.*, **87**, 275 (1965). e) R. E. Irland und R. C. Kierstead, *J. Org. Chem.*, **31**, 2543 (1966).

7) T. Mukaiyama, T. Inamoto, und S. Kobayashi, *Chem. Lett.*, **1973**, 261, 715; G. W. Klumpp, H. Bos, M. Shakel, R. F. Schmitz, und J. J. Vrielink, *Tetrahedron Lett.*, **1975**, 3429; M. Julia und C. Blasioli, *Bull. Soc. Chim. Fr.*, **1976**, 1941; S. F. Martin und T. S. Chou, *Tetrahedron Lett.*, **1978**, 1943.

8) Vorläufige Mitteilungen; M. Kobayashi und T. Matsumoto, *Chem. Lett.*, **1973**, 957; M. Kobayashi und T. Matsumoto., *Bull. Chem. Soc. Jpn.*, **48**, 2935 (1975).

9) Obwohl kein Unterschied zwischen HCO_2H und AcOH in der Tablelle-1 zu sehen ist, verläuft aber die Cyclisierung beim präparativen Ansatz in HCO_2H vielfach schneller als in AcOH.

10) W. S. Johnson, J. Ackerman, J. F. Eastman, und H. A. DeWalt, Jr., *J. Am. Chem. Soc.*, **78**, 6302 (1956); W. S. Johnson, J. J. Korst, R. A. Clement, und J. Dutta, *ibid.*, **82**, 614 (1960).

11) Die Konstitution der bekannten Verbindungen wurde durch den Vergleich der spektroskopischen sowie anderen physikalischen Daten ermittelt. Die Konstitution der unbekannten Substanzen wurde spektroskopisch aufgeklärt.

12) M. W. Cronyn und G. H. Riesser, *J. Am. Chem. Soc.*, **75**, 1664 (1953).

13) a) J. W. Apsimon, J. W. Hooper, und B. A. Laishes, *Can. J. Chem.*, **48**, 3064 (1970); C. H. Heathcock, J. E. Ellis, J. E. McMurray, und A. Coppolino, *Tetrahedron Lett.*, **1971**, 4995; K. L. Cook und A. J. Waring *J. Chem. Soc., Perkin Trans. 1*, **1973**, 529. b) E. Wenkert, N. F. Golob, und R. A. J. Smith, *J. Org. Chem.*, **38**, 4068 (1973).

14) R. Robinson, E. C. Feu, und F. J. McQuillin, *J. Chem. Soc.*, **1937**, 53.

15) O. I. Fedrova, G. S. Grienko, und V. I. Maskimov, *Zh. Org. Khim.*, **4**, 611, 614, 1219 (1968); *Chem. Abstr.*, **69**, 3061, 96945k (1968).

16) C. B. C. Boyce und J. C. Whitehurst, *J. Chem. Soc.*, **1959**, 2022.

17) M. Kobayashi, T. Minami, und T. Matsumoto, *Bull. Chem. Soc. Jpn.*, im Druck.

18) I. N. Nazarov, S. N. Anachenko, und I. V. Torogov, *Zh. Obshch. Khim.*, **26**, 819 (1956); *Chem. Abstr.*, **50**, 13843h (1956).

19) I. N. Nazarov und S. I. Zavyalov, *Izv. Akad. Nauk SSSR, Otd. Khim. Nauk*, **1952**, 300.

20) S. Swaminathan und M. S. Newman, *Tetrahedron*, **2**, 88 (1958).

21) K. Balasubramanian, J. P. John, und S. Swaminathan, *Synthesis*, **1974**, 51.

22) Eine asymmetrische Synthese, Vgl., U. Eder, G. Sauer, und R. Wiechert, *Angew. Chem.*, **83**, 492 (1971).

23) G. Bauduin und Y. Pietrasanta, *Tetrahedron*, **29**, 4225 (1973).

24) G. Stork und J. Singh, *J. Am. Chem. Soc.*, **96**, 6181 (1974).

25) F. Näf und R. Decorzant, *Helv. Chim. Acta*, **57**, 1317 (1974).

26) B. E. Denot und A. Bowers, *Steroid*, **1**, 257 (1963); M. Akthar und D. H. R. Barton, *J. Am. Chem. Soc.*, **86**, 1528 (1964); K. K. Pivnitsky und I. V. Torogov, *Tetrahedron*, **22**, 1407 (1966); N. S. Wulfson, V. I. Zavetskii, V. L. Sadovskaya, S. N. Anachenko, V. M. Rzheznikov, und V. I. Torogov, *ibid.*, **22**, 1885 (1966); P. Crabbé, A. Cruz, und J. Iriarte, *Can. J. Chem.*, **46**, 349 (1968); M. Rosenberger, R. Borer, und G. Saucy, *J. Org. Chem.*, **43**, 1550 (1978).

27) a) Übersichten: R. A. Ellison, *Synthesis*, **1973**, 397; S. Nimgirawath, E. Ritchie, und W. Taylor, *Aust. J. Chem.*, **29**, 339 (1976); G. Rio und A. Lecas-Nawrocka, *Bull. Soc. Chim. Fr.*, **1976**, 317. b) J. Tsuji, I. Shimizu, und K. Yamamoto, *Tetrahedron Lett.*, **1976**, 2975. c) M. Miyashita, T. Yanami, und A. Yoshikoshi, *J. Am. Chem. Soc.*, **98**, 4679 (1976). d) Y. Ito, T. Konoike, T. Harada, und T. Saegusa, *J. Am. Chem. Soc.*, **99**, 1487 (1977). e) H. Stetter, P. H. Schmitz, und M. Schreckenberg, *Chem. Ber.*, **110**, 1971 (1977).

28) E. J. Nienhous, R. M. Irwin, und G. R. Fimi, *J. Am. Chem. Soc.*, **89**, 4557 (1967).

29) P. A. Grieco und C. S. Pogonowski, *J. Org. Chem.*, **39**, 733 (1974); R. M. Dessau und E. I. Heiba, *ibid.*, **39**, 3457 (1974).

30) G. Stork und M. E. Jung, *J. Am. Chem. Soc.*, **96**, 3684 (1974).

31) Dagegen lieferte die Einwirkung von konz.H_2SO_4 auf **86** bei 0 °C das entsprechende 1,4-Diketon.

32) Th. Cuvigng, M. Larcheveque, und H. Normant, *Justus Liebigs Ann. Chem.*, **1975**, 719.

33) S. H. Huckin und L. Weiler, *J. Am. Chem. Soc.*, **96**, 1082 (1974).

34) G. Büchi und H. Wüest, *J. Org. Chem.*, **31**, 977 (1966).

35) C. S. Marvel und F. D. Hager, *Org. Synth.*, Coll. Vol. I, 248 (1956).

36) G. Stork, A. Brizzolara, H. Landesman, J. Szmuszkoviz, und R. Terrell, *J. Am. Chem. Soc.*, **85**, 207 (1963).

37) H. K. Dietl und K. C. Brannock, *Tetrahedron Lett.*, **1973**, 1273.

38) H, Stetter, "Newer Methods of Preparative Organic Chemistry," Academic Press, New York und London (1963), Vol. II, S. 51—100.

39) H. Stetter und W. Diericks, *Chem. Ber.*, **85**, 1061 (1952).

40) K. Nakazawa, M. Matsumura, und M. Kusuda, *Yakugaku Zasshi*, **74**, 495 (1954).

41) H. Hunsdiecker, *Chem. Ber.*, **75**, 455 (1942).

Conformational Equilibria of 8-Alkyl-8,9,10,11-tetrahydro-7*H*-cycloocta[*de*]naphthalenes

Toshihiro KAMADA* and Osamu YAMAMOTO

National Chemical Laboratory for Industry, Honmachi 1-1-5, Shibuya-ku, Tokyo 151

(Received November 30, 1978)

The conformations of 8-methyl (**4**) and 8-ethyl-8,9,10,11-tetrahydro-7*H*-cycloocta[*de*]naphthalenes (**5**) have been studied on the basis of the NMR spectra. It was found that both compounds exist as an equilibrium mixture of the axial-boat (**ab**) and the equatorial-boat (**eb**) conformers in solution. The ^{1}H spectra revealed that the boat conformations of all these isomers are somewhat in the distorted form due to the steric repulsion between the interior benzyl protons. The free-energy differences ($-\Delta G°$) between the two isomers (**ab**$\rightleftarrows$**eb**) in **4** and **5** were calculated from the ^{13}C spectra and found to be 0.09 and -0.07 kcal/mol, respectively. These results are discussed in terms of the structural and conformational features of the 8-membered pericyclized naphthalene ring and compared with the cyclohexane ring.

Recently, as a part of our studies on the chemistry of the 8,9,10,11-tetrahydro-7*H*-cycloocta[*de*]naphthalene system (**1**),[1-4] the conformations of 8-alkyl-9-oxo derivatives, **2** and **3**, were reported.[5] In the present paper, we have extended our study to the deoxo compounds **4** and **5** in order to examine in detail the effect of the alkyl substituent on the stability of the peri ring in these pericyclized naphthalene system. Here, we will report the conformational equilibria in these 8-alkylated compounds by a study of the ^{1}H- and ^{13}C-NMR spectra and make some discussion about the conformational and spectral features of the 8-membered pericyclized naphthalene system in comparison with the cyclohexane ring.

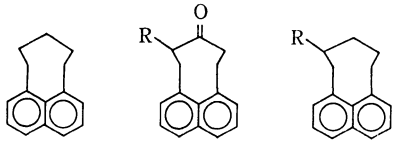

1 **2**; R=CH_3 **4**; R=CH_3
3; R=C_2H_5 **5**; R=C_2H_5

Results and Discussion

The room-temperature ^{1}H-NMR spectrum of 8-methyl-8,9,10,11-tetrahydro-7*H*-cycloocta[*de*]naphthalene-8,10,10-d_3 (**4**-d_3) in a *ca.* 10% solution in deuteriochloroform shows broad signals for both the methyl and the benzyl protons. As the temperature of the sample is progressively lowered, the methyl signal broadens and then splits into two different lines with a chemical-shift difference of 0.36 ppm, while the benzyl proton signal changes into four sets of AB quartets of different intensities, centered at δ 3.29, 3.38, 3.44, and 3.46 ppm, respectively. The proton-decoupled ^{13}C-NMR spectrum of **4** at 30 °C gives a broad line for each of the peri ring carbons and the methyl group, all of which split into a doublet of different peak heights on lowering the temperature. Similar spectral changes were observed for the ethyl compound **5**.

From these spectra it is apparent that both **4** and **5** assume two different forms interchanging to each other by the inversion of the peri ring. Analysis of the low-temperature spectra of **4** and **5** as well as their 8,10,10-trideuterated derivatives (**4**-d_3, **5**-d_3) affords the ^{1}H- and ^{13}C-data for each conformational isomer of these compounds which are summarized in Tables 1 and 2.

It has previously been shown[1-6] that the interior benzyl protons (H_{in}) in the 8-membered pericyclized naphthalene ring suffer a severe steric interaction and resonate at much lower field than the corresponding exterior protons (H_{ex}). Thus the strong vicinal couplings (J=13 Hz) observed in the lower-field signals of the C-11 methylene groups in all the conformations (Table 1) clearly suggest that only boat conformations are significantly populated in these 8-alkylated compounds, since, as can be seen in Fig. 1, the H_{in} proton of the boat conformation (**B**) is situated in a position trans to an adjacent equatorial proton (H_{eq}), and thus a strong coupling is expected between these two protons.

Table 1. ^{1}H-NMR data of conformational isomers of **4** and **5**[a,b]

Conformer	7-CH_2	11-CH_2	CH_3
4-eb	4.25 (J=−14.4, 6.1 Hz)	3.99 (J=−14.3, 13.0, 7.0 Hz)	0.84 *d* (J=6.8 Hz)
	2.64 (J=−14.4, 1.0 Hz)	2.92 (J=−14.3, 6.0 Hz)[d]	
4-ab	3.67 (J=−14.1, 12.7 Hz)	3.87 (J=−14.3, 13.0, 7.0 Hz)	1.20 *d* (J=7.0 Hz)
	2.90 (J=−14.1, 6.0 Hz)	2.90 (J=−14.3, 6.0 Hz)[d]	
5-eb	4.20 (J=−14.6, 6.1 Hz)	3.98 (J=−14.5, 13.0, 7.0 Hz)	*ca.* 1.0[c]
	2.75 (J=−14.6, 1.0 Hz)	2.93 (J=−14.5, 6.0 Hz)[d]	
5-ab	3.57 (J=−14.4, 11.5 Hz)	3.83 (J=−14.3, 13.0, 6.0 Hz)	*ca.* 1.0[c]
	2.89 (J=−14.4, 6.0 Hz)	2.96 (J=−14.3, 6.0 Hz)[d]	

a) At −45.1 °C in $CDCl_3$, δ in ppm from internal TMS. b) Signals due to the C-9 protons are buried under those of the methyl group. c) Because of overlapping of signals splitting of this signal was not observed. d) The coupling ($J_{ex,ax}$) is small enoguh not to be observed.

TABLE 2. CARBON-13 CHEMICAL SHIFTS OF CONFORMATIONAL ISOMERS OF **4** AND **5**[a]

Conformer	C-7	C-8	C-9	C-10	C-11	$\underline{C}H_3$[b]	$\underline{C}H_2$[b]
4-eb	42.6	33.2	29.6	29.4	35.9	22.0	
4-ab	44.6	34.1	26.9	24.4	36.3	20.0	
5-eb	39.5	40.7	26.6	29.2	36.5	12.4	27.7
5-ab	43.2	40.7	23.8	24.6	36.5	12.4	27.7

a) At −56.1 °C in $CDCl_3$, δ in ppm from internal TMS. b) Carbons due to the alkyl group.

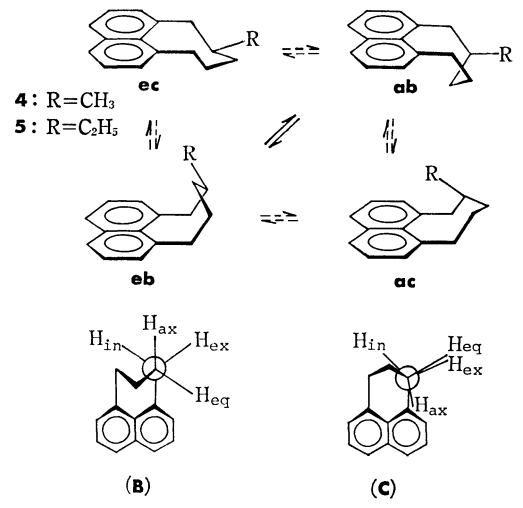

Fig. 1. The boat (**B**) (**eb**, **ab**) and the chair (**C**) (**ec**, **ac**) conformations for **4** and **5**, and their Newman projections about the C_{10}–C_{11} bond.

On the contrary, if the chair (**C**) would be the predominant conformation for **4** and **5**, then the strong vicinal coupling could be observed for the H_{ex} protons (see Newman projections in Fig. 1). The splitting pattern of the C-11 interior proton signal (J=14.3, 13.0, 7.0 Hz) in each conformer of **4** and **5** is analogous to that of the parent compound **1** (J=14.2, 12.9, 6.5 Hz),[4] which exists in the boat conformation alone.

Then the positions of the alkyl group in each conformation can be obtained from the magnitude of the vicinal couplings of the C-7 interior protons. Thus the isomers which have larger values (12.7 Hz in **4** and 11.5 Hz in **5**) have the alkyl groups at axial (**4-ab** and **5-ab**), while the others with smaller values (6.1 Hz in both **4** and **5**) have the equatorial alkyl groups (**4-eb** and **5-eb**).

This result is consistent with the ^{13}C chemical shifts in Table 2. Thus, high-field shifts of the C-7 carbons in the equatorial isomers (**eb**) relative to those in the axials (**ab**) ($\Delta\delta$=2.0—3.7 ppm) are caused by a gauche interaction between the alkyl substituent and the peri bond in the **eb** isomer (see Fig. 1), whereas marked shieldings of the C-9 ($\Delta\delta$=2.7—2.8 ppm) and C-10 carbons ($\Delta\delta$=4.6—5.0 ppm) in the **ab** conformations as compared to those in the **eb** result from the so-called γ-effect.[7] By these effects the chemical-shift differences in the C-8 ($\Delta\delta$=0.0—0.9 ppm) and in the alkyl carbons ($\Delta\delta$=0.0—2.0 ppm) between the axial (**ab**) and the equatorial (**eb**) isomers in these peri-8-membered ring system are rather small as compared to those observed in the cyclohexane system ($\Delta\delta$=4.5 and 6.0 ppm for the α and the methyl carbons, respectively).[7]

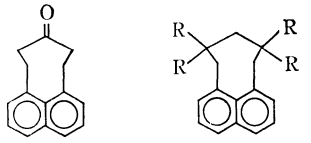

6 **7**

Consequently, compounds **4** and **5** exist as an equilibrium mixture of the axial-boat (**ab**) and the equatorial-boat (**eb**) conformers in solution. The unusually overwhelming preference of the boat conformations (**ab**, **eb**) over the chair (**ac**, **ec**) observed in these compounds results chiefly from much lower torsional energy about the C_7–C_8 and C_{10}–C_{11} bonds of the boat conformation (staggered) than the chair (eclipsed), which is one of the unique features in the peri-8-membered ring system of naphthalene (Fig. 1). All the other compounds of this ring system studied so far, including the substituted (**2**, **3**,[5] and **7**[1]) and unsubstituted (**1**[4] and **6**[2]) compounds exist solely in the boat conformation, too. The interconversion between **ab**⇄**eb** in **4** and **5** is likely to proceed by pseudorotations of the peri bonds *via* the twist-boat as in the parent compound **1**.[4,6]

TABLE 3. CONFORMATIONAL EQUILIBRIA BETWEEN **ab** ⇌ **eb** IN **4** AND **5**[a]

	R=CH_3		R=C_2H_5	
	4	**2**	**5**	**3**
K(**eb**/**ab**)	1.27		0.89	
$-\Delta G°$/(kcal/mol)	0.09	0.10[b]	−0.07	−0.59[b]
	1.70[c]	1.6—1.8[d]	1.75[c]	1.1—1.2[d]

a) Obtained from the intensity ratio of the C-7 carbon signal at −56.1 °C. b) Data taken from Ref. 5. c) For the alkylcyclohexane (Ref. 8). d) For the 2-alkylcyclohexanone (Ref. 10).

In order to determine the effect of the naphthalene moiety on the stabilities of isomers in **4** and **5** (the C-8–C-9–C-10 moiety of the boat has a geometry very similar to that of the cyclohexane ring;[1] Fig. 1), the isomer ratios (**eb**/**ab**) in these compounds were then calculated from the C-7 carbon signal intensities of each conformational isomer in the low-temperature ^{13}C spectra. The results are shown in Table 3 together with the corresponding free energy differences ($-\Delta G°$). In **4**, the equatorial methyl group at C-8 is slightly favored *vis-à-vis* the corresponding axial group, by *ca.* 0.09 kcal/mol, while the C-8 ethyl group in **5**, on the contrary, prefers the axial conformation by *ca.* 0.07 kcal/mol at −56.1 °C. This result is in striking contrast with the situation of the cyclohexane system, in which both the methyl and the ethyl substituting groups have a strong preference for the equatorial conformation ($-\Delta G°$=1.7 and 1.75 kcal/mol, respectively).[8]

The unusual high stability of the axial isomers (**ab**) observed in these 8-membered pericyclized naphthalenic compounds **4** and **5** as compared to those in the cyclohexane ring may be explained on the basis of molecular models as follows:[5] The axial alkyl group

in the **ab** conformation involves one gauche arrangement around the C_9–C_{10} bond and one *syn*-axial hydrogen at C-10 position. This corresponds to only one half of the steric interaction present in the axial isomer of the alkylcyclohexanes.[9] In the case of the equatorial isomer, however, the cyclohexane ring has no significant steric interaction within molecules,[9] while the equatorial alkyl group in the peri-8-ring (**eb**) involves one gauche arrangement with the C-7 peri bond.

Here, it is of interest to note that the bulkiness of the substituting group in the peri-8-ring system can play a more significant role in determining the conformational equilibria than in the cyclohexane ring, since, with increasing the steric bulkiness of the alkyl group, the conformation **eb** additionally suffers a non-bonded interaction between the alkyl group and the naphthalene nucleus, which is absent in the cyclohexane system. Thus, the $\Delta G°$ difference ($\Delta\Delta G° = -0.16$ kcal/mol) on going from the methyl (**4**) to the ethyl (**5**) derivative may be attributed chiefly to the alkyl-naphthalene interaction mentioned above, by which the stability of the **5-eb** conformation is further decreased as compared to that of the equatorial isomer of the alkylcyclohexane ($\Delta\Delta G° = 0.05$ kcal/mol).[8]

We have already studied[5] the NMR spectra of the 8-alkyl-8,9,10,11-tetrahydro-7*H*-cycloocta[*de*]naphthalen-9-ones (**2** and **3**) and shown that these compounds exist also as an equilibrium mixture of the **ab** and the **eb** conformers in solution. Comparison of the $\Delta G°$ values between the hydrocarbons (**4**, **5**) and the ketones (**2**, **3**) reveals that $-\Delta G°$ value of the methyl compound **4** (0.09 kcal/mol) is almost equal to that of the corresponding ketone **2** (0.10 kcal/mol), whereas in the case of the ethyl derivatives the $-\Delta G°$ value of the ketone **3** is considerably decreased (−0.59 kcal/mol) relative to the value of the deoxo compound **5** (−0.07 kcal/mol) (Table 3). This can be reasonably explained in terms of the so-called "2-alkylketone effect," since the geometry around the C-8–C-9–C-10 moiety of the peri-8-membered ring system is very similar to that of the cyclohexane ring.[1] That is, because of the eclipsed interaction between the equatorial ethyl group and the carbonyl function, the **3-eb** isomer is more destabilized than the **5-eb** isomer by the energy of *ca.* 0.5 kcal/mol, which is almost comparable to the value (0.55—0.65 kcal/mol)[10] found in the cyclohexane system.

The ^{1}H- and ^{13}C-data in the tables show other spectral and conformational features inherent in the 8-membered pericyclized naphthalene ring. The chemical-shift difference between the axial and the equatorial methyl protons in **4** ($\Delta\delta = 0.36$ ppm) is greatly increased relative to the value (0.07 ppm)[11] found in the cyclohexane system. This may be caused chiefly by the ring-current effect of the naphthalene nucleus, since, in the boat conformation of the peri-8-membered ring, the equatorial methyl group on C-8 has a position closer to the naphthalene ring than the corresponding axial methyl group (see Fig. 1). Actually, the magnitude of the shift difference of the two methyl protons observed in the spectrum (0.36 ppm) well agrees with the result of the calculation that the equatorial methyl protons resonate at *ca.* 0.46 ppm higher field than the axial methyl protons by the effect of the ring current of naphthalene.[1]

In all the isomers of **4** and **5**, the chemical shifts of the exterior benzyl protons ($\delta = 2.64$—2.96 ppm) are approximately equal to the values reported for the benzyl protons of 6,7,8,9-tetrahydro-5*H*-benzocycloheptene **8** ($\delta = 2.721$—2.827 ppm),[12] whereas the interior protons of **4** and **5** are deshielded markedly ($\delta = 3.57$—4.25 ppm) as a result of the steric compression effect. The calculation[4] revealed that the interatomic distance between the two interior protons of the boat conformation is 0.652 Å, much smaller than the sum of the van der Waals radii of the two hydrogens (2.4 Å). This suggests that although the boat (**ab**, **eb**) is the most favored conformation for **4** and **5**, it still involves severe steric repulsion between the two interior protons.

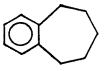

8

Thus it is expected that as in the case of the parent compound **1**,[4] the boat conformations of **4** and **5** are also in the distorted form [**B**], in which the two interior benzyl protons are pushed apart to relieve the steric repulsion between them. In this case, in view of the fact that the splitting patterns observed in the C-11 protons of **4** and **5** are very similar to those of **1** and **6**, it is reasonable to consider that the peri bonds of **4** and **5** undergo in-plane deformation as in the compounds **1**[4] and **6**[2,4] to result in the symmetric (C_s) conformation [**B**] as is shown in Fig. 2 (in studies on the peri-

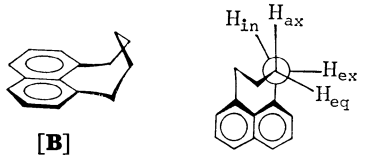

[**B**]

Fig. 2. The distorted boat conformation [**B**] for the 8,9,10,11-tetrahydro-7*H*-cycloocta[*de*]naphthalene ring and its Newman projection about the C_7–C_8 (C_{10}–C_{11}) bond (see text).

substituted naphthalenes, it was revealed that the peri bonds of 1,8-dimethylnaphthalene undergo in-plane deformation,[13,14] while, in 1,8-di-*t*-butylnaphthalene,[15,16] the peri bonds undergo out-of-plane deformation). Table 1 shows that in all the isomers the vicinal spin couplings between the C-11 exterior and the C-10 axial protons are very small (splitting is not observed) as compared to the values observed between the C-11 interior and the C-10 axial protons ($J = 6.0$ and 7.0 Hz). Similar trend is observed in the vicinal couplings about the C_7–C_8 bond of the **eb** isomer, where the axial protons are coupled more strongly with the interior benzyl protons ($J = 6.1$ Hz) than with the exterior protons ($J = 1$ Hz). These facts strongly support that all the isomers of **4** and **5** exist in the distorted boat [**B**] rather than in the normal boat (**B**), since as is seen in Fig. 2, the observed couplings are explained much

better by the space arrangement in the distorted molecule [**B**] (H_{ex}/H_{ax}; $\theta>60°$, H_{in}/H_{ax}; $\theta<60°$) than by the space arrangement in the normal boat conformation (**B**) ($\theta\approx60°$).

In our previous paper,[5] we have reported the NMR spectra of **2** and **3**. The interior benzyl protons in these compounds suffer also marked deshieldings (δ=4.22—4.89 ppm) and show splitting patterns (**2**; J=14.8, 13.4, 7.3 Hz, **3**; J=14.7, 13.5, 5.6 Hz) similar to those of the distorted conformations (**6**; J=14.8, 13.0, 5.9 Hz).[2,4] Thus, taking account of this fact, it is most probable that **2** and **3** also experience the ring distortions as in the deoxo compounds **4** and **5**, though the magnitude of the vicinal splitting ($J_{ex,ax}$) is not known in **2** and **3**. It should be noted here that the interior benzyl protons in the ketones (**2**, **3**) are *ca.* 0.5—0.7 ppm more deshielded than those of **4** and **5**, which makes the chemical-shift differences of the benzyl methylene protons in the former molecule much larger ($\Delta\delta$=1.21—2.11 ppm) than those in the latter molecules ($\Delta\delta$=0.68—1.61 ppm). Similar trend is observed between the unsubstituted compounds **1** and **6** ($\Delta\delta$= 1.03 and 1.55 ppm for **1** and **6**, respectively). This results probably from the differences in the steric interaction of the interior benzyl protons. A calculation reveals that the distance between the interior benzyl protons of the peri-8-ring system is somewhat shortened when the bond of the C-9 carbon changes from the sp^3 (0.652 Å)[4] into the sp^2 hybrid (0.632 Å). Thus it can be expected that the interior benzyl protons of the ketones (**2**, **3**, and **6**) suffer the steric repulsion larger than that of the hydrocarbons (**4**, **5**, and **1**) and are deshielded more largely than in the case of the latter compounds.

Comparison of the ^{13}C chemical shifts of **4** and **5** with those of the ketones (**2**, **3**) reveals that the axial methyl group in the ketone **2-ab** is only slightly shielded (0.9 ppm) relative to that of the hydrocarbon **4-ab**, whereas the methyl group in the equatorial isomer suffers a marked shielding (7.4 ppm) by introduction of the carbonyl group. Similar trend is observed in the ethyl derivative, where the methylene carbon of the equatorial ethyl group (**eb**) is greatly shielded (6.0 ppm) relative to that of the axial isomer (**ab**) by the effect of the carbonyl group. This chiefly arises from the eclipsed interaction of the carbonyl function and the alkyl group in the equatorial isomer as is noted in the cyclohexane system.[17] This interaction is also reflected in the chemical shifts of the peri ring carbons of both alkyl compounds, in which the C-8 and the carbonyl carbons of the equatorial isomers are shielded by 5.8—7.1 ppm relative to those of the axial isomers (for the other peri ring carbons, which are remote from the interacting groups, the effects are rather small (0.0—1.0 ppm)). This result is interesting in comparison with the result of the norbornane system previously reported.[18] In 3-methyl-2-norbornanones, in which the carbonyl group is nearly in the same orientation with respect to the exo- and the endo-methyl groups, the carbonyl substituent effects differ only by 0.9—2.3 ppm between the two isomers.

Table 5 shows the effect of the 8-alkyl group on the chemical shifts of the C-7 benzyl protons. In both hydrocarbon (**4**) and ketone (**2**), the exterior protons are shielded markedly (0.30—0.31 ppm) by the effect of the equatorial methyl group, whereas the interior protons, on the contrary, are markedly deshielded (0.25—0.28 ppm) by the same substituting group. On the other hand, the introduction of an axial methyl group shields both the interior and the exterior protons on C-7, but the effects for the former protons are much larger (0.30 and 0.33 ppm) than those for the latter protons (0.03 and 0.04 ppm). Similar effect was

TABLE 4. EFFECT OF THE CARBONYL GROUP ON THE CARBON-13 CHEMICAL SHIFTS OF 8-ALKYL-8,9,10,11-TETRAHYDRO-7*H*-CYCLOOCTA[*de*]NAPHTHALENES (in ppm)[a]

R	Isomer	C-7	C-8	C-9	C-10	C-11	$\underline{C}H_3$	$\underline{C}H_2$
Me	**eb**	1.9	−12.0	−185.0	−16.4	1.4	7.4	
	ab	1.9	−17.9	−190.8	−17.4	2.4	0.9	
	Δ[b]	0.0	5.9	5.8	1.0	−1.0	6.5	
Et	**eb**	1.7	−11.4	−187.4	−17.1	1.9	0.2	6.8
	ab	2.1	−18.5	−193.2	−17.9	2.5	0.2	0.8
	Δ[b]	−0.4	7.1	5.8	0.8	−0.6	0.0	6.0

a) $\Delta\delta=\delta^{Hydrocarbon}-\delta^{Ketone}$ (obtained from the data in Table 2 and in Ref. 5). b) Differences of the carbonyl substituent effect between the two isomers ($\Delta=\Delta\delta^{eb}-\Delta\delta^{ab}$)

TABLE 5. EFFECT OF 8-ALKYL GROUP ON THE CHEMICAL SHIFTS OF 7-BENZYL PROTONS IN THE 8,9,10,11-TETRAHYDRO-7*H*-CYCLOOCTA[*de*]NAPHTHALENE RING (in ppm)[a]

Isomer	R	H_{7in}[b]			H_{7ex}[b]		
eb	Me	0.28	0.25	(θ=166°)[c]	−0.30	−0.31	(θ=46°)[c]
	Et	0.23	0.07		−0.19	−0.17	
ab	Me	−0.30	−0.33	(θ=46°)[c]	−0.04	−0.03	(θ=74°)[c]
	Et	−0.40	−0.42		−0.05	−0.08	

a) A minus sign indicates a high-field shift. b) Figures in the left column are due to the hydrocarbons ($\Delta\delta=\delta$(**4**, **5**)$-\delta$(**1**)) (Ref. 4), and those in the right column are to the ketones ($\Delta\delta=\delta$(**2**, **3**)$-\delta$(**6**)) (Refs. 2 and 5). c) Torsional angle between the C_7-benzyl proton and the alkyl group (taken from the data of **1** in Ref. 4).

observed in the cyclohexane ring[11,19] and some theories to explain this were reported.[20,21] In the present case, although details are not known at present, the above results may be interpreted qualitatively in terms of carbon–carbon single-bond anisotropies.[19] Since the peri rings of **4** and **5** have a geometry analogous to that of the parent compound **1**, the torsional angle about the C_7–C_8 bond of **4** and **5** can be estimated from the data of **1** as follows; $H_{7in}/CH_3(ax)=H_{7ex}/CH_3(eq)=46°$, $H_{7ex}/CH_3(ax)=74°$ and $H_{7in}/CH_3(eq)=166°$ (the peri-eight-membered ring of 8,9,10,11-tetrahydro-7*H*-cycloocta[*de*]naphthalene system is more greatly distorted (internal dihedral angle $\Psi=46°$)[4] than the cyclohexane ring ($\Psi=58°$),[22] see Fig. 2). These angles could adequately explain the trend of the shift values of the C_7-benzyl protons of **4** described above. For the ethyl compounds (**3**, **5**), almost the same trend is observed except for the H_{7in} proton of the **eb** isomer (see Table 5). The small shift value (0.07 ppm) observed in the ketone **3-eb**, in contrast to the case of the hydrocarbon **5-eb** (0.23 ppm), might be related chiefly to the 2-alkylketone effect described above.

Experimental

The synthesis of 8-methyl-8,9,10,11-tetrahydro-7*H*-cycloocta[*de*]naphthalene (**4**) was reported previously.[3] 8-Ethyl-8,9,10,11-tetrahydro-7*H*-cycloocta[*de*]naphthalene (**5**) was synthesized from diethyl 9-oxo-8,9,10,11-tetrahydro-7*H*-cycloocta-[*de*]naphthalene-8,10-dicarboxylate (**9**)[3] as follows.

To a stirred solution of sodium ethoxide in ethanol (obtained by dissolving 1.7 g of sodium into 150 ml of absolute ethanol) was added a solution of 5 g of keto ester **9** in 50 ml of absolute ethanol and 30 ml of dry dimethyl sulfoxide. After 1 h heating, excess ethyl bromide was added and the mixture was refluxed overnight. The mixture was poured into ice–water and the resulting cloudy solution was extracted with ethyl acetate. The organic solution was worked up as usual to leave a brown oil, which then treated with alkaline solution. The solid precipitated was crystallized from ethanol to give 1.2 g of 8-ethyl-8,9,10,11-tetrahydro-7*H*-cycloocta[*de*]naphthalen-9-one (**3**) as white needles; mp 97—98 °C; Found: C, 85.87; H, 7.83%. Calcd for $C_{17}H_{18}O$: C, 85.67; H, 7.61%. Clemmensen reduction of the ketone **3** gave the hydrocarbon **5**. The product was obtained as white needles after recrystallization from aqueous ethanol; mp 38—39 °C; Found: C, 90.95; H, 8.70%. Calcd for $C_{17}H_{20}$: C, 91.01; H, 8.99%.

8-Methyl-8,9,10,11-tetrahydro-7*H*-cycloocta[*de*]naphthalene-8,10,10-d_3 (**4**-d_3) and 8-ethyl-8,9,10,11-tetrahydro-7*H*-cycloocta[*de*]naphthalene-8,10,10-d_3 (**5**-d_3) were synthesized by Clemmensen reduction of the corresponding 8,10,10-trideuterated derivatives[5] of **2** and **3**, which had been obtained by the deuterium exchange reactions described previously.[4] The structures of the deuterated compounds were confirmed based on TLC, mp (**4**-d_3; 39—40 °C, **4**; 40—41 °C,[3] **5**-d_3; 38—39.5 °C) and their spectra (IR and NMR).

^{1}H NMR spectra were determined on a Varian HA-100D spectrometer operating at 100 MHz. ^{13}C NMR spectra were determined on a Varian NV-14 spectrometer operating at 15.087 MHz with a Varian 620/L computer (16K) in the pulsed FT mode (pulse flipping angle, 48°; pulse repetition time, 1.3 s). The samples were dissolved in chloroform-*d* (*ca.* 10% (w/v) solution), and tetramethylsilane was used as an internal standard. The temperature was controlled by using cooled nitrogen and measured by calibrated copper–constantan thermocouple.

References

1) T. Kamada, N. Wasada, and O. Yamamoto, *Bull. Chem. Soc. Jpn.*, **49**, 275 (1976).
2) T. Kamada and O. Yamamoto, *Chem. Lett.*, **1976**, 843.
3) T. Kamada, *Bull. Chem. Soc. Jpn.*, **52**, 170 (1979).
4) T. Kamada and O. Yamamoto, *Bull. Chem. Soc. Jpn.*, **52**, 1159 (1979).
5) T. Kamada and O. Yamamoto, *Tetrahedron Lett.*, **1977**, 691.
6) S. F. Nelsen and J. P. Gillespie, *J. Am. Chem. Soc.*, **95**, 2940 (1973).
7) J. B. Stothers, "Carbon-13 NMR Spectroscopy," Academic Press, New York (1972).
8) J. A. Hirsch, "Topics in Stereochemistry," ed by E. L. Eliel and N. L. Allinger, Interscience Publishers, New York (1967), Vol. 1.
9) E. L. Eliel, "Stereochemistry of Carbon Compounds," McGraw-Hill, New York (1959).
10) H. Hanack, "Conformation Theory," Academic press, New York (1965).
11) D. Danneels and M. Anteunis, *Org. Magn. Reson.*, **6**, 617 (1974).
12) M. St-Jacqoues and C. Vaziri, *Org. Magn. Reson.*, **1**, 451 (1969).
13) V. Balasubramaniyan, *Chem. Rev.*, **66**, 567 (1966).
14) D. Bright, I. E. Maxwell, and J. de Boer, *J. Chem. Soc., Perkin Trans. 2*, **1973**, 2101.
15) J. E. Anderson, R. W. Franck, and W. L. Mandella, *J. Am. Chem. Soc.*, **94**, 4608 (1972).
16) J. Handal, J. G. White, R. W. Franck, Y. H. Yuh, and N. L. Allinger, *J. Am. Chem. Soc.*, **99**, 3345 (1977).
17) F. Weigert and J. D. Roberts, *J. Am. Chem. Soc.*, **92**, 1347 (1970).
18) J. B. Grutzner, M. Jautelat, J. B. Dence, R. A. Smith, and J. D. Roberts, *J. Am. Chem. Soc.*, **92**, 7107 (1970).
19) J. B. Lambert and Y. Takeuchi, *Org. Magn. Reson.*, **1**, 345 (1969).
20) E. Pretsch and W. Simon, *Helv. Chim. Acta*, **52**, 2133 (1969).
21) H. Boaz, *Tetrahedron Lett.*, **1973**, 55.
22) J. B. Lambert, *Acc. Chem. Res.*, **4**, 87 (1971).

Catalytic Efficiency of Synthetic Micellar Catalysts Bearing a Mercapto Group as the Reaction Center†

Yukito MURAKAMI,* Akio NAKANO, and Kiyoshi MATSUMOTO

Department of Organic Synthesis, Faculty of Engineering, Kyushu University, Hakozaki, Higashi-ku, Fukuoka 812

(Received December 25, 1978)

In order to obtain a clue to understanding the micro-environmental effect on the reactivity of a mercapto group placed in a reaction center of enzymes, micellar surfactants bearing a mercapto group were synthesized and their catalytic activity in the degradation of *p*-nitrophenyl carboxylates was studied. *N*-Hexadecyl-N^{α}-glutaryl-L-cysteinamide (AM·Cys-1) has an ability to form anionic micelles in aqueous media. The catalytic activity of AM·Cys-1 was compared with that of another synthetic surfactant, *N*-hexadecanoyl-L-cysteine (AM·Cys-2). These surfactants below their critical micelle concentrations markedly accelerated the degradation of several *p*-nitrophenyl carboxylates. On the contrary, the concentration-rate profiles for the degradation of *p*-nitrophenyl dodecanoate (PNPL) as catalyzed by the surfactants indicate that the reactivity of the mercapto group is reduced upon formation of the anionic micelles. The large rate retardation is primarily due to the decrease in concentration of the active thiolate anion. This was supported by the fact that the pK_a values for mercapto groups of the anionic micelles, for which the carboxyl group acts as an anionic head, were increased by 0.8—1.6 pK_a unit over those of the corresponding monomeric surfactants in the bulk phase. These surfactants showed profound reactivity even in a neutral pH region when mixed with cationic CTAB micelle. The electrostatic field effect provided by the cationic head of CTAB micelle seems to enhance the nucleophilicity of the mercapto group in the mixed micelles.

The mercapto group is located at the active site of thiol proteases such as papain, ficin, and bromelain and playes an important role in enzymatic reactions.[1] The reactivity of the mercapto groups of these enzymes, however, drastically changes from one to another depending on the nature of micro-environment where they are located. Because of the complexity of protein molecules, the difference in reactivity among various types of mercapto groups has not yet been satisfactorily clarified. Only a few studies on the reactivity of mercapto groups of non-enzymatic systems in the degradation of *p*-nitrophenyl acetate have been reported so far.[2] Some studies were carried out in cationic micelles such as hexadecyl- and octadecyltrimethylammonium bromide as enzyme model systems.[3] Shinkai and Kunitake introduced the concept of hydrophobic ion pair for the reaction of coenzyme A (CoASH) and glutathione (GSH) with *p*-nitrophenyl acetate in a cationic micelle in which the hydrophobic environment has an important role for the development of catalysis.[4] Recently, Moss and his coworkers synthesized self-contained thiol-functionalized surfactants and investigated their catalytic activity in the degradation of *p*-nitrophenyl acetate.[5] In their system, the mercapto group seems to be placed in the cationic Stern layer judging from the molecular structure of surfactants.

In order to clarify the various features of reactivity of the mercapto group in enzymatic reactions and to create more elaborated models of thiol proteases, we prepared in this work a novel type of surfactants, *N*-hexadecyl-N^{α}-glutaryl-L-cysteinamide (AM·Cys-1). The mercapto group is expected to be placed in a hydrophobic core of the micellar phase. The catalytic activity of AM·Cys-1 was compared with that of another synthetic surfactant, *N*-hexadecanoyl-L-cysteine (AM·Cys-2). The structural and micellar effects provided by the present cysteine-containing surfactants have been clarified in the deacylation of *p*-nitrophenyl carboxylates. The effective catalysis by mixed micelles composed of hexadecyltrimethylammonium bromide (CTAB) and either AM·Cys-1 or -2 in the deacylation has also been investigated here.

† Contribution No. 509 from this Department.

Experimental

Spectroscopic data were taken on a JASCO DS-403G grating IR spectrophotometer, a Varian A60 NMR spectrometer, and a Hitachi 124 spectrophotometer. pH-Measurements were carried out with a TOA HM-9A pH meter equipped with a TOA GC-125 combined electrode after calibration with a combination of appropriate aqueous standard buffers.

Materials. Hexadecyltrimethylammonium bromide (CTAB) of Nakarai Chemicals was recrystallized from ethanol, mp 237—239 °C (dec). Sodium dodecyl sulfate (SDS) and α-hydro-ω-dodecyloxytricosa(oxyethylene) (Brij 35) were purchased from Nakarai Chemicals as extra pure grade and used without further purification. 1-Dodecanethiol (C_{12}-SH) was obtained from Ishizu Pharmaceutical Co. and distilled under nitrogen, bp 145—147 °C/16 mmHg. 2-Mercaptoethanol was purchased from Nakarai Chemicals and distilled under nitrogen, bp 54.5 °C/13 mmHg. Glutathione (GSH, Wako Pure Chemical Industries), L-cysteine hydrochloride (Cys·HCl, Ishizu Pharmaceutical Co.), and 2,2′-dinitro-5,5′-dithiodibenzoic acid (DTNB, Nakarai Chemicals) of bio-analytical grade were used without further purification. Rhodamine 6G was purchased from Daiwa Chemicals as extra pure grade. *p*-Nitrophenyl carboxylates were prepared by the reaction of the corresponding carbonyl chlorides with *p*-nitrophenol. The esters were identified by elemental analyses and spectroscopic measurements.[6]

N-Hexadecanoyl-L-cysteine (AM·Cys-2). This was prepared by the condensation of hexadecanoic acid with *S*-benzyl-L-cysteine in the presence of ethyl chloroformate followed by elimination of the benzyl group in a manner reported by Heitmann.[7]

N-Hexadecanoyl-*S*-benzyl-L-cysteine: mp 79—81 °C. IR (KBr disc): 3320 (NH str.); 2920 and 2860 (CH str.); 1750 and 1650 (C=O str.); 825, 770, and 700 cm^{-1} (CH bend. of benzene). NMR ($CDCl_3$, TMS): δ 0.87 (3H, t, $C\underline{H}_3(CH_2)_{13}$-$CH_2$–), 1.24 (26H, broad, $CH_3(C\underline{H}_2)_{13}CH_2$–), 2.20 (2H, t,

$CH_3(CH_2)_{13}C\underline{H}_2CO$–), 2.91 (2H, d, –NHCH($C\underline{H}_2SCH_2Ph$)-$CO_2H$), 3.68 (2H, s, $-SC\underline{H}_2Ph$), 4.80 (1H, t, –NHC$\underline{H}$-(CO_2H)–), 6.37 (1H, d, –N$\underline{H}$–), and 7.51 (5H, s, phenyl H's).

N-Hexadecanoyl-L-cysteine: mp 83—85 °C, nitroprusside positive, Ellman positive, $[\alpha]_D^{21}$ −26.0° (*c* 1.00, C_2H_5OH); R_f (silica gel IB of J. T. Baker, methanol), 0.80; R_f (silica gel IB of J. T. Baker, butanol–water–acetic acid at 4: 2: 1 by volume), 0.87. IR (KBr disc): 3320 (NH str.); 2920 and 2860 (CH str.); 1750 and 1650 cm^{-1} (C=O str.). NMR ($CDCl_3$, TMS): δ 0.86 (3H, t, $C\underline{H}_3(CH_2)_{13}CH_2$–), 1.25 (26H, broad, $CH_3(C\underline{H}_2)_{13}CH_2$–), 2.28 (2H, t, $CH_3(CH_2)_{13}C\underline{H}_2CO$–), 2.96 (2H, dd, –NHCH($C\underline{H}_2SH$)$CO_2H$), 4.80 (1H, t, –NHC$\underline{H}$-($CH_2SH$)$CO_2H$), 6.25 (1H, d, –N$\underline{H}$–), and 8.18 (1H, s, $-CO_2\underline{H}$). Found: C, 63.55; H, 10.16; N, 3.80%. Calcd for $C_{19}H_{37}NO_3S$: C, 63.47; H, 10.37; N, 3.90%.

The synthetic procedures for *N*-hexadecyl-N^{α}-glutaryl-L-cysteinamide (AM·Cys-1) is outlined in Scheme 1.

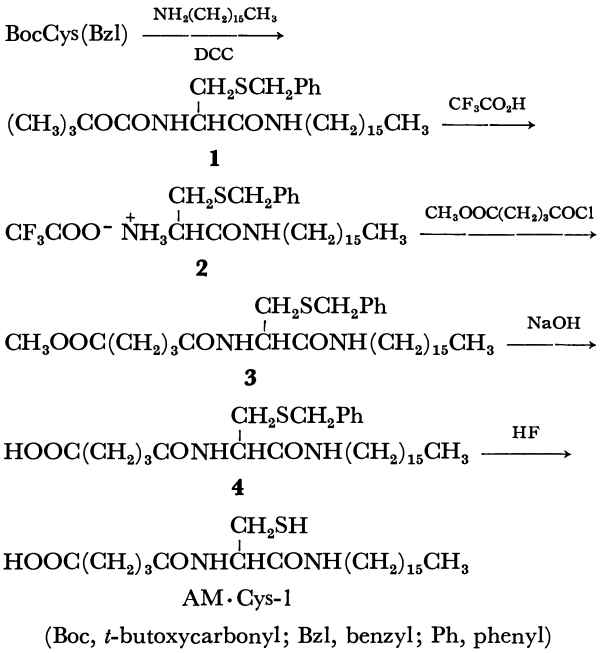

(Boc, *t*-butoxycarbonyl; Bzl, benzyl; Ph, phenyl)

Scheme 1. Synthetic procedures for AM·Cys-1.

N-*Hexadecyl*-N^{α}-t-*butoxycarbonyl*-S-*benzyl*-L-*cysteinamide* (*1*). *t*-Butoxycarbonyl-*S*-benzyl-L-cysteine (8.0 g, 23 mmol) and dicyclohexylcarbodiimide (4.7 g, 23 mmol) were dissolved in dichloromethane–acetonitrile (1: 1 by volume, 40 ml), and the solution was cooled down to 0 °C. Then, 1-aminohexadecane (5.5 g, 23 mmol) was added to the solution and the mixture was stirred for 3 h at 0 °C. Precipitated white solid was recovered by filtration and recrystallized from hexane–ethyl acetate (1: 1 by volume); yield 8.7 g (72%), mp 88—90 °C. IR (KBr disc): 3300 (NH str.); 2910 and 2850 (CH str.); 1695 and 1640 cm^{-1} (C=O str.). NMR ($CDCl_3$, TMS): δ 0.88 (3H, broad t, $C\underline{H}_3(CH_2)_{15}$–), 1.27 (28H, s, $CH_3(C\underline{H}_2)_{14}$-$CH_2NH(CO)$–), 1.45 (9H, s, $(C\underline{H}_3)_3CO$–), 2.82 (2H, d, $-C\underline{H}_2SCH_2Ph$), 3.23 (2H, broad t, $CH_3(CH_2)_{14}C\underline{H}_2NH$-(CO)–), 3.75 (2H, s, $-CH_2SC\underline{H}_2Ph$), 4.57 (1H, broad t, –NHC$\underline{H}$(CH_2SCH_2Ph)CO–), and 7.31 (5H, s, phenyl H's).

N-*Hexadecyl*-N^{α}-*methylglutaryl*-S-*benzyl*-L-*cysteinamide* (*3*). Trifluoroacetic acid (5.7 g) was added to a dichloromethane solution (16 ml) of **1** (534 mg, 1.0 mmol), and the mixture was stirred for 1 h at room temperature. Evaporation of the excess trifluoroacetic acid *in vacuo* below 40 °C gave pale yellow crystals (**2**), mp 72 °C. Elimination of the *t*-butoxycarbonyl group was confirmed by the NMR spectrum. The crystals were used for the following reaction without further purification. Amine component **2** (210 mg, 0.38 mmol) and triethylamine (115 mg, 1.14 mmol) were dissolved in dichloromethane (5 ml) and cooled down to 5 °C. Methyl 4-chloroformylbutanoate (81 mg) dissolved in dichloromethane (2 ml) was added to the solution in 15 min at this temperature. The mixture was stirred for 1 h at 0 °C, for 1 h at room temperature, and refluxed for 10 min; and then washed with water (5 ml), 5% aqueous sodium hydrogencarbonate (5 ml ×2), water (5 ml×2), and 5% aqueous citric acid (5 ml×2) in this sequence. After being dried over anhydrous sodium sulfate, the mixture was evaporated *in vacuo* at 50 °C to give a white solid which was then purified by gel-filtration chromatography (Sephadex LH-20, 1: 1 chloroform–methanol as an eluant); yield 180 mg (50%), mp 86—88 °C. IR (KBr disc): 3275 (NH str.); 2900 and 2830 (CH str.); 1740 and 1640 cm^{-1} (C=O str.). NMR ($CDCl_3$, TMS): δ 0.88 (3H, broad t, $C\underline{H}_3(CH_2)_{15}$–), 1.27 (30H, s, $CH_3(C\underline{H}_2)_{14}CH_2NH$– and $CH_3O_2CCH_2C\underline{H}_2CH_2CO$–), 1.75—2.55 (4H, m, CH_3O_2-$CC\underline{H}_2CH_2C\underline{H}_2CO$–), 2.71 (2H, d, –CHC$\underline{H}_2SCH_2$Ph), 3.24 (2H, broad t, $-NHC\underline{H}_2(CH_2)_{14}CH_3$), 3.66 (3H, s, $C\underline{H}_3O_2C$–), 3.74 (2H, s, $-SC\underline{H}_2Ph$), 4.57 (1H, t, –NHC$\underline{H}$(CH_2SCH_2Ph)-CO–), and 7.29 (5H, s, phenyl H's). Found: C, 67.96; H, 9.63; N, 4.87%. Calcd for $C_{32}H_{54}O_4N_2S$: C, 68.29; H, 9.67; N, 4.97%.

N-*Hexadecyl*-N^{α}-*glutaryl*-S-*benzyl*-L-*cysteinamide* (*4*). To a mixture of **3** (700 mg), dioxane (20 ml), and methanol (35 ml) was added 4% aqueous sodium hydroxide (9 ml). After being stirred for 6 h at room temperature, the mixture was evaporated *in vacuo* to remove methanol and then water (30 ml) was added to the residue. The solution was acidified to pH 5 by adding 10% aqueous citric acid. White precipitates were recovered by filtration and washed with water (5 ml× 10); yield 677 mg (99%), mp 101—102 °C. IR (KBr disc): 3250 (NH str.); 2900 and 2840 (CH str.); 1700, 1630, and 1525 cm^{-1} (C=O str.). NMR ($CDCl_3$, TMS): δ 0.88 (3H, broad t, $C\underline{H}_3(CH_2)_{15}$–), 1.26 (30H, s, $CH_3(C\underline{H}_2)_{14}CH_2$– and $HO_2CCH_2C\underline{H}_2CH_2CO$–), 1.73—2.57 (4H, m, $HO_2CC\underline{H}_2CH_2$-$C\underline{H}_2CO$–), 2.71 (2H, d, –CH($C\underline{H}_2SCH_2Ph$)–), 3.24 (2H, broad t, $-NHC\underline{H}_2(CH_2)_{14}CH_3$), 3.74 (2H, s, $-SC\underline{H}_2Ph$), 4.57 (1H, t, –NHC$\underline{H}$(CH_2SCH_2Ph)CO–), and 7.29 (5H, s, phenyl H's). Found: C, 67.23; H, 9.48; N, 5.06%. Calcd for $C_{31}H_{52}O_4N_2S$: C, 67.84; H, 9.55; N, 5.10%.

N-*Hexadecyl*-N^{α}-*glutaryl*-L-*cysteinamide* (*AM·Cys-1*). L-Methionine (180 mg) and **4** (600 mg) were placed in a reaction vessel into which hydrogen fluoride (20 ml) was introduced. The mixture was stirred for 1 h at 0 °C, for 30 min at room temperature, and then evaporated *in vacuo* to remove hydrogen fluoride completely. Dichloromethane (30 ml) was added to the residue and white precipitates were recovered by filtration; this treatment was repeated four times. The white solid was dissolved in ethanol–chloroform (1: 1 by volume, 5 ml) and purified by repeated gel-filtration chromatography (Sephadex LH-20, 1: 1 ethanol–chloroform as an eluant); yield 135 mg (27%), mp 98—101 °C, nitroprusside positive. IR (KBr disc): 3250 (NH str.); 2910 and 2830 (CH str.); 1710, 1635, and 1535 cm^{-1} (C=O str.). NMR ($CDCl_3$, TMS): δ 0.88 (3H, broad t, $C\underline{H}_3(CH_2)_{15}$–), 1.27 (30H, s, $CH_3(C\underline{H}_2)_{14}CH_2$– and $HO_2CCH_2C\underline{H}_2CH_2CO$–), 1.75—2.55 (4H, m, $HO_2CC\underline{H}_2$-$CH_2C\underline{H}_2CO$–), 2.82 (2H, dd, –CH($C\underline{H}_2SH$)–), 3.20 (2H, broad t, $CH_3(CH_2)_{14}C\underline{H}_2NH$–), and 4.60 (1H, broad t, –NH-C$\underline{H}$(CH_2SH)–). Found: C, 63.63; H, 9.89; N, 5.93%. Calcd for $C_{24}H_{46}N_2O_4S$: C, 62.84; H, 10.10; N, 6.11%.

Kinetic Measurements. The concentration of free thiol for AM·Cys-1 and -2 was determined by using the Ellman's reagent (DTNB)[8] before kinetic runs. The reaction between a thiol compound and DTNB in 10% (v/v) aqueous ethanol

at pH 8.0 (μ 0.10 with KCl) and room temperature was followed at 412 nm to completion and the amount of free thiol was evaluated by using cysteine hydrochloride and/or 2-mercaptoethanol as a reference. The concentration of free thiol for AM·Cys-1 and -2 decreases upon oxidation to the corresponding disulfides at alkaline pH's, and the oxidation rate for the mercapto group of AM·Cys-2 was roughly estimated at several pH's by the Ellman's method. For example, the acyl transfer from an ester substrate to AM·Cys-2 was completed within 1 min at pH 11.82 while only a 5% amount of AM·Cys-2 was oxidized in 5 min. Under every conditions used in this work, the reaction between surfactant and ester species was fast enough to neglect oxidation of the mercapto group of the surfactants.

Rates of *p*-nitrophenol liberation from *p*-nitrophenyl esters were measured at 317 nm (pH<6) and 400 nm (pH>6) with a Hitachi 124 spectrophotometer. Each run was initiated by adding a dry dioxane solution (30 μl) of a substrate ester to a mixture of a reaction medium (3.0 ml) and a dry ethanol solution (30 μl) of a catalyst which was pre-equilibrated at 30.0±0.1 °C in a thermostatted cell set in the spectrophotometer. The reaction medium was prepared as follows: 10.0 ml of 1.0 M aqueous potassium chloride, 10.0 ml of an appropriate aqueous buffer, and 10.0 ml of dry ethanol were placed in a 100-ml volumetric flask; and subsequently the flask was filled with deionized and distilled water. Aqueous buffer solutions adopted in the present study were as follows: 1/10 M potassium dihydrogenphosphate–1/20 M sodium borate for pH 6—9, 1/20 M sodium borate–1/20 M sodium carbonate for pH 10—11, and 1/10 M sodium hydroxide–1/10 M sodium hydrogenphosphate for pH 11—12.

Determination of pK_a *Values.* The pK_a value for a mercapto group involved in AM·Cys-1 and -2 depends on their concentrations. The extent of dissociation of the mercapto group was evaluated by Eq. 1.

$$\alpha = \Delta\text{Abs(pH x)}/\Delta\text{Abs(pH 13.26)} \quad (1)$$

where ΔAbs(pH x) refers to the difference between absorbances at 235 (maximum) and 265 nm (minimum) in 10.8% (v/v) aqueous ethanol at pH x. ΔAbs for the completely ionized mercapto group of AM·Cys-1 was evaluated at pH 13.26. The modified Henderson-Hasselbalch equation as represented by Eq. 2 was adopted to evaluate pK_a values.

$$\text{pH} = pK_a + n\log\{\alpha/(1-\alpha)\} \quad (2)$$

In order to determine the true pK_a value in a micellar phase, the pK_a value was plotted against the concentration of AM·Cys-1 as shown in Fig. 4.

CMC Measurements. The critical micelle concentrations for AM·Cys-1 and -2 were determined at 30.0±0.1 °C, pH 9.30, and μ 0.10 (KCl) in 15.6%(v/v) and 11.5%(v/v) aqueous ethanol, respectively. Rhodamine 6G was used as a dye probe at 1.0×10^{-5} M. The difference spectra between 520 (maximum) and 543 nm (minimum) were taken and the difference in absorption was plotted against the concentration of a surfactant in reference to the method used for the determination of CMC values for *N*-acyl-DL-cysteines.[7]

Results and Discussion

The catalytic efficiency of the surfactants in the deacylation of *p*-nitrophenyl carboxylates has been investigated by the kinetic method in 10.8%(v/v) ethanol–1.0%(v/v) dioxane–water at 30.0±0.1 °C and μ 0.10 (KCl). Apparent pseudo-first-order rate constants (k_{obsd}) were obtained by measuring the amount of liberated *p*-nitrophenol. The first-order kinetics was found to hold at least up to 80% conversion of the substrate for [C]≫[S]; C and S stand for catalyst and substrate species, respectively. Figure 1 shows the rate-concentration profile for the deacylation of *p*-nitrophenyl dodecanoate (PNPL) catalyzed by AM·Cys-1 and -2 at pH 9.3; k_1 refers to $k_{obsd}-k_{hyd}$. The apparent first-order rate constant (k_1) increases as the surfactant concentration is raised up to a certain concentration range which may be referred to the critical micelle concentration. The kinetic CMC values agree reasonably well with the corresponding values determined by the dye method as seen in Table 1. Beyond these concentration ranges, the k_1 values were nearly leveled off for both surfactant systems. The straight line portions below

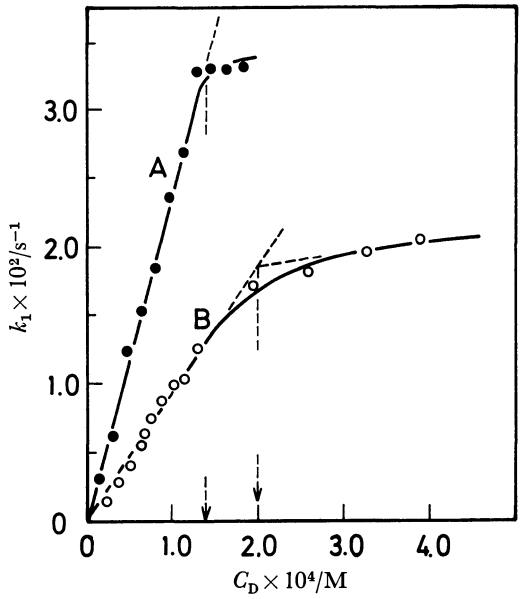

Fig. 1. Plots of first-order rate constant *vs.* surfactant concentration (C_D) for the deacylation of *p*-nitrophenyl dodecanoate in 10.8%(v/v) ethanol–1.0%(v/v) dioxane–water at 30.0±0.1 °C, pH 9.3, and μ 0.10 (KCl): $k_1=k_{obsd}-k_{hyd}$; initial concentration of PNPL, 0.984×10^{-5} M; A, AM·Cys-1; B, AM·Cys-2. The rate was not measured for the AM·Cys-1 system beyond this concentration range due to its limited solubility.

Table 1. Critical micelle concentrations for AM·Cys-1 and -2

Surfactant	CMC×10⁴/M	
	Dye method	Kinetic method
AM·Cys-1	3.76[a)]	1.33[b)]
AM·Cys-2	1.40[c)]	2.00[d)]

a) In 15.6%(v/v) aqueous ethanol at 30.0±0.1 °C, pH 9.30, and μ 0.10 (KCl). b) In 15.6%(v/v) ethanol–1.0%(v/v) dioxane–water at 30.0±0.1 °C, pH 9.28, and μ 0.10 (KCl); initial concentration of PNPL, 0.984×10^{-5} M. c) In 11.5%(v/v) aqueous ethanol at 30.0±0.1 °C, pH 9.30, and μ 0.10 (KCl). d) In 10.8%(v/v) ethanol–1.0%(v/v) dioxane–water at 30.0±0.1 °C, pH 9.30, and μ 0.10 (KCl); initial concentration of PNPL, 0.984×10^{-5} M. All the concentrations throughout this paper are given in M; 1 M=1 mol dm^{-3}.

Table 2. Kinetic parameters for the catalyzed deacylation of *p*-nitrophenyl dodecanoate and acetate[a)]

Catalyst RSH	[RSH]×10⁵ / M	pK_a^{app}	pH	k_2/M⁻¹ s⁻¹ PNPL	k_2/M⁻¹ s⁻¹ PNPA
AM·Cys-1	9.82(<CMC)	10.5[c)]; 10.5[d)]	9.28	4180	0
AM·Cys-2	10.5 (<CMC)	10.3[c)]; 10.4[d)]	9.30	1290	0
C_{12}-SH[b)]	5.01(<CMC)	12.0[c)]	12.41	1970	—
GSH	567	9.2[e)]	9.41	0.011	1.92
$HSCH_2CH_2OH$	98.3	9.4[e)]	9.41	—	4.28
	9830			0.012	—
OH^-[f)]				1.11	24.4

a) In 10.8% (v/v) ethanol–1.0% (v/v) dioxane–water at 30.0±0.1 °C and μ 0.10 (KCl). Initial concentrations: PNPL, 0.984×10⁻⁵ M; PNPA, 0.989×10⁻⁵ M. The relative rate (k_{obsd}/k_{hyd}) in the presence of AM·Cys(Bzl)-1 (39.9×10⁻⁵ M > CMC) is 0.48 at pH 11.13. b) In 10.8% (v/v) aqueous dioxane at 40.0±0.1 °C and μ 0.10 (KCl). c) Determined by the kinetic method (Eq. 3) as a dissociation constant for a mercapto group. d) Determined by the photometric titration as a dissociation constant for a mercapto group. e) Cited from literature: J. W. Ogilvie, J. T. Tildon, and B. S. Strauch, *Biochemistry*, **3**, 754 (1964). f) Alkaline hydrolysis.

CMC are referred to the apparent second-order kinetics with rate constant k_{2b} as catalyzed by the monomeric surfactants in the bulk phase, whereas those above CMC are due to the apparent second-order kinetics with rate constant k_{2m} as catalyzed by the micellar surfactants. The leveling-off behavior suggests that the micelle formation results in the loss of thiol-reactivity for the present surfactants.

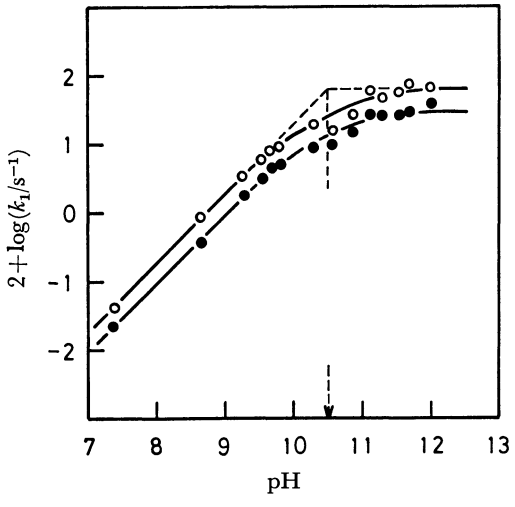

Fig. 2. pH-rate profiles for the deacylation of *p*-nitrophenyl dodecanoate as catalyzed by AM·Cys-1 above (○) and below (●) its CMC in 10.8% (v/v) ethanol–1.0% (v/v) dioxane–water at 30.0±0.1 °C and μ 0.10 (KCl). Initial concentrations: AM·Cys-1, 8.20×10⁻⁵ M (<CMC) and 1.63×10⁻⁴ M (>CMC); PNPL, 0.984×10⁻⁵ M.

The pH-rate profiles for the decomposition of *p*-nitrophenyl dodecanoate (PNPL) as catalyzed by AM·Cys-1 below and above its CMC are shown in Fig. 2. A plot of log k_1 against pH exhibited a straight line of slope 1.0 below pH 10.5, and log k_1 is leveled off beyond this pH. The behavior indicates that the active group of the surfactant for the degradation of PNPL is the thiolate anion. The apparent pK_a value evaluated from Fig. 2 agrees satisfactorily with that determined by the photometric titration as seen in Table 2. The pH-rate profile for the surfactant-catalyzed degradation of PNPL above its CMC is almost identical with that observed below CMC. The result again indicates that the reactivity of AM·Cys-1 above its CMC is primarily due to the monomeric species. The similar behavior was observed for AM·Cys-2.

Reactivity of the Mercapto Group Below CMC's. The initial rapid release of *p*-nitrophenol from PNPL was followed by the slow process at pH 9.28 for [S]>[C]. The absorbance increase due to *p*-nitrophenol at 400 nm in the slow rate region is almost identical with that observed in the absence of the surfactants. The result indicates that the deacylation of the thiol ester yielded by the reaction between PNPL and surfactants can not proceed to any detectable extent under present conditions. Thus, the net reaction pathway below CMC is given by Scheme 2, where P_1 and P_2 stand for phenol and carboxylic moieties, respectively; k_2 refers to the true second-order rate constant for the acylation step and k_{hyd} to the rate constant for the alkaline hydrolysis of PNPL.

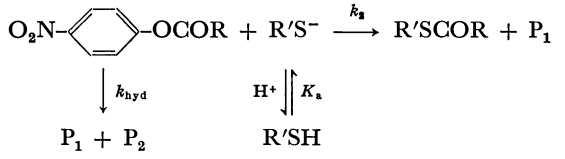

Scheme 2.

The true second-order rate constant for the below-CMC region was determined by the aid of Eq. 3, where k_2' is the apparent second-order rate constant at a given pH; $k_2'=k_1/[R'SH]_T$. A plot of $1/k_2'$ against $[H^+]$ is shown in Fig. 3 for the PNPL–AM·Cys-1 system.

$$\frac{1}{k_2'} = \frac{1}{k_2} + \frac{[H^+]}{k_2 K_a^{app}} \quad (3)$$

The k_2 values thus obtained are summarized in Table 2. The reactivity of the thiolate anion of the surfactants

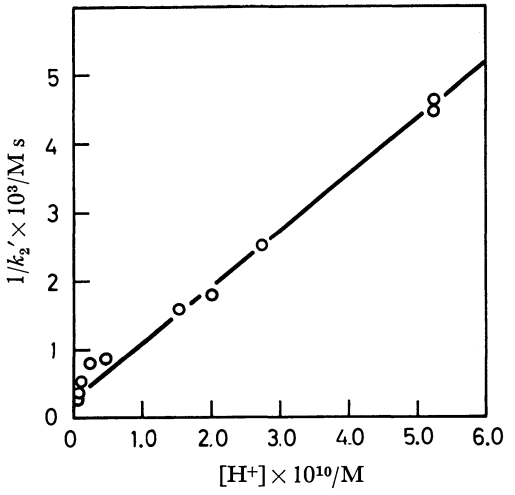

Fig. 3. A plot of $1/k_2'$ *vs.* $[H^+]$ for the deacylation of *p*-nitrophenyl dodecanoate as catalyzed by AM·Cys-1 in 10.8%(v/v) ethanol–1.0%(v/v) dioxane–water at 30.0±0.1 °C and μ 0.10 (KCl). Initial concentrations: AM·Cys-1, 8.20×10^{-5} M; PNPL, 0.984×10^{-5} M.

on a carboxylic ester which bears a long alkyl chain (PNPL) in the aqueous phase is remarkably larger than that of the hydroxide ion as seen in Table 2, but not so on PNPA. The result also indicates that the catalytic activity of AM·Cys-1 in the decomposition of *p*-nitrophenyl dodecanoate is greater than that of AM·Cys-2 by 3.3 fold. A carboxylate anion as the surfactant-head would destabilize the anionic tetrahedral intermediate formed from the thiolate anion and the substrate in a manner as observed for the paracyclophane catalysis.[9] Therefore, the distance between the carboxyl group and the mercapto group in the surfactant molecules must control the reactivity toward ester substrates. The difference in reactivity between AM·Cys-1 and -2 would be attributed to the greater hydrophobic interaction of the former with PNPL.

N-Hexadecyl-N^{α}-glutaryl-*S*-benzyl-L-cysteinamide [AM·Cys(Bzl)-1], in which the mercapto group is protected with a benzyl group, did not show any meaningful effect on the hydrolysis of PNPL below its CMC. On the other hand, AM·Cys(Bzl)-1 retarded the alkaline hydrolysis above its CMC. The result indicates that the anionic micelle may incorporate PNPL into its hydrophobic core and the ester bond of PNPL is masked from the hydroxide attack. Anionic micelles of sodium dodecanoate were found to behave similarly for the hydrolysis of several *p*-nitrophenyl esters as reported recently by Menger *et al.*[10] Thiol catalysts bearing a long alkyl chain such as AM·Cys-1, -2, and 1-dodecanethiol (C_{12}-SH) show catalytic activity in the decomposition of PNPL, but smaller thiols such as glutathione (GSH) and 2-mercaptoethanol give out little catalytic activity (Table 2). These smaller thiols, however, catalyzed the decomposition of *p*-nitrophenyl acetate (PNPA) by using them in a large amount. AM·Cys-1, -2, and C_{12}-SH were not used in higher concentrations for the reaction with PNPA because of their limited solubility. As we clarified previously,[11] the reactivity of monomeric esters decreases with increasing the alkyl chain length due to their self-coiling behavior so as to mask the ester bond from the hydroxide attack. Thus, the hydrophobic interaction between the catalyst and the substrate may cause not only the access of both reactants (proximity effect) but also the decoiling of the alkyl chain of PNPL.

Both AM·Cys-1 and -2 showed a marked catalytic activity in the deacylation of PNPL at pH 9.30 below

Table 3. Relative catalytic activity of AM·Cys-1 and -2 for the deacylation of *p*-nitrophenyl carboxylates[a]

Substrate R[b]	pH 9.30			pH 12.00		
	$k_{hyd} \times 10^5$/s^{-1}	k_{rel}[c] AM·Cys-1	k_{rel}[c] AM·Cys-2	$k_{hyd} \times 10^4$/s^{-1}	k_{rel}[c] AM·Cys-1	k_{rel}[c] AM·Cys-2
CH_3–	72.2	1	1			
$CH_3(CH_2)_4$–	32.0	9.8	4.4	587	3.0	1.9
$CH_3(CH_2)_8$–	5.23	575	199	65.7	43.8	19.9
$CH_3(CH_2)_{10}$–	1.82	1509	441	8.08	267	138
$CH_3(CH_2)_{14}$–	0.50	2397	801	0.88	1432	292
	11.3	13.9	5.2			
	13.6	11.4	3.6			
	1.75	13.0	5.7			
	140		3.5			
	530	18.0	6.6			

a) In 10.8%(v/v) ethanol–1.0%(v/v) dioxane–water at 30.0±0.1 °C and μ 0.10 (KCl). Initial concentrations: substrate, $0.984—1.00 \times 10^{-5}$ M; AM·Cys-1 and -2, 7.90×10^{-5} M. b) R for *p*-$NO_2C_6H_4OC(O)$R. c) $k_{rel} = k_{obsd}/k_{hyd}$: k_{obsd}, apparent first-order rate constant; k_{hyd}, hydrolysis rate constant in the absence of a catalyst.

their CMC's. These surfactants catalyzed not only the deacylation of *p*-nitrophenyl carboxylates bearing a long alkyl chain but also that of *p*-nitrophenyl esters of cyclohexane derivatives and *N*-benzyloxycarbonylglutarate as shown in Table 3. The present thiol catalysts exercise a significant activity toward hydrophobic substrates in their deacylation and the profound efficiency is observed selectively in the decomposition of esters bearing a longer alkyl chain.

Table 4. Effects of metal ions in the surfactant-catalyzed deacylation of *p*-nitrophenyl dodecanoate[a)]

Metal ion/M	$V_0 \times 10^8$/M s^{-1} [b)]	
	AM·Cys-1	AM·Cys-2
None	10.9	8.27
Cu^{2+} : 1.02×10^{-6}	10.4	7.20
1.02×10^{-5}	6.85	4.68
1.02×10^{-4}	0	0
Zn^{2+} : 1.01×10^{-6}	10.6	7.55
1.01×10^{-5}	7.38	6.60
1.01×10^{-4}	0	0
Mg^{2+}: 1.01×10^{-6}	10.9	8.27
1.01×10^{-5}	10.9	8.27
1.01×10^{-4}	10.9	8.27

a) In 10.8%(v/v) ethanol–1.0%(v/v) dioxane–water at 30.0±0.1 °C, pH 9.27, and μ 0.10 (KCl). Initial concentrations: AM·Cys-1, 3.33×10^{-4} M; AM·Cys-2, 3.92×10^{-4} M; PNPL, 0.984×10^{-5} M. All the metal ions were used as nitrates. b) V_0 stands for the initial velocity of reaction.

Effects of Metal Ions on the Catalysis. It is expected that an appropriate metal ion would show somewhat a unique effect on the reactivity of surfactants which involve effective donor groups. The metal ions used here (Cu^{2+}, Zn^{2+}, and Mg^{2+}) did not give out any effect on the alkaline hydrolysis of PNPL, while the surfactant-catalyzed deacylation of the ester was markedly retarded by Cu^{2+} and Zn^{2+} as shown in Table 4. Such a behavior of the synthetic surfactants bears a resemblance to those of thiol proteases. Thiol proteases such as papain are extremely sensitive to the presence of heavy metal ions, and metal ions of groups IB and IIB such as Cu^{2+}, Zn^{2+}, and Hg^{2+} cause reversible inhibition of the enzyme catalysis. The inhibition seems to occur through formation of the thiolate complexes. Since the thiolate anion is one of the soft bases, the hard acid (Mg^{2+}) does not form the corresponding complex and consequently show no effect on the surfactant-catalyzed reaction.

Evaluation of True pK_a *Values for the Mercapto Group in Micellar Phase.* In order to clarify the reason why the catalytic activity of the surfactants markedly decreases above CMC for the deacylation of *p*-nitrophenyl esters, we evaluated true pK_a values for the mercapto group in micellar phase from the pK_a-concentration profiles. The pK_a- and *n*-values determined by Eq. 2 were plotted against the concentration of the surfactants as shown in Fig. 4. The pK_a-value of each surfactant increases as the concentration increases

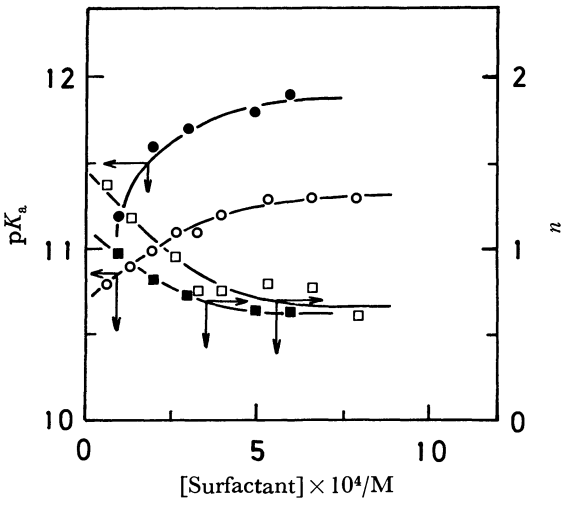

Fig. 4. Plots of pK_a- and *n*-values against concentration of the anionic surfactants. pK_a- and *n*-values were evaluated by the modified Henderson-Hasselbalch equation. For AM·Cys-1: ○, pK_a; □, *n*. For AM·Cys-2: ●, pK_a; ■, *n*.

to a certain extent which is considered to be the true pK_a in micellar phase: AM·Cys-1, 11.3; AM·Cys-2, 11.9. These values are larger than those for the corresponding monomeric surfactants. On the other hand, the *n*-value of each surfactant decreases as the surfactant concentration increases and levels off beyond a certain range: AM·Cys-1, 0.58; AM·Cys-2, 0.56. pK_a-Values are generally affected by electrostatic and hydrophobic fields. The result suggests that the electrostatic field effect overcomes the hydrophobic effect for the present surfactant systems since the evaluated pK_a-value for AM·Cys-2 is larger than that for AM·Cys-1 by 0.6 pK_a unit. The α-values for AM·Cys-1 and -2 are 3.57×10^{-4} and 2.30×10^{-5}, respectively, at pH 9.30. As a whole, the diminished reactivity observed for the micellar systems of AM·Cys-1 and -2 is primarily attributed to the decrease in pK_a of the mercapto group. The modified Henderson-Hasselbalch equation was applied to a micellar system of hexadecyl(imidazolylmethyl)-dimethylammonium chloride and a low *n*-value (0.8) was obtained.[12)]

Effects of CTAB Micelle on the Catalysis. The rate constant (k_{obsd}) for the deacylation of PNPL was measured in several micellar systems. Sodium dodecyl sulfate and α-hydro-ω-dodecyloxytricosa(oxyethylene) did not appreciably alter the rate relative to that for the alkaline hydrolysis, while a greater rate was observed in the presence of CTAB. Figure 5 shows the rate-concentration profiles for the decomposition of PNPA and *p*-nitrophenyl hexanoate (PNPH) as catalyzed by mixed CTAB–AM·Cys-1 micelle. A pronounced catalytic effect was observed with the mixed micelle and the profile is typical for the micellar catalysis. The reaction pathway for the decomposition of *p*-nitrophenyl esters as catalyzed by the mixed micelle is given by Scheme 3, where S stands for an ester substrate (PNPA or PNPH), CM for the mixed micelle formed with CTAB and a thiol surfactant, CM·S for a complex formed with the mixed micelle and a substrate, and P

Table 5. Kinetic parameters for the deacylation of *p*-nitrophenyl dodecanoate and acetate catalyzed by mixed micelles[a)]

Catalyst	[Catalyst]/[CTAB]	PNPH			PNPA		
		$k_m \times 10^2$ / s^{-1}	K_b / M^{-1}	k_m/k_{hyd}	$k_m \times 10^2$ / s^{-1}	K_b / M^{-1}	k_m/k_{hyd}
AM·Cys-1	1/20	4.41	885	3080	4.75	33.3	3320
AM·Cys-2	1/16	1.95	599	1360	0.874	71.4	611
	1/20	1.59	633	1110	0.526	117	368
C_{12}-SH	1/20	0.168	667	117	0.557	15.5	390

a) In 10.8%(v/v) ethanol–1.0%(v/v) dioxane–water at 30.0±0.1 °C, pH 7.60, and μ 0.10 (KCl). Apparent first-order rate constants for the hydrolyses of PNPH and PNPA in the absence of the mixed micelles are 1.43×10^{-5} s^{-1} at pH 7.60.

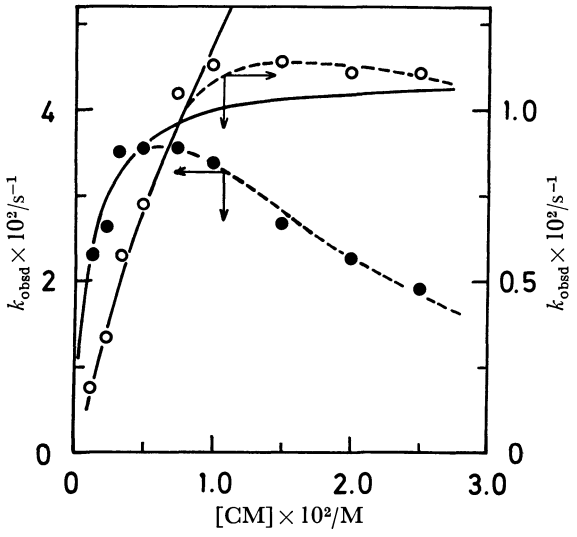

Fig. 5. Rate-concentration profiles for the deacylation of *p*-nitrophenyl hexanoate (●) and acetate (○) as catalyzed by CTAB–AM·Cys-1 mixed micelle in 10.8 %(v/v) ethanol–1.0%(v/v) dioxane–water at 30.0± 0.1 °C, pH 7.63, and μ 0.10 (KCl). Initial concentrations: PNPA, 0.989×10^{-5} M; PNPH, 0.983×10^{-5} M. [CM]=[CTAB]+[AM·Cys-1]; [AM·Cys-1]/[CTAB] =1/20. Solid lines are the theoretical curves calculated by Eq. 5. The maximum rate constants for the hydrolysis of PNPA and PNPH in the CTAB micelle (0.125—2.50×10^{-2} M) are 3.75×10^{-5} and 2.73×10^{-5} s^{-1}, respectively, under the same kinetic conditions.

and P′ for reaction products; k_{hyd} and k_m refer to rate constants for product formation in the bulk phase and in the mixed micelle, respectively; K_b represents a binding constant for formation of the micelle-substrate complex.

$$\mathrm{CM} + \mathrm{S} \overset{K_b}{\rightleftharpoons} \mathrm{CM{\cdot}S} \overset{k_m}{\longrightarrow} \mathrm{P}$$
$$\Big\downarrow k_{hyd}$$
$$\mathrm{P'}$$

Scheme 3.

Under the present experimental conditions the reaction in the micellar phase resulted in the formation of the acylated micelle and any further reaction was not detected. For [CTAB]>CMC and [CTAB]>[Thiol surfactant]≫[Substrate], the pseudo-first-order rate constant (k_{obsd}) is given by Eq. 4[13] on the basis of Scheme 3.

$$k_{obsd} = \frac{k_{hyd} + k_m K_b[\mathrm{CM}]}{1 + K_b[\mathrm{CM}]} \quad (4)$$

Rearrangement gives Eq. 5.

$$\frac{1}{k_{obsd} - k_{hyd}} = \frac{1}{k_m - k_{hyd}} + \frac{1}{(k_m - k_{hyd})K_b[\mathrm{CM}]} \quad (5)$$

where [CM] refers to the sum of the initial concentrations of CTAB and a thiol surfactant. A plot of $1/(k_{obsd}-k_{hyd})$ *vs.* 1/[CM] allows to evaluate k_m and K_b. The kinetic parameters thus evaluated are summarized in Table 5 for the reactions catalyzed by mixed micelles; CTAB–AM·Cys-1, CTAB–AM·Cys-2, and CTAB–C_{12}-SH.

The binding constant (K_b) for the mixed micelles with PNPA changes depending upon the nature of the thiol surfactants, whereas K_b is constant with PNPH regardless of the surfactants. This seems to suggest that PNPH is incorporated into the hydrophobic core of the mixed micelles while PNPA into the hydrophilic Stern layer. The value of k_m stands for the acyl transfer from the substrates to the mercapto group of the thiol surfactants, and the hydrolysis rate (k_{CM}^{OH}) for the esters with the concentrated hydroxide ion in the Stern layer of the mixed micelles** is negligibly small relative to the acyl transfer rate for a neutral pH region. The most effective micellar catalyst was constructed with AM·Cys-1 and CTAB and the k_m value for the deacylation of PNPH is 3080 times as large as the corresponding k_{hyd} value as shown in Table 5. Some plausible explanations for the difference in reactivity among the mercapto groups of AM·Cys-1, -2, and C_{12}-SH placed in micellar CTAB are as follows.

(1) If the pK_a value for the mercapto group of AM·Cys-1 in micellar CTAB decreases more than those for AM·Cys-2 and C_{12}-SH in micellar CTAB, the difference in catalytic activity is attributed to variation in concentration of the active thiolate anion. This may not be the case since the mercapto group of AM·Cys-1 must be located in a more hydrophobic region than those of AM·Cys-2 and C_{12}-SH. In other words, the mercapto groups of AM·Cys-2 and C_{12}-SH are most likely

** The k_{CM}^{OH} values were evaluated from the hydrolysis of *p*-nitrophenyl carboxylates as catalyzed by micellar CTAB under the same conditions.

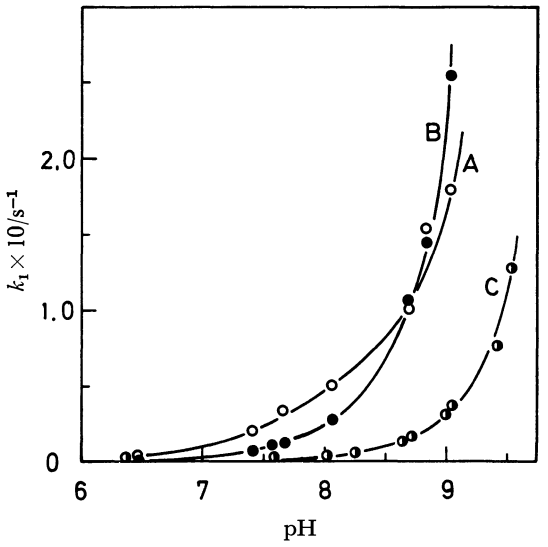

Fig. 6. pH-Rate profiles for the deacylation of PNPH as catalyzed by CTAB–AM·Cys-1 (A), CTAB–AM·Cys-2 (B), and CTAB–C_{12}-SH (C) mixed micelles in 10.8%(v/v) ethanol–1.0%(v/v) dioxane–water at 30.0±0.1 °C and μ 0.10 (KCl): $k_1=k_{obsd}-k_{CTAB}$; k_{CTAB}, apparent first-order rate constant for the hydrolysis of PNPH as catalyzed by hexadecyltrimethylammonium bromide. Initial concentrations: PNPH, 0.983×10^{-5} M; [CM]=[CTAB]+[Thiol surfactant], 0.50×10^{-2} M; [Thiol surfactant]/[CTAB]=1/20.

placed in the cationic Stern layer and, therefore, the pK_a values for these mercapto groups are expected to decrease more than that for the mercapto group of AM·Cys-1 in micellar CTAB. Figure 6 shows the pH-rate profiles for the deacylation of PNPH as catalyzed by the mixed micelles. These profiles indicate that the pK_a value for each thiol surfactant in the mixed micelle decreases by 1—2 pK_a unit relative to that for each surfactant monomer, and the greater reactivity of the thiol surfactants in mixed micelles is partly due to the pK_a effect. The pK_a value for AM·Cys-1 is almost comparable to that for AM·Cys-2 and *smaller than that for C_{12}-SH.*

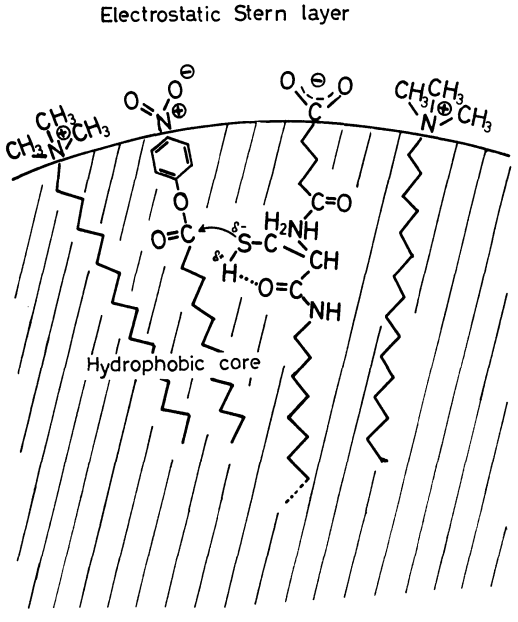

Fig. 7. Schematic representation of a plausible reaction mechanism for the deacylation of PNPH by CTAB–AM·Cys-1.

(2) The orientation of the ester bond of PNPH would be so arranged that an attack of the mercapto group on it is facilitated in the hydrophobic core.

(3) The intramolecular hydrogen bonding between the thiol and peptide-carbonyl groups as shown in Fig. 7 for the AM·Cys-1–CTAB system would enhance the nucleophilicity of the mercapto group in the effective hydrophobic core. Such development of a negative charge on the sulfur atom of the mercapto group in the hydrophobic core would be facilitated by the electrostatic field effect provided by the cationic micelle head in the transition state of acylation. Meanwhile, the mercapto groups of AM·Cys-2 and C_{12}-SH in the mixed micelle would not form an effective hydrogen bond since these may be placed in the more hydrophilic region. The reaction mechanism is analogous to that for papain catalysis proposed by Lowe[14] in which the nucleophilicity of a catalytic mercapto group is enhanced by its hydrogen bonding with an imidazolyl group.

Conclusion. The reactivity of mercapto groups drastically changes upon variation of their micro-environment. An electrostatic field provided by the Stern layer of an anionic micelle tends to increase pK_a of a mercapto group placed in such a micelle, so that the mercapto group is masked to reduce its reactivity in a neutral pH region against an ester substrate. However, pK_a of a mercapto group decreases when it is placed in a cationic micelle due to the effective electrostatic field effect provided by cationic heads. Furthermore, the nucleophilicity of the mercapto group placed in a hydrophobic core is enhanced by the intramolecular hydrogen bonding (Fig. 7) as well as by the electrostatic field effect transmitted into the hydrophobic core. These effects were demonstrated here with the mixed micelle composed of CTAB and AM·Cys-1 for the deacylation of ester substrates. The present results suggest that there are two kinds of mercapto groups; masked and super-reactive ones depending on their micro-environment and should be noted in connection with enzyme catalysis. In order to make a mercapto group more active in the hydrophobic region of micelles, it is required to introduce the second functional group at the juxtaposition of the mercapto group so that its nucleophilicity is much enhanced.

References

1) G. Lowe, *Tetrahedron*, **32**, 291 (1976).

2) (a) J. W. Ogilvie, J. T. Tildon, and B. S. Strauch, *Biochemistry*, **3**, 754 (1964); (b) J. R. Whitaker, *J. Am. Chem. Soc.*, **84**, 1900 (1962); (c) A. Williams, E. C. Lucas, and A. R. Rimmer, *J. Chem. Soc., Perkin Trans. 2*, **1972**, 621; (d) A. Williams, E. C. Lucas, and K. T. Douglas, *J. Chem. Soc., Perkin Trans. 2*, **1972**, 1493.

3) (a) P. Heitmann, *Eur. J. Biochem.*, **5**, 305 (1968); (b) W. Tagaki, T. Amada, Y. Yamashita, and Y. Yano, *J. Chem. Soc., Chem. Commun.*, **1972**, 1131.

4) S. Shinkai and T. Kunitake, *Bull. Chem. Soc. Jpn.*, **49**, 3219 (1976).
5) R. A. Moss, R. C. Nahas, and T. J. Lukas, *Tetrahedron Lett.*, **1978**, 507.
6) Y. Murakami, Y. Aoyama, M. Kida, and A. Nakano, *Bull. Chem. Soc. Jpn.*, **50**, 3365 (1977).
7) P. Heitmann, *Eur. J. Biochem.*, **3**, 346 (1968).
8) G. L. Ellman, *Arch. Biochem. Biophys.*, **82**, 70 (1959).
9) Y. Murakami, Y. Aoyama, and K. Dobashi, *J. Chem. Soc., Perkin Trans. 2*, **1977**, 24.
10) F. M. Menger and C. E. Portnoy, *J. Am. Chem. Soc.*, **89**, 4698 (1967).
11) Y. Murakami, Y. Aoyama, and M. Kida, *J. Chem. Soc., Perkin Trans. 2*, **1977**, 1947.
12) U. Tonellato, *J. Chem. Soc., Perkin Trans. 2*, **1976**, 771.
13) E. J. Fendler and J. H. Fendler, "Catalysis in Micellar and Macromolecular Systems," Academic Press, New York, N. Y. (1975), p. 88.
14) G. Lowe, *Phil. Trans. Roy. Soc. London, Ser. A.* **257**, 237 (1970).

^{11}B-NMR Study of the Complex Formation of Borate with Catechol and L-Dopa

Kazuo YOSHINO,* Masahiro KOTAKA, Makoto OKAMOTO, and Hidetake KAKIHANA

Research Laboratory for Nuclear Reactors, Tokyo Institute of Technology, Ookayama, Meguro-ku, Tokyo 152

(Received January 30, 1979)

In the solution of catechol and borax at pH 11, the equilibria between catechol and the monomeric borate anion to form the 1:1 and 2:1 (catechol: boron) anionic complexes have been demonstrated by the existence of ^{11}B-NMR signals for the two complexes and the monomeric borate anion. In the solution of L-dopa and borax at pH 11, however, the signal for the 2:1 anionic complex was not observed, though it was observed below pH 7. By the ^{11}B-NMR spectra at pH 6.5, the complex formation constants, log K_1 and log K_2, have been estimated as 3.9 and 4.4 for catechol, and as 4.3 and 5.0 for L-dopa, respectively.

The neutron-capture therapy requires a boron-10-containing compound which concentrates selectively in cancer tissue and does not in normal tissue in order to collect boron-10 selectively in the malignant tumor.[1-3] L-Dopa is one of the precursors of melanine, which is produced in a great quantity in malignant melanoma. Planning to carry the boron-10 into melanoma using L-dopa as a carrier, the compound "dopaborate," which has one boron atom per molecule, has been synthesized. The present authors have investigated the structure and reactivety of this compound in an aqueous solution by means of the UV spectroscopic method.[4] It was thus recognized that the solution of "dopaborate" was just the same as that of a mixture of 1:1 L-dopa and boric acid at about pH 8.5, and in an aqueous solution the catechol site of L-dopa coordinates to the monomeric borate anion.

In the equilibrium system of catechol and the monomeric borate anion, the equlibria may be represented by the following equations (Equilibria 1—3). The equilibrium constants for these equilibria can be represented by Eq. 6—8. Since catechol itself is an acid, the acidic strength of which is comparable to that of boric acid, its dissociation reactions must also be taken into consideration (Equilibria 4 and 5).

$$B(OH)_3 + H_2O \overset{K_a}{\rightleftharpoons} B(OH)_4^- + H^+ \quad (1)$$
(BH) (B$^-$)

$$B(OH)_4^- + \text{(C) } \mathbf{1} \overset{K_1}{\rightleftharpoons} \text{(BC}^-\text{) } \mathbf{2} + 2H_2O \quad (2)$$

$$B(OH)_4^- + 2\,\text{(C) } \mathbf{1} \overset{K_2}{\rightleftharpoons} \text{(BC}_2^-\text{) } \mathbf{3} + 4H_2O \quad (3)$$

$$\text{(C) } \mathbf{1} \rightleftharpoons \text{(C}^-\text{)} + H^+ \quad (4)$$

$$\text{(C}^-\text{)} \rightleftharpoons \text{(C}^{2-}\text{)} + H^+ \quad (5)$$

$$K_a = [B^-][H^+]/[BH] \quad (6)$$

$$K_1 = [BC^-]/[B^-][C] \quad (7)$$

$$K_2 = [BC_2^-]/[B^-][C]^2 \quad (8)$$

Two methods have been developed to identify the equilibrium system of catechol and the monomeric borate anion. One is the potentiometric method,[5-8] and the other is the UV spectroscopic method.[9] In the case of potentiometry, the evidence concerning the complex formation is largely indirect. In the case of the UV method, though, since the absorption spectrum of the catechol–borate complex, (**2** or **3**), is different from that of catechol (**1**), the method offers direct evidence concerning the complex formation; however, since the absorption spectrum of the 1:1 catechol–borate complex (**2**) seems to be the same as that of the 2:1 catechol–borate complex (**3**), this method does not give directly the concentrations of the two complexes.

In many equilibrium systems of diol and the monomeric borate anion, ^{11}B-NMR spectroscopy demonstrated that the 2:1 complex has a chemical shift different from that of the 1:1 complex, and the ^{11}B-NMR spectra give the concentrations of the each boron species directly, which makes it possible to calculate the equilibrium constants.[10,11] Therefore, we have used ^{11}B-NMR spectroscopy in order to elucidate the nature of the equilibria of the catechol–borate and L-dopa–borate systems.

Experimental

Preparation of Solutions for ^{11}B-NMR Studies. Twice-distilled deionized water was used throughout the experiments. Dissolving the weighed amount of borax into water, a weighed amount of L-dopa (or catechol) was slowly added to the solution. Thereby the pH of the solution was kept higher than 8 by adding sodium hydroxide. After the L-dopa (or catechol) had been completely dissolved, the pH of the solution was adjusted to the required value with sodium hydroxide or hydrochloric acid, and the solution was diluted with water to 50 ml. These preparations were carried out in an N_2 atmosphere, because both L-dopa and catechol are oxidized by atmospheric oxygen, especially in an alkaline solution. The 2—4 ml aliquots were put into 8 mmϕ NMR quartz probes and sealed in an N_2 atmosphere to avoid oxidation; these probes were then placed into 10 mmϕ quartz probes which had D_2O as a lock.

^{11}B-NMR Measurements. The FT-NMR spectrometer used was JEOL FX-100. The operation were performed at

Table 1. ^{11}B-NMR spectroscopic data

Diol	Diol-Boron ratio	pH	σ_4	σ_3	σ_2	σ_1	A_4	A_3	A_2	A_1
Catechol	0.5:1	11	—	—	8.9(27)	3.5(17)	—	—	51	49
	1:1	11	—	—	9.0(26)	3.4(45)	—	—	91	9
	2:1	11	—	14.5	9.0(28)	—	—	5	95	—
	1:1*	6.5	20.6(73)	14.4(20)	9.0(23)	—	34	9	57	—
L-Dopa	0.5:1	11	—	—	9.0(50)	3.4(12)	—	—	48	52
	1:1	11	—	—	9.0(57)	3.3(43)	—	—	87	13
	2:1	11	—	—	9.1(74)	—	—	—	100	—
	1:1	12	—	—	9.0(55)	3.1(24)	—	—	79	21
	1:1	10	—	—	9.1(62)	—	—	—	100	—
	1:1	9	—	—	9.2(64)	—	—	—	100	—
	1:1	8	—	13.7(sh)	9.1(63)	—	—	—	100	—
	1:1	7	19.8	14.5	9.1(67)	—	—	—	—	—
	1:1*	6.5	20.4	14.7	9.1(56)	—	28	12	60	—

The total concentration of boron is 0.5 mol dm^{-3}, except in the cases marked with *, which are 0.25 mol dm^{-3}. σ_n, the downfield chemical shift (in ppm) from sodium tetrafluoroborate; the width at half-height ($W_{0.5}$) is shown in brackets in Hz in cases where the values were obtained. A_n, the relative area of the signal at σ_n as % of the total area of the signals. In cases where the signals overlapped, the relative areas of the signals were obtained by computer simulation.[16]

31.96 MHz. The probe temperature was about 27 °C. The number of pulses (the repetition time is 1.0 s) was 100 except in the case of the 0.25 mol dm^{-3} boron concentration in which 400 pulses were needed. The solution of sodium tetrafluoroborate was used as an external reference.

Results and Discussion

The experimental conditions and the obtained data are summarized in Table 1.

A borax solution has only one ^{11}B-NMR signal in all the pH region, but the chemical shift of this signal changes from 20.6 ppm (pH 6.5) to 3.1 ppm (pH 12) with the increase in pH; these values are assigned to boric acid and the monomeric borate anion respectively.[10,12] The appearance of only one signal in the pH region in which both monomeric species exist indicates that Equilibrium 1 is rapidly interconverting.[10] Therefore, if any other boron species does not exist in this pH region, the chemical shift of the signal may be ascribed to the relative concentration of boric acid and the borate anion, and the line-width (the width at the half height) of the signal would be intermediate between those of the monomeric species. Figure 1 shows the ^{11}B-NMR spectra of the solution of borax at pH 7, 9, and 11. The boron concentration of each solution was 0.5 mol dm^{-3}. The signal at pH 11 is assigned to the almost monomeric borate anion. Since the signal at pH 7 has a shoulder peak, and since the line-width of the signal at pH 9 is broader than that of the signal at pH 7 and 11, there may be polyborates.[13,14]

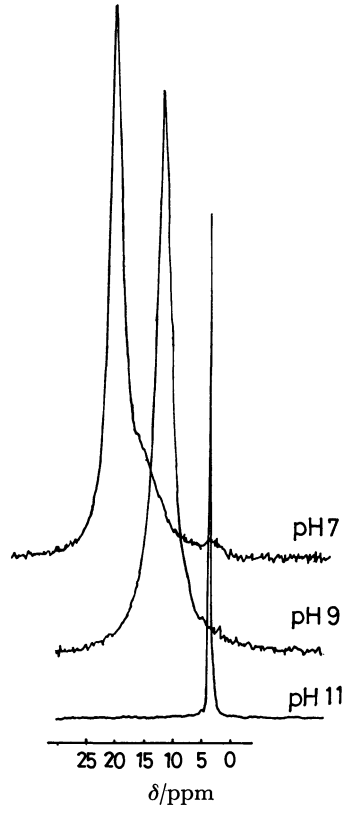

Fig. 1. ^{11}B-NMR spectra of borax solutions at pH 7, 9, and 11. The boron concentration of the solutions is 0.5 M (1 M=1 mol dm^{-3}). The reference signal of sodium tetrafluoroborate at δ 0.0 is not shown.

^{11}B-NMR Spectroscopic Examination at pH *11.*

The spectra of catechol–borax solutions (pH 11) at several molar ratios are illustrated in Fig. 2. The signal at 3.4 ppm corresponds exactly to that of the monomeric borate anion. The change in the signal intensity with the increase in the catechol concentration (the boron concentration is kept at 0.5 mol dm^{-3}) demonstrates that the low-field signals at 9.0 and 14.5 ppm can be assigned to the 1:1 (**1**) and 2:1 (**2**) complexes respectively. The line-width of the 1:1 catechol–borate complex has nearly the same value (27 Hz) in the spectra of three different molar ratios of catechol–boron.

Figure 3 shows the spectra of L-dopa–borax solutions (pH 11) at several molar ratios. The signal at 9.0 ppm,

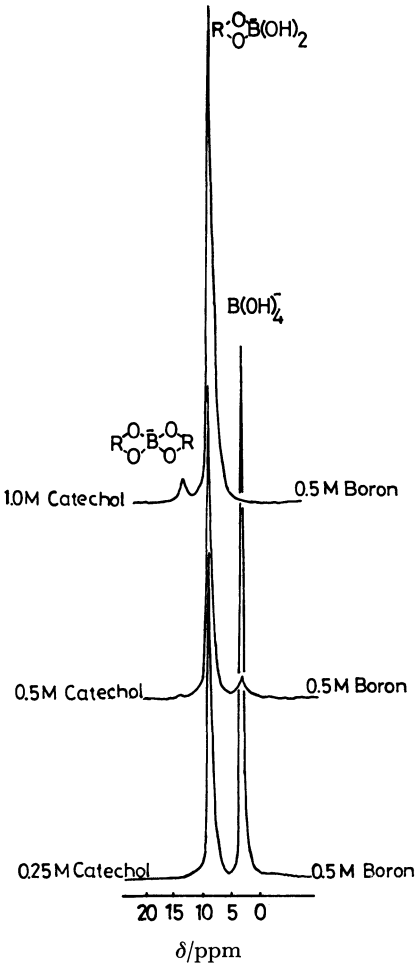

Fig. 2. ^{11}B-NMR spectra of catechol–borax solutions at 2: 1, 1: 1, and 0.5: 1 molar ratios of catechol and boron. In the solutions, the initial concentration of boron is 0.5 M (1 M=1 mol dm^{-3}) and pH is 11. The reference signal of sodium tetrafluoroborate at δ 0.0 is not shown.

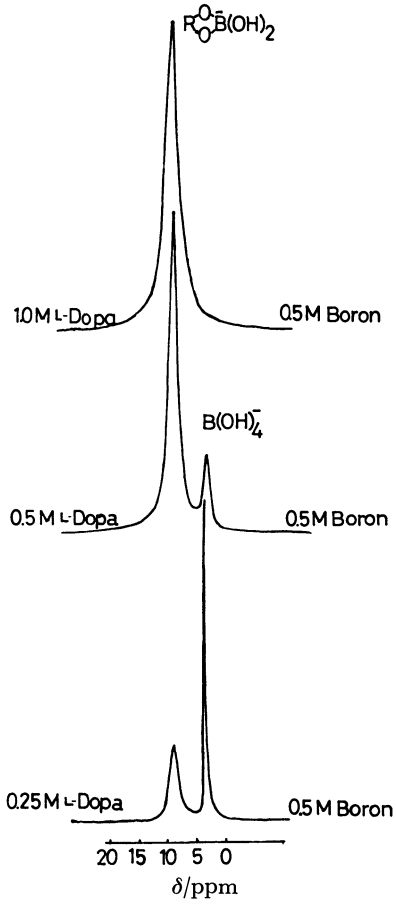

Fig. 3. ^{11}B-NMR spectra of L-dopa–borax solutions at 2: 1, 1: 1, and 0.5: 1 molar ratios of L-dopa and boron. In the solutions, the initial concentration of boron is kept 0.5 M (1 M=1 mol dm^{-3}) and pH is 11. The reference signal of sodium tetrafluoroborate at δ 0.0 is not shown.

which seems to be that of the 1: 1 L-dopa–borate complex, is not so sharp as that of catechol–borate complex, and the broadening of this signal with the increase in the molar ratio of L-dopa–boron is remarkable (the boron concentration is kept at 0.5 mol dm^{-3}). The signal of the 2: 1 L-dopa–borate complex could not be observed separately, not even in the L-dopa–borax solution with a L-dopa–boron ratio of 2: 1.

^{11}B-NMR Spectroscopic Examination for the 1: 1 L-Dopa–Boron Solution at Various pH *Values.* Figures 4 and 5 show the obtained spectra of the 1: 1 L-dopa–boron solutions at pH 12—pH 6.5. The boron concentration is kept at 0.5 mol dm^{-3}, except in the case with pH 6.5, in which the concentration is 0.25 mol dm^{-3}. In the case of pH 12—pH 9, the signal of the monomeric borate anion became smaller and at last disappeared at pH 10 with a decrease in the pH. There may be two reasons for this. One of these is that, in the dissociation equilibria in the catechol part of L-dopa, the amount of un-ionized dihydroxy species, which may coordinate with the monomeric borate anion, increases with the decrease in pH and the formation of the 1: 1 L-dopa–borate complex proceeds; as a result, the monomeric borate anion decreases by the corresponding amount. The other possible reason may be explained as follows. With a decrease in the pH, some monomeric borate anions become boric acid or polyborate anions, as was mentioned above, and the signals of these species overlap with that of the 1: 1 complex. The latter explanation is proved by the change in the line-width for the signal at 9.1 ppm. It becomes larger with a decrease in the pH. The constant chemical shift (9.1 ppm) in this pH region, however, makes it clear that most of the boron species is the 1: 1 L-dopa–borate complex. Figure 5 shows that, at pH 7, two signals (at 19.8 and 14.5 ppm) appear in addition to the signal of the 1: 1 complex. These signals are more clearly observed at pH 6.5. The signals at 19.8 (pH 7) and 20.4 (pH 6.5) ppm are ascribed to the free boron species, as is shown in Fig. 1, and that at 14.5 ppm, to the 2: 1 L-dopa–borate complex. The latter assignment is made by comparing this signal with that of the 2: 1 catechol–borate complex at 14.5 ppm, which was observed in Fig. 2. These assignments are also confirmed by a comparison of these spectra with the spectrum of the 1: 1 catechol–boron solution at pH 6.5, which is shown

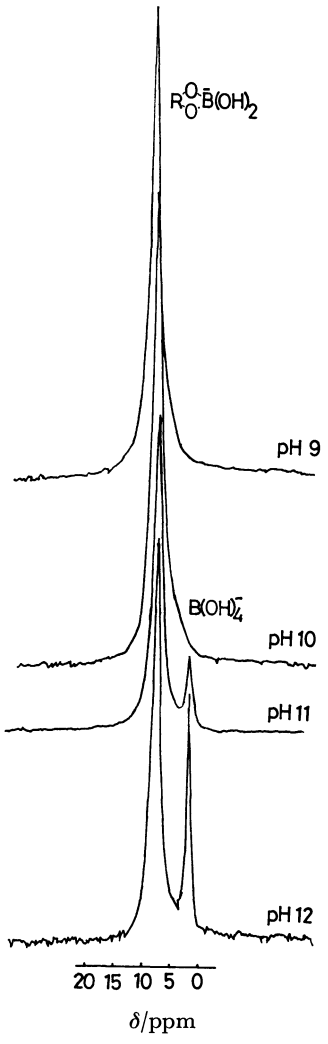

Fig. 4. ^{11}B-NMR spectra of L-dopa–borax solutions at pH 12—pH 9. In the solutions, the ratio of L-dopa and boron is kept 1: 1, and the initial concentration of boron is kept 0.5 M (1 M=1 mol dm^{-3}). The reference signal of sodium tetrafluoroborate at δ 0.0 is not shown.

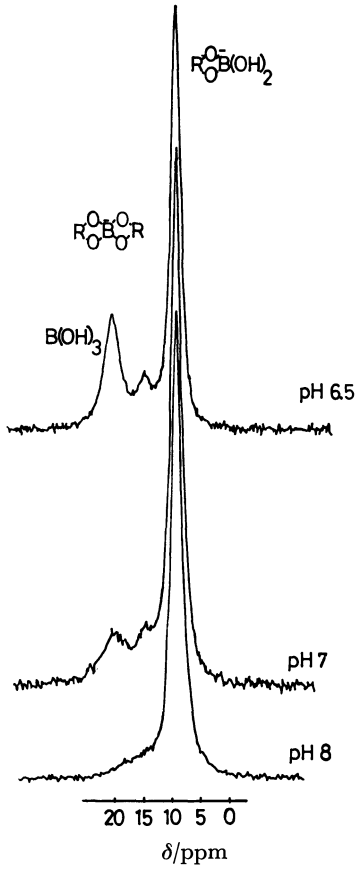

Fig. 5. ^{11}B-NMR spectra of L-dopa–borax solutions at pH 8—pH 6.5. In the solutions, the ratio of L-dopa and boron is kept 1: 1, and the initial concentration of boron is 0.5 M (1 M=1 mol dm^{-3}) except in the case at pH 6.5 in which 0.25 M. The reference signal of sodium tetrafluoroborate at δ 0.0 is not shown.

in Fig. 6 (the boron concentration is 0.25 mol dm^{-3}). The appearance of the 2: 1 L-dopa–borate complex might be explained as follows. As has been mentioned in the introduction, the complex formations may occur between the monomeric borate anion and the un-ionized catechol part of L-dopa. Therefore, under the present experimental conditions, in spite of the same initial concentrations of L-dopa and boron, the concentration of the monomeric borate anion is far less than that of the un-ionized catechol type of L-dopa. Therefore, the equilibrium not only for 1: 1 but also for 2: 1 L-dopa–borate complex formation is shifted to the right.

The Estimation of the Equilibrium Constants for the 1: 1 and 2: 1 Complex Formations. In the case of the catechol–borate complex formation, the equilibria which seem to take place in this experiment have already been summarized in Equilibria 1—5. In the case of L-dopa–borate complex formation, however, the equilibria are much more complicated, because L-dopa has an amino group, the acidic strength of which seems

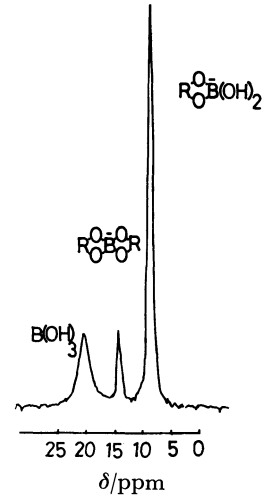

Fig. 6. ^{11}B-NMR spectrum of catechol–borax solution at pH 6.5. The ratio of catechol and boron is 1: 1, and the initial concentration of boron is 0.25 M (1 M =1 mol dm^{-3}). The reference signal of sodium tetrafluoroborate at δ 0.0 is not shown.

to be comparable to that of catechol or boric acid. Therefore, L-dopa has many dissociation equilibria

which must be taken into consideration; the equilibria for L-dopa–borate complex formation may be represented as follows in the experimental pH region:

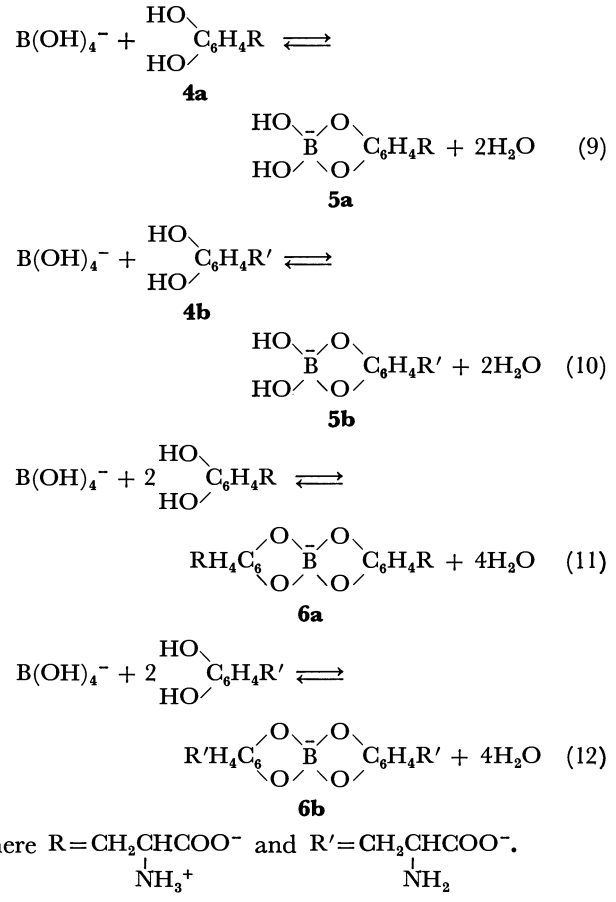

where R=CH_2CHCOO^- (NH_3^+) and R′=CH_2CHCOO^- (NH_2).

In order to estimate the equilibrium constants by using the ^{11}B-NMR spectra, the concentrations of the monomeric borate anion ($B(OH)_4^-$) and un-ionized dihydroxy catechol (**1**) or un-ionized dihydroxy L-dopa (**4a**) and (**4b**) should be obtained. At pH 11, the free boron species is regarded as almost entirely the monomeric borate anion, and its concentration is calculated directly from the signal area of the ^{11}B-NMR spectra. However, the concentration of (**1**) cannot be obtained without using the dissociation constants of Equilibria 4 and 5, and the concentrations of (**4a**) and (**4b**) are hard to obtain, because the dissociation constants of L-dopa, which are needed to calculate the concentrations of (**4a**) and (**4b**), have not yet been determined. On the other hand, at pH 6.5, since free catechol and free L-dopa are regarded as (**1**) and (**4a**) respectively, these concentrations can be obtained from the ^{11}B-NMR spectra and the ionization constant of boric acid (K_a).

Calculation of Equilibrium Constants. *Catechol*: The three signal areas of the ^{11}B-NMR spectrum at pH 6.5 correspond to $[BC^-]$, $[BC_2^-]$, and $[B]+[B^-]$ respectively. The combination of these concentrations with the following equations gives the concentrations of all the species:

$$[B]_0 = [BH] + [B^-] + [BC^-] + [BC_2^-]$$
$$[C]_0 = [C] + [BC^-] + 2[BC_2^-]$$
$$K_a = [B^-][H^+]/[BH]$$

where $[B]_0$ is the initial concentration of boron and $[C]_0$ is the initial concentration of catechol. 9.00 was used for log K_a.[15]

L-*Dopa*: The method is the same as that used in the case of catechol, but in this case [C], $[BC^-]$, and $[BC_2^-]$ correspond to the concentrations of (**4a**), (**5a**), and (**6a**) respectively, and $[C]_0$ is the initial concentration of L-dopa.

Table 2. Comparison of equilibrium constants (K_1 and K_2) calculated from this ^{11}B-NMR study for catechol and L-dopa with the values obtained from other methods

Diol	Method	Temp	log K_1	log K_2	Remarks
Catechol	pH-Change[8]	25 °C	3.97	4.26	
	UV[9]		4.3	—	pH 7.8
	^{11}B-NMR	27 °C	3.9	4.4	pH 6.5
L-Dopa	pH-Change		—	—	
	UV[9]		4.2	—	pH 7.8
	^{11}B-NMR	27 °C	4.3	5.0	pH 6.5

The values thus obtained, log K_1 and log K_2, are shown in Table 2, along with the values of the other methods. The values obtained for catechol are consistent with the values obtained by potentiometry. Among the results obtained, it is found for the first time that the 2:1 L-dopa–borate complex is formed between L-dopa and the monomeric borate anion.

The authors wish to thank Professor Atsuo Nishioka and Dr. Isao Ando of the Tokyo Institute of Technology for their helpful discussion, and also JEOL for measuring the ^{11}B-NMR spectra.

References

1) Y. Mishima, *Pigment Cell.* **1**, 215 (1973).
2) H. Kakihana and K. Yoshino, *Gendai Kagaku*, **71**, 42 (1977).
3) H. Hatanaka, *Shinkei Shinpo*, **22**, 142 (1978).
4) K. Yoshino, H. Kakihana, M. Okamoto, M. Kotaka, and T. Iizuka, 36th National Meeting of the Chemical Society of Japan, Osaka, April 1977, Abstr, No. 3U17.
5) G. L. Roy, A. L. Laferriere, and J. O. Edwards, *J. Inorg. Nucl. Chem.*, **4**, 106 (1957).
6) P. J. Antikainen and A. Kauppila, *Suom. Kemistil. B*, **31**, 255 (1958).
7) J. M. Conner and V. C. Bulgrin, *J. Inorg. Nucl. Chem.*, **29**, 1953 (1967).
8) P. J. Antikainen and I. P. Pitkanen, *Suom. Kemistil. B*, **41**, 65 (1968).
9) K. T. Yasunobu and E. R. Norris, *J. Biol. Chem.*, **227**, 473 (1957).
10) W. G. Henderson, M. J. How, G. R. Kennedy, and E. F. Mooney, *Carbohydr. Res.*, **28**, 1 (1973).
11) G. R. Kennedy and M. J. How., *Carbohydr. Res.*, **28**, 13 (1973).
12) M. J. How, G. R. Kennedy, and E. F. Mooney, *Chem. Commun.*, **1969**, 267.
13) R. K. Mommi and N. H. Nachtrieb, *Inorg. Chem.*, **6**, 1189 (1969).
14) H. D. Smith and R. J. Wiersema, *Inorg. Chem.*, **11**, 1152 (1972).
15) N. Ingri, *Acta Chem. Scand.*, **17**, 573 (1963).
16) Y. Kato, I. Ando, and A. Nishioka, *Kobunshi Ronbunshu*, **32**, 200 (1975).

p-Styrenesulfinic Acid and Its Polymer as Reactants

Hiroyoshi KAMOGAWA,* Hideaki INOUE, Hiromoto FUKUYAMA, and Masato NANASAWA

Department of Applied Chemistry, Yamanashi University, Takeda 4, Kofu, Yamanashi 400

(Received March 15, 1979)

The free-radical aqueous polymerizations of *p*-styrenesulfinates (Na, K, NH_4, $NHEt_3$-salts) provided water-soluble polymers with high molecular weights at low conversions. The polymers contained 62—84% of the sulfinate unit and indicated half-oxidation potentials ranging from 340 to 415 mV. The nucleophilic reactions of the sodium polysulfinate [poly(sulfinic acid)] prepared from cross-linked polystyrene are highly dependent upon the swelling nature of the solvent. The reactions consisting of (A) simple displacements with activated halomethyl groups, (B) reductive additions to quinonoid compounds such as TCNQ and alizarin, and (C) displacements of the activated aromatic nitro groups, *e.g.*, of 2,4,7-trinitrofluorenone have been investigated and the results compared with those of *p*-toluene and *p*-styrenesulfinates. The effect of the solvent on the reaction rate is in the order: DMSO>DMF> HMPA.

Arenesulfinic acids and their salts are of chemical interest since they are mild reductants and take the role of nucleophiles in many reactions.

From the standpoint of obtaining a novel and usefuel polymer reagent, *p*-styrenesulfinic acid and its salts have been synthesized and it has been shown that polymers of high-molecular weights are formed.[1)]

This paper summarizes the results of the investigations conducted on the redox properties of the pendant polymers synthesized from *p*-styrenesulfinates by free-radical polymerizations as well as the nucleophilic reactions of the *p*-styrenesulfinate (sulfinic acid) polymers prepared from polystyrene by means of polymer reactions, together with those of *p*-toluenesulfinate and *p*-styrenesulfinates (sulfinic acids).

The following nucleophilic reactions were examined:

(1) 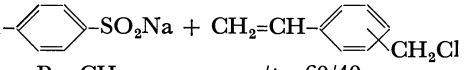

1a: R=CH_3 *m*/*p*=60/40 **2**
1b: R=CH_2=CH–
1c: R=···–CH_2–CH–···

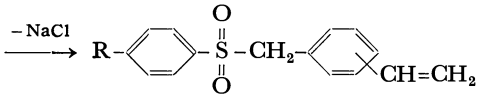

3a: R=CH_3
3b: R=CH_2=CH–
3c: R=···–CH_2–CH–···

(2) **1a, c** + $ClCH_2COOCH{=}CH_2$ **4**

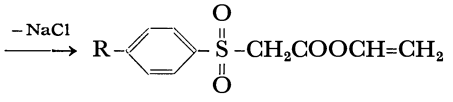

5a: R=CH_3
5c: R=···–CH_2–CH–···

(3) **1a, c** + 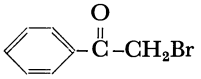 **5**

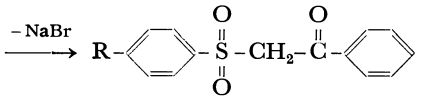

7a: R=CH_3
7c: R=···–CH_2–CH–···

(4) 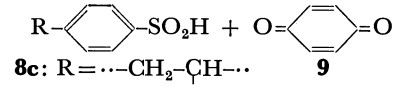

8c: R=···–CH_2–CH–··· **9**

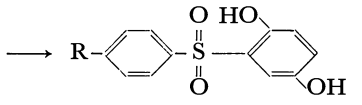

10c: R=···–CH_2–CH–···

(5) **1a—c** + 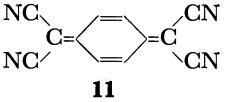 **11**

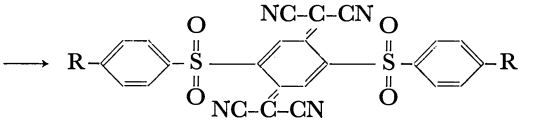

12a: R=CH_3
12b: R=CH_2=CH–
12c: R=···–CH_2–CH–···

(6) **1c** + 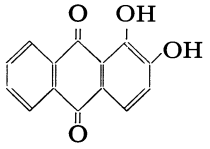 **13**

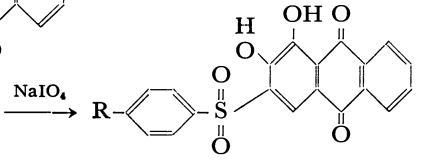

14c: R=···–CH_2–CH–···

(7) **1a, c** + 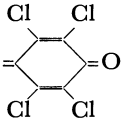 **15**

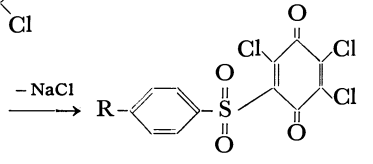

16a: R=CH_3
16c: R=···–CH_2–CH–···

(8) **1c** + 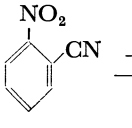 **17**

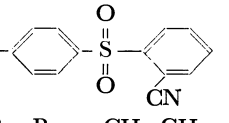

18c: R=···–CH_2–CH–···

(9) **1a—c** + 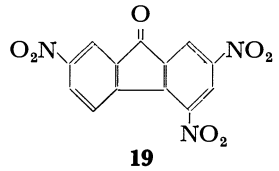

19

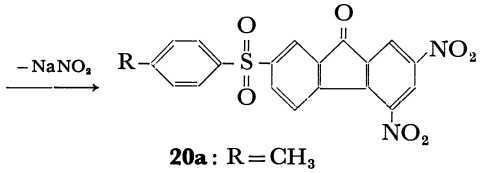

20a: R=CH_3
20b: R=CH_2=CH–
20c: R=···–CH_2–CH–···

(10) **1c** + 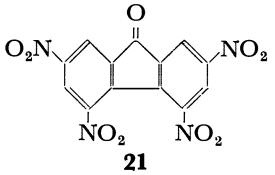

21

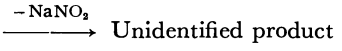

Table 1. Polymerization behavior of

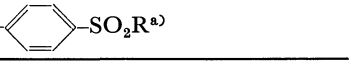

R	Conversion/%	Precipitant	$[\eta]$ [b] dl g^{-1}	Sulfinate[c] content/%	E_0 [d] mV
Na	29.7	MeOH	6.9	78	410
K	24.2	DMF	5.5	63	370
NH_4	31.0	EtOH	7.9	62	415
$NHEt_3$	45.6	*t*-BuOH	9.3	84	340

a) Aqueous solution with 10% monomer and 0.1% KPS. 70 °C×24 h. b) In water at 30 °C. c) By oxidative titration with bromine–water. d) Half-oxidation potential against a saturated calomel electrode at 20 °C.

Results and Discussion

The free-radical polymerizations of four *p*-styrenesulfinates as listed in Table 1 proceeded smoothly to afford water-soluble polymers of high molecular weights. The conversions were however rather low and the sulfinate contents in the polymers were reduced by possible side reactions:

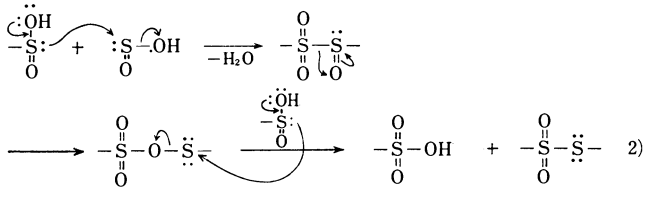

The low conversion data listed in Table 1 appear to be caused by the reductive actions of the sulfinates which lead to the disappearances of growing radicals as well as the physical loss of polymers into precipitants.

The values of $[\eta]$ are, nevertheless, high, a characteristic of the aqueous polymerizations of ionic vinyl monomers.

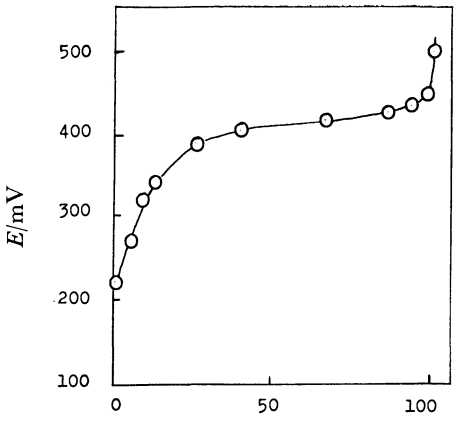

Fig. 1. Typical oxidative titration curve for sulfinate polymers. Sodium poly *p*-styrenesulfinate in aqueous solution (4×10^{-3} mol dm^{-3}) was titrated with aqueous bromine (0.0435 mol dm^{-3}) at 20 °C. *E*, oxidation potential against sat. calomel electrode.

The half-oxidation potential (E_0) for each sulfinate ranges from 340 to 410 mV and is comparable with that (375 mV) for hydroquinone under the same titration conditions, indicating that these polymers are weak reductants. Figure 1 illustrates a typical oxidative titration curve for a sulfinate polymer.

The nucleophilic reactions of the sulfinate polymers and their low-molecular weight homologs investigated have been classified into three categories.

Simple Displacements (Reactions 1, 2, 3, and 7). Reactions 1, 2, and 3 are quite simple nucleophilic reactions, in which the sulfinate anions attack the activated halomethyl groups with the elimination of sodium halides. Satisfactory yields are attained for **1a** and **1b** at room temperature in dipolar aprotic solvents such as DMSO, DMF, and HMPA. In polymer **1c**, on the other hand, which was prepared from a porous crosslinked polystyrene, the swelling ability of the solvent plays a decisive role in determining the extent of reaction. Thus, in Reaction 1 conducted for 72 h at room temperature with a large excess of **2**, the **3c**-contents were 92.7, 79.7, and 31.7% in DMSO, DMF, and HMPA, respectively (on the basis of the initial **1c** unit). DMSO, the most favorable swelling solvent for polymer **1c**, provided the best results throughout the reactions. Reaction 7 with chloranil (**15**) appears to be somewhat complicated due to possible inactivation of the sulfinates and **15** as a result of oxidation to the sulfonates and reduction to tetrachlorohydroquinone, respectively. The extent of side reaction, however, appears to be small and does not appreciably affect the yield of **16c**.

Reductive Additions to Quinonoids (Reactions 4, 5, and 6). The nucleophilic addition reaction of sulfinic acid to *p*-benzoquinone[3] was applied to polysulfinic acid (**8**) in ethanol–water (1:1) to afford a 91 mol% addition of the hydroquinone unit (Reaction 4). Similarly, the reaction of oxidized alizarin with sulfinate[4] was applied to the polymer **1c** and gave satisfactory extents of Reaction 6.

The reactions of **1a** *and* **1b** *with TCNQ* (**11**) *in* acetonitrile giving the disubstituted products **12a** and **12b** which were analytically pure (Reaction 5) appears to proceed as follows:

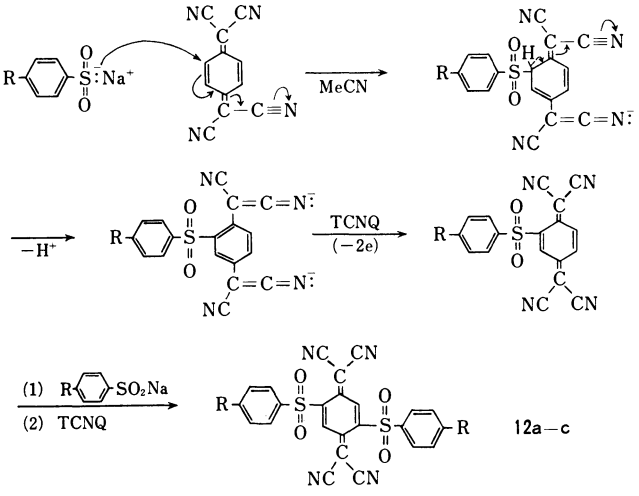

The reaction of polymer **1c** with TCNQ also appears to take place in a similar manner.

Displacement of Aromatic Nitro Groups (Reactions 8, 9, and 10). The displacement reactions of aromatic nitro groups with arenesulfinate[5] were applied to **1a**—**c**. Thus, *o*-nitrobenzonitrile (**17**) possessing an activated nitro group reacted with polymer **1c** in DMSO at room temperature (Reaction 8). In the reactions of **1a** and **1b** with TNF (**19**) (Reaction 9), only single monosubstituted products (**20a** and **20b**) were isolated, indicating that the most activated 7-nitro group of **19** was predominantly replaced. The effect of the solvent on the extent of reaction for polymer **1c** (70 °C, 12 h) was also in the order: DMSO >DMF >HMPA. As anticipated, the reaction of **1c** with tetranitrofluorenone (**21**) was easier than that with TNF, but a product of unidentified structure was obtained.

The results indicate that the nucleophilic reactions of **1a**—**c** are generally very easy and provide satisfactory yields of products, sometimes with apparent selectivity.

The polymerization behavior of the styrenesulfonyl derivatives synthesized here has also been examined. The results so far obtained, however, indicate the predominance of polymer reactions.

Experimental

The IR, ^{1}H-NMR, and mass spectra were recorded on a Hitachi 215 spectrophotometer, a JNM-PMX 60 spectrometer, and a Hitachi RMU-6 MG spectrometer, respectively, all under standard measurement conditions. Elemental analyses were conducted using a Perkin-Elmer 250 instrument.

p-Styrenesulfinates. *p*-Styrenesulfinic acid, synthesized as in a previous paper,[1] was neutralized in aqueous or *t*-butyl alcoholic solutions with equimolar sodium hydroxide, potassium hydroxide, ammonia, and triethylamine and the resulting solutions freeze-dried to isolate the respective salts.

Polymerization of p-Styrenesulfinates. A solution of the monomer (0.5 g) and potassium persulfate (KPS, 0.005 g) in water (5 ml) was placed in a glass ampoule, which was evacuated twice by a standard freeze-thaw method, sealed, and maintained at 70 °C for 24 h. The viscous solutions were precipitated into appropriate precipitants (Table 1) to afford the polymers.

Preparation of Sodium Polystyrenesulfinate (1c) from Crosslinked Polystyrene. To a suspension of crosslinked polystyrene beads (1.2 g; 10 mmol; Aldrich Macroporous) in chloroform (50 ml) was added dropwise chlorosulfuric acid (8 ml; 100 mmol) and the mixture refluxed overnight. The brown reaction mixture was filtered and washed with chloroform, acetonitrile, and finally with cold water to leave white beads. The weight increase and IR data [disappearance of the absorption peaks at 680 and 740 cm^{-1} attributable to the monosubstituted styrene and appearance of a strong 820 cm^{-1} peak (*p*-disubstitution)] indicated that reaction was practically quantitative.

Poly(*p*-styrenesulfonyl chloride) thus prepared (2.0 g, 10 mmol) was converted to sodium poly(*p*-styrenesulfinate) (**1c**) by stirring in a solution of sodium sulfite (13 g, 100 ml) in water (50 ml) at 50—60 °C for 24 h. The **1c**-polymer was filtered and washed with water thoroughly to leave light brown beads (2.0 g). Iodometry on the sample stirred in excess aqueous bromine at room temperature overnight provided 90.9% of the sulfinate unit on the basis of available reaction sites.

Oxidative Titration. Oxidative titrations of the soluble sulfinate polymers were conducted in aqueous solutions with bromine (0.05 mol dm^{-3}) potentiometrically (electrodes: Pt–sat. calomel at 20 °C). Figure 1 illustrates a typical titration curve.

Reaction 1. As a typical example, 4-(vinylbenzylsulfonyl)styrene (**3b**) was prepared as follows: a solution of sodium *p*-styrenesulfinate (1.0 g, 5 mmol; **1b**) and vinylbenzyl chloride (1.0 g, 7 mmol; **2**, Seibi Chem. Co., *m*/*p*=60/40) in DMF (30 ml) was stirred at room temperature overnight. The reaction mixture was poured into water and the resulting precipitates were filtered and recrystallized from benzene–hexane to afford colorless crystals (mp 162—165 °C) in 26% yield. Found: C, 71.15; H, 5.59%. Calcd for $C_{17}H_{16}O_2S$: C, 70.82; H, 5.67%. IR (KBr): 3100—3000 (aryl), 3000—2920 (alkyl), 1310, 1150 (SO_2), 990, 910 (vinyl) cm^{-1}. NMR ($CDCl_3$) δ 4.4 (s, 2H, CH_2), 5.0—6.2 (m, 4H, 2×(-CH=C$\underline{H}_2$)), 6.7 (m, 2H, 2×(-C$\underline{H}$=CH_2)), 7.1—7.8 (m, 8H, ArH) ppm. Mass (*m*/*e*): 284 (M^+, 1.5), 117 (100).

4-(Vinylbenzylsulfonyl)toluene (**3a**) was synthesized in the same manner to afford colorless crystals (mp 147—148 °C) in 46% yield. Found: C. 70.44; H, 6.02%. Calcd for $C_{16}H_{16}O_2S$: C, 70.56; H, 5.89%. IR (KBr): 3100—3000 (aryl), 2920—2980 (alkyl), 1310, 1150 (SO_2), 990, 910 (vinyl) cm^{-1}. NMR ($CDCl_3$) δ 2.5 (s, 3H, CH_3), 4.4 (s, 2H, CH_2), 5.3 (d, 1H, C$\underline{H}_2$=CH–), 5.8 (d, 1H, C$\underline{H}_2$=CH–), 6.7 (q, 1H, CH_2=C$\underline{H}$–), 7.1—7.8 (m, 8H, ArH) ppm. Mass (*m*/*e*): 273 (M^+, 2.4), 117 (100).

In the case of polystyrenesulfinate (**1c**; 0.1 g), 72 h-reactions at room temperature with a large excess of **2** (1 ml) provided 92.7, 79.7, and 31.7% of **3c**-content in DMSO, DMF, and HMPA (each 10 ml), respectively. These were determined by the remaining $-SO_2Na$ in IR (960 cm^{-1}) on the basis of the initial **1c** unit. IR (KBr) indicated vinyl (1620, 990, 910 cm^{-1}) and SO_2 (1310 cm^{-1}) absorptions.

Reaction 2. **1a** (1.5 g, 7 mmol) was reacted for 15 h with vinyl chloroacetate (**4**, 1.0 g, 8 mmol) in HMPA solution (20 ml) at room temperature. Subsequent purification of the product by extraction with ether–water, washing of the colorless organic layer with aqueous sodium hydrogencarbonate, drying over anhydrous sodium sulfate, removal of the ether, extraction of the residue with petroleum ether, and vacuum drying afforded a colorless viscous oil in 65% yield. Found:

C, 54.83; H, 5.21%. Calcd for $C_{11}H_{12}SO_4$: C, 55.00; H, 5.00%. IR ($CHCl_3$): 1760 (ester); 1640, 940 (vinyl); 1320 (SO_2), 1120 (SO_2) cm^{-1}. NMR ($CDCl_3$) δ 2.5 (s, 3H, CH_3), 4.3 (s, 2H, CH_2), 5.0 (t, 2H, $C\underline{H}_2$=CH–), 7.1—8.6 (m, 5H, CH_2=C<u>H</u>–+ArH) ppm. Mass (*m/e*): 240 (M^+).

In the case of polymer **1c** (0.1 g) using a large excess of **4** (1.0 g) in DMSO (10 ml) at room temperature, the extent of reaction (IR) was 86 mol % over 72 h. IR (KBr) indicated 1760 (ester), 1310 (SO_2), 1120 (SO_2), 990, 950 (vinyl) cm^{-1}.

Reaction 3. 4-(Phenacylsulfonyl)toluene (**8a**; mp 109—110 °C) was synthesized in quantitative yield by allowing a solution of **1a** (1.5 g, 7 mmol) and phenacyl bromide (1.0 g, 5 mmol; **6**) in DMSO (30 ml) to stand for 20 h at room temperature. Subsequent precipitation into water and recrystallization from benzene–petroleum ether gave the product as colorless crystals. Found: C, 65.35; H, 5.26%. Calcd for $C_{15}H_{14}SO_3$: C, 65.69; H, 5.11%. IR (KBr): 3050 (aromatic) 3000—2850 (alkyl), 1660 (C=O), 1580 (aromatic), 1305, 1140 (SO_2) cm^{-1}. NMR ($CDCl_3$) δ 2.5 (s, 3H, CH_3), 4.8 (s, 2H, CH_2), 7.2—8.2 (m, 9H, ArH) ppm. Mass (*m/e*): 274 (M^+).

In the case of polymer **1c** (0.2 g), a large excess of **6** (1.0 g) in DMSO (10 ml) at room temperature gave a quantitative yield in 72 h as determined by IR (960 cm^{-1}). IR (KBr) also indicated 1660 (C=O), 1600 (aromatic), and 1310 (SO_2) cm^{-1} absorptions.

Reaction 4. Crosslinked poly(*p*-styrenesulfinic acid) (0.2 g, **8c**) was stirred in a solution of *p*-benzoquinone (**9**, 1 g) in ethanol–water (30 ml, 1: 1 v/v) for 48 h at room temperature. The brown reaction mixture was filtered and extracted with acetone to afford a brown powder, in which the hydroquinone unit existed in 91 mol %, as determined by both remaining $-SO_2Na$ and weight increase. IR (KBr) indicated absorptions at 1450 (hydroquinone), 1300 (SO_2), and 1200 (hydroquinone) cm^{-1}.

Reaction 5. 7,7,8,8-Tetracyanoquinodimethane (TCNQ, **11**; 1 g, 5 mmol) and **1a** (1 g, 5 mmol) in acetonitrile (50 ml) were refluxed for 8 h. The dark green solution containing a precipitate was poured into aqueous hydrochloric acid and the resulting precipitate extracted with chloroform. The red extract was filtered and evaporated *in vacuo* at 50 °C to give a green powder (**12a**) in 15% yield. Found: C, 61.37; H, 3.63: N, 10.82%. Calcd for $C_{26}H_{16}N_4S_2O_4$: C, 60.82; H, 3.12; N, 10.92%. IR (KBr): 2200 (CN), 1590 (aromatic), 1340, 1140 (SO_2) cm^{-1}. NMR (DMSO-d_6+$CDCl_3$) δ 2.5 (s, 6H, 2 CH_3), 7.2—8.3 (m, 10H, ArH+quinonoid) ppm. Mass (*m/e*): 512 (M^+).

The same procedure was applied for **1b** also to afford the disubstituted product **12b**. Polymer **1c** (0.1 g) and TCNQ (**11**, 0.5 g) in acetonitrile (25 ml) were refluxed for 24 h. The dark green product was extracted with hot acetonitrile. The extent of reaction, as determined by the remaining $-SO_2Na$ in IR and N-analysis, was 48%. IR (KBr) indicated absorptions at 2150 (CN), 1600 (aromatic), 1330 (SO_2) cm^{-1}.

Reaction 6. To a solution of alizarin (**13**, 1 g) in DMSO (25 ml) was added a solution of sodium periodate (0.8 g) in water (5 ml). The mixture was stirred for a short time, then the polymer **1c** (0.2 g) was added. Stirring was continued at 70 °C overnight. The red reaction mixture was filtered and the polymer extracted with acetone to leave an orange powder. Weight increase and the remaining $-SO_2Na$ in IR indicated that the polymer contained 95 mol % of the **14c** unit. IR (KBr) indicated absorptions at 1660, 1630 (quinone), 1430 (phenol), 1340 (SO_2) cm^{-1}.

Reaction 7. A mixture of **1a** (1 g, 5 mmol), chloranil (**15**, 1.2 g, 5 mmol), and DMF (20 ml) was stirred at 50 °C for 15 h. The resulting brown solution containing a white precipitate was poured into water to give a gray powder. Recrystallization form benzene–petroleum ether containing bromine gave a yellow powder (**16a**, mp 140—142 °C) in 52% yield. Found: C, 42.89; H, 1.98%. Calcd for $C_{13}H_7SO_4Cl_3$: C, 42.68; H, 1.92%. IR (KBr): 1690 (quinone), 1580 (aromatic), 1370, 1160 (SO_2), 1100, 900 cm^{-1}. NMR ($CDCl_3$) δ 2.5 (s, 3H, CH_3), 7.0—8.3 (m, 4H, ArH) ppm. Mass (*m/e*): 290 (M^+—74).

Polymer **1c** (0.1 g) was stirred in a solution containing an excess of **15** (0.5 g) in DMSO (20 ml) for 24 h at room temperature. This was followed by filtration and subsequent extraction with acetone which gave a light orange powder. Weight increase and IR indicated that the extent of the reaction was 91% based on the available reaction sites of **1c**. IR (KBr) indicated characteristic absorptions at 1680 (quinone), 1580 (aromatic), 1370, 1180 (SO_2), 1120, 900 cm^{-1}.

Reaction 8. The polymer **1c** (0.1 g) was stirred in a solution of *o*-nitrobenzonitrile (**17**, 1 g) in DMSO (10 ml) for 72 h at room temperature. The reaction mixture was filtered and the polymer extracted with acetone to afford a light brown powder. IR and N-analysis indicated the presence of 43 mol % of the **18c** unit. IR (KBr) indicated 2200 cm^{-1} (CN) absorption.

Reaction 9. A solution of 2,4,7-trinitrofluorenone (**19**; 1 g, 32 mmol) and **1a** (0.57 g, 32 mmol) in DMSO (25 ml) was stirred at room temperature for 12 h. The brown solution was poured into iced hydrochloric acid to afford a white precipitate, which was recrystallized from acetonitrile–water. A yellow powder (**20a**) of mp 220—222 °C was isolated in 52% yield. Found: C, 56.49; H, 2.86; N, 6.78%. Calcd for $C_{20}H_{12}N_2SO_7$: C, 56.60; H, 2.83; N, 6.60%. IR (KBr): 3060 (aromatic), 2960—2840 (CH_3), 1720 (C=O), 1510 (NO_2), 1340, 1150 (SO_2) cm^{-1}. NMR (DMSO-d_6) δ 2.5 (s, 3H, CH_3), 7.5 (d, 2H, H_a, H_b), 8.0 (d, 3H, H_c, H_d, H_f), 8.4 (s, 1H, H_e), 8.7 (s, 2H, H_h, H_i), 8.9 (s, 1H, H_g) ppm. Mass (*m/e*): 424 (M^+, 11), 149 (100).

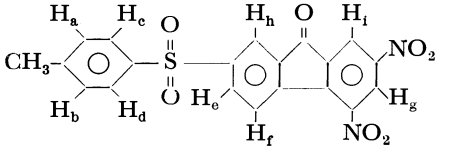

The same reaction procedure was applied to **1b** to afford a yellow powder (**20b**, mp 200—204 °C) in 44% yield. Found: C, 57.70; H, 2.79; N, 6.75%. Calcd for $C_{21}H_{12}N_2SO_7$: C, 57.80; H, 2.75; N, 6.42%. IR (KBr): 1720 (C=O), 1580 (aromatic), 1520 (NO_2), 1320, 1140 (SO_2), 990, 910 (vinyl) cm^{-1}. NMR (DMSO-d_6) δ 5.5 (d, 1H, $C\underline{H}_2$=CH–) 6.1 (d, 1H, $C\underline{H}_2$=CH–), 6.8 (q, 1H, CH_2=C<u>H</u>–), 7.8 (d, 2H, H_a, H_b), 8.2 (d, 3H, H_c, H_d, H_f), 8.4 (s, 1H, H_e), 8.7 (s, 2H, H_h, H_i), 9.0 (s, 1H, H_g) ppm. Mass (*m/e*): 436 (M^+, 30), 104 (100).

Polymer **1c** (0.1 g) was stirred in a solution of **19** (1 g) in DMSO (25 ml) at 70 °C for 12 h. The yellow-brown reaction mixture was filtered and the polymer extracted first with acetone, then with acetone–water (1: 1), and finally with acetone. A light yellow powder containing 77% of the **20c** unit, as determined by the remaining $-SO_2Na$ and N-analysis, was obtained. Reactions for 72 h at room temperature in DMSO, DMF, and HMPA provided 77.0, 57.8, and 35.0% extents of reaction, respectively. IR (KBr) indicated characteristic absorptions at 1730 (C=O), 1600 (aromatic), 1530 (NO_2), 1340 (SO_2) cm^{-1}.

Reaction 10. Polymer **1c** (0.2 g) was stirred in a solution of 2,4,5,7-tetranitrofluorenone (**21**, 1 g) in DMSO (25 ml) for 72 h at room temperature. The green reaction mixture was filtered and the polymer extracted first with acetone, then

with acetone–water (1: 1), and finally with acetone. A brown powder with the extent of reaction of 83 mol %, as determined by $-SO_2Na$ in IR, was obtained. IR indicated that the reaction proceeded *via* the formation of the SO_2 linkage (1350 cm^{-1}), but the number of replaced nitro groups in **21** was not established.

Characteristic absorptions in IR (KBr) were located at 1740 (C=O), 1600 (aromatic), 1540 (NO_2), 1350 (SO_2) cm^{-1}.

References

1) H. Kamogawa, T. Hayashi, and M. Nanasawa, *Chem. Lett.*, **1976**, 419.

2) F. Muth in Houben-Weyl, "Methoden der Organischen Chemie," 4th ed, Georg Thieme Verlag, Stuttgart (1955), Vol. 9, p. 299.

3) "The Chemistry of Quinonoid Compounds II," ed by S. Patai, Wiley, New York (1974), p. 881.

4) Ref. 3, p. 900.

5) N. Kornblum, L. Cheng, R. C. Kerber, M. M. Kestner, B. N. Newton, H. M. Pinnick, R. S. Smith, and P. A. Wade, *J. Org. Chem.*, **41**, 1560 (1976).

Photochemical Reaction at 3-*O*-Functional Group of Methyl 4,6-*O*-Cyclohexylidene-2-deoxy-2-methoxycarbonylamino-α-D-glucopyranoside Derivatives

Teruo KISHI, Tsutomu TSUCHIYA,* and Sumio UMEZAWA
Institute of Bio-organic Chemistry, 1614 Ida, Nakahara-ku, Kawasaki 211

(Received March 19, 1979)

3-*O*-Acetyl, 3-*O*-thiocarbonyl, and 3-*O*-sulfonyl derivatives of the titled compound have been irradiated in aqueous HMPT. Conversion of the 3-*O*-acetyl derivative to the corresponding 3-deoxy compound was most effective. 3-*O*-Dimethylthiocarbamoyl-, 3-*O*-(methylthio)thiocarbonyl- and 3-*O*-(1-imidazolyl)thiocarbonyl derivatives were found to give the 3-deoxy compound accompanied by 3-hydroxy compound, whereas the 3-*O*-phenyl(thiocarbonyl) derivative did not give the 3-deoxy compound. 3-*O*-Methylsulfonyl and 3-*O*-tolylsulfonyl derivatives gave the 3-hydroxy compound. Under low-energy irradiation, the (1-imidazolyl)thiocarbonyl derivative gave the 3-deoxy compound in moderate yield.

Deoxygenation of the hydroxyl group at C-3 of sugars and its application to aminoglycoside antibiotics[1] are of current interest, due to the marked activities of 3′-deoxy derivatives such as 3′-deoxykanamycin A,[2] 3′,4′-dideoxykanamycin B,[3] and 3′-deoxybutirosins[4] against resistant bacteria. In α-D-glucopyranosides, however, deoxygenation at C-3 is difficult[5] since the S_N2 process at this position is hindered in the majority of cases. Barton *et al.*[6] recently solved this problem by treating *O*-thiocarbonyl derivatives with tributylstannane and have synthesized the corresponding deoxy compounds in good yields. Pete *et al.*[7] succeeded in deoxygenation of the position by acetylating the 3-hydroxyl group followed by irradiation of the solution of the *O*-acetyl derivative in aqueous hexamethylphosphoric triamide (HMPT). Horton *et al.*[8] prepared the 2- and 3-deoxy sugars by irradiation of the methanol solution of 2- and 3-*O*-dimethylthiocarbamoyl derivatives. The present studies have been undertaken to investigate the photochemical treatment of several 3-*O*-thiocarbonyl and 3-*O*-sulfonyl sugars.

The starting materials, the 3-*O*-thiocarbonyl derivatives of methyl 4,6-*O*-cyclohexylidene-2-deoxy-2-methoxycarbonylamino-α-D-glucopyranoside[10] (**1**), namely, 3-*O*-dimethylthiocarbamoyl (**4**), 3-*O*-[(methylthio)thiocarbonyl] (**5**), 3-*O*-[(1-imidazolyl)thiocarbonyl] (**6**), and 3-*O*-phenyl(thiocarbonyl) (**7**) derivatives were prepared. In addition, the 3-*O*-acetyl derivative (**3**) was prepared.

In order to select the solvent for the photochemical reaction, compound **6**, a model compound, was dissolved in several solvents and each solution irradiated (with 2537 Å lamp) for 1.5 h in the manner described in the experimental. Photochemical reactions conducted in tetrahydrofuran, dioxane, methanol, ethanol, 2-propanol, 1-butanol, acetone, acetonitrile, dimethyl sulfoxide (all including the reactions in neat solvents and aqueous solvents=5: 95), *t*-butyl alcohol, benzene or sulforane gave the starting material (**6**) together with the formation of a slight amount of the 3-hydroxy compound (**1**). The low yield of the 3-deoxy compound (**2**) was found in the reactions in 2-propanol, 1-butanol,

TABLE 1. THE YIELDS (%) OF **2** AND **1** BY IRRADIATION OF **3**—**10** IN AQUEOUS HMPT (5: 95)

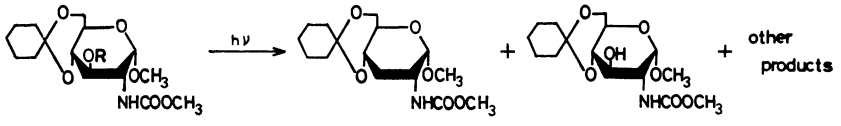

3-10 2 1

Compound	R	2537 Å Lamp Time/h	2	1	St. m. and other products	3000 Å Lamp Time/h	2	1	St. m. and other products
3	CH_3CO–	1.5	88	0	0	14	0	0	100[a] (**3**)
4	$(CH_3)_2NCS$–	14	72	10	0	14	0	0	100(**4**)
5	CH_3SCS–	2	57	12	14(**5**)	14	0	0	100(**5**)
6		1.5	54	17	5(**4**)	4	51	26	8(**4**)
7	C_6H_5CS–	3	0	≈30	>7(**7**) >17(**11**)	4	0	9	b)
8	$(CH_3)_2NSO_2$	4	0	0	100[a] (**8**)	14	0	0	100(**8**)
9	CH_3SO_2–	6	trace(?)	86	9(**9**)	14	0	0	100(**9**)
10	*p*-$CH_3C_6H_4SO_2$–	4	0	91	0	14	0	0	100(**10**)

a) The figure 100 indicates that no product other than the starting material (st. m.) was produced. b) A large amount of unidentified product was formed, but the formation of **11** was not observed.

sulforane, and dimethyl sulfoxide (all including the reactions in neat solvents and in aqueous solvents= 5: 95). In the reaction in *N,N*-dimethylformamide and aqueous *N,N*-dimethylformamide (5: 95), **6** was converted to the dimethylthiocarbamoyl derivative (**4**). The reaction mechanism is thought to that **6** reacts with dimethylamine produced from *N,N*-dimethylformamide during the irradiation. **1** and **2** were however formed in trace amounts. The solution of **6** however in aqueous HMPT (5: 95) when irradiated produced the 3-deoxy compound (**2**) in 54% yield.

On the basis of these results **3**—**7** were treated photochemically (2537 Å lamp) in aqueous HMPT, the results of which are summarized in Table 1. The acetyl derivative (**3**) gave the best result, the deoxy compound (**2**) being formed exclusively. In the case of **4**, **2** was formed in good yield, but the reaction required a longer period and the product was contaminated by the 3-hydroxy compound (**1**). In the cases of **5** and **6**, **2** and **1** were formed but in the case of **7** the expected **2** was not formed, the 3-hydroxy compound (**1**) and an unidentifiable product being formed. Interestingly the 3-*O*-benzyl product (**11**) was found to be formed in this reaction. This product was proved by synthesis from **1** and α-bromotoluene.

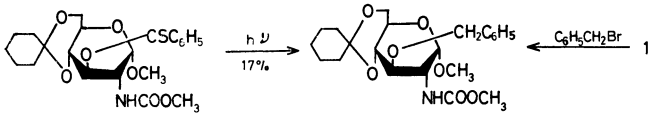

7 11

Under low-energy irradiation (3000 Å lamp), only the (1-imidazolyl)thiocarbonyl compound (**6**) was converted to the 3-deoxy compound (**2**) in moderate yield, but other compounds except **7** were all stable after 14 h irradiation (Table 1). This demonstrates that low-energy irradiation, only the (1-imidazolyl)-thiocarbonyl group can be removed to give the deoxy compound in the presence of acetyl, dimethylthiocarbamoyl), (methylthio)thiocabonyl, methylsulfonyl, and *p*-tolylsulfonyl groups.

The deoxygenation at C-3 of α-D-glucopyranosides by treatment of the 3-*O*-dimethylsulfamoyl derivatives with sodium metal in liquid ammonia has been reported.[10] The mechanism of photochemical reaction and the reaction with sodium metal are both considered to be radical reactions and consequently the photochemical treatment of the 3-sulfonic esters (**8**—**10**) of **1** in aqueous HMPT (5: 95) were examined. On photochemical treatment of the 3-*O*-dimethylsulfamoyl derivative[10] (**8**), however, no deoxy compound was formed and the starting material was recovered (Table 1). In the cases of the 3-*O*-methylsulfonyl (**9**) and 3-*O*-(*p*-tolylsulfonyl) derivative (**10**), the 3-hydroxy compound (**1**) was formed in good yield. The ready removal of the 3-*O*-tosyl group of **10** offers a facile method for detosylation. Zen *et al.*[11] reported the photochemical detosylation of sugar tosylates in methanol containing sodium methoxide.

Experimental

PMR spectra were recorded at 90 MHz with a Varian EM-390 spectrometer. Thin-layer chromatography (TLC) was performed on Wakogel B-5 using a sulfuric acid spray for detection. Silica gel (Wakogel C-200) was used for separation of the products by column chromatography.

General Procedure for Photochemical Reaction. Nitrogen was bubbled through an aqueous HMPT (5: 95, ≈10 ml) solution of the starting material (**3**—**10**, 0.04—0.05 mmol) in a quartz tube (PQV-5 or -7, 13×180 mm) for 10 min. The solution was stoppered, set in a photo-reactor (Rayonet ® RPR 208 Preparative Photochemical Reactor with MGR-100 Merry-Go-Round) and irradiated with a RUL-2537 Å or RUL-3000 Å lamp (in the latter case, a Pyrex RPV-8 tube was used instead of a quartz tube). All apparatus used was manufactured by The Southern New England Ultraviolet Company, England. The speed of reaction was influenced by both the concentration and the volume of the solution in the tube of the starting material.

*Photochemical Reaction of **3** (2537 Å Lamp).* A solution of **3** (55 mg) in aqueous HMPT (30 ml) was divided between three quartz tubes and, after nitrogen was bubbled through the solution, the solution was irradiated at room temperature with a 2537 Å lamp for 1.5 h. The TLC plate was prepared as follows: a small portion of the solution was poured into aqueous ether and, after shaking the mixture vigorously, the separated ethereal solution was spotted with a glass capillary on the plate and developed with benzene–ethyl acetate=5: 1. The solution showed a single spot at R_f 0.38 (**2**) (*cf.* **3**, R_f 0.2). The solution was poured into water (150 ml) and the mixture extracted with ether (150+50 ml). The ethereal solution was washed with water, dried (sodium sulfate), and concentrated. The residue was chromatographed with benzene–ethyl acetate (5: 1) to give a HMPT-free syrup of **2**, which crystallized on standing, 41 mg (88%). Recrystallization from hexane gave granular crystals; mp 118—119 °C, $[\alpha]_D^{25}$ +77° (*c* 1, chloroform); PMR ($CDCl_3$): δ 1.3—2.2 (12H), 3.40 (3H s, CH_3O), 3.72 (3H s, CH_3OCO), 4.60 (1H d, J=3.5 Hz, H-1).

Found: C, 57.28; H, 7.82; N, 4.28%. Calcd for $C_{15}H_{25}NO_6$: C, 57.13; H, 7.99; N, 4.44%.

Decyclohexylidenation of **2** as previously described[10] gave methyl 2,3-dideoxy-2-methoxycarbonylamino-α-D-glucopyranoside.[10]

*Photochemical Reaction of **6** (2537 Å Lamp).* An aqueous HMPT solution (40 ml) of **6** (73 mg) in four quartz tubes was irradiated for 1.5 h. The standard work-up as described above gave a mixture of products. The mixture showed, on TLC with cyclohexane–ethyl acetate (5: 1), spots of R_f 0.23 (major, **2**), 0.11 (trace, **4**), and ≈0.05 (minor) (*cf.* **6**, R_f 0.05). Separation by column-chromatography with cyclohexane–ethyl acetate (5: 1) as eluent gave **2** (28 mg, 54%) and **4** (3.2 mg, 5%). Further elution with ethyl acetate gave **1** (9.1 mg, 17%).

*Photochemical Reaction of **6** (3000 Å Lamp).* An aqueous HMPT solution (40 ml) of **6** (41 mg) in four Pyrex tubes was irradiated with a 3000 Å lamp for 4 h. The standard work-up gave **2** (14.7 mg, 51%), **4** (2.9 mg, 8%), and **1** (7.9 mg, 26%).

*Photochemical Reaction of **7** (2537 Å Lamp).* A solution of **7** (183 mg) in aqueous HMPT (90 ml) was irradiated for 3 h. The solution was poured into water (500 ml) and the mixture extracted with ethyl acetate (150 ml×2, 50 ml×3). The combined solutions were washed with water, dried (sodium sulfate) and concentrated. The residue was chromatographed on a column of silica gel with cyclohexane–ethyl acetate (5: 1). **7** (12 mg, 7%, R_f 0.46 with benzene–ethyl acetate=5: 1), a mixture of **7** and **11** (6.8 mg), and **11** (29 mg, 17%, R_f 0.33) were eluted in this order. A change of eluent to ethyl acetate gave **1** (43 mg, 32%) and to methanol gave an unidentified product (≈130 mg).

Compound **11** was purified by column chromatography with benzene–ethyl acetate (15: 1) to give colorless powder, $[\alpha]_D^{25}$ +98° (*c* 1, chloroform); IR (KBr): 1735 cm^{-1}; PMR ($CDCl_3$): δ 1.3—2.5 (10H, cyclohexylidene), 3.37 (3H s, C_1OCH_3), 3.71 (3H s, CO_2CH_3); 2H AB q centered at 4.87 (J=12 Hz, $C_6H_5C\underline{H}_2O$), 4.74 (1H d, J=4 Hz, H-1), 4.83 (1H d, J=10 Hz, NH; disappeared on deuteration), 7.40 (5H s, C_6H_5).

Found: C, 62.86; H, 7.29; N, 3.15%. Calcd for $C_{22}H_{31}NO_7$: C, 62.69; H, 7.41; N, 3.32%.

Photochemical Reaction of ***10*** *(2537 Å Lamp).* An aqueous HMPT solution (20 ml) of **10** (41.5 mg) was irradiated for 4 h in the manner described. The solution was poured into water (100 ml) and the mixture extracted with ethyl acetate (100+50 ml). The organic solution was washed with water, dried, and concentrated. The residue was chromatographed with benzene–ethyl acetate (2: 1) to give **1**, 25.7 mg (91%), $[\alpha]_D^{25}$ +78° (*c* 1, chloroform).

*Methyl 3-O-Acetyl-4,6-O-cyclohexylidene-2-deoxy-2-methoxycarbonylamino-α-D-glucopyranoside (**3**).* Prepared from **1** with acetic anhydride in pyridine gave a yield of 76%, $[\alpha]_D^{25}$ +81° (*c* 1, chloroform); UV (ethanol): λ_{max} 203 nm (ε 270); PMR ($CDCl_3$): δ 2.10 (3H, s, Ac), 3.41 (3H s, CH_3O), 3.72 (3H s, CH_3OCO), 4.72 (1H d, J=3.5 Hz, H-1), 5.10 (1H t, J=10 Hz, H-3).

Found: C, 54.72; H, 7.10; N, 3.78%. Calcd for $C_{17}H_{27}NO_8$: C, 54.68; H, 7.29; N, 3.75%.

*Methyl 4,6-O-Cyclohexylidene-2-deoxy-3-O-(dimethylthiocarbamoyl)-2-methoxycarbonylamino-α-D-glucopyranoside (**4**).* To an ice-cold solution of **1** (106 mg) in tetrahydrofuran–HMPT (1: 1, 2 ml), 50% oily sodium hydride (net wt 15 mg) was added and the mixture stirred for 10 min under an atmosphere of nitrogen. Dimethylthiocarbamoyl chloride[12] (59 mg) was added and the mixture stirred for 1 h at room temperature. The reaction mixture was poured into water and the mixture extracted with ethyl acetate. The organic solution was washed with water, dried (sodium sulfate), and concentrated to give a residue. The residue was chromatographed with chloroform–ethyl acetate (10: 1) to give a pale-yellow syrup. The solution of the syrup in hexane was concentrated *in vacuo* to give a solid, 83.3 mg (62%), $[\alpha]_D^{25}$ +32° (*c* 1, chloroform); UV (ethanol): λ_{max} 285 nm (log ε 3.00), 248 (4.18), 203 (3.95); PMR ($CDCl_3$); δ 3.14 (3H s, CH_3N), 3.41 and 3.42 (each 3H s, CH_3N and CH_3O), 3.65 (3H s, CH_3OCO), 4.79 (1H d, J=3.5 Hz, H-1), 5.99 (1H t, J=10 Hz, H-3).

Found: C, 51.65; H, 7.06; N, 6.73; S, 7.69%. Calcd for $C_{18}H_{30}N_2O_7S$: C, 51.66; H, 7.23; N, 6.69; S, 7.66%.

*Methyl 4,6-O-Cyclohexylidene-2-deoxy-2-methoxycarbonylamino-3-O-[(methylthio)thiocarbonyl]-α-D-glucopyranoside (**5**).* To a solution of **1** (365 mg) in tetrahydrofuran (4.0 ml), 50% oily sodium hydride (net wt 55 mg) and imidazole (2 mg) were added and the mixture stirred for 30 min at room temperature. Carbon disulfide (0.50 ml) was added and the reaction mixture stirred for 1 h, then methyl iodide (0.12 ml) was added and stirring continued for further 30 min. After the addition of acetic acid (1.0 ml), the mixture was poured into a mixture of ice–water and chloroform and stirred vigorously. The chloroform solution was successively washed with a 5% potassium hydrogensulfate solution, sodium hydrogencarbonate solution, and water, dried (sodium sulfate) and concentrated. The residue was chromatographed with chloroform–ethyl acetate (5: 1) to give a pale-yellow syrup, which was dissolved in hexane and concentrated to give a solid, 373 mg (80%), $[\alpha]_D^{25}$ +48° (*c* 1, chloroform): UV (ethanol): λ_{max} 281 nm (log ε 4.00), 227 (3.78), 203 (3.85): PMR ($CDCl_3$): δ 2.60 (3H s, CH_3S), 4.77 (1H d, J=3.5 Hz, H-1), 6.15 (1H t, J=9 Hz, H-3).

Found: C, 48.69; H, 6.27; N, 3.23; S, 15.49%. Calcd for $C_{17}H_{27}NO_7S_2$: C, 48.44; H, 6.46; N, 3.32; S, 15.21%.

*Methyl 4,6-O-Cyclohexylidene-2-deoxy-3-O-[(1-imidazolyl)thiocarbonyl]-2-methoxycarbonylamino-α-D-glucopyranoside (**6**).* To a solution of **1** (457 mg, 1.38 mmol) in tetrahydrofuran (5 ml), *N,N'*-thiocarbonyldiimidazole[13] (490 mg, 2.75 mmol) was added and the mixture refluxed for 4.5 h under an atmosphere of nitrogen. After the addition of chloroform (30 ml), the organic solution was washed successively with 5% potassium hydrogensulfate solution, sodium hydrogencarbonate solution, and water, dried (sodium sulfate) and concentrated to give a solid. Recrystallization from benzene–hexane gave needles, 499 mg (82%); mp 172—173 °C, $[\alpha]_D^{25}$ +62° (*c* 1, chloroform); UV (ethanol): λ_{max} 276 nm (log ε 4.08), 219 (3.70), 201 (3.70); PMR ($CDCl_3$): δ 3.46 (3H s, CH_3O), 3.61 (3H s, CH_3OCO), 4.78 (1H d, J=4 Hz, H-1), 5.10 (1H d, J=10 Hz, NH; disappeared on deuteration), 6.00 (1H t, J=10Hz, H-3); 7.09, 7.69, and 8.41 (each 1H s, imidazolyl).

Found: C, 51.95; H, 6.22; N, 9.48; S, 7.37%. Calcd for $C_{19}H_{27}N_3O_7S$: C, 51.69; H, 6.17; N, 9.52; S, 7.26%.

*Methyl 4,6-O-Cyclohexylidene-2-deoxy-2-methoxycarbonylamino-3-O-phenyl(thiocarbonyl)-α-D-glucopyranoside (**7**).* A mixture of carboxymethyl dithiobenzoate[14] (157 mg) and 50% oily sodium hydride (net wt 36 mg) in tetrahydrofuran (20 ml) was stirred at room temperature for 5 min. Imidazole (101 mg) was added and the mixture refluxed for 5 min. Compound **1** (245 mg) dissolved in tetrahydrofuran (3 ml) was added and the mixture refluxed for a further 5 min. The reaction mixture was poured into a mixture of ice–water and chloroform and vigorously stirred. The separated organic layer was treated similarly as described for **5** to give a syrup. Chromatography with chloroform–ethyl acetate (10: 1) gave a pale-yellow solid of **7**, 200 mg (60%). Recrystallization from hexane gave yellow needles; mp 129—131 °C, $[\alpha]_D^{25}$ +48° (*c* 1, chloroform): UV (ethanol): λ_{max} 292 nm (log ε 4.00), 253 (3.90), 217 (3.90), 202 (4.04); PMR ($CDCl_3$): δ 3.48 (3H s), 3.57 (3H s), 4.80 (1H d, J=4 Hz, H-1), 5.15 (1H d, J=8 Hz, NH), 6.35 (1H t, J=9 Hz, H-3), 7.4—8.3 (5H).

Found: C, 58.32; H, 6.35; N, 2.86; S, 6.82%. Calcd for $C_{22}H_{29}NO_7S$: C, 58.52; H, 6.47; N, 3.10; S, 7.10%.

*Methyl 4,6-O-Cyclohexylidene-2-deoxy-3-O-dimethylsulfamoyl-2-methoxycarbonylamino-α-D-glucopyranoside[10] (**8**).* Mp 136—137 °C (recrystallized from hexane), $[\alpha]_D^{25}$ +51° (*c* 1, chloroform).

*Methyl 4,6-O-Cyclohexylidene-2-deoxy-3-O-methylsulfonyl-2-methoxycarbonylamino-α-D-glucopyranoside (**9**).* Prepared in the usual manner from **1** with methanesulfonyl chloride and pyridine; mp 147.5—148.5 °C (hexane), $[\alpha]_D^{25}$ +70° (*c* 1, chloroform); UV (ethanol): λ_{max} 223 nm (ε 160), 200 (200); PMR ($CDCl_3$): δ 3.10 (3H s, Ms), 3.42 (3H s), 3.74 (3H s), 4.66 (1H t, H-3), 4.78 (1H d, H-1).

Found: C, 47.07; H, 6.50; N, 3.43; S, 7.68%. Calcd for $C_{16}H_{27}NO_9S$: C, 46.93; H, 6.65; N, 3.42; S, 7.83%.

*Methyl 4,6-O-Cyclohexylidene-2-deoxy-2-methoxycarbonylamino-3-O-tosyl-α-D-glucopyranoside (**10**).* Prepared in the standard manner from **1** with tosyl chloride and pyridine to give a solid, $[\alpha]_D^{25}$ +44° (*c* 1, chloroform); UV (ethanol): λ_{max} 223 nm (log ε 4.00), 199 (3.88); PMR ($CDCl_3$): δ 2.44 (3H s, CH_3 of Ts), 3.41 (3H s), 3.69 (3H s), 4.72 (1H d, H-1), 4.75 (1H t, H-3).

Found: C, 54.70; H, 6.53; N, 2.67; S, 6.70%. Calcd for $C_{22}H_{31}NO_9S$: C, 54.42; H, 6.44; N, 2.89; S, 6.60%.

*Methyl 3-O-Benzyl-4,6-O-cyclohexylidene-2-deoxy-2-methoxycarbonylamino-α-D-glucopyranoside (**11**).* To a solution of **1** (121 mg) in tetrahydrofuran (3 ml), 50% oily sodium hydride (net wt 17 mg) and imidazole (1 mg) were added and the mixture stirred for 15 min in an ice bath. α-Bromotoluene

(0.065 ml) was added and the mixture stirred at room temperature for 47 h. After the addition of methanol (0.2 ml), the mixture was poured into water containing sodium chloride and the mixture extracted with ethyl acetate. Concentration of the extracts gave a residue which was chromatographed on a column of silica gel with benzene–ethyl acetate (10: 1) to give **11** (59 mg, 38%), which was identical with the product obtained by photochemical reaction of **7** in all respects. Changing the eluent to ethyl acetate gave recovered **1** (48 mg, 40%).

The authors are grateful to Prof. H. Umezawa, Director of the Institute of Microbial Chemistry, for his support and encouragement.

References

1) S. Umezawa, *Adv. Carbohydr. Chem. Biochem.*, **30**, 111 (1974); see also H. Umezawa, *ibid.*, **30**, 183 (1974).

2) S. Umezawa, T. Tsuchiya, R. Muto, Y. Nishimura, and H. Umezawa, *J. Antibiot.*, **24**, 274 (1971); S. Umezawa, Y. Nishimura, H. Hineno, K. Watanabe, S. Koike, T. Tsuchiya, and H. Umezawa, *Bull. Chem. Soc. Jpn.*, **45**, 2847 (1972).

3) H. Umezawa, S. Umezawa, T. Tsuchiya, and Y. Okazaki, *J. Antibiot.*, **24**, 485 (1971); S. Umezawa, H. Umezawa, Y. Okazaki, and T. Tsuchiya, *Bull. Chem. Soc. Jpn.*, **45**, 3624 (1972).

4) I. Watanabe, A. Ejima, T. Tsuchiya, D. Ikeda, and S. Umezawa, *Bull. Chem. Soc. Jpn.*, **50**, 487 (1977); I. Watanabe, T. Tsuchiya, and S. Umezawa, *ibid.*, **50**, 972 (1977).

5) For example, see: A. C. Richardson, *Carbohydr. Res.*, **10**, 395 (1969).

6) D. H. R. Barton and S. W. McCombie., *J. Chem. Soc., Parkin Trans. 1*, **1975**, 1574.; D. H. R. Barton and R. Subramanian, *ibid.*, **1977**, 1718.

7) H. Deshayes, J. Pete, C. Portella, and D. Scholler, *J. Chem. Soc., Chem. Commun.*, **1975**, 439; J. Pete, C. Portella, C. Monneret, J. Florent, and Q. Khuong-Huu, *Synthesis*, **1977**, 774.

8) R. H. Bell, D. Horton, D. M. Williams, and E. Winter-Mihaly, *Carbohydr. Res.*, **58**, 109 (1977).

9) D. H. R. Barton, C. Chavis, M. K. Kaloustian, P. D. Magnus, G. A. Poulton, and P. J. West, *J. Chem. Soc., Parkin Trans. 1*, **1973**, 1571.

10) T. Tsuchiya, I. Watanabe, M. Yoshida, F. Nakamura, T. Usui, M. Kitamura, and S. Umezawa, *Tetrahedron Lett.*, **1978**, 3365.

11) S. Zen, S. Tashima, and S. Koto, *Bull. Chem. Soc. Jpn.*, **41**, 3025 (1968).

12) R. H. Goshorn, W. W. Levis, Jr., E. Jaul, and E. J. Ritter, *Org. Synth.*, Coll. Vol. IV, 307 (1963).

13) J. J. Fox, N. Miller, and I. Wempen, *J. Med. Chem.*, **9**, 101 (1966).

14) A. Kjaer, *Acta Chem. Scand.*, **4**, 1347 (1950).

The Photochemical Dimerization of 2-Acyl-1,4-quinones

Yo MIYAGI,* Kazuhiro MARUYAMA,† Hideo ISHII, Sachie MIZUNO, Masao KAKUDO,††
Nobuo TANAKA,†† Yoshiki MATSUURA,†† and Shigeharu HARADA††

Faculty of Education, Kanazawa University, Kanazawa 920
†*Department of Chemistry, Faculty of Science, Kyoto University, Kyoto 606*
††*Institute for Protein Research, Osaka University, Suita, Osaka 565*

(Received March 28, 1979)

2-Acyl-1,4-benzoquinones and 2-acyl-1,4-naphthoquinones underwent a novel type of regiospecific and stereospecific cyclodimerization by photolysis. The reaction was general, being not affected by any variation in the substituents and solvents. The structure of the dimers was elucidated as 4aα-acyl-10β-alkyl-5,8-dihydroxy-4aα,10aα-dihydro-1,4,9(10*H*)-phenanthrenetriones and dibenzo[*b*,*h*]homologues (**8**). The structure of **8** suggests that the dimerization proceeds through *cis*-ring fusion, disposing two substituents of the dimer (an acyl and an alkyl group) to a *trans* configuration.

Many types of photochemical reactions have been reported for quinones and related compounds.[1] In the absence of other sustrates, 1,4-quinones undergo dimerization to give oxetanes and cyclobutanes. We wish to report here that acyl-1,4-quinones (**2**) suffer a novel and general type of dimerization upon irradiation.[2] For example, when a degassed solution of 2-butanoyl-1,4-benzoquinone (**2c**) in carbon tetrachloride was irradiated with a high-pressure mercury arc lamp in a Pyrex tube, a yellow solid product soon crystallized out, the yield of the product being up to 80% in 15 h. Elemental analysis and mass spectrometric data showed it to be a dimer of **2c**. When benzene was used as the solvent, none of the dimer crystallized out of the reaction solution, but the solution was deeply darkened because of the partial decomposition of the dimer formed. As is shown in Table 1, the reaction proceeded in the same fashion on acylquinones with a wide variety of substituents, and only a single compound was obtained in each case. The solutions of **2** gave no signs of affording such dimers after standing for a fairly long time without light at room temperature.

The isolation and purification of the dimers could not be performed under the same conditions since the dimers decomposed thermally or with a trace amount of water, sometimes even with moisture. Consequently, the yields of the purified dimers were of less constancy. This makes it hard to compare the each yields with others obtained under different conditions. However, there is a discernible tendency for the reaction to be considerably slower for acetylquinones **2** (R=H) than for the other acylquinones **2** (R≠H) (Table 1).

The Skeletal Structure of the Dimers. The structures of the dimers were determined by means of their ^{1}H NMR spectral data, which are listed in Table 2. They

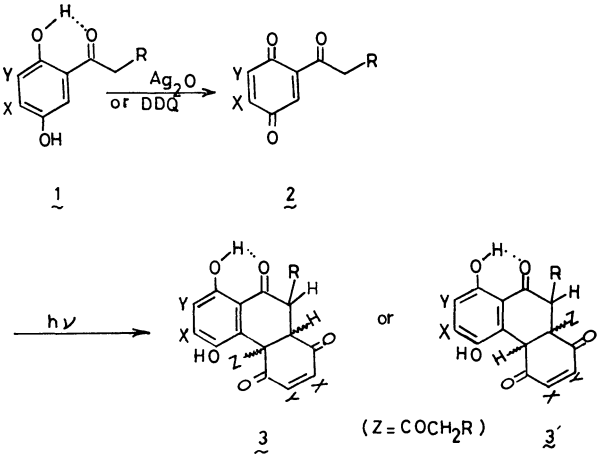

1 2 3 3′

are all consistent either with **3** or **3′** (the usual double-resonance technique was used to determine the identity of protons causing ^{1}H-^{1}H couplings). The spectrum of a dimer of **2g** in $CDCl_3$ is exemplified, illustrated with the atoms denoted in Table 2.

Four methyl signals were observed. Two of them had coupling constants of 7.5 Hz; the triplet at 0.99 and the doublet at 1.29 were assigned to Me_A and Me_B, respectively. Although the triplet suggests the existence of the $COCH_2Me_A$ group, the spectrum lacked a quartet normally expected for a methylene group. Instead, a lot of weak signals were observed at 2.1—2.6. This suggests that the $COCH_2Me_A$ group might be bound to an asymmetric carbon atom. The third methyl signal, arising at 1.99 as a doublet (J=1.5 Hz), may be ascribed to Me_C. The signal was split by coupling with H_C, which showed its signal at 6.77 as a quartet (J=1.5 Hz). The fourth methyl group, Me_D, and the aromatic

Table 1. Yields of the dimers **3**

	a	**b**	**c**	**d**	**e**	**f**	**g**	**h**	**i**	**j**	**k**	**l**	**m**
R	H	Me	Et	*n*-Pr	*n*-Bu	H	Me	Me	H	Me	H	Me	Et
X	H	H	H	H	H	Me	Me	Cl	Br	Br	}	−(CH=CH)$_2$−	
Y	H	H	H	H	H	H	H	H	H	H	}		
Yield/%	60	40	80	15	44	40	20	40	0	10	0	30	25
Irradiation time/h	100	15	15	10	13	70	15	40	30	15	20	10	10
Solvent[a)]	c	c	c	a	a	c	c	c	c	c	b	b	b

a) a, benzene–cyclohexane (1 : 4, v/v); b, benzene; c, carbon tetrachloride.

proton, H_D, showed their signals as singlets at 2.30 and 6.84, respectively. The double quartet at 2.81 may be due to H_B, which was coupled with Me_B (J=7.5 Hz) and H_A (J=3.5 Hz). The doublet at 3.84 (J=3.5 Hz) was assigned to H_A, which was coupled with H_B. A chelated and a non-chelated hydroxyl proton resonated at 12.28 and 6.10, respectively.

The other dimers showed similar spectra, but with partial variations dependent on their substituents.

i) The variation for R=H (the dimers of **2a** and **2f**). A set of signals of the ABX type was observed at about 3.0 (H_B and $H_{B'}$) and at about 4.1 (H_A). A singlet due to an acetyl group was observed at about 2.2.

ii) The variation for X=Y=H (the dimers of **2a**—**e**). Two AB quartets due to H_C and $H_{C'}$, and to H_D and $H_{D'}$, were observed at about 6.7 and about 7.1, respectively.

iii) The variation for X+Y=-(CH=CH)$_2$- (the dimers of **2l**—**m**). Two sets of four aromatic protons gave complex signals at 7.5—8.5.

The above assignments were substantiated by the spectra of the dimers (**6a**—**b** or **6'a**—**b**) of the partially deuterated monomers (**5a**—**b**), which were prepared from **4a**—**b**. The signals due to H_B and $H_{B'}$ (dABq at 3.08) and $COCH_3$ (s at 2.23) of **3a** disappeared, and the signal of H_A became a singlet upon deuteration. The doublets due to Me_B (1.45) and H_A (4.08) and the triplet due to Me_A (0.96) of **3b** all became singlets in **6b**.

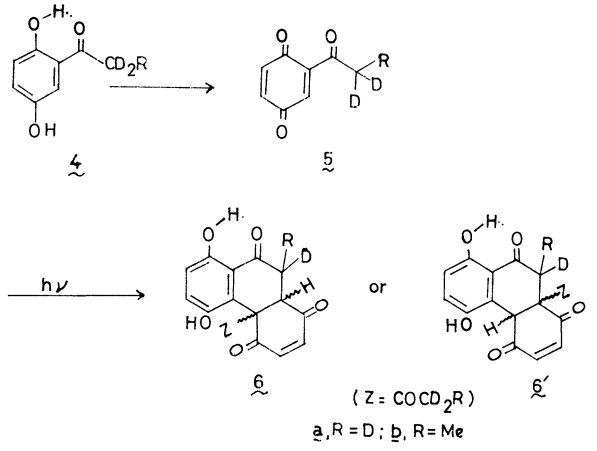

However, all the types of spectra illustrated above may be explained by the alternative structure, **3'**, *i.e.*, an orientational isomer of **3**, though **3** is more feasible for the following reason. The value of the ^1H-^1H coupling constant, which had been ascribed above to the H_A–C–C–H_B coupling of **3g**, was 3.5 Hz. The corresponding values of the other dimers were also in the range of 3.0—4.0 Hz. They are a little too large for the H–C–C–C–H couplings, which should be in **3'**. The ^{13}C NMR data of the dimer of **2h** was also either compatible with **3h** or **3'h**, shown with **3h** in Fig. 1. As was stated in a previous communication,[2] **3'** was excluded on the basis of chemical evidence by converting

Table 2. ^1H NMR data of the dimers **3** and **6**: δ/ppm

	Solv[a]	OH[b]	OH[c]	H_D and $H_{D'}$	H_C and $H_{C'}$	H_A	H_B (and $H_{B'}$)	R_B (R_B=H and $(CH_2)_nMe_B$ (n=0—3))	$COCH_2R_A$ (R_A=H and $(CH_2)_nMe_A$(n=0—3))
3a	A	12.30	9.28	7.18[d] (9 Hz)	6.76[d] (11 Hz)	4.09 (dd, 5 and 3 Hz)	3.08 (2H, dABq[e])	R_B=$H_{B'}$	2.23 (s, Ac): R_A=H
6a	A	12.59	8.91	7.30[d] (8.5 Hz)	6.88[d] (10 Hz)	4.15 (s)	H_B=$H_{B'}$ =D	R_B=$H_{B'}$=D	CH_2R_A=CD_3
3b	A	12.44	9.43	7.01[d] (9 Hz)	6.62[d] (10 Hz)	4.08 (d, 3.5 Hz)	unclear	1.46 (d, 7 Hz, Me_B): n=0	0.96 (t, 7 Hz, Me_A); CH_2–Me_A, unclear
6b	A	12.30	9.09	6.98[d] (8.5 Hz)	6.59[d] (10 Hz)	4.09 (s)	H_B=D	1.45(s, Me_B): n=0	0.95 (s, Me_A); CH_2R_A=CD_2Me_A
3c	A	12.42	9.18	7.01[d] (9 Hz)	6.60[d] (10 Hz)	4.18 (d, 3.5 Hz)	unclear	1.01 (t, 7 Hz, Me_B); $-CH_2Me_B$ and	0.80 (t, 7 Hz, Me_A); $-(CH_2)_2Me_A$, unclear
	C	12.34	5.82	6.98[d] (8 Hz)	6.68[d] (10 Hz)	3.94 (d, 3.5 Hz)	unclear	0.94 (t, 7 Hz, Me_B); $-CH_2Me_B$ and	0.78 (t, 7 Hz, Me_A); $-(CH_2)_2Me_A$, unclear
3d	C	12.35	5.90	6.95[d] (9 Hz)	6.63[d] (10 Hz)	3.95 (d, 3.5 Hz)	unclear	0.91 (t, 6 Hz, Me_B); $-(CH_2)_2Me_B$ and	0.82 (t, 7 Hz, Me_A); $-(CH_2)_3Me_A$, unclear
3e	C	12.41	6.12	7.00[d] (9 Hz)	6.69[d] (10 Hz)	4.06 (d, 3.5 Hz)	unclear	0.90 (t, 6 Hz, Me_B); $-(CH_2)_3Me_B$ and	0.83 (t, 6.5 Hz, Me_A); $-(CH_2)_4Me_A$, unclear

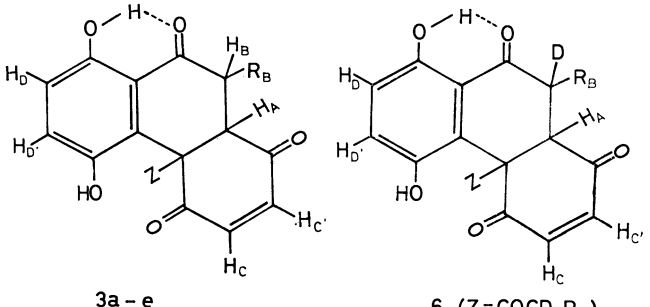

3a - e
(Z=COCH$_2$R$_A$)

6 (Z=COCD$_2$R$_A$)
a, R=D; b, R=Me

Table 2. (Continued)

	Solv[a]	OH[b]	OH[c]	H_D	H_C	H_A	H_B (and $H_{B'}$)	Me_D	Me_C	R_B (R_B=H and $(CH_2)_nMe_B$ (n=0—1))	$COCH_2R_A$ (R_A=H and $(CH_2)_nMe_A$ (n=0—1))
3f	A	12.81	8.03	6.81 (1H, s)	6.75 (1H, q, 1.5 Hz)	3.99 (dd, 5 and 4 Hz)	3.00 (2H, dABq[f])	2.14 (s)	1.81 (d, 1.5 Hz)	R_B=$H_{B'}$	2.34 (s, Ac): 2.35 (s, Ac): } R_A=H
	C	12.20	—	6.88 (1H, s)	6.83 (1H, q, 1.5 Hz)	3.76 (dd, 8.5 and 5 Hz)	2.95 (2H, dABq[g])	2.13 (s)	2.01 (d, 1.5 Hz)		
3g	A	12.41	7.84	6.76 (1H, s)	6.60 (1H, q, 1.5 Hz)	4.08 (d, 3 Hz)	2.82 (1H, dq, 7 and 3 Hz)	2.30 (s)	1.74 (d, 1.5 Hz)	1.43 (d, 7 Hz, Me_B)	0.94 (t, 7 Hz, Me_A); CH_2Me_A, unclear
	C	12.28	6.10	6.84 (1H, s)	6.77 (1H, q, 1.5 Hz)	3.84 (d, 3.5 Hz)	2.81 (1H, dq, 8 and 3.5 Hz)	2.30 (s)	1.99 (d, 1.5 Hz)	1.29 (d, 7.5 Hz, Me_B)	0.99 (t, 7.5 Hz, Me_A); CH_2Me_A, unclear
3h	C	12.54	5.78	7.15 (1H, s)	7.08 (1H, s)	4.10 (d, 3.5 Hz)	2.92 (1H, m)	—	—	1.52 (d, 7 Hz, Me_B)	1.06 (t, 7 Hz, Me_A); CH_2Me_A, nuclear
3j	A	12.44	8.64	7.42 (1H, s)	7.29 (1H, s)	4.19 (d, 3.5 Hz)	3.06 (1H, dq, 6 and 3.5 Hz)	—	—	1.48 (d, 6 Hz, Me_B)	0.98 (t, 7 Hz, Me_A); CH_2Me_A, unclear
3l	C	14.18	6.40	7.6—8.4 (8H, m)		4.11 (d, 4 Hz)	3.01 (1H, dq, 7 and 4 Hz)	—	—	1.30 (d, 7 Hz, Me_B)	1.02 (t, 7 Hz, Me_A); CH_2Me_A, unclear
3m	C	14.19	6.60	7.6—8.5 (8H, m)		4.16 (d, 3.5 Hz)	2.78 (1H, m)	—	—	0.92(t, 7 Hz,Me_B); CH_2Me_B and $(CH_2)_2Me_A$, unclear	0.77 (t, 7 Hz, Me_A);

a) A, CD_3COCD_3; C, $CDCl_3$. b) Chelated (1H). c) Non-chelated (1H). d) 2H, ABq. e) Analyzed as AMX: 2.90 (H_B, $J_{A,B}$=5 Hz), 3.26 ($H_{B'}$, $J_{A,B'}$=3 Hz); $J_{B,B'}$=18 Hz. f) Analyzed as AMX: 2.84 (H_B, $J_{A,B}$=5 Hz), 3.16 ($H_{B'}$, $J_{A,B'}$=4 Hz); $J_{B,B'}$=18.5 Hz. g) Analyzed as AMX: 2.81 (H_B, $J_{A,B}$=5 Hz), 3.09 ($H_{B'}$, $J_{A,B'}$=8.5 Hz); $J_{B,B'}$=18.5 Hz.

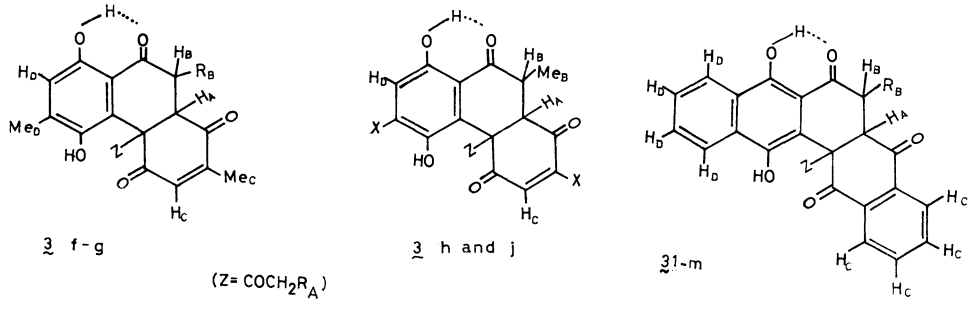

a dimer to a phenanthrenequinone derivative. Finally, **3** was confirmed by X-ray analysis.

The Stereochemistry of the Dimers. The structures of the dimers, including their stereochemistry, were unequinvocally resolved by X-ray structure analysis. It was carried out for the monoacetyl derivative of

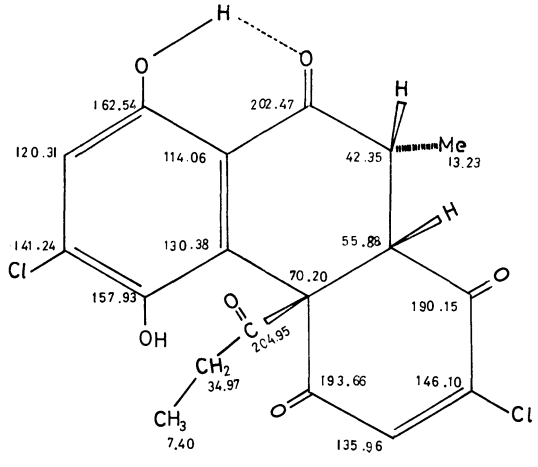

Fig. 1. Carbon chemical shifts of **3h** in $CDCl_3$(δ/ppm).

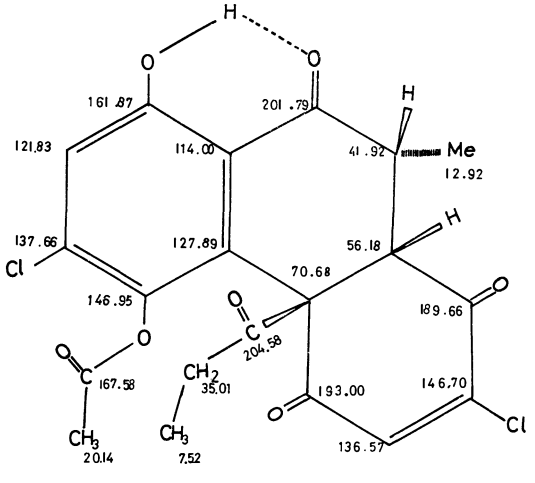

Fig. 2. Carbon chemical shifts of **7** in $CDCl_3$ (δ/ppm).

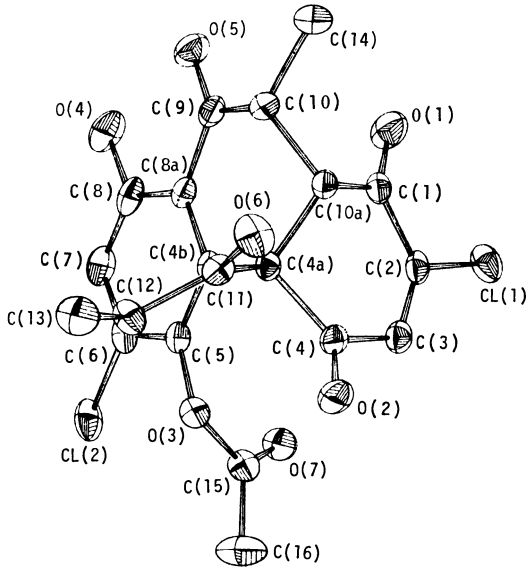

Fig. 3. Perspective view of **7**.

the dimer of **2h** because the dimer itself gave no satisfactory single crystals. The monoacetyl derivative was prepared by treating the dimer with Ac_2O–*p*-TsOH; it showed a ^1H NMR spectrum quite similar to that of the parent dimer (Table 2). Its ^{13}C NMR spectrum was also similar to that of the dimer (Fig. 2).

Figure 3 presents a stereoscopic view of one molecule. Here, the acetyl derivative has the structure and complete stereochemistry shown in **7**. Accordingly, those

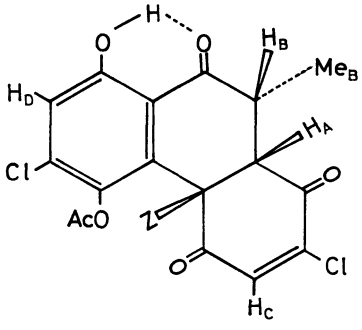

7 (Z=$COCH_2Me_A$)

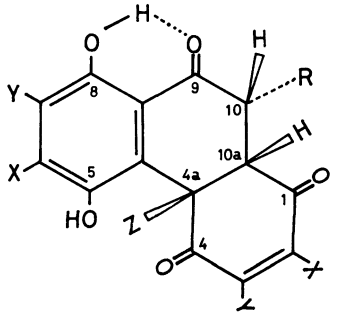

8 (Z=$COCH_2R$) 4aα-Acyl-10β-alkyl-5,8-dihydroxy-4aα,10aα-dihydro-1,4,9(10*H*)-phenanthrenetrione.

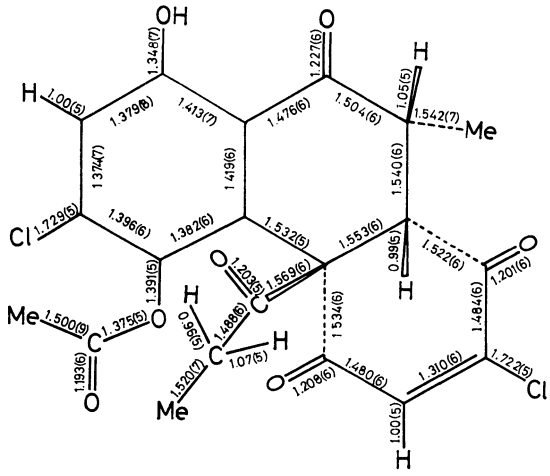

Fig. 4. Bond lengths of **7** (*l*/Å).

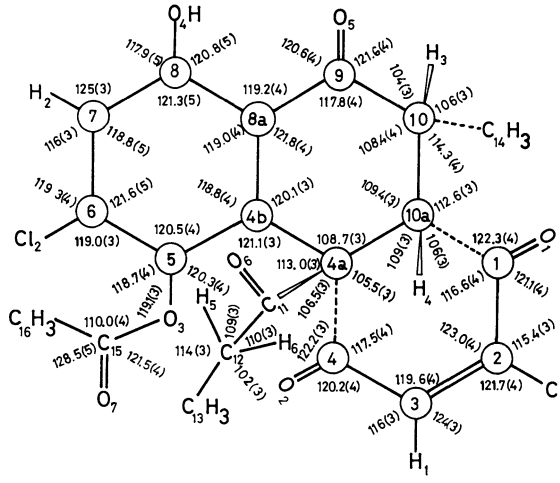

∠C(4)–C(4a)–C(4b), 114.2(3); ∠C(10a)–C(4a)–C(11), 108.5(3); ∠C(9)–C(10)–C(14), 114.4(4); ∠C(10a)–C(10)–H(3), 109(3); ∠C(10)–C(10a)–H(4), 109(3); ∠C(1)–C(10a)–C(4a), 109.6(3); ∠O(6)–C(11)–C(4a), 118.0(4); ∠O(6)–C(11)–C(12), 123.7(4); ∠C(4a)–C(11)–C(12), 118.3(3); ∠C(11)–C(12)–C(12)–C(13), 113.7(4); ∠H(5)–C(12)–H(6), 108(4).

Fig. 5. Numbering of atoms and bond angles (φ/°) of **7**.

of the dimers should be shown as **8**, confirming **3** as the sketletal structure. The *cis* disposition of the hydrogen atom at C_{10a} and the acyl group at C_{4a} indicates that the condensation proceeds through a *cis* addition. The disposition of the hydrogen atoms at C_{10} and C_{10a} was also clarified as *cis*.

Mechanistic Consideration. The following mechanism may be the most plausible. In many cases, the Diels-Alder reaction resulted in the preferential formation of a certain one of the possible orientational and stereochemical isomers. Photochemically formed enols have been known to undergo the Diels-Alder reaction with dienophiles.[3] If the above mechanism indeed holds, the condensation of the enol, **9**, with the other kinds of dienophiles should proceed. However, the expected products, **10**, **11**, or **12**, were not obtained and the dimer **8** was still the only isolable product when the

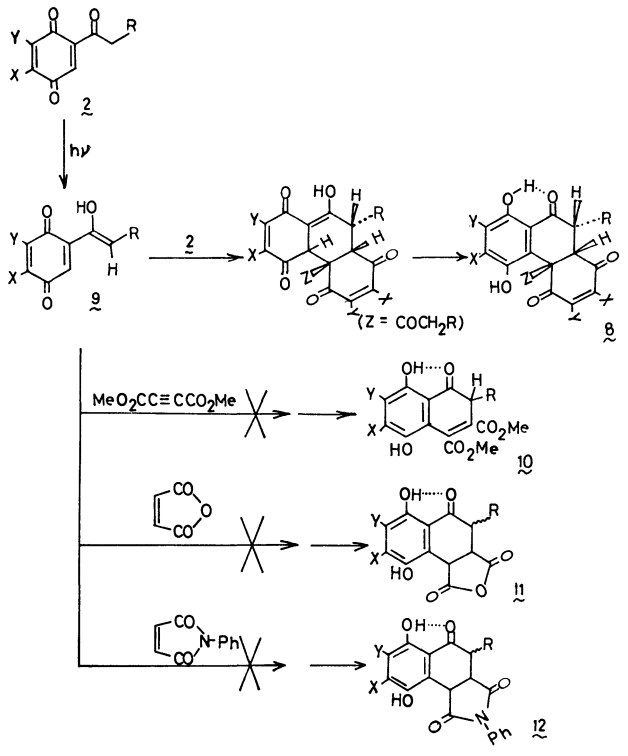

reaction was carried out in the presence of twice as many moles of maleic anhydride, *N*-phenylmaleimide, or dimethyl acetylenedicarboxylate.

In contrast to the above dimerization, the other type of dimer, **13**, was obtained by the irradiation of degassed solutions of **2a**—**c** in the presence of Rose Bengal.[4] The mechanisms of the above two dimerizations are now under investigation.

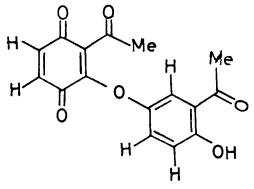

13

Experimental

2-Acylhydroquinones (1). **1a**—**j** were prepared from hydroquinones and carboxylic acids by known methods.[5-7] **1k**—**m** were photochemically prepared from 1,4-naphthoquinone and aldehydes by a known method.[8] All the new compounds gave satisfactory results in elemental analyses and

Table 3. Physical data of 2-acyl-1,4-quinones (**2**)

	X	Y	R	Mp/°C	Found (%) (Calcd (%)) C	H	X	Molecular formula	^{1}H NMR: δ ($CDCl_3$) Aliphatic	Aromatic	Method of prepn.	Yield %
a	H	H	H	62.5—65.5	Known compound[a]				2.57 (3H, s, Ac)	6.94 (2H, d[d]) 7.10 (1H, d[d])	A	90
b	H	H	Me	36—37	65.89 (65.85	5.04 4.91)	—	$C_9H_8O_3$	1.14 (3H, t, 7 Hz, Me) 2.88 (2H, q, 7 Hz, CH_2)	6.70 (2H, d[d]) 6.88 (1H, d[d])	A	80
c	H	H	Et	39—40.5	67.47 (67.40	5.63 5.66)	—	$C_{10}H_{10}O_3$	0.98 (3H, t, 7 Hz, Me) 1.70 (2H, sex, 7 Hz, CH_2) 2.85 (2H, t, 7 Hz, $COCH_2$)	6.88 (2H, d[d]) 7.02 (1H, s)	A	80
d	H	H	*n*-Pr	37.5—39	68.98 (68.73	6.21 6.29)	—	$C_{11}H_{12}O_3$	0.93 (3H, t, 7 Hz, Me) 1.2—1.7 (4H, m, $(CH_2)_2$) 2.87 (2H, t, 7 Hz, $COCH_2$)	6.81 (2H, d[d]) 6.93 (1H, d[d])	C	65
e	H	H	*n*-Bu	50.5—52	69.58 (69.88	6.95 6.84)	—	$C_{12}H_{14}O_3$	0.86 (3H, t, 7 Hz, Me) 1.2—1.6 (6H, m, $(CH_2)_3$) 2.70 (2H, t, 7 Hz, $COCH_2$)	6.60 (2H, d[d]) 6.74 (1H, d[d])	C	60
f	Me	H	H	78—80	65.90 (65.85	5.07 4.91)	—	$C_9H_8O_3$	2.10 (3H, d, 1.5 Hz, Me) 2.56 (3H, s, Ac)	6.64 (1H, q, 1.5 Hz) 7.00 (1H, s)	A	90
g	Me	H	Me	40—41	67.32 (67.40	5.59 5.66)	—	$C_{10}H_{10}O_3$	1.15 (3H, t, 7 Hz, Me) 2.10 (3H, d, 1.5 Hz, Me) 2.90 (2H, q, 7 Hz, CH_2)	6.62 (1H, q, 1.5 Hz) 6.92 (1H, s)	A	80
h	Cl	H	Me	51—54	54.70 (54.41	3.41 3.53	18.00 17.88)	$C_9H_7O_3Cl$	1.17 (3H, t, 7 Hz, Me) 2.91 (2H, q, 7 Hz, CH_2)	7.01 (1H, s) 7.10 (1H, s)	B	80
i	Br	H	H	93—96	42.74 (42.90	2.38 2.18	34.87 34.92)	$C_8H_5O_3Br$	2.57 (3H, s, Ac)	7.17 (1H, s) 7.30 (1H, s)	B	70
j	Br	H	Me	56—58	b			$C_9H_7O_3Br$	1.15 (3H, t, 7 Hz, Me) 2.87 (2H, q, 7 Hz, CH_2)	7.14 (1H, s) 7.33 (1H, s)	B	50
k	-(CH=CH)$_2$-		H	83.5—84	Known compound[c]				2.50 (3H, s, Ac)	6.92 (1H, d[d]) 7.5—7.6 (2H, m) 7.8—7.9 (2H, m)	A	90
l	-(CH=CH)$_2$-		Me	78.5—80	72.59 (72.89	4.98 4.71)	—	$C_{13}H_{10}O_3$	1.18 (3H, t, 6 Hz, Me) 2.96 (2H, q, 6 Hz, CH_2)	7.10 (1H, s) 7.8—7.9 (2H, m) 8.1—8.2 (2H, m)	A	80
m	-(CH=CH)$_2$-		Et	58—59	73.49 (73.67	5.37 5.30)	—	$C_{14}H_{12}O_3$	0.97 (3H, t, 7 Hz, Me) 1.68 (2H, sex, 7 Hz, CH_2) 2.87 (2H, t, 7 Hz, $COCH_2$)	7.06 (1H, s) 7.8—7.9 (2H, m) 8.1—8.2 (2H, m)	A	80

a) Ref. 12. b) Satisfactory results were not obtained because of the hygroscopic character of the sample. c) Ref. 9.
d) Slightly splitting.

the expected values of *m/e* for the molecular peaks in the mass spectroscopy. The melting points of **1a**—**m** were: **a**, 200—202 °C, lit, 201—203 °C,[6] 204 °C;[7] **b**, 97—99 °C, lit, 96 °C;[7] **c**, 91 °C;[7] **d**, 61—62.5 °C; **e**, 82—83 °C; **f**, 149—150 °C, lit, 141 °C;[7] **g**, 110—116 °C; **h**, 127—129 °C; **i**, 144—156 °C; **j**, 121—123 °C; **k**, 215—216 °C, lit, 210—211 °C,[9] 206 °C,[10] and 216—217 °C;[11] **l**, 187—189 °C;[8] **m**, 151—153 °C.

2-(Acetyl-d_3)hydroquinone (4a) and 2-(Propanoyl-2-d_2)hydroquinone (4b). A solution of **3a** or **3b** (1 g) in dioxane (30 ml) and a solution of NaOH (1 equiv) in D_2O (3 ml) were successively syringed into a flask equipped with a rubber-serum cap and purged with nitrogen. The solution immediately turned reddish yellow. After stirring for 0.5 h, deuteriochloric acid (1.5 equiv) was added (the color of the solution thereupon turned back yellow). The solution was concentrated to yellow crystals, which were subsequently recrystallized from aqueous acetone to give **4a** or **4b**, respectively; mp: **4a**, 200—202 °C; **4b**, 96—98 °C. They showed no ^1H NMR signals due to methyl or methylene protons adjacent to a carbonyl group and the expected values of *m/e* for the molecular peaks in the mass spectroscopy.

2-Acyl-1,4-benzoquinones (2). These substances were prepared by one of the following methods. The yields were usually high, but showed less constancy. Their physical data are tabulated in Table 3.

Method A: This was originally described by Kloetzel *et al.*[12] A solution of **1** (1 g) in benzene (20 ml; for **1a**—**c**, **f**, and **g**) or diethyl ether (100 ml; for **1k**—**m**) was stirred with silver oxide (3 g) and magnesium sulfate (1.5 g) for 0.5 h. The powder was then filtered off and washed with diethyl ether under a slightly reduced pressure to prevent moisture from being condensed on the filtrate. The residue obtained by the concentration of the filtrate was submitted to sublimation under a vacuum to give **2a**—**j**. **2k**—**m** were purified by recrystallization from ligroin.

The partially deuterated monomers (**5a**—**b**) were prepared from **4a**—**b**. **5a**—**b** were not subjected to elemental analysis, but they gave satisfactory results in the mass and ^1H NMR spectroscopies.

Method B: When **1h** and **1i** were oxidized by Method A, many unsublimable solids remained. The use of DDQ was successful for oxidation. A solution of the calculated amount of DDQ in acetonitrile (20 ml) was added to a stirred solution of **1h** or **1i** (1 g) in acetonitrile (20 ml). Immediately the solution became deeply colored, and a colorless powder soon began to precipitate. After *ca.* 15 min the solution turned yellow and precipitation had ended. After filtration, the filtrate was concentrated to a residue, which was submitted to sublimation under a vacuum to give **2h**—**i**.

Method C: **2d** and **2e** were very hygroscopic. When Method A was apllied, a dirty colored syrup was left by the concentration of the filtered reaction solution. A method to avoid to contact with moisture was devised as follows. A solution of **1d** or **1e** (1 g) in acetonitrile (20 ml) was charged into a two-necked flask equipped with a rubber-serum cap. The flask was connected to a vacuum line, and the solution was then degassed by the thaw-freeze-pump method. Through the serum cap a solution of the calculated amount of DDQ in acetonitrile (10 ml) was syringed in. The change in the color of the reaction was the same as in method B. After *ca.* 15 min, the solvent was evaporated by bulb-to-bulb distillation through the vacuum line. The residual powder, composed of dichlorodicyanohydroquinone and **2**, was submitted to sublimation under a vacuum to isolate **2a**—**e**.

Preparation of the Dimers (3). Solutions of **2** were sealed in Pyrex glass tubes after having been degassed by the thaw-freeze-pump method and irradiated externally by means of a 300W high-pressure Hg-arc lamp for the appropriate times. The homogeneous reaction solutions, or the filtrates when solid products had been crystallized out, were concentrated to semi-solid residues, which were then submitted to sublimation under a vacuum to recover the **2**. The residues on sublimation were repeatedly rinsed with benzene to remove any tarry materials.[13] The remaining dirty yellow crystals, combined with the crystals which had been filtered off from the reaction solutions, were dissolved chloroform by slight warming. The solvent was evaporated in a desiccator by connecting it through a calcium chloride tube to a water pump. The solid residues were repeatedly rinsed with benzene. This process was repeated several times to give the pure dimers (**3**), *i. e.* **8**, which decomposed on silica-gel chromatography.

Table 4. Elemental analyses of the dimers **3**[a]

	Mp/°C[b]	Found (%) (Calcd (%)) C	H	X	Formula ($C_lH_mO_nX_x$): *l-m-n-x*
a	154—156	63.96 (64.00	4.25 4.03)	—	16-12-6
c	c	67.52 (67.40	5.61 5.66)	—	20-20-6
d	137—142	68.79 (68.73	6.41 6.29)	—	22-24-6
e	c	69.91 (69.88	6.99 6.84)	—	24-28-6
f	159—161	65.61 (65.85	4.80 4.91)	—	18-16-6
h	c	54.13 (54.41	3.46 3.53	18.09 17.88)	18-14-6-2
l	c	73.09 (72.89	4.40 4.71)	—	26-20-6
m	c	73.94 (73.67	5.44 5.30)	—	28-24-6

a) For **3b**,[c] **g**,[c] and **j**,[c] satisfactory results were not obtained because of the contamination by a trace amount of tarry materials, which could not be eliminated by repeated purification. b) Measured in a vacuum-sealed capillary. c) Melting gradually because of thermal decomposition.

The results of the elemental analyses are shown in Table 4. All the dimers gave the expected values of the molecular peaks in the mass spectrometry. Some of the dimers showed their melting points sharply in vacuum sealed capillaries, but the others melted gradually because of thermal decomposition. All the dimers showed similar IR and UV spectral data. Those of **3c** are representative; IR (KBr): ν 3500 (broad), 2980, 2950 (shoulder), 2880, 1720, 1695, 1680, 1645, 1610 (shoulder), 1595 cm^{-1}; UV (EtOH): λ_{max} (ε) 388 (5930), 300 (3650), 275 (3900), 222 (31200) nm.

The partially deuterated dimers (**6**) were similarly prepared from **5**. Elemental analyses were not performed for **6**, but satisfactory results were obtained in the mass spectrometry.

The Monoacetyl Derivative of 3h (7). A homogeneous solution obtained by the occasional swirling of a suspension of **3h** (0.5 g) in acetic anhydride (20 ml) containing one crop of *p*-toluenesulfonic acid was left standing at room temperature for 2 days. The solvent was then evaporated by bulb-to-bulb distillation through a vacuum line. Upon standing *in vacuo* overnight, the strupy residue became a semi-solid, which was subsequently dissolved in chloroform after rinsing with benzene.[14] The solution was concentrated to a solid, which was

Table 5A. Final atomic coordinates ($\times 10^4$) and thermal parameters* ($\times 10^4$), with their estimated standard deviations in parentheses

	x	y	z	B_{11}	B_{22}	B_{33}	B_{12}	B_{13}	B_{23}
Cl(1)	7568(2)	−2130(1)	3896(1)	275(3)	56(1)	68(1)	36(2)	−67(2)	−3(1)
Cl(2)	2906(2)	344(1)	619(1)	329(3)	93(1)	33(1)	27(3)	−33(2)	−20(1)
O(1)	9036(4)	−230(3)	3835(3)	198(6)	78(3)	116(3)	52(6)	102(7)	54(4)
O(2)	3465(3)	226(3)	4148(2)	179(5)	98(3)	45(1)	−34(6)	66(4)	20(3)
O(3)	3032(3)	411(2)	2372(2)	159(4)	53(2)	38(1)	11(4)	12(3)	−18(2)
O(4)	8164(5)	1621(3)	1293(2)	316(8)	112(3)	68(2)	−19(8)	−184(7)	38(4)
O(5)	9365(4)	1897(3)	2737(2)	176(5)	88(3)	84(2)	−15(6)	94(5)	36(4)
O(6)	5151(4)	2221(3)	4559(2)	257(6)	92(3)	36(1)	31(7)	8(4)	−39(3)
O(7)	3332(3)	−1209(2)	2153(2)	183(5)	58(2)	67(2)	17(5)	29(5)	−20(3)
C(1)	7756(5)	−126(3)	3926(2)	147(6)	71(3)	41(2)	23(7)	16(5)	35(4)
C(2)	6729(5)	−987(3)	3895(2)	206(7)	54(2)	28(1)	−2(7)	−11(5)	15(3)
C(3)	5282(5)	−894(3)	3877(2)	193(7)	61(3)	32(2)	−26(7)	1(5)	14(3)
C(4)	4616(5)	106(3)	3883(2)	153(6)	76(3)	24(1)	−37(7)	21(4)	13(3)
C(4a)	5498(4)	972(3)	3601(2)	135(5)	50(2)	26(1)	−5(6)	20(4)	7(3)
C(4b)	5588(4)	958(3)	2696(2)	157(6)	39(2)	26(1)	26(5)	30(4)	10(3)
C(5)	4388(4)	651(3)	2132(2)	162(6)	46(2)	31(1)	31(6)	35(5)	0(3)
C(6)	4456(5)	694(3)	1306(2)	246(8)	49(2)	29(1)	51(7)	10(6)	−9(3)
C(7)	5712(6)	1026(4)	1027(3)	294(10)	69(3)	34(2)	33(9)	74(7)	4(4)
C(8)	6940(6)	1304(3)	1581(3)	260(9)	56(3)	46(2)	38(8)	120(7)	26(4)
C(8a)	6907(5)	1287(3)	2421(2)	157(6)	49(2)	41(2)	15(6)	61(5)	21(3)
C(9)	8218(5)	1648(3)	2986(3)	148(6)	52(3)	60(2)	12(7)	60(6)	38(4)
C(10)	8071(5)	1744(3)	3865(3)	143(6)	66(3)	46(2)	−46(7)	13(5)	18(4)
C(10a)	7107(4)	879(3)	4086(2)	149(6)	53(2)	34(1)	−17(6)	2(5)	15(3)
C(11)	4769(5)	1943(3)	3874(2)	158(6)	57(2)	31(1)	−24(6)	32(5)	−15(3)
C(12)	3615(5)	2451(3)	3280(3)	162(7)	63(3)	42(2)	46(7)	2(6)	−18(4)
C(13)	3034(5)	3403(4)	3599(3)	192(8)	67(3)	71(3)	29(8)	39(8)	−46(5)
C(14)	9569(6)	1875(4)	4441(4)	184(8)	106(5)	79(3)	−101(10)	−45(8)	32(6)
C(15)	2539(5)	−553(3)	2304(3)	178(7)	63(3)	44(2)	6(7)	1(6)	−23(4)
C(16)	952(6)	−609(5)	2452(4)	153(8)	106(5)	121(5)	−50(10)	83(10)	−72(8)

*The anisotropic thermal factors are of the form: $\exp\{-(h^2B_{11}+k^2B_{22}+l^2B_{33}+hkB_{12}+hlB_{13}+klB_{23})\}$.

Table 5B. Final atomic coordinates ($\times 10^3$), with their estimated standard deviations in parentheses

	x	y	z
H(1)	458(5)	−146(4)	386(3)
H(2)	563(6)	109(4)	43(3)
H(3)	747(5)	241(4)	390(3)
H(4)	706(5)	90(4)	467(3)
H(5)	284(6)	199(4)	308(3)
H(6)	410(6)	271(4)	278(3)

again rinsed with benzene. By repeating this process, faint yellow crystals of **7** were obtained; 150 mg. These crystals gradually melted at 180—190 °C. Found: C, 54.30; H, 3.48; Cl, 16.01%. Calcd for $C_{20}H_{16}O_7Cl_2$: C, 54.66; H, 3.64; Cl, 16.17%. ^{1}H NMR ($CDCl_3$): δ 1.06 (3H, t, J=7 Hz, Me_A), 1.49 (3H, d, J=7 Hz, Me_B), 2.23 (3H, s, OAc), 2.68 (1H, dq, J=7 and 3.5 Hz, H_B), 4.21 (1H, d, J=3.5 Hz, H_A), 7.16 (1H, s, H_C), 7.32 (1H, s, H_D), 12.88 (1H, s, chelated OH) ($COCH_2$–Me_A: unclear). MS: *m/e* 440 and 438 (M^+).

X-Ray Structure Analysis. The molecular structure of **7** was determined by X-ray structure analysis. The crystal data were: monoclinic, $P2_1/c$, a=9.052 (2), b=13.512 (2), c=16.750 (3) Å, β=99.39 (2)°, V=2021.1 (7) Å^3. Z=4, D_m=1.449, D_c=1.445 g·cm^{-3}. A single crystal of approximately 0.26×0.25×0.18 mm was used for the intensity measurement. The cell constants were determined by the least-squares treatment of the angular settings of 20 reflections measured on a Rigaku computer-controlled four-circle diffractometer with Ni-filtered Mo $K\alpha$ radiation. The intensities were measured by the θ-2θ scan technique, with a scan speed of 2° min^{-1} in θ. The intensities of 3248 independent reflections were collected within $\sin\theta/\lambda \leq 0.65$. The structure of **7** was solved by the heavy-atom method and refined by the blok-diagonal least-squares method. The difference Fourier synthesis computed after the anisotropic refinement of the non-hydrogen atoms revealed the positions of all the hydrogen atoms except the methyl and hydroxyl hydrogen atoms. The final refinement, including the contribution of these hydrogen atoms with isotropic temperature factors, reduced the R-value to 0.074 without F_{obsd}=0. The final atomic coordinates are given in Table 5, while the bond lengths and angles are shown in Figs. 4 and 5 respectively.

We wish to thank Dr. Yoshitaka Itatani, Faculty of Pharmaceutical Sciences, Kanazawa University, for the NMR measurements and for his valuable discussions. One of the authors (Y. M.) is also especially grateful to The Institute for Protein Research, Osaka University, for supporting his stay for X-ray analysis.

References

1) J. M. Bruce, *Quart. Rev.*, **21**, 405 (1967); "The Chemistry of the Quininoid Compounds," ed by S. Patai, John Wiley & Sons, London (1974), p. 465.

2) Y. Miyagi, K. Kitamura, K. Maruyama, and Y. L. Chow, *Chem. Lett.*, **1978**, 33.
3) N. C. Yang and C. Rives, *J. Am. Chem. Soc.*, **83**, 2213 (1961).
4) K. Maruyama, N. Narita, and Y. Miyagi, *Chem. Lett.*, **1978**, 1033.
5) E. C. Armstrong, R. L. Bent, A. Loria, J. R. Thirtle, and A. Weissberger, *J. Am. Chem. Soc.*, **82**, 1932 (1960).
6) G. C. Amin and N. M. Shah, *Org. Synth.*, Coll. Vol. III, 280 (1955).
7) E. Kurosawa, *Nippon Kagaku Zashii*, **78**, 312 (1957).
8) K. Maruyama, *Bull. Inst. Chem. Res. Kyoto Univ.*, **50**, 348 (1972).
9) G. Read and V. M. Ruiz, *J. Chem. Soc., Perkin Trans. 1*, **1973**, 235.
10) C. J. P. Spruit, *Recl. Trav. Chim. Pays-Bas*, **66**, 655 (1947).
11) D. J. Cram, *J. Am. Chem. Soc.*, **71**, 3953 (1949).
12) M. C. Kloetzel, R. P. Dayton, and B. Y. Abadir, *J. Org. Chem.*, **38**, 40 (1955).
13) The dimers were hardly soluble in benzene after having been purified once but they did not crystallize out from the reaction solutions in benzene.
14) The washings contained **7** and the diacetyl derivative, **14**.

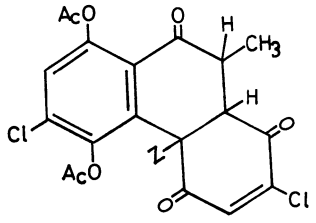

(Z=COC$_2$H$_5$)

14

Structure of a New Ionone Derivative, Nigakialcohol from *Picrasma ailanthoides* PLANCHON[1)]

Yayoi SUGIMOTO, Takaaki SAKITA, Toru IKEDA, Yoshihiko MORIYAMA, Tatsushi MURAE, Takahiko TSUYUKI, and Takeyoshi TAKAHASHI*

Department of Chemistry, Faculty of Science, The University of Tokyo, Hongo, Bunkyo-ku, Tokyo 113

(Received March 31, 1979)

A new ionone derivative, nigakialcohol, was isolated from the leaves of *Picrasma ailanthoides* PLANCHON (Simaroubaceae), the structure being found to be (4*R*,5*S*)-4-[(*R*)-3-hydroxybutyl]-5-hydroxymethyl-3,3-dimethyl-1-cyclohexanone. Nigakilactones E, F, and H and vomifoliol were also isolated from the leaves.

Bitter principles isolated from Simaroubaceae have been extensively investigated.[2-4)] Some of them show antileukemic activity.[5)] *Picrasma ailanthoides* PLANCHON (Japanese name: Nigaki) is one of two species belonging to Simaroubaceae grown in Japan. A number of bitter principles were isolated from the bark and stem of the plant and their structures elucidated.[3,4)] In connection with these studies, we examined constituents of the leaves of the plant and isolated vomifoliol[6)] (blumenol A[7)]) and a new ionone derivative (**1**, named nigakialcohol) as non-bitter principles, as well as three bitter principles, nigakilactones E,[3a)] F,[3a)] and H.[3b)] In this paper we wish to report on the determination of the structure of nigakialcohol (**1**).

Dried leaves of the plant were extracted with hot water. The aqueous extract was concentrated and extracted with benzene. The benzene extract was subjected to separation by chromatography to afford a new compound (**1**; yield 0.003%, $[\alpha]_D^{24}$ 0°), which is not bitter. The IR and ^{1}H NMR spectra suggested the presence of two tertiary methyls (δ 0.80 and 1.08, each 3H, s), a secondary methyl (δ 1.23, 3H, d), two hydroxyls (δ 2.26, 2H, s-like; disappeared on addition of D_2O; ν_{OH} 3400 cm^{-1}), three protons (δ 3.30—4.10, 3H, m) attached to carbon atoms bearing hydroxyls, a saturated carbonyl group ($\nu_{C=O}$ 1700 cm^{-1}), and α- and α'-methylene protons (δ 2.00—2.60, 4H, m) adjacent to the carbonyl group. The molecular formula, $C_{13}H_{24}O_3$, was inferred from elemental analysis and high resolution mass spectrum which gave no molecular ion peak but a fragment ion peak at *m/e* 210.1620 ($C_{13}H_{22}O_2$) due to dehydration.

The presence of a primary alcohol and a secondary alcohol was suggested for **1** from the spectral data. This is supported by the following evidence. Acetylation of nigakialcohol (**1**) with acetic anhydride and pyridine afforded nigakialcohol diacetate (**2**) and monoacetate I (**3**). The NMR spectrum of the diacetate (**2**) showed that one acetoxyl is attached to a methylene carbon and another to a methine carbon, while the spectrum of the monoacetate I (**3**) revealed the presence of a secondary alcohol and an acetoxyl group on methylene carbon. On the other hand, another monoacetate, nigakialcohol monoacetate II (**4**) could be obtained by partial hydrolysis of diacetate (**2**) with alumina. The NMR spectrum of **4** showed the presence of a primary alcohol and an acetoxyl group on methine carbon (*cf.* Experimental).

In the NMR measurement of **1** using Eu(dpm)$_3$ as a shift reagent, one of three protons (due to –C<u>H</u>OH and –C<u>H</u>$_2$OH) giving a multiplet at δ 3.30—4.10, appeared at δ 13.85—14.65, the doublet corresponding to the secondary methyl being observed at δ 4.78 (d, J= 6 Hz). On irradiation at δ 14.28 (due to –C<u>H</u>OH), the doublet changed into a singlet. This shows the presence of the partial structure CH_3–C<u>H</u>–OH for nigakialcohol (**1**).

The molecular formula, $C_{13}H_{24}O_3$, of nigakialcohol and a comparison of the IR and NMR spectra of nigakialcohol with those of vomifoliol[6,7)] suggest the presence of an ionone skeleton for nigakialcohol. The above observation could lead to a structure **1a** for nigakialcohol.

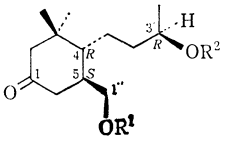

	R^1	R^2
1	H	H
2	Ac	Ac
3	Ac	H
4	H	Ac

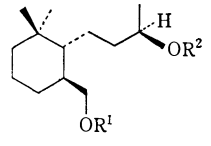

	R^1	R^2
5	H	H
11	Ac	Ac
12	Ac	H
13	H	Ac

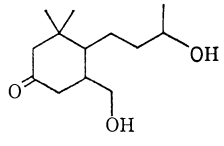

1a

The presence of the ionone skeleton for **1** was shown as follows. Nigakialcohol (**1**) was subjected to Huang-Minlon reduction to afford deoxonigakialcohol (**5**) as an oil, $[\alpha]_D^{30}$ −28°. (±)-Deoxonigakialcohol was synthesized from (±)-γ-ionone (**6**) in four steps. (±)-γ-Ionone (**6**)[8,9)] was epoxidized with *m*-chloroperbenzoic acid in chloroform to afford a mixture of epoxy ketones (**7**) quantitatively.[10)] The mixture of epoxy ketones (**7**) gave one spot on TLC and a single peak on GLC examination. However, NMR measurement revealed that the product consists of two isomeric epoxy ketones in a ratio of 2:1 (*cf.* Experimental). The coupling constant values of the olefinic protons in the side chain for two isomers are identical, indicating that they are

configurational isomers between the side chain and the oxirane ring.

A mixture of **7** was treated with boron trifluoride etherate in toluene at 0 °C. An unsaturated keto aldehyde (**8**) obtained in 70% yield was found to be a mixture of two isomers in a ratio of 3:2 (by NMR measurement) which, without further separation, was subjected to reduction with sodium borohydride.

The reduction product was purified by column chromatography to give two diols **9** (R_f 0.36) and **9'** (R_f 0.30) in a ratio of 3:1. The IR and MS spectra of **9** and **9'** were almost the same. On GLC examination, each diol was found to be a mixture of two isomeric diols. NMR measurement also revealed that each diol consists of two isomers (*cf.* Experimental). In the NMR measurement using Eu(fod)$_3$-d_{27} as a shift reagent for **9** and **9'**, a doublet appearing at δ 1.26, changed into a pair of doublets at δ 2.25 (d, J=6 Hz) and δ 2.30 (d, J=6 Hz), and at δ 2.20 (d, J=6 Hz) and δ 2.25 (d, J=6 Hz), respectively.

Finally, the unsaturated diols **9** and **9'** were catalytically hydrogenated to afford saturated diols **10** and **10'**, respectively. **10** and **10'** gave almost the same IR spectra, minute differences being observed in the MS and NMR spectra. Each diol was found to be a mixture of two isomeric diols by NMR, GLC, and HPLC examinations. Their retention times on GLC and HPLC together with those of deoxonigakialcohol (**5**) are given in Table 1. Diol **10** was subjected to separation by preparative HPLC to give diols **10a** and **10b**. The synthetic diol **10a** was identical with deoxonigakialcohol (**5**) with respect to IR, MS, NMR, R_f on TLC, and R_t on GLC and HPLC (Table 1).

Table 1. R_f and R_t values on TLC, GLC, and HPLC for **5**, **10**, **10'**, **10a**, **10b**

	5	**10**	**10'**	**10a**	**10b**
R_f[a]	0.34	0.34	0.32	0.34	0.34
R_t on GLC[b] (min)	16.75	{16.83 17.78	{16.47 17.60		
R_t on HPLC[c] (min)	31.0	{27.5 30.8	{33.2 35.1	30.8	27.5

a) Developed with ether. b) Column: 10% FFAP Uniport B, 1.5 m, temperature 200 °C, a flow rate of N_2: 60 ml/min. c) Column: μ-Porasil 1/8 (inch) × 1 (foot), solvent system: 2.5% methanol–dichloromethane, flow rate: 0.5 ml/min, pressure: *ca.* 450 psi, detection: an RI detector.

The absolute configurations of chiral centers at C-5 and C-3' for nigakialcohol (**1**) were determined by an MTPA ester method; this method was recently developed by Yamaguchi and Yasuhara in order to determine the absolute configurations of secondary alcohols[11] and primary alcohols with the chiral center at the 2-position.[12]

Acetylation of deoxonigakialcohol (**5**) yielded a diacetate (**11**), which was partially hydrolyzed over alumina to afford deoxonigakialcohol monoacetate I and II (**12** and **13**). Nigakialcohol monoacetate I and II (**3** and **4**) and deoxonigakialcohol monoacetate II

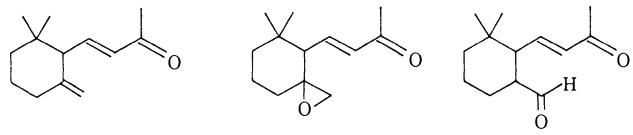

6 **7** **8**

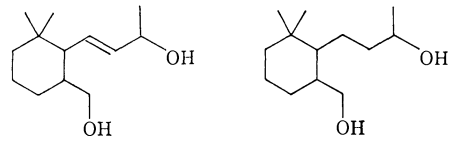

9 **10**

(**13**) were converted into the corresponding (*R*)-(+)-α-methoxy-α-trifluoromethylphenylacetic acid [(*R*)-(+)-MTPA; Mosher's reagent] esters (**A**) and (*S*)-(−)-MTPA esters (**B**), respectively, by Mosher's method.[13] The LIS (lanthanoid induced shift) values of the three pairs of diastereomeric esters are given in Table 2. The ΔLIS_{OMe} values[11,12] (−0.46 and −0.60) for MTPA esters of nigakialcohol monoacetate II (**4**) and deoxonigakialcohol monoacetate II (**13**) show a negative sign, indicating that the chiral center at C-5 of **4** is in *S*-configuration.[12] On the other hand, the positive sign of ΔLIS_{OMe} value (+2.06) was observed for MTPA esters of nigakialcohol monoacetate I (**3**). This indicates that the chiral center at C-3' is in *R*-configuration.[11] This is in line with the absolute configuration determination by Horeau's method.[14]

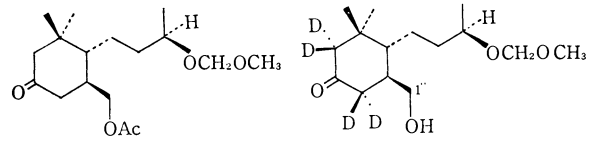

14 **15**-d_4

Table 2. Lanthanoide induced shift (LIS) values of the methoxyl group in the acid moiety for (*R*)-(+)- and (*S*)-(−)-MTPA esters[a]

Monoacetate	LIS_{OMe} value for (*R*)-(+)-MTPA ester, **A**	LIS_{OMe} value for (*S*)-(−)-MTPA ester, **B**	ΔLIS_{OMe} value ($LIS_A - LIS_B$)	Absolute configuration
3	4.89	2.83	+2.06	*R*(C-3')
4	1.09	1.55	−0.46	*S*(C-5)
13	3.33	3.93	−0.60	*S*(C-5)

a) Determined at the molar ratio of Eu(fod)$_3$-d_{27}/each ester (1:1) for a *ca.* 1.3 mmol/ml solution of each ester in CCl_4.

The absolute configuration of the asymmetric center at C-4 could be determined by the measurement of coupling constant between $C_{(4)}$–H and $C_{(5)}$–H in a tetradeuterio derivative (**15**-d_4) derived from nigakialcohol (**1**). Nigakialcohol monoacetate I (**3**) was treated with dimethoxymethane[15] and phosphorus pentaoxide to afford nigakialcohol monoacetate I methoxymethyl ether (**14**). Deuteriation of **14** proceeded

with concomitant hydrolysis of the acetoxyl group at C-1″ to give **15**-d_4. In the NMR measurement of **15**-d_4 using Eu(fod)$_3$-d_{27} as a shift reagent, a broad signal due to a proton on C-5 and a broad signal due to methylene protons (-C$\underline{H}_2$OH) appeared at δ 2.20—2.50 and δ 4.25—4.66, respectively. On irradiation at δ 4.46, the broad signal due to the proton on C-5 collapsed into a doublet, coupled with a proton on C-4 with a coupling constant, J=11.5 Hz. Since the large coupling constant suggests a *trans*-relationship between $C_{(5)}$–H and $C_{(4)}$–H, the asymmetric carbon atom at C-4 position could be concluded to be in *R*-configuration.

The structure including the absolute configuration of nigakialcohol should be represented by (4*R*,5*S*)-4-[(*R*)-3-hydroxybutyl]-5-hydroxymethyl-3,3-dimethyl-1-cyclohexanone.

Experimental

General Procedure. IR spectra were taken on a Hitachi 260-30 or a JASCO JIR-10 spectrometer. ^{1}H NMR spectra were measured on a Hitachi R-20B (60 MHz) or a JNM PS-100 (100 MHz) spectrometer (JEOL). Chemical shifts are expressed in δ (ppm) downfield from TMS as an internal standard and coupling constants in Hz. CD and ORD curves were measured on a JASCO Model J-20 spectrometer. Measurements of optical rotation $[\alpha]_D$ were carried out using a JASCO DIP-SL polarimeter. Mass spectra (MS) were obtained on a Hitachi RMU-6-Tokugata mass spectrometer and high resolution mass spectra on a Hitachi RMH-2 mass spectrometer. Gas chromatography (GLC) was carried out using Shimadzu 4A-PF equipped with a hydrogen flame ionization detector (column A: SP-1000, 2 m, N_2 60 ml/min; column B: 10% FFAP Uniport B, 1.5 m, N_2 60 ml/min). Liquid Chromatograph Model ALC/GPC 202/401 (Waters Assoc.) was used for high performance liquid chromatography (HPLC); column: μ-Porasil 1/8 (inch)×1 (foot). Thin layer chromatography (TLC) was carried out on Kieselgel GF_{254} and Kieselgel G (E. Merck) of 0.25 mm thickness for analytical and 0.5 mm thickness for preparative. Wakogel C-200 (Wako) and Activated Alumina mesh 200—300 (Showakagaku) were used for column chromatography.

*Isolation of Nigakialcohol (**1**).* Dried leaves (12 kg) of *Picrasma ailanthoides* PLANCHON were pulverized and extracted with hot water (90 °C, 70 L) for 4 h. Extraction under the same conditions was repeated twice. The combined extracts (*ca.* 200 L) were concentrated under reduced pressure to *ca.* 40 L and extracted continuously with benzene for 4 days. The benzene extracts (36.5 g), dissolved in benzene, were passed through a column of neutral alumina (2 kg, pretreated with dilute hydrochloric acid, washed with water until the washings became neutral, and then activated) and eluted with the following solvents (each fraction: 1 L). Fractions 1—4, benzene; frs 5—20, benzene–ether 1:1; frs 21—31, ether; frs 32—40, ether–ethyl acetate 1:1; frs 41—92, ethyl acetate. Fractions 60—90 (4.7 g) were subjected to separation by column chromatography on silica gel (300 g). Elution (each fraction: 40 ml) was carried out with benzene (100 ml), benzene–acetone, 4:1 (500 ml), 3:1 (800 ml), 2:1 (1.2 L), and then with 1:1 (1 L). Nigakialcohol (**1**; 306 mg) was obtained from fractions 46—76. Fractions 77—95 (129 mg) were combined and purified by rechromatography on silica gel (20 g) to afford additional nigakialcohol (**1**; 67 mg). Nigakialcohol (**1**): IR (neat) 3400 and 1700 cm^{-1}; $[\alpha]_D^{24}$ 0° (*c* 0.21, $CHCl_3$); CD (*c* 0.083, EtOH, at 24 °C) $[\theta]_{340}$ −50, $[\theta]_{323}$ 0, $[\theta]_{294}$ +310, $[\theta]_{278}$ 0, $[\theta]_{255}$ −460; ORD (*c* 0.083, EtOH, at 24 °C) $[\Phi]_{360}$ −27°, $[\Phi]_{345}$ 0°, $[\Phi]_{314}$ +180°, $[\Phi]_{298}$ 0°, $[\Phi]_{277}$ −410°, $[\Phi]_{260}$ 0°; NMR (60 MHz) δ ($CDCl_3$) 0.80, 1.08 (each 3H, s, *t*-CH_3), 1.23 (3H, d, J=6 Hz, *s*-CH_3), 2.00—2.60 (4H, m, -CH_2-CO-CH_2-), 2.26 (2H, s-like, 2×-OH; disappeared on addition of D_2O), and 3.30—4.10 (3H, m, -C$\underline{H}_2$OH and -$\underline{C}$HOH); High resolution MS, Found: *m/e* 210.1628. Calcd for $C_{13}H_{22}O_2$ $(M-H_2O)^+$: *m/e* 210.1620. Found: *m/e* 213.1456. Calcd for $C_{13}H_{21}O_3$ $(M-CH_3)^+$: *m/e* 213.1491; Found: C, 65.99; H, 10.67%. Calcd for $C_{13}H_{24}O_3 \cdot 1/2\ H_2O$: C, 65.79; H, 10.62%. NMR measurement using Eu(dpm)$_3$ as a shift reagent was effected for a 9% (w/v) solution of **1** in $CDCl_3$ in a molar ratio [**1**/Eu(dpm)$_3$] of 1:0.69.

Isolation of Vomifoliol and Nigakilactones E, F, and H. The benzene extracts (45 g), obtained from the dried leaves (15 kg) by the same procedure as described above, were dissolved in benzene and chromatographed on a column of neutral alumina (3 kg) using the following solvents (each fraction: 1 L) as eluents: benzene (frs 1—7), benzene–ether (1:1, frs 8—65), ether (frs 66—165), ether–ethyl acetate (3:1, frs 166—187), ether–ethyl acetate (2:1, frs 188—220), ether–ethyl acetate (1:1, frs 221—254), and ethyl acetate (frs 255—265).

Fractions 66—75 were combined and the solvent was distilled off. The residue (2.3 g) was further chromatographed on silica gel [dry column, 250 g, eluent: benzene–ether (from 1:1 to 1:3), each fraction 50 ml]. Fractions 27—34 were combined and crystallized from benzene to afford vomifoliol (1.2 g).[6,7]

Fractions 101—116 gave a residue (1 g) which was chromatographed on silica gel [dry column, 150 g, eluent: ethyl acetate–ether (1:4), each fraction 50 ml]. Fractions 31—33 were combined and crystallized from benzene and then from benzene–light petroleum to give nigakilactone E.[3a]

Fractions 144—170 were combined and the solvents were removed. The residue (1.5 g) was further chromatographed on silica gel [dry column, 200 g, eluent: benzene–acetone (3:1), each fraction 50 ml]. Fractions 7—9 gave a residue which was crystallized successively from benzene and aqueous methanol to yield nigakilactone F (153 mg).[3a]

Fractions 182—195 were combined (1.8 g) and chromatographed on silica gel [dry column, 200 g, eluent: benzene–acetone (from 3:1 to 1:1), each fraction 100 ml]. Fractions 7 and 8 were combined and crystallized from benzene and then from methanol to give nigakilactone H (17 mg).[3b]

*Acetylation of Nigakialcohol (**1**).* Nigakialcohol (**1**; 41.0 mg) was treated with acetic anhydride (3 ml) and pyridine (5 drops) at room temperature for 25 min. After addition of methanol, the reaction mixture was treated as usual to give a residue, which was dissolved in benzene and passed through a dry column of silica gel (5 g). On elution (each fraction: 1 ml) with ether, fractions 8—12 gave nigakialcohol diacetate (**2**; 24.4 mg, yield 43%) and fractions 15—26 afforded nigakialcohol monoacetate I (**3**; 26.7 mg, yield 55%). Nigakialcohol diacetate (**2**): IR (neat) 1740 and 1715 cm^{-1}; $[\alpha]_D^{27}$ +30° (*c* 0.098, $CHCl_3$); NMR (60 MHz) δ ($CDCl_3$) 0.81, 1.09 (each 3H, *t*-CH_3), 1.24 (3H, d, J=6 Hz, *s*-CH_3), 2.03, 2.07 (each 3H, s, CH_3COO-), 2.10—2.50 (4H, m, -CH_2-CO-CH_2-) 3.80—4.40 (2H, m, -C$\underline{H}_2$OAc), and 4.50—5.10 (1H, m, -$\underline{C}$HOAc); MS *m/e* 252 $(M-60)^+$; Found: C, 65.36; H, 8.93%. Calcd for $C_{17}H_{28}O_5$: C, 65.36; H, 9.03%. Nigakialcohol monoacetate I (**3**): IR (neat) 3450, 1740, and 1715 cm^{-1}; $[\alpha]_D^{26}$ +3° (*c* 0.094, $CHCl_3$); NMR (60 MHz) δ ($CDCl_3$) 0.82, 1.10 (each 3H, s, *t*-CH_3), 2.07 (3H, s, CH_3COO-), 1.22 (3H, d, J=6 Hz, *s*-CH_3), 1.67 (1H, s-like, -OH; disappeared on addition of D_2O), 2.05—2.70 (4H, m, -CH_2-CO-CH_2-), 3.45—4.05 (1H, m, -$\underline{C}$HOH), and 3.95—4.30 (2H, m,

$-C\underline{H}_2OAc$); MS *m/e* 210 $(M-60)^+$; High resolution MS, Found: *m/e* 210.1558. Calcd for $C_{13}H_{22}O_2$ $(M-CH_3COOH)^+$: *m/e* 210.1620.

Partial Hydrolysis of Nigakialcohol Diacetate (2) into Nigakialcohol Monoacetate II (4). A solution of nigakialcohol diacetate (**2**; 57.3 mg) in benzene was adsorbed on the neutral alumina (6 g, prepared by the same pretreatment as before) for 6 days at room temperature. Elution with ether afforded nigakialcohol monoacetate II (**4**; 22.4 mg, yield 46%), IR (neat) 3450, 1735, and 1715 cm^{-1}; $[\alpha]_D^{26}$ +21° (*c* 0.14, $CHCl_3$); NMR (60 MHz) δ ($CDCl_3$) 0.80, 1.08 (each 3H, s, *t*-CH_3), 1.25 (3H, d, J=6 Hz, *s*-CH_3), 2.01 (1H, s-like, –OH; disappeared on addition of D_2O), 2.05 (3H, s, CH_3COO–), 2.05—2.60 (4H, m, $-CH_2-CO-CH_2-$), 3.40—3.90 (2H, m, $-C\underline{H}_2OH$), and 4.60—5.20 (1H, m, $-\underline{C}\underline{H}OAc$); MS *m/e* 252 $(M-18)^+$; High resolution MS, Found: *m/e* 252.1727. Calcd for $C_{15}H_{24}O_3$ $(M-H_2O)^+$: *m/e* 252.1725, Found: *m/e* 210.1652. Calcd for $C_{13}H_{22}O_2$ $(M-CH_3COOH)^+$: *m/e* 210.1620.

Huang-Minlon Reduction of Nigakialchol (1). A mixture of nigakialcohol (**1**; 153.7 mg), diethylene glycol (16 ml), hydrazine hydrate (2.4 ml), and potassium hydroxide (1.6 g) was heated under reflux at 140 °C for 1 h under a nitrogen atmosphere, distillation being continued until the temperature of the vapor reached 218 °C. The reaction mixture was refluxed at 218 °C for 5 h, followed by extraction with chloroform and the usual treatment. The reaction product was dissolved in benzene and subjected to purification by chromatography on silica gel (5 g). Elution with ether afforded deoxonigakialcohol (**5**; 98.3 mg, yield 69%), IR (**5**; 3 mg/0.12 ml $CHCl_3$) 3380 cm^{-1}, (**5**; 12.5 mg/5.0 ml $CHCl_3$) 1450, 1388, 1088, 1061, and 945 cm^{-1}, $[\alpha]_D^{30}$ −28° (*c* 0.125, $CHCl_3$); NMR (60 MHz) δ ($CDCl_3$) 0.83, 0.94 (each 3H, s, *t*-CH_3), 1.19 (3H, d, J=6 Hz, *s*-CH_3), 2.27 (2H, s-like, 2× –OH; disappeared on addition of D_2O), and 3.35—4.05 (3H, m, $-C\underline{H}_2OH$ and $-\underline{C}\underline{H}OH$); High resolution MS, Found: *m/e* 196.1745. Calcd for $C_{13}H_{24}O$ $(M-H_2O)^+$: *m/e* 196.1827; GLC and HPLC (Table 1).

Acetylation of Deoxonigakialcohol (5). Deoxonigakialcohol (**5**; 110.3 mg) was treated with acetic anhydride (8 ml) and pyridine (10 drops) at room temperature for 6 h. After decomposition of excess acetic anhydride by addition of methanol and the usual work-up, the reaction product was dissolved in benzene and passed through a column of silica gel (5 g). On elution with benzene–ether (2: 1), deoxonigakialcohol diacetate (**11**; 122.0 mg, yield 79%) was obtained, IR (neat) 1742 cm^{-1}; $[\alpha]_D^{20}$ −17° (*c* 1.06, $CHCl_3$); NMR (60 MHz) δ ($CDCl_3$) 0.82, 0.93 (each 3H, s, *t*-CH_3), 1.21 (3H, d, J=6 Hz, *s*-CH_3), 2.02, 2.05 (each 3H, s, CH_3COO–), 3.60—4.40 (2H, m, $-C\underline{H}_2OAc$), and 4.60—5.10 (1H, m, $-\underline{C}\underline{H}$–OAc); MS *m/e* 238 $(M-60)^+$.

Partial Hydrolysis of Deoxonigakialcohol Diacetate (11). A solution of deoxonigakialcohol diacetate (**11**; 119.2 mg) in benzene was adsorbed on the neutral alumina (7 g, prepared by the same treatment as before) for 6 days. After benzene (20 ml) had been passed through the column, elution with benzene–ether (4: 1, each fraction: 10 ml) was followed. From fractions 1—5, the starting material (**11**; 26.0 mg) was recovered in 23% yield. Fractions 6—11 gave deoxonigakialcohol monoacetate II (**13**; 43.1 mg, yield 43%), IR (neat) 3430 and 1739 cm^{-1}; $[\alpha]_D^{30}$ −7° (*c* 0.40, $CHCl_3$); NMR (60 MHz) δ ($CDCl_3$) 0.81, 0.92 (each 3H, s, *t*-CH_3), 1.23 (3H, d, J=6 Hz, *s*-CH_3), 1.75 (1H, s-like, –OH; disappeared on addition of D_2O), 2.03 (3H, s, CH_3COO–), 3.30—3.90 (2H, m, $-C\underline{H}_2OH$), and 4.85 (1H, m, $-\underline{C}\underline{H}OAc$); MS *m/e* 196 $(M-60)^+$. Fractions 13—17 afforded deoxonigakialcohol monoacetate I (**12**; 10.4 mg, yield 10%), IR (neat) 3420 and 1739 cm^{-1}; $[\alpha]_D^{30}$ −36° (*c* 0.104, $CHCl_3$); NMR (60 MHz) δ ($CDCl_3$); 0.83, 0.94 (each 3H, s, *t*-CH_3), 1.20 (3H, d, J=6 Hz, *s*-CH_3), 1.65 (1H, s-like, –OH; disappeared on addition of D_2O), and 3.55—4.40 (3H, m, $-C\underline{H}_2OAc$ and $-\underline{C}\underline{H}OH$); MS *m/e* 196 $(M-60)^+$.

Epoxidation of (±)-γ-Ionone (6). (±)-γ-Ionone (**6**) was prepared from geraniol *via* Ψ-ionone[8] by the reported procedure.[9] The crude γ-ionone containing α- and β-ionones was chromatographed on a column of silica gel impregnated with 20% silver nitrate. Elution with 15% ether in hexane gave (±)-γ-ionone (**6**), the purity of which was examined by GLC (column: A, temperature 220 °C), IR (neat) 1676, 990, and 896 cm^{-1}; NMR (60 MHz) δ ($CDCl_3$) 0.89, 0.93 (each 3H, s, *t*-CH_3), 2.27 (3H, s, CH_3CO–), 2.59 (1H, s, $-\underline{C}\underline{H}$–CH=CH–), 4.57, 4.81 (each 1H, s, $-C=CH_2$), 6.10 (1H, d, J=16 Hz, $-CH=C\underline{H}-CO-$), and 6.97 (1H, dd, J=10 and 16 Hz, $-\underline{C}\underline{H}-C\underline{H}=CH$); MS *m/e* 192 (M^+) and 43 (base peak).

(±)-γ-Ionone (**6**; 987.1 mg) in chloroform (100 ml) was treated with *m*-chloroperbenzoic acid (975.7 mg) at room temperature for 2 days with agitation. After addition of chloroform (100 ml), the reaction was stopped by addition of 10% sodium sulfite solution and the reaction product was extracted with chloroform. The usual treatment gave a mixture of isomeric epoxy ketones (**7**) in a quantitative yield, which showed a single peak on GLC (R_t 4.3 min, column: A, temperature 220 °C) and a single spot on TLC (R_f 0.38, developed with hexane–ether, 1: 1); IR (neat) 3030, 1662, 1250, and 900 cm^{-1}; NMR (60 MHz) δ ($CDCl_3$) 0.92, 1.05 (each 3H×2/3, s, *t*-CH_3), 0.95, 1.01 (each 3H×1/3, s, *t*-CH_3), 2.24 (3H, s, CH_3CO–), 6.08 (1H×2/3, d, J=16 Hz, $-CH=C\underline{H}-CO-$), 6.05 (1H×1/3, d, J=16 Hz, $-CH=C\underline{H}-CO-$), 6.68 (1H×2/3, dd, J=10 and 16 Hz, $-\underline{C}\underline{H}-C\underline{H}=CH-$), 6.66 (1H×1/3, dd, J=10 and 16 Hz, $-\underline{C}\underline{H}-C\underline{H}=CH-$); MS *m/e* 208 (M^+) and 43 (base peak); Found: C, 74.68; H, 9.48%. Calcd for $C_{13}H_{20}O_2$: C, 74.96; H, 9.68%.

Keto Aldehyde (8). A few drops of boron trifluoride etherate solution were added with stirring to an ice-cooled solution of the epoxy ketone (**7**; 280.5 mg) in toluene (2.5 ml). After 15 min, 5% sodium hydroxide solution was added. The reaction product was then extracted with toluene and the extract was treated as usual to give a residue. The residue was subjected to purification by chromatography on a column of silica gel (6 g). Elution with ether afforded a mixture of isomeric keto aldehydes (**8**; 200.5 mg, yield 71.4%). The product showed one spot on TLC (R_f 0.44, developed with hexane–ether, 2: 3) and one peak on GLC (R_t 6.1 min, column: A, temperature 220 °C); IR (neat) 2830, 1715, and 1662 cm^{-1}; NMR (60 MHz) δ ($CDCl_3$) 0.94 (6H×3/5, s, *t*-CH_3), 0.87, 1.10 (each 3H×2/5, *t*-CH_3), 2.24 (3H, s, CH_3CO–), 2.45—2.80 (2H, m, $-\underline{C}\underline{H}$–), 6.05 (1H×3/5, d, J=16 Hz, $-CH=C\underline{H}-CO-$), 6.12 (1H×2/5, d, J=16 Hz, $-CH=C\underline{H}-CO-$), 6.66 (1H×3/5, dd, J=8 and 16 Hz, $-\underline{C}\underline{H}-C\underline{H}=CH-$), 6.70 (1H×2/5, dd, J=8 and 16 Hz, $-\underline{C}\underline{H}-C\underline{H}=CH-$), 9.45 (1H×3/5, d, J=3.5 Hz, –CHO), and 9.56 (1H×2/5, s-like, –CHO); MS *m/e* 208 (M^+) and 43 (base peak); High resolution MS, Found: *m/e* 208.1464. Calcd for $C_{13}H_{20}O_2$: *m/e* 208.1463.

Reduction of Keto Aldehyde (8) into Unsaturated Diol (9). A solution of the keto aldehyde (**8**; 40.8 mg) in methanol (1.5 ml) was cooled with an ice bath and sodium borohydride (7.7 mg) was added to the solution. After 30 min, the reaction was stopped by addition of aqueous acetic acid, methanol was removed and extraction with ether was followed. The ether extract was treated as usual and the reaction product was chromatographed on a column of silica gel (10 g) eluting with ether to afford isomeric diols **9** (7.3 mg) and **9′** (2.4 mg). **9**: TLC R_f 0.36 (developed with ether); GLC R_t 24.4 and 25.8

min with peak area in a ratio of 3:2 (column: A, temperature 200 °C), R_t 18.3 and 19.0 min with peak area in a ratio of 3:2 (column: B, temperature 210 °C); IR (neat) 3330 cm^{-1}; NMR (60 MHz) δ ($CDCl_3$) 0.85 (6H×3/5, s, *t*-CH_3), 0.80, 1.02 (each 3H×2/5, s, *t*-CH_3), 1.26 (3H, d, J=6 Hz, *s*-CH_3), 2.41 (2H, s-like, -OH), 3.15—3.65 (2H, m, -C$\underline{H}_2$OH), 4.05—4.50 (1H, m, -C$\underline{H}$OH), and 5.40—5.70 (2H, m, -CH=CH-); MS *m/e* 194 $(M-18)^+$ and 82 (base peak). **9′**: TLC R_f 0.30 (developed with ether); GLC R_t 26.1 and 27.1 min with peak area in a ratio of 5:3 (column: A, temperature 200 °C), R_t 18.4 and 18.8 min with peak area in a ratio of 5:3 (column: B, temperature 210 °C); IR (neat) 3330 cm^{-1}; NMR (60 MHz) δ ($CDCl_3$) 0.82 (6H×5/8, s, *t*-CH_3), 0.77, 1.02 (each 3H×3/8, s, *t*-CH_3), 1.26 (3H, d, J=6 Hz, *s*-CH_3), 2.82 (2H, s-like, -OH), 3.20—3.75 (2H, m, -C$\underline{H}_2$OH), 4.00—4.40 (1H, m, -C$\underline{H}$OH), and 5.18—5.78 (2H, m, -CH=CH-); MS *m/e* 194 $(M-18)^+$ and 82 (base peak). The NMR measurement using Eu(fod)$_3$-d_{27} as a shift reagent was carried out for a 10% (9%) solution of **9** (**9′**) in $CDCl_3$ in a molar ratio [**9** (**9′**)/Eu(fod)$_3$-d_{27}] of 1:0.25 (0.17).

*Hydrogenation of Unsaturated Diols (**9** and **9′**).* Unsaturated diol (**9**; 59.8 mg) in ethanol (4 ml) was hydrogenated in the presence of 5% palladium charcoal (4.9 mg) at room temperature overnight. The reaction product was purified by chromatography on a column of silica gel (7 g). Elution with ether gave a mixture of saturated diols (**10a** and **10b**; 20.1 mg, yield 33.3%), R_f value on TLC, R_t value on GLC, and R_t values on HPLC are listed in Table 1; IR (neat) 3320 cm^{-1}; NMR (60 MHz) δ ($CDCl_3$) 0.82, 0.90, 0.93, 1.00 (each s, total 6H, *t*-CH_3), 1.19 (3H, d, J=6 Hz, *s*-CH_3), 2.01 (2H, m, 2× -OH), and 3.55 (3H, m, -C$\underline{H}$OH and -C$\underline{H}_2$OH); MS *m/e* 196 $(M-18)^+$ and 69 (base peak).

Unsaturated diol (**9′**; 24.0 mg) in ethanol (4 ml) was hydrogenated in the presence of 5% palladium charcoal (4.9 mg) under the same conditions as above to afford a mixture of saturated diols (**10′a** and **10′b**; 9.8 mg, yield 40.5%), R_f value on TLC, R_t values on GLC, and R_t values on HPLC are shown in Table 1; IR (neat) 3320 cm^{-1}; NMR (60 MHz) δ ($CDCl_3$) 0.82, 0.90, 0.93, 1.00 (each s, total 6H, *t*-CH_3), 1.19 (3H, d, J=6 Hz, *s*-CH_3), 2.06 (2H, s-like, 2× -OH), 3.40—4.20 (3H, m, -C$\underline{H}$OH and -C$\underline{H}_2$OH); MS *m/e* 196 $(M-18)^+$ and 69 (base peak).

*Separation of Diols (**10a** and **10b**) by HPLC.* A mixture of the diols (**10a** and **10b**; 12.6 mg) was subjected to separation by preparative HPLC under the same conditions as given in Table 1 to give diols **10a** (2.5 mg) and **10b** (3.0 mg). **10a**: R_f value on TLC, R_t value on GLC, and R_t value on HPLC given in Table 1; IR (**10a**; 2.5 mg/0.12 ml $CHCl_3$) 3380 cm^{-1}, (**10a**; 2.5 mg/1.5 ml $CHCl_3$) 1450, 1388, 1088, 1061, and 945 cm^{-1}; NMR (60 MHz) δ ($CDCl_3$) 0.90, 1.00 (each 3H, s, *t*-CH_3), 1.21 (3H, d, J=6 Hz, *s*-CH_3), 1.80 (2H, s-like, 2× -OH), and 3.35—4.05 (3H, m, -C$\underline{H}$OH and -C$\underline{H}_2$OH); High resolution MS, Found: *m/e* 196.1830. Calcd for $C_{13}H_{24}O$ $(M-H_2O)^+$: *m/e* 196.1827. **10b**: R_f and R_t values given in Table 1; IR (**10b**; 3 mg/0.12 ml $CHCl_3$) 3380 cm^{-1}, (**10b**; 3.0 mg/1.5 ml $CHCl_3$) 1450, 1388, 1076, 1061, and 937 cm^{-1}; NMR (60 MHz) δ ($CDCl_3$) 0.83, 0.94 (each 3H, s, *t*-CH_3), 1.19 (3H, d, J=6 Hz, *s*-CH_3), 1.74 (2H, s-like, 2× -OH), 3.35—4.05 (3H, m, -C$\underline{H}$OH and -C$\underline{H}_2$OH); High resolution MS, Found: *m/e* 181.1590. Calcd for $C_{12}H_{21}O$ $(M-H_2O-CH_3)^+$: *m/e* 181.1592.

*(R)-(+)-MTPA Ester of Nigakialcohol Monoacetate I (**3**).* Pyridine (0.3 ml) and (+)-MTPACl (25 μl) were added to a solution of nigakialcohol monoacetate I (**3**; 17.8 mg) in carbon tetrachloride (0.3 ml). The mixture was stirred for 2 h at room temperature and then *N,N*-dimethyl-1,3-propanediamine (50 μl) was added. After the usual treatment, the reaction product was dissolved in benzene and subjected to purification by chromatography on a column of silica gel (2 g). Elution with ether gave (*R*)-(+)-MTPA ester of **3** (24.0 mg, yield 74%), IR (neat) 1742 and 1720 cm^{-1}; NMR (60 MHz) δ (CCl_4) 0.77, 1.02 (each 3H, s, *t*-CH_3), 1.30 (3H, d, J=6 Hz, *s*-CH_3), 2.01 (3H, s, CH_3COO-), 3.49 (3H, -OCH_3), 3.90—4.15 (2H, m, -C$\underline{H}_2$OAc), 4.70—5.20 (1H, m, -C$\underline{H}$-OMTPA), and 7.20—7.70 (5H, m, arom H's); MS *m/e* 253 and 189 (base peak).

*(S)-(-)-MTPA Ester of Nigakialcohol Monoacetate I (**3**).* The same treatment of nigakialcohol monoacetate I (**3**; 23.1 mg) with (-)-MTPACl (25 μl) gave (*S*)-(-)-MTPA ester of **3** (29.2 mg, yield 70%); IR (neat) 1740 and 1720 cm^{-1}; NMR (60 MHz) δ (CCl_4) 0.65, 0.88 (each 3H, s, *t*-CH_3), 1.37 (3H, d, J=6 Hz, *s*-CH_3), 2.01 (3H, s, CH_3COO-), 3.55 (3H, -OCH_3), 3.85—4.05 (2H, m, -C$\underline{H}_2$OAc), 4.80—5.20 (1H, m, -C$\underline{H}$-OMTPA), and 7.20—7.65 (5H, m, arom H's); MS *m/e* 253 and 189 (base peak).

*(R)-(+)- and (S)-(-)-MTPA Esters of Nigakialcohol Monoacetate II (**4**).* (*R*)-(+)-MTPA ester (17.0 mg, yield 67%) and (*S*)-(-)-MTPA ester (24.3 mg, yield 89%) were prepared by the same procedure from nigakialcohol monoacetate II (**4**; 14.1 mg and 15.0 mg), respectively. (*R*)-(+)-MTPA ester: IR (neat) 1740 and 1720 cm^{-1}; NMR (60 MHz) δ (CCl_4) 0.78, 1.03 (each 3H, s, *t*-CH_3), 1.18 (3H, d, J=6 Hz, *s*-CH_3), 1.97 (3H, s, CH_3COO-), 3.50 (3H, -OCH_3), 3.90—4.40 (2H, m, -C$\underline{H}_2$OAc), 4.45—4.95 (1H, m, -C$\underline{H}$-OMTPA), and 7.20—7.60 (5H, m, arom H's); MS *m/e* 253 and 189 (base peak). (*S*)-(-)-MTPA ester: IR (neat) 1742 and 1720 cm^{-1}; NMR (60 MHz) δ (CCl_4) 0.78, 1.03 (each 3H, s, *t*-CH_3), 1.17 (3H, d, J=6 Hz, *s*-CH_3), 1.98 (3H, s, CH_3COO-), 3.52 (3H, -OCH_3), 4.20—4.40 (2H, m, -C$\underline{H}_2$OAc), 4.45—5.00 (1H, m, -C$\underline{H}$-OMTPA), and 7.20—7.70 (5H, m, arom H's); MS *m/e* 253 and 189 (base peak).

*(R)-(+)- and (S)-(-)-MTPA Esters of Deoxonigakialcohol Monoacetate II (**13**).* (*R*)-(+)-MTPA ester (16.7 mg, yield 65%) and (*S*)-(-)-MTPA ester (30.7 mg, yield 87%) were prepared from deoxonigakialcohol monoacetate II (**13**; 13.8 mg and 19.1 mg). (*R*)-(+)-MTPA ester: IR (neat) 1740 cm^{-1}; NMR (60 MHz) δ (CCl_4) 0.82, 0.92 (each 3H, s, *t*-CH_3), 1.17 (3H, d, J=6 Hz, *s*-CH_3), 1.96 (3H, s, CH_3COO-), 3.52 (3H, -OCH_3), 3.70—4.95 (3H, m, -C$\underline{H}_2$OAc and -C$\underline{H}$-OMTPA), 7.20—7.70 (5H, m, arom H's); MS *m/e* 280 and 189 (base peak). (*S*)-(-)-MTPA ester: IR (neat) 1740 cm^{-1}; NMR (60 MHz) δ (CCl_4) 0.82, 0.92 (each 3H, s, *t*-CH_3), 1.16 (3H, d, J=6 Hz, *s*-CH_3), 1.97 (3H, s, CH_3COO-), 3.53 (3H, -OCH_3), 3.90—4.50 (2H, m, -C$\underline{H}_2$OAc), 4.50—5.00 (1H, m, -C$\underline{H}$-OMTPA), and 7.20—7.65 (5H, m, arom H's); MS *m/e* 280 and 189 (base peak).

*Determination of the Configuration at C-3′ in Nigakialcohol Monoacetate I (**3**) by Horeau's Method.* Racemic α-phenylbutyric anhydride (60.3 mg, 0.194 mmol) and nigakialcohol monoacetate I (**3**; 20.0 mg; 0.074 mmol) were dissolved in pyridine (0.3 ml). After the solution had been allowed to stand at room temperature overnight, water (0.5 ml) was added and the mixture was left to stand for 1.5 h at room temperature. Benzene was added, followed by extraction with saturated sodium hydrogencarbonate solution. The benzene layer was washed with dilute hydrochloric acid and then with brine, and dried over sodium sulfate. Concentration *in vacuo* afforded 28.5 mg (0.069 mmol, yield 93%) of an α-phenylbutyrate of **3**. An NMR spectrum of this ester indicated that **3** was totally esterified. The sodium hydrogencarbonate extract was acidified with 3M hydrochloric acid and the acidified solution was extracted with chloroform. The chloroform extract was

washed with brine and treated as usual to yield 47.1 mg (0.287 mmol, yield 91%) of α-phenylbutyric acid, which showed $[\alpha]_D^{28}$ +2.1° (*c* 0.471, $CHCl_3$, optical yield 12%), suggesting that the asymmetric center (C-3′) of the secondary alcohol possesses *R*-configuration.

*Preparation of Tetradeuterionigakialcohol Methoxymethyl Ether (**15**-d_4).* Phosphorus pentaoxide (*ca.* 500 mg) was added to a solution of nigakialcohol monoacetate I (**3**; 26.7 mg) in chloroform (3 ml, freshly distilled from phosphorus pentaoxide) and dimethoxymethane (1.5 ml), and the mixture was stirred for 30 min at room temperature. The reaction mixture was washed with cold saturated sodium carbonate solution and then with brine, dried over sodium sulfate, and evaporated to afford a residue. The residue was dissolved in hexane and purified by column chromatography over silica gel (4 g). On elution (each fraction: 1 ml) with hexane–ether (2: 3), fractions 7—21 gave nigakialcohol monoacetate I methoxymethyl ether (**14**; 20.5 mg, yield 66%); IR (neat) 1740 and 1715 cm^{-1}; $[\alpha]_D^{26}$ +5° (*c* 0.140, $CHCl_3$); NMR (60 MHz) δ ($CDCl_3$) 0.82, 1.10 (each 3H, s, *t*-CH_3), 1.19 (3H, d, J=6 Hz, *s*-CH_3), 2.10—2.50 (4H, m, $-CH_2-CO-\underline{C}H_2-$), 2.18 (3H, s, CH_3COO-), 3.40—3.80 (1H, m, $-\underline{C}H-O-CH_2-$), 3.48 (3H, s, $-OCH_3$), 4.00—4.20 (2H, m, $-\underline{C}H_2OAc$), and 4.46, 4.60 (2H, ABq, J=7.5 Hz, $-O-CH_2-O-$); MS *m/e* 299 $(M-15)^+$.

The methoxymethyl ether (**14**; 30.0 mg) was deuteriated by treatment with sodium methoxide [prepared from sodium (*ca.* 60 mg) and deuterium oxide (1.2 ml)] in methanol-*d* (9 ml). The reaction mixture was heated under reflux for 4 days under nitrogen atmosphere. Neutralization with dilute hydrochloric [*D*] acid, extraction with dichloromethane, and the usual work-up gave a residual oil. The same deuteriation procedure was repeated twice to afford a deuteriated nigakialcohol methoxymethyl ether (**15**-d_4; 23.1 mg); IR (neat) 3440 and 1700 cm^{-1}; NMR (60 MHz) δ ($CDCl_3$) 0.79, 1.08 (each 3H, s, *t*-CH_3), 1.20 (3H, d, J=6 Hz, *s*-CH_3), 2.17 (1H, s-like, -OH), 3.40—4.00 (3H, m, $-C\underline{H}_2OH$ and $-\underline{C}H-O-CH_2-$), 3.38 (3H, s, $-OCH_3$), and 4.58, 4.68 (2H, ABq, J= 7.5 Hz, $-O-CH_2-O-$); δ (CCl_4) 0.78, 1.08 (each 3H, s), 1.26 (3H, d, J=6 Hz), 2.60 (1H, s-like; disappeared on addition of D_2O), 3.30—3.90 (1H, m), 3.31 (3H, s), and 4.47, 4.61 (2H, ABq, J=7.5 Hz); NMR (100 MHz) [**15**-d_4/Eu(fod)$_3$-d_{27} =1: 0.07; for 7% (w/v) solution of **15**-d_4 in $CDCl_3$] δ 1.03, 1.24 (each 3H, s, *t*-CH_3), 1.31 (3H, d, J=6 Hz, *s*-CH_3), 2.20 —2.50 (1H, m, $-\underline{C}H-CH_2O\cdots Eu$), 3.58 (3H, s, $-OCH_3$), 3.75—4.10 (1H, m, $-\underline{C}H-O-CH_2-$), 4.25—4.66 (2H, m, $-C\underline{H}_2O\cdots Eu$), and 4.87, 4.94 (2H, ABq, J=7.5 Hz, $-O-CH_2-O-$).

References

1) This work was reported in a preliminary form: Y. Sugimoto, T. Sakita, Y. Moriyama, T. Murae, T. Tsuyuki, and T. Takahashi, *Tetrahedron Lett.*, **1978**, 4285; Y. Sugimoto, T. Murae, T. Sakita, T. Tsuyuki, and T. Takahashi, The 21st Symposium on the Chemistry of Perfumes, Terpenes, and Essential Oils, Tokushima, November 4, 1977, Abstract Papers p. 217; Y. Sugimoto, T. Murae, T. Sakita, Y. Moriyama, T. Tsuyuki, and T. Takahashi, The 22nd Symposium, Yokohama, October 14, 1978, Abstract Papers p. 203.

2) E. P. Clark, *J. Am. Chem. Soc.*, **59**, 927, 2511 (1937); Z. Valenta, S. Papadopoulos, and C. Podesva, *Tetrahedron*, **15**, 100 (1961); Z. Valenta, A. H. Gray, D. E. Orr, S. Papadopoulos, and C. Podesva, *ibid.*, **18**, 1433 (1962); J. Polonsky, *Planta Med., Suppl.*, **1966**, 107; C. Pascard, T. Prange, and J. Polonsky, *J. Chem. Res. (S)*, **1977**, 324; W. A. C. Brown and G. A. Sim, *Proc. Chem. Soc.*, **1964**, 293.

3) a) T. Murae, T. Tsuyuki, T. Ikeda, T. Nishihama, S. Masuda, and T. Takahashi, *Tetrahedron*, **27**, 1545 (1971); b) Idem, *ibid.*, **27**, 5147 (1971); c) T. Murae, A. Sugie, T. Tsuyuki, S. Masuda, and T. Takahashi, *ibid.*, **29**, 1515 (1973); d) T. Murae, T. Ikeda, A. Sugie, T. Nishihama, T. Tsuyuki, and T. Takahashi, *Bull. Chem. Soc. Jpn.*, **46**, 3621 (1973); e) T. Murae, A. Sugie, T. Tsuyuki, and T. Takahashi, *Chem. Pharm. Bull.*, **23**, 2188 (1975). And references cited therein.

4) H. Hikino, T. Ohta, and T. Takemoto, *Phytochemistry*, **14**, 2473 (1975), and the references cited therein.

5) S. M. Kupchan, R. W. Britton, M. F. Ziegler, and C. W. Siegel, *J. Org. Chem.*, **38**, 178 (1973); S. M. Kupchan, R. W. Britton, J. A. Lacadie, M. F. Ziegler, and C. W. Siegel, *ibid.*, **40**, 654 (1975); S. M. Kupchan and D. R. Streelman, *ibid.*, **41**, 3481 (1976); J. P. Tresca, L. Alais, and J. Polonsky, *C. R. Acad. Sci., Ser. C*, **273**, 601 (1971); K.-H. Lee and Y. Imakura, *J. Chem. Soc., Chem. Commun.*, **1977**, 69.

6) J. -L. Pousset and J. Poisson, *Tetrahedron Lett.*, **1969**, 1173.

7) M. N. Galbraith and D. H. Horn, *J. Chem. Soc., Chem. Commun.*, **1972**, 113; G. Weiss, M. Koreeda, and K. Nakanishi, *ibid.*, **1973**, 565.

8) J. W. Batty, A. Burawoy, S. H. Harper, I. M. Heilbron, and W. E. Jones, *J. Chem. Soc.*, **1938**, 175.

9) G. Ohloff and G. Schade, *Angew. Chem.*, **74**, 944 (1962).

10) F. Näf, R. Decorzant, B. Willhalm, A. Velluz, and M. Winter, *Tetrahedron Lett.*, **1977**, 1413.

11) S. Yamaguchi and F. Yasuhara, *Tetrahedron Lett.*, **1977**, 89; S. Yamaguchi, F. Yasuhara, and K. Kabuto, *Tetrahedron*, **32**, 1363 (1976).

12) F. Yasuhara and S. Yamaguchi, *Tetrahedron Lett.*, **1977**, 4085.

13) J. A. Dale and H. S. Mosher, *J. Am. Chem. Soc.*, **85**, 512 (1973); J. A. Dale, D. L. Dull, and H. S. Mosher, *J. Org. Chem.*, **34**, 2543 (1969).

14) T. J. Mabry, W. Renold, H. E. Miller, and H. B. Kagan, *J. Org. Chem.*, **31**, 681 (1966); A. Horeau, *Tetrahedron Lett.*, **1961**, 506.

15) K. Fujii, S. Nakano, and E. Fujita, *Synthesis*, **1975**, 276.

The Substituent Effect. 14.[1] The Solvolysis of 6- and 7-Substituted 1-(2-Naphthyl)ethyl Chlorides

Yuho Tsuno,† Masami Sawada,* Takahiro Fujii, and Yasuhide Yukawa

The Institute of Scientific and Industrial Research, Osaka University, Suita, Osaka 565

†*Department of Chemistry, Faculty of Science, Kyushu University, Hakozaki, Fukuoka 812*

(Received April 13, 1979)

Nine of the title compounds were synthesized, and their solvolysis rates were determined in 80% (v/v) aq acetone at 45 °C. The effects of the *pi*-donor substituents for each substituent position are shown to be excellently described in terms of inductive(*I*) and *pi*-electronic(*Pi*) effects by means of the LSFE equation ($\log k/k_0=\rho_i\sigma_i+\rho_\pi^+\sigma_\pi^+$), just as with those in the 1-naphthyl systems. When those data are joined with all our substituent effects data for the phenyl, 4-biphenylyl, 2-fluorenyl, and 1-naphthyl systems under identical conditions, it is clear that the overall correspondence between the ρ_i values and Dewar's simple-field-effect function ($1/r$) is satisfactory. On the other hand, the ρ_π^+ values appear to give slightly different responses (separate correlations for the 1- and 2-naphthyl systems) to the SCF-π charge difference values; this may be ascribed to the steric effects on the *Pi* effect in only the 1-naphthyl-solvolysis sets. Furthermore, the position constancy of the *I* effect ($\rho_{i,6\text{-X-}2}/\rho_{i,7\text{-X-}2}=0.85$) has been observed in the present solvolysis and the available data for dissociation of 2-naphthalenecarboxylic acids involving relatively weak *Pi* effects; the figure is in good agreement with the ratio of $\rho_{i,para}/\rho_{i,meta}=0.85$. Analogous results were also achieved by the same treatment to 2-benzo[*b*]thienyl reactivities. All the results are discussed with respect to the validity of the LSFE equation.

It has been the well-accepted concept that substituent effects on reactivities can be described in a good approximation as an additive function of two basic components, polar (inductive, *I*) and resonance (*pi*-electronic, *Pi*) effects, each of which is given as a $\rho\sigma$ product.[2-4] Provided that there exists a universal set of inductive and *pi*-electronic substituent constants, the constants should be applicable in principle to any kinds of extended *pi*-system for various reactions. The term of universal substituent constants refers to the unchanged (inherent) electron-donating or -withdrawing capabilities of their own substituents, independent of any different reactivity classes.[2]

We have long focused on such separation and separability problems and have continued our studies of substituent effects on reactivities in certain *pi*-electronic systems. LArSR Eq. 1, originally based upon the phenyl system,[8-10] has been applied to 3′-, 4′-substituted 4-biphenylyl,[5] 7-substituted 2-fluorenyl,[1] and 3-, 4-substituted 1-naphthyl systems:[7]

$$\log k/k_0=\rho(\sigma^0+r^+\Delta\bar{\sigma}_R^+ + r^-\Delta\bar{\sigma}_R^-) \quad (1)$$

LArSR Eq. 1, however, stands on the reference scale of σ^0 for unexalted phenyl reactivities as a standard, which is separable further into two basic terms, *I* and *Pi* effects. The σ^0 scale also implies the effect of the substituent position, such as the meta or para position. Therefore, LSFE Eq. 2[6,10-12] is expected to be appropriate to an understanding of the general scheme of the substituent effect in extended *pi*-systems.

$$\log k/k_0=\rho_i\sigma_i+\rho_\pi^+\sigma_\pi^+ + \rho_\pi^-\sigma_\pi^- \quad (2)$$

The σ_i values are the inductive substituent constants, while the σ_π^+ or σ_π^- values the *pi*-electronic substituent constants for *pi*-donor($-R$) or *pi*-acceptor($+R$) substituents respectively, which, we believe, may be regarded as universal constants independent of any different reactivity classes; the numerical values are defined by $\sigma_i=0.74\sigma'$, $\sigma_\pi^+=0.415\Delta\bar{\sigma}_R^+$, and $\sigma_\pi^-=0.73\ \Delta\bar{\sigma}_R^-$. These scales hold a simple association with σ_p^0 by means of:

$$\sigma_p^0=\sigma_i+\sigma_\pi^+ + \sigma_\pi^-.[15] \quad (3)$$

The substituent-effect parameters obtained by means of the LArSR treatment can, then, be interconverted into those obtained by means of the LSFE treatment:[1]

$$\rho_i=\rho,\ \rho_\pi^+=\rho(1+r^+/0.415),\ \rho_\pi^-=\rho(1+r^-/0.73).$$

It must be noted that the different susceptibilities to *Pi* effects for donor and acceptor substituents, even in a given reaction, are essentially expressed as in LSFE Eq. 2. The duality of such ρ_π's is a significant implication of LArSR Eq. 1 and the inevitable conclusion to be induced from it.

On the other hand, DSP Eq. 4 by Taft has been widely applied to many chemical reactivities and physical properties:[2,4,13]

$$\log k/k_0=\rho_I\sigma_I+\bar{\rho}_R\bar{\sigma}_R \quad (4)$$

We can point out there remain three important differences between our LSFE Eq. 2 and Taft's DSP Eq. 4: that is, (1) the existence of universal *pi*-electronic substituent constants,[6,14] (2) the dual susceptibilities to the *Pi* effects,[6,14,16] and (3) the scaling of the inductive substituent constants.[17] A principal objective of our current studies has been to obtain evidence for the existence of a universal set of *pi*-electronic substituent constants.

A naphthyl system is suitable for studies of substituent effects because of its various substituent positions.[2a] We have already reported the correlations for the solvolysis of the 5-, 6-, and 7-substituted 1-naphthyl systems and for the pK_a of the corresponding 1-naphthalenecarboxylic acids with respect to *pi*-donor substituents, *i.e.*, by means of Eq. 5:[18]

$$\log k/k_0=\rho_i\sigma_i+\rho_\pi^+\sigma_\pi^+ \quad (5)$$

Here, we have worked with the alternative 2-naphthyl system and have examined the substituent effects at the B-ring positions, namely, the solvolysis of 6- and 7-substituted 1-(2-naphthyl)ethyl chlorides.

Surprisingly few substituent effect data have been published on 2-naphthyl reactivities;[24] available are

only data sets as four reactions, in which at least both 6- and 7-substituent effects were studied systematically: (I) the present solvolysis in 80% aq acetone, (II) the detritiation of 2-tritionaphthalenes in CF_3COOH at 70 °C,[19] (III) the dissociation of 2-naphthalenecarboxylic acids in 50% aq EtOH at 25 °C,[2a,20] and (IV) the alkaline hydrolysis of methyl 2-naphthalenecarboxylates in 70% aq dioxane at 25 °C.[21] These 2-naphthyl reactivities belong to the σ^+-type (I and II) as well as the σ-type category (III and IV) and are appropriate for a study of the accurate reaction dependencies of the *I* and *Pi* effects. Further, LSFE Eq. 5 will also be tested for some electrophilic reactivities of the relevant heteroaromatics, such as 2-benzofuryl and 2-benzo[*b*]-thienyl systems.[22,23a]

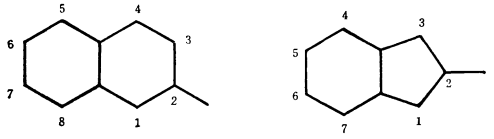

Chart 1.

Accordingly, the present results and discussion bear on the validity and utility of LSFE Eq. 2 in extended *pi*-systems and on the transmission efficiency of the *I* and *Pi* effects.

Experimental[25]

Materials. Commercial 2-acetylnaphthalene was purified through the recrystallization of its picrate (mp 82—83 °C), followed by the fractional distillation of the regenerated ketone using aq NH_3.

6-Substituted 2-Acetylnaphthalenes: 6-Methoxy-,[26] 6-methylthio-,[27] 6-methyl-,[28] and 6-bromo-2-acetylnaphthalenes[29] were prepared by following the literature methods of the Friedel-Crafts acetylation in nitrobenzene and were purified by fractional redistillation or by column chromatography over alumina (eluting with hexane–benzene) or by fractional recrystallization. The 6-bromo-2-acetylnaphthalene was converted to 6-cyano-2-acetylnaphthalene (mp 142—144 °C) by the ordinary method, using CuCN in DMF.[24c,30] The physical constants agreed well with the reported values, as is shown in Table 1.

7-Substituted 2-Acetylnaphthalenes: These compounds were prepared essentially by a combination of such well-known synthetic routes[31] of reactions as the following.

7-Methyl-2-acetylnaphthalene. 3-(*p*-Methylbenzoyl)propanoic acid was prepared by the Friedel-Crafts reaction of succinic anhydride with toluene and $AlCl_3$.[32] The acidification of the aq sodium salt solution gave colorless ppt (mp 129—131 °C; lit, 126—128 °C,[33] 124—126 °C),[34] which was then reduced by a Wolff-Kishner reaction with KOH, 80% aq NH_2NH_2 in diethylene glycol[35] to 4-(*p*-methylphenyl)-butanoic acid (recrystd from hexane, mp 57—58 °C; lit, 59—61 °C,[33] 60—61 °C)[31] and then esterified with 99% EtOH. Ethyl 4-(*p*-methylphenyl)butanoate was distilled at bp 97.5—98 °C/2 mmHg as a GLC pure sample. The ester (80 g) was treated with ethyl formate (64 g) and NaOEt in abs ether[36] to give ethyl 2-formyl-4-(*p*-methylphenyl)butanoate, along with about a half of the starting butanoate ester (43 g). The product was, then, cyclized to ethyl 3,4-dihydro-7-methyl-2-naphthoate, using phosphoric acid and concd H_2SO_4, according to the procedure described by Holmes and Trevoy.[36] The subsequent distillation of the desired ester gave a GLC

Table 1. Physical properties and analytical data of 2-acetylnaphthalenes, 1-(2-naphthyl)ethanols, and 1-(2-naphthyl)ethyl chlorides

Group	Subst	Mp or bp (°C or °C/mmHg)	Lit	Carbon Found (Calcd)	Hydrogen Found (Calcd)	Other Found (Calcd)
Ketone	H-2	55—56	56[44b]	84.81(84.68)	5.87(5.92)	
		133—135/5	171—173/17[44b]			
	6-MeO-2	109—110	106.5[26]	78.01(77.98)	5.56(6.04)	
			175—185/0.8[44a]			
	6-MeS-2	124.5—126.5	120[27]	72.19(72.19)	5.64(5.59)	
	6-Me-2	140—144/0.8	*ca.* 154/0.8[28]	84.61(84.75)	6.73(6.57)	
	6-Br-2	104.5—105.5	100.5[29]	58.15(57.86)	3.72(3.64)	(Br) 31.84(32.08)
	7-MeO-2	85.0—85.5		77.87(77.98)	5.98(6.04)	
	7-Me-2	95.5—96.0		84.66(84.75)	6.39(6.57)	
	7-Br-2	94.5—95.5		57.81(57.86)	3.36(3.64)	(Br) 31.69(32.08)
Alcohol[a]	H-2	75.5—76.0	74[38a]	83.45(83.69)	6.79(7.02)	
	6-Me-2	135—137/1		84.11(83.83)	7.40(7.58)	
	6-Br-2	142—144/0.7		57.49(57.39)	4.30(4.42)	
	6-CN-2	*ca.* 55—57				
	7-MeO-2	86.0—86.5		76.94(77.20)	6.82(6.98)	
	7-Me-2	70.5—71.5		83.64(83.83)	7.37(7.58)	
	7-Br-2	90—91		57.19(57.40)	4.18(4.42)	(Br) 31.53(31.82)
Chloride[b]	H-2	68.5—69.0	68[38a]	75.45(75.59)	5.74(5.82)	(Cl) 18.48(18.59)
	6-MeS-2	97.5—99.0		65.94(65.95)	5.48(5.53)	(Cl) 15.13(14.97)
	6-CN-2	82—83		72.51(72.39)	4.34(4.67)	(Cl) 16.17(16.44)
	7-MeO-2	75—76		70.71(70.75)	5.80(5.94)	(Cl) 16.01(16.06)
	7-Me-2	66—67		76.28(76.28)	6.16(6.40)	(Cl) 17.12(17.32)
	7-Br-2	76—77		53.64(53.47)	3.58(3.74)	(Cl) 12.92(13.15)

a) 6-MeS-2, mp 100—102 °C. b) 6-Me-2, bp 115—116 °C/1.2 mmHg. Both 6-MeO-2 and 6-Br-2 derivatives were used immediately after the preparation of the chlorides, without distillation.

pure, colorless liquid (27.6 g); bp 142—144 °C/4 mmHg; NMR (CCl_4) δ=1.33 (3H, t, J=7.1 Hz, $CH_2C\underline{H}_3$), 2.29 (3H, s, $C\underline{H}_3$), 2.4—2.9 (4H, m, $C\underline{H}_2C\underline{H}_2$), 4.20 (2H, q, J=7.1 Hz, $C\underline{H}_2CH_3$), 6.94 (3H, s, Ar), and 7.36 (1H, olefinic); Found: C, 77.78; H, 7.30%. Calcd for $C_{14}H_{16}O_2$: C, 77.75; H, 7.46%.

The ethyl dihydronaphthoate (27 g) was dehydrogenated with 2,3-dichloro-5,6-dicyano-*p*-benzoquinone (DDQ, 32 g) in xylene (250 ml) under refluxing for 24 h. After a usual work-up, a major fraction of the distillation (bp 133—140 °C/2 mmHg) was collected (solidified on standing) and recrystallized from hexane to give pure ethyl 7-methyl-2-naphthalenecarboxylate (15 g); mp 64.5—65 °C; NMR (CCl_4) δ=1.42 (3H, t, J=7.1 Hz, $CH_2C\underline{H}_3$), 2.50 (3H, s, $C\underline{H}_3$), 4.37 (2H, q, J=7.1 Hz, $C\underline{H}_2CH_3$), and 7.2—8.4 (6H, m, Ar); Found: C, 78.38; H, 6.65%. Calcd for $C_{14}H_{14}O_2$; C, 78.48; H, 6.59%.

7-Methyl-2-naphthalenecarboxylic acid, obtained from the alkaline hydrolysis, was recrystallized from aq EtOH; mp 208—209 °C (lit, 207—209 °C).[31] 7-Methyl-2-acetylnaphthalene was similarly synthesized (*via* 7-methyl-2-naphthoyl chloride, as has been described elsewhere)[7,8a,18] and purified by recrystallization from hexane; mp 85.0—85.5 °C; NMR (CCl_4) δ=2.5_5 (3H, s, $C\underline{H}_3$), 2.6_4 (3H, s, $COC\underline{H}_3$), and 7.4—8.4 (6H, m, Ar).

7-Methoxy-2-acetylnaphthalene. 3-(*p*-Methoxybenzoyl)-propanoic acid (mp 148—150 °C; lit, 148—149 °C),[37,38] 4-(*p*-methoxyphenyl)butanoic acid,[38] and ethyl 4-(*p*-methoxyphenyl)butanoate (bp 133.5—134 °C/3 mmHg) were prepared successively by methods similar to those used for the above 7-methyl derivatives. The cyclization of ethyl 4-(*p*-methoxyphenyl)butanoate (74 g) *via* ethyl 2-formyl-4-(*p*-methoxyphenyl)butanoate gave ethyl 3,4-dihydro-7-methoxy-2-naphthalenecarboxylate (17.5 g); bp 169—175 °C/5—6 mmHg; NMR (CCl_4) δ=1.33 (3H, t, J=7.1 Hz, $CH_2C\underline{H}_3$), 2.4—2.9 (4H, m, $C\underline{H}_2C\underline{H}_2$), 3.74 (3H, s, $OC\underline{H}_3$), 4.19 (2H, q, J=7.1 Hz, $C\underline{H}_2CH_3$), 6.6—7.0 (3H, m, Ar), and 7.36 (1H, s, olefinic); Found: C, 72.50; H, 6.70%. Calcd for $C_{14}H_{16}O_3$: C, 72.39; H, 6.94%.

The dehydrogenation of the dihydronaphthalene (28.5 g) with DDQ gave ethyl 7-methoxy-2-naphthalenecarboxylate (21.5 g); bp 188—195 °C/5 mmHg (lit, mp 36—36.5 °C);[39] NMR (CCl_4) δ=1.42 (3H, t, J=7.1 Hz, $CH_2C\underline{H}_3$), 3.88 (3H, s, $OC\underline{H}_3$), 4.37 (2H, q, J=7.1 Hz, $C\underline{H}_2CH_3$), and 7.1—8.4 (6H, m, Ar).

After alkaline hydrolysis, 7-methoxy-2-naphthalenecarboxylic acid was obtained; recrystd from aq EtOH, mp 200.5—201 °C (lit, 194—195 °C,[40] 195.5—196 °C).[39] The naphthalenecarboxylic acid was converted to 7-methoxy-2-acetylnaphthalene, being distilled at 183—189 °C/5 mmHg, and was then recrystallized from hexane–benzene as colorless needles; mp 95.5—96.0 °C; NMR (CCl_4) δ=2.61 (3H, s, $COC\underline{H}_3$), 3.90 (3H, s, $OC\underline{H}_3$), and 7.1—8.2 (6H, m, Ar).

7-Bromo-2-acetylnaphthalene. 3-(*p*-Bromobenzoyl)propanoic acid (mp 148.5—150.5 °C; lit, 148—149 °C),[41] 4-(*p*-bromophenyl)butanoic acid (mp 68.5—69.5 °C; lit, 71—72 °C),[41] and ethyl 4-(*p*-bromophenyl)butanoate (bp 115—117 °C/2 mmHg) were similarly prepared as the corresponding Me and MeO derivatives. The ester condensation and successive cyclization of the ester (89 g) gave ethyl 3,4-dihydro-7-bromo-2-naphthalenecarboxylate, which was distilled at bp 140—153 °C/1 mmHg (35 g) and then recrystallized from hexane to afford the above named substance (mp 67—67.5 °C) as colorless crystals (30 g); NMR (CCl_4) δ=1.33 (3H, t, J=7.1 Hz, $CH_2C\underline{H}_3$), 2.4—2.9 (4H, m, $C\underline{H}_2C\underline{H}_2$), 4.21 (2H, q, J=7.1 Hz, $C\underline{H}_2CH_3$), and 6.9—7.3 (4H, m, Ar and olefinic); Found: C, 55.51; H, 4.42; Br, 28.53%. Calcd for $C_{13}H_{13}O_2Br$: C, 55.54; H, 4.66; Br, 28.42%.

The dihydronaphthalene was dehydrogenated with DDQ to give ethyl 7-bromo-2-naphthalenecarboxylate as colorless needles (recrystd from ligroin; mp 92.5—94 °C); NMR (CCl_4) δ=1.4_6 (3H, t, J=7 Hz, $CH_2C\underline{H}_3$), 4.4_6 (2H, q, J=7 Hz, $C\underline{H}_2CH_3$), and 7.7—8.6 (6H, m, Ar); NMR ($CDCl_3$) δ=1.44 (3H, t, J=7.1 Hz, $CH_2C\underline{H}_3$), 4.45 (2H, q, J=7.1 Hz, $C\underline{H}_2CH_3$), and 7.6—8.5 (6H, m, Ar);[42a] C^{13}-NMR ($CDCl_3$) δ=14.40 ($CH_2\underline{C}H_3$), 61.38 ($\underline{C}H_2CH_3$), 120.80 (C_7), 125.93 (C_3), 128.27 (C_4),†,[42b] 129.00 (C_2), 129.59 (C_5),† 130.22 (C_1) 131.39 (C_8), 131.69 (C_6),† 133.84 and 134.03 (C_9 and C_{10}), and 166.60 ($\underline{C}OOEt$);[42b] Found: C, 55.93; H, 3.73; Br, 28.25%. Calcd for $C_{13}H_{11}O_2Br$: C, 55.94; H, 3.97; Br, 28.63%.

The alkaline hydrolysis of the ester afforded 7-bromo-2-naphthalenecarboxylic acid (mp 241—243 °C; lit, 238—240 °C),[40] which was similarly converted to 7-bromo-2-acetylnaphthalene, having been purified by distillation and then recrystallization from hexane; mp 94.5—95.5 °C; NMR (CCl_4) δ=2.6_5 (3H, s, $COC\underline{H}_3$) and 7.7—8.4 (6H, m, Ar).

1-(6- and 7-Substituted 2-naphthyl)ethanols and Their Chlorides. The alcohols and chlorides were prepared successively from the corresponding ketones with the standard method:[7,8a,18] (i) the reduction of the ketone with $LiAlH_4$ or $NaBH_4$ to give 1-(2-naphthyl)ethanol followed by (ii) the chlorination of the alcohol with dry HCl or $SOCl_2$ to provide 1-(2-naphthyl)ethyl chloride. The NMR data of 1-(7-substituted 2-naphthyl)-ethanols were as follows. 7-Me deriv; NMR (CCl_4) δ=1.47 (3H, d, J=6.3 Hz, $CHOHC\underline{H}_3$), 1.93 (1H, s, $O\underline{H}$), 2.48 (3H, s, $C\underline{H}_3$), 4.89 (1H, q, J=6.3 Hz, $C\underline{H}OHCH_3$), and 7.1—7.7

Table 2. Solvolysis data for 6- and 7-substituted 1-(2-naphthyl)ethyl chlorides in 80% aq acetone

Subst	Temp/°C	$10^5\,k_1/s^{-1}$
H-2	45.0	5.01[b]
	25.0	0.442
6-MeO-2	45.0	835[a]
	25.0	127[a]
	15.0	46.6
	0.0	7.78
	−15.0	1.30
6-MeS-2	45.0	224[a]
	25.0	24.0
	0.0	0.935
6-Me-2	45.0	34.5[c]
	25.0	3.73
6-Br-2	65.0	10.5
	45.0	1.18
	25.0	0.0993[a]
6-CN-2	90.0	3.68
	75.0	0.870
	45.0	0.0325[a]
	25.0	0.00253[a]
7-MeO-2	45.0	5.94[d]
7-Me-2	45.0	9.05[d]
7-Br-2	45.0	0.300[d]

a) Extrapolated from other temperatures by means of the Arrhenius equation. b) Previous value; 5.03 (5.18).[8a] c) Calculated from the LFER of (log k/k_0)$_{45\,°C}$ = 0.9436 (log k/k_0)$_{25\,°C}$ − 0.036 (r=0.9996, s=±0.057, n=5). d) For the 7-X-2 series, k_1=5.17×10^{-5} s^{-1} for the parent H-2 was used for the calculations of the relative rates because of the different batchs and different workers.

(6H, m, Ar). 7-MeO deriv; NMR (CCl_4) δ=1.48 (3H, d, J=6.4 Hz, CHOHC$\underline{H}_3$), 1.79 (1H, s, O$\underline{H}$), 3.85 (3H, s, OC$\underline{H}_3$), 4.89 (1H, q, J=6.4 Hz, C$\underline{H}$OHCH$_3$), and 7.0—7.7 (6H, m, Ar). 7-Br deriv; NMR (CCl_4) δ=1.49 (3H, d, J=6.4 Hz, CHOHC$\underline{H}_3$), 1.69 (1H, s, O$\underline{H}$), 4.94 (1H, q, J=6.4 Hz, C$\underline{H}$OHCH$_3$), and 7.4—7.9 (6H, m, Ar).

The physical properties and the microanalysis data of the ketones, alcohols, and chlorides are listed in Table 1.

Solvent and Kinetics: The 80% (v/v) aq acetone solvent was prepared by mixing 1 volume of deionized, distilled, and degassed water with 4 volumes of purified acetone at 25 °C, as has been described before.[7,8a,18] Different batches of the aq acetone solvent, which gave slightly different rate constants (Table 2), were employed without calibration for each series of measurements. The solvolysis reaction was followed by the usual titration method (chloride of *ca.* 0.02 M^{-1}, titer of *ca.* 0.02 M^{-1} aq NaOH, indicator of Bromocresol Purple). The bath temperature was controlled to $\pm$0.02 °C. At very low temperatures (−15 °C), the accuracy was estimated to be within 0.1 °C. The kinetic procedures were essentially the same as those reported before.[8a,45a]

All runs followed first-order kinetics, covering over 70—80% of the reaction, except for the 6-CN-2 derivative (50% reaction). The first-order rate constants were calculated by means of the least squares method using the mean infinity reading obtained after over 10 half-lives (corr coeff> 0.9999).[45b] The data points in a run were usually 12 points (2 for infinity reading), but in a few instances 7 points were used, covering up to *ca.* 70% of the reaction. The rate constants from duplicated runs were reproducible within $\pm$2% or better. Very reactive chloride, such as the 6-MeO-2 derivative, was used for the kinetic measurements immediately after the evaporation of the solvent and without purification.

The rate constants, $k_1(s^{-1})$, obtained at various temperatures are given in Table 2.

Results and Discussion

The logarithmic relative rates of 6- and 7-substituted 1-(2-naphthyl)ethyl chlorides with respect to the parent unsubstituted 2-naphthyl derivative in 80% aq acetone at 45 °C and 25 °C are summarized in Table 3, along with some activation parameters. The reaction conditions are our standard ones in our studies of a series of solvolysis reactions. The log k/k_0 values in Table 3 can, then, be directly compared with the other corresponding solvolysis sets in the phenyl,[8a] 4-biphenylyl,[5] 2-fluorenyl,[1] and 1-naphthyl systems.[7,18]

Table 3. log k/k_0 values for the solvolysis of substituted 1-(2-naphthyl)ethyl chlorides in 80% aq acetone

Subst	(log k/k_0) at 25 °C	(log k/k_0) at 45 °C	ΔH^* kcal/mol	$-\Delta S^*$ eu
H-2	0.000	0.000	22.3	8.3
6-MeO-2	2.46[a]	2.22[a]	17.1	14.4
6-MeS-2	1.735	1.65[a]	20.4	6.5
6-Me-2	0.926	0.84[c]	20.4	10.5
6-Br-2	−0.65[a]	−0.628	22.7	9.8
6-CN-2	−2.24[a]	−2.19[a]	23.4	14.6
7-MeO-2		0.060[d]		
7-Me-2		0.234[d]		
7-Br-2		−1.236[d]		

a), c), and d) are the same as in the footnotes in Table 2.

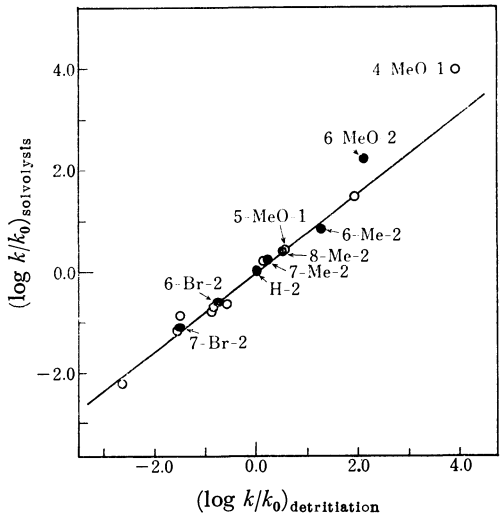

Fig. 1. A rate plot between the present solvolysis (45 °C) and the detritiation (70 °C) in the 2-naphthyl (closed circle) and in the 1-naphthyl (open circle) systems.

In the present 2-naphthyl series, the log k/k_0 varies widely not only with the substituent change, but also with the position change, just as in the 1-naphthyl series. Figure 1 shows a plot of the logarithmic relative rates for the present solvolysis, I (at 45 °C), against those for II (at 70 °C).[19a] Although common substituents are so limited, all the points except for the 6-MeO-2 derivative in the 2-naphthyl system (closed circle) fall on or near the line for the 1-naphthyl system (open circle).[18] The detritiation data for the 6-Cl-2 and 7-Cl-2 derivatives were employed in this figure instead of those for the Br derivatives.

The MeO group may be modified in CH_3COOH by hydrogen-bonding interaction, which appears to reduce mainly its ability to make a *pi*-electron donation.[18,46] The modification seems to be consistent with the fact that deviations are serious only in a strongly conjugative position, in which the *pi*-electronic contribution is important, but not appreciable in weakly conjugative (5-MeO-1) and essentially nonconjugative positions. The single correlation line for 1- and 2-naphthyl derivatives, except for such a single MeO group, reflects a similar blend of the *I*/*Pi* effects in the two naphthyl series between I and II.

On the contrary, Fig. 2 illustrates a plot of I (at 45 °C) against III (at 25 °C).[2a,20] Note that the plot does not show an overall linearity in the 2-naphthyl system from the MeO to the CN substituents (closed circle); the same is true in the 1-naphthyl system (open circle). This is similar to the plot of the σ^+ reactivity data against the σ values in the phenyl system: that is, (i) all the substituents at the conjugate position (7-MeO-2, 7-Br-2, 7-Me-2), the *pi*-acceptor ($+R$) substituents at the conjugate position (6-CN-2), and the unsubstituted one make a straight line, and (ii) the *pi*-donor ($-R$) substituents at the conjugate position (6-MeO-2, 6-Me-2, 6-Br-2) substantially deviate upward from the correlation line, the deviations depending upon the

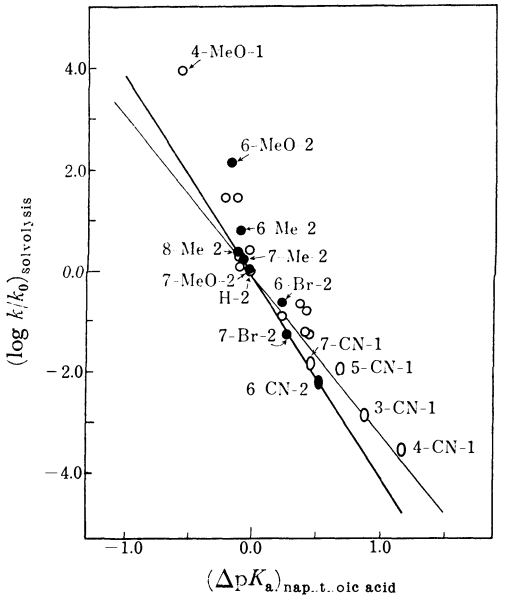

Fig. 2. A plot of the log k/k_0 in the present solvolysis (45 °C) *vs.* ΔpK_a in the corresponding naphthoic acids; closed circle for 2-naphthyl and open circle for 1-naphthyl systems.

order of the *pi*-donor ability: MeO>Me≥Br. Analogous phenomena have been observed in the 2-fluorenyl[1] and 4-biphenylyl systems.[5] As far as electrophilic reactivities are concerned, it can be generally deduced from extended *pi*-electron systems that the blend of the *I-Pi* effects of the donor substituents at the conjugate positions varies with the reactions of different electron demands, whereas the blend for acceptor substituents, even at conjugate positions, does not. All these facts are in line with the general features of the substituent effects observed in the Hammett-type treatment of general benzene reactivities.

The next feature of this figure is the separate slopes for the 2-naphthyl (a solid line) and 1-naphthyl (a fine line) systems; each line is drawn through the substituents for which no additional resonance exaltation effect can be expected. The slope for the 2-naphthyl system is 25% larger than that for the 1-naphthyl system. Any one of the three reactions (I, II, and III) has a higher sensitivity to the substituent changes in the 2-naphthyl than in the 1-naphthyl system. This probably arises from the different steric effects with the peri-hydrogen on the reaction center. Special care should be taken in the discussion of the apparent substituent constants in the 2-naphthyl system compared with the 1-naphthyl system, for example, the use of the ρ in the phenyl system. Since the ρ value for the solvolysis of 1-(3,4-X-1-naphthyl)ethyl chlorides (by LArSR or LSFE for 4-X-1) was found to be −5.1,[7] compatible with the ρ of −5.0 for the phenyl system,[8a] the separate lines in Fig. 2 imply the possibility that the treatment of the substituent effects for the dissociation of both 1- and 2-naphthalenecarboxylic acids with a single, common ρ[20] is not appropriate.

At the intermediate in the present solvolysis, where a positive charge is developed, the 6-X-2 naphthyl system can be stabilized by an extended quinoid structure throughout the A and B rings. The higher stability of 2,6-naphthoquinone than, for example, 1,7-naphthoquinone or 1,5-naphthoquinone[47] may tell us qualitatively of the larger contribution of such a 2,6-naphthoquinonoid structure. Our attempt to correlate the 6-X-2 reactivities with simple σ^+ parameters[48] appears to have been practically successful. It provides $\rho^+=-3.05$, with a correlation coefficient of 0.9990 ($s=\pm0.080$, $n=6$), suggesting quite a large *pi*-electronic exaltation effect in this series. The LArSR approach gives a more precise description (Fig. 3) by the use of:

$$\log k/k_0 = -3.275(\sigma_p^0+0.872\Delta\bar{\sigma}_R^+) - 0.053$$

with a corr coeff of 0.9997 and a standard deviation of ±0.044 ($n=6$).[49] On the basis of the ρ and r^+ values thus obtained, the LSFE ρ_i and ρ_π^+ values are estimated to be as listed in Table 4; the ρ_π^+/ρ_i ratio is *ca.* 3.1.

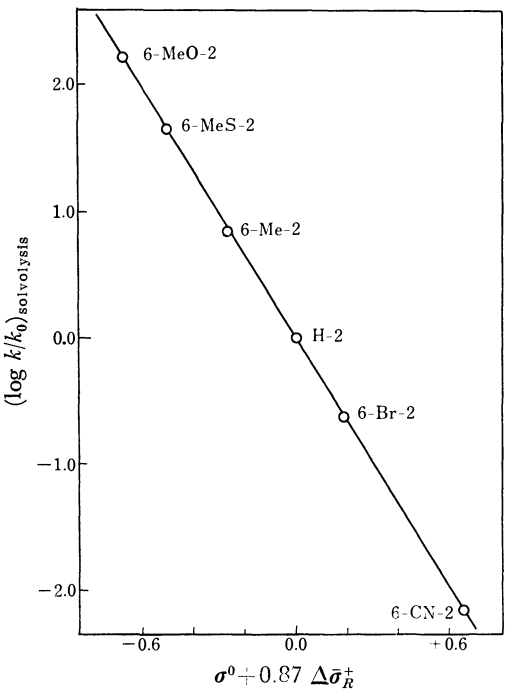

Fig. 3. The LArSR plot for the solvolysis of 6-substituted 1-(2-naphthyl)ethyl chlorides at 45 °C.

In the 7-X-2 naphthyl reactivities, there is no single σ-type parameter to describe the substituent effects. We arrived at the view that the effects for 7-X-2 of I may correlate well with the quantity of $(\sigma_p^0+\sigma_m)/2$ rather than with that of σ_p^0 or σ_m.[50] This indicates that the ρ_π^+/ρ_i ratio is close to 0.7 (rather than to 1.0 or 0.4).

For the present aim to ascertain the general features of the position dependency of the *I* and *Pi* components of substituents in extended *pi*-systems, it should be appropriate to use the LSFE approach, using their universal substituent constants. It would seem that a large number of data including both $-R$ and $+R$ substituents would give the most reliable statistical parameters of ρ_i, ρ_π^+, and ρ_π^- in LSFE Eq. 2 when three independent variables are used (σ_i, σ_π^+, and σ_π^-).[6,16,54] In the present cases, we have treated only *pi*-donor substituents and then utilized the simplified LSFE Eq. 5 for each substituent position in the naphthalene ring.

Table 4. Correlational parameters for the solvolysis of 1-(2-naphthyl)ethyl chlorides at 45 °C[a]

$\log k/k_0 = \rho_i\sigma_i + \rho_\pi^+\sigma_\pi^+ + (\rho_\pi^-\sigma_\pi^-)$

Series	Method[b]	ρ_i	ρ_π^+	ρ_π^-	$\pm s$[c]	R[d]	n(Subst)[e]
6-X-2	LArSR Eq. 1	−3.28	−10.2	(−3.3)	0.044	0.9998	6(MeO,MeS, Me, Br, H, CN)
	LSFE Eq. 5	−3.45	−10.4		0.069	0.9991	5(MeO, MeS, Me, Br, H)
	LSFE Eq. 5[f]	−3.49	−10.3		0.092	0.9991	4(MeO, Me, Br, H)
7-X-2	LSFE Eq. 5	−3.89	−2.96		0.121	0.9946	4(MeO, Me, Br, H)

a) See also Table 5. b) See Text. c) Standard deviation. d) Correlation coefficient. e) Substituents involved in calculation. f) Without SMe.

The regression parameters derived are given in Table 4. The substituent constants employed here are the same as those in previous reports.[18] The reliability of such statistically derived ρ_i and ρ_π^+ parameters depends greatly upon the variation in the electronic natures of the substituents as well as on those numbers.[2a,51,52] The present series involve four common, typical substituents—MeO, Me, Br, H. Such a variety should provide meaningful results for the present purpose.

In the case of the 6-X-2 naphthyl series, the parameters from LSFE Eq. 5 (without the CN group) agreed quite well with those from the LArSR treatment, including the CN group. The identity of the correlation parameters with and without the CN, associated with high correlation coefficients, suggests that the ρ_π^- value must be rather close to the ρ_i value. In a previous paper,[1] it has been demonstrated that the reactivities in the 6-X-2 naphthyl derivatives can generally be expressed by the LArSR approach, involving both *pi*-donor and *pi*-acceptor substituents (CN or NO_2). This means that $\rho_\pi^- \simeq \rho_i$ holds generally, as a good approximation, in spite of varying contributions by *Pi* effects of *pi*-donor groups.

To minimize the probability of an accidental correlation due to experimental error, *etc.*, we used here the correlation values of ρ_i and ρ_π^+, including the CN group, for wider coverage. The $-\rho_i$ value for 7-X-2 naphthyl has been shown to be larger than that for the 6-X-2 series. The $\rho_{i,6\text{-x-}2}/\rho_{i,7\text{-x-}2}$ ratio is calculated to be 0.85 by the use of −3.3/−3.9; this value is in good agreement with the $\rho_{i,para}/\rho_{i,meta}$ value of 0.85, but it seems to be slightly larger than the relevant values of $\rho_{i,6\text{-x-}1}/\rho_{i,7\text{-x-}1}$ or $\rho_{i,6\text{-x-}1}/\rho_{i,5\text{-x-}1}$ of *ca.* 0.75 in the 1-naphthyl series (see also Table 5).[18] It is apparent that the *I* effect of substituents from the 7-position is more effectively transmitted than that from the 6-position in the 2-naphthyl system. This can reasonably be related to the shorter distance or less intervening sp^2-carbons in the 7-X-2 system than in the 6-X-2 system. On the other hand, the resulting $-\rho_\pi^+$ for the 6-X-2 is larger by a factor of 3 than that for the 7-X-2 system; this is in qualitative accord with the prediction from MO calculations.[2a,3,19b,20,23]

In Table 5 are collected the full sets of ρ_i and ρ_π^+ values derived from our solvolysis rates. Figure 4 gives the overall correspondence of the empirical ρ_i sets to Dewar's $1/r$ function, which has been shown to be appropriate for 1-naphthyl reactivities.[18] The figure seems to justify again the soundness of the simple function, covering a wide enough range, from the phenyl to the 2-fluorenyl system. Although the deviation of the 7-X-2 naphthyl appears to be slightly large, no other complicated functions, such as $(\cos\theta)/r^2$ (Table 5), can provide any appreciable improvement in the correlation. Therefore, it is apparent that the angle factors are unimportant. Herein, the *r* refers to Dewar's simplest distance between the naphthyl carbons to which substituents and reaction site are attached,[3a] and θ is the angle between the above distance vector and a C–X dipole vector. It is characteristic that, instead of the 4-biphenylyl sets which had previously

Table 5. Comparisons between empirical and theoretical parameters for the solvolysis of 1-arylethyl chlorides in 80% aq acetone at 45 °C

Aryl system	Method[lit]	ρ_i	ρ_π^+	Ratio of $1/r$[d]	Ratio of $\cos\theta/r^2$[d]	MO index SCF-π Δq[c]
4-X-1 Phenyl	LArSR[8]	−4.95[a]	−18.7[a]	1.00	1.00	0.200
3-X-1 Phenyl	LArSR[8]	−5.79[b]	−2.48[b]	1.15	0.96	0.042
7-X-2 Fluorenyl	LArSR[1]	−2.28[a,c]	−6.79[a,c]	0.40	0.25	
4′-X-4 Biphenylyl	LArSR[5]	−1.56[a]	−4.71[a]	0.40	0.25	
3′-X-4 Biphenylyl	LArSR[5]	(−1.83)[b]		0.44	0.18	
3-X-1 Naphthyl	LSFE[18]	−6.96	−2.56	1.15	0.96	0.019
4-X-1 Naphthyl	LSFE[18]	−5.09	−17.6	1.00	1.00	0.225
5-X-1 Naphthyl	LSFE[18]	−3.82	−4.40	0.76	0.65	0.084
6-X-1 Naphthyl	LSFE[18]	−2.90	−2.43	0.67	0.67	0.043
7-X-1 Naphthyl	LSFE[18]	−3.66	−7.74	0.76	0.50	0.107
6-X-2 Naphthyl	LArSR[f]	−3.28	−10.2	0.56	0.42	0.116
7-X-2 Naphthyl	LSFE[f]	−3.89	−2.96	0.58	0.38	0.045

a) Calcd with $\rho_i = \rho$, $\rho_\pi^+ = \rho(1 + r^+/0.415)$.[1] b) Calcd with $\rho_{i,meta} = 1.17\rho_{i,para}$.[15] c) The temperature factor of 0.957 was used from 25 °C to 45 °C.[5] d) See Text. e) Ref. 23b. f) Present study.

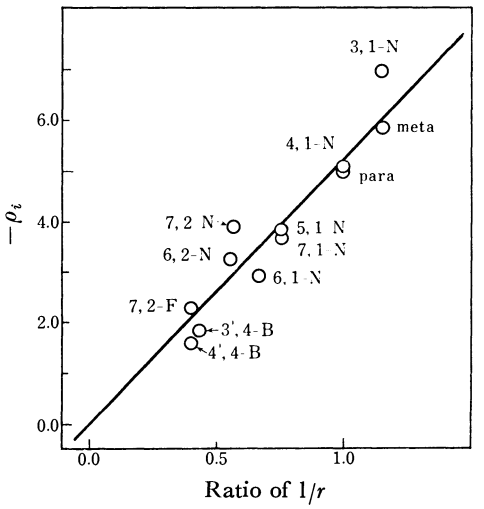

Fig. 4. A plot of the ρ_i values *vs.* a ratio of Dewar's $1/r$; N(Naphthyl), F(Fluorenyl), and B(Biphenylyl).

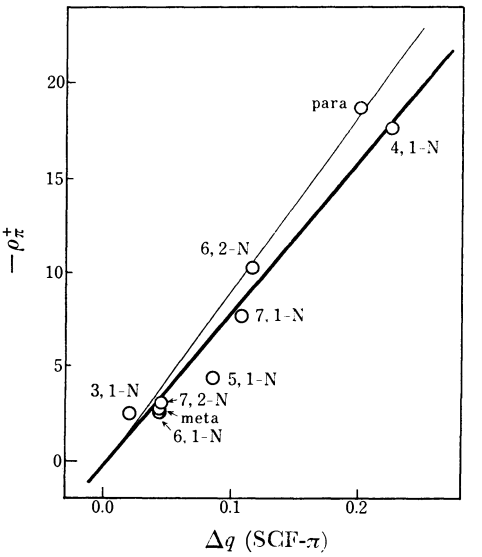

Fig. 5. A plot of the ρ_π^+ values *vs.* Δq of Forsyth's charge difference values by PPP SCF-π method.[23b]

been applied to Dewar's FM equation,[3a] the planar 2-fluorenyl set fits the line much more closely (Fig. 4). This observation is not inconsistent with our earlier conclusion of the $1/R^2$ dependence of the *I* effect in the 4-biphenylyl relative to the phenyl system.[5] Even bearing the crudeness of the approximation in mind, the inductive effect in various extended *pi*-systems for the present solvolysis series may be explicable in terms of Dewar's $1/r$ parameter (to a practical approximation) if the *peri*-hydrogen steric effect does not exert any observable effects on the ρ_i values. This conclusion will be further evaluated on the basis of available solvolysis data for heteroaromatics (see below).

In the solvolysis of 6-substituted bicyclo[4.4.0]dec-2-yl tosylates, which constitute a good model of the 6-X-2 naphthyl sigma skeleton, Tanida *et al.* suggested the importance of the field effect based upon the rate ratio of $k_{ax}/k_{eq}=0.7$—0.9.[55]

Previously, we noted a good relationship between the ρ_π^+ values and Forsyth's theoretical Δq_{ij} values (the regional charge difference at a substituent position).[53] Resently, Forsyth, Spear, and Olah have reported extensive sets of Δq; the change in charge density for the process of Ar→ArCH$_2^+$ was calculated by the use of a PPP SCF-π method.[23b,58] Figure 5 illustrates the correspondence between the empirical ρ_π^+ and the charge difference (Δq), giving two lines covering the 1- and 2-naphthyl and phenyl sets. The higher-slope line involves 4-X-1 phenyl and 6-X-2 naphthyl groups, while the lower line involves 4-X-1 naphthyl and 7-X-1 naphthyl groups; the four ρ_π^+ values of these groups are more reliable than the other groups in Fig. 5 because of their wider coverage of the reactivity change. The MO calculations do not involve any accounts of the steric effects. The separate response (Fig. 5) is explicable; that is, the 1-naphthyl ρ_π^+ sets, appreciably 4-X-1 and 7-X-1, are influenced more efficiently by steric effects caused by *peri*-hydrogen and give lower ρ_π^+ values than would be expected with other steric-free sets.

As a conclusion, the good coincidence between the empirical and theoretical coefficients with respect to the *I* and *Pi* effects, covering a wide range of *pi*-systems, provides evidence justifying the validity of the description of the substituent effects in terms of the *I* and *Pi* effects by means of the LSFE equation.

The LSFE approach has been further tested for other reactions[59] or other extended *pi*-systems: the III, IV, and the (V) solvolysis of 1-(2-benzofuryl)ethyl *p*-nitrobenzoates,[22] the (VI) solvolysis of 1-(2-benzo[*b*]-thienyl)ethyl *p*-nitrobenzoates,[23] the (VII) acetolysis of 2-(1-azulenyl)ethyl tosylates,[56a] and the (VIII) dissociation of 1-azulenecarboxylic acids.[56b] The correlation results are summarized in Table 6, in which almost all the series provide very satisfactory correlations ($R>0.995$).[61] Since common substituents are involved in most cases, the correlation parameters (ρ_i, ρ_π^+) can be estimated with a similar reliability without paying attention to improper substituent constants in certain groups.

In the case of the III and IV reactions, the $\rho_{i,7\text{-x-}2}$ is apparently larger than the $\rho_{i,6\text{-x-}2}$ and the $\rho_{i,6\text{-x-}2}/\rho_{i,7\text{-x-}2}$ ratio is calculated to be 0.85 for III and 0.87 for IV. The features are in line with that for the I solvolysis. The identical ρ_i ratio of 0.85, in spite of the obviously different amount of the *Pi* effect, means that the *I* effect in the 2-napthyl system also remains the position constant. At present, the meaning of the difference between the factor of the present 0.85 in the 2-naphthyl and the previous 0.75 in the 1-naphthyl[18] is not clear. The other sets of solvolysis data, such as for the 5-X-2 and 8-X-2 naphthyl systems, will clarify the significance of such a figure for the entire B-ring positions.

With this purpose in mind, the 2-benzofuryl and 2-benzothienyl reactivities have been chosen. These heteroaromatic systems are similar to the 2-naphthyl system; an oxygen or sulfur atom substituted for the CH=CH group. The empirical $-\rho_i$ values for 5- and 6-substituent positions in the two heteroaromatics are nearly equal: 4.1 ± 0.1 for V and 4.1 ± 0.2 for VI.

Table 6. Correlational parameters for reactivities in 2-naphthyl and relevant systems

	Reaction type[a]	Condition	Subst position	Method[b]	ρ_i	ρ_π^+	R	Subst and note
III:	2-Naph–COOH, pK_a[2a,20]	50E, 25 °C	6-X-2	A	0.74	0.97	0.995	NMe_2,MeO,Me,Br,Cl, F,H,CN,NO_2[c]
			7-X-2	A	0.87	0.57	0.993	NMe_2,NH_2,MeO,Me,Br, Cl,F,H,CN,NO_2[d]
IV:	2-Naph–COOMe+OH[21]	70D, 25 °C	6-X-2	C	1.72	2.43	0.995	MeO,Me,F,Cl,H,CN,NO_2[e]
			7-X-2	A	(1.97)	(3.56)	(0.996)	F,Cl,H,CN,NO_2[f]
V:	2-Benzofuryl–CH(OPNB)–Me, Solv[22]	80E, 75 °C	5-X-2	B	−4.21	−4.79	0.998	MeO,Me,Cl,H[g]
			6-X-2	B	−4.00	−11.5	0.999	MeO,Me,Cl,H[g]
VI:	2-Benzothienyl–CH(OPNB)–Me, Solv[23]	80E, 75 °C	4-X-2	B	−4.99	−7.15	0.993	MeO,Me,Cl,H
			5-X-2	B	−4.19	−4.81	0.997	MeO,Me,Cl,H[h]
			6-X-2	B	−3.88	−11.0	0.999	MeO,Me,Cl,H
			7-X-2	B	−4.61	−3.10	0.992	MeO,Me,Cl,H
VII:	1-Azulenyl–CH_2CH_2–OTs, Solv[56a]	AcOH, 25 °C	2-X-1	B	−4.49	−5.17	0.999	MeO,Me,Cl,Br,H
			3-X-1	A	−3.70	−3.80	0.995	MeO,Me,Br,H,CN,Ac,NO_2[i]
			6-X-1	B	−3.16	−4.39	0.993	MeO,Me,Br,H
VIII:	1-Azulenc–COOH, pK_a[56b]	50E, 25 °C	2-X-1	B	2.23	2.53	0.999	MeO,Me,Cl,Br,H
			3-X-1	A	1.58	0.89	0.999	MeO,Me,Cl,H,CN,Ac,NO_2[j]
			6-X-1	B	1.29	1.48	0.997	MeO,Me,Br,H

a) See text. b) A: Analysis with LSFE Eq. 2, B: with LSFE Eq. 5, C: calculation by means of the parameters of LArSR Eq. 1. c) $\rho_\pi^-=(0.96)$. d) Without OH; $\rho_\pi^-=(0.56)$. e) $r^+=0.17$[1] was used for the interconversion. f) Without NH_2; too limited data set. g) Too limited data sets for the 5-X-3 and 6-X-3 benzofuryl systems;[57] further, the data for the pK_a of 5,6-X-benzofurancarboxylic acids are not sufficient.[60] h) The log k/k_0 value for MeO (=0.53) was corrected and used; $(\log k/k_0)_{\text{benzofuryl}}=0.9842(\log k/k_0)_{\text{benzothienyl}}+0.013$. i) $\rho_\pi^-=-3.3$. j) $\rho_\pi^-=1.9$.

On the other hand, the $-\rho_i$ values for the 4- and 7-positions in the benzothienyl system are also nearly the same as the value of 4.9 ± 0.2 for VI. The ratio of the values is calculated to be 0.84 (by 4.1/4.9), identical with the position constant in the 2-naphthyl system. The ρ_i values thus obtained by the use of LSFE Eq. 5 may again be concluded to furnish the simple $1/r$ dependency well. Previously, Wells and Adcock argued for the requirement of some angle function, $(\cos\theta)/R^2$, in particular for the dissociation of the 8-X-2 naphthalenecarboxylic acids.[20] The orientational effect, if operative, may be expected to be relatively more important in the 4-X-2 benzothienyl system than in the 8-X-2 naphthyl system because of the larger angle of θ.[23a] However, no orientational factor can be detected in the present results. Further, the azulyl system gives a constant ratio of $\rho_{i,6\text{-x-}1}/\rho_{i,3\text{-x-}1}$ (0.84 for VII and VIII), independent of the different *Pi* effects. Since the reactivities are concerned with nonconjugate positions in the azulyl ring, more data at the conjugate positions would be of much interest.

From the values of ρ_π^+ relative to ρ_i in the series of the 2-benzothienyl system in Table 6, the 6-X-2 system ($\rho_\pi^+/\rho_i=2.8$) can be regarded as a system involving a strong *Pi* exaltation effect. Though the 7-X-2 benzothienyl system (0.7) also shows less exaltation than σ_p^0, as in the case of the 7-X-2 naphthyl, the 4-X-2 (1.4) and 5-X-2 (1.2) systems belong to the intermediate class, with a moderate *Pi* exaltation. These observations indicate the requirement of different resonance parameters of σ_R^+, σ_R^0, and σ_R(BA) for the respective sets to achieve the best fit to Taft's DSP Eq. 4. Generally speaking, however, there is no definite rule for the choice of the most appropriate parameters, especially for any intermediate class of reactivity ($\rho_\pi^+/\rho_i=2$—2.5). Since a different choice of $\bar{\sigma}_R$ causes different $\bar{\rho}_R$ values, the comparison of $\bar{\rho}_I$ and $\bar{\rho}_R$ between different sets of reactivity classes may be difficult. The present ρ_π^+ values, obtained for VI, satisfy not only the sequence, but also the magnitude of Δq, Forsyth's charge difference.[23a]

As has been mentioned before by us[18] and by others,[4] Dewar's FM[3] and many other modified methods for extended *pi*-systems[19,20,23] have, *a priori*, assumed transmission coefficients, especially for *Pi* effects, obtained by means of MO calculations and have then defined the substituent constants to fit the corresponding original phenyl set of reactivities. Although this kind of approach is successful with a very limited reactivity class, the approach can never handle variations in *Pi* effects depending on the types of reactions without any changes in substituent constants and/or model calculations.

In summary, it may be concluded that the electrophilic reactivity sets at B-ring positions in the 2-naphthyl and relevant extended systems can be adequately described by means of the LSFE equation. The resulting empirical ρ_i and ρ_π^+ parameters are reasonably correlated with certain physical properties characteristic of the system and are not inconsistent with our earlier conclusions with regard to the 1-naphthyl and other reactivities. The present discussion has been concerned

with the *pi*-donor substituents in electrophilic reactivities, but the treatment seems likewise promising for *pi*-acceptor substituents in nucleophilic reactivities.[50] We believe the present results provide further evidence for the significance of the LSFE equation as well as for the applicability of the universal substituent constants, independent of the reactivity classes.

References

1) Part 13; Y. Tsuno, Y. Tairaka, M. Sawada, T. Fujii, and Y. Yukawa, *Bull. Chem. Soc. Jpn.*, **51**, 601 (1978).

2) a) P. R. Wells, S. Ehrenson, and R. W. Taft, "Progress in Physical Organic Chemistry," **6**, 147 (1968); b) S. Ehrenson, R. T. C. Brownlee, and R. W. Taft, *ibid.*, **10**, 1 (1973); c) R. D. Topsom, *ibid.*, **12**, 1 (1976); d) For example, S. K. Dayal, S. Ehrenson, and R. W. Taft, *J. Am. Chem. Soc.*, **94**, 9113 (1972); e) See also O. Exner, *Collect. Czech. Chem. Commun.*, **31**, 65 (1966).

3) a) M. J. S. Dewar and P. J. Grisdale, *J. Am. Chem. Soc.*, **84**, 3539, 3546, 3548 (1962); b) M. J. S. Dewar, R. Golden, and J. M. Harris, *ibid.*, **93**, 4187 (1971).

4) J. Shorter, "Correlation Analysis in Chemistry," Plenum Press (1978), Chap. 4. The authors are indebted to Professor J. Shorter for making his recent review paper available to them prior to publication.

5) Y. Tsuno, W. -Y. Chong, Y. Tairaka, M. Sawada, and Y. Yukawa, *Bull. Chem. Soc. Jpn.*, **51**, 596 (1978).

6) Y. Tsuno, M. Fujio, M. Mishima, Y. Yukawa, and Y. Takai, to be published.

7) Y. Tsuno, M. Sawada, T. Fujii, and Y. Yukawa, *Bull. Chem. Soc. Jpn.*, **48**, 3347 (1975).

8) a) Y. Tsuno, Y. Kusuyama, M. Sawada, T. Fujii, and Y. Yukawa, *Bull. Chem. Soc. Jpn.*, **48**, 3337 (1975); b) Y. Tsuno, M. Sawada, M. Fujio, N. Shimizu, T. Uemura, M. Ichihara, T. Nakachi, and Y. Yukawa, *ibid.*, to be published.

9) a) Y. Yukawa and Y. Tsuno, *Bull. Chem. Soc. Jpn.*, **32**, 960, 965, 971 (1959); b) Y. Yukawa, Y. Tsuno, and M. Sawada, *ibid.*, **39**, 2274 (1966); **45**, 1198 (1972); c) M. Fujio, phD. thesis, Osaka Univ. (1972).

10) Y. Tsuno, M. Fujio, Y. Takai, and Y. Yukawa, *Bull. Chem. Soc. Jpn.*, **45**, 1519 (1972).

11) a) Y. Yukawa and Y. Tsuno, *Nippon Kagaku Zasshi*, **86**, 873 (1965); b) Y. Yukawa and Y. Tsuno, *Memoir, ISIR, Osaka Univ.*, **23**, 71 (1966).

12) M. Fujio, M. Mishima, Y. Tsuno, Y. Yukawa, and Y. Takai, *Bull. Chem. Soc. Jpn.*, **48**, 2127, 3324 (1975).

13) O. Exner, "Advances in Linear Free Energy Relationships," ed by N. B. Chapman and J. Shorter, Plenum Press (1972), Chap. 1; b) M. Fujio, Y. Tsuno, Y. Yukawa, and Y. Takai, *Bull. Chem. Soc. Jpn.*, **48**, 3330 (1975).

14) The authors are indebted to Prof. Taft for making his most recent papers available to them prior to publication. a) Taft and Brownlee have developed an improved DSP-2 equation; b) Recently, they have further developed a non-linear resonance effect treatment (DSP-NLR); J. Bromilow, R. T. C. Brownlee, D. J. Craik, M. Sadek, V. O. Lopez, and R. W. Taft, to be published.

15) The correlation of $\sigma_m = 1.17\,\sigma_i + 0.50\,\sigma_\pi^+ + 0.50\,\sigma_\pi^-$ has been derived statistically.[10-12]

16) a) M. Mishima, M. Fujio, R. Takeda, and Y. Tsuno, *Memoir, Fac. Sci., Kyushu Univ., Ser. C*, **11**, 85, 97 (1978); b) Y. Tsuno, M. Fujio, T. Nakachi, M. Mishima, R. W. Taft, J. Bromilow, and R. T. C. Brownlee, to be published; c) M. Sawada, M. Ichihara, Y. Yukawa, and Y. Tsuno, to be published; d) Y. Tsuno, M. Fujio, M. Mishima, Y. Takai, and Y. Yukawa, to be published.

17) Y. Tsuno, M. Fujio, T. Nakachi, and Y. Yukawa, 26th IUPAC Congress Abstract, Organic Chemistry Session (1977), p. 911.

18) Y. Tsuno, M. Sawada, T. Fujii, Y. Tairaka, and Y. Yukawa, *Bull. Chem. Soc. Jpn.*, **48**, 3356 (1975).

19) a) C. Eaborn and A. Fischer, *J. Chem. Soc., B*, **1969**, 152; b) C. Eaborn, P. Golborn, R. E. Spillett, and R. Taylor, *ibid., B*, **1968**, 1112.

20) P. R. Wells and W. Adcock, *Aust. J. Chem.*, **18**, 1365 (1965).

21) P. R. Wells and W. Adcock, *Aust. J. Chem.*, **19**, 221 (1966).

22) D. S. Noyce and R. W. Nichols, *J. Org. Chem.*, **37**, 4306 (1972).

23) a) D. A. Forsyth, *J. Am. Chem. Soc.*, **95**, 3594 (1973); b) D. A. Forsyth, R. J. Spear, and G. A. Olah, *ibid.*, **98**, 2512 (1976).

24) a) A. Bryson, *J. Am. Chem. Soc.*, **82**, 4862 (1960); b) A. Bryson and R. W. Matthews, *Aust. J. Chem.*, **16**, 401 (1963); c) V. Baliah and P. A. Nadar, *Indian J. Chem.*, **9**, 671, 1339 (1971).

25) All the mp's are uncorrected, as are the bp's. Elemental analysis was performed at the Material Analytical Center in ISIR, Osaka Univ. The IR absorption spectra were routinely recorded, to check the characteristic functional groups of the compounds prepared, on a JASCO model IR-G grating infrared spectrophotometer under neat or nujol conditions. Further, for most compounds, their purity was routinely checked with GLC or TLC (on silica gel). Analytical GLC was carried out on a Varian Aerograph, Model 2860-30, equipped with an integrator, using a column packed mainly with apieson grease L or silicone DC550 on Celite 545 (a TCD or FID mode detector was employed).

The proton NMR spectra were obtained using a Hitachi R-20 or R-24 spectrometer (60 MHz, CW) or JEOL JNM-FX100 (100 MHz, FT), with TMS as the internal standard. The carbon-13 NMR spectra were also obtained with the latter spectrometer at 25 MHz (FT). The chemical shifts are given in ppm downfield from TMS (δ value).

A programable Seiko 500 calculator was used to get k_1 and various correlational parameters by means of the least-squares method. For triple regression analysis, a Hewlett Packard 9821A calculator was employed.

26) R. B. Girdler, P. H. Gore, and J. A. Hoskins, *J. Chem. Soc., C*, **1966**, 181.

27) Ng. Ph. Buu-Hoi, Ng. Hoan, and D. Lavit, *J. Chem. Soc.*, **1953**, 485.

28) a) G. A. R. Kon and W. T. Weller, *J. Chem. Soc.*, **1939**, 792; b) P. R. Wells and P. G. E. Alcorn, *Aust. J. Chem.*, **16**, 1108 (1963).

29) R. B. Girdler, P. H. Gore, and J. A. Hoskins, *J. Chem. Soc., C*, **1966**, 518.

30) L. Friedmann and H. Shechter, *J. Org. Chem.*, **26**, 2522 (1961).

31) W. Adcock and P. R. Wells, *Aust. J. Chem.*, **18**, 1351 (1965).

32) L. F. Somerville and C. F. H. Allen, *Org. Synth.*, Coll. Vol. II, 81 (1943).

33) E. Ochiai, T. Okamoto, M. Sekijima, M. Nishikawa, and K. Shono, *Chem. Abstr.*, **51**, 16387i (1957).

34) J. Jacques and A. Horeau, *Chem. Abstr.*, **51**, 8048h (1957).

35) D. Todd, *Org. React.*, **4**, 378 (1949).

36) H. L. Holmes and L. W. Trevoy, *Org. Synth.*, Coll. Vol. III, 300 (1955).

37) N. Kharasch and S. H. Kaefayan, *J. Org. Chem.*, **21**,

929 (1956); H. O. House and R. J. McCaully, *ibid.*, **24**, 725 (1959); E. D. Bergmann and S. Yaroslavsky, *ibid.*, **25**, 1848 (1960).

38) L. F. Fieser and E. B. Hershberg, *J. Am. Chem. Soc.*, **58**, 2315 (1936).

39) C. C. Price and R. H. Michel, *J. Am. Chem. Soc.*, **74**. 3652 (1952).

40) R. E. Bowman, *J. Chem. Soc.*, **1950**, 322.

41) L. P. Fieser and A. M. Seligman, *J. Am. Chem. Soc.*, **60**, 170 (1938); K. Adachi and S. Tanaka, *Yuki Gosei Kagaku Kyokai Shi*, **29**, 1147 (1971).

42) a) As a first-order approximation, aromatic protons are assigned on the basis of irradiations and chemical shifts are obtained; 8.50 (H_1), 8.1$_2$ (H_8), 8.0$_7$ (H_3, $J_{1,3}$=1.5 Hz), 7.8$_5$ (H_4, $J_{3,4}$=8 Hz), 7.7$_4$ (H_5, $J_{5,6}$=8 Hz), and 7.6$_4$ (H_6, $J_{6,8}$= 2.0 Hz); b) The assignment of aromatic carbons was made mainly on the basis of the peak height and the selective decoupling spectra, with the aid of the H-NMR spectral data; the additivity rule was also employed for those carbons marked (†).[43] Here, the carbon bearing COOEt group is called C_2 and the carbon bearing Br group in the naphthalene, C_7 (ethyl 7-bromo-2-naphthalenecarboxylate). Concn of 0.13 M^{-1} (w/v); 5000 Hz/8 K.

43) W. Kitching, M. Bullpitt, D. Gartshore, W. Adcock, T. C. Khor, D. Doddrell, and I. D. Rae, *J. Org. Chem.* **42**, 2411 (1977).

44) a) S. R. Robinson and H. N. Rydon, *J. Chem. Soc.*, **1939**, 1394; b) "Dictionary of Organic Compounds," **1**, 11 4th ed, Eyre and Spottiswoode Publishers (1965).

45) a) J. F. Bunnett, "Investigation of Rates and Mechanisms of Reactions," Wiley (1974), Part 1, Chap. 4; b) For example, K. B. Wiberg, *ibid.*, Chap. 13.

46) For example, R. W. Taft, E. Price, I. R. Fox, I. C. Lewis, K. K. Anderson, and G. T. Davis, *J. Am. Chem. Soc.*, **85**, 709 (1963); P. E. Peterson, D. M. Chevli, and K. A. Sipp, *J. Org. Chem.*, **33**, 972 (1968).

47) H. L. K. Schmand and P. Boldt, *J. Am. Chem. Soc.*, **97**, 447 (1975).

48) L. M. Stock and H. C. Brown, "Advances in Physical Organic Chemistry," Academic Press (1963), Vol. 1.

49) σ_{CN}=0.653 was used; see Ref. 8b.

50) ΔpK_a of substituted 1-naphthylamines; Y. Tsuno, T. Nakachi *et al.*, to be published.

51) J. Shorter, "Correlation Analysis in Organic Chemistry," Clarendon Press (1973).

52) O. Exner, "Advances in Linear Free Energy Relationships," Plenum Press (1972), Chap. 1.

53) The numerical values used were estimated with a reasonable interconversion method.[18]

54) For example, N. R. Draper and H. Smith, "Applied Regression Analysis," Wiley (1966); see also Refs. 6, 16a, and 16b.

55) H. Tanida, S. Yamamoto, and K. Takeda, *J. Org. Chem.*, **38**, 2077 (1973).

56) a) R. N. McDonald, J. M. Richmond, J. R. Curtis, H. E. Petty, and R. J. Mobley, *J. Am. Chem. Soc.*, **99**, 5739 (1977); b) R. N. McDonald, R. R. Reitz, and J. M. Richmond, *J. Org. Chem.*, **41**, 1822 (1976).

57) D. S. Noyce and R. W. Nichols, *J. Org. Chem.*, **37**, 4311 (1972).

58) The PPP SCF-π and CNDO/2 regional charge values are almost identical (Ref. 23b).

59) The data for the detritiation[19] are insufficient to evaluate the ρ_i and ρ_π^+ values.

60) H. H. Jaffe and L. Jones, Adv. Heterocyclic Chem., **3**, 209 (1964); K. Bowden and D. C. Parkin, *Can. J. Chem.*, **44**, 1493 (1966).

61) Although the results by means of LSFE Eq. 2 are involved, the use of LSFE Eq. 5 for only $-R$ substituents provides nearly the same values.

The Transformation of 11-Deoxojervine into 18-Functional *C*-Nor-*D*-homosteroids[1,2]

Hiroshi SUGINOME,* Norio SATO, and Tadashi MASAMUNE*

Department of Chemistry, Faculty of Science, Hokkaido University, Sapporo 060

(Received April 23, 1979)

Deoxojervine, a *C*-nor-*D*-homosteroidal alkaloid, has been transformed into 17β-acetyl-12α-etiojervan-3β-ol acetate in 3 steps. Treatment with base gave the 17α-epimer. Reduction of the 17β-isomer with $NaBH_4$ afforded 17β-ethyl-12α-etiojervane-3β,20β-diol 3-acetate as a single product whereas reduction of the 17α-isomer afforded 17β-ethyl-12α-etiojervane-3β,20β-diol 3-acetate and the 20α isomer in an approximate 1 : 1 ratio. Irradiation of 17β-ethyl-12α-etiojervane-3β,20β-diol 3-acetate in cyclohexane in the presence of lead tetraacetate and iodine afforded a C-18 functional *C*-nor-*D*-homosteroid as a 18,20-epoxide which was oxidized to the corresponding γ-lactone with chromium trioxide. A mixture of the 17α-ethyl-12α-etiojervane-3β,20α-diol 3-acetate and its 20β isomer in contrast gave no 18-functional compounds upon irradiation under similar conditions.

Selective functionalization of inactive angular methyl groups by processes, which involve intramolecular free radical reactions[3] have been proven to be successful in steroids. There exists, however, no studies on the functionalization of inactive methyl groups by intramolecular radical processes in the field of *C*-nor-*D*-homosteroids. In this and subsequent papers the functionalization of the 13β-methyl group in the *C*-nor-*D*-homosteroid, derived from jerveratrum alkaloids by this process will be reported. These C-18 functional *C*-nor-*D*-homosteroids may be of value in further transformations of this important group of steroids.

Results

Catalytic hydrogenation of tetrasubstituted double bonds in (22*S*,25*S*)-5α-veratr-13(17)-enine-3β,23β-diol (**2**), prepared by the platinum-catalyzed hydrogenation[4] of 11-deoxojervine (**1**),[5] was affected using a rhodium–platinum catalyst.[6] The perhydro derivative (**3**), mp 219—221 °C, was obtained in a 35% yield. The NMR spectrum of **3** exhibited a 3-H singlet at τ 9.20 due to the 19-H, and three 3-H doublets centered at τ 9.23 (J=*ca.* 6 Hz, a signal of the doublet coincided with 19-H), 9.11 (J=6.3 Hz) and 8.99 (J=6.3 Hz) due to the three secondary methyl groups. At lower field, after D_2O exchange, a broad 2-H multiplet at τ 6.47, attributable to the 3α-H and the 23-αH, a 1-H doublet at τ 7.52 (J=9.6) and a 1-H double doublet at τ 7.08 (J=12 and 4) presented themselves. Irradiation at τ 6.47 caused the doublet at τ 7.52 to collapse to a singlet and thus the doublet has been assigned to the 22β-H. The double doublet is then assignable to one of the 27-methylene protons. The stereochemistry was assumed to be (22*S*,25*S*)-5α-veratranine-3β,23β-diol (**3**) on the basis of the *cis* addition of hydrogen atoms to an isolated olefinic center from the less-hindered side of steroid molecules and confirmed by its transformation into 17β-acetyl-12α-etiojervan-3β-ol[7] (**10**) identical with a specimen derived from a *C*-nor-*D*-homosapogenin by Johns and Laos.[8] The configurations at C-12, C-13, and C-17 in the 3β-ol **10** were established by further transformations as described later in this paper.

It was subsequently found that the diol **3** could be directly obtained by the catalytic hydrogenation of 11-deoxojervine in the presence of a rhodium–platinum catalyst or a large amount of Adams' platinum catalyst in acetic acid. From the hydrogenation product using the rhodium–platinum catalyst, perhydro compound (**4**), mp 178—180 °C, isomeric with the diol **3** was isolated in a 4% yield. The NMR spectra of **4** and compound **3** were very similar exhibiting a 3-H singlet at τ 9.25 due to the 19-H, and 4 singlets due to the overlap of three doublets centered at τ 9.13 (J=6), 9.08 (J=6), and 9.00 (J=6) assignable to three secondary methyl groups. A broad 2-H multiplet at τ 6.47 attributable to an overlap of the 3α-H and the 23-αH, a 1-H doublet at τ 7.73 (J=9.9 Hz, 22-βH), and a 1-H double doublet after D_2O exchange at τ 7.03 (J=12 and 4, one of 27-CH_2) were also present further downfield in the spectrum. No evidence is available on the configurations at the C-13 and the C-17 centers, but the structure has been tentatively assigned as (22*S*,25*S*)-5α,13α,17α-veratranine-3β,23β-diol (**4**) resulting from *cis* addition of hydrogen atoms from a more-hindered side.

The heterocyclic ring of diol **3** was removed by the procedure devised by Frank and Johnson.[9,10] Treatment of the diol **3** in dry THF with *N*-chlorosuccinimide for 1 h in an atmosphere of nitrogen afforded a *N*-chloro derivative (**6**). This was treated *in situ* with sodium methoxide in methanol for *ca.* 24 h at 0—10 °C to afford an aldehyde (**7**), mp 109—110 °C, in a 95% yield. The NMR spectral data was in agreement with the structure assigned. The mass spectrum exhibited a base peak at *m/e* 274 resulting from a loss of the C-17-substituent from the molecular ion involving a McLafferty rearrangement of a γ-hydrogen.

Treatment of the aldehyde **7** in THF with butyl nitrite in the presence of sodium methoxide afforded a ketone (**10**), mp 150—152 °C, in a 90% yield. Upon acetylation and oxidation with Jones reagent the 3-acetate (**11**), mp 116—118 °C, and a 3-one (**12**); mp 158—160 °C, were formed. The ketone **10** and acetate **11** were identical with the specimens[8] kindly provided by Dr. Johns. The corresponding oxime (**9**), mp 106—109 °C, which is characteristically obtained as the product in this reaction,[9] was isolated in only one experiment. Hydrolysis of the oxime with aq ethanolic HCl under reflux, however, gave an isomeric ketone which was identical with the ketone (**13**) obtained by treatment of the ketone **10** with base. It is assumed

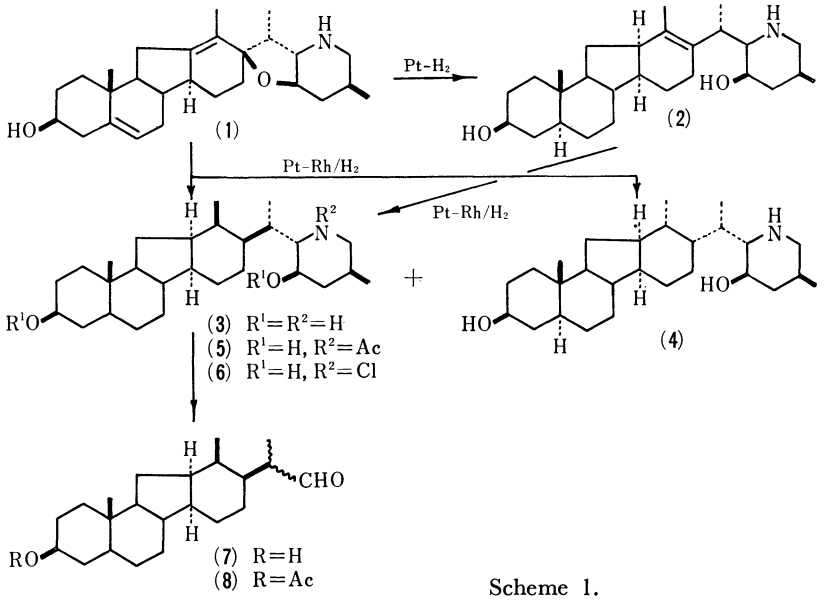

Scheme 1.

to be epimeric with the ketone **10** at the C-17.

The configurations at C-12 and C-13 in methyl ketone **10** have been established by Johns and Laos by transformation into 12α-etiojervane-3,17-dione (**17**) by Baeyer-villiger oxidation, followed by hydrolysis and oxidation with Jones' reagent. Repetition of these experiments afforded a diol (**16**)[11] and a dione (**17**) which were identical with the specimens prepared by Johns and Laos from a *C*-nor-*D*-homosapogenin, by direct comparison. As described by Johns and Laos,[8] treatment of the dione **17** with methanolic 5% KOH for 1 h under reflux resulted in partial epimerization at C-13 and afforded an equilibrium mixture of 12α-etiojervane-3,20-dione **17** and 12α,13α-dione (**18**). Recrystallization of this mixture from aq acetone afforded a pure dione **18**, mp 136—140 °C, identical with a specimen obtained from *C*-nor-*D*-homosapogenin by Johns and Laos.[8] The configurations at the C-17

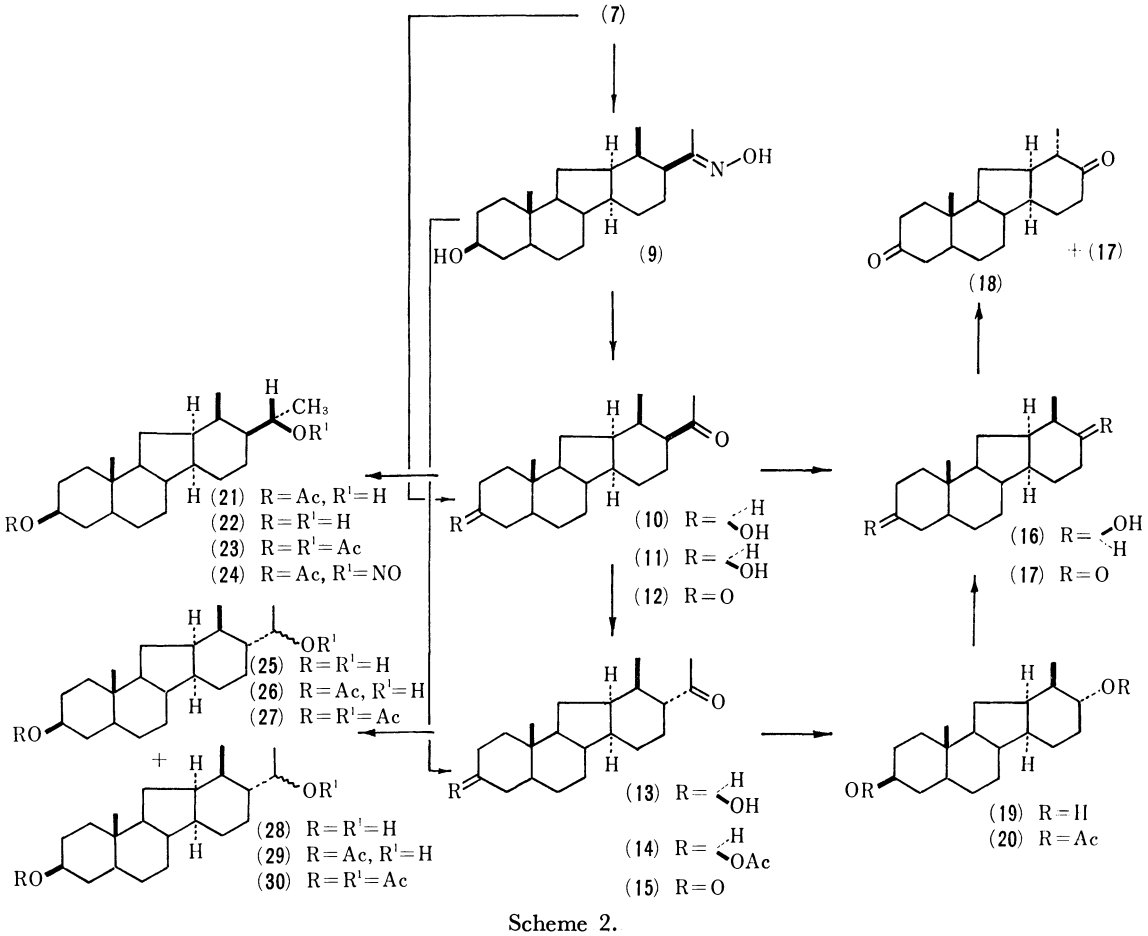

Scheme 2.

centers of methyl ketone **10** and consequently the diol **3**, and the aldehyde **7**, were confirmed as β on the basis of the following epimerization experiments.

Treatment of the methyl ketone **10** with methanolic potassium hydroxide (2.5%) for 12 h at room temperature gave an isomeric ketone **13**, mp 140.0—141.5 °C, the acetate (**14**), mp 88.0—90.0 °C, of which was isomeric with methyl ketone acetate (**11**).

On Baeyer-Villiger oxidation, the isomeric ketone **13** afforded a new diol (**19**), mp 179.0—179.5 °C, which gave an acetate (**20**), mp 96—98 °C. The diol **19** was shown to be epimeric at C-17 with the diol **16** in that Jones' oxidation of the diol **19** afforded the dione **17** identical with the dione obtained by oxidation of the diol **16**. The D-ring of the ketones **10** and **13** is assumed to adopt one of four possible conformations, two *quasi* chair and two *quasi* boat forms. Regardless of these conformations, the 13β-methyl and the 17-acetyl substituents in the more stable ketone **13** will occupy more stable equatorial positions.

It follows that the 13β-methyl and the 17-acetyl substituents in the D-ring of the less stable ketone **10** and hence in the aldehyde **7** and the diol **3**, should be either in β-equatorial and β-axial or in β-axial and β-equatorial orientations. Thus, the isomerization of methyl ketone **10** into methyl ketone **13** demonstrates that the two substituents at C-13 and C-17 in the D-ring of compounds **3**, **7**, and **10** are oriented in the *cis* direction. The structures of the isomeric diols **16** and **19** have thus been assigned as 12α-etiojervane-3β,17β-diol and 12α-etiojervane-3β,17α-diol respectively.

Reduction of methyl ketone **11** with $NaBH_4$ in a mixture of ethanol and ethyl acetate gave a single product (**21**), mp 126—129 °C, in greater than 95% yield. Under these conditions both the 3β-ol (**22**) and the 20ξ-epimer of **21** were not formed. Hydrolysis and acetylation of the 20ξ-ol afforded 3β,20ξ-diol, mp 252—254 °C, and the diacetate (**23**), mp 84.5—87.0 °C.

Reduction of isomeric 17α-acetyl-12α-etiojervan-3β-ol acetate with $NaBH_4$ under similar conditions afforded a mixture of 20ξ-ols (**26**)[4] and (**29**) which was hydrolyzed to a mixture of 3β,20ξ-diols. Separation by preparative TLC afforded 3β,20ξ-diol (**25**), mp 140.0—140.5 °C, and isomeric 3β,20ξ-diol (**28**), 187—189 °C, in 38 and 41% yields respectively.

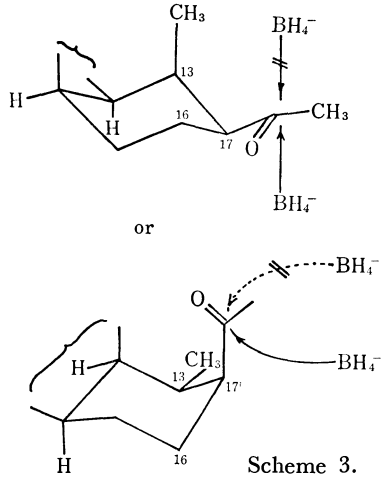

Scheme 3.

No unambiguous spectral evidence with regard to the configurations of the hydroxyl group in the C-17 side chain of the etiojervanes (**21**, **26**, and **29**) was available. The stereochemistry can however be reasonably explained by considering the steric course of the reduction with complex metal hydrides. Examination of models of 17β-acetyletiojervane **11** indicates that regardless of the *quasi*-chair or *quasi*-boat conformation of the D-ring, the preferred conformation of the 17β-acetyl group would be such that the C=O bond eclipses the C-16–C-17 bond when the 13-methyl is axial and the 17β-acetyl is equatorial. Alternatively, with the 13-methyl equatorial and the 17β-acetyl group axial, the preferred conformation is for the carbonyl to lie orthogonal to the C-16–C-17 bond. In the former case, hydride ion attack would occur predominantly from the α-face due to the presence of the 13β-methyl group (steric approach control)[12] giving predominantly the β-ol **21** (Scheme 3). In the latter case, the hydride ion would attack predominantly from the front, and aided by the presence of the 13β-methyl and the predominant product would be the β-ol **21** (Scheme 3). In such cases, formation of the α-ol is unlikely.

The situation is analogous to the reduction of 20-oxopregnanes with complex metal hydrides where the predominant product is the 20β-isomer.[13]

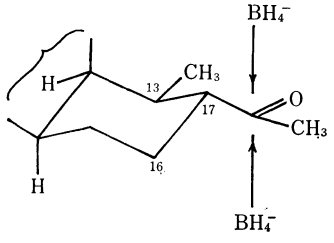

Scheme 4.

Examination of the model of 17α-etiojervane in which the 13β-methyl and the 17α-acetyl both occupy equatorial positions, shows that the preferred conformation of the 17α-acetyl group is when the C=O bond eclipses the C-13–C-18 bond in order to minimize the interaction between the skeletal part and the C-17 acetyl methyl. Thus, the hydride ion can approach the C=O bond equally from both the α- and β-sides affording a 1: 1 mixture of the observed α- and β-ols **26** and **29** (Scheme 4).

20β-ol **21** in pyridine readily afforded a crystalline nitrite (**24**), mp 102—106 °C, by treatment with nitrosyl chloride–pyridine.

Irradiation of the nitrite in benzene for 230 min under an atmosphere of nitrogen afforded a mixture of products. The product, hydrolyzed with methanolic 5% potassium hydroxide at room temperature and subjected to recrystallization and preparative TLC afforded 3β,20β-diol **22** (23%) and 17β-acetyl-3β-ol **10** (15%).

Examination of the NMR spectra of the other fractions from the preparative TLC failed to identify the 18-functionalized derivative. The failure in obtaining the 13β-methyl functionalized product contrasts with the results for the normal steroids.[14]

Functionalization of the 13β-methyl in the 20β-ol **21**

was, however, achievable by the hypoiodide reaction (Scheme 5). Thus, 20β-ol **21** in cyclohexane containing iodine and lead tetraacetate was irradiated for 0.5 h with a 450 W high pressure Hg arc. Preparative TLC of the product afforded a crystalline 18,20-epoxide (**32**), mp 76—79 °C, resulting from intramolecular hydrogen abstraction, (16% yield) together with an amorphous substance (**31**). The NMR spectrum of the former exhibited two 3-H singlets at τ 9.22 and 7.98 which have been assigned 10β-methyl and OAc and a 3-H doublet (J=6.3 Hz) at τ 8.75 which has been assigned to the methyl attached to a carbon having an ether oxygen. The spectrum disclosed the absence of a signal attributable to the 13β-methyl and the presence of a multiplet due to the AB part of the ABX system from τ 5.88 to 6.91 ascribable to the 18-methylene protons. The mass spectrum was in full accordance with the epoxide structure (**32**). Thus, the prominent fragment ions (B) at *m/e* 345 (65%) and 285 (73%, $M^+-CH_3CO_2H-CH_3$) result from the expulsion of a methyl group from the molecular ion (A) and the molecular ion peak at *m/e* 360 (2%) and base peak at *m/e* 300 arise from the loss of acetic acid from the molecular ion. The amorphous substance **31** exhibited aromatic and cyclopropane protons in the NMR spectrum and contained iodine. No satisfactory structure has been evaluated for this compound.

Oxidation of (20*S*)-18,20-epoxy-17β-ethyl-12α-etiojervane-3β,20β-diol 3-acetate (**32**) with chromium trioxide afforded the corresponding γ-lactone (**33**), mp 89—90 °C, characterized by IR and NMR spectra [10β-methyl at τ 9.15 and 20ξ-methyl at τ 8.60 (J=6.0

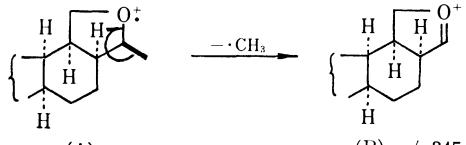

(A) (B) *m/e* 345 and 285

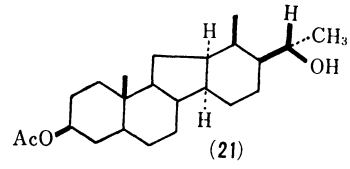

(21)

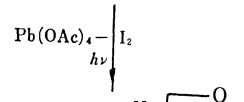

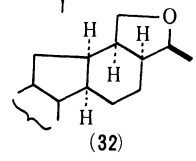

(32)

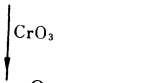

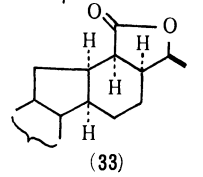

(33)

Scheme 5.

Table 1. NMR parameters for etiojervane derivatives in $CDCl_3$ solution
(Chemical shifts (τ) and splittings (Hz; in parentheses))

Compound	18-H	19-H	21-H	OAc	Other
7	8.97(d, 7.2)	9.20(s)	9.19(d, 7.2)	—	CHO, 0.42(d, 3.8)
8	8.96(d, 6.6)	9.16(s)	9.19(d, 6.6)	7.97(s)	CHO, 0.43(d, 3.8)
9	9.21(d, 6)	9.20(s)	8.12(s)	—	
10	9.20(d, 6.8)	9.20(s)	7.85(s)	—	
11[a)]	9.28(d, 7)	9.24(s)	7.93(s)	8.04(s)	
12	9.16(d, 6.6)	8.99(s)	7.84(s)	—	
13[a)]	9.21(d, 5.4)	9.21(s)	7.87(s)	—	
14[a)]	9.30(d, 6)	9.26(s)	7.93(s)	8.05(s)	
15	9.15(d, 6.0)	8.98(s)	7.86(s)	—	
16	9.03(d, 6.6)	9.20(s)	—	—	
17	9.01(d, 6.0)	9.09(s)	—	—	
18	9.00(d, 6.2)	9.00(s)	—	—	
19	8.96(d, 6.6)	9.21(s)	—	—	
20	9.04(d, 7.8)	9.19(s)	—	7.92 and 7.92(s)	
21[a)]	9.14(d, 7)	9.19(s)	8.81(d, 6.0)	7.99(s)	20-H 6.39(m)
23	9.22(d, 7.8)	9.18(s)	8.80(d, 6.0)	7.96 and 7.96(s)	
24	9.21(d, 6)	9.20(s)	8.63(d, 6.6)	7.98(s)	
25	9.08(d, 6.0)	9.20(s)	8.82(d, 6.0)	—	
27	9.13(d, 6)	9.19(s)	8.81(d, 6.0)	7.98 and 7.98(s)	
28	9.10(d, 5.3)	9.18(s)	8.86(d, 6.6)	—	
30	9.07(d, 4.5)	9.20(s)	8.85(d, 6.6)	7.99 and 7.99(s)	
32[a)]	13β-methylene, 6.05 (bt, 8), 6.57 (bt, 8)	9.25(s)	8.78(d, 6.0)	8.00(s)	20α-H, 6.37(m)
33	—	9.15(s)	8.60(d, 6.0)	7.97(s)	

a) Measured by 100 MHz instrument.

Hz)], in 19% yield.

A mixture of the isomeric 20ξ-ols (**26**) and (**29**) was subjected to the hypoiodite reaction but no 18-functional compound resulting from intramolecular hydrogen abstraction was obtained.

The foregoing results demonstrate that the functionalization of the 13β-methyl group in *C*-nor-*D*-homosteroids may be achieved by intramolecular hydrogen abstraction of the 20β-oxyl radical attached to the C-17β alkyl but not by 20α and 20β-oxyl radicals attached to the C-17 α-alkyl group.

Experimental

All melting points were determined with a hot-plate (Yanagimoto micro melting point) apparatus and are uncorrected. Unless stated otherwise, IR spectra were determined in Nujol with a JASCO DS-402G or JASCO model IR-E spectrophotometer. Unless stated otherwise, NMR spectra were determined with a JEOL 3H-60 high resolution spectrometer in deuteriochloroform solution using TMS as an internal reference. The course of reaction and column chromatography were followed by thin layer chromatography with Wakogel B-5. Mass spectra were determined with a RMU-6E spectrometer with the exception of the MS of compound **21** which was determined with a Hitachi JMS-D 300 spectrometer.

Catalytic Hydrogenation of (22S,25S)-5α-Veratr-13(17)-enine-3β,23β-diol (2). The diol **2** (1 g) in acetic acid (30 ml) containing a rhodium–platinum oxide catalyst (2 g) was hydrogenated with stirring. The theoretical amount of hydrogen was absorbed in 22 h. After the removal of the catalyst, the filtrate was made alkaline by the addition of aq 10% sodium carbonate solution. To the solution was added chloroform and the chloroform complex obtained was recrystallized from acetone to yield (22*S*,25*S*)-5α-veratratranine-3β,23β-diol (**3**), identical with the diol obtained by catalytic hydrogenation of 11-deoxojervine.

Catalytic Hydrogenation of 11-Deoxojervine (1). (a) Rhodium–Platinum Catalyst: 11-Deoxojervine (8 g) in glacial acetic acid (130 ml) containing rhodium–platinum oxide[6] (2.69 g) was hydrogenated with stirring. The absorption of hydrogen practically ceased after 69 h. The catalyst was removed by filtration and washed with hot methanol. The filtrate and methanol washings were combined and the solution concentrated. To this solution methanol was added followed by methanolic potassium hydroxide and finally a small volume of water to afford crude crystals of diol **3**. The total weight of crystals obtained (5 crops) was recrystallized to afford the pure diol (2.88 g). Specimens for analysis were obtained by recrystallization from methanol, mp 219—221 °C. IR: 3274 and 3338 (OH and NH), 1038, and 968 cm^{-1} NMR, see text. Found: C, 77.78; H, 11.25; N, 3.42%. Calcd for $C_{27}H_{47}O_2N$, C, 77.64; H, 11.34; N, 3.35%; MS (80 eV), *m/e* (rel. intensity) 417 (0.2, M^+), 402 (0.3, M^+-CH_3), 399 (0.4, M^+-H_2O), 384 (0.8, $M^+-CH_3-H_2O$), and 114 (100, 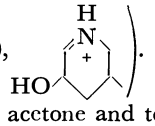). The residue from the filtrate was dissolved in acetone and to this solution a small volume of methanol was added to afford the crystals on standing. Recrystallization from aq methanol gave (22*S*,25*S*)-5α,13α,17α-veratranine-3β,23β-diol (**4**) (0.36 g). Specimens for analysis were obtained by recrystallization from acetone. Mp 178—180 °C: IR: 3112—3432 (OH and NH), 1040, and 883 cm^{-1}; NMR, see text. Found: C, 78.11; H, 11.27; N, 3.33%. Calcd for $C_{27}H_{47}O_2N$, C, 77.64; H, 11.34; N, 3.35%; MS (80 eV), *m/e* (rel. intensity), 417 (0.3, M^+), 402 (0.4, M^+-CH_3), 399 (0.5, M^+-H_2O), 384 (1.1, $M^+-CH_3-H_2O$), and 114 (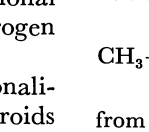). The yields of diol **3** from of hydrogenation conducted under different ratios of substrate and catalyst and under different concentrations, are tabulated below.

Weight ratio between deoxojervine and the catalyst	Concentration of deoxojervine (g/100 ml)	Yield of diol **3** (%)
1:0.3	5.0	39
1:0.33	6.2	36
1:0.66	5.0	42
1:1	3.3	46
1:1.4	2.5	46

(b) Platinum Catalyst: 11-Deoxojervine (2.0 g) in glacial acetic acid (20 ml) containing Adams platinum oxide (0.68 g) was hydrogenated for 60 h under atmospheric pressure with stirring. The solution was worked up as described in procedure (a). The diol **3** obtained, was recrystallized from methanol (0.613 g).

Preparation of N-Acetyl-(22S,25S)-5α-veratranine-3β,23β-diol (5). The diol **3** was acetylated with acetic anhydride and pyridine at 60—70 °C for 3 h. After the usual work-up, an amorphous 3-*O*,23-*O*,*N*-triacetyl derivative of diol **3** [NMR τ 9.20 (3-H, s, 19-H), 7.84 and 7.95 (3-H and 6-H, s, N–Ac, and OAc)] was obtained. This triacetyl derivative was hydrolyzed with methanolic 2.5% potassium hydroxide at room temperature overnight. The usual work-up afforded the *N*-acetyl derivative **5** which was recrystallized from aq acetone. Mp 227—229 °C: IR: 3153 and 3429 (OH), 1602 cm^{-1} (NAc), 1025, and 986 cm^{-1}. Found: C, 75.76; H, 10.69; N, 2.84%. for $C_{29}H_{49}O_3N$; C, 75.77; H, 10.74; N, 3.05%.

N-Chloro-(22S,25S)-5α-veratranine-3β,23β-diol (6). The diol **3** (50 mg) and *N*-chlorosuccinimide (22 mg) in dry THF (8 ml) were stirred for 1 h under dry nitrogen atmosphere. After the addition of water, the resultant precipitate was collected by filtration. The crude *N*-chloro derivative was dissolved in chloroform, the solution filtered and the residue recrystallized from acetone to yield the pure *N*-chloro derivative, mp over 290 °C, in an almost quantitative yield. IR: 3399 cm^{-1} (OH), 1036, and 1019 cm^{-1}. Found: N, 2.97%. Calcd for $C_{27}H_{46}O_2NCl$, N, 3.10%.

Degradation of Diol 3 to 20-Formyl-17β-ethyletiojervan-3β-ol (7). The diol **3** (1.4 g) and *N*-chlorosuccinimide (0.63 g) in dry THF (250 ml) were stirred for 1 h under an atmosphere of nitrogen. The reaction mixture was cooled to −20—−40 °C and to this solution a mixture of sodium (4.0 g) in dry methanol (70 ml) was added within a period of 0.5 h. The mixture was allowed to stand at −2—−10 °C for 15 h and then at 0 °C for 9 h. This procedure was conducted under an atmosphere of nitrogen. The solution was concentrated (<35 °C) and water (300 ml) added to the solution. The mixture was neutralized with 6 M-hydrochloric acid (50 ml) at *ca.* −7—−4 °C and then stirred for 2.5 h at room temperature. The reaction mixture was extracted three times with chloroform and the combined chloroform solution were washed with water, dried and evaporated to afford crude aldehyde **7**. The products from other two identical procedures were combined (3.1 g, 95%). The crude aldehyde **7** was recrystallized from aq ethanol. Mp 109—111 °C: IR: 3363

(broad, OH), 1708 and 2703 (CHO), and 1024 cm^{-1}. Found: C, 79.22; H, 10.72%. Calcd for $C_{22}H_{36}O_2$: C, 79.46; H, 10.92%; MS, (80 eV), *m/e* (rel. intensity), 332 (2.0, M^+), 317 (0.7, M^+-CH_3), 314 (1.6, M^+-H_2O), 274 (100, M^+-H-C-17-substituent), 259 (20.5, M^+-H-C-17-substituent$-CH_3$), 257 (19.6, M^+-C-17-substituent$-H_2O$), 149 (44.2), 148 (49.5), and 107 (35.3). The acetyl derivative **8** was prepared by the usual method. Mp 114—116 °C (methanol): IR: 1720 and 1735 cm^{-1} (CHO), 1242, and 1028 cm^{-1}. Found: C, 76.48; H, 9.98%. Calcd for $C_{24}H_{38}O_3$: C, 76.96; H, 10.23%; MS (80 eV), *m/e* (rel. intensity) 374 (1.1, M^+), 316 (100, M^+-C-17-substituent$-H$), 257 (30.9, M^+-C-17-substituent$-CH_3CO_2H$), 256 (42.4, M^+-C-17-substituent$-H-CH_3CO_2H$), 149 (57.4), 148 (62.3), 107 (56.0), and 93 (56.0).

*Preparation of 17β-Acetyl-12α-etiojervan-3β-ol (**10**) and the 3-Acetate.* To a solution of the aldehyde **7** (1.3 g) and butyl nitrite (5 ml) in THF (10 ml) was added sodium (460 mg) in dry methanol (10 ml) under an atmosphere of nitrogen at −20 °C over 20 min. The mixture was set aside 25 h at 2—3 °C and neutralized by the addition of hydrochloric acid (3 ml) at 0——4 °C. The solution was concentrated (<35 °C) and extracted with chloroform. The chloroform solution was washed with water, dried and evaporated and the viscous residue subjected to silica gel column chromatography (Mallincrodt, 100 mesh). The column was successively eluted with hexane, benzene, chloroform, and diethyl ether. The chloroform and diethyl ether fractions afforded a ketone **10**, mp 145—150 °C (1.14 g, 90%). Specimens for analysis were obtained by recrystallization from aq ethanol; mp 150—152 °C (lit,[8] 154—156 °C); IR: 1699 (acetyl), 3523 (OH), 1193, and 1063 cm^{-1}. The acetyl derivative **11** was obtained in the usual manner and recrystallized from aq methanol. Mp 116—118 °C (lit,[8] 131—133 °C); IR: 1692 (Ac), and 1720 cm^{-1} (OAc), 1241, and 1030 cm^{-1}. Methyl ketone **10** and its acetate **11** were identical with specimens prepared by Johns and Laos[8] by direct comparison.

*Preparation of 17β-Acetyl-12α-etiojervan-3β-ol Oxime (**9**) and the Acid-catalyzed Hydrolysis to 17α-Acetyl-12α-etiojervan-3β-ol (**13**).*

The oxime **9** was obtained only from this precedure. To a solution of the aldehyde **7** (50 mg) and butyl nitrite (0.5 ml) in methanol (1.5 ml) was added sodium metal (62 mg) in dry methanol (1.5 ml) over 3 min in an atmosphere of dry nitrogen at −20 °C. The mixture was set aside for 27.5 h at 0 °C. The pH of the mixture was adjusted to 4 by the addition of hydrochloric acid (*ca.* 6 drops) at −20 °C. After removal of the solvent, the residue was extracted with chloroform. After the usual work-up, the residue (42 mg) was purified by preparative TLC to afford a crude oxime (36 mg). The oxime was recrystallized from acetone to yield the pure oxime, mp 106—109 °C. IR: no carbonyl band, 3336 cm^{-1} (OH), 1040, and 879 cm^{-1}. The oxime (*ca.* 20 mg) in ethanol (10 ml) containing hydrochloric acid (1 ml) was refluxed for 2 h for 40 min. The reaction mixture was concentrated and extracted with diethyl ether and water. The organic layer was worked up to afford a residue (17 mg). After recrystallization from aq methanol it was shown to be identical with 17α-ethyl-12α-etiojervan-3β,20ξ-ol (**13**), obtained by the isomerization of 17β-ketone **10**.

*Oxidation of 17β-Acetyl-12α-etiojervan-3β-ol (**10**) with Chromium Trioxide.* To the 3β-ol **10** (105 mg) in acetone (5 ml), cooled in an ice-water bath, was added Jones' reagent (7 drops) and the mixture stirred for 1 h. After the usual work-up, the residue (120 mg) was recrystallized from acetone to afford the 3,20-dione **12** in 95% yield. Specimens for analysis were obtained by recrystallization from acetone. Mp 158—160 °C. Found: C, 79.58; H, 10.07%. Calcd for $C_{21}H_{32}O_2$: C, 79.90; H, 10.19%: MS (80 eV), *m/e* (rel. intensity); 316 (65, M^+), 301 (19, M^+-CH_3), 232 (42), 231 (44), 203 (30), 163(55), 107(58), 95(86), 85(100), 55(87), and 43(91).

*Preparation of 12α-Etiojervane-3β,17β-diol (**16**) by the Baeyer-Villiger Oxidation of 17β-Acetyl-12α-etiojervan-3β-ol.* A solution of the 20-one **10** (178 mg) and perbenzoic acid (90% purity, 105 mg) in chloroform (0.75 ml) were allowed to stand for 7 days at room temperature. The excess of perbenzoic acid was decomposed by the addition of 10% aq sodium hydrogen sulfite and the reaction mixture extracted with chloroform and water. The organic layer was washed with 10% aq sodium carbonate and water successively and dried. After evaporation of the solvent the residue (150 mg) was dissolved in methanolic 5% potassium hydroxide solution (10 ml) and allowed to stand for 3 h at room temperature. The usual work-up of the solution afforded a residue which was subjected to preparative TLC with a 1:1 mixture of chloroform and diethyl ether. The starting material (20 mg) and 13β-etiojervane-3β,17β-diol **16** (49 mg) were obtained. Recrystallization from acetone–cyclohexane, gave **16** which melted at 167—169 °C (lit,[8] mp 169—170 °C). The diol was proved to be identical with a specimen prepared by Johns and Laos[8] by direct comparison. IR: 3339 (OH), 1036, and 1069 cm^{-1}.

*Oxidation of 12α-Etiojervane-3β,17β-diol (**16**) with Chromium Trioxide.* To the diol **16** (50 mg) in acetone (10 ml) cooled by ice–water, was added Jones' reagent (3 drops). The reaction mixture was stirred for 1 h. After the excess chromium trioxide was decomposed by the addition of 10% aq sodium hydrogen sulfite, the solvent was evaporated and the reaction mixture worked up in the usual manner. The dione **17** was recrystallized from acetone (42 mg). Specimens for direct comparison were obtained by recrystallization from diethyl ether. Mp 169—170 °C (lit,[8] 169—170 °C). This specimen was identical with dione **17** prepared by Johns and Laos by a direct comparison. IR 1700 and 1713 cm^{-1} (carbonyl).

*Isomerization of 12α-Etiojervane-3,17-dione (**17**) with Base.*

The dione (20 mg) in methanolic 5% potassium hydroxide solution (10 ml) was refluxed for 1 h under an atmosphere of nitrogen. The solution was concentrated and the residue extracted with diethyl ether and water. After the usual work-up, the residue was recrystallized from aq acetone to yield crystals (18 mg); mp 115—125 °C which were largely an isomer **18**, epimeric at the C-13 and contaminated with a small amount of the starting ketone as evidenced by a weak singlet at τ 9.09 due to 19-H of **17** in the NMR spectrum. The mixture was recrystallized twice to afford pure 12α,13α-etiojervane-3,17-dione (1 mg), mp 136—140 °C (lit,[8] mp 143—145 °C). This compound was identical with the specimen prepared by Johns and Laos[8] by a direct comparison.

*Base-catalyzed Epimerization of 17β-Acetyl-12α-etiojervan-3β-ol (**10**).* The 3β-ol **10** (100 mg) in methanolic 2.5% potassium hydroxide (10 ml) was allowed to stand for 12 h under an atmosphere of nitrogen. The solution was neutralized by the addition of dilute hydrochloric acid and extracted with chloroform. The organic layer was washed with water, dried and evaporated. The residue was recrystallized from a diethyl ether–hexane mixture to yield 17α-acetyl-12α-etiojervan-3β-ol (**13**) (78 mg). Specimens (57 mg) for analysis were obtained by recrystallization from aq methanol. Mp 140.0—141.5 °C: IR: 3450 (OH), 1695 (acetyl), 1166, 1069, and 1045 cm^{-1}. Found: C, 78.54; H, 10.49%. Calcd for $C_{21}H_{34}O_2$: C, 79.19; H, 10.76%. The acetate (**14**) was prepared in usual way and was recrystallized from aq methanol. Mp 88—90 °C: IR: 1723 and 1701 cm^{-1}, (carbonyl and OAc), 1240, and 1030 cm^{-1}. Found: C, 76.67; H, 9.97%. Calcd for $C_{23}H_{36}O_3$: C, 76.62; H, 10.07%.

Oxidation of 17α-Acetyl-12α-etiojervan-3β-ol with Chromium Trioxide. To 17α-acetyl-12α-etiojervan-3β-ol (70 mg) in acetone (4 ml) cooled by ice-water, was added Jones' reagent and the solution stirred for 1 h. After the excess reagent was decomposed by the addition of 10% aq sodium hydrogen sulfite, the solution was worked up. The product (73 ml) was recrystallized from aq methanol to afford 17α-acetyl-12β-etiojervan-3-one, mp 87—88 °C, (48 mg). IR: 1700 cm^{-1} (broad, carbonyl). Found: C, 79.59; H, 10.12%. Calcd for $C_{21}H_{32}O_2$: C, 79.70; H, 10.19%.

*Preparation of 12α-Etiojervane-3β,17α-diol (**19**) by Baeyer-Villiger Oxidation of 17α-Acetyl-12α-etiojervan-3β-ol.* The reaction was conducted as described for the oxidation of the 17β-isomer **10**. The 20-one **13** (178 mg) afforded a crude product (200 mg) which was hydrolyzed in a manner similar to that for the 17β-isomer. The crude product was subjected to preparative TLC with a 5: 1 mixture of chloroform and acetone to afford the starting material (41 mg) and etiojervane-3β,17α-diol (83 mg). Specimens of the latter for analysis were obtained by recrystallization from aq methanol. Mp 179.0—179.5 °C; IR: 3240—3372 (OH) and 1034 cm^{-1}. Found: C, 78.05; H, 10.93%. Calcd for $C_{29}H_{32}O_2$: C, 78.03; H, 11.03%. Diacetate **20**, mp 96—98 °C, was prepared by the usual method. IR ($CHCl_3$), 1722 (broad, OAc), 1250, 1028, and 978 cm^{-1}. Found: C, 73.30, H, 9.82%; Calcd for $C_{23}H_{36}O_4$: C, 73.36; H, 9.64%.

*Reduction of 17β-Acetyl-12α-etiojervan-3β-ol Acetate (**11**) with $NaBH_4$.* 17β-Acetyl-12α-etiojervan-3β-ol acetate (300 mg) and $NaBH_4$ (160 mg) in absolute ethanol (26 ml) containing ethyl acetate (0.75 ml) were stirred for 2.5 h. After the excess reagent was decomposed by the addition of acetic acid, the solvent was removed to afford a residue which was extracted with chloroform. After the usual work-up, the product (310 mg) was examined by TLC which indicated the formation of virtually a single product. The product was recrystallized from a diethyl ether–hexane mixture to yield pure 17β-ethyl-12α-ethiojervane-3β,20ξ-diol 3-acetate (**21**), in greater than 95% yield. Specimens for analysis were obtained by recrystallization from aq methanol. Mp 126—129 °C: IR: ($CHCl_3$), 1719 (OAc), 3519 and 3401 (OH), 1457, 1393, 1269, and 1027 cm^{-1}. Found: C, 75.62; H, 10.45%. Calcd for $C_{23}H_{38}O_3$: C, 76.19; H, 10.57%. MS (70 eV) *m/e* (relative intensity), 344 (56.3, M^+-H_2O), 329 ($M^+-H_2O-CH_3$), 315 (18.4), 302 (22.5, M^+—AcOH), 274 (47.5), 269 (26.6), 257 (88.3, M^+—C-17-side chain—AcOH), 147 (56.1), 107 (100), 95 (82.2), 93 (91.9), 81 (78.0), and 43 (74.3).

*Hydrolysis of 17β-Ethyl-12α-etiojervane-3β,20ξ-diol 3-Acetate (**21**).* The 3-acetate (60 mg) in methanolic 2.5% potassium hydroxide (15 ml) was allowed to stand for 3 h at room temperature under an atmosphere of nitrogen. The solution was concentrated and extracted with chloroform. The usual work-up afforded a residue which was recrystallized to afford 3β,20ξ-diol **22** (53 mg). Specimens for analysis were obtained by further recrystallization from aq methanol. Mp 252—254 °C; IR: 3247 (OH), 1064, 1048, 1027, and 1010 cm^{-1}. Found: C, 78.06; H, 11.13%. Calcd for $C_{21}H_{36}O_2$: C, 78.69; H, 11.32 %; MS (80 eV), *m/e* (relative intensity), 302 (59, M^+-H_2O), 287 (18), 273 (21), 257 (77, M^+-H_2O—C-17 substituent), 147 (65), 107 (99), 95 (100), 81 (91), 67 (79), and 55 (86).

*Acetylation of 17β-Ethyl-12α-etiojervane-3β,20ξ-diol 3-Acetate (**21**).* The 3-acetate (43 mg) and acetic anhydride (0.5 ml) in pyridine (0.5 ml) were allowed to stand for 3 h at room temperature. The usual work-up afforded the diacetate **23** (35 mg). Recrystallization from aq methanol gave the pure product, mp 84.5—87.0 °C. IR: 1718 cm^{-1} (OAc), 1239, 1051, and 1024 cm^{-1}. Found: C, 74.36; H, 9.70%. Calcd for $C_{25}H_{40}O_4$: C, 74.21; H, 9.97%.

*Reduction of 17α-Acetyl-12α-etiojervan-3β-ol Acetate(**14**) with $NaBH_4$.* 17α-Acetyl-12α-etiojervan-3β-ol acetate (**14**) (300 mg) and $NaBH_4$ (160 mg) in absolute ethanol (26 ml) containing ethyl acetate (0.75 ml) were stirred for 3 h at room temperature. The addition of acetic acid to the reaction mixture and extraction with chloroform afforded a product (332 mg). A portion of the product (178 mg) was treated with methanolic 5% potassium hydroxide solution and allowed to stand for 1 h. The usual work-up afforded products which were subjected to preparative TLC with a 5: 1 mixture of chloroform and acetone to afford two fractions. The more mobile fraction (63 mg) was recrystallized from aq methanol to afford 3β,20ξ-diol **25** (55 mg), mp 140.0—140.5 °C. IR: 3170—3310 (OH), 1038, 1009, and 895 cm^{-1}. Found: C, 78.50; H, 11.31%. Calcd for $C_{21}H_{36}O_2$: C, 78.69; H, 11.32%. The less mobile fraction (70 mg) was recrystallized from aq methanol to afford 3β,20ξ-diol **28** (59 mg), mp 187—189 °C. IR: 3336 (OH), 1063, 1038, and 895 cm^{-1}. Found: C, 78.87; H, 11.42%. Calcd for $C_{21}H_{36}O_2$: C, 78.69; H, 11.32%. The diacetates **27** and **30** of the diols **25** and **28** were prepared by standard methods. The diacetate **27** from diol **25**, mp 131—132 °C (aq methanol). IR: ($CHCl_3$), 1739, 1241, 1042, and 1030 cm^{-1}. Found: C, 74.63; H, 9.84%. Calcd for $C_{25}H_{40}O_4$: C, 74.21; H, 9.97%. The diacetate **30** from diol **28** was amorphous. IR: ($CHCl_3$), 1725 (OAc), 1255, and 1028 cm^{-1}.

*17β-Ethyl-12α-etiojervane-3β,20ξ-diol 3-Acetate 20-Nitrite (**24**).* 20ξ-Ol **21** (290 mg) in pyridine (2 ml) was nitrosated with nitrosyl chloride in pyridine at −20 to −30 °C by the standard method. The crude nitrite **24** was recrystallized from methanol. Mp 102—106 °C: IR: 1734 (OAc), 1631, 794, 774, (ONO), 1242, and 1031 cm^{-1}.

*Photolysis of Nitrite **24**.* The nitrite (200 mg) in dry benzene (10 ml) in a Pyrex vessel was irradiated with a 100 W high pressure Hg arc for 3 h and 50 min under an atmosphere of nitrogen. After evaporation of the solvent, the residue was examined by TLC which indicated at least 6 spots. The product was dissolved in chloroform and the solution washed with water, dried and evaporated. The residue was hydrolyzed with methanolic 5% potassium hydroxide solution (5 ml) at room temperature and under an atmosphere of nitrogen for 3 h. The usual work-up afforded a residue which was dissolved in acetone to yield crystals (38 mg) of 17β-ethyl-12α-etiojervane-3β,20ξ-diol (**22**). The residue from the filtrate was subjected to preparative TLC with chloroform. The plates were developed three times and the major three fractions, A (13 mg), B (48 mg), and C (60 mg) were obtained. The NMR spectra of fraction A showed the absence of a C-18 functionalized product. The amorphous fraction B was recrystallized from acetone to afford 17α-acetyl-12α-etiojervan-3β-ol (**13**) (25 mg). Fraction C exhibited three spots on TLC examination and this was subjected again to preparative TLC with a 40: 1 mixture of diethyl ether–methanol to afford two major fractions C-1 (35 mg) and C-2 (18 mg). The more mobile fraction C-1 was a mixture and fraction C-2 showed a single spot on the TLC. The NMR spectra of both fractions, however, showed the absence of a C-18 functionalized product.

The Hypoiodite Reaction of 17β-Ethyl-12α-etiojervane-3β,20ξ-diol 3-Acetate. Freshly prepared lead tetraacetate (600 mg) and sodium carbonate (200 mg) in cyclohexane (18 ml) were refluxed for 1 h and the solution brought to room temperature. To this solution, were added 17β-ethyl-12α-etiojervane-3β,20ξ-diol 3-acetate (180 mg) and iodine (160 mg) and the solution irradiated under reflux for 0.5 h with a 450 W high pressure Hg arc. The insoluble material was removed by filtration and washed with hot cyclohexane. The filtrate and washings were combined and the solution washed with 10% aq sodium

hydrogen sulfite and water successively. The organic layer was dried and evaporated to afford a brownish residue (0.2 g) which was dissolved in methanolic 2.5% potassium hydroxide solution (10 ml). The solution was allowed to stand for 3 h under an atmosphere of nitrogen, concentrated under reduced pressure and extracted with chloroform and water. The usual work-up of the organic layer gave a residue which showed two major and a very minor spot on TLC. The residue was subjected to preparative TLC with chloroform. The TLC plates were developed three times to afford three fractions. The most mobile amorphous fraction (79 mg) could not however crystallize but gave a positive Beilstein test and the chloroform solution developed an yellow color by the addition of tetranitromethane. UV λ_{max} (ethanol) 262 nm; NMR τ 2.99 (2H, q, possibly ortho aromatic protons), 8.92 (s, 19-H), 7.97 (s, OAc), 7.68 (s, possibly the methyl group attached to the aromatic ring), 8.01 (s), 9.38 (1H, d, J=1.7 Hz, the proton possibly attached to the cyclopropane ring). IR ($CHCl_3$) no carbonyl or hydroxyl groups. The second mobile fraction (4 mg) was an unidentified gum. The least mobile amorphous fraction (48 mg) was a deacetylated product of a 18,20-epoxide **32**. This fraction was acetylated with acetic anhydride (2 ml) and pyridine (2 ml). After the usual work-up, the product was recrystallized from aq methanol to yield a 18,20-epoxide (**32**) (29 mg), amorphous. IR: 1732 (OAc), 1024, and 1237 cm^{-1}. Found: C, 76.50; H, 9.92%. Calcd for $C_{23}H_{36}O_3$: C, 76.62; H, 10.07%; MS (80 eV), *m/e* (rel. intensity) 360 (2.4 M^+), 345 (65.0, M^+-CH_3), 316 (16.7), 300 (100, $M^+-CH_3CO_2H$), 285 (73.4, $M^+-CH_3CO_2H-CH_3$), 149 (92.2), 148 (92.2), and 141 (98.4).

*Oxidation of 18,20-Epoxide (**32**) with Chromium Trioxide.* To the 18,20-epoxide (25 mg) in glacial acetic acid, was added dropwise chromium trioxide (50 mg) in aq acetic acid (90%) (2 ml) a period over 0.5 h while the solution refluxed. The reaction mixture was further refluxed for 0.5 h and the solvent removed under reduced pressure. The residue was extracted with chloroform and water and the organic layer washed with water and dried (Na_2SO_4). The residue (23 mg) from the solution was dissolved in methanolic hydrochloric acid (10 ml) to hydrolyze the 3β-acetoxyl group and allowed to stand overningt. After removal of the solvent, the residue was dissolved in chloroform. The chloroform solution was worked up in the usual way to afford the crude lactone (20 mg). The lactone was subjected to preparative TLC with a 1: 20 mixture of benzene and chloroform to afford 6 fractions. The third mobile fraction (4 mg) was the major product. The product in pyridine was subjected to acetylation in the usual way. The usual work-up of the reaction mixture afforded a crystalline lactone **33** (5 mg) which was recrystallized from diethyl ether. Mp 89—90 °C; IR: 1752 (γ-lactone), 1726 (OAc), 1238, and 1029 cm^{-1}. Found: C, 73.64; H, 9.21%. Calcd for $C_{23}H_{36}O_4$: C, 73.36; H, 9.64%.

The authors are grateful to Dr. W. F. Johns of C. D. Searle and Co., for the generous gift of several etiojervane samples for direct comparisons. Thanks are also due to Mr. S. Shimokawa of the Faculty of Engineering for the NMR measurements.

References

1) Photoinduced Transformations. Part 43. Part 42. H. Suginome and T. Uchida, *J. Chem. Soc., Chem. Commun.*, **1979**, 701.

2) Preliminary communication. H. Suginome, N. Sato, and T. Masamune, *Tetrahedron Lett.*, **1969**, 2671.

3) a) For review of Barton reaction, see A. L. Nussbaum and C. H. Robinson, *Tetrahedron*, **17**, 35 (1962); M. Akhtar, *Adv. Photochem.*, **2**, 263 (1964); R. O. Kan, "Organic Photochemistry," McGraw-Hill, New York (1966), p. 233; R. H. Hesse, *Adv. Free Radical Chem.*, **3**, 83 (1969); b) For review of the Hypoiodite reaction, see K. Heusler and J. Kalvoda, *Angew. Chem.*, **76**, 518 (1964); J. Kalvoda and K. Heusler, *Synthesis*, **1971**, 501; c) For review of lead tetraacetate oxidation, see K. Heusler and J. Kalvoda, "Organic Reaction in Steroid Chemistry," ed by J. Fried and J. A. Edwards, Van Nostrand Reinhold, New York (1972), Vol. 2, p. 237; K. Heusler and J. Kalvoda, *Angew. Chem., Int. Ed. Engl.*, **3**, 525 (1964).

4) T. Masamune, M. Takasugi, and Y. Mori, *Tetrahedron Lett.*, **1965**, 489.

5) T. Masamune, Y. Mori, M. Takasugi, A. Murai, S. Ohuchi, N. Sato, and N. Katsui, *Bull. Chem. Soc. Jpn.*, **38**, 1375 (1965); for stereochemistry, see G. N. Reeke, Jr., R. L. Vincent, and W. N. Lipscomb, *J. Am. Chem. Soc.*, **90**, 1663 (1968); S. M. Kupchan and M. I. Suffness, *ibid.*, **90**, 2730 (1968).

6) S. Nishimura, *Bull. Chem. Soc. Jpn.*, **33**, 566 (1960); P. N. Rylander, "Catalytic Hydrogenation over Platinum Metals," Academic Press, New York, N. Y. (1967), p. 23.

7) For nomenclature of *C*-nor-*D*-homosteroids, see S. M. Kupchan and M. J. Abu El-Haj; *J. Org. Chem.*, **33**, 647 (1968); F. C. Chang and R. C. Ebersole, *Tetrahedron Lett.*, **1968**, 3521.

8) W. F. Johns and I. Laos, *J. Org. Chem.*, **30**, 123 (1965).

9) R. W. Franck and W. S. Johnson, *Tetrahedron Lett.*, **1963**, 545; R. W. Franck, G. P. Rizzi, and W. S. Johnson, *Steroids*, **4**, 463 (1964).

10) An alternative method has been developed which involved radical fragmentation for the removal of heterocyclic rings from the veratranine framework. By this new procedure, removal of the heterocyclic ring can be executed under neutral conditions by the use of *N*-acetyl veratranines. H. Suginome, M. Murakami, and T. Masamune, *J. Chem. Soc., Chem. Commun.*, **1966**, 343; *Bull. Chem. Soc. Jpn.*, **41**, 468 (1968); H, Suginome, H. Umeda, S. Sugiura, and T. Masamune, *J. Chem. Res.*, (S), **1978**, 380; (M) 4520. Transformation of the jerveratrum alkaloid into 18-functional *C*-nor-*D*-homosteroids involving this new procedure will be described later.

11) The previous structural assignment[8] as 13β-etiojervane-3β,17α-diol for this diol should be revised to 13β-etiojervane-3β,17β-diol since an isomeric diol (**19**) has been obtained by Baeyer-Villiger oxidation of the isomeric ketone (**13**).

12) W. G. Dauben, G. J. Fonken, and D. S. Noyce, *J. Am. Chem. Soc.*, **78**, 2579 (1956).

13) W. Klyne and E. Miller, *J. Chem. Soc.*, **1950**, 1972; *J. K.* Norymberski and G. F. Woods, *J. Chem. Soc.*, **1955**, 3426; R. Gardi, R. Vitali, A. Ercoli, and W. Klyne, *Tetrahedron*, **21**, 179 (1965); F. Sondheimer, J. Romo, G. Rosenkranz, and C. Djerassi, U. S. Patent 2911403 (1959).

14) A. L. Nussbaum, F. E. Carlon, E. P. Oliveto, E. Townley, P. Kabasakalian, and D. H. R. Barton, *J. Am. Chem. Soc.*, **82**, 2973 (1960); *Tetrahedron*, **18**, 373 (1962).

Aminosugars. XXXI. Preparation of Benzyl 2-Acylamino-4-azido-2,4-dideoxy-ribo- and -lyxopyranosides by Inversion of Hydroxyl Group on C-3[1)]

Hironobu HASHIMOTO,* Koichi ARAKI, and Juji YOSHIMURA

Laboratory of Chemistry for Natural Products, Faculty of Science, Tokyo Institute of Technology, Nagatsuta, Midori-ku, Yokohama 227

(Received May 7, 1979)

Benzyl 2-acylamino-4-azido-2,4-dideoxypentopyranosides having α-D-*ribo*, β-L-*ribo*, α-D-*lyxo*, and β-L-*lyxo* configurations were derived from the corresponding α-D-*xylo*, β-L-*xylo*, α-D-*arabino*, and β-L-*arabino* isomers, respectively, by inversion of hydroxyl group on C-3. Displacement reaction of sulfonyloxy group with sodium acetate or benzoate in aqueous 2-methoxyethanol or anhydrous *N,N*-dimethylformamide, or oxidation-reduction method *via* ulose derivative was used properly according to the stereochemistry of the starting materials.

In the course of study on the relationship between the configuration and biological activity using diastereomers of an antifungal antibiotic, prumycin: 4-(D-alanyl)-amino-2-amino-2,4-dideoxy-L-arabinose, as model compounds, the *arabino* and *xylo* analogues could be synthesized *via* 2,3-anhydro-4-azido-4-deoxypentopyranosides.[1-3)] In order to complete the synthesis of the remaining diastereomers which have *ribo* and *lyxo* configurations, the inversion of hydroxyl group on C-3 was studied in this paper.

Being used often for the inversion of hydroxyl group, displacement reactions of its sulfonate on the pyranose ring are known to be restrained by the axial substituent on α- or β-carbon with respect to the sulfonyloxy group. Four isomers, namely, α-D-*arabino* (**9**), β-L-*arabino* (**10**), α-D-*xylo* (**11**), and β-L-*xylo* (**12**) diastereomers of benzyl 4-azido-2-benzyloxycarbonylamino-2,4-dideoxy-3-*O*-methylsulfonylpentopyranoside, were prepared from the corresponding ammonolysis products (**1**—**4**) of benzyl 2,3-anhydro-4-azido-4-deoxy-pentopyranosides[1-4)] *via* their *N*-benzyloxycarbonyl derivatives (**5**—**8**). In order to predict the reactivity, the predominant conformers of these 3-*O*-methylsulfonyl derivatives together with the corresponding 3-*O*-acetyl ones (**13**—**16**) were examined by NMR data (Table 1). The conformational equilibria were estimated by the method of averaging of spin coupling[5)] using the values of $J_{4,5a}$ or $J_{4,5e}$† and $J_{2,3}$. Although the standard values for $J_{a,a}$ and $J_{e,e}$ should be determined in each case because of dependency of spin coupling on the substituent groups of the concerned system,[7)] the following values reported for the similar aldopyranoside systems were used: 11.1 and 1.5 Hz for $J_{4a,5a}$ and $J_{4e,5e}$,[8)] and 11.0 and 3.6 Hz for $J_{2a,3a}$ and $J_{2e,3e}$, respectively.[9)] In the cases of α-*arabino* and β-*xylo* isomers whose hydrogens on C-1 and C-2 have *trans* relationship, the ratios of two chair

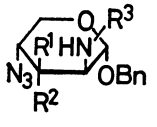

	R¹	R²	R³
1	H	OH	H
5	H	OH	Z
9	H	OMs	Z
13	H	OAc	Z
28	H	OBz	Z
41	H	OH	Ac
42	H	OH	CHO
43	H	OMs	Ac
44	H	OMs	CHO
45	OH	H	Ac
46	OH	H	CHO
50	OAc	H	Ac
51	OAc	H	CHO

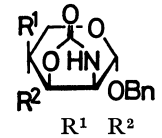

	R¹	R²
18	N_3	H
24	H	N_3

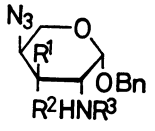

	R¹	R²	R³
2	OH	H	H
6	OH	H	Z
10	OMs	H	Z
14	OAc	H	Z
26	OBz	H	Z
29	OH	H	Ac
30	OH	H	Bz
31	OH	H	CHO
32	OMs	H	Ac
33	OMs	H	Bz
34	OMs	H	CHO
35	H	OH	Ac
36	H	OH	Bz
37	H	OH	CHO
38	H	OAc	Ac
39	H	OAc	Bz
40	H	OAc	CHO

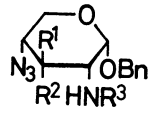

	R¹	R²	R³
3	OH	H	H
7	OH	H	Z
11	OMs	H	Z
15	OAc	H	Z
47	OH	H	Ac
48	OMs	H	Ac
49	H	OH	Ac
52	H	OAc	Ac
54	H	OH	Z
55	H	OAc	Z

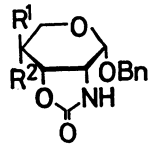

	R¹	R²
23	N_3	H
25	H	N_3

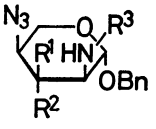

	R¹	R²	R³
4	H	OH	H
8	H	OH	Z
12	H	OMs	Z
16	H	OAc	Z
17	OH	H	Z
19	OAc	H	Z
20	OBz	H	Z
22	H	OBz	Z

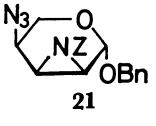

21

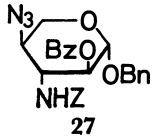

27

† The methylene protons on C-5, *i.e.*, H_{5a} and H_{5e} were assigned due to Lemieux's empirical rules[6)] that an axial proton resonates at higher field than an equatrial one.

conformers were also calculated from the observed values of $J_{1,2}$ using 7.9[10] and 2.0[9] Hz as standards for $J_{1a,2a}$ and $J_{1e,2e}$, respectively. The results and predominant conformers were shown in Table 2. The ratios obtained from coupling constants between different ring protons gave good agreement with one another indicating that the standard coupling constants used here for the estimation of conformer ratios seem to be also applicable to the here examined system. The conformational equilibria of benzyl 4-azido-2-benzyloxycarbonylamino-

Table 1. NMR data of benzyl 4-azido-2-benzyloxycarbonylamino-2,4-dideoxy-3-*O*-methylsulfonylpentopyranosides (**9**—**12**) and the corresponding 3-*O*-acetyl derivatives (**13**—**16**) at 100 MHz in $CDCl_3$

	Compounds							
	9	**10**	**11**	**12**	**13**	**14**	**15**	**16**
Chemical shifts, δ/ppm								
H-1	4.74 d	4.98 d	4.90 d	4.62 d	4.57 d	4.90 d	4.88 d	4.43 d
H-2	3.74 dd	4.36 dt	4.02 dt	3.50 — 3.80	*ca.* 3.95 —	4.28 dt	3.94 dt	3.79 dd
H-3	*ca.* 5.20 —	4.98 dd	4.62 —		5.24 dd	5.14 dd	*ca.* 5.10 —	4.94 t
H-4	4.10 nm	4.14 nm	3.60 — 3.80 m		*ca.* 3.95 —	3.92 m	*ca.* 3.70 —	3.66 dt
H-5[a]	3.60 dd	3.90 dd		3.29 dd	3.59 dd	3.87 dd	3.76 dd	3.24 dd
H-5′[a]	4.05 dd	3.70 dd		4.11 dd	4.04 dd	3.62 dd	3.54 dd	4.07 dd
CH_2 in Bn[b]	4.56, 4.88	4.46, 4.70	4.42, 4.68	4.51, 4.80	4.54, 4.86	4.41, 4.65	4.46, 4.70	4.54, 4.82
CH_2 in Z	5.08 s	5.10[c]	5.09 s	5.07 s	5.09 s	5.06[c]	5.06[c]	5.08 s
NH	5.28	5.21 d	5.26 d	*ca.* 5.18 —	*ca.* 4.85 d	*ca.* 5.04 d	*ca.* 5.10 —	—
Others	2.84 (Ms,s)	2.84 (Ms,s)	2.94 (Ms,s)	2.96 (Ms,s)	2.05 (Ac,s)	1.99 (Ac,s)	1.96 (Ac,s)	2.02 (Ac,s)
Coupling constants/Hz								
$J_{1,2}$	7.5	3.6	3.6	7.5	*ca.* 6.2	3.5	3.2	7.5
$J_{2,3}$	—[d]	10.5	10.4	—	9.3	10.5	10.5	9.3
$J_{3,4}$	—	3.5	—	—	3.3	3.5	—	9.0
$J_{4,5}$	1.5	1.5	—	9.4	1.7	2.1	2.0	9.2
$J_{4,5'}$	3.3	2.0	—	4.5	3.5	1.5	10.2	4.5
$J_{5,5'}$	*ca.* 12.5	12.6	—	11.5	12.2	12.4	11.7	11.6
J_{AB}[d]	12.0	11.9	12.0	11.4	12.0	12.0	11.9	12.0
$J_{NH,CH}$	7.8	10.5	9.1	—	—	10.8	—	—

a) H-5 and H-5′ designate pro *R* and pro *S* protons, namely, in $^4C_1$ conformation equatrially and axially oriented protons on C-5, respectively. b) AB quartet with coupling constant J_{AB}. c) Narrow AB quartet. d) Could not be obtained from the spectra. Abbreviation of functional groups: Bn=benzyl, Z=benzyloxycarbonyl, Ac=acetyl and Ms=methylsulfonyl. Observed signal multiplicities: s=singlet, d=doublet, t=triplet, m=multiplet, dd=double doublet, dt=double triplet, nm=narrow multiplet

Table 2. Ratios of conformers calculated from coupling constants

Compound	Configuration	Ratios of $^4C_1$ and $^1C_4$ conformers in %: Calculated from the values of $J_{1,2}$	$J_{2,3}$	$J_{4,5}$ or $J_{4,5'}$	for methyl tri-*O*-acetylpentopyranosides[a]	Predominant conformers R=Ms or Ac	
9	α-D-*arabino*	15:85	—[b]	19:81	17:83	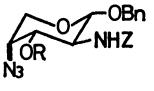	$^1C_4$
13	α-D-*arabino*	39:61—20:80[c]	23:77	21:79			
10	β-L-*arabino*	×[d]	93:7	100:0	97:3	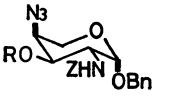	$^4C_1$
14	β-L-*arabino*	×	93:7	—			
11	α-D-*xylo*	×	92:8	—	>98: <2	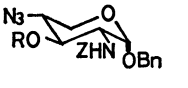	$^4C_1$
15	α-D-*xylo*	×	93:7	91:9			
12	β-L-*xylo*	15:85	—	18:82	19:81	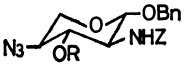	$^1C_4$
16	β-L-*xylo*	15:85	23:77	20:80			

a) see Ref. 11. b) Coupling constants could not be obtained from the spectra. c) Due to overlap of H_1 signal with a part of methylene proton, the exact ratio could not be obtained. d) This method cannot be applied for estimation of conformational equilibria because of *cis*-relationship of H-1 and H-2.

Table 3. Displacement reactions of β-L-*xylo* isomer (**12**)

Run	Reaction conditions					Yield/%						Recovered
	Base	Concentration M	Solvent[a]	Temperature °C	Time h	**17**	**18**	**19**	**20**	**21**	**22**	**12**/%
1	AcONa	0.2	A	95—100	40	44	14	—	—	—	—	28
2	AcONa	0.4	A	95—100	40	52	17	—	—	—	—	19
3	AcONa	0.8	A	95—100	40	62	23	—	—	—	—	0
4	AcONa	0.8	B	95—100	40	61	17	—	—	—	—	0
5	AcONa	1.5	B	95—100	40	60	25	—	—	—	—	0
6	AcONa	0.2	A	115—120	13	44	34	—	—	—	—	10
7	AcONa	0.2	B	115—120	13	37	35	—	—	—	—	14
8	AcONa	0.4	B	115—120	13	45	24	—	—	—	—	7
9	AcONa	0.8	B	115—120	13	41	24	—	—	—	—	10
10	AcONa	1.5	B	115—120	13	38	35	—	—	—	—	0
11	AcONa	0.2	C	95—100	13	—	—	57	—	25	—	0
12	AcONa	0.2	C	115—120	13	—	—	58	—	25	—	0
13	BzONa	0.2[b]	C	95—100	13	—	—	—	69	—	0	0
14	BzONa	0.2[b]	C	115—120	13	—	—	—	68	—	17	0

a) A, 2-methoxyethanol: water=19: 1; B, 2-methoxyethanol: water=4: 1; C, DMF. b) Not fully dissolved.

2,4-dideoxy-3-*O*-methylsulfonylpentopyranosides (**9**—**12**) accord with those of the corresponding 3-*O*-acetyl derivatives (**13**—**16**), and also with those of methyl tri-*O*-acetylpentopyranosides.[11] Among these predominant conformers only that of the β-L-*xylo* isomer (**12**) has no axial substituent on α- and β-carbons as shown in Table 2 (axial substituent with thick line) and seems to be most reactive for displacement reactions. Therefore, some displacement reactions of **12** were examined at first and the results were summarized in Table 3.

The S_N2 type displacements of methylsulfonyloxy group with hydroxyl and acyloxy groups in compound **12** were accomplished in the presence of sodium acetate in 2-methoxyethanol–water and by sodium acetate or benzoate in *N*,*N*-dimethylformamide (DMF), respectively. Under the first conditions, which are used generally for the similar conversion in acylamino sugar derivatives having *trans* vicinal amino alcohol structure in the aid of anchimeric assistance,[12] the desired compound, benzyl 4-azido-2-benzyloxycarbonylamino-2,4-dideoxy-β-L-ribopyranoside (**17**) was obtained as a major product together with benzyl 2-amino-4-azido-2-*N*: 3-*O*-carbonyl-2,4-dideoxy-β-L-ribopyranoside (**18**). Although configuration on C-3 in compound **17** was ascertained by the change of $J_{1,2}$ from the large value (7.5 Hz) in **12** to the small value (2.4 Hz)[3] in predominant $^4C_1$ conformation,[11] the structure was furthermore confirmed unambiguously by the NMR data of its 3-acetate (**19**) (Table 4). On the other hand, absence of benzyloxycarbonyl group ascertained by the NMR and

Table 4. NMR data of compounds **18**—**23** and **25**—**26** at 100 MHz in $CDCl_3$

	Compounds							
	18	**19**	**20**	**21**	**22**	**23**	**25**	**26**
Chemical shifts, δ/ppm								
H-1	4.64 d	4.87 d	4.93 d	5.09 s	4.64 d	4.78 d	4.77 d	5.01 d
H-2	3.82 dd	4.20 m	4.37 m	2.87 d	3.98 ddd	3.94 dd	4.82 dd	*ca.* 4.56 —
H-3	4.93 dd	5.31 t	5.57 t	3.18 dd	5.21 t	4.55 dd	4.85 dd	5.46 dd
H-4	3.94 —	3.92 m	4.10 nm	*ca.* 3.58 nm	3.80 dt	*ca.* 3.92 m	*ca.* 3.65 —	4.06 nm
H-5	—	3.72 dd	3.78 dd	3.91 dd	3.44 dd	3.51 dd	4.03 t	3.72 dd
H-5′	—	3.99 dd	4.10 dd	3.50 dd	4.20 dd	4.13 dd	3.70 —	3.98 dd
CH_2 in Bn	4.54, 4.79	4.49, 4.68	4.52, 4.72	4.55, 4.78	4.56, 4.84	4.56, 4.86	4.50, 4.80	4.48, 4.73
CH_2 in Z		5.10 s	5.10 s	5.16 s	5.03 s			5.00 s
NH	6.12 s	5.88 d	6.02 d		5.32 d	5.40 s	5.55 s	5.08 d
Others		2.02 (Ac, s)						
Coupling constants/Hz								
$J_{1,2}$	3.0	1.4	1.2	<0.5	*ca.* 6.0	3.6	4.2	5.3
$J_{2,3}$	7.6	4.2	4.3	5.8	7.4	7.2	6.0	11.0
$J_{3,4}$	3.3	4.2	4.3	6.2	7.4	4.5	4.5	3.8
$J_{4,5}$	—	1.9	2.3	6.0	7.4	6.0	4.5	2.1
$J_{4,5'}$	—	1.7	1.1	2.6	4.1	4.0	11.7	1.5
$J_{5,5'}$	—	12.0	12.5	13.5	11.9	12.0	11.7	12.5
J_{AB}	11.9	12.0	12.0	11.7	11.9	12.2	12.0	12.0
$J_{NH,CH}$	<0.5	10.1	10.1		*ca.* 9.0	<0.5	<0.5	—

IR spectra of **18** and presence of a typical absorption at 1760 cm^{-1} in the IR spectra assigned to carbonate supported its structure. Moreover the NMR data, especially the large value (7.6 Hz) for $J_{2,3}$, indicated that **18** exists in a boat conformation ($B_{4,1}$).

As shown in Table 3 the higher base concentration, the lower water content of the solvent, and the higher reaction temperature accelerated the formation of both **17** and **18** (Runs 1—10). The last factor, however, favored the formation of **18**, so the ratio of **17** and **18** was changed from 3: 1 at 95—100 °C to nearly 1—2: 1 at 115—120 °C. Although the formation of **18** could not be completely suppressed, among the reaction conditions tested the most suitable combination for preparation of **17** seems to be as follows: concentration of sodium acetate, 0.8—1.5 M; water content of solvent (2-methoxyethanol), 5—20%; reaction temperature, 95—100 °C. All these reactions were carried out in sealed tubes to maintain the constant water content, but for preparative purpose more convinient open air system was examined. It was found that the compound **12** was heated under gentle reflux (in oil bath at 110—115 °C) with sodium acetate (1.5 M) in 20% water containing 2-methoxyethanol to give **17** in unexpectedly good yield (80%) as reported earlier.[3] Considering the azeotropic point (99.5 °C/750 mmHg) of this binary solvent system, these conditions seem to be very similar to the best combination of reaction conditions described above. The difference between closed and open system, however, remains unclear. Furthermore, displacement reaction with sodium acetate or benzoate in DMF gave the corresponding 3-acetate (**19**) or 3-benzoate (**20**) of **17** in good yields (Runs 11—14), while in the former case the aziridine derivative (**21**) in *ca.* 25% yield, and in the latter only at higher temperature the corresponding 3-benzoate (**22**) of **8** were also formed (Run 14). The structure of **19** and **20**, especially the configuration on C-3, was confirmed by the characteristic small coupling constants of all ring protons as shown in Table 4 indicating also that they exist in $^4C_1$ conformation predominantly. The aziridine derivative (**21**) showed no N–H absorption in IR and NMR spectra, and the latter showed typical two protons attached to the aziridine ring at higher magnetic field (δ 2.87 and 3.18) than other pyranoside ring protons. The structure of **22** was also elucidated by NMR spectra in comparison with that of **12** and **16**. The compound **22** may be formed *via* **21** or by the neighboring group participation of urethane carbonyl. The former case may be more reasonable considering relatively weak polarization of benzyloxycarbonyl group. The structure of **22** was also confirmed by its identification with the alternatively prepared 3-benzoate of **8**.

Thus, in the case of β-L-*xylo* isomer (**12**) the inversion reactions in the presence of sodium acetate in 80% 2-methoxyethanol and with sodium benzoate in DMF gave good results and then the same reactions of the other three diastereomers of **12** were also examined (Table 5). As expected these isomers resisted the displacement of methylsulfonyloxyl group with both hydroxyl and benzoyloxyl ones. So at the lower temperature (95—100 °C) both reactions did scarcely proceed, and higher temperature (over 120 °C) and higher base concentration promoted decomposition of the starting material and also DMF. In the first reaction the product characterized was only the 2-*N*: 3-*O*-carbonate derivative in each case. The β-L-*arabino* isomer (**10**) gave the β-L-*lyxo* carbonate (**23**) in 22% yield, while the α-D-*arabino* and α-D-*xylo* isomers (**9** and **11**) gave the corresponding α-D-*lyxo* and α-D-*ribo* carbonate (**24** and **25**) in very low yield. The structure of these carbonate derivatives was easily ascertained by IR absorption of the cyclic carbamate (1755—1760 cm^{-1}) and by NMR signal of the proton attached to the nitrogen, which show a typical broad singlet. The NMR data of **23** and **25** confirmed their structures indicating also the predominance of $^{4,1}B$ conformation. The compound **24** was, however, characterized only by the IR absorption of cyclic carbamate. Moreover, the inversion reaction with benzoate gave no desired product, and those obtained (**26** and **27** from **10**, and **28** from **9**) seem to be derived *via* the corresponding aziridine intermediate as supposed for the formation of **22** from **12**.

As shown in the substitution reaction of **12**, benzyloxycarbonyl group can participate or assist the displacement reaction of the neighboring carbon atom, but such ability is not so strong as those of acetyl, benzoyl and formyl groups.[13] Then, the similar displacement reaction of *N*-acetyl, *N*-benzoyl, and *N*-formyl derivatives was investigated. Because β-L-*ribo* and α-D-*ribo* isomers could be prepared by the above mentioned displacement reactions or by oxidation-reduction method as described below, respectively, only *arabino* isomers were examined in detail. The *N*-acetyl (**29**), *N*-benzoyl (**30**), and *N*-formyl (**31**) derivatives of **2** were prepared in the usual manner by treatment with acetic anhydride, benzoyl chloride, or *p*-nitrophenyl formate, respectively. These compounds were converted into the corresponding

Table 5. Displacement reactions of α-D-*arabino* (**9**), β-L-*arabino* (**10**) and α-D-*xylo* (**11**) isomers

Run	Starting compound	Reaction conditions					Product (yield)
		Base	Concentration M	Solvent[a]	Temperature °C	Time h	
1	**9**	AcONa	0.4	A, B	110—115	144	**24** (low)
2	**9**	BzONa	0.4[b]	C	110—115	144	**28** (12%)
3	**10**	AcONa	0.4	A	110—115	120	**23** (22%)
4	**10**	BzONa	0.4[b]	C	130	36	**26** (4%), **27** (3%)
5	**11**	AcONA	0.4	A, B	110—115	216	**25** (trace)

a) A, 2-methoxyethanol: water=4: 1; B, 2-methoxyethanol: water=19: 1; C, DMF. b) Not fully dissolved.

Table 6. NMR data of compounds **28**, **32**—**34**, **36**, and **38**—**40** at 100 MHz in $CDCl_3$

	Compounds							
	28	**32**	**33**	**34**	**36**	**38**	**39**	**40**
Chemical shifts, δ/ppm								
H-1	4.68 d	4.90 d	5.08 d	4.98 d	5.00 d	4.72 d	*ca.* 4.86m	4.75 d
H-2	4.16 dt	4.62 m	4.84 ddd	*ca.* 4.70 m	4.52 m	*ca.* 4.64 —		—
H-3	5.52 dd	5.00 dd	5.18 dd	5.06 dd	3.69 nm	4.90 dd	5.05 dd	4.94 dd
H-4	*ca.* 4.05 —	4.12 nm	4.20 nm	4.20 nm	3.86 nm	3.72 dt	3.80 dt	4.74 ddd
H-5	3.68	3.72 dd	3.78 dd	3.76 dd	3.62 dd	3.42 dd	3.50 dd	3.42 dd
H-5′	*ca.* 4.08 —	3.92 dd	4.00 dd	3.95 dd	4.14 dd	4.10 dd	4.16 dd	4.12 dd
CH_2 in Bn	4.60, 4.91	4.45, 4.68	4.48, 4.71	4.50, 4.74	4.49, 4.76	4.50, 4.82	4.56, 4.86	4.52, 4.82
CH_2 in Z	5.08 s							
NH	5.08 d	5.72 d	6.38 d	6.16 d	6.80 d	5.94 d	6.51 d	6.34 d
Others		1.96 (Ac,s) 3.08 (Ms,s)	3.02 (Ms,s)	3.09 (Ms,s) 8.21 (HCO,s)		1.98 (Ac,s) 2.10 (Ac,s)	2.10 (Ac,s)	2.10 (Ac,s)
Coupling constants/Hz								
$J_{1,2}$	6.0	3.3	3.5	2.7	3.3	3.0	—	3.0
$J_{2,3}$	8.7	10.7	10.5	10.8	2.7	3.8	3.8	3.8
$J_{3,4}$	2.7	3.4	3.5	3.4	*ca.* 4.2	6.0	6.0	6.8
$J_{4,5}$	<0.5	2.2	2.0	1.6	3.0	5.3	5.4	6.0
$J_{4,5'}$	—	1.7	1.5	1.2	3.0	3.3	3.2	3.0
$J_{5,5'}$	10.4	12.3	12.0	12.0	13.5	12.2	12.0	12.0
J_{AB}	12.0	11.6	11.7	11.7	12.0	12.3	12.0	12.0
$J_{NH,CH}$	9.0	9.0	9.0	9.0	9.0	8.3	8.4	8.7

3-*O*-methylsulfonyl derivatives (**32**, **33**, and **34**) in high yields. The displacement reactions of **32**, **33**, and **34** using sodium acetate in 20% water-containing 2-methoxyethanol at 115 °C gave benzyl 2-acylamino-4-azido-2,4-dideoxy-β-L-lyxopyranosides; *N*-acetyl derivative (**35**) in quantitative yield, while, *N*-benzoyl one (**36**) in 60%, and *N*-formyl one (**37**) in 70—80% yield, respectively. The structure of these three compounds were ascertained by the NMR spectra of themselves and their 3-acetates (**38**, **39**, and **40**) as shown in Table 6. The coupling constants of ring protons supported the *β-lyxo* configuration and indicated the existence of nearly equal $^4C_1$ and $^1C_4$ conformers, which was deduced from the values of $J_{3,4}$ and $J_{4,5}$. In the case of *N*-benzoyl derivative an unidentified by-product was also obtained in 12% yield, which is deduced to be 2,3-oxazoline derivative having β-L-*lyxo* configuration by spectral data given in the Experimental. As *N*-acetyl and *N*-formyl derivative gave satisfactory results in the case of α-D-*arabino* isomer, only *N*-acetyl (**41**) and *N*-formyl (**42**) derivative of **1** were prepared. Although **41** could be converted into the corresponding 3-*O*-methylsulfonyl derivative (**43**) in high yield, the same conversion of **42** gave **44** in slightly lower yield (60%). Then, similar displacement reaction of *N*-acetyl derivative (**43**) in the presence of sodium acetate as described above gave the α-D-*lyxo* isomer (**45**) in quantitative yield, but the corresponding *N*-formyl derivative (**44**) did inversion product (**46**) in 54% yield. The slightly poor results of *N*-formyl derivative both in the 3-*O*-methylsulfonylation and the inversion reaction may be due to the fact that formyl group is not perfectly stable under these reaction conditions. Furthermore, *N*-acetyl derivative (**47**) of the α-D-*xylo* isomer (**3**) was converted into the corresponding α-D-*ribo* isomer (**49**) *via* the 3-methanesulfonate (**48**) in the same manner. The structures of these inversion reaction products (**45**, **46**, and **49**) were also elucidated by NMR data, especially by coupling constants of ring protons of the corresponding 3-acetates (**50**, **51**, and **52**, respectively).

On the other hand, the inversion of hydroxyl group *via* ulose derivative is also used widely for the synthetic purpose.[14] Then, all isomers (**1**—**4**) were subjected to oxidation with dimethyl sulfoxide–trifluoroacetic anhydride (DMSO–TFAA), which was applied recently to preparation of ulose by us.[15] To our surprise, all isomers gave only one ulose, benzyl 4-azido-2-benzyloxycarbonylamino-2,4-dideoxy-α-D-*erythro*-pentopyranosid-3-ulose (**53**), preferrentially in 80—85% yields. The IR spectrum of **53** shows a new absorption 1740 cm^{-1} due to carbonyl group and the signal of H-2 proton appears as a quartet indicating the proton has no vicinal one other than H-1 and NH. The structure of **53** was further ascertanied by conversion into the α-D-*ribo* derivative by reduction as described below. Thus, except the α-D-*xylo* isomer (**7**) the configuration of at least one substituent on C-2 and C-4 was inverted in the oxidation reaction. As the inversion of the axially oriented group adjacent to carbonyl group was observed often in DMSO oxidation,[16] the case of β-L-*arabino* isomer (**6**) could be explained in the same category. On the other hand, in the cases of α-D-*arabino* (**5**) and β-L-*xylo* (**8**) isomers the change of conformation from $^1C_4$ to $^4C_1$ at the intermediate stage of the reaction should occur, because the inverted groups have equatorial orientations originally. Such conformational change may be caused by the electrostatic attraction between the intermediate sulfonium ion and the lone pair of oxygen at C-1 as shown in Scheme 1.

Then, the reduction of **53** with sodium borohydride

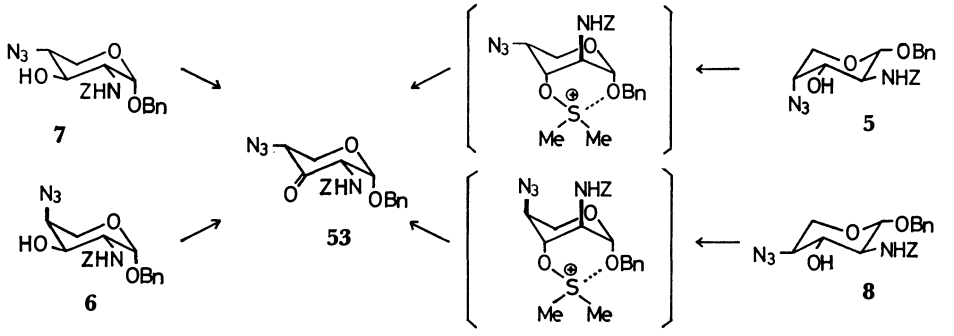

Scheme 1.

in methanol gave stereoselectively the corresponding α-D-*ribo* isomer (**54**) in high yield. The structure of **54** was confirmed by NMR data of its 3-acetate (**55**), which show typical coupling constants of ring protons for α-ribopyranosides.

In conclusion, the four isomers of benzyl 4-azido-2-acylamino-2,4-dideoxypentopyranosides having *ribo* and *lyxo* configurations were prepared from the corresponding *xylo* and *arabino* isomers, and the following facts must be useful. Inversion of hydroxyl group by nucleophilic substitution of its sulfonate with sodium carboxylate can be applied only to β-*xylo* isomer which have no axial substituent in its predominant conformer. On the other hand, inversion using the corresponding 2-acetylamino derivative in the aid of anchimeric assistance can be applied surely to all *xylo* and *arabino* isomers. Furthermore, DMSO oxidation of all four *xylo* and *arabino* isomers followed by sodium borohydride reduction gave α-*ribo* isomer selectively in good yields, respectively.

Experimental

General Methods. Melting points were determined with a Mel-Temp melting point apparatus and not corrected. Optical rotations were measured in chloroform at *c* 1.0, unless otherwise stated, using a 0.5-dm tube with Carl Zeiss LEP-Al or JASCO DIP-4 polarimeter. IR spectra were recorded with a Hitachi EPI-G2 grating spectrometer. NMR spectra were recorded with a JEOL JNM PS-100 spectometer in chloroform-*d* containing tetramethylsilane as the internal reference. Chemical shifts and coupling constants are recorded in δ and Hz units, and IR frequencies in cm^{-1}. Evaporations were conducted under diminished pressure. The products were recrystallized from ethanol unless otherwise stated.

*Benzyl 4-Azido-2-benzyloxycarbonylamino-2,4-dideoxypentopyranosides (**5**, **6**, **7**, and **8**).* To a solution of benzyl 2-amino-4-azido-2,4-dideoxy-pentopyranoside (10 mmol) and sodium hydrogencarbonate (20 mmol) in 1:1 dioxane–water (50 ml) was added benzyloxycarbonyl chloride (13 mmol) dropwise with vigorous stirring at room temperature and stirring was continued overnight. The crystals separated during the reaction was filtered and recrystallized from ethanol to give pure *N*-benzyloxycarbonyl derivative in *ca.* 80% yield. The filtrate was evaporated to give a crystalline residue, which was extracted with chloroform. The extract was washed with water, dried, and evaporated to give a further crop of the product. The combined yield of the product was almost quantitative. In the cases of α-D- and β-L-*arabino* isomers the ammonolysis mixture which contain 2- and 3-amino derivatives in the ratio of 3:2[4] was directly subject to this reaction because of difficulty of separation of each component on a column in large scale, and the 2-benzyloxycarbonylamino derivative was obtained in *ca.* 40% yield by fractional crystallization from ethanol.

*Benzyl 4-Azido-2-benzyloxycarbonylamino-2,4-dideoxy-α-D-arabinopyranoside (**5**)*: Mp 188—190 °C; $[\alpha]_D$ +24.2° (*c* 1.9 $CHCl_3$), +31.5° (*c* 0.7 MeOH): The reported value of −110° for the enantiomer of **5**[17] seems to be incorrect; IR (KBr): 3420 and 3320 (OH and NH), 2100 (N_3), 1690 and 1540 (urethane). Found: C, 60.12; H, 5.59; N, 14.02%. Calcd for $C_{20}H_{22}N_4O_5$: C, 60.29; H, 5.57; N, 14.06%. Acetylation of **5** with acetic anhydride in pyridine gave its 3-acetate (**13**) in quantitative yield. Mp 183—184 °C; $[\alpha]_D$ +18.8°; IR (KBr): 3300 (NH), 2100 (N_3), 1738 (ester), 1685 and 1540 (urethane), 730 and 698 (phenyl). Found: C, 59.66; H, 5.57; N, 12.83%. Calcd for $C_{22}H_{24}N_4O_6$: C, 59.99; H, 5.49; N, 12.72%.

*Benzyl 4-Azido-2-benzyloxycarbonylamino-2,4-dideoxy-β-L-arabinopyranoside (**6**)*: Mp 159—160 °C; $[\alpha]_D$ +143°; IR (KBr): 3315 (OH and NH), 2120 (N_3), 1690 and 1530 (urethane). Found: C, 60.45; H, 5.61; N, 13.99%. Calcd for $C_{20}H_{22}N_4O_5$: C, 60.29; H, 5.57; N, 14.06%. Acetylation of **6** in a usual manner gave its 3-acetate (**14**) in good yield. Mp 129—130 °C; $[\alpha]_D$ +134.0°; IR (KBr): 3340 (NH), 2120 (N_3), 1735 (ester), 1685 and 1515 (urethane), 735 and 703 (phenyl). Found: C, 60.09; H, 5.43; N, 12.63%. Calcd for $C_{22}H_{24}N_4O_6$: C,59.99; H, 5.49; N, 12.72%.

*Benzyl 4-Azido-2-benzyloxycarbonylamino-2,4-dideozy-α-D-xylopyranoside (**7**)*: Mp 114—115 °C; $[\alpha]_D$ +123.9°; IR (KBr): 3325 (OH and NH), 2100 (N_3), 1690 and 1530 (urethane), 733 and 695 (phenyl). Found: C, 60.00; H, 5.52; N, 13.87%. Calcd for $C_{20}H_{22}N_4O_5$: C, 60.29; H, 5.57; N, 14.06%. Acetylation of **7** in a usual manner gave its 3-acetate (**15**) in good yield. Mp 106—107 °C; $[\alpha]_D$ +157.3°; IR (KBr): 3400 (NH), 2098 (N_3), 1745 (ester), 1718 and 1502 (urethane), 735 and 690 (phenyl). Found: C, 59.90; H, 5.51; N, 12.24%. Calcd for $C_{22}H_{24}N_4O_6$: C, 59.99; H, 5.49; N, 12.72%.

*Benzyl 4-Azido-2-benzyloxycarbonylamino-2,4-dideoxy-β-L-xylopyranoside (**8**)* was already reported.[3] Acetylation of **8** in a usual manner gave its 3-acetate (**16**) in good yield. Mp 134—137 °C; $[\alpha]_D$ +13.6°; IR (KBr): 3305 (NH), 2110 (N_3), 1750 (ester), 1698 and 1540 (urethane), 738 and 695 (phenyl). Found: C, 60.10; H, 5.49; N, 12.76%. Calcd for $C_{22}H_{24}N_4O_6$: C, 59.99; H, 5.49; N, 12.72%.

*Benzyl 4-Azido-2-benzyloxycarbonylamino-2,4-dideoxy-3-O-methylsulfonylpentopyranosides (**9**, **10**, **11**, and **12**).* To a solution of the compound **5**, **6**, **7**, or **8** (2 mmol) in pyridine (5 ml) was added methylsulfonyl chloride (3 mmol) dropwise with stirring at 0 °C. Stirring was continued overnight at room temperature. The solution was poured into ice–water with

stirring. After 3 h, a crystalline precipitate separated was collected by filtration and recrystallized from ethanol to give the corresponding 3-*O*-methylsulfonyl derivative in 90—95% yield.

*Benzyl 4-Azido-2-benzyloxycarbonylamino-2,4-dideoxy-3-O-methylsulfonyl-α-D-arabinopyranoside (**9**)*: Mp 160—162 °C; $[\alpha]_D$ +3.5°; IR (KBr): 3320 (NH), 2100 (N_3), 1690 and 1535 (urethane), 1335 (SO_2), 733 and 695 (phenyl). Found: C, 53.33; H, 5.20; N, 11.41; S, 6.68%. Calcd for $C_{21}H_{24}N_4O_7S$: C, 52.94; H, 5.08; N, 11.76; S, 6.72%.

*Benzyl 4-Azido-2-benzyloxycarbonylamino-2,4-dideoxy-3-O-methylsulfonyl-β-L-arabinopyranoside (**10**)*: Mp 139—140 °C; $[\alpha]_D$ +137.0°; IR (KBr): 3360 (NH), 2130 (N_3), 1690 and 1535 (urethane), 1365 (SO_2), 740 and 700 (phenyl). Found: C, 52.50; H, 5.07; N, 11.82; S, 6.96%. Calcd for $C_{21}H_{24}N_4O_7S$: C, 52.94; H, 5.08; N, 11.76; S, 6.72%.

*Benzyl 4-Azido-2-benzyloxycarbonylamino-2,4-dideoxy-3-O-methylsulfonyl-α-D-xylopyranoside (**11**)*: Syrup; $[\alpha]_D$ +124.5°; IR (NaCl): 3375 (NH), 2110 (N_3), 1695 and 1523 (urethane), 1345 and 1175 (SO_2), 740 and 700 (phenyl). Found: C, 53.25; H, 5.31; N, 11.32%. Calcd for $C_{21}H_{24}N_4O_7S$: C, 52.94; H, 5.08; N, 11.76%.

*Benzyl 4-Azido-2-benzyloxycarbonylamino-2,4-dideoxy-3-O-methylsulfonyl-β-L-xylopyranoside (**12**)* was reported already.[3]

General Methods for Inversion Reaction with Sodium Acetate or Benzoate. All inversion reactions were carried out in sealed tubes or tightly stoppered test tubes at a temperature between 95 and 140 °C using 2-methoxyethanol–water or DMF as solvent.

Inversion Reaction with Sodium Acetate in 2-Methoxyethanol–Water: The starting 3-metanesulfonate (50 mg, 0.1 mmol) and sodium acetate (50—380 mg, 0.55—4 mmol) were dissolved or suspended in 2-methoxyethanol–water (19: 1 or 4: 1, 3 ml) and heated. Undissolved material went into the solution during the reaction. Then, the reaction solution was evaporated directly to give a residue, which was extracted with acetone. The extract was concentrated to a small volume, and subjected to preparative TLC on silica gel.

Inversion Reaction with Sodium Acetate or Benzoate in DMF: A suspension of the 3-methanesulfonate (50 ml, 0.1 mmol) and sodium acetate (41 mg, 0.5 mmol) or benzoate (85 mg, 0.5 mmol) in DMF (3 ml) was heated. Sodium benzoate did not dissolved completely even at higher temperature, and formation of resin-like material was observed by long time heating at higher than 130 °C. Work-up was done in the same manner as described above.

*Benzyl 4-Azido-2-benzyloxycarbonylamino-2,4-dideoxy-β-L-ribopyranoside (**17**) and Benzyl 2-Amino-4-azido-2-N: 3-O-carbonyl-2,4-dideoxy-β-L-ribopyranoside (**18**).* A mixture of **12** (95 mg, 0.2 mmol) and sodium acetate (656 mg, 80 mmol) in 80% 2-methoxyethanol (6 ml) was heated at 95—100 °C for 40 h. A mixture of products obtained as described above was separated on a silica gel TLC using 19: 1 benzene–methanol as a solvent to give **17** (51 mg) and **18** (14 mg), in 60 and 20% yields, respectively.

17: Syrup. The optical rotation, IR, and NMR spectra were identical with those reported previously.[3]

18: Syrup; $[\alpha]_D$ +71.0°; IR (NaCl): 3300 (NH), 2090 (N_3), 1760 (cyclic urethane), 735 and 695 (phenyl). Found: C, 53.44; H, 5.04; N, 18.93%. Calcd for $C_{13}H_{14}N_4O_4$: C, 53.79; H, 4.86; N, 19.30%.

*Benzyl 3-O-Acetyl-4-azido-2-benzyloxycarbonylamino-2,4-dideoxy-β-L-ribopyranoside (**19**) and Benzyl 4-Azido-N-benzyloxycarbonyl-2,3-epimino-2,3,4-trideoxy-β-L-ribopyranoside (**21**).* A mixture of **12** (50 mg, 0.1 mmol) and sodium acetate (54 mg, 0.65 mmol) in DMF (3 ml) was heated at 115—120 °C for 13 h. The similar work-up mentioned above gave **19** (27 mg) and **21** (10 mg) in 58 and 25% yields, respectively.

19: Syrup; $[\alpha]_D$ +76.6°; IR (NaCl): 3410 (NH), 2100 (N_3), 1745 (ester), 1720 and 1500 (urethane), 740 and 700 (phenyl). Found: C, 59.95; H, 5.48; N, 12.85%. Calcd for $C_{22}H_{24}N_4O_6$: C, 59.99; H, 5.49; N, 12.72%.

21: Syrup; The structure was ascertained only by NMR data (Table 4).

*Benzyl 4-Azido-3-O-benzoyl-2-benzyloxycarbonylamino-2,4-dideoxy-β-L-ribopyranoside (**20**) and -β-L-xylopyranoside (**22**).* A suspension of **12** (50 mg, 0.10 mmol) and sodium benzoate (85 mg, 0.5 mmol) in DMF (3 ml) was heated at 115—120 °C for 13 h. The similar work-up mentioned above gave **20** (39 mg, 68%) and **22** (10 mg, 17%). At lower reaction temperature (95—100 °C) only **16** was obtained in 69% yield.

20: Mp 88—90 °C; $[\alpha]_D$ +28.2°; IR (KBr): 3410 (NH), 2100 (N_3), 1720 (ester), *ca.* 1700 and 1500 (urethane), *ca.* 740 and 705 (phenyl). Found: C, 64.47; H, 5.26; N, 11.26%. Calcd for $C_{27}H_{26}N_4O_6$: C, 64.53; H, 5.22; N, 11.15%.

22: Mp 122.0—123.5 °C; $[\alpha]_D$ +25.5°; IR (KBr): 3330 (NH), 2110 (N_3), 1720 (ester), 1700, and 1520 (urethane), 710 and 698 (phenyl).

*Benzyl 2-Amino-4-azido-2-N: 3-O-carbonyl-2,4-dideoxy-β-L-lyxopyranoside (**23**).* A solution of **10** (128 mg, 0.26 mmol) and sodium acetate (170 mg) in 80% aqueous 2-methoxyethanol was heated at 110—115 °C and evaporated to dryness. The residue was shaken with chloroform and water. The chloroform layer was evaporated to give a dark brown syrup. The syrup was separated on preparative TLC with 8: 1 benzene–acetone to give **23** (18 mg, 23%). Mp 102—104 °C; $[\alpha]_D$ +126.0°; IR (KBr): 3300 (NH), 2090 (N_3), 1760 (cyclic urethane), 735 and 695 (phenyl). Found: C, 52.19; H, 4.88; N, 18.85%. Calcd for $C_{13}H_{14}N_4O_4 \cdot 1/2H_2O$: C, 52.17; H, 5.02; N, 18.71%.

*Benzyl 2-Amino-4-azido-2-N: 3-O-carbonyl-2,4-dideoxy-α-D-ribopyranoside (**25**).* Similarly, **25** was obtained from **11** in 17% yield. Mp 118—120 °C; $[\alpha]_D$ +130.0°; IR (KBr): 3260 (NH), 2100 (N_3), 1755 (cyclic urethane), 735 and 695 (phenyl). Found: C, 53.34; H, 4.88; N, 18.96%. Calcd for $C_{13}H_{14}N_4O_4$: C, 53.79; H, 4.86; N, 19.30%.

*Reaction of **10** with Sodium Benzoate.* A mixture of **10** (393 mg, 0.77 mmol) and sodium benzoate (540 mg) in DMF (20 ml) was heated at 140 °C for 17 h to give many products on TLC. Sodium benzoate did not dissolved completely during the reaction. The solution turned black was evaporated. The residue was shaken with chloroform and water. The chloroform layer was evaporated to give a black syrup. The syrup was separated on preparartive TLC with 8: 1 benzene–acetone to give benzyl 4-azido-2-benzyloxycarbonylamino-3-*O*-benzoyl-2,4-dideoxy-β-L-arabinopyranoside (**26**) and benzyl 4-azido-3-benzyloxycarbonylamino-2-*O*-benzoyl-3,4-dideoxy-β-L-xylopyranoside (**27**) in 3.8 and 3.0% yields, respectively. Besides **26** and **27**, benzyl 4-azido-3-*O*-benzoyl-2,4-dideoxy-2-(3,3-dimethylureido)-β-L-arabinopyranoside could be also obtained in 7.8% yield, but its structure was deduced only by the following spectral data. IR (NaCl): 3450 and 3470 (NH), 2120 (N_3), 1725 (ester), and 1660 and 1525 (amide), 710 (phenyl); NMR: 5.07 (H_1: d, $J_{1,2}$=3.0), 5.60 (H_3: dd, $J_{2,3}$=10.5, $J_{3,4}$=3.6), 5.12 (H_4: broad s), 4.06 (H_5: dd, $J_{4,5'}$=1.5, $J_{5,5'}$=12.8), 3.80 ($H_{5'}$: dd, $J_{4,5'}$=1.5), 2.74 (6H, *N*–CH_3: s).

26: Mp 85—87 °C; $[\alpha]_D$ +114.0°; IR (KBr): 3320 (NH), 2100 (N_3), 1715 (ester), 1685 and 1515 (urethane), 735, 705, and 695 (phenyl). Found: C, 64.83; H, 5.21; N, 11.30%. Calcd for $C_{27}H_{26}N_4O_6$: C, 64.53; H, 5.22; N, 11.15%.

27: Mp 142—144 °C; $[\alpha]_D$ +3.9°; IR (KBr): 3320 (NH), 2125 (N_3), 1715 (ester), 1695 and 1540 (urethane), 730, 700, and 690 (phenyl). Found: C, 64.60; H, 5.15; N, 10.96%.

Calcd for $C_{27}H_{26}N_4O_6$: C, 64.53; H, 5.22; N, 11.15%.

Reaction of **9** *with Sodium Benzoate.* A mixture of **9** (231 mg, 0.45 mmol) and sodium benzoate (278 mg) in DMF (10 ml) was heated at 110—115 °C for 5 days. The mixture of products obtained by the same work-up as described in the reaction of **10** was separated on preparative TLC with 7: 1 benzene–methanol to give benzyl 4-azido-3-*O*-benzoyl-2-benzyloxycarbonylamino-2,4-dideoxy-α-D-arabinopyranoside (**28**, 27 mg) in 13% yield. Mp 77—79 °C; $[\alpha]_D$ +29.9°; IR (KBr): 3325 (NH), 2105 (N_3), 1720 (ester), 1695 and 1530 (urethane), 735, 715 and 695 (phenyl). Found: C, 64.18; H, 5.36; N, 10.80%. Calcd for $C_{27}H_{26}N_4O_6$: C, 64.53; H, 5.22; N, 11.15%.

General Method for N-*Acetylation.* To a solution of 2-amino derivative (**2**, **1**, or **3**, 10 mmol) in ethanol (30 ml) was added acetic anhydride (15 mmol) dropwise with stirring at room temperature. After 30 min, water was added to a suspension of crystallized product, and this suspension was evaporated directly to give a crystalline residue, which was recrystallized from ethanol to give the corresponding *N*-acetyl derivative in 85—90%.

*Benzyl 2-Acetylamino-4-azido-2,4-dideoxy-β-*L*-arabinopyranoside (**29**)*: As in the preparation of **6** the ammonolysis mixture of benzyl 4-azido-2,3-anhydro-β-L-ribopyranoside was used, and **29** was obtained in *ca.* 40% yield by fractional crystallization from ethanol. Mp 178—180 °C; $[\alpha]_D$ +217.9° (MeOH); IR (KBr): 3455 and 3395 (OH and NH), 2130 (N_3), 1655 and 1550 (amide), 735 and 695 (phenyl). Found: C, 54.95; H, 5.83; N, 18.35%. Calcd for $C_{14}H_{18}N_4O_4$: C, 54.89; H, 5.92; N, 18.29%.

*Benzyl 2-Acetylamino-4-azido-2,4-dideoxy-α-*D*-arabinopyranoside (**41**)*: Mp 208—210 °C; $[\alpha]_D$ +47.2° (MeOH); IR (KBr): 3280 (OH and NH), 2110 (N_3), 1650 and 1550 (amide), 730 and 692 (phenyl). Found: C, 54.95; H, 5.84; N, 18.25%. Calcd for $C_{14}H_{18}N_4O_4$: C, 54.89; H, 5.92; N, 18.29%.

*Benzyl 2-Acetylamino-4-azido-2,4-dideoxy-α-*D*-xylopyranoside (**47**)*: Mp 160—161 °C; $[\alpha]_D$ +210.9° (MeOH); IR (KBr): 3500 and 3280 (OH and NH), 2105 (N_3), 1630 and 1525 (amide), 735 and 695 (phenyl). Found: C, 55.15; H, 5.95; N, 18.52%. Calcd for $C_{14}H_{18}N_4O_4$: C, 54.89; H, 5.92; N, 18.29%.

*Benzyl 4-Azido-2-benzoylamino-2,4-dideoxy-β-*L*-arabinopyranoside (**30**).* To a solution of **2** (2.0 g, 6.7 mmol) in 1: 1 dioxane–water (40 ml) was added potassium hydroxide (0.38 g, 6.7 mmol) and benzoyl chloride (1.54 g, 11 mmol) with stirring in an ice–water bath. After 3 h the solution was poured into ice-water. The crystalls separated were collected by filtration, washed with 1 M sodium hydroxide and recrystallized from ethanol to give **30** in a quantitative yield. Mp 167—170 °C; $[\alpha]_D$ +140.0° ($CHCl_3$); IR (KBr): 3275 (OH and NH), 2105 (N_3), 1630 and 1523 (amide), 732 and 692 (phenyl). Found: C, 62.24; H, 5.17; N, 14.91%. Calcd for $C_{19}H_{20}N_4O_4$: C, 61.94; H, 5.47; N, 15.21%.

*Benzyl 4-Azido-2,4-dideoxy-2-formylamino-β-*L*-arabinopyranoside (**31**) and -α-*D*-arabinopyranoside (**42**).* To a solution of 2-amino derivative (**2** or **1**, 1 mmol) in tetrahydrofuran (10 ml) was added a solution of *p*-nitrophenyl formate (2 mmol) in tetrahydrofuran (5 ml) dropwise with stirring at 0 °C. After standing overnight at room temperature, the solution was evaporated to give a crystalline residue, which was purified on a column of silica gel with 15: 1 benzene–ethanol to give the corresponding 2-formylamino derivative in good yield.

31: Mp 166—167 °C; $[\alpha]_D$ +205.0° (MeOH); IR (KBr): 3295 (OH and NH), 2140 (N_3), 1655 and 1545 (amide), 740 and 700 (phenyl). Found: C, 53.13; H, 5.54; N, 19.00%. Calcd for $C_{13}H_{16}N_4O_4$: C, 53.42; H, 5.52; N, 19.17%.

42: Mp 194—195 °C; $[\alpha]_D$ +44.7° (MeOH); IR (KBr): 3290 (OH and NH), 2110 (N_3), 1645 and 1530 (amide), 730 and 705 (phenyl). Found: C, 53.67; H, 5.53; N, 19.31%. Calcd for $C_{13}H_{16}N_4O_4$: C, 53.42; H, 5.52; N, 19.17%.

*Benzyl 2-Acetylamino-(or 2-Formylamino)-4-azido-2,4-dideoxy-3-O-methylsulfonylpentopyranosides (**32**, **34**, **43**, **44**, and **48**).* To a solution of the compound to be methylsulfonylated (**29**, **31**, **41**, **42** or **47**) (2 mmol) in pyridine (15 ml) was added methanesulfonyl chloride (3 mmol) dropwise with stirring at 0 °C. After stirring overnight at room temperature, water was added to the solution, and the solution was evaporated directly to give black syrupy residue. The residue was fractionated on a silica-gel column using 5: 1 benzene–acetone as eluant to give the corresponding 3-*O*-methylsulfonyl derivative in 80%—quantitative yield.

*Benzyl 2-Acetylamino-4-azido-2,4-dideoxy-3-O-methylsulfonyl-β-*L*-arabinopyranoside (**32**)*: Mp 137—138 °C; $[\alpha]_D$ +213.8° (*c* 1.0, MeOH); IR (KBr): 3305 (NH), 2120 (N_3), 1645 and 1530 (amide), 1365 and 1180 (SO_2), 735 and 698 (phenyl). Found: C, 46.58; H, 5.20; N, 14.95; S, 8.52%. Calcd for $C_{15}H_{20}N_4O_6S$: C, 46.87; H, 5.25; N, 14.58; S, 8.33%.

*Benzyl 4-Azido-2,4-dideoxy-2-formylamino-3-O-methylsulfonyl-β-*L*-arabinopyranoside (**34**)*: Syrup; IR (KBr): 3375 (NH), 2110 (N_3), 1665 (amide), 1345 (SO_2), 700 (phenyl). Beside spectral data (NMR data in Table 6), other characterization could not be done because of its unstability.

*Benzyl 2-Acetylamino-4-azido-2,4-dideoxy-3-O-methylsulfonyl-α-*D*-arabinopyranoside (**43**)*: Mp 148—150 °C; $[\alpha]_D$ +19.2° (*c* 1.0, MeOH); IR (KBr): 3250 (NH), 2100 (N_3), 1645 and 1545 (amide), 1360 and 1178 (SO_2), 750 and 695 (phenyl). Found: C, 47.13; H, 5.24; N, 14.87; S, 8.53%. Calcd for $C_{15}H_{20}N_4O_6S$: C, 46.87; H, 5.25; N, 14.58; S, 8.33%.

*Benzyl 4-Azido-2,4-dideoxy-2-formylamino-3-O-methylsulfonyl-α-*D*-arabinopyranoside (**44**)*: Mp 162—163 °C; $[\alpha]_D$ +15.4° (MeOH); IR (KBr): 3300 (NH), 2120 (N_3), 1662 and 1535 (amide), 1338 and 1175 (SO_2), 725 and 700 (phenyl). Found: C, 45.25; H, 4.92; N, 15.10; S, 8.53%. Calcd for $C_{14}H_{18}N_4O_6S$: C, 45.40; H, 4.90; N, 15.13; S, 8.45%.

*Benzyl 2-Acetylamino-4-azido-2,4-dideoxy-3-O-methylsulfonyl-α-*D*-xylopyranoside (**48**)*: Mp 115—117 °C; $[\alpha]_D$ +141.5° (*c* 1.0, MeOH); IR (KBr): 3275 (NH), 2100 (N_3), 1650 and 1510 (amide), 1345 (SO_2), 722 and 690 (phenyl). Found: C, 46.71; H, 5.15; N, 14.30; S, 8.17%. Calcd for $C_{15}H_{20}N_4O_6S$: C, 46.87; H, 5.25; N, 14.58; S, 8.33%.

*Benzyl 4-Azido-2-benzoylamino-2,4-dideoxy-3-O-methylsulfonyl-β-*L*-arabinopyranoside (**33**).* Compound **30** was methylsulfonylated as described in the preparation of **9**—**12** to give **33** in 95% yield. Mp 163—164 °C; $[\alpha]_D$ +150.7°; IR (KBr): 3320 (NH), 2140 (N_3), 1635 and 1530 (amide), 1362 and 1188 (SO_2), 730 and 695 (phenyl). Found: C, 54.03; H, 4.97; N, 12.37; S, 7.00%. Calcd for $C_{20}H_{22}N_4O_6S$: C, 53.81; H, 4.97; N, 12.55; S, 7.17%.

*Inversion Reaction of 2-Acylamino Derivatives (**32**, **33**, **34**, **43**, **44**, and **48**).* A solution of 2-acylamino derivative (1 mmol) and sodium acetate (5 mmol) in 80% 2-methoxyethanol was heated in a sealed tube overnight at 110—115 °C. The solution was evaporated and the residue was purified on a colomn of silica gel to give a product in various yields.

*Benzyl 2-Acetylamino-4-azido-2,4-dideoxy-β-*L*-lyxopyranoside (**35**)*: The inversion reaction of **32** as described above gave **35** in 89% yield. Mp 117—119 °C; $[\alpha]_D$ +116.8° (MeOH); IR (KBr): 3330 (OH and NH), 2110 (N_3), 1650 and 1520 (amide), 740 and 704 (phenyl). Found: C, 55.19; H, 5.95; N, 18.35%. Calcd for $C_{14}H_{18}N_4O_4$: C, 54.89; H, 5.92; N, 18.29%. A usual acetylation of **35** gave the corresponding 3-*O*-acetyl derivative (**38**): Only NMR spectra was taken (Table 6).

*Benzyl 4-Azido-2-benzoylamino-2,4-dideoxy-β-L-lyxopyranoside (**36**).* Similarly, **33** gave **36** in 60% yield. IR (KBr): 3420 (OH and NH), 2090 (N_3), 1630 (amide), 705 (phenyl). Further characterization was done as its 3-*O*-acetyl derivative (**39**): Syrup; $[\alpha]_D$ +62.4°; IR (NaCl): 3440 and 3360 (NH), 2105 (N_3), 1745 (ester), 1660 and 1510 (amide), 710 and 695 (phenyl). Found: C, 61.31; H, 5.48; N, 13.30%. Calcd for $C_{21}H_{22}N_4O_5$: C, 61.45; H, 5.40; N, 13.65%. The by-product obtained in a low yield and supposed to be an oxazoline derivative has the following spectral data. IR (NaCl): 2095 (N_3), 1720, 1640 and 695; NMR: 5.09 (H_1: d, $J_{1,2}$=4.0), 4.50 (H_2: dd, $J_{2,3}$=9.3), 4.70 (H_3: dd, $J_{3,4}$=6.8), 4.28 (H_4: ddd), 3.94 (H_{5a}: dd, $J_{4,5a}$=5.7, $J_{5a,5b}$=11.0), 3.43 (H_{5b}: t, $J_{4,5b}$=10.1), 4.83 and 4.65 (ABq. CH_2 in Bn), 7.26 (broad s, 5H), 7.48 (m, 2H) and 8.02 (m, 2H).

*Benzyl 4-Azido-2,4-dideoxy-2-formylamino-β-L-lyxopyranoside (**37**)*: Similarly, **34** gave **37** in 65% yield. Syrup, $[\alpha]_D$ +72.3° (MeOH); IR (NaCl), 3320 (OH and NH), 2100 (N_3), 1660 (amide), 735 and 695 (phenyl). Found: C, 53.21; H, 5.66; N, 18.81%. Calcd for $C_{13}H_{16}N_4O_4$: C, 53.42; H, 5.52; N, 19.17%. A usual acetylation of **37** gave the corresponding 3-*O*-acetyl derivative (**40**): Mp 99—101 °C; $[\alpha]_D$ +134.3°; IR (KBr): 3415 and 3180 (NH), 2105 (N_3), 1730 (ester), 1645 (amide), 695 (phenyl). Found: C, 53.68; H, 5.44; N, 16.65%. Calcd for $C_{15}H_{18}N_4O_5$: C, 53.88; H, 5.43; N, 16.76%.

*Benzyl 2-Acetylamino-4-azido-2,4-dideoxy-α-D-lyxopyranoside (**45**)*: Similarly, **43** gave **45** in quantitative yield. $[\alpha]_D$ +133.0° (MeOH); IR (KBr): 3325 (OH and NH), 2110 (N_3), 1645 and 1530 (amide), 728 and 700 (phenyl). Found: C, 53.72; H, 6.02; N, 17.74%. Calcd for $C_{14}H_{18}N_4O_4 \cdot 1/2H_2O$: C, 53.50; H, 6.05; N, 17.83%. NMR data of its 3-acetate (**50**): 4.74 (H_1: d, $J_{1,2}$=1.5), 4.65 (H_2: dq, $J_{2,3}$=4.5, $J_{NH,CH}$=9.0) 5.24 (H_3: dd, $J_{3,4}$=9.0)

*Benzyl 4-Azido-2,4-dideoxy-2-formylamino-α-D-lyxopyranoside (**46**)*: Similarly, **44** gave **46** in low yield. Mp 97—98 °C, $[\alpha]_D$ +72.9° (MeOH); IR (KBr): 3455, 3350 (NH and OH), 2080 (N_3), 1648 and 1505 (amide), 740 and 695 (phenyl). Found: C, 53.30; H, 5.83; N, 17.45%. Calcd for $C_{14}H_{18}N_4O_4 \cdot 1/2H_2O$: C, 53.33; H, 6.03; N, 17.78%.

*Benzyl 2-Acetylamino-4-azido-2,4-dideoxy-α-D-ribopyranoside (**49**)*: Similarly, **48** gave **49** in 83% yield. Mp 94—96 °C; $[\alpha]_D$ +72.9° (MeOH); IR (KBr): 3455 and 3350 (OH and NH), 2080 (N_3), 1648 and 1505 (amide), 740 and 695 (phenyl). Found: C, 53.30; H, 5.83; N, 17.45%. Calcd for $C_{14}H_{18}N_4O_4 \cdot 1/2H_2O$: C, 53.33; H, 6.03; N, 17.78%. NMR data of its 3-acetate (**52**): 4.70 (H_1: d, $J_{1,2}$=3.8), 4.39 (H_2: dt, $J_{2,3}$=3.8, $J_{NH,CH}$=9.5), 5.43 (H_3: t, $J_{3,4}$)=3.8).

*Benzyl 4-Azido-2-benzyloxycarbonylamino-2,4-dideoxy-α-D-erythro-pentopyranosid-3-ulose (**53**).* Dimethyl sulfoxide (2.65 g,34 mmol) and dichloromethane (5 ml) were put into Erlenmeyer flask with vigorous stirring at −76 °C. To this solution was added trifluoroacetic anhydride (3.56 g, 18 mmol) with vigorous stirring for 5 min at −76 °C and was added a solution of **6** (2.92 g, 6.75 mmol) in dichloromethane (20 ml). After 1 h, to this solution was added triethylamine (3 ml) dropwise. After 10 min, the solution was mixed with chloroform–water, and the chloroform layer was evaporated to give a crystalline, which was recrystallized from ethanol to give **44** in 81.7% yield (2.37 g): Mp 123—125 °C; $[\alpha]_D$ +173.8° ($CHCl_3$); IR (KBr): 3350 (OH and NH), 2100 (N_3), 1740 (ketone), 1720 and 1530 (urethane), 695 (phenyl). Found: C, 60.35; H, 5.13; N, 14.09%. Calcd for $C_{20}H_{20}N_4O_5$: C, 60.60; H, 5.09; N, 14.14%.

The stereoisomers of **6** (**5**, **7**, and **8**) were also oxidized in the same manner as described above to give the same ulose derivative (**53**) in 80—85% yields.

*Benzyl 4-Azido-2-benzyloxycarbonylamino-2,4-dideoxy-α-D-ribopyranoside (**54**).* To a solution of **53** (250 mg, 0.58 mmol) in methanol was added sodium borohydride (40 mg, 1.06 mmol) with stirring at room temperature. After 30 min, the solution was neutralized with 1 M hydrochloric acid. After evaporation of the solution the resulting residue was dissolved in chloroform. The chloroform solution was washed with water, dried with anhydrous sodium sulfate and evaporated to give a syrup. The syrup was first crystallized by evaporation of ethanol solution after decolorization with activated charcoal. Yield, 94.4%: $[\alpha]_D$ +97.2° ($CHCl_3$); IR (KBr): 3450 and 3340 (OH and NH), 2075 (N_3), 1680 and 1495 (urethane), 740 and 695 (phenyl). Found: C, 60.25; H, 5.57; N, 13.93%. Calcd for $C_{20}H_{22}N_4O_5$: C, 60.29; H, 5.57; N, 14.16%. Its 3-acetate (**55**); Syrup, $[\alpha]_D$ +70.8° ($CHCl_3$); NMR: 4.78 (H_1: d, $J_{1,2}$=3.3), 4.14 (H_2: dt, $J_{2,3}$=3.0, $J_{NH,CH}$=9.6), 5.75 (H_3: t, $J_{3,4}$=3.0) 3.94 (H_{5a}: dd, $J_{4,5a}$=3.6, $J_{5a,5b}$=12.3), 3.64 (H_{5b}: dd, $J_{4,5b}$=6.8).

This work was supported in part by a Scientific Research Grant from the Ministry of Education, Japan (No. 347023).

References

1) Aminosugars Part XXX. H. A. Khan, H. Hashimoto, and J. Yoshimura, *Bull. Chem. Soc. Jpn.*, **51**, 951 (1978).
2) J. Yoshimura, H. Hashimoto, and T. Nishide, *Chem. Lett.*, **1976**, 201; H, Hashimoto, T. Nishide, F. Chiba, and J. Yoshimura, *Carbohydr. Res.*, **60**, 75 (1978).
3) H. Hashimoto, F. Chiba, K. Araki, and J. Yoshimura, *Carbohydr. Res.*, **72**, 261 (1979.)
4) H. Hashimoto, K. Araki, and J. Yoshimura, *Carbohydr. Res.*, to be published.
5) F. A. L. Anet, *J. Am. Chem. Soc.*, **84**, 1053 (1962); H. Feltkamp and N. C. Franklin, *J. Am. Chem. Soc.*, **87**, 1616 (1965).
6) R. U. Lemieux and J. D. Stevens, *Can. J. Chem.*, **43**, 2059 (1965).
7) M. Karplus, *J. Am. Chem. Soc.*, **85**, 2870 (1963).
8) P. L. Durette and D. Horton, *Carbohydr. Res.*, **18**, 403 (1971).
9) H. Paulsen and M. Friedmann, *Chem. Ber.*, **105**, 705 (1972).
10) H. Paulsen and H. Koebernick, *Carbohydr. Res.*, **45**, 205 (1975).
11) P. L. Durette and D. Horton, *Adv. Carbohydr. Chem. Biochem.*, **26**, 46 (1971).
12) W. M. zu Reckendorf, *Methods Carbohydr. Chem.* **6**, 266 (1972); B. R. Baker and R. E. Schaub, *J. Org. Chem.*, **19**, 646 (1954).
13) F. L. Scott, R. E. Glick, and S. Winstein, *Experientia*, **15**, 183 (1957); L. Goodman, *Adv. Carbohydr. Chem. Biochem.*, **22**, 109 (1967).
14) J. D. Stevens, *Methods Carbohydr. Chem.*, **6**, 123 (1972).
15) J. Yoshimura, K. Sato, and H. Hashimoto, *Chem. Lett.*, **1977**, 1327.
16) Y. Ali and A. C. Richardson, *Carbohydr. Res.*, **5**, 441 (1967).
17) A. Hasegawa, N. Aritake, and M. Kiso, *Carbohydr. Res.*, **52**, 137 (1976).

The Hydrocracking of Solvent Refined Coals over Molten Salt Catalysts[1)]

Yohji NAKATSUJI,* Yasuhiko IKKAKU, Masakatsu NOMURA, and Shōichi KIKKAWA

Department of Applied Chemistry, Faculty of Engineering, Osaka University, Yamadakami, Suita, Osaka 565

(Received December 14, 1978)

The hydrocracking of Yūbari SRC and Tempoku SRC over $ZnCl_2$/CuCl or $ZnCl_2$ molten salt was examined at 350 or 400 °C for 3 h in a batch autoclave system. The reactivity of SRC under the hydrocracking conditions with the molten salts was estimated mainly by comparison with the results obtained in the study using a variety of polynuclear aromatic hydrocarbons. The presence of hetero atoms (especially, the hydroxyl group) in SRC may be supposed to play an important role in this hydrocracking using molten salts. In addition, the average structures of SRC, according to the CAMSC method, are offered, and the usefulness is examined from the point of view of the reactivity of SRC in the presence of molten salts.

Although the structure of coal has not been appreciably clarified in detail, some structural analyses suggest that coal is a natural polymer consisting mainly of condensed rings. Consequently, in order to obtain liquid fuels from coal, it is necessary to decompose the condensed rings in addition to effecting the scission of the bonds between structural units. From this standpoint, the hydrocracking of model substances of coal (that is, a heavy anthracene oil[2)] and polynuclear aromatic hydrocarbons[3)]) over molten salts was investigated. On the basis of detailed product analyses, $ZnCl_2$/CuCl molten salt was found to be a superior hydrocracking catalyst for coal-related substances. In this paper, we will apply this catalyst system to the hydrocracking of solvent refined coals (SRC), which are considered to be representative of some of structural units of coal, and will clarify the catalytic action for SRC in comparison with that of $ZnCl_2$.

Experimental

The NMR spectra were recorded on a JEOL JNM-PS-100 spectrometer, using tetramethylsilane as the internal standard. $CDCl_3$ was used as the solvent for all the substances. The GLC analyses were performed on a Shimadzu GC-3AH apparatus for gaseous products and on a GC-4BPTF apparatus for liquid and solid products. The GC-MS spectra were taken with a Hitachi RMU-6MG spectrometer at 20 eV connected with a Hitachi M 5201 apparatus using a 3 m×3 mm column of 5% Silicone OV-1 on Uniport KS. The average molecular weights were determined with a Hitachi-Perkin Elmer 115 vapour-pressure osmometer in chloroform, with bibenzyl as the calibration standard. The zinc chloride and copper(I) chloride were obtained from Nakarai Chemicals, Ltd.

Preparation of SRC. The experiments were carried out in a 500 ml SUS 32 autoclave; 50 g of Yūbari coal (−200 mesh) and 100 ml of tetralin were placed in it, and hydrogen was added up to a pressure of 80 kg/cm². The rate of the temperature rise was controlled to about 3 °C/min up to 400 °C, after which the temperature was held for 3 h. The autoclave was shaken in a horizontal direction (70 strokes/min). No attempts were made to maintain the hydrogen pressure at a constant level during the reaction. After the system had been cooled to room temperature, the gases were collected in a gas holder and analyzed by GLC (60—80 mesh silica-gel column, 3 m×3 mm, TCD, 120 °C, N_2 carrier). The product was filtered, and the residue was extracted with benzene by means of a Soxhlet extractor. The above procedure was repeated 3 times. The benzene and tetralin were then removed from the combined mixture of filtrates and extracted solutions. The yield of Yūbari SRC was 90 g. In the case of the Tempoku coal, the reaction time was 30 min and the autoclave experiment was repeated 4 times. The yield of Tempoku SRC was 70 g. All the properties of coals and their SRC are shown in Table 1.

Hydrocracking of SRC. A stainless-steel vessel containing 8 g of SRC and the catalyst was placed in a SUS 32 autoclave with a capacity of 200 ml. The air in the autoclave was replaced by hydrogen, and then the system was filled with hydrogen to 100 kg/cm²; thereafter, the autoclave was heated up to the desired temperature. The time taken to reach the stage was from 60—70 min. The reaction system shaken in a horizontal direction (68 strokes/min) was maintained at the reaction temperature for 3 h. No attempts were made to maintain the hydrogen pressure at a constant level during the reaction. After the system had been cooled to room temperature, the gases were collected in a gas holder and analyzed by GC. The liquid and solid products were extracted with pentane by means of a Soxhlet extractor, and the residues were subjected to benzene extraction. Moreover, the pentane extracts were separated into two fractions (PSL and PSH) by means of vacuum distillation (−190 °C/3 mmHg). The lighter fraction (PSL) was analyzed by GC (4.5 m×3 mm packed with 20% SE-30 on Uniport B 60—80 mesh, programmed from 30—270 °C, 5 °C/min, TCD, H_2 carrier).

Table 1. Properties of coal and SRC

	Ultimate analyses[a)]				Structural parameters[b)]			
	H	C	N	O[c)]	f_a	σ	Hau/Ca	mol wt[d)]
Yūbari coal	6.0	86.1	2.1	5.8	—	—	—	—
Yūbari SRC	6.4	88.9	2.2	2.6	0.73	0.28	0.63	506
Tempoku coal	5.4	69.8	1.9	22.9	—	—	—	—
Tempoku SRC	6.3	87.2	1.7	4.8	0.76	0.26	0.69	340

a) D.a.f. b) By Brown-Ladner's method.[5)] c) Difference. d) In $CHCl_3$.

Results and Discussion

Average Structure of SRC. The SRC consists of large numbers of compounds possessing different molecular weights; moreover, the constituents cannot be determined. However, as these compounds may be supposed to consist of similar types of compounds, the concept of the average structure has been employed for a variety of structural analyses. In this investigation, the average structure of the SRC was estimated according to the CAMSC method proposed by Oka *et al.*[4] This CAMSC method attempts to represent the average structure as a combination of aromatic and aliphatic groups, in accordance with the input data represented as integral numbers based on the experimental data from the elemental, NMR, and molecular-weight analyses. The oxygen atoms were considered as a phenolic OH, as an ether, or as a carbonyl group; on the other hand, the sulfur and nitrogen atoms were not considered. The determination of the average structures has been carried out by means of a computer program prepared according to the flow chart and the classification method of Oka *et al.* The results for Yūbari SRC and Tempoku SRC are shown in Figs. 1 and 2 respectively. It may be supposed to be unreasonable to represent the average structure by a single structure. It is preferable to divide the average structures obtained by the CAMSC method broadly into two types, that is, the type containing a direct bond between two aromatic rings (a) and the type containing a large ring structure (b).

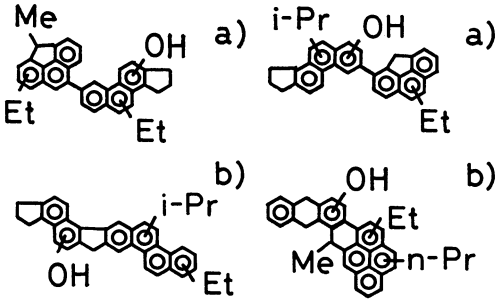

Experimental result: H_α=9.4, H_o=10.5, H_{al}=19.9, H_{ar}=12.2, C_{ar}=28.0, C_{al}=9.4, (OH=0.82).
Input data for CAMSC: H_α=9, H_o=11, H_{al}=20, H_{ar}=12, C_{ar}=28, C_{al}=9, (OH=1).

Fig. 1. Average structure of Yūbari SRC by CAMSC.

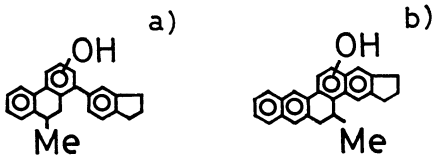

Experimental result: H_α=6.9, H_o=5.0, H_{al}=11.9, H_{ar}=9.6, C_{ar}=19.0, C_{al}=5.7, (OH=0.79).
Input data for CAMSC: a) H_α=7, H_o=5, H_{al}=12, H_{ar}=10, C_{ar}=18, C_{al}=6, (OH=1). b) C_{ar}=20.

Fig. 2. Average structure of Tempoku SRC by CAMSC.

Hydrocracking of SRC. The SRC, which underwent a thermal scission of the bonds between structural units and stabilization by hydrogen transfer from tetralin, is the primary hydrocracked product of coal and may be regarded as representative some of the structural units of coal. The difference in the structural parameters calculated using Brown-Ladner's method[5] and the average molecular weight between Yūbari SRC and Tempoku SRC suggest that the original structure of coal considerably influences the structure of SRC. On the other hand, as the SRC is molten at this reaction temperature and becomes a homogeneous liquid, the catalytic action of the molten salts on the SRC may be expected to be similar to that on polynuclear aromatic hydrocarbons (PAH). With these facts in view, the SRC was selected as a kind of model substance of coal.

The results of the hydrocracking of the SRC are shown in Table 2. The products were classified into Gas, PSL, PSH, and BS. The GC charts of the hydrocracked products (PSL) of Yūbari SRC are shown in Figs. 3 and 4. The products listed in Figs. 3 and 4 were identified by means of GC-MS and by reference to the GC charts of the hydrocracked products of PAH.[3] The structural parameters, the average molecular weight, and the nitrogen content of the hydrocracked products of Yūbari SRC are shown in Table 3. The catalytic action of molten salts will now be discussed on the basis of the product distribution shown in Table 2 and the properties shown in Table 3.

Table 2. Hydrocracking of Yūbari SRC[a]

	Run No.								
	1	2	3	4	5	6	7	8	9[b]
Catalyst	$ZnCl_2$	$ZnCl_2$/CuCl	—	$ZnCl_2$	$ZnCl_2$/CuCl	$ZnCl_2$	$ZnCl_2$/CuCl	$ZnCl_2$/CuCl	$ZnCl_2$/CuCl
(mol: mol)		(60:40)			(60:40)		(90:10)	(60:40)	(60:40)
Catalyst/Feed (wt/wt)	0.1	0.1	—	0.1	0.1	1	1	1	1
Reaction temp (°C)	350	350	400	400	400	400	400	400	400
Gas	2	3	9	13	14	25	29	36	40
PSL	2	2	7	16	19	32	32	24	34
PSH	25	34	19	39	41	28	22	13	8
BS	48	42	61	17	14	1	1	1	1

Reaction conditions: initial hydrogen pressure, 100 kg/cm²; reaction time, 3h; a) Yūbari SRC consists of 22% of PS, 61% of BS, and 17% of BIS. b) Tempoku SRC.

Table 4. Influence of OH substituent on the product distribution

Feed		Naphthalene		2-Naphthol	
Catalyst (mol: mol)		$ZnCl_2$	$ZnCl_2$/CuCl (60:40)	$ZnCl_2$	$ZnCl_2$/CuCl (60:40)
Products (wt %)	C_1–C_4 gases	3.4	45.7	26.3	56.0
	C_5–C_7 alkanes	—	3.7	1.1	2.9
	cycloalkanes	0.1	1.5	3.2	3.1
	monocyclic aromatics	2.0	46.4	18.7	33.7
	indans and tetralins	16.0	1.7	31.2	3.0
	naphthalene	77.9	0.5	9.3	0.7
	higher boiling products	0.7	—	10.3	0.6

Reaction conditions: initial hydrogen pressure, 100 kg/cm²; reaction time, 3h; reaction temperature, 400 °C. Catalyst/Feed=1(mol/mol).

At 350 °C (Runs 1 and 2), a difference in these two catalysts was observed in the yields of PSH and BS.

In the hydrocracking of PAH, it was clarified that the product distribution is dependent upon the original structure and that the methyl groups in the feed remarkably affect the compositions of monocyclic aromatics and of gases.[10] Based on the results obtained in the hydrocracking of SRC under conditions similar to those in the hydrocracking of PAH,[3] the structure of SRC will be discussed.

Table 5. Influence of ring size on the product distribution

Substance used for hydrocracking	Cycloalkanes/monocyclic aromatics[a]
Bicyclic compounds[b]	0.03—0.04
Tricyclic compounds[c]	0.14—0.42
Chrysene	0.70
Tempoku SRC[d]	0.82
Yūbari SRC[e]	1.11

a) wt/wt. b) Naphthalene, 1-methylnaphthalene, 2-methylnaphthalene, 2,6-dimethylnaphthalene. c) Anthracene, 2-methylanthracene, 9-methylanthracene, 9-propylanthracene, 9,10-dihydroanthracene, 9,10-dihydro-9-methylanthracene, 9,10-dihydro-9,10-dimethylanthracene, phenanthrene, 9-methylphenanthrene, 9,10-dihydro-9-methylphenanthrene, fluorene. d) Run 9. e) Run 8.

Monocyclic aromatics are relatively stable under these reaction conditions. On the other hand, cycloalkanes are mainly formed *via* highly hydrogenated compounds (for example, *unsym*-octahydrophenanthrene in the hydrocracking of phenanthrene[3]), and so the yield of cycloalkanes can be expected to increase as the size of the original ring structure increases. The ratio of the amounts of cycloalkanes to those of monocyclic aromatics in the hydrocracked products shown in Table 5 is considered to be a measure of the size of the ring structure. If the SRC consists of alkyl-substituted PAH, they are supposed to have larger a ring structure than chrysene, on the average. This finding suggests that the type containing a large ring structure (b) is more important than that containing a direct bond between two aromatic rings (a) in the average structures as determined by the CAMSC method. Table 5 also indicates that the average ring size of Yūbari SRC is larger than that of Tempoku SRC. The values shown in Table 5 are supposed to reflect the difference in the average structures, shown in Figs. 1 and 2, between these two SRC.

Table 6. Composition of monocyclic aromatics (mol %)

	Yūbari SRC[a]	Tempoku SRC[b]
A[c]	14.2	27.0
B[d]	25.0	27.7
C[e]	28.7	26.8
D[f]	20.2	12.3
E[g]	12.0	6.2
R[h]	0.57	0.97

a) Run 8. b) Run 9. c) Benzene. d) Toluene. e) Ethylbenzene and xylenes (C_2 alkylbenzenes). f) C_3 alkylbenzenes. g) Alkylbenzenes containing more than C_4. h) R=benzene/toluene (mol/mol).

Table 7. Composition of gases (mol %)

	Yūbari SRC[a]	Tempoku SRC[b]
C1[c]	40.0	39.1
C2[d]	17.7	17.7
C3[e]	19.3	20.7
C4[f]	22.9	22.5

a) Run 8. b) Run 9. c) Methane. d) Ethane. e) Propane. f) Butanes and butenes.

In the hydrocracking of alkyl-substituted PAH,[10] the behavior of the alkyl group attached to the condensed ring has been found to be different. The methyl group was not completely dealkylated in the initial stage, but remained in the products as monocyclic aromatics; the extent of dealkylation had been found to be dependent upon the type of starting materials. Table 6 suggests that Yūbari SRC possesses many more alkyl groups as substituents than does Tempoku SRC. On the other hand, Table 7 indicates that the extent of dealkylation is similar to that in the case of Tempoku SRC. These results seem to support the idea that the average structures shown in Figs. 1 and 2 reflect quite well the characteristics of the real structures of these two SRC.

References

1) Organic reaction in Fused Salts. Part XV, Part XIV: Y. Nakatsuji, Y. Ikkaku, M. Nomura, and S. Kikkawa, *Bull.*

Chem. Soc. Jpn., **51**, 3631 (1978); a part of this work was presented at the 45th Meeting of the Fuel Society of Japan, Osaka, October 1978.

2) Y. Nakatsuji, S. Fujioka, M. Nomura, and S. Kikkawa, *Bull. Chem. Soc. Jpn.*, **50**, 3406 (1977).

3) Y. Nakatsuji, T. Kubo, M. Nomura, and S. Kikkawa, *Bull. Chem. Soc. Jpn.*, **51**, 618 (1978).

4) M. Oka, H.-C. Chang, and G. R. Gavalas, *Fuel*, **56**, 3 (1977).

5) J. K. Brown and W. R. Ladner, *Fuel*, **39**, 87 (1960).

6) In the isomerization of cyclohexene at 400 °C over the molten salts,[7] the yield of isomerized products was found to be remarkably dependent upon the composition between $ZnCl_2$ and CuCl. The catalytic activity for the isomerization displayed its maximum in a ratio of 2: 1 ($ZnCl_2$: CuCl).

7) Y. Nakatsuji, K. Shigeta, M. Nomura, and S. Kikkawa, unpublished data.

8) M. Morita and K. Hirosawa, *Nippon Kagaku Kaishi*, **1975**, 1555.

9) C. W. Dewalt, Jr., and R. A. Glenn, *Anal. Chem.*, **24**, 1789 (1952). The hydroxyl groups were determined by acetylation using acetic anhydride. The values are shown in the experimental results of Figs. 1 and 2.

10) Y. Nakatsuji, Y. Ikkaku, M. Nomura, and S. Kikkawa, *Bull. Chem. Soc. Jpn.*, **51**, 3631 (1978).

Vapor-phase Hydrolysis of Chlorobenzene Catalyzed by Copper(II) Ion-exchanged Zirconium Phosphate

Yusuke IZUMI*,† and Yukio MIZUTANI

Research and Development Division, Tokuyama Soda Co., Ltd., Mikage-cho 1-1, Tokuyama 745

(Received January 18, 1979)

Copper(II) ion-exchanged zirconium phosphate (ZP–Cu(II)) effectively catalyzed the vapor-phase hydrolysis of chlorobenzene to phenol at 450 °C under atmospheric pressure. Per-pass conversion of chlorobenzene was between 12 and 18% with selectivity for phenol from 90 to 95 mol %. The catalytic activity was influenced by the content of copper, the ratio of phosphate to zirconium, and the pH at which copper(II) ions were introduced into zirconium phosphate. ZP–Cu(II) catalyst was amorphous and it turned inactive by thermal treatment at above 800 °C, resulting in a crystalline substance. The active site of ZP–Cu(II) for this hydrolysis reaction appears to be the phosphate groups of ZP bearing copper(II) ion. The reaction seems to proceed *via* a Rideal mechanism in which an adsorbed chlorobenzene molecule reacts with water in the vapor phase at the catalyst surface. The desorption of hydrogen chloride was rate controlling.

Ion-exchange properties of zirconium phosphate (ZP) as well as its crystallography have been the subject of a great deal of research in the field of inorganic and nuclear chemistry. On the other hand, little interest have been shown in the catalysis of ZP since Austerweil first tried to employ ZP as a catalyst for the Pechmann condensation of malic acid with phenol into cumarins in 1959.[1–6] Recently, acidic characteristics of ZP have been investigated in detail in connection with its catalysis in dehydration of 2-propanol and isomerization of 1-butene.[7,8]

Since amorphous ZP has a large surface area (100—350 m^2/g) and it is also considerably durable against thermal and chemical treatments, ZP would be expected to show unique catalytic performance in several organic reactions when combined with various transition metal ions or metals through ion exchange or subsequent reduction. The authors have previously reported that the acidic amorphous ZP loaded with a small amount of finely dispersed palladium metal is an efficient bifunctional catalyst for the direct synthesis of isobutyl methyl ketone by the liquid-phase reductive aldol condensation of acetone.[9–11] As another attempt of applying ZP to catalyst, we have examined the vapor-phase hydrolysis of chlorobenzene to phenol over the ZP incorporating copper(II) ions through ion exchange (ZP–Cu(II)).

The Raschig process, an existing commercial technology of phenol synthesis, involves oxychlorination of benzene to yield chlorobenzene and subsequent vapor-phase hydrolysis of the chlorobenzene to phenol:

$$C_6H_6 + 1/2O_2 + HCl \longrightarrow C_6H_5Cl + H_2O,$$
$$\Delta H = -43 \text{ kcal/mol at } 500 \text{ K} \quad (1)$$

$$C_6H_5Cl + H_2O \longrightarrow C_6H_5OH + HCl,$$
$$\Delta H = -0.64 \text{ kcal/mol}, \; K_p = 0.877 \text{ at } 700 \text{ K}. \quad (2)$$

Although silica has been found effective for the second step reaction (Eq. 2),[12–14] calcium hydroxyapatite, often promoted by copper(II) ion, is commercially employed at present.[15] But this "calcium phosphate" catalyst (CP) still has drawbacks such as poor thermal durability and loss of copper at high temperatures (375—450 °C). It is, therefore, interesting to examine the applicability of thermally stable ZP catalyst to this hydrolysis reaction.

The present study concerns itself with a general examination of ZP-Cu(II) catalyst in the hydrolysis of chlorobenzene, its nature, and possible reaction mechanism.

Experimental

Catalyst Preparation. ZP–Cu(II) catalyst was directly prepared by reacting phosphate ion with zirconium salt in the presence of copper(II) ion at a pH around 4.0, because ZP was fully ion-exchangeable even in a state of hydrous gel. This method was preferable to obtain such ZP as contained homogeneously distributed metal cations in it. The standard ZP–Cu(II) catalyst was prepared as follows: 0.6 g of copper(II) chloride ($CuCl_2 \cdot 2H_2O$) was added to an aqueous solution of zirconium dichloride oxide ($ZrOCl_2 \cdot 8H_2O$ 24 g/H_2O 100 ml). Separatly, 8.0 g of sodium hydroxide was added to an aqueous phosphoric acid (85 vol% H_3PO_4 14.8 g/H_2O 100 ml). The former solution was added to the latter under vigorous stirring at room temperature. The ratio of phosphate to zirconium (P/Zr) was 2: 1. The mixture was then allowed to stand for 44 h. A light blue gel was precipitated, leaving a colorless liquid, pH of which was 4.08. The hydrous gel was filtered, washed with water, dried at 110 °C, and finally calcined at 400 °C for 3 h to yield 20 g of ZP–Cu(II) catalyst. The copper content was 1.1% by weight.

Calcium hydroxyapatite was prepared by a known procedure.[16] Copper doping of the calcium hydroxyapatite was carried out after Reichle.[15]

Chlorobenzene Hydrolysis. The reaction was carried out using a fixed-bed flow apparatus under atmospheric pressure. A Pyrex tube reactor (20 mmϕ × 400 mm) was placed in a fluidized alumina bath. The catalyst (18—28 mesh) was placed in the middle of the reactor, and the remainder was filled with catalytically inactive porcelain chips. Reaction temperature was measured with a thermocouple inserted in a Pyrex thermowell (7.5 mmϕ) extending longitudinary through the center of the reactor. Both water and chlorobenzene were continuously metered into the reactor by means of microfeeders. The products were withdrawn as oil and aqueous condensates in a receiver held in an ice bath. When the reaction was carried out with a nitrogen flow to dilute the reactants, a trap containing water was connected with the receiver in order to completely recover the produced hydrogen chloride.

† Present address: Department of Synthetic Chemistry, Faculty of Engineering, Nagoya University, Furo-cho, Chikusa-ku, Nagoya 464.

Analytical Methods. The aqueous condensate was separated from the reaction products and extracted with benzene to recover the dissolving phenol. The extract was joined to the oil condensate and the mixture was analyzed by means of gas chromatography using a 3 m Silicone DC-550 column at 80 °C with a flow rate of carrier gas (H_2) 40 ml/min. The hydrogen chloride dissolving in the aqueous condensate was determined by means of alkalimetry. Thus the total per-pass conversion of chlorobenzene (x) was calculated from the amount of hydrogen chloride. The selectivity for phenol was calculated as $100\,m(1-x)/x$ (%), where m denotes the molar ratio of phenol to chlorobenzene in the reaction products that was determined by the above described analysis by gas chromatography.

Copper in catalyst was determined by means of iodometry. A powdered ZP–Cu(II) sample was previously treated with 1 M nitric acid at 80 °C to remove copper(II) ions.

The thermal analysis of catalyst was carried out by use of a differential thermal analyzer. A 20 mg sample was heated in an aerobic atmosphere at the rate of 10 °C/min using α-alumina as a reference.

Results and Discussion

Catalytic Activity. Figure 1 shows the results of the vapor-phase hydrolysis of chlorobenzene over ZP (P/Zr=2.0), standard ZP–Cu(II), CP and CP–Cu(II) (Cu 2.0 wt%). ZP–Cu(II) was very active compared with other catalysts. The rapid decrease in activity with the time on-stream observed for CP and CP–Cu(II) and the slow one for ZP–Cu(II) were both due to the formation of carbonaceous matter on the catalyst surface. The by-product was benzene. Each of the used catalysts nearly recovered its initial activity after it was regenerated with air to burn off the coke at 450 °C for 2 h. CP was considerably active without the aid of copper. But ZP itself was almost inactive,

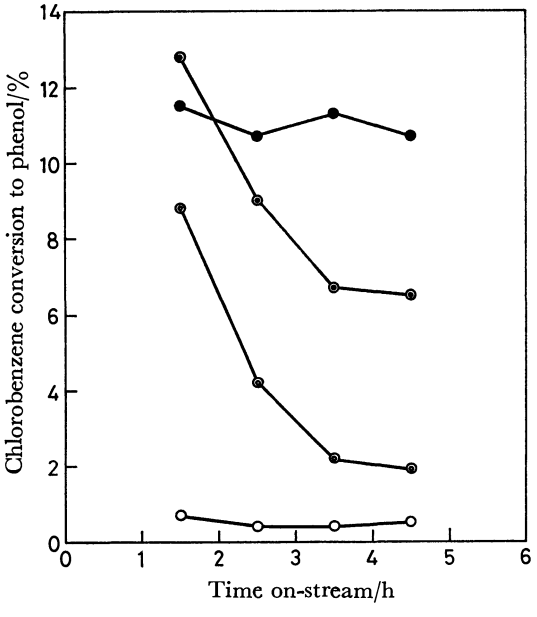

Fig. 1. Vapor-phase hydrolysis of chlorobenzene at 450 °C under atmospheric pressure. H_2O/C_6H_5Cl mole ratio: 3.84, contact time: 1.6 s.
●: ZP–Cu(II), ⊙: CP–Cu(II), ◎: CP, ○: ZP.

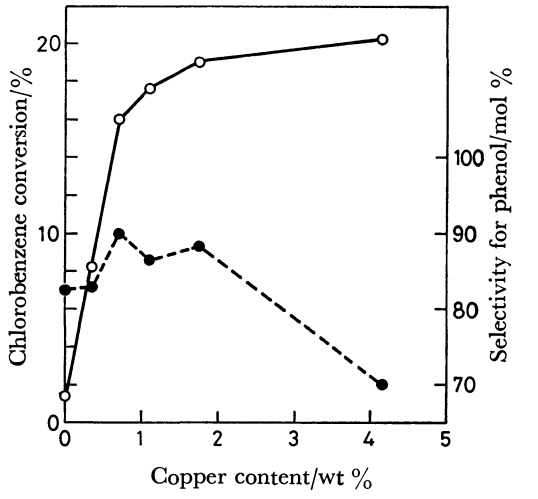

Fig. 2. Effect of copper content of ZP–Cu(II) on initial conversion (○) and selectivity (●). Reaction conditions: 450 °C, 1 atm, H_2O/C_6H_5Cl 3.8, contact time 1.8 s. Data represent the average values during the initial 2.75 on-stream hours.

and copper was essential to the catalysis of ZP for this hydrolysis reaction. These facts suggest that the catalytic performance of ZP is quite different from that of CP. Furthermore, the effect of copper seems to be specific to this reaction because other metal ions incorporated into ZP such as Ag(I), Ni(II), Fe(III), and Co(II) were all inactive except Ca(II) which was slightly effective (conversion=4.0%). The influence of copper content of ZP–Cu(II) (P/Zr=2.0) upon the activity is shown in Fig. 2 in more detail. The chlorobenzene conversion rapidly increased with the copper content until around 2.0% by weight (0.6 meq/g catalyst). On the other hand, the selectivity for phenol gradually decreased with the copper contents as a result of increasing catalytic decomposition of chlorobenzene to benzene. The optimum range of the copper content was between

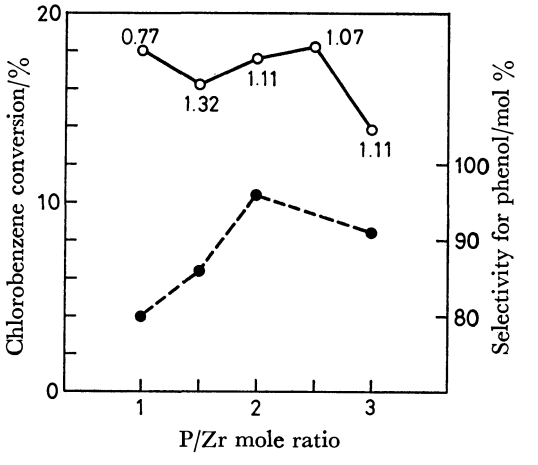

Fig. 3. Effects of P/Zr mole ratio of ZP–Cu(II) on initial conversion (○) and selectivity (●). Reaction conditions: 450 °C, 1 atm, H_2O/C_6H_5Cl 3.8, contact time 1.8 s. Data represent the average values during the initial 2.75 on-stream hours. The figure beside each conversion plot denotes copper content (wt %).

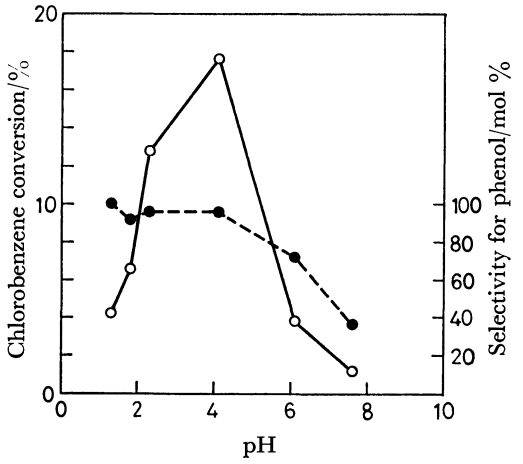

Fig. 4. Effect of pH at catalyst preparation on initial conversion (○) and selectivity (●). Reaction conditions: 450 °C, 1 atm, H_2O/C_6H_5Cl 3.8, contact time 1.8 s. Data represent the average values during the initial 2.75 on-stream hours.

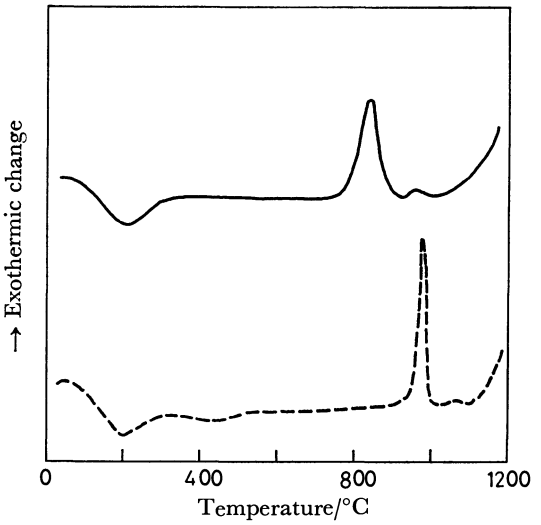

Fig. 5. DTA curves of ZP–Cu(II) (——) and ZP (-----).

1 and 2 wt % at which the maximum space-time yield of phenol was obtained.

Figure 3 shows the effect of the P/Zr molar ratio in ZP–Cu(II) catalyst. The ratio considerably affected the selectivity for phenol, though the conversion of chlorobenzene was almost unaffected except for a P/Zr ratio 3.0. The optimum P/Zr ratio was 2.0.

Characterization of ZP–Cu(II). The catalyst efficiency remarkably changed with the pH at which ZP–Cu(II) hydrous gel was precipitated (Fig. 4). The most active catalyst was obtained at a pH about 4.0 that was most preferable to introducing copper(II) ion into ZP hydrous gel through ion exchange. At a pH below 4.0 ion exchange became incomplete, while at a pH above 5.3 ineffective copper(II) hydroxide was deposited in ZP hydrous gel. Since not only fresh catalyst but also used one contained no chloride ion, ZP–Cu(II) catalyst appears to hold copper not as liberated copper(II) chloride but as copper(II) ion that is bound to its phosphate groups. In fact, it was experimentally found that both copper(II) chloride and copper(II) phosphate themselves were inactive for this reaction. The ion-exchange capacity of ZP (P/Zr=2.0) was measured 0.7 meq/g for copper(II) ion at a pH 4.0. This corresponded to 2.2 wt % as the copper content. Considering that the activity rapidly increased until around this value of copper content (Fig. 2), the active site of ZP–Cu(II) catalyst seems to be represented by the phosphate groups in ZP bearing a copper(II) ion.

Figure 5 illustrates the thermal change of the standard ZP–Cu(II) catalyst in an aerobic atmosphere, together with a thermogram of ZP (P/Zr=2.0). Although the catalyst was an amorphous solid, it was transformed into an unknown crystalline substance when heated at above around 800 °C, turning completely inactive. The ZP containing no copper was found to change into zirconium pyrophosphate (ZrP_2O_7) at above around 1000 °C.

Activity Maintenance. A continuous catalyst testing was performed by using ZP–Cu(II) (P/Zr=2.0, copper content=2.2 wt %). Although the catalyst was regenerated with air at 430 °C for 33 min every 3.5 h, the conversion of chlorobenzene gradually decreased with the time on-stream. This change in activity is mainly due to the loss of copper in catalyst because the surface area of catalyst was almost unchanged except for its rapid decrease observed during the initial 14 h (Table 1). The selectivity for phenol gradually increased due to the decrease in the copper content of catalyst with reaction time. The copper removed from the catalyst was detected as copper(II) chloride on the reactor wall. Probably, the copper(II) ion bonding to the phosphate groups in ZP reacted with hydrogen chloride to change into copper(II) chloride and vaporized out of the catalyst. Since the vapor pressure of copper(II) chloride is as much as 28 mmHg†† at 450 °C, the copper(II) chloride thus liberated on the catalyst surface seems to be liable to vaporize.

Table 1. Changes of surface area and copper content of ZP–Cu(II) with time on-stream of reaction

Time on-stream h	BET surface area m^2/g	Copper content wt %
0	169	2.16
14.3	118	1.06
47.5	114	0.39

In order to maintain the activity for longer duration, another catalyst testing with continual supply of copper was undertaken at 450 °C using a stainless steel reactor (28 mmϕ×400 mm). Preheated gaseous reactants had passed at 400 °C through a reactor zone packed with copper metal chips (15 mm in depth) before they reached the catalyst bed (40 mm in depth). The catalyst was regenerated with air at 450 °C for 33 min every 3.5 h, and at the same time the surface of the copper metal chips above the catalyst bed were also

†† (1 mmHg≈133.3 Pa).

oxidized. Copper(II) oxide thus formed catalyzed the decomposition of chlorobenzene and a small amount of hydrogen chloride was produced. The hydrogen chloride, in turn, reacted with the surface copper(II) oxide to form copper(II) chloride. The catalyst could be, therefore, continually supplied with the vapor of copper(II) chloride from the zone of copper metal chips. By means of such continual supply of copper, the ZP–Cu(II) catalyst maintained both the conversion and the selectivity at their stationary levels for 600 on-stream hours, except for a slight decrease in the conversion observed during the initial 140 h.

Reaction Mechanism. The kinetic data of the hydrolysis of chlorobenzene were obtained using small particles (18—24 mesh) of the standard ZP–Cu(II) catalyst. The linear velocity of the flow of gaseous reactants was kept above 22 cm/s at the reaction temperature. Under these conditions, the reaction rate was released from the influence of both external and internal mass-transport processes. The total pressure of the reactants was varied by the dilution with nitrogen. Figure 6 shows the changes in the initial reaction rate with the water to chlorobenzene molar ratio and with the total pressure of the reactants. The initial rate at each reaction temperature remained nearly unchanged under varied partial pressures of the reactants and different total pressures. At a reaction temperature as high as 400 to 450 °C, it is unlikely that the adsorption constant for chlorobenzene or for water is large enough to cancel the effect of the total pressure of the reactants on the initial rate. It is, therefore, probable that the desorption of one of the products was rate-controlling. Figure 7 gives the change in the initial rate when one of the products was added to the reactants beforehand. The rate again remained approximately constant with all the amount of hydrogen chloride added. On the other hand, the phenol in the feed clearly lowered the rate. Considering that the equilibrium constant for the over-all reaction

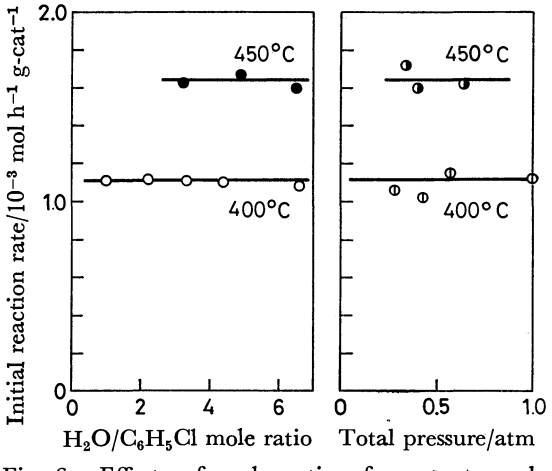

Fig. 6. Effects of mole ratio of reactants and total pressure on initial reaction rate. Data were obtained between initial 1.0 and 2.0 on-stream hours.
○: fresh catalyst, total pressure 1.0 atm; ●: regenerated catalyst, total pressure 0.7 atm; ⦶: fesh catalyst, H_2O/C_6H_5Cl 2.2; ◐: regenerated catalyst, H_2O/C_6H_5Cl 3.2.

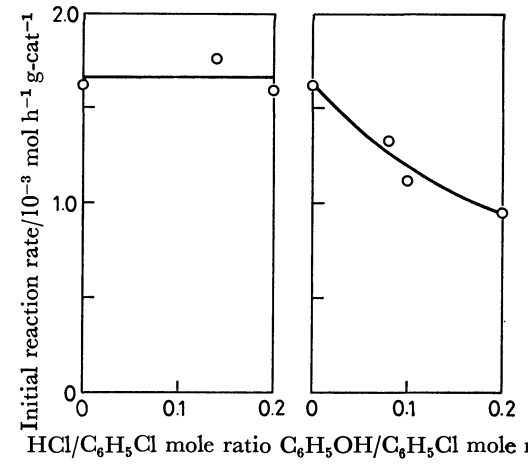

Fig. 7. Effects of hydrogen chloride and phenol on initial reaction rate at 450 °C. Data were obtained between initial 1.0 and 2.0 on-stream hours. Catalyst: regenerated, total pressure: 0.65 atm.

is less than unity at 400 to 450 °C, the above kinetic data are well interpreted by assuming that the desorption of hydrogen chloride is rate-controlling. The apparent activation energy was 8.6 kcal/mol at a reaction temperature between 400 and 450 °C.

Furthermore, in order to presume the reaction mechanism, it was examined at what stage in the reaction path phenol was formed. Water and chlorobenzene were alternately adsorbed on the catalyst surface and each desorbed product was analyzed (Fig. 8). It was found that phenol was formed only when water was supplied to the catalyst on which chlorobenzene had already been adsorbed, but on the other hand no phenol was detected in the reactor effluent when chlorobenzene was fed to the catalyst on which only water had been adsorbed. This experiment suggests that the reaction proceeded *via* a Rideal mechanism in which adsorbed chlorobenzene reacts with water in the vapor phase.

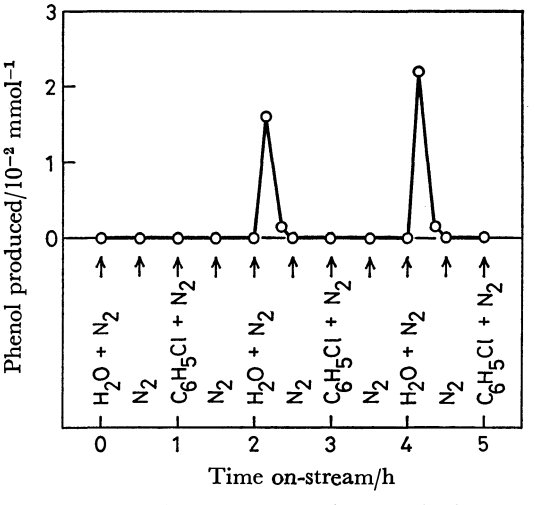

Fig. 8. Phenol formation by alternate feed of water and chlorobenzene at 305 °C.
Catalyst: standard fresh ZP–Cu(II) 2.0 g, H_2O flow rate: 0.0992 mol/h, C_6H_5Cl flow rate: 0.0306 mol/h.

Considering the structure of the active site in ZP–Cu(II) discussed above, the vapor-phase hydrolysis of chlorobenzene over ZP–Cu(II) catalyst appears to proceed as follows:

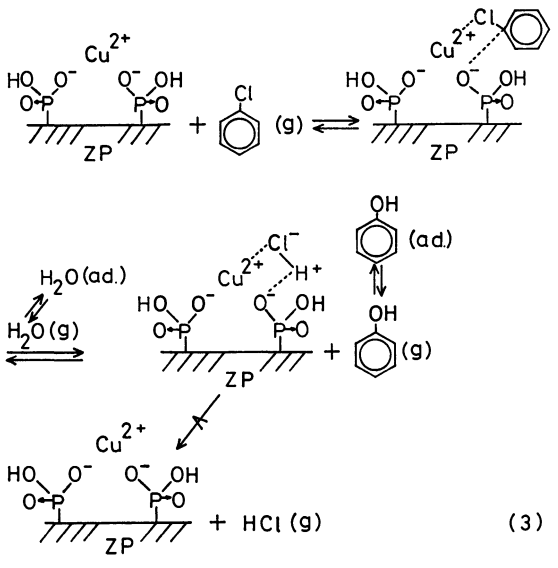

(3)

A chlorobenzene molecule is first adsorbed on the active site and activated by copper(II) ion and phosphate group. The activated molecule is then hydrolyzed with the water in the vapor phase at the catalyst surface, and finally converted into phenol, leaving adsorbed hydrogen chloride behind. The rate-determining step is the desorption of hydrogen chloride.

Reichle[15] has previously investigated the vapor-phase hydrolysis of chlorobenzene over calcium hydroxyapatite promoted by copper(II) ion and proposed a mechanism of nucleophilic displacement of chlorobenzene by the hydroxide ion of the apatite. The copper(II) ion held in the apatite crystal would activate the formation of a Meisenheimer type complex from chlorobenzene and hydroxide ion. Thus the calcium apatite catalyst works as a nucleophile by itself:

$$2C_6H_5Cl + Ca_{10}(OH)_2(PO_4)_6 \longrightarrow 2C_6H_5OH + Ca_{10}Cl_2(PO_4)_6 \quad (4)$$

$$2H_2O + Ca_{10}Cl_2(PO_4)_6 \longrightarrow 2HCl + Ca_{10}(OH)_2(PO_4)_6 \quad (5)$$

On the other hand, ZP–Cu(II) in the present study catalyzes the reaction presumably in this way that both copper(II) ion and the phosphate group concertedly activate or polarize a chlorobenzene molecule and facilitate a nucleophilic attack of water on the chlorobenzene molecule.

The authors wish to thank Mr. Noboru Idemoto of Tokuyama Soda Co., Ltd. for a great deal of experimental help.

References

1) G. V. Austerweil, *C. R. Acad. Sci.*, **248**, 1810 (1959).
2) T. Kagiya, T. Sano, T. Shimizu, and K. Fukui, *Kogyo Kagaku Zasshi*, **66**, 1893 (1963).
3) A. A. Balandin, A. I. Kukina, N. E. Malenberg, and M. M. Ermilova, *Dokl. Akad. Nauk SSSR*, **161**, 851 (1965).
4) N. E. Malenberg, A. I. Kukina, and T. N. Fadeeva, *Vestn. Mosk. Univ., Ser. II Khim.*, **21**, 107 (1966).
5) M. Giorgini, A. Lucchesi, F. Morelli, G. Stoppato, and R. Tartarelli, *Ann. Chim. (Rome)*, **1968**, 58.
6) L. Kh. Freidlin, V. Z. Sharf, E. N. German, N. K. Vorobeva and S. I. Shcherbakova, *Izv. Akad. Nauk SSSR, Ser. Khim.*, **1970**, 2130.
7) F. Nozaki, T. Itoh and S. Ueda, *Nippon Kagaku Zasshi*, **1973**, 674.
8) T. Hattori, A. Ishiguro, and Y. Murakami, *Nippon Kagaku Zasshi*, **1977**, 761.
9) Y. Onoue, Y. Mizutani, S. Akiyama, Y. Izumi, Y. Watanabe, and J. Maekawa, *Bull. Jpn. Petrol. Inst.*, **16**, 55 (1974).
10) Y. Watanabe, Y. Matsumura, Y. Izumi, and Y. Mizutani, *J. Catal.*, **40**, 76 (1975).
11) Y. Onoue, Y. Mizutani, S. Akiyama, Y. Izumi, and Y. Watanabe, *Chem. Technol.*, **7**, 36 (1977).
12) L. Kh. Freidlin, A. A. Balandin, and A. Fridman, *Chem. Abstr.*, **39**, 4792 (1945); **40**, 4576 (1946); **42**, 2241 (1948).
13) N. Ohta and T. Tezuka, *Kogyo Kagaku Zasshi*, **54**, 297, 328, 462, 509 (1951).
14) Y. Chiba, *Yuki Gosei Kagaku*, **11**, 466 (1953); **12**, 26, 139, 371, 408 (1954).
15) W. T. Reichle, *J. Catal.*, **17**, 297 (1970).
16) E. Hayek and H. Newesely, *Inorg. Synth.*, Vol. VII, 63 (1963).

Theoretical Studies of Some Nonbenzenoid Hydrocarbons. V. Benzazulenes and Benzofluoranthenes

Archana Das Gupta, Subrata Chatterjee, and Nanda K. Das Gupta*,**,†

Department of Chemistry, Visva-Bharati University, Santiniketan, West Bengal, India

***Department of Chemistry, University of Alberta, Edmonton, Alta, Canada*

(Received March 11, 1978)

The molecules benzazulenes and benzofluoranthenes have been studied by the semi-empirical method for π-molecular systems, similar to that of Pariser-Parr and Pople. Ground state properties and $\pi^* \leftarrow \pi$ spectra have been predicted and compared with experiment. Agreement between the theoretical values and observed ones is good; that between the experimental value of half-wave reduction potential and values calculated by SCF(d) method is very good.

Dewar and coworkers[1] and Lo and Whitehead[2] predicted the ground state properties of many conjugated systems using the self-consistent field molecular orbital (SCF MO) theory with core resonance integral values determined either by a hypothetical thermocycle[1a,2] or utilising a relation[1a] between overlap integral and resonance integral. By means of their methods not only the ground state properties of some nonbenzenoid hydrocarbons can be predicted but also the $\pi^* \leftarrow \pi$ spectral transitions can be obtained with reasonable accuracy.[3] In most cases this spectra thus predicted are better than those predicted by the 'β-variable' SCF method with core resonance integral proposed by Yamaguchi *et al.*[4a] and modified by Das Gupta and Birss.[4b]

In this paper we would like to report the results of our calculations on some benzazulenes and benzofluoranthenes using the semi-empirical SCF MO method with resonance integral proposed by Chung and Dewar,[1a] Lo and Whitehead,[2] and Dewar and Harget.[1c] The results are compared with those obtained by the 'β-variable' SCF method, the methods being designated as SCF(a), SCF(b), SCF(c), and SCF(d). The molecules (Fig. 1) have also been studied theoretically by others[5] using different sets of parameters. We have studied how the properties of azulene and fluoranthene change with the fusion of benzene nucleus to them.

Method and Parameters

The method used here is the Pariser and Parr[6] and Pople[7] method within the zero-differential approximation.[8] The choice of parameters and mode of evaluation of certain integrals were reported.[3] For molecule **6** experimental structure[9] is available and core resonance integral and the two-center two electron repulsion integrals were evaluated by means of the structure. For other molecules whose experimental structure is not known we have used a planar and regular geometry with each bond length equal to 1.40 Å as far as possible for the evaluation of integrals.

Results and Discussion

Bond Length. For monobenzazulenes the bond lengths calculated by the SCF(d) method is in good agreement with those of Dewar *et al.*[5f]

In the monobenzazulenes and dibenz[*a*,*e*]azulene the predicted bond lengths in the benzene ring have aromatic character, the bond length varying from 1.384

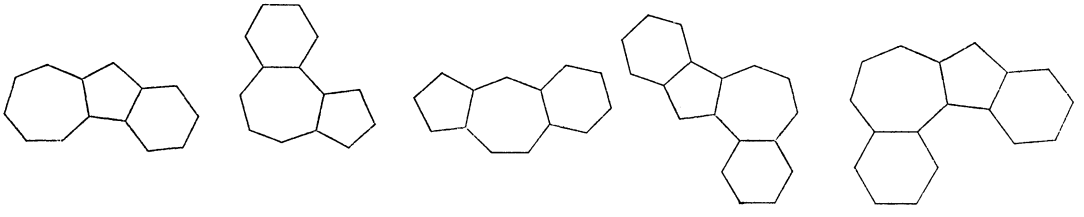

1 Benz[*a*]azulene **2** Benz[*e*]-azulene **3** Benz[*f*]-azulene **4** Dibenz[*a*,*e*]-azulene **5** Dibenz[*a*,*h*]azulene

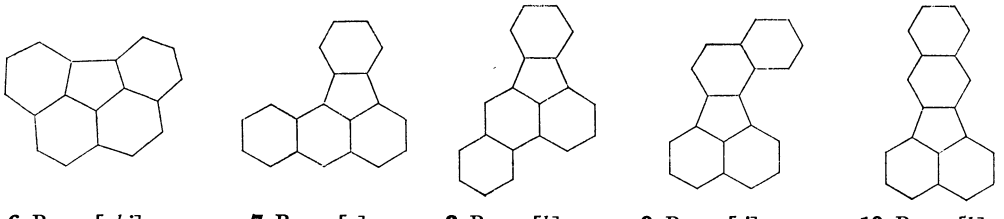

6 Benzo[*ghi*]-fluoranthene **7** Benzo[*a*]-fluoranthene **8** Benzo[*b*]-fluoranthene **9** Benzo[*j*]-fluoranthene **10** Benzo[*k*]-fluoranthene

Fig. 1.

† On leave of absence from Chemistry Department, Visva-Bharati University, Santiniketan, West Bengal, India.

to 1.413 Å. In dibenz[*a*,*h*]azulene, however, the bond lengths of one of the benzene ring maintain the aromatic character whereas the bonds of the other benzene nucleus have marked deviation from aromatic character. In the first case they vary from 1.38 to 1.425 Å and in the second case from 1.36 to 1.45 Å. Thus the two benzene nuclei of the two dibenzazulenes are quite different; in one (Molecule **4**) both the six-membered rings have aromatic nature whereas in the other (Molecule **5**) only the benzene ring attached to the seven-membered ring maintains the character. This is also exhibited in the prediction of resonance energy. Molecule **4** has a higher value of resonance energy.

The peripheral bonds in azulene[3b] lie between 1.394 and 1.408 Å and are predicted to have aromatic character, but the fusion of benzene nucleus to azulene destroys the aromatic nature of the peripheral bonds in the five and seven-membered rings of the benzazulenes, except molecule **5** where the bond lengths predicted by the SCF(a), SCF(b), and SCF(d) methods have aromatic nature. The SCF(c) method gives the results which disagree. In all the molecules the common bond between the five and seven-membered rings has single bond character similar to that of azulene, the value lying between 1.45 and 1.47 Å calculated by these methods compared to 1.46 to 1.47 Å of azulene.[3b]

In the molecules **7**—**10** the fusion of a benzene ring in a fluoranthene moiety alters the predicted bond lengths of the six-membered ring to a considerable extent where the fusion takes place, the other bond lengths remaining almost the same as those of fluoranthene.[3e]

Resonance Stabilization

The heats of atomization (ΔH_a) and π-bond energy ($E_{\pi b}$) for the molecules calculated by the SCF(a), SCF(b), and SCF(c) methods are given in Table 1. The resonance energy (E_R) calculated by the methods of Lo and Whitehead[2], Dewar *et al.*[1] and Hess and Schaad[10] is given in Table 2, together with the resonance energy per C–C bond (E_R/C–C) since it is more useful for predicting the stability or aromaticity of a molecule. In benzazulenes the fusion of a benzene nucleus in azulene increases the E_R/C–C over that of azulene, whereas in benzofluoranthenes E_R/C–C is almost the same as that of fluoranthene. This suggests that all the benzazulenes should be more stable than azulene. It is also clear from the values of resonance energy and E_R/C–C bond that molecule **4**

Table 1. Heat of atomization (eV) and π-bond energy (eV)

Molecule	Heat of atomization				π-Bond energy			
	SCF(a)	SCF(b)	SCF(c)	Other work[a]	SCF(a)	SCF(b)	SCF(c)	Other work
1	122.910	123.041	123.211	123.68[b]	19.920	19.600	19.596	18.24[b]
2	122.955	123.086	123.253	123.70[b]	19.964	19.644	19.628	18.25[b]
3	122.909	123.040	123.218	123.69[b]	19.919	19.598	19.604	18.25[b]
4	156.624	156.798	157.054		26.441	26.023	25.858	
5	156.147	156.321	156.432		25.962	25.546	25.205	
6	153.227	152.002	153.259		27.930	27.525	26.912	
7	171.650	171.850	172.003		30.471	30.001	29.426	
8	171.987	172.185	172.316		30.809	30.336	29.729	
9	171.818	172.016	172.164		30.639	30.168	29.600	
10	171.768	171.967	172.129		30.590	30.119	29.576	

a) Heat of formation. b) Ref. 5f.

Table 2. Resonance energy and resonance energy per C–C bond

Molecule	Resonance energy						Resonance energy per C–C bond				
	(a) (eV)	(b) (eV)	Other work[5f] (eV)	(c) (eV)	(d) (eV)	(e) (β)	(a) (eV)	(b) (eV)	(c) (eV)	(d) (eV)	(e) (β)
1	3.908	4.055	2.32	0.621	1.108	0.411	0.244	0.253	0.039	0.069	0.026
2	3.953	4.099	2.37	0.666	1.151	0.425	0.247	0.256	0.042	0.072	0.027
3	3.907	4.054	2.37	0.620	1.112	0.428	0.244	0.253	0.039	0.069	0.027
4	6.006	5.967		1.335	1.958	0.648	0.286	0.284	0.064	0.093	0.031
5	5.528	5.490		0.858	1.367	0.562	0.263	0.261	0.041	0.065	0.027
6	7.592	7.306		2.465	2.683	0.865	0.345	0.333	0.112	0.122	0.039
7	7.605	7.610		2.123	2.701	0.886	0.317	0.317	0.088	0.113	0.037
8	7.943	7.945		2.461	3.014	0.984	0.331	0.331	0.103	0.126	0.041
9	7.773	7.777		2.291	2.862	0.934	0.324	0.324	0.095	0.119	0.039
10	7.724	7.728		2.242	2.717	0.931	0.322	0.322	0.093	0.113	0.039

a, b, c, d, and e represent SCF(a), SCF(b), SCF(c), Dewar and de Lano[1b] and Hess and Schaad[10] methods, respectively.

Table 3. $\pi^* \leftarrow \pi$ Transitions and oscillator strength†††

Molecule	Experimental††		Sym.	SCF (a)		SCF (b)		SCF (d)		Sym.	CI		Other works					
	eV	log ε		eV	f	eV	f	eV	f		eV	f	eV	f	eV	f	eV	f
1	1.98	2.54		2.12	0.18	2.11	0.19	2.39	0.26		2.17	0.075	1.503[a]	0.029	2.39[b]		1.581[d]	0.030
	3.25	3.64		3.37	0.92	3.36	0.92	3.60	0.92		3.19	0.077	2.905	0.177	3.19		3.020	0.126
	4.25	4.78		4.26	0.44	4.24	0.44	4.44	0.44		4.30	1.05	3.977	1.339	3.99		4.114	1.344
													4.259	0.230	4.38		4.426	0.248
													4.301	0.566			4.457	0.454
	5.21	4.03		5.30	0.22	5.27	0.22	5.40	0.19		5.45	0.121						
2	2.15	2.5		2.10	0.15	2.09	0.15	2.37	0.19		2.18	0.060	1.444[a]	0.028	2.49[b]		1.550[d]	0.022
	3.12	3.51		3.32	0.67	3.30	0.66	3.52	0.65		3.13	0.068	2.82	0.057	3.24		3.016	0.104
				3.75	0.58	3.73	0.58	{3.98	0.59		3.89	0.036						
	4.09	4.46		4.24	0.65	4.22	0.65	{4.36	0.68		4.00	0.495	3.816	1.168	4.09		4.120	1.009
				4.42	0.11	4.40	0.11	4.45	0.16		4.40	0.758	4.197	0.196			4.375	0.080
													4.204	0.085			4.457	0.401
	4.90	4.32		4.67	0.38	4.64	0.38	4.77	0.34		4.86	0.537			4.40			
	5.44	4.23		5.30	0.10	5.27	0.10	5.36	0.08		5.41	0.215						
3	2.05			2.38	0.25	2.37	0.25	2.52	0.23		2.23	0.051	1.706[a]	0.040	2.44[b]			
				3.34	0.67	3.33	0.67				3.18	0.017	2.931	0.048				
	3.57	3.56		3.59	1.01	3.57	1.00	3.65	0.76		3.77	0.070	3.948	0.738	3.21			
	4.30	4.75		4.31	0.35	4.29	0.35	4.42	0.34		4.14	1.585	4.177	0.847	4.04			
	5.08	4.20		5.03	0.27	5.01	0.27	5.20	0.29		4.97	0.103	4.508	0.363	4.463			
4	1.83	2.47											1.747[a]					
				2.45	0.50	2.44	0.49	2.68	0.55		2.46	0.198						
	3.28	3.89		3.38	0.37	3.37	0.36	3.55	0.39		3.24	0.012	2.997					
	3.85	4.89		3.59	0.57	3.58	0.57	3.75	0.58		3.71	0.471	3.763					
											3.99	0.285	4.108					
				4.38	0.77	4.36	0.77	4.41	0.79		4.26	0.81	4.120					
	4.63	4.12		4.57	0.05	4.55	0.05	4.53	0.06		4.69	0.157						
				5.08	0.39	5.06	0.38	5.14	0.35		5.12	0.514						
5				1.69	0.13	1.68	0.13	1.65	0.13		1.36	0.031	0.940[a]	0.030				
	2.11										2.55	0.039	2.593	0.035				
	3.11			{3.09	0.77	{3.07	0.77	{3.05	0.84		3.46	1.338	3.451	1.308				
				{3.21	0.84	{3.20	0.83	{3.21	0.89									
	3.91			{3.99	0.03	{3.97	0.03	{3.82	0.02		3.98	0.140	3.607	0.166				
				{4.13	0.63	{4.11	0.63	{4.16	0.64				3.781	0.321				
	4.86			{4.55	0.41	{4.53	0.41	{4.58	0.40		4.82	0.571						
				{5.15	0.10	{5.12	0.10	{5.06	0.11									

TABLE 3. (Continued)

Molecule	Experimental†† eV	Experimental†† log ε	Sym.	SCF (a) eV	SCF (a) f	SCF (b) eV	SCF (b) f	SCF (d) eV	SCF (d) f	Sym.	CI eV	CI f	Other works eV	Other works f	Other works eV	Other works f	Other works eV	Other works f
6	2.93	2.47								B_2	3.23	0.043	3.283[a]	0.002				
	3.10	2.90	B_2			3.33	0	3.49	0	B_2	3.50	0.132	3.537	0.375				
	3.68	4.23	B_2			3.78	0.96	3.76	1.00	A_1	3.66	0.029	3.763	0.053				
										A_1	3.95	0.014	4.192	0.012				
	4.38	4.58	B_2	4.29	0.85	4.35	0.70	4.35	0.71	B_2	4.29	0.843	4.501	0.906				
7													2.730[a]	0.181				
	2.90	3.92		3.06	0.73	3.05	0.73	3.13	0.73		2.77	0.360	3.070	0.174				
	3.47	3.70		3.25	0.22	3.24	0.22	3.39	0.21		3.35	0.060	3.736	0.086				
	4.15	3.91		4.31	0.74	4.29	0.73	4.25	0.80		4.26	0.074	4.102	0.368				
	4.97	4.86		5.15	0.67	5.12	0.66	5.16	0.69		4.95	0.781	4.409	0.128				
8	3.36	3.86									3.32	0.233	3.346[a]	0.324				
	3.55	4.00		3.59	1.07	3.58	1.06	3.72	1.12		3.42	0.383	3.578	1.129				
													3.612	0.096				
	4.24	4.58		4.57	0.35	4.55	0.35	4.48	0.34		4.13	0.168	4.419	0.175				
	4.97	4.57		4.97	0.58	4.94	0.58	5.01	0.61		4.91	0.707	4.689	0.126				
				5.15	0.65	5.12	0.65	5.13	0.65									
9													2.764[a]	0.097				
	3.27	4.09		3.27	0.43	3.26	0.43	3.34	0.41		3.26	0.370	3.389	0.584				
	3.88	4.14		3.51	0.74	3.49	0.74	3.62	0.78		3.84	0.458	3.959	0.132				
				4.12	0.15	4.11	0.15											
	4.07	4.50		4.40	0.45	4.38	0.45	4.26	0.60		4.25	0.162	4.124	0.446				
	5.41	4.70		5.48	0.23	5.45	0.23	5.41	0.19		5.16	0.950	4.389	0.226				
											5.37	0.211						
10	3.16	4.09	A_1	3.49	0.96	3.48	0.96	3.51	1.01		3.13	0.499	3.237[a]	0.678	3.163[c]	0.134	3.22[e]	>0.5
			B_2								3.48	0.000	3.503	0.002			3.53	<0.1
	3.66		B_2	3.83	0.20	3.82	0.20	3.97	0.20		3.67	0.001	3.927	0.063	3.906	0.057	3.87	<0.1
	4.02	4.76	A_1	4.36	0.95	4.34	0.94	4.43	0.98		3.89	0.713	4.054	0.142	4.235		4.07	>0.5
			B_2	4.07	0.25	4.05	0.25	4.16	0.23		3.93	0.167			3.982		4.03	0.1—0.5
			A_1	4.81	0.03	4.79	0.03	4.69	0.02		4.51	0.227	4.131	0.85			4.65	0.1—0.5
			B_2	5.07	0.16	5.05	0.16	4.75	0.39		4.79	0.006					4.96	<0.1
			A_1	5.24	0.24	5.22	0.24	5.48	0.01		4.95	0.203					5.21	0.1—0.5
	4.93		B_2	4.97	0.39	4.94	0.39	5.07	0.16		5.04	1.062					5.24	>0.5
	5.27	4.79	A_1	5.26	0.45	5.22	0.44	5.07	0.22		5.20	0.423					5.08	>0.5

†† Molecule **1** Refs. 11, 12; **2** Refs. 12, 5a; **3** Refs. 11, 12, 13; **4** Ref. 5b; **5—9** Ref. 11; **10** Refs. 11, 22, 23.
††† Calculated using the relation in Ref. 20. a) Ref. 5b, b) Ref. 5a; c) Ref. 5c; d) Ref. 21; e) Ref. 22.

should be more stable than molecule **5**. All the methods agree that the monobenzazulenes should be equally stable as shown by Dewar and Gleicher.[5f]

Molecules **7**, **8** and **9** or **10** can be treated as either anthracene and benzene, phenanthrene and benzene, and two naphthalene molecules joined by single bonds respectively. The resonance energy for these molecules corresponds almost to the sum of the resonance energies of anthracene and benzene, phenanthrene and benzene, and two naphthalene molecules. The best result is obtained by the method of Dewar and Harget.[1c]

$\pi^*\leftarrow\pi$ Spectra, Ionization Energy and Electron Affinity. The $\pi^*\leftarrow\pi$ spectra calculated by the SCF methods (except the SCF(c)[3] method which is not as good as the other SCF methods in predicting the spectral transitions) with and without configuration interaction (CI) along with the experimental spectra[11-13] are given in Table 3. For the sake of comparison, the results of other workers[5] are given. In the CI procedure the final vectors and integrals obtained by the SCF(d) method were used, all the single excitations being included. For benzazulenes our results are in good agreement with the experimental value, in particular, the results predicted by the CI method which is better than those predicted by Koutecky *et al.*[5b] The same conclusion can be drawn for the benzofluoranthenes (**7**—**10**). However, for molecule **6** the agreement between our results and experimental values is not so good; the results predicted by the CI method are better than the results predicted by other workers.[5b]

Although SCF(a) and SCF(b) methods were parameterized to predict the ground state properties, the spectral transitions predicted by them are in better agreement with the experimental values than the SCF(d) method which was parameterized to predict the $\pi^*\leftarrow\pi$ spectra. The same has been observed.[3]

According to Koopmans' theorem[14] ionization potential (*IP*) is equal to the highest occupied orbital energy. But *IP* predicted in this way is 1 or 2 eV higher than the true ionization potential. Hence a correction should be introduced. The ionization potential can be given by the relation

$$IP = -(\varepsilon_i + c)\ \text{eV}$$

where ε_i is the highest occupied orbital energy and 'c' is the correction term. Bloor[15a] used a value of 1.33 for the correction term 'c' and we have used it in predicting the *IP* by the SCF(a) or SCF(b) method. For the SCF(d) method the value of the correction term is 1.06 as suggested by Kunii and Kuroda.[16] It has been found that a value of 1.88[15b] for 'c' gives very good prediction of *IP* in SCF(c) method. The calculated values of ionization potential are given in Table 4. According to Bloor[15a] the half-wave reduction potential, measured in 95% aqueous dioxane, can be fitted by a relation. If the SCF(d) method is used, the half-wave reduction potential for molecules **7**—**10** are well reproduced by the relation

$$\varepsilon_{1/2} = -(\varepsilon_j + 4.60)\ \text{eV}$$

where ε_j is the lowest unoccupied orbital energy. The predicted values of half-wave reduction potential, $\varepsilon_{1/2}$, using the SCF(d) method along with the experimental values of $\varepsilon_{1/2}$ where available and calculated values of π-dipole moment are also given in Table 4. The experimental value $(1+0.2D)$[19] has been reported only for molecule **10**. For comparison we have included the values of Dewar *et al.*[5f] for monobenzazulenes.

The authors wish to thank Professor F. W. Birss for his comments, helpful discussions and financial support. Computational facilities were provided by the Computing Services, University of Alberta.

References

1) (a) A. L. H. Chung and M. J. S. Dewar, *J. Chem. Phys.*, **42**, 756 (1965); (b) M. J. S. Dewar and C. de Llano, *J. Am. Chem. Soc.*, **91**, 789 (1969); (c) M. J. S. Dewar and A. J. Harget, *Proc. R. Soc. London, Ser. A*, **315**, 443 (1970) and other references therein.

2) D. H. Lo and M. A. Whitehead, *Can. J. Chem.*, **46**, 2027, 2041 (1968).

3) (a) F. W. Birss and N. K. Das Gupta, *Can. J. Chem.*, **49**, 2840 (1971); (b) A. Das Gupta and N. K. Das Gupta, *Can. J. Chem.*, **52**, 155 (1974), **53**, 915 (1975); (c) A. Das

Table 4. Ionization potential (eV), electron affinity (eV) and π-dipole moment (D)

Molecule	Ionization potential			Electron affinity		π-Dipole moment			Other work	
	SCF(a) or SCF(b)[a]	SCF(c)	SCF(d)	$\varepsilon_{1/2}$, Bloor, SCF(d)	$-\varepsilon_{1/2}$, expt.	SCF(a) or SCF(b)[a]	SCF(c)	SCF(d)	Ref. 5f	Ref. 21
1	7.36	7.23	7.23	−1.95		2.4	1.39	2.32	1.86, 1.32	2.24
2	7.77 (7.76)	7.54	7.60	−1.69		2.5 (2.4)	1.46	2.34	1.96, 1.41	2.40
3	7.65	7.46	7.49	−1.78		2.3	1.52	2.52	2.01, 1.41	
4	7.50 (7.49)	7.32	7.39	−1.83		2.0	1.79	1.16		
5	7.01	6.88	6.86	−1.27		3.7	2.37	3.76		
6	8.46 (8.15)	7.73	7.92	−2.08		0	0	0.10		
7	7.64 (7.63)	7.30	7.51	−1.66	1.495[b]	0.9	0.57	0.80		
8	8.11 (8.10)	7.72	7.95	−2.02	1.895[b]	0.6	0.41	0.67		
9	7.92	7.61	7.78	−1.85	1.685[b]	0.9	0.57	0.87		
10	7.74	7.43	7.60	−2.09	1.91[b]	0.5	0.26	0.38		0.522[c]

a) Values in parentheses obtained by the SCF(b) method. b) Ref. 17. The half-wave reduction potential has been lowered by 0.52V (Ref. 18). c) Ref. 5c.

Gupta and N. K. Das Gupta, *J. Mol. Struct.*, **27**, 113 (1975); (d) A. Das Gupta and N. K. Das Gupta, *Can. J. Chem.*, **53**, 3777 (1975); (e) A. Das Gupta and N. K. Das Gupta, *Can. J. Chem.*, **54**, 3227 (1976); (f) A. Das Gupta and N. K. Das Gupta, *Tetrahedron*, **33**, 169 (1977); (g) S. Chatterjee and N. K. Das Gupta, *Bull. Chem. Soc. Jpn.*, **49**, 1839 (1976).

4) (a) H. Yamaguchi, T. Nakajima, and T. L. Kunii, *Theor. Chim. Acta*, **12**, 349 (1968); (b) N. K. Das Gupta and F. W. Birss, *Bull. Chem. Soc. Jpn.*, **51**, 1211 (1978).

5) (a) E. Heilbronner and J. N. Murrell, *Mol. Phys.*, **6**, 1 (1963); (b) J. Koutecky, P. Hochman, and J. Michl, *J. Chem. Phys.*, **40**, 2439 (1964); (c) M. M. Mestechkin, L. S. Gutyrya, and V. N. Poltavets, *Opt. Spectrosc. (USSR)*, **30**, 547 (1971); (d) G. Troger and J. Fabian, *Z. Phys. Chem., Leipzig*, **247**, 139 (1971); (e) J. Michl and F. Muller, *J. Am. Chem. Soc.*, **98**, 4550 (1976); (f) M. J. S. Dewar and G. J. Gleicher, *Tetrahedron Lett.*, **1965**, 4503; (g) R. Zahradnik and J. Michl, *Collect. Czech. Chem. Commun.*, **31**, 3442 (1966); (h) J. Michl and R. Zahradnik, *ibid.*, **31**, 3453 (1966).

6) R. Pariser and R. G. Parr, *J. Chem. Phys.*, **21**, 466 (1953); **21**, 767 (1953).

7) J. A. Pople, *Trans. Faraday Soc.*, **49**, 1375 (1953).

8) R. G. Parr, "Quantum Theory of Molecular Electronic Structure," Benjamin, New York (1963).

9) H. W. Ehrlich and C. A. Beever, *Acta Crystallogr.*, **9**, 602 (1956).

10) B. A. Hess, Jr. and L. J. Schaad, *J. Am. Chem. Soc.*, **93**, 305 (1971); *J. Org. Chem.*, **36**, 3418 (1971).

11) E. Miller Layton, Jr. *J. Mol. Spectrosc.*, **5**, 181 (1960) and other references therein.

12) P. A. Plattner, A. Furst, and W. Keller, *Helv. Chim. Acta*, **32**, 2464 (1949).

13) E. Kloster-Jensen, E. Kovats, A. Eschenmoser, and E. Heilbronner, *Helv. Chim. Acta*, **39**, 1051 (1956).

14) T. Koopmans, *Physica*, **1**, 104 (1934).

15) (a) J. E. Bloor, *Can. J. Chem.*, **43**, 3026 (1965); (b) N. K. Das Gupta and F. W. Birss, unpublished results.

16) T. L. Kunii and H. Kuroda, *Theor. Chim. Acta*, **11**, 97 (1968).

17) I. Bergman, *Trans. Faraday Soc.*, **50**, 629 (1954).

18) G. J. Hoijtnik, *Recl. Trav. Chim. Pays-Bas*, **74**, 1525 (1955).

19) C. Sandorfy, N. Q. Trinh, A. Laforque, and R. Daudel, *J. Chim. Phys.*, **46**, 655 (1949).

20) L. Salem, "The Molecular Orbital Theory of Conjugated Systems," W. A. Benjamin, Inc. New York (1966), p. 358.

21) N. Tyutyulkov and F. Fratev, *Theor. Chim. Acta*, **5**, 376 (1966).

22) J. Michl and J. H. Eggers, *Tetrahedron*, **30**, 813 (1974).

23) K. F. Lang, H. Buffleb, and J. Kalowy, *Chem. Ber.*, **90**, 2888 (1957).

Conductometric Study of Ion-Ion and Ion-Solvent Interactions. I. Conductances of Silver Acetate in 0—50% (w/w) Methanol–Water Mixtures at 35 °C

J. Ananthaswamy, B. Sethuram, and T. Navaneeth Rao*
Department of Chemistry, Osmania University, Hyderabad 500007, India

(Received June 24, 1978)

Conductances of the solutions of silver acetate in 0 to 50% (w/w) methanol–water mixtures were measured at 35 °C. The association constants and molar conductances at infinite dilution were calculated using the Shedlovsky extrapolation technique and the Fuoss-Hsia equation with Fernandez-Prini coefficients. The log K_A *vs.* $1/D$ plot passes through the origin in accordance with the Denison-Ramsey theory of ion-pair formation. The results were interpreted in terms of the equilibrium between the solvent separated ion-pairs (SSIP) and contact ion-pairs (CIP).

Ion-association increases from lithium to cesium in solutions of alkali metal halides, and from cesium to lithium in solutions of alkali metal acetates, hydroxides and fluorides.[1] Ion-pair formation in solutions of alkali metal halides and halides of small metal ions has been extensively investigated[2] conductometrically both in aqueous and aquo-organic solvents. However, such studies on acetates[3] of small metal ions are very few. The electrical conductances of silver acetate were thus measured in order to understand the reverse trend of ion-association in acetates *etc.*, as compared to that in halides. The conductance data was analysed using the Fuoss-Hsia equation[4] with Fernandez-Prini coefficients[5] to evaluate the association parameters. The results were interpreted in terms of the equilibrium between the solvent separated ion-pairs (SSIP) and contact ion-pairs (CIP). The applicability of various theories of ion-pair formation such as those of Bjerrum,[6] Fuoss,[7] Denison-Ramsey[8] (DR), and Ebeling-Kraeft-Yokoyama and Yamatera[9,10] (EKYY) has been discussed.

Experimental

Silver acetate (Fluka: purum) was used after repeated recrystallizations from ethanol and drying. Methanol (BDH, electrolytic grade) was used without further purification. The specific conductance was found to be within $2-5\times10^{-8}$ S cm^{-1}. Water with a specific conductance less than 5×10^{-7} S cm^{-1} was used. Due correction was made for the solvent conductance in the conductance values of all the salt solutions. All solutions were prepared freshly just before use and protected from light by covering with a thick dark cloth. The experimental arrangement was the same as reported earlier.[11] The overall accuracy of the measured molar conductances was better than ±0.05%.

Results and Discussion

The molar conductances of the solutions of silver acetate in water and 10, 20, 30, 40, and 50% (w/w) methanol–water mixtures at 35 °C are given in Table 1. The dielectric constants and viscosities of methanol–water mixtures were taken from literature.[12a,b]

The conductance data were first analysed using the Shedlovsky extrapolation technique,[13]

$$1/\Lambda S(Z) = 1/\Lambda_0 + (K_A/\Lambda_0^2)(c\Lambda y_\pm^2 S(Z)), \quad (1)$$

where Λ and Λ_0 are the molar conductances at concentrations c mol dm^{-3} and zero (infinite dilution), respectively.

$$S(Z) = 1 + Z + Z^2/2 + Z^3/8 + \cdots, \quad (2)$$

$$Z = s(\Lambda c)^{1/2}/\Lambda_0^{3/2}, \quad (3)$$

s is the limiting law slope and K_A is the association constant. The activity coefficient ($y_\pm$) was calculated using the Debye-Hückel limiting law.[14]

$$\log y_\pm = -A(\propto c)^{1/2}, \quad (4)$$

where

$$A = 1.8246\times10^6/(DT)^{3/2}. \quad (5)$$

The degree of dissociation ($\propto$) is related to $S(Z)$ by

$$\propto = \Lambda S(Z)/\Lambda_0. \quad (6)$$

The association parameters obtained by this method are given in Table 2.

The conductance data was then analysed using the Fuoss-Hsia equation[4] with Fernandez-Prini coefficients[5] as in the following.

$$\Lambda = \Lambda_0 - s(\propto c)^{1/2} + E\propto c\ln(\propto c) + J_1(\propto c) - J_2(\propto c)^{3/2} - K_A\Lambda y_\pm^2\propto c \quad (7)$$

where the various symbols have their usual meanings. The activity coefficients ($y_\pm$) were calculated by the equation,

$$-\log y_\pm = A(\propto c)^{1/2}/\{1+Ba(\propto c)^{1/2}\}. \quad (8)$$

Equation 7 was solved as originally described by Justice[15] and subsequently clarified by Pethybridge and Spiers,[16] and Kubota and Yokoi.[17] The procedure envisages the replacement of the distance of closest approach of ions (a) by the Bjerrum critical distance (q). The standard deviation (σ) values were calculated from the relation:

$$\sigma = \{\sum(\Lambda_{exp}-\Lambda_{cal})^2/(N-3)\}^{1/2}. \quad (9)$$

All the calculations were done on TDC-12 computer and the results are given in Table 3.

We see from Table 2 that Λ_0 values obtained by the Shedlovsky method are higher than those obtained by use of the Fuoss-Hsia equation by 0.1—1.4%. The deviations in K_A values are 7.7—16.4% (50% methanol). Thus, the Λ_0 values obtained by the Shedlovsky method deviate to a lesser extent than the corresponding K_A values. Therefore, the Shedlovsky method may be used as a rapid first hand tool for evaluating Λ_0 values, even though the K_A values obtained by this method are not so reliable.

The functional dependence of log K_A on $1/D$ was used to test the applicability of the various theories

Table 1. Molar conductivities of silver acetate in methanol-water mixtures at 35 °C

$10^4\,c$ / mol dm^{-3}	Λ / S cm^2 mol^{-1}	$10^4\,c$ / mol dm^{-3}	Λ / S cm^2 mol^{-3}
50% Methanol		40% Methanol	
D=53.21		D=57.720	
η=0.01129 poise		η=0.01143 poise	
49.708	53.537	49.200	58.197
42.607	55.514	42.172	60.101
37.281	57.301	36.900	61.654
33.139	58.993	32.800	63.003
29.825	59.956	29.500	64.082
27.114	61.007	26.837	65.006
24.854	62.002	24.600	65.901
22.942	62.805	22.708	66.702
21.304	63.588	21.086	67.385
19.883	64.391	19.680	67.977
18.641	64.951	18.450	68.535
30% Methanol		20% Methanol	
D=62.20		D=66.52	
η=0.01119 poise		η=0.01005 poise	
48.230	65.709	48.956	74.754
41.340	66.472	41.654	76.773
36.173	68.963	36.447	78.214
32.153	70.002	32.398	79.425
28.938	71.221	29.158	80.418
26.307	72.143	26.507	81.325
24.115	73.001	24.298	82.101
22.260	73.616	22.429	82.802
20.670	74.302	20.827	83.417
19.292	74.861	19.439	84.001
18.086	75.259	18.224	85.487
10% Methanol		Water	
D=70.68		D=75.03	
η=0.00866 poise		η=0.00725 poise	
48.335	87.302	21.094	114.524
41.430	88.998	18.080	115.532
36.251	90.471	15.820	116.426
32.223	91.532	14.063	117.157
29.001	92.506	12.656	117.783
26.365	93.321	11.506	118.301
24.168	94.077	10.547	118.785
22.309	94.701	9.735 (6)	119.202
20.715	95.325	9.040 (2)	119.629
19.334	95.833	8.437 (5)	119.938
18.126	96.316		

of ion-pair formation. A linear plot passing through the origin is expected according to the Denison-Ramsey (DR) theory whereas Bjerrum and EKYY theories predict curves which are concave downwards. The Fuoss theory predicts a straight line with a finite intercept. The least square regression line required by the experimental points has a correlation coefficient of 0.997 with slope and intercept values of 120.4 and −0.0453 respectively (Fig. 1). When we neglect the small intercept (−0.0453), the plot of $\log K_A$ *vs.* $1/D$ becomes a straight line passing through the origin. The following simple expression of DR theory closely

Table 2. Λ_0 and K_A values calculated according to the Shedlovsky method and their deviations from the corresponding values obtained by use of the Fuoss-Hsia equation

Solvent	Λ_0 / S cm^2 mol^{-1}	Deviation in Λ_0/%	K_A / dm^3 mol^{-1}	Deviation in K_A/%
50% MeOH	80.888	1.36	132.0	16.4
40% MeOH	81.453	0.963	93.36	14.8
30% MeOH	86.438	0.704	68.71	13.6
20% MeOH	95.667	0.595	57.05	12.8
10% MeOH	105.84	0.377	37.93	11.8
Water	125.81	0.111	31.89	7.70

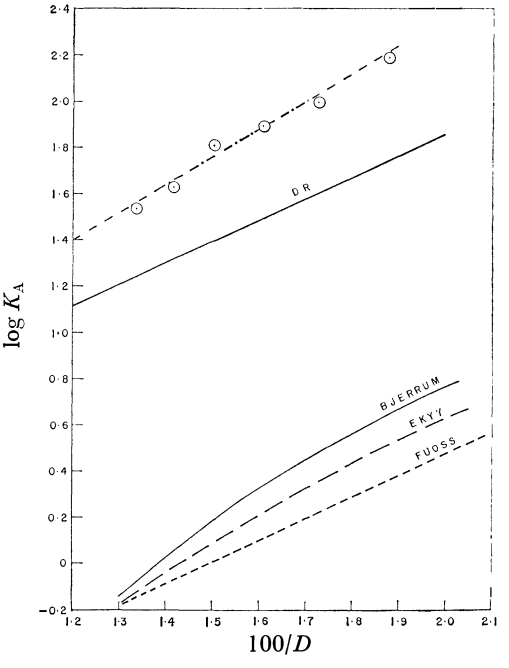

Fig. 1. $\log K_A$ *vs.* $100/D$.

reproduces the association constant data for silver acetate in 0—50% (w/w) methanol–water mixtures at 35 °C.

$$\log K_A = 120.4/D \tag{10}$$

or

$$K_A = \exp(277/D). \tag{11}$$

By comparing Eq. 10 with DR theory expression, we have

$$\log K_A = |Z_+Z_-|e^2/aDkT. \tag{12}$$

The distance of the closest approach of ions was found to be 2.02 Å. The ion-size parameters (a_K) required by various theories to give the experimental K_A values were also calculated. While the Fuoss, Bjerrum and EKYY theories require the a values to lie in the range 0.6—0.8 Å, the DR theory requires thom to be 2.01± 0.03 Å. Since the ionic radii of Ag^+ itself is 1.26 Å, an a value of 0.8 Å for silver acetate is incompatible. The DR theory is in better agreement with experimental results.

The ion-size parameter of the silver acetate was calculated[18] to be 2.53 Å from the known crystallographic data. The theoretical association constant

Table 3. Association parameters of silver acetate obtained by use of the Fuoss-Hsia equation

Solvent	q/Å	Λ_0 / S cm^2 mol^{-1}	K_A / dm^3 mol^{-1}	σ	$\Lambda_0\eta$
50% Methanol	5.095	82.006	157.9	0.121	0.9267
40% Methanol	4.697	82.245	109.6	0.072	0.9376
30% Methanol	4.358	87.051	79.49	0.097	0.9750
20% Methanol	4.075	96.240	65.40	0.382	0.9672
10% Methanol	3.835	106.24	43.01	0.054	0.9200
Water	3.613	125.95	34.55	0.091	0.9131

values for silver acetate according to Bjerrum, Fuoss, Denison-Ramsey (K_{DR}) and EKYY theories were calculated for various dielectric constants using the crystallographic ion-size parameter value, *i.e.* 2.53 Å. The plots of the logarithms of these theoretical association constants against $1/D$ are also shown in Fig. 1. It is evident that all the theories predict lower association constants than those obtained experimentally. However, K_{DR} values are comparatively nearer to the experimental values. The experimental results are in better agreement with the DR theory than the other theories. The same was concluded above from the nature of log K *vs.* $1/D$ plots. The experimental values are higher than the theoretical values, *i.e.* K_{DR}. This could be explained[19] by assuming the existence of two types of ion-pairs *i.e.* solvent separated ion-pairs (SSIP) and contact ion-pairs (CIP) in equilibrium. This involves a two step process:

$$M^+(S)_m + A^-(S)_n \underset{}{\overset{K_1}{\rightleftharpoons}} \underset{\text{(SSIP)}}{M^+SA^-(S)_{m+n-1}}$$

$$\Big\| K_2$$

$$\underset{\text{(CIP)}}{M^+A^-(S)_{m+n-1}} + S,$$

where S denotes a solvent molecule and m and n are the solvation numbers of ions. The overall association constant K_t for this process could be related to K_1 and K_2 by

$$K_t = K_1(1+K_2/[S]). \quad (13)$$

The values of K_2 were calculated by substituting the association constant values calculated using the DR theory with an a value of 2.53 Å for K_1 and experimentally obtained K_A values for K_t in Eq. 13. The results are given in Table 4. In Eq. 13, S was taken as the concentration of water in methanol–water mixtures since the medium activity coefficient data[20] shows that both Ag^+ and CH_3COO^- are preferentially hydrated in methanol–water mixtures.

The association constants of silver acetate increased from 34.55 in water (D=75.03) to 157.9 dm^3 mol^{-1} in 50% methanol (D=53.21). The values are unusually high as compared to those of alkali metal halides in these solvent systems. In a recent study[16] the K_A values of alkali metal fluorides in water at 25 °C were found to be 0.07 (CsF), 0.16 (RbF), 0.14 (KF), 0.47 (NaF) and 1.78 (LiF). In aqueous solutions[21] potassium, rubidium and cesium hydroxides are completely dissociated whereas lithium hydroxide (K_A= 0.81 dm^3 mol^{-1}) shows clear evidence of association.

Table 4. Equilibrium constants for the conversion of SSIP into CIP

Solvent	$K_1=K_{DR}$ / dm^3 mol^{-1}	$K_2=[S](K_t/K_1-1)$ / dm^3 mol^{-1}
50% Methanol	56.12	50.38
40% Methanol	40.97	55.87
30% Methanol	31.36	59.69
20% Methanol	25.06	71.54
10% Methanol	20.74	53.69
Water	17.40	54.76

An unusually high association constant of 200 dm^3 mol^{-1} was reported[22] for silver hydroxide. Similarly silver nitrate was found to be more associated than alkali metal nitrates in both methanol and ethanol.[23] This shows that ion-pair formation is higher in silver salts than in the corresponding alkali metal salts.

References

1) H. S. Harned and B. B. Owen, "The Physical Chemistry of Electrolyte Solutions," Reinhold, N. Y. (1950), pp. 369, 562, 563.

2) L. G. Sillén and A. E. Martell, "Stability Constants of Metal-Ion Complexes, Supplement No. 1," The Chemical Society, London (1971, Special Publication No. 25). See also Special Publication No. 17.

3) F. H. MacDougall and L. E. Topol, *J. Phys. Chem.*, **56**, 1090 (1952).

4) R. M. Fuoss and K. L. Hsia, *Proc. Natl. Acad. Sci. U.S.A.*, **57**, 1550 (1967); **58**, 1818 (1967).

5) R. Fernandez-Prini, *Trans. Faraday Soc.*, **65**, 3311 (1969).

6) N. Bjerrum, *Danske Vidensk. Selsk.*, **7**, 1 (1926).

7) R. M. Fuoss, *J. Am. Chem. Soc.*, **77**, 2615 (1958).

8) J. T. Denison and J. B. Ramsey, *J. Am. Chem. Soc.*, **77**, 2615 (1955).

9) H. Falkenhagen, W. Ebeling, and W. D. Kraeft, "Ionic Interactions," ed by S. Petrucci, Academic Press, N. Y. (1971), Vol. 1 p. 104.

10) H. Yokoyama and H. Yamatera, *Bull. Chem. Soc. Jpn.*, **48**, 1770 (1975).

11) J. Ananthaswamy, B. Sethuram, and T. Navaneeth Rao, *Indian J. Chem.*, **15A**, 9 (1977).

12) a) R. Parsons, "Handbook of Electrochemical Constants" Butterworths, London (1959), p. 11; b) E. W. Washburn, "International Critical Tables, Vol. V," McGraw Hill (1929), p. 22.

13) T. Shedlovsky, *J. Franklin Inst.*, **225**, 739 (1938).

14) R. A. Robinson and R. H. Stokes, "Electrolyte Solutions" 2nd ed, Butterworths, London (1965), p. 230.

15) J. C. Justice, *J. Chim. Pyhs.*, **65**, 353 (1968); *Electrochim.*

Acta, **16**, 701 (1971).
16) A. D. Pethybridge and D. J. Spiers, *J. Chem. Soc., Faraday Trans. 1*, **1976**, 64, 73; **1977**, 768.
17) E. Kubota and M. Yokoi, *Bull. Chem. Soc. Jpn.*, **49**, 2674 (1976); **50**, 1425 (1977).
18) J. Ananthaswamy, Thesis (Osmania University, India), 1978.
19) M. A. Matesich, J. A. Nadas, and D. F. Evans, *J. Phys. Chem.*, **74**, 4568 (1970).
20) J. E. Gordon, "Organic Chemistry of Electrolyte Solutions," John Wiley & Sons (1975), p. 226.
21) F. G. R. Gimblett and C. B. Monk, *Trans. Faraday Soc.*, **50**, 965 (1954); R. P. Bell and J. E. Prue, *J. Chem. Soc.*, **1949**, 362; L. S. Darken and H. F. Meier, *J. Am. Chem. Soc.*, **64**, 612 (1942).
22) J. Bjerrum, *Chem. Rev.*, **46**, 381 (1950); H. L. Johnston, F. Cuta, and A. B. Garrett, *J. Am. Chem. Soc.*, **55**, 2311 (1933).
23) R. L. Kay, *J. Am. Chem. Soc.*, **82**, 2099 (1960); R. E. Busby and V. S. Griffiths, *J. Chem. Soc.*, **1963** 902; V. S. Griffiths, K. S. Lawrence, and M. L. Pearce, *J. Chem. Soc.*, **1958**, 3998; G. D. Parfitt and A. L. Smith, *Trans. Faraday Soc.*, **59**, 257 (1963).

Thermochemistry of Copper(II) β-Diketonates. II.† Bis(benzoylacetonato)copper(II)

Manuel A. V. Ribeiro da Silva* and Ana Maria M. V. Reis

Chemistry Department, Faculty of Sciences, University of Oporto, P-4000 Porto, Portugal

(Received July 22, 1978)

The standard enthalpy of formation of crystalline bis(benzoylacetonato)copper(II) has been determined at 298.15 K by solution calorimetry: $\Delta H_f^\circ[Cu(bzac)_2]$ (c) $= -143.6 \pm 2.2$ kcal mol^{-1}. Enthalpy changes at 298.15 K for the following hypothetical gaseous reactions have been subsequently derived:

$$Cu(g) + 2bzac\cdot(g) = [Cu(bzac)_2](g) \qquad \Delta H = -165.9 \pm 14.3 \text{ kcal mol}^{-1}$$

$$Cu^{2+}(g) + 2bzac^-(g) = [Cu(bzac)_2](g) \qquad \Delta H = -747.3 \pm 14.4 \text{ kcal mol}^{-1}$$

The corresponding homolytic($\overline{E}$) and heterolytic($\overline{E}'$) copper(II)-oxygen mean bond energy parameters were calculated as

$$\overline{E}_{Cu-O} = 41 \pm 3 \text{ kcal mol}^{-1} \quad \text{and} \quad \overline{E}'_{Cu-O} = 187 \pm 3 \text{ kcal mol}^{-1}$$

respectively.

In a previous paper,[1] the standard enthalpy of formation of bis(tropolonato)copper(II) and the Cu(II)–O homolytic and heterolytic bond energies were presented. As it was pointed out in the discussion, the lack of knowledge of similar parameters for the Cu(II)–O bonds of other compounds, made it very difficult to discuss the calculated values of the Cu(II)–O bonds.

To close the gap we examine here the corresponding benzoylacetonate†† complex in order to compare the ligand structural effects in the copper–oxygen bond. The crystal structure of bis(benzoylacetonato)copper-(II) has been determined[2] and shows that the crystals are formed from separate components and that in each molecule the four oxygen atoms lie in the same plane as the copper atoms.

Experimental

The Solution Calorimeter. The LKB 8700 Reaction and Solution Precision Calorimeter was used for all solution reactions. The operation and calculation methods have been described before.[1]

Thermochemical functions are expressed in terms of the thermochemical calorie (defined as 4.184 J exactly) and refer to the isothermal process at 298.15 K and the true mass, calculated using the atomic weights of 1966 based on the isotope ^{12}C. A check on the accuracy of the calorimeter was carried out by determining the enthalpy of solution of *N,N′,N″*-tris(hydroxymethyl)methanetriamine, (tham) in excess 0.1 M hydrochloric acid. The result, -7110.2 ± 0.7 cal mol^{-1} is in excellent agreement with previous results[3] (-7115.4 ± 0.6 cal mol^{-1}).

The uncertainty range is twice the standard deviation of the mean (five determinations were made for each compound).

Materials. Benzoylacetone (Hbzac): 'AnalaR' Koch-Light benzoylacetone was recrystallized from ethanol-water and dried over silica gel; mp = 55 °C (lit, 56 °C[4]).

Found: C, 73.87; H, 6.26%. Calcd for $C_{10}H_{10}O_2$: C, 74.06; H, 6.22%.

Bis(benzoylacetonato)copper(II): $[Cu(bzac)_2]$ was prepared by a modification of the method of Hammond *et al*:[5] a solution of 'AnalaR' copper(II) sulfate (2.5 g) in water (100 cm^3) was buffered with sodium acetate (7.5 g) and then mixed with a solution of benzoylacetone (5 g) in ethanol (80 cm^3). The precipitated complex was washed on the filter with water and cold ether, filtered off, dried in the air, recrystallised from chloroform and stored in a desiccator over silica gel; mp = 189—190 °C.

Found: C, 62.00; H, 4.68; Cu, 16.41%. Calcd for $C_{20}H_{18}O_4Cu$: C, 62.25; H, 4.70; Cu, 16.46%.

Copper(II) Sulfate Pentahydrate: 'AnalaR' grade copper(II) sulfate pentahydrate was powdered and dried in a desiccator over silica gel for 48 h. Its composition was determined by means of a electrogravimetric copper analyses and found to be $CuSO_4 \cdot 5.00\, H_2O$. Periodical analyses showed no change in composition.

Sulfuric Acid: A molar solution of 'AnalaR' grade sulfuric acid was made up, by using a BDH concentrated volumetric solution; the concentration was checked by acid-base titration against $Na_2B_4O_7 \cdot 10H_2O$ and found to be (series of six titrations) 1.0000 ± 0.0004 M which corresponds[4] to the composition $H_2SO_4 \cdot 53.539(1)\ H_2O$.

1,4-Dioxane: 'AnalaR' dioxane was purified according to Refs. 6 and 7.

Constant Boiling Hydrochloric Acid, was prepared from 'AnalaR' HCl by dilution with distilled water. The concentration of the HCl solution was determined by titration against $Na_2B_4O_7 \cdot 10H_2O$. A series of six different determinations gave the result of 4.2172 ± 0.0004 M *i.e.* $HCl \cdot 11.911\ H_2O$.[4]

Analyses: All carbon and hydrogen analyses were carried out in the Microanalytical Service of the University of Surrey; copper in the complex was analysed by atomic absorption spectroscopy.

Method for Solution Calorimetry: Preliminary tests of solubility showed that although some species would dissolve very slowly in dilute acid solutions, satisfactory results were obtained using a solution of dioxane (75%) and 4.2 M HCl (25%) as calorimetric solvent, and dissolving stoichiometric quantities of the reactants and products in this mixed solvent.

Calculation: The standard enthalpy of formation of the bis(benzoylacetonato)copper(II) complex can be determined from reaction between the benzoylacetone and the copper(II) sulfate pentahydrate to give a solution of the copper(II) complex and sulfuric acid:

$$2Hbzac(c) + CuSO_4 \cdot 5H_2O(c) \xrightarrow{\Delta H_R} [Cu(bzac)_2](c) + H_2SO_4 \cdot 5H_2O(aq). \qquad (1)$$

The difference between the enthalpies of solution of the products and reactants in the same stoichiometric ratio gives the required enthalpy of formation, provided equilibrium is

† Part I is Ref. 1.

†† Benzoylacetone(Hbzac) = 1-phenyl-1,3-butanedione.

reached from either side within the period of the experiment.

To the calorimetric solvent (100.0 cm^3) ampoules with the appropriate amounts of water, benzoylacetone and $CuSO_4 \cdot 5H_2O$ were added consecutively and ΔH_1, ΔH_2, and ΔH_3 were measured. To a second portion of the same solvent (100.0 cm^3) were added consecutively ampoules of $H_2SO_4 \cdot 53.54\ H_2O$ and bis(benzoylacetonato)copper(II) and ΔH_4 and ΔH_5 were measured. The general procedure together with the general thermochemical cycle, is given in the Scheme. The quantities of reactants in a series of experiments were determined by the amount of bis(benzoylacetonato)copper(II) in a particular ampoule (about 2.5×10^{-4} mol); exact control of stoicheiometry was maintained throughout each series. When this procedure is used the value calculated for ΔH_R refers to the reaction indicated in the first line of the Scheme, provided that solutions (A_3) and (B_2) are identical and that the value of ΔH_6 is zero. As a check of the validity of this, ampoules of solutions (B_2) were broken into solution (A_3) in the calorimeter; no detectable heat exchange occurred.

Results and Discussion

The experimental data are presented in Table 1, leading to the value $\Delta H_R = +10.13 \pm 0.31$ kcal mol^{-1}.

The following values were taken from the literature:

$\Delta H_f^\circ[CuSO_4 . 5H_2O(c)] = -544.85$ kcal mol^{-1},[8]

$\Delta H_f^\circ[Hbzac(c)] = -81.2 \pm 1.1$ kcal mol^{-1},[9]

$\Delta H_f^\circ[H_2SO_4 \cdot 53.54H_2O(aq)] = -3869.5509$ kcal mol^{-1},[10]

$\Delta H_f^\circ[H_2O(l)] = -68.315$ kcal mol^{-1},[10]

and, according to the first line of the Scheme, the standard enthalpy of formation of crystalline bis(benzoylacetonato)copper(II) at 25 °C was calculated to be $\Delta H_f^\circ[Cu(bzac)_2](c) = -143.6 \pm 2.2$ kcal mol^{-1}.

Although the enthalpy of sublimation of the bis(benzoylacetonato)copper(II) has not yet been experimentally and accurately measured, the consideration of the existing data on similar compounds (other metal β-diketonates[11,12]) makes possible a reasonable estimate[1]; however, the uncertainty must be large, but if we take the upper value of ±10 kcal mol^{-1}, this only produces an uncertainty of *ca.* 2.5 kcal in the bond energy. Accordingly, if we assume $\Delta H_{sub}^\circ[Cu(bzac)_2](c) = 32.0 \pm 10.0$ kcal mol^{-1}, the standard enthalpy of formation of the gaseous complex is $\Delta H_f^\circ[Cu(bzac)_2](g) = -111.6 \pm 10.2$ kcal mol^{-1}.

As discussed previously,[11,12] the metal–oxygen bond strength can be equated to be the energy needed to break the molecule into the metal and ligand radicals, all referred to the gaseous state (Eq. 2), in order to remove the condensed state effects.

$$[Cu(bzac)_2](g) \xrightarrow{\Delta H_f(r)} Cu(g) + 2bzac\cdot(g) \qquad (2)$$

Since the oxygens in β-diketonates are known to be equivalent,[13] which is again supported by the crystal structure of this particular complex[2], the mean copper(II)–oxygen homolytic bond energy $\overline{E}$(Cu–O), is $\Delta H_f^\circ(r)/4$.

The value of the standard enthalpy of formation of the benzoylacetone radical itself can be calculated from the knowledge of the dissociation energy of the enolic hydrogen of benzoylacetone, that is the enthalpy of reaction of process(3)

$$Hbzac(g) \longrightarrow H\cdot(g) + bzac\cdot(g) \qquad (3)$$

According to previous work[1,11,14,15] we take 100±5 kcal mol^{-1} for the enolic hydrogen dissociation energy of gaseous Hbzac. Hence, from ΔH_{sub}°(Hbzac) =

Table 1. Calorimetric study of $[Cu(bzac)_2]$

(a) Addition of H_2O to solvent (dioxane–HCl)

H_2O 10^2 amount/mol	$10^3(\Delta R/R_m)$	ε	ΔH_1/kcal mol^{-1}
1.2446	1.8124	1566.2	−0.228
1.2416	1.7986	1569.0	−0.227
1.2463	1.6979	1565.6	−0.213
1.2111	1.7363	1562.4	−0.224
1.2102	1.7262	1570.4	−0.224

Mean: $\Delta H_1 = -0.223 \pm 0.006$ kcal mol^{-1}

(b) Addition of Hbzac to solution A_1

Hbzac 10^4 amount/mol	$10^3(\Delta R/R_m)$	ε	ΔH_2/kcal mol^{-1}
5.0046	2.0179	1567.7	+6.321
5.0583	2.0686	1575.2	+6.442
5.0348	2.0417	1576.6	+6.393
4.9824	2.0318	1564.6	+6.380
4.9676	2.0275	1568.2	+6.400

Mean: $\Delta H_2 = +6.39 \pm 0.04$ kcal mol^{-1}

(c) Addition of $CuSO_4 \cdot 5H_2O$ to solution A_2

$CuSO_4 \cdot 5H_2O$ 10^4 amount/mol	$10^4(\Delta R/R_m)$	ε	ΔH_3/kcal mol^{-1}
2.4860	9.9760	1562.4	+6.270
2.5276	9.9381	1558.7	+6.129
2.5152	9.8559	1577.7	+6.182
2.4824	9.6201	1575.7	+6.106
2.5124	9.6803	1606.5	+6.190

Mean: $\Delta H_3 = +6.18 \pm 0.06$ kcal mol^{-1}

(d) Addition of $H_2SO_4 \cdot 53.54H_2O$ to solvent (dioxane–HCl)

$H_2SO_4 \cdot 53.54H_2O$ 10^4 amount/mol	$10^3(\Delta R/R_m)$	ε	ΔH_4/kcal mol^{-1}
2.5172	2.0177	1574.2	−12.618
2.6236	2.1124	1574.4	−12.676
2.5076	2.0235	1575.2	−12.711
2.5078	2.0625	1557.1	−12.806
2.5223	2.0371	1573.5	−12.708

Mean: $\Delta H_4 = -12.70 \pm 0.06$ kcal mol^{-1}

(e) Addition of $[Cu(bzac)_2]$ to solution B_1

$[Cu(bzac)_2]$ 10^4 amount/mol	$10^3(\Delta R/R_m)$	ε	ΔH_5/kcal mol^{-1}
2.4739	1.6856	1576.8	+10.744
2.4104	1.6284	1572.3	+10.622
2.5369	1.7427	1566.8	+10.763
2.5188	1.7096	1569.0	+10.649
2.5146	1.7138	1580.5	+10.772

Mean: $\Delta H_5 = +10.71 \pm 0.06$ kcal mol^{-1}

$$CuSO_4\cdot 5H_2O(c) + 2Hbzac(c) + 48.54H_2O(l) \xrightarrow{\Delta H_R} H_2SO_4\cdot 53.54H_2O(l) + [Cu(bzac)_2](c)$$

$\downarrow \Delta H_3$ $\downarrow \Delta H_2$ $\downarrow \Delta H_1$ $\downarrow \Delta H_4$ $\downarrow \Delta H_5$

Solvent (75% Dioxane+25% HCl, 4.2 M) Solvent (75% Dioxane+25% HCl, 4.2 M)

$$\text{Solution } A_3 \xrightarrow{\Delta H_6=0} \text{Solution } B_2$$

$$\text{Solvent} + H_2O \xrightarrow{\Delta H_1} \text{Solution } A_1$$

$$\text{Solution } A_1 + \text{Hbzac} \xrightarrow{\Delta H_2} \text{Solution } A_2$$

$$\text{Solution } A_2 + CuSO_4\cdot 5H_2O \xrightarrow{\Delta H_3} \text{Solution } A_3$$

$$\text{Solvent} + H_2SO_4\cdot 53.54H_2O \xrightarrow{\Delta H_4} \text{Solution } B_1$$

$$\text{Solution } B_1 + [Cu(bzac)_2] \xrightarrow{\Delta H_5} \text{Solution } B_2$$

$$\Delta H_R = 48.54\Delta H_1 + 2\Delta H_2 + \Delta H_3 - \Delta H_4 - \Delta H_5 + \Delta H_6$$

Scheme 1.

Table 2. (all values in kcal mol^{-1})

Complex	ΔH_f°(c)	ΔH_r(r)	$\overline{E}$(Cu–O)	$\Delta H_f'$(i)	$\overline{E}'$(Cu–O)
$[Cu(trop)_2]$[24]	−99.13±0.42	−146.9±14.1	37±3	−728.0±11.4	182±3
$[Cu(bzac)_2]$	−143.6 ±2.2	−165.9±14.3	41±3	−747.3±14.4	187±3

20.02±0.10[16] kcal mol^{-1} one calculates ΔH_f°(Hbzac, g) = −61.2±1.1 kcal mol^{-1} and from the above values and ΔH_f°(H·,g) = 52.095 kcal mol^{-1},[10] the standard enthalpy of formation of the gaseous benzoylacetone radical, is derived as ΔH_f°(bzac·,g) = −13.3±5.1 kcal mol^{-1}.

As ΔH_f°(Cu,g) = 80.86 kcal mol^{-1},[8] the calculated value for the hypothetical gaseous reaction 2 is ΔH_r(r) = 165.9±14.3 kcal mol^{-1} and hence, the mean copper(II)–oxygen homolytic bond energy, $\overline{E}$(Cu–O) = 41±3 kcal mol^{-1} was calculated.

The bond energy in terms of the ions in defined by Eq. 4.

$$Cu^{2+}(g) + 2bzac^-(g) \xrightarrow{\Delta H_f(i)} [Cu(bzac)_2](g) \qquad (4)$$

Estimating the electron affinity of the β-diketonates[1] to be approximately equal to that of the oxygen atom for one electron (E_L = 1.465 eV = 33.8 kcal mol^{-1}),[17] the enthalpy of formation of the gaseous anion benzoylacetone is calculated as ΔH_f(bzac$^-$)(g) = −47.1± 5.1 kcal mol^{-1}, and using the literature value ΔH_f° (Cu^{2+})(g) = 729.93 kcal mol^{-1},[8] one calculates the value of ΔH_f(i) = 747.3±14.4 kcal mol^{-1} and hence the so called heterolytic copper(II)–oxygen mean bond energy, $\overline{E}'_{Cu-O} = \Delta H_f(i)/4$, is calculated as $\overline{E}'_{Cu-O}$ = 187±3 kcal mol^{-1}.

The stability of a co-ordination compound is commonly interpreted as referring to the process

$$M^{n+} + nL^- \longrightarrow [ML_n]$$

occurring in solution, which is a Lewis acid-base reaction and therefore the stability of the compound should increase as the strength of the Lewis base increases. One would expect therefore that the stability should be in the order of increasing dissociation constant pK of the ketone, *i.e.*, in the case of copper(II) β-diketonates, tropolone(7.0)[18] and benzoylacetone (8.94).[19] There is little data from stability constant studies which related directly to this system: copper(II) tropolonate has an overall stability constant of 15.4, at 30 °C in 50% dioxane–water[20–22] and copper(II) benzoylacetonate has an overall stability constant of 17.02 at 25 °C in 75% dioxane–water,[23] from which the free energies can be derived: $\Delta G[Cu(trop)_2]$ = −21.4 kcal mol^{-1} and $\Delta G[Cu(bzac)_2]$ = −23.2 kcal mol^{-1}.

This is quite a significant difference in free energy but the lack of values for the entalpy of formation of the complexes in solution prevents other conclusions.

However, the large value for the enthalpy of formation of copper(II) benzoylacetonate from its ions in the vapour state (−747 kcal mol^{-1}) shows the large importance of solvation effects in solution processes, and so, it is apparent from this, that stability constants can give very little direct information of metal–ligand bond energies.

Table 2 summarizes the relevant parameters for the copper(II) complexes of benzoylacetone and tropolone.[24]

Whether the Cu–O bond energy is expressed in terms of dissociation into radicals or ions, the uncertainty arising from the use of the estimated auxiliary data is sufficiently large to obscure any clear difference effect of ligand parameters, but it is noteworthy that a change in the dissociation constant of the ligand by almost 2 pK units causes a change in the heterolytic bond energy of less that 5 kcal (3%). Unfortunatly, the uncertainties ascribed to the bond energy parameters (±3 kcal mol^{-1}) are big enough to prevent one to conclude that the Cu–O bond energy is definitely larger in the benzoylacetonate complex than in the tropolonate one. Nevertheless, it seems reasonable to think that these results are in agreement with the Nakamoto's[25] statement that the value of the metal–oxygen bond energy in substituted β-diketonates increases with the introduction of a phenyl group in

the β-diketones and disagrees with Collman's[26] opposite statement.

Thanks are due to the Instituto Nacional de Investigação Científica, Lisboa, Portugal, for partial financial support of the research project.

References

1) M. A. V. Ribeiro da Silva and R. J. Irving, *Bull. Chem. Soc. Jpn.*, **50**, 734 (1977).
2) P. K. Hon, C. E. Pfluger, and R. L. Belford, *Inorg. Chem.*, **5**, 516 (1966).
3) E. J. Prosen and M. V. Kilday, *J. Res. Nat. Bur. Stand., Sect A*, **77**(5), 581 (1973).
4) "Handbook of Chemistry and Physics," 55th ed, ed by R. C. Weast, The Chemical Rubber Co., Cleveland, Ohio (1974).
5) G. S. Hammond, D. C. Nonhebel, and C. H. S. Wu, *Inorg. Chem.*, **2**, 73 (1963).
6) J. O. Hill and R. J. Irving, *J. Chem. Soc., A*, **1966**, 1971.
7) D. D. Perrin, W. L. Armarego, and R. D. Perrin, "Purification of Laboratory Chemicals," Pergamon Press, Oxford (1966).
8) D. D. Wagman *et al.*, "Selected Values of Chemical Thermodynamic Properties," Technical-Note 270-4, U. S. Nat. Bur. Stand., Washington, D. C. (1969).
9) D. T. Farrar and M. M. Jones, *J. Phys. Chem.*, **68**, 1717 (1964).
10) D. D. Wagman *et al.*, "Selected Values of Chemical Thermodynamic Properties," Technical-Note 270-3, U. S. Nat. Bur. Stand., Washington, D. C. (1968).
11) R. J. Irving and M. A. V. Ribeiro da Silva, *J. Chem. Soc., Dalton. Trans.*, **1976**, 1940.
12) R. J. Irving and M. A. V. Ribeiro da Silva, *J. Chem. Soc., Dalton. Trans.*, **1975**, 1257.
13) E. C. Lingafelter and R. L. Braun, *J. Am. Chem. Soc.*, **88**, 2951 (1966).
14) J. O. Hill and R. J. Irving, *J. Chem. Soc., A*, **1966**, 971.
15) C. A. Coulson, personal communication (1973).
16) A. Aihara, *Bull. Chem. Soc. Jpn.*, **32**, 1242 (1959).
17) L. M. Branscomb, D. S. Burch, S. Geltman, and S. J. Smith, *Phys. Rev.*, **111**, 504 (1955).
18) J. C. James and J. C. Speakman, *Trans. Faraday Soc.*, **48**, 474 (1952).
19) S. P. Patel, "Ph. D. Thesis," University of Surrey (1973).
20) B. E. Bryant, W. C. Fernelius, and B. E. Douglas, *Nature*, **170**, 247 (1952).
21) Y. Dutt, R. P. Singh, and M. Katyal, *Talanta*, **16**, 1369 (1969).
22) B. E. Bryant and W. C. Fernelius, *J. Am. Chem. Soc.*, **76**, 3783, (1954).
23) B. Rao and M. B. Mathur, *J. Inorg. Nucl. Chem.*, **33**, 2919 (1971).
24) Recalculated from the experimental values of Ref. 1.
25) K. Nakamoto, Y. Morimoto, and A. E. Martell, *J. Phys. Chem.*, **66**, 346 (1962).
26) H. F. Holtzlaw, Jr. and J. P. Collman, *J. Am. Chem. Soc.*, **79**, 3318 (1957).

Oxidation of Benzaldehydes by Peroxomonophosphoric Acid. A Kinetic and Mechanistic Study in Acid and Alkaline Media

G. P. PANIGRAHI* and Radhasyam PANDA

Department of Chemistry, Berhampur University, Berhampur 760007, Orissa, India

(Received October 7, 1978)

The oxidation of benzaldehydes by peroxomonophosphoric acid has been found to proceed by

(i) $-d[\text{peroxomonophosphoric acid}]/dt \propto [\text{benzaldehyde}][\text{peroxomonophosphoric acid}][H^+]^x$

where x=a fraction at $[H^+]<0.5$ M and $x=0$ at $[H^+]>0.5$ M and

(ii) $-d[\text{peroxomonophosphate}]/dt \propto [\text{benzaldehyde}][\text{peroxomonophosphate}][OH^-]^y$

where y=a fraction at $[OH^-]<0.1$ M and $y=0$ at $[OH^-]>0.1$ M.

In the alkaline oxidation Hammett relationship is obeyed excellently, unlike the oxidation in the acid medium. The oxidation mechanisms are discussed in terms of a nucleophilic attack of the peroxomonophosphoric acid species on the carbonyl carbon centre. Thermodynamic parameters have been evaluated to substantiate the mechanisms.

Peroxomonophosphoric acid (PMPA) is known to function through a polar mechanism in spite of the fact that these compounds are sources of free radicals due to homolysis of O–O bonds not only in homogeneous media but also in some heterogeneous reactions.[1-3] Operation of a polar mechanism in oxidations by peroxo compounds was first recognised by Swern.[4] Kinetics of oxidation of halide ions[5] by peroxomonophosphoric acid, peroxomonosulfuric acid and peracetic acid, and of iodide ion[6] by peroxomonophosphoric acid involve both H^+-dependent and H^+-independent terms.

A survey of literature, however, reveals that studies relating to PMPA oxidation of organic substrates are quite few. Hence it was thought worthwhile to investigate the possibility of the use of PMPA as an oxidant for organic substrates. More interesting is the use of PMPA in alkaline medium which is probably for the first time we have attempted to undertake. This report deals with the kinetics of oxidation of aromatic aldehydes by PMPA in acid and alkaline media.

Experimental

All the chemicals used were of Analar grade. Benzaldehydes used were freshly distilled or recrystallized samples. PMPA was prepared by the acid hydrolysis[5-7] of $K_4P_2O_8$. The acidity of the medium was adjusted with $HClO_4$ or H_2SO_4 as the case may be and the ionic strength of the medium was maintained by adding requisite amounts of $NaClO_4$ or $NaHSO_4$. In the case of experiments in alkaline medium, the acid after hydrolysis of peroxodiphosphate was first neutralised by adding a calculated amount of alkali and then a known excess of alkali was added so as to obtain the required hydroxide concentration. Reactions were followed by measuring the rate of disappearance of PMPA, the estimation of which was done in an acetic acid–acetate buffer of pH 4—5 by the usual iodometric procedure. In separate experiments, the oxidation rates followed by the disappearance of PMPA were found to check within 2—6% with the rates followed by measuring the formation of benzoic acid spectrophotometrically. The self decomposition of the oxidant was routinely checked and found to be either nil or negligibly small under our experimental conditions. The aerial oxidation of benzaldehyde was found to be negligible because the rates of oxidation in an atmosphere of nitrogen, in representative runs, agreed with in 3—5% to those in the presence of air.[8,9]

Results and Discussion

Reactions in Acid Medium. Stoichiometry: Experiments conducted with excess of PMPA, in the presence of air or under a nitrogen atmosphere, showed that the stoichiometry of aldehyde to PMPA is 1: 1 and the product is the corresponding benzoic acid.

Benzaldehyde has been oxidised by PMPA in aqueous medium in the presence of $HClO_4$ and H_2SO_4 at 35 °C at constant ionic strength. The reaction is found to be first order with respect to the disappearance of PMPA and to the substrate (Table 1).

Dependence on $[H^+]$: The variation of $[H^+]$ ($HClO_4$ or H_2SO_4) is accompanied by a variation of rate in the same direction suggesting the reaction to be acid-catalysed. However, this catalysis is observed upto $H^+=0.5$ M beyond which the rate tends to become independent of the acid concentration.

Effect of Added Substances: A change in the ionic strength of the medium or the addition of acrylamide or Cu^{2+} does not affect the oxidation rate. The decrease in the rate in the presence of HPO_4^{2-} may be due to the removal of H^+ from the reaction medium (Table 1).

Effect of Substituents: The second order rate constants (k_2') for the oxidation of benzaldehydes are summarised in Table 2. It is interesting to note that the substituent effect on the reaction rate is insignificant in acid medium; the electron-withdrawing *p*-nitro substituent and the electron-releasing *p*-methyl substituent only marginally influence the rate whereas the other substituents are without any effect. Such observations on anomalous substituent effect have been reported earlier.[10,10a] It might have arisen because of the operation of a preliminary hydration equilibrium,[10a]

$$XC_6H_4CHO + H_2O \overset{K_p}{\rightleftharpoons} XC_6H_4CH(OH)_2,$$

competing with the oxidation steps; an electron withdrawing *p*-nitro substituent would favour the formation of the hydrate, but would retard the oxidation process because of a fall in the effective concentration of benzaldehyde available for oxidation (benzaldehyde is prefered to the hydrate in the oxidation steps because otherwise the substituent effects would have been in the same direction; *e.g.*, an electron-withdrawing substituent

Table 1.[a] Oxidation of benzaldehydes by PMPA in acid medium

Substrate (S)	10^3 S / M	10^3 PMPA / M	$HClO_4$ / M	HOAc–Water (% v/v)	$10^2 k_2'$ / dm^3 mol^{-1} s^{-1}
Benzaldehyde	5.29	4.27	0.1	20—80	0.62
	5.31	8.60	0.1		0.63
	5.31	6.42	0.1		0.66
	2.74	4.16	0.3		1.90
	5.11	4.28	0.3		1.66
	10.63	4.16	0.3		1.76
	25.56	4.16	0.3		1.83
	5.29	4.17	0.3	30—70	1.61
	5.26	0.64	0.05	Aqueous	0.59 (1.07)[b]
	5.43	4.56	0.1		0.94 (1.5)
	5.26	0.57	0.2		1.43 (2.0)
	5.14	4.27	0.3		2.02 (2.2) 1.89[c]
	5.14	4.34	0.3		1.78[d]
	5.43	4.38	0.5		2.56 (2.42)
	5.27	1.14	0.75		2.64 (2.53)
	5.37	0.59	0.5[e]		3.6
	5.23	1.08	0.5[e]		3.48
	5.21	4.07	0.5[e]		3.63
	2.46	4.41	0.5[e]		4.75
	5.29	4.41	0.5[e]		3.66
	10.52	4.41	0.5[e]		3.70
p-Nitrobenzaldehyde	2.07	0.59	0.05		1.20 (1.27)
	2.09	1.10	0.1		1.50 (1.83)
	2.07	0.60	0.2		2.32 (2.35)
	2.13	1.19	0.3		2.58 (2.60)

a) At I=1.5 M and 35 °C. b) (In parentheses) $10^2 k_2'$ calcd dm^3 mol^{-1} s^{-1}. c) Rate of formation of benzoic acid. d) In the presence of added HPO_4^{2-} (5.02×10^{-2} M). e) At 0.5 M H_2SO_4.

Table 2.[a] Oxidation of benzaldehydes by PMPA: effect of substituents

Substrate	$10^2 k_2'$[b] / dm^3 mol^{-1} s^{-1}	$10^2 k_2''$[c] / dm^3 mol^{-1} s^{-1}	$10^2 k_2'''$[d] / dm^3 mol^{-1} s^{-1}
Benzaldehyde(H–)	1.66	2.95	7.30
p-Nitro-	2.33	4.15	63.56
m-Nitro-	1.75	2.91	58.26
p-Chloro-	1.61	2.51	15.45
m-Chloro-	—	—	22.05
o-Chloro-	—	—	6.93
p-Bromo-	1.68	2.56	18.31
m-Bromo-	—	—	22.55
p-Methyl-	3.03	5.15	3.81
p-Methoxy-	1.78	—	2.48

a) At 35 °C. b) $HClO_4$, 0.3 M; HOAc: water, 20: 80; I=0.5 M. c) H_2SO_4, 0.5 M; HOAc: water 20: 80; I=2.0 M. d) OH^-, 0.2 M; aqueous medium, I=0.5 M.

would have enhanced the rate and an electron-releasing substituent would have retarded it).

Solvent Effect: The oxidation rate is found to decrease marginally with increase in acetic acid content in the solvent mixture (Table 1). The marginal decrease in the rate with decrease in dielectric constant of the medium is to be expected for a reaction involving a neutral molecule and an ion[11] to which the present reactions probably conform.

Rate Law: The various equilibria involving PMPA in the solution are

$$H_3PO_5 \overset{K_1}{\rightleftharpoons} H_2PO_5^- + H^+, \quad (1)$$

$$H_2PO_5^- \overset{K_2}{\rightleftharpoons} HPO_5^{2-} + H^+, \quad (2)$$

$$HPO_5^{2-} \overset{K_3}{\rightleftharpoons} PO_5^{3-} + H^+. \quad (3)$$

K_1, K_2, and K_3 values are 8.0×10^{-2}, 4.2×10^{-6}, and 1.6×10^{-13} respectively at 25 °C.[7] Since in the [H$^+$] range used, PMPA exists[7] as H_3PO_5 and $H_2PO_5^-$, the oxidation steps may be written as

$$XC_6H_4CHO + H_2O \overset{K_p}{\rightleftharpoons} XC_6H_4CH(OH)_2, \quad (A)$$

$$H_2PO_5^- + H^+ \overset{K}{\rightleftharpoons} H_3PO_5, \quad (4)$$

$$H_2PO_5^- + XC_6H_4CHO \xrightarrow{k_1} XC_6H_4COOH + H_2PO_4^-, \quad (5)$$

and

$$H_3PO_5 + XC_6H_4CHO \xrightarrow{k_2} XC_6H_4COOH + H_3PO_4. \quad (6)$$

The reaction sequence leads to the rate law

$$-\frac{d[PMPA]}{dt} = [PMPA][XC_6H_4CHO]\left\{\frac{k_1+k_2K[H^+]}{1+K[H^+]}\right\} \times(1+K_p[H_2O]), \quad (7)$$

where

$$k_2' = \left\{\frac{k_1+k_2K[H^+]}{1+K[H^+]}\right\}(1+K_p[H_2O]). \quad (8)$$

Since $1/K_1=K$, and $K_p[H_2O]\ll1$,[15] Eq. 8 becomes

$$k_2' = \frac{K_1k_1+k_2[H^+]}{K_1+[H^+]}. \quad (9)$$

This rate law (Eq. 9) is in agreement with the experimental findings. The values of k_1 and k_2 have been calculated by the method of least squares from Eq. 9. The values of k_2 for benzaldehyde and *p*-nitrobenzaldehyde are 2.80×10^{-2} and 3.29×10^{-2} dm^3 mol^{-1} s^{-1} respectively. For both the compounds, the values of k_1 are small and negative and thus can be approximated to zero. Therefore the Eq. 9 reduces to

$$k_2' = \frac{k_2[H^+]}{K_1+[H^+]}. \quad (10)$$

The rate constants (k_2' calcd) as obtained from Eq. 10 at different [H$^+$] are recorded in Table 1. It appears that in the lower [H$^+$], k_2' calcd values for benzaldehyde are significantly higher than the experimental ones (k_2') and this can probably be ascribed to the contribution of the k_1 term at lower [H$^+$] to the observed k_2' as defined by Eq. 9. It is now evident that the species H_3PO_5 is important in the reaction. It is also natural

Table 3.[a] Oxidation of benzaldehydes by PMP in alkaline medium

Substrate (S)	10^3 S / M	10^4 PMP / M	OH^- / M	I/M	$10^2 k_2''$ / dm^3 mol^{-1} s^{-1}
Benzaldehyde	2.80	5.37	0.204	0.5	7.30
	5.38	5.37	0.204	0.5	7.60
					7.45[b]
	10.27	4.85	0.205	0.5	7.83
	24.98	5.57	0.204	0.5	7.28
	9.98	4.66	0.050	0.1	1.95
	10.41	5.03	0.05	0.302	2.88
	9.72	5.01	0.05	0.503	3.41
	10.06	3.94	0.017	0.5	1.40
	10.06	4.33	0.031	0.5	2.43
	10.22	4.11	0.105	0.5	5.95
	2.61	4.74	pH 10	—	0.52
p-Nitro-benzaldehyde	2.62	3.80	0.019	0.5	29.15 (30.52)[c]
	2.62	3.91	0.0387	0.5	46.21 (44.79)
	2.61	4.24	0.058	0.5	55.73 (54.25)
	2.61	4.56	0.098	0.5	65.08 (66.61)

a) At 35 °C in aqueous medium. b) Rate of formation of benzoate ion. c) (In parentheses) $10^2 k_2''$ calcd dm^3 mol^{-1} s^{-1}.

to expect a very insignificant value of k_1, since in the range of [H$^+$] used, PMPA would mainly exist as H_3PO_5.[7]

Peroxo compounds are known to act as nucleophiles since the peroxo group can attach itself to a reactive site (*i.e.*, a p-orbital of carbon). Thus the peroxomonophosphoric acid can attack the carbonyl carbon of the aldehyde giving rise to transition state of the form:

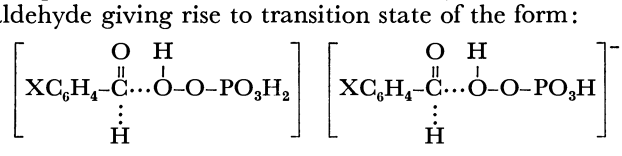

(I) (II)

This is consistent with the idea of Edwards[12] that in the reactions of peroxo compounds with inorganic and organic substrates, a fair degree of covalent bonding developes between the redox pair. The activation parameters calculated (Table 4) are also in agreement with the mechanism.

Table 4.[a] Oxidation of benzaldehydes by PMP: thermodynamic parameters

Substrate	$\Delta H^{\neq}$[b] / kJ mol^{-1}	$\Delta S^{\neq}$[b] / J mol^{-1} K^{-1}	$\Delta H^{\neq}$[c] / kJ mol^{-1}	$\Delta S^{\neq}$[c] / J mol^{-1} K^{-1}
Benzaldehyde(H–)	39.4	−145.3	35.8	−150.6
p-Nitro-	33.4	−161.4	48.6	− 91.0
p-Methyl-	33.4	−160.5	35.8	−156.1
p-Methoxy-	32.3	−163.7	—	—

a) Calculated at 298 K. b) H_2SO_4, 0.5 M; aqueous medium, I=1.5 M. c) OH^-, 0.2 M, aqueous medium, I=0.5 M.

Reactions in the Alkaline Medium: The oxidation of benzaldehydes by peroxomonophosphate (PMP) in alkaline medium follows a first order dependence each on oxidant and substrate as shown by the constancy of the pseudo first order rate constants (k_1'') upto a high percentage of the reaction in any single run and the constancy of $k_1''/[S]$ ($=k_2''$) values respectively. The dependence of rate on [OH$^-$] is peculiar; the rate increases with an increase in the [OH$^-$] at lower [OH$^-$] and tends to reach a limiting value at higher [OH$^-$] (Table 3).

Substituent Effect: Substituent effect in alkaline medium is another important observation made which is kinetically different from that in acid medium. The substituents manifest their influence implying electronic effects are prominent for the oxidation in alkaline medium. The rate variation is essentially in agreement with the Hammett's substituent constants, σ (Table 2); a plot of log k_2'' *vs.* σ is linear (r=0.992) with a positive slope (ρ=1.27), which is indicative of a developing negative charge in the side chain of the benzaldehyde molecule.[13] The magnitude of the ρ value is close to that observed for the ionization of benzoic acids (ρ=1.0).

Effect of Temperature: Identical enthalpy and entropy of activation observed for benzaldehyde and the *p*-methyl derivative (Table 4) suggest that oxidation of both the compounds are isoentropic; however, *p*-nitro derivative requires higher energy of activation and much higher entropy of activation compared to the other two derivatives, inspite of the higher reactivity of the *p*-nitro derivative. This is probably due to the reason that a greater concentration of *p*-nitrobenzaldehyde will be available in the hydrate form compared to that for benzaldehyde or *p*-methylbenzaldehyde.

Rate Law and Mechanism: At pH>11, peroxomonophosphate exists[7] as HPO_5^{2-} and PO_5^{3-}.

$$HPO_5^{2-} + OH^- \overset{K_4}{\rightleftharpoons} PO_5^{3-} + H_2O \qquad (11)$$

In alkaline medium benzaldehydes also exist[15,16] in the hydrated form because of the following equilibria:

$$XC_6H_4CHO + OH^- \overset{K_5}{\rightleftharpoons} XC_6H_4CH(OH)O^-, \qquad (12)$$

$$XC_6H_4CH(OH)O^- + H_2O \overset{K_6}{\rightleftharpoons} XC_6H_4CH(OH)_2 + OH^-. \qquad (13)$$

Even though the equilibrium (13) has been considered to be unimportant by earlier workers;[16] Sayer,[14] and Bell and Sorensen[15] attach significance to this equilibrium and have evaluated the formation constant for $XC_6H_4CH(OH)_2$. An examination of the formation constants though reveals the predominance of $XC_6H_4CH(OH)O^-$, $XC_6H_4CH(OH)_2$ is considered to be the reactive species in this oxidation process. This arises mainly from the following reasons (i) that the OH^--dependence would have been more than unity had the reacting species been the hydrate mono anion because of the participation of OH^- in steps (Eqs. 11 and 12), (ii) that there would have been a marked ionic strength effect if the reaction involved two ions. The marginal effect of ionic strength on rate points the reaction to involve at least one neutral molecule[17] and

(iii) that the attack of the PMP species on the more electrophilic $XC_6H_4CH(OH)_2$ will be favoured.

So the reaction would involve a nucleophilic attack of the peroxo di- and tri-anions on the carbonyl carbon of the aldehyde hydrate molecule giving rise to the transition states III and IV respectively. The thermodynamic parameters calculated are in the range expected for a bimolecular substitution reaction.

$$HPO_5^{2-} + XC_6H_4CH(OH)_2 \xrightarrow{k_3} \left[O_3P\text{–}O\text{–}O\cdots C(H,XC_6H_4)\cdots OH(H) \right]^{2-}$$

(III)

$$\longrightarrow XC_6H_4COO^- + H_2PO_4^- + H_2O \qquad (14)$$

$$PO_5^{3-} + XC_6H_4CH(OH)_2 \xrightarrow{k_4} \left[O_3P\text{–}O\text{–}O\cdots C(XC_6H_4)\cdots OH(H) \right]^{3-}$$

(IV)

$$\longrightarrow XC_6H_4COO^- + HPO_4^{2-} + H_2O \qquad (15)$$

On the basis of the proposed mechanism the rate law can be derived as:

$$-\frac{d[PMP]}{dt} = \left\{\frac{k_3K_hK_5K_6 + k_4K_5K_6[OH^-]}{K_h + [OH^-]}\right\} \times [PMP][XC_6H_4CHO], \qquad (16)$$

where

$$k_2'' = \frac{k_3K_hK_5K_6 + k_4K_5K_6[OH^-]}{K_h + [OH^-]} \qquad (17)$$

and

$$\frac{K_4}{[H_2O]} = \frac{1}{K_h}.$$ ($K_h = K_w/K_3$, where K_w is the ionic product of water and K_3 is the dissociation constant of HPO_5^{2-})

Rearrangement of Eq. 17 would give

$$k_2''(K_h + [OH^-]) = k_3K_hK_5K_6 + k_4K_5K_6[OH^-]. \qquad (18)$$

On plotting $k_2''(K_h + [OH^-])$ against $[OH^-]$, linearity ($r = 0.99$) is observed for both benzaldehyde and *p*-nitrobenzaldehyde.

From the intercept and slope of the plot, and employing the reported K_5 and K_6 values,[15] the values of k_3 and k_4 for *p*-nitrobenzaldehyde are calculated to be 0.34 $dm^3\,mol^{-1}\,s^{-1}$ and 6.76 $dm^3\,mol^{-1}\,s^{-1}$ respectively. The higher k_4 value is quite in agreement with the higher nucleophilic reactivity of PO_5^{3-} in alkaline medium. With these k_3 and k_4 values, the rate constants k_2'' (calcd) from Eq. 17 are collected in Table 3. In the case of benzaldehyde, since the least squares plot results in a very small and negative intercept, the value of k_3 is approximated to zero. The value of $k_4K_5K_6$, as given by the slope is 1.07×10^{-1}. The value of k_4 for benzaldehyde could not be calculated because of the non-availability of the K_5 and K_6 values.

The authors are thankful to Prof. P. S. Radhakrishna Murti, Dr. S. N. Mahapatro and Dr. R. K. Panda of this Department for helpful discussions and encouragement. Dr. Y. K. Gupta, Department of Chemistry, University of Rajasthan is gratefully acknowledged for the gift of the sample of peroxodiphosphate. One of the authors (R. S. P.) is grateful to C. S. I. R. (New Delhi) for the award of a Junior Research Fellowship.

References

1) (a) R. Curci and J. O. Edwards, "Organic Peroxides," ed by D. Swern, Wiley Interscience, New York (1970), Vol. I, p. 212: (b) L. S. Silbert, "Organic Peroxides," ed by D. Swern, Wiley Interscience, New York, (1970), Vol. 2, p. 637.

2) J. A. Kerr, *Chem. Rev.*, **66**, 465 (1966).

3) (a) E. Boyland and D. Manson, *J. Chem. Soc.*, **1957**, 4689; (b) Y. Ogata, I. Urasaki, K. Nagura, and N. Satomi, *Tetrahedron*, **30**, 3021 (1974); (c) Y. Ogata, K. Tomizawa, and T. Ikeda, *J. Org. Chem.*, **43**, 2417 (1978).

4) D. Swern, *J. Am. Chem. Soc.*, **69**, 1692 (1947).

5) D. H. Fortnum, C. J. Battaglia, S. R. Cohen, and J. O. Edwards, *J. Am. Chem. Soc.*, **82**, 778 (1960).

6) F. Secco and M. Venturini, *J. Chem. Soc. Dalton Trans.*, **1976**, 1410.

7) C. J. Battaglia and J. O. Edwards, *Inorg. Chem.*, **4**, 552 (1965).

8) K. B. Wiberg and Ross Stewart, *J. Am. Chem. Soc.*, **77**, 1786 (1955).

9) G. T. E. Graham and F. H. Westheimer, *J. Am. Chem. Soc.*, **80**, 3030 (1958).

10) D. A. Blackadder and C. Hinshelwood, *J. Chem. Soc.*, **1958**, 2720; (a) Y. Ogata, H. Tezuka, and Y. Sawaki, *Tetrahedron*, **23**, 1007 (1967).

11) K. B. Wiberg, "Physical Organic Chemistry," John Wiley, New York (1966), p. 389.

12) E. Chaflee and J. O. Edwards, "Inorganic Reaction Mechanism," ed by J. O. Edwards, Interscience, New York (1969), p. 205.

13) J. E. Leffler and E. Grunwald, "Rates and Equilibria of Organic Reactions," Wiley, New York (1963), p. 177

14) J. M. Sayer, *J. Org. Chem.*, **40**, 2545 (1975).

15) R. P. Bell and P. E. Sorensen, *J. Chem. Soc. Perkin Trans. 2*, **1976**, 1594.

16) W. J. Bover and P. Zuman, *J. Chem. Soc. Perkin Trans. 2*, **1973**, 786.

17) K. J. Laidler, "Chemical Kinetics," Tata McGraw Hill, (1965), p. 229.

Preparation and Characterization of Complexes of Dichlorobis-(cyclopentadienyl)zirconium(IV) with Bidentate, Terdentate, and Quadridentate Schiff Bases

Gopal GUPTA, Ram SHARAN, and Ramesh N. KAPOOR*
Department of Chemistry, University of Delhi, Delhi-110007, India
(Received May 12, 1978)

Bis(cyclopentadienyl)zirconium(IV) Schiff base derivatives have been synthesized by treating dichlorobis-(cyclopentadienyl)zirconium(IV) (Cp_2ZrCl_2) with bidentate Schiff bases (SBH) *viz.*, *N*-salicylidenaniline, *N*-salicylidene-*o*-toluidine, *N*-salicylidene-*m*-toluidine, *N*-salicylidene-*p*-toluidine, and *N*-(2-hydroxyl-1-naphthyl-iden)aniline, terdentate Schiff bases ($SB'H_2$) *viz.*, *N*-(3-oxo-1-methylbutyliden)-*o*-aminophenol and *N*-(3-oxo-1-phenylbutyliden)-*o*-aminophenol; quadridentate Schiff base ($SB''H_2$) *N,N'*-disalicylidene-*o*-phenylenediamine, in THF, in the presence of triethylamine at room temperature. The resulting derivatives of the type $Cp_2Zr(SB)Cl$, $Cp_2Zr(SB)_2$, $Cp_2Zr(SB')$, $Cp_2Zr(SB'')$, and $(Cp_2ZrCl)SB''$ [where $[SB]^-$, $[SB']^{2-}$, and $[SB'']^{2-}$ represent the anion of corresponding Schiff bases SBH, $SB'H_2$, and $SB''H_2$] have been characterised by their elemental analysis and by IR, electronic spectra, electrical conductance and molecular weight determinations.

A number of transition metal complexes of Schiff bases have been synthesized and characterized during recent years.[1,2] In view of the interesting synthetic and structural aspects of these complexes, interest in the study of Schiff base complexes continues to increase. However, few Schiff base complexes of organometallic derivatives such as dichlorobis(cyclopentadieyl)zirconium(IV) and dichlorobis(cyclopentadieyl)titanium(IV) have been studied.[3,4] Recently, a series of complexes of dichlorobis(cyclopentadienyl)-titanium(IV) with Schiff bases has been reported.[5] Now these studies have been extended to the complexes of dichlorobis(cyclopentadienyl)zirconium(IV) with bidentate, terdentate and quadridentate Schiff bases. Such a study appears to be useful in view of the fact that organometallic compounds of titanium[6] and zirconium[7] are found to be capable of activating molecular nitrogen. In one instance, alkoxy derivatives of zirconium(IV) have been investigated as potential agent in the nitrogen fixation processes.[8]

Experimental

Dichlorobis(cyclopentadienyl)zirconium(IV) was prepared by CpNa method.[9,10] Schiff bases were synthesised by the usual methods[11-13] and recrystallized from absolute ethanol.

THF (Baker AR) was dried by storage on sodium wire overnight and then refluxed until it gave a blue colouration with benzophenone. It was finally dried by distilling over $LiAlH_4$. Hexane was dried by distilling over sodium wire. Triethylamine was purified by the given method.[14] All the reactions were carried out in anhydrous conditions.

Zirconium was estimated gravimetrically as ZrO_2, chlorine as AgCl, and nitrogen was estimated by Kjeldahl's method. Analytical data of these complexes are given in Tables 1—3. The IR spectra were recorded on Perkin-Elmer IR-621 and IR-137 instruments in KBr phase in the ranges of 4000—200 cm^{-1} and 4000—700 cm^{-1}. The electronic spectra of the complexes were run on Perkin-Elmer 4000A in the range of 400—750 $cm.^{-1}$ Molecular weight of the complexes were determined by Gallen-Kamp Ebulliometer, W. G. Pye & Co. Electrical conductance measurements were carried out in nitrobenzene on a Beckmann conductivity Bridge Model RC-18A.

Reactions of Dichlorobis(cyclopentadienyl)zirconium(IV) (1 mol) with N-*Salicylidene*-p-*toluidine (1 mol).* Schiff base (0.64 g) was added to a solution of dichlorobis(cyclopentadienyl)-ziroconium(IV) (0.89 g) in dry THF (80 g). To this triethylamine (0.50 g) was added, the mixture was stirred for 24 h. Precipitated $Et_3N \cdot HCl$ was removed by filtration and the complex was crystallised by a hexane/THF mixture (yield 85%).

Reaction of Dichlorobis(cyclopentadienyl)zirconium(IV) (1 mol) with N-*Salicylidene*-p-*toludidine (2 mol).* To dichlorobis(cyclopentadienyl)zirconium(IV) (0.72 g) and Schiff base (1.05 g) dissolved in THF (80 g) was added triethylamine (0.51 g) and the mixture was stirred for 18 h. $Et_3N \cdot HCl$ which precipitated was removed by filtration. After distilling the solvent under reduced pressure, the product was recrystallised from a hexane/THF mixture (yield=82%).

Reaction of Dichlorobis(cyclopentadienyl)zirconium(IV) (1 mol) with N-*(3-Oxo-1-methylbutylidene)*-o-*aminophenol (1 mol).* A mixture of dichlorobis(cyclopentadienyl)zirconium(IV) (1.20 g) and Schiff base (0.72 g) was dissolved in THF (80 g) and triethylamine (0.84 g) was added. The mixture was stirred for 24 h. Precipitated $Et_3N \cdot HCl$ was removed by filtration and complex was crystallised from a hexane/THF mixture (yield 80%).

Reaction of Dichlorobis(cyclopentadienyl)zirconium(IV) (2 mol) with N,N'-*Disalicylidene*-o-*phenylenediamine (1 mol).* Schiff base (0.68 g) was added to a solution of Cp_2ZrCl_2 (1.27 g) in dry THF(75 g). To this triethylamine (0.88 g) was added, and the mixture was stirred for 30 h. $Et_3N \cdot HCl$ which precipitated out was removed and solvent was removed under reduced pressure. The complex was crystallized from a hexane/THF mixture (yield 83%).

Results and Discussion

Dichlorobis(cyclopentadienyl)zirconium(IV) reacts with bidentate Schiff bases (1:1 and 1:2 molar ratios) in anhydrous THF, in the presence of triethylamine.

$$Cp_2ZrCl_2 + SBH + Et_3N \xrightarrow[\text{room temp}]{\text{THF}} Cp_2Zr(SB)Cl + Et_3N \cdot HCl,$$

$$Cp_2ZrCl_2 + 2SBH + 2Et_3N \xrightarrow[\text{room temp}]{\text{THF}} Cp_2Zr(SB)_2 + 2Et_3N \cdot HCl,$$

where SB^- represents the anion of corresponding bidentate Schiff bases SBH.

Table 1. Reactions of Cp_2ZrCl_2 with bidentate Schiff bases

Reactants (Molar ratio)	Stirring time (h)	Product, colour and dec temp	Mol wt Found (Calcd)	Found (Calcd) % Zr	N	Cl
Cp_2ZrCl_2 + SBH + Et_3N (1:1:1)	26	$Cp_2Zr(SB)Cl$ Reddish brown, 138	491 (453)	19.8 (20.1)	2.95 (3.1)	7.5 (7.8)
Cp_2ZrCl_2 + SBH + Et_3N (1:2:2)	24	$Cp_2Zr(SBH_2)$ Dark brown, 112	668 (613)	14.8 (14.9)	4.4 (4.6)	— —
Cp_2ZrCl_2 + SB'H + Et_3N (1:1:1)	18	$Cp_2Zr(SB')Cl$ Brownish red, 152	— —	19.2 (19.5)	2.8 (3.0)	7.3 (7.6)
Cp_2ZrCl_2 + SB'H + Et_3N (1:2:2)	24	$CpZr(SB')_2$ Light brown, 95	— —	13.9 (14.2)	4.2 (4.4)	— —
Cp_2ZrCl_2 + S'BH + Et_3N (1:1:1)	24	$Cp_2Zr(S'B)Cl$ Brown, 165	— —	19.1 (19.5)	2.8 (3.0)	7.3 (7.6)
Cp_2ZrCl_2 + S'BH + Et_3N (1:2:2)	30	$Cp_2Zr(S'B)_2$ Yellowish brown 130	676 (641.4)	14.0 (14.2)	4.3 (4.4)	— —
Cp_2ZrCl_2 + S'B'H + Et_3N (1:1:1)	24	$Cp_2Zr(S'B')Cl$ Yellow orange, 115	483 (466.9)	19.3 (19.5)	2.9 (3.0)	7.4 (7.6)
Cp_2ZrCl_2 + S'B'H + Et_3N (1:2:2)	18	$Cp_2Zr(S'B')_2$ Yellowish brown 103	— —	13.9 (14.2)	4.24 (4.4)	— —
Cp_2ZrCl_2 + S''B''H + Et_3N (1:1:1)	24	$Cp_2Zr(S''B'')Cl$ Light brown, 228	— —	17.8 (18.1)	2.7 (2.8)	6.7 (7.05)
Cp_2ZrCl_2 + S''B''H + Et_3N (1:2:2)	30	$Cp_2Zr(S''B'')_2$ Dark yellow, 203	759 (713.5)	12.6 (12.8)	3.85 (3.9)	— —

SBH = *N*-salicylidenaniline, SB'H = *N*-salicylidene-*o*-toludine, S'BH = *N*-salicylidene-*m*-toludine, S'B'H = *N*-salicylidene-*p*-toluidine and S''B''H = *N*-(2-hydroxy-1-naphthyliden)aniline.

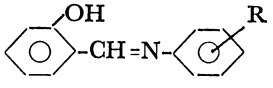

[R = H, *o*-Me, *m*-Me, and *p*-Me]

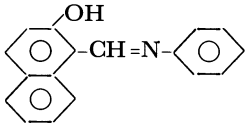

These Schiff base complexes are yellow to dark brown in colour and are soluble in benzene, tetrahydrofuran, chloroform and acetone. Analytical data and physical measurements are given in Table 1.

Reactions of Cp_2ZrCl_2 with terdentate Schiff bases (1:1 molar ratio) in THF, in the presence of triethylamine yielded complexes of the type $Cp_2Zr(SB')$.

$$Cp_2ZrCl_2 + SB'H_2 + 2Et_3N \xrightarrow[\text{room temp}]{\text{THF}} Cp_2Zr(SB') + 2Et_3N\cdot HCl$$

$[SB']^{2-}$ represents the anion of terdentate Schiff base $SB'H_2$

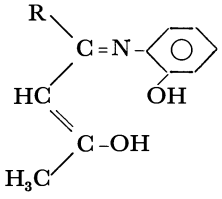

[R = Me, Ph]

These complexes are yellowish green and orange in colour and are soluble in organic solvents. Analytical data and physical properties are given in Table 2.

Quadridentate Schiff base reacts with Cp_2ZrCl_2 (1:1 and 1:2 molar ratios) in anhydrous THF, in the presence of triethylamine giving soluble products.

$$Cp_2ZrCl_2 + SB''H_2 + 2Et_3N \xrightarrow[\text{room temp}]{\text{THF}} Cp_2Zr(SB'') + 2Et_3N\cdot HCl$$

$$2Cp_2ZrCl_2 + SB''H_2 + 2Et_3N \xrightarrow[\text{room temp}]{\text{THF}} (Cp_2ZrCl)_2SB'' + 2Et_2N\cdot HCl$$

$[SB'']^{2-}$ represents the anion of quadridentate Schiff base $SB''H_2$

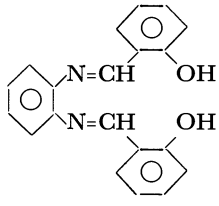

These complexes are brown or dark brown in colour and are soluble in organic solvents. The analytical data of these complexes is given in Table 3.

All the above reactions are quite facile and the resulting compounds could be isolated in almost quantitative yields. The complexes are involatile, very senstive to oxygen but relatively stable in an inert atmosphere and decomposes on heating between 95—325 °C. All complexes are monomeric except binuclear complex(E) with a dimeric structure (Tables 1—3). Electrical conductance measured in nitrobenzene showed them to be essentially nonelectrolytes.

On the basis of elemental analysis, IR and electronic spectra, molecular weight determination and electrical conductance, following structures are tentatively assigned for the complexes of the type (A) $Cp_2Zr(SB)Cl$; (B) $Cp_2Zr(SB)_2$; (C) $Cp_2Zr(SB')$; (D) $Cp_2Zr(SB'')$ and (E) $(Cp_2ZrCl)_2SB$.

Complexes with bidentate Schiff bases:

Table 2. Reactions of Cp_2ZrCl_2 with terdentate Schiff bases

Reactants (Molar ratio)	Stirring time (h)	Product, colour and dec temp	Mol wt Found (Calcd)	Found (Calcd) % Zr	N
$Cp_2ZrCl_2 + SBH_2 + Et_3N$ (1:1:2)	24	$Cp_2Zr(SB)$ Dark yellow, 225 °C	435 (410.4)	22.0 (22.2)	3.2 (3.4)
$Cp_2ZrCl_2 + SB'H_2 + Et_3N$ (1:1:2)	24	$Cp_2Zr(SB')$ Orange, 245 °C	— —	19.0 (19.3)	2.7 (3.0)

SBH_2 = *N*-(3-oxo-1-methylbutyliden)-*o*-aminophenol and SB'H = *N*-(3-oxo-1-phenylbutyliden)-*o*-aminophenol.

Table 3. Reactions of Cp_2ZrCl_2 with quadridentate Schiff base

Reactants (Molar ratio)	Stirring time (h)	Product, colour and dec temp	Mol wt Found (Calcd)	Found (Calcd) % Zr	N	Cl
$Cp_2ZrCl_2 + SB''H_2 + Et_3N$ (1:1:2)	36	$Cp_2Zr(SB'')$ Yellowish green, 290	—	16.9 (17.0)	5.1 (5.2)	— —
$Cp_2ZrCl_2 + SB''H_2 + Et_3N$ (2:1:2)	30	$(Cp_2ZrCl)_2SB''$ Dark brown, 325	885 (827.4)	22.4 (22.05)	3.3 (3.4)	8.3 (8.6)

$SB''H_2$ = *N*,*N*'-disalicylidene-*o*-phenylenediamine.

Table 4. IR frequencies (cm^{-1}) for bis(π-cyclopentadienyl)zirconium(IV) Schiff base complexes

Complex	ν(C-H)	ν(C-C)	$\delta^{i.p.}$(-CH)	$\delta^{o.p.}$(-CH)	ν(C=N)	ν(C=O)
Cp_2ZrCl_2	3100 s	1435 s	1020m	820 mb	—	—
$Cp_2Zr(SB)Cl$	3000 s	1442 s	1010 b	800 b	1590 s	1315m
$Cp_2Zr(SB)_2$	2995 w	1445 s	1005 b	810 b	1590 s	1305 b
$Cp_2Zr(SB')Cl$	3000 w	1440 s	1015m	800 s	1600 s	1305 s
$Cp_2Zr(SB')_2$	2995 s	1435 s	1015m	800 b	1600 s	1305 s
$Cp_2Zr(S'B)Cl$	2995m	1440 s	1020 w	805 w	1600 s	1310 w
$Cp_2Zr(S'B)_2$	3000 s	1440 s	1018 b	800 b	1595 s	1305 w
$Cp_2Zr(S'B')Cl$	2990 s	1440 s	1016 s	800 b	1590 s	1220 s
$Cp_2Ze(S'B')_2$	3000 w	1445 s	1016 s	810 b	1595 s	1340 w
$Cp_2Zr(S''B'')Cl$	2990 s	1430 s	1018m	820 b	1613 w	1335 s
$Cp_2Zr(S''B'')_2$	3000 w	1425 s	1018m	820 b	1613 w	1345 s
$Cp_2Zr(SB)$	2910 w	1430m	1018 s	805m	1580 s	1305 w
$Cp_2Zr(SB')$	2930 w	1430 s	1020 s	800 s	1588 s	1310m
$Cp_2Zr(SB'')$	2960 w	1445 s	1018 s	815 b	1610 s	1315 s
$(Cp_2ZrCl)_2SB''$	2970 b	1445 s	1018 s	810 s	1605 s	1310 s

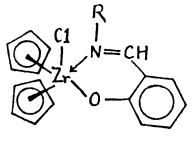

(A)

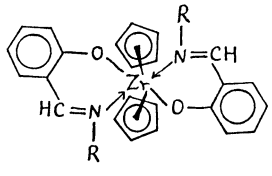

(B)

[R = C_6H_5, *o*-$CH_3C_6H_5$, *m*-$CH_3C_6H_5$, and *p*-$CH_3C_6H_5$]

Complexes with terdentate Schiff bases:

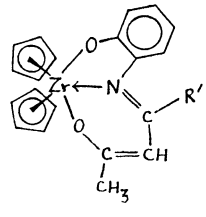

(C)

[R' = CH_3 and C_6H_5]

Complexes with quadridentate Schiff base:

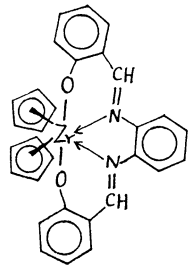

(D)

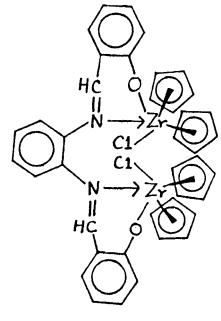

(E)

Similar structures have been reported for oximate complexes of dichlorobis(cyclopentadienyl)ziroconium.[15] In all complexes having structures (A), (C), and (E), the coordination number of zirconium appears to be five. This coordination number is well known for zirconium complexes.[15,16] For complexes with structures (A) and (E), the appearance of band at $\approx$350 cm^{-1} due to ν(Zr–Cl) confirms the presence of coordinated chlorine. In complexes having structures (B) and (D)

zirconium attains the well known coordination number six.[15,17] In the structure (B) the Schiff base acts as a bidentate ligand while in the case of (D) the denticity of the ligand is four *i.e.* it behaves as quadridentate ligand. Both these complexes are examples of twenty-electron system which has been reported for several other titanium[18,19] and zirconium[15] complexes. A twenty-electron system is also well documented for nickelocene.[20]

In all the complexes the cyclopentadienyl rings are *cis*, as their IR frequencies in the complexes coincide with those of dichlorobis(cyclopentadienyl)zirconium-(IV), supporting "angular" sandwich structure as reported by Giddings *et al.*[21]

Infrared Spectra. The important IR frequencies are given in Table 4. Absorption bands occurring at $\approx 3000\ cm^{-1}$ ν(C–H), $\approx 1435\ cm^{-1}$ ν(C–C), $\approx 1020\ cm^{-1}$ $\delta^{i.p.}$(–CH), and at $\approx 810\ cm^{-1}$ $\delta^{o.p.}$(–CH) indicated the presence of the cyclopentadienyl groups. All these bands are similar to these of dichlorobis-(cyclopentadienyl)zirconium(IV).[22]

In the spectra of Schiff bases, a strong band is observed in the 1617—1613 cm^{-1} region, which can be assigned to the absorption basd of the azomethine group (>C=N–). In these complexes, this band is slightly shifted to the lower side as given in Table 4. Similar observations have also been made by a number of workers.[23,24] But in case of complexes with Schiff base, *N*-(2-hydroxy-1-naphtyliden)aniline, there is no appreciable shift in ν(C=N) band compared to Schiff base as reported by Bailar.[25]

The strong band in the region of 1300—1282 cm^{-1} in the Schiff bases is attributed to the phenolic ν(C–O) in view of previous assignments. This ν(C–O) band shifts by $\approx 30\ cm^{-1}$ towards higher frequency upon complexation, suggesting bonding between zirconium and oxygen as observed by Poddar *et al.*[26]

The disappearance of the weak and broad bands in the region 3300—3100 cm^{-1} (–OH) in the complexes suggests that the (–OH) group of the Schiff base has taken part in the bond formation, and confirms the complex formation. Bands in the region 570—530 cm^{-1} and 520—420 cm^{-1} are attributed to ν(Zr–N) and ν(Zr–O), respectively as reported.[27,28]

Electronic Spectra. The electronic spectra of all the Schiff base complexes of dichlorobis(cyclopentadienyl)zirconium(IV) complexes were recorded in chloroform and acetone. All complexes show a single band in the region 25250—24280 cm^{-1} which can be assigned to the charge transfer band,[29] and is in accordance with their $(n-1)d^0ns^0$ electronic configuration.

Two of the authors (G.G.) and (R.S.) thank the Council of Scientific and Industrial Research, New Delhi, for the award of junior Research Fellowship.

References

1) R. H. Holm, G. W. Everett, Jr., and A. Chakravarty, *Prog. Inorg. Chem.*, **7**, 83 (1966).
2) L. Sacconi, *J. Am. Chem. Soc.*, **74**, 4503 (1952); **76**, 3400 (1954).
3) P. C. Walies, R. S. P. Coutts, and M. Weigold, "Organometallic Chemistry of Titanium, Zirconium and Hafnium," Academic Press (1974).
4) J. A. Labinger, *J. Organomet. Chem.*, **138**, 185 (1977). P. C. Bharara, V. D. Gupta, and R. C. Mehrotra, *J. Organomet. Chem. Rev.*, **1977**, 259.
5) R. Sharan, G. Gupta, and R. N. Kapoor, *Transition Metal Chem.*, **3**, 282 (1978).
6) M. E. Volpin and V. B. Shur, *Nature*, **209**, 1236 (1966). E. E. Van Tamelen, D. Seeley, S. Schneller, M. Rudler, and W. Cretney, *J. Am. Chem. Soc.*, **92**, 5251 (1970).
7) D. R. Gray and C. H. Brubaker, *Chem. Commun.*, **1969**, 1239.
8) D. R. Gray and C. H. Brubaker, *Inorg. Chem.*, **10**, 2143 (1971).
9) W. L. Jolly, "Synthetic Inorganic Chemistry," Prentice Hall, New Delhi (1965), p. 176.
10) G. Wilkinson and J. M. Birmingham, *J. Am. Chem. Soc.*, **76**, 4281 (1954).
11) J. Uttamchandani, S. K. Mehrotra, A. M. Bhandari, and R. N. Kapoor, *Monath. Chem.*, **108**, 735 (1977).
12) J. Uttamchandani, S. K. Mehrotra, A. M. Bhandari, and R. N. Kapoor, *Transition Metal Chem.*, **1**, 249 (1976).
13) I. A. Savich, A. K. Pikaev, I. A. Lebedev, and V. L. Spitsyn, *Vestn. Mosk. Univ, Fiz. Khim.*, **1**, 225 (1956).
14) A. I. Vogel, "A Textbook of Practical Organic Chemistry" Longman, London (1948).
15) G. Gupta, R. Sharan, and R. N. Kapoor, *Transition Metal Chem.*, **3**, 211 (1978).
16) P. Prashar and J. P. Tandon. *Z. Anorg. Allg. Chem.*, **383**, 81 (1971).
17) P. Prashar and J. P. Tandon. *J. Less-Common Met.*, **15**, 219 (1968).
18) R. Sharan, G. Gupta, and R. N. Kapoor, *J. Less-Common Met.*, **60**, 171 (1978).
19) B. Bhushan, G. Chhatwal, and N. K. Kaushik, *Transition Metal Chem.*, **3**, 215 (1978).
20) R. B. King, "Transition-Metal Organometallic Chemistry," Academic Press, (1969), p. 7.
21) S. A. Gidding and R. J. Bert, *J. Am. Chem. Soc.*, **83**, 2393 (1961).
22) H. P. Fritz., *Adv. Organomet. Chem.*, **1**, 262 (1964).
23) J. Uttamchandani and R. N. Kapoor, *Transition Metal Chem.*, **3**, 79 (1978).
24) R. N. Prasad and J. P. Tandon, *J. Inorg. Nucl. Chem.*, **36**, 1473 (1974).
25) B. D. Sharma and J. C. Bailar, *J. Am. Chem. Soc.*, **77**, 5476 (1955).
26) S. N. Poddar and N. S. Das, *Indian J. Chem.*, **12**, 1105 (1974).
27) K. Issleib and G. Bätz, *Z. Anorg. Allg. Chem.*, **369**, 83 (1969).
28) D. R. Gray and C. H. Drabaker, *Inorg. Chem.*, **10**, 2143 (1971).
29) P. B. Dorain, H. H. Patterson, and P. C. Jordon, *J. Chem. Phys.*, **49**, 3845 (1968).

Reactions of 2-Ethoxycarbonyl-1,3-indandione with Aromatic Amines, Diazonium Salts, and Phenols

El-Sayed Afsah* and Tawfik Zimaity

Department of Chemistry, Faculty of Science, Mansoura University, Mansoura, A. R. Egypt

(Received March 6, 1978)

2-Ethoxycarbonyl-1,3-indandione (**1**) was treated with primary aromatic amines in acetic acid to afford 3-hydroxy-1-(arylimino) derivatives (**2**). Treatment of **1** with excess *p*-toluidine gave 3-tolylimino-4′-methyl-indancarboxanilide (**3**). With *o*- or *p*-phenylenediamine it yielded 3,3′-dihydroxy-1′-(*o*- or *p*-phenylenedinitrilo)di-2-indenecarboxylate. The tetraazacycloeicosene derivative was obtained by the action of *p*-phenylenediamine on **1** in a 1:1 molar ratio. In boiling toluene **1** gave the corresponding 2-carboxanilides (**8**) which cyclized to the diazepinone or to the quinolone. The coupling of **1** and **8** with diazonium salts was also investigated. The condensation of **1** with phenols afford **14**, which were hydrolysed to 3-aryl-1-indenones.

Many reactions of 1,3-indandione and its derivatives with various reagents have been reported.[1-5] However, little work has been done on the reactions of 2-ethoxycarbonyl-1,3-indandione.[6-7] The compound is considered to be an easily available starting material for the synthesis of some new 1,3-indandione derivatives.

We have found that 2-ethoxycarbonyl-1,3-indandione (**1**)[8] reacts with aromatic amines to give various products depending upon the reaction conditions. In hot acetic acid **1** reacts with primary aromatic amines to give ethyl 3-hydroxy-1-(arylimino)-2-indenecarboxylate (enolic form A; **2a**—**d**). Structure of **2** was elucidated on the basis of elemental analysis and IR spectra, which showed bands attributable to (C=N) 1630, enolised *β*-keto ester 1670, 3080 and (C=O) 1705 cm^{-1}. Furthermore, the lack of IR bands characteristic of the (NH) stretching mode ruled out the alternative structure B. Thus, it can be concluded that the structure of **2** is best represented by the enolic form A.

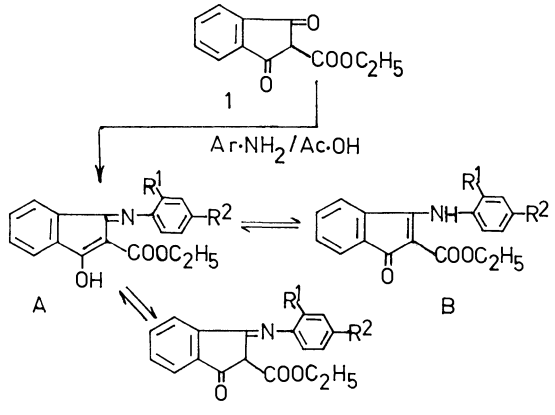

2 a: $R^1=R^2=H$
b: $R^1=H$, $R^2=OCH_3$
c: $R^1=H$, $R^2=CH_3$
d: $R^1=NH_2$, $R^2=H$

Treatment of **1** with excess *p*-toluidine in hot acetic acid gave 1-oxo-3-(*p*-tolylimino)-4′-methyl-2-indancarboxanilide (**3**). The IR spectrum of **3** indicated bands characteristic of the secondary amide group at 3400 (–NH) and 1630, 1540 cm^{-1} (–NHCO–). In particular, the presence of a –NHCO– grouping is confirmed by the NMR spectrum (*δ* 8.1, 1H, s). Attempts to prepare ethyl 1,3-bis(tolylimino)-2-indancarboxylate (**4**) failed.

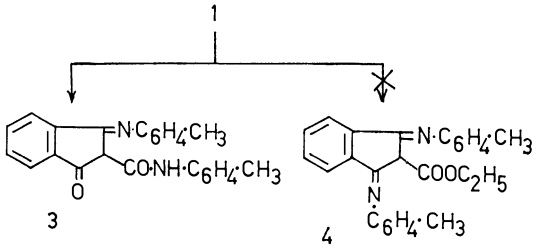

Condensation of **1** with aromatic diamines was also investigated. The reaction of **1** with *o*-phenylenediamine in a 2:1 molar ratio in hot acetic acid yielded a mixture of two compounds, which were separated by their different solubilities in ethanol. The insoluble compound was found to be diethyl 3,3′-dihydroxy-1,1′-(*o*-phenylenedinitrilo)di-2-indenecarboxylate (**5**), while the ethanol soluble one was identified to be **2d** by elemental analysis, mixed mp and IR spectrum. Under essentially the same conditions, condensation of **1** with *p*-phenylenediamine afforded diethyl 3,3′-dihydroxy-1,1′-(*p*-phenylenedinitrilo)di-2-indenecarboxylate (**6**). The assigned structure for the two compounds, **5** and **6**, is inferred from their elemental analyses and the IR spectra. In the mass spectra of both compounds, the basic peak was *m/e* 362 corresponding to the splitting of the two ethoxycarbonyl groups.

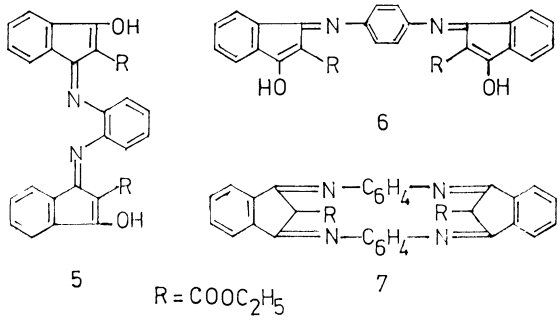

Treatment of **1** with *p*-phenylenediamine in 1:1 molar ratio in acetic acid at 80 °C for 1 h, gave diethyl 7,10:19,22-diethano-5,24:12,17-dimethanodibenzo-[*c*,*m*][1,6,11,16]tetraazacycloeicosene-25,28-dicarboxylate (**7**). The results of the elemental analysis and the mass spectrum were in line with the molecular formula $C_{36}H_{28}N_4O_4$. The structure **7** was assigned

on the basis of its IR spectrum which shows bands at 1725 (ester group), 1200 (C–O stretching), and 1665 cm^{-1} (C=N), its mass spectrum showing a peak at mass *m/e* 490 ($M^+-2(OC_2H_5)$).

On the other hand, treatment of **1** with primary aromatic amines in boiling toluene afforded the corresponding 1,3-dioxo-2-indancarboxanilides (**8a—i**). The products **8** were characterized by analysis and spectral data. They all showed characteristic absorptions at 1680—1700 (C=O) and 1625, 1560 cm^{-1} (–NHCO–). The NMR spectra also exhibited one proton singlet at δ 8.1 due to (–NHCO–). Further, the identity is established by converting **8b** into **3**, by treatment with *p*-toluidine in acetic acid. The action of *o*-, or *p*-phenylenediamine on **1** in boiling toluene gave in each case a single product (**8f** and **g**), respectively. The mass spectra of both compounds, *m/e* 280 (M^+) and 173 ($M^+-NHC_6H_4NH_2$), confirm their structures. Upon treatment with boiling acetic acid, **8f** or **2d** afforded 10,10a,11,12-tetrahydrobenz-[*b*]indeno[1,2-*e*][1,4]diazepine-10,11-dione (**9**). The formation of the diazepine derivative **9** is in line with the work of Ried and Draisbach[9] on the condensation of ethyl 2-oxocyclohexanecarboxylate with *o*-phenylenediamine.

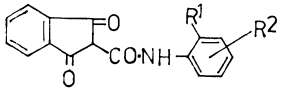

(8) a: $R^1=R^2=H$
b: $R^1=H$, $R^2=CH_3$-p
c: $R^1=H$, $R^2=Cl$-p
d: $R^1=H$, $R^2=Cl$-m
e: $R^1=H$, $R^2=NO_2$-p
f: $R^1=NH_2$, $R^2=H$
g: $R^1=H$, $R^2=NH_2$-p
h: $R^1=H$, $R^2=COCH_3$-p
i: $R^1=H$, $R^2=COOC_2H_5$-p

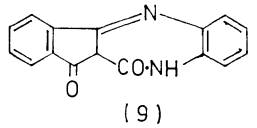

(9)

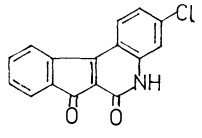

(10)

The synthesis of quinolones by the condensation between *β*-keto esters and primary aromatic amines was described in earlier reports.[10,11] The nature of the product depends on the conditions. Compounds **2** and **8** are considered to be suitable starting materials for the synthesis of new quinolones fused to the indanone and/or indenone nuclues. Thus, **8d** was cyclized according to the Knorr quinolone synthesis[10] by hot sulfuric acid to give 3-chloro-5*H*-indeno[2,1-*c*]quinoline-6,7-dione (**10**).

The structure of the quinolone derivative (**10**) was confirmed by elemental analysis and IR spectrum. An attempt to cyclize **2a** under conditions similar to those for Conrad-Limpach synthesis[11] gave only a black, intractable tar.

Treatment of **1** with diazotised *p*-nitroaniline or bis-(diazotised) benzidine, in basic medium, gave the expected result of a Japp-Klingemann reaction.[12] The ethoxycarbonyl group was cleaved with the formation of 1,2,3-indantrione 2-*p*-nitrophenylhydrazone (**11**), and 4,4′-bis(1,3-dioxo-2-indanylidenehydrazono) biphenyl (**12**) respectively. The melting point of **11** and **12** showed no depression on being mixed with an authentic sample.[13]

On the other hand, coupling of **8a—b** with diazotised

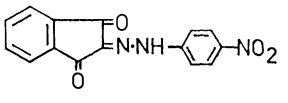

11

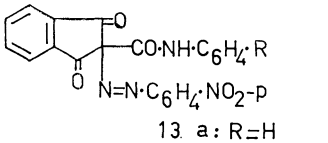

13 a: R=H
b: R=CH_3-p

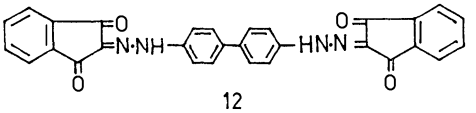

12

p-nitroaniline in methanol afforded 2-(*p*-nitrophenylazo)-1,3-dioxo-2-indancarboxanilide (**13a**) and 2-(*p*-nitrophenylazo)-1,3-dioxo-4′-methyl-2-indancarboxanilide (**13b**), respectively. Structure of **13** was confirmed by elemental analysis and IR spectra. The coupling of *β*-keto anilides has been reported.[14] The formation of the azo derivatives (**13**) is in line with the work of Linstead and Wang[15] on the coupling of 2-oxocyclohexan-1-carboxanilide with benzenediazonium chloride.

The observation that *β*-keto esters react with phenols to form coumarin derivatives (Pechmann reaction),[16] prompted us to investigate the behaviour of **1** under similar reactions in order to obtain 3-arylindenones. Compound **1** was treated with resorcinol[17] and *p*-cresol in ethanolic-hydrogen chloride to give 3-hydroxy-, and 2-methyl-benz[*b*]indeno[1,2-*d*]pyran-6,7-diones (**14a—b**), respectively. Alkaline hydrolysis of **14**, followed by treatment with boiling hydrochloric acid afforded 3-(2-hydroxyphenyl)-1-indenones (**15**). The structure of indenones **15** has been confirmed by analytical data and IR spectroscopy.

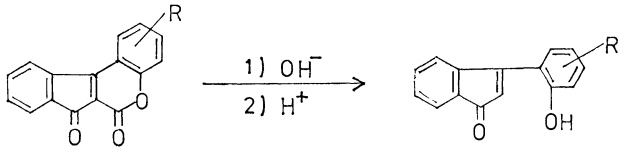

14 15

a: R=OH-m
b: R=CH_3-p

Experimental

All melting points were determined in a capillary and are uncorrected. IR spectra were determined on KBr discs with a Unicam SP 2000 Infrared spectrophotometer. The NMR spectra in $CDCl_3$ solution were obtained on a Varian 60 MHz spectrometer with TMS as an internal standard. The mass spectra were obtained on MS 902 at 70 eV using a direct insertion probe at 250—300 °C.

Ethyl 3-Hydroxy-1-(arylimino)-2-indenecarboxylate (2). *General Procedure*: A mixture of **1** (1.1 g, 0.005 mol) and appropriate primary aromatic amine (2 g) in 10 ml acetic acid was heated at 60 °C for 5 min. After cooling and dilution with water the solid was filtered and crystallized from ethanol.

Ethyl 3-Hydroxy-1-(phenylimino)-2-indenecarboxylate (2a): Orange crystals, yield, 0.8 g (54.8%), mp 152 °C. IR: 3080, 1705, 1670, 1630, and 1040 cm^{-1}. Found: C, 73.81; H, 5.36; N, 4.31%. Calcd for $C_{18}H_{15}NO_3$: C, 73.70; H, 5.15; N, 4.77%.

Ethyl 3-Hydroxy-1-(p-methoxyphenylimino)-2-indenecarboxylate (2b): Brown crystals, yield, 1 g (62.5%), mp 162 °C (dec).

IR: 3085, 1700, 1665, 1630, and 1045 cm^{-1}. Found: C, 70.34; H, 5.11; N, 4.10%. Calcd for $C_{19}H_{17}NO_4$: C, 70.57; H, 5.30; N, 4.32%.

*Ethyl 3-Hydroxy-1-(*p*-tolylimino)-2-indenecarboxylate (**2c**)*: Orange crystals, yield, 0.9 g (58.8%), mp 174 °C. IR: 3080, 1700, 1660, 1625, and 1050 cm^{-1}. Found: C, 74.48; H, 5.61; N, 4.33%. Calcd for $C_{19}H_{17}NO_3$: C, 74.24; H, 5.57; N, 4.55%.

*Ethyl 3-Hydroxy-1-(*o*-aminophenylimino)-2-indenecarboxylate (**2d**)*: Dark brown crystals, yield, 0.5 g (32.4%), mp>300 °C. IR: 3280, 3100, 1690, 1650, and 1625 cm^{-1}. Found: C, 69.82; H, 5.13; N, 8.88%. Calcd for $C_{18}H_{16}N_2O_3$: C, 70.11; H, 5.20; N, 9.08%.

*1-Oxo-3-(*p*-tolylimino)-4'-methyl-2-indancarboxanilide (**3**)*: From 1.1 g (0.005 mol) of **1** and 3 g of *p*-toluidine dissolved in (10 ml) acetic acid, **3** was obtained by the same procedure as that for **2**. Recrystallization from methanol gave 0.8 g (43%) of **3** as a brown crystalline powder; mp 205 °C (dec). IR: 3400, 2920, 1670, 1630, 1540, 1525, and 1250 cm^{-1}; NMR ($CDCl_3$): δ; 2.6 (1H s, –CO–CH–CO–); 2.41 (6H s, $C_6H_4CH_3$); 7.33 (8H s, $C_6H_4CH_3$); 7.62 (4H d, *o*-substituted C_6H_4) and 8.1 ppm (1H s, –NH–CO–). Found: C, 78.31; H, 5.50; N, 7.31%. Calcd for $C_{24}H_{20}N_2O_2$: C, 78.23; H, 5.47; N, 7.60%.

*Diethyl 3,3'-Dihydroxy-1,1'-(*o*-phenylenedinitrilo)di-2-indenecarboxylate (**5**)*: A mixture of 1.1 g (0.005 mol) of **1** and 0.3 g (0.0025 mol) of *o*-phenylenediamine in 10 ml acetic acid was heated with stirring for 15 min. The reaction mixture gave a dark brown solid (0.8 g) on dilution with water, which on treatment with boiling ethanol gave **5** as an insoluble red solid (0.5 g). Recrystallization from acetic acid afforded **5** as red crystals; mp>300 °C. IR: 3100, 1700, 1650, and 1635 cm^{-1}. MS, *m/e* 362 (base, M^+-2 $COOC_2H_5$), 274, 104, and 76. Found: C, 71.00; H, 4.95; N, 5.37%. Calcd for $C_{30}H_{24}N_2O_6$: C, 70.85; H, 4.75; N, 5.51%.

Concentration of the ethanolic filterate after separation of **5** gave 0.14 g of **2d** as dark brown crystals, the IR spectrum of which was identical with that of the authentic sample of **2d** obtained above.

*Diethyl 3,3'-Dihydroxy-1,1'-(*p*-phenylenedinitrilo)di-2-indenecarboxylate (**6**)*: From 1.1 g (0.005 mol) of **1** and 0.3 g (0.0025 mol) of *p*-phenylenediamine dissolved in 10 ml acetic acid, **6** was obtained according to the same procedure as that for **5**. Recrystallization from benzene–ethanol gave 0.7 g (27.5%) of **6** as dark brown powder; mp>300 °C. IR: 3105, 1690, 1655, and 1640 cm^{-1}. MS, *m/e* 362 (base, M^+-2 $COOC_2H_5$), 274, 104, and 76. Found; C, 70.91; H, 4.66; N, 5.40%. Calcd for $C_{30}H_{24}N_2O_6$: C, 70.85; H, 4.75; N, 5.51%.

Diethyl 7,10:19,22-Dietheno-5,24:12,17-dimethanodibenzo [c,m]-*[1,6,11,16]tetraazacycloeicosene-25,28-dicarboxylate (**7**)*: A mixture of 1.1 g (0.005 mol) of **1** and 0.6 g (0.006 mol) of *p*-phenylenediamine in 20 ml acetic acid was heated at 80 °C for 1 h with stirring. The reaction mixture was diluted with water, and filtered to give dark green material (0. 6g). Crystallization from ethanol–benzene (1:1) afforded **7** as a dark green powder (0.4 g); mp 255 °C, IR: 1725, 1665, and 1200 cm^{-1}; MS, *m/e* 490 ($M^+-2(OC_2H_5)$), 366, 169, and 76. Found: C, 74.60; H, 4.90; N, 9.42%. Calcd for $C_{36}H_{28}N_4O_4$: C, 74.46; H, 4.86; N, 9.65%.

*1,3-Dioxo-2-indancarboxanilides (**8a—i**)*: A mixture of 1.1 g (0.005 mol) of **1** and 0.0055 mol of the appropriate primary aromatic amine in 50 ml toluene was refluxed for 30 min. The solid obtained after concentration and cooling was filtered. Recrystallization from benzene gave **8a—i** as yellow crystalline solids. The results are summarized in Table 1.

*Formation of **3** from **8b***: A mixture of 0.28 g (0.001 mol) of **8b** and 0.11 g (0.001 mol) of *p*-toluidine in 10 ml acetic acid was heated at 70 °C for 10 min. The solid obtained on dilution with water was filtered and crystallized from benzene to give 0.08 g of **3**. The IR spectrum of the product was identical with that of the authentic sample of **3**.

10,10a,11,12-Tetrahydrobenz [b] *indeno* [1,2-e] [1,4] *diazepine-10,11-dione (**9**)*: 0.5 g of **8f** or **2d** was refluxed in 30 ml acetic acid. The dark red solid obtained on cooling was filtered and recrystallized from acetic acid to give 0.22 g of **9** as a red crystalline solid; mp>300 °C. IR: 3210, 1705, 1650, 1630, and 1575 cm^{-1}. Found: C, 73.34; H, 4.10; N, 10.31%. Calcd for $C_{16}H_{10}N_2O_2$: C, 73.27; H, 3.84; N, 10.68%.

*3-Chloro-5H-indeno[2,1-c]quinoline-6,7-dione (**10**)*: 0.5 g of **8d** was heated with 20 ml of H_2SO_4 (85%) in an oil bath at 110 °C for 1 h. After cooling, the reaction mixture was diluted with 80 ml cold water, and the brown solid obtained was filtered. Crystallization from benzene–ethanol gave 0.16 g of **10**; mp>300 °C. IR: 2900, 1725, 1670, 1620, 1590, and 1450 cm^{-1}. Found: C, 67.91; H, 3.01; N, 4.66%. Calcd for $C_{16}H_8NO_2Cl$: C, 68.22; H, 2.86; N, 4.97%.

*Coupling of **1** with* p*-Nitrobenzenediazonium Chloride and Bis-(diazotised) Benzidine*: Diazotised *p*-nitroaniline (0.005 mol), or bis(diazotised) benzidine (0.0025 mol), was added with stirring to a cold solution of **1** (0.005 mol) in 50 ml 2.5% aq NaOH. Sodium acetate (2 g) was added, and the reaction mixture was left to stand under cooling overnight. The brown solid obtained was crystallized from acetic acid to give **11** and **12**, respectively, in a 75% yield. Compounds **11** and **12** were identical with the corresponding authentic samples prepared from 1,3-indandione by the method of Das and Ghosh.[13]

*Coupling of **8a—b** with Diazotised* p*-Nitroaniline*: Diazotised *p*-nitroaniline (0.003 mol) was added with stirring to a cold solution of **8a** or **8b** (0.003 mol) in 60 ml methanol, followed by addition of lg of sodium acetate in 5 ml water. The

Table 1. 1,3-Dioxo-2-indancarboxanilides (**8**)

Compound No.	Mp °C	Yield %	Formula	Found (%) C	H	N	Calcd (%) C	H	N	IR(KBr) ν_{max}/cm^{-1}
8a	148	61	$C_{16}H_{11}NO_3$	72.11	4.23	5.00	72.44	4.18	5.27	3402, 1680, 1560
8b	188	43	$C_{17}H_{13}NO_3$	73.31	4.37	5.15	73.10	4.69	5.01	3400, 1685, 1560
8c	200	77	$C_{16}H_{10}NO_3Cl$	64.33	3.41	4.52	64.10	3.36	4.67	3390, 1680, 1565
8d	170	70	$C_{16}H_{10}NO_3Cl$	64.25	3.51	4.53	64.10	3.36	4.67	3390, 1680, 1560
8e	228	53	$C_{16}H_{10}N_2O_5$	61.56	3.50	8.95	61.93	3.24	9.03	3400, 1685, 1560
8f	>300	45	$C_{16}H_{12}N_2O_3$	68.43	4.11	10.03	68.56	4.31	9.99	3400, 1685, 1550
8g	280	41	$C_{16}H_{12}N_2O_3$	68.37	4.20	10.01	68.56	4.31	9.99	3400, 1680, 1550
8h	185	66	$C_{18}H_{13}NO_4$	70.26	4.31	4.38	70.35	4.26	4.55	3400, 1700, 1555
8i	161	52	$C_{19}H_{15}NO_5$	67.41	4.20	4.00	67.64	4.48	4.15	3400, 1740, 1560

solid obtained was crystallized from methanol to give **13a—b**, respectively.

*2-(p-Nitrophenylazo)-1,3-dioxo-2-indancarboxanilide (**13a**)*: Orange crystals, yield, 0.19 g (15.3%), mp 132 °C. IR: 3060, 1700, 1650, 1580, 1340, and 890 cm^{-1}. Found: C, 63.61; H, 3.17; N, 13.68%. Calcd for $C_{22}H_{14}N_4O_5$: C, 63.76; H, 3.40; N, 13.52%.

*2-(p-Nitrophenylazo)-1,3-dioxo-4′-methyl-2-indancarboxanilide (**13b**)*: Yellow crystals, yield, 0.16 g (12.5%), mp 158 °C. IR: 3065, 1700, 1640, 1585, 1345, and 890 cm^{-1}. Found: C, 64.22; H, 3.68; N, 12.88%. Calcd for $C_{23}H_{16}N_4O_5$: C, 64.48; H, 3.76; N, 13.07%.

*Condensation of **1** with Phenols*: Cold saturated ethanolic hydrogen chloride (10 ml) was added with stirring to a mixture of 2 g of **1** and resorcinol or *p*-cresol (6 g) in 30 ml ethanol. After 24 h the yellow crystalline product was filtered, washed with ethanol and acetone to give **14a—b** respectively.

3-Hydroxybenz[b]*indeno*[*1,2*-d]*pyran-6,7-dione (**14a**)*: Yellow crystals, yield, 1 g (37.8%). Its mp and IR spectrum were identical with those of an authentic sample.[17]

2-Methylbenz[b]*indeno*[*1,2*-d]*pyran-6,7-dione (**14b**)*: Recrystallized form ethanol, pale yellow crystals, yield, 0.5 g (19%), mp 265 °C. IR: 1740, 1720, 1590, and 1470 cm^{-1}. Found: C, 77.67; H, 4.00%. Calcd for $C_{17}H_{10}O_3$: C, 77.85; H, 3.84%.

*3-(2-Hydroxyphenyl)indenones (**15**)*: A solution of aq NaOH (5%, 20 ml) was added to boiling solution of **14a** or **14b** (0.002 mol) in ethanol (40 ml). The reaction mixture was refluxed for 1 h, acidified with dil hydrochloric acid and the resulting precipitates were filtered and dried to give **15a**, 0.15 g (32%). Recrystallization from methanol afforded greenish-yellow crystals; mp 177 °C. IR: 3410, 1740, 1630, 1375, 1270, and 1180 cm^{-1}. Found: C, 75.46; H, 4.06%. Calcd for $C_{15}H_{10}O_3$: C, 75.62; H, 4.23%.

*3-(2-Hydroxy-*m*-tolyl)indenone (**15b**)*: Orange crystals from methanol, yield, 0.2 g (42%), mp 147 °C. IR: 3400, 1735, 1620, 1370, 1270, and 1185 cm^{-1}. Found: C, 81.16; H, 5.22%. Calcd for $C_{16}H_{12}O_2$: C, 81.33; H, 5.12%.

We wish to express our sincere gratitude to Dr. A. M. Dawidar for the NMR and mass measurements.

References

1) W. Wislicenus and H. Pfannenstiel, *Chem. Ber.*, **50**, 183 (1917).
2) S. Sastry and B. Ghosh, *J. Chem. Soc.*, **1915**, 1442.
3) A. Cirulis, *Justus Liebigs Ann. Chem.*, **522**, 278 (1936).
4) C. Marchase, *Gazz. Chim. Ital.*, **37**, 303 (1907); *J. Chem. Soc. Abstr.*, i, **1907**, 941.
5) K. Ezoe and K. Kurosawa, *Bull. Chem. Soc. Jpn.*, **50**, 443 (1977).
6) V. Demselben, *Justus Liebigs Ann. Chem.*, **246**, 355 (1888).
7) M. T. El-Zimaity, E. M. Kandeel, S. El-Morsi, and M. H. Elnagdi, *Z. Naturforsch., Teil B*, **32**, 698 (1977).
8) W. Wislicenus, *Justus Liebigs Ann. Chem.*, **246**, 349 (1888).
9) W. Ried and A. Draisbach, *Chem. Ber.*, **92**, 949 (1959).
10) L. Knor, *Justus Liebigs Ann. Chem.*, **236**, 83 (1886).
11) M. Conrad and L. Limpach, *Chem. Ber.*, **20**, 944 (1887).
12) F. Japp and F. Klingemann, *Chem. Ber.*, **21**, 549 (1888); *J. Chem. Soc.*, **1888**, 519.
13) A. Das and B. Ghosh, *J. Am. Chem. Soc.*, **43**, 1739 (1921).
14) S. M. Parmerter, "Organic Reactions," ed by R. Adams, E. Krieger Publishing Company Huntington, New York (1975), Vol. X, Chap. 1, p. 13.
15) R. P. Linstead and A. B. Wang, *J. Chem. Soc.*, **1937**, 807.
16) H. Von Pechmann and C. Duisberg, *Ber.*, **16**, 2119 (1883).
17) H. Appel, W. Baker, H. Hagenbach, and R. Robinson, *J. Chem. Soc.*, **1937**, 738.

Synthesis and Absorption Spectra of Some 6-Hydroxythiazolo[3,2-*a*]-benzimidazoles and Their Quaternary Derivatives

R. P. Soni and J. P. Saxena*

Department of Chemistry, University of Jodhpur, Jodhpur, India

(Received January 30, 1979)

A series of substituted 6-Hydroxythiazolo[3,2-*a*]benzimidazoles has been synthesized. Their quaternary derivatives showed characteristic absorption maxima at longer wavelengths in visible region. The spectral study of parent compounds in the visible region shows a red shift at higher pH which is attributed to the dipolar nature of these compounds.

The chemotherapeutic importance of imidazole derivatives is well recognized.[1–3] The effectiveness of condensed heterocycles containing thiazole and imidazole rings as antiprotozoal agents,[4] anticonvulsants,[5] antidepressants,[6] antihelminthic agents,[7–10] antidiabetic,[11] and as inhibitors of dihydrofolate[12] led us to synthesize a new series of thiazolobenzimidazoles in a manner analogous to Schmid and Czerney's[13] synthesis of 8-hydroxypyrido[1,2-*a*]benzimidazole. Rudner[14] synthesized some of the 6-hydroxy-substituted thiazolo[3,2-*a*]benzimidazoles by the condensation of substituted 2-aminothiazoles with *p*-benzoquinone in acetic acid. We followed the same procedure and obtained more new compounds of the above series. A study of their finer structure through spectral analysis was made. The thiazolobenzimidazoles so obtained were quaternized with ethyl bromide giving the corresponding 9-ethyl-6-hydroxythiazolo[3,2-*a*]benzimidazolium bromides. These quaternary compounds gave intense yellow color with dilute aqueous alkali due to the formation of phenol betaines.[15–16] The colored betaines could be extracted in the chloroform layer giving a deep violet color. The color was discharged on acidification which is the reversal of the mode of formation of these betaines.

Experimental

All the reagents were thoroughly dried and purified before use. All melting points were determined on Kofler instrument and were uncorrected. IR spectra were recorded on a Perkin-Elmer 577 spectrophotometer in KBr. UV absorption spectra were scanned in Beckman spectrophotometer, Model DU-2.

2-Aminothiazoles: These compounds were prepared by known method.[17]

*6-Hydroxythiazolo[3,2-*a*]benzimidazoles (I).* A solution of *p*-benzoquinone (0.01 mol) in glacial acetic acid (10 ml) was added in small portions to the substituted 2-aminothiazole (0.01 mol) in acetic acid (10 ml) with shaking. The mixture was left aside for 30 min. After addition of 20 ml of 50% aq HCl, the solution was diluted with water, and extracted with ether to remove any unreacted quinone and hydroquinone. The resulting solution was made alkaline with aq sodium carbonate when the desired compound precipitated. After treatment with charcoal in ethanol, the compound was recrystallized from ethanol. The yields, mp; *etc.* are given in Table 1.

*9-Ethyl-6-hydroxythiazolo[3,2-*a*]benzimidazolium Bromides (II).* A mixture of I (0.01 mol) and ethyl bromide (0.01 mol) in a minimum quantity of acetone was boiled under reflux for 1 h. The solvent was evaporated to dryness under reduced pressure and the residue was crystallized from ethanol–ether. The yields, mp *etc.* are given in Table 2.

Discussion

All these compounds are deep colored powdery substances, insoluble in water but are readily soluble in ethanol. They do not melt upto 330 °C. The structure of these compounds has been determined on the basis of IR spectra and elemental analysis. The IR spectra of these compounds showed bands at 3210, 1200 (phenolic OH), 1610(C=N), 1310(C–N), and 1440 cm^{-1} (aromatic

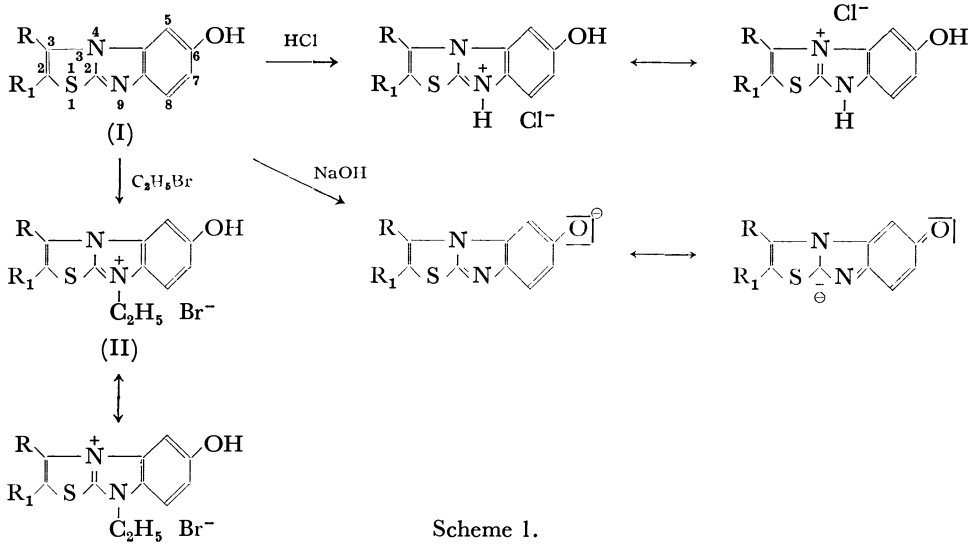

Scheme 1.

Table 1. 6-Hydroxythiazolo[3,2-*a*]benzimidazoles (I)

Compd No.	R	R_1	Molecular formula	Analysis (%)		Yield %	UV spectra: Ethanol λ_{max} nm	Ethanol log ε	0.1 M HCl λ_{max} nm	0.1 M HCl log ε	0.1 M NaOH λ_{max} nm	0.1 M NaOH log ε
				Calcd	Found							
1	C_6H_5	H	$C_{15}H_{10}N_2OS$	C, 67.6	67.4	55	230	4.13				
				H, 3.7	3.6		258	3.93	315	3.40	312	3.53
				N, 10.5	10.4		350	3.39	375	3.47	450	3.55
2	CH_3	H	$C_{10}H_8N_2OS$	C, 58.8	58.6	40	236	4.01				
				H, 3.9	3.7		253	3.95	310	3.43	305	3.54
				N, 13.7	13.5		357	3.56	366	3.71	435	3.43
3	CH_3	$COOC_2H_5$	$C_{13}H_{12}N_2O_3S$	C, 56.5	56.4	57	240	3.98				
				H, 4.3	4.1		255	3.90	313	3.41	308	3.51
				N, 10.1	9.9		361	3.78	372	3.35	415	3.29
4	H	CH_3	$C_{10}H_8N_2OS$	C, 58.8	58.5	36	244	3.80				
				H, 3.9	3.8		272	3.74	321	3.37	310	3.48
				N, 13.7	13.5		355	3.40	370	3.5	427	3.35
5	CH_3	C_6H_5	$C_{16}H_{12}N_2OS$	C, 68.5	68.1	25	245	3.60				
				H, 4.28	4.1		278	3.57	329	3.8	324	3.2
				N, 10.0	9.8		364	3.60	385	3.3	450	3.7
6	*p*-$CH_3C_6H_4$	H	$C_{16}H_{12}N_2OS$	C, 68.5	68.3	40	238	3.76				
				H, 4.28	4.20		275	3.54	325	3.6	318	3.3
				N, 10.0	9.7		362	3.65	380	3.5	445	3.46
7	*p*-BrC_6H_4	H	$C_{15}H_9N_2OSBr$	C, 52.1	52.0	39	245	3.69				
				H, 2.5	2.3		267	4.35	319	3.38	312	3.43
				N, 8.1	8.1		357	3.81	384	3.40	449	3.61
8	*p*-HOC_6H_4	H	$C_{15}H_{10}N_2O_2S$	C, 63.8	63.5	48	248	4.01				
				H, 3.54	3.32		272	4.41	315	3.46	308	3.28
				N, 9.95	9.67		352	3.87	377	3.38	438	3.72
9	2-Thienyl	H	$C_{13}H_8N_2OS_2$	C, 57.3	57.1	53	251	4.31				
				H, 2.94	2.78		277	4.13	334	3.84	325	3.63
				N, 10.2	10.1		368	3.61	387	3.61	453	3.57
10	2-Naphthyl	H	$C_{19}H_{12}N_2OS$	C, 72.1	71.8	35	254	3.84				
				H, 3.78	3.52		279	4.12	339	3.51	322	3.31
				N, 8.86	8.75		372	3.71	383	3.47	451	3.57

Note: Compounds No. **1**, **2**, **4**, **5** are reported.[14]

Table 2. 9-Ethyl-6-hydroxythiazolo[3,2-*a*]benzimidazolium bromides (II)

Compd No.	R	R_1	Molecular formula	Mp °C	Yield %	Analysis (%) Calcd	Analysis (%) Found	UV, Ethanol λ_{max} nm	UV, Ethanol log ε
1	C_6H_5	H	$C_{17}H_{15}N_2OSBr$	310	40	N, 7.43	7.41	260	3.84
						Br, 21.3	21.2	510	4.00
2	CH_3	H	$C_{12}H_{13}N_2OSBr$	299	35	N, 8.94	8.89	265	3.65
						Br, 25.5	25.4	525	3.90
3	CH_3	$COOC_2H_5$	$C_{15}H_{17}N_2O_3SBr$	317	25	N, 7.27	7.16	257	3.45
						Br, 20.7	20.5	515	3.85
4	H	CH_3	$C_{12}H_{13}N_2OSBr$	285	25	N, 8.94	8.92	253	3.50
						Br, 25.5	25.3	530	3.64
5	CH_3	C_6H_5	$C_{18}H_{17}N_2OSBr$	360	30	N, 6.88	6.86	250	3.50
						Br, 19.5	19.3	512	3.81
6	*p*-$CH_3C_6H_4$	H	$C_{18}H_{17}N_2OSBr$	293	40	N, 6.88	6.85	264	3.72
						Br, 19.5	19.4	526	3.94
7	*p*-BrC_6H_4	H	$C_{17}H_{14}N_2OSBr_2$	288	37	N, 7.48	7.37	260	3.40
						Br, 21.3	21.0	512	3.81
8	*p*-HOC_6H_4	H	$C_{17}H_{15}N_2O_2SBr$	280	41	N, 7.17	7.09	255	3.38
						Br, 20.5	20.1	508	3.63
9	2-Thienyl	H	$C_{15}H_{13}N_2OS_2Br$	326	51	N, 7.34	7.31	271	3.71
						Br, 20.9	20.6	535	3.56
10	2-Naphthyl	H	$C_{21}H_{17}N_2OSBr$	304	45	N, 6.58	6.37	276	3.51
						Br, 18.5	18.3	519	3.87

ring breathing).

A study of the absorption spectra of various substituted 6-hydroxythiazolo[3,2-*a*]benzimidazoles in ethanol at different pH shows a bathochromic shifting of the absorption maxima in both acidic and alkaline media. The observed bathochromic shift might be explained by the canonical quinonoid structure shown in Scheme 1. Same phenomenon is observed when these compounds are quaternized with ethyl bromide which results into further red shifting of absorption maxima in visible region.

For the sake of comparison of the absorption spectra of these title compounds (I), 8-hydroxypyrido[1,2-*a*]-benzimidazole was synthesized by the method described by Schmid and Czerney.[13] A study of its absorption spectra in ethanol under various conditions (Table 3) also shows a red shifting of absorption band in the longer wavelengths in alkaline medium whereas in acid medium the spectra remain practically unaltered.

Table 3. Absorption spectra of 8-hydroxy-pyrido[1,2-*a*]benzimidazole

S. No.	Compound	λ_{max}/nm (log ε)			
1	Parent base in ethanol	—	360 (3.78)	300 (3.76)	248 (4.5)
2	Parent base in alkaline ethanol	405 (3.87)	—	268—270 (4.49)	242 (4.36)
3	Parent base in acidic ethanol	—	358 (3.94)	292 (3.71)	238 (4.17)

It has been observed by Edger *et al.*[18] that the 5- or 6-chlorobenzimidazoles do not show any shifting of absorption maxima in ethanolic solution of different pH. It indicates that the presence of 6-hydroxyl group in these title compounds which being more acidic causes the molecule to attain greater dipolar character at different pH thereby facilitating absorption in the longer wavelengths.

Thanks are due to Professor R. C. Kapoor for providing necessary laboratory facilities and to the U. G. C., New Delhi for awarding a research scholarship to one of them (R. P. S). We are also thankful to the Director, C. D. R. I. Lucknow for the IR spectra and elemental analysis.

References

1) P. K. Smith and A. C. Hollinshead, *J. Pharmacol. Exp. Ther.*, **54**, 123 (1958).
2) A. F. Wagner, P. E. Wihereich, A. Luisi, and K. Folkers, *J. Org. Chem.*, **27**, 3236 (1962).
3) E. W. Bernadt, H. U. Esser, and B. G. Held, *J. Med. Chem.*, **12**, 371 (1969).
4) J. M. Singh, *J. Med. Chem.*, **13**, 1019 (1970).
5) C. J. Sharpe, R. S. Shadbolt, A. Ashferd, and J. W. Ross, *J. Med. Chem.*, **14**, 977 (1971).
6) L. F. Miller and R. E. Bambory, *J. Med. Chem.*, **15**, 415 (1972).
7) R. K. Robins and G. H. Hitchings, *J. Am. Chem. Soc.*, **80**, 3449 (1958).
8) A. H. M. Raeymakers, F. T. N. Alleuigin, J. Vandenherk, P. J. A. Domoen, T. T. T. V. Ottenwert, and P. A. J. Janssen, *J. Med. Chem.*, **9**, 545 (1966).
9) J. S. Remders, *Neth. J. Vet. Sci.*, **91**, 967 (1966).
10) M. H. Fisher and A. Lusi, *J. Med. Chem.*, **15**, 983 (1972).
11) K. Okamato, T. Taii, H. Koso, N. Takenaka, T. Hayakawa, and T. Ibaraki, *J. Exptl. Med.*, **61**, 31 (1955).
12) B. S. Hurbert, R. Perone, T. A. Hermann, and G. H. Hitchings, *J. Med. Chem.*, **11**, 711 (1968).
13) L. Schmid and H. Czerney, *Monatsh. Chem.*, **83**, 31 (1952).
14) B. Rudner, *Chem. Abstr.*, **51**, 13934a (1957).
15) J. P. Saxena, *J. Sci. Ind. Res.*, **22**, 81 (1963).
16) J. P. Saxena, W. H. Stafford, and W. L. Stafford, *J. Chem. Soc.*, **1959**, 1579.
17) (a) B. C. Dash and G. N. Mahapatra, *Indian J. Chem.*, **5**, 40 (1967); (b) B. L. Carrollking and R. J. Hlavacer, *J. Am. Chem. Soc.*, **72**, 3722 (1950).
18) A. S. Edgar, C. N. Frederick, W. E. Galen, and H. G. Nancy, *J. Am. Chem. Soc.*, **70**, 3406 (1948).

NOTES

BULLETIN OF THE CHEMICAL SOCIETY OF JAPAN, VOL. 52 (10), 3099—3100 (1979)

Formation of Benzyl Radicals by Pulse Radiolysis of Benzyltriphenylphosphonium Chloride in Aqueous Solutions

Hideo Horii,* Shinichi Fujita, Toshiaki Mori, and Setsuo Taniguchi

Department of Chemistry, Radiation Center of Osaka Prefecture, Shinke-cho, Sakai, Osaka 593

(Received February 19, 1979)

Synopsis. The reaction of benzyltriphenylphosphonium ion ($PhCH_2P^+Ph_3$) with e^-_{aq} has been studied. The benzyl radical and triphenylphospine are formed by the reaction: $PhCH_2P^+Ph_3+e^-_{aq}\rightarrow PhCH_2\cdot+Ph_3P$, with the rate constant $(2.7\pm0.3)\times10^{10}$ M^{-1} s^{-1}. The benzyl radical decays in a bimolecular reaction with $2k=(2.7\pm0.4)\times10^9$ M^{-1} s^{-1}.

Tetraphenylphosphonium ions (Ph_4P^+) are reduced with hydrated electrons to form $Ph_4P\cdot$ radicals which decay by disproportionation.[1]

On the other hand, optically active tertiary phosphines have been prepared without racemization by electrochemical reduction of quaternary phosphonium salts having the benzyl group.[2,3] This indicates that the electron is transferred directly to the benzyl group and not to the phosphorus atom, causing fission to form a tertiary phosphine and benzyl radical, since nucleophilic attack on phosphorus leads to inversion of configuration.[4] The present investigation deals with the direct confirmation of this scheme by the pulse radiolysis method.

Experimental

The experimental details and dosimetry were reported.[5] A 500 W Xe lamp was used to follow the decay of the hydrated electron and observe other transient and permanent absorptions. All solutions were prepared from triply distilled water. The solutions were buffered with 1 mM phosphate. Deaeration of solutions was performed by argon bubbling for about 2 h. The reagents were of analytical grade and used without further purification. A fresh solution was used for each pulse. Ph_3P aqueous solution used for the absorption spectra was prepared by mixing 5×10^{-5} M Ph_3P EtOH solution with H_2O.

Results and Discussion

Pulse radiolysis of deaerated neutral aqueous solutions of benzyltriphenylphosphonium chloride yielded a transient species and products. Figure 1 shows the spectra observed immediately and 5 ms after the cessation of pulse in a buffered solution at pH 7 of 2×10^{-5} M benzyltriphenylphosphonium chloride containing 0.2 M *t*-butyl alcohol as an OH radical scavenger. The absorption at 5 ms after cessation of the pulse seems to be permanent from oscilloscopic tracing. On saturating the solution with dinitrogen oxide which converts e^-_{aq} into OH radicals, the transient absorption almost disappeared. Thus, transient and permanent absorptions are caused by the reaction of the phosphonium ion with e^-_{aq}.

Figure 2 shows the spectrum of the intermediate

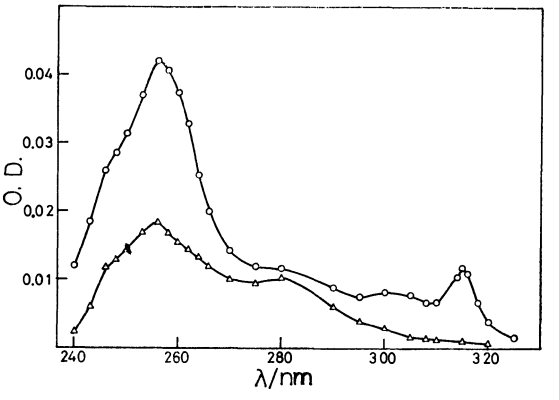

Fig. 1. Absorption spectra observed after pulse irradiation in a deaerated aqueous solution of 2×10^{-5} M benzyltriphenylphosphonium chloride, 0.2 M *t*-butyl alcohol at pH 7. Dose, 430 rad: (○) end of the pulse; (△) 5 ms after the pulse.

obtained by subtraction of the absorption taken 5 ms after cessation of the pulse from that taken immediately on cessation (Fig. 1). The spectrum has three maxima at 258, 305, and 315 nm with the estimated extinction coefficients 13300, 3400, and 5900 M^{-1} cm^{-1}, respectively, taking $G(e^-_{aq})=2.7$. The spectrum is very similar to that of the benzyl radical[6] in aqueous solutions, which has three maxima at 258, 307, and 317.5 nm with extinction coefficients 14000, 3300, and 5500 M^{-1} cm^{-1}, respectively.

Figure 3 shows the absorption spectrum at 5 ms after the pulse corrected for the depletion of the solute ($PhCH_2P^+Ph_3Cl^-$), and that of aqueous Ph_3P solution

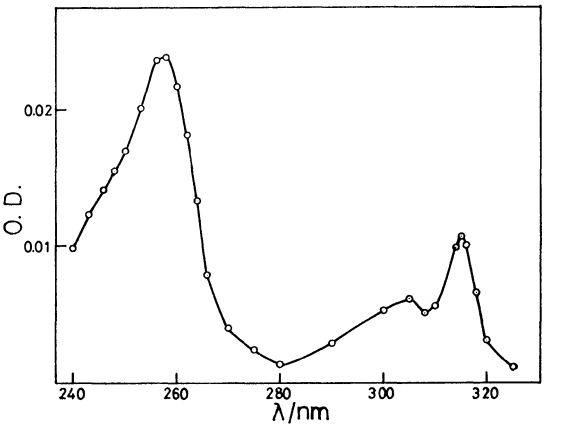

Fig. 2. Transient spectrum corrected for the permanent absorption obtained from Fig. 1.

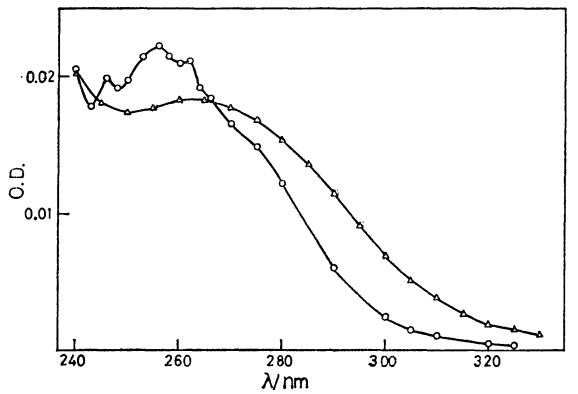

Fig. 3. Absorption spectra of the stable products corrected for depletion of the substrate obtained from Fig. 1 (○) and that of ethanolic aqueous solution of Ph_3P corresponding to the e^-_{aq} concentration in Fig. 1 (△).

corresponding to the concentration of the e^-_{aq} produced under the conditions of Fig. 1. The absorption spectrum of Ph_3P in Fig. 3 was obtained from that of 9×10^{-6} M Ph_3P aqueous solution containing 20 vol% EtOH, which has an absorption maximum at 260—265 nm with $\varepsilon=10300\ M^{-1}\ cm^{-1}$. The permanent absorption spectrum formed by pulse radiolysis probably comes from PPh_3, since the two spectra are considerably similar. The small difference in the absorption spectra below 260 nm may be due to bibenzyl[7] produced by the recombination of benzyl radicals and the one beyond 270 nm may arise from undissolved triphenylphosphine in water.

The transient absorption at 315 nm (Fig. 2) disappears in a bimolecular reaction with $2k=(2.7\pm0.4)\times10^9\ M^{-1}\ s^{-1}$. The absorption at 258 nm, which is corrected for the permanent one, decays by a second-order kinetics with the same rate constant as that at 315 nm within an experimental error. This indicates that the permanent absorption takes place immediately on cessation of the pulse. The rate constant agrees with the previous values $(3.1\pm0.3)\times10^9$,[6] $2.4\times10^9\ M^{-1}\ s^{-1}$.[8]

The results suggest that the $PhCH_2P^+Ph_3$ ion is reduced with e^-_{aq} to dissociate into the benzyl radical and triphenylphosphine. The following reaction scheme may be suggested:

$$H_2O \rightsquigarrow e^-_{aq},\ H,\ OH,\ etc. \quad (1)$$

$$OH + t\text{-BuOH} \longrightarrow t\text{-BuOH radical} + H_2O \quad (2)$$

$$PhCH_2P^+Ph_3 + e^-_{aq} \longrightarrow PhCH_2\cdot + Ph_3P \quad (3)$$

$$PhCH_2\cdot + PhCH_2\cdot \longrightarrow \text{Products} \quad (4)$$

$$e^-_{aq} + N_2O \longrightarrow OH + OH^- + N_2 \quad (5)$$

The rate constant for the reaction of the $PhCH_2P^+Ph_3$ ion with e^-_{aq} is $(2.7\pm0.3)\times10^{10}\ M^{-1}\ s^{-1}$, which was determined from the decay of e^-_{aq}. The rate constant is diffusion controlled, similar to that[1] of Ph_4P^+ with e^-_{aq}.

The phosphoranyl radical $PhCH_2\dot{P}Ph_3$ might not be sufficiently stable to be observed in the microsecond pulse radiolysis. It seems reasonable to assume that e^-_{aq} attacks the $PhCH_2$ group, and causing release of the benzyl radical before the electron is delocalized to form the phosphoranyl radical.

The reaction mechanism might be similar to that of the electroreduction of quaternary ammonium compound.[9,10]

References

1) H. Horii, S. Fujita, T. Mori, and S. Taniguchi, *Int. J. Radiat. Phys. Chem.*, **8**, 521 (1976).
2) L. Horner, H. Winkler, A. Rapp, A. Mentrup, H. Hoffmann, and P. Beck, *Tetrahedron Lett.*, **1961**, 161.
3) L. Horner and H. Winkler, *Tetrahedron Lett.*, **1964**, 175.
4) R. F. Hudson, "Structure and Mechanism in Organophosphorus Chemistry," Academic Press, London (1965), pp. 211—212.
5) S. Fujita, H. Horii, and S. Taniguchi, *J. Phys. Chem.*, **77**, 2868 (1973).
6) H. C. Christensen, K. Sehested, and E. J. Hart, *J. Phys. Chem.*, **77**, 983 (1973).
7) H. C. Christensen and R. Gustafsson, *Acta Chem. Scand.*, **26**, 937 (1972).
8) K. Sehested, H. Corfitzen, H. C. Christensen, and E. J. Hart, *J. Phys. Chem.*, **79**, 310 (1975).
9) M. Finkelstein, R. C. Petersen, and S. D. Ross, *J. Am. Chem. Soc.*, **81**, 2361 (1959); **82**, 1582 (1960).
10) J. S. Mayell and A. J. Bard, *J. Am. Chem. Soc.*, **85**, 421 (1963).

BULLETIN OF THE CHEMICAL SOCIETY OF JAPAN, VOL. 52 (10), 3101—3102 (1979)

Phase Transition of $[(C_6H_5)_3PCH_3]_{1-x}^+$ $[(C_6H_5)_3AsCH_3]_x^+$ $(TCNQ)_2^-$, $(0 \leq x \leq 1)$, Anion Radical Salts. Thermodynamical Stability of the Solid Solutions

Yôichi IIDA

Department of Chemistry, Faculty of Science, Hokkaido University, Sapporo 060

(Received April 28, 1979)

Synopsis. The phase transition and the thermodynamic properties of solid solutions were studied with anion radical salts of $[(C_6H_5)_3PCH_3]_{1-x}^+$ $[(C_6H_5)_3AsCH_3]_x^+$ $(TCNQ)_2^-$, $(0 \leq x \leq 1)$. The stability condition of the solid solutions was examined in both the low- and high-temperature phases.

Much attention has been paid to solid anion radical salts of 7,7,8,8-tetracyanoquinodimethane (TCNQ) because of their prominent electronic properties.[1-12] In particular, the anion radical salt of methyltriphenylphosphonium, $[(C_6H_5)_3PCH_3]^+$ $(TCNQ)_2^-$, undergoes a solid-state phase transition at 315.7 K.[1-8] The methyltriphenylarsonium salt, $[(C_6H_5)_3AsCH_3]^+$ $(TCNQ)_2^-$, although it exhibits electronic properties very similar to those of the phosphonium salt, shows no such phase transition up to the decomposition temperature at 1 atm pressure.[1-3,6-11] Moreover, one can prepare the salts containing the mixed cations represented by $[(C_6H_5)_3PCH_3]_{1-x}^+$ $[(C_6H_5)_3AsCH_3]_x^+$ $(TCNQ)_2^-$, $(0 \leq x \leq 1)$.[1,2,6-11] The phase transitions of these mixed anion radical salts have been studied, as a function of the composition parameter, by observing anomalies in the temperature dependence of the static magnetic susceptibilities and the electrical conductivities and also by means of thermal analyses.[2,6-8] The experimental relation between the transition temperature and the composition parameter (x) at 1 atm pressure is illustrated in Curve (a) of Fig. 1. In order to understand the thermodynamic behavior of the phase transitions against the composition parameter, we proposed in a previous paper a thermodynamical theory of binary regular solid solution model for those TCNQ mixed crystals.[11] In the present paper, we shall examine the condition of the thermodynamical stability of the solid solutions and investigate the mechanism of the phase transitions.

According to the previous paper,[11] a thermodynamical theory of binary regular solid solution model is applicable to $[(C_6H_5)_3PCH_3]_{1-x}^+$ $[(C_6H_5)_3AsCH_3]_x^+$ $(TCNQ)_2^-$, $(0 \leq x \leq 1)$. This model assumes an ideal mixing of the two components of $[(C_6H_5)_3PCH_3]^+$ $(TCNQ)_2^-$, $(x=0.00)$, and $[(C_6H_5)_3AsCH_3]^+$ $(TCNQ)_2^-$, $(x=1.00)$, because the crystal structure and the chemical properties of the phosphonium salt are very similar to those of the arsonium salt. The model further assumes that the phase transition of a solid solution does not change the manner of ideal mixing of the two components. In this respect, it is important to note that the phase transition of our system is not the usual order-disorder type with respect to the mixing of the two components. Moreover, we could well assign the low- and high-temperature phases of the solid solutions at 1 atm pressure as $\alpha\gamma$ and $\beta\gamma$ phases, respectively.[9-11] Their Gibbs free energies per mol were expressed by

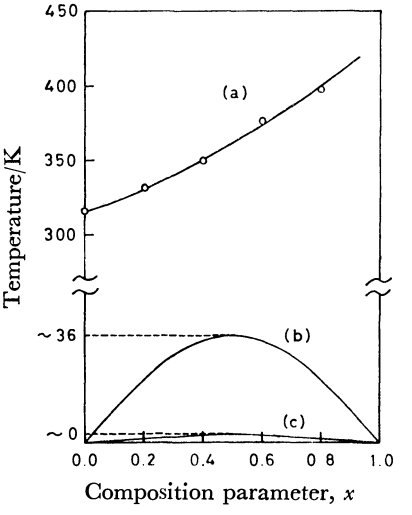

Fig. 1. Curve (a) shows the experimental relation between the temperature of the $\alpha\gamma \rightarrow \beta\gamma$ phase transition and the composition parameter (x) of the solid solutions of $[(C_6H_5)_3PCH_3]_{1-x}^+$ $[(C_6H_5)_3AsCH_3]_x^+$ $(TCNQ)_2^-$, $(0 \leq x \leq 1)$, anion radical salts at 1 atm pressure. Curves (b) and (c) show boundaries between the solid solution and the segregated region for the $\beta\gamma$ and $\alpha\gamma$ phases of the solid solutions, respectively. See text.

$$G^{i\gamma}(T,p,x) = (1-x)G_1^{i}(T,p) + xG_2^{\gamma}(T,p) + H_m^{i\gamma}(1-x)\cdot x + RT\{(1-x)\ln(1-x) + x\ln x\}, \quad (i=\alpha,\beta), \tag{1}$$

where T and p represent temperature and pressure, respectively, and where $(1-x)$ and x are the mole fractions of the component $[(C_6H_5)_3PCH_3]^+$ $(TCNQ)_2^-$ and $[(C_6H_5)_3AsCH_3]^+$ $(TCNQ)_2^-$, respectively. $G_1^{\alpha}(T,p)$ and $G_1^{\beta}(T,p)$ are the Gibbs free energies per mol for the low-temperature (α) and high-temperature (β) phases of pure phosphonium salt, respectively, while $G_2^{\gamma}(T,p)$ is that of the (γ) phase of pure arsonium salt at 1 atm pressure. $H_m^{i\gamma}$ is the heat of mixing per mol for each phase, and is assumed to be independent of temperature. The phase transitions of the solid solutions at 1 atm pressure can then be assigned to the $\alpha\gamma \rightarrow \beta\gamma$ process. By analyzing the experimental relation between the transition temperature of the $\alpha\gamma \rightarrow \beta\gamma$ phase transition and the composition parameter (Curve (a) of Fig. 1), we obtained the difference of the heat of mixing between the $\alpha\gamma$ and $\beta\gamma$ phases as $H_m^{\beta\gamma} - H_m^{\alpha\gamma} = 0.594 \pm 0.021$ kJ/mol.[11]

For either of the low-temperature ($\alpha\gamma$) or high-temperature ($\beta\gamma$) phase of our solid solutions, if the value of $H_m^{i\gamma}$, (i=α or β), is positive, the solid solutions are unstable below certain critical temperature and the segregation into the phosphonium salt and the arsonium salt should take place. It is well known that the theoretical relation between the mole fraction of the two components and the critical temperature at which the breaking of solid solution occurs can be determined by solving the equation

$$H_m^{i\gamma}(1-2x) + RT\ln\frac{x}{1-x} = 0. \quad (2)$$

In the region above critical temperature the solid solutions are thermodynamically stable with ideal mixing of the two components, while the solid solutions do not exist below critical temperature. In the temperature region above $T_m^{i\gamma}=H_m^{i\gamma}/2R$, the solid solutions can be obtained with all compositions ranging from $x=0.00$ to $x=1.00$.

In the case of $[(C_6H_5)_3PCH_3]_{1-x}^+[(C_6H_5)_3AsCH_3]_x^+(TCNQ)_2^-$, ($0\leq x\leq 1$), anion radical salts, although we have no information about the individual value of $H_m^{\alpha\gamma}$ or $H_m^{\beta\gamma}$, we can safely assume that the value of $H_m^{\alpha\gamma}$ may be very nearly equal to zero kJ/mol for the low-temperature ($\alpha\gamma$) phase, because the crystal and molecular structures of the α phase of the phosphonium salt are almost identical with those of the γ phase of the arsonium salt.[12] Moreover, there acts no specific interaction between the methyltriphenylphosphonium and methyltriphenylarsonium cations in the $\alpha\gamma$ phase and the chemical properties of the phosphonium salt are very similar to those of the arsonium salt. The assumption of $H_m^{\alpha\gamma}\approx 0$ kJ/mol is also strongly supported by the reason to be mentioned in the following. Then, we have $H_m^{\beta\gamma}\approx 0.594$ kJ/mol for the high-temperature ($\beta\gamma$) phase of the solid solutions. This positive $H_m^{\beta\gamma}$ value is reasonable, because the molecular and crystal structures of the β phase of the phosphonium salt are closely related to those of the γ phase of the arsonium salt but a difference was found in the conformation of the methyltriphenylphosphonium cation with respect to the intramolecular rotation of the phenyl groups.[12]

First, we neglect the effect of the $\alpha\gamma\rightarrow\beta\gamma$ phase transition, and only consider the $\beta\gamma$ phase of the solid solutions. By the use of $H_m^{\beta\gamma}\approx 0.594$ kJ/mol, together with Eq. 2, the boundary between the solid solutions and the segregated region is obtained as shown in Curve (b) of Fig. 1. In the region above Curve (b) the solid solutions composed of ideally mixed β form of the phosphonium salt and the γ form of the arsonium salt are stable, while they have to be segregated into two components below Curve (b). $T_m^{\beta\gamma}$ at $x=0.50$ is calculated to be about 36 K.

In view of these results, we can understand the importance of the $\beta\gamma\rightarrow\alpha\gamma$ phase transitions (Curve (a) of Fig. 1) of the solid solutions. If there were no such phase change, the $\beta\gamma$ phase would become unstable in going to low temperatures and the crystals of the solid solutions would break. Actually, however, the solid solutions change into the $\alpha\gamma$ phase at Curve (a) of Fig. 1, which lies in the temperature region much higher than does Curve (b) of Fig. 1. As for the $\alpha\gamma$ phase, since $H_m^{\alpha\gamma}\approx 0$ kJ/mol and thus $T_m^{\alpha\gamma}\approx 0$ K, the boundary between the solid solutions and the segregated region is schematically given by Curve (c) of Fig. 1, that is, the solid solutions composed of the α form of the phosphonium salt and the γ form of the arsonium salt will be stable down to 0 K in all compositions. This prediction may be supported by the experimental results by Kosaki *et al.*[8] For example, the fact that the observed heat capacity *versus* temperature curve of the $\alpha\gamma$ phase of the solid solution with the composition $x=0.449$ is smooth down to about 10 K means that the solid solution does not break and that the $\alpha\gamma$ phase is stable at least down to 10 K. This experimental result also implies very small value (less than 0.17 kJ/mol) for $H_m^{\alpha\gamma}$ in the $\alpha\gamma$ phase.

Our investigation clearly shows that, because of the $\beta\gamma\rightarrow\alpha\gamma$ phase transition, the solid solutions of $[(C_6H_5)_3PCH_3]_{1-x}^+[(C_6H_5)_3AsCH_3]_x^+(TCNQ)_2^-$, ($0\leq x\leq 1$), anion radical salts are stable both in the temperature range from 0 K up to decomposition temperatures and in the whole composition range from $x=0.00$ to $x=1.00$. So far, this conclusion agrees well with the experimental observations.[1-8] Another important conclusion is concerned with the mechanism of the phase transition of the solid solutions. The existence of the $\beta\gamma\rightarrow\alpha\gamma$ phase change is necessary to avoid breaking of the $\beta\gamma$ phase at low temperatures.

References

1) L. R. Melby, R. J. Harder, W. R. Hertler, W. Mahler, R. E. Benson, and W. E. Mochel, *J. Am. Chem. Soc.*, **84**, 3374 (1962).

2) R. G. Kepler, *J. Chem. Phys.*, **39**, 3528 (1963).

3) A. W. Merkl, R. C. Hughes, L. J. Berliner, and H. M. McConnell, *J. Chem. Phys.*, **43**, 953 (1965).

4) Y. Iida, M. Kinoshita, M. Sano, and H. Akamatu, *Bull. Chem. Soc. Jpn.*, **37**, 428 (1964).

5) A. Kosaki, Y. Iida, M. Sorai, H. Suga, and S. Seki, *Bull. Chem. Soc. Jpn.*, **43**, 2280 (1970).

6) Y. Iida, *Bull. Chem. Soc. Jpn.*, **43**, 3685 (1970); **46**, 683 (1973).

7) Y. Iida, *J. Chem. Phys.*, **59**, 1607 (1973).

8) A. Kosaki, M. Sorai, H. Suga, and S. Seki, *Bull. Chem. Soc. Jpn.*, **50**, 817 (1977).

9) Y. Iida, *J. Phys. Chem.*, **80**, 2944 (1976).

10) Y. Iida, *Mol. Cryst. Liq. Cryst.*, **39**, 195 (1977); **43**, 259 (1977).

11) Y. Iida, *J. Chem. Soc., Faraday Trans. 1*, **74**, 190 (1978).

12) A. T. McPhail, G. M. Semeniuk, and D. B. Chesnut, *J. Chem. Soc., A*, **1971**, 2174; M. Konno and Y. Saito, *Acta Crystallogr., Sect. B*, **29**, 2815 (1973).

BULLETIN OF THE CHEMICAL SOCIETY OF JAPAN, VOL. 52 (10), 3103—3104 (1979)

Decomposition of Ozone on Natural Sand

Shin SUZUKI,* Yoshio HORI, and Osamu KOGA

Department of Synthetic Chemistry, Faculty of Engineering, Chiba University, Yayoi-cho 1-33, Chiba 260

(Received December 11, 1978)

Synopsis. Ozone decomposition on natural sand has been studied with a flow system. Ozone decomposed significantly on natural sand and in particular on iron sand. Silica, alumina, and iron oxides, the major components of the sand, were also capable of decomposing ozone.

Ozone is one of the major photochemical pollutants and its behavior in the environment has been reported. Ozone is reactive, which suggests that ozone may be decomposed on terrestrial substances on the ground or in airborne dusts. There have been several reports describing the heterogeneous decomposition of ozone on solids. Harteck and Dondes reported the decomposition of ozone on glass wool,[1] and Mahieux studied the decomposition of ozone on glass, aluminium, copper, silica gel, and active charcoal.[2] These investigations were qualitative and conducted at relatively high concentration (several %). No report has been published concerning the decomposition of ozone at low levels of concentration *e.g.*, several ppm.

The present paper describes the decomposition of ozone on natural sea sand in order to clarify the decomposition of ozone on terrestrial substances. Natural sea sand was used since it is easy to handle and has a relatively uniform composition.

Experimental

Materials. *Natural Sea Sand*: The sample was supplied from the seashore of Futsu Cape, Tokyo Bay, Japan. The sample was sieved between 80 and 120 mesh, and dried at 150 °C for three hours in an electric furnace.

Iron Sand and Remainder-sand: Natural sea sand was subdivided into iron sand and remainder-sand by means of a magnet and dried identically.

Silica, Fe_2O_3, Fe_3O_4, and Al_2O_3: Commercial reagents were employed; silica(α-quartz), α-Fe_2O_3(hematite), Fe_3O_4 (magnetite), and α-Al_2O_3(corundum). They were dried identically.

Instruments. Reactions were conducted in a flow system. An ozone generator (Tokyo Kogyo Co.) supplied a given concentration of ozone (0—5 ppm). The air containing ozone was blown into the reaction cell, filled with the appropriate sample powder. Sample powders were supported on glass frit and Teflon filters. The concentration of ozone was measured by a UV absorption type ozone monitor (Dasibi Co.) at the inlet and the outlet of the reactor. The flow rate of the ozonized air was regulated at 2 l/min by the suction pump of the ozone monitor.

Results and Discussion

Ozone Decomposition on Natural Sea Sand. No ozone was decomposed in blank tests in the absence of sample materials in the reactor. Ozone decomposition was seen to take place on the natural sand sample charged in the reactor. Figure 1 shows the variation

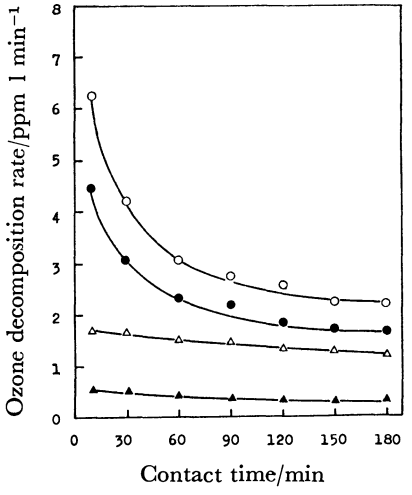

Fig. 1. Decomposition rate of ozone on natural sand (5 ml) *versus* contact time.
Concentration of ozone at inlet; -○-: 5 ppm, -●-: 3.5 ppm, -△-: 1.0 ppm, -▲-: 0.25 ppm.

in the rate of decomposition of ozone with contact time on the natural sand (5 ml). The decomposition rate was determined as follows:

$$\text{Decomposition rate} = ([O_3]_i - [O_3]_o) \times f$$

$[O_3]_i$: Inlet ozone concentration (ppm)
$[O_3]_o$: Outlet ozone concentration (ppm)
f: Flow rate of air (l/min)

The rate of decomposition decreased gradually with increase in concentration, whereas the rate remained almost constant at low ozone concentration.

The decomposition rate of ozone at constant concentration (3.5 ppm) increased in proportion to the volume

Table 1. Analysis of sand

Component	Sieved sand[a] (wt %)	Original sand[b] (wt %)	Analytical method
SiO_2	57.18	68.21	alkaline fusion, $HF+H_2SO_4$
Fe_2O_3[c]	21.73	13.43	EDTA chelatometry
Al_2O_3	10.11	9.09	EDTA chelatometry
CaO	3.30	4.59	EDTA chelatometry
MgO	3.76	3.44	EDTA chelatometry
$H_2O(-)$	0.66	0.59	
$H_2O(+)$	1.25	2.27	
Mn	0.33		atomic absorption photometry
Cr	0.01		atomic absorption photometry
Zn	0.01		atomic absorption photometry

a) Natural sand sieved between 80 and 120 mesh, and provided for exposure to ozone. b) The original natural sand was used without sieving. c) Fe content expressed as Fe_2O_3.

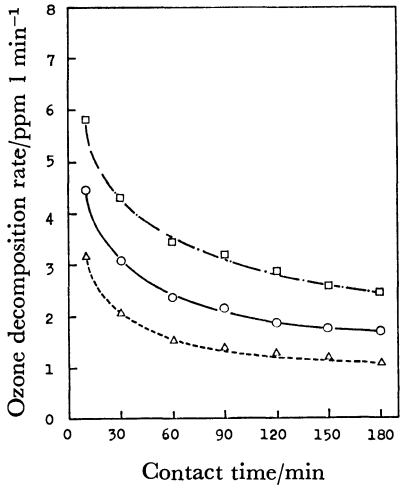

Fig. 2. Decomposition rate of ozone on various components of the sand *versus* contact time.
-○-: Natural sand (5 ml), ---□---: iron sand (5 ml) ---△---: remainder-sand (5 ml).

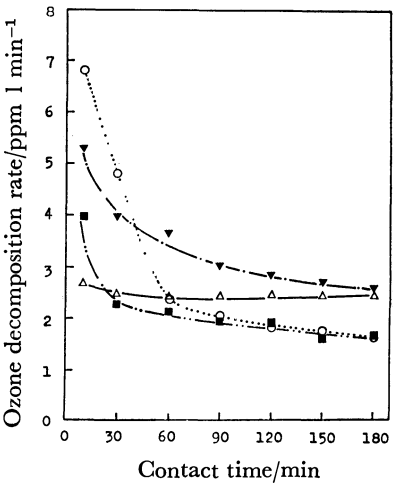

Fig. 3. Decomposition rate of ozone on several materials *versus* contact time.
···○···: Fe_2O_3 (5 ml), ---▼---: Fe_3O_4 (1 g), ---■---: Al_2O_3 (1 g) -△-: SiO_2 (5 ml)

of the sand.

Individual Activity of the Components of Natural Sand in Ozone Decomposition. The decomposition was studied on several components of sand; iron sand, remainder-sand and some reagents. The reagents are those which were found by chemical analysis to be the major components of the sand; *i.e.* silica, iron oxides, and alumina. The major component of iron sand is known to be Fe_3O_4, so that α-Fe_2O_3 and magnetite were investigated.

Natural sand was analyzed by chelatometry and atomic absorption spectrometry, the results of which are given in Table 1. The sand used in the experiments contained more iron oxides than the original non-sieved sand probably because the iron sand grain size is mainly distributed in the 80—120 mesh range. In measurements of ozone decomposition the amounts of samples used were: remainder-sand (5 ml), iron sand (5 ml), silica (5 ml), Fe_2O_3 (5 ml), alumina (1 g), and Fe_3O_4 (1 g). Figure 2 shows the rates of ozone decomposition on iron sand, remainder-sand and natural sand. The rate on iron sand was higher than that on natural sand suggesting that iron sand more effectively decomposes ozone than remainder-sand.

The decomposition rates on alumina, Fe_2O_3 and Fe_3O_4 were lower, whereas that on silica remained almost constant as shown in Fig. 3. The decomposition on Fe_3O_4, a major component of iron sand, behaved very similarly to that on iron sand as shown in Figs. 2 and 3.

The authors wish to express their sincere thanks to Dr. Ryozo Nakagawa for the analysis of natural sand. Thanks are also due to Mr. Hiroo Takagi and Miss Hiromi Miyamoto for their collaboration in the experimental works. The present work was supported by a Grant-in-Aid for Scientific Research from the Ministry of Education, Science and Culture.

References

1) P. Harteck and S. Dondes, *J. Chem. Phys.*, **21**, 2240 (1953).
2) F. Mahieux, *Genie Chim.*, **87**, 15 (1962).

BULLETIN OF THE CHEMICAL SOCIETY OF JAPAN, VOL. 52 (10), 3105—3106 (1979)

The Polarographic Reduction and UV Spectral Properties of Pentaamminecarboxylatoruthenium(III) Complexes

Akira OHYOSHI* and Kenichiro YOSHIKUNI
Department of Industrial Chemistry, Kumamoto University, Kumamoto 860
(Received January 22, 1979)

Synopsis. Pentaamminecarboxylatoruthenium(III) complexes are reversibly reduced to the corresponding Ru(II) complexes by means of a one-electron transfer at the dropping mercury electrode in aqueous solutions. The absorption maxima, which ranged from 34.6×10^3 cm^{-1} (trichloroacetato complex) to 33.6×10^3 cm^{-1} (glycinato complex) were assigned to the charge-transfer from ligand to metal; they were linearly related to the reversible half-wave potential.

Recent polarographic reduction studies of ruthenium(III) carboxylato complexes[1-3] have revealed that the complexes are reversibly reduced at the dropping mercury electrode through the process of one-electron-transfer. For the series of ammineruthenium(II, III) complexes,[4-9] formal reduction potentials (E_f) were measured and a linear relationship was found to exist between the E_f and the charge-transfer energy from metal to ligand.[8] Hence, it seemed of interest to check whether or not a similar relationship exists between the $E_{1/2}$ and the CT-energy from ligand to metal for ruthenium(III) complexes. In the present paper, a similar relationship was confirmed between them for the series of Ru(III) complexes.

Experimental

Reagents and Materials. All the chemicals used were of a reagent grade. Twice-distilled water was used in all the experiments. The ionic strength and the acidity of the electrolyte solution were adjusted with *p*-toluenesulfonic acid and its sodium salt. Pentaammineformatoruthenium(III) and other carboxylato complexes were prepared by the method described in the literature[10] starting from pentaamminechlororuthenium(III) chloride, the corresponding buffer solution, and zinc amalgam. The complexes thus prepared were analyzed by the usual elemental analysis, and their chemical purities were confirmed.

Apparatus and Procedures. A Shimadzu RP-50 polarograph was employed with a circuit for an extendable and adjustable applied potential. An H-cell with a saturated calomel electrode (SCE) was used. The capillary used had an *m*-value of 1.82 mg s^{-1} and a drop time of 5.0 s in distilled water at a mercury height of 61.5 cm with an open circuit. All the measurements were carried out in a thermostat of (25.0±0.1) °C. Gelatin was used as the maximum suppressor. Polarographic measurements were made after the removal of oxygen by bubbling nitrogen gas through the electrolyte solution. The half-wave potentials were determined from the extended polarograms by means of the plotting. The potential values were corrected for the *iR* drop by using the minimum value of the cell resistance. A Shimadzu UV-200 spectrophotometer was used to measure the electronic spectra of the ruthenium complexes.

Results and Discussion

Electrode Process in the Polarographic Reduction of a Complex. Each complex exhibits a single well-defined reduction wave at a potential near zero volt *vs.* SCE. The limiting current, i_l, was proportional to the concentration of the complex ion. Plots of i_l *vs.* the square root of the mercury head, h, were linear. Thus, the electrode process posseses a high degree of diffusion control. The plots of $E_{d.e.}$ *vs.* log $[i/(i_d-i)]$ are almost linear for all the complexes (Fig. 1). The numbers of electrons involved in the reduction was determined to be almost one from the slope of this plot. Thus, each low-spin $(t_{2g})^5$ ruthenium(III) complex was found to undergo a ready one-electron reduction, which might be regarded as completing the metal t_{2g} subshell. In each case, the reciprocal slope of the logarithmic plot is (60±2) mV, indicating that the electrode reaction is a reversible step, with a one-electron transfer. The half-wave potentials measured in solutions of pH 5.0—7.5 and at an ionic strength of 0.1 mol dm^{-3} are almost constant; they are given in Table 1. However, the half-wave potentials shifted slightly in a positive direction with a lowering of the pH of the solution, as is exemplified in Fig. 1. This fact may be attributable to the increase in the reversibility of the electrode reaction resulting from the stabilization of the reduced Ru(II) species.

The redox potential of the Ru(III)/Ru(II) couple for the complexes of the $[Ru(O_2CR)(NH_3)_5]$ type shifts in a negative direction in this ligand order: $O_2CCCl_3<O_2CCHCl_2\approx O_2CCH_2F<O_2CCH_2Cl\approx O_2CCH_2Br\approx O_2CCH_2I<O_2CH<O_2CCH_2NH_2<$

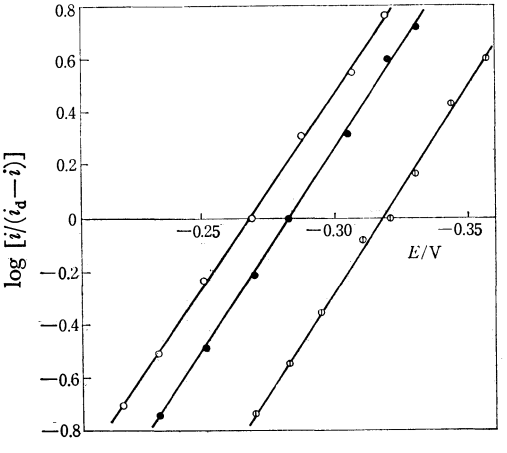

Fig. 1. Plots of log $[i/(i_d-i)]$ *vs.* $E_{d.e.}$.
$[Ru(O_2CH)(NH_3)_5]^{2+}$, ○: 0.008 mol dm^{-3} *p*-toluene sulfonic acid, 0.092 mol dm^{-3} sodium *p*-toluenesulfonate, ●: 0.1 mol dm^{-3} sodium *p*-toluenesulfonate.
$[Ru(O_2CCH_2OH)(NH_3)_5]^{2+}$ ⊕: 0.1 mol dm^{-3} sodium *p*-toluenesulfonate.

$O_2CCH_2OH < O_2CCH_3 \approx O_2CC_2H_5 \approx O_2CCH(CH_3)_2$. This order agrees with that for the increasing pK_a values of the ligand acids, except for the glycinato complex.

When the complex ion reacts with the electrode as a depolarizer, the reduction is regarded as comprising the acceptance of an electron into the lowest unoccupied orbital of the complex. For the reduction process, the rate and mechanism of the overall process will be dictated by the localization and energy of the lowest orbital.[12] The Ru(III) complex with an electronic configuration of $(t_{2g})^5$ tends to take the $(t_{2g})^6$ configuration because of the high electron affinity of the unoccupied orbital, partly filled with one electron. Thus, the values of the redox potentials measured in this experiment are correlated with the energy level of the lowest unoccupied orbital of Ru(III) in the coordination sphere of pentaamminecarboxylato complexes.

Electronic Spectra of Ru(III) Complexes. The electronic spectra of all the complexes measured in a solution of 0.1 mol dm^{-3} *p*-toluenesulfonate at 25 °C exhibit an intense band in the energy region from 34.6×10^3 cm^{-1} to 33.6×10^3 cm^{-1}, as is shown in Table 1. These bands are assigned to the charge-transfer transition from ligand $p\pi$ to Ru(III) $d\pi$ orbitals on the basis of their intensity and spectral energies, and on the basis of a comparison of these data with those of the other related complexes.[13] The $p\pi$-$d\pi$ charge-transfer energy in $[Ru^{III}O_2CR(NH_3)_5]$ complexes regularly decreases upon R-substituents of RCO_2 ligands in this order: $O_2CCCl_3 > O_2CCHCl_2 > O_2CCH_2F > O_2CCH_2Cl > O_2CCH_2Br \approx O_2CCH_2I > O_2CH \approx O_2CCH_2OH > O_2CCH_3 \approx O_2CC_2H_5 > O_2CCH(CH_3)_2 > O_2CCH_2NH_2$. This order agrees with that of the increasing pK_a values of the ligand acids except for the case of iso-butyric acid and glycine (Table 1).

It is of interest to examine whether or not there exists a direct relationship between the electrochemical stabilization of Ru(III) towards cathodic reductions, as expressed in terms of $E_{1/2}$ values, and the LMCT

Table 1. Half-wave potentials and optical parameters of pentaammineruthenium(III) complexes and dissociation constants of ligand acids

Complex ion	$-(E_{1/2}$ *vs.* SCE)[a] / V	ν_{max} / 10^3 cm^{-1}	ε[b]	pK_a of ligand acid[c] (Ionic strength / mol dm^{-3})
$Ru(O_2CCCl_3)(NH_3)_5^{2+}$	$0.20_2\pm0.01$	34.6 ± 0.1	1380	0.635(0.003—0.01)
$Ru(O_2CCHCl_2)(NH_3)_5^{2+}$	$0.23_5\pm0.01$	34.4 ± 0.1	1490	1.257(0.001—0.2)
$Ru(O_2CCH_2F)(NH_3)_5^{2+}$	$0.23_8\pm0.01$	34.2 ± 0.1	1470	2.586(0.0003—0.0015)
$Ru(O_2CCH_2Cl)(NH_3)_5^{2+}$	$0.26_6\pm0.01$	34.1 ± 0.1	1510	2.854(0.0001—0.03)
$Ru(O_2CCH_2Br)(NH_3)_5^{2+}$	$0.27_0\pm0.02$	34.0 ± 0.1	1300	2.902(0.0003—0.001)
$Ru(O_2CCH_2I)(NH_3)_5^{2+}$	$0.27_5\pm0.02$	34.0 ± 0.1	710	3.175(0.0001—0.001)
$Ru(O_2CH)(NH_3)_5^{2+}$	$0.28_2\pm0.01$	33.9 ± 0.1	1540	3.752(0.01—0.2)
$Ru(O_2CCH_2OH)(NH_3)_5^{2+}$	$0.31_1\pm0.01$	33.9 ± 0.1	1480	3.831(0.005—0.08)
$Ru(O_2CCH_3)(NH_3)_5^{2+}$	$0.33_1\pm0.02$	33.8 ± 0.1	1590	4.756(0.01—0.2)
$Ru(O_2CCH_2CH_3)(NH_3)_5^{2+}$	$0.33_8\pm0.01$	33.8 ± 0.1	1660	4.874(0.01—0.09)
$Ru(O_2CCH(CH_3)_2)(NH_3)_5^{2+}$	$0.34_3\pm0.01$	33.7 ± 0.1	1770	4.862(0.01—0.02)
$Ru(O_2CCH_2NH_2)(NH_3)_5^{2+}$	$0.28_8\pm0.02$	33.6 ± 0.1	1560	2.350(0.01—0.36)

a) Supporting electrolyte solution: 0.1 mol dm^{-3} sodium *p*-toluenesulfonate. b) mol^{-1} dm^3 cm^{-1}. c) From Ref. 11.

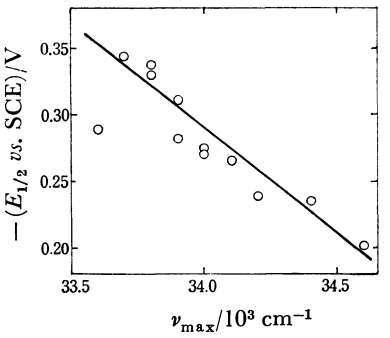

Fig. 2. Plot of half-wave potential $E_{1/2}$ of the $Ru(O_2CR)(NH_3)_5^{2+/+}$ couples *vs.* the wave number of the ligand-to-metal charge-transfer maxima for the $Ru(O_2CR)(NH_3)_5^{2+}$ complexes.

spectral energies. The plots of $E_{1/2}$ *vs.* ν_{max} (LMCT) are approximately linear for various pentaammine-carboxylatoruthenium(III) complexes, as is shown in Fig. 2. A linear relationship between the formal redox potential and the absorption maximum of the metal to ligand charge-transfer (MLCT) has been found to exist for various benzonitrile and pyridine complexes of Ru(II).[8] The charge-transfer energy is related only to the energy difference between $p\pi$ and $d\pi$ orbitals. On the contrary, the reversible half-wave potential is directly related to the energy level of a singly occupied $d\pi$ orbital. Therefore, this $d\pi$ orbital energy level may be a determinant factor for both the redox potential and the charge-transfer energy for pentaammine-carboxylatoruthenium(III) complexes.

References

1) F. A. Cotton, J. F. Norman, A. Spencer, and G. Wilkinson, *Chem. Commun.*, **1971**, 967.
2) M. Mukaida, T. Nomura, and T. Ishimori, *Bull. Chem. Soc. Jpn.*, **45**, 2143 (1972).
3) A. Ohyoshi, S. Hamaoka, and Y. Hiroshima, *Chem. Lett.*, **1973**, 737.
4) H. S. Lim, D. J. Barclay, and F. C. Anson, *Inorg. Chem.*, **11**, 1460 (1972).
5) P. E. Dumas and E. E. Mercer, *Inorg. Chem.*, **11**, 531 (1972).
6) G. M. Coleman, J. W. Gesler, F. A. Shirley, and J. R. Kuempel, *Inorg. Chem.* **12**, 1036 (1973).
7) C. M. Elson, I. J. Itzkovitch, J. Mckenney, and J. A. Page, *Can. J. Chem.*, **53**, 2922 (1975).
8) T. Matsubara and P. C. Ford, *Inorg. Chem.*, **15**, 1107 (1976).
9) J. A. Marchant, T. Matsubara, and P. C. Ford, *Inorg. Chem.*, **16**, 2160 (1977).
10) J. A. Stritar and H. Taube, *Inorg. Chem.*, **8**, 2281 (1969).
11) G. Kortum, W. Vogel, and K. Andrussow, "Dissociation Constants of Organic Acid in Aqueous Solution," Butterworths, London (1961), pp. 240—315.
12) D. R. Crow, "Polarography of Metal Complexes," Academic Press, London and New York (1969), p. 147.
13) S. W. Lin and A. F. Schreiner, *Inorg. Chim. Acta*, **5**, 290 (1971).

BULLETIN OF THE CHEMICAL SOCIETY OF JAPAN, VOL. 52 (10), 3107—3108 (1979)

Metal-substitution of 12-Heteropolymolybdate with Iron Atoms

Kenji NOMIYA, Motoki SUGAYA, and Makoto MIWA*

Department of Industrial Chemistry, Faculty of Engineering, Seikei University, Musashino-shi, Tokyo 180

(Received April 6, 1979)

Synopsis. Triheteropolymolybdates of $[XFeMo_{11}O_{40}H_2]$- and $[XFeMo_{11}O_{40}H_3]$-type have been synthesised by the metal-substitution reaction of 12-heteropolymolybdate of $[XMo_{12}O_{40}]$-type (X is Si or P) and their properties have been investigated.

Although triheteropolymolybdate, a mixed-metal polyoxoanion, was expected to be a new catalyst of reversible oxidation in homogeneous system,[1] the compound, generally prepared in only a narrow pH range, is more easily hydrolyzed than the corresponding saturated heteropolymolybdate. We have examined the metal substitution of 12-heteropolymolybdate possessing well-known Keggin structure with Fe(II) and Fe(III) ions. We report on the isolation of the reaction products, the anions of $[XFeMo_{11}O_{40}H_2]$- and $[XFeMo_{11}O_{40}H_3]$-type as tetrabutylammonium salts, where X is Si or P. So far as Fe-ion substituted products derived from heteropolyanions of $[XMo_{12}O_{40}]$-type are concerned, no precedent has been reported except for $[SiFeMo_{11}O_{40}H_2]^{5-}$.[2]

The reaction of $[SiMo_{12}O_{40}]^{4-}$ with $FeCl_3$ in aqueous solution containing potassium acetate and glacial acetic acid gave mainly $[SiFeMo_{11}O_{40}H_2]^{4-}$, where Fe is tervalent and all Mo are sexivalent cations. The complex was isolated as a stable tetrabutylammonium salt. The reaction of $[SiMo_{12}O_{40}]^{4-}$ with $FeCl_2$ under similar conditions gave $[SiFeMo_{11}O_{40}H_3]^{5-}$, where Fe is also tervalent, only one Mo being quinquevalent and the others sexivalent cations. During the course of substitution, bivalent Fe ion turns into a tervalent cation by the intrinsic strong oxidation property of the parent anion. Such a compound has also been isolated as a tetrabutylammonium salt and purified by recrystallization from acetonitrile. By the reaction of $[PMo_{12}O_{40}]^{3-}$ with Fe(II) or Fe(III) ion, the corresponding one iron substituted derivatives were obtained. In these reactions no further substitution of Mo ion was observed.

The K^+, Na^+, and NH_4^+ salts of heteropolymolybdate containing an iron atom, once formed in aqueous solutions of limited pH range, are sparingly recrystallized from an aqueous solution because of their extremely low solubility and hydrolytic instability. However, by using tetrabutylammonium cation as precipitants, such unstable anions were converted into stable compounds for recrystallization from a nonaqueous solvent such as acetonitrile. The treatment makes the determination of anionic charge, elemental analysis, spectroscopic characterization easy, giving good yield of compounds. Furthermore, in a nonaqueous solvent, these compounds obtained as a tetrabutylammonium salt do not decompose even in the presence of an organic base such as pyridine and triphenylphosphine.

The heteropolyanions obtained are formulated as follows;

$[SiFe^{III}Mo^{VI}_{11}O_{40}H_2]^{5-}$ (yellow, **1**),
$[SiFe^{III}Mo^{V}Mo^{VI}_{10}O_{40}H_3]^{5-}$ (yellow-green, **2**),
$[PFe^{III}Mo^{VI}_{11}O_{40}H_2]^{4-}$ (pale yellow, **3**),
$[PFe^{III}Mo^{V}Mo^{VI}_{10}O_{40}H_3]^{4-}$ (dark green, **4**),

their analytical data being given in Table 1.

Yellow compounds **1** and **3** are written as $[XFeMo_{11}O_{40}H_2]$ (X=Si, P), where "H_2" is included in the formula not only to make the total oxidation number consistent; X (+4 or +5 corresponding to Si or P), Fe (+3), Mo (+6), O (−2) and two H (+1), but is arised from the hydrogen part of coordinating water molecule. Existence of a coordinating water molecule was determined by IR study. The complexes were recrystallized several times from dry acetonitrile in order to remove solvated water molecules entirely. In this case, the characteristic bands of coordinating water at *ca.* 3400 and 1630 cm^{-1} were observed, but not in the case of parent anion $[XMo_{12}O_{40}]$-type. Thus if Fe ion is considered as a central ion, the compounds obtained are considered to be a hexa-coordination complex of Fe coordinated by quinquedentate ligand "$XMo_{11}O_{39}$" and unidentate ligand H_2O.

The green compounds **2** and **4** with the formula $[XFeMo_{11}O_{40}H_3]$-type also possess the water molecule coordinated to tervalent Fe ion and one hydroxyl group coordinated to one quinquevalent Mo ion in quinquedentate ligand "$XMo_{11}O_{39}$." The presence of the coordinating hydroxyl group is strongly suggested from the reduction of parent anion $[SiMo_{12}O_{40}]^{4-}$ by alcohols leading to the formation of the blue anion of $[SiMo_{12}O_{40}H_n]$-type, where n=2—4 and Mo ions of the corresponding numbers are quinquevalent.[3]

IR and electronic spectral data of heteropoly anion obtained together with parent molybdosilicate and molybdophosphate, are given in Tables 2 and 3,

TABLE 1. ANALYTICAL DATA

Formula		Found (%)				Calcd (%)			
		C	H	N	Fe	C	H	N	Fe
$K[(C_4H_9)_4N]_4[SiFeMo_{11}O_{40}H_2]\cdot CH_3CN$	**1**	28.09	5.57	2.17	1.41	27.99	5.27	2.47	1.97
$K[(C_4H_9)_4N]_4[SiFeMo_{11}O_{40}H_3]$	**2**	26.90	5.23	2.10	1.64	27.53	5.27	2.01	2.00
$[(C_4H_9)_4N]_4[PFeMo_{11}O_{40}H_2]\cdot 12H_2O$	**3**	25.89	5.04	1.87	1.82	25.89	5.73	1.89	1.88
$[(C_4H_9)_4N]_4[PFeMo_{11}O_{40}H_3]\cdot 9H_2O$	**4**	26.46	5.19	1.81	1.63	26.34	5.66	1.92	1.92

Table 2. IR data (KBr)

$[(C_4H_9)_4N]_4[SiMo_{12}O_{40}]$	1	2	$[(C_4H_9)_4N]_3[PMo_{12}O_{40}]$	3	4
			1057s	1053s	1053s
980m	980m	980m			
			960s	970w(sh)	970w(sh)
			950vs	950vs	948vs
940s	937s	936s		940vs	938vs
898vs	894vs	887vs			
863m	863m	860m	875s	863s	868s
800vs	800vs	788vs	804vs	803vs	805vs
730m(sh)	730m(sh)	730m(sh)	735w	735w	735m(sh)
633m	633m	633m		710w	
			605w	588w	590w
527m	527m	525m			
503m	505m	500m	495w	495w	500w

respectively. Typical electronic spectra are dominated by two or three bands in the 240—500 nm region, which are based on the charge transfer transition of intra-ligand, *viz.* intra-"$XMo_{11}O_{39}$" moiety. The absorption due to the low spin Fe(III) complex under such ligand fields is extremely weak, the whole spectral aspect resembling that of the parent anion. However, the intensity at near 300 nm strongly reflects the effect of metal substitution and/or the degree of reduction of molybdenum atom. The characteristic spectra of compounds **2** and **4** containing a reduced molybdenum ion have weak intensity bands in a longer wave-length region than 700 nm. The data (Table 2) reveal that the metal substitution and/or heteroatom substitution directly influence the IR bands due to the M–O–M, X–O and M–O stretching modes.[4] All such bands are shifted to the low frequency region on replacement of one Mo ion in $[XMo_{12}O_{40}]$ with one Fe ion.

Table 3. Electronic spectral data[a]

	λ_{max}/nm($\varepsilon_{max}\times10^{-4}$)
$[(C_4H_9)_4N]_4[SiMo_{12}O_{40}]$	250sh (7.26), 292 (2.40)
1	245sh (4.45), 300 (1.64), 420sh (0.04)
2	245sh (5.35), 300 (2.06), 420sh (0.08)
$[(C_4H_9)_4N]_4[PMo_{12}O_{40}]$	307 (2.24), 400sh (0.19)
3	307 (6.30), 360sh (2.54)
4	307 (3.24), 360sh (1.29)

a) In acetonitrile.

Experimental

IR spectra (KBr and Nujol) were recorded with a JASCO IR-G spectrophotometer and electronic spectra with a Hitachi 124-Model spectrophotometer. In the measurements of the tetraalkylammonium salts of heteropolyanions, both the KBr pellet method and the Nujol mull method gave the same results. $[SiMo_{12}O_{40}]^{4-}$ was prepared according to the method of North and Haney.[5] Its tetrabutylammonium salt was obtained by adding excess tetrabutylammonium halide. Commercial $[PMo_{12}O_{40}]^{3-}$ (Wako Pure Chemicals Co., Ltd.) was used. Its tetrabutylammonium salt was prepared by a similar work-up. The contents of Fe in the heteropolymolybdates was determined by the analytical method in the presence of Mo.[6]

Preparation. $K[(C_4H_9)_4N]_4[SiFeMo_{11}O_{40}H_2]\cdot CH_3CN$, ***1***: A solution of 1 g (0.478 mmol) $H_4[SiMo_{12}O_{40}]\cdot15H_2O$ dissolved in 3 ml water was gently heated to 60 °C. To this were added in succession a 1 ml solution mixture of 15 g (0.15 mol) CH_3COOK and 25 ml water containing 1 ml glacial acetic acid, and a 2 ml solution of 1.2 g (7.39 mmol) $FeCl_3$ dissolved in 20 ml water. The mixture was refrigerated overnight. The white precipitate produced was filtered off. The filtrate was evaporated under 50 °C until some crystal appeared, and then refrigerated overnight. The resulting yellow needle compound of $K_5[SiFeMo_{11}O_{40}H_2]$ was dissolved in a small amount of warm water, and then an aqueous solution containing excess tetrabutylammonium bromide was added. The product was washed several times with water, dried *in vacuo*, and recrystallized from dry acetonitrile (yield 35%, pale yellow).

$K[(C_4H_9)_4N]_4[SiFeMo_{11}O_{40}H_3]$, ***2***: 0.94 g (7.39 mmol) of $FeCl_2$ was dissolved in 20 ml water containing 0.5 ml concd HCl. Except for use of this solution instead of the $FeCl_3$ aqueous solution in the preparation of **1**, the product was obtained by a similar work-up (yield 38%, yellow-green).

$[(C_4H_9)_4N]_4[PFeMo_{11}O_{40}H_2]\cdot12H_2O$, ***3***: A solution of 1 g $H_3[PMo_{12}O_{40}]$ in 3 ml water was gently heated to 65 °C. A 1 ml solution of 15 g (0.15 mol) CH_3COOK in 25 ml water containing 1 ml glacial acetic acid was added and stirred thoroughly. A 2 ml solution of 1.2 g (7.39 mmol) $FeCl_3$ in 20 ml water was then added and refrigerated overnight. The precipitate was dissolved in water. To this yellow clear solution was added a small amount of solution containing excess tetrabutylammonium bromide. The product was thoroughly washed with water and dried *in vacuo* (yield 95%, pale yellow).

$[(C_4H_9)_4N]_4[PFeMo_{11}O_{40}H_3]\cdot9H_2O$, ***4***: 0.94 g (7.39 mmol) of $FeCl_2$ was dissolved in 20 ml water containing 0.5 ml concd HCl. Except for use of the solution mixture instead of the $FeCl_3$ aqueous solution in the preparation of **3**, the product was obtained by a similar work-up (yield 62%, dark green).

References

1) M. Otake and T. Onoda, *Shokubai*, **18**, 169 (1976).
2) A. M. Qureshi, S. A. Zubairi, and S. A. Malik, *J. Inorg. Nucl. Chem.*, **38**, 879 (1976).
3) K. Nomiya, T. Ueno, and M. Miwa, under submission.
4) C. R. Deltcheff, R. Thouvenot, and R. Franck, *Spectrochim. Acta, Part A*, **32**, 587 (1976).
5) E. O. North and W. Haney, *Inorg. Synth.*, **1**, 127 (1939).
6) V. R. R. Rao, K. V. Rao, and P. V. R. B. Sarma, *Talanta*, **16**, 277 (1969).

BULLETIN OF THE CHEMICAL SOCIETY OF JAPAN, VOL. 52 (10), 3109—3110 (1979)

Studies of Tritylated Pentoses and 6-Deoxyhexoses. II. Trityl Ethers of Methyl α- and β-L-Rhamnopyranoside and Their Derivatives[1)]

Toshiki OTAKE,* Toru SONOBE,** and Tetsuo SUAMI***

Department of Food and Nutrition, Yamanashi Gakuin Junior College, 502, Sakaori-machi, Kofu 400

***Tobishi Pharmaceutical Co., Ltd., Omori-Nishi, Ota-ku, Tokyo 143*

****Department of Applied Chemistry, Faculty of Engineering, Keio University, Hiyoshi, Kohoku-ku, Yokohama 223*

(Received April 14, 1978)

Synopsis. Mono-*O*-trityl derivatives of methyl α- and β-L-rhamnopyranoside have been prepared and the structures established by PMR analysis.

Hockett and Hudson[2)] described the tritylation of methyl α-L-fucopyranoside which contains only secondary hydroxyl groups.

Recently, the preparation of methyl 2-*O*- and 3-*O*-trityl-α-D-fucopyranoside has been reported.[3)] This paper represents on extention of that work and reports the tritylation of methyl α- and β-L-rhamnopyranoside.

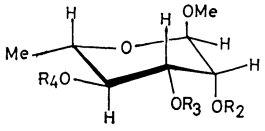

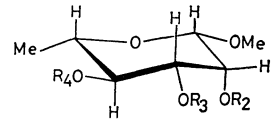

1	$R_2=R_3=R_4=H$	**2**	$R_2=R_3=R_4=H$
3a	$R_3=Tr, R_2=R_4=H$	**11a**	$R_3=Tr, R_2=R_4=H$
3b	$R_3=Tr, R_2=R_4=Ac$	**11b**	$R_3=Tr, R_2=R_4=Ac$
3c	$R_3=Tr, R_2=R_4=Me$	**11c**	$R_3=Tr, R_2=R_4=Me$
4a	$R_4=Tr, R_2=R_3=H$	**12a**	$R_4=Tr, R_2=R_3=H$
4b	$R_4=Tr, R_2=R_3=Ac$	**12b**	$R_4=Tr, R_2=R_3=Ac$
4c	$R_4=Tr, R_2=R_3=Me$	**12c**	$R_4=Tr, R_2=R_3=Me$
5a	$R_2=Tr, R_3=R_4=H$	**13a**	$R_3=H, R_2=R_4=Me$
5b	$R_2=Tr, R_3=R_4=Ac$	**13b**	$R_3=Ac, R_2=R_4=Me$
6	$R_3=H, R_2=R_4=Ac$	**14a**	$R_4=H, R_2=R_3=Me$
7	$R_4=H, R_2=R_3=Ac$	**14b**	$R_4=Ac, R_2=R_3=Me$
8	$R_2=H, R_3=R_4=Ac$	Tr:	$-C-(C_6H_5)_3$
9a	$R_3=H, R_2=R_4=Me$		
9b	$R_3=Ac, R_2=R_4=Me$		
10a	$R_4=Ac, R_2=R_3=Me$		
10b	$R_4=Ac, R_2=R_3=Me$		

Results and Discussion

The reaction of **1** with 2.5 molar equivalents of trityl chloride in pyridine afforded three mono-*O*-trityl ethers: the 3-*O*- (**3a**), 4-*O*- (**4a**) and 2-*O*-trityl derivative (**5a**) in 57, 2.8 and 1.4% yields, respectively, which were converted to the corresponding di-*O*-acetates **3b**, **4b**, and **5b**. The PMR spectra were analyzed with a favorable 1C conformation[4)] confirming the structure. The PMR data for the compounds described are summarized in Tables 1 and 2. Detritylation of **3b**, **4b**, and **5b** with HBr in glacial acetic acid at low temperature gave the corresponding di-*O*-acetates: **6**, **7**, and **8**. Methylation of **3a** and **4a**, followed by detritylation and acetylation gave the *O*-acetyl-di-*O*-methyl derivatives **9b** and **10b**, the structures of which were established by PMR analysis. Gas chromatography-mass (GC-MS) spectra of the intermediary di-*O*-methyl derivatives (**9a** and **10a**) were similar to the

Table 2. Chemical shifts (ppm) of methyl protons

	OAc (s, 3H)	OMe (s, 3H)	H-6 (d, 3H)
3b	1.85, 2.18	3.12	1.10
4b	1.18, 1.85	3.18	1.08
5b	1.88, 2.02	2.93	1.25
6	2.09, 2.13	3.33	1.19
7	2.04, 2.10	3.36	1.35
8	2.02, 2.06	3.37	1.20
3c		3.10, 3.14, 3.57	1.25
4c		2.85, 3.37, 3.43	1.05
9b	2.13	3.36, 3.45, 3.48	1.33
10b	2.08	3.40, 3.42, 3.52	1.20
11b	1.72, 1.92	3.32	1.19
12b	1.20, 1.92	3.34	1.16
11c		3.26, 3.26, 3.58	1.33
12c		2.84, 3.40, 3.43	1.09
13b	2.17	3.50, 3.52, 3.57	1.37
14b	2.07	3.42, 3.53, 3.62	1.25

Table 1. PMR parameters of methine protons

	Chemical shifts, δ/ppm					Coupling constants/Hz				
	H-1	H-2	H-3	H-4	H-5	$J_{1,2}$	$J_{2,3}$	$J_{3,4}$	$J_{4,5}$	$J_{5,6}$
3b	4.43 (d)	4.18 (dd)	3.88 (dd)	5.27 (dd)	3.47 (qd)	1.9	3.2	10.0	9.7	6.0
4b	4.42 (d)[a)]	*ca.*5.2	*ca.*5.3	3.18 (dd)[b)]	4.03 (qd)	1.5	—	9.0	9.0	6.1
5b	3.53 (d)	3.88 (dd)	5.07 (dd)[c)]	5.44 (dd)	*ca.*3.7 (m)[d)]	1.6	3.0	10.5	9.0	6.0
6	4.63 (d)	5.02 (dd)	3.98 (dd)	4.82 (dd)	3.77 (qd)	1.5	4.0	9.8	10.0	6.0
7	4.58 (d)	4.9—5.3 (m)		3.4—3.9 (m)		1.8	—	—	—	6.0
8	4.66 (d)	4.01 (dd)	4.8—5.3 (m)		3.82 (qd)	1.6	3.0	—	9.5	6.0
9b	4.66 (d)	3.60 (dd)[f,g)]	5.08 (dd)	3.22 (dd)[g)]	3.67 (qd)	2.0	3.4	9.5	9.5	6.0
10b	4.75 (d)	3.3—3.6 (overlapped)		5.06 (dd)	3.85 (qd)	1.3	—	9.5	9.5	6.4
11b	3.89d (bs)	4.74 (d,bs)	3.48 (dd)	5.27 (dd)	*ca.*3.1 (m)	*ca.*0.5	3.4	10.0	10.0	6.2
12b	4.51 (d)	5.33 (dd)	5.01 (dd)	3.23 (dd)	3.70 (qd)	*ca.*0.7	3.3	9.5	9.5	6.0
13b	4.37 (d,bs)	3.1—4.1 (m)	4.77 (dd)	3.1—4.1 (m)		*ca.*0.5	3.0	10.0	—	6.0
14b	4.32 (d,bs)	3.1—3.9 (m)		5.02 (dd)	3.1—3.9 (m)	*ca.*0.5	—	10.0	10.0	6.2

Mutiplicity in nuclear magnetic double resonance (irradiated protons are in parentheses): a) s (H-2 and H-3); b) d (H-2and H-3); c) d (H-2); d) d (H-6); e) s (H-2); f) d (H-1); g) d (H-3); bs: broad singlet.

methyl 2,4- and 2,3-di-*O*-methyl-α-D-fucopyranosides,[3] respectively, supporting the proposed structures. The analogous triethylation of **2** gave a 2:1 mixture of two mono-*O*-trityl ethers: 3-*O*- (**11a**) and 4-*O*- (**12a**), in a combined yield of 52%. The structures were established by PMR analysis of the corresponding di-*O*-acetates (**11b** and **12b**) and *O*-acetyl-di-*O*-methyl derivatives (**13b** and **14b**) of **2**. The equatorial OH-3 having a vicinal cis hydroxyl group (OH-2) was most reactive towards tritylation as shown in the selective acetylation of the pyranosides.[4]

Experimental

General Methods. The solution were evaporated under reduced pressure below 40 °C. Optical rotations were measured with a Japan Spectroscopic DIP-SL polarimeter. PMR spectra were recorded on a NEVA NV-14 (60 MHz) or Varian EM-360 (60 MHz) spectrometer, deuteriochloroform being used as the solvent and tetramethylsilane as an internal standard. The multiplicities of the signals have been designated s for a singlet, d for a doublet, dd for a doublet of doublets, qd for a quartet of doublets and m for a multiplet. GC-MS was conducted using the Varian MAT 111 GC/MS system. An electron energy of 80 eV was applied. A glass column (5′×1/8″) packed with 5% NPGS/Chromosorb W was used for the GC. TLC and preparative column chromatography were performed with Wakogel B-10 and C-300 (Wako Junyaku Co., Ltd.), respectively.

Tritylation of Methyl α- (1) and β-L-Rhamnopyranoside (2). Rhamnosides **1** and **2** were prepared from commercial L-rhamnose monohydrate. A mixture of **1** or **2** and trityl chloride in a molar ratio of 1:2.5 dissolved in dry pyridine (×5) was allowed to stand for five days at room temperature. A small amount of water was added to the solution. After concentration, the residue was dissolved in (×5) toluene. Triphenylmethanol was filtered from the toluene solution and the triphenylmethanol-free concentrate subjected to recycling column chromatography five-times on silica gel (50 g) with 5% acetone/benzene. Evaporation of the solvent fractions having R_f values of 0.45, 0.42, and 0.39 on TLC in 15% acetone/benzene gave 973 mg (57.2%) of **3a**, 62 mg (3.7%) of **4a** and 29 mg (1.6%) of **5a**, respectively, as an amorphous solid. $[\alpha]_D^{20}$ in chloroform: **3a**, −50.6° (*c* 2.7); **4a**, −88.4° (*c* 1.0); **5a**, +45.0° (*c* 1.1). Found: **3a**, C, 74.26; H, 6.82%; **4a**, C, 74.37; H, 6.79%; **5a**, C, 73.86; H, 6.73%. Calcd for $C_{26}H_{28}O_5$: C, 74.26; H, 6.71%.

The triphenylmethanol-free concentrate from **2** (1780 mg) was chromatographed on silica gel (50 g) with 5% acetone/benzene three-times. Concentration of the fractions having R_f values of 0.56 and 0.37 on TLC with 12.5% acetone/benzene two developments gave 1522 mg (36.5%) of **11a** and 633 mg (16.7%) of **12a** as an amorphous solid, respectively. $[\alpha]_D^{20}$ in chloroform: **11a**, +55.2° (*c* 0.9); **12a**, +13.2° (*c* 0.7). Found: **11a**, C, 74.26; H, 6.71%; **12a**, C, 73.94; H, 6.80%. Calcd for $C_{26}H_{28}O_5$: C, 74.26; H, 6.71%. Compound **12a** was recrystallized as a monobenzene complex from benzene: $[\alpha]_D^{20}$ +14.7° (*c* 1.2, chloroform), mp 67—68 °C. Found as a benzene complex: C, 77.65; H, 7.07%. Calcd for $C_{32}H_{34}O_5$: C, 77.52; H, 6.87%.

Acetylation of Methyl O-Tritylrhamnopyranoside. Each sample was acetylated under standard conditions for 2 days. After chromatographic purification, the acetates were recrystallized (except **4b** and **5b**) from 80% aqueous acetone in yields of 70—80%. Mp: **3b**, 127—130 °C; **11b**, 188—190 °C; **12b**, 186—188 °C. $[\alpha]_D^{20}$ in chloroform: **3b**, −7.9° (*c* 3.3); **4b**, −86.7° (*c* 0.7); **5b**, +31.6° (*c* 0.5); **11b**, +53.6° (*c* 1.1); **12b**, −42.3° (*c* 1.35). Found: **3b**, C, 71.12; H, 6.61%; **4b**, C, 71.16; H, 6.44%; **5b**, C, 71.11; H, 6.51%; **11b**, C. 71.16; H, 6.46%; **12b**, C, 71.15; H, 6.46%. Calcd for $C_{30}H_{32}O_7$: C, 71.41; H, 6.40%.

Detritylation of Tritylacetyl Derivatives of Methyl Rhamnopyranosides. The detritylation procedure for **3b**, **4b**, and **5b** was almost identical to that for the tritylacetylsucroses.[6] The corresponding di-*O*-acetates were purified on a silica-gel column eluted with 5% acetone/benzene. The yields of detritylation products were 80—85%. Recrystallization (except 7) from 80% aqueous acetone gave the products as needles. Mp: **6**, 116 °C; **8**, 119—120 °C. $[\alpha]_D^{20}$ in chloroform: **6**, −106.5° (*c* 1.7); **8**, −97.4° (*c* 1.0). Found: **6**, C, 75.24; H, 7.12%; **8**, C, 74.91; H, 7.17%. Calcd for $C_{28}H_{32}O_5$: C, 74 97; H, 7.19%.

Methylation of Methyl O-Tritylrhamnopyranosides. Methylation was conducted according to the Purdie method.[7] The products were purified on a silica-gel column eluted with 1% acetone/benzene, after the column was washed with benzene. The yields were approximately 70%. Recrystallization from 80% aqueous acetone gave the products as needles Mp: **3c**, 101—104 °C; **4c**, 138—139 °C; **11c**, 158—159 °C; **12c** 174—178 °C. $[\alpha]_D^{20}$ in chloroform: **3c**, −30.0° (*c* 6.7); **4c**, −96.5° (*c* 0.7); **11c**, +67.3° (*c* 2.7); **12c**, +18.5° (*c* 1.5). Found: **3c**, C, 75.24; H, 7.12%; **4c**, C, 74.81; H, 7.17%; **11c**, C, 74.72; H, 7.17%; **12c**, C, 74.81; H, 7.19%. Calcd for $C_{28}H_{32}O_5$: C, 74.97; H, 7.19%.

Detritylation of Methyl O-Trityl-di-O-methylrhamnopyranoside and Acetylation of the Corresponding Methyl Ethers. Detritylation was conducted by heating the sample with 80% aqueous acetic acid at 90 °C for 1 h. The corresponding methyl ethers were purified on a silica-gel column eluted with 20% acetone/benzene. After acetylation of the methyl ethers, the corresponding acetates were purified on a silica-gel column, the acetates being eluted with 3% acetone/benzene after the column was washed with benzene. The yields of detritylation and acetylation products were greater than 90%. Mp: **13a**, 73.5 °C; **14a**, 63—64 °C; **14b**, 83—84 °C. $[\alpha]_D^{20}$: **9a**, −63.2° (*c* 1.2, methanol); −53.3° (*c* 1.2, chloroform); lit,[8] $[\alpha]_D^{22}$ −68.0° (*c* 4.1, methanol); **9b**, −46.5° (*c* 0.8, chloroform); lit,[8] −51.1° (*c* 0.8, chloroform); **10a**, −22.8° (*c* 1.0, methanol); −18.2° (*c* 1.0, chloroform); lit,[9] $[\alpha]_D$ −14° (*c* 1.94, methanol); **10b**, −32.5° (*c* 1.4, chloroform); **13a**, +88.2° (*c* 1.4, chloroform); **13b**, +89.9° (*c* 1.4, chloroform); **14a**, +68.3° (*c* 3.2, chloroform); **14b**, +89.2° (*c* 2.3, chloroform). Found: **10b**, C, 53.40; H, 7.60%, **13b**, C, 53.17; H, 7.92%, **14b**, C, 53.72; H, 7.49%. Calcd for $C_{11}H_{20}O_6$: C, 53.21; H, 8.12%.

References

1) Presented in part at the 32nd National Meeting of the Chemical Society of Japan, Tokyo, April 1975.
2) R. C. Hockett and C. S. Hudson, *J. Am. Chem. Soc.*, **56**, 1414 (1936).
3) T. Otake and T. Sonobe, *Bull. Chem. Soc. Jpn.*, **49**, 1050 (1976).
4) A. H. Haines, *Adv. Carbohydr. Chem. Biochem.*, **33**, 11 (1976).
5) E. Hemmer and Liaaen-Jensen, *Acta Chem. Scand.*, **24**, 3019 (1970).
6) T. Otake, *Bull. Chem. Soc. Jpn.*, **43**, 3199 (1970).
7) T. Purdie and J. C. Irvine, *J. Chem. Soc.*, **83**, 104 (1903).
8) B. P. F. Lloyd and M. Stacey, *J. Chem. Soc.*, **1955**, 1531.
9) F. Brown, L. Hough, and J. K. N. Jones, *J. Chem. Soc.*, **1950**, 1125.

BULLETIN OF THE CHEMICAL SOCIETY OF JAPAN, VOL. 52 (10), 3111—3112 (1979)

A Synthetic Method for *N*-Benzyloxycarbonyl Hydroxy Amino Acid *t*-Butyl Esters

Hideki KINOSHITA,* Hajime ISHIKAWA, and Hiroshi KOTAKE

Department of Chemistry, Faculty of Science, Kanazawa University, Kanazawa 920

(Received September 13, 1978)

Synopsis. A preparative method for the *N*-benzyloxycarbonyl hydroxy amino acid *t*-butyl esters using the acetoacetyl group as a protecting group for the hydroxyl group of hydroxy amino acids is described. The acetoacetyl group is readily introduced into the hydroxyl group with diketene and effectively deprotected from the O-protected compounds using hydrazine.

Recently, a new method for the synthesis of a peptide lactone as exemplified in the preparation of *N*-(3-hydroxypicolinyl) threonyl-D-leucyl-propylsarcosyl-leucyl-alanyl-alanine threonine lactone, *via* peptide cyclization between sarcosine and leucine (Fig. point A) has been reported.[1] The peptide lactone has also been synthesized by an alternative route, in which peptide cyclization was achieved by peptide bond formation between threonine and D-leucine (Fig. point B).[2] In the latter case it was necessary to prepare *N*-benzyloxycarbonyl threonine *t*-butyl ester (**4a**) as a starting material.

N-benzyloxycarbonyl amino acids are readily esterified by treating the acid with isobutylene in the

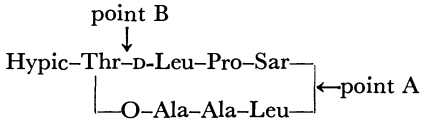

presence of an acid catalyst. In the case of *N*-benzyloxycarbonyl hydroxy amino acids, however, this method is accompanied by simultaneous *O*-alkylation. A novel preparation of *t*-butyl ester of the hydroxy amino acids **4a**—**c** *via* protection of the hydroxyl group of **1a**—**c** effectively overcomes this problem. For the O-protection the acetoacetyl (AcA) group proved very effective for this purpose, the synthetic route of which is shown in Scheme 1. A practical example will be given to illustrate the route for the case of threonine derivatives. The reaction of Z–Thr–OH (**1a**) with diketene was conducted in dichloromethane in the presence of an equimolar amount of triethylamine at room temperature to give Z–Thr(AcA)–OH (**2a**) in 96% yield. Esterification of **2a** with isobutylene in the presence of a catalytic amount of concd sulfuric acid gave the *t*-butyl ester **3a** in 65% yield.

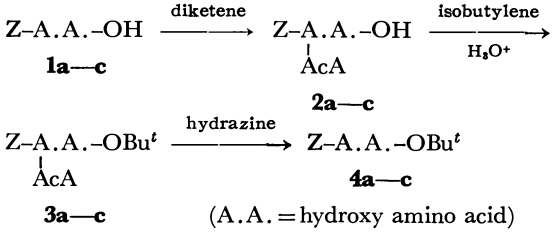

Scheme 1.

Similarly, but without isolation of **2b**—**c**, compounds **1b**—**c** were converted into the corresponding esters **3b**—**c**. Attempts to protect the hydroxyl group of **1a**—**c** by acetylation gave unsatisfactory results.

Removal of the protecting group from compound **3a** was achieved by treatment with a twicemolar amount of hydrazine in ethanol for 30 min, the yield of deprotected product **4a** being 94%. Similarly, the deacylated products **4b**—**c** were prepared from compounds **3b**—**c**, the results of which are listed in Table 1.

Table 1. Preparation of *N*-benzyloxycarbonyl hydroxy amino acid *t*-butyl esters **4a**—**c** from *N*-benzyloxycarbonyl hydroxy amino acids **1a**—**c**

Starting material	Yield/%	
	3a—**c**	**4a**—**c**
Z–Thr–OH (**1a**)	65[a]	94
Z–Ser–OH (**1b**)	65[b]	96
Z–Hyp–OH (**1c**)	80[b]	quant.

a) Yield based on **2a**. b) Yields based on the corresponding **1b**—**c**.

Experimental

All melting points are uncorrected. The NMR spectra were recorded on a JEOL/MH-60. The chemical shifts are reported on the δ scale relative to TMS as an internal standard. The IR spectra were measured with a JASCO IRA-1 diffraction grating infrared spectrometer. The optical rotation values were measured with a JASCO DIP-SL polarimeter.

Z-Thr(AcA)-OH (2a). To a suspension of Z–Thr–OH (**1a**) (506 mg, 2 mmol) in dichloromethane (10 ml) was added triethylamine (202 mg, 2 mmol). To the resulting clear solution, diketene (168 mg, 2 mmol) was added. After stirring at room temperature for several hours, the reaction mixture was evaporated to dryness under reduced pressure. The residual oil was dissolved in ethyl acetate and the organic layer washed with 1M HCl (2.2 ml) and water, and dried over Na_2SO_4. After evaporation of the solvent, the desired product was obtained as an oil (96% yield; 646 mg): IR (neat) 3300, 2990, 1710, 1530, 1060 cm^{-1}; NMR ($CDCl_3$) δ 1.30 (d, 3H, J=7 Hz), 2.14 (s, 3H), 3.36 (s, 2H), 4.30—4.65 (dd, 1H, J=9 Hz), 5.07 (s, 2H), 5.27—5.90 (m, 2H), 7.24 (s, 5H), 8.75 (bs, 1H). DCHA salt of **2a**: mp 140—141 °C; $[\alpha]_D^{25}$ +3.0° (0.67, absEtOH); Found: C, 64.80; H, 8.26; N, 5.26%. Calcd for $C_{28}H_{42}N_2O_7$: C, 64.84; H, 8.16; N, 5.40%.

Z-Thr(AcA)-OBu^t (3a). Compound **2a** (337 mg, 1 mmol) was dissolved in dichloromethane (10 ml) and the solution saturated with isobutylene in the presence of concd sulfuric acid (0.05 ml). The reaction mixture was allowed to stand at room temperature for 65 h, evaporated *in vacuo* and the residue dissolved in ethyl acetate. The organic layer was washed with 10% $NaHCO_3$ and water, dried over Na_2SO_4

and filtered. Then it was evaporated to dryness *in vacuo* to give the crude product. The crude oil was subjected to preparative TLC using benzene–ethanol (10: 1 v/v) as solvent to give the desired product **3a** as an oil in 65% yield (254 mg): IR (neat) 3320, 2960, 1720, 1510, 1150, 1060 cm^{-1}; NMR (CCl_4) δ 1.25 (d, 3H, J=7 Hz), 1.37 (s, 9H), 2.09 (s, 3H), 3.22 (s, 2H), 4.10—4.42 (bd, 1H, J=9 Hz), 5.00 (s, 2H), 5.17—5.75 (m, 2H), 7.20 (s, 2H).

*Z–Ser(AcA)–OBu^t (**3b**)*: Oil, IR (neat) 3320, 2960, 1715, 1420, 1050 cm^{-1}; NMR (CCl_4) δ 1.39 (s, 9H), 2.08 (s, 3H), 3.25 (s, 2H), 4.32 (m, 3H), 4.97 (s, 2H), 5.62—5.95 (m, 1H), 7.19 (s, 5H).

*Z–Hyp(AcA)–OBu^t (**3c**)*: Oil, IR (neat) 2960, 1740, 1700, 1050 cm^{-1}; NMR (CCl_4) δ 1.39 (d, 9H, J=8 Hz), 2.12 (s, 2H), 2.30 (m, 2H), 3.29 (s, 2H), 3.65 (m, 2H), 4.18 (t, 1H, J=7 Hz), 5.01 (s, 2H), 5.22 (bs, 1H), 7.20 (s, 5H).

*Z–Thr–OBu^t (**4a**)*. To a solution of **3a** (100 mg, 0.25 mmol) in ethanol (2 ml), was added a solution of hydrazine hydrate (25 mg, 0.50 mmol) in ethanol. The reaction mixture was stirred at room temperature for 30 min, and evaporated to dryness under reduced pressure. The residue was dissolved in ethyl acetate and filtered. After evaporation of the solvent, the residue was subjected to preparative TLC using benzene–ethanol (10: 1 v/v) as solvent to give the desired product **4a** (74 mg, 94%), which was recrystallized from benzene–hexane: mp 66—67 °C; $[\alpha]_D^{26}$ −20.6° (1.07, absEtOH); IR (KBr) 3400, 3180, 1738, 1705, 1220, 1090, 1065 cm^{-1}; NMR (CCl_4) δ 1.15 (d, 3H, J=7 Hz), 1.43 (s, 9H), 2.70 (d, 1H, J=4 Hz), 3.29—4.23 (m, 2H), 5.03 (s, 2H), 5.64 (bd, 1H, J=9 Hz), 7.26 (s, 5H); Found: C, 61.90; H, 7.32; N, 4.68%. Calcd for $C_{16}H_{23}NO_5$: C, 62.12; H, 7.49; N, 4.53%.

*Z–Ser–OBu^t (**4b**)*: Mp 93—95 °C; $[\alpha]_D^{26}$ −16.5° (1.03, absEtOH); IR (KBr) 3400, 3260, 1710, 1704, 1235, 1045 cm^{-1}; NMR (CCl_4) δ 1.46 (s, 9H), 2.60 (s, 1H), 3.83 (d, 2H, J=4 Hz), 4.20 (m, 1H), 5.03 (s, 2H), 5.70 (d, 1H, J=8 Hz), 7.86 (s, 5H); Found: C, 61.32; H, 7.04; N, 4.58%. Calcd for $C_{15}H_{21}NO_5$: C, 61.00; H, 7.17; N, 4.74%.

*Z–Hyp–OBu^t (**4c**)*: Mp 62—63 °C; $[\alpha]_D^{27}$ −68.6° (1.09, absEtOH); IR (KBr) 3440, 1730, 1665, 1370, 1040 cm^{-1}; NMR (CCl_4) δ 1.31 (d, 9H, J=7 Hz), 2.20 (m, 2H), 3.39 (m, 2H), 3.73—4.38 (m, 3H), 4.89 (s, 2H), 7.02 (s, 5H); Found: C, 63.66; H, 6.96; N, 4.31%. Calcd for $C_{17}H_{23}NO_5$: C, 63.53; H, 7.21; N, 4.36%.

References

1) H. Kinoshita and H. Kotake, *Bull. Chem. Soc. Jpn.*, **50**, 280 (1977).

2) H. Kinoshita, H. Ishikawa, and H. Kotake, 36th National Meeting of the Chemical Society of Japan, Higashi-oosaka, April 1977, Abstr. No. 3U37.

3) The abbreviations used in this work are those recommended by the IUPAC-IUB commission on Biochemical Nomenclature, as published in *J. Biol. Chem.*, **247**, 977 (1972): Hypic for 3-hydroxypicolinyl.

BULLETIN OF THE CHEMICAL SOCIETY OF JAPAN, VOL. 52 (10), 3113—3114 (1979)

Novel Lactonization of γ-Cyclopropyl Carboxylic Acid *via* Acid-catalyzed Cleavage of Cyclopropane Ring

Haruo SEKIZAKI,* Masaaki ITO, and Shoji INOUE**

Chemistry Laboratory, Department of General Education, Higashi Nippon Gakuen University, Onbetsu-cho, Hokkaido 088-01

***Faculty of Pharmacy, Meijo University, Tenpaku-ku, Nagoya 468*

(Received November 13, 1978)

Synopsis. 4,6,10,10-Tetramethyltricyclo[4.4.0.0^{1,3}]-undec-4-ene-5-carboxylic acid has been converted to a tricyclic γ-butyrolactone by perchloric acid catalyzed isomerization. Acetalization of the ketocarboxylic acid afforded an acetal derivative of γ-butyrolactone.

The acid-catalyzed rearrangement of cyclopropylcarbonyl or cyclopropylcarbinyl systems have been extensively investigated. Most of these reactions have known to undergo acid-catalyzed cleavage of the cyclopropane ring and migration of the angular methyl group and/or one of a *gem*-dimethyl groups. For example, under acid conditions, *cis*-thujopsene (**1**) is converted by ring enlargement and angular methyl group migration into a diene (**2**).[1] The acid-catalyzed isomerization of 6,10,10-trimethyl-4-oxotricyclo-[4.4.0.0^{1,3}]decane (**3**) caused ring enlargement and *gem*-dimethyl group migration giving the product **4**.[2]

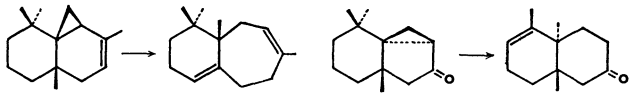

1 **2** **3** **4**

Marshall and Ellison[3] reported that cyclopropylmethanols were subjected to solvolysis in aqueous acid to give γ-butyrolactones fused with cycloheptene and cyclohexene rings. Interest in these reactions prompted the authors to investigate the acid-catalyzed isomerization of 4,6,10,10-tetramethyltricyclo[4.4.0.0^{1,3}]undec-4-ene-5-carboxylic acid (**8**) and its related compound (**5**). It was found that compounds **5** and **8** were converted into the γ-butylolactones (**9** and **11**) *via* cleavage of the cyclopropane ring, and that migration of the angular methyl or *gem*-dimethyl group of **5** and **8** did not occur.

The starting materials (**5** and **8**) were synthesized from *cis*-thujopsene (**1**) as follows. Ozonolysis of *cis*-thujopsene (**1**) in acetic acid gave **6** (47.5%) and **5** (26.6%). The IR and NMR spectra of **6** were identical with those of the sensitized photo-oxidation products of *cis*-thujopsene (**1**).[4] Compound **5** was identical with the spectra of the ozonolysis products of *cis*-thujopsene (**1**) obtained in methanol and ethyl acetate by Norin.[5] One of the ozonolysis products (**6**) was converted into a carboxylic acid (**8**) *via* the aldehyde (**7**)[4,6] as reported by Ohloff *et al.*[6]

The reaction of tricyclic carboxylic acid (**8**) with 70% perchloric acid in benzene gave a γ-butyrolactone (**9**) in 65.5% yield. The structure of **9** was deduced from the spectral data together with the following evidence. The IR absorption of **9** at 1760 cm^{-1} shows the presence of γ-butyrolactone. The presence of a methyl group

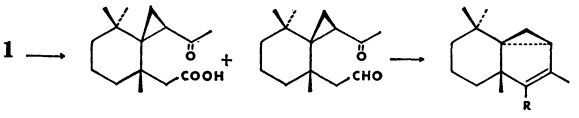

5 **6** **7**: R=CHO **8**: R=COOH

on the olefinic carbon, a C_5–H proton, and a vinyl proton are indicated by the NMR signals at δ 1.80, 2.35, and 5.45 ppm, respectively. Reduction of **9** with lithium aluminium hydride in ether gave an alcohol (**10**). The IR absorptions of **10** at 3260 and 3100 cm^{-1} show the presence of a hydroxyl group. The presence of a methyl group on the olefinic carbon, a vinyl proton, and a hydroxymethyl group are indicated by the NMR signals at δ 1.75, 5.41, and 2.78 ppm (d, J=3.0 Hz), respectively.

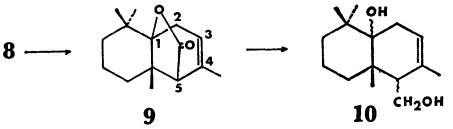

9 **10**

The other ozonolysis product (**5**) was refluxed for 10 h with ethylene glycol and *p*-toluenesulfonic acid in benzene and the reaction mixture chromatographed to give compound **11**. The structure of **11** was deduced from the spectral data as well as the following evidence. The IR absorption of **11** at 1755 cm^{-1} shows the presence of an γ-butyrolactone ring. Reduction of **11** with lithium aluminium hydride in ether at room temperature gave the lactol (**12**). The lithium aluminium hydride reduction of **11** in ether at boiling point however for 2 h gave the diol (**13**).

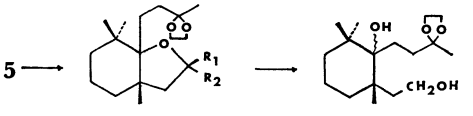

11: R_1=R_2=O **12**: R_1=H, R_2=OH **13**

Experimental

The melting points were determined on a Yanagimoto micro melting point apparatus and are uncorrected. The NMR spectra were recorded on a JEOL PMX-60 spectrometer at 60 MHz, using Me_4Si as an internal standard. The IR spectra were determined on a Shimadzu IR-400 spectrometer. Elemental analyses were performed by a Hitachi 026 CHN analyzer. The analytical GLC was performed on a Shimadzu GC-4B apparatus with a 3 m stainless steel column packed with 3% SE-30, at 10 °C/min 150—250 °C.

Ozonolysis of cis-*Thujopsene (1).* A stream of ozone at 20—35 °C was passed through a stirred solution of **1** (20.4 g, 0.1 mol) in acetic acid (200 ml), until all the starting material had disappeared. The reaction mixture was subsequently treated with zinc dust (30 g) for 1 h at 60—70 °C to reduce the ozonide, filtered, and concentrated. The residue was dissolved in ether (500 ml) and the ether solution washed with 5% aqueous NaOH (50 ml×3), water, dried (Na_2SO_4), and evaporated to give an oily residue (16.2 g). The product was purified by column chromatography using silica gel. Elution with benzene gave **6** (11.2 g) as a colorless liquid. **6**; NMR ($CDCl_3$) δ 0.72 (s, 3, CH_3), 1.13 (s, 3, CH_3), 1.30 (s, 3, CH_3), 2.37 (s, 3, CH_3), 3.00 (dd, 1, J=10.0 and 3.5 Hz), and 9.68 (t, 1, J=3.0 Hz). The combined water layer was acidified with 10% HCl, and extracted with ether. The ether solution was washed with water, dried (Na_2SO_4), and evaporated to give a solid residue (7.9 g). A pure sample of **5** was obtained by recrystallization from hexane. **5**; mp 165—168 °C (lit,[6] mp 166—168 °C).

Cyclization of 6. To a stirred solution of **6** (10.5 g, 40 mmol) in ethanol (200 ml), maintained at 15 °C was added powdered KOH (50 mg, 10 mmol). The solution was stirred for 2 h at room temperature, and then the solvent evaporated under reduced pressure and the residue diluted with water and extracted with ether. The ether solution was washed with water, dried (Na_2SO_4), and evaporated to give an oily residue (9.8 g). The product was separated by column chromatography using silica gel. Elution with benzene gave colorless crystals (**7**) (5.2 g). A pure sample of **7** was obtained by recrystallization from hexane. **7**; mp 73.5—75 °C (lit,[6] mp 73—74 °C).

Oxidation of 7. Compound **7** (2.16 g, 10 mmol) was oxidized in acetone (25 ml) with Jones reagent (8 mole ratio, 2.8 ml) at room temperature for 1 h. The mixture was evaporated and ice-cooled water poured into the resulting residue, which was then extracted with ether. The extract was washed with water, dried (Na_2SO_4), and evaporated to give crude crystals (1.98 g). Recrystallization from hexane gave pure **8**. **8**; mp 148—149 °C (lit,[6] mp 147—149 °C).

Lactonization of 8. A mixture of **8** (1.16 g, 5 mmol) and perchloric acid (70%, 0.5 ml) in benzene was refluxed for 5 min. The reaction mixture was washed with water, dried (Na_2SO_4), and evaporated to give an oily residue (1.1 g). The product was separated by column chromatography using silica gel. Elution with benzene gave colorless crystals **9** (0.81 g). A pure sample of **9** was obtained by recrystallization from hexane. **9**; mp 122—125 °C; IR (KBr) ν 1760 cm^{-1} (γ-butyrolactone); NMR ($CDCl_3$) δ 1.03 (s, 6, $2CH_3$), 1.10 (s, 3, CH_3), 1.80 (d, 3, CH_3, J=3.0 Hz), 2.35 (s, 1, C_5–H), 2.48 (m, 2, C_2–H), and 5.45 (m, 1). Found: C, 76.97; H, 9.35%. Calcd for $C_{15}H_{22}O_2$: C, 76.88; H, 9.46%.

Reduction of 9. A mixture of **9** (117 mg, 0.5 mmol) and $LiAlH_4$ (46 mg, 1.2 mmol) in ether was refluxed for 3 h. To the stirred reaction mixture was added water (2 ml), and extracted with ether. The ether solution was washed with water, dried (Na_2SO_4) and evaporated to give a solid residue (116.5 mg). A pure sample of **10** was obtained by recrystallization from hexane. **10**; mp 140—141 °C; IR (KBr) ν 3250 and 3100 cm^{-1}; NMR ($CDCl_3$) δ 0.95 (s, 3, CH_3), 1.13 (s, 6, $2CH_3$), 1.75 (broad s, 3, CH_3), 2.78 (d, 2, $-CH_2OH$, J= 3.0 Hz), and 5.41 (m, 1).

Lactonization of 5. A benzene solution of **5** (2.52 g, 10 mmol), ethylene glycol (740 mg, 12 mmol), and *p*-TsOH (19 mg, 0.1 mmol) was refluxed for 10 h. The reaction mixture was washed with water, dried (Na_2SO_4), and evaporated to give an oily residue (3.17 g). The product was separated by column chromatography using silica gel. Elution with benzene gave colorless crystals (**11**) (1.58 g). A pure sample of **11** was obtained by recrystallization from hexane. **11**; mp 65—67 °C; IR (KBr) ν 1755 cm^{-1} (γ-butyrolactone); NMR ($CDCl_3$) δ 1.10 (s, 6, $2CH_3$), 1.25 (s, 3, CH_3), 1.32 (s, 3, CH_3), and 3.95 (s, 4, $-CH_2CH_2-$). Found: C, 69.02; H, 9.56%. Calcd for $C_{17}H_{28}O_4$: C, 68.89; H, 9.52%.

Reduction of 11 at Room Temperature. To a stirred solution of **11** (296 mg, 1 mmol) in ether (3 ml), maintained at 10 °C, $LiAlH_4$ (45.6 mg, 1.2 mmol) was added and the solution stirred for 2 h at room temperature. Water (1 ml) was added to the stirred solution, and the aqueous solution extracted with ether. The ether solution was washed with water, dried (Na_2SO_4), and evaporated to give an oily residue (294.2 mg). **12**; IR (neat) ν 3400 cm^{-1} (–OH); NMR ($CDCl_3$) δ 0.98 (s, 6, $2CH_3$), 1.10 (s, 3, CH_3), 1.33 (s, 3, CH_3), 3.97 (s, 4, $-CH_2CH_2-$), and 5.33 (m, 1).

Reduction of 11 at Boiling Point. A mixture of **11** (296 mg, 1 mmol) and $LiAlH_4$ (91 mg, 2.4 mmol) in ether (3 ml) was refluxed for 2 h. Water (2 ml) was added to the stirred solution and the aqueous solution extracted with ether. The ether solution was washed with water, dried (Na_2SO_4) and evaporated to give an oily residue (116.5 mg). **13**; IR (neat) ν 3395 cm^{-1} (–OH); NMR ($CDCl_3$) δ 0.95 (s, 3, CH_3), 1.07 (s, 6, $2CH_3$), 1.32 (s, 3, CH_3), 2.90 (broad s, 2, –OH), 3.68 (t, 2, $-CH_2OH$, J=6.0 Hz), and 3.97 (s, 4, $-CH_2CH_2-$).

References

1) W. G. Dauben and L. E. Friedrich, *J. Org. Chem.*, **37**, 241 (1972).

2) H. Sekizaki, M. Ito, and S. Inoue, *Chem. Lett.*, **1978**, 811.

3) J. A. Marshall and R. H. Ellison, *J. Org. Chem.*, **40**, 2070 (1975).

4) S. Ito, H. Takeshita, T. Muroi, M. Ito, and K. Abe, *Tetrahedron Lett.*, **1969**, 3091.

5) T. Norin, *Acta Chem. Scand.*, **15**, 1676 (1961).

6) G. Ohloff, H. Strickler, B. Willhalm, C. Borer, and M. Hinder, *Helv. Chim. Acta*, **53**, 623 (1970).

BULLETIN OF THE CHEMICAL SOCIETY OF JAPAN, VOL. 52 (10), 3115—3116 (1979)

Notiz über die Säurekatalysierte Umwandlung von 7a-Methyl-5,6,7,7a-tetrahydroindan-1,5-dion in 1-Methylbrexan-4,9-dion

Makoto KOBAYASHI, Takashi MINAMI, und Takeshi MATSUMOTO*

Department of Chemistry, Faculty of Science, Hokkaido University, Sapporo 060

(Eingegangen November 20, 1978)

Synopsis. Beim Erhitzen in HCO_2H mit Mineralsäure wurde 7a-Methyl-5, 6, 7, 7a-tetrahydroindan-1, 5-dion sauer katalysiert in 1-Methylbrexan-4,9-dion umgewandelt. Ein Zwischenprodukt, 7a-Methylhexahydro-2-inden-1,5-dion konnte gaschromatographisch abgetrennt werden.

Wir haben schon berichtet, dass α-(3-Chlor-2-butenyl)ketone wie **1** unter Rückfluss in HCO_2H in Anwesenheit von Mineralsäure 2-Cyclohexenon-Derivate liefern.[1] Unter diesen Bedingungen der modifizierten Wichterle-Reaktion wurde aus **1** 7a-Methyl-5,6,7,7a-tetrahydroindan-1,5-dion (**2**) in mässiger Ausbeute erhalten, wobei 1-Methylbrexan-4,9-dion (**4**) (1-Methyltricyclo[4.3.0.0^{3,7}]nonan-4,9-dion) als Nebenprodukt entstand, dessen Konstitution ohne Diskussion bereits erwähnt wurde.[1b] Aus der weiteren Untersuchung zeigte sich, dass **4** nicht direkt aus **1**, sondern aus **2** durch die sauer katalysierte Umwandlung entsteht. Hier beschreiben wir eingehend die spektroskopisch aufgeklärte Konsitution von **4** sowie einem Zwischenprodukt, das gaschromatographisch in geringer Ausbeute isoliert wurde.

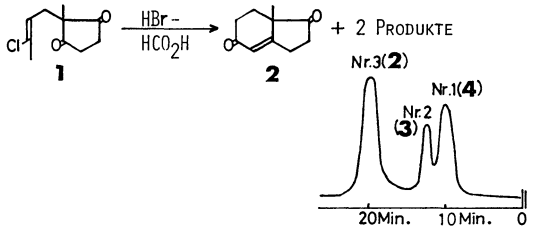

GASCHROMATOGRAMM: QF-1, 180 °C

Abb.-1

Im analytischen Gaschromatogramm des durch die Behandlung von **1** mit HBr–HCO_2H erhaltenen Rohproduktes erschienen 3 Peaks (Abb. 1). Die GC-MS-Messung zeigte, dass alle diese Substanzen das selbe Molekulargewicht (M^+ 164) besitzen. Es wurde durch Vergleich mit der authentischen Probe festgestellt, dass der dritte Peak mit der längsten Retentionszeit dem erwünscheten Produkt **2** entspricht. Durch Säulenchromatographie an SiO_2 wurde das Rohprodukt vorsichtig abgetrennt und die dem Peak Nr. 1 entsprechende Substanz **4** wurde in 10%-iger Ausbeute rein isoliert. Die Analyse zeigte eine Molekularformel $C_{10}H_{12}O_2$. Im IR-Spektrum erscheint eine charakteristische Band für gesättigtes 5-gliedriges Keton (1740 cm^{-1}). Ausserdem war kein besonderes Band für C=C-Doppelbindung, Hydroxy-, Ester-, sowie Ethergruppen zu beobachten. Dies zeigt, dass zwei Sauerstoffatome an zwei Cyclopentanringen vorliegen. Im NMR-Spektrum waren erkennbar: ein Singulett für eine anguläre Methylgruppe bei 1.18 ppm, ein Dublett (1H) mit J=15 Hz bei 1.36 ppm, ein doppeltes Dublett (1H) mit J=6 und 15 Hz bei 1.85 ppm, ein breites Singulett (5H) bei 2.35 ppm und ein Multiplett (2H) bei 2.65 ppm. Durch Einstrahlen bei 2.65 ppm geht das doppeltes Dublett bei 1.85 ppm in ein Dublett mit J=15 Hz über. Diese Daten weisen auf das Vorliegen der Teilkonstitutionen A, B, C, und D hin (Abb. 2).

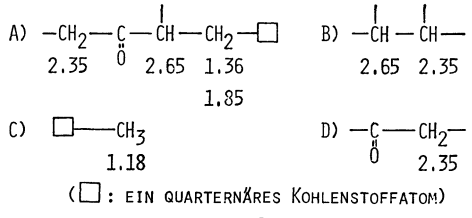

(□: EIN QUARTERNÄRES KOHLENSTOFFATOM)

Abb.-2

Wie schon erwähnt, enthält diese Substanz 10 Kohlenstoffatome. Da in den Teilkonstitutionen A—D insgesamt 11 Kohlenstoffatome vorliegen, so müssen die Zeichen □ in A und C das gleiche Kohlenstoffatom darstellen. Daraus folgt, dass die Verbindung **4** ein tricyclisches Molekül mit zwei Cyclopentanringen ist. Aufgrund dieser spektroskopischen Befunde und der mechanistischen Überlegung sowie Annahme, dass **4** ein Folgeprodukt von **2** sein sollte, folgt für diese

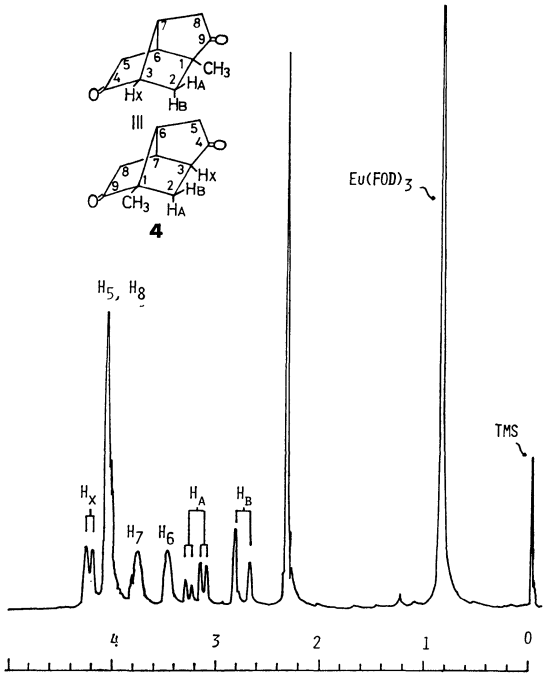

Abb.-3 Ein mit Eu(Fod)$_3$[15 mol %] verschobenes NMR-Spektrum von **4**.

Substanz die Konstitution eines 1-Methylbrexan-4,9-dions (**4**).[2] Die nicht beobachtete Kopplungskonstante J_{BX} wird dadurch erklärt, dass das H_B-Atom am C-2 zum H_x-Atom am C-3 in einem Winkel ≈90° steht. Das Molekülmodell zeigte, dass die beide Winkel $\angle H_{8\alpha}C_8H_{8\beta}$ und $\angle H_{5\alpha}C_5H_{5\beta}$ durch die Carbonylgruppen halbiert werden. Im Einklang damit bleiben diese Methylenprotonen im mit Eu(Fod)$_3$(Tris(heptafluorbutanoylpivaloylmethan)europium) verschobene NMR-Spektrum auch fast äquivalent (Abb. 3). In der demethylierten analogen Verbindung von **4** sollten die Protonen H_A und H_B bzw. H_6 und H_7 äquivalent sein.[3] Bei **4** ist die Symmetrie durch die Methylgruppe am C-1 erniedrigt. Wegen deren C–CH_3 Bindungsanisotropie sind die H_B und H_6-Protonen zu höherem Feld verschoben als H_A- und H_7-Protonen.

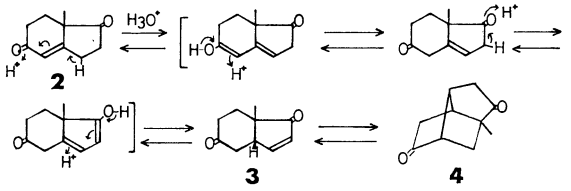

Abb.-4

Ein denkbarer Bildungsmechanismus von **4** ist in Abb.-4 wiedergegeben.[4] **1** wurde zuerst mit HBr–HCO_2H zum **2** cyclisiert, das unter der Umwandlung der Doppelbindung zum **3** isomerisiert. **3** liess sich durch sauer katalysierte intramolekulare Michael-Reaktion weiter in **4** umwandeln. Das oben angenommene Reaktionsbild konnte in der Tat bestätigt werden. Die Behandlung von **2** in HCO_2H mit HBr ergab auch **4** in einer Ausbeute von 6% neben polymeren Produkten. Das Gaschromatogramm war identisch mit dem in Abb. 1 gezeigten. Es wurde dann versucht, die dem Peak Nr. 2 entsprechende Substanz **3** abzutrennen. Diese konnte mit Hilfe der präparativen Gaschromatographie isoliert werden. Das NMR-Spektrum dieser Verbindung zeigt ein Singulett für eine anguläre Methylgruppe bei 1.24 ppm, ein Singulett (1H) mit Feinstruktur bei 2.99 ppm und zwei doppelte Dubletts bei 6.25 ppm (1H, J=1.5, 6 Hz) bzw. 7.52 (1H, J=2, 6 Hz). Durch Einstrahlen bei 7.52 ppm geht das Signal bei 6.25 ppm in ein Dublett mit J=1.5 Hz über. Demgemäss wurden die zwei doppelten Dubletts dem AB-Teil eines ABX-Systems zugeordnet. Entsprechend erscheint im IR-Spektrum die Absorption der α,β-ungesättigten Carbonylgruppe bei 1710 cm^{-1}. Der Substanz könnte somit die Konstitution von *cis*-7a-Methylhexahydro-2-inden-1,5-dion (**3**) zugewiesen werden, die auch durch den Basis-Peak des MS-Spektrums bei *m/e* 55 (O^+≡C–CH=CH_2) bekräftigt wird.

Experimenteller Teil

Vorbemerkungen. Die Schmelzpunkte sind nicht korrigiert. IR-Spektren: JASCO IR-S; NMR-Spektren: Hitachi R-20B bzw. JEOL PS-100 (interner Standard; TMS=0 ppm); MS-Spektren: Hitachi RMU-6E bzw. RMS-4; Gaschromatographie: Hitachi 063 (analytisch) und AEROGRAPH 700 (präparativ).

1-Methylbrexan-4,9-dion (4). *a*): Eine Lösung von 1.89 g **1**[1] in 100 ml HCO_2H wurde mit 10 ml 47% HBr versetzt und 1.5 h unter Rückfluss gekocht. Nach Abdampfen von HCO_2H wurde der Rückstand in AcOEt aufgenomen und mit gesätt. $NaHCO_3$-Lösung neutralgewaschen. Nach Eindampfen des Lösungsmittels wurde das Rohprodukt an der 100-fachen Menge SiO_2 chromatographiert. AcOEt–Benzol (1:4) eluierte 150 mg (10%) **4**, und dann folgten 620 mg **2**, das als Verunreinigung **3** enthielt.

b): Eine Lösung von 164 mg **2** in 3 ml HCO_2H wurde mit 0.3 ml 47% HBr versetzt und 3 h rückfliessend erhitzt. Nach der oben beschriebenen Aufarbeitung und Reinigung erhielt man 10 mg **4**; Schmp. 106—108 °C (Hexan–Isopropylether); IR (Nujol): 1740 cm^{-1}; NMR ($CDCl_3$): 1.18 (3H, s), 1.36 (1H, d, J=15 Hz), 1.85 (1H, dd, J=6, 15 Hz), 2.35 (5H, bs), 2.65 (2H, m); MS: 164 (M^+); Gef: C, 72.90; H, 7.39%. Ber. für $C_{10}H_{12}O_2$: C, 73.14; H, 7.37%.

cis-7a-Methylhexahydro-2-inden-1,5-dion (3). Die Mutterlauge von **2**[1] wurde an SiO_2 chromatographiert und man erhielt eine Fraktion, die **3** relativ viel enthält. Dann wurde das Gemisch von **2** und **3** gaschromatographisch (DGSP, bei 150 °C) abgetrennt. Man isolierte 20 mg **3** (1.2% aus 2 g **1**); Schmp. 84.5—86 °C; IR ($CHCl_3$): 1710, 1675, 1595 cm^{-1}; NMR ($CDCl_3$): 1.24 (3H, s), 2.99 (1H, bs), 6.25 (1H, dd, J=1.5, 6 Hz), 7.52 (1H, dd, J=2, 6 Hz); MS: 164 (M^+); Gef: C, 73.20; H, 7.42%. Ber. für $C_{10}H_{12}O_2$: C, 73.14; H, 7.37%.

Literatur

1) a) M. Kobayashi und T. Matsumoto, *Chem. Lett.*, **1973**, 957. b) M. Kobayashi und T. Matsumoto, *Bull. Chem. Soc. Jpn.*, **52**, 2978 (1979).

2) A. Nickon, H. Kwanski, T. Swartz, R. O. Williams, und J. B. DiGiorgio, *J. Am. Chem. Soc.*, **87**, 1613, 1615 (1955); A. Nickon, F-chih Huang, R. Weglein, K. Matsuo, und H. Yagi, *ibid.*, **96**, 5264 (1974); A. Nickon, D. F. Corey, G. D. Pandit, und J. J. Frank, *Tetrahedron Lett.*, **1975**, 3681; R. S. Bly, P. K. Bly, J. B. Hamilton, J. N. C. Hsu, und P. K. Lillis, *J. Am. Chem. Soc.*, **99**, 204, 216 (1977).

3) NMR-Spektrum von Brexan; G. Brieger, und D. R. Anderson, *J. Org. Chem.*, **36**, 243 (1970).

4) Eine ähnliche Isomerisierung; D. J. Collins und C. W. Tomkins, *Aust. J. Chem.*, **30**, 443 (1977).

BULLETIN OF THE CHEMICAL SOCIETY OF JAPAN, VOL. 52 (10), 3117—3118 (1979)

New Synthesis of Alkyl Polysulfides by Treatment of Thiols, Disulfides and Thionitrites with Anhydrous Copper(II) Chloride

Yong Hae KIM, Kōichi SHINHAMA, and Shigeru OAE*

Department of Chemistry, University of Tsukuba, Niiharigun, Ibaraki 300-31

(Received January 16, 1979)

Synopsis. Reaction of several divalent organic sulfur compounds with copper(II) chloride in acetonitrile gave the corresponding disulfides or other polysulfides in good yields under mild conditions.

In the course of our studies on the synthetic applications of thionitrites, the initial intermediates in the oxidation of either thiols or disulfides, we found that *t*-alkyl thionitrites were readily converted to the trisulfides upon treatment with anhydrous copper(II) chloride. Various other divalent organic sulfur compounds such as *t*-BuSH and di-*t*-butyl disulfide have now been found to react similarly with anhydrous copper(II) chloride under mild conditions to give either the corresponding disulfides or other polysulfides in good yields, as shown in Table 1. This paper deals with these reactions.

A few dialkyl trisulfides or tetrasulfides have been prepared either by the reaction of the corresponding disulfides[1] or thiols[2] with sulfur, by treatment of alkanesulfenyl chlorides with hydrogen sulfide,[3] or by the reaction of sulfur monochloride with alkanethiols.[4] Our new method which involves only mixing anhydrous copper(II) chloride with divalent organic sulfur compounds is simple and especially useful to prepare di-*t*-alkyl trisulfides or di-*t*-alkyl tetrasulfides. This method is also quite useful to prepare various disulfides from corresponding thiols upon slight modifications.

Di-*t*-butyl disulfide was added to a stirred mixture of acetonitrile and anhydrous copper(II) chloride at room temperature. After 5 h under nitrogen, the starting material disappeared completely and di-*t*-butyl trisulfide and di-*t*-butyl tetrasulfide were obtained (Run 1). The trisulfide and the tetrasulfide were separated by distillation, and then identified by elemental analysis. The main product was the tetrasulfide (63%).

Meanwhile, treatment of anhydrous copper(II) chloride with *t*-BuSH or *t*-BuSNO in acetonitrile was found to afford di-*t*-butyl trisulfide as the main product (Runs 2 and 5).

When di-*t*-butyl disulfide was treated with anhydrous iron(III) chloride in ether, the corresponding tri- and tetrasulfides were also obtained, though the reaction was slow and a small amount of the starting material always remained even after a prolonged reaction time (Run 8).

Treatment of *s*-BuSH with anhydrous copper(II) chloride at room temperature afforded di-*s*-butyl disulfide in a good yield without forming any di-*s*-butyl trisulfide or di-*s*-butyl tetrasulfide (Run 11). However, the same treatment of *s*-BuSH or di-*s*-butyl disulfide at a high reaction temperature (under reflux) gave di-*s*-butyl trisulfide in 66—79% yields (Runs 12 and 13).

Primary and aromatic divalent sulfur compounds did not give the corresponding trisulfides and tetrasulfides even after a prolonged reaction time, but gave the corresponding disulfides selectively only in several

Table 1. Synthesis of polysulfides from several organic sulfur compounds with metal halides in acetonitrile

Run	Substrate	Halide	[Halide][a]/[Substrate]	Temp °C	Time min	Yield/%[b] R_2S_2[c]	R_2S_3	R_2S_4
1	$(t\text{-Bu})_2S_2$	$CuCl_2$	2	25	300	0	25[e]	63[e]
2	*t*-BuSH	$CuCl_2$	4	25	90	trace	51[e]	43[e]
3	$t\text{-}C_5H_{11}SH$	$CuCl_2$	4	25	180	trace	49[e]	47[e]
4	$t\text{-}C_9H_{19}SH$	$CuCl_2$	4	25	150	trace	37[e]	55[e]
5	*t*-BuSNO	$CuCl_2$	1	25	20	trace	81[e]	3[e]
6	$t\text{-}C_5H_{11}SNO$	$CuCl_2$	1.5	25	10	9[e]	59[e]	8[e]
7	$t\text{-}C_9H_{19}SNO$	$CuCl_2$	1	25	20	trace	77[e]	4[e]
8	$(t\text{-Bu})_2S_2$	$FeCl_3$[g]	2	25[g]	840	10[e]	49[e]	41[e]
9	*t*-BuSH	CuCl	4	25[h]	20	quant.[e]	0	0
10	$t\text{-}C_5H_{11}SH$	CuCl	1	25[h]	40	88[e]	0	0
11	*s*-BuSH	$CuCl_2$	4	25	15	84[d]	0	0
12	*s*-BuSH	$CuCl_2$	6	82[f]	240	23[e]	66[e]	trace
13	$(s\text{-Bu})_2S_2$	$CuCl_2$	3	82[f]	360	20[e]	79[e]	trace
14	*s*-BuSNO	$CuCl_2$	1	25	5	91[e]	0	0
15	*n*-BuSH	$CuCl_2$	3	25	10	84[d]	0	0
16	$(n\text{-Bu})_2S_2$	$CuCl_2$	2	82[f]	720	quant.[d]	0	0
17	$n\text{-}C_9H_{17}SH$	$CuCl_2$	3	25	10	85[d]	0	0
18	$C_6H_5CH_2SH$	$CuCl_2$	3	25	10	quant.[d]	0	0
19	$C_6H_5CHMeSH$	$CuCl_2$	3	25	10	quant.[d]	0	0
20	*p*-TolSH	$CuCl_2$	3	25	10	quant.[d]	0	0

a) Molar ratio. b) Yield of 100% is achieved when 2/3 mol of the trisulfide or 1/2 mol of the tetrasulfide is obtained from 1 mol of the disulfide, or when 1/2 mol of the disulfide or 1/3 mol of the trisulfide or 1/4 mol of the tetrasulfide is afforded from 1 mol of the thiol or the thionitrite. c) Spectroscopic data of all the disulfides were identical with those of the authentic samples. d) Yield isolated. e) Yield determined by GLC. f) Refluxed in acetonitrile. g) Ethyl ether was used as the solvent. h) Air was bubbled into the solution.

Table 2. Spectral data of polysulfides

Compound	IR (neat, cm^{-1})	NMR (CCl_4, δ)	MS (70 eV, *m/e*, M^+)
$(t\text{-Bu})_2S_3$	1450, 1360, 1260	1.36(s) (lit,[7] 1.34)	210
$(t\text{-Bu})_2S_4$	1450, 1360, 1159	1.37(s) (lit,[7] 1.37)	242
$(t\text{-}C_5H_{11})_2S_3$	1450, 1378, 1150	0.95(t, 6H), 1.30(s, 12H), 1.68(q, 4H)	238
$(t\text{-}C_5H_{11})_2S_4$	1455, 1380, 1153	0.97(t, 6H), 1.35(s, 12H), 1.70(q, 4H)	270
$(t\text{-}C_9H_{19})_2S_3$	1452, 1373, 1135	0.6—2.1(m)	350
$(t\text{-}C_9H_{19})_2S_4$	1459, 1380, 1135	0.6—2.1(m)	382
$(s\text{-Bu})_2S_3$	1462, 1373, 1217	0.99(t, 6H), 1.37 (d, J=7 Hz, 6H) 1.50—1.92(m, 4H), 2.69—3.18 (m, 2H)	210

Table 3. Boiling points, and analytical data of polysulfides

Compound	Bp/°C(Torr) (bath temp)	Found(%)			Calcd(%)		
		C	H	S	C	H	S
$(t\text{-Bu})_2S_3$	65—75/2	45.75	8.69	45.82	45.66	8.62	45.71
$(t\text{-}C_5H_{11})_2S_3$	85—90/2	50.30	9.32	—	50.36	9.29	—
$(t\text{-}C_5H_{11})_2S_4$	95—100/2	44.02	7.81	—	44.39	8.19	—
$(t\text{-}C_9H_{19})_2S_3$	120—125/2	61.93	11.30	—	61.65	10.92	—
$(t\text{-}C_9H_{19})_2S_4$	130—135/2	56.14	9.85	—	56.48	10.00	—

minutes (Runs 15, 16, 17, 18, and 20). It is interesting to note that the treatment of *t*-BuSH with anhydrous copper(I) chloride in the presence of air at the room temperature also gave selectively di-*t*-butyl disulfide, no formation of the trisulfide or the tetrasulfide being confirmed (Run 9). Oxidation of thiols with CuCl was found to require atomospheric oxygen, while oxidation with $CuCl_2$ proceeded under nitrogen. Thus, the reaction is quite useful to prepare symmetrical polysulfides.

These experimental observations seem to suggest that the C–S bond in *t*-alkyl compounds is readily cleaved to form the relatively stable *t*-alkyl cation upon treatment with copper(II) ion.

Thus the following mechanism may be conceivable for the reaction with di-*t*-alkyl disulfide. Other *t*-alkyl sulfur compounds would behave similarly. Copper(II) chloride would be reduced to Cu^0 or copper(I) chloride.

$$\underset{\mathbf{1}}{R\text{–}S\text{–}S\text{–}R} + Cu^{II} \longrightarrow \underset{\mathbf{2}}{R\text{–}S\text{–}S\text{–}R} \longrightarrow R^+ + \underset{\mathbf{3}}{Cu^{II}\text{–}SSR}$$
$$\qquad\qquad\qquad\qquad\quad \downarrow Cu^{II}$$

$$\mathbf{3} + \mathbf{1} \longrightarrow R\text{–}S\text{–}S\text{–}S\text{–}R + \underset{\mathbf{5}}{RS\text{–}Cu^{II}}$$
$$\qquad\qquad\quad \mathbf{4}$$

$$\mathbf{5} + \mathbf{1} \longrightarrow R^+ + \mathbf{4} + [Cu^0] \xrightarrow{Cu^{II}} [Cu^I]$$
$$\qquad\qquad\qquad\qquad\quad \mathbf{6} \qquad\quad \mathbf{7}$$

$$\mathbf{5} + \mathbf{4} \longrightarrow R^+ + R\text{–}S\text{–}S\text{–}S\text{–}S\text{–}R + \mathbf{6} \xrightarrow{Cu^{II}} \mathbf{7}$$

The gas evolved during the reaction of di-*t*-butyl disulfide with anhydrous copper(II) chloride was analyzed through mass spectroscopy which gave a strong peak of 56 (C_4H_8). Thus *t*-butyl cation was found to be converted to the olefin. Meanwhile, the lack of C–S bond cleavage in primary and aromatic sulfur compounds and the low reactivities of the secondary sulfur compounds are also in keeping with the relative stabilities of the respective carbonium ions.

Experimental

All the melting points and boiling points were uncorrected. Elemental analysis of sulfur was carried out by Sagami Chemical Research Center and the analyses of other elements were carried out by the analytical labolatory in our university. Analytical determinations by GLC were performed on a Hitachi 163 gas chromatograph fitted with the following column (3 mm o.d. ×3 m): 10% SE-30 on Chromosorb W. ^{1}H-NMR spectra were taken at 60 MHz on a Hitachi R-24 A apparatus. IR spectra were recorded with a Hitachi 215 spectrometer. Mass spectra were recorded with a Hitachi RMU-6M spectrometer. Thionitrites were prepared from corresponding thiols by the method reported by us.[5] The followings are typical runs.

Reaction of Di-t-butyl Disulfide and Anhydrous Copper(II) Chloride. Di-*t*-butyl disulfide 3.56 g (20 mmol) was added to a stirred mixture of anhydrous copper(II) chloride 5.38 g (40 mmol) in 50 ml of anhydrous acetonitrile. The mixture was stirred at room temperature for 5 h. A saturated NaCl aq solution was added to the dark brown mixture and extracted with ether. The ethereal extract was dried ($MgSO_4$), concentrated, and distilled, giving pure trisulfide and tetrasulfide. The amounts of the products were estimated by GLC: Di-*t*-butyl trisulfide 0.69 g (25%), di-*t*-butyl tetrasulfide 1.52 g (63%). Di-*t*-butyl trisulfide; mp 14—15 °C (lit,[6] 16.63 °C). Di-*t*-butyl tetrasulfide; bp (bath temperature), 80—90 °C/2 mmHg (lit,[6] 70 °C/2 mmHg).

t-Butyl thionitrite and *t*-BuSH were found to react similarly, and the results are shown in Table 1 while the physico-chemical properties are listed in Tables 2 and 3.

Reaction of Di-s-butyl Disulfide with Anhydrous Copper(II) Chloride. Di-*s*-butyl disulfide 1.16 g (6.5 mmol) and anhydrous copper(II) chloride 2.62 g (19.5 mmol) was refluxed in anhydrous acetonitrile for 6 h under nitrogen. The saturated NaCl aq solution was added into the mixture which was extracted with ether. The amount of di-*s*-butyl trisulfide was calibrated by GLC: 0.694 g (79%). The ethereal extract was dried ($MgSO_4$), concentrated and distilled giving 0.623 g of trisulfide: bp (bath temperature) 100—110 °C/2 mmHg (lit,[3] bp 79—80 °C/0.4 mmHg).

Primary and secondary thiols were found to react similarly and the results, physical properties and analytical data on the resulted products are listed in Tables 1, 2, and 3 respectively.

References

1) W.A. Schulze and W.W. Crouch, U.S. Patent 2529355. *Chem. Abstr.*, **45**, 2966g (1951).
2) B. D. Vineyard, *J. Org. Chem.*, **31**, 601 (1966).
3) H. Brinzinger and M. Langheck, *Chem. Ber.*, **86**, 557 (1953); *ibid.*, **87**, 325 (1954).
4) J. F. Harris, Jr., *(Ann Arbor, Mich.)* pub. No. 4927, p. 111, *Dissertation Abstr.*, **13**, 177 (1953). *Chem. Abstr.*, **48.**, 2636 (1954).
5) S. Oae, Y. H. Kim, D. Fukushima, and K. Shinhama, *J. Chem. Soc., Perkin Trans. 1*, **1978**, 913.
6) T. V. Cullum and R. A. Dean, *J. Inst. Petroleum*, **39**, 206 (1953); *Chem. Abstr.*, **48**, 4429a (1954).
7) D. Grant and J. R. Van Wazer, *J. Am. Chem. Soc.*, **86**, 3012 (1964).

BULLETIN OF THE CHEMICAL SOCIETY OF JAPAN, VOL. 52 (10), 3119—3120 (1979)

Enantioselective Alkylation Using Optically Active Phase Transfer Catalyst

Kazuhiko SAIGO,* Hiroshi KODA, and Hiroyuki NOHIRA

Department of Applied Chemistry, Faculty of Engineering, Saitama University, Shimo-ohkubo, Urawa, Saitama 338

(Received February 1, 1979)

Synopsis. Synthesis of optically active benzyl[*cis*-2-(hydroxymethyl)cyclohexyl]dimethylammonium bromide (**3**) and its application to asymmetric synthesis were studied. It was found that **3** was as effective as (−)-*N*-benzyl-*N*-methylephedrinium bromide in the enantioselective alkylation of active methylene compounds when it was employed as a chiral phase transfer catalyst.

As part of ongoing program of study on the use of optically active benzyl[*cis*-2-(hydroxymethyl)cyclohexyl]amine (**1**), prepared by the lithium aluminium hydride reduction[1] of optically active *cis*-2-benzamidocyclohexanecarboxylic acid,[2] application of **1** to the asymmetric synthesis and induction was initiated. Among many papers about asymmetric synthesis and induction, there is only one report concerning enantioselective alkylation of active methylene compounds using a chiral phase transfer catalyst.[3] This prompted us to prepare a new chiral catalyst from **1** and to employ it in the enantioselective alkylation.

Both enantiomers, (+)- and (−)-**1**, were prepared in 30—40% overall yields and in high optical purities from commercially available *cis*-1,2-cyclohexanedicarboxylic anhydride *via* six steps as reported.[1,2]

Treatment of **1** with aq formaldehyde and formic acid under gentle refluxing gave *N*-methylated product, namely, benzyl[*cis*-2-(hydroxymethyl)cyclohexyl]methylamine (**2**) in a good yield. By the quaternization of **2** with methyl bromide, benzyl[*cis*-2-(hydroxymethyl)-cyclohexyl]dimethylammonium bromide (**3**) was obtained in a moderate yield.

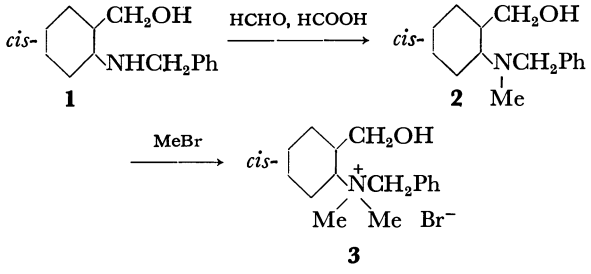

These reaction conditions are completely free from epimerization and/or racemization. Therefore, (+)- and (−)-**3** are considered to be optically pure when optically pure **1** is used as a starting material.

In the next stage, the enantioselective alkylation of active methylene compounds (**4**) was carried out using (+)- or (−)-**3** as an asymmetric phase transfer catalyst.

The solvent effect on the alkylation of ethyl 2-oxocyclohexanecarboxylate (**4a**) with allyl bromide was studied in ether, benzene, dichloromethane, and chloroform, and chloroform was found to be a suitable solvent. Both chemical yield and optical purity of ethyl 1-allyl-2-oxocyclohexanecarboxylate (**5a**) were fairly improved when the alkylation was carried out in

TABLE 1. ENANTIOSELECTIVE ALKYLATION OF ACTIVE METHYLENE COMPOUNDS

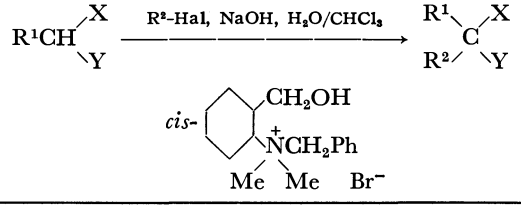

Run	Active Methylene Compound	Halide	**3**/**4** Ratio mol%	Solvent	Temp	Product	Yield/%	$[\alpha]_D$/°
1	**4a**	CH_2=$CHCH_2Br$	3	Et_2O	r.t.	**5a**	0	—
2[a]	**4a**	CH_2=$CHCH_2Br$	3	C_6H_6	r.t.	**5a**	18	+0.1
3	**4a**	CH_2=$CHCH_2Br$	3	CH_2Cl_2	r.t.	**5a**	54	−0.9
4	**4a**	CH_2=$CHCH_2Br$	3	$CHCl_3$	r.t.	**5a**	60	−3.3
5	**4a**	CH_2=$CHCH_2Br$	3	$CHCl_3$	0 °C	**5a**	74	−7.0
6	**4a**	CH_2=$CHCH_2Br$	5	$CHCl_3$	0 °C	**5a**	84	−7.4
7[a]	**4a**	CH_2=$CHCH_2Br$	5	$CHCl_3$	0 °C	**5a**	79	+7.7
8[a]	**4a**	CH_5CH_2Br	5	$CHCl_3$	0 °C	**5a′**	71	+4.7
9[a]	**4b**	CH_2=$CHCH_2Br$	5	$CHCl_3$	0 °C	**5b**	68	+18.2
10[b]	**4c**	CH_3I	5	$CHCl_3$	0 °C	**5c**	65	+1.7
11[b]	**4d**	CH_2=$CHCH_2Br$	5	$CHCl_3$	0 °C	**5d**	86	+0.4

a) (+)-Ammonium bromide, (+)-**3**, was used, and in the other runs (−)-**3** was employed. b) 5% Aq NaOH (40 ml) was used. Runs (5—11) were carried out twice, and comparing their specific rotations lower ones are listed.

chloroform at 0 °C. No reaction proceeded when allyl chloride was employed as an alkylating agent.

Under optimum conditions, the enantioselective alkylation of ethyl 2-oxocyclohexanecarboxylate (**4a**), 2-acetylcyclohexanone (**4b**), ethyl 2-oxocyclopentanecarboxylate (**4c**), and ethyl 2-cyano-2-phenylacetate (**4d**) was carried out giving ethyl 1-allyl-2-oxocyclohexanecarboxylate (**5a**), ethyl 1-benzyl-2-oxocyclohexanecarboxylate (**5a'**), 2-acetyl-2-allylcyclohexanone (**5b**), ethyl 1-methyl-2-oxocyclopentanecarboxylate (**5c**),[4] and ethyl 2-cyano-2-phenyl-4-pentenoate (**5d**).[5] The results are summarized in Table 1.

Fiaud reported that specific rotations of **4a** and **4b** were −8.2° and −23.5°, respectively, when (−)-*N*-benzyl-*N*-methylephedrinium bromide (**6**) was used as a catalyst.[3] Thus, **3** is considered to be as effective as **6** in the enantioselective alkylation of active methylene compounds. In contrast to that only one enantiomer, namely, (−)-**6** is usually available because it is derived from a natural product, both enantiomers of **3** are conveniently prepared, and alkylated products having the desired configuration are easily given choosing the suitable enantiomer. In this respect, **3** is considered to be advantageous as a chiral phase transfer catalyst.

Experimental

The melting points were determined on a Laboratory Devices Mel-Temp apparatus and are uncorrected. The boiling points are also uncorrected. The NMR spectra were recorded on a Varian A-60 spectrometer at 60 MHz using Me_4Si as an internal standard. The IR and MS spectra were determined on a JASCO IR-2A spectrometer and on a JEOL-01SG instrument, respectively. The values of specific rotation were obtained on JASCO DIP-181 digital polarimeter. Optically active **1** was prepared as reported.[1,2] (+)-Form: mp 68—69 °C, $[\alpha]_D^{32}$ +40.4° (*c* 1.00, dry Et_2O). (−)-Form: mp 68—69 °C, $[\alpha]_D^{24}$ −40.6° (*c* 1.00, dry Et_2O).

Benzyl[cis-*2-(hydroxymethyl)cyclohexyl*]*methylamine* (**2**). To (+)-**1** (5.48 g, 25 mmol) was added under cooling with an ice bath 35% aq formaldehyde (2.15 g, 25 mmol) followed by dropwise addition of formic acid (4.14 g, 90 mmol). Then, the mixture was allowed to stand at room temperature for 15 min, and was gently refluxed for 8 h. To the ice cooled reaction mixture was added concd HCl (13 ml), and the solution was concentrated under reduced pressure to give viscous brown residue. The residue was treated with 4 M NaOH (50 ml) and was extracted with three 30 ml portions of ether. The ethereal extract was dried ($MgSO_4$), concentrated, and distilled giving 4.59 g (79%) of (+)-**2**: bp 141—142 °C/0.2 Torr; $[\alpha]_D^{30}$ +22.8° (*c* 1.14, $CHCl_3$); IR (neat) 3300 (OH), 1030 (OH), 740 (Ph), and 695 cm^{-1} (Ph); NMR (CCl_4) δ=1.1—2.1 (8H, m), 2.10 (3H, s), 2.2—2.7 (2H, m), 3.3—4.3 (4H, m), 4.87 (1H, *quasi* s) and 7.22 (5H, s); MS *m/e* 233 (M^+); Found: N, 6.31%. Calcd for $C_{15}H_{23}NO$: N, 6.00%.

In a similar manner, (−)-**2** was obtained in 75% yield: bp 130—132 °C/0.08 Torr; $[\alpha]_D^{24}$ −22.4° (*c* 0.98, $CHCl_3$); MS *m/e* 233 (M^+).

Benzyl[cis-*2-(hydroxymetyl)cyclohexyl*]*dimethylammonium Bromide* (**3**). To a solution of (+)-**2** (4.00 g, 17 mmol) in methanol (30 ml) was bubbled methyl bromide gas for about 8 h at 0 °C. After removal of the solvent, the residual crystals were recrystallized from 2-propanol giving 3.87 g (69%) of (−)-**3**: mp 176—177 °C; $[\alpha]_D^{29}$ −34.6° (*c* 1.00, $CHCl_3$); IR (KBr) 3450 (OH), 1040 (OH), 730 (Ph) and 700 cm^{-1} (Ph); NMR ($CDCl_3$) δ=1.1—2.5 (8H, m), 2.6—3.0 (1H, bs), 3.17 (3H, s), 3.67 (3H, s), 3.7—4.2 (3H, m), 4.7—5.2 (3H, m) and 7.2—7.7 (5H, m); Found: N, 4.29%. Calcd for $C_{16}H_{26}BrNO$: N, 4.27%.

Similarly, (+)-**3** was prepared from (−)-**2** in 54% yield: mp 175—176 °C; $[\alpha]_D^{21}$ +34.6° (*c* 1.04, $CHCl_3$); Found: N, 4.21%. Calcd for $C_{16}H_{26}BrNO$: N, 4.27%.

General Procedure for the Alkylation of Active Methylene Compounds (**4**). To an ice cooled solution of active methylene compound (**4**) (20 mmol), alkylating agent (22 mmol), and (+)- or (−)-**3** (328 mg, 1.0 mmol) in chloroform (20 ml) was added 10% NaOH (20 ml), and the mixture was stirred overnight at 0 °C. After separation of the chloroform layer, the aqueous layer was extracted with three 40 ml portions of chloroform. The chloroform solution combined was concentrated under reduced pressure. Ether (about 100 ml) was added to the concentrated oily product, and residue was separated by decantation. The ethereal solution was dried (Na_2SO_4), evaporated, and distilled giving **5**.

5a: Yield 3.53 g (84%); bp 84—85 °C/2 Torr; $[\alpha]_D^{25}$ −7.4° (*c* 1.51, $CHCl_3$); IR (neat) 1740 (shoulder, C=O), 1705 (C=O) and 1200 cm^{-1} (C–O–C); NMR (CCl_4) δ=1.23 (3H, t, *J*=7 Hz), 1.4—2.2 (6H, m), 2.2—2.7 (4H, m), 4.15 (2H, q, *J*=7 Hz), 4.7—5.0 (1H, m), 5.0—5.2 (1H, m), and 5.4—6.1 (1H, m).

5a': Yield 3.69 g (71%); bp 140—141 °C/3 Torr; $[\alpha]_D^{25}$ +4.7° (*c* 1.15, $CHCl_3$); IR (neat) 1730 (C=O), 1710 (C=O), 1190 (C–O–C), 740 (Ph) and 700 cm^{-1} (Ph); NMR (CCl_4) δ=1.12 (3H, t, *J*=7 Hz), 1.4—2.2 (6H, m), 2.2—2.6 (2H, m), 2.77 (1H, d, *J*=13.5 Hz), 3.19 (1H, d, *J*=13.5 Hz), 4.01 (2H, q, *J*=7 Hz) and 7.10 (5H, s).

5b: Yield 2.44 g (68%); bp 119—120 °C/11 Torr; $[\alpha]_D^{28}$ +18.2° (*c* 1.48, $CHCl_3$); IR (neat) 1710 (C=O) and 1695 cm^{-1} (C=O); NMR (CCl_4) δ=1.3—2.2 (6H, m), 1.99 (3H, s), 2.2—2.6 (4H, m), 4.8—5.0 (1H, m), 5.1 (1H, *quasi* s) and 5.2—5.8 (1H, m).

5c: yield 2.21 g (65%); bp 101—102 °C/14 Torr; $[\alpha]_D^{22}$ +1.7° (*c* 10.33, $CHCl_3$); IR (neat) 1745 (C=O) and 1725 cm^{-1} (C=O); NMR (CCl_4) δ=1.22 (3H, s), 1.25 (3H, t, *J*=7 Hz), 1.6—2.6 (6H, m) and 4.08 (2H, q, *J*=7 Hz).

5d: yield 3.95 g (86%); bp 111—112 °C/1 Torr; $[\alpha]_D^{20}$ +0.4° (*c* 10.0, $CHCl_3$); IR (neat) 2250 (C≡N) and 1740 cm^{-1} (C=O); NMR (CCl_4) δ=1.17 (3H, t, *J*=7 Hz), 2.5—3.3 (2H, m), 4.15 (2H, q, *J*=7 Hz), 5.0—6.1 (3H, m) and 7.2—7.7 (5H, m).

References

1) 2-Benzamidocyclohexanecarboxylic acid was resolved by preferential crystallization after it was converted to benzylamine salt. H. Nohira, K. Watanabe, and M. Kurokawa, *Chem. Lett.*, **1976**, 299.

2) J. Nishikawa, T. Ishizaki, F. Nakayama, H. Kawa, K. Saigo, and H. Nohira, *Nippon Kagaku Kaishi*, **1979**, 754.

3) J.-C. Fiaud, *Tetrahedron Lett.*, **1975**, 3495.

4) This compound is expected to be applicable in optically active illudin S synthesis.

5) Disubstituted cyanoacetate is employed to synthesize barbital.

BULLETIN OF THE CHEMICAL SOCIETY OF JAPAN, VOL. 52 (10) 3121—3122 (1979)

Methylation of Purine 2′-Deoxynucleosides with Trimethyl Phosphate

Toshizumi TANABE,* Kiyoshi YAMAUCHI, and Masayoshi KINOSHITA

Department of Applied Chemistry, Osaka City University, Sumiyoshi-ku, Osaka 558

(Received February 2, 1979)

Synopsis. Trimethyl phosphate was found to methylate deoxyadenosine (N-1) and deoxyguanosine (N-1, N-7, and O-6) in a homogeneous aqueous phase at 37 and 60 °C, giving the corresponding methyl derivatives.

The alkylation of nucleic acids, especially deoxyribonucleic acid (DNA) *in vivo*, is considered to be closely related to carcinogenesis or mutagenesis, and various alkylating agents have been employed for alkylation studies of nucleic acids and their components.[1-8]

Methylation reactions of nucleic acid-bases,[9] pyrimidine 2′-deoxynucleosides,[10] and ribonucleosides[11] were carried out successfully in a homogeneous aqueous phase using trimethyl phosphate (TMP) as a methylating agent.

In this paper, we wish to describe the reactions of deoxyadenosine (**1**) and deoxyguanosine (**4**) with TMP in an aqueous phase.

The reactions were carried out at 37 and 60 °C by stirring a mixture of 2′-deoxynucleoside and TMP in water at an appropriate pH (7—10 for **1** and 10—11 for **4**). The products were conveniently identified by comparison of their R_f values and UV spectra with those of the authentic samples, their yields being determined by means of UV spectra. The results are summarized in Table 1.

TABLE 1. METHYLATION OF PURINE 2′-DEOXYNUCLEOSIDES (dNu) WITH TRIMETHYL PHOSPHATE (TMP)[a]

dNu[b]	Temp °C	Mole ratio (TMP/dNu)	pH	Product[b]	UV-yield/% 24 h	48 h	72 h
dA (**1**)	37	15	7	1-Methyl-dA (**2**)	4	8	10
				N^6-Methyl-dA (**3**)	0	0	3
	37	60	7	**2**	5	9	13
				3	0	1	1
	37	15	10	**2**	3	3	3
				3	3	7	11
	37	60	10	**2**	4	7	8
				3	3	6	9
	60	15	7	**2**	38	52	58
				3	0	5	7
	60	15	10	**2**	5	6	7
				3	32	48	54
				Unknown A	2	3	3
				Unknown B	1	1	3
dG (**4**)	37	15	10	1-Methyl-dG (**5**)	27	35	32
				Imidazole ring opened 7-methyl-dG (**6**)	7	15	16
				Imidazole ring opened 1,7-dimethyl-dG (**7**)	7	15	25
				O^6-Methyl-dG (**8**)	2	3	9
	37	15	11	**5**	32	48	41
				6	11	14	17
				7	6	12	24
				8	3	3	6
	37	60	11	**5**	42	43	44
				6	16	9	10
				7	14	30	37
				8	3	3	2

a) Reaction size: deoxyadenosine (0.25 mmol)+TMP (3.8 or 15.0 mmol)+H_2O (2.5 ml); deoxyguanosine (0.05 mmol)+TMP (0.7 or 3.0 mmol)+H_2O (0.5 ml). b) dA and dG refer to deoxyadenosine and deoxyguanosine, respectively.

Compound **1** and adenosine are generally alkylated with methyl iodide[1] or diazomethane[6] at the N-1 position. Singer *et al.* reported the formation of 1-ethyl- and 7-ethyladenosine in the reaction of adenosine with diethyl sulfate.[3]

TMP also alkylates **1** at the N-1 position to give 1-methyldeoxyadenosine (**2**) and N^6-methyldeoxyadenosine (**3**) which arose from **2** by the Dimroth rearrangement under alkaline conditions. Two minor products obtained in the reaction at 60 °C, pH 10, were considered to be 5′ (or 3′)-*O*-methylated products found also in methylation of pyrimidine 2′-deoxynucleosides under similar conditions.[10]

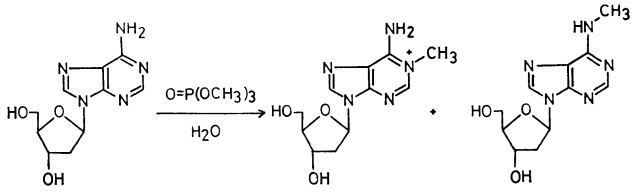

1 2 3

In deoxyguanosine (**4**), the N-1 and N-7 positions are subjected to alkylation in preference to the other positions by alkylating agents.[1,2,4,7,8]

In the present method with TMP, **4** was methylated at the N-1, N-7, and O-6 positions giving 1-methyl- (**5**), imidazole ring opened 7-methyl- (**6**), imidazole ring opened 1,7-dimethyl- (**7**), and O^6-methyldeoxyguanosines (**8**). Identification of **5**, **6**, and **7** was based on comparison of their R_f values and UV spectra with those of the authentic samples, **8** being tentatively assigned through its UV spectra and characterestic fluorescence under UV light.

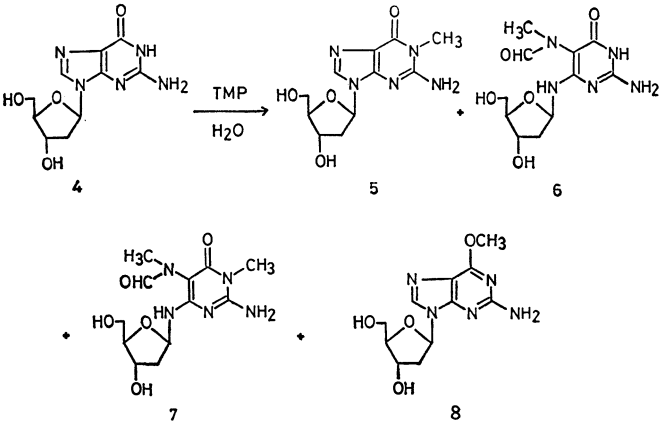

4 5 6 7 8

Thus, methylation of the N-1 position of **4** was found to be accelerated by the increase of pH of the reaction medium, the reactivities of the N-1 position of **1** and the N-7 position of **4** being independent of pH.

Occurrence of O^6-methylation of **4** may be worth remarking, since O^6-alkylation of guanine moiety in DNA seems to be related closely to the mutagenecity and the carcinogenecity through atypical base-pairing.[12]

Experimental

Melting points are uncorrected. UV spectra were recorded on a Hitachi 3T spectrometer, and NMR spectra on a Hitachi Perkin-Elmer R-20 spectrometer with a dilute solution in deuterioxide and sodium 3-(trimethylsilyl)propionate-d_4 as an internal standard. Thin-layer chromatography was performed on silica gel [GF_{254}(type 60), Merck] or cellulose (13254, Eastman) using the following solvents; A: chloroform–methanol, 5: 1, B: 2-propanol–water, 7: 3. Column chromatography was carried out using silica gel (Merck, Art. 7734, 70—230 mesh).

Commercial deoxyadenosine (**1**) and deoxyguanosine (**4**) were used without further purification. Trimethyl phosphate (TMP) was distilled prior to use.

Methylation of Deoxyadenosine (1). A mixture of **1** (125 mg, 0.5 mmol) and TMP (7.5 or 30 mmol) in water (5 ml) was stirred at 37 or 60 °C at an appropriate pH maintained throughout the reaction by occasional addition of 2 M sodium hydroxide. At an appropriate reaction time, 4 μl of the reaction mixture was spotted on silica gel TLC plate, which was developed immediately using solvent A. Two UV-absorbing products (**2** and **3**) were observed (R_f; **1**: 0.29, **2**: 0.01, **3**: 0.41). In the reaction at 60 °C, pH 10, additional two spots (Unknown A and B) appeared (R_f; A: 0.54, B: 0.60). Each product was identified by a comparison of its R_f and UV spectrum with those of the authentic sample and the yield was calculated from its UV spectrum in a similar way to that reported.[9] The results are summarized in Table 1.

The authentic sample of 1-methyldeoxyadenosine was prepared according to the procedure of Jones and Robins.[1]

N^6-Methyldeoxyadenosine was isolated as follows.

A mixture of **1** (1.0 g, 4.0 mmol) and TMP (8.4 g, 60.0 mmol) in water (10 ml, pH 10, NaOH) was stirred at 60 °C for 48 h. After the reaction mixture had been neutralized by concentrated hydrochloric acid, the solvent was removed by evaporation. The residue was purified by silica gel column chromatography (2.5×50 cm). Elution with chloroform afforded unchanged TMP, **3** being obtained by subsequent elution with chloroform–methanol (7: 1) (349 mg, 33%); mp 200—201 °C (lit,[1] 206—208 °C); UV λ_{max} (H_2O) nm: pH 1, 262.0, pH 7, 265.0, pH 13, 265.0 (lit,[1] pH 1, 261.0, pH 7, 265.0, pH 11, 265.0).

Methylation of Deoxyguanosine (4). The reaction of **4** (0.05 mmol) with TMP (0.7 or 3.0 mmol) in water (0.5 ml) at 37 °C, pH 10 or 11 afforded four UV-absorbing products (**5**, **6**, **7**, and **8**) on cellulose TLC which was developed using solvent B (R_f; **4**: 0.46, **5**: 0.67, **6**: 0.59, **7**: 0.73, **8**: 0.83). At an appropriate reaction time, the yield of each product was calculated in a similar way to that mentioned above. The UV spectrum of each product was as follows; **5**: λ_{max} (H_2O) nm: pH 1, 257.0, 280.0 (shoulder), pH 7, 255.5, 271.0 (shoulder), pH 13, 255.5, 272.0 (shoulder) (lit,[2] pH 1, 257.0, pH 11, 254.0); **6**: λ_{max} (H_2O) nm: pH 1, 272.0, pH 7, 273.0, pH 13, 266.0 (lit,[13] pH 1, 270.5, pH 11, 265.0); **7**: λ_{max} (H_2O) nm: pH 1, 272.0, pH 7, 273.0, pH 13, 273.0 (lit,[4] pH 1, 272.0, pH 13, 273.0); **8**: λ_{max} (H_2O) nm: pH 1, 241.0, 286.0, pH 7, 249.0, 279.0 (lit,[7] pH 1, 244.0, 286.0 pH 7, 248.0, 277.0, pH 13, 247.0, 278.0). The R_f and UV spectrum of each product agreed with those of the authentic sample or reported values. Products and their distribution are summarized in Table 1.

The authentic sample of **5** was prepared from the reaction of **4** with trimethylsulfonium hydroxide,[14] and that of **6** was given by the alkaline treatment of 7-methyldeoxyguanosine prepared according to the procedure of Jones and Robins.[1]

Compound **7** was prepared as follows. A mixture of **5** (57 mg, 0.2 mmol) and TMP (0.84 g, 6.0 mmol) in water (2 ml, pH 10, NaOH) was stirred at 60 °C for 30 h. The TLC of the reaction mixture showed only one UV-absorbing spot whose aqueous extract had λ_{max} at 273.0 nm. After the reaction mixture had been neutralized with concentrated hydrochloric acid, unchanged TMP was removed by extraction with chloroform. Evaporation of the water layer gave the residue which was washed with acetone several times. The acetone solution was concentrated and poured into a large excess of ether, giving white hydroscopic precipitate of **7** (31 mg, 49%); NMR (DMSO-d_6) δ=2.65 and 2.71 (0.8 H+2.2 H, two s, N(CHO)CH_3), 3.05 (3H, s, N–CH_3), 5.05—5.60 (1H, complex m, 1′-CH), and 7.55 and 7.62 (0.25H +0.75H, two s, N(CHO)CH_3); UV λ_{max} (H_2O) nm: pH 1, 272.0, pH 7, 273.0, pH 13, 273.0.

References

1) J. W. Jones and R. K. Robins, *J. Am. Chem. Soc.*, **85**, 193 (1963).

2) A. D. Broom, L. B. Townsend, J. W. Jones, and R. K. Robins, *Biochemistry*, **3**, 494 (1964).

3) B. Singer, L. Sun, and H. Fraenkel-Conrat, *Biochemistry*, **13**, 1913 (1974).

4) B. Singer, *Biochemistry*, **11**, 3939 (1972).

5) P. Brookes and P. D. Lawley, *J. Chem. Soc.*, **1962**, 1348; **1960**, 539.

6) J. A. Haines, C. B. Reese, and L. Todd, *J. Chem. Soc.*, **1964**, 1406; **1962**, 5281.

7) O. M. Friedman, G. N. Mahapatra, B. Dash, and R. Stevenson, *Biochim. Biophys. Acta*, **103**, 286 (1965).

8) P. B. Farmer, A. B. Foster, M. Jarman, and M. J. Tisdale, *Biochem. J.*, **135**, 203 (1973).

9) K. Yamauchi, T. Tanabe, and M. Kinoshita, *J. Org. Chem.*, **41**, 3691 (1976).

10) T. Tanabe, K. Yamauchi, and M. Kinoshita, *Bull. Chem. Soc. Jpn.*, **52**, 204 (1979).

11) K. Yamauchi and M. Kinoshita, *J. Chem. Soc. Perkin Trans. 1*, **1978**, 762.

12) A. Loveless, *Nature*, **223**, 206 (1969).

13) L. B. Townsend and R. K. Robins, *J. Am. Chem. Soc.*, **85**, 242 (1963).

14) K. Yamauchi, T. Tanabe, and M. Kinoshita, *J. Org. Chem.*, **44**, 638 (1979).

BULLETIN OF THE CHEMICAL SOCIETY OF JAPAN, VOL. 52 (10), 3123—3124 (1979)

Reactive Troponoids and *o*-Aminophenol. IV. The Synthesis of 8-Arylazocyclohepta[*b*][1,4]benzoxazine by the Reaction of Arylazotropolone with *o*-Aminophenol[1)]

Taichi SOMEYA

Central Research Laboratory of Takasago Perfumery Co., Ltd., Kamata, Ohta-ku, Tokyo 144

(Received February 17, 1979)

Synopsis. 8-Phenylazocyclohepta[*b*][1,4]benzoxazine was obtained by the dehydration of 5a-hydroxy-8-phenylhydrazonocyclohepta[*b*][1,4]benzoxazine, which had itself been obtained by the reaction of 5-phenylazotropolone with *o*-aminophenol.

In previous papers, we have reported the formation of cyclohepta[*b*][1,4]benzoxazine (**1a**) and its derivatives by the reactions with *o*-aminophenol of troponoids which have one or two leaving groups.[2-4)] Many years ago, Nozoe and his coworkers found that 5-nitrosotropolone (**2a**) and 5-arylazotropolone (**2b**) reacted with *o*-phenylenediamine to give quinoxalotropone derivatives,[5)] while 5-nitrosotropolone gave the condensation products (**3a**) by a reaction with *o*-aminophenol; the latter reaction has not, however, been examined in detail.[6)]

In this paper, the present author wishes to describe the results of the reactions of 5-phenylazo- and 5-(*p*-tolylazo)tropolone with *o*-aminophenol.

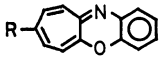

1a R=H

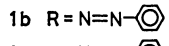

1b R=N=N-C6H5

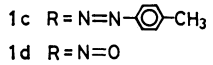

1c R=N=N-C6H4-CH3

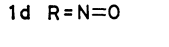

1d R=N=O

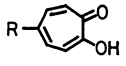

2a R=N=O

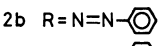

2b R=N=N-C6H5

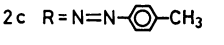

2c R=N=N-C6H4-CH3

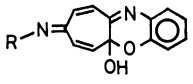

3a R=OH

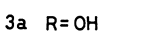

3b R=NH-C6H5

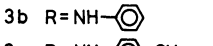

3c R=NH-C6H4-CH3

Results and Discussion

The heating of 5-phenylazotropolone (**2b**) with *o*-aminophenol (**4**) in ethanol under reflux resulted in the repid, quantitative precipitation of sparingly soluble crystals (**3b**). From elemental analysis ($C_{19}H_{15}N_3O_2$), the mass-spectral determination of mol wt (*m/e* 317 (M^+)), and other spectral data, **3b** seems to be 5a-hydroxy-8-phenylhydrazonocyclohepta[*b*][1,4]benzoxazine. Similarly, 5a-hydroxy-8-(*p*-tolylhydrazono)cyclohepta[*b*][1,4]benzoxazine (**3c**) was obtained from 5-(*p*-tolylazo)tropolone (**2c**) and **4**. It is because of the contribution of the arylazo or nitroso group that **3b,c** and **3a** do not undergo dehydration to form **1b,c** and **1d** respectively under these reaction conditions.

When **3b** and **3c** were left in acetic acid in the presence of sulfuric acid, they underwent dehydration to form 8-phenylazo- (**1b**) and 8-(*p*-tolylazo)cyclohepta[*b*][1,4]benzoxazine (**1c**) respectively. These structures were determined by mass and elemental analyses and by means of the spectral data. When **1b,c** were allowed to stand in ethanol, upon the addition of 1 M NaOH or 1 M HCl at room temp. for 3 h, **1b,c** reverted to **3b,c**, which were then decomposed into **2b,c** and **4** when heated with an excess of alkali for 2 h.

The dehydration of **3a** failed to produce 8-nitrosocyclohepta[*b*][1,4]benzoxazine (**1d**) under the same reaction conditions as were used in the case of **3b,c** to **1b, c**.

The NMR data of **1b** measured in trifluoroacetic acid and chloroform-*d* show a sflift of the seven-membered ring protons by 0.86—1.07 ppm and that of the benzene ring protons by only 0.10—0.22 ppm towards a lower magnetic field. This indicates that the positive charge of the cation (**5**) derived from **1b** is delocalized over both the seven-membered ring and the heterocyclic part, as in the case of cyclohepta[*b*][1,4]-benzoxazine (**1a**).[2)]

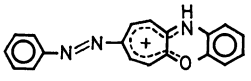

5

Experimental

If not otherwise stated, the instruments and methods were as previously described.[2)]

5a-Hydroxy-8-phenylhydrazonocyclohepta[b][*1,4*]*benzoxazine(3b)*: A mixture of 5-phenylazotropolone (**2b**) (2.0 g, 8.7 mmol), *o*-aminophenol (**4**) (2.0 g, 18.3 mmol), and ethanol (16 ml) was refluxed for 3 h. After cooling, the resulting red crystals (3.2 g) were filtered and recrystallized from ethanol to give 2.7 g (96%) of **3b**; red needles; mp 198 °C; λ_{max}^{MeOH} nm (log ε): 205 (4.73), 234 (4.36), 278 (4.06), and 440 (4.32); $\lambda_{max}^{MeOH+NaOH}$ nm (log ε): 277 (4.05), 410 (4.00)^{sh}, and 472 (4.20); IR (KBr): 3300 (NH) and 3200 cm^{-1} (OH); NMR (60 MHz in DMSO-d_6): δ 9.72 (br. s, 1H, OH), 9.09 (s, 1H, NH), and 6.2—8.0 ppm (m, 13H). Found: C, 71.88; H, 4.86; N, 13.50%; M^+, 317. Calcd for $C_{19}H_{15}N_3O_2$: C, 71.91; H, 4.76; N, 13.24%; M, 317.

*5a-Hydroxy-8-(*p*-tolylhydrazono)cyclohepta*[b][*1,4*]*benzoxazine (3c)*. A mixture of 5-(*p*-tolylazo)tropolone (**2c**) (2.0 g, 8.2 mmol), **4** (1.8 g, 16.4 mmol), and ethanol (4.5 ml) was refluxed for 9 h. After cooling, the resulting crystals were filtrated. Recrystallization from ethyl acetate gave 2.3 g (87 %) of **3c** as orange red needles; mp 231 °C; λ_{max}^{MeOH} nm (log ε): 205 (4.72), 250 (4.35), 300 (4.04), and 442 (4.33); $\lambda_{max}^{MeOH+NaOH}$

nm (log ε): 293 (4.05), 405 (4.09), and 480 (4.26); IR (KBr): 3400 (NH) and 3250 cm^{-1} (OH); NMR (60 MHz in DMSO-d_6): δ 9.40 (s, 1H, NH), 6.9—8.2 (m, 12H), and 2.40 ppm (s, 3H, CH_3). Found: C, 72.20; H, 5.13; N, 12.33%; M^+, 331. Calcd for $C_{20}H_{17}N_3O_2$: C, 72.49; H, 5.17; N, 12.33%; M, 331.

5a-Hydroxy-8-(hydroxyimino)cyclohepta[b][*1,4*]*benzoxazine (**3a**).* A mixture of 5-nitrosotropolone (**2a**) (400 mg, 2.6 mmol), **4** (290 mg, 2.66 mmol), and MeOH (40 ml) was stirred at room temp. The suspension became clear once, and then yellow crystals were precipitated. After filtration, recrystallization from ethyl acetate gave 540 mg (86%) of **3a**; pale yellow needles; mp 198 °C.

8-Phenylazocyclohepta[b][*1,4*]*benzoxazine (**1b**).* A mixture of **3b** (800 mg, 2.5 mmol), acetic acid (15 ml), and concd sulfuric acid (1.4 ml) was allowed to stand at room temp for 1 day. The solution was then neutralized with aq $NaHCO_3$ and extracted with ether. The extract was concentrated, and the residue was chromatographed on a silica-gel column. From the benzene fraction, 600 mg (80%) of **1b** was obtained as brown, triangular structures; mp 210 °C (from benzene); λ_{max}^{MeOH} nm (log ε): 205 (4.45), 231 (4.32), 263 (4.44), 322 (4.30), 450 (4.43)^{sh}, 471 (4.48), 500 (4.40)^{sh}, and 570 (3.76)^{sh}; $\lambda_{max}^{MeOH+HCl}$ nm (log ε): 205 (4.38), 235 (4.37), 265 (4.38), 274 (4.41), 333 (4.26), and 535 (4.39); $\lambda_{max}^{MeOH+NaOH}$ nm (log ε): 258 (4.32), 321 (4.14), 448 (4.52), 505 (4.28)^{sh}, and 570 (4.16)^{sh}; NMR (100 MHz in $CDCl_3$): δ 7.76 (2H, m, $C_{2',6'}$–H), 7.43 (3H, m, $C_{3',4',5'}$–H), 7.14 (1H, dd, J=13.0, 2.0 Hz, C_9–H), 6.89 (1H, dd, J=10.5, 2.0 Hz, C_7–H), 6.86 (3H, m, $C_{1,2,3}$–H), 6.51 (1H, m, C_4–H), 6.29 (1H, d, J=13.0 Hz, C_{10}–H), and 5.72 ppm (1H, d, J=10.5 Hz, C_6–H); NMR (100 MHz in $CDCl_3$+CF_3COOD): δ 8.06 (C_9–H, $\Delta\delta$=0.92 ppm), 7.90 ($C_{2',6'}$–H, $\Delta\delta$=0.14 ppm), 7.88 (C_7–H, $\Delta\delta$=0.99 ppm), 7.53 ($C_{3',4',5'}$–H, $\Delta\delta$=0.10 ppm), 7.15 (C_{10}–H, $\Delta\delta$=0.86 ppm), 6.96 ($C_{1,2,3}$–H, $\Delta\delta$=0.10 ppm), 6.79 (C_6–H, $\Delta\delta$=1.07 ppm), and 6.73 ppm (C_4–H, $\Delta\delta$=0.22 ppm). Found: C, 76.23; H, 4.19; N 13.77%; M^+, 299. Calcd for $C_{19}H_{13}N_3O$: C, 76.24; H, 4.38; N, 14.04%; M, 299.

8-(p-Tolylazo)cyclohepta[b][*1,4*]*benzoxazine (**1c**).* A mixture of **3c** (400 mg, 1.2 mmol), acetic acid (10 ml), and concd sulfuric acid (0.5 ml) was heated at 75—80 °C for 2 h After standing over night, water (50 ml) was added to the solution, and it was neutralized with $NaHCO_3$ and extracted with benzene. The extract was chromatographed on a silica-gel column. From the benzene–ethyl acetate (20: 1) fraction, 250 mg (64%) of **1c** was obtained as brown needles; mp 219 °C (from benzene); λ_{max}^{MeOH} nm (log ε): 206 (4.39), 230 (4.25), 264 (4.41), 328 (4.28), 455 (4.45)^{sh}, 474 (4.49), 500 (4.41)^{sh}, and 560 (4.37)^{sh}; $\lambda_{max}^{MeOH+HCl}$ nm (log ε): 206 (4.31), 233 (4.28), 265 (4.36), 275 (4.39), 341 (4.17), and 540 (4.37); $\lambda_{max}^{MeOH+NaOH}$ nm (log ε): 268 (4.35), 333 (4.21), 475 (4.50), 510 (4.37)^{sh}, and 570 (4.02)^{sh}; NMR (60 MHz in $CDCl_3$): δ 7.70 (2H, m, $C_{2',6'}$–H), 7.30 (2H, m, $C_{3',5'}$–H), 7.10 (1H, m, C_9–H) 6.87 (1H, m, C_7–H), 6.80 (3H, m, $C_{1,2,3}$–H), 6.45 (1H, m, C_4–H), 6.27 (1H, d, J=13 Hz C_{10}–H), 5.70 (1H, d, J=10 Hz C_6–H), and 2.38 ppm (3H, s, CH_3). Found: C, 76.67; H, 4.63; N, 13.06%; M^+, 313. Calcd for $C_{20}H_{15}N_3O$: C, 76.66; H, 4.83; N, 13.41%, M, 313

*Conversion of **1b,c** into **3b,c**.* A solution of **1b,c** (5 mg) in ethanol (1 ml) and three drops of 1 M HCl or 1 M NaOH was allowed to stand at room temp for 3 h. The neutralized solution was found to be **3b,c** by means of the TLC and UV absorptions

A solution of **1b,c** or **3b,c** (5 mg) in ethanol (1 ml) and 1 M NaOH (1 ml) was refluxed or 2 h. The neutralized solution was found to be a mixture of **2b,c** and **4** by means of the TLC and UV absorptions.

The author wishes to express his deep gratitude to Professor Emeritus Tetsuo Nozoe and Professor Kahei Takase (Tohoku University) for their encouragement and advice, and also to Dr. Haruki Tsuruta (Takasago Perfumery Co., Ltd.) for his valuable discussion.

References

1) A part of this work was presented at the 34th National Meeting of the Chemical Society of Japan, Kanagawa, April 1976; Abstr. II, p. 738.

2) T. Nozoe, H. Okai, and T. Someya, *Bull. Chem. Soc. Jpn.*, **51**, 2185 (1978).

3) T. Nozoe and T. Someya, *Bull. Chem. Soc. Jpn.*, **51**, 3316 (1978).

4) T. Nozoe, T. Someya, and H. Okai, *Bull. Chem. Soc. Jpn.*, **52**, 1156 (1979).

5) T. Nozoe, "Daiyuki Kagaku," Asakura, Tokyo (1961), Vol. 13, p. 600.

6) T. Nozoe, T. Asao, and J. Tsunetsugu, unpublished results.

BULLETIN OF THE CHEMICAL SOCIETY OF JAPAN, VOL. 52 (10), 3125—3126 (1979)

Mesomorphic 4-Alkylphenyl 4-Benzoyloxybenzoate Bearing a Terminal Vinyl Group

Hiroyoshi KAMOGAWA,* Masayuki SEKIGAWA, Tomohiro NAKANO, Shin IZAWA, and Masato NANASAWA

Department of Applied Chemistry, Yamanashi University, Takeda 4, Kofu, Yamanashi 400

(Received March 31, 1979)

Synopsis. 4-Alkylphenyl 4-(4-vinyl-, methacryloyloxy-, and methacrylamido-benzoyloxy)benzoates have been synthesized by the reactions of 4-alkylphenyl 4-hydroxybenzoates with the corresponding substituted benzoyl chloride in pyridine. The mesomorphic ranges of these novel monomers are highly dependent upon the type of substituent at both ends of the molecules.

Phenyl 4-benzoyloxybenzoates such as 4-hexylphenyl 2-chloro-4-(4-hexylbenzoyloxy)benzoate have been reported[1] to possess low mesomorphic ranges as well as to be more stable against hydrolysis as compared with the Schiff bases commonly used for liquid crystal applications.

In the course of synthetic studies of mesomorphic organic compounds bearing terminal vinyl groups and their polymers,[2,3] several novel 4-alkylphenyl 4-benzoyloxybenzoates bearing terminal vinyl groups have been synthesized.

The synthetic route adopted was as follows.

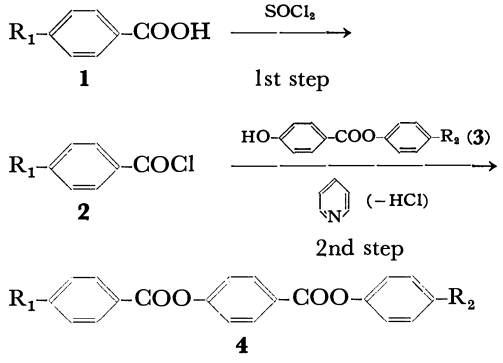

The 4-vinyl-, methacryloyloxy-, and methacrylamido-benzoic acids (**1**) synthesized were converted to the respective acyl chlorides (**2**), which were subsequently reacted with 4-alkylphenyl 4-hydroxybenzoate (**3**) in

TABLE 1. MESOMORPHIC RANGE FOR SUBSTITUTED PHENYL 4-BENZOYLOXYBENZOATES

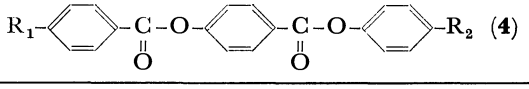

Monomer	R_1	R_2	Yield[a]/%	Mesomorphic range[b]/°C
4-1	CH_2=CH–	CH_3CH_2–CH(–CH_3)–	36	C 88—90 N 169—170 I
4-2	CH_2=CH–	CH_3–C(CH_3)(CH_3)–	16	C 115—118 S 128 N 151—154 I
4-3	CH_2=CH–	CH_3–C(CH_3)(CH_3)–CH_2–C(CH_3)(CH_3)–	52	C 117—118 I
4-4	CH_2=CH–	$CH_3CH_2CH_2$–CH(CH_3)–	45	C 79 S 96 N 130 I
4-5	CH_2=CH–	CH_3CH_2–C(CH_3)(CH_3)–	19	C 102 N 107 I
4-6	CH_2=C(CH_3)–COO–	CH_3CH_2–CH(CH_3)–	18	C 125—126 N 134—135 I
4-7	CH_2=C(CH_3)–COO–	$CH_3CH_2CH_2$–CH(CH_3)–	9	C 121—122 S 126 N 157—158 I
4-8	CH_2=C(CH_3)–CONH–	CH_3CH_2–CH(CH_3)–	18	C 162—165 N 175—176 I
4-9	CH_2=C(CH_3)–CONH–	CH_3CH_2–C(CH_3)(CH_3)–	20	C 170—171 N 176—177 I

a) For purified products. b) C: crystal; S: smectic; N: nematic; I: isotropic.

anhydrous pyridine to afford the desired product **4**. The yields however were not high. The success of this synthetic route depends on the 2nd step. The nature of R_1 appears to markedly affect the yield and the extent of side reactions, *e.g.*, the use of acryloyloxyl or acrylamido groups as R_1 resulted in little reaction or polymerization. Substitution of *N,N*-dimethylaniline for pyridine as the HCl-acceptor did not give satisfactory results.

The novel vinyl monomers thus synthesized are listed in Table 1, where it may be seen that the effect of R_1 and R_2 on the mesomorphic range is large. It is anticipated that branching in the alkyl group R_2 brings about a narrower mesomorphic range. Normal alkyl groups were however not introduced due to the lack of raw materials. The use of vinyl (**4-1**—**4-5**), methacryloyloxyl (**4-6** and **4-7**), and methacrylamido (**4-8** and **4-9**) as R_1 markedly affected the mesomorphic range. The vinyl group appears to afford the lowest CN or SN transition temperature and the widest nematic range, which appear to be comparable with those with freely rotatable alkyl groups.[1)]

The compounds not only indicate mesomorphic ranges as they are, but also they might afford polymers with mesomorphic ranges due to pendant portions by suitable polymerization methods.

Experimental

Mesomorphic ranges were determined by means of a Yamato MP-21 melting point apparatus. 4-Alkylphenyl 4-hydroxybenzoates (**3**) were synthesized according to the reported method.[1)]

*4-s-Butylphenyl 4-(4-Vinylbenzoyloxy)benzoate (**4-1**).* To a solution of 4-*s*-butylphenyl 4-hydroxybenzoate (**3**, 1.3 g, 4.7 mmol) and 4-*t*-butylcatechol (50 mg) in anhydrous pyridine (25 ml), 4-vinylbenzoyl chloride (**2**, 0.8 g, 5.0 mmol) prepared by the room temperature reaction of 4-vinylbenzoic acid (**1**) and thionyl chloride was added with ice-cooling. The solution was allowed to stand at room temperature for 18 h with the exclusion of moisture. The reaction mixture was then poured into iced water and the precipitated crude product was recrystallized three times from ethanol to afford colorless crystals (0.7 g, 36% yield). Found: C, 77.49; H, 6.05%. Calcd for $C_{26}H_{24}O_4$: C, 77.98; H, 6.04%. IR (KBr) 1720 (C=O), 995, 900 (vinyl) cm^{-1}. ^{1}H-NMR ($CDCl_3$) δ 0.8 (t, 3H, CH_3), 1.2 (d, 3H, CH_3), 1.6 (t, 2H, CH_2), 2.6 (q, 1H, CH), 5.4 (d, 1H, $C\underline{H}_2$=CH–), 5.8 (d, 1H, $C\underline{H}_2$=CH–), 6.7 (q, 1H, CH_2=C$\underline{H}$–), 7.3 (q, 8H, ArH), 8.2 (t, 4H, ArH) ppm. Mass (*m/e*) 400 (M^+, 6), 131 (100).

The monomers **4-2**—**4-5** were synthesized in the same manner, their analytical data being also satisfactory.

*4-(1-Methylbutyl)phenyl 4-[4-(Methacryloyloxy)benzoyloxy]benzoate (**4-7**).* The same procedure as that for monomer **4-1** was applied for **3** (R_2=1-methylbutyl; 1.3 g, 5.0 mmol) prepared from 4-(methacryloyloxy)benzoic acid (**1**), which was itself synthesized by the reaction of sodium 4-hydroxybenzoate with methacryloyl chloride in aqueous solution, to afford colorless crystals (0.2 g, 9% yield). Found: C, 73.74; H, 5.49%. Calcd for $C_{29}H_{28}O_6$: C, 73.69; H, 5.99%. IR (KBr) 1740 (C=O), 950, 885 (CH_2=CCH_3) cm^{-1}. NMR ($CDCl_3$+DMSO-d_6) δ 0.8 (t, 3H, CH_3), 1.3 (d, 3H, CH_3), 1.6 (m, 4H, CH_2CH_2), 2.1 (s, 3H, CH_2=C$C\underline{H}_3$), 2.5 (m, 1H, CH), 5.8 (s, 1H, CH_2=), 6.4 (s, 1H, CH_2=), 7.4 (m, 8H, ArH), 8.3 (d, 4H, ArH) ppm. Mass (*m/e*) 472 (M^+, 2), 190 (100).

Monomer **4-6** was synthesized in the same manner with satisfactory analytical data.

*4-t-Pentylphenyl 4-[4-(Methacrylamido)benzoyloxy]benzoate (**4-9**).* Compound **3** (R_2=*t*-pentyl; 1.3 g, 4.7 mmol) and 4-(methacrylamido)benzoyl chloride (**2**, 1.1 g, 5.0 mmol), prepared by the reaction of sodium 4-aminobenzoate with methacryloyl chloride in aqueous solution, when subjected to the same reaction procedure as described above, gave colorless crystals (0.4 g, 20% yield). Found: C, 73.80; H, 6.50; N, 3.16%. Calcd for $C_{29}H_{29}NO_5$: C, 73.87; H, 6.20; N, 2.97%. IR (KBr) 1740 (ester), 1680 (amide), 960, 860 (CH_2=CCH_3) cm^{-1}. NMR ($CDCl_3$) δ 0.7 (t, 3H, CH_3), 1.3 (s, 6H, 2 CH_3), 1.6 (t, 2H, CH_2), 2.1 (s, 3H, CH_2=C$C\underline{H}_3$), 5.5 (s, 1H, CH_2=), 5.8 (s, 1H, CH_2=), 7.0—8.3 (m, 13H, ArH+CONH) ppm. Mass (*m/e*) 471 (M^+, 3), 190 (100).

Monomer **4-8**, synthesized in the same manner, also provided satisfactory analytical data.

References

1) J. P. Van Meter and A. K. Seidel, *J. Org. Chem.*, **40**, 2998 (1975).
2) H. Kamogawa, *Polym. Lett.*, **10**, 7 (1972).
3) H. Kamogawa, O. Yanagihara, Y. Ohkubo, Y. Haramoto, and M. Nanasawa, *Reports of the ASAHI Glass Foundation for Industrial Technology*, **32**, 21 (1978).

BULLETIN OF THE CHEMICAL SOCIETY OF JAPAN, VOL. 52 (10), 3127—3128 (1979)

A New Triterpene Glucoside from *Terminalia arjuna*. Arjunglucoside III

Takahiko TSUYUKI, Yuriko HAMADA, Tadashi HONDA, Takeyoshi TAKAHASHI,* and Kazuhiro MATSUSHITA**

Department of Chemistry, Faculty of Science, The University of Tokyo, Hongo, Bunkyo-ku, Tokyo 113
***Application Center, Scientific Instrument Project, JEOL Ltd., Nakagami, Akishima, Tokyo 196*

(Received April 24, 1979)

Synopsis. The structure of a new triterpene glucoside, arjunglucoside III, isolated from *Terminalia arjuna* was found to be β-D-glucopyranosyl 2α,3β,19α-trihydroxy-11-oxoolean-12-en-28-oate.

The isolation and structure determination of sitosterol, ellagic acid, D-(+)-mannitol, (+)-leucocyanidin, (+)-leucodelphinidin, oleanolic acid, arjunic acid (**1**), arjunolic acid (**2**), and arjunetin (**3**) from *Terminalia arjuna* have been reported.[1,2] In a previous paper,[3] a report was given on three new constituents, arjungenin (**4**) and arjunglucosides I (**5**) and II (**6**) from the bark of plant. We describe the structure determination of a minor glucoside, arjunglucoside III (**7**), isolated from the same plant.

Arjunglucoside III (**7**) was obtained from the methanol extract of the bark of *Terminalia arjuna* in *ca.* 0.01% yield based on the bark. Crystallization from methanol gave a crystal, mp 241.5—243.5 °C, $[\alpha]_D^{19}$ +4.8°; UV λ_{max} 255.5 nm (ε 9600). The ^{13}C NMR spectra of arjunglucoside III (**7**) together with those of arjunetin (**3**) and arjunglucoside II (**6**) are given in Table 1. The results led to the proposal[4,5] that the structure of arjunglucoside III (**7**) can be formulated as glucopyranosyl 2,3,19-trihydroxy-11-oxoolean-12-en-28-oate.

The ^{13}C NMR spectrum of methyl 3β-acetoxy-11-oxoolean-12-en-29-oate shows its C-9 signal at δ 61.9, C-11 signal at δ 200.2, and C-12 signal at δ 128.9, while that of the corresponding 11-deoxo derivative, methyl 3β-acetoxyolean-12-en-29-oate shows its C-9 signal at δ 47.7, C-11 signal at δ 23.6, and C-12 signal at δ 123.0.[5] The ^{13}C NMR and UV spectra strongly suggest the 11-oxoolean-12-ene structure for arjunglucoside III (**7**); this was confirmed by the following evidence.

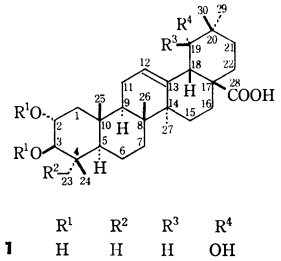

	R^1	R^2	R^3	R^4
1	H	H	H	OH
2	H	OH	H	H
4	H	OH	H	OH

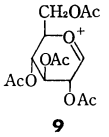

9

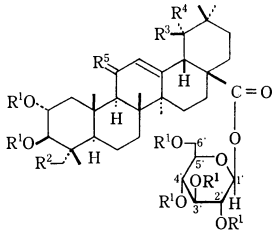

	R^1	R^2	R^3	R^4	R^5
3	H	H	H	OH	H_2
5	H	OH	H	OH	H_2
6	H	OH	H	H	H_2
7	H	H	H	OH	O
8	Ac	H	H	OH	O
10	Ac	H		=O	O
11	Ac	H	H	OH	H_2

Arjunglucoside III (**7**) was treated with acetic anhydride in pyridine to afford an acetate (**8**), mp 272—275 °C, UV λ_{max} 250 nm (ε 11500). The mass spectrum showed a molecular ion peak at *m/e* 916 and a base peak at *m/e* 331. The molecular ion peak together with elemental analysis led to the molecular formula, $C_{48}H_{68}O_{17}$, the base peak due to a fragment ion (**9**)[6] suggesting the presence of a glucosyl moiety in the molecule. The ^1H NMR spectrum showed the presence of seven tertiary methyls, two acetoxyls, an α-proton (at C-9) adjacent to the carbonyl group, an allylic proton (at C-18β), and a proton attached to a carbon atom (C-19) bearing a hydroxyl group (the presence of which was supported by the IR spectrum at 3540 cm^{-1}), besides a tetra-*O*-acetyl-D-glucopyranosyl moiety (*cf.* Experimental). The acetate (**8**), on oxidation with the Collins reagent,[7] gave an oxidation product (**10**), mp 215—218 °C, which was found to be identical with the 11,19-dioxoolean-12-ene derivative obtained by the same oxidation reaction of known arjunetin hexaacetate

TABLE 1. CARBON-13 CHEMICAL SHIFTS δ_c OF ARJUNGLUCOSIDE III (**7**) ARJUNETIN (**3**), AND ARJUNGLUCOSIDE II (**6**)

Carbon number	**7**	**3**	**6**	Carbon number	**7**	**3**	**6**
C-1	48.3	47.5	46.9	C-19	80.3	80.9	46.1
C-2	68.3	68.5	68.8	C-20	35.6	35.5	30.7
C-3	83.4	83.7	78.2	C-21	28.3	29.9	34.0
C-4	39.9	39.8	43.5	C-22	32.1	32.1	32.5
C-5	55.6	55.9	48.1	C-23	28.7	28.7	66.6
C-6	17.9	19.0	18.5	C-24	17.5	16.8	14.2
C-7	33.4	32.9	32.8	C-25	17.9	17.5	17.5
C-8	44.5	39.8	40.0	C-26	19.6	17.5	17.4
C-9	62.6	48.3	47.6	C-27	24.3	28.9	26.0
C-10	38.9	38.6	38.4	C-28	176.7	177.1	176.3
C-11	200.1	24.2	23.9	C-29	29.2	29.9	33.0
C-12	129.0	123.4	122.8	C-30	22.9	24.6	23.6
C-13	170.7	144.2	144.0	C-1′	95.9	95.7	95.6
C-14	45.9	42.1	42.2	C-2′	74.0	74.0	74.0
C-15	28.3	29.2	28.1	C-3′	79.2	79.1	79.0
C-16	27.6	24.9	23.3	C-4′	71.0	71.0	71.1
C-17	46.6	46.3	48.0	C-5′	78.7	78.7	78.7
C-18	45.5	44.5	41.7	C-6′	62.1	62.1	62.2

^{13}C FT NMR spectra were measured with a JEOL FX-100 spectrometer at 25.05 MHz using pyridine-d_5 solutions (*ca.* 100 mg/cm^3) in 10 mm o.d. egg-shape cells. FT conditions: spectral width, 5 kHz; pulse flipping angle, 60°; pulse repetition time, 1.0 s; number of data points, 4 K; number of transients, 5 K—40 K. Chemical shifts are expressed by δ (ppm downfield from internal TMS).

(**11**), tetra-*O*-acetyl-β-D-glucopyranosyl 2α,3β-diacetoxy-19α-hydroxyolean-12-en-28-oate.[1,3] Arjunglucoside III should be β-D-glucopyranosyl 2α,3β,19ξ-trihydroxy-11-oxoolean-12-en-28-oate.

Since the tetra-*O*-acetyl-D-glucopyranosyl group preferentially exists as C1 form, the ^{1}H NMR spectrum of the hexaacetate (**8**) ($J_{1',2'}$=8 Hz) provides support for the presence of a β-glucosyl linkage in the molecule.[8] The α-orientation of the hydroxyl group at C-19 was suggested from the ^{1}H NMR spectrum of the acetate (**8**), which showed a broad signal ($W_{1/2}$ 6 Hz) at δ 3.20 due to a proton on C-18 (β-axial) and a triplet-like signal ($W_{1/2}$ 6 Hz) at δ 3.47 (β-equatorial) due to a proton on C-19. The values are in good accord with those of 18β- and 19β-protons of arjunetin hexaacetate (**11**) and arjungenin methyl ester triacetate,[3,9] suggesting the α(axial)-orientation of the hydroxyl group of arjunglucoside III (**7**).

In conclusion, the structure of arjunglucoside III (**7**) is β-D-glucopyranosyl 2α,3β,19α-trihydroxy-11-oxo-olean-12-en-28-oate.

Experimental

The general procedure is the same as described in a previous paper[3] except UV measurement, which was carried out on a Hitachi 340 spectrometer. High resolution mass spectrum was taken on a JEOL JMS-D300 mass spectrometer.

Isolation of Arjunglucoside III (7). The bark (1.5 kg) of *Terminalia arjuna* was pulverized and extracted with methanol (8 l) for 10 days. The methanol extract afforded a residue (10.5 g), which was subjected to separation by column chromatography on silica gel (500 g). Elution was carried out with chloroform containing methanol of the following concentration: frs 1—13, 2%, each 200 ml; frs 14—17, 4%, each 250 ml; frs 18 and 19, 6%, each 500 ml; frs 20—24, 8%, each 200 ml; frs 25—30, 10%, each 200 ml; frs 31—35, 12%, each 160 ml; frs 36—43, 14%, each 200 ml; frs 44—51, 16%, each 200 ml; frs 52—60, 18%, each 160 ml. After arjunic acid (**1**), arjunolic acid (**2**), and arjungenin (**4**) had been eluted, arjunetin (**3**; 2.4 g) was eluted in frs 41—49 and a mixture (102 mg) of arjunetin (**3**) and arjunglucoside III (**7**) was eluted in fr 50. Fr 51 mainly consisted of arjunglucoside III (**7**; 96 mg) and frs 52—58 afforded arjunglucoside II (**6**; 1.4 g). The mixture containing arjunglucoside III (**7**) was subjected to separation by column chromatography under the same conditions as above to give additional arjunglucoside III (**7**; *ca.* 20 mg). Two crops of crude arjunglucoside III were combined and purified by crystallization from methanol to give 64 mg of arjunglucoside III (**7**), mp 241.5—243.5 °C (with decomposition); $[\alpha]_D^{19}$ +4.8° (*c* 0.83, C_2H_5OH); IR (Nujol) 3380, 1725, and 1630 cm^{-1}; UV (C_2H_5OH) λ_{max} 255.5 nm (ε 9600); ^{13}C NMR (Table 1); MS *m/e* 470, 455, 410, 395, and 69 (base peak) (no molecular ion peak was observed), characterized as its hexaacetate (**8**).

Acetylation of Arjunglucoside III (7). Arjunglucoside III (**7**; 45 mg) was treated with acetic anhydride (0.2 ml) and pyridine (0.2 ml) at room temperature overnight. After the usual treatment, crystallization from ethanol gave arjunglucoside III hexaacetate (**8**; 42 mg), mp 272—275 °C; $[\alpha]_D^{20}$ +12.6° (*c* 1.9, $CHCl_3$); IR (Nujol) 3540, 1765, 1755, 1730, 1660, and 1240 cm^{-1}; UV ($CHCl_3$) λ_{max} 250 nm (ε 11500); ^{1}H NMR (100 MHz) δ ($CDCl_3$) 0.92 (6H, s), 0.96, 1.25 (each 3H, s), 0.99 (9H, s), 1.99 (3H, s), 2.05 (9H, s), 2.08 (6H, s), 2.55 (1H, s), 3.20 (1H, br s), 3.47 (1H, t-like, $W_{1/2}$ 6 Hz), 3.82 (1H, m), 4.06 (1H, as A part of ABX-system, $J_{6',6'}$=12 and $J_{5',6'}$=2 Hz), 4.32 (1H, as B part of ABX-system, $J_{6',6'}$=12 and $J_{5',6'}$=4 Hz), 4.74 (1H, d, $J_{2\beta,3\alpha}$=10 Hz), 5.20 (4H, m), 5.62 (1H, d, $J_{1',2'}$=8 Hz), and 5.77 (1H, s); MS *m/e* 916 (M$^+$), 856, 796, 649, 483, 465, 335, 331 (base peak), 271, and 169; Found: C, 62.76; H, 7.62%. Calcd for $C_{48}H_{68}O_{17}$: C, 62.87; H, 7.47%.

Oxidation of Arjunglucoside III Hexaacetate (8). Chromium trioxide (160 mg) was added to a mixture of pyridine (0.4 ml) and dichloromethane (4 ml) with stirring for 15 min.[7] To the solution was added arjunglucoside III hexaacetate (**8**; 28 mg) in dichloromethane (0.3 ml) and the reaction mixture was stirred at room temperature for 1.5 h. The usual treatment and crystallization from ethanol gave tetra-*O*-acetyl-β-D-glucopyranosyl 2α,3β-diacetoxy-11,19-dioxoolean-12-en-28-oate (**10**; *ca.* 20 mg), as white needles, mp 215—218 °C; $[\alpha]_D^{23}$ +21° (*c* 0.85, $CHCl_3$); the IR, UV, ^{1}H NMR, and MS spectra were identical with those of the sample prepared from arjunetin hexaacetate (**11**).

Oxidation of Arjunetin Hexaacetate (11). Arjunetin hexaacetate[1,3] (**11**; 36 mg, mp 233.5—235.5 °C) was oxidized with the Collins reagent according to the same procedure as above. The reaction product was crystallized from ethanol to give tetra-*O*-acetyl-β-D-glucopyranosyl 2α,3β-diacetoxy-11,19-dioxoolean-12-en-28-oate (**10**; *ca.* 20 mg) as white needles, mp 215—218 °C; $[\alpha]_D^{23}$ +13° (*c* 0.93, $CHCl_3$); IR (Nujol) 1760, 1750, 1712, 1663, and 1230 cm^{-1}; UV ($CHCl_3$) λ_{max} 246 nm (ε 8300); ^{1}H NMR (100 MHz) δ ($CDCl_3$) 0.92 (9H, s), 1.17, 1.25 (each 3H, s), 1.22 (6H, s), 1.99 (3H, s), 2.02 (9H, s), 2.08 (6H, s), 2.53 (1H, s), 3.82 (1H, m), 4.06 (1H, as A part of ABX-system, $J_{6',6'}$=12 and $J_{5',6'}$=2 Hz), 4.30 (1H, as B part of ABX-system, $J_{6',6'}$=12 and $J_{5',6'}$=4 Hz), 4.72 (1H, d, $J_{2\beta,3\alpha}$=10 Hz), 5.23 (4H, m), 5.60 (1H, s), and 5.68 (1H, d, $J_{1',2'}$=8 Hz); MS *m/e* 914 (M$^+$), 854, 794, 647, and 522; Found: *m/e* 914.4162. Calcd for $C_{48}H_{66}O_{17}$: M 914.4298; Found: C, 62.40; H, 7.22%. Calcd for $C_{48}H_{66}O_{17}\cdot 1/2\ H_2O$: C, 62.39; H, 7.31%.

The authors wish to express their thanks to Dr. Kazuo Tori, Shionogi Research Laboratory, for his helpful discussion.

References

1) L. R. Row, P. S. Murty, G. S. R. S. Rao, C. S. P. Sastry, and K. V. J. Rao, *Indian J. Chem.*, **8**, 716, 772 (1970); L. R. Row and G. S. R. S. Rao, *J. Indian Chem. Soc.*, **39**, 89 (1962).

2) F. E. King, T. J. King, and J. M. Ross, *J. Chem. Soc.*, **1954**, 3995.

3) T. Honda, T. Murae, T. Tsuyuki, T. Takahashi, and M. Sawai, *Bull. Chem. Soc. Jpn.*, **49**, 3213 (1976).

4) S. Seo, Y. Tomita, and K. Tori, *J. Chem. Soc., Chem. Commun.*, **1975**, 954.

5) G. S. Ricca, B. Danieli, and G. Palmisano, *Org. Magn. Reson.*, **11**, 163 (1978); H. Duddeck and M. H. A. Elgamal, *ibid.*, **11**, 130 (1978).

6) K. Biemann, D. C. DeJongh, and H. K. Schnoes, *J. Am. Chem. Soc.*, **85**, 1763 (1963).

7) R. Ratcliffe and R. Rodehorst, *J. Org. Chem.*, **35**, 4000 (1970).

8) R. U. Lemieux, R. K. Kulling, H. J. Bernstein, and W. G. Schneider, *J. Am. Chem. Soc.*, **80**, 6098 (1958).

9) *Cf.* D. H. R. Barton, N. J. Holness, K. H. Overton, and W. J. Rosenfelder, *J. Chem. Soc.*, **1952**, 3751; R. T. Aplin, W. H. Hui, C. T. Ho, and C. W. Yee, *J. Chem. Soc., C*, **1971**, 1067.

BULLETIN OF THE CHEMICAL SOCIETY OF JAPAN, VOL. 52 (10), 3129—3130 (1979)

Convenient Preparation of Furanoeremophilane and Menthofuran[1)]

Toshichika SATO, Masahiro TADA,** and Takeyoshi TAKAHASHI*

Department of Chemistry, Faculty of Science, The University of Tokyo, Hongo, Bunkyo-ku, Tokyo 113

***Laboratory of Bioorganic Chemistry, Tokyo University of Agriculture and Technology, Fuchu, Tokyo 183*

(Received April 27, 1979)

Synopsis. Pulegone was transformed into isopulegone enol acetate or isopulegone ethylene acetal, which was treated with *m*-chloroperbenzoic acid and then with acid to give menthofuran. Fukinone was converted into furanoeremophilane by the same procedure.

It has been reported that oxidation of isopulegone (**1**) with perbenzoic acid and subsequent treatment of a keto epoxide (**2**) with hot dilute acid give menthofuran (**3**) in 13% yield.[2)] The present paper deals with a convenient preparation of **3** from pulegone (**4**) *via* isopulegone enol acetate (**5**) or isopulegone ethylene acetal (**6**). Although the preparation is similar to that reported, the yield was much improved. Preparation of furanoeremophilane (**7**) from fukinone (**8**) by the same procedure is described.

Enol acetylation of pulegone (**4**) gave a mixture of **5** and pulegone enol acetate (**9**) quantitatively in a *ca.* 5:3 ratio. Enol acetate (**5**) with isopropenyl double bond was isolated in 59% yield, epoxidized with *m*-chloroperbenzoic acid in the presence of phosphate buffer solution (pH 7.2),[3)] and the reaction mixture was treated with *p*-toluenesulfonic acid to afford menthofuran (**3**)[4)] in 68% yield. The reaction of **5** to form **3**[1,5)] may proceed through an epoxide (**10**) and (or) a hydroxy ketone (**11**)[6)] as an intermediate. However, no information could be obtained about the intermediate due to its labile nature.

Similarly, fukinone (**8**)[7)] was enol acetylated to give two enol acetates **12** and **13** in 27% and 40% yields, respectively. The enol acetate (**13**) was treated successively with *m*-chloroperbenzoic acid and *p*-toluenesulfonic acid to afford furanoeremophilane (**7**)[8)] in 42% yield.

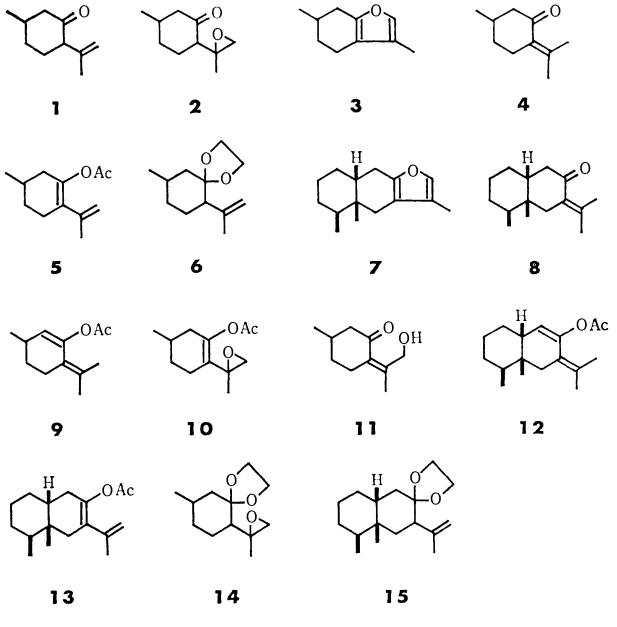

Acetalization of pulegone (**4**) proceeded quantitatively to give **6**. Epoxidation of **6** with *m*-chloroperbenzoic acid gave an epoxide (**14**) in 89% yield showing two peaks in a *ca.* 2:1 ratio on GLC examination. The major epoxide was separated by means of preparative TLC and converted into menthofuran (**3**) by acid treatment (2 M hydrochloric acid–pentane).[9)] When the reaction was carried out without separation of the intermediates **6** and **14**, **3** was obtained from **4** in 90% yield.

An ethylene acetal (**15**) with terminal double bond was formed as the sole product on acetalization of fukinone (**8**). Treatment of **15** with peroxy acid and then with acid gave furanoeremophilane (**7**) in 74% yield from **15**.

These two methods are useful for the synthesis of 3-methylfuran derivatives from α-isopropylidene ketones.

Experimental

UV spectra were measured on a Hitachi 124 spectrophotometer, and high resolution mass (MS) spectra on a JEOL JMS-D300 spectrometer. Other details are the same as described in a previous paper.[10)]

Enol Acetylation of Pulegone (4). A mixture of **4** (3.60 g), isopropenyl acetate (4.17 g), and *p*-toluenesulfonic acid (0.5 g) was stirred under nitrogen at room temperature for 15 h. The reaction mixture was passed through a column of silica gel (100 g). An excess of isopropenyl acetate was eluted with pentane. Elution with pentane–ether (50:1) afforded isopulegone enol acetate (**5**; 2.69 g; yield 59%), an oil (one spot on TLC), bp 74.5—77 °C/533 Pa; IR (neat) 1760, 1635, and 900 cm^{-1}; UV_{max} (EtOH) 223 nm (ε 5700); NMR (CS_2) δ 0.88 (3H, d, J=6 Hz), 1.74 (3H, d-like, J=1.5 Hz), 1.92 (3H, s), and 4.73 (2H, m); NMR (CCl_4) δ 1.03 (3H, d, J=6 Hz), 1.78 (3H, d-like, J=1.5 Hz), 1.98 (3H, s), and 4.77 (2H, m). Found: *m/e* 194.1308. Calcd for $C_{12}H_{18}O_2$: M, 194.1307. Successive elution with the same solvents gave pulegone enol acetate (**9**; 1.50 g; yield 33%), an oil (one spot on TLC); IR (neat) 1760 cm^{-1}; UV_{max} (EtOH) 241 nm (ε 3400); NMR (CCl_4) δ 1.00 (3H, d, J=6.5 Hz), 1.74 (3H, br. s), 1.82 (3H, br. s), 2.00 (3H, s), and 5.07 (1H, d, J=3 Hz). Found: *m/e* 194.1278. Calcd for $C_{12}H_{18}O_2$: M, 194.1307.

Menthofuran (3) from Isopulegone Enol Acetate (5). A buffer solution (pH 7.2; 20 ml; prepared from KH_2PO_4–NaOH–H_2O) and *m*-chloroperbenzoic acid (2.3 g) in ether (30 ml) were added to a solution of **5** (250 mg) in ether (10 ml) at 0 °C, and the mixture was stirred for 30 min. The organic layer was washed with a 10% aqueous sodium thiosulfate solution and treated with *p*-toluenesulfonic acid (30 mg) in ether at room temperature for 2 min. The ethereal solution was washed with a 5% sodium hydroxide solution and brine, dried ($MgSO_4$) and evaporated, giving a residue which was chromatographed (silica gel, 5 g; elution with pentane) to

afford menthofuran (**3**; 132 mg; yield 68%), an oil (one spot on TLC); IR (neat) 1635 and 1560 cm^{-1}; NMR (CS_2) δ 1.09 (3H, d, J=5.5 Hz), 1.85 (3H, d, J=2 Hz), and 6.84 (1H, m); NMR (CCl_4) δ 1.06 (3H, d, J=5.5 Hz), 1.86 (3H, d, J=2 Hz), and 6.88 (1H, m). Found: *m/e* 150.1032. Calcd for $C_{10}H_{14}O$: M, 150.1045.

Furanoeremophilane (7) from Fukinone (8). Fukinone (**8**; 351 mg) was treated with isopropenyl acetate (300 mg) in the presence of *p*-toluenesulfonic acid (50 mg) under nitrogen with stirring at room temperature for 15 h. The reaction mixture was passed through a column of silica gel (10 g). An excess of isopropenyl acetate was eluted with pentane. Elution with pentane–ether (25: 1) gave an enol acetate (**13**; 164 mg; yield 40%), an oil (one spot on TLC); IR (neat) 1760 and 895 cm^{-1}; NMR (CS_2) δ 0.88 (3H, d, J=6.5 Hz), 0.91 (3H, s), 1.73 (3H, d-like, J=1.5 Hz), 1.92 (3H, s), 4.68 (1H, m), and 4.77 (1H, m); MS *m/e* 262 (M^+). Successive elution with the same solvent mixture gave another enol acetate (**12**; 114 mg; yield 27%), an oil (one spot on TLC); IR (neat) 1760 cm^{-1}; NMR (CS_2) δ 0.70 (3H, d, J=6 Hz), 0.90 (3H, s), 1.74 (3H, br s), 1.81 (3H, br s), 2.00 (3H, s), and 4.80 (1H, d, J=3 Hz); MS *m/e* 262 (M^+).

The enol acetate (**13**; 85 mg) was dissolved in ether (10 ml), and treated with *m*-chloroperbenzoic acid (650 mg) in ether (50 ml) at 0 °C for 1 h with stirring in the presence of the phosphate buffer solution (10 ml; *vide supra*). The organic layer was treated as described above (including the treatment with *p*-toluenesulfonic acid, 10 mg) to give a residue which was chromatographed (silica gel, 5 g; elution with pentane) to give furanoeremophilane (**7**; 30 mg; yield 42%). The IR and NMR spectra were identical with those of an authentic **7**.[8]

Acetalization of Pulegone (4). Ethylene glycol (2.5 ml) and *p*-toluenesulfonic acid (100 mg) were added to a solution of **4** (2.24 g) in benzene (20 ml) and the mixture was refluxed under nitrogen for 7.5 h using a Dean-Stark water separator. The organic layer was washed with aqueous sodium hydrogencarbonate solution and brine, dried ($MgSO_4$), and evaporated, giving a residue. This was passed through a column of silica gel (30 g) [elution with hexane–ether (20: 1)] to give isopulegone ethylene acetal (**6**; 2.84 g; yield 98%), an oil showing one spot on TLC and one peak at R_t=8.7 min on GLC examination [column, SP-1000 (10%), 3(mm)×2(m); 160 °C; N_2 flow rate, 40 ml/min]; IR (neat) 1640 and 890 cm^{-1}; NMR (CCl_4) δ 0.90 (3H, d, J=6 Hz), 1.74 (3H, m), 3.78 (4H, br s), and 4.74 (2H, m). Found: *m/e* 196.1455. Calcd for $C_{12}H_{20}O_2$: M, 196.1464.

Menthofuran (3) from Isopulegone Ethylene Acetal (6). A solution of *m*-chloroperbenzoic acid (266 mg) in ether (20 ml) was added to **6** (304 mg) in ether (10 ml) at 0 °C, and the mixture was stirred for 15 h. The ethereal solution was washed with a 10% aqueous sodium thiosulfate solution, aqueous sodium hydroxide solution and brine, and dried ($MgSO_4$). The solvent was removed under reduced pressure (at below 20 °C) to give a residue which was chromatographed on a column of Florisil (5 g). Elution with pentane–ether (5: 1) gave an epoxide (**14**; 294 mg; yield 89%) as an oil. The epoxide (**14**) showed two spots on TLC and two peaks at R_t=10.1 min (a major epoxide) and R_t=10.8 min (a minor epoxide) in a ratio of *ca.* 2: 1 on GLC examination under the same conditions as described above. Epoxide (**14**) was further chromatographed [silica gel, 3 g; elution with pentane–ether (5: 1)] to afford the major epoxide, an oil (one spot on TLC); NMR (CCl_4) δ 0.89 (3H, d, J=6 Hz), 1.19 (3H, s), 2.46 and 2.67 (each 1H, J=6 Hz, CH_2 in an oxirane ring), and 3.86 (4H, m, O–CH_2–CH_2–O). Found; C, 68.05; H, 9.58%. Calcd for $C_{12}H_{20}O_3$: C, 67.89: H, 9.50%. The minor epoxide could not be obtained as a pure sample.

To this major epoxide (1024 mg) in pentane (15 ml) was added 2 M hydrochloric acid (15 ml), and the mixture was stirred at room temperature for 1.5 h. The pentane layer was separated and the aqueous layer was further extracted with pentane (total 50 ml). A combined pentane solution was washed with aqueous sodium hydrogencarbonate solution and brine, dried ($MgSO_4$), and evaporated (at below 28 °C), giving a residue which was chromatographed on a column of Florisil (5 g). Elution with pentane afforded menthofuran (**3**; 674 mg) in 93% yield, identical (IR, NMR, MS, and TLC) with the authentic sample (*vide supra*).

Acetalization of Fukinone (8). Fukinone (160 mg) in benzene (7 ml) was acetalized with ethylene glycol (1 ml) in the presence of *p*-toluenesulfonic acid (30 mg; in benzene, 5 ml) under reflux (12 h) using a Dean-Stark water separator. After the usual work-up, the residue was chromatographed [silica gel, 10 g; elution with hexane–ether (20: 1)] to give an ethylene acetal (**15**; 112 mg) in 58% yield, an oil (one spot on TLC); IR (neat) 1635 and 890 cm^{-1}; NMR (CCl_4) δ 0.88 (3H, d, J=5 Hz), 0.97 (3H, s), 1.78 (3H, m), 3.78 (4H, m), and 4.50 (2H, m); MS *m/e* 264 (M^+). Further elution with the same solvents gave fukinone.

Furanoeremophilane (7) from the Ethylene Acetal (15). A solution of **15** (44 mg) in ether (10 ml) was epoxidized with *m*-chloroperbenzoic acid (55 mg; in ether, 20 ml) at 0 °C (4.5 h). The ether solution was washed with a 10% aqueous sodium thiosulfate solution, a 5% sodium hydroxide solution, and brine, and then treated with 2M hydrochloric acid (10 ml) under nitrogen at room temperature for 20 min. The ether layer was separated and the aqueous layer was further extracted with ether (total 20 ml). The combined ether solution was treated as usual to give a residue which was chromatographed on a column of silica gel (2 g). Elution with pentane afforded furanoeremophilane (**7**; 27 mg; yield 74%), identical with the authentic specimen.[8]

References

1) A part (preparation of **3** from **4** *via* **5**) of this work was presented at the 35th National Meeting of the Chemical Society of Japan, Sapporo, August 31, 1976, Abstr. No. 4K12.

2) H. Fritel and M. Fetizon, *J. Org. Chem.*, **23**, 481 (1958).

3) Buffer solution was used in order to maintain the reaction mixture neutral.

4) H. Wienhaus and H. Dewein, *Angew. Chem.*, **47**, 415 (1934); W. Treibs, *Ber.*, **70**, 85 (1937); W. Treibs, *Justus Liebigs Ann. Chem.*, **581**, 59 (1953).

5) Preparation of **3** from **4** *via* **5** or **6** was recently announced: T. Sato, H. Tsuruta, and T. Yoshida (Takasago Perfumery Co., Ltd.), 22nd Symposium on the Chemistry of Perfumes, Terpenes, and Essential Oils, Yokohama, October 13, 1978, Abstr. No. B30.

6) In steroids, a 3-acetoxy-3,5-diene was treated with peroxy acid in aqueous dioxane to give a 6-hydroxy-4-en-3-one derivative: D. N. Kirk and J. M. Wiles, *Chem. Commun.*, **1970**, 518 and 1015.

7) K. Naya, I. Takagi, Y. Kawaguchi, Y. Asada, Y. Hirose, and N. Shinoda, *Tetrahedron*, **24**, 5871 (1968).

8) H. Ishii, T. Tozyo, and H. Minato, *J. Chem. Soc., C*, **1966**, 1545; Y. Ishizaki, Y. Tanahashi, Y. Moriyama, T. Takahashi, and H. Koyama, *Phytochemistry*, **13**, 674 (1974).

9) Preparation of 3-methylfuran by treatment of 3,4-epoxy-3-methylbutan-1-al diethyl acetal with dilute sulfuric acid was reported: J. W. Cornforth, *J. Chem. Soc.*, **1958**, 1310.

10) M. Namikawa, T. Murae, and T. Takahashi, *Bull. Chem. Soc. Jpn.*, **51**, 3616 (1978).

BULLETIN OF THE CHEMICAL SOCIETY OF JAPAN, VOL. 52 (10), 3131—3132 (1979)

Selective Spectrophotometric Determination of Zinc with Di-2-pyridylmethanone 2-Pyrimidylhydrazone

R. B. SINGH, H. KULSHRESHTHA, B. S. GARG, and R. P. SINGH*

Department of Chemistry, University of Delhi, Delhi 110007, India

(Received December 4, 1978)

Synopsis. Synthesis of a new 2-pyrimidylhydrazone *i.e.* di-2-pyridylmethanone 2-pyrimidylhydrazone (DPMPH) and its application in the selective determination of micro-amounts of zinc is presented. DPMPH reacts with zinc to form a yellow complex in the pH range 7.9—11.1 with molar absorptivity 5.2×10^4 l mol^{-1} cm^{-1} at 430 nm. Beer's law is obeyed upto 1.56 ppm of zinc. Zinc has also been determined in several alloys.

In recent years many nitrogen containing heterocyclic hydrazones derived from 2-hydrazinopyridine[1-4] and 2-hydrazinoquinoline[5-8] have been prepared and tested as possible analytical reagents. Lions *et al.*[9,10] first reported the analytical properties of these compounds. However, hydrazones derived from 2-hydrazinopyrimidine have not been investigated in detail for analytical purpose.

In this note, synthesis of di-2-pyridylmethanone 2-pyrimidylhydrazone (DPMPH, I) and its application in the determination of micro-amounts of zinc is described.

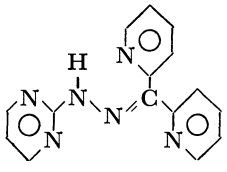

DPMPH, I

This method is based upon a differential demasking technique proposed by Platte and Marcy.[11] According to this technique utilized here zinc was determined with DPMPH in the presence of interfering metals, such as iron and copper. The cyanide complexes of the metals present in the solution were formed and the zinc complex was preferentially destroyed by chloral hydrate. The zinc–DPMPH complex formed by the liberated zinc was measured spectrophotometrically, before interfering metals were liberated from its cyanide complex. It was reported[12-14] that the cyanide complexes of Cu(II) and Fe(III) are not stable enough to prevent interferences of copper and iron in the determination of zinc according to the above procedure and the reduction of Cu(II) and Fe(III) with ascorbic acid was proposed.[15] The Cu(I) and Fe(II) cyanide complexes are more stable against chloral hydrate.

Experimental

Apparatus. A Unicam SP600 spectrophotometer was used for measuring absorbance and a Beckman Expandomatic SS-2 pH meter was used for pH measurements.

Reagents. *Synthesis of Di-2-pyridylmethanone 2-Pyrimidylhydrazone*: 2-Chloropyrimidine was prepared by the method of Kogon *et al.*[16] and converted to 2-hydrazinopyrimidine by the method of Shirakawa *et al.*[17] An ethanolic solution of equimolar quantities of 2-hydrazinopyrimidine and di-2-pyridylmethanone (Fluka A. G.) was refluxed for 6 h. The residue obtained after the removal of ethanol, by using a rotatory evaporator, was crystallized from benzene to give pale yellow crystals (mp 160 °C). Purity was checked by TLC. Elemental analysis confirmed the synthesis (Calcd: C, 65.2; H, 4.3%. Found: C, 65.5; H, 4.9%).

DPMPH solutions were prepared in ethanol (95%) and stored in amber glass bottles. Such solutions are stable for several weeks.

Ascorbic Acid Solution (10% w/v): This solution was prepared on alternate days and stored in amber glass bottles.

Buffer Solution: Borax (4.5 g) and KCN (0.2 g) were dissolved in 20 ml of 4 M NaOH and the solution was diluted to 50 ml with distilled water. When 1 ml of buffer is mixed with 5 ml of working standard or blank, the resulting pH should fall between 8.5—9.5 usually. If it does not, the preparation must then be repeated by changing the amount of alkali added and the pH is checked again. Once the final conditions have been established for this solution, it is easy to prepare new buffer when it is needed.

Standard Zinc Solution: A standard solution of zinc was prepared by dissolving the analytical reagent grade zinc sulfate heptahydrate in doubly distilled water.

Chloral Hydrate Solution (1.5%): Chloral hydrate solution was prepared for differential demasking of zinc from cyanide complex.

All other solutions were prepared with analytical grade reagents in doubly distilled water.

Recommended Procedure. To an aliquot containing 2.6—13.0 μg of Zn(II), add 1 ml of ascorbic acid solution, followed by 2 ml of buffer solution. Then add 1 ml of ethanolic 10^{-2} M solution of DPMPH and dilute the contents to 10 ml. Measure the absorbance of the solution within 25 min after the addition of DPMPH at 430 nm against reagent blank prepared under the identical conditions.

Absorption Spectra, Effect of pH *and Reagent Concentration*: A pH study of the complexation of DPMPH with Zn(II) showed that the yellow complex (λ_{max}=430 nm) gives a constant absorbance in the pH range 7.9—11.1. Carrying out the proposed procedure it has been found that the pH adjustment in the desirable range was more effectively achieved when the buffer solution and the masking agent *i.e.* the cyanide, are added simultaneously. It was observed that a separate addition of cyanide and buffer, irrespective of their order of addition, did not give good results in pH adjustments. For complete complexation 6-fold excess of reagent is necessary. The absorbance of the reagent at the wavelength of maximum absorbance of its zinc complex *i.e.* at 430 nm, is negligible. This is advantageous because the excess of reagent is not critical.

Stability of the Complex. It was also observed that addition of chloral hydrate is not necessary after the addition of DPMPH, for the destruction of zinc–CN complex and for full colour development. The zinc–CN complex is completely

destroyed within 5 min and zinc–DPMPH is formed even in the absence of chloral hydrate. This must be related to the strength of the stability constants of zinc–CN and zinc–DPMPH complexes. This complex is stable upto 25 min. While by addition of chloral hydrate (1.5%) solution, zinc–DPMPH complex is formed as soon as it is added and remains stable for 5 min, then it diminishes. However, full colour development takes place in both the cases. Hence readings of the absorbance of the test solution should be taken within 5—25 min after the addition of DPMPH in the first case and within 5 min in the second case.

Effect of Diverse Ions: Synthetic solutions containing known amounts of zinc(II) and varying amounts of diverse ions were prepared and the recommended procedure was followed for the determination of zinc(II). An error of $\pm 2\%$ in the absorbance reading was considered tolerable. In the determination of 0.65 ppm of zinc, the ions tolerated (given in ppm in parentheses) are as follows:

Chloride, bromide, iodide, fluoride, citrate, tartrate, thiourea, acetate, sulfite, nitrite, nitrate (2000 ppm each); thiocyanate (1000 ppm); thiosulfate, oxalate (500 ppm each); phosphate (150 ppm); Ca(II), Sr(II), Ba(II), Mg(II), Pb(II), Mo(VI), W(VI) (1000 ppm each); Al(III), Sn(II), Be(II), Sb(III), (800 ppm each); Ru(III), Rh(III), Ir(III), Au(III), Os(VIII), Ti(IV), Mn(II), Ag(I) (500 ppm each); Pd(II), Ni(II), Co(II), Cd(II), Hg(II), V(V) (200 ppm each); Cu(II) and Fe(II) (100 ppm each). However, EDTA interferes seriously.

Calibration Curve: Beer's law is obeyed upto 1.56 ppm of Zn(II) in presence or absence of chloral hydrate. The optimum concentration range evaluated by Ringbom's method is 0.26—1.30 ppm. The Sandell's sensitivity is 0.0012 μg Zn cm^{-2} and the molar absorptivity is 5.2×10^4 l mol^{-1} cm^{-1} at 430 nm. The composition of the complex as determined by Job's method of continuous variations shows that metal to ligand ratio is 1 : 2.

Determination of Zinc in Alloys. Dissolve 1.0 g of brass or gun metal in 10 ml of concentrated nitric acid, evaporate to dryness, extract with 4 ml of concentrated sulfuric acid and dilute to 250 ml.

Table 1. Determination of zinc (in %) in alloys

Alloy	Zn reported	Zn found	n[a)]	R.s.d. (%)
Brass (BCS No. 5g)	30.0	29.8	6	1.40
Gun metal (BCS No. 6g)	1.5	1.43	6	2.96
6% Zn–Al alloy (BCS No. 300)	5.98	5.76	6	1.49

a) The average of n determinations is reported with the relative standard deviation.

Dissolve 1.0 g of the aluminium alloy in aqua regia, evaporate to small volume, add 10 ml of concentrated hydrochloric acid and dilute to 250 ml.

Suitable aliquot solution is taken and recommended general procedure is followed for the determination of zinc in alloys. The results of alloy analysis are summarized in Table 1.

Selective and sensitive method for the determination of zinc is proposed. Determination can be carried out in aqueous solutions and there is no need of extraction *etc.* Zinc can be determined in alloys, without its separation from other metals present in the alloys.

Authors are thankful to the Centre of Advanced Studies in Chemistry, University of Delhi (India) for the award of teacher-fellowship to one of them (RBS).

References

1) J. E. Going and R. T. Pflaum, *Anal. Chem.*, **42**, 1098 (1970).
2) R. T. Pflaum and E. S. Tucker, *Anal. Chem.*, **43**, 458 (1971).
3) V. Zatka, J. Abrahm, J. Holzbecker, and D. E. Ryan, *Anal. Chim. Acta*, **54**, 65 (1971).
4) H. Alexaki-Tzivanidou, *Anal. Chim. Acta*, **75**, 231 (1975).
5) M. L. Heit and D. E. Ryan, *Anal. Chim. Acta*, **34**, 407 (1966).
6) S. P. Singhal and D. E. Ryan, *Anal. Chim. Acta*, **37**, 91 (1967).
7) B. K. Afghan and D. E. Ryan, *Anal. Chim. Acta*, **41**, 167 (1968).
8) R. W. Frei, G. H. Jamro, and O. Navratil, *Anal. Chim. Acta*, **55**, 125 (1971).
9) F. Lions and K. Martin, *J. Am. Chem. Soc.*, **80**, 3858 (1968).
10) J. F. Geldard and F. Lions, *J. Am. Chem. Soc.*, **84**, 2262 (1962); *Inorg. Chem.*, **2**, 270 (1963).
11) J. A. Platte and V. M. Marcy, *Anal. Chem.*, **31**, 1226 (1959).
12) R. E. Peterson and M. E. Bollier, *Anal. Chem.*, **27**, 1195 (1955).
13) L. A. Williams, J. S. Cohen, and B. Zak, *Clin. Chem.*, **8**, 502 (1962).
14) B. Zak, R. M. Nalbandian, L. A. Williams, and J. Cohen, *Clin. Chim. Acta*, **7**, 634 (1962).
15) R. Watkins, L. M. Weiner, and B. Zak, *Microchem. J.*, **16**, 14 (1971).
16) I. C. Kogon, R. Minin, and C. G. Overberger, *Org. Synth.*, **35**, 34 (1955).
17) K. Shirakawa, S. Ban, and M. Yoneda, *Yakugaku Zasshi*, **73**, 598 (1953).

BULLETIN OF THE CHEMICAL SOCIETY OF JAPAN, VOL. 52 (10), 3133 (1979)

On Thallium(I) Chelates of 1,2-Cyclohexanediamine-*N,N,N',N'*-tetraacetic Acid and Diethylenetriaminepentaacetic Acid

Giorgio ANDEREGG* and Emilio BOTTARI
Laboratorium für Anorganische Chemie, ETHZ, 8092-Zürich, Switzerland

(Received February 8, 1979)

Synopsis. The stability constants of the complexes mentioned in the title obtained by us by potentiometric pH measurements are compared with those of Kodama *et al.* Because sodium ion forms quite a stable 1,2-cyclohexanediamine-*N,N,N',N'*-tetraacetate (CyDTA) complex, the discrepancy of the values can be explained. Further new calculations confirm the formation of protonated chelate with CyDTA but in a very limited pH range.

Kodama *et al.* have determined the stability constants of thallium(I) complexes with diethylenetriaminepentaacetate (DTPA)[1] and 1,2-cyclohexanetetraacetate (CyDTA)[2] ions using polarographic measurements. Their values (K. and T.) are given together with those obtained by us[3] (A. and B.) with pH measurements in the Table 1. The difference between the results of the two works can be partly caused by the different ionic strengths used but the discrepancies with CyDTA as ligand is too large to be explained in this manner. The preference given by us to the potassium nitrate as inert salt is justified by the fact that potassium ion forms very weak complexes with amino polycarboxylate ligands and the ligand protonation constants in this medium at $I=0.1$ are known.[4,5] Kodama and Tominaga have preferred $NaClO_4$ solutions ($I=0.4$ resp. 0.3) in spite of the greater stability of the sodium complexes[4,7] and have calculated the dissociation constants of the acids using the pK values of Schwarzenbach and Ackermann,[6] correcting for the change in the ionic strength by means of the Davies equation. The calculation of the activity coefficients of high charged ions as those involved here can only give very approximative results. Further the pK value of $HCyDTA^{3-}$ of the above work was found to be too low.[5] The better agreement of the results in the case of DTPA indicates that the discrepancies for CyDTA cannot be due only to these reasons.

K. and T. followed from the constancy of $(E_{1/2})_{Tl^{Z}}$ in the pH range from 10 to 11.7 the formation of the protonated chelate $TlHZ^{2-}$. This constancy is due to the fact that beside the unprotonated complex TlZ^{3-} "uncomplexed" ligand is mainly present as sodium complex NaZ^{3-} in that pH range. Indeed from our pK values[4,5] and some new measurements—the pK of $HCyDTA^{3-}$ at $I=0.1$ ($NaNO_3$) and 20 °C is found to be 9.80—for that complex a stability constant of approximately $10^{2.7}$ is estimated. Therefore in 0.3 ($NaClO_4$) and pH=10 already more than 80% of the uncomplexed ligand is present as NaZ^{3-}. As described in our work[3] for the determination of the stability of the thallium(I) complexes alkalimetric titration have been used, in which solutions containing the diprotonated ligand H_2Z^- and thallium(I) nitrate have been titrated with 0.1 M KOH. In Fig. 1 of reference[3] the curve obtained with EDTA as ligand is given. Starting from 100 ml of a solution containing 10^{-4} mol H_2CyDTA and Tl^+ by addition of 0.1 M KOH the following data have been obtained: (ml/pH): 0.4/5.919: 0.6/6.259: 0.8/6.686: 0.9/6.986: 0.95/7.178: 1.0/7.409: 1.05/7.637: 1.1/7.823: 1.2/8.136: 1.3/8.399: 1.4/8.626: 1.5/8.858: 1.6/9.098: 1.65/9.218: 1.7/9.478: 1.8/9.605. The calculations were done considering the following equilibria:

$$H_2L^{2-} \overset{pK_3}{\rightleftharpoons} HL^{3-} \overset{pK_4}{\rightleftharpoons} L^{4-}$$

$$Tl^+ + H_2L^{2-} \rightleftharpoons TlHL^{2-} \rightleftharpoons TlL^{3-}$$

and inserting for pK_3 6.12 and pK_4 12.3.

New calculations show that in the solutions at lower pH, between 5 and 8, also $TlHL^{2-}$ is formed, being its maximal concentration always lower than 10% of the total amount of the metal ion. The values given in the table are calculated using differents titration curves. As found by K. and T. Tl^+ forms with CyDTA also an hydrogen complex $TlHL^{2-}$, with a limited pH range of existence (pK of $TlHL^{2-}$=7.32).

References

1) M. Kodama, T. Noda, and M. Murata, *Bull. Chem. Soc. Jpn.*, **41**, 354 (1968).
2) K. Kodama and Y. Tominaga, *Bull. Chem. Soc. Jpn.*, **42**, 72 (1969).
3) G. Anderegg and E. Bottari, *Helv. Chim. Acta*, **50**, 2341 (1967).
4) G. Anderegg, *Helv. Chim. Acta*, **50**, 2333 (1967).
5) G. Anderegg, *Helv. Chim. Acta*, **46**, 1833 (1963).
6) G. Schwarzenbach and H. Ackermann, *Helv. Chim. Acta*, **30**, 1798 (1947).
7) H. Irving and J. J. R. F. Da Silva, *J. Chem. Soc.*, **1963**, 488.
8) D. L. Wright, J. H. Holloway, and C. N. Reilley, *Anal. Chem.*, **37**, 884 (1965).

TABLE 1. STABILITY CONSTANTS OF SOME Tl(I) COMPLEXES[a]

		$\log \frac{[ML]}{[M][L]}$	$\log \frac{[MHL]}{[M][HL]}$	pK of MHL	Ionic medium
DTPA	K. and T.	5.45	4.24	8.8	$I=0.4$ ($NaClO_4$)
	A. and B.	5.97±0.05	4.2±0.1	8.8±0.1	$I=0.1$ (KNO_3)
CyDTA	K. and T.	3.85	3.71	11.29	$I=0.3$ ($NaClO_4$)
	A. and B.	6.7±0.05	1.7±0.2	7.3±0.2	$I=0.1$ (KNO_3)

a) Unit of concentration used is mol dm^{-3}.

An Ultrasonic Absorption Study of the DMF–Water System

Fumio KAWAIZUMI,* Hiroyasu NOMURA, Makoto OHNO, and Yutaka MIYAHARA

Department of Chemical Engineering, Faculty of Engineering, Nagoya University, Chikusa-ku, Nagoya 464

(Received September 12, 1978)

Using the pulse method, the ultrasonic absorption was measured for binary mixtures of water and *N*,*N*-dimethylformamide (DMF) at 5.5 and 57 MHz in the temperature range of 5—45 °C. At lower temperatures α/f^2 as a function of the concentration produces a plateau up to x (x is the mole percent of DMF in solution)= 1.5, a minimum point at $x=6$, and a maximum point at $x=25$. An increase in the temperature causes these characteristic features of α/f^2 to disappear. At 45 °C the values of α/f^2 increase monotonically. No relaxation process is observed in the frequency range of this work. The general features of the concentration dependence of α/f^2 resemble those of the urea–water system in a water-rich region and those of the dioxane–water system in a DMF-rich region. The mechanism of the plateau can be explained by the cooperative nature of the formation and breaking of water clusters. The maximum of α/f^2 is ascribed to the complex formation between DMF and water molecules, while the minimum of α/f^2 arises from the competition between the breaking-down of the water structure and the complex formation in solution. The maximum behavior in the ultrasonic absorption can be interpreted in terms of a kinetic model, $DMF+mH_2O \rightleftharpoons DMF\cdot(H_2O)_m$. m is determined to be 3, and the following values have been obtained for the model mentioned above: $\Delta V_m \simeq 1$ cm³/mol, $K_m=10\pm2$.

In a previous paper[1] the ultrasonic and volumetric behavior of aqueous solutions of amides (*N*-methylformamide, *N*,*N*-dimethylformamide and *N*,*N*-dimethylacetamide) was studied at 25 and 35 °C over the entire concentration range. The velocity maxima were observed for all three of the amide solutions, while the minima in the partial molar volume were observed for DMF and DMAA. A tentative interpretation has been proposed that the velocity maxima are ascribable to the complex formation between water and amide molecules, while the minima in the partial molar volume are to be ascribed to the competition between the volume increase due to the complex formation and the volume decrease due to the breaking-down of the water structure.

In order to obtain further information on the interaction between water and amide molecules, ultrasonic absorption measurements have been carried out on the DMF–water system. From among three types of amide–water systems investigated previously, the DMF–water system is chosen because this system is one of the most widely used systems of polar mixed solvents.

Experimental

The DMF used was of a spectral grade obtained from Nakarai Chemicals and was used without further purification. The distilled water was degassed prior to each measurement.

The ultrasonic pulse method was used for the measuremet of the absorption coefficients of solutions. The details of the apparatus and the experimental procedures have been reported previously.[2,3] The measurements of the absorption coefficient were done at 5.5 and 57 MHz in the temperature range of 5—45 °C. The data are reproducible within ±1% at 57 MHz and within 5% at 5.5 MHz. The temperature was controlled to ±0.1 °C.

Results

Temperature and Concentration Dependences of α/f^2. Figure 1 shows the concentration dependences of α/f^2 at various temperatures. At lower temperatures, the curves show a minimum point at x (x is the mole percent of DMF in solution)=5—8 and a maximum point at *ca.* $x=25$. With the rise in the temperature, the height of $(\alpha/f^2)_{max}$ and the depth of $(\alpha/f^2)_{min}$ decrease, and the width of the maximum peak shows a broadening with a slight shift of PSAC (the peak sound absorption concentration) towards higher concentrations of DMF. At temperatures higher than 35 °C, the minimum and the maximum points disappear and the values of α/f^2 increase monotonically. The appearance of the minimum point in the relation of α/f^2 *vs.* concentration in a small concentration of solute has not been observed in other aqueous solutions of nonelectrolytes except the work of Takenaka *et al.*[4] who found the appearance of the minimum in the α/f^2 *vs.* concentration curves for this system (20 and 25 °C, 15—45 MHz), but who mentioned nothing further about it.

Figure 2 is an expanded representation of Fig. 1 in the water-rich region. Two characteristic features should be noted regarding the temperature dependence of α/f^2 in this region. The first is, as has been described above, the appearance of the minimum point, while the second is the appearance of the plateau, in which α/f^2 is relatively insensitive to the quantity of DMF added. With a decrease in the temperature, this region increases from $x=0$ at 45 °C to $x=2$ at 5 °C. At 35 °C, the values of α/f^2 remain constant up to $x=7$, but this constant-value region does not correspond to the true plateau. From the comparison of the plateau region at different temperatures, it may be concluded that the constant-value region observed at 35 °C is the result of the opposite effects of the decrease of α/f^2 in the 2—6 mol% concentration range and the increase of α/f^2 in the concentration range of more than 6 mol%. The overlooking of the plateau in this system by Takenaka *et al.*[4] is due to the incompleteness of their measurements.

The general behavior of the DMF–water system in a small concentration of a solute shown in Fig. 2 resembles the results observed by Arakawa *et al.*[5] in the aqueous solutions of urea and guanidine hydrochloride. In urea solutions, the magnitudes of α/f^2 first decreased very slowly (it is more correct to say that the α/f^2 remains constant) with the concentration, and then, decreased rapidly in the range *ca.* 0.5 to

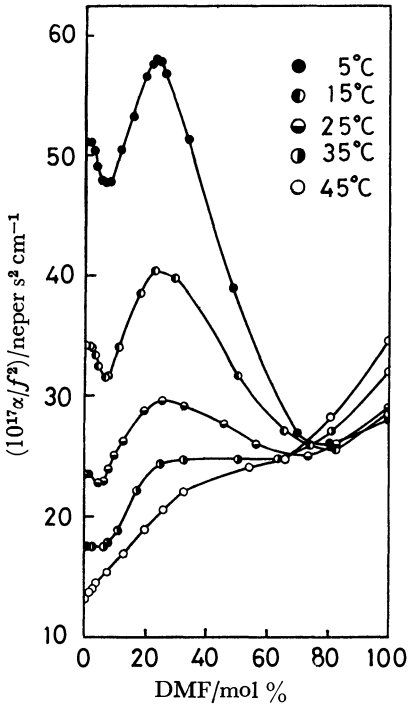

Fig. 1. Temperature and concentration dependence of α/f^2 in DMF–water system.

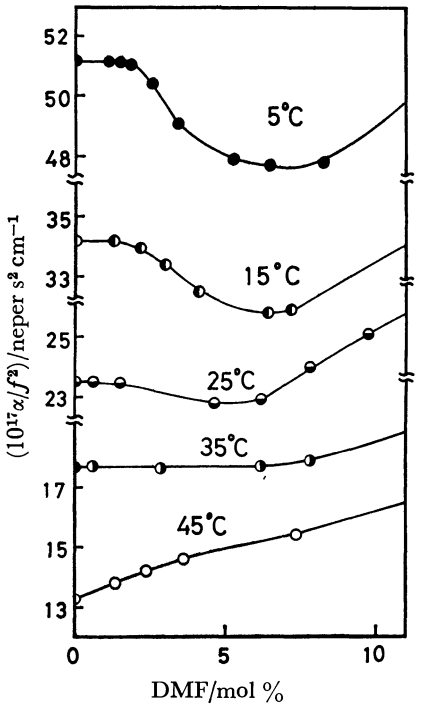

Fig. 2. Expanded representation of Fig. 1 in water-rich region.

3 M. The temperature rise causes these concentration dependences to disappear. The similarities between the urea–water system and the present one will be clearer if the results shown in Fig. 2 are represented in a molar scale (see Fig. 6(a) of Ref. 5).

As is shown in Fig. 1, in the DMF-rich region the values of α/f^2 measured at higher temperatures are larger than those measured at lower temperatures. These phenomena correspond well to those observed in the dioxane–water system.[5]

Frequency Dependence of α/f^2. The values of α/f^2 at 5.5 MHz are always larger than those at 57 MHz. However, the differences are so small (at most 4×10^{-17} neper s^2 cm^{-1} at 25 °C) that it is reasonable to conclude that the relaxation process does not exist in the present frequency range. Takenaka *et al.*[4] have also reported that the relaxation process is not observed in the frequency range of 15—45 MHz.

Discussion

Plateau and Minimum in the Water-rich Region. In spite of many theories of water structure and the ambiguities involved in them, it is widely recognized that the temperature-rise breaks down the hydrogen-bonding of water, resulting in increases in the fraction of unbonded or smaller-cluster molecules in water. The ultrasonic absorption coefficient of water, expressed as α/f^2 decreases monotonically with the temperature. The variation in the relation of α/f^2 *vs.* concentration in a small concentration of solute reflects the effects of the addition of DMF upon the water structure. The present experimental results indicate that the added DMF molecules have the same effects as the temperature-rise upon the ultrasonic absorption coefficient. Therefore, DMF molecules act as a structure breaker in water. Some experimental evidences have been found that DMF is a water-structure breaker.[7–9]

As has already been mentioned in the preceding section, the behavior of α/f^2 observed in the urea–water system and in the present one in their water-rich regions is very similar. Urea acts as a water-structure breaker. Both urea and DMF molecules have the $\rangle$N–C– group. These facts led us to adopt
O
the same interpretation of the concentration dependence of α/f^2 in the DMF–water system in a small concentration region of the solute as that proposed for the urea–water system.[5] Arakawa *et al.*[5] have argued that the characteristic feature in the α/f^2 *vs.* concentration curve found in the small concentration region is attributable to the cooperative nature of the formation and breaking of water clusters. When a very small amount of DMF is added to water, the influence of the DMF molecules upon the structure of water is isolated and the cooperative formation of clusters is not affected by the added DMF. When the amount of DMF is greater, however, the influence becomes appreciable and DMF affects the clusters cooperatively, disrupting them into unbonded monomers and/or small clusters.

Blandamer[6] has insisted that, if the liquid clathrate model is accepted, the plateau region is the zone of the enhanced water structure in the system of water–alcohols (alcohols are water-structure formers). His interpretation, however, can not be applied in the present system, for the DMF molecule is a water-structure breaker.[7–9]

The minimum sound absorption concentration

(hereafter abbreviated as MSAC) corresponds to the concentration at which the partial molar volume of DMF reaches a minimum point. MSAC becomes more remarkable with a decrease in the temperature. This phenomenon suggests that MSAC is intimately related to the structure of water. In the preceding paper,[1] the minimum in the partial molar volume of DMF in the aqueous solution is ascribed to the competition between the volume increase due to the complex formation and the volume decrease due to the breaking-down of the water structure. A similar conclusion can be drawn in the case of MSAC observed in the present work. In other words, MSAC arises from the competition between the decrease in α/f^2 due to the breaking-down of the water structure and the increase in α/f^2 due to the complex formation in DMF with water, which will be discussed below from another point of view.

PSAC and Excess Absorption due to the Complex Formation between DMF and Water. Two different approaches are possible to account for the abnormal ultrasonic absorption in the liquid mixture. One is the fluctuation theory proposed by Romanov *et al.*,[10] while the other is a kinetic model of complex formation between solute and solvent. The following factors indicate that the interpretation based on the complex formation is more suitable in the present system. First, Assarsson and Eirich[11] have shown the complex formation of such alkyl-substituted amides as *N,N*-dimethylacetamide with water from the data of viscosity and the phase diagram of these systems. Therefore, the complex formation in the DMF-water system is higly probable. Second, PSAC agrees fairly well with the concentration of the velocity maximum, *ca.* $x=20$. Third, the peak in the ultrasonic absorption observed in the present system is less steep than in the system consisting of water and alcohols, to which the fluctuation theory has been applied. Finally, the effects of the temperature rise on the PSAC and the width of the maximum peak in the ultrasonic absorption are small in comparison with those found in the aqueous solutions of alcohols.

Various kinetic models of complex formation have been put forward.[12] The model adopted by the present authors to interpret the ultrasonic absorption behavior observed in the DMF–water system is represented by this equation:

$$\mathrm{A} + m\mathrm{B} \underset{k_b}{\overset{k_f}{\rightleftharpoons}} \mathrm{AB}_m \qquad \text{(I)}$$

The principal reason for adopting this model is the extreme unsymmetry in the relationships of α/f^2 with the concentration of DMF. In Model (I), it is assumed that the DMF molecule, represented by the symbol A, combines in a single step with m water molecules, represented by the symbol mB. Let the mole fraction, x, of the solute and the z of the complex be such that when the total number of solute and water molecules, including those in the complex, is unity, x is the total number of solute molecules and z is the number of complexes in the A+B⇌AB model. If the variables x and z are transformed to

$$x_m = \frac{x}{x+(1-x)/m} \quad \text{and} \quad z = \frac{z}{x+(1-x)/m},$$

PSAC is situated at $x_m=0.5$ or PSAC$=x=1/(1+m)$. Therefore, in this model, $m=(1-\mathrm{PSAC})/\mathrm{PSAC}$ is the optimum water-to-solute ratio. Using the usual analysis of the ultrasonic absorption data, the following physical properties concerning the excess absorption can be obtained;

$$\mu_{\max}^{\mathrm{excess}} = \frac{\pi}{4}\cdot\frac{dc^2}{V_m RT}(\Delta V_m)^2\frac{(1-\beta_m)}{K_m\beta_m} \qquad (1)$$

$$\Delta V_m = (\partial V/\partial z_m)_{p,T} \qquad (2)$$

$$\beta_m{}^2 = 1 - 4x_m(1-x_m)K_m{}^2/(1+K_m)^2 \qquad (3)$$

and;

$$K_m = z_m/(x_m-z_m)(1-x_m-z_m), \qquad (4)$$

where $\mu_{\max}^{\mathrm{excess}}$, V_m, and K_m refer to the excess absorption per wavelength at the maximum, the molar volume of the complex, and the equilibrium constant in Model (I) respectively. The theory enables a match to be made of the position of the experimental absorption peak by adjusting the value of m, of the height of the peak, by adjusting ΔV_m, and of the mean width of the peak by adjusting K_m. Here m is taken to be 3, as PSAC is found at *ca.* $x=25$ in Fig. 1. μ^{excess} is given by this relation; $\mu^{\mathrm{excess}}=(\alpha/f^2)^{\mathrm{excess}}\cdot fc$, where f is the frequency, and c, the velocity of the ultrasonics.

In the course of calculation, the values of the ultrasonic velocity, c, and the density, d, introduced on the right-hand side of Eq. 1 should not be the real values, but the ones at the "*hypothetical state*" of the solution without complex formation, because only the excess contribution originating from the complex formation is considered. The values of d and c at these "*hypothetical state*," d_{hyp}, and c_{hyp} respectively, were estimated on the basis of the ideal additivity of the volume of solution and the ideal additivity of the compressed volume in solution:

$$V_{\mathrm{hyp}} = x_1V_1 + x_2V_2 = \frac{M_1x_1+M_2x_2}{d_{\mathrm{hyp}}} \qquad (5)$$

$$V_1x_1\kappa_1 + V_2x_2\kappa_2 = V_{\mathrm{hyp}}\kappa_{\mathrm{hyp}} = \frac{M_1x_1+M_2x_2}{d_{\mathrm{hyp}}}\cdot\frac{1}{(c_{\mathrm{hyp}})^2d_{\mathrm{hyp}}} \qquad (6)$$

The final results of calculation are shown in Fig. 3, where PSAC is at $x_m=0.5$, as predicted by Eqs. 1 and 3. The improper choice of m does not lead to the results shown in Fig. 3. The small non-symmetry in the curve of Fig. 3 is not significant and the variation in the mean width of the peak with the temperature can be taken to be negligible if due consideration is paid to the experimental errors and the analysis of the data. The average values of $(x_m)_{1/2}$ are found to be 0.72 and 0.28. As $(x_m)_{1/2}$ is obtained by solving Eq. 3 at $\mu_{\max}^{\mathrm{excess}}/2$, the sum of the two values of $(x_m)_{1/2}$ is always 1. The most appropriate values of K_m compatible with these values of $(x_m)_{1/2}$ were numerically determined through the use of Eqs. 1 and 3: $K_m=10\pm2$. This value and the values of μ^{excess} at PSAC make possible the evaluation of ΔV_m. At this stage, the sign of ΔV_m remains undetermined. It is, however, the same as that of ΔH_m (see Eq. 7 below). The temperature dependence of the latter leads to the assignment of the negative sign to ΔH_m. The values of ΔV_m thus obtained are

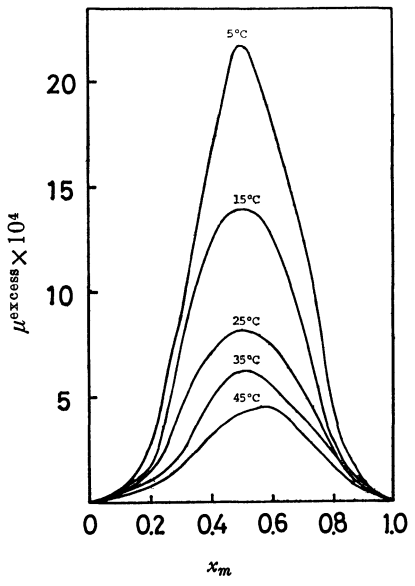

Fig. 3. Excess absorption plotted against x_m at various temperatures.

T/°C	5	15	25	35	45
ΔV_m/cm^3 mol^{-1}	1.12	0.93	0.74	0.67	0.61

These values have been determined on the assumption that the thermal contribution to the relaxation strength of the ultrasonic absorption is negligible compared with the isothermal one. In other words, the observed behavior in the ultrasonic absorption has been ascribed to the volume changes of complex formation between DMF and water. Denote these values of ΔV_m by ΔV_m^{ls}. If we consider that the thermal contribution is dominant in the ultrasonic absorption behavior, the contribution denoted by the enthalpy change, ΔH_m^{th}, can also be estimated. ΔH_m^{th} is obtained with recourse to this equation:

$$V\theta\Delta H_m^{th} = C_p\Delta V_m^{ls} \quad (7)$$

where θ is the volume expansibility of the solution. The basis of Eq. 7 is that the same value of μ_{max}^{excess} is produced either by ΔV_m^{ls} or ΔH_m^{th}. Therefore, the values of ΔH_m^{th} determined by Eq. 7 correspond to those at the maximum contribution. Using the values of $\Delta V_m \simeq 1$ cm^3/mol and θ and C_p data at $x=25$ found in the literature,[13] $\Delta H_m^{th} \simeq 5.06$ J/mol. This value gives the temperature dependence of K_m: 10.7 at 5 °C and 9.4 at 45 °C. The small variations in K_m with the temperature well correspond to the experimental fact that the mean width of the peak in Fig. 3 is almost independent of the temperature in the present system.

The values of ΔV_m^{ls} is small in comparison with the results found in the systems of acetone–, dimethylamine–, methyldiethylamine–, and *n*-amylamine–water.[14] The complex formation in the aqueous solution of DMF produces rather minor changes in the intermolecular distances between DMF and water molecules. The complex formed in the solution becomes looser with an increase in the temperature, as is seen in the variation of ΔV_m with the temperature. This fact confirms the views described in our preceding paper[1] that the structure of the complex in amide–water systems may not be similar to those in an ordinary clathrate-like 17 hydrate or $8X \cdot 136H_2O$.

A part of the cost of this work was defrayed by the support given to F. K. from Hattori Ho-ko-kai.

References

1) F. Kawaizumi, M. Ohno, and Y. Miyahara, *Bull. Chem. Soc. Jpn.*, **50**, 2229 (1977).
2) H. Nomura, S. Kato, and Y. Miyahara, *Memoirs of the Faculty of Engineering, Nagoya Univ.*, **27**, 72 (1975).
3) H. Nomura, S. Kato, and Y. Miyahara, *Nippon Kagaku Zasshi*, **90**, 30 (1969).
4) N. Takenaka, K. Sasaki, and H. Arakawa, 18th Meeting of Ultrasound Physics and Chemistry of Japan, Osaka, November 1973, Abstr. p. 7.
5) K. Arakawa, N. Takenaka, and T. Sasaki, *Bull. Chem. Soc. Jpn.*, **43**, 636 (1970).
6) M. J. Blandamer, "Water," ed by F. Franks, Plenum Press, Vol. 2, Chap. 9.
7) G. E. Rodgers and R. A. Plane, *J. Chem. Phys.*, **63**, 818 (1975).
8) C. A. Swenson, *Arch. Biochem. Biophys.*, **117**, 494 (1966).
9) D. D. Macdonald, M. E. Estep, M. D. Smith, and J. B. Hyne, *J. Solution Chem.*, **3**, 713 (1974).
10) V. P. Romanov and V. A. Solovyev, *Sov. Phys. Acoust.*, **11**, 68, 219 (1965).
11) P. Assarsson and F. R. Eirich, *J. Phys. Chem.*, **72**, 2710 (1968): *Adv. Chem. Ser.*, **84**, 1, (1968).
12) J. Lamb, "Physical Acoustics," ed by W. P. Mason, Academic Press, New York (1965), Vol. 2, Part A, p. 273.
13) θ; from the data given in Ref. 1. C_p; O. D. Bonner and P. J. Cerutti, *J. Chem. Thermodyn.*, **8**, 105 (1976).
14) J. H. Andreae, P. D. Edmond, and J. F. McKellar, cited in Ref. 12, p. 275.

Effect of Diffusion Layers on Bi-ionic Potentials across Liquid Ion-exchange Membranes

Nobuo YOSHIDA

Department of Chemistry, Faculty of Science, Kyushu University, Fukuoka 812

(Received September 28, 1978)

In a bi-ionic system in which a liquid membrane is interposed between aqueous solutions containing different counterions, the solution composition is often not maintained uniform right up to the membrane–solution interface owing to the presence of diffusion layers adjacent to the interface. Taking the effect of the diffusion layers into account, an expression is derived for the bi-ionic potential across a membrane having completely dissociated ion-exchange sites and counterions. The expression contains as an empirical parameter the ratio between the thicknesses of the diffusion layers at the solution and membrane sides of the interface. The expression is found to agree with experimental data, with the parameter given a single value.

The electric potential difference, V, between two aqueous solutions (′) and (″) separated by a liquid ion-exchange membrane is usually given in the form of the following empirical equation:[1–3]

$$V = \frac{RT}{F} \ln \frac{a_i' + \sum_j K_{i,j}^{pot} a_j'}{a_i'' + \sum_j K_{i,j}^{pot} a_j''}, \quad (1)$$

where a_i and a_j are the activities of univalent counterions i and j, respectively, in solutions (′) and (″), and $K_{i,j}^{pot}$ is the potentiometric selectivity coefficient of ion j over ion i. In particular, when ion-exchange sites and counterions are completely dissociated in the membrane, Eq. 1 was also derived theoretically by Conti and Eisenman,[4] who showed that the selectivity coefficient is given by

$$K_{i,j}^{pot} = \frac{\bar{u}_j k_j}{\bar{u}_i k_i}, \quad (2)$$

where $\bar{u}_i$ and $\bar{u}_j$ are the mobilities of ions i and j, respectively, in the membrane, and k_i and k_j are the single-ion distribution coefficients between the membrane solvent and water. However, Eq. 1 is sometimes observed to be only approximate, since the selectivity coefficient changes with the solution concentration and composition. In a previous study,[5] electric potentials were measured for liquid membranes having dissociated sites and counterions, and the results were compared with those predicted by the Conti-Eisenman theory. The theory was found to be applicable only when the concentrations of aqueous solutions were sufficiently high in comparison with that of an ion exchanger in the membrane. Deviation from the theory occurring in other cases was attributed to the ionic composition at the membrane–solution interface differing from that in the bulk solution owing to the presence of diffusion layers adjacent to the interface. The effect of diffusion layers on the membrane potential has been discussed quantitatively for solid ion-exchange membranes,[6–8] but not for their liquid counterpart.

In the present paper, the Conti-Eisenman theory is extended so as to incorporate the effect of the diffusion layers, and an expression is derived for the membrane potential in a bi-ionic system. The validity of this expression is examined by a comparison with experimental results.[5]

Theoretical

The system considered is a bi-ionic cell in which a liquid membrane with an ion exchanger RY is interposed between two aqueous solutions (′) and (″) containing different counterions X and Y of equal valence z, respectively, but with a common co-ion M of valence z_M:

Solution (′)	Liquid membrane	Solution (″)
MX	RY	MY .

(3)

(The treatment given below can be readily extended to more general systems in which the solutions and membrane contain both counterions.) It is assumed that the ion-exchange sites (R) and counterions are completely dissociated in the membrane and that the aqueous and membrane phases are impermeable to R and M, respectively. In cell (3), a continuous exchange of the counterions occurs across the membrane–solution (′) interface. As a result, the concentrations of the counterions at the interface generally differ from those in the bulk phases, since two diffusion layers (through which the transport of the ions can take place by diffusion only) are present adjacent to the interface. The situation is schematically shown in Fig. 1, where C is the concentration of the counterions; a and b refer to the membrane–solution (′) and membrane–solution (″) interfaces, respectively; a superscript bar refers to the membrane phase; and δ and $\bar{\delta}$ are the thicknesses of the diffusion layers at the solution and membrane sides of interface a, respectively. Contamination of the bulk phases by the counterion exchange, however, is assumed to be negligible in the present treatment.

In order to obtain an expression for the total membrane potential in cell (3), the two phase-boundary potentials ($\bar{\phi}^a - \phi^a$) and ($\phi'' - \bar{\phi}^b$) and the two dif-

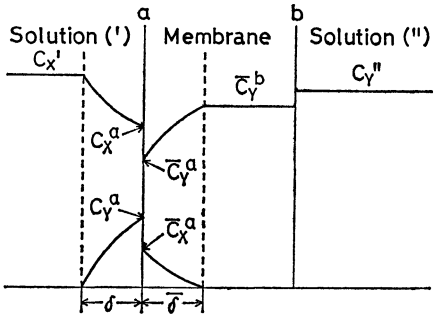

Fig. 1. Concentration profiles of counterions X and Y in the bi-ionic system (schematic).

fusion potentials within the diffusion layers ($\phi^a - \phi'$) and ($\bar{\phi}^b - \bar{\phi}^a$) should be evaluated, where ϕ is the electric potential. If thermodynamic equilibrium is assumed to be established at the membrane–solution interfaces, the electrochemical potentials of the counterions are continuous at the interfaces. Thus we have at interface a,

$$\mu_X^\circ + RT\ln y_X' C_X^a + zF\phi^a = \bar{\mu}_X^\circ + RT\ln \bar{y}_X \bar{C}_X^a + zF\bar{\phi}^a, \quad (4)$$

$$\mu_Y^\circ + RT\ln y_Y' C_Y^a + zF\phi^a = \bar{\mu}_Y^\circ + RT\ln \bar{y}_Y \bar{C}_Y^a + zF\bar{\phi}^a, \quad (5)$$

where μ° is the standard chemical potential and y the activity coefficient, for which the superscript a is not used since it is assumed to be constant throughout the diffusion layers. Rearrangement of Eq. 4 yields

$$\bar{\phi}^a - \phi^a = \frac{RT}{zF}\ln\frac{k_X y_X' C_X^a}{\bar{y}_X \bar{C}_X^a}, \quad (6)$$

where k is the single-ion distribution coefficient defined by

$$k = \exp\left(\frac{\mu^\circ - \bar{\mu}^\circ}{RT}\right). \quad (7)$$

Subtraction of Eq. 4 from Eq. 5 gives

$$\frac{C_Y^a \bar{C}_X^a}{C_X^a \bar{C}_Y^a} = K, \quad (8)$$

where K is the equilibrium selectivity coefficient given by

$$K = \frac{k_X y_X' \bar{y}_Y}{k_Y y_Y' \bar{y}_X}. \quad (9)$$

At interface b, we get an equation corresponding to Eq. 6:

$$\phi'' - \bar{\phi}^b = \frac{RT}{zF}\ln\frac{\bar{y}_Y \bar{C}_Y^b}{k_Y a_Y''}, \quad (10)$$

where a_Y'' is the activity of counterion Y in solution ('').

The diffusion potentials can be evaluated by considering the steady transport of the ions inside the diffusion layers. Expressing the ionic fluxes by the Nernst-Planck equations, we have, for the diffusion layer at the solution side of interface a,

$$J_X = -u_X C_X \frac{d}{dx}(RT\ln C_X + zF\phi) = \text{const}, \quad (11)$$

$$J_Y = -u_Y C_Y \frac{d}{dx}(RT\ln C_Y + zF\phi) = \text{const}, \quad (12)$$

$$J_M = -u_M C_M \frac{d}{dx}(RT\ln C_M + z_M F\phi) = 0, \quad (13)$$

where J is the ionic flux, u the mobility (assumed to be constant throughout the diffusion layer), and x the space coordinate perpendicular to the membrane–solution interfaces. Since no electric current flows through the present system,

$$J_X + J_Y = 0. \quad (14)$$

Substitution of Eqs. 11 and 12 into Eq. 14 yields

$$\frac{d\phi}{dx} = -\frac{RT}{zF}\frac{d\ln(u_X C_X + u_Y C_Y)}{dx}. \quad (15)$$

Integration of Eq. 15 across the diffusion layer leads to

$$\phi^a - \phi' = \frac{RT}{zF}\ln\frac{u_X C_X'}{u_X C_X^a + u_Y C_Y^a}. \quad (16)$$

Alternatively, the electric potential gradient $d\phi/dx$ can be expressed from Eq. 13 as

$$\frac{d\phi}{dx} = -\frac{RT}{z_M F}\frac{d\ln C_M}{dx}, \quad (17)$$

so that

$$\phi^a - \phi' = \frac{RT}{z_M F}\ln\frac{C_M'}{C_M^a}. \quad (18)$$

The diffusion layer at the membrane side of interface a can be treated by regarding the co-ions as the sites in the above calculation. Thus, we get an equation corresponding to Eq. 16:

$$\bar{\phi}^b - \bar{\phi}^a = \frac{RT}{zF}\ln\frac{\bar{u}_X \bar{C}_X^a + \bar{u}_Y \bar{C}_Y^a}{\bar{u}_Y \bar{C}_Y^b}. \quad (19)$$

Combining Eqs. 6, 10, 18, and 19 and using Eqs. 8 and 9, we have the total membrane potential V:

$$V = \phi'' - \phi' = \frac{RT}{F}\left\{\frac{1}{z}\ln\frac{y_Y'(K\bar{r}C_X^a + C_Y^a)}{a_Y''} + \frac{1}{z_M}\ln\frac{C_M'}{C_M^a}\right\}, \quad (20)$$

where

$$\bar{r} = \bar{u}_X/\bar{u}_Y. \quad (21)$$

With the use of the electroneutrality condition

$$zC_X + zC_Y + z_M C_M = 0, \quad (22)$$

Eq. 20 is written as

$$V = \frac{RT}{zF}\ln\left[\frac{y_Y' C_X'}{a_Y''}\left\{(K\bar{r}-1)\frac{C_X^a}{C_X'} + \frac{C_M^a}{C_M'}\right\}\left(\frac{C_M^a}{C_M'}\right)^{-z/z_M}\right]. \quad (23)$$

For the calculation of V the concentrations C_X^a and C_M^a at interface a are required. They can be determined in the following way. It follows from Eqs. 15 and 17 that within the diffusion layer at the solution side,

$$C_M^{-z/z_M}(u_X C_X + u_Y C_Y) = \text{const}. \quad (24)$$

Applying Eq. 24 to both ends of the diffusion layer and taking Eq. 22 into account, we get

$$C_X^a = \frac{z_M}{z}\frac{1 - r(C_M^a/C_M')^{z/z_M - 1}}{r-1}C_M^a \quad (25)$$

or

$$\frac{C_X^a}{C_X'} = \frac{r(C_M^a/C_M')^{z/z_M - 1} - 1}{r-1}\frac{C_M^a}{C_M'}, \quad (26)$$

where

$$r = u_X/u_Y. \quad (27)$$

Likewise, the following relation holds inside the diffusion layer at the membrane side:

$$\bar{C}_R^{-z/z_R}(\bar{u}_X \bar{C}_X + \bar{u}_Y \bar{C}_Y) = \text{const}, \quad (28)$$

so that

$$\bar{C}_X^a = \frac{z_R}{z}\frac{1 - (\bar{C}_R^a/\bar{C}_R^b)^{z/z_R - 1}}{\bar{r}-1}\bar{C}_R^a, \quad (29)$$

where the electroneutrality condition in the membrane

$$z\bar{C}_X + z\bar{C}_Y + z_R\bar{C}_R = 0 \quad (30)$$

has been used. Introducing Eqs. 25 and 29 into Eq. 8, taking Eqs. 22 and 30 into account, we obtain

$$\left(\frac{\bar{C}_R{}^a}{\bar{C}_R{}^b}\right)^{z/z_R-1}=\frac{(K\bar{r}-1)r(C_M{}^a/C_M{}')^{z/z_M-1}-K\bar{r}+r}{(K-1)r(C_M{}^a/C_M{}')^{z/z_M-1}-K+r}. \quad (31)$$

It is now necessary to derive another relationship between the unknown quantities $C_M{}^a$ and $\bar{C}_R{}^a$. Combination of Eqs. 11, 12, and 22 gives

$$\frac{J_X}{u_X}+\frac{J_Y}{u_Y}=\frac{z_M}{z}RT\frac{dC_M}{dx}+z_MFC_M\frac{d\phi}{dx}. \quad (32)$$

Using Eqs. 14 and 17 to eliminate J_Y and $d\phi/dx$ and integrating, we have

$$J_X=\left(1-\frac{z_M}{z}\right)RT\frac{u_X}{r-1}\frac{C_M{}^a-C_M{}'}{\delta}. \quad (33)$$

A similar expression is valid for the diffusion layer at the membrane side:

$$\bar{J}_X=\left(1-\frac{z_R}{z}\right)RT\frac{\bar{u}_X}{\bar{r}-1}\frac{\bar{C}_R{}^b-\bar{C}_R{}^a}{\bar{\delta}}. \quad (34)$$

In the steady state ($J_X=\bar{J}_X$), it follows from Eqs. 33 and 34 that

$$\frac{(C_M{}^a/C_M{}')-1}{1-(\bar{C}_R{}^a/\bar{C}_R{}^b)}=\frac{(1-z_R/z)\bar{u}_X(r-1)\delta\bar{C}_R{}^b}{(1-z_M/z)u_X(\bar{r}-1)\bar{\delta}C_M{}'}. \quad (35)$$

Thus, the membrane potential can be calculated from Eqs. 23, 26, 31, and 35, if the mobilities of the counterions and the quantities K and $\delta/\bar{\delta}$ are known. The effect of the diffusion layers appears through the parameter on the right-hand side of Eq. 35. Two limiting cases are noted. When the parameter is very small, it is seen from Eqs. 35, 31, and 26 that $C_M{}^a/C_M{}'$ and $C_X{}^a/C_X{}'$ approach unity, *viz.*, the effect of the diffusion layers becomes negligible. Under such circumstances Eq. 23 is reduced to the form of Eq. 1 with the selectivity coefficient $K_{Y,X}^{pot}$ given by $\bar{r}(k_X\bar{y}_Y/k_Y\bar{y}_X)$. The latter equation is identical with that of Conti and Eisenman[4] for the system in question, if the ratio of the activity coefficients in the membrane $\bar{y}_Y/\bar{y}_X$ is taken as equal to unity (see Eq. 2). On the other hand, when the above parameter is extremely large, it is found from Eqs. 35, 31, and 26 that $(C_M{}^a/C_M{}')^{1-z/z_M}\to r$ and $C_X{}^a/C_X{}'\to 0$. In other words, the concentration gradient of counterion X (in the diffusion layer at the solution side) reaches its maximum value, and there are no concentration gradients within the membrane. The situation corresponds to what is known as "film diffusion control" in solid membrane systems.[6] For this case the membrane potential is obtained from Eq. 23 as

$$V=\frac{RT}{zF}\ln\frac{ry_Y{}'C_X{}'}{a_Y{}''}. \quad (36)$$

In particular, when the mobilities of the counterions are the same in both solutions and membrane ($u_X=u_Y=u$ and $\bar{u}_X=\bar{u}_Y=\bar{u}$), Eq. 23 takes a simpler form. Since Eqs. 22 and 24 show that the concentration C_M of the co-ions is constant across the diffusion layer, Eq. 23 becomes

$$V=\frac{RT}{zF}\ln\frac{y_Y{}'C_X{}'\{(K-1)(C_X{}^a/C_X{}')+1\}}{a_Y{}''}. \quad (37)$$

Here $C_X{}^a/C_X{}'$ is evaluated as follows. From the constancy of C_M and Eqs. 22, 17, and 11, we get

$$C_Y{}^a=C_X{}'-C_X{}^a, \quad (38)$$

$$J_X=RTu(C_X{}'-C_X{}^a)/\delta. \quad (39)$$

Similarly, for the diffusion layer at the membrane side, we have

$$\bar{C}_Y{}^a=\bar{C}_Y{}^b-\bar{C}_X{}^a, \quad (40)$$

$$\bar{J}_X=RT\bar{u}\bar{C}_X{}^a/\bar{\delta}. \quad (41)$$

Equating Eq. 39 with Eq. 41, we get

$$\bar{C}_X{}^a=(u\bar{\delta}/\bar{u}\delta)(C_X{}'-C_X{}^a). \quad (42)$$

Introducing Eqs. 38, 40, and 42 into Eq. 8 and solving the result with respect to $C_X{}^a/C_X{}'$, we find that

$$\frac{C_X{}^a}{C_X{}'}=\left(\left\{K\left(1-\frac{\bar{u}\delta\bar{C}_Y{}^b}{u\bar{\delta}C_X{}'}\right)-2\right\}+\left[\left\{K\left(1-\frac{\bar{u}\delta\bar{C}_Y{}^b}{u\bar{\delta}C_X{}'}\right)-2\right\}^2+4(K-1)\right]^{1/2}\right)\Big/2(K-1). \quad (43)$$

In this case, the effect of the diffusion layers is given in terms of the parameter $\bar{u}\delta\bar{C}_Y{}^b/u\bar{\delta}C_X{}'$. It is negligible when $\bar{u}\delta\bar{C}_Y{}^b/u\bar{\delta}C_X{}'\to 0$, and largest when $\bar{u}\delta\bar{C}_Y{}^b/u\bar{\delta}C_X{}'\to\infty$.

Comparison with Experimental Results

Experimental data were reported for the bi-ionic potentials across liquid anion membranes [nitrobenzene solutions of a Crystal Violet (CV) salt] separating aqueous solutions containing $NaClO_4$, NaSCN, or NaI.[5] Values of k_X/k_Y were also determined by measuring the distribution coefficients of the counterions between nitrobenzene and water. The results are as follows: $k(ClO_4^-)/k(I^-)=84.7$, $k(ClO_4^-)/k(SCN^-)=27.0$, $k(SCN^-)/k(I^-)=3.13$. The assumptions made in the present treatment seem to be satisfactory for these membrane systems. The counterions have approximately the same mobility in both water and nitrobenzene, the ratio being less than 1.16 and 1.12 at infinite dilution in water[9] and nitrobenzene,[10] respectively. The experimental potentials are therefore compared with those expected from Eqs. 37 and 43. (The small difference between the counterion mobilities is disregarded here and hence Eq. 23 is not employed, in view of the approximate nature of the assumption involved in the theory that the counterion mobilities are constant throughout the diffusion layers.)

In the calculation of membrane potentials, the data on k_X/k_Y given above were used to obtain the selectivity coefficient K. The activity coefficient y in solutions was calculated from the Debye-Hückel equation with Kielland's ion-size parameters.[11] In the membrane the activity coefficient $\bar{y}$ was assumed to be the same for all the counterions. The mobility ratio $\bar{u}/u$ was evaluated from the mobilities of iodide ions estimated from the equivalent conductance data for NaI[12] in water and CV–I[13] in nitrobenzene by assuming that their transport numbers are independent of concentrations and equal to those at infinite dilution. The value of $\delta/\bar{\delta}$ can be determined by means of Eqs. 37 and 43 from one potential measurement with a system of known values of K and $\bar{u}/u$, and can be used to predict all other membrane potentials, as long as cell geometry and stirring conditions in the membrane

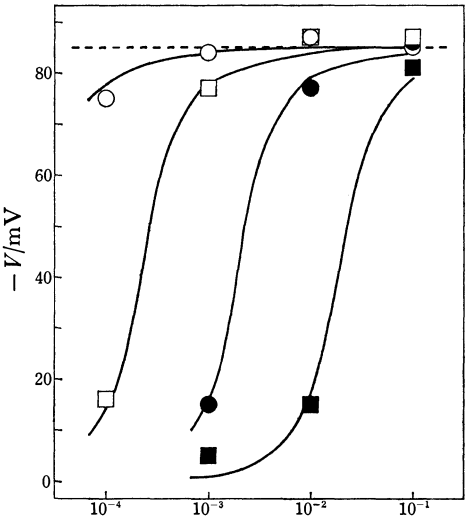

Fig. 2. Comparison of experimental potentials (points) with those calculated from Eqs. 37 and 43 (solid curves) for the bi-ionic system $NaClO_4$(′)/CV–SCN in nitrobenzene/NaSCN (″). The value of the empirical parameter $\delta/\bar{\delta}$ (see Fig. 1) is taken as 1.8. Exchanger (CV–SCN) concentrations: ○, 5×10^{-5} M; □, 5×10^{-4} M; ●, 5×10^{-3} M; ■, 5×10^{-2} M. The broken line indicates the value of the potential expected from the Conti-Eisenman theory, or from Eq. 37 when the effect of diffusion layers is neglected, *i.e.*, $C_X^a/C_X' = 1$.

and solutions remain unchanged. In the experimental work mentioned above, neither the membrane nor the solution phases were stirred. The value of $\delta/\bar{\delta}$ was taken here as 1.8.

Figure 2 shows membrane potentials in the bi-ionic system $NaClO_4$–NaSCN in which a membrane (nitrobenzene solution of CV–SCN) is interposed between aqueous solutions of the two counterions (ClO_4^- and SCN^-) at the same concentration and at the same activity.* The experimental potentials are indicated by points. When the effect of diffusion layers is absent, the membrane potential for this system is calculated from the Conti-Eisenman theory, or from Eq. 37 with $C_X^a/C_X' = 1$. It is independent of the concentrations of the aqueous solutions and of the ion exchanger in the membrane. The calculated value is 85 mV and is given by a broken line. The Conti-Eisenman theory is seen to be valid only when the solution concentration is more than *ca.* 20 times as high as the exchanger concentration. The solid curves, on the other hand, represent values of the potential predicted from Eqs. 37 and 43.[14] They reproduce the experimental values quantitatively.

In Figs. 3 and 4, membrane potentials observed with the systems $NaClO_4$–NaI and NaSCN–NaI are plotted as a function of iodide ion activity.[15] The curves represent the values calculated by Eqs. 37 and 43. Agreement between the calculated and experimental potentials is good. The effect of diffusion layers is absent only in systems of the type:

* In this paper 1 M = 1 mol dm^{-3}.

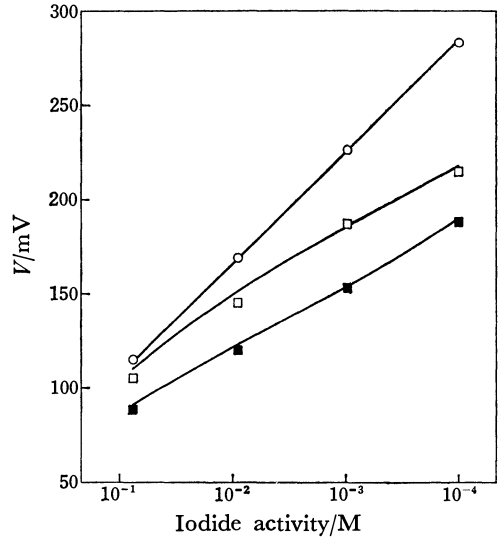

Fig. 3. Comparison of experimental potentials (points) with those calculated from Eqs. 37 and 43 with $\delta/\bar{\delta}=1.8$ (curves) for systems of the types: ○, 0.1 M $NaClO_4$ (′)/5×10^{-4} M CV–I in nitrobenzene/NaI (″); □, NaI (′)/5×10^{-4} M CV–ClO_4 in nitrobenzene/0.1 M $NaClO_4$ (″); ■, NaI (′)/10^{-2} M CV–ClO_4 in nitrobenzene/0.1 M $NaClO_4$ (″). The potentials are shown as positive.

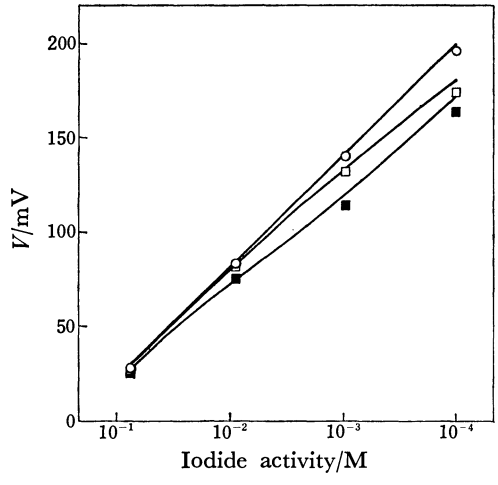

Fig. 4. Comparison of experimental potentials (points) with those calculated from Eqs. 37 and 43 with $\delta/\bar{\delta}=1.8$ (curves) for systems of the types: ○, 0.1 M NaSCN (′)/5×10^{-4} M CV–I in nitrobenzene/NaI (″); □, NaI (′)/5×10^{-4} M CV–SCN in nitrobenzene/0.1 M NaSCN (″); ■, NaI (′)/10^{-2} M CV–SCN in nitrobenzene/0.1 M NaSCN (″). The potentials are shown as positive.

0.1 M NaX (′)/5×10^{-4} M CV–I in nitrobenzene/NaI (″) where $X = ClO_4^-$ or SCN^-.

The results indicate that the concept of diffusion layers is useful in the theoretical interpretation of liquid membrane potentials.

References

1) J. W. Ross, Jr., "Ion-Selective Electrodes," National Bureau of Standards Special Publication, No. 314, ed by

R. A. Durst, U. S. Government Printing Office, Washington, D. C. (1969), Chap. 2.

2) K. Srinivasan and G. A. Rechnitz, *Anal. Chem.*, **41**, 1203 (1969).

3) P. R. Danesi, F. Salvemini, G. Scibona, and B. Scuppa, *J. Phys. Chem.*, **75**, 554 (1971); P. R. Danesi, G. Scibona, and B. Scuppa, *Anal. Chem.*, **43**, 1892 (1971); C. Fabiani, P. R. Danesi, G. Scibona, and B. Scuppa, *J. Phys. Chem.*, **78**, 2370 (1974); C. Fabiani, *Anal. Chem.*, **48**, 865 (1976).

4) F. Conti and G. Eisenman, *Biophys. J.*, **6**, 227 (1966); J. Sandblom, G. Eisenman, and J. L. Walker, Jr., *J. Phys. Chem.*, **71**, 3862 (1967).

5) N. Yoshida and N. Ishibashi, *Bull. Chem. Soc. Jpn.*, **50**, 3189 (1977).

6) F. Helfferich, *Discuss. Faraday Soc.*, **21**, 83 (1956); "Ion Exchange," McGraw-Hill, New York (1962), pp. 378—384.

7) D. Mackay and P. Meares, *Kolloid Z.*, **171**, 139 (1960).

8) D. K. Hale and K. P. Govindan, *J. Electrochem. Soc.*, **116**, 1373 (1969).

9) "Landolt-Börnstein Tabellen," 6th ed, Springer-Verlag, Berlin, Göttingen, and Heidelberg (1960), Vol. II, Part 7, p. 259.

10) Ref. 9, p. 680; F. R. Longo, J. D. Kerstetter, T. F. Kumosinski, and E. C. Evers, *J. Phys. Chem.*, **70**, 431 (1966).

11) J. Kielland, *J. Am. Chem. Soc.*, **59**, 1675 (1937).

12) P. A. Lasselle and J. G. Aston, *J. Am. Chem. Soc.*, **55**, 3067 (1933).

13) N. Ishibashi, H. Kohara, and K. Horinouchi, *Talanta*, **20**, 867 (1973).

14) The value of $\bar{u}$ at an exchanger concentration of 5×10^{-2} M was estimated from the equivalent conductance of CV-I at 10^{-2} M.

15) Taken in part from unpublished results.

A Vapor-Liquid Equilibrium Still Suitable for Small Amounts of Samples*

Sadao TAKAGI**

Department of Chemistry, Faculty of Science, Osaka City University, Sumiyoshi-ku, Osaka 588

(Received November 16, 1978)

Details are described for the apparatus and procedures for the accurate measurement of vapor–liquid equilibria by use of small amounts of samples. The new recirculation still described is a modification of the Brown's still (*Aust. J. Sci. Res., A*, **5**, 530 (1952)) and its total amount of operating charge is *ca.* 53 cm³, of which each 7 cm³ is in the vapor- and liquid-sample traps and *ca.* 23 cm³ is in the boiler. A method of determining an optimum value of the heating current of the boiler is described. Partial condensation of the vapor and entrainment of the liquid phase into the vapor were eliminated. Some results obtained for the system hexane+chlorobenzene at 338.15 K agreed with the thermodynamically consistent values of Brown, showing the reliability of this still operating with the samples having relative volatilities up to 13. The construction of a thermostatted sample vessel without vapor space for a Pulfrich refractometer is also illustrated which is suitable for small quantity of volatile or hygroscopic solution.

Vapor pressures of binary solutions may be measured[1,2] by the static method, the boiling-point method, the gas-saturation method, the isopiestic method, the dew-point method, the method used with the so-called vapor phase osmometer or vapor pressure osmometer, and others. Of those the first two methods are most widely used. The boiling-point method is preferred when both components of a binary solution are volatile, because the sufficient amounts of representative samples of vapor and liquid phases can easily be obtained if the apparatus is properly handled, and hence the thermodynamic consistency among the values obtained for the temperature, pressure, and compositions of vapor and liquid phases can be checked by means of the Gibbs-Duhem relation. In this paper the author will describe a recirculation still which was constructed to obtain sufficient amounts of representative samples of both vapor and liquid phases with use of relatively small amounts of solution.

After a survey of literatures of existing stills, including some actual trials, the equilibrium still of Brown (the still No. 2)[3] was selected as a basis for modification. The Brown's still incorporates many refinements designed to ensure that the samples of condensate and liquid accurately reflect the equilibrium compositions at a well-defined temperature and pressure. Using his still, Brown obtained the thermodynamically consistent results for miscible systems having a relative volatility in the range 1.0 to 14.[3] The amount of operating charge of his still is, however, approximately 200 cm³.

Apparatus

Description of the Vapor–Liquid Equilibrium Still. The design of the new still is shown in Fig. 1. This still was made of borosilicate glass. Its total amounts of operating charge are approximately 53 cm³, of which 7 cm³ is in each trap and about 23 cm³ is in a boiler. On the inner surface of boiler B finely powdered borosilicate glass was sintered to promote even bubbling which ensures effective stirring of the content. The outer heater O is a nichrome ribbon heater wound on the outer wall. The internal heater P is a closely coiled platinum wire[4] whose diameter is *ca.* 0.1 mm. It was spot-welded with tungsten wires which had been sealed with a glass ground joint S. For being insulated thermally and increasing the heat capacity, the boiler was pasted thick with asbestos leaving each peep slit in front and behind, through which condition of the platinum coil and mode of bubbling were observed. The Cottrell pump C is *ca.* 39 cm long and its inside diameter is *ca.* 3.5 mm. The equilibrium chamber A has a thermometer well Q whose depth is *ca.* 9.0 cm and inside diameter is 10 mm. A spiral guide made of glass cane was welded on the outside wall of the thermometer well to ensure sufficient thermal contact of the liquid and vapor with the well. Three concentric tubes in the equilibrium chamber form two annular spaces, of which the outer space is *ca.* 6 to 7 mm wide and it serves as a vapor jacket to prevent fractional condensation of the vapor phase in the inner space. The inner annular space of *ca.* 5 mm width may contribute to eliminate entrainment of liquid phase into the vapor. The upper end of the middle tube was slightly bent toward the center to prevent entering of sprays. The narrowest width of this annular space is 3 mm. Special care was taken to eliminate spattering of sprays as follows. The middle and lower portions of the middle tube were gently tapered. The bottom of the innermost tube was slightly made narrower so as to drain for the liquid gently along the wall of the middle tube. The equilibrium chamber was completely enclosed in a vacuum jacket R whose wall was silvered except vertical peep slits. The inside diameter of condenser D is *ca.* 12 mm. A vertical condenser E (shown as B in Fig. 2) is a total condenser whose vacuum jacket has been silvered leaving peep slits. Inside diameters of the tubes designated U and L are *ca.* 4 mm and *ca.* 5 mm, respectively. The extended portion I, *ca.* 20 mm i.d., and the constriction J in a return path were inserted so as to reduce fluctuations of the liquid level. About 8.5 cm long U-shaped tube K was required to avoid flowing upstream. Inside diameters of this portion are 2 to 3 mm. The vertical extension of a capillary,

* Presented at the 15th National Meeting of the Chemical Society of Japan, Kyoto, April 1962.

** Present address: Department of Chemistry, Faculty of Science and Technology, Kinki University, Kowakae 3-4-1, Higashi-osaka, Osaka 577.

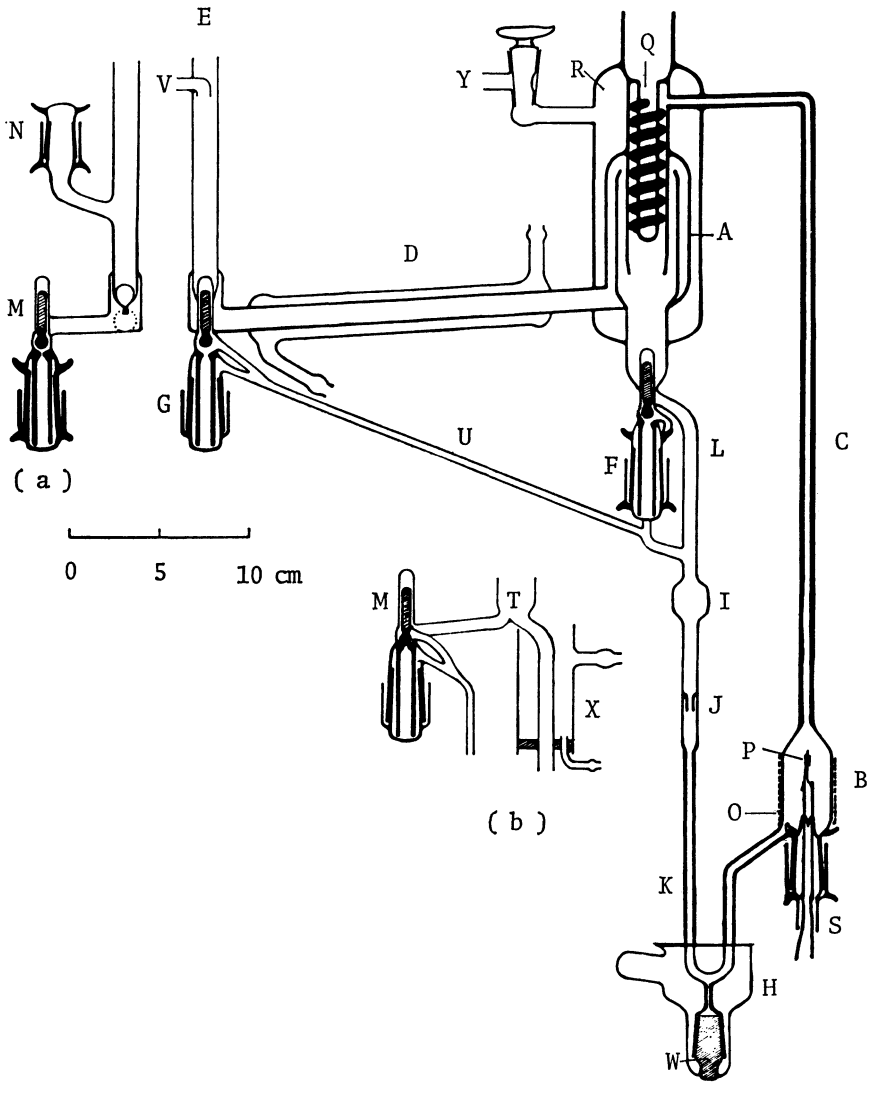

Fig. 1. Equilibrium still. (a) and (b) are side views of the sample traps G and F and their neighbors.
A: Equilibrium chamber, B: boiler, C: Cottrell pump, D: condenser, E: to a total condenser (shown in Fig. 2, B), F: liquid sample trap, G: vapor sample trap, H: cup for collecting the contents, I and J: devices for reducing fluctuations of the liquid level, K: U-shaped tube, L: path of a main flow of the liquid, M: magnetically operated ball valve, N: opening for filling, O: outer heater, P: internal heater, Q: thermometer well, R: vacuum jacket, S: tapered ground stopper, T: ridge for dividing liquid into two 2 : 1 portions, U: path of the returning condensate, V: vent for filling by distillation, W: ground stopper, X: cooler, Y: to a diffusion pump through a liquid nitrogen trap.

ca. 3.5 cm long and *ca.* 0.1 mm i.d., was connected with a ground tapered joint. A cup H with the core of ground joint W for collecting the contents of the still was copied from that originally introduced by Smit and Ruyter.[5] Both the vapor trap G and the liquid trap F are essentially similar to those introduced by Brown:[3] each trap has a small vapor hold-up, a small area of free surface of liquid, and a magnetically operated ball valve M. The both surfaces of the ball and the top of the trap were well ground. In the design of this still a spiral heat-exchanger B of the Brown's still was omitted for simplification of the design and reduction of the volume of dead space. However, a small cooler of *ca.* 6 cm long was mounted on L as shown in Fig. 1, (b) after the construction was completed. A vent V was provided for filling hygroscopic liquids by distillation through a mercury cut-off (shown in Fig. 2). All tapered joints of F, G, and N and the ground stoppers S and W were supported with springs and hooks and sealed with mercury in use.

Measurement of Pressure. The apparatus for the control and measurement of pressure was essentially the same as that used by Scatchard *et al.*[6] It is illustrated schematically in Fig. 2. The maintenance of constant pressure was ensured by connecting the still with a manostat through a liquid nitrogen trap D. The manostat F filled with dry nitrogen is a

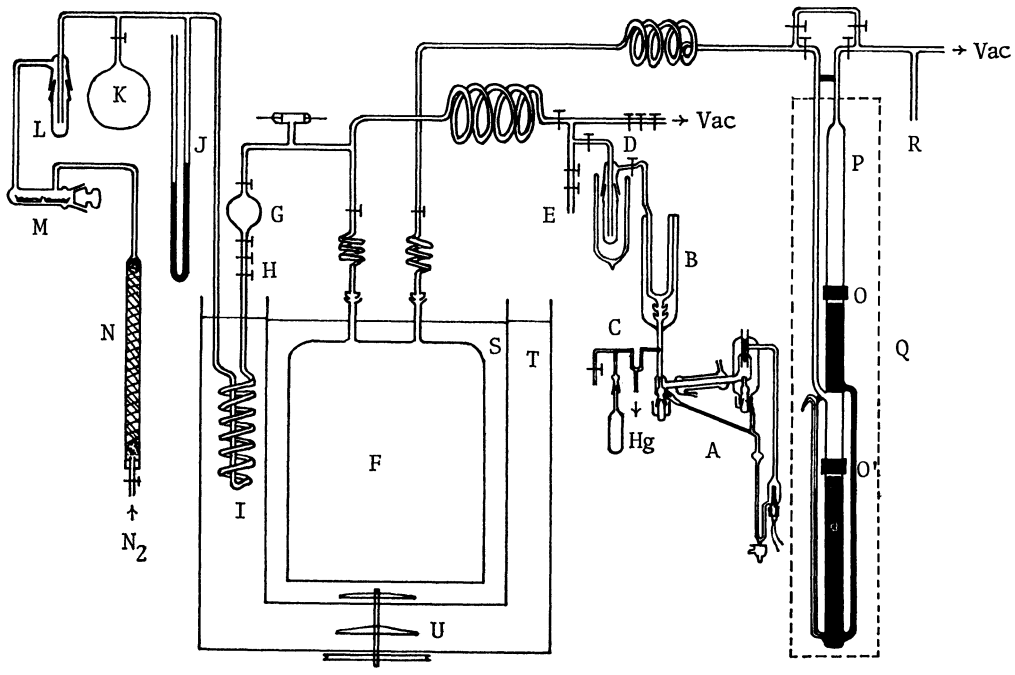

Fig. 2. Arrangement of pressure measuring apparatus.
A: Main part of the still, B: total condenser, C: distillation device for hygroscopic liquid, D: liquid nitrogen trap, E: openning for atmosphere or a dry nitrogen reservoir, F: manostat, G and H: bulb and stopcocks for fine adjustment of nitrogen pressure, Hg: to a mercury reservoir, I: heat-exchanger for nitrogen, J: rough manometer, K: dry nitrogen reservoir, L: liquid nitrogen trap for drying nitrogen gas, M: P_2O_5, N: silica-gel column, N_2: nitrogen from a cylinder, O and O': tubular brass screens, P: precision manometer, Q: thermostat, R: to a rotatable McLeod gauge, S and T: inner and outer baths of a double water thermostat, U: stirrer, Vac: to a high vacuum system.

painted 100-dm³ iron tank submerged in a double thermostat S and T made of tinplate whose temperature was regulated to within ±0.001 K. The pressure of dry nitrogen in the manostat F was measured with a precision manometer P immersed in a thermostat Q in which the thermostatted water in the outer thermostat T was circulated. The circulating water was ejected through three nozzles as jet streams into the thermostat Q and the water was gently stirred with a stirrer driven with a synchronous motor so as to prevent any temperature difference along the manometer P. A high quality plate glass for mirror was used for the front window of the thermostat. A good quality tubing with constant bore size, 20 mm i.d., and uniform thickness was used for making the precision manometer. Two brass collars O and O' painted black were fitted around the tubes and connected to an adjustment device. The readings of mercury menisci were made with a 1-m Shimazu cathetometer readable to 0.05 mm under illumination of a diffuse pale yellow, vertically parallel light from behind; an angular displacement of *ca.* 30° from the diametrical position. The pressure in the vacuum side of manometer was checked with a rotatable McLeod gauge. The temperature of the scale was read with a thermometer immersed in a mercury pool attached to the cathetometer.

Measurement of Temperature. Temperatures were measured with a specially constructed platinum resistance thermometer of the four-lead type,[7,8] a Yokogawa P-7 vernier potentiometer, and a calibrated 100-ohm standard resistance of four-lead type. A lead storage battery was lagged with foamed polystyrene boards. The thermometer was calibrated at the triple point of water[9] and compared with a Leeds and Northrup No. 8163 platinum resistance thermometer calibrated by the National Bureau of Standards, U.S.A. The values obtained of the coefficients of the Callendar equation:[7]

$$t/°\mathrm{C} = \frac{R_t - R_0}{\alpha R_0} + \delta\left(\frac{t/°\mathrm{C}}{100} - 1\right)\frac{t/°\mathrm{C}}{100} \qquad (1)$$

were

$$\frac{R_{100}}{R_0} = 1.39145, \quad \alpha = 0.0039145_1, \quad \text{and} \quad \delta = 1.49225, \qquad (2)$$

which indicated the platinum to be of the requisite purity. A clearance of *ca.* 0.7 mm wide between the outer wall of thermometer and the inside wall of thermometer well was filled with silicone oil. A space between the thermometer and a wide tube welded on the top of thermometer well was plugged with cotton wool.

Operation of the Still

After the solution was charged, the still was evacuated and kept to boil below the room temperature for a few minutes. Then, it was isolated from the vacuum line and connected to the manostat whose pressure had been adjusted to an approximately predicted value.

Heating was commenced adjusting the pressure to the value corresponding to the required temperature by using a calibrated mercury-in-glass thermometer at first and finally the platinum resistance thermometer. After the still was allowed to make steady boiling, the valves on the traps were closed, and the samples were withdrawn for analysis.[3)]

The measured height h_T between the menisci was converted to the pressure P given in the standard mm of mercury† by Eqs. 3 and 4.[10)] The corrections due to the capillary depressions of the mercury were found to be negligible.

$$\frac{h^{\circ}_{273.15}}{\text{mm}} = \frac{h_T}{\text{mm}} \times \frac{1+1.84\times10^{-5}\{(T_S/\text{K})-293.15\}}{1+1.818\times10^{-4}\{(T/\text{K})-273.15\}} \quad (3)$$

$$\frac{P}{\text{mmHg}^{\dagger}} = \frac{h^{\circ}_{273.15}}{\text{mm}} - 0.0974_8\left(\frac{h^{\circ}_{273.15}/\text{mm}}{100}\right) \quad (4)$$

Here T_S and T are the temperatures of the cathetometer scale and the manometer, respectively.

Performance Tests

Optimum Value of Heating Current. Electric currents were supplied to the outer and internal heaters under observation on each ammeter. A fine adjustment was made with each autotransformer whose input voltage was adjusted to ten volts. The heating current of the internal heater was fixed so as to ensure smooth bubbling of the liquid. The current through the outer heater was changed and the plots of equilibrium temperature *vs.* heating current were made. A range of the optimum heating currents was determined from a horizontal portion of the curve where the equilibrium temperature was independent of the value of current supplied. As the range of optimum values of heating current was dependent on the concentration of solution, boiling temperature, or systems to be measured, this test was carried out before the measurement. Portions of the Cottrell pump were wrapped with asbestos ropes, if necessary.

Entrainment of the Liquid Phase into the Vapor. A saturated ethanolic solution of fluorescein at a room temperature (296 K) was charged into the boiler and a lower portion of the return line by means of a syringe fitted with a bent needle. The liquid trap was filled with this solution and the vapor trap was filled with pure ethanol. After 5-h recirculation at atmospheric, 542-mmHg, and 330-mmHg pressures, no color could be detected in the vapor trap.

Comparison with the Reported Values of Hexane+Chlorobenzene at 338 K. *Materials*: Reagent grade hexane was passed through a column filled with silica gel six times to remove aromatics. The hexane obtained was rectified and the portion of distillates boiling at 341 to 342 K was collected. This material was shaken with chlorosulphonic acid to remove methylcyclopentane by means of the method described by Brown,[3,11)] and finally rectified over phosphorus pentaoxide through a 1-m column packed with Dixon packing. The boiling temperature of the purified material was 341.83 K. Gas-chromatography analysis showed that the impurities having shorter retention times than hexane were completely removed and methylcyclopentane was almost completely removed. Reagent grade chlorobenzene showed only very small peaks of a gas-chromatography curve in the shorter side of retention time apart from the main peak. It was rectified, shaken with 10% aqueous solution of sodium hydroxide, washed with water, dried over anhydrous calcium chloride and then phosphorus pentaoxide, and finally rectified over phosphorus pentaoxide through the column described above. The boiling temperature was 404.85 K.

† Throughout this paper 1 mmHg=133.3224 Pa.

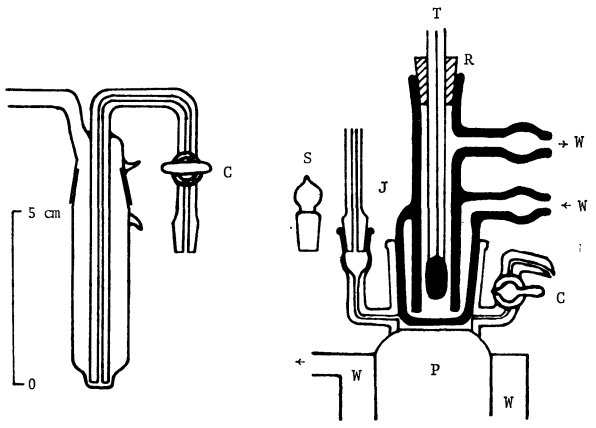

Fig. 3. Thermostatted sample vessel without vapor space suitable for small amounts of volatile or hygroscopic solutions for a Pulfrich refractometer and a device for the transfer of samples.
The both equipments were made of borosilicate glass.
C: stopcocks, J: tapered ground joint, P: prism, R: rubber stopper, S: ground stopper, T: thermometer, W: thermostatted water.

Table 1. Mole fractions x_1 and y_1 of hexane in liquid and vapor phases, equilibrium vapor pressures P, and relative volatilities $\alpha=y_1x_2/y_2x_1$ for the system hexane(1)+chlorobenzene(2) at 338.15 K
(1 mmHg=133.3224 Pa)

x_1	y_1	P/mmHg	α
0.089	0.564	174.2_1	13.2
0.321	0.822	344.7_0	9.8
0.442	0.870	410.1_6	8.4

Procedures and Results: Since the refractive indices of both components agreed with those reported by Brown,[3)] the equilibrium compositions were determined by the refractive index *vs.* mole fraction curve which had been drawn from his data. The refractive indices of small quantities of samples were accurately measured on a Pulfrich refractometer by use of the thermostatted liquid vessel without gas phase designed by the author as shown in Fig. 3. The results of vapor–liquid equilibria obtained are given in Table 1. These values agreed well with the Brown's data[3)] within the experimental error. Since the Brown's data for this system satisfied the Gibbs-Duhem relation well,[3)] the vapor–liquid equilibrium still for small sample size, *ca.* 52 cm^3, here described is also reliable to operate

with the samples having relative volatilities up to $\alpha=13$.

The author wishes to thank Professor Emeritus Ryoichi Fujishiro of Osaka City University, and Professor Syûzô Seki of Osaka University for their continuing interest and encouragements. He is also thankful to Professor Syûzô Seki, Dr. Hiroshi Suga, and Dr. Minoru Sakiyama, Osaka University, for the loan of their precision platinum resistance thermometer, Leeds and Northrup No. 8163.

References

1) "Jikken Kagaku Koza," ed by The Chemical Society of Japan, Maruzen, Tokyo (1958), Vol. 5, pp. 376—395.
2) "Experimental Thermodynamics," ed by B. Le Neindre and B. Vodar, Butterworths, London (1975), Vol. 2, pp. 749—786.
3) I. Brown, *Aust. J. Sci. Res.*, *A*, **5**, 530 (1952).
4) I. Brown and A. H. Ewald, *Aust. J. Sci. Res.*, *A*, **3**, 306 (1950), foot note in p. 308.
5) W. M. Smit and J. H. Ruyter, *Rec. Trav. Chim. Pays-Bas*, **79**, 1244 (1960).
6) G. Scatchard, C. L. Raymond, and H. H. Gilmann, *J. Am. Chem. Soc.*, **60**, 1275 (1938).
7) "Temperature, Its Measurement and Control in Science and Industry," ed by American Institute of Physics, Reinhold Publishing Corporation, New York (1941).
8) "Jikken Kagaku Koza," ed by The Chemical Society of Japan, Maruzen, Tokyo (1958), Vol. 5, pp. 93—142.
9) H. F. Stimson, *J. Res. Nat. Bur. Stand.*, **42**, 209 (1949).
10) "Physical Methods of Organic Chemistry," 2nd ed, ed by A. Weissberger, Interscience Publishers, Inc., New York (1949), Part 1, p. 141.
11) A. F. Shepard, A. L. Henne, and T. Midgley, Jr., *J. Am. Chem. Soc.*, **53**, 1948 (1931); A. F. Shepard and A. L. Henne, *Ind. Eng. Chem.*, **22**, 356 (1936).

^{35}Cl-NQR of Some Chlorocarbons and Oxochlorocarbons with a Small Ring†

Koichi MANO, Takefumi MATSUKURA,** and Akira FUJINO*

Research Institute for Atomic Energy, Osaka City University, Sugimoto-cho, Sumiyoshi-ku, Osaka 558

(Received December 25, 1978)

^{35}Cl-NQR of two chlorocarbons and six oxochlorocarbons, all having a small ring, were measured in the temperature range 77—300 K. The NQR line groups for the allylic and vinylic chlorine atoms appear separately in the five-membered ring compounds, whereas they are concentrated in a rather narrow region near 38 MHz in the four-membered ones. Perchlorocyclopropene possesses at least three crystal modifications at 77 K, the most stable one of which has only two lines in the temperature range examined. The line assignments, and the hyperconjugative effect in some of them, are discussed with reference to the CNDO/2 MO calculation data.

By means of ^{35}Cl-NQR we can discuss the hyperconjugative effects in the ground state of an organic molecule. Unexpected lowering of the observed frequencies in chlorofluoromethanes, chloromethyl ethers,[1,2] and benzyl chlorides[3] was explained by the interaction between the C–Cl σ bond and the p-orbital of the adjacent first-row substituents. Considering the fitness of chlorocarbons (no hydrogen bond in or between the molecule(s)) for the purpose, we examined the ^{35}Cl-NQR of some cyclic chloro- and oxochlorocarbons in which all the chlorine atoms on the ring carbons have a rigid conformation. We found that in some of them the hyperconjugative effect causes a significant frequency shift from the expected value.

Experimental

Except for commercial perchlorocyclopropene, all the specimens were prepared according to the methods described.[4-8] They were purified by monitoring their IR spectra and elemental analyses. Melting points are: perchloro-4-cyclopentene-1,3-dione (**1**), 68 °C; perchloro-2-cyclopentenone (**2**), 28 °C; perchloro-3-cyclopentenone (**3**), 89 °C, perchloro-3,4-dimethylenecyclobutane-1,2-dione (**4**), 167 °C; perchloro-2,3-dimethylenecyclobutanone (**5**), 68 °C; perchloro-2-cyclobutenone (**6**), −1 °C (by DSC); perchlorocyclobutene (**7**), 50 °C.

A Decca Radar NQR Spectrometer and a superregenerative spectrometer were used. Temperature dependence of the NQR signals was measured by Hashimoto's method.[9] Resonance frequency values obtained by extrapolating the observed variation to 0 K were taken for minimizing the thermal effect of the crystalline lattice on frequencies.

Results and Discussion

The resonance frequencies of six oxochlorocarbons (**1**—**6**) and two chlorocarbons (**7** and **8**) at several temperatures are given in Table 1. The stick diagram (Fig. 1) shows the values at 0 K together with those of the related compounds, perchlorocyclopentene (**9**) and perchloro-1,2-dimethylenecyclobutane (**10**).

Five-membered Ring Compounds. The resonance lines of all oxo compounds as well as the reference chlorocarbon **9** fall into two clearly separated frequency regions, one lower than 38.1 MHz, and the other above 39.1 MHz. The lower group corresponds to the vinylic (*v*-), and the higher to the allylic (*a*-) chlorine substituents. The numbers of observed lines for **1** and **3** were two and three, respectively, indicating that the former molecule has a C_2 and/or two C_s, and the latter a C_2 or C_s symmetry element(s) in their crystals.

The lowest line ν_6 in **2** is easily assigned to a *v*-Cl, β-positioned to the carbonyl group. The two-paired *a*-Cl's resonate in sufficiently separated regions, re-

TABLE 1. TEMPERATURE DEPENDENCES OF NQR LINES IN SOME CHLOROCARBONS AT SEVERAL TEMPERATURES

		77 K	195 K	288 K	0 K[a]
1	ν_1	39.848	39.272	38.765	40.07
	ν_2	36.573[b]	36.105	35.692	36.72
2	ν_1	40.362	40.060	39.749	40.45
	ν_2	40.157	39.789	39.429	40.30
	ν_3	39.333	39.077	38.810	39.38
	ν_4	39.178	38.905	38.632	39.28
	ν_5	38.014	37.684	37.381	38.14
	ν_6	37.266	36.905	36.587	37.39
3	ν_1	39.414	38.921	38.403	39.55
	ν_2	39.082	38.577	38.036	39.22
	ν_3	37.674	37.376	36.997	37.75
4	ν_1	37.948	37.372	37.508	38.02
	ν_2	37.389	37.115	36.836	37.45
5	ν_1	38.304	37.874[c]	37.447	38.40
	ν_2	37.921	37.465[c]	37.006	38.01
	ν_3	37.798	37.494[c]	37.190	37.86
	ν_4	37.723	37.425[c]	37.104	37.80
	ν_5	37.562	37.153[c]	36.701	37.64
	ν_6	37.562	37.254[c]	36.950	37.62
6	ν_1	37.780[b]	37.461	37.420[d]	37.90
	ν_2	37.645[b]	37.354	37.319[d]	37.75
	ν_3	37.296[b]	36.971	36.940[d]	37.42
	ν_4	36.707[b]	36.371	36.337[d]	36·82
7	ν_1	38.482	38.151	37.789	38.55
	ν_2	38.412[b]	38.037	37.637	38.50
	ν_3	38.352[b]	38.011	37.637	38.42
	ν_4	38.230[b]	37.843	37.439	38.34
	ν_5	36.647[b]	36.259	35.843	36.74
	ν_6	36.480[b]	36.105	35.711	36.57
8	ν_1	38.730	38.308	38.144[c]	38.80
	ν_2	36.471	36.131	35.933[c]	36.54

a) Extrapolated values. b) *Cf.* C. Brevard and J. M. Lehn, *J. Chim. Phys. Physicochim. Biol.*, **1968**, 727. Their ν_2 value for **1** differs exactly 1000 kHz from ours. However, their values for **6** and **7** and those we obatined are in good agreement. c) At 200 K. d) At 206 K. e) At 233 K.

† Presented in part at the Third International Symposium on Nuclear Quadrupole Resonance, Tampa, Fla., U. S. A., April 1975.

** The Toyo Linoleum Manufacturing Company Limited, 5-125 Higashi-arioka, Itami 664.

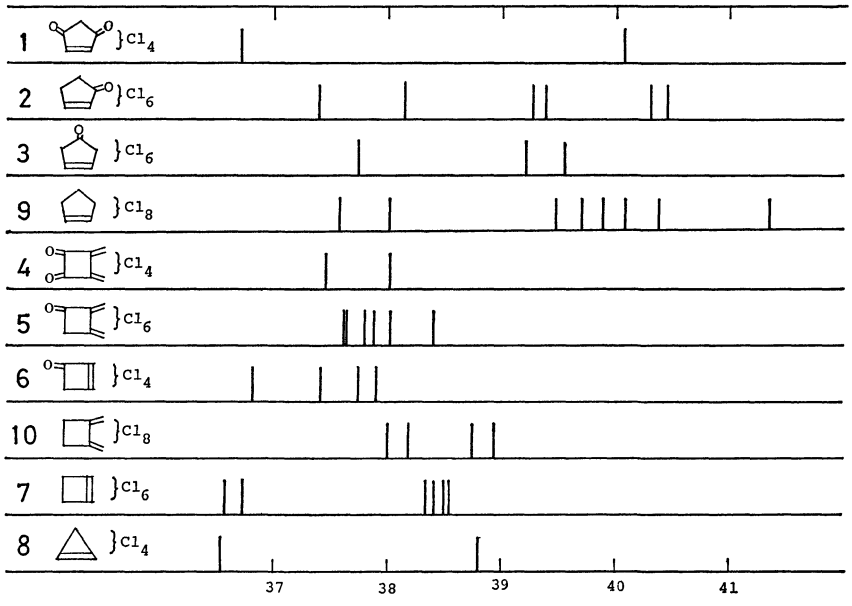

Fig. 1. Resonance lines obtained by extrapolating the thermal variation to 0 K.

spectively *ca.* 39.3 and 40.4 MHz. The highest two among them can be explained in terms of the hyperconjugative interaction between the C_5–Cl bond and the carbonyl group which unusually decreases the ionicity of the allylic chlorine (the term "allylic" is also applied to the chlorine atom α-positioned to the carbonyl group). The remaining pairing lines, ν_3 and ν_4, can be assigned to the *a*-Cl's at C_4.

The *a*-Cl (ν_1) in **1** appears in a region similar to the highest one in **2**. In this case, we see no additive effect of hyperconjugation due to the second carbonyl group.

The frequency of *v*-Cl in **3** is situated roughly at an average of the highest two lines for **9**. The *a*-Cl's resonate in the same frequency region as do the *a*-Cl's at C_4 in **2**. Thus, the carbonyl seems to have no influence on all the resonance frequencies.

Four-membered Ring Compounds. In contrast to the above, all the NQR lines of oxochlorocarbons **4**—**6** were observed in a narrow range near 38 MHz. Dioxo compound **4** gave two lines which suggest a C_2 and/or a C_s symmetry in the crystal, its splitting (*ca.* 600 kHz) due to inner and outer *v*-Cl's being appreciably larger than the corresponding one in chlorocarbon **10**. The large splitting suggests a difference in contribution of each carbonyl group to the conjugation with chlorine atoms between the inner *v*-Cl and the outer one. Preliminary MO calculation data (CNDO/2)[11] indicate that the lower line corresponds to the inner substituent.

Mono oxo compound **5** has five lines at 77 K. However, temperature dependence observation of these lines revealed that **5** has essentially six lines in the range 77—310 K; three (ν_1, ν_2, and ν_3) of them having a steeper temperature gradient, *ca.* 4.2 kHz/K, and the rest having *ca.* 2.9 kHz/K. All the lines appear in the *v*-Cl region after 0 K extrapolation, suggesting that the hyperconjugation with C=C double bond would be dominant over that with the C=O group. Reflecting this situation, the calculation gave an appreciably large N_z (1.233, AO population of p_z) of the *a*-Cl. Such a polarization in the Cl at C_4 is due to the contribution of a stabilized allylic cation with full π-conjugation. It was difficult to assign the six lines because of their concentration in a narrow range within crystal field effects. However, the calculated line pattern for **5** with a twisted geometry of $C{=}Cl_2$ groups resembles the observed one.[11,12]

Compound **6**, having four NQR lines all in the *v*-Cl region (below 38.0 MHz), shows an almost simultaneous fade-out at around 210 K, which seems to be related to the phase transition at 220 K evidenced by DSC analysis. The extraordinary low values for the *a*-Cl's suggest the contribution, in the ground state, of some stabilized structure, perhaps an aromatized one as shown below, rather than a hyperconjugated. In a compound like **7**, where no similar contribution can be expected, six lines appear in two groups well separated.

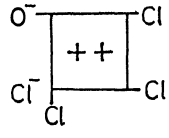

Three-membered Ring Compound. Perchlorocyclopropene **8** is an interesting compound in view of NQR spectra. Lucken and Mazeline reported six lines at 77 K, falling into two frequency groups (four: 38.2—38.8; two: 36.4—36.8 MHz).[13] They assigned the higher line group to *a*-, and the lower to *v*-Cl's. Smith and West later gave a completely inversed assignment on the basis of the data for some chlorocyclopropene derivatives.[14] We found from both NQR and DSC studies that **8** possesses at least three crystal modifications at 77 K. The most stable form, obtained by annealing **8** at Dry Ice temperature for 72 h, has only two NQR lines with very strong intensities in the temperature range 77—233 K (mp). Thus, it should have a C_2 and/or two C_s symmetry in the crystal.

Prediction from MO calculation strongly supports West's assignment.[14] The inversion of the frequency region between *a*- and *v*-Cl is attributed to both an extraordinary increase in N_z of the *a*-Cl (1.261) and a decrease in that of *v*-Cl (1.181).[11] The former is caused by the hyperconjugation with the C=C bond which stabilizes its cyclopropenium cationic structure in the ground state of the molecule.

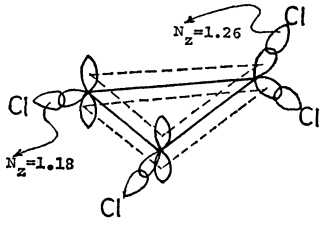

References

1) E. A. C. Lucken, *J. Chem. Soc.*, **1959**, 2954.
2) Z. Ardalan and E. A. C. Lucken, *Helv. Chim. Acta*, **56**, 1715 (1973).
3) J. S. Dewar and M. L. Herr, *Tetrahedron*, **27**, 2377 (1971).
4) H. M. Molotsky and E. G. Ballweber, *Chem. Abstr.*, **52**, 426 (1958).
5) A. Fujino, K. Kusuda, and T. Sakan, *Bull. Chem. Soc. Jpn.*, **39** 160 (1966).
6) K. Kusuda, K. Mano, A. Fujino, and T. Sakan, *Bull. Chem. Soc. Jpn.*, **40**, 1188 (1967).
7) W. C. Solomon, L. A. Dee, and D. W. Schults, *J. Org. Chem.*, **31**, 1511 (1966).
8) G. Maahs, *Justus Liebigs Ann. Chem.*, **686**, 55 (1965).
9) M. Hashimoto, Thesis, Osaka University (1975).
10) M. Hashimoto and K. Mano, *Bull. Chem. Soc. Jpn.*, **45**, 706 (1972).
11) T. Matsukura, Thesis, Osaka City University (1975).
12) K. Mano, *J. Magn. Reson.*, **26**, 393 (1977).
13) E. A. C. Lucken and C. Mazeline, *J. Chem. Soc., A*, **1968**, 153.
14) R. M. Smith and R. West, *Tetrahedron Lett.*, **1969**, 2141.

On the Phase Transitions in Ammonium Hexafluoroaluminate(III)

Keiichi MORIYA,* Takasuke MATSUO, Hiroshi SUGA, and Syûzô SEKI
Department of Chemistry, Faculty of Science, Osaka University, Toyonaka Osaka 560

(Received January 5, 1979)

The heat capacities of $(NH_4)_3[AlF_6]$ were measured between 11 and 300 K with an adiabatic calorimeter. Two anomalies were found at (193.0±0.3) K and (220.79±0.05) K. The enthalpy and entropy of the phase transitions are (790±150) J mol^{-1} and (4.2±0.8) J K^{-1} mol^{-1} for the former, and (4030±150) J mol^{-1} and (18.5±0.7) J K^{-1} mol^{-1} for the latter, respectively. The total anomalous entropy, (22.7±1.5) J K^{-1} mol^{-1}, is in agreement with $R \ln 16 = 23.05$ J K^{-1} mol^{-1} predicted by a model involving orientational disorder of the hexafluoroaluminate(III) and the ammonium ions. Discontinuities in fluorine T_1 and $T_{1\rho}$ at 221 K by pulse NMR measurement also support this model. The potential barrier height of the hindered rotation of the NH_4^+ ion was estimated to be 7 kJ mol^{-1} from the heat capacity data. The intermediate phase undercooled and coexisted with the low temperature phase in a limited range of temperature. The upper phase transition is of the first order but the anomalous heat capacity follows the Landau theory of the phase transitions of the second kind. The high symmetry of the crystal structure of the present crystal at room temperatures in comparison with that of the alkali cryolites was discussed in terms of the hydrogen bonding, molecular disorder and packing consideration.

There is currently a considerable interest in the phase transitions of crystals containing $[AX_6]^{n-}$ ions, where A is a multivalent atom and X halogen. The phase transitions hitherto studied of this type of compound appear to be displacive if X is chlorine, *e.g.*, $K_2[SnCl_6]$,[1,2] $(NH_4)_2[SnCl_6]$,[3] $K_2[ReCl_6]$,[4] $K_2[OsCl_6]$,[4] and $(NH_3CH_3)_2[SnCl_6]$.[5] Spectroscopic studies have shown that low-frequency rotational vibrations of $[ACl_6]^{2-}$ ion play an important role in the phase transitions in these crystals.[2,3,5] The entropy of transition, in case where calorimetric data are available, is relatively small in agreement with the displacive mechanism of the transitions. For X= fluorine, we have shown that the phase transition is of order-disorder type in $(NH_4)_3[FeF_6]$ crystal.[6] The large entropy of transition ($\Delta S \simeq 24.8$ J K^{-1} mol^{-1}) was accounted for in terms of a model involving orientational disorder of both the ammonium and hexafluoroferrate (III) ions. It was pointed out that the same orientational disorder explains, albeit qualitatively, why ammonium hexafluoroferrate(III) crystal is cubic at room temperature while alkali hexafluoroferrates(III) are not.

In the present paper we will report a calorimetric and NMR study of phase transitions in ammonium hexafluoroaluminate (ammonium cryolite), $(NH_4)_3[AlF_6]$. It will be shown that this crystal is very similar to ammonium hexafluoroferrate(III) in regard to the ionic disorder but the low temperature behavior, having an additional phase transition, is more complicated than in the iron compound.

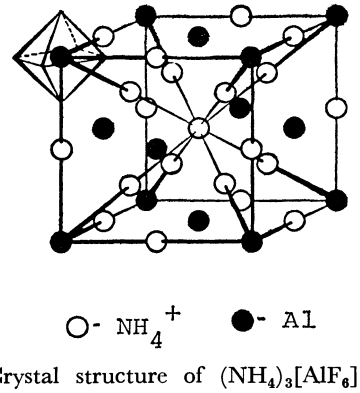

Fig. 1. Crystal structure of $(NH_4)_3[AlF_6]$.

$(NH_4)_3[AlF_6]$ at room temperature is isomorphous with cubic $(NH_4)_3[FeF_6]$. The structure[7] is illustrated in Fig. 1. The aluminum atoms occupy the corner (0,0,0) and face-center (1/2,1/2,0) of the cube. The fluorines are placed tentatively on the four-fold axis of the crystal to form a regular octahedron around the aluminum. There are two sites for the ammonium ions. One is on the edge of the cube (1/2,0,0) and the other (1/4,1/4,1/4). There are four of the former in the unit cell of the fcc Bravais lattice and eight of the latter.

The crystal is not cubic at 93 K. Steward and Rooksby[7] called it pseudo tetragonal. Schwarzmann[8] found that $(NH_4)_3[InF_6]$ belongs to the monoclinic system (C_{2h}^5-$P2_1/n$) and that $(NH_4)_3[AlF_6]$ undergoes a phase transition at 224 K which he described as displacive. Thus it has been known that there is a phase transition between the room temperature and 93 K. It will be shown below that there are in fact two phase transitions.

Comparison of the crystal structure of alkali and ammonium hexafluoroaluminates and analogous hexafluoroferrates(III) shows that there is similar behavior as the size of cation increases in these two families. In Table 1[9] which summarizes the crystal system and the molar volume of the cryolite family, it is shown that smaller alkali cations excluding lithium tend to form less symmetric crystals. The molar volume of the ammonium cryolite is intermediate between those of Rb and Cs compounds. The fcc symmetry of the ammonium cryolite is thus anomalously high in

TABLE 1. THE CRYSTAL SYSTEM AND MOLAR VOLUME OF CRYOLITE-TYPE COMPOUNDS $A(I)_3[AlF_6]$ AT ROOM TEMPERATURE

A(I)	Crystal system	Molar volume / cm^3 mol^{-1}
Li	orthorhombic	58.9
Na	monoclinic	72.0
K	tetragonal	90.4
Rb	tetragonal	102.0
Cs	tetragonal	117.4
NH_4	cubic	107.2

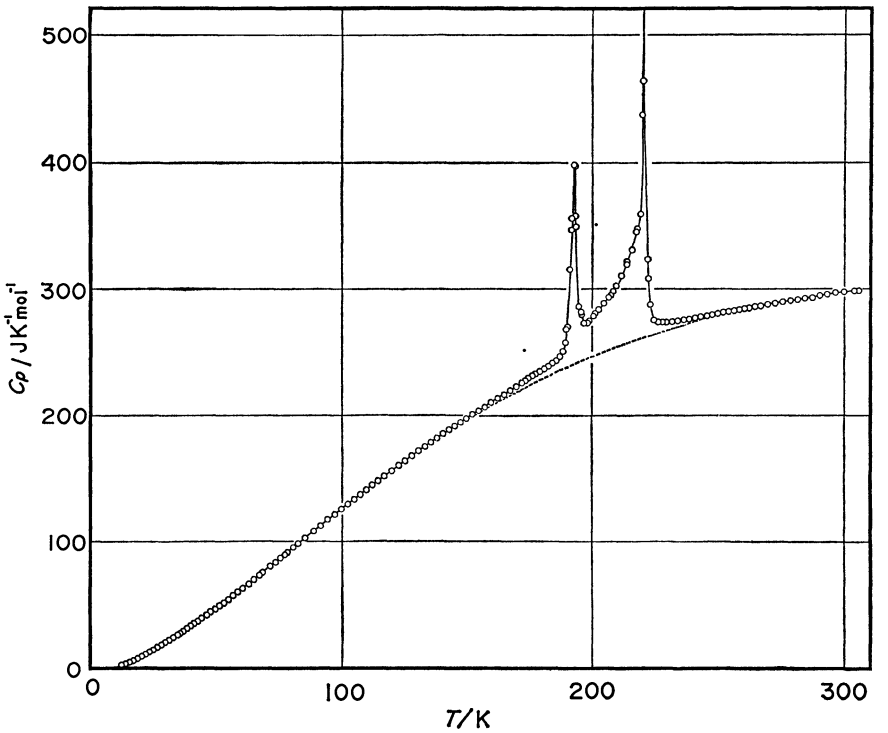

Fig. 2. Molar heat capacity of $(NH_4)_3[AlF_6]$.

this family. It will be shown below that the anomalous property of the ammonium compound is closely related to the orientational disorder and packing of the ions.

Experimental

Sample Preparation. Metallic aluminum of stated 99.99% purity was dissolved in extra-pure reagent of hydrofluoric acid (Wako Pure Chemical Industries, Ltd.). The aluminum fluoride solution thus prepared was added to the aqueous solution of the 1.5 times equivalent amount of extra-pure reagent of ammonium fluoride (Wako Pure Chemical Industries, Ltd.). The reaction was performed at 60 °C. The precipitated crystal, $(NH_4)_3[AlF_6]$, was repeatedly digested at 90 °C. The crystal obtained was separated by filtration, washed with methanol and dried *in vacuo* at 90 °C. Polyethylene or teflon laboratory ware was used exclusively throughout the sample preparation. The crystal was kept in an evacuated desiccator together with calcium oxide before heat capacity measurement. The elemental analysis was made by oxine gravimetric method for Al, by thorium nitrate titration for F and gravimetric method for N and H. The values given below in parentheses are calculated for the chemical formula $(NH_4)_3[AlF_6]$; Al: 13.80±0.04 (13.83%), F: 58.3±0.4 (58.5%), H: 6.17±0.20 (6.20%), N: 21.3±0.2 (21.54%).

Differential Thermal Analysis and X-Ray Powder Photograph. The thermal behavior was first examined by differential thermal analysis (DTA).[10] Only one exothermic peak was detected at 220 K on cooling at the rate of 3 K/min down to 100 K. On the other hand two peaks were observed in the heating run around 190 K and 220 K, respectively. This behavior was reproducible with the same crystal. X-Ray powder photographs taken at 125, 216 and 293 K gave different diffraction patterns. The pattern at 293 K was fully indexed with the fcc lattice. The intermediate and the lowest-temperature patterns were increasingly complicated and could not be indexed. However, by the DTA and the Debye-photograph data it became evident for the first time that ammonium hexafluoroaluminate is trimorphic below the room temperature. The hysteresis phenomenon in DTA was confirmed in the heat capacity measurement as will be discribed below.

Heat Capacity Measurement. The heat capacity was measured from 11 K to 300 K with an adiabatic calorimeter. The calorimeter consists of the sample cell and double adiabatic jackets surrounding it. They are suspended in a vacuum chamber. The temperature of the cell was measured with a platinum resistance thermometer calibrated in terms of the IPTS-68. Precision of the heat capacity measurement was ±0.05% in the temperature range above 50 K, and the estimated accuracy ±1% at 20 K and 0.1% above 50 K. Details of the construction of the calorimeter were published elsewhere.[11]

The calorimeter cell, a chromium plated thin-walled copper cylinder with the thermometer and heater, was loaded with 44.296 g (0.22706 mol) of the $(NH_4)_3[AlF_6]$ crystal, evacuated to approximately 1 Pa, filled with 10^5 Pa of He gas at 20 °C and then sealed off with low melting solder. The increment of the temperature in one measurement of the heat capacity was 1—3 K in the normal temperature region and less than 0.1 K in the transition region. The experimental heat capacity values are given in Table 2 and shown in Fig. 2. Two heat capacity peaks were found at (193.0±0.3) K and (220.79±0.05) K, respectively. These temperatures agree well with the DTA result. The high temperature anomaly has a premonitory effect already at 193 K where the peak height of the low temperature anomaly reaches maximum. The apparent heat capacity reached 23000 J K^{-1} mol^{-1} at the upper phase transition. The time required for thermal equilibration in the neighbourhood of both phase transitions increased to about an hour, compared with ten minutes normally required in normal region. Such a behavior is often observed in the first order transitions. Figure 3 shows the cooling curve obtained by slow removal

TABLE 2. HEAT CAPACITY OF $(NH_4)_3AlF_6$

T_{av}/K	C_p/J K^{-1} mol^{-1}	T_{av}/K	C_p/J K^{-1} mol^{-1}	T_{av}/K	C_p/J K^{-1} mol^{-1}	T_{av}/K	C_p/J K^{-1} mol^{-1}
1 st series		65.60	71.53	200.49	278.5	198.64	274.7
11.99	2.13	68.35	75.84	202.82	283.8	199.76	276.9
13.07	2.77	71.11	80.08	205.12	289.6	201.47	280.3
13.93	3.38	73.43	83.73	207.38	295.4	203.07	284.4
14.65	3.93	75.64	87.27	209.60	302.2	204.90	288.9
15.41	4.55	78.20	91.37	211.78	310.5	206.52	293.2
16.20	5.18	80.66	95.35	213.91	319.8	208.19	298.1
16.96	5.93	3 rd series		215.99	331.7	210.16	303.9
17.77	6.71	80.15	94.56	217.99	347.7	212.10	311.9
18.58	7.51	82.52	98.46	219.81	437.1	213.98	320.9
19.38	8.38	85.28	102.9	220.69	7349	215.85	330.4
20.19	9.29	88.57	108.1	220.78	23300	217.66	345.1
20.96	10.26	91.47	112.8	221.10	1378	219.12	359.9
21.76	10.87	94.31	117.1	222.48	308.2	220.16	464.5
22.56	11.95	97.10	121.6	224.72	274.5	220.68	5605
23.30	12.77	99.81	125.7	227.06	273.2	220.75	15540
24.09	13.74	102.38	129.7	229.40	273.3	220.78	22050
24.94	14.68	104.92	133.6	231.73	273.7	220.80	23130
25.72	15.67	107.38	137.3	234.05	274.4	221.07	963.3
26.46	16.49	109.79	141.0	236.37	275.1	221.94	323.5
27.18	17.40	112.14	144.5	238.68	275.8	223.23	287.3
27.93	18.30	114.44	148.0	240.98	276.8	224.60	275.0
28.76	19.35	117.00	151.7	243.27	277.5	226.17	273.6
29.55	20.34	119.80	156.0	245.56	278.4	228.08	273.4
30.29	21.17	122.54	160.4	247.83	279.1	230.17	273.5
31.09	22.16	125.22	159.9	250.03	279.9	5 th series	
31.93	23.29	127.86	167.7	252.23	281.0	262.52	284.6
32.73	24.36	130.46	171.3	254.48	281.5	264.75	285.6
33.57	25.39	133.02	174.9	256.73	282.8	267.15	286.2
34.44	26.52	135.51	178.4	258.96	283.5	269.91	287.8
35.44	27.86	137.97	181.7	261.18	284.0	272.85	288.0
36.79	29.67	140.38	185.1	4 th series		275.78	289.2
38.27	31.57	142.76	188.3	172.07	225.6	278.70	290.3
39.66	33.45	145.11	191.4	173.50	227.5	281.60	291.2
41.07	35.29	147.42	194.4	174.91	229.1	284.49	292.4
42.46	37.08	149.70	197.5	176.32	231.0	287.39	292.9
44.08	39.37	152.12	200.9	177.73	232.5	290.28	294.3
45.97	41.91	154.60	203.7	179.29	234.5	293.22	295.0
47.65	44.38	157.08	206.9	181.02	236.3	296.37	295.9
49.39	46.91	159.69	210.2	182.73	238.8	299.83	297.0
51.17	49.52	162.27	213.5	184.35	241.1	6 th series	
52.92	51.09	164.80	216.7	185.78	243.1	187.49	254.8
54.66	54.67	167.32	219.9	187.15	246.1	188.69	255.9
56.61	57.44	169.81	222.8	188.34	250.2	190.05	258.8
58.38	60.30	172.26	226.0	189.32	257.2	191.57	261.4
60.33	63.34	174.69	229.0	190.27	269.9	193.27	264.3
62.69	66.73	177.09	231.8	191.15	315.6	195.12	267.9
64.67	70.14	179.47	235.0	191.95	356.1	197.10	271.7
66.81	73.51	181.92	237.9	192.68	398.7	199.15	275.8
71.33	80.47	184.42	241.2	193.38	397.6	201.08	280.2
75.47	87.10	187.37	247.0	194.11	358.3	203.08	284.6
77.15	89.66	189.39	268.0	194.88	285.9	7 th series	
79.13	92.91	191.61	346.9	195.83	279.8	181.59	244.5
81.04	96.05	193.59	349.8	196.75	272.6	182.88	246.5
2 nd series		195.76	281.7	197.67	272.8	184.53	249.6
62.66	66.98	198.13	272.9			186.30	252.0

TABLE 2. Continued.

T_{av}/K	C_p/J K^{-1} mol^{-1}	T_{av}/K	C_p/J K^{-1} mol^{-1}
188.05	255.3	190.74	282.4
189.96	258.8	192.67	313.7
192.01	265.9	194.64	278.9
194.03	267.9	196.71	271.1
196.04	269.5	198.77	275.1
198.03	273.5	200.82	279.3
199.97	277.5	9 th series	
201.91	281.8	175.52	231.1
8 th series		176.93	232.9
174.61	232.4	178.31	235.3
176.26	234.1	179.68	236.4
178.39	237.4	181.04	238.6
180.50	240.2	182.39	240.4
182.59	243.2	184.08	242.9
184.68	246.4	186.09	246.2
186.70	250.4	188.06	252.3
188.75	256.4	189.67	266.2

of heat from the specimen. The cooling rate 0.7 K/h at the normal region was effected by introduction of an appropriate back-up potential in the cell-jacket thermocouple circuit. The temperature arrest occurred at (220.79±0.05) K which was in good agreement with the temperature of the heat capacity peak. No temperature halt was observed, however, at the lower temperature where the low temperature transition was expected to occur. This is consistent with the DTA result that the low temperature anomaly is observed only in the heating run. The hysteresis was then studied by the heat capacity measurement. The crystal was first cooled down to 186.8 K, 6.2 K below the lower transition temperature. Subsequent measurement of the heat capacity gave the curve that joins smoothly to the heat capacity of the intermediate phase, as shown by the Series 2 curve in Fig. 4. The crystal was cooled then to 180.9 K and again the heat capacity was measured, giving the Series 3 curve. There occurred a small anomaly at 193.0 K in this series. Similar series of measurements after precooling to increasingly lower temperatures gave Series 4 (173.9 K)- and 5 (171.3 K)- curves in Fig. 4, respectively. In these measurements, the temperature drift was less than the observational limit, 0.1 mK h^{-1}. It is therefore concluded that the two phases (the intermediate and the low temperature phases) coexist side by side indefinitely in the temperature range between 193.0 K and the temperature of the precooling. The heat capacity values above 80.15 K plotted in Fig. 2 and given as the 3rd series in Table 2 pertain to the crystal cooled to 78 K and are believed to represent the crystal fully converted to the low temperature phase.

Thermodynamic Quantities. The tempered enthalpy, entropy and heat capacity of $(NH_4)_3[AlF_6]$ crystal are given in Table 3. These values refer to the stabilized crystal.

The Proton and Fluorine Nuclear Relaxation Times.† The

† More detailed NMR study was presented at the Symposium on Molecular Structures and Molecular Electronic States, Tokyo, 1976 (Title: "Nuclear magnetic relaxation and molecular motion of ^{1}H, ^{19}F, ^{27}Al in $(NH_4)_3[AlF_6]$" by Yoshihiro Furukawa, Hideko Kiriyama, Keiichi Moriya and Takasuke Matsuo).

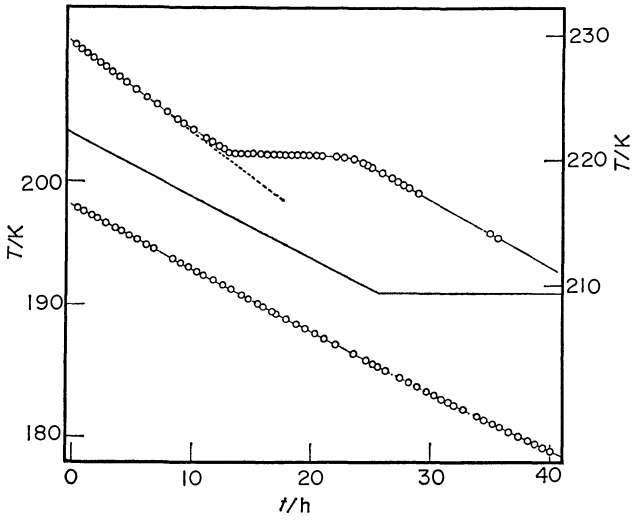

Fig. 3. Cooling curve of $(NH_4)_3[AlF_6]$.

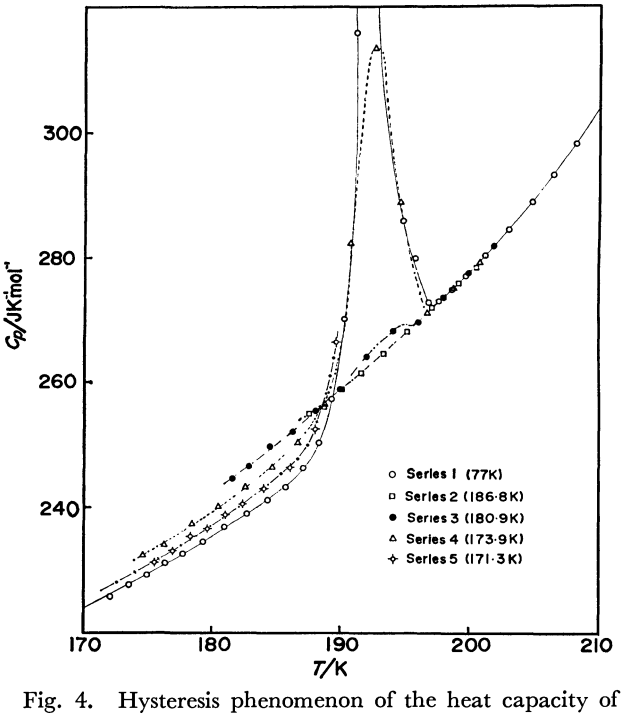

Fig. 4. Hysteresis phenomenon of the heat capacity of $(NH_4)_3[AlF_6]$ around the lower phase transition.

spin relaxation time T_1 was measured for the proton and fluorine nucleus by use of a pulse NMR spectrometer, Brucker Model BK-322S, in the temperature range between 15 and 350 K. The T_1 was measured at 60 and 20 MHz by the 180°-τ-90° method, and, at lower temperatures, by the 90°-τ-90° method. $T_{1\rho}$ in the rotating frame was also measured by the method of Look *et al.*[12] The powder sample was sealed in a thin-wall glass ampule of 5 mm diameter together with He gas. The sample temperature was measured with either a copper-constantan or copper cobalt-doped-gold thermocouples, depending on the temperature region. The temperature was stabilized at least 30 min in each of the measurements.

The T_1 and $T_{1\rho}$ for the proton are shown in Fig. 5. On cooling the crystal from the room temperature, T_1 decreased gradually and underwent a jump at 222 K to a lower value. The gradually decreasing portion of the curve was fitted to the Arrhenius equation and gave an activation enthalpy

Table 3. Thermodynamic function of $(NH_4)_3[AlF_6]$

T / K	C_p° / J K^{-1} mol^{-1}	$S^\circ - S_0^\circ$ / J K^{-1} mol^{-1}	$[H^\circ - H_0^\circ]/T$ / J K^{-1} mol^{-1}	$-[G^\circ - H_0^\circ]/T$ / J K^{-1} mol^{-1}
10	(1.24)	(0.30)	(0.31)	(0.10)
20	9.04	3.23	2.41	0.83
30	20.85	9.09	6.55	2.54
40	33.80	16.83	11.22	5.11
50	47.79	25.81	17.47	8.34
60	62.75	35.84	23.76	12.08
70	78.40	46.69	30.45	16.24
80	94.30	58.19	37.43	20.76
90	110.3	70.22	44.65	25.58
100	126.0	82.67	52.00	30.66
110	141.2	95.39	59.43	35.97
120	156.1	108.3	66.87	41.45
130	170.7	121.4	74.30	47.10
140	184.6	134.6	81.69	52.87
150	198.0	147.8	88.99	58.77
160	210.6	160.9	96.20	64.74
170	223.1	174.1	103.3	70.79
180	235.6	187.2	110.3	76.89
190	265.2	200.4	117.3	83.04
200	277.6	216.2	126.9	89.30
210	303.5	230.3	134.6	95.68
220	441.0	245.7	143.6	102.1
230	273.5	270.0	160.8	109.2
240	276.3	281.6	165.6	116.1
250	279.9	293.0	170.1	122.9
260	283.8	304.1	174.4	129.7
270	287.4	314.8	178.5	136.4
280	290.9	325.3	182.4	142.9
290	294.2	335.6	186.2	149.4
300	297.1	345.6	189.9	155.8
273.15	288.5	318.2	179.7	138.4
298.15	296.6	343.8	189.2	154.6

of 14.6 kJ mol^{-1}. The T_1 at 20 MHz reached the maximum value at approximately 357 K, indicating onset of another relaxation mechanism operating at higher temperature. The same relaxation mechanism showed itself in $T_{1\rho}$ which reached the maximum value at 250 K and decreased with the increasing temperature. The activation enthalpy derived from the $T_{1\rho}$ is 22.5 kJ mol^{-1}. This is assigned tentatively to diffusional motion of the ammonium ion, as the AC conductivity[13] increased rapidly above the room temperature.

In the intermediate phase, a T_1 minimum of the proton of 5.4 ms occurred at (200±2) K for $\omega_0/2\pi=20$ MHz. The corresponding T_1 minimum for $\omega_0/2\pi=60$ MHz, as calculated by the BPP equation, will be 16.2 ms and may be identified with the experimental value of 16.2 ms at (213±2) K.

The T_1 value shows a hysteresis at the lower transition consistently with the calorimetric observations. The cooling run gave slightly larger T_1. Below 200 K, T_1 remained more or less constant down to 78 K with shallow minima in the T_1 *vs.* $1/T$ curve. In the temperature range from 111 to 197 K, slight deviation from the exponential law was observed in the magnetization *vs.* τ curve. This may be reasonable in view of the presence of the proton and fluorine nuclei in the crystal. It was not possible, however, to evaluate separately the two T_1 values characterizing the cross relaxations. The values plotted in Fig. 5 are those of the faster relaxation process.

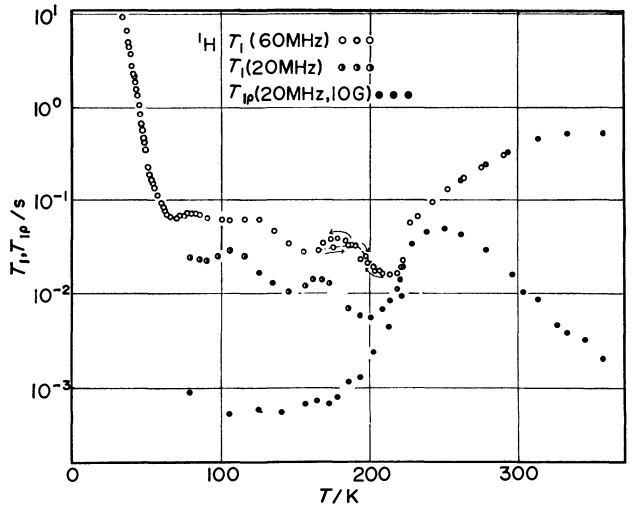

Fig. 5. Proton T_1 and $T_{1\rho}$ in $(NH_4)_3[AlF_6]$, plotted semi-logarithmically against temperature.

The temperature dependence of the fluorine T_1 (Fig. 6) is similar to that of the proton. In the high temperature phase, the T_1 at 20 MHz and 60 MHz are the same at least to 291 K. It increased with the increasing temperature,

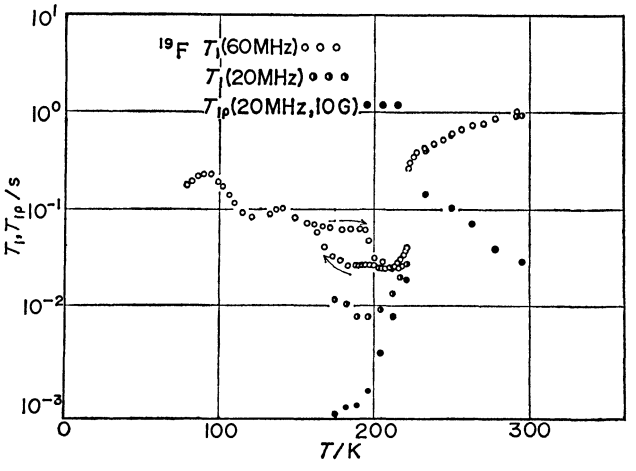

Fig. 6. Fluorine T_1 and $T_{1\rho}$ in $(NH_4)_3[AlF_6]$, plotted semi-logarithmically against temperature.

while the $T_{1\rho}$ measured at $H_1=10$ G decreased with the increasing temperature. There is a large jump of the fluorine T_1 at the upper transition temperature. The ratio of the T_1 of the high temperature phase to that of the intermediate phase at the transition temperature is four times as large for the fluorine resonance as for the proton. A T_1 minimum of 8.7 ms for 20 MHz occurred at (193±2) K. This value pertains to the intermediate phase because the data was taken in a cooling run. A hysteresis behavior was found again around the intermediate-to-the-low-temperature phase transition. The difference in the T_1 values obtained in the cooling and heating runs is larger for the fluorine resonance than for the proton.

Discussion

Heat Capacity of the High Temperature Phase. One does not expect that the heat capacity of a complex compound should be equal to the sum of the heat capacities of the components of the compound. However, approximate equality holds between the heat capacity of an alloy and that of the component metals and is known as the Neumann-Kopp law. We have examined the validity of the additivity of the heat capacity of the hexafluoroaluminates as shown in Fig. 7 where the difference (ΔC_p) between the experimental value and the Neumann-Kopp sum are plotted in ordinate. The heat capacity data were taken from Furukawa, Saba and Ford ($Li_3[AlF_6]$)[14], Clusius, Goldmann and Perlick (LiF)[15], and King ($Na_3[AlF_6]$, NaF, and AlF_3)[16]. ΔC_p is very small for these hexafluoroaluminates between 220 and 300 K considering that the total heat capacity amounts to 200 J K^{-1} mol^{-1} of $M_3[AlF_6]$, although the fractional difference increases with the decreasing temperature at lower temperature as Furukawa, Saba and Ford noted. Similar calculation was done for the high temperature phase of $(NH_4)_3[AlF_6]$ by using the present heat capacity data and those by Benjamins and Westrum (NH_4F)[17] and King (AlF_3)[16]. There is a large positive deviation from the Neumann-Kopp law as shown in Fig. 7. The internal vibrations of the $[AlF_6]^{3-}$ and NH_4^+ ions are practically independent of their environment as far as their contribution to the heat capacity is

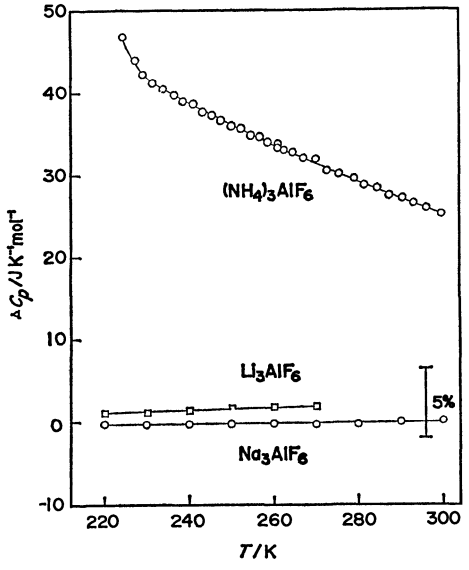

Fig. 7. Additivity of the heat capacity of hexafluoroaluminates.
$3C_p(3M(I)F)+C_p(AlF_3)=C_p(M(I)_3[AlF_6])$

concerned. One may, therefore, attribute the positive deviation from the Neumann-Kopp law to the difference in the external vibrations of the ammonium ions in NH_4F and $(NH_4)_3[AlF_6]$. There are two types of the external vibrations, translational and rotational. Translational vibrations of the cation are involved also in $Li_3[AlF_6]$ and $Na_3[AlF_6]$. But the Neumann-Kopp law holds to a good approximation for these substances. Therefore, the rotational motion of the ammonium ions is responsible to the non-additivity of the heat capacity. It is very reasonable to assume that the rotational motion of the ammonium ion is much more hindered in NH_4F than in $(NH_4)_3[AlF_6]$ in view of the strong NH···F hydrogen bonding in the former crystal[18]. The fluorine atoms in fluorocomplex ions such as $[SiF_6]^{2-}$, $[PF_6]^-$ and $[BF_4]^-$ are generally poor hydrogen-bond acceptors in comparison with the fluoride ion F^-, as is evident from the higher N–H stretching frequencies in these compounds.[19–21]

An estimate of the rotational heat capacity of NH_4^+ ion in $(NH_4)_3[AlF_6]$ crystal is obtained by addition of three times the rotational heat capacity of the ammonium ion in NH_4F to the heat capacity difference given in Fig. 7. The former is calculated by the harmonic approximation by using the three-fold degenerate frequency of 523 cm^{-1}.[18] The result of the calculation for the present crystal is plotted in Fig. 8 (data designated by (B)) for one mole of NH_4^+ ion.

A slightly different estimate of the rotational heat capacity is obtained by subtraction of the heat capacity of $Na_3[AlF_6]$ from that of $(NH_4)_3[AlF_6]$ and making a small correction for the internal vibration of the ammonium ion. This is equivalent to assuming that all the translational vibrations and the internal vibrations and rotational parts of the external vibrations of the $[AlF_6]^{3-}$ anion in $(NH_4)_3[AlF_6]$ crystal are the same as the corresponding vibrations in $Na_3[AlF_6]$ crystal, as far as their contributions to the heat capacity are concerned. The difference between the C_p and

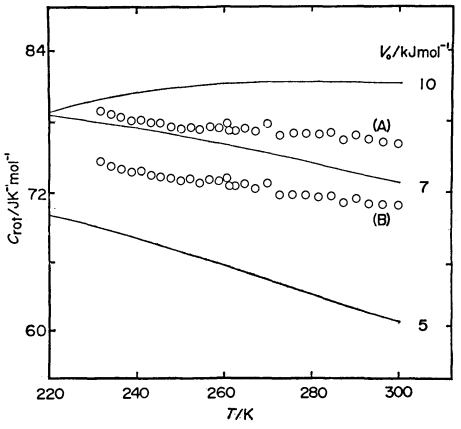

Fig. 8. NH_4^+ ion rotational heat capacity in $(NH_4)_3[AlF_6]$ by two methods
(A) $C_{rot}=C((NH_4)_3[AlF_6])-C(Na_3[AlF_6])-3C(NH_4^+$ internal).
(B) $C_{rot}=C((NH_4)_3[AlF_6])-C(AlF_3)-3C(NH_4F)+9C$(Harmonic, $\sigma=523$ cm^{-1}).

C_v is also assumed to cancel out by the subtraction. The estimated rotational heat capacity is plotted also in Fig. 8 as data (A). Accuracy of the assumptions made here is difficult to assess. But the good agreement of two independent estimates (difference 7%) indicates the essential correctness of the derived rotational heat capacity. The derived value is approximately equal to the heat capacity of three harmonic oscillators in the classical limit. However, it decreases with increasing temperature. This behavior is often observed in a high-temperature heat capacity of a hindered rotator. In Fig. 8, approximate calculations for the hindered rotational heat capacity are plotted for the hindering potential V_0 of 5, 7 and 10 kJ mol^{-1}. The calculation with $V_0=7$ kJ mol^{-1} reproduces fairly well the experimental heat capacity. Here, three dimensional rotation of the ion was approximated as the sum of one dimensional rotations[22] and the two ammonium ions at (1/2,0,0) and at (1/4, 1/4,1/4) were assumed to have the same heat capacity. In spite of these limitation one may conclude that the barrier hindering the rotation of the ammonium ion is much lower in $(NH_4)_3[AlF_6]$ than in NH_4F[23] for which the barrier height of 42 kJ mol^{-1} was reported. This may be another instance of a general observation that fluorocomplex ions are poor hydrogen-bond acceptors.

The activation enthalpy derived from the T_1 measurement, 14.6 kJ mol^{-1} differs from the calorimetric barrier height. Quantitative comparison of the two values will be justified when quantum mechanical calculation of three dimensional motion[24] of the ion is performed for the present compound.

Ionic Motion in the Intermediate and Low Temperature Phases. The T_1 minimum of the proton for $\omega_0/2\pi=20$ MHz indicates that the correlation time of the reorientational motion of the ammonium ion is 4.9 ns at (200±2) K. The activation enthalpy from the temperature dependence of T_1 near the minimum is ≈23 kJ mol^{-1} and the pre-exponential factor of the correlation time τ_0 4.8 fs. An approximately equal value is obtained from the T_1 value at 60 MHz. The minimum value of T_1, 5.4 ms, at 20 MHz is comparable with 3.1—4.3 ms calculated for a reasonable range of the proton–proton distance in ammonium ion by use of the BPP mechanism involving random reorientation of the ion.[25,26] The second moment of the proton resonance absorption is 5.4 G^2 in the intermediate phase[27] and supports the rapid reorientation model. In the calculation of the T_1 minimum all of the ammonium ions are assumed to have the same correlation time. The fair agreement of the experimental and calculated values appears to support this simplification. The relatively short T_1 found in the low temperature phase suggests the occurrence of some reorientational motion of the ammonium ions in this phase. However, detailed interpretation of the shallow T_1 minima is not possible at present because of lack of the structural information.

The T_1 minimum of 8.7 ms of the fluorine resonance occurs in the intermediate phase for $\omega_0/2\pi=20$ MHz. The activation enthalpy derived from the fluorine T_1 is 23 kJ mol^{-1} and equal to that derived from the proton T_1. This suggests that the same mechanism (reorientation of NH_4^+) is involved in the proton and fluorine relaxations, though reorientation of hexafluoroaluminate ion cannot be ruled out. In the cubic $(NH_4)_2[SiF_6]$, reorientation of $[SiF_6]^{2-}$ octahedron begins to take part in the fluorine relaxation above 360 K and the fluorine second moments retains its rigid lattice value up to 300 K.[28] On the other hand, fluorine T_1 minimum occurs in the temperature range 130—245 K for the low temperature phase of $Na[PF_6]$, $K[PF_6]$ and $Rb[PF_6]$.[29] These minima are caused by reorientation of the fluorine octahedron. In $NH_4[PF_6]$ both proton and fluorine T_1's show minima due to the reorientation of $[PF_6]^-$[30] at 125 K. The second moment of the fluorine resonance of $(NH_4)_3[AlF_6]$ is 3.1 G^2 in the intermediate phase.[23] It is evident that the $[AlF_6]^{3-}$ ion reorients rapidly and that the same motion can well contribute to the nuclear relaxation at some appropriate temperature. T_1 measurements of $(ND_4)_3[AlF_6]$ will be interesting in this respect. This will disentangle the probable complication arising from the motion of ammonium and hexafluoroaluminate ions and cross relaxation through the interaction of the proton and fluorine.

Increase of the proton T_1 in the temperature range 30—50 K gives an activation enthalpy of 2.5—3 kJ mol^{-1}. It is not clear if this really corresponds to a potential barrier hindering another reorientational motion of the ammonium ion. Effect of the tunnelling motion of the ammonium ion is excluded because the second moment of the proton resonance increases toward the rigid lattice value around 80 K[27] and the T_1 value becomes very high (≈100 s) at 15.8 K. Interestingly, the activation energy corresponds to 210—250 cm^{-1} of the wave number or the frequency of typical optical lattice vibration of translational or rotational origin. Physical implication of the coincidence of these two energy parameters is not clear at present.

Mechanism of the Phase Transitions. The enthalpy and entropy of the phase transitons were evaluated

Table 4. "Normal" heat capacity of $(NH_4)_3AlF_6$

T/K	C_p/J K^{-1} mol^{-1}	T/K	C_p/J K^{-1} mol^{-1}
150	196.5	210	254.4
160	207.9	220	261.6
170	218.7	230	268.0
180	228.7	240	273.8
190	237.9	250	279.2
200	246.5	260	283.6

Table 5. Phase transitions of $(NH_4)_3[AlF_6]$

T/K	ΔH/J mol^{-1}	ΔS/J K^{-1} mol^{-1}
193.0 ±0.3	790±150	4.2±0.8
220.79±0.05	4030±150	18.5±0.7

by integrating the excess heat capacity over the normal value. The normal heat capacity was determined by smooth interpolation of the low and the high temperature heat capacities into the anomalous region. The normal heat capacity employed here is given in Table 4. The entropies and enthalpies of both transitions are given in Table 5.

If one assumes that the orientation of the ions is uniquely fixed in the low temperature phase, the entropy of transition ΔS is related to the number W of different orientations allowed to the ions in the high temperature phase through the equation, $\Delta S = R \ln W$, provided that the vibrational entropy is adequately taken into account by the lattice heat capacity. The sum of the entropies of the two transitions (22.7± 1.5) J K^{-1} mol^{-1} corresponds to $W=15.3\pm3.0$. An approximately equal value was found for the entropy of transition in $(NH_4)_3[FeF_6]$.[6] One interpretation of $W=16$ is to ascribe it entirely to the disorder of the ammonium ion. $[AlF_6]^{3-}$ ion having the O_h symmetry occupies the site of O_h symmetry, the (0,0,0) position in the fcc Bravais lattice, and is assumed to have uniquely fixed orientation. There are two types of the ammonium ions, one in the (1/2,0,0) position and the other in the (1/4,1/4,1/4). One formula unit of $(NH_4)_3[AlF_6]$ contains one of the former ammonium and two of the latter. The experimental transition entropy may be interpreted formally by allowing four orientations to each of the former ammonium and two to the latter, or $W=4\times2\times2=16$. However, four equivalent orientations of the NH_4^+ ion in the (1/2, 0,0) position is inconceivable from the geometrical viewpoint. Moreover, absence of phase transitions in the cubic $(NH_4)_2[SiF_6]$ disfavors this model. In the cubic $(NH_4)_2[SiF_6]$, the ammonium ions are all equivalent and occupy the (1/4,1/4,1/4) positions. In this case the site symmetry is T_d so that the ammonium ions occupy the site without two-fold disorder. As will be discussed below, the ammonium ion in the (1/4,1/4,1/4) position appears to stabilize the cubic structure energetically. Another interpretation of $W=16$ proposed earlier[6] will be appropriate to the present crystal also. It involves orientational disorder of the $[AlF_6]^{3-}$ ion. Because of the O_h symmetry of the Al site, the orientational disorder has to be one-fold (ordered) or eight-fold. The latter corresponds to rigid rotation of the fluorine octahedron which shifts the fluorine atom from (x,0,0) to a general position. There are eight different orientations of this type.[6] Allowing two orientations to the (1/2,0,0) ammonium in conformity with the site (O_h) and ionic (T_d) symmetries one of which is related to the other by a 90° flipping, one obtains $8\times2=16$ states for one formula unit of $(NH_4)_3[AlF_6]$.

These two models of ionic disorder in the cubic phase predict the same entropy of transitions $\Delta S = R \ln 16 = 23.05$ J K^{-1} mol^{-1} which is in agreement with the experimental data. In addition to the symmetry argument, the NMR result favors the second model. It was pointed out that discontinuity in T_1 at the upper transition is much larger for the fluorine resonance than for the proton. One should not expect the large T_1 change in the fluorine resonance if the phase transition involved only the orientational disorder of the ammonium ions. Thus the NMR data supports the second model rather than the first.

Comparison with the Alkali Cryolites. As shown in Table 1, $(NH_4)_3[AlF_6]$ alone is cubic in the cryolite family at the room temperature. This high symmetry is a result of replacement of the spherical alkali ion by the tetrahedral ammonium ion. Three reasons may be advanced for explanation of this fact. The first is that the ammonium occupying the (1/4,1/4,1/4) position will stabilize the cubic structure. The twelve fluorine atoms surrounding the ammonium ion are grouped into four clusters of three. The four clusters, each belonging to different $[AlF_6]^{3-}$ ion, form a regular tetrahedron around the ammonium. The (1/2,0,0) ammonium and the equivalents occupy the corners of another tetrahedron which forms, together with the four aluminum atoms, the cube of the one-eighth volume of the fcc unit cell. Thus there are positive charges (NH_4^+ ions) at the four of the eight corners of the cube and negative charges (cluster of fluorine atoms) at the other four corners. The central ammonium ion will be situated stably in this tetrahedral field with its hydrogen atoms pointing toward the negative corners. Consequently, the cubic structure is stabilized by the presence of the (1/4,1/4,1/4) ammonium. This will also explain the fact that the cubic $(NH_4)_2[SiF_6]$ remains cubic at least down to 25 K:[31] the crystal has ammonium ions only in the (1/4,1/4,1/4) positions which favors the stability of the cubic lattice without orientational disorder. In alkali cryolites, the alkali ions in the (1/4,1/4,1/4) position do not offer any particular advantage for the cubic structure because the spherical alkali ions have no special reason to favor the tetrahedral environment. The structure of alkali cryolites will be dominated by the packing consideration and (at higher temperatures) by the entropy effect of the $[AlF_6]^{3-}$ disorder.

The second of the explanations for the stability of the cubic structure of the ammonium cryolite is that the orientational disorder of the (1/2,0,0) ammonium ion will decrease the free energy of the cubic phase relative to the non-cubic phase at sufficiently high temperature. Position of the (1/2,0,0) ammonium ion is not known at present. However, it will be reason-

able to suppose that orientational disorder (and decrease of the free energy) is possible only in the cubic phase, as the experimental transition entropy indicates. Such a stabilization of the cubic phase is not available to the alkali cryolites because alkali ions lack orientational degree of freedom. In passing it may be interesting to note here that $A[PF_6]$ crystals, where A is alkali or ammonium ion, are all cubic (except for Li salt) at room temperatures and undergo phase transitions at lower temperature.[1,29,30] It may be argued that orientational disorder of $[PF_6]^-$ ions stabilizes the cubic phase of these crystals.

Finally, the third of the factors contributing to the stability of the cubic ammonium cryolite is that the ionic radius of the ammonium ion may be favorable for the packing of the ions in the cubic lattice. Comparison of the unit cell dimensions of the ammonium, rubidium and caesium cryolites gives some support to this view. If we define the cubicity ratio $\gamma_c=c/(\sqrt{2}\,a)$ where a and c are unit cell lengths of the tetragonal crystal, we obtain $\gamma_c=1.0098$ for $Rb_3[AlF_6]$ and 0.9945 for $Cs_3[AlF_6]$ from the X-ray data of Holm.[32] Linear interpolation between the Rb and Cs gives $\gamma_c=1.0043$ for $(NH_4)_3[AlF_6]$ where the cubic cell dimension (0.893 nm) was taken from Steward and Rooksby.[7] The calculated cubicity ratio of the ammonium cryolite is not exactly equal but closer to the ideal cubic value 1 than the corresponding ratios of the rubidium and caesium cryolites are. Thus, it may be argued that as the size of cation increases the tetragonal cell changes from prolate to oblate and the ammonium happens to have the size that is favorable for the cubic packing. This will decrease the anisotropy of the environment of the ammonium ion and thus increase the tendency toward disordering of the ion discussed above.

We have presented triple reasons, the first energetic, second entropic and the third due to packing consideration, to explain the apparently contradictory fact that less symmetric ammonium ion forms more symmetric crystal in the cryolite family. Alkali cryolites undergo phase transition at higher temperatures.[32,33] It will be interesting to study the heat capacity of these substances to see if the orientational disorder of $[AlF_6]^{3-}$ ion proposed here will be substantiated by the experimental data for the entropy of transition.

Temperature Dependence of the Anomalous Entropy. In Fig. 9, the excess entropy $\Delta S(T)$ is plotted against the temperature. This quantity was calculated by integrating the excess heat capacity,

$$\Delta S(T) = \int^{T} \{\Delta C(T')/T'\} \cdot \mathrm{d}T'.$$

The anomalous entropy increases gradually in the intermediate phase and jumps discontinuously at the upper transition temperature to the high temperature value. Thus, the phase transition is of the first order in agreement with the T_1 discontinuity at the transition. The discontinuous part of the anomalous entropy is 13.2 J K^{-1} mol^{-1} in the total of 22.7±1.5 J K^{-1} mol^{-1}. This behavior is very similar to that observed in $(NH_4)_3[FeF_6]$[6] (discontinuity 18.5 J K^{-1} mol^{-1}, total 24.8±1.9 J K^{-1} mol^{-1}).

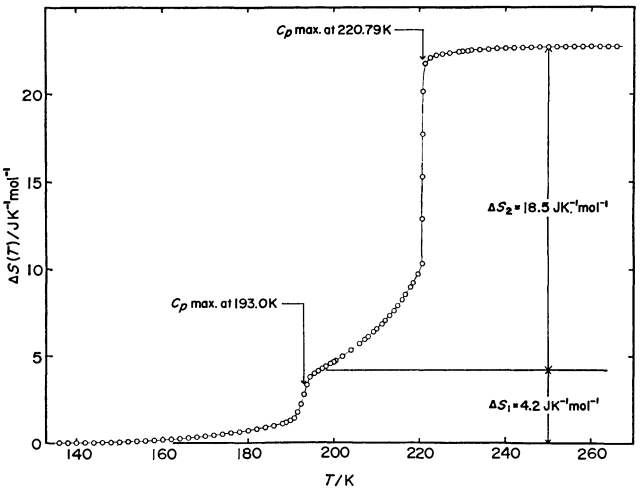

Fig. 9. Temperature dependence of the anomalous entropy $\Delta S(T)$.

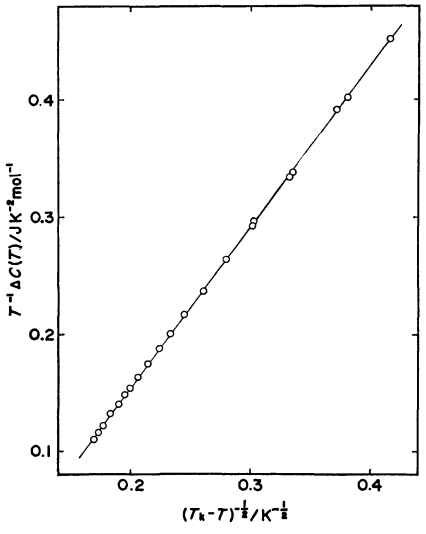

Fig. 10. $\Delta C(T)/T$ plotted against $(T-T_k)^{-1/2}$ with $T_k=224.9$ K.

The gradual increase of the entropy near the upper phase transition will be described by the Landau theory of the phase transition. The free energy of a crystal is expanded in powers of a certain order parameter.

$$G = (T-T_c)a\eta^2 + \frac{1}{2}b\eta^4 + \frac{1}{3}c\eta^6.$$

By differentiation of the free energy, one obtains the heat capacity. Figure 10 shows the plot of the anomalous encraty $(\Delta C_p/T)$ against $(T_k-T)^{-1/2}$ for $T_k=$ 224.9 K. The linearity of the plot between 190 K and 220 K is very satisfactory up to the onset of the first order transition. The parameter values derived from the best fit are as follows.

$a = 18.4\,\mathrm{J\,K^{-1}\,mol^{-1}}$, $b = -995\,\mathrm{J\,mol^{-1}}$, $c = 819\,\mathrm{J\,mol^{-1}}$.

In the lower temperature region between 180 K and 200 K of the intermediate phase where the extent of the disorder is small, the anomalous heat capacity will be expressed as

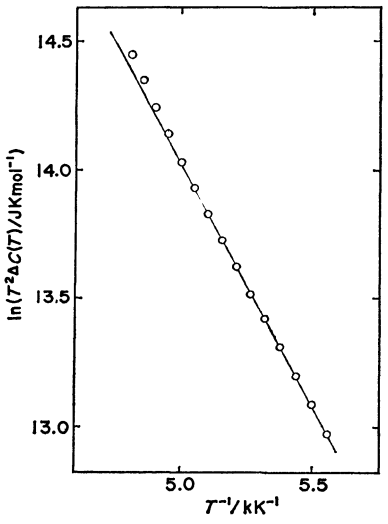

Fig. 11. $\ln(T^2\Delta C(T))$ plotted against inverse temperature.

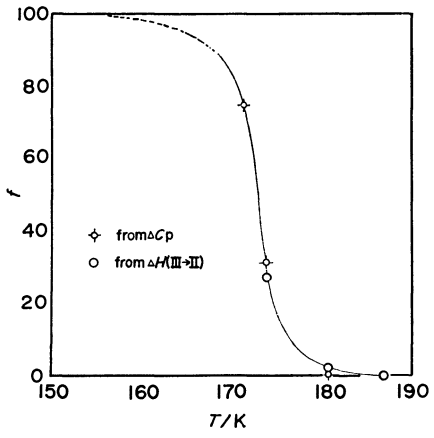

Fig. 12. Fraction of the low temperature phase *vs.* the lowest temperature to which the crystal was precooled before each measurement.

$$\Delta C(T) = R\left(\frac{\varepsilon}{RT}\right)^2 \exp[S^*/R]\cdot\exp[-\varepsilon/RT],$$

where R is the gas constant, S^* an entropic parameter (not equal to the total transition entropy and ε the molar energy required to excite the ion to the "misoriented" state in the ordered crystal. In Fig. 11, $\ln T^2\Delta C(T)$ is plotted against $1/T$. As expected the experimental heat capacity satisfies the linearity in this plot. The parameter values are $\varepsilon=15.6$ kJ mol^{-1} $S^*=51.8$ J K^{-1} mol^{-1}. In the same low temperature approximation, the anomalous entropy is given by the expression,

$$\Delta S(T) = R(\varepsilon/RT+1)\exp[S^*/R]\exp[-\varepsilon/RT].$$

By use of this equation, one can calculate the entropy which the crystal would acquire if the anomalous heat capacity of the intermediate phase continued down to zero Kelvin without being disrupted by the low temperature phase transition. $\Delta S(T=197.10\text{ K})$ calculated by this equation is equal to 2.86 J K^{-1} mol^{-1}, where the temperature 197.10 K corresponds to the minimum of the anomalous heat capacity just above the lower phase transition. The experimental value of the anomalous entropy (Fig. 9) determined by the integration of the anomalous heat capacity including that due to the lower phase transition is 3.2 J K^{-1} mol^{-1} at 197.10 K. Thus large fraction of the entropy of the lower phase transition is accounted for by the disrupted part of the upper phase transition.

It is tempting to assume that ammonium and hexafluoroaluminate ions contribute to the lower and the upper transitions separately, but the entropy of the lower transition is too small as compared with R ln 2 to support this view. At present we have no ready explanation to the fact that the phase transition in $(NH_4)_3[AlF_6]$ proceeds in two steps while the isomorphous $(NH_4)_3[FeF_6]$ has only one phase transition.

Undercooling of the Intermediate Phase. It was pointed out in the experimental section that the intermediate phase undercools and that the heat capacity of the intermediate phase was measured in its metastable temperature region. Undercooling of the present substance is very different in its character from that of typical first order transitions, *e.g.* crystallization of a simple liquid. Once the nucleation takes place in a typical undercooled liquid, the crystallization proceeds to completion consuming the liquid phase entirely, as the Gibbs phase rule dictates. In contrast, the present crystal exists in two different forms over a range of temperature. In Fig. 12, the fraction (f) of the low temperature phase is plotted against the temperature to which the crystal was cooled just before the heat capacity measurement. The measurement after precooling to 78 K gave the same heat capacity as after the precooling down to 13 K. This was taken to represent the completely transformed crystal. The fraction of the low temperature phase was calculated by two methods, one from the enthalpy of the low-temperature-to-intermediate phase transition and the other from the heat capacity difference at 184 K (see Fig. 4). The two methods gave a consistent result. A similar suspended phase change was reported in $K_4Fe(CN)_6\cdot 3H_2O$.[34] In this case, a monotropic transformation (in contrast to enantiotropic of the present crystal) from the metastable tetragonal phase to the stable low temperature phase stops in the midway depending on the temperature to which the tetragonal crystal is cooled. A simple interpretation of these anomalous metastabilities would be that slow atomic motion hinders the progress of the phase transition in these crystals. The fact that simple liquids never exhibit the anomalous metastability seems to support this interpretation because the molecular motion is certainly rapid there. However, the nuclear relaxation data presented above shows that the ionic motion is very rapid at the temperature where the under cooling of the intermediate phase occurs. Therefore the immobility of the ions cannot be the explanation of the anomalous metastability. It should be added that similar hysteresis phenomena have been reported in $Rb[PF_6]$ and $Cs[PF_6]$.[29,35] Most probably, interfacial and strain free energies caused by coexistance of the two phases will have to be taken into account for correct understanding of these phenomena.

We should like to express our best thanks to Professor Ryôichi Kiriyama, Professor Hideko Kiriyama and Dr. Masahiro Furukawa for the kind cooperation in the NMR measurement and for the fruitful discussion of the result. The X-ray powder photographs were taken with the help of Associate Professor Yôzô Chatani to whom we are grateful for his kindness. We are also indebted to Messers Masakazu Okumiya and Hiroshi Minari for the chemical analysis.

References

1) R. G. S. Morfee, L. A. K. Staveley, S. T. Walters and D. L. Wigley, *J. Phys. Chem. Solids*, **13**, 132 (1960).
2) J. Winter, K. Rossler, J. Bolz, and J. Pelzl, *Phys. Status Solidi B*, **74**, 193 (1976).
3) A. Sasane, D. Nakamura, and M. Kubo, *J. Magn. Reson.*, **3**, 76 (1970).
4) V. Novotny, C. A. Martin, R. L. Armstrong, and P. P. M. Meincke, *Phys. Rev. B*, **15**, 382 (1977).
5) Y. Furukawa, H. Kiriyama, and R. Ikeda, *Bull. Chem. Soc. Jpn.*, **50**, 1927 (1977).
6) K. Moriya, T. Matsuo, H. Suga, and S. Seki, *Bull. Chem. Soc. Jpn.*, **50**, 1920 (1977).
7) E. G. Steward and H. P. Rooksby, *Acta Crystallogr.*, **6**, 49 (1953).
8) S. Schwarzmann, *Fortschr. Mineral.*, **42**, 231 (1966).
9) The data are taken from H. Bode and E. Voss, *Z. Anorg. Allg. Chem.*, **290**, 1 (1957); D. Babel, *Structure and Bonding*, **3**, 21 (1967).
10) H. Suga, H. Chihara, and S. Seki, *Nippon Kagaku Zasshi*, **82**, 24 (1961).
11) T. Matsuo, H. Suga, and S. Seki, *J. Phys. Soc. Jpn.*, **30**, 785 (1971).
12) D. C. Look, I. J. Lowe, and J. A. Northby, *J. Chem. Phys.*, **44**, 3441 (1966).
13) Unpublished data by K. Moriya *et al.*
14) G. T. Furukawa, W. G. Saba, and J. C. Ford, *J. Res. Natl. Bur. Stand.*, **74A**, 631 (1970).
15) K. Clusius, J. Goldmann, and A. Perlick, *Z. Naturforsch., Teil A*, **4**, 424 (1949).
16) E. G. King, *J. Am. Chem. Soc.*, **79**, 2056 (1957).
17) E. Benjamins and E. F. Westrum, Jr., *J. Am. Chem. Soc.*, **79**, 287 (1957).
18) R. C. Plumb and D. F. Hornig, *J. Chem. Phys.*, **23**, 947 (1955).
19) M. Trefler and G. R. Wilkinson *Faraday Discuss. Chem. Soc.*, **48**, 108 (1969).
20) A. M. Heyns and G. J. van Schalkwyk, *Spectrochim. Acta, Part A*, **29**, 1163 (1973).
21) G. L. Cote and H. W. Thompson, *Proc. R. Soc. London, Ser. A*, **210**, 217 (1951).
22) K. S. Pitzer and W. D. Gwinn, *J. Chem. Phys.*, **10**, 428 (1942).
23) L. E. Drain, *Faraday Discuss. Chem. Soc.*, **19**, 200 (1955).
24) D. Smith, *Chem. Phys. Lett.*, **25**, 348 (1974).
25) C. A. McDowell, P. Raghunathan, and R. Srinivasan, *Mol. Phys.*, **29**, 815 (1975).
26) W. Mandema and N. J. Trappeniers, *Physica*, **76**, 102 (1974).
27) M. Guido and C. Franconi, *Ann. Chim. (Rome)*, **53**, 1048 (1963).
28) R. Blinc and G. Lahajnar, *J. Chem. Phys.*, **47**, 4146 (1967).
29) H. S. Gutowsky and S. Albert, *J. Chem. Phys.*, **58**, 5446 (1973).
30) S. Albert and H. S. Gutowsky, *J. Chem. Phys.*, **59**, 3585 (1973).
31) C. C. Stephenson, C. A. Wulff, and O. R. Lundell, *J. Chem. Phys.*, **40**, 967 (1964).
32) J. L. Holm, *Acta Chem. Scand.*, **19**, 261 (1965).
33) J. L. Holm, *Acta Chem. Scand.*, **20**, 1167 (1966).
34) M. Oguni, T. Matsuo, H. Suga, and S. Seki, *Bull. Chem. Soc. Jpn.*, **48**, 379 (1975).
35) L. A. K. Staveley, N. R. Grey, M. J. Layzell, *Z. Naturforsch., Teil A*, **18**, 148 (1963).

Film Dichroism. II. Linearly-polarized Absorption Spectra of Acridine Dyes in the Stretched Poly(vinyl alcohol) Films[1)]

Yukio MATSUOKA and Kiwamu YAMAOKA*

Faculty of Science, Hiroshima University, Higashisenda-machi, Hiroshima 730

(Received January 5, 1979)

The linear dichroic absorption spectra of the protonated and quaternized acridine dyes were measured in the UV and visible regions by the stretched film technique. The dyes examined were acridine, 10-methylacridine, Proflavine, Trypaflavine, Acridine Yellow, 10-Methylacridine Yellow, Acridine Orange, and 10-Methylacridine Orange, all of which belong to the C_{2v} point symmetry group. Poly(vinyl alcohol) was used as a film matrix. The absorption spectrum of each dye was resolved into the long-axis and short-axis polarized components. Two orthogonally-polarized electronic transitions (the ^1L_a and ^1L_b bands) of 3,6-disubstituted acridine dyes were reduced to overlap in the visible region of the spectra. The orientation factors K_y and K_z of each dye were evaluated at a constant degree of stretching and were related to the geometry of the dye molecule.

Studies of the interaction between acridine dyes and natural or synthetic polymers have been carried out by various optical methods.[2-8)] However, the optical properties of the dyes *per se* were treated qualitatively in those studies. To obtain useful and unambiguous information on the optical properties of those polymer-dye complexes, it is imperative to accumulate the detailed data on the polarization direction of the electronic bands of individual dyes.[9-11)]

One promising technique is the measurement of the linear dichroism of dyes oriented in a film by mechanical stretching. The importance of this method has been recognized in the assignment of the polarization directions of absorption bands.[12-18)] Tanizaki[12)] derived a theoretical expression which relates the dichroic ratio to the stretch ratio of a matrix film, and applied it to the absorption band of naphthols[13)] and acridine[14)] to determine the relative directions of their transition moments. Thulstrup *et al.*[15)] reported a method (the reduction procedure) for the quantitative evaluation of "reduced spectra" from the dichroic absorption spectra of planar molecules belonging to the C_{2v} or D_{2h} point symmetry group.

The first paper of this series has established the groundwork for the measurement and analysis of the dichroic spectra.[19)] The purposes of this paper are, therefore, (1) to determine the relative direction of the transition moment of eight acridine dyes,[20,21)] (2) to divide the isotropic spectrum of each dye into the long-axis and short-axis polarized components (the reduced spectra), (3) to evaluate the orientation factors K_y and K_z for each dye, and (4) to relate the molecular shape of the dye with the orientation factors. The major findings are as follows: (1) Isotropic spectra of acridine and 10-methylacridine contain a short-axis polarized (^1L_a) and two long-axis polarized transitions (^1B_b and ^1L_b). (2) The isotropic spectrum of each 3,6-disubstituted acridine dye consists of two orthogonally-polarized transitions (^1B_a and ^1B_b) in the UV region, a dominant long-axis polarized transition (^1L_b) and a weak short-axis polarized transition (^1L_a) in the visible region. (3) The values of K_y and K_z obtained for acridine and 10-methylacridine change remarkably upon substitution of the amino or dimethylamino groups at the 3,6-positions of the acridine nucleus. (4) Both Acridine Yellow and 10-Methylacridine Yellow behave like a rod-shaped molecule as regards their orientation property.

Experimental

Materials. Acridine dyes were all in the monocationic form, the anion being chloride (for details, see Ref. 20): Acridine (Acr) and 10-methylacridine (MeAcr), 3,6-diaminoacridine or Proflavine (PF) and 3,6-diamino-10-methylacridine or Trypaflavine (TF), 3,6-diamino-2,7-dimethylacridine or Acridine Yellow (AY) and 3,6-diamino-2,7-dimethyl-10-methylacridine or 10-Methylacridine Yellow (MeAY), 3,6-bis(dimethylamino)acridine or Acridine Orange (AO) and 3,6-bis(dimethylamino)-10-methylacridine or 10-Methylacridine Orange (MeAO). All these dyes were purified by recrystallization from ethanol and their purity was confirmed by the method of thin layer chromatography. The powdered poly(vinyl alcohol) (PVA) samples were obtained from Tokyo Kasei Co., Ltd., and Kuraray Co. (Kuraray Poval 117-H). Their nominal degrees of polymerization were 1750 and 1680, respectively.

Preparation of Sample Films. A stock aqueous PVA solution (*ca.* 9.1 wt %) was prepared as described elsewhere.[19)] To the stock PVA solution (5×10^{-2} dm^3), an aqueous dye solution (*ca.* 1×10^{-3} mol dm^{-3}) was added dropwise. The mixture was then stirred for 20—30 min to make a dye-PVA solution (the final dye concentration was about 1×10^{-5} mol dm^{-3}). (Each solution spectrum was measured at this stage to compare with the corresponding film spectrum.) To prepare a nonoriented sample film, the dye-PVA solution was spread onto a glass plate and kept for 7—10 days in an open room to ensure dryness. The glass plate was adjustable horizontally by screws and equipped with four removable sides (10×10 cm) which allowed the dried film to be detached easily from the glass surface. The reference film was prepared from an aqueous PVA solution which contained no dye under the same conditions.

Measurements and Analyses of Dichroic Spectra. Dichroic spectra were measured on a Hitachi EPS-3T double beam recording spectrophotometer equipped with a mechanical stretcher that could stretch both sample and reference films simultaneously inside the cell compartment.[19)] In each optical path, a schlieren-free grade Glan-Taylor calcite polarizer (Karl Lambrecht Corp., Chicago) was mounted in front of the stretcher. The stretch ratio, S, of the film was defined as the axial ratio, a/b, (a and b are the semi-major and -minor axes) of an ellipse deformed from a circle of radius r which was initially drawn on the film.[12,19)] Uniform stretching of the film was tested at each S by comparing an imaginary volume of $4\pi ab^2/3$ with the initial volume of $4\pi r^3/3$. These two volumes agreed within an experimental

uncertainty of 4%.

The absorbances of dye molecules in the film, with polarizers arranged parallel, $A_{\parallel}$ and perpendicular, $A_{\perp}$ to the direction of stretch, should satisfy the relation

$$k \times A_0 = \frac{A_{\parallel} + 2A_{\perp}}{3} \tag{1}$$

where k is the normalization factor, which depends on S, and A_0 is the absorbance of the nonstretched film. The dichroic ratio, R_d, or the reduced dichroism, $\Delta A/A$, of partially oriented rod-shaped molecules can be related to the transition moment angle, θ, which is defined as the angle between the direction of the transition moment and the orientation axis of a molecule, as[19,22]

$$R_d = \frac{A_{\parallel}}{A_{\perp}} = \frac{2+2(3\cos^2\theta-1)\Phi}{2-(3\cos^2\theta-1)\Phi}, \tag{2}$$

or

$$\frac{\Delta A}{A} = \frac{3(A_{\parallel}-A_{\perp})}{A_{\parallel}+2A_{\perp}} = \frac{3}{2}(3\cos^2\theta-1)\Phi, \tag{3}$$

where Φ is called the *orientation function* which represents the degree of orientation of an assembly of like molecules. An orientation function was derived for the rod-shaped molecule as[19]

$$\Phi(S) = \frac{3}{2}\frac{S^2-S^2(S^2-1)^{-1/2}\tan^{-1}(S^2-1)^{1/2}}{S^2-1} - \frac{1}{2}. \tag{4}$$

By using Eqs. 2 and 4 or Eqs. 3 and 4, the transition moment angle can be determined according to the method of Tanizaki.[12]

Since the acridine dyes studied in the present work belong to the C_{2v} point symmetry group, the reduction procedure[15] can be employed for evaluating the A_y-spectrum (the short-axis polarized component of isotropic spectrum) and the A_z-spectrum (the long-axis polarized component) from the observed dichroic spectra. In the spectral region between 220 and 550 nm, the out-of-plane polarized component may be ignored (*i.e.*, $A_x=0$); therefore, if the molecules in the film are oriented uniaxially, the formulas necessary for the procedure are as follows:[15]

$$A_{\perp} - d_{\perp}A_{\parallel} = \frac{K_z-K_y}{2K_z}A_y$$

and (5)

$$A_{\parallel} - d_{\parallel}A_{\perp} = \frac{K_z-K_y}{1-K_y}A_z,$$

where $d_{\perp}$ and $d_{\parallel}$ are the reduction factors. The constants K_y and K_z are termed the *orientation factors* and are given by[15]

$$K_y = \frac{d_{\parallel}}{d_{\parallel}+2} \quad \text{and} \quad K_z = \frac{1}{2d_{\perp}+1} \tag{6}$$

Results and Discussion

Isotropic, Dichroic, and R_d-Spectra. Figures 1 to 4 show the *dichroic spectra, i.e.*, the $A_{\parallel}$-spectrum (dotted curve) and the $A_{\perp}$-spectrum (dashed curve), of eight acridine dyes at a particular stretch ratio, together with the wavelength dependence of the dichroic ratio R_d (filled circles), which is termed the R_d-spectrum. An error bar on the dichroic ratio indicates the experimental uncertainty. The dichroic ratio can be converted into the reduced dichroism,[19] which should be referred to the left ordinate of each figure. Two

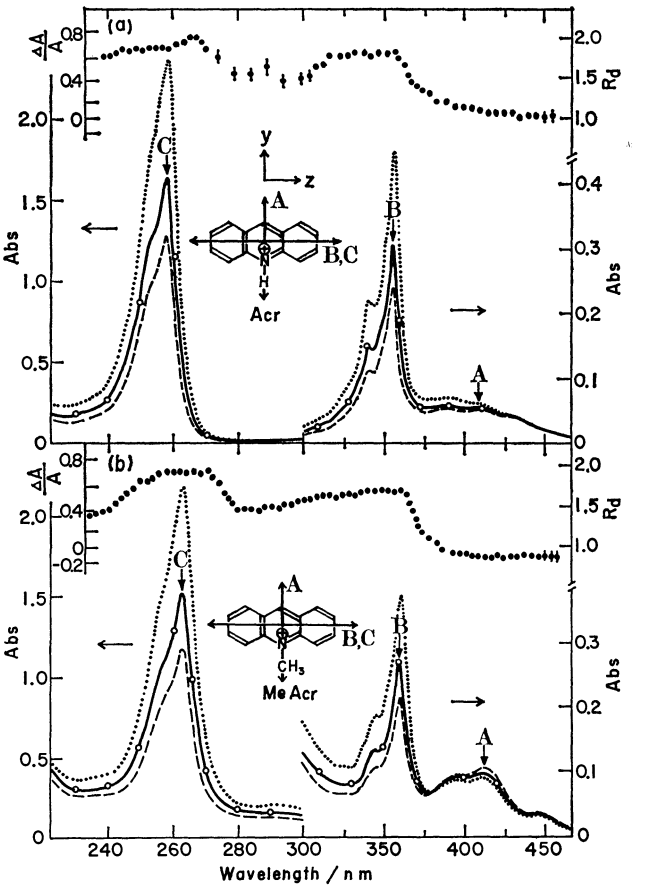

Fig. 1. Isotropic, dichroic, and R_d-spectra of Acr and MeAcr in the stretched PVA film. Symbols are: the isotropic spectrum (——), the parallel (·····) and perpendicular (----) polarized spectra, the R_d-spectrum (••••) and the normalized isotropic absorbance (○). Letters **A** to **F** indicate the apparent peak or shoulder positions in each isotropic spectrum and the polarization directions in the acridine nucleus. Acr at $S=4.3$ and $\bar{k}=0.62$. MeAcr at $S=4.3$ and $\bar{k}=0.65$. Factor $\bar{k}$ is an average of the values of k at about 30 wavelengths.

kinds of isotropic spectra are also shown in each figure: one, $k\times A_0$ (open circles), was obtained from the left hand side of Eq. 1 and the other, A (solid curve), was calculated from the right hand side of the same equation. An excellent agreement between these two isotropic spectra suggests that the dye molecules are indeed oriented uniaxially in the stretched film. The observed isotropic spectra of all the acridine dyes in the PVA film were similar to the spectra of the dyes in aqueous PVA solution. The apparent band positions of each dye are shown in Table 1.

The dye AO has drawn special attention because of its strong ability of dimerization in aqueous solution. The "monomer" spectrum, which was unmasked by the monomer-dimer analysis, gave a value of 1.5—1.6 for the ratio of the peak intensity (492 nm) to the shoulder intensity (≈470 nm).[23,24] The spectrum of AO in an aqueous PVA solution (2.5×10^{-5} mol dm^{-3} in 9.1 wt %) also gave nearly the same value, which indicates AO is probably in the monomeric form.

Table 1. The apparent band positions (**A**—**F**) in the isotropic spectra and the transition moment angles (θ_A—θ_F) at the corresponding band positions of eight acridine dyes

Dyes	Positions[a]/nm			Angles/deg		
	A	**B**	**C**	θ_A	θ_B	θ_C
Acr	408 (403)	356 (354)	258	54±1	41±1	40±1
MeAcr	412 (416)	360 (358)	263	58±1	40±1	38±1
	D	**E**	**F**	θ_D	θ_E	θ_F
PF	465 (452)	305	263 (261)	8±2	—	22±2
TF	470	305	265	8±2	—	24±2
AY	467 (453)	314	266 (265)	—	—	—
MeAY	471 (461)	317	270 (267)	8±2	—	23±2
AO	502 (496)	330	272 (271)	12±2	70±2	23±2
MeAO	506 (500)	335	274 (272)	10±2	—	27±2

a) The values in the parentheses are the corresponding positions in the aqueous PVA solution.

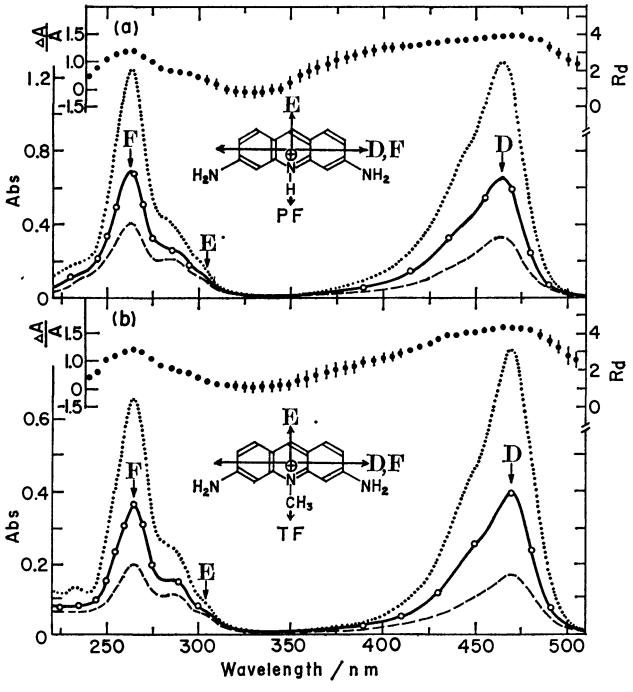

Fig. 2. Isotropic, dichroic, and R_d-spectra of PF and TF in the stretched PVA film. Symbols are the same as in Fig. 1. PF at $S=3.7$ and $\bar{k}=0.65$. TF at $S=3.7$ and $\bar{k}=0.65$.

In the isotropic spectrum of AO in the PVA film (Fig. 4a), the ratio was as high as 2.0. This value compares favorably with the values of 2.1 in chloroform ($1—10\times10^{-6}$ mol dm^{-3}) and 1.9 in ethanol (2×10^{-5} mol dm^{-3}). These data suggest that AO is also in the monomeric form in the PVA film. Results similar to the above were observed for such associative dyes as PF,[25,26] TF,[26] and MeAO. Therefore, the isotropic spectra in Figs. 1 to 4 were concluded to be essentially the monomer spectra of the respective dyes.

Acridines: Both the dichroic and R_d-spectra of Acr and MeAcr are shown in Fig. 1. In order to ascertain that Acr is fully protonated, an appropriate amount of HCl (0.1 mol dm^{-3}) was added to the aqueous dye–PVA solution prior to casting. The isotropic spectrum of Acr in the film resembles the solution spectrum of the acridinium ion. The $A_\parallel$-spectrum of Acr is always more intense than the $A_\perp$-spectrum, except for the long-wavelength region. The R_d-spectrum of Acr is nearly flat in 460—400 nm ($R_d=1.0$—1.1) and again in 360—320 nm ($R_d\approx1.7$), sharply changing at about 370 nm. Another plateau region is observed in 260—240 nm ($R_d\approx1.8$). These dichroic features are in excellent agreement with a previous report.[27] The isotropic spectrum of MeAcr shifts toward the red, as compared with the spectrum of Acr, because of the substitution of a methyl group on the ring nitrogen. The R_d-spectrum is constant over 460—390 nm ($R_d\approx0.9$), 360—330 nm ($R_d\approx1.8$), and 270—250 nm ($R_d\approx1.9$).

3,6-Diaminoacridines: Figure 2 shows the dichroic and R_d-spectra of PF and TF, which are 3,6-diamino derivatives of Acr and MeAcr, respectively. The isotropic spectra of PF and TF differ from those of Acr and MeAcr in that PF and TF show a deceptively simple absorption peak in the visible region and two conspicuous shoulders in 280—320 nm. In spite of the simple isotropic absorption in the visible region, the R_d-spectra of PF and TF are not flat: the largest values occur near 465 nm and 470 nm, respectively. They descend rather sharply on the long-wavelength side and slowly but irregularly on the short-wavelength side. These descending trends are well beyond the experimental uncertainty.

3,6-Diamino-2,7-dimethylacridines: Figure 3 shows the dichroic data of AY and MeAY, which are 3,6-diamino-2,7-dimethyl derivatives of Acr and MeAcr, respectively. In the isotropic spectrum of AY, there are at least three humps at *ca.* 445, 428, and 400 nm, and a shoulder at *ca.* 255 nm. The profile of the isotropic spectrum of MeAY resembles that of AY in the visible and UV regions. A new feature was discovered for MeAY in the 340—310 nm region, where the $A_\perp$-spectrum is more intense that the $A_\parallel$-spectrum (inset of Fig. 3). Such a reverse trend is always found for more heavily substituted dyes, such as AO and MeAO. The R_d-spectra of AY and MeAY give the highest value near the main peak in the visible region and show the lowest value in the 340—310 nm region.

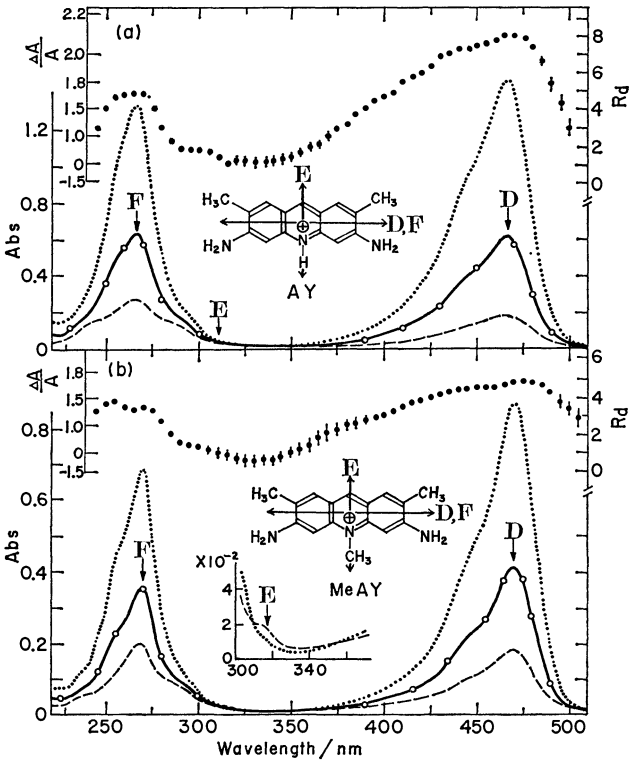

Fig. 3. Isotropic, dichroic, and R_d-spectra of AY and MeAY in the stretched PVA film. Symbols are the same as in Fig. 1. AY at $S=4.3$ and $\bar{k}=0.57$. MeAY at $S=4.3$ and $\bar{k}=0.62$.

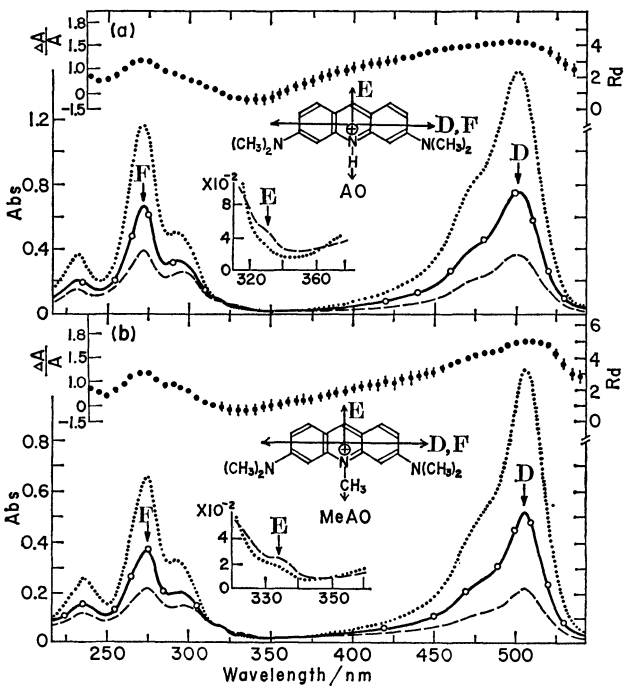

Fig. 4. Isotropic, dichroic, and R_d-spectra of AO and MeAO in the stretched PVA film. Symbols are the same as in Fig. 1. AO at $S=4.3$ and $\bar{k}=0.55$. MeAO at $S=4.3$ and $\bar{k}=0.60$.

Especially, the R_d-value becomes smaller than unity for MeAY, indicating that a weak absorption band exists in 340—310 nm. On the analogy of the R_d-spectrum of MeAY in 340—310 nm, all AY, TF, and PF should also have such a weak band in the same region.

3,6-Bis(dimethylamino)acridines: The dichroic and R_d-spectra of AO, which is the 3,6-bis(dimethylamino) derivative of Acr, are shown in Fig. 4a. The $A_\parallel$-spectrum is more intense than the $A_\perp$-spectrum in the entire spectral region, except for the 360—320 nm region, where the behavior of the $A_\parallel$- and $A_\perp$-spectra is reversed. Such a reverse trend has also been reported.[28,29] The R_d-spectrum of AO descends on the long-wavelength side of the 502 nm principal band, while it decreases irregularly on the short-wavelength side and becomes smallest at *ca.* 330 nm. Figure 4b shows the dichroic data of MeAO. The isotropic spectrum of MeAO is bathochromic relative to AO; the spectral features are almost the same. The reverse trend of the dichroic spectra was also observed in the 350—320 nm region. The changes in the R_d-spectrum on both sides of the 506 nm principal band become more pronounced than those of AO. The change of the R_d-spectrum of MeAO in the visible region can be explained reasonably well by introducing the short-axis polarized transition (the ^1L_a band) with a vibrational structure which is overlapped by the 506 nm band (the ^1L_b band). Similar interpretations can be put on the changes of the R_d-spectra of all 3,6-disubstituted dyes: AO, AY, MeAY, PF, and TF.

Determination of Transition Moment Angles. If a planar molecule has at least one C_2 symmetry axis in the molecular plane, the observed isotropic spectrum can be divided into two components (*i.e.*, the divided spectra)[13] which are polarized parallel and perpendicular to the symmetry axis, respectively. In order to obtain the divided spectra of each acridine dye, the transition moment angle must be evaluated correctly.[13,30] For this purpose, the dichroic spectra were analyzed, in the first place, by Tanizaki's method.[12] As examples, the dependences of R_d (and $\Delta A/A$) on S are shown for Acr and AY in Fig. 5. The transition moment angles, θ, relative to the orientation axis are given in Table 1, together with those of the remaining acridine dyes.

The sums of the transition moment angles of θ_A and θ_C, and θ_A and θ_B, for Acr are 94° and 95°, respectively. These values are in good agreement with the results obtained by Yoshino *et al.*,[27] and assure the equal precision of the experimental procedures of the present work. From the symmetry consideration, the transition moments of the **A** and **C** bands of Acr or MeAcr (each band can be regarded as a single transition from the flatness of the R_d-spectrum) should be orthogonal *i.e.*, $\theta_A+\theta_C=90°$. However, the values are 94° for Acr and 96° for MeAcr, always larger than 90°. The deviation from the orthogonality is more conspicuous for MeAcr than Acr; this implies that those transition moment angles contain some kind of systematic error which is associated with the molecular shape, *i.e.*, the shape of Acr or MeAcr can not be generally represented by a rod, but is more likely to be planar. The most unrealistic example is AY, for which the dependence of R_d (or $\Delta A/A$) on S at position **D** exceeds the theoretically permissible curve

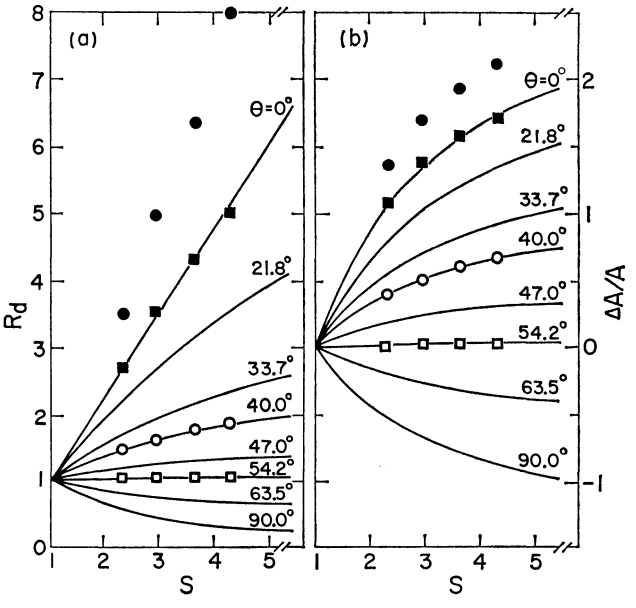

Fig. 5. Dependence of (a) the observed R_d and (b) $\Delta A/A$ on S for Acr and AY. Symbols (□ and ○) denote the values of Acr at wavelength positions **A** and **C**; and (■ and ●) denote the values of AY at **F** and **D**, respectively. Solid curves are theoretical and calculated with the angle θ specified for respective curves by the use of Eqs. 2, 3, and 4.

($\theta=0°$), as shown in Fig. 5. In fact, the R_d-values of AY are very large in the visible absorption peak, as compared with those of PF and AO. (The dichroic spectra of AY were measured several times to confirm the reproducibility of the R_d-values.)

The above findings suggest that the orientation function given by Eq. 4 does not represent the degree of orientation of AY and Acr correctly. Since this equation was derived from the distribution of unit vectors and contains the variable S only, no consideration has been given to the geometrical shape of a particular guest molecule. For instance, the large R_d-values of AY at two main peaks (467 and 266 nm), as compared with those of MeAY, can be accounted for by assuming that AY is better oriented than MeAY at a given S. Hence, the actual orientation mechanism of dyes in the stretched polymer film seems to be more complex than that described by the orientation function (Eq. 4). The stretch ratio S may need a more critical evaluation: the true stretch ratio for AY could possibly be greater than the macroscopic S. The discrepancy between the true and calculated angles of a transition moment may become pronounced, if any transition moment of the molecule is nearly parallel or perpendicular to the orientation axis, *i.e.*, if the angle θ approaches either 0° or 90°. Because of the reasons cited in this section, the reduction procedure,[15] which does not need to assume the degree of orientation of the guest molecules, was employed to determine the reduced spectra of each dye.

Reduced Spectra of Eight Acridine Dyes. Since each dye belongs to the C_{2v} point symmetry group, its transition moment should be in the molecular plane and along the long (z) or short (y) axis in the visible and UV regions. According to many film dichroism measurements, the molecules embedded in the PVA matrix are generally known to orient predominantly with their long axes aligned to the direction of stretch. This means that an absorption band whose transition moment is polarized along the long axis rather than the short axis should give a larger R_d-value. For example, in the dichroic spectra of Acr and MeAcr (Fig. 1), the change of each R_d-curve indicates the existence of at least one short-axis polarized (denoted as **A**) and two long-axis polarized (denoted as **B** and **C**) transitions. In contrast, the R_d-curves of the 3,6-disubstituted acridine dyes (Figs. 2 to 4) reveal the existence of at least one short-axis polarized (**E**) and two long-axis polarized (**D** and **F**) transitions. On the basis of these apparent spectral features, the reduced spectra of each dye were determined with a HITAC-8700 computer according to the reduction procedure.[15]

The resultant reduced spectra of Acr are shown in the upper half of Fig. 6a. As expected from Fig. 1, the A_z-spectrum (solid curve) gives rise to two strong long-axis polarized transitions at *ca.* 356 and 258 nm (the ^1L_b and ^1B_b bands), while the A_y-spectrum (dotted curve) manifests a short-axis polarized transition at *ca.* 408 nm (the ^1L_a band). These assignments are in excellent agreement with the results of fluorescence polarization[31] and film dichroism.[27] It is interesting to note that the A_y-spectrum is much better resolved with the reduction procedure than the D_y-spectrum,[27] which appears to contain some remaining contributions from the intense D_x-spectrum between 370 and 320 nm. The reduced spectra of MeAcr are shown in the lower half of Fig. 6a. Just as noted for Acr, the A_z-spectrum of MeAcr gives two long-axis polarized transitions at *ca.* 360 and 263 nm (the ^1L_b and ^1B_b bands), whereas the A_y-spectrum shows a short-axis polarized transition at *ca.* 412 nm (the ^1L_a band).[32] The higher-energy transition polarized along the short axis (the ^1B_a band) is rather obscured in the reduced spectra, but can possibly be at 260 nm for Acr and at 280 nm for MeAcr, as was shown for Acr previously,[27] or it may be hidden in the higher-energy region, as in anthracene.[33]

The reduced spectra of 3,6-disubstituted acridine dyes are shown in Figs. 6b to 6d. As already expected from the R_d-spectra in Figs. 2 to 4, there are generally two strong long-axis polarized transitions (the ^1L_b and ^1B_b bands) in the A_z-spectrum and a short-axis polarized transition (the ^1B_a band) in the A_y-spectrum.[34] In addition to these transitions, there is definitely a short-axis polarized, weak transition (probably the ^1L_a band)[34] in the visible region, the presence of which has long been a point of controversy.[35] It should be this transition, hidden in the isotropic spectrum, that is responsible for the decrease in the R_d-values on both sides of the principal peak in the visible region.

From comparison of the reduced spectra between Acr and PF or between MeAcr and TF, it is clear that the ^1L_a and ^1L_b bands of Acr or MeAcr are shifted, on the substitution of amino groups at 3,6-positions, toward the long wavelength in such a way that the ^1L_b band overtakes the ^1L_a band.[36] The ^1B_a transition is definitely unraveled in the UV regions of PF and

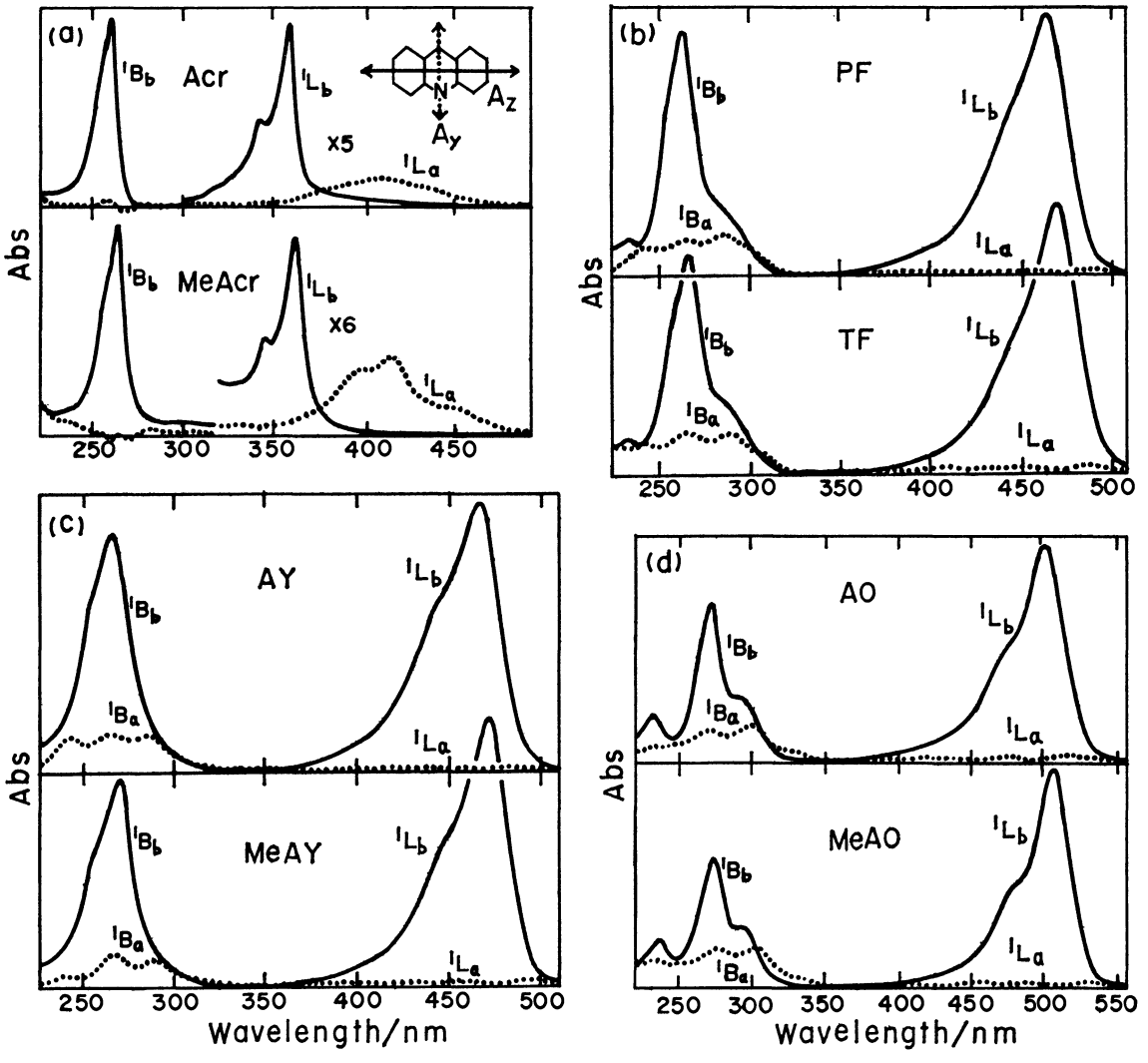

Fig. 6. The reduced spectra (the A_z-spectrum and the A_y-spectrum) of eight acridine dyes at $S=4.3$. The long-axis (z-axis) and short-axis (y-axis) polarized absorbances (arbitrary units) are shown by the solid and the dotted curves, respectively. (a) Acr and MeAcr (The absorbance between 320 and 480 nm is expanded as indicated.), (b) PF and TF, (c) AY and MeAY, and (d) AO and MeAO.

TF, in contrast to the reduced spectra of Acr and MeAcr. These features of the reduced spectra are also evident from Figs. 6c and 6d for AY and AO relative to Acr and for MeAY and MeAO relative to MeAcr.

The A_y-spectrum of AO shows the ^1L_a band in 550—400 nm (probably the 0-0 transition near 518 nm). This 0-0 transition of the ^1L_a band is mostly responsible for the decrease of the R_d-spectrum of AO (also PF, TF, AY, MeAY, and MeAO) on the long-wavelength side of the visible peak. In 350—310 nm, the A_y-spectra of AO and MeAO are more intense than the corresponding A_z-spectra. This trend is in excellent accord with the result that the R_d-spectra of AO and MeAO become smallest at *ca.* 330 nm. (This statement is also valid for PF, TF, AY, and MeAY.) Since the 330 nm band is expected to be an in-plane transition, it may be assigned to be the 0-0 transition of the ^1B_a band.

A comprehensive assignment of polarization was tentatively carried out for the reduced spectra of 3,6-disubstituted acridine dyes on the basis of the data of Acr and MeAcr. In order to obtain the complete and detailed assignment of all the transition moments of those dyes, each reduced spectrum should be resolved into individual component bands, the isotropic spectrum should then be reconstructed from those decomposed bands, and above all, the observed R_d-spectrum should be reproduced fully by simulation. The details will be reported shortly.

Relation between Molecular Shape and Orientation Factors. The orientation factors K_y and K_z were determined from the reduction factors $d_\parallel$ and $d_\perp$ with the aid of Eq. 6. The values of $d_\parallel$, $d_\perp$, K_y, and K_z obtained for each dye at $S=4.3$ are listed in Table 2. In order to find out the relation between the molecular shape and the orientation factors, the points (K_y,K_z) for all the dyes are plotted in Fig. 7. All these points lie either inside or on the periphery of the "orientation triangle".[18] The accuracy of each point is roughly indicated by its size.

The location of each point in the orientation triangle

Table 2. The average values of the reduction factors ($d_{\parallel}$ and $d_{\perp}$) and the orientation factors (K_y and K_z) at $S=4.3$ of eight acridine dyes

Dyes	$d_{\parallel}$	$d_{\perp}$	K_y	K_z
Acr	0.95	0.54	0.322	0.481
MeAcr	0.88	0.53	0.305	0.485
PF	0.52	0.21	0.206	0.704
TF	0.47	0.18	0.190	0.735
AY	0.23	0.12	0.099	0.806
MeAY	0.30	0.19	0.130	0.725
AO	0.47	0.24	0.190	0.676
MeAO	0.37	0.18	0.156	0.735

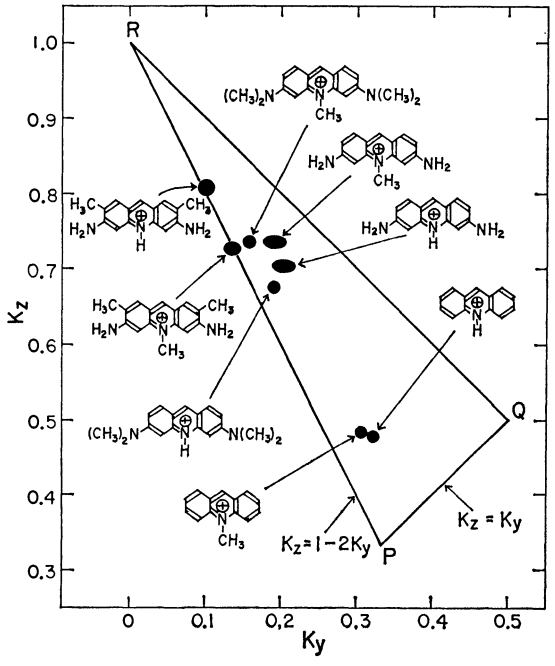

Fig. 7. The orientation factors K_y and K_z of eight acridine dyes at $S=4.3$ in the coordinates (K_y, K_z). The orientation triangle is denoted by PQR.

is clearly related to the molecular shape of dye. For example, the points for Acr and MeAcr are closest to the apex P (1/3,1/3), indicating that both Acr and MeAcr are the least orientable among those dyes studied here. This is probably due to their molecular shape, which lacks the 3,6-substituents and, as a result, is least prolate. The distance between the apex P and each point increases remarkably on the substitution of the amino or dimethylamino groups at the 3- and 6-positions of acridine nucleus (AO, PF, TF, MeAO, MeAY, and AY in this order). Since these dyes are oriented more favorably than Acr and MeAcr, the increase in the distance is attributable to the lengthening of the molecular shape. The factor K_z is larger for AY than for the quaternized, 10-methyl substituted MeAY, which implies that the quaternization of AY may alter the orientability along the z-axis. However, this tendency is reversed for pairs of PF and TF, and AO and MeAO, which possess the same substituents (either amino or dimethylamino) at 3- and 6-positions but a different one at 10-position (hydrogen or methyl). The reason for this reversal is not yet clear.

Since the points for AY and MeAY are nearly on the line PR ($K_z=1-2K_y$), these two dyes can be approximated as a rod-like molecule in their orientation property.[18] It may then be concluded that AY and MeAY are geometrically more symmetric than PF and TF with respect to the z-axis and, accordingly, the orientation axis nearly coinsides with the z-axis. The points for Acr, MeAcr, PF, TF, AO, and MeAO lie not on the line PR but inside the orientation triangle. This result indicates that the orientation axis of each of those six dyes does not coincide with the z-axis but should be somewhere between the y- and z-axes in the molecular plane. Thus the locations of the points in Fig. 7 are related to the molecular shape and, as a consequence, to the orientability of dyes. With the location of those points determined at a single S value, however, the degree of orientation of an assembly of like molecules can not be specified as yet. In this connection, a more comprehensive theory of the film dichroism must be developed under due consideration of the dependence of the degree of orientation on the geometrical shape of the guest molecules.

Conclusion

The film dichroism method has proved to be powerful for obtaining information on the polarization directions and the presence of weak bands for 3,6-disubstituted acridine dyes. From the dependence of R_d on S, the transition moment angle relative to the orientation axis could be determined, only when the R_d-values are near unity. By the reduction procedure, the reduced spectra and the orientation factors for acridine dyes of C_{2v} symmetry could be estimated at a given S without recourse to the orientation function of the guest molecules. The orientation factors of these dyes could be related to their molecular shapes.

The authors thank Mr. Takumi Matsuda for his skilled computer programming, which was used in calculating the reduced spectra.

References

1) Part of this work was presented at the Meeting of the Molecular Structures (Bunshikozosogotoronkai) of the Chemical Society of Japan held at Hiroshima in October, 1978, Abstr. p. 590.

2) D. F. Bradley and M. K. Wolf, *Proc. Natl. Acad. Sci. U.S.A.*, **45**, 945 (1959).

3) M. K. Pal and M. Schubert, *J. Phys. Chem.*, **67**, 1821 (1963).

4) K. Yamaoka, M. Takatsuki, and M. Miura, *Bull. Chem. Soc. Jpn.*, **48**, 2739 (1975).

5) G. Weill and M. Calvin, *Biopolymers*, **1**, 401 (1963).

6) H. Ito and Y. J. I'Haya, *Int. J. Quantum Chem.*, **2**, 5 (1968).

7) K. Jackson and S. F. Mason, *Trans. Faraday Soc.*, **67**, 966 (1971).

8) E. Fredericq and C. Houssier, *Biopolymers*, **11**, 2281 (1972).

9) K. Yamaoka and R. A. Resnik, *J. Phys. Chem.*, **70**, 4051 (1966).

10) C. Houssier, B. Hardy, and E. Fredericq, *Biopolymers*, **13**, 1141 (1974).

11) G. R. Kelly and T. Kurucsev, *Biopolymers*, **15**, 1481 (1976).
12) Y. Tanizaki, *Bull. Chem. Soc. Jpn.*, **32**, 75 (1959); **38**, 1798 (1965).
13) Y. Tanizaki and S. Kubodera, *J. Mol. Spectrosc.*, **24**, 1 (1967).
14) H. Inoue, T. Hoshi, T. Masamoto, J. Shiraishi, and Y. Tanizaki, *Ber. Bunsenges. Phys. Chem.*, **75**, 441 (1971).
15) E. W. Thulstrup and J. H. Eggers, *Chem. Phys. Lett.*, **1**, 690 (1968); E. W. Thulstrup, J. Michl, and J. H. Eggers, *J. Phys. Chem.*, **74**, 3868 (1970); J. Michl, E. W. Thulstrup, and J. H. Eggers, *ibid.*, **74**, 3878 (1970).
16) A. Davidsson and B. Nordén, *Chem. Phys. Lett.*, **28**, 221 (1974).
17) C. C. Bott and T. Kurucsev, *J. Chem. Soc., Faraday Trans. 2*, **71**, 749 (1975).
18) E. W. Thulstrup and J. Michl, *J. Am. Chem. Soc.*, **98**, 4533 (1976); J. Michl and E. W. Thulstrup, *Spectrosc. Lett.*, **10**, 401 (1977).
19) K. Yamaoka and Y. Matsuoka, *J. Sci. Hiroshima Univ., Ser. A*, **40**, 105 (1976).
20) K. Yamaoka, *Biopolymers*, **11**, 2537 (1972).
21) K. Yamaoka, Y. Matsuoka, and M. Miura, *J. Phys. Chem.*, **78**, 1040 (1974).
22) R. L. Rill, *Biopolymers*, **11**, 1929 (1972).
23) M. E. Lamm and D. M. Neville, Jr., *J. Phys. Chem.*, **69**, 3872 (1965).
24) T. Kurucsev and U. P. Strauss, *J. Phys. Chem.*, **74**, 3081 (1970).
25) G. R. Haugen and W. H. Melhuish, *Trans. Faraday Soc.*, **60**, 386 (1964).
26) M. Takatsuki and K. Yamaoka, *J. Sci. Hiroshima Univ., Ser. A*, **40**, 387 (1976).
27) J. Yoshino, T. Hoshi, T. Masamoto, H. Inoue, and K. Ota, *Nippon Kagaku Kaishi*, **1972**, 2227.
28) H. Jacobi and H. Kuhn, *Z. Elektrochem.*, **66**, 46 (1962).
29) B. Nordén, G. Lindblom, and I. Jonáš, *J. Phys. Chem.*, **81**, 2086 (1977).
30) H. Hiratsuka, Y. Tanizaki, and T. Hoshi, *Spectrochim. Acta, Part A*, **28**, 2375 (1972).
31) W. Seiffert, H. H. Limbach, V. Zanker, and H. Mantsch, *Histochemie*, **23**, 220 (1970).
32) V. Zanker and H. Cnobloch, *Z. Naturforsch., Teil B*, **17**, 819 (1962).
33) J. Michl, E. W. Thulstrup, and J. H. Eggers, *Ber. Bunsenges. Phys. Chem.*, **78**, 575 (1974).
34) A. Wittwer and V. Zanker, *Z. Phys. Chem. (Frankfurt am Main)*, **22**, 417 (1959).
35) A. Gafni, J. Schlessinger, and I. Z. Steinberg, *Israel J. Chem.*, **11**, 423 (1973).
36) H. Lang and G. Löber, *Tetrahedron Lett.*, **46**, 4043 (1969).

The Determination of the Formation Constant of Triiodide Ion in Micellar Solution of Dodecyltrimethylammonium Chloride

Katumitu HAYAKAWA,* Mitsuo KANDA, and Iwao SATAKE

Department of Chemistry, Faculty of Science, Kagoshima University, Korimoto, Kagoshima 890

(Received January 27, 1979)

Spectrophotometric measurements were undertaken at 360 nm in order to estimate the formation constant of triiodide ion in micellar solution of dodecyltrimethylammonium chloride. The absorption spectra of the solutions suggested that both iodine molecule and triiodide ion are solubilized in a hydrophilic surface region of the surfactant micelle. The apparent formation constant of triiodide ion, K_a, was found to be much larger in micellar solution than in water. It was also shown that the value of K_a decreases regularly with increasing surfactant concentration. A tentative estimation based on a lamellar micelle model led to the intrinsic formation constant of triiodide ion of 650 mol^{-1} dm^3 or less at 30 °C, which is comparable with that in water. The thermodynamic consideration revealed that the formation reaction of triiodide ion from iodine and iodide ion in micellar solution is accompanied by an anomalous entropy decrease.

In a previous paper,[1] we have reported the spectrophotometric measurements of the effect of solvent composition on the formation constant, K_c, of triiodide ion in water–methanol and water–ethanol mixed solvents. We found that in both systems the value of K_c increases remarkably with increasing mole fraction of alcohol, *e.g.*, it varies rapidly with methanol concentration from 730 in water to 12200 mol^{-1} dm^3 in methanol at 25 °C. Similar increases in K_c were also found in 2-propanol[2] and acetonitrile.[2,3]

In connection with a remarkable effect of solvent properties on K_c, it is of great interest to study the formation constant of triiodide ion in a solution of surfactant, since this provides an aqueous as well as a hydrophobic environment by forming a micelle, which consists of a hydrocarbon core with polar groups at the surface. In particular, the cationic surfactant micelle may be anticipated to affect K_c significantly through a strong coulombic interaction with iodide and triiodide ions. However, such studies have not been performed so far. The estimation of K_c in micellar solution is also essential for the clear understanding of our recent studies on the rate of catalytic oxidation of formate ion by iodine in micellar solutions.[4]

The present paper is concerned with the spectrophotometric determination of the formation constant of triiodide ion in a micellar solution of dodecyltrimethylammonium chloride.

Experimental

Materials. Dodecyltrimethylammonium chloride (DTAC), purchased from Tokyo Kasei Kogyo Co., Ltd., was recrystallized twice from methanol. Other chemicals were of guaranteed grade. Sodium iodide was dried at 120 °C and used without further purification. Iodine was purified further by sublimation.

Measurements. The apparent formation constant of I_3^- in a mixed solution of I_2, NaI, and DTAC was determined spectrophotometrically at 360 nm. The absorption spectra were recorded on a Hitachi spectrophotometer model 200-20 equipped with a thermoregulated cell compartment. The change in absorbance at 360 nm was followed as a function of NaI concentration at constant concentrations of I_2 and DTAC.

The chloride ion activity in DTAC solution was measured potentiometrically by using a National chloride ion selective ceramic electrode IE-510103. The electromotive force was measured with an Orion digital pH/mV meter model 701A with an accuracy of ±0.1 mV. In the concentration range below the critical micelle concentration (CMC) of DTAC, the semilogarithmic plots of electromotive force *versus* chloride ion activity taken from Kieland's data[5] gave a linear relation with an ideal Nernst slope, suggesting that the electrode responds exclusively to chloride ions.

All measurements were conducted at 21, 30, and 40 °C.

Results and Discussion

The Absorption Spectra. In the presence of DTAC micelles, the absorption spectrum of the solution of I_2 and NaI is characterized by an absorption band at 360 nm. Figure 1 shows the typical change in

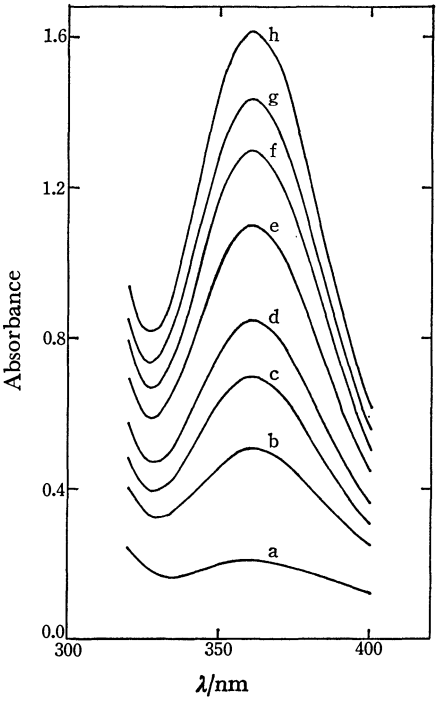

Fig. 1. The dependence of the absorbance spectrum of iodine in DTAC micellar solution on the concentration of sodium iodide at 30 °C; I_2 7.82×10^{-5} mol dm^{-3}, DTAC 0.13 mol dm^{-3}, NaI a: 0, b: 3.36, c: 6.71, d: 10.1, e: 16.8, f: 25.2, g: 33.6, h: 58.2×10^{-5} mol dm^{-3}.

absorption spectrum with NaI concentration, under the condition where concentrations of I_2 and DTAC are kept constant. Similar results were also obtained at the different DTAC concentrations studied. The important aspects of Fig. 1 are that the absorbance at 360 nm increases progressively with increasing NaI concentration, while the peak location is independent of NaI and DTAC concentrations. Unfortunately, only limited data are available in the concentration range of DTAC below CMC, since the occurrence of an appreciable amount of precipitate makes it difficult to obtain the reliable absorption spectra. However, the measurement of I_2 solution, though it was somewhat less accurate, showed that the absorption peak shifts successively from 460 to 360 nm with increasing DTAC concentration. At higher DTAC concentrations above CMC, the complex redissolved and the peak location remained at 360 nm. These observations suggest that an iodine molecule can interact strongly with a DTAC ion to give rise to a complex which is sparingly soluble in water but is easily solubilized in DTAC micelle.

The absorption spectrum of an iodine molecule is known to depend significantly on the polarity of the surrounding medium. Thus, an iodine molecule has the absorption band with a peak at 525 nm in a hydrophobic medium such as hexane,[6] but at 460 nm in water.[7] It is, therefore, reasonable to assume that the iodine molecules in micellar solution of DTAC are solubilized not in the hydrocarbon core but in a hydrophilic surface region of the DTAC micelle. The pronounced blue shift in peak location from 460 nm in water to 360 nm in micellar solution would provide additional evidence for the strong interaction between the iodine molecule and the ionic head group of DTAC.

As is shown in Fig. 1, the addition of sodium iodide results in a successive increase in absorbance but in no shift in peak location. This change can reasonably be ascribed to the formation of triiodide ion. Since, however, the peak location is red-shifted by 8 nm in micellar solution as compared with that in water,[7] triiodide ion is also considered to be solubilized in the surface region of the DTAC micelle.

The Formation Constant of Triiodide Ion. The foregoing considerations suggest that the formation reaction of triiodide ion in micellar solution will take place at the micellar surface, *i.e.*, between the iodine molecules solubilized in the surface region of DTAC micelle and the surrounding iodide ions in the close neighborhood of the micellar surface. Thus, if the inside and outside regions of micellar surface are denoted by suffix m and s respectively, the formation reaction of triiodide ion can be written as

$$I_{2,m} + I_s^- \rightleftharpoons I_{3,m}^-. \tag{1}$$

By taking into account the fact that the electrical potential at I_s^- is virtually identical with that at $I_{3,m}^-$, we can safely set the activity coefficient ratio of these ions equal to unity without introducing serious errors. Moreover, the activity coefficient of $I_{2,m}$ may probably be set equal to unity, since the total concentration of I_2 is sufficiently small as compared with that of DTAC under our experimental conditions. With this simplification, the intrinsic formation constant of triiodide ion may be written as

$$K_c = [I_3^-]_m/[I_2]_m[I^-]_s, \tag{2}$$

where the bracket represents an equilibrium concentration in moles per liter of the respective phase. Denoting the electrical potential at the micellar surface by ψ_0, the concentration of iodide ion near the micellar surface, $[I^-]_s$, can be described in terms of the apparent iodide ion concentration, $[I^-]_t$, as

$$[I^-]_s \exp(-e\psi_0/kT) = \gamma_-[I^-]_t, \tag{3}$$

where γ_- is the activity coefficient of the iodide ion. Since both iodine molecule and triiodide ion are solubilized in the same surface region of the DTAC micelle, their concentration ratio $[I_3^-]_m/[I_2]_m$ in Eq. 2 may be replaced by the ratio of the number of moles of solubilized triiodide ions per mole of iodine molecules. Therefore, if we denote an apparent concentration in moles of solubilized species per liter of solution by suffix t, we have

$$[I_3^-]_m/[I_2]_m = [I_3^-]_t/[I_2]_t. \tag{4}$$

Substitution of Eqs. 3 and 4 into Eq. 2 gives

$$K_c = K_a/\gamma_- \exp(e\psi_0/kT), \tag{5}$$

where K_a represents an apparent formation constant of triiodide ion defined by

$$K_a = [I_3^-]_t/[I_2]_t[I^-]_t. \tag{6}$$

It is worth noting here that in micellar solution the counterion concentration is a primary determinant of ψ_0 and γ_-. Accordingly, K_a can be regarded as constant at a given concentration of DTAC, because the iodide ion does not contribute appreciably to the total counterion concentration. Denoting $[I_3^-]_t$ by x, and the total concentrations of iodine and sodium iodide by a and b, we have

$$K_a = x/(a-x)(b-x). \tag{7}$$

Substituting $y=x/a$ and $z=b/a$, Eq. 7 may be rearranged to

$$y/(1-y) = K_a a(z-y). \tag{8}$$

Eq. 8 suggests that $y/(1-y)$ should be proportional to $(z-y)$. Since sodium iodide and DTAC do not show an appreciable absorption at 360 nm, the absorption coefficient of the solution, A, may be written as

$$A = \varepsilon_0(a-x) + \varepsilon_1 x = A_0 + (A_1-A_0)y \tag{9}$$

with

$$A_0 = \varepsilon_0 a, \qquad A_1 = \varepsilon_1 a, \tag{10}$$

where ε_0 refers to the molar absorption coefficient of iodine and ε_1 to that of triiodide ion, respectively. Equation 9 allows one to estimate the value of y as a function of b or z, with the knowledge of $\Delta A_\infty (= A_1-A_0)$ which corresponds to an increment in absorbance of a hypothetical solution in which iodine molecules are converted completely to triiodide ions. In order to estimate ΔA_∞, therefore, the increment in absorbance, $\Delta A (= A-A_0)$, was conveniently plotted against the reciprocal of sodium iodide concentration and was extrapolated to infinite iodide concentration. Using the value of y so determined, we can easily evaluate the apparent formation constant at a given

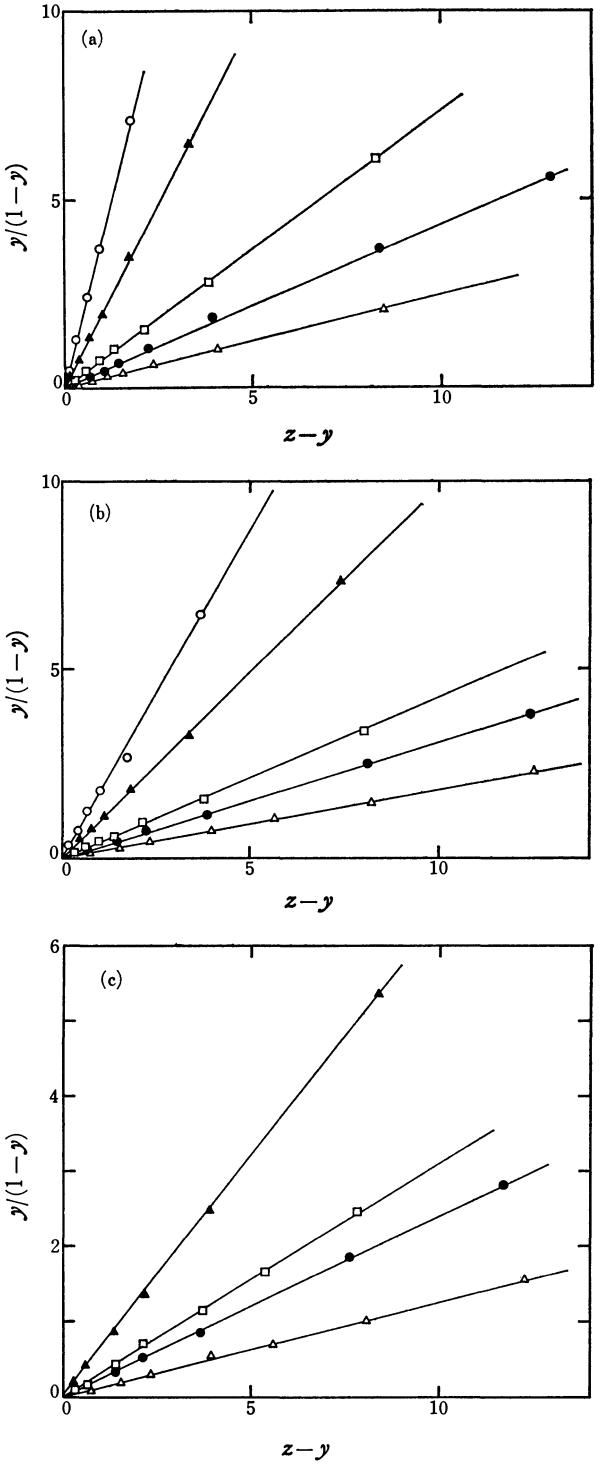

Fig. 2. The plot of $y/(1-y)$ *versus* $z-y$. (a): 21 °C, (b): 30 °C, (c): 40 °C; [DTAC] ○: 0.03, ▲: 0.04, □: 0.06, ●: 0.08, △: 0.13 mol dm^{-3}.

surfactant concentration from the slope of $y/(1-y)$ *versus* $(z-y)$ plots according to Eq. 8. Equation 5 then serves to estimate the intrinsic formation constant, K_c, provided that an appropriate expression is available for ψ_0.

Figure 2 shows $y/(1-y)$ *versus* $(z-y)$ plots at the given concentrations of iodine and surfactant. In all cases, the linearity of the plots is satisfactory over the whole concentration range of sodium iodide studied.

Table 1. The apparent formation constant of triiodide ion in DTAC micellar solution

[DTAC] / mol dm^{-3}	$10^{-4}K_a$/mol^{-1} dm^3 (21 °C)	(30 °C)	(40 °C)
0.03	10.4	4.35	—
0.04	4.97	2.47	1.8
0.06	2.05	1.16	0.80
0.08	1.20	0.82	0.60
0.13	0.67	0.48	0.32

Standard deviation: 2% at 21 and 30 °C, 7% at 40 °C.

The values of K_a calculated from Eq. 8 are summarized in Table 1. According to Eq. 5, K_a should decrease with increasing surfactant concentration, since both ψ_0 and γ_- are decreasing functions with respect to surfactant concentration. This is the case for the present results. The value of K_a shown in Table 1 tends to decrease regularly with increasing DTAC concentration, reflecting the significant contribution of electrostatic term in Eq. 5. It should also be noted that even in the highest concentration of DTAC studied the observed values of K_a are much larger than those in water.

Information regarding the intrinsic formation constant of triiodide ion can now be obtained by introducing an appropriate expression for the electrical work, $e\psi_0$, into Eq. 5. To this end, we applied an expression based on the lamellar micelle with uniformly charged surface. It is well known that the lamellar model can account for most of the interesting features of ionic surfactant solutions, *e.g.*, the effect of added salt on CMC, and a linear dependence of log CMC on the number of carbon atoms, m, for the homologous series of surfactants described as[8]

$$\log \mathrm{CMC} = A - Bm. \tag{11}$$

In his theoretical study of ionic surfactant solutions, Shinoda[8] has derived the following expression for the effective electrical work, E_{el}, needed to introduce a unit charge e into the surface of a lamellar micelle, by taking into consideration the counterion fixation effect of a highly charged micellar surface.

$$E_{el} = K_g kT \ln(2000\pi\sigma^2/\varepsilon_r N_A kTC_g) \tag{12}$$

where, σ is the surface charge density, ε_r the relative permittivity of the solution, and C_g the total counterion concentration in equivalents per liter; other symbols than K_g have their usual meanings. For a given homologous series of surfactants, K_g is an experimental constant which can be correlated to the constant B in Eq. 11 by

$$B = \omega/2.303(1+K_g)kT, \tag{13}$$

where ω refers to the cohesive energy change involved in transferring one methylene group from a hydrocarbon environment to an aqueous medium.[8] The value of ω was estimated by Shinoda[9] to be $1.08\,kT$. By introducing the critical micelle concentrations reported for dodecyltrimethyl- and hexadecyltrimethylammonium chlorides,[10] K_g for alkyltrimethylammonium chloride may be estimated from Eqs. 11 and 13 to be 0.62 at 30 °C. It is to be noted that K_g is nearly

Table 2. The formation constant of triiodide ion in some solvents

Medium	K_c/mol^{-1} dm^3			ΔH/kJ mol^{-1}
DTAC	910 (21 °C)	650 (30 °C)	430 (40 °C)	−30
H_2O	1010 (9.5 °C)	730 (25 °C)	550 (38 °C)	−15.4
MeOH	13600 (20 °C)	10900 (31 °C)	9590 (39 °C)	−14.3
EtOH	28700 (17 °C)	20700 (28 °C)	15100 (39 °C)	−21.4

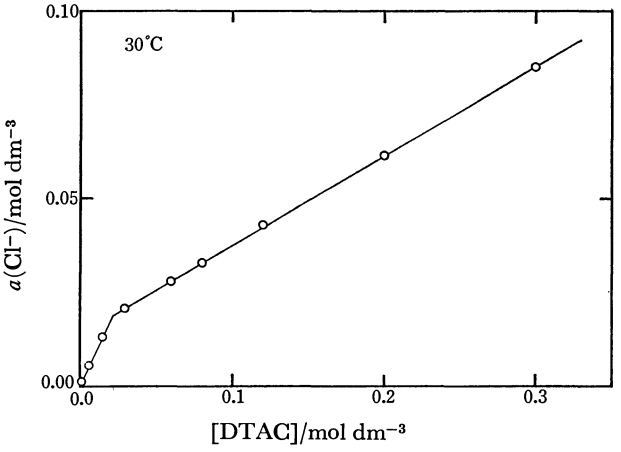

Fig. 3. The plot of chloride ion activity *versus* the total concentration of DTAC at 30 °C.

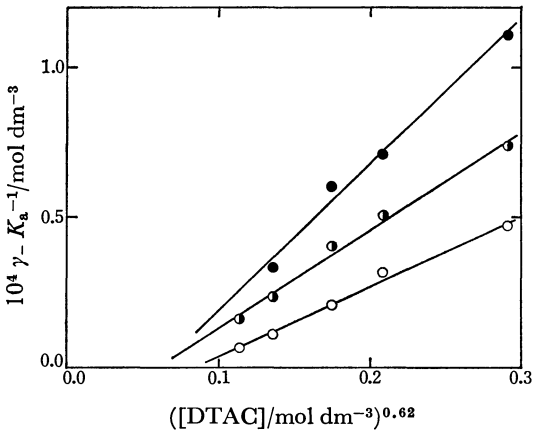

Fig. 4. The plot of γ_-/K_a *versus* $C_g^{0.62}$. ●: 40 °C, ◑: 30 °C, ○: 21 °C.

independent of temperature.[8]

Substituting E_{el} for $e\phi_0$ in Eq. 5, we have

$$\frac{\gamma_-}{K_a} = \frac{1}{K_c}\left(\frac{\varepsilon_r N_A kT}{2000\pi\sigma^2}\right)^{K_g}(C_g)^{K_g}. \qquad (14)$$

This equation implies that γ_-/K_a should be proportional to $(C_g)^{K_g}$ if surface charge density σ remains constant over the concentration range of DTAC studied. Though C_g in Eq. 14 can safely by replaced by the total concentration of DTAC, the use of this equation still requires a knowledge of the activity coefficient of an iodide ion in the presence of excess chloride ions, which is experimentally rather difficult to estimate. Therefore, on the assumption that the activity coefficient of iodide ion is equal to that of chloride ion, we made the potentiometric measurements of chloride ion activity in a solution of DTAC alone. Figure 3 shows the typical plot of chloride ion activity *versus* the total concentration of DTAC at 30 °C. Similar results were also obtained at different temperatures. In agreement with the results reported for counterion activities in solutions of various ionic surfactants,[11] the observed chloride ion activity first increases almost linearly with increasing DTAC concentration up to CMC, then it continues to increase linearly but less steeply with further increases in DTAC concentration. According to the earlier assumption, this chloride ion activity divided by total DTAC concentration gives γ_- in Eq. 14. In Fig. 4, γ_-/K_a is plotted against $C_g^{0.62}$. As would be expected, the plots are linear, but the straight lines do not converge to the origin. At the present time, no conclusive explanation can be offered as to whether the observed deviation in the intercept comes from the underlying lamellar model which assumes an infinitely extended plane surface with uniform charge density or from the assumption of equal activity coefficients for iodide and chloride ions. In fact, the micellar aggregation number of DTAC was determined from a light scattering experiment to be 57 in 0.05 mol dm^{-3} sodium chloride solution.[12] However, in view of the fact that the predicted linear relationship is found between γ_-/K_a and $C_g^{0.62}$, Eq. 14 can presumably be applied for a tentative estimation of the intrinsic formation constant of triiodide ion, K_c. On the basis of geometric considerations, Tanford[13] has calculated the surface area per polar head group of micelle forming surfactant molecules, S, for various micelle shapes as a function of micellar aggregation number. According to his calculation for globular micelles, the micellar aggregation number of 57 corresponds to the value of S of 78 A^2. Substituting e/S for σ and assuming that S is independent of temperature, the values of K_c were tentatively estimated from the slopes of straight lines given in Fig. 4. The results are summarized in Table 2 together with those in various solvents.[1] It should be emphasized that the value of K_c estimated above depends considerably on the selected value of S. For instance, it decreases up to 190 at 30 °C if we assume $S \approx 30$ A^2, which corresponds to the surface area per polar head group of a lamellar micelle.[13] With these reservations in mind, the intrinsic formation constant of triiodide ion in DTAC micellar solution is expected to be comparable with or slightly less than that in water, but small enough as compared with those in alcohols. This result supports well the assumption that the formation reaction of the triiodide ion in the micellar solution will take place at a hydrophilic surface region of the micelle. Thus the remarkable increase in the apparent formation constant of triiodide ion may be ascribed to an increase in surface concentration of iodide ions due to the strong coulombic interaction between iodide

ion and polyvalent micellar ion. Other factors seem to play at best a minor role.

Apart from a plausible estimation of K_e, we can easily evaluate the enthalpy change for Reaction 1 from the change in the slope of the straight line in Fig. 4 with temperature. As can be seen from Eq. 14, the enthalpy change so calculated is independent of the value of σ, so long as it remains constant over the temperature range studied.

It is worth noting that the enthalpy change in micellar solution shown in Table 2 is not only negative but about twice as large as that in water. Nevertheless, the values of K_e are nearly the same in both solvents. This implies that the formation reaction of triiodide ion in micellar solution is accompanied by an anomalous entropy decrease, contrary to the increases observed in water and alcohols.[1] The situation is somewhat complicated by the fact that in micellar solution both iodine molecule and triiodide ion are solubilized in the surface region of the micelle. It seems probable that the solubilized triiodide ions are restricted in their molecular motion through a strong coulombic interaction with highly charged micellar surface.

The authors wish to express their thanks to Associate Professor Norinobu Yonehara, Kagoshima University, for use of the Hitachi Spectrophotometer.

References

1) K. Hayakawa and S. Nakamura, *Bull. Chem. Soc. Jpn.*, **50**, 566 (1977).
2) A. A. Ramadan, P. K. Agasyan, and S. I. Petrov, *Zh. Obshch. Khim.*, **44**, 983 (1974).
3) C. Barraqué, J. Vedel, and B. Tremillon, *Anal. Chim. Acta*, **46**, 263 (1969).
4) K. Hayakawa, M. Kanda, and I. Satake, *Bull. Chem. Soc. Jpn.*, to be published.
5) J. Kielland, *J. Am. Chem. Soc.*, **59**, 1675 (1937).
6) F. H. Getman, *J. Am. Chem. Soc.*, **50**, 2883 (1928).
7) A. D. Awtrey and R. E. Connick, *J. Am. Chem. Soc.*, **73**, 1842 (1951).
8) K. Shinoda, T. Nakagawa, B. Tamamushi, and T. Isemura, "Colloidal Surfactants," Academic Press, New York (1963), Chap. 1.
9) K. Shinoda, *Bull. Chem. Soc. Jpn.*, **26**, 101 (1953); K. Shinoda, *J. Phys. Chem.*, **59**, 432 (1955).
10) A. W. Ralston, D. N. Eggenberger, and P. L. Du Brow, *J. Am. Chem. Soc.*, **70**, 977 (1948).
11) C. Botré, V. L. Crescenzi, and A. Male, *J. Phys. Chem.*, **63**, 650 (1959); L. Shedlovsky, C. W. Jacob, and M. B. Epstein, *ibid.*, **67**, 2075 (1963); P. Stenius and P. Ekwall, *Acta Chem. Scand.*, **21**, 1643 (1967); I. Satake, T. Tahara, and R. Matsuura, *Bull. Chem. Soc. Jpn.*, **42**, 319 (1969); T. Sasaki, M. Hattori, J. Sasaki, and K. Nukina, *ibid.*, **48**, 1397 (1975); M. Koshinuma and T. Sasaki, *ibid.*, **48**, 2755 (1975).
12) M. F. Emerson and A. Holtzer, *J. Phys. Chem.*, **71**, 1898 (1967).
13) C. Tanford, *J. Phys. Chem.*, **76**, 3020 (1972).

Disintegration of Sulfonated Poly(1,4-piperazinediylterephthaloyl) Microcapsules by 1-Dodecylpyridinium Chloride

Shiro SUZUKI, Takashi NAKAMURA, and Tamotsu KONDO*,†

Department of Domestic Science, Ferris Women's College, Naka-ku, Yokohama 231

† *Faculty of Pharmaceutical Sciences, Science University of Tokyo, Shinjuku-ku, Tokyo 162*

(Received February 19, 1979)

Partially sulfonated poly(1,4-piperazinediylterephthaloyl)(SPP) microcapsules were found to undergo disintegration by the action of dodecylpyridinium ions when the surfactant cation concentration exceeded a certain value which was dependent on pH of the medium. At their lower concentrations, dodecylpyridinium ions interacted with negatively charged SPP microcapsules to produce aggregation of the latter. A polyelectrolyte-type viscosity behavior was observed with the complex formed between SPP and dodecylpyridinium ions in the disintegration process of the microcapsules. Crosslinking of the terminal amino groups of SPP microcapsules prevented disintegration from taking place.

Since the earliest work was carried out on protein-anionic surfactant systems in the 1940's,[1] interactions in aqueous media between polyelectrolytes and oppositely charged surfactants have been under study for more than 30 years.[2–8] In almost all systems studied so far, the interaction causes precipitation of a complex which can be resolubilized by excess surfactant. In general, maximum precipitation seems to correspond to a single layer of surfactant adsorbed on the polymer, and the resolubilized form to a double layer of surfactant.

Meanwhile, it has become possible to prepare microcapsules composed of polyelectrolytes and to study their various physical properties.[9] Since such an electrically charged microcapsule can be regarded as a matrix of polyelectrolyte molecules assembled in a very thin spherical shell the interaction of the microcapsule with oppositely charged surfactants in aqueous media will be worth studying on the ground that understanding of this type of interaction should help us elucidate the mechanisms of the action of ionic surfactants on biological cells such as erythrocytes.[10]

The present paper deals with the interaction between partially sulfonated poly(1,4-piperazinediylterephthaloyl)(SPP) microcapsules and 1-dodecylpyridinium chloride(C_{12}PyCl) as a function of the cationic surfactant concentration at different degrees of sulfonation and pH of the medium, which leads to disintegration of the microcapsules at high concentrations of the surfactant. The effect of crosslinking with glutaraldehyde of the terminal amino groups of the polymers constituting the microcapsules on the interaction will also be discussed.

Experimental

Preparation of Microcapsules. SPP microcapsules were prepared by the method described in a previous paper.[11] The degree of sulfonation was varied by changing the molar ratio of 4,4′-diaminostilbene-2,2′-disulfonic acid to piperazine in the diamine mixture to be used as the water-soluble monomer in the preparation. When the ratio was fixed at 1:2, 1:3, and 1:5, the microcapsules obtained were named SPP-2, -3, and -5 microcapsules, respectively.

Microscopic Observation of Disintegration. To a dialyzed suspension of each of SPP-2, -3, and -5 microcapsules (*ca.* 5×10^7 capsules cm^{-3}) in test tubes was added an equal volume of various concentrations of aqueous C_{12}PyCl solution. The pH and ionic strength of the medium were adjusted by the addition of HCl or NaOH and NaCl, respectively.

The mixtures were then allowed to stand for 1 h with shaking in a thermostated water bath maintained at 35 °C. At the end of this period, a small portion of each of the mixtures was withdrawn by a capillary tube and placed on a slide glass to observe if SPP capsules were disintegrated or not.

Treatment of Microcapsules with Glutaraldehyde. The terminal amino groups of SPP microcapsules were crosslinked with glutaraldehyde in the same way as in the previous work.[11]

Adsorption of Dodecylpyridinium Ions to Microcapsules. Adsorption of C_{12}Py ions to noncrosslinked and crosslinked SPP microcapsules was measured by an equilibrium dialysis technique in the following manner.

Seventy cm^3 each of surfactant solution and microcapsule suspension were placed respectively in two compartments separated by a Cellophane membrane of an equilibrium dialysis cell made of methacrylate. The cell was immersed in a constant temperature bath kept at 35 °C. The content of each compartment was stirred with a two-blade glass stirrer. Equilibrium was attained within 4 h in all cases.

After equilibration, an aliquot of solution was withdrawn by a pipet from the compartment containing surfactant solution and its concentration was determined by the Few-Ottewill method.[12]

The amount of adsorption was calculated from the difference between the surfactant concentrations before and after adsorption.

Viscosity of Solubilized Complex. An Ostwald viscometer was used to measure the viscosity of solutions containing the solubilized complex formed between SPP and C_{12}Py ions. All measurements were made at 35 °C.

Sample solutions were prepared by diluting the solubilized complex solution with NaCl solutions of appropriate concentrations. The ratio of the specific viscosity to the dilution was defined as the viscosity number.

Results

Microscopic Observation. Disintegration of SPP microcapsules by C_{12}Py ions was dependent greatly on the surfactant cation concentration and slightly on the pH of the medium. The degree of sulfonation and the ionic strength of the medium had no effect on the disintegration phenomenon.

SPP microcapsules were disintegrated by the action of C_{12}Py ions when their concentration exceeded a certain value at all pH studied. Lower concentrations

Table 1. Disintegration of SPP microcapsules by $C_{12}PyCl$[a)]

$C_{12}PyCl$ concn M	pH 2.0		pH 4.0		pH 7.0	
	Microcapsule					
	SPP-2	SPP-5	SPP-2	SPP-5	SPP-2	SPP-5
1×10^{-6}	−	−	−	−	−	−
1×10^{-5}	−	−	−	−	−	−
1×10^{-4}	−	−	−	−	−	−
1×10^{-3}	−	−	−	−	−	−
1×10^{-2}	−	−	−	−	−	−
3×10^{-2}	−	−	−	−	−	−
5×10^{-2}	−	−	−	−	+−	+−
7×10^{-2}	+−	+−	+−	+−	+	+
1×10^{-1}	+	+	+	+	+	+

a) −, aggregation; +−, partial disintegration; +, disintegration.

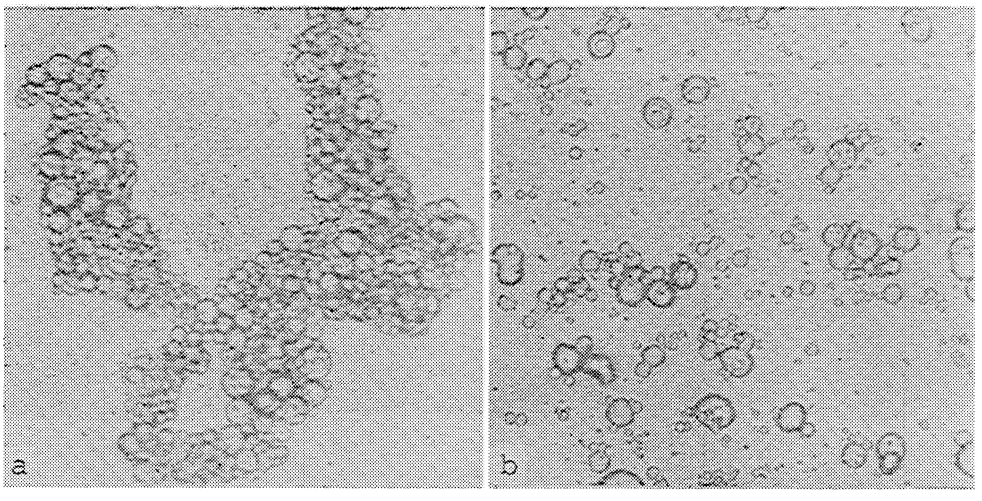

Fig. 1. Photomicrographs of SPP-5 microcapsules aggregated by 10^{-4} M $C_{12}PyCl$ (a) and partially redispersed by 10^{-2} M $C_{12}PyCl$ (b) at pH 7.0 and ionic strength 0.1.

of the surfactant cation caused aggregation of the microcapsules. Complete disintegration of the microcapsules was observed at surfactant concentrations higher than 7×10^{-2} M.** The minimum surfactant concentration needed for complete disintegration slightly decreased with increasing pH of the medium.

Table 1 gives the dependence of the phenomenon on the two variables at an ionic strength of 0.1.

Disintegration of glutaraldehyde-treated SPP microcapsules was never observed even when the highest concentration of $C_{12}PyCl$ was used. Instead, redispersion of the crosslinked microcapsules aggregated by low concentrations of $C_{12}PyCl$ took place in the presence of a large excess of the surfactant as shown in Fig. 1.

Surfactant Adsorption. Adsorption of $C_{12}Py$ ions on SPP microcapsules was affected by the surfactant cation concentration, the pH of the medium, the degree of sulfonation, and crosslinking of the terminal amino groups.

All adsorption isotherms exhibited a definite step in the surfactant concentration range of 10^{-2} to 10^{-3} M. The number of $C_{12}Py$ ions adsorbed on the microcapsules increased with increasing pH of the medium. This trend was more remarkable at low concentrations than at high concentrations of the surfactant cation. Increase in the degree of sulfonation gave rise to an increase in the amount adsorbed of $C_{12}Py$ ions.

Some of the adsorption isotherms for SPP-2 and SPP-5 microcapsules at an ionic strength of 0.1 are shown in Figs. 2 and 3, respectively, where the number of $C_{12}Py$ ions adsorbed on unit weight of the microcapsules is plotted against the initial surfactant concentration in logarithmic scale.

Crosslinking with glutaraldehyde of the terminal amino groups of SPP microcapsules caused a significant decrease in the number of adsorbed $C_{12}Py$ ions. Examples of the adsorption isotherms obtained at pH 7.0 and an ionic strength of 0.1 are given in Fig. 4 where isotherms for noncrosslinked SPP microcapsules are also shown for comparison.

Viscosity Behavior. The viscosity of solubilized complex formed between SPP molecule and $C_{12}Py$ ions exhibited a concentration dependence which is characteristic of polyelectrolytes.

The viscosity number of the solubilized complex

** 1 M=1 mol dm^{-3}.

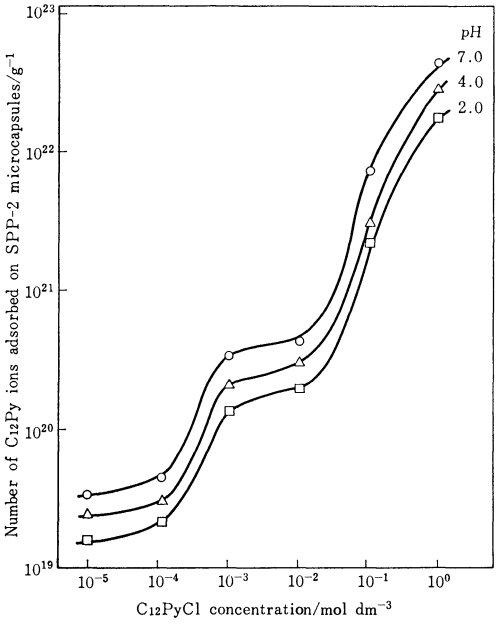

Fig. 2. Adsorption isotherms of $C_{12}Py$ ions on SPP-2 microcapsules at different pH and ionic strength 0.1 (35 °C).

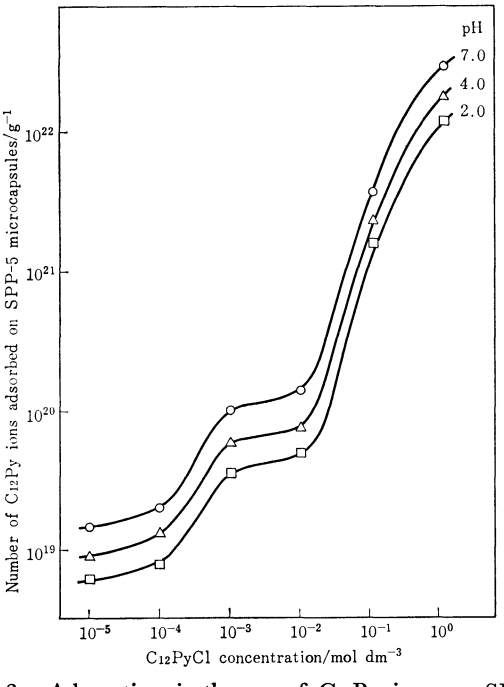

Fig. 3. Adsorption isotherms of $C_{12}Py$ ions on SPP-5 microcapsules at different pH and ionic strength 0.1 (35 °C).

at high ionic strength decreased linearly with increasing dilution while that at low ionic strength showed an uprising tendency at high dilutions. At intermediary ionic strength, the viscosity curve lay on a position between those at lower and higher ionic strengths. An example is illustrated in Fig. 5.

Discussion

It is quite obvious that aggregation of SPP microcapsules observed at low surfactant concentrations is

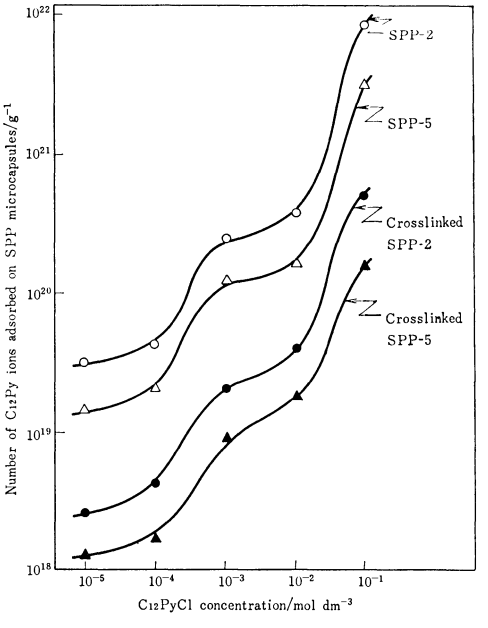

Fig. 4. Adsorption isotherms of $C_{12}Py$ ions on crosslinked and noncrosslinked SPP microcapsules at pH 7.0 and ionic strength 0.1 (35 °C).

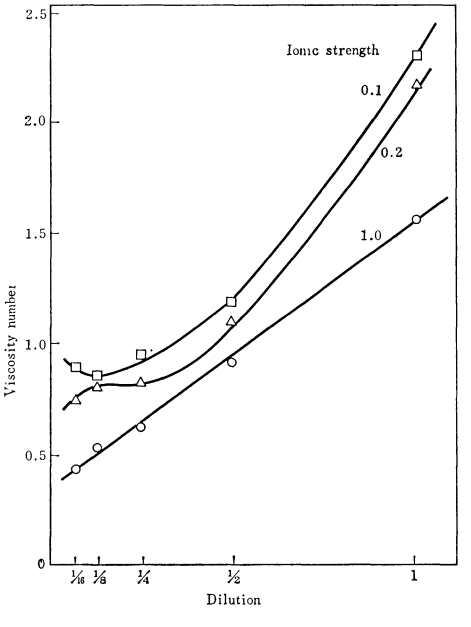

Fig. 5. Viscosity of solubilized $C_{12}Py$-SPP complex as a function of dilution at 35 °C.

caused by adsorption of $C_{12}Py$ cations with their hydrophobic tails directing outwards on sulfonato groups of the polymers constituting the microcapsules to form a hydrophobic complex. As the number of sulfonato groups on the polymers is slightly pH dependent, this head-to-head adsorption is also slightly pH dependent. This type of adsorption of the surfactant cations diminishes the electrostatic repulsion and at the same time augments the van der Waals attraction between the microcapsules, thus causing their aggregation.

When the $C_{12}Py$ ion concentration is increased beyond a value of 10^{-2} M adsorption of the surfactant cations rises steeply to form a step on the adsorption

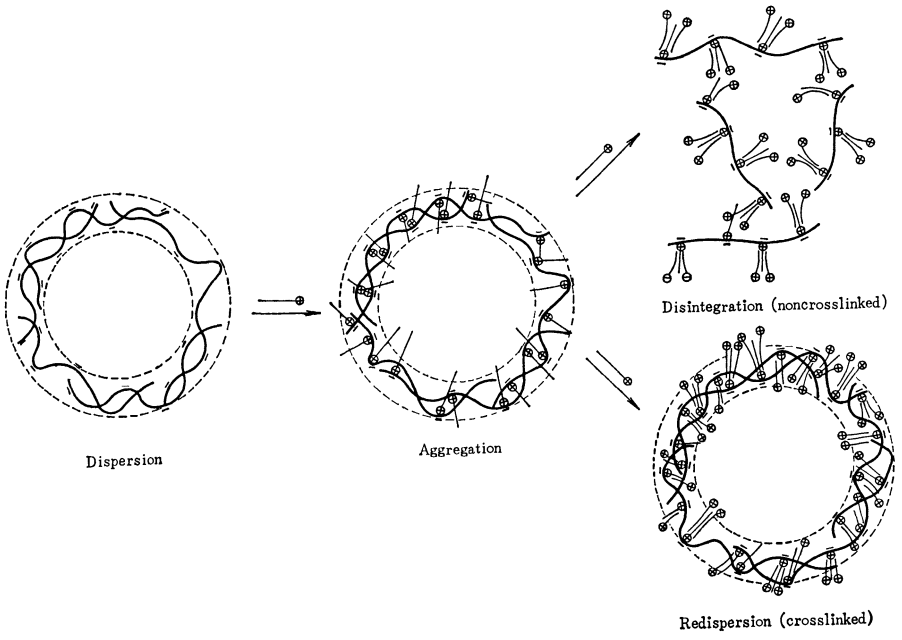

Fig. 6. Model for aggregation, disintegration, and redispersion of SPP microcapsules caused by $C_{12}Py$ ions.

isotherm (Figs. 2 and 3). The rise in adsorption is likely to correspond to the start of tail-to-tail adsorption onto the anionic sites modified by head-to-head adsorption and hydrophobic binding onto lipophilic sites on the polymer chains of $C_{12}Py$ ions. This view is supported by the fact that the number of the surfactant cations adsorbed at the concentration of 10^{-2} M on the capsules is comparable to that of anionic sites on the polymer chains.[11] Both types of adsorption generate positive charges on the polymer chains. The number of positive charges thus created will be larger, though not remarkably, at higher pH of the medium because the number of anionic sites along the polymer chains increases slightly with increasing pH as dissociation of sulfonato groups on the polymer proceeds while the number of lipophilic sites is independent of pH. It continues to increase with further rise in the surfactant cation concentration and the amount of adsorbed surfactant cations will then be enough to solubilize the polymer chains since the number of adsorbed surfactant cations reaches a value far larger than that of sulfonato groups on the polymer chains (Figs. 2 and 3).[11]

As the degree of sulfonation rises the number of sulfonato groups on the polymer chains also increases, and this in turn brings about an increase in the number of adsorbed $C_{12}Py$ ions as indicated from comparison of Fig. 2 with Fig. 3.

Increase in the number of positive charges on the constituent polymer chains of the microcapsules will cause dissociation of the chains, which leads to disintegration of the microcapsules, owing to the increased electrostatic repulsion between the chains. As is seen from Fig. 5, the viscosity of solubilized complex undergoes a marked increase with dilution when the ionic strength of the medium is low. This behavior of viscosity is characteristic of polyelectrolytes. Hence, each of the dissociated and solubilized polymer chains can be regarded as a polyelectrolyte.

Crosslinking of the constituent polymer chains prevents them from separating each other though they acquire some positive charges as a result of adsorption of $C_{12}Py$ ions on them. Consequently, disintegration of the microcapsules is never observed and instead redispersion occurs. Adsorption is rather limited in this case as the positively charged polymer chains are connected to each other by covalent bonds, and hence, an electric field exists around each capsule which is strong enough to repel the free surfactant cations approaching from the bulk of solution after adsorption proceeds to a certain degree (Fig. 4).

Figure 6 gives a proposed model for disintegration and redispersion of SPP microcapsules by the action of $C_{12}Py$ ions based on the experimental findings described in the previous section and the arguments made so far.

References

1) F. W. Putnam and H. Neurath, *J. Am. Chem. Soc.*, **66**, 672, 1992 (1944).
2) F. Karush and M. Sonenberg, *J. Am. Chem. Soc.*, **71**, 1369 (1949).
3) E. D. Goddard and B. A. Pethica, *J. Chem. Soc.*, 2659 (1951).
4) S. Saito, *Kolloid Z.*, **143**, 66 (1955).
5) M. N. Jones, *J. Colloid Interface Sci.*, **23**, 36 (1967).
6) E. D. Goddard, T. S. Phillips, and R. B. Hannan, *J. Cosmet. Chem.*, **26**, 461 (1975).
7) E. D. Goddard and R. B. Hannan, *J. Colloid Interface Sci.*, **55**, 73 (1976).
8) E. D. Goddard and R. B. Hannan, *J. Am. Oil Chem. Soc.*, **54**, 561 (1977).
9) T. Kondo, "Surface and Colloid Science", ed by E. Matijevic, Plenum Press, New York and London (1978), Vol. 10, pp. 1—43.
10) T. Kondo, *Adv. Colloid Interface Sci.*, **6**, 139 (1976).
11) S. Suzuki and T. Kondo, *Bull. Chem. Soc. Jpn.*, **52**, 1330 (1979).
12) A. V. Few and R. H. Ottewill, *J. Colloid Sci.*, **11**, 34 (1956).

Polarized Absorption and Reflection Spectra of the Single Crystals of Benzidine–7,7,8,8-Tetracyano-*p*-quinodimethane Molecular Complexes

Kyuya YAKUSHI, Masaaki IGUCHI, and Haruo KURODA*

Department of Chemistry, Faculty of Science, The University of Tokyo, Hongo, Tokyo 113

(Received March 9, 1979)

Polarized absorption and reflection spectra were observed on the single crystals of the solvent-free and solvent-containing modifications of benzidine (BD)–7,7,8,8-tetracyano-*p*-quinodimethane (TCNQ) molecular complex, by using the microspectrophotometers of transmission and reflection types. The absorption spectra obtained by the dispersion analyses of the reflection spectra agreed fairly well with those directly observed by the transmission method. The spectra showed that the BD–TCNQ complex has non-ionic ground state in all modifications although the intermolecular interaction is considerably strong and is appreciably affected by the inclusion of solvent molecules. In all modifications, the second charge-transfer band was confirmed to be polarized in the direction almost perpendicular to the direction of the donor-acceptor stack, while the first charge transfer band is polarized in the direction of the donor-acceptor stack as it is usually found for a typical charge-transfer complex. This anomaly of the polarization direction of the second charge-transfer band was concluded to be due to a strong mixing between the charge-transfer excitation and the local excitation associated with TCNQ.

The charge-transfer complex which involves benzidine (BD) as electron donor and 7,7,8,8-tetracyano-*p*-quinodimethane (TCNQ) as electron acceptor, exhibits anomalous behaviors in several respects. First, BD–TCNQ is not a radical salt, but a charge-transfer complex with essentially non-ionic ground state, although BD is an electron donor with considerably low ionization potential (7.0 eV) and TCNQ is an electron acceptor with very high electron affinity (2.8 eV).[1] Second, when BD–TCNQ complex is crystallized from solution, it forms either a crystal including solvent molecules in the crystal lattice or a crystal of the solvent-free form, depending on the solvent used, and the semiconductive properties of the solvated modifications are markedly different from those of the solvent-free modification.[2,6] The crystal structure analyses revealed that, in the solvated modifications, solvent molecules are included in the channel-like free space in the BD–TCNQ host-lattice, while BD and TCNQ molecules are closely packed without leaving any space to accommodate solvent molecules in the case of the solvent-free modification.[3–5] From these structural studies, the solvated modifications of BD–TCNQ complex were concluded to be a new type of the inclusion compound where the intermolecular hydrogen bonds and intermolecular charge-transfer interaction are responsible for the formation of the channeled structure of the host lattice. The third point of interest is that, according to our preliminary study on the absorption spectrum of BD–TCNQ crystal,[1] the polarization direction of the second charge-transfer band is perpendicular to the direction of the BD–TCNQ stack while the first charge transfer band is parallel to the stacking direction as it is usually expected for a typical charge-transfer band.

In view of those anomalous behaviors of BD–TCNQ system, it seemed of great interest to investigate the optical properties of the single crystals of the solvent-free and solvated modifications of BD–TCNQ complex.

As we have pointed out in our previous papers,[3–5] the obtainable modifications of BD–TCNQ complex can be classified into three types according to the difference as regards the structure of the BD–TCNQ sub-lattice: the one is the solvent free modification, the second is the modification which includes an aliphatic solvent molecule such as dichloromethane and the third is the one which includes benzene or its derivatives. Thus, in the present study, we have taken up one representative example for each of these three types: the solvent-free crystal (BD–TCNQ–[n]), the dichloromethane-containing crystal (BD–TCNQ–[CH_2Cl_2]), and the benzene-containing crystal (BD–TCNQ–[C_6H_6]). We will show the absorption and reflection spectra of these crystals measured by means of the microspectrophotometric technique. Discussion will be given on the interpretation of the observed spectra and on the charge-transfer interaction between BD and TCNQ molecules, using the results of the molecular orbital calculations on the models of isolated BD–TCNQ molecular pair.

Experimental

Materials. The crystals of the solvent-free modification of BD–TCNQ complex were obtained by crystallizing the complex from chloroform solution. The crystals of each solvated modification were prepared from the solution where appropriate amounts of BD and TCNQ were dissolved in the solvent which was to be included in the crystal. The details of the procedure of preparation and the characterization of each modification were described in our previous paper.[6]

Absorption Spectrum. The absorption spectrum was measured on very small single crystals by use of plane-polarized light, using the Olympus MSP-A-IV microspectrophotometer which we had modified for the purpose of the measurement of crystal spectrum. The details of this apparatus and the procedure of measurement have been described elsewhere.[7] All absorption spectra were observed at room temperature.

Reflection Spectrum and Its Analysis. We have newly constructed an apparatus for the measurement of the reflection spectrum of a very small single crystal. Figure 1 shows the block diagram of this apparatus. We used Sylvania 650 W halogen lamp as the light source for infrared and visible region. The light is monochromatized by means of JASCO-CT52 grating monochromator with the focal length of 50 cm and the *f*-number of 4.5. The monochromatic light is put into the microscope optical system, Olympus

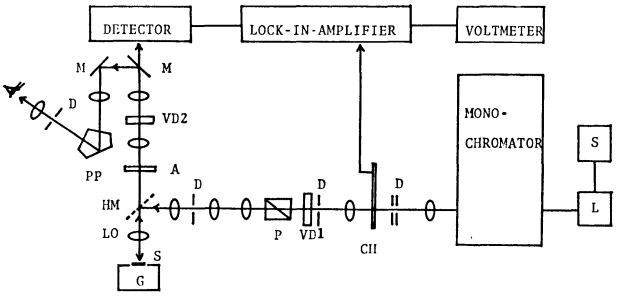

Fig. 1. The optical system of the Olympus MMSP-RK and the block diagram of the microspectrophotometer for reflection spectra. S: A.c. stabilizer, L: 650 W halogen lamp, D: diaphragm, CH: chopper, VD: variable diaphragm, P: polarizer, HM: half mirror, M: mirror, A: analyzer, PP: pentaprism, S: sample, G: goniometer head.

MMSP-RK, the structure of which is schematically illustrated in Fig. 1. In this optical system, the light which has passed through a variable diaphragm (VD1), is converted to a plane-polarized light by a Glan-Thompson prism (P), reflected by a half-mirror (HM), and focussed down onto the sample crystal through an objective lens (LO). The size of the light spot on the sample can be varied from 10 $\mu m\phi$ to 196 $\mu m\phi$ by changing the opening of the variable diaphragm (VD1) and the magnification of the objective lens. The reflected light passes again through the same objective lens, is focussed at the second variable diaphragm (VD2), and the intensity of the light passes through the above diaphragm is measured by the detector. Three detectors, having different spectral sensitivities, are installed and selectively used depending on the wavelength by changing the optical path by means of a mirror system: A photomultiplier tube HTV R435 is used for 400—700 nm region, another tube HTV R316 for 700—1100 nm region and a PbS photoconductive cell, cooled with Dry Ice–methanol mixture, for 1100—2500 nm region.

The output signal from the detector is amplified by a lock-in-amplifier, Brookdeal M9503, by being synchronized to the signals from the remote sensor which detects the rotation of the light chopper (CH), and the final output is read with a digital voltmeter.

The sample crystal is mounted on a goniometer head so that we can select out the crystal face on which the measurement of reflection spectrum is carried out, and can orient the observing crystal face exactly normal to the light axis. The goniometer head is transferable to X-ray diffraction camera to examine the crystallographic character of the observing crystal face. The goniometer head mentioned above is mounted on a rotatable sample stage which also has a mechanism to move in two horizontal directions.

Strictly speaking, the condition of normal incidence is not filled in our optical system, since the light is focussed down onto the sample through the objective lens. The reflectance we are observing, is the one averaged over the contributions of the *s*- and *p*-polarized components of the light beams with the incident directions within the cone of the focusing light. Naturally, the deviation from the normal incidence condition will be larger as the aperture angle of the objective lens is larger. The aperture angles of our lenses are 5.8°, 14.5°, and 23.6° for the magnifications of ×5, ×10, and ×20, respectively. We carried out numerical calculation by computer on the variation of reflectance with incident angle for *s*- and *p*- polarizations.[8] This calculation showed that, when the deviation from the normal incidence direction is less than 24°, the average of the reflectances of the *s*- and *p*-components remains at almost the same value, because the reflectance increases for the *s*-polarization while decreases for the *p*-polarization on increasing the deviation from the normal direction. In effect, the reflectance data which were obtained on the same sample by using the three lenses mentioned above, agreed with each other within the experimental error. Thus we concluded that the reflectance data which are obtainable with our microspectrophotometer can be regarded to be effectively the same as those obtained under the normal incidence condition.

To obtain absolute reflectance values, we have to compare the intensity of the light reflected from the sample with that reflected from a standard reflector of known reflectivity. The single crystals of silicon[9] and saphire[10,11] were used as the standard reflector, since the reflectances of their polished surfaces, in the near-infrared and visible region, are of the same order of magnitude with those of our samples and their surfaces are very stable so that their reflectance values do not vary with time.

On each modification of BD–TCNQ complex, we carried out the measurement on several different crystals. Although the obtained spectral shape were almost the same, the absolute reflectance values were different at most 10% ($\Delta R/R<0.1$) from crystal to crystal depending on the quality of the crystal surface. We considered that the spectrum showing the highest reflectance value at each reflectance maximum, are the best observed result.

There are several different method to obtain optical constants from a reflection spectrum. The Kramers-Kronig analysis is the most direct way if one can use reflectance data over a wide wavelength region. However, in the present study, the observation was limited only in the near-infrared and visible region, and, furthermore, our samples had strong absorption bands around the long and short wavelength limits of the observed range. These situations make it difficult to perform a direct Kramers-Kronig analysis. The method proposed by Roessler[12] and its modification[13] are also hard to be used in the present case. Therefore, we used the so-called dispersion analysis method, describing the complex dielectric function $\varepsilon(\omega)$ by the following equation based on the model of uncoupled Helmholtz-Kettler oscillators:[8]

$$\varepsilon(\omega) = \varepsilon_c + \sum_{j=1}^{N} \frac{S_j\omega_j^2}{(\omega_j^2-\omega^2)-i\gamma_j\omega_j\omega} \tag{1}$$

There is the following relation between the reflectance $R(\omega)$ and the complex dielectric function $\varepsilon(\omega)$.

$$R(\omega) = \frac{|\varepsilon(\omega)|+1-\sqrt{2}\{|\varepsilon(\omega)|+\mathrm{Re}[\varepsilon(\omega)]\}^{1/2}}{|\varepsilon(\omega)|+1+\sqrt{2}\{|\varepsilon(\omega)|+\mathrm{Re}[\varepsilon(\omega)]\}^{1/2}} \tag{2}$$

Treating the constants ε_c and (ω_j, γ_j, S_j), as adjustable parameters, we determined their values so as to give the best agreement between the observed and calculated reflectance. In this curve-fitting procedure, we defined an error function as $\sum_k[R_{obsd}(\omega_k)-R_{calcd}(\omega_k)]^2$, and looked for the set of the parameter values which minimize the above error function, by means of the Fletcher-Powell method,[14] using computer. By use of the known relations, $\mathrm{Re}[\varepsilon(\omega)]=n(\omega)^2-k(\omega)^2$ and $\mathrm{Im}[\varepsilon(\omega)]=2n(\omega)k(\omega)$, we calculated the optical constants, $n(\omega)$ and $k(\omega)$, from the obtained complex dielectric function. Then, the molar extinction coefficient $\mu(\omega)$ was calculated by Eq. 3

$$\mu(\omega) = \frac{2\omega k(\omega)}{c}\cdot\frac{1000d}{M}, \tag{3}$$

where c is the light velocity in vacuum, d is the density of

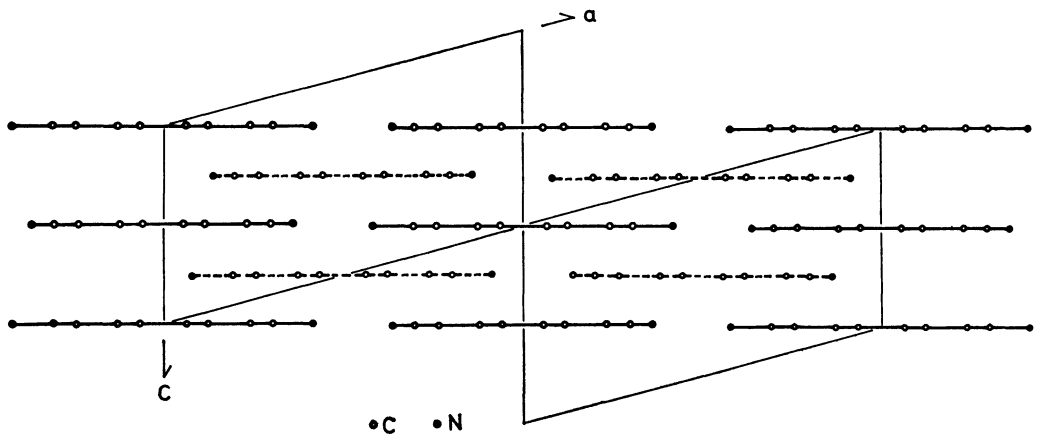

Fig. 2. The crystal structure of BD–TCNQ–[n] projected onto the (010) plane.

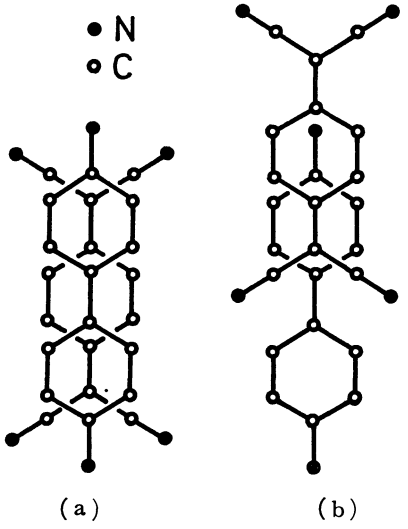

Fig. 3. (a) Molecular overlap between BD and TCNQ (Type A). (b) Molecular overlap between BD and TCNQ (Type B).

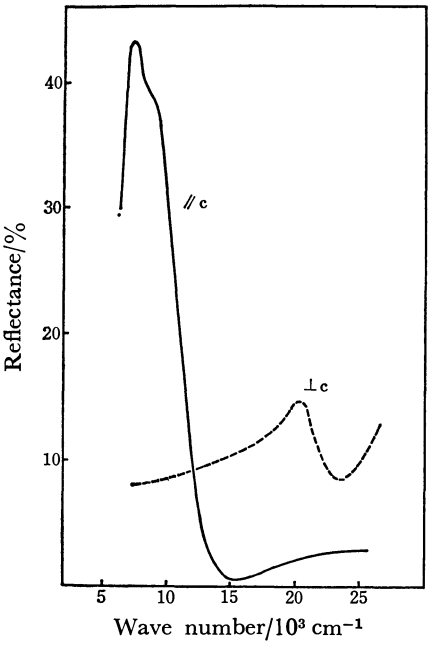

Fig. 4. Reflection spectra on the (010) plane of BD–TCNQ–[n].

the crystal, and M is the molecular weight of the complex. In practice, we used one oscillator function for each transition in describing the complex dielectric function by Eq. 1. The oscillator strength of the j-th electronic transition was calculated by the following equation.

$$f(j) = \frac{m}{2\pi^2 e^2 n} \int_0^\infty \mathrm{Im}\varepsilon^{(j)}(\omega)\omega \mathrm{d}\omega \qquad (4)$$

where $\varepsilon^{(j)}(\omega) = S_j\omega_j^2/[(\omega_j^2-\omega^2)-i\gamma\omega_j\omega]$, n is the number density of electrons concerned with the j-th transition, m is the electron mass, and e is the electron charge.

Results and Discussion

Solvent-free Modification, BD–TCNQ–[n]. The crystal of BD–TCNQ–[n] is monoclinic with the space group C2/m. The lattice constants are $a=12.231$ Å, $b=12.679$ Å, $c=6.477$ Å, and $\beta=104.84°$. Two molecular units are contained in the unit cell. As shown in the projection of the structure onto the (010) planes (Fig. 2), BD and TCNQ molecules are alternately stacked along the c axis, orienting their molecular planes almost perpendicular to the axis, and their long molecular axes are in the [201] direction. The overlap of BD and TCNQ molecules in this crystal is of the type A shown as Fig. 3(a), having the average intermolecular separation of 3.24 Å, between BD and TCNQ. We measured the reflection spectrum as well as the transmission spectrum on the (010) face of this crystal.

The observed reflection spectra are shown in Fig. 4, and the absorption spectra directly observed by the transmission method are shown in Fig. 5 (solid lines). It should be noted in Fig. 5 that the absorption spectra obtained by the two entirely different experimental methods are in satisfactory agreement with each other. As we will show later, a similarly good agreement between the spectra obtained by the two methods could be found in all cases studied in the present study. This fact provides an evidence for the validity of the procedure which we have adopted for the measurement and analysis of reflectance data.

As shown in Fig. 5, the //c absorption spectrum exhibits a strong absorption band with a maximum at 7.4×10^3 cm^{-1} and a shoulder at about 9×10^3

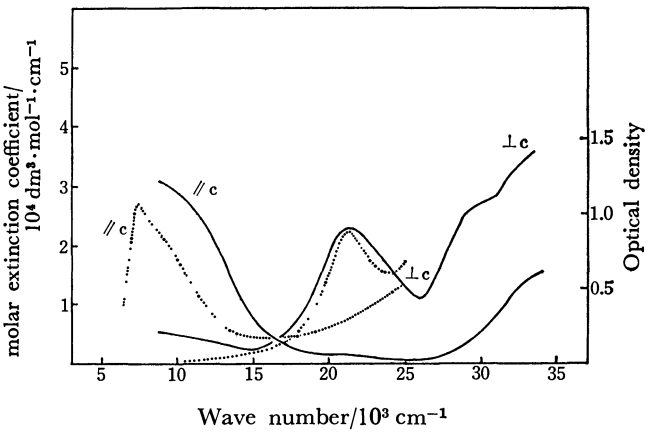

Fig. 5. Absorption spectra on the (010) plane of BD–TCNQ–[n]. The solid lines are the absorption spectra measured by the transmission method. The ordinate is optical density. The dotted lines are absorption spectra calculated by the reflection spectra. The ordinate is molar extinction coefficient.

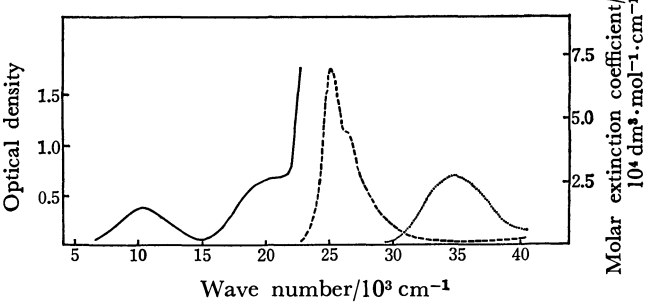

Fig. 6. Absorption spectra of BD (·····) and TCNQ (----) in the dichloromethane solution. The ordinate is molar extinction coefficient. Absorption spectra of BD–TCNQ complex (——) in the chloroform solution. The ordinate is optical density.

cm^{-1}. This infrared absorption band is strongly polarized in the c axis direction (BD–TCNQ stacking direction). On the other hand, the ⊥c spectrum shows an absorption band at 21.2×10^3 cm^{-1}, completely polarized in the [201] direction. The ⊥c spectrum measured by the transmission method shows another two absorption bands in the ultraviolet region, the one being at 29×10^3 cm^{-1} and the other at above 33×10^3 cm^{-1}. Figure 6 shows the absorption spectra of BD and TCNQ molecules observed on their dichloromethane solutions, and the charge-transfer bands of the BD–TCNQ complex formed in the chloroform solution. The absorption spectrum of BD shows a broad absorption band in the region from 30×10^3 cm^{-1} to 40×10^3 cm^{-1} (the maximum is at 35×10^3 cm^{-1}). This band can be assigned mainly to the π-π^* transition ($^1B_{3u}\leftarrow{}^1A_g$) polarized along the long molecular axis of BD. According to the molecular orbital calculation, there must be a weak absorption band associated with the short-axis polarized π-π^* transition ($^1B_{2u}\leftarrow{}^1A_g$) in the same region. Seemingly, this weak band is hidden under the strong absorption band mentioned above. In the solution spectrum of TCNQ, the absorption band at 25.4×10^3 cm^{-1} is due to the lowest π-π^* transition ($^1B_{3u}\leftarrow{}^1A_g$), polarized in the long-axis direction. BD and TCNQ molecules form a stable charge-transfer (CT) complex in the chloroform solution. As shown in Fig. 6, this molecular complex exhibits the first CT band at 10.3×10^3 cm^{-1} and the second one at 20×10^3 cm^{-1}. It was found in our previous study that the energy separation between the first and second CT bands was always about 1.3 eV in the solution spectra of a series of the molecular complexes which involve BD as the donor, irrespective of the acceptor, and the separation of the two CT bands is approximately equal to the energy difference between the highest and second highest occupied orbitals of BD. These facts indicate that the second CT band of the solution spectrum of BD–TCNQ complex is associated with the charge transfer from the second highest occupied molecular orbital (second HOMO) of BD to the lowest unoccupied molecular orbital (LUMO) of TCNQ, while the first CT band is associated with that from the HOMO of BD to the LUMO of TCNQ.

Let us compare the crystal spectrum of BD–TCNQ–[n] with the solution spectra discussed above. The 7.4×10^3 cm^{-1} band of the //c spectrum undoubtedly corresponds to the first CT band of the solution spectrum of BD–TCNQ complex, although its shift, 3×10^3 cm^{-1}, to lower energy is a little larger than the shift usually found for a typical CT complex.

From the simple comparison of the crystal spectrum with the solution spectra of BD, TCNQ, and their complex, we could conclude that the 21.2×10^3 cm^{-1} band of the crystal spectrum corresponds to the second CT band of the solution spectrum of BD–TCNQ complex, and the 29×10^3 cm^{-1} band and the band above 33×10^3 cm^{-1} are the local-excitation bands associated with the transitions in TCNQ and BD, respectively. However, it should be noted that the 21.2×10^3 cm^{-1} band of the crystal spectrum is polarized perpendicular to the direction of the BD–TCNQ stack. This is unusual for a CT band. On the other hand, if the 21.2×10^3 cm^{-1} band is due to the $^1B_{3u}\leftarrow{}^1A_g$ transition of TCNQ, we must consider that it is shifted by 4×10^3 cm^{-1} to lower energy as compared with the solution spectrum.

A BD molecule overlaps with the adjacent TCNQ molecule, in the manner shown in Fig. 3(a). In this case, the overlap integral between the HOMO (b_1) of BD and the LUMO (b_1) of TCNQ is large, but the overlap integral between the second HOMO (a_1) of BD and the LUMO (b_1) of TCNQ must be zero. This means that the absorption band, which has been tentatively attributed to the charge transfer from the second HOMO of BD to the LUMO of TCNQ, cannot appear unless the above CT configurations is mixed with another excited configuration which gives a strong absorption band. The most probable mechanism would be the mixing of the local excitation associated with the lowest π-π^* transition ($^1B_{3u}\leftarrow{}^1A_g$) of TCNQ. In order to confirm this idea, we carried out a molecular orbital calculation on the isolated BD–TCNQ pair of the geometry found in the crystal. The method of calculation is the same as the one which was previously used by Ohta, Kuroda, and Kunii for the molecular complexes of polycyclic aromatic hydrocarbon

TABLE 1. TRANSITIONS PREDICTED BY THE SCF·MO·CI CALCULATION ON A BD·TCNQ PAIR CORRESPONDING TO BD-TONQ-[n] CRYSTAL

	Transition[a]	Wave number $\nu/10^3$ cm^{-1}	f[b]	Transition dipole[c]			Character of transition				Assignment
				M_x	M_y	M_z	$(DD)_m$	$(AA)_m$	$(DA)_m$	$(AD)_m$	
(1)	(16→17)	12.51	0.356	—	—	1.619	0.13	0.13	0.69	0.03	CT(D→A)
(2)	(15→17)	17.55	0.802	2.052	—	—	0.08	0.38	0.43	0.07	CT(D→A)+LE(A*)
(3)	(14→17)	24.52	0.559	1.450	—	—	0.09	0.39	0.42	0.07	CT(D→A)+LE(A*)
(4)	(16→19)	26.96	0.124	—	0.651	—	0.00	0.19	0.75	0.00	CT(D→A)
(5)	(16→20)	28.07	0.196	0.802	—	—	0.01	0.20	0.77	0.01	CT(D→A)
(6)	(15→20)	31.22	0.018	—	—	0.235	0.00	0.46	0.50	0.00	CT(D→A)+LE(A*)
(7)	(15→18)	32.35	0.143	—	0.638	—	0.04	0.37	0.46	0.01	CT(D→A)+LE(A*)
(8)	(16→21)	33.91	0.494	—	1.157	—	0.06	0.15	0.56	0.04	CT(D→A)
(9)	(16→22)	34.21	1.850	2.233	—	—	0.80	0.01	0.01	0.15	LE(D*)

a) The main excitation is indicated here: $(i\rightarrow j)$ stands for the electron excitation from the i-th orbital to the j-th orbital. b) Oscillator strength. c) x and y are parallel to the long and short axes of BD and TCNQ; z axis is parallel to the direction connecting the centers of BD and TCNQ.

with tetracyanoethylene.[15] A π-orbital of a supermolecule, BD–TCNQ pair, is expressed by the linear combination of $2p_z$ AO's as follows.

$$\phi_i = \sum_{\mu=1}^{n_d+n_a} C_{i\mu}\phi_\mu \tag{5}$$

where ϕ_μ with $\mu=1$—n_d are the AO's associated with the donor and those with $\mu=n_d+1$—n_d+n_a are the AO's associated with the acceptor. In order to see the contributions of the donor and acceptor for the i-th molecular orbital, we define D_i and A_i as follows.

$$D_i = \sum_{\mu=1}^{n_d} C_{i\mu}^2 \qquad A_i = \sum_{\mu=n_a+1}^{n_d+n_a} C_{i\mu}^2 \tag{6}$$

The π-orbital scheme calculated for the BD–TCNQ pair and those for the constituent molecules are illustrated in Fig. 7, where the values (D_i, A_i) are given for each molecular orbital of BD–TCNQ pair. With the aid of D_i and A_i values and the symmetry consideration, we derived the correlation between the orbitals of BD–TCNQ pair and those of BD and TCNQ molecules as illustrated in Fig. 7 with dotted lines.

The excited states of BD–TCNQ pair were calculated by taking into account the configuration interaction of all singly-excited configurations. The results of this calculation are summarized in Table 1. The electronic transitions in a molecular pair DA can be classified into four categories: (a) the local excitation LE(D*) associated with a transition in the donor molecule D, (b) the local excitation LE(A*) associated with a transition in the acceptor molecule A, (c) the charge-transfer excitation CT(D→A), (d) the back charge-transfer excitation CT(A→D). The excitation of an electron from the i-th orbital to the j-th orbital of the molecular pair, Φ_{ij}, generally has a character that LE(D*), LE(A*), CT(D→A), and CT(A→D) are mixed with the weights proportional to D_iD_j, A_iA_j, D_iA_j and A_iD_j, respectively. When the CI (configuration interaction) wavefunction of the m-th excited state, Ψ_m, is expressed as,

$$\Psi_m = \sum_{ij} b_{ij,m}\Phi_{ij} \tag{7}$$

we define the following quantities.

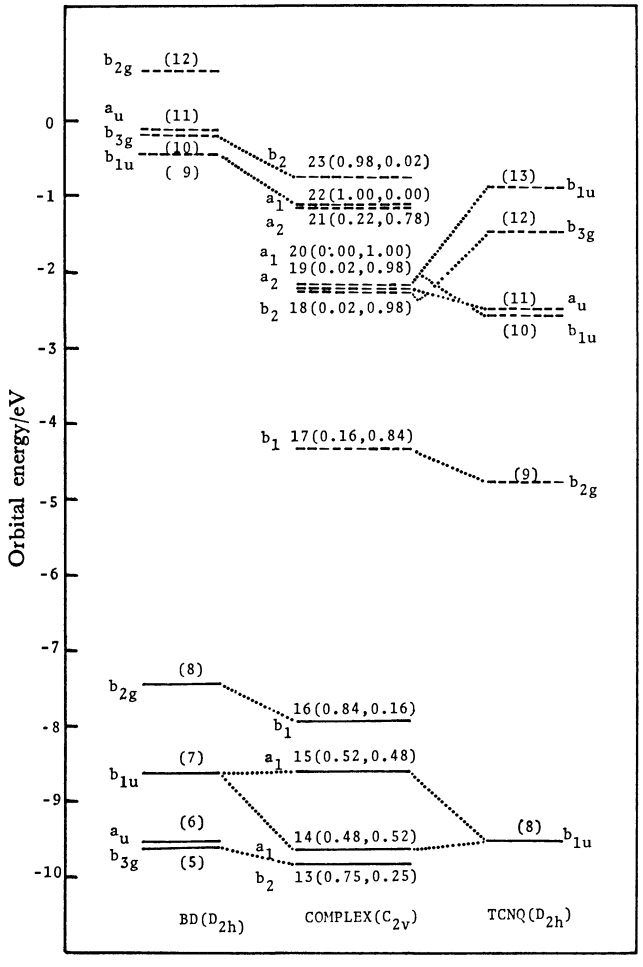

Fig. 7. Molecular orbitals of BD, TCNQ, and BD-TCNQ complex. The numerical values in the parenthesis correspond to the weight of the donor and acceptor character.

$$\begin{aligned}(DD)_m &= \sum_{ij} b^2_{ij,m}D_iD_j \\ (AA)_m &= \sum_{ij} b^2_{ij,m}A_iA_j \\ (DA)_m &= \sum_{ij} b^2_{ij,m}D_iA_j \\ (AD)_m &= \sum_{ij} b^2_{ij,m}A_iD_j\end{aligned} \tag{8}$$

The values of $(DD)_m$, $(AA)_m$, $(DA)_m$, and $(AD)_m$ give the weights of the characters of LE(D*), LE(A*), CT(D→A), and CT(A→D) in the m-th excited state, respectively. The above values of each transition are also given in Table 1. For example, in the case of the transition (1) which is predicted at 12.51×10^3 cm^{-1}, the $(DA)_m$ value is about 0.7, which indicates that this transition is mainly associated with a charge transfer from BD to TCNQ. In effect, the transition moment is predicted to be in the direction connecting the centers of BD and TCNQ molecules. The result for the transition (2) is most interesting. This transition is predicted to have its transition moment parallel to the long axes of BD and TCNQ molecules. In this case, $(DA)_m$ is 0.43 and $(AA)_m$ is 0.38. This means that the transition has a character that CT (D→A) and LE(A*) are mixed with almost equal weights. The same can be said for the third transition predicted at 24.52×10^3 cm^{-1}. When we calculate the transitions in TCNQ molecule using the same method, the lowest π-π^* transition ($^1B_{3u}\leftarrow{}^1A_g$) is predicted at 22.18×10^3 cm^{-1}, which is lower by about 3×10^3 cm^{-1} than the experimental value. From the comparison of the results of the calculation on BD–TCNQ pair and those on TCNQ molecule, we can conclude that the CT configuration associated with the charge transfer from the second HOMO of BD to the LUMO of TCNQ and the LE(A*) configuration associated with the lowest singlet π-π^* excitation of TCNQ, are strongly mixed with each other in BD–TCNQ pair to give the transitions (2) and (3).

Although the crystal of BD–TCNQ–[n] is not composed of isolated BD–TCNQ pairs, the results of the above calculation can be used to interprete the crystal spectrum, since the main features of the crystal spectrum of a CT complex is determined by the interaction between neighboring donor and acceptor molecules. The z and x axes in Table 1 correspond to the //c and ⊥c directions of the crystal of BD–TCNQ–[n], respectively. Consequently, the transition (1) which is predicted to be polarized in the z axis direction will appear in the //c spectrum, while the x axis polarized transitions, (2), (3), (5), and (9) are expected to appear in the ⊥c spectrum. Therefore, we can assign the 7.4×10^3 cm^{-1} band in the //c spectrum to the transition (1), and the 21.2×10^3 cm^{-1} and 29×10^3 cm^{-1} bands in the ⊥c spectrum to the transitions (2) and (3), respectively. The strong absorption band at above 33×10^3 cm^{-1} in the ⊥c spectrum is likely to correspond to the transition (9) which is mainly associated with the lowest π-π^* transition of BD. We were not able to observe any absorption maximum corresponding to the transition (5). Seemingly, it is hidden under the strong absorption bands corresponding to the transitions (3) and (9).

The low frequency dielectric constants of the microcrystalline powders of molecular complexes were studied by Ishii *et al.*[16] by use of the microwave cavity perturbation method. It was revealed that the observed dielectric constants are always larger than the values estimated under the assumption that the molecular polarization of a complex is equal to the simple sum of the molecular polarizations of the

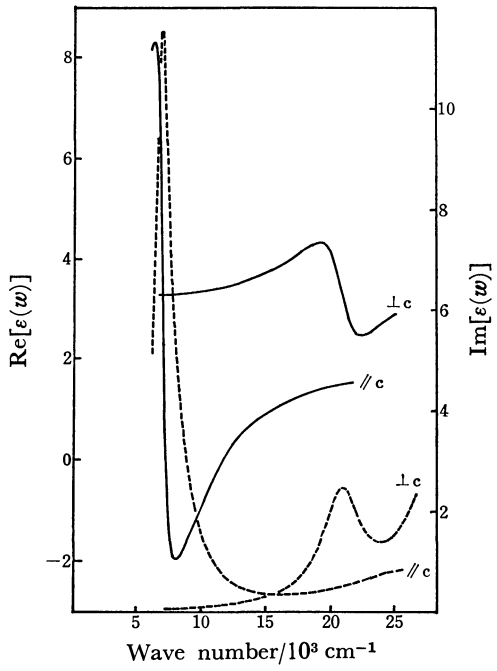

Fig. 8. The real (——) and the imaginary (----) parts of the dielectric function of BD–TCNQ–[n].

constituent molecules. The dielectric constant of the BD–TCNQ–[n] powder is 6—7 according to the above paper. If we estimate the molecular polarization of BD–TCNQ system as the simple sum of the molecular polarizations of BD and TCNQ, and assume the Clausius-Mossotti equation, the dielectric constant of BD–TCNQ–[n] is estimated to be about 4, which is smaller by 2—3 than the observed dielectric constant. This difference must be due to the enhancement of dielectric constant by the intermolecular interaction. It is most likely that the above enhancement arises mainly from the CT interaction between BD and TCNQ. To confirm this idea, we carried out the following analysis.

Fig. 8 shows the real and imaginary parts of the frequency-dependent dielectric functions obtained from the //c and ⊥c reflection spectra. The static dielectric constant $\varepsilon(0)$ can be estimated from the complex dielectric function $\varepsilon(\omega)$ by means of the Kramers-Kronig equation for an insulator.

$$\varepsilon(0) = 1 + \frac{2}{\pi}\int_0^\infty \frac{\mathrm{Im}\varepsilon(\omega)}{\omega}\mathrm{d}\omega \tag{9}$$

According to this relation, the contribution of the CT transitions to $\varepsilon(0)$ can be expressed as follows.

$$\Delta\varepsilon(\mathrm{CT}) = \frac{2}{\pi}\int_{\omega_1}^{\omega_2} \frac{\mathrm{Im}\varepsilon(\omega)}{\omega}\mathrm{d}\omega \tag{10}$$

where ω_1 and ω_2 are the low- and high-frequency limits of the region of CT band. Taking $\omega_1=4\times10^3$ cm^{-1} and $\omega_2=24\times10^3$ cm^{-1}, we performed the above integration using the complex dielectric functions obtained from the //c and ⊥c reflection spectra. The $\Delta\varepsilon$(CT) value thus calculated was 3.0 and 0.5 for the //c and ⊥c polarizations, respectively. The $\Delta\varepsilon$ (CT) value must be zero for the //b polarization since the CT transitions concerned here has no //b component. In order to compare with the dielectric behavior

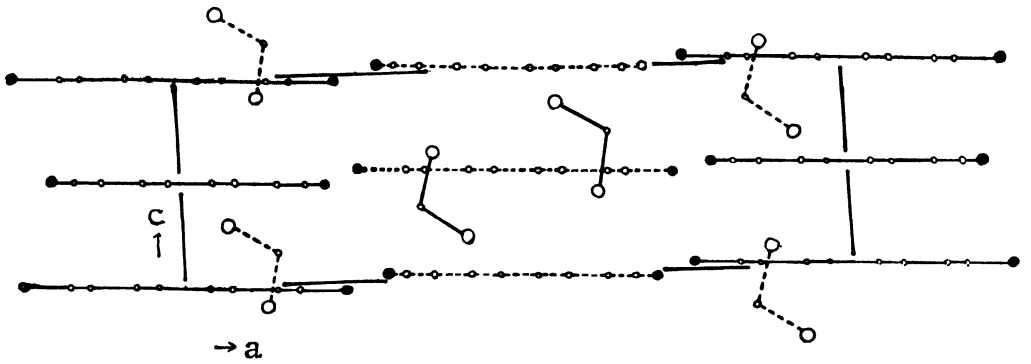

Fig. 9. The crystal structure of BD–TCNQ–[CH_2Cl_2] projected onto the (010) plane.

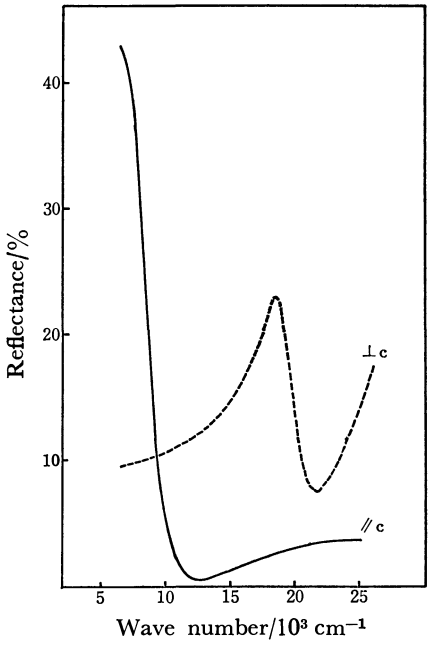

Fig. 10. Reflection spectra on the (010) plane of BD–TCNQ–[CH_2Cl_2].

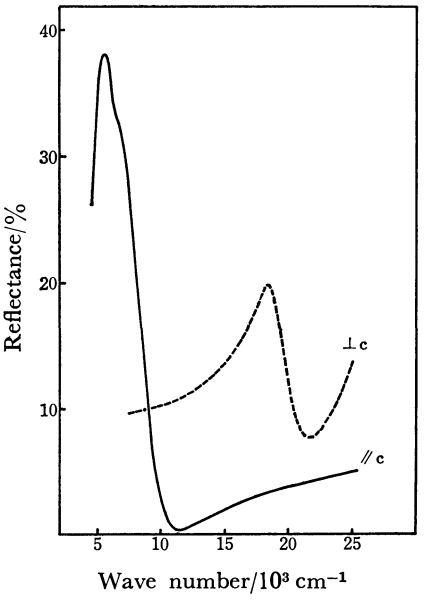

Fig. 11. Reflection spectra on the (100) plane of BD–TCNQ–[CH_2BrCH_2Br].

of the microcrystalline powder, we have to take the average of the $\Delta\varepsilon$(CT) values for the three polarizations. This average value is calculated to be 1.2. Although it is a little smaller than the enhancement of dielectric constant, estimated from the data by the microwave cavity perturbation method, the above result indicates that the enhancement of dielectric constant is indeed mainly due to the intermolecular charge-transfer interaction.

BD–TCNQ–[CH_2Cl_2] and BD–TCNQ–[CH_2BrCH_2Br]. The crystal of BD–TCNQ–[CH_2Cl_2] is monoclinic, with the space group I2/m. The lattice constants are $a=20.892$ Å, $b=9.950$ Å, $c=6.445$ Å, and $\beta=91.92°$.[3] Two molecular units are contained in the unit cell as shown in Fig. 9. The BD and TCNQ molecules are alternately stacked along the c axis to form a BD–TCNQ column, in which the molecular overlap of BD and TCNQ are almost the same as that in BD–TCNQ–[n] except that the average separation of the molecular planes, 3.22 Å, is a little smaller than that in the latter. The main difference between BD–TCNQ–[CH_2Cl_2] and BD–TCNQ–[n] is that, in the former crystal, there are channels surrounded by four BD–TCNQ columns, in which dichloromethane molecules are included, while BD–TCNQ columns are closely packed in the crystal of BD–TCNQ–[n]. The adjacent BD–TCNQ columns in BD–TCNQ–[CH_2Cl_2] are connected with each other by the intermolecular hydrogen bonds between C≡N group of TCNQ and NH_2 group of BD. These hydrogen bonds seem to contribute to the stabilization of the channeled structure of BD–TCNQ sublattice of the solvated modification.

The crystal of BD–TCNQ–[CH_2BrCH_2Br] is orthorhombic with the space group Immm. The lattice constants are $a=10.205$ Å, $b=20.785$ Å, and $c=6.525$ Å. The a and b axes in this crystal correspond to the b and a axes of BD–TCNQ–[CH_2Cl_2], respectively, and the structure of BD–TCNQ sub-lattice is almost the same as that of the latter crystal, except that the average separation between the molecular planes of BD and TCNQ is 3.26 Å.

The reflection spectrum measured on the (010) face of BD–TCNQ–[CH_2Cl_2] and that measured on the corresponding crystal face, (100), of BD–TCNQ–[CH_2BrCH_2Br] are shown in Fig. 10 and Fig. 11, respectively. From the analyses of these spectra, we obtained the absorption spectra shown in Figs. 12 and 13. In Fig. 12, we have also shown the absorption

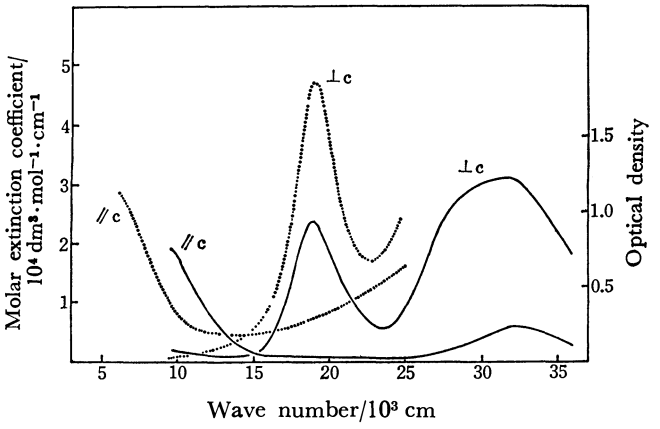

Fig. 12. Absorption spectra on the (010) plane of BD-TCNQ-[CH_2Cl_2]. The continuous lines are the absorption spectra measured by transmission method. The ordinate is optical density. The dotted lines are absorption spectra calculated by the reflection spectra. The ordinate is molar extinction coefficient.

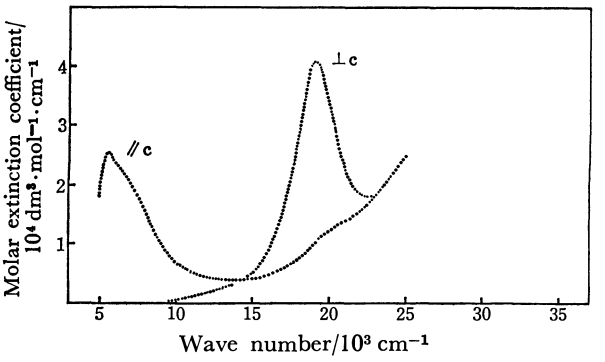

Fig. 13. Absorption spectra on the (100) plane of BD-TCNQ-[CH_2BrCH_2Br] calculated by the reflection spectra. The ordinate is molar extinction coefficient.

spectrum measured on the same crystal face directly by the transmission experiment.

The spectra of BD-TCNQ-[CH_2Cl_2] and BD-TCNQ-[CH_2BrCH_2Br] are very similar to each other as we can expect from the similarity of BD-TCNQ sub-lattice in these two crystal forms. In both cases, the //c spectrum exhibits a strong absorption band in the near-infrared region. The maximum of this band is located at 5.7×10^3 cm^{-1} in the case of BD-TCNQ-[CH_2BrCH_2Br]. Seemingly the absorption maximum is at almost the same wave number in the case of BD-TCNQ-[CH_2Cl_2]. This infrared band is the CT band corresponding to the 7.4×10^3 cm^{-1} band of BD-TCNQ-[n]. There are three absorption bands in the ⊥c spectrum: a relatively sharp one at 19.0×10^3 cm^{-1} and two broad ones at 27×10^3 and 32×10^3 cm^{-1}, respectively. These bands must correspond to the absorption bands observed at 21.2×10^3, 29×10^3, and above 33×10^3 cm^{-1}, respectively, in the ⊥c spectrum of BD-TCNQ-[n]. It should be noted that all absorption bands are shifted to lower wave number by about 2×10^3 cm^{-1} in the spectrum of BD-TCNQ-[CH_2Cl_2] as compared with the spectrum of BD-TCNQ-[n], and the intensity of 19.0×10^3 cm^{-1} band is markedly enhanced in the solvated modifications.

We carried out the molecular orbital calculation on the BD-TCNQ pair taking the separation of the molecular planes as 3.22 Å as in the crystal of BD-TCNQ-[CH_2Cl_2]. This calculation shows that the transitions which are responsible for the observed absorption bands, are shifted to lower wave number on decreasing the molecular separation from 3.24 Å to 3.22 Å. But the predicted shift is 50 and 300 cm^{-1} for the transitions (1) and (2), respectively, and 600 cm^{-1} for the transitions (3) and (8) of Table 1. These

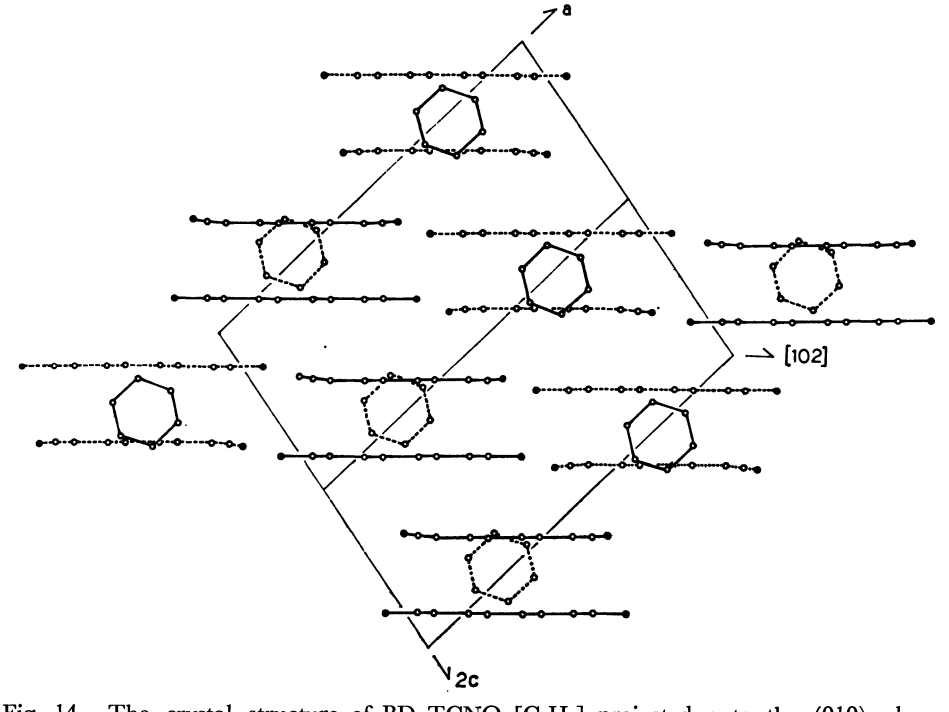

Fig. 14. The crystal structure of BD-TCNQ-[C_6H_6] projected onto the (010) plane.

TABLE 2. TRANSITION PREDICTED BY SCF·MO·CI CALCULATIONS ON THE TWO STRUCTURES OF BD·TCNQ PAIR CORRESPONDING TO BD-TCNQ-[C_6H_6]; SEE Fig. 3 (a) AND (b) FOR THE OVERLAPPING OF BENZIDINE AND TCNQ IN EACH MODEL

	Transition	Wave number $\nu/10^3$ cm^{-1}	f	Transition dipole			Charabter of transition				Assignment
				M_x	M_y	M_z	$(DD)_m$	$(AA)_m$	$(DA)_m$	$(AD)_m$	
Model (a)											
(1)	(16→17)	13.83	0.467	—	—	1.762	0.18	0.18	0.56	0.06	CD(D→A)
(2)	(15→17)	17.35	0.964	2.263	—	—	0.11	0.40	0.34	0.12	CT(D→A)+LE(A*)
(3)	(14→17)	24.98	0.266	0.989	—	—	0.08	0.49	0.28	0.12	LE(A*)
(4)	(16→19)	28.21	0.144	—	0.685	—	0.02	0.26	0.69	0.01	CT(D→A)
(5)	(16→20)	29.08	0.244	0.898	—	—	0.02	0.27	0.67	0.02	CT(D→A)
(6)	(15→20)	30.77	0.023	—	—	0.262	0.03	0.46	0.46	0.04	CT(D→A)+LE(A*)
(7)	(15→18)	30.79	0.166	—	0.705	—	0.03	0.46	0.43	0.01	CT(D→A)+LE(A*)
(8)	(15→19)	31.96	0.102	—	0.542	—	0.04	0.46	0.42	0.02	CT(D→A)+LE(A*)
(9)	(16→21)	33.22	1.663	2.148	—	—	0.72	0.00	0.02	0.23	LE(D*)
(10)	(16→22)	33.56	0.295	—	0.900	—	0.27	0.19	0.47	0.09	CT(D→A)
Model (b)											
(1′)	(16→17)	10.16	0.505	1.595	—	1.429	0.13	0.10	0.73	0.02	CT(D→A)
(2′)	(15→17)	20.47	0.230	0.788	—	0.642	0.09	0.29	0.53	0.05	CT(D→A)
(3′)	(14→17)	21.32	1.159	2.210	—	0.358	0.06	0.54	0.29	0.09	LE(A*)
(4′)	(16→19)	25.98	0.427	1.224	—	0.131	0.00	0.14	0.82	0.00	CT(D→A)
(5′)	(16→20, 21, 23)	31.40	0.230	—	0.823	—	0.23	0.09	0.55	0.05	CT(D→A)
(6′)	(16→22)	32.19	1.196	1.840	—	0.199	0.81	0.03	0.02	0.11	LE(D*)
(7′)	(16→25) (14→18)	35.86	0.506	—	1.141	—	0.30	0.40	0.22	0.00	LE(A*)+LE(D*)

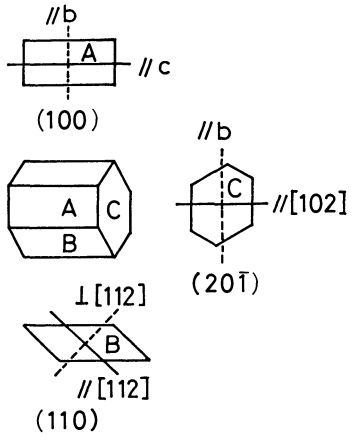

Fig. 15. Crystal morphology and principal axis directions for BD-TCNQ-[C_6H_6] single crystal.

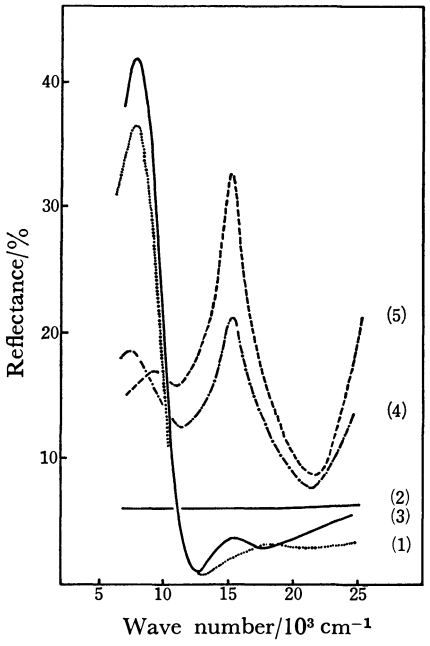

Fig. 16. Reflection spectra of BD-TCNQ-[C_6H_6]. The numbers correspond to the spectra polarized to (1) //c on the (100) (2) //b on the (100) (3) ⊥[112] on the (110) (4) //[112] on the (110) (5) //[102] on the (201).

are too small to explain the observed difference between the spectra of BD-TCNQ-[CH_2Cl_2] and BD-TCNQ-[n]. The oscillator strength of the transition (2) is predicted to increase only by about 15 percent on decreasing the molecular separation from 3.24 Å to 3.22 Å, while the observed oscillator strength of the 19.0×10^3 cm^{-1} band of BD-TCNQ-[CH_2Cl_2] is almost twice that of the 21.2×10^3 cm^{-1} band of BD-TCNQ-[n]. Thus, the observed differences between the spectra of BD-TCNQ-[CH_2Cl_2] and BD-TCNQ-[n] cannot be simply explained from the decrease of the intermolecular separation. Seemingly, it is necessary to take into account the effects of the intermolecular hydrogen bonds and the presence of solvent molecules in order to fully understand the observed differences.

BD-TCNQ-[C_6H_6]. The crystal of BD-TCNQ-[C_6H_6] is monoclinic with the space group $P2_1/m$, the lattice constants being $a=17.184$ Å, $b=9.852$ Å, $c=7.680$ Å, and $\beta=100.3°$.[5] The unit cell contains two molecular units. The structure of BD-TCNQ sub-lattice in this crystal is quite different from

Table 3. Comparison between the predicted and observed absorption bands in the //c and //b spectra of the (100) plane of BD-TCNQ-[C_6H_6]

//c Spectrum					//b Spectrum				
$\nu/10^3$ cm^{-1}	f_c[a]		Ttansition[c]	observed band $\nu/10^3$ cm^{-1}	$\nu/10^3$ cm^{-1}	f_b[b]		Transition[c]	Observed band $\nu/10^3$ cm^{-1}
10.16	0.48	(1′)	CT(D→A)	4—15 (max. 7.5)					
13.83	0.20	(1)	CT(D→A)						
17.35	0.32	(2)	CT(D→A)+LE(A)	15—24 (max. 17.3 shoulder: 20)					
20.47	0.21	(2′)	CT(D→A)						
21.32	0.22	(3′)	LE(A*)						
24.98	0.09	(3)	LE(A*)	>25	28.21	0.14	(4)	CT(D→A)	25—30
25.98	0.10	(4′)	CT(D→A)		30.79	0.17	(6)	CT(D→A)+LE(A*)	
29.08	0.08	(5)	CT(D→A)		31.40	0.23	(5′)	CT(D→A)	
					31.96	0.10	(8)	CT(D→A)+LE(A*)	
32.19	0.28	(6′)	LE(D*)		33.56	0.30	(10)	CT(D→A)	≈33
33.22	0.05	(9)	LE(D*)		35.86	0.51	(7′)	LE(A*)+LE(D*)	

a) //c component of oscillator strength predicted for each transition. //b component of oscillator strength predicted for each transition. c) Refer Table 2 for the numberings of transitions.

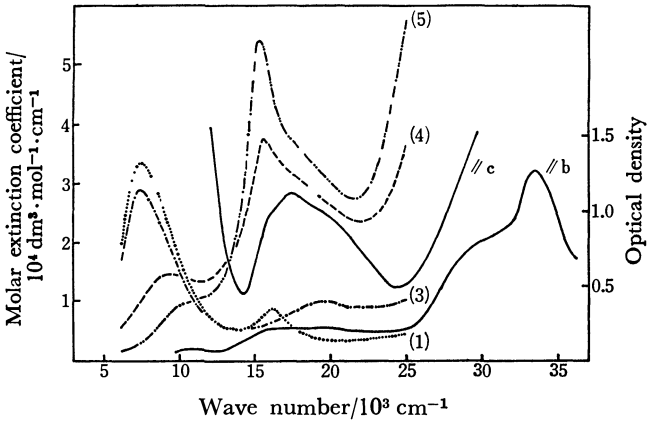

Fig. 17. Absorption spectra of BD-TCNQ-[C_6H_6]. The continuous lines are the absorption spectra on the (100) plane measured by the transmission method. The ordinate is optical density. The other lines are the absorption spectra calculated by the reflection spectra. The ordinate is molar extinction coefficient. The numbers correspond to those in Fig. 16.

Table 4. Comparison between the observed and predicted oscillator strength of BD-TCNQ-[C_6H_6]

	Spectrum[a] (1)	(2)	(3)	(4)	(5)
[Infrared band]					
$\nu_m/10^3$ cm^{-1}	7.5	—	7.5	9.4	≈10
f_{obsd}[b]	1.2	0.0	0.9	0.7	0.2
$f(1)$	0.308	0.000	0.427	0.000	0.000
$f(1')$	0.476	0.000	0.256	0.242	0.296
$f(1)+f(1')$	0.784	0.000	0.683	0.242	0.296
[Visible band]					
$\nu_m/10^3$ cm^{-1}	16.1	—	19.5	15.6	15.3
f_{obsd}[b]	0.1	0.0	0.2	2.1	2.8
$f(2)$	0.334	0.000	0.015	0.789	0.964
$f(2')$	0.211	0.000	0.106	0.119	0.145
$f(3')$	0.207	0.000	0.003	0.914	1.117
$f(2)+f(2')+f(3')$	0.752	0.000	0.124	1.822	2.226

a) The numbers of the spectrum correspond to those in Fig. 17. b) f_{obsd} is the oscillator strength obtained from each reflection spectrum. $f(a)$ is the projected value of the predicted oscillator strength of the transition (a) on each observed polarization-direction.

the cases discussed above. The BD-TCNQ sub-lattice is definitely composed of BD-TCNQ pairs (see Fig. 14). The molecular overlap within the BD-TCNQ pair is of the same type as those in BD-TCNQ-[n] and BD-TCNQ-[CH_2Cl_2], which are shown in Fig. 3(a), but with a very short intermolecular separation of 3.09 Å. On the other hand, the BD-TCNQ overlap between the adjacent pairs is of the type shown in Fig. 3(b) with an intermolecular separation of 3.27 Å. Here again, the hydrogen bonds between C≡N group of TCNQ and NH_2 group of BD stabilize the channeled structure of the BD-TCNQ sub-lattice.

The typical shape of the crystal of BD-TCNQ-[C_6H_6] is a hexagonal prism with the developed crystal faces (100), (110), and (201) as shown in Fig. 15. The reflection spectra were measured on all of the above three crystal faces. Fig. 16 shows the observed spectra. The spectra (1) and (2) were obtained on the (100) face for the light polarizations parallel to the c and b axes, respectively; the spectra (3) and (4) were obtained on the (110) face for the polarizations parallel and perpendicular to the [112] direction; the spectrum (5) is the one obtained on the (201) face for the polarization parallel to the [102] direction. The spectrum (1) shows two reflectance maxima at 7.6×10^3 and 15.5×10^3 cm^{-1}, while the spectrum (2) exhibits no indication of dispersion in the whole observed range. The spectra (3) and (4) also exhibit a reflectance maximum at about 7.6×10^3 cm^{-1}, but the spectrum (5) shows a small maximum at 9.0×10^3 cm^{-1} instead of 7.6×10^3 cm^{-1}. This fact indicates that there are two kinds of transitions in the infrared region. In the visible region, the spectra (1), (4), and (5) exhibit a reflectance maximum at 15.5×10^3 cm^{-1}, but the spectrum (3) shows a maximum at 19×10^3 cm^{-1}. We note

also in the spectra (4) and (5), the shape of the reflectance curve at the high energy side of the 15.5×10^3 cm^{-1} maximum suggests the presence of another dispersion.

The absorption spectra obtained by the analysis of the reflectance data are shown in Fig. 17, together with the absorption spectra directly observed by the transmission experiment on the (100) plane of the relatively thick crystal.

We carried out the molecular orbital calculations on the two models of BD–TCNQ pair corresponding to the two kinds of BD–TCNQ molecular overlap in BD–TCNQ–[C_6H_6]. The model (a) is the one corresponding to the arrangement of BD and TCNQ molecules within the BD–TCNQ pair and the model (b) is the one corresponding to that between adjacent pairs. The transitions which are predicted for the two models are listed in Table 2. Since the short molecular axis of TCNQ has been taken as the y axis direction in the above Table, the transition polarized in the y axis direction are expected to appear only in the //b spectrum, while other transitions are expected to have their transition moments within the (010) plane. Thus the comparison of the observed absorption band with the predicted transitions can be made as shown in Table 3. As indicated in this table, it is most likely that the absorption bands in the infrared region is associated with the transitions (1) and (1′), and those in the visible region are associated with the transitions (2), (2′), and (3′). Using the predicted oscillator strengths and the crystal structure data, we estimated the components of the oscillator strengths parallel to the polarization direction of each observed spectrum. The results are listed in Table 4 together with the observed values. Naturally it is difficult to expect a good quantitative agreement between the experimental and predicted values. But the general features of the absorption spectra can be understood from the results of the calculation. The results shown in Table 4 suggest that the absorption band at about 9×10^3 cm^{-1} observed in the spectra (4) and (5) of Fig. 17 is the one associated with the transition (1′), while the strong infrared band in the spectra (1) and (3), is due to the superimposition of the bands associated with the transitions (1) and (1′). This means that the absorption band corresponding to the transition (1) is located at about 7×10^3 cm^{-1}, and is energetically lower than the one corresponding to the transition (1′), although the transition (1′) is predicted to be energetically lower than the transition (1), according to the calculation on the models of isolated BD–TCNQ pair. For the visible region, we can conclude that the weak absorption band at 19×10^3 cm^{-1} in the spectrum (3) is due to the transition (2′), while, in the spectra (4) and (5), the strong peak at 15.5×10^3 cm^{-1} is associated with the transition (2) and its high-energy tail is associated with the transition (3′). There exists a discrepancy as regards the spectral shape in the visible region between the spectrum (1) and the absorption spectrum measured directly by the transmission method on the same crystal plane (100). In this case, the absorption spectrum derived from the reflectance data seems to be less reliable since the reflectance of the (100) face in the above region is very small for the //c polarization, so that there could be relatively large errors in the process of their analysis. We consider that the absorption spectrum directly observed on a thick crystal is more reliable in this case than the spectrum derived from the reflectance data. The former shows a weak and broad visible absorption band with an indication that it is actually composed of three transitions. Indeed this is consistent with the results of calculation shown in Table 4.

Summary and Conclusion. In the present study, we have observed the absorption and reflection spectra on the known crystallographic faces of the single crystals of BD–TCNQ–[n], BD–TCNQ–[CH_2Cl_2], BD–TCNQ–[CH_2BrCH_2Br], and BD–TCNQ–[C_6H_6]. Usually in the case of the direct measurement of absorption spectrum by the transmission experiment with a microspectrophotometer, there remains some ambiguity as regards the identification of the crystallographic nature of the observing crystal face since it is hard to identify it directly by X-ray diffraction. On the other hand, in the case of the measurement of reflection spectrum by the microspectrophotometric technique, we can use a relatively large crystal, so that we can directly determine the observing crystal face by means of the X-ray diffraction, and it is also possible to observe the reflection spectrum on several different crystal faces. Thus we can determine the direction of the transition moment of an absorption band without any ambiguity. By this method, we confirmed that the first absorption band at about $6—8\times10^3$ cm^{-1} is polarized in the direction of BD–TCNQ stack, but the second absorption band at about 17×10^3 cm^{-1} is polarized parallel to the direction of the long molecular axes of BD and TCNQ in the cases of BD–TCNQ–[n], BD–TCNQ–[CH_2Cl_2], and BD–TCNQ–[CH_2BrCH_2Br]. The situation is a little complicated in the case of BD–TCNQ–[C_6H_6]. The transmission experiment was possible only on the (100) face of the crystal of this modification, and the observed absorption spectra indicated that both the first and second band appear in the //c spectrum. However, by examining the reflection spectra obtained on three different crystal faces, we revealed that there exist two absorption bands of different polarizations in the infrared region, and three bands in the visible region. We carried out molecular-orbital calculations on the models of BD–TCNQ pair, and showed that the observed spectra can be satisfactorily interpreted by using the results of these calculations. It has been thus concluded that, in BD–TCNQ complexes, the infrared absorption band is associated with the charge transfer from the HOMO of BD to the LUMO of TCNQ, but the second CT excitation associated with the charge transfer from the second HOMO of BD to the LUMO of TCNQ is strongly mixed with the local excitation from the HOMO to the LUMO of TCNQ to give a visible absorption band and an absorption band at about 29×10^3 cm^{-1}. This can be understood as follows from the consideration of the orbital symmetries. BD and TCNQ molecules overlap on each other as shown in Fig. 3(a), having their molecular axes exactly on each

Table 5. Observed oscillator strengths of the charge-transfer bands of BD-TCNQ complexes

	CT1		CT2[a]		Intermolecular spacing	
	$\nu_{max}/10^3$ cm^{-1}	f	$\nu_{max}/10^3$ cm^{-1}	f	Å	
BD-TCNQ-[n]	7.4	0.8	21.3	0.7	3.24	
BD-TCNQ-[CH_2Cl_2]	<6.2	(0.8)	19.1	1.6	3.22	H-bond
BD-TCNQ-[CH_2BrCH_2Br]	5.7	0.8	19.8	1.5	3.26	H-bond
BC-TCNQ-[C_6H_6] (a)	7.5	≈1.2	15.3	(<2.8)[b]	3.09	H-bond
(b)	≈10		19.5		3.29	

a) This is not a pure charge-transfer band. Refer the text for the nature of this band. b) The contribution of the transition (3′) is included in this value.

other. As shown in Fig. 7, the HOMO of TCNQ and the second HOMO of BD have the same orbital symmetry b_{1u}. Therefore, the electronic excitations from these orbitals to the LUMO (b_{2g}) of TCNQ belong to the same symmetry, and can strongly mix with each other. On the other hand, because of the above orbital symmetries, the overlap integral between the second HOMO of BD and the LUMO of TCNQ must be zero. Thus the moments of the optical transition where the above two excitations are mixed, will be entirely due to the contribution of the excitation from the HOMO to the LUMO of TCNQ. This is the reason why the visible absorption band, which was tentatively considered as the second CT band in our previous study, is polarized perpendicular to the direction of BD–TCNQ stack.

We noted that the CT bands are very strong in the crystal spectra of BD–TCNQ complex as compared with the crystals of typical CT complexes such as pyrene–TCNE. From the analysis of reflectance data, we can determine the absolute oscillator strength of each absorption band. The values thus determined are given in Table 5. It should be noted that the oscillator strength of the first CT band is as large as 0.8. Interestingly, this is about twice the oscillator strength predicted for a BD–TCNQ pair by the molecular orbital calculations. The experimentally determined oscillator strength is much larger for the second CT band. This is primarily due to the effect of the mixing of the local excitation associated with the strong $^1B_{3u} \leftarrow {}^1A_g$ transition of TCNQ.

Finally, we wish to point out that, when dichloromethane or dibromoethane is included in the BD–TCNQ lattice, the absorption bands are shifted to lower energy by about 2×10^3 cm^{-1}. Since the strucuture within the BD–TCNQ stack remains almost the same except a slight change of the intermolecular separation, the above shifts must be due to the effect of included solvent molecules and/or to that of the formation of intermolecular hydrogen bonds.

We wish to thank Dr. T. Ohta in our laboratory for helping us to use his computer program for the molecular orbital calculation of supermolecule system.

We are grateful to Olympus Optical Co., Ltd. for their generous offer of Olympus MMSP-RK used in this study.

References

1) T. Amano, H. Kuroda, and H. Akamatsu, *Bull. Chem. Soc. Jpn.*, **42**, 671 (1969).
2) H. Ohmasa, M. Kinoshita, and H. Akamatsu, *Bull. Chem. Soc. Jpn.*, **44**, 391, 395 (1971).
3) I. Ikemoto, K. Chikaishi, K. Yakushi, and H. Kuroda, *Acta Crystallogr., Sect. B.*, **28**, 3502 (1972).
4) K. Yakushi, I. Ikemoto, and H. Kuroda, *Acta Crystallogr., Sect. B*, **30**, 835 (1974).
5) K. Yakushi, I. Ikemoto, and H. Kuroda, *Acta Crystallogr., Sect. B*, **30**, 1738 (1974).
6) N. Takahashi, K. Yakushi, K. Ishii, and H. Kuroda, *Bull. Chem. Soc. Jpn.*, **49**, 182 (1976).
7) H. Kuroda, T. Kunii, S. Hiroma, and H. Akamatsu, *J. Mol. Spectrosc.*, **22**, 1 (1967).
8) For the method of calculation, see, for example, the following reference. F. Stern, "Elementary Theory of the Optical Properties of Solids," *Solid State Phys.*, **15**, 299 (1963).
9) H. W. Verleur, *J. Opt. Soc. Am.*, **58**, 1356 (1968).
10) I. H. Malison, *J. Opt. Soc. Am.*, **52**, 1377 (1962).
11) The single crystal of saphire were mounted on the small vessel in which 1-chloronaphthalene mixed with the powder of active charcoal was filled in order to avoid the reflection from the back surface of the crystal.
12) D. M. Roessler, *Brit. J. Appl. Phys.*, **16**, 1119, 1359 (1965); **17**, 1313 (1966).
13) R. K. Ahrenkiel, *J. Opt. Soc. Am.*, **61**, 1651 (1971).
14) Y. Oyanagi, Subprogram POWl, Program Library, Computer Centre, Univ. of Tokyo.
15) T. Ohta, H. Kuroda, T. L. Kunii, *Theor. Chim. Acta (Berl.)*, **19**, 167 (1970).
16) K. Ishii, M. Kinoshita, and H. Kuroda, "Energy and Charge Transfer in Organic Semiconductors," ed by K. Masuda and M. Silver, Plenum Press (1974), p. 177.

Metathesis of 1,5-Cyclooctadiene over Supported Rhenium Oxide Catalysts

Kaizaburo SAITO, Tsutomu YAMAGUCHI, Kozo TANABE,*
Toshimasa OGURA,** and Misao YAGI**

Department of Chemistry, Faculty of Science, Hokkaido University, Sapporo 060
***Central Research Laboratory, Takasago Perfumery Co., Kamata 5, Ohta-ku, Tokyo 144*

(Received March 10, 1979)

The metathesis of 1,5-cyclooctadiene (COD) was investigated over supported rhenium oxide catalysts in terms of carrier effects, acid properties of the catalysts, product distributions, and the reversibility of the reaction. Only alumina plays an effective role as a support. The reaction of COD over rhenium oxide–alumina catalyst yields oligomers, C_{8n}, sesqui-oligomers, C_{8n+4}, and polymers. The important results are as follows: 1) The product distribution in terms of the carbon number of the products shows a decay curve with maxima around C_{12}, C_{16}, and C_{20}. 2) The reaction of oligomers gives COD and some products similar to those of COD. 3) The reactivity of 1,5,9-cyclododecatriene (CDT) was low compared with COD, 1,5,9,13-cyclohexadecatetraene (CHT), and 1,5,9,13,17-cycloeicosapentaene (CEP). 4) A reaction of a mixture of macrocyclic polyenes and polymers gave appreciable amounts of CDT, CHT, and CEP, whereas no COD was obtained. On the basis of the results, we conclude that the products, oligomers, sesqui-oligomers, and polymers, are formed independently from the active intermediary polymers which are formed from COD.

The metathesis of acyclic alkenes has been investigated extensively both in homogeneous and heterogeneous systems. It is known that the effective catalysts for this reaction include compounds or complexes of Mo, W, and Re.[1–3]

One of the characteristics in the metathesis reaction of cyclic alkenes is to form two kinds of homologues, cyclic oligomers and polyalkenes,[4,5] which are not obtained in the disproportionation of acyclic alkenes. Though some studies on the polyalkenenes have been reported[6] and put into practical applications in high polymer industries because of their high selectivity for ring-opening polymerization,[6] less attention has been paid to the formation of cyclic oligomers.

1,5-Cyclooctadiene (COD) was reportedly catalyzed by homogeneous metal complexes to yield not only cyclic oligomers and poly(octadiene) but "sesqui-oligomers."[5–8] In a previous paper,[8] we briefly reported a heterogeneous catalytic metathesis of COD on Re_2O_7–Al_2O_3, yielding oligomers and sesqui-oligomers, in which the distribution of C_{12}—C_{32} cyclopolyenes was different from that in homogeneous catalyst system.

It will also be quite interesting to investigate how the sesqui-oligomers (C_{8n+4}) are formed from COD (eight membered ring diene) and what kind of reaction path is dominant and will give the three types of products: poly(octadiene) (polymers), cyclic oligomers (oligomers), and sesqui-oligomers.

In this study, supported rhenium oxides were used in the metathesis of COD; their catalytic activities and selectivities are compared with surface properties. The reactivity of 1,5,9-cyclododecatriene (CDT, C_{12}), 1,5,9,13-cyclohexadecatetraene (CHT, C_{16}), and 1,5,9,13,17-cycloeicosapentaene (CEP, C_{20}), and the reversibility of the reaction are discussed and a probable reaction path is proposed.

Experimental

Materials. *Catalyst Preparation*: Supported molybdenum and rhenium oxide catalysts were prepared by impregnating various metal oxide supports with aqueous solutions of ammonium heptamolybdate (Wako Pure Chemical Ind., Ltd., GR) and ammonium perrhenate (Engelhard), respectively, followed by drying and calcining at desired temperatures in air for more than two hours. The supports tested here were SiO_2–Al_2O_3, Al_2O_3, MgO, TiO_2, ZnO, ZrO_2, SnO_2, La_2O_3, ThO_2, WO_3, and MgO–ZnO. SiO_2–Al_2O_3 was obtained from Nikki Chemical Co., and contained 15 wt% of Al_2O_3. Magnesium oxide was the GR grade of Kanto Chemical Co. Aluminas were "an activated alumina" from Nishio Industry Co., Ltd, N611 from Nikki Chemical Co., A022 and TK13R from Tokai Konetsu Kogyo, Neobead MSC from Mizusawa Chemical Co., Ltd., and Albes FE and FF from Showa Tansan Kaisha, Ltd. An alumina was prepared by neutral hydrolysis of aluminum triisopropoxide (Wako Pure Chemical Ind. Ltd.). Titanium dioxide, ZnO, ZrO_2, SnO_2, and La_2O_3 were prepared by hydrolysis of titanium tetrachloride (Wako, GR), zinc nitrate (Nakarai Chemicals, Ltd., GR), zirconium(IV) dichloride oxide (Wako, GR), tin(IV) chloride (Wako, GR), and lanthanum nitrate (Nakarai Chemicals, Ltd., extra pure) with aqueous ammonia, respectively, followed by washing, drying, and calcining in air at 500 °C for 3 h. Thorium oxide and WO_3 were obtained by thermal decomposition of thorium nitrate (Wako, GR) at 550 °C for 1 h and of ammonium dodecatungstate (Wako, GR) at 550 °C for 10 h, respectively. A mixed oxide MgO–ZnO (1:9 in molar ratio) was provided by hydrolysis of aqueous mixture of $Zn(NO_3)_2$ and $MgCl_2$ with 28% aqueous ammonia, followed by washing, drying, and calcining in air at 500 °C for 3 h.

6.5 wt% of Re_2O_7 was mounted on all carriers except Al_2O_3, on which the amount of Re_2O_7 was varied from 0.5 to 10 wt%. The amount of MoO_3 supported was 5.1 wt%.

Reactants and Solvents: COD (Shell) was distilled under atmospheric pressure without using any drying reagents.

CDT, CHT, and CEP were obtained by fractional distillation from the reaction mixture of COD. Polymers which contain the open-chain polymers and macrocyclics higher than C_{56} were also prepared from COD products by distillation.

Solvent purifications are as follows. Benzene and cyclohexane (Wako, GR) were distilled over metallic sodium. 1,2-Dichloroethane (Wako, GR) was distilled over phosphorus pentaoxide. Heptane and ethyl alcohol (Wako, GR) were dried over molecular sieves; carbon tetrachloride (Wako, Pure Grade) was dried over calcium chloride. Hexane, ethyl acetate (Wako, GR), and dioxane (Kanto, GR) were used without further purifications.

Procedure. The reactions were carried out at 0 to

80 °C with continuous stirring in a round bottom flask which contained 0.5 ml of COD with 5 ml of solvent and 0.2 g of catalyst. Small amounts of samples for analysis were taken out from the reaction mixture at appropriate time intervals.

The reaction products were analyzed by three sets of gas chromatographs: (A) equipped with a 3 m column of Silicone DC 200 at 200 °C for lower molecular weights macrocyclics (C_8—C_{20}) analysis. (B) equipped with a 1 m column of SE-30 with temperature programming for the analysis of an internal standard and C_8—C_{28} macrocyclics. (C) equipped with a 1 m column of Dexsil 300 GC (3%) with temperature programming for C_{16}—C_{56} macrocyclics analysis.

Products were identified by gas chromatography, IR, and mass spectra, in comparison with their authentic samples. Quantitative analyses were made by using an absolute calibration curve.

Measurement of Surface Acidity. Acidic properties of the catalysts were examined by the butylamine titration method using Hammett indicators.

Definition of Terms. The term "the conversion of COD" was defined as a percentage ratio of the converted COD to the initial amount of COD. The term "the amount of polymers" was defined as the difference between the amount of COD converted and the total amount of the products which can be analyzed by gas chromatography. "Catalytic activity" and "selectivity" were defined as the ratio of the total amount of macrocyclics to the initial amount of COD and the ratio of macrocyclics to the converted COD, respectively.

$$\text{Conversion} = \frac{\text{Converted COD}}{\text{Initial COD}} \times 100\%$$

$$\text{Amount of Polymers} = (\text{Converted COD}) - (\text{Total Product})$$

$$\text{Catalytic Activity} = \frac{\text{Total Macrocyclics}}{\text{Initial COD}}$$

$$\text{Selectivity} = \frac{\text{Macrocyclics Individual}}{\text{Converted COD}}$$

Results and Discussion

Effect of Carriers on Catalytic Activity. The reactions were carried out over single or impregnated oxides. Only Re_2O_7–Al_2O_3 showed an activity for the formation of macrocyclic polyenes and polymers; the following catalysts were completely inactive: MoO_3, WO_3, Re_2O_7, Al_2O_3, Re_2O_7–MgO, Re_2O_7–TiO_2, Re_2O_7–ZnO, Re_2O_7–ZrO_2, Re_2O_7–SnO_2, Re_2O_7–La_2O_3, Re_2O_7–ThO_2, Re_2O_7–MgO–ZnO, and Re_2O_7–SiO_2·Al_2O_3 or MoO_3–Al_2O_3. The high catalytic activity of Re_2O_7–Al_2O_3 implies that only alumina plays a special role in the formation of the active sites. Such a specific role of Al_2O_3 is also reported in the disproportionation of propylene over MoO_3–Al_2O_3[9] and Re_2O_7–Al_2O_3.[10] Various aluminas, which were supplied by different industries, were examined to investigate the role of Al_2O_3. Table 1 lists the names of these aluminas, their crystal forms, and their surface areas. The numbers correspond to that of Fig. 1. As Fig. 1 shows, catalytic activities are well correlated with the surface area of supports and do not depend on crystal forms (α, γ, *etc.*). Therefore, in the following studies, the alumina which had the largest surface area was used as the carrier of rhenium oxide.

Table 1. List of Alumina Used

No.	Name	Crystal form	Surface area / $m^2\,g^{-1}$
1	Albes-FF	(fibrillar)	330
2	TK-13R	γ-	230
3	Albes-FE	(fibrillar)	110
4	N-611	γ-	200
5	Neobead M6C	γ-	210
6	A-022	α-	1

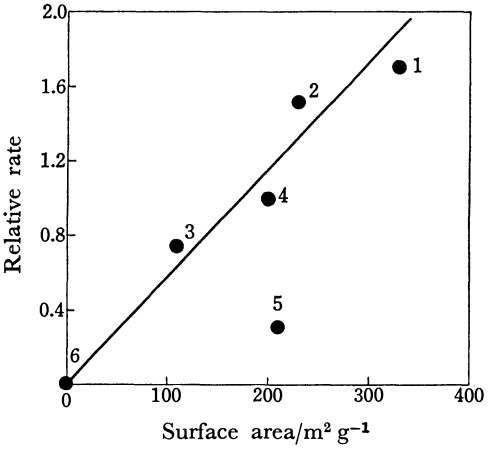

Fig. 1. Correlation between surface area and relative rate. Numbers correspond to those in Table 1.

The amount of Re_2O_7 supported was varied from 0.5 to 10 wt% to Al_2O_3. The catalytic activity increased up to 3 wt% and became constant above this range.

Optimum and reproducible activity was obtained by calcining the catalyst at 600 °C in air for more than 2 h.

Catalytic Activities and Acid-Base Properties of Catalysts. Since some relationships were suggested between the acidic properties of catalysts and the catalytic activities for the metathesis of alkenes,[11–15] the acidic strength and the acidity (number of acid sites) of the catalytically active Re_2O_7–Al_2O_3 and the inactive MoO_3–Al_2O_3 were compared. These catalysts have strong acid sites ($pK_a = -5.6$) which were not found on the component oxides themselves, *i.e.*, the strong acid sites were created by the combination of those oxides. Though both catalysts have fairly large amounts of acid sites, one of the catalysts, MoO_3–Al_2O_3, does not show any catalytic activity. However, the activity of Re_2O_7–Al_2O_3 was decreased with the increase of the amount of NaOH added and completely lost by the addition of 1.24 mmol/g NaOH. These results seem to indicate that the acidic property does not directly dominate the catalytic activity, but is one of the important factors which control the activity.

Effect of Solvent on Catalytic Activity. It is known that some particular solvents are favorable for a high conversion or a high selectivity in metathesis.[16,17] The solvents used in this study are listed in Table 2, together with the conversion of COD, the catalytic

Table 2. Effect of solvents[a)]

Solvent	Reaction time / min	Conversion / %	Activity / %	Selectivity / %
Benzene	80	37	11	30
Carbon tetrachloride[b)]	75	38	8	21
Cyclohexane[b)]	60	24	7	29
Hexane[b)]	60	23	4	17
1,2-Dichloroethane	60	20	0.8	4
Dioxane	120	0	0	—
Ethyl acetate	120	0	0	—
Ethyl alcohol	120	0	0	—

a) Reaction conditions: temp=40 °C, solvent=5.0 ml, COD=0.5 ml. b) White polymer was found on glass wall.

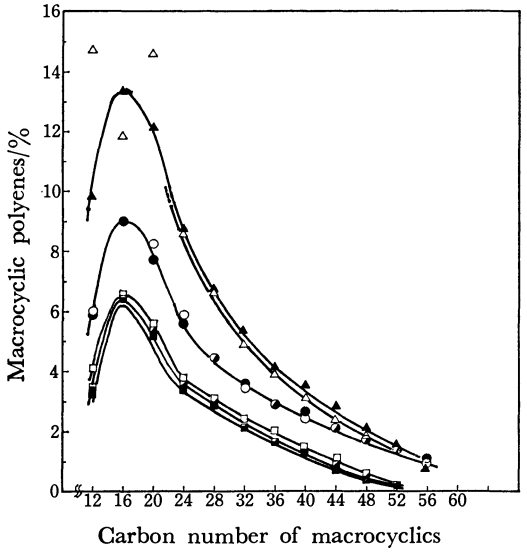

Fig. 2. Product distributions in terms of the carbon number of the products.
■, ◪, □: after 5, 10, and 15 min reaction, respectively, of 2 wt% solution of COD in heptane. △, ▲: After 0.5 and 9 h reaction, respectively, of 5 wt% solution of COD in benzene. ○, ●: After 4 and 51 h reaction, respectively, of 10 wt% of COD in heptane.

activity, and the selectivity. Besides benzene and cyclohexane, which are known as suitable solvents in homogeneous systems, carbon tetrachloride is also a good solvent for obtaining high conversion, activity, and selectivity. On the other hand, in ethyl alcohol, dioxane, and ethyl acetate, no product was obtained. Product distributions did not depend on the solvents used. Though the effective solvents seem to be good for polymers as well as oligomers, further studies should be done to clarify the role of solvents.

Product Distributions. As in the case of homogeneous systems, the metathesis of COD over Re_2O_7–Al_2O_3 yields oligomers, C_{8n}, sesqui-oligomers, C_{8n+4}, and polymers. Figure 2 shows the dependency of the product distribution in terms of the carbon number of macrocyclics. The spectrum seems to be a decay curve over C_{20} product, with an ambiguous maximum around the first three products: CDT, CHT, and

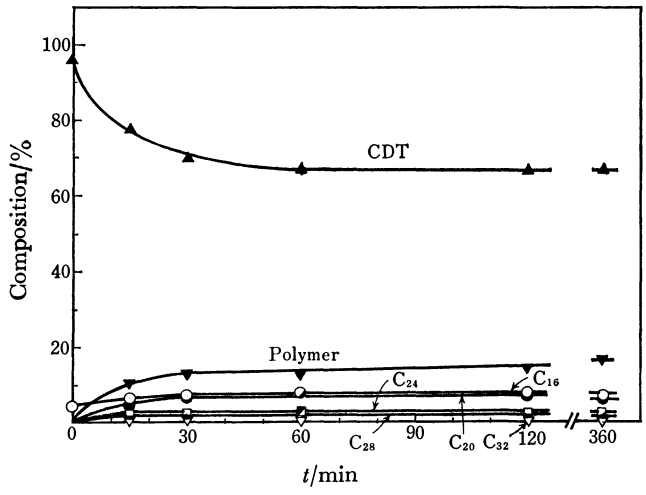

Fig. 3. Reaction of CDT ▲: CDT, ▼: polymer, ○: C_{16}, ●: C_{20}, □: C_{24}, ■: C_{28}, ▽: C_{32}.

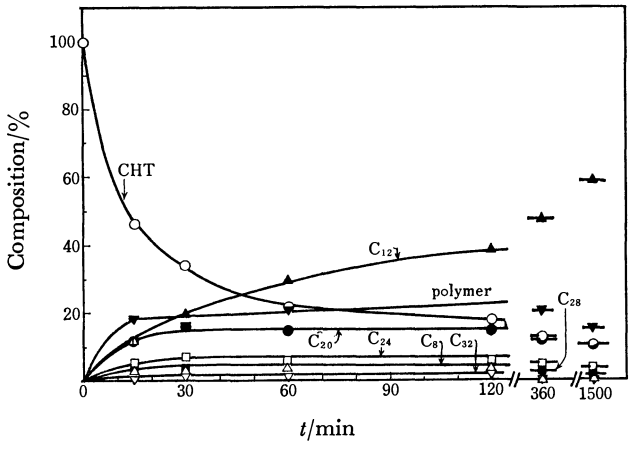

Fig. 4. Reaction of CHT ○: CHT, ▲: C_{12}, ▼: polymer, ○: C_{20}, □: C_{24}, △: C_8, ■: C_{28}, ▽: C_{32}.

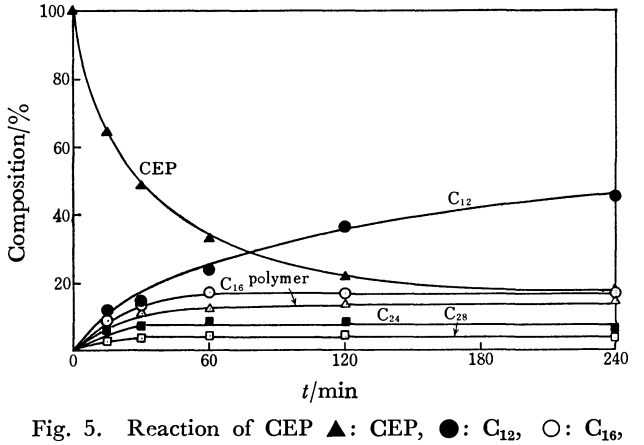

Fig. 5. Reaction of CEP ▲: CEP, ●: C_{12}, ○: C_{16}, △: polymer, ■: C_{24}, □: C_{28}.

CEP. The product distributions were essentially unchanged through the entire reaction period, until most of the COD was consumed. These results suggest that oligomers and sesqui-oligomers are formed by parallel paths but not by a consecutive reaction path.

The Reaction of Oligomers and Sesqui-oligomers. The results of the individual reactions of CDT, CHT,

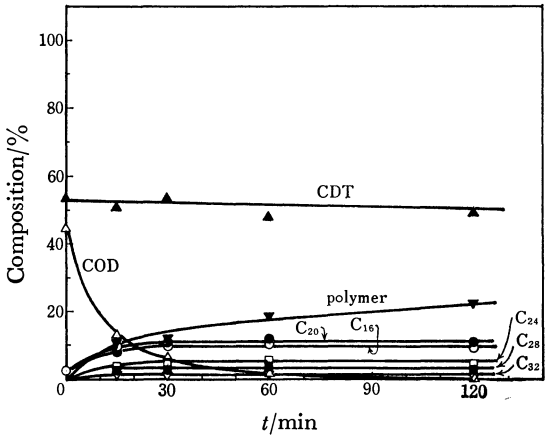

Fig. 6. Competition reaction of COD and CDT ▲: CDT, △: COD, ▽: polymer, ●: C_{20}, ○: C_{16}, □: C_{24}, ■: C_{28}, ▽: C_{32}.
Reaction mixture contains 0.4% of COD, 0.5% of CDT, and benzene as solvent.

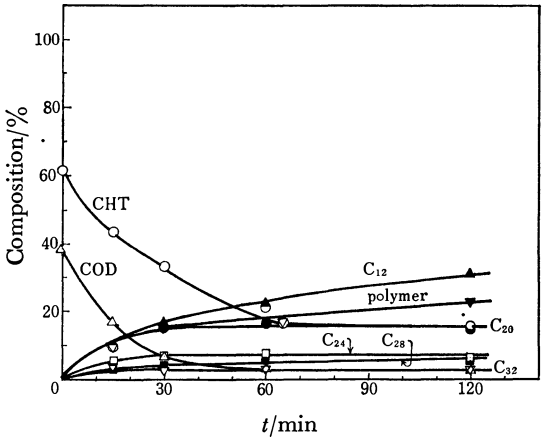

Fig. 7. Competition reaction of COD and CHT ○: CHT, △: COD, ▲: C_{12}, ▼: polymer, ●: C_{20}, □: C_{24}, ■: C_{28}, ▽: C_{32}.

and CEP are shown in Figs. 3, 4, and 5, respectively. Sesqui-oligomers react and give similar products to those of oligomers, except there is no production of COD. Such results are consistent with the results shown in Fig. 2, which indicate that the product distributions of both oligomers and sesqui-oligomers produced by the metathesis of COD are on the same line.

If we assume that those products were formed by a consecutive oligomerization reaction, it is expected that the product distribution may be different in reactions in which CDT, CHT, or CEP is used as a reactant, since they are supposed to be the intermediate reaction products in the consecutive reaction. Thus, the data which suggest similar product distributions (Figs. 3, 4, and 5) lead us to conclude that each product, CDT, CHT, or CEP, is formed independently and not by a consecutive step.

In the competitive reaction of CDT or CHT with COD, the product distributions hardly differed from those in the reaction of individual materials, as shown in Figs. 6 and 7. This reveals that the competitive reaction is the simple superposition of two independent

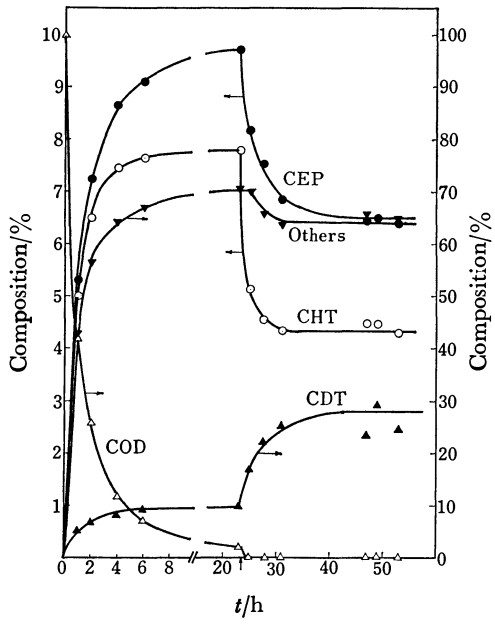

Fig. 8. Reaction of COD △: COD, ▲: CDT, ○: CHT, ●: CEP, ▼: polymer. An arrow on the time scale indicates the addition of a new catalyst.

reactions of COD and other cyclic polyenes.

The reactivity of macrocyclics can be estimated from the competitive reactions and the individual ones. COD is the most reactive and is followed by CHT and CEP. The low reactivity of CDT is indicated by the following observations. (1) the reaction seems to stop at about 30% conversion within 1 h, when CDT is used as the reactant, while CHT and CEP react over 70% within 1 h and keep converting to the products. (2) CDT is continuously formed as the product during the reaction, while the additional formation of other products such as C_{20}, C_{24}, and C_{28} was not observed after 1 h. (3) in a competitive reaction of COD and CDT, only COD was a reactive component.

Though CHT gives a small amount of COD (about 3%), CDT and CEP do not give any. No production of COD in the latter case may be due to the absence of a reverse reaction or to the rapid disappearance of the COD formed. Since the reactivity and the distribution of the products from CHT do not differ markedly from that of CEP or CDT, it will be reasonable to conclude that no reverse reaction takes place from CDT or CEP to COD. The formation of COD from oligomers, such as CHT, will be a simple deoligomerization. The difficulty in the formation of COD from sesqui-oligomers will be understood by considering that such a reaction must accompany the C_4 fragments.

Depolymerization and Equilibrium. A depolymerization of macrocyclic polyenes and polymers was examined to elucidate the reversibility of the reaction; a 1 wt% mixture containing 75.5 wt% of C_{24}—C_{52} macrocyclics and 24.5 wt% of polymers was used at 40 °C. The composition of the mixture after 4 h reaction was as follows: 13.5% of CDT, 8.5% of CHT, 12% of CEP, 35% of macrocyclics, and 31% of polymers. No COD was obtained. These results are coin-

cident with those which have been obtained in homogeneous catalyst systems. Scott *et al.* found the formation of C_{12}—C_{32} materials in the reaction of a diluted solution of the "extracted high molecular weight COD polymers" by using the system WCl_6–$EtAlCl_2$–EtOH.[7]

Figure 8 shows the result of the prolonged reaction of COD. When the amount of COD is sufficient (more than 5%), the ratios of the first three products, CDT, CHT, and CEP, are held almost constant at about 9.5:8:9.5, and the reaction seems to reach equilibrium. However, after the amount of COD decreased below 5%, an addition of a fresh catalyst leads a remarkable change in the ratio of the first three products. The amount of CDT increases abruptly and the amounts of CHT and CEP decrease rapidly, while the amount of the higher molecular weight products becomes a little smaller. After a long period, COD disappeared completely from the reaction mixture and the reaction seems to reach equilibrium again, where the composition of the products is CDT=25, CHT=4.5, CEP=6.5, and others=64.

Reaction Route. Before presenting a probable reaction route, it will be convenient to summarize the important findings.

a) COD is formed by a degradation of the oligomers (dimer, trimer, tetramer, *etc.*) but not from the sesqui-oligomers.

b) Some oligomers and sesqui-oligomers are formed by the back reaction of the polymers which contain chained species of high molecular weight and large ring-size polyenes.

c) The consecutive reaction is unlikely.

The following reaction scheme interprets the observations.

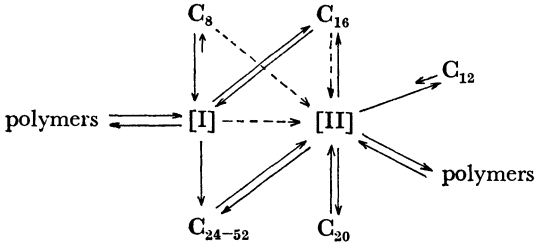

I and II represent active intermediary polymers (AIP). An assumption of two intermediates is based on the observations that CDT and CEP did not give any COD. Arrows with different lengths between C_8 and I and between C_{12} and II mean that, for instance, the rate of formation of I from C_8 is faster than that of C_8 from I. The dotted arrows indicate that it is uncertain whether II is formed directly from C_8 and C_{16} or indirectly *via* II.

Formation of Polymers. The polymers will be formed either as the desorption products of one part of the "active intermediary polymers" (AIP) or as the product of the ring-opening polymerization of COD with the AIP. A sufficient amount of COD will give a large amount of polymers by the latter reaction. The polymers produced may readsorb on the sites to form the AIP and may give the oligomers. A large amount of polymers produced may inhibit the reaction by covering the active sites.[18]

Formation of Oligomers and Sesqui-oligomers. Oligomers will be formed by an intramolecular disproportionation of the AIP. COD does not participate in this reaction process. The oligomers produced can be reconverted to the AIP and give polymers or other oligomers with a new product distribution. The AIP from the oligomers can produce COD by an intramolecular reaction of the AIP, while the AIP from the sesqui-oligomers does not. Presumably, the latter AIP is different from the others.

The oligomers and the sesqui-oligomers will be formed by the intramolecular reaction process, *i.e.*, by the "pinch off" process proposed by Scott *et al.*[7] As already shown in Fig. 2, the distribution of the reaction products shows a decay curve, as the ring-size of the products increases. Especially, the distribution of the products which have larger ring-size than C_{20} is expressed very well by a single curve. This indicates that the product distribution will dominantly depend on the "pinch off" probability of the intramolecular reaction in the formation of the individual products, where the production of the smaller polyenes is much higher than that of the higher ones. The deviation of the product distribution of the three products, C_{12}, C_{16}, and C_{20}, from this plot will be brought about from the following reactions: CDT (C_{12}), which is the product of the intramolecular reaction of polyenes, reacts with COD (C_8) to form CEP (C_{20}) or dimerizes to give C_{24} species. The former reaction ($C_{12}+C_8$) will take place more easily than the latter ($C_{12}+C_{12}$), because COD is more reactive than CDT (C_{12}). Dimerization of COD to form CHT (C_{16}) should also be taken into consideration.

Formation of AIP. Though the AIP are supposed to be the macrocyclic polyenes[19] or open-chain polymers which are adsorbed on the catalyst at multiple points, it is not clear how the AIP forms from COD. One possible way is to assume a chain reaction, as Chauvin has proposed,[20] in which a carbene intermediate mechanism was proposed for the polymerization of cycloolefins. Considering the reaction time-course, the AIP is supposed to be formed at a very early stage of the reaction.

References

1) G. C. Bailey, *Catal. Rev.*, **3**, 37 (1969).
2) J. C. Mol and J. A. Moulijin, *Adv. Catal.*, **24**, 131 (1975).
3) R. J. Haines and G. J. Leigh, *Chem. Soc. Rev.*, **14**, 155 (1975).
4) G. Dall'Asta, *Makromol. Chem.*, **154**, 1 (1972).
5) N. Calderon, E. A. Ofstead, and W. A. Judy, *J. Polym. Sci.*, **5**, 2209 (1967).
6) K. W. Scott, N. Calderon, E. A. Ofstead, W. A. Judy, and J. P. Ward, *Adv. Chem. Ser.*, **91**, 399 (1969).
7) Yu. V. Korshak, L. M. Vardanian, and B. A. Dolgoplosk, *Dokl. Akad. Nauk. SSSR*, **208**, 1138 (1973).
8) H. Kumobayashi, T. Ogura, S. Akutagawa, K. Saito, T. Yamaguchi, and K. Tanabe, *Chem. Lett.*, **1976**, 317.
9) E. Echigoya and R. Nakamura, *Nippon Kagaku Kaishi*, **1972**, 500.
10) R. Nakamura, H. Iida, and E. Echigoya, *Nippon Kagaku Kaishi*, **1976**, 221.

11) British Patent 1 106 015; 1 106 016.
12) Japan Patent Sho-44-5543.
13) Dutch Patent 1966, 6610196.
14) T. Takahashi, *Kogyo Kagaku Zasshi*, **73**, 718 (1970).
15) R. Nakamura and E. Echigoya, *Bull. Jpn. Petro. Inst.*, **14**, 187 (1972).
16) V. M. Kothari and J. J. Tazuma, *J. Org. Chem.*, **36**, 2951 (1971).
17) L. Hocks, A. J. Hubert, and Ph. Teyssié, *Tetrahedron Lett.*, **1973**, 2719.
18) N. Calderon, *J. Macromol. Sci.*, **1972**, C7, 105.
19) E. Wasserman, D. A. Ben-Eftain, and R. Wolovsky, *J. Am. Chem. Soc.*, **90**, 3286 (1968).
20) J. L. Herisson and Y. Chauvin, *Makromol. Chem.*, **141**, 161 (1971).

A Thermodynamic Study on the Hydrolysis of Beryllium Ion in Dioxane–Water Mixed Solvents

Shin-ichi ISHIGURO and Hitoshi OHTAKI*

Department of Electronic Chemistry, Tokyo Institute of Technology at Nagatsuta, Nagatsuta-cho, Midori-ku, Yokohama 227

(Received March 18, 1979)

The hydrolytic reactions of beryllium(II) ions were calorimetrically studied at 25 °C in aqueous solution and dioxane–water mixtures, both containing 3.0 mol dm^{-3} (Li)ClO_4 as a constant ionic medium. On the basis of the formation constants previously determined,[10–12] the enthalpy and entropy changes for the reaction, $qBe^{2+}+pH_2O=Be_q(OH)_p^{(2q-p)+}+pH^+$, were estimated for the Be_2OH^{3+} and $Be_3(OH)_3^{3+}$ complexes in aqueous solution and 0.1 mole fraction dioxane–water mixture and for Be_2OH^{3+}, $Be_3(OH)_3^{3+}$, and $Be_2(OH)_2^{2+}$ complexes in 0.2 mole fraction dioxane–water mixture. The enthalpy and entropy changes of formation of the $Be_q(OH)_p^{(2q-p)+}$ complex obtained in solutions of various mole fractions of dioxane were as follows: $2Be^{2+}+H_2O=Be_2OH^{3+}+H^+$; ΔH_{12} (mole fraction: 0.0)$=18.6\pm0.2$ kJ mol^{-1}, $T\Delta S_{12}$(mole fraction: 0.0)$=1.3\pm0.2$ kJ mol^{-1}, ΔH_{12} (0.1)$=15.2\pm0.2$ kJ mol^{-1}, $T\Delta S_{12}(0.1)=-3.4\pm0.2$ kJ mol^{-1}, $\Delta H_{12}(0.2)=8.4\pm0.4$ kJ mol^{-1}, $T\Delta S_{12}(0.2)=-12.4\pm0.4$ kJ mol^{-1}, $3Be^{2+}+3H_2O=Be_3(OH)_3^{3+}+3H^+$; $\Delta H_{33}(0.0)=61.7\pm0.2$ kJ mol^{-1}, $T\Delta S_{33}(0.0)=12.2\pm0.2$ kJ mol^{-1}, $\Delta H_{33}(0.1)=59.4\pm0.2$ kJ mol^{-1}, $T\Delta S_{33}(0.1)=10.0\pm0.2$ kJ mol^{-1}, $\Delta H_{33}(0.2)=59.0\pm0.4$ kJ mol^{-1}, $T\Delta S_{33}(0.2)=9.1\pm0.4$ kJ mol^{-1}, $2Be^{2+}+2H_2O=Be_2(OH)_2^{2+}+2H^+$; $\Delta H_{22}(0.2)=42.3\pm0.4$ kJ mol^{-1}, $T\Delta S_{22}(0.2)=1.3\pm0.4$ kJ mol^{-1}. The enthalpy and entropy changes of the reaction, $H_2O=H^++OH^-$, in the solutions of the same compositions were also determined as $\Delta H_w(0.0)=56.6\pm0.1$ kJ mol^{-1}, $T\Delta S_w(0.0)=-22.6\pm0.1$ kJ mol^{-1}, $\Delta H_w(0.1)=58.1\pm0.1$ kJ mol^{-1}, $T\Delta S_w(0.1)=-25.3\pm0.1$ kJ mol^{-1}, $\Delta H_w(0.2)=61.2\pm0.1$ kJ mol^{-1}, $T\Delta S_w(0.2)=-26.6\pm0.1$ kJ mol^{-1}. These results were discussed in connection with interactions between the hydroxo complexes and the solvent molecules and with those between solvent molecules in the mixed solvents.

It has been said that the thermodynamic parameters of transfer of electrolytes from aqueous to aqueous organic mixed solvents would be a measure of solute–solvent and solvent–solvent interactions.[1–4] The change in strength of carboxylic acids in mixed solvents may be a typical example, where the acidity usually decreases with increasing mole fraction of organic component.[5,6] On the other hand, the acidity of ammonium ion and its homologues increases with the concentration of an organic solvent and then sharply decreases after passing through a maximum.[7–9] In the preceding studies of hydrolytic reactions of metal ions in mixed solvents,[10–12] we pointed out that hydrated metal ions behave in different manner from these two types of acids, that is, the acid dissociation (*i.e.*, hydrolysis) constant of a hydrated metal ion is not practically influenced by the solvent composition of aqueous organic mixtures.

Since no data have been available for the enthalpy and entropy changes of hydrolytic reactions of metal ions in aqueous organic mixtures, we carried out calorimetric measurements of hydrolytic reactions of metal ions in order to investigate solute–solute and solute–solvent interactions in the reactions. Beryllium ion was first chosen as a target of the aim, because it has been investigated in detail in aqueous and aqueous organic mixtures containing various ionic media.[10–12] Since the complex formation proceeds rather slowly at a high pH range,[12] the experiments in this study were carried out in the range pH$\lesssim$4.

Experimental

Reagents and Analysis. *Beryllium Perchlorate*: Beryllium oxide of reagent grade was heated for several hours with an excess of perchloric acid. Residual beryllium oxide was filtered off with a glass filter and beryllium perchlorate thus prepared was recrystallized three times from water. The concentration of beryllium ions in the stock solution was determined gravimetrically.[13]

Lithium Perchlorate: Lithium perchlorate was prepared as described in Ref. 14. Crystals of lithium perchlorate were dried at about 200 °C in an electric oven.

Lithium Hydroxide: A lithium hydroxide solution was prepared by electrolysis of an aliquot of the lithium perchlorate stock solution under an atmosphere of nitrogen in a polyethylene bottle. The concentration of hydroxide ions thus prepared was determined by Gran's method[15] by titrating with a standard perchloric acid solution.

Perchloric Acid: Perchloric acid of super special grade was used without further purification.

Dioxane: Dioxane was purified by the method described in Ref. 10.

The concentrations of hydrogen ions contained in the stock solutions were coulometrically determined by Gran's method.[15]

Preparation of Test Solutions. Test solutions were contained 3.0 mol dm^{-3} perchlorate ions as a constant ionic medium. In each titration, two test solutions were prepared, both containing the same total concentration of beryllium ion at a given concentration of dioxane in the solutions. One (Solution S) contained hydrolyzed beryllium ions and the other (Solution T) contained unhydrolyzed beryllium ions and a known concentration of perchloric acid, and the former was titrated by the latter. The total concentration of beryllium ion was kept practically constant during the titration.

The Method of Measurements. The measurements were carried out in a thermostated room at 25.0±0.5 °C. All the cells used were Dewar vessels, which were immersed in a thermostated water bath. The temperature fluctuated by ±0.0007 °C at 25.00±0.05 °C. First, about 150 cm^3 of test solution S was placed in a titration vessel. The temperature change in the titration vessel was detected by use of a micro volt meter (Model AM-1001, Ohkura Electric Co., Ltd.) and a couple of thermisters which were introduced into the titration and reference vessels. Temperature in

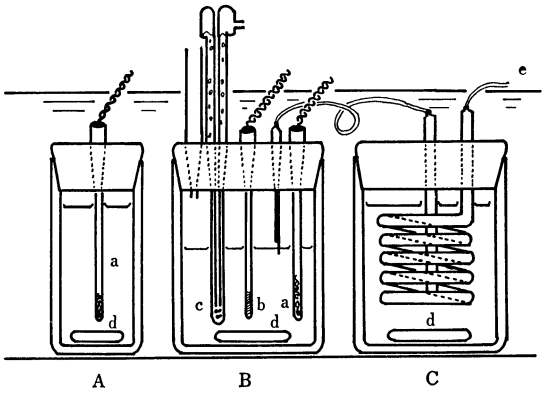

Fig. 1. The cell arrangement used for the enthalpy titration. A: The reference vessel, B: the titration vessel, C: the cell used as a heat exchanger, a: thermister, b: heater, c: cooler which is filled with methanol and is connected with an air pump, d: stirring bar, e: titrant from a piston buret.

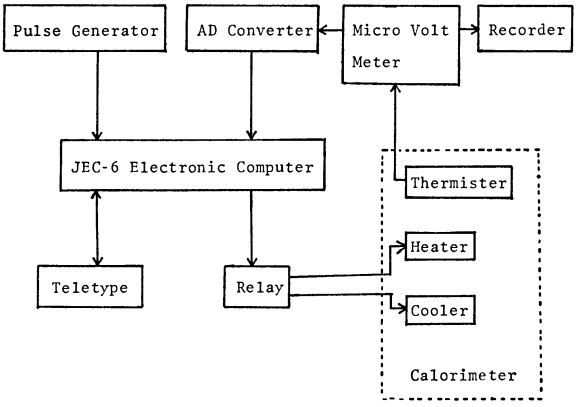

Fig. 2. The on-line controlled enthalpy titration system. The arrows indicate the direction of signals.

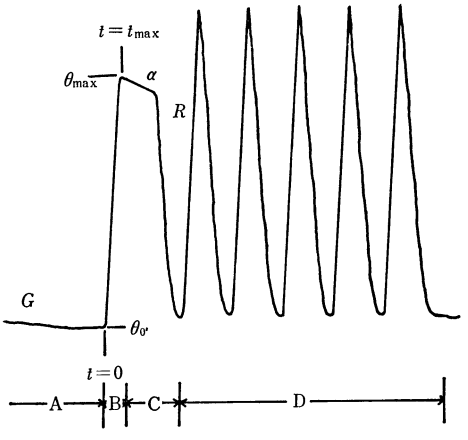

Fig. 3. Determination of heat evolved per addition of the titrant.

the reference vessel, to which the temperature change in the titration vessel was referred, was kept constant throughout the titration. At the thermal equilibrium, temperature in the titration vessel was usually slightly higher than that in the thermostated water bath because of joule heat by agitation. Therefore, in order to keep temperature of the titrant practically the same as that of the test solution, another cell was used as a heat exchanger through which the titrant T was introduced into the titration vessel. The heat exchanger was also agitated with a stirring bar to keep the same temperature in the heat exchanger with that in the titration vessel. The cell arrangement was depicted in Fig. 1. Heat evolved per addition of the titrant was about 6—20 J, which corresponded to the change of about 200—700 μV. The estimated uncertainty (σ) of the heat measurements was about $\pm 0.4\,\mu$V or ± 0.00005 °C. The on-line controlled enthalpy titration system was developed in order to make precise determinations of heat evolved and to spare time for measurements.

The On-line Controlled Enthalpy Titration System. The on-line controlled enthalpy titration system is schematically shown in Fig. 2. The temperature change in the titration vessel was monitored by a JEC-6 spectrum computer (JEOL Co., Ltd.) through a micro volt meter and a 10-bit AD converter. Throughout the measurements, time was controlled by means of a pulse generator.

The procedure of a heat measurement per addition of the titrant consisted of four steps, A through D, as is shown in Fig. 3.

A Region: Before addition of the titrant, the temperature difference between the titration and reference vessels was measured every 10 seconds and a set of continued 50 data was analyzed to give the temperature gradient G ($=\mathrm{d}\theta/\mathrm{d}t$) by assuming the temperature (θ) changing linearly with time, and, at the same time, the uncertainty δG was estimated. If G and δG obtained did not fall within specified ranges, one more temperature-difference was measured, and the same procedure was repeated using a new set of 50 data. When G and δG fell within given ranges, and thus the test solution was reached the thermal equilibrium with the thermostated bath, the temperature at the equilibrium θ_0 and its uncertainty $\delta\theta_0$ were recorded.

B Region: When the test solution was reached the thermal equilibrium with the thermostated bath, the titrant T was added from a piston buret to the test solution. The operation of adding the titrant usually took a few minutes. When the temperature in the titration vessel rose over a level of $10\delta\theta_0$, the temperature change was read every second. The procedure was continued until the temperature in the titration vessel started to decrease, and the time (t_{max}) when the temperature reached the maximum was determined (the maximum temperature: θ_{max}).

C Region: The temperature in the titration vessel decreased approximately linearly after passing through the maximum. The temperature change in the C region could be expressed by the following equation:

$$\theta(t) = (\theta_{max}-\theta_0)\{1-\alpha(t-t_{max})\} \quad (1)$$

where α denotes a constant. The values of θ_{max} and α were determined using a set of 100 data in this region which were measured every second. Then, a cooler was operated to cool the test solution to approximately the same temperature as θ_0.

D Region: When the cooling of the test solution was finished, the test solution was heated by using a standard heater which evolved a constant joule heat q. During the evolution of heat, the temperature change was read every second. The heating of the test solution was continued until a set of 100 data was recorded, then the cooler was again operated. The set of 100 data was analyzed by assuming that temperature rose with a constant rate, and the rate R ($=\mathrm{d}\theta/\mathrm{d}t$) was determined. The determination of R was repeated five times and the mean value was used to estimate the heat capacity C_p of the test solution $C_p=q/RV$, where V denotes the volume of the test solution. The un-

certainty in R was usually within $\pm 0.3\%$. Thus, the heat evolved in the course of one titration q was determined by the following equation:

$$q = k_1 C_p V f(\theta_{max} - \theta_0) + k_2 \quad (2)$$

where f stands for a correction of heat escaped from the titration vessel until temperature reached the maximum in the B region,

$$f = 1/(1 - \alpha t_{max}/2 + \alpha^2 t_{max}^2/3) \quad (3)$$

and k_1 and k_2 represent empirical constants (k_1 was nearly unity and k_2 was nearly zero) which had been determined by separate experiments using a standard heater.

All procedures were automatically operated under the controll by the JEC-6 electronic computer. A least-squares method was employed for the analysis of the sets of data obtained. One procedure of the measurement from A to D usually finished within 40 min. In one run of the whole titration, ten experimental points were usually measured with the total volume of the titrant of about 20 cm³.

Results

The Enthalpy Change for the Autoprotolysis Reaction of Solvents. The enthalpy change for the autoprotolysis reaction of the solvents were measured by titrating a standard lithium hydroxide solution with perchloric acid in mixed solvents containing 3.0 mol dm^{-3} perchlorate ions. The enthalpy change ΔH_w for the reaction, $H_2O = H^+ + OH^-$, is given by the equation:

$$Q = \sum q = \Delta H_w c_H v \quad (4)$$

where Q, q, c_H, and v stand for the total heat evolved, the heat evolved per addition of the titrant, the concentration of hydrogen ions in the titrant and the total volume of the titrant added, respectively. A plot of Q/c_H against v might give a straight line. The plots in various solvents are shown in Fig. 4, and ΔH_w was given as the slope of the straight line.

The Enthalpy Changes of Formation of the Hydroxo Complexes of Beryllium(II). In aqueous solution and 0.1 mole fraction dioxane–water mixture, the only Be_2OH^{3+} and $Be_3(OH)_3^{3+}$ complexes were formed in the pH range examined (pH$\lesssim$4). Therefore, the heat evolved was expressed as follows:

$$Q = \sum q = \Delta H_{12}\delta n_{12} + \Delta H_{33}\delta n_{33} \quad (5)$$

where δn_{pq} denotes the total change in the number of moles of the $Be_q(OH)_p^{(2q-p)+}$ complex when the titrant was added. The δn_{pq} was calculated on the basis of the formation constants previously determined.[10–12] Plots of $Q/\delta n_{33}$ against $\delta n_{12}/\delta n_{33}$ gave a straight line with the slope of ΔH_{12} and the intercept of ΔH_{33}. The plots are shown in Fig. 5.

In 0.2 mole fraction dioxane–water mixture, the $Be_2(OH)_2^{2+}$ complex was formed together with the Be_2OH^{3+} and $Be_3(OH)_3^{3+}$ complexes. Therefore, the heat evolved was expressed as follows:

$$Q = \Delta H_{12}\delta n_{12} + \Delta H_{33}\delta n_{33} + \Delta H_{22}\delta n_{22} \quad (6)$$

When we applied a least-squares method to Eq. 6 in order to evaluate the values ΔH_{12}, ΔH_{33}, and ΔH_{22}, reasonable values were not obtained. A possible reason may be that δn_{22} was approximately proportional to δn_{33} under the experimental conditions examined. Since the formation of the $Be_2(OH)_2^{2+}$ complex was small (about 20%) compared with that of the $Be_3(OH)_3^{3+}$ complex, we assumed at a first step of approch that the only Be_2OH^{3+} and $Be_3(OH)_3^{3+}$ complexes were present. Thus, the same plots as those demonstrated for the aqueous solution and 0.1 mole fraction dioxane–water mixture were possible and are shown in Fig. 6. A relatively good straight line was obtained to give approximate values of ΔH_{12} and ΔH_{33}. Using the value of ΔH_{12} thus obtained, the values of ΔH_{33} and ΔH_{22} were estimated by Eq. 7:

$$(Q - \Delta H_{12}\delta n_{12})/\delta n_{33} = \Delta H_{33} + \Delta H_{22}(\delta n_{22}/\delta n_{33}) \quad (7)$$

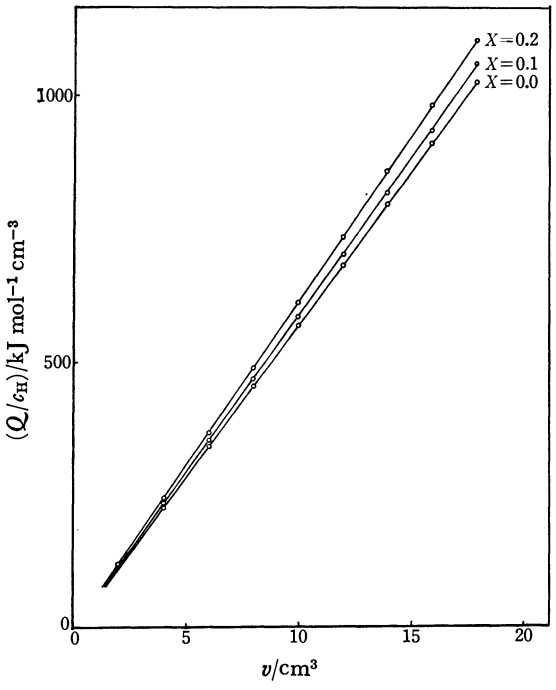

Fig. 4. Determination of the enthalpy change for the autoprotolysis reaction of water in dioxane–water mixture. X represents mole fraction of dioxane in the mixture.

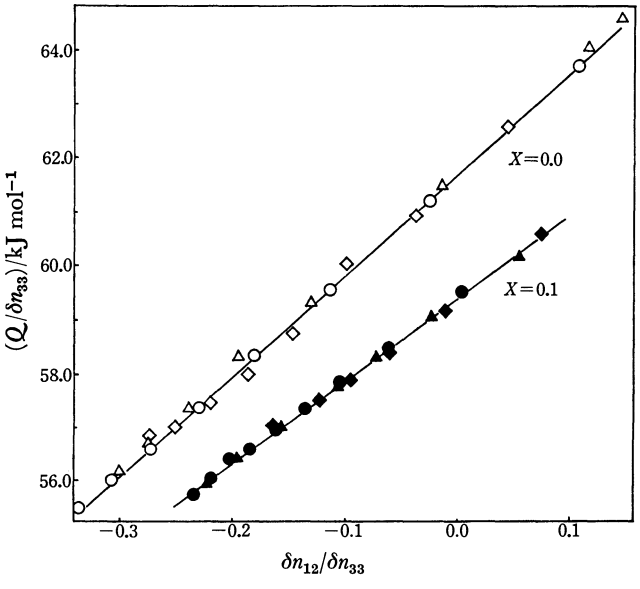

Fig. 5. Determinations of the enthalpy changes of formation of the Be_2OH^{3+} and $Be_3(OH)_3^{3+}$ complexes in aqueous solution and 0.1 mole fraction dioxane–water mixture. Total concentration of beryllium ions c_{Be} (mol dm^{-3}): ○ 0.1620, △ 0.0967, ◇ 0.0506 ▲ 0.0995, ◆ 0.0831, ● 0.0652. X represents mole fraction of dioxane in the mixture.

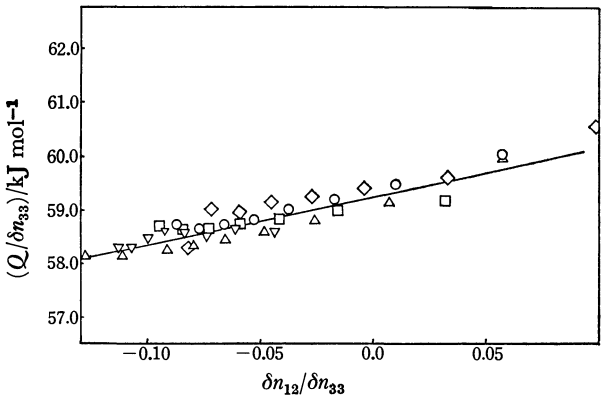

Fig. 6. Determination of the enthalpy changes of formation of the Be_2OH^{3+} and $Be_3(OH)_3{}^{3+}$ complexes in 0.2 mole fraction dioxane–water mixture. Total concentration of beryllium ions c_{Be} (mol dm^{-3}): ○ 0.1183, △ 0.0855, □ 0.0847, ▽ 0.0646, ◇ 0.0390.

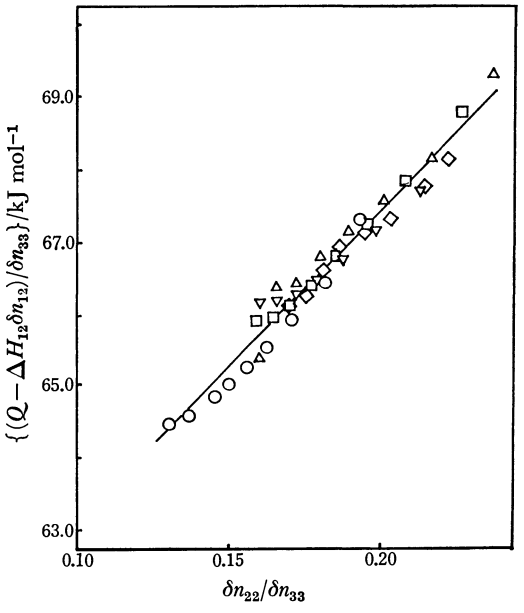

Fig. 7. Determination of the enthalpy changes of formation of the $Be_2(OH)_2{}^{2+}$ and $Be_3(OH)_3{}^{3+}$ complexes in 0.2 mole fraction dioxane–water mixture. Total concentration of beryllium ions c_{Be} (mol dm^{-3}): ○ 0.1183, △ 0.0855, □ 0.0847, ▽ 0.0646, ◇ 0.0390.

The plots of $(Q-\Delta H_{12}\delta n_{12})/\delta n_{33}$ against $\delta n_{22}/\delta n_{33}$ for a given total concentration of beryllium ions gave a straight line with the slope of ΔH_{22} and the intercept of ΔH_{33}. By changing ΔH_{12} around the value firstly obtained, the procedure was repeated until the plots for all given total concentrations of beryllium ions examined were converged on the same line. The plots are shown in Fig. 7. The value of ΔH_{33} finally obtained was 59.0 kJ mol^{-1}, which was in good agreement with the value of 59.2 kJ mol^{-1} firstly approximated. The thermodynamic parameters for the formation of the hydroxo complexes of beryllium ions and for the autoprotolysis reaction of the solvents thus obtained are summarized in Table 1. The results obtained in aqueous solution are in good agreement with those obtained previously.[16,17]

Discussion

Ion–solvent and solvent–solvent interactions in dioxane–water mixtures have so far been studied by using various methods and the following conclusions are generally accepted. 1) The hydrogen bonded structure of water is broken down by the addition of dioxane (it has also been reported that the structure of water may be enhanced by the addition of dioxane less than 0.05 mole fraction[18]). The fact is directly confirmed by means of NMR. The PMR signal of the water molecules shifts to the higher magnetic field on dilution with dioxane.[19] 2) The interaction between cations and solvent molecules is enhanced as the dioxane content of the solvent increases, while the reverse is the case for the interaction between anions and solvent molecules. The cation–solvent interaction is usually larger than the anion–solvent interaction. It has been shown that the enthalpy changes of transfer of most electrolytes from aqueous solution to dioxane–water mixture are negative (exothermic) and become more negative as the dioxane content of the mixtures increases.[20–22] The results are explained as follows: Solvent structure plays an important role in determining the thermodynamic parameters of transfer of electrolytes.[23,24] A dioxane–water mixture is less structured than an aqueous solution, and therefore, ions have a larger solvent-ordering effect (or an enhanced solvation structure of ions) in the dioxane–water mixture. 3) The inner-sphere structure of a complex ion is not practically influenced by the addition of dioxane. It has been found that metal ions are primarily solvated with water molecules in water-rich dioxane–water mixtures (*e.g.*, the dioxane content less than 0.5 mole fraction).[25,26]

On the basis of these facts, the solvent effects on the autoprotolysis of water and the formation of hydroxo complexes of beryllium ion are discussed in the following sections.

Autoprotolysis Reaction of the Solvents. The difference between the enthalpy changes for the autoprotolysis reaction of water, $H_2O=H^+ + OH^-$, in a dioxane–water mixture and an aqueous solution is represented as follows:

$$\Delta H_w^t = \Delta H_w(\text{mixed}) - \Delta H_w(\text{aqueous}) = \Delta h_H^t + \Delta h_{OH}^t - \Delta h_{H_2O}^t \quad (1)$$

where Δh_i^t stands for the partial molar enthalpy change of transfer of species i from aqueous solution to a dioxane–water mixture. As is seen from Table 1, the enthalpy changes in both aqueous solution and dioxane–water mixtures were positive. ΔH_w^t was also positive and became more positive with increasing concentration of dioxane. This result for ΔH_w^t is in contrast to those of dissociation reactions of weak acids (*e.g.*, acetic acid), in which ΔH_w^t is usually negative.[5] Since the sum of the partial molar enthalpy changes of transfer of H^+ and OH^- ions from water to a dioxane–water mixture is negative,[20] the positive ΔH_w^t obtained indicated that $\Delta h_{H_2O}^t$ must be more negative than the sum of Δh_H^t and Δh_{OH}^t. Since the hydrogen bonded structure of water is broken down by the addition of dioxane, the negative $\Delta h_{H_2O}^t$ may be caused by enhancement of the intramolecular interaction of a water molecule (*i.e.*, the strength of the O–H bond) in dioxane–water mixtures.

Formation of Hydroxo Complexes of Beryllium Ion. A hydrolytic reaction of beryllium ions may be expressed as follows:

$$q\mathrm{Be}^{2+} + p\mathrm{H_2O} = \mathrm{Be}_q(\mathrm{OH})_p^{(2q-p)+} + p\mathrm{H}^+ \quad (2)$$

Similar to Eq. 1, Eq. 3 can be represented as follows:

$$\Delta H^{\mathrm{t}}_{pq} = \Delta H_{pq}(\mathrm{mixed}) - \Delta H_{pq}(\mathrm{aqueous}) = \Delta h^{\mathrm{t}}_{pq} + p\Delta h^{\mathrm{t}}_{\mathrm{H}} - q\Delta h^{\mathrm{t}}_{\mathrm{Be}} - p\Delta h^{\mathrm{t}}_{\mathrm{H_2O}} \quad (3)$$

In order to estimate the extent of the direct beryllium–dioxane interaction, Raman spectra of aqua beryllium ions in dioxane–water mixtures were measured. Raman bands of aqua beryllium ions in aqueous solution were held at the same frequencies in dioxane–water mixtures examined, and therefore, beryllium ions may be preferentially solvated with water molecules in the mixtures. Although no direct evidence has been given for hydroxo complexes, beryllium ions within the hydroxo complexes may also be preferentially solvated with water molecules in water-rich dioxane–water mixtures, and the structure of the skeleton (*i.e.*, –Be–OH– bonds) of the hydroxo complexes may not be appreciably influenced by the solvent composition. Therefore, we assumed that $\Delta h^{\mathrm{t}}_{pq}$, as well as those of simple ions, reflected the change in the solvation structure of the $\mathrm{Be}_q(\mathrm{OH})_p^{(2q-p)+}$ complex when the hydroxo complex was transferred from water to a dioxane–water mixture. Solvation of the hydroxo complex may occur at the beryllium ions within the complex. Charges of beryllium ions within the $\mathrm{Be}_q(\mathrm{OH})_p^{(2q-p)+}$ complex may partially be compensated with those of hydroxide ions, and therefore, the charge per beryllium ion of the $\mathrm{Be}_q(\mathrm{OH})_p^{(2q-p)+}$ complex may be smaller than +2. Thus, the relation $\Delta h^{\mathrm{t}}_{pq} > q\Delta h^{\mathrm{t}}_{\mathrm{Be}}$ may generally be held.

As is seen from Table 1, the enthalpy changes of formation of the $\mathrm{Be_2OH^{3+}}$ complex in aqueous solution and dioxane–water mixtures were both positive, but $\Delta H^{\mathrm{t}}_{12}$ became negative with the increase in the concentration of dioxane. On the contrary, the enthalpy changes of the $\mathrm{Be_3(OH)_3^{3+}}$ complex was practically independent of the concentration of dioxane, and $\Delta H^{\mathrm{t}}_{33}$ was approximately zero. The different tendencies in $\Delta H^{\mathrm{t}}_{pq}$ between $\mathrm{Be_2OH^{3+}}$ and $\mathrm{Be_3(OH)_3^{3+}}$ complexes may be caused by the difference in $\Delta h^{\mathrm{t}}_{pq}$, or in other words, the different solvation structures of the complexes.

Table 1. The formation constants and the changes in enthalpy (ΔH_{pq}/kJ mol^{-1}) and entropy ($T\Delta S_{pq}$/kJ mol^{-1}) of the hydrolytic reaction of beryllium ion in dioxane–water mixtures

$$q\mathrm{Be}^{2+} + p\mathrm{H_2O} = \mathrm{Be}_q(\mathrm{OH})_p^{(2q-p)+} + p\mathrm{H}^+$$
$$\beta^*_{pq} = [\mathrm{Be}_q(\mathrm{OH})_p^{(2q-p)+}][\mathrm{H}^+]^p/[\mathrm{Be}^{2+}]^q$$

		Mole fraction of dioxane 0.0	0.1	0.2
$\mathrm{Be_2OH^{3+}}$	$-\log\beta^*_{12}$	3.04[11]	3.29[11]	3.64[10]
	ΔH_{12}	18.6	15.2	8.4
	$T\Delta S_{12}$	1.3	−3.4	−12.4
$\mathrm{Be_3(OH)_3^{3+}}$	$-\log\beta^*_{33}$	8.671[11]	8.65[11]	8.763[10]
	ΔH_{33}	61.7	59.4	59.0
	$T\Delta S_{33}$	12.2	10.0	9.1
$\mathrm{Be_2(OH)_2^{2+}}$	$-\log\beta^*_{22}$	—	—	7.11
	ΔH_{22}	—	—	42.3
	$T\Delta S_{22}$	—	—	1.3
$\mathrm{H_2O=H^+ + OH^-}$	pK_w	13.867[6]	14.610[6]	15.376[6]
	ΔH_w	56.6	58.1	61.2
	$T\Delta S_w$	−22.6	−25.3	−26.6

In order to compare $\Delta h^{\mathrm{t}}_{12}$ and $\Delta h^{\mathrm{t}}_{33}$ with $\Delta h^{\mathrm{t}}_{\mathrm{Be}}$, the values of $\Delta H^{\mathrm{t}}_{\mathrm{A}}$ and $\Delta H^{\mathrm{t}}_{\mathrm{B}}$ of the following reactions were calculated, where the contributions of hydrogen ions and water molecules to the reactions are same.

$$6\mathrm{Be}^{2+} + 3\mathrm{H_2O} = 3\mathrm{Be_2OH^{3+}} + 3\mathrm{H}^+; \quad \Delta H^{\mathrm{t}}_{\mathrm{A}} = 3\Delta H^{\mathrm{t}}_{12} \quad (4)$$

$$3\mathrm{Be_2OH^{3+}} + 3\mathrm{H_2O} = 2\mathrm{Be_3(OH)_3^{3+}} + 3\mathrm{H}^+; \quad \Delta H^{\mathrm{t}}_{\mathrm{B}} = 2\Delta H^{\mathrm{t}}_{33} - 3\Delta H^{\mathrm{t}}_{12}. \quad (5)$$

The values of $\Delta H^{\mathrm{t}}_{\mathrm{A}}$ and $\Delta H^{\mathrm{t}}_{\mathrm{B}}$ from water to 0.2 mole fraction dioxane–water mixture were −30.6 and 25.2 kJ mol^{-1}, respectively. Equations 6 and 7 can be derived by using partial molar enthalpy changes of transfer of the relevant species as follows:

$$\Delta H^{\mathrm{t}}_{\mathrm{A}} = 3(\Delta h^{\mathrm{t}}_{12} - 2\Delta h^{\mathrm{t}}_{\mathrm{Be}}) + 3(\Delta h^{\mathrm{t}}_{\mathrm{H}} - \Delta h^{\mathrm{t}}_{\mathrm{H_2O}}) \quad (6)$$

$$\Delta H^{\mathrm{t}}_{\mathrm{B}} = (2\Delta h^{\mathrm{t}}_{33} - 3\Delta h^{\mathrm{t}}_{12}) + 3(\Delta h^{\mathrm{t}}_{\mathrm{H}} - \Delta h^{\mathrm{t}}_{\mathrm{H_2O}}) \quad (7)$$

and

$$\Delta H^{\mathrm{t}}_{\mathrm{A}} < \Delta H^{\mathrm{t}}_{\mathrm{B}} \quad (8)$$

Therefore, the relation

$$2\Delta h^{\mathrm{t}}_{33} - 3\Delta h^{\mathrm{t}}_{12} > 3\Delta h^{\mathrm{t}}_{12} - 6\Delta h^{\mathrm{t}}_{\mathrm{Be}} \quad (9)$$

or

$$0 > 2\Delta h^{\mathrm{t}}_{33} \gg 3\Delta h^{\mathrm{t}}_{12} > 6\Delta h^{\mathrm{t}}_{\mathrm{Be}} \quad (10)$$

was readily obtained.

As has been pointed out by earlier workers,[18–26] the enthalpy change of transfer of an ion from water to dioxane–water is due to the change in secondary or more hydration spheres of the ion and the enthalpy change of transfer becomes large for ions having a large charge density. Therefore, the relationship given in Eq. 10 leads to the charge density per metal ion of aqua and hydroxo complexes of beryllium ions decreasing in the order of $\mathrm{Be^{2+}}$, $\mathrm{Be_2OH^{3+}}$, and $\mathrm{Be_3(OH)_3^{3+}}$. Although the formal charges calculated on the beryllium atoms within the aqua and hydroxo complexes are +2, +1.5, and +1 for $\mathrm{Be^{2+}}$, $\mathrm{Be_2OH^{3+}}$, and $\mathrm{Be_3(OH)_3^{3+}}$, respectively, the results given in Eq. 10 suggested that much more positive charges might locate at the beryllium atoms within the hydroxo complexes.

The charge distributions within the $\mathrm{Be_2OH^{3+}}$ and $\mathrm{Be_3(OH)_3^{3+}}$ complexes may be represented as follows:[27]

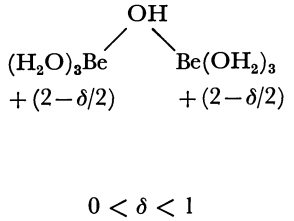

$0 < \delta < 1$

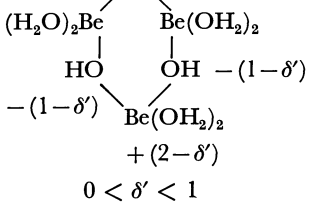

$0 < \delta' < 1$

In the models it was simply assumed that solvation of a hydroxo complex of beryllium ions occurred at the beryllium ion, and a hydroxide ion within the complex acted as a joint between beryllium atoms and as to decrease their charges.

The interaction between a beryllium ion and solvent molecules may be essentially electrostatic, so that the bond energy (or the enthalpy of solvation) may be approximately proportional to $z\mu/r^2$, where z, μ, and r stand for the formal charge of beryllium ion in the complex, the dipole moment of the water molecule and the distance between the beryllium ion and the water molecule, respectively. If we assumed that the enthalpy of solvation of a beryllium ion within a hydroxo complex is proportional to the charge of the beryllium ion, the relationship $\delta<\delta'$ may be derived from Eq. 9. Thus, the charge on the hydroxide ions within the Be_2OH^{3+} complex may be larger than that within the $Be_3(OH)_3{}^{3+}$ complex.

Raman spectroscopic measurements of aqua beryllium ions in aqueous solution showed a band at 527 cm^{-1} due to the total symmetric stretching vibration of $Be(OH_2)_4{}^{2+}$.[28] Corresponding frequencies(ν) of the Be–OH_2 stretching vibration within the Be_2OH^{3+} and $Be_3(OH)_3{}^{3+}$ complexes shifted to 497 and 408 cm^{-1}, respectively.[28] The shift of the band of the Be_2OH^{3+} complex is comparatively less than that of the $Be_3(OH)_3{}^{3+}$ complex. If we simply assumed that the interaction between a beryllium ion and water molecules within a complex is purely electrostatic, and thus, ν^2 is approximately proportional to the charge of the beryllium ion, the formal charge of the beryllium ions within the Be_2OH^{3+} and $Be_3(OH)_3{}^{3+}$ complexes were estimated to be $+1.78$ and $+1.20$, respectively, or $\delta=0.44$ and $\delta'=0.80$. The results coincided with that derived from a qualitative comparison between Δh_{12}^{t} and Δh_{33}^{t} described above.

Although these considerations were very approximate, the results obtained suggested that the charge distribution within the hydroxo complexes may be strongly related to the enthalpy of solvation, and thus the partial molar enthalpy change of transfer of the complexes from one solvent to another.

References

1) R. G. Bates, "Hydrogen-bonded Solvent Systems," Taylor and Francis Ltd., London (1968), p. 49.
2) R. G. Bates, *J. Electroanal. Chem.*, **29**, 1 (1971).
3) B. K. Das and P. K. Das, *J. Chem. Soc. Faraday Trans. 1*, **1978**, 22.
4) G. H. Parsons and C. H. Rochester, *J. Chem. Soc. Faraday Trans. 1*, **1972**, 523.
5) H. S. Harned and L. D. Fallon, *J. Am. Chem. Soc.*, **61**, 2377 (1939).
6) T. Kawai, The Doctoral Thesis, Tokyo Institute of Technology (1975).
7) M. Paabo, R. G. Bates, and R. A. Robinson, *J. Phys. Chem.*, **70**, 247 (1968).
8) H. Ohtaki and N. Tanaka, *J. Phys. Chem.*, **75**, 90 (1971).
9) H. Ohtaki, *Bull. Chem. Soc. Jpn.*, **42**, 1537 (1969).
10) H. Ohtaki, *Inorg. Chem.*, **6**, 808 (1967).
11) H. Ohtaki and H. Kato, *Inorg. Chem.*, **6**, 1935 (1967).
12) H. Tsukuda, T. Kawai, M. Maeda, and H. Ohtaki, *Bull. Chem. Soc. Jpn.*, **48**, 691 (1975).
13) T. P. Prasad and N. N. Sastri, *Talanta*, **13**, 1517 (1966).
14) G. Biedermann and L. Ciavatta, *Acta Chem. Scand.*, **15**, 1347 (1961), *Arkiv Kemi*, **22**, 253 (1964).
15) G. Gran, *Analyst*, **77**, 661 (1952).
16) R. Arnek and W. Kakolowicz, *Acta Chem. Scand.*, **21**, 2180 (1967).
17) B. Carell and Å. Olin, *Acta Chem. Scand.*, **16**, 2357 (1962).
18) D. R. Underdown, S. S. Yun, and J. L. Bear, *J. Inorg. Nucl. Chem.*, **36**, 2043 (1974).
19) D. N. Glew, H. D. Mak, and N. S. Rath, "Hydrogen-bonded Solvent Systems," Taylor and Francis Ltd., London (1968), p. 195.
20) H. P. Bennetto, D. Feakins, and K. G. Lawrence, *J. Chem. Soc. A*, **1968**, 1493.
21) D. Feakins and C. T. Allan, *J. Chem. Soc. Faraday Trans 1*, **1976**, 314.
22) A. Gregery and T. Kiss, *J. Inorg. Nucl. Chem.*, **39**, 109 (1977).
23) F. Franks and D. S. Reid, *J. Phys. Chem.*, **74**, 3152 (1969).
24) C. M. Criss, R. P. Held, and E. Luksha, *J. Phys. Chem.*, **72**, 2970 (1968).
25) L. S. Frankel, T. R. Stengle, and C. H. Langford, *Can. J. Chem.*, **46**, 3183 (1968).
26) Y. Sze and D. E. Irish, *J. Solution Chem.*, **7**, 417 (1978).
27) R. Faure, F. Bertin, H. Loiseleur, and G. Thomas-David, *Acta Crystallogr., Sect. B*, **30**, 462 (1974).
28) S. Ishiguro, M. Maeda, S. Ono, and H. Kakihana, *Denki Kagaku*, **46**, 553 (1974).

Molecular Structure of Trimethylphosphine-boron Trichloride by Gas Electron Diffraction

Kinya IIJIMA and Shuzo SHIBATA*

Department of Chemistry, Faculty of Science, Shizuoka University, Oya, Shizuoka 422

(Received March 22, 1979)

The molecular structure of trimethylphosphine-boron trichloride $(CH_3)_3P\cdot BCl_3$ has been determined from gas electron-diffraction data. The structure parameters and uncertainties are r_g(P–B) = 1.941(16) Å, r_g(B–Cl) = 1.851(7) Å, r_g(C–P) = 1.800(4) Å, r_g(C–H) = 1.099(5) Å, r_g(Cl···Cl) = 3.022(5) Å, and r_g(C···C) = 2.936 (10) Å. The potential barrier about the P–B axis is 3.8±0.7 kcal mol^{-1} in the gas phase. The data show that the molecular structure in the gas phase is nearly equal to that in the solid phase.

The molecular structures of several phosphorus-boron donor-acceptor complexes have been investigated in the gas and solid phases by microwave spectroscopy[1–5] and X-ray diffraction,[6] respectively. According to these studies the distances of the P–B dative bond in the complexes are very different from each other. The experimental data showed that the P–B distances in $F_3P\cdot BH_3$[1] and $H_3P\cdot BH_3$[2] are 1.836±0.006 Å and 1.937±0.005 Å, respectively, and the P–B distances of the other complexes are somewhat between these values. Therefore, the P–B dative bond appears to considerably change in length according to circumstances surrounding the bonded atoms. It has been noted that there appears to be no correlation between the distance of the P–B dative bond and the stability of the complex.[4] For example, the $F_3P\cdot BH_3$ complex is extensively dissociated in the gas phase at room temperature, while the $(CH_3)_3P\cdot BH_3$ complex, which has a greater P–B distance, 1.901±0.007 Å,[4] is more stable and can be heated to approximately 200 °C without appreciable decomposition.[7] Rudolph and Parry have proposed a theory to account for the unusual properties of the P–B bond,[8] but more structural data appears to be necessary in order to understand the nature of the P–B dative bond. It has been reported that the distance of the N–B dative bond in trimethylamine-boron trihalide is significantly larger in the gas phase than in the solid phase.[9–11] It is therefore of interest to compare the P–B distance of trimethylphosphine-boron trihalide in the gas phase with that in the solid phase.[6] Thus the present study was undertaken in order to determine the molecular structure of gaseous trimethylphosphine-boron trichloride $(CH_3)_3P\cdot BCl_3$.

Experimental

Trimethylphosphine was prepared by the dropwise addition of phosphorus trichloride into an ethereal solution of methyllithium, and the distilled trimethylphosphine solution added to an ethereal solution of boron trichloride. After removal of the ether, the trimethylphosphine-boron trichloride complex was recrystallized from acetone and water, and sublimed under vacuum. The purity of the complex was verified by IR analysis.[12] In the electron-diffraction experiment the sample was vaporized at approximately 190 °C by means of a high temperature nozzle, and photographs taken with an r^3-sector at camera distances of 144 and 294 mm. The accelerating voltage was 40 kV, and the exposure time for the long camera distance was 25 s using an electron-beam current of 0.7 μA. For the short camera distance the exposure time was 80 s using a beam current of 0.9 μA. The pressure in the diffraction chamber was approximately 1×10^{-5} Torr during the experiment. The electron wavelength was measured by means of diffraction patterns of thallium chloride powder.[13] Photographs were recorded on Kodak electron-image plates, and the optical densities of the three plates taken at each camera distance were measured at 0.4 mm intervals by means of a digital microphotometer. The electron-diffraction unit and digital microphotometer used in the present study have been described elsewhere.[14]

Analysis and Results

The scattering intensities were obtained in the ranges of s = 2.5—17.3 Å^{-1} and 5.0—34.2 Å^{-1} from the photographic plates at long and short camera distances, respectively. The intensities were divided by the theoretical backgrounds, and the leveled intensities of several plates for each camera distance were averaged. The elastic and inelastic scattering factors were taken from the tables prepared by Schäfer *et al.*[15] and Cromer and Mann,[16] respectively. The background curves were drawn by hand for the long distance data and fitted to a 7th degree polynomial for the short distance data. The molecular intensities for each camera distance were joined at s = 14.8 Å^{-1}, and the curve, shown in Fig. 2, used for the analysis. Figure 3 shows the radial distribution curve, which suggests that the molecular structure of $(CH_3)_3P\cdot BCl_3$ is staggered.

The molecular parameters were determined by a least-squares analysis of the molecular intensities. It was assumed that the $(CH_3)_3P\cdot BCl_3$ molecule has C_{3v} symmetry in the staggered form, and that the methyl group has local C_{3v} symmetry and is staggered with respect to the P–B bond. The mean amplitudes and the corrections for the shrinkage effects,[17] $r_a - r_\alpha$, were calculated on the basis of the force field for $(CH_3)_3P\cdot BCl_3$[12] and are given in Table 1. The

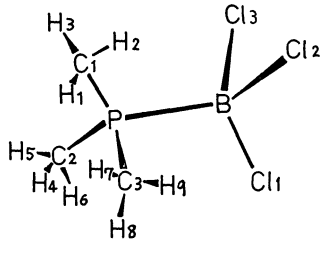

Fig. 1. Numbering of atoms in trimethylphosphine-boron trichloride (symmetry C_{3v}).

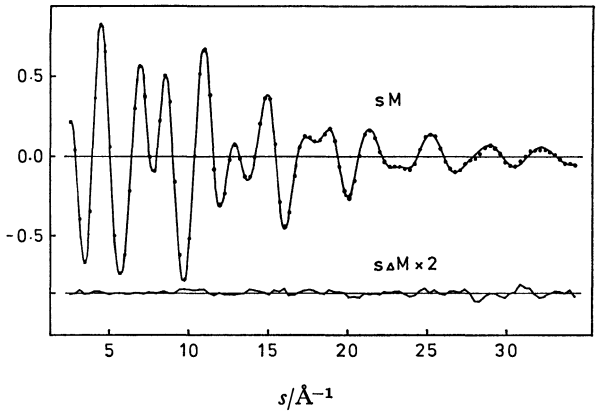

Fig. 2. Molecular intensities for trimethylphosphine-boron trichloride. Solid curve, calculated; dotted curve, experimental. Lower curve, two times the residuals with respect to the experimental curve.

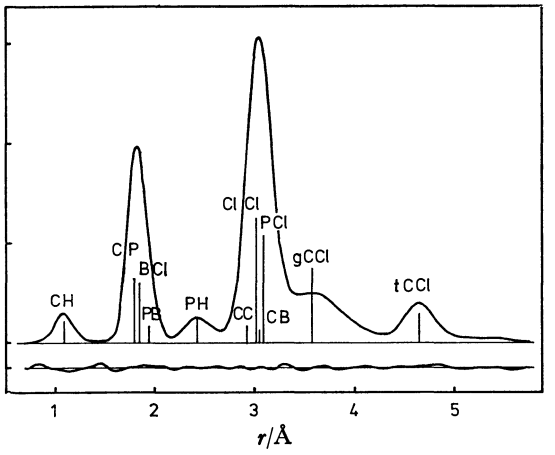

Fig. 3. Radial distribution curve for trimethylphosphine-boron trichloride. Solid curve, experimental; lower curve, 2.5 times the residuals.

geometrical parameters and the mean amplitudes determined by the least-squares analysis are as follows: r(B–Cl), r(P–B), r(C–P), r(C–H), r(Cl···Cl), r(C···C), ∠PCH, l(B–Cl), l(C–P), l(C–H), l(Cl···Cl), l(*trans* C···Cl), l(*gauche* C···Cl), l(P···H). The mean amplitudes for the other atomic pairs were fixed to the calculated values shown in Table 1. The asymmetry parameter, κ, for the C–H bond was assumed to be 1.2×10^{-5} Å^3 by a diatomic approximation.[18] The asymmetry parameters for the other atomic pairs were neglected.

Table 1. Calculation of mean amplitudes and shrinkage effects for $(CH_3)_3P \cdot BCl_3$ (in 10^{-4} Å)

	l	$r_a - r_\alpha$		l	$r_a - r_\alpha$
B-Cl	696	62	P-C_1	534	277
B-P	645	3	P···H_1	1181	428
B···C_1	1187	117	C_1···C_2	1189	410
B···H_1	1340	242	C_1-H_1	782	518
B···H_2	2276	253	C_1···H_4	2329	401
Cl_1···Cl_2	808	93	C_1···H_5	2341	450
Cl_1···P	1001	15	C_1···H_6	1330	685
Cl_1···C_1	1160	20	H_1···H_2	1299	900
Cl_1···C_2	2390	3	H_1···H_4	3292	356
Cl_1···H_1	1498	111	H_1···H_5	3621	271
Cl_1···H_2	2141	107	H_1···H_6	2373	665
Cl_1···H_4	2476	123	H_2···H_5	2319	740
Cl_1···H_5	3850	−106	H_2···H_6	1561	889
Cl_1···H_6	3456	112	H_2···H_9	3360	363

The numbering of the atoms is shown in Fig. 1.

In the force field treatment by Drake *et al.*[12] the torsional vibrations around the C–P and P–B bonds were not taken into consideration. In the present study the force constant for the torsional vibration around the C–P bond was assumed to be 0.08 mdyne Å. This value was estimated from the potential barrier for trimethylphosphine, 2.6 kcal mol^{-1}.[19] Since the torsional vibration around the P–B bond contributes considerably to the mean amplitude of the *gauche* C···Cl pair, the force constant for this motion, Y(P–B), was adjusted to fit the calculated mean amplitude of the *gauche* C···Cl pair to the observed one from the analysis of electron-diffraction intensities.[11] Thus Y(P–B) was estimated to be 0.12± 0.02 mdyne Å, and the potential barrier of the torsional vibration around the P–B bond was evaluated as 3.8±0.7 kcal mol^{-1}.

The r_α parameters and mean amplitudes determined by the analysis are given in Tables 2 and 3 together

Table 2. Molecular parameters

	$(CH_3)_3P \cdot BCl_3$ (gas)[a]			(solid)[c]	$(CH_3)_3P$[d]	BCl_3[e]
	r_α[b]	r_g	σ[f]	r	r_g	r_g
B-Cl	1.843	1.851	0.007	1.855 (5)		1.742 (4)
P-B	1.939	1.941	0.016	1.957 (5)		
C-P	1.771	1.800	0.004	1.81 (1)	1.846 (3)	
C-H	1.042	1.099	0.005		1.091 (6)	
Cl···Cl	3.010	3.022	0.005			3.013 (6)
C···C	2.890	2.936	0.010		2.800 (5)	
∠PCH	113.7		0.9		110.7 (5)	
∠ClBCl	109.5		0.4	111.4 (4)		120
∠CPC	109.3		0.3	107.9 (4)	98.6 (3)	

Bond distance: Å unit; bond angle: degree unit. a) Present study. b) Angles were calculated using r_α parameters. c) Ref. 6. d) Ref. 21. e) Ref. 22. f) See text.

Table 3. Root-mean-square amplitudes for $(CH_3)_3P\cdot BCl_3$ (in Å unit)

	l_{obsd}	l_{calcd}
B-Cl	0.067 (6)	0.070
C-P	0.048 (4)	0.053
C-H	0.073 (5)	0.078
C···Cl	0.092 (4)	0.081
trans C···Cl	0.106 (8)	0.116
gauche C···Cl	0.238 (10)	0.239
P···H	0.113 (10)	0.118

with their 99% confidence errors, respectively. The errors were estimated from random errors in the least-squares calculations and systematic errors originating from the measurements of camera distance and electron wavelength. The comparatively large errors of r(B–Cl), r(P–B), and l(B–Cl) are attributable to the large correlations between other parameters. The correlation matrix is listed in Table 4, and the best-fit theoretical intensity curve is shown in Fig. 2.[20] The calculations of mean amplitudes, shrinkage effects, and method of least-squares were conducted on a HITAC 8800/8700 computer in the Computer Center of the University of Tokyo.

Discussion

From a comparison of the molecular structure of the $(CH_3)_3P\cdot BCl_3$ complex to those of the component molecules of $(CH_3)_3P$[21] and BCl_3[22] (Table 2), it can be seen that complex formation increases the CPC angle by 11% and the B–Cl distance by 6%, and decreases the C–P distance by 3% and the ClBCl angle by 9%. Both the CPC and the ClBCl angles in the complex are almost tetrahedral. The above changes can be interpreted in terms of the valence-shell electron-pair repulsion theory.[23]

The structural change of the donor molecule by the formation of $(CH_3)_3P\cdot BCl_3$ is quite different from that by the formation of the trimethylamine complex, since in the former the CPC angle increases and the C–P distance decreases while in the latter the CNC angle decreases (2°) and the C–N distance increases (0.04 Å).[10] With respect to the acceptor molecule, however, the structural change is rather similar in both complexes (a decrease of 8% in the ClBCl angle and an increase of 6% in the B–Cl distance in the $(CH_3)_3N\cdot BCl_3$ complex[10]). There is another difference between both complexes. The molecular structure of $(CH_3)_3N\cdot BCl_3$ in the gas phase[10] differs from that in the solid phase.[24] For example, the N–B dative bond is much greater in the gas phase than in the solid phase. The molecular structure of gaseous $(CH_3)_3P\cdot BCl_3$ is however nearly equal to that in the solid phase.[6]

The rotational barrier of $H_3P\cdot BH_3$ about the P–B bond is 2.47±0.05 kcal mol^{-1} according to a MW spectroscopic study.[2] The fluorine-substituted compounds of $F_3P\cdot BH_3$ and $H_3P\cdot BF_3$ have slightly larger barriers, 3.24±0.15 and 3.39±0.40 kcal mol^{-1}, respectively.[1,3] The H···H distance in $H_3P\cdot BH_3$, the F···H distance in $F_3P\cdot BH_3$ and that in $H_3P\cdot BF_3$ are virtually identical, which suggests that the increment in the barrier for the fluorine-substituted compounds is probably due to the large steric repulsion of the fluorine atoms. On this bases, it might be expected that in $(CH_3)_3P\cdot BCl_3$ the methyl groups and chlorine atoms increase the barrier around the P–B bond through large steric effects. The barrier was however found to be 3.8±0.7 kcal mol^{-1}, which is equal to that reported for $F_3P\cdot BH_3$ and $H_3P\cdot BF_3$ within the limits of experimental error. This could be attributed to the considerably large C···Cl distances in $(CH_3)_3P\cdot BCl_3$.

References

1) R. L. Kuczkowski and D. R. Lide, *J. Chem. Phys.*, **46**, 357 (1967).

Table 4. Correlation matrix of $(CH_3)_3P\cdot BCl_3$

	r(BCl)	r(PB)	r(CP)	r(CH)	r(ClCl)	r(CC)	∠PCH	l(CH)	l(tCCl)	l(gCCl)	l(PH)	l(BCl)	l(CP)	l(ClCl)	R_1[a]	R_2[a]
r(BCl)	1.0															
r(PB)	−0.95	1.0														
r(CP)	−0.65	0.51	1.0													
r(CH)	−0.06	0.07	−0.03	1.0												
r(ClCl)	0.12	−0.27	−0.01	−0.04	1.0											
r(CC)	−0.18	0.18	0.49	−0.02	−0.32	1.0										
∠PCH	0.17	−0.18	−0.16	−0.33	0.03	−0.11	1.0									
l(CH)	−0.10	0.11	0.10	−0.02	−0.20	0.07	−0.03	1.0								
l(tCCl)	−0.07	0.09	0.06	0.03	−0.15	0.05	−0.07	0.18	1.0							
l(gCCl)	0.03	−0.09	−0.03	−0.09	0.13	−0.09	0.18	−0.09	−0.10	1.0						
l(PH)	0.02	−0.01	−0.04	−0.04	0.10	−0.02	0.05	−0.14	−0.10	0.00	1.0					
l(BCl)	0.25	−0.39	0.46	−0.05	0.04	0.33	−0.01	0.15	0.10	−0.04	−0.13	1.0				
l(CP)	−0.75	0.79	0.22	0.09	−0.31	−0.01	−0.12	0.25	0.19	−0.10	−0.13	−0.42	1.0			
l(ClCl)	−0.44	0.23	0.57	0.00	0.33	0.10	−0.09	0.20	0.14	0.00	−0.14	0.37	0.30	1.0		
R_1	−0.30	0.33	0.24	0.02	−0.41	0.04	0.06	0.32	0.24	−0.28	−0.09	0.19	0.45	0.30	1.0	
R_2	−0.22	0.24	0.21	0.06	−0.42	0.14	−0.08	0.48	0.35	−0.17	−0.32	0.32	0.53	0.42	0.63	1.0

a) R_1 and R_2 are indices of resolution for the long and short camera distance data, respectively. The indices and uncertainties are R_1=0.88 (1) and R_2=1.00 (5).

2) J. R. Durig, Y. S. Li, L. A. Carreira, and J. D. Odom, *J. Am. Chem. Soc.*, **95**, 2491 (1973).
3) J. D. Odom, V. F. Kalasinsky, and J. R. Durig, *Inorg. Chem.*, **11**, 2837 (1975).
4) P. S. Bryan and R. L. Kuczkowski, *Inorg. Chem.*, **11**, 553 (1972).
5) J. P. Pasinski and R. L. Kuczkowski, *J. Chem. Phys.*, **54**, 1903 (1971).
6) D. L. Black and R. C. Taylor, *Acta Crystallogr., Sect. B*, **31**, 1116 (1975).
7) A. B. Burg and R. I. Wagner, *J. Am. Chem. Soc.*, **75**, 3872 (1953).
8) R. W. Rudolph and R. W. Parry, *J. Am. Chem. Soc.*, **89**, 1621 (1967).
9) S. Shibata and K. Iijima, *Chem. Lett.*, **1977**, 29.
10) M. Hargittai and I. Hargittai, *J. Mol. Struct.*, **39**, 79 (1977).
11) K. Iijima and S. Shibata, *Bull. Chem. Soc. Jpn.*, **52**, 711 (1979).
12) J. E. Drake, J. L. Hencher, and B. Rapp, *Inorg. Chem.*, **16**, 2289 (1977).
13) W. Witt, *Z. Naturforsch., Teil A*, **19**, 1363 (1964).
14) S. Shibata, K. Iijima, R. Tani, and I. Nakamura, *Rep. Fac. Sci. Shizuoka Univ.*, **9**, 33 (1974).
15) L. Schäfer, A. C. Yates, and R. A. Bonham, *J. Chem. Phys.*, **55**, 3055 (1971).
16) D. T. Cromer and J. B. Mann, *J. Chem. Phys.*, **47**, 1892 (1967); D. T. Cromer, *ibid.*, **50**, 4857 (1969).
17) K. Kuchitsu and S. J. Cyvin, "Molecular Structures and Vibrations," ed by S. J. Cyvin, Elsevier, Amsterdam (1972), Chap. 12.
18) K. Kuchitsu, *Bull. Chem. Soc. Jpn.*, **40**, 505 (1967).
19) "Kagaku Binran," 2nd ed, ed by the Chemical Society of Japan, Maruzen, Tokyo (1975), p. 1330.
20) Numerical experimental data of the leveled total intensity and background have been deposited with the Chemical Society of Japan (Document No. 7931).
21) L. S. Bartell and L. O. Brockway, *J. Chem. Phys.*, **32**, 512 (1960).
22) S. Konaka, Y. Murata, K. Kuchitsu, and Y. Morino, *Bull. Chem. Soc. Jpn.*, **39**, 1134 (1966).
23) R. J. Gillespie, *J. Chem. Educ.*, **40**, 295 (1963).
24) P. H. Clippard, J. C. Hanson, and R. C. Taylor, *J. Cryst. Mol. Struct.*, **1**, 363 (1971).

Anodic Oxidation of 2-Aminofluorene at a Platinum Electrode in Acetonitrile Solutions

Kazuo YASUKOUCHI, Isao TANIGUCHI,* Hiroko YAMAGUCHI, Katsuji MIYAGUCHI, and Koji HORIE

Department of Industrial Chemistry, Faculty of Engineering, Kumamoto University, 2-39-1, Kurokami, Kumamoto 860

(Received April 16, 1979)

Anodic oxidation of 2-aminofluorene in acetonitrile solutions at a Pt electrode was investigated by using electrochemical techniques and by preparative-scale electrolyses. The cyclic voltammogram of 2-aminofluorene exhibited two anodic waves, which had peak potentials at 0.45 V (I_a) and 1.15 V (II_a) *vs.* Ag/0.01 M $AgClO_4$. Wave II_a was due to oxidation of protonated 2-aminofluorene. In the voltammogram of repetitive sweeps, another redox couple (III_a/III_c) was observed at 0.13 V for III_a and 0.06 V for III_c, respectively. This indicates that at wave I_a, a species which is more easily oxidized than 2-aminofluorene was produced by follow-up chemical steps. By controlled-potential electrolysis at 0.5 V of a 2-aminofluorene solution containing pyridine as a proton acceptor, a dark green product, 3-(2-fluorenylimino)-2,3-dihydro-2-fluorenimine (**5**) (or 1-(2-fluorenylimino)-1,2-dihydro-1-fluorenimine (**5′**)), precipitated as the main product in more than 70% yield. The oxidation pathway of 2-aminofluorene (Eqs. 1—4) has been proposed on the bases of the following results: (i) The apparent *n*-value was 1.95, (ii) two protons/molecule of 2-aminofluorene were released in the follow-up chemical steps, and (iii) the peak potential for oxidation of 2′-amino-2,3′-difluorenylamine (**3**) (or 2-amino-1,2′-difluorenylamine (**3′**)) was in good agreement with that of wave III_a, and the anodic oxidation of **3** (or **3′**) gave the same product as that obtained by oxidation of 2-aminofluorene.

Anodic oxidation of aromatic amines has been extensively studied in both aqueous and nonaqueous solutions, and some general rules for reaction pathways have been obtained for mononuclear aromatic amines.[1—5] For polynuclear aromatic amines, however, little is known about the oxidation pathway. This is partially because in many cases the oxidation products film the electrode surface and no product could be isolated. Most investigations of these compounds have been limited to the measurement of the oxidation half-wave potentials which are correlated with the HMO energies of the highest occupied molecular orbitals.[6,7] Recently, however, electrochemical pathways of polynuclear aromatic amines have become increasingly important biologically. This is because, (i) since these compounds are typical carcinogens and their azo and/or hydrazo derivatives are important metabolic intermediates of the carcinogens,[8,9] information which elucidates the carcinogenic mechanism may be obtained, and (ii) an electrochemical technique for the synthesis of biologically important compounds can be developed. Furthermore, it would be worthwhile to study the oxidation of polynuclear aromatic amines to examine whether or not the general rules for the oxidation mechanism proposed for mononuclear aromatic amines can be applicable for polynuclear ones.

In the present study, anodic oxidation of 2-aminofluorene, whose reaction pathway has not yet been reported, was investigated.

Experimental

Reagents were analytical GR grade and used without further purification unless otherwise noted. Sodium perchlorate was recrystallized twice from ethanol, dried overnight under a reduced pressure (400 Pa), and stored over silica gel. Acetonitrile was purified by distillation with P_2O_5 and with K_2CO_3, and then twice by slow fractional distillation. The MeCN was used within two weeks after purification. The water concentration of the test solution was determined to be less than 0.2 wt% by the Karl-Fischer titration.

The cyclic voltammograms were measured at a Pt disk electrode (2.0×10^{-3} cm^2) using a Yanaco P8 polarograph. The electrode was polished with an oil stone before each measurement. Rotating disk electrode (RDE) voltammetry was carried out using a commercially available instrument constructed by Nikko Keisoku. The kinematic viscosity (ν) of the solution used was 0.00441 cm^2 s^{-1}. The diffusion coefficient (D) of 2-aminofluorene was estimated to be 1.55×10^{-5} cm^2 s^{-1} by the Levich equation.

Controlled-potential electrolysis was undertaken using a Nikko Keisoku NPGS 301 potentiostat. A two-compartment cell with a fine glass frit was used. The working (50 cm^2) and the counter electrodes were Pt plates. During electrolysis, cyclic voltammograms of the solution were measured to check the change of the composition of the solution. The working electrode for preparative-scale electrolysis was reactivated, when necessary, by burning, because the product which adhered on the electrode surface caused a steep decrease in current. In the time scale for voltammetric measurements, however, no serious adsorption of the product was observed.

An Ag/0.01 M $AgClO_4$ couple in MeCN was used as the reference electrode and potentials appearing in this paper are referred to this electrode. All electrochemical experiments were carried out at 25±0.5 °C under an atmosphere of nitrogen. Throughout this paper, 1 M=1 mol dm^{-3}.

After exhaustive electrolysis of 2-aminofluorene, the solution was concentrated and water was added to precipitate a dark green product. The precipitate was separated by centrifugation and filtered off. The crude product was washed more than six times with each 10 ml of water to remove trace amounts of 2-aminofluorene which remained unreacted, and then recrystallized from either aqueous methanol or aqueous *N*,*N*-dimethylformamide. Thus, for example, 19 mg of the product (I) was obtained by electrolysis of 27 mg of 2-aminofluorene (150 ml of 1 mM solution); the yield is more than 70%. The product I was then chromatographed on both silica gel (Wako B-10) and alumina (Wako B-10) with either benzene, acetone, or ethanol, and detected with iodine. In each case only a single spot was

observed. The analytical data on the product I are: mp> 300 °C; UV-Vis$_{max}$ (MeCN) 277 (log ε 4.3) and 660 nm (log ε 3.4); NMR (C_5D_5N) δ=3.76 (4H, s, CH_2) and 6.9—7.8 (13H, m, Ar–H); IR (KBr) 3370 (ν N–H) and 1610 cm^{-1} (ν C=N). Found: C, 87.2; H, 5.4; N, 7.4%; M$^+$, 358. Calcd for $C_{26}H_{18}N_2$: C, 87.1; H, 5.1; N, 7.8%; M, 358.4. The product I was easily soluble in *N*,*N*-dimethylformamide, fairly soluble in pyridine, soluble in MeCN, methanol, and ethanol, but almost insoluble in water.

Acetylation of I was performed by a method similar to that described by Bridger *et al.*[10] In the IR spectrum of the acetylated product, the absorption of N–H stretching at 3370 cm^{-1} disappeared, and those of C=O stretching and C–CH_3 bending appeared at 1720 and 1370 cm^{-1}, respectively (=NH→=N–C(=O)–CH_3). The number of NH groups was estimated to be one by the ratios of the number of methyl protons introduced by acetylation to those of methylene protons and aromatic protons of the fluorene ring in the NMR spectrum of the acetylated product.

2′-Amino-2,3′-difluorenylamine (**3**) was prepared according to the literature,[11] where it had not been determined whether the compound was **3** or 2-amino-1,2′-difluorenylamine (**3′**). No data for distinguishing between **3** and **3′** were obtained in the present study; we denote this compound as **3** just for convenience. Oxidation of **3** was carried out electrochemically by a method similar to that used for the oxidation of 2-aminofluorene, except for the applied potential.

The IR and UV spectra were obtained using a Hitachi 125-G (using KBr pellet technique) and a Hitachi 200-10 spectrophotometer, respectively. The NMR spectra were measured using a JEOL MH-100 spectrometer in either pyridine-d_5 or $CDCl_3$ containing TMS as an internal standard. The mass spectra were recorded using a JEOL JMS D-100 spectrometer.

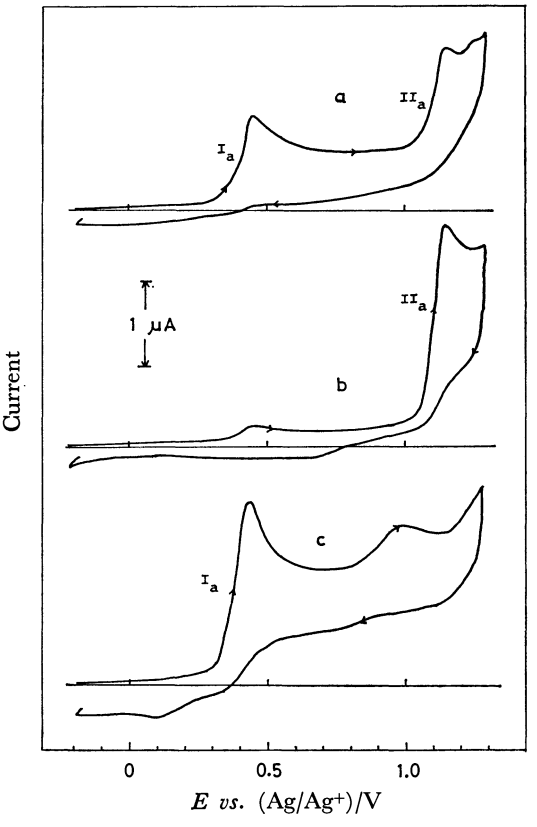

Fig. 1. Cyclic voltammograms of 1 mM 2-aminofluorene in 0.1 M $NaClO_4$–MeCN at the scan rate of 0.2 V s^{-1}. a; With no additive, b; with 1 mM $HClO_4$, and c; with 2 mM pyridine. The direction of the potential sweep is shown by arrows on the voltammograms.

Results and Discussion

The cyclic voltammogram of 2-aminofluorene showed two anodic waves having peak potentials, E_p, of 0.45 (I_a) and 1.15 (II_a) (Fig. 1a). Wave II_a was due to oxidation of protonated 2-aminofluorene. When the concentration of proton added was equal to that of 2-aminofluorene, only this wave was observed (Fig. 1b). Further increase in proton concentration did not cause appreciable change in the shape or height of the wave. On the other hand, the height of wave I_a increased with increasing amounts of pyridine added. Finally, in the solution containing twice as much pyridine as the concentration of 2-aminofluorene, the peak current of I_a became twice the value observed in the solution with no pyridine, whereas wave II_a disappeared and a wave due to oxidation of pyridine at E_p=0.95 V was observed (Fig. 1c). These cyclic voltammetric data show that 2-aminofluorene acted as a base in the follow-up chemical steps, but pyridine replaced 2-aminofluorene as a proton acceptor.

By controlled-potential electrolysis of 1 mM 2-aminofluorene solution with no pyridine, the *n*-value (electrons consumed/molecule of the starting amine) observed was 0.5—0.6, and a dark green precipitate and protonated 2-aminofluorene were produced. During electrolysis, the color of the solution turned green and then reddish purple. The latter color was due to protonated species of the dark green product, because an acetonitrile solution of the green product changed from green to reddish purple when perchloric acid was added to the solution. Thus, in order to reduce the complication caused by the protonation of both the starting amine and the product, preparative-scale electrolyses at 0.5 V of 1 mM 2-aminofluorene solution containing 2—5 mM pyridine were carried out. During electrolysis, the dark green product was generated as the main product in a yield of more than 70%, and the *n*-value of 1.95 was obtained by coulometry. The color of the solution became dark green and no further change to reddish purple was observed even at the end of the electrolysis. In the cyclic voltammograms of the solution during electrolysis, the peak current of I_a decreased and a new reduction wave (IV_c) due to reduction of protonated pyridine appeared (Fig. 2). The peak current of wave IV_c observed at the end of the electrolysis indicates that two protons per molecule of 2-aminofluorene were released in the follow-up chemical steps. No appreciable change in the results was observed by varying the concentration of pyridine (2—5 mM).

Oxidation Product. The structure of the dark green product is now considered in detail. In general, anodic oxidation of aromatic amine gives three types of compounds, namely, azo type (which is formed by N–N coupling of the intermediates), ortho-semidine type (by ortho C–N coupling), and benzidine type

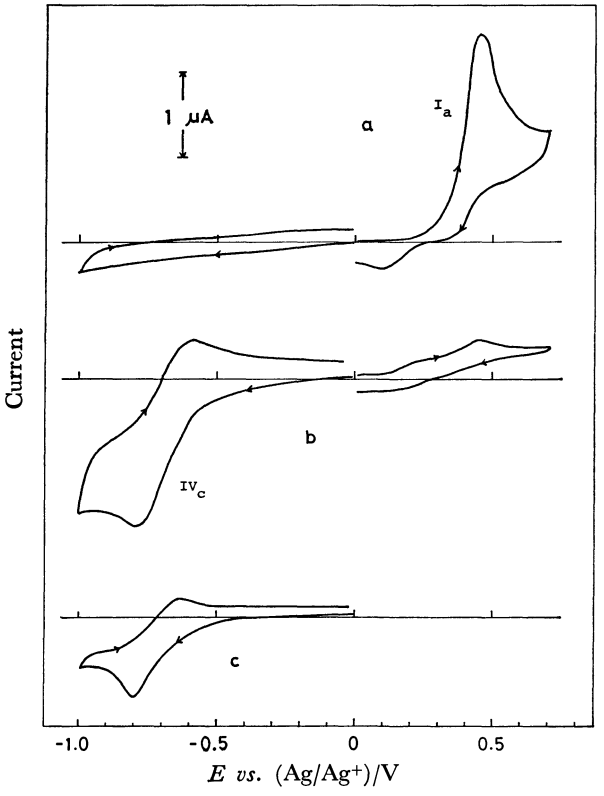

Fig. 2. Cyclic voltammograms of 1 mM 2-aminofluorene in 0.1 M $NaClO_4$–MeCN containing 3 mM pyridine (a and b), and of 1 mM protonated pyridine (c) in 0.1 M $NaClO_4$–MeCN. a; Before, and b; after exhaustive oxidation at 0.5 V. c; 1 mM pyridine solution containing 1 mM $HClO_4$. Scan rate: 0.2 V s^{-1}.

compounds (by C–C coupling). For product I, 2,2′-azofluorene must be rejected because no appreciable UV absorption for 2,2′-azofluorene or 2,2′-hydrazofluorene[12] was observed. A benzidine type compound may also be unlikely because of the structural hindrance of 2-aminofluorene. Thus, an ortho-semidine type is most probable, and 2′-amino-2,3′-difluorenylamine (**3**), which seems to be an intermediate in the present reaction, was synthesized according to the literature[11] (see experimental section).

By anodic oxidation of **3** at 0.3 V, the slightly orange-colored solution turned green and a product was obtained, which was identical with that obtained by oxidation of 2-aminofluorene, judging from their NMR, IR, and UV spectra. Thus, the following structure, **5**, is suggested for product I:

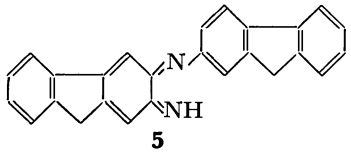

5

To further clarify the structure, the product was analyzed by several methods (see experimental section). The following analytical data support the structure **5**: (i) In the IR spectrum of I, N–H stretching absorptions for 2-aminofluorene at 3360 and 3450 cm^{-1} changed to a single band at 3370 cm^{-1} and a C=N

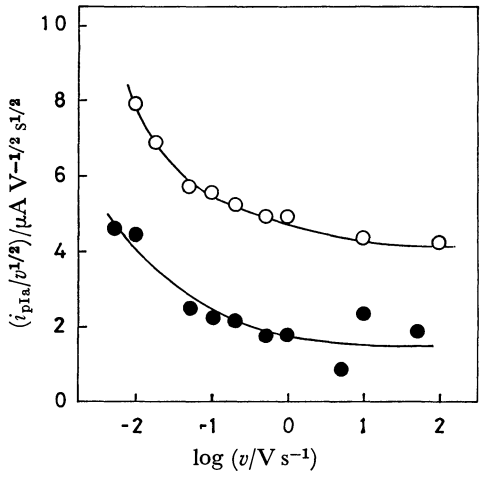

Fig. 3. The ratio of the peak current for wave I_a of 1 mM 2-aminofluorene solution to the square root of the scan rate, $i_{pIa}/v^{1/2}$, as a function of the scan rate in 0.1 M $NaClO_4$–MeCN. (○); With 2 mM pyridine, and (●); without.

stretching absorption at 1610 cm^{-1} was observed ($-NH_2 \rightarrow >C=NH$). (ii) Acetylation of I took place, and the number of N–H groups per molecule of I was estimated to be one from the NMR spectrum of the acetylated product. (iii) Results of elementary analysis and molecular weight (=358) are in good agreement with those calculated for **5**. (iv) The NMR spectrum showed that the number of aromatic protons and that of methylene protons are reasonably explained in terms of the structure of **5**, though no appreciable peak for N–H protons was observed.

Oxidation Pathway. To clarify the mechanism for the formation of **5**, further cyclic voltammetric investigations were carried out. The ratio of the peak current of wave I_a to the square root of the scan rate of the potential, $i_{pIa}/v^{1/2}$, decreased with an increase in the scan rate (Fig. 3). In repetitive cyclic voltammograms, a couple of waves (III_a/III_c) at potentials less anodic than that of wave I_a were observed (Fig. 4). These results indicate that for oxidation at wave I_a a primary one-electron transfer occurred to form a cation radical, and then a species which is more easily oxidized than the starting amine was produced by a chemical reaction and was further oxidized; this would be like a so-called ECE mechanism. Wave III_a in the cyclic voltammogram of 2-aminofluorene was in good agreement with the oxidation wave of **3** in both the peak potential and the wave shape (Fig. 4). The differences in shape and the peak potential observed between wave III_c and the corresponding re-reduction wave of **3** are probably because the oxidation product adsorbed on the electrode shifts the re-reduction wave of **3** to more negative potentials (Fig. 4c). During controlled-potential electrolysis of **3** at 0.3 V, two electrons per molecule of **3** were consumed, and the number of protons liberated was estimated to be two from the peak current for the reduction of protonated pyridine.

Thus, taking into account the results that (i) the over-all *n*-value for oxidation of 2-aminofluorene was two, and (ii) two protons with respect to the starting

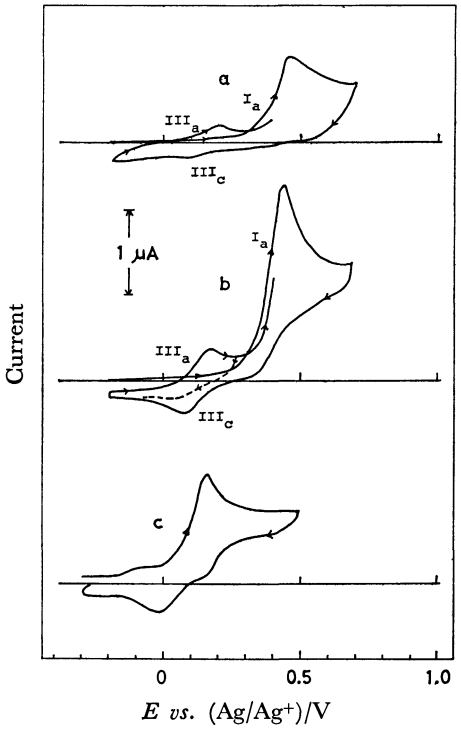

Fig. 4. Repetitive cyclic voltammograms of 1 mM 2-aminofluorene (a and b), and of 0.5 mM of **3** (c) in 0.1 M $NaClO_4$–MeCN containing a; 0 mM, b; 2 mM, and c; 5 mM pyridine. Scan rate: 0.2 V s^{-1}.

amine were released in the follow-up chemical steps to produce **5**, we propose that **5** is formed by the following reactions in a solution containing pyridine (Py):

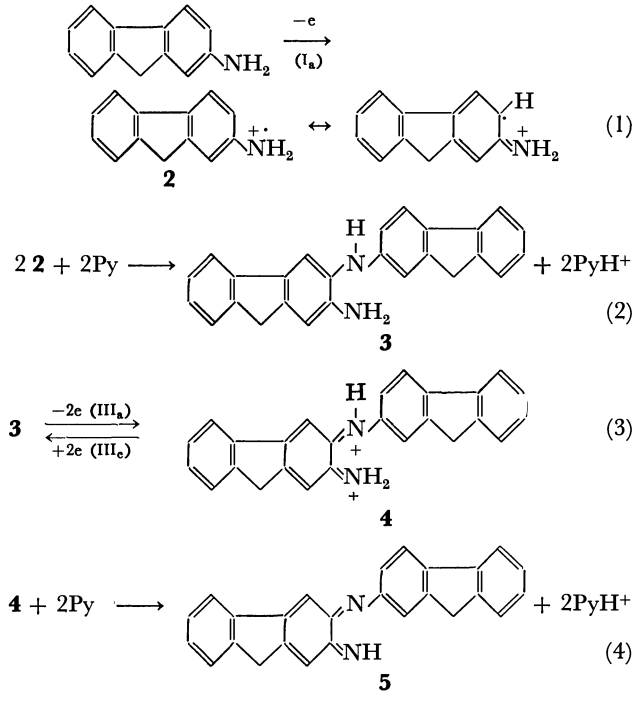

where the formation of **5′**, an isomer of **5**, is also possible *via* similar reactions. In the present experiment, no data for distinguishing between **5** and **5′** have yet been obtained; to determine the correct structure of the product I, further experiments, for example ^{13}C NMR measurements, are required, and some investigations are now in progress.

Table 1. RDE[a] data for oxidation of 2-aminofluorene in 0.1 M $NaClO_4$–MeCN

Concn / mM	ω / rad s^{-1}	$i_l\omega^{-1/2}$ [b] / μA rad$^{-1/2}$ $s^{1/2}$	n_{app}	k [c] / s^{-1}
0.6	20.7	3.99	1.05	0.20
	30.4	3.94	1.04	0.22
	40.3	3.87	1.02	0.16
	49.8	3.83	1.01	—
	61.3	3.79	1.00	—
	mean[d]	3.79	1.00	—
0.8	20.7	5.46	1.05	0.19
	30.2	5.41	1.04	0.23
	40.2	5.36	1.03	0.23
	50.0	5.29	1.02	0.16
	61.4	5.19	0.998	—
	mean[d]	5.20	1.00	—
1.0	11.0	6.99	1.07	0.15
	20.7	6.77	1.04	0.15
	30.6	6.71	1.03	0.17
	40.2	6.64	1.02	0.15
	50.3	6.56	1.01	—
	mean[d]	6.51	1.00	—
1.2	20.7	8.68	1.05	0.20
	30.4	8.51	1.03	0.17
	40.4	8.45	1.02	0.17
	50.2	8.43	1.02	0.19
	mean[d]	8.26	1.00	—
				Av. 0.18

a) The area of the electrode was 0.0707 cm^2. b) The values adopted are the average of more than five independent experiments. c) The values of k were estimated using Eq. 7 of Ref. 14, where $D=1.55\times10^{-5}$ cm^2 s^{-1} and $\nu=0.00441$ cm^2 s^{-1}. d) The mean of the values obtained at $83.8<\omega<314.2$ rad s^{-1}.

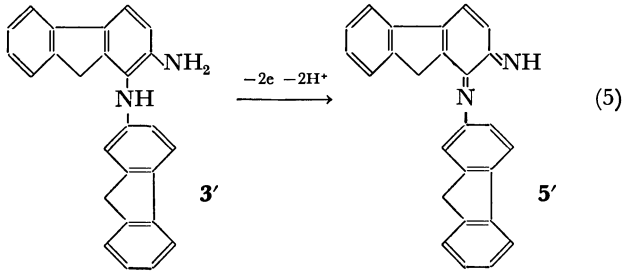

Since the potentials for the waves III_a/III_c and I_a were not affected by the presence of pyridine, similar reactions to those described above (Eqs. 1—4) also occurred in the solution with no pyridine, except that the protonations of the starting amine and of the product **5** occurred in this solution. The proposed reactions for 2-aminofluorene are similar to those usually observed for mononuclear aromatic amines. However, the predominant formation of the ortho-semidine type dimer should be noted because several compounds involving polymers are usually formed for mononuclear amines. This probably results from the structures of 2-aminofluorene and its generated cation radical.

Preliminary Information for the Chemical Steps. Due to protonations of both 2-aminofluorene and the product, it appears difficult to measure kinetic data on the chemical steps. However, some preliminary information on the rate of chemical steps may be obtained. Since the peak current of the wave III_c increased when pyridine was added, the deprotonation in Eq. 2 was accelerated by pyridine, whereas the deprotonation in Eq. 4 was probably slow and the addition of pyridine did not affect the rate. Thus, in the solution with no pyridine, the step of deprotonation of the cation radical generated by the primary electron transfer,

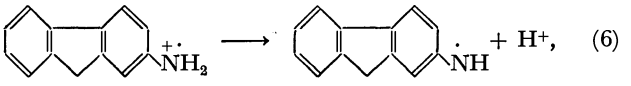

(6)

becomes a rate-determining step for oxidation at wave I_a. To confirm this consideration, RDE voltammetry was applied for 2-aminofluorene solution with no pyridine. The value of $i_l/\omega^{1/2}$, where i_l is the limiting current at an RDE and ω is the rotation speed of the electrode, decreased to a limiting value ($I_{l\lim}$) with an increase in the rotation speed (Table 1). The limiting value, $I_{l\lim}$, corresponds to the initial one-electron oxidation. The values of n_{app} ($=i_l\omega^{-1/2}/I_{l\lim}$) for lower rotation speeds depend on the rotation speed but are independent of the concentration of 2-aminofluorene. This is explained in terms of a first-order reaction for the chemical step,[13,14] namely, deprotonation. The rate constant of the deprotonation in Eq. 6 was thus estimated to be about 0.2 s^{-1} using Eq. 7 of Ref. 14 (Table 1).

This work was supported in part by the Asahi Glass Foundation for the Contribution to Industrial Technology.

References

1) R. N. Adams, "Electrochemistry at Solid Electrodes," Marcel Dekker, New York (1969), pp. 327—363.
2) S. D. Ross, M. Finkelstein, and E. J. Rudd, "Anodic Oxidation," Academic Press, New York (1975), Chap. 8.
3) R. F. Nelson, "Technique of Electroorganic Synthesis," ed by N. L. Weinberg, Interscience, New York (1974), Part I, Chap. 5.
4) R. L. Hand and R. F. Nelson, *J. Electrochem. Soc.*, **125**, 1059 (1978).
5) P. Berkenkotter and R. F. Nelson, *J. Electrochem. Soc.*, **120**, 346 (1973).
6) E. S. Pysh and N. C. Yang, *J. Am. Chem. Soc.*, **85**, 2124 (1963).
7) C. Parkanyi and R. Zahradnik, *Collect. Czech. Chem. Commun.*, **30**, 4287 (1965).
8) M. J. Namkung and T. L. Fletcher, *J. Chem. Soc., Chem. Commun.*, **1969**, 1052.
9) H. Pan and T. L. Fletcher, *J. Med. Chem.*, **13**, 567 (1970).
10) R. F. Bridger, D. A. Law, D. F. Bowman, B. S. Middleton, and K. U. Ingold, *J. Org. Chem.*, **33**, 4329 (1968).
11) F. E. Cislak, I. M. Eastman, and J. K. Senior, *J. Am. Chem. Soc.*, **49**, 2318 (1927).
12) T. L. Fletcher and M. J. Numkung, *J. Org. Chem.*, **35**, 4231 (1970).
13) L. S. Marcoux, R. N. Adams, and S. W. Feldberg, *J. Phys. Chem.*, **73**, 2611 (1969).
14) P. A. Malachesky, L. S. Marcoux, and R. N. Adams, *J. Phys. Chem.*, **70**, 4068 (1966).

Emission Spectra of 1,4-Naphthoquinone and Its 2-Methyl Derivative in the Vapor Phase

Takao ITOH and Hiroaki BABA*

Division of Chemistry, Research Institute of Applied Electricity, Hokkaido University, Sapporo 060

(Received April 21, 1979)

The emission spectra of 1,4-naphthoquinone (NQ) and 2-methyl-1,4-naphthoquinone (MNQ) vapors have been investigated at various temperatures in the presence of added foreign gases ($\approx$100 Torr). The results indicate that in both NQ and MNQ the emission consists of $T_1(n, \pi^*) \rightarrow S_0$ phosphorescence and weak E-type delayed fluorescence, $S_1(n, \pi^*) \rightarrow S_0$, the latter lying at higher frequencies. This new interpretation of the vapor-phase emission spectra of the naphthoquinones, which is substantially different from the interpretations given by previous authors, is based on and consistent with the following observations: (1) When the temperature is raised, the ratio of the fluorescence intensity to the phosphorescence intensity increases; (2) the S_1—T_1 energy separations, 1365$\pm$60 and 1500$\pm$200 cm^{-1} for NQ and MNQ, respectively, determined from the temperature dependence of the emission intensities agree with the corresponding values obtained from spectral data; (3) the emission lifetimes obtained by monitoring the fluorescence and phosphorescence are identical.

1,4-Naphthoquinone (NQ) is one of the representative quinones and shows strong emission in the visible region in rigid glass solution at 77 K. This emission has been identified as the phosphorescence from the lowest triplet state of n, π^* type, on the basis of the prominent progression in the C–O stretching vibration, the short lifetime, and the band position.[1] A comparison of the phosphorescence and absorption spectra of NQ indicates that the energy difference between the lowest excited singlet and triplet states is very small.

It is known that NQ exhibits weak emission in the vapor phase, and studies have been made on both emission[2,3] and absorption spectra[4] of NQ vapor. The vapor-phase emission spectrum of NQ was obtained in the presence of added benzene by Singh and Singh[2] and by Longin[3] with the aid of discharge excitation, but their assignments of the emitting states are inconsistent with each other. The former authors interpreted the emission spectrum in terms of fluorescence from a $^1(n, \pi^*)$ state and phosphorescence from a $^3(n, \pi^*)$ state, with the origins at 21945 and 18782 cm^{-1}, respectively, while the latter regarded the spectrum as due to two kinds of fluorescence from different n, π^* states with the origins at 22163 and 21974 cm^{-1}.

The emission and absorption spectra of 2-methyl-1,4-naphthoquinone (MNQ) vapor also were reported by Baruah *et al.*[5] They interpreted the emission as consisting of fluorescence from a $^1(n, \pi^*)$ state and phosphorescence from a $^3(n, \pi^*)$ state, with origins at 22075 and 20262 cm^{-1}, respectively.

Since the phosphorescent carbonyl compounds having a small S_1-T_1 energy separation often show weak E-type delayed fluorescence at room temperature,[6] one must take this into account in the assignment of the emitting states of NQ or MNQ vapor.

The purpose of the present study is to clarify the emitting states of NQ and MNQ in the vapor phase. Particular attention has been directed to the change of emission spectra with temperature. It is shown that, at high total pressure ($\approx$100 Torr) in the presence of a foreign gas, the emission spectra of NQ and MNQ vapors consist of $T_1(n, \pi^*) \rightarrow S_0$ phosphorescence and weak E-type delayed fluorescence, $S_1(n, \pi^*) \rightarrow S_0$. The S_1-T_1 energy gaps obtained from the temperature dependence of emission spectra are in agreement with those obtained from the band positions. The results of the decay measurement also support the present assignment.

Experimental

Materials. 1,4-Naphthoquinone (NQ), obtained from Wako Pure Chemical Industries, was recrystallized several times from ethanol, passed through a silica-gel column with benzene or petroleum benzine as the solvent, and finally sublimed *in vacuo*. 2-Methyl-1,4-naphthoquinone (MNQ) from Tokyo Chemical Industries was recrystallized several times from ethanol and sublimed *in vacuo*. It was confirmed that the emission spectra of these purified materials in a rigid glass at 77 K agree well with those reported previously.[1,7] Carbon tetrachloride of spectroscopic quality from Merck and benzene of chromatographic quality from Nakarai Chemicals were used as foreign gases without further purification.

Apparatus and Procedure. Emission and excitation spectra were measured with a high-sensitivity spectrophotometer based on the photon-counting method; it is equipped with a xenon lamp and a double monochromator for excitation, and with an HTV R-585 photomultiplier.[8] Two reflecting concave mirrors were placed beside the sample cell so as to intensify the emission signal. Absorption spectra were obtained with a Hitachi EPS-3 or a Cary-15 spectrophotometer. Emission decays were measured with a spectrophosphorimeter which was specially designed for measuring lifetimes ranging from 10^{-2} to 10^{-5} s by means of the photon-counting method.[9] Quartz cells of 35-mm path length were used for measuring emission and excitation spectra as well as emission decays. Samples were degassed in a mercury-free vacuum system.

Emission spectra were corrected for the spectral sensitivity of the monochromator-photomultiplier system with a solution of quinine in 0.5 M sulfuric acid as a standard. Excitation spectra were corrected for the spectral intensity distribution of the exciting light by the use of an aqueous solution of rhodamine B as a quantum counter. Emission quantum yields were determined by comparing the corrected emission spectra of the sample vapors with that of quinine in 0.5 M sulfuric acid, which is known to have an emission quantum yield of 0.51.[10]

Results

Figure 1 shows the corrected emission spectra in

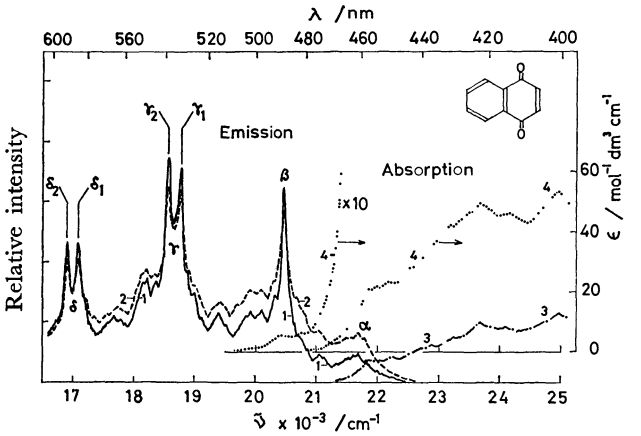

Fig. 1. Vapor-phase emission spectra (corrected) in the presence of benzene vapor (≈100 Torr) at different temperatures (1 and 2) and absorption spectra (3 and 4) of 1,4-naphthoquinone: (1) at 15 °C; (2) at 85 °C; (3) in the vapor phase; (4) in isopentane solution at room temperature. The intensity of spectrum 2 is arbitrarily chosen with no relation to that of spectrum 1. Emission spectra were obtained with a bandwidth of 1.0 nm.

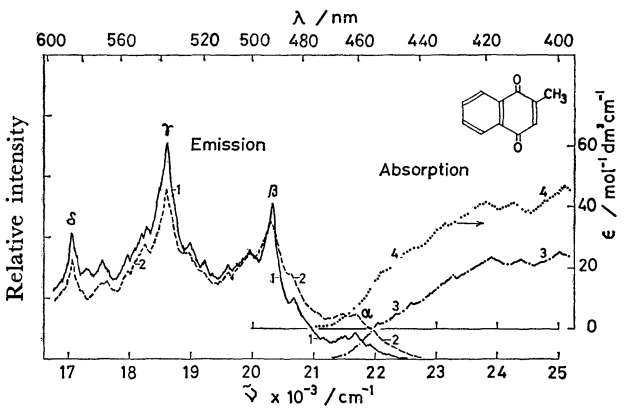

Fig. 2. Vapor-phase emission spectra (corrected) in the presence of benzene vapor (≈100 Torr) at different temperatures (1 and 2), vapor-phase excitation spectrum (3), and absorption spectrum in isopentane at room temperature (4) of 2-methyl-1,4-naphthoquinone: (1) at 25 °C; (2) at 80 °C. The intensity of spectrum 2 is arbitrarily chosen with no relation to that of spectrum 1. Emission spectra were obtained with a bandwidth of 2.0 nm.

the presence of benzene (≈100 Torr) at two temperatures and the absorption spectrum of NQ vapor, where the main emission bands are denoted by α, β, γ, and δ. Bands γ and δ split into doublets, *i.e.* γ_1 and γ_2, and δ_1 and δ_2, respectively. When the temperature is raised, the ratio of the intensity of band α to that of band β, γ, or δ increases. Band α has a sort of mirror-image relation to the vapor-phase absorption spectrum. Band β agrees in position with the very weak band which appears at about 20500 cm^{-1} in the absorption spectrum in isopentane solution (Fig. 1). This weak absorption band can be attributed to $S_0 \rightarrow T_1(n, \pi^*)$ transition on account of its small molar extinction coefficient ($\varepsilon \simeq 0.4$ mol^{-1} dm^3 cm^{-1}). The excitation spectra monitored at bands α, β, γ_1, and γ_2 agree well with the absorption spectrum. The absorption spectrum of NQ vapor ranging from 2.1 to 2.8×10^4 cm^{-1} can safely be assigned as the $S_0 \rightarrow S_1(n, \pi^*)$ transition on the basis of the molar extinction coefficients for the corresponding absorption in isopentane, although Singh and Singh[4] regarded it as consisting of transitions from the ground state to a $^1(n, \pi^*)$ state and a $^3(n, \pi^*)$ state with the origins at 23161 and 21944 cm^{-1}, respectively.

Figure 2 shows the corrected emission spectra of MNQ vapor in the presence of benzene (≈100 Torr) at two temperatures, the vapor-phase excitation spectrum, and the absorption spectrum in isopentane solution. As is seen in Fig. 2, the intensity distribution of the emission spectrum changes with temperature in much the same way as that of NQ vapor. Band α for MNQ vapor also has a sort of mirror-image relation to the vapor-phase excitation spectrum and to the absorption in isopentane solution in the $S_0 \rightarrow S_1(n, \pi^*)$ region. The absorption spectrum of MNQ vapor in the $S_0 \rightarrow S_1$ region could not be obtained. It is assumed that the vapor-phase excitation spectrum, which resembles the absorption spectrum in isopentane, can be used as a substitute for the vapor-phase absorption spectrum. The excitation spectrum of MNQ vapor in the $S_0 \rightarrow S_2(\pi, \pi^*)$ region ($2.8—3.6 \times 10^4$ cm^{-1}) was found to agree well with the corresponding vapor-phase absorption spectrum. The emission spectra of NQ and MNQ vapors obtained in the present study are somewhat different in structure from the previous results.[2,3,5]

In the present experiment, carbon tetrachloride as well as benzene was used as a foreign gas. These compounds have the same effect on NQ and MNQ vapors with respect to the temperature dependence of the emission spectra and to the relation between excitation and absorption spectra. Both benzene and carbon tetrachloride are considered to induce collisional deactivation of excited vibronic levels of NQ and MNQ vapor. Benzene, however, has an additional effect: When NQ (or MNQ) vapor is excited in the presence of benzene at wavelengths where benzene absorbs (<260 nm), intense emission is observed. The spectrum of this emission is identical with the emission spectrum of NQ (or MNQ), but the excitation spectrum for the emission agrees with the absorption spectrum of benzene vapor. On reference to the electronic energy levels of NQ (or MNQ) and benzene, one is led to the conclusion that actually the emission in question occurs through energy transfer from benzene to NQ (or MNQ). We thus utilized benzene not only as an inert foreign gas but also as an energy donor in order to obtain strong emission from NQ (or MNQ).

Figure 3 shows the emission spectra of NQ and MNQ in rigid glass solution at 77 K. Except for the absence of band α, these spectra resemble the corresponding vapor-phase emission spectra. With NQ in the rigid glass solution, however, the second and third bands, which belong to the prominent progression in the C–O stretching vibration, do not show such doublets as observed in the case of the vapor-phase emission spectrum (bands γ_1 and γ_2, and δ_1 and δ_2 in Fig. 1).

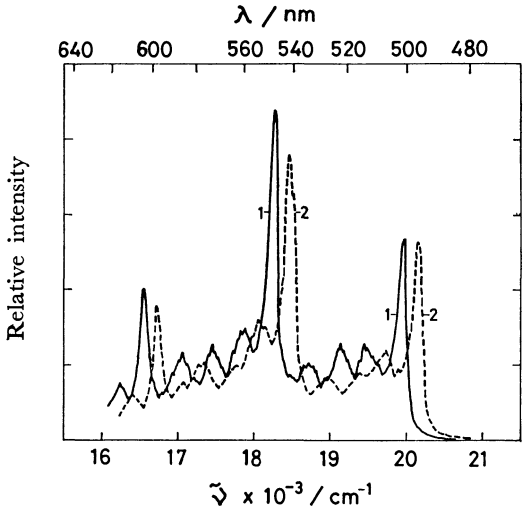

Fig. 3. Emission spectra (corrected) of 1,4-naphthoquinone (1) and 2-methyl-1,4-naphthoquinone (2) in an isopentane-methylcyclohexane (1:1) mixture at 77 K.

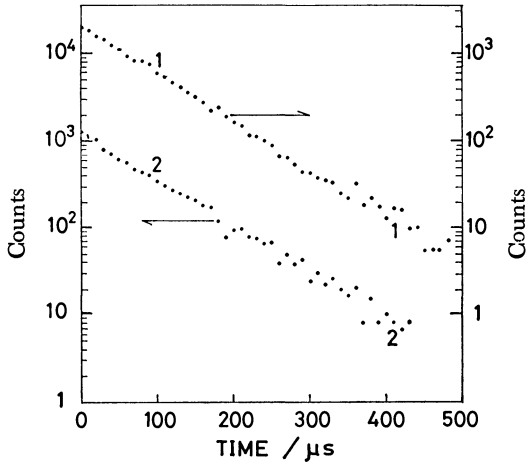

Fig. 4. Typical semilogarithmic plots of emission intensity vs. time for 1,4-naphthoquinone vapor in the presence of added CCl_4 ($\approx$100 Torr) at 80 °C: (1) monitored at band α; (2) at band β. Emission decays were obtained with a bandwidth of 20 nm for the detection monochromator.

Emission decays of NQ vapor in the presence of carbon tetrachloride ($\approx$100 Torr) are shown in Fig. 4. The lifetimes monitored at bands α, β, and γ_1 were found to be the same (84 μs) and independent of the excitation energy. The decay of the emission of MNQ vapor could not be measured because of its low quantum yield. The emission quantum yields were determined to be 1.5×10^{-2} for NQ and 9.5×10^{-4} for MNQ vapor at 80 °C in the presence of carbon tetrachloride.

Discussion

The vapor-phase emission spectra of NQ and MNQ obtained in the present study show characteristic temperature dependence; that is, the ratios of the intensity of band α to those of the other bands increase, when

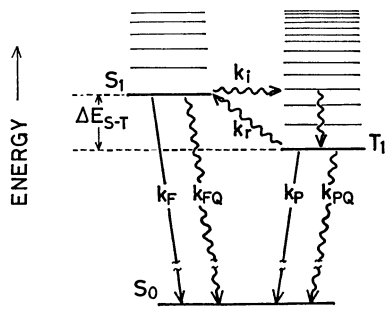

Fig. 5. Kinetic scheme and the rate constants for the radiative (→) and nonradiative (⇝) processes of naphthoquinone vapors in the presence of an added foreign gas.

the temperature is raised. We assign band α to the $S_1(n, \pi^*)\rightarrow S_0$ fluorescence and bands β, γ, and δ to the $T_1(n, \pi^*)\rightarrow S_0$ phosphorescence. This assignment is based on the mirror-image relation between vapor-phase emission and absorption spectra and on the similarity between the emission spectrum in the vapor and the phosphorescence spectrum in the rigid glass. For both NQ and MNQ vapors (Figs. 1 and 2), band β can be taken as the origin of the phosphorescence; and the peak on the higher-wavenumber side of band α is taken as the fluorescence origin, since it coincides in position with a peak that appears in the vapor-phase absorption or excitation spectrum. Thus, the origins of phosphorescence are located at 20460 and 20340 cm^{-1}, and those of fluorescence at 21830 and 21950 cm^{-1}, respectively, for NQ and MNQ vapors. The S_1-T_1 energy separations, ΔE_{S-T}, are thus found to be 1370 cm^{-1} for NQ and 1610 cm^{-1} for MNQ vapor. It then follows from Figs. 1 and 2 that the ratio of the fluorescence intensity to the phosphorescence intensity increases with temperature. In view of this observation, we assign the fluorescence of the naphthoquinone vapors to E-type delayed fluorescence.

The kinetic scheme for the electronic relaxation processes in the naphthoquinone vapors, including E-type delayed fluorescence, is illustrated in Fig. 5 together with various rate constants: k_F and k_P are the radiative rate constants, and k_{FQ} and k_{PQ} are the nonradiative rate constants, respectively, from S_1 and T_1 to the ground state, S_0; k_I represents the rate constant for the intersystem crossing; k_r is the rate constant for thermal activation to upper vibrational levels of T_1 followed by reverse intersystem crossing to S_1, and it can be written in the form[11]

$$k_r = k_r^0 \exp\left(\frac{-\Delta E_{S-T}}{kT}\right), \quad (1)$$

where k and T are the Boltzmann constant and absolute temperature, respectively, and k_r^0 represents a temperature-independent term.

According to the kinetic scheme, the ratio of the quantum yield of the delayed fluorescence, Φ_{DF}, to that of phosphorescence, Φ_P, is given by

$$\frac{\Phi_{DF}}{\Phi_P} = \frac{k_F k_r^0}{k_P(k_F+k_{FQ}+k_I)} \exp\left(\frac{-\Delta E_{S-T}}{kT}\right). \quad (2)$$

Therefore, ΔE_{S-T} can be derived from the variation

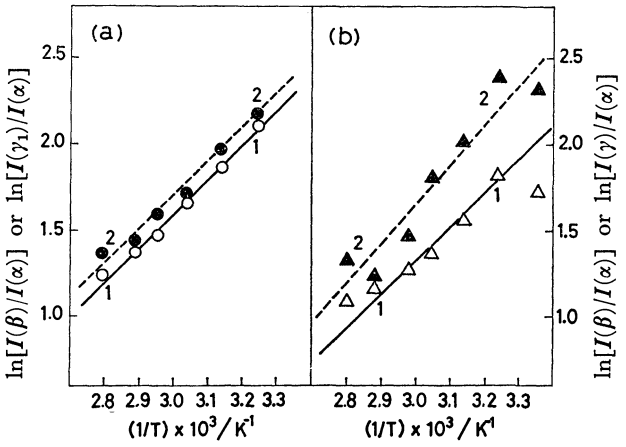

Fig. 6. Temperature dependence of ratios between band intensities for (a) 1,4-naphthoquinone and (b) 2-methyl-1,4-naphthoquinone vapors: (1) $\ln[I(\beta)/I(\alpha)]$ *vs.* $1/T$; (2) $\ln[I(\gamma_1)/I(\alpha)]$ or $\ln[I(\gamma)/I(\alpha)]$ *vs.* $1/T$. Essentially the same results were obtained by using benzene and carbon tetrachloride as foreign gases.

of Φ_{DF}/Φ_P with T. We use peak-intensity ratios instead of the quantum-yield ratios; the peak intensities of bands α, β, and γ will be denoted by $I(\alpha)$, $I(\beta)$, and $I(\gamma)$, respectively.

Figure 6 shows the plots of $\ln[I(\beta)/I(\alpha)]$ and $\ln[I(\gamma)/I(\alpha)]$ against $1/T$ for NQ and MNQ vapors. In the case of NQ, the peak intensity of band γ_1 is used instead of $I(\gamma)$. The plots give straight lines, and the values of ΔE_{S-T} calculated from the slopes are 1365 ± 60 and 1500 ± 200 cm^{-1} for NQ and MNQ vapors, respectively. These values agree well with the spectroscopically estimated gaps of 1370 cm^{-1} for NQ and 1610 cm^{-1} for MNQ, thus confirming the occurrence of E-type delayed fluorescence. Since the intensities of the emission bands other than band α change in the same way when the temperature is changed, the main emission bands located at wavenumbers lower than about 2.1×10^4 cm^{-1} can be regarded as due to a single electronic transition, $T_1\rightarrow S_0$, for both NQ and MNQ vapors.

The fact that the lifetimes of NQ vapor monitored at bands α and β are the same also supports our interpretation of the emission spectra, because according to the kinetic scheme in Fig. 5 the concentration of the S_1 molecule is to be proportional to that of the T_1 molecule. It is certain that the T_1 state is of an n, π^* type on account of its relatively short lifetime.

Our assignment for NQ vapor differs entirely from the ones presented by the previous authors. There are marked differences between the present and previous assignments also for MNQ vapor. The previous authors[5] assigned a relatively weak band of MNQ at 20262 cm^{-1} to the origin of phosphorescence and some of very strong bands at wavenumbers lower than 2.1×10^4 cm^{-1} to fluorescence. Moreover, none was pointed out as to the mechanism of the occurrence of fluorescence emission. Although our spectral measurement was performed with lower resolution, the temperature dependence of the emission spectra along with the results of the lifetime measurement indubitably indicates that the emission spectra of NQ and MNQ vapors at high total pressures consist of phosphorescence and E-type delayed fluorescence.

References

1) A. Kuboyama and S. Yabe, *Bull. Chem. Soc. Jpn.*, **40**, 2475 (1967).
2) S. N. Singh and R. S. Singh, *Indian J. Pure Appl. Phys.*, **5**, 394 (1967).
3) P. Longin, *C. R. Acad. Sci., Ser. B*, **t. 271**, 292 (1970).
4) S. N. Singh and R. S. Singh, *Indian J. Pure Appl. Phys.*, **6**, 187 (1968).
5) G. D. Baruah, S. N. Singh, and R. S. Singh, *Bull. Chem. Soc. Jpn.*, **42**, 3572 (1969).
6) M. Stockburger, *Z. Phys. Chem. (Frankfurt am Main)*, **31**, 350 (1962).
7) A. Kuboyama, Preprints of the International Conference on Photochemistry, Tokyo, **1965**, 117.
8) K. Chihara and H. Baba, *Bull. Chem. Soc. Jpn.*, **48**, 3039 (1975).
9) T. Takemura, M. Aikawa, H. Baba, and Y. Shindo, *J. Am. Chem. Soc.*, **98**, 2205 (1976).
10) W. H. Melhuish, *J. Phys. Chem.*, **65**, 229 (1961).
11) J. L. Kropp and W. R. Dawson, *J. Phys. Chem.*, **71**, 4499 (1967).

Competitive Redox Reactions at the ZnO Semiconductor Photoelectrode

Tooru INOUE,* Akira FUJISHIMA, and Kenichi HONDA
Department of Synthetic Chemistry, Faculty of Engineering,
The University of Tokyo, 7-3-1 Hongo, Bunkyo-ku, Tokyo 113
(Received April 23, 1979)

The study of the photoanodic reaction at the ZnO electrode in an electrolyte solution containing redox agents was carried out by means of the rotating ring-disk electrode technique. The competition reactions between the photocorrosion of ZnO and the oxidation of reducing agents were discussed focusing on the potentials of the electroactive species at the semiconductor-solution interface. The ZnO photoelectrode was stabilized in the course of the oxidation of a strong reducing agent dissolved in a solution.

Photo-induced redox reaction at the semiconductor-liquid junction have been extensively investigated with photoelectrolytic synthesis or solar energy conversion in mind.[1-6] The most recent interest in the electrochemical photocells has been the suppression of the photocorrosion of the semiconductor electrode itself during the operation.[7] The stabilization of the photocorrosive semiconductor electrode has been much investigated from several experimental approaches[7-18] and also discussed from the point of view of thermodynamic points.[19,20] However, the charge-transfer kinetics of a photogenerated hole-electron pair is not well understood, so the investigation of photoelectrochemical competitive oxidations at the ZnO electrode by means of the rotating ring-disk electrode (RRDE) is the subject of this work.

The photoanodic reaction of the ZnO electrode in the supporting electrolyte solution is known to consist of the photocorrosion[21-23] of the electrode *per se* by photoholes (p^+):

$$ZnO + 2\,p^+ \longrightarrow Zn^{2+} + 1/2O_2 \qquad (1)$$

Though ZnO has a demerit as the photoelectrode in an electrochemical photocell because of its large bandgap (*ca.* 3.2 eV), the stabilization of ZnO under operation in a solution is necessary for it to be used as a semiconductor-solution photodiode. When we introduce a certain reducing agent into an electrolyte solution, the oxidation (2) of a reducing agent can occur in competition with Process 1:

$$\underset{\text{form}}{\text{reduced}} + n\,p^+ \longrightarrow \underset{\text{form}}{\text{oxidized}} \qquad (2)$$

By using the rotating ring-disk electrode with a semiconductor disk and a metal ring, one can instantaneously ascertain the competition efficiencies of Processes 1 and 2 under illumination by comparing the collection ring currents caused by the reduction of the oxidized products with the geometrical collection current.[10,17,22]

Experimental

The semiconductor electrode used in this experiment was sintered polycrystal ZnO which had been prepared by pressing the reagent-grade ZnO powder at 1.0 t/cm^2 and then heated at 1300 °C for 3 h in the air. The sintered polycrystal was shaped into a disk 6.0 mm in diameter and 1.0 mm in thickness. Indium–gallium alloy was painted onto one face of the polycrystal in order to insure an ohmic contact with the copper conducting wire. Then, the ZnO disk was mounted on a Teflon rod using epoxy resin, together with a Au ring 7.0 mm in inner diameter and 9.0 mm in outer diameter, thus producing a ring-disk electrode system. Sometimes a Au-ring electrode was also amalgamated. The polycrystal face of ZnO was polished with alumina powder, etched in 6 M (M=mol dm^{-3}) HCl for 10 s, and washed with water. The ring-disk electrode thus prepared was connected into an RRDE measurement system (Nikko Keisoku), which has been described elsewhere.[7,10,11,22,24] The light source was a 500 W high pressure mercury arc lamp, while the illuminating wavelengths was selected with a glass filter from 300 to 400 nm. The supporting electrolyte was 0.2 M Na_2SO_4, and all the redox agents used were reagent-grade.

Results

The curves of the ring current, I_R, *vs.* the ring potential, E_R, where the disk photocurrents are constant at the disk potential of 1.0 V *vs.* SCE, are shown in Fig. 1.

Photogenerated carriers (holes) produced by the illumination of the absorbable light, whose energy is greater than a bandgap (3.2 eV) of ZnO, are forced to the surface by the electric field in a space charge layer and then oxidize the electroactive species at the interface. The collection current at the ring electrode caused by the discharge of the oxidized product which flows from the disk electrode gives information about the photoassisted oxidation, the photocorrosion of ZnO, and the oxidation of reducing agents. Cathodic currents which appear at the Au ring electrode in the solution without reducing agents indicate the reduction of the oxygen produced by the photocorrosion process (1). In the presence of a reducing agent in an electrolyte solution, a two-step cathodic current appears at the Au ring electrode, where the first wave of the cathodic current depends on the reduction of an oxidized redox agent produced by Process 2, while the second wave depends on the reduction of the oxygen produced by Process 1. Therefore, we can calculate the competition ratios[6,24] between Processes 1 and 2 from the height of the reduction current at the Au ring electrode.

Figure 2 shows the relation curves of the competitive oxidation ratios of various reducing agents *versus* their concentrations. The competition ratio increases in general with an increase in the concentration of a redox agent, while its value is different for different kinds of reducing agents. When a redox agent is present in a high concentration (*ca.* 1.0 M) in the solution, it is nearly 100%, oxidized by photogenerated holes, while the ZnO photoelectrode is stabilized against

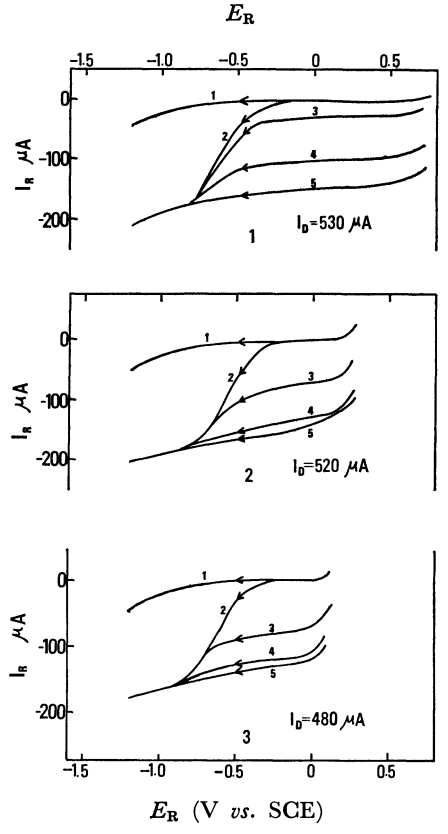

Fig. 1. Current-potential (I_R-E_R) curves at the Au ring electrode at the rotational speed of 1000 rpm with reducing agents in the electrolyte solution. Potential of the ZnO disk electrode was 1.0 V *vs.* SCE. (1) In addition of Br^-, (2) in addition of I^-, (3) in addition of $Fe(CN)_6^{4-}$: 1, in dark with and without reducing agents (red.); 2, in a supporting electrolyte solution; 3, in addition of 10^{-3} M red.; 4, in addition of 10^{-2} M red.; 5, in addition of 10^{-1} M red.; 2—5, under illumination.

the photocorrosion process (1).

Figure 3 shows the competitive oxidation ratios (stability ratios) of a variety of reducing agents (10^{-2} M) as a function of their redox potentials. The results indicate that the reducing agent with a more negative redox potential has a larger competition ratio and can better stabilize the photoelectrocorrosive ZnO electrode.[9]

Discussion

For charge transfer across the semiconductor-solution junction, the statistical equations have been established by several investigators.[26] The photocurrent at the illuminated n-type semiconductor electrode is determined by the overlap of the relative distributions of states in the valence band holes and of the reducing agents in the electrolyte solution; that is,

$$I_{ox} = k^\circ [\mathrm{Red}] \int_{-\infty}^{0} K^\circ(\mathrm{E}) D_+(\mathrm{E}) W_R(\mathrm{E}) \mathrm{d}E \qquad (3)$$

where I_{ox} is the anodic photocurrent, [Red] is the concentration of a reducing agent in a solution, $D_+(\mathrm{E})$ is the density of photogenerated holes in a semiconductor, and $W_R(\mathrm{E})$ is the distribution function of

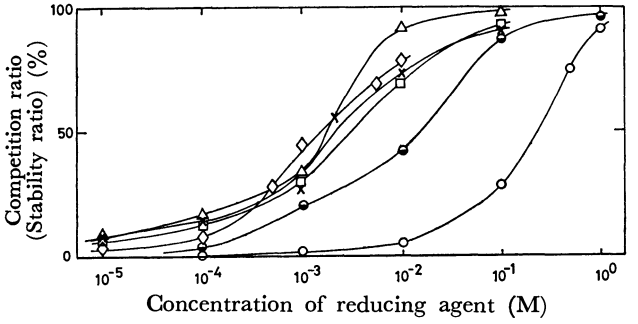

Fig. 2. Concentration dependences of competition ratios for various reducing agents.
×, $S_2O_3^{2-}$; □, SO_3^{2-}; ◇, $Fe(CN)_6^{4-}$; △, I^-; ◒, Br^-; ○, Cl^-.

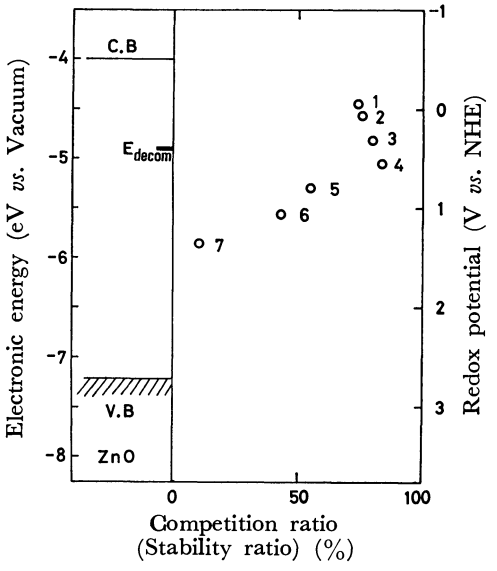

Fig. 3. Competition ratios (stability ratios) of various reducing agents (0.01 M) as a function of their redox potentials. E_{decom} denotes the oxidative decomposing potential of ZnO, C. B. the conduction band, V. B. the valence band of ZnO, respectively.
1, $S_2O_3^{2-}$; 2, SO_3^{2-}; 3, $Fe(CN)_6^{4-}$; 4, I^-; 5, Fe^{2+}; 6, Br^-; 7, Cl^-.

a reducing agent. Figure 4 shows the schematic distributions between the states of the ZnO electrode and a redox agent ($Fe(CN)_6^{3-/4-}$) in the solution. The distribution functions (W_{ox}, W_{red}) of this redox couple are given by;

$$W_{red} = \exp[-\lambda(E-E^\circ_{F,el}+\lambda)^2/4kT]$$

$$W_{ox} = \exp[-(E-E^\circ_{F,el}-\lambda)^2/4kT\lambda]$$

where λ denotes a reorganization energy (*ca.* 0.75 eV[27,28]), $E^\circ_{F,el}$ denotes the Fermi level of the electrolytes, and E denotes the energy level. It can be expected from the mapping between $D_+(\mathrm{E})$ and $W_{red}(\mathrm{E})$ that it will be difficult for $Fe(CN)_6^{4-}$ to be oxidized by the photogenerated holes in the valence band, whereas $Fe(CN)_6^{3-}$ will be reduced by the electrons in the conduction band. However, $Fe(CN)_6^{4-}$ is actually oxidized well by the photogenerated holes at the ZnO photoelectrode, as is shown in Fig. 3.

Therefore, for the elucidation of the photo-hole

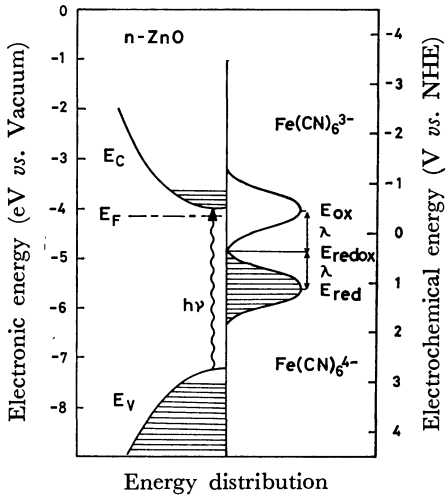

Fig. 4. Schematic illustration of the energy distributions between ZnO and a redox agent ($Fe(CN)_6^{3-/4-}$) in the solution.

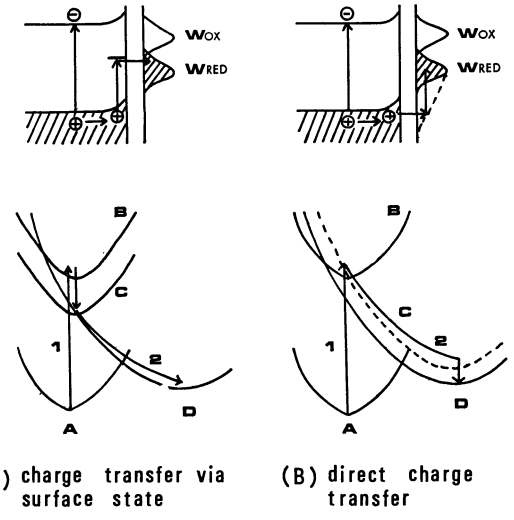

Fig. 5. Schematic explanation for charge transfer kinetics, upper illustration for hole transfer and lower one for reaction coodinations. (A) Charge transfer via surface state, (B) direct charge transfer. A, initial state; B, photoexcited state; C, intermediate state; D, final state. 1, Photoexciting process; 2, relaxation process.

transfer across the semiconductor-solution interface, the following two schemes are considered to be probable. One process is the charge transfer *via* surface states within a bandgap, when the overlap between distributions of surface states and of reducing species is necessary. For the explanation of this scheme, some investigators have reported that positively charged holes could transfer to reducing species *via* the surface states at the ZnO photoelectrode.[29,30] Another process is the direct transfer of a positively charged hole to the excited states of reducing species, when the distribution of reducing species becomes an unsymmetrical one. Figure 5 presents schematic representations of the above two processes. However, from this experiment it is hard to decide which process is more acceptable.

As for the stability of the photoelectrodes, the guidance has been presented from the point of view of thermodynamics[19,20] and on the basis of the experimental results,[10,31] focusing upon the redox reactivities of electroactive species at the semiconductor-solution interface. The stability of an n-type semiconductor photoelectrode in a supporting electrolyte solution is determined by the potentials of the competitive oxidations between the photocorrosion of a semiconductor and the oxidation of water, as schematically shown in Fig. 6. From this consideration, while TiO_2 is a stable photoelectrode because this oxidative decomposition potential is more positive than the oxidation potential of water, the ZnO photoelectrode becomes a stable photoanode in the course of the competitive oxidation of dissolved reducing agents whose redox potentials are more negative than the decomposing potential of ZnO.

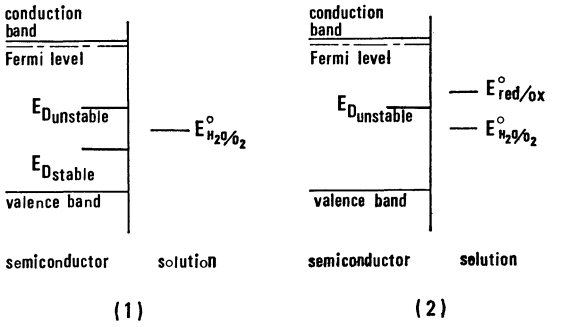

Fig. 6. Enegetic elucidation for stability of photoelectrodes in the course of redox reactions at the interface. E_D denotes the decomposition potential of a semiconductor electrode *per se*.
(1) Stable or unstable case of semiconductor photoelectrodes *versus* photoelectrolytic oxidation of water.
(2) Stabilized case of an unstable photoelectrode in the course of photoelectrolytic oxidation of reducing agents.

Conclusion

Many semiconductor electrodes cause photocorrosion by means of an action of photogenerated carriers when they are illuminated in water. However, once a photocorrosive semiconductor electrode is stabilized, a new way of its use may be developed, for example, as photosensitive devices,[32] including the photoelectrode in the electrochemical photocell.

References

1) "Semiconductor-Liquid Junction Solar Cells: Proceedings of a Conference on the Electrochemistry and Physics of Semiconductor-Liquid Interfaces under Illumination," 77-3, ed by A. Heller, Electrochem. Soc., Princeton (1977).
2) A. Fujishima, K. Kohayakawa, and K. Honda, *J. Electrochem. Soc.*, **122**, 1487 (1975).
3) H. Yoneyama, H. Sakamoto, and H. Tamura, *Electrochim. Acta*, **20**, 341 (1975).
4) H. Gerischer, *Ber. Bunsenges. Phys. Chem.*, **80**, 1046 (1976).
5) A. J. Bard, *J. Photochem.*, **10**, 59 (1979).
6) M. Halmann, *Nature*, **275**, 115 (1978).
7) T. Inoue, T. Watanabe, A. Fujishima, K. Honda,

and K. Kohayakawa, *J. Electrochem. Soc.*, **124**, 719 (1977).
8) H. Minoura, M. Tsuiki, and T. Oki, *Ber. Bunsenges. Phys. Chem.*, **81**, 588 (1977).
9) H. Minoura and M. Tsuiki, *Nippon Kagaku Kaishi*, **1977**, 487.
10) A. Fujishima, T. Inoue, T. Watanabe, and K. Honda, *Chem. Lett.*, **1978**, 357.
11) T. Inoue, T. Watanabe, A. Fujishima, and K. Honda, *Bull. Chem. Soc., Jpn.*, **52**, 1243 (1979).
12) H. Gerischer and J. Gobrecht, *Ber. Bunsenges. Phys. Chem.*, **80**, 327 (1976).
13) A. B. Ellis, S. W. Kaiser, J. M. Bolts, and M. S. Wrighton, *J. Am. Chem. Soc.*, **99**, 2839 (1977).
14) B. Miller and A. Heller, *Nature*, **262**, 680 (1976).
15) H. Morisaki, M. Haraya, and K. Yazawa, *Appl. Phys. Lett.*, **30**, 7 (1977).
16) H. Tributsch, *Ber. Bunsenges. Phys. Chem.*, **81**, 361 (1977).
17) R. Memming, *Ber. Bunsenges. Phys. Chem.*, **81**, 732 (1977).
18) Y. Nakato, T. Ohnishi, and H. Tsubomura, *Chem. Lett.*, 883 (1975).
19) H. Gerischer, *J. Electroanal. Chem.*, **82**, 133 (1977).
20) A. J. Bard and M. S. Wrighton, *J. Electrochem. Soc.*, **124**, 1706 (1977).
21) S. R. Morrison and T. Freund, *Electrochim. Acta*, **13**, 1343 (1968).
22) A. Fujishima, E. Sugiyama, and K. Honda, *Bull. Chem. Soc. Jpn.*, **44**, 304 (1971).
23) B. Pettinger, R. Schoeppel, and H. Gerischer, *Ber. Bunsenges. Phys. Chem.*, **78**, 1024 (1974).
24) T. Inoue, T. Watanabe, A. Fujishima, and K. Honda, *Chem. Lett.*, **1977**, 1073.
25) A. Fujishima, T. Inoue, and K. Honda, *J. Am. Chem. Soc.*, in press.
26) H. Gerischer, "Physical Chemistry: An Advanced Treatise," ed by H. Eyring *et al.*, Academic Press, New York (1970), pp. 467—478.
27) M. Gleria and R. Memming, *Electroanal. Chem.*, **65**, 163 (1975).
28) F. Willig and G. Scherer, *Z. Naturforsch., Teil A*, **31**, 981 (1976).
29) B. Pettinger, H. R. Schoppel, and H. Gerischer, *Ber. Bunsenges. Phys. Chem.*, **80**, 849 (1976).
30) H. Gerischer, *J. Electrochem. Soc.*, **125**, 218C (1978).
31) K. Honda, A. Fujishima, and T. Inoue, "Electrode Process and Its New Approach to Chemical Energy Problems; The Extended Abstracts of the 3rd Japan-USSR Seminar on Electrochemistry," Electrochem. Soc., Jpn. (1978), 139.
32) T. Inoue, A. Fujishima, and K. Honda, *Chem. Lett.*, **1978**, 1197.

An Interpretation of the "Molecular Space" on the Basis of Quantum Chemical Calculations of Hydrated Ions

Shizuo FUJIWARA* and Bernd M. RODE**

Department of Chemistry, Faculty of Science, The University of Tokyo, Hongo, Bunkyo-ku, Tokyo 113

(Received April 25, 1979)

Quantum chemical calculation has been made for the sizes of the hydration shells of the metal ions as well as for the binding energies of water molecules in the hydration shells. The results of the both calculations give the basis of the size of the molecular space.[1] Although the experimental value of the molecular space, $(20\pm 5\text{A})^3$, does not exactly agree with the calculated value, we assume that the quantum chemically obtained hydration sphere refers to the molecular space.

Several experimental results concerning aqueous solutions of salts have indicated that there exists a well defined minimal volume of solvent which is needed by each ion to maintain "regular" behavior in a thermodynamic as well as in a kinetic sense.[1,2] ESR investigations of aqueous solutions in gels allowed to determine this volume to be $(20\pm 5\text{A})^3$ for copper and some other simple organic molecules.[1] Hence this apparently essential volume was named "molecular space."[1] Within this context it is of particular interest that the concentration of salt in the sea water as well as the salt concentration in "biosolutions" as human blood serum is adjusted to an amount, which still corresponds to the maintenance of this "molecular space" for the ions.

Previous quantum chemical calculations on ions linked to linear water polymers have shown that the upper limit of ion solvent interaction corresponds to the size of the experimentally determined molecular space for a series of monovalent and divalent ions.[3] These calculations could give, however, only an estimation of upper limit of interaction range and, due to methodical simplification, not yet reflect well the situation of a fully solvated ion in solution.

Using the common *ab-initio* MO-SCF calculation method, the treatment of such large systems (an ion surrounded by several hydration layers) will lead to dimensions of the calculation, which cannot be managed so far. On the other hand, semiempirical methods are also not suitable for the correct description of such systems[4,5] and also lead to rather ambiguous results due to the neglect of most 2-electron integrals and introduction of numerous empirical parameters.

The recently developed MESQUAC (Mixed Electrostatic Quantum Chemical) MO-SCF method allows a treatment of quite large complex systems at a reasonable computational effort.[6,7] The results obtained for some hydrated ions[6] are in very satisfactory agreement with experimental values and with results obtained by *ab initio* calculations near HF-limit. It was to be expected, therefore, that this method should be the most useful way for calculating ions with several hydration layers and to obtain therby a theoretical explanation for the experimental facts concerning molecular space.

Experimental

MESQUAC Concept. The details of the method have been published already elsewhere,[6] so that at this point a very brief survey will be given. The principle of the method is a separation of the total system into an "essential" part (usually the ion +1 or several ligands) and a second part ("outer part"), including the other ligands or even some bulk solvent. The "essential part" is calculated within the framework of the all-electron *ab initio* MO-SCF method, the "outer part" introduced as electrostatic perturbation term to the Hamiltonian, constructed according to the molecular geometry of the ligands in this outer part. The electrostatic fractional charges used in building up this perturbation terms are those being obtained from previous *ab initio* calculations on smaller ion-ligand-systems, performing a MULLIKEN population analysis.[6]

The method could be shown recently to work also satisfactorily in the case of transition metal ions,[8] and even for these systems computing times are still quite short. For this reason, we have chosen the monovalent ions of Li(I), Na(I) and K(I), and the divalent ions of Mg(II), Ca(II), Mn(II) and Zn(II) for this work. Mn(II) and Zn(II) seemed to be a useful supplement to the main group metal ions, since they also possess a "symmetrical" electron configuration (d^5 and d^{10}, respectively), one being a typical open shell (high spin) system, the other one a closed shell system, but containing d electrons.

Performance of the Calculations. The Gaussian basis sets being used for ions and ligands have been given already in the references.[5,6,8] The geometries of the first hydration shells have been chosen according to experimental results of X-ray investigations of aqueous salt solutions[9,10] or to optimized MO-SCF geometries.[12,13] The geometries of the further solvation layers were constructed assuming hydrogen bonding of each water molecule to two water molecules in the next higher shell (0···0 distance 2.70 Å), in a 90° twisted configuration. For most of the ions both tetrahedral and octahedral coordinations have been considered. Some data obtained for Ti(III) aquacomplexes[8] are included for comparison of the results of this work with those of a tervalent ion.

The calculations were performed in part at the HITAC 8700/8800 computer of the University of Tokyo, in part at the CDC Cyber 174 computer of the Vienna TU computer center.

Results and Discussion

In Table 1, the binding energies per water molecule, calculated for the first, second and third hydration shells of the ions, are listed. For the discussion of

** On leave from Institut für Anorganische und Analytische Chemie Uuiversität Innsbruck, Innrain 52a, A-6020, Innsbruck, Austria.

Table 1. Calculated binding energies per water molecule of the first (E-I), second (E-II), and third (E-III) hydration shells, for tetrahedral (Td) and octahedral (Oh) coordinations, in kcal/mol

Ion	Coordination	E-I	E-II	E-III
Li(I)	Td	25.7	9.8	1.5
	Oh	22.1	9.4	1.6
Na(I)	Td	17.3	7.6	1.5
	Oh	15.4	7.6	1.5
K(I)	Td	14.7	7.2	1.5
	Oh	14.2	6.4	1.3
Mg(II)	Td	59.4	21.6	3.3
	Oh	50.5	20.9	3.2
Ca(II)	Td	47.1	19.9	3.0
	Oh	46.9	18.3	3.0
Mn(II)	Oh	73.8	22.1	5.4
Zn(II)	Oh	71.0	22.4	5.5
Ti(III)	Oh	100.0	34.5	8.8

Table 2. Calculated volumes for the hydrated ions including hydration layers, n being the number of hydration shells

Values are given in (hartree)^3.

Ion	V_1	V_2	V_3	V_4	V_5
Li(I)	457	2668	9209	24300	46870
Na(I)	681	3352	10730	27160	51271
K(I)	1051	4361	12860	31000	57160
Mg(II)	475	2668	9209	24300	46870
Ca(II)	754	3561	11182	27900	52540
Mn(II)	612	4151	10292	26340	50020
Zn(II)	537	2922	9775	25390	48550

these energy values, the hydrogen bond energy between the solvent molecules themselves (6.8 kcal/mol with the basis set used) represents a crucial limit, since stabilization and structural influence of the ion by full or partial formation of a hydration shell is not to be expected, if the energy gain by solvation does not exceed this value to some extent. The larger the difference between binding energy in the hydration layer and hydrogen bond level is, the more stable and rigid the hydration shell will be.

According to our results (Table 1), almost all ions show such a stabilization up to the second hydration shell, I(I) and Ti(III) ion being the lower and upper limit, showing possibly a somewhat different behavior (no influence on second shell for K(I), partial formation of a third shell for Ti(III)).

These results are in good agreement with some preliminary calculations one on the hydrated divalent ions Fe(II), Co(II), Ni(II), and Cu(II), which also let expect a quite strong influence on the second shell, and the other on the binding energies for the third shell below hydrogen bond level.[14]

Experimental X-ray investigations of aqueous salt solutions[9–11,15] also support our results, showing a significant structural influence of the ions up to a radius of about 5 Å around the ion, which corresponds to the distance including two hydration layers. X-Ray data have been evaluated, however, usually only for the first shell, for which the peaks are more strong and easier to analyze. The existence of the second shell (and sometimes even of a third shell) has been pointed out, however, by some of the authors.[11,15]

Discussing now the results of our calculations in connection with the concept of molecular space, another consideration will be useful and necessary, namely that of the volume occupied by an ion surrounded by 1,2,3, or more solvation layers. In Table 2, these volumes are given, as they result from the geometries being used in the MESQUAC MO calculations.

From the values for the necessary volume being assigned to an ion including 1, 2, or more solvation layers we can see that the volume corresponding to an ion with two layers —which are expected according to the calculations for most of the ions— is always smaller than 6800 hartree^3, corresponding to a sphere of 10 Å diameter. The volume needed after addition of a third shell will exceed, however, in all cases this value. It can be concluded, therefore, that the space being "structured" by the ions in aqueous solution corresponds to a sphere of about 10 Å in diameter.

Summarizing the results of the calculations presented here, we believe that they seem to give a reasonable theoretical foundation for the experimentally observed size of the molecular space. They are expected also to be a useful basis for further investigations of aqueous and nonaqueous electrolyte solutions by means of the calculation method being employed.

References

1) S. Fujiwara, K. Nagashima, H. Morita, and Y. Kanaoka *Bull. Chem. Soc. Jpn.*, **50**, 2851 (1977).
2) S. Fujiwara, *J. Am. Chem. Soc.*, in press.
3) B. M. Rode, S. Fujiwara, and R. Fujikura, unpublished work.
4) P. Russegger and P. Schuster, *Chem. Phys. Lett.*, **19**, 254, (1973); *Theor. Chim. Acta*, **24**, 191, (1972).
5) B. M. Rode, *Mh. Chemie*, **106**, 339, (1975).
6) B. M. Rode and F. J. Reibnegger, *J. Chem. Soc., Faraday Trans. 2*, **75**, 178, (1979).
7) B. M. Rode and R. Fussenegger, *Mh. Chemie*, **108**, 703, (1977).
8) G. J. Reibnegger and B. M. Rode, *Mh. Chemie*, in press.
9) H. Ohtaki, T. Yamaguchi, and M. Maeda, *Bull. Chem. Soc. Jpn.*, **49**, 701, (1976).
10) R. M. Laurence and R. F. Kruh, *J. Chem. Phys.*, **47**, 4758, (1967).
11) J. N. Albright, *J. Chem. Phys.*, **56**, 3783, (1972),
12) H. Kistenmacher, H. Popkie, and E. Clementi, *J. Chem. Phys.*, **61**, 799, (1974); **58**, 1689, (1973).
13) P. A. Kollman and I. D. Kuntz, *J. Am. Chem. Soc.*, **94**, 9236, (1972).
14) G. J. Reibnegger and B. M. Rode, unpublished work.
15) H. Ohtaki, private communication.

Photoelectron Spectra of Hydrogen-bonded Complexes

Chikatoshi UTSUNOMIYA, Tsunetoshi KOBAYASHI,† and Saburo NAGAKURA*

The Institute for Solid State Physics, The University of Tokyo, Roppongi, Minato, Tokyo 106

†*The Institute of Physical and Chemical Research, Wako, Saitama 351*

(Received April 26, 1979)

The photoelectron spectra of typical hydrogen-bonded complexes, CF_3COOH–$(C_2H_5)_2NCH_3$, CF_3COOH–$(n\text{-}C_3H_7)_3N$, CF_3CF_2COOH–$(C_2H_5)_2NCH_3$, and CF_3CF_2COOH–$(n\text{-}C_3H_7)_3N$ were observed in the gas phase. It was found that the nonbonding orbital of the proton acceptor is stabilized significantly by hydrogen-bond formation while the three higher occupied orbitals of the proton donor are destabilized. The large orbital energy changes due to hydrogen-bond formation strongly support the charge-transfer model for the hydrogen bond.

Photoelectron spectroscopy is expected to give effective informations concerning the electronic structure of hydrogen-bonded systems and also concerning the nature of hydrogen bond. This is because the photoelectron spectrum of the hydrogen-bonded complex gives the orbital energy shifts due to hydrogen-bond formation within the limitation of Koopmans' theorem.

In a previous paper,[1] we reported the photoelectron spectra of some electron donor-acceptor complexes in the gas phase, and found that this technique was quite effective for the study of the intermolecular interaction. In this paper, in order to clarify the nature of hydrogen bond, we have studied the He I photoelectron spectra of hydrogen-bonded complexes between carboxylic acids as proton donors and alkylamines as proton acceptors in the gas phase. In actuality, *N,N*-diethylmethylamine and tripropylamine are taken as proton acceptors, and trifluoroacetic acid and pentafluoropropionic acid as proton donors.

Experimental

N,N-Diethylmethylamine (DEMA) and tripropylamine (TPA) were purified by distillation. Commercially available trifluoroacetic acid (TFAA) and pentafluoropropionic acid (PFPA) were used without further purification. Purity of the amines and the carboxylic acids was checked by NMR spectroscopy. An aliphatic amine and a carboxylic acid were introduced through needle valves into a 5-liter gas reservoir and were mixed with each other. The nonexistence of chemical products except for hydrogen-bonded complexes in the mixtures was checked by NMR spectroscopy for the liquid phase. The mixed gas was introduced into the ionization chamber of a photoelectron spectrometer, the details of which were described in a previous paper.[2] The photoelectron spectra of the hydrogen-bonded complexes and their component molecules were measured at room temperature, the He I resonance line being used as the excitation source. At the initial stage of the measurement of the mixed gases, the bands of the free amines added in slight excess appear strongly in addition to those of the hydrogen-bonded complexes. The bands of the free amines, however, rapidly decreased in intensity, and the spectra turned out to be composed almost completely of the bands of the hydrogen-bonded complexes.

Results and Discussion

The photoelectron spectra of hydrogen-bonded systems such as TFAA–DEMA, PFPA–DEMA, TFAA–TPA, and PFPA–TPA are shown in Fig. 1, together with those of component molecules. The measurements were performed with very high sensitivity for the hydrogen-bonded complexes because of their low vapour pressure. This is the reason why the signal of only a trace of water appears in the spectra of the complexes. The vertical ionization potentials (I_v) of the hydrogen-bonded complexes and the component molecules are summarized in Table 1.

Thomas[3] has assigned the first band of TFAA to the nonbonding (n) orbital mainly localized on the oxygen atom of the carbonyl group, the second band to a π orbital, and the third band to a σ orbital which is denoted by n′ hereafter. The shapes of the higher occupied molecular orbitals of TFAA obtained by the CNDO/2 calculation are schematically shown in Fig.

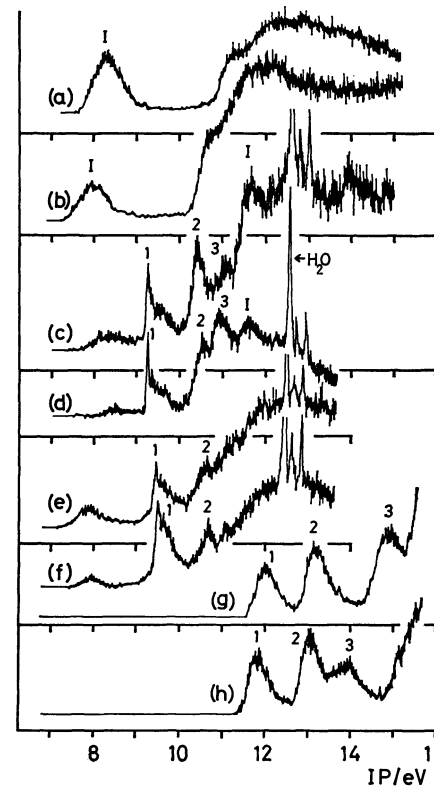

Fig. 1. Photoelectron spectra of hydrogen-bonded complexes and their component molecules: curve (a), DEMA; curve (b), TPA; curve (c), TFAA–DEMA complex; curve (d), PFPA–DEMA complex; curve (e), TFAA–TPA complex; curve (f), PFPA–TPA complex; curve (g), TFAA; curve (h), PFPA.

Table 1. Vertical ionization potentials, $I_v(J)$, of hydrogen-bonded complexes and their component molecules

Species	$I_v(J)$/eV			
J[a)]	1	2	3	I
TFAA	12.00	13.16	14.83	
PFPA	11.94	13.09	14.04	
DEMA				8.32
TPA				7.94
TFAA-DEMA	9.26	10.41	11.23	11.64
PFPA-DEMA	9.24	10.38	10.94	11.63
TFAA-TPA	9.53	10.71		
PFPA-TPA	9.49	10.67		

a) J shows the numbering of the photoelectron spectral band given in Fig. 1 from which the vertical ionization potential in this table was obtained.

Table 2. Photoelectron spectral band shifts, $\Delta I_v(J)$, due to hydrogen-bond formation

Species	$\Delta I_v(J)$/eV			
	Carboxylic acid			Amine
J[a)]	1(n)	2(π)	3(n′)	I(n)
TFAA-DEMA	−2.74	−2.75	−3.60	3.32
PFPA-DEMA	−2.70	−2.71	−3.10	3.31
TFAA-TPA	−2.47	−2.45		
PFPA-TPA	−2.45	−2.42		

a) See the footnote a) for Table 1.

2. The ordering of the first three bands of PFPA may safely be regarded to be the same as in the case of TFAA judging from the band shapes and positions. The first band of the alkylamine is assigned to the nonbonding orbital localized on the nitrogen atom.

Let us turn to amine–carboxylic acid systems. As is seen in Fig. 1 which shows the photoelectron spectra of the TFAA–DEMA, PFPA–DEMA, TFAA–TPA, and PFPA–TPA systems, each of the amine–carboxylic acid systems has several bands pertinent to the corresponding hydrogen-bonded complex, in addition to the band around 8 eV due to the corresponding free amine added in excess. The bands due to the complex are numbered as shown in Fig. 1. The energy separation between bands 1 and 2 of the hydrogen-bonded complex is nearly equal to that of the free carboxylic acid. This means that bands 1 and 2 of the hydrogen-bonded complex correspond to bands 1 and 2 of the carboxylic acid, respectively. The CNDO/2 calculations made for the TFAA–DEMA system taken as an example show that the energy separation is almost unaffected by hydrogen-bond formation (1.51 eV for the free acid; 1.49 eV for the weak complex with the N–H distance of 1.6 Å; 1.42 eV for the strong complex with the distance of 1.2 Å). This is consistent with the present assignment. According to this assignment, the shifts of bands 1 and 2 due to hydrogen-bond formation amount to 2.70—2.75 eV for the systems containing DEMA and to 2.42—2.47 eV for the systems containing TPA (see Table 2).

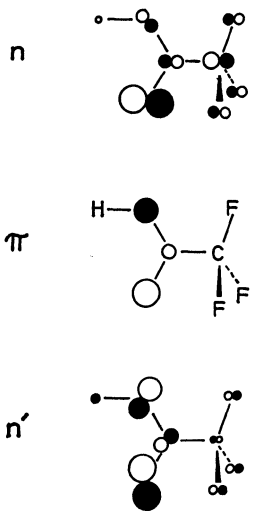

Fig. 2. Schematic representation of the higher occupied molecular orbitals of trifluoroacetic acid.

Another possible assignment of bands 1 and 2 of the hydrogen-bonded complexes is to assign one of them to the n orbital of the amine and the other band to the n orbital of the carboxylic acid. This assignment, however, may lead to unreasonable band shifts. Let us consider, as an example, the case in which bands 1 and 2 are assigned to the n orbitals of the amine and the carboxylic acid, respectively. The shift of the amine band due to complex formation with TFAA is 0.94 eV for DEMA and 1.59 eV for TPA. This apparently indicates that TPA is stronger as proton acceptor than DEMA. On the other hand, the shift of the carboxylic acid band due to complex formation with the amine is 1.59 eV for DEMA and 1.29 eV for TPA. This seems to show that TPA is weaker as proton acceptor than DEMA. From the above consideration, the assignment of either of bands 1 and 2 to the n orbital of the amine is unacceptable.

Judging from the orbital shape of the carboxylic acid shown in Fig. 2, the shift due to hydrogen-bond formation is larger for band 3 (n′ band) than for band 1 (n band). Therefore, it is expected that band 3 of PFPA at 14.04 eV appears below 11.34 eV for the PFPA–DEMA hydrogen-bonded system. Thus, the third and fourth bands of the system are assigned to the shifted bands of the third band of PFPA and of band I of DEMA, respectively. From an analogy with the PFPA–DEMA system, the third and fourth bands of the TFAA–DEMA system are tentatively correlated with band 3 of TFAA and band I of DEMA, respectively. In the TFAA–TPA and PFPA–TPA complexes, bands 3 and I are covered with a background band and their exact positions can not be decided.

The band shifts due to hydrogen-bond formation are summarized in Table 2. We can see that the n bands of the proton acceptors (amines) shift towards the higher-IP region by hydrogen-bond formation while the n bands, π bands, and n′ bands of the proton donors (carboxylic acids) shift towards the lower-IP region. These tendencies can well be explained by the contribution of the dative structure (–COO⁻···

H–$N^{+}\leftarrow$) as is expected from the charge-transfer mechanism[4] of hydrogen-bond formation. The large energy shifts of the bands of the component molecules due to hydrogen-bond formation indicate that the contribution of the dative structure to these hydrogen-bonded complexes is quite significant.

The n, π, and n′ bands of the proton donor and the n band of the proton acceptor shift a little more in the system containing TFAA as the proton donor than in the system containing PFPA. This suggests that TFAA is slightly stronger as the proton donor than PFPA. Concerning proton acceptors, the band shift due to hydrogen-bond formation is less in the system containing TPA. This is reverse to the order of the proton-accepting ability expected from their ionization potentials. This contradiction may be explained in terms of the steric hindrance effect.

References

1) C. Utsunomiya, T. Kobayashi, and S. Nagakura, *Chem. Phys. Lett.*, **39**, 245 (1976).

2) T. Kobayashi, K. Yokota, and S. Nagakura, *J. Electron Spectrosc.*, **2**, 449 (1973).

3) R. K. Thomas, *Proc. R. Soc. London, Ser. A*, **331**, 249 (1972).

4) R. S. Mulliken and W. B. Person, "Molecular Complexes," Wiley-Interscience, New York (1969).

Vibrational Distribution of $CS(X^1\Sigma^+)$ Fragments Formed in the UV Flash Photolysis of CS_2

Takayuki EBATA, Masahiro KAWASAKI†, Kin-ichi OBI, and Ikuzo TANAKA*

Department of Chemistry, Tokyo Institute of Technology, Ohokayama, Meguro-ku, Tokyo 152

(Received April 26, 1979)

The vibrational distribution of the CS(X) fragment has been studied by the UV flash photolysis and kinetic spectroscopic technique. The CS fragment was generated by the flash photolysis of CS_2 at $\approx$200 nm. The vibrational distribution is well represented by a sum of two modified Poisson distributions with different mean values. This distribution is explained by assuming the following two photodissociation processes of CS_2; one is a predissociation through a triplet state and the other is a direct photodissociation.

$$CS_2 + h\nu \begin{cases} \rightarrow CS_2(\tilde{A}^1B_2) \rightarrow CS_2(T) \rightarrow CS(X^1\Sigma^+, v'') + S(^3P), \\ \rightarrow CS(X^1\Sigma^+, v'') + S(^1D). \end{cases}$$

The photodissociation dynamics of triatomic molecules has been of theoretical interest and simple models for the vibrational distribution have been developed.[1] The vibrational distribution of CS fragments in the photodissociation of CS_2 is a good test for these models. Early works[2–4] reported that the vibrationally excited $CS(X^1\Sigma^+)$ radicals are formed in the flash photolysis of CS_2. Lee and Judge[5] pointed out that the vibrational population of $CS(A^1\Pi)$ produced in the vacuum-UV photolysis of CS_2 is approximately represented by a modified Poisson distribution. Bersohn and co-laborators[6] measured the translational energy distribution of photofragments, CS and S, by photodissociating a CS_2 molecular beam with a pulsed ArF excimer laser at 193 nm. They observed that the translational energy distribution can be represented by a sum of two distributions.

In this study, using the flash photolysis and kinetic spectroscopic technique, the vibrational distribution of $CS(X^1\Sigma^+)$ has been determined in the photolysis of CS_2 at quartz UV region.

Experimental

The set-up of quartz UV flash photolysis and kinetic spectroscopic system has been described previously.[7] In brief, the mixture of CS_2 (0.2 Torr) and Ar (5.0—200 Torr) was flash-photolyzed in a quartz cell which contained a multiple reflection mirror system. The 1000 J photolysis and 50 J spectroscopic flash lamps gave 8 and 5 μs light pulses, respectively. The absorption spectra of CS were photographed with a Nikon G-500 spectrograph on Kodak 2475 recording films in the wavelength range between 255 and 275 nm. We assumed that in this wavelength range the spectral sensitivity of the film was constant. The absorption intensity of each vibrational band at "no delay" was obtained by extrapolating the decay curve to $t=0$.

CS_2 (Wako Chemical) was degassed under vacuum and Ar (Takachiho Chemical Ind., 99.99%) was used without further purification. The mixture was left in a 20-l glass bulb for 4 h before photolysis. Under our experimental conditions, the absorption spectrum of CS ($A^1\Pi$, $v'=0 \leftarrow X^1\Sigma^+$, $v''=0$) could be observed even a few minutes after one flashing because of its stability. Therefore after each flashing, the mixture was pumped out.

† Present address: Chemistry Department of Industry and Resources, Faculty of Engineering, Mi'e University, Kamihama-cho, Tsu 514.

Results and Discussion

Vibrational Distribution of the $CS(X^1\Sigma^+)$ Photofragment. Figure 1 shows relative excited population density which is determined by folding the lamp spectral irradiance into the absorption spectrum of the CS_2 molecule. The population density is centered at $\approx$200 nm. The FWHM is $\approx$1700 cm^{-1} which corresponds to less than two vibrational quanta of CS $(X^1\Sigma^+)$.

The absorption spectra of the $CS(X^1\Sigma^+)$ fragment formed in the photodissociation of CS_2 by quartz flash lamp were observed up to five vibrational quanta. The pressure effect of Ar buffer gas was not observed under our experimental conditions. In order to obtain the vibrational population of $CS(X^1\Sigma^+)$ at $t=0$, the optical density of each vibrational band is plotted against delay time as shown in Fig. 2, where $OD_t(0, 0)$ is normalized to unity. The plots show good linear relations between $\log[OD_t(v', v'')/OD_t(0, 0)]$ and delay time. Using the extrapolated values of the optical

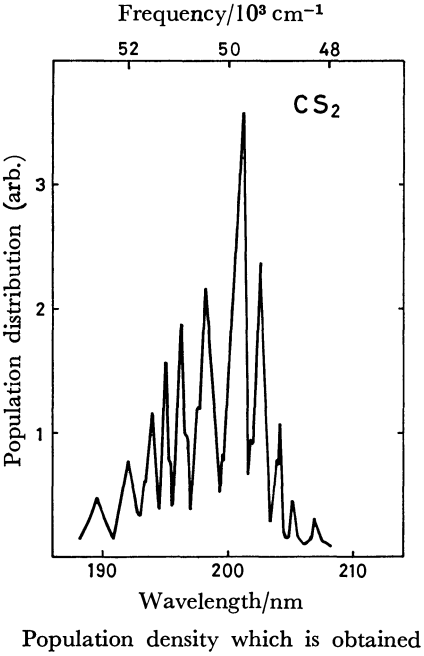

Fig. 1. Population density which is obtained by multiplying the absorption spectra of CS_2 by the lamp spectral irradiance.

Table 1. Vibrational distribution of $CS(X^1\Sigma^+)$ formed by photodissociation of CS_2

v'-v''	λ/nm	$OD_0(v', v'')/OD_0(0, 0)$	$q_{v'v''}$[a]	$N_{v''}$(rel.)	$q_{v'v''}$[b]	$N_{v''}$(rel.)	$N_{v''}$(rel.)
0-0	257.7	1.00	0.830	1	0.75	1	1
0-1	266.4	0.43	0.151	2.9	0.17	2.2	2.1±0.4
1-1	259.1	1.08	0.514	1.8	0.59	1.4	
1-2	267.9	0.38	0.268	1.5	0.23	1.5	1.5±0.1
2-2	260.7	0.57	0.261	1.9	0.35	1.2	
2-3	269.4	0.43	0.306	1.5	0.34	1.2	1.3±0.2
3-4	271.0	0.32	0.292	1.2	0.35	0.8	1.0±0.2
4-5	272.7	0.22	0.242	1.0	0.36	0.6	0.8±0.2

a) Ref. 8. b) Corrected for the change of the electronic transition moment according to Ref. 5. c) Averaged population relative to $v''=0$.

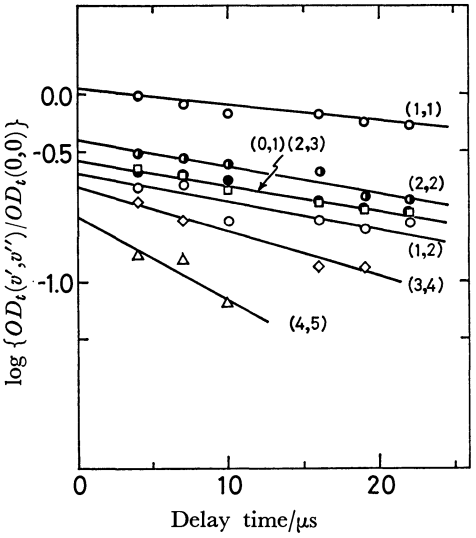

Fig. 2. Time variation of the relative absorption intensity of CS, $A^1\Pi(v')\leftarrow X^1\Sigma^+(v'')$ bands. The (0, 0) band is normalized to unity.

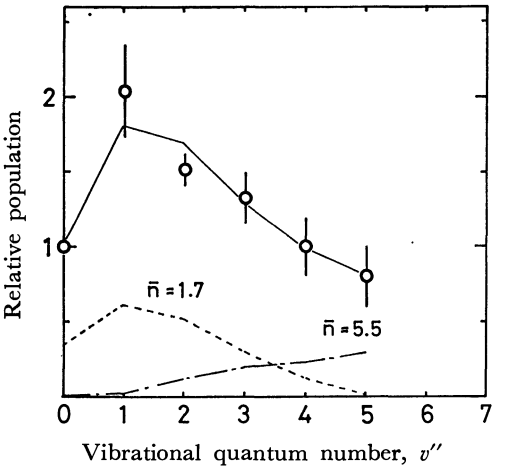

Fig. 3. The vibrational population of the $CS(X^1\Sigma^+)$ state formed in photodissociation. The solid line shows the best fit curve obtained by summing up the two distributions. See text.

density at $t=0$, the vibrational population $N_{v''}$ is obtained by,

$$\frac{N_{v''}}{N_0}=\frac{OD_0(v', v'')}{OD_0(0, 0)}\frac{q_{00}}{q_{v'v''}}\frac{R_e^2(\bar{r}_{00})}{R_e^2(\bar{r}_{v'v''})} \quad \text{(I)}$$

where $q_{v'v''}$ is the Franck-Condon factor of CS(A-X) and R_e is the electronic transition moment which is given by $R_e(\bar{r}_{v'v''})=c(1-0.39\bar{r}_{v'v''})$ with the r-centroid in Ångstrom units. In order to evaluate the ratio $N_{v''}/N_0$, we used the Franck-Condon factors which were calculated by Coxon *et al.*[8] with the RKR potential and obtained experimentally by Lee and Judge[5] with correction for the change of the electronic transition moment (Table 1). The averaged values of $N_{v''}/N_0$ against vibrational quantum numbers are plotted in Fig. 3. A population inversion between $v''=0$ and 1 levels is evident. The FWHM is approximately four vibrational quanta which is wider than that of the population density of the parent molecule of Fig. 1, indicating vibrational excitation of CS in photodissociation processes.

The vibrational excitation of the CS fragment is explained both in terms of the comparison of the CS internuclear distance of CS_2* with that of the electronically ground state of CS radical and in terms of the dynamical energy transfer during photodissociation.[9] If we assume that both the vibrational levels $i=0$ and 1, are *initially* populated and the energy transferred by dynamical interaction is the same for two vibrational states, the population in the vibrational level v'' is given by "modified Poisson distribution" in the impulsive half-collision model[1]

$$N_{v''}=(\bar{n})^{v''}\frac{(\bar{n})^2+(\alpha-2v'')\bar{n}+v''^2}{v''![(\bar{n})^2+(\alpha-2)\bar{n}+1]}\exp(-\bar{n}) \quad \text{(II)}$$

where α is the ratio of the population in the $i=0$ state to that in the $i=1$ state, and $\bar{n}$ is the averaged vibrational state.[5] Assuming two photodissociation processes, *i.e.*, two vibrational distributions, the result of the best fit to the observed populations using Eq. II is shown in Fig. 3. The best fit curve was obtained by summing up two distributions of the ($\bar{n}$, α) values of (1.7, ∞) and (5.5, 19.0) almost equally weighted. The former means that CS fragments are not *initially* vibrationally excited, while the latter indicates the *initial* vibrational excitation of the CS photofragments.

Photodissociation Processes. The vibrationally hot CS fragments may be directly produced by the photolysis of CS_2. Since the absorption of light is centered at ≈200 nm in this experiment, photolysis occurs with sufficient energy to leave an excess of ≈40 kcal/mol after production of electronically ground state fragments. In the photolysis of the CS_2 molecular beam

at 193 nm,[6] the translational energy distribution of the fragments consists of two distributions; one peaks sharply at ≈8 kcal/mol and the other extends broadly with its peak at ≈15 kcal/mol. From both these data and ours, it is expected that there are two photodissociation processes of CS_2 at ≈200 nm and that the CS fragment is vibrationally and/or rotationally excited.

The absorption spectrum of gaseous CS_2 around at 200 nm consists of a single progression of bands superimposed on the continuum. The variation of the contours of the bands may result from varying degrees of predissociation.[10] The maximum quantum yield of $\approx 10^{-3}$ has been reported for the fluorescence of CS_2 and it is concluded that the main fate of CS_2^* is photodissociation.[11]

The following two processes are energetically possible in the photolysis at ≈200 nm,

$$CS_2 \begin{cases} \rightarrow CS(X^1\Sigma^+) + S(^3P), & \Delta H_0^\circ = 102.9 \text{ kcal/mol} \quad (1) \\ \rightarrow CS(X^1\Sigma^+) + S(^1D). & 129.3 \quad (2) \end{cases}$$

Concerning the photodissociation process (1) which is spin-forbidden, it is postulated that CS_2 is decomposed through a triplet excited state[4]

$$CS_2 + h\nu \rightarrow CS_2(\tilde{A}^1B_2) \rightarrow CS_2(T) \rightarrow CS(X^1\Sigma^+) + S(^3P). \quad (1a)$$

The CS_2 absorption band near 200 nm has been assigned to the transition to the $\tilde{A}^1B_2$ state[10] which is nonlinear with a C–S bond distance of $r_e = 1.66$ Å. Once this singlet state crosses over to the repulsive triplet state, CS_2 will simultaneously decompose to the fragments. If this is the case, the CS fragment is vibrationally excited before photodissociation because the CS equilibrium bond distance of the excited $CS_2(\tilde{A}^1B_2)$ is longer than that of $CS(X^1\Sigma^+)$ by 0.13 Å. Furthermore, during dissociation the fragment is vibrationally excited by the actual repulsive force, *i.e.*, dynamical excitation. Because the $\tilde{A}^1B_2$ state has the S–C–S angle of 153°, the CS fragments are thought to be rotationally excited. The spectator model predicts that the rotational energy will be one fourth of the vibrational energy.[12]

Concerning the photodissociation process (2), Donovan *et al.*[13] reported the preliminary results which showed the yields of $S(^1D_2)$ in the photolysis of CS_2 at 200 nm. As the process (2) is thought to be the direct photodissociation, the singlet excited state must have very short lifetime in which the linear structure of the ground state of $CS_2(\tilde{X}^1\Sigma^+)$ is retained during the decomposition. Although no rotational excitation is possible in this case, $\bar{n}$ is smaller because available energy for the process (2) is smaller than that for (1) by 26.4 kcal/mol.[14] Because the CS bond distance (1.55 Å) of $CS_2(\tilde{X})$ is almost same as that of CS(X) (1.53 Å), the value of α in Eq. II is expected to be infinite, *i.e.* only $i=0$ is *initially* populated. From the above discussion it is concluded that the vibrational distribution with the lower vibrational quanta $(\bar{n}, \alpha) = (1.7, \infty)$ corresponds to the process (2), while that with $(\bar{n}, \alpha) = (5.5, 19.0)$ corresponds to the process (1) because of the *initial* excitation of the CS fragment.

References

1) (a) Y. Band and K. F. Freed, "Excited States," ed by E. C. Lim Academic Press, New York (1977); b) W. M. Gelbart, *Ann. Rev. Phys. Chem.*, **28**, 323 (1977).
2) G. Porter, *Proc. R. Soc. London, Ser. A*, **200**, 284 (1950).
3) A. B. Callear and R. G. W. Norrish, *Nature*, **188**, 53 (1960).
4) A. B. Callear, *Proc. R. Soc. London, Ser. A*, **276**, 401 (1963).
5) L. C. Lee and D. L. Judge, *J. Chem. Phys.*, **63**, 2782 (1975).
6) R. Bersohn, *J. Photochem.*, **9**, 87 (1978); A. Freedman, S. Yang, M. Kawasaki, and R. Bersohn, to be published.
7) K. Shibuya, T. Ebata, K. Obi, and I. Tanaka, *J. Phys. Chem.*, **81**, 2292 (1977).
8) J. A. Coxon, P. J. Marcoux, and D. W. Setser, *Chem. Phys.*, **17**, 408 (1976).
9) M. J. Berry, *Chem. Phys. Lett.*, **29**, 329 (1974).
10) A. E. Douglas and I. Zanon, *Can. J. Phys.*, **42**, 627 (1964).
11) K. Hara and D. Phillips, *Trans. Faraday Soc.*, **74**, 1441 (1978).
12) G. E. Bush and K. R. Wilson, *J. Chem. Phys.*, **56**, 3626 (1972).
13) M. C. Addison, C. D. Byrne, and R. J. Donovan, *Chem. Phys. Lett.*, **64**, 57 (1979).
14) H. Okabe, "Photochemistry of Small Molecules," Wiley-Interscience (1978).

Proton Magnetic Relaxation Study of Oxalic Acid Dihydrate

Takehiko CHIBA

Department of Chemistry, Nihon University, Sakurajosui, Setagaya-ku, Tokyo 156

(Received May 26, 1979)

Proton magnetic relaxation times T_1, $T_{1\rho}$, and T_{1D} were measured on a single crystal of α-form oxalic acid dihydrate in two modes: temperature dependence at one or two specific crystal orientations, and angular dependence at several temperatures. Results were compared with the calculation based on an isolated three proton system for the assumed modes of motions. The temperature dependence of T_1 and that of $T_{1\rho}$ and T_{1D} in the low temperature range are reasonably accounted for by the 180°-flip of the water molecule. The activation energy for the motion of 43.6 kJ mol^{-1} is obtained. $T_{1\rho}$ and T_{1D} above about 35 °C decreased as the temperature was raised. The comparison of the observed results in this temperature range with the calculated ones suggests that there is exchange motion among the three spins. An activation energy for this motion of 80.8 kJ mol^{-1} is obtained. This three spin exchange motion may be considered as a combination of a jump of carboxyl proton to a higher potential trough corresponding to the ionic configuration and the three-fold reorientation of the hydronium ion thus formed.

Because nuclear magnetic relaxation in a low field can be very effectively caused by a slow nuclear motion, measurement of $T_{1\rho}$ is an important means to study such motion. In the course of $T_{1\rho}$ and T_{1D} measurements on powdered samples of oxalic acid dihydrate, we found a decrease in these relaxation times with temperature which cannot be accounted for by the familiar 180°-flip of the water molecule of hydration. Our primary purpose in this paper is to elucidate the motion responsible for the above finding from the relaxation time study on single crystals.

We will describe first the calculation of relaxation times for assumed modes of motion, then experimental procedures, results of temperature and magnetic-field-direction dependence of relaxation times, and comparison of these results with the calculated values.

Calculation of the Relaxation Rates

The crystal of α-form oxalic acid dihydrate is monoclinic, and its structure is accurately known.[1] Hydrogen atoms in this crystal are incorporated in a hydrogen bond network, as shown in Fig. 1. For simplicity, calculations of relaxation rates are made for an isolated three spin system of H_1, H_2, and H_3. The atomic positions obtained from neutron diffraction studies are used.[2] For proton resonance, an isolated three spin system may be a reasonable approximation, because inter-proton distances within the three spin group are 2.05, 2.12, and 1.53 Å, while those between the adjacent groups are 3 Å or greater, except the $H_3\cdots H_3'$ value of 2.78 Å.

Calculation of Relaxation Rates due to 180°-Flip of Water Molecule. Relaxation Rate in the Laboratory Frame: Along the line of Look and Lowe's standard treatment,[3] the relaxation rate T_1^{-1} due to random modulation of the dipole interaction between the carboxyl proton and two protons of a water molecule executing 180°-flip motion with a probability w_I can easily be calculated as

$$T_1^{-1} = \frac{3}{4}\gamma^4\hbar^2\left\{\frac{\tau_I}{1+\omega_0^2\tau_I^2}[|\chi_{12}^{(1)}|^2+|\chi_{13}^{(1)}|^2 - 2\mathrm{Re}(\chi_{12}^{(1)*}\chi_{13}^{(1)})]+\frac{\tau_I}{1+4\omega_0^2\tau_I^2}\times[|\chi_{12}^{(2)}|^2+|\chi_{13}^{(2)}|^2-2\mathrm{Re}(\chi_{12}^{(2)*}\chi_{13}^{(2)})]\right\} \quad (1)$$

where $\tau_I=1/2w_I$ defines the correlation time of the motion. χ's are given by

$$\left.\begin{aligned}\chi_{\alpha\beta}^{(1)} &= r_{\alpha\beta}^{-3}\sin\theta_{\alpha\beta}\cos\theta_{\alpha\beta}\exp(-i\varphi_{\alpha\beta}),\\ \chi_{\alpha\beta}^{(2)} &= r_{\alpha\beta}^{-3}\sin^2\theta_{\alpha\beta}\exp(-2i\varphi_{\alpha\beta}),\end{aligned}\right\} \quad (2)$$

where $r_{\alpha\beta}$, $\theta_{\alpha\beta}$, and $\varphi_{\alpha\beta}$ are the polar coordinates of a vector joining site α to site β in the coordinate system with its polar axis along the static field H_0, site 1 for carboxyl proton, sites 2 and 3 for those of a water molecule. ω_0 is the Larmor angular frequency and other symbols have their usual meanings.

Relaxation Rate in the Rotating Frame: In a same manner $T_{1\rho}^{-1}$ can be calculated for the present case.[3] Since $T_{1\rho}\ll T_1$ in the present experiment, we retain only the dominant terms in the expression of $T_{1\rho}^{-1}$ involving ω_1 and neglect those terms involving ω_0 and $2\omega_0$, where $\omega_1=\gamma H_1$. $T_{1\rho}^{-1}$ is then given by

$$T_{1\rho}^{-1} = 3\gamma^4\hbar^2\frac{\tau_I}{1+4\omega_1^2\tau_I^2}d_0^2, \quad (3)$$

where

$$d_0 = \frac{1}{4}(\chi_{12}^{(0)}-\chi_{13}^{(0)}), \quad (4)$$

with

$$\chi_{\alpha\beta}^{(0)} = r_{\alpha\beta}^{-3}(1-3\cos^2\theta_{\alpha\beta}). \quad (5)$$

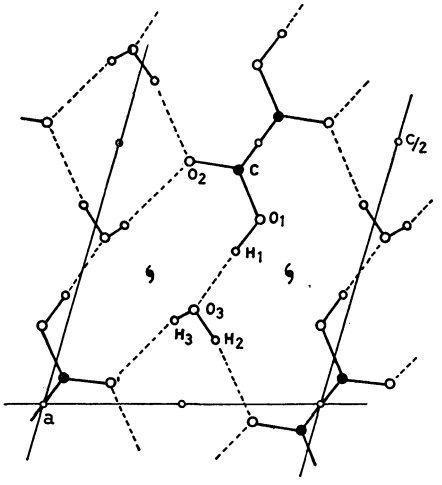

Fig. 1. Crystal structure of α-oxalic acid dihydrate: b axis projection.

When $\omega_1\tau_1 \ll 1$, we have

$$T_{1\rho}^{-1} = 3\gamma^4\hbar^2\tau_I d_0^2. \tag{6}$$

Relaxation Rate in the Dipole Field in the Rotating Frame: Because under the conditions of the present measurement of T_{1D}, τ_I is always much smaller than the Larmor period in the local field, we only consider the case of the short correlation time limit. We start from the general perturbation equation of relaxation rate[4] in which the dipole Hamiltonian in the rotating frame is divided into two parts: $\mathcal{H}_{d_0}$, the motion averaged part, and $\mathcal{H}_{d_1}$, the time-varying part (perturbation term).

$$T_{1D}^{-1} = -[2\hbar^2\mathrm{Tr}\{(\mathcal{H}_{d_0})^2\}]^{-1} \times \int_{-\infty}^{+\infty} d\tau \mathrm{Tr}\{\langle[\mathcal{H}_{d_1}^*(\tau), \mathcal{H}_{d_0}] \times [\mathcal{H}_{d_1}^*(0), \mathcal{H}_{d_0}]\rangle\}, \tag{7}$$

where

$$\mathcal{H}_{d_0} = a_0(D_{IJ}+D_{IK}) + b_0 D_{JK}, \tag{8}$$

$$\mathcal{H}_{d_1} = d(t)(D_{IJ}-D_{IK}), \tag{9}$$

$$\mathcal{H}_{d_1}^*(t) = \exp\left(-i\frac{\mathcal{H}_{d_0}}{\hbar}t\right)\mathcal{H}_{d_1}(t)\exp\left(i\frac{\mathcal{H}_{d_0}}{\hbar}t\right), \tag{10}$$

and

$$\left.\begin{aligned} a_0 &= \frac{1}{4}(\chi_{12}^{(0)}+\chi_{13}^{(0)}), \\ b_0 &= \frac{1}{2}\chi_{23}^{(0)}. \end{aligned}\right\} \tag{11}$$

D_{IJ} *etc.* are of the form,

$$D_{IJ} = \gamma^2\hbar^2(3I_Z J_Z - \boldsymbol{I}\cdot\boldsymbol{J}). \tag{12}$$

I is a spin at site 1, J and K are those flipping between sites 2 and 3, and

$d(t)=d_0$ if J spin is in site 2 at time t,
$=-d_0$ if J spin is in site 3 at time t.

In the short correlation time limit it is permissible to replace $\exp\left(i\frac{\mathcal{H}_{d_0}}{\hbar}t\right)$ in Eq. 10 by 1. We then have

$$T_{1D}^{-1} = -[2\hbar^2\mathrm{Tr}\{(\mathcal{H}_{d_0})\}^2]^{-1}\mathrm{Tr}\{[(D_{IJ}-D_{IK}), \mathcal{H}_{d_0}]^2\} \times \int_{-\infty}^{+\infty}\langle d(\tau)d(0)\rangle dt. \tag{13}$$

The integral gives $2\tau_I d_0^2$. Traces in Eq. 13 are evaluated straightforwardly, leading to the final expression

$$T_{1D}^{-1} = \frac{3}{2}\gamma^4\hbar^2\tau_I d_0^2, \tag{14}$$

which is 1/2 the $T_{1\rho}^{-1}$ of Eq. 6.

It is noted here that when $\mathcal{H}_{d_0}+\mathcal{H}_Z$ is used instead of $\mathcal{H}_{d_0}$ in Eq. 7, where $\mathcal{H}_Z = -\gamma\hbar H_1(I_x+J_x+K_x)$ is the effective Zeeman Hamiltonian in the rotating frame, a straightforward calculation similar to the above yields

$$T_{1\rho}^{-1} = \frac{3}{2}\gamma^4\hbar^2\tau_I d_0^2(H_L^2+2H_1^2)/(H_L^2+H_1^2), \tag{15}$$

where the local field in the rotating frame H_L is by definition

$$H_L^2 = [3/N\gamma^2\hbar^2 I(I+1)(2I+1)^N]\mathrm{Tr}\{(\mathcal{H}_{d_0})^2\},$$

and expressed in this case as

$$H_L^2 = \frac{1}{2}\gamma^2\hbar^2(2a_0^2+b_0^2). \tag{16}$$

Equations 6 and 14 are the two limiting cases of Eq. 15 for $H_L \ll H_1$ and $H_1 \to 0$, respectively.

Relaxation due to Slow Motional Processes. Relaxation Rate in the Rotating Frame due to Exchange between Carboxyl and Water Protons, or a Three-fold Reorientation: In the present work, in the temperature range where relaxation effects of slow motion appear, we consider the situation where exchange between H_1 and H_2 or H_3 occurs. This may be viewed as a slow three-fold reorientation in addition to the rapid flip motion of the water molecule. We will discuss the actual mode of motion later.

We assume that exchange occurs among the spin arrangements i, ii, and iii with a probability w_{II}.

	site 1	sites 2 and 3
i	I	J, K
ii	J	K, I
iii	K	I, J

Look and Lowe's treatment[3] is again followed and $T_{1\rho}^{-1}$ is expressed by

$$T_{1\rho}^{-1} = \frac{2}{3}\gamma^4\hbar^2(a_0-b_0)^2\frac{\tau_{II}}{1+(4\omega_1\tau_{II}/3)^2}, \tag{17}$$

or

$$T_{1\rho}^{-1} = \frac{3}{8}\gamma^4\hbar^2\frac{(a_0-b_0)^2}{\omega_1^2}\cdot\frac{1}{\tau_{II}} \tag{18}$$

in the limit of slow motion ($\omega_1\tau_{II} \gg 1$). Here we take the correlation time of the exchange motion as $\tau_{II} = 1/w_{II}$.

When $T_{1\rho}^{-1}$ of Eq. 18 is compared with T_{1D}^{-1} of Eq. 24 to be given in the next section, we have

$$T_{1\rho}^{-1}/T_{1D}^{-1} = \frac{3}{4}H_L^2/H_1^2. \tag{19}$$

According to Slichter and Ailion,[5] for the relaxation by slow motion

$$T_{1\rho}^{-1}/T_{1D}^{-1} = H_L^2/(H_1^2+H_L^2), \tag{20}$$

when H_1 is comparable to or less than H_L, and

$$T_{1\rho}^{-1}/T_{1D}^{-1} = \frac{3}{4}H_L^2\Big/\left(H_1^2+\frac{3}{4}H_L^2\right), \tag{21}$$

when H_1 is sufficiently greater than H_L so that cross-relaxation between the Zeeman and the secular part of the dipole energy in the rotating frame can be neglected. In the present experiment the largest H_L amounts to $\approx$3.7 G, while the H_1 used is 6.2 G. Rigorously, $T_{1\rho}^{-1}$ of Eq. 18 needs adjustment for H_L due to the relation given by Eq. 20 or 21. These correction factors, however, turn out to be small (estimated to be not more than 20% in the worst case) and are therefore neglected.

Relaxation Rate in the Dipole Field in the Rotating Frame due to Slow Exchange between the Carboxyl and Water Protons: T_{1D}^{-1} in the present case can be given by[5]

$$T_{1D}^{-1} = (1-p)\frac{1}{\tau_{II}}, \tag{22}$$

with

$$(1-p) = \sum_{q,s} A_q(A_q-A_s)/\sum_{q,s} A_q^2, \tag{23}$$

where A's are the lattice part of the dipole interaction (a_0 between sites 1 and 2 or 3, and b_0 between sites

2 and 3), q denotes a spin pair before the reorientational jump and s denotes that after the jump, and the summation is carried out over all possible processes and possible spin pairs. For each jump from one of the arrangements, i, ii, and iii, to another the numerator of Eq. 23 will be given by $(a_0—b_0)^2$ because in the process of i→ii, for instance, one of the three spin pairs (IJ) makes no contribution to it while for the others, (IK) has $a_0(a_0—b_0)$ and (JK) has $b_0(b_0—a_0)$. Each jump contribution to the denominator of Eq. 23 is simply $2a_0^2+b_0^2$; thus we have

$$T_{1D}^{-1} = \frac{(a_0-b_0)^2}{(2a_0^2+b_0^2)} \cdot \frac{1}{\tau_{II}}. \tag{24}$$

Relaxation Rate due to Diffusion. Diffusion of water molecules or carboxyl protons may be another motion which is likely to exist at high temperatures. Here we consider the following two cases of diffusional jump (the three-spin system is considered as before):

Case 1: all dipole interactions are destroyed.

Case 2: dipole interactions between carboxyl protons and water protons are destroyed but that within the water molecule is retained. As will be described later, these diffusion mechanisms do not give satisfactory angular dependence of relaxation rates; thus only the proportionality relations resulting from these mechanisms, which are necessary for later discussion, will be presented.

When an expression for relaxation rate by slow motion similar to Eq. 22 is applied, we have for Case 1,

$$T_{1D}^{-1} \propto \frac{2a_0^2+b_0^2}{2a_0^2+b_0^2} \cdot \frac{1}{\tau_d} = \frac{1}{\tau_d}, \tag{25}$$

independent of the field direction, because the entire dipole interaction is destroyed by a diffusional jump. τ_d denotes the correlation time for diffusion. From the relation of $T_{1\rho}^{-1}$ and T_{1D}^{-1} mentioned before we can expect to have an approximate relation:

$$T_{1\rho}^{-1} \propto \frac{2a_0^2+b_0^2}{\omega_1^2} \cdot \frac{1}{\tau_d}. \tag{26}$$

A similar argument for Case 2 leads to

$$T_{1D}^{-1} \propto \frac{2a_0^2}{2a_0^2+b_0^2} \cdot \frac{1}{\tau_d}, \tag{27}$$

and

$$T_{1\rho}^{-1} \propto \frac{a_0^2}{\omega_1^2} \cdot \frac{1}{\tau_d}. \tag{28}$$

Experimental

Single crystals of α-form oxalic acid dihydrate $(COOH)_2 \cdot 2H_2O$ are grown by slowly cooling a saturated aqueous solution. The crystal is mounted on a teflon holder which fits in the probe head. Alignment of the crystalline axes in the probe head is made visually. The alignment error is estimated to be less than 2°. Measurements are made at the Larmor frequency of 30 MHz. A single coil coupling arrangement is used. Recovery time of the receiving system is about 8 μs. T_1 is measured by 90° pulse comb-90° pulse sequence. For rotating frame experiments the spin locking state is prepared by turning on H_1 slowly (in a time of ≈1 ms), and at the same time the initially offset rf frequency is swept to the exact resonance.

Accuracy of the relaxation time measurement depends strongly on the appearance of free induction decay signals. In most unfavorable cases the error in the relaxation time probably amounts to 20%, but in most cases the estimated error is 10% or less.

Temperature control below room temperature is made by regulation of intermittent flushing of liquid nitrogen directly onto the thick-wall copper shield casing of the sample coil.[6]

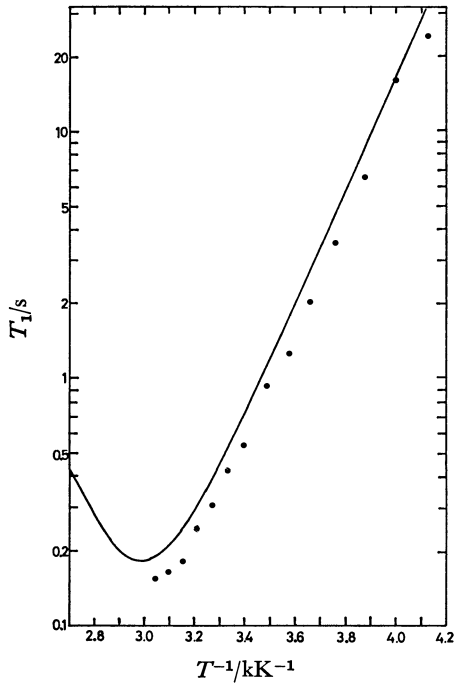

Fig. 2. Temperature dependence of T_1 at $\varphi_H=172°$, φ_H being defined in the text.

Results

T_1. Temperature dependence of T_1 as shown in Fig. 2 is measured at $\varphi_H=172°$, where φ_H denotes the angle of rotation of H_0 from the a axis toward the c axis in the ac plane. To avoid damage of the sample due to dehydration the measurement is not carried out to the point of T_1 minimum. However, from the appearance of Fig. 2, we estimate this to occur at about 61 °C. The theoretical T_1 curve of Eq. 1 with τ_I of Arrhenius form is fit to the observed one in the following two respects: (1) the slope of log T_1 against $1/T$, and (2) the temperature of the T_1 minimum. The following parameters are obtained:

$$\left.\begin{aligned} &\tau_I = 4.37 \times 10^{-16} \exp(\Delta E_I/RT), \\ &\Delta E_I = 43.6\ \mathrm{kJ\ mol^{-1}}. \end{aligned}\right\} \tag{29}$$

The calculated T_1 from Eq. 1, also shown in Fig. 2, is in satisfactory agreement with the observed value, considering that only isolated three-proton system is taken into account.

In Fig. 3, T_1^{-1} at 1.4 °C with H_0 in the ac plane, and that with H_0 in the b axis are compared with the theoretical curve with τ_I of Eq. 29. The agreement is generally satisfactory.

$T_{1\rho}$ and T_{1D}. The temperature dependence of $T_{1\rho}$ and T_{1D} is measured at $\varphi_H=47°$ and 172° where the free induction decay signal is not exceedingly short,

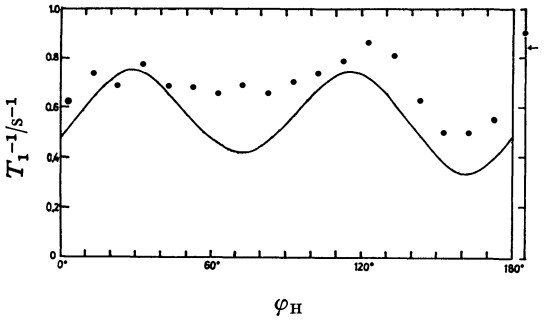

Fig. 3. Angular dependence of T^{-1} at 1.4 °C. The calculated curve from Eq. 1 is also shown. The value with H_0 along the b axis is shown at the far-right of the figure; an arrow indicates a calculated value.

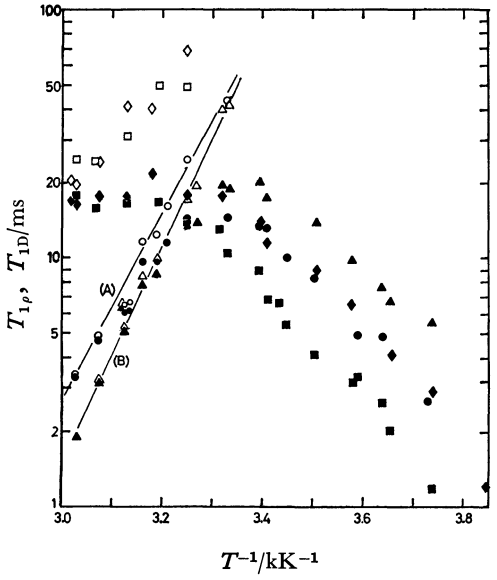

Fig. 4. Temperature dependence of $T_{1\rho}$ and T_{1D}. ■, ●: $T_{1\rho}$ and T_{1D}, respectively, measured at φ_H= 172°. ◆, ▲: those measured at φ_H=47°. The values corrected for relaxation rates due to 180°-flip are indicated by open marks, □, *etc.*

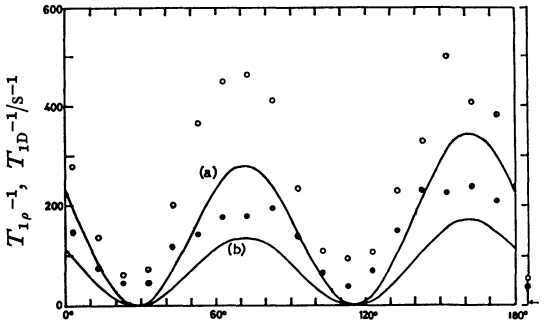

Fig. 5. Angular dependence of $T_{1\rho}^{-1}$(○) and T_{1D}^{-1} (●) at 0 °C. (a): $T_{1\rho}^{-1}$ from Eq. 6, (b): T_{1D}^{-1} from Eq. 14. Values at the b axis are presented at the far-right (calculated $T_{1\rho}^{-1}$ value indicated by an arrow).

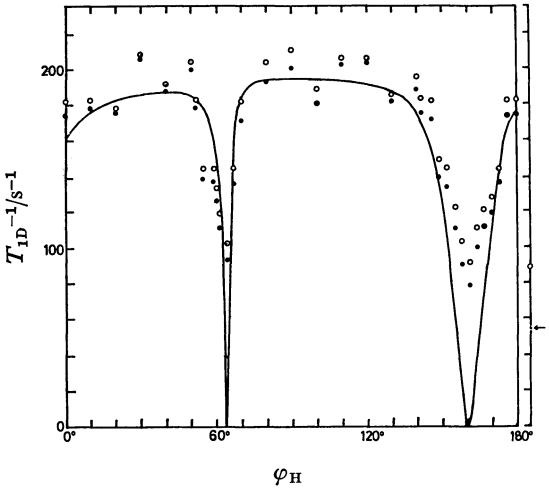

Fig. 6. Angular dependence of T_{1D}^{-1} at 47 °C (solid circles) with H_0 in the ac plane and along the b axis, the latter being shown at the far-right of the figure. Open circles are those corrected for contribution from 180°-flip motion. Calculated curve from Eq. 24 is also shown.

so that a relatively accurate measurement of relaxation time is possible. The results are shown in Fig. 4 as a semilog plot against $1/T$. Each curve shows a maximum, indicating the presence of at least two different modes of motion.

Positively Temperature Dependent Range. The slopes of the curves in this range are nearly the same as that of Fig. 2. This indicates that the relaxation times are governed by the fast 180°-flip of water molecule ($\tau_I\gamma H_1 \ll 1$ or $\tau_I\gamma H_L \ll 1$). The ΔE_I values derived from $T_{1\rho}$, ≈47 kJ mol^{-1} (φ_H=172°), and ≈41 kJ mol^{-1} (φ_H=47°) are in satisfactory agreement with ΔE_I of Eq. 29. Calculated $T_{1\rho}$ and T_{1D} from Eqs. 6 and 14 with τ_I from Eq. 28 are a factor of about 1.5 greater than the observed values of φ_H=172° and a factor of about 2.2 greater than those of φ_H=47°.

The angular dependences of $T_{1\rho}^{-1}$ and T_{1D}^{-1} measured at 0 °C are shown in Fig. 5. Calculated angular dependences due to fast 180°-flip from Eqs. 6 and 14 with Eq. 28 are also shown in the same figure. The agreement with the experimental values is generally satisfactory. Discrepancies may be partly ascribed to the assumption of the isolated three spin system.[7]

Negatively Temperature Dependent Range. At temperatures above the T_{1D} maximum, relaxation rates due to the high-temperature-mode motion are estimated by subtracting the contribution due to the 180°-flip motion of water molecule from the observed relaxation rates. The latter values are estimated by extrapolating relaxation rates from the low temperature values, by assuming the activation energy determined above. The corrected values are also shown in Fig. 4. An average value of activation energy for the high-temperature-mode motion of 80.8 kJ mol^{-1} is obtained from lines (A) and (B) fit to the temperature dependence of T_{1D} of Fig. 4. The same trend at high temperatures is apparent for both $T_{1\rho}$ and T_{1D} but the high temperature mode motion has less effect on $T_{1\rho}$. Therefore, $T_{1\rho}$ data are not used for deriving the activation energy.

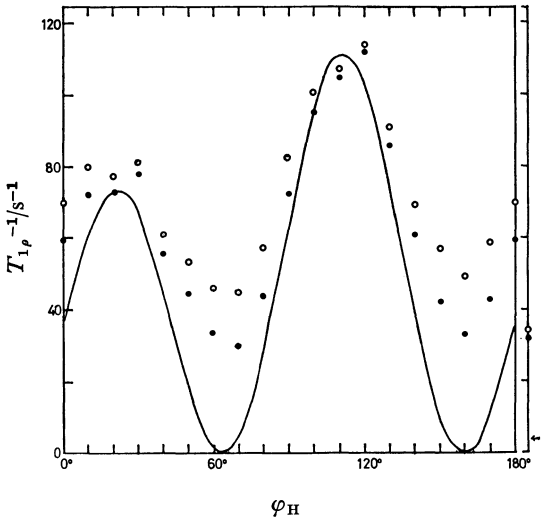

Fig. 7. Angular dependence of $T_{1\rho}^{-1}$ at 55.3 °C (solid circles) with H_0 in the ac plane and along the b axis. Open circles are values corrected for contribution from 180°-flip motion. Calculated curve from Eq. 18 is also shown.

To understand the mode of motion responsible for the high temperature relaxation, angular dependences of T_{1D} at 47 °C and $T_{1\rho}$ at 55.3 °C are measured. These relaxation rates are shown in Figs. 6 and 7. Also shown in these figure are the rates corrected for the small contribution due to the 180°-flip. The amounts of correction at these temperatures are assumed to be the fraction theoretically expected from the temperature variation in correlation time of the relaxation rates of Fig. 5 at 0 °C.

Theoretical curves of the angular dependence of relaxation rates due to carboxyl–water proton exchange motion from Eqs. 18 and 24 are also shown in Figs. 6 and 7. Numerical values of τ_{II} used in drawing these curves are to be described later. Except for the field direction in which the second moment of the three spin system becomes very small and where such an approximation is by no means a good one, the agreement of angular dependence between observed T_{1D}^{-1} and the one calculated for the three spin exchange motion appears excellent. The observed angular dependence of $T_{1\rho}^{-1}$ in Fig. 7 is also in satisfactory agreement with the curve for the exchange mechanism.

Before concluding that the exchange mechanism is the high temperature motional mode of this crystal, however, we need to examine whether a diffusion mechanism can also explain the observed results. The angular dependences of diffusion mechanisms expected from relations (25)—(28) are shown in Fig. 8. Diffusional motion of Case 2 can be definitely eliminated from the appearance of the curve. As for Case 1, though T_{1D}^{-1} from (25), which is angular independent, disagrees with the observed curve of Fig. 6, two dips on the curve which are located around the second moment minimum might be a consequence of inappropriate assumption of the isolated three spin system at these angles. Unfortunately, this cannot be decided by the angular dependence of $T_{1\rho}^{-1}$, because the curves of Fig. 7 and Fig. 8 (d) have similar appearance.

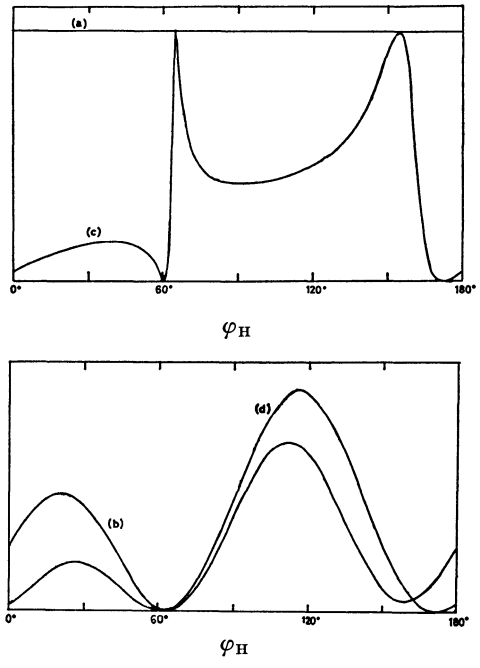

Fig. 8. Angular dependence of T_{1D}^{-1} and $T_{1\rho}^{-1}$, in the ac plane from assumed diffusional mechanisms. (a) and (b) represent T_{1D}^{-1} and $T_{1\rho}^{-1}$, respectively, for Case 1 ((25) and (27)). (c) and (d) represent T_{1D}^{-1} and $T_{1\rho}^{-1}$, respectively, for Case 2 ((26) and (28)). Each curve is drawn to arbitrary scale.

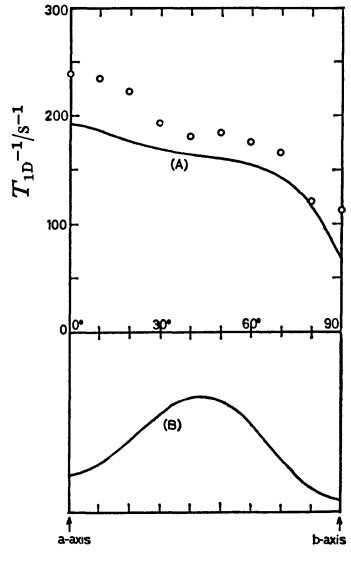

Fig. 9. T_{1D}^{-1} at 49 °C as H_0 is rotated from the a to b axis. (A): Calculated curve from Eq. 24. (B): calculated angular dependence of second moment (scale arbitrary); this curve is to show no extremely small values of H_L is present in these directions.

In order to draw a definite conclusion to this problem, the angular dependence of T_{1D} with H_0 in the ab plane is measured. In this case the three spin system has two different orientations with respect to H_0, and T_{1D}^{-1} is calculated as the mean value for these two orientations, as shown in Fig. 9. It is noted that the theoretical T_{1D}^{-1} due to three spin exchange motion decreases steadily as the field is rotated from

the a axis to the b axis. The observed values of T_{1D}^{-1}, also shown in Fig. 9, are in satisfactory agreement with the curve calculated for the exchange mechanism,[8] but they disagree with the diffusional motion of Case 1, where a constant value over the whole range is expected. A diffusion mechanism is therefore excluded.

From the maximum value of T_{1D}^{-1} at 47 °C of Fig. 6, $\tau_{II}=7.7$ ms is obtained using Eq. 24. With this τ_{II} and the activation energy obtained above, we have

$$\left.\begin{aligned}&\tau_{II} = 5.3 \times 10^{-16} \exp(\Delta E_{II}/RT),\\ &\Delta E_{II} = 80.8 \text{ kJ mol}^{-1}.\end{aligned}\right\} \quad (30)$$

Similarly, from the maximum value of $T_{1\rho}^{-1}$ at 55.3 °C of Fig. 7, $\tau_{II}=2.8$ ms is obtained using Eq. 18; this is in fair agreement with 3.5 ms at that temperature from Eq. 30.

Discussion

T_1 and the low temperature part of $T_{1\rho}$ and T_{1D} are consistently explained by a 180°-flip motion of water molecule. The activation energy for this motion has been obtained from the temperature dependence of T_1 of the deuteron in the α-form $(COOD)_2 \cdot 2D_2O$ crystal to be 9.7 kcal mol^{-1} (=40.6 kJ mol^{-1}).[9] There is a small difference in ΔE_I of the previous report from the present result; this may be ascribed to experimental error rather than indicating an isotope effect.[10]

While relaxation rates in the rotating frame are most sensitive to slow motion at $H_1 \to 0$, for a rapid motion this is not the case. As seen in Eqs. 6 and 14, T_{1D} is twice the $T_{1\rho}$ in the case of rapid two-fold reorientation.[11] The relation may be utilized to detect slow motion in the presence of rapid reorientation, for $T_{1D}/T_{1\rho}$ may be a sensitive measure of additional slow motional processes.

The case dealt with in the present study revealed an interesting three spin exchange motion in a system in which H_3O^+ is not formed. It seems more reasonable to consider this motion as involving the following excited configuration rather than a simple three-fold reorientation. The system in the ground configuration (I) is first excited to the excited configuration (II),

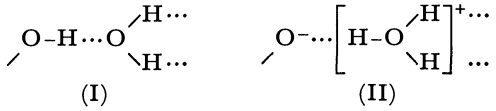

(I) (II)

followed by a three-fold reorientation of H_3O^+ in that state, and then it returns to (I). Schematic illustration of the potential curve of the system is shown in Fig. 10. The observed ΔE_{II} may be interpreted as the sum of E_1+E_3 if $E_2 \lesssim E_3$, or interpreted as E_1+E_2 if $E_2>E_3$; in the latter case the jump of the carboxyl proton to the upper state and the three-fold reorientation take place in one step. The activation energy for the three-fold reorientation of H_3O^+ is reported to be 4.82 kcal mol^{-1} (=20.17 kJ mol^{-1}) in H_3O^+-ClO_4^-,[12] and that of 34 kJ mol^{-1} is obtained for $H_3O^+HSO_4^-$ from our T_1 measurement.[13] Though the interpretation of the energy relations given here is very approximate, with E_3 in the range of activation energy of H_3O^+ reorientation quoted above, a reasonable estimate of the upper limit of E_1 may be around 60 kJ mol^{-1}.

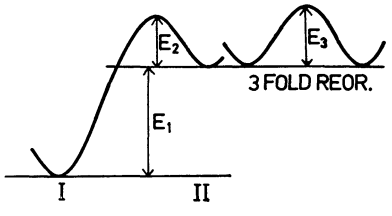

Fig. 10. Schematic illustration of the potential curves for water and carboxyl proton exchange motion.

The mechanism of motion proposed above involves jumps between unequal levels of the carboxyl proton. Usually in a case like this the motion is relatively ineffective for relaxation due to the short residence time in the less stable site.[14] In the present case, however, the carboxyl proton which moved to the high energy site can exchange position with the water protons by the three-fold reorientation and therefore the whole sequence can provide an efficient mechanism for relaxation.[15]

From the positive temperature dependence of the deuteron quadrupole coupling of carboxyl deuteron in deuterated oxalic acid dihydrate, a weakening of the hydrogen bond with temperature is suggested.[9] If this is the case it would result in an increase in the activation energy ΔE_{II} with temperature. However, if such an effect is taken into consideration, the resulting pre-exponential factor, τ_{II}^0, becomes unreasonably small. For instance, a linear temperature dependence of ΔE_{II} of only 4.2 kJ mol^{-1}/100 °C leads to ΔE_{II} at 350 K of 88 kJ mol^{-1} and τ_{II}^0 of 10^{-17}. Though there seems to be thus some incongruity between the previous deuteron resonance result and the present work, for which at the moment no explanation is available, we conclude that ΔE_{II} of Eq. 30 is substantially correct and that the positive temperature dependence in ΔE_{II}, if it exists, is not large.

The chemical shift of oxalic acid dihydrate at room temperature has been measured by high resolution NMR in solids.[16] Because the chemical shift spectrum is also sensitive to slow motional processes, it is hoped that such study will be extended to higher temperatures to see if supporting results can be obtained.

References

1) a) R. G. Delaplane and J. A. Ibers, *Acta Crystallogr., Sect. B*, **25**, 2423 (1969); b) T. M. Sabine, G. W. Cox, and B. M. Craven, *ibid.*, **25**, 2437 (1969).

2) Ref. 1 b).

3) D. C. Look and I. J. Lowe, *J. Chem. Phys.*, **44**, 2995 (1966).

4) A. Abragam, "The Principles of Nuclear Magnetism," Oxford University Press, London (1961), p. 359.

5) C. P. Slichter and D. Ailion, *Phys. Rev. A*, **135**, 1099 (1964).

6) M. O. Norris and J. H. Strange, *J. Phys. E*, **2**, 1106 (1969).

7) For the calculation of $T_{1\rho}^{-1}$, Eq. 6 is used throughout, and no correction (Eq. 15) due to nonvanishing H_L is made. In directions where $T_{1\rho}^{-1}$ becomes large, H_L is relatively

small, and the theoretical curve is not greatly influenced by this correction.

8) Some discrepancy of theoretical and observed T_{1D}^{-1} is seen in the vicinity of the a axis direction. This might be due to a small error in crystal orientation, because crystal setting in this case was more difficult than in the case of the b axis rotation. Therefore, theoretical curves for up to 10° misalignment in the a axis were also examined and found not to affect the above conclusion.

9) T. Chiba, *Bull. Chem. Soc. Jpn.*, **44**, 1703 (1971).

10) We calculated the deuteron T_1 at the experimental conditions of the previous measurement, using the quadrupole coupling tensor and τ_I of Eq. 29. The calculation reproduced the measured values rather satisfactorily.

11) The same relation can be seen to hold for rapid reorientation of an isolated three-spin system (T. Chiba, unpublished).

12) D. E. O'Reilly, E. M. Peterson, and J. M. Williams, *J. Chem. Phys.*, **54**, 96 (1971).

13) T. Chiba, unpublished.

14) D. C. Look and I. J. Lowe, *J. Chem. Phys.*, **44**, 3437 (1966).

15) A case somewhat like the present one is found in the work of D. E. O'Reilly *et al.* on chloroauric acid tetrahydrate [*J. Chem. Phys.*, **55**, 5629 (1971)]. Here the proton motion in $(H_5O_2)^+$ of the jump between symmetric double minimum equilibrium positions plus hydronium reorientation is treated.

16) S. Sagnowski, S. Aravamudhan, and U. Haeberlen, *J. Chem. Phys.*, **66**, 4697 (1977), and Refs. 1 and 2 quoted therein.

Theory of A.c. Polarization and A.c. Polarography and Voltammetry of Surface Redox Reaction

Tadaaki KAKUTANI* and Mitsugi SENDA

Department of Agricultural Chemistry, Faculty of Agriculture, Kyoto University, Kyoto 606

(Received May 30, 1979)

Theoretical equations are presented of the a.c. polarization and of the a.c. polarography and voltammetry for the surface redox reaction ($O_{ad}+ne\rightleftharpoons R_{ad}$) in which charge transfer reaction takes place exclusively between the adsorbed reactants O_{ad} and R_{ad}, and both reactants are adsorbed so strongly that the amount of O or R brought to or removed from the electrode surface can be neglected. The interaction between adsorbed molecules is assumed to be expressed by Frumkin's *a*-parameters. Also the effect of the double layer impedance is taken into account. Some simplified cases are discussed in detail.

Electrochemistry with electroactive reactants irreversibly or strongly adsorbed on or chemically bonded to electrode surface is an active field of current research (for reviews, see Refs. 1 and 2). In the majority of cases the electrochemical behavior of such electrodes has been studied by using linear sweep cyclic voltammetry and differential pulse polarography. Also the coulostatic technique[3] and the second harmonic a.c. voltammetric technique[4] were used for the study of electron transfer reactions between reactants irreversibly or strongly adsorbed on or chemically bonded to electrode surface. We have applied the a.c. polarographic technique to elucidate the electrode processes of ferredoxins irreversibly adsorbed on the surface of mercury electrode.[5a] The results indicated that the a.c. polarography is a powerful technique, in particular, for determining the electrochemical kinetic parameters.

Theory of the faradaic impedance or a.c. polarography of the electrode processes with specific adsorption has been given in a general form[6] which involves terms of mass transfer, adsorption and charge transfer. Although the general expressions are very involved, the expressions will become very simple[7] when the charge transfer reaction takes place exclusively between adsorbed molecules and the amount of electroactive species (O or R) brought to or removed from the electrode surface by mass transfer can be neglected in comparison with the amount which remains adsorbed. These conditions will be satisfied in the case of strongly or irreversibly adsorbed or chemically bonded species.

In this paper, we present theoretical expressions of the faradaic impedance and of the a.c. polarography and voltammetry of the electrode processes with reactants irreversibly adsorbed on or chemically bonded to electrode surface (hereafter we call this the "surface redox reaction") on the basis of the general expressions[6]. In the following derivation we shall make several assumptions: (a) the charge transfer reaction takes place exclusively between the adsorbed molecules, (b) both O and R are adsorbed so strongly (irreversibly) that the amount of O or R brought to or removed from the electrode surface can be neglected, and (c) the interaction between adsorbed molecules can be expressed by Frumkin's *a*-parameters. The effect of the double layer impedance is also considered.

Theory of Faradaic and Non-faradaic Currents

We consider an *n*-electron surface redox reaction,

$$O_{ad} + ne \rightleftharpoons R_{ad}. \tag{1}$$

Since the surface redox reaction proceeds exclusively between the adsorbed molecules (assumption (a)), the faradaic current density I_F is a function of the electrode potential, E, and the surface concentrations of the adsorbed species O and R, Γ_O and Γ_R; $I_F=g(E, \Gamma_O, \Gamma_R)$. For small variations of the potential, δE, superimposed on the "d.c." potential, E_{dc}, ($E=E_{dc}+\delta E$), the surface concentration will change around the mean ("d.c.") value, $\overline{\Gamma}_i$, with small variations, $\delta\Gamma_i$; $\Gamma_i=\overline{\Gamma}_i+\delta\Gamma_i$ (i=O and R) and the faradaic current will be given by[6]

$$I_F = I_{dc} + \delta I_F. \tag{2}$$

Thus we have for the first harmonic of faradaic current, $\delta_1 I_F$,

$$\delta_1 I_F = (\partial I/\partial E)\delta_1 E + (\partial I/\partial \Gamma_O)\delta_1\Gamma_O + (\partial I/\partial\Gamma_R)\delta_1\Gamma_R, \tag{3}$$

where $\delta_1 E$ and $\delta_1\Gamma_i$'s represent the first harmonic variations of E and Γ_i's respectively. From the assumption (b) we further have[6]

$$d(\delta_1\Gamma_i)/dt = j\omega\delta_1\Gamma_i = \pm(\delta_1 I_F/nF). \tag{4}$$

Here the upper and lower sings correspond to O and R, respectively, j is the operator $(-1)^{1/2}$, and ω the angular frequency of sinusoidal variations.

By combination of Eqs. 3 and 4 we obtain the *I-E* characteristic for sinusoidal variations of small amplitude,

$$\delta_1 I_F = \delta_1 I_F^{real} + j\delta_1 I_F^{imag} = (r-jy)^{-1}\delta_1 E, \tag{5a}$$

$$\delta_1 I_F^{real} = \frac{(r/y)^2}{1+(r/y)^2}\cdot\frac{1}{r}\delta_1 E, \tag{5b}$$

and

$$\delta_1 I_F^{imag} = \frac{1}{1+(r/y)^2}\cdot\frac{1}{y}\delta_1 E, \tag{5c}$$

where $\delta_1 I_F^{real}$ and $\delta_1 I_F^{imag}$ are the real and imaginary components of the faradaic a.c. current, respectively, and r and y are given by

$$r = 1/(\partial I/\partial E), \tag{6a}$$

and

$$y=y_O + y_R = (1/nF\omega)[-(\partial I/\partial\Gamma_O)/(\partial I/\partial E) + (\partial I/\partial\Gamma_R)/(\partial I/\partial E)]. \tag{6b}$$

In harmony with the assumption (b) (see Eq. 4) the general theory[6] would give the same expressions as above when

$$(\partial\phi_O/\partial\Gamma_R) = (\partial\phi_R/\partial\Gamma_O) = 0, \quad |\zeta_i| \ll 1,$$
$$\text{and } (\omega/2D_i)^{1/2}(\partial\Gamma_i/\partial C_i^\circ) \gg 1$$

(see Ref. 6 regarding the notations).

Because of adsorption of O and R, the double layer impedance, *i.e.*, the non-faradaic impedance may differ from that observed in the absence of O and R. In this case we can assume that the surface charge density on the electrode, q, is a function of E, Γ_O, and Γ_R only, so that for sinusoidal variations of the non-faradaic current-density we have for the first harmonic[6,8]

$$\delta_1 I_{NF} = (dq/dt)_{ac} = j\omega[(\partial q/\partial E)\delta_1 E + (\partial q/\partial\Gamma_O)\delta_1\Gamma_O + (\partial q/\partial\Gamma_R)\delta_1\Gamma_R]. \quad (7)$$

From Eqs. 4 and 7, we obtain for the non-faradaic ac current

$$\delta_1 I_{NF} = (1/nF)[(\partial q/\partial\Gamma_O) - (\partial q/\partial\Gamma_R)]\delta_1 I_F + j\omega(\partial q/\partial E)\delta_1 E. \quad (8)$$

Thus we have for the total (faradaic and non-faradaic) ac current

$$\delta_1 I_t = \delta_1 I_F + \delta_1 I_{NF} = \{1 + (1/nF)[(\partial q/\partial\Gamma_O) - (\partial q/\partial\Gamma_R)]\}\delta_1 I_F + j\omega(\partial q/\partial E)\delta_1 E, \quad (9)$$

and the observable real and imaginary components are

$$\delta_1 I_{obsd}^{real} = \{1 + (1/nF)[(\partial q/\partial\Gamma_O) - (\partial q/\partial\Gamma_R)]\}\delta_1 I_F^{real}, \quad (10a)$$

and

$$\delta_1 I_{obsd}^{imag} = \{1 + (1/nF)[(\partial q/\partial\Gamma_O) - (\partial q/\partial\Gamma_R)]\}\delta_1 I_F^{imag} + \omega(\partial q/\partial E)\delta_1 E, \quad (10b)$$

respectively. The second term on the right-hand side of Eq. 10b, $\omega(\partial q/\partial E)\delta_1 E$, (*i.e.*, so-called "wahre Käpazität" term[8]) can be estimated from double-layer capacity measurements employing very high frequencies. This term is generally a reverse-S-shaped or S-shaped variation of the capacity current and for practical purpose can approximately be eliminated by a conventional method of correction for ac base current as usually used in a.c. polarographic technique:

$$\delta_1 I_{corr}^{imag} = \delta_1 I_{obsd}^{imag} - \omega(\partial q/\partial E)\delta_1 E = \{1 + (1/nF)[(\partial q/\partial\Gamma_O) - (\partial q/\partial\Gamma_R)]\}\delta_1 I_F^{imag}. \quad (10c)$$

On the other hand it is very difficult to estimate the term $[(\partial q/\partial\Gamma_O) - (\partial q/\partial\Gamma_R)]$ experimentally. However, since the potential range in which the faradaic current appears does not exceed a few tenths of a volt, it can be assumed that this term is practically a constant within the range studied:

$$\delta_1 I_{obsd}^{real} = (m/n)\delta_1 I_F^{real}, \quad (11a)$$
$$\delta_1 I_{corr}^{imag} = (m/n)\delta_1 I_F^{imag}, \quad (11b)$$
$$(m/n) = \{1 + (1/nF)[(\partial q/\partial\Gamma_O) - (\partial q/\partial\Gamma_R)]\} \quad (11c)$$

We call the constant, m, defined by Eq. 11c the apparent number of electrons associated with the surface redox reaction (1).

Equations for Faradaic Impedance and A.c. Polarography and Voltammetry

Laitinen and Randles[9] first gave theoretical expressions of the faradaic impedance for the surface redox reaction. However, they did not take the interaction between the adsorbed molecules into account. We assume that the current-potential-concentration characteristic can be written as[7]

$$(I_F/nF) = \overleftarrow{V} - \overrightarrow{V}, \quad (12a)$$

$$\overleftarrow{V} = k_s'(1-f)\theta_t B_R^{-1} \exp[\beta(nF/RT)(E-E_0)] \times \exp[-a_{RR}(1-f)\theta_t - a_{RO} f\theta_t], \quad (12b)$$

$$\overrightarrow{V} = k_s' f\theta_t B_O^{-1} \exp[-\alpha(nF/RT)(E-E_0)] \times \exp[-a_{OO} f\theta_t - a_{OR}(1-f)\theta_t], \quad (12c)$$

where B_i is the constant representing the adsorption energy of i on the electrode surface at $E=E_0$, E_0 being the reference electrode potential (see below), a_{ij} the Frumkin's a-parameter of interaction between the adsorbed molecules i and j (a_{ij} is positive for an attraction and negative for a repulsion),[10] θ_t the total coverage defined by $\theta_t = \Gamma_t/\Gamma_m = \theta_O + \theta_R$ with $\theta_O = \Gamma_O/\Gamma_m$, $\theta_R = \Gamma_R/\Gamma_m$, and $\Gamma_t = \Gamma_O + \Gamma_R = \overline{\Gamma}_O + \overline{\Gamma}_R$, Γ_m the maximum value of the total surface concentration, $f = \theta_O/\theta_t$, $k_s' = k_s\Gamma_m$ and k_s (in s^{-1}) the rate constant of the charge transfer reaction at the standard potential of the surface redox reaction, E_0', which is defined by

$$E_0' = E_0 + [RT/(\alpha+\beta)nF][\ln(B_R/B_O) - (1/2)(a_{OO} - a_{RR} + a_{OR} - a_{RO})\theta_t]. \quad (13)$$

The equilibrium dc potential, E_{eq}, at $I_F=0$ is given by

$$E_{eq} = E_0' + [RT/(\alpha+\beta)nF][\ln(f/(1-f)) + (1/2)(1-2f)G\theta_t]_{eq} \quad (14)$$

where G is defined by Eq. 19. α and β are the transfer coefficients for cathodic and anodic charge transfer reaction, respectively. Similar expression of the current-potential-concentration characteristic has been used by Conway *et al.*[11,12] in the kinetic theory of the linear sweep voltammetry of the surface redox reaction, and by Laviron,[13] Brown and Anson,[14] and Murray *et al.*[15] in theoretical expressions of the reversible linear sweep voltammogram of the surface redox reaction. It can generally be shown that the peak potential of the d.c. reversible (*i.e.*, d.c. Nernstian) linear sweep voltammogram, E_p^{dc}, is equal to E_0' defined by Eq. 13. In the following we assume that the a_{ij}-parameters are independent of the electrode potential. In Eqs. 12b and 12c the terms $\exp[\beta(nF/RT)(E-E_0)]$ and $\exp[-\alpha(nF/RT)(E-E_0)]$ represent the dependence of both the activation free energy of charge transfer and the adsorption free energy of reactants on the electrode potential. The quadratic dependence of these energies on the electrode potential has been described. In the following, however, we assume in the first approximation that the coefficients α and β are independent of the electrode potential. The reference electrode potential, E_0, may be considered as corresponding to the standard potential of the redox couple

supposedly in the bulk of solution.

From Eqs. 6a, 6b, 12a, 12b, and 12c we obtain

$$r = (1/nF)[\beta(nF/RT)\overleftarrow{V}_{dc}+\alpha(nF/RT)\overrightarrow{V}_{dc}]^{-1} \quad (15)$$

and

$$y = (r/\omega)\{\overrightarrow{V}_{dc}[(1/\overline{\Gamma}_O)-(a_{OO}-a_{OR})(\theta_t/\Gamma_t)] + \overleftarrow{V}_{dc}[(1/\overline{\Gamma}_R)-(a_{RR}-a_{RO})(\theta_t/\Gamma_t)]\}. \quad (16)$$

Here $\overleftarrow{V}_{dc}=\overleftarrow{V}(E=E_{dc}, f=\bar{f})$ and $\overrightarrow{V}_{dc}=\overrightarrow{V}(E=E_{dc}, f=\bar{f})$ with $\bar{f}=\overline{\Gamma}_O/\Gamma_t$ and these are related to the dc faradaic current by

$$(I_F)_{dc}/nF = \overleftarrow{V}_{dc} - \overrightarrow{V}_{dc}. \quad (17a)$$

When the surface redox reaction is d.c. reversible (dc Nernstian), *i.e.*, $(4RTk_s/nF\nu)\gg 1$ in a.c. voltammetry with the potential sweep rate, ν, or $k_s\tau\gg 1$ in a.c. polarography with the drop time, τ, $\bar{f}$ or $\overline{\Gamma}_O$, and $\overline{\Gamma}_R$ can be estimated by

$$(\overleftarrow{V}_{dc}-\overrightarrow{V}_{dc})_{dc\ reversible} = 0 \quad (17b)$$

and given by

$$E_{dc} = E_0' + [RT/(\alpha+\beta)nF] \times [\ln(\bar{f}/(1-\bar{f}))+(1/2)(1-2\bar{f})G\theta_t], \quad (18)$$

with

$$G = a_{OO} + a_{RR} - a_{OR} - a_{RO}. \quad (19)$$

In this case r and y are given by

$$r = \frac{1}{(\alpha+\beta)}\cdot\frac{RT}{nF}\cdot\frac{1}{I_0}, \quad (20)$$

and

$$y = \frac{1}{(\alpha+\beta)nF(nF/RT)\omega\Gamma_t}\cdot\frac{1-G\theta_t(1-\bar{f})\bar{f}}{(1-\bar{f})\bar{f}}, \quad (21)$$

where I_0 is the exchange current density at $E=E_{dc}$ and given by

$$I_0 = nFk_s\Gamma_t\bar{f}^{\beta/(\alpha+\beta)}(1-\bar{f})^{\alpha/(\alpha+\beta)}B_O^{-\beta/(\alpha+\beta)}B_R^{-\alpha/(\alpha+\beta)} \times \exp\{-(\beta/(\alpha+\beta))[a_{OO}\bar{f}+a_{OR}(1-\bar{f})]\theta_t\} \times \exp\{-(\alpha/(\alpha+\beta))[a_{RR}(1-\bar{f})+a_{RO}\bar{f}]\theta_t\}. \quad (22)$$

The phase angle, ψ, is given by

$$\cot\psi = (r/y) = (\delta_1 I_F^{real}/\delta_1 I_F^{imag}) = (\delta_1 I_{obsd}^{real}/\delta_1 I_{corr}^{imag}) = \frac{\omega}{\phi_0}\cdot\frac{(1-\bar{f})\bar{f}}{1-G\theta_t(1-\bar{f})\bar{f}}, \quad (23)$$

with $\phi_0=I_0/nF\Gamma_t$.

These equations 18, 20, 21, and 23 are applicable without alteration to a.c. polarization of the surface redox reaction at the equilibrium (dc) potential.

Simplified Cases

In the following we shall consider several simplified cases, in which the surface redox reaction is assumed to be dc reversible.

A.c. Reversible Case. When the rate constant is so large that the condition $(r/y)\ll 1$ is satisfied, Eqs. 5a, 5b, and 5c are reduced to

$$(\delta_1 I_F)_{rev} = (\delta_1 I_F^{imag})_{rev} = \frac{1}{y}\delta_1 E = (\alpha+\beta)nF(nF/RT)\omega\Gamma_t\cdot\frac{\bar{f}(1-\bar{f})}{1-G\theta_t(1-\bar{f})\bar{f}}\delta_1 E, \quad (24)$$

and $\cot\psi=0$. That is, $\delta_1 I_F^{real}$ becomes vanishingly small and ψ approaches 90°. The a.c. wave has a maximum at $\bar{f}=1/2$ and is symmetrical with respect to the peak potential. The peak current, $(\delta_1 I_F^p)_{rev}$, peak potential, E_p^{rev}, and half-peak width, $\Delta E_{p/2}^{rev}$, are given by

$$(\delta_1 I_F^p)_{rev} = (\alpha+\beta)nF(nF/RT)\omega\Gamma_t(4-G\theta_t)^{-1}\delta_1 E, \quad (25)$$

$$E_p^{rev} = E_0', \quad (26)$$

and

$$\Delta E_{p/2}^{rev} = \frac{2RT}{(\alpha+\beta)nF}\left|\ln\frac{1+\gamma}{1-\gamma}-(1/2)G\theta_t\gamma\right| \quad (27)$$

with

$$\gamma = \sqrt{(4-G\theta_t)/(8-G\theta_t)}. \quad (28)$$

As seen from these equations, both $(\delta_1 I_F^p)_{rev}$ and $\Delta E_{p/2}^{rev}$ depend remarkably on the adsorption parameter $G\theta_t$ and also on the coefficient $(\alpha+\beta)$. It is noted that these equations are the same as those of the reversible linear sweep voltammogram[13] if the term $\omega\delta_1 E$ is replaced by the sweep rate ν. Namely, in this case the shape of the a.c. wave is the same as that of the reversible linear sweep voltammogram and E_p^{rev} coincides with E_p^{dc}.

Case of $a=a_{OO}=a_{RR}=a_{OR}=a_{RO}$. In this case r and y are reduced to

$$r = [(\alpha+\beta)nF(nF/RT)k_{sap}\Gamma_t\rho^{\beta/(\alpha+\beta)}(1+\rho)^{-1}]^{-1}, \quad (29)$$

and

$$y = [(\alpha+\beta)nF(nF/RT)\omega\Gamma_t\rho(1+\rho)^{-2}]^{-1}, \quad (30)$$

where

$$k_{sap} = k_s B_O^{-\beta/(\alpha+\beta)}B_R^{-\alpha/(\alpha+\beta)}\exp(-a\theta_t), \quad (31)$$

$$\rho = \exp[(\alpha+\beta)(nF/RT)(E_{dc}-E_0')], \quad (32)$$

with $E_0'=E_0+[RT/(\alpha+\beta)nF]\ln(B_R/B_O)$, because $a_{OO}-a_{RR}+a_{OR}-a_{RO}=0$ in this simplified case (see Eq. 13). Introducing Eqs. 29 and 30 into Eqs. 5b and 5c leads to equations of the two components of the a.c. wave, from which the two peak potentials, E_p^{real} and E_p^{imag}, are given as functions of the kinetic parameters, α, β and k_{sap}, which implicitly depends on the adsorption parameter a, as shown, for example, for the case of $\alpha+\beta=1$ in Fig. 1.

For the phase angle we obtain

$$\cot\psi = (\delta_1 I_F^{real}/\delta_1 I_F^{imag}) = (\omega/k_{sap})\rho^{\alpha/(\alpha+\beta)}(1+\rho)^{-1}. \quad (33)$$

Accordingly a plot of $\cot\psi$ against E_{dc} at any frequency has a maximum at the potential

$$[E_{dc}]_{\cot\varphi=max} = E_0' + [RT/(\alpha+\beta)nF]\ln(\alpha/\beta) \quad (34)$$

with a magnitude

$$[\cot\psi]_{max} = (\omega/k_{sap})[(\alpha/\beta)^{-\alpha/(\alpha+\beta)} + (\alpha/\beta)^{\beta/(\alpha+\beta)}]^{-1}. \quad (35)$$

The relations 33 to 35 are important because we do not need the knowledge on $[(\partial q/\partial\Gamma_O)-(\partial q/\partial\Gamma_R)]$.

When $\alpha+\beta=1$, we can determine the kinetic param-

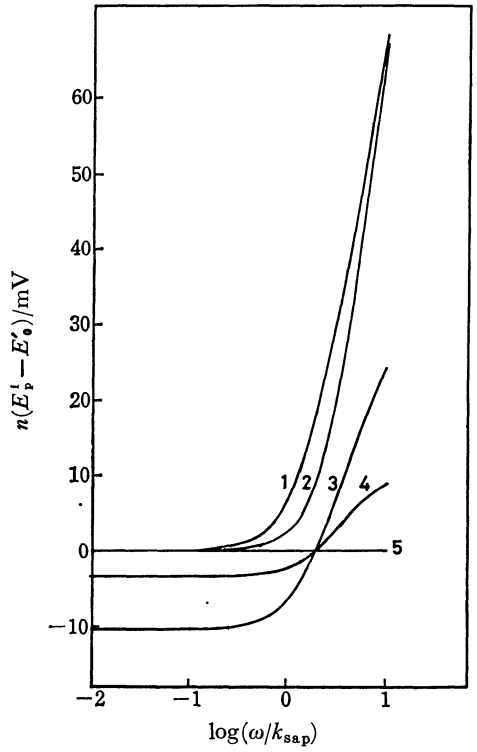

Fig. 1. Variations of E_p^{real} and E_p^{imag} as a function of $\log(\omega/k_{sap})$ for the case (2) with $\alpha+\beta=1$. E_p^{imag}: (1) $\alpha=0.2$, (2) $\alpha=0.4$, (5) $\alpha=0.5$ E_p^{real}: (3) $\alpha=0.2$, (4) $\alpha=0.4$, (5) $\alpha=0.5$.

eters, k_{sap} and α, from the relations 33 to 35. Then the adsorption parameter, a, can be determined from the slope of a plot of ln k_{sap} *versus* θ_t. Furthermore if $\alpha=\beta=0.5$, we have the following simplified relations for the half-peak widths of the two a.c. components, $\Delta E_{p/2}^{real}$ and $\Delta E_{p/2}^{imag}$, and the half-peak width of the cot ψ *versus* E_{dc} curve, $\Delta E_{p/2}(\cot\psi)$:

$$\Delta E_{p/2}^{i}(\text{i=real or imag}) = (2RT/nF)\,|\ln[(1+\eta^i)/(1-\eta^i)]|, \quad (36)$$

$$\Delta E_{p/2}(\cot\psi) = 5.27(RT/nF), \quad (37)$$

In Eq. 36 $\eta^{real}=\sqrt{1-4\xi_{real}}$ with ξ_{real} representing the solution of the equation,

$4[4+(\omega/k_{sap})^2]\xi_{real}^{3/2}=(\omega/k_{sap})^2\xi_{real}+1$, and

$\eta^{imag}=\sqrt{[4+(\omega/k_{sap})^2]/[8+(\omega/k_{sap})^2]}$.

When $\alpha+\beta=1$ and $a=0$, theoretical equations of the a.c. wave are reduced to

$$\delta_1 I_F^{real} = nF(nF/RT)\omega\Gamma_t\frac{\rho}{(1+\rho)^2}\cdot\frac{\omega/(\vec{k}+\overleftarrow{k})}{[(\omega/(\vec{k}+\overleftarrow{k}))^2+1]}\delta_1 E, \quad (38)$$

$$\delta_1 I_F^{imag} = nF(nF/RT)\omega\Gamma_t\frac{\rho}{(1+\rho)^2}\cdot\frac{1}{[(\omega/(\vec{k}+\overleftarrow{k}))^2+1]}\delta_1 E, \quad (39)$$

where $\vec{k}=k_s B_O^{-\beta/(\alpha+\beta)}B_R^{-\alpha/(\alpha+\beta)}\rho^{-\alpha}$ and $\overleftarrow{k}=k_s B_O^{-\beta/(\alpha+\beta)}B_R^{-\alpha/(\alpha+\beta)}\rho^{\beta}$. If $B_O=B_R=1$, Eqs. 38 and 39 are reduced to the equations which were previously

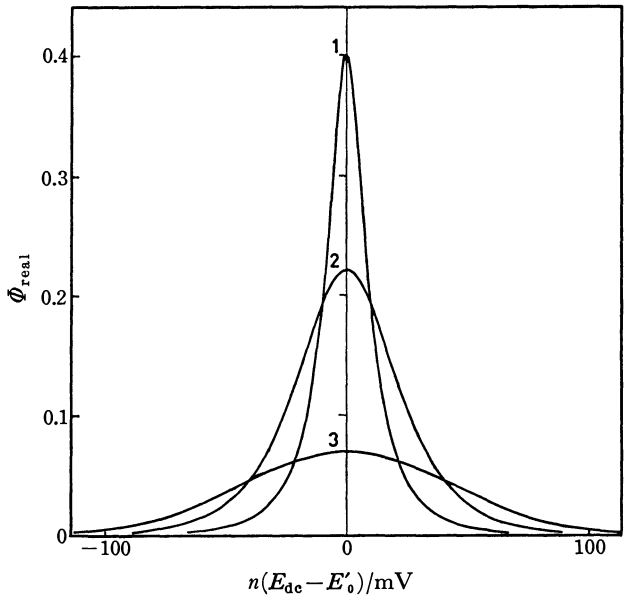

Fig. 2. Normalized real component of a.c. wave calculated by Eqs. 5b, 40, 41 and 44 with $\alpha=\beta=0.5$ and $(\omega/k_{sap})=1$. $G\theta_t$: (1) 3, (2) 1, (3) −1.

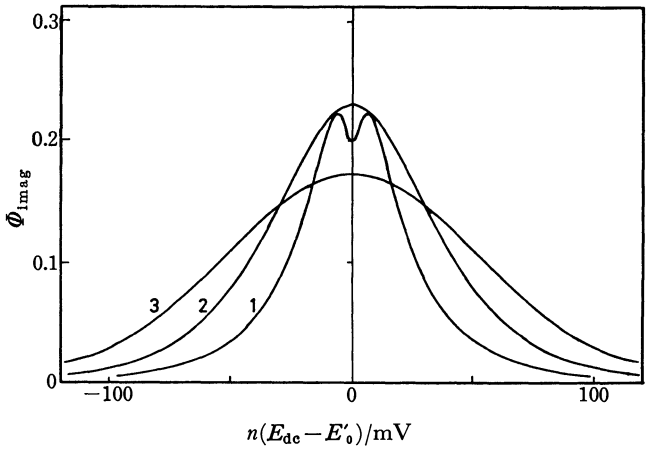

Fig. 3. Normalized imaginary component of a.c. wave calculated by Eqs. 5c, 40, 41 and 44 with $\alpha=\beta=0.5$ and $(\omega/k_{sap})=1$. $G\theta_t$: (1) 3, (2) 1, (3) −1.

derived for analysing the electrode processes of ferredoxins irreversibly adsorbed on the mercury electrode.[5a,5b] Quite recently theoretical equations, essentially the same as Eqs. 38 and 39, have been reported by Laviron.[16]

Case of $a_{ii}=a_{OO}=a_{RR}$, $a_{ij}=a_{OR}=a_{RO}$ *and* $\alpha=\beta$. In this case the terms r and y are reduced to

$$r = [2\alpha nF(nF/RT)k_{sap}\Gamma_t\bar{f}^{1/2}(1-\bar{f})^{1/2}]^{-1}, \quad (40)$$

$$y = \left[2\alpha nF(nF/RT)\omega\Gamma_t\frac{(1-\bar{f})\bar{f}}{1-G\theta_t(1-\bar{f})\bar{f}}\right]^{-1}. \quad (41)$$

where

$$k_{sap} = k_s(B_O B_R)^{-1/2}\exp[-(1/2)(a_{ii}+a_{ij})\theta_t] \quad (42)$$

and

$$G = 2(a_{ii}-a_{ij}). \quad (43)$$

The relation between E_{dc} and $\bar{f}$ is given by

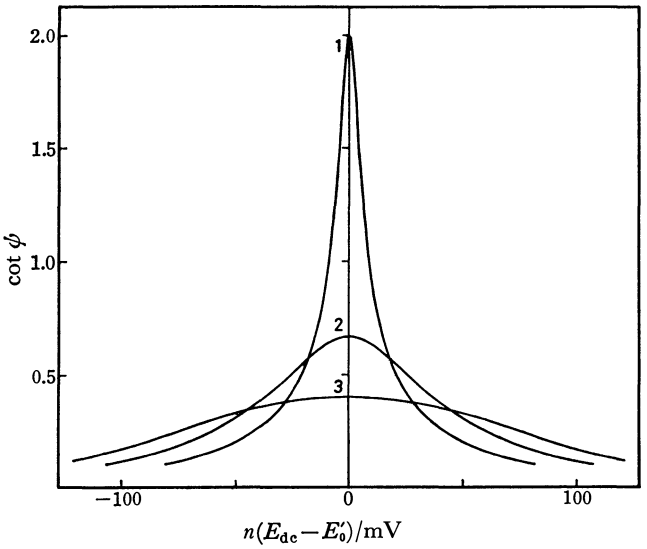

Fig. 4. D.c. dependece of phase angle calculated by Eqs. 45 and 44 with $\alpha=\beta=0.5$ and $(\omega/k_{sap})=1$. $G\theta_t$: (1) 3, (2) 1, (3) -1.

$$E_{dc} = E'_0 + (RT/2\alpha nF)[\ln(\bar{f}/(1-\bar{f})) + (1/2)(1-2\bar{f})G\theta_t] \tag{44}$$

with $E'_0=E_0+(RT/2\alpha nF)\ln(B_R/B_O)$, because $a_{OO}-a_{RR}+a_{OR}-a_{RO}=0$ in this simplified case. Thus the a.c. wave is expressed by Eqs. 5a, 5b, and 5c with Eqs. 40, 41, and 42 and is shown to be symmetrical with respect to the potential $E'_0=E_p^{dc}$. Also Eq. 42 predicts that ln k_{sap} depends lineally on θ_t. The normalized a.c. waves, $\Phi_{real}\equiv\delta_1 I_F^{real}/nF(nF/RT)\omega\Gamma_t\delta_1 E$ and $\Phi_{imag}\equiv\delta_1 I_F^{imag}/nF(nF/RT)\omega\Gamma_t\delta_1 E$, for different values of $G\theta_t$ at $\alpha=\beta=0.5$ and $(\omega/k_{sap})=1$ are illustrated in Figs. 2 and 3.

Furthermore we obtain

$$\cot\psi = \frac{\omega}{k_{sap}}\cdot\frac{(\bar{f})^{1/2}(1-\bar{f})^{1/2}}{1-G\theta_t(1-\bar{f})\bar{f}} \tag{45}$$

This equation predicts that the $\cot\psi$ *versus* E_{dc} curve has a maximum for $4>G\theta_t\geqslant -4$ or minimum for $G\theta_t<-4$ at E'_0 with a magnitude

$$[\cot\psi]_{E_{dc}=E'_0} = (\omega/k_{sap})[2/(4-G\theta_t)] \equiv \lambda. \tag{46}$$

Figure 4 shows the $\cot\psi$ *versus* E_{dc} curves for different values of $G\theta_t$ at $\alpha=\beta=0.5$ and $(\omega/k_{sap})=1$.

In this case we can determine the kinetic and adsorption parameters by the following two methods if α is known.

Method (a): When $\alpha=\beta=$A, $\Delta E_{p/2}^{i}$ is given by (for $G\theta_t\neq 0$)

$$\Delta E_{p/2}^{i} = (RT/AnF)\left|\ln\frac{1+\sqrt{1-4\xi_i}}{1-\sqrt{1-4\xi_i}} - (1/2)G\theta_t\sqrt{1-4\xi_i}\right|. \tag{47}$$

In this equation i=real or imag and ξ_{real} and ξ_{imag} respectively are the solutions of the following two equations; $(4-G\theta_t)^2(1+\lambda^2)\xi_{real}^{3/2}=(1-G\theta_t\xi_{real})^2+(\lambda/2)^2(4-G\theta_t)^2\xi_{real}$ and $(1-G\theta_t\xi_{imag})^2+(\lambda/2)^2(4-G\theta_t)^2\xi_{imag}=2(4-G\theta_t)(1+\lambda^2)(1-G\theta_t\xi_{imag})\xi_{imag}$, where λ is defined by Eq. 46. Dependences of $\Delta E_{p/2}^{i}$'s on $G\theta_t$ for different values of λ at $\alpha=\beta=0.5$ are shown in Figs. 5 and 6. Since λ can be estimated from

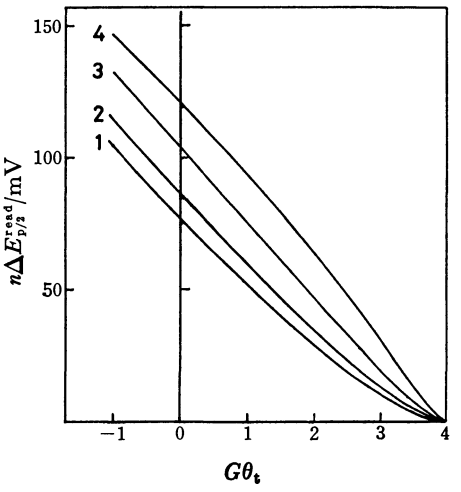

Fig. 5. Variations of $n\Delta E_{p/2}^{real}$ as a function of $G\theta_t$ calculated by Eqs. 36 and 47 with $\alpha=\beta=0.5$. λ: (1) 0.5, (2) 1, (3) 2, (4) 4.

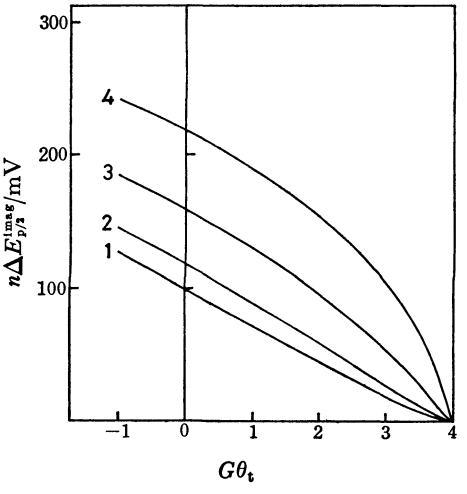

Fig. 6. Variations of $n\Delta E_{p/2}^{imag}$ as a function of $G\theta_t$ calculated by Eqs. 36 and 47 with $\alpha=\beta=0.5$. λ: (1) 0.5, (2) 1, (3) 2, (4) 4.

$(\delta_1 I_F^{real}/\delta_1 I_F^{imag})_{E_{dc}=E'_0}$ and $\Delta E_{p/2}^{i}$'s are functions of $G\theta_t$ and λ only, we can determine k_{sap} and $G\theta_t$ from λ and either $\Delta E_{p/2}^{real}$ or $\Delta E_{p/2}^{imag}$. As shown in Fig. 3, $\delta_1 I_F^{imag}$ has a maximum or minimum at $E_{dc}=E'_0$. When $\delta_1 I_F^{imag}$ has a minimum at $E_{dc}=E'_0$, $\Delta E_{p/2}^{imag}$ of Eq. 47 means a difference between the dc potentials at which the current value is one-half that observed at $E_{dc}=E'_0$.

Method (b): The half-peak width of the $\cot\psi$ *versus* E_{dc} curve, $\Delta E_{p/2}$ $(\cot\psi)$, depends on $G\theta_t$ ($G\theta_t\neq 0$ in this case) only and is given by

$$\Delta E_{p/2}(\cot\psi) = (RT/AnF) \times\left|\ln[(1+\sqrt{1-4\delta})/(1-\sqrt{1-4\delta})] - (1/2)G\theta_t\sqrt{1-4\delta}\right| \tag{48}$$

with

$$\delta = [1/2(G\theta_t)^2]\{[2G\theta_t+(4-G\theta_t)^2] - \sqrt{[2G\theta_t+(4-G\theta_t)^2]^2-4(G\theta_t)^2}\}.$$

Thus we can determine $G\theta_t$ from this relation and

finally k_{sap} from λ when $G\theta_t$ is given. As described above, the cot ψ *versus* E_{dc} curve has a minimum at E'_0 when $G\theta_t<-4$. In this case $\Delta E_{p/2}(\cot\psi)$ of Eq. 48 means a difference between the dc potentials at which the value of cot ψ is one-half that observed at $E_{dc}=E'_0$.

Finally since the sum of the parameters, $(a_{ii}+a_{ij})$, can be determined from the slope of a plot of ln k_{sap} against θ_t, the two parameters, a_{ii} and a_{ij}, can be determined when G is given.

Application of these simplified equations to the electrode processes of ferredoxins irreversibly adsorbed on the surface of the dropping mercury electrode[17] will be reported in a succeeding paper.

References

1) W. R. Heineman and P. T. Kissinger, *Anal. Chem.*, **50**, 166R (1978).

2) D. K. Roe, *Anal. Chem.*, **50**, 9R (1978).

3) A. P. Brown and F. C. Anson, *J. Electroanal. Chem. Interfacial Electrochem.*, **92**, 133 (1978).

4) A. F. Diaz and K. K. Kanazawa, *J. Electroanal. Chem. Interfacial Chem.*, **86**, 441 (1978).

5) a) T. Ikeda, K. Toriyama, and M. Senda, *Bull. Chem. Soc. Jpn.*, **52**, 1937 (1979); b) T. Ikeda, K. Toriyama, M. Senda, Paper Presented at the Polarographic Meeting, Oct. 7—8, 1976, Nagano; abstract, *Rev. Polarogr. (Kyoto)*, **22**, 80 (1976).

6) M. Senda and P. Delahay, *J. Phys. Chem.*, **65**, 1580 (1961).

7) T. Kakutani, T. Ikeda, and M. Senda, Paper Presented at the Polarographic Meeting, Nov. 4—5, 1977, Osaka; abstract, *Rev. Polarogr. (Kyoto)*, **23**, 6 (1977).

8) W. Lorenz and F. Möckel, *Z. Elektrochem.*, **60**, 507 (1956).

9) H. A. Laitinen and J. E. B. Randles, *Trans. Faraday Soc.*, **51**, 54 (1955).

10) B. B. Damaskin, O. A. Petrii, and V. V. Batrakov, "Adsorption of Organic Compounds on Electrodes," Plenum, New York (1971).

11) B. E. Conway, E. Gileadi, and M. Dzieciuch, *Electrochim. Acta*, **8**, 143 (1963).

12) H. Angerstein-Kozlowska, J. Klinger, and B. E. Conway, *J. Electroanal. Chem. Interfacial Chem.*, **75**, 45 (1977).

13) E. Laviron, *J. Electroanal. Chem. Interfacial Chem.*, **52**, 395 (1974).

14) A. P. Brown and F. C. Anson, *Anal. Chem.*, **49**, 1589 (1977).

15) D. F. Smith, K. Willman, K. Kuo, and R. W. Murray, *J. Electroanal. Chem. Interfacial Chem.*, **95**, 217 (1979).

16) E. Laviron, *J. Electroanal. Chem. Interfacial Chem.*, **97**, 135 (1979).

17) T. Ikeda, K. Toriyama, and M. Senda, Paper Presented at the Polarographic Meeting, Nov. 4—5, 1977, Osaka; extended abstract, *Rev. Polarogr. (Kyoto)*, **23**, 26 (1977).

A Molecular Orbital Calculation of Chemically Interacting Systems. Recombination of Two Methyl Radicals

Shinichi YAMABE,* Tsutomu MINATO,** Hiroshi FUJIMOTO,** and Kenichi FUKUI**

Department of Chemistry, Nara University of Education, Takabatake-cho, Nara 630

***Faculty of Engineering, Kyoto University, Sakyo-ku, Kyoto 606*

(Received March 13, 1978)

A molecular orbital (MO) approach to a radical-radical reacting system is proposed within the isolated molecule approximation. The interaction energy, ΔW, is defined as the sum of four components, Coulomb, exchange, charge transfer and polarization energies. The four terms are calculated in the recombination of two methyl radicals. The origin of the deformation of methyl radical ($D_{3h} \rightarrow C_{3v}$) and the rotational barrier (staggered→eclipsed) in the course of the recombination was found to be the exchange energy caused by the interaction of both doubly occupied MO's. The difference-density map shows the characteristic role of exchange and charge transfer interactions for charge redistribution.

The molecular orbital (MO) method has been found to be fairly satisfactory for describing a reasonable reaction path and the activation energy of ionic[1] and addition[2] reactions, but not those of radical-radical reactions. Multi-determinantal wave functions such as those obtained by the MCSCF[3] and natural orbital[4] methods have also been utilized. However, enormous computer time is required for molecules with size of chemical interest, and difficulty in convergence is sometimes encountered. In addition, the methods give no vivid orbital picture which appeals to organic chemists as regards the interpretation of reactivity. In view of the fact that the path of the radical-radical reaction does not yet seem to be understood theoretically,[5] a new means to analyze the mechanism with a clear orbital concept is desirable.

In 1968, two of us (K.F. and H.F.) proposed a method for the general reactivity index ("ΔW method") based on the isolated molecule approximation.[6] Various calculations of model reacting systems showed that the ΔW method is effective for interpreting the reactivity of closed-shell molecules.[7]

In view of the applicability of this method to the elucidation of the reaction mechanism and the necessity to investigate the radical-radical reaction theoretically, an extension of the method was carried out, the aim of the work being to simulate and analyze the reaction within the framework of the MO calculation. Since the ΔW method is based on the *static* model, dynamic processes in the reaction such as the relaxation of vibration energy are beyond the scope of the present approach.

Definition of Interaction Energy

The derivation of the interaction energy (ΔW) is based on the configuration interaction (CI) procedure in terms of the electronic structure of two independent radicals, essentially similar to the case of the reaction between two closed-shell molecules.[6] The wave function ($\Psi^{s,t}$) of the whole reacting system is represented by a linear combination of various configuration functions (Fig. 1).

$$\Psi^{s,t} = C_0\Psi_0^{s,t} + \sum_p C_p\Psi_p^{s,t} \qquad (1)$$

Each Slater determinant of $\Psi_0^{s,t}$ and $\Psi_p^{s,t}$ is composed of the MO's, a_l,[8] a_o, b_k, and b_o, which are the solutions of the doublet spin state of two *independent* radicals. Once they are included within one Slater determinant and the electron exchange between them is allowed, the non-orthogonality condition makes the evaluation of expected values difficult. The tedious derivation was carried out in this work. Configurations other than $\Psi_0^{s,t}$ in Eq. 1 are all possible one-electron transferred (from i→l to o→o′) and excited (from i→j to o′→l) ones which have the forms as the eigenstate of the spin augular momentum $\hat{S}^2$. The minimum total energy of $\langle\Psi^{s,t}|\mathbf{H}|\Psi^{s,t}\rangle/\langle\Psi^{s,t}|\Psi^{s,t}\rangle$ is determined by the secular equation according to the usual CI procedure. In order to get a succinct expression of the interaction energy (ΔW), the secular determinant is expanded perturbationally. We obtain ΔW in the following partitioned form.

$$\Delta W = E_Q + E_K - D - \Pi \qquad (2)$$

E_Q is the classical Coulombic energy and E_K the exchange energy caused by the overlap of the electron cloud between two radicals. These two are the first-order energies in the sense of the Rayleigh-Schrödinger perturbation. On the other hand, fourteen terms of the second-order perturbation form corresponding to the electron configurations (except $\Psi_0^{s,t}$) (Fig. 1) are divided into two groups, D and Π, according to the type of electron jumping. D is the stabilization energy due to the mixing of the one-electron transferred configurations and Π the stabilization energy by the one-electron excited configurations. ΔW is a general index of the reactivity for both singlet and triplet radical-radical interactions. This simplified form of interaction energy which can be grasped intuitively is based on the idea of *isolated molecule approximation.* The mode of molecular interaction is entirely dependent on the electronic structure of two monomers. In order to get a more explicit form of the four terms in Eq. 2, we rewrite them as the sum of various molecular integrals, taking into account the possible permutation of electrons within each Slater determinant. Thus, E_K, D, and Π are generally represented as a power series of the MO overlap (s_{ik}). As long as the interaction is weak enough to be dealt with by perturbation, the MO overlap of the high order caused by the multiple permutation is negligible. The validity of this

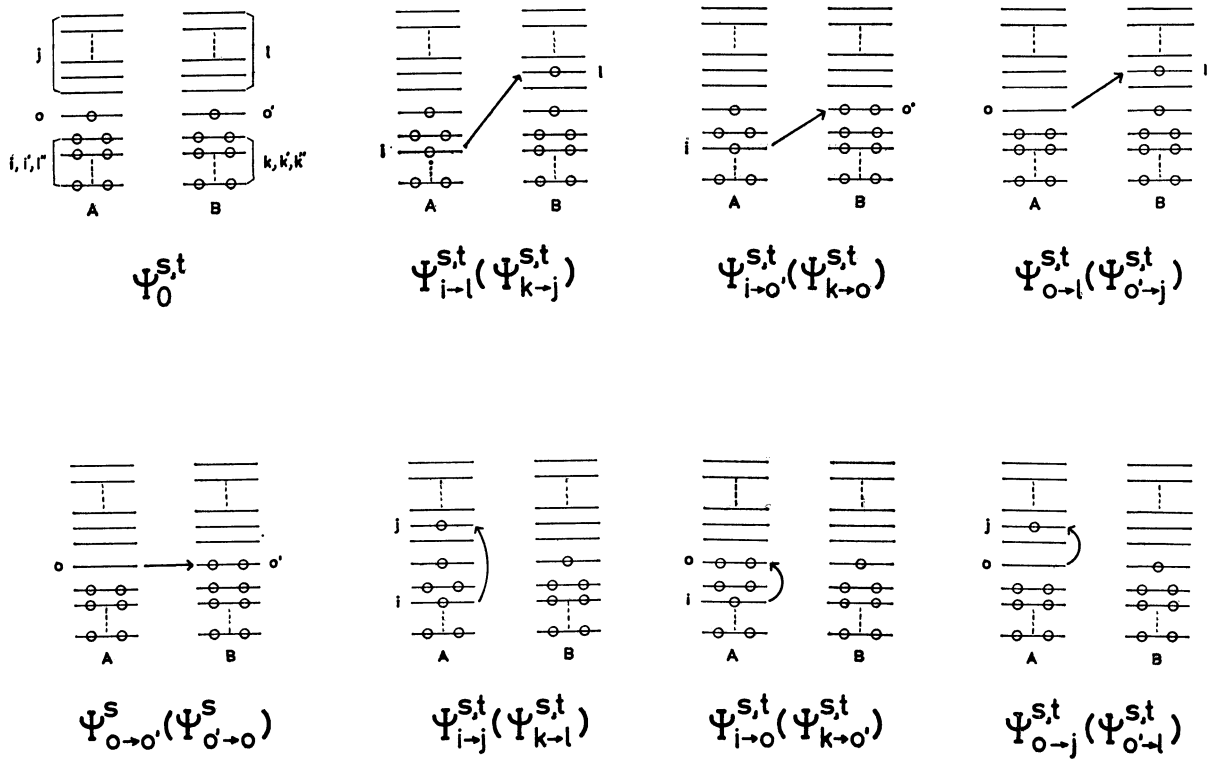

Fig. 1. Electronic configurations adopted for the present CI procedure. The "zero confiuration." $\Psi_0^{s,t}$, retains the original electronic structure at the infinite separation between two radical monomers, A and B.

truncation can be confirmed numerically by calculating some terms of MO overlap.

Coulomb Energy E_Q. This energy depends only on the occupation number of electrons in each MO regardless of the spin multiplicity of the system. The derivation is straightforward.

Exchange Energy E_K. In the present scheme, E_K can be partitioned into four pairs of occupied MO's.

$$E_K = E_K(i', k') + E_K(i', o') + E_K(o, k') + E_K(o, o') \quad (3)$$

Their schematic representation is shown in Fig. 2. $E_K(i',k')$ expresses the interaction between doubly occupied MO's, working repulsively. Both $E_K(i',o')$ and $E_K(o,k')$ are also repulsive energies (>0). Whether $E_K(o,o')$ is repulsive or attractive depends on the spin multiplicity of the system. When the spin coupling between the electrons of MO's, a_o and $b_{o'}$, gives the singlet state, $E_K(o,o')$ represents attraction, when it gives the triplet state, $E_K(o,o')$ represents repulsion.

Charge Transfer Energy D. D consists of eight different terms of the second-order perturbational form corresponding to charge-transferred configurations (Fig. 1). The difference in the normalization factors (*e.g.*, $\langle\Psi_{i\to l}^{s,t}|\Psi_{i\to l}^{s,t}\rangle$ and $\langle\Psi_0^{s,t}|\Psi_0^{s,t}\rangle$) for expected values are explicitly considered. For the sake of convenience, D is represented as the sum of eight components.

$$D = D(i\to l) + D(k\to j) + D(i\to o') + D(k\to o) + D(o\to l) + D(o'\to j) + D(o\to o') + D(o'\to o) \quad (4)$$

In line with the fact that $\Psi_{o\to o'}$ and $\Psi_{o'\to o}$ have only singlet spin state that can not mix with Ψ_0^t, the stabilization energies $D(o\to o')$ and $D(o'\to o)$ are zero for triplet. D is usually positive, acting as the stabilization energy in ΔW of Eq. 2. The denominator of each component of Eq. 4 becomes negative in some cases.[9]

Polarization Energy Π. In Eq. 2, the residual part of the second-order perturbational form, Π, consists of six different terms corresponding to local one-electron excited configurations (Fig. 1). Π can be represented by the sum of six components.

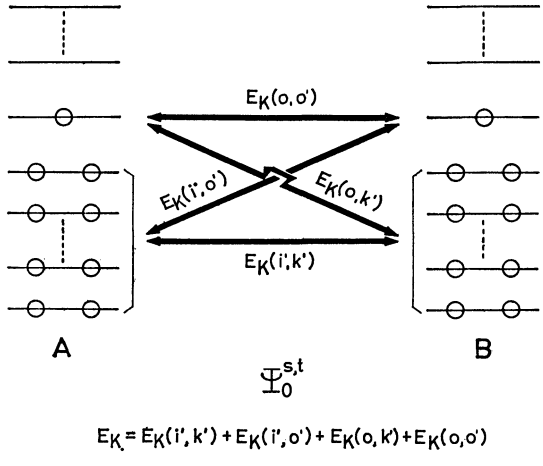

Fig. 2. The schematic representation of four types of exchange interaction. The reason why the doubly occupied MO's, i and k, have the prime in the figure is that exchange energy is caused by the electron permutation for which the prime is imposed on MO's.

$$\Pi = \Pi(\mathrm{i}\to\mathrm{j}) + \Pi(\mathrm{k}\to\mathrm{l}) + \Pi(\mathrm{i}\to\mathrm{o}) + \Pi(\mathrm{k}\to\mathrm{o}') + \Pi(\mathrm{o}\to\mathrm{j}) + \Pi(\mathrm{o}'\to\mathrm{l}) \quad (5)$$

Difference Density. The difference density map of the radical-radical reaction system visualizes the change of the electron density during the course of reaction. Here, the case of singlet interaction is dealt with. The spinless difference density $\Delta\rho(1|1)_{E_K}$ which includes the exchange interaction is derived by the use of Eq. (A.3),[10] and is partitioned into four components according to the decomposition of E_K in Eq. 3.

$$\Delta\rho(1|1)_{E_K} = \Delta\rho(1|1)_{E_K(\mathrm{i}',\mathrm{k}')} + \Delta\rho(1|1)_{E_K(\mathrm{i}',\mathrm{o}')} + \Delta\rho(1|1)_{E_K(\mathrm{o},\mathrm{k}')} + \Delta\rho(1|1)_{E_K(\mathrm{o},\mathrm{o}')} \quad (6)$$

The difference density including the exchange and charge-transfer interactions, $\Delta\rho(1|1)$, is also given as

$$\Delta\rho(1|1) = \mathrm{M}\int \Psi'^{s}(1,2,\cdots,\mathrm{M})\Psi'^{s}(1,2,\cdots,\mathrm{M})\mathrm{d}\xi_1\mathrm{d}\tau_2\cdots\mathrm{d}\tau_{\mathrm{M}} - \rho(1|1)_{\mathrm{A}} - \rho(1|1)_{\mathrm{B}} \quad (7)$$

where $\Psi'^{s}(1,2,\ldots,\mathrm{M})$ is the wavefunction of Eq. 1 without the six polarization-type configurations and M the total number of electrons of the system. $\Delta\rho(1|1)$ can be obtained numerically.[11]

Recombination of Methyl Radicals

As a test of the ΔW method, the recombination between two methyl radicals was examined. In the assumed model of the D_{3d} symmetry (*i.e.*, elongated staggered ethane), two variables (R and θ) are changed to simulate the reaction. R is the C···C distance and θ is the <HCC angle. The C–H bond length (1.079 Å)[12] of the monomer radical is kept constant throughout the calculation. The interaction energy is computed approximately in terms of the semi-empirical all-valence-electron UHF MO including overlap integrals. In a strict sense, the RHF MO which is the doublet spin eigenfunction should be employed as MO's, i, k, j, and so forth (Fig. 1). However, the MO gives unacceptable physical properties such as ionization potential and electron affinity. Since the orbital energy is crucial to evaluate the second-order terms (D and Π), we are obliged to use the UHF MO instead of the RHF MO. The former MO, although somewhat deviated from the spin eigenfunction, can reproduce the property well. The way of estimating semi-empirical parameters to evaluate MO integrals is the same as that used in a previous paper.[7a] Calculated results of the singlet ΔW along the approaching path of two radicals with plausible values of R and θ are given in Fig. 3a and Table 1 and those of the triplet ΔW in Fig. 3b and Table 2. R is restricted to the range 2.85 Å—2.40 Å, since the perturbational expansion of the CI matrix elements was used in this work. The two methyl radicals approach in an eclipsed manner (D_{3h}), the other models having D_{3d} symmetry.

First, the singlet ΔW is examined. E_Q is found to have a positive (repulsive) and small value throughout the adopted models (Table 1). Since the present neutral system consists of only carbon and hydrogen atoms, E_Q is obviously small, the positive value being caused by the C···C electrostatic repulsion, overcoming the C···H attraction.

The singlet E_K in Eq. 2 is also positive. Of its four components the largest (absolute value) at R=

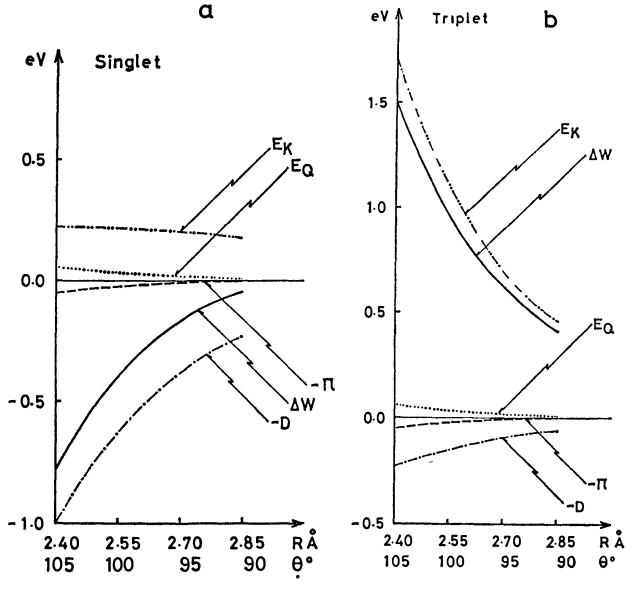

Fig. 3a. The change of the singlet interaction energies along the adopted staggered path with the deformation of the methyl-radical geometry. The deformation of methyl radical is found to smooth the increase of the global E_K as R becomes smaller, and consequently the stabilization of the system becomes large.

3b. The change of the triplet interaction energies along the adopted staggered path with the deformation of the methyl-radical geometry.

Table 1. Caluculated singlet interaction energies for the recombination of two methyl radicals

R/Å	2.85	2.85(E)[b]	2.40	2.40
θ/°	90.00	90.00	105.00	90.00
E_Q[a]/eV	0.0134 (0.0216)	0.0145 (0.0235)	0.0626 (0.0858)	0.0269 (0.0435)
E_K(i′, k′)	0.1678	0.1821	0.3779	0.7401
E_K(i′, o′), E_K(o, k′)	0.0756	0.0757	0.2703	0.3251
E_K(o, o′)	−0.1372	−0.1373	−0.6964	−0.5730
E_K/eV	0.1818	0.1962	0.2221	0.8173
D(i→l), D(k→j)	0.0004	0.0001	0.0113	0.0072
D(o→l), D(o′→j)	0.0008	0.0008	0.0002	0.0099
D(i→o′), D(k→o)	0.0283	0.0283	0.0937	0.1130
D(o→o′), D(o′→o)	0.0842	0.0842	0.3962	0.3170
D/eV	0.2274	0.2268	1.0028	0.8942
Π(i→j), Π(k→l)	0.0002	0.0002	0.0044	0.0012
Π(i→o), Π(k→o′)	0.0019	0.0019	0.0205	0.0269
Π(o→j), Π(o′→l)	0.0000	0.0000	0.0003	0.0006
Π/eV	0.0042	0.0042	0.0504	0.0574
ΔW/eV	−0.0364	−0.0203	−0.7685	−0.1074

a) Values in parentheses evaluated by net charge approximation. b) Eclipsed approach model with R= 2.85 Å.

Table 2. Calculated triplet interaction energies for the recombination of two methyl radicals

R/Å	2.85	2.40
θ/°	90.00	105.00
E_Q/eV	0.0134 (0.0216)	0.0626 (0.0858)
E_K(i′, k′)	0.1696	0.3994
E_K(i′, o′), E_K(o, k′)	0.0764	0.2857
E_K(o, o′)	0.1386	0.7361
E_K/eV	0.4610	1.7069
D(i→l), D(k→j)	0.0004	0.0123
D(o→l), D(o′→j)	0.0008	0.0002
D(i→o′), D(k→o)	0.0288	0.1017
D(o→o′), D(o′→o)	0	0
D/eV	0.0600	0.2284
Π(i→j), Π(k→l)	0.0002	0.0044
Π(i→o), Π(k→o′)	0.0019	0.0223
Π(o→j), Π(o′→l)	0.0000	0.0000
Π/eV	0.0042	0.0534
ΔW/eV	0.4102	1.4877

2.85 Å is E_K(i′,k′), while that at R=2.40 Å is E_K(o,o′). This shows that a_o-b_o' MO interaction grows discriminatively along the progress of the reaction. Such remarkable growth of a particular MO interaction plays a key role to determine the reaction path. Thus, the repulsive character of the exchange energy which is unfavorable to the enhancement of the reaction is considerably weakened by E_K(o,o′).

D is found to give the largest attractive energy throughout the adopted staggered models, the increase of the energy along the C···C approach being drastically large. It is noteworthy that D(i→l) [or D(k→j)] has a small value in spite of many (a_i,b_l) pairs. This is because both a_1 and b_1 do not have their spatial extension toward the intermolecular C···C region, the MO overlap between them thus being small. The strength of the MO overlap is a crucial criterion to determine the extent of the (a_i→b_l) charge transfer (CT) interaction. Since the "symmetry-forbidden" CT interaction (*e.g.*, from the a_1-symmetry MO of one radical to the e-symmetry MO of the other) has no contribution to D, the non-zero components of D(i→l) are actually limited to three. D(o→l) and D(o′→j) have also small values for the following reason. The singly occupied (SO) MO's, a_o and b_o', which are of $a_1(\sigma)$-symmetry, can overlap only one unoccupied a_1 MO with its spatial extension localized on three hydrogens. However, owing to the largest separation between the density of a_o (or b_o') and that of the one σ type a_1 MO, no effective CT interaction occurs. As for D(i→o′) [or D(k→o)] there is only one occupied $a_1(\sigma)$ MO with its substantial localization on the carbon 2s atomic orbital,[13] which is able to mix with the a_1 type MO, a_o or b_o'. Contrary to the case of D(i→l), the combination of a_1 and b_o' gives an appreciable MO overlap, s_{io}', resulting in the large value of D(i→o′) (Fig. 4a). The largest two equivalent CT terms, D(o→o′) and D(o′→o),

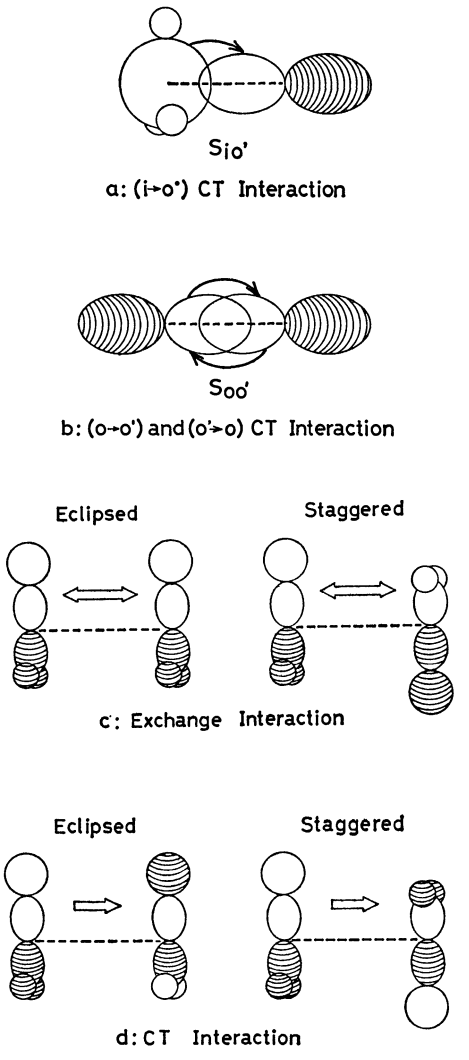

Fig. 4. Schematic representation of the mode of dominant MO interactions.

have their common origin from the huge MO overlap, s_{oo}', shown in Fig. 4b. In view of this, the MO overlap, s_{oo}', is a crucial factor to give the large stabilization energies, D(o→o′) and D(o′→o) as well as E_K(o,o′) in the case of singlet interaction. Thus, the important role of the particular MO interaction to control the reaction is demonstrated.

The polarization energy Π (Table 1) has the smallest absolute value among the four terms of ΔW regardless of the C···C distance R, reflecting the "neutral" character of the system without heteroatoms.

Summing up E_Q, E_K, D, and Π according to Eq. 2, we obtain the total singlet energy, ΔW (Table 1). Its value indicates that the electronic interaction energy gives considerable stabilization energy at the perturbational region between two radicals. Comparing the two ΔW's (θ=90° and 105°) at R=2.40 Å, we see a remarkable difference in E_K. Thus, the geometrical deformation of methyl radical (planar→pyramidal) in the course of the reaction brings about the decrease in the exchange repulsion resulting in the decrease of ΔW and ease in recombination. Terms other than E_K are not influenced so much by the θ variation. Of the four terms of E_K, E_K(i′,k′) of θ=90° differs a

great deal from that of $\theta=105°$ at $R=2.40$ Å. Thus, for the progress of the reaction it is very important to avoid the exchange repulsion of doubly occupied MO's by deformation. The enlargement of lobes of SOMO's (a_o and $b_{o'}$) which makes $E_K(o,o')$, $D(o\rightarrow o')$ and $D(o'\rightarrow o)$ more attractive terms is found to be a secondary factor for this acceleration. Even if the geometrical deformation is accompanied by the destabilization of the monomer total energy in its isolated state, it is covered entirely by the electronic stabilization energy.[14]

A comparison of the interaction energy between the D_{3d} staggered and the D_{3h} eclipsed models is made at $R=2.85$ Å. As expected, the staggered path gets more stabilization energy ($\Delta W=-0.0364$ eV) than the eclipsed path ($\Delta W=-0.0203$ eV). What is the origin of this rotational barrier in the course of the reaction? Comparing all the components of ΔW, we find that the sole component, E (i',k'), gives the energy difference. This is because the σ type MO overlap such as $s_{oo'}$ is insensitive to the rotation of the π type electronic cloud around the C···C σ axis. Only the π-π' type exchange interaction which is included in E_K(i',k') depends on the rotation angle. The mode of the MO overlap, the origin of E_K(i',k'),[15] for the two approaching models is shown in Fig. 4c. It is evident that the eclipsed approach gets the larger MO overlap than the staggered one. On the other hand, CT interaction does not give a large energy difference between the two approaches (Fig. 4d). The negligible difference in CT interaction arises from the nodal property of the π type unoccupied MO. Sovers and his coworkers made an extensive study on the internal rotation barrier of ethane by use of the bond-orbital wavefunction and concluded that the main source of the barrier is the overlap repulsion between localized C–H bond orbitals with the closed shell.[16] Although ethane itself is not dealt with in this work, the present result seems to help to elucidate the origin of the rotational barrier.

The sharp increase of ΔW is due mostly to E_K (Fig. 3b). This indicates that the triplet interaction makes the recombination (D_{3d}) path unfavorable. The triplet E_K (Table 2) differs considerably from the singlet E_K (Table 1). The greater destabilization due to the triplet E_K is ascribed to the change of the sign attached to $E_K(o,o')$. The minor difference of E_K(i',k'), E_K(i',o') and E_K(o,k') between singlet and triplet is due to that of the normalization factor of Ψ_0. Contrary to the case of singlet, the triplet a_o-$b_{o'}$ MO interaction contributes to the exchange energy as repulsive. The triplet D is much smaller than the singlet D, which is mostly due to the absence of both $\Psi^{s}_{o\rightarrow o'}$ and $\Psi^{s}_{o'\rightarrow o}$ configurations in Eq. 1. However, the triplet Π is almost the same as the singlet Π. The global term, ΔW, of triplet is positively large. This reflects the fact that two electrons with parallel spins can not occupy the same space (along the C···C axis) according to the Pauli exclusion principle.

The density distribution is analyzed in terms of the various difference densities given by Eqs. 6 and 7. Of the four terms of Eq. 6, $\Delta\rho(1|1)_{E_K(i',k')}$ of the singlet radical-radical interaction is shown in Fig. 5a. This is regarded as the electron rearrangement through the mutual overlap between both doubly occupied MO's, i' and k'. We see a large amount of decreased density in the C···C region. This quantity corresponding to the positive E_K(i',k') usually appears when the exchange interaction is taken up in the system of closed-shell molecules. Instead, the electron density, shifting from the central C···C region, is piled up around respective carbon and hydrogen atoms. In the case of $\Delta\rho(1|1)_{E_K(i',o')}$ (Fig. 5b), E_K(i',o') is the repulsive energy (Table 1). The repulsive character is reflected in the large area of the negative density along the C···C line (Fig. 5b). However, the center of the negative part is located almost at the left end of the C···C region. The shift of the region of the intermolecular decreased density is due to the fact that the differential MO overlap, i'(1)o'(1), which is the main origin of the $\Delta\rho(1|1)_{E_K(i',o')}$ has a maximum in the region. The trend always appears in the overlap between the s type and p type orbitals.[17] The counterpart of the decreased density is accumulated at each carbon site, which is similar to the case of $\Delta\rho(1|1)_{E_K(i',k')}$. As regards $\Delta\rho(1|1)_{E_K(o,o')}$ (Fig. 5c), since $E_K(o,o')$ is a considerable stabilization energy, $\Delta\rho(1|1)_{E_K(o,o')}$ is expected to give the large bonding density at the central C···C region, competing with the decrease by $\Delta\rho(1|1)_{E_K(i,'k')}$, $\Delta\rho(1|1)_{E_K(i',o')}$ and $\Delta\rho(1|1)_{E_K(o,k')}$. An egg-shaped increased density is observed in the middle of the C···C line. This also demonstrates the important role of the a_o-$b_{o'}$ MO interaction on bond formation. The decreased quantity opposing the drastic bonding density is found just around each carbon atom. Thus, the change in density distribution is interpreted as follows. The MO overlap, $s_{oo'}$, absorbs the electron density from the MO's a_o and $b_{o'}$.

Of the four components of $\Delta\rho(1|1)_{E_K}$ the origin of the geometrical deformation. ($D_{3h}\rightarrow C_{3v}$) of methyl radical is brought about by $\Delta\rho(1|1)_{E_K(i',k')}$ (Fig. 5-a).[18] The other three difference densities exhibit a nearly equivalent electron redistribution around both hydrogen and carbon atoms or represent only the motion of translation of the C–H bond. However, $\Delta\rho(1|1)_{E(i',k')}$ has a positive contour line just around the front side of the pyramidal methyl carbon which pulls the carbon atom so as to decrease the C···C distance,[19] whereas the hydrogen atom does not move toward any direction. The discussion based on the "force" criterion[20] is in line with the result of interaction energy. E_K(i',k') affects mostly nuclear deformation of the methyl radical among the four energy terms of E_K.

The change of the electron distribution due to the exchange and CT interactions in Eq. 7 is shown in Fig. 5d. No polarization interaction is taken into account in the present analysis, since the reacting system is neutral and the interaction is not so important. A huge accumulation of the intermolecular bonding density in the central C···C region is noteworthy. As compared with that of $E_K(o,o')$, the global bonding density in the C···C region is much more increased. This indicates the significant role of the $a_o\rightarrow b_{o'}$ and

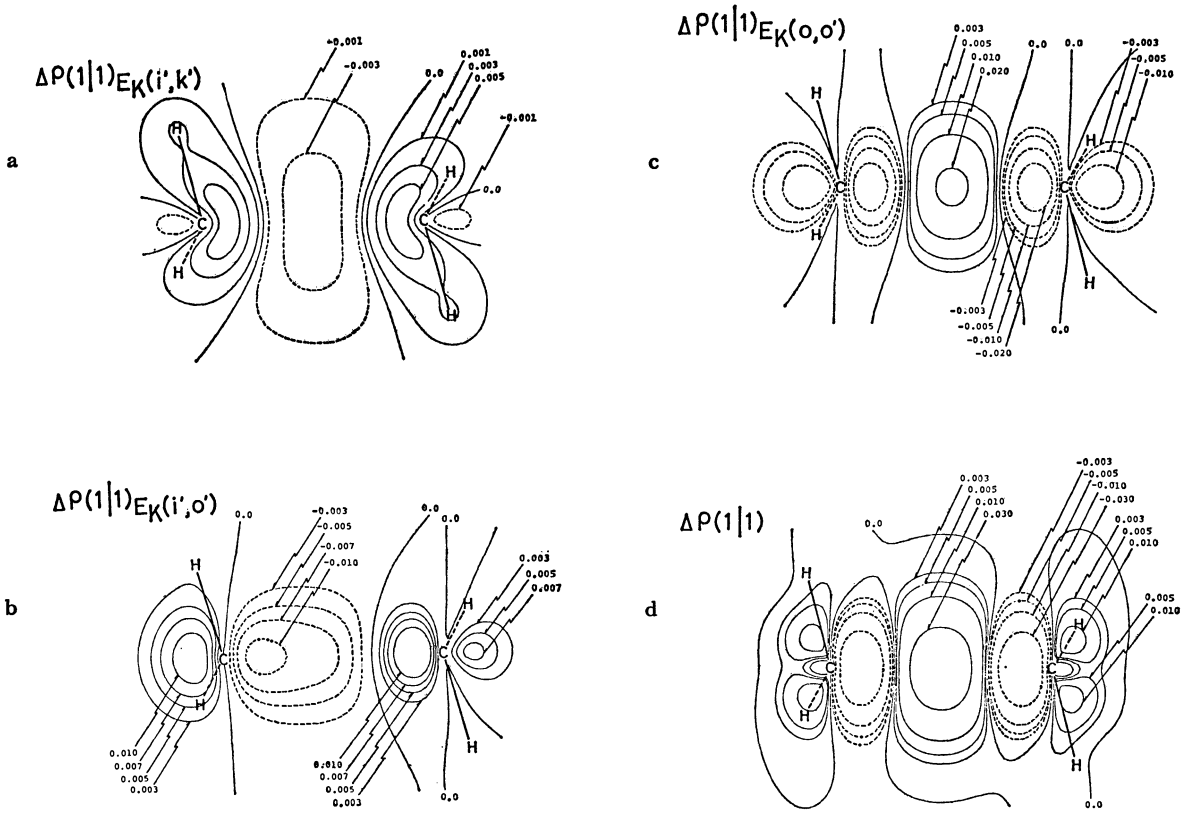

Fig. 5a. The difference density map of $\Delta\rho(1|1)_{E_K(i',k')}$ for the singlet interaction. The value attached to each contour line is in $e/Å^3$.

5b. The difference density map of $\Delta\rho(1|1)_{E_K(i',o')}$ for the singlet interaction. The map of $\Delta\rho(1|1)_{E_K(o,k')}$ is obtained through the 180° rotation of this figure around the center of C···C line in the cut plane.

5c. The difference density map of $\Delta\rho(1|1)_{E_K(o,o')}$ for the singlet interaction.

5d. The difference density map due to the singlet exchange and charge transfer interactions in Eq. 7.

its reverse $b_o' \rightarrow a_o$ CT interactions to pile up the density. The decreased density which sandwiches the central increased density arises, to a great extent, from the exchange interaction, $\Delta\rho(1|1)_{E_K(o,o')}$.

Conclusion

In the present work, a means to investigate the mode of interaction between two radicals has been proposed. The interaction energy, ΔW, has been partitioned into four terms, E_Q, E_K, D, and Π.

As a result of analysis of its four components for the $CH_3 \cdots CH_3$ reaction, the ease of the recombination in this neutral system is attributed to the SOMO–SOMO interaction. If the deformation ($D_{3h} \rightarrow C_{3v}$) is added to each methyl radical, the singlet W gains a greater stabilization. The deformation enlarges the a_o-b_o' MO interaction and reduces the exchange repulsion between both doubly occupied MO's. The latter effect in particular is remarkable. The rotational barrier between staggered and eclipsed approaches was examined and found to be almost due to the exchange interaction of both doubly occupied MO's.

A density map of the same system has been constructed, in order to examine the role of the four components of E_K. Accumulation of the bonding density in the $\Delta\rho(1|1)_{E_K(o,o')}$ is remarkable, contributing to the new C–C bond formation.

Since the present study is made within the scope of perturbation procedure with the use of semi-empirical MO, each term calculated so far should be regarded as qualitative. The ΔW method employed simplifies the reaction as a static model, the energy obtained thus having hardly anything to do with measurable property. In spite of these handicaps, the present method seems to give an idea of how to interpret and understand the radical-radical reaction in terms of the partitioned energies. Applicability of the orbital picture to this reaction could be successfully demonstrated. We may take up two important types of interaction contributing to the progress of recombination, $E_K(i',k')$ which has a role to deform the monomer radical, and the a_o-b_o' MO overlap [$E_K(o,o')$, $D(o \rightarrow o')$, and $D(o' \rightarrow o)$] which operates to make the new C···C bond.

Permission to use the FACOM 230-75 computer at the Data Processing Center of Kyoto University is gratefully acknowledged. The MO calculations were carried out with Grant-in-Aid No. 139012 from the Ministry of Education.

References

1) A. Dedieu and A. Veillard, *J. Am. Chem. Soc.*, **94**, 6730 (1972).

2) M. J. S. Dewar and E. Haselbach, *J. Am. Chem. Soc.*, **92**, 590 (1970).
3) A. C. Wahl and G. Das, *Adv. Quantum Chem.*, **5**, 261 (1970).
4) C. F. Bender and E. R. Davidson, *J. Phys. Chem.*, **70**, 2675 (1966).
5) For instance, S. W. Benson and W. DeMore, *Ann. Rev. Phys. Chem.*, **16**, 397 (1965).
6) K. Fukui and H. Fujimoto, *Bull. Chem. Soc. Jpn.*, **41**, 1989 (1968).
7) a) K. Fukui, H. Fujimoto, and S. Yamabe, *J. Phys. Chem.*, **76**, 232 (1972); b) H. Fujimoto, S. Yamabe, T. Minato, and K. Fukui, *J. Am. Chem. Soc.*, **94**, 9205 (1975).
8) The notation for the MO, "i", is used interchangeably with a_i.
9) Attention should be paid to the level of the unoccupied MO's which are unreliable as a virtual solution of the Hartree-Fock equation. The orbital energy of the unoccupied MO's sometimes gives a physically meaningless result. Even the combination of very inactive donor and acceptor monomers can give a negative D when the energy of the unoccupied MO's is deliberately changed.
10) H. Fujimoto, S. Yamabe, and K. Fukui, *Bull. Chem. Soc. Jpn.*, **44**, 2936 (1971).
11) H. Fujimoto and N. Kosugi, *Bull. Chem. Soc. Jpn.*, **50**, 2209 (1977).
12) G. Herzberg, "Molecular Spectra and Molecular Structure," D. Van Nostrand Co., Inc., New York (1966).
13) The present calculation was carried out with use of the semi-empirical MO. Thus, the lowest occupied MO with localization on the carbon 1 s atomic orbital does not appear.
14) Many rigorous *ab initio* calculations have been carried out for the planarity of a methyl radical. Chang *et al.* showed that the destabilization energy due to the out-of-plane bending by 15 degree is *ca.* 2 kcal/mol. S. Y. Chang, E. R. Davidson, and G. Vincow, *J. Chem. Phys.*, **52**, 5596 (1970).
15) H. Fujimoto, S. Yamabe, and K. Fukui, *Bull. Chem. Soc. Jpn.*, **45**, 1566 (1972).
16) O. J. Sovers, C. W. Kern, R. M. Pitzer, and M. Karplus, *J. Chem. Phys.*, **49**, 2592 (1968). See also J. P. Lowe, *J. Am. Chem. Soc.*, **92**, 3799 (1970).
17) S. Yamabe and K. Morokuma, *J. Am. Chem. Soc.*, **97**, 4458 (1975).
18) H. Umeyama and K. Morokuma, *J. Am. Chem. Soc.*, **98**, 7208 (1976).
19) $\Delta\rho(1|1)_{E_K(i',k')}$ has a density of $i'(1)o(1)s_{i'k'}s_{ok'}$ type which is a coupling term between (i',k') and (o,k') exchange interactions.
20) H. Nakatsuji, T. Kuwata, and A. Yoshida, *J. Am. Chem. Soc.*, **95**, 6894 (1973); H. Fujimoto and T. Sugiyama, *ibid.*, **99**, 15 (1977).

Temperature Dependence of Reorientational and Vibrational Relaxation Times of Benzene and Benzene-d_6 in Solid and Liquid Phases

Hiroyasu NOMURA,* Shinobu KODA,** and Yutaka MIYAHARA

Department of Chemical Engineering, Faculty of Engineering, Nagoya University, Chikusa-ku, Nagoya 464

***Department of Synthetic Chemistry, Faculty of Engineering, Nagoya University, Chikusa-ku, Nagoya 464*

(Received December 26, 1978)

The temperature dependences of reorientational and vibrational relaxation times of benzene and benzene-d_6 in the solid and liquid phases were measured by means of Raman line shape analysis. The temperature dependence of the reorientational relaxation times was in very good agreement with that published previously. The vibrational relaxation times of benzene changed drastically at the solid to liquid phase transition point both in C_6H_6 and C_6D_6. We consider that this effect is due to the non-radiative energy transfer and the pure dephasing process by molecular collisions in the liquid state.

Some time ago, the ultrasonic technique was the only method available to measure the vibrational relaxation times of molecules in the liquid state.[1] However, more recently some other methods have been used to study the molecular orientational and vibrational relaxation processes in the liquid phase. In particular, it is known that one may analyse separately the effects of reorientational and vibrational motions from the profiles of the isotropic and anisotropic Raman scattering. Also, spectroscopic techniques using high powered pulsed laser have been applied to the investigation of vibrational relaxation in liquids.[2-5]

Recently, Griffiths, Clerc, and Rentzepis applied the Raman and picosecond pulsed spectroscopic methods to study the intermolecular vibrational energy transfer between C_6H_6 and C_6D_6.[6]

Several mechanisms may contribute to the shape of the vibrational correlation function, but the two most common interpretations are energy relaxation to lower vibrational levels (the lowest of which is the ground vibrational state) through a collisional non-radiative mechanism, and phase relaxation, which also involves a collision induced process. Both mechanisms are subject to molecular collisions in the liquid phase.

An intuitive argument suggests that the molecules in the solid phase freeze out orientational motions and collisions, which are effective for the exchange of the energy. Therefore the vibrational relaxation time in the solid state is expected to be much longer than in the liquid state. A discontinuity in the vibrational relaxation times is expected at the solid-liquid phase change.

In this work, we report the experimental results of the temperature dependence of the reorientational and vibrational relaxation times of C_6H_6 and C_6D_6 in solid and liquid phases and discuss the process of the vibrational energy transfer of C_6H_6 and C_6D_6 in the liquid phase.

Experimental Details and Data Analysis

The apparatus used consisted of an argon ion laser (800 mW at 488 nm) produced by the Coherent Radiation Co., Ltd., and a Laser Raman Spectrometer of JRS-U1 type JEOL, Ltd., Japan.

In order to obtain the reorientational and vibrational relaxation times, the Raman line shapes of the $\nu_2(a_{1g})$ and $\nu_1(a_{1g})$ fundamental modes of ring and C–H or C–D stretching were analyzed. The Raman spectrum was observed at 90° with respect to the linearly polarized incident light. With $I_{\parallel}(\omega)$ and $I_{\perp}(\omega)$ respecting the strong and weak components of the scattered light, one can write:

$$I_{\parallel}(\omega) = I_{\mathrm{isot}}(\omega) + 4/3\, I_{\mathrm{anis}}(\omega) \quad (1)$$

$$I_{\perp}(\omega) = I_{\mathrm{anis}}(\omega) \quad (2)$$

$$\rho_s = I_{\perp}(\omega)/I_{\parallel}(\omega) \quad (3)$$

where ρ_s is the depolarization ratio. $I_{\mathrm{isot}}(\omega)$ represents the intrinsic vibrational line shape, and $I_{\mathrm{anis}}(\omega)$ is a convolution of the vibrational line shape and the orientational spectrum.

The Raman lines of C_6H_6 and C_6D_6 were measured using a constant mechanical slit width, 30 μm. The Raman bands obtained are broadened by the slit and the spectrum measured is a convolution of the true Lorentzian spectrum and the slit function, $S(\omega)$. As the spectral slit function is well approximated by a Gaussian function,[7] one can write

$$I(\nu) = N\int_{-\infty}^{\infty} \frac{1}{\beta_L^2 + (\nu-\nu')^2} \exp\left\{-\left(\frac{\nu'}{\beta_g}\right)^2\right\} d\nu' \quad (4)$$

where β_L is the true half-width and $\beta_g = S/2\sqrt{\ln 2}$,[8] where S is the spectral slit width; $S = 0.741\ \mathrm{cm^{-1}}$ at 30 μm. By curve fitting of Eq. 4 to the measured spectrum, we determined the true half-width β_L of each measured Raman line. $\omega_{\mathrm{isot}}(1/2)$ and $\omega_{\mathrm{anis}}(1/2)$, hereafter, refer to the true half-width, β_L, of the isotropic and anisotropic Raman line, respectively. From $I_{\parallel}(\omega)$ of the $\nu_2(a_{1g})$ band of C_6D_6 in the liquid phase, the $\omega_{\mathrm{isot}}(1/2)$ obtained was $0.73\ \mathrm{cm^{-1}}$, corresponding to a vibrational relaxation time of 7.42×10^{-12} s. This value is in excellent agreement with that obtained by Griffiths *et al.* from direct measurements using picosecond spectroscopy and the Raman line width.

Temperatures were in the range from −50 to 60 °C. A variable temperature Raman cell of the Harney-Miller type was used.

Results

The temperature dependence of $\omega_{\mathrm{isot}}(1/2)$ and $\omega_{\mathrm{anis}}(1/2)$ of ν_1 and ν_2 bands of C_6H_6 are shown in Fig. 1 and those of ν_1 and ν_2 bands of C_6D_6 are shown in Fig. 2, together with the values obtained by Griffiths *et al.*[9] In Figs. 1 and 2, in the solid phase, $\omega_{\mathrm{anis}}(1/2)$ apparently equals $\omega_{\mathrm{isot}}(1/2)$ for C_6H_6 and C_6D_6 at each Raman line but, as pointed out by many workers,[10,11] we can not directly reduce the above relation in the crystalline state from this experimental

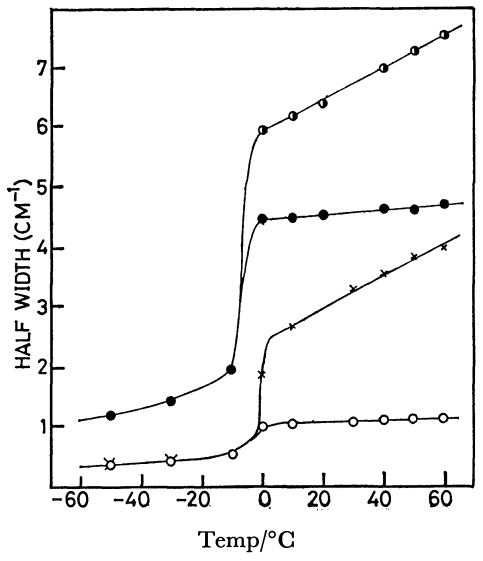

Fig. 1. Temperature dependences of half-width of ν_1 and ν_2 bands of C_6H_6. ●; $\omega_{isot}(1/2)$ of ν_1 band, ◑; $\omega_{anis}(1/2)$ of ν_1 band, ○; $\omega_{isot}(1/2)$ of ν_2 band, ×; $\omega_{anis}(1/2)$ of ν_2 band.

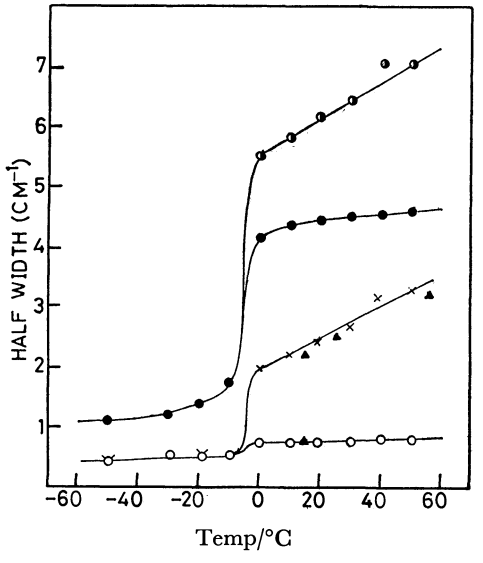

Fig. 2. Temperature dependences of half-width of ν_1 and ν_2 bands of C_6D_6. ▲; $\omega_{anis}(1/2)$ of ν_2 band (Griffiths *et al.*) and the other symbols are the same as those in Fig. 1.

data. However, as the Raman intensities of the isotropic light were very much stronger than those of the anisotropic light, the values of $\omega_{isot}(1/2)$ in the solid state may be considered significant.

As is seen in Figs. 1 and 2, the values of $\omega_{isot}(1/2)$ are dependent on the vibrational modes and increase slightly with increasing temperature in the solid and liquid phases.

From these results, we can obtain the vibrational and reorientational relaxation times from the following equations:

$$\tau_v = (2\pi c\omega_{isot}(1/2))^{-1} \quad (5)$$

$$\tau_{or} = (2\pi c\omega_{or}(1/2))^{-1} \quad (6)$$

where $\omega_{or}(1/2)=\omega_{anis}(1/2)-\omega_{isot}(1/2)$.

Discussion

Reorientational Relaxation Times of C_6H_6 and C_6D_6. The relationship between ln τ_{or} and $10^3/T$ is shown in Fig. 3. As is seen in Fig. 3, the reorientational relaxation times of C_6H_6 and C_6D_6 obtained from the ν_2 bands are in good agreement with those obtained from their ν_1 bands. The isotope effect, $\tau_{or}(C_6D_6)/\tau_{or}(C_6H_6)=1.102$, is in good agreement with the value calculated for the small step Brownian diffusion (1.10).

The relationship between ln τ_{or} and T can be expressed by

$$\ln \tau_{or} = A + \Delta U/RT \quad (7)$$

The values of ΔU are 2.83 and 2.76$_4$ kcal/mol for C_6H_6 and C_6D_6, respectively. These values are in very good agreement with those published previously.[9]

Vibrational Relaxation Times of ν_1 and ν_2 Modes. As is seen in Figs. 1 and 2, the half-widths of ν_2 fundamentals in C_6H_6 and C_6D_6 are 1.09 and 0.72 cm^{-1} at 30 °C and slightly depend on the temperature.

Griffiths *et al.* explained this difference as follows.[6] During collisions, the vibrational energy from one molecule is more readily transferred to a lower neighboring energy level in a second molecule if the vibrational energy levels are close together. In C_6H_6, there are two vibrational levels, ν_7 at 985 (b_{2g}) and ν_{19} at 970 (e_{2u}) cm^{-1}. During collisions, the near resonance energy condition would favor the non-radiative transition. On the contrary, the closest level in C_6D_6 is the $\nu_{17}(e_{2g})$ fundamental at 867 cm^{-1}. The energy difference between the $\nu_2(a_{1g})$ and the $\nu_{17}(e_{2g})$ fundamental modes is $\Delta E=78$ cm^{-1} in C_6D_6. This value is much larger than the energy differences $\Delta E=6$ cm^{-1} between the $\nu_2(a_{1g})$ and the $\nu_7(b_{2g})$, and $\Delta E=21$ cm^{-1} between the $\nu_2(a_{1g})$ and the $\nu_{19}(e_{2u})$. Therefore, in C_6D_6 a non-radiative transition such as is observed in C_6H_6 should not contribute significantly to a change in life time of the ν_2 state of C_6D_6. Although there is one more level, $\nu_6(b_{1u})$, at 963 cm^{-1} near the ν_2 fundamental, this excitation energy level is higher

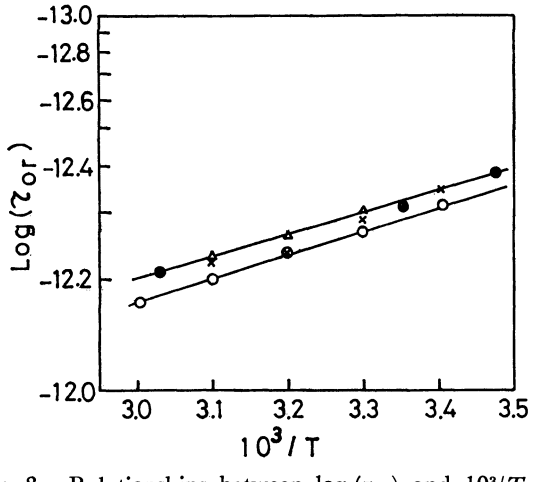

Fig. 3. Relationships between log (τ_{or}) and $10^3/T$. ○; C_6H_6, obtained from ν_2 band, ●; C_6D_6, obtained from ν_2 band, △; C_6D_6, Griffiths *et al.*, ×; C_6D_6, obtained from ν_1 band.

than ν_2 at 945 cm^{-1}; so this level may not contribute significantly to the relaxation mechanism of the ν_2 mode of C_6D_6.

At the transition point, the values of $\omega_{isot}(1/2)$ for C_6D_6 changed from 0.52 in solid state to 0.72 cm^{-1} in liquid state. This broadening can only be interpreted by considering some other mechanisms besides those proposed by Griffiths *et al.*

Similarly, as is seen in Figs. 1 and 2, the half-widths of the ν_1 fundamental mode are broader than those of the ν_2 mode in liquid phase. The differences in $\omega_{isot}(1/2)$ of ν_1 solid and liquid phases are about 2.8 cm^{-1}, which is about 6 and 10 times those of the ν_2 band of C_6H_6 and C_6D_6, respectively.

As mentioned above, there is one more dominant mechanism which contributes to the vibrational relaxation, that is, the phase relaxation or so-called "pure dephasing process,"

Fischer and Laubereau[12] have presented the following expression for the vibrational dephasing relaxation time:

$$\tau_{ph} = \frac{2}{9}\frac{M^2\omega^2L^2}{\mu\gamma^4k_BT}\tau_c \tag{8}$$

where M is the reduced mass of the oscillator with frequency ω, and L measures the range of interactions between colliding molecules. The μ and γ are parameters defined by them.[12]

As a first approximation, the energy dissipation and pure dephasing which are caused by the molecular collisions in liquid phase are considered to be an independent process. The vibrational relaxation time of this mechanism, τ_v', can be written as follows:

$$1/\tau_v' = 1/\tau_{ph} + 1/\tau_e \tag{9}$$

in a practical case, $(1/\tau_v')$ can be estimated from the difference of $\omega_{isot}(1/2)$ between the solid and the liquid phase. In ultrasonic studies of liquid C_6H_6 and C_6D_6, the relaxation process was found to have the frequency of about 2 GHz.[13,14] This relaxation has been considered to be due to the vibrational process. The total relaxation strength of the ultrasonic relaxation was found to be in very good agreement with those calculated from the Einstein equation, assuming the relaxation to be that of vibrational specific heats. From these ultrasonic data and a liquid model, τ_e in Eq. 8 can be estimated as about 0.79×10^{-13} s.[1]

Recently, Tanabe and Jonas have reported that the line broadening effects of Raman lines can be interpreted by the pure dephasing model as caused by the molecular collisions in the liquid phase, using Eq. 8.[15,16] The values obtained are summarized in Table 1. The vibrational relaxation mechanism of ν_2 band in the liquid C_6H_6 involves the non-radiative transition mentioned above. So, as is seen in Table 1, the difference of the $\omega_{isot}(1/2)$ of ν_2 band between in C_6H_6 and C_6D_6, about 0.3 cm^{-1}, can be considered to be due to the non-radiative transition mechanism proposed by Griffiths *et al.* In the case of ν_1 band, the value of δ_v' of C_6H_6 is comparable to that of C_6D_6.

As indicated in Table 1, the values of δ_v' obtained in this experiment are quite different from those of δ_{ph} estimated from Eq. 8. In the dephasing mechanism explained by Eq. 8, a binary collision is assumed and only the repulsive part of the intermolecular potential is considered. Intrinsically, the above dephasing mechanism should be applied to the diatomic molecule. In a polyatomic molecule such as benzene, the interactions between intramolecular modes should be involved. Recently, the vibrational dephasing of polyatomic molecules was treated by the intermolecular vibrational energy exchange model.[17] In the exchange model, the dephasing arises from random modulation of the vibrational frequency caused by intramolecular anharmonic coupling to low frequency modes which are undergoing intermolecular energy exchange with the bath. Therefore, the δ_v' obtained in this experiment could not be explained by the dephasing mechanism expressed by Eq. 8.

Table 1. Estimated vibrational widths (cm^{-1})

Mode	Assignment	C_6H_6		C_6D_6	
		δ_v'	δ_{ph}	δ_v'	δ_{ph}
$\nu_1(a_{1g})$	C-H or C-D stretching	2.8	6.3_5[a]	2.8	3.5_5[a]
$\nu_2(a_{1g})$	C-C stretching	0.5	0.4_0[a]	0.2	0.4_5[a]

a) The dephasing widths calculated by Tanabe and Jonas.[15]

$\delta_v' = (2\pi c\tau_v')^{-1}$ and $\delta_{ph} = (2\pi c\tau_{ph})^{-1}$.

In the C–H or C–D stretching vibration region, there are a few Raman forbidden bands; for example, the 2264 and 2294 cm^{-1} bands which lie close to ν_1 band of C_6D_6. At this stage, it is impossible to rule out the energy transfer mechanism due to the non-radiative transition as in the case of ν_2 band of C_6H_6.

As indicated above, the vibrational relaxation mechanism of benzene is very complicated. Further theoretical and experimental investigations are needed and continuing.

The authors are grateful to Prof. D. Nakamura of Nagoya University for many stimulating discussions. This work was financially supported by a Grant-in-Aid for Scientific Research from the Ministry of Education.

References

1) K. F. Herzfeld and T. A. Litovitz, "Absorption and Dispersion of Ultrasonic Waves," Academic Press, New York (1950).

2) A. Laubereau, D. von der Linde, and W. Kaiser, *Phys. Rev. Lett.*, **28**, 1162 (1972).

3) R. R. Alfano and S. L. Shapiro, *Phys. Rev. Lett.*, **29**, 1655 (1972).

4) A. Laubereau, L. Kirshner, and W. Kaiser, *Opt. Commun.*, **9**, 128 (1973).

5) P. R. Monson, S. Patumtevatibal, K. J. Kaufmann, and G. W. Robinson, *Chem. Phys. Lett.*, **28**, 312 (1974).

6) J. E. Griffiths, M. Clerc, and P. M. Rentzepis, *J. Chem. Phys.*, **60**, 3824 (1974).

7) R. E. Meredith. *J. Quant. Spectros. Radiant. Transfer*, **12**, 455 (1972).

8) J. S. Seshadri and R. Norman Jones, *Spectrochim. Acta*, **19**, 1013 (1963).

9) K. T. Gillen and J. E. Griffiths, *Chem. Phys. Lett.*, **17**, 359 (1972).

10) B. J. Bulkin, *J. Opt. Soc. Am.*, **59**, 1387 (1969).
11) D. W. Johnson and D. Sutton, *Can. J. Chem.*, **49**, 671 (1971).
12) S. F. Fischer and A. Laubereau, *Chem. Phys. Lett.*, **35**, 6, (1975).
13) K. Takagi, P-K Choi, and K. Negishi, *Acoustica*, **34**, 336 (1976).
14) K. G. Plass, *Acoustica*, **19**, 236, (1967/68).
15) K. Tanabe and J. Jonas, *J. Chem. Phys.*, **67**, 4222 (1977).
16) K. Tanabe and J. Jonas, *Chem. Phys. Lett.*, **53**, 278 (1978).
17) R. M. Shelby, C. B. Harris, and P. A. Cornelius, *J. Chem. Phys.*, **70**, 34 (1979).

Resistmetric Study of the Potential-sensitive Surface Layer Formed on VO_2 Electrode in a Neutral Solution

Toyohisa NAKAMURA* and Shiro HARUYAMA**

Technical High School, Faculty of Engineering, Tokyo Institute of Technology, 3-3-6, Shibaura, Minato-ku, Tokyo 108

***Faculty of Engineering, Tokyo Institute of Technology, 2-12-1, Ookayama, Meguro-ku, Tokyo 152*

(Received December 27, 1978)

The formation of a potential-dependent surface layer on VO_2 electrode has been investigated from the change in conductance of a thin VO_2 film electrode by galvanostatic polarization. The VO_2 electrode dissolved as vanadate with 100% current efficiency by anodic polarization. At potentials negative to the immersion potential, the VO_2 electrode functioned as an insoluble electrode with the formation of the potential-dependent surface layers of the vanadium oxides by lower valence. The change in composition of the surface layers was traced by resistmetry and coulometry, and illustrated against the amount of electric charge passed, taking V_7O_{13}, V_6O_{11}, V_5O_9, V_4O_7, V_3O_5, and V_2O_3 as the possible oxides. The composition at vanadium oxides of outer-most layer was plotted against the electrode potential. The plot shows a multi-step figure as in the equilibrium partial pressures of oxygen on vanadium oxides at high temperatures, suggesting a model in which the composition of the outer-most layer of the oxide responds to the electrode potential applied.

Resistmetry, a method based on the resistance measurement of a thin film electrode, was first applied to the studies of anodic oxide film on metals by Haruyama and Tsuru[1-4] as an *in-situ* method of measuring the thickness and the electric properties of anodic oxide film.

The potentiostatic transient current on VO_2 electrodes in the cathodic potentials between -0.30 and -1.00 V (SCE) decreases in proportion to the inverse of time asymptotically, the stationary cathodic being below 10^{-5} A/cm^2.[5] In this potential region, the VO_2 electrode functions as an insoluble electrode. A similar behavior has often been observed on transition metals in passive potentials, anodic current flowing in this case.

Iron in passive potentials carries a thin duplex oxide film which consists of an outer γ-Fe_2O_3 and an inner Fe_3O_4 layer.[4-6] It was found by resistmetric studies on passive iron that the structure of the cation-vacant outer-most layer responds to the applied potential.[4] We have applied resistmetry to the thin VO_2 electrode in order to establish the structure of the surface layer formed at the potentials negative to the immersion potential, where the VO_2 electrode works as an insoluble electrode.

Method

When no dissolution process takes place, cathodic polarization of VO_2 electrode yields a thin oxide layer with lower valence on the surface. The conductance of a VO_2 film electrode changes during the course of cathodic reduction. The total conductance of the film electrode is assumed to be the sum of the conductance of the VO_2 substrate and that of the surface layers thus formed. The conductance of each layer is given by

$$K_j = 1/R_j = wt_j/\rho_j l, \tag{1}$$

where t_j and ρ_j are the thickness and the resistivity of j-th layer, respectively, w and l are the width and length of the electrode, respectively. Thus, when a vanadium oxide VO_n is reduced giving VO_{n-x} according to the electrochemical reaction

$$VO_n + 2xH^+ + 2xe^- = VO_{n-x} + xH_2O, \tag{2}$$

the change in conductance Δk_1 during the reduction is given by

$$\Delta k_1 = \frac{W}{2xFl}\left[\frac{M_{n-x}}{\sigma_{n-x}\rho_{n-x}} - \frac{M_n}{\sigma_n\rho_n}\right]Q_1, \tag{3}$$

where M is the molecular weight, ρ the electric resistivity, σ the density, Q the amount of charge passed (C/cm^2), x the number of electron concerned, and suffixes n and $n-x$ represent VO_n and VO_{n-x}, respectively. When the VO_{n-x} formed is reduced to $VO_{n-(x+y)}$,

$$VO_{n-x} + 2yH^+ + 2ye^- = VO_{n-(x+y)} + yH_2O, \tag{4}$$

the change in conductance Δk_2 dealing with Eq. 4 is given by

$$\Delta k_2 = \frac{w}{2yFl}\left[\frac{M_{n-(x+y)}}{\sigma_{n-(x+y)}\rho_{n-(x+y)}} - \frac{M_{n-x}}{\sigma_{n-x}\rho_{n-x}}\right]Q_2, \tag{5}$$

Therefore, the change in conductance Δk ($=\Delta k_1+\Delta k_2$) caused by the reactions of Eqs. 2 and 4 is given by

$$\frac{Q_1}{x}\left[\frac{1}{\rho_{n-x}} - \frac{1}{\rho_n}\right] + \frac{Q_2}{y}\left[\frac{1}{\rho_{n-(x+y)}} - \frac{1}{\rho_{n-x}}\right] = \frac{2Fl\sigma\Delta k}{Mw}, \tag{6}$$

$$Q_1 + Q_2 = Q, \tag{7}$$

where Q represents the total amount of charge passed.

Since the resistivities of vanadium oxides differ a great deal from each other in comparison with the differences in the molecular weight or the density of oxides, the latter differences can be neglected. Thus, we have

$$M \fallingdotseq M_{n-x} \fallingdotseq M_{n-(x+y)} \tag{8}$$

$$\sigma \fallingdotseq \sigma_{n-x} \fallingdotseq \sigma_{n-(x+y)} \tag{9}$$

According to Eqs. 6 and 7, it is possible to separate Q into Q_1 and Q_2 by using the Δk *vs.* Q diagrams and the data of resistivity of oxides. The change in the composition of surface layer of the VO_2 electrode during the course of galvanostatic polarization can be estimated from the k *vs.* time curve and chronopotentiogram. A similar treatment is also possible for the anodic oxidation of the surface layer in a reduced

state.

Experimental

Specimen. The VO_2 film electrode was prepared by the dry oxidation of a vanadium foil. A pure vanadium foil (99.98%) of 0.125 mm thick was oxidized at first in a stream air (1.2 m^3/h) at 873 K for 4 h. The X-ray diffraction pattern of the oxidized surface layer of vanadium shown in Fig. 1-A indicates that the oxidation product consists of V_2O_5, V_6O_{13}, and VO_2. The oxidized vanadium was then reduced in a stream of SO_2 gas (1.2 m^3/h) at 773 K for 2 h. The oxide layer changed to a single phase of VO_2 (Fig. 1-B).[7-8] Since the oxidation process proceeds *via* the vacancy diffusion mechanism, a number of voids should be concentrated at the metal-oxide boundary. The oxide layer can be easily removed from the metallic substrate. In order to prepare the VO_2 film electrode, the oxidized vanadium sample was covered first with an epoxy resin, and then with an acryl resin plate. After the elapse of 12 h for the solidification of the epoxy resin, the VO_2 layer was taken off with the acryl plate from the vanadium substrate. The dimension of the VO_2 electrode thus prepared was 0.015×0.02 m and 10^{-5} m thick. Both ends of the specimen were connected to lead wires by an electric conductive cement and then covered with epoxy resin. The electrode surface was a sort of cleavage surface of black color and moderate brightness.

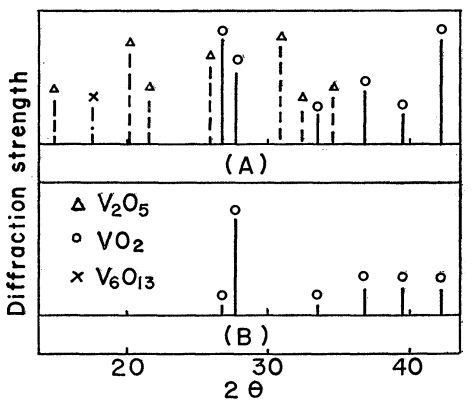

Fig. 1. X-Ray diffraction patterns of vanadium oxides. Preparation of specimen; (A) oxidation of vanadium in air at 873 K for 4 h; (B) reduction of specimen (A) in SO_2 at 773 K for 2 h.

Solution. A mixture of 0.2 mol/l boric acid and 0.05 mol/l sodium borate solution (pH 8.39) was used as an electrolyte solution. Reagent grade chemicals and twice-distilled water were used to prepare the solution. The solution was kept in a storage vessel and deaerated for more than 20 h by bubbling nitrogen gas purified through an active copper bed at 473 K. The solution was transferred from the vessel to the cell or removed from the cell under a nitrogen atmosphere.

Electrical Circuit. The electrical circuit of the resistance measurement is shown in Fig. 2. The change in conductance of the film electrode was traced by recording the unbalanced output voltage of the bridge through a pre-amplifier and a rectifier. The a-c signal between both ends of the film electrode was maintained below 0.005 V in order to minimize an undesirable change in film composition and the by-pass current through the solution. Polarization experiments were carried out with an electronic galvanostat and a counter

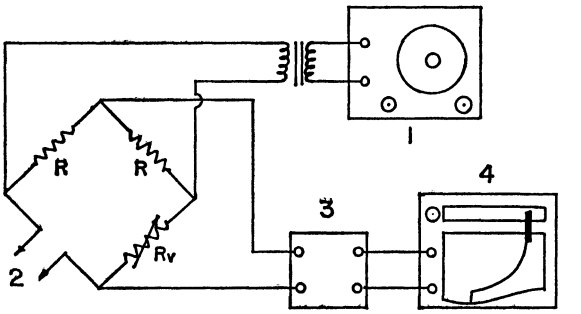

Fig. 2. Diagram of electrical cirucit for conductance measurement.
(1) Oscillator (1 kHz), (2) connected to electrode or standard resistance box, (3) amplifier and rectifier, (4) recorder.

electrode made of a platinum plate. The potential of the film electrode was measured against a saturated calomel electrode *via* a Luggin capillary and a salt bridge. A two-pen recorder was used to record the change in both the potential and the conductance of the film electrode.

Procedure. All the experiments were carried out after anodic treatment at a constant current density of 10^{-5} A/cm^2. After the electrolyte solution had been replaced, the specimen was polarized cathodically at 10^{-5} A/cm^2. The VO_2 electrode did not dissolve except at the final stage of the anodic polarization. The amount of vanadium ion dissolved was analyzed by a colorimetric analysis using the 4-(2-pyridylazo) resorcinol method.[9] The experiments were carried out under a nitrogen atmosphere at 298 K. In order to confirm semiconductive property, the experiment was carried out also under illumination with a 500 W lamp. Illumination effected neither the potential nor the conductance of the film electrode.

Results

Chronopotentiogram of VO_2 Electrode. The VO_2 electrode did not dissolve, functioning as an insoluble electrode at the potentials negative to 0.05 V (SCE) in a solution of pH 8.39.[5] The potentiostatic transient current decreased in proportion to the inverse of time.[5] This indicates the formation of an oxide layer with low valence on the VO_2 electrode, since a similar transient phenomenon is often observed in a film-forming reaction.[6] The VO_2 film electrode was cathodically reduced at first until the potential reached a certain value and then anodically oxidized at a constant current density of 10^{-5} A/cm^2. The chronopotentiograms of the galvanostatic polarization of the VO_2 electrode are shown in Fig. 3. The cathodic polarization of VO_2 electrode was terminated at various potentials, followed by anodic polarization. In the initial periods of cathodic polarization, the potential decreased steeply toward the negative direction to reach E_1, then showing an asymptotic behavior. The chronopotentiogram of the succeeding anodic polarization exhibits two potential arrests E_2 and E_3. Potential E_3 corresponds to a stationary state of the anodic polarization where the anodic dissolution of VO_2 occurred. The amount of electric charge relating to the arrest E_2 increases with the extension of the periods of cathodic polarization.

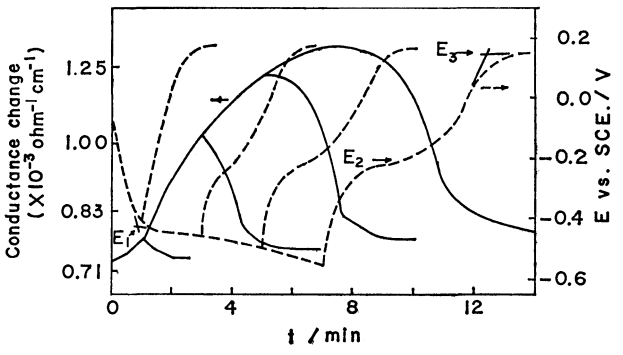

Fig. 3. Change in potential and conductance of VO_2 film during cathodic and anodic polarization at 10^{-5} A/cm².
Solid lines —— conductance change; dashed lines – – potential change.

Anodic Dissolution of VO_2. The VO_2 electrode dissolved at the final stage of anodic polarization. In order to determine the dissolution scheme, the solution after the anodic polarization was examined by colorimetry. The amount of vanadium dissolved and that of the electric charge passed are summarized in Table 1, together with the calculated value of the number of electron in the anodic dissolution of VO_2 electrode. The sample solution for the spectrophotometric analysis was prepared by the anodic dissolution of the VO_2 electrode at a constant current density of 5.0×10^{-5} A/cm² for 21 min. The expected concentration of vanadate(V) was 4.1×10^{-5} mol/l. The absorbance curve of the solution, shown in Fig. 4, is in good agreement with the data of vanadate HVO_4^{2-} reported by Newman *et al.*[10] The anodic dissolution of VO_2 (Fig. 4 and Table 1) proceeds with one electron,

$$VO_2 + 2H_2O = HVO_4^{2-} + 3H^+ + e^-. \quad (10)$$

Table 1. Number of electrons in the anodic dissolution of VO_2 at 298 K (pH 8.39)

I_a/A cm^{-2} a)	$10^3\,Q_d$/C cm^{-2} b)	$10^6\,W_{s.l.}$/g cm^{-2} c)	N d)
10^{-5}	7.143	3.798	0.993
10^{-5}	9.091	4.833	0.993
5×10^{-5}	7.500	4.026	0.983
5×10^{-5}	5.000	2.607	1.013

a) Current density. b) Amount of anodic charge. c) Weight of vanadium dissolved. d) Number of electrons.

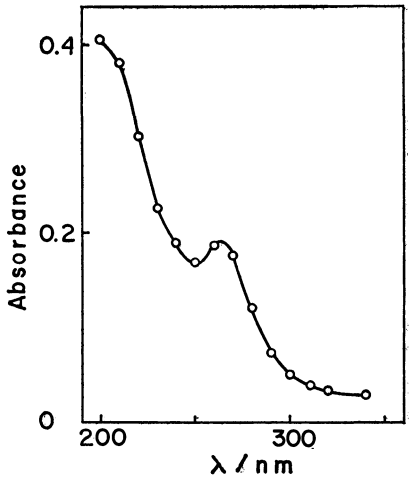

Fig. 4. Absorption spectrum of electrolyte solution after anodic dissolution of VO_2 (4.1×10^{-5} mol/l, pH 8.39).

Change in Conductance on VO_2 Film Electrode During Galvanostatic Polarization. The change in conductance of the VO_2 film electrode during polarization is plotted against the amount of charge passed in Fig. 3, together with corresponding change in potential. In the initial periods of polarization where a steep change in potential is observed, the conductance changes slowly with time. After the potential reaches the arrest E_1, the conductance increases steeply, then exhibiting an asymptotic behavior. The conductance *vs.* time curves of the subsequent anodic polarization are nearly symmetrical to those of the cathodic branch. The conductance of the electrode reverts nearly to the original value at the end of anodic polarization and the electric charge needs to reach the original conductance value increased with extension of the periods of cathodic polarization.

Discussion

Since the VO_2 electrode did not dissolve during the course of polarization at the potentials negative to 0.05 V, the change in conductance (Fig. 3 and Fig. 5-A) is attributed to the formation and the reduction of the oxide layers with different electric resistivity.

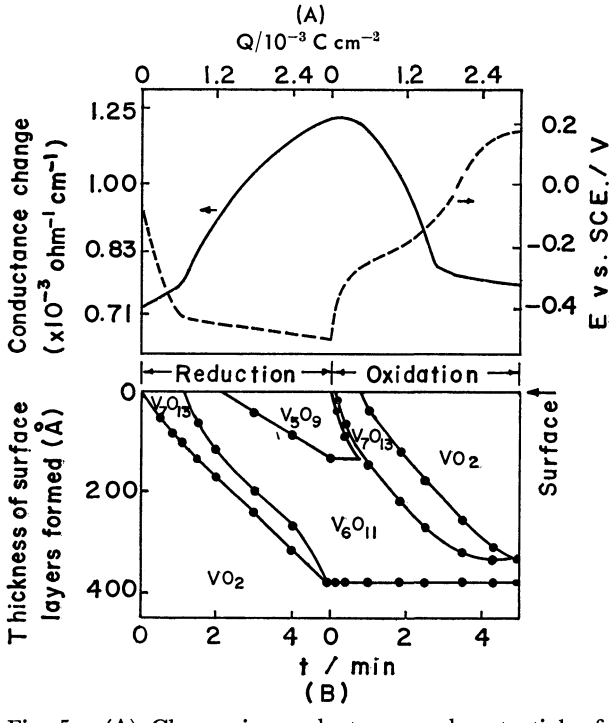

Fig. 5. (A) Change in conductance and potential of VO_2 film during cathodic and anodic polarization curves at 10^{-5} A/cm².
(B) Change in composition of surface layers during cathodic reduction and anodic oxidation of VO_2 film.

TABLE 2. ELECTRIC RESISTIVITY OF VANADIUM OXIDES[11]

Oxide form	Resistivity/Ω cm
VO_2	250
V_7O_{13}	50
V_6O_{11}	4.4
V_5O_9	142
V_4O_7	13.3
V_3O_5	1000
V_2O_3	0.04

In order to estimate the constitution of the surface layers formed by the cathodic polarization, Eqs. 6 and 7 were solved for Q_1 and Q_2, by using the change in conductance and the electric resistivities of vanadium oxides.

The values of resistivity of vanadium oxides show an appreciable scattering. The data given in Table 2[11] were chosen in the following calculation. The thickness of each layer was calculated from Q_1 and Q_2, by means of Eqs. 2 and 4, and the densities of oxides. The species and thicknesses of oxide layers were estimated on the following assumptions.

(1) The VO_2 electrode is reduced in the decreasing order of oxidation state with formation of a multilayer film on surface

$$VO_2 \underset{Q'_1}{\overset{Q_1}{\rightleftharpoons}} V_7O_{13} \underset{Q'_2}{\overset{Q_2}{\rightleftharpoons}} V_6O_{11} \underset{Q'_3}{\overset{Q_3}{\rightleftharpoons}} V_5O_9 \underset{Q'_5}{\overset{Q_4}{\rightleftharpoons}} V_4O_7$$

$$\underset{Q'_5}{\overset{Q_5}{\rightleftharpoons}} V_3O_5 \underset{Q'_6}{\overset{Q_6}{\rightleftharpoons}} V_2O_3$$

where Q'_n is the amount of charge concerned with respective reaction.

(2) The thickness of each layer increases or decreases monotonically with time, the total thickness of the surface layers being nearly proportional to the duration of cathodic reduction.

(3) The calculation based on Eqs. 6 and 7 can be applied to the thicknesses of V_7O_{13} and V_6O_{11} in the initial stage of reduction, where only two layers are formed. When the third layer participates in the growth with the progress of reduction, a supplementary procedure is used in the calculation. The growth of the V_7O_{13} layer (Fig. 5-A) follows the following equation in the initial stage of cathodic reduction

$$d = 2.47 \times t^{0.85} \qquad (11)$$

where d represents the thickness of the V_7O_{13} layer (Å) and t the time (s). It was assumed that the thickness of the V_7O_{13} layer increases according to Eq. 11 even after the V_5O_9 layer has appeared. The thickness of the V_6O_{11} and V_5O_9 layers was calculated by means of Eqs. 6 and 7 and that of V_5O_9 layer was estimated by Eq. 11.

The results of calculation are illustrated against time in Fig. 5-B. The unit time (1 min) corresponds to 6×10^{-4} C/cm^2, since the polarization experiment was carried out at a constant current density of 10^{-5} A/cm^2. The surface of the VO_2 electrode is seen to be reduced first to V_7O_{13}, and then to V_6O_{11}, which is further reduced to V_5O_9. During the course of reduction process, the VO_2 substrate is consecutively reduced to the low-valence oxides, the total thickness of the oxide layer increasing in proportion to the amount of electric charge passed. The V_7O_{13} layer vanishes after 5 min of cathodic polarization (3×10^{-3} C/cm^2), the final structure of surface layer consisting of V_5O_9 and V_6O_{11}.

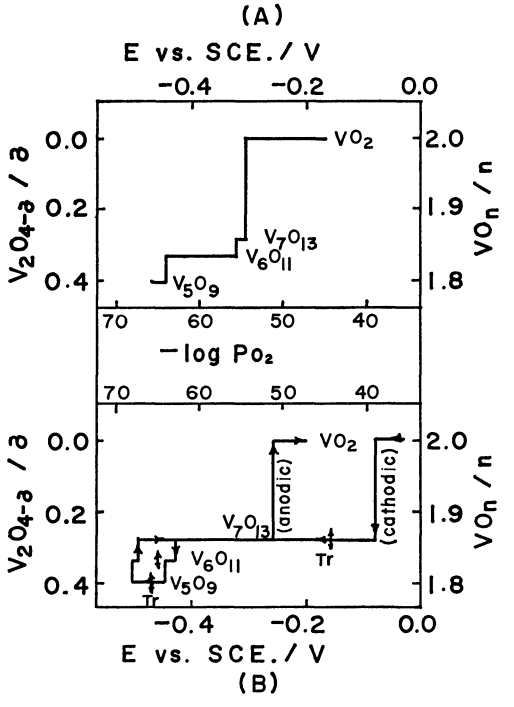

Fig. 6. (A) Relation between vanadium oxides and their eqilibrium pressures of oxygen (from Okinaka's data).
(B) Potential dependency of surface oxides on VO_2 (present work). Tr: Transition potential.

In the subsequent anodic oxidation, V_5O_9 is oxidized to VO_2 *via* V_6O_{11} and V_7O_{13}. Using Fig. 5-B, the oxidation state of the outer-most layer of the VO_2 electrode is plotted against the potential in Fig. 6-B. Since the ohmic drop inside the oxide electrode was estimated to be of the order of 10^{-4} V at the current density chosen, the potential difference should appear mainly at the oxide/electrolyte interface.

The transition from VO_2 to V_7O_{13} occurs at -0.08 V (SCE) in the cathodic process, and at -0.26 V in the anodic process. A similar hysteresis of the transition potential between the cathodic and anodic branch is observed on the transition between V_7O_{13} and V_6O_{11} on that between V_6O_{11} and V_5O_9. Further experiments are necessary to explain, the hysteresis in the transition potential, since it is a sort of underpotential phnomenon.

Thermodynamic properties of vanadium oxides were reported[12-14] mainly from the measurement of the equilibrium partial pressure of oxygen p_{O_2} at high temperature. The composition *vs.* log p_{O_2} diagram of vanadium oxides at 298 K (Fig. 6-A) was estimated by the extrapolation of the data at high temperature to those at 298 K according to the Van't Hoff equation. The log p_{O_2} scale at 298 K was also converted into the potential scale, by considering the Nernst equation

Table 3. Thermodynamic data of vanadium oxides

	Data extrapolated from high temperature measurement (Okinaka *et al.*[13])			Data calculated from transition potential (present work)		
	ΔG°_{298} / kJ mol^{-1}	$-\log p_{O_2}$	E(SCE) pH 8.39	ΔG°_{298} / kJ mol^{-1}	$-\log p_{O_2}$	E(SCE) pH 8.39
VO_2	−658			−658		
		54.6	−0.312		45.1	−0.170
V_7O_{13}	−4447			−4474		
$VO_{13/7}$	−653			−639		
		55.7	−0.328		64.5	−0.465
V_6O_{11}	−3789			−3809		
$VO_{11/6}$	−631			−635		
		64.1	−0.452		67.9	−0.505
V_5O_9	−3127			−3142		
$VO_{9/5}$	−626			−628		

on the reversible potential of oxygen, thus

$$O_2 + 2H_2O + 4e^- = 4OH^- \quad (12)$$

$$E^{rev}_{O_2} = 1.229 + 0.015 \log p_{O_2} - 0.060\ pH \quad (13)$$

Figure 6-A and B are so arranged that the scale of $\log p_{O_2}$ and that of potential correspond to each other according to Eq. 13.

Transition potentials and the $(-\log p_{O_2\ 298K})$ at the equilibrium between two oxides are summarized in Table 3, together with the free energy of the formation $\Delta G_{f'298K}$ of the vanadium oxides. The free energy of formation was calculated from $(-\log p_{O_2\ 298K})$ and the transition potentials, assuming that $\Delta G_{f'298K}$ of VO_2 is −314.3 kcal/mol. There is an appreciable disagreement between the values of $\Delta G^\circ_{f'298K}$ calculated from the data of equilibrium partial pressure of oxygen at high temperatures and those from the transition potentials. The former values might be less reliable since they are based on an extended extrapolation from the data at temperatures over 1273 K by using the Van't Hoff equation. On the other hand, uncertainity also exists in the latter method especially on the hysteresis of the transition potentials.

The potential dependency of the surface layer on the VO_2 electrode estimated from the resistmetry (Fig. 5-B) exhibits a quite reasonable behavior as compared with that obtained from the equilibrium partial pressures of oxygen at high temperatures. The results strongly support the model in which the composition of the outer-most layer oxide electrodes changes responding to the applied potential.

The authors wish to thank Prof. Masao Taniguchi, Dr. Tooru Tsuru, and Dr. Masataka Wakihara for their discussions.

References

1) S. Haruyama and T. Tsuru, *Corros. Sci.*, **13**, 275 (1973).
2) T. Tsuru and S. Haruyama, *J. Jpn. Inst. Metals*, **39**, 1098 (1975).
3) T. Tsuru and S. Haruyama, *J. Jpn. Inst. Metals*, **40**, 1172 (1976).
4) S. Haruyama and T. Tsuru, "Passivity and Its Breakdown on Iron and Base Alloys," ed by R. W. Staehle and H. Okada, National Association of Corrosion Engineers, Houston (1976), p. 41.
5) T. Nakamura and S. Haruyama, *Denki Kagaku*, **45**, 309 (1977).
6) M. Nagayama and M. Cohen, *J. Electrochem. Soc.*, **109**, 781 (1962).
7) T. Nakamura, *Report of Technical High School, Faculty of Engineering, Tokyo Institute of Technology*, **8**, 113 (1977).
8) K. Kawashima, K. Kosuge, and S. Kachi, *Chem. Lett.*, **1975**, 1131.
9) Y. Yojou and T. Takeuchi, *Bunseki Kagaku*, **14**, 115 (1965).
10) L. Newman, W. J. Lafleur, J. Brousaides, and A. M. Ross, *J. Am. Chem. Soc.*, **80**, 4491 (1958).
11) S. Kachi, T. Takada, and K. Kosuge, *J. Phys. Soc. Jpn.*, **18**, 1839 (1963).
12) H. Okinaka, K. Kosuge, and S. Kachi, *Trans. Jpn. Inst. Met.*, **12**, 44 (1971).
13) H. Endo, M. Wakihara, M. Taniguchi, and T. Katsura, *Bull. Chem. Soc. Jpn.*, **46**, 2087 (1973).
14) H. Endo, M. Wakihara, and M. Taniguchi, *Chem. Lett.*, **1974** 905.

Hydrogen–Deuterium Equilibration Reaction over Platinum Supported on Polyamide-6

Yasunobu INOUE,* Seiji HACHO, Eizo MIYAZAKI, and Iwao YASUMORI

Department of Chemistry, Tokyo Institute of Technology, Ookayama, Meguro-ku, Tokyo 152

(Received January 27, 1979)

Catalysis by platinum supported on polyamide-6 was examined for the H_2–D_2 equilibration reaction at 0 °C in the pressure range of 5—20 Torr (1 Torr=133.3 Pa). Three kinds of polyamides with different molecular weights were prepared as support; the concentration of platinum varied from 0.5 to 2.7 wt%. With preadsorption of hydrogen at 0 °C, the rate of the reaction was found to increase up to 10 times as high as the original level. The rate k_m (HD molecule s^{-1}Pt $atom^{-1}$) showed a maximum, depending on surface area of the polyamides used, in the range 0.8—1.0 wt% of Pt content and its dependence on total pressure is represented by $k_m=K_1P/(1+K_2\sqrt{P})^2$ irrespective of Pt content. No significant isotope effect was observed at 0 °C. It was found that a linear relationship exists between the enhancement of k_m and the amount of hydrogen preadsorbed, indicating an important role of the preadsorbed hydrogen in activation of the catalysts. In contrast to k_m, the turn-over frequency k_t (HD molecule s^{-1} $site^{-1}$) was nearly independent of Pt concentration. The exchange reaction is explained in terms of the Bonhoeffer-Farkas mechanism. XPS spectra provided the evidence for the presence of Pt(II) complexes on the surface. The structure of active sites is discussed.

Catalysis by metals dispersed on organic polymers has been the subject of particular interest, because the catalytically active sites are different in electronic and geometric factors from metals on inorganic supports. The pioneering work on this subject has been done by Izumi,[1] who employed silk fibroins as supports for palladium and studied the hydrogenation of various organic compounds. Harrison and Rase[2] studied the hydrogenation of benzene on platinum supported on polyamides. They reported the capacity of the catalysts to produce cyclohexene, which is scarcely formed at all on silica-supported platinum. They used polymers with different periodic structures, and pointed out the importance of the geometric arrangement of Pt metal atoms correlating to the position of the amide group in the polymer chains. Dini *et al.*[3] examined the number of chlorine atoms remaining in the catalysts and showed the presence of bivalent platinum ions which are available as sites for the formation of cyclohexene.

The structures and distributions of active sites on polyamides are of interest. So we will examine systematically the effect of platinum metal dispersion upon catalytic activity, since the number of the active sites is likely to depend on that of NHCO and/or NH_2 groups exposed to the surface to which Pt is considered to be bonded. Further information is obtained from the change in catalytic activity which occurs when the polyamides which differ as much in molecular weight as possible are used.

In our preliminary study[4] on the hydrogenation of acetylene and butadiene over the Pt–polyamide catalysts, it was found that the major products of the reactions were the saturated hydrocarbons instead of the corresponding monoolefins, indicating that the reactions are quite different in selectivity from those on metal powder and silica-supported catalysts reported earlier.[5] Preadsorbed hydrogen promoted the reactions and there were optimum conditions to give the stable and high catalytic activity, which is apparently associated with the pretreatment by hydrogen. These results led to the consideration that an interaction of hydrogen with Pt on the polymer is characteristic, but no extensive study has been done so far. Thus, the present study was undertaken to examine the equilibration reaction between H_2 and D_2 on Pt–polyamide catalysts and to determine the effect of Pt dispersion on catalytic activity. In order to get information on the states of Pt supported on polyamides, X-ray photoelectron Spectroscopy (XPS) was employed in this study.

Experimental

Catalyst Preparations. Polyamide-6 (PA) was obtained by the polymerization of ε-caprolactam (Wako Pure Chemical Co.) initiated with 1.0 wt% of 6-aminohexanoic acid at 250 °C in a stream of nitrogen. Unreacted monomer, oligomers, and cyclic oligomers were eliminated from the products with hot water. The polyamide-6 was dissolved into formic acid of extra pure grade, and then the PA powder was obtained by transferring the solution to ion-exchanged water and drying *in vacuo* at room temperature. Three kinds of polyamide-6 with different molecular weights of 6.8×10^3, 3×10^3, and 1.7×10^3 (as denoted by L, M, and S hereafter) were prepared and found to have surface areas of 5.7, 5.5, and 4.6 m^2/g, respectively.

The polymers were immersed in an aqueous solution of H_2PtCl_6 of about 8×10^{-3} Pt g/l in concentration, heated at 90 °C for 2 h and then washed thoroughly with ion-exchanged water. The catalysts were dried *in vacuo* at room temperature. The concentration of Pt dispersed on PA was determined according to the procedure described in the reference.[6] The catalysts with Pt concentration of 0.5 to 2.7 wt% were prepared. Elemental analysis showed that the amount of chlorine atoms remaining on the treated 2.7 wt% Pt–PA-M catalyst was estimated, in terms of the Cl/Pt ratio, at 1.7.

Characterization of Catalyst. In order to examine the valence states of Pt bonded to PA, a Hewlett-Packard 5950A ESCA spectrometer with a monochromatic Al $K\alpha$ X-ray was used and a flood gun was operated at 0.3 mA with 0—0.7 eV to avoid the charging of the samples. The binding energy of C 1 s of CH_2 group in PA, 284.8 eV, was taken as standard. X-Ray diffraction and electron microscopic studies were done to ascertain the presence of Pt crystallites and also their distributions on the surface.

Equilibration Reaction. The equilibration reaction be-

tween H_2 and D_2 was studied using a closed circulating apparatus which was similar to that used before.[7] Hydrogen, hydrogen deuteride, and deuterium were analyzed by a gas chromatograph connected to the system.[7] Prior to the kinetic run, a fresh catalyst was evacuated at 150 °C for 1 h and then cooled to the reaction temperature, 0—35 °C. Hydrogen (99.98% pure), and deuterium (containing less than 0.5% HD) were obtained from Takachiho Chemical Co. and used without further purification.

Results

Figure 1 shows the time course of the equilibration reaction at 0 °C using the catalyst evacuated at 150 °C. The rate of equilibration is expressed as

$$\ln (X_o - X_e)/(X_t - X_e) = k_e t \qquad (1)$$

where X_o, X_t, and X_e are, respectively, the fraction of HD at $t=0$, t, and equilibrium. In the initial stage of the first run (curve a), the experimental values were considerably off the linearity but, after three or more successive runs, they turned out to fit a linear expression. The reaction rate k_e is derived from the slope and then k_m is defined as

$$k_m = nk_e/N_{Pt} \quad \text{(molecule s}^{-1}\text{ Pt atom}^{-1}\text{)} \qquad (2)$$

where n is the number of molecules in the gas phase and N_{Pt} the number of Pt atoms. Figure 2 shows the dependence of the reaction rate upon the time of exposure of the catalyst to hydrogen of 20 Torr at 0 °C after evacuation at 150 °C. The catalytic activity increased with the contact time and no further increase was observed after 24 h. The highest activity, about 10 times as high as the original one of the first run without H_2-preadsorption, was diminished by evacuation at 150 °C for 3 h to the original level, but the treatment with hydrogen at 0 °C promoted again the activity to the highest level. This cycle

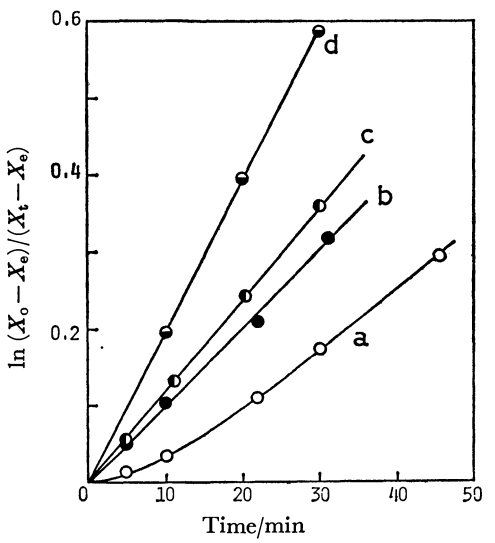

Fig. 1. H_2-D_2 exchange reaction on 0.5 wt% Pt-PA-M. ○: First run, ●: second, ◐: third, ◒: fourth. Between each run, the catalyst was evacuated at 0 °C for 10 min. The reaction conditions are as follows unless otherwise stated. Total pressure=20 Torr, $H_2/D_2=1$, reaction temperature=0 °C.

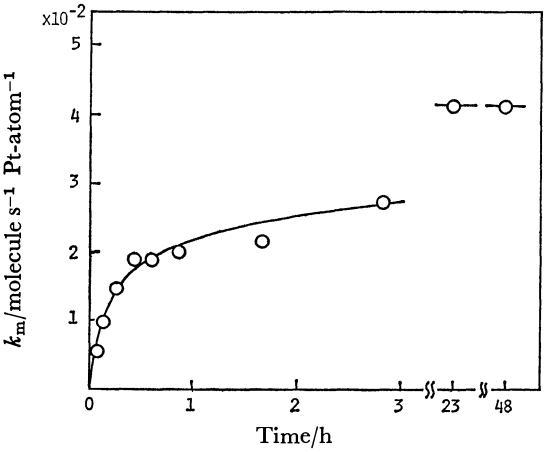

Fig. 2. Increase in k_m as a function of time exposed to hydrogen.
Catalyst: 0.5 wt% Pt-PA-M, $P_H=20$ Torr, temperature=0 °C.

of activation and deactivation was quite reversible and reproducible. Evacuation at 0 °C for less than 30 min caused no significant change in the highest activity, which was taken as the measure for comparison of catalytic activity, unless otherwise stated.

The dependence of k_m on Pt concentration for three catalysts, Pt–PA-L, -M, and -S, is shown in Fig. 3. Each catalyst has a maximum k_m value around 0.8—1.0 wt% of Pt. The activity beyond the maximum declined sharply. Figure 4 shows Arrhenius plots for the H_2–D_2 equilibration on 0.5, 0.8, 1.0, and 2.0 wt% Pt–PA-M catalysts. The evaluated activation energies were almost constant as 7.2±0.2 kcal/mol (1 kcal=4.184 kJ) irrespective of Pt content. The total pressure dependence of the exchange rate for these four catalysts using an equimolar mixture of H_2 and D_2 as reactant is shown in Fig. 5. The reciprocals of the square root of both total pressure P and k_m provided a linear relationship for each catalyst, indicating that k_m can be represented as $K_1P/(1+K_2\sqrt{P})^2$

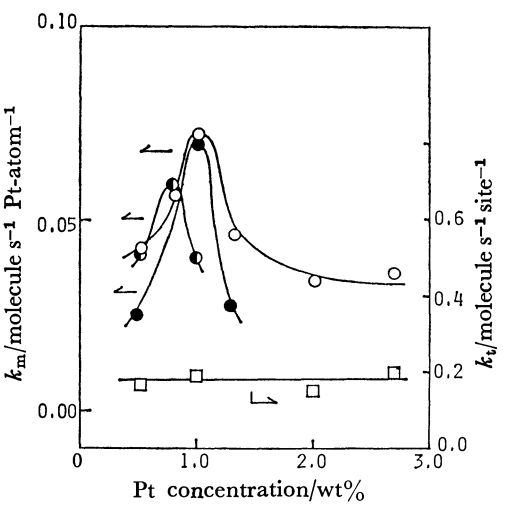

Fig. 3. Change in k_m and invariance of k_t with Pt concentration.
k_m, ○: Pt-PA-M, ◐: -S, ●: -L. k_t, □: Pt-PA-M.

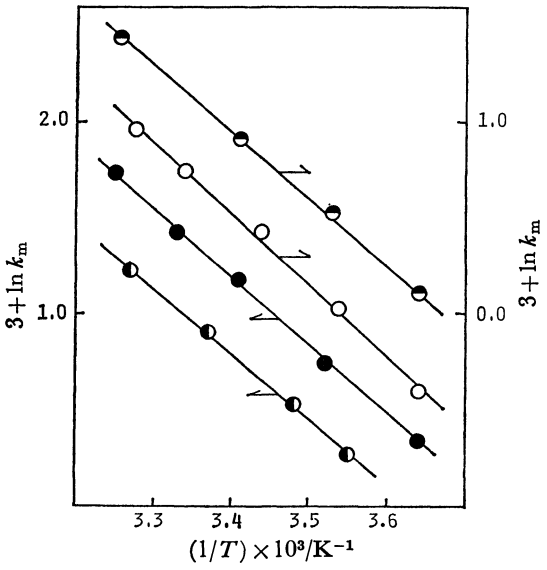

Fig. 4. Arrhenius plots for H_2–D_2 exchange reaction.
◐: 0.5 wt% Pt-PA-M, ◓; 0.8, ●; 1.0, ○; 2.0.

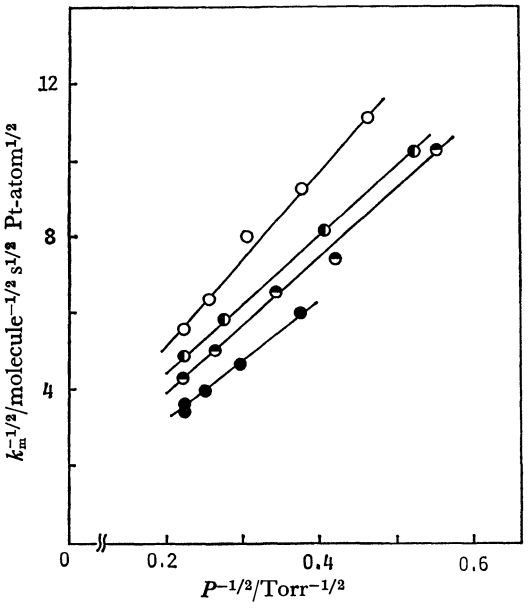

Fig. 5. Total pressure dependence of k_m at 0 °C.
◐: 0.5 wt% Pt-PA-M, ◓; 0.8, ●; 1.0, ○; 2.0.

where K_1 and K_2 are constants.

In order to see the detailed kinetic behavior of the reaction and also to ascertain whether the isotope effect is present or not, the partial pressure dependence was investigated at 0 °C. For 1.0 wt% Pt–PA-M catalyst, the reaction order with respect to hydrogen pressure, P_H, was about 0.5 in a range from 2 to 4.7 Torr at a fixed deuterium pressure, P_D, of 7 Torr, and the deuterium order was the same as that of hydrogen in a range of P_D from 0.4 to 4.5 Torr at a fixed P_H of 5 Torr. This close similarity in the partial pressure dependence between H_2 and D_2 predicts that there exists little isotope effect at the reaction temperature.

The adsorption of hydrogen at 0 °C in an activation process occurred in a slow manner analogous to the increase of activity observed in Fig. 2; thus we can obtain a correlation between the amount of the preadsorbed hydrogen and the corresponding catalytic activity. The results are shown in Fig. 6. The linear relationship between k_m and the H/Pt ratio reflects the direct contribution of hydrogen to the activation of catalysts. The saturation of the preadsorbed hydrogen took place after 24 h, and evacuation of the surface at 0 °C for 10 min caused negligible desorption of the hydrogen, since no further adsorption of hydrogen was observed after the introduction of hydrogen following the evacuation. For Pt–PA-M catalysts with Pt loading ranging from 0.5 to 2.7 wt%, the saturated amount of the adsorbed hydrogen per gram Pt increased with the content, passed through a maximum at 1.0 wt%, and decreased. This change is in a close parallel to that observed in the catalytic activity. The number of active sites can be calculated from that of the hydrogen atoms preadsorbed. The turn-over frequency, k_t, in terms of molecules s^{-1} site^{-1}, is given in Fig. 3.

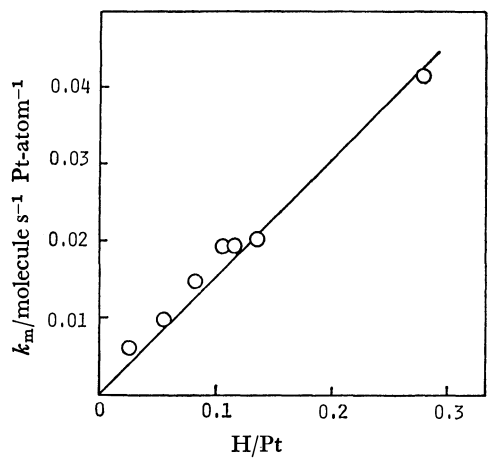

Fig. 6. Relationship between k_m and H/Pt ratio.
Catalyst: 0.5 wt% Pt-PA-M.

The effects of the preadsorbed hydrogen on the exchange reaction of catalyst hydrogen with gaseous deuterium were examined at 0 °C. Hydrogen of 3.6×10^{-6} mol was preadsorbed at 0 °C, evacuated for 10 min, and then deuterium of 2.4 Torr was introduced. The rate of HD formation is much the same in the cases of both the presence and the absence of the preadsorbed hydrogen, but smaller by a factor of about 40 compared to the ordinary rate in the steady reactions. In order to confirm whether or not the slow exchange is attributable to the reaction between the structural hydrogen in PA and gaseous deuterium, 1.0 wt% Pt–PA-M catalyst was exposed to a deuterium atmosphere at 150 °C. The number of the exchanged hydrogen atoms was found to amount to approximately 300 times that of Pt atoms, indicating that hydrogens in bulk organic groups participated in the exchange. After the exchange, the catalyst was examined by means of infrared spectroscopy, and, in addition to ordinary bands due to PA, new strong bands at 2400 and 2460 cm^{-1} and also weak bands at 2090 and 2190 cm^{-1} were observed. The former group corresponds to the bands of the characteristic region ascribable to the N–D stretching vibration. The latter

two bands are reasonably assigned to the C–D stretching vibration.

For 2.7 wt% Pt–PA-M catalyst without evacuation at high temperature after preparation, the Pt 4f region of X-ray photoelectron spectra showed three peaks, the central one of which is apparently derived from a superposition of two peaks (Fig. 7 and Table 1). From the comparison with binding energies of Pt complexes reported earlier,[8] these peaks can be associated with the 4f level of Pt(IV) and Pt(II). It was found that three peaks gradually changed to two stable peaks, $4f_{7/2}$ and $4f_{5/2}$, during the course of the photoemission measurement and that X-ray irradiation caused the reduction of Pt(IV) to Pt(II), which is analogous to the phenomena observed in XPS studies on Pt complexes.[8,9] For 2.7 wt% Pt–PA-M catalyst, which was evacuated at 150 °C, only two 4f peaks appeared at the binding energies of 72.5 and 75.7 eV, which are higher by 1.3—1.2 eV than those of Pt metal, indicating the presence of Pt(II) on PA. Further exposure of the surface to a hydrogen atmosphere at 0 °C for 24 h gave rise to no significant change in the spectra. The chlorine 2p level was monitored

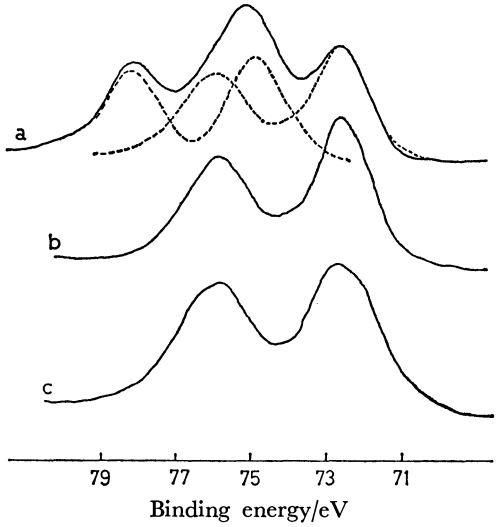

Fig. 7. Pt 4f region of XPS spectra of 2.7 wt% Pt–PA-M.
a: Evacuated at room temperature, b: evacuated at 150 °C and then exposed to 20 Torr of hydrogen at 0 °C, c: exposed to X-ray for 6.5 h after a.

but no strong peak was observed. This is probably attributed either to the low intensity of the level or to the loss of chlorine with X-ray exposure, which occurred in the case of Cl-containing Pt complexes.[8] For N ls and O ls levels, neither a significant shift of the peaks nor broadening was observed between PA and Pt–PA.

No appreciable change was observed in the infrared spectra of the organic groups characteristic in PA when the platinum complex was deposited on it. The X-ray diffraction measurement provided only a diffused peak due to PA crystallites and showed unambiguous evidence for the absence of large Pt metal particles. Electron microscopy was applied to the catalysts under a magnification of more than 90000, but failed to detect the presence of large Pt particles.

Discussion

The platinum–PA catalysts are characterized by a gradual increase in the activity for H_2–D_2 equilibration as the catalysts are exposed to a hydrogen atmosphere. One might argue that such an activity enhancement is ascribable to metal particles produced by the reduction of the Pt complexes. This is unlikely, because the activity was lost upon heat-treatment at 150 °C but again restored to the same level as before when they were exposed to a hydrogen atmosphere at 0 °C. XPS results gave no sign of a Pt 4f peak due to the metallic state, but showed the presence of bivalent platinum cation. The results obtained by electron microscopy and X-ray diffraction also support this view. The reversible change in catalytic activity mentioned above clearly shows that the preadsorbed hydrogen played an important role in the formation of catalytically active sites.

It is of interest to see that the position of peak activity shown in Fig. 3 can be correlated with the surface area of PA used as support; for both PA-L and PA-M catalysts having the surface areas of 5.7 and 5.5 m^2/g, each peak appears at a Pt content of 1 wt%, whereas for PA-S the downward shift of the position occurs by a factor of 0.2, almost the same ratio as the decrease in the surface area. This correlation indicates that the functional organic groups of PA exposed on the surface, but not those in bulk, are of importance in catalysis, and also predicts that the number of active

Table 1. Binding energy of Pt 4f, N 1s, and O 1s levels of 2.7 wt% Pt-PA-M catalyst

Samples	Binding energy/eV[b]					
	Pt $4f_{7/2}$		Pt $4f_{5/2}$		N 1s	O 1s
1) PA-6	—		—		399.6	531.1
2) 2.7 wt% Pt-PA-M evacuated at room temperature[a]	72.7	75.4	78.1		399.6	531.1
	(72.7		76.0	Pt(II)		
	75.0)		78.2	Pt(IV))		
3) 2.7 wt% Pt-PA-M evacuated at 150 °C	72.5		75.7		399.5	531.2
4) After 3), exposed to H_2 at 0 °C	72.7		76.0		399.5	531.2
5) Pt metal	71.2		74.5		—	—

a) Prolonged exposure to X-ray gives the values of 72.8 and 76.0 eV for the Pt 4f region. b) C 1s=284.8 eV as standard. The error in binding energy is within 0.2 eV.

sites is proportional to that of such groups.

The (010) face of a polyamide-6 crystal consists of a unit cell with a dimension of 17.2 Å×4.78 Å and involves two NHCO groups. For 1.0 wt% Pt–PA-M catalyst, a calculation gave the ratio of Pt atoms to surface NHCO groups to be 2.3. Since even the highest value of the H/Pt ratio reaches only 0.4, not all the Pt atoms on PA can work as active sites for both the equilibration and the adsorption of hydrogen. This low ratio of H/Pt is consistent with the results obtained by Dini *et al.*;[3] their 0.6 and 3.8 wt% Pt supported on nylon-6 catalysts gave 0.08 and 0.11, respectively, at 25 °C. It should be noted that no metal crystallites as large as 100 Å, which would be anticipated in such low degrees of exposure, were detected.

The kinetic results showed that the turn-over frequency k_t for the exchange reaction is apparently independent of Pt content and that kinetic behavior such as activation energy and reaction order are almost the same over the whole range of the loading. Thus, it is suggested that there is a single kind of catalytically active site on the surface. For this view, the presence of a maximum in k_m appears somewhat puzzling, but is explained by the model on the basis of the following assumptions. The fundamental unit of polyamide-6 (α-type) is given below, where x and y represent the positions corresponding to the spacing between neighboring polymer chains.

It is likely that an NHCO group (position x) is involved in the coordination with the Pt complex, whereas a CH_2 group (position y) has a weak interaction with the complex upon its access. It is assumed that such characteristics in the structure of PA-6 lead to the formation of cluster complexes consisting of two and three Pt metal atoms, denoted as $(Pt)_2$ and $(Pt)_3$ respectively, and that only $(Pt)_3$ is catalytically active. The ratio of existing $(Pt)_3$ to $(Pt)_2$ depends on the numbers of the positions having suitable spacing

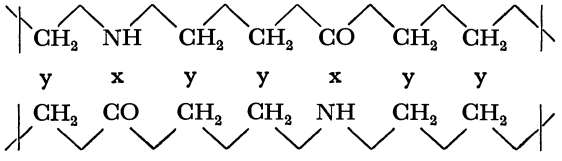

in the vicinity of NHCO group; thus it follows that the catalytic activity becomes the highest when one unit is occupied by one $(Pt)_3$ and one $(Pt)_2$. Further deposition of Pt beyond this distribution results in the decrease of the catalytic activity per gram Pt. Table 2 shows the results of calculations obtained on the basis of the distribution of $(Pt)_3$ and $(Pt)_2$ on the polyamide-6 with a periodicity of three units which contain six NHCO and fifteen $CH_2\cdots CH_2$ groups in them. The rather good agreement between the calculated and experimental values shows that the structures of the active sites are well represented by the cluster model.

Reaction Mechanism. The adsorption of hydrogen in the formation of the catalytically active sites is undoubtedly slow and irreversible at 0 °C, but induces a drastic rise in activity. The following process seems to take place.

$$(Pt)_3 + H_2 \longrightarrow (Pt^*)_3 \tag{3}$$

where $(Pt^*)_3$ represents the catalytically active sites. The H_2–D_2 equilibration on this surface is considered in terms of the Bonhoeffer-Farkas mechanism which is shown below.

$$H_2(g) \underset{k_d^H}{\overset{k_a^H}{\rightleftharpoons}} 2H(a) \tag{4}$$

$$HD(g) \underset{k_d^{HD}}{\overset{k_a^{HD}}{\rightleftharpoons}} H(a) + D(a) \tag{5}$$

$$D_2(g) \underset{k_d^D}{\overset{k_a^D}{\rightleftharpoons}} 2D(a) \tag{6}$$

The rate constants of adsorption and desorption are denoted as k_a^i and k_d^i, respectively, where i=H, HD, or D. The changes in surface concentration of hydrogen and deuterium atoms as a function of time can be represented by the following equations:

$$\frac{d\theta_H}{dt} = 2k_a^H P_H(1-\theta_H-\theta_D)^2 + k_a^{HD}P_{HD}(1-\theta_H-\theta_D)^2 - 2k_d^H\theta_H^2 - k_d^{HD}\theta_H\theta_D \tag{7}$$

$$\frac{d\theta_D}{dt} = 2k_a^D P_D(1-\theta_H-\theta_D)^2 + k_a^{HD}P_{HD}(1-\theta_H-\theta_D)^2 - 2k_d^D\theta_D^2 - k_d^{HD}\theta_H\theta_D \tag{8}$$

TABLE 2. THE H/Pt RATIO AND THE NUMBER OF Pt ATOMS ON Pt–PA CATALYSTS

Catalysts	(N_n+N_c)[a]	wt%	Obsd		Calcd[b]	
			Pt (atom/g)	H/Pt	Pt (atom/g)	H/Pt
Pt-PA-L	4.9×10^{19}	1.0	3.1×10^{19}	—	3.5×10^{19}	—
Pt-PA-M	4.7×10^{19}	1.0	3.1×10^{19}	0.40	3.3×10^{19}	0.40
		0.5	1.5×10^{19}	0.27	1.6×10^{19}	0.27
Pt-PA-S	3.9×10^{19}	0.8	2.5×10^{19}	—	2.8×10^{19}	—

a) The total number of NHCO and CH_2 surface groups per gram of catalyst. b) At the maximum activity, the surface of three units distributes fifteen Pt atoms on twenty one positions (=x+y). Numbers of Pt atoms per gram catalyst were calculated by multiplying (N_n+N_c) by 15/21. The H/Pt ratio is given by 2×(number of $(Pt)_3$)/(number of Pt atoms) under the assumption that a hydrogen molecule occupies a $(Pt)_3$. From the distribution of the cluster described in the text, the H/Pt value is calculated to be $2\times3/15=0.4$ for 1.0 wt% and $2\times1/7.5=0.27$ for 0.5 wt%. This model permits the comparison of k_m; for 1.0 wt%, k_m is given by $(3/15)k_t$, whereas for 0.5 wt% by $(1/7.5)k_t$. The ratio of k_m(1.0 wt%)/k_m(0.5 wt%), 1.5, is close to the observed one, 1.7.

where θ_H and θ_D are, respectively, the fractions of hydrogen and deuterium occupying the active sites in the complex. The neglect of the isotope effect leads to the simple relations, $k_a^H=k_a^D=k_a^{HD}=k_a$ and $2k_d^H=2k_d^D=k_d^{HD}=k_d$. The factor 2 in the desorption rate constants k_d^H and k_d^D comes from the fact that the probability of making an atom pair HD is twice as large as that of making a pair H_2 or D_2. Since the amount of hydrogen adsorbed on a catalyst surface was negligibly small compared to that in the gas phase, P_{HD} is represented by 2 $(P_H^\circ-P_H)$ or 2 $(P_D^\circ-P_D)$, where P_H° and P_D° are hydrogen and deuterium pressures at $t=0$, respectively. By introducing the steady-state approximation, $d\theta_H/dt=d\theta_D/dt=0$, and the relations described above, one can obtain the following equations:

$$(1-\theta_H-\theta_D)^2 2KP_H^\circ = \theta_H(\theta_H+\theta_D) \tag{9}$$

and

$$(1-\theta_H-\theta_D)^2 2KP_D^\circ = \theta_D(\theta_D+\theta_H) \tag{10}$$

where K denotes k_a/k_d.

Total Pressure Dependence. The rate equation which describes the time course of the reaction is given by

$$\left(\frac{N_aV}{RTN_{pt}}\right)\frac{dP_{HD}}{dt} = k_d\theta_H\theta_D - k_aP_{HD}(1-\theta_H-\theta_D)^2 \tag{11}$$

where N_a is Avogadro's number, V the volume of the reaction system, and R the gas constant. Since the equimolar mixtures of H_2 and D_2 were used as the reactants, the relations, $\theta_H=\theta_D=\theta/2$ and $P_H^\circ=P_D^\circ=P^\circ/2$, always hold in this case. Equation 9 or 10 is then transformed into

$$\theta_H + \theta_D = \theta = \frac{\sqrt{2KP^\circ}}{1+\sqrt{2KP^\circ}} \tag{12}$$

The insertion of Eq. 12 into Eq. 11 provides

$$\left(\frac{N_aV}{RTN_{Pt}}\right)\frac{dP_{HD}}{dt} = \frac{k_dKP^\circ}{(1+\sqrt{2KP^\circ})^2}\left(\frac{1}{2}-\frac{P_{HD}}{P^\circ}\right) \tag{13}$$

By introducing the fraction of HD in the gas phase, $X_{HD}=P_{HD}/P^\circ$ and that in equilibrium, $X_e=P_{HD}^e/P^\circ=1/2$, Eq. 13 can be rewritten as

$$\frac{dX_{HD}}{dt} = k_e(X_e-X_{HD}) \tag{14}$$

where

$$k_e = \frac{k_dKRTN_{Pt}}{N_aV(1+\sqrt{2KP^\circ})^2} \tag{15}$$

The integration of Eq. 14 gives the experimental relation (1), and Eq. 2 on k_m is correlated with k_e in Eq. 15 as

$$k_m = \frac{nk_e}{N_{Pt}} = \frac{k_dKP^\circ}{(1+\sqrt{2KP^\circ})^2} \tag{16}$$

This equation accords well with the observed kinetic behavior shown in Fig. 5.

Partial Pressure Dependence. By solving Eq. 9 and 10, one can obtain the following expressions for θ_H and θ_D:

$$\theta_H = \frac{\sqrt{2KP_H^\circ}}{\sqrt{(P_H^\circ+P_D^\circ)}\,[1+\sqrt{2K(P_H^\circ+P_D^\circ)}]} \tag{17}$$

$$\theta_D = \frac{\sqrt{2KP_D^\circ}}{\sqrt{(P_H^\circ+P_D^\circ)}\,[1+\sqrt{2K(P_H^\circ+P_D^\circ)}]} \tag{18}$$

The measurements on the partial pressure dependence of the rate were carried out only at the initial stage of reaction and then P_{HD} in Eq. 11 was safely omitted from the expression.

$$\left(\frac{N_aV}{RTN_{pt}}\right)\frac{dP_{HD}}{dt} = k_m' = k_d\theta_H\theta_D = \frac{2k_dKP_H^\circ P_D^\circ}{(P_H^\circ+P_D^\circ)[1+\sqrt{2K(P_H^\circ+P_D^\circ)}]^2} \tag{19}$$

where $k_m'=k_m/2$ when $P_H^\circ=P_D^\circ$. This equation can be transformed into

$$\sqrt{\frac{P_H^\circ P_D^\circ}{k_m'(P_H^\circ+P_D^\circ)}} = \sqrt{\frac{1}{2k_dK}} + \sqrt{\frac{1}{k_d}}(P_H^\circ+P_D^\circ)^{1/2} \tag{20}$$

Figure 8 shows the plot of experimental values of $\sqrt{P_H^\circ P_D^\circ/k_m'(P_H^\circ+P_D^\circ)}$ against $(P_H^\circ+P_D^\circ)^{1/2}$. Besides, the values of k_d and K were evaluated at 2.2 molecule s^{-1} Pt atom^{-1} and 3.6×10^{-3} Torr^{-1}, respectively, from the observed rate shown in Fig. 5. These values were inserted into Eq. 20 and the line thus obtained is also shown in Fig. 8. In spite of the lower accuracy in the values of initial rate, the correspondence between the results of the separate studies seems fairly good and suggests that the proposed mechanism is an acceptable one. The equation derived on the basis of the Rideal-Eley mechanism did not fit with the experimental pressure dependence.

It is of interest to compare the present kinetic results with those on metal platinum. The value of k_m is smaller by a factor of about 10^3 at 0 °C than the absolute equilibration rate (molecule s^{-1} Pt atom^{-1}) on Pt wire cleaned by outgassing around 1100 °C,[10] and the activation energy of about 7 kcal/mol in the present study makes a contrast to the negligibly small value for Pt wire at temperatures higher than −73 °C.[10] The detailed analysis of energy level of the adsorbed hydrogen is permitted by use of the thermal desorption technique and will be presented in a subsequent paper.

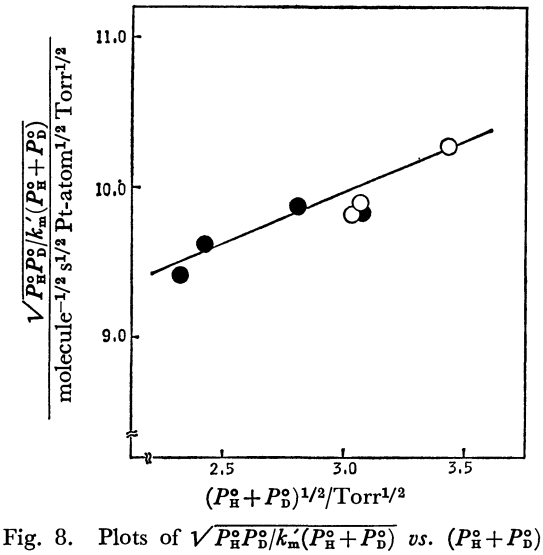

Fig. 8. Plots of $\sqrt{P_H^\circ P_D^\circ/k_m'(P_H^\circ+P_D^\circ)}$ *vs.* $(P_H^\circ+P_D^\circ)^{1/2}$.
○: $P_D=7$ Torr, $2\leq P_H\leq4.7$ Torr, ●: $P_H=5$ Torr, $0.4\leq P_D\leq4.5$ Torr. ——: Calculated line from k_d and K obtained from the total pressure dependence of the rate.

Structures of Active Sites and Role of Preadsorbed Hydrogen. There are several possibilities about the structures of the active sites of Pt–polyamide catalysts. The monoatomic dispersion of platinum metal with a suitable arrangement of appropriate amide group spacing was first proposed in order to explain the formation of cyclohexene in the benzene hydrogenation,[2] but confirmative support has not been so far obtained by other workers. Bernard *et al.*[11] observed the formation of Pt metal crystallites on nylon-66 upon heating, but showed that such an aggregation is due to the specific structure of nylon-66. Such formation is not the case in polyamide-6. On the other hand, the importance of platinum complexes containing chlorine atoms has been pointed out; Dini *et al.* reported the ratio of Cl/Pt to be 2 for 0.6 wt% Pt–nylon-6 catalyst.[3] From the diamagnetic properties of Pt on nylon, Rasadkina *et al.* concluded that platinum is non-metallic in character.[12] These results indicating the presence of Pt(II) are consistent with our XPS results.

The present kinetic results for the equilibration are well explained by the Bonhoeffer-Farkas mechanism. Since the mechanism involves the dissociative adsorption of both hydrogen and deuterium and needs at least four sites available in the neighborhood, it seems unlikely that a complex of single Pt atom can work as the active site. The requirement of such multiple sites and of the presence of a bivalent cation provides further support to the existence of the cluster such as $(Pt)_3$ which was proposed on the basis of the model discussed earlier. Although no experimental evidence has yet been obtained, it seems plausible that the clusters are analogous to complexes with bridging metal–halogen bonds. The process of activation of the catalysts probably involves the dissociation of hydrogen molecules into atoms. The splitting of the hydrogen molecule is likely to take place, since UV spectra on Rh–polyamide catalysts showed the formation of a hydride complex when the catalysts in an aqueous alcoholic solution were exposed to a hydrogen atmosphere.[13] However, the exchangeable hydrogen takes a different configuration and location on the surface from those of the preadsorbed hydrogen used for activation, because the exchange of the former hydrogen is very rapid. The difinite structure of the clusters and the conformation of the hydrogen on them have to await further study. The loss of the activity upon heating at 150 °C can be explained by a reverse process to reproduce the original complex by the desorption of hydrogen.

Exchange of Hydrogen in PA with Deuterium. The exchange rate of the structural hydrogen in PA support with gaseous deuterium at 0 °C was lower than that of H_2–D_2 equilibration by a factor of about 40 under ordinary conditions, and showed no enhancement even for the activated catalysts. The infrared spectra of Pt–PA-M systems in which hydrogen was replaced by deuterium to different extents showed that the exchange of hydrogen atoms in NH and NH_2 groups was preferentially invoked as a first step, followed by the exchange of hydrogen in the CH_2 group. These results together with those of the measurement of electric conductivity of polyamides by Eley and Spivey[14] suggest that the slow exchange described here takes place with proton diffusing on the surface and also in the bulk of the polyamide.

References

1) Y. Izumi, *Bull. Chem. Soc. Jpn.*, **32**, 932, 936, 942 (1959).
2) D. P. Harrison and H. F. Rase, *Ind. Eng. Chem. Fundam.*, **6**, 161 (1967).
3) P. Dini, D. Dones, S. Montelatini, and N. Giordano, *J. Catal.*, **30**, 1 (1973).
4) M. Yoshida, Y. Inoue, and I. Yasumori, to be published.
5) G. C. Bond, "Catalysis by Metals," Acad. Press, New York (1962), p. 315; G. C. Bond and P. B. Wells, *Adv. Catal.*, **15**, 299 (1964).
6) "Treatise on Analytical Chemistry," ed by I. M. Kolthoff and P. J. Elving, Interscience, New York (1963), Part II, Vol. 8; G. H. Ayres and A. S. Meyer, *Anal. Chem.*, **23**, 299 (1951).
7) S. Ohno and I. Yasumori, *Bull. Chem. Soc. Jpn.*, **41**, 2227 (1968).
8) P. Burroughs, A. Hamett, J. F. McGilp, and A. F. Orchard, *J. Chem. Soc., Faraday Trans. 2*, **71**, 177 (1975).
9) D. Cahen and J. E. Lester, *Chem. Phys. Lett.*, **18**, 108 (1973).
10) R. J. Breakspere, D. D. Eley, and P. R. Norton, *J. Catal.*, **27**, 215 (1972).
11) J. R. Bernard, C. Hoang-Van, and S. J. Teichner, *J. Chim. Phys.*, **72**, 735, 1217 (1975).
12) E. N. Rasadkina, A. T. Teleshev, I. D. Rozhdestvenskaya, and I. V. Kalechits, *Kinet. Catal.*, **14**, 1065 (1973).
13) E. N. Rasadkina, I. D. Rozhdestvenskaya, and I. V. Kalechits, *Kinet. Catal.*, **17**, 799 (1976).
14) D. D. Eley and D. I. Spivey, *Trans. Faraday Soc.*, **57**, 2280 (1961).

The Origin of the Polarity of a Radical in Hydrogen Abstraction Reactions

Hiroyuki SHINOHARA* and Akira IMAMURA**

Department of Radiology, Fujigaoka Hospital, Showa University, Fujigaoka, Midori-ku, Yokohama 227

***Department of Chemistry, Shiga University of Medical Science, Seta Tsukinowa-cho, Otsu 520-21*

(Received February 14, 1979)

The electrophilicity of the H atom in hydrogen abstraction reactions was studied by the CNDO/2 method. The origin of the electrophilicity of the H atom was well understood using the stabilization energy due to the delocalization of electrons (SEDE) between the radical and substrate; this energy was calculated along the reaction path. The electrophilic energy (SEDE from the substrate to the radical) governs the relative reactivities of substrates, $CH_4<CH_3CH_3<CH_3CH_2CH_3<(CH_3)_3CH$, which correspond to the order of the increase in the electron density. The electrophilic energy is also important in hydrogen abstraction by the H atom from aliphatic alcohols. In the case of the Cl_2^- radical, the nucleophilic energy (SEDE from the radical to the substrate) determines the relative reactivities of substrates, $CH_3OH<C_2H_5OH<i\text{-}C_3H_7OH$. The polarity of a free radical is tentatively clarified by using its ionization potential.

The polarities of free radicals in abstraction reactions (nucleophilicity or electrophilicity) have been examined experimentally by the Hammett or the Taft equation.[1-4] Although the equation does allow the determination of the polarity, its origin has not been clarified theoretically. In previous papers,[5] we attempted to explain the polarity of a free radical by the stabilization energy due to the delocalization of electrons (SEDE) between the radical and substrate; this was calculated by the CNDO/2 method.[6,7] The nucleophilic stabilization energy, defined by the SEDE from the radical to substrate (contribution of the structure **1** in the reacting system R···H···X), and the electrophilic stabilization energy, defined by the SEDE from substrate to the radical (structure **2** in Eq. 2), contribute in determining the relative reactivities of substrates (RH: hydrogen donor, X: radical).

$$RH + X \longrightarrow [R\cdots H\cdots X] \longrightarrow R + HX \quad (1)$$

$$[\overset{\delta-}{R}\cdots\overset{\delta+}{H}\cdots\overset{\delta+}{X} \longleftrightarrow \overset{\delta+}{R}\cdots\overset{\delta+}{H}\cdots\overset{\delta-}{X}] \quad (2)$$

1 **2**

The polarity of a free radical is correlated with the relative importance of these structures. Thus the radical is a nucleophile if the relative reactivities of substrates are governed by the nucleophilic energy (nucleophilic stabilization energy) and an electrophile when the reactivities are governed by the electrophilic energy (electrophilic stabilization energy). The electrophilicity of the OH and CH_3 radicals in hydrogen abstractions with methane derivatives or the nucleophilicity of the CH_3 radical in hydrogen abstraction with chlorinated methanes is well understood by using the SEDE.[5]

In the present work, we examined the polarity of the H atom in hydrogen abstractions with aliphatic hydrocarbons. The hydrocarbon–H system is useful to check our ideas on the polarity because the reaction path for CH_4–H system was deduced by the *ab initio* MO method,[8] which enabled us to calculate the SEDE in detail along the reaction path. The electrophilic energy changes remarkably from one substrate to another substrate, compared with the change in nucleophilic energy. The former thus plays a dominant role in determining the relative reactivities of substrates, $CH_4<CH_3CH_3<CH_3CH_2CH_3<(CH_3)_3CH$, which correspond to the order of the increase in the electron density. On the other hand, in hydrogen abstractions by the Cl_2^- radical from aliphatic alcohols, the nucleophilic energy changes remarkably compared with the electrophilic energy, although the absolute magnitude of these energies changes with a change of the geometry in the reacting system. The ionization potential of the radical is found to be the important factor determining the polarity, judging from the present results obtained in the reactions of the H atom and Cl_2^- radical.

Method of Calculation

The total energies for the reacting systems were calculated by the UHF method[9] in the CNDO/2 approximation.[6,7] The values of the parameters included in the method are the same as those used in the original papers.

Geometries used for calculation are as follows: for CH_4,[10] CH_3CH_3, $CH_3CH_2CH_3$, and $(CH_3)_3CH$, r(C–H)=1.09 Å and r(C–C)=1.54 Å; for CH_3OH,[11] C_2H_5OH, and $i\text{-}C_3H_7OH$, r(C–H)=1.094 Å, r(C–O)=1.425 Å, r(O–H)=0.945 Å, ∠COH=108.53°. The bond angles HCH for these compounds were assumed to be 109.47°.

Procedure of Analysis.[5] (i) The total energy of the reacting system [R···H···X] without the delocalization of electrons is calculated with the UHF method in the CNDO/2 approximation after dropping all the resonance integrals (I_{rs}) between atomic orbitals (AO's) on the fragment RH and those on the fragment X. Thus we obtain the MO's localized on the fragment RH and those on the fragment X. (ii) By using the MO's obtained in step (i), the modified resonance integrals between AO's (I'_{rs}) are calculated according to Eq. 3 in order to take the delocalization of electrons between particular MO's into account.

$$I'_{rs} = \sum_{(i_1-j_1)} C_{RHi_1,r} C_{Xj_1,s} I_{i_1j_1} \quad (3)$$

where $C_{RHi_1,r}$ is the coefficient of AO in the i-th MO of the substrate RH and $C_{Xj_1,s}$ is for the radical X. $\sum_{(i_1-j_1)}$ denotes the summation over a particular orbital

TABLE 1. THE SCHEMATIC REPRESENTATION OF THE ORBITAL INTERACTION BETWEEN SUBSTRATE RH AND RADICAL X[a)]

Interaction	α-Spin			β-Spin		
Electrostatic (Zero)	RH	Occ	Vac	RH	Occ	Vac
	X	Occ	Vac	X	Occ	Vac
Nucleophilic (*N*)	RH	Occ	Vac	RH	Occ	Vac
	X	Occ	Vac	X	Occ	Vac
Electrophilic (*E*)	RH	Occ	Vac	RH	Occ	Vac
	X	Occ	Vac	X	Occ	Vac

a) The orbital interaction which includes the $I_{i_1 j_1}$ is represented by a solid line. The symbol for the interaction used in the text is given in the parentheses.

set (i_1, j_1). (iii) I'_{rs} values are employed to calculate the total energy of the reacting system with the delocalization of electrons, which corresponds to the nucleophilic or the electrophilic nature of the radical in question. (iv) When the vacant MO's of the substrate and occupied MO's of the radical are chosen for i_1 and j_1, respectively, in Eq. 3, the difference between two energies obtained in steps (i) and (iii) corresponds to the SEDE from the radical to the substrate. This energy should be the nucleophilic energy; it is represented by the symbol *N*. When the occupied MO's of the substrate and the vacant MO's of the radical are chosen for i_1 and j_1, respectively, the electrophilic energy *E* is obtained. Table 1 shows the schematic representation of intermolecular interaction between the MO's of RH and X obtained by dropping the I_{rs} (they interact electrostatically with each other, but the delocalization of electrons is prohibited).

Results and Discussion

The Electrophilicity of the H Atom. The coordinate system for a hydrogen abstraction reaction by the H atom from aliphatic hydrocarbons is shown in Fig. 1. We specify the reaction path with a notation (r_1, r_2), where r_1 is the distance (in Å) between the carbon atom C^1 and the hydrogen atom H^5 to be abstracted, while r_2 is the distance between this hydrogen atom H^5 and the incoming H atom. Calculations were carried out at six path points: A(1.2, 1.1), B(1.3, 0.95), C(1.365, 0.873), D(1.38, 0.85), E(1.5, 0.80), and F(1.7, 0.75), which are very nearly on the potential valley deduced by *ab initio* calculations.[8)] Figure 2a shows the correlation of the activation energy[12)] and the electron density on the hydrogen atom. The activation energy decreases with an increase in the electron density. The origin of the electrophilicity of the H atom can be understood by *N* and *E*, as summarized in Tables 2a—2f. *E* is about 6—10 times larger than *N* before transition state (C) and after the state, the difference becomes nearly constant as the reaction proceeds. When the substrate changes from CH_4 to CH_3CH_3, $CH_3CH_2CH_3$, or $(CH_3)_3CH$,

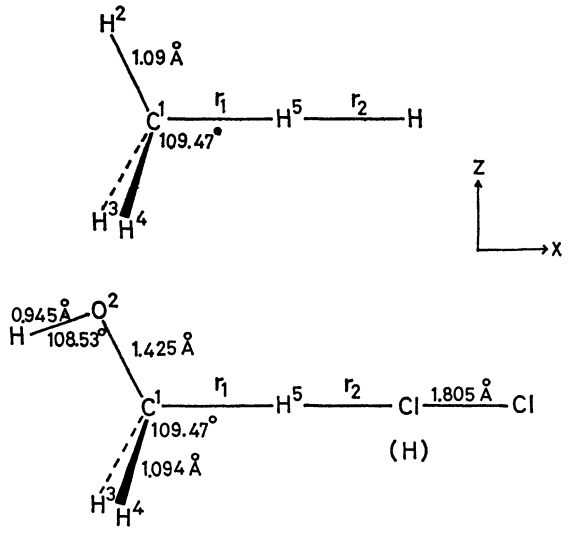

Fig. 1. The coordinate systems for hydrogen abstractions by the H atom and the Cl_2^- radical from CH_4 and CH_3OH, respectively.

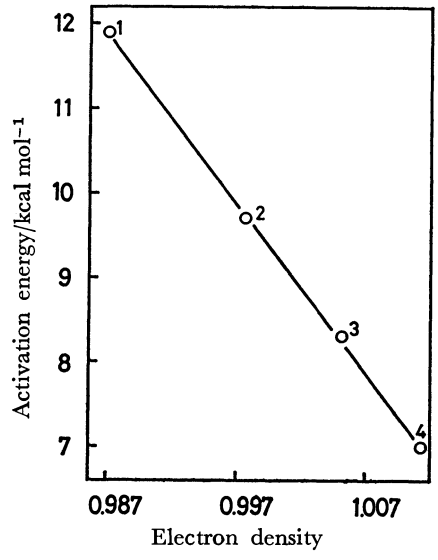

Fig. 2a. The correlation of the activation energy[12)] and the electron density in hydrogen abstraction by the H atom from aliphatic hydrocarbons. 1: CH_4, 2: CH_3CH_3, 3: $CH_3CH_2CH_3$, 4: $(CH_3)_3CH$.

E increases remarkably with the increasing number of electron donating CH_3 groups, while *N* does not change significantly in any substrate. The contribution of the structure **2** in the reacting system is an important factor in determining the relative reactivities of substrates, and thus the reactivities are explained by *E*, as is shown in Fig. 2b. The electrophilicity of the H atom suggested by the electron density is ascribable to the correlation of the electron density and *E* in Fig. 2c.

The Nucleophilicity of the Cl_2^- Radical. Radical anions $(Br_2^-$, $(CNS)_2^-$, CO_3^-, and $Cl_2^-)$ are known as the free radical probes which attack specific residues in enzymes[13,14)] and give the information on the active sites. In comparison with OH radical, the radical anions are highly selective in reactions with amino acid residues. The polarity of the radical anion is

Table 2a. The SEDE for hydrocarbon-H system in the path point A(1.2, 1.1)

Substrates	Orbital[a] interaction	Total[b] energy	SEDE[b]	ET[c]
CH_4	Zero	−10.7030	0	0
	N	−10.7075	0.0045	0.0079
	E	−10.7473	0.0443	−0.0718
CH_3CH_3	Zero	−19.3987	0	0
	N	−19.4033	0.0046	0.0081
	E	−19.4437	0.0450	−0.0762
$CH_3CH_2CH_3$	Zere	−28.0894	0	0
	N	−28.0941	0.0047	0.0083
	E	−28.1349	0.0455	−0.0801
$(CH_3)_3CH$	Zero	−36.7764	0	0
	N	−36.7811	0.0047	0.0085
	E	−36.8223	0.0459	−0.0829

a) See the notes in Table 1. b) Atomic units. c) Electron transfer quantities due to delocalization of electrons. Positive values correspond to those from the radical to substrate and negatives, *vice versa*.

Table 2b. The SEDE for hydrocarbon-H system in the path point B(1.3, 0.95)

Substrates	Orbital[a] interaction	Total[b] energy	SEDE[b]	ET[c]
CH_4	Zero	−10.6445	0	0
	N	−10.6530	0.0085	0.0168
	E	−10.7085	0.0640	−0.1087
CH_3CH_3	Zero	−19.3414	0	0
	N	−19.3500	0.0086	0.0170
	E	−19.4066	0.0652	−0.1158
$CH_3CH_2CH_3$	Zero	−28.0332	0	0
	N	−28.0419	0.0087	0.0170
	E	−28.0993	0.0661	−0.1209
$(CH_3)_3CH$	Zero	−36.7213	0	0
	N	−36.7300	0.0087	0.0173
	E	−36.7882	0.0669	−0.1263

a)—c) See the notes in Table 2a.

Table 2c. The SEDE for hydrocarbon-H system in the path point C(1.365, 0.873)

Substrates	Orbital[a] interaction	Total[b] energy	SEDE[b]	ET[c]
CH_4 (11.9)[d]	Zero	−10.5959	0	0
	N	−10.6078	0.0120	0.0249
	E	−10.6723	0.0765	−0.1338
CH_3CH_3 (9.7)	Zero	−19.2936	0	0
	N	−19.3056	0.0120	0.0252
	E	−19.3717	0.0781	−0.1426
$CH_3CH_2CH_3$	Zero	−27.9862	0	0
(8.3)	*N*	−27.9983	0.0121	0.0256
	E	−28.0656	0.0794	−0.1489
$(CH_3)_3CH$	Zero	−36.6751	0	0
(7.0)	*N*	−36.6873	0.0121	0.0260
	E	−36.7556	0.0805	−0.1554

a)—c) See the notes in Table 2a. d) Activation energy (kcal/mol).[12]

Table 2d. The SEDE for hydrocarbon-H system in the path point D(1.38, 0.85)

Substrates	Orbital[a] interaction	Total[b] energy	SEDE[b]	ET[c]
CH_4	Zero	−10.5808	0	0
	N	−10.5939	0.0131	0.0276
	E	−10.6616	0.0808	−0.1418
CH_3CH_3	Zero	−19.2789	.	0
	N	−19.2920	0.0131	0.0279
	E	−19.3613	0.0824	0.1510
$CH_3CH_2CH_3$	Zero	−27.9716	0	0
	N	−27.9849	0.0133	0.0283
	E	−28.0555	0.0839	−0.1577
$(CH_3)_3CH$	Zero	−36.6607	0	0
	N	−36.6740	0.0133	0.0282
	E	−36.7457	0.0850	−0.1645

a)—c) See the notes in Table 2a.

Table 2e. The SEDE for hydrocarbon-H system in the path point E(1.5, 0.80)

Substrates	Orbital[a] interaction	Total[b] energy	SEDE[b]	ET[c]
CH_4	Zero	−10.5051	0	0
	N	−10.5251	0.0200	0.0462
	E	−10.5950	0.0898	−0.1680
CH_3CH_3	Zero	−19.2051	0	0
	N	−19.2250	0.0199	0.0465
	E	−19.2973	0.0922	−0.1791
$CH_3CH_2CH_3$	Zero	−27.8997	0	0
	N	−27.9195	0.0198	0.0469
	E	−27.9937	0.0940	−0.1883
$(CH_3)_3CH$	Zero	−36.5903	0	0
	N	−36.6102	0.0199	0.0475
	E	−36.6859	0.0959	−0.1962

a)—c) See the notes in Table 2a.

Table 2f. The SEDE for hydrocarbon-H system in the path point F(1.7, 0.75)

Substrates	Orbital[a] interaction	Total[b] energy	SEDE[b]	ET[c]
CH_4	Zero	−10.3827	0	0
	N	−10.4176	0.0349	0.0913
	E	−10.4857	0.1030	−0.2156
CH_3CH_3	Zero	−19.0863	0	0
	N	−19.1213	0.0350	0.0925
	E	−19.1929	0.1066	−0.2289
$CH_3CH_2CH_3$	Zero	−27.7841	0	0
	N	−27.8191	0.0350	0.0936
	E	−27.8934	0.1093	−0.2393
$(CH_3)_3CH$	Zero	−36.4776	0	0
	N	−36.5130	0.0354	0.0947
	E	−36.5890	0.1114	−0.2474

a)—c) See the notes in Table 2a.

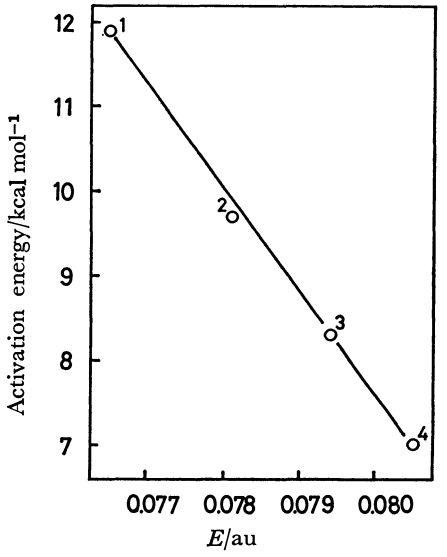

Fig. 2b. The correlation of the activation energy and the electrophilic energy E (in path point C) in hydrogen abstraction by the H atom from aliphatic hydrocarbons. 1—4, see the caption in Fig. 2a.

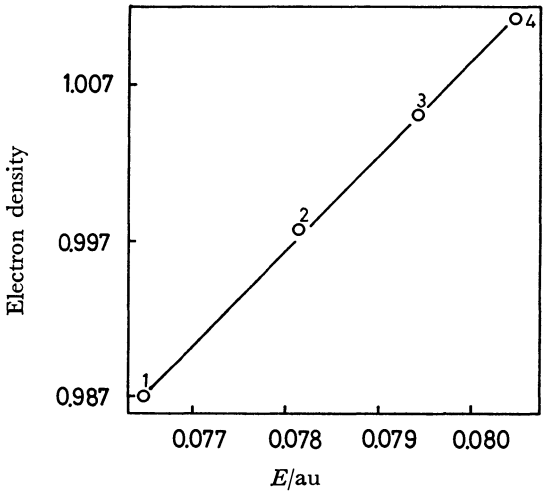

Fig. 2c. The correlation of the electron density and the electrophilic energy E (in path point C) in hydrogen abstraction by the H atom from aliphatic hydrocarbons. 1—4, see the caption in Fig. 2a.

interesting from a theoretical point of view since it has a negative charge, unlike a neutral radical. In the present work, we calculated the SEDE in hydrogen abstraction by the Cl_2^- radical from aliphatic alcohols[15] by assuming the following reaction paths: A(1.2, 1.4), B(1.3, 1.4), C(1.4, 1.3), and D (1.5, 1.27). Calculations were also carried out for hydrogen abstraction by the H atom from aliphatic alcohols[16] to study the factors which determine the polarity of a radical. The coordinate systems for these reactions are shown in Fig. 1. The optimized Cl–Cl distance of the Cl_2^- radical is 1.805 Å. It is slightly longer than that of Cl_2 molecule (1.75 Å).[17] Table 3 shows the result for the H atom. As is shown in the previous section, the electrophilic energy governs the relative reactivities of alcohols, which confirms the electrophilicity of the H atom (Fig. 3). Although the points A, B, C, and

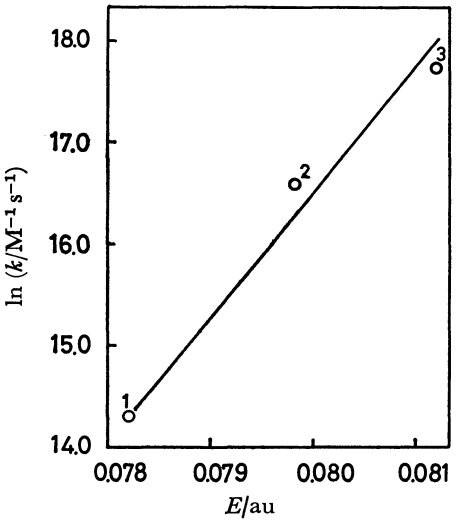

Fig. 3. The correlation of the rate constant[16] and the electrophilic energy E (in path point C) in hydrogen abstraction by the H atom from aliphatic alcohols. 1: CH_3OH, 2: C_2H_5OH, 3: i-C_3H_7OH.

TABLE 3. THE SEDE IN ALCOHOL-H SYSTEM

Path point	Substrates	Orbital[a] interaction	Total[b] energy	SEDE[b]	ET[c]
B	CH_3OH	Zero	−29.0907	0	0
		N	−29.0991	0.0084	0.0165
		E	−29.1559	0.0652	−0.1153
	C_2H_5OH	Zero	−37.7878	0	0
		N	−37.7962	0.0084	0.0165
		E	−37.8542	0.0664	−0.1222
	i-C_3H_7OH	Zero	−46.4778	0	0
		N	−46.4861	0.0083	0.0167
		E	−46.5453	0.0675	−0.1283
C	CH_3OH (1.6)[d]	Zero	−29.0431	0	0
		N	−29.0550	0.0119	0.0249
		E	−29.1213	0.0782	−0.1421
	C_2H_5OH (16)[d]	Zero	−37.7411	0	0
		N	−37.7528	0.0117	0.0249
		E	−37.8209	0.0798	−0.1504
	i-C_3H_7OH (50)[d]	Zero	−46.4319	0	0
		N	−46.4436	0.0117	0.0251
		E	−46.5131	0.0812	−0.1578
D	CH_3OH	Zero	−29.0285	0	0
		N	−29.0413	0.0128	0.0276
		E	−29.1110	0.0825	−0.1505
	C_2H_5OH	Zero	−37.7266	0	0
		N	−37.7394	0.0128	0.0276
		E	−37.8109	0.0843	−0.1593
	i-C_3H_7OH	Zero	−46.4176	0	0
		N	−46.4304	0.0128	0.0278
		E	−46.5034	0.0858	−0.1669

a)—c) See the notes in Table 2a. d) Rate constant (10^6 M^{-1} s^{-1}).[16]

D were tentatively chosen for the reaction of the Cl_2^- radical, an interesting result was obtained, as is shown in Table 4. When the C^1–H^5 bond is not elongated far from the equilibrium C–H bond distance, the electrophilic energy is larger than the nucleophilic

Table 4. The SEDE for alcohol-Cl_2^- system

Path point	Substrates	Orbital[a] interaction	Total[b] energy	SEDE[b]	ET[c]
A	CH_3OH	Zero	−60.9592	0	0
	(0.035)[d]	*N*	−61.0001	0.0409	0.0906
		E	−61.0186	0.0594	−0.0646
	C_2H_5OH	Zero	−69.6550	0	0
	(0.45)[d]	*N*	−69.6978	0.0428	0.0967
		E	−69.7146	0.0596	−0.0656
	i-C_3H_7OH	Zero	−78.3439	0	0
	(1.2)[d]	*N*	−78.3879	0.0440	0.1028
		E	−78.4037	0.0598	−0.0666
B	CH_3OH	Zero	−60.9341	0	0
		N	−60.9894	0.0553	0.1309
		E	−60.9892	0.0551	−0.0630
	C_2H_5OH	Zero	−69.6308	0	0
		N	−69.6875	0.0567	0.1395
		E	−69.6861	0.0553	−0.0642
	i-C_3H_7OH	Zero	−78.3205	0	0
		N	−78.3788	0.0583	0.1482
		E	−78.3761	0.0556	−0.0653
C	CH_3OH	Zero	−60.8363	0	0
		N	−60.9177	0.0814	0.1951
		E	−60.9001	0.0638	−0.0769
	C_2H_5OH	Zero	−69.5339	0	0
		N	−69.6175	0.0836	0.2071
		E	−69.5981	0.0642	−0.0784
	i-C_3H_7OH	Zero	−78.2247	0	0
		N	−78.3104	0.0857	0.2189
		E	−78.2891	0.0644	−0.0797
D	CH_3OH	Zero	−60.7704	0	0
		N	−60.8751	0.1047	0.2521
		E	−60.8341	0.0637	−0.0805
	C_2H_5OH	Zero	−69.4691	0	0
		N	−69.5765	0.1074	0.2729
		E	−69.5332	0.0641	−0.0821
	i-C_3H_7OH	Zeru	−78.1609	0	0
		N	−78.2708	0.1099	0.2869
		E	−78.2254	0.0645	−0.0833

a)—c) See the notes in Table 2a. d) Rate constant ($10^4\ M^{-1}\ s^{-1}$).[15]

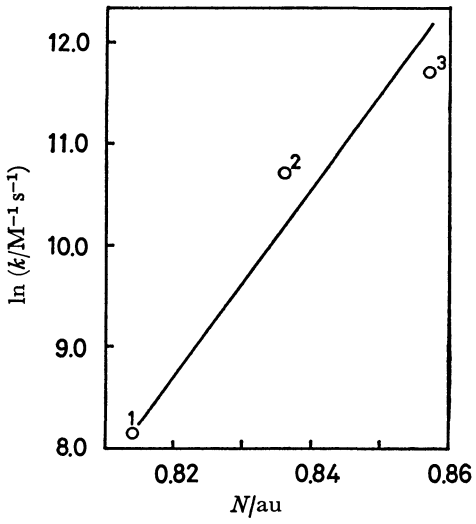

Fig. 4. The correlation of the rate constant[15] and the nucleophilic energy *N* (in path point C) in hydrogen abstraction by the Cl_2^- radical from aliphatic alcohols. 1—3, see the caption in Fig. 3.

Table 5. The correlation of the ρ values in hxdrogen abstractions and the ionization potentials

Radicals	Ionization[a] potential/eV	Electron[b] affinity/eV	ρ value[c]
t-C_4H_9	7.07		1.0
i-C_3H_7	7.90		0.8
n-C_3H_7	8.69	0.69	
C_2H_5	8.67	0.94	
CH_3	9.86	1.4	−0.1—0
C_6H_5	9.90	2.21	−0.1
H	13.16	0.80	−0.3
CCl_3	8.78	1.22	−1.46
CF_3	8.90, 10.15	1.85	
OH	13.18	1.83	−0.96[d]
Cl	13.01	3.61	−0.8——1.9

a) Ref. 19. b) Ref 20. c) Ref 4d. d) ρ value for hydrogen abstraction with substituted methanes. Ref. 4e.

energy, but the latter increases as the C^1–H^5 bond is elongated. Thus, at the initial stage, the SEDE from the substrate to the radical is a driving force of the reaction; but as the reaction proceeds, the SEDE from the radical to the substrate is an important force in completing the reaction. It is noteworthy that although the absolute magnitude of *N* or *E* changes along the reaction path, the nucleophilic energy governs the relative reactivities of alcohols, as is shown in Fig. 4.[5c,5] Therefore the Cl_2^- radical reacts as a nucleophile.

Both frontier electron densities of HOMO (f_{HOMO}) and LUMO (f_{LUMO}) on the α hydrogen atom of alcohol[18] increase as follows: CH_3OH (f_{HOMO}: 0.234, f_{LUMO}: 0.185); C_2H_5OH (f_{HOMO}: 0.297, f_{LUMO}: 0.347); *i*-C_3H_7OH (f_{HOMO}: 0.314, f_{LUMO}: 0.592). In the case of the Cl_2^- radical, the electrophilic or the nucleophilic energy increases with an increase in f_{HOMO} or f_{LUMO}, respectively, while the nucleophilic energy does not increase in hydrogen abstractions by the H atom. The SOMO of the Cl_2^- radical (an electron occupies the LUMO of Cl_2 molecule) is high enough so that the increase of f_{LUMO} contributes largely to the increase in the nucleophilic energy, while the SOMO of the H atom is so low that the above situation is not attainable. The result obtained here leads to the conclusion that a radical having a low ionization potential is a nucleophile and one having a high potential is an electrophile. Table 5 shows the correlation of the ρ values in hydrogen abstractions by radicals[4d] and the ionization potentials. It is expected that C_2H_5 radical will react as a weak nucleophile with substituted toluenes. Although the CH_3 radical reacts as an electrophile in this case, it reacts as a nucleophile in hydrogen abstractions with chlorinated methanes.[5d] As the ionization potential of the CH_3 radical is not

so high as that of the electrophilic OH radical or Cl atom, the nucleophilic energy will change largely from substrate to substrate in a nucleophilic reaction. Therefore a radical having a moderate ionization potential reacts as an electrophile or a nucleophile according to the nature of the substrate.

We would like to express our gratitude to the Computer Center, Tokyo University, for its generous permission to use the HITAC 8700/8800 computer.

References

1) C. Walling, "Free Radicals in Solution," Wiley, New York, N. Y. (1957), pp. 132—140, 365—369, 375—376, 474—491.

2) W. A. Pryor, "Free Radicals," McGraw-Hill, New York, N. Y. (1966), p. 170 ff.

3) L. E. Leffler and E. Grunwald, "Rates and Equilibria of Organic Reaction," Wiley, New York, N. Y. (1963), p. 177 ff.

4) a) J. A. Howard and K. U. Ingold, *Can. J. Chem.*, **41**, 1744 (1963); b) G. A. Russel and R. C. Williamson, *J. Am. Chem. Soc.*, **86**, 2357 (1964); c) M. A. DaRooge and L. R. Mahoney, *J. Org. Chem.*, **32**, 1 (1967), and references cited therein; d) ρ values for hydrogen abstractions by radicals from substituted toluenes are summarized by W. A. Pryor, T. H. Lin, J. P. Stanley, and R. W. Henderson, *J. Am. Chem. Soc.*, **95**, 6993 (1973); e) M. Anbar, D. Meyerstein, and P. Neta, *J. Chem. Soc., B*, **1966**, 742; f) Y. Nagai, K. Yamazaki, I. Shiojima, N. Kobori, and M. Hayashi, *J. Organomet. Chem.*, **9**, 21 (1967); g) H. Sakurai and K. Mochida, *J. Organomet. Chem.*, **42**, 339 (1972).

5) a) H. Shinohara, A. Imamura, T. Masuda, and M. Kondo, *Bull. Chem. Soc. Jpn.*, **51**, 1917 (1978); b) A. Imamura and K. Hirao, *ibid.*, **52**, 287 (1979); c) H. Shinohara, A. Imamura, T. Masuda, and M. Kondo, *ibid.*, **52**, 974 (1979); d) H. Shinohara, A. Imamura, T. Masuda, and M. Kondo, *ibid.*, **52**, 2801 (1979).

6) J. A. Pople, D. P. Santry, and G. A. Segal, *J. Chem. Phys.*, **43**, s129 (1965); J. A. Pople and G. A. Segal, *ibid.*, **43**, s136 (1965).

7) J. A. Pople and G. A. Segal, *J. Chem. Phys.*, **44**, 3289 (1966).

8) K. Morokuma and R. E. Davis, *J. Am. Chem. Soc.*, **94**, 1060 (1972).

9) J. A. Pople and P. K. Nesbet, *J. Chem. Phys.*, **33**, 571 (1954).

10) H. C. Allen and E. K. Plyler, *J. Chem. Phys.*, **26**, 972 (1957).

11) "Molecular Structures and Dimensions," ed by O. Kennard and D. G. Watson, Crystallographic Data Centre Cambridge, International Union of Crystallography, N. V. A. Oosthoek's Uitegevers Mij Utrecht (1972), Vol. Al.

12) R. R. Baldwin and R. W. Walker, *J. Chem. Soc., Perkin Trans. 2*, **1973**, 362.

13) G. A. Adams, R. B. Cundall, and R. L. Willson, "Chemical Reactivity and Biological Role of Functional Groups in Enzymes," ed by R. M. Smellie, Academic Press, New York (1970), p. 71.

14) J. E. Aldrich, R. B. Cundall, G. E. Adams, and R. L. Willson, *Nature*, **221**, 1049 (1969).

15) K. Hasegawa and P. Neta, *J. Phys. Chem.*, **82**, 854 (1978).

16) A. Appleby, G. Scholes, and M. Simic, *J. Am. Chem. Soc.*, **85**, 3891 (1963).

17) The experimental value of Cl–Cl bond distance in Cl_2 molecule is 1.988 Å. "Tables of Interatomic Distances and Configuration in Molecules and Ions," ed by L. E. Sutton, Chemical Society, London (1958).

18) The α hydrogen atoms of aliphatic alcohols are reported to more reactive than β or γ hydrogen atoms, therefore the SEDE was calculated for α hydrogen atoms. Ref. 4e; H. Shinohara, A. Imamura, T. Masuda, and M. Kondo, *Bull. Chem. Soc. Jpn.*, **51**, 98 (1978).

19) "Mass Spectrometry of Organic Ions," ed by F. W. McLatterty, Academic Press, N. Y. (1963), Chap. 5.

20) F. M. Page, "Hand Book of Chemistry and Physics," 53rd ed, CRC Press (1972—1973).

The Reaction of Recoil ^{35}S Atoms with Organic Compounds. II. The Insertion Reaction of Recoil ^{35}S Atoms into the C–H and C–C Bonds in Ethane in the Gas Phase

Kazuhiro NIISAWA* and Ko TAKI

Faculty of Industrial Hygiene, Kitasato University, Asamizodai, Sagamihara, Kanagawa 228

(Received March 3, 1979)

The sulfur atoms produced by the nuclear transformation of $^{35}Cl(n,p)^{35}S$ were allowed to react with gaseous ethane in the presence or in the absence of radical scavengers. The products were hydrogen sulfide, methanethiol, ethanethiol, dimethyl sulfide, and other sulfur-containing compounds. The yield of the C–H insertion product (ethanethiol) increased upon the addition of a small amount of the scavenger and then decreased with an increase in the amount of the scavenger to give a constant value, but the yield of the C–C insertion product (dimethyl sulfide) did not vary. The increase in the ethanethiol yield at low concentrations of the scavenger may be ascribed to a protective effect by the scavenger. By the addition of ethanethiol before thermal-neutron irradiation, the yield of ethanethiol was increased, but that of dimethyl sulfide was not increased, therefore the primary yield of ethanethiol could be determined. The spin state of the reactive sulfur atoms in the thermal-insertion reaction was also estimated to be the ^3P state upon the addition of COS and C_2H_4.

Recently, there have been intensive investigations of the reactivities of the sulfur atoms generated by the photolysis of COS and by nuclear transformations. Kremer and Spicer have studied the reactions of recoil ^{35}S or ^{38}S atoms produced from ^{34}S or ^{40}Ar atoms with several reactants.[1,2]

Church and Rowland have also investigated the reaction of ^{35}S atoms produced from ^{35}Cl atoms with propane; they found that the atoms are predominantly inserted into the secondary C–H bond in the triplet state.[3]

The sulfur atoms generated photolytically from COS can be inserted into the C–H bond of hydrocarbons to produce the corresponding thiols. These insertion reactions have been investigated in detail by Strausz and Gunning;[4] they have established that the atoms can be inserted into the C–H bond in ethane in the singlet state.

In our previous paper,[5] it has been demonstrated that the recoil sulfur atoms produced by the nuclear transformation of $^{35}Cl(n,p)^{35}S$ in the liquid phase are capable of being inserted into the C–C bond of 2-methylbenzothiazole by the energetic process, and that the insertion into the C–H bond of benzothiazole takes place not only in the energetic process but also in other processes, such as the thermal and the dissociation processes.

In this paper, the primary yield of sulfur compounds in the reaction of the sulfur atoms produced by the nuclear transformation of $^{35}Cl(n,p)^{35}S$ process with gaseous ethane will be estimated, and the ratio of the insertion rate of the C–H bond to that of the C–C bond will be decided. Also, the spin state of the sulfur atoms in this reaction will be discussed.

Experimental

Materials. Ethane (purchased from the Takachiho Chem. Co.; purity, 99.9%) and dichlorodifluoromethane as a chlorine source (Asahi Glass Co., Ltd.; purity, 99.8%) were purified by trap-to-trap distillation.

Methanethiol, ethanethiol, and dimethyl sulfide were also purified by trap-to-trap distillation before use. Carbonyl sulfide (prepared from KSCN and sulfuric acid) and hydrogen sulfide (prepared from NaSH and hydrochloric acid) were purified by gas-chromatographic separation using a silica-gel column.

Nitrogen monoxide was purified by trap-to-trap distillation, while oxygen from the tank was purified by passing it through a NaOH trap to remove a trace amount of carbon dioxide.

Thermal-neutron Irradiation. Thermal neutron irradiation was carried out by means of a Triga Mark II nuclear reactor (Institute for Atomic Energy, Rikkyo University) at a thermal-neutron flux of about 1.5×10^{12} n cm^{-2} s^{-1} for 1 h.

A mixture of ethane and dichlorodifluoromethane was irradiated in a quartz ampoule (about 5 ml) at a total pressure of about 700 Torr.†

The ratio of the ethane pressure to the dichlorodifluoromethane pressure was 2.05 ± 0.02. Additives were also added to this system. The irradiation was carried out in the gas phase and at a reactor temperature of about 40 °C. The irradiated samples were stored below −78 °C and then at −196 °C until analysis.

The Separation and the Purification of the Reaction Products. Carriers [carbonyl sulfide, hydrogen sulfide, methanethiol, ethanethiol, dimethyl sulfide, carbon disulfide, ethyl methyl sulfide, and diethyl sulfide (about 0.2×10^{-5}—0.5×10^{-5} mol each; Tokyo Kasei Co.; purity, above 98% except for hydrogen sulfide and carbonyl sulfide)] were added to avoid the loss of trace amounts of ^{35}S-labeled compounds during separation and purification. The separation and the purification of the products were performed by means of a gas-chromatograph equipped with a thermal conductivity cell, using hydrogen as the carrier gas. The column contained 15% tritolyl phosphate, 15% *m*-bis(*m*-phenoxy phenoxy) benzene (polyphenyl ether, 5 rings), 15% squalane and 10% α-[4-(1,1,3,3-tetramethyl butyl)phenyl]-ω-hydroxy poly(oxy-1,2-ethanediyl) [Triton-X 305] on Chromosorb-T (40—60 mesh) in stainless steel tubes (3-mm diameter; 7 m, 5 m, 3 m, and 2 m long).

The Reduction of the Reaction Products to $H_2{}^{35}S$.[6] Each eluted sulfur compounds from the gas-chromatograph was passed through quartz tube containing platinized quartz wool as a catalyst and heated above 800 °C to produce hydrogen sulfide-^{35}S. The hydrogen sulfide thus produced was trapped at the temperature of liquid nitrogen. The reduction efficiency was about 60—80%.

The Radioassay of the Reaction Products. The amount and the radioactivity of hydrogen sulfide was measured by

† 1 Torr=133.3 Pa.

means of a radio-gas-chromatograph equipped with a thermal conductivity cell and with a proportional flow counter. The specific radioactivity of each product was determined by comparing the mass peak area with the radioactivity of the hydrogen sulfide.

The radiochemical yield was determined from the specific radioactivity of each product and the standard hydrogen sulfide obtained by the simultaneous irradiation of ammonium chloride in the following processes:

$$NH_4Cl \xrightarrow{\text{irradiation with thermal neutrons}} {}^{35}S \xrightarrow[\text{oxidation by } HNO_3]{Na_2SO_4\text{(carrier)}} {}^{35}SO_4^{2-} \xrightarrow{BaCl_2\ aq} Ba^{35}SO_4 \xrightarrow[Pt\text{(catalyst)}]{H_2 \text{ at } 900\,^\circ C} Ba^{35}S^{9)} \xrightarrow[H_3PO_4]{} H_2{}^{35}S^{10)}$$

The column for the quantitative determination of the hydrogen sulfide consisted of silica gel (60—80 mesh) in a stainless steel tube (2 m long, 3-mm diameter).

No isotopic exchange was found between the products and the carriers, as confirmed by the following experimental fact. The methanethiol separated gas-chromatographically from a mixture of labeled hydrogen sulfide-^{35}S, ethanethiol-^{35}S and non-radioactive methanethiol did not show any radioactivity under the same experimental conditions as those in the analysis of the reaction product. The standard deviation in the figures represents the experimental error in 2 or more runs.

Results and Discussion

The Effects of the Radical Scavenger. When recoil sulfur atoms react with an organic compound, roughly two processes (thermal and energetic) must be considered. In order to eliminate the thermal process, radical scavengers have been used in a number of recoil and radiation chemical studies. Nitrogen monoxide has been used as a radical scavenger by Hyder and Markowitz in the reactions of recoil sulfur atoms with hydrogen sulfide and other reactants.[11] Oxygen has been also used by Lee and his coworkers in the reactions of recoil sulfur atoms with CO and CO_2 to produce $CO^{35}S$, especially, it may be said that oxygen reacts fast with the triplet sulfur atoms.[13]

The effects of the scavenger on the formations of the two insertion products are shown in Fig. 1. The formation of dimethyl sulfide was not affected by the addition of NO, but the yield of ethanethiol was affected by the addition of NO.

The results of the effects of the scavenger show that both the thermal and energetic processes are obviously involved in the formation of ethanethiol, but the thermal process sensitive to NO may not be involved in the formation of dimethyl sulfide. This sulfide formation seems to be inserted directly by means of the recoil sulfur atoms with excess translational energy into the C–C bond.[14] The insertion of a diradical into the C–C bond in the thermal reaction has not been known. The fact that the C–C insertion takes place only in the energetic process may not conflict with usual chemical reactions. This finding had already been discussed in a previous paper.[5]

Figure 1 shows that the yield of ethanethiol increases slightly at the low concentration of NO, but as the concentration of NO is increased the yield decreases

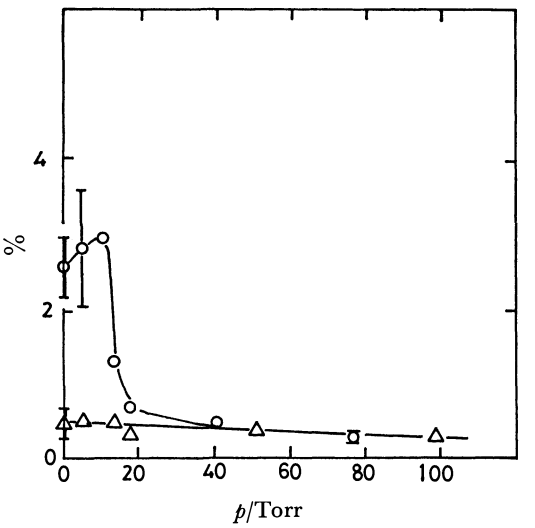

Fig. 1. Plots of the yield of ethanethiol and dimethyl sulfide as a function of NO pressure.
○: Ethanethiol, △: dimethyl sulfide.

to about 0.4%. This may be considered to show that the increase is due to a protective effect by the radical scavenger. The main characteristic of the action of NO may be the high reactivity with radicals or fragments, which reduce the thiol yield.

Thiols are easily decomposed by radicals and by some other fragments formed in an irradiated system. These types of behavior have also been seen in the reaction of recoil tritium atoms with pure ethane[16] in the presence of oxygen and in the reactions of recoil carbon atoms with methane[17] and ammonia,[18] in which the increases the yields of ethylene-t and methylamine have been ascribed to the protective effect of oxygen.[19]

The Addition of Thiols and Dimethyl Sulfide. If an additive which is identical with a product is present in the reaction system before the irradiation, the product may be protected from the attack of radicals formed by radiation, and then the primary yield may be estimated, because the number of additive molecules is much greater than that of the product molecules formed in the system. The effects of the additives on the formation of ethanethiol and dimethyl sulfide are shown in Figs. 2—4 in the presence or in the absence of *ca.* 20 Torr oxygen as a radical scavenger. By the addition of ethanethiol the yield of radioactive ethanethiol increased in both the presence and the absence of the radical scavenger.

This increase suggests that the sulfur atoms also react with added thiol by means of the collisional exchange with the sulfur in the added ethanethiol. Then the intercept of the plots of the thiol yield in the scavenged and non-scavenged systems in Fig. 2 may give the primary yield of ethanethiol in the energetic and the sum of the energetic and thermal processes.

The values are 0.4% and 3.7% respectively. The difference in the yield (dotted line) of ethanethiol between that in the presence and that in the absence of the scavenger in Fig. 2 increases slightly. This

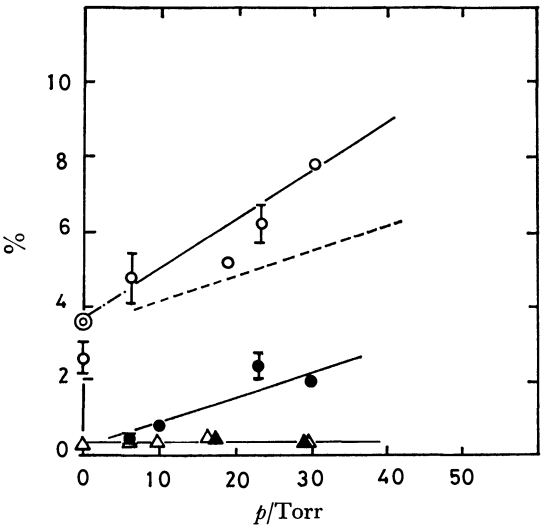

Fig. 2. Plots of the yield of ethanethiol and dimethyl sulfide as a function of the pressure of added ethanethiol or the added dimethyl sulfide in the presence or in the absence of O_2.
○: Ethanethiol in the absence of O_2, ●: ethanethiol in the presence of *ca.* 20 Torr O_2, △: dimethyl sufide in the absence of O_2, ▲: dimethyl sulfide in the presence of *ca.* 20 Torr O_2, ◎: intercept of the plots of ethanethiol yield in the absence of O_2, ……: difference between the yield in the absence of O_2 and in the presence of O_2.

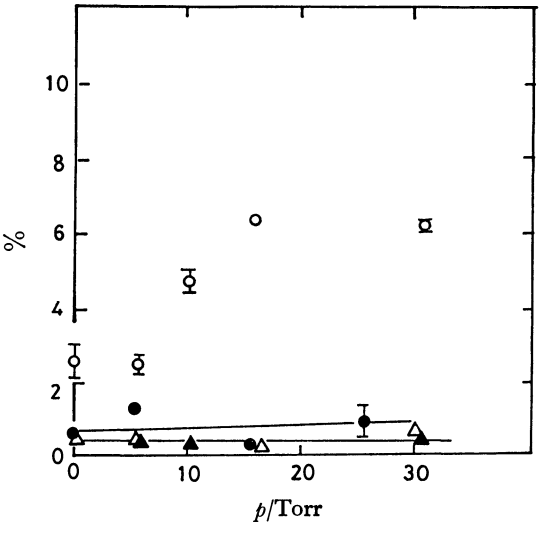

Fig. 3. Plots of the yield of ethanethiol and dimethyl sulfide as a function of the pressure of added methanethiol.
○: Ethanethiol in the absence of O_2, ●: ethanethiol in the presence of *ca.* 20 Torr O_2, △: dimethyl sulfide in the absence of O_2, ▲: dimethyl sulfide in the presence of *ca.* 20 Torr O_2.

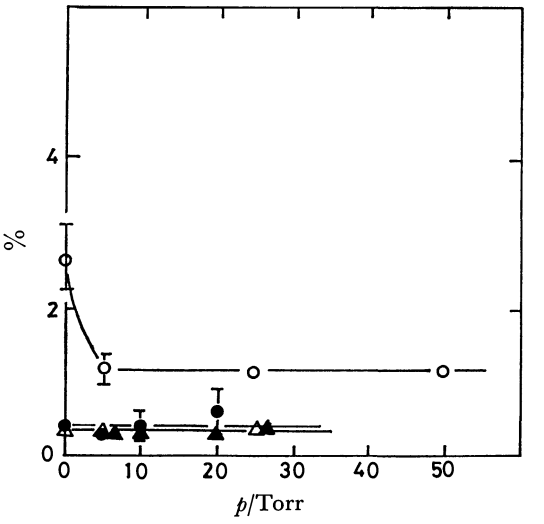

Fig. 4. Plots of the yield of ethanethiol and dimethyl sulfide as a function of the pressure of added hydrogen sulfide.
○: Ethanethiol in the absence of O_2, ●: ethanethiol in the presence of *ca.* 20 Torr O_2, △: dimethyl sulfide in the absence of O_2, ▲: dimethyl sulfide in the presence of *ca.* 20 Torr O_2.

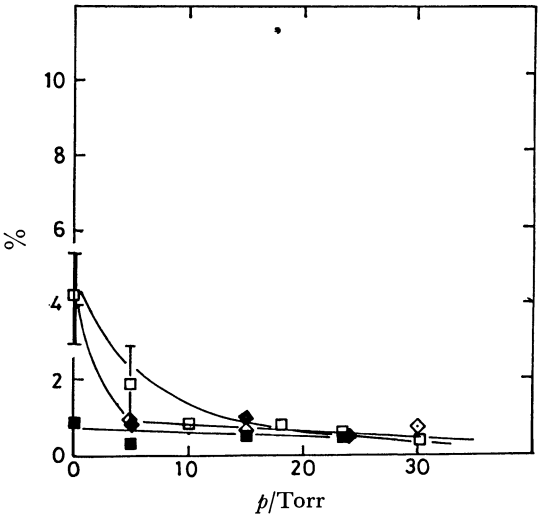

Fig. 5. Plots of the yield of diethyl sulfide as a function of the pressure of added methanethiol and added ethanethiol in the presence or in the absence of *ca.* 20 Torr O_2.
◇: Diethyl sulfide in the presence of methanethiol and in the absence of O_2, ◆: diethyl sulfide in the presence of methanethiol and in the presence of *ca.* 20 Torr O_2, □: diethyl sulfide in the presence of ethanethiol and in the absence of O_2, ■: Diethyl sulfide in the presence of ethanethiol and in the presence of *ca.* 20 Torr O_2.

indicates that there are other thermal processes involved in the formation of ethanethiol. One of these processes may be the hydrogen exchange of $C_2H_5{}^{35}S\cdot$ species with the added thiols. The radioactive ethylthio radical may react with ethanethiol to give radioactive ethanethiol, as in (1); it also reacts with methanethiol to give the ethanethiol, as in (2), by almost the same S–H bond dissociation energy as that of ethanethiol, as is shown in Fig. 3.

$$C_2H_5{}^{35}S\cdot + C_2H_5SH \longrightarrow C_2H_5{}^{35}SH + C_2H_5S\cdot \quad (1)$$

$$C_2H_5{}^{35}S\cdot + CH_3SH \longrightarrow C_2H_5{}^{35}SH + CH_3S\cdot \quad (2)$$

However it does not react with hydrogen sulfide by means of a higher S–H bond dissociation energy than that of the thiols ($\Delta D = 17.7$ kJ mol^{-1}).[20]

Figure 4 shows the decrease in the ethanethiol yield as the hydrogen sulfide is increased. The existence of the ethylthio radical is also supported by the following experimental fact.

The yield of diethyl sulfide decreases drastically in the presence of ethanethiol and methanethiol as is shown in Fig. 5.

The formation mechanism of this sulfide may be mainly considered to be the combination of ethylthio and ethyl radicals, because the yield of the sulfide was very much affected by the radical scavenger. The addition of the thiol may reduce the yield of the sulfide by the hydrogen donation. Accordingly, the existence of the ethylthio radical in the reaction system is confirmed by the above experimental findings but it can not become the precursor of ethanethiol without the help of the thiol additives. On the other hand, the radiochemical yield of dimethyl sulfide was not affected both in the presence and in the absence of the added dimethyl sulfide carrier.

The dimethyl sulfide thus does not seem to react with the radicals and the fragments formed in the reaction system.

The Effects of Carbonyl Sulfide and the Spin State of the Sulfur Atoms. The electronic states of the sulfur atoms produced by the nuclear transformation are not known. At a high initial recoil energy, many higher electronic states and S^{n+} ions may be possible. However, the sulfur in the higher excited states and in the ionic states may be quickly deactivated to the lowest electronic states by elastic and non-elastic collisions with its surroundings, and then chemical reactions may occur. These states are $^3P_2$ (ground state (0.00 kJ mol^{-1}), $^3P_1$ (4.76 kJ mol^{-1}), $^3P_0$ (6.85 kJ mol^{-1}), $^1D_2$ (110.46 kJ mol^{-1}) and $^1S_0$ (265.22 kJ mol^{-1}).[4] Although some differences in reactivity may exist in the three triplet states, it may be difficult to discriminate among them by usual chemical means.

For convenience, the sulfur atoms will be considered simply to have a ^3P ground-state and the two excited singlet-states, which are both metastable with transitions among them.[4]

Strausz and Gunning have proposed the following reaction schemes for the sulfur atoms produced by the photolysis of COS with hydrocarbons:[4]

$$\mathrm{COS} \xrightarrow{h\nu} \mathrm{S(^1D)} + \mathrm{CO} \quad (3)$$

$$\mathrm{S(^1D)} + \mathrm{RH} \begin{cases} \longrightarrow \mathrm{RSH} & (4a) \\ \longrightarrow \mathrm{S(^3P)} + \mathrm{RH} & (4b) \end{cases}$$

$$\mathrm{S(^1D)} + \mathrm{COS} \begin{cases} \longrightarrow \mathrm{S_2} + \mathrm{CO} & (5a) \\ \longrightarrow \mathrm{S(^3P)} + \mathrm{COS^*} & (5b) \end{cases}$$

$$\mathrm{S(^3P)} + \mathrm{COS} \longrightarrow \mathrm{S_2} + \mathrm{CO} \quad (6)$$

$$\mathrm{S(^3P)} + \mathrm{S(^3P)} \longrightarrow \mathrm{S_2} \quad (7)$$

$$\mathrm{S(^3P)} + \mathrm{S(^3P)} + \mathrm{M} \longrightarrow \mathrm{S_2} + \mathrm{M} \quad (8)$$

$$n\mathrm{S_2} \longrightarrow \mathrm{S}_{2n} \quad (9)$$

The rate constants of several steps have been reported: $k_{4a}=5\times10^7$ M^{-1} s^{-1},[21] $k_{5a}\geqslant4\times10^{10}$ M^{-1} s^{-1},[22] and $k_6=1.8\times10^6$ M^{-1} s^{-1},[23] then, the disappearance of the S(^{1}D) atoms is about 1000 times greater than that of the corresponding thiol formation. In the

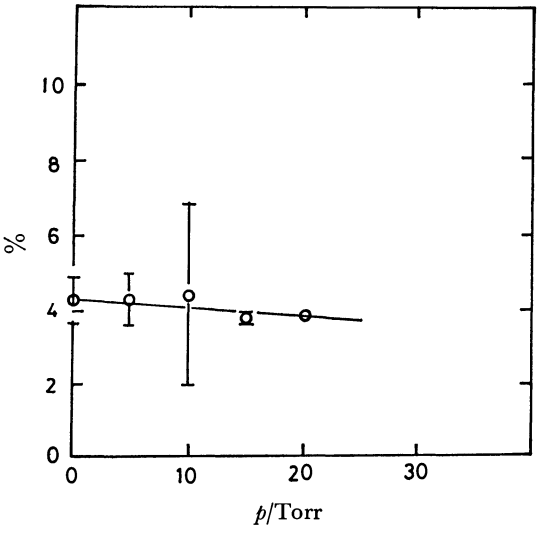

Fig. 6. Plots of the yield of ethanethiol as a function of COS pressure in the presence of 10 Torr ethanethiol.
The plots were corrected for the yield of ethanethiol-^{35}S in the collisional exchange reaction by the addition of 10 Torr ethanethiol as a protecting agent.

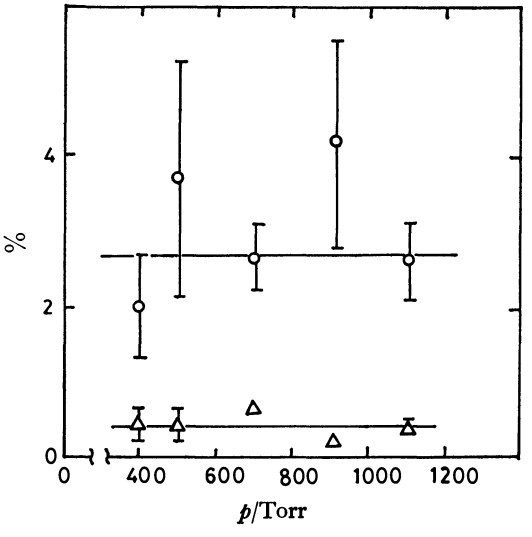

Fig. 7. Plots of the yield of ethanethiol and dimethyl sulfide as a function of total pressure.
○: Ethanethiol, △: dimethyl sulfide.

^{35}Cl(n,p)^{35}S reaction, the sulfur atoms produced are carrier-free, so the sulfur-sulfur combination reaction is improbable. Therefore, Schemes 7, 8, and 9 can be excluded.

The radiochemical yield of ethanethiol in the reaction of sulfur atoms with ethane in the presence of COS is shown in Fig. 6. The yield of ethanethiol is 0.4% for an energetic reaction and 3.3% for a thermal reaction, as has been mentioned above. Therefore, the formation of ethanethiol proceeds mostly by means of a thermal process. The electronic states of the sulfur atoms for the formation of ethanethiol may be considered to be those of thermal sulfur atoms. The formation of ethanethiol was not affected by the addition of COS, and the yield kept constant. Such

a constancy of the yield may imply that the contribution of $S(^1D)$ atoms to the formation of ethanethiol is negligible in the thermal process.

Moreover, the formation of ethanethiol was not affected with the variation of the reaction pressure from 400 Torr to 1100 Torr, as is shown in Fig. 7. Strausz and Gunning have shown that the deactivation of the $S(^1D)$ state to the $S(^3P)$ state increases when the pressure of the reaction system is increased (300—2000 Torr).[4]

The yield of ethanethiol was reduced from about 2.6% to 1.1% by the addition of a small amount of ethylene. Davis and his coworkers have reported that ethylene reacts fast with the $S(^3P)$ atoms (rate constant, 5×10^8 M^{-1} s^{-1}).[13] Also, thermochemically, the insertion reaction of the $S(^3P)$ atoms into the C–H bond of ethane is 231.8 kJ mol^{-1} exothermic.

From the above facts and the thermochemical calculation, the insertion of $S(^3P)$ atoms into the C–H bond may be possible, although the $S(^3P)$ atoms must be accompanied by a spin conversion in the formation of the C–^{35}S–H bond.

Church and Rowland[3] have also reported that the $S(^3P)$ atoms can be inserted into the secondary C–H bond of propane in the presence of a large amount of argon as a moderator.

Furthermore, Ring and Rabinovitch[25,26] have reported that the reaction of the triplet CH_2 (a diradical) produced by the photolysis of diazomethane in a large excess of inert N_2 can be inserted into the C–H bond of propane and isobutane in the gas phase. On the other hand, Gunning and his co-workers have concluded that the $S(^3P)$ atoms do not insert into the C–H bond of hydrocarbons in the photolysis of COS; they concluded this from the marked decrease in the thiol yield in the presence of a large amount of CO_2.[4] This discrepancy can not be explained clearly, but it may presumably be expected that, in this system, a small yield of a sulfur compound is detectable, even if the reaction rate of the insertion by the $S(^3P)$ is extremely slow as compared with that of the $S(^1D)$ atoms; a small excess of the translational energy in this thermal reaction may then cause the insertion, even in the $S(^3P)$ states.

The Ratio of the C–H and C–C Insertions. The insertion yield of the C–H bond in ethane is about 0.4% as an energetic process, and about 3.3% as a thermal process and the insertion yield of the C–C bond is about 0.3% as an energetic process.

Therefore the ratio of the rate constant in the energetic reaction can be represented as the ratio of the yields per bond, *i.e.*, (0.4/6)/0.3. The insertion into the C–C bond is about 5 times faster than that of the C–H insertion in the energetic process. In a previous paper,[5] it was pointed out that the insertion rate of the 2-position of the C–H bond in benzothiazole to that of the C–C bond in 2-methylbenzothiazole was slightly larger in the C–H bond.

In general, the insertion reaction of diradical into the C–H bond always takes place more easily in a weaker bond than a strong bond. For instance, the insertion rate in the reaction of CH_2, generated from the photolysis of diazomethane, into the primary C–H bond relative to that of the secondary in the propane molecule is 1:1.22.[27] The bond dissociation energy is 410.0 kJ mol^{-1} for the primary C–H bond and 395.4 kJ mol^{-1} for the secondary C–H bond in the propane molecule.[28]

Even in the energetic reaction, a similar fact was shown by Church and Rowland,[3] they concluded that the recoil sulfur atoms are inserted predominantly into the secondary C–H bond rather than the primary C–H bond in propane.

Moreover, it has been reported that the formation of the tritiated hydrogen (abstraction reaction) is reduced as the bond dissociation energy of hydrocarbons becomes greater.[29]

The above insertion and abstraction reactions are discussed in just the C–H bond in both the thermal and energetic processes. In the energetic reaction, it may be considered that the insertion reaction occurs also in the C–C bond, and a comparison of the insertion rate into the C–H bond with that of the C–C bond seems to show that it is also affected by the bond-dissociation energy. The bond-dissociation energy of the C–C bond is smaller than that of the C–H bond by about 41.8 kJ mol^{-1} in ethane.[28]

This work was supported by the Visiting Researchers Program in the Rikkyo Reactor. The authors wish to express their appreciation to Dr. S. Harasawa and others for their kind cooperation in the thermal-neutron irradiation.

References

1) L. N. Kremer and L. D. Spicer, *J. Am. Chem. Soc.*, **97**, 5021 (1975).

2) L. N. Kremer, PhD. Thesis, University of Utah, 1974.

3) L. B. Church and F. S. Rowland, *Radiochim. Acta*, **16**, 55 (1971).

4) H. E. Gunning and O. P. Strausz, *Adv. Photochem.*, **4**, 143 (1966).

5) K. Niisawa and K. Taki, *Bull. Chem. Soc. Jpn.*, **50**, 57 (1977).

6) Mlinkó and his coworkers[7] have studied the radioactivity measurement of the $H_2^{35}S$ produced from ^{35}S-labeled compounds by reduction in hydrogen gas. This was modified in order to determine the specific radioactivity of ^{35}S-labeld products in the recoil reaction system using an internal-flow proportional detector.[8]

7) S. Mlinkó, I. Gács, and T. Szarvas, *Int. J. Appl. Radiat. Isot.*, **18**, 457 (1967).

8) K. Niisawa and K. Taki, IAERU-7601 Report, Yokosuka, Jpn., March.

9) G. B. Heisig and R. Holt, *J. Am. Chem. Soc.*, **74**, 1597 (1952).

10) C. W. Bills and A. R. Ronzio, *J. Am. Chem. Soc.*, **72**, 5510 (1950).

11) M. L. Hyder and S. S. Markowitz, *J. Inorg. Nucl. Chem.*, **26**, 257 (1964).

12) E. K. C. Lee, Y. N. Tang, and F. S. Rowland, *J. Phys. Chem.*, **68**, 318 (1968).

13) D. D. Davis, R. B. Klemm, and M. Pilling, *Int. J. Chem. Kinet.*, **4**, 367 (1972).

14) The initial recoil energy of the sulfur atoms, as given by the nuclear transformation of ^{35}Cl(n, p)^{35}S process is

31.2 keV.[15]
15) R. H. Herber, "Chemical Effects of Nuclear Transformations," I. A. E. A., Vienna (1961), Vol. 2, p. 201.
16) D. S. Urch and M. J. Welch, *Trans. Faraday Soc.*, **62**, 388 (1966).
17) G. Stöcklin, H. Stangle, D. R. Christman, J. B. Cumming, and A. P. Wolf, *J. Phys. Chem.*, **67**, 1735 (1963).
18) F. Cacace and A. P. Wolf, *J. Am. Chem. Soc.*, **87**, 5301 (1965).
19) R. T. K. Baker and R. L. Wolfgang, *Trans. Faraday Soc.*, **65**, 1842 (1969).
20) S. Patai, "The Chemistry of the Thiol Group," Part I, John Wiley and Sons, London (1974).
21) E. Leppin and K. Gollnick, *J. Am. Chem. Soc.*, **92**, 2221 (1970).
22) R. J. Donovan, L. J. Krish, and D. Husain, *Nature*, **222**, (1970).
23) R. B. Klemm and D. D. Davis, *J. Phys. Chem.*, **78**, 1137 (1974).
24) R. J. Donovan and D. Husain, *Chem. Rev.*, **70**, 506 (1970).
25) D. F. Ring and B. S. Rabinovitch, *J. Am. Chem. Soc.*, **88**, 4285 (1966).
26) D. F. Ring and B. S. Rabinovitch, *Can. J. Chem.*, **46**, 2435 (1968).
27) G. Z. Whitten and B. S. Rabinovitch, *J. Phys. Chem.*, **69**, 4348 (1956).
28) J. A. Kerr, *Chem. Rev.*, **66**, 465 (1968).
29) F. Schmidt-Bleek and F. S. Rowland, *Angew. Chem., Int. Ed. Engl.*, **3**, 769 (1964).

Kinetics of the Formation and Transformation of Alkoxy-derived Calcium Metasilicate

Osamu YAMAGUCHI,* Muneaki KAMATA, and Kiyoshi SHIMIZU*

Department of Applied Chemistry, Faculty of Engineering, Doshisha University, Karasuma Imadegawa, Kamigyo-ku, Kyoto 602

(Received January 10, 1979)

Wollastonite(β-$CaSiO_3$) was formed directly from the mixed powder prepared by simultaneous hydrolysis of calcium and silicon alkoxides. Crystallization isotherms were described by the Avrami equation $\ln(1-\alpha)=-kt^n$ with $n=3$ and the activation energy was determined as 284.5 kJ/mol. The kinetics of transformation of β- into α-$CaSiO_3$ was best interpreted by the contracting cube equation $1-(1-\alpha)^{1/3}=kt$. The value of the activation energy was 983.2 kJ/mol.

Calcium metasilicate($CaSiO_3$) exists in three polymorphic modifications; wollastonite(triclinic, β-$CaSiO_3$), pseudowollastonite(triclinic, α-$CaSiO_3$), and parawollastonite (monoclinic). Parawollastonite has been recognized as a mineral. Many investigations[1-7] have been made on the solid state reaction of an equimolar mixture of silica and either calcium carbonate or calcium oxide. It is shown that calcium orthosilicate (Ca_2SiO_4) is always one of the first products at any reaction temperature. For example, Jander and Hoffmann[3] reported that Ca_2SiO_4 and $Ca_3Si_2O_5$ are the first-formed products and gradually convert into $CaSiO_3$, the final product. They observed also a strong effect of grinding on the formation of $CaSiO_3$.

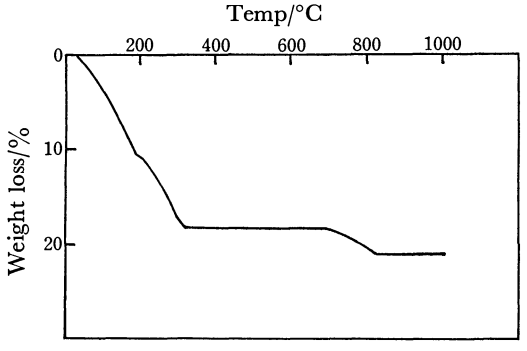

Fig. 1. TG curve of the starting powder.
Sample weight: 20 mg.

This indicates that the contact of reactants in the powder mixture plays an important role. On the other hand, though it has been reported that β-$CaSiO_3$ transforms into α-$CaSiO_3$ at 1125±10 °C,[8] 1180 °C,[5] or 1190 °C,[9] no kinetic study has been carried out.

In the present study, it was found that β-$CaSiO_3$ is formed directly from the mixed powder prepared by simultaneous hydrolysis of calcium and silicon alkoxides. On the basis of this result, kinetic studies have been made on the formation of β-$CaSiO_3$ and the transformation of β- into α-$CaSiO_3$. The kinetic data were analyzed with available solid state models.

Experimental

Materials and Procedure. Silicon ethoxide used was of guaranteed purity. Calcium methoxide was synthesized by heating calcium metal in an excessive amount of dehydrated methanol at 65 °C for 5 h. The purity of calcium metal was 99.9%. A mixture of these alkoxides with the mole ratio of $Ca^{2+}/Si^{4+}=1:1$ was prepared, and then poured into aqueous ammonia solution at 30 °C. The temperature was slowly raised up to 85 °C while being stirred. The resulting mixed powder was washed repeatedly with hot water and dried at 60 °C under reduced pressure. The mixed powder, in the description below, is termed starting powder. The average particle size of the starting powder is *ca.* 400 Å.

Measurement. Thermal analyses (TG, DTA) were carried out in air at a heating rate of 10 °C/min. Alpha-alumina was used as a standard material in DTA. On

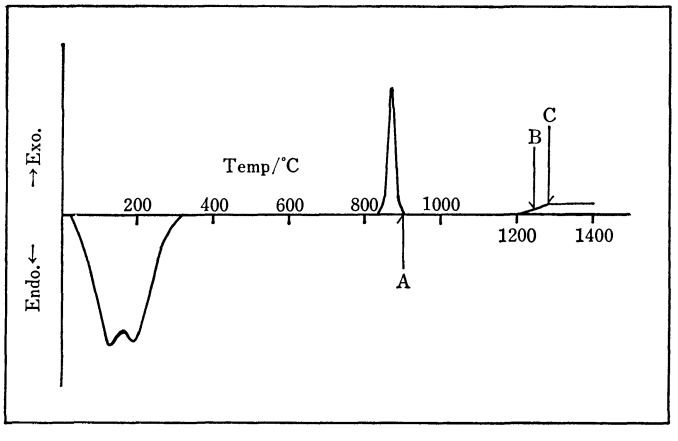

Fig. 2. DTA curve of the starting powder.
Sample weight: 20 mg.
Arrows show the temperatures at which the starting powder was heated in order to obtain several specimens for X-ray diffraction.

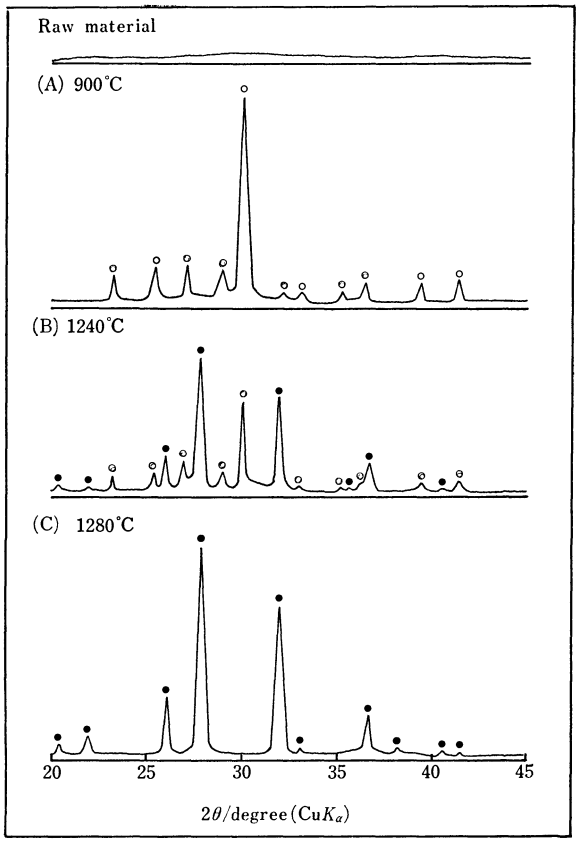

Fig. 3. X-ray diffraction patterns of specimens with increasing temperature.
○: β-$CaSiO_3$, ●: α-$CaSiO_3$.

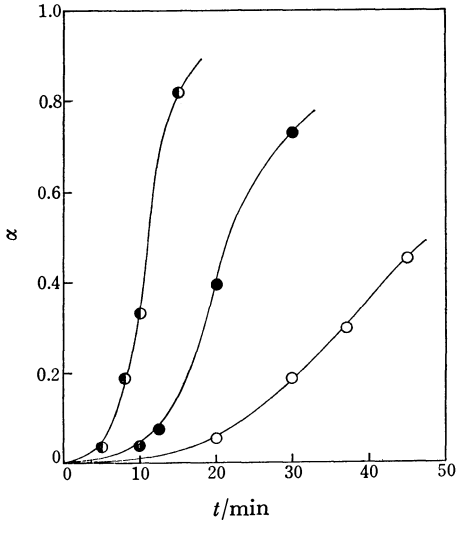

Fig. 4. Formation of β-$CaSiO_3$ as a function of time at different temperatures.
○: 820 °C, ●: 840 °C, ◐: 870 °C.

the basis of the DTA data, the starting powder was heated in an electric furnace up to a desired temperature at a heating rate of 10 °C/min, and then cooled rapidly to room temperature. The specimens were examined by means of X-ray diffractometer using nickel filtered copper K_α. The fractional transformation was determined from the heights of the main peaks characteristics of α-(d=3.20 Å) and β-$CaSiO_3$ (d=2.97 Å), using the calibration curve prepared with known compositions.

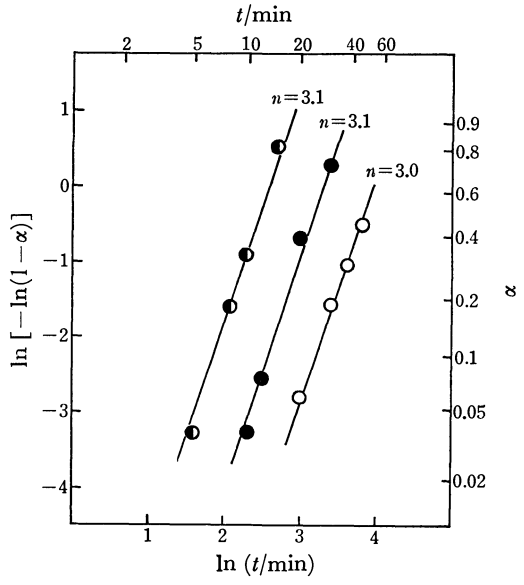

Fig. 5. Plots of ln $(1-\alpha)$ *vs.* time t of the data shown in Fig. 4.
○: 820 °C, ●: 840 °C, ◐: 870 °C.

Results and Discussion

Thermal Analysis. Figure 1 shows a TG curve of the starting powder. The weight loss of 18.2% up to 320 °C is attributed to the loss of ammonia, surface-absorbed methanol and ethanol, absorbed water, and hydrated water. Continued weight loss, 2.8%, was observed between 690 and 820 °C. The specimens heated in this temperature range were grayish. This may be due to the alcoholic hydrocarbon occluded in powders and/or free carbon produced by heating, which reacts with oxygen of bulk at the surface, resulting in the evolution of the decomposition products such as carbon monoxide, carbon dioxide, and water vapor.[10-11]

A DTA curve of the starting powder is shown in Fig. 2. Two exothermic reactions were observed at 830—900 °C and 1200—1280 °C. From the results of X-ray diffraction, the reactions were found to be the crystallization of β-$CaSiO_3$ from an amorphous phase and the transformation of β- into α-$CaSiO_3$, respectively.

X-Ray Analysis. Figure 3 shows the variation of X-ray diffraction patterns of $CaSiO_3$ with increasing temperature. The starting powder was amorphous, and no significant changes were observed up to 800 °C. The peaks corresponding to β-$CaSiO_3$ appeared after heating at 820 °C for 10 min, and the intensity increased rapidly up to 900 °C. No other peaks were identified except for the β-$CaSiO_3$ spectrum up to 1170 °C. The peaks of α-$CaSiO_3$ began to appear when heated at 1180 °C for 20 min, and the specimen heated at 1280 °C showed an X-ray diffraction pattern characteristic of α-$CaSiO_3$.

Kinetics of the Formation of β-$CaSiO_3$. Figure 4 shows the fraction of the crystallized β-$CaSiO_3$ at 820, 840, and 870 °C. The starting powder was preheated at 500 °C for 1 h. The fractional crystallization of each specimen was determined from the height


(×20000)

Fig. 6. Electron micrograph of the β-$CaSiO_3$ powder.

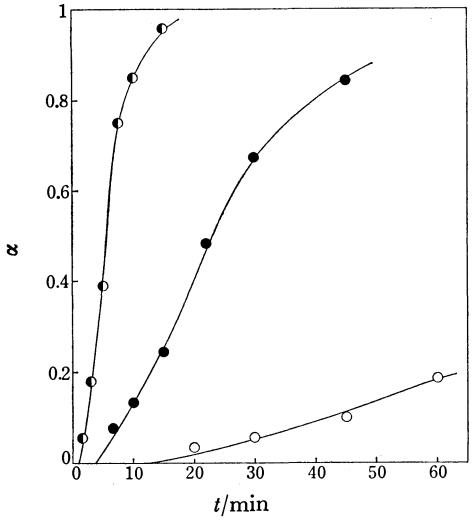

Fig. 7. Phase transformation from β- into α-$CaSiO_3$ as a function of time at different temperatures.
○: 1180 °C, ●: 1210 °C, ◐: 1240 °C.

of d=2.97 Å which is the strongest peak of the β-$CaSiO_3$ spectrum. A well-crystallized specimen was obtained by heating the starting powder at 1150 °C for 20 min. Quartz was used as an internal standard material. Crystallization isotherms were characterized by sigmoidal shape (Fig. 4), the kinetics being best described by the Avrami equation[12] (Fig. 5),

$$\ln(1-\alpha) = -kt^n \qquad (n=3\text{—}3.1\fallingdotseq 3) \qquad (1)$$

where α, t, k, and n are the fractional crystallization, time, rate constant and a constant related to the reaction mechanism, respectively. Electron micrograph of the β-$CaSiO_3$ powder consisting of nearly spherical particles is shown in Fig. 6. In view of this fact and also the fact that the Avrami equation with n=3 was fitted over the whole range of crystallization

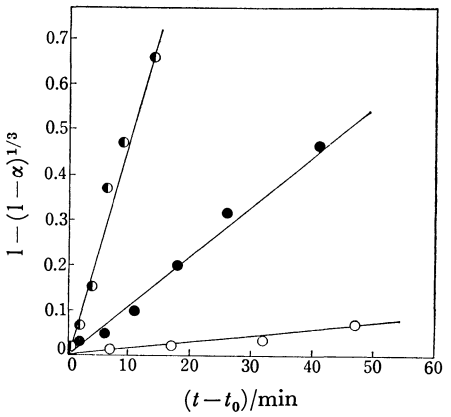

Fig. 8. Plots of $1-(1-\alpha)^{1/3}$ *vs.* time $t-t_0$ of the data shown in Fig. 7.
○: 1180 °C, ●: 1210 °C, ◐: 1240 °C.

curves, three-dimensional growth of β-$CaSiO_3$ with site-saturation for nucleation is probably the rate-determining step. The activation energy calculated from the Arrhenius plot was 284.5 kJ/mol.

Kinetics of the Transformation of β- into α-$CaSiO_3$. Figure 7 shows the fractional transformation of β- into α-$CaSiO_3$ as a function of time at different temperatures. The specimens heated at 1150 °C for 20 min were used as a starting material. Induction periods were observed, attempts being made to fit the results to kinetic laws by considering the induction periods. As shown in Fig. 8, transformation isotherms are best described by the contracting cube equation,[13]

$$1-(1-\alpha)^{1/3} = k(t-t_0) \qquad (2)$$

where α is the fractional transformation, t time and t_0 induction period. This indicates that the transformation is controlled by the rate of advance of the reaction interface. The rate constants were determined from the slopes of the straight lines and the activation energy was determined as 983.2 kJ/mol.

References

1) J. W. Cobb, *J. Soc. Chem. Ind.*, **26**, 250 (1910).
2) W. Maskill, G. H. Whiting, and W. E. S. Turner, *J. Soc. Glass Technology*, **16**, 94 (1932).
3) W. Jander and E. Hoffmann, *Z. Anorg. Allg. Chem.*, **218**, 211 (1934).
4) L. Heller and H. F. W. Taylor, "Crystallographic Data for the Calcium Silicates," Majesty's Stationery Office, London (1956), pp. 16—17.
5) S. Kakitani and M. Fujisaka, *Yogyo Kyokai Shi*, **66**, 133 (1958).
6) H. F. W. Taylor, "The Chemistry of Cements," Academic Press, New York (1964), Vol. 2, pp. 363—364.
7) W. A. Klemm and R. L. Berger, *J. Am. Ceram. Soc.*, **55**, 485 (1972).
8) E. F. Osborn and J. E. Schairer, *Am. J. Sci.*, **239**, 715 (1941); *Chem. Abstr.*, **21**, 50 (1942).
9) "Kagaku Dai-Jiten," ed by S. Mizushima, Kyoritsu Shuppan, Tokyo (1960), Vol. 3, p. 103.
10) O. Yamaguchi, H. Tonami, and K. Shimizu, *Chem. Lett.*, **1976**, 796.
11) O. Yamaguchi, S. Nakamura, and K. Shimizu, *Nippon Kagaku Kaishi*, **1979**, 5.
12) N. Avrami, *J. Chem. Phys.*, **7**, 1103 (1939); **8**, 212 (1940).
13) For example, D. Dollimore and D. Tinsely, *J. Chem. Soc., A*, **1971**, 3043.

Pressure Effects on the Base Hydrolysis Reaction Rates of α-, β-[Co(edda)$(NH_3)_2]^+$ and α-[Co(edda)$(NO_2)_2]^-$ in a Carbonate Buffer

Yoichi KITAMURA

Department of Chemistry, Faculty of Science, Ehime University, Matsuyama, Ehime 790

(Received January 20, 1979)

The pressure effects on the base hydrolysis reaction rates of α-, β-[Co(edda)$(NH_3)_2]^+$ and α-[Co(edda)-$(NO_2)_2]^-$ in a carbonate buffer were measured up to 1500 kg/cm² (1 kg/cm²=98.0665 kPa). The activation volumes at normal pressure were found to be 16.6, 22.3, and 11.9 cm³/mol respectively. These values are consistent with those expected from the S_N1 CB mechanism, where the conjugate bases dissociate *via* the I_d mechanism.

The pressure dependence of a reaction rate gives the value of the activation volume (ΔV^*). In the base hydrolysis reaction of a Co(III)-complex, the magnitude of ΔV^* is comparatively large (20±10 cm³/mol) for the S_N1 CB mechanism, since the volume change in the pre-equilibrium to produce the conjugate base amounts to about 20 cm³/mol.[1] In contrast, it is smaller than 9 cm³/mol for the S_N2 mechanism.[2] Thus, the activation volume is a useful quantity for use in discriminating the mechanisms for a base hydrolysis reaction.

It has been shown by Kuroda *et al.* that, in a carbonate buffer, the base hydrolysis reactions of α-, β-[Co(edda)$(NH_3)_2]^+$ and α-[Co(edda)$(NO_2)_2]^-$,

$$\alpha\text{-}[Co(edda)(NH_3)_2]^+ + OH^- \rightarrow \alpha\text{-}[Co(edda)(NH_3)OH] + NH_3, \quad (1)$$

$$\beta\text{-}[Co(edda)(NH_3)_2]^+ + OH^- \rightarrow \beta\text{-}[Co(edda)(NH_3)OH] + NH_3, \quad (2)$$

$$\alpha\text{-}[Co(edda)(NO_2)_2]^- + OH^- \rightarrow \alpha\text{-}[Co(edda)(NO_2)OH]^- + NO_2^-, \quad (3)$$

are followed by successive carbonation steps (ethylenediamine-*N*,*N*′-diacetic acid=H_2edda).[3-5] The rates of the carbonation step are relatively high for the reactions of α-[Co(edda)$(NH_3)_2]^+$ and α-[Co(edda)-$(NO_2)_2]^-$, and relatively low for that of β-[Co(edda)-$(NH_3)_2]^+$, compared to the base hydrolysis rates. By assuming a first-order reaction for the base hydrolysis, the rate constants of Reactions 1,[3] 2,[6] and 3[5] have been calculated at a normal pressure.

In this experiment, the pressure dependences of the rate constants of Reactions 1, 2, and 3 were examined up to 1500 kg/cm². The mechanisms are discussed from the standpoint of the activation volume.

TABLE 1. THE PREPARATIVE METHODS AND THE ABSORPTION MAXIMA OF THE COMPLEXES USED IN THIS STUDY

Complex	λ_{max}/nm(ε_{max}) This work	Lit	Ref. a)	Ref. b)
α-[Co(edda)$(NH_3)_2]\cdot ClO_4\cdot H_2O$	538 (92.5) 363 (116)	538 (92.0) 363 (118)	7)	7)
β-[Co(edda)$(NH_3)_2]\cdot ClO_4\cdot 1.5H_2O$	502 (140) 359 (154)	499 (153) 358 (159)	8)	9)
α-Cs[Co(edda)$(NO_2)_2]\cdot H_2O$	520 (148)	520 (150)	10)	10)

a) Ref. for preparations. b) Ref. for spectra.

Experimental

Materials. The preparative methods and the absorption maxima of the complexes used in this study are summarized in Table 1. The buffer solutions were made from reagent-grade chemicals. The water was distilled after passing it through an ion-exchange column.

Kinetic Measurement. The procedures were the same as those in a previous work.[11]

Results

The first-order rate constant, k_1, of the base hydrolysis was determined by

$$\ln[(D_\infty - D_{t'})/(D_\infty - D_t)] = k_1(t - t'),$$

where $D_{t'}$ and D_t represent the optical densities at the moment when the high pressure is reached, and at the moment when the high pressure is released, respectively. For the reaction of α-[Co(edda)$(NH_3)_2]^+$, D_∞ represents the optical density (OD) at equilibrium. For the reactions of β-[Co(edda)$(NH_3)_2]^+$ and α-[Co(edda)-$(NO_2)_2]^-$, D_∞ represents the estimated OD values of the base hydrolysis products: β-[Co(edda)(NH_3)OH] and α-[Co(edda)(NO_2)OH]$^-$ respectively. Kuroda's D_∞/D_0 values are used, where D_0 represents the OD at the moment of the dissolution of the initial complex. The D_∞/D_0 values (λ(nm) used to follow the reaction) are 1.9 (540) for Reaction 1,[3] 0.7 (500) for Reaction 2,[6] and 4.86 (590) for Reaction 3.[5] ($t-t'$) is the reaction time. The k_1 values at each pressure are summarized in Table 2. An increase in pressure by 1000 kg/cm² reduces the k_1 values below half, from which large positive magnitudes (*ca.* 20 cm³/mol) of the activation volumes can be expected for these reactions. They were fitted to the formula, $\ln(k_1/k_{10}) = aP + bP^2$, where k_{10} is the rate constant at a normal pressure and where P is expressed in kg/cm² (Fig. 1).

At a normal pressure, the k_1 values are proportional to [OH$^-$] *i.e.*, $k_1 = k_2[OH^-]$.[3,5,6] Then, the activation volume and its pressure dependence are given by[2]

$$\Delta V^* = -RT\frac{d\ln k_2}{dP} = -RT\frac{d\ln k_1}{dP} + RT\frac{d\ln[OH^-]}{dP}$$

$$= -RT(a+2bP) + RT\frac{d\ln K_w}{dP} - RT\frac{d\ln K_2}{dP}$$

$$\frac{d\Delta V^*}{dP} = -2bRT + RT\frac{d^2\ln K_w}{dP^2} - RT\frac{d^2\ln K_2}{dP^2},$$

where K_w and K_2 represent the ionic product of water and the second dissociation constant of carbonic acid respectively. By using the known pressure dependences

of the K_w and K_2, the values of ΔV^* and $d\Delta V^*/dP$ at the normal pressure are calculated.[2] El'yanov and Hamann have proposed a formula for the pressure dependence of the volume change of an acid-base equilibrium:

$$d\Delta V/dP=(-1.80\times10^{-4}\ cm^2/kg)\Delta V,$$

where ΔV is the volume change at a normal pressure.[11] The second derivatives of K_w and K_2 are estimated following their method. The results are summarized in Table 3.

Discussion

From the proportionality of the k_1 values to $[OH^-]$, the S_N2 and S_N1 CB mechanisms are possible for these reactions. In the case of the S_N2 mechanism, ΔV^* is estimated to be smaller than 9 cm³/mol.[2] The large positive values of ΔV^* obtained for Reactions 1 and 2 can then be considered as evidence for the S_N1 CB mechanism. For Reaction 3, the obtained magnitude of ΔV^* is not large enough. However, this complex ion has a negative charge, and so the formation of a seven-coordinated intermediate or an ion pair with an OH^- ion would be improbable. Therefore, Reaction 3 should also proceed *via* the S_N1 CB mechanism.

In this mechanism, the reaction series for Reactions 1 and 2 are

$$\alpha\text{-, }\beta\text{-}[Co(edda)(NH_3)_2]^+ + OH^- = \alpha\text{-, }\beta\text{-}[Co(edda)(NH_2)(NH_3)] + H_2O$$

$$\alpha\text{-, }\beta\text{-}[Co(edda)(NH_2)(NH_3)] \rightarrow \alpha\text{-, }\beta\text{-}[Co(edda)(NH_2)] + NH_3$$

$$\alpha\text{-, }\beta\text{-}[Co(edda)(NH_2)] + H_2O \rightarrow \alpha\text{-, }\beta\text{-}[Co(edda)(NH_3)OH],$$

where the first and the third steps are rapid and where

Table 2. $k_1\times10^3$ (min^{-1}) for the base hydrolysis reactions in a carbonate buffer

α-[Co(edda)(NH₃)₂]⁺				
in 0.2 M Na_2CO_3–0.2 M $NaHCO_3$, $pH_{65\,°C}$=9.38, t[a)]=65.6 °C.				
P/kg cm⁻²	1	500	1000	1500
	11.3(41.2)	7.5(50)	4.0(50)	2.4(50)
	11.8(50.6)	7.9(60)	4.6(60)	2.2(60)
	11.8(60.6)	7.7(70)	4.0(70)	2.3(70)
Average	11.6	7.8	4.2	2.3
β-[Co(edda)(NH₃)₂]⁺				
in 0.2 M Na_2CO_3–0.2 M $NaHCO_3$, $pH_{45\,°C}$=9.54, t=42.8 °C.				
P/kg cm⁻²	1	500	1000	1500
	7.4(40.7)	4.4(50)	2.4(60)	1.3(70)
	7.2(50.5)	4.3(60)	2.7(70)	1.6(80)
	7.2(60.6)	4.3(70)	2.5(80)	1.4(90)
Average	7.3	4.3	2.5	1.4
α-[Co(edda)(NO₂)₂]⁻				
in 0.3 M Na_2CO_3–0.1 M $NaHCO_3$, $pH_{65\,°C}$=9.86, t=65.6 °C.				
P/kg cm⁻²	1	500	1000	1500
	10.3(30.8)	8.0(40)	5.3(40)	3.4(50)
	10.1(40.9)	7.5(50)	5.7(50)	3.3(60)
	11.5(50.9)	7.4(60)	4.7(60)	3.2(70)
Average	10.6	7.6	5.2	3.3

a) Reaction temperature. The numbers in parentheses denote the reaction time in min. M=mol/dm³.

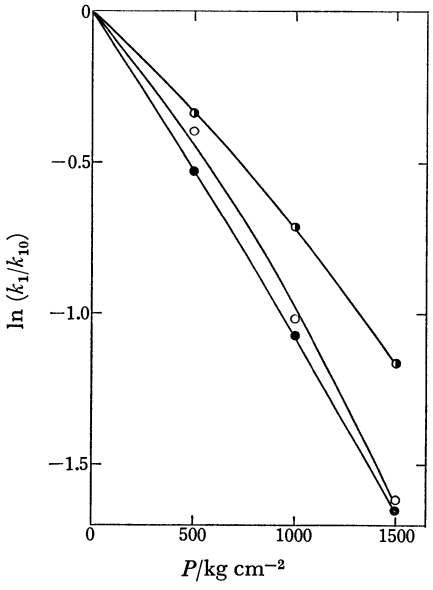

Fig. 1. The pressure dependence of the k_1-value.
○: α-[Co(edda)(NH₃)₂]⁺ $\ln(k_1/k_{10})=-7.60\times10^{-4}P-2.18\times10^{-7}P^2$,
●: β-[Co(edda)(NH₃)₂]⁺ $\ln(k_1/k_{10})=-10.3\times10^{-4}P-0.497\times10^{-7}P^2$,
◑: α-[Co(edda)(NO₂)₂]⁻ $\ln(k_1/k_{10})=-5.96\times10^{-4}P-1.21\times10^{-7}P^2$.

Table 3. Activation parameters for reactions 1—5

a)	Complex	ΔV^*	ΔV_{pre}	$\Delta V^{*\prime}$	$\frac{d\Delta V^*}{dP}$	$\frac{d\Delta V^{*\prime}}{dP}$	E_a	ΔS^*	b)
1	α-[Co(edda)(NH₃)₂]⁺	16.6	16.9	−0.3	13.4	16.4	157	145	3)
2	β-[Co(edda)(NH₃)₂]⁺	22.3	16.9	5.4	3.6	6.6	172	213	6)
3	α-[Co(edda)(NO₂)₂]⁻	11.9	13.9	−2.0	7.9	10.4	161	143	5)
4	β-[Co(edda)(tn)]⁺	14.7	16.9	−2.2	0.2	3.2	151	124	17)
5	β-[Co(edda)(en)]⁺	20.0	16.9	3.1	−1.4	1.6	176	195	4)

a) Reaction number. b) Ref. for E_a and ΔS^*. The units are: ΔV^*, ΔV_{pre}, $\Delta V^{*\prime}$ (cm³/mol); $\frac{d\Delta V^*}{dP}$, $\frac{d\Delta V^{*\prime}}{dP}$ (10^{-3} cm⁵ mol⁻¹ kg⁻¹); E_a (kJ/mol); and ΔS^* (J K⁻¹ mol⁻¹).

the second is the rate-determining process. Analogously, the series for Reaction 3 is

$$\alpha\text{-}[Co(edda)(NO_2)_2]^- + OH^- = \alpha\text{-}[Co(edda^*)(NO_2)_2]^{2-} + H_2O$$

$$\alpha\text{-}[Co(edda^*)(NO_2)_2]^{2-} \rightarrow \alpha\text{-}[Co(edda^*)(NO_2)]^- + NO_2^-$$

$$\alpha\text{-}[Co(edda^*)(NO_2)]^- + H_2O \rightarrow \alpha\text{-}[Co(edda)(NO_2)OH]^-,$$

where edda* represents the conjugate base of the edda ligand. Thus, the activation volume is given by $\Delta V^* = \Delta V_{pre} + \Delta V^{*\prime}$, where ΔV_{pre} is the volume change in the pre-equilibrium and $\Delta V^{*\prime}$ is the activation volume of the second step.

The isomerization reactions in a carbonate buffer,

$$\beta\text{-}[Co(edda)(tn)]^+ \rightarrow \alpha\text{-}[Co(edda)(tn)]^+, \quad (4)$$

$$\beta\text{-}[Co(edda)(en)]^+ \rightarrow \alpha\text{-}[Co(edda)(en)]^+, \quad (5)$$

also proceed *via* the S_N1 CB mechanism. In a previous report, the ΔV_{pre} value for Reactions 4 and 5 was estimated as 18.8 cm³/mol.[2] Later, for the equilibrium,

$$\alpha\text{-}[Co(edda)(H_2NCH_2CH_2OH)]^+ + OH^- = \alpha\text{-}[Co(edda)(H_2NCH_2CH_2O)]^0 + H_2O, \quad (6)$$

the volume change ($\Delta V = 16.9 \pm 0.7$ cm³/mol) was obtained at 25 °C and a low ionic strength.[1] This equilibrium is analogous to the pre-equilibria of Reactions 1, 2, 4, and 5, and the ΔV_{pre} values for these reactions may be taken approximately as 16.9 cm³/mol. In Equilibrium 6, $\Delta Z^2 = -1$, where Z is the charge of the complex ion; the contribution (ΔV_{el}) of the electrostrictive volume change of the complex ion is positive. In contrast, in the pre-equilibrium for Reaction 3 ($\Delta Z^2 = 3$), ΔV_{el} would be negative and ΔV_{pre} would be smaller than 16.9 cm³/mol. Values of $\Delta V = 19.9 \pm 1$ cm³/mol are known for the neutralization equilibria of trivalent complex ions ($\Delta Z^2 = -5$) such as $[Fe(H_2O)_6]^{3+}$, $[Co(NH_3)_5(H_2O)]^{3+}$, and $[Cr(H_2O)_6]^{3+}$.[1] Since ΔV_{el} is proportional to ΔZ^2, the ΔV_{pre} value for Reaction 3 must be approximately 13.9 cm³/mol.[1] The magnitudes of $\Delta V^{*\prime}$ thus obtained for Reactions 1, 2, and 3 are comparable to those for Reactions 4 and 5. In the activated states of Reactions 4 and 5, the $-NH_2$ group liberated from the conjugate base must remain in the vicinity of the five-coordinated intermediate, since it is linked to the intermediate through the molecular chain of tn or en. Therefore, the conjugate bases in Reactions 1, 2, and 3 may dissociate *via* the I_d mechanism; *i.e.*, in the activated state the leaving group remains in the second coordination sphere.

The aquo-exchange reaction,

$$[Co(NH_3)_5H_2O]^{3+} + H_2O^* \rightarrow [Co(NH_3)_5H_2O^*]^{3+} + H_2O, \quad (7)$$

also proceeds *via* the I_d mechanism and $\Delta V^* = 1.2$ cm³/mol is known at 25 °C.[13] In the activation step of Reaction 7, the electrostrictive volume change is not involved. In the dissociative activation steps for Reactions 1 and 2, a neutral NH_3 departs from the neutral conjugate base, and the electrostrictive volume change is also ignored. In that of Reaction 3, only a separation of charge occurs, and the electrostrictive volume change may be insignificant. Therefore, the $\Delta V^{*\prime}$ values for the I_d dissociation in Reactions 1, 2, and 3 may be expected to be comparable to the ΔV^* for Reaction 7. The experimentally obtained magnitudes of $\Delta V^{*\prime}$ are consistent with this expectation.

If the conjugate bases completely dissociate in the activated state (D mechanism), $\Delta V^{*\prime}$ can be estimated from the partial molar volumes ($\overline{V}$) by

$$\Delta V^{*\prime} = \overline{V}(\alpha\text{-},\beta\text{-}[Co(edda)(NH_2)]) - \overline{V}(\alpha\text{-},\beta\text{-}[Co(edda)(NH_2)(NH_3)]) + \overline{V}(NH_3),$$

and

$$\Delta V^{*\prime} = \overline{V}(\alpha\text{-}[Co(edda^*)(NO_2)]^-) - \overline{V}(\alpha\text{-}[Co(edda^*)(NO_2)_2]^{2-}) + \overline{V}(NO_2^-).$$

Stranks assumes that the intrinsic volume difference between the five-coordinated intermediate and its six-coordinated precursor is zero.[14] This volume difference may be estimated from the volume difference between a square pyramid or a trigonal bipyramid and an octahedron, with each center-apex length 3 Å. This leads to the intrinsic volume difference of -10.8 and -7.6 cm³/mol. $\overline{V}(NH_3)$ is *ca.* 24.9 cm³/mol.[15] Then, in the D mechanism, the $\Delta V^{*\prime}$ values for Reactions 1 and 2 would be 14.1 cm³/mol or larger. $\overline{V}(NO_2^-)$ is *ca.* 31.6 cm³/mol.[16] Taking account of the electrostrictive volume expansion (*ca.* 2.3 cm³/mol) of the complex, the $\Delta V^{*\prime}$ value for Reaction 3 would be 23.1 cm³/mol or larger in the D mechanism. Thus, the values of $\Delta V^{*\prime}$ to be expected from the D mechanism are considerably larger than those obtained from the experimental results.

The values of $d\Delta V^{*\prime}/dP$ are calculated from $d\Delta V^*/dP$ (Table 3):

$$(d\Delta V^{*\prime}/dP) = (d\Delta V^*/dP) - (d\Delta V_{pre}/dP),$$

where $d\Delta V_{pre}/dP$ is -3×10^{-3} and -2.5×10^{-3} cm⁵ mol^{-1} kg^{-1} for $\Delta V_{pre} = 16.9$ and 13.9 cm³/mol respectively (estimated after El'yanov and Hamann).[12] The values of $d\Delta V^{*\prime}/dP$ are comparatively small for Reactions 4 and 5, where the liberated $-NH_2$ group is linked to the five-coordinated intermediate. In contrast, they are comparatively large for Reactions 1, 2, and 3, where the leaving group is not linked to the intermediate. Hence, the increases in the $\Delta V^{*\prime}$ with the increase in the pressure are caused by the enhancement of the separation of the leaving group from the five-coordinated intermediate at high pressures. In other words, the mechanism of the dissociation of the conjugate base changes from the I_d mechanism at a normal pressure to the D mechanism at higher pressures. A possible factor promoting the separation at high pressures may be the increasing stability of the hydrogen bonds between the leaving group and the water molecules, which decreases the interaction between the leaving group and the intermediate.

The activation energies (E_a) obtained by Kuroda are listed in Table 3. In the S_N1 CB mechanism, $E_a \simeq \Delta H_{pre} + E_a'$, where ΔH_{pre} is the enthalpy change for the pre-equilibrium and where E_a' is the activation energy for the dissociation of the conjugate base. ΔH_{pre} would be negative, since an evolution of heat was noticed in the analogous neutralization Equilibrium 6.[1] The abnormally large magnitudes of E_a'

can be understood only by considering the Co–N bond rupture to be the activation step.[3] There can be found an qualitative correspondence relation between the magnitude of E_a and the position of the first absorption band.[9,17] This indicates that the ligand-field strength is one factor which influences the activation energy. The activation entropies calculated from the first-order rate constants are listed in Table 3. An ordinary compensation relation is found between the magnitudes of E_a and ΔS^*. This relation is often found for a series of related reactions and is interpreted as indicating that the essential reaction mechanism is the same for all of a given series.[18] Another linear correlation is found between ΔS^* and ΔV^* except for Reaction 3. Thus, the values of $\Delta V^{*\prime}$, E_a, and ΔS^* for Reactions 2 and 5 are comparatively larger than those for Reactions 1 and 4. One possible interpretation of this may be that, in the activated states for Reactions 2 and 5, the leaving group is more separated from the five-coordinated intermediate than in those for Reactions 1 and 4. Then, the smaller magnitude of $d\Delta V^{*\prime}/dP$ for Reaction 2 than that for Reaction 1 may be interpreted as showing that, for Reaction 2, the separation increases rather moderately with the pressure, since it is already considerable at the normal pressure.

The author wishes to thank Professor Kashiro Kuroda of Ehime University for permission to refer to his unpublished results and for his valuable suggestions throughout this work. The author is also indebted to Mr. Yoshifumi Noma for his co-work in the preliminary experiments on the reaction of α-$[Co(edda)(NH_3)_2]^+$.

References

1) Y. Kitamura, *Bull. Chem. Soc. Jpn.*, **52**, 3453 (1979). The references cited therein.
2) Y. Kitamura, *Bull. Chem. Soc. Jpn.*, **49**, 1002 (1976).
3) K. Kuroda, *Chem. Lett.*, **1972**, 1153.
4) K. Kuroda and F. Mohri, *Chem. Lett.*, **1972**, 719.
5) K. Kuroda, Preprint presented for the 28th National Meeting of the Chemical Society of Japan, Tokyo, April 1973, Vol. 1., p. 542.
6) The first-order rate constants ($k_1 \times 10^3$ min^{-1}) obtained by K. Kuroda for the base hydrolysis of β-$[Co(edda)(NH_3)_2]^+$ in carbonate buffers are as follows at a normal pressure:

Condition (pH at 60 °C)	40 °C	45 °C	50 °C
0.1 M Na_2CO_3–0.3 M $NaHCO_3$ (9.48)	3.3	10	25
0.2 M Na_2CO_3–0.2 M $NaHCO_3$ (9.81)		15	
0.3 M Na_2CO_3–0.1 M $NaHCO_3$ (10.18)		30	

7) K. Kuroda and K. Watanabe, *Bull. Chem. Soc. Jpn.*, **44**, 1034 (1971).
8) K. Igi and D. E. Douglas, *Inorg. Chem.*, **13**, 425 (1974).
9) K. Kuroda, *Bull. Chem. Soc. Jpn.*, **45**, 2176 (1972). For β-$[Co(edda)(en)]ClO_4$, λ_{max}=494 nm.
10) K. Kuroda and K. Watanabe, *Bull. Chem. Soc. Jpn.*, **44**, 2550 (1971).
11) Y. Kitamura, *Bull. Chem. Soc. Jpn.*, **50**, 2097 (1977).
12) B. S. El'yanov and S. D. Hamann, *Aust. J. Chem.*, **28**, 945 (1975).
13) H. R. Hunt and H. Taube, *J. Am. Chem. Soc.*, **80**, 2642 (1958).
14) D. R. Stranks, *Pure Appl. Chem.*, **38**, 303 (1974).
15) R. H. Stokes, *Aust. J. Chem.*, **28**, 2109 (1975).
16) "Water and Aqueous Solutions, Structure, Thermodynamics and Transport Processes," ed by R. A. Horn, Wiley-Interscience, New York (1972), pp. 519—560.
17) K. Kuroda, *Chem. Lett.*, **1974**, 17. For β-$[Co(edda)(tn)]ClO_4$, λ_{max}=503 nm.
18) T. W. Swaddle, *Coord. Chem. Rev.*, **14**, 217 (1974).

Heteropolyanions of Methylarsonate and Dimethylarsinate: The Crystal Structures of Guanidinium Hexamolybdomethylarsonate Hexahydrate, $(CN_3H_6)_2[CH_3AsMo_6O_{21}(H_2O)_6]\cdot 6H_2O$ and Guanidinium Tetramolybdodimethylarsinate Monohydrate, $(CN_3H_6)_2[(CH_3)_2AsMo_4O_{14}(OH)]\cdot H_2O$

Kazuko Y. MATSUMOTO

Department of Chemistry, Faculty of Science, The University of Tokyo, Hongo, Bunkyo-ku, Tokyo 113

(Received February 1, 1979)

The crystal and molecular structures of polymolybdo complexes of methylarsonate and dimethylarsinate have been determined by the X-ray diffraction technique. The crystal of $(CN_3H_6)_2[CH_3AsMo_6O_{21}(H_2O)_6]\cdot 6H_2O$ is trigonal, with the space group R3 and the cell dimensions of $a=9.653(6)$ Å, $\alpha=87.01(15)°$, and $Z=1$. The anion is an assemblage of six MoO_6 octahedra and a tetrahedral CH_3AsO_3 group. The six MoO_6 octahedra constitute a ring with alternate edge- and corner-sharing, and the tetrahedral CH_3AsO_3 group joins the anion, with its three oxygen atoms shared with the ring. Each molybdenum atom has two terminal oxygen atoms in the *cis* position and is coordinated by one water molecule. $(CN_3H_6)_2[(CH_3)_2AsMo_4O_{14}(OH)]\cdot H_2O$ crystallizes in the space group $P2_1/c$ of the monoclinic system, with the cell dimensions of $a=8.530(5)$, $b=8.532(4)$, $c=30.121(15)$ Å, $\beta=95.50(16)°$, and $Z=4$. The $Mo_4O_{14}(OH)$ moiety in the $[(CH_3)_2AsMo_4O_{14}(OH)]^{2-}$ anion is formed with two face- and two edge-sharings of MoO_6 octahedra into an almost flat rectangle. The oxygen atom located at the center of the anion and bonded to all the four molybdenum atoms is protonated and is, in fact, a hydroxyl group.

It is well known that arsenic acid reacts with molybdic acid to yield various heteropoly acids. Some of them have been structurally elucidated by X-ray diffraction: $AsMo_{12}O_{40}^{3-}$ with the Keggin structure,[1,2] $H_4AsMo_{12}O_{50}^{4-}$[3] with the "reversed" Keggin structure, $AsMo_9O_{34}^{9-}$,[4] $As_2Mo_{18}O_{62}^{6-}$,[5,6] and $As_2Mo_5O_{23}^{6-}$.[7] Alkyl- or arylarsonic acids and -arsinic acids, $RAsO_3H_2$ and R_2AsO_2H, seem to be similar to phosphoric or arsenic acid in their chemical properties in the following respects: they form dimers of the pyrophosphoric-acid type and are weak acids (the pK values of $RAsO_3H_2$ are 3—4, whereas pK_1 is 2.1 for phosphoric acid and 2.3 for arsenic acid). In view of the fact that the heteropolyanions containing phosphorus or arsenic atoms are formed through dehydration between phosphoric or arsenic acid and molybdic acid, these organo-arsenic acids can be expected to react with molybdic acid to give organo-heteropolyanions.

Such anions are noteworthy from the following points of view: the organo-heteropolyanions have their heteroatoms, that is, As(V) in the present case, partly coordinated by organic groups. Therefore, the arsenic atoms can not be coordinated by four oxygen atoms, unlike those in non-alkylated arsenic acids, as long as the former keep their coordination number of 4. Otherwise, they may increase the coordination number from 4 to 6. Whichever of the two may be the case, new structural types may be expected for these anions. Recently, the present author has reported the crystal and molecular structure of $(CN_3H_6)_4[(C_6H_5As)_2Mo_6O_{25}H_2\cdot 4H_2O$,[8] whose anion's interconversion with $[(C_6H_5As)_2Mo_6O_{24}]^{4-}$ in an aqueous solution[9] has added valuable knowledge concerning the intermediate species involved in the formation of these anions and the pH regions where they are stable.

In this paper the author will report on the crystal and molecular structures of guanidinium polymolybdomethylarsonate and polymolybdodimethylarsinate, $(CN_3H_6)_2[CH_3AsMo_6O_{21}(H_2O)_6]\cdot 6H_2O$ and $(CN_3H_6)_2[(CH_3)_2AsMo_4O_{14}(OH)]\cdot H_2O$. The first synthetic description of these complexes was made by Gibbs as early as in 1883[10] and later by Rosenheim and Bilecki,[11] but their analytical results are unsatisfactory and the molecular formulae they gave seem doubtful. As for the heteropolyanions containing methylarsonic acid, the synthesis and the structure of $[(CH_3As)_2Mo_6O_{24}]^{4-}$ have recently been reported,[12] but the author has independently obtained a hexamolybdomethylarsonate anion which seems to have a different molecular formula, *i.e.*, $[CH_3AsMo_6O_{21}(H_2O)_6]^{2-}$. Thus, the formation conditions and structural differences of these anions are of interest and would give information about the reactions occurring in an aqueous solution containing molybdic acid and methylarsonic acid. On the other hand, regarding the heteropolyanion containing dimethylarsinic acid, a short communication on the crystal structure of $(CN_3H_6)_2[(CH_3)_2AsMo_4O_{14}(OH)]\cdot H_2O$ recently appeared;[13] it briefly discusses the anion's structure. In this paper, the whole crystal structure, together with the anion's structure, will be discussed, and the full and detailed data on the bond distances, bond angles, and the crystal packings, including the network of hydrogen bondings, will be presented.

Experimental

$(CN_3H_6)_2[CH_3AsMo_6O_{21}(H_2O)_6]\cdot 6H_2O$. *Preparation*: 4.3 g (0.03 mol) of MoO_3 was gradually added to 75 cm³ of a boiling aqueous solution containing 1.46 g (5 mmol) of $Na_2AsCH_3O_3$, and the pH of the solution was decreased to *ca.* 2 with HCl. After the solution has been boiled for a few minutes, it was filtered to remove a small amount of unreacted MoO_3 and the filtrate was condensed on a water bath to 12.5 cm³. The addition of 1 g of CN_3H_6Cl to the solution readily gave a lolorless precipitate, which was subsequently filtered, recrystallized from hot water, and air-dried. The reaction is expressed as follows:

$$CH_3AsO_3^{2-} + 6MoO_3 + 6H_6O \longrightarrow [CH_3AsMo_6O_{21}(H_2O)_6]^{2-}$$

Found: C, 2.69; H, 2.94; N, 6.48%. Calcd for $(CN_3H_6)_2[CH_3AsMo_6O_{21}(H_2O)_6]\cdot 6H_2O$: C, 2.73; H, 2.80; N, 6.37%.

The addition of $(CH_3)_4NBr$ or KCl instead of CN_3H_6Cl

Table 1. Final positional parameters ($\times 10^4$) for $(CN_3H_6)_6[CH_3AsMo_6O_{21}(H_2O)_6]\cdot 6H_2O$, with their estimated standard deviations in parentheses

	x	y	z
Mo (1)	40 (6)	2265 (6)	−2956 (6)
Mo (2)	2965 (5)	−145 (6)	−2245 (5)
As	300[a)]	= x	= x
C	1345 (58)	= x	= x
O (1)	844 (35)	629 (36)	−1312 (37)
O (2)	2041 (69)	1381 (71)	−3223 (70)
O (3)	1373 (53)	3538 (60)	−1545 (61)
O (4)	392 (58)	3612 (56)	−4156 (56)
O (5)	−1155 (76)	2718 (82)	−1584 (76)
O (6)	−882 (53)	949 (55)	−3863 (51)
O (7)	3735 (36)	787 (42)	−1203 (36)
O (8)	4185 (54)	−435 (63)	−3482 (51)
O (9)	1429 (46)	−1577 (48)	−3345 (46)
C (1)	3204 (306)	= x	= x
C (2)	−3133 (243)	= x	= x
N (1)	2079 (85)	4063 (99)	3206 (106)
N (2)	−1890 (92)	−3994 (72)	−3146 (87)
H_2O (1)	−4040 (53)	2496 (53)	−4076 (50)
H_2O (2)	−2273 (64)	4035 (59)	4161 (59)

a) The coordinates for As are arbitrarily fixed at 300.

Table 2. Final temperature factors for $(CN_3H_6)_2[CH_3AsMo_6O_{21}(H_2O)_6]\cdot 6H_2O$ with their estimated standard deviations

The β_{ij}'s are defined by $\exp[-(\beta_{11}h^2+\beta_{22}k^2+\beta_{33}l^2+2\beta_{12}hk+2\beta_{13}hl+2\beta_{23}kl)]$. ($\times 10^4$ for Mo and As and $\times 10^3$ for the others).

	β_{11}	β_{22}	β_{33}	β_{12}	β_{13}	β_{23}
Mo (1)	73 (7)	50 (6)	46 (6)	19 (5)	11 (5)	27 (4)
Mo (2)	27 (5)	76 (7)	35 (5)	12 (5)	18 (4)	11 (4)
As	12 (3)	12 (3)	12 (3)	4 (3)	4 (3)	4 (3)
C	5 (4)	5 (4)	5 (4)	−1 (4)	−1 (4)	−1 (4)
O (1)	3 (4)	2 (4)	3 (4)	2 (3)	2 (3)	0 (3)
O (2)	12 (9)	15 (9)	14 (9)	8 (8)	−3 (7)	−6 (8)
O (3)	5 (5)	11 (7)	13 (8)	−1 (5)	5 (5)	1 (6)
O (4)	11 (7)	9 (7)	9 (7)	1 (6)	3 (6)	5 (6)
O (5)	14 (9)	18 (10)	13 (9)	4 (8)	8 (7)	−1 (8)
O (6)	8 (6)	11 (7)	7 (6)	0 (5)	2 (5)	2 (5)
O (7)	2 (4)	6 (5)	2 (3)	5 (3)	3 (3)	3 (3)
O (8)	8 (6)	14 (8)	6 (6)	2 (6)	5 (5)	−1 (5)
O (9)	6 (5)	7 (5)	6 (5)	3 (4)	2 (4)	1 (4)
C (1)	29 (16)	29 (16)	29 (16)	12 (11)	12 (11)	12 (11)
C (2)	9 (19)	9 (19)	9 (19)	7 (23)	7 (23)	7 (23)
N (1)	18 (12)	32 (17)	37 (19)	10 (12)	23 (13)	24 (15)
N (2)	30 (16)	11 (10)	24 (14)	14 (11)	13 (12)	8 (9)
H_6O (1)	12 (7)	13 (7)	11 (6)	0 (5)	−2 (5)	5 (5)
H_6O (2)	18 (8)	13 (7)	15 (8)	−4 (7)	−6 (7)	4 (6)

precipitated the corresponding salts of the anion. The potassium salt was recrystallized from hot water. However, the tetramethylammonium salt is insoluble in most aqueous and organic solvents. The addition of $(n\text{-}C_4H_9)_4NBr$ to the solution gave a yellow-green precipitate, which was a mixture of several polyanions. By the fractional recrystallization of this mixture from CH_3NO_2, the $[(CH_3As)_4Mo_{12}O_{46}]^{4-}$ anion was obtained together with other polyanions, such as $[CH_3AsMo_6O_{21}(H_2O)_6]^{2-}$ and $Mo_6O_{19}^{2-}$. The $[(CH_3As)_4Mo_{12}O_{46}]^{4-}$ [12] and $Mo_6O_{19}^{2-}$ [14] anions were identified by elemental analyses and IR spectra.

Crystal Data: Although many kinds of salts of the $[CH_3AsMo_6O_{21}(H_2O)_6]^{2-}$ anion were prepared, as has been described above, most of them were obtained in powder or microcrystalline form. Among them, guanidinium salt seemed likely to give a single crystal of an appropriate size, though it would not do so easily. Thus, attempts were made to obtain it by a diffusion method, and a crystal with approximate dimensions of $0.1\times 0.08\times 0.08$ mm was used for X-ray measurements. Although this crystal gives slightly smeared diffraction spots, it is fairly stable in air and against X-ray irradiation, at least for the period of X-ray data collection. Such smeared spots have been observed in other isopoly- and heteropolyanions; they are probably attributed to the loose packings of large anions and the existence of easily mobile water of crystallization occupying the cavities between the large anions.[15,16] Although a crystal structure analysis with a high precision can not be expected for this crystal, X-ray measurement was undertaken, because at least the structure of the anion could be elucidated and this would be valuable information for the chemistry of heteropolyanions containing methylarsonic acid. The lattice constants were refined with twelve 2θ values measured on a diffractometer with Mo $K\alpha$ radiation ($\lambda=0.7107$ Å). The crystal data for $(CN_3H_6)_2[CH_3AsMo_6O_{21}(H_2O)_6]\cdot 6H_2O$ are: trigonal, R3, $a=9.653(6)$ Å, $\alpha=87.01(15)°$, $V=895.9$ Å^3, $M.W.=1338.0$, $Z=1$, $D_m=2.45$ g cm^{-3}, $D_x=2.48$, $\mu=13.3$ cm^{-1}.

Data Collection: All the intensities were measured on a Philips automatic four-circle diffractometer with graphite-monochromated Mo $K\alpha$ radiation. The ω-2θ scan mode was employed with the scan rate of 1 ° min^{-1} in 2θ. The scan width was determined for each reflection according to this formula $\omega=(1.4+0.6\tan\theta)°$. Background counts of 20 s were taken at each scan end. Three standard reflections were monitored every 3 h, but no significant intensity loss was observed throughout the data collection. The data were corrected for Lorentz and polarization effects. Absorption and extinction corrections were not applied. The intensities were collected up to $2\theta=60°$, of which 1094 independent reflections with $|F_o|\geq 3\sigma(|F_o|)$ were used for the structural analysis.

Solution and Refinement of the Structure: Two independent molybdenum atoms were located from the Patterson map, and successive Fourier syntheses revealed the positions of all non-hydrogen atoms in the anion. At this stage, a problem arose concerning the space group of this crystal. Although this anion itself is, strictly speaking, dissymmetric, a close examination of the atomic coordinates (Table 1) exhibits that this anion is approximately centrosymmetrical except the part of the As–C bond. For instance, many atoms in the anion are related to each other nearly centrosymmetrically, *i.e.*, Mo(1) and Mo(2), O(3) and O(9), O(4) and O(8), and O(6) and O(7). Moreover, when the structure analysis had proceeded further, it was found that the cations and water molecules also occupy centrosymmetric positions (C(1) and C(2), N(1) and N(2), and H_2O(1) and H_2O(2)). As the R3 and R$\bar{3}$ space groups can not be distinguished from the systematic absence of reflection, two different refinements were attempted, one based on the R3 space group, and the other, on R$\bar{3}$, assuming a statistical distribution of the anions in the right-handed and left-handed orientations, with an equal weight for each. Disorder of

Table 3. Final positional coordinates ($\times 10^4$) for $(CN_3H_6)_2[(CH_3)_2AsMo_4O_{14}(OH)]\cdot H_2O$, with their estimated standard deviations in parentheses

	x	y	z
Mo (1)	1896 (2)	1989 (2)	3202 (1)
Mo (2)	3606 (2)	−1073 (2)	3550 (1)
Mo (3)	1720 (2)	−1161 (2)	4458 (1)
Mo (4)	−32 (2)	1942 (2)	4114 (1)
As	−367 (2)	−1375 (2)	3413 (1)
O (1)	3744 (16)	748 (15)	3155 (4)
O (2)	4120 (22)	−2518 (18)	3180 (5)
O (3)	5407 (20)	−764 (19)	3887 (5)
O (4)	2458 (15)	952 (14)	3923 (4)
O (5)	2546 (16)	−2190 (15)	3961 (4)
O (6)	3508 (20)	−932 (19)	4778 (5)
O (7)	737 (19)	−2628 (17)	4712 (5)
O (8)	683 (16)	735 (15)	4629 (4)
O (9)	807 (18)	3671 (17)	4282 (5)
O (10)	−298 (16)	−656 (14)	3920 (5)
O (11)	−2029 (17)	2197 (17)	4153 (5)
O (12)	−67 (15)	2138 (14)	3472 (4)
O (13)	2752 (18)	3723 (18)	3349 (6)
O (14)	1175 (19)	2176 (19)	2654 (5)
O (15)	1205 (15)	−703 (15)	3186 (4)
O (16)	4960 (17)	2335 (16)	4434 (5)
C (1)	−348 (37)	−3636 (24)	3435 (10)
C (2)	−2220 (27)	−623 (26)	3063 (8)
C (3)	6612 (30)	6234 (27)	4634 (8)
C (4)	6446 (25)	4093 (23)	2942 (7)
N (1)	5352 (26)	5770 (23)	4392 (7)
N (2)	7651 (31)	5169 (27)	4841 (8)
N (3)	6996 (25)	7738 (22)	4691 (7)
N (4)	6263 (24)	3873 (23)	3374 (7)
N (5)	7708 (22)	3476 (21)	2766 (6)
N (6)	5401 (23)	4940 (22)	2686 (6)

Table 4. Final temperature factors ($\times 10^4$) for $(CN_3H_6)_2[(CH_3)_2AsMo_4O_{14}(OH)]\cdot H_2O$, with their estimated standard deviations

The β_{ij}'s are defined by: $\exp[-(\beta_{11}h^2+\beta_{22}k^2+\beta_{33}l^2+2\beta_{12}hk+2\beta_{13}hl+2\beta_{23}kl)]$

	β_{11}	β_{22}	β_{33}	β_{12}	β_{13}	β_{23}
Mo (1)	48 (2)	29 (2)	5 (1)	6 (2)	5 (1)	3 (1)
Mo (2)	46 (2)	31 (2)	4 (1)	12 (2)	4 (1)	1 (1)
Mo (3)	54 (2)	28 (2)	4 (1)	11 (2)	3 (1)	1 (1)
Mo (4)	46 (2)	23 (2)	4 (1)	10 (1)	3 (1)	0 (1)
As	45 (2)	26 (2)	4 (1)	−7 (2)	2 (1)	−1 (1)
O (1)	64 (17)	39 (15)	4 (1)	18 (13)	11 (4)	1 (3)
O (2)	184 (29)	50 (19)	6 (2)	−22 (19)	20 (6)	0 (4)
O (3)	68 (23)	81 (22)	10 (2)	−1 (18)	1 (5)	4 (5)
O (4)	38 (16)	37 (15)	5 (1)	4 (12)	3 (3)	−1 (3)
O (5)	73 (18)	39 (15)	4 (1)	7 (14)	5 (4)	1 (4)
O (6)	92 (24)	93 (23)	7 (2)	18 (19)	−2 (5)	−3 (5)
O (7)	106 (23)	34 (17)	9 (2)	39 (16)	12 (5)	2 (4)
O (8)	65 (17)	37 (15)	5 (1)	31 (13)	10 (4)	1 (4)
O (9)	80 (20)	30 (17)	12 (2)	20 (16)	−12 (5)	−4 (5)
O (10)	56 (17)	13 (14)	7 (2)	−13 (13)	−2 (4)	−1 (4)
O (11)	56 (19)	53 (18)	9 (2)	22 (15)	9 (4)	−2 (5)
O (12)	46 (16)	9 (13)	6 (1)	2 (12)	1 (4)	0 (4)
O (13)	45 (20)	52 (19)	16 (2)	17 (17)	−3 (5)	−2 (6)
O (14)	77 (22)	114 (23)	7 (2)	15 (19)	8 (5)	7 (5)
O (15)	31 (15)	38 (15)	6 (2)	6 (13)	3 (3)	−4 (4)
O (16)	54 (18)	33 (17)	10 (2)	−11 (14)	2 (4)	1 (4)
C (1)	107 (48)	19 (22)	18 (3)	17 (27)	10 (11)	−2 (7)
C (2)	79 (30)	63 (27)	10 (3)	−10 (24)	0 (7)	−1 (7)
C (3)	115 (35)	54 (28)	9 (3)	45 (27)	−3 (8)	−4 (8)
C (4)	82 (27)	51 (24)	5 (2)	1 (21)	−1 (6)	0 (6)
N (1)	120 (32)	52 (25)	11 (3)	17 (23)	−8 (7)	−3 (7)
N (2)	183 (42)	62 (30)	16 (3)	52 (30)	−24 (10)	0 (9)
N (3)	100 (30)	47 (24)	11 (3)	−15 (22)	−7 (7)	1 (6)
N (4)	94 (28)	79 (25)	8 (2)	−13 (23)	4 (6)	8 (6)
N (5)	69 (23)	55 (22)	8 (2)	23 (19)	4 (5)	1 (6)
N (6)	88 (26)	72 (24)	6 (2)	33 (21)	4 (6)	0 (6)

this kind has sometimes been observed in crystals of isopoly- and heteropoly acids and their salts,[16,17] and is considered as one of their specific properties. The R value for R3 was 0.20, whereas that for $R\bar{3}$ was 0.21. Therefore the R3 space group was assumed to be the true one. After several cycles of refinement with isotropic temperature factors by the block-diagonal least-squares method using the UNICS program,[18] anisotropic temperature factors were applied for all the atoms; further refinements reduced the R value to 0.16 ($R=\sum||F_o|-|F_c||/\sum|F_o|$). All the cations and water of crystallization were located on the basis of the difference synthesis, and the structure was finally refined to $R=0.14$. Although the final R value is not low enough, this is because of the unsatisfactory quality of the crystal, as has been mentioned, and does not basically obviate the elucidated anion's structure.

The atomic coordinates and temperature factors are listed in Tables 1 and 2. The final F_o-F_c table is available at the Office of Chemical Society of Japan as Document No. 7930A. The atomic scattering factors were taken from Ref. 19, while the corrections of the effect of the anomalous dispersion for molybdenum and arsenic atoms were based on Ref. 20. The calculation was performed on a HITAC 8700/8800 computer at the Computer Center of the University of Tokyo.

$(CN_3H_6)_2[(CH_3)_2AsMo_4O_{14}(OH)]\cdot H_2O$. *Preparation*: This compound was prepared according to the method described in Ref. 11. Found: C, 5.41; H, 2.51; N, 9.90; Mo, 45.52%. Calcd for $(CN_3H_6)_2[(CH_3)_2AsMo_4O_{14}(OH)]\cdot H_2O$: C, 5.54; H, 2.44; N, 9.68; Mo, 44.22%.

Cyrstal Data: A colorless rectangular crystal with the approximate dimensions of $0.2\times0.2\times0.1$ mm was used. The cell dimensions were obtained from twelve 2θ values measured on a diffractometer with Mo $K\alpha$ radiation. The crystal data for $(CN_3H_6)_2[(CH_3)_2AsMo_4O_{14}(OH)]\cdot H_2O$ are: monoclinic $P2_1/c$, $a=8.530(5)$ Å, $b=8.532(4)$, $c=30.121(15)$, $\beta=95.50(16)°$, $M.W.=867.9$, $Z=4$, $D_m=2.63$ g cm^{-3}, $D_x=2.64$, $\mu=41.0$ cm^{-1}.

Data Collection: All the intensity measurements were performed on a Rigaku four-circle diffractometer with graphite-monochromated Mo $K\alpha$ radiation. The conditions for the data collection were basically the same as those described above. The scan rate was 2° min^{-1} in 2θ, and the scan range was determined according to this formula: $\omega=(1.4+0.6\tan\theta)°$. A background count was made for 10 s at the end of each scan. Three standard reflections, monitored every 50 measurements, remained essentially constant during the data collection. The data were corrected for Lorentz and polarization effects. Absorption and extinction cor-

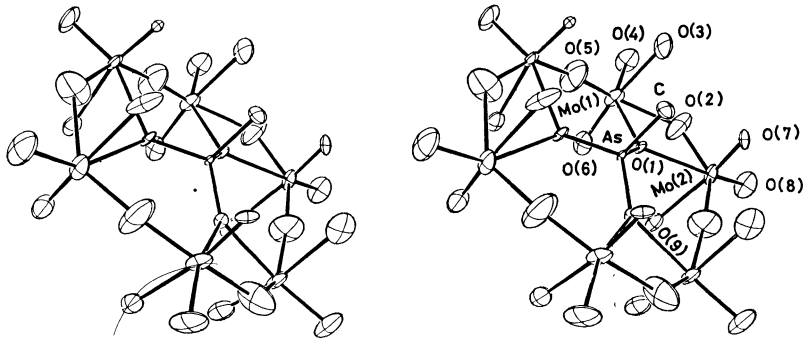

Fig. 1. Stereoscopic view of the $[CH_3AsMo_6O_{21}(H_2O)_6]^{2-}$ anion with vibrational ellipsoids drawn at the 30% probability level. (ORTEP Johnson, 1971)

TABLE 5. THE BOND LENGTHS FOR THE ANION AND THE CATIONS IN $(CN_3H_6)_2[CH_3AsMo_6O_{21}(H_2O)_6]\cdot 6H_2O$, WITH THEIR ESTIMATED STANDARD DEVIATIONS IN PARENTHESES

	l/Å		*l*/Å
MO(1)-O(1)	2.33(4)	Mo(2)-O(1)	2.29(4)
O(2)	2.08(7)	O(2)	1.91(7)
O(3)	2.35(6)	O(7)	1.62(4)
O(4)	1.73(6)	O(8)	1.66(5)
O(5)	1.77(8)	O(9)	2.40(5)
O(6)	1.87(6)	O(5′)	1.72(7)
As-O(1)	1.64(4)	Mo(1)···Mo(2)	3.63(1)
C	1.84(6)	Mo(1)···Mo(2′)	3.48(1)
C(1)-N(1)	1.33(27)		
C(2)-N(2)	1.42(24)		

The prime refers to the transformation, (y, z, x).

rections were not applied. 5222 independent reflections with $|F_o| \geq 3\sigma(|F_o|)$ up to $2\theta=60°$ were used for the computation.

Solution and Refinement of the Structure: The coordinates for the four independent molybdenum atoms were deduced from the Patterson map. All the remaining non-hydrogen atoms were located from the successive Fourier maps. A few cycles of refinement with individual isotropic temperature factors for all the atoms, followed by several further cycles of anisotropic refinement, resulted in a final R value of 0.091. The final coordinates and temperature factors are listed in Tables 3 and 4, while the F_o-F_c table is kept at the office of this Bulletin as Document No. 7930B.

Description of the Structure and Discussion

$(CN_3H_6)_2[CH_3AsMo_6O_{21}(H_2O)_6]\cdot 6H_2O$. The structure of the anion is illustrated in Fig. 1. The anion consists of six MoO_6 octahedra, which form a ring by alternate corner- and edge-sharing (the shared corner is O(5) and the shared edge is O(1)–O(2)), and a CH_3AsO_3 tetrahedron connected to the ring with its three oxygen atoms shared with the ring. The six molybdenum atoms are not coplanar and deviate from the best plane by about 0.4 Å, upward and downward alternately. Only Mo(1), Mo(2), As, C, and the nine oxygen atoms coordinated to these molybdenum and arsenic atoms are crystallographically independent; the remaining part of the anion is related

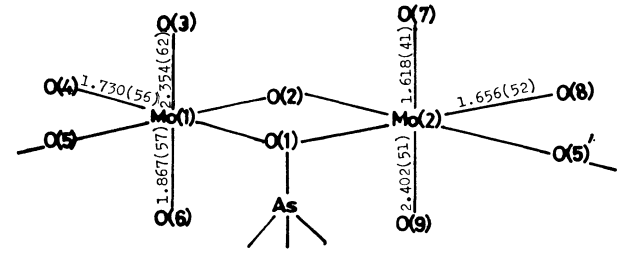

∠O(3)-Mo(1)-O(4)	82.5(2.3)°	∠O(8)-Mo(2)-O(9)	90.4(2.1)°
∠O(4)-Mo(1)-O(6)	107.4(2.4)°	∠O(7)-Mo(2)-O(8)	102.7(2.2)°
∠O(3)-Mo(1)-O(6)	168.5(2.2)°	∠O(7)-Mo(2)-O(9)	166.6(1.8)°

Fig. 2. The geometry of the terminal oxygen atoms around Mo(1) and Mo(2) in the $[CH_3AsMo_6O_{21}(H_2O)_6]^{2-}$ anion.

to the independent atoms by a three-fold axis which coincides with the As–C bond axis. The bond lengths in the anion and cations are listed in Table 5. It is noteworthy that each molybdenum atom seemingly possesses three terminal oxygen atoms. However, for the reasons to be presented below, it is concluded that each molybdenum atom is surrounded not by three terminal oxygen atoms, but by two terminal ones and a water molecule. One of the reasons is concerned with the distances of the terminal Mo–O bonds. As is illustrated in Fig. 2, the Mo(1)–O(3) and Mo(2)–O(9) distances are obviously longer than the other four terminal ones (Mo(1)–O(4), Mo(1)–O(6), Mo(2)–O(7), and Mo(2)–O(8)). The distances, 2.35 Å for Mo(1)–O(3) and 2.40 Å for Mo(2)–O(9), are comparable to the Mo–OH_2 distances of 2.28 Å in $MoO_3\cdot 2H_2O$[21] and of 2.33 Å in $K_2(Mo_2O_5(C_2O_4)_2(H_2O)_2)$.[22] The second reason is concerned with the arrangement of the oxygen atoms coordinated to the molybdenum atoms and the bond angles. In the present polyanion, the three terminal oxygen atoms occupy the *mer* position, whereas the mononuclear and binuclear oxo-complexes of Mo(VI) with three terminal oxygen atoms investigated thus far possess the oxygen atoms in the *fac* position.[22,23] The angles between these three Mo–O bonds are given in Fig. 2. It is generally accepted that the repulsion between two terminal oxygen atoms always, without exception, causes fairly large O(terminal)–Mo–O(terminal) bond angles, ranging from 101° to 108°,[22,24] while the O(terminal)–Mo–H_2O angle in $K_2(Mo_2O_5(C_2O_4)_2(H_2O)_2)$ is reduced to

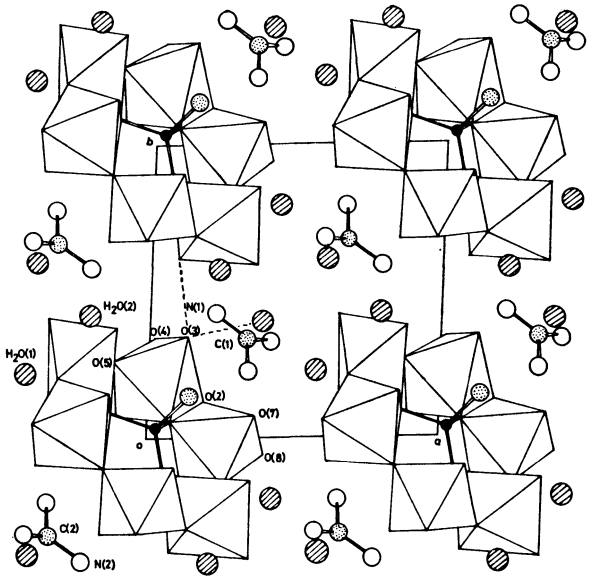

Fig. 3. The crystal structure of $(CN_3H_6)_2[CH_3AsMo_6O_{21}(H_2O)_6]\cdot 6H_2O$ viewed normal to a and b axes.

85.50°.[22] Considering the fact that the O(3)–Mo(1)–O(4) and O(8)–Mo(2)–O(9) angles in the present anion are as small as the latter, O(3) and O(9) can be identified as water molecules without any risk of serious mistake. This assignment is also supproted by the fact that each molybdenum atom is coordinated by two terminal oxygen atoms in the cis position, which is the usual geometry not only in polyacids but also in mono- and binuclear oxo-complexes of Mo(VI). Trans terminal oxygens have been found only in d^2 complexes, such as in $(MoO_2(CN)_4)^{4-}$,[25] but not in Mo(VI) complexes.

Although there have been some reports concerning the coordination of water molecules to heteroatoms in polyanions and their substitution reactions,[26,27] the present anion would seem to be one of the few examples of water molecules coordinating to addenda atoms, that is, molybdenums; another example is found in $Na_3[PMo_9O_{31}(H_2O)_3]\cdot nH_2O$.[28]

The crystal structure is shown in Fig. 3, while selected interionic distances are listed in Table 6. The anions, water molecules, and cations form a three-dimensional network of hydrogen bondings.

$(CN_3H_6)_2[(CH_3)_2AsMo_4O_{14}(OH)]\cdot H_2O$. Figure 4 illustrates the structure of the $[(CH_3)_2AsMo_4O_{14}(OH)]^{2-}$ anion, which consists of four MoO_6 octahedra joined to form a flat group of Mo_4O_{15}, with two face-sharings (the shared faces are O(4)–O(8)–O(10) and O(1)–O(4)–O(15)) and two edge-sharings (the shared edges are O(4)–O(5) and O(4)–O(12)). A $(CH_3)_2AsO_2$ tetrahedron shares two oxygen atoms (O(10) and O(15)) with the Mo_4O_{15} moiety. The bond lengths and angles in the anion are listed in Tables 7 and 8. O(4) is common to all four octahedra, and the Mo(n)–O(4) (n=1, 2, 3, and 4) bond lengths are noticeably large; the distance of Mo(3)–O(4) is 2.538 Å in the present work, one of the largest Mo–O lengths recorded, so far as the author knows. Not many examples of face-sharing of octahedra, as is seen in the present anion, are known, either; other examples are the Mo_2O_9 part of the mannitol-molybdate complex, $H_2Mo_2O_9C_6H_8(OH)_2$,[29] and the molybdocerate anion, $[CeMo_{12}O_{42}]^{8-}$.[30]

Table 6. Bond lengths in the $[(CH_3)_2AsMo_4O_{14}(OH)]^{2-}$ anion and in the guanidinium cations, $CN_3H_6^+$, with their estimated standard deviations in parentheses

	l/Å		l/Å
Mo(1)–O(1)	1.916(14)	Mo(2)–O(1)	1.960(14)
O(4)	2.351(15)	O(2)	1.720(17)
O(12)	1.934(15)	O(3)	1.709(19)
O(13)	1.690(16)	O(4)	2.369(15)
O(14)	1.713(17)	O(5)	1.911(16)
O(15)	2.371(13)	O(15)	2.326(15)
Mo(3)–O(4)	2.538(14)	Mo(4)–O(4)	2.407(15)
O(5)	1.926(16)	O(8)	1.912(15)
O(6)	1.736(19)	O(9)	1.696(15)
O(7)	1.726(16)	O(10)	2.298(13)
O(8)	1.938(14)	O(11)	1.732(15)
O(10)	2.290(17)	O(12)	1.939(14)
Mo(1)···Mo(2)	3.163(5)	As–O(10)	1.642(15)
Mo(2)···Mo(3)	3.353(9)	O(15)	1.665(15)
Mo(3)···Mo(4)	3.166(5)	C(1)	1.930(20)
Mo(4)···Mo(1)	3.334(9)	C(2)	1.924(25)
C(3)–N(1)	1.30(3)	C(4)–N(4)	1.34(3)
N(2)	1.38(3)	N(5)	1.35(3)
N(3)	1.33(3)	N(6)	1.33(3)
O(1)–O(2)	2.81(2)	O(5)–O(10)	2.75(2)
O(3)	2.82(2)	O(15)	2.81(2)
O(4)	2.66(2)	O(6)–O(7)	2.76(2)
O(13)	2.76(2)	O(8)	2.80(2)
O(14)	2.82(2)	O(7)–O(8)	2.88(2)
O(15)	2.51(2)	O(10)	2.98(2)
O(2)–O(3)	2.74(2)	O(8)–O(9)	2.72(2)
O(5)	2.83(2)	O(10)	2.52(2)
O(15)	2.93(2)	O(11)	2.89(2)
O(3)–O(4)	2.92(2)	O(9)–O(11)	2.72(2)
O(5)	2.75(2)	O(12)	2.81(2)
O(4)–O(5)	2.68(2)	O(10)–O(11)	2.97(2)
O(6)	3.10(2)	O(12)	2.76(2)
O(8)	2.73(2)	O(11)–O(12)	2.77(2)
O(9)	2.97(2)	O(12)–O(13)	2.81(2)
O(10)	2.72(2)	O(14)	2.77(2)
O(12)	2.64(2)	O(15)	2.83(2)
O(13)	2.96(2)	O(13)–O(14)	2.72(2)
O(15)	2.76(2)	O(14)–O(15)	2.93(2)
O(5)–O(6)	2.74(2)		
O(7)	2.88(2)		
C(1)···C(2)	3.17(3)		
O(10)···O(15)	2.66(2)		
C(1)–O(10)	2.93(4)		
O(15)	2.96(3)		
C(2)–O(10)	2.92(3)		
O(15)	2.91(3)		

Considering the fact that the distances of As–O (terminal) are generally smaller than those of the As–O(bridging) distances in pyroarsenic acids,[31,33,34] the As–O(bridging) distances in the present anion are

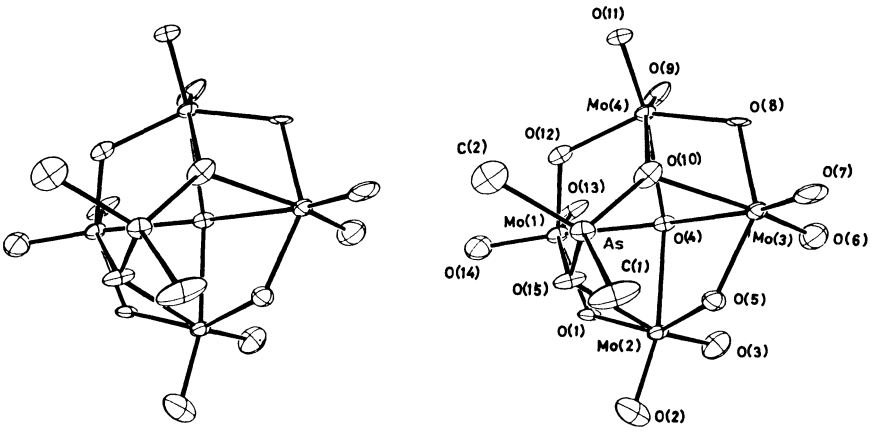

Fig. 4. The structure of the $[(CH_3)_2AsMo_4O_{14}(OH)]^{2-}$ anion.
The vibrational ellipsoids are drawn at the 50% probability level. (ORTEP Johnson, 1971)

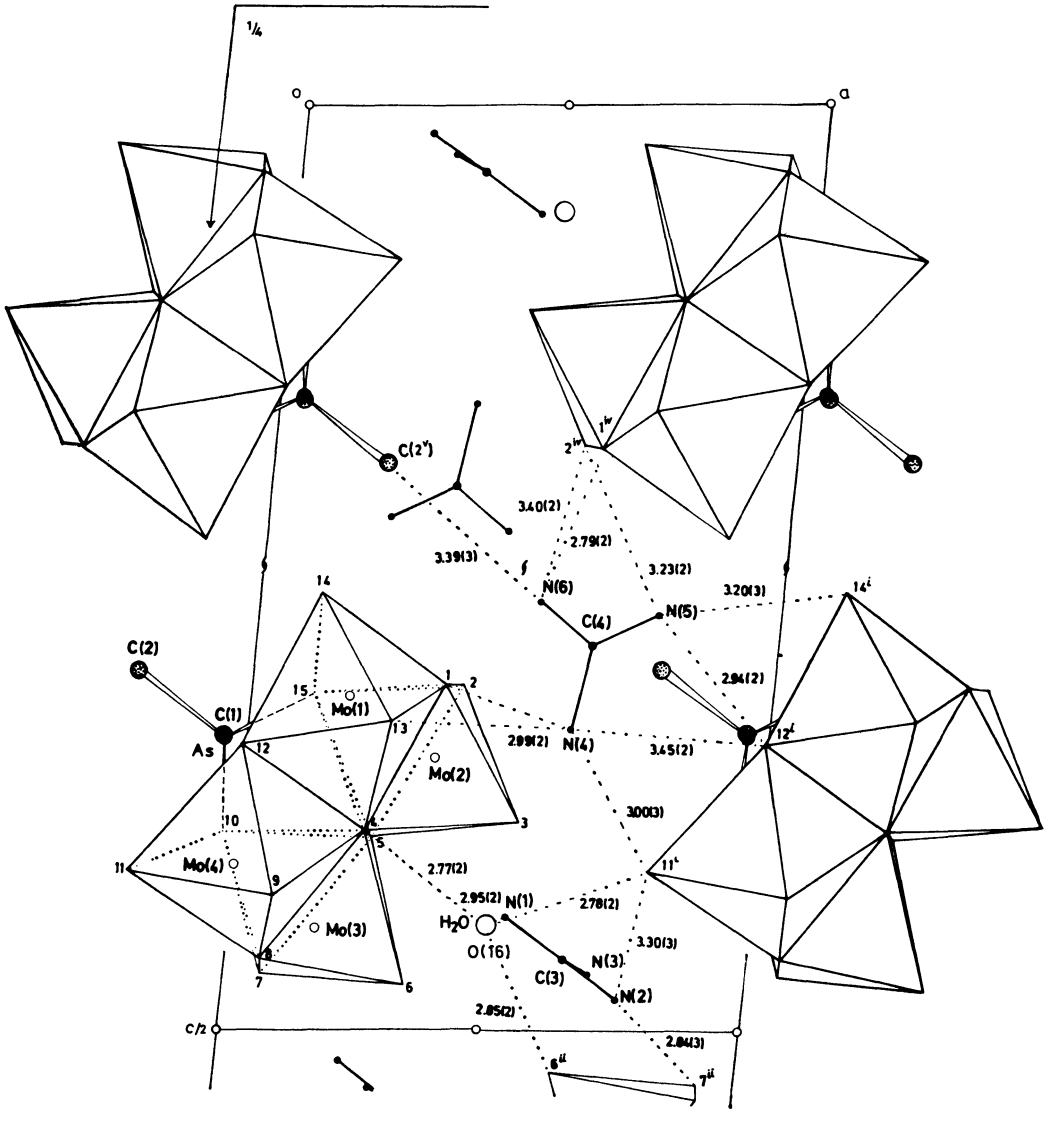

Fig. 5. The crystal structure of $(CN_3H_6)_2[(CH_3)_2AsMo_4O_{14}(OH)]\cdot H_2O$ viewed along b axis.

rather short, with lengths comparable to the As–O (terminal) distances. The O–As–O angles do not deviate significantly from the usual values in AsO_4^{3-} anions.[32,34]

It is of interest to know where the unique hydrogen atom is located and what kind of role it plays in the crystal. Barkigia *et al.* reported[13] that IR absorption is observed at 3615 cm^{-1} in unhydrated tetrabutylammonium salt; this absorption can be identified as O–H stretching. They also reported that the anion

Table 7. Bond angles in the $[(CH_3)_2AsMo_4O_{14}(OH)]^{2-}$ anion and in the guanidinium cations with their estimated standard deviations in parentheses

	θ/°		θ/°
O(1)-Mo(1)-O(4)	76.3(5)	O(5)-Mo(3)-O(7)	104.1(6)
O(12)	145.0(6)	O(8)	142.9(6)
O(13)	99.5(6)	O(10)	80.9(5)
O(14)	101.7(7)	O(6)-Mo(3)-O(7)	105.9(7)
O(15)	70.6(5)	O(8)	99.0(6)
O(4)-Mo(1)-O(12)	75.3(5)	O(10)	158.9(6)
O(13)	92.5(6)	O(7)-Mo(3)-O(8)	103.5(6)
O(14)	161.4(6)	O(10)	94.9(6)
O(15)	90.2(6)	O(8)-Mo(3)-O(10)	72.5(5)
O(12)-Mo(1)-O(13)	101.7(6)	O(4)-Mo(4)-O(8)	77.6(5)
O(14)	98.8(6)	O(9)	91.1(6)
O(15)	81.3(5)	O(10)	70.6(4)
O(13)-Mo(1)-O(14)	106.1(7)	O(11)	163.0(6)
O(15)	97.2(6)	O(12)	73.8(5)
O(14)-Mo(1)-O(15)	90.2(6)	O(8)-Mo(4)-O(9)	97.7(6)
O(1)-Mo(2)-O(2)	99.2(6)	O(10)	72.7(5)
O(3)	100.1(6)	O(11)	104.7(6)
O(4)	75.1(5)	O(12)	146.0(5)
O(5)	145.9(6)	O(9)-Mo(4)-O(10)	160.7(6)
O(15)	71.0(5)	O(11)	105.1(7)
O(2)-Mo(2)-O(3)	106.2(7)	O(12)	100.8(6)
O(4)	163.6(6)	O(10)-Mo(4)-O(11)	93.7(6)
O(5)	102.3(7)	O(12)	80.7(5)
O(15)	91.6(6)	O(11)-Mo(4)-O(12)	97.7(6)
O(4)-Mo(2)-O(4)	90.0(6)	O(10)-As-O(15)	107.2(7)
O(5)	98.9(7)	C(1)	110.0(7)
O(15)	161.3(6)	C(2)	109.9(8)
O(4)-Mo(2)-O(5)	76.9(5)	O(15)-As-C(1)	110.7(7)
O(15)	72.0(4)	C(2)	108.1(8)
O(5)-Mo(2)-O(15)	82.3(5)	C(1)-As-C(2)	110.8(9)
O(4)-Mo(3)-O(5)	72.5(5)	N(1)-C(3)-N(2)	121.0(21)
O(6)	90.8(6)	N(3)	123.1(20)
O(7)	163.3(6)	N(2)-C(3)-N(3)	115.9(18)
O(8)	73.9(5)	N(4)-C(4)-N(5)	119.9(19)
O(10)	68.4(4)	N(6)	120.2(20)
O(5)-Mo(3)-O(6)	96.7(7)	N(5)-C(4)-N(6)	119.9(19)

can not be neutralized by alkali; instead, it is directly decomposed. On the other hand, a close contact of 2.77(2) Å is observed between O(4) and the water molecule O(16), which suggests a hydrogen bonding. These facts all together lead to the conclusion that O(4) is, in fact, a hydroxyl group and is hydrogen-bonded to O(16).

Guanidinium cations are almost flat triangles. The close contacts between nitrogen and oxygen atoms in the polyanions water molecules suggest probable hydrogen bondings (see Fig. 5). Table 9 lists the interionic distances less than 3 Å.

The author wishes to thank Professor Yukiyoshi Sasaki of the University of Tokyo for his continual interest in the present work and for his valuable discussions. Thanks are also due to Professor Hisao Kuroya and Dr. Keiji Matsumoto of Osaka City University for the use of a Philips automatic diffractometer.

References

1) K. Nishikawa, unpublished data.
2) J. F. Keggin, *Proc. R. Soc. London, Ser. A*, **114**, 75 (1934).
3) H. Nishikawa and Y. Sasaki, *Chem. Lett.*, **1974**, 1185.
4) R. Strandberg, *Acta Chem. Scand., Sect. A*, **28**, 217 (1974).
5) B. Dawson, *Acta Crystallogr.*, **6**, 113 (1953).
6) K. Y. Matsumoto and Y. Sasaki, *Chem. Commun.*, **1975**, 691.
7) R. Strandberg, *Acta Chem. Scand.*, **27**, 1004 (1973).
8) K. Y. Matsumoto, *Bull. Chem. Soc. Jpn.*, **51**, 492 (1978).
9) W. Kwak, L. M. Rajkovic, M. T. Pope, C. O. Quicksall, K. Y. Matsumoto, and Y. Sasaki, *J. Am. Chem. Soc.*, **99**, 6463 (1977).
10) W. Gibbs, *Am. Chem. J.*, **5**, 363 (1883).
11) A. Rosenheim and R. Bilecki, *Chem. Ber.*, **4**, 543 (1913).
12) W. Kwak, L. M. Rajković, J. K. Stalick, M. T. Pope, and C. O. Quicksall, *Inorg. Chem.*, **15**, 2778 (1976).
13) K. M. Barkigia, L. M. Rajković, M. T. Pope, and C. O. Quicksall, *J. Am. Chem. Soc.*, **97**, 4146 (1975).

Table 8. Interionic distances less than 3 Å in $(CN_3H_6)_2[(CH_3)_2AsMo_4O_{14}(OH)]\cdot H_2O$, with their estimated standard deviations in parentheses

		l/Å
O(16)	·····O(4)	2.77(2)
	O(11^{i})	2.78(2)
	O(6^{ii})	2.86(2)
N(1)	·····O(16)	2.95(2)
N(2)	·····O(7^{ii})	2.84(3)
N(3)	·····O(3^{iii})	2.95(3)
N(4)	·····O(13)	2.99(3)
N(5)	·····O(12^{i})	2.94(3)
N(6)	·····O(2^{iii})	2.90(3)
	O(1^{iv})	2.93(3)

Symmetry code

i	1.0+x,	y,	z
ii	1.0−x,	−y,	1.0−z
iii	x,	1.0+y,	z
iv	1.0−x,	0.5+y,	0.5−z

14) V. R. Mattes, H. Bierbüsse, and J. Fuchs, *Z. Anorg. Allg. Chem.*, **385**, 230 (1971).
15) K. Y. Matsumoto, A. Kobayashi, and Y. Sasaki, *Bull. Chem. Soc. Jpn.*, **48**, 3146 (1975).
16) Y. Sasaki and K. Matsumoto, *Kagaku No Ryoiki*, **29**, 853 (1975).
17) D. D. Dexter and J. V. Silverton, *J. Am. Chem. Soc.*, **90**, 3589 (1968).
18) "The Universal Crystallographic Computation Program System," Crystallographic Society of Japan (1967).
19) "International Tables for X-Ray Crystallography," Kynoch Press, Birmingham (1974), Vol. IV.
20) D. T. Cromer, *Acta Crystallogr.*, **18**, 17 (1965).
21) B. Krebs, *Acta Crystallogr., Sect. B*, **28**, 2222 (1972).
22) F. A. Cotton, S. M. Morehous, and J. S. Wood, *Inorg. Chem.*, **3**, 1603 (1964).
23) F. A. Cotton and R. C. Elder, *Inorg. Chem.*, **3**, 397 (1964).
24) A. Perloff, *Inorg. Chem.*, **9**, 2228 (1970).
25) V. W. Day and J. L. Hoard, *J. Am. Chem. Soc.*, **90**, 3374 (1968).
26) L. C. W. Baker and J. S. Figgis, *J. Am. Chem. Soc.*, **92**, 3794 (1970).
27) T. J. R. Weakley, H. T. Evans, Jr., J. S. Showell, G. F. Tourné, and C. M. Tourné, *J. Chem. Soc. Chem. Commun.*, **1973**, 139.
28) H. d'Amour, *Acta Crystallogr., Sect. B*, **32**, 729 (1976).
29) L. Pettersson, Ph. D. Thesis, Umeå University (1974).
30) D. D. Dexter and J. V. Silverton, *J. Am. Chem. Soc.*, **90**, 3589 (1968).
31) K. Y. Leung and C. Calvo, *Can. J. Chem.*, **51**, 2082 (1073).
32) G. Ferraris and M. F. Angela, *Acta Crystallogr., Sect. B*, **29**, 286 (1973).
33) M. Catti and G. Ferraris, *Acta Crystallogr., Sect. B*, **29**, 90 (1973).
34) G. Ferraris and M. F. Angela, *Acta Crystallogr., Sect. B*, **29**, 859 (1973).

The Thermal Decomposition of Vanadium(III) Chloride Oxide and Its Reaction with Oxygen

Akimasa YAJIMA, Ryoko MATSUZAKI, and Yuzo SAEKI*

Research Laboratory of Resources Utilization, Tokyo Institute of Technology, 4259, Nagatsuta-cho, Midori-ku, Yokohama 227

(Received March 15, 1979)

The thermogravimetry and differential thermal analysis of VClO in an argon stream were carried out. The products obtained by heating VClO in an argon stream at various temperatures were examined by chemical analysis and X-ray analysis. Also, the reaction between VClO and oxygen was examined in the same manner. When VClO is heated in an argon stream, it decomposes above about 400 °C to form V_2O_3 and VCl_3, $3VClO(s) \rightarrow V_2O_3(s)+VCl_3(s)$. Subsequently, the resulting VCl_3 disproportionates to form VCl_2 and VCl_4, $2VCl_3(s) \rightarrow VCl_2(s)+VCl_4(g)$. VClO reacts with oxygen above about 120 °C to form V_2O_5 and VCl_3O, $6VClO(s)+3O_2(g) \rightarrow 2V_2O_5(s)+2VCl_3O(g)$; this reaction is accompanied by the $4VClO(s)+3O_2(g) \rightarrow 2V_2O_5(s)+2Cl_2(g)$ reaction.

As regards the thermal decomposition of vanadium(III) chloride oxide(VClO), McCarley and Roddy[1] have examined the thermal stability of VClO at a pressure of *ca.* 10^{-3} mmHg in the course of their investigation of the reduction of vanadium(V) trichloride oxide(VCl_3O) with hydrogen, and have estimated that, when VClO is heated, the $3VClO=V_2O_3+VCl_3$ and $6VClO=2V_2O_3+VCl_2+VCl_4$ reactions probably occur simultaneously above 650 °C, although at a higher temperature the latter reaction should become relatively more important since vanadium(III) chloride (VCl_3) becomes increasingly unstable with an increase in the temperature. Schäfer and Wartenpfuhl[2] have briefly reported that, when VClO is heated at a pressure of 10^{-5} mmHg, the thermal decomposition of VClO occurs above 620 °C. In addition to these reports, Oppermann[3] has reported that the thermal decomposition of VClO, $7VClO(s)=2V_2O_3(s)+2VCl_2(s)+VCl_3O(g)$, occurs above 600 °C; he has also given the equilibrium pressure of the above reaction in the temperature range of 750—850 °C, based on vapor-pressure measurements by a static method using a Bourdon-type sickle gauge. As has been mentioned above, the thermal decomposition of VClO was not clarified. Also, there has been no report on the reaction between VClO and oxygen.

In this paper, the thermal decomposition process of VClO in an argon stream and the reaction process between VClO and oxygen will be revealed.

Experimental

The VClO used was obtained by heating vanadium(IV) chloride oxide (VCl_2O) at 370 °C in an argon stream, based on the results of a previous investigation concerning the disproportionation of VCl_2O;[4] it was confirmed to be VClO[5] by X-ray analysis. The chemical analysis gave V, 49.8; Cl, 34.6% (Calcd for VClO: V, 49.75; Cl, 34.62%). VCl_3 was obtained by the thermal decomposition of VCl_4, which had been prepared by the reaction between vanadium (V, 99.8% up) and chlorine at 500 °C,[6] at 180 °C in an argon atmosphere;[7] it was confirmed to be VCl_3[8] by X-ray analysis. The chemical analysis gave V, 32.4; Cl, 67.6% (Calcd for VCl_3: V, 32.38; Cl, 67.62%). The oxygen was dried by passing it through concd sulfuric acid and over phosphorous(V) oxide.

The sensitivity of the quartz helix used for the thermogravimetry(TG) was approximately 67 mm/g. 0.15—0.20 g of the sample was heated at a rate of 2.5 °C/min. The flow-rate of argon or oxygen was maintained at 50 cm³/min. The differential thermal analysis (DTA) was performed in an argon stream at the same heating rate for TG. α-Al_2O_3 was used as a reference.

The X-ray analysis of the solid sample was performed using Ni-filtered Cu radiation. The sample chamber of the diffractometer was maintained under a dry nitrogen atmosphere to prevent the contamination of the sample with moisture in the air during the irradiation.

The products obtained by heating VClO in an argon stream at various temperatures were examined by the following procedures. The sample (1.0 g) in a quartz boat (60 mm length, 13 mm width, 7 mm depth) was placed in a straight reaction tube (16 mm i.d.) with a water-cooled condenser. Argon was introduced into the reaction tube at a flow-rate of 50 cm³/min. The sample part was then placed in the centre of an electric furnace (300 mm in heating length) maintained at a specified temperature for a specified period. The temperature of the sample part was controlled to within ±2 °C.

The products obtained by heating VClO in an oxygen stream at various temperatures were examined in the manner described above, except that oxygen was introduced into the reaction tube instead of argon at the same flow-rate as that of argon.

The liquid product (VCl_4 or VCl_3O) was collected in a trap cooled in solid carbon dioxide through the condenser. The chlorine formed was absorbed in a KI solution through the trap and was determined by iodometry. The total amount of chlorine formed during the reaction was determined by adding the above value and the amount of chlorine dissolved in the liquid product in the trap cooled in solid carbon dioxide.[9,10] The determination of the amount of chlorine dissolved in the liquid product will be described later.

The chemical analysis of solid and liquid products was performed as follows. The vanadium content in the sample was determined by chelatometric titration,[11] while the chlorine content was gravimetrically determined as AgCl after dissolving the sample in dilute nitric acid. When the sample contained vanadium chloride, the chloride oxide, and the oxide, the water-soluble chloride (VCl_2, VCl_3) was dissolved in water and filtered, and the water-insoluble residue (V_2O_3, unreacted VClO) was dissolved in dilute nitric acid. The vanadium and chlorine contents in the both solutions were determined as has been described above.

The amount of chlorine dissolved in the liquid product in the trap cooled in solid carbon dioxide was determined as

Table 1. Thermal decomposition products of VClO in an argon stream

Temp/°C	Heating time/h	Product/% In the boat			Outside the heating zone			Unreacted VClO/%
		V_2O_3	VCl_2	VCl_3	VCl_4	VCl_3	Cl_2	
420	6	5	2	<1	3	<1	<0.1	89
700	1	28	11	—	16	2	0.4	42

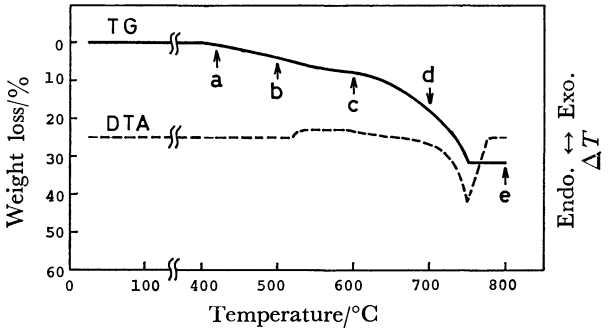

Fig. 1. TG and DTA curves of VClO in an argon stream.

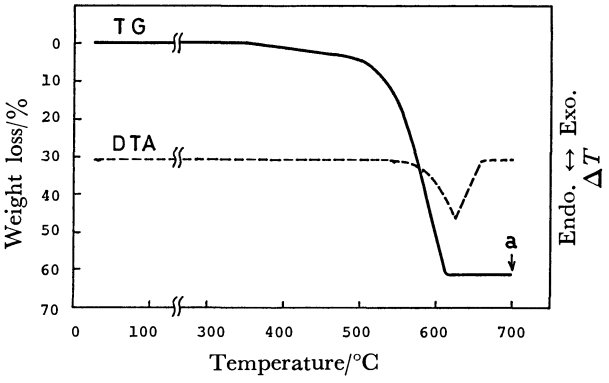

Fig. 2. TG and DTA curves of VCl_3 in an argon stream.

follows. After the reaction was over, the liquid product was allowed to warm to room temperature in an argon atmosphere in order to liberate the chlorine from the liquid product. The liberated chlorine was absorbed in a NaOH solution. A small amount of the liquid product which vaporized during the above procedure was also absorbed in the NaOH solution. The total amount of chlorine in the NaOH solution was gravimetrically determined as AgCl, while the vanadium content in the NaOH solution was also determined by chelatometric titration. From the vanadium content, the amount of the liquid product absorbed in the NaOH solution was calculated. The amount of chlorine dissolved in the liquid product was calculated by subtracting the amount of chlorine corresponding to the liquid product absorbed in the NaOH solution from the total amount of chlorine in the NaOH solution. Also, the total amount of the liquid product formed was corrected by adding the amount of the liquid product absorbed in the NaOH solution to the amount of the liquid product in the trap.

Throughout this work, the chlorides and chloride oxides of vanadium were handled in an argon atmosphere or *in vacuo* to prevent any contamination with moisture.

Results and Discussion

Thermal Decomposition Process of Vanadium(III) Chloride Oxide in an Argon Stream. The TG and DTA curves of VClO in an argon stream are shown in Fig. 1.

The TG curve showed that VClO gradually lost weight above about 400 °C. The samples heated up to Point a (420 °C), Points b (500 °C) and c (600 °C), Point d (700 °C), and Point e (800 °C) in Fig. 1 were found by X-ray analysis to be VClO, a mixture of vanadium(III) oxide(V_2O_3)[12] and unreacted VClO, a mixture of V_2O_3, VCl_2,[13] and unreacted VClO, and a mixture of V_2O_3 and VCl_2, respectively. A weak exothermic effect followed by an endothermic peak was observed in the DTA curve. The weight loss at Point e in Fig. 1 was 31.4%. This value was in good agreement with the calculated value, 31.37%, based on the assumption that the $3VClO(s) \rightarrow V_2O_3(s) + VCl_3(s)$ and $2VCl_3(s) \rightarrow VCl_2(s) + VCl_4(g)$[14-17] reactions occur when VClO is heated. However, VCl_3 was not observed by X-ray analysis.

Then, the products formed by heating VClO at various temperatures for a specified period were examined by chemical analysis and X-ray analysis. The results are shown in Table 1. The amount of each product is shown as a weight percentage of the product to the initial weight of VClO.

The results showed that a small amount of VCl_3 was formed as a solid product, in addition to V_2O_3 and VCl_2, at 420 °C. The gaseous product formed was confirmed to be VCl_4. Also, the formation of small amounts of VCl_3 and chlorine outside the heating zone was considered to be due to the thermal decomposition of the gaseous VCl_4 formed, $2VCl_4(g) \rightarrow 2VCl_3(s) + Cl_2(g)$,[18] since the molar ratio of the amount of VCl_3 to that of chlorine was calculated to be approximately 2 : 1.

From the above-mentioned results, the solid products on heating VClO were found to be V_2O_3, VCl_2, and VCl_3. Among these products, VCl_3 is unstable on heating. It has been reported that, when VCl_3 is heated, the disproportionation, $2VCl_3(s) \rightarrow VCl_2(s) + VCl_4(g)$, occurs above 380 °C,[14] 400 °C,[15] 425 °C,[16] or 450 °C.[17]

To confirm the disproportionation of VCl_3, the following experiments were carried out.

The TG and DTA curves of VCl_3 in an argon stream are shown in Fig. 2. The TG curve showed that VCl_3 gradually lost weight above about 350 °C. The sample heated up to Point a (700 °C) in Fig. 2 was found by X-ray analysis to be VCl_2. The weight loss at Point a was 61.3%. This value was in good agreement with the calculated value, 61.27%, based

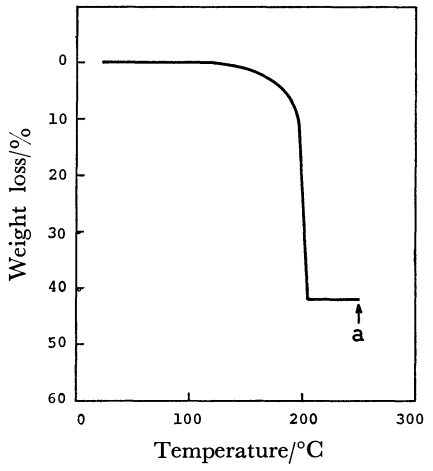

Fig. 3. TG curve of VClO in an oxygen stream.

on the disproportionation of VCl_3, $2VCl_3(s) \rightarrow VCl_2(s) + VCl_4(g)$. Also, the gaseous product was confirmed to be VCl_4 by the chemical analysis of the product obtained outside the heating zone by heating VCl_3 (1.0 g) in an argon stream at 600 °C for 1 h.

From these results, it is clarified that VCl_3 disproportionates above about 350 °C with an endothermic effect, according to the $2VCl_3(s) \rightarrow VCl_2(s) + VCl_4(g)$ reaction.

Considering the above-mentioned results, it is found that, when VClO is heated in an argon stream, the $3VClO(s) \rightarrow V_2O_3(s) + VCl_3(s)$ reaction occurs above about 400 °C. Subsequently, the resulting VCl_3 disproportionates according to the $2VCl_3(s) \rightarrow VCl_2(s) + VCl_4(g)$ reaction, since the disproportionation of VCl_3 occurs as early as about 350 °C.

The exothermic effect observed in the DTA curve, shown in Fig. 1, is considered to be due to the $3VClO(s) \rightarrow V_2O_3(s) + VCl_3(s)$ reaction, since the disproportionation of VCl_3 is accompanied by an endothermic effect. It was considered that the observed exothermic effect was very weak, because the $3VClO(s) \rightarrow V_2O_3(s) + VCl_3(s)$ reaction proceeded slowly at the lower temperature and was accompanied by the disproportionation of the resulting VCl_3, with an endothermic effect.

As has been mentioned above, Oppermann[3] has reported that the thermal decomposition, $7VClO(s) \rightarrow 2V_2O_3(s) + 2VCl_2(s) + VCl_3O(g)$, occurs when VClO is heated in a sealed tube. On the other hand, the formation of VCl_3O was not observed on heating VClO in an argon stream. It may be considered that the VCl_3O was formed by the reaction between unreacted VClO and gaseous VCl_4,[2] which had itself been formed *via* the thermal decomposition of VClO, as has been revealed in this work.

Reaction Process between Vanadium(III) Chloride Oxide and Oxygen. The TG curve of VClO in an oxygen stream is shown in Fig. 3.

The results showed that VClO reacted with oxygen before decomposing and that the reaction proceeded rapidly above about 200 °C. The sample heated up to Point a (250 °C) was found by X-ray analysis to be a mixture of vanadium(V) oxide(V_2O_5)[19] and a small amount of vanadium(IV) oxide(VO_2).[20]

Table 2. Reaction products between VClO and oxygen at various temperatures

Temp/°C	Reaction time/h	Product/% In the boat		Product/% Outside the heating zone		Unreacted VClO/%
		V_2O_5	VO_2	VCl_3O	Cl_2	
120	0.5	<1	—	0.2	<0.1	>99
	1	<1	—	0.4	0.1	99
	3	2	—	1.2	0.3	97
150	0.5	2	—	1.2	0.2	97
	1	5	—	3.6	0.5	92
	3	9	—	5.6	1.2	86
170	0.5	5	—	4.1	0.3	91
	1	8	—	6.6	0.4	87
	3	22	—	16.5	1.7	64
190	0.5	26	<1	21.3	1.3	57
	1	40	2	34.5	2.4	31
	3	55	4	48.1	3.4	3
200	0.5	42	15	51.9	1.6	2
230	0.5	46	13	52.3	1.9	0
250	0.5	52	7	52.5	1.9	0

Table 3. Solid products between VClO and oxygen at various flow-rates of oxygen

O_2 flow-rate / $cm^3\ min^{-1}$	Solid product/% V_2O_5	Solid product/% VO_2	Unreated VClO/%
50	89	9	2
100	94	5	1
200	>99	—	<1

To obtain more detailed information on the reaction between VClO and oxygen, the products formed by heating VClO for a specified period at various temperatures in an oxygen stream were examined by X-ray analysis and chemical analysis.

At 110 °C, no reaction product was observed. The reaction products obtained at various temperatures above 120 °C and their weight percentages relative to the initial VClO were determined by chemical analysis and X-ray analysis.[5,19,20] The results are shown in Table 2.

These results indicate that the reaction between VClO and oxygen proceeds above about 120 °C. V_2O_5, VCl_3O, and a small amount of chlorine were formed below 170 °C. Above 190 °C, VO_2 was also formed in addition to these products.

The most stable oxide phase of vanadium under the conditions of this work is V_2O_5,[21] and, as is shown in Table 2, VO_2 was not formed below 170 °C. However, the formation of VO_2 in addition to V_2O_5 was observed above 190 °C. As is shown in Table 2, the reaction between VClO and oxygen proceeded markedly above 190 °C to form a large amount of gaseous VCl_3O. Consequently, the concentration of oxygen decreased temporarily in the neighborhood of the sample VClO in the boat. Under such a low concentration of oxygen, the oxidation of VClO has been thought to yield VO_2. Then, the solid products obtained by heating VClO (0.25 g) at 200 °C under various flow-rates of oxygen for 0.5 h were examined.

The results are shown in Table 3.

From the results, it was observed that VO_2 was not formed under a high flow-rate of oxygen. This confirms the above consideration of the formation of VO_2.

Based on the experimental results presented above, the reaction process between VClO and oxygen will now be discussed.

The experimental results for the reaction products between VClO and oxygen at various temperatures, shown in Table 2, showed that V_2O_5 and VCl_3O were the main products. This fact was considered to indicate that the main reaction which occurred upon heating VClO in an oxygen stream was

$$6VClO(s) + 3O_2(g) \rightarrow 2V_2O_5(s) + 2VCl_3O(g). \quad (1)$$

The reactions which possibly gave the chlorine (in Table 2) were considered to be

$$4VClO(s) + 3O_2(g) \rightarrow 2V_2O_5(s) + 2Cl_2(g) \quad (2)$$

and the reaction between gaseous VCl_3O formed by Reaction 1 and oxygen,

$$4VCl_3O(g) + 3O_2(g) \rightarrow 2V_2O_5(s) + 6Cl_2(g).^{22)} \quad (3)$$

It has previously been reported that Reaction 3 does not proceed below 400 °C.[22] The present authors also confirmed that Reaction 3 began at about 400 °C and proceeded almost completely above about 700 °C. On the basis of these results, the formation of a small amount of chlorine obtained by heating VClO in an oxygen stream was considered to be due to Reaction 2.

Based on the assumption that the formation of chlorine was due to Reaction 2, the amount of V_2O_5 formed by Reaction 2 was calculated from the amount of chlorine formed (in Table 2). The molar ratio of the amount of VCl_3O to the amount of V_2O_5 obtained by subtracting the amount of V_2O_5 formed by Reaction 2 from the total amount of V_2O_5 formed was calculated to be approximately 1 : 1. In this calculation, the amount of VO_2 formed was converted into that of V_2O_5 on the assumption that VO_2 was oxidized to V_2O_5. These results confirmed that the main reaction which occurred when VClO was heated in an oxygen stream was Reaction 1 and that this reaction was accompanied by Reaction 2.

The above-mentioned results reveal that VClO reacts with oxygen above about 120 °C according to Reaction 1 and that this reaction is accompanied by Reaction 2. As a result, V_2O_5 (under a low concentration of oxygen, VO_2 is formed in addition to V_2O_5), VCl_3O, and a small amount of chlorine are formed.

References

1) R. E. McCarley and J. W. Roddy, *J. Inorg. Nucl. Chem.*, **15**, 293 (1960).
2) H. Schäfer and F. Wartenpfuhl, *J. Less-Common Met.*, **3**, 29 (1961).
3) H. Oppermann, *Z. Anorg. Allg. Chem.*, **351**, 127 (1967).
4) A. Yajima, R. Matsuzaki, and Y. Saeki, Preprint of the 37th National Meeting of Chemical Society of Japan, I (1978), p. 36, *Bull. Chem. Soc. Jpn.*, in press.
5) Joint Committee on Powder Diffraction Standards, Powder Diffraction File, 23-1472.
6) C. Starr, F. Bitter, and A. R. Kaufmann, *Phys. Rev.*, **58**, 977 (1940).
7) R. E. McCarley and J. W. Roddy, *Inorg. Chem.*, **3**, 60 (1964).
8) Joint Committee on Powder Diffraction Standards, Powder Diffraction File, 15-382.
9) A. Morette, *C. R. Acad. Sci.*, **202**, 1846 (1936).
10) F. E. Brown and J. E. Snyder, *J. Am. Chem. Soc.*, **47**, 2671 (1925).
11) J. Krtil, *Z. Anal. Chem.*, **219**, 412 (1965).
12) ASTM X-Ray Powder Data File, 1-1293.
13) Joint Committee on Powder Diffraction Standards, Powder Diffraction File, 15-215.
14) P. Ehrlich and H. J. Seifert, *Z. Anorg. Allg. Chem.*, **301**, 282 (1959).
15) H. Funk and W. Weiss, *Z. Anorg. Allg. Chem.*, **295**, 327 (1958).
16) M. A. Oranskaya, Yu. S. Lebedev, and I. L. Perfilova, *Russ. J. Inorg. Chem.*, **6**, 132 (1961).
17) A. B. McIntosh, *Ind. Chem.*, **32**, 195 (1956).
18) J. H. Simons and M. G. Powell, *J. Am. Chem. Soc.*, **67**, 75 (1945).
19) ASTM X-Ray Powder Data File, 9-387.
20) Joint Committee on Powder Diffraction Standards, Powder Diffraction File, 19-1398.
21) H. Endo, M. Wakihara, and M. Taniguchi, *Chem. Lett.*, **1974**, 905.
22) N. I. Vorob'ev, V. V. Pechkovskii, F. N. Kozlov, and Yu. A. Raikov, *Izv. Vyssh. Uchebn. Zaved., Tsvetn. Metall.*, **12** (3), 86 (1969).

A Proton Conductive Coordination Polymer. I. [*N,N'*-Bis(2-hydroxyethyl)-dithiooxamido]copper(II)[15]

Seiichi KANDA,* Kenichi YAMASHITA,** and Kuwako OHKAWA†

Department of Applied Chemistry, Faculty of Engineering, Tokushima University, Minamijosanjima 2-1, Tokushima 770

(Received April 4, 1979)

In a family of *catena*-μ-*N,N'*-disubstituted dithiooxamidocopper(II) complexes which have been assumed as two-dimensional coordination polymers, one complex with HOC_2H_4– substituents is an electronic conductor as well as others, and also a protonic conductor uniquely. The latter property was proved both by spectroscopic detection of the hydrogen molecules evolved from d.c. electrolysis of pressed pellets of the powder specimen and by observation of the anomalous increase (three orders of magnitude) of the electric conductivity as an effect of 10^3 Pa of H_2O or D_2O vapor on the dehydrated specimen in an evacuated conductivity cell. A novel conduction mechanism was suggested for such a solid system with both conjugated double bonds and extended hydrogen bonds.

The [*N,N'*-disubstituted dithiooxamido]copper(II) complexes, abbreviated as R_2-dtoa-Cu(earlier as R-DTOA-Cu),[1] have been regarded as two-dimensional polymers from several experimental facts[1,2] as shown in Fig. 1. Those copper containing polymers with a pair of CH_3–, $C_6H_5CH_2$–, C_6H_{11}–, $C_{12}H_{25}$– radicals as the two substituents on the two nitrogen atoms of a dithiooxamide molecule are the amorphous semiconductors in which the delocalized electrons on the two-dimensional atomic network constructed from carbon, nitrogen, sulfur, and copper atoms take part.

An anomalous time dependence of electric conductivity of $(HOC_2H_4)_2$-dtoa-Cu is observed which implies a part of the conductance at least originated from the characteristic behavior of the hydroxyl protons. The proton conduction in solid has recently attracted attention from the view point of both pure and applied sciences;[3-7] as a consequence a few comprehensive reviews have been published.[8]

In this report we try to prove the proton conduction, and propose a possibility of a novel mechanism of the charge transfer in solid which is attributed to the cooperation of electrons and protons due to the specific structure of the compound.

Experimental

Materials. Ligand, *N,N'*-bis(2-hydroxyethyl)dithiooxamide, abbreviated as $(HOC_2H_4)_2$-dtoa-H_2, was of a commercial preparation, purified by recrystallization from distilled water. Copper(II) sulfate pentahydrate of reagent grade was recrystallized from distilled water. The coordination polymer was precipitated by addition of 5% ligand ethanol solution to a lukewarm copper aqueous solution with stirring, followed by washing several times with distilled water and ethanol alternatively. The gelatinous precipitate was centrifugated and dried in an evacuated desiccator. The analytical values will be discussed in detail later.

Measurements of Conductance. The measurements were made on the pressed disk (13 mm diameter × 1.5—2.0 mm thick) prepared in a press and a die at 1.3×10^8 Pa for 30 s. Electrical leads were silver pasted on the disk from the both sides with an area of 0.7—0.8 cm^2. The measurements were carried out in a cell which could be evacuated to 10^{-2} Pa and kept the blank value of resistance more than 10^{17} Ω. In order to improve an electrical insulation, the electrical leads for the electrodes entered the cell through Teflon plugs (a). A vacuum tight of the Teflon plugs to the metal plate and to the brass bolts(d) was made with O-rings(b) and with O-stat-seals 660(c), respectively, as shown in Fig. 2. The other leads for a thermocouple and a heater were connected to hermetic seals on the plate.

After installation of the specimen in position the cell was evacuated and flushed with nitrogen several times to remove the gas molecule such as H_2O adsorbed on the specimen,

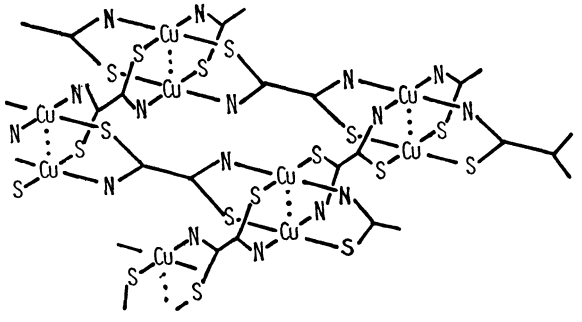

Fig. 1. The two-dimensional molecular model of copper acetate Type R_2-dtoa-Cu. For simplicity, substituents R on nitrogen atoms are omitted. See Ref. 2.

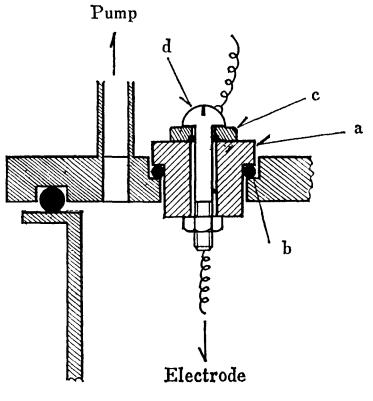

Fig. 2. Teflon plug of high resistance conductivity cell. a) Teflon plug, b) O ring, c) stat-O-seal 660 (Manuf. by Parker Seal Company, U.S.A.), d) brass bolt.

† Present address: Training Institute for Environmental Pollution Control, Tokorozawa 526, Saitama 359.

** Present address: Osaka Titanium Co., Ltd., Amagasaki, Hyogo 660.

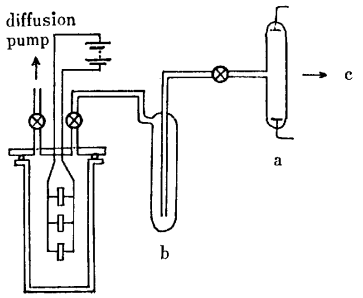

Fig. 3. Electrolysis cell and vacuum line for gas identification by atomic spectra. a) Geisler tube operated by neon trans (6000 V, 60 Hz), b) gas trap at 77 K, c) spectrograph.

before admitting dry nitrogen of 10^4 Pa as heat conductor for temperature control. In addition to nitrogen, H_2O or D_2O vapor of 10^3 Pa was introduced for confirmation of effects of water vapor.

For electrolysis the three pellets were connected in parallel in an evacuated cell (Fig. 3) and d.c. (6.8×10^{-1} C) was passed under 300—500 V for 170 h. After the procedure mentioned above, the gas in the vessel was transported to the Geissler tube(a) in Fig. 3 through a 77 K trap(b) to remove leaked gases, H_2O and CO_2, if any. By application of an a.c. voltage (6000 V, 60 Hz) an atomic spectrum was taken on a photographic film (Fuji SSS) with a spectrograph (Shimadzu-OC-50) using a mercury lamp as a calibration source. The blank test was performed for the same processes without the application of the d.c. voltage.

DTA and TGA measurements were carried out simultaneously by a derivatograph (Rigakudenki 8002) with α-Al_2O_3 as a reference, at a rate of temperature rise of 5 °C/min.

Results and Discussion

Chemical Constitution and the Structure. Analysis of $(HOC_2H_4)_2$-dtoa-Cu, Found: C, 25.7; N, 9.77; H, 3.91; Cu, 23.0%. And a weight loss in TGA up to 150 °C; 3.3%. In the light of the coordination chemistry, the constitutional formula of $(HOC_2H_4)_2$-dtoa-Cu is proposed as $Cu((HOC_2H_4)_2\text{-dtoa})_{0.985}(OH)_{0.03}(OH_2)_{0.5}$: Calcd for the constituents: C, 25.7; N, 9.99; H, 3.97; Cu, 23.00; H_2O, 3.26%. These values are in excellent agreement with each other except those for nitrogen. The discrepancy is not serious for the proposed formula, as the nitrogen atom coordinated directly to copper ion has a tendency to result in a lower value in the analysis than expected. The other homologous complexes R_2-dtoa-Cu's are assumed to have a two-dimensional structure of sheet polymer on the basis of several experimental facts.[1,2] Assuming the same two-dimensional structure for this compound, the nonstoichiometric 0.03 mol hydroxide in the formula suggests that the molecules were terminated by coordination of two of OH instead of $(HOC_2H_4)_2$-dtoa at some parts of the edge of the sheet polymer. One half mole of OH_2 is assumed to be the coordinated water on copper(II) ions as the water is not removed even in an evacuated desiccator but is lost at the temperatures up to 150 °C as observed in the TGA analysis.

From IR study of the complex in KBr pellets the following results were obtained; 1) no peak between

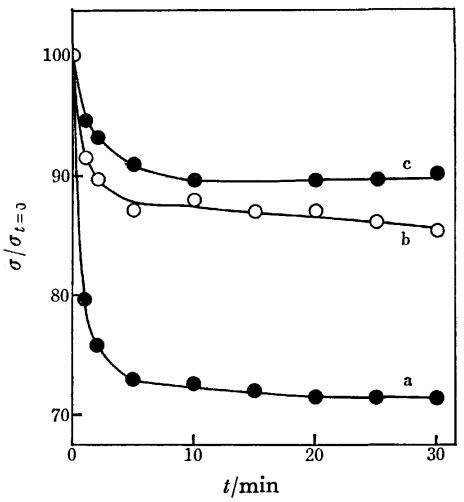

Fig. 4. Time decrease(%) of conductivity, at a) 22 °C, b) 50 °C, and c) 78 °C.

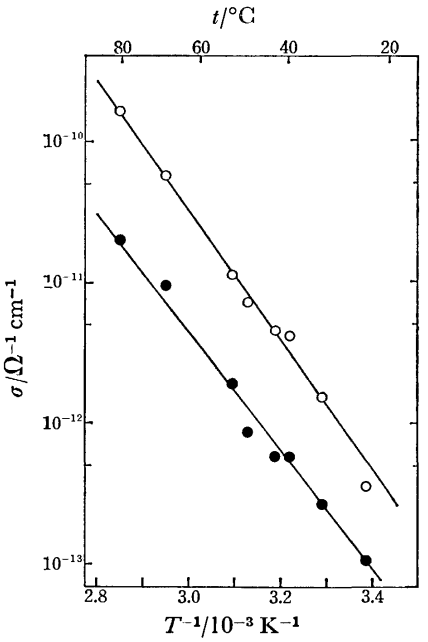

Fig. 5. Effects of temperature on specific conductivities for both σ_e and σ_H°. ○: σ_e, ●: σ_H°.

4000 and 3400 cm^{-1} and 2) a broad intense band around 3340 cm^{-1} with a half-value width of *ca.* 400 cm^{-1}. These results suggest the followings; 1) Free $HOCH_2CH_2$–, H_2O and/or –NH groups (which should indicate ν_{OH} at 3600 cm^{-1}) do not exist, 2) almost all nitrogen atoms separate protons for coordination to the copper ions, and 3) the HOC_2H_4– and H_2O form inter- and/or intramolecular hydrogen bonds to the oxygen, nitrogen, or sulfur atoms, which are proved by the peak shifted to 3340 cm^{-1} assigned to $\nu_{OH\cdots X}$. Provided that the macromolecules are the two-dimensional sheets as mentioned before,[1,2] intermolecular hydrogen bonds would connect the parallel macromolecules on their both sides of the lamellar layer.

Electric Conductivity. Figure 4 shows the typical time dependence of the electric current through the pellet of the specimen at applying d.c. voltage of 32 V/1.5—2.0 mm. As shown in Fig. 4 the current

Table 2. Non-Ohmic behavior in $(HOC_2H_4)_2$-dtoa-Cu, contrasted with $(C_6H_5CH_2)_2$-dtoa-Cu

Sample	Temp °C	Ohm's law deviation %	Applied voltages V/cm
$(HOC_2H_4)_2$-dtoa-Cu	22	18	1800
	42	18	1800
	64	10	1800
	79	8.3	1800
$(C_6H_5CH_2)_2$-dtoa-Cu	20	2.7	1700
	57	1	1700
	79	1	1700

The current values are taken at 30 s after applied voltage.

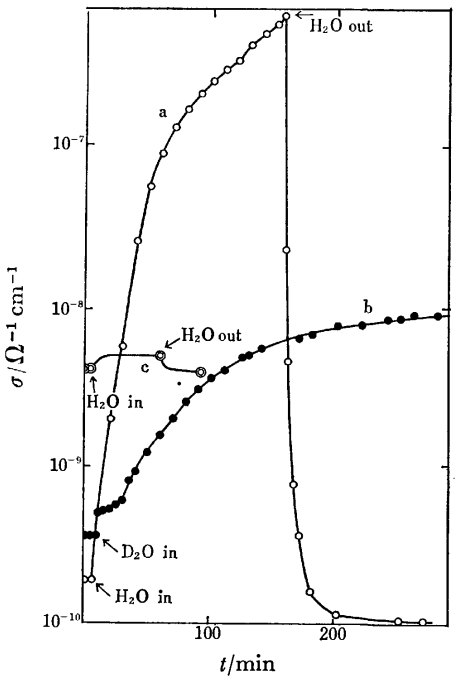

Fig. 8. Effect of water vapor on the conductivity of $(HOC_2H_4)_2$-dtoa-Cu. a) Vapor of H_2O (white circle), b) vapor of D_2O (black circle), c) contrasted with that of $(C_6H_5CH_2)_2$-dtoa-Cu.

voltage relation deviates to higher current side at a higher voltage region as shown in Table 2 together with that of $(C_6H_5CH_2)_2$-dtoa-Cu for comparison; the deviations are expressed as a percentage, 100 $(i_o-i_c)/i_o$ where i_o is the observed current and i_c is that calculated from the initial slope assuming Ohm's law.

In the case of trap-limited or ionic conduction, the current has non-Ohmic character and follows an eq. $i=A \sinh bV$ which has a non-linear character.[9] The values for $(HOC_2H_4)_2$-dtoa-Cu in Table 2 support the proton conduction mechanism.

Figure 8 illustrates the marked effects of water vapor (*ca.* 10^3 Pa) on the conductivity of the hydroxyethyl homologue and that of benzyl-substituted one for comparison. Conductivity of the former compound increases gradually by a factor of 10^3 in 2 h, whereas that of the latter increases only by 10%, levels off within 10 min and decreases to original value by re-evacuation of the water vapor. As is shown in Fig. 8, by a reevacuation the conductivity of the former rapidly decreases not to the initial but to 50% of the initial value, probably because the crack of the pellet or the partial peeling of the cathode causes a decrease of the apparent conductivity. Introduction of deuterated water in the cell results in the slower increase of the conductivity than in the case of normal water. The difference between the effects of H_2O and D_2O would be attributed to that in the diffusion coefficients of the water molecules in the pellets and in the mobilities of H^+ and D^+ in an electric field through hydrogen bonds, although these data are not sufficient for quantitative analysis. The slow effects of water vapor imply that the increment of the current originates not only from the water molecules adsorbed on the surface of the pellets but also from that absorbed into the pellets.

In order to confirm a proton conduction mechanism in $(HOC_2H_4)_2$-dtoa-Cu complex, three pellets connected in parallel were subjected to d.c. voltage (av. 400 V) for 170 h, resulting in a charge flow of *ca.* 0.7 C and a certain amount of electrolytically generated gas. From the spectrogram of the gas, H_β (486.1 nm) medium line, H_γ (434.0 nm) very strong line, and H_δ (410.1 nm) weak line of Balmer series of hydrogen atom were assigned by comparison with the line spectra of mercury as a standard for wavelength determination. This fact proves directly the generation of hydrogen gas by applying d.c. voltage on the specimen. Now it became apparent that the generated hydrogen causes the cracks of the pellets and the peeling of the cathodes observed only in case of the $(HOC_2H_4)_2$-dtoa-Cu compound.

The experimental facts on this compound can be summarized as follows: 1) H_2 is generated at a cathode, 2) the charge carrier other than electrons will be protons, and 3) the charge drift and the gas evolution seem to occur not only on surface but also in the inner part of the pellet as well. The third conclusion needs more consideration in detail. The pellet is an aggregate of the microscopic amorphous grains, and the "inner part of the pellet" mentioned above could mean both the surface and the interior of the grain. However, they are indistinguishable because the surface of the grain and that of the two-dimensional amorphous macromolecule located inside behave almost in the same manner as far as the proton conduction mechanism is concerned.

In order to elucidate the hydrogen evolution at the location remote from the cathode, an appropriate mechanism should be proposed. The conventional mechanisms of electric conduction by linked chain of hydrogen bonds are reviewed and classified as follows:[10] Type 1, through chains of hydrogen bonds π-electrons drift without evolution of hydrogen gas to give rise the steady current as was proposed by Eley and his school for protein and amino acids.[11] Type 2, a hydrogen bonded proton transfers from molecule A to molecule B sequentially followed by reorientation processes of the chain, that is, the molecular rotation of B by which further transfer of the proton takes place from B to C through a newly formed hydrogen bond between them. The arrangement of

A, B, and C is more or less parallel to the electric field. In such case that the reorientation processes are energetically difficult, the step could be substituted by the intramolecular proton migration. The transition of the mechanism from type 1 to type 2 at about 100 °C was reported in the polyamides.[12] The generation of molecular hydrogen at the locations other than cathode is hard to be explained by both the types.

The $(HOC_2H_4)_2$-dtoa-Cu specimen containing nonstoichiometric H_2O and OH^- provides the several possible paths for the electric conduction due to either electrons or protons, or both (Fig. 9). That is, the serial bondings $\{S–C–C–S–Cu\}_n$, $\{N–C–C–N–Cu\}_n$, and $\{S–C–C–N–Cu\}_n$ in the framework of the macromolecule could operate as the pure π-electronic macroscopic conduction paths independently from the hydrogen bond chain. As the figure shows, a set of the complicated hydrogen bonds could be composed between $-C_2H_4OH$, coordinated water, nitrogen and sulfur of ligand molecules; the bonds could construct a) extended chains of the hydrogen bonds solely, and b) mixed chains of the hydrogen bonds and the conjugate double bonds, both resulting the macroscopic paths. In case (a) the protons move to the cathode and are discharged there to evolve hydrogen molecules, whereas in case (b) the protons could be discharged at the contact points between the hydrogen bond chains and the conjugate double bond paths as well as at the metallic cathode. Especially the D-defect (doppel Besetzung) in the hydrogen bonds[13] presents a probable opportunity of the H_2 generation in the interior of the specimen. Many studies[14] on cooperative phenomena of H^+-jump and e^--transfer in microscopic scale have been done as a kind of redox reactions in the liquid phases. Coexistence of conjugated double bonds and extended hydrogen bonds in solid phases makes a following conduction mechanism possible in macroscopic scales (type 3); the sequence of the proposed mechanism is shown in Fig. 10 by way of a simple example (peptide bonds), which is adoptable easily for any other systems with H^+-bonds and conjugate π-bonds. In this case neither the conduction band of π-electrons in an extended hydrogen bond system (type 1) nor the molecular rotation mechanism with hydrogen evolution on the electrode (type 2) are needed. The cyclic sequence (1, 2, 3, and 4), type 3A, is that of no hydrogen evolution and of the time independence of the conductivity, whereas the other sequence (1, 2, 3, and 5), type 3B, is that of the hydrogen evolution on a positive electrode surface and/or in the interior of the solid. In type 3B the electric conduction path through hydrogen bonding chains will be bleached gradually. Consequently 3A mechanism allows the time independent part of the whole electric current. Although some residual possibility of type 2 mechanism can not be ruled out, the hydrogen evolution from the interior of the specimen suggested by its cracking induces us to conclude the functioning of the type 3B mechanism. At the present stage the type 3 mechanism is presented as a working hypothesis which should be ascertained quantum-mechanically and experimentally in future.

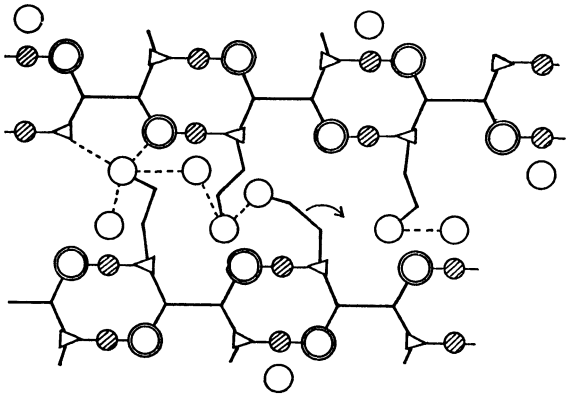

Fig. 9. The possible conduction paths by both electron and proton. Shaded circle, double circle, and triangle exhibit copper, sulfur, and nitrogen atoms respectively. White circles are OH and/or water molecule. All carbon atoms are abbreviated. Covalent bonds and coordinate bonds are represented by broad and narrow lines. Dotted lines are hydrogen bonds and the circled arrow exhibits an internal rotation of the hydroxyethyl group to transfer of hydrogen bond.

References

1) S. Kanda, A. Suzuki, and K. Ohkawa, *Ind. Eng.*

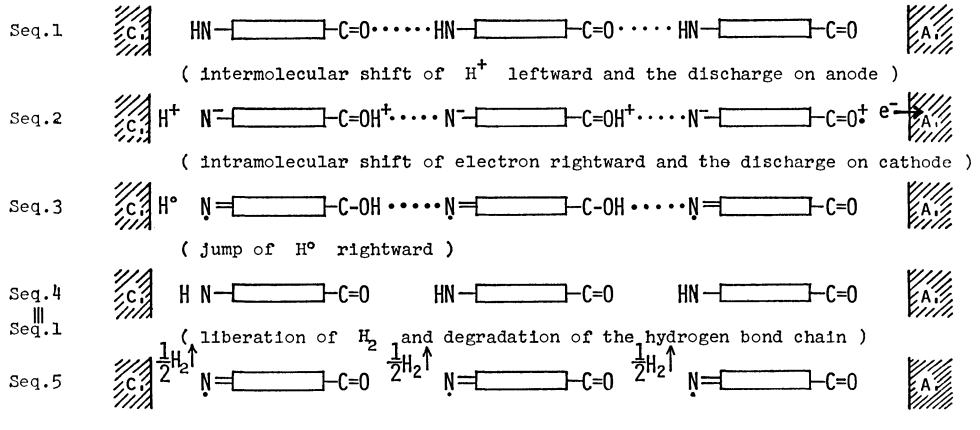

Fig. 10. A consolidated model for electric conduction through hydrogen bond ($\rangle C{=}O\cdots HN\langle$) and π-electron conjugate double bond system ($-\square-$) following the sequence (1, 2, 3, and 4) or (1, 2, 3, and 5). C. and A. are the cathode and anode respectively.

Chem., Prod. Res. Dev., **12**, 88 (1973).

2) S. Kanda, *Nippon Kagaku Zasshi*, **83**, 560 (1962); S. Kanda, K. Ito, and T. Nogaito, *J. Polym. Sci., Polym. Symp.*, **17**, 151 (1967); A. Suzuki, K. Ohkawa, S. Kanda, M. Emoto, and S. Watari, *Bull. Chem. Soc. Jpn.*, **48**, 2634 (1975); A. Suzuki, K. Ohkawa, and S. Kanda, *Bull. Faculty Eng., Tokushima Univ.*, **14**, 59 (1977).

3) M. G. Shilton and T. Howe, *Mater. Res. Bull.*, **12**, 701 (1977).

4) M. Sharon and A. K. Kalia, *J. Solid State Chem.*, **21**, 171 (1977).

5) H. Ohbayashi, M. Yoshida, and T. Kudo, Japan Patent 120286 (1977), 120287 (1977); *Chem. Abstr.*, **88**, 81087a, 81088b (1978).

6) R. Lutze, W. Gieseke, and W. Schröter, *Solid State Commun.*, **23**, 215 (1977).

7) E. R. Mognaschi and A. Chierico, *J. Chem. Soc., Faraday Trans. 1*, **74**, 2333 (1978).

8) L. Glasser, *Chem. Rev.*, **75**, 21 (1975); *Mineral. Sci. Eng.*, **5**, 135 (1972).

9) D. A. Seanor, *J. Polym. Sci., Polym. Phys. Ed.*, **6**, 468 (1968); D. D. Eley and D. I. Spivey, *Trans. Faraday Soc.*, **56**, 1432 (1960).

10) The classification of the type of the electrical conductive properties by hydrogen bonding was attempted by L. Glasser in the section 3 of his review: Ref. 8.

11) D. D. Eley, G. D. Parfitt, M. J. Perry, and D. H. Taysum, *Trans. Faraday Soc.*, **49**, 79 (1953); D. D. Eley, and D. I. Spivey, *ibid.*, **56**, 1432 (1960); D. D. Eley and W. P. Williams, *ibid.*, **64**, 1528 (1968); M. H. Cardew and D. D. Eley, *Discuss. Faraday Soc.*, **27**, 115 (1957).

12) D. D. Eley and D. I. Spivey, *Trans. Faraday Soc.*, **57**, 2280 (1961).

13) C. Jaccard, "Water and Aqueous Solutions," ed by R. A. Horne, Wiley-Interscience, New York, N. Y. (1972) Chap. 2.

14) Refer for example: F. J. Kristine and R. E. Shepherd, *Inorg. Chem.*, **17**, 3145 (1978).

15) Parts of this paper were presented at the 25th Symposium of the Coordination Chemistry held in Tokyo in 1975.

The Crystal Structure of Ethylenediaminebis[2-(aminomethyl)pyridine]-cobalt(III) Hexacyanocobaltate(III) Dihydrate

Masao SEKIZAKI* and Shunji UTSUNO†

College of Liberal Arts, Kanazawa University, Marunouchi, Kanazawa 920

† *Department of Chemistry, Faculty of Science, Shizuoka University, Oya, Shizuoka 422*

(Received April 23, 1979)

The crystal structure of ethylenediaminebis[2-(aminomethyl)pyridine]cobalt(III) hexacyanocobaltate(III) dihydrate, $[Co(H_2NCH_2CH_2NH_2)(C_5H_4NCH_2NH_2)_2][Co(CN)_6]\cdot 2H_2O$, has been determined by the X-ray diffraction method and subsequently refined by a block-diagonal least-squares method to give $R=0.050$ for 5238 non-zero reflections. The crystals are triclinic with a space group $P\bar{1}$; $a=9.034(2)$, $b=17.267(2)$, $c=8.395(2)$ Å, $\alpha=87.1(3)$, $\beta=96.2(3)$, $\gamma=104.6(3)°$, and $Z=2$. The crystal is ionic, comprising the $[Co(H_2NCH_2CH_2NH_2)(C_5H_4NCH_2NH_2)_2]^{3+}$ cation and the $[Co(CN)_6]^{3-}$ anion. The complex cation is a slightly distorted octahedron with three five-membered chelate rings in a *lel* conformation. The two pyridine nitrogen atoms occupy *trans* positions. Thus, the cation has an approximate twofold axis of rotation. The anion is also a distorted octahedron, with the coordination of CN^- through the carbon atom. The cobalt atoms of the anions occupy the special positions. Two cations in the unit cell are connected by these anions through hydrogen bonds to form a three-dimensional network typical of an ionic crystal.

The cobalt(III) complexes of bidentate 2-(aminomethyl)pyridine (2-picolylamine, abbreviated as pic) have been reported from the synthetic and spectroscopic points of view.[1-5] In a previous investigation,[4] a mixed-ligand complex, the ethylenediaminebis[2-(aminomethyl)pyridine]cobalt(III) cation, $[Co(en)(pic)_2]^{3+}$, was prepared and separated into all three possible geometrical isomers by means of a chromatographic method. The structures were assumed from the elution order and the PMR spectra. In the present investigation, a crystal-structure analysis has been carried out to confirm the previous assumption. One of the isomers has been selected in which two pyridine groups may occupy *trans* positions of the octahedron, and its hexacyanocobaltate(III) salt has been used.

Experimental

The complex was prepared and separated by the previously reported method.[4] Orange prismatic crystals were obtained by a diffusion method using aqueous solutions of the complex chloride and $K_3[Co(CN)_6]$. A crystal of $0.2\times0.2\times0.2$ mm was selected, and the X-ray diffraction intensities were measured on a Philips PW 1100 four-circle automatic single-crystal diffractometer with Mo $K\alpha$ radiation monochromated by a graphite plate. The θ-2θ scan technique was used at a scan rate of 0.0668°/s in θ with a scan width of $(0.90+0.30\tan\theta)°$. The intensities of three reference reflections monitored every 2 h remained constant during the data collection. Of 5326 observed independent reflections measured up to $\theta=30°$, 5238 with $|F_o|>3\sigma$ were used for the structure analysis. No corrections were made for absorption and extinction effects ($\mu r=0.14$). The cell dimensions were obtained from the least-squares method, based on 14 2θ values. The crystal data are listed in Table 1.

Determination and Refinement of the Structure

The coordinates of the three cobalt atoms were determined from the Patterson map; successive Fourier synthesis gave the approximate skeletal structure. The block-diagonal least-squares refinement was carried out based on 5238 non-zero reflections with the weight of 1.0 for $|F_o|>3.5$ and that of 0.5 for the others. The atomic scattering factors were taken from the International Tables for X-Ray Crystallography.[6]

At the beginning stage of refinement, both atoms of each cyano group were assumed to be carbon. After several cycles of refinement with isotropic temperature factors, the R-value was 0.088. Anisotropic temperature factors were, then, introduced for all the non-hydrogen atoms. At this stage, if the coordination atom of each cyano group was assumed to be nitrogen, the R-value was 0.073. On the other hand, if it was carbon, the R-value was lowered to 0.058. It was thus concluded that the cyano groups coordinate through the carbon atoms.

The positional parameters of all the hydrogen atoms except for those of the water molecules were calculated using sp^2 and sp^3 models. They were refined with the isotropic temperature factors fixed at 4.0 Å^2. The final R-value was 0.050.

The final atomic parameters are listed in Table 2. The observed and calculated structure amplitudes are deposited with the Chemical Society of Japan (Document No. 7933).

The refinement of the structure and the drawing of the thermal ellipsoids were carried out with HBLS-IV[7] and ORTEP[8] programs respectively. The other calculations were carried out with programs written by one of the present authors (M. S.). A FACOM 230-75 computer at the Computation Center of Nagoya University and a FACOM M-160 computer at the

Table 1. The crystal data

$[Co(H_2NCH_2CH_2NH_2)(C_5H_4NCH_2NH_2)_2][Co(CN)_6]\cdot 2H_2O$
$F.\ W.=586.39$.
Triclinic, $P\bar{1}$.
$a=9.034(2)$, $b=17.267(2)$, $c=8.395(2)$ Å,
$\alpha=87.1(3)$, $\beta=96.2(3)$, $\gamma=104.6(3)°$.
$V=1258$ Å^3.
$D_x=1.547$ g cm^{-3}, $Z=2$.
$\mu=14.2$ cm^{-1} (Mo $K\alpha$ radiation, $\lambda=0.7107$ Å).

Table 2a. Final atomic parameters with their estimated standard deviations in parentheses
Thermal parameters are in the form: $\exp -(h^2\beta_{11}+k^2\beta_{22}+l^2\beta_{33}+hk\beta_{12}+hl\beta_{13}+kl\beta_{23})$.
Values are multiplied by 10^4.

Atom	x	y	z	β_{11}	β_{22}	β_{33}	β_{12}	β_{13}	β_{23}
Co(1)	0	0	0	62 (2)	17 (1)	61 (2)	12 (1)	7 (2)	1 (1)
Co(2)	1/2	1/2	0	81 (2)	16 (1)	81 (2)	24 (1)	5 (2)	−2 (1)
Co(3)	3388 (1)	2346 (1)	5015 (1)	62 (1)	16 (1)	66 (1)	16 (1)	6 (2)	−1 (1)
N(1)	1993 (5)	2806 (3)	3579 (5)	65 (5)	17 (2)	104 (7)	14 (5)	9 (9)	9 (5)
C(2)	1827 (6)	2781 (4)	1952 (7)	80 (7)	27 (2)	101 (8)	21 (6)	13 (12)	23 (7)
C(3)	832 (7)	3149 (4)	1045 (7)	100 (8)	35 (3)	115 (9)	27 (7)	−33 (13)	23 (8)
C(4)	−32 (7)	3554 (4)	1796 (9)	99 (8)	39 (3)	201 (13)	67 (8)	−2 (16)	39 (10)
C(5)	110 (7)	3570 (4)	3449 (8)	87 (7)	31 (3)	174 (11)	48 (7)	45 (14)	12 (8)
C(6)	1112 (6)	3183 (3)	4309 (7)	73 (7)	24 (2)	137 (9)	29 (6)	38 (12)	12 (7)
C(7)	1369 (7)	3170 (4)	6117 (7)	119 (8)	34 (3)	116 (9)	61 (7)	70 (14)	−19 (8)
N(8)	2110 (5)	2515 (3)	6634 (6)	85 (6)	23 (2)	107 (7)	20 (5)	44 (10)	5 (6)
N(11)	4527 (5)	1771 (3)	6555 (5)	74 (5)	20 (2)	85 (6)	24 (5)	15 (9)	11 (5)
C(12)	5703 (6)	2097 (4)	7672 (7)	99 (7)	28 (2)	95 (8)	40 (7)	−4 (12)	−10 (7)
C(13)	6414 (7)	1628 (4)	8694 (7)	103 (8)	38 (3)	98 (8)	55 (7)	−30 (13)	−5 (8)
C(14)	5934 (7)	804 (4)	8603 (8)	117 (9)	40 (3)	134 (10)	73 (8)	29 (14)	42 (8)
C(15)	4753 (7)	469 (4)	7466 (8)	102 (8)	26 (2)	143 (10)	41 (7)	52 (14)	30 (7)
C(16)	4065 (6)	964 (3)	6465 (5)	82 (7)	21 (2)	92 (8)	20 (6)	41 (11)	5 (6)
C(17)	2830 (7)	643 (3)	5164 (8)	127 (9)	18 (2)	150 (10)	30 (6)	−38 (15)	−6 (7)
N(18)	2082 (5)	1276 (3)	4520 (5)	85 (6)	20 (2)	86 (6)	14 (5)	−15 (10)	−10 (5)
N(21)	4753 (5)	3422 (3)	5400 (5)	90 (6)	19 (2)	94 (7)	22 (5)	14 (10)	−2 (5)
C(22)	6206 (6)	3513 (4)	4623 (7)	72 (7)	24 (2)	114 (9)	−0 (6)	19 (12)	5 (7)
C(23)	5751 (6)	3090 (4)	3074 (6)	85 (7)	29 (2)	85 (8)	15 (6)	33 (11)	1 (7)
N(24)	4799 (5)	2271 (3)	3436 (5)	73 (6)	21 (2)	91 (6)	24 (5)	3 (9)	−2 (5)
C(101)	1962 (6)	691 (3)	537 (6)	85 (7)	20 (2)	76 (7)	22 (6)	26 (11)	−4 (6)
N(101)	3124 (6)	1120 (3)	948 (6)	96 (7)	32 (2)	137 (9)	1 (6)	30 (12)	−39 (7)
C(102)	−275 (6)	629 (3)	−1850 (6)	69 (6)	22 (2)	98 (8)	16 (5)	19 (11)	6 (6)
N(102)	−403 (6)	999 (3)	−3025 (6)	105 (7)	33 (2)	97 (7)	12 (6)	6 (11)	28 (6)
C(103)	−800 (6)	652 (3)	1267 (6)	69 (6)	21 (2)	81 (7)	11 (5)	−4 (10)	−4 (6)
N(103)	−1231 (6)	1047 (3)	2074 (6)	123 (8)	34 (2)	134 (9)	45 (7)	43 (13)	−31 (7)
C(201)	4535 (6)	3905 (3)	−470 (6)	104 (7)	22 (2)	78 (7)	36 (6)	9 (11)	3 (6)
N(201)	4222 (6)	3245 (3)	−804 (6)	147 (8)	24 (2)	98 (7)	33 (6)	25 (12)	−12 (6)
C(202)	4189 (6)	4790 (3)	2021 (7)	92 (7)	17 (2)	112 (8)	20 (6)	16 (12)	12 (6)
N(202)	3740 (6)	4691 (3)	3265 (6)	140 (8)	29 (2)	129 (9)	27 (7)	48 (13)	9 (7)
C(203)	3023 (7)	5011 (4)	−1021 (7)	106 (8)	24 (2)	124 (9)	44 (7)	9 (13)	−4 (7)
N(203)	1837 (7)	4988 (4)	−1673 (8)	121 (8)	44 (3)	203 (11)	64 (8)	−54 (15)	−18 (9)
O(1w)[a]	7335 (6)	1556 (4)	4533 (6)	194 (9)	75 (3)	129 (8)	177 (9)	62 (13)	16 (8)
O(2w)[a]	−1350 (7)	4085 (4)	−2260 (9)	205 (11)	65 (4)	410 (18)	76 (10)	−211 (22)	−177 (12)

a) Oxygen atoms of water molecules.

Table 2b. Positional parameters of the hydrogen atoms ($\times 10^3$)

	x	y	z		x	y	z
H(C2)	250 (9)	252 (5)	139 (8)	H(C17-a)	214 (9)	17 (5)	557 (8)
H(C3)	76 (9)	311 (5)	−18 (8)	H(C17-b)	334 (9)	47 (5)	429 (8)
H(C4)	−68 (9)	382 (5)	114 (8)	H(N18-a)	117 (9)	121 (5)	502 (8)
H(C5)	−47 (9)	388 (5)	407 (8)	H(N18-b)	192 (9)	125 (5)	344 (8)
H(C7-a)	37 (9)	312 (5)	663 (8)	H(N21-a)	427 (9)	382 (5)	493 (8)
H(C7-b)	211 (9)	374 (5)	651 (8)	H(N21-b)	494 (9)	353 (5)	656 (8)
H(N8-a)	143 (9)	208 (5)	680 (8)	H(C22-a)	690 (9)	328 (5)	537 (8)
H(N8-b)	279 (9)	264 (5)	771 (8)	H(C22-b)	674 (9)	409 (5)	455 (8)
H(C12)	601 (9)	271 (5)	778 (8)	H(C23-a)	661 (9)	302 (5)	249 (8)
H(C13)	721 (9)	193 (5)	959 (8)	H(C23-b)	507 (9)	332 (5)	227 (8)
H(C14)	636 (9)	45 (5)	937 (8)	H(N24-a)	542 (9)	197 (5)	388 (8)
H(C15)	431 (9)	−14 (5)	738 (8)	H(N24-b)	427 (9)	201 (5)	246 (8)

Table 3. Bond distances (l/Å) and angles (φ/°)

Co(3)-N(1)	1.938(4)	Co(3)-N(11)	1.953(4)
Co(3)-N(8)	1.953(4)	Co(3)-N(18)	1.961(4)
N(1)-C(2)	1.360(7)	N(11)-C(12)	1.364(7)
N(1)-C(6)	1.356(7)	N(11)-C(16)	1.354(6)
C(2)-C(3)	1.372(8)	C(12)-C(13)	1.371(8)
C(3)-C(4)	1.386(9)	C(13)-C(14)	1.381(9)
C(4)-C(5)	1.381(9)	C(14)-C(15)	1.381(9)
C(5)-C(6)	1.380(9)	C(15)-C(16)	1.380(8)
C(6)-C(7)	1.510(8)	C(16)-C(17)	1.493(8)
C(7)-N(8)	1.480(7)	C(17)-N(18)	1.476(7)
Co(3)-N(21)	1.974(4)	Co(3)-N(24)	1.966(4)
N(21)-C(22)	1.498(7)	N(24)-C(23)	1.494(7)
C(22)-C(23)	1.490(8)		
Co(1)-C(101)	1.892(5)	Co(2)-C(201)	1.882(5)
Co(1)-C(102)	1.881(5)	Co(2)-C(202)	1.903(5)
Co(1)-C(103)	1.902(5)	Co(2)-C(203)	1.900(6)
C(101)-N(101)	1.150(7)	C(201)-N(201)	1.144(7)
C(102)-N(102)	1.158(7)	C(202)-N(202)	1.150(7)
C(103)-N(103)	1.147(7)	C(203)-N(203)	1.141(8)
C(2)-H	1.01(8)	C(12)-H	1.04(8)
C(3)-H	1.03(8)	C(13)-H	1.04(8)
C(4)-H	0.95(8)	C(14)-H	0.98(8)
C(5)-H	1.03(8)	C(15)-H	1.03(8)
C(7)-Ha	1.02(8)	C(17)-Ha	0.96(8)
C(7)-Hb	1.09(8)	C(17)-Hb	1.01(8)
N(8)-Ha	0.86(8)	N(18)-Ha	0.94(8)
N(8)-Hb	1.04(8)	N(18)-Hb	0.90(8)
N(21)-Ha	0.95(8)	N(24)-Ha	0.90(8)
N(21)-Hb	0.99(8)	N(24)-Hb	0.97(8)
C(22)-Ha	0.98(8)	N(23)-Ha	1.00(8)
C(22)-Hb	0.99(8)	C(23)-Hb	0.99(8)
N(1)-Co(3)-N(8)	83.2(2)	N(1)-Co(3)-N(11)	171.7(2)
N(11)-Co(3)-N(18)	84.4(2)	N(8)-Co(3)-N(24)	174.8(2)
N(21)-Co(3)-N(24)	84.8(2)	N(18)-Co(3)-N(21)	176.8(2)
Co(3)-N(1)-C(2)	126.3(4)	Co(3)-N(11)-C(12)	127.0(4)
Co(3)-N(1)-C(6)	115.1(4)	Co(3)-N(11)-C(16)	114.4(4)
C(2)-N(1)-C(6)	118.6(5)	C(12)-N(11)-C(16)	118.5(5)
N(1)-C(2)-C(3)	121.6(5)	N(11)-C(12)-C(13)	121.6(6)
C(2)-C(3)-C(4)	119.6(6)	C(12)-C(13)-C(14)	119.7(6)
C(3)-C(4)-C(5)	119.2(7)	C(13)-C(14)-C(15)	119.1(6)
C(4)-C(5)-C(6)	119.0(6)	C(14)-C(15)-C(16)	119.3(6)
N(1)-C(6)-C(5)	122.0(6)	N(11)-C(16)-C(15)	121.8(5)
N(1)-C(6)-C(7)	114.6(5)	N(11)-C(16)-C(17)	116.0(5)
C(5)-C(6)-C(7)	123.4(6)	C(15)-C(16)-C(17)	122.1(5)
C(6)-C(7)-N(8)	108.3(5)	C(16)-C(17)-N(18)	110.3(5)
Co(3)-N(8)-C(7)	110.4(4)	Co(3)-N(18)-C(17)	111.4(4)
Co(3)-N(21)-C(22)	110.1(4)	Co(3)-N(24)-C(23)	109.1(4)
N(21)-C(22)-C(23)	106.2(5)	N(24)-C(23)-C(22)	107.3(5)
C(101)-Co(1)-C(102)	90.3(3)	C(201)-Co(2)-C(202)	92.8(3)
C(102)-Co(1)-C(103)	91.6(3)	C(202)-Co(2)-C(203)	90.6(3)
C(101)-Co(1)-C(103)	87.2(3)	C(201)-Co(2)-C(203)	87.3(3)
Co(1)-C(101)-N(101)	175.9(5)	Co(2)-C(201)-N(201)	177.6(5)
Co(1)-C(102)-N(102)	176.8(5)	Co(2)-C(202)-N(202)	177.3(5)
Co(1)-C(103)-N(103)	177.3(5)	Co(2)-C(203)-N(203)	176.9(6)

Data Processing Center of Kanazawa University were used.

Description of the Structure and Discussion

The crystal is ionic, comprising $[Co(en)(pic)_2]^{3+}$ and $[Co(CN)_6]^{3-}$ ions and water molecules. The arrangement of the ions in the crystal is shown in Fig. 1. The unit cell has two formula units, which are related to each other by an inversion center. The cobalt atoms of the cations occupy the general positions, while those of the anions occupy the special positions, (0, 0, 0) and (1/2, 1/2, 0), of the triclinic cell.

The structure of the cation is shown in Fig. 2, together with the anisotropic thermal ellipsoids of the non-hydrogen atoms. Each of the 2-(aminomethyl)pyridine molecules acts as a bidentate ligand through the amino nitrogen and pyridine nitrogen atoms. The two pyridine nitrogen atoms are located at *trans* positions, while the two amino nitrogen atoms are at *cis* positions of the octahedron. The remaining two coordination positions are occupied by the ethylenediamine nitrogen atoms. Thus, the cation has an approximate twofold axis of rotation through the cobalt atom and bisecting the C–C bond of ethylenediamine. This structural feature agrees with the assumption by

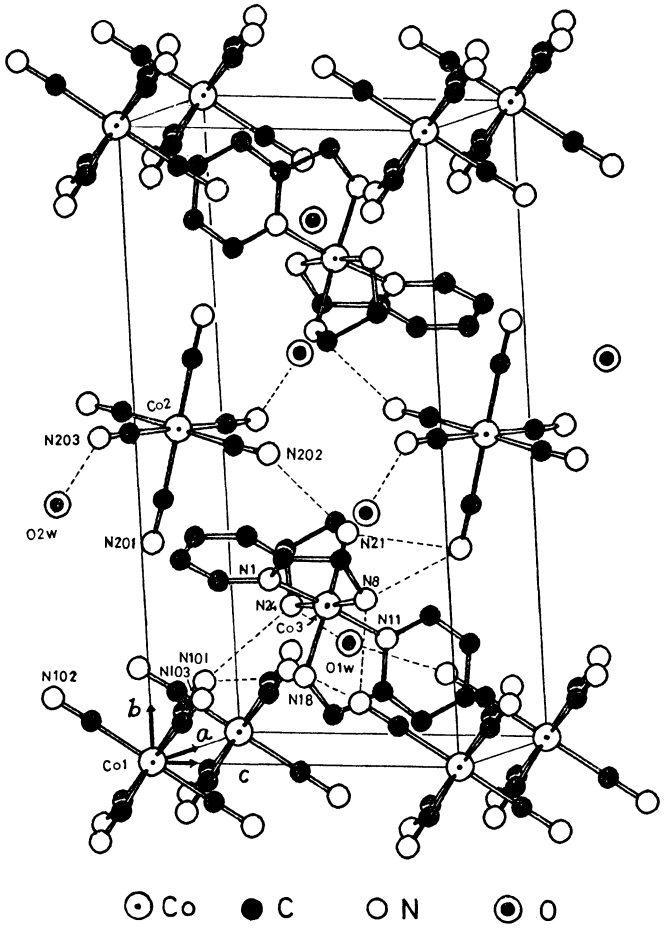

Fig. 1. Atomic arrangement in the crystal. Dashed lines exhibit hydrogen bonds.

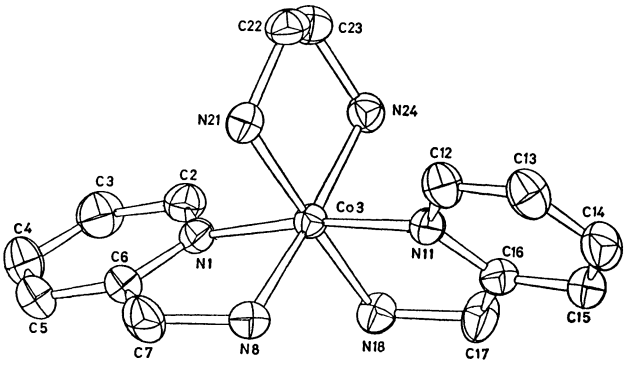

Fig. 2. The structure of the cation with the anisotropic thermal ellipsoids of the non-hydrogen atoms at the 50% probability level.

Table 4. Hydrogen bonds

D – H ··· A[a]			D-A (*l*/Å)	H-A (*l*/Å)
N(18)	Hb	N(101)[b]	3.282	2.50
N(21)	Ha	N(202)	3.020	2.11
N(24)	Hb	N(101)	2.969	2.04
N(24)	Ha	O(1w)	2.913	2.04
O(2w)	H	N(203)	2.910	—
O(1w)	H	N(103)^{i}	2.836	—
N(8)	Ha	N(102)^{ii}	3.025	2.17
N(8)	Hb	N(201)^{ii}	2.833	1.85
N(18)	Ha	N(102)^{ii}	3.143	2.24
N(21)	Hb	N(201)^{ii}	3.262	2.37
O(1w)	H	N(102)^{iii}	3.033	—
O(2w)	H	N(202)^{iv}	3.402	—

a) D, Hydrogen donor; A, Hydrogen acceptor.
b) Key to symmetry operation:

No mark	x	y	z
i	$1+x$	y	z
ii	x	y	$1+z$
iii	$1+x$	y	$1+z$
iv	$-x$	$1-y$	$-z$

the previous investigation.[4,5]

Three five-membered chelate rings exhibit the *lel* conformation. The value of the dihedral angle between the N(21)C(22)C(23) and C(22)C(23)N(24) planes is 51.2°. On the other hand, those between the C(6)C(7)N(8) and N(1)C(6)C(7) planes and between the C(16)C(17)N(18) and N(11)C(16)C(17) planes give smaller values of 19.6° and 15.3° respectively. These values indicate that 2-(aminomethyl)pyridine nearly forms a plane in contrast to the usual *gauche* conformation of ethylenediamine.

The bond distances and angles are listed in Table 3. The coordination bond distances of the cation show an average value of 1.96 Å; the coordination bond angles in the chelate rings are smaller than 90° (average, 84°). These results are similar to those for $[Co(en)_3]^{3+}$.[9] All the three coordination bond angles in *trans* positions of the octahedron deviate from 180°. Especially the N(1)–Co–N(11) angle is considerably small (171.7°). Thus, the octahedron of the cation is distorted.

The octahedral coordination in the anion is also

slightly distorted. The Co–C and C–N bond distances are normal,[9] with the mean values of 1.89 and 1.15 Å respectively. The average value of the Co–C–N angles is 177°.

The complex cations and anions are connected to one another through hydrogen bonds between amino and cyano nitrogen atoms, in addition through electrostatic interactions. The water molecules are also hydrogen-bonded with these ions. These hydrogen bonds are summarized in Table 4 and are also shown in Fig. 1. No contacts shorter than 3.5 Å are observed between any cations or between any anions. Thus, a three-dimensional network typical of the ionic crystal is completed by these intermolecular interactions.

The authors are grateful to Professor Yoichi Iitaka of the University of Tokyo for the measurements of the intensities with the diffractometer.

References

1) G. J. Sutton, *Aust. J. Chem.*, **13**, 473 (1960).
2) S. Utsuno and K. Sone, *Bull. Chem. Soc. Jpn.*, **37**, 1038 (1964).
3) K. Michelsen, *Acta Chem. Scand.*, **24**, 2003 (1970); **26**, 769 (1972); *ibid.*, *Sect. A*, **28**, 428 (1974).
4) S. Utsuno and M. Sekizaki, *Inorg. Nucl. Chem. Lett.*, **15**, 259 (1979).
5) M. Utsumi and S. Utsuno, The 28th Symposium on Coordination Chemistry, Matsuyama, (1978).
6) "International Tables for X-Ray Crystallography," Kynoch Press, Birmingham (1974), Vol. IV.
7) T. Ashida, "Universal Crystallographic Computation Program System (UNICS)," ed by T. Sakurai, The Crystallographic Society of Japan, Tokyo (1967).
8) C. K. Johnson, Oak Ridge National Laboratory Report ORNL-3794 (1965).
9) M. Iwata, K. Nakatsu, and Y. Saito, *Acta Crystallogr., Sect. B*, **25**, 2562 (1969).

The Crystal Structure and Absolute Configuration of $(-)_{589}$-Bis(2,4-pentanedionato)(1,3-propanediamine)chromium(III) Iodide Monohydrate

Keiji MATSUMOTO* and Shun'ichiro OOI

Department of Chemistry, Faculty of Science, Osaka City University, Sumiyoshi-ku, Osaka 558

(Received May 15, 1979)

The crystal structure of $(-)_{589}$-$[Cr(acac)_2(tn)]I\cdot H_2O$ has been determined from the X-ray diffraction data collected on a diffractometer. The crystal is orthorhombic, with the space group $P2_12_12_1$ and with $a=20.834(6)$, $b=12.015(3)$, $c=7.621(2)$ Å, and $Z=4$. Block-diagonal least-squares refinement for 1426 independent reflections with $F_o^2>3\sigma(F_o^2)$ converged to $R=4.91\%$. The complex cation has the Λ absolute configuration. The 1,3-propanediamine ligand assumes a chair conformation. One of the 2,4-pentanedionato chelate rings is almost planar, while in the other the 2,4-pentanedionato plane is bent away from the plane defined by Cr and 2 O donor atoms because of the intramolecular repulsion, the interplanar angle being 9.4°. The interrelation between the absolute configuration and the circular dichroism was discussed for the $[Cr(acac)_n(tn)_{3-n}]^{(3-n)+}$-type complexes.

The optically pure $(-)_{589}$-$[Cr(acac)_3]$ (acac=2,4-pentanedionate anion) was isolated by Mason *et al.*[1] using asymmetric synthesis. The circular dichroism spectrum(CD) of the complex had previously been related to those of Λ-$(+)_{589}$-$[Cr((+)\text{-atc})_3]$[2] ((+)-atc=(+)-3-acetylcamphorate anion) and *Λ-trans*-$(-)_{589}$-$[Cr(d\text{-hmc})_3]$[3] (*d*-hmc=*d*-hydroxymethylene-camphorate anion) the structures of which had already been determined by means of X-ray analysis and stereoselectivity respectively. The Δ configuration had thus been given to $(-)_{589}$-$[Cr(acac)_3]$. Recent X-ray work has confirmed that the assignment of the Δ configuration to $(-)_{589}$-$[Cr(acac)_3]$ is correct.[4]

The $(-)_{589}$-$[Cr(acac)_2(tn)]^+$ (tn=1,3-propanediamine) complex was prepared and resolved by Nakano and Kawaguchi.[5] The CD curve of the complex is similar in shape to that of Λ-$(+)_{589}$-$[Cr(acac)_3]$, although the former is shifted to a higher wave number. Therefore, the Λ configuration could be assigned to the $(-)_{589}$-$[Cr(acac)_2(tn)]^+$ complex. The $(-)_{589}$-$[Cr(acac)_2(tn)]I\cdot H_2O$ crystal was subjected to X-ray structure analysis in order to confirm the absolute configuration of the complex cation.

Experimental

X-Ray Data Collection. Preliminary photographic data obtained using a Weissenberg camera indicated that the Laue symmetry was mmm and that the space group was $P2_12_12_1$. The specimen employed for the data collection was an approximate sphere, the diameter of which was 0.3 mm. The crystal was mounted on a glass fibre along the c axis.

The cell dimensions were obtained by the least-squares refinement of the θ values of 26 automatically centered reflections by means of a Philips PW1100 four-circle diffractometer.

Crystal Data: $(-)_{589}$-$[Cr(C_5H_7O_2)_2(C_3H_{10}N_2)]I\cdot H_2O$, *F.W.*=469.3, orthorhombic, $a=20.834(6)$ Å, $b=12.015(3)$ Å, $c=7.621(2)$ Å, $U=1907.7(9)$ Å^3, $Z=4$, $D_x=1.63$, $D_m=1.62$ g·cm^{-3}, space group $P2_12_12_1$, μ(Mo $K\alpha$)=22.8 cm^{-1}, λ(Mo $K\alpha$)=0.7107 Å.

The intensity data ($2\theta\leqq55°$) were collected at room temperature by the use of graphite-monochromated Mo $K\alpha$ radiation. The ω-scan mode was employed, since the reflections were rather broad. The scan range was (1.6+0.5 tan θ)°, and the scan speed, 2°/min; the background was counted for 10 s at each side of the scan range. During the data collection, the intensities of three standard reflections were monitored every 180 min in order to check the orientation and stability of the crystal. No appreciable decay was observed. A total of 1426 reflections with $F_o^2>3\sigma(F_o^2)$ were observed and used in the subsequent structure determination and refinement. The observed intensities were corrected for Lorentz-polarization and absorption effects (r=0.015 cm), and the relative structure factors were derived.[6]

Structure Determination and Refinement. The crystal structure was solved by the heavy-atom method. The parameters of all the non-hydrogen atoms were refined by

TABLE 1. POSITIONAL AND THERMAL PARAMETERS

Atom	10^4x	10^4y	10^4z	$10B$/Å^2
I	3959.0(5)	901.3(7)	212.1(14)	a
Cr	3930(1)	6720(1)	606(2)	a
O(1)	3445(4)	5447(7)	1492(12)	36(2)
O(2)	3939(4)	6080(6)	−1754(10)	34(1)
O(3)	3158(4)	7542(6)	−64(12)	34(2)
O(4)	3919(4)	7415(6)	2950(10)	31(1)
N(1)	4784(5)	5914(8)	1181(13)	30(2)
N(2)	4461(5)	8041(8)	−293(14)	31(2)
C(1)	2947(7)	3680(13)	1713(21)	46(3)
C(2)	3262(5)	4583(9)	616(16)	26(2)
C(3)	3369(7)	4448(12)	−1130(20)	42(3)
C(4)	3678(6)	5169(11)	−2235(19)	34(2)
C(5)	3725(8)	4997(15)	−4198(23)	53(3)
C(6)	2223(7)	8696(12)	100(23)	50(3)
C(7)	2788(6)	8109(10)	956(17)	30(2)
C(8)	2882(6)	8234(11)	2790(17)	32(2)
C(9)	3450(6)	7916(10)	3625(17)	28(2)
C(10)	3521(7)	8235(12)	5592(19)	42(3)
C(11)	5314(6)	5965(11)	−89(19)	41(2)
C(12)	5519(7)	7126(11)	−578(19)	40(2)
C(13)	5023(7)	7799(12)	−1520(19)	39(3)
O(H_2O)	4813(5)	3400(9)	1269(14)	47(2)

a) Anisotropic thermal parameters($\times10^5$) in the form of: $\exp[-(B_{11}h^2+B_{22}k^2+B_{33}l^2+B_{12}hk+B_{13}hl+B_{23}kl)]$.

Atom	B_{11}	B_{22}	B_{33}	B_{12}	B_{13}	B_{23}
I	289(2)	564(4)	2387(17)	30(7)	−115(15)	−81(18)
Cr	161(4)	382(10)	1236(32)	1(14)	17(25)	−124(32)

Table 2. Observed and calculated structure amplitudes of some Bijvoet pairs

h k l	$\|F_c(hkl)\|$	Obsd	$\|F_c(\bar{h}\bar{k}\bar{l})\|$
1 1 1	42.5	<	69.3
3 1 1	22.3	>	18.0
3 2 1	227.0	>	212.0
8 2 1	24.5	>	14.0
1 5 1	105.3	>	96.5
5 1 2	22.3	>	19.8
1 3 2	10.0	<	14.3
2 3 2	174.8	>	166.5
3 3 2	27.0	>	23.0
4 3 2	52.8	>	39.0
3 4 2	23.0	<	32.6

the block-diagonal least-squares method, using the anisotropic temperature factors for the I and Cr atoms. Although the difference Fourier map computed at this stage showed the positions of all the hydrogen atoms except for those of the hydrogen atoms of the CH_3 groups and the water of crystallization, the hydrogen atoms were located in geometrically calculated positions (N–H, C–H=1.03 Å, B=4.0 Å^2) and their contributions to the structure factors were taken into account. However, their parameters were not refined. The final agreement indices R and $R'=[\sum w\Delta F^2/\sum wF_o^2]^{1/2}$, were 0.0491 and 0.0640 respectively. A weighting scheme of $w=(44.4/F_o)^2$ for $F_o>44.4$, $w=1$ for $17.8\leqq F_o\leqq 44.4$, and $w=0.6$ for $17.8>F_o$ was used to make $w\Delta F_o^2$ approximately constant over the whole range of F_o values. All the parameter shifts in the final cycle refinement were less than 0.2σ. The atomic scattering factors were taken from Ref. 7. The real and imaginary parts of the anomalous dispersion correction were applied for the I and Cr atoms.[7] The final difference Fourier map was rather flat, the largest peak being 0.6 e/Å^3. The atomic coordinates and the temperature factors are listed in Table 1. A complete list of the observed and calculated structure factors is preserved by the Chemical Society of Japan (Document No. 7934).

The absolute configuration of the complex cation was determined by the anomalous dispersion technique. Table 2 gives the calculated structure amplitudes of several Bijvoet pairs and the observed inequality relationships which were obtained from Weissenberg photographs taken with Cu $K\alpha$ radiation. The observed relationships indicate that the absolute configuration of the complex cation is Λ.

The computer programs used in the calculations included the local version of the UNICS.[8] All the calculations were performed on a FACOM 230-60 computer at Osaka City University.

Results and Discussion

Figure 1 shows a view of the $(-)_{589}$-$[Cr(acac)_2(tn)]^+$ complex. The absolute configuration of the complex cation has been determined as Λ. The projections of the three chelate rings are given in Fig. 2, along with the deviations(Å) of the atoms from the planes formed by the Cr and two ligator atoms. One of the Cr-acac six-membered chelate rings is nearly planar, and the [Cr, O(1), O(2)] and [O(1), O(2), C(1), C(2), C(3), C(4), C(5)] planes make an angle of 2.6°, while the other somewhat deviates from a plane, the interplanar angle between the [Cr, O(3), O(4)] and

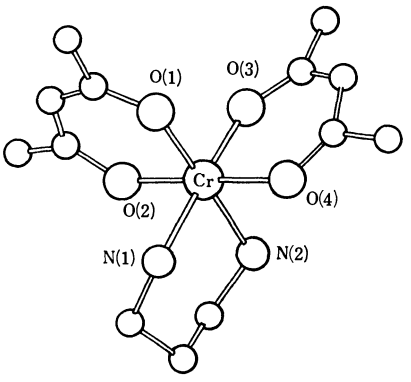

Fig. 1. A perspective view of $(-)_{589}$-$[Cr(acac)_2(tn)]^+$.

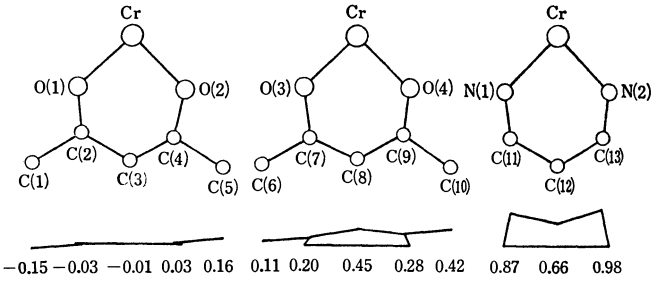

Fig. 2. Projections of the three chelate rings.

[O(3), O(4), C(6), C(7), C(8), C(9), C(10)] planes being 9.4°. The Cr-tn chelate ring is of a chair form. The average length of the Cr–O bonds is 1.96(1) Å, which is in agreement with the 1.951(7), 1.97 (1), and 1.964(5) Å found in $[Cr(acac)_3]$,[9] Λ-$(+)_{589}$-$[Cr((+)\text{-atc})_3]^{3+}$,[2] and $(-)_{589}$-$[Cr(acac)_3]$[4] respectively. The chelate bite angle (90.6(4)°) in the Cr-acac ring is slightly smaller than 91.9(6)[9] and 91.9(1)°[2] in these related complexes, but it agrees well with 90.8(2)° in $(-)_{589}$-$[Cr(acac)_3]$.[4] Both the Cr–N distance (2.06(1) Å) and the N–Cr–N angle (88.2(4)°) are normal compared with the values previously reported.[10,11] The bond distances and angles are given in Table 3.

Figure 3 gives the CD spectra of the four $[Cr(acac)_n(tn)_{3-n}]^{(3-n)+}$-type complexes in the octahedral $^4A_{2g}\rightarrow {}^4T_{2g}$ transition, whose absolute configurations are considered to be Λ. The X-ray diffraction study of $(-)_{589}$-$[Cr(acac)_3]$ indicates that this complex has the Δ absolute configuration. The Λ configuration is, therefore, given to the enantiomeric form $(+)_{589}$-$[Cr(acac)_3]$ of the complex. The present X-ray study has revealed that the configuration of $(-)_{589}$-$[Cr(acac)_2(tn)]^+$ is Λ. In the case of $(+)_{589}$-$[Cr(acac)(tn)_2]^{2+}$, the structure of the corresponding Co(III) complex was determined by the X-ray method.[12] The $(+)_{589}$-$[Co(acac)(tn)_2]^{2+}$ complex, which shows a positive CD peak in the first absorption band region, has the Λ configuration. As the CD curve of $(+)_{589}$-$[Cr(acac)(tn)_2]^{2+}$ is similar to that of the cobalt analogue, the configuration of $(+)_{589}$-$[Cr(acac)(tn)_2]^{2+}$ is Λ. In the CD spectrum of $(-)_{589}$-$[Cr(tn)_3]^{3+}$, the positive CD peak was identified as the ^4E component from the ion-pairing effect.[13] Therefore, the configuration may be Λ.

Table 3. Interatomic distances and bond angles

Bond length(l/Å)		Bond angle(φ/°)	
Cr-O (1)	1.95 (1)	O (1)-Cr-O (2)	90.9 (4)
Cr-O (2)	1.96 (1)	O (3)-Cr-O (4)	90.7 (4)
Cr-O (3)	1.96 (1)	N (1)-Cr-N (2)	88.2 (4)
Cr-O (4)	1.97 (1)	Cr-O (1)-C (2)	127.1 (8)
Cr-N (1)	2.07 (1)	Cr-O (2)-C (4)	126.6 (8)
Cr-N (2)	2.05 (1)	Cr-O (3)-C (7)	127.0 (8)
O (1)-C (2)	1.29 (2)	Cr-O (4)-C (9)	125.6 (8)
O (2)-C (4)	1.28 (2)	Cr-N (1)-C (11)	119.1 (8)
O (3)-C (7)	1.29 (2)	Cr-N (2)-C (13)	118.1 (8)
O (4)-C (9)	1.26 (2)	O (1)-C (2)-C (3)	123.6 (12)
N (1)-C (11)	1.47 (2)	O (2)-C (4)-C (3)	124.5 (13)
N (2)-C (13)	1.53 (2)	O (3)-C (7)-C (8)	124.6 (11)
C (1)-C (2)	1.52 (2)	O (4)-C (9)-C (8)	127.1 (12)
C (2)-C (3)	1.36 (2)	N (1)-C (11)-C (12)	114.5 (11)
C (3)-C (4)	1.37 (2)	N (2)-C (13)-C (12)	109.9 (11)
C (4)-C (5)	1.51 (2)	C (2)-C (3)-C (4)	127.2 (13)
C (6)-C (7)	1.52 (2)	C (7)-C (8)-C (9)	122.4 (11)
C (7)-C (8)	1.42 (2)	C (11)-C (12)-C (13)	115.0 (11)
C (8)-C (9)	1.40 (2)	O (1)-C (2)-C (1)	114.7 (11)
C (9)-C (10)	1.55 (2)	O (2)-C (4)-C (5)	111.9 (12)
C (11)-C (12)	1.51 (2)	O (3)-C (7)-C (6)	116.8 (11)
C (12)-C (13)	1.50 (2)	O (4)-C (9)-C (10)	116.0 (11)
		C (1)-C (2)-C (3)	121.6 (12)
		C (5)-C (4)-C (3)	123.6 (13)
		C (6)-C (7)-C (8)	118.7 (11)
		C (10)-C (9)-C (8)	116.9 (11)

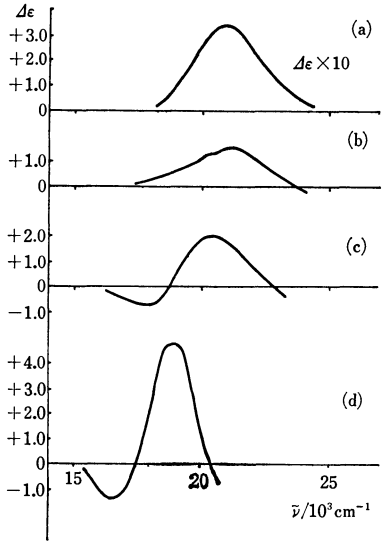

Fig. 3. CD spectra of $[Cr(acac)_n(tn)_{3-n}]^{(3-n)+}$-type complexes in the region of the octahedral $^4A_{2g}$-$^4T_{2g}$ absorption.
(a) $(-)_{589}$-$[Cr(tn)_3]^{3+}$, (b) $(+)_{589}$-$[Cr(acac)(tn)_2]^{2+}$, (c) $(-)_{589}$-$[Cr(acac)_2(tn)]^+$, (d) $(+)_{589}$-$[Cr(acac)_3]$.

In the CD spectrum of $(+)_{589}$-$[Cr(acac)_3]$, the negative CD peak at the lower wave number is assigned to the $^4A_1$ component, and the positive CD peak at the higher wave number, to the ^4E component.[14] The CD spectrum of $(-)_{589}$-$[Cr(acac)_2(tn)]^+$ is similar in shape to that of $(+)_{589}$-$[Cr(acac)_3]$, although the former is shifted to a higher wave number. Therefore, the positive CD peak of $(-)_{589}$-$[Cr(acac)_2(tn)]^+$ is mainly due to the ^4E component of the $^4T_{2g}$ transition of $(+)_{589}$-$[Cr(acac)_3]$. The $(+)_{589}$-$[Cr(acac)(tn)_2]^{2+}$ complex gives two positive CD components in the region of the octahedral $^4T_{2g}$ absorption. The two components are due to the combined $^4A_1$, $^4B_2$, and $^4B_1$ components derived from the octahedral $^4T_{2g}$ transition of Cr(III)[15,16] and seem to have a sign reflecting that of the positive CD peak of $(-)_{589}$-$[Cr(acac)_2(tn)]^+$. The combined $^4A_1$, $^4B_2$, and $^4B_1$ components of $(+)_{589}$-$[Cr(acac)(tn)_2]^{2+}$ have the same sign as the CD of $(-)_{589}$-$[Cr(tn)_3]^{3+}$, and the CD peaks of the two complexes are observed at approximately equal energies. Therefore, the positive CD peaks of $(+)_{589}$-$[Cr(acac)(tn)_2]^{2+}$ and $(-)_{589}$-$[Cr(tn)_3]^{3+}$ are likely to have the same origin. Consequently, the absolute configuration of $(-)_{589}$-$[Cr(tn)_3]^{3+}$ is Λ, in accordance with the assignment from the ion-pairing effect.[13]

Table 4. Possible hydrogen bonds(l/Å)

I···O(H_2O)			3.58 (1)
N(1)···O(H_2O)			3.02 (2)
O(4)···O(H_2O)$(1-x,\ 1/2+y,\ 1/2-z)$			2.96 (2)
N(2)···I$(x,\ 1+y,\ z)$			3.61 (1)
N(1)-H	1.02	H···O(H_2O)	2.07
N(2)-H	1.03	H···I$(x,\ 1+y,\ z)$	2.97

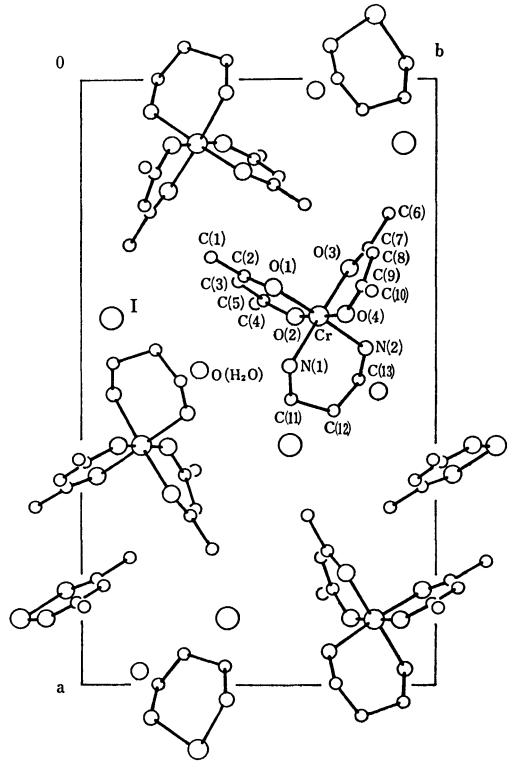

Fig. 4. A projection of the crystal structure along the c axis.

Figure 4 gives the crystal structure viewed down the c axis. Possible hydrogen bonds are summarized in Table 4. The Cr-acac six-membered chelate ring containing the O(3) and O(4) atoms is bent away

from the [Cr, O(3), O(4)] plane to C(1)($1/2-x$, $1-y$, $1/2+z$) by 9.4° (Fig. 2). As the interatomic distances between C(10) and C(1) ($1/2-x$, $1-y$, $1/2+z$) and that between C(10) and C(11) ($1-x$, $1/2+y$, $1/2-z$) are 3.92 and 4.11 Å respectively, the large deviation of the acac ring from the coordination plane (9.4°) may result from an intramolecular repulsion.

We wish to thank Professor Shinichi Kawaguchi for providing the sample and for his continuing interest in this study. This research was supported by a Grant-in-Aid from the Ministry of Education.

References

1) S. F. Mason, R. D. Peacock, and T. Prosperi, *J. Chem. Soc., Dalton Trans.*, **1977**, 702.
2) W. D. Horrocks, Jr., D. L. Johnston, and D. Macinnes, *J. Am. Chem. Soc.*, **92**, 7620 (1970).
3) "Fundamental Aspects and Recent Developments in Optical Rotatory Dispersion and Circular Dichroism," ed by F. Ciardelli and P. Salvadori, Heyden & Son (1973), p. 231; J. H. Dunlop, R. D. Gillard, and R. Ugo, *J. Chem. Soc., A*, **1966**, 1540.
4) R. Kuroda and S. F. Mason, *J. Chem. Soc., Dalton Trans.*, **1979**, 273.
5) M. Nakano and S. Kawaguchi, *Bull. Chem. Soc. Jpn.*, **52**, 2897 (1979).
6) J. Hornstra and B. Stubbe, PW1100 Data Processing Programs, Philips Research Laboratories, Eindhoven, Holland.
7) "International Tables for X-Ray Crystallography," Kynoch Press, Birmingham (1974), Vol. IV, pp. 71, 148.
8) "The Universal Crystallographic Computation Program System," The Crystallographic Society of Japan (1969).
9) B. Morosin, *Acta Crystallogr.*, **19**, 131 (1965).
10) F. A. Jurnak and K. N. Raymond, *Inorg. Chem.*, **13**, 2387 (1974).
11) E. N. Duesler and K. N. Raymond, *Inorg. Chim. Acta*, **30**, 87 (1978).
12) K. Matsumoto, H. Kawaguchi, H. Kuroya, and S. Kawaguchi, *Bull. Chem. Soc. Jpn.*, **46**, 2424 (1973).
13) P. G. Beddoe and S. F. Mason, *Inorg. Nucl. Chem. Lett.*, **4**, 433 (1968).
14) T. S. Piper and R. L. Carlin, *J. Chem. Phys.*, **36**, 3330 (1962).
15) H. Yamatera, *Bull. Chem. Soc. Jpn.*, **31**, 95 (1958).
16) A. J. McCaffery, S. F. Mason, and B. J. Norman, *J. Chem. Soc.*, **1965**, 5094.

Quantification of Phenols in Gas from Rotten Liquid Swine Manure by Computer-controlled Gas Chromatography-Mass Spectrometry

Akio YASUHARA* and Keiichiro FUWA

Division of Chemistry and Physics, National Institute for Environmental Studies, Yatabe, Tsukuba-gun, Ibaraki 300-21

(Received April 10, 1979)

Analytical studies on phenol, *o*-cresol, *m*-cresol, *p*-cresol, and *p*-ethylphenol from liquid swine manure were performed with selected ion monitoring in computer-controlled gas chromatography-mass spectrometry. Phenol, *p*-cresol, and *p*-ethylphenol in effluent gas from liquid swine manure and in the head-space gas over liquid swine manure were determined.

Some odorous phenols have already been detected in liquid swine manure.[1] Phenols contributed greatly to malodor of liquid swine manure, because there is a relationship between the nature of the putrid odor and the quantity of phenols present.[2] Phenols are present at a relatively high concentration in liquid swine manure. It is very valuable to quantify phenols in gas from rotten liquid manure in order to estimate the role of phenols on the malodor from the piggery. The analytical methods reported for phenols are mainly gas chromatography (GC).[3-5] Selected ion monitoring (SIM) in gas chromatography-mass spectrometry however has the advantage of higher selectivity and sensitivity, when compared to GC. SIM controlled by computer has been shown to have sufficient accuracy and stability for long-time measurement in the quantification of geosmin.[6]

This paper reports an analytical method for phenols by SIM and the results of measurements on phenols in the gas from liquid swine manure.

Experimental

Gas Chromatography. A 3 m×2 mm i.d. glass column packed with KG-02[7] was used. The column temperature was 170 °C, the injection port temperature was 250 °C and the carrier gas was helium at a flow-rate of 30 ml/min (2.4 kg/cm^2).

Computer-controlled Selected Ion Monitoring. A JEOL Model JMS-D 100 mass spectrometer was connected with a JEOL Model JGC-20 K gas chromatograph and a JEOL Model JMA-2000 mass data analysis system. The mass spectrometer was operated with a resolution (10% valley) of *ca.* 1000. The magnetic field was set at *m/e* 93 and the accelerating voltage and electric field were changed at intervals of 0.3 s. Six-time repetitions of a small range sweep (1 mass unit) on each mass number setting (94, 105, 107) were carried out and the latter four values were averaged for the correction of deviations of the magnetic field. The ionizing current was 3×10^{-4} A and the ionizing energy was 75 eV.

Absorption Process and Extraction of Phenols. A fixed volume of gas was passed through a glass filter and then into sodium hydroxide solution (20 ml, 1 M) to trap phenols. After acidification of the solution with concd hydrochloric acid (5 ml), phenols were extracted with dichloromethane (10 ml) twice. The combined solution after drying over anhydrous sodium sulfate was concentrated to a few millilitres using a Kuderna-Danish concentrator under atmospheric pressure. One μg of butyl benzoate was added as an internal standard to 1 ml of the sample solution.

Isolation of Phenols from Rotten Liquid Manure by a Gas-stripping Method. Liquid swine manure (2.5 l) which had been digesting anaerobically or acrobically was transfered to a three-necked flask (3 l) and warmed to 35 °C. Nitrogen or air was passed into the flask at a rate of 220 ml/min for 3 h. The effluent gas was treated with the absorption process described above.

Isolation of Phenols from Head-space Gas over Rotten Liquid Swine Manure in the Pigsty. The head-space gas over the reservoir of liquid manure in a pigsty near Tsukuba New Town, Ibaraki, was passed into sodium hydroxide (20 ml, 1 M) at a rate of 1 l/min for 1 h. Subsequent procedures were the same as described above.

Results and Discussion

It has already been reported that the column packing material, KG-02, used here had excellent ability for the separation of several phenols.[8]

The mass numbers used for ion detection were 94 for phenol and 107 for three cresols and *p*-ethylphenol. As the dynamic range in the mass spectrometer is very narrow and injection of an exact volume with a microsyringe is not sufficiently accurate, quantitative analysis was carried out using an internal standard method. Butyl benzoate was selected as the internal standard, since the retention times of phenols and butyl benzoate in the gas chromatogram were close and a base peak at *m/e* 105 in the mass spectrum of butyl benzoate was close to the mass numbers of the selected ions for phenols.

Extended measurements by SIM with a magnet-type mass spectrometer has been considered to be difficult until a few years ago, because the magnetic field is not so stable at a resolution (10% valley) over 1000. Improvements of instruments have now enabled

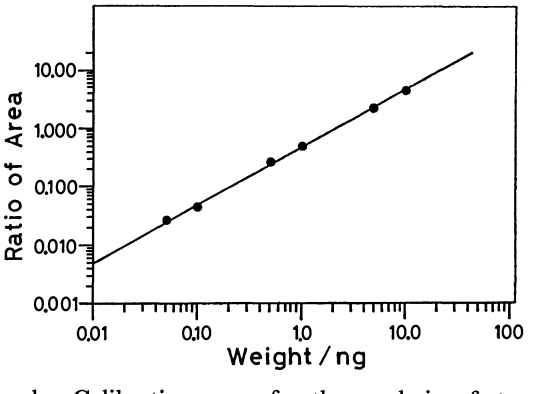

Fig. 1. Calibration curve for the analysis of *p*-cresol by selected ion monitoring.

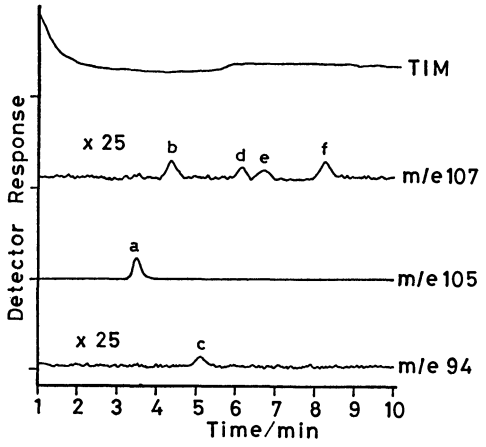

Fig. 2. Typical example of selected ion monitoring in GC/MS.
a: Butyl benzoate (1 μg/ml), b: *o*-cresol (50 ng/ml), c: phenol (50 ng/ml), d: *p*-cresol (50 ng/ml), e: *m*-cresol (50 ng/ml), f: *p*-ethylphenol (50 ng/ml).

TABLE 1. COEFFICIENT OF VARIATION FOR MEASUREMENT OF PHENOLS BY SELECTED ION MONITORING

Concentration	Phenol	Cresol			*p*-Ethylphenol
		o-	*m*-	*p*-	
10 μg/ml	13.5%	8.1%	8.7%	9.2%	7.4%
5 μg/ml	12.9	6.0	10.4	12.5	10.6
1 μg/ml	8.2	2.8	5.4	5.7	3.8
500 ng/ml	8.4	2.8	8.3	17.3	8.9
100 ng/ml	3.1	7.1	12.2	7.5	5.9
50 ng/ml	5.9	1.6	15.7	14.9	7.6

TABLE 2. RECOVERY OF PHENOLS FROM ALKALINE AQUEOUS SOLUTION

Run No.	Recovery/%				
	Phenol	*o*-Cresol	*m*-Cresol	*p*-Cresol	*p*-Ethylphenol
1	86	89	89	92	95
2	92	93	95	97	99
Average	89	91	92	95	97

extended measurements over 10 h to become possible, since deviations of the magnetic field can now be corrected by computer. This is achieved by generating the electric field and accelerating voltage as a continuously varying triangular wave function which sweeps over a small mass range (1 mass unit). The sweep correction technique is described in the experimental section.

The calibration curve for each phenol was prepared using the ratio of the peak areas of the component and butyl benzoate. An example of the calibration curves is shown in Fig. 1. The detection limit of each compound was 50 ng/ml and an example of SIM is shown in Fig. 2. The precision of measurement was obtained by making measurements on six samples five times respectively. The coefficients of variation are shown in Table 1.

A standard gas containing a fixed amount of phenols

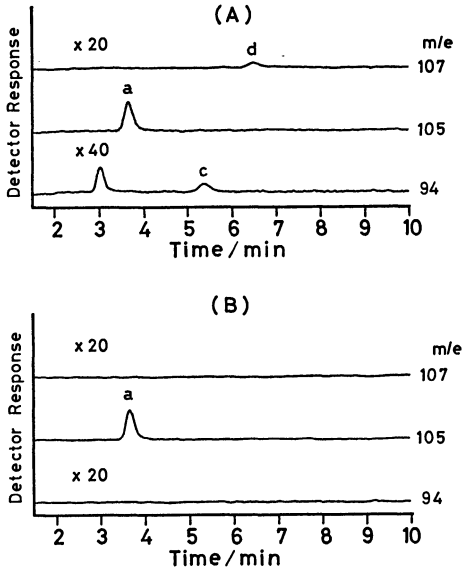

Fig. 3. Selected ion monitoring for phenols in effluent gas from liquid swine manure.
(A): The case of aerobic digestion, (B): background.
a: Butyl benzoate, c: phenol, d: *p*-cresol.

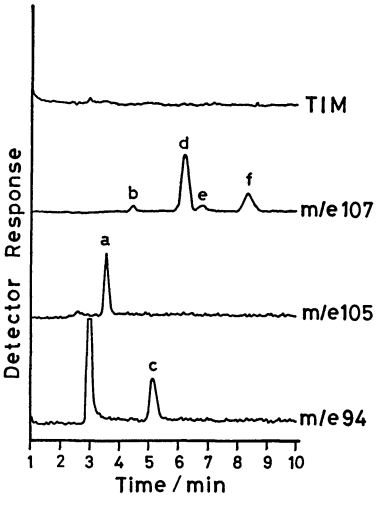

Fig. 4. Selected ion monitoring for phenols in effluent gas from anaerobically digested liquid swine manure.
a: Butyl benzoate, b: *o*-cresol, c: phenol, d: *p*-cresol, e: *m*-cresol, f: *p*-ethylphenol.

cannot be prepared because of the low volatility of phenols and also because of adsorption loss on the container walls. Therefore, a fixed volume of gas containing a suitable amount of phenols was passed consecutively through two bottles containing sodium hydroxide solution (20 ml, 1 M). This extraction procedure was the same as those of the samples and extracted phenols were measured by SIM. Phenols were not detected from the second trap so that subsequent experiments utilized only one bottle containing sodium hydroxide solution (20 ml, 1 M).

Next, to test whether phenols trapped in alkaline aqueous solution are oxidized by aeration, air was passed into 1 M aqueous solution (20 ml) of sodium hydroxide containing phenol (6.2 μg), *o*-cresol (4.2

Table 3. Concentration of phenols in the effluent gas from anaerobically or aerobically digested liquid swine manure by gas-stripping method[a)]

Run No.	Anaerobically			Aerobically	
	Phenol	*p*-Cresol	*p*-Ethyl-phenol	Phenol	*p*-Cresol
1	27.4	163	16.6	ND	3.0
2	33.1	201	20.1	ND	5.1
3	35.8	215	22.1	6.3	13.1
4	39.3	225	24.2	7.1	15.2
5	37.4	191	19.3	ND	3.5
6	42.8	201	19.9	ND	3.5
7	43.0	212	21.9	ND	9.7
8	46.3	219	27.1	ND	5.5
9	47.3	218	28.4	ND	4.4
10	44.1	222	24.0	ND	10.1
11	40.9	226	22.6	ND	3.7
12	41.7	237	24.8	ND	6.4
13	44.1	233	28.4	ND	3.0
14	42.5	232	26.7	ND	3.7
15	42.8	245	25.9	ND	3.5
16	39.8	212	23.0	ND	9.7

a) Unit of concentration is volume ppb (10^{-9}). ND means "not detected."

μg), *m*-cresol (6.9 μg), *p*-cresol (8.3 μg), and *p*-ethylphenol (19.4 μg) under the same conditions as those of measurements. The results are shown in Table 2.

Figures 3 and 4 show the SIM for the phenols isolated from aerobically or anaerobically digested liquid manure by gas stripping. Phenol and *p*-cresol were detected under aerobic digestion, whereas five phenols were sometimes detected from anaerobically digested manure. Phenol, *p*-cresol, and *p*-ethylphenol were always detected at a higher concentration under anaerobic digestion than under aerobic digestion. The results of measurements are shown in Table 3.

Phenols in the head-space gas over the reservoir of liquid manure, in which a small amount of fresh manure was continuously poured, were measured according to this procedure. The results are shown in Table 4. The concentration of phenol was greater than that of *p*-ethylphenol in the head-space gas, compared with the gas-stripping method.

Table 4. Concentration of phenols in head-space gas over the reservoir of liquid swine manure[a)]

Run No.	Phenol	*p*-Cresol	*p*-Ethylphenol
1	13	0.83	0.86
2	11	0.35	0.38
3	9	ND	0.31
4	13	ND	ND

a) Unit of concentration is volume ppb (10^{-9}). ND means "not detected."

Quantification of carboxylic acids by SIM was unsuccessful, because the concentration of carboxylic acids in liquid manure or head-space gas was lower than that of phenols. For the analysis of carboxylic acids it is necessary to use an adsorption method with a precolumn rather than the absorption method with an alkaline aqueous solution.

The authors wish to thank Mr. Minoru Kuriyama, a hog raiser near Tsukuba New Town, Ibaraki Prefecture, for his offer of liquid swine manure and for his permission on the measurements in his pigsty.

References

1) A. Yasuhara and K. Fuwa, *Bull. Chem. Soc. Jpn.*, **50**, 731 (1977).
2) A. Yasuhara and K. Fuwa, *Bull. Chem. Soc. Jpn.*, **52**, 114 (1979).
3) S. Naito, M. Kaneko, S. Setsuda, J. Matsuzaki, S. Fukui, and S. Kanno, *J. Hyg. Chem.*, **16**, 41 (1970).
4) W. A. Dietz, *J. Chromatogr. Sci.*, **10**, 423 (1972).
5) Y. Hoshika and G. Muto, *J. Chromatogr.*, **157**, 277 (1978).
6) A. Yasuhara and K. Fuwa, *J. Chromatogr.*, **172**, 453 (1979).
7) KG-02 is a column packing material coated with some derivative of polyethylene glycol on UNIPORT HP and was obtained from Gasukuro Kogyo Co., Ltd.
8) A. Yasuhara and K. Fuwa, *Agric. Biol. Chem.*, **43**, 313 (1979).

Peri Interaction in Naphthalene Ketones

Masao KUBO and Takeo SATO*

Department of Chemistry, Tokyo Metropolitan University, Setagaya-ku, Tokyo 158

(Received June 24, 1978)

Peri interaction in several naphthalene ketones was investigated using the carbon-13 NMR, IR, and UV spectra. The carbonyl carbon resonances for 7*H*,14*H*-cycloocta[1,2,3-*de*:5,6,7-*d'e'*]dinaphthalene-7,14-dione and its 7-oxa analog were found to be shifted upfield by 27 and 24 ppm respectively compared with those of model compounds. The anomalous shift for the former was attributed to π-orbital compression, which inhibited the polarization of carbonyl groups because of a forced parallel geometry, while the latter was attributed to field effects. The conclusion was supported by UV and IR data.

Recently we have observed the unusual chemical shifts for the sterically perturbed sp^2 carbon resonances in certain cyclophanes.[1] Unlike the conventional steric effects on the carbon chemical shifts,[2] which in general lead a resonance upfield through the charge polarization of the C–H bonds induced by the steric compression, this new type of steric effect seems to be caused by the interactions between π-orbitals along the orbital axis. In order to distinguish these two sterically induced shifts with opposite signs, we call the former (conventional) shifts "σ-orbital compression shifts" and the latter (new), "π-orbital compression shifts."

As the π-compression shifts may conveniently be used to assess the steric perturbation of π-orbitals, we have studied the proximity effects on the carbonyl carbon chemical shifts of naphthalene peri ketones, whose peri positions are only 2.4—2.5 Å apart.[3] The structural features of these ketones were also investigated in order to obtain collaborative evidence of the π-orbital compression effect.

Experimental

Spectral Measurements. The carbon-13 NMR spectra were recorded using a JEOL JNM FX-60 spectrometer equipped with a JFA-100 data system (8 K) operating at 15.00 MHz. The sample was dissolved in $CDCl_3$. The concentration was *ca.* 0.2 M except for **3**, for which a saturated solution was used. The samples were contained in 10 mm o.d. tubes. The spectra were obtained by storing the free induction decays produced by a series of 9 μs r.f. pulses (45° pulse), followed by the Fourier transformation. The sample temperature was 25 °C. Generally, 4 K data points (real 2 K points) were collected for a sweepwidth of 4 kHz, giving an effective resolution of 2 Hz (±0.13 ppm). The delay between pulses was 3—5 s, and 500—1000 transients were required to obtain a good signal-to-noise ratio. The chemical shifts are shown in a δ value downfield from the internal TMS.

The carbonyl stretching frequencies in the IR spectra were recorded using a Perkin-Elmer 225 spectrometer on samples dissolved in $CHCl_3$ (0.25 and 0.5% solutions) using a 1-mm cell. A symmetrical carbonyl band was observed in the expanded spectrum (×8) except for **4a**, which showed low-intensity bands at 1632 and 1623 cm^{-1} in addition to a strong band at 1653 cm^{-1}. The data are collected in Table 1, together with the shift and frequency differences from **1**.

The UV spectra were recorded on a Hitachi-124 spectrometer, using 95% ethanol as the solvent. The data are summarized in Table 3, while some representative curves are shown in Fig. 1.

*7-Oxa-7H,14H-cycloocta[1,2,3-de : 5,6,7-d'e']dinaphthalene-14-one (**4a**).* A mixture of 6.3 g (0.02 mol) of 8-(1-naphthyloxy)naphthalene-1-carboxylic acid (mp 128.5—130 °C), prepared by the Ullmann reaction between ethyl 8-bromonaphthalene-1-carboxylate[4] and sodium 1-naphthoate in DMF, using cupric oxide as the condensing reagent, followed by hydrolysis, and 300 g of polyphosphoric acid was warmed at 100 °C for 30 min. A usual work-up subsequently gave pale yellow needles; mp 210—212 °C; recrystallized from benzene; *m/e* 296; δ (C), 118.7, 123.4, 124.4, 124.9, 126.0, 127.0, 128.0, 128.6, 129.6, 130.4, 131.9, 133.2, 134.0, 134.5, 135.8, 136.9, and 173.2. Found: C, 84.31; H, 4.07%. Calcd for $C_{21}H_{12}O$: C, 85.12; H, 4.08%.

*7-Thia-7H,14H-cycloocta[1,2,3-de : 5,6,7-d'e']dinaphthalene-14-one (**4b**).* A mixture of 2.1 g (6.4 mmol) of 8-(1-naphthylthio)naphthalene-1-carboxylic acid (mp 202—203.5 °C), prepared by the Ullmann reaction between ethyl 8-bromonaphthalene-10-carboxylate and sodium 1-naphthalenethiolate, followed by hydrolysis, and 77 g of polyphosphoric acid was heated at 120 °C for 7.5 h after the literature method.[6] Pale yellow needles; mp 235.5—236.5 °C; recrystallized from benzene; *m/e* 312; δ (C), 123.1, 126.0, 127.3, 128.3, 129.9, 130.9, 133.2, 134.5, 137.7, 146.2, 200.5. Found: C, 80.69; H, 3.81%. Calcd for $C_{21}H_{12}S$: C, 80.74; H, 3.87%.

*12H-Benzo[f]naphtho[1,8-bc]oxepin-12-one (**5c**).* The acyl chloride obtained from 8-phenoxy-1-naphthoic acid (21.5 g, 0.082 mol) was dissolved in 100 ml of benzene, and to this we added 22 g (0.10 mol) of aluminum chloride. Column chromatography on silica gel gave pale yellow needles; mp 97.5—98.5 °C; 10% yield. Found: C, 83.33; H, 4.05%. Calcd for $C_{17}H_{10}O_2$: C, 82.91; H, 4.09%.

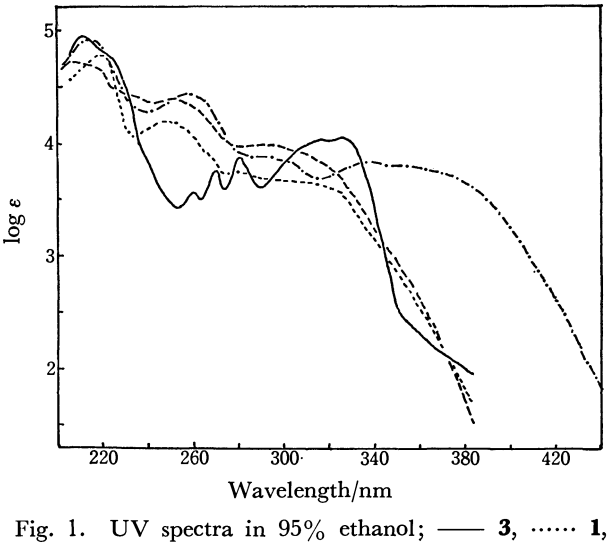

Fig. 1. UV spectra in 95% ethanol; —— **3**, ····· **1**, ---- **2**, and -·-·- **4a**.

Table 1. Carbon-13 NMR and IR data

Compound			Carboon-13 NMR, δ/ppm		IR, ν/cm^{-1}	
			C=O	$\Delta\delta$[a)]	$\nu_{C=O}$	$\Delta\nu_{C=O}$[b)]
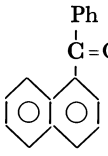	**1**		197.6	—	1660	—
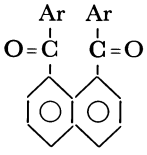		Ar				
	2a	Ph	197.6	0	1660	0
	2b	*p*-tolyl	197.3	−0.3	1656	−4
	2c	1-naphthyl	198.4	+0.8	1660	0
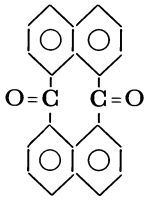	**3**		170.9	−26.7	1685	+25
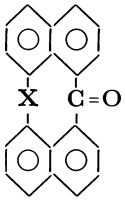		X				
	4a	O	173.2	−24.4	1653	−7
	4b	S	200.5	+2.9	1662	+2
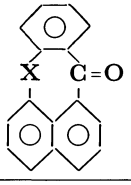		X				
	5a	CH_2	198.9	+1.3	1654	−6
	5b	CO	196.0	−1.6	1658	−2
	5c	O	193.8	−3.8	1659	−1

a) Chemical-shift differences for carbonyl carbons with respect to the shift for **1**. b) Difference in carbonyl stretching frequencies compared with **1**.

Table 2. Carbon-13 NMR chemical shifts, δ[a)]

Compound	Chemical shift, δ/ppm		
	C=O	Ar-C	CH_3
1	197.6	*136.2*, *133.6*, *132.4*, 133.0, 131.0, 130.3(×2), 128.3(×2), 127.7 127.1, 126.4, 125.6, 124.1	
2a	197.6	*137.7*, *137.1*, *135.1*, *132.7*, 131.9, 130.4(×2), 128.8, 128.0, 124.9	
2b	197.3	*143.5*, *137.3*, *135.1*, 131.7, 130.6(×2), 129.6, 128.8(×2), 124.8	21.7
2c	198.4	*153.2*, *141.9*, *135.6*, *134.9*, 133.6(×2), 132.5, 131.5, 129.2, 127.9, 127.4(×2), 125.2, 124.1	
3	170.9	129.9, *128.4*, 126.1, *125.2*, 124.4, *120.4*	
5c	196.0	*138.3*, *136.2*, 135.1, *133.8*, 132.8, 132.2, 127.8, 126.0	

a) Numbers in italic denote non-protonated carbons. Resonances due to the doubly overlapped carbons are shown by 2 in parentheses.

Results and Discussion

The naphthalene peri ketones examined in this paper, **1**—**5**, are shown in Table 1. 1-Benzoyl- (**1**)[5] and 1,8-diaroyl-naphthalenes (**2**),[6] 7*H*,14*H*-cycloocta[1,2,3-*de*:5,6,7-*d'e'*]dinaphthalene-7,14-dione (**3**),[7] 7(12*H*)-pleiadenone (**5a**),[8] and 7,12-pleiadenedione (**5b**)[8] were prepared according to the reported method. 7-Oxa-7*H*,14*H*-cycloocta[1,2,3-*de* : 5,6,7-*d'e'*]dinaphthalene-14-one (**4a**) and sulfur analog **4b**,[9] and 12*H*-benzo[*f*]naphtho[1,8-*bd*]oxepin-12-one (**5c**) were prepared from ethyl 8-bromonaphthalene-1-carboxylate (see Experimental section).

The chemical shift of the carbonyl-carbon resonances for these compounds are shown in Table 1, in which are also shown the chemical-shift differences, $\Delta\delta$'s, from that of the reference compound **1**. The carbon-

TABLE 3. UV SPECTRA DATA IN 95% ETHANOL

Compound	λ_{max}/nm (log ε)
1	220(4.79), 250(4.20), 280 sh(3.75), 290 sh(3.69), 306(3.67), 320 sh(3.60)
2a	206(4.72), 230 sh(4.40), 250(4.40), 290(3.99), 310 sh(3.91)
2c	216(5.02), 230 sh(4.79), 250 sh(4.35), 316(4.28)
3	212(4.95), 226(4.73), 250 sh(3.49), 259(3.56), 269(3.77), 280(3.87), 3.16(4.03), 326(4.05)
4a	215(4.89), 257(4.42), 293(3.87), 303 sh(3.82), 333(3.81), 356 sh(3.76)
4b	214(4.89), 253 sh(4.28), 258 sh(4.27), 270 sh(4.09), 293(4.01), 308(3.98), 333(3.84)
5a	210(4.63), 245(4.26), 336(3.92)
5b	206(4.66), 240(4.47), 280 sh(3.62), 335(3.39)

13 NMR data for selected compounds are summarised in Table 2. Quaternary carbon resonances were assigned by means of the ^1H single-frequency off-resonance decoupling (SFORD) technique. The protonated aryl carbon resonances having double intensity are designated in Table 2. The carbon-13 NMR spectra for the less symmetrical **4a**, **4b**, **5a**, and **5b** were too complex to analyze. The data for these compounds are, therefore, not included in Table 2.

Taking compound **3** as an example, the procedures of the assignment will now be illustrated. Compound **3** showed a carbonyl resonance at δ 170.9, together with six aromatic carbon resonances. The aromatic carbon peaks at δ 120.4, 125.2, and 128.4 were attributed to the protonated carbons by means of the SFORD technique. The lowest field resonance, at δ 120.4, was assigned to the carbon directly bonded to the carbonyl group, since it appeared as the double intensity peak. The resonances at δ 124.4, 126.1, and 129.9 all appeared as double-intensity peaks which were split into doublets in the SFORD spectrum.

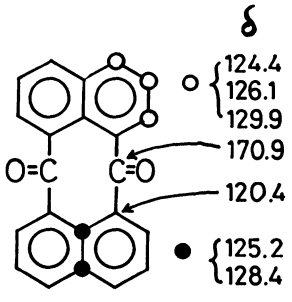

The chemical shifts of the carbonyl carbons depend strongly upon the conjugative interactions between the adjacent unsaturated bonds. The chemical shifts of the carbonyl carbons in the conjugated systems usually appear at a higher field than those in the non-conjugated systems. For example, the carbonyl carbon for di-*t*-butyl ketone at δ 215.8 is shifted to δ 195.2 for benzophenone.[10]

Carbonyl-carbon resonances for **1**, **2a**, **2b**, and **2c** at δ 197—198 are only slightly downfield from those of the unhindered aryl ketone ($\Delta\delta$ *ca.* 3 ppm). These slight downfield shifts may result from the peri interactions, which might inhibit the conjugation between the naphthalene ring and the carbonyl group. Because of additional conjugation in the benzoyl moiety, the extent of conjugation inhibition by the peri interaction in these systems could not be correctly estimated. The situation, however, may not be as serious as in the case of 9-acetylanthracene ($\Delta\delta$ 11 ppm),[10] in which two peri interactions exist. The UV spectral data for **1** and **2** in Table 3 revealed that the conjugations between the naphthalene ring and carbonyl groups were quite similar to each other, as is shown in Fig. 1.

With the 8-membered cyclic compound **3**, the carbonyl carbon resonance appeared at δ 170.9, which is, to our best knowledge, the highest field signal thus far reported for ketones. The shift difference, $\Delta\delta$, from compound **1** was −26.7 ppm. This observation is somewhat surprising, since the compound has a rigid structure in which two carbonyl groups are parallel to each other and are nearly perpendicular to the naphthalene ring plane.[11] The UV spectrum of **3** shows that the naphthalene chromophores are in an unfavorable geometry for conjugation (Table 2, Fig. 1). Furthermore, the 8-membered ketones have been known to show the $\delta_{C=O}$ at the lowest field among the other cycloalkanones.[12] Both the electronic and ring-size considerations call for downfield shifts of carbonyl carbons, the opposite of what we have observed. It is, therefore, apparent that a possible angle strain can not be responsible for the observed anomalous chemical shift.

Instead, we attribute the primary origin of the unusual up-field shift to the increased double-bond character of the carbonyl group in **3**, possibly caused by the inhibition of the carbonyl-bond polarization. In this compound, not only do two carbonyl groups come into a parallel geometry, but also the π electrons interact directly by means of the forced paralled orientation. The latter situation can not be expected for the related *s-cis* α-diketone, in which the nordal planes of the carbonyl carbons lie nearly on a single plane.

Carbon-13 upfield shifts were observed for all the other naphthalene carbon resonances in **3**, indicating the increased electron density of the aryl carbons in **3**. Especially, the resonance due to the carbons directly bonded to the carbonyl group was shifted upfield by more than 10 ppm from the equivalent resonances for 1 and 2. This may indicate a partial inhibition of the conjugation between carbonyls and aryl rings, which in turn increases the electron density of the aryl rings in **3** relative to those in **1** and **2**.

The carbonyl-stretching frequency of **3** was shifted by 25 cm^{-1} to 1685 cm^{-1} compared to that of the model compound **1**, indicating the increased double-bond character of the carbonyl group, again caused by the conjugation inhibition. Part of this frequency shift should also be ascribed to the $\angle$C–CO–C deformation

characteristic of the medium-sized cyclic ketones, which also show $\nu_{C=O}$ at a high frequency. The IR as well as UV spectral data are consistent with our interpretation of the anomalous chemical shift of the carbonyl carbons for **3**.

In order to obtain further insight into the stereochemical features of **3**, we have examined two analogs, **4a** and **4b**, in which one of the carbonyl groups in **3** is replaced by oxygen or by sulfur respectively. The carbonyl carbon in **4a** was observed at δ 173.3, at a field higher by 24.4 than that of **2a**. Unlike **3**, however, $\delta_{C=O}$ of **4a** appeared at a frequency lower by -7 cm^{-1} than that of **1**. Nakashima and Maciel[14] observed the $\nu_{C=O}$ in 4-oxacyclooctanone shifted by 3.9 ppm compared to cyclooctanone and attributed the phenomenon to the electric-field effect. As the nitrogen analog showed an upfield shift of 13 ppm, they considered this upfield shift to be caused by the transannular effect arising from the through-space charge-neutralization proposed by Leonard *et al.*[15] The upfield shift for **4a** may also be due to the transannular effects. The **4b**, sulfur analog, gave a less anomalous chemical shift for the carbonyl carbon, perhaps because of the enlarged ring size and also the poor electron-donating ability of sulfur compared to oxygen. Because of the substantial geometrical difference, no further comparison between acyclic models and **4** was attempted.

The **4a**, oxygen analog, showed a high intensity plateau at a long wavelength, indicative of substantial conjugation. The sulfur analog **4b** also exhibited an UV absorption similar to that of **4a** but the long wave band fell off to a shorter wavelength. The conformational rigidity of an 8-membered ring in **4b** was confirmed by Johnson *et al.*[6] using a derivative of **4b**.

The pleiadene ketones, **5a**, **5b**, and **5c**, are less anomalous with respect to the carbon-13 NMR and IR data. That these have conformational mobility and undergo inversion at an appreciable rate is shown by the variable temperature NMR spectra.[16] Two carbonyl groups are not in a parallel geometry, but point outward in **5b**. Conjugation between carbonyl and aryl groups dominates these compounds, as is shown by the data in Tables 1 and 3.

References

1) T. Sato, T. Takemura, and M. Kainosho, *J. Chem. Soc., Chem. Commun.*, **1974**, 97; T. Takemura and T. Sato, *Can. J. Chem.*, **21**, 3412 (1976); T. Sato, H. Matsui, and R. Komaki, *J. Chem. Soc., Perkin Trans. 1*, **1976**, 2051.

2) D. M. Grant and B. V. Cheney, *J. Am. Chem. Soc.*, **89**, 5315 (1967).

3) J. Meinwald, S. Knapp, S. K. Obendorf, and R. E. Hughes, *J. Am. Chem. Soc.*, **98**, 6643 (1976); A. R. Miller and D. Y. Curtin, *ibid.*, **98**, 1860 (1976); R. L. Clough, P. Mison, and J. D. Roberts, *J. Org. Chem.*, **41**, 2252 (1976); R. L. Clough, W. J. Kung, R. E. Marsh, and J. D. Roberts, *ibid.*, **41**, 3603 (1976); for review, see V. Balasubramaniyan, *Chem. Rev.*, **66**, 567 (1966).

4) H. C. Rule, W. Pursell, and R. R. H. Brown, *J. Chem. Soc.*, **1934**, 168.

5) L. F. Fieser and M. Fieser, *Reagents Org. Synth.*, **1**, 23 (1967).

6) E. J. Moriconi, W. F. O'Conner, L. P. Kuhn, E. A. Kenealy, and F. T. Wallenberger, *J. Am. Chem. Soc.*, **81**, 6472 (1959).

7) R. Letzinger and J. A. Gilpin, *J. Org. Chem.*, **29**, 243 (1964).

8) P. T. Lansbury, J. F. Bieron, and M. Klein, *J. Am. Chem. Soc.*, **88**, 1477 (1966).

9) C. R. Johonson and D. C. Vegh, *Chem. Commun.*, **1969**, 557.

10) J. B. Stothers, "Carbon-13 NMR Spectroscopy," Academic Press, New York (1972), p. 279.

11) W. C. Agosta, *Tetrahedron Lett.*, **1966**, 3685; W. C. Agosta, *J. Am. Chem. Soc.*, **89**, 3926 (1967).

12) F. J. Weigert and J. D. Roberts, *J. Am. Chem. Soc.*, **92**, 1347 (1970).

13) J. O. Halford, *J. Chem. Phys.*, **24**, 830 (1956).

14) T. T. Nakashima and G. E. Maciel, *Org. Magn. Reson.*, **4**, 321 (1972).

15) N. J. Leonard, M. Oki, J. Brader, and H. Boaz, *J. Am. Chem. Soc.*, **77**, 6237 (1955).

16) M. E. Biffin, L. Crombie, T. M. Connor, and J. A. Elvidge, *J. Chem. Soc., B*, **1967**, 841; P. T. Lansbury and J. F. Bieron, *J. Am. Chem. Soc.*, **86**, 2524 (1964).

A New Method for the Synthesis of 2-Substituted 2-Buten-4-olide *via* α-Substituted β-Phenylthio-γ-butyrolactone

Mikio WATANABE, Kozo SHIRAI, and Takanobu KUMAMOTO*

Department of Chemistry, Faculty of Science, Tokai University, Kitakaname, Hiratsuka, Kanagawa 259-12

(Received January 5, 1979)

The addition reaction of lithium benzenethiolate to 2-buten-4-olide in the presence of aldehydes and ketones afforded α-substituted β-phenylthio-γ-butyrolactones (**4a—f**). The dehydrosulfenylation of **4a—d** proceeded smoothly to give 2-substituted 2-buten-4-olide by the reflux of α-substituted β-phenylsulfinyl-γ-butyrolactone, which was prepared by the oxidation of **4a—d**, in the presence of triethylamine.

A number of methods for the preparation of 2- or 3-buten-4-olides[1a-d] exist because of the interest in the synthesis of natural products. In a previous paper, a covenient method for the preparation of 3-substituted 2-buten-4-olide using α,α-bis(phenylthio)-γ-butyrolactone was reported which was readily prepared by the reaction of γ-butyrolactone with *N*-phenylthiophthalimide.[2]

In the present study, the introduction of substituent groups to the α-position of 2-buten-4-olide (**1**) was investigated by the reaction of the lithium salt of β-phenylthio-γ-butyrolactone (**2**) with aldehydes and ketones and subsequent dehydrosulfenylation.

Results and Discussion

*Synthesis of α-Substituted β-Phenylthio-γ-butyrolactones (**4a—f**).* The Michael addition reaction of lithium benzenethiolate to **1** afforded **2**. However, when lithium benzenethiolate was allowed to react with **1** in THF at −50 °C and the reaction mixture quenched with 10% hydrochloric acid, **2** was obtained in only 52% yield because of the addition reaction of the resulting lithium salt of **2** to unreacted **1** to yield the lactone derivative (**3**). Therefore, in order to avoid the undesired addition reaction, the reaction was conducted in the presence of phenol, which neutralized the resulting lithium salt of **2** to give **2** quantitatively.

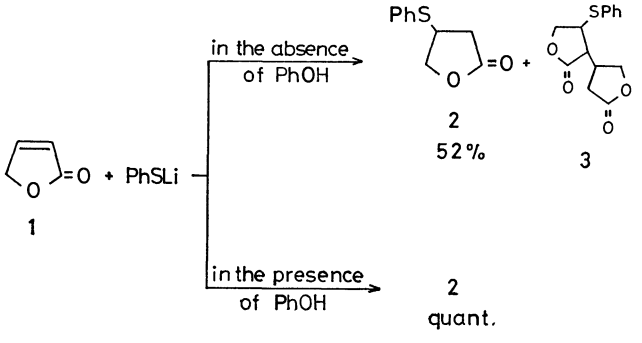

The alkylation of **2** with alkyl halides (methyl iodide, benzyl bromide, butyl bromide) in the presence of lithium diisopropylamide was examined, but this attempt was unsuccessful due to the formation of alkyl phenyl sulfide. This shows that the α-anion of **2** decomposes to the benzenethiolate anion and **1**.

The synthesis of α-substituted β-phenylthio-γ-butyrolactones was established by the reaction of the α-anion of **2** with aldehydes and ketones as electrophiles. The reaction of **2** with benzaldehyde in the presence of lithium diisopropylamide in THF at −50 °C for 2 h afforded α-(1-hydroxybenzyl)-β-phenylthio-γ-butyrolactone (**4a**) in 52% yield. Furthermore, it was found that the yield of **4a** was increased to 92% when a mixture of benzaldehyde and **1** was added to a solution of lithium benzenethiolate in THF at −50 °C. This reaction involves two different addition reactions, *i.e.*, the α-anion of **2** generated by the addition of lithium benzenethiolate to **1** underwent subsequent addition to benzaldehyde to give **4a**.

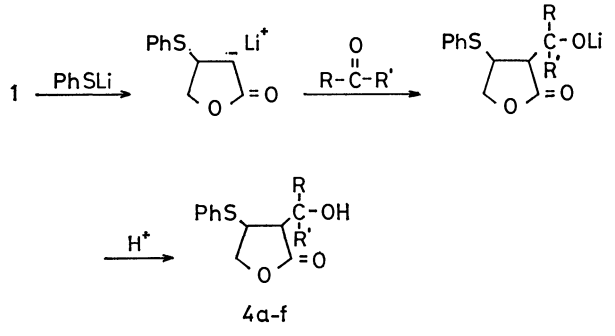

a: R=Ph, R'=H d: R=$CH_3(CH_2)_6$, R'=H
b: R=$CH_3(CH_2)_2$, R'=H e: R=Ph, R'=CH_3
c: R=$CH_3(CH_2)_4$ R'=H f: R=R'=C_2H_5

Scheme 1.

In a similar manner, the reactions with other aldehydes and ketones were investigated and these results are given in Table 1. As shown in Table 1, the reaction with acetophenone or 3-pentanone gave unsatisfactory results compared with the other aldehydes.

Dehydrosulfenylation. Dehydrosulfenylation[3] of **4a—d** to **8a—d** was achieved by elimination of the sulfinyl group of the α-substituted β-phenylsulfinyl-γ-butyrolactones (**7a—d**) prepared by the oxidation of **4a—d**. Oxidation of **4a** to α-(1-hydroxybenzyl)-β-phenylsulfinyl-γ-butyrolactone (**7a**) with *m*-chloroperbenzoic acid was conducted in dichloromethane at 0 °C for 1 h. Subsequent elimination of the sulfinyl group of **7a** without further purification in refluxing THF for 3 h in the presence of one equivalent of triethylamine afforded 2-(1-hydroxybenzyl)-2-buten-4-olide (**8a**) in 75% yield. Substitution of lead acetate as the eliminating agent in refluxing methanol gave **8a** in 60% yield. The results of dehydrosulfenylation of **4a—d** to **8a—d** are summarized in Table 2. For **8b**, **8c**, and **8d**, where the reaction time was longer than 1.5 h in the

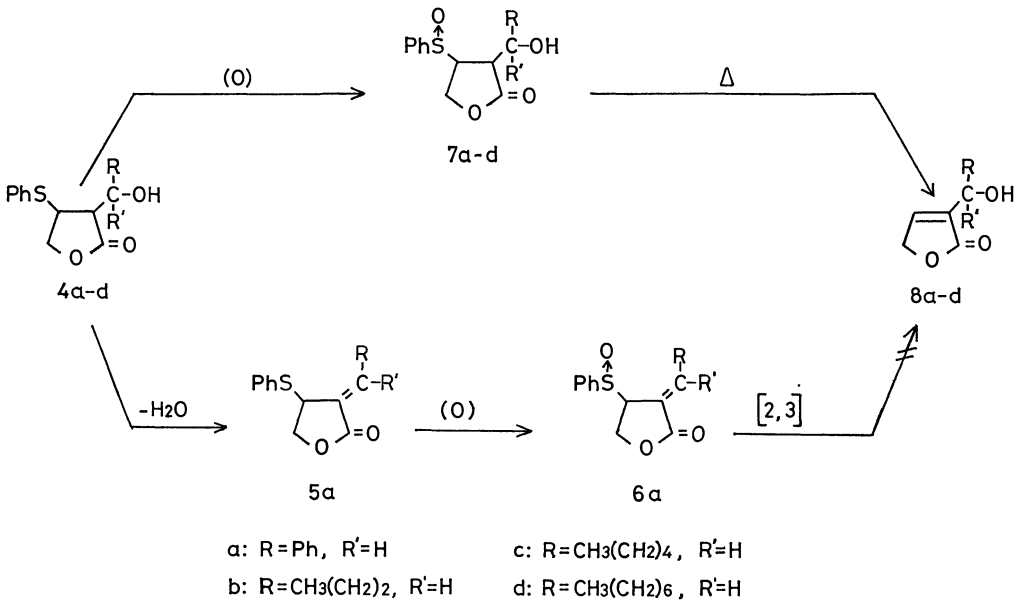

a: R=Ph, R'=H c: R=$CH_3(CH_2)_4$, R'=H
b: R=$CH_3(CH_2)_2$, R'=H d: R=$CH_3(CH_2)_6$, R'=H

Scheme 2.

Table 1. The reaction of **1** with aldehydes and ketones

Entry	Aldehyde or ketone	Temp °C	Time h	Product	Yield[a] %
1	Benzaldehyde[b]	−50	2	**4a**	92
2	Butanal[b]	−50	1.5	**4b**	61
3	Hexanal[b]	−50	1.5	**4c**	73
4	Octanal[b]	−50	1.5	**4d**	56
5	Acetophenone[c]	−50 −40	1 1	**4e**	17
6	3-Pentanone[c]	−40 −30	1 1	**4f**	7

a) The yields are based on **1**. b) For entry 1, 2, 3, and 4, 1.5 equiv of aldehyde was used. c) For entry 5 and 6, 2 equiv of ketone was used.

Table 2. Formation of **8a—d**

Entry	Oxidation[a] Sulfenyl lactone	Oxidation[a] Sulfinyl lactone	Thermolysis[b] Time h	Product	Yield[c] %
1	**4a**	**7a**	3	**8a**	65
2	**4b**	**7b**	1.5	**8b**	84
3	**4c**	**7c**	1.5	**8c**	58
4	**4d**	**7d**	1.5	**8d**	69

a) Oxidation was conducted in dichloromethane at 0 °C and the oxidation products were used for the subsequent thermolysis without further purification. b) Thermolysis was conducted in refluxing THF in the presence of triethelamine. c) Yields are calculated from sulfenyl lactones **4a—d**.

thermolysis step, dehydration products were obtained.

In addition, a second method of dehydrosulfenylation, which involves [2,3] sigmatropic rearrangement of allyl sulfoxide (**6a**),[4] was attempted. The conversion of **4a** to **6a** was conducted as follows. Compound **4a** was treated with one equivalent of sulfuric acid in refluxing benzene with azeotropic removal of water to give α-benzylidene-β-phenylthio-γ-butyrolactone (**5a**) (90% yield). Oxidation of **5a** with *m*-chloroperbenzoic acid in dichloromethane afforded **6a** quantitatively. Several reaction conditions for the [2,3] sigmatropic rearrangement were examined, however, but the desired **8a** could not be obtained, the starting material **6a** being recovered in almost cases. The use of trimethylphosphite as the thiophile gave the reduction product, **5a**.

Thus a convenient method for the preparation of **8a—d** was established. Several reports exist of the introduction of substituent groups on the α-position of α,β-unsaturated ketones and esters.[5] In the reaction studied here the α-anion of **2** serves as an α-anion of **1**. The advantages of this method are (1) the starting materials are inexpensive and readily available; (2) there is no need to isolate the intermediate **2** and (3) the generation of the α-anion of **2** is performed by a week base, lithium benzenethiolate.

Experimental

Preparation of β-Phenylthio-γ-butyrolactone (2). To a solution of benzenethiol (1.10 g, 0.01 mol) in THF (10 ml) was added dropwise a hexane solution of butyllithium (15%, 6.3 ml, 0.01 mol) at −50 °C under nitrogen and the mixture stirred for 15 min. A THF (8 ml) solution of 2-buten-4-olide (**1**)[6] (0.84 g, 0.01 mol) and phenol (0.94 g, 0.01 mol) was added to this mixture over 10 min, and the mixture stirred for 1 h at −50 °C. The reaction mixture was warmed to room temperature and washed with 10% sodium carbonate to remove the phenol and extracted with three 30 ml portions of ether and dried over sodium sulfate. After removal of the solvent, the residual oil was chromatographed on silica gel using benzene as an eluting agent to yield 1.90 g (98%) of **2**: mp 51—52 °C (recrystallized from 2-propanol). IR 1770 cm^{-1}. NMR ($CDCl_3$) δ 6.98—7.27 (5H, m), 3.70—4.50 (3H, m), 2.06—3.00 (2H, m). MS 194 (M^+). Found: C, 61.55; H, 5.15; S, 16.46%. Calcd for $C_{10}H_{10}O_2S$: C, 61.83; H, 5.19; S, 16.50%.

α-(1-Hydroxybenzyl)-β-phenylthio-γ-butyrolactone (4a).

To a THF (8 ml) solution of benzenethiol (550 mg, 5 mmol) was added butyllithium (in hexane, 15%, 3.2 ml, 5 mmol) at −50 °C and the mixture stirred for 15 min. To this solution was added dropwise over 15 min a mixture of **1** (420 mg, 5 mmol) and benzaldehyde (795 mg, 7.5 mmol) in THF (10 ml) and the reaction mixture stirred for 1.5 h at −50 °C. The reaction mixture was poured with stirring into cold saturated ammonium chloride solution and extracted with three 30 ml portions of ether and the extracts dried over anhydrous sodium sulfate. After removal of the solvent, the residual oil was chromatographed on silica gel using benzene as an eluting agent to give 1344 mg (92%) of **4a**. Further purification of **4a** was conducted by recrystallization from 2-propanol: mp 127—127.5 °C. IR 3420, 1758 cm^{-1}. NMR (DMSO-d_6) δ 6.83—7.20 (10H, m), 6.02 (1H, d), 4.00—4.85 (3H, m), 3.30 (1H, s), 2.45 (1H, br). MS 300 (M^+). Found: C, 67.84; H, 5.37; S, 10.65%. Calcd for $C_{17}H_{16}O_3S$: C, 67.99; H, 5.37; S, 10.67%.

In a similar manner, α-(1-hydroxybutyl)-β-phenylthio-γ-butyrolactone (**4b**), α-(1-hydroxyhexyl)-β-phenylthio-γ-butyrolactone (**4c**), α-(1-hydroxyoctyl)-β-phenylthio-γ-butyrolactone (**4d**), α-(1-hydroxy-1-phenylethyl)-β-phenylthio-γ-butyrolactone (**4e**), and α-(1-ethyl-1-hydroxypropyl)-β-phenylthio-γ-butyrolactone (**4f**) were obtained in 61%, 73%, 56%, 17%, and 7% yields respectively. The reaction temperature and time for each aldehyde or ketone are as follows: −50 °C for 1.5 h for butanal, hexanal, and octanal; −50 °C for 1 h, −40 °C for 1 h for acetophenone; −40 °C for 1 h, −30 °C for 1 h for 3-pentanone. **4b**: IR 3450, 1758 cm^{-1}. NMR ($CDCl_3$) δ 7.20—7.60 (5H, m), 3.37—4.70 (4H, m) 2.42—2.85 (2H, m), 1.30—1.80 (4H, m), 0.93 (3H, t). MS 266 (M^+). **4c**: IR 3450, 1760 cm^{-1}. NMR ($CDCl_3$) δ 7.10—7.38 (5H, m), 3.70—4.68 (4H, m), 3.15 (1H, s) 2.52 (1H, t), 1.30 (8H, br), 0.88 (3H, t). MS 294 (M^+). **4d**: IR 3450, 1770 cm^{-1}. NMR ($CDCl_3$) δ 7.10—7.38 (5H, m), 3.72—4.68 (4H, m), 3.41 (1H, s), 2.52 (1H, t), 1.25 (12H, br), 0.88 (3H, t). MS 322 (M^+). **4e**: IR 3490, 1770 cm^{-1}. NMR (DMSO-d_6) δ 6.90—7.20 (10H, m), 4.50 (1H, s), 2.93—3.75 (3H, m), 2.38 (1H, d), 1.63 (3H, s). MS 314 (M^+). **4f**: IR 3500, 1775 cm^{-1}. NMR ($CDCl_3$) δ 7.35—7.65 (5H, m), 3.92—4.40 (2H, m), 2.20—3.35 (3H, m), 1.22—1.82 (4H, m), 0.83 (6H, dt). MS 280 (M^+).

*Preparation of α-Benzyliden-β-phenylthio-γ-butyrolactone (**5a**).* A solution of **4a** (3.00 g, 0.01 mol) in benzene (50 ml) in the presence of one equivalent of *p*-toluenesulfonic acid or concd sulfuric acid was heated under reflux for 8 h using a water separator. The reaction mixture was cooled to room temperature, washed with 10% sodium carbonate solution, extracted with THF–$CHCl_3$ (1:1), and dried. Removal of the solvent under reduced pressure and recrystallization from 2-propanol gave 2.54 g (90%) of **5a**: mp 218—219 °C. IR 1760 cm^{-1}. NMR (DMSO-d_6) δ 6.20—7.20 (11H, m), 3.50—4.65 (3H, m). MS 282 (M^+). Found: C, 72.27; H, 5.00; S, 11.35%. Calcd for $C_{17}H_{14}O_2S$: C, 72.53; H, 4.94; S, 11.40%.

*Preparation of α-Benzyliden-β-phenylsulfinyl-γ-butyrolactone (**6a**).* To a solution of **5a** (564 mg, 2 mmol) in dichloromethane (20 ml) was added dropwise a dichloromethane (15 ml) solution of *m*-chloroperbenzoic acid (414 mg, 2.4 mmol) at 0 °C. The reaction mixture was stirred for 1 h. The reaction mixture was washed with 10% sodium hydrogencarbonate, extracted with dichloromethane and dried over anhydrous sodium sulfate. Evaporation of the solvent gave an oil of **6a** and treatment with ether provided crystals of **6a** (578 mg, 97%): mp 169 °C (dec). IR 1780 cm^{-1}. NMR (DMSO-d_6) δ 6.80—7.60 (11H, m), 3.60—4.65 (3H, m). MS 298 (M^+). Found: C, 68.87; H, 4.92; S, 10.77%. Calcd for $C_{17}H_{14}O_3S$: C, 68.44; H, 4.73; S, 10.75%.

*General Procedure for Oxidation of **4a—d**.* To a solution of the β-phenylthio lactone derivative in dichloromethane (15 ml, for 1 g of the lactone) was added dropwise a dichloromethane solution of *m*-chloroperbenzoic acid (1.2 equiv) at 0 °C. The reaction mixture was stirred for 1 h at 0 °C, washed with 10% aqueous sodium hydrogencarbonate and dried. Evaporation of the solvent under reduced pressure gave the β-phenylsulfinyl derivative in quantitative yield. The products thus obtained, **7a—d** were used for subsequent thermolysis without further purification.

*General Procedure for Thermolysis of β-Phenylsulfinyl-γ-butyrolactones (**7a—d**).* A solution of the β-phenylsulfinyl-γ-butyrolactone derivative in THF (20 ml for 1 g of the lactone) in the presence of one equivalent of triethylamine was heated under reflux for 1.5—3 h. After removal of the solvent under reduced pressure the residue was chromatographed on silica gel using benzene–ether (3:1) as an eluent to give the 2-substituted 2-buten-4-olide.

Analytical and spectral results are as follows:

*2-(1-Hydroxybenzyl)-2-buten-4-olide (**8a**).* 75%. IR 3425, 1740 cm^{-1}. NMR ($CDCl_3$) δ 6.95—7.25 (6H, m), 5.40 (1H, s) 4.65 (2H, t), 3.37 (1H, br). MS 190 (M^+). Found: C, 69.97; H, 5.38%. Calcd for $C_{11}H_{10}O_3$: C, 69.46; H, 5.30%.

*2-(1-Hydroxybutyl)-2-buten-4-olide (**8b**).* 84%. IR 3425, 1730 cm^{-1}. NMR ($CDCl_3$) δ 7.18—7.30 (1H, m), 4.76 (2H, t), 4.42 (1H, br), 4.10 (1H, s), 1.08—1.98 (4H, m), 0.90 (3H, t). MS 138 (M−18). The spectral data of the dehydration product, 2-(1-butenyl)-2-buten-4-olide, of **8b** was shown since the elemental analysis of **8b** gave unsatisfactory results. IR 1745 cm^{-1}. NMR (CCl_4) δ 5.92—7.22 (3H, m), 4.80 (2H, s) 2.15 (2H, q), 1.08 (3H, t). MS 138 (M^+).

*2-(1-Hydroxyhexyl)-2-buten-4-olide (**8c**).* 58%. IR 3425, 1735 cm^{-1}. NMR ($CDCl_3$) δ 7.31—7.35 (1H, m), 4.80 (2H, t), 4.45 (1H, br), 3.55 (1H, br), 1.33 (8H, brs), 0.90 (3H, t). MS 166 (M−18). Found: C, 64.90; H, 9.04%. Calcd for $C_{10}H_{16}O_3$: C, 65.19; H, 8.75%.

*2-(1-Hydroxyoctyl)-2-buten-4-olide (**8d**).* 69%. IR 3425, 1750 cm^{-1}. NMR ($CDCl_3$) δ 7.10—7.25 (1H, m), 4.80 (2H, t), 4.38 (1H, br), 3.10 (1H, br), 1.30 (12H, brs), 0.90 (3H, t). MS 194 (M−18). Due to the difficulty in the further purification of **8d**, elemental analysis was achieved by dehydration product, 2-(1-octenyl)-2-buten-4-olide, of **8d** as follow. Found: C, 74.04; H, 9.31%. Calcd for $C_{12}H_{18}O_2$: C, 74.19; H, 9.34% [IR 1750 cm^{-1}. NMR (CCl_4) δ 5.90—7.23 (3H, m), 4.76 (2H, s), 1.35 (10H, brs), 0.90 (3H, t). MS 194 (M^+).]

References

1) (a) Y. S. Rao, *Chem. Rev.*, **76**, 625 (1975); (b) K. Iwai, H. Kosugi, H. Uda, and M. Kawai, *Bull. Chem. Soc. Jpn.*, **50**, 242 (1977); (c) B. M. Trost and T. N. Salzmann, *J. Am. Chem. Soc.*, **95**, 6840 (1973); (d) S. Inayama and T. Kawamata, *Chem. Pherm. Bull.*, **21**, 461 (1973).

2) M. Watanabe, K. Shirai, and T. Kumamoto, *Chem. Lett.*, **1975**, 855.

3) Ref. 1 (c). Ref. 1 (b). P. Brownbridge and S. Warren, *J. Chem. Soc., Chem. Commun.*, **1977**, 465.

4) D. A. Evance, G. C. Andrews, and C. L. Sims, *J. Am. Chem. Soc.*, **93**, 4956 (1971).

5) D. J. Ager and I. Freming, *J. Chem. Soc., Chem. Commun.*, **1978**, 177.

6) C. C. Price and J. M. Judge, *Org. Synth.*, Coll. Vol. V, 255 (1973).

The Oxidation of Toluene by Cobalt-Copper-Bromide System. A Side-chain Acetoxylation

Toshihiko OKADA* and Yoshio KAMIYA

Department of Reaction Chemistry, Faculty of Engineering, The University of Tokyo, Hongo, Tokyo 113

(Received January 27, 1979)

The liquid-phase oxidation of toluene catalyzed by the cobalt(II) ion and the bromide ion in the presence of the copper(II) ion has been studied. Benzyl acetate was obtained in a good yield (50—70%) with mixed catalysts of metal acetates and sodium bromide in acetic acid at 100—150 °C, accompanied by small amounts of benzaldehyde and benzoic acid. The product distribution was greatly dependent on the NaBr concentration, which can be explained in terms of the high oxidizing ability of the copper(II) ion coordinated by the bromide ion. A synergistic effect was found on the yield of benzyl acetate upon the addition of copper(II) acetate with a high NaBr concentration, the maximum yield being obtained at the Co:Cu:NaBr ratio of 1:1:5—10. A change in the oxygen partial pressure also varied the product distribution, suggesting that the competitive reaction of the copper(II) ion with the oxygen molecule for the benzyl radical was simultaneously taking place at a diffusion-controlled rate. Benzyl acetate was considered to result from the oxidation of the benzyl radical by copper(II) bromide and the subsequent solvolysis by acetic acid. The addition of acetic anhydride had a negative effect on the formation of benzyl acetate.

The transition metal ion-catalyzed autoxidation of alkylbenzenes, especially with the cobalt(II) ion and the bromide ion, in acetic acid has been widely studied.[1-6] The autoxidation of *p*-xylene catalyzed by the cobalt(II) ion and the bromide ion to terephthalic acid is important from the viewpoint of the petrochemical industry. The oxidation products, however, are mainly acids or carbonyl compounds, although in rare cases in the presence of acetic anhydride,[2,3] they also include acetoxylated compounds.

Hay[2] has reported that methylbenzenes were converted to the acetoxylated compounds in the oxidation catalyzed by the cobalt(II) ion and the bromide ion in the presence of acetic anhydride, *e.g.*, the oxidation of toluene gave benzyl acetate in a 44% yield, but not in the absence of acetic anhydride. On the other hand, copper(II) acetate is well known to act as an inhibitor[9] in the cobalt(III) ion-catalyzed autoxidation and to behave as an oxidizing reagent for alkyl radicals.[8]

We previously suggested that the deactivation of cobalt(III) acetate by copper(II) acetate in the oxidation of toluene is due to the formation of a binuclear complex.[9] Therefore, it seems difficult to obtain benzyl acetate by the oxidation of toluene, which has a relatively high ionization potential, by copper(II) acetate. Recently, Imamura reported the oxidation of 1,2,3,4-tetrahydronaphthalene catalyzed by copper(II) acetate with a high LiCl concentration; in this case, the copper(II) ion, bearing the Cl ion, was considered to be a monomer species that is capable of oxidizing 1,2,3,4-tetrahydro-1-naphthyl hydroperoxide.[10]

We attempted to obtain benzyl acetate by means of the oxidation of toluene in the presence of cobalt–copper catalysts and found that a side-chain acetoxylation of toluene occurred and that the yield was dependent on the reaction conditions.

Experimental

Materials. The acetic acid, copper(II) acetate, cobalt(II) acetate, and other metal acetates were used without further purification. The sodium bromide were dried under a vacuum at 150 °C for 5 h. The toluene was purified by the usual method: distillation after washing with concentrated sulfuric acid, an aq alkaline solution, and water and drying over ($CaCl_2$ and sodium metal).

Procedure. The oxidation was carried out with two methods.

Method A: A 200 ml three-necked round-bottomed flask equipped with a gas inlet, a thermometer, and a condenser was used. Oxygen was blown onto the surface of the reaction mixture.

Method B: A 200 ml autoclave made of Ti was used. The reaction was carried out with a batch method; the total pressure of the mixed gas was 40 kg/cm^2.

Analysis. The reaction mixture, with an internal standard (1-chloronaphthalene), was poured into ice water and then extracted with ether. The extract was submitted to GC analysis after having been washed with water and aqueous Na_2CO_3 and then dried (Na_2SO_4). The benzoic acid was analyzed by GC directly or after esterification with a MeOH–BF_3 reagent. The products were identified by means of IR, NMR, and GC-MS. PhCHO: 9.9 ppm (1H), 7.7 ppm (5H), 2750 cm^{-1}, 1690 cm^{-1}, M$^+$ 106 (*MW* 106). $PhCH_2OCOCH_3$: 7.3 ppm (5H), 5.1 ppm (2H), 2.1 ppm (3H), 1730—1760 cm^{-1}, 1220—1260 cm^{-1}, M$^+$ 150 (*MW* 150). $PhCH_2Br$: M$^+$ 171 (*MW* 171). A gas chromatograph (Shimadzu GC-3BT) was mainly used for the analysis of the products.

Column: PEG 20 M 10% on Celite 545, 1 m, 2 m, 145 °C, 180 °C, He gas, 40 ml/min.

Results and Discussion

Effect of Bromide-ion Concentration on the Co–Cu Catalysis. The effect of the Br-ion concentration on the product distribution in the presence of cobalt(II) acetate and copper(II) acetate was investigated (Fig. 1). The ratio of the bromide ion to the cobalt(II) ion drastically affected the product distribution. At ratios lower than four, the major product was benzoic acid, while benzyl acetate was formed in only a minor amount. When the ratios were higher than five, the major products were benzyl acetate and benzyl bromide.

On the oxidation of alkyl radicals by copper(II) salts, Kochi[8] clarified that there is an equilibrium between the monomeric and dimeric copper(II) ion,

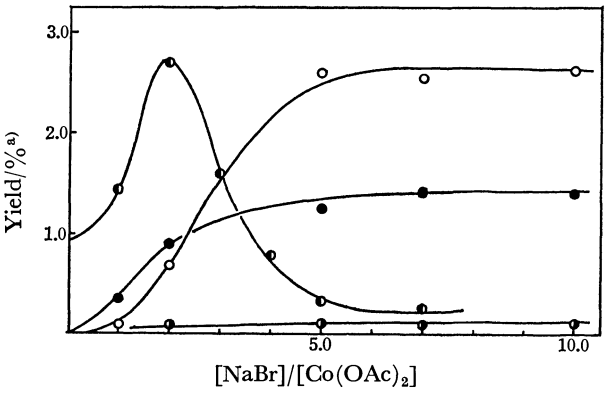

Fig. 1. Oxidation products of toluene catalyzed by Co-Cu-Br as a function of the ratio of [NaBr]/[$Co(OAc)_2$].
Reaction conditions: 100 °C, 20 h, [$Co(OAc)_2$]=[$Cu(OAc)_2$]=5.71×10^{-2} M, [toluene]=1.39 M, method A. a) Based on initial toluene.
○: $PhCH_2OAc$, ●: $PhCH_2Br$, ◑: PhCHO, ◐: PhCOOH.

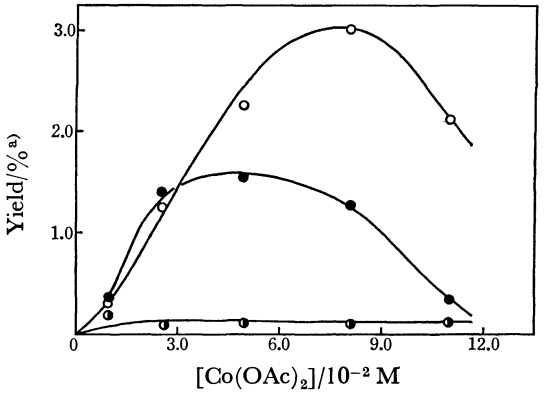

Fig. 2. Oxidation products of toluene catalyzed by Co-Cu-Br as a function of catalyst concentration.
Reaction conditions: 100 °C, 20 h, [$Co(OAc)_2$]:[$Cu(OAc)_2$]:[NaBr]=1:1:7, [toluene]=1.39 M, method A. a) Based on initial toluene.
○: $PhCH_2OAc$, ●: $PhCH_2Br$, ◑: PhCHO.

and that the active species in the oxidation is the monomeric one. Upon the addition of the acetate ion[8] or the chloride ion,[10-12] this dimer-monomer equilibrium becomes favorable to the monomer side. In our experiments, this equilibrium may be present, and the monomer with the bromide ion is predominant upon the addition of the bromide ion to the cobalt–copper system at ratios higher than five; thus, the benzyl radical was oxidized by the monomeric copper(II) ion to benzyl acetate and benzyl bromide. On the other hand, Gaevskii[13] recently discussed the active species in the oxidation of ethyl benzene catalyzed by the cobalt(II) ion and the bromide ion; he concluded that cobalt(III) monobromide is an active species, for it has a high stability constant. Accordingly, at a low ratio of the bromide ion to the cobalt(II) ion, the main reaction may be an abstraction of the α-hydrogen of toluene by cobalt(III) monobromide. Figure 1 indicates that the ratio of the amount of benzyl acetate to that of benzyl bromide retains constant, even when the bromide-ion concentration is increased by a factor of two. This fact suggests that the oxidation of the benzyl radical proceeds not through the carbonium ion but through a so-called ligand-transfer reaction.

Table 1. Effect of sodium salts on the reaction products in the oxidation of toluene by the Co-Cu system

Sodium salts	Products (mol %)a)
None	—b)
NaOAc	
NaCl	—
NaBr	$PhCH_2OAc$ (64.3)
	$PhCH_2Br$ (11.4)
	PhCHO (1.2)
	PhCOOH (23.1)
NaI	PhCOOH (100)

Reaction conditions: Method A, 100 °C, 24 h, [$Co(OAc)_2$]=[$Cu(OAc)_2$]=5.71×10^{-2} M, [NaX]=0.4 M, [toluene]=1.39 M. a) Based on the total amounts of all oxidation products. b) No reaction occurred.

Effect of Catalyst Concentration. Figure 2 shows the effect on the oxidation of the catalyst concentration at the ratio of Co : Cu : Br^- = 1 : 1 : 7. The maximum yield of benzyl acetate was obtained at the 0.08 M cobalt concentration.

According to Kochi,[8] this ligand-transfer reaction determines the rate of diffusion control. It seems that a higher catalyst concentration is required since the copper(II) ion and oxygen will be competing for the benzyl radical. However, when the concentration of the catalyst was higher than 0.08 M, low yields of benzyl bromide and benzyl acetate were observed. This phenomenon can be explained in terms of an aggregation of metal acetates[14] or a complex formation between metal acetates and hydroperoxide.[15]

As the concentration of a catalyst becomes higher, the ratio of benzyl acetate to benzyl bromide increases, suggesting that the reaction of benzyl bromide with cobalt(II) acetate is playing a part, an idea supported by Hay.[2]

Effect of Sodium Salts. The effect of sodium salts on the product distribution was also investigated. As may be seen from Table 1, it is obvious that the bromide ion is the most effective for the synthesis of benzyl acetate. According to the studies by Imamura[10-12] of the liquid-phase oxidation catalyzed by the Cu–Cl system, the main reaction is a decomposition of hydroperoxide by Cu–Cl compounds and no significant oxidation by the Co–Cu–Cl system seems to occur, since hydrogen abstraction is important in this reaction. The addition of sodium acetate did not change the oxidizing activity of the Co–Cu system and resulted in the recovery of toluene. These results may be attributed to their redox potentials being lower than that of the Co–Cu–Br systems.

When sodium iodide was added to the Co–Cu system, a small amount of benzoic acid was obtained, perhaps for the same reason as in the case of the chloride ion.

Recycling of the Bromide Ion in the Course of the Oxidation. Figure 3 shows the time dependence on the yield of products in the oxidation of toluene in acetic acid at 100 °C. In the early stage of the oxidation, benzyl bromide was primarily formed and benzyl acetate increased gradually. After 20 h, benzyl acetate turned into the major product. Many workers[1-6] have suggested that the reaction of benzyl bromide with acetic acid proceeds easily at 100 °C. In our study, however, this reaction was very slow, presumably because of the high bromide-ion concentration. The formation of benzyl bromide in the early stage suggests that the ligand transfer by the copper(II) ion is mainly bromide-ion transfer; consequently, the structure of the copper(II) ion might be $CuBr_n^{m-}$. Here, $m=0$—2 and $n=2$—4, according to Imamura.[10-12] The Br ion concentration decreases in the course of the oxidation; hence, the activity of the copper(II) ion is gradually lost. Under these conditions (method A), benzoic acid and benzaldehyde were minor products, since the oxygen concentration in the reaction media was very low. The dependence of the reaction temperature on the product distribution was also investigated (Table 2).

It was found that the selectivity changes drastically with the reaction temperature and that benzyl bromide disappears at temperatures above 140 °C. As reported by Hay,[2] the solvolysis of benzyl bromide in the oxidation catalyzed by the cobalt(II) ion and the bromide ion in acetic acid is quite difficult at temperatures lower than 100 °C. In our study, benzoic acid was formed at low reaction temperatures; that is, the oxidizing ability of the cobalt(III) ion was maintained because of the high additional bromide-ion concentration. The amount of products which can be regarded as resulting from the oxidation of the benzyl radical by the copper(II) ion was relatively small because of the deterioration of the copper(II) ion. At low temperatures, the monomeric copper(II) ion gradually turns to a dimer, becoming inactive for the oxidation of the benzyl radical in the course of the oxidation, because the bromide ion in the reaction media decreases because of the slow rate in the solvolysis of benzyl bromide. At 150 °C for 1—5 h, the yield of benzyl acetate was at its maximum. The solvolysis of benzyl bromide may proceed easily at these temperatures.

Therefore, the activity of the catalyst in the oxidation can be maintained. On the other hand, at temperatures higher than 150 °C, the oxidation of benzyl acetate and benzyl bromide can not be ignored, for it results in a lower yield of benzyl acetate.

According to the study by Howard and his coworkers[16] of the hydrogen abstraction at the α-position of toluene, benzyl bromide, and benzyl acetate by the *t*-butylperoxyl radical at 30 °C, though there is a small difference in the reactivity between the *t*-butylperoxyl radical and cobalt(III) bromide acetate, their rates are 0.012, 0.0075, and 0.006 $M^{-1}\,s^{-1}$ respectively.

Benzyl acetate is oxidized to benzaldehyde *via* benzylidene diacetate. Thus, it is obvious that the optimum reaction temperature is about 150 °C for the synthesis of benzyl acetate.

Effect of the Oxygen Partial Pressure. The dependence of the oxygen partial pressure on the product yields is shown in Table 3. As has been mentioned above, the ligand-transfer is a competitive reaction with the oxygen molecule for the benzyl radical. Therefore, when a low oxygen partial pressure was used, the yield of benzyl acetate was high. However, it should be mentioned that the oxidant in this reaction

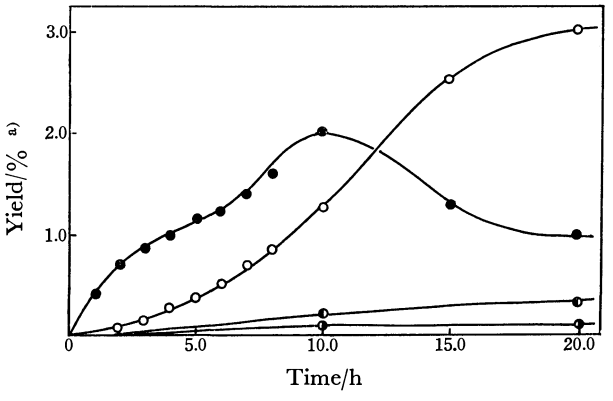

Fig. 3. Oxidation products of toluene catalyzed by Co-Cu-Br as a function of reaction time.
Reaction conditions: 100 °C, $[Co(OAc)_2]=[Cu(OAc)_2]=5.71\times10^{-2}$ M, [NaBr]=0.4 M, [toluene]=1.39 M, method A. a) Based on initial toluene.
○: $PhCH_2OAc$, ●: $PhCH_2Br$, ◑: PhCHO, ◐: PhCOOH.

Table 2. Effect of the reaction temperature on the reaction products in the oxidation of toluene by the Co-Cu-Br system

Temperature °C	Toluene conversion %	Products (mol %)[a]			
		$PhCH_2OAc$	$PhCH_2Br$	PhCHO	PhCOOH
80	12	2	9	34	54
100	54	17	12	49	20
120	66	42	2	29	26
140	64	44	—[b]	23	43
150	77	49	—	15	33
170	61	48	—	21	30

Reaction conditions: method B, 5 h, total pressure, 40 kg/cm², $(O_2/N_2=1/3)$, $[Co(OAc)_2]=[Cu(OAc)_2]=5.71\times10^{-2}$ M, [NaBr]=0.4 M, [toluene]=1.39 M. a) Based on toluene consumed. b) Not detected.

Table 3. Effect of the partial pressure of oxygen on the reaction products in the oxidation of toluene by the Co-Cu-Br system

Partial pressure of oxygen	Toluene conversion	Products (mol %)[a]		
kg/cm²	%	$PhCH_2OAc$	PhCHO	PhCOOH
20	83	29	13	56
10	77	49	15	33
5	34	60	27	12
0	0	Trace	0	0

Reaction conditions: method B, 150 °C, 5 h, $[Co(OAc)_2]=[Cu(OAc)_2]=5.71\times10^{-2}$ M, [NaBr]=0.4 M, [toluene] =1.39 M. a) Based on toluene consumed.

Table 4. Effect of the $[Cu(OAc)_2]/([Co(OAc)_2]+[Cu(OAc)_2])$ ratio on the reaction products in the oxidation of toluene by the Co-Cu-Br system

[Cu]/([Co]+[Cu])	Toluene conversion	Products (mol %)		
mol %	%	$PhCH_2OAc$	PhCHO	PhCOOH
0.00	98	6	2	88
0.25	91	25	8	66
0.50	77	49	15	33
0.75	76	45	15	37
1.00	65	38	13	48

Reaction conditions: method B, 150 °C, 5 h, $[Co(OAc)_2]+[Cu(OAc)_2]=1.14\times10^{-1}$ M, [NaBr]=0.4 M, [toluene]= 1.39 M; total pressure, 40 kg/cm² ($O_2/N_2=1/3$). a) Based on toluene consumed.

is ultimately oxygen; hence, benzyl acetate was not obtained under a nitrogen atmosphere, that is, the active species could not be generated from the reaction between cobalt(II) acetate bromide and the benzylperoxyl radical.

Effect of the Ratio of [Cu]/([Co]+[Cu]). The effect of the copper(II) acetate concentration in the constant NaBr and metal acetate concentrations on the oxidation was also studied (Table 4).

A remarkable synergistic effect was observed at the [Cu]/([Co]+[Cu]) ratio of 0.5; that is, Co : Cu=1 : 1. With an increase in the concentration of copper(II) acetate, the products changed from benzoic acid to benzyl acetate and the conversion of toluene went down little by little. In the region of [Cu]/([Co]+[Cu])=0—0.5, the benzyl radical may react with the oxygen molecule; consequently, the main product was benzoic acid.

On the other hand, the product distribution was similarly changed in the ratio of the 0.5—1.0 region. In the copper(II)-ion and bromide-ion system, although the oxidizing ability was small, as has been shown by Shigeyasu,[17] benzyl acetate was also obtained as well as a large amount of benzoic acid, and precipitates of presumably copper(II) oxide or hydroxide were formed in a manner similar to the oxidation of naphthalene catalyzed by the palladium–copper–chloride system in acetic acid.[18] The reason for the synergistic effect is not clear, but it might be due to the formation of a binuclear complex between cobalt(III) acetate and copper(II) acetate. In a study of the additive effect of metal acetates to cobalt(III) acetate, Kawai[9] suggested that the formation of the binuclear complex was caused by the lowering of the activity and the redox potential of cobalt(III) acetate.

We found that toluene can not be oxidized by cobalt–copper system without the bromide ion, although it was easily oxidized to benzyl acetate by the addition of NaBr.

Additive Effect on the Product Distribution. The additive effects of other transition-metal acetates, acetic anhydride, ethyl methyl ketone, and paraacetaldehyde, were also investigated.

No remarkable effects on the product selectivity were found upon the addition of $Ni(OAc)_2$, $Ce(OAc)_3$, $Cr(OAc)_3$, and $Mn(OAc)_2$.

The synergistic effect of Mn^{2+} in the oxidation of alkylbenzenes catalyzed by the cobalt ion and the bromide ion has previously been reported.[5]

In our study, however, no additive effect of Mn^{2+} on this system was observed, suggesting that the reaction between the peroxyl radical and the metal ion is not very important. Replacing 0.01 part of acetic acid partly with acetic anhydride reduced the yield of benzyl acetate at 150 °C for 5 h. The same effect was observed with ethyl methyl ketone and paraacetaldehyde.

A reaction between these additives and catalyst seems to occur.

Mechanistic Consideration. A plausible mechanism is shown in the Scheme except for the formation of a binuclear complex between cobalt(III) acetate and copper(II) acetate. The present reaction is considered to be substantially a ligand transfer of the benzyl radical with the copper(II) ion based on the studies by Kochi[8] in Eqs. 6 and 7. Very recently, the oxidation of methylbenzenes with cerium(IV) pyridinium salt was reported by Rol;[19] a ligand-transfer reaction similar to that in the case of the copper(II) ion occurs and arylalkyl chloride and arylalkyl methoxide were

obtained. The active species in a hydrogen abstraction has been proposed by many workers.[2-6]

One of the present authors[20] also clarified that the active species, cobalt(III) acetate bromide, produced by the reaction of cobalt(II) acetate bromide with the peroxyl radical has a reactivity similar to that of the Br radical toward various alkylbenzenes (Eqs. 1 and 3).

$$PhCH_3 + Co(III)Br \longrightarrow PhCH_2\cdot + Co(II)BrH \quad (1)$$

$$PhCH_2\cdot + O_2 \rightleftharpoons PhCH_2OO\cdot \quad (2)$$

$$PhCH_2OO\cdot + Co(II)BrH \longrightarrow PhCHO + Co(III)Br + H_2O \quad (3)$$

$$PhCHO + O_2 \longrightarrow PhCOOH + H_2O \quad (4)$$

$$[Cu(OAc)_2]_2 + y\mathrm{NaBr} \rightleftharpoons 2Cu(OAc)_xBr_y + y\mathrm{NaOAc} \quad (5)$$

$$PhCH_2\cdot + Cu(OAc)_xBr_y \longrightarrow PhCH_2OAc + Cu(I) \quad (6)$$

$$PhCH_2\cdot + Cu(OAc)_xBr_y \longrightarrow PhCH_2Br + Cu(I) \quad (7)$$

$$PhCH_2Br + AcO^- \longrightarrow PhCH_2OAc + Br^- \quad (8)$$

$$Cu(I) + O_2 + HX \longrightarrow Cu(II)(OAc)_xBr_y \quad (9)$$

(HX=HOAc, HBr. x=0,1,2,3,4. y=0,1,2,3,4.)

Scheme 1. Oxidation mechanism of toluene catalyzed by Co-Cu-Br.

The coupling reaction between the benzyl radical and the oxygen molecule proceeds at the rate of diffusion control, although it is considered that this reaction may proceed to the reverse side in Eq. 2 and the concentration of the benzyl radical in the reaction media will be high at higher temperatures.[21]

References

1) D. A. S. Ravens, *Trans. Faraday Soc.*, **55**, 1768 (1959).
2) A. S. Hay and H. S. Blanchard, *Can. J. Chem.*, **43**, 1305 (1965).
3) a) Japan Patent Kokai 51-45572; b) T. Nakayama, E. Nakamura, K. Oguchi, and Y. Kamiya, Presented at the 9th Symposium on Oxidation, Tokyo, Japan, November 25—26, 1975.
4) Y. Kamiya, *Tetrahedron*, **22**, 2029 (1966).
5) Y. Kamiya, "Oxidation of Organic Compounds," Am. Chem. Soc. (1968), Vol. 2, p. 193.
6) C. E. H. Bawn and T. K. Wright, *Discuss. Faraday Soc.*, **46**, 164 (1969).
7) R. Hasegawa and Y. Kamiya, *Bull. Chem. Soc. Jpn.*, **51**, 1490 (1978).
8) a) C. L. Jenkins and J. K. Kochi, *J. Am. Chem. Soc.*, **94**, 856 (1972); b) J. K. Kochi and R. V. Subramanian, *J. Am. Chem. Soc.*, **87**, 4855 (1965).
9) R. Kawai and Y. Kamiya, *Nippon Kagaku Kaishi*, **1974**, 933.
10) S. Imamura, M. Teramoto, T. Sumi, H. Aomi, H. Teranishi, and Y. Takegami, *Bull. Chem. Soc. Jpn.*, **49**, 1650 (1976).
11) S. Imamura, T. Banba, and Y. Takegami, *Bull. Chem. Soc. Jpn.*, **46**, 856 (1973).
12) S. Imamura, T. Otani, and H. Teranishi, *Bull. Chem. Soc. Jpn.*, **48**, 1245 (1975).
13) V. F. Gaevskii, N. P. Evmenenko, and L. I. Budarin, *Kinet. Katal.*, **17**, 307 (1976).
14) K. Kagami, *Bull. Chem. Soc. Jpn.*, **41**, 1552 (1968).
15) J. F. Black, *J. Am. Chem. Soc.*, **100**, 5271 (1978).
16) J. A. Howard, *Ad. Free Radical. Chem.*, **4**, 55 (1972).
17) M. Shigeyasu and M. Inoue, *Kogyo Kagaku Zasshi*, **73**, 1155 (1970).
18) G. G. Arzovmanidis and F. C. Rauch, *J. Org. Chem.*, **38**, 4443 (1973).
19) S. Maini and C. Rol, *J. Org. Chem.*, **43**, 3236 (1978).
20) Y. Kamiya, *J. Catal.*, **33**, 480 (1974).
21) S. W. Benson, *J. Am. Chem. Soc.*, **87**, 972 (1965).

Studies of Unusual Amino Acids and Their Peptides. XI. The Resolution of β-(2-Furyl)-β-alanine and β-(2-Thienyl)-β-alanine and Their Absolute Configurations

Shigeru KUWATA, Takashi YAMADA, Tatsuya SHINOGI,** Naoki YAMAGAMI,*** Fumio KITABASHI,**** Toshifumi MIYAZAWA, and Hiroshi WATANABE*

Laboratory of Chemistry, Faculty of Science, Kōnan University, Okamoto, Higashinada, Kobe 658

(Received February 5, 1979)

(+)-β-(2-Furyl)-β-alanine and (+)-β-(2-thienyl)-β-alanine were obtained by resolving the *N*-benzyloxycarbonyl-DL-amino acids with quinine and by removing the protecting group from them. It was concluded, from the changes in their ORD curves depending on the pH, and also from the sign of the Cotton effects of their DCHA salts of the *N*-ethylthiocarbonothioyl derivatives, that both the compounds belong to the L-series. This conclusion was supported by the fact that the aspartic acid obtained by the oxidation of these amino acids belongs to the D-series.

In connection with β-(2-thiazolyl)-β-alanine,[1] present in a peptide antibiotic bottromycin as a C-terminal amino acid, we had an interest in the β-amino acids bearing a heterocycle in the β-position. Among these amino acids, we attempted to prepare β-(2-furyl)- and β-(2-thienyl)-β-alanine as analogs of the thiazolylalanine. Both the compounds are known,[2,3] but no attempt has been made to resolve them or to determine the absolute configuration of their optically active form.

These β-amino acids were prepared by the reaction of 2-furaldehyde or 2-thiophenecarbaldehyde with malonic acid in the presence of ammonium acetate according to the literature.[2a,3b] The racemates could be successfully resolved by treating the *N*-benzyloxycarbonyl derivatives with quinine in ethyl acetate or ethanol. From the crystalline quinine salts, separated out from the solution, the alkaloid base was removed; the following optically active compounds were thus obtained: *N*-benzyloxycarbonyl-(+)-β-(2-furyl)-β-alanine, mp 123—125 °C, $[\alpha]_D^{20}$ +55.9° (*c* 1, MeOH), *N*-benzyloxycarbonyl-(+)-β-(2-thienyl)-β-alanine, mp 128—129 °C, $[\alpha]_D^{20}$ +45.4° (*c* 1, MeOH). The *N*-protecting group could be removed by hydrobromic acid in acetic acid in the usual way, though the yields were unexpectedly low in both cases. The amino acids obtained were: (+)-β-(2-furyl)-β-alanine, $[\alpha]_D^{20}$ +12.9° (*c* 1, H_2O), (+)-β-(2-thienyl)-β-alanine, $[\alpha]_D^{20}$ +15.3° (*c* 1, H_2O). By hydrogenolytic deprotection, the former amino acid of $[\alpha]_D^{20}$ +13.7° (*c* 1, H_2O) was obtained in a much better yield than in the case of acidolysis.

In previous papers we proposed two empirical rules for the determination of the absolute configuration of the β-amino acid. One is that the value of the molecular rotation of L-β-amino acid[4] in water at various pH decreases in the order of neutral>acidic>alkaline media.[5] The other is that the dicyclohexylamine (DCHA) salt of the *N*-ethylthiocarbonothioyl (ETCT) derivative of the L-β-amino acid shows a negative Cotton effect.[6] In order to apply these rules to the optically active β-amino acids obtained here, their ORD spectra in water at different pH values were measured; it was found that the values decreased in both the β-amino acids in the order of neutral> acidic>alkaline media. On the other hand, the CD spectra of the DCHA salts of the *N*-ETCT-β-amino acids in some solvents showed negative Cotton effects in all the cases, as is shown in Table 1. Both the results denote that these β-amino acids belong to the L-series. It should be pointed out that solvents have a remarkable influence on the Cotton effects of the *N*-ETCT-β-aromatic β-amino acids, depending on the structure of the aromatic ring (Table 1).

Table 1. Cotton effects of *N*-ETCT-L-β-aromatic β-amino acids ($C_2H_5SSC-NH\underset{\displaystyle X}{\underset{|}{C}}HCH_2COOH$) and their DCHA salts in several solvents

X	Free acid			DCHA salt		
	MeOH	C_6H_6	$CHCl_3$	MeOH	C_6H_6	$CHCl_3$
Phenyl-[6]	−	−	−	−	−	−
2-Thiazolyl-	−	−, +	+	−	−	−
2-Thienyl	−	+	+	−	−	−
2-Furyl-	+	+	+	−	−	−

Terent'ev reported that *N*-benzoyl-DL-β-(2-furyl)-β-alanine or its amide was oxidized with alkaline permanganate to the benzoyl derivative of aspartic acid[7] or asparagine[2c] in a good yield. We also observed that β-(2-furyl)-α-alanine was easily converted into aspartic acid.[8] These facts suggest another route for determining the configuration of β-(2-furyl)- or β-(2-thienyl)-β-alanine by oxidizing it and by examining the chirality of the resulting aspartic acid. The β-amino acids belonging to the L-series should give D-aspartic acid upon the oxidation.

The oxidation of *N*-benzyloxycarbonyl-(+)-β-(2-furyl)-β-alanine with alkaline permanganate proceeded very smoothly and afforded *N*-(benzyloxycarbonyl) aspartic acid almost quantitatively; it was determined to be the D-isomer by a comparison of the optical rotation of the dimethyl ester with that of a sample derived from L-aspartic acid. On the other hand, the oxidation of *N*-benzyloxycarbonyl-(+)-β-(2-

** Present address: Star Rubber Ind. Co., Ltd., No. 2-3, 1-Chome, Nishishiriike-cho, Nagata-ku, Kobe 658.

*** Present address: The Green Cross Corporation, 2-2-11, Gokodori, Fukiai-ku, Kobe 651.

**** Present address: Amagasaki Chemical Industries Co., Ltd., 24-1-Chome, Rinkaicho, Izumiotsu-shi 595.

thienyl)-β-alanine to an aspartic acid derivative did not proceed so smoothly, and it was accompanied by many by-products. From the oxidation products obtained at 40 °C, *N*-(benzyloxycarbonyl)aspartic acid was isolated in a 12% yield after repeated purification by preparative silica gel TLC; benzoic acid was also isolated in a 51% yield. The configuration of the aspartic acid obtained here was confirmed to be the D-form, quite similar to the above case. Consequently, the original (+)-β-(2-furyl)- and (+)-β-(2-thienyl)-β-alanine could be attributed to the L-series.

The identity of the conclusions deduced both from the empirical rules and from the chemical evidences would demonstrate the usefulness of these rules.

Experimental

The melting points are uncorrected. The optical rotations were measured on a JASCO DIP-4 polarimeter. The ORD and CD curves were recorded on a JASCO ORD/UV-5 spectropolarimeter.

DL-β-(2-Furyl)-β-alanine (I). This compound was synthesized in a 28% yield by the condensation of 2-furaldehyde, malonic acid, and ammonium acetate according to the literature;[2a] mp 199—201 °C (dec), lit,[2a] mp 200—201 °C (dec).

N-Benzyloxycarbonyl-DL-β-(2-furyl)-β-alanine (II). I was acylated with benzyloxycarbonyl chloride and sodium hydroxide as usual; 79% yield; mp 143—143.5 °C (from aq EtOH).

Found: C, 62.31; H, 5.29; N, 4.71%. Calcd for $C_{15}H_{15}NO_5$: C, 62.28; H, 5.23; N, 4.84%.

Optical Resolution of DL-β-(2-Furyl)-β-alanine. *N-Benzyloxycarbonyl-(+)-β-(2-furyl)-β-alanine (III)*: II (8.7 g) and quinine (9 g) were dissolved in ethyl acetate (150 ml) and then allowed to stand for several days in a refrigerator. The crystals thus separated were collected and recrystallized from ethyl acetate: mp 109—111 °C, $[\alpha]_D^{20}$ −86.0° (*c* 1, MeOH).

By the removal of quinine from this salt with hydrochloric acid, optically active *N*-benzyloxycarbonyl-β-(2-furyl)-β-alanine was obtained; mp 123—125 °C (from aq EtOH), $[\alpha]_D^{20}$ +55.9° (*c* 1, MeOH). The overall yield from II was 70%.

(+)-β-(2-Furyl)-β-alanine (IV). Debenzyloxycarbonylation by Acidolysis: A 25% hydrogen bromide solution in acetic acid was added to III (600 mg), which dissolved immediately, forming a deep blue solution. After about ten minutes, the solution was concentrated under reduced pressure, and the resulting residue was washed with dry ether several times. After the remaining viscous, deep blue material had been dissolved in water and decolorized, the aqueous solution was passed through an Amberlite CG-120 (H^+ form) column. The amino acid was then eluted with aq ammonia, and the eluate was, after decolorization, concentrated to dryness under reduced pressure; yield, 44%. Recrystallization from water afforded large plates; mp 205—207 °C (dec), $[\alpha]_D^{20}$ +12.9° (*c* 1, H_2O).

Debenzyloxycarbonylation by Hydrogenolysis:[9] In a quantitative hydrogenation apparatus, a solution of III (723 mg; 2.5 mmol) in a mixture of 1 M NaOH (7 ml) and methanol (4 ml) was hydrogenated in the presence of 5% Pd–C (80 mg) at room temperature. Hydrogenation was stopped when 50 ml of hydrogen (*ca.* 2.2 mmol) had been absorbed. The reaction mixture was then filtered, and the catalyst was washed thoroughly with water. The filtrate and the washings were combined, acidified with hydrochloric acid, and extracted with ethyl acetate. The aqueous layer neutralized with 1 M NaOH to pH 6, was passed through the Amberlite CG-120 (H^+ form) column, which had been thoroughly washed with water. The amino acid was eluted with aq ammonia, and the eluate was concentrated to dryness under reduced pressure: 360 mg (93%). The NMR spectrum of this compound was identical with that of the (+)-β-(2-furyl)-β-alanine obtained by acidolysis and showed no peak attributable to the tetrahydrofuran ring. Recrystallization from water afforded large plates; $[\alpha]_D^{20}$ +13.7° (*c* 1, H_2O).

DL-β-(2-Thienyl)-β-alanine (V). This compound was synthesized in a 43% yield by the condensation of 2-thiophenecarbaldehyde,[10] malonic acid, and ammonium acetate according to the literature;[3b] mp 199—201 °C (dec), lit,[3b] mp 201—203 °C.

N-Benzyloxycarbonyl-DL-β-(2-thienyl)-β-alanine (VI). V was benzyloxycarbonylated as usual in an 86% yield; mp 118—118.5 °C (from aq EtOH).

Found: C, 59.02; H, 4.94; N, 4.34%. Calcd for $C_{15}H_{15}NO_4S$: C, 59.00; H, 4.95; N, 4.59%.

Optical Resolution of DL-β-(2-Thienyl)-β-alanine. The resolution was carried out in a manner similar to that used in the case of the furan derivative.

Easily crystallizable quinine salt of *N*-benzyloxycarbonyl-β-(2-thienyl)-β-alanine was obtained in a 60% yield; mp 155—156 °C (from EtOH), $[\alpha]_D^{20}$ −29.3° (*c* 1, MeOH).

N-Benzyloxycarbonyl-(+)-β-(2-thienyl)-β-alanine (VII). Yield, 95%; mp 128—129 °C (from aq EtOH), $[\alpha]_D^{20}$ +45.4° (*c* 1, MeOH).

(+)-β-(2-Thienyl)-β-alanine (VIII). VII was debenzyloxycarbonylated with hydrogen bromide in acetic acid and worked up similarly to the case of furylalanine. Yield, 54%; mp 206—208 °C (dec), $[\alpha]_D^{20}$ +15.3° (*c* 1, H_2O).

Measurement of CD Spectra of N-ETCT-amino Acids and Their DCHA Salts. Both β-amino acids, IV and VIII, and (+)-β-(2-thiazolyl)-β-alanine[1] were converted to the corresponding ethyl dithiocarbamates as well as their DCHA salts according to the literature.[11] The signs of the Cotton effects of their CD spectra in several solvents are summarized in Table 1.

Oxidation of N-Benzyloxycarbonyl-(+)-β-(2-furyl)-β-alanine. III (289 mg) was dissolved in a sodium hydroxide solution (NaOH 40 mg, H_2O 5 ml), into which an alkaline potassium permanganate solution ($KMnO_4$ 1.6 g, NaOH 0.5 g, H_2O 50 ml) was added, drop by drop, under ice-cooling until the violet color of the reaction mixture had come to persist. The residual permanganate was destroyed with aqueous sodium sulfite, the precipitated manganese dioxide was filtered off, and the filtrate was extracted with ethyl acetate after having been acidified with hydrochloric acid. The organic layer was then washed with water and dried over anhydrous sodium sulfate. The evaporation of the solvent gave white crystals (mp 110—114 °C), the IR spectrum of which agreed well with that of *N*-benzyloxycarbonyl-L-aspartic acid; the yield was 266 mg (quantitative). The optical rotation was measured after converting it to dimethyl ester with diazomethane; $[\alpha]_D^{20}$ +15.3° (*c* 1.7, MeOH), $[\alpha]_D^{20}$ −29.5° (*c* 1.3, $CHCl_3$). (*N*-Benzyloxycarbonyl-L-aspartic acid dimethyl ester:[12] $[\alpha]_D^{20}$ −20.4° (*c* 1, MeOH), $[\alpha]_D^{20}$ +27.5° (*c* 1, $CHCl_3$)).

Oxidation of N-Benzyloxycarbonyl-(+)-β-(2-thienyl)-β-alanine. VII (600 mg) was oxidized with alkaline permanganate similarly to the case of the furan derivative, except that the reaction temperature was kept at about 40 °C. The color change of the reaction mixture was very slow compared

with that of the furan derivative, so a large excess of the oxidizing reagent was added to ensure the oxidation. The separation of the crude oxidation products was carried out by preparative TLC (adsorbent: Merck silica gel GF_{254}; developing solvent, $CHCl_3$:MeOH:AcOH=95:15:3). The zone of the chromatogram containing *N*-(benzyloxycarbonyl)-aspartic acid was scraped off and extracted with methanol. The extract was then concentrated and purified again in the same manner. The methanol extract was then dissolved in ethyl acetate, and the solution was washed with water and dried over sodium sulfate. The subsequent evaporation of the solvent gave white crystals (mp 114—115 °C), the IR spectrum of which agreed well with that of *N*-benzyloxycarbonyl-L-aspartic acid; the yield was 64 mg (12%); dimethyl ester, $[\alpha]_D^{20}$ +17.7° (*c* 1.2, MeOH), $[\alpha]_D^{20}$ −20.3° (*c* 1.2, $CHCl_3$). Another component of the oxidation product, with a larger R_f value than that of the aspartic acid derivative, was also isolated in a similar manner. This compound melted at 119—121 °C after recrystallization from water and showed no depression of the melting point when admixed with benzoic acid. The yield was 122 mg (51%).

References

1) Y. Seto, K. Torii, K. Bori, K. Inabata, S. Kuwata, and H. Watanabe, *Bull. Chem. Soc. Jpn.*, **47**, 151 (1974).

2) a) B. R. Baker, F. J. McEvoy, R. E. Schaub, J. P. Joseph, and J. H. Williams, *J. Org. Chem.*, **18**, 153 (1953); b) V. M. Rodionov, F. Blanko, S. V. Bragin, A. M. Fedorova, A. B. Ershler, and A. I. Gryaznov, *Tr. Mosk. Khim.-Technol. Inst.*, **1956**, No. 23, 13; *Chem. Abstr.*, **52**, 20117c (1958); c) A. P. Terent'ev, R. A. Gracheva, and N. M. Mikhailova, *Zh. Obshch. Khim.*, **33**, 581 (1963); *Chem. Abstr.*, **59**, 2935f (1963); d) T. Posner, *Justus Liebigs Ann. Chem.*, **389**, 107 (1912); e) A. Ahmed, P. B. Marshall, and D. M. Shepherd, *J. Pharm. Pharmacol.*, **10**, 672 (1958).

3) a) V. P. Mamaev, N. N. Suvorov, and E. M. Roklin, *Dokl. Akad. Nauk SSSR*, **101**, 269 (1955); *Chem. Abstr.*, **50**, 3387d (1956); b) Y. L. Gol'dfarb, B. P. Fabrichnyĭ, and I. F. Schalavina, *Zh. Obshch. Khim.*, **28**, 213 (1958); *Chem. Abstr.*, **52**, 12838f (1958).

4) The L-β-amino acid means the acid which could be derived from the corresponding L-α-amino acid by inserting CH_2 between the α-asymmetric carbon atom and the carboxyl group.

5) Y. Seto, T. Yamada, K. Niwa, S. Miwa, F. Tanaka, S. Kuwata, and H. Watanabe, *Chem. Lett.*, **1973**, 151.

6) T. Yamada, S. Kuwata, and H. Watanabe, *Tetrahedron Lett.*, **1978**, 1813.

7) A. P. Terent'ev, R. A. Gracheva, and V. A. Dorokhov, *Zh. Obshch. Khim.*, **29**, 3474 (1959); *Chem. Abstr.*, **54**, 15262h (1960).

8) H. Watanabe, S. Kuwata, S. Nakajima, K. Koshida, and M. Hayashi, *Bull. Chem. Soc. Jpn.*, **38**, 1461 (1965).

9) The debenzyloxycarbonylation by hydrogenolysis was carried out similarly to that of *N*-benzyloxycarbonyl-β-(2-furyl)-α-alanine; H. Watanabe and S. Kuwata, Proceedings of the 2nd Symposium on Peptide Chemistry, Japan (1963), p. 1.

10) A. W. Weston and R. J. Michaelis, Jr., *Org. Synth.*, Coll. Vol. IV, 915 (1963).

11) K. Ishikawa, K. Achiwa, and S. Yamada, *Chem. Pharm. Bull.*, **19**, 912 (1971).

12) T. Yamada, N. Isono, A. Inui, T. Miyazawa, S. Kuwata, and H. Watanabe, *Bull. Chem. Soc. Jpn.*, **51**, 1897 (1978).

Pyrrolizidine Alkaloids. The Synthesis and Absolute Configuration of All Stereoisomers of Monocrotalic Acid

Takashi MATSUMOTO,* Makoto TAKAHASHI, and Yutaka KASHIHARA

Department of Chemistry, Faculty of Science, Hiroshima University, Higashisenda-machi, Hiroshima 730

(Received March 7, 1979)

All stereoisomers (**3a, b**—**6a, b**) of monocrotalic acid have been synthesized. Methylation of (±)-*cis*-2,3,4-trimethyl-2-pentenedioic acid with diazomethane followed by *cis*-hydroxylation with potassium permanganate afforded two epimeric γ-lactone esters in a ratio of *ca.* 1:5. These esters were then hydrolyzed with dilute hydrochloric acid to the corresponding acids, (±)-**3** and racemic monocrotalic acid (**4**). Optical resolution of (±)-**3** with brucine afforded **3a** (2*R*,3*R*,4*S*) and **3b** (2*S*,3*S*,4*R*). The racemic monocrotalic acid was also resolved by means of brucine to give natural monocrotalic acid (**4a**: 2*R*,3*R*,4*R*) and its enantiomer (**4b**: 2*S*,3*S*,4*S*). Subsequently, (±)-*trans*-2,3,4-trimethyl-2-pentenedioic acid was resolved with cinchonidine to give **8a** and **8b**, whose stereochemistry was assigned respectively as *S*- and *R*-configuration by correlation to the known (*R*)-(−)-2-phenylpropanoic acid. Methylation of **8a** followed by *cis*-hydroxylation and hydrolyses afforded γ-lactone acids, **5a** (2*R*,3*S*,4*S*) and **6b** (2*S*,3*R*,4*S*). Similarly, the enantiomer **8b** was also converted into the corresponding acids, **5b** (2*S*,3*R*,4*R*) and **6a** (2*R*,3*S*,4*R*). The stereochemical course of the above hydroxylations with potassium permanganate was well explained by a modification of Cram's rule of asymmetric induction. The CD spectra of **3a,b**—**6a,b** were also discussed.

The pyrrolizidine alkaloid monocrotaline (**1**) has been isolated from *Crotalaria spectabilis* Roth.,[1,2] *C. retusa* L.,[2-4] and *C. grahamiana* Wight *et* Arn.[5] Hydrogenolysis of **1** produced a necic acid component, monocrotalic acid (**2**), which possesses three asymmetric carbons in the molecule. Therefore, eight stereoisomers (**3a,b**—**6a,b**) are possible for **2**. The structure of monocrotalic acid was established by degradation and synthesis by Adams *et al.*[6,7] On the basis of the stereospecificity of the synthetic reaction,[7] they assigned the relative configuration of methyl groups on C-2 and C-3 to be *cis* (2*R*,3*S* or 2*S*,3*R*). This means that the stereostructure of monocrotalic acid is shown as one of four diastereomers (**5a**, **5b**, **6a**, and **6b**).

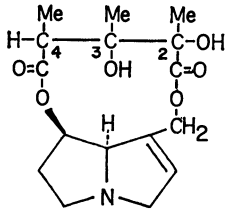

1

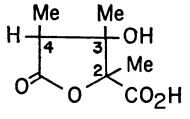

2

Cervinka *et al.*[8,9] also studied the stereochemistry of monocrotalic acid and assigned the absolute configuration of C-2 to be *R* by the method of asymmetric transformation and by means of the optical rotatory dispersion. On the other hand, Crout *et al.*[10,11] disagreed with the result of Adams *et al.*[7] and found the chirality of three asymmetric centers in monocrotalic acid to be 2*R*,3*R*,4*R* (**4a**) by comparing the rate constant of dehydration of methyl monocrotalate with those of methyl trichodesmate,[12] 3-hydroxy-4-butyrolactone, and mevalonolactone, and by correlation of C-2 and C-4 to the known compounds, (2*R*,3*S*)-2,3-dihydroxy-2-methylbutanoic acid and (*S*)-3-hydroxy-2-methylpropanohydrazide. Although this discrepancy concerning the configuration of C-3 had been explained by Crout *et al.*,[10] it was desirable to obtain the direct confirmation of the stereochemistry of C-3 by an unambigous synthesis. The key step in the reported synthesis[7] was the stereospecific hydroxylation of (±)-*cis*-2,3,4-trimethyl-2-pentenedioic acid (**7**) with pertungstic acid, which is known to give predominantly *trans*-hydroxylation of olefinic double bonds. However, Crout *et al.*[10] have reported that the above hydroxylation actually proceeded in

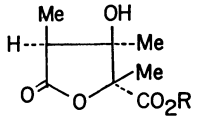

3a R=H
11a R=Me

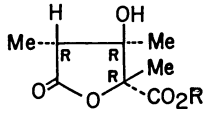

4a R=H
12a R=Me

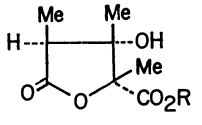

5a R=H
13a R=Me

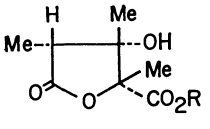

6a R=H
14a R=Me

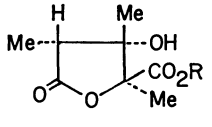

3b R=H
11b R=Me

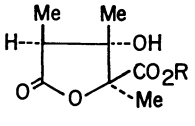

4b R=H
12b R=Me

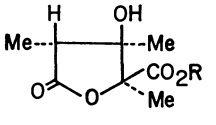

5b R=H
13b R=Me

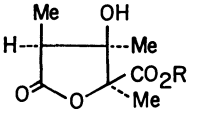

6b R=H
14b R=Me

a stereospecifically *cis* manner. This confusion about the stereochemical course of the synthetic reaction seemed to have occurred because of using the acidic compound (**7**) which did not react with potassium permanganate or osmium tetraoxide.[7] In previous papers,[13] we have reported that similar compounds, methyl *trans*-3-methoxycarbonyl-2-methyl-3-pentenoate and its *cis*-isomer, were easily hydroxylated with potassium permanganate in a *cis* manner. Therefore, it was of interest to study the hydroxylation of dimethyl *cis*-2,3,4-trimethyl-2-pentenedioate (**9**) and its *trans*-isomer (**10**) with potassium permanganate. We were further interested in studying the steric course of the hydroxylation to the olefinic double bonds directly bonded to asymmetric carbon atoms. This paper describes the syntheses and absolute configurations of all stereoisomers of monocrotalic acid, and the stereochemistry of the potassium permanganate hydroxylations. In addition, the relationship between the absolute configurations and the circular dichroism (CD) spectra of the synthetic γ-lactone acids was also discussed.

A mixture of racemic *cis*- (**7**) and *trans*-2,3,4-trimethyl-2-pentenedioic acid (**8**) was prepared by the procedure of Adams *et al.* and then successfully separated by column chromatography on silica gel. The NMR spectrum of (±)-**7** showed a methine proton quartet at δ 4.43 ppm and two methyl singlets at δ 1.75 and 1.90 ppm, while that of (±)-**8** showed the corresponding signals at δ 3.74 (q) ppm and at δ 1.94 (6H, s) ppm. The appearance of the methine proton signal of (±)-**7** in the field lower than that of (±)-**8** suggested that these dioic acids, (±)-**7** and (±)-**8**, have respectively *cis*- and *trans*-configuration. Methylation of the *cis*-isomer, (±)-**7**, with diazomethane afforded the dimethyl ester (**9**), which was submitted to oxidation with aqueous potassium permanganate in the presence of magnesium sulfate at −20 °C. Purification of the crude product by column chromatography on silica gel produced, as expected, two epimeric γ-lactone esters, (±)-**11** and (±)-**12**, in a ratio of *ca.* 1:5. The IR and NMR spectra of the major product, (±)-**12**, were identical with those of natural methyl monocrotalate. Since it is well known that potassium permanganate reacts with olefins to add two hydroxyl functions to the double bond in a *cis* manner, the relative configuration of the methyl groups on C-2 and C-3 in both (±)-**11** and (±)-**12** is *trans*, supporting the assignment of Crout *et al.*[10] The γ-lactone esters, (±)-**11** and (±)-**12**, were hydrolyzed with dilute hydrochloric acid to the corresponding acids, (±)-**3** and (±)-**4**, which were subsequently methylated back into (±)-**11** and (±)-**12** with diazomethane. This proved that there was no configurational change during the hydrolyses. The (±)-**4** acid was then resolved by means of brucine to give monocrotalic acid (**4a**), $[\alpha]_D$ −5.6° (EtOH), and its enantiomer (**4b**), $[\alpha]_D$ +5.3° (EtOH). Methylation of **4a** and **4b** with diazomethane, followed by dehydration of the resulting esters, **12a** and **12b**, with phosphoryl chloride in pyridine afforded respectively methyl (*R*)-(+)-anhydromonocrotalate (**15a**),[10,11] $[\alpha]_D$ +205° ($CHCl_3$), and its (*S*)-(−)-enantiomer (**15b**), $[\alpha]_D$ −195° ($CHCl_3$). From the above synthesis the absolute configuration of monocrotalic acid was conclusively assigned as being 2*R*,3*R*,4*R* (**4a**). The (±)-**3** acid was also resolved by means of brucine to give **3a**, $[\alpha]_D$ −32° (EtOH), and **3b**, $[\alpha]_D$ +22° (EtOH),[14] which, after methylation with diazomethane, were dehydrated with phosphoryl chloride in pyridine to afford **15a** and **15b** respectively. Thus, the absolute configurations of **3a** and **3b** were also assigned as being 2*R*,3*R*,4*S* and 2*S*,3*S*,4*R* respectively.

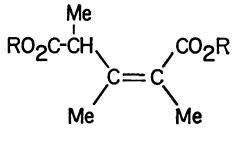

7 R=H
9 R=Me

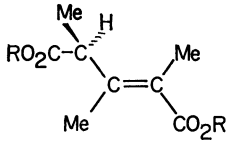

8a R=H
10a R=Me

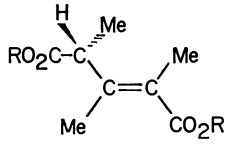

8b R=H
10b R=Me

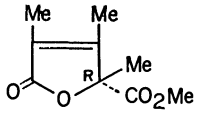

15a

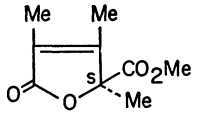

15b

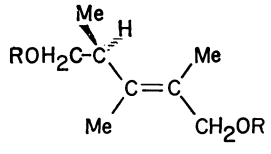

16 R=H
17 R=Ac

Subsequently, our attention was directed toward the syntheses of the other four diastereomers. For this purpose, (±)-**8** was resolved by means of cinchonidine to give **8a**, $[\alpha]_D$ +121° (ether), and **8b**, $[\alpha]_D$ −120° (ether), which were methylated with diazomethane to yield dimethyl esters, **10a** and **10b**. The absolute configurations of **8a** and **8b** were determined by the following correlation. Reduction of **10a**[15] with lithium aluminium hydride, followed by acetylation of the resulting diol (**16**) with acetic anhydride in

pyridine, afforded a diacetate (**17**), $[\alpha]_D$ +9.1° ($CHCl_3$). This was then submitted to ozonization to yield 4-acetoxy-3-methyl-2-butanone (**18**). The Grignard reaction of the crude **18** with methylmagnesium iodide gave a diol (**19a**) which was characterized as its monoacetate, 3-hydroxy-2,3-dimethylbutyl acetate (**20a**), $[\alpha]_D$ +16.9° ($CHCl_3$). Transformation of the known (*R*)-(−)-2-phenylpropanoic acid (**21**)[16] into **20a** or its enantiomer (**20b**) was also carried out as follows. Methylation of **21** with diazomethane afforded the corresponding methyl ester (**22**), which was converted into (*R*)-(−)-2-phenylpropyl acetate (**24**) by reduction with lithium aluminium hydride and subsequent acetylation of the resulting alcohol (**23**) with acetic anhydride in pyridine. Ozonization of **24** followed by methylation of the resulting acid (**25**) with diazomethane afforded methyl (*S*)-(+)-3-acetoxy-2-methylpropanoate (**26**), $[\alpha]_D$ +18.2° ($CHCl_3$), which was then converted into (*S*)-(−)-3-hydroxy-2,3-dimethylbutyl acetate (**20b**), $[\alpha]_D$ −27.1° ($CHCl_3$), by the Grignard reaction with methylmagnesium iodide and subsequent acetylation. The IR and NMR spectra of **20b** was identical in every respect with those of **20a**. Thus, the stereochemistry of **20a** was assigned to be *R*-configuration and **8a** and **8b** consequently have *S*- and *R*-configuration respectively.

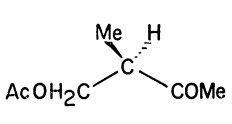

18

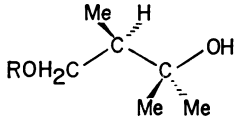

19a R=H
20a R=Ac

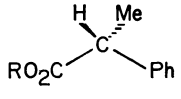

21 R=H
22 R=Me

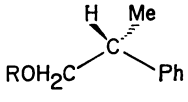

23 R=H
24 R=Ac

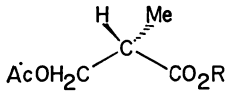

25 R=H
26 R=Me

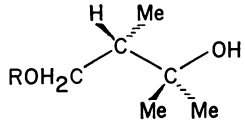

19b R=H
20b R=Ac

Oxidation of **10b** with potassium permanganate afforded two γ-lactone esters, **13b** and **14a**, in a ratio of *ca.* 5:2. The NMR spectrum of **13b** showed a quartet at δ 3.04 ppm due to a methine proton at C-4, while that of **14a** showed the corresponding signal at δ 2.61 ppm. These chemical shifts suggested that the relative configuration of the methine proton and a hydroxyl group at C-3 is *cis* in **13b** and *trans* in **14a**. From the above spectral data and the consideration of the stereochemical course of the oxidation, the absolute configurations of **13b** and **14a** were assigned as 2*S*,3*R*,4*R* and 2*R*,3*S*,4*R* respectively. These assignments were further supported by the dehydration of **13b** and **14a** with phosphoryl chloride in pyridine, yielding **15b** and **15a** respectively. Hydrolyses of **13b** and **14a** with dilute hydrochloric acid yielded the corresponding acids, **5b** (2*S*,3*R*,4*R*), $[\alpha]_D$ +60° (EtOH), and **6a** (2*R*,3*S*,4*R*), $[\alpha]_D$ −5.1° (EtOH). The enantiomers, **5a** (2*R*,3*S*,4*S*) and **6b** (2*S*,3*R*,4*S*), were also synthesized from **10a** by oxidation and subsequent

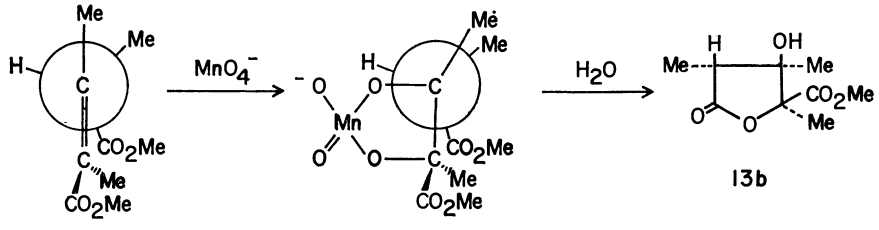

10b (A)

13b

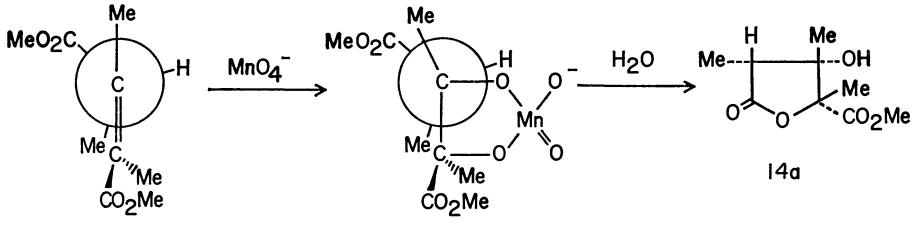

10b (B)

14a

Fig. 1.

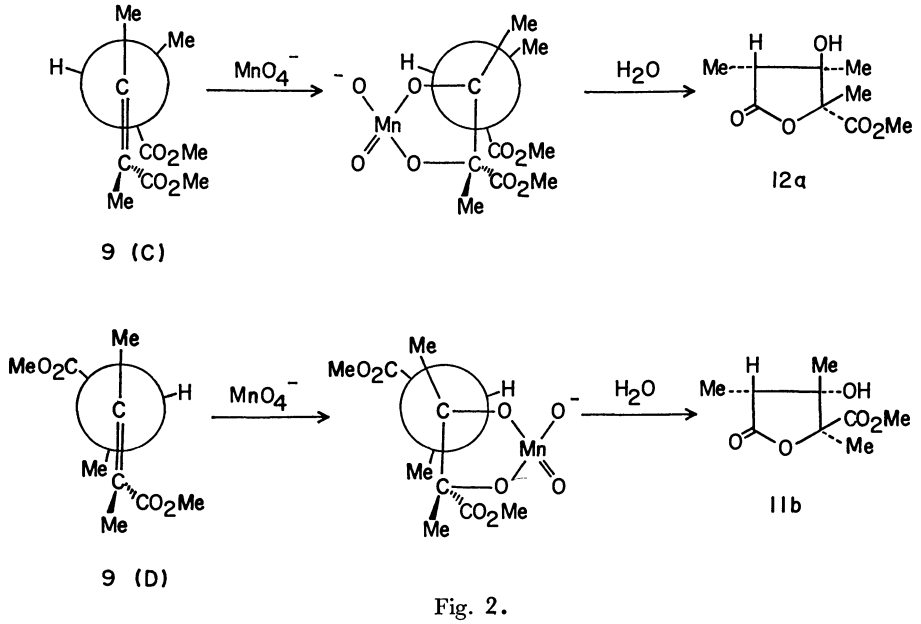

Fig. 2.

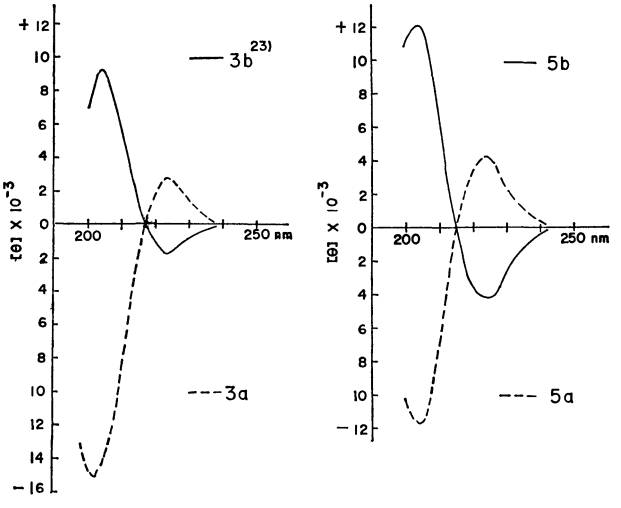

Fig. 3. The CD spectra of **3a**, **b** and **5a**, **b** in H_2O.

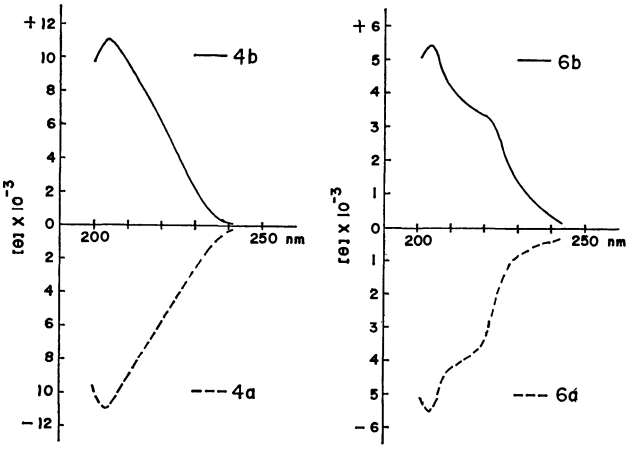

Fig. 4. The CD spectra of **4a**, **b** and **6a**, **b** in H_2O.

hydrolyses of the resulting γ-lactone esters, **13a** and **14b**. Further, (±)-**10** prepared from (±)-**8** was also converted into (±)-**5** and (±)-**6** *via* (±)-**13** and (±)-**14**. Resolution of (±)-**5** by means of cinchonidine afforded **5a** and **5b**, whereas that of (±)-**6** was unsuccessful. Thus, the syntheses of all stereoisomers of monocrotalic acid were successfully achieved.

The stereochemical course of the potassium permanganate hydroxylation of olefinic esters having an asymmetric carbon atom adjacent to the double bond can be well explained by a modification of Cram's rule of asymmetric induction (open-chain model)[17,18] as shown in Figs. 1 and 2. For example, in the *trans* ester **10b** and its *cis*-isomer **9** which is shown only one enantiomer of the racemate, the A and C conformations should be more stable than the corresponding B and D conformations, as has been reported by Karabatsos,[18] because the effective steric size of three substituents on the asymmetric carbon atom is Me>CO_2Me>H.[19] Therefore, the double bonds in the A and B conformations are attacked by the permanganate anion from the side of the smallest hydrogen atom, as pictured, leading to the major product **13b** and the minor one **14a**. Similarly, the C and D conformations also lead to the major product **12a** and the minor one **11b** respectively.

It has been reported that the sign of the Cotton effect in the CD spectra of γ-lactones depends on the configuration of C-4,[20-22] while in the cases of γ-lactones possessing a carboxyl group at C-2 it depends on the configuration of C-2.[8,9] On the other hand, we have also reported that when γ-lactones possess a carboxyl group at C-3, the sign is influenced by the configuration of C-4.[13] In connection with these previous works, the CD spectra of our synthetic acids (**3a,b**—**6a,b**) were also measured to obtain further information on the relationship between the absolute configuration and the sign of the CD spectrum. The CD spectra of the present samples may be divided into two classes. The compounds of the first class, **3a,b** and **5a,b**, which have the opposite absolute configurations at C-2 and C-4 (2*R*,4*S* or 2*S*,4*R*), show two distinct Cotton effects at 204 and 224 nm; these respectively represent the configurations of C-2

and C-4. Those of the second class, **4a,b** and **6a,b**, which have the same absolute configurations at C-2 and C-4 (2*R*,4*R* or 2*S*,4*S*), exhibit only one effect at 204 nm. It is clear that when the absolute configuration of C-2 or C-4 is *R*, the sign is negative, and when *S*, it is positive. It is also evident that the Cotton effect due to the configuration of C-2 is superior to that of C-4, as has been reported by Cervinka *et al.*[8,9] In the cases of **4a,b** and **6a,b**, the two Cotton effects are apparently overlapped and, consequently, only the strong effect due to the configuration of C-2 is observed at 204 nm. These results in the CD study seemed to be very useful for the prediction of the absolute configurations of both C-2 and C-4 in γ-lactones carrying a carboxyl group at C-2.

Experimental

All melting points are uncorrected. The IR spectra and optical rotations were measured in chloroform, and the NMR spectra in carbon tetrachloride at 60 MHz, with tetramethylsilane as the internal standard, unless otherwise stated. The chemical shifts are presented in terms of δ values; s: singlet, bs: broad singlet, d: doublet, dd: double doublet, q: quartet, m: multiplet. The CD spectra were recorded on a JASCO J-40CS spectropolarimeter. Column chromatography was performed using Merck silica gel (0.063 mm).

(±)-cis-2,3,4-Trimethyl-2-pentenedioic Acid (7) and Its (±)-trans-Isomer (8). A mixture of (±)-**7** and (±)-**8** prepared by the procedure of Adams *et al.*[7] was chromatographed on silica gel[24] using acetone-benzene (3:97) as the eluent to give an anhydride of (±)-**7**; IR: 1790, 1736, 1657 cm^{-1}; NMR: 1.51 (3H, d, J=7 Hz, $C\underline{H}_3CH$–), 1.95 and 2.01 (each 3H and s, 2=CCH_3), 3.25 (1H, q, J=7 Hz, $CH_3C\underline{H}$–). Further elution gave (±)-**7**, which was recrystallized from ether-petroleum benzine: mp 118—120 °C; NMR (CD_3COCD_3): 1.20 (3H, d, J=7 Hz, $C\underline{H}_3CH$–), 1.75 and 1.90 (each 3H and bs, 2=CCH_3), 4.43 (1H, q, J=7 Hz, $CH_3C\underline{H}$–). Found: C, 55.71; H, 7.18%. Calcd for $C_8H_{12}O_4$: C, 55.80; H, 7.03%.

Further elution with acetone-benzene (1:9) afforded (±)-**8**, which was recrystallized from ether-petroleum benzine: mp 132—133 °C; NMR (CD_3COCD_3): 1.23 (3H, d, J=7 Hz, $C\underline{H}_3CH$–), 1.94 (6H, s, 2=CCH_3), 3.74 (1H, q, J=7 Hz, $CH_3C\underline{H}$–). Found: C, 55.97; H, 6.96%. Calcd for $C_8H_{12}O_4$: C, 55.80; H, 7.03%.

The above anhydride was hydrolyzed with aqueous sodium hydroxide at 40 °C for 2 h to give (±)-**7**.

Dimethyl (±)-cis-2,3,4-Trimethyl-2-pentenedioate (9) and Its (±)-trans-Isomer (10). *a)*: A sample of (±)-**7** in ether was methylated with diazomethane to give the corresponding dimethyl ester (**9**); NMR: 1.20 (3H, d, J=7 Hz, $C\underline{H}_3CH$–), 1.68 and 1.85 (each 3H and s, 2=CCH_3), 3.60 and 3.68 (each 3H and bs, 2–CO_2CH_3), 4.34 (1H, q, J=7 Hz, $CH_3C\underline{H}$–).

b): Similarly, (±)-**8** was methylated with diazomethane to afford the corresponding ester (**10**); NMR: 1.16 (3H, d, J=7 Hz, $C\underline{H}_3CH$–), 1.79 and 1.81 (6H, m, 2=CCH_3), 3.58 and 3.62 (each 3H and s, 2–CO_2CH_3), *ca.* 3.6 (1H, overlap, $CH_3C\underline{H}$–).

Oxidation of (±)-9 with Potassium Permanganate. A solution of potassium permanganate (182 mg) and magnesium sulfate heptahydrate (254 mg) in water (9.0 ml) was added at −20±2 °C into a solution of (±)-**9** (170 mg) in methanol (5.0 ml) with stirring. The mixture was further stirred for 3 h at this temperature, and sodium hydrogensulfite was then added. After the methanol had been evaporated under a vacuum, the mixture was extracted with ether. The ether extract was washed with brine, dried over sodium sulfate, and then evaporated under a vacuum. The residue was purified by column chromatography on silica gel using ether–benzene (15:85) as the eluent to give a γ-lactone ester (**11**) (19 mg: 11.1%) as an oil; IR: 3590, 3450, 1777, 1737 cm^{-1}; NMR ($CDCl_3$): 1.16 (3H, d, J=7 Hz, C_4–CH_3), 1.23 (3H, s, C_3–CH_3), 1.59 (3H, s, C_2–CH_3), *ca.* 2.4 (1H, bs, –OH), 2.76 (1H, q, J=7 Hz, C_4–H), 3.77 (3H, s, $-CO_2CH_3$). Found: C, 53.20; H, 7.06%. Calcd for $C_9H_{14}O_5$: C, 53.46; H, 6.98%.

Further elution gave another γ-lactone ester (**12**) (91 mg: 53.0%) which was recrystallized from ether-petroleum benzine: mp 76—77 °C; IR: 3580, 3450, 1780, 1732 cm^{-1}; NMR ($CDCl_3$): 1.18 (3H, d, J=7 Hz, C_4–CH_3), 1.19 (3H, s, C_3–CH_3), 1.62 (3H, s, C_2–CH_3), *ca.* 2.5 (1H, bs, –OH), 2.87 (1H, q, J=7 Hz, C_4–H), 3.78 (3H, s, $-CO_2CH_3$). Found: C, 53.47; H, 6.97%. Calcd for $C_9H_{14}O_5$: C, 53.46; H, 6.98%. The IR and NMR spectra of (±)-**12** were identical with those of natural methyl monocrotalate.

Hydrolyses of (±)-11 and (±)-12. *a)*: A mixture of (±)-**11** (826 mg) and dilute hydrochloric acid (4 mol dm^{-3}: 33 ml) was refluxed for 2 h and then evaporated with benzene under a vacuum to dryness. The residue was chromatographed on silica gel[24] using acetone-benzene (1:4) as the eluent to give an acid (**3**) (587 mg: 76.4%) which was recrystallized from acetone-petroleum benzine; mp 156—158 °C; NMR (CD_3COCD_3): 1.13 (3H, d, J=7 Hz, C_4–CH_3), 1.38 (3H, s, C_3–CH_3), 1.57 (3H, s, C_2–CH_3), 2.80 (1H, q, J=7 Hz, C_4–H). Found: C, 51.16; H, 6.51%. Calcd for $C_8H_{12}O_5$: C, 51.06; H, 6.43%. Methylation of (±)-**3** with diazomethane yielded (±)-**11**.

b): A mixture of (±)-**12** (1.738 g) and dilute hydrochloric acid (4 mol dm^{-3}: 65 ml) was refluxed for 2 h and then treated as described for the preparation of (±)-**3**. The crude product was recrystallized from acetone-petroleum benzine to give the racemic monocrotalic acid (**4**) (659 mg: 40.8%); mp 187—189 °C; NMR (CD_3COCD_3): 1.14 (3H, d, J=7 Hz, C_4–CH_3), 1.27 (3H, s, C_3–CH_3), 1.62 (3H, s, C_2–CH_3), 2.84 (1H, q, J=7 Hz, C_4–H). Found: C, 51.30; H, 6.53%. Calcd for $C_8H_{12}O_5$: C, 51.06; H, 6.43%. The mother liquor of the above crystallization was evaporated under a vacuum and the residue was chromatographed on silica gel[24] using acetone-benzene (1:4) as the eluent to give some additional (±)-**4** (451 mg: 27.9%). Methylation of (±)-**4** with diazomethane afforded (±)-**12**.

Resolution of (±)-3. A mixture of (±)-**3** (551 mg) and brucine dihydrate (1.262 g) was dissolved in ethanol (100 ml) by heating. The solution was concentrated, allowed to stand at room temperature, and then filtered to give colorless crystals (870 mg), which were recrystallized three times from ethanol to give a brucine salt (464 mg); mp 218—225 °C dec; $[\alpha]_D$ −39.4°.

The salt was suspended in dilute hydrochloric acid and extracted with ether. The ether extract was washed with brine, dried over sodium sulfate, and then evaporated to dryness. The residue was purified by column chromatography on silica gel[24] to give **3a** (2*R*,3*R*,4*S*) (120 mg); $[\alpha]_D$ −32° (EtOH); CD (H_2O): $[\theta]_{204}$ −15000, $[\theta]_{224}$ +2700.

The filtrate from the above salt was evaporated under a vacuum and the residue was recrystallized from ethanol to yield another brucine salt (550 mg); mp 165—168 °C;

$[\alpha]_D$ −11.1°.

This salt was also treated with dilute hydrochloric acid as described above and the crude product was purified by column chromatography on silica gel[24] to give **3b** (2*S*,3*S*,4*R*) (103 mg); $[\alpha]_D$ +22° (EtOH); CD (H_2O):[23] $[\theta]_{204}$ +9200, $[\theta]_{224}$ −1800.

Resolution of (±)-4. A mixture of (±)-**4** (1.112 g) and brucine dihydrate (2.545 g) in ethanol (150 ml) was refluxed, concentrated, and then allowed to stand at room temperature. The crystals (1.790 g, mp 207—208 °C dec) were collected by filtration and recrystallized twice from ethanol to give a brucine salt (1.165 g); mp 208—209 °C dec; $[\alpha]_D$ −11.4°.

The salt was suspended in dilute hydrochloric acid, extracted with ether, and the ether extract was washed with brine. After drying over sodium sulfate, the solution was evaporated to afford a colorless solid (210 mg), which was recrystallized from acetone–petroleum benzine, giving monocrotalic acid (**4a**) (2*R*,3*R*,4*R*); mp 185—187 °C; $[\alpha]_D$ −5.6° (EtOH) (lit, mp 181—182 °C,[2] $[\alpha]_D$ −4.65±0.5° (EtOH)[7]); CD (H_2O): $[\theta]_{204}$ −11000.

The filtrate from the above salt was evaporated and the residue was recrystallized from ethanol to give another salt (1.145 g); mp 214—216 °C dec; $[\alpha]_D$ −32°.

This salt was also treated with dilute hydrochloric acid and the product (228 mg) was recrystallized from acetone–petroleum benzine to give **4b** (2*S*,3*S*,4*S*); mp 185—187 °C; $[\alpha]_D$ +5.3° (EtOH); CD (H_2O): $[\theta]_{204}$ +11000.

Dehydration of 11a and 11b. *a)*: A sample of **3a** (59 mg) was methylated with diazomethane to yield the corresponding methyl ester (**11a**), which was dissolved in a mixture of phosphoryl chloride (246 mg) and pyridine (0.6 ml). The solution was refluxed for 30 min, cooled, diluted with a mixture of ice and dilute hydrochloric acid, and then extracted with ether. The ether extract was washed with brine, dried over sodium sulfate, and evaporated. The residue was chromatographed on silica gel using ether–benzene (2:98) as the eluent to give methyl (*R*)-(+)-anhydromonocrotalate (**15a**) as an oil (35 mg: 60%); $[\alpha]_D$ 203°; IR: 1757, 1732, 1675 cm^{-1}; NMR ($CDCl_3$): 1.64 (3H, s, C_2–CH_3), 1.83 and 1.99 (each 3H and s, 2=CCH_3), 3.76 (3H, s, $-CO_2CH_3$). Found: C, 58.58; H, 6.67%. Calcd for $C_9H_{12}O_4$: C, 58.69; H, 6.57%.

b): A sample of **3b** (60 mg: $[\alpha]_D$ +18° (EtOH)) was methylated with diazomethane to afford a methyl ester (**11b**), which was refluxed with a mixture of phosphoryl chloride (248 mg) and pyridine (0.5 ml) for 30 min. After the same work-up as described in a) above the crude product was purified by column chromatography on silica gel to give methyl (*S*)-(−)-anhydromonocrotalate (**15b**) (47 mg: 76%) as an oil, $[\alpha]_D$ −101°, whose IR and NMR spectra were identical with those of **15a**.

Dehydration of 12a and 12b. *a)*: A sample of monocrotalic acid (**4a**) (143 mg) was methylated with diazomethane to give methyl monocrotalate (**12a**), which was refluxed with phosphoryl chloride (560 mg) in pyridine (1.2 ml) for 30 min. After the same work-up as described above, the crude product was purified by column chromatography on silica gel to afford an oil (100 mg: 72%), $[\alpha]_D$ +205°, whose IR and NMR spectra were identical with those of methyl (*R*)-(+)-anhydromonocrotalate (**15a**).

b): Methylation of **4b** (43 mg) with diazomethane gave the corresponding methyl ester (**12b**), which was dehydrated with phosphoryl chloride (170 mg) in pyridine (0.5 ml) as described above. Purification of the crude product by column chromatography on silica gel afforded methyl (*S*)-(−)-anhydromonocrotalate (**15b**) (35 mg: 83%) as an oil, $[\alpha]_D$ −195°.

(S)-(+)-3-Acetoxy-2-methylpropanoic Acid (25). (*R*)-(−)-2-Phenylpropanoic acid (**21**)[16] (6.136 g, $[\alpha]_D$ −63.8°) was methylated with diazomethane to give a methyl ester (**22**) (6.701 g), $[\alpha]_D$ −85°.

A sample of **22** (6.137 g) was reduced with lithium aluminium hydride (852 mg) in ether (60 ml) at room temperature for 2 h. After the usual work-up, the crude alcohol (**23**) (5.038 g: $[\alpha]_D$ +4.5°) was immediately acetylated at 80 °C for 1.5 h with acetic anhydride (19 ml) in pyridine (25 ml) to give (*R*)-(−)-2-phenylpropyl acetate (**24**) (6.254 g); $[\alpha]_D$ −4.5°; NMR: 1.30 (3H, d, J=7 Hz, $C\underline{H}_3CH$–), 1.96 (3H, s, $-OCOCH_3$), 3.05 (1H, m, $CH_3C\underline{H}$–), 4.10 (2H, bd, J=7 Hz, $-CH_2O$–), 7.21 (5H, s, $-C_6H_5$).

A solution of **24** (5.810 g) in chloroform (30 ml) was ozonized at 0—15 °C for *ca.* 70 h. The solution was evaporated under a vacuum and the residue was chromatographed on silica gel[24] using ether–benzene (1:9) as the eluent to afford an acid (**25**) as an oil (1.813 g); $[\alpha]_D$ +16.2°; NMR: 1.25 (3H, d, J=7 Hz, $C\underline{H}_3CH$–), 2.23 (3H, s, $-OCOCH_3$), 2.78 (1H, m, $CH_3C\underline{H}$–), 4.16 (2H, d, J=7 Hz, $-CH_2O$–).

Methyl (S)-(+)-3-Acetoxy-2-methylpropanoate (26). A solution of **25** (1.508 g) in ether (10 ml) was methylated with diazomethane to give the corresponding methyl ester (**26**) (1.567 g); $[\alpha]_D$ +18.2°; NMR: 1.19 (3H, d, J=7 Hz, $C\underline{H}_3CH$–), 2.00 (3H, s, $-OCOCH_3$), 2.70 (1H, m, $CH_3C\underline{H}$–), 3.69 (3H, s, $-CO_2CH_3$), 4.13 (2H, d, J=7 Hz, $-CH_2O$–).

(S)-(−)-3-Hydroxy-2,3-dimethylbutyl Acetate (20b). The Grignard reagent, prepared from methyl iodide (5.0 ml) and magnesium (1.306 g) in dry ether (10 ml), was diluted with dry benzene (15 ml), and then the ether was distilled off. After the addition of a solution of **26** (1.323 g) in dry benzene (3.0 ml), the mixture was stirred at room temperature for 30 min and then refluxed for 1.5 h. The reaction mixture was poured into a mixture of ice and dilute hydrochloric acid, and extracted with ether. The aqueous layer was further extracted continuously with ether for *ca.* 2.5 h. The ether extracts were combined, washed successively with aqueous sodium thiosulfate and brine, dried over sodium sulfate, and then evaporated. The residual oil (925 mg) was purified by column chromatography on silica gel using ether–chloroform (1:1) as the eluent to give (*S*)-2,3-dimethyl-1,3-butanediol (**19b**) (615 mg); NMR: 0.82 (3H, d, J=7 Hz, $C\underline{H}_3CH$–), 1.12 and 1.19 (each 3H and s, $(CH_3)_2C$–), 3.58 (2H, d, J=7 Hz, $-C\underline{H}_2OH$).

The above diol **19b** (64.8 mg) was acetylated with acetic anhydride (0.3 ml) in pyridine (0.5 ml) at room temperature for 36 h. After the usual work-up, the crude product was purified by column chromatography on silica gel using ether–chloroform (1:9) as the eluent to give (*S*)-(−)-3-hydroxy-2,3-dimethylbutyl acetate (**20b**) (54.3 mg) as an oil: $[\alpha]_D$ −27.1°; IR: 3605, 3460, 1725 cm^{-1}; NMR: 0.94 (3H, d, J=7 Hz, $C\underline{H}_3CH$–), 1.12 and 1.17 (each 3H and s, $(CH_3)_2C$–), 2.00 (3H, s, $-OCOCH_3$), 3.6—4.4 (2H, m, $-CH_2O$–). Found: C, 59.69; H, 9.78%. Calcd for $C_8H_{16}O_3$: C, 59.98; H, 10.07%.

Resolution of (±)-trans-2,3,4-Trimethyl-2-pentenedioic Acid (8). A mixture of (±)-**8** (3.455 g) and cinchonidine (11.812 g) was dissolved in ethyl acetate (2.3 l) by refluxing, concentrated to about half volume, and then allowed to stand at room temperature. The colorless crystals (8.14 g) were collected by filtration and recrystallized twice from ethyl acetate to afford a cinchonidine salt (5.537 g); mp 185—187 °C; $[\alpha]_D$ −64°.

An aliquot of the above salt (500 mg) was suspended in dilute hydrochloric acid, extracted with ether, and the ether extract was washed with brine. After drying over sodium sulfate, the solution was evaporated to give (*S*)-(+)-*trans*-2,3,4-trimethyl-2-pentenedioic acid (**8a**) (121 mg), which was recrystallized from ether-petroleum benzine; mp 108—110 °C; $[\alpha]_D$ +121° (ether).

The filtrate from the above salt was evaporated under a vacuum and the residue was recrystallized several times from ethyl acetate to give another cinchonidine salt (1.787 g); mp 166—168 °C; $[\alpha]_D$ −97°.

This salt was also treated with dilute hydrochloric acid to afford (*R*)-(−)-*trans*-2,3,4-trimethyl-2-pentenedioic acid (**8b**) (375 mg); mp 108—110 °C; $[\alpha]_D$ −120° (ether).

*Methylation of **8a** and **8b**.* *a)*: Methylation of **8a** with diazomethane afforded dimethyl (*S*)-(+)-*trans*-2,3,4-trimethyl-2-pentenedioate (**10a**) as an oil, $[\alpha]_D$ +114° (ether), whose IR and NMR spectra were identical with those of (±)-**10**.

b): Methylation of **8b** with diazomethane afforded dimethyl (*R*)-(−)-*trans*-2,3,4-trimethyl-2-pentenedioate (**10b**) as an oil, $[\alpha]_D$ −111° (ether), whose IR and NMR spectra were identical with those of (±)-**10**.

*(S)-(+)-1,5-Diacetoxy-2,3,4-trimethyl-2-pentene (**17**).* A solution of **10a** (1.670 g, $[\alpha]_D$ +102° (ether)) in dry ether (15 ml) was added dropwise to a suspension of lithium aluminium hydride (950 mg) in dry ether (20 ml) with stirring. The mixture was refluxed for 2 h, poured into a mixture of ice and dilute hydrochloric acid, and extracted with ether. The ether extract was washed with brine, dried over sodium sulfate, and then evaporated to give a diol (**16**) (1.101 g) as an oil, $[\alpha]_D$ +7.4° (ether).

The above crude diol (**16**) (1.101 g) was immediately acetylated with acetic anhydride (4.4 ml) in pyridine (6.0 ml) at 80 °C for 2 h. After the usual work-up, the crude product was purified by column chromatography on silica gel using ether-benzene (2:98) as the eluent to give a diacetate (**17**) (665 mg) as an oil: $[\alpha]_D$ +9.1°; IR: 1725 cm^{-1}; NMR: 0.98 (3H, d, J=7 Hz, $C\underline{H}_3CH$–), 1.70 (6H, br, 2=CCH_3), 1.95 and 1.99 (each 3H and s, 2–$OCOCH_3$), 3.92 (2H, d, J=7 Hz, $-CH_2O$–), 4.51 (2H, s, =CCH_2O–). Found: C, 63.02; H, 9.13%. Calcd for $C_{12}H_{20}O_4$: C, 63.13; H, 8.83%.

*(R)-(+)-3-Hydroxy-2,3-dimethylbutyl Acetate (**20a**).* A solution of **17** (323 mg) in chloroform (10 ml) was ozonized at −10 °C for 3 h and then evaporated to give a crude ketone (**18**) (331 mg).

A solution of the above ketone (**18**) (321 mg) in dry benzene (3.0 ml) was refluxed for 1.5 h with the Grignard reagent, prepared from methyl iodide (1.1 ml) and magnesium (345 mg) in dry ether (5.0 ml) and benzene (5.0 ml). After the same work-up as described for the preparation of **19b**, the crude product was purified by column chromatography on silica gel using ether-chloroform (1:1) as the eluent to give a diol (**19a**) (83 mg) whose IR and NMR spectra were identical with those of **19b**.

The above diol **19a** (68 mg) was acetylated with acetic anhydride (0.3 ml) in pyridine (0.5 ml) at room temperature for 36 h. After the same work-up as described for the preparation of **20b**, the crude product was purified by column chromatography on silica gel to afford (*R*)-(+)-3-hydroxy-2,3-dimethylbutyl acetate (**20a**) (52 mg) as an oil, $[\alpha]_D$ +16.9°, whose IR and NMR spectra were identical with those of **20b**. Found: C, 59.73; H, 10.17%. Calcd for $C_8H_{16}O_3$: C, 59.98; H, 10.07%.

*Oxidation of **10b** with Potassium Permanganate.* A solution of **10b** (355 mg) in methanol (10 ml) was oxidized at −20±2 °C with a solution of potassium permanganate (380 mg) and magnesium sulfate heptahydrate (531 mg) in water (18 ml) as described above. The crude product was purified by column chromatography on silica gel using ether-benzene (15:85) as the eluent to give a γ-lactone ester (**13b**) (2*S*,3*R*,4*R*) (104 mg), which was recrystallized from ether-petroleum benzine; mp 93—95 °C; $[\alpha]_D$ +28.5°; IR: 3450, 1780, 1740 cm^{-1}; NMR ($CDCl_3$): 1.19 (3H, d, J=7 Hz, C_4–CH_3), 1.28 (3H, s, C_3–CH_3), 1.58 (3H, s, C_2–CH_3), 3.04 (1H, q, J=7 Hz, C_4–H), 3.82 (3H, s, $-CO_2CH_3$). Found: C, 53.62; H, 6.84%. Calcd for $C_9H_{14}O_5$: C, 53.46; H, 6.98%.

Further elution gave another γ-lactone ester (**14a**) (2*R*, 3*S*,4*R*) (44 mg) which was recrystallized from ether; mp 133—135 °C; $[\alpha]_D$ +5.1°; IR: 3450, 1780, 1730 cm^{-1}; NMR ($CDCl_3$): 1.22 (3H, d, J=7 Hz, C_4–CH_3), 1.53 (3H, s, C_3–CH_3), 1.58 (3H, s, C_2–CH_3), 2.61 (1H, q, J=7 Hz, C_4–H), 3.83 (3H, s, $-CO_2CH_3$). Found: C, 53.58; H, 7.18%. Calcd for $C_9H_{14}O_5$: C, 53.46; H, 6.98%.

*Dehydration of **13b** and **14a**.* *a)*: A sample of **13b** (86 mg) was dehydrated with phosphoryl chloride (324 mg) in pyridine (0.8 ml) as described above. The crude product was purified by column chromatography on silica gel to afford methyl (*S*)-(−)-anhydromonocrotalate (**15b**) (40 mg: 51%) as an oil, $[\alpha]_D$ −199°.

b): A sample of **14a** (39 mg) was also dehydrated with phosphoryl chloride (148 mg) in pyridine (0.5 ml) to yield methyl (*R*)-(+)-anhydromonocrotalate (**15a**) (13 mg: 35%) as an oil, $[\alpha]_D$ +170°.

*Hydrolyses of **13b** and **14a**.* *a)*: A sample of **13b** (88 mg) was refluxed with dilute hydrochloric acid (4 mol dm^{-3}:4.0 ml) for 2 h. The product (71 mg) was recrystallized from acetone-petroleum benzine to give the corresponding γ-lactone acid (**5b**) (2*S*,3*R*,4*R*); mp 185—188 °C; $[\alpha]_D$ +60° (EtOH); NMR (CD_3COCD_3): 1.11 (3H, d, J= 7 Hz, C_4–CH_3), 1.28 (3H, s, C_3–CH_3), 1.53 (3H, s, C_2–CH_3), 3.09 (1H, q, J=7 Hz, C_4–H). Found: C, 51.08; H, 6.46%. Calcd for $C_8H_{12}O_5$: C, 51.06; H, 6.43%.

Methylation of **5b** with diazomethane gave **13b**.

b): A sample of **14a** (39 mg) was hydrolyzed with dilute hydrochloric acid. The product (27 mg) was recrystallized from acetone-petroleum benzine to give the corresponding γ-lactone acid (**6a**) (2*R*,3*S*,4*R*); mp 185—187.5 °C; $[\alpha]_D$ −5.1° (EtOH); CD (H_2O): $[\theta]_{204}$ −5500; NMR (CD_3COCD_3): 1.13 (3H, d, J=7 Hz, C_4–CH_3), 1.53 (3H, s, C_3–CH_3), 1.56 (3H, s, C_2–CH_3), 2.82 (1H, q, J=7 Hz, C_4–H). Found: C, 51.10; H, 6.45%. Calcd for $C_8H_{12}O_5$: C, 51.06; H, 6.43%.

Methylation of **6a** with diazomethane gave **14a**.

*Oxidation of **10a** with Potassium Permanganate.* A solution of **10a** (1.075 g) in methanol (32 ml) was oxidized at −20±2 °C with a solution of potassium permanganate (1.150 g) and magnesium sulfate heptahydrate (1.607 g) in water (60 ml), as described for (±)-**9**. The crude product was chromatographed on silica gel using ether-benzene (15:85) as the eluent to give a γ-lactone ester (**13a**) (2*R*, 3*S*,4*S*) (432 mg), which was recrystallized from ether-petroleum benzine; mp 94—96 °C; $[\alpha]_D$ −29.6°. The IR and NMR spectra of **13a** were identical with those of **13b**.

Further elution gave another γ-lactone ester (**14b**) (2*S*, 3*R*,4*S*) (188 mg), which was recrystallized from ether: mp 133—135 °C; $[\alpha]_D$ −5.4°. The IR and NMR spectra of **14b** were identical with those of **14a**.

*Hydrolyses of **13a** and **14b**.* *a)*: A sample of **13a** was refluxed with dilute hydrochloric acid for 2 h. Purification of the product gave **5a** (2*R*,3*S*,4*S*); mp 186—189 °C; $[\alpha]_D$ −69° (EtOH). The NMR spectrum of **5a** was identical

with that of **5b**.

Methylation of **5a** with diazomethane gave **13a**.

b): A sample of **14b** was hydrolyzed with dilute hydrochloric acid to afford **6b** (2*S*,3*R*,4*S*); mp 185.5—188 °C; $[\alpha]_D$ +6.3° (EtOH); CD (H_2O): $[\theta]_{204}$ +5400. The NMR spectrum of **6b** was identical with that of **6a**.

Methylation of **6b** with diazomethane gave **14b**.

Oxidation of (±)-10 with Potassium Permanganate. A sample of (±)-**10** was oxidized with potassium permanganate as described for (±)-**9**. Chromatographic purification of the crude product yielded a γ-lactone ester, (±)-**13**, which was recrystallized from ether-petroleum benzine: mp 93—94.5 °C. Found: C, 53.73; H, 6.96%. Calcd for $C_9H_{14}O_5$: C, 53.46; H, 6.98%.

Further elution gave another γ-lactone ester, (±)-**14**, which was recrystallized from ether, mp 110—111.5 °C. Found: C, 53.55; H, 7.06%. Calcd for $C_9H_{14}O_5$: C, 53.46; H, 6.98%.

Hydrolyses of (±)-13 and (±)-14. *a)*: A sample of (±)-**13** was hydrolyzed with dilute hydrochloric acid to give (±)-**5**, mp 161—165 °C. Found: C, 50.78; H, 6.50%. Calcd for $C_8H_{12}O_5$: C, 51.06; H, 6.43%.

b): A similar hydrolysis of (±)-**14** afforded (±)-**6**, mp 199—203 °C. Found: C, 51.10; H, 6.45%. Calcd for $C_8H_{12}O_5$: C, 51.06; H, 6.43%.

Resolution of (±)-5. A mixture of (±)-**5** (1.048 g) and cinchonidine (1.639 g) was dissolved in hot ethyl acetate (600 ml) and then concentrated. The crystals were collected by filtration and recrystallized from ethyl acetate to afford a cinchonidine salt (930 mg); mp 199.5—201 °C dec; $[\alpha]_D$ −77.2°.

The salt was suspended in dilute hydrochloric acid and extracted with ether. The ether extract was washed with brine, dried over sodium sulfate, and then evaporated to give **5b** (2*S*,3*R*,4*R*) (311 mg), which was recrystallized from acetone-petroleum benzine; mp 186—189 °C; $[\alpha]_D$ +70.0° (EtOH); CD (H_2O): $[\theta]_{204}$ +12000, $[\theta]_{224}$ −4200.

The filtrate from the above salt was evaporated and the residue was recrystallized from ethyl acetate to give another cinchonidine salt (788 mg); mp 187—189 °C; $[\alpha]_D$ −62.9°.

This salt was also treated with dilute hydrochloric acid to give **5a** (2*R*,3*S*,4*S*) (279 mg), which was recrystallized from acetone-petroleum benzine; mp 186—189 °C; $[\alpha]_D$ −69.4° (EtOH); CD (H_2O): $[\theta]_{204}$ −12000, $[\theta]_{224}$ +4200.

The authors wish to express their thanks to Professor D. H. G. Crout, University of Exeter, for his generous gift of monocrotalic acid. This work was supported by a Grant-in-Aid for Scientific Research from the Ministry of Education.

References

1) W. M. Neal, L. L. Rusoff, and C. F. Ahmann, *J. Am. Chem. Soc.*, **57**, 2560 (1935).
2) R. Adams and E. F. Rogers, *J. Am. Chem. Soc.*, **61**, 2815 (1939).
3) M. Greshoff, *Ber.*, **23**, 3537 (1890).
4) S. Kumari, K. K. Kapur, and C. K. Atal, *Current Sci. (India)*, **35**, 546 (1966); *Chem. Abstr.*, **66**, 17040 (1967).
5) R. N. Gandhi, T. R. Rajagopalan, and T. R. Seshadri, *Current Sci. (India)*, **35**, 514 (1966); *Chem. Abstr.*, **66**, 11076 (1967).
6) R. Adams and T. R. Govindachari, *J. Am. Chem. Soc.*, **72**, 158 (1950).
7) R. Adams, B. L. VanDuuren, and B. H. Braun, *J. Am. Chem. Soc.*, **74**, 5608 (1952).
8) O. Cervinka and L. Hub, *Collect. Czech. Chem. Commun.*, **33**, 2933 (1968).
9) O. Cervinka, L. Hub, A. Klasek, and F. Santavy, *Chem. Commun.*, **1968**, 261.
10) D. J. Robins and D. H. G. Crout, *J. Chem. Soc., C*, **1969**, 1386.
11) D. J. Robins and D. H. G. Crout, *J. Chem. Soc., C*, **1970**, 1334.
12) J. D. Edwards, Jr., and T. Matsumoto, *J. Org. Chem.*, **32**, 2561 (1967).
13) T. Matsumoto, T. Okabe, and K. Fukui, *Chem. Lett.*, **1972**, 29; **1973**, 773.
14) Because of insufficient material, it was not possible to obtain the optically pure **3b**.
15) The dimethyl ester **10a**, $[\alpha]_D$ +102° (ether), was used.
16) P. A. Levene, L. A. Mikeska, and K. Passoth, *J. Biol. Chem.*, **88**, 27 (1930); G. Fodor and G. Csepreghy, *J. Chem. Soc.*, **1961**, 3222; C. L. Arcus and J. Kenyon, *J. Chem. Soc.*, **1939**, 916.
17) D. J. Cram and F. A. Abd Elhafez, *J. Am. Chem. Soc.*, **74**, 5828 (1952).
18) G. J. Karabatsos, *J. Am. Chem. Soc.*, **89**, 1367 (1967).
19) J. A. Hirsch, "Topics in Stereochemistry," ed by N. L. Allinger and E. L. Eliel, Interscience, New York (1967), Vol. 1, p. 199.
20) M. Kinoshita, S. Aburaki, and S. Umezawa, *J. Antibiot. (Tokyo)*, **25**, 373 (1972).
21) T. Okuda, S. Harigaya, and A. Kiyomoto, *Chem. Pharm. Bull.*, **12**, 504 (1964).
22) A. F. Beecham, *Tetrahedron Lett.*, **1968**, 2355.
23) The low molecular ellipticity arose from the low optical purity of the sample used.
24) Silica gel (Mallinckrodt, Silic AR CC-4) was used.

Acyl Cyanide. VI. The Synthesis of 1-Cyano-1-alkenyl Esters by the Reaction of Acyl Cyanides with Acid Chlorides. Synthesis and Mechanism

Akira Oku* and Shingo Arita

Department of Chemistry, Kyoto Institute of Technology, Matsugasaki, Sakyo-ku, Kyoto 606

(Received March 16, 1979)

The reactions of enolizable acyl cyanides (acetyl, propionyl, isobutyryl, and diphenylacetyl cyanide) with acid chlorides (acetyl, propionyl, benzoyl, *p*-nitrobenzoyl, diphenylcarbamoyl, and dimethylcarbamoyl chloride) in the presence of tertiary amines gave the corresponding 1-cyano-1-alkenyl carboxylates or carbamates in good yields. Among several solvents and amines examined in the reaction of acetyl cyanide with propionyl chloride, benzene and pyridine seem to be most appropriate. The maximum yield (98%) of the ester was attained in benzene when both the chloride and pyridine were used in excess amounts (1.2—1.4 times the amount of the cyanide). The rate of reaction depended little on the concentration of the chloride but on both the cyanide and the amine being of first order in each reactant; it was also influenced by the basicity of tertiary amines and, in the case of weak bases, additionally by their nucleophilic power.

In the preceding paper,[1] we reported that 1-cyano-1-alkenyl esters can be easily synthesized by simply mixing acid anhydrides with primary or secondary acyl cyanides under the influence of amine catalysts. In the present study, we have extended the choice of acylating reagent from acid anhydride to acyl chloride including not only carboxylic acid chlorides but also carbamoyl chlorides, and have carried out their reactions with potentially enolizable acyl cyanides in the presence of stoichiometric amount of tertiary amines. In this report, solvent effects, base catalysis, and reaction mechanisms are discussed together with the synthesis.

Results and Discussion

The results of the reactions between four enolizable acyl cyanides and nine acid chlorides are listed in Table 1. Tertiary amines were adopted as the base, tetrahydrofuran (THF) and dichloromethane were used as solvents. The yields listed in this table are based upon the products isolated by fractional distillation and are not necessarily the best ones (as for improving product yields, see the following sections).

$$R^1R^2CH\text{-}CO\text{-}CN + R^3\text{-}CO\text{-}Cl \xrightarrow{\text{amine}} R^1R^2C{=}C(CN)\text{-}OCOR^3 + \text{amine}\cdot HCl$$

Although a stoichiometric amount of amine is required in this reaction in contrast to its catalytic amount in the reaction with acid anhydrides,[1] the product esters were obtained in relatively high yields and in pure states not contaminated by such by-products as the dimer of acyl cyanide.

Solvents. In order to increase the reaction rates and also the product yields in this synthesis, the choice of appropriate solvents is important. As a model reaction, the reaction of acetyl cyanide with propionyl chloride in the presence of pyridine was chosen and the effect of solvents (acetonitrile, dichloromethane, benzene, and THF) were examined by plotting the product yields against reaction time (see Fig. 1). With this figure it becomes evident that the solvent effect on the rate of reaction is in the following order $CH_3CN \approx CH_2Cl_2 > C_6H_6 > THF$.[2] On the other hand, the yield was the highest in benzene (80% when the reactant ratio was cyanide/chloride/amine=1/1/1) but in CH_3CN or CH_2Cl_2 the yield hit a ceiling at *ca.* 60%, possibly due to the faster consumption of the chloride[3] than of the cyanide. Therefore, benzene seems to be most useful among the four solvents examined.

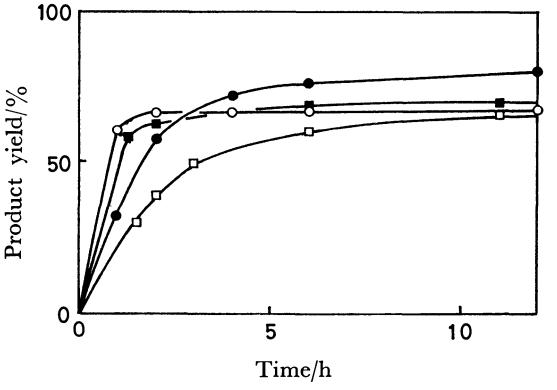

Fig. 1. The effect of solvent on the formation of 1-cyanovinyl propionate.[a]
CH_3CN (■), CH_2Cl_2 (○), C_6H_6 (●), THF (□).
a) Reactant ratio: cyanide/chloride/pyridine=1/1/1, 0.02 mol/18 ml for each reagent, at 25 °C. Product yields were determined by VPC using the method of calibration curves.

Reactant Ratios. At the last stage of average reactions where the initially charged reactant ratios were [cyanide]/[chloride]/[amine]=1/1/1 as in the cases of the reactions of Table 1, usually the chloride was completely consumed while some amount of the cyanide remained unreacted. This implied that some side reactions were taking place competingly to consume the chloride.[3] Thus we thought that the increase in the initial amount of chloride relative to that of the cyanide would improve the yield. We inspected this effect in the reaction of acetyl cyanide with propionyl chloride in the presence of pyridine, and the results are shown in Table 2. This table clearly indicates that acetyl cyanide can be converted into 1-cyanovinyl propionate almost quantitatively when an excess amount of the chloride and amine (both 1.2—1.4 times more than the cyanide) are used. Proved also is the necessity of an equivalent amount of amine to that of chloride

Table 1. Preparation of 1-cyano-1-alkenyl carboxylates by the reaction of acyl cyanides with acyl chlorides

$R^1R^2C{=}C(CN)OCOR^3$

Compd	R^1	R^2	R^3	Amine[d]	Solvent	Time/h	Yield/%[b]
1	H	H	CH_3	Pyr	CH_2Cl_2	24	65
2	H	H	CH_2Cl	DMA	CH_2Cl_2	21	76
3	H	H	C_2H_5	Pyr	CH_2Cl_2	24	56
4	H	H	OC_2H_5	Pyr	CH_2Cl_2	20	36
5	H	H	C_6H_5	Pyr	CH_2Cl_2	25	68
6	H	H	*p*-NO_2-C_6H_4	Pyr	THF	24	49
7	H	H	$N(CH_3)_2$	Pyr	THF	24	c)
8	H	H	$N(C_6H_5)_2$	Pyr	THF	24	c)
9	CH_3	H	CH_3	Pyr	CH_2Cl_2	24	70
	CH_3	H	CH_3	Dabco	CH_2Cl_2	2	75
	CH_3	H	CH_3	DBU	CH_2Cl_2	2	61
10	CH_3	H	CH_2Cl	DMA	CH_2Cl_2	28	77
11	CH_3	H	OC_2H_5	Pyr	CH_2Cl_2	21	50
12	CH_3	H	*p*-NO_2-C_6H_4	Pyr	THF	24	60
13	CH_3	H	$N(CH_3)_2$	Pyr	THF	24	33
14	CH_3	H	$N(C_6H_5)_2$	Pyr	THF	24	25
15	CH_3	CH_3	CH_3	Pyr	THF	21	78
16	CH_3	CH_3	*p*-NO_2-C_6H_4	Pyr	THF	24	68
17	CH_3	CH_3	$N(CH_3)_2$	Pyr	THF	24	33
18	CH_3	CH_3	$N(C_6H_5)_2$	Pyr	THF	24	50
19	C_6H_5	C_6H_5	$CH(C_6H_5)_2$	Crown[e]	DME	20	48

a) Reactant molar ratio: cyanide/chloride/amine = 1.0/1.0/1.0. b) Isolated yields after distillation or column chromatography. c) Only a trace amount of the corresponding cyanoalkenyl carbamate was formed whereas the major product was the dimer of the cyanide. d) Pyr = pyridine, DMA = *N*,*N*-dimethylaniline, Dabco = 1,4-diazabicyclo[2.2.2]octane, DBU = 1,8-diazabicyclo[5.4.0]undec-7-ene, Crown = dicyclohexyl-18-crown-6. e) This ester was prepared directly by the reaction of diphenylacetyl chloride with potassium cyanide in the presence of crown ether catalyst.

Table 2. The influence of reactant ratios on the ester formation[a]

Run	Relative reactant ratio			Yield of ester[b] %/Time(h)
	CH_3COCN	C_2H_5COCl	C_5H_5N	
1	1.0	1.0	1.0	80/10
2	1.0	1.4	1.0	81/10
3	1.0	1.4	1.4	96/10, 98/26
4	1.0	1.6	1.4	90/10, 97/24

a) In dry benzene at 25 °C. Standard reactant concentration for the cyanide was 0.02 mol in 16 ml of benzene. b) Determined by VPC analysis, calibrating with authentic compounds.

in this improved method.

Reaction Rate. In Table 3 are shown the effects of reactant ratios on the initial rates of reaction. Evidently, the rates seem to be dependent on the concentration of both the cyanide and the amine, being of first order in the concentration of each of these reactants, and hardly dependent on the concentration of the chloride.

Based on the above observations and subsidiarily on the fact that the chloride reacts rapidly with the amine to form a pyridinium salt **20**,[4,5] the following reaction channel is proposed.

$$C_2H_5COCl + \text{pyridine} \underset{}{\overset{K}{\rightleftharpoons}} \underset{\mathbf{20}}{[C_2H_5CO\text{-pyridine}]^+Cl^-} \quad (1)$$

$$CH_3COCN + \text{pyridine} \xrightarrow[\text{slow}]{k} \underset{\mathbf{21}}{[CH_3COCN][\text{pyridine}]} \quad (2)$$

$$[CH_3COCN][\text{pyridine}] + C_2H_5COCl \xrightarrow[\text{fast}]{} CH_2{=}C(CN)OCOC_2H_5 + \text{pyridine}\cdot HCl \quad (3)$$

Equation 1 means a rapidly established equilibrium prior to the condensation reaction. In Eq. 2 an intermediate (or a transition state) **21** consisting of the cyanide and pyridine is formed, whose structure will be discussed in the following section.

According to this mechanism, the initial rate of reaction R_0 is calculated and expressed by

$$R_0 = \frac{k}{2K}A_0[-\{1+K(E_0-P_0)\}+\sqrt{\{1+K(E_0-P_0)\}^2+4KP_0}] \quad (4)$$

where E_0, P_0, A_0 are the initial concentration of the chloride, pyridine, and cyanide respectively. By substituting the observed values of Runs 1 and 4 in Table 3 for Eq. 4, $k = 3.06\times10^{-2}$ L/mol·s and $K = 0.10$ were obtained. With these two constants we calculated the initial rates R_0(calcd) which agreed well with the observed R_0(obsd), thus the reaction channel proposed above seems to be compatible with the experimental results.

Base Catalysis. In this reaction it must be noticed that the rate of reaction depends markedly upon the choice of amine catalysts. To find a general

Table 3. Effect of the molar ratios of reactants on the initial rates of reaction R_0

Run	Reactant molar ratio			R_0(obsd)	Rel. rate	R_0(calcd)
	Cyanide	Chloride	Pyridine	mol·L^{-1}·min^{-1}		
1	0.396	0.396	0.396	4.7×10^{-3}	1.0	4.6×10^{-3}
2	0.770	0.385	0.385	8.2×10^{-3}	1.7	8.7×10^{-3}
3	0.382	0.764	0.382	4.5×10^{-3}	0.95	4.2×10^{-3}
4	0.384	0.384	0.762	8.5×10^{-3}	1.8	8.6×10^{-3}
5	0.371	0.742	0.742	9.3×10^{-3}	1.95	7.9×10^{-3}

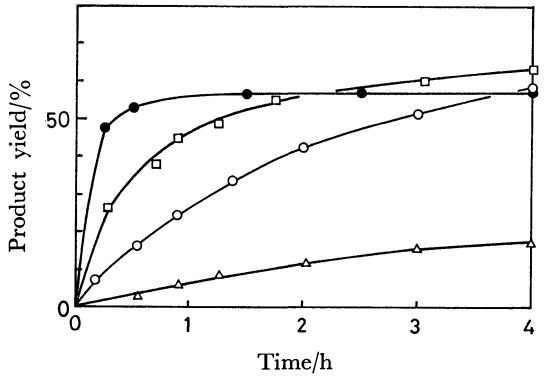

Fig. 2. The effect of tertiary amines on the rates of formation of 1-cyanovinyl propionate in benzene.[a]
2-Picoline (△), pyridine (○), 2,6-lutidine (□), 1,4-diazabicyclo[2.2.2]octane (●).
a) Reactant ratio: cyanide/chloride/amine=1/1/1, 0.02 mol/18 mL for each reagent, at 25±0.5 °C. Product yields were determined by VPC using the method of calibration curves.

rule in this catalysis along the line of solving the reaction mechanism, the influence of five tertiary amines, *i.e.*, 1,4-diazabicyclo[2.2.2]octane (Dabco), 4-(dimethylamino)pyridine, 2,6-lutidine, 2-picoline, and pyridine, upon the reaction rate were examined by means of direct measurements by NMR and also by VPC analysis using the internal reference technique. The tendencies of the base catalysis obtained in triplicate experiments were reproducible and the same in both methods. Results are shown in Fig. 2. Amines with strong basicity (and possibly with strong nucleophilicity), *e.g.*, Dabco (pK_a 8.7) and 4-(dimethylamino)-pyridine (pK_a 9.71),[6] showed the greatest rate-enhancement whereas the product yields were relatively low, probably due to some side reactions such as polymerization of the ester. In contrast, the best yield was attained when pyridine, a weaker base than the others, was adopted.

Looking at Figure 3, one notices that the effect of methyl-substituted pyridines on the rate acceleration is in the order of 2,6-lutidine (pK_a 6.75)>pyridine (5.27)>2-picoline (5.97),[6] which is not in laccord with the order of basicity nor nucleophilic power. Therefore, the rate is not solely dependent on either character of amines but seems to be controlled by both of them.

As a rational structure of the transition state which is compatible not only with the behavior of bases but also with the rate Eq. 4, a base-catalysis model **22** is postulated where the proton-abstraction composes the rate-determining step. According to Eq. 1 the concentration of free amine must depend upon its nucleophilic power which, in the reaction of methyl-substituted pyridines toward acyl chloride, seems to be in the order of 2-picoline (steric factor is conformationally negligible with regard to its pyridinium structure) > pyridine > 2,6-lutidine. Therefore, the equilibrium constant K must be small for 2,6-lutidine, and large enough for 2-picoline to cancell out its higher basicity than pyridine's. As for strong bases above p$K_a\approx8$, the nucleophilicity may not change so much as the pK_a does that the basicity plays an important role in the transition state.

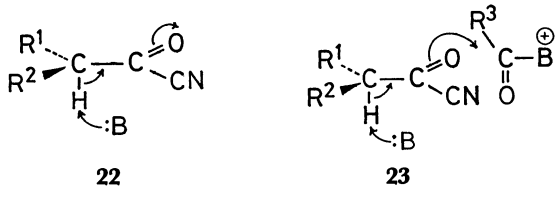

Scheme 1.

As an alternative transition state, a push-pull model **23** seems to be proposable where the ionic character of the N–CO bond in pyridinium ion plays a part of the rate acceleration. In this, 2,6-lutidine acts as a strong base and simultaneously as a weak nucleophile that enhances the ionization of the N–CO bond, whereas 2-picoline acts in the opposite way. The nucleophilicity of pyridine, though being a weaker base than picoline, may lie in between the other two amines as explained above. Although, at a glance, the rate seems to be dependent on the concentration of the chloride in this sort of general acid-base catalysis, the possibility of rate acceleration by the increase in acyl chloride must be cancelled out by the decrease in free amine concentration at the other reacting terminus. Therefore, the rate may become almost insensitive to the change in the chloride concentration.

Experimental

General. NMR chemical shifts and coupling constants are expressed by δ and Hz unit respectively. Acyl cyanides (acetyl, propionyl, isobutyryl, and diphenylacetyl cyanide) were prepared according to the reported method.[1] Other reagents were commercially available.

Reaction of Acyl Cyanide with Acyl Chloride; A General Synthetic Procedure. Under ice-cooling, tertiary amine (0.04 mol) dissolved in 10 mL of a solvent was added to a mixture of an acyl cyanide (0.04 mol) and an acyl chloride (0.04 mol)

both dissolved in 10 mL of the same solvent. Immediate formation of the pyridinium salt was observed. After stirring the mixture at ambient temperature for several hours, the solution was filtered, the filtrate was washed with water three times and dried over anhyd $MgSO_4$. Fractional distillation of the solution gave the expected 1-cyano-1-alkenyl ester. The product yields and amines used are listed in Table 1. In the following paragraphs, the spectroscopic data of some 1-cyano-1-alkenyl esters are listed. For the other esters, see the preceding report.[1]

*1-Cyanovinyl Chloroacetate (**2**)*: Bp 70—75 °C/4 Torr. IR 2240, 1780 cm^{-1}. NMR ($CDCl_3$) 5.93 (2H, a pair of d, J=3.2), 4.27 (2H, s).

*1-Cyanovinyl Ethyl Carbonate (**4**)*: Bp 46—50 °C/3 Torr. IR 2230, 1765 cm^{-1}. NMR ($CDCl_3$) 5.70 (2H, a pair of d, J=3.0), 4.25 (2H, q, J=7.3), 1.40 (3H, t, J=7.3).

*1-Cyanovinyl p-Nitrobenzoate (**6**)*: Mp 132—135 °C. IR 1760 cm^{-1}. NMR ($CDCl_3$) 8.47 (4H, m), 6.03 (2H, a pair of d, J=3.5).

*1-Cyanovinyl Benzoate (**5**)*: Mp 35.5—38 °C. Bp 88—95 °C/0.4 Torr. IR 2220, 1740 cm^{-1}. NMR ($CDCl_3$) 8.2—7.3 (5H, m), 5.87 (2H, a pair of d, J=2.5).

*1-Cyano-1-propenyl Chloroacetate (**10**)*: Bp 75—84 °C/3 Torr. IR 2220, 1780 cm^{-1}. NMR ($CDCl_3$) *Z*-isomer 6.30 (1H, q, J=7.3), 4.27 (2H, s), 1.80 (3H, d, J=7.3); *E*-isomer 6.35 (1H, q, J=7.4), 4.23 (2H, s), 2.00 (3H, d, J=7.4). Z/E=5.

*1-Cyano-1-propenyl Ethyl Carbonate (**11**)*: Bp 67—69 °C/5 Torr. NMR ($CDCl_3$) *Z*-isomer 6.20 (1H, q, J=7.1), 4.35 (2H, q, J=7.0), 1.85 (3H, d, J=7.1), 1.40 (3H, t, J=7.0); *E*-isomer 6.85 (1H, q, J=7.1), 4.32 (2H, q, J=7.0), 1.97 (3H, d, J=7.1), 1.37 (3H, t, J=7.0). Z E=7.0.

*1-Cyano-1-propenyl p-Nitrobenzoate (**12**)*: Mp 153—154 °C (*Z*-isomer). IR 2220, 1780 cm^{-1}. NMR ($CDCl_3$) *Z*-isomer 8.35 (4H, s), 6.38 (1H, q, J=7.3), 1.87 (3H, d, J=7.3); *E*-isomer 8.32 (4H, s), 6.47 (1H, q, J=7.3), 2.09 (3H, d, J=7.3). Z/E=6.7.

*1-Cyano-1-propenyl Dimethylcarbamate (**13**)*: Bp 75—78 °C/0.6 Torr. IR 2230, 1725 cm^{-1}. NMR (CCl_4) *Z*-isomer 1.77 (3H, d, J=7.1), 3.01 (6H, bs), 6.08 (1H, q, J=7.1); *E*-isomer 1.99 (3H, d, J=7.4), 2.98 (6H, bs), 6.11 (1H, q, J=7.4). Z/E=2.4. 1,1-Dicyanopropyl dimethylcarbamate was also formed (8%), NMR (CCl_4) 1.30 (3H, t, J=7.2), 2.35 (2H, q, J=7.2), 3.00 (6H, bs), MS (*m/e*) 181 (M^+).

*1-Cyano-1-propenyl Diphenylcarbamate (**14**)*: Mp 213—216 °C. IR 2220, 1720 cm^{-1}. NMR (CCl_4) *Z*-isomer 7.25 (10H, s), 5.92 (1H, q, J=7.1), 1.60 (3H, d, J=7.1); *E*-isomer 7.25 (10H, s), 6.04 (1H, q, J=7.1), 1.80 (3H, d, J=7.1). Z/E=2.8.

*1-Cyano-2-methyl-1-propenyl Dimethylcarbamate (**17**)*: IR 2220, 1720 cm^{-1}. NMR ($CDCl_3$) 1.83 (3H, s), 2.05 (3H, s), 3.01 (6H, bs).

*1-Cyano-2-methyl-1-propenyl Diphenylcarbamate (**18**)*: Mp 110—112 °C. IR 2230, 1730 cm^{-1}. NMR ($CDCl_3$) 7.27 (10H, s), 1.98 (3H, s), 1.73 (3H, s).

*1-Cyano-2,2-diphenylvinyl Diphenylacetate (**19**)*: Mp 126—126.5 °C. IR 2220, 1773 cm^{-1}. NMR ($CDCl_3$) 5.03 (1H, s), 7.1—7.4 (10H, m). Found: C, 84.03; H, 4.79; N, 3.17%. Calcd for $C_{29}H_{21}NO_2$: C, 83.83; H, 5.09; N, 3.37%.

Examination of Solvents. To a mixture of purified acetyl cyanide and propionyl chloride (0.02 mol each) in 10 mL of purified solvent (acetonitrile, THF, CH_2Cl_2, or benzene) was added the solution of pyridine (0.02 mol) dissolved in the same solvent (8 mL), and successively isobutyl isobutyrate (0.02 mol, as the internal standard for VPC analysis). The reaction mixture was kept at 25 or 0 °C and an aliquot of the mixture was sucked up by a syringe at specified time intervals and analyzed by VPC.

Kinetics. Reagents: Methyl benzoate (as the internal standard) and acetyl cyanide were dried over anhyd $CaSO_4$ and distilled. Propionyl chloride was purified according to Paul's method.[7] Pyridine was purified by the reported method.[8] Each of the reagents thus purified was divided into several 0.5 mL portions which were stored in ampule tubes. In each experimental run, reagents from new ampules were used.

Procedure: Into a NMR tube which was preliminarily flushed by dry N_2 and sealed with a septum cap, the specified amounts of benzene-d_6, methyl benzoate, acetyl cyanide, and propionyl chloride were injected and mixed. Then pyridine was added, the solution was vigorously mixed for a few seconds at 25 °C, the tube was inserted into the NMR cavity whose temperature was controlled at 35 °C. The rates of formation of 1-cyanovinyl propionate (**3**) were measured at specified time intervals by integrating the relative intensity of the methylene protons to the internal standard. The number of data collections per reaction was more than eight in all cases.

Data Analysis: Molar change of **3** *vs.* reaction time was plotted and from this curve the fractions of yield per minute ($\Delta Y/\Delta t$) for the first 6 min were measured. These fractions were extrapolated to t=0 to obtain Δ[product]/Δt=R_0, the initial rate of reaction. These R_0(obsd) values are listed in Table 3.

Derivation of R_0*(calcd)*: Based on the reaction Eqs. 1, 2, and 3, the initial rate of reaction R_0(calcd) was derived as follows. Abbreviations: E, P, A are the concentrations of propionyl chloride, pyridine, and acetyl cyanide respectively, E_0, P_0, A_0 are the corresponding initial concentrations.

$$R_0 = \frac{\mathrm{d[product]}}{\mathrm{d}t} = kAP \tag{5}$$

Since the equilibrium (Eq. 1) is established at the initial stage of the reaction and the concentrations of **21**, **3**, and pyridine·HCl are negligible, P_0, E_0, and A_0 are expressed by

$$E_0 = E + KPE,\ P_0 = P + KPE,\ A_0 = A \tag{6}$$

From Eq. 6, P is expressed by the following equation

$$P = \frac{1}{2K}[-\{1+K(E_0-P_0)\}+ \sqrt{\{1+K(E_0-P_0)\}^2+4KP_0}] \tag{7}$$

Substituting Eqs. 6 and 7 for Eq. 5, R_0 is obtained as expressed by Eq. 4.

Examination of the Effect of Amines. Reagents: Three amines (2,6-lutidine, 2-picoline, pyridine) were purified by the reported method.[8] Purified *o*-dichlorobenzene was used as the internal standard in VPC analysis. For the other reagents, see the preceding paragraph.

Procedure: In a 50 mL flask equipped with a septum cap, a 0.02 mol each of acetyl cyanide, propionyl chloride, and *o*-dichlorobenzene were mixed in 10 mL of dry benzene under dry N_2 atmosphere. The flask was held in a bath controlled at 20±0.5 °C, and then the solution of a tertiary amine (0.02 mol in 8 mL of benzene) was added to the mixture at one time. An aliquot of the solution was then periodically analyzed by VPC by means of calibration curves independently prepared from authentic compounds.

The authors are indebted to Dr. Masaaki Teramoto of Kyoto Institute of Technology for his helpful discussion on the results of kinetics.

References

1) A. Oku, S. Nakaoji, T. Kadono, and H. Imai, *Bull. Chem. Soc. Jpn.*, **52**, 2966 (1979).

2) The rate-acceleration effect of CH_2Cl_2 seems to be explainable in terms of the gausche effect proposed by Y. Imami, *J. Am. Chem. Soc.*, **83**, 4745 (1961).

3) The reason is ascribed to the hydrolysis of acid chloride (or to the carboxylic acid in the chloride) as demonstrated by the formation of propionic anhydride as a by-product. The formation of the anhydride can be minimized, but not completely, by using purified reagents and consequently the yield of the ester can be increased. For the formation of anhydride, see D. P. U. Satchell and R. S. Satchell, "The Chemistry of Acyl Halides," ed by S. Patai, Interscience (1972), pp. 123—124.

4) D. Cook, *Can. J. Chem.*, **40**, 2362 (1962).

5) S. L. Johnson, *J. Phys. Chem.*, **68**, 3149 (1964).

6) (a) H. C. Brown and X. R. Mihm, *J. Am. Chem. Soc.*, **77**, 1723 (1955); (b) J. M. Essery and K. Shofield, *J. Chem. Soc.*, **1961**, 3939.

7) R. C. Paul, D. Singh, and S. S. Sandhu, *J. Chem. Soc.*, **1959**, 315.

8) P. J. R. Bryant and A. W. H. Wardrop, *J. Chem. Soc.*, **1957**, 895.

Syntheses of Alkylphosphonic Esters by the Reactions of Aliphatic Thiones with Trialkyl Phosphites

Tokuzo KAWASE, Shigeo YONEDA, and Zen-ichi YOSHIDA*

Department of Synthetic Chemistry, Kyoto University, Yoshida, Kyoto 606

(Received February 5, 1979)

Aliphatic thiones were found to react with trialkyl phosphites to give (alkylthio)- and/or mercapto-alkylphosphonic esters. The reaction is interpreted in terms of the carbophilic attack with trialkyl phosphites at the carbon atom of the thiocarbonyl group, and the subsequent migration mechanism *via* the betaine intermediate.

Reactions of thiocarbonyl compounds with nucleophiles are different from those of carbonyl compounds.[1] For example, though Grignard reagents normally attack at the carbon atom of a carbonyl group (carbophilic attack), they may attack at the sulfur atom of a thiocarbonyl group (thiophilic attack) rather than at the carbon atom.[2] The reactions of thiocarbonyl compounds with phosphites have been the focus of interest in the past several years, because phosphites have both "carbophilicity" and "thiophilicity"[3] toward organosulfur compounds. When trivalent phosphorus compounds such as phosphines and phosphites are employed as nucleophiles, they have generally been regarded as thiophiles, not as carbophiles, in the previously reported works.[4] However, in our preceding papers,[5] it was elucidated that cycloalkanethiones react with trialkyl phosphites at the carbon atom of the thiocarbonyl group to give phosphonic esters.

In this work, we have carried out the reactions of aliphatic thiones with trialkyl phosphites and succeeded in the syntheses of sulfur-containing phosphonic esters. This reaction is also explained by the initial carbophilic attack of phosphites at the thiocarbonyl carbon atom to form the betaine intermediate.

Results and Discussion

The syntheses of 1-(alkylthio)- and 1-mercaptocycloalkylphosphonic esters by the reactions of cycloalkanethiones with trialkyl phosphites were reported in our previous papers.[5] Similar reactions of aliphatic thioketones with trialkyl phosphites successfully yielded new sulfur containing alkylphosphonates.

In our preceding papers,[5] cycloalkanedithiols were utilized as precursors of cycloalkanethiones because of the instability of the latter. Cycloalkanethiones were easily generated from the corresponding dithiols at elevated temperatures. Similarly, the *gem*-dithiols[6] (**1**—**4**), as precursors of thioacetone, methyl ethyl thioketone, diethyl thioketone, and methyl isopropyl thioketone, were also employed in this study.

When a solution of propane-2,2-dithiol (**1**) and 4 equiv of trimethyl phosphite in toluene was heated under refluxing, hydrogen sulfide evolved vigorously and the reaction mixture became pink. The evolution of hydrogen sulfide and the pink coloration indicate the formation of thioacetone. After the complete decoloration, distillation gave a mixture of *O*,*O*-dimethyl 1-methyl-1-(methylthio)ethylphosphonate (**5a**) and *O*,*O*-dimethyl 1-mercapto-1-methylethylphosphonate (**6a**), which were separated by gas chromatography. The structures were determined by the elemental analyses and spectral data.

The reaction of **1** with triethyl phosphite also gave a mixture of *O*,*O*-diethyl 1-(ethylthio)-1-methylethylphosphonate (**5b**) and *O*,*O*-diethyl 1-mercapto-1-methylethylphosphonate (**6b**). The reaction of **1** with triisopropyl phosphite gave only *O*,*O*-diisopropyl 1-mercapto-1-methylethylphosphonate (**6c**), but no esters

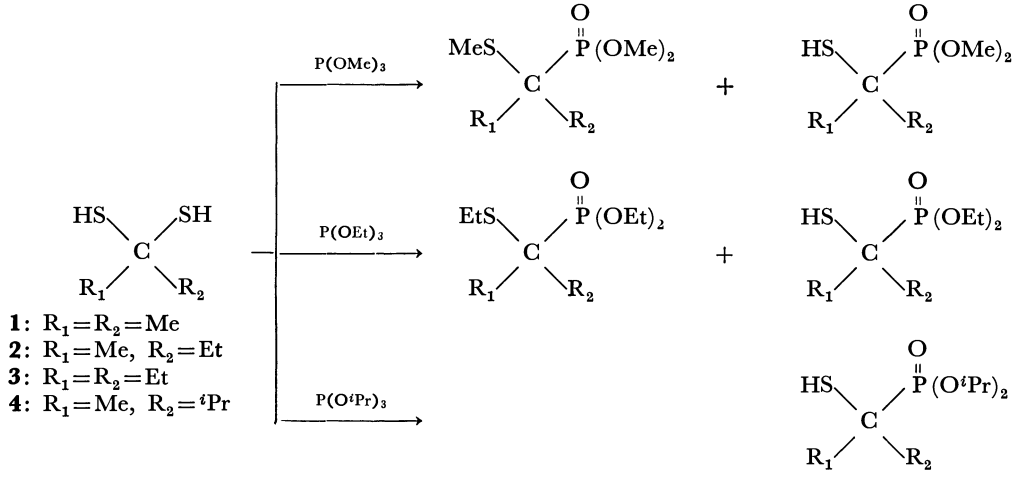

1: $R_1=R_2=Me$
2: $R_1=Me$, $R_2=Et$
3: $R_1=R_2=Et$
4: $R_1=Me$, $R_2={}^i Pr$

5: $R_1=R_2=Me$
7: $R_1=Me$, $R_2=Et$
9: $R_1=R_2=Et$
11: $R_1=Me$, $R_2={}^i Pr$

6: $R_1=R_2=Me$
8: $R_1=Me$, $R_2=Et$
10: $R_1=R_2=Et$
12: $R_1=Me$, $R_2={}^i Pr$

Scheme 1.

Table 1. Reaction conditions and yields of products in the reactions of aliphatic alkanedithiols with trialkyl phosphites

Substrates (Dithiols)	Reactants (Phosphites)	Reaction time/h	Products (Yield/%)	
			Alkylthio	Mercapto
Propane-2,2-dithiol (**1**)[a]	$P(OMe)_3$	20	23	23
	$P(OEt)_3$	20	25	17
	$P(O^iPr)_3$	20	0	62
Butane-2,2-dithiol (**2**)	$P(OMe)_3$	20	35	18
	$P(OEt)_3$	25	17	24
	$P(O^iPr)_3$	20	0	76
Pentane-3,3-dithiol (**3**)	$P(OMe)_3$	30	43	11
	$P(OEt)_3$	30	24	29
	$P(O^iPr)_3$	20	0	80
2-Methylbutane-3,3-dithiol (**4**)	$P(OMe)_3$	30	22	10
	$P(OEt)_3$	35	18	10
	$P(O^iPr)_3$	25	0	46

a) Hexamethyltrithiane was obtained in 30—40% yields.

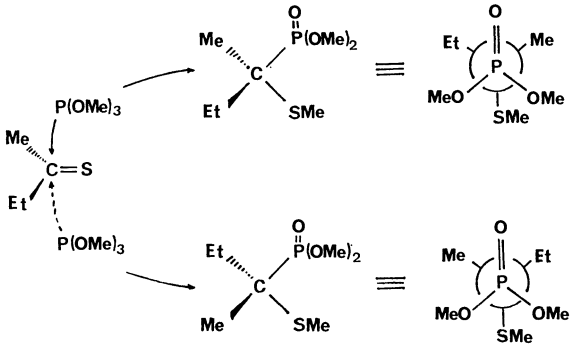

Fig. 1. Projection formulas of **7a** with respect to the C–P bond (staggered conformers).

having an alkylthio group were obtained.

In these reactions, a side reaction (trimerization) also occurred to afford hexamethyltrithiane in 30—40% yield.

The reactions of butane-2,2-dithiol (**2**) with trialkyl phosphites were carried out under similar conditions. The reaction with trimethyl phosphite gave a mixture of *O,O*-dimethyl 1-methyl-1-(methylthio)propylphosphonate (**7a**) and *O,O*-dimethyl 1-mercapto-1-methylpropylphosphonate (**8a**). In the NMR spectrum of **7a**, the protons of the methyl group attached to the oxygen atom appeared as two doublets at δ 3.73 and 3.79 in the ratio 1 : 1 with $J_{P-H}=10.0$ Hz. As seen in Fig. 1, in the staggered conformer of the projection formulas of **7a** with respect to the C–P bond, the two methyl groups attached to the oxygen atoms are situated in different environments, which accounts for the appearance of two doublets in the NMR spectrum. In addition, the attacks of trimethyl phosphite at the thiocarbonyl group of methyl ethyl thioketone from the different sides of the molecular plane should also yield two isomers possessing different configurations (*R*- and *S*-) in the ratio 1 : 1. Such an indication could be obtained with the aid of chiral shift reagent [europium(III)-tris(3-trifluoroacetyl-1*R*-campherate)], that is, the methyl protons attached to the oxygen atom appeared as two kinds of two doublets.[7]

The reactions of pentane-3,3-dithiol (**3**) and 2-methylbutane-3,3-dithiol (**4**) with trialkyl phosphites

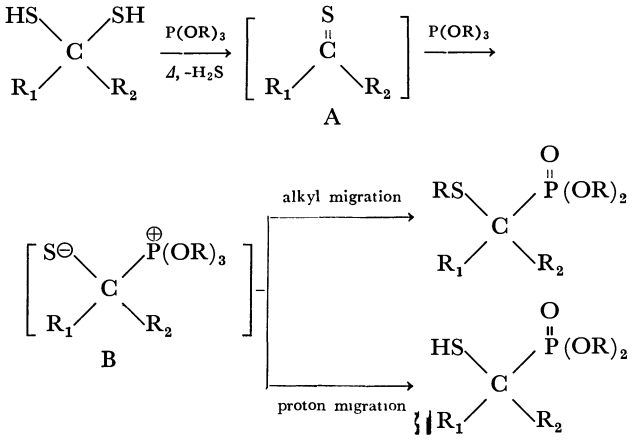

Scheme 2.

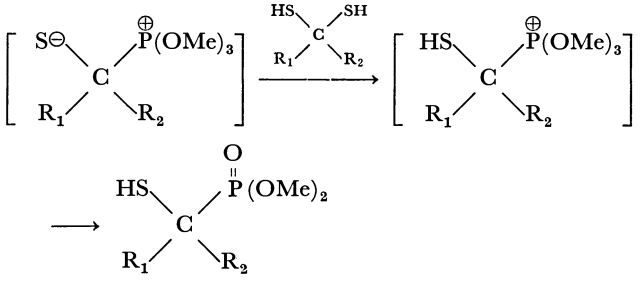

Scheme 3.

were carried out under similar conditions.[8] The results are summarized in Scheme 1 and Table 1.

The mechanistic interpretation of the reactions of aliphatic thioketones with trialkyl phosphites is outlined in Scheme 2. The reaction is initiated by the removal of hydrogen sulfide from *gem*-dithiols to form the corresponding thioketones (A). The resulting thioketones might immediately react with excess trialkyl phosphites. The phosphites should attack at the carbon atom of thiocarbonyl group and from the betaine intermediate (B). From the intermediate B the migration of an alkyl group or proton would afford the phosphonic esters containing a sulfur atom in alkylthio and/or mercapto groups. When the phosphites are trimethyl and/or triethyl phosphites, the negatively charged sulfur

atom would intramolecularly attack the alkyl group attached to the oxygen atom; this would result in the formation of alkylthio phosphonic esters. When triisopropyl phosphite was used, this nucleophilic attack should be hindered, and so the proton migration would occur to afford the mercapto phosphonic esters.

However, even when the trimethyl phosphite was used, the mercapto phosphonic esters were obtained in fair yields; their formation can be explained by Scheme 3.

Experimental

The infrared spectra were recorded on a Hitachi EPI-G3 grating infrared spectrophotometer; the ^1H NMR spectra were recorded on a Varian Associates AH-100 spectrometer with TMS as an internal standard. Mass spectra were taken on a Hitachi RMU-6C mass spectrometer. Gas-liquid chromatography was carried out with a Shimadzu gas chromatograph Model GC-6A, using a stainless steel column packed with 20% silicon DC-550 on Celite 545, and the preparative VPC was carried out with a Varian Aerograph Model 920 using 20% Silicon DC-550. Elemental analyses were carried out at the Elemental Analytical Center of Kyoto University.

Materials. Propane-2,2-dithiol (**1**), butane-2,2-dithiol (**2**), pentane-3,3-dithiol (**3**), and 2-methylbutane-3,3-dithiol (**4**) were prepared from the ketimines and hydrogen sulfide according to the literature procedure by Magnusson,[6] and distilled under reduced pressure at temperatures below 70 °C. Trimethyl and triethyl phosphites were commercial matrials and were used after distillation. Triisopropyl phosphite was prepared utilizing the procedure of Ford-Moore.[9]

*General Procedure for the Reactions of Alkanedithiols (**1**—**4**) with Trialkyl Phosphites.* A mixture of 0.01 mol of alkanedithiol (**1**—**4**) and 0.04 mol of trialkyl phosphite in 30 ml of toluene was heated at reflux temperature under nitrogen for 20—30 h. When the temperature of the mixture exceeded 80 °C, gas evolution and pink coloration were observed. After removal of toluene and excess phosphite, the residue was distilled under reduced pressure to give a colorless viscous liquid. In the reactions with trimethyl and triethyl phosphites, the distillates were mixtures of the (alkylthio)- and mercapto-alkylphosphonates. They were separated by gas chromatography to determine the yields.

The boiling points, IR, ^1H NMR, and mass spectral data, and the results of elemental analyses are as follows.

O,O-*Dimethyl 1-Methyl-1-(methylthio)ethylphosphonate (**5a**)*: Bp 78—80 °C (14 Torr) as a mixture of **5a** and **6a**; 23% yield; IR (Neat) 1255 (P=O), 1180, 1060, 1030, 830, and 800 cm^{-1}. NMR (CCl_4) δ=1.49 (d, 6H, J_{P-H}=15.5 Hz, CH_3), 2.28 (s, 3H, SCH_3) and 3.80 (d, 6H, J_{P-H}=10.0 Hz, $POCH_3$); MS *m/e* 198 (M^+). Found: C, 36.53; H, 7.86; P, 15.66%. Calcd for $C_6H_{15}O_3PS$: C, 36.36; H, 7.63; P, 15.63%.

O,O-*Dimethyl 1-Mercapto-1-methylethylphosphonate (**6a**)*: 23% yield; IR (Neat) 2500 (SH), 1250 (P=O), 1180, 1060, 1025, 830, and 790 cm^{-1}. NMR (CCl_4) δ=1.59 (d, 6H, J_{P-H}=15.5 Hz, CH_3), 2.16 (d, 1H, J_{P-H}=4 Hz, SH) and 3.78 (d, 6H, J_{P-H}=10.0 Hz, $POCH_3$); MS *m/e* 184 (M^+). Found: C, 32.43; H, 7.07; P, 16.85%. Calcd for $C_5H_{13}O_3PS$: C, 32.60; H, 7.11; P, 16.82%.

O,O-*Diethyl 1-(Ethylthio)-1-methylethylphosphonate (**5b**)*: Bp 82—83 °C (9 Torr) as a mixture of **5b** and **6b**; 25% yield; IR (Neat) 1250 (P=O), 1060, 1030, and 963 cm^{-1}. NMR (CCl_4) δ=1.13 (t, 3H, J=7.5 Hz, $SCH_2C\underline{H}_3$), 1.25 (t, 6H, J_{H-H}=7.0 Hz, $POCH_2C\underline{H}_3$), 1.30 (d, 6H, J_{P-H}=15 Hz, CH_3), 2.78 (q, 2H, J=7.5 Hz, $SC\underline{H}_2CH_3$), and 4.03 (dq, 4H, J_{H-H}=7.0 Hz, J_{P-H}=8.0 Hz, $POC\underline{H}_2CH_3$); MS *m/e* 240 (M^+). Found: C, 44.65; H, 9.08; P, 12.69%. Calcd for $C_9H_{21}O_3PS$: C, 44.98; H, 8.81; P, 12.89%.

O,O-*Diethyl 1-Mercapto-1-methylethylphosphonate (**6b**)*: 17% yield; IR (Neat) 2503 (SH), 1245 (P=O), 1050, 1023, and 955 cm^{-1}. NMR (CCl_4) δ=1.26 (t, 6H, J_{H-H}=7.0 Hz, $POCH_2C\underline{H}_3$), 1.40 (d, 6H, J_{P-H}=15 Hz, CH_3), 2.16 (d, 1H, J_{P-H}=4 Hz, SH), and 4.05 (dq, 4H, J_{H-H}=7.0 Hz, J_{P-H}=8.5 Hz, $POC\underline{H}_2CH_3$); MS *m/e* 212 (M^+). Found: C, 39.67; H, 8.11; P, 14.41%. Calcd for $C_7H_{17}O_3PS$: C, 39.61; H, 8.07; P, 14.59%.

O,O-*Diisopropyl 1-Mercapto-1-methylethylphosphonate (**6c**)*: Bp 92—93 °C (11 Torr); 62% yield; IR (Neat) 2500 (SH), 1250 (P=O), 1005, and 985 cm^{-1}. NMR (CCl_4) δ=1.33 [d, 12H, J_{H-H}=6.5 Hz, $POCH(C\underline{H}_3)_2$], 1.45 (d, 6H, J_{P-H}=15 Hz, CH_3), 2.24 (d, 1H, J_{P-H}=4 Hz, SH), and 4.64 [dsep, 2H, J_{H-H}=6.5 Hz, J_{P-H}=8.5 Hz, $POC\underline{H}(CH_3)_2$]; MS *m/e* 240 (M^+). Found: C, 44.65; H, 9.13; P, 12.51%. Calcd for $C_9H_{21}O_3PS$: C, 44.98; H, 8.81; P, 12.89%.

O,O-*Dimethyl 1-Methyl-1-(methylthio)propylphosphonate (**7a**)*: Bp 98—99 °C (13 Torr) as a mixture of **7a** and **8a**; 35% yield; IR (Neat) 1249 (P=O), 1185, 1060, 1031, 823, and 780 cm^{-1}. NMR (CCl_4) δ=0.97 (t, 3H, J=7.1 Hz, $CH_2C\underline{H}_3$), 1.27 (d, 3H, J_{P-H}=15.5 Hz, CH_3), 1.58—1.97 (m, 2H, $C\underline{H}_2CH_3$), 2.19 (s, 3H, SCH_3), and 3.73 and 3.79 (two d, 6H, J_{P-H}=10.0 Hz, $POCH_3$); MS *m/e* 212 (M^+). Found: C, 39.58; H, 8.14; P, 14.49%. Calcd for $C_7H_{17}O_3PS$: C, 39.61; H, 8.07; P, 14.59%.

O,O-*Dimethyl 1-Mercapto-1-methylpropylphosphonate (**8a**)*: 18% yield; IR (Neat) 2520 (SH), 1252 (P=O), 1186, 1060, 1034, 830, and 782 cm^{-1}. NMR (CCl_4) δ=1.04 (t, 3H, J=7.5 Hz, $CH_2C\underline{H}_3$), 1.40 (d, 3H, J_{P-H}=15.0 Hz, CH_3), 1.61—2.01 (m, 2H, $C\underline{H}_2CH_3$), 2.07 (d, 1H, J_{P-H}=5 Hz, SH), and 3.76 and 3.80 (two d, 6H, J_{P-H}=10.5 Hz, $POCH_3$); MS *m/e* 198 (M^+). Found: C, 36.52; H, 7.42; P, 15.28%. Calcd for $C_6H_{15}O_3PS$: C, 36.36; H, 7.63; P, 15.63%.

O,O-*Diethyl 1-(Ethylthio)-1-methylpropylphosphonate (**7b**)*: Bp 98—103 °C (5.5 Torr) as a mixture of **7b** and **8b**; 17% yield; IR (Neat) 1245 (P=O), 1058, 1030, and 960 cm^{-1}. NMR (CCl_4) δ=0.98 (t, 3H, J=7.0 Hz, $CH_2C\underline{H}_3$), 1.20 (t, 3H, J=7.5 Hz, $SCH_2C\underline{H}_3$), 1.28 (d, 3H, J_{P-H}=15 Hz, CH_3), 1.32 and 1.33 (two t, 6H, J_{H-H}=7.0 Hz, $POCH_2C\underline{H}_3$), 1.61—1.97 (m, 2H, $C\underline{H}_2CH_3$), 2.73 and 2.83 (two q, 2H, J=7.5 Hz, $SC\underline{H}_2CH_3$), and 4.08 and 4.13 (two dq, 4H, J_{H-H}=7.0 Hz, J_{P-H}=8.0 Hz, $POC\underline{H}_2CH_3$); MS *m/e* 254 (M^+). Found: C, 47.10; H, 9.23; P, 12.25%. Calcd for $C_{10}H_{23}O_3PS$: C, 47.23; H, 9.12; P, 12.18%.

O,O-*Diethyl 1-Mercapto-1-methylpropylphosphonate (**8b**)*: 24% yield; IR (Neat) 2510 (SH), 1250 (P=O), 1055, 1030, and 963 cm^{-1}. NMR (CCl_4) δ=1.06 (t, 3H, J=7.0 Hz, $CH_2C\underline{H}_3$), 1.34 (t, 6H, J_{H-H}=7.0 Hz, $POCH_2C\underline{H}_3$), 1.40 (d, 3H, J_{P-H}=15.5 Hz, CH_3), 1.60—1.93 (m, 2H, $C\underline{H}_2CH_3$), 2.04 (d, 1H, J_{P-H}=6 Hz, SH), 4.12 and 4.15 (two dq, 4H, J_{H-H}=7.0 Hz, J_{P-H}=8.0 Hz, $POC\underline{H}_2CH_3$); MS *m/e* 226 (M^+). Found: C, 42.62; H, 8.64; P, 13.47%. Calcd for $C_8H_{19}O_3PS$: C, 42.46; H, 8.46; P, 13.69%.

O,O-*Diisopropyl 1-Mercapto-1-methylpropylphosphonate (**8c**)*: Bp 100—101 °C (6.7 Torr); 76% yield; IR (Neat) 2505 (SH), 1246 (P=O), 1108, 1005, and 980 cm^{-1}. NMR (CCl_4) δ=1.04 (t, 3H, J=7.0 Hz, $CH_2C\underline{H}_3$), 1.32 [d, 12H, J_{H-H}=6 Hz, $POCH(C\underline{H}_3)_2$], 1.40 (d, 3H, J_{P-H}=13.0 Hz, CH_3), 1.54—1.97 (m, 2H, $C\underline{H}_2CH_3$), 2.07 (d, 1H, J_{P-H}=6 Hz, SH), and 4.35—4.96 [m, 2H, $POCH(CH_3)_2$]; MS *m/e* 254 (M^+). Found: C, 47.31; H, 9.36; P, 11.92%. Calcd for $C_{10}H_{23}O_3PS$: C, 47.23; H, 9.12; P, 12.18%.

O,O-*Dimethyl 1-Ethyl-1-(methylthio)propylphosphonate (**9a**)*;

Bp 111—112 °C (6.5 Torr) as a mixture of **9a** and **10a**; 43% yield; IR (Neat) 1246 (P=O), 1182, 1060, 1031, 824, and 770 cm^{-1}. NMR (CCl_4) δ=0.95 (t, 6H, J=7.1 Hz, $CH_2C\underline{H}_3$), 1.54—1.97 (m, 4H, $C\underline{H}_2CH_3$), 2.18 (s, 3H, SCH_3), and 3.76 (d, 6H, J_{P-H}=10.2 Hz, $POCH_3$); MS *m/e* 226 (M^+). Found: C, 42.37; H, 8.62; P, 13.90%. Calcd for $C_8H_{19}O_3PS$: C, 42.46; H, 8.46; P, 13.69%.

O,O-*Dimethyl 1-Ethyl-1-mercaptopropylphosphonate (**10a**)*: 11% yield; IR (Neat) 2500 (SH), 1245 (P=O), 1060, 1030, 820, and 770 cm^{-1}. NMR (CCl_4) δ=1.00 (t, 6H, J=6.5 Hz, $CH_2C\underline{H}_3$), 1.73 and 1.87 (dq, 4H, J_{H-H}=6.5 Hz, J_{P-H}=13.5 Hz, $C\underline{H}_2CH_3$), 2.03 (d, 1H, J_{P-H}=6 Hz, SH), and 3.77 (d, 6H, J_{P-H}=10.1 Hz, $POCH_3$); MS *m/e* 212 (M^+). Found: C, 39.51; H, 8.00; P, 14.79%. Calcd for $C_7H_{17}O_3PS$: C, 39.61; H, 8.07; P, 14.59%.

O,O-*Diethyl 1-Ethyl-1-(ethylthio)propylphosphonate (**9b**)*: Bp 123—124 °C (6.7 Torr) as a mixture of **9b** and **10b**; 24% yield; IR (Neat) 1250 (P=O), 1060, 1032, and 960 cm^{-1}. NMR (CCl_4) δ 0.98 (t, 6H, J=7.0 Hz, $CH_2C\underline{H}_3$), 1.21 (t, 3H, J=7.5 Hz, $SCH_2C\underline{H}_3$), 1.33 (t, 6H, J_{H-H}=7.0 Hz, $POCH_2C\underline{H}_3$), 1.73 and 1.88 (dq, 4H, J_{H-H}=7.0 Hz, J_{P-H}=14 Hz, $C\underline{H}_2CH_3$), 2.78 (q, 2H, J=7.0 Hz, $SC\underline{H}_2CH_3$), 4.05 (dq, 4H, J_{H-H}=7.0 Hz, J_{P-H}=8.1 Hz, $POC\underline{H}_2CH_3$); MS *m/e* 268 (M^+). Found: C, 46.24; H, 8.97; P, 10.71%. Calcd for $C_{11}H_{25}O_3PS$: C, 46.16; H, 8.80; P, 10.82%.

O,O-*Diethyl 1-Ethyl-1-mercaptopropylphosphonate (**10b**)*: 29% yield; IR (Neat) 2500 (SH), 1245 (P=O), 1060, 1025, and 965 cm^{-1}. NMR (CCl_4) δ=1.01 (t, 6H, J=7.0 Hz, $CH_2C\underline{H}_3$), 1.32 (t, 6H, J_{H-H}=7.0 Hz, $POCH_2C\underline{H}_3$), 1.74 and 1.87 (dq, 4H, J_{H-H}=7.0 Hz, J_{P-H}=13.5 Hz, $C\underline{H}_2CH_3$), 2.10 (d, 1H, J_{P-H}=5.5 Hz, SH), and 4.03 (dq, 4H, J_{H-H}=7.0 Hz, J_{P-H}=8.0 Hz, $POC\underline{H}_2CH_3$); MS *m/e* 240 (M^+). Found: C, 45.11; H, 8.90; P, 12.67%. Calcd for $C_9H_{21}O_3PS$: C, 44.98; H, 8.81; P, 12.89%.

O,O-*Diisopropyl 1-Ethyl-1-mercaptopropylphosphonate (**10c**)*: Bp 120—121 °C (5.5 Torr); 80% yield; IR (Neat) 2502 (SH), 1243 (P=O), 1108, 1004, and 980 cm^{-1}. NMR (CCl_4) δ=1.00 (t, 6H, J=7.0 Hz, $CH_2C\underline{H}_3$), 1.32 [d, 12H, J_{H-H}=6.1 Hz, $POCH(C\underline{H}_3)_2$], 1.71 and 1.84 (dq, 4H, J_{H-H}=7 Hz, J_{P-H}=13.4 Hz, $C\underline{H}_2CH_3$), 2.05 (d, 1H, J_{P-H}=6 Hz, SH), and 4.63 [dsep, 2H, J_{H-H}=6.1 Hz, J_{P-H}=7.2 Hz, $POC\underline{H}(CH_3)_2$]; MS *m/e* 268 (M^+). Found: C, 46.29; H, 9.01; P, 10.57%. Calcd for $C_{11}H_{25}O_3PS$: C, 46.14; H, 8.80; P, 10.82%.

O,O-*Dimethyl 1,2-Dimethyl-1-(methylthio)propylphosphonate (**11a**)*: Bp 101—104 °C (7.8 Torr) as a mixture of **11a** and **12a**; 22% yield; IR (Neat) 1250 (P=O), 1178, 1060, and 1030 cm^{-1}. NMR (CCl_4) δ=1.04 [d, 6H, J=6.5 Hz, $(C\underline{H}_3)_2CH$], 1.23 (d, 3H, J_{P-H}=15.5 Hz, CH_3), 1.75—2.45 [m, 1H, $(CH_3)_2C\underline{H}$], 2.19 and 2.20 (two s, 3H, SCH_3), 3.73 and 3.79 (two d, 6H, J_{P-H}=10.0 Hz, $POCH_3$); MS *m/e* 226 (M^+). Found: C, 42.26; H, 8.66; P, 13.58%. Calcd for $C_8H_{19}O_3PS$: C, 42.46; H, 8.46; P, 13.69%.

O,O-*Dimethyl 1-Mercapto-1,2-dimethylpropylphosphonate (**12a**)*: 10% yield; IR (Neat) 2500 (SH), 1248 (P=O), 1180, 1060, and 1028 cm^{-1}. NMR (CCl_4) δ=1.03 and 1.13 [two d, 6H, J=6.5 Hz, $(C\underline{H}_3)_2CH$], 1.41 and 1.43 (two d, 3H, J_{P-H}=15.5 Hz, CH_3), 1.7—2.4 [m, 1H, $(CH_3)_2C\underline{H}$], 2.04 (d, 1H, J_{P-H}=7 Hz, SH), 3.77 and 3.85 (two d, 6H, J_{P-H}=10.1 Hz, $POCH_3$); MS *m/e* 212 (M^+). Found: C, 39.45; H, 8.17; P, 14.55%. Calcd for $C_7H_{17}O_3PS$: C, 39.61; H, 8.07; P, 14.59%.

O,O-*Diethyl 1,2-Dimethyl-1-(ethylthio)propylphosphonate (**11b**)*: Bp 98—101 °C (6.2 Torr) as a mixture of **11b** and **12b**; 18% yield; IR (Neat) 1250 (P=O), 1055, and 1030 cm^{-1}. NMR (CCl_4) δ=1.00 and 1.10 [two d, 6H, J=6.5 Hz, $(C\underline{H}_3)_2CH$], 1.21 (t, 3H, J=7.5 Hz, $SCH_2C\underline{H}_3$), 1.32 and 1.34 (two t, 6H, J_{H-H}=7.0 Hz, $POCH_2C\underline{H}_3$), 1.33 and 1.35 (two d, 3H, J_{P-H}=15.5 Hz, CH_3), 1.8—2.4 [m, 1H, $(CH_3)_2C\underline{H}$], 2.79 and 2.88 (two q, 2H, J=7.5 Hz, $SC\underline{H}_2CH_3$), 4.07 and 4.11 (two dq, 4H, J_{H-H}=7.0 Hz, J_{P-H}=8.1 Hz, $POC\underline{H}_2CH_3$); MS *m/e* 268 (M^+). Found: C, 46.22; H, 8.96; P, 10.67%. Calcd for $C_{11}H_{25}O_3PS$: C, 46.14; H, 8.80; P, 10.82%.

O,O-*Diethyl 1-Mercapto-1,2-dimethylpropylphosphonate (**12b**)*: 10% yield; IR (Neat) 2510 (SH), 1250 (P=O), 1058, and 1030 cm^{-1}. NMR (CCl_4) δ=1.04 and 1.15 [two d, 6H, J=6.5 Hz, $(C\underline{H}_3)_2CH$], 1.30 and 1.31 (two t, 6H, J_{H-H}=7.0 Hz, $POCH_2C\underline{H}_3$), 1.35 and 1.38 (two d, 3H, J_{P-H}=15.5 Hz, CH_3), 1.7—2.4 [m, 1H, $(CH_3)_2C\underline{H}$], 2.05 (two d, 1H, J_{P-H}=6.5 Hz, SH), 4.01 and 4.05 (two dq, 4H, J_{H-H}=7.0 Hz, J_{P-H}=8.0 Hz, $POC\underline{H}_2CH_3$); MS *m/e* 240 (M^+). Found: C, 44.73; H, 9.01; P, 12.79%. Calcd for $C_9H_{21}O_3PS$: C, 44.98; H, 8.81; P, 12.89%.

O,O-*Diisopropyl 1-Mercapto-1,2-dimethylpropylphosphonate (**12c**)*: Bp 105—106 °C (6 Torr); 46% yield; IR (Neat) 2505 (SH), 1243 (P=O), 1003, and 980 cm^{-1}. NMR (CCl_4) δ=0.99 and 1.08 [two d, 6H, J=6.5 Hz, $(C\underline{H}_3)_2CH$], 1.30 and 1.33 [two d, 12H, J_{H-H}=6.3 Hz, $POCH(C\underline{H}_3)_2$], 1.37 and 1.38 (two d, 3H, J_{P-H}=15.5 Hz, CH_3), 1.7—2.4 [m, 1H, $(CH_3)_2C\underline{H}$], 2.06 (two d, J_{P-H}=7 Hz, SH), and 4.44—5.04 [m, 2H, $POC\underline{H}(CH_3)_2$]; MS *m/e* 268 (M^+). Found: C, 45.98; H, 9.01; P, 10.88%. Calcd for $C_{11}H_{25}O_3PS$: C, 46.14; H, 8.80; P, 10.82%.

References

1) For reviews, "Organic Chemistry of Sulfur," ed by S. Oae, Plenum Press, London (1974), Chap. 5.

2) P. Beak and J. W. Worley, *J. Am. Chem. Soc.*, **92**, 4142 (1970).

3) D. B. Denny and M. J. Boskin, *J. Am. Chem. Soc.*, **82**, 4736 (1960).

4) a) E. J. Corey and G. Märkl, *Tetrahedron Lett.*, **1967**, 3201; b) W. J. Middleton and W. H. Scharkey, *J. Org. Chem.*, **30**, 1385 (1965); c) E. J. Corey and R. A. E. Winter, *J. Am. Chem. Soc.*, **85**, 2677 (1963); d) H. D. Hartzler, *ibid.*, **95**, 4379 (1973); e) M. G. Miles, J. S. Wager, and J. D. Wilson, *J. Org. Chem.*, **40**, 2577 (1975); f) Y. Ogata, M. Yamashita, and M. Mizutani, *Tetrahedron*, **30**, 3709 (1974); g) C. U. Pittman, Jr., M. Narita, and Y. F. Liang, *J. Org. Chem.*, **41**, 2855 (1976); h) S. Yoneda, T. Kawase, M. Inaba, and Z. Yoshida, *ibid.*, **43**, 595 (1978).

5) a) Z. Yoshida, T. Kawase, and S. Yoneda, *Tetrahedron Lett.*, **1975**, 235; b) S. Yoneda, T. Kawase, and Z. Yoshida, *J. Org. Chem.*, **43**, 1980 (1978).

6) B. Magnusson, *Acta Chem. Scand.*, **16**, 1536 (1962); **17**, 273 (1963).

7) A similar feature (appearance of two kinds of signals in the ratio 1:1) was also observed in the NMR spectra of reaction products of **2** with triethyl and triisopropyl phosphites.

8) In the NMR spectra of **11** and **12**, similar to **7** and/or **8**, two kinds of signals, assigned to the alkyl protons attached to the oxygen atom, were observed.

9) A. H. Ford-Moore and B. J. Perrey, *Org. Synth.*, Coll. Vol. IV, 955 (1963).

Replacement of Methoxyl Group on the Grignard Reaction of *N*-(*o*-Methoxybenzylidene)aniline

Masao Ōkubo* and Sonoko Ueda

Department of Chemistry, Faculty of Science and Engineering, Saga University, Honjo-machi, Saga 840

(Received March 17, 1979)

The methoxyl group of the title imine was replaced by the phenyl group on treatment with PhMgBr, the same group of *N*-benzylidene-*o*-anisidine remaining. The result was discussed on the basis of radical chain mechanism involving the initial electron-transfer.

The Grignard reaction of >C=N– compounds has not been extensively studied. Gilman and his co-workers reported that *N*-(diphenylmethylene)aniline (**1**) on the "forced" reaction with phenylmagnesium bromide (PhMgBr) affords the *o*-phenylation product (**2**) as the result of 1,4-addition (Scheme 1).[1] The characteristic deep-red coloration of the reaction mixture seems to indicate the presence of radical species. From the results of recent studies on the Grignard reaction of hindered benzophenones,[2,3] a similar, more facile *o*-phenylation is expected if the substrate has an *o*-methoxyl group. We thus attempted to realize the replacement reaction of Scheme 2.

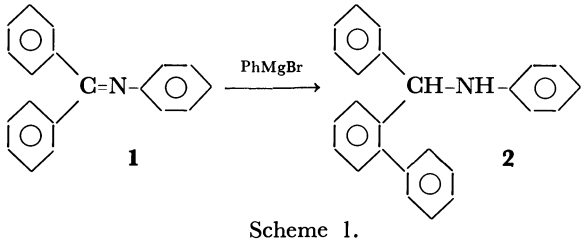

Scheme 1.

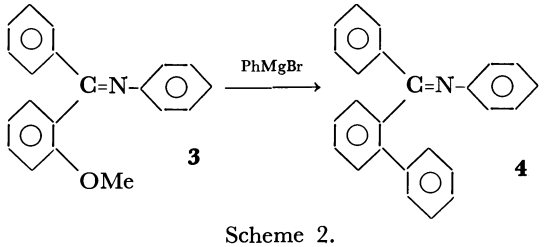

Scheme 2.

For the preparation of **3**, however, attempts to condense the benzophenone and aniline by use of some Lewis' acid catalysts ($POCl_3$,[4] $ZnCl_2$,[5] and BF_3[6]) were unsuccessful. In the course of studies on the Grignard reaction of *o*-methoxy-substituted *N*-benzylideneanilines in order to find another preparative route (Scheme 3), an interesting replacement of *o*-methoxyl group was found. The results are reported in this paper.

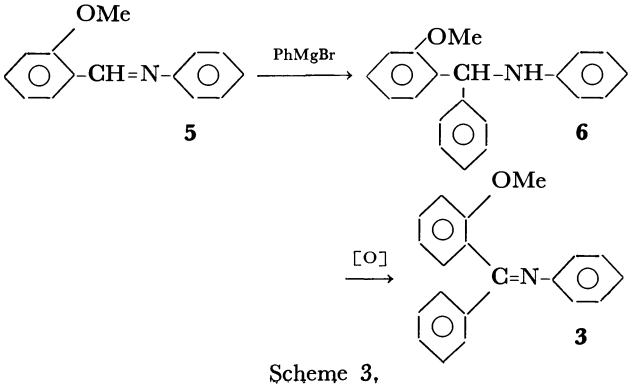

Scheme 3.

Results and Discussion

Preparation of o-*Methoxy-substituted* N-*Benzylideneanilines.* *N*-(*o*-Methoxybenzylidene)aniline (**5**) and *N*-benzylidene-*o*-anisidine (**7**) were prepared by the condensation of the corresponding benzaldehydes and anilines in methyl alcohol.[7] However, in both cases the colorless crystalline products obtained after recrystallization from the same solvent were found by NMR to be 1:1-molecular complexes, **5** with methyl alcohol and **7** with *o*-anisidine. In order to obtain purified pale-yellow imines, the alcohol combined with **5** should be removed by evacuation at 70 °C for about 1 h and **7** distilled under reduced pressure.

Grignard Reaction. The reaction was carried out in tetrahydrofuran(THF) under N_2. On reaction of **5** with five molar equivalents of PhMgBr at 50—55 °C for 5 h, the products isolated by column chromatography on silica gel (petroleum ether : diethyl ether : benzene=10 : 1 : 1) were the Gilman product **2** (58%) and the dimer **8** (0.5%) (Scheme 4). 25% of **5** recovered. Formation of **2** is obviously the result of the methoxy-replacement accompanied by 1,2-addition. Absence of the simple addition product **6** was confirmed by comparing the thin-layer chromatogram of the product mixture of this reaction with that of the independent reaction: 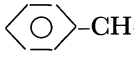 + 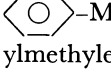 -MgBr→**6** and other products. *N*-(2-Biphenylylmethylene)aniline (**9**), prepared according to Scheme 5,[8] was not detected in the reaction mixture, nor recognized as an intermediate product. Formation of **8** suggests that the radical chain mechanism is involved.

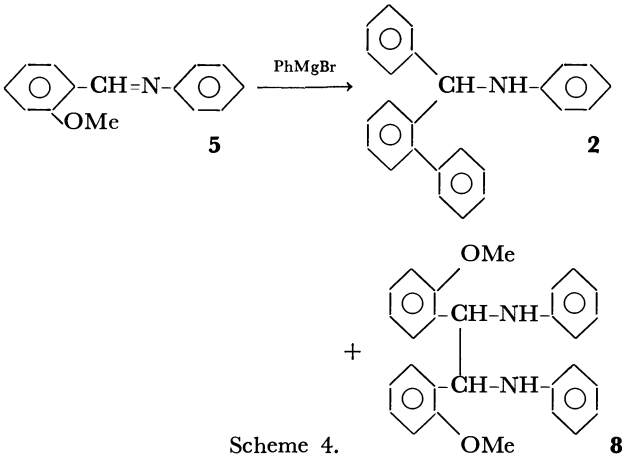

Scheme 4.

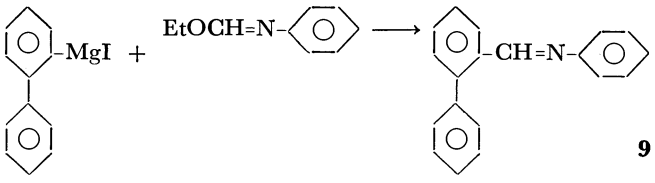

9

Scheme 5.

In contrast, the *o*-methoxyl group of **7** was not replaced at all even by treatment with five molar equivalents of PhMgBr at 50—55 °C for 5 h (Scheme 6). A fair yield of the secondary amine **11**[9] (64%) and the dimer **12** (0.8%) were isolated. 28% of **7** recovered. Two isomeric dimers giving the same TLC spot were obtained: **12a**, mp 135—138 °C, NMR ($CDCl_3$), δ=6.24—7.22 (18H, m, aromatic), 5.15 (2H, broad d, NH), 4.9 (2H, d, >CH), and 3.80 (6H, s, OCH_3); **12b**, mp 198—201 °C, NMR ($CDCl_3$), δ= 6.22—7.22 (18H, m, aromatic), 5.15 (2H, broad s, NH), 4.58 (2H, d, >CH), and 3.80 (6H, s, OCH_3). No stereochemical assignment was made. Formation of **12** suggests the intermediate formation of the radical derived from **7** *via* initial electron-transfer.

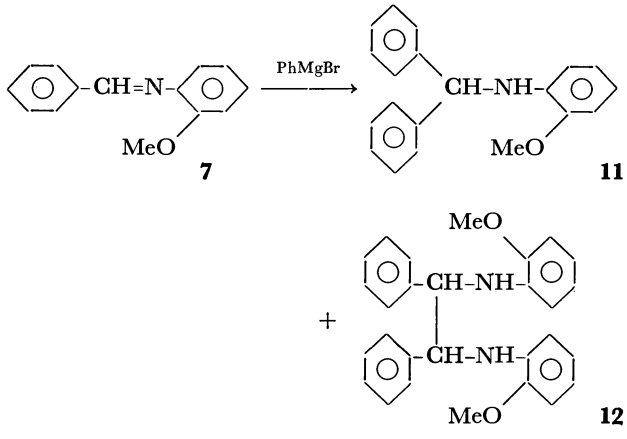

Scheme 6.

The low reactivity of *N*-benzylideneanilines and *N*-(diphenylmethylene)anilines towards PhMgBr should be noted. This is demonstrated by the fact that no heat evolution usually observed in the reaction of >C=O compounds was detectable in all the reactions of >C=N- compounds examined, and about 50% of **7** was recovered after it had been treated with 1.3 molar equivalents of PhMgBr at 50—55 °C for 30 min. Such a low reactivity of >C=N- compounds can be interpreted by their much lower electrophilic character as compared to that of >C=O compounds due to the lower electronegativity of nitrogen atom.

ESR Study. Attempts to detect radical species in the reaction of **5** and **7** were unsuccessful. No ESR signal was detected at lower temperatures (−20 °C and −40 °C) and at higher one (+40 °C) even by the use of concentrated reaction solutions.

However, in the reaction of Scheme 1, an ESR signal gradually became very strong at room temperature accompanied by deep purple coloration; no resolvable hyperfine splitting was observed probably because of the non-planarity of the diphenylmethylene moiety. In the reaction of *N*-fluorenylidene-*p*-anisidine(**13**) with PhMgBr (Scheme 7), a strong ESR signal accompanied by deep green coloration was detected, hyperfine splitting being observed when the reaction mixture was diluted. The well-resolved spectrum consists of 45 lines expected solely from the number of protons of the planar fluorenylidene moiety (**14**, $2p+2o+4m$). The same hyperfine splitting was observed in the reaction of *N*-fluorenylideneaniline.[6]

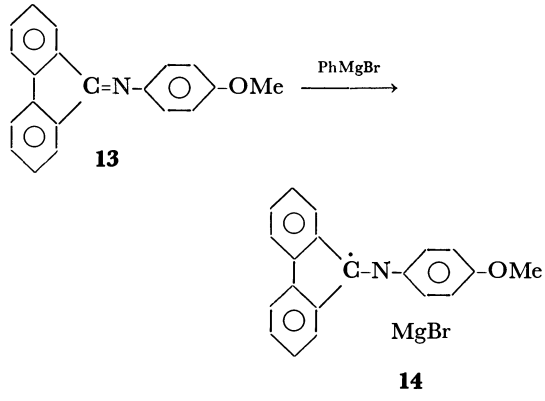

Scheme 7.

General Discussion. From the observation of strong ESR signals in the reactions of **1** and **13**, the original suggestion that Gilman's reaction of **1** (Scheme 1) proceeds *via* initial electron-transfer was verified.

On the basis of discussion on the steric hindrance effect on the amount of radicals detectable in the Grignard reaction of >C=O compounds,[2] failure to detect radical species in the reactions of **5** and **7** is attributed to their less crowded molecular structures as compared to those of **1** and **13**. The radical formed as the result of initial electron-transfer would accumulate if the subsequent reactions involving the attack of another Grignard molecule are hindered by the crowded molecular structure of substrate such as **1** and **13**. In contrast, the radicals formed from the less crowded **5** and **7** would be rapidly consumed by the subsequent reactions.

The failure to detect ESR signals in the cases of **5** and **7** is also attributable to their low electrophilicity in contrast to that of >C=O compounds. The success to detect ketyl radicals of unhindered benzophenones at lower temperatures[2] is due to their high electrophilicity and to the suppression of the subsequent reactions by the lowered temperature. In cases of much less electrophilic >C=N- compounds, it is reasonable to consider that even the application of low temperature is ineffective since the velocity of electron-transfer is retarded. The higher temperature is ineffective due to the shortened life time of radicals.

Attempts to detect CINDP signal were abandoned since a similar attempt on the reaction of hindered benzophenones failed in spite of very high radical concentrations detected by ESR. The reaction probably proceeds *via* "radical-anion" mechanism of S_{RN}-type[10,11] and not *via* "radical-pair" mechanism.

Scheme 8 could be proposed for explaining the formation of Gilman product **2** in the reaction of Scheme 4. Formation of the dimeric product **8** indi-

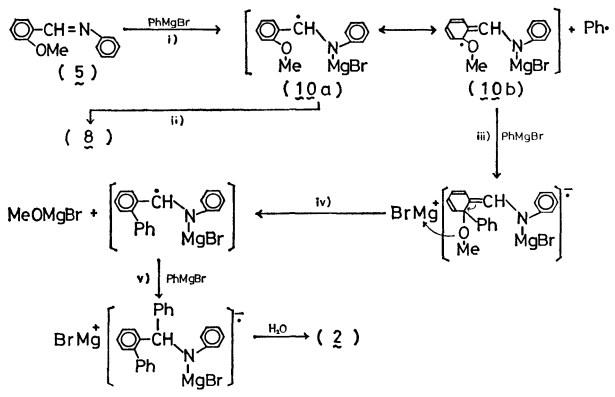

Scheme 8.

cates that the initial electron-transfer (step i) and the dimerization (step ii) are involved. The fate of Ph· produced by a step similar to i was discussed.[2] The step subsequent to the initial electron-transfer should be the replacement (steps iii and iv) but not the 1,2-addition. If the latter is the case, the radical chain will terminate leading to the originally expected product **6**. However, this was not the case. The release of the methoxyl anion (step iv) should be easy due to its coordination to $^{+}$MgBr species.[3] The final addition (step v) leads to the formation of the main product **2**.

The result of ESR measurement in the reaction of **13** indicates that the free spin of the radical **14** delocalizes mainly on the fluorenylidene moiety. Thus in the reaction of Scheme 1, the subsequent addition of another PhMgBr to the initially formed radical in the 1,4-manner could be facilitated by the relatively high spin-density at the *ortho*-position. Similarly, the free spin in the radical **10** and that derived from **7** are considered to delocalize mainly on the respective benzylidene moieties. This mode of spin-distribution is responsible for the effective release of the methoxyl anion from the benzylidene moiety as well as for the survival of the group on the aniline moiety.

Experimental

All melting and boiling points are uncorrected.

Materials. Commercial benzophenone, fluorenone, benzaldehyde, *o*-anisaldehyde, aniline, *o*- and *p*-anisidine (reagent grade) were used. *N*-Fluorenylidene-*p*-anisidine (**13**) was prepared by the method of Taylor and Fletcher:[6] mp 135—136 °C. *N*-(*o*-Methoxybenzylidene)aniline (**5**) was prepared by the usual method.[7] The molecular complex with methyl alcohol melted in the range 85—88 °C, and the purified imine at 42—43 °C: NMR ($CDCl_3$), δ=8.85 (1H, s, –CH=), 6.80—8.18 (9H, m, aromatic), and 3.82 (3H, s, OCH_3). *N*-Benzylidene-*o*-anisidine (**7**) was prepared by the same method. The molecular complex with *o*-anisidine melted in the range 62.5—74 °C, and the oily pure imine was obtained by distillation: bp 158—159 °C/2 mmHg; NMR ($CDCl_3$), δ=8.30 (1H, s, –CH=), 6.70—7.88 (9H, m, aromatic), and 3.78 (3H, s, OCH_3). *N*-(2-Biphenylylmethylene)aniline (**9**) was prepared by the method of Smith and Nichols.[8] The method has been established for aldehyde synthesis, but the treatment of the Grignard reaction mixture with aqueous NH_4Cl and not aqueous HCl directly afforded **9**: mp 137—138 °C; NMR ($CDCl_3$), δ=8.16 (1H, s, –CH=), and 6.86—7.36 (14H, m, aromatic). Tetrahydrofuran for the ordinary Grignard reaction was dried over sodium wire, distilled, and stored on sodium wire. The same solvent for ESR measurement was dried by sodium hydride, frozen, degassed repeatedly, and distilled into the storage vessel on a vacuum line containing sodium-potassium alloy.

Procedures. Phenylmagnesium bromide (0.05 mol) was prepared in the usual way in THF (25 ml), imine **7** (0.01 mol) dissolved in THF (20 ml) being added at room temperature. No heat evolution took place. The resulting yellow mixture was stirred at 50—55 °C for 5 h, and quenched with saturated aqueous NH_4Cl. The residue obtained after the usual work-up was chromatographed on silica gel. Appropriate fractions were combined, solvent was removed, and the residue was recrystallized from methyl alcohol: **11**, mp 90.5—92 °C; NMR ($CDCl_3$), δ=7.12—7.36 (10H, m, phenyl), 6.20—6.72 (4H, m, *o*-substd phenyl), 5.40 (1H, s, –CH), 4.65 (1H, broad s, NH), and 3.75 (3H, s, OCH_3).

The reaction of **5** and product separation were carried out in a similar way. The Gilman product **2**: mp 140 °C; NMR ($CDCl_3$), δ=6.20—7.60 (19H, m, aromatic), 5.52 (1H, s, >CH), and 4.0 (1H, s, NH). The dimeric product **8**: mp 206—209 °C; NMR ($CDCl_3$), δ=6.44—7.20 (18H, m, aromatic), 5.35 (2H, d, >CH), 4.84 (2H, broad s, NH), and 3.68 (3H, s, OCH_3).

ESR-Spectrum was recorded on JEOL ME-1X model spectrometer. The apparatus for the measurement was constructed and used as reported.[12]

References

1) H. Gilman, J. E. Kirby, and C. R. Kinney, *J. Am. Chem. Soc.*, **51**, 2252 (1929).
2) M. Ōkubo, *Bull. Chem. Soc. Jpn.*, **48**, 1327, 2057 (1975).
3) M. Ōkubo, *Bull. Chem. Soc. Jpn.*, **50**, 2379 (1977).
4) W. Weston and P. J. Michael, Jr., *J. Am. Chem. Soc.*, **73**, 1381 (1951).
5) J. H. Billman and K. M. Tai, *J. Org. Chem.*, **23**, 535 (1958).
6) M. E. Taylor and T. L. Fletcher, *J. Org. Chem.*, **26**, 940 (1956).
7) L. A. Bigelow and H. Eatough, *Org. Synth.*, Coll. Vol. I, 80 (1956).
8) L. I. Smith and J. Nichols, *J. Org. Chem.*, **6**, 489 (1941).
9) M. Busch and A. Rink, *Ber.*, **38**, 1770 (1905).
10) N. Kornblum, *Angew. Chem. Int. Ed. Engl.*, **1975**, 734.
11) J. F. Bunnett, *Acc. Chem. Res.*, **11**, 413 (1978).
12) K. Maruyama, *Bull. Chem. Soc. Jpn.*, **37**, 1013 (1964).

Halogenated Sesquiterpene Phenols and Ethers from the Red Alga *Laurencia glandulifera* Kützing[1]

Minoru Suzuki and Etsuro Kurosawa*

Department of Chemistry, Faculty of Science, Hokkaido University, Sapporo 060

(Received March 31, 1979)

Several brominated sesquiterpene phenols and the related ethers were isolated from the red alga *Laurencia glandulifera* Kützing. The structures of these compounds were determined on the basis of spectroscopic evidence and chemical correlation.

In the course of our continuing studies of the constituents of the red algae genus *Laurencia* (Rhodomelaceae), we have reported a variety of metabolites which have been isolated from *L. glandulifera* Kützing, *i.e.*, laurencin,[2] several halogenated chamigrenes,[3,4] spirolaurenone,[5] two bromocuparenes,[6] and laurene.[7] In a previous communication[8] we reported the isolation and structural elucidation of three brominated aromatic sesquiterpene ethers as minor components from this alga. The isolation of these ethers prompted us to investigate the remaining portion of the neutral oil of this alga, and three brominated phenols were isolated. We wish to report herein the isolation and structures of these minor brominated sesquiterpene phenols, (**1a**), (**2a**), and (**3a**), and the related ethers, (**8**), (**9**), and (**10**).

Freshly collected and half-dried algae were extracted with MeOH in the usual manner. The neutral MeOH extracts, which, on silica gel TLC, reveal a chromatogram similar to that of the previous extracts, were fractionated by column chromatography on neutral alumina.

Sesquiterpene Phenols: Diethyl ether fractions, which consisted of a mixture of alcohols, were rechromatographed on a silica-gel column. The earlier benzene eluates afforded a mixture of phenols which, following acetylation, was further submitted to preparative TLC on silica gel to yield three acetylated products, (**1b**), (**2b**), and (**3b**).

The major compound (**2b**) was identified as the acetate of laurenisol (**2a**), isolated from *L. nipponica* Yamada,[9] by a direct comparison of their physical properties.

One of the minor compounds, **1b**, $C_{17}H_{20}O_2Br_2$ (*m/e* 418, 416, and 414; M^+), had the following spectral characteristics: ν_{max} 1760 cm^{-1}; δ 0.73 (3H, d, J= 7 Hz), 1.14, 2.25, 2.36 (each 3H, s), 2.85 (1H, q, J=7), 6.01 (1H, br s), 6.85, and 7.27 (each 1H, s). The IR and NMR spectra of **1b** are very similar to those of laurenisol acetate (**2b**). In the NMR spectra of **1b** and **2b**, however, distinct differences were observed in the lower-field region; *e.g.*, in the spectrum of **2b**, absorptions due to three aromatic protons appeared at 6.75 (1H, br s), 6.85 (1H, br d, J=8), and 7.01 (1H, d, J=8) instead of two aromatic protons in the spectrum of **1b**. Hence, **1b** must be a bromo analog of laurenisol acetate (**2b**). Saponification of **1b** with 5% methanolic KOH gave the original phenol (**1a**). The structure of **1a** was confirmed by the following reaction: laurenisol (**2a**) was treated with bromine in acetic acid under the same conditions as the bromination of debromolaurinterol (**6a**)[10] to yield a brominated product, which was found to be identical with **1a** in all respects.

Another minor compound (**3b**), $C_{17}H_{21}O_2Br$ (*m/e* 338 and 336; M^+), $[\alpha]_D^{25}$ +45°, indicates in its IR and NMR spectra the presence of a secondary methyl group [0.66 (3H, d, J=7) and 2.70 (1H, q, J=7)], which was shifted to the higher magnetic field as same as **1b** and **2b**, a tertiary methyl group [1.12 (3H, s)], an aromatic methyl group [2.27 (3H, s)], a 2,4,5-trisubstituted phenyl acetate grouping [1763 cm^{-1}; 2.36 (3H, s), 6.84 and 7.25 (each 1H, s)], and a terminal methylene group [1655 and 885 cm^{-1}; 4.80 and 4.90 (each 1H, br s)]. These spectral data reveal that **3b** has a structure similar to that of **1b** except for a terminal methylene group instead of a bromomethylene group in **1b** and would, therefore, be represented by formula **3b**, an isomer of laurinterol acetate (**5b**) and isolaurinterol acetate (**7b**).[10] The spectral properties were identical to those reported[11] for the acetate of allollaurinterol (**3a**), isolated from *L. filiformis* as a major metabolite[11,12] and *L. subopposita* as a minor one.[13] Debromoallolaurinterol (**4a**) was also isolated from *L. subopposita*.[13]

Although the stereochemistry of a double bond between C-3 and C-6 in **2a** has remained unsettled, the assignment of the *Z*-configuration to this double bond can now be made with the aid of chemical shifts of the proton at C-2 in the NMR spectra of **1a**, **2a**, **3a**, and **4a**. In these spectra, the signals of C_2–H in **1a** (δ 3.11 q) and **2a** (δ 3.15 q) appear in a lower-field region than those in **3a** (δ 2.95 q) and **4a** (δ 2.95 q). These low-field chemical shifts in **1a** and **2a** are due to the deshielding being caused by C_6–Br, which is situated close to C_2–H.

Sesquiterpene Ethers: The hexane fraction was repeatedly chromatographed on a silica-gel column and subsequently on a PLC to yield three bromo ethers, (**8**), (**9**), and (**10**), along with laurene, isolaurene, bromocuparenes, and halo-chamigrenes.[4]

One of the three bromo ethers, **8**, $C_{15}H_{19}OBr$ (*m/e* 296 and 294; M^+), was identified as the ether isomerized from laurenisol (**2a**)[9] by comparisons of the spectral data.

The second bromo ether, **9**, mp 86—87 °C, $[\alpha]_D^{23}$ +22°, $C_{15}H_{18}OBr_2$ (*m/e* 376, 374, and 372; M^+), shows in its NMR spectrum the presence of three methyl groups at 0.74 (3H, d, J=7), 1.38 (3H, s), and 2.29 (3H, s), a $BrCH_2$-group at 3.41 and 3.55 (each 1H, AB-q, J=10), and two aromatic protons at 6.55 and 7.08 (each 1H, s). The IR and NMR spectra of **9** are very similar to those of **8**, suggesting that **9** must be a bromo analog of **8**. The structure

of **9** was confirmed by the following reactions. Treatment of **8** with bromine in acetic acid yielded a dibromo compound, which was identical with **9** in all respects. Although, on treatment with *p*-toluenesulfonic acid in acetic acid at room temp (2 h), **1a** was recovered, treatment of **1a** with TsOH in acetic acid under reflux gave **9** in a low yield.

The third bromo ether, **10**, mp 125—126 °C, $[\alpha]_D^{21}$ +79°, $C_{15}H_{18}OBr_2$ (*m/e* 376, 374, and 372; M^+), shows in its IR and NMR spectra the presence of three methyl groups [0.68 (3H, d, J=7), 1.35 (3H, s), and 2.22 (3H, s)], a Br_2CH-group [5.65 (1H, s)], and a 2,5-substituted aryl ether moiety [1622, 1577, 1505, 1245, and 815 cm^{-1}; 6.50 (1H, br s), 6.50 (1H, br d, J=8), and 6.82 (1H, d, J=8)].

The NMR spectrum of **10** displays signals comparable to those of **8** except for the absorptions due to a two-proton quartet at δ 3.40 and 3.52 (attributed to the $BrCH_2$-group in **8**) instead of a one-proton singlet at δ 5.65 (attributed to the Br_2CH-group in **10**). Thus, formula **10** can completely interpret all spectral properties. The related compounds, filiformin (**11**) and filiforminol (**12**), were also isolated from *L. filiformis*.[11,12]

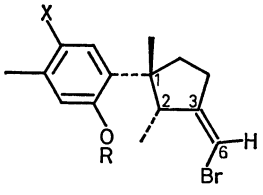

1a: X = Br, R = H
1b: X = Br, R = Ac
2a: X = H, R = H
2b: X = H, R = Ac

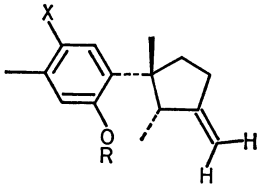

3a: X = Br, R = H
3b: X = Br, R = Ac
4a: X = H, R = H

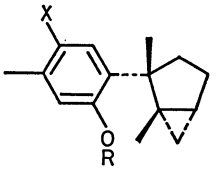

5a: X = Br, R = H
5b: X = Br, R = Ac
6a: X = H, R = H

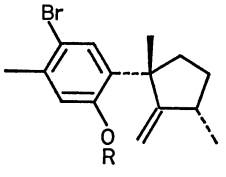

7a: R = H
7b: R = Ac

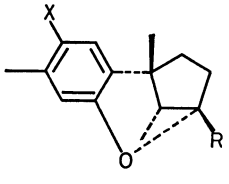

8: X = H, R = CH_2Br
9: X = Br, R = CH_2Br
10: X = H, R = $CHBr_2$
11: X = Br, R = CH_3
12: X = Br, R = CH_2OH

Experimental

All the mps were uncorrected. The IR spectra were measured on a Nihon-Bunko IR-S spectrometer in a $CHCl_3$ soln. The NMR spectra were recorded on a JEOL JNM-PS-100 spectrometer, TMS being used as the internal reference in a CCl_4 soln. The optical rotations were measured in a $CHCl_3$ soln. Alumina (Merck, activity II—III) and silica gel (Mallinckrodt, 100 mesh) were used for the column chromatography. Silica gel (Merck, Kieselgel GF_{254} (Type 60)) was used for the preparative TLC (PLC).

Isolation. *L. glandulifera* was collected at Oshoro Bay Hokkaido, early in August, 1978. The half-dried algae (600 g) were extracted with methanol. After the separation of the acidic and basic components by shaking with 1M aqueous KOH and 1M aqueous HCl respectively, a neutral oil (7.3 g) was obtained; this oil was subsequently chromatographed on a neutral alumina column. Elution with hexane gave an oily substance, which consisted of a mixture of hydrocarbons, aromatic ethers, and fatty acid methyl esters. Elution with ether gave a mixture of alcohols, which was then rechromatographed on a silica-gel column. The earlier benzene eluates gave a mixture of phenolic compounds, which was acetylated with acetic anhydride in pyridine at room temp in the usual manner and subsequently chromatographed on a PLC plate to give **1b** (0.5% of neutral oil), **2b** (0.2%), and **3b** (0.07%). These acetates were converted to the original phenols, (**1a**), (**2a**), and (**3a**), by treatment with 5% KOH in methanol. The above oily substance eluted with hexane was rechromatographed on a silica-gel column. The later hexane eluates were further repeatedly chromatographed on a PLC plate to yield **8** (0.07%), **9** (0.05%), and **10** (0.05%). These phenols and ethers were also obtained from the previous extracts but in different ratios.

1a: Colorless oil; $[\alpha]_D^{22}$ +74° (*c* 0.58); IR, ν_{max} 3680, 3360, 1640, 1610, 1500, 1397, 1380, 1255, 1150, 1070, and 885 cm^{-1}; NMR, δ 0.73 (3H, d, J=7 Hz), 1.19 (3H, s), 2.28 (3H, s), 3.11 (1H, q, J=7 Hz), 4.60 (s: OH), 5.98 (1H, br s), 6.47 (1H, s), and 7.13 (1H, s); MS, *m/e* (rel. intensity) 376, 374, 372 (7, M^+), 361, 359, 357 (2), 295, 293 (21), 253, 251 (7), 214 (53), 199 (21), 149 (47), 115 (16), 91 (18), 77 (18), 71 (58), 57 (55), and 43 (100). Acetate **1b**: colorless oil; $[\alpha]_D^{20}$ +76° (*c* 0.95); IR, ν_{max} 1760, 1642, 1375, 1190, 1147, 1070, and 908 cm^{-1}; MS, *m/e* 418, 416, 414 (4, M^+), 403, 401, 399 (1), 376, 374, 372 (10), 337, 335 (46), 295, 293 (53), 294, 292 (51), 279, 277 (23), 265, 263 (14), 214 (100), 201 (25), 199 (28), 159 (10), 145 (11), 115 (11), 91 (13), 77 (10), and 43 (65).

2a and **3a**: **2a** and **3a** were identified as laurenisol and allolaurinterol respectively by comparisons of the spectral data of the corresponding acetates, **2b** and **3b**. Attempts to crystallize **3b** [white solid, $[\alpha]_D^{25}$ +45° (*c* 0.35)] failed; allolaurinterol acetate,[11] mp 86.6—89.1 °C (from methanol), $[\alpha]_D$ +48.2° (*c* 1.03 in $CHCl_3$).

8: The IR and NMR spectra were superimposable on those of an authentic sample (**8**).[9]

9: Mp 86—87 °C (from methanol); $[\alpha]_D^{23}$ +22° (*c* 1.16); IR, ν_{max} 1612, 1557, 1395, 1380, 1357, 1240, 1152, 1085, 1020, 935, and 880 cm^{-1}; MS, *m/e* 376, 374, 372 (8, M^+), 295, 293 (17), 239, 237 (14), 214 (29), 201 (13), 199 (15), 107 (100), 95 (43), and 91 (27).

10: Mp 125—126 °C (from methanol); $[\alpha]_D^{21}$ +79° (*c* 0.38); IR, ν_{max} 1622, 1577, 1505, 1390, 1355, 1308, 1245, 1175, 1150, 1083, 1017, 965, 872, and 815 cm^{-1}; MS, *m/e* 376, 374, 372 (46, M^+), 295, 293 (35), 214 (40), 213 (100), 201 (50), 159 (51), 135 (30), 133 (20), 121 (30), 105 (15), and 91 (20).

Conversion of ***2a*** *to* ***1a***. One molar equivalent of bromine (8 mg) in acetic acid (2 ml) was added to a soln of **2a** (15 mg) in acetic acid (1 ml). The mixture was allowed to stand at room temp for 15 min and then extracted with ether. The ether soln was successively washed with water, 5% aqueous $NaHCO_3$, and saturated brine, and dried over Na_2SO_4. A crude substance obtained after the removal of the solvent was chromatographed on a PLC plate to give **1a** (18 mg); The IR and NMR spectra were superimposable on those of natural **1a**.

*Conversion of **8** to **9**.* One molar equivalent of bromine (21 mg) in acetic acid (2 ml) was added to a soln of **8** (40 mg) in acetic acid (1 ml). The mixture was allowed to stand at room temp for 15 min and then worked up as has been described above. Crude crystalline products were chromatographed on a PLC plate to give **9** (38 mg); crystals; mp 85 °C; The IR and NMR spectra were superimposable on those of natural **9**.

*Conversion of **1a** to **9**.* A soln of **1a** (16 mg) and *p*-toluenesulfonic acid (15 mg) in acetic acid (1 ml) was refluxed for 30 min. The mixture was then poured into water and extracted with ether. The ether soln was successively washed with water, 5% aqueous $NaHCO_3$, and saturated brine, and dried over Na_2SO_4. Crude products were chromatographed on a PLC plate to give **9** (6 mg).

References

1) Part XXXIV of "Constituents of Marine Plants." Part XXXIII: T. Suzuki and E. Kurosawa, *Chem. Lett.*, **1979**, 301.
2) T. Irie, M. Suzuki, and T. Masamune, *Tetrahedron*, **24**, 4193 (1968).
3) M. Suzuki, E. Kurosawa, and T. Irie, *Tetrahedron Lett.*, **1974**, 821, 1807.
4) M. Suzuki, A. Furusaki, and E. Kurosawa, *Tetrahedron*, **35**, 823 (1979).
5) M. Suzuki, E. Kurosawa, and T. Irie, *Tetrahedron Lett.*, **1970**, 4995.
6) T. Suzuki, M. Suzuki, and E. Kurosawa, *Tetrahedron Lett.*, **1975**, 3057.
7) T. Irie, T. Suzuki, Y. Yasunari, E. Kurosawa, and T. Masamune, *Tetrahedron*, **25**, 459 (1969).
8) M. Suzuki and E. Kurosawa, *Tetrahedron Lett.*, **1976**, 4817.
9) T. Irie, A. Fukuzawa, M. Izawa, and E. Kurosawa, *Tetrahedron Lett.*, **1969**, 1343.
10) T. Irie, M. Suzuki, E. Kurosawa, and T. Masamune, *Tetrahedron*, **26**, 3271 (1970).
11) R. Kazlauskas, P. T. Murphy, R. J. Quinn, and R. J. Wells, *Aust. J. Chem.*, **29**, 2533 (1976).
12) R. Kazlauskas, P. T. Murphy, R. J. Wells, J. J. Daly, and W. E. Oberhänsli, *Aust. J. Chem.*, **30**, 2679 (1977).
13) S. J. Wratten and D. J. Faulkner, *J. Org. Chem.*, **42**, 3343 (1977).

Halogenated and Non-halogenated Aromatic Sesquiterpenes from the Red Algae *Laurencia okamurai* Yamada[1)]

Minoru Suzuki and Etsuro Kurosawa*

Department of Chemistry, Faculty of Science, Hokkaido University, Sapporo 060

(Received March 31, 1979)

The taxonomic reexamination of the red alga '*L. intermedia* Yamada,' previously collected at Oshoro Bay, Hokkaido, showed that this alga consistd of a mixture of *L. intermedia* Yamada, *L. capituliformis* Yamada, and *L. okamurai* Yamada. Within the Japanese species of genus *Laurencia*, laurinterol and debromolaurinterol were found to be characteristic metabolites of *L. okamurai*, not of *L. intermedia*. In the course of this examination, dibromophenol and debromoaplysinol were newly isolated.

Red algae of the genus *Laurencia* (Rhodomelaceae) are a rich source of halogenated sesquiterpenes, diterpenes, and non-terpenoid C_{15} acetylenic ethers,[2-5)] and various species of *Laurencia* contain unique halogenated metabolites with some overlap ("species-specific"). Since species separation in the genus *Laurencia* is complicated by the high degree of morphological variation within the species, halogenated secondary metabolites might be useful for taxonomic purposes at the species level.[6)]

Previously we reported that laurinterol (**1**) and debromolaurinterol (**2**) were the major components of *L. okamurai* Yamada, specimens of which were collected in two different locations, Hakata-shima, the Inland Sea of Japan[7)] and Okino-shima, Kochi Prefecture,[8)] and also of '*L. intermedia* Yamada,' collected at Oshoro Bay, Hokkaido.[9)] Recently we collected *L. intermedia* Yamada at Inomisaki, Tosa Bay, and examined its neutral oil. There was no halogenated compound in this alga. The above-mentioned results conflicted with the concept of "species-specificity." Therefore, we carried out a taxonomical reexamination of the alga '*L. intermedia*,' previously collected at Oshoro Bay, to reveal that this material consisted of a mixture of *L. intermedia* Yamada, *L. capituliformis* Yamada, and *L. okamurai* Yamada. An examination of fresh algae *L. intermedia* and *L. capituliformis*, collected at Oshoro Bay, showed that these species did not contain any halogenated compound. On the other hand, the freshly collected alga *L. okamurai* was extracted with methanol, and the methanol extracts were subjected to separation by a combination of column and thin-layer chromatography to give laurinterol (**1**), debromolaurinterol (**2**), isolaurinterol (**3**), debromoisolaurinterol (**4**), aplysinol (**9**), isoaplysin (**11**), cuparene-type ether (**13**), bromocuparene (**23**), isobromocuparene (**24**), and isolaurene (**25**). Furthermore, dibromophenol (**5**) and debromoaplysinol (**10**) were newly isolated.

The structure of debromoisolaurinterol (**4**), $C_{15}H_{20}O$, $[\alpha]_D^{23}$ −104°, which has not been obtained in the pure state,[9)] was confirmed by the chemical correlation with aplysin (**7**). Treatment of **4** with bromine in acetic acid afforded a bromo compound, which was found to be identical with aplysin (**7**) by a comparison of the spectral data. The structure of debromoaplysinol (**10**), $C_{15}H_{20}O_2$, $[\alpha]_D^{23}$ −32°, was deduced by a comparison of the spectral data with those of aplysinol (**9**).[7)]

Dibromophenol (**5**), $C_{15}H_{18}OBr_2$ (*m/e* 376, 374, 372; M+), mp 50—52 °C, $[\alpha]_D^{23}$ +8°, exhibited the same intense sharp hydroxyl absorption in the IR spectrum at ν_{max} 3570 cm^{-1} as that of neolaurinterol (**6**), isolated from *L. okamurai* in Okino-shima.[8)] The NMR spectrum exhibited the signals due to a cyclopropane ring at δ 0.2—1.1 (3H, m), two tertiary methyl groups at 1.30 and 1.38 (each 3H, s), an aromatic methyl group at 2.51 (3H, s), and one aromatic proton at 7.59 (1H, s). The signal of the aromatic methyl group was shifted to a lower magnetic field region than those due to the methyl groups of **1** (δ 2.22), **6** (δ 2.33), and other bromophenols. The IR and NMR spectra suggest that dibromophenol should be represented by formula **5**. The structure of **5** was confirmed by the chemical correlation with laurinterol (**1**). Treatment of **1** with *N*-bromosuccinimide in CCl_4[8)] gave a dibromo compound, which was found to be identical with natural **5** in all respects.

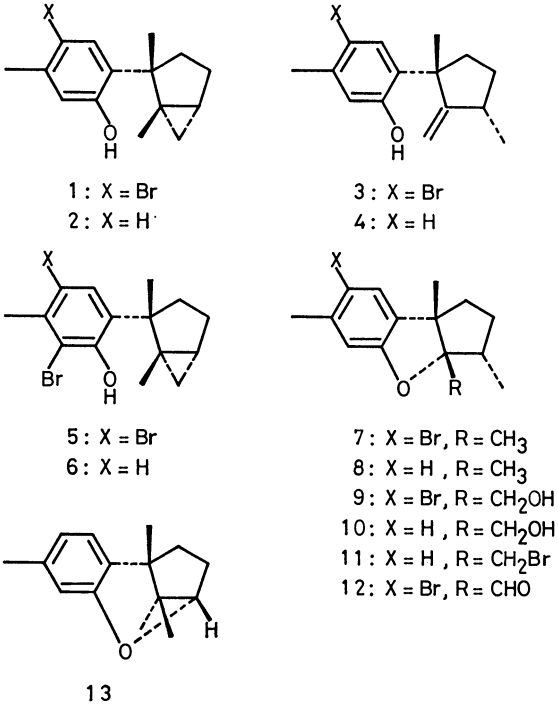

The similarities of the components (Table 1) between the algae *L. okamurai* in Okino-shima[8)] and in Oshoro Bay led to a reexamination of the previous extracts of *L. okamurai* in Hakata-shima[7)] and '*L. intermedia*' in Oshoro Bay.[9)] The results of the reexamination will be described in the experimental section and

Table 1. Aromatic sesquiterpenes from *Laurencia* species

Species	Location	Compounds
L. okamurai	Oshoro Bay (Japan)	**1, 2, 3, 4, 5, 9, 10, 11, 13, 23, 24, 25**
L. okamurai	Okino-shima (Japan)	**1, 2, 3, 4, 6, 11, 13, 23, 24, 25**
L. okamurai	Hakata-shima (Japan)	**1, 2, 5, 7, 8, 9, 10, 11, 13, 23, 24, 25**
L. pacifica	La Jolla, Calif. (USA)	**1**
L. pacifica	Ensenada (Mexico)	**3**
L. nidifica	Kahala Reef, Hawaii (USA)	**1, 7**
L. desidua	Alpha Helix Baja (Mexico)	**1, 3, 7, 9**
L. nipponica	Moheji, Hokkaido (Japan)	**15, 24, 25, 26**
L. glandulifera	Oshoro Bay (Japan)	**14, 15, 16, 18, 19, 20, 23, 24, 25, 26**
L. filiformis	Port MacDonnell (Australia)	**16, 21, 22, 26**
L. subopposita	La Jolla, Calif. (USA)	**16, 17, 26**
L. species (?)	Cape Omaezaki (Japan)	**1, 3, 7, 9, 12**

summarized in Table 1. As shown in Table 1, laurinterol (**1**) and debromolaurinterol (**2**) are characteristic major metabolites of Japanese species *L. okamurai*, and several aromatic compounds are common metabolites with only slight differences. Only Hakata-shima's species contained a chamigrene-type sesquiterpene, johnstonol.[10]

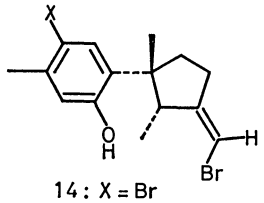

14: X = Br
15: X = H

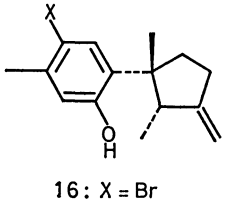

16: X = Br
17: X = H

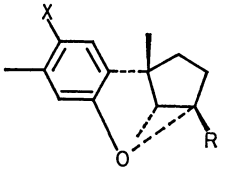

18: X = Br, R = CH_2Br
19: X = H , R = CH_2Br
20: X = H , R = $CHBr_2$
21: X = Br, R = CH_3
22: X = Br, R = CH_2OH

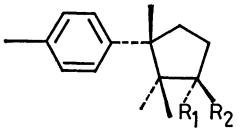

23: R_1 = H , R_2 = Br
24: R_1 = Br, R_2 = H

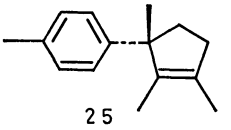

25

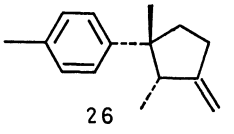

26

Laurinterol (**1**) was also isolated from *L. pacifica*,[11] *L. nidifica*,[12] and *L. desidua*.[13] Isolaurinterol (**3**) was also isolated from *L. pacifica*[14] and *L. desidua*.[13] On the other hand, allolaurinterol-type phenols and the related ethers have been obtained from several *L.* species. Allolaurinterol (**16**) and the related ethers, **21** and **22**, were isolated from *L. filiformis*.[15,16] **16** was also isolated from *L. subopposita*[17] along with debromoallolaurinterol (**17**). *L. nipponica*,[18] a Japanese species of *Laurencia*, contained a bromo phenol, laurenisol (**15**), which was also isolated from *L. glandulifera*[20] together with other bromo phenols, **14** and **16**, and the related ethers, **18**, **19**, and **20**. It is interesting to note that these *Laurencia* species contained not only allolaurinterol-type metabolites but also halo-chamigrene derivatives,[19,20] other halo-sesquiterpene derivatives,[16,17] and C_{15} acetylenic ethers.[17,19,20]

Among other Japanese species of the genus *Laurencia*, *L. papillosa* and *L. undulata* did not contain any halogenated compound, and *L. majuscula* contained only halo-chamigrene derivatives.[21,22] Ohta and Takagi have reported the isolation of several aromatic sesquiterpenes, **1**, **3**, **7**, **9**, and **12**, from the red algae *Marginisporum aberrans*, *Amphiroa zonata*, and *Corallina pilulifera* (Corallinaceae), collected at Cape Omaezaki, Shizuoka Prefecture, Japan.[23] As has been described by the authors, these compounds may be derived from *Laurencia* species, for some *Laurencia* species grow in the vicinity of Cape Omaezaki.

Experimental

All the mps were uncorrected. The IR spectra were measured on a Nihon-Bunko IR-S and a A-102 spectrometer. The NMR spectra were recorded on a JEOL JNM-PS-100 spectrophotometer, TMS being used as the internal reference in a CCl_4 soln. The optical rotations were measured in a $CHCl_3$ soln. Alumina (Merck, activity II—III) and silica gel (Mallinckrodt, 100 mesh) were used for the column chromatography. Silica gel (Merck, Kieselgel GF_{254} (Type 60)) was used for the preparative TLC (PLC).

Isolation. *L. okamurai* was collected at Oshoro Bay, Hokkaido, early in August, 1978. The half-dried algae (250 g) were extracted with methanol and then worked up as has previously been described.[9] After the separation of the acidic and basic components, a neutral oil (4 g) was obtained and submitted to column chromatography on neutral alumina.

Hexane Fraction: This fraction consisted of a mixture of hydrocarbons, aromatic ethers, and fatty acid methyl esters. Repeated chromatography on a silica-gel column and a PLC plate yielded isoaplysin (**11**) (0.4% of the neutral oil), cuparene-type ether (**13**) (0.8%), bromocuparene (**23**) (2%), isobromocuparene (**24**) (0.2%), and isolaurene (**25**) (0.6%).

Hexane/Benzene (10 : 1) Fraction: This fraction was rechromatographed on a silica gel column to give dibromophenol (**5**) (0.3%) upon elution with hexane. A benzene eluate gave a mixture of fatty acid methyl esters.

Benzene Fraction: This fraction consisted of laurinterol

(**1**), debromolaurinterol (**2**), isolaurinterol (**3**), and debromoisolaurinterol (**4**). As has previously been described,[9] the isolation and purification of these compounds were carried out *via* their acetates by repeated silica-gel column chromatography and PLC; **1** (40%), **2** (15%), **3** (3.5%), and **4** (2.5%) were thus obtained.

Ether Fraction: This fraction consisted of aplysinol (**9**), debromoaplysinol (**10**), and cholesterol. Repeated chromatography on a PLC plate gave **9** (0.3%) and **10** (0.3%).

Previous Extracts: The neutral oil of '*L. intermedia*,' which was previously collected at Oshoro Bay[9] and stored in an ice box in a N_2 atmosphere, was subjected to separation as described above to give **1** (20%), **2** (10%), **3** (0.6%), **4** (0.3%), **9** (0.1%), **10** (0.2%), **11** (0.1%), **13** (0.7%), **23** (1.1%), **24** (0.3%), and **25** (1.3%). The neutral oil of *L. okamurai*, collected at Hakata-shima,[7] was subjected to separation to give **1** (30%), **2** (13%), **5** (0.1%), **7** (3%), **8** (3%), **9** (0.7%), **10** (0.2%), **11** (0.3%), **13** (0.4%), **23** (0.3%), **24** (0.1%), **25** (1.7%), and johnstonol (0.7%).

*Debromoisolaurinterol (**4**)*: Colorless oil; $[\alpha]_D^{23}$ $-104°$ (*c* 1.10); IR (film), ν_{max} 3490, 3070, 1642, 1620, 1575, 1505, 1380, 1291, 1247, 1160, 1138, 950, 901, 889, and 807 cm^{-1}; NMR, δ 1.20 (3H, d, J=7 Hz), 1.43 (3H, s), 2.23 (3H, s), 4.91 (1H, br s), 5.05 (1H, br s), 5.20 (br s: OH), 6.52 (1H, br s), 6.56 (1H, br d, J=8), and 7.08 (1H, d, J=8); MS, *m/e* (rel. intensity) 216 (34, M^+), 201 (100), 173 (15), 160 (20), 159 (60), 115 (3), 91 (45), and 77 (4).

Acetate: Colorless oil; $[\alpha]_D^{23}$ $-91°$ (*c* 1.43); IR (film) ν_{max} 3075, 1773, 1650, 1622, 1577, 1510, 1380, 1200, 1143, 1070, 1020, 955, 900, and 822 cm^{-1}; NMR, δ 1.13 (3H, d, J=7), 1.23 (3H, s), 2.19 (3H, s), 2.30 (3H, s), 4.71 (1H, br s), 4.99 (1H, br s), 6.70 (1H, br s), 6.79 (1H, br d, J=8), and 7.20 (1H, d, J=8); MS, *m/e* 258 (8, M^+), 216 (20), 201 (100), 173 (6), 160 (8), 159 (16), 115 (3), 91 (4), 77 (3), and 43 (10).

*Dibromophenol (**5**)*: Mp 50—52 °C (from MeOH–H_2O); $[\alpha]_D^{23}$ $+8°$ (*c* 1.0); IR ($CHCl_3$), ν_{max} 3570, 1593, 1395, 1380, 1315, 1290, 1187, 1160, 1130, and 890 cm^{-1}; NMR, δ 0.2—1.1 (3H, m), 1.30 (3H, s), 1.38 (3H, s), 2.51 (3H, s), 5.66 (s: OH), and 7.59 (1H, s); MS, *m/e* 376, 374, 372 (45, M^+), 361, 359, 357 (67), 319, 317, 315 (20), 308, 306, 304 (100), 280, 278 (28), 254, 252 (50), 212 (24), 199 (25), 173 (66), 158 (28), 115 (33), 109 (32), 93 (30), 91 (30), and 77 (30).

*Debromoaplysinol (**10**)*: Mp 85—87 °C (from hexane); $[\alpha]_D^{21}$ $-32°$ (*c* 0.44); IR ($CHCl_3$), ν_{max} 3590, 1620, 1595, 1501, 1280, 1267, 1159, 1100, 1081, 1035, 1000, 948, 855, and 805 cm^{-1}; NMR, δ 1.07 (3H, d, J=7), 1.24 (3H, s), 2.26 (3H, s), 3.57, 3.75 (each 1H, br AB-q, J=12), 6.44 (1H, br s), 6.52 (1H, br d, J=8), and 6.78 (1H, d, J=8); MS, *m/e* 232 (86, M^+), 201 (55), 199 (38), 173 (15), 159 (100), 115 (4), 91 (4), and 77 (3).

*Conversion of **4** to Aplysin (**7**)*. One molar equivalent of bromine (9 mg) in acetic acid (2 ml) was added to a soln of **4** (12 mg) in acetic acid (1 ml). The mixture was allowed to stand at room temp for 15 min and then extracted with ether. The ether soln was successively washed with water, 5% aqueous $NaHCO_3$, and saturated brine. After drying over Na_2SO_4, the solvent was removed to yield a colorless oil, which was purified by PLC to give aplysin (**7**) (11 mg); crystals; mp 85 °C (from MeOH). The IR and NMR spectra were superimposable on those of an authentic sample (**7**).

*Conversion of **1** to **5**.* A soln of **1** (30 mg) and *N*-bromosuccinimide (18 mg) in CCl_4 (2.5 ml) was stirred for 1 h at room temp, and then ether was added. The subsequent removal of the solvent, after filtering from an insoluble substance, gave a residual substance, which was chromatographed on a PLC plate to give dibromophenol (**5**) (33 mg); crystals; mp 50 °C (from MeOH–H_2O). The IR and NMR spectra were superimposable on those of natural **5**.

The authors are grateful to Dr. Hiroshi Yabu and Dr. Yuzuru Saito, Faculty of Fisheries, Hokkaido University, for collecting and identifying the algae *Laurencia* species.

References

1) Part XXXV of "Constituents of Marine Plants." Part XXXIV: M. Suzuki and E. Kurosawa, *Bull. Chem. Soc. Jpn.*, **52**, 3349 (1979).
2) W. Fenical, *J. Phycol.*, **11**, 245 (1975).
3) D. J. Faulkner, *Tetrahedron*, **33**, 1421 (1977).
4) S. M. Waraszkiewicz, H. H. Sun, K. L. Erickson, J. Finer, and J. Clardy, *J. Org. Chem.*, **43**, 3194 (1978).
5) B. M. Howard and W. Fenical, *J. Org. Chem.*, **43**, 4401 (1978).
6) W. Fenical and J. N. Norris, *J. Phycol.*, **11**, 104 (1975).
7) T. Irie, M. Suzuki, and Y. Hayakawa, *Bull. Chem. Soc. Jpn.*, **42**, 843 (1969).
8) M. Suzuki and E. Kurosawa, *Tetrahedron Lett.*, **1978**, 2503.
9) T. Irie, M. Suzuki, E. Kurosawa, and T. Masamune, *Tetrahedron*, **26**, 3271 (1970).
10) J. J. Sims, W. Fenical, R. M. Wing, and P. Radlick, *Tetrahedron Lett.*, **1972**, 195.
11) J. J. Sims, W. Fenical, R. M. Wing, and P. Radlick, *J. Am. Chem. Soc.*, **93**, 3774 (1971).
12) S. M. Waraszkiewicz and K. L. Erickson, *Tetrahedron Lett.*, **1974**, 2003.
13) J. A. McMillan, I. C. Paul, S. Caccamese, and K. L. Rinehart, Jr., *Tetrahedron Lett.*, **1976**, 4219.
14) W. Fenical, *Phytochemistry*, **15**, 511 (1976).
15) R. Kazlauskas, P. T. Murphy, R. J. Quinn, and R. J. Wells, *Aust. J. Chem.*, **29**, 2533 (1976).
16) R. Kazlauskas, P. T. Murphy, R. J. Wells, J. J. Daly, and W. E. Oberhänsli, *Aust. J. Chem.*, **30**, 2679 (1977).
17) S. J. Wratten and D. J. Faulkner, *J. Org. Chem.*, **42**, 3343 (1977).
18) T. Irie, A. Fukuzawa, M. Izawa, and E. Kurosawa, *Tetrahedron Lett.*, **1969**, 1343.
19) T. Suzuki, A. Furusaki, N. Hashiba, and E. Kurosawa, *Tetrahedron Lett.*, **1977**, 3731, and the related references cited therein.
20) Part XXXIV of this series: M. Suzuki and E. Kurosawa, *Bull. Chem. Soc. Jpn.*, preceding paper, and the related references cited therein.
21) M. Suzuki and E. Kurosawa, *Tetrahedron Lett.*, **1978**, 4805.
22) M. Suzuki, A. Furusaki, N. Hashiba, and E. Kurosawa, *Tetrahedron Lett.*, **1979**, 879.
23) K. Ohta and M. Takagi, *Phytochemistry*, **16**, 1062 (1977).

Diels-Alder Reaction of 2-Substituted Tropones with Ethylene. HMO Level Aspect of the Regioselectivity

Tadao UYEHARA* and Yoshio KITAHARA†

Department of Chemistry, Faculty of Science, Tohoku University, Aoba, Aramaki, Sendai 980

(Received April 6, 1979)

2-Chloro-, 2-methoxy-, 2-phenyl-, and 2-methyltropones (2,4,6-cycloheptatrien-1-ones) and benzoate of tropolone (2-hydroxy-2,4,6-cycloheptatrien-1-one) reacted with ethylene affording Diels-Alder type 1,4-addition products, bicyclo[3.2.2]nona-3,6-dien-2-ones. The regioselectivities of the cycloaddition are quite random, while they are reproduced by the calculated interaction energies based on Salem's PMO equation which includes the closed-shell repulsion term.

Recently we have reported that tropone (2,4,6-cycloheptatrien-1-one, **1**) reacts relatively easily with alternant hydrocarbons (neutral olefins), such as ethylene, styrene and acenaphthylene giving Diels-Alder type 1,4-addition products.[1] The HOMO-LUMO orbital arrangements of the reactions indicate that the interaction between $HOMO_{dienophile}$—$LUMO_{tropone}$ is dominant in each case. On the basis of Sustmann's classification,[2] those reactions are of the "inverse electron demand" type.

From a theoretical point of view, a diene synthesis utilizing ethylene as the dienophile is of interest. We can treat the Diels-Alder reaction quantitatively because of absence of complicated secondary interactions. We now like to describe the regioselectivities of the Diels-Alder reaction of 2-substituted tropones with ethylene and perturbational MO (PMO) approach to the selectivities based on Eqs. 1 and 2.

The stabilization energy through the interconjugation between a diene and a dienphile at the transition state is evaluated by Eq. 1, based on which the frontier orbital approach was derived.[3]

$$\Delta E = 2\left(\sum_{i}^{occ}\sum_{j}^{unocc} - \sum_{l}^{unocc}\sum_{j}^{occ}\right)\frac{(C_{lr}^{l}C_{2r}^{j}+C_{ls}^{l}C_{2s}^{j})^2}{E_{1l}-E_{2j}}\gamma^2 \qquad (1)$$

Equation 2, derived by Salem,[4] consists of the closed-shell repulsion term (the first term, E_{rep}) and the overlap stabilization terms (E_{stab}) which are similar to Eq. 1. Here subscripts r and r′ refer to a pair of atoms in a diene and a dienophile at which a bond is formed. q is the charge density and S denotes the overlap integral. k is the value of the ratio of interaction integral to overlap integral.

$$\left.\begin{aligned} E_{int} = {} & -k\sum_{rr'}(q_r+q_{r'})S_{rr'}^2 \\ & -2\sum_{j}^{occ}\sum_{k'}^{unocc}\Big(\sum_{rr'}C_{jr}C_{k'r'}S_{rr'}\Big)^2[k^2/(E_{k'}-E_j) \\ & \qquad + (E_{k'}-E_j)/4] \\ & -2\sum_{j'}^{occ}\sum_{k}^{unocc}\Big(\sum_{rr'}C_{kr}C_{j'r'}S_{rr'}\Big)^2[k^2/(E_k-E_{j'}) \\ & \qquad + (E_k-E_{j'})/4] \end{aligned}\right\} \qquad (2)$$

Results and Discussion

The dienophile, ethylene, is able to add to the 4- and 7-positions of 2-substituted tropones giving 3-substituted bicyclo[3.2.2]nona-3,6-dien-2-ones (A-type adducts) and to the 2- and 5-positions affording 1-substituted ones (B-type adducts). A reaction of 2-substituted tropones (**2**—**6**) with ethylene was carried out in a stainless steel autoclave. The reaction conditions and the results are listed in Table 1.

Table 1. The reaction conditions and the results of Diels-Alder reaction of 2-substituted tropones with ethylene

Tropone	Conditions (°C, day)	Product (ratio)[a]	Total yield[a]
2	135, 3.5	**2a** (40.5), **2b** (59.5)	100
3	140, 3	**3a** (12.3), **3b** (87.7)	100
4	135, 3	**4a** (100)	87.5
5	140, 3	**5a** (58), **5b**(42)	91.5
6	135, 3	**6a** (60), **6b**(40)[b]	78[b]

a) By VPC analysis using 1 m×3 mm columns containing 5% PDEGS on Diasolid H or 10% SE-30 on Diasolid H. b) After isolation.

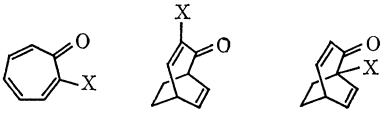

		A-type	B-type
X=H	**1**		
X=Cl	**2**	**2a**	**2b**
X=OCH_3	**3**	**3a**	**3b**
X=Ph	**4**	**4a**	(**4b**)
X=CH_3	**5**	**5a**	**5b**
X=OCOPh	**6**	**6a**	**6b**

A reaction of 2-chlorotropone (**2**) with ethylene gave the two types of adducts (**2a** and **2b**) in a ratio of 40.5 to 59.5, which were separated by chromatography on silica gel. Struture elucidation of the products was performed easily by means of their NMR spectra. A reaction of 2-methoxytropone (**3**) with ethylene proceeded regioselectively giving **3a** (12.3%) and **3b** (87.7%). 2-Phenyltropone (**4**) afforded only the A-type adduct (**4a**), while 2-methyltropone (**5**) gave both types of adducts (**5a** and **5b**: 58 and 42% respectively). The adducts (**6a** and **6b**) were obtained from benzoate of tropolone (**6**) in 60 and 40%, respectively. Thus, regioselectivities of the Diels-Alder reactions are quite random. The cycloadditions should be kinetically controlled: compound **2b** was completely recovered under the cycloaddition conditions, and when it was heated in C_6D_6 (in a sealed tube) at 135 °C for 3 d.

† Deceased February 4, 1976.

Table 2. Caluculated interaction energies (β) based on Eq. 2[a)]

Adduct	E_{int}	E_{repul}	E_{stab}
2a	0.0125	−0.4393	0.4518
2b	0.0128	−0.4382	0.4510
3a	0.0116	−0.4395	0.4511
3b	0.0123	−0.4372	0.4495
4a	0.0101	−0.4401	0.4502
(**4b**)	0.0024	−0.4400	0.4424
5a	0.0093	−0.4400	0.4493
5b	0.0087	−0.4367	0.4454

a) The overlap integral is 0.2. The ratio of the interaction integral to the overlap integral is 2.85 β.

The frontier orbital approach[2)] to the regioselectivity of the reaction of the tropones (**2**—**5**) did not reproduce the experimental results, when we used the Hückel MO calculations based on Streitwieser's parameters.[5)] Our calculations[6)] based on Eq. 1 indicated preferred formation of the A-type adduct in every case. In reality, **2a** and **3a** are not predominant adducts. Thus the stabilization energy concept through the interconjugation is not sufficient to explain the regioselectivities.

It has been mentioned by Salem that the repulsion energy term must be included in a quantitative evaluation of interaction energies.[4)] The interaction energies calculated from Eq. 2 for the transition states of the present Diels-Alder reactions are shown in Table 2. The differences in E_{int} between the A- and B-type adduct formations are uniformly small, and yet they are qualitatively in line with the observed preponderance of one adduct isomer over the other.

The overlap energies (E_{stab}), from the second and third terms of Eq. 2, also show that the predominant adducts are A-type ones in all cases. Thus, the closed-shell repulsion is not negligible in PMO approach to the regioselectivities.

Experimental

General. Melting points were determined on a Thomas Hoover MP apparatus, and are not corrected. Infrared spectra were recorded on Hitachi EPI-3 and Model 215 spectrophotometers. Ultraviolet spectra were recorded on a Hitachi EPS-2T spectrometer. NMR spectra were obtained on Varian A-60 and HA-100 spectrometers equipped with spin decouplars, using tetramethylsilane as the internal standard. The mass spectral studies were conducted using a Hitachi RMU-6D spectrometer. VPC analyses were carried out on a Hitachi gas chromatograph K-53 equipped with a FID. Preparative GLC were done on a Varian Aerograph Model 700 gas chromatograph equipped with a TCD.

*Diels-Alder Reaction of Tropones (**2**—**6**) with Ethylene.* A solution of a tropone (1—2.5 g) in toluene (10—15 ml) was placed in a stainless steel autoclave (100 ml), and heated with excess of ethylene (*ca.* 13 MPa, at 130 °C). After removal of the solvent *in vacuo*, the adducts were isolated by respective way.

*3- and 1-Chlorobicyclo[3.2.2]nona-3,6-dien-2-ones (**2a** and **2b**, respectively).* A mixture of **2a** and **2b**, obtained from 1.65 g of 2-chlorotropone, was chromatographed on silica gel (Wako C-200, 50 g). Elution with hexane gave 245 mg of **2a** and that with benzene gave 450 mg of **2b**. **2a**: Colorless oil; UV_{max} (CH_3OH) 238 (log ε 3.69), 265 (3.44)[sh] and 330 nm (1.94); IR (CCl_4) 1689, 1630 and 1600 cm^{-1}; NMR (CCl_4) δ=7.23 (d, J=9.4 Hz, H_4), 6.54 (ddd, J=8.0, 7.2 and 1.2 Hz, H_6), 6.06 (ddd, J=8.2, 7.6, and 1.2 Hz, H_7), 3.65 (m, H_1), 3.40 (m, H_5), and 2.1—1.5 (4H, m). 2,4-DNP of **2a**: 203—205 °C (dec). Found: C, 51.70; H, 3.92; N, 15.69%. Calcd for $C_{15}H_{13}ClN_4O_4$: C, 51.51; H, 3.75; N, 15.62%. **2b**: Colorless needles; mp 55—56 °C; UV_{max} (CH_3OH) 226.5 (log ε 3.82) and 330 nm (1.97); IR (KBr) 1680 and 1615 cm^{-1}; NMR ($CDCl_3$) δ=7.12 (dd, J=11.2 and 8.9 Hz, H_4), 6.55 (dd, J=9.0 and 7.2 Hz, H_6), 6.01 (dd, J=9.0 and 0.8 Hz, H_7), 5.89 (dd, J=11.2 and 0.8 Hz, H_3), 3.43 (m, H_5), 2.4 (2H, m), and 1.9 (2H, m). Found: C, 64.08; H, 5.35%. Calcd for C_9H_9ClO: C, 64.10; H, 5.38%.

*3- and 1-Methoxybicyclo[3.2.2]nona-3,6-dien-2-ones (**3a** and **3b**, respectively).* Isolation of the adducts was performed by preparative GLC using a 10 ft × 3/8 in aluminium column containing 5% PDEGE on Diasolid H at 180 °C. **3a**: Colorless prisms (from hexane–ether); mp 48—49 °C; UV_{max} (CH_3OH) 234.5 (log ε 3.64), 276.5 (3.68) and 335 nm (2.43)[sh]; IR (CCl_4) 1686, 1635 and 1620 cm^{-1}; NMR ($CDCl_3$) δ=6.60 (ddd, J=8.3, 7.5 and 1.0 Hz, H_6), 6.06 (bd, J=9.5 Hz, H_4), 5.95 (ddd, J=8.3, 6.5 and 1.0 Hz, H_7), 3.65 (m, H_1), 3.52 (3H, s), 3.40 (m, H_5), and 2.0—1.6 (4H, m). Found: M+, 164. Calcd for $C_{10}H_{12}O_2$: M, 164. 2,4-DNP of **3a**: mp 207 °C (dec). **3b**: Colorless oil; UV_{max} (CH_3OH) 228 (log ε 3.77) and 340 nm (2.22); IR (CCl_4) 1685 and 1635 cm^{-1}; NMR ($CDCl_3$) δ=7.02 (dd, J=11.1 and 8.5 Hz, H_4), 6.54 (dd, J=9.0 and 7.1 Hz, H_6), 6.03 (dd, J=9.0 and 0.9 Hz, H_7), 5.83 (dd, J=11.4 and 0.8 Hz, H_3), 3.49 (3H, s), 3.38 (m, H_5), and 2.2—1.7 (4H, m). 2,4-DNP of **3b**: mp 217 °C (dec). Found: C, 55.71; H, 4.79; N, 16.64%. Calcd for $C_{16}H_{16}N_4O_5$: C, 55.81; H, 4.68; N, 16.77%.

*3-Phenylbicyclo[3.2.2]nona-3,6-dien-2-one (**4a**).* Recrystallization of the crude product, from 1 g of 2-phenyltropone (**4**), was performed from hexane–ether yielding 750 mg of **4a**. The mother liquor gave 270 mg of **4a** and trace of **4**, after chromatography on silica gel. **4a**: Colorless needles (from ethanol); mp 93—95 °C; UV_{max} 223.5 (log ε 4.07), 275 (3.56) and 335 nm (2.05)[sh]; IR (KBr) 1670 and 1628 cm^{-1}; NMR ($CDCl_3$) δ=7.24 (5H, m), 7.07 (d, J=9.0 Hz, H_4), 6.58 (ddd, J=8.1, 7.2 and 1.0 Hz, H_6), 6.13 (ddd, J=8.1, 8.1 and 1.1 Hz, H_7), 3.68 (m, H_1), 3.46 (m, H_5), and 2.15—1.6 (4H, m). Found: C, 85.97; H, 6.86%. Calcd for $C_{15}H_{14}O$: C, 85.69; H, 6.71%.

*3- and 1-Methylbicyclo[3.2.2]nona-3,6-dien-2-ones (**5a** and **5b**, respectively).* A mixture of **5a** and **5b**, and unreacted 2-methyltropone (**5**, 8.5%) were separated by preparative GLC (5% PDEGS). The adducts **5a** and **5b** were separated by preparative GLC using a 20 ft × 3/8 in column containing 20% SE-30, at 180 °C. **5a**: Colorless oil; UV_{max} (CH_3OH) 231.5 (log ε 3.82), 255 (3.68)[sh] and 330 nm (2.10); IR (CCl_4) 1668 and 1638 cm^{-1}; NMR ($CDCl_3$) δ=6.91 (dq, J=9.0 and 1.5 Hz, H_4), 6.53 (ddd, J=8.3, 6.3 and 1.2 Hz, H_6), 6.06 (ddd, J=8.3, 7.3 and 1.0 Hz, H_7), 3.55 (m, H_1), 3.30 (m, H_5), 2.0—1.6 (4H, m), and 1.72 (3H, d, J=1.5 Hz); MS (25 eV), *m/e* (rel intensity), 148 (69, M+), 133 (96), 131 (73), 106 (62), 105 (99), 93 (48), 92 (100), and 91 (89). 2,4-DNP of **5a**: mp 193—194.5 °C. Found: C, 58.22; H, 4.81; N, 16.94%. Calcd for $C_{16}H_{16}N_4O_4$: C, 58.53; H, 4.91; N, 17.07%. **5b**: Colorless oil; UV_{max} (CH_3OH) 227.5 (log ε 3.90) and 326 nm (2.17); IR (CCl_4) 1665 and 1633

cm^{-1}; NMR ($CDCl_3$) δ=7.01 (dd, J=11.2 and 8.6 Hz, H_4), 6.53 (dd, J=8.8 and 6.2 Hz, H_6), 5.77 (dd, J=8.8 and 1.0 Hz, H_7), 5.65 (dd, J=11.2 and 0.5 Hz, H_3), 3.30 (m, H_5), 2.0—1.6 (4H, m), and 1.29 (3H, s); MS (25 eV), *m/e* (rel intensity), 148 (69, M^+), 133 (96), 131 (73), 106 (62), 105 (99), 93 (48), 92 (100), 91 (89), 79 (64), and 55 (60).

*2-Oxobicyclo[3.2.2]nona-3,6-dien-3-yl and 7-yl Benzoates (**6a** and **6b**, Respectively).* Chromatography of a mixture of **6a** and **6b**, obtained from 1 g of benzoate of tropolone (**6**), on 50 g of silica gel (elution with benzene–ether, 10:1) gave 320 mg of **6a** and a mixture of **6a** and **6b**. The latter was chromatographed on Florisil (eluted with benzene) yielding 165 mg of **6a**, 363 mg of **6b** and 95 mg of 1 : 1 mixture of them. **6a**: Colorless needles; mp 104—105 °C (from ethanol); UV_{max} (CH_3OH) 232 (log ε 4.37) and 330 nm (2.04); IR (KBr) 1740, 1675, 1643, and 1625 cm^{-1}; NMR ($CDCl_3$) δ=8.2—7.95 (2H, m), 7.65—7.4 (3H, m), 6.87 (d, J=9.8 Hz, H_4), 6.67 (ddd, J=8.7, 7.2 and 1.0 Hz, H_6), 6.15 (ddd, J=8.7, 7.6 and 1.0 Hz, H_7), 3.72 (m, H_1), 3.45 (m, H_5), and 2.2—1.7 (4H, m). Found: C, 75.57; H, 5.57%. Calcd for $C_{16}H_{14}O_3$: C, 75.57; H, 5.55%. **6b**: Colorless needles (from ethanol); mp 74—75 °C; UV_{max} (CH_3OH) 230.5 (log ε 4.33) and 333 nm (1.83); IR (KBr) 1722, 1672 and 1635 cm^{-1}; NMR ($CDCl_3$) δ=8.2—8.0 (2H, m), 7.6—7.35 (3H, m), 7.00 (dd, J=11.2 and 8.5 Hz, H_4), 6.52 (dd, J=9.0 and 7.0 Hz, H_6), 6.28 (bd, J=9 Hz, H_7), 5.92 (d, J=11.2 Hz, H_3), 3.42 (m, H_5), and 2.8—1.75 (4H, m). Found: C, 75.52; H, 5.48%. Calcd for $C_{16}H_{14}O_3$: C, 75.57; H, 5.55%.

References

1) T. Uyehara and Y. Kitahara, *Chem. Ind. (London)*, **1971**, 354.

2) R. Sustmann, *Tetrahedron Lett.*, **1971**, 2721.

3) K. Fukui "Molecular Orbitals in Chemistry, Physics, and Biology," ed by P.-O. Lowdin and B. Pullman, Academic Press Inc., New York (1964), p. 573.

4) L. Salem, *J. Am. Chem. Soc.*, **90**, 543 (1968).

5) A. J. Streitwieser, Jr., *J. Am. Chem. Soc.*, **82**, 4123 (1960).

6) PMO calculations in this paper were performed using NEAC-2200-700 at Tohoku University Computer Center.

The Crystal and Molecular Structure of (±)-2-Methylamino-4,5-bis(*p*-chlorophenyl)-4-hydroxy-4*H*-imidazole

Hiroaki TAKAYANAGI, Haruo OGURA, Keinosuke MATSUZAKI, Koji KITAJIMA,† and Tamio NISHIMURA†,*

School of Pharmaceutical Sciences, Kitasato University, Shirokane, Minato-ku, Tokyo 108

† *Department of Chemistry, School of Hygienic Sciences, Kitasato University, Kitasato, Sagamihara-shi 228*

(Received April 9, 1979)

The crystal and molecular structure of (±)-2-methylamino-4,5-bis(*p*-chlorophenyl)-4-hydroxy-4*H*-imidazole has been determined by the single-crystal X-ray diffraction method. The crystals are monoclinic with space group $P2_1/c$, cell dimensions: $a=14.872(5)$, $b=9.216(7)$, $c=12.945(11)$ Å, $\beta=99.53(5)°$, and $Z=4$. The structure was determined by the symbolic addition method and refined by the least-squares method to give the final R factor of 0.072 for 1616 non-zero reflections.

In conection with the development of the new synthetic method of 2-aminoimidazoles,[1-3] 4,5-diaryl-4-hydroxy-4*H*-imidazoles (**1**) were prepared by the reaction of the corresponding benzils with methylguanidine.[4] The NMR spectra of these compounds (**1**) show a slightly broad singlet for the *N*-methyl protons indicating the structure of 4,5-diaryl-4-hydroxy-2-imino-1-methyl-5-imidazoline (**1b**).[4] On the other hand, the fact that hydrogenation of **1** produced 4,5-diaryl-2-methylaminoimidazoles suggests isomeric 4,5-diaryl-4-hydroxy-2-methylamino-4*H*-imidazoles (**1a**) as the structure of **1**.[4] Since structural interconversion between **1a** and **1b** in solution is possible,[2] it is difficult

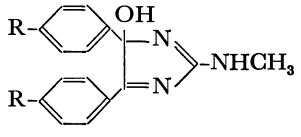

1a

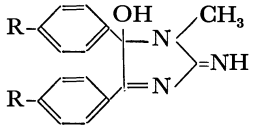

1b

to determine which isomeric structure **1a** or **1b** corresponds to compounds (**1**). Thus, an X-ray crystallographic analysis of the bis(*p*-chlorophenyl) derivative (**1**, R=Cl) was undertaken to determine the position of the methyl group and the conformation of the molecule.

Experimental

Preparation of 2-Methylamino-4,5-bis(p-chlorophenyl)-4-hydroxy-4H-imidazole (1). A mixture of 4,4′-dichlorobenzil (2.70 g) and methylguanidine (0.73 g) in 16 ml of methanol was stirred at room temperature for 30 min. The presipitate was filtered, washed with methanol, chloroform, and then ether and air-dried at room temperature. Colorless powder, mp *ca.* 295 °C dec (gradual darkening ≳125 °C), yield 3.03 g (91%). Recrystallization of **1** with methanol gave pale yellowish crystals; mp >280 °C (gradual darkning ≳126 °C); NMR (DMSO-d_6) $\delta=2.87$ (3H, s, NCH_3), 3.19 (3H, s, OCH_3), *ca.* 4.1 (2H, broad, disappeared on addition of D_2O, OH), *ca.* 7.1 (1H, broad, disappeared on addition of D_2O, NH), 7.30 (4H, s, 4-C_6H_4Cl), 7.50 (2H, d, $J=9.3$ Hz, $H_{3,5}$ of 5-C_6H_4Cl), 7.97 (2H, d, $J=9.3$ Hz, $H_{2,6}$ of 5-C_6H_4Cl). The NMR spectrum was recorded with a Hitachi R-24 (60 MHz) spectrometer. The size of crystal used for obtaining X-ray data was $0.3\times0.2\times0.4$ mm. The data are given in Table 1. The cell constants were determined by the least-squares procedure from the 2θ values of 25 reflections measured on a diffractometer using monochromated Mo $K\alpha$ radiation. The density was determined by the flotation method. The integrated intensities of the reflections were collected on a Rigaku automatic four circle diffractometer with Mo $K\alpha$ radiation monochromatized by a graphite plate. Background was counted for 10 s at both sides of each peak. Three standard reflections were measured every 50 reflections during the couse of collection. The intensities of unique reflections with 2θ values than 69° were collected, a total of 1616 reflections with $|F|>3\sigma(|F|)$ being obtained. The data were corrected for Lorentz and polarization factors, but not for absorption. The atomic scattering factors for C, O, N, and Cl were given by Cromer and Mann,[5] and that for H by Stewart *et al.*[6]

TABLE 1. CRYSTAL DATA

$C_{16}H_{13}ON_3Cl_2\cdot CH_3OH$	
Monoclinic	Space group $P2_1/c$
$a=$ 14.872 (5) Å	$D_m=1.39$ g·cm^{-3}
$b=$ 9.216 (7) Å	$D_c=1.391$ g·cm^{-3}
$c=$ 12.945 (11) Å	$Z=4$
$\beta=$ 99.53 (5)°	
$V=$ 1749.7 Å^3	

Determination of Structure

The structure was determined by the symbolic addition method.[7] The distribution and statistics of $|E|^s$ agree with the theoretical values for the centrosymmetric case. The resulting E map revealed the location of all the 24 non-hydrogen atoms including methanol molecule. Several cycles of least-squares refinement of the coordinates with isotropic temperature factors gave an R value of 0.15. Anisotropic thermal parameters were introduced for all non-hydrogen atoms, the R value being reduced to 0.11. Of seventeen hydrogen atoms, the two hydrogen atoms of the hydroxyl group of compound **1** and the methylamino group were located on the difference map, but the other hydrogen atoms could not be identified. Refinement of the coordinates with anisotropic temperature factors for non-hydrogen atoms and isotropic thermal factors for hydrogen atoms gave the final R value 0.072. At the final stage of the refinement the difference electron density map showed only featureless peaks, which were about half of those of the two hydrogen atoms H(1) and H(2). The complete F_o-F_c data are deposited as Document No. 7932 at the Chemical Society of Japan.

TABLE 2. FINAL ATOMIC PARAMETERS ($\times 10^4$), WITH THEIR STANDARD DEVIATIONS IN PARENTHESES

(a) Fractional atomic coordinates and anisotropic temperature factors[a] for non-hydrogen atoms.

Atom	x	y	z	U_{11}	U_{22}	U_{33}	U_{12}	U_{13}	U_{23}
Cl(1)	175(2)	−230(2)	3129(2)	703(15)	559(15)	1195(20)	217(11)	272(14)	103(13)
Cl(2)	809(2)	8649(2)	−435(2)	747(15)	732(14)	767(16)	−205(12)	−29(12)	−243(12)
C(1)	5142(5)	7836(8)	4830(6)	684(54)	550(45)	564(53)	229(40)	−41(39)	4(39)
C(2)	3981(4)	6011(7)	4170(5)	423(41)	355(36)	476(45)	−11(30)	78(31)	29(32)
C(3)	3004(4)	4414(7)	3529(5)	437(42)	350(35)	453(47)	−14(29)	0(31)	−5(31)
C(4)	3390(4)	5109(7)	2632(5)	461(42)	454(38)	352(44)	9(31)	79(30)	70(32)
C(5)	2315(4)	3266(7)	3417(6)	407(42)	356(35)	588(50)	0(30)	62(33)	−19(33)
C(6)	1944(5)	2834(8)	4304(6)	613(53)	582(48)	736(58)	128(41)	169(43)	−19(43)
C(7)	1274(6)	1745(9)	4231(7)	744(59)	530(49)	828(65)	171(44)	137(47)	64(44)
C(8)	999(5)	1127(7)	3244(7)	393(44)	372(39)	989(66)	31(32)	89(41)	−2(40)
C(9)	1349(5)	1515(8)	2345(6)	534(50)	477(44)	806(61)	98(37)	56(41)	−24(41)
C(10)	2014(5)	2612(7)	2434(6)	519(46)	417(38)	538(48)	38(33)	46(35)	−5(35)
C(11)	2686(4)	5896(7)	1829(5)	367(40)	408(36)	418(44)	41(29)	26(30)	−10(31)
C(12)	1986(5)	6638(8)	2170(6)	452(45)	524(42)	526(51)	−76(35)	75(34)	87(36)
C(13)	1388(5)	485(8)	1452(6)	546(48)	574(46)	541(50)	−58(37)	35(36)	−3(38)
C(14)	1528(5)	7539(8)	432(6)	465(45)	516(42)	504(47)	−2(33)	−72(34)	−110(36)
C(15)	2213(5)	6762(9)	63(6)	538(51)	722(52)	556(54)	−146(41)	58(38)	−103(42)
C(16)	2805(5)	5926(8)	788(6)	591(48)	641(48)	401(48)	−64(40)	73(35)	−74(38)
C(17)	6286(6)	4735(9)	2661(7)	805(63)	587(51)	822(67)	−110(46)	154(49)	16(46)
O(1)	3849(3)	4064(5)	2105(4)	465(30)	517(28)	541(32)	−87(24)	67(23)	167(25)
O(2)	5644(3)	3633(5)	2840(4)	495(30)	556(30)	482(32)	75(24)	28(23)	−34(24)
N(1)	4446(4)	6733(6)	4981(4)	592(39)	473(33)	436(39)	54(30)	−42(28)	51(29)
N(2)	3351(4)	4943(6)	4420(4)	519(37)	444(32)	403(38)	28(28)	50(27)	2(28)
N(3)	4037(4)	6176(6)	3197(4)	455(34)	473(32)	331(34)	27(27)	24(25)	47(27)

a) The anisotropic temperature factors are expressed in the from: $\exp[-2\pi^2(U_{11}h^2a^{*2}+U_{22}l^2c^{*2}+U_{33}l^2c^{*2}+2U_{12}hka^*b^*+2U_{13}hla^*c^*+2U_{23}klb^*c^*)]$.

(b) Atomic coordinates ($\times 10^3$) and isotopic temperature factors ($\times 10^2$) for hydrogen atoms.

Atom	x	y	z	U
H(1)	459(6)	421(10)	226(7)	14(4)
H(2)	434(5)	633(9)	571(6)	11(3)

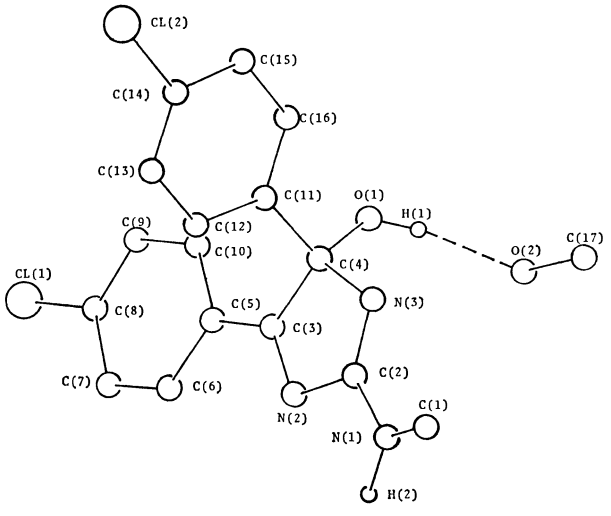

Fig. 1. The molecular structure and numbering of (±)-2-methylamino-4,5-bis(*p*-chlorophenyl)-4-hydroxy-4*H*-imidazoles.

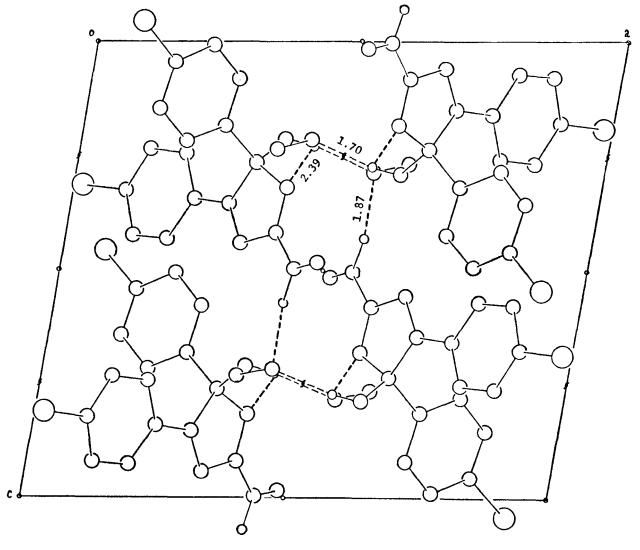

Fig. 2. The molecular arrangement in this crystal viewed along the b axis. The dotted lines show the hydrogen bonds. Their distances are given in Å.

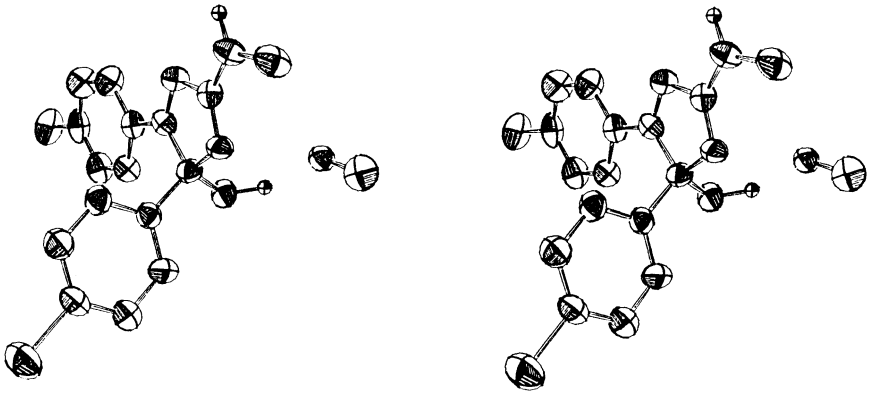

Fig. 3. Stereoscopic view of the compound **1**.

TABLE 3. BOND ANGLES AND THEIR STANDARD DEVIATIONS

C(3)-C(4)-C(11)	114.6(6)°	C(1)-N(1)-C(2)	121.2(6)°
C(3)-C(5)-C(6)	119.0(6)	C(2)-N(2)-C(3)	104.0(6)
C(3)-C(5)-C(10)	120.7(7)	C(2)-N(3)-C(4)	104.6(5)
C(4)-C(11)-C(12)	119.0(6)	C(3)-C(4)-N(3)	102.3(5)
C(4)-C(11)-C(16)	119.1(6)	C(3)-C(4)-O(1)	110.7(5)
C(4)-C(3)-C(5)	125.2(6)	C(4)-C(3)-N(2)	112.4(6)
C(5)-C(6)-C(7)	121.0(7)	C(5)-C(3)-N(2)	122.5(6)
C(6)-C(7)-C(8)	116.7(8)	C(11)-C(4)-N(3)	109.2(5)
C(7)-C(8)-C(9)	124.4(7)	C(11)-C(4)-O(1)	108.9(5)
C(8)-C(9)-C(10)	118.0(7)	C(7)-C(8)-Cl(1)	117.8(7)
C(9)-C(10)-C(5)	119.6(7)	C(9)-C(8)-Cl(1)	117.8(6)
C(10)-C(5)-C(6)	120.3(6)	C(13)-C(14)-Cl(2)	117.7(6)
C(11)-C(12)-C(13)	119.4(7)	C(15)-C(14)-Cl(2)	119.1(6)
C(12)-C(13)-C(14)	118.3(7)	C(1)-N(1)-H(2)	125.1(43)
C(13)-C(14)-C(15)	123.2(7)	C(2)-N(1)-H(2)	113.1(44)
C(14)-C(15)-C(16)	117.8(7)	C(4)-O(1)-H(1)	112.1(49)
C(15)-C(16)-C(11)	119.5(7)	N(1)-C(2)-N(2)	116.0(6)
C(16)-C(11)-C(12)	121.7(6)	N(1)-C(2)-N(3)	127.2(6)
		N(2)-C(2)-N(3)	116.8(5)
		N(3)-C(4)-O(1)	110.8(5)

TABLE 4. BOND LENGTHS AND THEIR STANDARD DEVIATIONS

C(3)-C(4)	1.519(10) Å	C(1)-N(1)	1.487(10) Å
C(5)-C(6)	1.412(11)	C(2)-N(1)	1.335(8)
C(6)-C(7)	1.406(11)	C(2)-N(2)	1.432(9)
C(7)-C(8)	1.397(12)	C(2)-N(3)	1.309(9)
C(8)-C(9)	1.398(12)	C(3)-N(2)	1.279(9)
C(9)-C(10)	1.406(10)	C(4)-N(3)	1.473(8)
C(11)-C(12)	1.378(10)	C(4)-O(1)	1.419(8)
C(12)-C(13)	1.411(10)	C(17)-O(2)	1.439(10)
C(13)-C(14)	1.372(11)	C(8)-Cl(1)	1.740(7)
C(14)-C(15)	1.392(11)	C(14)-Cl(2)	1.747(7)
C(15)-C(16)	1.405(11)		
C(3)-C(5)	1.463(9)	N(1)-H(2)	1.05(8)
C(4)-C(11)	1.530(9)	O(1)-H(1)	1.10(8)
C(5)-C(10)	1.412(10)		
C(11)-C(16)	1.389(10)		

TABLE 5. EQUATIONS OF LEAST-SQUARES PLANES IN THE $AX+BY+CZ+D=0$[a] FORM DISPLACEMENTS (1/Å) OF ATOMS FROM THE PLANES ARE GIVEN IN SQUARE BRACKETS

Benzene plane I

$0.690X+0.693Y+0.207Z=7.075$

[C(5) 0.002, C(6) 0.000, C(7) 0.000, C(8) 0.002, C(9) 0.004, C(10) 0.004]

Benzene plane II

$0.581X+0.788Y+0.205Z=-0.422$

[C(11) 0.012, C(12) −0.007, C(13) −0.007, C(14) 0.014, C(15) −0.008, C(16) −0.005]

Imidazole plane

$0.719X+0.689Y+0.090Z=6.626$

[C(2) 0.004, N(2) −0.001, C(3) −0.002, C(4) 0.004, N(3) −0.004]

a) X, Y, and Z are orthogonal coordinates in Å related to the crystal axes by

$$\begin{bmatrix} X \\ Y \\ Z \end{bmatrix} = \begin{bmatrix} 1 & 0 & \cos\beta \\ 0 & 1 & 0 \\ 0 & 0 & \sin\beta \end{bmatrix} \begin{bmatrix} ax \\ by \\ cz \end{bmatrix}$$

TABLE 6. SELECTED DIHEDRAL ANGLES (°)

C(5)-C(3)-C(4)-C(11)	61.55	C(3)-C(4)-O(1)-H(1)	71.8
C(1)-N(1)-C(2)-N(2)	1.96	C(11)-C(4)-O(1)-H(1)	55.1
C(1)-N(1)-C(2)-N(3)	2.24	N(2)-C(2)-N(1)-H(2)	6.6
C(3)-N(2)-C(2)-N(1)	0.26	N(3)-C(2)-N(1)-H(2)	6.3
C(4)-N(3)-C(2)-N(1)	0.50	N(3)-C(4)-O(1)-H(1)	4.7
C(2)-N(3)-C(4)-O(1)	62.61		
N(2)-C(3)-C(4)-O(1)	62.28		

Dihedral angles between the planes (°)

Benzene plane I and benzene plane II	95.9
Benzene plane I and imidazole plane	6.9
Benzene plane II and imidazole plane	96.2

Results and Discussion

The molecular structure and numbering are shown in Fig. 1. The methyl group was found to be bonded with the 2-amino group. The final atomic coordinates and thermal parameters with their standard deviations are given in Table 2, and bond distances and angles with their standard deviations in Tables 3 and 4, respectively. The sum of the bond angles around the N(1) atom is 359.4°, and the bond length of N(1)–C(2) is 1.34 Å. The values suggest that the atomic configuration of N(1) is sp^2 hybridized, and that the N(1)–C(2) bond is conjugated with the imidazole ring. The crystal structure projected along the b axis is shown in Fig. 2. The crystal of compound **1** contains four methanol molecules in an unit cell. The

oxygen atom of the methanol molecule is hydrogen-bonded with the hydrogen atom of the hydroxy group of compound **1** and the methylamino group. The N(3) atom is also hydrogen-bonded with the H(1) atom. A stereoscopic view of compound **1** is shown in Fig. 3. The dihedral angles are given in Table 6. The dihedral angle between two phenyl groups is 95.5° and that between the imidazole ring and the phenyl group attached to C(3) and the phenyl group attached to C(4) is 6.88° and 96.2°, respectively. The least-squares planes and deviations of atoms from these planes are given in Table 5. The benzene ring attached to C(3) and the imidazole ring are nearly coplanar. C(1), N(1), and H(2) are almost of the imidazole ring plane, and H(2) is on the N(2) side and C(1) on the N(3) side of the imidazole ring.

References

1) T. Nishimura, K. Nakano, S. Shibamoto, and K. Kitajima, *J. Heterocycl. Chem.*, **12**, 471 (1975).
2) T. Nishimura and K. Kitajima, *J. Org. Chem.*, **41**, 1590 (1976).
3) T. Nishimura and K. Kitajima, *J. Org. Chem.*, **44**, 818 (1979).
4) T. Nishimura and K. Kitajima, unpublished work.
5) D. Cromer and J. Mann, *Acta Crystallogr., Sect. A*, **24**, 321 (1968).
6) R. F. Stewart, E. R. Davidson, and W. T. Simpson, *J. Phys. Chem.*, **42**, 3175 (1965).
7) I. L. Karle and J. Karle, *Acta Crystallogr., Sect. A*, **16**, 969 (1963); **21**, 894 (1966).

Syntheses of Cationic Mononucleotide Analogs and Their Interaction with Polynucleotide and Polynucleotide Analogs

Takeo SHIMIDZU,* Akira MURAKAMI, Kazushige YAMANA, and Yoshiyuki KONISHI

Department of Hydrocarbon Chemistry, Faculty of Engineering, Kyoto University, Yoshida, Sakyo-ku, Kyoto 606

(Received April 9, 1979)

Cationic mononucleotide analogs were synthesized through a quaternization reaction of *N*-halogenoethylated derivatives of nucleic acid bases or 5′-halogeno-5′-deoxynucleoside. When they interacted with polynucleotide and polynucleotide analogs with negative charges, base-base interactions were observed. The interactions between complementary bases were stronger than the others. It is suggested that an anionic field originating from the polynucleotide or polynucleotide analog contributes to the interaction of complementary bases.

Several polynucleotide analogs with positive charges have been synthesized.[1,2] Their interactive properties with nucleic acid bases,[3] nucleotides,[2,4] polynucleotides,[3] and nucleotide analogs with negative charges[5,6] have also been investigated. In these studies, the mode of interactions was predominantly the base-base stacking. This evidence for the contribution of stacking interaction has also been found in the interaction of nucleotides or nucleotide analogs with negative charges in the cationic polyelectrolyte.[5] The mode of the interaction was also affected by the hydrophobic polymer domain. The cross-linked cationic polynucleotide analogs have a tendency to interact with the complementary nucleotide,[4] and so template-directed syntheses of oligonucleotides were carried out.[7]

In comparison with those phenomena, it is significant to elucidate the effect of the ionic field originating from the polynucleotide. For this purpose, some nucleotide analogs with the charge opposite to that of the nucleotide were synthesized. The present paper will give the details of the syntheses of the cationic mononucleotide analogs and the interactive properties with polynucleotides and their analogs with negative charges. Some consideration regarding the contribution of the ionic field to the base-base interaction will also be paid.

Results and Discussion

The cationic mononucleotide analogs shown in Fig. 1 were synthesized in the following manner. Nucleic acid bases were first converted to the corresponding *N*-halogenoethylated derivatives by the literature method.[8] 5′-Halogeno-5′-deoxynucleoside was synthesized by the literature procedure.[9] To *N*-halogenoethylated derivatives and 5′-halogeno-5′-deoxynucleosides, pyridine and trimethylamine were added; cationic mononucleotide analogs were then obtained through a quaternization reaction. In general, it is recommended that the reactions are carried out without any solvent. In the case of trimethylammonium derivatives, though, a good result was also yielded by using ethanol as a solvent. The precipitates during the reaction were almost purely the desired substances. These derivatives were hygroscopic.

The UV characteristics, R_f values, and electropho-

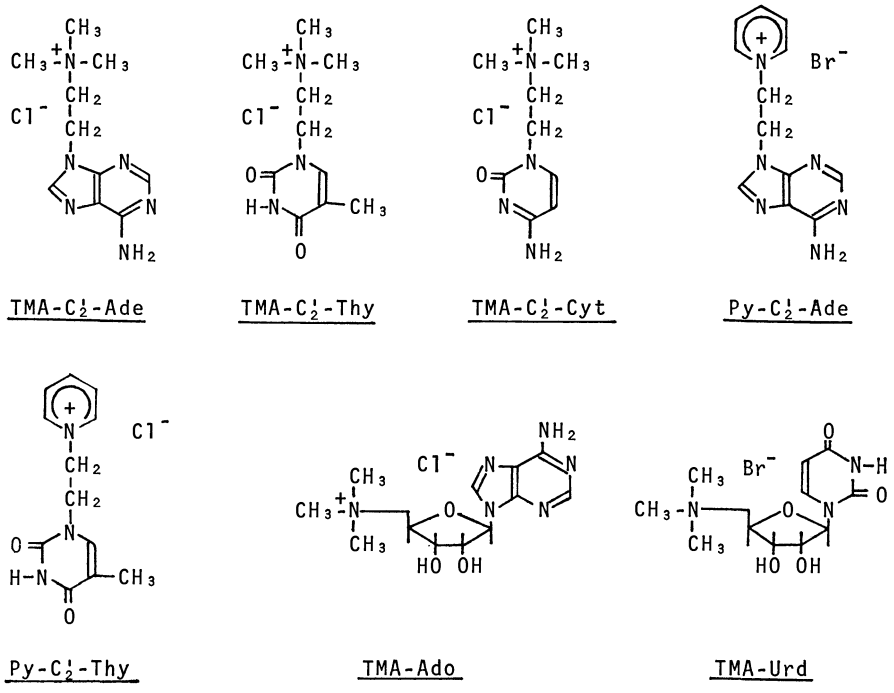

Fig. 1. Cationic mononucleotide analogs.

Table 1. λ_{max}, R_f values, and electrophoretical mobilities of cationic mononucleotide analogs

Analog	λ_{max} (H_2O)[a]	Paper chromatography[b] Solvent A	Paper chromatography[b] Solvent B	Paper electrophoresis[c] Relative mobility
TMA-C_2'-Ade	261	0.35	0.46	−2.0
TMA-C_2'-Thy	266	0.65	0.35	−2.0
TMA-C_2'-Cyt	272	0.57	0.55	−1.9
Py-C_2'-Ade	260	0.10	0.44	−2.5
Py-C_2'-Thy	266	0.28	0.66	−2.2
TMA-Ado	261	0.53		−2.4
TMA-Urd	262	0.24	0.62	−1.6

a) The UV measurements were carried out in water. The pH of the unbuffered solutions were 5.4—5.6. b) The solvent systems have been shown in the text. c) Electrophoresis was carried out in a 0.1 M phosphate buffer(pH 7.0). The relative mobility was based on the corresponding nucleotides.

Table 2. Apparent hypochromicities in the mixing curves of cationic mononucleotide analogs and polynucleotides[a]

Polynucleotide	Analog	Hypochromicity[b] %
Poly A	TMA-C_2'-Ade	2.8
	TMA-C_2'-Thy	4.5
	TMA-C_2'-Cyt	3.3
	Py-C_2'-Ade	3.3
	Py-C_2'-Thy	5.0
	TMA-Ado	4.9
	TMA-Urd	5.6
Poly U	TMA-C_2'-Ade	2.6
	TMA-C_2'-Thy	1.5
	TMA-C_2'-Cyt	0.0
	Py-C_2'-Ade	4.3
	Py-C_2'-Thy	3.0
	TMA-Ado	2.1
	TMA-Urd	2.5

The total concentration of nucleic acid bases in the mixture was 5.4×10^{-5} mol dm^{-3}.
a) Potassium salts of polynucleotides were used. b) The hypochromicities were calculated at 260 nm.

retical mobilities of cationic mononucleotide analogs are shown in Table 1. Their mobilities were almost twofold in the opposite direction, based on the corresponding nucleotides. This result indicates that they have a cationic charge even in neutral aqueous media.

The interactive properties of the present cationic mononucleotide analogs have also been investigated. Evidence for interaction between cationic mononucleotide analogs and polynucleotides came from the apparent hypochromicities in mixtures of them. When solutions of polynucleotides were mixed with solutions of cationic mononucleotide analogs, apparent hypochromicities down to a low percentage were observed. The results are shown in Table 2. Generally, a UV hypochromicity is not observed in a mixture of polynucleotide and nucleotide at the present concentration

Table 3. Apparent hypochromicities in the mixing curves of cationic mononucleotide analogs and anionic polynucleotide analogs[a]

Anionic polynucleotide analog	Cationic mononucleotide analog	Hypochromicity[b] %
PAA-Ado_8 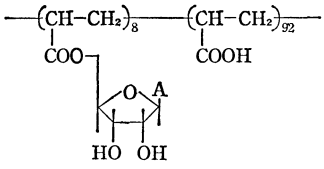	TMA-C_2'-Ade	1.0
	TMA-C_2'-Thy	5.8
	TMA-C_2'-Cyt	2.5
	Py-C_2'-Ade	0.0
	Py-C_2'-Thy	1.5
	TMA-Ado	1.0
	TMA-Urd	2.3
PAA-Urd_{15} 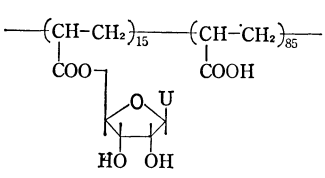	TMA-C_2'-Ade	2.5
	TMA-C_2'-Thy	1.0
	TMA-C_2'-Cyt	0.0
	Py-C_2'-Ade	1.6
	Py-C_2'-Thy	0.0
	TMA-Ado	2.4
	TMA-Urd	0.0

The total concentration of nucleic acid bases in the mixture was 5.4×10^{-5} mol dm^{-3}.
a) Anionic polynucleotide analogs were synthesized by the condensation reaction of poly(acrylic acid) with nucleoside. The content of adenine or uridine was determined by a UV measurement. b) The hypochromicities were calculated at 260 nm.

range. Such an interaction suggests a dominant contribution of Coulombic forces in the interaction between the cationic mononucleotide analog and the polynucleotide.

The observed hypochromicities of the complementary base's sets (Poly A-T derivative, Poly A-U derivative, and Poly U-A derivative) were larger than those of the incomplementary base's sets (Poly A-A derivative, Poly A-C derivative, and Poly U-C derivative, Poly U-T derivative, and Poly U-U derivative). This fact indicates that both a base stacking and a hydrogen bonding contribute to the mode of intermolecular base-base interaction.

The apparent hypochromicities in the mixing curves of the cationic mononucleotide analogs and the anionic polynucleotide analogs are shown in Table 3. A mode of interaction similar to that of polynucleotide was observed. This shows that hydrogen bonding between complementary bases takes place in the intermolecular interaction of the bases. As the contrary, previous studies of the interaction between nucleotides and cationic polynucleotide analogs showed that the stacking interaction was overwhelming.[2,4]

Now we can deduce that the anionic field originating from polynucleotides and polynucleotide analogs makes a large contribution to the base-base interaction; the anionic field contributes to the hydrogen bonding in the complementary base-base interaction.

Experimental

General Method. Paper chromatographies were carried out by the descending technique using Whatman 3 MM

paper in the following solvent systems: A, 2-propanol–concentrated ammonia–water (7:1:2, v/v); B, ethanol–1 M ammonium acetate (pH 7.5) (7:3, v/v). Paper electrophoresis was carried out on the same paper at 35 V cm^{-1} in a 0.1 M phosphate buffer (pH 7.0). The UV absorption spectra were obtained on a Hitachi EPS-3T spectrophotometer. The NMR spectra were recorded with a Varian HR-220 spectrometer.

Reagents. The pyridine was distilled by a general method. A 30% trimethylamine–ethanol solution was obtained by dissolving a dry trimethylamine gas in ice-cooled ethanol.

Materials. The 9-(2-bromoethyl)adenine, 9-(2-chloroethyl)adenine, and 1-(2-chloroethyl)thymine were synthesized by the literature procedure.[8] The 1-(2-chloroethyl)cytosine was synthesized by the modification of the literature method:[8] 15 cm^3 of thionyl chloride was added to 1 g of 1-(2-hydroxyethyl)cytosine, and the mixture was stirred for 90 min at 35 °C and then was refluxed for 30 min. After the removal of the excess thiony chloride under reduced pressure, the residue was dissolved in water and treated with 5% of a sodium carbonate solution, and the precipitate thus formed was filtered off and dried. Recrystallization from ethanol gave 1-(2-chloroethyl)cytosine as pale yellow needles (48% yield). Found: C, 41.38; H, 4.69; N, 23.81; Cl, 19.63%. Calcd for $C_6H_8N_3OCl$: C, 41.51; H, 4.65; N, 24.20; Cl, 20.42%. The 5′-bromo-5′-deoxyuridine was synthesized by the literature method.[9] The 5′-chloro-5′-deoxyadenosine was kindly given by the Tanabe Pharmacy Company, Ltd.

2-(Adenin-9-yl)ethyltrimethylammonium Chloride, TMA-C_2'-Ade: In 25 cm^3 of a 30% trimethylamine–ethanol solution, 0.6 g of 9-(2-chloroethyl)adenine was dissolved. The mixture was sealed in a thick glass tube and then heated at 80 °C for 48 h. A white precipitate was filtered, washed with ethanol, then dried (63% yield). Found: C, 44.24; H, 6.86; N, 31.43; Cl, 13.48%. Calcd for $C_{10}H_{17}N_6Cl$: C, 46.78; H, 6.62; N, 32.74; Cl, 13.84%. NMR (D_2O) δ 8.45 (1H, s, 2 position of adenine), 8.43 (1H, s, 8 position of adenine), 4.93 (2H, t, 2 position of ethylene), 4.23 (2H, t, 1 position of ethylene), 3.23 (9H, s, trimethylammonium).

2-(Thymin-1-yl)ethyltrimethylammonium Chloride, TMA-C_2'-Thy: In 10 cm^3 of a 30% trimethylamine–ethanol solution, 0.5 g of 1-(2-chloroethyl)thymine was dissolved. The mixture was sealed in a thick glass tube and then heated at 80 °C for 70 h. A white precipitate was obtained after cooling. It was washed with ethanol and then dried (26% yield). Found: C, 43.26; H, 7.44; N, 15.29; Cl, 12.70%. Calcd for $C_{10}H_{18}N_3O_2Cl$: C, 47.74; H, 7.16, N, 16.70; Cl, 14.12%. NMR (D_2O) δ 7.92 (1H, s, 6 position of thymine), 4.74 (2H, t, 2 position of ethylene), 4.12 (2H, t, 1 position of ethylene), 3.69 (9H, s, trimethylammonium).

2-(Cytosin-1-yl)ethyltrimethylammonium Chloride, TMA-C_2'-Cyt: In 15 cm^3 of a 30% trimethylamine–ethanol solution, 0.2 g of 1-(2-chloroethyl)cytosine was dissolved. The mixture was sealed in a thick glass tube and then heated at 80 °C for 72 h. Pale yellow needles were filtered out, washed with ethanol, and then dried (52% yield). Found: C, 45.45; H, 7.37; N, 23.89; Cl, 14.96%. Calcd for $C_9H_{17}N_4OCl$: C, 46.45; H, 7.31; N, 24.09; Cl, 15.27%. NMR (D_2O) δ 7.98 (1H, d, 6 position of cytosine), 6.30 (1H, d, 5 position of cytosine), 4.49 (2H, t, 2 position of ethylene), 3.86 (2H, t, 1 position of ethylene), 3.41 (9H, s, trimethylammonium).

1-[2-(Adenin-9-yl)ethyl]pyridinium Bromide, Py-C_2'-Ade: In 2 cm^3 of a freshly distilled pyridine, 0.11 g of 9-(2-bromoethyl)-adenine was dissolved. The mixture was sealed under nitrogen and then heated in boiling water for 78 h. A white precipitate was filtered out, washed with ethyl acetate, and then dried (28% yield). Found: C, 44.80; H, 3.97; N, 26.02; Br, 25.03%. Calcd for $C_{12}H_{13}N_6Br$: C, 44.87; H, 4.08; N, 26.17; Br, 24.88%. NMR (D_2O) δ 8.86 (2H, d, α proton of pyridinium), 8.80 (1H, dd, γ proton of pyridinium), 8.29 (1H, s, 8 position of adenine), 8.18 (2H, dd, β proton of pyridinium), 8.10 (1H, s, 2 position of adenine), 5.29 (2H, t, 2 position of ethylene), 5.02 (2H, t, 1 position of ethylene).

1-[2-(Thymin-1-yl)ethyl]pyridinium Chloride, Py-C_2'-Thy: In 5 cm^3 of a freshly distilled pyridine, 0.1 g of 1-(2-chloroethyl)-thymine was dissolved. The mixture was then refluxed on a steam bath for 5 h. White needle crystals were obtained after cooling. They were washed with ethanol and then dried (17% yield). Found: C, 52.33; H, 5.34; N, 15.14; Cl, 13.15%. Calcd for $C_{12}H_{14}N_3O_2Cl$: C, 53.84; H, 5.27, N, 15.70; Cl, 13.24%. NMR (D_2O) δ 9.09 (2H, d, α proton of pyridinium), 8.82 (1H, dd, γ proton of pyridinium), 8.30 (2H, dd, β proton of pyridinium), 7.57 (1H, s, 6 position of thymine), 5.09 (2H, t, 2 position of ethylene), 4.05 (2H, t, 1 position of ethylene).

(Adenosin-5′-yl)trimethylammonium Chloride, TMA-Ado: In 15 cm^3 of a 30% trimethylamine–ethanol solution, 0.2 g of 5′-chloro-5′-deoxyadenosine was dissolved. The mixture was sealed in a thick glass tube and then heated at 55 °C for 70 h. A white precipitate was filtered, washed with ethanol, and then dried (38% yield). Found: C, 45.63; H, 6.35; N, 23.96; Cl, 10.43%. Calcd for $C_{13}H_{21}N_6O_3Cl$: C, 45.28; H, 6.10; N, 24.38; Cl, 10.30%. NMR (D_2O) δ 8.16 (1H, s, 8 position of adenine), 8.14 (1H, s, 2 position of adenine), 3.18 (9H, s, trimethylammonium).

(Uridin-5′-yl)trimethylammonium Bromide, TMA-Urd: In 20 cm^3 of a 30% trimethylamine–ethanol solution, 0.7 g of 5′-bromo-5′-deoxyuridine was dissolved. The mixture was sealed in a thick glass tube and then heated at 55 °C for 70 h. A white precipitate was filtered, washed with ethanol, and then dried (12% yield). Found: C, 38.74; H, 5.65; N, 10.96; Br, 22.36%. Calcd for $C_{12}H_{20}N_3O_5Br$: C, 39.36; H, 5.74; N, 11.48; Br, 21.84%. NMR (D_2O) δ 7.50 (1H, d, 6 position of uracil), 6.82 (1H, d, 5 position of uracil), 3.19 (9H, s, trimethylammonium).

UV Measurements. The measurements were carried out in water at 15 °C. The pH of the unbuffered solutions was 5.4—5.6. Absorbances were obtained in a 10-mm quartz cell. The apparent hypochromicity was calculated according to the following equation:[10]

$$\% \text{ Hypochromicity} = \left(1 - \frac{I_{a+b}}{mI_a + nI_b}\right) \times 100$$

where m and n are the volume fractions of the solutions of Compounds a and b, and where I_a, I_b, and I_{a+b} are the absorbances of the solutions of Compound a, Compound b, and the mixture of Compounds a and b respectively.

The authors are indebted to Prof. Kenichi Fukui for his encouragement. This investigation was supported by a Grant-in-Aid of the Ministry of Education.

References

1) T. Okubo and N. Ise, *Polym. J.*, **4**, 674 (1974).
2) T. Shimidzu, Y. Konishi, and A. Murakami, *Makromol. Chem.*, **178**, 2581 (1977).
3) T. Okubo, K. Ban, and N. Ise, *Makromol. Chem.*, **175**, 49 (1974).
4) T. Shimidzu, A. Murakami, Y. Konishi, and M. Minami, *Bull. Chem. Soc. Jpn.*, **51**, 821 (1978).

5) T. Shimidzu, Y. Konishi, and A. Murakami, *Nucleic Acids Res.*, Sp. **2**, 35 (1976).
6) T. Shimidzu, A. Murakami, and K. Yamana, *Nucleic Acids Res.*, Sp. **5**, 379 (1978).
7) T. Shimidzu, A. Murakami, and Y. Konishi, *J. Chem. Soc., Perkin Trans. 1*, **1979**, 20.
8) N. Ueda, K. Kondo, M. Kono, K. Takemoto, and M. Imoto, *Makromol. Chem.*, **120**, 13 (1968).
9) P. A. Levene and R. S. Tipson, *J. Biol. Chem.*, **106**, 113 (1934).
10) M. N. Lipsett, L. A. Happel, and D. F. Bradley, *J. Biol. Chem.*, **236**, 857 (1961).

A Synthesis of 7α-Methoxycephalosporins through Selenenamides

Takeo KOBAYASHI and Tetsuo HIRAOKA*

Central Research Laboratories, Sankyo Co., Ltd., 1-2-58, Hiromachi, Shinagawa-ku, Tokyo 140

(Received April 16, 1979)

The *o*-nitrobenzeneselenenamides were oxidized with active manganese dioxide to give the imines, which were converted to the 7α-methoxycephalosporins **3** by the reaction with lithium methoxide. The selenenamides **3** were acylated with phenoxyacetyl chloride to afford the desired cephamycin derivatives **4** *via* tertiary amide **5**, which was not isolable. This methoxylation reaction was also carried out in penicillin series to give the desired 6α-methoxypenicillin **8** although the ring opening compound **9** was a major product. The difference between sulfenamides and selenenamides in their acylation reactions was discussed.

Much attention has been focused on 7α-methoxycephalosporins after isolation of cephamycins from cultures of *streptomyces* species[1] and subsequent modification of the original compound to those with enhanced activity.[2] Several methods have been developed for introduction of a methoxyl group at the seven position of cephalosporins starting from 7-aminocephalosporins or 7-acylaminocephalosporins.[3] However, some difficulties still remain in the synthesis of 7α-methoxycephalosporins having a complex 7β-acylamino side chain.[4] Recently, we have shown that 7β-sulfenamidocephalosporins and 7β-sulfinamidocephalosporins were converted to 7α-methoxycephalosporins *via* the intermediacy of novel 7-sulfenylimine β-lactams.[5]

As a part of program to device a new method for introduction of a methoxyl group at the seven position of cephalosporins, we were interested in a synthesis of an analog of the sulfenamide in which the sulfur atom is suitably substituted by selenium atom. We now describe a method for a synthesis of 7α-methoxycephalosporins utilizing selenenamidocephalosporins *via* selenenylimine intermediates.

The chemistry of selenenamides (amide of selenenic acid) has been little studied and only a very limited number of examples of this class are known[6-8] owing to the lack of the stabilities of those compounds. In view of the scope and limitations of selenenamides, a study of selenenamidocephalosporins is of considerable interest. A recent study of selenenamides has suggested that the Se–N bond is hydrolyzed slowly at room temperature and rapidly with acids or at an elevated temperature.[6] The method generally used for the preparation of selenenamides is the reaction of corresponding amines with selenenyl halides. Of several possible starting materials, first, we chose benzeneselenenamidocephalosporins. Treatment of *t*-butyl 7β-amino-3-methyl-3-cephem-4-carboxylate with benzeneselenenyl chloride in the presence of triethylamine gave a spot ascribable to the benzeneselenenamide **1c** on silica gel thin layer chromatography, by short time development, but this spot vanished on further development. The isolation of the benzeneselenenamide **1c** also failed by chromatography on silicic acid. Difficulty in isolation of benzeneselenenamide **1c** probably results from the known instability of Se–N bond.

It is frequently observed that benzeneselenenyl compounds without *o*-substituent exhibit properties differing from those of the corresponding *o*-substituted derivatives with higher stabilities.[9] Thus we examined *o*-nitrophenylselenenamidocephalosporin which has an electron-withdrawing group on the ortho position of the aromatic ring, expecting more stable Se–N bond. Treatment of *t*-butyl 7β-amino-3-methyl-3-cephem-4-carboxylate with *o*-nitrophenylselenenyl chloride in the presence of triethylamine afforded *o*-nitrophenylseleneamide **1a** in 79.0% yield after silica-gel chromatography. This procedure using ortho-nitrophenylselenenyl compound, also worked well in the case of benzhydryl 3-acetoxymethyl-7β-amino-3-cephem-4-carboxylate and *p*-bromophenacyl 6β-aminopenicillanate to give **1b** and **6** in 60.0% and 53.3% yields, respectively. When *p*-nitrophenylselenenyl bromide was used in place of *o*-nitrophenylselenenyl chloride in the reaction with *t*-butyl 7β-amino-3-methyl-3-cephem-4-carboxylate, a clear spot ascribable to the desired selenenamide was observed in thin layer chromatography; however, attempted isolation of selenenamide **1d** by chromatography on silica gel resulted in decomposition of the product. Thus the synthesis of selenenamides of cephalosporins and penicillin derivatives was successful only in *o*-nitrophenylselenenamide series.

Next our effort was directed to the conversion of selenenamides **1** to selenenylimines **2**. Only a few selenenylimines have been reported in the literature and they were prepared by addition of benzeneselenenyl and *p*-nitrophenylselenenyl chlorides to 1,1-di-*p*-tolylmethanimine in the presence of triethylamine.[8] These crystalline selenenylimines were observed to decompose to an oil after several weeks under nitrogen in the dark. So, we had a great concern about the stability of the selenenyliminocephalosporins. Treatment of *o*-nitrophenylselenenamidocephalosporins **1a** and **1b** with active manganese dioxide in benzene solution according to the sulfenamide oxidation[5a] gave the corresponding selenenyliminocephalosporins **2a** and **2b** in 60.0% and 41.0% yields, respectively, which were crystalline solids and stable on exposure to air at room temperature for several weeks. The structure of the imines **2a** and **2b** was unambiguous on the basis of their NMR spectra which showed a sharp singlet at 5.32 and 5.42 ppm, respectively, due to the hydrogen at the six position. In the penicillin series the reaction leading to the selenenylimine took place similarly as in the cephalosporin series. Thus, the reaction of the selenenamidopenicillin **6** with active manganese dioxide gave the selenenyliminopenicillin **7** as an amorphous solid in 49.7% yield, which was also stable under the same conditions as the selenenylimines of cephalosporins.

Treatment of the selenenylimines **2a** and **2b** with

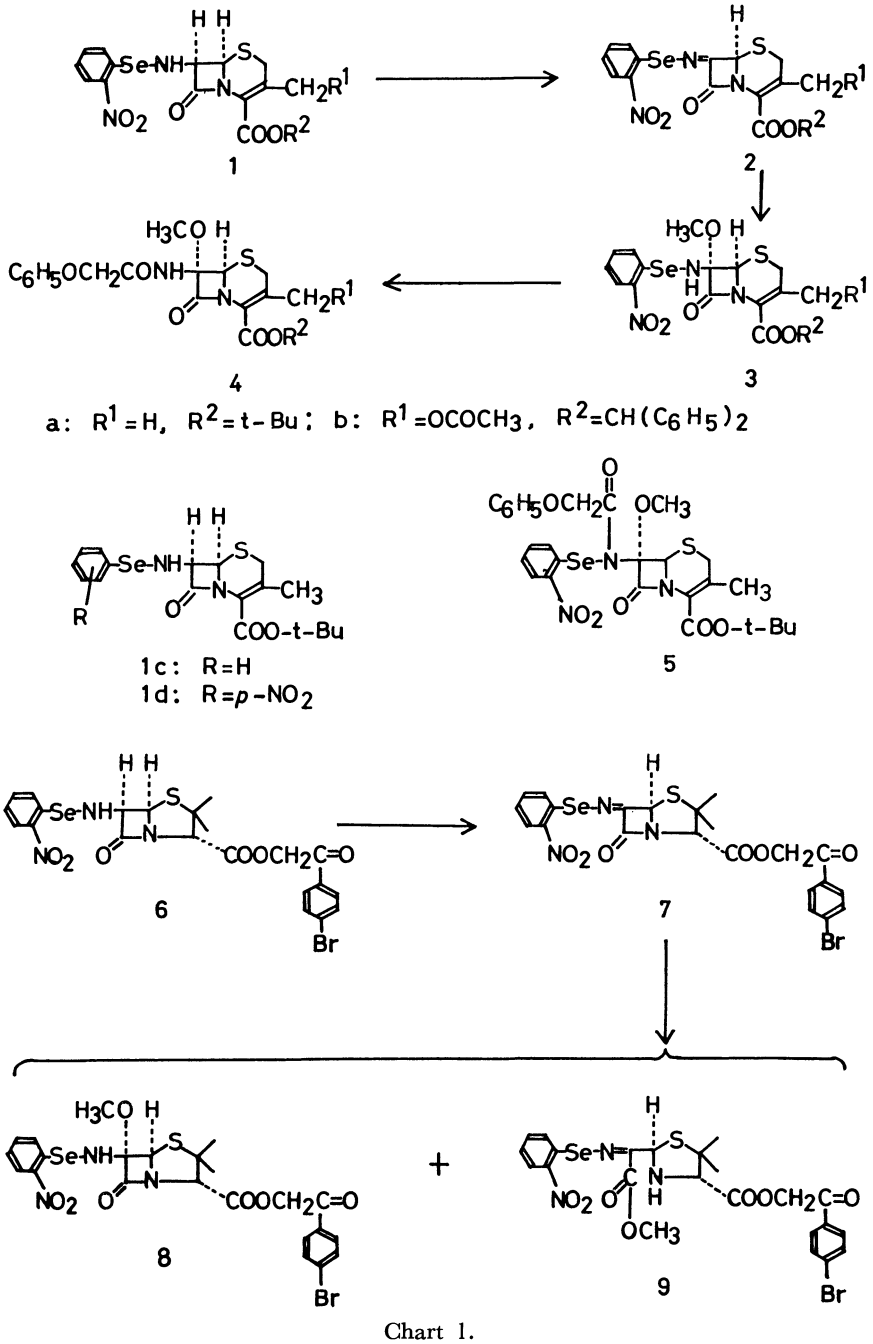

Chart 1.

excess of lithium methoxide in methanol and tetrahydrofuran at −78 °C for 3 h afforded 7α-methoxyselenenamidocephalosporins **3a** and **3b** in 87.1% and 21.6% yields, respectively. The low yield of **3b** was due to the production of 2-cephem isomer (benzhydryl 3-acetoxymethyl-7α-methoxy-7β-*o*-nitrophenylselenenylamino-2-cephem-4-carboxylate) (26.8%), whose formation was frequently observed in the compound having 3-acetoxymethyl group in a basic medium. As in the case of the sulfenyliminocephalosporins[5a] only α-methoxy isomers were obtained by attack of methoxide anion from less hindered α-face of the molecules. Methoxylation of the selenenyliminopenicillin **7** under the same reaction conditions gave the desired 6α-methoxy-6β-(selenenylamino)-penicillin **8** only in 8.8% yield together with the ring opened diester **9** (79.9%) as a major product. It should be noted that the ratio of **8**/**9** (8.8/79.9) was significantly small as compared with the case of the corresponding sulfenyliminopenicillin in which the ratio of the methoxylated product to the ring cleaved compound was 30.9/58.4. This difference might arise from the less effective overlapping of the d-orbital of the selenium of the compound **7** with the imine part and *o*-nitrobenzene ring. Thus, electrophilicity at the six position of **7** would decrease as compared with the corresponding sulfenyliminopenicillin. We should also note that the ring opened selenenylimine **9** was not attacked by methoxide any more.

Acylation of 7α-methoxyselenenamide **3a** with phenoxyacetyl chloride in dichloromethane in the absence of any base gave **5** judging from silica gel thin

TABLE 1.

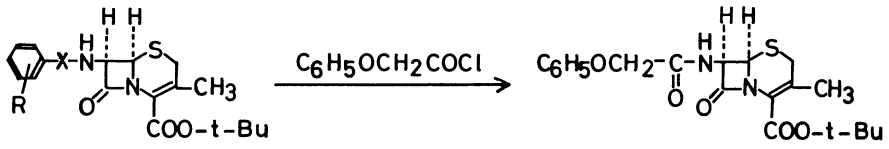

(10a,b,c,1a) (11)

run	cephalosporin	condition	product(11)
1	o-nitrobenzenesulfenamide(10a) R=o-NO_2 ,X=S	rt,24h	trace[a]
2	p-nitrobenzenesulfenamide(10b) R=p-NO_2 ,X=S	0°C,90min	96.3%[b]
3	2,4-dinitrobenzenesulfenamide(10c) R=2,4-NO_2,X=S	rt,24h	trace[a]
4	o-nitrobenzeneselenenamide(1a) R=o-NO_2 ,X=Se	0°C,30min	92.9%[b]

a) the reaction was checked by silica gel TLC plate
b) isolated yield

layer chromatography, which showed a less polar spot ascribable to the tertiary amide **5**. Attempted purification of **5** by chromatography on silica gel resulted in decomposition. Therefore the obtained compound was used in the subsequent reaction without further purification. The crude compound **5** was treated with lithium methoxide or sodium benzenethiolate to furnish 7α-methoxy-7β-phenoxyacetamidocephalosporin **4** in 18% and 15% yields, respectively. The physical properties of **4** were identical in all respects with an authentic sample.[5]

A comparison of selenenamidocephalosporins with sulfenamidocephalosporins in the reaction with an acyl chloride is interesting in connection with the bonding character between nitrogen and sulfur or selenium. Thus we examined the reaction of sulfenamides and selenenamide with phenoxyacetyl chloride in dichloromethane. Results are summarized in Table 1. *o*-Nitrophenylselenenamide **1a** was found to be more reactive than *p*-nitrophenylsulfenamide **10b**, which was the most reactive in the sulfenamide series. Namely, ortho-substituted benzenesulfenamides **10a** and **10c** did not react with phenoxyacetyl chloride, while the *p*-nitro derivative **10b**, was easily converted into phenoxyacetamide **11**, and in the case of the selenenamide ortho-substitution gave no effect on the reaction with phenoxyacetyl chloride to afford the desired amide **11** with great ease without detection of the tertiary amide corresponding to **5**.

Although the Se–N bond in selenenamide is generally unstable and sensitive to nucleophiles, the method *via* the intermediacy of selenenyliminocephalosporins provides a versatile and useful alternative to functionalization at the 7(6) position of cephalosporins (penicillins).

Experimental

All melting points are not corrected. IR spectra were recorded on a JASCO A-2 spectrometer. NMR spectra were measured on Hitachi R-24 spectrometer using tetramethylsilane as an internal standard. The abbreviations in the NMR spectra are as follows: s, singlet; bs, broad singlet; d, doublet; dd, doublet of doublets; q, quartet; m, multiplet.

*t-Butyl 3-Methyl-7β-o-nitrophenylselenenylamino-3-cephem-4-carboxylate (**1a**).* A solution of *t*-butyl 7β-amino-3-methyl-3-cephem-4-carboxylate (6.50 g, 24 mmol) and triethylamine (3.36 ml, 24 mmol) in chloroform (150 ml) was stirred and cooled to 0—5 °C. To this solution was added *o*-nitrophenylselenenyl chloride (4.73 g, 20 mmol) dissolved in chloroform (50 ml) over a period of 10 min. The mixture was then stirred for an additional 2 h at 0—5 °C. The mixture was diluted with ethyl acetate, washed successively with saturated $NaHCO_3$ solution and water. Evaporation of the dried ($MgSO_4$) organic phase *in vacuo* provided a residue, which was chromatographed on silica gel using benzene–EtOAc (10:1) to give *o*-nitrophenylselenenamide **1a** (7.25 g, 79.0%) as yellow crystals. **1a**: mp 133—134 °C (EtOAc–diisopropyl ether); IR ($CHCl_3$) 1780 cm^{-1}; NMR ($CDCl_3$) δ=1.55 (9H, s), 2.10 (3H, s), 3.35 and 3.60 (2H, ABq, J=18 Hz), 3.53 (1H, d, J=13.5 Hz), 4.95 (1H, dd, J=13.5 and 4.5 Hz), 5.08 (1H, d, J=4.5 Hz), 7.3—8.7 (4H, m).

*Benzhydryl 3-Acetoxymethyl-7β-o-nitrophenylselenenylamino-3-cephem-4-carboxylate (**1b**).* To a mixture of benzhydryl 7β-amino-3-acetoxymethyl-3-cephem-4-carboxylate hydrochloride (10.4 g, 22 mmol) and triethylamine (5.85 ml, 42 mmol) in dry chloroform (150 ml) under nitrogen was added *o*-nitrophenylselenenyl chloride (4.73 g, 20 mmol) in chloroform (25 ml) at 0—5 °C over a period of 10 min. The mixture was stirred for 3 h at 0—5 °C, and then EtOAc was added. The organic phase was washed with saturated $NaHCO_3$ solution and water, dried over $MgSO_4$, and evaporated *in vacuo* to give a residue. Subsequent chromatography on silica gel using benzene–EtOAc (10 : 1) provided *o*-nitrophenylselenenamide **1b** (7.61 g, 60.0%) as yellow crystals: **1b**: mp 124—125 °C ($CHCl_3$–diisopropyl ether); IR ($CHCl_3$) 1780 cm^{-1}; NMR ($CDCl_3$) δ=1.90 (3H, s), 3.35 and 3.50 (2H, ABq, J=18 Hz), 3.50 (1H, d, J=13.5 Hz), 4.75 and 4.98 (2H, ABq, J=13.5 Hz), 4.90 (1H, dd, J=13.5 and 4.5 Hz), 4.93 (1H, d, J=4.5 Hz), 6.97 (1H, s), 7.1—8.5 (14H, m).

p-*Bromophenacyl 6β-o-Nitrophenylselenenylaminopenicillanate (6).* To a stirred solution of *p*-bromophenacyl 6β-aminopenicillanate hydrochloride (4.95 g, 11 mmol) and triethylamine (2.79 ml, 20 mmol) in $CHCl_3$ (75 ml) was added a solution of *o*-nitrophenylselenenyl chloride (2.36 g, 20 mmol) in $CHCl_3$ (25 ml) at 0 °C. After 3 h at 0 °C, EtOAc was added and organic solution was washed successively with saturated $NaHCO_3$ solution and water, and then dried ($MgSO_4$). Evaporation of the organic part and chromatography of the residue using benzene–EtOAc (5 : 1) afforded *o*-nitrophenylselenenamide **6** (3.27 g, 53.3%) as amorphous solid. **6**: IR ($CHCl_3$) 1780 cm^{-1}; NMR ($CDCl_3$) δ=1.73 (3H, s), 1.77 (3H, s), 3.58 (1H, d, J=12 Hz), 4.63 (1H, s), 4.75 (1H, dd, J=12 and 4.5 Hz), 5.38 and 5.53 (2H, ABq, J=16.5 Hz), 5.65 (1H, d, J=4.5 Hz), 7.3—8.6 (8H, m).

t-*Butyl 3-Methyl-7-o-nitrophenylselenenylimino-3-cephem-4-carboxylate (2a).* To a solution of selenenamide **1a** (2.0 g, 4.25 mmol) in benzene (100 ml) was added active manganese dioxide (100 g) at room temperature and reaction mixture was stirred at room temperature for 60 min. The solid substance was filtered off, washed with benzene, and evaporation of the combined filtrates *in vacuo* afforded selenenylimine **2a** (1.20 g, 60.0%) which was practically pure judging by NMR and used for the next step without any purification. **2a**: mp 185—186 °C ($CHCl_3$–diisopropyl ether); IR ($CHCl_3$) 1780 cm^{-1}; NMR ($CDCl_3$) δ=1.58 (9H, s), 2.17 (3H, s), 3.25 and 3.52 (2H, ABq, J=18 Hz), 5.32 (1H, s), 7.2—8.8 (4H, m).

Benzhydryl 3-Acetoxymethyl-7-o-nitrophenylselenenylimino-3-cephem-4-carboxylate (2b). A solution of selenenamide **1b** (2.3 g, 3.6 mmol) in benzene (100 ml) was stirred at room temperature with active manganese dioxide (115 g). After 1 h the reaction mixture was filtered and active manganese dioxide was washed with benzene. The combined filtrates were evaporated *in vacuo* to give selenenylimine **2b** (944 mg, 41.0%), which was pure judging by NMR and used in the next reaction without further purification. **2b**: mp 126—127 °C (EtOAc–diisopropyl ether); IR ($CHCl_3$) 1790 cm^{-1}; NMR ($CDCl_3$) δ=2.03 (3H, s), 3.45 and 3.61 (2H, ABq, J=18 Hz), 4.90 and 5.08 (2H, ABq, J=13.5 Hz), 5.42 (1H, s), 6.26 (1H, s), 7.3—8.9 (14H, m).

p-*Bromophenacyl 6-o-Nitrophenylselenenyliminopenicillanate (7).* A solution of selenenamide **6** (1.0 g, 1.63 mmol) in benzene (50 ml) was stirred at room temperature with active manganese dioxide (50 g) for 60 min. Active manganese dioxide was filtered off and the filtrate was evaporated *in vacuo* to give selenenylimine **7** (497 mg, 49.7%), which was found to be pure by NMR and used in the subsequent reaction without further purification. **7**: amorphous solid; IR ($CHCl_3$) 1780 cm^{-1}; NMR ($CDCl_3$) δ=1.60 (3H, s), 1.67 (3H, s), 4.85 (1H, s), 5.50 (2H, s), 5.98 (1H, s), 7.3—8.8 (8H, m).

t-*Butyl 7α-Methoxy-3-methyl-7β-o-nitrophenylselenenylamino-3-cephem-4-carboxylate (3a).* A stirred solution of selenenylimine **2a** (939 mg, 2.0 mmol) in dry MeOH (30 ml) and dry THF (60 ml) was cooled to −78 °C, and lithium methoxide (prepared from 77 mg of lithium, 11 mmol) in dry MeOH (10 ml) was added with vigorous stirring. The mixture was stirred for 3 h at −78 °C, and then glacial AcOH was added. After dilution with EtOAc, the organic solution was washed successively with water, saturated $NaHCO_3$ solution, and water, dried ($MgSO_4$) and evaporated *in vacuo* to afford a residue. Purification by chromatography on silica gel using benzene–EtOAc (10:1) gave 7α-methoxyselenenamide **3a** (870 mg, 87.1%) as a yellow oil. **3a**: IR ($CHCl_3$) 1770 cm^{-1}; NMR ($CDCl_3$) δ=1.50 (9H, s), 2.12 (3H, s), 3.18 and 3.35 (2H, ABq, J=18 Hz), 3.58 (3H, s), 4.18 (1H, s), 4.93 (1H, s), 7.2—8.6 (4H, m).

Benzhydryl 3-Acetoxymethyl-7α-methoxy-7β-o-nitrophenylselenenylamino-3-cephem-4-carboxylate (3b). To a solution of selenenylimine **2b** (204 mg, 0.32 mmol) in dry MeOH (5 ml) and dry THF (10 ml) was added lithium methoxide in methanol (5 ml) (from 14.7 mg of lithium, 2.1 mmol) at −78 °C and the solution was vigorously stirred for 3 h. The reaction mixture was quenched with glacial AcOH and diluted with EtOAc. The organic solution was washed with water, aqueous $NaHCO_3$, and again water. Evaporation of the solvents (dried over $MgSO_4$) and chromatography of the residue gave 7α-methoxy-*o*-nitrophenylselenenamide **3b** (46.0 mg, 21.6%; R_f=0.39: benzene–EtOAc 10:1) and benzhydryl 3-acetoxymethyl-7α-methoxy-7β-*o*-nitrophenylselenenylamino-2-cephem-4-carboxylate (57.3 mg, 26.8%; R_f=0.33: benzene–EtOAc 10:1), which were eluted from the column with benzene–EtOAc (10:1). **3b**: yellow oil; IR ($CHCl_3$) 1770 cm^{-1}; NMR ($CDCl_3$) δ=2.05 (3H, s), 3.38 and 3.53 (2H, ABq, J=18 Hz), 3.63 (3H, s), 4.33 (1H, s), 4.90 and 5.03 (2H, ABq, J=13.5 Hz), 4.98 (1H, s), 7.03 (1H, s), 7.3—8.7 (14H, m). Benzhydryl 3-acetoxymethyl-7α-methoxy-7β-*o*-nitrophenylselenenylamino-2-cephem-4-carboxylate: yellow oil: IR ($CHCl_3$) 1775 cm^{-1}; NMR ($CDCl_3$) δ=1.97 (3H, s), 3.50 (3H, s), 4.22 (1H, s), 4.67 (2H, bs), 5.22 (2H, s), 6.48 (1H, bs), 6.98 (1H, s), 7.2—8.6 (14H, m).

p-*Bromophenacyl 6α-Methoxy-6β-nitrophenylselenenylaminopenicillanate (8).* To a cold solution of selenenylimine **7** (201 mg, 0.33 mmol) in dry MeOH (5 ml) and dry THF (10 ml) was added lithium methoxide (prepared from 17.4 mg of lithium, 2.5 mmol) in dry MeOH (5 ml) at −78 °C. After vigorous stirring for 3 h, glacial AcOH was added. After dilution with EtOAc the organic solution was washed successively with water, saturated $NaHCO_3$ solution, and again water. The organic phase was dried ($MgSO_4$), evaporated, and the residue was chromatographed on silica gel. 7α-Methoxy-*o*-nitrophenylselenenamide **8** (18.7 mg, 8.84%; R_f=0.47: benzene–EtOAc 5:1) and diester **9** (169 mg, 79.9%, R_f=0.56: benzene–EtOAc 5:1) were eluted with benzene–EtOAc (5:1). **8**: yellow oil; IR ($CHCl_3$) 1780 cm^{-1}; NMR ($CDCl_3$) δ=1.58 (3H, s), 1.62 (3H, s), 3.53 (3H, s), 4.28 (1H, s), 4.67 (1H, s), 5.40 (2H, s), 5.48 (1H, s), 7.3—8.7 (8H, m). **9**: yellow oil; IR ($CHCl_3$) 1755 cm^{-1}; NMR ($CDCl_3$)[10] δ=1.49 (3H, s), 1.63 (3H, s), 3.98 (3H, s), 4.26 (1H, s), 5.59 (2H, s), 5.93 (1H, s), 7.2—8.9 (8H, m).

t-*Butyl 7α-Methoxy-3-methyl-7β-phenoxyacetamido-3-cephem-4-carboxylate (4).* To a solution of 7α-methoxyselenenamide **3a** (50.0 mg, 0.10 mmol) in CH_2Cl_2 (5 ml) was added phenoxyacetyl chloride (0.08 ml, 0.58 mmol). The mixture was stirred for 3 h at room temperature and then the solvent was evaporated. The residue was dissolved again in dry THF (5 ml), and lithium methoxide (prepared from 8 mg of lithium, 1.2 mmol) in dry MeOH (3 ml) was added. The reaction mixture was stirred vigorously at −78 °C for 2.5 h, and quenched with glacial AcOH. After dilution with EtOAc the organic solution was washed with water, aqueous $NaHCO_3$, and water, and dried over $MgSO_4$. Evaporation of the solvents *in vacuo* and chromatography (solvent: benzene–EtOAc 10:1) afforded phenoxyacetamide **4** (8.0 mg, 18.0%). **4**: IR ($CHCl_3$) 1780 cm^{-1}; NMR ($CDCl_3$) δ=1.53 (9H, s), 2.12 (3H, s), 3.08 and 3.33 (2H, ABq, J=18 Hz), 3.55 (3H, s), 4.60 (2H, s), 5.07 (1H, s), 6.8—7.5 (6H, m).

t-*Butyl 3-Methyl-7β-phenoxyacetamido-3-cephem-4-carboxylate (11).* A stirred solution of *t*-butyl 3-methyl-7β-*o*-nitrophenylselenenylamino-3-cephem-4-carboxylate **1a** (47.8

mg, 0.10 mmol) in dry dichloromethane (5 ml) was cooled to 0 °C, and phenoxyacetyl chloride (0.06 ml, 0.35 mmol) was added under vigorous stirring. The mixture was stirred 30 min at 0 °C. Evaporation of the solvent *in vacuo* gave a residue, which was purified by preparative chromatography on silica gel to provide 7β-phenoxyacetamide **11** (38.2 mg, 92.9%) using benzene–EtOAc (5:1). **11**: oil: IR ($CHCl_3$) 1780 cm^{-1}; NMR ($CDCl_3$) δ=1.53 (9H, s), 2.10 (3H, s), 3.15 and 3.50 (2H, ABq, J=19 Hz), 4.57 (2H, s), 5.01 (1H, d, J=4.5 Hz), 5.85 (1H, dd, J=4.5 and 10 Hz), 6.8—7.8 (6H, m).

We are grateful to Dr. Y. Kishida, the director of chemical research, for his encouragement through this work.

References

1) (a) R. Nagarajan, L. D. Boeck, M. Gorman, R. L. Hamil, C. E. Higgens, M. M. Hoehn, W. M. Stark, and J. G. Whitney, *J. Am. Chem. Soc.*, **93**, 2308 (1971); (b) E. O. Stapley, M. Jackson, S. Hernandez, S. B. Zimmerman, S. A. Currie, S. Mochales, J. M. Mata, H. B. Woodruff, and D. Hendlin, *Antimicrob. Agents Chemother.*, **2**, 122 (1972); (c) T. W. Miller, R. T. Goegelman, R. G. Weston, I. Putter, and F. J. Wolf, *ibid.*, **2**, 132 (1972).

2) (a) P. P. K. Ho, R. D. Towner, J. M. Indelicato, W. J. Wilham, W. A. Spitzer, and G. A. Koppel, *J. Antibiot (Tokyo)*, **26**, 313 (1973); (b) A. K. Miller, E. Celozzi, Y. Kong, B. A. Pelak, D. Hendlin, and E. O. Stapley, *Antimicrob. Agents Chemother.*, **5**, 33 (1974); (c) H. Nakao, H. Yanagisawa, B. Shimizu, M. Kaneko, M. Nagano, and S. Sugawara, *J. Antibiot. (Tokyo)*, **29**, 554 (1976); (d) R. M. DeMarinis, J. V. Uri, J. A. Weisbach, *ibid.*, **29**, 973 (1976); (e) H. E. Applegate, C. M. Cimarusti, J. E. Dolfini, W. H. Koster, M. A. Ondetti, W. A. Slusarchyk, and M. G. Young, *ibid.*, **31**, 561 (1978).

3) Y. Sugimura, K. Iino, Y. Iwano, T. Saito, and T. Hiraoka, *Tetrahedron Lett.*, **1976**, 1307 and references cited therein.

4) Acylation of 7α-methoxy-7β-aminocephalosporins with a carboxylic acid having complex functional groups using DCC or mixed anhydride methods gave poor results. So a carboxylic acid whose acid chloride cannot be prepared is difficult to condense with 7α-methoxy-7β-aminocephalosporins.

5) (a) T. Kobayashi and T. Hiraoka, *Chem. Pharm. Bull. (Tokyo)*, submitted; (b) T. Kobayashi, K. Iino, and T. Hiraoka, *ibid.*, submitted; (c) T. Kobayashi, K. Iino, and T. Hiraoka, *J. Am. Chem. Soc.*, **99**, 5505 (1977).

6) (a) H. Pheinboldt, "Houben Weyl. Methoden der Organischen Chemie, Schwefel-, Selen-, Tellurverbindungen," (1955), Vol. IX; (b) "Organic Selenium Compounds: Their Chemistry and Biology," ed by D. L. Klayman and W. H. H. Gunther, Weily, New York, N. Y. (1973).

7) H. J. Reich and J. M. Renga, *J. Org. Chem.*, **40**, 3313 (1975).

8) F. A. Davis and E. W. Kluger, *J. Am. Chem. Soc.*, **98**, 302 (1976).

9) R. Eriksen, *Acta Chem. Scand.*, **26**, 1274 (1972) and references cited therein.

10) The compound **9** is a mixture of two isomers (*ca.* 2:1) due to *syn-anti* isomerism of seleno-oxime or isomerization at 2 or 4 position during methoxylation. Only NMR spectrum of the major isomer was described here.

Enantioface-differentiating Reactions Using (2*S*,2′*S*)-2-Hydroxymethyl-1-[(1-alkyl-2-pyrrolidinyl)methyl]pyrrolidines as Chiral Ligands. Addition of Lithium Derivatives of Methyl Phenyl Sulfide, Acetonitrile, *N*-Nitrosodimethylamine, and 2-Methylthiothiazoline to Aldehydes

Kenso SOAI and Teruaki MUKAIYAMA*

Department of Chemistry, Faculty of Science, The University of Tokyo, Hongo, Bunkyo-ku, Tokyo 113

(Received May 2, 1979)

Optically active oxiranes, β-hydroxy nitrile, β-hydroxy *N*-nitrosoamine, and thiirane were obtained (up to 72% optical purity) by the enantioface-differentiating addition of lithium derivatives of methyl phenyl sulfide, acetonitrile, *N*-nitrosodimethylamine, and 2-methylthiothiazoline to aldehydes using (2*S*,2′*S*)-2-hydroxymethyl-1-[(1-alkyl-2-pyrrolidinyl)methyl]pyrrolidines (**1a**—**f**) as chiral ligands. Optical purity of the products depended greatly on the reaction medium (dimethoxymethane or dimethyl ether gave the best results) and the structure of pyrrolidine moieties of **1a**—**f**.)

One of the current interests in organic chemistry is asymmetric syntheses, and recently there have been many investigations reported on various types of asymmetric synthesis.[1] Among these, *enantioselective* reactions are one of the most difficult problems.

Concerning the enantioselective asymmetric reactions of organolithium compounds, several reports have been given on asymmetric reductions using metal hydride complexes.[2] However, on the *enantioselective* addition of organolithium compounds to aldehydes, very few investigations have been reported.[3] Recently, (+)-2,3-dimethoxy-*N*,*N*,*N*′,*N*′-tetramethyl-1,4-butanediamine (**2**) was reported as an effective chiral ligand for the enantioface-differentiating addition of butyllithium to aldehydes by Seebach *et al.*[4] In the synthesis, the highest optical yield of the alcohols obtained is 40%, probably due to the rather weak interaction of the chiral ligand **2** with the reactants.

In the preceding papers,[5] it was shown that **1** and (2*S*,2′*S*,2″*S*)-2-hydroxymethyl-1-[[1-[(1-methyl-2-pyrrolidinyl)methyl]-2-pyrrolidinyl]methyl]pyrrolidine (**3**), easily derived from (*S*)-proline, are very effective chiral ligands for the enantioface-differentiating addition of alkyl-, alkynyllithium, and dialkylmagnesium to aldehydes, and that the corresponding secondary alcohols of very high optical purity are obtained (Fig. 1). The explosive increase of the use of lithium compounds in organic synthesis[6] during the last decade prompted us to extend the above enantioface-differentiating reaction to addition of some lithium derivatives of various functionalized organic compounds such as methyl phenyl sulfide, acetonitrile, *N*-nitrosodimethylamine, and 2-methylthiothiazoline (Eq. 1).

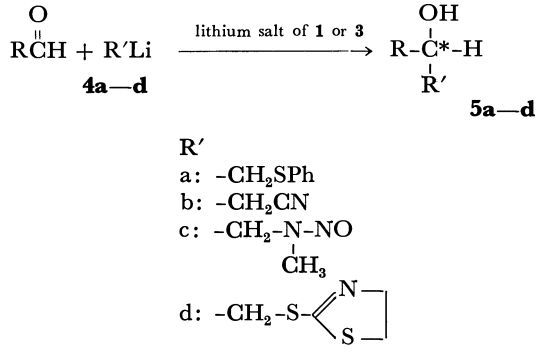

(1)

In this paper, we wish to describe the scope and limitations of the enantioface-differentiating additions of these functionalized lithium compounds to aldehydes.

Optically active **5a**—**d** are known to be converted respectively to the corresponding optically active compounds (oxirane, thiirane, *etc.*). The conventional methods are as follows.

Optically active β-hydroxy sulfides (**5a**) can be converted to optically active oxiranes with little racemization by the use of trimethyloxonium tetrafluoroborate and aq sodium hydroxide (Eq. 2).[7a]

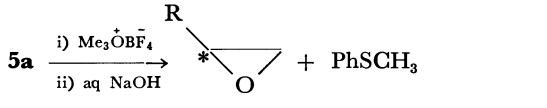

(2)

Since optically active oxiranes play an important role in metabolic processes,[8] many attempts have been reported on the asymmetric syntheses of the oxiranes.[9] For example, epoxidation of olefins by optically active peroxy acids,[9a] or by hydrogen peroxide in the presence of an optically active phase transfer catalyst,[9b] nucleophilic alkylidene transfer by optically active oxosulfonium ylides,[9c] and optically active metal complex catalyzed epoxidation of allylic alcohols with alkyl hydroperoxide,[9d] however, optical yields of oxiranes obtained by these methods are not high in general (maximum 50% e.e.[9d]).

As to the formation of β-hydroxy nitrile (**5b**), a report was given in 1974 utilizing aldehydes and the

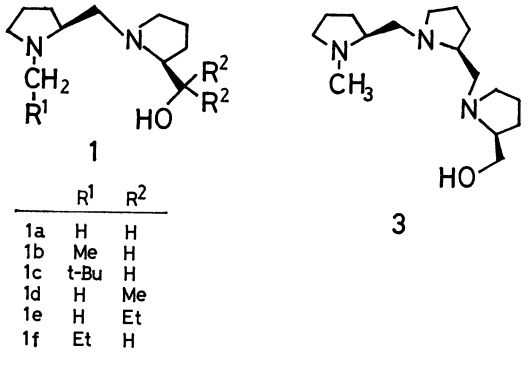

	R^1	R^2
1a	H	H
1b	Me	H
1c	t-Bu	H
1d	H	Me
1e	H	Et
1f	Et	H

Fig. 1.

Table 1. Effects of solvents in the enantioface-differentiating addition of phenylthiomethyllithium to benzaldehyde

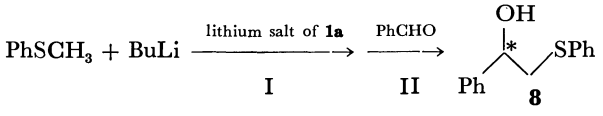

Entry[a]	I			II		8	
	Solvent	Temp/°C	Time/h	Solvent[c]	Temp/°C	Yield/%	Opt. yield/% e.e.[b]
1	Me_2O	−40	2	Me_2O	−123	22	12
2	Et_2O	0	overnight	Et_2O	−123	68	10
3	Pr_2O	0	overnight	Pr_2O	−123	67	0
4	THF	0	1	THF	−78	85	21
5	Hexane	0	overnight	Hexane	−78	50	15
6	$CH_2(OMe)_2$	0	overnight	$CH_2(OMe)_2$	−100	72	60
7	$CH_2(OMe)_2$	0	overnight	$CH_2(OMe)_2$[d]	−100	67	25
8	$CH_2(OMe)_2$	0	overnight	$CH_2(OMe)_2$[e]	−100	63	24
9	$CH_2(OMe)_2$	0	overnight	$CH_2(OMe)_2$ Me_2O(1 : 1)	−123	74	33
10	$CH_2(OMe)_2$	0	overnight	1,3-Dioxolane	−95	74	15
11	$CH_2(OMe)_2$	0	overnight	DME[f]	−78	80	11

a) Molar ratio of the reactants. [PhCHO] : [$PhSCH_3$] : [BuLi] : [**1a**] = 1.0 : 2.7 : 6.7 : 4.0. b) Optical yields were determined by quantitative analyses of NMR spectra of the corresponding esters of (*R*)-(+)-α-methoxy-α-trifluoromethylphenylacetic acid. c) Otherwise noted, the amount of solvent was 20 ml. d) The amount of solvent was 120 ml. e) The amount of solvent was 10 ml. f) 1,2-Dimethoxyethane.

lithium salt of **1a**. It was also found that the enantiomeric excess of **8** depended on the concentrations and β-hydroxy carboxylic acid (Eq. 3), no report has appeared on the asymmetric synthesis of **5b** itself, to our knowledge.

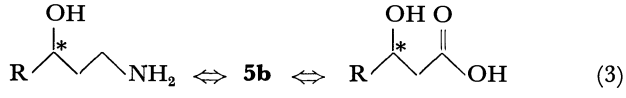

(3)

Moreover **5c** is obtained by the reaction of aldehydes and the lithium derivative of *N*-nitrosodimethylamine, a masked nucleophilic α-(alkylamino)methylating reagent[11] (Eq. 4).

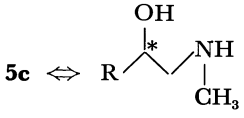

Halostahine **11**
(R=Ph)

(4)

Seebach *et al.* reported the asymmetric synthesis of **5c** (15% optical purity) by the enantioface-differentiating addition of **4c** to benzaldehyde using **2** as a chiral media.[6]

The compound **5d** is known as an intermediate for the formation of thiirane.[12] Concerning the asymmetric synthesis of thiirane, there have been two methods reported, namely, (a) the reaction of chiral 2-methylthiooxazoline (**6**)[13a] and (b) the reaction utilizing the chiral lithiocarboxylate (**7**).[13b] Reactants possessing a chiral moiety are employed in both methods (a) and (b), and as yet no method for the preparation of optically active thiiranes by enantioface-differentiating reactions utilizing chiral ligands has been reported. Therefore this report deals with the first example of enantioface-differentiating reactions using chiral ligands.

Results and Discussion

Oxiranes. As for the generation of phenylthiomethyllithium (**4a**) from methyl phenyl sulfide, Corey and Seebach reported a method using 1,4-diazabicyclo-[2.2.2]octane (DABCO).[14] However, it was found in the preliminary study, that the reaction of equimolar amounts of methyl phenyl sulfide, butyllithium, and the lithium salt of (2*S*,2′*S*)-2-hydroxymethyl-1-[(1-methyl-2-pyrrolidinyl)methyl]pyrrolidine (**1a**) in THF at 0 °C for 45 min or in dimethoxymethane at 0 °C overnight produced **4a** in 95% yield, as determined by subsequent quenching with deuterium oxide and quantitative NMR analysis.

To a mixture of **4a** and the lithium salt of **1a**, formed under the above reaction conditions, benzaldehyde in various solvents was added at low temperatures (−78—−123 °C), and the reaction mixture was stirred for 1 h. Usual work-up gave 1-phenyl-2-phenylthioethanol (**8**), of which enantiomeric excess was determined by quantitative analysis of NMR spectra of the corresponding esters of (+)-α-methoxy-α-trifluoromethylphenylacetic acid (Table 1).

As shown in Table 1, effects of solvents were remarkable. The best result was obtained when the reaction was carried out in dimethoxymethane (entry 6). Moreover it is noted that the enantiomeric excesses of the alcohols obtained became higher as the solvating ability of the reaction media increased (entry 1, 2, and 3), and this tendency was the same as that of alkyllithium, reported in the preceding papers.[5b,d] This might suggest that solvation plays an important role in the formation of the complex of **4a** and the

Table 2. Effects of structures of chiral ligands

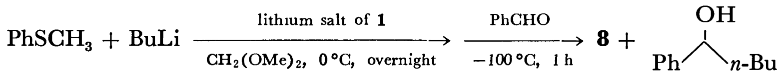

Entry	Chiral ligand	8 Yield/%	8 Opt. yield/% e.e.	1-Phenyl-1-pentanol Yield/%
1	**1a**	72	60	—
2	**1b**	56	54	20
3	**1c**	30	72	34
4	**1d**	48	28	—
5	**3**	31	60	29

Table 3. Asymmetric synthesis of oxiranes

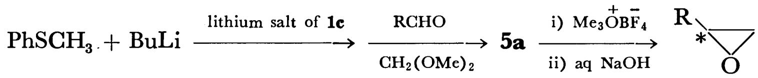

R[a)]		5a Yield/%	5a $[\alpha]_D$ (c, CH_2Cl_2)	5a Enantiomeric ratio[b)]	Oxirane Yield/%	Oxirane $[\alpha]_D$ (c, solvent)	Oxirane Opt. purity/%
Ph	**8**	83	$[\alpha]^{28}$ +7.96°(8.7)	84 : 16	54	$[\alpha]^{26}$ +4.5°(4.0, acetone)	68[c)]
i-Pr	**9**	57	$[\alpha]^{28}$ −28.2°(3.8)	70 : 30			
n-$C_{11}H_{23}$	**10**	54	$[\alpha]^{29}$ −6.79°(2.7)	69 : 31	83	$[\alpha]^{28}$ +3.3°(1.2, THF)	35[d)]

a) Molar ratio of reactants. [RCHO] : [BuLi] : [$PhSCH_3$] : [Ligand **1c**] = 1.0 : 6.7 : 2.7 : 4.0. b) Determined by quantitative analysis of NMR spectra of the corresponding esters of (+)-α-methoxy-α-trifluoromethylphenylacetic acid. c) Calculated from optical rotation based upon the value available. $[\alpha]^{22}_D$ +6.64° (c 4.9, acetone), See Ref. **7b**. d) Calculated from optical rotation based upon the value available. $[\alpha]^{22}_D$ +9.61° (c 1.2, THF). J. L. Coke and A. B. Richon, *J. Org. Chem.*, **41**, 3516 (1976).

lithium derivative of acetonitrile.[10)] Though **5b** is a synthetic equivalent to optically active γ-amino alcohol of the reactants (entry 6, 7, and 8), and that the most suitable concentration of benzaldehyde was found to be 5 M (entry 6). In the preceding paper[5)] it was shown that optical purity of secondary alcohols obtained by asymmetric addition of alkyllithium or dialkylmagnesium to aldehydes are greatly influenced by the structure of chiral ligands. Therefore we examined asymmetric addition of **4a** to benzaldehyde in dimethoxymethane using various kinds of chiral ligands (**1a**—**d**, **3**). (Table 2).

The highest enantiomeric excess (72% e.e.) of **8** was achieved by the use of (2*S*,2′*S*)-2-hydroxymethyl-1-[(1-neopentyl-2-pyrrolidinyl)methyl]pyrrolidine (**1c**) which has bulky neopentyl substituent at the nitrogen atom (entry 3). However, in this case, 1-phenyl-1-pentanol was also produced in 34% yield by the side reaction of butyllithium with benzaldehyde. These results suggest that steric hindrance of the neopentyl group at the nitrogen atom of **1c** decreased the rate of the formation of **4a**. After a number of unsuccessful attempts to develop a satisfactory method, we devised an excellent method; the formation of the complex of **4a** with **1c** was carried out in petroleum ether at 25—30 °C overnight, and the asymmetric addition was carried out at −100 °C after the substitution of petroleum ether for dimethoxymethane.

When benzaldehyde was employed under the above mentioned reaction conditions, optically active (+)-**8** was obtained in 83% yield $[\alpha]^{28}_D$ + 7.96° (c 8.7, CH_2Cl_2) and its enantiomeric ratio (84:16) was determined by quantitative NMR (100 MHz) analysis of the corresponding ester of (+)-α-methoxy-α-trifluoromethylphenylacetic acid. According to the procedure of Shanklin *et al.*,[7a)] the compound **8** thus obtained was converted without racemization to (*R*)-(+)-2-phenyloxirane (54%, $[\alpha]^{26}_D$ +4.5° (c 4.0, acetone), 68% optical purity).[7b)]

In a similar manner, several optically active 2-substituted oxiranes were obtained from the corresponding aldehydes and the results are summarized in Table 3.

Lithium Derivatives of Acetonitrile and N-*Nitrosodimethylamine.* It is well known that the abstraction of a proton from acetonitrile by butyllithium at −78 °C easily produces lithium derivatives (**4b**).[10)] The reaction conditions of the enantioface-differentiating addition of **4b** to benzaldehyde were studied by varying both, type of solvents and structure of chiral ligands. The results are summarized in Table 4.

The highest enantiomeric excess (40% e.e.) of β-hydroxy nitrile (**5b**) was achieved when the reaction was carried out in dimethyl ether at −123 °C using the lithium salt of **1d** as a chiral ligand (Table 4, entry 3).

As to the asymmetric addition of the lithium derivative of *N*-nitrosodimethylamine (**4c**) to benzaldehyde in dimethoxymethane at −100 °C, the corresponding 2-(*N*-nitrosomethylamino)-1-phenylethanol (**5c**)[15)] was

Table 4. Enantioface-differentiating addition of lithium derivative of acetonitrile

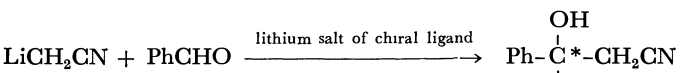

4b **5b**

Entry[a]	Ligand	Solvent	Temp/°C	Yield/%	Opt. yield/%[b]
1	**1c**	$CH_2(OMe)_2$	−100	80	26
2	**1d**	$CH_2(OMe)_2$	−100	94	35
3	**1d**	Me_2O	−123	76	40
4	**1d**	Et_2O	−123	52	9
5	**1e**	$CH_2(OMe)_2$	−100	78	17
6	**1f**	$CH_2(OMe)_2$	−100	86	16
7	**3**	$CH_2(OMe)_2$	−100	83	0
8	**1c**	$CH_2(OMe)_2$	−100	76	0

a) Molar ratio of the reactant; [PhCHO] : [BuLi] : [CH_3CN] : [Ligand] = 1.0 : 6.7 : 2.7 : 4.0. b) Determined by quantitative analysis of NMR spectra of the corresponding ester of (+)-α-methoxy-α-trifluoromethylphenylacetic acid.

obtained in 96% yield ($[\alpha]_D^{25}$ +12.46°), and subsequent denitrosation gave 2-methylamino-1-phenylethanol (**11**) Halostahine, $[\alpha]_D^{24}$ +11.9° (*c* 1.68, EtOH), opt. purity 25%.[16]

The reason that enantiomeric excesses of the adducts **4b** and **4c** are not so high as those of the addition of alkyllithium as reported in the previous papers[5] may be explained as follows; it is clear that efficient complexes of lithium derivatives with chiral ligand should be tight and stable for achievement of higher enantioselectivity. It is also well known that ionic character of the lithium–carbon bond of lithium derivatives increases as the pK_a value of the parent compound decreases. Hence, the lithium–carbon bond of **4b** and **4c** becomes looser than that of alkyllithium. Therefore, the enantiomeric excesses of the adducts obtained may depend on the decrease in the stability of the chelated complexes of **4b** and **4c** with chiral ligand **1** as compared with that of alkyllithium.

Thiirane. Enantioface-differentiating addition of lithium compound (**4d**) to benzaldehyde was carried out in dimethoxymethane at −100 °C for 1 h in the presence of lithium salt of **1a**. The optical purity of the obtained (*R*)-(−)-2-methylthiirane was 20%[17] (Eq. 5).

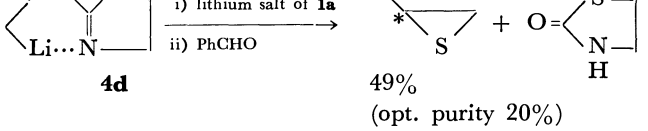

4d 49% (opt. purity 20%) (5)

It is noticeable that **4d** has a rather rigid structure because of the coordination between the nitrogen atom and the lithium atom.[18]

This rigidity of **4d** may interfere in the formation of the complex between **4d** and the lithium salt of **1a**, and decreases enantioselectivity. Though optical purity of this procedure is comparable to that of the previously reported method using chiral **6**,[13a] this procedure has an advantage over previous methods in that there is no need to synthesize chiral thiazoline derivatives.

In conclusion, the chiral ligands **1** and **3**, easily prepared from (*S*)-proline, are efficient for the enantioface-differentiating addition of a wide variety of organolithium compounds to aldehydes. Optical yields of the various products thus obtained are higher than those illustrated in the previous methods. Furthermore, this method has an advantage over previous methods of asymmetric syntheses, in the simplicity of the reaction procedure, namely, there is no necessity of introducing and removing chiral moieties in the reactants at any stage.

Experimental

General. NMR spectra were taken on a Hitachi R-24B Spectrometer. Infrared spectra were taken on a Hitachi EPI-G2 spectrometer. Optical rotation was taken on a JASCO DIP-SL automatic polarimeter. THF, dimethoxyethane, dimethoxymethane, diethyl ether, and dipropyl ether were distilled from $LiAlH_4$ prior to use. Dimethyl ether was dried by passing the gas through a tube packed with calcium chloride. Reactions involving air-sensitive compounds were carried out under an atmosphere of argon. For evaporative bulb-to-bulb distillation, a Büchi Kugelrohrofen was used. According to the reported procedure,[5d] preparation of chiral ligands from (*S*)-proline and recovery of them after the asymmetric reactions were carried out.

*Asymmetric Addition of Phenylthiomethyllithium (**4a**) to Aldehydes Using **1c** as Chiral Ligand.* Methyl phenyl sulfide (0.670 g, 5.4 mmol) in 8 ml of petroleum ether (bp 37 °C) was added to a mixture of hexane (8.65 ml) solution of butyllithium (13.5 mmol) and petroleum ether (36 ml) solution of **1c** (2.057 g, 8.1 mmol) at 0 °C, and the mixture was stirred at room temperature (25—30 °C) for 17 h. Solvent was removed by evaporation with vacuum pump (1 mmHg) for 10 min at room temperature.[19] The residue was dissolved in 40 ml of dimethoxymethane, and was added a dimethoxymethane solution (4 ml) of benzaldehyde (0.212 g, 2 mmol) at −100 °C, and the stirring was continued for 1 h. The reaction was quenched with 3 M hydrochloric acid, extracted with ether and dried over Na_2SO_4. After removal of the solvent, the residue was purified by silica-gel TLC (CH_2Cl_2) and the isolated product was further purified by short-path distillation. 1-Phenyl-2-phenylthioethanol (**8**) (0.384 g, 83%, $[\alpha]_D^{28}$ +7.96° (*c* 8.7, CH_2Cl_2), optical yield

68%e.e.) was obtained as a yellow oil of which enantiomeric excess was determined according to Mosher's method.[20] In a similar manner, isobutyraldehyde and dodecanal were employed and the spectra data of the adducts were as follows; **8**; IR (neat) 3400, 3050, 2900, 1580, 1485, 1475, 1450, 1435, 1055, and 1025 cm^{-1}; NMR ($CDCl_3$) δ=2.77—3.30 (3H, m), 4.66 (1H, m) and 7.23 (10H, m). **9**; IR (neat) 3420, 3050, 2960, 2950, 2870, 1590, 1480, 1440, 1100, 1050, 1030, and 1000 cm^{-1}; NMR ($CDCl_3$) δ=0.90 (6H, d, J=6 Hz), 1.46—2.06 (1H, m), 2.30—3.65 (4H, m), and 7.16 (5H, m). **10**; Mp 52—53 °C IR (KBr) 3380, 2920, 2840, 1585, 1475, 1460, 1435, 1345, 1090, 1065, 1060, 735, 730, and 690 cm^{-1}, NMR ($CDCl_3$) δ=1.22—1.60 (23H, m), 2.44 (1H, broad), 2.75—3.35 (2H, m), and 3.70 (1H, m).

Optically Active 2-Substituted Oxiranes. According to the procedure of Shanklin *et al.*,[7a] **8a** was converted to 2-phenyloxirane (0.107 g, 54%, optical purity 68%).[7b] Optically active 2-undecyl oxirane was obtained in a similar manner. The structures of these compounds were identified by their IR and NMR spectra.

*Asymmetric Addition of Lithium Derivative of Acetonitrile to Benzaldehyde Using **1d**.* Diethyl ether (0.5 ml) solution of **1d** (0.915 g, 4.0 mmol) was added to dimethyl ether (20 ml) at −78 °C, and butyllithium (6.7 mmol) was added subsequently. After the reaction mixture was stirred for 15 min, acetonitrile (0.111 g, 2.7 mmol) in Et_2O (1 ml) was added. Stirring was continued for further 15 min, then benzaldehyde (0.106 g, 1.0 mmol) in Et_2O (1 ml) was added at −123 °C to the reaction mixture. After the mixture was stirred for 30 min, the reaction was quenched by adding 3 M hydrochloric acid, and the mixture was extracted with diethyl ether, dried over Na_2SO_4. The organic layer was concentrated under reduced pressure. The residue, subjected to preparative TLC on silica gel (CH_2Cl_2) yielded 3-hydroxy-3-phenylpropanenitrile (0.111 g, 76%), $[\alpha]_D^{18}$ +24.4° (c 4.1, CH_2Cl_2). The enantiomeric exess (40%e.e.) was determined by Mosher's method.[20] The structure was identified by IR and NMR.

*Asymmetric Addition of Lithium Derivative of N-Nitrosodimethylamine Using **1a** as Chiral Ligand.* Butyllithium (6.7 mmol) was added to dimethoxymethane (12 ml) solution of **1a** at 0 °C, and the mixture was stirred for 30 min. Then, *N*-nitrosodimethylamine[21] (0.200 g, 2.7 mmol) in dimethoxymethane (4 ml) was added to the mixture at −100 °C and the stirring was continued for 10 min. To the reaction mixture, benzaldehyde (0.106 g, 1.0 mmol) in dimethoxymethane (1.5 ml) was added at −100 °C. After the reaction mixture was stirred for 1.5 h, the reaction was quenched with water (5 ml), then the aqueous layer was adjusted to pH 5. The mixture was extracted with diethyl ether, and the extract was dried over anhydrous sodium sulfate. After the extract was concentrated under reduced pressure, the residue was purified by preparative TLC on silica gel [CH_2Cl_2–AcOEt (1 : 1)]. 2-(*N*-nitrosomethylamino)-1-phenylethanol (**5c**) (0.172 g, 96%, $[\alpha]_D^{25}$ +12.5° (c 5.8, CH_2Cl_2) was obtained which was further purified by short-path distillation. The structure of **5c** was identified by IR and NMR spectra.

*Halostahine (**11**).* According to the procedure of denitrosation[15] reported by Seebach and Enders, **5c** was converted to halostahine. $[\alpha]_D^{24}$ +11.9° (c 1.7, EtOH). Optical purity 25% [based upon the reported rotation $[\alpha]_D$ −47.03°].[16] Mp 74—75 °C [lit, 75—76 °C][16] IR (KBr) 3320, 1445, 1345, 1200, 1140, 1115, 1085, 1065, 930, 760, 750, and 700 cm^{-1}. NMR ($CDCl_3$) δ=2.40 (3H, 5), 2.72 (2H, d, J=6 Hz), 3.56 (2H, s), 4.75 (1H, t, J=6 Hz), and 7.34 (5H, s).

Asymmetric Addition of Lithium Derivative of 2-Methylthiothiazoline to Benzaldehyde. Butyllithium (6.7 mmol) was added to a dimethoxymethane (15 ml) solution of **1a** (0.803 g, 4.0 mmol) at 0 °C, and the mixture was stirred for 30 min. After the mixture was cooled to −78 °C, 2-methylthiothiazoline[22] (0.359 g, 2.7 mmol) in dimethoxymethane (2 ml) was added, and the stirring was continued for 1 h. Then, benzaldehyde (0.106 g, 1.0 mmol) in dimethoxymethane (2 ml) was added at −100 °C to the reaction mixture. The mixture was stirred for 1 h, the reaction was quenched with water (15 ml). Organic layer was extracted with ether, and the extract was dried over anhydrous sodium sulfate. After the concentration of the extract under reduced pressure, the residue was subjected to silica gel column chromatography (CH_2Cl_2) to remove chiral ligand **1a**. Further purification utilizing preparative silica-gel TLC (hexane) gave 2-phenylthiirane (0.067 g, 50%) $[\alpha]_D^{27}$ −8.8° (c 2.6, heptane). Optical purity 20% [based upon the reported value, lit $[\alpha]_D$ −43.85° (heptane)].[17] IR (neat) 2930, 1600, 1500, 1495, 1450, 1070, 1045, 760, 695, and 665 cm^{-1}, NMR ($CDCl_3$) δ= 2.43 (1H, dd, J=6 Hz, 2 Hz), 2.70 (1H, dd, J=6 Hz, 2 Hz), 3.70 (1H, t, J=6 Hz), and 7.05 (5H, s).

The present work was partially supported by a Grant-in-Aid for Scientific Research from the Ministry of Education.

References

1) a) J. D. Morrison and H. S. Mosher, "Asymmetric Organic Reactions," Prentice-Hall, Englewood Cliffs., N. J. (1971); b) Y. Izumi, A. Tai, K. Hirota, and T. Harada, *Kagaku Sosetsu*, **4** (1971).

2) a) R. S. Brinkmeyer and V. M. Kappor, *J. Am. Chem. Soc.*, **99**, 8339 (1977); b) M. Asami, H. Ohno, S. Kobayashi, and T. Mukaiyama, *Bull. Chem. Soc. Jpn.*, **51**, 1869 (1978), and references cited therein.

3) See Ref. 1a) pp. 415—419.

4) D. Seebach, H. Kalinowski, B. Bastani, G. Grass, H. Daum, H. Dorr, N. P. Dupreez, W. Langer, C. Nussler, H.-A. Oei, and M. Schmidt, *Helv. Chim. Acta*, **60**, 301 (1977).

5) a) T. Mukaiyama, K. Soai, and S. Kobayashi, *Chem. Lett.*, **1978**, 219; b) K. Soai and T. Mukaiyama, *ibid*, **1978**, 491; c) T. Sato, K. Soai, K. Suzuki, and T. Mukaiyama, *ibid*, **1978**, 601; d) T. Mukaiyama, K. Soai, T. Sato, H. Shimizu, and K. Suzuki, *J. Am. Chem. Soc.*, **101**, 1455 (1979); e) T. Mukaiyama, K. Suzuki, K. Soai, and T. Sato, *Chem. Lett.*, **1979**, 447.

6) D. Seebach and K.-H. Greiss, "New Application of Organometallic Reagents in Organic Synthesis," Elsevier, Amsterdam (1976).

7) a) J. R. Shanklin, C. R. Johnson, J. Ollinger, and R. M. Coates, *J. Am. Chem. Soc.*, **95**, 3429 (1973); b) C. R. Johnson and C. W. Schroeck, *J. Am. Chem. Soc.*, **95**, 7418 (1973).

8) T. Shishibori, T. Fukui, and T. Suga, *Chem. Lett.*, **1973**, 1137, and references cited therein.

9) a) W. H. Pirkle and P. L. Rinaldi, *J. Org. Chem.*, **42**, 2080 (1977); b) R. Helder, J. C. Hummelen, R. W. P. M. Laane, J. S. Wiering, and H. Wynberg, *Tetrahedron Lett.*, **1976**, 1831; c) C. R. Johnson and C. W. Schroeck, *J. Am. Chem. Soc.*, **95**, 7418 (1973); d) S. Yamada, T. Mashiko, and S. Terashima, *J. Am. Chem. Soc.*, **99**, 1988, (1977); R. C. Michaelson, R. E. Palermo, and K. B. Sharpless, *ibid.*, **99**, 1990 (1977).

10) D. S. Watt, *Tetrahedron Lett.*, **1974**, 707.

11) D. Seebach and D. Enders, *Angew. Chem. Int. Ed.*

Engl., **14**, 15 (1975).
12) C. R. Johnson, A. Nakanishi, N. Nakanishi, and K. Tanaka, *Tetrahedron Lett.*, **1975**, 2865.
13) a) A. I. Meyers and M. Ford, *J. Org. Chem.*, **41**, 1735 (1976); b) C. R. Johnson and K. Tanaka, *Synthesis*, **1976**, 413.
14) E. J. Corey and D. Seebach, *J. Org. Chem.*, **31**, 4097 (1966).
15) D. Seebach and D. Enders, *Chem. Ber.*, **108**, 1293 (1975).
16) G. P. Men'shikov and G. M. Borodina, *J. Gen. Chem. USSR*, **17**, 1569 (1947); *Chem. Abstr.*, **42**, 2245a (1948).
17) E. Chiellini, M. Marchetti, and G. Ceccarelli, *Int. J. Sulfur Chem., Part A*, **1**, 73 (1971).
18) K. Narasaka, M. Hayashi, and T. Mukaiyama, *Chem. Lett.*, **1972**, 259.
19) The enantiomeric excess of β-hydroxy sulfide is greatly influenced by the presence of petroleum ether. In order to evaporate petroleum ether completely, the use of a larger reaction vessel (300-ml) is preferable.
20) J. A. Dale and H. S. Mosher, *J. Am. Chem. Soc.*, **95**, 512 (1973).
21) H. H. Hatt, *Org. Synth.*, Coll. Vol. II, 211 (1948).
22) K. Hirai, H. Matsuda, and Y. Kishida, *Chem. Pharm. Bull.*, **20**, 2067 (1972).

F-Propene-Dialkylamine Reaction Products as Fluorinating Agents

Akio TAKAOKA, Hiroshi IWAKIRI, and Nobuo ISHIKAWA*

Department of Chemical Technology, Tokyo Institute of Technology, Ookayama, Meguro-ku, Tokyo 152

(Received May 15, 1979)

The reaction products of *F*-propene and dialkylamines, mixtures of α,α-difluoroalkylamine and α-fluoro enamine, were found to be useful fluorinating agents for alcohols and carboxylic acids. These reagents were superior to the adduct of chlorotrifluoroethene and diethylamine, the so-called Yarovenko reagent, for their readier preparation and higher stability.

2-Chloro-1,1,2-trifluorotriethylamine (**1**), the adduct of chlorotrifluoroethene and diethylamine, has been known as a useful fluorinating agent for alcohols.[1] This agent, which is sometimes called as "Yarovenko reagent,"[2] can replace a hydroxyl group with a fluorine atom under mild conditions and has been used especially for the syntheses of fluoro steroids.[1]

$$Et_2NH + CF_2{=}CFCl \longrightarrow \underset{\mathbf{1}}{Et_2NCF_2CHFCl}$$

$$ROH + \mathbf{1} \longrightarrow R\text{-}F + Et_2NC(=O)CHFCl + HF$$

However, the addition reaction of chlorotrifluoroethene with diethylamine to give (**1**) is not so easy and it requires rather long time in a sealed vessel in order to get a good yield. Further, the adduct (**1**) is not so stable at room temperature and it can not be stored more than a few days.

For the past several years, we have been studying on the nucleophilic reactions of *F*-propene and its oligomers, and it has been known that *F*-propene reacts with dialkylamines much more easily than with chlorotrifluoroethene. We now wish to report on the utility of the reaction products of the *F*-propene and dialkylamines as fluorinating agents of alcohols and carboxylic acids.

Results and Discussion

Reaction between F-*Propene and Dialkylamines.* Many years ago the nucleophilic reaction of *F*-propene with diethylamine giving addition and substitution products was reported by Knunyants *et al.*, though not in detail.[3] We carried out the reaction of *F*-propene with a number of secondary amines in diethyl ether, and determined the ratios of fluoroalkylamine (**2**) to fluoro enamine (**3**) from the signal intensities of ^{19}F NMR spectra.

$$R_2NH + CF_2{=}CFCF_3 \longrightarrow \underset{\mathbf{2}}{R_2NCF_2CHFCF_3} + \underset{\mathbf{3}}{\begin{matrix} R_2N & & F \\ & \diagdown\!\!=\!\!\diagup & \\ F & & CF_3 \end{matrix}}$$

The assignment of the NMR signals for **2** and **3** (R=Et) was done as shown in Fig. 1. Regarding the geometric isomers of **3**, only *E*-isomer was found in the product. Thus the F-F coupling constant was determined as 117 Hz (R=Et), which agrees to the expected value for *trans* F-F coupling constant, 109—131 Hz, and is quite different form that for *cis* F-F, 19—58 Hz.[4]

The formation of *E*-form rather than *Z*-form can

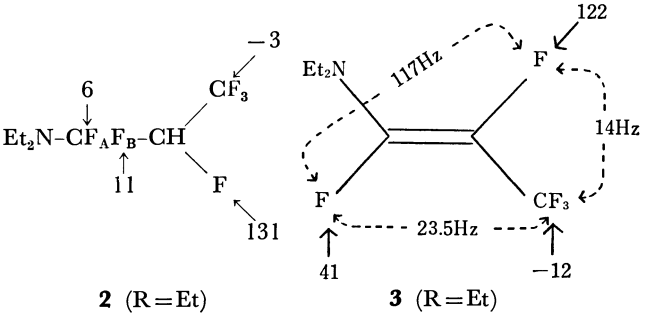

Fig. 1. The ^{19}F NMR spectra for **2** and **3** (R=Et). (Chemical shifts are given in δ ppm up field from external CF_3CO_2H).

be explained by considering the conformation of the intermediate carbanion (**4**). The *E*-isomer should be formed by the *trans*-elimination of fluoride ion from **4a**, whereas the *Z*-isomer should be from **4b**. However, **4b** must be less stable than **4a** due to the electronic replusion between lone pair electrons of the nitrogen atom and those of the fluorine atom of CF_3. Thus the formation of (*E*)-**3** through **4a** would predominate over the formation of (*Z*)-**3** through **4b**. We have already observed similar phenomenon in the case of nucleophilic aryloxylation of *F*-propene.[5]

$$R_2NH + CF_2{=}CFX \longrightarrow \underset{\mathbf{4}}{R_2N\text{-}CF_2\text{-}\overline{C}FX}$$

$$\xrightarrow{+H^+} R_2N\text{-}CF_2\text{-}CHFX \quad (\mathbf{1}\ X=Cl_3;\ \mathbf{2}\ X=CF_3)$$

$$\xrightarrow{-F^-} R_2N\text{-}CF{=}CFX \quad (\mathbf{3}\ X=CF_3)$$

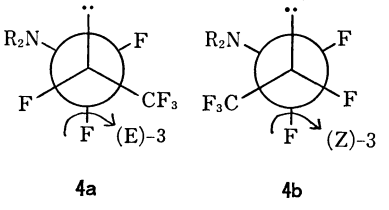

4a **4b**

As was shown in Table 1, the ratio **2** to **3** in the reaction products increased in the order of the bulkiness of the used amines, *i.e.*, piperazine<diethylamine< dibutylamine. Thus the bulkier the nucleophile is, the more enamine (**3**), which is more released from the steric hindrance than alkylamine (**2**), is formed.

Nucleophilic Reactivities and Reaction Products. Several methods for the preparation of **1**, the "Yarovenko reagent," were reported in the literature. A typical procedure is to have diethylamine and chlorotrifluoroethene react in a sealed vessel at room temperature for 48 h using dichloromethane as solvent[6]

Table 1. C_3F_6/R_2NH reaction products

R_2N	Product		
	Bp/°C (mmHg)	**2** : **3**[a]	Yield/%[b]
Et_2N	56—57(58)	3 : 1	72
n-Bu_2N	55—57(5)	2 : 1	78
Piperidino	49—50(7)	(2 only)	80

a) Determined by ^{19}F NMR. b) Isolated yield.

or without solvent.[7] Another procedure is to bubble chlorotrifluoroethene gas through diethylamine at atmospheric pressure.[2] However, we observed almost no reaction occurred by the latter procedure. In contrast, we found that *F*-propene reacted much more easily with diethylamine, and the perfluoroolefin was exothermally absorbed at room temperature by a solution of diethylamine in diethyl ether. As a result the reaction mixture itself could be used as a fluorinating agent without further purification by distillation.

The reaction product of *F*-propene and diethylamine was, as mentioned above, a mixture of fluoroalkylamine **2** and fluoro enamine **3** (R=Et), whereas that of chlorotrifluoroethene was almost pure fluoroalkylamine **1**. These facts can be explained by the difference between electronic effects of a Cl and a CF_3 group. Chlorine as a substituent group is known to manifest an electron-donative R-effect (or electron-repelling I_π effect by lone pairs) as well as an electron-withdrawing I_σ effect. On the other hand, a trifluoromethyl group behaves solely as an electron-withdrawing group by its strong negative I_σ effect. Therefore, the intermediate carbanion **4** (X=CF_3) formed by the reaction of *F*-propene and dialkylamine should be rather stable than that of chlorotrifluoroethene and dialkylamine, **4** (X=Cl). These effects should result in the higher reactivity of *F*-propene compared with that of chlorotrifluoroethene. Further, the negative charge of the carbanion **4** (X=Cl) is less delocalized than that of **4** (X=CF_3), and hence the former should be more strongly protophilic. Consequently, chlorotrifluoroethene gave predominantly the alkylamine **1**, while the *F*-propene gave a mixture of the alkylamine **2** and the enamine **3**.

The chlorotrifluoroethene–diethylamine adduct, **1**, is a rather unstable liquid, and it colored gradually

Table 2. Fluorination of primary-alcohols

$$R\text{-}OH \xrightarrow[Et_2O,\ 20\,h,\ r.t.]{C_3F_6/R'_2NH} R\text{-}F$$

R	Yields[a] of RF with R'_2N			Ref. for R-F
	Et_2N	*n*-Bu_2N	Piperidino	
$EtOCH_2CH_2$	60	76	78	c)
n-C_8H_{17}	87	90	76	d)
o-$C_{16}H_{33}$	78	72	91	e)
$HOC_{10}H_{20}$	82[b]	72[b]	81[b]	f)
$PhCH_2CH_2$	89	82	80	g)

a) Yields were determined by ^{19}F NMR unless otherwise noted. b) The product was $FC_{10}H_{20}F$, of which the yield was determined by GLC. c) E. G. Trochimouski, A. Sorzynski, and J. Wnuk, *Recl. Trav. Chim. Pays-Bas*, **66**, 413 (1947). d) Y. Kobayashi and C. Akashi, *Chem. Pharm. Bull. (Tokyo)*, **16**, 1009 (1968). e) E. D. Bergmann and A. M. Cohen, *Isr. J. Chem.*, **8**, 925 (1970). f) R. G. Woolford, F. L. M. Pattison, J. B. Stothers, and A. I. Vogel, *J. Am. Chem. Soc.*, **78**, 2255 (1956). g) J. Hayamizu, N. Mizuno, and A. Kaji, *Nippon Kagaku Zasshi*, **92**, 87 (1971).

Table 3. Fluorination of secondary and tertiary-alcohols

$$R\text{-}OH \xrightarrow{C_3F_6/Et_2NH} R\text{-}F + \text{alkene} + R_2O$$

R	Reaction conditions			Product yields[a]/%			Ref. for R-F
	Solv.	Temp/°C	Time/h	R-F	Alkene	R_2O	
$C_6H_{13}CH(Me)$	Et_2O	r.t.	20	62 (57)	Octene,[b] 25 (25)	—	e)
$C_6H_{13}CH(Me)$	MeCN	r.t.	20	18	Octene,[b] 52	—	
Cyclohexyl	Et_2O	r.t.	10	—	Cyclohexene, 78	—	
2-Me·cyclohexyl	Et_2O	r.t.	20	—	1- & 3-Methyl-cyclohexene, 31 & 27	—	
PhCH(Me)	Et_2O	r.t.	20	56 (57)	—	29 (25)	f)
PhCH(Et)	Et_2O	r.t.	20	65 (62)	—	27 (20)	f)
$PhCH_2$	Et_2O	r.t.	20	60	—	25	g)
$PhCH(CO_2Et)$	Et_2O	r.t.	20	66	—	—	h)
Bornyl	Et_2O	r.t.	5	58[c]	Camphene, 19	—	i)
Cholesteryl	CH_2Cl_2	0—5	16	83[d]	—	—	j)
t-Bu	CCl_4	r.t.	20	78 (61)	Isobutylene, 9 (8)	—	k)
1-Adamantyl	THF	refl.	5	81	—	—	l)

a) Yields were determined by ^{19}F and ^1H NMR, or by GLC, unless otherwise noted. Figures in parentheses are those obtained with "Yarovenko reagent" under similar conditions. b) *trans*-2-Octene : *cis*-2-octene : 1-octene = 4 : 3 : 1. c) The product is 3-fluoro-2,2-dimethylbicyclo[2.2.1]heptane. d) Isolated yields. e) E. D. Bergmann and I. Shahk, *Bull. Res. Counc. Isr.* **10A**, 91 (1961). f) K. Wiechert, *Z. Chem.*, **8**, 64 (1968). g) Ref. 6). h) K. Fendenberg, *Ann.*, **601**, (1933). i) W. J. Middleton, *J. Org. Chem.*, **40** (5), 575 (1975). j) J. C. Brial and M. Mousseron-Canet, *Bull. Soc. Fr.*, **1968**, 3321. k) K. A. Coper and E. D. Hughes, *J. Chem. Soc.*, **1973**, 1183. l) G. A. Olah, M. Nojima, and I. Kerckes, *Synthesis*, **1973**, 786.

Table 4. The yields of acyl fluorides

$$RCO_2H \xrightarrow[Et_2O,\ 2\ h,\ r.t.]{C_3F_6/Et_2NH} RCOF$$

R	Yield/% I[a]	Yield/% II[b]	^{19}F NMR δ/ppm[c]	Ref. for RCOF
Et	64	61 (40)[d]	−116	e)
n-C_6H_{13}	73		−118	f)
Ph	86	60 (90)[d]	−90	g)
p-MeC_6H_4	71		−91	h)
m-MeC_6H_4	88		−92	h)
p-HOC_6H_4	75		−88	i)

a) Yields determined by ^{19}F NMR. b) Isolated yield. c) Upfield from ext. CF_3CO_2H. d) Yield obtained with the "Yarovenko reagent." e) Ref. 2. f) G. A. Olah, S. Kuhn, and S. Beke, *Chem. Ber.*, **89**, 862 (1956). g) Z. Arnold, *Collect. Czech. Chem. Commun.*, **28**, 2047 (1963). h) H. S. Albert, *Act. Phys. Aust.*, **1**, 352 (1948). i) R. W. Taft, Jr., *J. Chem., Phys.*, **38**, 380 (1963).

in several days even by storage in a refrigerator. It also fumed strongly by contact with atmospheric moisture, and it is recommended to be prepared just before the use.[1] In contrast, the *F*-propene–diethylamine reaction product (**2**+**3**) was so stable that no coloration was observed by storage at room temperature. Even after half a year, it could be used without any deterioration, and it could be handled much easier than **1**.

Fluorination of Alcohols. Fluorination of various alcohols using the *F*-propene–diethylamine reaction product (**2**+**3**) mentioned above was carried out. In these reactions, we found that the pure **3**, which was prepared in another route, has no fluorinating ability. Nevertheless, when a mixture of **2** and **3** was used, hydrogen fluoride which was formed by the reaction of **2** and an alcohol added to **3** giving **2**. As a whole, all of **3** was consumed as a fluorinating agent through **2**.

$$ROH + \underset{\mathbf{2}}{Et_2NCF_2CHFCF_3} \longrightarrow RF + Et_2NC(=O)CHFCF_3 + HF$$

6

$$Et_2NCF{=}CFCF_3 + HF \longrightarrow \mathbf{2}$$

Several other *F*-propene–dialkylamine reagents were also examined for fluorination, however, there were no differences among their abilities as a fluorinating agent. From the practical point of view, however, it was necessary to choose an appropriate amine component, otherwise the fluorinated product and the formed amide might have similar boiling points, which would make the separation of them difficult.

Various primary alcohols were subjected to the fluorination using *F*-propene–dialkylamine reaction products, using diethyl ether as a solvent. After 20 h's reaction at room temperature, the yields of the fluorinated products were determined based on the signal intensities of ^{19}F NMR (Table 2). Most of the primary alcohols were fluorinated in good yields. However, benzyl alcohol, which readily gives a benzyl cation, formed 25% of dibenzyl ether.

Secondary and tertiary alcohols, which also tend to form carbonium ions, gave considerable amounts of alkenes and dialkyl ethers (Table 3). For example, 2-octanol in diethyl ether gave 25% of a mixture of *trans*-2-octene, *cis*-2-octene, and 1-octene (4 : 3 : 1), besides 62% of 2-fluorooctane. When the reaction was carried out in acetonitrile, a highly polar solvent, the formation of alkene reached up to 52%.

Borneol gave a fluorinated product formed through carbonium rearrangement. α-Hydroxycarboxylic acid ester such as ethyl DL-mandelate gave α-fluoro carboxylic acid ester in a good yield. Choresterol also afforded the expected cholesteryl fluoride by fluorination in dichloromethane at low temperature. The fluorination of *t*-butyl alcohol was notable, as it afforded *t*-butyl fluoride in 78% of yield. 1-Adamantanol also gave 1-fluoroadamantane in a high yield.

The reaction mechanism of the fluorination by chlorotrifluoroethene–diethylamine reagent is suggested to involve S_N1, S_N2, or S_Ni, though no diethylamine reagent is suggested to involve S_N1, S_N2, or S_Ni, though no kinetic investigation has been done.

The fluorination of alcohols with the *F*-propene–diethylamine reagent should also undergo through the following pathway.

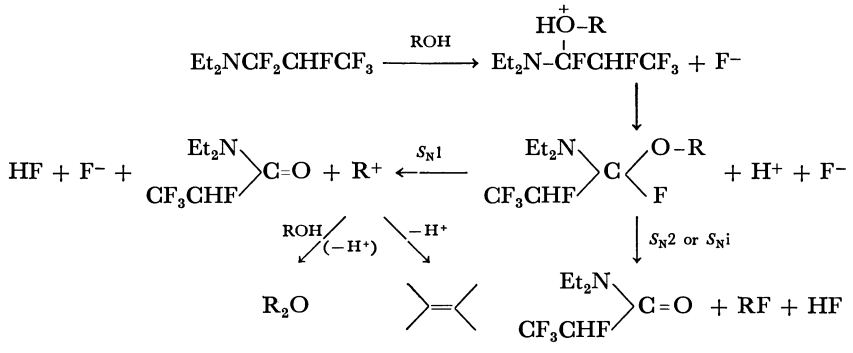

Fluorination of Carboxylic Acids. Carboxylic acids are known to be converted directly to their fluorides by using chlorotrifluoroethene–diethylamine reagent.[2,10] The *F*-propene–diethylamine reagent could also be used for the fluorination of aliphatic or aromatic carboxylic acids into their fluorides (Table 4).

Experimental

Reaction of F-*Propene with Diethylamine.* *a) Reaction under Pressure*: Diethylamine (11 mg, 0.15 mol) and dried

diethyl ether (30 ml) were placed in a glass pressure-vessel, and the whole was cooled to ≈ −70 °C by means of a Dry Ice–acetone bath. Liquefied *F*-propene (25 g, 0.17 mol) was introduced to the vessel and sealed. The cooling bath was removed and the mixture was brought to room temperature with magnetical stirring. After stirring over a night, the reaction mixture was filtered to remove the crystals of diethylamine hydrofluoride, and the solvent was evaporated. Resulting residue was subjected to distillation in a vacuum, and a liquid (23.7 g, 72%) bp 56—57 °C/58 mmHg, was obtained. The ^{19}F NMR spectrum revealed that this oil is a mixture of **2** and **3** in a ratio 3 : 1. When the vessel is stoppered tight, this material could be stocked at room temperature for more than half a year with only a slight discoloration.

b) Reaction at Atmospheric Pressure: A solution of diethylamine (105 g) in dried diethyl ether (200 ml) was placed in a three-necked flask which was equipped with a Dry Ice–acetone-cooled reflux condenser and a gas inlet tube. The whole was cooled to 0—5 °C with an ice-bath and *F*-propene gas (240 g) was bubbled through the mixture. Vigorous stirring was continued throughout this process and the temperature was kept below 10 °C. The whole gas was completely absorbed by 2 h's bubbling. After removing the ice-bath, the reaction mixture was allowed to stand overnight. The mixture thus obtained can be used as a fluorinating agent. However, for further purification, the solvent was evaporated and the residue was distilled in a vacuum giving an oil (273 g, 89%), bp 51—53 °C/40 mmHg. This liquid was a mixture of **2** and **3** in the ratio 1 : 1.

1-Fluorooctane. A solution of the *F*-propene–diethylamine reagent (13 g, 60 mmol) in diethyl ether (50 ml) was dropped into a solution of 1-octanol (6.5 g, 50 mmol) in diethyl ether (30 ml) at 0—5 °C. After stirring for 4 h, the reaction mixture was thrown into water and an oily layer was extracted with diethyl ether. The extract was washed with water, dried over magnesium sulfate, and evaporated to remove the solvent. The residue was distilled to give 1-fluorooctane (5.4 g, 82%), bp 145—146 °C.

Other primary alcohols were fluorinated in similar manners.

2-Fluorooctane. Fluorination of 2-octanol was carried out similarly to that of 1-octanol. The reaction product was subjected to gas chromatographic analysis using benzotrifluoride as a standard material. Following products were found in the reaction mixture: 2-fluorooctane (62%), 2-octene (22%, *trans*/*cis*=3/1), and 1-octene (3%).

Cholesteryl Fluoride. Into a solution of cholesterol (1.17 g) in dichloromethane (7 ml), a solution of *F*-propene–diethylamine reagent (0.81 g) in dichloromethane (3 ml) was dropped at 0—5 °C. Stirring was continued further several hours at that temperature, and the reaction mixture was thrown into water. An oily layer was extracted with dichloromethane, and the extract was washed with water, dried over magnesium sulfate and subjected to column chromatography on silica gel. Petroleum ether was used as the eluent, and the main elution was subjected to evaporation, affording white crystals (0.96 g, 83%) of cholesteryl fluoride, mp 92—93 °C (lit,[11] mp 93—94 °C).

Propionyl Fluoride. Into *F*-propene–diethylamine reagent (11.9 g, 56 mmol), propionic acid (3.9 g, 50 mmol) was dropped at room temperature. The mixture was stirred at 60 °C for 1 h and subjected to distillation. Propionyl fluoride (2.4 g, 62%) came out at bp 43—45 °C (lit,[1] bp 44 °C), followed by *N*,*N*-diethyl-2,3,3,3-tetrafluoropropionamide (10.5 g, 89%), bp 86—89 °C/11 mmHg.

References

1) See review, C. M. Sharts and W. A. Sheppard, *Org. React.*, **21**, 158 (1974).
2) N. N. Yarovenko and M. S. Raksha, *Zh. Obshch. Khim.*, **29**, 2159 (1959).
3) I. L. Knunyants, L. S. German, and B. L. Dyatkin, *Bull. Acad. Sci. USSR, Div. Chem. Sci.*, **1956**, 1387.
4) H. Harada and N. Ishikawa, *J. Fluorine Chem.*, **11**, 87 (1978).
6) E. D. Bergamann and A. M. Cohen, *Isr. J. Chem.*, **8**, 925 (1970).
7) D. E. Ayer, U. S. Patent, 3153644 (1964).
8) D. E. Ayer, *Tetrahedron Lett.*, **1962**, 1065.
9) M. Mousseron-Canet and J. L. Borgna, *Bull. Soc. Chim. Fr.*, **1969**, 613.
10) Z. Arnold, *Collect. Czech. Chem. Commun.*, **28**, 2047 (1963).
11) J. C. Brial and M. Mousseron-Canet, *Bull. Soc. Chim. Fr.*, **1968**, 3321.

Reactions of 1-Halo-1-nitroso- and 1-Halo-1-nitrocycloalkanes with Triphenylphosphine. A New Synthesis of Lactam[1]

Ikuo SAKAI,[††] Norio KAWABE,[†††] and Masaji OHNO*,[†]

Basic Research Laboratories, Toray Industries, Inc., Tebiro, Kamakura 248

(Received May 16, 1979)

Reactions of 1-halo-1-nitroso- and 1-halo-1-nitrocycloalkanes with triphenylphosphine have been carried out. The Perkov reaction and Beckmann rearrangement occurred successively with the formation of lactams in high yields. The reaction of cycloalkanone oxime with halogen in the presence of triphenylphosphine also gave lactams in one step.

Many works have been carried out on the Perkov reaction since 1955.[2] However, little is known about the reaction of halonitroso- and halonitroalkanes with trivalent organophosphorus compounds. The reactions of 2-chloro-1-nitrosopropane with 1 mol of triethyl phosphite and 2-chloro-2-nitropropane with 2 mol of triethyl phosphite afforded diethyl isopropylideneamino phosphate, but no Beckmann rearrangement product was obtained by its pyrolysis.[3] The reaction of bromonitromethane and triphenylphosphine smoothly forms a phosphonium salt that gives triphenylphosphine oxide and fulminic acid[4] with aqueous alkali at 0 °C. Treatment of 1-bromo-1-nitroalkanes with triphenylphosphine generally gives nitriles.[5] However, no investigation has been carried out on the Perkov type reaction of 1-halo-1-nitroso- and 1-halo-1-nitrocycloalkanes with trivalent organophosphorus compounds.[2]

We wish to report the first successful Beckmann rearrangement of 1-halo-1-nitroso- and 1-halo-1-nitrocycloalkanes (**2** and **6**) with triphenylphosphine.

All 1-halo-1-nitrosocycloalkanes (**2**) were prepared by the reaction of cycloalkanone oximes (**1**) with halogens according to the method of Piloty and Stork.[6] 1-Chloro-1-nitrocyclohexane was prepared by the reaction of sodium salt of nitrocyclohexane and chlorine according to the method of Robertson.[7] 1-Chloro-1-nitrocycloalkanes of 8- and 12-membered rings were prepared by the oxidation of the corresponding compound **2** with nitric acid according to the method of Iffland *et al.*[8]

Reaction of 1-Halo-1-nitrosocycloalkanes. 1-Chloro-1-nitrosocycloalkanes (**2**) were dissolved in nonpolar solvents such as benzene, toluene, ether, or tetrahydrofuran, and treated with 1 mol equivalent of triphenylphosphine at room temperature. The reaction was exothermic, the deep blue color characteristic of the nitroso group disappearing gradually. The reaction temperature reached 40—70 °C. After 30—60 min, the reaction mixture was hydrolyzed, the corresponding lactams (**5**) being obtained in moderate to excellent yields. When the temperature was kept at 0—10 °C, a very hygroscopic precipitate (the IR spectrum shows an absorption at 1655 cm^{-1}, characteristic of C=N group) was formed, which was then heated in dry benzene at 60 °C. The reaction mixtures were worked up in the same way as described above. Lactam (**5**) and triphenylphosphine oxide were obtained in high yields. The results of reactions of compound **2** with triphenylphosphine are summarized in Table 1.

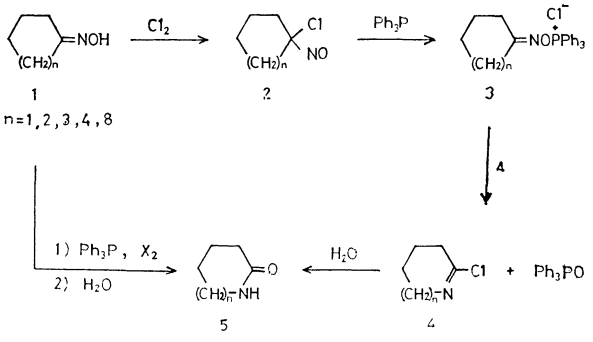

Scheme 1.

In order to simplify the reaction, compounds **1** were directly treated with halogens in the presence of equivalent amount of triphenylphosphine. The corresponding lactams **5** were obtained in good yields in the case of chlorine and bromine, and in fair yields in the case of iodine. The results are also summarized in Table 1.

Reaction of 1-Halo-1-nitrocycloalkanes. On the basis of the reaction of compound **2** with triphenylphosphine, reactions of 1-chloro-1-nitrocycloalkane (**6**) with triphenylphosphine were studied. 1-Chloro-1-nitrocyclohexane was treated with 2 mol of triphenylphosphine in benzene under reflux for 5 h. After the reaction mixture had been treated with 2 M hydrochloric acid, the benzene solution afforded triphenylphosphine oxide in 86% yield and the aqueous solution afforded ε-caprolactam in 55—60% yield. Treatment with 1 mol and 3 mol of triphenylphosphine gave ε-caprolactam in 34 and 77% yields, respectively. It seems reasonable to assume that 2 mol of triphenylphosphine are required to remove two oxygen atoms of the nitro group. The same reaction of 1-chloro-1-nitrocyclooctane and 1-chloro-1-nitrocyclododecane with 2 mol of triphenylphosphine afforded perhydroazonin-2-one in 43% yield and azacyclotridecan-2-one in 32% yield, respectively.

Mechanisms. The reactions of 1-chloro-1-nitroso- and 1-chloro-1-nitrocycloalkanes with triphenylphosphine provide a new synthetic method of lactams. The mechanisms of the new reactions are explained in Schemes 1 and 2.

† Present address: Faculty of Pharmaceutical Sciences. The University of Tokyo, Hongo, Tokyo 113.

†† Present address: Toray Research Center, Inc., Tebiro, Kamakura 248.

††† Present address: Pioneering R & D Labs., Toray Industries, Inc., Sonoyama, Otsu 520.

Table 1. Reactions of 1-halo-1-nitroso- and 1-halo-1-nitrocycloalkanes with triphenylphosphine

Starting material	Reagent	Product[a)]	Yield/%
1-Chloro-1-nitrosocyclopentane	$(C_6H_5)_3P$	δ-Valerolactam	57
1-Chloro-1-nitrosocyclohexane	$(C_6H_5)_3P$	ε-Caprolactam	96
1-Chloro-1-nitrosocycloheptane	$(C_6H_5)_3P$	Perhydroazonin-2-one	76
1-Chloro-1-nitrosocyclooctane	$(C_6H_5)_3P$	Perhydroazonin-2-one	83
1-Chloro-1-nitrosocyclododecane	$(C_6H_5)_3P$	Azacyclotridecan-2-one	78
Cyclopentanone oxime	$(C_6H_5)_3P,Cl_2$	δ-Valerolactam	76
Cyclohexanone oxime	$(C_6H_5)_3P,Cl_2$	ε-Caprolactam	86
Cyclohexanone oxime	$(C_6H_5)_3P,Br_2$	ε-Caprolactam	74
Cyclohexanone oxime	$(C_6H_5)_3P,I_2$	ε-Caprolactam	39
Cyclooctanone oxime	$(C_6H_5)_3P,Br_2$	Perhydroazonin-2-one	74
Cyclooctanone oxime	$(C_6H_5)_3P,I_2$	Perhydroazonin-2-one	60
Cyclododecanone oxime	$(C_6H_5)_3P,Br_2$	Azacyclotridecan-2-one	81
Cyclododecanone oxime	$(C_6H_5)_3P,I_2$	Azacyclotridecan-2-one	48
1-Chloro-1-nitrocyclohexane	$(C_6H_5)_3P$	ε-Caprolactam	77
1-Chloro-1-nitrocyclooctane	$(C_6H_5)_3P$	Perhydroazonin-2-one	42
1-Chloro-1-nitrocyclododecane	$(C_6H_5)_3P$	Azacyclotridecan-2-one	32

a) All lactams were confirmed to be identical with authentic samples prepared by the usual Beckmann rearrangement.

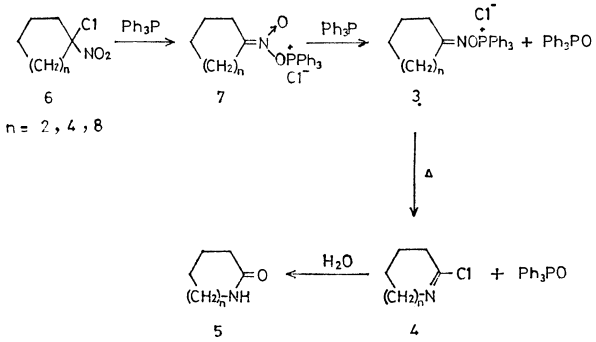

Scheme 2.

In the case of compound **2**, the mechanism includes initial attack of phosphorus on oxygen to give phosphonium salts (**3**) directly followed by thermal rearrangement to chloro imine (**4**) which could not be isolated, and in line with the present understanding of the reactions of α-bromo ketone with triphenylphosphine.[9)]

The reaction of compound **6** with triphenylphosphine differs a great deal from that of compound **2**. The former is endothermic, requiring drastic conditions, but the latter is exothermic and can be carried out smoothly at room temperature. The evidences combined with the fact that no blue coloration takes places during the course of reaction suggest that the reaction mechanism is not by way of compound **2**, but by the formation of Perkov type intermediate (**7**) followed by transformation into a phosphonium salt (**3**) and then the Beckmann rearrangement.

Experimental

Melting points and boiling points are uncorrected. IR spectra were taken on a Hitachi EPI-S2 spectrometer.

1-Chloro-1-nitrosocyclohexane. In a 1-litre three-necked, round-bottomed flask, equipped with a gas inlet tube and a mechanical stirrer, were placed 500 ml of cyclohexane and 56.5 g of cyclohexanone oxime. The flask was covered with a black cloth so as to prevent exposure to sun-light. Chlorine gas was passed into the solution with stirring at room temperature in the course of about 2 h. A solution of a deep blue color was obtained. The excess chlorine remaining in the flask was removed under reduced pressure. The solution was washed successively with water, 1 M sodium hydroxide, and water; dried over anhydrous sodium sulfate. Cyclohexane was removed by distillation, and the residue was distilled under reduced pressure. The yield of **2** was 63.5 g (86%) of dark blue liquid, bp 75 °C/41 mmHg. IR (liquid film): 1570 cm^{-1} (NO).

Of 1-chloro-1-nitrosocycloalkanes prepared by the same procedure, 5-, 6-, 7-, and 8-membered ring compounds are dark blue liquids. Only 1-chloro-1-nitrosocyclododecane is a blue crystalline material which melts at 53—55 °C after recrystallization from ethanol.

Their infrared spectra show an absorption at 1570—1580 cm^{-1}, characteristic of monomeric nitroso group.

Reaction of 1-Chloro-1-nitrosocyclohexane with Triphenylphosphine. In a 300 ml three-necked, round-bottomed flask fitted with a condenser, a dropping funnel, and a mechanical stirrer were placed 10 g (0.068 mol) of 1-chloro-1-nitrosocyclohexane and 100 ml of benzene. A solution of 17.8 g (0.068 mol) of triphenylphosphine in 100 ml of benzene was slowly added from the dropping funnel, with stirring for 30 min at room temperature. The deep blue color of the solution disappeared within 15 min and the temperature rose as high as 70 °C. After 30 min, the reaction mixture was treated with 100 ml of 1 M hydrochloric acid. Triphenylphosphine oxide was obtained in 95% yield (18.5 g) from the organic layer. The aqueous fraction was evaporated to dryness under reduced pressure on a water bath. The residue was neutralized with 2 M sodium hydroxide, and extracted with three 100 ml portions of dichloromethane–ether (1 : 1). The extract was dried with anhydrous sodium sulfate and evaporated to dryness under reduced pressure on a water bath. The residual solid was 7.6 g (99%) of crude ε-caprolactam and was distilled under reduced pressure. The main fraction was distilled at 165—167 °C/33 mmHg. Its infrared spectrum and mp were identical with those of an authentic sample.

Other 1-halo-1-nitrosocycloalkanes were treated with triphenylphosphine in a similar way. Lactams of 6- to 8-membered ring showed a single characteristic absorption (1650—1660 cm^{-1}). Those of 9- and 13-membered ring

showed two characteristic absorptions (1635—1655 cm^{-1} and 1535—1550 cm^{-1}).

Reaction of Cyclohexanone Oxime with Chlorine in the Presence of Triphenylphosphine. In a 300 ml three-necked, round-bottomed flask, fitted with a gas inlet tube, a mechanical stirrer, and a condenser, were placed a solution of 5.7 g (0.05 mol) of cyclohexanone oxime and 13.1 g (0.05 mol) of triphenylphosphine in 100 ml of benzene. Chlorine gas was passed into the solution with stirring at room temperature, the reaction temperature rising as high as 50—60 °C. After the temperature had fallen to room temperature, bubbling of chlorine was stopped. The reaction mixture was worked up in a similar way to that above. ε-Caprolactam was obtained in 86% yield (4.9 g) from the aqueous layer and triphenylphosphine oxide being obtained quantitatively from the benzene layer. A solution of bromine or iodine in benzene could also be used instead of chlorine gas.

1-Chloro-1-nitrocyclohexane. In a 100 ml Erlenmeyer flask provided with a magnetic stirrer was placed 10 g (0.08 mol) of nitrocyclohexane. A solution of 5 g (0.123 mol) of sodium hydroxide in 60 ml of water was added dropwise with stirring at room temperature. After being stirred for 3 h, the reaction mixture became homogeneous. Chlorine gas was then passed into the solution which had been cooled to −5—0 °C in an ice–salt bath. Pale blue oil separated out after 1.5 h. The reaction mixture was extracted three times with 60 ml portions of dichloromethane–ether (1 : 1). The extract was dried with anhydrous sodium sulfate and evaporated to dryness. The oily residue (12.3 g) was distilled under reduced pressure. The principal fraction was 10 g of 1-chloro-1-nitrocyclohexane, a colorless oil boiling at 53.5 °C/1 mmHg.

1-Chloro-1-nitrocyclododecane. In a 200 ml separatory funnel was placed a solution of 5.00 g (0.022 mol) of 1-chloro-1-nitrosocyclododecane in 50 ml of cyclohexane, and 12.5 ml of concentrated nitric acid was added. The funnel was then shaken until the blue color of the solution disappeared. The reaction mixture was washed successively with 50 ml of water, 50 ml of 5% aqueous sodium hydroxide, and 50 ml of water. After being dried over anhydrous sodium sulfate, the cyclohexane was removed under atmospheric pressure, and 5.44 g of the oily residue was distilled under reduced pressure. The product of 1-chloro-1-nitrocyclododecane was 3.62 g (68%) of colorless crystal boiling at 118—119 °C/0.2 mmHg and melting at 49.5—50.5 °C after recrystallization from acetone. IR (KBr): 1556, 1348 cm^{-1} (NO_2). 1-Chloro-1-nitrocyclooctane was also prepared in a similar way. The product was 5.52 g (44.2%) of colorless liquid boiling at 74 °C/0.6 mmHg. IR (liquid film): 1563, 1333 cm^{-1} (NO_2).

Reaction of 1-Chloro-1-nitrocyclohexane with Triphenylphosphine. In a 100 ml flask fitted with a reflux condenser was placed a solution of 4.8 g (0.0294 mol) of 1-chloro-1-nitrocyclohexane in 40 ml of benzene and a solution of 16.2 g (0.0618 mol) of triphenylphosphine in 20 ml of benzene. The mixture was refluxed for 4 h on a steam bath. The reddish reaction mixture was washed three times with 180 ml portions of 2 M hydrochloric acid. The yellow organic layer was dried with anhydrous sodium sulfate and evaporated. Triphenylphosphine oxide was obtained in 86% yield (14.0 g). The aqueous layer was evaporated. The oily residue was made basic to litmus with 2 M sodium hydroxide and was extracted with dichloromethane–ether (1 : 1). After the extract had been dried over anhydrous sodium sulfate, the dichloromethane and ether were removed by distillation. ε-Caprolactam was obtained in 58% yield (1.93 g).

Reactions of 1-chloro-1-nitrocyclooctane and 1-chloro-1-nitrocyclododecane with triphenylphosphine were also carried out in a similar way.

References

1) Preliminary reports of this work appeared in M. Ohno and I. Sakai, *Tetrahedron Lett.*, **1965**, 4541, and M. Ohno and N. Kawabe, *ibid.*, **1966**, 3935.
2) F. W. Lichtenthaler, *Chem. Rev.*, **61**, 607 (1961).
3) J. F. Allen, *J. Am. Chem. Soc.*, **79**, 3071 (1957).
4) S. Trippett and D. M. Walker, *J. Chem. Soc.*, **1959**, 3874.
5) S. Trippett and D. M. Walker, *J. Chem. Soc.*, **1960**, 2976.
6) O. Piloty and A. Stork, *Ber.*, **35**, 3093 (1902).
7) J. A. Robertson, *J. Org. Chem.*, **13**, 395 (1948).
8) D. C. Iffland, G. X. Criner, M. Koral, F. J. Lotspecich, Z. B. Papanastassiou, and S. M. White Jr., *J. Am. Chem. Soc.*, **75**, 4044 (1953).
9) I. J. Borowitz and R. Virkhaus, *J. Am. Chem. Soc.*, **85**, 2183 (1963).

A Kinetic Study of the Reaction of Arylthiotrimethylsilane with Carboxylic Acid Giving Acyloxytrimethylsilane and Arenethiol

Seizi KOZUKA* and Takuro KITAMURA

Department of Applied Chemistry, Faculty of Engineering, Osaka City University, Sugimotocho, Sumiyoshi, Osaka 558

(Received May 18, 1979)

The mechanism of the reactions of arylthiotrimethylsilanes with carboxylic acids has been studied kinetically. The reaction was found to obey a second-order kinetic equation. The substituent effects of the aryl moiety ($\rho=-2.4$) and of the silicon atom, the hydrogen-deuterium kinetic isotope effect of the acid ($k_H/k_D=3$) were observed. A mechanism involving the 5-coordination of the silicon atom prior to the rate-determining protonation of the sulfur atom has been suggested for the reaction. A remarkable base catalysis was observed. The formation of the coordinated intermediate has been suggested to be the slow step in the presence of a bese.

The kinetic behavior of silicon–sulfur bond cleavage has scarcely been studied at all. Only one kinetic study, to the best of our knowledge, has been reported dealing with the hydrolysis of the Si–S bond in aqueous dioxane.[1] On the other hand, we have ourselves

$$R_3Si\text{-}SAr + H^+ \rightleftharpoons R_3Si\text{-}S^+(H)Ar$$

$$R_3Si\text{-}S^+(H)Ar + nH_2O \xrightarrow{\text{slow}} R_3Si\text{-}OH + ArSH + H^+ + (n-1)H_2O$$

reported a kinetic aspects of the acyloxy-exchange reaction of acyloxysilane with carboxylic acid, which involves Si–O bond fission.[2] In the mean time, an analogous reaction of carboxylic acid with thiosilane

$$RCOO\text{-}SiR'_3 + R''COOH \rightleftharpoons RCOO\text{-}Si^-(R'_3)\text{-}O\overset{+OH}{\overset{\|}{C}}R'' \xrightarrow{\text{slow}} RCO\text{-}Si^-(R'_3)\text{-}OCOR'' \rightleftharpoons RCOOH + R'_3Si\text{-}OCOR''$$

has also been known to give the acyloxysilane in a Si–S bond cleavage reaction.[3] We have now extended our kinetic study to this reaction: *i.e.*, the reaction of

$$RCOOH + (Me_3Si)_2S \longrightarrow H_2S + 2RCOO\text{-}SiMe_3$$

$$RCOOH + EtS\text{-}SiMe_3 \longrightarrow EtSH + RCOO\text{-}SiMe_3$$

arylthiotrimethylsilane with carboxylic acid in order to obtain more knowledge about the mechanism of the Si–S bond fission.

Results and Discussion

The reaction of arylthiosilane with carboxylic acid in chloroform was found to proceed smoothly at room temperature to give arenethiol and acyloxytrimethylsilane in high yields. The product was isolated and characterized.

$$Me_3Si\text{-}SAr + RCOOH \longrightarrow Me_3Si\text{-}OCOR + ArSH$$

The reverse reaction, *i.e.*, that giving the thiosilane from the acyloxysilane and arenethiol, was not found to proceed at all under the conditions used. Small amounts of hexamethyldisiloxane (8—10%) and trimethylsilanol (2%) were detected in the reaction mixture by NMR analysis, as in the acyloxy exchange reaction,[2] but the amounts were found to be unchanged during the reaction. This suggests that these side products are independent of the reaction of thiosilane with acid. They may be formed by the interaction of the thiosilane with moisture, giving silanol, while the subsequent dehydration of the silanol results in the formation of the disiloxane.[4]

The rate of the reaction of thiosilane with two equivalents of carboxylic acid was measured by monitoring the decrease in the ^1H NMR trimethyl signal of the starting thiosilane (δ 0.25—0.27 ppm) and the increase in that of acyloxysilane (δ 0.32—0.40 ppm). A good second-order rate constant was obtained with satisfactory reproducibility. The rate of the reaction with acetic acid could not be obtained by this kinetic procedure because the trimethyl signal of acetoxytrimethylsilane (δ *ca.* 0.3 ppm) appeared rather close to that of the starting material, therefore, the amounts of the two components could not be measured with a high accuracy. Accordingly, chloro-, dichloro-, and trichloroacetic acids were used in the present study. The results are given in Table 1. Good Hammett correlations were found for the reactions with each carboxylic acid with apparently negative ρ value ($\rho_{(\sigma)}=-2.4$, with $CHCl_2COOH$). The value thus obtained appeared quite similar in magnitude to those of the dissociation constants of arenethiols with the opposite sign ($\rho=+2.24$).[5] This would suggest that the present reaction involves the formation of a sulfonium ion.

The effect of the acid strength of the attacking carboxylic acids was observed on the rate of the reaction. A plot of the results given in Table 1 against the σ^* constants gave a straight line with a ρ^* value of $+1.34$ ($X=OCH_3$; $\gamma=0.968$; similar ρ^* values were obtained

Table 1. Rate constants for the reactions of p-X-C_6H_4-S-$SiMe_3$ (0.60 mol/dm^3) with RCOOH (1.20 mol/dm^3) in $CHCl_3$ at 34 °C[a]

	k_2/dm^3 mol^{-1} s^{-1}		
	R in RCOOH		
X	CH_2Cl ($\times 10^4$)	$CHCl_2$ ($\times 10^3$)	CCl_3 ($\times 10^2$)
OCH_3	2.58±0.07	1.47±0.14	4.70±0.80
CH_3	1.13±0.05	0.64±0.01	1.65±0.03
H	0.50±0.02	0.30±0.01	0.64±0.03
Cl	0.15±0.01	0.10±0.01	0.30±0.03
		$\rho_{(\sigma)}=-2.4$	
		$\gamma=0.993$	

a) NMR probe temperature, Hitachi-Perkin Elmer R-20 spectromerer.

Table 2. Rate constants and activation parameters for the reaction of Me_3SiSPh (0.60 mol/dm³) with $CHCl_2COOH$ (1.20 mol/dm³) in $CHCl_3$

Temp/°C[a]	$k_2 \times 10^4$/dm³ mol⁻¹ s⁻¹	ΔH^* kcal/mol	ΔS^* e.u.
28	2.89±0.21		
38	3.89±0.16		
45	6.99±0.27	8.8	−45.6
56	10.9 ±1.1		

a) JEOL PS-100 VT probe; the temperatures were calibrated by measuring the chemical shift of 1,2-ethanediol at the temperatures.

Table 3. Rates of the reactions of $Me_2RSiSPh$ (0.60 mol/dm³) with $CHCl_2COOH$ and $CHCl_2COOD$ (1.20 mol/dm³) in $CHCl_3$ at 34 °C[a]

R	$k_2 \times 10^4$/dm³ mol⁻¹ s⁻¹	k_{rel}	k_{rel}, $Me_2RSiOAc$[b]
CH_3	2.96±0.09 (H)	3.08	2.66
CH_3	1.08±0.05 (D)		(k_H/k_D=1.6)
	k_H/k_D=2.7		
$PhCH_2$	1.15±0.09 (H)	1.20	1.11
			(k_H/k_D=1.7)
Ph	0.96±0.04 (H)	1.00	1.00
Ph	0.29±0.01 (D)		
	k_H/k_D=3.3		

a) NMR probe temperature (Hitachi-Perkin Elmer, R-20). b) Rate of $Me_2RSiOAc + CHCl_2COOH \rightarrow Me_2RSiOCOCHCl_2 + AcOH$.[2]

for each substituent, X). The ρ^* value appeared quite similar to that observed for the acyloxy exchange reaction of acyloxytrimethylsilane with various carboxylic acids.[2]

In order to obtain the activation parameters, the rate of the reaction of trimethyl(phenylthio)silane with dichloroacetic acid in chloroform was measured at various temperatures. The results are shown in Table 2. An Arrehnius plot of the data gave 8.8 kcal/mol (4.184 J) and −45.6 e.u. for the enthalpy and entropy values respectively. Here again, the values appeared to be quite similar to those observed for the acyloxy exchange reaction.[2] The large negative entropy value suggests a tight transition state for the reaction, but it does not suggest a 4-centered reaction, since a remarkably negative ρ value was observed in the present study, as has been mentioned above. The tight transition state may be explained in terms of an ionic reaction which is forced to proceed in a nonpolar solvent, as was suggested for the reaction of thiostannane with haloalkane, in which a large negative entropy value was observed when the reaction was carried out in a nonpolar solvent, while the value fell to a normal magnitude in a polar solvent.[6]

The steric and electronic effects of the silicon substituent were examined by carrying out the reaction of dichloroacetic acid with alkyl (or aryl)dimethyl(phenylthio)silanes. The results obtained can be explained in terms of the steric effect rather than the electronic effect of the substituent. The hydrogen-deuterium kinetic isotope effect was also examined,

Table 4. Effect of base on the rate of the reaction of Me_3SiSPh (0.60 mol/dm) with $CHCl_2COOH$ (1.20 mol/dm³) in $CHCl_3$ at 34 °C[a]

Base	Mole ratio Base/Sulfide	k_2 dm³ mol⁻¹ s⁻¹	k_{rel}
None	0	$3.0\pm0.1\times10^{-4}$	1.0
Et_3N	0.1	$1.3\pm0.1\times10^{-2}$	43
C_5H_5N	0.1	$7.6\pm0.8\times10^{-3}$	25

a) NMR probe temperature (Hitachi-Perkin Elmer R-20).

Table 5. Rates of the reactions of p-X-$C_6H_4SSiMe_3$ (0.31 mol/dm³) with $CHCl_2COOH$ (0.65 mol/dm³) in $CHCl_3$ at 34 °C[a] in the presence of C_5H_5N (0.03 mol/dm³)

X	$k_2 \times 10^3$/dm³ mol⁻¹ s⁻¹	
OCH_3	2.05±0.13	
CH_3	2.53±0.11	
H	2.86±0.27	$\rho_{(\sigma)}$=+0.74
Cl	4.61±0.15	γ=0.983

a) NMR probe temperature (Hitachi-Perkin Elmer R-20).

and a positive isotope effect was observed. The results are summarized in Table 3. The positive kinetic isotope effect and the negative ρ value suggest a rate-determining protonation of the sulfur atom. In the meantime, the steric effect of the bulky substituent on the silicon atom appeared almost the same as those observed in the acyloxy exchange reactions of the corresponding acyloxysilanes, as is shown in Table 3. These results, together with the similarity of the ρ^* value, the activation parameters, and the positive kinetic isotope effect to those of the acyloxy exchange reaction,[2] strongly suggest that these two reactions are similar in their mechanisms; *i.e.*, the reaction involves the 5-coordination of the silicon atom prior to the rate-determining proton transfer. Thus, the most plausible mechanism for the reaction can be formulated as follows. The first step of the reaction

$$ArS\text{-}SiMe_3 + RCOOH \rightleftharpoons \left[ArS\text{-}Si^{-}(Me_3)\text{-}O\text{-}\overset{+OH}{\overset{\|}{C}}R\right] \xrightarrow{\text{slow}} \left[ArS^{+}(H)\text{-}Si^{-}(Me_3)\text{-}O\text{-}\overset{O}{\overset{\|}{C}}R\right] \longrightarrow ArSH + Me_3Si\text{-}O\text{-}\overset{O}{\overset{\|}{C}}R$$

would be the formation of a 5-coordinated intermediate by a reversible reaction. Thus, the bulky substituent on the silicon atom disfavors the formation of the intermediate. The second step is the rate-determining proton migration from the carbonyl oxygen to the sulfur atom. An electron-withdrawing substituent on the aryl moiety would destabilize the second intermediate of the sulfonium ion, resulting in a deceleration of the reaction and bringing forth a negative ρ value. The sulfonium intermediate would rapidly col-

lapse into the products.

According to the mechanism, one can expect the base catalysis of the reaction, since the carboxylate ion would be a better reagent than the conjugate acid for the formation of a 5-coordinated silicon atom. Furthermore, an opposite substituent effect of the aryl ring, that is, a positive ρ value, would be expected for the base-catalyzed reaction because of the lack of the protonation step. The rate of the reaction was found to be markedly accelerated by the addition of a base, as is shown in Table 4. The rates of the reactions of arylthiotrimethylsilanes with dichloroacetic acid in the presence of pyridine as the base are given in Table 5. As expected, a small but clearly positive substituent effect ($\rho = +0.74$) was observed. The reaction scheme in the presence of a base is formulated below:

$$RCOOH + :B \rightleftharpoons RCOO^- + BH^+$$

$$RCOO^- + Me_3Si\text{-}SAr \rightleftharpoons RCOO\text{-}Si^-(Me_3)\text{-}SAr$$

$$RCOO\text{-}Si^-(Me_3)\text{-}SAr \longrightarrow RCOO\text{-}SiMe_3 + ArS^-$$

The substituent on the aryl ring affects the stability of the coordinated silicon atom with a formal anionic character through the sulfur linkage. As a result, a positive ρ value would result in a moderate magnitude.

Experimental

Materials. The arylthiotrimethylsilanes were prepared from chlorotrimethylsilane and lead arenethiolates.[7] Benzyl (or phenyl)dimethyl(phenylthio)silane was prepared similarly from the corresponding chlorodimethylsilane; bp 142—146°C/1 mmHg (133.332 Pa), NMR ($CDCl_3$) δ(ppm), 0.46 s(6H), 2.36 s(2H), and 7.00—7.23 m(10H). The carboxylic acids were purified by distillation. Dichloroacetic acid-*d* was obtained by the hydrolysis of the corresponding anhydride with D_2O. The deuterium content was measured by the integration of the NMR signals (90%).

Product Analysis. Trimethyl(phenylthio)silane (48 mg, 0.26 mmol) and dichloroacetic acid (70 mg, 0.56 mmol) were dissolved in chloroform-*d* (0.37 cm^3), and then the mixture was allowed to stand for 5 h at room temperature. Trimethyl(dichloroacetoxy)silane (75%), benzenethiol(81%), haxamethyldisiloxane ($\simeq$10%), and trimethylsilanol (2%) wew detected in the reaction mixture by NMR analysis. No other compound was detected. The assignmemt of these signals was performed by comparing them to those of the authentic samples. The latter two compounds were found in almost the same amounts even at the beginning of the reaction and in the absence of the acid. Thus, these two compounds were concluded to be formed by the hydrolysis of the thiosilane during work-up. Trimethyl(dichloroacetoxy)silane was isolated by GLC separation (SE-30, 2 m, 150°C), and the structure was characterized by comparison with an authentic sample.[8]

Kinetics. Trimethyl(phenylthio)silane (48 mg, 50 mm^3, 0.26 mmol) was dissolved in chloroform (0.37 cm^3), after which the solution, in a sample tube was placed in a NMR probe. Dichloroacetic acid (70 mg, 46 mm^3, 0.56 mmol) was then added to the solution. Immediately after the addition, trimethyl signals of the starting thiosilane (δ 0.25 ppm) and the product (δ 0.36 ppm) were recorded repeatedly at short time intervals. Twenty to thirty measurements were done for each run until the completed conversion exceeded a half. After the reaction, the total volume of the solution was measured, and the concentrations of each component were calculated. The second-order rate constant, k, was obtained by means of the following equation, where a and b are the initial concentrations of the thiosilane and the acid respectively, and where x is the amount of the acetoxysilane formed at time t. A good reproducibility was obtained ($\pm$10% error established by a duplicate run). The kinetics of the base-catalyzed reactions were done by using half concentrations of the starting materials.

$$kt = \frac{l}{b-a} \ln \frac{a(b-x)}{b(a-x)}$$

References

1) R. Danieli and A. Ricci, *J. Chem. Soc., Peckin Trans. 2*, **1972**, 1471.
2) S. Kozuka, T. Kitamura, N. Kobayashi, and K. Ogino, *Bull. Chem. Soc. Jpn.*, **52**, 1950 (1979).
3) E. W. Abel, *J. Chem. Soc.*, **1961**, 4933.
4) W. Patnode and D. F. Wilcock, *J. Am. Chem Soc.*, **68**, 358 (1964).
5) H. H. Jaffe, *Chem. Ber.*, **53**, 191 (1953).
6) S. Kozuka and S. Ohya, *Bull. Chem. Soc. Jpn.*, **51**, 2651 (1978).
7) E. W. Abel, *J. Chem. Soc.*, **1960**, 4406.
8) W. McFarlane and J. H. Seaby, *J. Chem. Soc., Perkin Trans. 2*, **1972**, 1561.

1,3-Dipolar Cycloadditions to 2-Phenyl-1-azaspiro[2.2]pent-1-ene[1)]

Otohiko TSUGE,* Hiroyuki WATANABE, and Yōko KIRYU

Research Institute of Industrial Science, Kyushu University 86, *Hakozaki, Higashi-ku, Fukuoka 812*

(Received May 19, 1979)

Benzonitrilium-*p*-nitrobenzylide undergoes 1,3-dipolar cycloaddition to highly strained 2-phenyl-1-azaspiro-[2.2]pent-1-ene, yielding the cycloadduct which is thermally converted to the dihydrobenzo[*f*]quinazoline and pyrimidine. In the reaction with α,*N*-diarylnitrone, the spiroazapentene gives 1-(benzylideneamino)-1-(*N*-phenylbenzamido)cyclopropane arising from the initial cycloadduct.

It seemed of interest to investigate the cycloadditions of highly strained 2-phenyl-1-azaspiro[2.2]pent-1-ene (**1**)[2)] having an 1-azirine moiety, because it is known that 1-azirines are useful reagents for the synthesis of a large number of heterocyclic systems.[3)] However, no studies on the cycloadditions to **1** have so far been

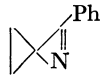

1

reported. We now wish to report on the reactions of **1** with benzonitrilium-*p*-nitrobenzylide (**2**) and α,*N*-diarylnitrones (**8**).

Reaction with Benzonitrilium-p-nitrobenzylide. Schmid and his co-workers[4)] reported that benzonitrilium-*p*-nitrobenzylide (**2**) undergoes 1,3-dipolar cycloaddition to 2-phenyl- and 2,3-diphenyl-1-azirines, yielding the bicyclic adducts. However, 3,3-dimethyl-2-phenyl-1-azirine does not react with **2**. Although **1** is a 3,3-disubstituted 2-phenyl-1-azirine, **1** might react with **2** due to its highly strained structure.

When **1** was allowed to react with 1 equivalent of **2** generated *in situ* from *N*-*p*-nitrobenzylbenzimidoyl chloride and triethylamine in benzene under nitrogen at room temperature, the 1:1 cycloadduct **3** was obtained as the major product, along with by-products **4**, **5**, and **6** (Scheme 1). Structural elucidation of these products, **3**—**6**, was accomplished on the basis of their spectral data and chemical correlations.

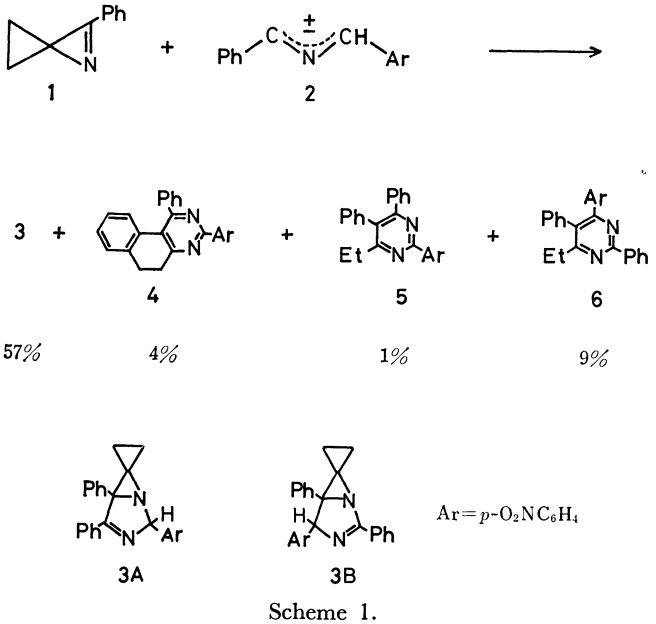

Scheme 1.

Although ^{1}H- and ^{13}C-NMR spectra of **3** (see Scheme 2 and Experimental Section) do not permit a clear assignment as to which structures, 2′-(*p*-nitrophenyl)-4′,5′-diphenylspiro[cyclopropane-1,6′-[1,3]diazabicyclo-[3.1.0]hex-3′-ene] (**3A**) or 4′-(*p*-nitrophenyl)-2′,5′-diphenylspiro[cyclopropane-1,6′-[1,3]diazabicyclo[3.1.0]-hex-2′-ene] (**3B**), would be more reasonable for **3**, **3** was assigned to be **3A** on the basis of results of chemical conversions which will be described below.

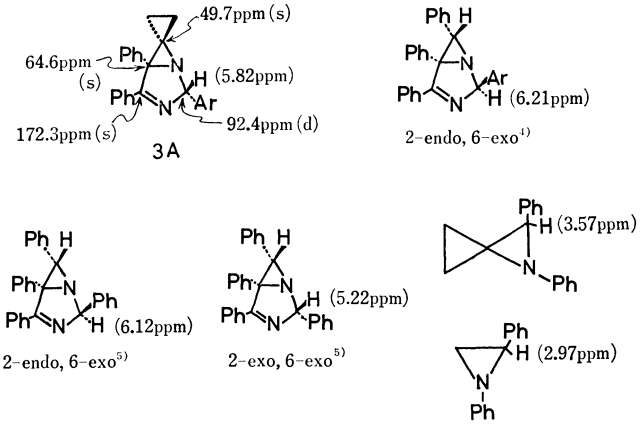

Scheme 2.

The stereochemistry of **3A** is hereinafter described. As illustrated in Scheme 2, the value of chemical shift of benzylic methine proton in **3A** is situated between those of *endo*- and *exo*-benzylic methine protons in other reported 1,3-diazabicyclo[3.1.0]hex-3-enes. On the other hand, the benzylic methine proton of 1,2-diphenyl-1-azaspiro[2.2]pentane[6)] appears at a lower field than that of 1,2-diphenylaziridine,[7)] because of anisotropy effect of cyclopropyl ring of the azaspiropentane. From a consideration of anisotropy effect of cyclopropyl ring in **3A**, it seems most reasonable to conclude that **3A** is the 2-*exo* structure.

Hydrolysis of **3** with 10% hydrochloric acid afforded 3,4-dihydro-5,6-diphenyl-2-pyridone (**7**) and *p*-nitrobenzaldehyde in 26 and 20% yields respectively. The structure of **7** was confirmed by the identification with an authentic sample prepared by a modification of the reported method.[8)] This result strongly supports that **3** is **3A** but not **3B**.[9)] The pathway for the formation of **7** from **3A** is illustrated in Scheme 3. The compound **3A** undergoes hydrolysis with concurrent ring expansions to form **C** through **A** and then **B**. This is followed by further hydrolysis of the cyclic amidine **C** to yield the benzaldehyde and amide **D**, and subsequent cyclization of **D** with dehydration leads to the formation of **7**.

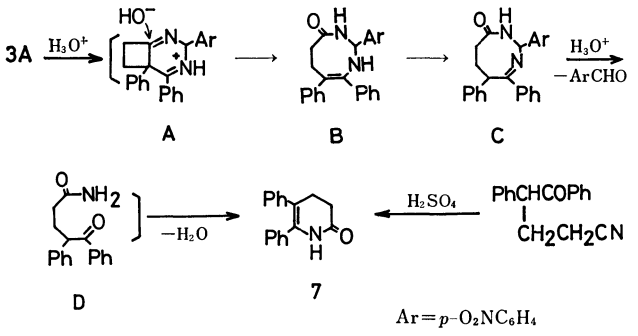

Scheme 3.

Contrary to the formation of pyridazine compound from the bicyclic adduct of **2** to 2,3-diphenyl-1-azirine,[4] thermolysis of **3A** in boiling xylene afforded 5,6-dihydro-3-*p*-nitrophenyl-1-phenylbenzo[*f*]quinazoline (**4**) and 6-ethyl-2-*p*-nitrophenyl-4,5-diphenylpyrimidine (**5**) in 64 and 8% yields respectively. It is thus evident that the products **4** and **5** of the reaction are derived from **3A**.

The product **6** which is an isomer of **5** was deduced to be 6-ethyl-4-*p*-nitrophenyl-2,5-diphenylpyrimidine.

The pathways for the formation of **4**, **5**, and **6** are illustrated in Scheme 4. The initial adduct **3A** is subjected to ring expansion to form **E**. This is followed by homolytic rupture of the cyclobutane ring of **E** to yield biradical **F**, which can lead to **4** through **G** and to **5**. The formation of **6** can be also interpreted as arising from the initial reversed cycloadduct **3B** through biradical **H**. It is thought that **3B** whose structure is a cyclic amidine could not be isolated owing to its lability.

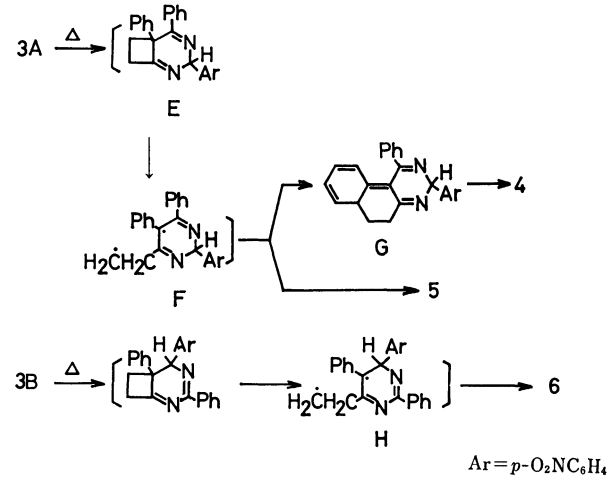

Scheme 4.

Reaction with α,N-Diarylnitrones. Although nitrones undergo 1,3-dipolar cycloaddition to C=N bonds of heterocumulenes such as isocyanates, isothiocyanates, and carbodiimides,[10] no studies on the cycloaddition of nitrones to simple C=N bonds have been reported. As mentioned above, the C=N bond of **1** exhibited high reactivity toward **2**. Thus our attention was directed to the reaction of **1** with α,*N*-diarylnitrones (**8**).

After **1** was allowed to react with 1 equivalent of α,*N*-diphenylnitrone (**8a**) in boiling benzene, the reaction mixture was chromatographed on silica gel to give 1-amino-1-(*N*-phenylbenzamido)cyclopropane (**10**), benzaldehyde, and benzanilide. A similar reaction of **1** with α-(*p*-nitrophenyl)-*N*-phenylnitrone (**8b**) afforded 1 : 1 adduct, 1-(*p*-nitrobenzylideneamino)-1-(*N*-phenylbenzamido)cyclopropane (**9b**), *p*-nitrobenzaldehyde, and benzanilide (Scheme 5). Structural elucidation of **9b** and **10** was accomplished on the basis of spectral data as well as of chemical conversions. Hydrolysis of **9b** gave **10** and *p*-nitrobenzaldehyde, while **10** reacted with the benzaldehyde to give **9b**.

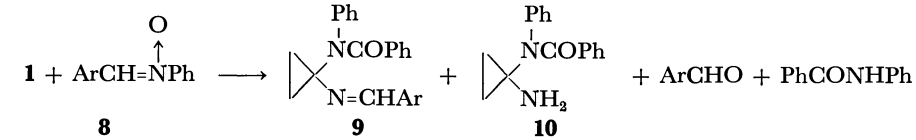

a : Ar=Ph	—	51%	14%	39%
b : Ar=*p*-$O_2NC_6H_4$	16%	—	33%	23%

9b ⇌ **10** + ArCHO

Scheme 5.

The pathways for the formation of products are assumed as depicted in Scheme 6. The nitrone **8** undergoes 1,3-dipolar cycloaddition to **1**, yielding labile cycloadduct **I**. The formation of **9** can be understood as proceeding through the oxaziridine **J** which is arising from **I**, since it is known that *C,N*-diaryloxaziridines are readily isomerized into the amides.[11]

As described above, hydrolysis of **9b** afforded **10** and the benzaldehyde, but not benzanilide. This fact suggests that benzanilide obtained from the reaction is derived from hydrolysis of a compound other than **9**. Although mechanistic considerations are still speculative, a possible pathway is also shown in Scheme 6. The rearrangement of **I** to the diaziridine **K**,

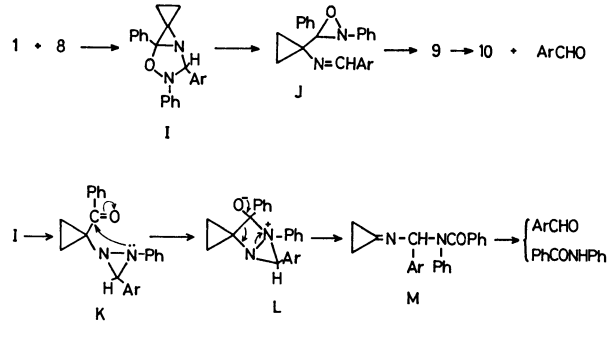

Scheme 6.

followed by a nucleophilic attack of the nitrogen atom on the carbonyl carbon atom yields the tricyclic betaine **L**. This is followed by ring cleavage to give **M**, which on hydrolysis gives the benzaldehyde and benzanilide. The process (**K**→**L**→**M**) is similar to that proposed for the formation of *N,N*-dibenzoylaniline from the photooxygenation of 1,2-diphenyl-2-(phenylimino)-1-ethanone.[12,13]

Experimental

All melting points are uncorrected. IR, NMR, and mass spectra were obtained on a JASCO IRA-1 spectrometer, Hitachi R-40, JEOL SX-100 spectrometers, and a Hitachi RMS-4 spectrometer, respectively.

Materials. Azaspiropentene **1**,[2] *N*-*p*-nitrobenzylbenzimidoyl chloride,[14] and α,*N*-diarylnitrones **8a**,[15] **8b**[16] were prepared by the reported methods respectively.

*Reaction of Azaspiropentene **1** with Benzonitrilium*-p-*nitrobenzylide (**2**).* To a vigorously stirred solution of **1** (0.44 g, 3 mmol) and *N*-*p*-nitrobenzylbenzimidoyl chloride (0.85 g, 3 mmol) in benzene (30 ml) was dropwise added a solution of NEt_3 (1.75 g, 17.3 mmol) in benzene (10 ml) at 0 °C over a period of 1 h under nitrogen. The reaction mixture was stirred at room temperature for 24 h, and then filtered to remove formed triethylammonium chloride. The filtrate was concentrated *in vacuo*, and the residue was chromatographed on silica gel (Wako gel C-300) using benzene as the eluent.

The first fraction gave crystals which were recrystallized from benzene to give 53 mg (4%) of 5,6-dihydro-3-*p*-nitrophenyl-1-phenylbenzo[*f*]quinazoline (**4**), mp 225—226 °C, as yellow needles. ^{1}H-NMR ($CDCl_3$) δ 3.09 (s, 4H), 6.8—7.8 (m, 9H), 8.28 8.73 (each d, 2H, *J*=9 Hz). ^{1}H-NMR (C_6D_6) δ 2.4—3.0 (m, 4H), 6.6—7.4 (m, 7H), 7.6—7.8 (m, 2H), 8.08, 8.67 (each d, 2H, *J*=9 Hz). ^{13}C-NMR ($CDCl_3$) δ 28.3 (t), 32.0 (t), 123.5, 125.1, 126.1, 127.9, 128.4, 128.6, 128.9, 129.5, 129.6, 130.5, 138.3, 138.9, 143.3, 149.0, 159.2, 162.1, 169.3. MS *m/e* 379 (M^+, base peak). Found: C, 76.05; H, 4.43; N, 10.92%. Calcd for $C_{24}H_{17}N_3O_2$: C, 75.97; H, 4.52; N, 11.08%.

The second fraction afforded crystals which were recrystallized from hexane to give 108 mg (9%) of 6-ethyl-4-*p*-nitrophenyl-2,5-diphenylpyrimidine (**6**), mp 134—135 °C, as colorless needles. ^{1}H-NMR ($CDCl_3$) δ 1.28 (t, 3H, *J*=7 Hz), 2.75 (q, 2H, *J*=7 Hz), 6.9—7.7 (m, 10H), 8.03 (d, 2H, *J*=9 Hz), 8.45—8.80 (m, 2H). ^{13}C-NMR ($CDCl_3$) δ 12.7, 28.9, 122.8, 128.0, 128.5, 128.8, 129.9, 130.8, 135.7, 137.5, 145.0, 147.5, 161.1, 162.8, 171.0. MS *m/e* 381 (M^+), 380 (base peak). Found: C, 75.50; H, 4.85; N, 10.89%. Calcd for $C_{24}H_{19}N_3O_2$: C, 75.57; H, 5.02; N, 11.02%.

The third fraction gave 12.3 mg (1%) of 6-ethyl-2-*p*-nitrophenyl-4,5-diphenylpyrimidine (**5**), mp 194—195 °C, as colorless needles (from EtOH). ^{1}H-NMR ($CDCl_3$) δ 1.28 (t, 3H, *J*=7.6 Hz), 2.76 (q, 2H, *J*=7.6 Hz), 6.6—7.5 (m, 10H), 8.27, 8.77 (each d, 2H, *J*=9 Hz). ^{13}C-NMR ($CDCl_3$) δ 12.7, 28.9, 123.5, 127.8, 128.5, 128.8, 129.0, 129.8, 130.0, 130.9, 136.2, 138.2, 143.9, 149.1, 160.4, 163.8, 170.8. MS *m/e* 381 (M^+), 380 (base peak). Found: C, 75.42; H, 5.05; N, 11.13%. Calcd for $C_{24}H_{19}N_3O_2$: C, 75.57; H, 5.02; N, 11.02%.

The fourth fraction gave crystals which were recrystallized from ether to give 2′-(*p*-nitrophenyl)-4′,5′-diphenylspiro-[cyclopropane-],6′-[1,3]diazabicyclo[3.1.0]hex-3′-ene] (**3A**), mp 167—169 °C, as colorless prisms. IR (KBr) 1602 (C=N), 1575, 1339 cm^{-1}. ^{1}H-NMR ($CDCl_3$) δ 0.8—1.2 (m, 2H), 1.4—2.1 (m, 2H), 5.82 (s, 1H), 7.2—7.5 (m, 8H), 7.5—7.9 (m, 4H), 8.22 (d, 2H, *J*=9 Hz). ^{13}C-NMR ($CDCl_3$) δ 0.6 (t), 9.4 (t), 49.7 (s), 64.6 (s), 92.4 (d), 123.7, 128.0, 128.4, 128.5, 129.0, 131.1, 131.9, 135.1, 147.5, 148.0, 172.3. MS *m/e* 381 (M^+). Found: C, 75.60; H, 4.98; N, 11.08%. Calcd for $C_{24}H_{19}N_3O_2$: C, 75.57; H, 5.02; N, 11.02%.

*Hydrolysis of 1 : 1 Adduct **3A**.* A suspension of **3A** (110 mg) in 10% HCl (10 ml) was stirred at room temperature for 30 h. Filtration gave crystals which were recrystallized from EtOH to give 18.2 mg (26%) of 3,4-dihydro-5,6-diphenyl-2-pyridone (**7**), mp 220—221 °C, as colorless needles. This compound was identical with an authentic sample prepared by the method described below.

The filtrate was concentrated *in vacuo*, and the residue was chromatographed on silica gel using benzene as the eluent, giving 9 mg (20%) of *p*-nitrobenzaldehyde.

*3,4-Dihydro-5,6-diphenyl-2-pyridone (**7**).* A solution of deoxybenzoin (3.0 g) in THF (50 ml) was treated with NaH (0.8 g, 50% suspension in oil) at 60—70 °C for 1 h, and then a solution of 3-chloropropionitrile (1.4 g) in THF (10 ml) was added to the resultant solution at 0 °C. The reaction mixture was stirred at room temperature for 2 h, and refluxed for 2 h, and then poured into water to give solid (1.9 g). After a solution of the solid (1.9 g) in concd H_2SO_4 (50 ml) was stirred at room temperature for 12 h, the solution was poured into water to give crystals which were recrystallized from EtOH to afford 1.95 g (51%) of **7**, mp 220—221 °C (lit,[8] mp 218—219 °C). Found: C, 81.79; H, 5.83; N, 5.72%. Calcd for $C_{17}H_{15}NO$: C, 81.90; H, 6.06; N, 5.62%.

*Thermolysis of 1 : 1 Adduct **3A**.* A solution of **3A** (100 mg) in xylene (4 ml) was refluxed for 15 h. The solvent was evaporated *in vacuo* to leave the residue which was chromatographed on silica gel using benzene as the eluent to give 64 mg (64%) of **4** and 8 mg (6%) of **5**.

*Reaction of Azaspiropentene **1** with α,*N*-Diarylnitrones (**8**).* A solution of **1** (326 mg, 2.28 mmol) and α,*N*-diphenylnitrone (**8a**) (450 mg, 2.28 mmol) in benzene (10 ml) was refluxed for 3 h under nitrogen. The reaction mixture was concentrated *in vacuo*, and the residue was chromatographed on silica gel using $CHCl_3$ as the eluent. From the first and second fractions, 40 mg (14%) of benzaldehyde and 78 mg (39%) of benzanilide were obtained respectively. The third fraction gave 215 mg (51%) of 1-amino-1-(*N*-phenylbenzamido)cyclopropane (**10**) as colorless oil. IR (neat) 3400, 3320 (NH), 1650 cm^{-1} (C=O). ^{1}H-NMR (CCl_4) δ 0.5—1.4 (m, 4H), 2.27 (broad, 2H), 6.8—7.5 (m, 10H). MS *m/e* 252 (M^+), 147 (M^+—PhCO, base peak), 105.

A similar reaction of **1** (400 mg, 2.81 mmol) and α-(*p*-nitrophenyl)-*N*-phenylnitrone (**8b**) (680 mg, 2.81 mmol) in benzene (10 ml) for 5 h afforded 140 mg (33%) of *p*-nitrobenzaldehyde, 184 mg (23%) of benzanilide, and 170 mg (16%) of 1-(*p*-nitrobenzylideneamino)-1-(*N*-phenylbenzamido)cyclopropane (**9b**), mp 185—186 °C, as colorless prisms (from EtOH). IR (KBr) 1662 cm^{-1} (C=O). ^{1}H-NMR ($CDCl_3$) δ 1.20—1.83 (m, 4H), 6.8—7.5 (m, 10H), 7.90, 8.25 (each d, 2H, *J*=9 Hz), 8.51 (s, 1H, N=C**H**). ^{13}C-NMR ($CDCl_3$) δ 21.3, 62.6, 123.7, 126.5, 127.9, 128.6, 128.8, 129.0, 130.1, 135.9, 141.5, 142.9, 151.9, 170.7. MS *m/e* 385 (M^+). Found: C, 71.72; H, 4.93; N, 10.84%. Calcd for $C_{23}H_{19}N_3O_2$: C, 71.67; H, 4.97; N, 10.90%.

The reaction of **10** with 1 equivalent of *p*-nitrobenzaldehyde in boiling EtOH for 3 h afford **9b** in 36% yield.

*Hydrolysis of 1 : 1 Adduct **9b**.* A suspension of **9b** (47 mg) in EtOH (6 ml) was stirred with concd HCl (2 drops) at room temperature. After 1 h the suspension turned to a clear solution. After the solution was concentrated *in vacuo*, water was added to the residue and then the mixture was extracted with ether. The extract was concentrated

to give 7 mg (38%) of *p*-nitrobenzaldehyde. The aqueous layer was made basic with NaOH aq solution, and then extracted with ether. The extract was evaporated *in vacuo* to leave 30 mg (100%) of **10**.

References

1) Studies of Highly Strained Heterocycles. Part 3. Part 2 of this series: O. Tsuge and H. Watanabe, *Heterocycles*, **7**, 907 (1977).
2) H. J. Bestmann and R. Kunstmann, *Chem. Ber.*, **102**, 1816 (1969).
3) D. J. Anderson and A. Hassner, *Synthesis*, **1975**, 483.
4) N. S. Narasimhan, H. Heimgartner, H.-J. Hansen, and H. Schmid, *Helv. Chim. Acta*, **56**, 1351 (1973).
5) A. Padwa, S. Clough, and E. Glazer, *J. Am. Chem. Soc.*, **92**, 1778 (1970).
6) J. K. Crandall and W. W. Conover, *J. Org. Chem.*, **39**, 63 (1974).
7) M. Ohtsuru and K. Tori, *J. Mol. Spectry.*, **27**, 296 (1968).
8) O. Yu. Magidson, *Zh. Obshch. Khim.*, **33**, 2137 (1963); *Chem. Abstr.*, **59**, 13942f (1963).
9) 3,4-Dihydro-6-*p*-nitrophenyl-5-phenyl-2-pyridone should be formed from hydrolysis of **3B**.
10) D. St. C. Black, R. F. Crozier, and V. C. Davis, *Synthesis*, **1975**, 205.
11) J. S. Splitter and M. Calvin, *J. Org. Chem.*, **30**, 3427 (1965).
12) R. O. Kan and R. L. Furey, *Tetrahedron Lett.*, **1966**, 2573.
13) A. Padwa, *J. Am. Chem. Soc.*, **87**, 4365 (1965).
14) R. Huisgen, H. Stangl, H. J. Sturm, R. Raab, and K. Bunge, *Chem. Ber.*, **105**, 1258 (1972).
15) O. H. Wheeler and P. H. Gore, *J. Am. Chem. Soc.*, **78**, 3363 (1956).
16) K. Koyano and H. Suzaki, *Bull. Chem. Soc. Jpn.*, **42**, 3306 (1969).

Oxygen-17 Nuclear Magnetic Resonance. III.[1] Oxygen Atoms with a Coordination Number of Two

Tadashi SUGAWARA, Yuzo KAWADA, Morimatsu KATOH, and Hiizu IWAMURA*

Division of Applied Molecular Science, Institute for Molecular Science, Myodaiji, Okazaki 444

(Received May 23, 1979)

Fourier transform ^{17}O NMR spectra have been measured for a number of alcohols, ethers, acetals, formates, acetates, and esters of inorganic acids in natural abundance at 10.8 MHz. The ^{17}O chemical shifts which cover a range as large as several hundred ppm are primarily governed by the sum of electronegativity of the first atoms or groups attached to the central oxygen. The downfield shift due to β-methyl groups in alcohols and ethers is in parallel with decrease in their ionization potentials, demonstrating the importance of the paramagnetic screening term in the ^{17}O shifts of these compounds. Diamagnetic shift due to γ-carbons and -oxygens has also been disclosed.

The first observation of ^{17}O nuclear magnetic resonance signals was reported as early as in 1951.[2] Chemical shifts of more than one hundred organic compounds of relatively small molecular weight were documented by Christ *et al.* in 1961.[3] Wider applications of the ^{17}O NMR technique have since been hampered both by a low natural abundance (0.037%) and by an appreciable electric quadrupole moment ($Q=-2.6\times10^{-26}$ cm^2) which effects line broadening of the ^{17}O isotope. Recent advances in FT-NMR instrumentation together with rf units with a frequency synthesizer and probe heads with a tunable preamplifier have made observation of ^{17}O NMR routinely available on samples with ^{17}O isotope in natural abundance.[4] In view of an important role of oxygen-containing functions in chemistry, establishment of a useful ^{17}O NMR shifts *vs.* structure correlation is indispensable. We wish to report here the ^{17}O NMR shifts of a variety of alcohols, ethers, acetals, formates, acetates, and esters of inorganic acids, and review a number of empirical rules governing the shift data of these compounds as well as the literature values[4] for some typical compounds with dicoordinated oxygen functions.

Results and Discussion

A General Trend in ^{17}O Shifts. The ^{17}O NMR shift data of dicoordinated oxygen functions are given in Table 1. Firstly we note that the ^{17}O shifts have a wide range of several hundred ppm. This is quite large in reference to 10 and 200 ppm of the ^1H and ^{13}C shift ranges, respectively, of ordinary organic compounds and will give the impression that ^{17}O NMR spectra can be most informative as a structural probe. Strictly speaking, however, we have also to take into account of the wide ^{17}O NMR line-width unprecedented in ^1H and ^{13}C NMR. The amount of information derivable from chemical shift is approximately given by the shift range (Δ) divided by the spectral line width ($\Delta_{1/2}$). When the ^1H, ^{13}C, and ^{17}O NMR are compared, Δ can be taken as 0.8, 4, and 8 kHz for example and $\Delta_{1/2}$ may be typically 1, 1, and 100 Hz, respectively. Therefore, the capacity of information derivable from chemical shift data of ^1H, ^{13}C, and ^{17}O NMR spectroscopies would be ($\Delta/\Delta_{1/2}=$) 800, 4000, and 80, respectively. The widest shift range observed for the ^{17}O NMR should not necessarily be overemphasized.

It may be noted in the second place that the water molecule has the oxygen atom which resonates at one of the highest field region,[5] and the resonance for the central oxygen atom of ozone appears at the extreme downfield. Other data on the oxygens attached to various kinds of elements are scattered in between. Changes in the oxygen-17 chemical shift appear to be due primarily to alterations in the electron density at oxygen caused by changes in the electronegativity of α-atoms attached to the central oxygen atom. As illustrated by an approximately linear correlation in Fig. 1, downfield shift is produced as more electronegative atoms are introduced. The line has a slope of about 270 ppm/electronegativity unit which is about six times as steep as those obtained by similar plots of the ^{13}C shifts *vs.* the electronegativity of the adjacent hetero atoms.[6] We point out that, whereas the diamagnetic electric current which is directly affected by the electronegativity of ligands plays a major role in controlling the chemical shifts of ^1H, the ^{13}C and ^{17}O NMR shifts are governed by the paramagnetic screening and decrease of shielding with the increasing electronegativity of the substituents may be provided by increase in the mean inverse cube of the 2p electron radius $\langle r^{-3}\rangle_{oxygen}$ and the orbital term Q_{AA} (*vide infra*).[7]

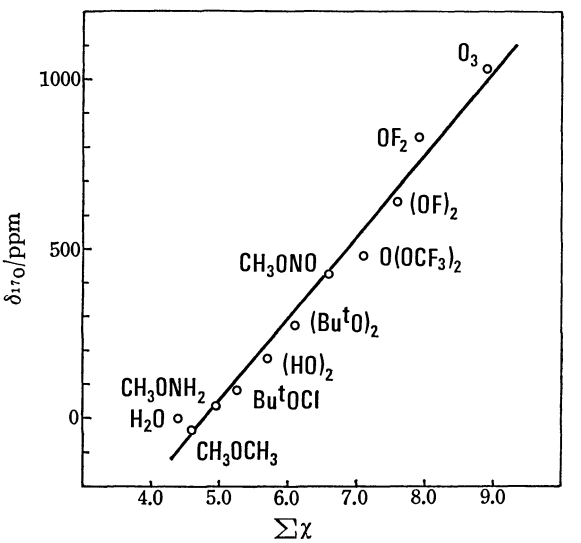

Fig. 1. Plots of ^{17}O NMR shifts *vs.* the sum of the electronegativities for dicoordinated oxygen compounds. Electronegativities (which are group values where relevant) are from Ref. 20.

Table 1. ^{17}O Chemical shifts (ppm downfield from water) of dicoordinated oxygen compounds

	$\delta^{17}O$	$\Delta_{1/2}$ [c] / Hz	Solvent	Temp / °C
Alcohols and phenols				
Methaol	−38	60	neat	amb
1-Butanol	−3	172	CCl_4 (1:1) [a]	70
1-Butanol	−1	168	neat	62
3-Methyl-1-butanol	−2	244	neat	75
Benzyl alcohol	4		CCl_4 (1:1)	70
Citronellol	5		CCl_4 (1:1)	80
Ethanol	8	128	neat	amb
2-Pentanol	30		CCl_4 (1:1)	70
2-Butanol	36	160	CCl_4 (1:1)	70
Cyclohexanol	36		CCl_4 (1:1)	70
2-Propanol	39	280	neat	amb
2-Methyl-2-butanol	55	200	CCl_4 (1:1)	70
2,3-Dimethyl-2-butanol	55	200	CCl_4 (1:1)	70
α-Terpineol	55		CCl_4 (1:1)	70
t-Butyl alcohol	63	180	CCl_4 (1:1)	68
t-Butyl alcohol	68		neat	amb
Phenol	79		C_6H_6 (1:2)	76
o-Nitrophenol	87		C_6H_6 (1:2)	76
Hydrogen peroxide	174		30% aq.	amb
Ethers				
Ethylene oxide	−49		neat	amb
Dimethyl ether	−42		$CDCl_3$ (1:1)	−40
Oxetane	−12	48	neat	amb
Tetrahydropyran	10		$CDCl_3$ (1:1)	amb
Oxepane	14	80	neat	amb
Diethyl ether	16		neat	amb
Tetrahydrofuran	18		neat	amb
Tetrahydrofuran	18		$CDCl_3$ (1:1)	amb
Anisole	50	180	neat	amb
Diisopropyl ether	64		neat	amb
7-Oxanorbornane	86		$CDCl_3$ (1:1)	amb
Di-*t*-butyl ether	88	140	CCl_4 (1:1)	amb
Di-*t*-butyl ether	90		neat	amb
1,2-Dimethoxyethane	−23		neat	amb
Diethylene glycol dimethyl ether	−27 (center) −3 (end)		neat	70
1,4-Dioxane	0	85	$CDCl_3$ (1:1)	amb
15-Crown-5	0		DMF	128
Furan	240		neat	amb
Furfural	237		neat	amb
Trimethyloxonium tetrafluoroborate	−29	180	CH_3NO_2	amb
Diethyl ether–BF_3	31		neat	amb
Hexamethyldisiloxane	43		neat	amb
Acetals and orthoestes				
Dimethoxymethane	10	60	neat	amb
1,3-Dioxolane	34		$CDCl_3$ (1:1)	amb
1,3-Dioxane	37		$CDCl_3$ (1:1)	amb
1,3-Dioxane	38		neat	amb
Bis(methoxymethyl) ether	65 (center) 10 (end)	100 100	neat	amb
1,3,5-Trioxane	65		$CDCl_3$	amb
(2*H*-)1,3-Benzodioxole	82		$CDCl_3$	amb
Trimethyl orthoformate	30		neat	amb
2,8,9-Trioxaadamantane	67	200	$CDCl_3$	amb

Table 1. (Continued)

	$\delta_{^{17}O}$	$\Delta_{1/2}$ / Hz	Solvent	Temp / °C
1,4,6,9-Tetraoxaspiro[4.4]nonane	75		neat	amb
Esters				
Methyl formate	143 (364) [b]		neat	amb
Ethyl formate	173 (364)		neat	amb
Isopropyl formate	200 (364)		neat	amb
t-Butyl formate	212 (380)		neat	amb
Methyl acetate	148 (355)		neat	amb
Ethyl acetate	169 (363)		neat	amb
Isopropyl acetate	196 (363)		neat	amb
t-Butyl acetate	207 (375)		neat	amb
Methyl acrylate	132 (345)		neat	amb
Diethyl oxalate	166 (359)		neat	amb
γ-Butyrolactone	176 (335)		neat	amb
Diethyl carbonate	123 (242)		neat	amb
Trimethyl phosphite	44 ($J_{O-P}=183$ Hz)		neat	amb
Trimethyl phosphate	65 ($J_{O-P}=164$ Hz) (19)		$CDCl_3$	amb
2,8,9-Trioxa-1-phospaadamantane	82		CD_2Cl_2	amb
Methyl nitrite	420 (790) [18]			
Propyl nitrite	455 (803) [3]			
Isopentyl nitrite	467 (819)		$CDCl_3$ (1:1)	amb
t-Butyl nitrite	513 (838) [3]			
Dimethyl sulfate	142 (101)		$CDCl_3$ (1:1)	amb
Others				
O-Methylhydroxylamine	35 [3]			
t-Butyl hypochlorite	79			
Di-*t*-butyl peroxide	276 269 [3]			
$(CF_3O)_2O$	479 (center) [19] 321 (end)			
FOOF	647 [19]			
F_2O	830 [19]			
Ozone	1032 (center) [19] 1598 (end)			

a) An approximate ratio in volume. b) Shift values in parentheses are for doubly bonded oxygens. c) No window function was applied for the measurement except for alcohols where a sensitivity enhancement parameter was set at -0.02 s throughout.

Simple Alcohols and Ethers. Shifts to lower field in the ^{17}O resonance are observed as the α-carbon is substituted with alkyl groups. Primary, secondary, and tertiary alcohols, for example, have their characteristic shift ranges: -3—10 (except for -38 ppm of methanol), 30—40 and 55—70 ppm downfield relative to water, respectively. We have so far met no exception to the above rule on the ^{17}O shifts brought about by the alkyl substitution. The presence of diamagnetic γ-effect is suggested by a slightly high field shift of 1-butanol and 2,3-dimethyl-2-butanol as compared to ethanol and *t*-butyl alcohol, respectively. An example which would violate the above shift ranges could be found in sterically congested alcohols. Changes in chemical shifts are steeper in ethers than in alcohols and esters.

The findings have two facets of importance. One is as a new method for differentiating among primary, secondary, and tertiary structures of unknown alcohols, ethers and esters. The method appears quite unique and useful, but let us point out that there is a certain limitation to the practical application of this rule to the structural elucidation of complex organic molecules. Since the oxygen-17 nucleus ($I=5/2$) has electric quadrupole moment and the line width of resonance signals is directly proportional to correlation time τ_c for the overall rotation of the molecules which in turn is correlated to solution viscosity η, a fairly fluid sample solution must be employed. When isotropic molecular tumbling is rapid on the NMR time scale, the line width ($1/T_1$) determined by quadrupole relaxation is given by Eq. 1, where q and η stand for the electric field gradient and the asymmetry parameter at the nuclear site. The Stokes-Einstein-Debye equation (Eq. 2) relates τ_c to temperature T. The measurement at elevated solution temperature is thus preferred. A

$$\frac{1}{T_1} = \frac{3}{125}\left(1+\frac{\eta}{3}\right)\left(\frac{e^2Qq}{h}\right)^2\tau_c \quad (1)$$

$$\tau_c = \frac{4\pi\eta a^3}{3kT} \quad (2)$$

sample of relatively large molecular weight ($M>150$) for which a solution of considerably high concentration may be required by the sensitivity of the present instrument often tends to be hard to measure because of line-broadening. The limitation could be avoided in principle by the use of a spectrometer with higher magnetic field and/or isotopically enriched samples.

The other is on the origin of the observed ordering of chemical shifts. There are ample examples which show that electron density at the oxygen atom increases as we go from methanol *via* ethanol and 2-propanol to *t*-butyl alcohol. The polar substituent, constants σ^* for the methyl, ethyl, isopropyl, and *t*-butyl groups are 0 (by definition), −0.1, −0.19, and −0.3, respectively. The observed shifts in Table 1 show that ^{17}O screening decreases on going from methanol to *t*-butyl alcohol, and is not compatible with the electron density at oxygen dominating the ^{17}O shifts as was the case in the previous section.

According to the Pople-Karplus theory on paramagnetic screening,[7] the screening constant of atom A bound to other atom B is given by Eq. 3. The Q's are orbital terms related to charge density on atom

$$\sigma_p^A = -\frac{e^2\hbar^2\langle r^{-3}\rangle}{2m^2c^2(\Delta E)}[Q_{AA}+\sum_{B\neq A}(Q_{AB})] \quad (3)$$

A and bond order between A and B, and ΔE is a mean or effective excitation energy. If the diamagnetic screening or the $\langle r^{-3}\rangle$ and Q_{AA} terms in the paramagnetic screening were the determining factor, tertiary alcohols and ethers which have highest electron density at oxygen should have given the highest field shifts in the ^{17}O resonance. Resonance can move downfield as the lowest-energy electronic transition is shifted to longer wavelength. The $n\rightarrow\pi^*$ transition has been shown to be crucial to the shift differences in the ^{17}O NMR of carbonyl compounds.[8] In the present case of aliphatic alcohols and ethers, the excited states to be mixed with the ground state by an external magnetic field is either the $n\rightarrow\sigma^*$ or Rydberg states.[9] Since the corresponding transition appears in the vacuum ultraviolet region and is not unambiguously characterized, let us take the adiabatic ionization potentials of these compounds as a measure of ΔE. A reasonably smooth correlation is found in the ^{17}O chemical shifts *vs.* the inverse of the ionization potentials plots both for alcohols and ethers as shown in Fig. 2.

Whereas there is no strict meaning in the apparent linearity of the plots, the correlation appears to demonstrate that the energy levels of the oxygen n-electrons are more sensitive to the structural changes in the alkyl groups than the terminating orbital levels of oxygen and that ΔE gets smaller on going from the methyl through ethyl and isopropyl to *t*-butyl groups. The paramagnetic contribution to the total screening constant is concluded to be important in simple alcohols and ethers.

Simple cyclic ethers present no anomaly in that

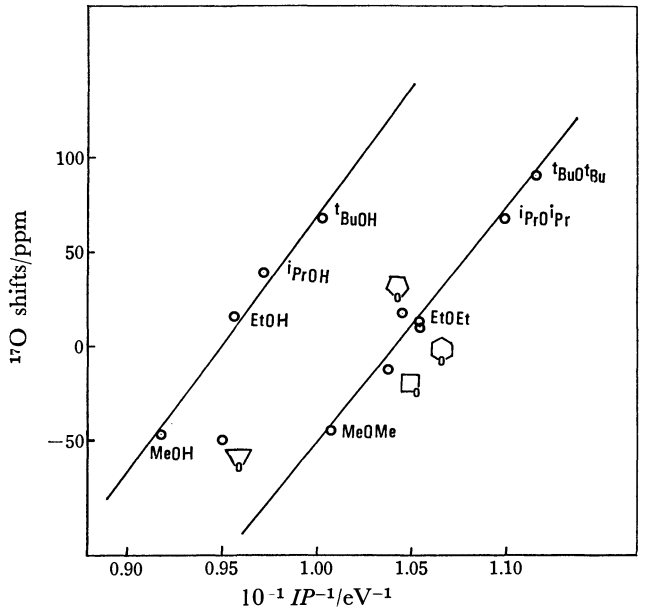

Fig. 2. Plots of ^{17}O chemical shifts *vs.* the inverse of adiabatic ionization potentials (from Ref. 11) of alcohols and ethers.

their ^{17}O shifts *vs.* $1/IP$ plots conform to a line given by acyclic ethers. Oxiranes form a conspicuous exception to this trend. Just as the well-known case of the ^1H and ^{13}C shielding of three membered rings, the ^{17}O resonance of oxiranes shows a marked shielding effect. The diamagnetic shielding is, however, not as strong as it should be expected from the ^{17}O shifts *vs.* $1/IP$ plots for other ethers. These anomalies of oxiranes will be discussed separately in the forthcoming paper in view of the importance of the epoxide functions in many fields of chemistry.

Acetals and Orthoesters. When the β-methylene group in methyl propyl ether (δ −18)[10] is replaced by oxygen to make dimethoxymethane (δ 10), downfield shift by 28 ppm is obtained. The downfield shift of a similar amount ($\Delta\delta$ 27 ppm) is observed on going from tetrahydropyran (δ 10) to 1,3-dioxane (δ 37). An approximate additivity appears to hold for this downfield shift due to introduction of the β-oxygen atoms. A shift by 56 ppm on going from dipropyl ether (δ 7)[10] to bis(methoxymethyl) ether (δ 65) is just twice as large as 28 ppm. The ^{17}O resonances for 1,3,5-trioxane and 2,8,9-trioxaadamantane appear at 54 and 56 ppm downfield of tetrahydropyran, respectively.

γ-Effects. Effects of the γ-carbon atom on the ^{17}O NMR shifts have been pointed out;[10] replacement of β-hydrogens in ethyl methyl ether with the methyl groups produces a stepwise highfield shift by 6, 1.5, and 2.5 ppm. Now, replacement of the γ-carbon atom in butyl methyl ether (δ −18)[10] by oxygen to give 1,2-dimethoxyethane accompanies 5 ppm upfield shift. Similar upfield shifts are observed also in diethylene glycol dimethyl ether (6.5 ppm from dibutyl ether (δ 3.5)) and *p*-dioxane (11 ppm from tetrahydropyran).

The observed diamagnetic shifts of 6 and 12 ppm of ethylene glycol and 2-chloroethanol, respectively,

relative to 1-propanol (δ 0) may be additional examples of γ-effect due to a hetero atom.

Esters. The effect of alkyl groups on ^{17}O shifts of the ethereal oxygen of esters is similar to that in alcohols and ethers but is less pronounced. The shift differences between two extreme alkyl groups, namely, the methyl and *t*-butyl derivatives, are 130 and 106 in ethers and alcohols, respectively, and only 93, 70, and 60 ppm in nitrites, formates, and acetates, respectively. The results may be a manifestation of resonance interaction as depiced in Eq. 4 serving as a buffer of the electronic effect of alkyl groups R. Contribution of the zwitterionic canonical structure in each resonance hybrid will be in the order: acetates>formates>nitrites.

$$\begin{array}{l} R'-\underset{\underset{O}{\|}}{C}-\dot{O}-R \leftrightarrow R'-\underset{\underset{O^-}{|}}{C}=\overset{+}{O}-R \\ \\ O=N-O-R \leftrightarrow {}^-O-N=\overset{+}{O}-R \end{array} \qquad (4)$$

We conclude that, in spite of some difficulties inherent in natural-abundance ^{17}O NMR measurements, this new technique has a number of merits worth the effort. Firstly, the technical difficulties are partly compensated by the short spin-lattice relaxation times of the quadrupolar ^{17}O which enable us to accumulate a large number of transients in a given time. Often a spectrum with good S/N ratios is obtained within a time period shorter than that necessary for measuring ^{13}C NMR signals due to quaternary carbons of relatively long T_1 and with almost no NOE effect. Secondly, we have pointed out that ^{17}O NMR spectra are highly informative as a structural probe. Shift ranges as large as 1000 ppm for dicoordinated oxygens are governed by the paramagnetic screening and can be interpreted in terms of empirical rules basically similar to the familiar ones employed in ^{13}C NMR spectroscopy.

Experimental

Spectral Measurements. The measurements were made with the ^{17}O nuclei in natural abundance (0.037 %) on a Varian FT-80A spectrometer at 10.782 MHz. For a 8000 Hz spectral width, 320 data points in the time-domain spectra were used, the Fourier number being kept at 16384. The number of transients accumulated with a 90° pulse and an acquisition time of 0.02 s was in the range 10^4—10^5 to get spectra of reasonable S/N ratios. When a longer acquisition time (AT) of 0.1 s was employed, the number of data points (DP) increased to 1600 according to equation $DP=2AT\cdot SW$ (SW is a spectral width). The measurement under these conditions was found to be worse with respect to the S/N of spectra, not only because it required the accumulation time five times as long as the previous one to get the same sum of the number of transients, but also because it sampled mostly noise signals after the free induction signals practically decayed at $5T_1$(<0.02 s). The ^{17}O shifts and half-band-widths did not differ at all from those obtained under the standard conditions. Since quadrupole relaxation of ^{17}O nuclei is rapid, the use of long delay times between the end of each rf pulse and the beginning of data collection is not in principle necessary. However, some baseline distortions in transformed frequency-domain signals often resulted due to incomplete spectrometer recovery following rf pulse, when too short delay times were employed.[12] This was more pronounced in ^{17}O NMR, as the rf frequency was lower than those of ^{1}H and ^{13}C spectroscopy. Alpha delay was usually set at 800—1000 μs.

Chemical shifts were measured as frequency shifts from the rf synthesizer frequency (8.532000 MHz) and expressed in ppm relative to the oxygen of water which resonated at 10.78321 MHz when measured in a capillary tube placed concentrically within a sample tube of 10 mm o.d. Chemical shifts are accurate to $\pm$1 ppm. The sample temperature was at 34—36 °C unless otherwise stated in Table 1. The half-band-widths of alcohols and ethers were 60—280 Hz under these conditions.

Materials. The following compounds were prepared according to the literature and their purity was confirmed by VPC and/or spectral data: di-*t*-butyl ether,[13] trimethyloxonium tetrafluoroborate,[14] bis(methoxymethyl) ether,[15] 2,8,9-trioxaadamantane,[16] and 2,8,9-trioxa-1-phosphaadamantane.[17] The samples of (2*H*-)1,3-benzodioxole and 1,4,6,9-tetraoxaspiro[4.4]-nonane were kindly supplied by Prof. Dr. S. Smoliński of Jagellonian University, Kraków, Poland. Pure samples from commercial sources were used otherwise.

References

1) Presented in part at the ACS/CSJ Chemical Congress, Honolulu, Hawaii, April 2—6, 1979. For Part II, see: Y. Kawada, T. Sugawara, and H. Iwamura, *J. Chem. Soc., Chem. Commun.*, **1979**, 291.

2) F. Alder and F. C. Yu, *Phys. Rev.*, **81**, 1067 (1951). See also: H. E. Weaver, B. M. Tolbert, and R. C. LaForce, *J. Chem. Phys.*, **23**, 1956 (1955).

3) H. A. Christ, P. Diel, HR. Schneider, and H. Dahn, *Helv. Chim. Acta*, **44**, 865 (1961).

4) T. Sugawara, Y. Kawada, and H. Iwamura, *Chem. Lett.*, **1978**, 1371; W. G. Klemperer, *Angew. Chem. Int. Ed. Engl.*, **17**, 246 (1978) and the papers cited therein.

5) J. Reuben, *J. Am. Chem. Soc.*, **91**, 5725 (1969).

6) P. C. Lauterbur, *Ann. N. Y. Acad. Sci.*, **70**, 841 (1958); J. B. Lambert, D. A. Netzel, H. Sun, and K. K. Lilianstrom, *J. Am. Chem. Soc.*, **98**, 3778 (1976).

7) M. Karplus and J. A. Pople, *J. Chem. Phys.*, **38**, 2803 (1963).

8) C. Delseth and J.-P. Kintzinger, *Helv. Chim. Acta*, **59**, 466 (1976); D. J. Sardella and J. B. Stothers, *Can. J. Chem.*, **47**, 3089 (1969); B. N. Figgis, R. G. Kidd, and R. S. Nyholm, *Proc. R. Soc. London. Ser. A.*, **269**, 469 (1962); K. K. Ebraheem and G. A. Webb, *J. Magn. Reson.*, **25**, 399 (1977).

9) M. B. Robin, "Higher Excited States of Polyatomic Molecules," Academic Press, New York and London (1974), Vol. 1, Chap. 3.

10) C. Delseth and J.-P. Kintzinger, *Helv. Chim. Acta*, **61**, 1327 (1978). Shift data in this paper are referenced to the oxygen of acidified water[5] in an external capillary and should be displaced by 10.5 ppm downfield to compared with our data.

11) B. J. Cocksey, H. H. D. Eland, and C. J. Danby, *J. Chem. Soc., B*, 790 (1971); F. Broglim, E. Heilbronner, J. Wirz, E. Kloster-Jensen, R. G. Bergman, K. P. C. Vollhardt, and A. J. Ashe III, *Helv. Chim. Acta*, **58**, 2620 (1975).

12) D. Canet, C. Goulon-Ginet, and J. P. Marchal, *J. Magn. Reson.*, **22**, 537 (1976).

13) J. L. E. Erickson and W. H. Ashton, *J. Am. Chem. Soc.*, **63**, 1769 (1941).

14) H. Meerwein, *Org. Synth.*, Coll. Vol. V, 1096 (1973).

15) L. R. Evans and R. E. Martin, *J. Org. Chem.*, **23**, 744 (1958).

16) *r*-1,*c*-3,*c*-5-Cyclohexanetriol was prepared according to the method of Smith and Stump (*J. Am. Chem. Soc.*, **83**, 2739 (1961)), and the triol was treated with triethyl orthoformate under the catalysis of *p*-toluenesulfonic acid.

17) T. L. Browm, J. G. Verkade, and T. S. Piper, *J. Phys. Chem.*, **65**, 2051 (1961).

18) L. -O. Andersson and J. Mason, *J. Chem. Soc., Dalton Trans.*, **1974**, 202.

19) I. J. Solomon, A. J. Kacmarek, and J. Raney, *Inorg. Chem.*, **11**, 195 (1972); I. J. Solomon, J. N. Keith, A. J. Kacmarek, and J. K. Raney, *J. Am. Chem. Soc.*, **90**, 5408 (1968); I. J. Solomon, J. K. Raney, A. J. Kacmarek, R. M. Maguire, and G. A. Noble, *ibid.*, **89**, 2015 (1967).

20) J. Hinze and H. H. Jaffe, *J. Am. Chem. Soc.*, **84**, 540 (1962); J. Hinze, M. A. Whitehead, and H. H. Jaffe, *ibid.*, **85**, 148 (1963); J. E. Huheey, *J. Phys. Chem.*, **69**, 3284 (1965); J. R. Van Wazer and J. H. Letcher, "Topics in Phosphorus Chemistry," Interscience, New York (1967), Vol. 5, Chap. 3.

The Stereoisomerization of *N,N'*-Diacyl Derivatives of Indigo

Yoshimori OMOTE,* Satoshi IMADA, Ryuichi MATSUZAKI, Kiyoko FUJIKI,†
Takehiko NISHIO, and Choji KASHIMA

Department of Chemistry, University of Tsukuba, Sakuramura, Niihari, Ibaraki 300-31
† *Department of Agricultural Chemistry, Faculty of Agriculture, Meiji University, Ikuta, Kawasaki 214*

(Received June 11, 1979)

The *cis*-isomers of *N,N'*-diacylindigo (*e.g.*, *cis-N,N'*-diacetyl-, distearoyl-, dibenzoyl-, and bis(3,5-dinitrobenzoyl)-indigo) were found to separate out in a crystalline form from a solution of the corresponding *trans*-isomer upon irradiation. The kinetics of the *cis*-to-*trans* isomerization of these four *cis-N,N'*-diacylindigos was studied, the relative rates being 7.9, 11.0, 1.0, and 5.1 respectively. Several amines were found to accelerate the *cis*-to-*trans* isomerization in the order of: $Et_2NH > PrNH_2 > Et_3N > i\text{-}Pr_2NH$ in the case of *cis-N,N'*-diacetylindigo and in the order of: $Et_2NH > i\text{-}Pr_2NH > PrNH_2 > Et_3N$ in the case of *cis-N,N'*-dibenzoylindigo.

Photochemical and thermal isomerizations are of interest in the field of natural products, including retinal,[1] bilirubin,[2] phytochrome,[3] and trichochrome.[4] During the course of an investigation of melanins, we have interested indigoid pigments as model compounds of trichochromes.

Indigo is a *trans* compound: attempts to convert it photochemically to the corresponding *cis*-isomer have been unsuccessful.[5] This photostability was first explained by hydrogen-bonding,[6] and the explanation was substantiated by the observation that the *N,N'*-diacetyl-[5,7] and *N,N'*-dimethylindigo[8,9] show phototropic behavior. Wyman[10] later suggested the contribution of a fast proton transfer in the excited state, and also reported the existence of a photochemical equilibrium between *cis*- and *trans*-thioindigo in an inert solvent. Recently, the preparation and spectroscopic properties of a basic chromophore of thioindigo have been reported.[11]

As far as indigo derivatives are concerned, the separation of the *cis*-isomer has been unsuccessful, while the isomerization of *cis-N,N'*-diacylindigo has not yet been examined. This paper will be concerned with the isolation of *cis*-isomers of *N,N'*-diacylindigo and with a kinetic study of the *cis*-to-*trans* isomerization in the dark as well as the effect of amines on the *cis*-to-*trans* isomerization of *N,N'*-diacylindigo.

Results and Discussion

Isolation of cis-N,N'-*Diacylindigo.* We found that *cis-N,N'*-diacetyl-, distearoyl-, dibenzoyl-, and bis(3,5-dinitrobenzoyl)indigo separated in crystalline form from a solution of the corresponding *trans*-isomer on irradiation. The yield of the *cis*-isomer was almost quantitative after repeated irradiation and concentration.

The structure of each *cis*-isomer was confirmed by elemental analyses and UV and IR spectra. The IR spectra show two carbonyl bands characteristic of the *cis*-isomer.[11] The UV spectrum of *cis-N,N'*-diacetylindigo was almost superimposable with the calculated spectrum.[12] All four *cis-N,N'*-diacylindigos changed quantitatively into the corresponding *trans*-isomers when dissolved in a solvent.

The cis-*to*-trans *Isomerization of* cis-N,N'-*Diacylindigo.* It is generally accepted that the size and the structure of substituents on the two nitrogen atoms of the indigo molecule (I) sterically affect the *cis-trans* isomerization of this compound. In order to ascertain the effects of the substituents, we prepared benzene solutions of *cis-N,N'*-diacetyl-, distearoyl-, dibenzoyl-, and bis(3,5-dinitrobenzoyl)indigo, which were then kept at a constant temperature in the dark. The change in the absorption curve with the time showed the isomerization of the *cis*-isomer to the *trans*-isomer. From the change in the *cis*-isomer percentage with the time, the reaction-rate constants were calculated: the other kinetic parameters were also calculated, as is shown in Table 1.

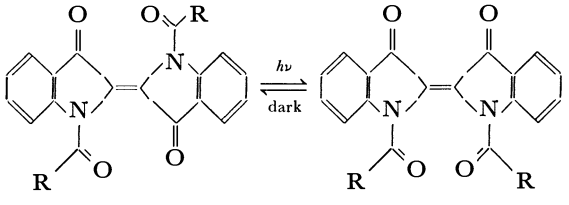

I II

a. R=CH_3 b. R=$CH_3(CH_2)_{16}$ c. R=C_6H_5
d. R=3,5-$(NO_2)_2C_6H_3$

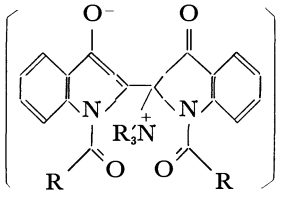

III

The relative rate shows that alkyl substituents correspond to a faster rate than do the aryl substituents. The value of the activation free energy is almost 20 kcal/mol, while the activation energy is between 19 and 23 kcal/mol. The value of the activation energy is far less than that of stilbene, 42.8 kcal/mol,[13] or methyl cinnamate, 41.6 kcal/mol.[14] Substituents on stilbene decrease the activation energy.[15] These facts reveal that *cis-N,N'*-diacylindigos are less stable than *cis*-stilbene or *cis*-cinnamate because the structure of the latter can be planar.

Effects of Amines on the cis-*to*-trans *Isomerization of* cis-N,N'-*Diacylindigo.* We found that amines accelerate the *cis*-to-*trans* (IIa to Ia) isomerization of *cis-N,N'*-diacetylindigo. In order to clarify the rela-

TABLE 1. KINETIC DATA FOR *cis*-TO-*trans* ISOMERIZATION OF *cis*-*N,N'*-DIACYLINDIGOS (IIa—d)

II	k[a)] / s^{-1}	Rel. rate	ΔG^{*}[a)] kcal/mol	E_a kcal/mol	ΔH^{*} kcal/mol
a	4.92×10^{-4}	7.9	23.5	19.5	18.8
b	6.84×10^{-4}	11.0	23.3	19.9	19.2
c	6.21×10^{-5}	1.0	24.5	23.1	22.4
d	3.14×10^{-4}	5.1	23.8	19.4	18.8

a) At 45.2 °C.

TABLE 2. RELATIVE RATES OF *cis*-TO-*trans* ISOMERIZATION OF *cis*-*N,N'*-DIACETYL- AND DIBENZOYLINDIGO IN THE PRESENCE OF AMINES

Amine[a)]	Diacetylindigo[b)]	Dibenzoylindigo[c)]
Et_3N	3.7	1.0
i-Pr_2NH	3.4	1.7
Et_2NH	18.2	6.1
$PrNH_2$	14.7	1.5
$PhNH_2$	1.1	1.0
None	1.0	1.0

a) Equimolar amount of amines. b) At 25.0 °C. c) At 50.0 °C.

tion between the effectiveness and the amount of amines for the *cis*-to-*trans* isomerization, the rate was measured in the presence of an equimolar amount of triethylamine under various concentrations. The reaction was found to be pseudo-first-order for the indigo, and the amine concentration was constant during the reaction. These facts reveal that the amine acts as a catalyst.

Also, the observed reaction rate constant was proportional to the concentration of triethylamine. This suggests that equimolar amounts of the indigo and the amine make up the reaction intermediate (III).

Furthermore, the effects of several kinds of amines were compared in the case of *cis*-*N,N'*-diacetylindigo (IIa) as well as in the case of *cis*-*N,N'*-dibenzoylindigo (IIc). Their relative rates are summarized in Table 2. It can be concluded that the order of acceleration by these amines is roughly in accord with the basicity of the amines except when steric hindrance plays an important role, as in the case of diisopropylamine or triethylamine.

Experimental

trans-N,N'-*Diacetylindigo (Ia).* Ia was prepared by the modified method reported by Blanc and Ross[12] and was recrystallized from benzene: mp 256—257 °C. IR (KBr): 1690, 1680, 1595 cm^{-1}. UV (C_6H_6) max: 562 nm (ε 7000).

trans-N,N'-*Distearoylindigo (Ib).* A mixture of indigo (1.0 g) and stearoyl chloride (11.6 g) in pyridine (10 ml) was refluxed for 20 min to give Ib, which was then recrystallized from petroleum ether: 28% yield: mp 101—102 °C. IR (KBr): 1690, 1670, 1600 cm^{-1}. UV (C_6H_6) max: 567 nm (ε 7100). Found: C, 78.28; H, 9.65; N, 3.43%. Calcd for $C_{52}H_{78}N_2O_4$: C, 78.54; H, 9.88; N, 3.52%.

trans-N,N'-*Dibenzoylindigo (Ic).* Ic was prepared by the modified method reported by Posner.[12b] Mp 256—257 °C. IR (KBr): 1700, 1660, 1590 cm^{-1}. UV (C_6H_6) max: 574 nm (ε 7700).

trans-*Bis(3,5-dinitrobenzoyl)indigo (Id).* Id was prepared from indigo (1.0 g) and 3,5-dinitrobenzoyl chloride (8.89 g) and was recrystallized from hexane–chloroform. 50% yield. Mp 249—252 °C. IR (KBr): 1700, 1680, 1620, 1600, 1550, 1345 cm^{-1}. UV (C_6H_6) max: 552 nm (ε 6200). Found: C, 55.38; H, 2.14; N, 12.23%. Calcd for $C_{30}H_{14}N_6O_{12}$: C, 55.39; H, 2.16; N, 12.92%.

General Method for the Isolation of cis-N,N'-*Diacylindigo.* The *trans*-isomer was dissolved in a slightly soluble solvent, such as benzene, petroleum ether, or hexane, and was then irradiated with visible light, the wave length being more than 550 nm, the light source being a mercury lamp (100 W), and the filter solution being cobalt sulfate 60 g+potassium chromate 3.24 g+sodium carbonate 12 g/750 ml water, for an appropriate period. This afforded precipitates of the corresponding *cis*-isomer.

cis-N,N'-*Diacetylindigo (IIa).* Ia was dissolved in benzene by heating, and then an equivalent volume of hexane was added (5×10^{-4} mol/l). The solution was irradiated with visible light for 5 h. Crimson needles; mp 244—246 °C. IR (KBr): 1720, 1690, 1590 cm^{-1}. UV (C_6H_6) max: 438 nm (ε 4500). Found: C, 69.29; H, 3.95; N, 7.99%. Calcd for $C_{20}H_{14}N_2O_4$: C, 69.36; H, 4.07; N, 8.08%.

cis-N,N'-*Distearoylindigo (IIb).* Ib was dissolved in petroleum ether by heating, and an approximately saturated solution was irradiated by visible light for 30 min. Orange needles; mp 101—103 °C. IR (KBr): 1720, 1700, 1600 cm^{-1}. UV (C_6H_6) max: 435 nm (ε 3900). Found: C, 78.58; H, 9.92; N, 3.48%. Calcd for $C_{52}H_{78}N_2O_4$: C, 78.54; H, 9.88; N, 3.52%.

cis-N,N'-*Dibenzoylindigo (IIc).* Ic was dissolved in benzene by heating, and then petroleum ether was added to the mixture. After cooling, precipitates were filtered off, and the filtrate was irradiated with visible light for 10 h: mp 245—247 °C. IR (KBr): 1725, 1675, 1595 cm^{-1}. UV (C_6H_6) max: 460 nm (ε 3900). Found: C, 76.01; H, 3.71; N, 5.82%. Calcd for $C_{30}H_{18}N_2O_4$: C, 76.58; H, 3.85; N, 5.95%.

cis-N,N'-*Bis(3,5-dinitrobenzoyl)indigo (IId).* Id was dissolved in benzene by heating (4×10^{-4} mol/l), and then the solution was irradiated with visible light for 4 h to afford orange needles; mp 205—210 °C. IR (KBr): 1730, 1680, 1620, 1600, 1540, 1340 cm^{-1}. UV (C_6H_6) max: 436 nm (ε 2800). Found: C, 55.93; H, 2.18; N, 12.48%. Calcd for $C_{30}H_{14}N_6O_{12}$: C, 55.39; H, 2.16; N, 12.92%.

Kinetics for the cis-*to*-trans *Isomerization of* N,N'-*Diacylindigo.* The *cis*-isomer was dissolved in benzene, the concentration being in the order of 10^{-4} mol/l. The sample solution was sealed in several ampoules, each aliquot being 3 ml. Each ampoule was wrapped in aluminum foil and kept in a thermostat. After an appropriate time, each ampoule was pulled out from the thermostat and the *cis*-isomer percentage was measured from the change in the visible absorption curve of each ampoule solution. From the change in the *cis*-isomer percentage with the time pseudo-first-order rate constant, k, was calculated at 45.2 °C, from which the activation free energy, ΔG^{*}, was subsequently calculated. The activation enthalpy, ΔH^{*}, was derived from the activation energy, E_a, which was itself calculated from the rate constants at different temperatures, 45.2 °C and 54.6 °C.

Acceleration Effect of Amines on the cis-*to*-trans *Isomerization of* cis-N,N'-*Diacetylindigo. Concentration of Amines*: A

benzene solution (5 ml) of *cis-N,N'*-diacetylindigo (IIa) with a concentration of 6.54×10^{-4}, 7.52×10^{-4}, 8.18×10^{-4}, and 1.02×10^{-3} mol/l, and a benzene solution of triethylamine with an equivalent mol/l concentration were prepared. Each indigo solution was mixed with 5 ml of a triethylamine solution of the corresponding concentration. Then the absorbance at 562 nm was scanned by the recorder at time intervals of 15 min. For each concentration, the rate constants were found to be 3.85×10^{-5}, 4.90×10^{-5}, 5.74×10^{-5}, and $7.74\times10^{-5}/s^{-1}$.

Acceleration Effect and Structure of Amines. The relation between the acceleration effect and the structures of the amines was examined by measuring the reaction rate of the *cis*-to-*trans* isomerization of *cis-N,N'*-diacetylindigo or *cis-N,N'*-dibenzoylindigo in a benzene solution to which an equimolar amount of each amine had been added.

References

1) K. van der Meer, J. J. C. Mulder, and J. Lugtenburg, *Photochem. Photobiol.*, **24**, 363 (1976).

2) a) R. Bonnett, J. E. Davies, and M. B. Hursthouse, *Nature*, **262**, 326 (1976); b) C. F. Foote and T. Y. Ching, *J. Am. Chem. Soc.*, **97**, 6209 (1975); c) D. A. Lightner, *Photochem. Photobiol.*, **26**, 427 (1977).

3) a) R. E. Kendrick and C. J. P. Spruit, *Photochem. Photobiol.*, **26**, 201 (1977); b) G. Struckmeier, U. Thewalt, and J. H. Fuhrhop, *J. Am. Chem. Soc.*, **98**, 278 (1976).

4) a) R. A. Nicolaus, G. Prota, C. Santacroce, G. Scherillo, and D. Sica, *Gazzetta*, **99**, 323 (1969); b) G. Prota, A. Suarato, and R. A. Nicolaus, *Experientia*, **27**, 1381 (1971); c) F. Giordano, L. Mazzasella, G. Prota, C. Santacroce, and D. Sica, *J. Chem. Soc., C*, **1971**, 2610.

5) W. R. Brode, E. G. Pearson, and G. M. Wyman, *J. Am. Chem. Soc.*, **76**, 1034 (1954).

6) W. Lüttke and M. Klessinger, *Chem. Ber.*, **97**, 2342 (1964).

7) G. M. Wyman and A. F. Zenhäusern, *J. Org. Chem.*, **30**, 2348 (1965).

8) J. Weinstein and G. M. Wyman, *J. Am. Chem. Soc.*, **78**, 4007 (1956).

9) C. R. Giuliano, L. D. Hess, and J. D. Margerum, *J. Am. Chem. Soc.*, **90**, 587 (1968).

10) a) G. M. Wyman, *J. Chem. Soc., Chem. Commun.*, **1971**, 1332; b) G. M. Wyman and B. M. Zarneger, *J. Phys. Chem.*, **77**, 1204 (1973); c) G. M. Wyman and W. R. Brode, *J. Am. Chem. Soc.*, **73**, 1487 (1951); d) D. A. Rogers, J. D. Margerum, and G. M. Wyman, *J. Am. Chem. Soc.*, **79**, 2469 (1957).

11) a) U. Luhmann and W. Lüttke, *Chem. Ber.*, **111**, 3246 (1978); b) U. Luhmann, F. G. Wentz, B. Knieriem, and W. Lüttke, *Chem. Ber.*, **111**, 3233 (1978).

12) a) J. Blanc and D. L. Ross, *J. Phys. Chem.*, **72**, 2818 (1968); b) T. Posner, *Ber. B*, **59**, 1977 (1926).

13) G. B. Kistiakowsky and W. R. Smith, *J. Am. Chem. Soc.*, **56**, 638 (1934).

14) G. B. Kistiakowsky and H. A. Smith, *J. Am. Chem. Soc.*, **57**, 269 (1935).

15) M. Calvin and H. W. Alter, *J. Chem. Phys.*, **19**, 768 (1951).

A Novel Carbonization of Naphthalene and Other Aromatic Compounds in a Molten Mixture of $AlCl_3$–NaCl–KCl[1)]

Etsuro OTA,* Sadao INOUE, Masahiro HORIGUCHI,† and Sugio OTANI†

College of Technology, Gunma University, Kiryu, Gunma 376

† *Faculty of Technology, Gunma University, Kiryu, Gunma 376*

(Received December 25, 1978)

The use of molten salt as the solvent made it possible to carry out the carbonization process throughout in the liquid state. The process proceeded at a lower temperature than conventional ones, resulting in higher yields. The carbon was deposited from the reaction mixture as powder or flakes; it was similar to "raw coke" in its composition. Thus, 12.8 g of naphthalene was treated in a mixed melt (mp 95 °C) of $AlCl_3$, NaCl, and KCl (60:26:14 mol%) at 300 °C for 10 h, yielding 11.3 g of carbon. Anthracene, phenanthrene, substituted naphthalene, and biphenyl also gave carbon in yields 69—99% of the theoretical yields, while N-containing heterocycles hardly reacted at all. The X-ray parameters of the carbons, the d_{002} spacing and the crystal thickness, L_c, varied with the kind of compound used and with other factors; after heat-treatment at 2800 °C, these values were 3.37—3.52 and 20—700 Å respectively. As the mode of reaction, an acid-catalyzed ionic mechanism was proposed, and the role of hydrogen-disproportionation was discussed.

Carbonization in a homogeneous liquid system is interesting in many aspects. It would seem to favor, at least, theoretical studies facilitating the introduction of powerful analytical methods into the carbon chemistry. The coking of pitch is a typical process involving liquid carbonization, but in this case the whole system can not avoid solidifying as the reaction proceeds, since the reaction solvent is the reactant itself. Therefore, an inert solvent which is not incorporated into the resulting carbon is desirable for the carbonization in question.

Lewis and Singer[2)] presented *m*-quinquephenyl as an inert solvent for carbonization, but according to Evans and Marsh[3)] this compound polymerized and pyrolysed and did react with the reactant during carbonization. This seems to indicate that an organic material ultimately can not be an inert carbonization solvent.

On the other hand, some Lewis acids are known to be effective catalysts for the polycondensation of aromatic compounds.[4–6)] One of the present authors previously studied the effect of the aluminium chloride catalyst on the carbonization of coal-tar pitches.[7)] The catalyst acted to lower the carbonization temperature and to give graphitizable carbon. Recently Mochida and his coworkers[8)] reported similar effects of this catalyst on the carbonization of aromatic compounds.

On the basis of these facts, we attempted carbonization in an inorganic melt containing aluminium chloride as the reaction solvent. Among many reports on the use of inorganic melts for organic reactions, only a few[9)] have mentioned the formation of carbonaceous matter as an undesired by-product, and none have mentioned the use of a melt specially planned for the purpose of carbonization.

As the melt, a mixture of 60 mol% of anhydrous aluminium chloride and 40 mol% of alkali metal chlorides was used. The reasons for this choice were its relatively low melting point, its strong acidity, its low cost, and the ease of handling. According to Kikkawa *et al.*,[10)] this molten system is believed to be in an equilibrium state, as is shown in Scheme 1, and to exhibit the catalytic action of aluminium chloride only when its content is over 50 mol% because of the very large equilibrium constant. In this melt, therefore, about 20 mol% of aluminium chloride can be expected to be present as active Lewis acid.

$$0.6\,AlCl_3 + 0.4\,MCl \rightleftharpoons 0.4\,AlCl_4^- + 0.4\,M^+ + 0.2\,AlCl_3 \quad (1)$$

M: K and Na

As the raw material, naphthalene was mostly used, among other carbocyclic and heterocyclic aromatic compounds.

In consequence, carbonization was successfully carried out throughout in the liquid state; a remarkable lowering of the carbonization temperature as well as a high carbon yield also resulted. Here we wish to describe this quite new method of carbonization.

Experimental

Materials. *Phenanthrene*: Prepared from a raw product of technical grade (90% pure) by purifying[11)] it to a purity of 99% or more; mp 99 °C (ethanol).

Tetrabenzo[a,c,h,j]*phenazine*(*PZ*): Prepared according to Pschorr;[12)] mp 480 °C(nitrobenzene).

Other Aromatic Compounds and Inorganic Salts: Commercially available reagents of an extra pure and guaranteed grade were used without further purification.

Standard Procedure. A 100-cm³ three-necked flask was fitted with a stirrer, a thermometer, and an air condenser with a calcium chloride tube on the top. In the flask a mixture of 0.6 mol of anhydrous aluminium chloride, 0.26 mol of sodium chloride, and 0.14 mol of potassium chloride was placed, after which the mixture was heated to melt (mp 95 °C). With vigorous stirring 0.01 mol of a raw material was then added at once. The temperature was raised to 300 °C for 2 h at a constant rate, and held there (±5 °C) for an additional 10 h. After some cooling, but before solidification, the mass was poured into a mixture of 500 g of crushed ice and 50 cm³ of 1 mol dm^{-3}-hydrochloric acid. The resulting black precipitate was filtered with suction, washed thoroughly with 0.1 mol dm^{-3}-hydrochloric acid and distilled water successively, and dried on calcium chloride in a vacuum. The crude product thus obtained was refluxed with 100 cm³ of benzene for 1 h and filtered while still hot to separate it into benzene-soluble (BS) and benzene-insoluble (BI) portions. The BI was dried in air and then on phosphorus pentaoxide in a vacuum. Hereafter, the BI shall be called "carbon" for reasons to be

Table 1. Yields and elemental analyses of products

No. of runs	Raw material	Yield of products		Elemental analysis of BI					
		BS (%)[a]	BI(%)[b]	C (%)	H (%)	N (%)	Ash (%)	Total (%)	Atom. ratio H/C
1	Anthracene	6	96	87.93	3.64	—	3.40	94.97	0.50
2	Phenanthrene	22	71	86.51	3.48	—	0.51	90.50	0.48
3	Naphthalene	10	92	83.33	3.27	—	0.66	87.26	0.47
4	Biphenyl	19	69	84.86	3.71	—	1.36	89.93	0.52
5[c]	1-Bromonaphthalene	trace	98	82.96	2.76	—	0.27	85.99	0.40
6[g]	1-Naphthol	7	92	83.82	3.22	—	0.47	87.51	0.46
7[d]	1-Nitronaphthalene	trace	99	70.20	2.02	4.35	0.50	77.07	0.35
8	1-Methylnaphthalene	7	91	82.96	3.51	—	0.44	86.91	0.51
9	PZ[e]	46[f]	59	77.08	2.69	3.23	3.84	86.84	0.42
10[i]	Quinoline	0	0	—	—	—	—	—	—
11	*trans*-Stilbene	11	89	84.32	3.34	—	0.54	88.20	0.48
12[j]	Benzene	trace	0	—	—	—	—	—	—
13[h]	Naphthalene	6.3	94.1	85.92	3.28	—	0.61	89.81	0.45

a) Calcd for the amount of the raw meterial used, based on the assumption that BS is the unchanged raw material. b) Calcd for the theoretical amount of carbon in the raw material used, based on the assumption that BI consists of pure carbon. c) The evolution of HBr was obserbed at 150 °C. d) The evolution of a brown gas was observed at 120 °C. e) Tetrabenzo(*a,c,h,j*)phenazine. f) Extracts by nitrobenzene (not by benzene), almost pure PZ. g) The evolution of HCl was observed soon after the mixing. h) A run specially designed to obtain precise quantitative data with a scale 10 times the others. i) No reaction. j) Almost no reaction.

described later.

All the runs were carried out by this procedure unless otherwise stated.

Estimation of the Reactivity of the Raw Materials. During the reaction, a series of specimens of the reaction mixture were taken out at regular intervals and poured into 0.1 mol dm^{-3}-hydrochloric acid; the mode of the resulting precipitate was observed. The first substance to be yielded was a floating brown precipitate, which consisted of tar or pitch; then a sinking black precipitate was yielded, with an increase in the reaction time. The time necessary for the first appearance of such a heavy precipitate was regarded as a measure of the reactivity of the raw materials.

Evaluation of Graphitizability of the Carbon. The carbons obtained were heated at 2800 °C in an argon stream for 15 min. The X-ray parameters for the carbons before and after the heat-treatment were calculated from the 002-diffraction profiles.

Results and Discussion

Properties of the Carbon Obtained. Outline: Most of the BI's formed black powder or flakes, and most were insoluble in usual organic solvents. Even upon hot-quinoline extraction they lost only a small percentage of their weight. At red-heat they were infusible, and they only slowly disappeared after prolonged heating. As is shown in Fig. 1 as an example, the X-ray diffraction profile of every BI exhibited a rather broad peak near the diffraction angle (2θ) of 25°, indicating that every BI has a layer structure similar to those of known carbon materials. The results of the elemental analysis of the BI's, given in Table 1, show that the values of the atomic hydrogen-to-carbon ratio (H/C) fall mostly within a range of 0.4—0.5.[13] These values correspond with those of carbonaceous mesophase isolated from various carbon materials made by simple heating in the temperature range of 390—490 °C.[14] Raw coke[15a] and so-called carboid coke[15b] have been reported to have similar H/C values, 0.49 and 0.41 respectively. All these facts support the idea of calling the BI's "carbon material" or "carbon" in a broader sense.

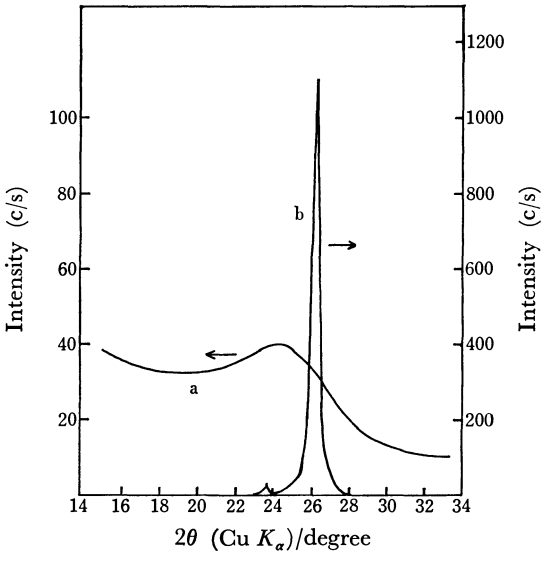

Fig. 1. 002-Diffraction profiles of a BI from naphthalene a) before and b) after heat-treatment at 2800°C.

The total value of the elemental analysis of each BI is short of 100%. The deficiency can be partly ascribed to the water and oxygen content. For example, the BI from anthracene (Run 1 in Table 1) lost 5.5% of its weight when heated in a glass tube over a small flame, yielding water drops on the cold wall of the tube. Regarding the oxygen content, no direct evidence has yet been obtained. However, as will be described below, some facts suggest that the

Table 2. X-Ray parameters of BI's before and after heating at 2800 °C

No. of runs	Raw Material	Parameters (Å)[b] Before heating d_{002}	Before heating L_c	After heating d_{002}	After heating L_c	Graphitizability
1	Anthracene	3.50	15	3.42	150	medium
2	Phenanthrene	3.70	20	3.37	700	high
3	Naphthalene	3.56	10	3.37	700	high
4	Biphenyl	3.68	10	3.45	60	low
5	1-Bromonaphthalene	3.74	15	3.40	200	medium
6	1-Naphthol	3.45	20	3.40	200	medium
7	1-Nitronaphthalene	3.72	10	3.52	20	low
8	1-Methylnaphthalene	3.56	15	3.40	200	medium
9	PZ	3.62	10	3.36[a] 3.44	—	low
11	*trans*-Stilbene	3.56	15	3.46	70	low

a) A composite profile. b) Throughout this paper 1 Å=0.1 nm.

BI's have a tendency to take in oxygen in some way.

Graphitizability: The results of the X-ray analysis, given in Table 2, show that the graphitizability of the carbons ranged widely. As factors influencing the graphitizability, besides the kind of raw material, the atmosphere during the reaction and the after-treatment proved important. An oxidative atmosphere showed a tendency to make the carbon nongraphitizable. About this problem a detailed investigation is now in progress.

Shape and Size: As Fig. 2 shows, the carbons were of various types as to their shape and size; that is, one type formed a fine powder, and another, rough films or plates. Some of the largest of the latter were 4—5 mm in diameter. The type seems to be determined mainly by the kind of raw material. The more reactive raw materials, such as bromonaphthalene and naphthol, gave large flakes, while the moderately reactive ones, such as naphthalene and anthracene, yielded fine particles. However, this is not always the case. A compound could often give different types of carbons when the reaction conditions are modified.

These results, considered together with those of the graphitizability, indicate the possibility of controlling the properties of the carbon by a proper combination of raw material and reaction conditions.

Mode of the Reaction. The standard melt is a colorless, clear liquid of a low viscosity in the temperature range of 95—400 °C, while it is immediately colored by the addition of a raw material. Only a few miligrams of every compound were enough for the coloration. The hue varied depending on the nature of the raw material; for example, it was deep blue with anthracene and dull orange with biphenyl. At the same time, the temperature of the reaction mixture rose by several degrees. No appreciable gas evolution was observed during all the period of reaction except in the cases described in the footnote in Table 1.

The temperature rise mentioned above indicates the dissolution of the raw material with a large heat of solution due to the strong solvation, and suggests, together with the coloration, the formation of some reactive intermediate.

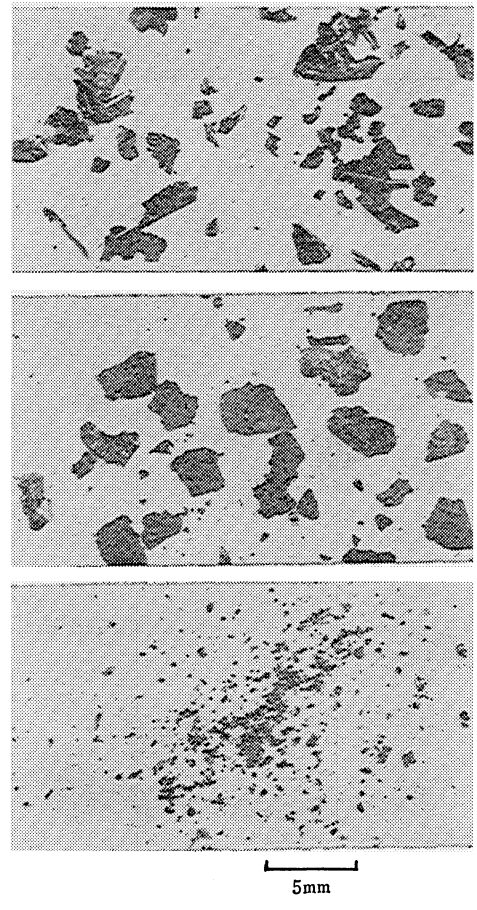

Fig. 2. Shape of BI's from a) 1-bromonaphthalene, b) 1-naphthol, and c) anthracene.

In the majority of cases, a reaction period of 4—8 h at 300 °C was almost enough for the first appearance of carbon in the reaction mixture. A longer reaction time increased the carbon yield.

In the case of naphthalene, during the first 1—2 h the reaction mixture was a homogeneous brown liquid, which yielded a tarry matter after the salts have been washed off; after 30 h, the mixture separated into

black precipitates and a clear, almost colorless medium. The BS from naphthalene, represented in Table 1, proved soluble in the melt at 100 °C, with a brown color.

From these facts, the reaction seems to proceed in solution, at least during the important stages.

Generally, in the precipitation polymerization of a linear polymer, the precipitating polymer does not grow further because the reactive chain end is deactivated by the entanglement of the chain. On the other hand, carbon is usually constructed from planar polymer, which is thought to be free from entanglement. The carbon here obtained is probably like this. Therefore, the fringe of the plate of carbon just produced should be still reactive for further polymerization, and the plate will continue to grow. Secondary aggregation among the plates may also be important for the growth to a visible size.

Regarding the mode of reaction, another possible one is as follows: the molten raw material is dispersed, not dissolved, in the melt as small oil drops, and inside of these oil drops the reaction proceeds under the catalytic action of aluminium chloride. In this case, the character of the reaction is essentially the same as that of the reactions mentioned above.[4-8] We can, however, find little support for this mode of reaction, but much counterevidence. For example, it can hardly explain why anthracene reacts far below its melting point, and yet more actively than naphthalene.

Reactivity of the Raw Materials. A rough evaluation of the reactivity of the raw materials was made from the estimation of the ease of carbonization. The carbon yields were also taken to consideration.

About this problem, an additional series of experiments were carried out with a shortened reaction time and at various reaction temperatures. The carbon (BI) yields of these runs, as is given in Table 3, clearly indicate the differences in reactivity among the compounds used.

From these results, the following sequences as to the reactivity may be drawn;

a) anthracene>naphthalene>phenanthrene>stilbene >biphenyl>PZ>benzene>quinoline

and b) 1-nitronaphthalene>1-bromonaphthalene>1-naphthol>1-methylnaphthalene>naphthalene.

The a) sequence indicates roughly that the larger conjugation system of the aromatic skeleton makes the compound more reactive. One of the reasons for the very small reactivities of PZ and quinoline is their general properties being inactive toward an electrophilic reagent. Another is probably the lack of a neutral molecule as the substrate for electrophilic attack. This lack can be caused by the almost complete formation of such a type of complex as $[-\overset{+}{N}=\cdots AlCl_3^-]$. The b) sequence is not likely to reflect simply the polar effect of substituents, but to show the reactivity of an individual compound in a complicated specific reaction involving the displacement and/or decomposition of the substituent itself. This view is based on the facts that nitronaphthalene decomposed soon after the mixing with the melt, evolving a brown gas; similarly, bromonaphthalene evolved hydrogen bromide. Moreover, bromonaphthalene gave carbon in a good yield at such a low temperature as 200 °C, as is shown in Table 3. These two compounds are generally less reactive toward the electrophilic reagent than naphthalene. These particular reactions present a tangential but interesting problem.

Table 3. Reaction temperatures and the yields of products[a]

No. of runs	Raw material	Reaction temp (°C)	Yield of products BS (%)[b]	BI (%)[b]
14	Naphthalene	350	8	92
15	Naphthalene	300	23	67
16	Phenanthrene	350	11	83
17	Phenanthrene	300	56	42
18	Quinoline	350	trace	3
19[c]	Quinoline	300	—	—
20	1-Bromonaphthalene	250	trace	100
21	1-Bromonaphthalene	200	8	92

a) All the runs were carried out in the same way as in the standard procedure, except that various reaction temperatures and a fixed reaction time of 2 h were employed and except that the raw material was added to the melt when the temperature of the melt became constant at the desired point b) Calcd, respectively, as stated in Table 1. c) No reaction.

Table 4. Compositions of melts and the yields of products[a]

No. of runs	Raw material	Composition of melt (mol)	Yield of products BS (%)[b]	BI (%)[b]
22[c]	Anthracene	$ZnCl_2$-NaCl-KCl (0.6 : 0.2 : 0.2)	—	—
1[d]	Anthracene	$AlCl_3$-NaCl-KCl (0.6 : 0.26 : 0.14)	6	96
23	Anthracene	$AlCl_3$-NaCl-KCl (0.49 : 0.35 : 0.16)	19	84
24	Anthracene	$AlCl_3$-NaCl-KCl (0.4 : 0.3 : 0.3)	25	76
25	Biphenyl	$AlCl_3$-NaCl-KCl (0.4 : 0.3 : 0.3)	91	2
26	Naphthalene	$AlCl_3$-NaCl-KCl (0.4 : 0.3 : 0.3)	80	16

a) All the runs were carried out in the same way as in the standard procedure, except for the use of melts of different compositions. b) Calcd, respectively, as stated in Table 1. c) The anthracene was recovered quantitatively. d) Transferred from Table 1 for the convenience of comparison.

Effect of the Acidity of Melt. Table 4 shows the effect of the acidity of various melts on the carbon yield. In the cases with [$AlCl_3$–NaCl–KCl] systems, the decreasing content of aluminium chloride resulted in a decrease in the yield of carbon. A melt containing 60 mol% of zinc chloride, known as a weaker Lewis acid than aluminium chloride, was quite inactive. These facts indicate the critical importance of the acidity of the melt.

It is also noteworthy that, although weaker, the

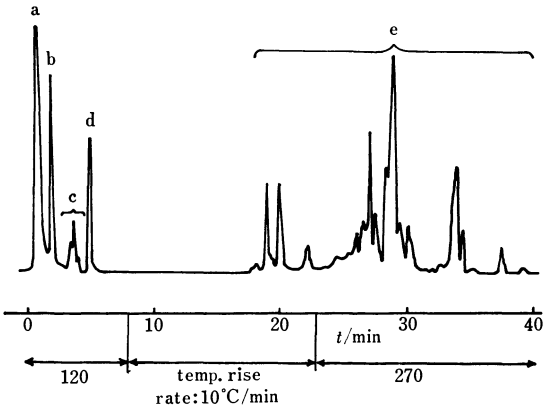

Fig. 3. Gas liquid partition chromatogram of a tar obtained from naphthalene by a reaction at 100 °C for 30 min. a: Solvent, b: *p*-dichlorobenzene as an internal standard, c: low boiler (Y: 1.02 mol%), d: naphthalene (Y: 2.78 mol%), e: high boiler (Y: 24.7 mol%).
Column: OV-17 5% on Chromosorb WAW DMCS 80—100 mesh, 3 mm×3 m; carrier gas: He, 60 cm³/min; detecter: TCD.

activity of the melt still remained when the content of aluminium chloride was lower than 50 mol%. This can be ascribed partly to the small amounts of aluminium chloride free in the equilibrium, and partly to the strong affinity of the compounds used to the Lewis acid. In the melt containing 40 mol% of aluminium chloride, anthracene, naphthalene, and biphenyl gave carbons, in yields decreasing in that order, in accordance with their decreasing basicity.

Products in the Earlier Stage of Reaction. Some runs with naphthalene were carried out with the standard procedure but at a fixed low temperature of 100 °C to yield the titled products. The tarry products were analyzed by TLC, GLPC, IR, UV, and NMR.

The results from GLPC, given in Fig. 3 as an example, show that the naphthalene reacted very fast, diminishing to a small percentage of the original amount during the first 30 min of the reaction. The products can be classified into three groups. The first (low-boiling, 1.02%) and the second (high-boiling, 24.7%) consists of substances with shorter and longer retention time than naphthalene respectively. The third (*ca.* 70%) consists of substances which did not give any peaks in the chromatogram because of their small volatility. The last two groups together form the greater part of the tar and can be accepted as consisting of polymerization products. The low-boiling group will be dicussed below.

The NMR spectrum of the tar, given in Fig. 4, shows that the tar contains aliphatic hydrogen atoms amounting to 50—60% for aromatic ones. This indicates that the polymerized naphthalene is partially hydrogenated. The IR spectrum of the tar supports this view. It shows a strong absorption band at 2920 cm^{-1} which can be assigned to the aliphatic C–H stretching vibration.

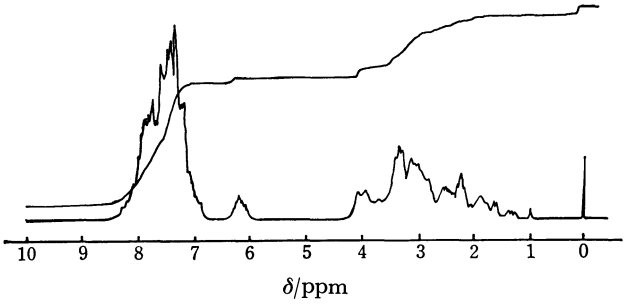

Fig. 4. ^{1}H-NMR Spectrum (60 MHz, in $CDCl_3$) of a tar obtained from naphthalene by a reaction for 30 min at 100 °C.

By TLC with the [silica gel–hexane] system, the tar was revealed to contain a number of substances which enamate a strong visible fluorescence when irradiated with ultraviolet rays. This indicates the formation of an aromatic condensed-ring structure with four or more rings. In fact, perylene was detected by a TLC-UV combined technique (R_f: 0.22, blue fluorescence; λ_{max}: 434 nm in ethanol).

The formation of the low-boiler is noteworthy, though the amount was small. The GLPC analysis of the tar using a glass capillary column revealed that the low-boiler consists of 1,2,3,4-tetrahydronaphthalene, 1,2-dihydronaphthalene, and several other compounds.

Possible Reaction Mechanism and Pathway. Many of the facts mentioned above all indicate that the reaction proceeds through an ionic mechanism. No evidence has been obtained to support a radical mechanism, which is believed to control the carbonization by simple heating.

The first step in the polycondensation toward carbon must be a C–C bond formation between two aromatic nuclei. This reaction probably involves an electrophilic attack by a positively charged aromatic nucleus, which is produced from an aromatic molecule and Lewis acid or proton, on a remaining neutral aromatic molecule. Similar ideas have been presented[6] and supported[16] by several authors concerning the condensation of aromatic compounds in the presence of Lewis acid. In the present system the mechanism is thought to be essentially the same. The coloration of the melt seems consistent with this mechanism. This assumption regarding the coloration finds supports in Morita and Hirosawa's report[17] and in the studies[18-19] referred to therein.

In parallel with the C–C bond formation, hydrogen disproportionation must take place. The hydrogen atoms necessary for the formation of the hydronaphthalenes must be supplied from the condensation. This reaction is probably also catalyzed by acids, probably in a manner similar to that described by Wristers[20] in the hydrogenation of benzene in superacid systems. It is important to recognize that this hydrogen transfer occurs not only between monomers, but also between any organic species in the system, and that, therefore, it plays a certain role in all stages of the reaction.

From these facts, the reaction, for example, with naphthalene should proceed as is shown in Scheme 2.

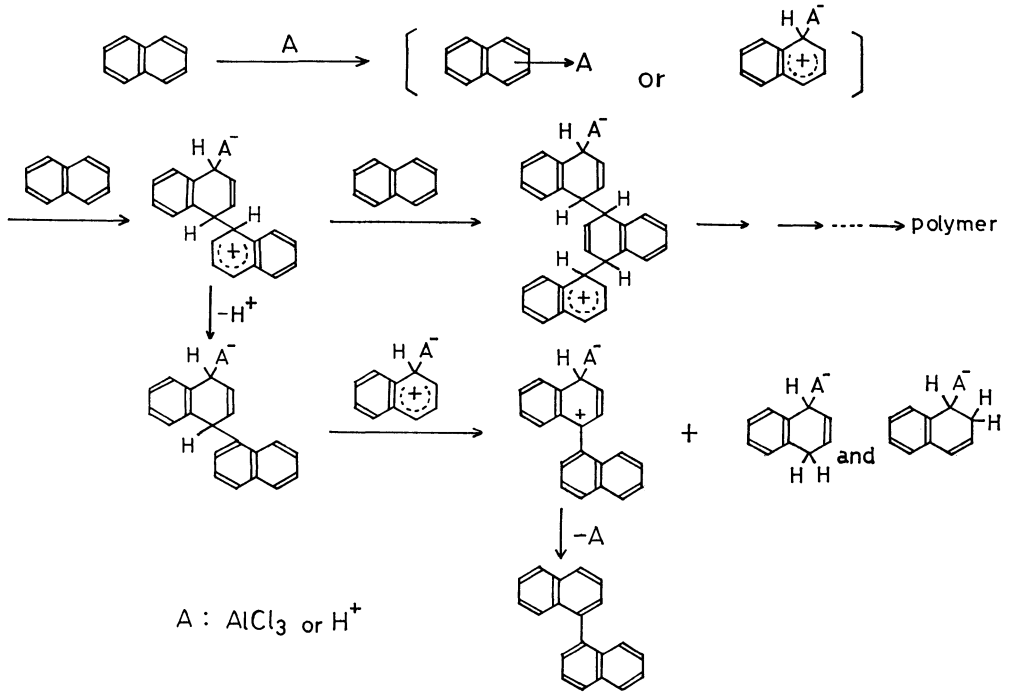

Scheme 2.

The 1,1′-type of condensation product may be predominant at first, while it may rearrange to the 2,2′-type in a thermodynamically controlled reaction.[6]

The fluorescent substances mentioned above seem to be formed by the intra- and intermolecular condensation of the naphthalene polymers. This type of condensation will become more important in the middle and later stages of reaction, and the combination of all the types of reactions mentioned above should produce carbon at last.

The true character of the catalyst is not clear. Throughout this series of experiments the invasion of the reaction system by moisture could not be prevented, and as a result the evolution of hydrogen chloride occurred. Therefore, it is reasonable to postulate that the catalytic action of the melt is partly attributable to that of a superacid system of [hydrogen chloride–aluminium chloride].

Features of This Process. The present process is characterized as *a solution reaction* through *an ionic mechanism*, resulting in *a low carbonization temperature* and *a high carbon yield.*

When simply heated, most polycyclic aromatic compounds first begin to be carbonized near 500 °C;[21] therefore, the compounds boiling below that temperature can not be carbonized under an ordinary pressure. The addition of aluminium chloride lowers the carbonization temperature. For example, by the $AlCl_3$-addition process Mochida *et al.*[8] succeeded in obtaining "coke" from polycyclic aromatic compounds with 2—4 rings under an ordinary pressure at 300 and/or 380 °C. However, the carbon yield does not appear to be high.[22] In our experiment, by the $AlCl_3$-addition process with naphthalene under conditions (with 5 mol% of aluminium chloride at 300 °C for 10 h) similar to those employed by Mochida *et al.*, the yields of BI and quinoline-insoluble matter (QI) were 39 and 7% respectively for the theoretical yield of carbon, while by the present process these yields were determined to be 94 and 85% (Run 13). The observed high yield—in other words, the high reaction velocity— in the present process can be ascribed mostly to the highly ionic character of the solvent, including the strong acidity, although the details of how these properties influenced the reaction machanism are not clear. The molten salt system should, at least, be more favorable for the formation of the positively charged species, the assumed reaction intermediates, than the organic system in the $AlCl_3$-addition process. One of the reasons for the occurrence of nongraphitizable carbons in the present study may be the too fast reaction, which is believed often to prevent the growth of a layer structure.

In practice, being a solution reaction makes the inspection of a reaction easy. The low carbonization temperature made the use of an autoclave unnecessary for the carbonization of materials with low boiling points.

This process can be modified in use. When the reaction stops halfway, tar or pitch is generally obtained. For example, naphthalene gave a pitch suitable for making graphitizable carbon. Methylnaphthalenes proved to isomerize and disproportionate quickly through the migration of the methyl group in the earlier stage of reaction; as a result, tars with a fixed composition were obtained from the different isomers.[23] These may be of importance for the commercial use of this process.

The present work was partially supported by a Grant-in-Aid for Scientific Research from the Ministry of Education. Project Number 155315 (1977).

References

1) A brief note on this subject was reported by two of the present authors, E. Ota and S. Otani, in *Chem. Lett.*, **1975**, 241.

2) L. S. Singer and I. C. Lewis, *Carbon*, **2**, 115 (1964).

3) S. Evans and H. Marsh, *Carbon*, **9**, 733 (1971).

4) H. Minato, N. Higosaki, and C. Isobe, *Bull. Chem. Soc. Jpn.*, **42**, 779 (1969).

5) M. Makabe, Y. Katayama, H. Itoh, and G. Takeya, *Nippon Kagaku Kaishi*, **1974**, 742.

6) P. Kovacic and F. Koch, *J. Org. Chem.*, **30**, 3176 (1965); P. Kovacic and C. Wu, *J. Polym. Sci.*, **47**, 45 (1960).

7) S. Otani and A. Oya, *Kogyo Kagaku Zasshi*, **73**, 1110 (1970); *Bull. Chem. Soc. Jpn.*, **45**, 623 (1972).

8) I. Mochida, K. Kudo, N. Fukuda, and K. Takeshita, *Carbon*, **13**, 135 (1975); I. Mochida, N. Fukuda, K. Maeda, and K. Takeshita, *Bull. Chem. Soc. Jpn.*, **49**, 260 (1976).

9) For example, P. C. Johnson and S. Swann, *Ind. Eng. Chem.*, **38**, 990 (1946).

10) S. Kikkawa, T. Hayashi, T. Miura, and T. Tani, Abstr. No. 11006, 22th National Meeting of the Chemical Society of Japan, Tokyo, April 1969.

11) J. Feldman, P. Pantages, and M. Ortchn, *J. Am. Chem. Soc.*, **73**, 4341 (1951).

12) R. Pschorr, *Ber.*, **35**, 2739 (1902).

13) The range should be shifted lower if the water content in the BI's is taken to account.

14) Y. Sanada, T. Furuta, J. Kumai, and H. Kimura, *Sekiyu Gakkai Shi*, **16**, 902 (1973).

15) a) Private communication from H. Sunago (Nittetsu Chemical Industrial Co.; Tobata, Kitakyushu 804); b) "Carbon and Graphite Handbook," ed by C. L. Mantell Interscience Publishers, New York (1968), p. 150, Table 6.

16) I. Mochida, E. Nakamura, K. Maeda, and K. Takeshita, *Carbon*, **13**, 489 (1975).

17) M. Morita and K. Hirosawa, *Nippon Kagaku Kaishi*, **1975**, 1555.

18) H. H. Perkampus and Th. Kranz, *Z. Phys. Chem., Neue Folge.*, **34**, 213 (1962); **38**, 295 (1963).

19) H. Sato and Y. Aoyama, *Bull. Chem. Soc. Jpn.*, **46**, 631 (1973).

20) J. Wristers, *J. Am. Chem. Soc.*, **97**, 4312 (1975).

21) T. Edstrom and I. C. Lewis, *Carbon*, **7**, 85 (1969).

22) Mochida *et al.* mentioned the BI content in the coke but not the yield of the coke.

23) The details will be reported in a subsequent paper, *Nippon Kagaku Kaishi*, submitted for publication.

Crystal Structure and Related Physical Properties of [*N,N,N,N',N',N'*-Hexamethylhexamethylenediammonium]$^{2+}$-[Tetracyanoquinodimethane]$_4^{2-}$: as a Two-dimensional Magnetic System

Serge FLANDROIS,* Daniel CHASSEAU,† Pierre DELHAES, Jacques GAULTIER,† Jacques AMIELL, and Christian HAUW†

Centre de Recherche Paul Pascal, Domaine Universitaire, 33405 Talence Cedex, France

† *Laboratoire de Cristallographie, Université de Bordeaux I, 33405 Talence Cedex, France*

(Received July 24, 1978)

The crystal structure, electrical conductivity and magnetic properties of (HMHDA)(TCNQ)$_4$ are studied. It appears that this ion-radical salt consists of planar arrays of (TCNQ)$_2^-$ dimers (diads) in weak interaction. The structure may thus be considered as quasi two-dimensional, the magnetic behavior being in line with two-dimensionality.

Organic radical-ion salts and charge transfer complexes, especially those based on tetracyanoquinodimethane (TCNQ), have received considerable attention in recent years.[1] As shown by crystallographic studies these compounds are often formed in linear chains of molecules. Physical properties such as electrical conductivity exhibit a high degree of anisotropy, makes these systems considered as quasi one-dimensional electronic substances.

Some questions have arisen as to the existence of a real electronic one-dimensionality.[2] There is always some interchain coupling whatever the mechanism is, and at 0 K the system must be three-dimensional. Many experimental and theoretical works deal with the cross-over from a one-dimensional behavior to a three-dimensional one, but at the present stage the situation is far from clear.

Our purpose was to investigate the dimensionality effects by synthesizing an homologous series of compounds, in which we would be able to vary the distance between the radical-ion chains. One way to accomplish this could be the use of cations such as polymethylene-diammoniums: $R_3N^+-(CH_2)_n-N^+R_3$. According to the length of the polymethylene chain we could expect a gradual variation of distances between TCNQ stacks. Thus the larger the number of CH_2 groups, the more rigorous should be the one-dimensionality of the electronic or magnetic system.

Hadek *et al.*[3] synthesized a series of TCNQ salts with *N,N,N,N',N',N'*-hexamethylpolymethylenediammonium cations model compounds for polymeric TCNQ salts. However, only the electrical conductivity was measured on powdered samples. This study incited us to prepare TCNQ salts of cations $(CH_3)_3N^+-(CH_2)_n-N^+(CH_3)_3$ and examine their crystal structure and physical properties on single crystals.

In this paper we will report a detailed study of the salt with $n=6$:

$$[(CH_3)_3N^+-(CH_2)_6-N^+(CH_3)_3](TCNQ)_4^{2-}$$

or (HMHDA)(TCNQ)$_4$. Contrary to our expectation TCNQ molecules in this salt do not crystallize in one-dimensional stacks. Actually the structure consists of diads with two-dimensional magnetic interactions.

Table 1. Crystal data for (HMHDA)(TCNQ)$_4$

$(C_{12}H_{30}N_2)(C_{12}H_4N_4)_4$—Molecular mass=1016		
Triclinic—Space group $P\bar{1}$		
$a=14.172$ (8) Å	$\alpha=77.67$ (5)°	$V=1371.2$ Å^3
$b=13.487$ (8) Å	$\beta=99.20$ (5)°	$Z=1$
$c=7.785$ (4) Å	$\gamma=75.51$ (5)°	$D_c=1.304$ g·cm^{-3}
$F(000)=530$	Cu $K\alpha$($\lambda=1.5418$ Å)	$\mu=6.33$ cm^{-1}

Experimental

Preparation of (HMHDA)(TCNQ)$_4$. To a hot methanol solution (40 ml) of Li-TCNQ (420 mg) was added a hot methanol solution (20 ml) of *N,N,N,N',N',N'*-hexamethylhexamethylenediammonium diiodide (460 mg). The solution was allowed to cool slowly down to room temperature. The resulting complex (700 mg) was collected and washed with water, methanol and ether. A deep blue crystalline product of (HMHDA)(TCNQ)$_2$ was obtained.

To a hot acetonitrile solution (40 ml) of (HMHDA)-(TCNQ)$_2$ obtained as above was added a solution (40 ml) of neutral TCNQ (408 mg) in acetonitrile heated at the same temperature. After being cooled down to room temperature the crystalline precipitate (600—700 mg) was filtered and washed successively with acetonitrile and ether.

The stoichiometry of the complexes was checked by electronic absorption spectroscopy with a Cary spectrophotometer, using acetonitrile as a solvent.

Crystal Data. The space group and unit cell dimensions were obtained initially from oscillation and Weissenberg photographs by using Cu $K\alpha$ radiation. The cell constants were subsequently refined on a Siemens computer-controlled three-circle diffractometer. Intensity data of 4763 independent reflexions were collected on this diffractometer from a crystal of dimensions $0.1\times0.22\times0.35$ mm with a $\theta/2\theta$ scan, a scintillation counter and Cu $K\alpha$ radiation; 2793 reflexions are significantly above zero. The c direction is the growth

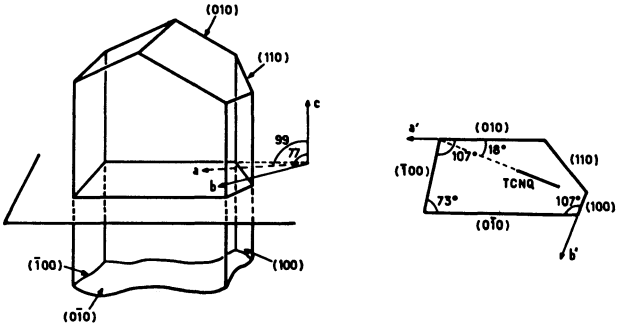

Fig. 1. Crystal morphology.

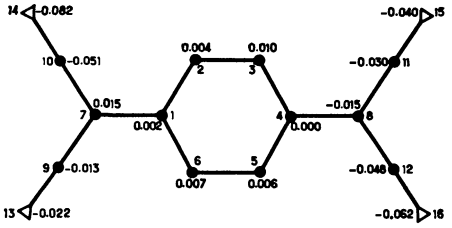

$0.2115x+0.9458y-0.2463z=1.6033$

TCNQ A

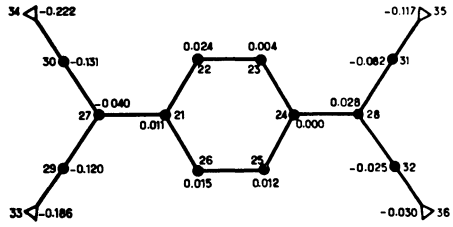

$0.2061x+0.9486y-0.2402z=8.2296$

TCNQ B

Fig. 2. Details of molecular planes and equations to the planes.

TABLE 2. FINAL POSITIONAL AND THERMAL PARAMETERS FOR NON-HYDROGEN ATOMS

(The figures in parentheses indicate standard deviations.)

	x	y	z	B/Å^2
C (1)	0.0736 (3)	0.1081 (3)	0.1639 (5)	3.7
C (2)	0.0693 (3)	0.1114 (3)	0.3453 (5)	4.0
C (3)	−0.0188 (3)	0.1327 (3)	0.3967 (5)	4.1
C (4)	−0.1117 (3)	0.1517 (3)	0.2708 (5)	3.6
C (5)	−0.1070 (3)	0.1489 (3)	0.0890 (5)	3.8
C (6)	−0.0189 (3)	0.1281 (3)	0.0385 (5)	3.7
C (7)	0.1651 (3)	0.0852 (3)	0.1129 (6)	4.2
C (8)	−0.2024 (3)	0.1720 (3)	0.3230 (5)	4.0
C (9)	0.1714 (3)	0.0815 (3)	−0.0667 (6)	4.1
C (10)	0.2559 (3)	0.0631 (4)	0.2406 (6)	4.6
C (11)	−0.2082 (3)	0.1745 (4)	0.5036 (6)	4.9
C (12)	−0.2940 (3)	0.1889 (4)	0.2016 (6)	4.9
N (13)	0.1754 (3)	0.0783 (4)	−0.2115 (6)	6.1
N (14)	0.3285 (3)	0.0455 (4)	0.3463 (6)	6.3
N (15)	−0.2132 (3)	0.1765 (4)	0.6485 (5)	6.3
N (16)	−0.3685 (3)	0.2034 (4)	0.1029 (6)	6.9
C (21)	0.1748 (3)	0.5907 (3)	−0.0094 (5)	3.8
C (22)	0.1740 (3)	0.5933 (3)	0.1728 (5)	4.0
C (23)	0.0875 (3)	0.6117 (3)	0.2287 (5)	4.1
C (24)	−0.0066 (3)	0.6313 (3)	0.1088 (5)	3.9
C (25)	−0.0058 (3)	0.6306 (3)	−0.0746 (5)	3.9
C (26)	0.0810 (3)	0.6111 (3)	−0.1310 (5)	3.8
C (27)	0.2647 (3)	0.5663 (3)	−0.0653 (6)	4.1
C (28)	−0.0952 (3)	0.6493 (3)	0.1692 (5)	4.1
C (29)	0.2683 (3)	0.5581 (4)	−0.2441 (6)	4.6
C (30)	0.3582 (3)	0.5394 (4)	0.0596 (6)	4.9
C (31)	−0.0964 (3)	0.6472 (4)	0.3528 (6)	5.2
C (32)	−0.1907 (3)	0.6701 (4)	0.0536 (6)	4.4
N (33)	0.2705 (4)	0.5513 (4)	−0.3860 (6)	6.4
N (34)	0.4325 (3)	0.5167 (4)	0.1620 (6)	6.7
N (35)	−0.0974 (3)	0.6458 (4)	0.4987 (6)	7.0
N (36)	−0.2681 (3)	0.6862 (4)	−0.0352 (6)	6.2
C (41)	0.5038 (6)	0.3337 (6)	−0.0403 (1)	8.6
C (42)	0.4876 (5)	0.2096 (6)	−0.5829 (8)	7.3
C (43)	0.3445 (4)	0.3098 (5)	−0.5133 (8)	6.7
C (44)	0.4775 (5)	0.1747 (6)	−0.0262 (1)	8.4
C (45)	0.4286 (6)	0.1028 (7)	−0.0233 (1)	9.3
C (46)	0.4492 (4)	0.0294 (6)	−0.0361 (8)	7.1
N (47)	0.4524 (3)	0.2561 (3)	−0.4413 (5)	5.0

TABLE 3. FINAL POSITIONAL AND THERMAL PARAMETERS FOR HYDROGEN ATOMS

(The figures in parentheses indicate standard deviations.)

	x	y	z	B/Å^2
H (17)	0.133 (3)	0.098 (3)	0.438 (5)	4.0
H (18)	−0.021 (3)	0.135 (3)	0.526 (5)	4.0
H (19)	−0.168 (3)	0.159 (3)	−0.002 (5)	4.0
H (20)	−0.019 (3)	0.128 (3)	−0.087 (5)	4.0
H (37)	0.239 (3)	0.580 (3)	0.259 (5)	4.0
H (38)	0.089 (3)	0.610 (3)	0.358 (5)	4.0
H (39)	−0.070 (3)	0.645 (3)	−0.162 (5)	4.0
H (40)	0.080 (3)	0.611 (3)	−0.256 (5)	4.0
H (54)	0.547 (4)	0.156 (4)	−0.214 (7)	8.5
H (64)	0.452 (4)	0.232 (4)	−0.165 (7)	8.5
H (55)	0.354 (4)	0.132 (4)	−0.266 (7)	9.0
H (65)	0.453 (4)	0.053 (4)	−0.300 (7)	9.0
H (56)	0.432 (4)	0.076 (4)	0.051 (7)	7.0
H (66)	0.407 (4)	−0.020 (4)	−0.028 (7)	7.0
H (71)	0.563 (4)	0.299 (4)	−0.428 (7)	8.6
H (81)	0.474 (4)	0.408 (4)	−0.483 (7)	8.6
H (91)	0.515 (4)	0.338 (4)	−0.272 (7)	8.6
H (73)	0.332 (4)	0.380 (4)	−0.612 (7)	6.7
H (83)	0.312 (4)	0.263 (4)	−0.574 (7)	6.7
H (93)	0.310 (4)	0.327 (4)	−0.418 (7)	6.7
H (72)	0.547 (4)	0.160 (4)	−0.514 (7)	7.5
H (82)	0.441 (4)	0.175 (4)	−0.640 (7)	7.5
H (92)	0.501 (4)	0.263 (4)	−0.682 (7)	7.5

direction of the crystals; the a and b directions, which belong respectively to the large and small lateral faces of the crystal, are tilted from the plane perpendicular to the c direction (Fig. 1).

Structure Determination. The structure was solved from a three dimensional Patterson synthesis and refined by block diagonal least squares. Refinement of the positional and isotropic thermal parameters of the 39 non-hydrogen atoms gave the residual $R=0.15$.

Positional parameters of the 23 hydrogen atoms were found on the difference Fourier synthesis. Further refinement of the non-hydrogen and hydrogen atoms with the aid of anisotropic and isotropic thermal parameters respectively gave a final value of 0.07 for R. The following weighting scheme was used

$$\sqrt{\omega} = 1 \qquad \text{if } |P_0| < P_1$$

$$\sqrt{\omega} = \frac{P_1}{P_0} \qquad \text{if } |P_0| > P_1$$

where $P_1=40$.

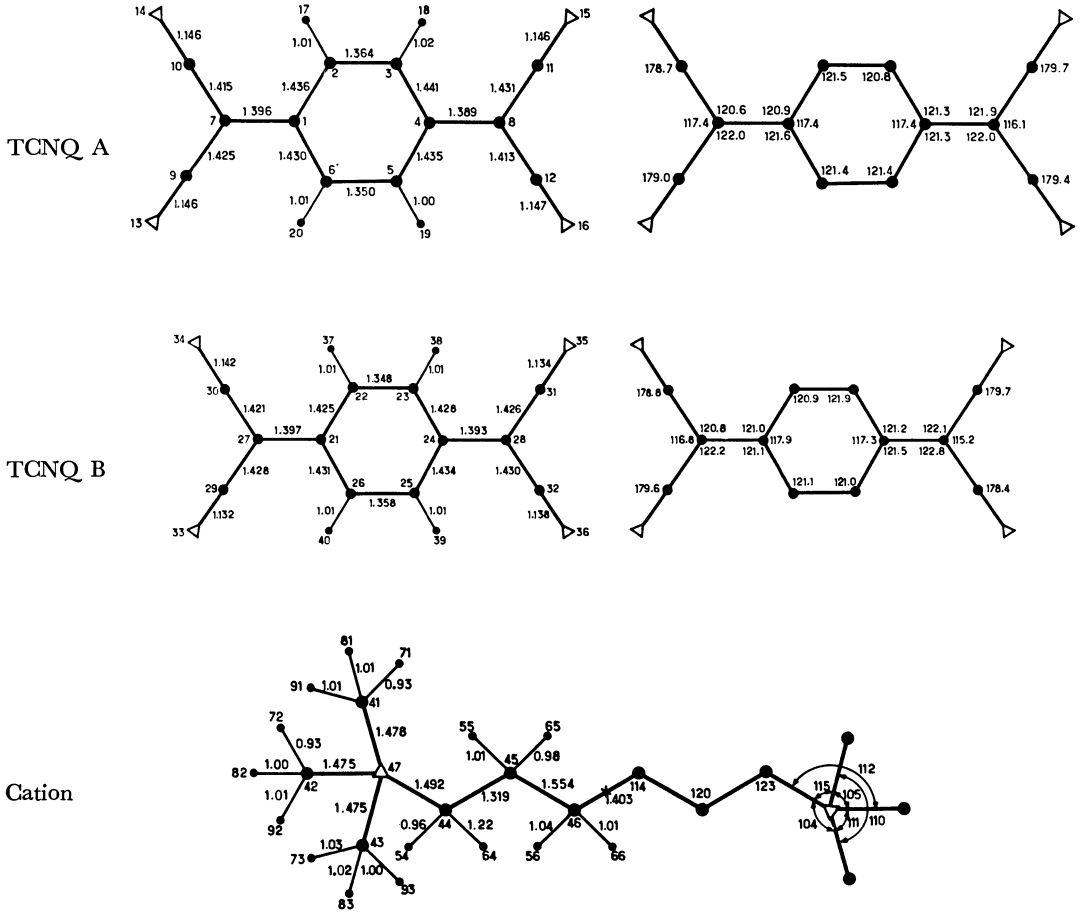

Fig. 3. Bond lengths (Å) and angles of TCNQ (A), TCNQ (B) and the cation.

The final positional and thermal parameters, together with their standard deviations, are listed in Tables 2 and 3.

Least squares planes were calculated through each quinonoid ring of the TCNQ molecules;** the distances of the atoms from these planes are shown in Fig. 2.

Electrical and Magnetic Measurements. The d.c. conductivities of single crystals (typical dimensions: $2\times0.2\times0.05$ mm) were determined by using a classical four-electrode technique. The electrical contacts were made with silver wires and silver paint.

Magnetic susceptibilities were obtained on microcrystalline samples by using Faraday's method in the temperature range 2.5—362 K. The core diamagnetism (-5.7×10^{-4} emu/mol) was calculated from Pascal's constants and from the value measured for TCNQ molecule.[4]

EPR measurements were carried out on single crystals with a Varian X-band spectrometer equipped with thermal variation accessories.

Results

Molecular and Crystal Structure. The dimensions of the two crystallographically independent types of TCNQ moiety are shown in Fig. 3. The average bond lengths of molecules A and B are nearly equal within experimental error, the differences between the averaged lengths of chemically equivalent bonds not exceeding 0.01 Å. The electronic charge of each TCNQ, calculated by the method developed by Flandrois and Chasseau,[5] is 0.46 electron and 0.50 electron for A and B, respectively. The negative charge is thus delocalized, leaving a half negative charge on each TCNQ molecule.

TCNQ A: The carbon atoms of the quinonoid ring are nearly in the same plane, the C–$(CN)_2$ groups being out of this plane and on the same side (Fig. 2). The dihedral angles between the plane of the quinonoid ring and the planes of the C(7)–$(CN)_2$ and C(8)–$(CN)_2$ groups are respectively 1.8° and 1.6°. The twist angles of the cyanomethylene groups around the C(1)–C(7) and C(4)–C(8) bonds are respectively 0.8° and 0.3°.

TCNQ B: The carbon atoms of the quinonoid ring are in the same plane : the C–$(CN)_2$ groups are clearly out of this plane, particularly the C(27)–$(CN)_2$ group, and on the same side. The dihedral angles between the plane of the quinonoid ring and the planes of the C(27)–$(CN)_2$ and C(28)–$(CN)_2$ groups are respectively 7.1° and 2.2°. The twist angles of the cyanomethylene groups around the C(21)–C(27) and C(24)–C(28) bonds are respectively 0.5° and 1.2°.

In each TCNQ, both –$C(CN)_2$ groups lie entirely on the same side of the quinonoid skeleton of the TCNQ molecule, so that the molecule has the shape of a shallow boat. In TCNQ B, the stronger deformation may be explained by a very short intermolecular distance

** XYZ are orthogonal atomic coordinates in Å where X is along a, Y in the (ab) plane orthogonal to a and Z orthogonal to the (XY) plane.

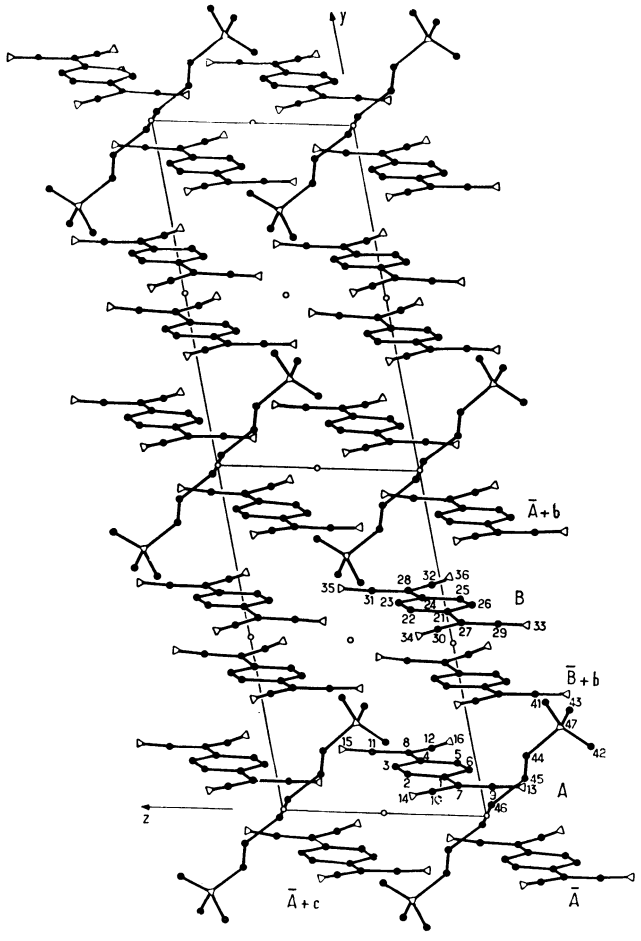

Fig. 4a. Projection of the crystal structure along the a axis.

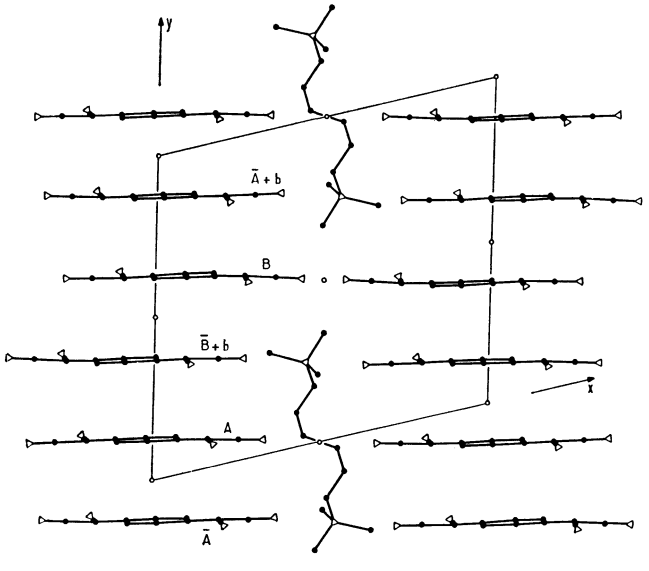

Fig. 4b. Projection of the crystal structure along the c axis.

between the N(34) atom and the C(41) atom of a cation methyl group (C–N=3.21 Å).

These results also confirm the general correlation found between the rotation of the $C(CN)_2$ groups and the length of the C–C bond adjacent to the quinonoid ring:[5] if this bond is shorter than 1.41 Å as

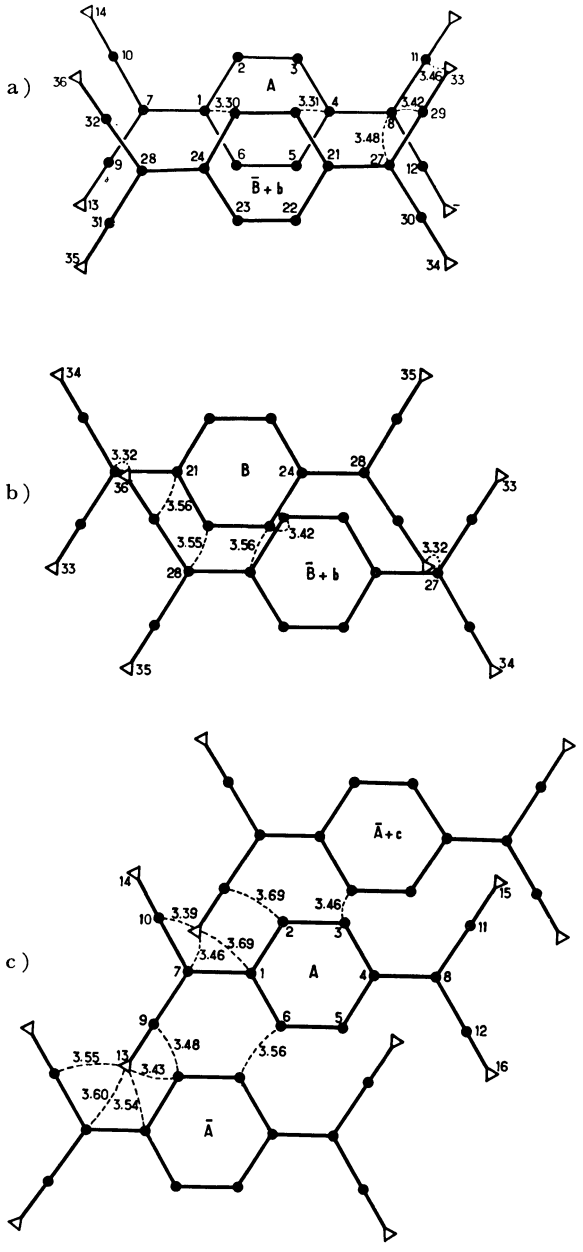

Fig. 5. Projection along the normal to the quinonoid ring of TCNQ molecules: a) $\overline{B}$+b on A; b) $\overline{B}$+b on B; c) $\overline{A}$ and $\overline{A}$+c on A. Some short distances between atoms of neighboring molecules are given.

in the present case the rotation is sligth, always less than 2°.

In the methylene chain, we found unusual and anomalous bond lengths (Fig. 3); the very short distance (1.32 Å) between the C(44) and C(45) atoms does not characterize a localized double bond; in the same way, the distance 1.40 Å of C(46)–C(46), cannot be a conjugated bond. Disorder, suggested by the high values of the temperature factors, may be a good explanation of these anomalous results. For the sake of comparison, the C–C bond lengths are 1.48, 1.56, and 1.48 Å in *N,N,N,N′,N′,N′*-hexamethylhexamethylenediammonium dibromide[6] and 1.53, 1.55, and 1.50 Å in *N,N,N,N′,N′,N′*-hexamethylhexamethylene-

diammonium dichloride dihydrate.[7]

Figures 4a and 4b show a general view of the crystal structure projected respectively along the a and c axes. The unit cell contains one cation and four roughly parallel TCNQ molecules, A, $\bar{B}$, B, $\bar{A}$,*** with two crystallographically independent molecules; the dihedral angle between the planes of the molecules A and B is 0.6°.

Cations, centered at 1/2, 0, 0 alternate in the a direction with the TCNQ groups; these groups make an angle of 56° with the best plane through the hexamethylene chain and an angle of 38° with the N(47)–$\bar{N}$(47) direction.

A good insight of the molecular arrangement is given by the projection of TCNQ moieties along the normal to the quinonoid ring (Fig. 5). This figure gives evidence for the pairing in (A, $\bar{B}$+b) diads. Within the (A, $\bar{B}$+b) dimer, the mode of overlap looks like those found, for example, in morpholinium–TCNQ salts:[8,9] the double bond of the quinonoid ring of one molecule is placed above the ring of the second one. The interplanar distance is 3.22 Å.

Between dimers there is only very weak overlap. The centrosymmetric pair of molecules B and $\bar{B}$+b has an interplanar separation of 3.38 Å. Only two short intermolecular contacts exist:

$$C_{25}(B) - C_{25}(\bar{B}+b) = 3.42\ \text{Å}$$

$$N_{36}(B) - C_{27}(\bar{B}+b) = 3.32\ \text{Å}$$

Between molecules A and $\bar{A}$, related by the symmetry operation −x, −y, −z, there is no real overlap, but the interplanar spacing is short (3.22 Å). Two short intermolecular contacts of 3.48 Å and 3.56 Å exist between C(9, A)–C(2, $\bar{A}$) and C(6, A)–C(3, $\bar{A}$) respectively. Similarly the $\bar{A}$+c molecule, related to A by the symmetry operation −x, −y, −z+1, has a short contact of 3.46 Å between the C(6, $\bar{A}$+c) and C(3, A) atoms, the interplanar spacing A−$\bar{A}$+c being 3.38 Å.

Thus the lattice appears to be constituted of diads in weak interaction in a plane parallel to the (b c) plane. Each diad D_1=(A, $\bar{B}$+b) is surrounded by five other diads in this plane: D_2=($\bar{A}$, B−b), D_3=($\bar{A}$+c, B−b+c), D_4=($\bar{A}$+b, B), D_5=(A+c, $\bar{B}$+b+c) and D_6=(A−c, $\bar{B}$+b−c),†† the distances between the centres of gravity of these diads being respectively D_1-D_2=7.44 Å, D_1-D_3=7.95 Å, D_1-D_4=7.17 Å, D_1-D_5=7.78 Å=D_1-D_6.

The planes containing these arrays of diads are separated by sheets of *N,N,N,N′,N′,N′*-hexamethylhexamethylenediammonium cations, giving rise to a quasi two-dimensional molecular lattice.

*** $\bar{A}$ and $\bar{B}$ are related to A and B respectively by the symmetry operation −x, −y, −z.

†† A, B x, y, z $\bar{B}$+b −x, −y+1, −z
$\bar{A}$, $\bar{B}$ −x, −y, −z $\bar{A}$+c −x, −y, −z+1
A+c x, y, z−1 B−b+c x, −y+1, −z
A−c x, y, z−1 B−b+c x, y−1, z+1
B−b x, y−1, z $\bar{B}$+b−c −x, −y+1, −z−1

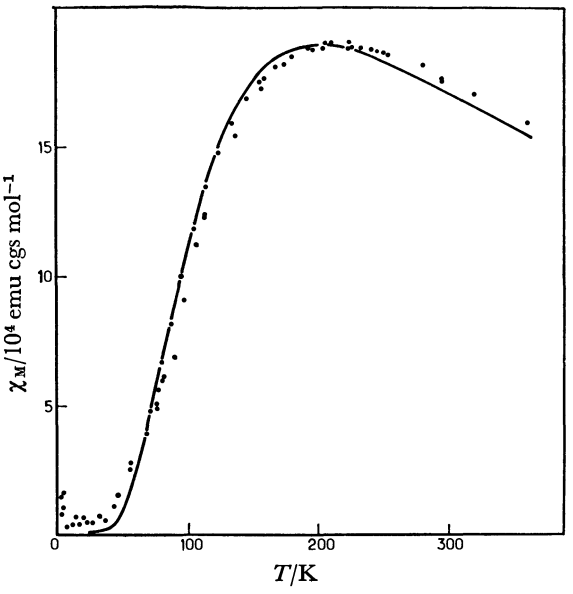

Fig. 6. Temperature dependence of paramagnetic susceptibility. The continuous line is a singlet-triplet fitting with J=0.028 eV.

In this way, (HMHDA)(TCNQ)$_4$ differs from most other radical anion salts in which the TCNQ molecules occur in continuous columns within which there is closer molecular contact than between adjacent columns. Nevertheless a structure exhibiting similar features has already been observed in some other 1:4 TCNQ salts such as *N,N′*-Diethyl-4,4′-bipyridinium–(TCNQ)$_4$.[10]

Electrical Conductivity. The conductivity at 300 K along the long crystal axis (c axis, Fig. 1) is *ca.* 4×10^{-3} $(\Omega\ \text{cm})^{-1}$. The radical-anion salt behaves as a typical semiconductor in the range 150—330 K, with an exponential dependence of conductivity on temperature obeying the equation: $\sigma=\sigma_0\ \exp(-E_a/kT)$, with a continuous dependence of E on temperature from 0.15 eV at *ca.* 150 K to 0.30 eV near room temperature.

Magnetic Properties. The temperature dependence of paramagnetic susceptibility is shown in Fig. 6 after substracting the diamagnetic part from the measured susceptibility. The curve exhibits a maximum at *ca.* 210 K. Below this temperature the susceptibility decreases to zero, although a slight increase appears at very low temperatures (T>10 K). The behavior is typical for semiconducting TCNQ salts [10] and may be interpreted in terms of an excited triplet state lying above the singlet diamagnetic ground state. The χ upright at low temperatures is probably due to impurities or lattice defects and corresponds to *ca.* 0.1% of the spins giving a slight Curie contribution.

For a compound with two electrons per mole, the susceptibility due to an excited triplet state is given by

$$\chi_M = 2Ng^2\mu_B^2/[kT(3+\exp(J/kT)] \quad (1)$$

where J is the energetic singlet-triplet separation, μ_B the Bohr magneton, g the g-factor, N the Avogadro number and k the Boltzmann constant.

The paramagnetic susceptibility of (HMHDA)-(TCNQ)$_4$ can be fitted by this expression within a

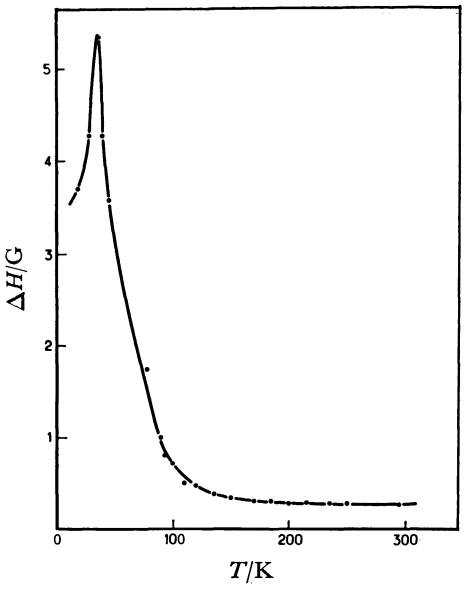

Fig. 7. Temperature dependence of EPR linewidth for the orientation of single crystal giving the largest variation with temperature.

good approximation (Fig. 6); the continuous line corresponds to a J-value of 0.028 eV.

The triplet character of the paramagnetic excitation is generally evidenced by a splitting of EPR spectra, caused by the dipole-dipole interaction of the electrons in the triplet state: [11] at high temperatures EPR spectra show an exchange-narrowed single line, but as the temperature is lowered the line broadens until finally it splits into a doublet. Actually no fine structure splitting could be detected in (HMHDA)(TCNQ)$_4$. The spectra showed a single line at all temperatures, although a rapid increase of linewidth was observed for some crystal orientations, when the temperature was lowered below 100 K (Fig. 7). The sharp maximum between 30 and 40 K reflects the disappearance of the activated part of the susceptibility and the prominence of the Curie contribution.

The linewidth exhibited a temperature dependent anisotropy. The variations shown in Fig. 8 correspond to rotations of the crystal around the c axis. When $\theta=0$ the magnetic field is along b′ axis (Fig. 1). Similar results were obtained at Q-band with a Varian spectrometer: the linewidth behavior is thus field independent. Figure 8 shows that the results can be fitted with the empirical expression:

$$\Delta H = a + b(3\cos^2\theta - 1) + c(3\cos^2\theta - 1)^2 \qquad (2)$$

where a, b, and c are temperature-dependent parameters.

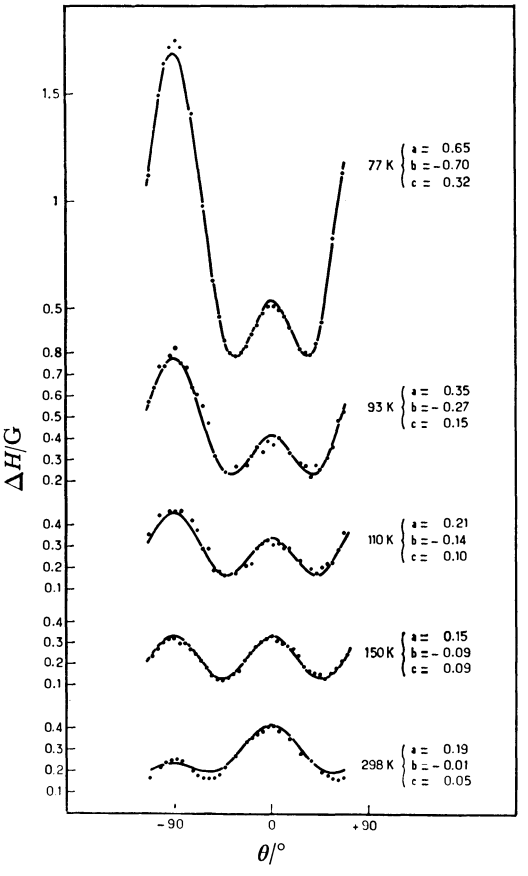

Fig. 8. Angular variation of the EPR linewidth at different temperatures for a single crystal. The rotation axis is the c axis. The parameters a, b, and c are in: $\Delta H=a+b(3\cos^2\theta-1)+c(3\cos^2\theta-1)^2$.

Discussion

Electrical Conductivity and Structure. Since the structure is two-dimensional the electrical conductivity should be isotropic in the corresponding plane. However, because of the smallness of crystals it was impossible to measure the conductivity along the b′-direction (Fig. 1).

The value of σ at room temperature along the c axis is very close to that of TCNQ salts of 1:4 stoichiometry with similar crystal structures.[10] This value is surprisingly high in comparison with other diadic compounds having a very weak overlap between the diads.

From a systematic examination of conductivities and structural data[12] it appears that the electrical conductivity depends on the plane-to-plane distances of TCNQ molecules, their types of overlap and the electronic charge distribution between TCNQ molecules (for a number of electrons smaller than the number of TCNQ molecules). A non-uniform distribution indicates that some charge localization occurs, leading to a smaller conductivity. In (HMHDA)(TCNQ)$_4$ the charge seems to be distributed uniformly, each TCNQ bearing a half electronic charge. The apparent delocalization compensates for the poor molecular overlaps and some rather large distances (3.38 Å) (Fig. 4), giving rise to a conductivity value better than expected.

Magnetic Properties and Structure. Thermal Variation of χ_p: A singlet-triplet behavior of χ_p is generally found for TCNQ salts in which each spin interacts strongly with only one adjacent spin. This occurs when TCNQ molecules form alternating stacks, composed of diads, triads or tetrads. The triplet character of the magnetic excitations is well understood[11] and clearly indicated experimentally by the dipolar splitting observed in EPR spectra at lowexcitati on concentra-

tion.

Another class of radical-anion salts and charge transfer complexes is known to crystallize in regular stacks with equal exchange interaction between neighbors along a given stack. In some of them an activated paramagnetic susceptibility $\chi_p \propto T^{-1} \exp(-\Delta E_p/kT)$ has been found. To our knowledge only charge transfer complexes with mixed stacks (···AD AD···) are concerned, such as TMPD–chloranil,[13] PD–chloranil[14] or TMPD–TCNQ.[15] No satisfactory explanation has been given concerning the origin of ΔE_p, but experimental results are interpreted by assuming a Wannier spin exciton model[16] where spin excitations are spatially uncorrelated.

At first view (HMHDA)(TCNQ)$_4$ seems to belong to none of the above classes. The lattice appears to be constituted of diads in weak interaction inside a plane. Moreover each diad bears an $S=1/2$ spin which is equally distributed on the two TCNQ molecules. So the spins appear to be delocalized on diads, the closest contacts of which are nearly van der Waals distances (3.42 Å to 3.51 Å). However, careful examination of the structure for C–C distances shows that there are more numerous close contacts between B molecules of two successive diads than between A molecules. So a slight tendency to the formation of tetrads AB BA is observed. If we calculate the zero-field parameter D for this arrangement from the approximately known spin-density distribution,[17] we get a value of several gauss. The value is small, but a splitting should be observed on the EPR spectra, which is not realized and thus seems to confirm the magnetic two-dimensionality of this system.

Angular Dependence of EPR Linewidth: The angular dependence of EPR linewidth shown in Fig. 8 is unusual. However, several similar features have been found for some TCNQ salts[18,19] and for charge transfer complexes of TMPD with TCNQ[15] and chloranil.[20] Two explanations have been proposed.

It has been shown that the angular variation, $\Delta H(\theta)$, of EPR linewidth in two-dimensional magnetic systems such as K_2MnF_4[21] or $(C_2H_{10}N_2)(MnCl_4)$[22] is approximately described by an expression of the form $\Delta H(\theta)=A+B(3\cos^2\theta-1)^2$, where θ is the angle between the applied magnetic field and the normal to the plane of the two-dimensional magnetic systems. For several TCNQ salts Takagi and Kawabe[18,19] fitted their results with the empirical relation:

$$\Delta H(\theta) = \alpha(3\cos^2\theta-1)^2 + \beta\sin^4\theta \qquad (3)$$

In spite of the lack of detailed structural information they inferred that the TCNQ salts studied are two-dimensional.

On the other hand, Soos and coworkers[20] showed that the linewidth anisotropy of TMPD–chloranil for which the one-dimensionality is firmly established was accurately reproduced by the secular part of the electron dipolar interaction. The angular dependence could be expected for spatially uncorrelated spin excitations.

Both explanations could be convenient for (HMHDA)(TCNQ)$_4$. From the crystal stucture data it looks like a nearly two-dimensional magnetic system. However, it is quite certain that the angular dependence of linewidth could be fitted by the angular dependence in the second moment of the secular part of the electron dipolar interaction, if the spin-densities distributions were accurately known, which is not the case.[20] The thermal variation of the angular dependence of linewidth could reflect either a change of spin distribution with temperature or a continuous thermal modification of the lattice, or, more probably, both together.

Contrary to the recent assertion of Takagi and Kawabe,[23] the temperature dependence of the linewidth does not seem to be related to the structural symmetry of the cation. From the study of several TCNQ salts with cyanine dyes as cations they deduced that for symmetrical cations the linewidth decreases when the temperature is lowered, while it increases for salts with unsymmetrical cations. Actually HMHDA is structurally symmetrical and the linewidth increases sharply with decreasing temperature (Fig. 7). Thus the behavior of ESR linewidths is not well understood, for both semiconducting salts as well as conducting ones.[24]

g*-*Tensor Anisotropy: Since two-dimensionality could not be evidenced by electrical measurements for experimental reasons, we thought that it could be reflected by the ***g***-tensor anisotropy. Actually the results show that the principal axis directions correspond to the molecular symmetry axes and not to the crystal axes.

The *g*-value perpendicular to the TCNQ molecular plane is found to be $g_{zz}=2.0021\pm0.0003$, the *g*-value along the in-plane molecular long axis is $g_{yy}=2.0028\pm0.0003$ and the third value $g_{xx}=2.0033\pm0.0003$. The average of this tensor: $\bar{g}\simeq 1/3\ (g_{xx}+g_{yy}+g_{zz})=2.0027\pm0.0003$ corresponds closely to the isotropic *g*-value of TCNQ anions in solution: 2.00263 ± 0.00005.[25]

Conclusion

From structural data it appears that (HMHDA)(TCNQ)$_4$ consists of planar arrays of $(TCNQ)_2^-$ dimers (diads) in weak interaction. Thus the structure may be considered as quasi two-dimensional, unlike most other TCNQ compounds for which a quasi one-dimensionality is generally assumed and sometimes established. The magnetic properties are in line with the two-dimensionality, although the linewidth behavior could be interpreted differently.

The study of this compound is interesting from another point of view. We recently obtained [26] a TCNQ salt with a parent cation: *N,N,N′,N′*-tetramethylhexamethylenediammonium (TMHDA). The salt, the stoichiometric formula of which is: (TMHDA)(TCNQ)$_2$(I)$_2$, has a metallic behavior above 120 K and contains iodine chains, although the method of preparation is the same. The reason why iodine is retained in the structure is not clear. The only difference with HMHDA is the substitution of two CH_3 groups by hydrogen atoms. A structural comparison between these compounds will be very useful. The study is in process.

We are grateful to Mrs. M. Joussot-Dubien and

M. L. Choukroun for preparing the samples.

References

1) J. J. Andre, A. Bieber, and F. Gautier, *Ann. Phys.*, **1**, 145 (1976).
2) H. R. Zeller, *Festkörperprobleme*, **13**, 31 (1973).
3) V. Hadek, H. Noguchi, and A. Rembaum, *Macromolecules*, **4**, 494 (1971).
4) P. Dupuis, S. Flandrois, and J. Neel, *C. R. Acad. Sci., Ser. C*, **269**, 1091 (1969).
5) S. Flandrois and D. Chasseau, *Acta Crystallogr., Sect. B*, **33**, 2744 (1977).
6) K. Lonsdale, H. L. Milledge, and L. M. Pant, *Acta Crystallogr.*, **19**, 827 (1965).
7) Y. Barrans, PhD Thesis, 1971, University of Bordeaux.
8) T. Sundaresan and S. C. Wallwork, *Acta Crystallogr., Sect. B*, **28**, 491 (1972).
9) T. Sundaresan and S. C. Wallwork, *Acta Crystallogr., Sect. B*, **28**, 3507 (1972).
10) G. J. Ashwell, D. D. Eley, S. C. Wallwork, and M. R. Willis, *Proc. R. Soc. London, Ser. A*, **343**, 461 (1975).
11) Z. G. Soos and D. J. Klein, "Molecular Association," ed by R. Foster, Academic Press, New York (1975), p. 1.
12) D. Chasseau, PhD Thesis, 1979, University of Bordeaux.
13) G. J. Pott and J. Kommandeur, *Mol. Phys.*, **13**, 373 (1967); P. L. Nordio, Z. G. Soos, and H. M. McConnell, *Ann. Rev. Phys. Chem.*, **17**, 237 (1966).
14) R. C. Hughes and Z. G. Soos, *J. Chem. Phys.*, **48**, 1066 (1968).
15) B. M. Hoffman and R. C. Hughes, *J. Chem. Phys.*, **52**, 4011 (1970).
16) Z. G. Soos, *J. Chem. Phys.*, **46**, 4284 (1967).
17) S. Flandrois and J. Boissonade, *Chem. Phys. Lett.*, **58**, 596 (1978).
18) S. Takagi and K. Kawabe, *Solid State Commun.*, **18**, 1467 (1976).
19) S. Takagi and K. Kawabe, *Phys. Lett. A*, **59**, 70 (1976).
20) T. Z. Huang, R. P. Taylor, and Z. G. Soos, *Phys. Rev. Lett.*, **28**, 1054 (1972).
21) P. M. Richards and M. B. Salamon, *Phys. Rev. B*, **9**, 32 (1974).
22) D. B. Losee, J. W. Hall, and W. E. Hatfield, *Solid State Commun.*, **16**, 389 (1975).
23) S. Takagi and K. Kawabe, *J. Phys. Soc. Jpn.*, **45**, 84 (1978).
24) G. Keryer, J. Amiell, S. Flandrois, P. Delhaes, E. Torreilles, J. M. Fabre, and L. Giral, *Solid State Commun.*, **26**, 541 (1978).
25) M. T. Jones and W. R. Hertler, *J. Am. Chem. Soc.*, **86**, 1881 (1964).
26) P. Dupuis, S. Flandrois, P. Delhaes, and C. Coulon, *J. Chem. Soc., Chem. Commun.*, **1978**, 337.

Polarographic Determination of Bismuth, Copper, Iron(III), Palladium, and Uranium(VI) after Extraction into Molten Naphthalene with Oxine

B. K. PURI,* Mamta GAUTAM, and Taitiro FUJINAGA†

Department of Chemistry, Indian Institute of Technology, Hauz Khas, New Delhi-29, India

† *Department of Chemistry, Faculty of Science, Kyoto University, Kyoto 606*

(Received December 27, 1978)

A rapid extraction-polarographic method has been developed for the direct determination of bismuth, copper, iron(III), palladium, and uranium(VI) extracted into the organic phase. Oxinates of metals were extracted into molten naphthalene at different pH values. With lowering of temperature, naphthalene separated out as a solid containing the metal oxinates. The solid mass was dissolved in DMF and the polarograms were recorded in the presence of a suitable supporting electrolyte. The metal oxinates give well defined waves. The relation between diffusion current and concentration is linear over a wide range of concentration with an average relative error not more than 1.05%. Interferences of various ions have been studied of the anions studied, only EDTA interfered in the extraction of bismuth, copper, iron(III), and uranium(VI). Of the cations studied, palladium interfered in the determination of bismuth, copper, iron(III), and uranium(VI). However, the intereference was eliminated by carrying out extraction first at low pH. In the determination of bismuth only copper interfered but its interference can also be eliminated as in the case of palladium. In the case of copper determination, only iron(III) interfered. In the determination of iron, copper interfered but interference can be eliminated by using a suitable masking agent. The determination of palladium and uranium(VI) is free from all interferences.

Of the heterocyclic nitrogen compounds, 8-quinolinol (oxine) reacts with more than fifty elements.[1] Studies on the use of this reagent in solvent extraction revealed that even with proper control of pH, the reagent is not selective in extracting specific elements, although many masking agents have also been examined.[2] The selectivity can be achieved by polarographic determination of metals after extracting into the organic phase. All the methods involve the use of mixed solvents, *i.e.* the extract is mixed with some other solvent in order to obtain well defined waves.[3-5] There are two disadvantages: (a) the sensitivity is much decreased since the amount of organic solvent used for the extraction is large, (b) the pH of the extract has to be readjusted in order to match the conditions with the standard.

We have developed a new method in which the metal complex is extracted with molten naphthalene and separated from the aqueous phase by solidification and subsequent filteration or decantation. Since the extraction is carried out at high temperature, the equilibrium in the two phases is attained rapidly and the complexes are extracted merely by contact with molten naphthalene. The main advantage is that a very small amount of the organic phase is required for complete extraction in order to get well defined waves and better sensitivity. The method has been tested and found successful for the extraction and polarographic determination of cadmium,[6] lead,[6] molybdenum,[7] indium,[8] and nickel.[9] In the present study, bismuth, copper, iron(III), palladium, and uranium(VI) have been extracted by this technique and determined polarographically. Elements such as Be(II), Hg(II), Sn(IV), Ti(IV), V(V), Cr(III), W(VI), Ce(IV), Co(II), Ga(III), Mn(II), Zn(II), and Zr(IV) can also be extracted by this technique, but they are not reduced at the dropping mercury electrode under these conditions, *i.e.* from 0.0 to −1.1 V. Above this potential oxine itself starts giving its own current. Interferences of various ions have been studied in detail. The method can be applied to the determination of these metals in complex materials.

Experimental

Reagents. All the metal salts solutions were prepared from G. R. samples in double distilled water, metal contents being controlled by classical methods (10). 0.1 M solution of oxine was prepared in alcohol. 2 M solution of pyridine, sodium perchlorate and perchloric acid were prepared as according to indicated in Table 2. Naphthalene and *N*,*N*-dimethylformamide (DMF) were also of G.R. grade and tested polarographically before use. Ammonia and perchloric acid were used for controlling the pH of the solutions.

Equipment. Polarograms in all cases were recorded at 25±0.5 °C with a Yanagimoto polarograph P-8 with three electrode systems. An H-type cell with fine porosite sintered glass disk between the two compartments was used. A saturated calomel electrode used as a reference electrode was connected to one compartment of the polarographic cell through potassium chloride agar-bridge. Dropping mercury electrode had the following characteristics, m: 1.52 mg/s, t: 4.78 s, and H: 60 cm in DMF with open circuit. In all instances the solution was deaerated with nitrogen for five minutes before recording the polarogram. A Hitachi pH-meter with glass electrode was used.

Metal Oxinates Standard in DMF. Aliquots of metal solutions were taken and precipitated with oxine,[11] filtered, washed with cold water, dissolved in DMF, transferred to 100 ml measuring flasks and made exactly 100 ml with DMF in each case. The solutions were used for studying the polarographic behaviour of metal oxinates in DMF.

General Procedure. An aliquot of each metal solution was taken separately. To this was added 1.0 ml of the reagent (oxine), the pH being adjusted as given in Fig. 2 after being transferred to round bottomed flasks with stopper and heated in a water bath at about 60 °C, 2 g of naphthalene was added, heating in the water bath being continued till naphthalene melted and formed a separate liquid layer. This was stirred vigorously till the naphthalene separated out as a solid mass. Once again the contents were heated in the water bath to remelt the naphthalene, shaken vigorously and allowed to stand. Naphthalene was separated from the aqueous phase by filteration, dried in the folds of the filter paper and dissolved in warm DMF (*ca.* 40 °C).

Table 1. Effect of naphthalene on the polarograms of iron(III) and palladium oxinates

Amount of naphthalene added, g	Amount of Fe(III) added: 168.00 μg Perchloric acid: 0.1 M Pyridine: 0.1 M				Amount of Pd(II) added: 106.00 μg Sodium perchlorate: 0.1 M Pyridine: 0.1 M			
	Specific conductivity $\Omega^{-1}\,cm^{-1}$ at 35 °C	Viscosity of the solution centipoise at 35 °C	i_d for Fe(III) in mm	$E_{1/2}$ for Fe(III) in V	Specific conductivity $\Omega^{-1}\,cm^{-1}$ at 35 °C	Viscosity of the solution centipoise at 35 °C	i_d for Pd(II) in mm	$E_{1/2}$ for Pd(II) in V
0.00	4.000×10^{-3}	1.164	—	—	4.545×10^{-3}	1.036	—	—
0.30	3.906×10^{-3}	1.205	76.00	−0.10	4.166×10^{-3}	1.055	78.00	−0.25
0.60	3.846×10^{-3}	1.210	76.00	−0.10	4.000×10^{-3}	1.063	70.00	−0.20
0.90	3.787×10^{-3}	1.218	76.00	−0.10	3.937×10^{-3}	1.073	69.00	−0.18
1.20	3.676×10^{-3}	1.234	76.00	−0.12	3.846×10^{-3}	1.095	68.00	−0.18
1.50	3.521×10^{-3}	1.247	75.00	−0.12	3.703×10^{-3}	1.109	68.00	−0.18
1.80	3.333×10^{-3}	1.284	72.00	−0.12	3.597×10^{-3}	1.129	66.00	−0.18
2.10	3.184×10^{-3}	1.320	68.00	−0.12	3.448×10^{-3}	1.145	63.00	−0.18

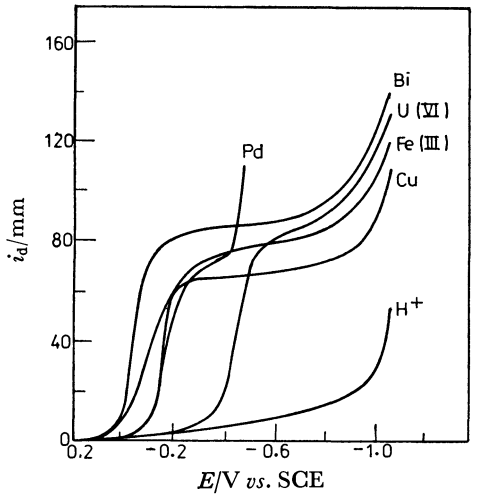

Fig. 1. Polarographic waves of metal oxinates in DMF. Bismuth: 82.80 μg, perchloric acid: 0.1 M, naphthalene: 1.0 g drope time: 4.78 s, H: 60 cm and the recorder sensitivity: 5×10^{-9} A/mm. Copper: 79.37 μg, sodium perchlorate: 0.1 M, recorder sensitivity: 10×10^{-9} A/mm, rest of the conditions are the same as for bismuth. Iron(III): 168.00 μg, pyridine: 0.1 M + 0.1 M perchloric acid, recorder sensitivity: 7×10^{-9} A/mm, rest of the conditions are the same as for bismuth. Palladium: 106.00 g, 0.1 M sodium perchlorate + 0.1 M pyridine, recorder sensitivity: 3×10^{-9} A/mm, rest of the conditions are the same as for bismuth. Uranium(VI): 95.21 μg, recorder sensitivtiy: 3×10^{-9} A/mm, rest of the conditions are the same as for iron(III).

A supporting electrolyte of appropriate type was added in each case, the volume being made exactly 20 ml with DMF in a measuring flask. 10 ml of the solution was taken separately in the polarographic cell and deaerated with pure nitrogen for 5 min. The polarogram was recorded, in each case i_d being referred to the calibration curve prepared under similar conditions.

Preliminary observations indicated that the metal oxinates give well defined waves (Fig. 1). Bismuth: 0.1 M perchloric acid (solution prepared in DMF), copper: 0.1 M $NaClO_4$ (solution of $NaClO_4$ in H_2O), iron and uranium: both in 0.1 M $HClO_4$ in DMF + 0.1 M pyridine in H_2O (waves were not diffusion controlled when both the electrolytes solutions were prepared in DMF) and palladium: 0.1 M pyridine + 0.1 M $NaClO_4$ (both electrolytes in DMF, aqueous solutions of the electrolytes gave distorted waves for palladium). In the case of palladium two waves appeared in the supporting electrolytes. Only the first wave was used for the analysis since a large maximum appeared on the second wave which was not supressed with the use of common maxima supressors.

Effect of Naphthalene on the Polarograms of Metal Oxinates. Aliquots of the metal oxinates solutions were taken individually (Bi: 82.80 μg, Cu: 79.37 μg, Fe(III): 168.00 μg, Pd: 106.00 μg, and U(VI): 95.21 μg) in the polarographic cell. The amount of naphthalene was varied from 0.0—2.1 g by adding a different volume of its 30% solution in DMF. The supporting electrolytes were added, the final volume being made 10 ml with DMF. The solution was deaerated and the polarograms were recorded. In case of bismuth, copper and uranium(VI), i_d remained constant up to 1.8 g of naphthalene added. Above this amount, i_d started decreasing slightly due to the increase in the viscosity of the medium given in Table 1. The wave for iron(III) and palladium developed only in the presence of naphthalene, *i.e.* in the absence of naphthalene a large current appeared. The large current might be due to the streaming effect eliminated in the presence of naphthalene which increases the viscosity of the medium (Table 1). In case of iron(III), i_d remained constant in the range 0.3—1.5 g of naphthalene and 0.6—1.5 g of palladium. In general, $E_{1/2}$ remained almost constant in all cases but i_d started decreasing when the amount of naphthalene exceeded a certain amount, obviously due to the further increase in the viscosity of the medium.

Effect of the Chelating Agent on the Polarograms of Metal Oxinates. Aliquots of the metal oxinates solutions were taken under conditions similar to those described above. To these were added supporting electrolytes, 1 g of naphthalene in the form of 30% solution. The amount of oxine being varied from 0.0—75.0 mg by adding different volume of its 5% solution in DMF. In all the cases except palladium, $E_{1/2}$ shifted towards negative direction. This indicates that the metals form stable oxinate complexes in the presence of excess of oxine, while palladium oxinate might be decomposed under these conditions. i_d remained constant in the range 0.0—11.5 mg for bismuth, 0.0—18.25 mg for copper, 0.0—15.0 mg for iron(III), 0.0—75.0 mg for palladium and uranium(VI). Above this concentration of the oxine added,

Table 2. Polarographic characteristics of metal oxinates in the presence of 1 g of naphthalene in DMF

Metal	Supporting electrolyte	$E_{1/2}$/V from log plot	I	Range of concentration in μg/20 ml	Value of slope from log plot in mV	Remarks	Average relative error %
Bismuth	0.1 M $HClO_4$ in DMF	−0.05	2.399	10.35—248.40	65.0	Irreversible	0.95
Copper	0.1 M $NaClO_4$ in H_2O	−0.14	3.858	3.96—198.40	38.0	Slightly irreversible	0.78
Iron(III)	0.1 M $HClO_4$ in DMF + 0.1 M Pyridine in H_2O	−0.11	1.466	11.20—324.80	87.0	Irreversible	0.97
Palladium	0.1 M Pyridine + 0.1 M $NaClO_4$ both in DMF	−0.18	1.259	10.60—212.00	76.85	Irreversible	0.05
Uranium(VI)	0.1 M $HClO_4$ in DMF + 0.1 M Pyridine in H_2O	−0.45	1.398	5.95—190.40	64.75	Reversible	0.88

Drop time: 4.78 s, m: 1.52 mg/s, H: 60 cm. Recorder sensitivity, bismuth: 5×10^{-9} A/mm, copper: 10×10^{-9} A/mm, iron(III): 7×10^{-9} A/mm, palladium: 3×10^{-9}, and uranium(VI): 3×10^{-9} A/mm.

the lower plateau in the case of bismuth and iron(III) became distorted. A prewave might start appearing in the presence of higher amount of oxine before the actual wave which was not fully developed. In the case of copper a maximum appeared in the higher amount of oxine added.

Effect of Water on the Polarograms of Metal Oxinates: Aliquots of each metal oxinate solution were taken separately in a polarographic cell. The amount of water was varied from 0.0—1.5 ml in different steps. The total volume of the solution was kept 10 ml in each case. In the case of bismuth 0.4 ml of water had no effect on i_d on the shape of the polarogram but above this amount of water, i_d started decreasing. A part of naphthalene might be separated in the colloidal state which would hinder the diffusion of the metal ions. The wave was drawn out at 1.5 ml of the water added. For this amount of water, naphthalene was separated out which increases the resistance of the medium, giving a drawn out wave for bismuth. 0.5 ml of water can be tolerated in case of copper, above this volume i_d started decreasing but $E_{1/2}$ remained constant. In the case of iron(III), 0.7 ml of water can be tolerated but above this volume a maximum appearing might be due to the streaming effect. Only 0.2 ml of water can be tolerated in the case of palladium above this amount i_d started decreasing though $E_{1/2}$ remained constant. The wave of palladium is very sensitive to water as indicated in the preliminary observations. In the case of uranium(VI), i_d started decreasing and $E_{1/2}$ started shifting towards positive potential when the amount of water exceeded 0.4 ml. The uranium complex might be decomposed under these conditions.

The linear dependence of the limiting current on the square root of the height of mercury column indicates that the rate of reduction of these metal oxinates is diffusion controlled. The plot of $\log i/i_d - i_d$ *vs.* E gives a straight line. The values of slopes and $E_{1/2}$ calculated from the plot are given in Table 2. Copper undergoes reduction slightly irreversible with two electron change while uranium(VI) undergoes reduction reversibly with one electron change, bismuth, iron(III), and palladium are reduced irreversibly. The graph plotted between the concentrations of metal oxinates and diffusion currents give straight lines over a wide range of concentration. The diffusion current constants were calculated using the Ilkovic equation, $I=i_d/Cm^{2/3}t^{1/6}$

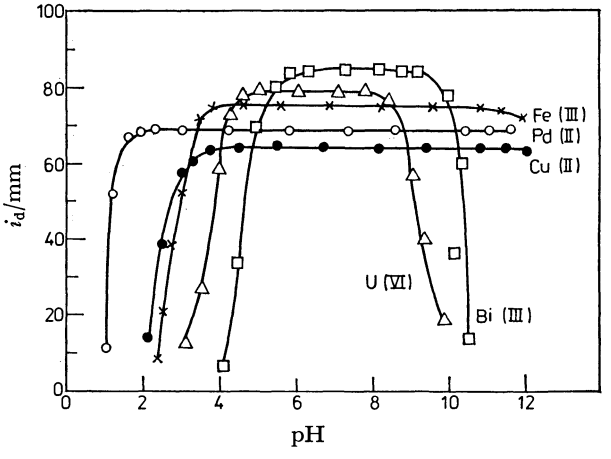

Fig. 2. Effect of pH on the extraction of bismuth, copper, iron(III), palladium, and uranium(VI). Naphthalene taken for each extraction: 2.0 g. Oxine used in each case: 1.0 ml of 1% solution in ethanol. Rest of the conditions are the same as Fig. 1.

and are also given in Table 2. They are constant, indicating that the method is as sensitive as most of the polarographic method in the aqueous media. The average relative error did not exceed 1.05%.

Effect of pH *on the Extraction of Metals.* Extraction was carried out by the general procedure but at different pH. The effect is shown in Fig. 2.

Effect of the Chelating Agent on the Extraction of Metals. Extraction was carried out at different concentration of oxine. It was found that extraction was complete; Bi: 7—20 mg, Cu: 2.5—15.0 mg, Fe(III): 4.0—20 mg, Pd: and U(VI): 6.0—18 mg of the oxine added.

Effect of Naphthalene on the Extraction of Metals. Extraction was complete in all cases when the amount of naphthalene used was higher than 0.8 g, so 2.0 g was used for safe side.

Effect of Aqueous Phase on the Extraction of Metals. The volume of the aqueous phase was varied from 20 ml to 250 ml. The extraction was more than 99% when the volume of the aqueous phase did not exceed the following amounts:

Table 3. Effect of anions on the determination of bismuth, copper, iron(III), palladium, and uranium(VI)[a]

Salt added	Amount of ion added in mg	Bismuth found in μg	Copper found in μg	Iron found in μg	Palladium found in μg	Uranium found in μg	Remarks
Sodium citrate	31.45	80.50	42.50	160.50	106.00	30.25	Extraction completed
	7.85	—	79.50	167.50	—	94.50	at low concentration
Sodium oxalate	33.60	80.75	65.20	122.50	105.50	35.50	Same as above
	3.36	—	80.50	166.66	—	94.00	
Sodium borate	20.20	81.25	79.50	168.00	106.00	95.50	—
Sodium azide	32.30	80.00	79.25	168.50	105.00	95.00	—
Sodium fluoride	22.60	81.00	75.25	167.75	105.50	35.40	Extraction complete
	11.30	—	79.50	—	—	94.00	at low concentration
Sodium thiosulfate	21.10	81.75	79.25	167.00	105.75	84.50	—
Sodinm phosphate	25.00	80.75	50.75	166.75	106.50	35.75	Extraction complete
	6.50	—	79.00	168.00	—	94.25	at low concentration
Disodium EDTA	40.00	nil	nil	nil	105.00	10.25	No extraction in case of Cu, Bi, and Fe
Sodium potassium	39.40	80.25	50.25	167.50	105.50	60.25	Extraction complete
tartrate	10.00	—	79.00	—	105.50	94.00	at low concentration
Sodium sulfate	40.00	80.00	79.50	168.50	106.00	95.25	—
Potassum thiocyanate	29.85	80.50	79.00	168.00	105.75	95.50	—
Potassium chloride	23.80	80.50	79.50	167.50	105.75	95.50	—
Potassium bromide	33.60	80.00	79.75	167.75	106.50	96.00	—
Potassium iodide	38.25	82.25	79.00	168.50	107.00	94.50	—

a) Conditions the same as those given in Fig. 2.

Table 4. Effect of cations on the determination of bismuth, copper, iron(III), palladium, and uranium(VI)[a]

Salt	Amount of foreign ion added in mg	Bismuth found in μg	Copper found in μg	Iron found in μg	Palladium found in μg	Uranium(VI) found in μg
Palladium chloride	00.60	81.50[b]	80.75[b]	169.50[b]	—	95.00[b]
Uranyl acetate	00.56	80.50	80.00	168.25	106.50	—
Tin(IV) chloride	00.42	80.00	79.25	168.00	107.00	95.00
Lead(II) nitrate	0.66	81.00	79.50	169.00	106.25	95.75
Sodium tungstate	00.56	80.50	79.00	169.50	106.50	95.25
Chromium(III) nitrate	00.36	80.75	79.75	166.50	106.00	95.50
Iron(III) chloride	00.20	81.75	c)	—	107.00	95.50
Copper(II) sulfate	00.25	81.00[b]	—	c)	107.25	95.00
Sodium vanadate	00.43	80.75	79.75	168.00	106.50	95.25
Bismuth nitrate	00.43	—	79.50	168.75	106.75	95.00
Thallium(I) nitrate	00.76	80.50	79.00	168.25	106.00	95.50
Mercury(II) chloride	00.70	81.00	80.25	168.50	106.50	96.00
Sodium molybdate	00.39	80.25	79.00	167.50	105.00	94.50
Nickel chloride	00.25	81.00	78.50	167.50	106.75	96.00
Cadmium chloride	00.66	80.75	79.50	168.00	106.50	95.25
Zinc nitrate	00.22	79.75	80.00	169.00	106.00	95.25
Manganese sulfate	00.27	80.50	80.25	169.75	107.50	96.00

a) Conditions the same as those given in Fig. 2. b) Interfering cation removed by extraction at low pH. c) Determination not possible.

Bi: 120 ml, Cu: 100 ml, Fe(III): 105 ml, Pd: 190 ml, and U(VI): 150 ml. Extraction was not quantitative above the volume of the aqueous phase.

Effect of Diverse Ions on the Determination of Metals. The effect is given in Tables 3 and 4. Among the anions examined the extraction of bismuth, copper, iron(III), and uranium(VI) is not possible in the presence of EDTA. In the presence of citrate, oxalate, tartrate, phosphate, and fluoride, the results are low in the case of copper, iron(III), and uranium(VI). However, they are satisfactory in the presence of a relatively low concentrations of the anions. In the determination of bismuth, copper, iron(III), and uranium(VI), palladium interfered, but its interference can be eliminated by extracting palladium first at low pH and then the other metal ions were extracted from the aqueous phase at their proper pH values (Fig. 2). In the determination of bismuth only copper interfered but its interference can be eliminated as in the case of palladium. In the determination of copper,

only iron(III) interfered while in the determination of iron(III), only copper interfered. The interference can be eliminated by using suitable masking agents.[12] There is no interference in the determination of palladium and uranium(VI).

References

1) F. J. Welcher, "Organic Analytical Reagents," D. Van. Nostrand Co. Inc., Princeton N. J. (1947), Vol. I.
2) J. Stary, *Anal. Chim. Acta*, **28**, 132 (1963).
3) R. M. Dagnall and S. K. Hasanuddin, *Talanta*, **15**, 1025 (1968).
4) T. Fujinaga, T. Nagai, and K. Yamashita, *J. Chem. Soc., Jpn.*, **84**, 506 (1963).
5) I. V. Pyatnitskii and R. P. Ruzhanskaya, *Zh. Anal. Khim.*, **25** (6), 1063 (1970).
6) T. Fujinaga and B. K. Puri, *Bull. Inst. Chem. Res., Kyoto Univ.*, **51**, (5), 253 (1973).
7) T. Fujinaga and B. K. Puri, *Z. Anal. Chem*, **269**, 340 (1974).
8) T. Fujinaga and B. K. Puri, *Talanta*, **22**, 71 (1975).
9) T. Fujinaga and B. K. Puri, *Indian J. Chem.*, **14A**, 72 (1976).
10) A. I. Vogel, "A Textbook of Quantitative Inorganic Analysis," Longmans, Green and Co., London (1964).
11) W. Geilman and F. J. Weibke, *Anorg. Allg. Chem*, **199**, 347 (1931).
12) D. D. Perrin, "Masking and Demasking of Chemical Reactions," Wiley-Interscience, New York (1970).

Bis(*N*-acetyl-DL-leucinate)copper(II) Complexes and Their Amine Adducts

G. MARCOTRIGIANO,* L. MENABUE,† P. MORINI, and G. C. PELLACANI†

Istituto di Chimica, Facoltá di Medicina-Veterinaria, University of Bari, Via Gentile 182, 70126 Bari, Italy

† *Istituto di Chimica Generale e Inorganica, University of Modena, Via Campi 183, 41100 Modena, Italy*

(Received April 9, 1979)

A compound of the type $Cu(AcLeu)_2$ and its amine adducts of the type $Cu(AcLeu)_2B_n$ (AcLeu=*N*-acetyl-DL-leucinato ion; $n=2$ and B=pyridine, 3- and 4-methylpyridine, *N*-methylpiperazine, morpholine, and piperidine; $n=1$ and B=1,10-phenanthroline, 2,2′-bipyridyl, piperazine, and pyridazine) were prepared and investigated by means of electronic, infrared and EPR spectroscopy and magnetic moment measurements. The results suggest a tetragonal configuration for the $Cu(AcLeu)_2$ complex and the amine adducts with CuO_4 and CuO_2N_2 chromophores, respectively. For the green $Cu(AcLeu)_2 \cdot pid$ complex a binuclear configuration similar to that observed for the bis(acetato)copper(II) monohydrate complex is suggested. The amino acid in all the complexes is found to coordinate toward the carboxylato group. In the assignment of the way in which the carboxylato group coordinates, in addition to the difference between their antisymmetric and symmetric stretching frequencies, we also pay special attention to the position of the symmetric stretch, which is directly connected with the oxygen atom linked to the metal ion.

The amino acids containing terminal *N*-acetyl residues are of great interest not only because they are present in protein, albumin, mosaic virus, ovalbumin, cytochrome C, and other natural proteins and peptides, but also because it is possible that an acetylamino acid might be the starting unit in the biosynthesis of some peptide chains which grow the stepwise addition of acylamino residues to the acetylated N-terminal amino acid.[1]

Being interested in the donor properties of amino acids as models for metal-protein interaction, we have paid particular attention to the interaction of some transition metal ions with simple *N*-protected amino acids containing a peptide group, as the *N*-acetyl and *N*-benzoyl derivatives of the glycine, alanine and valine.[2]

In this paper we have now investigated the coordination properties of the *N*-acetyl-DL-leucine (hereafter abbreviated as AcLeuH) with the copper(II) ion and the effect of additional ligands, such as saturated and aromatic heterocyclic amines, on the amino acid coordination.

Experimental

All the reagents used were of the best chemical grade.

Preparation of the Compounds. The *Cu(AcLeu)*$_2$ complex, which was used as starting material for the adduct preparations, was obtained by adding a copper(II) perchlorate hexahydrate (2×10^{-2} mol) solution in anhydrous ethanol (10 ml) to a *N*-acetyl-DL-leucine (4×10^{-2} mol) solution (50 ml) neutralized with a stoichiometric amount of potassium hydroxide. From the cooled solution (4—5 °C) the potassium perchlorate precipitated was filtered off and the green solution was slowly concentrated (20 ml). A blue solid compound separated by cooling after 24 h. *Cu(AcLeu)*$_2$*B*$_n$ ($n=1$ and B=bpy, phen pid; $n=2$ and B=py, Mepipz, morph, pipd) complexes were prepared by adding an excess of amine to a methanolic $Cu(AcLeu)_2$ solution. Solid compounds precipitated from the concentrated solutions on adding diethyl ether and on cooling. *Cu(AcLeu)*$_2$*B*$_2$ (B=3-pic and 4-pic) complexes were prepared in ethanol as reported above. *Cu(AcLeu)*$_2$*·pipz* complex instantaneously precipitated on mixing $Cu(AcLeu)_2$ (1.5×10^{-3} mol) and piperazine (3×10^{-3} mol) in ethanol.

Physical Measurements. The IR spectra of the compounds in KBr or Nujol (4000—250 cm^{-1}) were recorded with a Perkin-Elmer 180 spectrophotometer. The room temperature spectra of the solid compounds were recorded as mull transmission spectra with a Shimadzu MPS 50L spectrophotometer. The room temperature magnetic moments were measured with the Gouy method, using $Ni(en)_3S_2O_3$ as calibrant and correcting for diamagnetism with the appropriate Pascal constant. The EPR spectra were recorded on a JEOL PE-3X spectrometer. Quartz sample tubes were employed for polycrystalline samples. Spectra were calibrated with 2,2′-diphenyl-1-picrylhydrazyl (DPPH, $g=2.0036$) as a field marker.

Analyses. Nitrogen, carbon, and hydrogen were analyzed by Mr. Giuseppe Pistoni, using a Perkin-Elmer 240 Elemental Analyser.

Results and Discussion

The analytical results are reported in Table 1. The room temperature EPR spectrum of the bis(*N*-acetyl-DL-leucinato)copper(II) complex (Table 2 and Fig. 1), which is of axial type, shows g values of a typical isolated compound having a CuO_4 chromophore.[3,4] The broad EPR line excludes the possibility of exchange interaction between copper ions.[5] Its room temperature electronic spectrum (Table 1 and Fig. 2) also strongly resembles those reported for tetragonal copper(II)–oxygen systems.[4] By correlating the g values and the electronic spectrum, which shows two d-d bands at 12990 and 16950 cm^{-1} tentatively assigned to the $d_{xy}\rightarrow d_{x^2-y^2}$ and $d_{xz,\,yz}\rightarrow d_{x^2-y^2}$ transitions,[4] respectively, values of the molecular orbital coefficients ($k_\parallel=0.58$, $k_\perp=0.61$) are obtained. Since $k_\perp>k_\parallel$, this indicates the presence of more π bonding of the d_{xy} orbitals than of the d_{xz}, d_{yz} orbital. A tetragonal distortion in our complex greater than that found for some copper(II)–oxygen systems[4] may be suggested from the comparison of their g and k values and d-d band positions.

All the amine adducts, which have "normal" magnetic moments, show EPR spectra (Table 2) of axial type, except the pipd adduct which presents a rhombic spectrum. For these adducts the observed EPR line shapes are quite similar to each other and indicate a normal elongated tetragonal structure, while for the pipd adduct they indicate a rhombically-distorted

Table 1. Conventional chemical analysis

		C, %		H, %		N, %	
		calcd	found	calcd	found	calcd	found
$Cu(AcLeu)_2$	blue	47.55	47.75	5.99	6.02	6.94	6.47
$Cu(AcLeu)_2(py)_2$	blue	55.13	54.82	6.77	7.08	9.91	9.95
$Cu(AcLeu)_2(3pic)_2$	blue	56.57	57.24	7.13	6.80	9.43	10.03
$Cu(AcLeu)_2(4pic)_2$	blue	56.57	57.20	7.13	7.02	9.43	9.62
$Cu(AcLeu)_2 \cdot pid$	green	49.20	48.65	6.61	6.25	11.49	11.20
$Cu(AcLeu)_2 \cdot bpy$	blue	55.33	55.19	6.43	6.52	9.93	10.04
$Cu(AcLeu)_2 \cdot phen$	blue	57.16	56.83	6.17	6.23	9.53	9.65
$Cu(AcLeu)_2 \cdot pipz$	lilac	48.59	47.97	7.76	7.86	11.35	11.24
$Cu(AcLeu)_2(Mepipz)_2$	blue	50.77	51.31	9.04	8.62	13.75	13.82
$Cu(AcLeu)_2(morph)_2$	lilac	49.49	50.04	7.97	8.53	9.63	9.95
$Cu(AcLeu)_2(pipd)_2$	blue	53.98	54.28	8.72	8.93	9.69	9.88

Abbreviations: AcLeu=*N*-Acetyl-DL-leucinato ion; py=pyridine; 3- or 4-pic=3- or 4-methylpyridine; pid=pyridazine; bpy=2,2′-bipyridyl; phen=1,10-phenanthroline; pipz=piperazine; Mepipz=*N*-methylpiperazine; morph=morpholine; pipd=piperidine.

Table 2. Electronic spectra, magnetic moments, and EPR spectra of the solid complexes

	d-d bands/cm^{-1}			μ_{eff}/B.M.	$g_\parallel$	$g_\perp$	g_0		
$Cu(AcLeu)_2$	12990	16950		1.78	2.297	2.051	2.133		
$Cu(AcLeu)_2(py)_2$	13330 sh	16670		1.89	2.202	2.048	2.098		
$Cu(AcLeu)_2(3pic)_2$	13330 sh	16000		1.80	2.238	2.041	2.107		
$Cu(AcLeu)_2(4pic)_2$	13330 sh	16390		1.85	2.203	2.059	2.107		
$Cu(AcLeu)_2 \cdot bpy$	14290 sh	16670	23810 sh	1.83	2.257	2.053	2.121		
$Cu(AcLeu)_2 \cdot phen$	14290 sh	17390		1.80	2.234	2.055	2.115		
$Cu(AcLeu)_2 \cdot pipz$	15390 sh	19420		1.78	2.222	2.050	2.107		
$Cu(AcLeu)_2(Mepipz)_2$	13160 sh	15630		1.86	2.223	2.051	2.108		
$Cu(AcLeu)_2(morph)_2$	14820 sh	17860		1.77	2.249	2.053	2.118		
					g_3	g_2	g_1	g_0	
$Cu(AcLeu)_2(pipd)_2$	9520 sh	14290		1.85	2.201	2.133	2.048	2.127	
					Monomer		Dimer		D
					$g_\parallel$	$g_\perp$	$g_\parallel$	$g_\perp$	cm^{-1}
$Cu(AcLeu)_2 \cdot pid$	13510		24390 sh	1.38	2.234	2.066	2.40	2.09	0.39

a) $\lambda = -825\ cm^{-1}$.

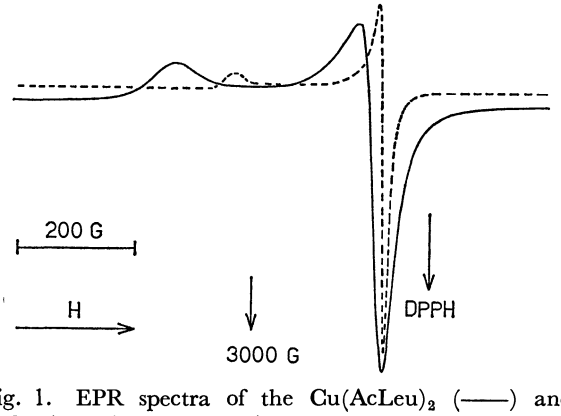

Fig. 1. EPR spectra of the $Cu(AcLeu)_2$ (——) and $Cu(AcLeu)_2 \cdot pipz$ (·····) complexes.

tetragonal configuration. Their g values are lower than those found for the bis(*N*-acetyl-DL-leucinato)-copper(II) complex, suggesting a chromophore change from CuO_4 to CuO_2N_2 as a consequence of the amine coordination.[4,6] From the shape and positions of the d-d bands (Table 2) a tetragonal distortion in the aliphatic heterocyclic amine adducts greater than in the aromatic heterocyclic amine adducts may be generally proposed, in agreement with the pK_a values of the former amines greater than those of the latter.

A correlation between EPR and electronic spectra[7] gives an approximate measure (k_0^2=0.45—0.58) of the degree of covalency for the copper(II)–ligand bondings, which are strictly similar to those reported for copper(II) complexes of other amino acids with an essentially CuO_2N_2 chromophore.[7]

The narrow EPR line in the pipz adduct (Fig. 1) ($\Delta H_\parallel$=20 G; $\Delta H_\perp$=5 G) is suggestive of a fairly strong spin exchange interaction through the piperazine molecules "bridging" two copper(II) ions.[5,8]

The "anomalous" room temperature magnetic moment and the EPR spectrum (Fig. 3) of the green $Cu(AcLeu)_2 \cdot pid$ complex are indicative of a binuclear structure.[9,10] In particular the EPR spectrum shows zero field splitting of 0.39 cm^{-1} and the presence of magnetically dilute copper(II) impurities. Its room temperature electronic spectrum (Fig. 2) are also strictly similar to those of the dimeric carboxylates.[9,11,12] It also presents a band at 24390 cm^{-1}, which is considered characteristic of dimeric carboxylate and similar

TABLE 3. RELEVANT IR BANDS (cm^{-1}) OF THE SOLID COMPLEXES

	ν(NH)	$\nu(OCO)_{as}$	$\nu(OCO)_s$	$\Delta\nu$
AcLeuH	3380 vs	1694 vs	1238 vs	456
AcLeuNa	3285 s	1590 vs	1403 s	187
AcLeuK	3278 s	1590 vs	1390 s	200
$Cu(AcLeu)_2$	3250 m	1580 vs	1390 vs	190
$Cu(AcLeu)_2(py)_2$	3282 s 3250 m	1600 vs	1390 vs	210
$Cu(AcLeu)_2(3pic)_2$	3328 m 3293 m 3245 m	1615 vs	1368 vs	247
$Cu(AcLeu)_2(4pic)_2$	3300 m 3245 m	1590 vs	1373 vs	217
$Cu(AcLeu)_2 \cdot bpy$	3242 m	1600 vs	1400 vs	200
$Cu(AcLeu)_2 \cdot phen$	3250 s	1590 vs	1393 vs	197
$Cu(AcLeu)_2 \cdot pipz$	3240 s (3195 mb)[a]	1586 vs	1396 vs	190
$Cu(AcLeu)_2(Mepipz)_2$	3275 s (3135 mb)[a]	1580 vs	1382 vs	198
$Cu(AcLeu)_2(morph)_2$	3240 s (3188 s)[a]	1582 vs	1390 vs	192
$Cu(AcLeu)_2(pipd)_2$	3275 s (3230 m)[a]	1588 vs	1390 vs	198
$Cu(AcLeu)_2 \cdot pid$	3252 s	1614 vs	1410 vs	204

a) ν(NH) of the saturated heterocyclic amines.

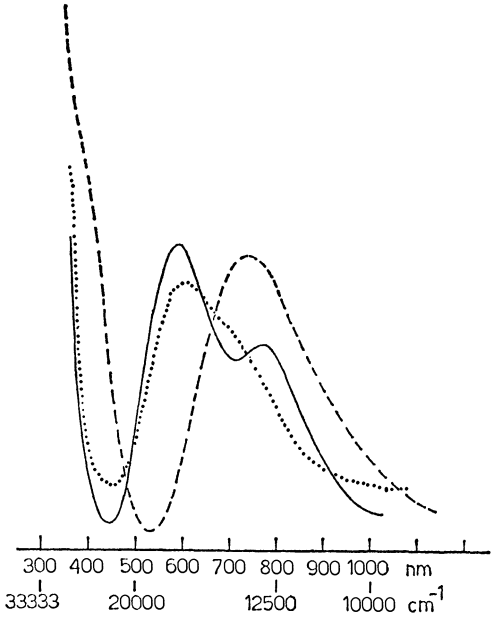

Fig. 2. Exemplifying electronic spectra of the $Cu(AcLeu)_2$ (——), $Cu(AcLeu)_2 \cdot pid$ (– – –), and $Cu(AcLeu)_2(pyridines)_2$ (·····) complexes.

Fig. 3. EPR spectrum of the $Cu(AcLeu)_2 \cdot pid$ complexes.

complexes.[9,11,12]

The electronic spectrum (14140 cm^{-1}, $\varepsilon = 188$ $l \cdot mol^{-1} \cdot cm^{-1}$) of the green methanolic solution of the $Cu(AcLeu)_2$ complex is very different to that of the solid state complex. The blue $Cu(AcLeu)_2B_2$ (B= py, 3pic, 4pic, morph, Mepipz, pipd) adducts in methanolic solution ($1 \div 3 \cdot 10^{-2}$ $mol \cdot dm^{-3}$) also give rise to green solutions, which show electronic spectra (14100—14600 cm^{-1} and $\varepsilon = 75 \div 90$ $l \cdot mol^{-1} \cdot cm^{-1}$) different to those of the solid state complexes. The color of the solutions and the position of the d-d bands suggest the presence of binuclear species due to a dissociation equilibrium involving the solvent molecules of this type:

$$2Cu(AcLeu)_2B_2 + 2Solv \rightleftharpoons [Cu(AcLeu)_2 \cdot Solv]_2 + 4B$$

This may be confirmed as an amine excess addition in the methanolic adduct solutions results in a blue shift of the d-d band (15350—15870 cm^{-1}) and generally in a decrease of the molar extinction (57—80 $l \cdot mol^{-1} \cdot cm^{-1}$). The lower d-d band positions of the blue solution complexes than those of the solid complexes (16000—17800 cm^{-1}) indicate that they are different and a lower tetragonal distortion in the former than in the latter complexes, being probably four amines entered in the coordination sphere around the metal ion.

The assignments of the more relevant infrared bands (Table 3) for emphasizing the amino acid coordination are made by comparing the amino acid, its sodium and potassium salts and their deuterated analogues. The coordination sites of the amino acid may be securely evidentiated, as the IR spectra of the complexes are very similar in shape and position to those of the sodium and potassium *N*-acetyl-DL-leucinato salts (Table 3).

This suggests that the carboxylato group is the only group of the ligand involved in the coordination of the metal ion, confirming the previous results obtained from the electronic spectra.

Trends in positions of and separation ($\Delta\nu$) between antisymmetric and symmetric carboxylate stretching bands provide a useful observation for assigning its

coordination type. In fact a large splitting of the carboxylate stretching frequencies is often an indication of a monodentate coordination, as the CO bonds become inequivalent, and a small splitting is indicative of bidentate coordination or bidentate "bridging" coordination.[10,13] In bidentate coordination $\Delta\nu$ values consistent with the above considerations may be obtained only in the absence of any strong hydrogen bonding effects.[13,14]

For the assignment of bidentate or monodentate coordination of our complexes we have also taken into consideration the position of the symmetric stretching band of the carboxylato group, as this band is directly connected with the oxygen atom certainly linked to the metal ion. Values of $\nu(OCO)_s$ at the same or lower energies than those found for the alkali metal salts are considered indicative of the presence of "symmetric" or "asymmetric" bidentate coordination of the carboxylato group, while values greater than 1410 cm^{-1} may be associated with a bridging bidentate behaviour of the carboxylato group, as has been experimentally found in some polynuclear complexes.[10] This also agrees with a greater double bond character of the symmetric CO bond when the carboxylato group links two metal ions, acting as "bridging" bidentate ligand, than when it links one metal ion, acting as a simple bidentate ligand.

By considering the $\Delta\nu$ values and the $\nu(OCO)_s$ position we may suggest the presence of "bridging" bidentate carboxylato groups in the $Cu(AcLeu)_2 \cdot pid$ complex and "asymmetric" bidentate groups in all the other complexes. These conclusions are also in agreement with the EPR and electronic results, and confirm the presence of an essentially CuO_2N_2 chromophore in the amine adducts.

The coordination of the amines is confirmed by the shift to lower frequencies of the $\nu(NH)_B$ (Table 3), with respect to the free amines,[15,16] in the saturated heterocyclic amine adducts, and by the shifts of the bands in the 800—500 cm^{-1} region, with respect to the free amines,[17–19] in the aromatic amine adducts.

The Authors are grateful to the Centro Strumenti of the University of Modena for the recording of the IR spectra and to the Consiglio Nazionale delle Ricerche of Italy for a financial support.

References

1) F. Haurowitz, "The Chemistry and Function of Protein," Academic Press, New York, N. Y. (1963), p. 404.
2) See for example: G. Marcotrigiano, L. Menabue, G. C. Pellacani, and M. Saladini, *Inorg. Chim. Acta*, **32**, 149 (1979); G. Marcotrigiano, L. Menabue, and G. C. Pellacani, *J. Chem. Soc., Dalton. Trans.*, **1976**, 1627; G. Marcotrigiano, L. Menabue, and G. C. Pellacani, *J. Inorg. Nucl. Chem.*, **40**, 753 (1978); L. P. Battaglia, A. Bonamartini Corradi, G. Marcotrigiano, and G. C. Pellacani, *Acta Crystallogr. Sect. B.*, **33**, 3886 (1977).
3) D. W. Smith, *J. Chem. Soc., A*, **1970**, 3108.
4) D. E. Billing, B. J. Hathaway, and P. Nicholls, *J. Chem. Soc. A*, **1969**, 316.
5) R. Gaura, G. Kokoszka, K. E. Hyde, and R. Lancione, *J. Coord. Chem.*, **5**, 105 (1976).
6) D. Attanasio, I. Collamati, and C. Ercolani, *J. Chem. Soc. Dalton. Trans.*, **1974**, 2442.
7) H. Yokoi, M. Sai, T. Isobe, and S. Ohsawa, *Bull. Chem. Soc. Jpn.*, **45**, 2189 (1972).
8) B. J. Hathaway and D. E. Billing, *Coord. Chem. Rev.*, **5**, 143 (1970).
9) J. R. Wasson, Chin-I Shyr, and C. Trapp, *Inorg. Chem.*, **7**, 469 (1968).
10) J. Catterick and P. Thornton, *Adv. Inorg. Chem. Radiochem.*, **20**, 291 (1977) and refserences cited therein.
11) D. Hibdon and J. H. Nelson, *Inorg. Chim. Acta*, **7**, 629 (1973) and references cited therein.
12) W. Harrison, S. Retting, and J. Trotter, *J. Chem. Soc. Dalton*, **1972**, 1852 and references cited therein.
13) S. T. Chow and C. A. McAuliffe, *Progr. Inorg. Chem.*, **19**, 51 (1975).
14) N. F. Curtis, *J. Chem. Soc. A*, **1968**, 1579.
15) I. S. Ahuja, *Inorg. Chim. Acta*, **3**, 110 (1969).
16) I. S. Ahuja and A. Garg, *Inorg. Nucl. Chem. Lett.*, **7**, 937 (1971).
17) N. N. Greenwood and K. Wade, *J. Chem. Soc.*, **1960**, 1130.
18) E. Konig and E. Lindner, *Spectrochim. Acta, Part A*, **28**, 1393 (1972) and references cited therein.
19) F. Micheel and B. Schleppinghof, *Chem. Ber.*, **88**, 763 (1955).

Super Exchange in Copper(II) Dimers. II. Synthesis, Characterization and Magnetic Properties of Binuclear Adducts of Copper(II) Halides with 1,2-Benzoquinone Dioximes. Ligand-induced Ferromagnetic Exchange Coupling

Michel Megnamisi BÉLOMBÉ†

Department of Physics, Stanford University, Stanford, California 94305, U. S. A.

(Received April 26, 1979)

Various 1,2-benzoquinone dioximes (bqdH) have been combined with $CuCl_2$ or $CuBr_2$ to afford the following new dimeric adducts: di-μ-chlorobis[chloro(1,2-benzoquinone dioxime)copper(II)], $[CuCl_2(bqdH)]_2$; di-μ-chlorobis[chloro(4-chloro-1,2-benzoquinone dioxime)copper(II)], $[CuCl_2(ClbqdH)]_2$; di-μ-chlorobis[chloro(4-methyl-1,2-benzoquinone dioxime)copper(II)], $[CuCl_2(MebqdH)]_2$; di-μ-chlorobis[chloro(4,5-dimethyl-1,2-benzoquinone dioxime)copper(II)], $[CuCl_2(Me_2bqdH)]_2$; di-μ-bromobis[bromo(1,2-benzoquinone dioxime)-copper(II)], $[CuBr_2(bqdH)]_2$; di-μ-bromobis[bromo(4-chloro-1,2-benzoquinone dioxime)copper(II)], $[CuBr_2$-$(ClbqdH)]_2$; di-μ-bromobis[bromo(4,5-dimethyl-1,2-benzoquinone dioxime)copper(II)], $[CuBr_2(Me_2bqdH)]_2$. These brown solids were characterized by variable-temperature magnetic susceptibility measured within 4.2—300 K, as well as by room temperature near infrared and electron spin resonance spectra from which the dimeric structure of the compounds was inferred. The intradimer magnetic exchange interaction was found to occur by a super exchange mechanism mediated by the valence p wave functions of the bridging halide ions. It was observed that the electrophilic character of the benzoquinonoid ligands affects the magnetic exchange *via* backbonding and through mesomeric π electron delocalization. It was found, most interestingly, that the tendency to ferro-magnetic exchange interaction within a dimer is the stronger, the more electrophilic the bqdH ligands can be made.

We present here part II of our investigations of magnetic super exchange in di-μ-halobridged copper(II) dimers. In part I[1] we showed that this category of magnetic clusters provides the simplest solids that appear to be best suited for reliable studies of magnetic exchange effects within the frame of the molecular field approximation or Heisenberg-Dirac-Van Vleck (HDVV) model.[2] To test the existing theoretical models,[2,3] new materials with possibly flexible properties are needed.[4] We therefore focus our efforts primarily on the development of novel synthetic routes aimed at establishing a means for bringing about desirable changes in the magnetic properties of solids by a systematic chemical modification of the constituent molecules. Thus, part I of this research series dealt with the isomorphous dimers,[5,6] $[CuX_2(dmgH)]_2$, where $X=Cl^-$ or Br^-, and dmgH=dimethylglyoxime (or 2,3-butanedione dioxime). The results obtained there had revealed that the substantial difference noted in the super exchange effects of the two dimers ought to be linked to the nature of the halogen atom involved in the bridges, a result which is, in fact, quite consistent with a general trend.[7]

In the present work as well as in a recent note,[8] we have employed a series of 1,2-benzoquinone dioxime (bqdH) ligands (Fig. 1) instead of dimethylglyoxime (dmgH). The purpose is to check that the reported nephelauxetic effect[9] induced at the central metal site by the electrophilic benzoquinonoid ligands is likely to affect the intradimer exchange coupling. This ligand-induced nephelauxetic effect was first observed while searching for new Krogmann type one-dimensional conductors,[9–11] of interest in the study of high temperature superconductivity according to the hypothetical excitonic model of Little.[12] It was shown that the effect arises because the electrophilicity of the partially oxidized aromatic ligands couples more or less to the d-shell electron density of the central metal ions by means of backbonding[13] and mesomeric delocalization

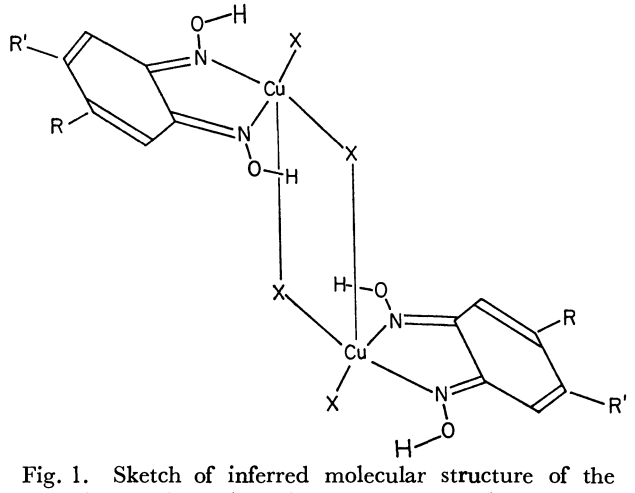

Fig. 1. Sketch of inferred molecular structure of the $[CuX_2(RR'bpdH)]_2$ dimers, with the planes of the individual molecules nearly perpendicular to the plane of the drawing. The *molecular planes* and the *intermolecular Cu–X bond direction* are taken roughly as the perpendicular ($\perp$) and parallel (//) orientations, respectively.[8]

$X=Cl^-$:

a)	R=R'=H	$[CuCl_2(bpdH)]_2$
b)	R=Cl, R'=H	$[CuCl_2(ClbpH)]_2$
c)	R=Me(=CH_3), R'=H	$[CuCl_2(MebpdH)]_2$
d)	R=R'=Me	$[CuCl_2(Me_2bpdH)]_2$

$X=Br^-$:

e)	R=R'=H	$[CuBr_2(bpdH)]_2$
f)	R=Cl, R'=H	$[CuBr_2(ClbpdH)]_2$
g)	R=R'=Me	$[CuBr_2(Me_2bpdH)]_2$

† Present address: Department of Chemistry, University of Ife, Ile-Ife, Nigeria.

of π electrons.[9] The effect is reminiscent of the through-bond phenomenon developed by Hoffmann.[14] Thus, the coupling between metal d-shell and ligand π-system provides a mechanism for d-shell "electron clouds" to be delocalized on to the spheres of the electrophilic benzoquinonoid rings. The degree of delocalization may be enhanced or reduced by appropriate substitution of these rings with electron withdrawing or electron releasing groups.

The objective of the present contribution, therefore, is three-fold: first to describe the synthesis of new di-μ-halobridged copper(II) dimers, second to examine the role of the bridging halide ion, third and most importantly, to check the impact of the ligand-induced nephelauxetic effect upon the super exchange coupling.

Experimental

Preparation of Materials. *The Reactants*: The commercially available anhydrous $CuBr_2$ crystals (Baker Analyzed Reagents, 99.4%) were used without further purification. $CuCl_2 \cdot 2H_2O$ crystals (90%+) from the same source were recrystallized from 99.5% acetone, finely ground and dehydrated at 105 °C over three consecutive nights to yield a dark-brown powder. The 1,2-benzoquinone dioxime ligands used were of analytical grade.[9]

Synthesis of the Compounds: The complexes listed in Table 1 were prepared according to the method reported earlier.[8] A general trend, however, was observed in the reaction yield which was found to be highest for the derivatives with less electrophilic bqdH ligands. The compounds decompose when heated above 200 °C.

Spectroscopic Experiments and Magnetic Susceptibility Measurements. The molar magnetic susceptibility data were collected at 36 closely spaced temperature points in the range 4.2—300 K, and near infrared and X-band electron spin resonance spectra were recorded at room temperature with the techniques described earlier.[1,15] A non-linear least-squares fitting procedure with a double-precision computer program[1,16] was employed to fit the susceptibility data to the conventional singlet-triplet Heisenberg equation.

Results

The Compounds. All the complexes listed in Table 1 crystallize as shiny, dark-brown tiny prisms or flakes. The ease of complex formation is apparently determined by the electrophilic character of the benzoquinonoid rings involved, since the reaction yield decreases noticeably with increasing electrophilic character of these rings (87% for the derivatives with methyl-substituted, and about 54% for those with chloro-substituted bqdH ligands). The stability of the complexes decreases in the same sense, particularly in the case of bromine-containing derivatives whose decomposition is obvious after a few weeks of exposure to air and light. The black body that results from this decomposition very probably consists of molecules with the Cu ions chelated by the quasi-coplanar 1,2-benzoquinone dioximate ligands, much like in $Cu(bqd)_2$[17] or in $Cu(dmg)_2$.[18] Note that the dimeric clusters reported here are very stable in vacuum or in a nitrogen atmosphere at room temperature. In solution, however, the likelihood of their decomposition increases considerably, especially at temperatures appreciably above ambient. For this reason, it is recommended that the syntheses be carried out at room temperature or lower.

In general the new materials are poorly soluble in the cold, even in water or in acetone and similar organic solvents. When a powdered sample of $[CuCl_2(bqdH)]_2$, for instance, is stirred for a while in H_2O at room temperature, it is rather transformed into the equally sparingly soluble $Cu(bqd)_2$ complex, presumably according to the reaction

$$[CuCl_2(bpdH)]_2 \xrightarrow{(2H_2O)} Cu(bpd)_2 + CuCl_2 \cdot 2H_2O + 2HCl,$$

as the resulting greenish-brown solution is strongly acidic. In hot acetone, the solubility is substantially higher, but the likelihood of chemical decomposition at that temperature is increased as well. The chemical decomposition taking place in the solution is recognizable by the formation of tear-causing bromoacetone in the case of the bromine-based derivatives. This suggests a redox reaction similar to the one noted previously on the related $[CuX_2(dmgH)]_2$ dimers.[1] The occurrence of this reaction is also indicated by the change in color of the solution which turns from dark-brown to light yellow-green after a few days. The true nature of this

Table 1. Microanalytical data of the $CuX_2(RR'bqdH)$ compounds

Compound	Element, %[a]					
	C	H	N	Br	Cl	Cu
$CuCl_2(bqdH)$	26.35 (26.44)	2.19 (2.22)	10.16 (10.28)		25.82 (26.01)	23.11 (23.31)
$CuCl_2(ClbqdH)$	23.52 (23.47)	1.55 (1.64)	8.84 (9.12)		34.64 (34.64)	20.30 (20.70)
$CuCl_2(MebqdH)$	29.47 (29.34)	2.81 (2.81)	9.44 (9.77)		24.56 (24.74)	21.98 (22.17)
$CuCl_2(Me_2bqdH)$	31.29 (31.96)	3.36 (3.35)	9.16 (9.32)		23.45 (23.59)	20.65 (21.14)
$CuBr_2(bqdH)$	20.09 (19.96)	1.64 (1.67)	7.68 (7.75)	43.63 (44.21)		17.50 (17.58)
$CuBr_2(ClbqdH)$	18.20 (18.20)	1.33 (1.27)	6.95 (7.08)	40.12 (40.37)	8.90 (8.95)	15.70 (16.50)
$CuBr_2(Me_2bqdH)$	25.92 (24.68)	2.63 (2.60)	6.97 (7.19)	39.73 (41.03)		15.80 (16.31)

a) Calculated values are given in parentheses.

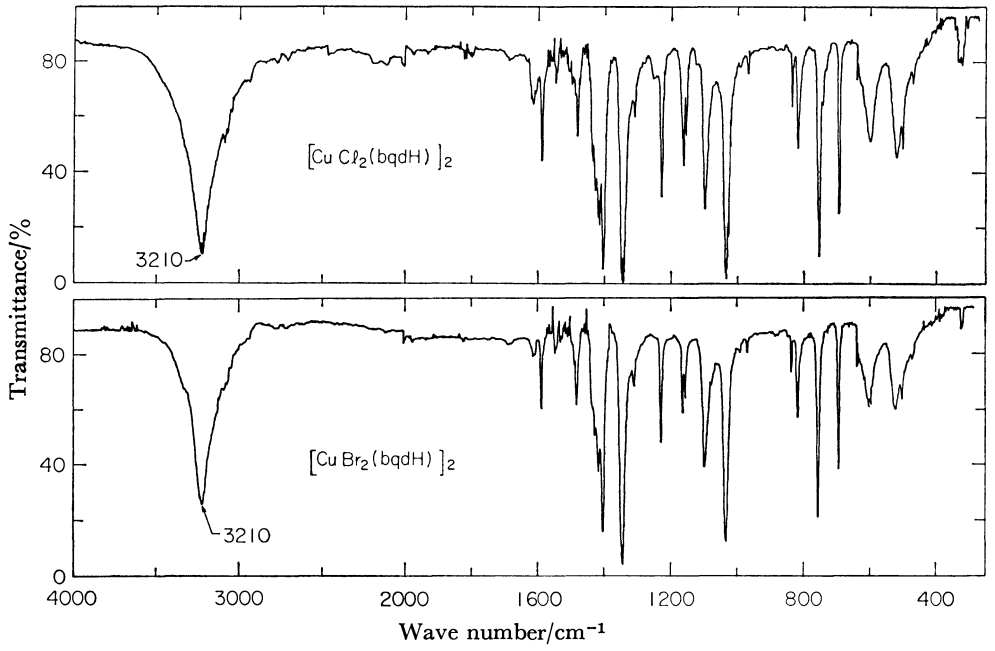

Fig. 2. Virtually identical near infrared spectra of $[CuCl_2(bpdH)]_2$ and $[CuBr_2(bpdH)]_2$ reflecting the matching structures of the compounds.

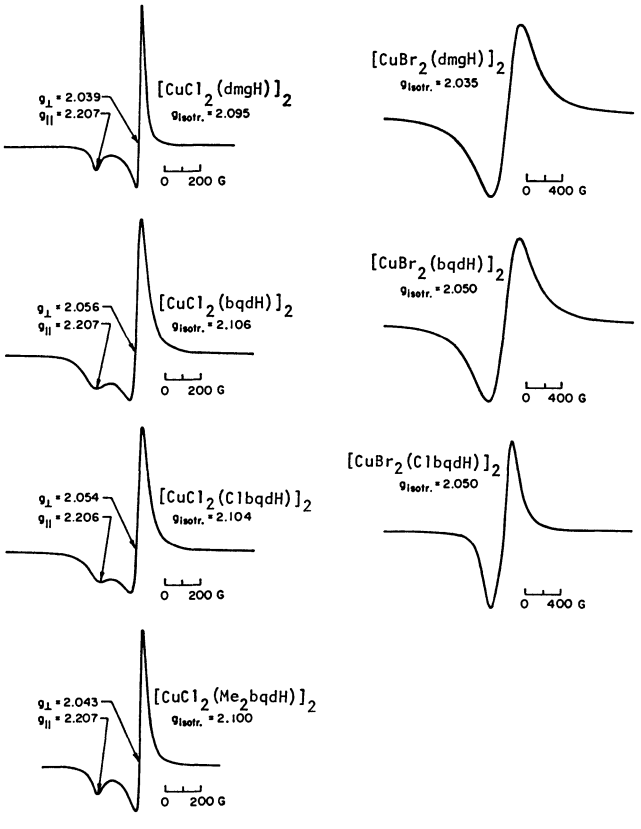

Fig. 3. *Row on the left*: Polycrystalline X-band ESR spectra of three representative chloro dimers, $[CuCl_2(RR'bpdH)]_2$, recorded at room temperature. The striking resemblance with the spectrum of the well-characterized dimer,[6] $[CuCl_2(dmgH)]_2$ (top of the row), reflects the dimeric structural similarity.
Row on the right: ESR spectra of two representative bromo dimers, $[CuBr_2(RR'bpdH)]$ demonstating their structural analogy to the well-characterized $[CuBr_2(dmgH)]_2$ dimer[1,5] (top of the row).

chemical process has not been established as yet.

Spectroscopic Results. Figure 2 shows the near infrared spectra[19] of $[CuCl_2(bqdH)]_2$ and $[CuBr_2(bqdH)]_2$, which exhibit a striking resemblance reminiscent of that observed previously on the $[CuX_2(dmgH)]_2$ dimers.[1] Nevertheless, the doublet splitting of the O–H stretching absorption band characteristic of the latter is not observed in the former pair of dimers.

In Fig. 3 are displayed the ESR spectra of both the $[CuX_2(dmgH)]_2$ and the $[CuX_2(RR'bqdH)]_2$ dimeric clusters. The absorption lines of four chloro compounds are presented in the row on the left, and the lines of three bromo derivatives in the row on the right side of the figure. In either case, the line shapes are characterized by their remarkable similarity. For the chloro compounds, the anisotropy of the $\boldsymbol{g}$ tensor is well-resolved into the parallel ($g_{//}$) and the perpendicular ($g_{\perp}$) components. Note, in particular, that $g_{//}$ remains equal to 2.207 as the ligand is varied from compound to compound, whereas $g_{\perp}$ does change markedly. The line shapes of the bromo derivatives, on the other hand, exhibit no obvious evidence for such a resolution of the $\boldsymbol{g}$ tensor which appears rather isotropic with the lines being considerably broader. In both categories of the $[CuX_2(RR'bqdH)]_2$ dimers, however, a significant narrowing of the lines is observed. This is obviously the result of substituent effects induced at the benzoquinonoid rings. Hence, the linewidth for the perpendicular absorption varies, *e.g.*, from $\Delta H_{\perp}=70$ G in $[CuCl_2(bqdH)]_2$ to $\Delta H_{\perp}=50$ G in $[CuCl_2(Me_2bqdH)]_2$. Likewise the width decreases from $\Delta H_{isotr}=330$ G in $[CuBr_2(bqdH]_2$ to $\Delta H_{isotr}=230$ G in $[CuBr_2(ClbqdH)]_2$.

Static Magnetic Results. The variable-temperature diamagnetic molar susceptibility of $Pt(bqd)_2$[9,10] (Table 2), along with Pascal's constants for H, Cl^-, and Br^-

TABLE 2. VARIABLE-TEMPERATURE DIAMAGNETIC MOLAR SUSCEPTIBILITY OF $Pt(bqd)_2$

Temp K	$10^{-3}\chi_m$ cgs emu mol^{-1}	Temp K	$10^{-3}\chi_m$ cgs emu mol^{-1}
4.2	0.057	34.1	−0.031
4.8	0.033	36.2	−0.035
5.7	0.021	38.3	−0.035
6.9	0.004	40.4	−0.044
8.0	−0.009	45.4	−0.044
9.4	−0.017	50.4	−0.061
10.6	−0.024	55.3	−0.044
12.5	−0.034	60.3	−0.026
15.0	−0.041	65.3	−0.013
16.2	−0.041	70.1	−0.017
17.6	−0.041	80.2	−0.020
19.7	−0.046	100.2	−0.039
21.8	−0.041	120.2	−0.035
23.8	−0.041	150.3	−0.044
25.7	−0.044	179.9	−0.044
27.6	−0.037	220.4	−0.050
29.8	−0.026	259.8	−0.052
31.9	−0.024	298.9	−0.068

atoms were used to correct for the diamagnetism of the ligands.

The corrected molar susceptibility data, χ_m, and the corresponding effective moments, μ_{eff}/Cu(II), of three representative dimers are listed in Tables 3, 4, and 5. The magnetic behavior of all three compounds is very similar over the temperature range examined. No maximum susceptibility is observed above 4.2 K, suggesting small J values in these materials. The trend in μ_{eff} data, on the contrary, is noticeably different. Whereas the effective moment per Cu(II) ion in $[CuCl_2(bqdH)]_2$ and in $[CuBr_2(bqdH)]_2$ remains virtually unchanged and close to the spin 1/2 value throughout the temperature range, the μ_{eff}/Cu(II) of $[CuBr_2(ClbqdH)]_2$ drops rather sharply in the lowest temperature region. A similar, though less dramatic, dropoff was observed in $[CuCl_2(ClbqdH)]_2$ as well. In all three cases, plots of inverse molar susceptibilities, $1/\chi_m$, *versus* temperature yielded nearly straight lines. From the slopes of these lines, the Curie constants of 0.804 for $[CuBr_2(ClbqdH)]_2$, 0.761 for $[CuBr_2(bqdH)]_2$,

TABLE 3. VARIABLE-TEMPERATURE MOLAR MAGNETIC SUSCEPTIBILITY (CORRECTED) χ_m, AND EFFECTIVE MOMENT, μ_{eff}/Cu(II), FOR $[CuBr_2(ClbqdH)]_2$

Temp K	$10^{-3}\chi_m$ cgs emu mol^{-1}		μ_{eff}/Cu(II) B.M.	
	Exper.	Theor.	Exper.	Theor.
4.2	100.144	100.556	1.296	1.299
4.8	94.308	94.090	1.345	1.343
5.7	85.195	85.599	1.393	1.396
6.9	77.292	76.153	1.459	1.449
8.0	69.150	69.001	1.486	1.485
9.4	61.597	61.512	1.521	1.519
10.6	56.510	56.210	1.546	1.542
12.5	48.738	49.394	1.559	1.570
15.0	42.203	42.537	1.590	1.596
16.2	39.751	39.865	1.603	1.605
17.6	36.681	37.136	1.605	1.615
19.7	33.411	33.668	1.620	1.627
21.8	30.547	30.786	1.630	1.636
23.8	28.296	28.462	1.639	1.644
25.7	26.459	26.555	1.647	1.650
27.6	24.616	24.886	1.646	1.655
29.8	22.990	23.197	1.653	1.660
31.9	21.770	21.785	1.664	1.664
34.1	20.747	20.479	1.679	1.668
36.2	19.928	19.370	1.695	1.671
38.3	18.792	18.375	1.693	1.674
40.4	17.743	17.477	1.690	1.677
45.4	15.779	15.655	1.689	1.682
50.4	14.358	14.178	1.697	1.686
55.3	13.009	12.979	1.692	1.690
60.3	12.157	11.948	1.707	1.693
65.3	11.348	11.069	1.716	1.695
70.1	10.432	10.339	1.705	1.697
80.2	8.993	9.081	1.692	1.700
100.2	7.237	7.321	1.695	1.705
120.2	6.029	6.135	1.693	1.708
150.3	4.969	4.936	1.717	1.712
179.9	4.126	4.144	1.710	1.714
220.4	3.506	3.401	1.742	1.716
259.8	3.104	2.899	1.778	1.717
298.9	2.748	2.530	1.792	1.718

TABLE 4. VARIABLE-TEMPERATURE MOLAR MAGNETIC SUSCEPTIBILITY (CORRECTED) χ_m, AND EFFECTIVE MOMENT, μ_{eff}/Cu(II) FOR $[CuBr_2(bqdH)]_2$

Temp K	$10^{-3}\chi_m$ cgs emu mol^{-1}		μ_{eff}/Cu(II) B.M.	
	Exper.	Theor.	Exper.	Theor.
4.2	176.114	176.044	1.719	1.719
4.8	154.271	153.349	1.720	1.715
5.7	127.168	128.505	1.702	1.711
6.9	105.738	105.682	1.707	1.707
8.0	89.986	90.889	1.696	1.704
9.4	77.463	77.148	1.705	1.702
10.6	68.587	68.299	1.704	1.700
12.5	57.888	57.804	1.700	1.699
15.0	47.997	48.086	1.695	1.697
16.2	44.567	44.496	1.698	1.696
17.6	41.752	40.932	1.713	1.696
19.7	36.090	36.543	1.684	1.695
21.8	33.070	33.005	1.696	1.694
23.8	30.449	30.219	1.700	1.694
25.7	28.235	27.977	1.701	1.693
27.6	26.219	26.045	1.699	1.693
29.8	24.212	24.117	1.696	1.693
31.9	22.401	22.526	1.688	1.692
34.1	21.395	21.071	1.705	1.692
36.2	20.182	19.847	1.706	1.692
38.3	19.166	18.758	1.710	1.692
40.4	17.137	17.782	1.661	1.692
45.4	15.939	15.824	1.697	1.691
50.4	14.135	14.256	1.684	1.691
55.3	12.930	12.995	1.687	1.691
60.3	11.929	11.920	1.691	1.691
65.3	11.133	11.010	1.700	1.690
70.1	10.335	10.258	1.697	1.690
80.2	8.920	8.972	1.685	1.690
100.2	6.908	7.190	1.656	1.690
120.2	5.903	6.002	1.675	1.690
150.3	4.760	4.811	1.680	1.689
179.9	4.012	4.029	1.686	1.689
220.4	3.560	3.299	1.756	1.689
259.8	3.007	2.808	1.749	1.689
298.9	2.535	2.448	1.720	1.689

TABLE 5. VARIABLE-TEMPERATURE MOLAR MAGNETIC SUSCEPTIBILITY (CORRECTED) χ_m, AND EFFECTIVE MOMENT, μ_{eff}/Cu(II) FOR $[CuCl_2(bqdH)]_2$

Temp / K	$10^{-3}\chi_m$ / cgs emu mol^{-1}		μ_{eff}/Cu(II) / B.M.	
	Exper.	Theor.	Exper.	Theor.
4.2	162.086	162.475	1.649	1.651
4.8	143.859	142.929	1.661	1.656
5.7	120.282	121.084	1.655	1.660
6.9	101.503	100.591	1.673	1.665
8.0	86.410	87.084	1.662	1.668
9.4	74.630	74.376	1.674	1.671
10.6	65.801	66.109	1.669	1.673
12.5	55.869	56.219	1.670	1.675
15.0	46.486	46.975	1.668	1.677
16.2	43.733	43.539	1.682	1.678
17.6	39.868	40.117	1.673	1.679
19.7	35.825	35.888	1.678	1.680
21.8	32.516	32.466	1.682	1.680
23.8	30.128	29.764	1.691	1.681
25.7	27.739	27.584	1.686	1.681
27.6	25.902	25.702	1.688	1.682
29.8	24.072	23.821	1.691	1.682
31.9	22.608	22.266	1.696	1.683
34.1	20.949	20.841	1.687	1.683
36.2	20.031	19.642	1.700	1.683
38.3	18.919	18.574	1.699	1.683
40.4	17.999	17.616	1.702	1.684
45.4	15.423	15.690	1.670	1.684
50.4	13.780	14.146	1.662	1.684
55.3	12.681	12.902	1.670	1.685
60.3	11.582	11.840	1.666	1.685
65.3	10.855	10.941	1.679	1.685
70.1	10.129	10.198	1.680	1.685
80.2	8.933	8.924	1.686	1.686
100.2	7.175	7.158	1.688	1.686
120.2	6.000	5.979	1.689	1.686
150.3	4.717	4.795	1.673	1.687
179.9	3.980	4.017	1.679	1.687
220.4	3.296	3.290	1.688	1.687
259.8	2.958	2.801	1.735	1.687
298.9	2.589	2.442	1.738	1.687

TABLE 6. ROOM TEMPERATURE PARAMAGNETIC MASS SUSCEPTIBILITY, χ_g, AS A FUNCTION OF THE APPLIED FIELD, H FOR THE $[CuCl_2(bqdH)]_2$ DIMER

H/kG	$10^{-6}\chi_g$/emu g^{-1}
2.10	4.36
3.13	4.20
4.11	4.16
5.12	4.19
6.12	4.17
7.13	4.36
8.10	4.24

and 0.754 for $[CuCl_2(bqdH)]_2$ were calculated.

Table 6 shows the field-dependence of the mass susceptibility, χ_g, for $[CuCl_2(bqdH)]_2$ at room temperature.[19] It is clearly seen that the magnetic susceptibility is independent of the applied field, H.

Discussion

By analogy to the previously well-characterized $[CuX_2(dmgH)]_2$ dimers,[1,5,6] the spectroscopic results of this study reflect conclusive evidences for a closely related dimeric structure of the present $[CuX_2(RR'bqdH)]_2$ clusters sketched in Fig. 1.[8]

The observations of a constant parallel g value in the ESR spectra of all chloro-bridged dimers (Fig. 3, row on the left) may be taken as good grounds to believe that the axial Cu–X bonds (which coincide roughly with the molecular parallel orientation) do not vary in character, no matter how radically the organic ligands lying in the horizontal direction (perpendicular orientation of the molecule) may be chemically modified. In other words, the structural element defined by the CuXCuX quadrangle in Fig. 1 remains virtually the same for all the dimers. From the well-known structure of $[CuCl_2(dmgH)]_2$ dimer,[6] therefore, it is reasonable to conclude that the present chlorobridged clusters have fairly the same structure, the specific difference residing merely in the replacement of the dmgH by the RR'bqdH ligands.

Likewise the ESR spectra of the bromobridged dimers (Fig. 3, row on the right) suggest that the structure of these derivatives is analogous to that of $[CuBr_2(dmgH)]_2$ (top of the row) which, in turn, has been shown to be isomorphous with the $[CuCl_2(dmgH)]_2$ dimer.[1,5,6]

Just as was found in that pair of dimers, it is demonstrated here that the new pair, $[CuCl_2(bqdH)]_2$ and $[CuBr_2(bqdH)]_2$, exhibit quasi-identical infrared spectra (Fig. 2). Yet, the doublet splitting of the O–H stretching absorption band characteristic of the former pair is not observed in the latter pair of dimers, thus suggesting that in the latter case, the hydroxyimino hydroxyl groups of the bqdH ligands find themselves in crystallographically equivalent positions. On the basis of these matching spectroscopic results, the dimeric structure of the new clusters is most reasonably assumed to be as sketched in Fig. 1, with the bridging angle CuXCu approximately 85°—88°.

Bearing in mind this structural similarity, it appears interesting next to examine the role of the halogen ligands in the super exchange effect. Considering, again, the pair of dimers, $[CuCl_2(bqdH)]_2$ and $[CuBr_2(bqdH)]_2$ (which differ only in their halogen ligands), it is seen that the variation of the exchange parameter, J, between the two compounds follows consistently the trend observed previously on the pair, $[CuCl_2(dmgH)]_2$ and $[CuBr_2(dmgH)]_2$.[1] For either dimer pair, the exchange coupling in the bromo derivative turns out to be antiferromagnetic ($J=-1.51$ cm^{-1} for the dmgH-based dimer, $J=-0.11$ cm^{-1} for the bqdH-based dimer), whilst in the chloro derivative it is found to be ferromagnetic ($J=+0.31$ cm^{-1} for the dmgH-based dimer, $J=+0.14$ cm^{-1} for the bqdH-based dimer). These observations indicate that, at least for the particular dimeric structure sketched in Fig. 1, bromo ligands are more likely to induce antiferromagnetic exchange coupling, while chloro ligands tend to drive a ferromagnetic coupling of the single electron spins at very low temperatures.

When, however, the ligand-induced nephelauxetic effect introduced above is modulated by appropriate substitutions of the benzoquinonoid rings, remarkable variations in the value of the exchange parameter result.[8] Considering the following dimers: $[CuCl_2(MebqdH)]_2$, $[CuCl_2(bqdH)]_2$, $[CuCl_2(ClbqdH)]_2$, where the electrophilic character of the benzoquinonoid rings is progressively enhanced in the same order, the corresponding J values of -3.32 cm^{-1}, $+0.14$ cm^{-1} and $+0.38$ cm^{-1} are observed. For $[CuBr_2(bqdH)]_2$ and $[CuBr_2(ClbqdH)]_2$ likewise, the exchange coupling constant changes from $J=-0.11$ cm^{-1} to $J=+4.63$ cm^{-1}, respectively. Clearly, electron releasing groups such as Me (methyl) at the bqdH moities are likely to induce antiferromagnetic exchange coupling, whereas electron withdrawing substituents such as Cl definitely drive the exchange process towards a ferromagnetic ordering of the intradimer single electron spins. In other words, the more electrophilic the bqdH ligands can be made, the more ferromagnetic the exchange coupling at lowest temperatures is expected to be. This finding constitutes the innovation of central interest in the present research.

The overall magnetic behavior of the binuclear Cu(II) clusters studied here is very much alike for the temperature region appreciably above 4.2 K. In particular the μ_{eff}/Cu(II) for $[CuCl_2(bqdH)]_2$ and $[CuBr_2(bqdH)]_2$ remains comparable to the spin 1/2 value over the temperature range considered. This indicates Curie-like behavior and agrees well with the small J values observed on these derivatives. The μ_{eff}/Cu(II) for $[CuBr_2(ClbqdH)]_2$, by contrast, departs markedly from this behavior at lowest temperatures, which is consistent with the larger J value found for this compound. Thus, it turns out that when the effect of the bridging halogen and the ligand-induced nephelauxetic effect are considered together with respect to their impact upon the exchange interaction within a dimer, the latter effect dominates overwhelmingly.

Although the dmgH-based copper(II) dimers on the one hand, and the bqdH-based dimers on the other hand, exhibit very similar magnetic and hence analogous structural features, the colors of the two compound classes differ radically. The blue-green crystals of the first class exhibit a color that is common to and characteristic of copper(II) derivatives of this type. The dark-brown color of the second class of compounds, by contrast, is rather unusual for such copper(II) derivatives.

The observed narrowing of the ESR lines upon substitution of the bqdH ring may be interpreted as a tangible manifestation of the ligand-induced nephelauxetic effect acting at the microscopic level. These observations indicate that there is a finite degree of involvement of the paramagnetic electrons in the phenomenon of ligand-induced nephelauxetic effect.

As a novel aspect of scientific interest, one may view the experimental evidence gained here on the basis of this nephelauxetic effect as a potential input to guide new developments in the field of magnetism. It is hoped that such developments might lead to the derivation of a model generally valid for predicting the occurrence of ferromagnetism in magnetic coordination compounds. Other effects such as the degree of coplanarity of the individual molecules, the magnitude of the bridging angle, the degree of the copper-halogen bondings, as well as the extent of the Cu–Cu contacts, considered together or separately, may play a non-negligible role in the intradimer exchange interactions. Detailed structural analyses, however, must be awaited in order to assess the importance of these factors. For more accurate and quantitative correlations of anisotropic spin-lattice relaxation processes, magnetic measurements on single crystals—possibly supplemented by neutron diffraction studies— are needed.

This work was supported by the National Science Foundation through Grant No. DMR-76-28087-A01.

I am indebted to Professor W. A. Little under whose auspices the work was done. I am grateful to Dr. E. J. Laskowski and M. A. Novotny for their invaluable experimental assistance. I wish to thank Professor R. H. Holm for the use of his magnetic susceptibility and ESR equipments, and Professor H. Taube for the use of his infrared instrument. Very useful conversations with Professors R. Hoffmann of Cornell and Z. G. Soos of Princeton are sincerely appreciated.

References

1) M. M. Bélombé and M. A. Novotny, *Inorg. Chem.*, submitted for publication.

2) P. A. M. Dirac, *Proc. R. Soc. London, Ser. A*, **1926**, 112, 661; *ibid.*, **1929**, 123, 714; W. Heisenberg, *Z. Phys.*, **38**, 411 (1926); *ibid*, **49**, 619 (1928); J. H. Van Vleck, "Theory of Electric and Magnetic Susceptibilities," Oxford University Press, London (1932); P. W. Anderson, *Solid State Phys.*, **14**, 99 (1963). For a review of magnetic exchanges in transition metal cluster compounds, see literature cited in Ref. 1.

3) P. J. Hay, J. C. Thibeault, and R. Hoffmann, *J. Am. Chem. Soc.*, **97**, 4884 (1975).

4) N. T. Watkins, E. E. Dixon, van H. Crawford, K. T. McGregor, and W. E. Hatfield, *J. Chem. Soc., Chem. Commun.*, **1973**, 133; M. V. Hanson, C. B. Smith, and G. O. Carlisle, *Inorg. Nucl. Chem. Lett.*, **12**, 917 (1976); J. S. Smart, in "Magnetism," ed by G. T. Rado and H. Suhl, Academic Press, New York (1963), Vol. 3, Chap. 2, p. 63.

5) H. Endres, *Acta Crystallogr., Sect B*, **34**, 3736 (1978).

6) D. H. Svedung, *Acta Chem. Scand.*, **23**, 2865 (1969).

7) E. J. Laskowski, D. M. Duggan, and D. N. Hendrickson, *Inorg. Chem.*, **14**, 2449 (1975); L. F. Larkworthy and A. Yavari, *J. Chem. Soc., Chem. Commun.*, **1977**, 172 and literature cited in Ref. 1.

8) M. M. Bélombé, *Bull. Chem. Soc. Jpn.*, **52**, 645 (1979).

9) M. M. Bélombé, *Ann. N. Y. Acad. Sci.*, **313**, 633 (1978).

10) M. M. Bélombé, *J. Solid State Chem.*, **22**, 151 (1977); M. M. Bélombé, *ibid.*, **27**, 389 (1979).

11) J. W. Brill, M. M. Bélombé, and M. Novotny, *J. Chem. Phys.*, **68**, 585 (1978).

12) W. A. Little, *Phys. Rev. A*, **134**, 1416 (1964); D. Davis, H. Gutfreund and W. A. Little, *Phys. Rev. B*, **13**, 4766 (1976); H. Gutfreund and W. A. Little, "Highly Conducting One-dimensional Solids," ed by J. T. Devreese, R. Evrard, and V. E. Van Doren, Plenum Press, New York (1979).

13) K. Krogmann, *Angew. Chem. Int. Ed. Engl.*, **8**, 35 (1969); see also, *e.g.*, F. A. Cotton and G. Wilkinson,

"Advanced Inorganic Chemistry," 3rd ed, John Wiley, New York, London (1972), Chaps. 20, 22, 23.

14) R. Hoffmann, *Acc. Chem. Res.*, **4**, 1 (1971); R. Gleiter, *Angew. Chem.*, **86**, 770 (1974).

15) E. J. Laskowski, R. B. Frankel, James A. Ibers, W. O. Gillum, G. C. Papaefthymiou, J. Renaud, and R. H. Holm, *J. Am. Chem. Soc.*, **100**, 5322 (1978); I. L. Mulay, *Anal. Chem.*, **46**, 490 (1974).

16) P. Gill, W. Murray, and Picken, Report DNAC 24, National Physical Laboratory, Teddington (England), August 1972.

17) K. Burger and I. Ruff, *Acta Chim. Acad. Sci.*, **49**, 1 (1966).

18) E. Frasson, R. Bardi, and S. Bezzl, *Acta Crystallogr.*, **12**, 201 (1957), and references cited therein.

19) The author thanks Ms B. Krickl for her kind assistance with the recording of the IR spectra, and Dr. D. Baumann of Heidelberg for checking the field-dependence of the magnetic susceptibility.

Studies on Xanthylium Salts. Behaviour of 9-Vinylidenexanthenes in Acid Media

Nadia Fouad ABDUL-MALIK, Sami Bassili AWAD, and Alfy Badie SAKLA*

Department of Chemistry, Faculty of Science, University of Cairo, Giza, Egypt

(Received June 5, 1978)

Unsymmetrical allenes namely, 1,1-diaryl-2-(9′-xanthenylidene)ethylenes (**1**) reacted readily with perchloric acid, hydrogen chloride, and acetic acid to give the corresponding highly coloured 9-vinylxanthylium salts (**3**). The latter derivatives (**3**) thermally rearranged in acid media to give spiro[indene-1,9′-xanthene]s (**7**). Structures of compounds **3** and **7** were established from chemical and spectral evidences. A new route for synthesis of allenes (**1**) was reported.

Orientation of polar addition of acids to substituted allenes to give carbonium ions has been shown to be controlled by the nature of substituents present.[1,2] A study is now reported on the behaviour of unsymmetrical allenes[3,4] (**1**) namely, 1,1-diaryl-2-(9′-xanthenylidene)ethylenes in acid media. These allenes (**1**, R=H, CH_3O, C_2H_5O, or *i*-C_3H_7O) added perchloric acid (in either acetic acid or methanol) to give crystalline, deeply coloured mono-perchlorate derivatives namely, 9′-[2,2-bis(*p*-substituted phenyl)vinyl]xanthylium perchlorates (**3**, R=H, CH_3O, C_2H_5O, or *i*-C_3H_7O; X=ClO_4). The structure of **3** (X=ClO_4) was established from analytical data and from the following findings: (i) The perchlorate **3** (R=H; X=ClO_4), derived from the corresponding allene (**1**, R=H), was identical with an authentic sample prepared by treatment of 1,1-diphenyl-2-(9′-hydroxy-9′-xanthenyl)ethylene (**2**, R=H) with perchloric acid in methanol at −5 °C; (ii) Reduction of perchlorate **3** (R=C_2H_5O; X=ClO_4) with sodium borohydride gave mainly 1,1-bis(*p*-ethoxyphenyl)-2-(9′-xanthenyl)ethylene (**6**, R=C_2H_5O); (iii) NMR spectrum of the *p*-alkoxy perchlorate **3** (R=*i*-C_3H_7O; X=ClO_4) revealed the equivalency of the 2,2-diaryl residues.

Allene **1** (R=H) added hydrogen chloride to yield deep red crystals of 9-(2,2-diphenylvinyl)xanthylium chloride (**3**, R=H; X=Cl). Synthesis of an authentic sample of **3** (R=H; X=Cl) was achieved by adding 9,9-dichloroxanthene (**4**) to 2,2-diphenylethylene (**5**, R=H). The reaction likely proceeded *via* an intermediate (scheme) which spontaneously eliminated hydrogen chloride on heating. The latter addition reaction was extended to prepare allenes **1** (R=H, CH_3O, C_2H_5O, or *i*-C_3H_7O) by using the appropriate ethylene (**5**, R=H, CH_3O, C_2H_5O, or *i*-C_3H_7O), and treatment of the intermediate products, without being isolated, with pyridine.

Electrophilic addition of hydrogen halides to substituted allenes has been reported to give monohalogenated products that were probably derived from vinylic cations formed by protonation of central carbon atom of these allenes.[1,2,5] Selective addition of acids to π bond attached to xanthene residue of allenes (**1**) seemed to take place initially *via* a similar mechanism that followed by cyclic conjugation[6] to give xanthylium derivatives (**3**). The deep colour of such perchlorates or chlorides (**3**, X=ClO_4 or Cl) in crystalline form or in solution might account for such conjugation. A similar chromophoric effect was noticed when colourless allenes (**1**) were dissolved in acetic acid (deep red, R=H, and bluish violet, R=alkoxy). This was probably due to similar type of protonation to give xanthylium acetate derivatives (**3**, X=OAc). UV spectra for both perchlorates (**3**, X=ClO_4) and acetates (**3**, X=OAc) were consistent with this observation.

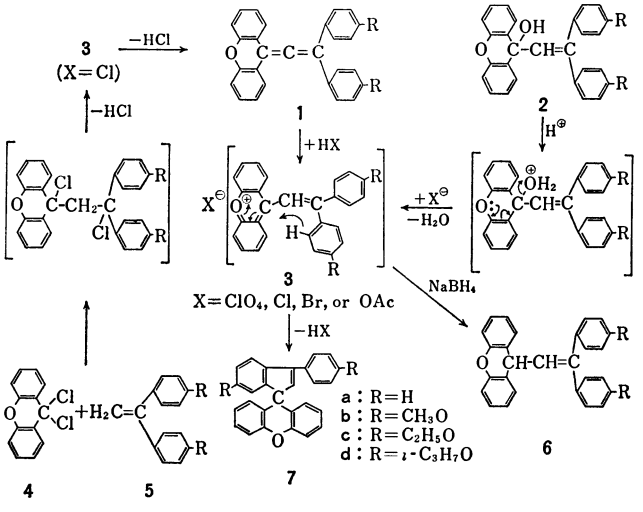

Allenes **1** (R=H, CH_3O, C_2H_5O, or *i*-C_3H_7O) rearranged in boiling acetic acid to afford colourless crystalline products namely, 6-substituted-3-(*p*-substituted phenyl)spiro[indene-1,9′-xanthene]s (**7**, R=H or alkoxy). This rearrangement could also be brought about by heating a solution of allene **1** (R=H, CH_3O or C_2H_5O) in either ethanol containing hydrochloric acid or in ether saturated with hydrogen bromide. The reaction pathway for this rearrangement would require an initial formation of xanthylium ion intermediate (**3**, X=OAc, Cl, or Br) that cyclized through an internal electrophilic substitution[7,8] of one of the 2,2-diaryl residues to give spiroindene (**7**). This was evidenced by: (i) the perchlorate **3** (R=H or C_2H_5O; X=ClO_4) converted in boiling acetic acid to yield typical indene **7** (R=H or C_2H_5O); (ii) 1,1-diphenyl-2-(9′-hydroxy-9′-xanthenyl)ethylene (**2**, R=H) cyclized in acid medium to give indene **7** (R=H), and (iii) NMR of *p*-alkoxy indenes (**7**, R=alkoxy) revealed the nonequivalency of the two *p*-alkoxyphenyl residues, and that one of them became trisubstituted. For example, the methoxyl groups of **7** (R=CH_3O) appeared as two singlets (δ, 3.71 and 3.53, each 3H), whereas the same groups were

shown as overlapped singlet in the spectrum of each of the parent allene (**1**, R=CH_3O, δ, 3.90, 6H) and of 1,1-bis(*p*-methoxyphenyl)ethylene (**5**, R=CH_3O, δ, 3.75, s, 6H). The above findings were also in support of structure **7** for indenes rather than the alternative structure **8**. Furthermore, the latter **8**, by analogy with the behaviour of 9-xanthenylidene derivatives,[9,10] might be expected to add acids to give the corresponding xanthylium salt. This was not the case with our indenes; they failed to add acetic acid or perchloric acid and recovered mainly unchanged. Further relevant evidence was obtained from UV measurements in methanol or in acid medium (in acetic acid or in acetic acid/perchloric acid). Indene **7** (R=H) showed the same single absorption maximum at λ_{max} 290 nm in either solvent, whereas 9-benzylidenexanthene, as a reference example, showed: λ_{max} (CH_3OH) 341 nm; and λ_{max} (AcOH) 288, 336 nm; and λ_{max} (AcOH/$HClO_4$) 296, 384, 474, and 500 (shoulder) nm.

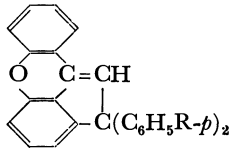

8

Experimental

NMR spectra were measured with a Varian T 60 instrument and mass spectra with an A.E.I. MS9 spectrometer, and UV spectra with a Beckman DK-1 spectrophotometer. The infrared spectra were recorded with a Pye-Unicam SP 1000 spectrometer. All melting points were determined in open capillary tubes.

*9,9-Dichloroxanthene (**4**).* This was prepared by refluxing a solution of xanthone (2 g) in excess of thionyl chloride (10 ml) for 5 h. Excess thionyl chloride was recovered by distillation under reduced pressure. The residue obtained was mixed with 10 ml of petroleum ether (bp 60—80 °C), and the solvent was again removed under reduced pressure. The procedure was repeated for 5 times. All the processes were carried out under complete protection of moisture, and the final residue kept under dry conditions, mp 101—103 °C (lit, mp[11] 103 °C).[11]

*1,1-Diaryl-2-(9-xanthenylidene)ethylene (**1a—d**).* A mixture of 9,9-dichloroxanthene (prepared from 2 g xanthone) and 1,1-diphenylethylene (1.8 g) was heated on a steam bath for 2 h. The mixture was further heated in benzene for 15 min and filtered. The insoluble reddish-brown material, mp 155—157 °C (dec) showed no depression in mp when admixed with an authentic sample. The sample was prepared by passing hydrogen chloride for 10 min into a solution of 1,1-diphenyl(9-xanthenylidene)ethylene (**1a**, 0.5 g) in benzene (15 ml) and the deep red crystals formed were collected by filtration to give **3a** (X=Cl), mp 157 °C.

After a solution of **3a** (0.5 g) in pyridine (10 ml) had been refluxed for 10 min, water was added to the reaction mixture and worked up in the usual way. The product was recrystallized from methanol to give **1a**, mp and mixed mp[3] 205 °C in *ca.* 50% overall yield.

In the case of a mixture of 1,1-bis(*p*-alkoxyphenyl)ethylene (0.01 mol) and 9,9-dichloroxanthene (0.01 mol), extensive evolution of hydrogen chloride was observed on heating, and the reaction mixture was directly treated with pyridine and worked up to give 1,1-bis(*p*-alkoxyphenyl)-2-(9-xanthylidene)-ethylene (**1**): **1b**, mp and mixed mp[3] 125 °C; **1c**, mp and mixed mp[3] 125 °C; and **1d**, mp and mixed mp[3] 147 °C in *ca.* 40% yield. IR spectra of these allenes were superimposable with that of authentic samples. UV and visible spectra measurements which performed in glacial acetic acid showed for **1a**: λ_{max}: 515, 371, 346, 330, 257 nm and for **1b**: λ_{max}: 628, 478, 373, 355, 277 nm.

*9-(2,2-Diarylvinyl)xanthylium Perchlorates (**3a—d**).* Perchloric acid (2 ml, 70%) was added gradually to a stirred solution of 1,1-diaryl-2-(9-xanthenylidene)ethylene **1** (1.0 g) in either acetic acid or methanol (25 ml) and the mixture was further stirred for 30 min. The mixture diluted with ether and cooled to give the corresponding perchlorates **3a—d**, which separated as highly coloured crystals in *ca.* 90% yield. Thus were obtained: **3a**, mp 181 °C, λ_{max} (AcOH): 533, 380, 278 nm; Found: Cl, 7.8%. Calcd for $C_{27}H_{19}ClO_5$: Cl, 7.73%. This perchlorate (**3a**) could be prepared by adding perchloric acid (0.5 ml) to a cold solution (−5 °C) of compound (**2a**) (0.2 g) in methanol (25 ml). The mixture was stirred for 10 min and the red crystals deposited were collected by filtration, mp and mixed mp 181 °C.

3b, mp 170 °C, λ_{max} (AcOH): 612, 497, 367, 271 nm; Found: Cl, 6.9%. Calcd for $C_{29}H_{23}ClO_7$: Cl, 6.83%.

3c, mp 172 °C, λ_{max} (AcOH): 619, 490, 367, 271 nm; Found: Cl, 6.6%. Calcd for $C_{31}H_{27}ClO_7$: Cl, 6.48%.

3d, mp 157 °C, Found: Cl, 6.2%. Calcd for $C_{33}H_{31}ClO_7$ Cl, 6.17%.

*Reduction of 9-(2,2-Diarylvinyl)xanthylium Perchlorates (**3a, c**).* To a cold stirred suspension of each of the title compound (0.5 g) in methanol (10 ml), sodium borohydride (0.2 g) was added at once. The deep colour (red or blue violet) disappeared immediately and colourless crystals deposited. After stirring for 15 min, the mixture diluted with water (2 ml) was cooled and the solid precipitated was collected by filtration. It was crystallized from methanol to give the corresponding 1,1-diaryl-2-(9′-xanthenyl)ethylene (**6**) in *ca.* 90% yield. Thus were obtained: **6a**, mp and mixed mp[3] 164 °C and **6c**, mp and mixed mp[3] 115 °C.

*Action of Pyridine on 9′-(2,2-Diarylvinyl)xanthylium Perchlorates (**3**).* A solution of the perchlorate **3a—d** (1.0 g) in pyridine (10 ml) was heated to boiling for 10 min. The mixture diluted with water was extracted with ether. The ether phase was washed thoroughly with water, separated, dried ($MgSO_4$), and the solvent was distilled off. The residue crystallized from methanol, from which the allene (**1**) separated as colourless crystals in *ca.* 90% yield. Thus were obtained: **1a**, mp and mixed mp[3] 205 °C; **1b**, mp and mixed mp[3] 125 °C; **1c**, mp and mixed mp[3] 125 °C; and **1d**, mp and mixed mp[3] 147 °C.

*6-Substituted-3-(p-substituted phenyl)spiro[indene-1,9′-xanthene]s (**7**).* These compounds were obtained as follows: A solution of 1,1-diaryl-2-(9′-xanthenylidene)ethylene (0.5 g) in acetic acid (20 ml) was heated to boiling until the deep colour developed on dissolution (red in case of **1a**, and blue violet with **1b—d**) almost discharged (*ca.* 4 h). The solution was cooled, diluted with water and extracted with ether. The extract was washed successively with water, sodium carbonate solution (5%), and water and dried ($MgSO_4$). The residue obtained by evaporation of the solvent was crystallized from methanol to give colourless crystals of compound **7** in *ca.* 90% yield. Thus were obtained: **7a**, mp 174 °C, δ (CCl_4) 7.07 (s, C_6H_5) superimposed on 7.51—6.61 (m, 8H, of xanthene plus 3H, indene), *m/e* 358 (M^+); Found: C, 90.5; H, 5.1%. Calcd for $C_{27}H_{18}O$: C, 90.47; H, 5.06%. λ_{max} 290 nm (AcOH/Ac_2O, 9: 1, v/v) or in AcOH/Ac_2O/$HClO_4$ (70%) (9: 0.9: 0.1, v/v/v).

7b, mp 174 °C;[13] δ (CCl_4) 7.67—6.42 (m, 15H, Ar), 6.35 (s, 1H, indene H-2) and 3.71, 3.53 (2s, 6H, $2CH_3O$); *m/e* 418 (M^+); Found: C, 83.3; H, 5.4%. Calcd for $C_{29}H_{22}O_3$: C, 83.23; H, 5.30%.

7c, mp 157 °C; δ (CCl_4) 7.58—6.46 (m, 15H, Ar), 6.41 (s, 1H, indene H-2), 3.94, 3.78 (2 overlapped q, J=8 Hz, each 2H of C_2H_5O), 1.38 and 1.24 (2 overlapped t, J=8 Hz, each 3H of C_2H_5O); *m/e* 446 (M^+); Found: C, 83.4; H, 5.8%. Calcd for $C_{31}H_{26}O_3$: C, 83.38; H, 5.87%.

7d, mp 122 °C, *m/e* 474 (M^+); Found: C, 83.4; H, 6.4%. Calcd for $C_{33}H_{30}O_3$: C, 83.51; H, 6.37%.

When a solution of **3a** or **3c** (0.5 g) in acetic acid (20 ml) heated to boiling for 5 h and worked up as above, spiroindenes **7a**, mp and mixed mp 174 °C and **7c**, mp and mixed mp 157 °C were obtained respectively in *ca.* 80% yield.

To each solution of **1a** or **1c** (0.5 g) in ethanol (10 ml) concentrated hydrochloric acid (2 ml) was added. Each mixture was heated to boiling for 10 h. The colourless crystals separated on cooling the mixture were collected by filtration and were recrystallized from methanol to give the corresponding indenes **7a** and **7c**, mp and mixed mp 174 and 157 °C respectively.

Hydrogen bromide was bubbled in a cold ethereal solution of **1b** (0.5 g in 15 ml ether) until no more absorption of gas was observed. The mixture was refluxed for 30 min and left overnight. The solvent was recovered and the residue obtained was recrystallized from methanol to give **7b**, mp and mixed mp 174 °C.

9-Benzylxanthylium Perchlorate. To a cold solution of 9-benzylidenexanthene (0.5 g) in a mixture of acetic acid (4 ml)/acetic anhydride (1 ml), perchloric acid (70%, 0.5 ml) was added. The mixture was left for 30 min at room temperature and then was diluted with ether. The deep yellow crystals precipitated were collected by filtration and were washed with ether. They had mp 226 °C which showed no depression when admixed with an authentic sample of 9-benzylxanthylium perchlorate prepared from 9-benzyl-9-hydroxyanthene according to the procedure reported by Conant *et al.*;[13] λ_{max} 288, 336 nm ($AcOH/Ac_2O$, 9: 1 v/v) and λ_{max} 296, 384, 474, and 500 (shoulder) nm ($AcOH/Ac_2O/HClO_4$, 8.9: 1: 0.1 v/v/v) were shown in the spectra of 9-benzylidenexanthene. The same absorption maxima in acetic acid perchloric acid, were obtained when 9-benzylxanthylium perchlorate was measured in acetic acid.

We are indebted to Dr. R. S. Atkinson, Department of Chemistry, University of Leicester, England, for his help to carry out mass and NMR spectra.

References

1) T. L. Jacobs and R. N. Johnson, *J. Am. Chem. Soc.*, **82**, 6397 (1960).
2) A. V. Federova, *J. Gen. Chem., USSR*, **33**, 3508 (1963).
3) W. Tadros, A. B. Sakla, S. B. Awad, and N. F. Abdul-Malik, *Helv. Chim. Acta*, **56**, 1829 (1973).
4) S. B. Awad, N. F. Abdul-Malik, and S. Abdou, *Bull. Chem. Soc., Jpn.*, **48**, 2200 (1975).
5) B. S. Thyagarajan, "Selective Organic Transformations;" M. C. Caserio "Selectivity in Addition Reactions of Allenes," John Wiley and Sons Inc., (1970), Vol. 1, p. 248.
6) H. Prest, "Oxonium Ions in Organic Chemistry," Verlag Chemie, Academic Press, (1971).
7) P. Maitland and W. H. Mills, *J. Chem. Soc.*, **1963**, 987.
8) H. Fischer and H. Fischer, *Chem. Ber.*, **97**, 2975 (1964); D. Vorlander and C. Siebert, *ibid.*, **39**, 1024 (1906); K. Ziegler and W. Sauormilch, *ibid.*, **63**, 1851 (1930).
9) R. Wizinger and M. L. Coenen, *J. Prakt. Chem.*, **153**, 127 (1939).
10) R. Wizinger and Y. Al-Attar, *Helv. Chim. Acta.*, **30**, 189 (1947).
11) M. M. Hafez, N. Latif, and I. F. Zeid, *J. Org. Chem.*, **26**, 3988 (1961).
12) R. Wizinger and G. Renckhoff, *Helv. Chim. Acta.*, **24**, 369 (1941).
13) J. B. Conant and A. W. Sloan, *J. Am. Chem. Soc.*, **47**, 576 (1925).

Synthesis of *cis*-Aryl Cyclopropyl Sulfones

T. BALAJI and D. Bhaskar REDDY*

Department of Chemistry, Sri Venkateswara University, Tirupati 517502, India

(Received March 17, 1979)

Some new *cis*-1-(arylsulfonyl)-2-phenylcyclopropanes have been synthesized by the addition of arylthiocarbenes to styrene in presence of excess potassium *t*-butoxide at low temperatures. The (arylthio)cyclopropanes thus obtained are subsequently oxidized with 30% hydrogen peroxide in acetic acid to corresponding sulfones. The IR and PMR spectra of all these compounds were recorded. Their IR spectra displayed bands in the region 1033—1008 cm^{-1} which are considered to be the most characteristic of the cyclopropane ring. They have also exhibited bands in the region 850—820 cm^{-1} characteristic of *cis*-configuration. The PMR spectra gave complex multiplets in the region 1.4—3.1 ppm. A study of these chemical shifts for ring protons and other substituents reveals that all the substituents tend to cause protons *cis*-to them to appear at higher fields than those *trans*-to them. Thus the differences of the chemical shifts can be used as a criterion to distinguish between *cis*- and *trans*-1-(arylsulfonyl)-2-phenylcyclopropanes.

One of the important methods[1] of preparing cyclopropanes is by the utility of dimethylsulfoxonium methylide (I) and dimethylsulfonium methylide (II).[2] A wide variety of Michael acceptors have been explored with I and II. α,β-Unsaturated ketones, nitriles, isocyanides and nitro compounds gave good to excellent yields for the preparation of cyclopropanes.[3] The utility of II as a co-reactant with α,β-unsaturated sulfones for the synthesis of cyclopropyl sulfones[4–8] seemed to be stereoselective and the cyclopropane derivatives thus obtained appeared to have *trans*-configuration.

The reaction of carbenes, derivatives of bivalent carbon with carbon-carbon multiple bonds provides one of the important methods for the preparation of cyclopropane compounds. Schoellkopf *et al.*[9–13] reported the preparation of cyclopropanes by treating olefins with chloromethyl phenyl ether ($PhOCH_2Cl$) and chloromethyl phenyl sulfide ($PhSCH_2Cl$) through phenoxycarbene and phenylthiocarbene intermediates respectively. These reactions were considered to proceed stereospecifically *cis*.

Although the synthesis and study of quite a number of *trans*-1-(arylsulfonyl)-2-arylcyclopropanes are known,[4–8] there are no reports about the synthesis and study of corresponding *cis*-compounds in the literature except *cis*-1-(phenylsulfonyl)-2-phenylcyclopropane.[4] It was therefore felt that the preparation of *cis*-1-(arylsulfonyl)-2-arylcyclopropanes would be of quite interest and of significance.

Results and Discussion

The first synthesis[14] of cyclopropyl sulfones was reported by α,γ-dehydrohalogenation of 3-chloropropyl sulfones. A few more cyclopropyl sulfones were reported according to various methods.[4,9,15,16] The synthesis of *cis*- and *trans*-1-(phenylsulfonyl)-2-phenylcyclopropane was reported first, by Truce and Badiger[4] in 1964.

A series of new *cis*-1-(arylsulfonyl)-2-phenylcyclopropanes (see Table 1) were synthesized by the addition of different aryl chloromethyl sulfides to excess of styrene at low temperature (−5 to −10 °C) in presence of excess potassium *t*-butoxide. The *cis*-1-(arylthio)-2-phenylcyclopropanes thus formed were subsequently oxidized with 30% hydrogen peroxide in acetic acid to obtain *cis*-1-(arylsulfonyl)-2-phenylcyclopropanes. Fairly high yields of *cis*-1-(arylsulfonyl)-2-phenylcyclopropanes have been obtained by refluxing for longer periods during the oxidation.

The IR spectra of most of these compounds showed medium to weak intensity bands in the region 1033—1008 cm^{-1} (see Table 2) which were considered to be the most characteristic of the cyclopropane deformation mode of the ring.[8,17–20] These compounds also displayed two high frequency bands in the region 3085—3060 cm^{-1} (ν CH_2 symmetric) and 3025—3000 cm^{-1} (ν CH_2 asymmetric) which in addition to the 1033—1008 cm^{-1} bands confirm the presence of cyclopropane ring system. All these compounds exhibited strong to medium intensity bands in the region 852—820 cm^{-1}, characteristic of *cis*-1-(arylsulfonyl)-2-phenylcyclopropanes.[21] These compounds have also exhibited very strong peaks characteristic of sulfonyl groups[22–25] in the regions 1342—1300 cm^{-1} and 1150—1136 cm^{-1}.

The PMR spectra of the compounds under present investigation exhibited complex multiplets in the region 1.40 to 2.45 ppm (methylene) and 2.36 to 3.12 ppm (methine) (see Table 3). The phenyl and arylsulfonyl groups showed signals in the regions 6.96 to 8.20 ppm. The chemical shifts data have been used[26–28] for the structural problems of cyclopropane derivatives. A study of the chemical shifts for ring protons and other substituent groups in cyclopropanes has indicated generally that all substituents tend to cause protons *cis*-to them to appear at higher fields than those *trans*-to them.

In the structure III both H_A and H_B are having substituents *cis*-to them. Hence H_A and H_B resonate at higher frequency with a small difference of chemical shifts between them, as is observed[7] in *trans*-1-(2-thienylsulfonyl)-2-phenylcyclopropane (H_A 1.50 ppm; H_B 1.89 ppm; H_C 2.77 ppm; H_D 2.89 ppm). Where

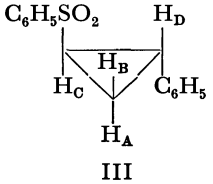

III

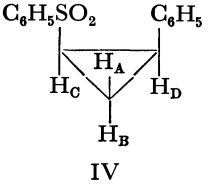

IV

TABLE 1. *cis*-1-(ARYLSULFONYL)-2-PHENYLCYCLOPROPANES

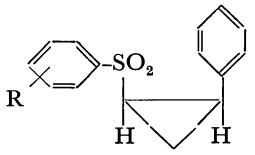

S. No.	R	Yield/%	Mp/°C	Formula	Analysis (%) Calcd C	Calcd H	Found C	Found H
1.	H	88.5	65.5— 66[a)]					
2.	*p*-Cl	78.6	90— 91	$C_{15}H_{13}ClO_2S$	61.53	4.47	61.40	4.58
3.	*p*-Br	80.3	109—110	$C_{15}H_{13}BrO_2S$	53.41	3.88	53.26	3.82
4.	*p*-CH_3	82.2	80— 81	$C_{16}H_{16}O_2S$	70.36	5.92	70.33	5.93
5.	*p*-OCH_3	86.1	114—115	$C_{16}H_{16}O_3S$	66.64	5.59	66.59	5.59
6.	*p*-NO_2	83.7	144—145	$C_{15}H_{13}NO_4S$	59.39	4.33	59.00	4.41
7.	3,4-Cl_2	78.1	95— 96	$C_{15}H_{13}Cl_2O_2S$	55.05	3.70	54.99	3.77

a) W. E. Truce and Badiger, *J. Org. Chem.*, **29**, 3277 (1964); report mp 67—68 °C, yield 83%.

TABLE 2. CHARACTERISTIC IR BANDS EXHIBITED BY

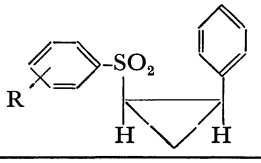

S. No.	R	ν CH_2 (cm^{-1}) 3100—3070 region	ν CH_2 (cm^{-1}) 3033—2955 region	Ring deformation (cm^{-1}) 1026 region	ν SO_2 (cm^{-1}) 1300 region	ν SO_2 (cm^{-1}) 1150 region	Absorption band at 848 (cm^{-1})
1.	H	—	3010 (m)	1020 (w)	1308 (s)	1136 (s)	835 (m)
2.	*p*-Cl	3085 (w)	3025 (m)	1033 (w)	1328 (s)	1150 (s)	830 (s)
3.	*p*-Br	3060 (w)	3000 (w)	1030 (w)	1300 (s)	1140 (s)	820 (s)
4.	*p*-CH_3	—	3020 (w)	1015 (w)	1315 (s)	1142 (s)	850 (m)
5.	*p*-OCH_3	—	3010 (w)	1022 (m)	1320 (m)	1142 (s)	842 (m)
6.	*p*-NO_2	3084 (w)	3020 (w)	1008 (w)	1342 (s)	1140 (s)	855 (m)

TABLE 3. CHEMICAL SHIFTS OF

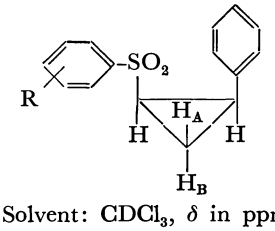

Solvent: $CDCl_3$, δ in ppm.

S. No.	R	Cyclopropyl CH_2(A)	Cyclopropyl CH_2(B)	Cyclopropyl CH	Aryl and arylsulfonyl
1.	H	1.42—1.64	2.00—2.24	2.36—2.88	6.97—7.58
2.	*p*-Cl	1.44—1.79	2.10—2.38	2.46—2.92	7.06—7.38
3.	*p*-Br	1.46—1.74	2.08—2.32	2.52—2.93	7.00—7.94
4.	*p*-CH_3	1.26—1.67	2.06—2.30	2.40—2.88	7.00—7.94
5.	*p*-OCH_3	1.42—1.72	2.00—2.27	2.52—2.90	6.72—6.86; 7.05—7.36
6.	*p*-NO_2	1.58—1.84	2.20—2.42	2.53—2.92	6.95—7.50; 8.02—8.20
7.	3,4-Cl_2	1.42—1.84	2.12—2.45	2.54—3.12	7.00—7.57

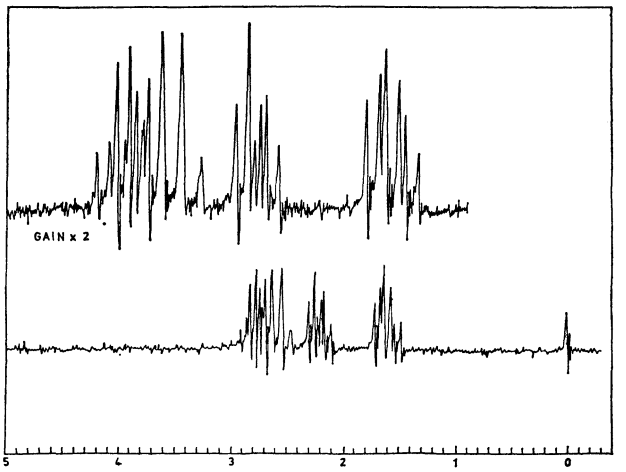

Fig. 1. 100 MHz ^1H NMR spectrum of **3** in the high field region (measured in $CDCl_3$).

as in IV H_A has substituents *cis*-to it but H_B is not having likewise. As a result of this, the chemical shift of H_A is observed at higher fields. There is a marked difference between chemical shifts of H_A and H_B in IV in comparison to III.

A representative spectra of these compounds in high field region in $CDCl_3$ is given in Fig. 1. Thus the chemical shifts data of ring protons of cyclopropane derivatives discussed above may be used as a criterion for the configurational assignments of *cis*- and *trans*-1-(arylsulfonyl)-2-phenylcyclopropanes.

The stereospecific synthesis adopted for these aryl cyclopropyl sulfones, IR and PMR spectral data, confirm that all these compounds are *cis*-isomers.

Experimental

All melting points were determined on a Mel-Temp apparatus and are uncorrected. The elemental analyses were performed by Dr. R. D. MacDonald, Australian Micro Analytical Service. The IR spectra were recorded on Perkin-Elmer model 257 in KBr discs. The PMR spectra were obtained at 100 MHz and on a Varian XL-100 spectrometer in deuteriochloroform using TMS as an internal reference. Chemical shifts were recorded in parts per million downfield from tetramethylsilane and IR frequencies in cm^{-1}.

Starting Materials. Styrene is obtained commercially and purified by distillation under reduced pressure.

Thiophenols. The arenesulfonyl chlorides were obtained by the chlorosulfonylation of the corresponding hydrocarbons as described by Huntress and Carten.[30] The arenesulfonyl chlorides were reduced to the corresponding thiophenols with zinc dust and dilute sulfuric acid. The procedure adopted was a modification of the method described by Vogel.[31] To a mixture of crushed ice and concentrated sulfuric acid the arenesulfonyl chloride was added with stirring. The zinc dust was added in portions as rapidly as possible to the cooled mixture without allowing the temperature to rise above 10 °C. The distillate obtained after the steam distillation of the mixture was extracted with ether. The product obtained after evaporation of ether was purified. Thiophenol: bp 168—169 °C, *p*-chlorothiophenol: mp 52—53 °C, *p*-bromothiophenol: mp 74—76 °C, *p*-thiocresol: bp 195—196 °C, *p*-methoxythiophenol: bp 225—227 °C, 3,4-dichlorothiophenol: bp 80—81 °C/8 mmHg. The *p*-nitrothiophenol: mp 73—74 °C, was prepared according to the procedure of Price and Stacy.[32]

Aryl Chloromethyl Sulfides: The aryl chloromethyl sulfides were prepared following the procedure of Francher.[33] A mixture of paraformaldehyde and benzene was taken in a conical flask and to this, concentrated hydrochloric acid was added rapidly with stirring. After a while, the mixture was kept at 40 °C and the appropriate thiol in benzene was added slowly. The resulting mixture was maintained slightly above 40 °C for 2 h. After removing the solvent the products were purified by distillation under reduced pressure. Phenyl chloromethyl sulfide: bp 109—110 °C/11 mmHg, *p*-chlorophenyl chloromethyl sulfide: bp 131—132 °C/12 mmHg, *p*-bromophenyl chloromethyl sulfide: bp 164—165 °C/18 mmHg, *p*-methoxyphenyl chloromethyl sulfide: bp 175—176 °C/20 mmHg, *p*-nitrophenyl chloromethyl sulfide: mp 54—55 °C, 3,4-dichlorophenyl chloromethyl sulfide: bp 144—145 °C/8 mmHg.

General Procedure for the Preparation of cis-*1-(Arylsulfonyl)-2-phenylcyclopropanes*: In a 250 ml three necked flask equipped with magnetic stirrer and fitted with a dropping funnel and calcium chloride guard tube was placed 25 ml of styrene. Small portions of potassium *t*-butoxide (5 g, 20% excess than 0.025 mol) was added with stirring to styrene at −5 to −10 °C. The aryl chloromethyl sulfide was added dropwise to the above mixture. After the complete addition the reaction mixture was stirred for 3 h and was diluted with water. The oily layer was separated and dried over anhydrous calcium chloride. It was then subjected to fractional distillation under reduced pressure and the product *cis*-1-(arylthio)-2-phenylcyclopropane was collected.

The sulfide (2.0 g) was dissolved in 20 ml of glacial acetic acid and 9 ml of 30% hydrogen peroxide was added to the mixture at ice-cold temperature. The mixture was refluxed for 25 to 48 h. It was then poured on to crushed ice and the solid separated was filtered off and dried. The product *cis*-1-(arylsulfonyl)-2-phenylcyclopropane was recrystallized from 2-propanol. The relevant data on the compounds synthesized are given in Table 1.

One of the authors (T.B.) is thankful to CSIR, India, for awarding him a Junior Research Fellowship.

References

1) E. J. Corey and M. Chaykovsky, *J. Am. Chem. Soc.*, **87**, 1353 (1965).
2) E. J. Corey and M. Chaykovsky, *J. Am. Chem. Soc.*, **84**, 3782 (1962).
3) B. M. Trost and L. S. Melvin, Jr., "Sulfur Ylides," Academic Press, New York (1975), p. 97.
4) W. E. Truce and V. V. Badiger, *J. Org. Chem.*, **29**, 3277 (1964).
5) W. E. Truce and C. T. Goralski, *J. Org. Chem.*, **33**, 3849 (1968).
6) W. E. Truce and C. T. Goralski, *J. Org. Chem.*, **34**, 3324 (1969).
7) C. T. Goralski, *J. Org. Chem.*, **37**, 2355 (1972).
8) D. Bhaskar Reddy, Ph. D. Thesis, Sri Venkateswara University, Tirupati, India, Dec. 1974.
9) U. Schoellkopf and G. J. Lehmann, *Tetrahedron Lett.*, **1962**, 165.
10) U. Schoellkopf, A. Lerch, and J. Paust, *Chem. Ber.*, **96**, 2206 (1963).
11) U. Schoellkopf and G. L. Lehman, J. Paust, and H. D. Haertl, *Chem. Ber.*, **97**, 1527 (1964).
12) U. Schoellkopf and J. Paust, *Chem. Ber.*, **98**, 2221

(1965).
13) U. Schoellkopf, F. P. Woerner, and E. Wiskott, *Chem. Ber.*, **99**, 806 (1966).
14) H. E. Zimmerman and B. S. Thyagarajan, *J. Am. Chem. Soc.*, **82**, 2505 (1960).
15) W. E. Parham, H. G. Braxton, Jr., and D. R. Theissen, *J. Org. Chem.*, **27**, 2632 (1962).
16) A. M. Van Leusen, R. J. Mulder, and J. Strating, *Recl. Trav. Chim., Pays-Bas*, **86**, 225 (1967).
17) H. Weitkamp, U. Hasserodt, and F. Korte, *Chem. Ber.*, **95**, 2280 (1962).
18) S. E. Wiberley and S. C. Bunce, *Anal. Chem.*, **24**, 623 (1952).
19) J. M. Derfer, E. E. Picket and C. E. Boord, *J. Am. Chem. Soc.*, **71**, 2482 (1949).
20) C. F. Wilcox, Jr., and R. R. Craig, *J. Am. Chem. Soc.*, **83**, 3866 (1961).
21) H. E. Simmons and R. D. Smith, *J. Am. Chem. Soc.*, **81**, 4256 (1959).
22) D. Barnard, J. M. Fabian, and H. P. Koch, *J. Chem. Soc.*, **1949**, 2442.
23) P. M. G. Bavin, G. W. Gray, and A. Stephenson, *Spectrochim. Acta*, **16**, 1312 (1960).
24) E. A. Robinson, *Can. J. Chem.*, **39**, 247 (1961).
25) M. Seshapathi Rao Naidu and D. Bhaskar Reddy, *Bull. Chem. Soc., Jpn.*, **48**, 1091 (1975).
26) A. Pavia, J. Wylde, R. Wylde, and E. Arnal, *Bull. Soc. Chim. Fr.*, **1965**, 2709, 2718.
27) L. Vo-Quang and M. P. Simonnin, *Bull. Soc. Chim. Fr.*, **1965**, 1534.
28) J. Seyden-Penne and T. Strazalko, *C. R. Acad. Sci.*, **260**, 5059 (1965).
29) K. L. Williamson, C. A. Landford, and C. R. Nicholson, *J. Am. Chem. Soc.*, **86**, 762 (1964).
30) E. H. Huntress and F. H. Carten, *J. Am. Chem. Soc.*, **62**, 511 (1940).
31) A. I. Vogel "A text book of Practical Organic Chemistry," Longmanns, Green and Co., Ltd. London (1968), p. 827.
32) C. C. Price and G. W. Stacy, *J. Am. Chem. Soc.*, **68**, 498 (1946).
33) L. W. Franchar, *Chem. Abstr.*, **52**, 16296d (1958).

Stereochemistry of Diels-Alder Reactions at High Pressure. II. Influence of High Pressure on Asymmetric Induction in Condensation of (−)-Di-(*R*)-menthyl Fumarate with Butadiene and Isoprene[1)]

Janusz Jurczak

Institute of Organic Chemistry, Polish Academy of Sciences, 01-224 Warszawa, Poland

(Received December 18, 1978)

The high-pressure Diels-Alder condensation of (−)-di-(*R*)-menthyl fumarate with butadiene and isoprene, followed by reduction of the adducts with lithium aluminium hydride, produced (1*S*,2*S*)-(+)-4-cyclohexene-1,2-dimethanol and (1*S*,2*S*)-(+)-4-methyl-4-cyclohexene-1,2-dimethanol in 6.2—12.8% optical yield, depending on the pressure applied. Results of asymmetric synthesis were discussed in light of the concept of parallel transition states. An interpretation of the thermal and Lewis-acid-catalyzed asymmetric Diels-Alder condensations using (−)-di-(*R*)-menthyl fumarate was proposed.

The Diels-Alder reaction is one of the best known organic reactions.[2)] In recent years the effect of pressure on the course of the (2+4) cycloaddition reaction has been widely studied.[3)] Cycloaddition reactions are characterized by negative values of activation volume ΔV^{*} defined as the difference between the volume occupied by the transition state and that occupied by the reactants. The large negative activation volume means that the reaction ought to be accelerated by an increase in pressure. Although this concept is very clear and simple from the theoretical standpoint, there are so far few studies dealing with the utilization of high pressure in organic synthesis.[4—6)] This is due to the relative inaccessibility of high-pressure equipment permitting work on a preparative scale.

High-pressure kinetics are much more frequently studied.[3,7,8)] High-pressure kinetics in solution permit observation of the activation volume ΔV^{*} whose changes are a convenient tool for interpretation of the mechanism of the reaction.

$$\Delta V^{*} = -RT(\partial \ln k/\partial P)_T$$

McCabe and Eckert[7)] have shown that the mechanism of the Diels-Alder reaction is of the nature of a concerted process, according to Woodward and Hoffmann.[9)] The (2+4) cycloaddition reaction is characterized by a large negative activation volume, and in some cases the activation volume is more negative than the volume change of reaction, ΔV_r ($\Delta V_r = V_{\text{products}} - V_{\text{reactants}}$). That is, in this case, the transition state is actually more compact than the product, probably due to the occurance of secondary π interactions in the transition state.[10)]

Recently we have observed an effect, heretofore unreported, of high pressure on the direction and magnitude of asymmetric induction in the Diels-Alder condensation of 1-methoxy-1,3-butadiene with (*R*)-(−)-menthyl glyoxylate.[1)] Satisfactory results of these preliminary investigations led us to undertake systematic studies on the effect of high pressure on the stereochemistry of the Diels-Alder reaction, especially on asymmetric induction.

In the present study we report the reaction between butadiene or isoprene and (−)-di-(*R*)-menthyl fumarate. Historically, this is the system for which Korolev and Mur[11)] first demonstrated the possibility of asymmetric induction in diene synthesis in 1948.

Results

The pioneering work of Korolev and Mur[11)] was repeated and extended by Walborsky *et al.*[12)] who studied the effect of a Lewis acid catalyst on asymmetric induction. Thermal condensation of butadiene or isoprene with (−)-di-(*R*)-menthyl fumarate was carried out by these authors at 25—180 °C in benzene as solvent (Scheme 1).

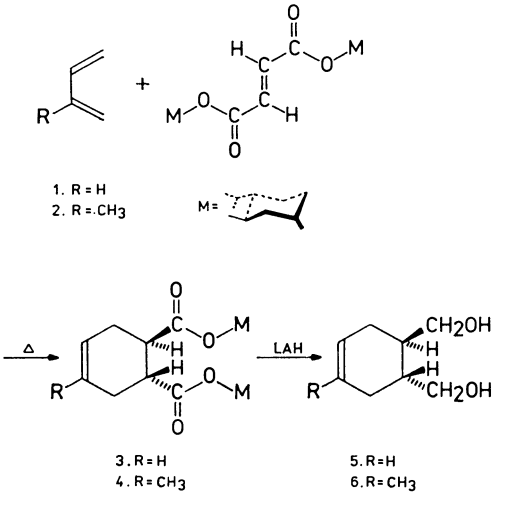

Scheme 1.

Optical yield and the direction of asymmetric induction were studied by measurements of the optical rotation of glycols **5** and **6** whose absolute configurations were established to be (−)-(1*R*,2*R*) by chemical correlations. Specific rotations of pure enantiomers were for **5** $[\alpha]_{589}^{22}$ −70.4° (*c* 3.0, in chloroform) and for **6** $[\alpha]_{589}^{25}$ −78.8° (*c* 3.4, in chloroform). In non-catalyzed reactions carried out at room temperature the products showed no induced optical activity. Elevation of temperature brought about formation of optically active products (0.8% optical yield at 65 °C and 3% at 180 °C), with predominance of the adduct with a 1*R*,2*R* configuration. Longer reaction time increased the total yield of the product, without changing the optical yield. The effect of solvent on the optical yield was slight. Reactions carried out in the presence of Lewis acids afforded predominantly

Table 1. Condensations of butadiene (**1**) and/or isoprene (**2**) with (−)-di-(*R*)-menthyl fumarate in different solvents under high pressure at 25 °C

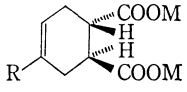

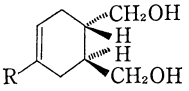

Diene	Solvent	ΔP/kbar	Yield/%	$[\alpha]_{589}^{20}$ in $CHCl_3$	c	Abs. conf.	Optical yield/%
1	$C_6H_5CH_3$	6.9	100	+9.0°	3.14	1*S*,2*S*	12.8
1	CH_2Cl_2	6.9	100	+5.2°	3.22	1*S*,2*S*	7.4
1	CH_2Cl_2	7.4	100	+5.7°	3.14	1*S*,2*S*	8.1
2	$C_6H_5CH_3$	4.0	75	+4.9°	3.20	1*S*,2*S*	6.2
2	$C_6H_5CH_3$	6.1	88	+7.2°	3.22	1*S*,2*S*	9.2
2	$C_6H_5CH_3$	7.5	100	+8.7°	3.05	1*S*,2*S*	11.0
2	$C_6H_5CH_3$	8.4	100	+9.8°	3.00	1*S*,2*S*	12.4
2	CH_2Cl_2	4.5	69	+5.0°	3.08	1*S*,2*S*	6.4
2	CH_2Cl_2	5.9	81	+6.7°	3.10	1*S*,2*S*	8.5
2	CH_2Cl_2	7.0	100	+7.8°	3.27	1*S*,2*S*	9.9
2	CH_2Cl_2	7.8	100	+8.8°	3.34	1*S*,2*S*	11.2

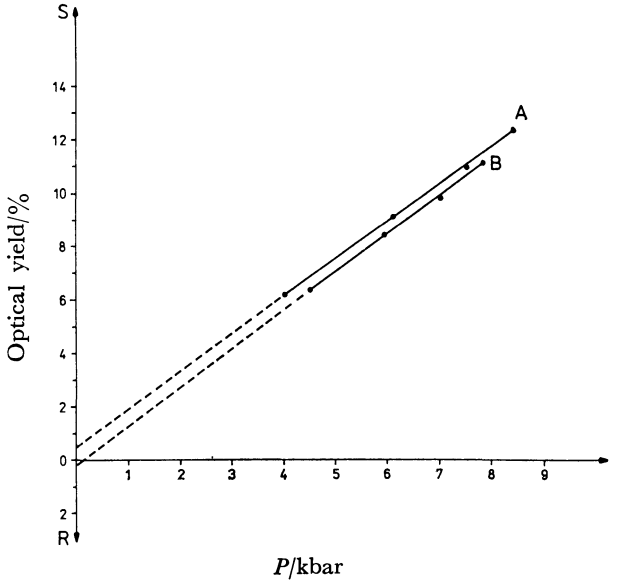

Fig. 1. Dependence of optical yield on pressure in the reactions between isoprene and (−)-di-(*R*)-menthyl fumarate carried out in toluene (A) and dichloromethane (B).

the adducts with opposite absolute configuration, 1*S*,2*S*; optical yields of the asymmetric synthesis were very high—about 75%.

For high-pressure studies of the stereochemistry of the Diels-Alder reaction, earlier observations[13] and preliminary experiments showed that the optimal conditions for the reactions of (−)-di-(*R*)-menthyl fumarate with dienes is at 25 °C and about 7 kbar for 20 h, which afforded a $\sqrt{100}$% yield of the product. These conditions were accepted for all high-pressure reactions presented in this study.

In the present studies toluene and dichloromethane were employed as solvents (solidification pressures at room temperature are about 8.8 kbar and about 8 kbar, respectively). We selected these two solvents also because previous work[14] showed that there is a change in the direction of asymmetric induction in the Diels-Alder reaction of 1-methoxy-1,3-butadiene with (*R*)-(−)-menthyl glyoxylate upon changing from an aromatic solvent to dichloromethane or chloroform. Results are presented in the Table showing the yields of adducts **3** or **4**, optical yields and configurations at C-1 and C-2.

The reaction of butadiene (**1**) with (−)-di-(*R*)-menthyl fumarate in toluene or dichloromethane at approximately 7 kbar gives adduct **3** in a quantitative yield. In all cases *S* configuration is induced at C-1 and C-2; the optical yield is higher in toluene than in dichloromethane. For systematic studies of the effect of pressure on the optical yield of the reaction, isoprene (**2**) was selected as a solvent. In all four reactions carried out in toluene (4.0—8.4 kbar), we obtained product **4** with predominance of the diastereomer of 1*S*,2*S* configuration. The optical yield increased from 6.2% at 4.0 kbar to 12.4% at 8.4 kbar. Similar results were obtained in reactions carried out in dichloromethane. Comparison of the dependence of optical yield on pressure in both solvents is presented graphically in Fig. 1.

The plots clearly testify to the same linear nature of the dependence of optical yield on pressure for both solvents; under the same pressure, optical yields are somewhat higher in toluene than in dichloromethane.

Discussion

Walborsky[12] has accepted the conformational model of Prelog[15] for (−)-di-(*R*)-menthyl fumarate as well as the concept of a rigid transition state in the Diels-Alder reaction[2] (Scheme 2).

The dienophile and diene approach each other in parallel planes, which results in two possible transition states of the reaction: "A", in which the diene is situated above the dienophile plane from the side of the smaller substituent M, giving an adduct of 1*R*,2*R* configuration, and "B", in which the diene is situated

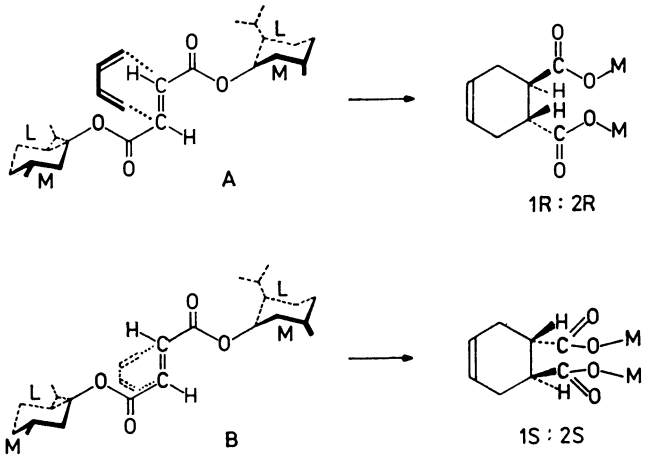

Scheme 2.

under the dienophile plane, from the side of larger substituent L, giving an adduct of 1*S*,2*S* configuration. The optical activity of the product is due to the difference in the steric ease of mutual approach of the reactants from one or the other side.

Conformational analysis of dienophile leads to the conclusion that three low-energy conformations are prefered: *s-trans*, *s-trans* (**7**), *s-cis*, *s-cis* (**8**), and *s-trans*, *s-cis* (**9**) (Scheme 3). Transoid-transoid conformation **7** prefers the approach of diene "from above," yielding the 1*R*,2*R* product. Cisoid-cisoid conformation **8** brings about formation of the 1*S*,2*S* product. In case of the transoid-cisoid conformation **9**, no asymmetric induction can be expected in reactions with symmetric dienes (*e.g.* butadiene).

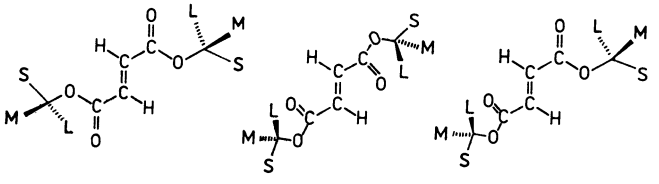

Scheme 3.

Acceptance of the concept of parallel transition states, as proposed by us,[14] permits elucidation of the stereochemical course of asymmetric diene synthesis, without severe deviation from the rules of Prelog[15] and Cram.[16]

For interpretation of the present results of condensations at room temperature, we assume that the optical yield is the result of the population of conformers **7** and **8** in the ground state. It is intuitively obvious that the probabilities of formation of transition states with the participation of conformers **7** and **8** are almost the same, and thus the difference between the activation energies of both transition states is only slight. Therefore, asymmetric induction should depend on the population of conformers **7** and **8**, which at constant temperature ought to be affected by the solvent used. Indeed, we found differences between the absolute configuration and optical yields of the products of the reaction of isoprene with (−)-di-(*R*)-menthyl fumarate run in toluene (2*S*,6*S*, 0.6%) and in dichloromethane (2*R*,6*R*, 0.4%);[17] this seems to confirm the accepted assumption.

Similar results have been obtained by Sauer and Kredel[18] in reactions of cyclopentadiene with (−)-di-(*R*)-menthyl fumarate (Scheme 4), carried out at 35 °C in several solvents. Using acetone and dioxane, these authors have obtained product **10** with optical yields of 2.8% and 1.5%, respectively; the resulting glycols **11** were dextrorotatory. Upon use of dichloromethane, the optical yield was 3.6%, and the resulting glycol was levorotatory.

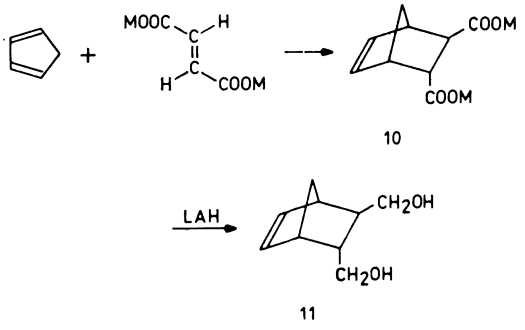

Scheme 4.

Results of the high-temperature condensations of Walborsky[12] can be interpreted using the above concept. Elevation of temperature changes the conformational equilibrium of the dienophile, in this case in favor of transoid, transoid form **7**, which is responsible for the formation of the adduct of 1*R*,2*R* configuration. The tendency for an increase in optical yield with elevation of temperature[12] confirms our interpretative approach.

In high-pressure reactions we obtained, irrespective of the solvent, adducts of 1*S*,2*S* configuration, with optical yields much higher as compared with atmospheric-pressure reactions carried out at the same temperature. Optical yields increase distinctly with an increase in pressure. We shall consider these facts in light of the concept of parallel transition states[14] (Scheme 5).

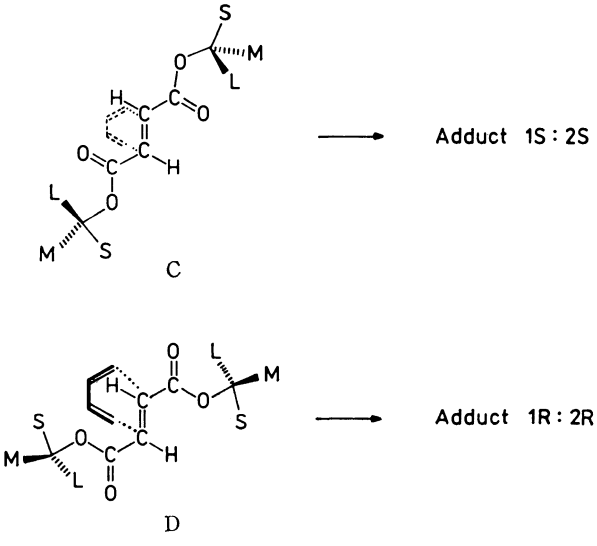

Scheme 5.

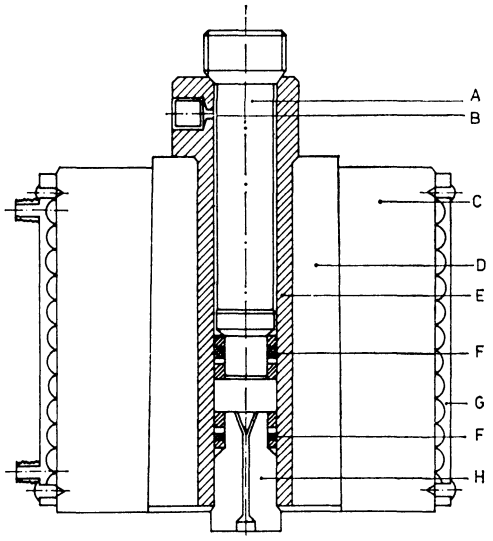

Fig. 2. Sketch of high-pressure apparatus.

Induction of the 1*S*,2*S* configuration in the high-pressure reaction indicates clearly that the active complex of the "C" type is favored, which suggests that it is more compact than "D". The probability of formation of active complex "C" increases with increasing pressure which is in practice the sole parameter determining the optical yield.

The direction of asymmetric induction in high-pressure reactions is identical to that in the reactions catalyzed by Lewis acids; in either case adducts of absolute 1*S*,2*S* configuration are formed. This may suggest that in both cases transition states of a similar type, *i.e.* with a cisoid-cisoid conformation of the dienophile, are preferred.

This conclusion is supported by high-pressure studies of the catalyzed Diels-Alder reaction between 2,3-dimethyl-1,3-butadiene and butyl acrylate, carried out by Poling and Eckert.[19] According to these authors, the activation volume for the reaction catalyzed by $AlCl_3$ is $\Delta V^{\neq} = -25.7$ cm^3/mol and for the non-catalyzed reaction it is $\Delta V^{\neq} = -28.6$ cm^3/mol. Comparison of these two values clearly points to similarities in the structures of the transition states of both reactions.

Experimental

Bps refer to air-bath temperatures. Mps (uncorrected) were determined on a Kofler block. Polarimetric measurements were performed with a Perkin-Elmer 141 automatic polarimeter. Silica gel G Merck was used for TLC, and silica gel 100—200 mesh Macherey-Nagel for column chromatography. All reactions and chromatographic separations were monitored in TLC. All high-pressure reactions were carried out in a piston-cylinder type apparatus. Initial working volume was about 10 ml. The details of this apparatus, previously applied to various investigations on the metal-hydrogen system,[20,21] are presented in the Fig. 2. The internal part (E) consisted of a beryllium brass vessel supported by two external steel rings (C,D). A jacket (G) supplied by flowing water served thermostatic conditions. It could be maintained within ±1 °C. The electrical leads for pressure and temperature measurements (manganine manometer, thermocouple) were led through a conical electrode placed in the stopper (H) of beryllium brass. The mobile piston (A) was made of special steel composition with an ending of beryllium brass. The sealing (F) of the mobile piston and the stopper was conventional character (O-ring and metallic Bridgeman type sealing) as described previously[22]. The reaction can be done under any gaseous atmosphere. The gas was introduced into the working volume through the capillary inlet (B), being initially compressed to 1—1.5 kbar in a separate multiplier.[21] The pressure inside the working volume was measured by a calibrated manganine coil with accuracy ±0.1 kbar.

Butadiene and isoprene were redistilled commercial (Fluka) reagents. (—)-Di-(*R*)-menthyl fumarate was prepared according to earlier procedure,[11] mp 59—60 °C, $[\alpha]_{589}^{20}$ −103.1° (*c* 1.55, in chloroform).

Condensations of butadiene and/or isoprene with (—)-di-(*R*)-menthyl fumarate.

Partial asymmetric synthesis of *trans*-4-cyclohexene-1,2-dimethanol (**5**) and *trans*-4-methyl-4-cyclohexene-1,2-dimethanol (**6**) was effected using both the atmospheric- and high-pressure methods.

Procedure A; *Atmospheric-pressure Method.* To a solution of 1.96 g (5 mmol) (—)-di-(*R*)-menthyl fumarate and 10 mg hydroquinone in 20 ml of toluene, 0.68 g (10 mmol) isoprene was added and the mixture was left at room temperature for 300 h. Solvent was removed and residue was dissolved in anhydrous ether and added to a refluxing slurry of 2.2 g (6 mmol) lithium aluminium hydride in 100 ml anhydrous ether. The reaction mixture was dried ($MgSO_4$) and filtered. The solvent was evaporated and the product isolated by column chromatography. Menthol was eluted using a mixture of ligroin and ether (9 : 1, v/v) and the glycol **6** was eluted using a mixture of ligroin and ether (7 : 3, v/v). After removal of the solvents the residue was distilled to give **6** (70%), bp 128—130 °C/0.2, mp 54—57 °C (from ether).

Procedure B; *High-pressure Method.* The high-pressure apparatus, closed on the bottom with a stopper, was filled with the reaction mixture (2.5 mmol (—)-di-(*R*)-menthyl fumarate, 5 mmol butadiene and 5 mg hydroquinone in 10 ml of dichloromethane) and a mobile piston was inserted. Then the whole assembly was placed between the pistons of a hydraulic press and the pressure was elevated up to 7.3 kbar. After stabilization of the pressure the heater was switched on, whereupon the temperature was raised to 25 °C and pressure to 7.4 kbar. The reaction mixture was kept under these conditions for 20 h. Pressure was released and the solvent was evaporated. The residue (100% yield of adduct **3**) was treated with 1 g (2.7 mmol) of lithium aluminium hydride in anhydrous ether for 12 h and the glycol **5** isolated (78%), bp 103—105 °C/0.2. The glycol **5** solidified on standing, mp 49—53 °C.

The author is very indebted to Professors B. Baranowski and A. Zamojski for stimulating interest and helpful discussions and to Mrs. M. Zajaczkowska and Mr. M. Tkacz for fruitful cooperation. This work was supported by grants from the Polish Academy of Sciences (MR I-12.1.1.1 and 03.10.7.01.01).

References

1) Part I, J. Jurczak and B. Baranowski, *Polish J. Chem.*, **52**, 1857 (1978).

2) J. Sauer, *Angew. Chem. Int. Ed. Engl.*, **5**, 211 (1966); **6**, 16 (1967).

3) T. Asano and W. J. le Noble, *Chem. Rev.*, **78**, 407

(1978).
4) W. G. Dauben and H. O. Krabbenhoft, *J. Org. Chem.*, **42**, 282 (1977) and references quoted therein.
5) J. Jurczak, M. Chmielewski and S. Filipek, *Synthesis*, **1979**, 41.
6) J. Jurczak and M. Tkacz, *Synthesis*, **1979**, 42.
7) J. R. McCabe and C. A. Eckert, *Acc. Chem. Res.*, **7**, 251 (1974).
8) G. Jenner, *Angew. Chem. Int. Ed. Engl.*, **14**, 137 (1975).
9) R. B. Woodward and R. Hoffmann, *Angew. Chem. Int. Ed. Engl.*, **8**, 781 (1969).
10) R. B. Woodward and T. J. Katz, *Tetrahedron*, **5**, 70 (1959).
11) A. Korolev and V. Mur, *Dokl. Akad. Nauk SSSR*, **59**, 251 (1948).
12) H. M. Walborsky, L. Barash, and T. C. Davis, *J. Org. Chem.*, **26**, 4778 (1961); *Tetrahedron*, **19**, 2333 (1963).
13) B. S. Eljanov, E. J. Klabunovskij, M. G. Gonikberg, G. M. Parfenova, and L. F. Godunova, *Izv. Akad. Nauk SSSR, Ser. Chim.*, **1971**, 1658.
14) J. Jurczak and A. Zamojski, *Tetrahedron*, **28**, 1505 (1972).
15) V. Prelog, *Helv. Chim. Acta*, **36**, 308 (1953).
16) D. J. Cram and F. A. Abd Elhafez, *J. Am. Chem. Soc.*, **74**, 5828 (1952).
17) Optical yields were reproducible with accuracy $\pm 0.2\%$; for either solvent three reactions under same conditions were carried out.
18) J. Sauer and J. Kredel, *Tetrahedron Lett.*, **1966**, 6359.
19) B. F. Poling and C. A. Eckert, *Ind. Eng. Chem., Fundam.*, **11**, 451 (1972).
20) B. Baranowski and W. Bujnowski, *Roczniki Chem.*, **44**, 2271 (1970).
21) M. Tkacz and B. Baranowski, *Roczniki Chem.*, **50**, 2159 (1976).
22) S. Majchrzak, B. Baranowski, W. Bujnowski, and M. Krukowski, *Roczniki Chem.*, **46**, 1173 (1972).

NOTES

BULLETIN OF THE CHEMICAL SOCIETY OF JAPAN, VOL. 52 (11), 3443—3444 (1979)

SO_2-Produced Acidic Hydroxyl Groups and the Catalytic Activities of Alkaline Earth X Zeolites

Kiyoshi Otsuka,* Yuji Wada, Kimiaki Tanaka, and Akira Morikawa

Department of Chemical Engineering, Tokyo Institute of Technology, Ookayama, Meguro-ku, Tokyo 152

(Received January 30, 1979)

Synopsis. The generation of Brönsted acid sites by SO_2-adsorption on alkaline earth X zeolites has been examined by infrared spectroscopy. The SO_2-induced catalytic activities of the zeolites in the double-bond isomerization of butenes can be ascribed to both the increase in the number of acidic hydroxyl groups and the enhancement in the catalytic activities of the groups after the SO_2 adsorption.

The kinetic studies of the SO_2-induced isomerization of 2-butene over various cation-exchanged X zeolites have been reported in the previous paper.[1,2] It was inferred that the promoting action of SO_2 on the rate of double-bond isomerization of butenes is caused by the generation of acidic hydroxyl groups. The formation of acidic hydroxyl groups by the adsorption of NO_2, SO_2, or Cl_2 has been confirmed on CaY zeolites, and the induced catalytic acitivity of the zeolite in dehydration of 2-propanol by these inorganic gases has been attributed to the formation of the acidic hydroxyl groups.[3] The object of the present work is to examine these suggestions by studying the generation of the Brönsted acid sites after SO_2-adsorption by infrared spectroscopy.

Experimental

The alkaline earth X zeolites used were prepared by a conventional ion exchange of a NaX zeolite (13X from Linde) with aqueous solution of the appropriate chlorides. The percentages of cation exchange, expressed by 100 ([Al]—[Na])/[Al], were as follows: MgX (78), CaX (78), SrX (94), and BaX (93).

The apparatus and the materials used and the analysis of butene isomers were described elsewhere.[1]

Prior to every run, the catalyst in the reactor was degassed under vacuum for 2 h at the required temperature. After the adsorption of SO_2 at 25 °C for 30 min, the isomerization was started at the same temperature by feeding *cis*-2-butene (1.29×10^{-3} mol) and circulating the gas through the catalyst bed.

Infrared-spectra measurements were made with the zeolite in the form of a self-supporting wafer (3—4 mg/cm^2). The sample wafer was calcined in dried oxygen at 400 °C in the IR-cell and degassed in a vacuum at the same temperature for 1 h. The wafer was then brought into contact with 15 Torr of D_2O vapor for 1 h at 200 °C to exchange OH by OD groups, because the broad OH stretching band around 3600 cm^{-1}, probably due to adsorbed water molecules on the zeolites, makes it difficult to identify the different kinds of OH groups. After this treatment, the wafer was outgassed again in a vacuum for 1 h at 400 °C. The spectra of the wafer were recorded, before and after a required amount of SO_2 was adsorbed at 100 °C, using a Shimadzu IR-430 grating spectrometer. It was confirmed that all the SO_2 introduced was adsorbed on the zeolites under the experimental conditions applied here.

Results and Discussion

Figure 1 shows the infrared spectra of the zeolites at the region of OD-stretching vibration, taken before and after the adsorption of SO_2. For all the zeolites, the intensities of the bands for OD groups around 2695 cm^{-1}, corresponding to the band at ≈3640 cm^{-1} due to acidic OH groups in the super cage for the undeuterated alkaline earth faujasites,[4-6] increased after the adsorption of SO_2. The shift in the frequency of the acidic OD band to a lower frequency of about 4 cm^{-1} has been confirmed by repeated experiments for the infrared spectra of the MgX zeolite. This shift caused by SO_2 was not clear within experimental error (±2 cm^{-1}) for the other three zeolites.

The increase in the absorbance of the acidic OD band at the maximum caused by the SO_2-adsorption and the rate of SO_2-induced double-bond isomerization of *cis*-2-butene have been plotted in Fig. 2 as functions of the amount of SO_2 on the zeolites. The dotted-lines or curve for the rate of the isomerization were from the data for the zeolites pretreated at 500 °C in the previous work.[2] For the CaX zeolite pretreated

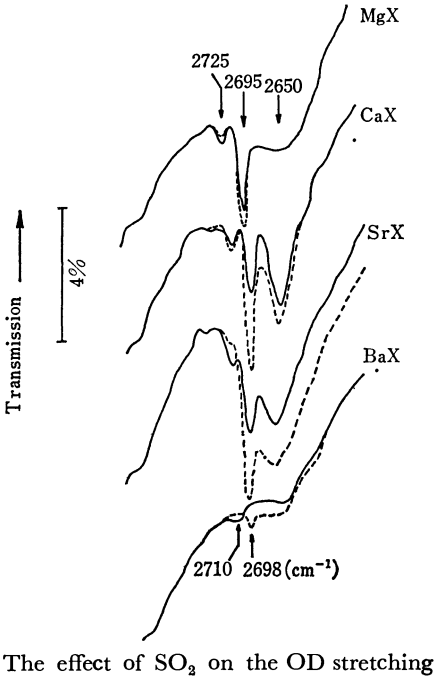

Fig. 1. The effect of SO_2 on the OD stretching bands of the alkaline earth zeolites: ——, without adsorbed SO_2; ----, after the addition of SO_2. The amount of SO_2 adsorbed (10^{-4} mol g^{-1}): MgX, 1.3; CaX, 1.5; SrX, 3.2; BaX, 1.3.

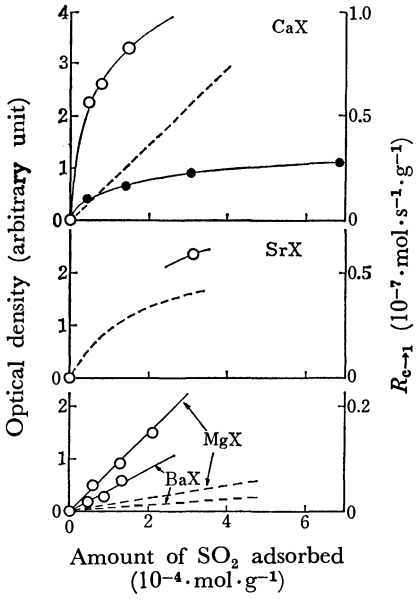

Fig. 2. The optical density of the acidic OD band generated by SO_2 and the rate of the double-bond isomerization as a function of the amount of pre-adsorbed SO_2: ○, optical density of the SO_2-induced acidic OD band; ●, the rate of double-bond conversion, $R_{c\rightarrow 1}$, over the CaX pretreated at 400 °C; ----, $R_{c\rightarrow 1}$ obtained for the zeolites pretreated at 500 °C.

at 400 °C, the catalytic activity in the isomerization increases with a rise in the concentration of SO_2 adsorbed in the similar way as that of the increase for the absorbance of acidic OD groups. Although the pretreatment temperatures for MgX, SrX, and BaX zeolites are different in the experiments of activity test and infrared spectra measurement, the identical order observed in the SO_2-induced activities among the four zeolites, *i.e.*, CaX≃SrX>MgX>BaX, has been confirmed in the generation of acidic OD groups.

The schemes proposed for the formation of Brönsted acid sites are as follows:[2,3]

$$M^{2+}(H_2O)_x + SO_2 \longrightarrow M^{2+}[SO_3]^{2-} + 2H^+ + (H_2O)_{x-1} \quad (1)$$

or

$$M^{2+}(OH)^- + SO_2 \longrightarrow M^+\text{-}O\text{-}S(=O)\text{-}O^- + H^+ \quad (2)$$

where, $M^{2+}(H_2O)_x$ is the divalent cation coordinated by water, and $M^{2+}(OH)^-$ is the basic hydroxyl groups formed through the following reaction:[5,7]

$$M^{2+} + H_2O \rightleftharpoons M^{2+}(OH)^- + H^+ \quad (3)$$

Mirodatos, Pichat, and Barthomeuf have suggested that the OH band at 3685 (MgY) (2710 cm^{-1} in the case of the corresponding OD band) or 3675 cm^{-1} (CaY) should be attributed to the basic OH group of M^{2+}-$(OH)^-$ which is responsible for the generation of acidic OH group after CO_2 addition.[8] The OD bands at 2725—2710 cm^{-1} shown in Fig. 1 correspond to the band due to the basic OD groups. In fact, for MgX, SrX, and BaX, the intensities of these OD bands decreased after the introduction of SO_2, accompanying the increase in intensities of acidic OD groups at ≈2695 cm^{-1} as shown in Fig. 1. However, the relatively greater increase in the intensities of the latter bands compared to the decrease in the former bands suggests that the generation of acidic OH groups cannot be attributed only to the reaction of Scheme 2. We believe that Scheme 1 is also important for the generation of the acid sites.

The spectra in Fig. 1 demonstrate the presence of OD groups at ≈2695 cm^{-1} even in the absence of SO_2 on MgX, CaX, and SrX. These OD groups, however, do not catalyse the isomerization of *cis*-2-butene at 100 °C. The reactivity of the acidic OH group at ≈3640 cm^{-1} with *cis*-2-butene has been examined at 100 °C for MgX before and after the adsorption of SO_2. In the absence of SO_2, the intensity of the OH band did not change by the addition of *cis*-2-butene. On the other hand, the intensity of the band decreased considerably with time in the presence of SO_2. These results suggest that the reactivity of the acidic OH group at ≈3640 cm^{-1} or of the OD group at ≈2695 cm^{-1} increases after the addition of SO_2. Hence, the favorable action of SO_2 on the catalytic activities of the zeolites can be ascribed not only to the increase in the number of acidic hydroxyl groups but also to the enhancement in the catalytic activities of the groups. The little or no change in the frequency of the OD band after the adsorption of SO_2 does not give us any information about the difference in the nature of the OD groups in the presence and absence of SO_2. A possible explanation for the increase in the reactivities of OD groups is that the acidic strength of the OD groups has been totally enhanced through the inductive effect of SO_2 adsorbed on the surface. An alternative explanation is that SO_2 may release the OD or OH groups which had been inhibited in regard to catalysis by the basic $M^{2+}(OD)^-$ or $M^{2+}(OH)^-$ species (Eq. 3).[9] Further studies are needed to clarify these points.

Addition of SO_2 onto alkaline earth hydroxides, such as $Mg(OH)_2$, $Ca(OH)_2$, and $Sr(OH)_2$, which contain a large number of basic hydroxyl groups and water molecules, causes neither the catalytic activities of these compounds in the double-bond isomerization of butene nor the generation of new hydroxyl groups. These tests have been carried out at 25 °C on the hydroxides pretreated at various temperatures between 100 and 400 °C. These results indicate that the reactions of Schemes 1 and 2 are found specifically on zeolites. A strong electrostatic field in the zeolite cavity must play an important role for the generation of the acidic OH groups.

References

1) K. Otsuka and A. Morikawa, *J. Catal.*, **46**, 71 (1977).
2) K. Otsuka and A. Morikawa, *J. Catal.*, **56**, 88 (1979).
3) Y. Ishinaga, K. Otsuka, and A. Morikawa, *Bull. Chem. Soc. Jpn.*, **52**, 933 (1979).
4) C. L. Angell and P. C. Schaffer, *J. Phys. Chem.*, **69**, 3463 (1965).
5) J. W. Ward, *Adv. Chem. Ser.*, **101**, 380 (1971).
6) J. W. Ward, *J. Phys. Chem.*, **72**, 4211 (1968).
7) A. E. Hirschler, *J. Catal.*, **2**, 428 (1963).
8) C. Mirodatos, P. Pichat, and D. Barthomeuf, *J. Phys. Chem.*, **80**, 1335 (1976).
9) C. Mirodatos, A. A. Kais, J. C. Vedrine, P. Pichat, and D. Barthomeuf, *J. Phys. Chem.*, **80**, 2366 (1976).

BULLETIN OF THE CHEMICAL SOCIETY OF JAPAN, VOL. 52 (11), 3445—3446 (1979)

Studies on the Aqueous Solutions of Guanidinium Salts. X. Activity Coefficients of Biguanide Salts in Aqueous Solutions at 25 °C

Koichiro MIYAJIMA,* Shigeo NAKANISHI, and Masayuki NAKAGAKI
Faculty of Pharmaceutical Sciences, Kyoto University, Yoshida-shimoadachi-cho, Sakyo-ku, Kyoto 606
(Received April 10, 1979)

Synopsis. Activity coefficients and molar conductivities of biguanide salts (Bg·HX) in aqueous solutions were determined at 25 °C. The values of mean activity coefficients of these salts were relatively low and lay in the order Bg·HOAc>Bg·HCl>Bg·HBr>ButylBg·HCl. These results were discussed in terms of the ion-ion interactions and the concomitant structural change of water.

Biguanide is a condensed compound of two molecules of guanidine and its salts are known to induce a significant change of conformation of protein in aqueous solutions.[1] Some of its alkyl and arylalkyl derivatives have been used clinically as hypoglycemic agents.

In a previous paper,[2] we reported that there was a close relation between $\gamma_\pm$ values and the denaturation abilities of various guanidinium salts with different counter anions, that is, the lower the $\gamma_\pm$ values are, the stronger the denaturation abilities are. The minimum concentration of a biguanide salt to produce the denaturation of BSA is about a half of that of the guanidinium salt.[3] On the basis of the similarities of functional group and the molecular structure between these two kinds of salts, the denaturation mechanism of biguanide salts seems to be similar to that of the guanidinium salts. As for the protein denaturation, the structure breaking action of the guanidinium salt is considered to be the most important factor. From these points of view, we determined the osmotic and activity coefficients of some biguanide salts and discussed their effects on the structure of water by using the cosphere overlap model of Desnoyers.[4]

Experimental

Materials. Biguanide hydrochloride, hydrobromide, and acetate were prepared from biguanide sulfate monohydrate obtained from Aldrich Chemical Co., Ltd. The crude compounds were recrystallized twice or more from ethanol. Butylbiguanide hydrochloride was obtained from Sankyo Co., Ltd. and used without further purification. The purities of these salts were described elsewhere.[3] These salts were dissolved in redistilled and deionized water.

Methods. Osmotic and activity coefficients were determined at 25±0.02 °C by the isopiestic comparison method described elsewhere.[3] From the osmotic coefficient (ϕ), mean activity coefficient ($\gamma_\pm$) was calculated from Eq. 1.

$$\ln \gamma_\pm = (\phi - 1) + 2\int_0^{\sqrt{m}} \frac{\phi - 1}{\sqrt{m}} d\sqrt{m} \qquad (1)$$

where m is the molality of salt. Buoyancy corrections were made for biguanide salts using the densities of solid salts reported previously.[3] For the determination of isopiestic molality, buoyancy correction was also made to the aqueous solution on the assumption that the densities of aqueous solutions were all unity. The isopiestic molalities of aqueous solutions of potassium chloride (reference solute) and the biguanide salts are shown in Table 1. The experimental determination of isopiestic concentrations is precise to ±0.2%. Conductance was measured by the universal bridge manufactured by Yokogawa-Hewlet-Packard Co., Ltd. at 25± 0.05 °C. The conductance of the solution was obtained by subtracting the experimental value of conductance of water from that of the solution to avoid the effect of CO_2 dissolved in water. The molar conductivity at infinite dilution was obtained graphically by using the Fuoss-Onsager equation.[5]

Results and Discussion

The values of ϕ and $\gamma_\pm$ are shown in Table 2. The values of log $\gamma_\pm$ *vs.* $\sqrt{m}$(mol kg^{-1})$^{1/2}$ curves for various biguanide salts approach the Debye-Hückel limiting line (DHL-L) from above at low concentration, indicating the absence of such ion pairs as seen in the case of cadmium sulfate. The relatively low values of log $\gamma_\pm$ for Bg·HOAc, Bg·HCl, and Bg·HBr as compared with the alkali metal salts with the same counter anions, may be attributed to the nature of structure breaking of the biguanide ion. The values of log $\gamma_\pm$ for three biguanide salts lie in the same order ($OAc^- > Cl^- > Br^-$) as the guanidinium salts with the corresponding counter anions.[2] The values of log $\gamma_\pm$ for Bg·HCl and Bg·HBr are smaller than those of guanidinium chloride and bromide respectively, while the value of log $\gamma_\pm$ of Bg·HOAc is larger than that of guanidinium acetate. The order of log $\gamma_\pm$ is consistent with the order predicted by the cosphere overlap model on the assumption that the biguanide ion is a structure breaker and cation-anion interaction predominate over the other interactions. The differences of log $\gamma_\pm$ values between biguanide and guanidinium salts imply that the biguanide ion breaks water structure more significantly than the guanidinium ion does. Butyl Bg·HCl shows the lowest value among the four salts. On the basis of the cosphere overlap model, this result can be attributed to the hydrophobic cation-cation interaction. As the concentration increases and two butylbiguanide ions approach each other, the water-structure-enforced ion pairing would occur to compensate the decrease of the entropy based on the hydrophobic hydration, leading to the decrease of $\gamma_\pm$ value. Therefore cation-cation interaction is the most predominant factor for the decrease of $\gamma_\pm$ value of butylbiguanide hydrochloride, while cation-anion interactions for the other three salts.

The molar conductivities of biguanide salts and ions at infinite dilution are shown in Table 3. Using the Λ° values in Table 3, the Stokes' radius (γ_s) of

Table 1. Molality of isopiestic solutions

m/mol kg^{-1} (KCl)	m/mol kg^{-1} (Bg·HCl)	m/mol kg^{-1} (KCl)	m/mol kg^{-1} (Bg·HCl)	m/mol kg^{-1} (KCl)	m/mol kg^{-1} (Bg·HCl)
0.1214	0.1229	0.5891	0.6384	0.9658	1.0986
0.2031	0.2085	0.6785	0.7440	0.9895	1.1262
0.3328	0.3488	0.7071	0.7808	1.0092	1.1524
0.3487	0.3666	0.7777	0.8639	1.0255	1.1747
0.4383	0.4657	0.8101	0.9047	1.0578	1.2153
0.5267	0.5669	0.9370	1.0615	1.3766	1.6380
m/mol kg^{-1} (KCl)	m/mol kg^{-1} (Bg·HBr)	m/mol kg^{-1} (KCl)	m/mol kg^{-1} (Bg·HBr)	m/mol kg^{-1} (KCl)	m/mol kg^{-1} (Bg·HBr)
0.1214	0.1229	0.5891	0.6469	0.9895	1.1536
0.2031	0.2085	0.6785	0.7551	1.0092	1.1797
0.3328	0.3486	0.7074	0.7940	1.0255	1.2006
0.4054	0.4346	0.7777	0.8795	1.0578	1.2457
0.4383	0.4709	0.8101	0.9204	1.2384	1.4954
0.5267	0.5723	0.9370	1.0853	1.3766	1.6917
0.5514	0.6040	0.9658	1.1261		
m/mol kg^{-1} (KCl)	m/mol kg^{-1} (Bg·HOAc)	m/mol kg^{-1} (KCl)	m/mol kg^{-1} (Bg·HOAc)	m/mol kg^{-1} (KCl)	m/mol kg^{-1} (Bg·HOAc)
0.1214	0.1214	0.6785	0.6914	0.9895	1.0138
0.2031	0.2040	0.7074	0.7207	1.0092	1.0350
0.3328	0.3367	0.7777	0.7932	1.0578	1.0862
0.4383	0.4425	0.8101	0.8272	1.2384	1.2764
0.5514	0.5595	0.9370	0.9614	1.3766	1.4223
0.5891	0.5971	0.9658	0.9923		
m/mol kg^{-1} (KCl)	m/mol kg^{-1} (ButylBg·HCl)	m/mol kg^{-1} (KCl)	m/mol kg^{-1} (ButylBg·HCl)	m/mol kg^{-1} (KCl)	m/mol kg^{-1} (ButylBg·HCl)
0.1319	0.1354	0.6785	0.7780	0.9658	1.1774
0.2031	0.2117	0.7074	0.8200	0.9895	1.2088
0.3328	0.3579	0.7777	0.9123	1.0092	1.2371
0.4383	0.4797	0.8101	0.9557	1.0578	1.3086
0.5514	0.6207	0.9370	1.1338	1.3766	1.8094

Table 2. Activity and osmotic coefficients of biguanide salts at 25 °C

m	Bg·HCl		Bg·HBr		Bg·HOAc		ButylBg·HCl	
mol kg^{-1}	ϕ	$\gamma_\pm$	ϕ	$\gamma_\pm$	ϕ	$\gamma_\pm$	ϕ	$\gamma_\pm$
0.1	0.760	0.918	0.753	0.914	0.771	0.926	0.744	0.908
0.2	0.693	0.891	0.684	0.885	0.714	0.908	0.670	0.876
0.3	0.649	0.872	0.635	0.864	0.681	0.898	0.619	0.853
0.4	0.614	0.856	0.601	0.847	0.655	0.892	0.581	0.834
0.5	0.585	0.843	0.571	0.836	0.637	0.887	0.550	0.817
0.6	0.561	0.832	0.547	0.822	0.621	0.884	0.524	0.802
0.7	0.541	0.822	0.526	0.811	0.608	0.881	0.501	0.789
0.8	0.524	0.813	0.508	0.801	0.597	0.879	0.480	0.777
0.9	0.508	0.804	0.491	0.792	0.587	0.877	0.462	0.766
1.0	0.493	0.797	0.475	0.783	0.579	0.876	0.446	0.756
1.2	0.468	0.782	0.450	0.767	0.565	0.874	0.418	0.736
1.4	0.447	0.770	0.426	0.752	0.553	0.872	0.393	0.718
1.6	0.429	0.759	0.406	0.739	0.543	0.871	0.372	0.701
1.8	0.412	0.748	0.389	0.726	0.531	0.871	0.344	0.678
2.0					0.528	0.871		

each biguanide ion and butylbiguanide ion calculated from Eq. 2 were 2.57 and 3.52 Å.

$$\gamma_s = \frac{0.82|z|}{\Lambda^\circ \eta_0} \qquad (2)$$

where z and η_0 are the valency of ion and the viscosity of water, respectively. Partial molar volumes at infinite dilution of biguanide ion and butylbiguanide ion were 69.8 and 137.1 cm^3/mol at 25 °C, respectively.[3] Assuming that these ions are spherical, the ionic radii of biguanide ion and butylbiguanide ion

Table 3. Molar conductivities of biguanide ions and salts at 25 °C

Salts or ions	Λ° / cm^2 Ω^{-1} mol^{-1}
Bg·HCl	112.4
Bg·HBr	114.3
Bg·HOAc	76.2
ButylBg·HCl	102.5
Bg·H$^+$	35.8
ButylBg·H$^+$	26.2

are calculated to be 2.55 and 3.20 Å, respectively. The ionic radius of the biguanide ion obtained from the partial molar volume is almost the same as that obtained from Eq. 2. But as for the butylbiguanide ion, the former is smaller than the latter indicating the hydrophobic hydration of butyl group.

The denaturation abilities for the three biguanide salts lie in the order $Br^- > Cl^- > OAc^-$, which is the reverse order of $\gamma_\pm$ values. This fact supports that the structure breaking actions of the biguanide salts contribute to the denaturation of protein in aqueous solutions. As reported previously,[3] butyl Bg·HCl has the strongest denaturation ability, but the denaturation mechanism may be different from the other three salts on the basis of the consideration of the mean activity coefficients. In other word, the hydrophobic interaction between the butyl group of butylbiguanide and the hydrophobic moiety of protein may play an important role as observed in the interaction of tetraalkylammonium salts and DNA.[6]

From the analysis of viscosity B-coefficients, the biguanide ion was concluded to be neither a structure maker nor a structure breaker.[3] But thermodynamically the biguanide ion should be a structure breaker. We have no idea to account for the discrepancy at the present stage. Now we are planning NMR study for solving this problem.

References

1) F. J. Castellio and R. Barker, *Biochem.*, **7**, 4135 (1968).
2) K. Miyajima, K. Inari, N. Hamaguchi, H. Yoshida, and M. Nakagaki, *Nippon Kagaku Kaishi*, **1975**, 1447.
3) K. Miyajima, S. Nakanishi, and M. Nakagaki, *Nippon Kagaku Kaishi*, **1976**, 205.
4) J. E. Desnoyers, M. Arel, G. Perron, and C. Jolicoeur, *J. Phys. Chem.*, **73**, 3346 (1969).
5) R. A. Robinson and R. H. Stokes "Electrolyte Solutions," Butterworth, London (1959) p. 143.
6) P. H. Von Hippel and T. Schleich, "Structure and Stability of Macromolecules," ed by Tismasheff and G. F. Fasman, Marcel Dekker, New York (1969), Vol. 2, p. 444.

BULLETIN OF THE CHEMICAL SOCIETY OF JAPAN, VOL. 52 (11), 3447—3448 (1979)

Resonance Energy Stabilization in Crystalline Ion Radical Salts

Yôichi IDA

Department of Chemistry, Faculty of Science, Hokkaido University, Sapporo 060

(Received April 20, 1979)

Synopsis. In solid ion radical salts, the ion radical molecules form a segregated stacking into columns, and the charge-transfer interaction occurs between ion radicals. The resonance energy stabilization due to the charge-transfer interaction was estimated for non-alternant one-dimensional system of solid ion radical salts.

The prominent magnetic, electrical, and optical properties of solid ion (cation or anion) radical salts have been the subject of many theoretical and experimental investigations over the past seventeen years.[1-5] In such solid ion radical salts, the planar ion radical molecules are known to form, in themselves, a segregated stacking into columns so as to make a large overlap between their half-occupied molecular orbitals.[2,3] In this case, any individual radical molecule interacts through charge transfer most strongly with other neighboring radicals, and the electronic and magnetic properties of the solid salts differ distinctly from those of ion radical monomer. In previous papers,[4,5] we applied half-filled Hubbard Hamiltonian to one-dimensional system of ion radical molecules, and explained the optical and magnetic properties of solid ion radical salts in terms of such a model. In the present paper, by using the same model, we examine the magnitude of the resonance energy stabilization due to the charge-transfer interaction in one-dimensional system of solid ion radical salts and apply this approach to certain crystalline ion radical salt such as Würster's Blue perchlorate cation radical salt.

Since every ion radical salt belongs to a kind of ionic crystals, Madelung energy is the most important factor for the cohesive energy. However, in contrast to typical ionic crystals such as alkali halides, resonance energy stabilization due to intermolecular charge-transfer interaction between ion radical molecules is the next important factor for the total cohesive energy in solid ion radical salts. In other words, because of half-occupied molecular orbital of the ion radical, there acts intermolecular covalent bonding between the ion radicals along infinite one-dimensional column. Calculation of the Madelung energy of solid ion radical salt is rather difficult, but we have found a way to estimate the magnitude of the resonance energy stabilization on the basis of a many-body problem. For this purpose, we consider only one-dimensional column of ion radicals in simple ion radical salt, where each ion radical carries one unpaired electron. The half-occupied molecular orbital of unpaired electron is taken for one site of ion radical molecule. We assume a model of non-alternant one-dimensional system composed of infinite number of such sites and neglect the effect of intramolecular electronic transitions of ion radical. In this model, each ion radical site has one identical molecular orbital with equal energy level, and there is one electron per each site. Along such one-dimensional column, an unpaired electron transfers from one site to another site, but a strong repulsive potential will take place when an electron happens to come onto a site which is already occupied by another electron with opposite spin. Let us denote the intra-site Coulomb repulsive energy as I, and consider a system of electrons described by the following Hamiltonian, which is often called the Hubbard Hamiltonian,[6]

$$\mathscr{H} = \sum_{i,j,\sigma} T_{ij} C_{i\sigma}^{+} C_{j\sigma} + I \sum_{i} n_{i\downarrow} n_{i\uparrow}, \tag{1}$$

where $n_{i\sigma} = C_{i\sigma}^{+} C_{i\sigma}$, and $C_{i\sigma}^{+}$ and $C_{i\sigma}$ are the creation and annihilation operators of an electron with σ-spin at the i-th site, respectively, and where T_{ij} is the transfer matrix element between the i-th and j-th sites, and the repulsive potential, I, appears only when two electrons with up and down spins are at the same site. Since each ion radical has identical molecular orbital with equal energy level, we put $T_{ii}=0$ without loss of generality. In the case of non-alternant one-dimensional model, we further assume that the transfer matrix elements exist only between nearest neighbor sites, and the value of this transfer matrix element is denoted by T (<0).

It is rather difficult to obtain the ground state energy of Eq. 1 in general case. However, Takahashi showed that, in the case of half-filled Hubbard model with $I \gg |T|$, the Hamiltonian of Eq. 1 becomes equivalent to the following effective Hamiltonian,[7]

$$\mathscr{H}_{\text{eff}} = \frac{4T^2}{I} \sum_{i} \left(\boldsymbol{S}_i \cdot \boldsymbol{S}_{i+1} - \frac{1}{4} \right) + 0\left(\frac{T^3}{I^2} \right), \tag{2}$$

where $\boldsymbol{S}_i$, ($S=1/2$), is the spin operator of an electron at the i-th site. In other words, in the limit of $I/|T| = \infty$, we can neglect such higher terms as $0(T^3/I^2)$, and the one-dimensional half-filled Hubbard model is reduced to one-dimensional Heisenberg antiferromagnetic model with exchange interaction, $J=2T^2/I$. Hereafter, we denote the number of sites in one-dimensional system as N. If we know the ground-state energy of the following non-alternant one-dimensional Heisenberg antiferromagnet,

$$\mathscr{H}' = 2J \sum_{i} \boldsymbol{S}_i \cdot \boldsymbol{S}_{i+1}, \qquad (J = 2T^2/I > 0), \tag{3}$$

we can obtain the value of the ground-state energy of Eq. 2 in the limit of $I/|T| = \infty$. It is well known that the exact ground-state energy of Eq. 3, as indicated by E', was obtained by Bethe and Hulthén.[8] For infinite number of sites, the value of E' is given by

$$E' = -2NJ \ln 2 + \frac{1}{2} NJ. \tag{4}$$

Therefore, if in the limit of $I/|T| = \infty$ we denote the exact ground-state energy of Eq. 2 as E, we can obtain

$$E = E' - \frac{1}{2}J\sum_{i} 1 = E' - \frac{1}{2}NJ$$
$$= -2NJ\ln 2 = -4N\frac{T^2}{I}\ln 2. \quad (5)$$

When we go back to our original system of ion radicals, we can see that the magnitude of E in Eq. 5 corresponds to the resonance energy stabilization due to charge-transfer interaction between ion radicals in one-dimensional system of solid ion radical salts and that the value of $E/N=-4(T^2/I)\ln 2$ is the resonance energy per one site of ion radical molecule. Obviously, if $T=0$, that is, if no electron transfer occurs between ion radical molecules, we have $E=0$ in Eq. 5, and no resonance energy stabilization takes place in such a system.

In the following, we shall estimate the magnitudes of E and E/N for certain system of solid ion radical salt. For example, we apply the present method to the high-temperature phase of Würster's Blue perchlorate crystal, which is one of stable cation radical salts derived from *N,N,N',N'*-tetramethyl-*p*-phenylenediamine. Although a solid-state phase transition occurs at 186 K,[3,9] the crystal structure of the high-temperature (room-temperature) phase of Würster's Blue perchlorate is known to be orthorhombic and to be built up from non-alternant one-dimensional columns composed of segregated stacking of equivalent Würster's Blue cation radicals along the a-axis, the intermolecular spacing between nearest neighbor cation radicals being 3.550 Å.[3] In a previous paper,[5] we examined the electronic state of the system of the cation radicals on the basis of the above-mentioned non-alternant one-dimensional Hubbard model. We could well understand the optical and magnetic properties of this Würster's Blue perchlorate salt in terms of the parameter values of $I=11900$ cm^{-1} and $T=-650$ cm^{-1}. In this case, since the magnitude of $I/|T|=18.3$ is much larger than unity, we can apply, in place of Eq. 1, the effective Hamiltonian of Eq. 2 to the one-dimensional system of Würster's Blue cation radicals. Then, in the approximation of $I/|T|=\infty$ limit, the magnitude of E in Eq. 5 was estimated by using the $I=11900$ cm^{-1} and $T=-650$ cm^{-1} values. The calculated resonance energy of the high-temperature phase of Würster's Blue perchlorate was $E=-277$ cal/mol or $E/N=-97$ cm^{-1} per one site of the cation radical. On the other hand, for this salt, Metzger performed calculation of Madelung energy by using Ewald's method in order to clarify the mechanism of the phase transition at 186 K.[10] Although the Madelung energy is rather sensitive to details in the atomic charge distribution, he estimated the Madelung energy for the 300 K (high-temperature phase) Würster's Blue perchlorate crystal to be -94550 ± 690 cal/mol. Therefore, the total cohesive energy is found to be -94827 ± 690 cal/mol by summing the Madelung energy and the resonance energy. Although the resonance energy is very small compared to the Madelung energy and is only 0.29% of the total cohesive energy in Würster's Blue perchlorate, it is important to note that the resonance energy stabilization does not take place in usual ionic crystals but only takes place in solid ion radical salts.

References

1) Y. Iida, *Bull. Chem. Soc. Jpn.*, **50**, 1445 (1977), and the references cited therein.
2) J. Tanaka, M. Tanaka, T. Kawai, T. Takabe, and O. Maki, *Bull. Chem. Soc. Jpn.*, **49**, 2358 (1976), and the references cited therein.
3) J. L. DeBoer and Aafje Vos, *Acta Crystallogr., Sect. B*, **28**, 835, 839 (1972).
4) Y. Iida, *Bull. Chem. Soc. Jpn.*, **51**, 2523, 3637 (1978); **52**, 1523 (1979).
5) Y. Iida, *Bull. Chem. Soc. Jpn.*, **52**, 689 (1979).
6) J. Hubbard, *Proc. R. Soc. London, Ser. A*, **276**, 238 (1963); **281**, 401 (1964).
7) M. Takahashi, *Prog. Theor. Phys. (Kyoto)*, **42**, 1098 (1969).
8) H. A. Bethe, *Z. Phys.*, **71**, 205 (1931); L. Hulthén, *Arkiv. Mat. Astron. Fysik*, **26A**, 1 (1938).
9) W. Duffy, Jr., *J. Chem. Phys.*, **36**, 490 (1962); K. Okumura, *J. Phys. Soc. Jpn.*, **18**, 69 (1963); D. D. Thomas, H. Keller, and H. M. McConnell, *J. Chem. Phys.*, **39**, 2321 (1963).
10) R. M. Metzger, *J. Chem. Phys.*, **64**, 2069 (1976).

BULLETIN OF THE CHEMICAL SOCIETY OF JAPAN, VOL. 52 (11), 3449—3450 (1979)

Photolysis of Water on Illuminated Strontium Titanium Trioxide

Hiroshi YONEYAMA,* Masashi KOIZUMI, and Hideo TAMURA

Department of Applied Chemistry, Faculty of Engineering, Osaka University, Yamadakami, Suita, Osaka 565

(Received May 17, 1979)

Synopsis. The photolysis of water was demonstrated in an illuminated strontium titanium trioxide suspension. Electrochemical mechanism takes place in the decomposition reaction.

The photolysis of water by the use of light from a xenon lamp was accomplished by Fujishima and Honda in a photoelectrochemical cell using a semiconducting titanium dioxide photoanode.[1] It was found that the photolysis occurs at illuminated titanium dioxide suspended in an aqueous solutions.[2] Schrauser and Guth[3] reported the quantitative photodecomposition of chemisorbed water on titanium dioxide.

It has been revealed from electrochemical studies on photocatalysis of n-type semiconductors[4–11] that electrochemical mechanisms are occasionally involved in heterogeneous photocatalytic reactions using semiconductor catalysts. In these cases, the photocatalytic reaction consists of a photosensitized oxidation process coupled with a reduction process thermodynamically regulated, the onset potential of the photosensitized oxidation being more negative than that of the reduction process. The coupled processes proceed spontaneously on an illuminated n-type semiconductor accompanied by local cell action. This principle is basically the same as that for construction of photoelectrochemical cells.[12]

If such a mechanism prevail in photolysis of water at illuminated n-type semiconductor catalysts, the following reaction schemes are established for pure water.

photosensitized oxidation

$$H_2O + 2p^+ \longrightarrow 1/2O_2 + 2H^+ \quad (1)$$

reduction

$$2H_2O + 2e^- \longrightarrow H_2 + 2OH^- \quad (2)$$

overall

$$H_2O \longrightarrow H_2 + 1/2O_2 \quad (3)$$

where p^+ and e^- represent a positive hole in the valence band and an electron in the conduction band, respectively. The oxidation of water (Reaction 1) should then occur at potentials negative to the reversible hydrogen electrode potential (RHE).

It is well known in semiconductor electrochemistry[12–14] that photosensitized oxidation on a semiconductor electrode sets on at its flat-band potential. Thus, photodecomposition of water is expected if a semiconductor having a flat-band potential more negative than RHE is used as a photocatalyst. Strontium titanium trioxide (Strontium titanate) satisfies this prerequisite for the flat-band potential.[14–16]

Experimental

The decomposition experiments were carried out in an air-tight cell made of pyrex glass, with gas inlet and outlet, a flat window (dia. 30 mm) and a mouth in a tubular form for sampling the gas. The mouth was sealed in the lower portion with silicone rubber packing (dia. 5 mm, height 8 mm), water being filled on the packing (height 10 mm) in order to make a perfect seal during the course of gas sampling.

Strontium titanium trioxide powder, purity 99.9%, was reduced by hydrogen at 900 °C for 3 h, giving the surface area 0.67 m^2/g, and stored in a desiccator under humid nitrogen for a week. 1 g was suspended in 20 cm^3 of distilled water and the suspension was magnetically stirred overnight in the cell into which prepurified nitrogen was continuously bubbled. Stop cocks of the gas inlet and outlet were then closed, and the light from an 1 kW xenon lamp was illuminated on the suspension. The light was so focused as to fit with the cell window, its intensity being *ca.* 3 W as measured by a laser power meter (Coherent Radiation, model 201). The gas was analyzed at intervals with a gas chromatograph using a molecular sieve 5A coloum.

A strontium titanium trioxide single crystal (Nakazumi Crystal Co., Ltd.) was used as an electrode in order to confirm govering of photodecomposition by the electrochemical processes given by Eqs. 1 and 2. The electrode was prepared in the same way as reported by Watanabe *et al.*[15] The effective area of the electrode was 0.3 cm^2.

Results and Discussion

Figure 1 shows the evolution of gases as a function of illumination time. With no illumination, no gas evolution took place. Illumination without strontium titanium trioxide caused no decomposition. The results (Fig. 1) satisfy the stoichiometry of the decomposition reaction. However, the rate of the decomposition showed a tendency to diminish with illumination time.

The cause of the decline in the evolution rate is not clear. This may reflect some change in the surface condition of the catalyst. However, judging from the volume ratio of the evolved gases, the reduction of the catalyst surface does not seem probable. It might

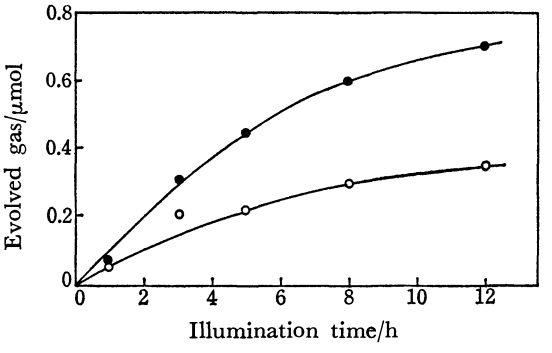

Fig. 1. Amount of oxygen and hydrogen evolved as a function of illumination time. —●—: H_2, —○—: O_2.

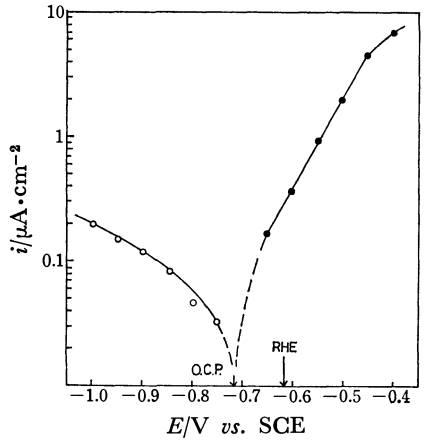

Fig. 2. Polarization curves of a single crystal $SrTiO_3$ electrode in 0.5 mol·dm^{-3} Na_2SO_4 (pH=6.4).
—●—: Anodic curve under illumination, —○—: cathodic curve in the dark, O.C.P.: open circuit potential under illumination. Illumination: 1 kW xenon lamp.

be postulated that the mode of reaction changed from water decomposition to a cycled reaction of oxygen evolution and reduction of the evolved oxygen. However, this does not seem to be the case. From Henry's law, the amount of evolved oxygen seems to be too small to dissolve into water in an appreciable amount.

Figure 2 shows polarization curves of the single crystal electrode in 0.5 mol·dm^{-3} Na_2SO_4. The anodic curve obtained under illumination (a) is related to the oxygen evolution reaction.[14,15] On the other hand, the cathodic curve in the dark (b) seems to be due to the hydrogen evolution reaction, since small bubbles were observed to stick on the electrode surface when a relatively high cathodic polarization was made. The open circuit potential of the illuminated strontium titanium trioxide electrode shown by arrow was in the potential region where the hydrogen evolution is thermodynamically feasible. Although these polarization curves were obtained in the solution of pH=6.3 and not in the pure water, almost the same situation should take place in pure water. The flat-band potential at which the oxidation of water sets on has the same pH dependency as RHE.

The decomposition rate is 0.03—0.05 μA/cm^2 (Fig. 2), corresponding to the water photolysis of 0.001 μmol/h per unit surface area of the catalyst at most. Since light was concentrated into a cell window of *ca.* 7 cm^2, the decomposition rate of 0.007 μmol/h can be expected for a single crystal having an area equal to that of the cell window. However, the rate estimated is low, suggesting that the quantum yield of water photolysis is too low to be significant. The potential at which the photolysis proceeds is near the flat-band potential, resulting in a weak field strength to anihilate photo-generated carriers.[13]

The surface area can be increased greatly with use of powder catalyst. However, attempts to increase the surface area do not always bring about a proportional increase in the photodecomposition rate. The decomposition rate of 0.1 μmol/h was observed in the initial stage of the experiment (Fig. 1). This gives only fourteen times the value estimated above for the single crystal catalyst having the area of the cell window. The increase in the surface area can in principle enhances the cathodic process, but the anodic process is usually controlled by the number of incident photons rather than by the surface area. Thus, the result seems to be reasonable.

This suggests that the photolysis of water can be carried out on illuminated n-type semiconductors having flat-band potentials more negative than RHE, if they are stable against both anodic and cathodic decomposition.

References

1) A. Fujishima and K. Honda, *Nature*, **238**, 37 (1972).
2) H. Tamura, S. Murakami, M. Murata, H. Ikeda, and H. Yoneyama, Presented at US-Japan Joint Seminor on "Key Technologies for the Hydrogen Energy System," (1975), Tokyo.
3) G. N. Schrauser and T. D. Guth, *J. Am. Chem. Soc.*, **99**, 7189 (1977).
4) S. R. Morrison and T. Freund, *J. Chem. Phys.*, **47**, 1543 (1967).
5) T. Freund and W. P. Gomes, "Catalysis Review," ed by H. Heinemann, Marcel Dekker, New York (1969), Vol. 3, p. 1.
6) H. Yoneyama, Y. Toyoguchi, and H. Tamura, *J. Phys. Chem.*, **72**, 3460 (1972).
7) F. Mollers, H. J. Tolle, and R. Memming, *J. Electrochem. Soc.*, **121**, 1160 (1974).
8) M. Miyake, H. Yoneyama, and H. Tamura, *Electrochim. Acta*, **22**, 1065 (1976).
9) M. Miyake, H. Yoneyama, and H. Tamura, *Bull. Chem. Soc. Jpn.*, **50**, 1492 (1977).
10) S. N. Frank and A. J. Bard, *J. Phys. Chem.*, **81**, 1484 (1977).
11) B. Kraeutler and A. J. Bard, *J. Am. Chem. Soc.*, **100**, 5895 (1978).
12) H. Gerischer, *J. Electroanal. Chem.*, **58**, 263 (1975).
13) T. Ohnishi, Y. Nakato, and H. Tsubomura, *Ber. Bunsenges. Phys. Chem.*, **79**, 523 (1975).
14) J. M. Bolt and M. S. Wrighton, *J. Phys. Chem.*, **80**, 2641 (1976).
15) T. Watanabe, A. Fujishima, and K. Honda, *Bull. Chem. Soc. Jpn.*, **49**, 355 (1976).
16) M. A. Butler and D. S. Ginley, *Chem. Phys. Lett.*, **47**, 319 (1977).

BULLETIN OF THE CHEMICAL SOCIETY OF JAPAN, VOL. 52 (11), 3451—3452 (1979)

Photoisomerization of Bis(*t*-butyl isocyanide)dichlorobis-(triphenylphosphine)ruthenium(II)

Tamotsu TSUIHIJI, Takeo AKIYAMA, and Akira SUGIMORI*

Department of Chemistry, Faculty of Science and Technology, Sophia University, Kioi-cho 7, Chiyoda-ku, Tokyo 102

(Received March 24, 1979)

Synopsis. UV-irradiation of bis(*t*-butyl isocyanide)-dichlorobis(triphenylphosphine)ruthenium(II) brings about isomerization. The composition of the photo-stationary state is wavelength-dependent. A mechanism *via* the photo-elimination of triphenylphosphine is proposed.

Photochemical redox and ligand substitution reactions of ruthenium complexes have been extensively investigated.[1,2] However, only a few studies have been done on the photoisomerization. Jeffery and Mawby observed the isomerization of dicarbonyldiiodobis(triphenylphosphine)ruthenium(II) by sunlight.[3] We report here the photochemical mutual conversion of bis(*t*-butyl isocyanide)dichlorobis(triphenylphosphine)-ruthenium(II) isomers with light from 254 to 436 nm.

Experimental

Materials. *af*-Bis(*t*-butyl isocyanide)-*bd*-dichloro-*ce*-bis(triphenylphosphine)ruthenium(II) (**1**) was prepared by the reaction of dichlorotris(triphenylphosphine)ruthenium-(II) with *t*-butyl isocyanide. *ad*-Bis(*t*-butyl isocyanide)-*bf*-dichloro-*ce*-bis(triphenylphosphine)ruthenium(II) (**2**) was prepared by refluxing **1** in benzene for 2 days according to the preparation of corresponding ethyl isocyanide complex.[4] Elemental analyses: **1**, Found: C, 63.85; H, 5.65; N, 3.34%. **2**, Found: C, 63.75; H, 5.50; N, 3.00%. Calcd for $C_{46}H_{48}Cl_2N_2P_2Ru$: C, 64.03; H, 5.61; N, 3.25%. The structures of **1** and **2** were established from the comparison of their IR spectra and color with those of dichlorobis(ethyl isocyanide)bis(triphenylphospine)ruthenium(II).[4] **1**, Yellow; IR: 2110 (ν_{NC}) and 320 cm^{-1} (ν_{RuCl}). **2**, Colorless; IR: 2135 and 2090 cm^{-1} (ν_{NC}); no absorption of ν_{RuCl} was observed above 300 cm^{-1}. Ruthenium(II) complexes in which two chlorine atoms are situated in *trans*-position have an IR band above 300 cm^{-1} and those in which two chlorine atoms are in *cis*-position have two IR absorption bands below 300 cm^{-1}.[4,5]

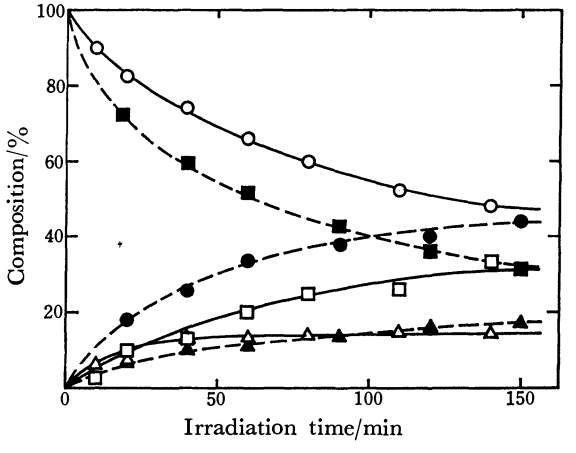

Fig. 1. Dependence of the composition of products on irradiation time (Irradiated with 254 nm).
Products in the irradiation of **1** —○—, **1**; —□—, **2**; —△—, **X**. Products in the irradiation of **2** —●—, **1**; —■—, **2**, —▲—, **X**.

Photoreaction. The photoreaction was followed by the change of NMR spectra. Solutions containing 5.8—8.5 mmol dm^{-3} of **1** or **2** in CD_2Cl_2 in quartz NMR sample tubes were irradiated with UV-light. For the irradiation with 254 nm, a low pressure mercury lamp was employed. For the irradiation with 313, 365, and 436 nm, the light from a high pressure mercury lamp was filtered with interference filters M-313, M-365, and M-436 of Karl Zeiss Co., respectively.

After the irradiation, five proton NMR peaks were observed. The peak at $\delta=7.75$—8.06 (multiplet) is assigned to the *o*-proton of coordinated triphenylphosphine (PPh_3), and the peak at $\delta=7.29$—7.57 (multiplet) to *m*- and *p*-protons of coordinated and *o*-, *m*-, and *p*-protons of free PPh_3. The peaks at $\delta=0.76$ (singlet) and 1.04 (singlet) are due to *t*-butyl of **2** and **1**, respectively. The peak at $\delta=1.34$ is ascribed to *t*-butyl of an unidentified product (**X**).

Results and Discussion

UV-irradiation of bis(*t*-butyl isocyanide)dichlorobis-(triphenylphosphine)ruthenium(II) isomers brings about the mutual isomerization and the formation of a complex **X**. No reaction occurs in the dark at room temperature. Over the wide range of the wavelength of the irradiating light (254—436 nm), almost no other photoproducts are formed.

Complex **X** which has an NMR peak at $\delta=1.34$ can be assigned to a dimer of the five-coordinate complex **3** or **4**, which is formed by the photochemical elimination of a molecule of PPh_3 from **1** or **2**. The area of the NMR absorption ascribed to *t*-butyl of **X** corresponds well with the increase in the area ascribed to the free PPh_3. The shift of the *t*-butyl peak to lower field can be explained by the increase in the positive charge of the central metal caused by the elimination of a PPh_3 molecule.

The change in the composition of the products with the irradiation time is shown in Fig. 1, as exemplified by the 254 nm irradiation. The prolonged irradiation gives photo-stationary mixtures, the composition of which depends on the wavelength of the irradiating light. Results are summarized in Table 1.

Photochemical conversion of **X** to **1** and **2** is suggested, because the quantity of **X** showed a maximum or saturation at the earlier stage of the photoreaction. The mechanism shown in Scheme 1 is proposed. The intermediacy of the five-coordinate complexes (**3** and **4**) is supported by the suppression of the formation of **X** by the addition of excess PPh_3. Similar five-coordinate complexes have been postulated in the

Table 1. Photoreactions of bis(*t*-butyl isocyanide)-dichlorobis(triphenylphosphine)ruthenium(II)

Wavelength nm	$\varepsilon_2/\varepsilon_1$	Starting complex	Additive	Composition at photo-stationary state $[1]_s/[2]_s$	Composition at photo-stationary state $[X]_s/([1]_s+[2]_s+[X]_s)$
254	1.3	**1**		1.3	0.17
		2		1.5	0.22
		1	PPh_3[a)]	1.5	0.07
313	0.85	**1**		0.11	0.04
		2		0.05	0.03
365	6.7	**1**		5.4	0.11
		2		3.0	0.06
436	0.01	**1**		0.05	0.02
		2		≈0	≈0

a) $[PPh_3]/[1]=10$.

photoisomerization of tetracarbonylbis(triphenylphosphine)molybdenum(0).[6] The fact that the addition of PPh_3 does not retard the photoisomerization of the ruthenium complex indicates that the conversion between **3** and **4** occurs efficiently.

If the reaction giving the dimer is neglected, we can obtain an approximate equation for the composition at the photo-stationary state as

$$\frac{[1]_s}{[2]_s}=\frac{k_2k_5k_{-7}\,(k_3+k_1)}{k_1k_6k_7\,(k_4+k_2)}\,\frac{\varepsilon_2}{\varepsilon_1}$$

where suffix s represents the stationary state, the k's are rate constants of the specified reactions in Scheme 1, and ε_1 and ε_2 are the molar absorption coefficients of **1** and **2**, respectively. In the equation, $[1]_s/[2]_s$ is independent on the concentration of free PPh_3. The fact that the addition of PPh_3 does not change the value supports the mechanism in Scheme 1.

Complex **1** has three electronic absorption bands at 268 (ε=26900 $dm^3\,mol^{-1}\,cm^{-1}$), 315 (ε=3200 $dm^3\,mol^{-1}\,cm^{-1}$), and 439 nm (ε=165 $dm^3\,mol^{-1}\,cm^{-1}$), which could be assigned to the excitations of coordinated PPh_3, CT, and d-d, respectively. For **2** the separation of CT and d-d bands is not enough, and **2** has no absorption in the visible region.

The value $[1]_s/[2]_s$ does not follow the ratio of molar absorption coefficients. Especially, in the irradiation with 313 nm, the isomerization from **1** to **2** occurs efficiently, whereas almost no reverse reaction occurs. This suggests that the irradiation with different wavelength produces different excited states, and each excited state has different efficiency of the elimination of PPh_3. For 254 nm irradiation, by which **1** and **2** are brought to excited states of a similar character (the excitation of coordinated PPh_3), $[1]_s/[2]_s$ is almost equal to $\varepsilon_2/\varepsilon_1$. This indicates that the overall efficiency from **1** to **2** is equal to that from **2** to **1** in the photoisomerization with 254 nm light.

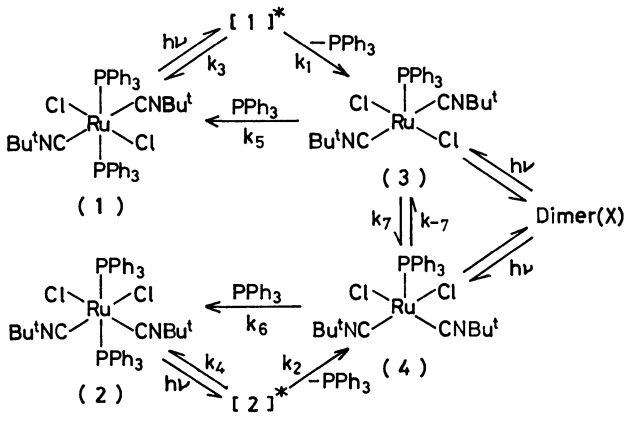

Scheme 1.

References

1) V. Balzani and V. Carassiti, "Photochemistry of Coordination Compounds," Academic Press, London (1970), p. 307.

2) P. Ford, R. E. Hintze, and J. D. Petersen, "Photochemistry of Heavier Elements" in "Concepts in Inorganic Photochemistry," ed by A. W. Adamson and P. D. Fleischauer, John Wiley, N. Y. (1975), p. 203.

3) J. Jeffery and R. J. Mawby, *J. Organomet. Chem.*, **40**, C42 (1972).

4) B. E. Prater, *J. Organomet. Chem.*, **34**, 379 (1972).

5) J. D. Gilbert and G. Wilkinson, *J. Chem. Soc.*, *A*, **1969**, 1749.

6) D. J. Darensbourg and M. A. Murphy, *J. Am. Chem. Soc.*, **100**, 463 (1978).

BULLETIN OF THE CHEMICAL SOCIETY OF JAPAN, VOL. 52 (11), 3453—3454 (1979)

The pK_a Value and Volume Change for the Neutralization of [Co(edda)($H_2NCH_2CH_2OH$)]$^+$

Yoichi KITAMURA

Department of Chemistry, Faculty of Science, Ehime University, Matsuyama, Ehime 790

(Received January 16, 1979)

Synopsis. The pK_a value of [Co(edda)($H_2NCH_2CH_2OH$)]$^+$at 25 °C has been determined spectrophotometrically to be 5.01±0.05. The volume change for the equilibrium: [Co(edda)($H_2NCH_2CH_2OH$)]$^+$+OH^-=[Co(edda)($H_2NCH_2CH_2O$)]^0+H_2O has been found to be 16.9±0.7 cm^3/mol at 25 °C at an ionic strength of *ca.* 5 mM (1 mM $=10^{-3}$ mol dm^{-3}).

The volume change (ΔV) for the neutralization equilibrium of a complex ion is essential for the interpretation of the activation volume for a reaction of a complex ion, proceeding *via* the S_N1 CB mechanism.[1,2] Values of ΔV for three such equilibria of trivalent complex ions are known:

$$[Co(NH_3)_5H_2O]^{3+} + OH^- = [Co(NH_3)_5OH]^{2+} + H_2O \quad (1)$$

ΔV_1=20.6 cm^3/mol at 30 °C;[3]

$$[Cr(H_2O)_6]^{3+} + OH^- = [Cr(H_2O)_5OH]^{2+} + H_2O \quad (2)$$

ΔV_2=18.3 cm^3/mol at 25 °C;[4]

$$[Fe(H_2O)_6]^{3+} + OH^- = [Fe(H_2O)_5OH]^{2+} + H_2O \quad (3)$$

ΔV_3=20.9 cm^3/mol.[5]

A value of ΔV for the analogous equilibrium of a univalent complex ion is however not known and is of interest with respect to the charge effect on the magnitude of ΔV.

α-*cis*-Ethylenediamine-*N*,*N*′-diacetato(2-aminoethanol)cobalt(III) perchlorate, α-*cis*-[Co(edda)(Hame)]ClO_4 was obtained by Kuroda.[6] The aqueous solution of this complex gives a low pH value (3.94 in a 2.5 mM solution) and the indication is that in water there exists an acid dissociation equilibrium:[6]

$$[Co(edda)(Hame)]^+ = [Co(edda)(ame)]^0 + H^+, \quad (4)$$

where Hame=$H_2NCH_2CH_2OH$ and ame=$H_2NCH_2CH_2O^-$.

The determination of the pK_a value of 4 is significant *per se*, since the pK_a values of Co(III) complex ions are known only for ones with the aqua ligand so far.[7] The volume change (ΔV_5) for the equilibrium:

$$[Co(edda)(Hame)]^+ + OH^- = [Co(edda)(ame)]^0 + H_2O \quad (5)$$

has been measured in relation to the interpretation of the activation volume for the base hydrolysis reactions of α-, β-*cis*-[Co(edda)(NH_3)$_2$]$^+$.[8]

Experimental

α-*cis*-[Co(edda)(Hame)]ClO_4 was obtained by the standard method and identified by the visible absorption spectrum of a 5 mM aqueous solution.[6] The λ_{max} (ε_{max}) values were 536 nm(89.2), 380 nm(84.4) which compare to the values reported by Kuroda of 535 nm(90.3), 377 nm(85.1) respectively. A Hitachi-Horiba M-5 pH meter was used and a Carlsberg dilatometer for the measurement of the volume change. The procedures were essentially the same as those described by Spiro *et al.*[3] Two liquids separated by kerosene were mixed and the volume change obtained from the change of the kerosene level in the capillary. 10 min was required for the establishment of the thermal equilibrium. In some experiments slow linearly time-dependent variations of the kerosene level were observed before and after mixing. The dilatometer readings were extrapolated to the time of mixing. The radius of the capillary was calibrated with mercury (0.0202±0.0003 cm) and the kerosene level read by a cathetometer. The thermostat was maintained at 25.02±0.02 °C with a variation of less than 0.002 °C. Boiled out water was used. The kerosene was purified.

Results and Discussion

The color of a solution of [Co(edda)(Hame)]ClO_4 in 0.01 M HCl is reddish pink and in 0.01 M KOH it is pale blue violet (1 M=1 mol dm^{-3}). The color changes instantaneously and reversibly by the addition of an acid or an alkali, which indicates that the color change is caused by a shift of the chemical equilibrium. The absorption spectrum is illustrated in Fig. 1. The absorption maxima (*ca.* 570 and 384 nm) of [Co(edda)(ame)]^0 (in 0.01 M KOH) lie at longer wavelengths relative to those (536 and 380 nm) of [Co(edda)(Hame)]$^+$ (in 0.01 M HCl). This tendency is analogous to the relative position of bands of the complexes with a hydroxo ligand to those of the corresponding complexes with an aqua ligand. In pure water the spectrum is similar to that in 0.01 M HCl and the complex exists mostly in the acid form, [Co(edda)(Hame)]$^+$.

The pK_a value was determined from the optical densities (OD) at 300 nm in a 1 mM solution of the complex in acetate buffers (Table 1). The absorption coefficients at 300 nm of [Co(edda)(Hame)]$^+$ and [Co-

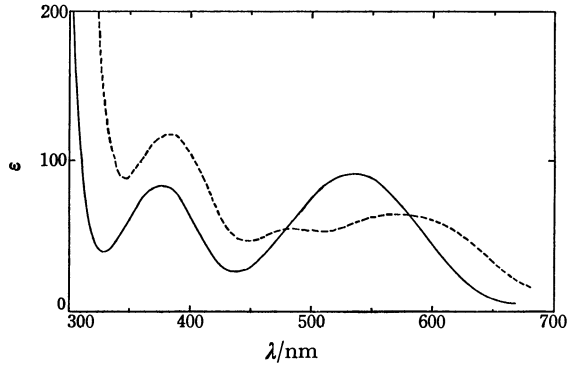

Fig. 1. Visible absorption spectra of 5 mM-[Co(edda)(Hame)]ClO_4. ——: in 0.01 M HCl, ----: in 0.01 M KOH.

Table 1. Spectrophotometric determination of the pK_a value at 25 °C

Solvent[a)]	pH[b)]	OD[b)]	pK_a
5.5/54.5	5.60	0.701	5.06
8.0/52.0	5.42	0.660	5.03
12.0/48.0	5.26	0.613	5.03
16.7/43.3	5.05	0.563	4.99
23.1/36.9	4.86	0.505	4.99
30.0/30.0	4.67	0.457	4.96
0.008 M HCl	2.18	0.290	
0.008 M KOH	11.75	0.842	

a) CH_3COOH(mM)/CH_3COONa(mM). b) Measured at 25 °C.

(edda)(ame)]^0 are 290 and 842 l mol^{-1} cm^{-1}, respectively. The activity coefficients of H^+ may be estimated according to the method of Davies.[9)] The magnitude of pK_a 5.01±0.05 is small compared with those of a Co(III) complex with an aqua ligand.[7)]

An aqueous solution of [Co(edda)(Hame)]ClO_4 (25 cm^3) was mixed with 0.035 M KOH (10 cm^3). Values of the volume change were [given as the initial concentration of the complex/mM, volume change/μl]: 5.21, 2.31; 5.13, 2.10; 5.20, 2.25; and 5.14, 2.18. Heat was evolved in the mixing. As a blank test, water (25 cm^3) was mixed with 0.035 M KOH (10 cm^3) and the volume change found to be negligibly small (0.00±0.11 μl, average for five runs). Thus, a value of 17.1±0.7 cm^3/mol is obtained for $\alpha\Delta V(H_2O)+(1-\alpha)\Delta V_5$, where $\Delta V(H_2O)$ is the volume change (22.07 cm^3/mol at 25 °C) for the equilibrium, $H^+ + OH^- = H_2O$ and α is the degree of dissociation (0.04) of [Co(edda)(Hame)]$^+$ in the 5.2 mM solution.[10)] Thus, ΔV_5 at 25 °C is evaluated as 16.9± 0.7 cm^3/mol. The magnitude of ΔV_5 is comparable to those of ΔV_1, ΔV_2, and ΔV_3, which indicates that the difference between the molar volume of water and the partial molar volume of OH^- (*ca.* 1.4 cm^3/mol) is the major contribution for the volume changes.[11)] The intrinsic volumes of the complex ions would be little affected by protonation and hence the somewhat smaller magnitude of ΔV_5 compared to those of ΔV_1, ΔV_2, and ΔV_3 may be qualitatively explained by the smaller contribution of the electrostrictive volume change (ΔV_{el}) of the complex in Equilibrium 5. To a first approximation, neglecting the compressibility of the complex ion[5)] and the dielectric saturation of water,[12)] the electrostrictive volume (V_{el}) for an ion of radius r and charge Ze in water is given by; $V_{el}=-(NZ^2e^2)(dD/dP)/(2rD^2)$, where N and D represent Avogadro's number and the bulk dielectric constant for water, respectively.[5)] Hence, ΔV_{el} in Equilibria 1, 2, and 3 ($\Delta Z^2=-5$) is larger than that in Equilibrium 5 ($\Delta Z^2=-1$). This difference in ΔV_{el} is evaluated as 5.5 cm^3/mol for $r=3$ Å, using the value of $(1/D^2)(dD/dP)$ at 1 bar (6.0×10^{-7} bar^{-1}).[13)] The water molecules around the ion however are under high pressure due to the electrostriction and this pressure is higher for ions of higher valency.[5)] Thus, values of $(1/D^2)(dD/dP)$ at high pressures must be used. Since, $(1/D^2)(dD/dP)$ decreases with increase in pressure, the difference in ΔV_{el} would be smaller than as simply estimated above.[13)]

The author would like to thank Professor Kashiro Kuroda of Ehime University for his continuous interest in the present work.

References

1) Y. Kitamura, *Bull. Chem. Soc. Jpn.*, **49**, 1002 (1976).
2) Y. Kitamura, *Bull. Chem. Soc. Jpn.*, **50**, 2097 (1977).
3) T. G. Spiro, A. Revesz, and J. Lee, *J. Am. Chem. Soc.*, **90**, 4000 (1968).
4) T. W. Swaddle and Pi-Chang Kong, *Can. J. Chem.*, **48**, 3223 (1970). For $[Cr(H_2O)_6]^{3+}=[Cr(H_2O)_5OH]^{2+}+H^+$, $\Delta V=-3.8$ cm^3/mol is given at an ionic strength of 0.5 mol/kg. Taking $\Delta V(H_2O)$ as 22.07 cm^3/mol, ΔV_2 was calculated by the present author.
5) D. R. Stranks, *Pure Appl. Chem.*, **38**, 303 (1974). For $[Fe(H_2O)_6]^{3+}=[Fe(H_2O)_5OH]^{2+}+H^+$, $\Delta V=-1.2$ cm^3/mol is given. ΔV_3 was calculated by the present author.
6) K. Kuroda, *Bull. Chem. Soc. Jpn.*, **45**, 2176 (1972).
7) F. Basolo and R. G. Pearson, "Mechanisms of Inorganic Reactions," 2nd ed, John Wiley and Sons, New York (1967), p. 32.
8) Y. Kitamura, *Bull. Chem. Soc. Jpn.*, **52**, 3280 (1979).
9) C. W. Davies, *J. Chem. Soc.*, **1938**, 2093.
10) F. J. Millero, E. V. Hoff, and L. Cahn, *J. Solution Chem.*, **1**, 309 (1972).
11) "Water and Aqueous Solutions, Structure, Thermodynamics, and Transport Processes," ed by R. A. Horn, Wiley-Interscience, New York (1972), pp. 519—560.
12) R. A. Robinson and R. H. Stokes, "Electrolyte Solutions," 2nd ed, Butterworths, London (1970), p. 19.
13) K. R. Srinivasan and R. L. Kay, *J. Chem. Phys.*, **60**, 3645 (1974). $(1/D^2)(dD/dP)=(2.746\times10^{-3})/(4574+P)$bar^{-1} at 25 °C up to 3 kbar (1 bar=10^5 Pa).

BULLETIN OF THE CHEMICAL SOCIETY OF JAPAN, VOL. 52 (11), 3455—3456 (1979)

Preparation of a Rare Earth Ion Selective Electrode

Yoshihiro TAKASAKA† and Yasuo SUZUKI*

Department of Industrial Chemistry, Faculty of Engineering, Meiji University, Ikuta, Tama-ku, Kawasaki 214

(Received May 9, 1979)

Synopsis. A new rare earth-ion selective electrode with a cerium(IV) oxide membrane has been prepared. The electrode was selective for the trivalent rare earths with a slope as great as 58 mV. The electrode was less selective for bi- and quadrivalent cations.

The conventional cation-selective electrodes with solid-state membranes have been prepared from insoluble salts, the iron(III)-selective electrode with a chalcogenide glass membrane[1] being the only exception. The fluoride-selective electrodes, containing lanthanum fluoride as the membrane, are possibly sensitive to lanthanum(III) ion,[2] but are of little analytical importance because of a small slope of 20 mV. The solid-membrane electrodes containing either a quadri- or bivalent rare-earth compound are possible sensors for the rare earths(III), with a slope as great as 59 mV. The present work includes the preparation and properties of the cerium(IV) oxide membrane electrodes as rare-earth(III) sensors. Since the trivalent rare earths behave similarly in aqueous solutions, the new electrodes should have identical selectivity for any of the rare earths.

Experimental

All the rare-earth oxides of 99.9% or higher purity were supplied by Shin-etsu Chemical Industries Co., Ltd. The solutions of rare-earth(III) nitrates were prepared by dissolving the respective oxides with nitric acid. Cerium(III) perchlorate and nitrate solutions were prepared from the corresponding salts of I. C. N. Pharmaceuticals Inc. Other reagent solutions were prepared from reagent-grade chemicals.

The electromotive force measurements were performed on a Beckman Model 3500 pH meter with an Orion 90-02 double junction reference electrode. The pH measurements were made by a Denki Kagaku Keiki Model HG-3 pH meter. Electric resistances of the membranes were measured by a Yokokawa Denki Model L-6B insulation-resistance tester.

The appropriate amounts of cerium(IV) oxide and Rapid Araldite, an epoxy adhesive from Ciba-Geigy, were mixed homogeneously, and coated on the copper plate of the electrode body, as shown in Fig. 1. All the electrode behaviors were studied at 25.0°C with an electrode system of: CeO_2 electrode|Solution X|Salt bridge|Ag–AgCl reference electrode.

Results and Discussion

The values of the activity coefficients of the rare-earth ions were selected[3,4] assuming that the mean activity coefficients of the rare-earth ions do not vary appreciably from ion to ion under identical conditions.

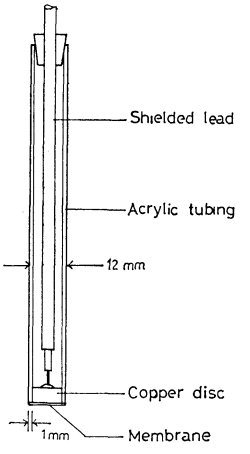

Fig. 1. A cerium(IV) oxide membrane electrode.

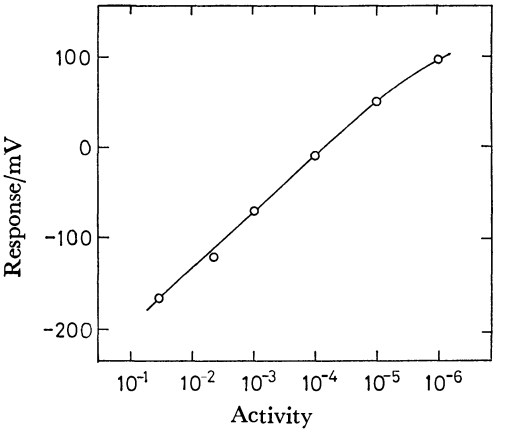

Fig. 2. Response of cerium(IV)-oxide electrode to the cerium(III) activity.

Of the electrodes having membranes of various cerium(IV) oxide concentrations, the ones containing 55% oxide and 45% adhesive in weight exhibited the closest response to the Nernstian theory. The slope of the electrode for cerium(III)-ion concentration ranged from 43 to 58 mV within a concentration range of 10^{-1} to 10^{-6} mol dm^{-3}, while the linear relationship between the response and concentration held only in a range of 10^{-3} to 10^{-5} mol dm^{-3} with a slope of 58 mV. By taking the activity scale, however, the linearity extended from 10^{-1} to 10^{-5}, as shown in Fig. 2. Considering the overall properties studied, the 55-% electrode was found to be superior to the other electrodes of 30—70%, and has thus been used in subsequent work.

The response time of the electrode was determined for several cerium(III) concentrations as 5 to 10 min.

† Present address: Japan Scientific Instrument Co., Ltd., Ichiban-cho, Chiyoda-ku, Tokyo 102.

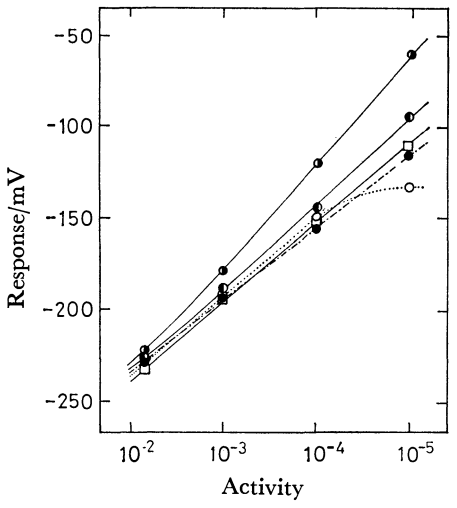

Fig. 3. Response curves of cerium(IV)-oxide electrode for some rare-earth(III) ions.
●: Lanthanum, ○: praseodymium, □: dysprosium, ◐: lutetium, ◑: yttrium.

The effect of the membrane thickness at 55-% cerium(IV) oxide concentration was also examined, and an electrode having a 0.100 g membrane, *i.e.* a 0.13 g cm^{-2} thickness, exhibited the optimum response. The electric resistance of the membrane ranged from 0.2 to 9 MΩ. No appreciable variation in the response behavior was observed within several months of repeated use.

The response behavior of the electrode against five trivalent rare-earth ions, including lanthanum, praseodymium, dysprosium, lutetium, and yttrium, were investigated, and the activity-response relations are shown in Fig. 3. It is remarkable that lanthanum and praseodymium, both adjacent elements to cerium, exhibited lower responses than the heavy rare earths, while yttrium exhibited the highest response among the rare earths examined.

The effect of pH was studied within the pH range of 2 to 9, where it was shown that the electrode could be useful in solutions of pH 3 to 5.5. Both higher hydrogen-ion concentrations and hydroxide precipitation apparently interfere in the measurements in solutions of pH less than 2 and above 6, respectively.

The selectivity coefficients for several cations, determined by separate and mixed solution methods,[5-9] are shown in Table 1. As might be expected, the rare-earth(III) ions exhibited selectivity coefficients as great as unity. Though barium(II) and zirconium(IV) ions did not interfere appreciably, the alkali metals, such as sodium and potassium, did interfere considerably. The latter fact is apparently not desirable when using the electrode in determining stability constants of the rare-earth complexes, where the solutions usually contain appreciable amounts of alkali metal salts, such as potassium nitrate, as the supporting electrolyte.

Though the present results are not sufficient for elucidating the response mechanism, it is probable that the oxidation-reduction reaction of cerium in the membrane and in solution predominates, at least in the case of cerium(III) solutions.

Table 1. Selectivity coefficients for several cations at 10^{-3} M

Cation	Selectivity coefficients	
	Separate solution method	Mixed solution method
Na(I)	1.0×10^{-2}	0.44
K(I)	2.5×10^{-2}	0.10
Ba(II)	0.11	3.5×10^{-3}
Fe(III)	0.20	1.4×10^{-2}
Zr(IV)	—	1.4×10^{-3}
La(III)	1.0	—
Ce(III)	1.0	—
Pr(III)	1.0	—
Dy(III)	1.0	—
Lu(III)	1.0	—
Y(III)	1.0	—

The cerium(IV) oxide-membrane electrode may thus be used as a sensor for the rare-earth(III) ions, with further possible improvements. The current work also includes research on the application of quadri- and bivalent rare-earth compounds as sensing materials, which would account for the response mechanism of the electrodes of the present type.

The authors wish to express their thanks to Shinetsu Chemical Industries Co., Ltd. for supplying the rare-earth oxides, to Dr. Kazuo Hiiro, Government Industrial Research Institute, Osaka, for his helpful advice, and to Mr. Hiroshi Itoh, Department of Electrical Engineering, Meiji University, for his assistance in the measurements of membrane resistance. The present work was partially supported by a Grant-in-Aid for Scientific Research from the Institute of Science and Technology, Meiji University.

References

1) C. T. Baker and I. Trachtenberg, *J. Electrochem. Soc.*, **118**, 571 (1971).
2) J. W. Ross, Jr., "Solid-State and Liquid Membrane Ion-Selective Electrodes," in "Ion Selective Electrodes," ed by R. A. Durst, NBS Special Publication 314, National Bureau of Standards, Washington, D. C. (1969), p. 75.
3) "Electrochemical Data," ed by D. Dobos, Elsevier, Amsterdam (1975).
4) H. S. Harned and B. B. Owen, "The Physical Chemistry of Electrolytic Solutions," Reinhold, New York (1957).
5) G. J. Moody and J. D. R. Thomas, "Selective Ion Sensitive Electrodes," Merrow, Watford (1971).
6) G. Eisenman, D. O. Rudin, and J. V. Cosby, *Science*, **126**, 831 (1957).
7) T. S. Light and J. L. Swartz, *Anal. Lett.*, **1**, 825 (1968).
8) K. Srinivasan and G. A. Rechnitz, *Anal. Chem.*, **41**, 1203 (1969).
9) G. J. Moody and J. D. R. Thomas, "Selectivity and Sensitivity of Ion-Selective Electrodes," in "Ion-Selective Electrodes," ed by E. Pungor, Akadémiai Kiadó, Budapest (1973), p. 97.

BULLETIN OF THE CHEMICAL SOCIETY OF JAPAN, VOL. 52 (11), 3457—3458 (1979)

Semiconducting Bis(dialkyldithiocarbamato)copper(III) Cation–TCNQ Radical Anion and –Bis(1,2-dicyano-1,2-ethylenedithiolato)nickel(III) Anion Salts: $[Cu(S_2CNR_2)_2]^+TCNQ^-$ and $[Cu(S_2CNR_2)_2]^+$-$[Ni(S_2C_2(CN)_2)_2]^-$ (R=Et, *n*-Pr, and *n*-Bu)

Yoshiji YUMOTO and Toshio TANAKA*

Department of Applied Chemistry, Faculty of Engineering, Osaka University, Suita, Osaka 565

(Received May 25, 1979)

Synopsis. The title salts were synthesized. Segregated columnar structures of the salts are suggested from their electronic spectra and electrical resistivities; 10^4—10^5 Ω cm range at 25 °C with activation energies of 0.24—0.33 eV as compact samples.

In a previous paper, a report was given on the preparation and electrical resistivity of simple and complex salts formed by the reaction between bis(dialkyldithiocarbamato)gold(III) cations and $TCNQ^-$ radical anion; $[Au(S_2CNR_2)_2]^+TCNQ^-$ (R=Me, Et, *n*-Pr, *n*-Bu, *n*-C_6H_{13}, *n*-C_8H_{17}, and $CH_2C_6H_5$), $[Au(S_2CN(CH_2C_6H_5)_2)_2]^+(TCNQ)_2^-$, and $[Au(S_2CN(CH_2C_6H_5)_2)_2]^+(TCNQ)_2^-\cdot MeCN$, all of which showed semiconducting behavior.[1] This paper describes the preparation, electronic spectra, and electrical resistivity of some bis(dialkyldithiocarbamato)copper(III) cation–TCNQ radical anion and –bis(1,2-dicyano-1,2-ethylenedithiolato)nickel(III) anion simple salts; $[Cu(S_2CNR_2)_2]^+TCNQ^-$ and $[Cu(S_2CNR_2)_2]^+[Ni(S_2C_2(CN)_2)_2]^-$ (R=Et, *n*-Pr, and *n*-Bu).

Experimental

Bis(dialkyldithiocarbamato)copper(III) perchlorates, $[Cu(S_2CNR_2)_2]^+ClO_4^-$ (R=Et, *n*-Pr, and *n*-Bu),[2] and tetraethylammonium bis(1,2-dicyano-1,2-ethylenedithiolato)-nickelate(III), $[Et_4N]^+[Ni(S_2C_2(CN)_2)_2]^-$,[3] were prepared by the methods reported.

*Bis(dialkyldithiocarbamato)copper(III)–TCNQ, $[Cu(S_2CNR_2)_2]^+TCNQ^-$ (R=Et (**1**), n-Pr (**2**), and n-Bu (**3**)).* To a boiling ethanol (30 ml) solution of Li^+TCNQ^- (0.39 g, 1.8 mmol) was added a hot acetonitrile (40 ml) solution of $[Cu(S_2CNEt_2)_2]^+ClO_4^-$ (0.82 g, 1.8 mmol). The mixture was allowed to stand in a refrigerator overnight to afford dark green needles of **1** in a 60% yield. **2** and **3** were similarly obtained both as dark green needles in 58 and 55% yields, respectively, by the equimolar reaction of $TCNQ^-$ in ethanol with the appropriate bis(dialkyldithiocarbamato)copper(III) cations in acetonitrile.

No complex salt was obtained by the reaction of **1**—**3** with neutral TCNQ in acetonitrile, only the starting materials being recovered.

*Bis(dialkyldithiocarbamato)copper(III) Bis(1,2-dicayno-1,2-ethylenedithiolato)nickelate(III), $[Cu(S_2CNR_2)_2]^+[Ni(S_2C_2(CN)_2)_2]^-$ (R=Et (**4**), n-Pr (**5**), and n-Bu (**6**)).* To an acetone (50 ml) solution of $[Cu(S_2CNEt_2)_2]^+ClO_4^-$ (0.67 g, 1.5 mmol) was added $[Et_4N]^+[Ni(S_2C_2(CN)_2)_2]^-$ (0.68 g, 1.5 mmol) in acetone (30 ml). After being stirred for 1 h, the mixture was concentrated to about half the volume under reduced pressure, followed by cooling to *ca.* 5 °C to give dark brown microcrystals of **4** in a 80% yield. Two analogues with R=*n*-Pr and *n*-Bu were similarly prepared as black and dark brown microcrystals in 71 and 85% yields, respectively.

Physical Measurements. Electrical resistivities, electronic spectra, and magnetic susceptibilities were measured as described previously.[1]

Results and Discussion

Linearity holds between log ρ (ρ: electrical resistivity) and $1/T$ for all the salts in the range 293—373 K (Table 1), indicating semiconducting behavior. Figure 1 shows the electronic absorption spectra of **1** and **4** in the solid state and **4** in acetonitrile; solid **1** exhibits three absorption maxima at 8800, 14800, and 24500 cm^{-1}. Similar spectra were observed in **2** and **3**. The spectral patterns of **1**—**3** closely resemble those of gold analogues, $[Au(S_2CN(n\text{-}Bu)_2)_2]^+TCNQ^-$ (λ_{max}: 8900, 13900, and 22400 cm^{-1}) and $[Au(S_2CN(n\text{-}C_8H_{17})_2)_2]^+TCNQ^-$ (λ_{max}: 10800, 14500, and 25100 cm^{-1}), both of which have been reported to involve dimeric $(TCNQ)_2^{2-}$.[1] The existence of the $(TCNQ)_2^{2-}$ dimer in **1**—**3** is supported by their diamagnetic properties at room temperature. Thus, **1**—**3** seem to have a segregated columnar stacking of $TCNQ^-$ radical anion in the crystalline state. This is in line with the ρ values of these salts in the order of 10^4 Ω cm. The columnar structure of **1** and **2** is in contrast to the corresponding gold salts, $[Au(S_2CNR_2)_2]^+TCNQ^-$ (R=Et and *n*-Pr), in which the cation and the anion are stacked alternatively: $D^+A^-D^+A^-\cdots$.[1]

The electronic spectrum of solid **4** shows absorption maxima at 8000, 13500, 16800, 22600, and 30200 cm^{-1}, of which the 22600 cm^{-1} band is due to the $[Cu(S_2CNEt_2)_2]^+$ cation and the remaining four bands to the $[Ni(S_2C_2(CN)_2)_2]^-$ anion. Thus, the solid state spectrum of **4** coincides with a superimposition of the spectra of the cation and anion moieties, indicating

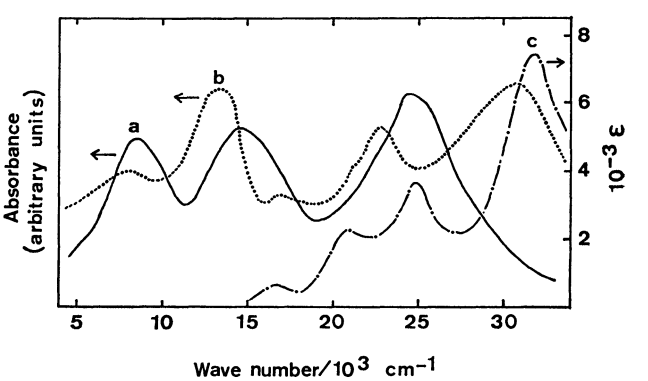

Fig. 1. Electronic absorption spectra of **1** (a) and **4** (b) in Nujol mulls, and **4** in acetonitrile (c).

Table 1. Analytical data, electrical resistivity (ρ), and activation energy (E_a) of the salts[a)]

No.	Salt	%C Found (Calcd)	%H Found (Calcd)	%N Found (Calcd)	$\rho_{25\,°C}$ / Ω cm	E_a [b)] / eV
1	$[Cu(S_2CNEt_2)_2]^+TCNQ^-$	47.11 (46.83)	4.15 (4.29)	14.66 (14.89)	4.6×10^4	0.24
2	$[Cu(S_2CN(n\text{-}Pr)_2)_2]^+TCNQ^-$	50.05 (50.34)	5.17 (5.20)	13.70 (13.55)	7.1×10^4	0.28
3	$[Cu(S_2CN(n\text{-}Bu)_2)_2]^+TCNQ^-$	53.08 (53.26)	5.80 (5.96)	12.30 (12.42)	8.5×10^4	0.30
4	$[Cu(S_2CNEt_2)_2]^+[Ni(S_2C_2(CN)_2)_2]^-$	30.59 (30.92)	2.86 (2.88)	11.61 (12.02)	3.1×10^5	0.31
5	$[Cu(S_2CN(n\text{-}Pr)_2)_2]^+[Ni(S_2C_2(CN)_2)_2]^-$	34.88 (34.99)	3.69 (3.74)	11.09 (11.13)	4.0×10^5	0.31
6	$[Cu(S_2CN(n\text{-}Bu)_2)_2]^+[Ni(S_2C_2(CN)_2)_2]^-$	38.20 (38.49)	4.20 (4.47)	10.17 (10.36)	8.9×10^5	0.33

a) Mp (dec) >300 °C for all the salts. b) Calculated by the equation $\rho=\rho_0\exp(E_a/kT)$.

that in the solid state the anion and the cation are segregated from each other. This is supported by the fact that **4** in acetonitrile exhibits an additional band at 25000 cm^{-1} (Fig. 1), which may be due to an anion-cation interaction. The interaction of this type has been reported in some double complex salts, such as $[Pt(CNR)_4]^{2+}[Pt(CN)_4]^{2-}$ (R=Me, Et, and *t*-Bu), in solution.[4)] Segregation between the anion and the cation is suggested also for solids **5** and **6** on the basis of their electronic spectra. Some bis(1,2-dithiolato)nickel(III) salts such as $[Et_4N]^+[Ni(S_2C_2(CN)_2)_2]^-$ ($\rho=3.5\times10^5$ and 4.9×10^7 Ω cm for two crystalline forms) have been reported to adopt a segregated columnar structure.[5)] Such a structure can be assumed in the crystals of **4**—**6**, since the ρ values (Table 1) are of the same orders as or smaller than those of $[Et_4N]^+$ salts.

In both series **1**—**3** and **4**—**6**, the ρ and E_a values trend to increase to some extent as the alkyl substituents on the carbamato nitrogen atom become bulky. A similar trend has been reported for a series of *N,N*-dialkyl-1,3-dithiolan-2-iminium–$TCNQ^-$ simple salts.[6)]

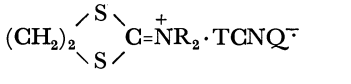

(R=Me, *n*-Pr, *n*-C_6H_{13}, and *n*-C_8H_{17})

The interplanar distance between the cation moieties in segregated columnar structures significantly influences electrical conduction, where the cation behaves as a matrix for the arrangement or packing of the planar anion moieties.[7)] It can be concluded that bulky substituents on the nitrogen atom of the cationic moieties increase the interplanar distances not only between the cation moieties but also between the anion moieties, raising electrical resistivity of the present salts.

The authors wish to express their thanks to the Central Research Institute, Matsushita Electric Industrial Co., Ltd. for supplying a sample of TCNQ. This work was carried out with a Grant-in-Aid for Scientific Research No. 347066 from the Ministry of Education, Science and Culture.

References

1) Y. Yumoto, F. Kato, and T. Tanaka, *Bull. Chem. Soc. Jpn.*, **52**, 1072 (1979).
2) R. M. Golding, C. M. Harris, K. J. Jessop, and W. C. Tennant, *Aust. J. Chem.*, **25**, 2567 (1972).
3) A. Davison and R. H. Holm, *Inorg. Synth.*, **10**, 8 (1967).
4) H. Isci and W. R. Mason, *Inorg. Chem.*, **13**, 1175 (1974).
5) A. Kobayashi and Y. Sasaki, *Bull. Chem. Soc. Jpn.*, **50**, 2650 (1977).
6) S. Araki, H. Ishida, and T. Tanaka, *Bull. Chem. Soc. Jpn.*, **51**, 407 (1978); S. Araki and T. Tanaka, *ibid.*, **51**, 1311 (1978).
7) A. F. Garito and A. J. Heeger, *Acc. Chem. Res.*, **7**, 232 (1974).

BULLETIN OF THE CHEMICAL SOCIETY OF JAPAN, VOL. 52 (11), 3459—3460 (1979)

Synthesis and Magnetism of Cobalt(II)–Manganese(II)–Cobalt(II) Trinuclear Complexes with *N,N'*-Disalicylidenealkanediamines

Visit KASEMPIMOLPORN, Hisashi OKAWA,* and Sigeo KIDA

Department of Chemistry, Faculty of Science, Kyushu University, Hakozaki, Higashi-ku, Fukuoka 812

(Received May 31, 1979)

Synopsis. Cobalt(II)–manganese(II)–cobalt(II) trinuclear complexes were synthesized by reacting *N,N'*-disalicylidenealkanediaminatocobalt(II) and manganese(II) halide in a 2:1 mole ratio. Cryomagnetic measurements indicated an antiferromagnetic spin-exchange interaction operating between the low-spin cobalt(II) and the high-spin manganese(II) ions, exchange integrals being estimated at -8——-12 cm^{-1}.

Recently we have reported the preparation and the characterization of the mixed-spin trinuclear cobalt(II) complexes with *N,N'*-disalicylideneethylenediamine and its homologues.[1] A considerably strong antiferromagnetic spin-exchange interaction ($J=-10$——-14 cm^{-1}) in these complexes prompted us to synthesize new trinuclear complexes of Co(II)($s=1/2$)–Mn(II)($s=5/2$)–Co(II)($s=1/2$) system in order to obtain further informations of spin-exchange in polynuclear complexes containing low-spin cobalt(II) ion.

N,N'-Disalicylidenealkanediamines are abbreviated as $H_2(R_1,R_2\text{-L})$ (R_1,R_2=H, CH_3; L=en, pn), where R_1 and R_2 denote the substituents attached to the 5- and the α-positions of salicylaldehyde moiety, respectively, and L is the chain connecting two imino-nitrogens.

Experimental

Syntheses. Mononuclear cobalt(II) complexes were obtained by the method of Bailes and Calvin.[2] Syntheses of the trinuclear complexes are practically the same and exemplified by $[Co(H,H\text{-en})]_2MnBr_2$. A mixture of Co(H,H-en) (500 mg) and manganese(II) bromide tetrahydrate (287 mg) in ethanol (80 ml) was stirred for 3 h under reflux in an atmosphere of nitrogen and allowed to stand overnight. Orange crystals which separated were collected by suction, washed with ethanol and dried.

Elemental analyses of the complexes are given in Table 1.

Measurements. Electronic spectra of powder samples were measured with a Shimadzu multipurpose spectrophotometer Model MSP-5000. Infrared spectra were measured with a Hitachi grating infrared spectrophotometer Model 215 in the region 4000—650 cm^{-1} on a KBr disk. Magnetic susceptibilities were measured by the Faraday method over the range from liquid nitrogen temperature to room temperature. Effective magnetic moments were calculated from the equation, $\mu_{eff}=2.828(\chi_M \cdot T)^{1/2}$, where χ_M is the molar magnetic susceptibility corrected for diamagnetisms using Pascal's constants.

TABLE 1. ELEMENTAL ANALYSES OF COMPLEXES

	Found (%)					Calcd (%)				
	C	H	N	Co	Mn	C	H	N	Co	Mn
$[Co(H,H\text{-en})]_2MnBr_4$	44.38	3.32	6.41	13.89	6.13	44.42	3.26	6.47	13.62	6.34
$[Co(H,Me\text{-en})]_2MnCl_4$	51.74	4.49	6.60	14.76	6.55	51.94	4.35	6.73	14.16	6.60
$[Co(Me,Me\text{-en})]_2MnCl_4$	53.50	4.96	6.17	12.82	6.23	54.07	4.99	6.30	13.26	6.18
$[Co(H,H\text{-pn})]_2MnBr_4$	45.43	3.53	6.19	13.70	6.40	45.71	3.61	6.27	13.19	6.15

Results and Discussion

Infrared spectra of the complexes display a skeletal vibration around 1530—1545 cm^{-1}, which is higher in frequency compared with that of the mononuclear cobalt(II) complexes. The high-frequency shift of this band has been utilized as a diagnosis of the bridging mode of the phenolic oxygen.[3] The similarity in infrared spectrum between $[Co(R_1,R_2\text{-L})]_2MnX_2$ and $[Co(R_1,R_2\text{-L})]_2CoX_2$[1] are indicative of the same structure between them. Since two molecules of $Co(R_1, R_2\text{-L})$ can not coordinate to a metal in a square plane because of the steric requirement of the molecule,[1,4,5] the most likely structure of the trinuclear complexes is *cis*-octahedral around the central manganese(II) ion (Fig. 1).

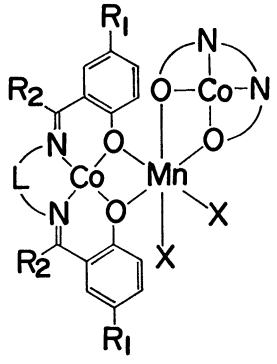

Fig. 1. Probable structure of $[Co(R_1,R_2\text{-L})]_2MnX_2$.

Powder reflectance spectra of the trinuclear complexes are nearly the same as those of the mononuclear cobalt(II) complexes except for Co(H,H-en), showing d-d bands at 8000 and 19000 cm^{-1}. Monomeric square-planar[6] and dimeric square-pyramidal[7] modifications are known for Co(H,H-en), and the electronic spectra of the present complexes are substantially the same as that of monomeric Co(H,H-en).[8] Since high-spin manganese(II) complexes show no spin-allowed d-d bands, the electronic spectra indicate that the electronic configuration of the low-spin cobalt(II) in $[Co(R_1,R_2\text{-L})]_2MnX_2$ is identical with that of Co(H,H-en), whose $(d_{x^2-y^2})^2(d_{yz})^1$ ground state electronic configuration was already demonstrated.[9,10]

Magnetic moments of the trinuclear complexes depend upon temperature (Table 2). This fact can be attributed to an antiferromagnetic spin-exchange interaction between the cobalt(II) and the manganese(II) ions. Molar magnetic susceptibility for the Co(II)($s=1/2$)–Mn(II)($s=5/2$)–Co(II)($s=1/2$) system is given by

Table 2. Temperature variation of molar magnetic susceptibility (c.g.s./mol) and molar magnetic moment(B.M.)

$[Co(H,H\text{-}en)]_2MnBr_2$												
T/K	81.1	95.1	115.6	135.4	155.6	176.2	196.1	216.7	236.5	256.3	276.6	296.6
$\chi_M \times 10^6$	53664	46543	40131	35006	31399	28307	25993	23814	22180	20721	19379	18212
μ_{eff}	5.90	5.97	6.09	6.16	6.25	6.32	6.38	6.42	6.48	6.52	6.55	6.57
$[Co(H,Me\text{-}en)]_2MnCl_2$												
T/K	82.8	102.5	122.5	141.9	161.3	180.9	200.5	219.6	239.5	258.4	278.3	297.6
$\chi_M \times 10^6$	46261	38907	34559	30764	28380	25808	23943	22308	20707	19492	18250	17223
μ_{eff}	5.53	5.65	5.82	5.91	6.05	6.11	6.20	6.26	6.30	6.35	6.37	6.40
$[Co(Me,Me\text{-}en)]_2MnCl_2$												
T/K	81.7	93.0	113.2	134.5	154.4	175.1	195.1	215.5	236.1	256.8	277.3	297.1
$\chi_M \times 10^6$	54620	50750	43996	38064	34415	30841	27750	25375	23262	21468	19973	18776
μ_{eff}	5.97	6.14	6.31	6.40	6.52	6.57	6.58	6.61	6.63	6.64	6.66	6.68
$[Co(H,H\text{-}pn)]_2MnBr_2$												
T/K	83.4	102.0	121.1	140.7	160.0	179.2	198.3	217.3	237.6	256.5	276.3	296.1
$\chi_M \times 10^6$	50857	42979	37638	33150	29946	27335	25193	23312	21693	20230	19133	17984
μ_{eff}	5.82	5.92	6.04	6.11	6.19	6.26	6.32	6.37	6.42	6.44	6.50	6.53

$$\chi_M = \frac{Ng^2\beta^2}{4kT} \times \frac{35+10\exp(-7J/kT)+35\exp(-2J/kT)+84\exp(5J/kT)}{3+2\exp(-7J/kT)+3\exp(-2J/kT)+4\exp(5J/kT)} + N\alpha,$$ [11]

where J is the exchange integral between the low-spin cobalt(II) and the high-spin manganese(II) ions and other symbols have their usual meanings. This expression is applicable to the present complexes. Agreement between the theoretical and the experimental χ_M *versus* T curves is satisfactory. An example of this is shown in Fig. 2. The magnetic parameters, g and J, were determined by the best fit technique on estimating the temperature-independent paramagnetism, $N\alpha$, at 120×10^{-6} c.g.s./mol. The results are as follows. $[Co(H,H\text{-}en)]_2MnBr_2$: $g=2.13$, $J=-10$; $[Co(H,Me\text{-}en)]_2MnCl_2$: $g=2.12$, $J=-12$; $[Co(Me,Me\text{-}en)]_2MnCl_2$: $g=2.14$, $J=-8$; $[Co(H,H\text{-}pn)]_2MnBr_2$: $g=2.13$, $J=-11$ cm^{-1}.

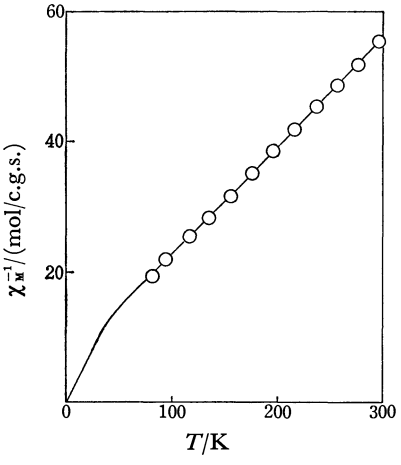

Fig. 2. Temperature variation of inverse molar magnetic susceptibility of $[Co(H,H\text{-}en)]_2MnBr_2$. The solid line represents the theoretical inverse susceptibility with $J=-10$ cm^{-1}, $g=2.13$ and $N\alpha=120\times10^{-6}$ c.g.s./mol.

The present complexes quite differ from the cobalt(II)–manganese(II) complexes, $CoMn(fsaR)(py)_3$,[12] in magnetic property (where H_4fsaR represents *N,N'*-bis(3-carboxysalicylidene)alkanediamines). In $CoMn(fsaR)(py)_3$ the low-spin cobalt(II) ion possesses an unpaired electron in its d_{z^2} orbital and no spin-exchange interaction is operating between the metal ions. Thus, we may conclude that an antiferromagnetic spin-exchange interaction in the present complexes results from the π-superpathway of $d_\pi(Co)$-$p_\pi(O)$-$d_\pi(Mn)$ overlapping.

Authors are grateful to the Ministry of Education for the Scientific Research Grant-in-Aid. One of the authors, V. Kasempimolporn, also wishes to express his thanks to the Ministry of Education for the Scholarship.

References

1) V. Kasempimolporn, H. Okawa, and S. Kida, *Bull. Chem. Soc. Jpn.*, **52**, 1928 (1979).
2) R. H. Bailes and M. Calvin, *J. Am. Chem. Soc.*, **69**, 1886 (1947).
3) C. M. Harris, J. M. James, P. J. Milham, and E. Sinn, *Inorg. Chim. Acta*, **3**, 81 (1969).
4) G. H. W. Hilburn, H. R. Truter, and B. L. Vickery, *Chem. Commun.*, **1968**, 1188.
5) J. M. Epstein, B. N. Figgis, A. H. White, and A. C. Willis., *J. Chem. Soc., Dalton Trans.*, **1974**, 1954.
6) W. P. Schaeffer and R. E. Marsh, *Acta Crystallogr., Sect. B*, **25**, 1675 (1969).
7) R. De Iasi, S. L. Holt, and B. Post, *Inorg. Chem.*, **10**, 1498 (1969).
8) H. Nishikawa and S. Yamada, *Bull. Chem. Soc. Jpn.*, **37**, 8 (1964).
9) Y. Nishida and S. Kida, *Bull. Chem. Soc. Jpn.*, **51**, 143 (1978).
10) M. A. Hitchman, *Inorg. Chem.*, **16**, 1985 (1977).
11) S. J. Gruber, C. M. Harris, and E. Sinn, *J. Chem. Phys.*, **49**, 2183 (1968).
12) N. Torihara, H. Okawa, and S. Kida, *Chem. Lett.*, **1979**, 683.

BULLETIN OF THE CHEMICAL SOCIETY OF JAPAN, VOL. 52 (11), 3461—3462 (1979)

A Catalytic Effect of Amines on the Reaction of α-Toluenethiol with *N,N'*-Thiodiphthalimide[1]

Yasuo ABE,* Toyokazu HORII, Shun-ichi KAWAMURA, and Takeshige NAKABAYASHI
Radiation Center of Osaka Prefecture, Shinke-cho, Sakai 593

(Received March 5, 1979)

Synopsis. In the presence of catalytic amounts of several amines, *N,N'*-thiodiphthalimide has been allowed to react with α-toluenethiol in benzene and dichloromethane giving *N*-(benzyldithio)phthalimide. *N*-(Benzyldithio)-phthalimide has been obtained in excellent yields with 2,4- or 2,6-lutidine as the catalyst in benzene.

Harpp *et al.*[2] prepared the *N*-(alkyldithio)- and *N*-(aryldithio)phthalimides in good yields by the reaction of thiols with *N,N'*-thiodiphthalimide(**2**) in refluxing benzene. In a previous paper,[3] it was shown that a catalytic amount of imidazole markedly accelerates Harpp's reaction in dichloromethane. This has lead to the present examination as to whether amines act as catalysts in the present reaction.

A mixture of α-toluenethiol (**1**) (5 mmol), **2** (5 mmol), and amine (0.5 mmol) was refluxed for 30 min in benzene (100 ml). The starting material **2** was not sufficiently soluble in hot benzene, but the product, *N*-(benzyldithio)phthalimide (**3**), and phthalimide were soluble. Consequently, the dissolution of **2** promotes the reaction. The product **3** was isolated from the reaction mixture by fractional dissolution in cold benzene and cold ethanol, and weighed. The remaining reaction mixture was subjected to column chromatography. The eluate obtained gave a mixture of the unchanged thiol and a by-product, dibenzyl trisulfide (**4**), which were identified and evaluated from NMR analysis,[4] the results of which are summarized in Table 1. As shown in the material balance of the benzyl group in Table 1, the compounds stemming from **1** collected exceeded 90% with few exceptions.

The unchanged thiol (93%) was recovered in the absence of amine in the reaction mixture (Run 1). Regardless of the functional group, *i.e.*, primary, secondary, or tertiary, all amines accelerated the present reaction. The product distribution varied with the amine employed, the results of which are given in Table 1. The results can be classified into three categories: (1) the thiol remaining practically unchanged (Runs 1—5); (2) the thiol being quantitatively changed into **3** (Runs 6—10); (3) the thiol being consumed to give mainly **3** but the remaining (over 20%) was changed into **4** (Runs 11—16). The variety in product distribution appears directly related to the pK_a value of the amine used. With the amine having a pK_a value of 5.06 or less, the unchanged thiol was recovered in over 25% of the initially charged amount. When 2,6- or 2,4-lutidine having a pK_a value of 6.75 or 6.79, respectively, was applied to the reaction system, **3** was obtained almost quantitatively. A pK_a value of 6.95 or greater caused a decrease in the yield of **3**. The yield of **4** increased with an increase in the pK_a value of the amine.[5]

Recently, Yamabe *et al.*[6] reported that 1 : 1 S–H–N type hydrogen bonding is formed between 1-propanethiol and several amines, and that the strength of the hydrogen bonding enhances with increase in the pK_a value of the amine. Therefore, the present reaction is expected to proceed rapidly to give **3** in a good yield since the nucleophilicity of the thiol toward **2** would increase in the presence of a strongly basic amine.

Table 1 shows that, in spite of the reaction of **2** with one equivalent of **1**, an undesirable trisulfide **4** was produced. This suggests that the thiol reacted competitively with the starting material **2** and product **3** (Eqs. 1 and 2). The thiol predominantly reacted

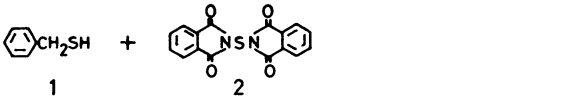

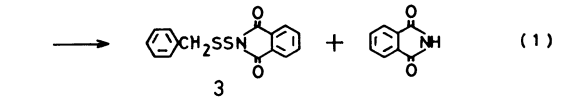

(1)

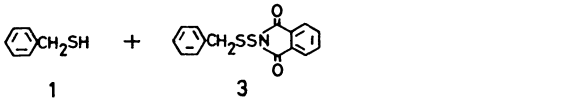

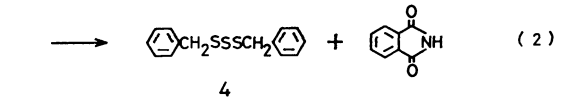

(2)

with **2** to give **3** when the nucleophilicity was suitable; this corresponds to a pK_a value of the amine of approximately 6.7 (Runs 7 and 8). As the nucleophilicity of the thiol increases, the two reactions occur giving both **3** and **4**. A second interpretation in formation of **4** is as follows. The starting material **2** does not dissolve adequately in hot benzene, and consequently the reaction rate of the thiol having a large nucleophilicity toward **2** may be limited by the rate of solution **2** into the benzene, and thus the reaction with **3** will increase giving **4**. The formation of **4** in the case of weak amines (Runs 2—6) is impossible to explain completely by the above reaction mechanisms. Amines having large pK_a values abstract protons from arylalkyl hydrodisulfide but amines having small pK_a values attack the sulfur atoms of the compound.[7] There is a possibility in the present reaction that the amine having a small pK_a value attacks the electron-deficient sulfur atom of **2** and **3** as a nucleophile but the actual reaction mechanism remains obscure.[8]

In order to increase the yield of **3** but to decrease that of **4**, a mixture of **1** and **2** was refluxed for 20

Table 1. Reactions of **1** with **2** in the presence of amines[a]

Run	Amine	pK_a	Solvent	Recovered **1** (mmol)	Products **3** (mmol)[b]	Products **4** (mmol)	Material Balance of benzyl group[c]
1	None	—	Benzene	4.65	0.12 (3)	0	4.89
2	Aniline	4.60	Benzene	3.01	1.09 (22)	0.32	4.74
3	2-Aminophenol[d]	4.72	Benzene	2.04	2.38 (48)	0.09	4.60
4	*N*-Methylaniline	4.85	Benzene	2.48	0.79 (16)	0.43[e]	4.13
5	*N*,*N*-Dimethylaniline	5.06	Benzene	1.08	1.55 (31)	0.49	3.61
6	Pyridine	5.17	Benzene	Trace	3.44 (69)	0.68[f]	4.80
7	2,6-Lutidine	6.75	Benzene	0	4.84 (97)	0.08	5.00
8	2,4-Lutidine	6.79	Benzene	0	4.82 (96)	0.09	5.00
9	Imidazole	6.95	Benzene	0	4.45 (89)	0.31[e]	5.07
10	*N*-Methylmorpholine	7.41	Benzene	0	4.47 (89)	0.20	4.87
11	Morpholine	8.36	Benzene	0	3.92 (78)	0.50	4.92
12	Butylamine	10.60	Benzene	0	3.20 (64)	0.90	5.00
13	Triethylamine	10.67	Benzene	0	1.98 (40)	1.52	5.01
14	Tributylamine	10.87	Benzene	0	2.70 (54)	1.15	5.00
15	Piperidine	11.22	Benzene	0	0.82 (16)	2.02	4.86
16	Dibutylamine	11.25	Benzene	0	2.14 (43)	1.39	4.93
17	None	—	Dichloromethane	3.60	0.44 (9)	0	4.04
18	Aniline	4.60	Dichloromethane	0	4.43 (89)	0.08	4.61
19	Imidazole	6.95	Dichloromethane	0	4.26 (85)	0.17	4.60
20	Triethylamine	10.67	Dichloromethane	0	3.60 (72)	0.70	5.00
21	Piperidine	11.22	Dichloromethane	0	2.96 (59)	0.81	4.58

a) All the reactions were performed by the use of **1** (5 mmol), **2** (5 mmol), amine (0.5 mmol) in a solvent (100 ml) at boiling point for 30 min in benzene and 20 min in dichloromethane. b) Values in parentheses show the yield based on **2** used. c) Summation of mmol of recovered **1** and **3** and two-fold mmol of **4**. The Theoretical value is 5.00. d) The pK_a value of phenol group is 9.71. e) The product unidentified was detected other than listed. f) The value includes dibenzyl polysulfide besides trisulfide.

min in dichloromethane which is able to dissolve **2** completely. It is expected that the nucleophilicity of the thiol in polar solvents increases because the hydrogen bonding between thiol and amine is enhanced by the polar solvent.[6] As seen in Run 17 of Table 1, the reaction without amine proceeded hardly as in benzene. Even with amines possesing small pK_a values, the reaction was significantly accelerated and gave **3** in good yield (Run 18). The formation of the by-product **4** was not sufficiently depressed by use of this reaction system.

References

1) Chemistry of *N*-(Organothio)imides. VI. For part V of this series, see Y. Abe, K. Oka, R. Kiritani, R. Akaki, and T. Fukumoto, *Ann. Rep. Rad. Ctr. Osaka*, **18**, 77 (1977).

2) D. N. Harpp and D. K. Ash, *Int. J. Sulfur Chem.*, *A*, **1**, 57 (1971).

3) Y. Abe and K. Oka, *Ann. Rep. Rad. Ctr. Osaka*, **18**, 75 (1977).

4) S. Kawamura, T. Kitao, T. Nakabayashi, T. Horii, and J. Tsurugi, *J. Org. Chem.*, **33**, 1179 (1968).

5) In the cases of triethylamine and piperidine, **4** was isolated in better yield than that expected from the respective pK_a values. A possible explanation is that the pK_a value of the amines cited in Table 1 were determined in aqueous solution whereas the present reaction was conducted in benzene.

6) T. Yamabe, K. Akagi, T. Hashimoto, S. Nagata, and K. Fukui, *J. Chem. Soc., Faraday Trans. 1*, **73**, 1860 (1977).

7) J. Tsurugi, Y. Abe, T. Nakabayashi, S. Kawamura, T. Kitao, and M. Niwa, *J. Org. Chem.*, **35**, 3263 (1970).

8) It has been known that the reaction of **2** with one equivalent of secondary amines gives *N*-(secondary aminothio)-phthalimides, and with two equivalent of those affords *N*,*N*'-thiodiamines. D. N. Harpp and T. G. Back, *Tetrahedron Lett.*, **1972**, 1481.

BULLETIN OF THE CHEMICAL SOCIETY OF JAPAN, VOL. 52 (11), 3463—3464 (1979)

Nucleophilic Substitution on Dialkoxy Disulfides. II.[1] Reactions with Hydrazine Derivatives

Hiroaki KAGAMI and Shinichi MOTOKI*

Department of Chemistry, Faculty of Science, Science University of Tokyo, Kagurazaka, Shinjuku-ku, Tokyo 162

(Received January 12, 1979)

Synopsis. Diethoxy disulfide (**1**) reacted with arylhydrazines to give arylbenzenes, diaryl sulfides, and aryl ethoxy tetrasulfides. The reaction of **1** with hydrazobenzenes gave azobenzenes in quantitative yields. The treatment of **1** with 1,5-diphenylthiocarbonohydrazide or 1,5-diarylthiocarbazones afforded 2,3-diaryltetrazolium-5-thiolates.

Dialkoxy disulfides (**1**) are reactive toward some nucleophilic reagents.[2,3] Previously, we have also found that the alkoxyl group of **1** is readily displaced by secondary amines,[1] thiols,[1] or thiocarboxylic acids[4] to give several unsymmetrical polysulfides. Further, the reaction of primary amines with **1** afforded *N*-thiosulfinylamine (**2a**) by the intramolecular elimination of alcohol (Scheme 1).[1] We have now studied the reaction of **1** with hydrazine derivatives, and found that not only the substitution of the alkoxyl group, but also the elimination of sulfur and nitrogen, takes place.

$$\underset{\mathbf{1}}{\mathrm{ROSSOR}} \xrightarrow[-\mathrm{ROH}]{\mathrm{XH}} \mathrm{ROSSX} \xrightarrow[-\mathrm{ROH}]{\mathrm{YH}} \mathrm{YSSX}$$

(XH, YH: R'_2NH, R'SH, R'C(=O)SH)

$$\mathbf{1} + \mathrm{R'NH_2} \xrightarrow[-\mathrm{ROH}]{} [\mathrm{R'NH\text{-}S\text{-}S\text{-}OR}] \xrightarrow[-\mathrm{ROH}]{} \underset{\mathbf{2}}{\mathrm{R'N{=}S{=}S}}$$

Scheme 1.

4-Nitrophenylhydrazine was allowed to react with **1** in refluxing benzene. Ethanol was eliminated, and 4-nitrobiphenyl, ethoxy 4-nitrophenyl tetrasulfide, and bis(4-nitrophenyl) disulfide were obtained. The other monosubstituted hydrazines reacted similarly. The results are shown in Table 1. Considering the formation of the thiosulfinyl compound (**2a**) from **1** and primary amines, it seems reasonable to assume that the reaction of **1** with hydrazines proceed *via* a thiosulfinyl intermediate (**2b**) in the following way: arylhydrazines and **1** initially afford **2b**, followed by the transfer of a proton to give an azo intermediate (**3**).

$$\mathrm{Ar\text{-}NHNH_2} \xrightarrow[-2\ \mathrm{EtOH}]{\mathrm{EtOSSOEt\ (1)}}$$

$$[\underset{\mathbf{2b}}{\mathrm{Ar\text{-}NH\text{-}N{=}S{=}S}} \rightleftharpoons \underset{\mathbf{3}}{\mathrm{Ar\text{-}N{=}N\text{-}S\text{-}S\text{-}H}}] \xrightarrow[-\mathrm{EtOH}]{\mathbf{1}}$$

$$[\underset{\mathbf{4}}{\mathrm{Ar\text{-}N{=}N\text{-}S_4\text{-}OEt}}] \xrightarrow[-\mathrm{N_2}]{} \mathrm{Ar\cdot} + \mathrm{EtOSSSS\cdot}$$

$$\mathrm{Ar\cdot} + \bigcirc \longrightarrow \mathrm{Ar\text{-}}\bigcirc + \mathrm{H\cdot}$$

$$\mathrm{Ar\cdot} + \mathrm{EtOSSSS\cdot} \longrightarrow \mathrm{Ar\text{-}S_4\text{-}OEt}$$

$$2\ \mathrm{Ar\text{-}S_4\text{-}OEt} \longrightarrow \mathrm{Ar\text{-}S_4\text{-}Ar} + \mathbf{1} + 2\ \mathrm{S}$$

Scheme 2.

Table 1. Reaction of diethoxy disulfide (**1**) with monosubstituted hydrazine

Hydrazine ($ArNHNH_2$) Ar	Benzene refluxing time / h	Products Isolated yield/% Ar-C_6H_5	Ar-S_4-OEt	Ar-S_x-Ar
4-$NO_2C_6H_4$	10	21	29	13 (x=2)[a]
2-ClC_6H_4	30	27	10	48 (x=4)
4-BrC_6H_4	20	0[b]	5[b]	39 (x=4)[a]
C_6H_5	12	8[b]	0[b]	37 (x=4)
4-$CH_3C_6H_4$	15	20	0[b]	31 (x=4)
2-$C_{10}H_7$	15	5[b]	0[b]	47 (x=4)

a) Diaryl tetrasulfides are relatively unstable compounds, and especially careful handling is necessary for bis(4-bromophenyl) tetrasulfide to prevent its thermal decomposition to the disulfide during recrystallization. Presumably, the formation of bis(4-nitrophenyl) disulfide is due to the elimination of sulfur from the tetrasulfide during the operation. b) In these cases, the complete separation of the products by chromatography is extremely difficult. The low yields of the biphenyl and aryl ethoxy tetrasulfide are mainly the result of the loss of these products during the operation.

The azo intermediate (**3**) then replaces the ethoxyl group in **1** to give the intermediate arylazo ethoxy tetrasulfide (**4**) (Scheme 2). The formation of the aryl radical by the decomposition of diazonium salts is well known.[5] Therefore, the intermediate, **4**, presumably decomposes to the aryl radical with the evolution of nitrogen, and the resulting radical reacts immediately with benzene (solvent) or the ethoxy tetrasulfanyl radical to give biphenyl or aryl ethoxy tetrasulfides respectively. Symmetrical diaryl sulfides would be formed by the thermal decomposition of aryl ethoxy tetrasulfides.

On the other hand, hydrazobenzene reacted with **1** to give azobenzene in a quantitative yield, with the elimination of ethanol and sulfur. 2,2′-Dibromohydrazobenzene reacted similarly. It can be assumed that hydrazobenzene reacts with **1** to give a cyclic disulfide (**5**), followed by the elimination of sulfur to form azobenzene (Scheme 3). In these reactions, the sulfur of **1** serves as an oxidizing agent, whereas divalent sulfur compounds such as dialkyl sulfoxylates

$$\mathrm{Ar\text{-}\underset{\mathrm{H}}{\underset{|}{N}}\text{-}\underset{\mathrm{H}}{\underset{|}{N}}\text{-}Ar} \xrightarrow[-\mathrm{EtOH}]{\mathrm{EtOSSOEt\ (1)}} \left[\mathrm{Ar\text{-}\underset{\mathrm{H}}{\underset{|}{N}}\text{-}\underset{\mathrm{H\ S\text{-}S\text{-}OEt}}{\underset{|}{N}}\text{-}Ar}\right] \xrightarrow[-\mathrm{EtOH}]{}$$

$$\left[\underset{\mathbf{5}}{\mathrm{Ar\text{-}\underset{\mathrm{S\text{-}S}}{\underset{|}{N}}\text{-}\underset{\mathrm{S\text{-}S}}{\underset{|}{N}}\text{-}Ar}}\right] \xrightarrow[-\mathrm{S}]{} \mathrm{Ar\text{-}N{=}N\text{-}Ar}$$

Ar: C_6H_5, 2-BrC_6H_4

Scheme 3.

are known as reducing agents.[6,7] Such conflicting dual properties of sulfur compounds has aroused interest.

In contrast to hydrazobenzene or phenylhydrazine, 1,1-diphenylhydrazine and **1** gave diphenylamine with ethanol and sulfur. However, the mechanism of the reaction has not yet been elucidated.

A related compound of hydrazine 1,5-diphenylthiocarbonohydrazide (**6a**) reacted with 2 mols of **1** to give 2,3-diphenyltetrazolium-5-thiolate (**9a**).[8] Similarly, 1,5-diphenylthiocarbazone (**7a**) or 1,5-di-2-naphthylthiocarbazone (**7b**) reacted readily with **1** to give **9a** or 2,3-di-2-naphthyltetrazolium-5-thiolate (**9b**). It is considered that these reactions proceed *via* azo compounds (**7**,**8**), much like the formation of azobenzene from hydrazobenzene.

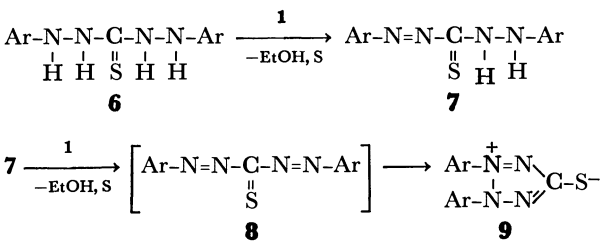

a) Ar: C_6H_5 b) Ar: 2-$C_{10}H_7$

Scheme 4.

Experimental

The IR spectra were measured with a Hitachi 260-10 spectrometer. The NMR spectra were determined in a $CDCl_3$ solution with a JEOL JNM-PMX-60 spectrometer. The mass spectra were obtained on a Hitachi RMU-7 M at 70 eV. Diethoxy disulfide (**1**)[3] and 2,2′-dibromohydrazobenzene[9] were prepared by the method of the literature.

Reaction of ***1*** *with Arylhydrazine.* A solution of arylhydrazine (0.02 mol) and **1** (0.04 mol) in 50 cm³ of benzene was refluxed for 10—30 h. The reaction mixture was then evaporated, and the residue was chromatographed on silica gel, using hexane or benzene–hexane (1:2) as an eluent, to give arylbenzene, aryl ethoxy tetrasulfide, and diaryl sulfide. Ethoxy 4-nitrophenyl tetrasulfide: light yellow liq.; NMR ($CDCl_3$) δ 1.32 (m, 3H), 3.93 (m, 2H), 7.36—8.40 (aromatic, 4H); MS *m/e* 295 (M^+). Found: N, 4.80; S, 43.74%. Calcd for $C_8H_9NO_3S_4$: N, 4.74; S, 43.41%. Bis(4-nitrophenyl) disulfide, mp 180 °C. Found: C, 46.90; H, 2.68%. Calcd for $C_{12}H_8N_2O_4S_2$: C, 46.74; H, 2.62%. 2-Chlorophenyl ethoxy tetrasulfide; light yellow liq., NMR ($CDCl_3$) δ 1.28 (m, 3H), 3.98 (m, 2H), 7.03—8.00 (aromatic, 4H). Found: C, 33.48; H, 2.92%. Calcd for $C_8H_9OClS_4$: C, 33.73; H, 3.18%. Bis(2-chlorophenyl) tetrasulfide, light yellow liq. Found: C, 41.10; H, 2.50%. Calcd for $C_{12}H_8Cl_2S_4$: C, 41.02; H, 2.30%. 4-Bromophenyl ethoxy tetrasulfide; light yellow liq., NMR ($CDCl_3$) δ 1.30 (m, 3H), 3.95 (m, 2H), 7.20—7.67 (aromatic, 4H). Found: C, 28.92; H, 2.52%. Calcd for $C_8H_9OBrS_4$: C, 29.18; H, 2.75%. Bis(4-bromophenyl) tetrasulfide, light yellow liq. Found: C, 32.95; H, 2.01%. Calcd for $C_{12}H_8Br_2S_4$: C, 32.74; H, 1.83%. Diphenyl tetrasulfide, light yellow liq. Found: C, 50.88; H, 3.66%. Calcd for $C_{12}H_{10}S_4$: C, 51.03; H, 3.57%. Ditolyl tetrasulfide, light yellow liq. Found: C, 54.03; H, 4.32%. Calcd for $C_{14}H_{14}S_4$: C, 54.15; H, 4.55%. Dinaphthyl tetrasulfide, light yellow liq. Found: C, 62.56; H, 3.41%. Calcd for $C_{20}H_{14}S_4$: C, 62.79; H, 3.69%.

Reaction of ***1*** *with Hydrazobenzene.* A solution of 9.2 g (0.05 mol) of hydrazobenzene and 7.7 g (0.05 mol) of **1** in 50 cm³ of benzene was refluxed for 20 h. The color of the solution turned red. The reaction mixture was then evaporated, and 60 cm³ of hexane was added. The precipitated sulfur (2.3 g) was filtered off, and the filtrate was evaporated. The residue was chromatographed on silica gel, using hexane as an eluent, to give 9.03 g (99%) of azobenzene (mp 67—68 °C) and 0.2 g of sulfur. A total of 2.5 g (78%) of sulfur was obtained. Similarly, 2,2′-dibromohydrazobenzene (3.42 g, 0.01 mol) and **1** (1.54 g, 0.01 mol) gave 2,2′-dibromoazobenzene (3.35 g, 99%) by column chromatography. 2,2′-Dibromoazobenzene; mp 131—132 °C; reddish orange needles from ethanol. A total of 0.63 g (98%) of sulfur was obtained.

Reaction of ***1*** *with 1,1-Diphenylhydrazine.* To a suspension of 2.21 g (0.01 mol) of 1,1-diphenylhydrazine hydrochloride in 30 cm³ of benzene, a solution of 1.51 g (0.01 mol) of triethylamine was added. After that, a solution of 1.54 g (0.01 mol) of **1** in 10 cm³ of benzene was added to the reaction mixture and the mixture was refluxed for 3 h. Triethylamine hydrochloride was then filtered off, and the filtrate was evaporated. The residue was chromatographed on silica gel, using benzene–hexane (1:2) as an eluent, to give 1.36 g (80%) of diphenylamine; mp 52 °C.

Reaction of ***1*** *with 1,5-Diphenylthiocarbonohydrazide (**6a**).* A suspension of 2.58 g (0.01 mol) of **6a** and 3.08 g (0.02 mol) of **1** in 50 cm³ of benzene was refluxed for 3 h. The color of the solution gradually turned reddish brown. Upon cooling to room temperature, a red solid precipitated from the solution. This red solid was collected and was recrystallized from ethanol to give 2.1 g (83%) of **9a** as red needles; mp 180 °C dec (lit,[8] 180 °C); MS *m/e* 254 (M^+, 18), 226 (M^+-N_2, 18), 167 (11), 105 (25), 77 (100); IR (KBr) 1320 cm^{-1} (very strong). Found: C, 61.25; H, 4.01%. Calcd for $C_{13}H_{10}N_4S$: C, 61.40; H, 3.96%.

Reaction of ***1*** *with 1,5-Diphenylthiocarbazone (**7a**).* A suspension of 2.56 g (0.01 mol) of **7a** and 1.54 g (0.01 mol) of **1** in 50 cm³ of benzene was refluxed for 0.5 h. The color of the suspension immediately turned from dark green to red. A red solid was collected and recrystallized to give 2.38 g (94%) of **9a**. Similarly, 1,5-di-2-naphtylthiocarbazone (**7b**) (1.1 g, 0.003 mol) and **1** (0.48 g, 0.003 mol) gave **9b** (0.8 g, 73%); red prisms from ethanol; mp 167—168 °C dec; MS *m/e* 354 (M^+, 11), 326 (M^+-N_2, 18), 267 (15), 131 (18), 127 (100); IR (KBr) 1310 cm^{-1} (very strong). Found: C, 71.33; H, 4.14; N, 15.66%. Calcd for $C_{21}H_{14}N_4S$: C, 71.16; H, 3.98%; N, 15.81%.

References

1) Part I: H. Kagami and S. Motoki, *J. Org. Chem.*, **42**, 4139 (1977).
2) A. Meuwsen and H. Gebhardt, *Ber. B*, **69**, 937 (1936).
3) Q. E. Thompson, M. M. Crutchfield, M. W. Dietrich, and E. Pierron, *J. Org. Chem.*, **30**, 2692 (1965).
4) H. Kagami, H. Satsumabayashi, and S. Motoki, *J. Org. Chem.*, **42**, 958 (1977).
5) D. H. Hey and W. A. Waters, *J. Chem. Soc.*, **1948**, 882.
6) B. S. Cambell, D. B. Denny, D. Z. Denny, and L. S. Shih, *J. Am. Chem. Soc.*, **97**, 3850 (1975).
7) H. Kagami and S. Motoki, *J. Org. Chem.*, **43**, 1267 (1978).
8) J. W. Ogilvie and A. H. Corwin, *J. Am. Chem. Soc.*, **83**, 5023 (1961).
9) H. R. Snyder, C. Weaver, and C. D. Marshall, *J. Am. Chem. Soc.*, **71**, 289 (1949).

BULLETIN OF THE CHEMICAL SOCIETY OF JAPAN, VOL. 52 (11), 3465—3466 (1979)

Photochemical Ethoxycarbonylmethylation of Anisole with Ethyl Chloroacetate in the Presence of Zinc Chloride

Yasuji IZAWA,* Hideo TOMIOKA, Masato KUTSUNA, and Yasuo TOYAMA

Chemistry Department of Industry and Resources, Faculty of Engineering, Mie University, Tsu, Mie 514

(Received April 5, 1979)

Synopsis. Irradiation of ethyl acetate solution of anisole and ethyl chloroacetate in the presence of $ZnCl_2$ gave ethyl *o*-, *m*-, and *p*-methoxyphenylacetates (**3**) (28.6—48%). The similar ethoxycarbonylmethylation in anisole–ethyl acetate (9:1) resulted in higher yields (80—81%) of **3**. The results on the positional and substrate selectivities imply that $ZnCl_2$-participated attacking species would play an important role in the present ethoxycarbonylmethylation.

It has been well known that in the Friedel-Crafts reactions of ordinary carboxylic acids or their esters with aromatic compounds a carboxymethylation or alkoxycarbonylmethylation is difficult. In previous studies,[1] however, we reported that the photochemical ethoxycarbonylmethylation of benzene with ethyl chloroacetate in the presence of metallic halides, such as $SbCl_3$, $AlCl_3$, $ZnCl_2$, and $FeCl_3$, was possible and gave ethyl phenylacetate (2.3—24.4%) as a sole product. We assumed that the reaction might proceed *via* an electrophilic aromatic substitution by such a C-T exciplex as $(MCl^-_{n+1}\cdots\cdots{}^+CH_2CO_2Et)^*$. If this is the case, the similar reaction of anisole, one of electron rich benzenes, could occur more efficiently and show a high positional selectivity. Thus, it was hoped that this reaction would provide greater mechanistic insight into the course of the photochemical ethoxycarbonylmethylation of aromatic compounds with ethyl chloroacetate in the presence of metallic halides. Herein we wish to report the results of our study on the photochemical ethoxycarbonylmethylation of anisole with ethyl chloroacetate in the presence of $ZnCl_2$ and discuss a probable mechanism.

Reaction Products. Irradiation of ethyl acetate solution of anisole (**1**) and ethyl chloroacetate (**2**) in the presence of $ZnCl_2$ with an unfiltered low pressure mercury lamp at room temperature for 37 h gave isomeric ethyl methoxyphenylacetates (28.6—48.1% yield) (**3**) accompanied by a trace of diethyl succinate (**4**). As shown in Table 1, addition of $ZnCl_2$ to the reaction significantly increases the yield of ethyl methoxyphenylacetates (**3**), which increases as the concentration of $ZnCl_2$ increases, and at the same time produces noticeable change in the isomer distribution. No photochemical interconversion between each methoxyphenylacetate was observed. The similar ethoxycarbonylmethylation was performed in anisole–ethyl acetate (9 : 1). This resulted in higher yields (80—81%) of methoxyphenylacetates (**3**) and no detection of **4** which eliminates the participation of ethoxycarbonylmethyl radicals. In absence of $ZnCl_2$ **4** was detected, but only in a trace.

TABLE 1. PHOTOCHEMICAL REACTION OF **1** WITH **2**

$[ZnCl_2]$/M	Convn of **2**	**3** yield[c]	Isomer distribution/%		
	%	%	*o*-	*m*-	*p*-
0[a]	48	14	61.0	25.5	13.5
0.09[a]	50	29	66.1	19.2	14.7
0.18[a]	44	38	69.2	12.5	18.3
0.5[a]	38	48	74.4	9.1	16.3
0[b]	33	38	66.1	14.6	19.3
0.1[b]	51	80	69.8	10.2	20.2
0.5[b]	57	81	70.5	11.4	18.1

a) Used ethyl acetate solutions of 1 M **1** and 0.1 M **2**. b) Used anisol-ethyl acetate (9 : 1) solutions of 0.1 M **2**. c) Based on consumed **2**.

Positional and Substrate Selectivities. Data of Table 1 show the effect of $ZnCl_2$ on positional selectivity (as shown with isomer distributions). The isomer distributions did not show any measurable change during irradiation from 3 to 37 h. Thus, the positional selectivity is safely shown with the isomer distribution. Addition of ethyl vinyl ether as a radical scavenger to the reaction without $ZnCl_2$ gave no detectable amounts of **3**. This result, together with the formation of **4** derived from ethoxycarbonylmethyl radicals and results for related reaction,[2] suggests the radical nature of the reaction without $ZnCl_2$. Thus, the relative high proportion of meta isomer in the absence of $ZnCl_2$ may be attributed to a radical substitution by the ethoxycarbonylmethyl radicals.

As shown in Table 2, striking is the significant increase in the values for the Selectivity Factor (S_f), as defined by Brown and Smoot,[3] in the reactions with $ZnCl_2$, when compared with those in the absence of $ZnCl_2$. From the S_f values it is possible to say that the reactions in the presence of $ZnCl_2$ proceed *via* competitive radical and non-radical mechanisms, the relative contributions of which depend on the concentration of $ZnCl_2$. The $k_{anisole}/k_{benzene}$ rate ratio ($=k_a/k_b$) in the presence of $ZnCl_2$ is found to be 5.9 from the competitive method. The lower substrate selectivity in the form of low k_a/k_b suggests the reaction to be an electrophilic aromatic substitution involving strongly electrophilic reagent.[4] These results on the positional and substrate selectivities imply that in the non-radical mechanism the carbon atom undergoing attack develops a partial positive charge and may have considerable carbonium ion charactor. Thus, $ZnCl_2$-participated attacking species, as expected previously,[1] would play an important role in the present reaction.

Fluorescence Quenching of Anisole by Ethyl Chloroacetate. In order to examine whether the reactions are induced by energy transfer from singlet anisole to **2**, fluorescence quenchings of **1** by **2** were carried out in cyclohexane and cyclohexane–ethyl acetate (1:1) containing $ZnCl_2$. Both solutions showed structureless fluorescence spectra

with a maximum at 296 nm. The fluorescences of **1** in cyclohexane and cyclohexane–ethyl acetate containing $ZnCl_2$ are quenched by **2** to give linear Stern-Volmer plots, whose slopes are 18[5] and 7.0 M^{-1} at 13 °C, respectively. The fluorescence quenching with the different efficiency cannot be inferred from the different viscosities of the solutions. The lower efficiency in the presence of $ZnCl_2$ may be attributed to weak interaction between $ZnCl_2$ and **2** in the ground state, although it has been shown that the basicity of ethyl acetate is higher than that of **2**.[6] No fluorescence quenching by only $ZnCl_2$ was observed. Thus, it seems likely that the present reactions are induced by energy transfer from singlet anisole to **2** or that interacting weakly with $ZnCl_2$.[7]

Reaction Schemes. Prior to discussing the reaction schemes, the UV spectra of ethyl acetate solutions of anisole in the presence of $ZnCl_2$ were measured. The results show that the spectra do not change by addition of $ZnCl_2$. This implies that there is no interaction between a ground state anisole and $ZnCl_2$ in ethyl acetate. On the basis of the facts mentioned above and before, the possible reaction schemes are outlined as follows:

: without $ZnCl_2$:

$$\text{Anisole} \xrightarrow{h\nu} (\mathbf{1})^S$$

$$(\mathbf{1})^S + \mathbf{2} \longrightarrow (\mathbf{2})^S \longrightarrow Cl\cdot + \cdot CH_2CO_2Et \longrightarrow$$

$$\text{radical aromatic substitution}$$

$$(\mathbf{2})^T$$

: with $ZnCl_2$:

$$\mathbf{2}^*_{S \text{ or } T} \longrightarrow Cl\cdot + \cdot CH_2CO_2Et \longrightarrow \text{radical substitution}$$

$$(\mathbf{1})^S + (ZnCl_2\cdots ClCH_2CO_2Et) \longrightarrow$$

ground state

$$(\overset{\delta-}{Z}nCl_2\cdots Cl\cdots \overset{\delta+}{C}H_2CO_2Et)^*$$

2a

$$\longrightarrow \text{electrophilic aromatic substitution}$$

Thus, in the presence of $ZnCl_2$, an electrophilic aromatic substitution by electronically excited attacking species (**2a**) having considerable carbonium ion charactor may compete with a radical substitution by ethoxycarbonylmethyl radicals. **2a** can be produced by an energy transfer from singlet anisole to **2** interacting weakly with $ZnCl_2$, assuming that the low-lying reactive excited state for **2** is n,π^*.[8]

Table 2. S_f in ethyl acetate

$[ZnCl_2]$/M	[1]/M	[2]/M	S_f[a]
0	0.9	0.09	0.025
0.09	1.0	0.1	0.185
0.18	1.0	0.1	0.476
0.5	1.0	0.1	0.560

a) Calculated from the isomer distribution (Table 1).[3]

Experimental

Materials. Ethyl chloroacetate (**2**), bp 142—143 °C, and authentic diethyl succinate, bp 108—108.5 °C/19 Torr, were prepared as previously described.[1a] Authentic ethyl *p*-methoxyphenylacetate was prepared by the conventional esterification of *p*-methoxyphenylacetic acid: bp 136—139 °C/9.5 Torr. *p*-Methoxyphenylacetic acid, mp 85—86 °C (lit, 84; 87 °C[9]) was prepared by hydrolysis of *p*-methoxybenzyl cyanide obtained by cyanation of *p*-methoxybenzyl chloride. Authentic ethyl *o*- and *m*-methoxyphenylacetates were similarly prepared: ethyl *o*-methoxyphenylacetate, bp 137 °C/14 Torr; ethyl *m*-methoxyphenylacetate, bp 135—138 °C/7 Torr. The *o*- and *m*-methoxybenzyl chlorides were prepared by crossed Cannizzaro reaction between the corresponding anisaldehydes and formaldehyde followed by chlorination with hydrochloric acid.

Irradiation for Analytical Purposes. The irradiations were conducted using a Halos 30 W low-pressure mercury lamp without filter. The solutions (5 mL) outlined in Table 1 were placed in 12 mm o.d. quartz tubes, and these were capped with polyethylene-stopples after flushing with nitrogen for about 5 min, then irradiated at 13—23 °C for 37 h. After irradiation, analysis of the reaction mixtures was performed by means of GC.

Fluorescence Quenching of ***1***. A stock solution of **1** in cyclohexane was prepared and varying amounts of **2** were added to aliquots of the stock: [**1**]=30 mM, [**2**]=3.8—30 mM. Five solutions were used for the quenching experiment. The fluorescence spectra were recorded at about 13 °C and the relative intensities (I_0/I) at 296 nm in the absence and presence of **2** were plotted with concentration of **2**. A linear Stern-Volmer plot was obtained. Similarly, fluorescence quenching of **1** by **2** containing $ZnCl_2$ (molar ratio= 1:1) was carried out in cyclohexane–ethyl acetate (1:1).

References

1) (a) Y. Ogata, T. Itoh, and Y. Izawa, *Bull. Chem. Soc. Jpn.*, **42**, 794 (1969); (b) Y. Izawa, T. Ishihara, and Y. Ogata, *Tetrahedron*, **28**, 211 (1972).

2) (a) O. Yonemitsu and S. Naruto, *Tetrahedron Lett.*, **1969**, 2387; (b) Y. Ogata, E. Hayashi, and H. Kato, *Bull. Chem. Soc. Jpn.*, **51**, 3657 (1978).

3) H. C. Brown and C. R. Smoot, *J. Am. Chem. Soc.*, **78**, 6255 (1956).

4) G. A. Olah, S. Kobayashi, and M. Tashiro, *J. Am. Chem. Soc.*, **94**, 7448 (1972), and references cited therein.

5) Assuming that the quenching is diffusion-controlled, from the slope (18 M^{-1}) τ_f is estimated to be 3.4×10^{-9} s (lit, 8.3×10^{-9} s: I. B. Berlman, "Handbook of Fluorescence Spectra of Aromatic Molecules," 2nd ed, Academic Press, New York (1971), p. 139).

6) D. G. Lee and M. H. Sadar, *J. Am. Chem. Soc.*, **96**, 2862 (1974).

7) Alternatively, although the fluorescence quenching by an exciplex formation might be considered, the obserbed positional and substrate selectivities could not be explained by a pathway *via* the exciplex.

8) It has been reported that the reactive excited state is n,π^* triplet state for some organic esters: see, J. A. Bartrop and J. D. Coyle, *J. Chem. Soc., B*, **1971**, 251; A. A. Scala, J. P. Colangelo, G. E. Hussey, and W. T. Stolle, *J. Am. Chem. Soc.*, **96**, 4069 (1974), and references cited therein.

9) "Handbook of Tables for Organic Compound Identification," The Chemical Rubber, Cleveland, Ohio (1967), p. 196.

BULLETIN OF THE CHEMICAL SOCIETY OF JAPAN, VOL. 52 (11), 3467—3468 (1979)

The BF_3 Catalyzed Decomposition of Diazo Compounds in the Presence of Carbonyl Compounds

Toshikazu IBATA,* Kazuo MIYAUCHI, and Seiji NAKATA

Institute of Chemistry, College of General Education, Osaka University, Toyonaka, Osaka 560

(Received April 9, 1979)

Synopsis The BF_3 catalyzed decomposition of diazo compounds such as α-diazoacetophenones, ethyl diazoacetate, and diphenyldiazomethane in the presence of cyclic β-diketones gave the corresponding enol ether. Used as a substrate, cyclohexanone gave the ring expanded homologation product.

The reactions of diazo compounds with carboxylic acids have been extensively studied as a preparative method for esters.[1] Few papers have however been published on the Lewis acid catalyzed reaction of diazo compounds with carbonyl compounds. For example, the BF_3 catalyzed decomposition of ethyl diazoacetate in carbonyl compounds was reported to give homologation products (**1**).[2-5]

$$\text{R-C(=O)-R} + N_2CHCOOC_2H_5 \xrightarrow[-N_2]{BF_3} \text{R-C(=O)-CH(COOC}_2\text{H}_5\text{)-R}$$

(**1**)

In this paper a further type of reaction observed in the BF_3 catalyzed decomposition of diazo compounds in the presence of β-diketones such as dimedone (5,5-dimethyl-1,3-cyclohexanedione) and 1,3-cyclohexanedione will be reported. A catalytic amount of BF_3 etherate when added to a solution of α-diazoacetophenone and dimedone (1 : 3 molar ratio) in benzene at 60 °C gave a vigorous evolution of nitrogen gas. Column chromatography (silica gel–benzene) of the reaction mixture gave two products. The first fraction was identified as α-hydroxyacetophenone (**3a**, 28%) by comparison of the IR and NMR spectra with those of authentic samples prepared by the decomposition of the diazoacetophenone in dilute sulfuric acid. The second product was characterized as 5,5-dimethyl-3-phenacyloxy-2-cyclohexene-1-one (**2a**: R^1=Ph, R^2=CH_3, 63%) on the basis of the results of elemental analysis and spectral properties. The IR spectrum shows the carbonyl band of the benzoyl group at 1700 cm^{-1} and bands of the enone group at 1650 and 1600 cm^{-1}. The NMR spectrum exhibits a singlet of the vinyl proton at δ 5.22 and three methylenes at 5.12, 2.43, and 2.22 ppm besides two methyl signals and a phenyl signal. Similar results were observed in the reactions of substituted diazoacetophenones with dimedone or 1,3-cyclohexanedione (Table 1, Runs a—f and h—j). Ethyl diazoacetate gave the corresponding enol ethers (**2g** and **2k**: R^1=OC_2H_5) in the reactions with dimedone and 1,3-cyclohexanedione.

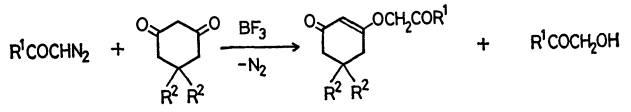

(**2**) (**3**)

In these reactions, no ring expanded homologation product, *e.g.*, **4** or **5** was found in detectable amounts despite detailed inspection of the reaction mixture by column chromatography.

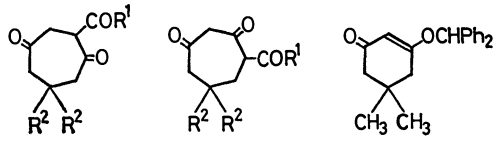

(**4**) (**5**) (**10**)

An excess of BF_3 etherate,[6] did not give the homologation product. In these cases **2** and **3** were accompanied by α-ethoxyacetophenone (**9**) which is thought formed by attack of the reaction intermediate (**6**) on diethyl ether through betaine (**8**). An increase in the amount of BF_3 etherate used caused a decrease in the yields of **2** and **3** an increase in the yield of **9**. The use of a five molar amount of BF_3 etherate gave only one product **9**, (69%), **2** and **3** were not detected.

TABLE 1. YIELDS, MELTING POINTS, AND ANALYTICAL DATA OF THE PRODUCTS (**2** and **3**)

Run	R^1	R^2	**2** Yield %	**2** Mp °C	**2** Found (%) C	**2** Found (%) H	**2** Calcd (%) C	**2** Calcd (%) H	**2** Molecular formula	**3** Yield %
a	C_6H_5	CH_3	63	109—110	74.18	7.06	74.39	7.02	$C_{16}H_{18}O_3$	28
b	*p*-BrC_6H_4		72	182—183	56.79	5.15	56.99	5.05	$C_{16}H_{17}O_3Br$	20
c	*p*-$NO_2C_6H_4$		60	187—189	63.32	5.66[a]	63.36	5.65	$C_{16}H_{17}O_5N$	11
d	*p*-$CH_3OC_6H_4$		65	102—105	70.97	6.92	70.81	6.99	$C_{17}H_{20}O_4$	23
e	*p*-$CH_3C_6H_4$		53	133—134	74.71	7.42	74.97	7.40	$C_{17}H_{20}O_3$	18
f	*m*-$CH_3C_6H_4$		44	57—58	74.61	7.34				29
g	C_2H_5O		55	oil						
h	C_6H_5	H	73	140—141	72.96	6.17	73.02	6.13	$C_{14}H_{14}O_3$	25
i	*p*-BrC_6H_4		49	182—183	54.15	4.26	54.39	4.24	$C_{14}H_{13}O_3Br$	43
j	*p*-$NO_2C_6H_4$		40	193—194	61.21	4.82[b]	61.09	4.76	$C_{14}H_{13}O_5N$	25
k	C_2H_5O		40	oil						

a) N: Found 4.53%, Calcd 4.62%. b) N: Found 4.92%, Calcd 5.09%.

TABLE 2. THE IR AND NMR DATA OF **2**

Compd	IR (KBr, ν/cm^{-1}) C=O	IR (KBr, ν/cm^{-1}) enone	NMR ($CDCl_3$, δ/ppm) CH_3	CH_2	CH_2	OCH_2	=CH	Others[a]
2a	1700	1650, 1660	1.07	2.22	2.43	5.12	5.22	
2b	1710	1640, 1600	1.02	2.20	2.42	5.13	5.27	
2c	1710	1630, 1595	1.10	2.23	2.47	5.23	5.30	
2d	1690	1645, 1600	1.10	2.23	2.43	5.14	5.31	3.88(s) OCH_3
2e	1700	1650, 1600	1.40	2.20	2.40	5.03	5.24	2.40(s) CH_3
2f	1705	1655, 1600	1.07	2.20	2.40	5.20	5.30	2.40(s) CH_3
2g	1760	1660, 1600	1.07	2.22	2.38	4.47	5.23	1.29(t), 4.29(q) CH_2CH_3
2h	1695	1640, 1600	—	m	m	5.20	5.28	
2i	1695	1640, 1600	—	m	m	5.20	5.30	
2j	1705	1635, 1600	—	m	m	5.18	5.30	
2k	1760	1650, 1605	—	m	m	4.45	5.23	1.27(t), 4.23(q) CH_2CH_3

a) Signals of the aromatic protons have been omitted.

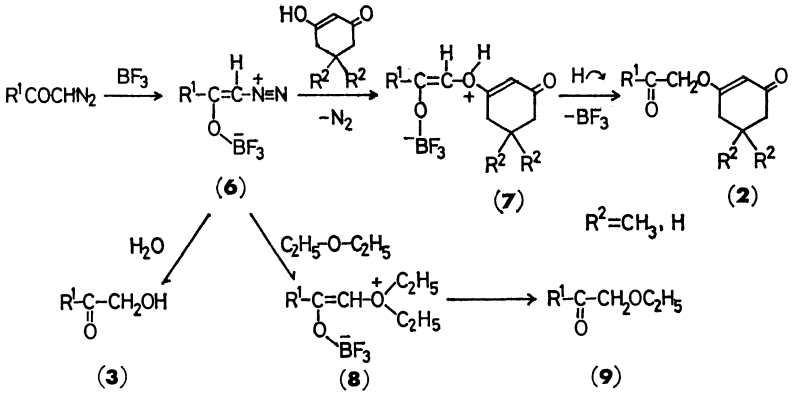

Scheme 1.

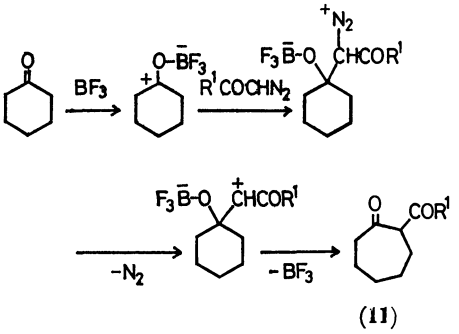

Scheme 2.

The reactions are explained in terms of the attack of the diazonium ion type intermediate (**6**) on the enol oxygen of the β-diketones to give the intermediate **7** which by the elimination of BF_3 and hydrogen migration gives the product **2**. An alternative mechanism which can not be excluded is the attack by **6** on the carbonyl oxygen of the keto form of the β-diketones. The formation of α-hydroxyacetophenones (**3**) may be explained by the attack of **6** on the water contained in the reaction system. Diphenyldiazomethane also gave the corresponding enol ether (**10**, 44%) in a similar reaction accompanying benzhydryl alcohol and tetraphenylethylene. Cyclohexanone however changes the mode of the reaction. The decomposition of *p*-methoxydiazoacetophenone in cyclohexanone in the presence of catalytic amounts of BF_3 occurs vigorously even at temperatures as low as 0 °C, affording the homologation product (**11**: R^1=*p*-$CH_3OC_6H_4$, 92%). A small broad singlet at 16.6 ppm in the NMR spectrum shows the partial existence of the enol form in **11**. This reaction may be initiated by the attack of BF_3 on the oxygen of cyclohexanone as shown in the following Scheme 2.

The difference in reaction between cyclohexanone and the cyclic β-diketones may be attributed to differences in affinity of these ketones to BF_3. The affinity appears to be in the order: cyclohexanone> diazoacetophenone>dimedone≈1,3-cyclohexanedione.

Experimental

All melting points are not corrected. The IR spectra were measured on a Hitachi Spectrometer Model 215. The ^{1}H-NMR spectra were recorded in $CDCl_3$ solution at 60 MHz on a Varian Spectrometer Model EM-360 using TMS as an internal standard.

Materials. All diazo compounds were prepared by the methods described in the literature.[7,8]

General Procedure of the BF_3 Catalyzed Decomposition of Diazoacetophenones in the Presence of Cyclic β-Diketones. To a benzene solution (50 ml) of diazoacetophenone (5 mmol) and the carbonyl compound (15 mmol) a catalytic amount of BF_3 etherate (20 mg) was added under magnetic stirring at 60°C. Vigorous evolution of N_2 occurred and the reaction mixture changed from yellow to dark red. The reaction mixture was added to water (50 ml) and the benzene layer washed with H_2O (10 ml), dried over Na_2SO_4, and column chromatographed on silica gel.

The BF_3 Catalyzed Decomposition of Diphenyldiazomethane in the Presence of Dimedone. To a benzene solution (50 ml) of diphenyldiazomethane (0.51 g, 2.6 mmol) and dimedone (0.63 g, 4.5 mmol) two drops of BF_3 etherate were added and the mixture stirred at room temperature. After the evolution of N_2 ceased, the reaction mixture was treated as described above. Column chromatography of the reaction mixture gave three products. Benzhydryl alcohol (35%) and tetraphenylethylene (8%) were characterized by direct comparison with authentic samples. Enol ether (**10**): colorless crystals; yield 44%; mp 57—58°C; IR (KBr) 1650, 1600 cm^{-1} (enone); NMR ($CDCl_3$) δ 1.03 (s, 6H, CH_3), 2.17 (s, 2H, CH_2), 2.45 (s, 2H, CH_2), 5.41 (s, 1H, =CH), 6.17 (s, 1H, OCH), and 7.33 ppm (s, 10H, Ph). Found: C, 82.10; H, 7.31%. Calcd for $C_{21}H_{22}O_2$: C, 82,37; H, 7.24%.

Reaction of p-*Methoxydiazoacetophenone with Cyclohexanone.* To a solution of *p*-methoxydiazoacetophenone (0.53 g, 3 mmol) in cyclohexanone (5 ml) three drops of BF_3 etherate were added. After the usual workup, 2-(*p*-anisoyl)cycloheptanone (**11**: R^1=*p*-$CH_3OC_6H_4$) was obtained; yield 92%, colorless needles; mp 125.0—126.5°C; IR (KBr) 1700, 1670 cm^{-1} (C=O); NMR ($CDCl_3$) δ 1.2—2.9 (m, 10H, CH_2), 3.85 (s, 3H, OCH_3), 4.5 (broad t, 1H, CH), 6.95, 7.97 (ABq, 4H, Ar), and 16.6 ppm (broad s, 0.1H, enol-H). Found: C, 72.94; H, 7.32%. Calcd for $C_{15}H_{18}O_3$: C, 73.14; H, 7.37%.

References

1) H. Zollinger, "Azo and Diazo Chemistry," Interscience Publishers, Inc., New York (1961), pp. 69, 103.

2) W. T. Tai and E. W. Warnhoff, *Can. J. Chem.*, **42**, 1333 (1964).

3) W. L. Mock and M. E. Hartman, *J. Am. Chem. Soc.*, **92**, 5767 (1970).

4) H. J. Liu and T. Ogino, *Tetrahedron Lett.*, **1973**, 4937.

5) H. J. Liu and S. P. Majumar, *Synth. Commun.*, **5**, 125 (1975).

6) Tai *et al.* obtained the homologation products using an excess of BF_3.[2]

7) M. S. Newman and P. F. Beal, III, *J. Am. Chem. Soc.*, **71**, 1506 (1949).

8) L. I. Smith and K. L. Howard, *Org, Synth.*, Coll. Vol. III, 351 (1955).

BULLETIN OF THE CHEMICAL SOCIETY OF JAPAN, VOL. 52 (11), 3469—3470 (1979)

Reaction of Thiobenzamides with Arylmagnesium Bromides

Takayuki KARAKASA, Takashi HANZAWA, and Shinichi MOTOKI*

Department of Chemistry, Faculty of Science, Science University of Tokyo, Kagurazaka, Shinjuku-ku, Tokyo 162

(Received April 12, 1979)

Synopsis. Reactions of thiobenzamide, *p*-methylthiobenzamide, *p*-methoxythiobenzamide, and *p*-chlorothiobenzamide with 4 equivalents of phenyl-, *p*-tolyl-, *p*-methoxyphenyl-, and *p*-chlorophenylmagnesium bromides gave the corresponding diphenylmethyleneamine and thiobenzophenone as 1,2-addition produsts in good yields.

Thiones, thioesters, and dithioesters are known to react with organometallic reagents to give thioethers and their derivatives.[1] However little is known of reactions of thioamides with organometallic reagents.[2] *N*-Phenyl-2,2-diphenylthioacetamide does not react with excess ethylmagnesium bromide.[2a] However, highly basic carbanions such as phenyllithium react with *N*,*N*-dimethylthiobenzamide to give *N*,*N*-dimethyltriphenylmethylamine, triphenylmethanol, and a small amount of benzophenone.[2b] *N*,*N*-Dialkyl-α,β-unsaturated thioamides undergo the 1,4-addition reaction with organolithium and magnesium compounds.[2c] We were interested in the reaction of thioamides with Grignard reagents as part of our study on thiocarbonyl compounds.[3]

Treatment of *N*-substituted thioamide such as *N*-morpholino(thiobenzamide) or *N*-methyl(thiobenzamide) with excess phenylmagnesium bromide in ether at room temperature resulted in the recovery of unchanged thioamide. In contrast, the reaction of primary thioamides with arylmagnesium bromides proceeded readily under the same conditions. When thiobenzamide was allowed to react with 4 equivalents of phenylmagnesium bromide, diphenylmethyleneamine (**5a**) and thiobenzophenone (**6a**) were obtained. Hydrogen sulfide was evolved after being hydrolyzed with aqueous ammonium chloride. The results are summarized in Table 1.

The formation of **5** and **6** can be explained by the following mechanisms.

When thiobenzamide was treated with 2 equivalents of phenylmagnesium bromide, unchanged thioamide was recovered. This indicates that the reaction proceeds *via* an initial dimetallation of the thioamide affording an intermediate (**3**).[4a] The reaction of **3** with **2** would give the intermediates (**4**) and/or (**7**)[4b,4c] (Scheme 1).

Path A involves the addition of **2** to the carbon–nitrogen double bond of **3** to give an intermediate (**4**) which cleaves to afford **5** and **6** by hydrolysis.

Alternative path B involves the replacement of the sulfur moiety of **3** by the aryl group of **2** to give **7** and **8** which afford **5** and hydrogen sulfide by hydrolysis. In this pathway, **6** may be formed by the reaction of **5** with hydrogen sulfide.[5]

If the reaction proceeds along either path A or B, the ratio of the products (Imine/Thione) in run **b** (or **c**) is approximately equal to that in run **e** (or **f**) since both runs **b** and **e** (**c** and **f**) give rise to the formation of an identical intermediate. However, the actual ratios are quite different as shown in Table 1.

An explanation is given by assuming that the reaction proceeds *via* both pathway A and B. The ratio of the products (Imine/Thione) from the intermediate **4** would not be the same as that from the intermediate **7**, the formation ratio of **4** and **7** depending on the nucleophilicity of the Grignard reagents.

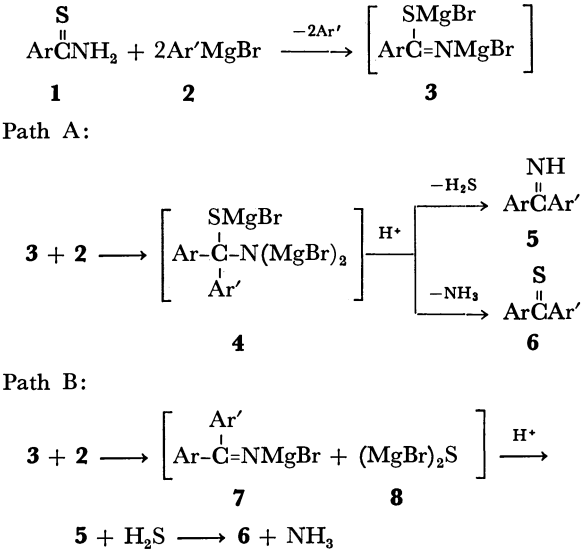

Scheme 1. Reaction route.

Experimental

Thiobenzamide (**1a—d**)[6] and *N*-morpholino(thiobenzamide)[7] were synthesized by the methods reported. *N*-Methyl(thiobenzamide) was prepared by the reaction of methyl isothiocyanate with phenylmagnesium bromide.[4]

A Typical Procedure for the Reaction of Thiobenzamides with Arylmagnesium Bromides. Thiobenzamide (0.1 mol) was added gradually to a solution of phenylmagnesium bromide (0.4 mol) in 300 cm^3 dry ether at room temperature under nitrogen atmosphere. After being allowed to stand overnight, the reaction mixture was quenched with saturated aqueous ammonium chloride at −10 °C and filtered, the solvent then being evaporated. The deep blue residue was dissolved in 150 cm^3 petroleum ether. Dry hydrogen chloride was bubbled into the solution until precipitation was complete. Precipitated diphenylmethyleneamine hydrochloride (13.56 g)(sublimed at 230—270 °C (230—250 °C)[8b]) was filtered off and the filtrate was evaporated. The deep blue residue was distilled to give thiobenzophenone (2.97 g) (120 °C/1 Torr (120—125 °C/1 Torr)[8a]).

The products (Table 1) were identified by comparing their boiling points, IR spectra, and/or GLC (Silicone Gum SE-30) with those of authentic compunds.[8]

Table 1. Reaction of thiobenzamides with arylmagnesium bromides

Run No.	Thioamide Ar	Grignard reagent Ar′	Yield/%[a]		Imine/Thione
			Imine	Thione	
a	C_6H_5	C_6H_5	66	15	4.4
b	p-CH_3O-C_6H_4	C_6H_5	58	12	4.8
c	p-Cl-C_6H_4	C_6H_5	63	26	2.4
d	p-CH_3-C_6H_4	C_6H_5	56	22	2.5
e	C_6H_5	p-CH_3O-C_6H_4	87	6	14.5
f	C_6H_5	p-Cl-C_6H_4	52	6	8.7

a) Yields of diphenylmethyleneamines and thiobenzophenones were determined by conversion into their hydrochlorides and oximes, respectively.

References

1) D. Paquer, *Bull. Soc. Chim. Fr.*, **1975**, 1439; K. Nakamura and A. Ohno, *Kagaku No Ryoiki*, **32**, 74 (1978).

2) a) T. Fujinami, N. Otani, and S. Sakai, *Nippon Kagaku Kaishi*, **1978**, 265; b) P. Beak, J. Yamamoto, and C. J. Upton, *J. Org. Chem.*, **40**, 3052 (1975); c) Y. Tamaru, T. Harada, H. Iwamoto, and Z. Yoshida, *J. Am. Chem. Soc.*, **100**, 5221 (1978); d) H. Wuyts and A. Lacourt, *Bull. Soc. Chim .Belg.*, **45**, 445 (1936).

3) T. Karakasa and S. Motoki, *J. Org. Chem.*, **43**, 4147 (1978).

4) a) G. Alliger, G. E. P. Smith Jr., E. L. Carr, and H. P. Stevens, *J. Org. Chem.*, **14**, 962 (1949); b) H. Gilman and C. R. Kinney, *J. Am. Chem. Soc.*, **46**, 493 (1924); T. Yamaguchi, Y. Shimizu, and T. Suzuki, *Chem. Ind. (London)*, **1972**, 380.

5) Actually, **6a** was formed by the reaction of **5a** with hydrogen sulfide in ether at room temperature; D. S. Tarbell and V. P. Wystrock, *J. Am. Chem. Soc.*, **68**, 2110 (1946). Since the reaction is carried out under acidic conditions, the reaction of thiobenzophenones with ammonia can be ruled out.

6) A. E. S. Fairfull, J. L. Lowe, and D. A. Peak, *J. Chem. Soc.*, **1952**, 742.

7) R. N. Hurd and G. DeLaMater, *Chem. Rev.*, **61**, 52 (1961).

8) a) K. Kimura, H. Niwa, and S. Motoki, *Bull. Chem. Soc. Jpn.*, **50**, 2751 (1977); b) A. Lachman, *Org. Syn.*, Coll. Vol. II, 234 (1943); c) P. L. Pickard and T. L. Tolbert, *Org. Syn.*, Coll. Vol. V, 520 (1973).

BULLETIN OF THE CHEMICAL SOCIETY OF JAPAN, VOL. 52 (11), 3471—3472 (1979)

Studies on the Configuration of *N*-Cyclohexylideneanilines with ^{13}C-NMR Spectroscopy

Masato YOSHIDA and Michio KOBAYASHI*

Department of Chemistry, Faculty of Science, Tokyo Metropolitan University, Fukazawa, Setagaya-ku, Tokyo 158

(Received May 1, 1979)

Synopsis. ^{13}C-NMR chemical shifts and the rates of thermal *E*-*Z* isomerizations of *N*-cyclohexylideneanilines have been determined and the substituent effects discussed.

In a previous paper the existence of two types of conjugation[1] in *N*-benzylideneanilines (**1a**) was reported. One is conjugation between the π-electrons of the carbon-nitrogen double bond and aromatic ring (**1b**), and the other is conjugation between the lone pair electrons of the nitrogen and aromatic ring (**1c**).

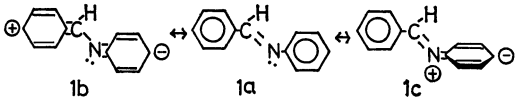

1b 1a 1c

There is no type **1c** conjugation when the dihedral angle between the >C=N– plane and imino benzene ring is 0°, whereas an angle of 90° represents the optimum conditions. *N*-Cyclohexylideneanilines appear to be suitable compounds to study this type of conjugation since the imino benzene rings are known to rotate by about 90° out of the >C=N– plane.[2] The ^{13}C-NMR spectra of substituted *N*-cyclohexylideneanilines (**2**—**6**) have been studied at several temperatures and the substituent effects discussed in connection with the thermal isomerism between the *E* and *Z* forms.

Results and Discussion

Thermal isomerization between the *E* and *Z* forms of the *N*-benzylideneanilines is known to readily occur. In *N*-cyclohexylideneaniline, thermal isomerization between the forms **A** and **B** shown below is expected.

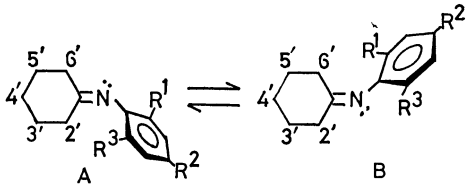

A B

	2	**3**	**4**	**5**	**6**
R^1	H	H	H	H	Me
R^2	NO_2	COOEt	H	OMe	NO_2
R^3	H	H	H	H	Me

The ^{13}C-NMR spectra of **2**—**5** were measured at room temperature in $CDCl_3$, and the δ_C values for **2**—**5** are given in Table 1. The differences in value of $\delta_{C-2'}$ and $\delta_{C-6'}$ (or $\delta_{C-3'}$ and $\delta_{C-5'}$) for **2**—**5** indicates that the configurations of **2**—**5** are fixed within the NMR time scale at room temperature. As shown in Fig. 1b the ^{13}C-NMR of C-2′-6′ of compound **6** could not be observed as a set of five signals. Five ^{13}C-NMR signals of each C-2′-6′ were observed at −50 °C, while at 100 °C the signals of C-2′ and C-6′ (also C-3′ and C-5′) coalesced and the ^{13}C-NMR signals of C-2′-6′ appeared as three signals. This indicates that the thermal isomerization between **6A** and **6B** is slower at −50 °C and faster at 100 °C than the

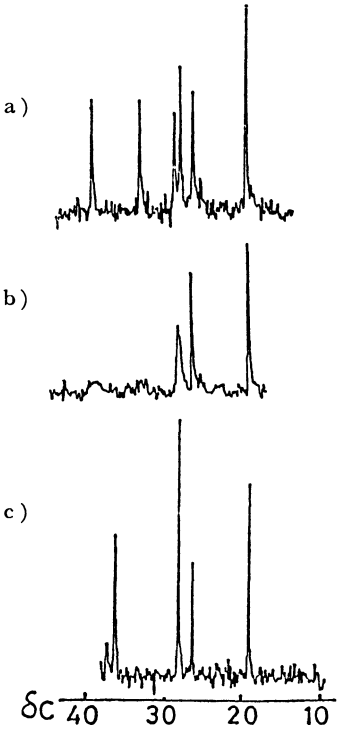

Fig. 1. ^{13}C-NMR spectra of compound **6** at a) −50 °C in $CDCl_3$, b) at room temperature in $CDCl_3$, and c) at 100 °C in DMSO-d_6.

TABLE 1. CARBON-13 CHEMICAL SHIFTS OF **2**—**6** AT ROOM TEMPERATURE

	2	**3**	**4**	**5**	**6**[a]
C-1	157.0	154.9	150.0	144.0	154.5
C-2,6	120.0	119.3	119.6	120.9	127.2
C-3,5	125.0	130.4	128.5	114.1	123.1
C-4	143.5	124.9	122.7	155.7	142.2
C-1′	176.4	175.2	174.5	175.2	175.6
C-2′	32.1	31.5	31.1	31.2	32.1
C-3′	27.8	27.4	27.4	27.7	26.9
C-4′	25.6	25.4	25.6	25.9	25.2
C-5′	27.8	27.6	27.7	27.9	27.7
C-6′	39.3	39.0	39.2	39.5	38.3

a) At −50 °C.

Table 2. Coalescence temperatures (T_c) of $C_{2'}$, $C_{6'}$ and ΔG^* values for **2**—**6**[a]

	$\nu C_{2'}-\nu C_{6'}$	T_c/K[b]	ΔG^*/kcal mol^{-1}
2	106.20	348	16.7
3	109.86	398	19.2
4	118.14	>413	>19.7
5	124.51	>413	>19.7
6	92.77	328	15.7

a) Solv. DMSO-d_6 for **2**—**5** and $CDCl_3$ for **6**. b) Accuracy: ±5 K.

NMR time scale. Consequently, at elevated temperatures, the thermal isomerizations in **2**—**5** are expected to be observable by NMR. The ^{13}C-NMR spectra of **2**—**6** were measured at several temperatures, and the coalescence temperatures (T_c) for C-2′ and C-6′ signals determined, and the ΔG^* values calculated. The results are summarized in Table 2.

Type **1b** conjugation should not be possible when the imino benzene ring is rotated out of the >C=N– plane by approximately 90°. Interaction between the *N*-lone pair and imino benzene ring however becomes important. Table 1 shows that $\delta_{C-1'}$ is very little affected by the substituents of the aromatic ring in comparison with $\delta_{C-\alpha}$ of *N*-benzylideneanilines (PhCH=N–C_6H_4–R-*p*) whose imino benzene rings are rotated approximately 50°.[3] This suggests that the substituents of the aromatic ring do not affect the electron density on the carbon atom of >C=N– when the imino benzene ring is rotated out of the >C=N– plane by approximately 90°. As shown in Table 2, the ΔG^* of **2** and **3** having electron-withdrawing groups are smaller than those of **4** and **5**. This can be explained by assuming a linear transition state **C** for the thermal isomerization between forms **A** and **B**.[4]

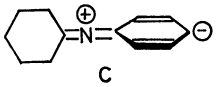

C

In this transition state, the hybridization of the N atom is of the sp type. The transition state (**C**) should be stabilized by the electron-withdrawing substituent on the imino benzene ring to a greater extent than in the ground state, since the delocalization of the *N*-lone pair into the imino benzene ring will be easier with a linear structure. Electron-withdrawing substituents on the imino benzene ring will assist this delocalization and decrease ΔG^*.

Experimental

N-Cyclohexylideneanilines[2] were prepared by condensation between the corresponding anilines and cyclohexanone diethyl acetal:[5] bp (mp): **2**; 176 °C/6 mmHg, **3**; 187 °C/5 mmHg, **4**; 140 °C/18 mmHg, (lit,[2] 156 °C/30 mmHg), **5**; 76—77 °C (mp), **6**; 57—58 °C (mp).

^{13}C-NMR chemical shifts were determined at room temperature in $CDCl_3$ with a JEOL Fx-60 FT spectrometer. The accuracies of chemical shifts were approximately 0.1 ppm (data points; 4096, sampling time; 900 ms, pulse flipping angle; 45°). The coalescence temperatures were determined in DMSO-d_6 well-dried with molecular sieves, and the values of the activation free energy calculated using the following equation,[6]

$$k = \pi\nu_{ab}/\sqrt{2} = (KT/h)\exp(-\Delta G^*/RT).$$

References

1) M. Yoshida, H. Minato, and M. Kobayashi, *Chem. Lett.*, **1976**, 1097.
2) H. Saito and K. Nukada, *Tetrahedron*, **22**, 3313 (1966).
3) $\delta_{C-\alpha}$ of *N*-benzylideneanilines; R=NO_2 162.79, R=H 160.01, R=OMe 157.95. N. Inamoto, K. Kushida, S. Masuda, H. Ohta, S. Satoh, Y. Tamura, K. Tokumaru, K. Tori, and M. Yoshida, *Tetrahedron Lett.*, **1974**, 3617.
4) C. G. McCarty, "The Chemistry of The Carbon-Nitrogen Double Bond," ed by S. Patai, Interscience, London (1970), Chap. 9.
5) U. Schmidt and P. Grafen, *Justus Liebigs Ann. Chem.*, **656**, 97 (1962).
6) D. K. Dalling, D. M. Grant, and L. F. Johnson, *J. Am. Chem. Soc.*, **93**, 3678 (1971).

BULLETIN OF THE CHEMICAL SOCIETY OF JAPAN, VOL. 52 (11), 3473—3474 (1979)

Reduction of Alloxan by Cyanide Ion. Isolation of Alloxan Radical Anion Salts and Alloxantin

Takeshi ENDO,* Akira KUDO, and Makoto OKAWARA
Research Laboratory of Resources Utilization, Tokyo Institute of Technology, Nagatsuta-cho, Midori-ku, Yokohama 227

(Received May 2, 1979)

Synopsis. Potassium or pyridinium salts of alloxan radical anion were isolated by the one-electron reduction of alloxan monohydrate with potassium cyanide or 1-benzyl-4-cyano-1,4-dihydronicotinamide at room temperature, respectively.

Alloxan(A) is known as one of vicinal tricarbonyl compounds, of which central carbonyl group activated by adjacent two carbonyl groups is so reactive that easily combines one mole of water to form hydrate (A-hydrate).[1] It has been also reported that A-hydrate can be easily reduced by hydrogen sulfide[2] or 1-alkyl-1,4-dihydronicotinamide[3] (NADH model) to obtain AT and dialuric acid(D) by one-electron or two-electron reduction of A-hydrate, respectively.

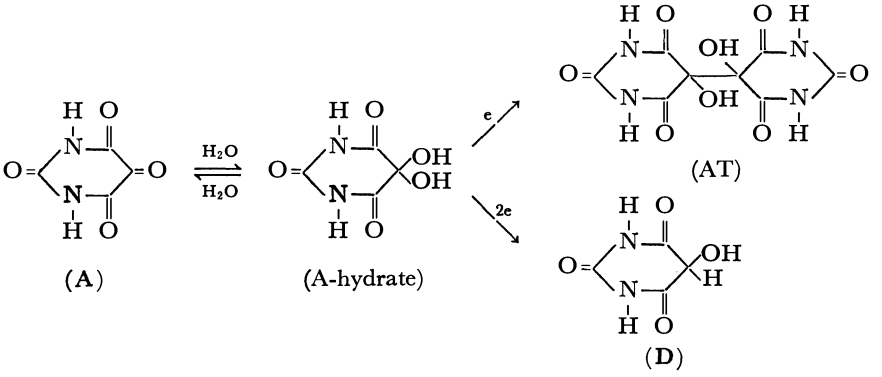

A is also known as one of "reductones" as same as ascorbic acid which plays important roles in the biological oxidation-reduction system.

In this paper, we wish to report the isolation of alloxan radical anion salts obtained by the reduction of A-hydrate with potassium cyanide and 1-benzyl-1,4-dihydronicotinamide.

Reduction of A-Hydrate by Potassium Cyanide. The reduction of nitro compounds[4] and sulfoxides[5] by cyanide ion have been reported. We found that A-hydrate could be reduced by potassium cyanide in water (pH 6.8) at room temperature to give a yellow precipitate in good yield. The esr spectrum of the precipitate in bulk showed the broad singlet line at 25 °C, as shown in Fig. 1. The precipitate was shown to be the 1 : 1 salt of potassium ion and alloxan radical anion by elemental analyses. Upon treating the precipitate with aq hydrochloric acid, AT was obtained in excellent yield. Based on the results described above, the reasonable structure of the precipitate is considered to the salt ($A^{\cdot-}$ K^+) of potassium ion and alloxan radical anion.

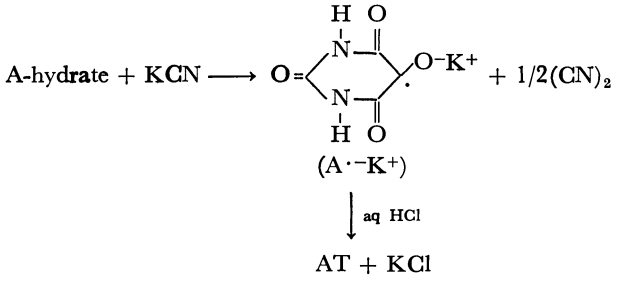

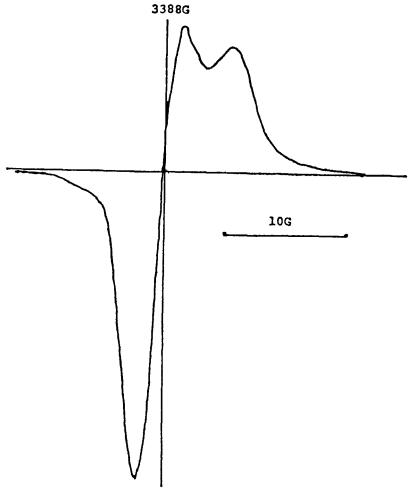

Fig. 1. ESR spectrum of potassium salt ($A^{\cdot-}K^+$) of alloxan radical anion (bulk, 25 °C).

Cyanogen (bp −21.2 °C, mp −27.9 °C[6]) could be also detected by IR (2200 cm^{-1}) qualitatively by trapping in ethanol by bubbling nitrogen gas into the reaction mixture during the reaction.

The formation of alloxan radical anion ($A^{\cdot-}$) has been observed by the reduction of A-hydrate with sodium dithionite in water or methylsulfinylmethanide ($CH_3SOCH_2^-$) in dimethyl sulfoxide (DMSO), and the esr was analyzed in detail. Further, $A^{\cdot-}$ was effectively produced by the dissociation of AT in DMSO.[7]

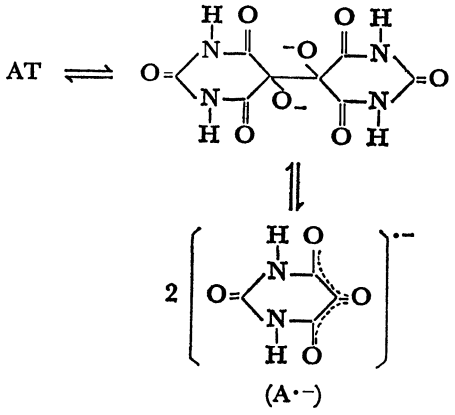

A·⁻ K⁺ was also prepared by treating AT with triethylamine in the presence of excess potassium chloride.

$$AT \rightleftharpoons 2[A\cdot] + 2KCl \xrightarrow{Et_3N} 2A\cdot^{-}K^{+} + 2Et_3N\cdot HCl$$

Reduction of A-Hydrate by 1-Benzyl-4-cyano-1,4-dihydronicotinamide. Whereas 1-benzyl-4-cyano-1,4-dihydronicotinamide (BNA–CN) shows the absorption maximum at 333—337 nm (dihydro form) in acetonitrile or dichloromethane, it exhibits both 337 (BNA–CN) and 265 nm (BNA⁺CN⁻) bands in methanol or ethanol, indicating the presence of equilibrium between BNA–CN and BNA⁺CN⁻.

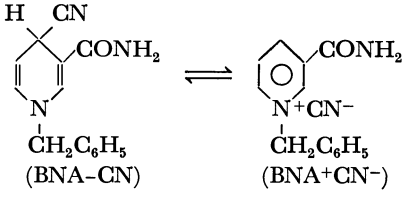

The reaction of A-hydrate and BNA–CN was tried in ethanol at room temperature to yield a yellow precipitate in a good yield. The yellow precipitate was found to be the pyridinium salt (A·⁻Py⁺) of alloxan radical anion which was obtained by the reduction of A-hydrate with 1-benzyl-1,4-dihydronicotinamide (BNAH) or the reaction of AT and 1-benzyl-3-carbamoylpyridinium chloride (BNA⁺Cl⁻) in the presence of triethylamine.[3] The production of cyanogen during the reaction was also detected by IR spectrum qualitatively. A·⁻Py⁺ was treated with aq. HCl to give and BNA⁺Cl⁻ in excellent yields. A·⁻K⁺ and A·⁻Py⁺ are insensitive to oxygen in solid state, but they are easily oxidized in solution to give alloxan.

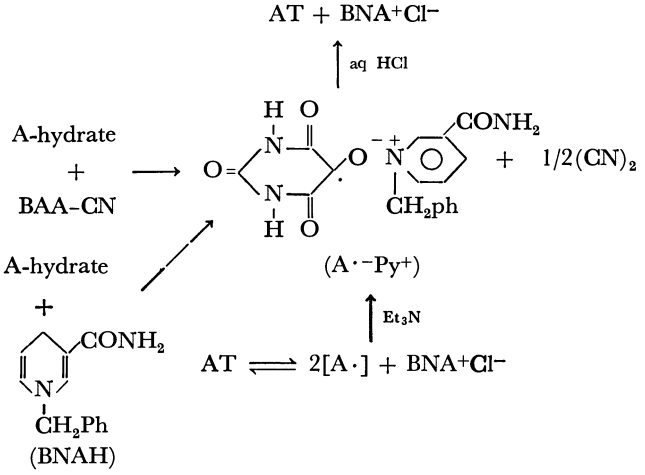

Experimental

Materials. Alloxan monohydrate(A-hydrate) (mp 253 °C (dec)) was prepared by the oxidation of barbituric acid with chromium trioxide.[8] Alloxantin(AT) (mp 230—231 °C) used in this study was prepared by the reduction of A-hydrate with hydrogen sulfide.[9] 1-Benzyl-3-carbamoylpyridinium chloride (BNA⁺Cl⁻) (mp 230—232 °C)[10] was synthesized by the reaction of benzyl chloride and nicotinamide in *N,N*-dimethylformamide. 1-Benzyl-4-cyano-1,4-dihydronicotinamide (BNA–CN) was prepared by the reaction of BNA⁺Cl⁻ and potassium cyanide in water and recrystallized from acetonitrile. Mp 113—133 °C (dec).[11]

The Reaction of A-Hydrate and Potassium Cyanide. To a solution of 0.8 g (5 mmol) of A-hydrate in 30 ml of water (buffer solution; pH 6.8), was added a solution of potassium cyanide (0.39 g, 6 mmol) in 10 ml of distilled water with stirring at room temperature to yield a precipitate immediately. After stirring for 2 h, the precipitate was filtered off and dried in vacuo to give alloxan radical anion salt (A·⁻K⁺) in 65% yield. Mp 270—273 °C (dec). IR (KBr, cm^{-1}): 3250 (N–H), 1670 (C=O). Found: C, 26.31; H, 1.61; N, 15.26%. Calcd for $C_4H_2O_4N_2K_1$: C, 26.50; H, 1.67; N, 15.46%.

AT (mp 229—231 °C) was also isolated from the filtrate in 15% yield.

The Reaction of AT and Potassium Chloride in the Presence of Triethylamine. To a solution of 1.6 g (5 mmol) of AT and 1.8 g (25 mmol) of potassium chloride in 100 ml of water, was added a solution of 1 g (10 mmol) of triethylamine dropwise with stirring at room temperature to obtain A·⁻K⁺ (5.6 g, 70%).

The Reaction of A-Hydrate and BNA–CN. To a solution of 0.8 g (5 mmol) of A-hydrate in 20 ml of ethanol, was added a solution of 1.2 g (5 mmol) of BNA–CN in 20 ml of ethanol in the atmosphere of nitrogen at room temperature to give 1.1 g (70%) of pyridinium salt (A·⁻Py⁺) of alloxan radical anion. IR (KBr, cm^{-1}): 3350, 3180 (N–H), 1700, 1590 (C=O). Found: C, 57.30; H, 4.57; N, 15.72%. Calcd for $C_{17}H_{15}O_5N_2$: C, 57.25; H, 4.52; N, 15.46%.

References

1) M. B. Rubin, *Chem. Rev.*, **75**, 155 (1975).
2) S. Tipson and L. H. Cretcher, *J. Org. Chem.*, **16**, 1091 (1951).
3) T. Endo and M. Okawara, *Chem. Lett.*, **1977**, 1487.
4) D. N. Kramers and G. Guilbault, *J. Org. Chem.*, **31**, 1103 (1966).
5) S. Tamagaki, H. Hirota, and S. Oae, *Bull. Chem. Soc. Jpn.*, **47**, 2057 (1974).
6) R. P. Cook and P. L. Robinson, *J. Chem. Soc.*, **1935**, 1001.
7) G. A. Russel and M. C. Young, *J. Am. Chem. Soc.*, **88**, 2007 (1966).
8) A. V. Holmgren and W. Wenner, *Org. Synth.*, Coll. Vol. IV, 23 (1963).
9) S. Tipson, *Org. Synth.*, Coll. Vol. IV, 25 (1963).
10) P. Karrer and F. J. Stare, *Helv. Chim. Acta*, **20**, 418 (1937).
11) A. S. Pietro, *J. Biol. Chem.*, **217**, 579 (1955).

BULLETIN OF THE CHEMICAL SOCIETY OF JAPAN, VOL. 52 (11), 3475—3476 (1977)

^{17}O Nuclear Magnetic Resonance Studies. V.[1] ^{17}O Shieldings of Some Substituted Anisoles

Morimatsu KATOH, Tadashi SUGAWARA, Yuzo KAWADA, and Hiizu IWAMURA*

Division of Applied Molecular Science, Institute for Molecular Science, Myodaiji, Okazaki 444

(Received June 4, 1979)

Synopsis. Fourier transform ^{17}O NMR spectra have been measured for a number of meta and para substituted anisoles in natural abundance at 10.8 MHz. The shielding of the methoxyl oxygen nucleus decreases as the electron-withdrawing substituents are introduced to the ring. A good linear correlation is obtained for a plot of the ^{17}O shifts *versus* the Hammett σ^- constants.

Proton nuclear magnetic resonance studies have shown that methoxyl proton shifts are linearly related to the Hammett σ parameter.[2] A similar but only a slight dependence of methoxyl ^{13}C shifts on the nuclear substitution has been reported.[3] In order to investigate the effects of nuclear substitution on the methoxyl oxygen shielding, we have now measured the ^{17}O NMR shifts of a series of sixteen anisoles.

It is apparent from the observed data collected in Table 1 that the oxygen shifts are highly sensitive to meta and para substitution on the ring; they cover a rather wide total range of 30 ppm. It is easily expected that electron-withdrawing groups on the ring decrease the shielding at the oxygen nucleus, since the conjugative electron release from the oxygen will be enhanced. This general trend is exactly what was observed for the ^{17}O chemical shifts of anisoles. A plot of the methoxyl oxygen shifts *versus* the Hammett σ^- values reveals a good linear correlation between the two parameters ($\rho=16.2$ ppm, correlation coefficient r of 0.963). Analyses of the data according to the Yukawa-Tsuno equation, $\Delta\delta=\rho\{\sigma^\circ+\gamma(\sigma^- -\sigma^\circ)\}$, give the following values: $\rho=17.2$ ppm and $\gamma=0.881$.[4] A quantitative measure of the resonance interaction of the methoxyl group with para substituents is thus obtained. These results may be compared with the Hammett σ dependence of the methoxyl hydrogen ($\rho=0.24$ ppm)[2] and carbon chemical shifts.[3]

TABLE 1. ^{17}O NMR SHIFTS OF *p*- AND *m*-SUBSTITUTED ANISOLES

Substituent	$\delta^{17}O$/ppm	π-Bond order $\times 10^2$	π-Electron density
p-NH_2	139[a]	4.03	1.905
p-OCH_3	141	4.16	1.902
p-$C(CH_3)_3$	147		
p-CH_3	147	4.32	1.899
p-F	148	4.27	1.900
H	151	4.36	1.898
p-Cl	151		
p-Br	154		
p-CF_3	157		
p-CN	163	4.49	1.894
p-NO_2	170	4.72	1.888
m-NH_2	149		
m-Cl	154		
m-Br	155		
m-F	156		
m-NO_2	166		

a) Subtract 103 ppm from the shift values to convert them into the data referenced to external H_2O.

Theoretical reasoning of the shielding pattern observed here is not so easy as it would be understood intuitively. The diamagnetic electric current about the nucleus which is directly affected by polar substituents play a major role in governing the chemical shifts of ^1H NMR, but not of ^{13}C and ^{17}O nuclei. The paramagnetic screening is considered to dominate the chemical shifts of the latter nuclei. Decrease of shielding with the increasing electron-withdrawal should be explained by increase in the mean inverse cube of the 2p electron radius $\langle r^{-3}\rangle_{\text{oxygen}}$ and/or in the orbital terms $[Q_{AA}+\Sigma Q_{AB}]$ in the Karplus-Pople expression of the paramagnetic screening (Eq. 1).[5]

$$\sigma_p^A = -\frac{e^2\hbar^2\langle r^{-3}\rangle}{2m^2c^2(\Delta E)}[Q_{AA}+\sum_{A\neq B}(Q_{AB})] \quad (1)$$

Decreasing charge density at the oxygen is expected to lead to a contraction of the 2p orbitals and thereby an increase in the paramagnetic screening. The good linear correlations were obtained between the observed ^{17}O chemical shifts on the one hand and the π-electron densities at the oxygen (2040 ppm/π-electron, $r=0.993$) or the π-bond orders between the oxygen and the aromatic carbon attached to it (4770 ppm/π-bond order, $r=0.974$) calculated by the CNDO/2 methods on the other.[6]

The trend observed here for the anisoles is just the opposite to that of the oxygen nuclei of the aliphatic ethers in which the more electron-donating tertiary alkyl ethers are deshielded compared to less electron-donating primary alkyl ethers.[7] Whereas the change in the effective excitation energy ΔE in Eq. 1 was a dominant factor in the paramagnetic screening there,[7] both the n- and π^*-levels would be affected simultaneously by the ring substituents in the anisoles, leaving the effect of ΔE term less obvious.

We conclude that one of the most direct experimental evidence for the dependence of the electron density about the methoxyl oxygen nucleus on the ring substituents was obtained by the ^{17}O NMR shifts.

Experimental

Pulsed Fourier transform spectra were obtained on a Varian FT-80A spectrometer at 10.8 MHz. A pulse width

of 35 μs with an acquisition time of 0.02 s was employed with a spectral width of 8000 Hz. Anywhere between 3×10^6 and 4×10^7 transients were accumulated depending on the sample. Chemical shifts were read as frequency shifts from the synthesizer setting (8.53200 MHz), expressed in ppm, and judged to be accurate to ±1 ppm (the Fourier number was at 1,6384). The spectra were run at 80 °C on pure, natural-abundance samples (1.0—1.4 g) dissolved in chloroform-*d* (0.9—1.2 ml) which also provided an internal deuterium lock signal.

p-*t*-Butyl- and *m*-chloroanisoles were prepared from the corresponding phenols by the standard methylation with dimethyl sulfate. The others were commercial samples of reliable grade and were used directly.

The π-electron densities and π-bond orders were calculated by the CNDO/2 methods with the aid of the program No. 141 of QCPE on a HITAC M-180 system of this institute. Molecular geometries employed for the framework of anisoles were basically those reported for 4,4′-anisoin[8] and the standard bond lengths and angles[6] were used otherwise.

References

1) For Part IV of this series see: H. Iwamura, T. Sugawara, Y. Kawada, K. Tori, R. Muneyuki, and R. Noyori, *Tetrahedron Lett.*, **1979**, 3449.

2) C. Heathcock, *Can. J. Chem.*, **40**, 1865 (1962).

3) K. S. Dhami and J. B. Stothers, *Can. J. Chem.*, **44**, 2855 (1966).

4) Y. Tsuno, T. Ibata, and Y. Yukawa, *Bull. Chem. Soc. Jpn.*, **32**, 960 (1959); Y. Yukawa, Y. Tsuno, and M. Sawada, *ibid.*, **39**, 2274 (1966).

5) M. Karplus and J. A. Pople, *J. Chem. Phys.*, **38**, 2803 (1963).

6) J. A. Pople and D. L. Beveridge, "Approximate Molecular Orbital Theory," McGraw-Hill, New York (1970).

7) T. Sugawara, Y. Kawada, and H. Iwamura, *Chem. Lett.*, **1978**, 1371; T. Sugawara, Y. Kawada, M. Katoh, and H. Iwamura, *Bull. Chem. Soc. Jpn.*, **52**, 3391 (1979); C. Delseth and J.-P. Kintzinger, *Helv. Chim. Acta*, **61**, 1327 (1978).

8) H. G. Norment and I. L. Karle, *Acta Crystallogr.*, **15**, 873 (1962).

Calculation of the H_4 Potential Energy Surface by a Semi-empirical Method

Noboru TANAKA

Department of Chemistry, Hachinohe Institute of Technology, Hachinohe 031

(Received December 27, 1978)

A semi-empirical method recently proposed for the calculation of the potential energy surface of the H_3 system is extended to a larger polyatomic H_4 system. The energy formula is based on the valence-bond formulation and is expressed as functions of many multiple exchange integrals. These integrals can be decomposed into "diatomic" contributions by using the Mulliken approximation. The diatomic contributions are estimated from accurate values of the H_2 molecule. Calculations of the H_4 potential energy for the symmetric linear, linear equidistant, and square planar configurations are presented. The present method is of use for dynamical studies of the H_2+D_2 exchange reaction.

In a previous paper, the author has proposed a new semi-empirical method for the calculation of the H_3 potential surface,[1] and has shown that this simple method yields a satisfactory and useful surface when compared with Liu's detailed *ab initio* calculation of the H_3 system.[2] It is interesting to extend the method to the case of larger polyatomic systems. In the present note the application to the H_4 potential surface calculation is presented.

There have been many *ab initio* calculations of the H_4 system at its special configurations, and the results have been discussed in connection with the mechanism of the $H_2+D_2\rightarrow 2HD$ exchange reaction. Experimental results for this reaction have often been interpreted in terms of a vibrational excitation mechanism,[3] which assumes a four-center H_4 transition state. The recent extensive *ab initio* calculation of Silver and Stevens (SS)[4] yielded potential barriers for the four-center transition state larger than the H_2 dissociation energy, which is in disagreement with the experimental activation energy, 42 kcal/mol.[3] Thus we are very much interested in the reaction dynamics study of the H_2+D_2 reaction, in order to examine the effect of vibrational activation on the reaction cross section. For such a study, we must have a complete reliable potential surface of the H_4 system. The author believes that the present note provides a practically useful method of calculating the surface, since it requires less computer time than *ab initio* calculations.

In the following section, we proceed in much the same way as the case of H_3.[1] By making use of the Mulliken approximation,[5] Slater's energy formula[6] is shown to be expressed in terms of "diatomic" contributions, *i.e.*, diatomic Coulomb (Q_i), exchange (α_i), and overlap (S_i) integrals. Hence we obtain the energy formula involving several empirical parameters. The surface thus calculated is compared with the results of the *ab initio* calculations of the H_4 surface,[4,7] in the last section.

Theoretical

Slater's energy formula[6] for the four-orbital four-electron system corresponding to H_4 is

$$E_{\pm} = (1/C_1)[-C_2 \pm (C_2^2 - C_1C_3)^{1/2}]. \tag{1}$$

The quantities C_1, C_2, C_3 are expressed in terms of the matrix elements:

$$\begin{aligned} C_1 &= (\mathrm{I}|\mathrm{I})(\mathrm{II}|\mathrm{II}) - (\mathrm{I}|\mathrm{II})^2, \\ C_2 &= (\mathrm{I}|H|\mathrm{II})(\mathrm{I}|\mathrm{II}) - \frac{1}{2}\{(\mathrm{I}|H|\mathrm{I})(\mathrm{II}|\mathrm{II}) \\ &\quad - (\mathrm{II}|H|\mathrm{II})(\mathrm{I}|\mathrm{I})\}, \\ C_3 &= (\mathrm{I}|H|\mathrm{I})(\mathrm{II}|H|\mathrm{II}) - (\mathrm{I}|H|\mathrm{II}), \end{aligned} \tag{2}$$

where the bond functions Ψ_{I} and Ψ_{II} correspond to the bonding schemes (a—b, c—d) and (a—d, b—c) respectively, and H is the Hamiltonian of the system,

$$H = \sum_{i=1}^{4}\left(-\frac{1}{2}\nabla_i^2 - \sum_{\nu=1}^{4}\frac{1}{r_{i\nu}} + \sum_{j>i}\frac{1}{r_{ij}}\right) + \sum_{\kappa=1}^{6}\frac{1}{R_\kappa}. \tag{3}$$

The subscripts i, j refer to the electrons, ν=a, b, c, d represent the four hydrogen nuclei, and R_1, R_2, R_3, R_4, R_5, and R_6 are the a—b, a—c, a—d, b—c, b—d, and c—d internuclear distances respectively. In terms of the functions Ψ_{I} and Ψ_{II}, the matrix elements can be written as

$$\begin{aligned} (\mathrm{I}|H|\mathrm{I}) &= 4Q + 2(2\alpha_1' - \alpha_2' - \alpha_3' - \alpha_4' - \alpha_5' + 2\alpha_6') \\ &\quad + 4(\beta_{25}+\beta_{34}+\beta_{16}) - 4(\gamma_{214}+\gamma_{153}+\gamma_{326}+\gamma_{465}) \\ &\quad + 4(\delta_{2543}+\delta_{3425}) - 2(\delta_{1526}+\delta_{2165}+\delta_{3146}-\delta_{1463}), \\ (\mathrm{II}|H|\mathrm{II}) &= 4Q - 2(\alpha_1' + \alpha_2' - 2\alpha_3' - 2\alpha_4' + \alpha_5' + \alpha_6') \\ &\quad + 4(\beta_{16}+\beta_{25}+\beta_{34}) - 4(\gamma_{214}+\gamma_{465}+\gamma_{153}+\gamma_{326}) \\ &\quad + 4(\delta_{2165}+\delta_{1526}) - 2(\delta_{2543}+\delta_{3425}+\delta_{3146}+\delta_{1463}), \\ (\mathrm{II}|H|\mathrm{I}) &= -2Q - 2(\alpha_1' - 2\alpha_2' + \alpha_3' + \alpha_4' - 2\alpha_5' + \alpha_6') \\ &\quad - 2(\beta_{16}+\beta_{34}+\beta_{25}) + 2(\gamma_{465}+2\gamma_{153}+\gamma_{326}+\gamma_{214} \\ &\quad -\gamma_{315}-\gamma_{546}) + 2(2\delta_{3146}+\delta_{1463}-\delta_{2165}-\delta_{1526} \\ &\quad -\delta_{2543}-\delta_{3425}), \\ (\mathrm{I}|\mathrm{I}) &= 2\{(1-S_2^2)(1-S_5^2) + (1-S_3^2)(1-S_4^2) \\ &\quad + (S_1S_6-S_3S_4)^2 - 2(S_1-S_3S_5)(S_2S_4-S_1) \\ &\quad + (S_1S_6-S_2S_5)^2 - 2(S_6-S_2S_3)(S_4S_5-S_6)\}, \\ (\mathrm{II}|\mathrm{II}) &= 2\{(1-S_1^2)(1-S_6^2) + (1-S_2^2)(1-S_5^2) \\ &\quad + (S_3S_4-S_2S_5)^2 - 2(S_4-S_1S_2)(S_5S_6-S_4) \\ &\quad + (S_1S_6-S_3S_4)^2 - 2(S_3-S_2S_6)(S_1S_5-S_3)\}, \\ (\mathrm{I}|\mathrm{II}) &= 2\{(S_4-S_1S_2)(S_5S_6-S_4) + (S_3-S_1S_5)(S_2S_6-S_3) \\ &\quad + (S_1-S_3S_5)(S_2S_4-S_1) + (S_6-S_2S_3)(S_4S_5-S_6) \\ &\quad - (S_2-S_1S_4)(S_3S_6-S_2) - (S_5-S_4S_6)(S_1S_3-S_5) \\ &\quad - (S_1S_6-S_3S_4)^2 - (1-S_2^2)(1-S_5^2)\}, \end{aligned} \tag{4}$$

where Q is the Coulomb integral, α_i' are single-exchange integrals, β_{ij} are double-exchange integrals, γ_{ijk} are triple-exchange integrals, δ_{ijkm} are quadruple-exchange

integrals, and S_i are overlap integrals. These are defined by the relations,

$$\begin{aligned}
&Q = (\mathrm{abcd}|H|\mathrm{abcd}),\\
&\alpha_1' = (\mathrm{abcd}|H|\mathrm{bacd}), \quad S_1 = (\mathrm{a}|\mathrm{b}),\\
&\alpha_2' = (\mathrm{abcd}|H|\mathrm{cbad}), \quad S_2 = (\mathrm{a}|\mathrm{c}),\\
&\alpha_3' = (\mathrm{abcd}|H|\mathrm{dbca}), \quad S_3 = (\mathrm{a}|\mathrm{d}),\\
&\alpha_4' = (\mathrm{abcd}|H|\mathrm{acbd}), \quad S_4 = (\mathrm{b}|\mathrm{c}),\\
&\alpha_5' = (\mathrm{abcd}|H|\mathrm{adcb}), \quad S_5 = (\mathrm{b}|\mathrm{d}),\\
&\alpha_6' = (\mathrm{abcd}|H|\mathrm{abdc}), \quad S_6 = (\mathrm{c}|\mathrm{d}),\\
&\beta_{16} = (\mathrm{abcd}|H|\mathrm{badc}),\\
&\beta_{25} = (\mathrm{abcd}|H|\mathrm{cdab}),\\
&\beta_{34} = (\mathrm{abcd}|H|\mathrm{dcba}),\\
&\gamma_{142} = (\mathrm{abcd}|H|\mathrm{bcad}) = \gamma_{214},\\
&\gamma_{153} = (\mathrm{abcd}|H|\mathrm{bdca}),\\
&\gamma_{263} = (\mathrm{abcd}|H|\mathrm{cbda}) = \gamma_{326},\\
&\gamma_{315} = (\mathrm{abcd}|H|\mathrm{dacb}),\\
&\gamma_{465} = (\mathrm{abcd}|H|\mathrm{acdb}) = \gamma_{546},\\
&\delta_{2165} = (\mathrm{abcd}|H|\mathrm{cadb}) = \delta_{1526},\\
&\delta_{1463} = (\mathrm{abcd}|H|\mathrm{bcda}) = \delta_{3146},\\
&\delta_{2543} = (\mathrm{abcd}|H|\mathrm{cdba}) = \delta_{3425}.
\end{aligned} \tag{6}$$

The Coulomb integral Q is written as a sum of the diatomic Coulombic contributions Q_i:

$$Q = 4E_{\mathrm{H}} + \sum_{i=1}^{6} Q_i, \tag{7}$$

where E_{H} represents the energy of a hydrogen atom.

The exchange integrals α_i', β_{ij}, γ_{ijk}, and δ_{ijkm} can also be decomposed into "diatomic" contributions Q_i, α_i, and S_i by using the Mulliken approximation:[5]

$$\begin{aligned}
&\alpha_i' \simeq \alpha_i + S_i^2(Q-Q_i),\\
&\beta_{ij} \simeq S_i^2S_j^2\{\alpha_i/S_i^2+\alpha_j/S_j^2+(Q-Q_i-Q_j)\},\\
&\gamma_{ijk} \simeq \frac{1}{2}S_iS_jS_k\{\alpha_i/S_i^2+\alpha_j/S_j^2+\alpha_k/S_k^2+2Q\\
&\qquad -(Q_i+Q_j+Q_k)\},\\
&\delta_{ijkm} \simeq \frac{1}{2}S_iS_jS_kS_m\{\alpha_i/S_i^2+\alpha_j/S_j^2+\alpha_k/S_k^2+\alpha_m/S_m^2\\
&\qquad +2Q-(Q_i+Q_j+Q_k+Q_m)\}.
\end{aligned} \tag{8}$$

Eventually, the energy, Eq. 1, is evaluated in terms of the diatomic integrals Q_i, α_i, and S_i. Following Porter and Karplus,[8] we write the Q_i, α_i, and S_i as

$$\begin{aligned}
Q_i &= [(E^1+E^3)+S_i^2(E^1-E^3)]/2,\\
\alpha_i &= [(E^1-E^3)+S_i^2(E^1+E^3)]/2,
\end{aligned} \tag{9}$$

where

$$\begin{aligned}
E^1 &= D_1\{\exp[-2\alpha(R_i-R_e)]-2\exp[-\alpha(R_i-R_e)]\},\\
E^3 &= D_3\{\exp[-2\beta(R_i-R_e)]+\exp[-\beta(R_i-R_e)]\},
\end{aligned} \tag{10}$$

and

$$S_i = (1+\zeta_iR_i+\zeta_i^2R_i^2/3)\exp(-\zeta_iR_i), \tag{11a}$$

where

$$\zeta_i = 1.0 + \kappa\exp(-\lambda R_i). \tag{11b}$$

Results and Discussion

The parameters D_1, D_3, α, β, and R_e in Eqs. 10 have been determined from the results of the accurate *ab initio* calculation on H_2 by Kołos and Wolniewicz[9] (see Ref. 1 for details). The screening parameter ζ_i appearing in Eq. 11a for the overlap integral S_i is given as a function of the internuclear distance R_i by Eq. 11b, which involves two parameters κ and λ. In their calculation of the H_3 system, Porter and Karplus[8] determined the values of κ and λ from early calculations of the H_2 molecule by Wang and Rosen.[10] In the present paper, however, κ and λ have been determined by fitting Eq. 1 to the *ab initio* calculations on the linear symmetric H_4 by Bender and Schaefer III (BS).[7] The values of the parameters thus determined are shown in Table 1. The values of the screening parameter ζ_i determined by Eq. 11b with the values of κ and λ in Table 1 are slightly higher than the values of ζ_i by Porter and Karplus (Table 2). This difference of the two sets of ζ_i values seems to be due to the difference

Table 1. The parameters used to calculate the H_4 potential energy[a]

D_1=0.174475 a.u.	κ=1.00
D_3=0.072900 a.u.	λ=0.40
α=1.050000 a.u.$^{-1}$	
β=1.036000 a.u.$^{-1}$	
R_e=1.401000 a.u.	

a) For definitions see the text.

Table 2. Comparison of the values of the screening parameter ζ_i

R_i	ζ_i (present paper)	ζ_i (Porter and Karplus)
1.5	1.549	1.226
2.0	1.449	1.164
2.5	1.368	1.118
3.0	1.301	1.085
4.0	1.202	1.045
5.0	1.135	1.023
6.0	1.091	1.012

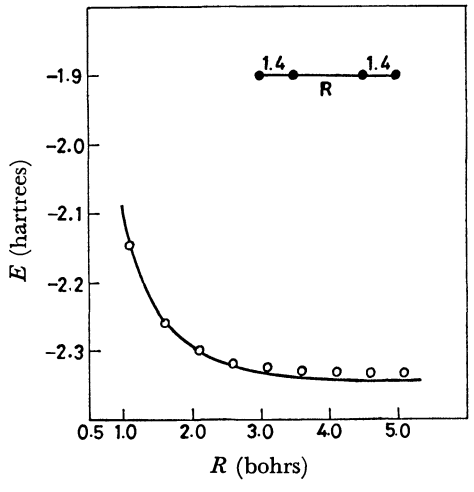

Fig. 1. Potential energies of symmetric linear H_4 as a function of distance of approach R with two H_2 molecule at equilibrium.
BS ○○○○;[7] ——, the present work.

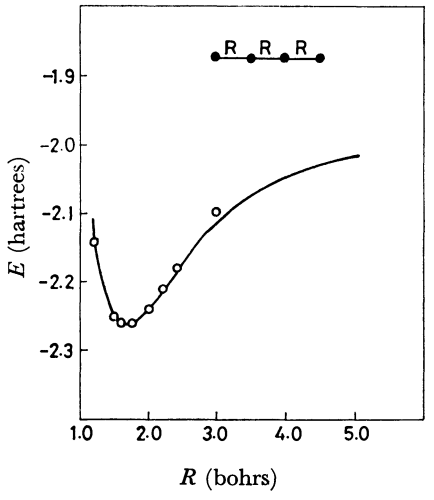

Fig. 2. Potential energies of linear equidistant H_4 as a function of R. R is the distance between H atoms. BS ○○○○;[7] ——, the present work.

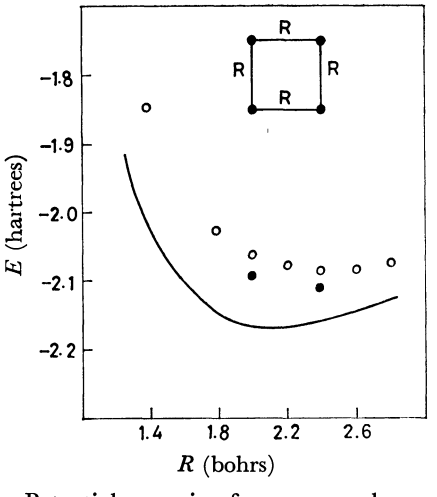

Fig. 3. Potential energies for square planar H_4. R measures the side of the square.
SS ○○○○, used orbital basis s,s′; SS ••••, used orbital basis s,s′, p;[4]— , the present work.

in the methods by which the values of κ and λ have been determined (see above).

In the case of linear symmetric and linear equidistant configurations, the results obtained here are compared with those of BS[7] in Figs. 1 and 2: The agreement is satisfactory. A similar calculation for square planar configuration is shown in Fig. 3, where we compare the results with those of SS.[4] The agreement is not so good as in the case of Figs. 1 and 2. It should be remembered that the values of κ and λ have been adjusted for the linear symmetric H_4. However it does not seem worthwhile to try to improve the above disagreement by readjusting the values of κ and λ for the square H_4, because the precision of the SS calculation is not as high as that of the BS calculation. In fact, it has been pointed out that the SS energies can be lowered by more than 0.025 hartrees by extending the orbital basis and by optimizing the orbital exponents.[4]

The author wishes to thank Professor T. Nakamura of Hokkaido University for many helpful discussions and suggestions. The numerical calculations were performed on the FACOM 230-75 computer at the Hokkaido University Computing Center.

References

1) N. Tanaka, *Chem. Phys. Lett.*, **54**, 551 (1978).
2) B. Liu, *J. Chem. Phys.*, **58**, 1925 (1973).
3) S. H. Bauer and E. Ossa, *J. Chem. Phys.*, **45**, 434 (1966) S. H. Bauer, D. M. Lederman, E. L. Resler. Jr., and E. R. Fisher, *Int. J. Chem. Kinet.*, **5**, 93 (1973).
4) D. M. Silver and R. M. Stevent, *J. Chem. Phys.*, **59**, 3378 (1973).
5) R. S. Mulliken, *J. Chem. Phys.*, **46**, 497 (1949).
6) J. C. Slater, *Phys. Rev.*, **38**, 1109 (1931). S. Glasstone, K. J. Laidler, and H. Eyring, "The Theory of Rate Processes" McGraw-Hill Book Company, Inc. New York, (1941).
7) C. F. Bender and H. F. Schaefer III, *J. Chem. Phys.*, **57**, 217 (1972).
8) R. N. Porter and M. Karplus, *J. Chem. Phys.*, **40**, 1105 (1964).
9) W. Kołos and L. Wolniewicz, *J. Chem. Phys.*, **43**, 2429 (1965).
10) S. C. Wang, *Phys. Rev.*, **31**, 579 (1928); N, Rosen, *Phys. Rev.*, **38**, 2099 (1931).

On the Magnetic Susceptibility of Interacting Spin-pair Systems

Hiroaki OHYA-NISHIGUCHI

Department of Chemistry, Faculty of Science, Kyoto University, Kyoto 606

(Received February 8, 1979)

Modifying a general theory of antiferromagnetism proposed by Oguchi, the parallel and perpendicular magnetic susceptibilities ($\chi_{//}$ and $\chi_{\perp}$ respectively) of antiferromagnetically interacting spin-pair systems have been formulated. As the parameter of the equations, $\kappa=z|J'|/|J|$, approaches zero, both of them coincide with a familiar equation of isolated spin-pairs. In the $0<\kappa\leq 1$ range the maximum susceptibility and the Weiss constant are compared with those estimated exactly by the alternating antiferromagnetic linear-chain model. For $1<\kappa\leq 2$, they can be characterized by a broad maximum and a transition to the antiferromagnetically ordered state. For $\kappa>2$, $\chi_{//}$ and $\chi_{\perp}$ show curves similar to those of a typical three-dimensional antiferromagnet. The $\chi_{//a}$ and $\chi_{\perp a}$ of the 2,2-diphenyl-1-picrylhydrazyl–benzene (1 : 1) complex have been examined based on the theoretical results for $\kappa=1.3$. The magnetic susceptibilities of the other organic free radicals have been compared with the results calculated in the $0\leq\kappa<1$ range.

Since the first observation of two-spin clusters in $Cu(CH_3COO)_2$ by means of electron paramagnetic resonance (EPR) and magnetic susceptibility (χ) measurements, many examples of such spin-pair systems in organic and inorganic materials have been studied by a number of investigators.[1] The χ or the EPR intensity has usually been characterized by a familiar equation:

$$\chi = \frac{N(g\mu)^2S(S+1)}{2kT[3+\exp(2|J|/kT)]} \tag{1}$$

where J is the interaction between two spins coupled antiferromagnetically; μ, the Bohr magneton, and g, the Lande g-factor, and where the other notations have the usual meanings. This equation, however, cannot be applied to systems with comparatively large inter-pair interactions. In 1955 Oguchi[2] developed a general theory of ferromagnetism and antiferromagnetism, based on the Heisenberg model of two-spin clusters. Modifying this theory, one can calculate analytically and tractably the susceptibility of interacting spin-pair systems. In this paper this theory will be extended to antiferromagnetically interacting spin-pair systems in order to understand qualitatively their physical behavior by relatively simple formulations. Based on the theoretical results thus derived, first we will examine the magnetic susceptibility of 2,2-diphenyl-1-picrylhydrazyl–benzene (1 : 1) complex (DPPH–Bz) measured by Fujito.[3] Recently it was shown for the complex that none of the isolated spin-pair, linear chain, or quadratic net Heisenberg models give a satisfactory agreement with the experimental results.[4] The main object of applying our model to DPPH–Bz, therefore, is to examine its magnetic property in relation to spin-cluster models. Secondly, the χ values of some organic free radicals with small or intermediate inter-pair interactions are compared with the theoretical results obtained by our model and the alternating linear-chain model developed by Duffy and Barr.[5]

Theoretical

We treat here a spin-pair, whose spin operators are denoted by $\boldsymbol{S}_i$ and $\boldsymbol{S}_j$, interacting with each other with a negative exchange interaction $-|J|$. For the sake of simplicity, it is assumed hereafter that g is isotropic and S is 1/2. Such assumptions can reasonably be accepted in spin systems consisting of usual organic free radicals. In addition to J inter-pair exchange interaction, $J'(|J'|<|J|)$, is introduced in the system. Then, the Hamiltonian can be written as

$$\mathcal{H} = 2|J|(\boldsymbol{S}_i\cdot\boldsymbol{S}_j) + 2|J'|[\sum_k(\boldsymbol{S}_i\cdot\boldsymbol{S}_k)+\sum_l(\boldsymbol{S}_j\cdot\boldsymbol{S}_l)] + g\mu H^z(S_i^z+S_j^z), \tag{2}$$

where the sums k and l go over the nearest neighbors of the i-spin except for the j-spin, and of the j-spin except for the i-spin, respectively. Here, the last term is the Zeeman energy of the system with an external magnetic field, H^z, along the easy axis, hereafter denoted as the z-axis. According to the usual molecular field approximation, $\boldsymbol{S}_k$ and $\boldsymbol{S}_l$ are replaced by their thermal mean expectation values, $-\bar{S}$ and $+\bar{S}$, respectively, which change to $\mp\bar{S}+\delta\bar{S}^z$ by the application of the magnetic field along the z-axis. Thus, the Hamiltonian can simply be written as

$$\mathcal{H} = 2|J|(\boldsymbol{S}_i\cdot\boldsymbol{S}_j) + aS_i^z + bS_j^z, \tag{3}$$

where

$$\begin{aligned} a &= 2|J'|z(-\bar{S}+\delta S^z) - g\mu H^z, \\ b &= 2|J'|z(+\bar{S}+\delta S^z) - g\mu H^z, \end{aligned} \tag{4}$$

and where z is the number of the nearest neighbors of the i-spin, excluding the j-spin. Next, we define a new parameter, $\kappa=z|J'|/|J|$, which means the strength of the molecular field. For simplicity in the description, we adopt the exchange interaction, $|J|$, as the unit of the energy. Then,

$$\mathcal{H} = 2(\boldsymbol{S}_i\cdot\boldsymbol{S}_j) + [2\kappa(-\bar{S}+\delta S^z)-h]S_i^z + [2\kappa(\bar{S}+\delta S^z)-h]S_j^z, \tag{3'}$$

where $h=g\mu H/|J|$. Using the spin states $\alpha_i\alpha_j$, $(1/\sqrt{2})(\alpha_i\beta_j+\beta_i\alpha_j)$, $\beta_i\beta_j$ and $(1/\sqrt{2})(\alpha_i\beta_j-\beta_i\alpha_j)$, the eigen values of Eq. 3′ are derived as

$$\begin{aligned} E_1 &= (1+4\kappa\delta S^z-2h)/2, \\ E_2 &= (-1/2) + R, \\ E_3 &= (1-4\kappa\delta S^z+2h)/2, \\ E_4 &= (-1/2) - R, \end{aligned} \tag{5}$$

where

$$R = (1+4\kappa^2\bar{S}^2)^{1/2}. \tag{6}$$

Now the magnetization in the external magnetic field along z-axis is defined self-consistently as

$$\bar{S} + \delta S^z = \mathrm{Tr}\, S^z e^{-\beta\mathcal{H}} / \mathrm{Tr}\, e^{-\beta\mathcal{H}} \tag{7}$$

where $\beta = 1/t = |J|/kT$. By substituting Eq. 5 into Eq. 7, we obtain

$$\bar{S} + \delta S^z = \frac{1}{2} \cdot \frac{\frac{2\kappa}{R}\bar{S}e^{\beta}\sinh\beta R + \sinh(h - 2\kappa\delta S^z)}{\cosh(h - 2\kappa\delta S^z) + e^{\beta}\cosh\beta R}. \tag{8}$$

As the terms containing h and S^z are small quantities of the first order, one can divide Eq. 8 into two parts. The zeroth-order term is

$$\bar{S} = \frac{\kappa\bar{S}\sinh\beta R}{R(e^{-\beta} + \cosh\beta R)} \tag{9}$$

which leads to the non-zero solution of $\bar{S}$. At the limit of $R=1$, the Néel temperature, $T_N = |J|/k\beta_N$, can be calculated from:

$$e^{-\beta_N} + \cosh\beta_N = \kappa\sinh\beta_N \tag{10}$$

As a function of κ, the solution of this equation is shown in Fig. 1. The lower part of the solid line of the figure is the antiferromagnetically ordered state, denoted as AF, while its upper part is the paramagnetic region (P). It should be noted here that in the $0 \leq \kappa < 1$ range no antiferromagnetic transition occurs.[6]

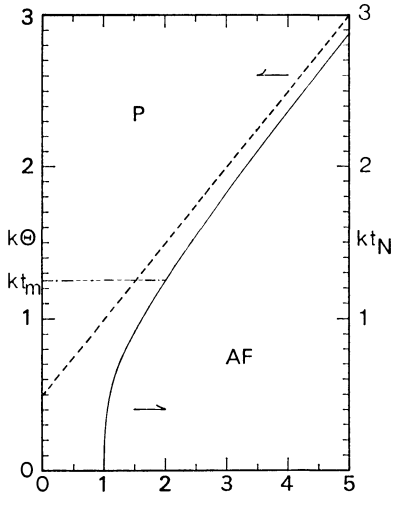

Fig. 1. The reduced Néel temperature (t_N: solid line), Weiss temperature (Θ: broken line), and temperature showing broad maximum of the susceptibility (t_m: dotted broken line) *versus* the molecular field parameter κ. AF: Antiferromagnetic state, P: Paramagnetic state.

From the first-order term of Eq. 8:

$$\chi_{\parallel} = Ng\mu\left(\frac{\delta S^z}{\delta H}\right)_{H=0} = \frac{1}{2}\,\frac{N(g\mu)^2\beta}{\kappa\beta + 1 + e^{\beta}\cosh\beta R}. \tag{11}$$

By a manner similar to that used with $\chi_{/\!/}$, the magnetic susceptibility perpendicular to the z-axis ($\chi_{\perp}$) is given as:

$$\chi_{\perp} = \frac{(R-1)^2 e^{\beta}\cosh\beta R + 2R - (R^2+1)e^{\beta(1-R)}}{\{2\kappa[(R-1)^2 e^{\beta}\cosh\beta R + 2R(R^2+1)e^{\beta(1-R)}] + 2R(R^2-1)(1+e^{\beta}\cosh\beta R)\}}. \tag{12}$$

In the paramagnetic region ($\bar{S}=0$), Eq. 12 coincides with Eq. 11 if we take the limit of $R = 1+\delta$ as δ approaches 0. Furthermore, for $\kappa=0$ Eqs. 11 and 12 coincide with Eq. 1 for $S=1/2$. In Fig. 2 the powder susceptibilities $\chi = (\chi_{/\!/} + 2\chi_{\perp})/3$, are shown as functions of the reduced temperature, t. The numbers in the figure are the values of κ.

We will now show some typical cases of Eqs. 11 and 12. At high temperatures ($t \gg 1/k$), χ becomes a simple form:

$$\chi = \frac{N(g\mu)^2}{4k} \cdot \frac{1}{t - (-\Theta)}, \tag{13}$$

where $\Theta(=(\kappa+1)/2k)$ is called the Weiss temperature. The dependence of Θ on κ is also shown in Fig. 1 by a broken line which coincides with the asymptote of the solid line.

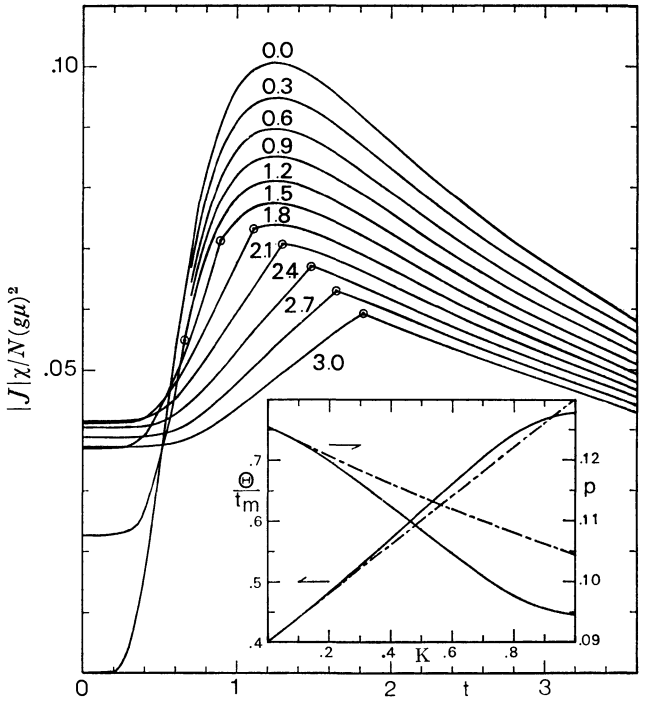

Fig. 2. The powder magnetic susceptibility *versus* the reduced temperature for $\kappa=0.0$ to 3.0. The Néel temperatures are indicated by the circles in the figure. The inset shows the Weiss temperature divided by t_m and the product of maximum susceptibility times t_m, $p = \chi_m k t_m / Ng^2\mu^2$, *versus* the molecular field parameter κ (broken line) compared with the alternating linear chain model (solid line) (Ref. 5).

At moderate temperatures comparable to $|J|/k$, χ depends sensitively on κ. For $0 \leq \kappa < 1$, Θ shows a broad maximum at a constant temperature, $t_m(=1.2473/k)$, without any phase transition. The inset in Fig. 2 shows the variations in the dimensionless Θ/t_m and of

$$p = \chi_m k t_m / N(g\mu)^2 \tag{14}$$

as functions of κ. In this range of κ for $z=1$, our results can be compared with the magnetic susceptibility of the alternating linear chain calculated exactly by Duffy and Barr.[5] Also shown by the solid line in the inset of Fig. 2 are the results of their theoretical calculations. Θ/t_m is in good agreement with their value, while p deviates upward as κ increases, the deviation being

about 10% at $\kappa=1$. For $\kappa<0.3$, however, our susceptibility calculations agree well with those by Duffy and Barr with the deviation of only 2%. The deviation of p for κ values larger than 0.3 in the inset is mainly due to the energy separation between the singlet ground state and the excited triplet states (Δ). In our model, Δ can be derived from Eq. 5 for $h=0$ and $R=1$ as $\Delta=2$ in units of $|J|$. This constant value of Δ in the paramagnetic state is one of the features of our simple model. For a more quantitative analysis of χ, it is desirable that Δ be explicitly expressed as a function of J' or κ, as will be discussed later. In the case of the alternating linear-chain model, on the other hand, Δ for $h=0$ depends on the continuous-energy spectrum, which is expressed as $\Delta(k)=2-\kappa\cos k$.[5]

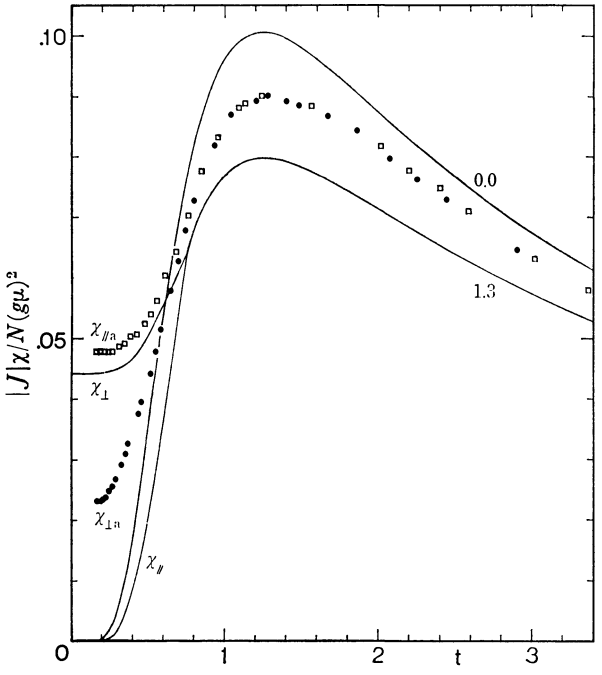

Fig. 3. The magnetic susceptibilities of the DPPH–Bz complex along a-axis (square) and perpendicular to a-axis (full circle) *versus* the reduced temperature t for $|J|/k=0.54$ K. Solid lines are the theoretical calculations by Eqs. 11 and 12 for $\kappa=0.0$ and 1.3.

In the antiferromagnetic region ($t>t_N$, $R>1$) $\chi_{//}$ decreases rapidly with a decrease in the temperature, while $\chi_\perp$ gives a constant value near absolute zero. Its magnitude depends approximately on κ as follows:

$$\chi_\perp(0) \fallingdotseq (\kappa-1)/4\kappa^2 \qquad (15)$$

As an illustrative example, the calculated $\chi_{//}$ and $\chi_\perp$ values for $\kappa=1.3$ are shown in Fig. 3 as functions of t. Such special susceptibilities can be experimentally visualized by a stable free radical, DPPH–Bz, as will be shown in the following section. In the antiferromagnetic region, Eq. 5 explicitly includes J', even for $h=0$. Therefore, our model is considered to be a good approximation compared with the case in the paramagnetic region mentioned above.

By a comparison of Eqs. 11 and 12 with the experimental results, one can estimate J' in addition to J, provided that z can be derived crystallographically. It should be noted, however, that the estimated J' is fundamentally not the real value, because, in the approximation treated here, we use a mean value of the molecular field produced by the neighbors.

Comparison with Experiments

Magnetic Susceptibility of DPPH–Bz Single Crystal. We will examine here the magnetic susceptibilities along the a-axis and perpendicular to the a-axis of the DPPH–Bz complex, hereafter denoted as $\chi_{//a}$ and $\chi_{\perp a}$ respectively.[3] In a previous paper[7] the powder susceptibility of DPPH–Bz at temperatures lower than 1.7 K, which were measured by a bridge method in a zero static field, were fitted to the value at 1.7 K measured by a force method in the field of 0.829 T. By this procedure, however, the values below 1.7 K were overestimated, because the $\chi_{//}$(also $\chi_\perp$) values of spin-pair systems with a singlet ground state depends on the applied magnetic field. In the paramagnetic region ($R=0$), for example, one can simply derive the χ as a function of the external field from Eq. 8 as

$$\frac{|J|\chi(t,h')}{N(g\mu)^2} = \frac{\beta j 2}{1+\kappa\beta+e^{\beta}\cosh\beta/\cosh\beta h'} \qquad (16)$$

where $h'=h-2\kappa\delta S^z$ is the effective field including the contribution from the induced magnetization. At temperatures higher than $|J|/k$, this contribution can be neglected ($h'=h$). $|J|/k$ was estimated to be 0.54 ± 0.02 K from the temperature (T_m) at which χ reached χ_m. By substituting this value into Eq. 16, the χ of DPPH–Bz at 1.7 K in 0.829 T is estimated to be 10% larger than that in the zero field. The experimental data in Fig. 3, measured by the bridge method were, therefore, calibrated by the value measured by the force method at 4.22 K which was corrected using Eq. 16. The anisotropy of the susceptibility ($\chi_{//a}-\chi_{\perp a}$) appeared at around 0.42 K at which the low-field EPR absorption line disappeared.[3] This behavior coincided with that which occurs around the Néel temperature of antiferromagnetic materials.[8] Therefore, we tentatively adopted 0.42 K as the T_N of DPPH–Bz. The ratio of T_m to T_N, 1.62, was used to determine the value of κ. The theoretical susceptibilities calculated for $|J|/k=0.54$ K and $\kappa=1.3$ are compared with $\chi_{\perp a}$ and $\chi_{//a}$ in Fig. 3. $\chi_\perp$ reproduces well the temperature dependence of $\chi_{//a}$. $\chi_{\perp a}$ also shows a value similar to $\chi_{//a}$ at t near t_N, but approaches a finite value as the temperature decreases. This is probably due to the lack of coincidence of the observed axis with the easy axis of the crystal.

Above t_N, on the other hand, the experimental values in Fig. 3 are just in the middle between those for $\kappa=0$ and 1.3. Such a deviation from our theoretical calculations for $\kappa=1.3$ in the paramagnetic region may indicate: 1) a cooperative phenomenon caused by J' and similar to those in the magnetic linear-chain and quadratic net Heisenberg models, or 2) the energy splittings of the degenerate triplet states by J', even in the range of the paramagnetic state. Recently Duffy, Strandburg and Deck[4] reported the susceptibility and

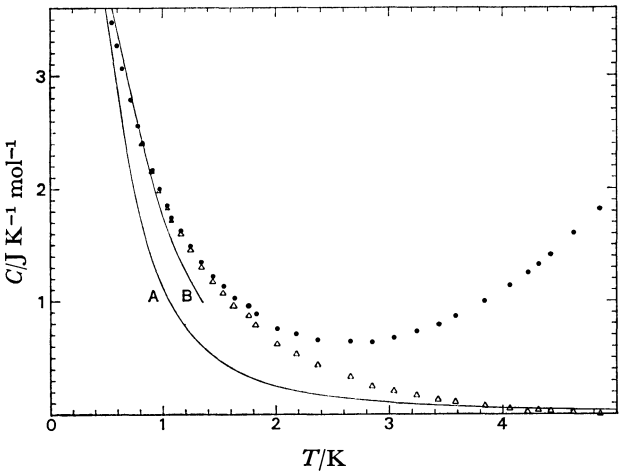

Fig. 4. Comparison of theoretical calculations of heat capacity with experimental data of DPPH–Bz measured by Duffy *et al.* (Ref. 4). A: Eq. 17, B: Two-spin-pair model calculated by Duffy and Barr (Ref. 5), ●: total heat capacity, △ magnetic part of the heat capacity.

the heat capacity (C_v) of DPPH–Bz from 0.4 K to room temperature, with which neither the linear-chain nor the quadratic net Heisenberg model gives satisfactory agreement. Therefore, the latter possibility described above may contribute to the deviation from the theoretical values.

Their heat-capacity data, shown in Fig. 4, are helpful in understanding the magnetic interactions of DPPH–Bz. Using Eq. 5, C_v of our model can be derived as

$$C_v = 6kN\beta^2|J|^2/(3e^{-\beta|J|}+e^{\beta|J|})^2 \qquad (17)$$

which coincides with the C_v of the isolated spin-pair systems, because in the paramagnetic state the energy levels under consideration are equal to those of the isolated spin-pair systems. A in Fig. 4 is calculated by means of Eq. 17 for $|J|=0.54\,k$. As has already been pointed out for the susceptibility data, the experimental data of C_v also deviate upward from A. For the linear-chain model, the magnitude of the theoretical heat capacity and the $\chi_m T_m$ values are quite low.[4] One of the possible ways to interpret both the susceptibility and heat capacity is to include J' in Eq. 5 explicitly, even in the paramagnetic region. Dufly and Barr[5] calculated the C_v of an alternative four-membered ring with $J'=0.8\,J$, a kind of two-spin-pair model, which is also shown in Fig. 4 as B for the sake of comparison. The agreement of B with the experimental results is better than that of A. The two-spin-pair model, therefore, is an improvement of the model for DPPH–Bz. Thus, one can conclude that our simple model well explains the appearance of t_N in addition to the temperature dependence of the magnetic susceptibilities of DPPH–Bz if we adopt 0.42 K as the T_N of DPPH–Bz. For the quantitative agreement of the susceptibilities, however, it is desirable to take into account the energy splittings in the triplet states. Some formulations according to such a modification are now in progress.

Table 1. Molecular-field parameter, κ, estimated from the maximum susceptibility of some organic free radicals

Compound	$\frac{T_m}{K}$	$\frac{\lvert J\rvert}{K}$	$\chi_m \times 10^4$ g)	$\frac{\lvert J\rvert\chi_m}{N(g\mu)^2}$	κ
Sulfite[a)]	15	12	127	0.101	0.02
DPPH-free[b)]	11	8.8	170	0.10	0.05
DPPH-free[c)]	10.5	8.75	177	0.099	0.06
TEMPAD[d)]	16.5	13.2	100	0.089	0.72
Porphyrexide[e)]	7.2	5.8	228	0.088	0.73
PAC[f)]	70	55	23.3	0.087	0.77
$D(NO_2)_2$[f)]	9.7	7.8	167	0.0863	0.82

a) A. Nakajima, H. Ohya-Nishiguchi, and Y. Deguchi, *Bull. Chem. Soc. Jpn.*, **45**, 713 (1972). b) Ref. 6. c) P. Grobet, L. Van Gerven, and A. Van den Bosch, *J. Chem. Phys.*, **68**, 5225 (1978). d) A. Nakajima, H. Nishiguchi, and Y. Deguchi, *J. Phys. Soc. Jpn.*, **24**, 1175 (1968). e) T. Fujito, H. Nishiguchi, Y. Deguchi, and J. Yamauchi, *Bull. Chem. Soc. Jpn.*, **42**, 3334 (1969). f) W. Duffy and D.L. Strandburg, *J. Chem. Phys.* **46**, 456 (1967). g) Corrected for the magnetic "impurities" as required.

Examples of Other Organic Free Radicals. In order to show the applicability of our model, the χ values of other compounds are compared with those calculated by means of Eq. 11. Table 1 summarizes the compounds with the values of $\kappa<1$. We can also derive the values of the parameter from Θ, but this method is not so reliable because of the large experimental errors. The $|J|$ values were estimated from T_m. It has been concluded that the sulfite and the DPPH-free are mostly isolated spin-pairs, while the others have comparatively large inter-pair interactions. For comparison with the experimental results on 2,2-bis(*p*-nitrophenyl)-1-picrylhydrazyl ($D(NO_2)_2$), Duffy and Barr estimated the alternation parameter (a) of the alternating linear-chain model as $a=0.6$, which corresponds to our value of $\kappa=0.9$ in the inset of Fig. 2. Thus, the molecular-field approximation of interacting spin-pair systems is useful for a physical understanding of complicated organic free radicals.

References

1) J. S. Smart, "Magnetism III," ed by G. T. Rado and H. Suhl, Academic Press, NY (1963), p. 63.
2) T. Oguchi, *Prog. Theor. Phys.*, **13**, 148 (1955).
3) T. Fujito, *Bull. Chem. Soc. Jpn.*, to be published.
4) W. Duffy, Jr., D. L. Stranburg, and J. F. Deck, *J. Chem. Phys.*, **68**, 2097 (1978).
5) W. Duffy, Jr., and K. P. Barr, *Phys. Rev.*, **165**, 647 (1968).
6) In the $0<\kappa<1$ range Yamashita and Amaya discussed the thermodynamical properties of the interacting spin-pair systems, including the perpendicular part of the molecular field, and pointed out another type of spin ordering. See N. Yamashita and K. Amaya, *J. Phys. Soc. Jpn.*, **41**, 419 (1976), and other references cited therein.
7) T. Fujito, T. Enoki, H. Ohya-Nishiguchi, and Y. Deguchi, *Chem. Lett.*, **1972**, 557.
8) See, for example, S. Foner, "Magnetism I," ed by G. T. Rado and H. Suhl, Academic Press, NY (1963), p. 383.

Polarized Two-photon Absorption Spectra of Naphthalene in Durene Single Crystal with Two Synchronized Tunable Dye Lasers

Naohiko MIKAMI*,† and Hwai-Kwan HONG

Department of Chemistry and Radiation Laboratory, University of Notre Dame, Notre Dame, Indiana 46556, U.S.A.††

(Received February 15, 1979)

Polarized two-photon absorption spectra of naphthalene in a single crystal of durene were observed with one and two beams of tunable dye lasers. Diagonal elements of the two-photon transition tensor were determined by one beam experiments with different incident polarizations on different faces of an oriented single crystal. The off-diagonal elements of the two-photon transition tensor were determined with two synchronized beams of different wavelengths and polarizations on the same sample. It was found that most of the vibronic states have large σ_{LL} consistent with an overall vibronic A_g symmetry and a long axis polarized $^1B_{2u}$ intermediate state. The intermediate states of the two-photon process of the strongest vibronic origin have been discussed on the basis of the observed values of the two-photon transition tensor elements. The band also has a small but non-vanishing off-diagonal tensor element (σ_{LM}). A crystal field perturbation due to reduced site symmetry by a B_{3g} two-photon allowed state is postulated.

Two-photon spectroscopic measurements of polyatomic molecules have become popular for observing new states inaccessible to the usual one-photon spectroscopy. A considerable amount of work has been done on the lowest singlet state of benzene.[1-7] The two-photon excitation spectra of a benzene crystal at very low temperature and of benzene vapor reveal new vibronic structures identified as u-type vibrations in the electronically two-photon forbidden state. In order to determine the symmetry species of these vibrations in the excited state, polarization measurements in the gas phase were performed with high resolution. Unlike one-photon spectroscopy, two-photon spectroscopy has the advantage that the polarization effects can be measured in isotropic media such as gases, since a molecule interacts with two photons simultaneously. Assignments of the vibronic transition in benzene vapor *via* polarization measurements have been carried out by several groups.[4-7]

Similarly, polarization measurements of two-photon spectra in crystals provide us direct and detailed information concerning tensors of two-photon transition amplitudes for crystals or molecules in the crystals. The tensor is composed of nine elements. Each element in the tensor can be determined uniquely by polarization measurements on crystals.[8,9] Studies on the polarized two-photon spectra have been made for crystals of aromatic molecules such as naphthalene,[10] pyrazine[14] and biphenyl.[15] However, the experiments were carried out by using only one exciting beam. Hochstrasser and Sung[12] utilized crystal birefringence to obtain two beams of identical photon energies but different polarizations inside the crystal and were able for the first time to obtain information on both the diagonal and off-diagonal elements of the two-photon transition tensors. If the diagonal elements of the tensor for a particular transition are large as compared with the off-diagonal elements, the two-photon signals are dominated by the absorption of the two photons of the same polarization. The determination of a small off-diagonal contribution due to the absorption of two photons of different polarizations becomes difficult. Thus, a two beam experiment with independent photons in frequencies and polarizations is particularly suitable for the detection of off-diagonal elements of the two-photon transition tensors. The frequencies of the two beams should be so chosen that neither $2\nu_1$ and $2\nu_2$ are in resonance with the transition but $\nu_1+\nu_2$ is. This requires sharp transitions and clear window area. Only mixed crystals at low temperatures such as naphthalene in durene reported here are amenable.

The only experiment using two different light sources on an unisotropic crystal was carried out by Froehlich and Mahr on the single crystal of anthracene.[16] The two beam experiment of the two-photon transition of benzene vapor was carried out by Hampf, Neusser and Schlag.[17]

We have measured polarized two-photon excitation spectra of the lowest singlet excited state of naphthalene in a durene single crystal at very low temperature by using two exciting light beams of different wavelength and polarization. The two-photon spectra of naphthalene in this spectral region has been thoroughly studied in the gas phase[18] and crystalline phase at low temperature.[12,13] The strongest false origin is known to be vibronically induced by a u-type vibration of b_{2u} symmetry in the excited state, all experimental evidence being consistent with this assignment. However, there is some uncertainty as to the mechanism for the appearence of the false origin. Careful polarization measurements of both the single crystals of naphthalene and naphthalene in a durene single crystal by Hochstrasser and Sung[12] shed some light on the nature of intermediate states, crystal field mixing and vibronic coupling in these systems. Our two beam experiment is complimentary to their one beam experiments. The polarization measurements include not only all the possible crystal faces but also new results with two synchronized dye laser beams of different wavelength and polarization. It is thus possible to obtain information on the relative ratio of the individual elements of

† Present address: Department of Chemistry, Faculty of Science, Tohoku University, Sendai 980.

†† The research was supported by the Division of Physical Research of the U. S. Energy Research and Development Administration. This paper is Document No. NDRL-1777 from the Notre Dame Radiation Laboratory.

the two-photon transition tensor. We will discuss the intermediate states of the two-photon process of the strongest vibronic origin and also the crystal field perturbation on two-photon states based on our results for the two-photon transition tensor.

Experimental

Apparatus for the two-photon excitation spectra with two beams of parallel incidence is shown in Fig. 1. Two dye lasers were pumped simultaneously by a nitrogen laser (Molectron UV-1000) with a beam splitter, reflection-transmission ratio being *ca.* 2:3. A home-made dye laser (laser 1) of almost the same design as Molectron DL-200 generated a lasing line with a fixed wavelength. After passing through a 90° prism and an iris, the output beam (beam 1) was polarized horizontally by a Glan-Thompson prism (P_1). A halfwave plate (H) made of thin mica was used in order to change the polarization of beam 1. Suitable selection of the angle between the axis of the plate and the horizontal axis afforded a horizontally or vertically polarized beam without any beam walk-off. A neutral density filter N_1 was used to control the light intensity. Beam 2, frequency of which was tuned continuously and which exits from dye laser 2 (Molectron DL-200), was polarized vertically by another Glan-Thompson prism (P_2). The two beams were adjusted close to each other, the distance between centers being *ca.* 7 mm, and kept parallel to each other by a mirror M_2. Mirrors M_1 and M_2 constitute an optical delay line to synchronize the two light pulses. The two beams were focused onto a sample by a spherical mirror M_3 of 300 mm focal length, spatial matching between the two beams also being accomplished at the same time. As long as the angle between the axis of the incident beam and the normal axis of the mirror is small ($<5°$), good focusing can be achieved. Polarization of the two beams was carefully checked at the point where the dewar was to be placed. No scrambling of polarization was observed. The sample was held on a rotatable holder and suspended in a sample compartment of a variable temperature cryostat (Cryogenic Associate CT-72) which was cooled by thermal conduction of cool helium gas down to *ca.* 5 K.

The optical arrangement using two beams with 90 degree incidence is shown in Fig. 2. The crystal should be carefully placed at the exact position where the two beams cross each other since only in this small area do we have sufficient intensities in both beams to observe two-photon signals.

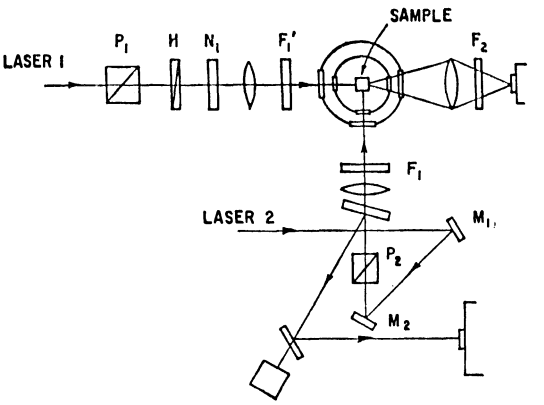

Fig. 2. Optical arrangement for two-photon excitation spectra by two beams with 90 degree incidence.

The fluorescence from the sample was focused onto a small monochromator (Bausch and Lomb) and detected with a photomultiplier (EMI 9635QB) connected to a boxcar integrator (PAR 162). A UV cut-off filter (F_1; Schott GG-22) and a visible cut-off filter (F_2; Corning 7-54) were used to eliminate undesirable photons. The output intensity of beam 2 was monitored by a biplanar photodiode (ITT FW114 with S-20 spectral response). Wavelength of the lasing line was calibrated by a monochromator (Spex 1402).

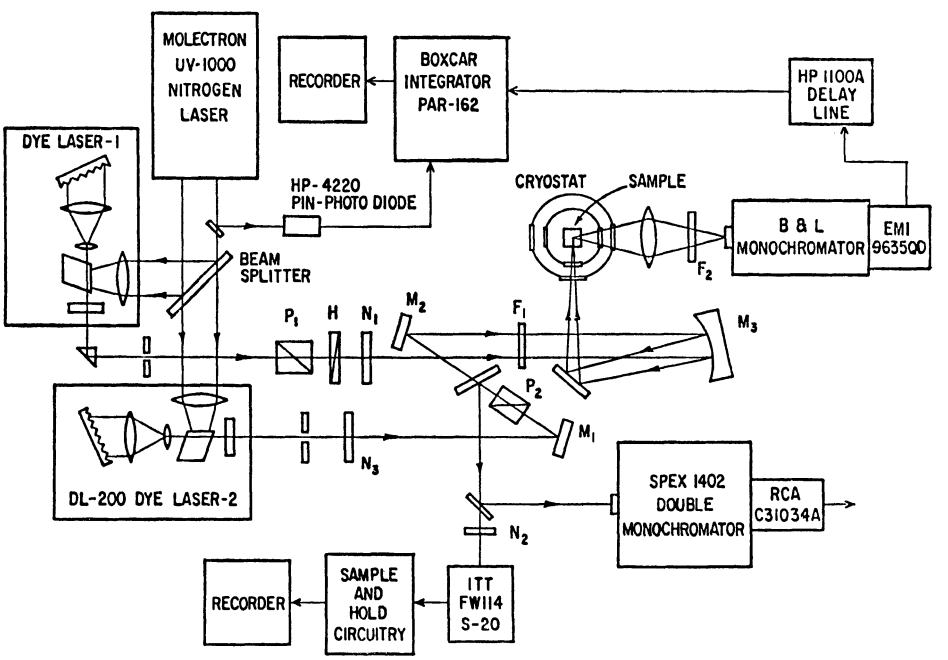

Fig. 1. Experimental set-up for two-photon excitation spectra by two synchronized tunable dye lasers with parallel beam incidence. Notice that the laser beams actually enter the cryostat from the bottom window. The last mirror reflects the beam propagation vector from horizontal to vertical.

Dye solutions were as follows: Cresyl violet perchlorate +Rhodamine-B in EtOH 6600—6200 Å, Rhodamine-B in EtOH 6450—5900 Å, Rhodamine-6G in EtOH 6050—5700 Å. Line width of dye laser 1 in these spectral region was 0.5—0.7 Å, that of laser 2 being less than 0.5 Å.

Naphthalene was purified by fusion with sodium followed by zone refining. Durene (1,2,4,5-tetramethylbenzene) was also purified by the zone melting method. Mixed crystals of durene with *ca.* 1% of naphthalene were grown by the simple Bridgman method. The actual concentration of naphthalene in durene is presumed to be less than 10^{-2} mol/mol. The (ab) crystal plane of durene was cleaved easily. Extinction directions on the (ab) plane were observed under a polarizing microscope. A cube of the crystal with edges parallel to the two extinction axes in the (ab) face (a and b axes) was cut with a razor blade. Examination of the conoscopic pattern of a small flake of the plane showed axis a to differ from axis b. All the directions along the edges of the crystal cube were therefore identified as a, b, and c′ (perpendicular to (ab) face) axes. The X-ray diffraction pattern in precession photographs along each axis confirmed the optical determination of these axes.

One of the principal axes denoted by X is almost parallel to axis a (the angle between it and axis X is known to be −0°54′ in Robertson's axis choice).[19,20] Since axis b coincides with the optical axis Y, all the three crystallographic axes a, b and c′, parallel to the edges of the crystal cube in this work, are parallel to the optical axes X, Y, and Z, respectively. We were able to use the crystallographic axes as reference axes for the polarization experiments.

Results

One Beam Experiment. The two-photon fluorescence excitation spectra of naphthalene in durene crystal with one laser beam was first observed by Hochstrasser, Sung, and Wessel.[10] We have observed almost the same spectra (Figs. 3 and 4). The relative intensities of these absorption peaks are not normalized with respect to the intensity distribution of the dye laser output, since the polarization ratios of the partially polarized laser output varied considerably in the tuning range. The 0-0 transition in this spectral region was

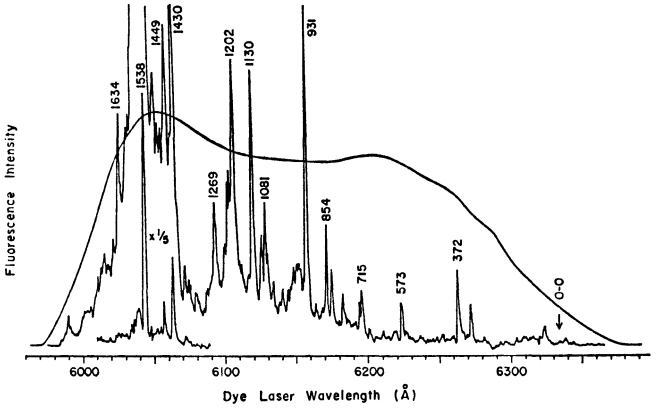

Fig. 3. Unpolarized two-photon excitation spectrum of naphthalene on the (bc′) face of durene crystal at 5 K taken with one laser beam. The smooth curve indicates the intensity distribution of the dye laser (rhodamine-B). The arrow indicates the position of the 0-0 transition.

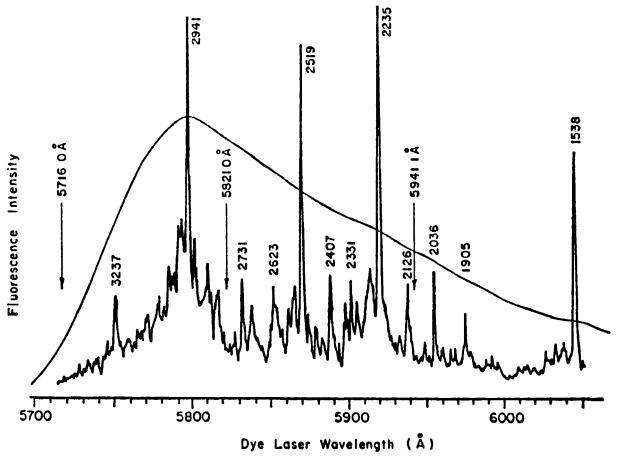

Fig. 4. Unpolarized two-photon excitation spectrum of naphthalene on the (bc′) face of durene crystal at 5 K by using one laser beam. The smooth curve indicates the intensity distribution of the dye laser (rhodamine 6G). The arrows indicate the frequency of the high energy photon in two beam experiments.

measured at 31554 cm^{-1} by McClure.[21] The arrow in Fig. 3 shows the position of the 0-0 transition forbidden in two-photon transition. Energy differences of the main bands from the 0-0 band are summarized in Table 1. Many bands observed in the lower energy side of the strongest false origin at 0+1538 cm^{-1} can be attributed to vibronic bands induced by non-totally symmetric vibrations of u-type. Most bands at the higher energy side of the false origin can be attributed to combinations of u-vibrations and totally symmetric vibrations in the excited state.

The polarized excitation spectra with one beam (Figs. 5—7) are essentially the same as those observed by Hochstrasser and Sung.[12] Due to the wavelength dependence of the polarization of the laser output, the spectra had to be taken in four sections separately for comparison of the two spectra. Usually, one polarized component of the dye laser output is attenuated with respect to the other so that the two polarizations have comparable intensities. The attenuation ratio changes from one spectral section to another, so that one should not compare the intensities of two peaks from different spectral sections. Figure 5 shows a part of the polarized spectra of the strongest vibronic origin at 0+1538 cm^{-1} and a band at 0+1430 cm^{-1} taken on the three principal crystal faces of durene. In the spectra on the (ab) face in which the propagation vector of the incident light is parallel to the c′ axis ($k//c'$), the peak intensity of the a-polarized spectrum ($E//a$) of 1538 cm^{-1} is as intense as that of the b-polarized component ($E//b$). However, in the (ac′) spectra the a-component of the band is more than twice as intense as the c′-component. On the other hand, the 1430 cm^{-1} band is the opposite of that of the 1538 cm^{-1} band in polarization behavior, being predominantly polarized along the c′ axis. Similar characteristics of the polarization spectra in the lower energy regions than the 1430 cm^{-1} band can be seen in Figs. 6 and 7. The polarization ratios are given in Table 2.

Table 1. Observed frequencies of two-photon excitation spectra of naphthalene in durene crystal

λ/Å	$2\bar{\nu}_{vac}$/cm^{-1}	$\Delta\bar{\nu}$[a)]/cm^{-1}	Assignment	$\Delta\bar{\nu}$(obsd)−$\Delta\bar{\nu}$(calcd)
6232.2	31621	67		
6271.6	31881	327		
6262.7	31926	372	372	
6223.6	32127	573		
6196.2	32269	715	715	
6194.3	32279	725		
6182.9	32338	784		
6173.3	32389	835		
6169.6	32408	854	854	
6155.0	32485	931	931	
6149.7	32513	959	931+28 (lattice mode)	
6139.2	32569	1015		
6132.7	32603	1049		
6126.7	32635	1081	1081	
6124.5	32647	1093		
6117.5	32684	1130	1130	
6104.1	32756	1202	1202	
6091.6	32823	1269	1269	
6079.4	32889	1335		
6074.4	32916	1362		
6071.1	32934	1380		
6061.8	32984	1430	1430	
6058.3	33003	1449		
6049.4	33052	1498		
6042.0	33092	1538	1538	
6037.0	33120	1566	1538+28	
6035.1	33130	1576		
6029.7	33160	1606		
6023.3	33196	1642		
5989.9	33380	1826	1130+697	−1
5975.8	33459	1905	1202+697	+6
5952.5	33590	2036	1538+498	0
5938.3	33670	2116	1130+981	+5
5936.6	33680	2126	1430+697	−1
5917.5	33789	2235	1538+697	0
5912.0	33820	2266	1538+697+28	+3
5903.8	33867	2313		
5900.7	33885	2331	931+1403	−3
5896.9	33907	2353		
5887.4	33961	2407	1430+981	−4
5882.6	33989	2435		
5877.5	34019	2465		
5873.0	34045	2491		
5868.2	34073	2519	1538+981	0
5864.8	34092	2538	1538+981+28	−9
5850.3	34177	2623	1430+498+697	−2
5838.0	34249	2695		
5831.8	34285	2731	1538+498+697	−2
5826.3	34318	2764		
5815.7	34380	2826	1430+2×697	+2
5809.6	34416	2862		
5800.7	34469	2915		
5796.3	34495	2941	1538+1403	0
5792.2	34520	2966	1538+1403+28	−3
5784.0	34569	3015	1538+498+981	−2
5777.0	34610	3056		
5747.0	34791	3237	1538+698+981(?)	+21

a) Frequency difference from the 0-0 transition at 31554 cm^{-1}.[21]

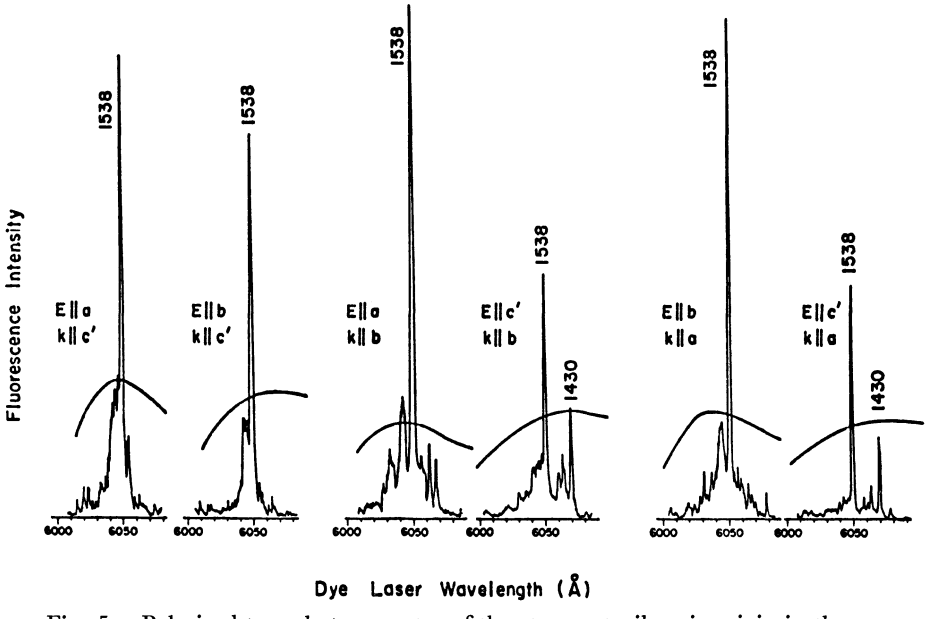

Fig. 5. Polarized two-photon spectra of the strongest vibronic origin in three different crystal faces of durene, with one laser beam. Smooth curves indicate intensity distributions.

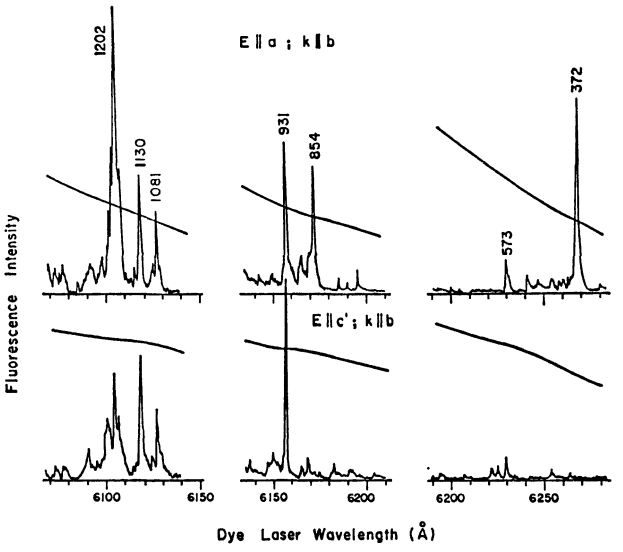

Fig. 6. A part of polarized two-photon excitation spectra in the (ac′) face of durene. Smooth curves indicate dye laser intensity distributions. One cannot compare the relative intensities in different spectral regions.

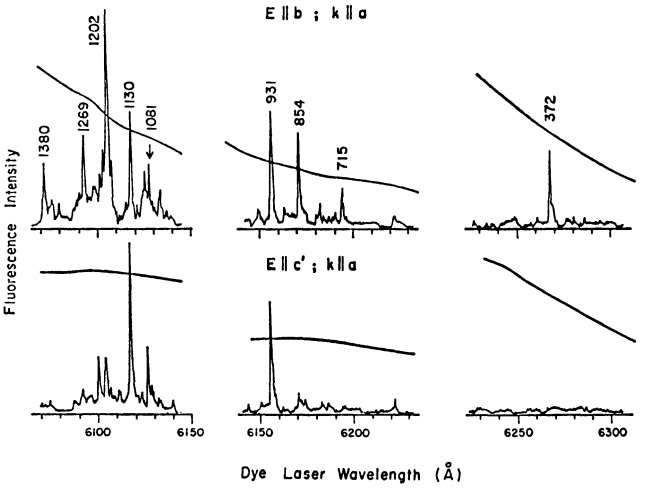

Fig. 7. A part of the polarized two-photon excitation spectra in the (bc′) face of durene. Smooth curves indicate dye laser intensity distributions. One cannot compare the relative intensities in different spectral regions.

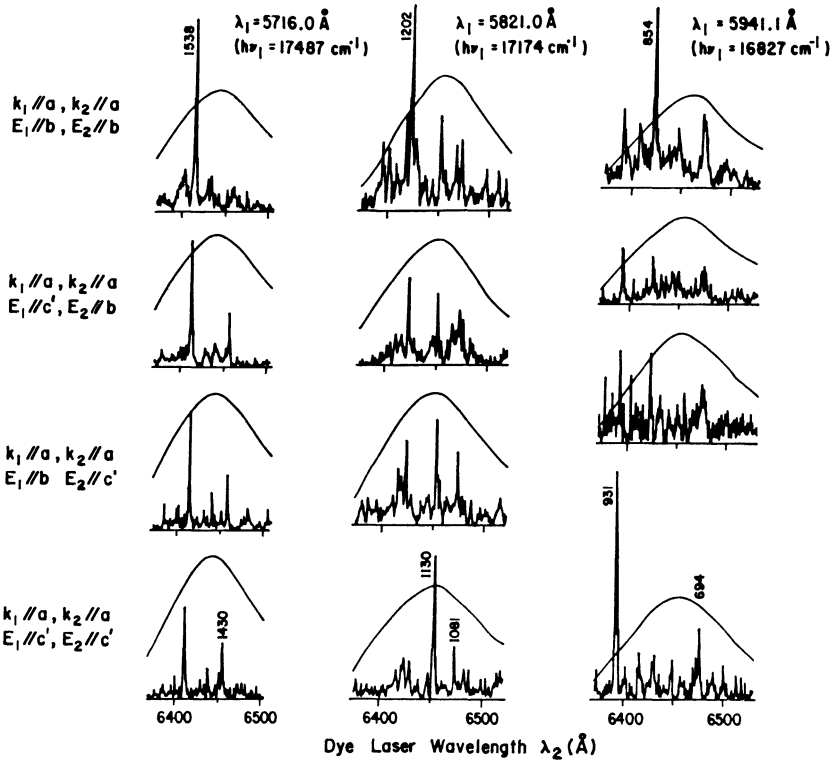

Fig. 8. A part of the polarized two-photon excitation spectra with two dye lasers of different frequencies and different polarizations and parallel beam incidence. The spectra were taken on the (bc′) face of durene at 5 K. k_1, E_1, and λ_1 indicate the k-vector, the polarization and the wavelength of the incident photon with higher energy, respectively. k_2, E_2, λ_2 indicate those of the lower energy photon. One cannot compare the relative intensities in different spectral regions. Smooth curves indicate intensity distributions of dye laser with lower-energy (Cresyl violet+ Rhodamine-B).

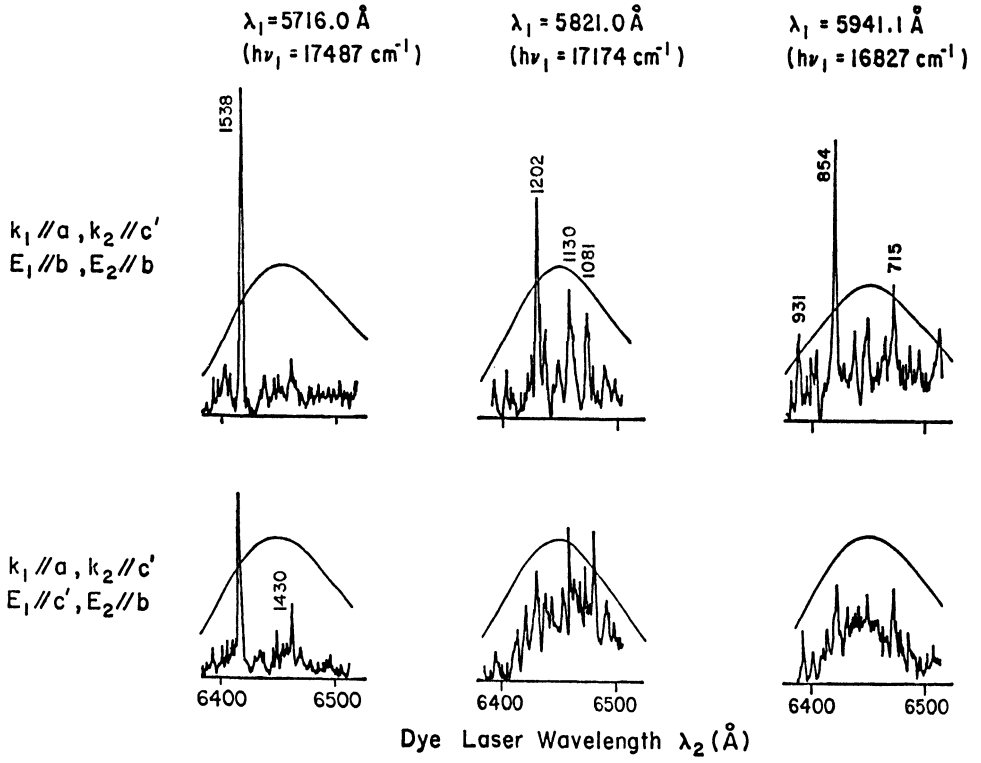

Fig. 9. A part of the polarized two-photon excitation spectra using two beams with 90 degree incidence. k_1, k_2 indicate k-vectors of the high energy photon λ_1 with the polarization E_1 and the lower energy photon λ_2 with the polarization E_2 respectively.

We can distiguish at least three kinds of bands with different polarization behavior (Figs. 5—7). The vibronic bands at 372, 715, 854, 1202, and 1269 cm^{-1} (type I) are polarized predominantly along the a-component on the (ac') spectra and also along the b-component on the (bc') spectra. Another group including 931, 1130, and 1430 cm^{-1} (type III) are apparently polarized along the c'-component in the (ac') or (bc') spectra. The strongest false origin at 1538 cm^{-1} and a band at 1081 cm^{-1} (type II) which are polarized weakly along the a axis in the (ac') plane and also along the b axis in the (bc') plane.

Two Beam Experiment. The excitation spectra taken with two beams of different frequencies and polarizations are shown in Figs. 8 and 9. λ_1 refers to the wavelength of the laser beam with higher energy and λ_2 to that of lower energy photons (Fig. 1). The sum of the frequencies of these two lights should coincide with the excitation energy of the transition. Since the lower frequency photon (λ_2) was tuned in the range where the molecule was not excited by the absorption of the two quanta of λ_2, the two-photon energy of λ_1 should always be higher than the transition energy. Thus, λ_1 beam necessarily induces a constant background on the excitation spectra. However, we were able to find suitable wavelengths of λ_1 to minimize the background (the wavelength λ_1 is indicated by arrow in Fig. 4).

Figure 8 shows the observed spectra using two beams of parallel incidence. The top two spectra in each

Table 2. Observed intensity ratios of the main vibronic bands

$\Delta\tilde{\nu}$ / cm^{-1}	$\left[\frac{I(bb)}{I(c'c')}\right]_1$ a)	$\left[\frac{I(bc')}{I(bb)}\right]_2$ b)	$\left[\frac{I(c'b)}{I(c'c')}\right]_2$ b)	$\left[\frac{I(bb)}{I(c'c')}\right]_2$ b)	$\left[\frac{I(aa)}{I(c'c')}\right]_1$ a)	$\left[\frac{I(ac')}{I(aa)}\right]_2$ b)	$\left[\frac{I(c'a)}{I(c'c')}\right]_2$ b)	$\left[\frac{I(aa)}{I(c'c')}\right]_2$ b)
372	>25	—	—	—	>80	—	—	—
715	7.9	0.48	0.91	1.9	7.7	—	—	—
854	11	0.27	5.0	19	38	—	—	—
931	<1.2	0.82	0.34	0.41	0.31	—	—	—
1081	1.5	0.86	1.27	1.5	3.5	0.68	1.60	2.35
1130	<1.4	0.81	0.62	0.76	2.3	0.88	1.64	1.86
1202	6.7	0.42	1.82	4.5	7.7	1.13	>3.0	>2.65
1269	4.6	0.15	2.78	18	—	—	—	—
1430	0.32	2.69	1.05	0.38	0.84	>1.60	0.67	<0.42
1538	1.8	0.62	1.25	2.0	2.5	0.68	1.57	2.31

a) Value taken from one beam experiment. b) Value taken from two beam experiment.

column were taken by simply changing the polarization of beam 1 without disturbing the optics or changing the sensitivity of the detection system. The lower two spectra were taken after a 90° rotation of the crystal along the axis of incident beams (the incident beams enter the cryostat from the bottom window, see Fig. 1). Thus we can directly measure the ratio for an individual band, $I(\mathrm{bc}')/I(\mathrm{bb})$, by using the normarized peak of the upper two spectra and also $I(\mathrm{c'b})/I(\mathrm{c'c'})$ by using the lower two spectra in Fig. 8. We can assume that the middle two spectra, *i.e.* $I(\mathrm{bc}')$ and $I(\mathrm{c'b})$, are identical when the frequency difference between the photons λ_1 and λ_2 is so small that the asymmetric property of the two-photon transition tensor can be neglected. We can then obtain the polarization ratio $I(\mathrm{bb})/I(\mathrm{c'c'})$ with two beams on the (bc') plane. Observed polarization ratios in the two beam experiment are summarized in Table 2 together with the ratios in the one beam experiments. The reproduced intensity ratios $I(\mathrm{bb})/I(\mathrm{c'c'})$ or $I(\mathrm{aa})/I(\mathrm{c'c'})$ for the two beam experiments are in line with those measured directly from the one beam experiment.

A part of the polarized spectra using two beams with 90 degree incidence is shown in Fig. 9. Each spectrum is similar to its counterpart in Fig. 8. It can be concluded that the polarized spectra do not depend on the direction of propagation of the incident laser beams.

Discussion

Estimation of the Two-photon Transition Tensor. Polarization dependence of two-photon transition can be expressed in terms of a 3×3 tensor. Consider the probability of a two-photon transition i→f. A component of the matrix element of the two-photon transition is expressed as follows:

$$(\sigma^{\mathrm{if}})_{\mathrm{AB}} = \sum_{\mathrm{e}}\left\{\frac{\langle \mathrm{i}|\vec{\mathrm{p}}\cdot\hat{\mathrm{e}}_{\mathrm{A}}|\mathrm{e}\rangle\langle \mathrm{e}|\vec{\mathrm{p}}\cdot\hat{\mathrm{e}}_{\mathrm{B}}|\mathrm{f}\rangle}{\Delta E_{\mathrm{ie}}-\hbar\omega_{\mathrm{A}}+i\Gamma_{\mathrm{e}}} + \frac{\langle \mathrm{i}|\vec{\mathrm{p}}\cdot\hat{\mathrm{e}}_{\mathrm{B}}|\mathrm{e}\rangle\langle \mathrm{e}|\vec{\mathrm{p}}\cdot\hat{\mathrm{e}}_{\mathrm{A}}|\mathrm{f}\rangle}{\Delta E_{\mathrm{ie}}-\hbar\omega_{\mathrm{B}}+i\Gamma_{\mathrm{e}}}\right\}, \tag{1}$$

where $|\mathrm{e}\rangle$ is an intermediate state for the two-photon process with its excitation energy ΔE_{ie} and a line width Γ_{e}. A and B denote the polarization of the incident photons with energy $\hbar\omega_{\mathrm{A}}$ and $\hbar\omega_{\mathrm{B}}$, respectively. The complete form of the tensor can be expressed by using molecular symmetric axes (L, M, N) as basis axes. We have

$$\sigma^{\mathrm{if}} \equiv \begin{bmatrix} \sigma_{\mathrm{LL}} & \sigma_{\mathrm{LM}} & \sigma_{\mathrm{LN}} \\ \sigma_{\mathrm{ML}} & \sigma_{\mathrm{MM}} & \sigma_{\mathrm{MN}} \\ \sigma_{\mathrm{NL}} & \sigma_{\mathrm{NM}} & \sigma_{\mathrm{NN}} \end{bmatrix}_{\mathrm{if}} \tag{2}$$

Generally, σ^{if} is an asymmetric tensor. It can be split into two parts,[8] symmetric and antisymmetric:

$$\sigma^{\mathrm{if}} = \sigma_{\mathrm{s}}^{\mathrm{if}} + \sigma_{\mathrm{a}}^{\mathrm{if}}$$

$$\sigma_{\mathrm{s}}^{\mathrm{if}} = \begin{bmatrix} \sigma_{\mathrm{LL}} & \frac{(\sigma_{\mathrm{LM}}+\sigma_{\mathrm{ML}})}{2} & \frac{(\sigma_{\mathrm{LN}}+\sigma_{\mathrm{NL}})}{2} \\ \frac{(\sigma_{\mathrm{ML}}+\sigma_{\mathrm{LM}})}{2} & \sigma_{\mathrm{MM}} & \frac{(\sigma_{\mathrm{MN}}+\sigma_{\mathrm{NM}})}{2} \\ \frac{(\sigma_{\mathrm{NL}}+\sigma_{\mathrm{LN}})}{2} & \frac{(\sigma_{\mathrm{NM}}+\sigma_{\mathrm{MN}})}{2} & \sigma_{\mathrm{NN}} \end{bmatrix}_{\mathrm{if}}, \tag{3}$$

$$\sigma_{\mathrm{a}}^{\mathrm{if}} = \begin{bmatrix} 0 & \frac{(\sigma_{\mathrm{LM}}-\sigma_{\mathrm{ML}})}{2} & \frac{(\sigma_{\mathrm{LN}}-\sigma_{\mathrm{NL}})}{2} \\ \frac{(\sigma_{\mathrm{ML}}-\sigma_{\mathrm{LM}})}{2} & 0 & \frac{(\sigma_{\mathrm{MN}}-\sigma_{\mathrm{NM}})}{2} \\ \frac{(\sigma_{\mathrm{NL}}-\sigma_{\mathrm{LN}})}{2} & \frac{(\sigma_{\mathrm{NM}}-\sigma_{\mathrm{MN}})}{2} & 0 \end{bmatrix}_{\mathrm{if}} \tag{4}$$

If the energy separation between the initial state and the intermediate state ΔE_{ie} is large as compared with the incident photon energies, *i.e.* off-resonance condition or energy difference between the two photons $\hbar\omega_{\mathrm{A}}$ and $\hbar\omega_{\mathrm{B}}$ is negligible as compared with the ΔE_{ie}, $\sigma_{\mathrm{a}}^{\mathrm{if}}$ can be neglected. Therefore, σ^{if} will be adequately approximated by the symmetric form $\sigma_{\mathrm{s}}^{\mathrm{if}}$. We assume that the transition tensor is symmetric even in the case of the two beam experiment with different photon energies, because the difference of these photon energies is very small as compared with the ΔE_{ie}.

The electronic state in the crystal can be described in terms of molecular states in the crystal lattice, *i.e.* the oriented gas model. Knowing the direction cosines of the molecular axes in the crystal, we can express the polarization characteristics of the two-photon transition in an oriented crystal in terms of the molecular two-photon transition tensor. The intensity ratio between the two polarized spectra $I(\alpha\beta)$ and $I(\gamma\delta)$ can be written as

$$\frac{I(\alpha\beta)}{I(\gamma\delta)} = \frac{|\sum_{\mathrm{AB}}\sigma_{\mathrm{AB}}\cos\theta_{\alpha}^{\mathrm{A}}\cos\theta_{\beta}^{\mathrm{B}}|^2}{|\sum_{\mathrm{AB}}\sigma_{\mathrm{AB}}\cos\theta_{\gamma}^{\mathrm{A}}\cos\theta_{\delta}^{\mathrm{B}}|^2}, \tag{5}$$

where α, β, or γ, δ denote the crystal axes, and A and B the molecular axes. σ_{AB} denotes the AB elements of molecular tensor of the two-photon transition amplitude in Eq. 2, $\cos\theta_{\alpha}^{\mathrm{A}}$ being the direction cosine between the crystal axis α and molecular axis A. Orientational factor of the two-photon transition of naphthalene in durene crystal can be easily obtained since the guest molecules are known to be embedded substitutionally in the lattice. L and M indicate the molecular long and short axes, respectively, in the molecular plane of naphthalene. a, b, and c' indicate the crystal axes of durene which are very close to the optical axes. Since the projection of axis N, which is perpendicular to the molecular plane, are very similar to those of axis L, we cannot distinguish their contributions. However, the contribution from axis N can be safely neglected since there are no dipole allowed transitions along it for the low-lying electronic states of the molecule. Under these conditions, we can easily find a leading term of the molecular tensor component in the two-photon spectra. As an example,

$$\begin{aligned} I(\mathrm{bb}) &= C\cdot(0.317)\sigma_{\mathrm{LL}}^2 \\ I(\mathrm{c'c'}) &= C\cdot(0.972)\sigma_{\mathrm{MM}}^2 \\ I(\mathrm{c'b}) &= I(\mathrm{bc}') = C\cdot(0.555)\{\sigma_{\mathrm{LM}}^2+\sigma_{\mathrm{ML}}^2\} \\ I(\mathrm{aa}) &= C\cdot(0.184)\sigma_{\mathrm{LL}}^2 \\ I(\mathrm{ab}) &= I(\mathrm{ba}) = C\cdot(0.241)\sigma_{\mathrm{LL}}^2 \\ I(\mathrm{ac}') &= I(\mathrm{c'a}) = C\cdot(0.423)\{\sigma_{\mathrm{LM}}^2+\sigma_{\mathrm{ML}}^2\} \end{aligned} \tag{6}$$

where C is a constant.

We can estimate the relative magnitudes of the squared elements of the tensor in the first approxima-

tion. If the relative signs of the elements are known, iterations using Eq. 5 can be employed to obtain more precise values. However, our experimental values are not sufficiently accurate to do so and the signs of the elements are not known. Corrections on the first approximation cannot exceed 10% of the original values and are thus ignored. The relative magnitude of the squared molecular two-photon transition amplitudes are given in Table 3.

Table 3. Relative magnitude of the tensor elements for two-photon transitions

$\Delta\tilde{\nu}$ / cm^{-1}	$\left\|\frac{\sigma_{MM}}{\sigma_{LL}}\right\|^2$	$\left\|\frac{\sigma_{LM}}{\sigma_{LL}}\right\|^2$	Type
715	0.04	0.14	I
854	0.02	0.08	I
931	0.78	0.23	III
1081	0.22	0.25	II
1130	0.42	0.23	III
1202	0.07	0.12	I
1269	0.02	0.04	I
1430	0.86	0.77	III
1538	0.16	0.18	II

We can draw the following conclusions: (1) The gross features of the polarization measurements indicate that σ_{LL} is the predominant tensor element. This might be due to the fact that most intense low-lying transitions of naphthalene are long-axis polarized. Since two-photon transition should gain intensity from one-photon transitions, the behavior is not unexpected. (2) Type I bands can be associated with the smallest σ_{MM}; type II with slightly larger σ_{MM} and type III with even larger σ_{MM}, with respect to σ_{LL}. The naphthalene guest molecules are so oriented that even a small σ_{MM} gives rise to a large $I(c'c')$. (3) The relatively large σ_{LM} is somewhat unexpected. For type I and II bands, all the assignments so far are in line with a b_{2u} vibration in a $^1B_{2u}$ electronic state to yield an overall A_g vibronic state. No σ_{LM} is expected within the oriented gas model. We can either relax the symmetry selection rules by introducing the crystal field perturbations or assume higher order radiation field-molecule coupling schemes. It appears that the former interpretation is more reasonable. (4) Type III bands can be interpreted as either a (LL+MM) mechanism of an A_g vibronic symmetry or LM mechanism of a B_{3g} vibronic symmetry. The crystal field perturbation could be operating here also with the net effect that polarization behavior becomes less distinct.

Assignments for Prominent Lines Based on the Dominant Tensor Elements. Assignments have been made by Hochstrasser and Sung[12] and by Mikami and Ito[13] for the individual vibronic transitions of naphthalene based on polarization experiments on crystals and by Boesel *et al.*[18] for the spectrum in vapor. Let us discuss these assignments (Table 3).

(1) 1538 cm^{-1}: This is the strongest vibronic origin of the spectrum. The dominant tensor element is σ_{LL} of an A_g two-photon tensor, which confirms the results reported by the others 1538 cm^{-1} in this work corresponds to 1540 cm^{-1} in durene crystal and 1542 cm^{-1} in neat crystal given by Hochstrasser and Sung, to 1535 cm^{-1} in pure crystal given by Mikami and Ito, and to 1559 cm^{-1} in vapor spectrum given by Boesel *et al.* The vibrational assignment of this band seems to be well established, *i.e.* 1538 cm^{-1} in the excited state has been assigned to a b_{2u} species which corresponds to 1375 cm^{-1} (ν_{14}) of a b_{2u} type vibration in the ground state. Although this is polarized strongly along the LL-component in the neat crystal, we have observed a non-vanishing amount of MM-component (σ_{MM}) in the durene crystal. In the study by Hochstrasser and Sung the same characteristics have been observed (*cf.* Ref. 12, Table IV) while the ratio of σ_{MM} to σ_{LL} in the neat crystal should be much less than the ratio in durene (*cf.* Ref. 12, Table V). Another remarkable point is existence of the unexpected off-diagonal two-photon tensor element σ_{LM}. This would not be the case on the basis of the assignment described above.

(2) 1430 cm^{-1}: Two-photon tensor shows mixed polarization. Like other type III bands, assignment of this band could not be made unequivocally. This could be attributed to LM-polarization, characteristic of a B_{3g} tensor with a b_{1u} vibration. Hochstrasser and Sung assigned their 1433 cm^{-1} band to a b_{2u} vibration with a dominant MM-component of an A_g tensor. No corresponding band was observed in the gas phase.

(3) 1269 cm^{-1}: This is polarized dominantly in LL-component which means an A_g tensor with a b_{2u} vibration. This agrees with the assignment by Hochstrasser and Sung for their 1276 cm^{-1} band. No corresponding band was observed in vapor.

(4) 1202 cm^{-1}: This polarized in the LL-component of an A_g tensor although an unnegligible amount of LM-component was observed. This corresponds to 1207 cm^{-1} by Hochstrasser and Sung and 1206 cm^{-1} in vapor by Boesel *et al.*, which have also been assigned as an A_g vibronic transition with a b_{2u} vibration.

(5) 1130 cm^{-1}: Mixed components were observed. The polarization characteristics of this band are similar to those of 1430 cm^{-1}. This could be assigned as LM-mechanism of a B_{3g} vibronic state, although an A_g tensor with mixed components (LL+MM) are also possible. Hochstrasser and Sung also observed 1140 cm^{-1} band with a similar polarization behavior to their 1433 cm^{-1}. They pointed out that the appropriate tensor is an A_g type on the basis of polarization in the neat crystal.

(6) 1081 cm^{-1}: The tensor pattern is similar to that of 1538 cm^{-1}. No corresponding band was observed by others.

(7) 931 cm^{-1}: Mixed polarization was observed. The tensor pattern is similar to that of 1430 cm^{-1}. We assigned this to A_g with mixed polarization (LL+MM) confirming the assignment for their 941 cm^{-1} by Hochstrasser and Sung. Boesel *et al.* assigned their 940 cm^{-1} band in vapor spectrum to a B_{3g} vibronic band induced by b_{1u} vibration, and Mikami and Ito also assigned their 901 cm^{-1} band in neat crystal to a B_{3g} state. The discrepancy might be due to the complicated tensor pattern of this band which cannot be clarified by simple one beam experiments.

TABLE 4. ASSIGNMENTS AND MECHANISMS OF TWO-PHOTON TRANSITIONS OF THE MAIN VIBRONIC BANDS (in cm^{-1})

Hochstrasser and Sung[a] (in durene)	Mikami and Ito[b] (in pure crystal)	Boesl, Neusser and Schlag[c] (in gas)	This work (in durene)
390(b_{1u})	365(b_{1u})	355(b_{1u})	372
		592(b_{2u})	573
			715(b_{2u}) LL
863(b_{3u})	847(b_{2u})	865(b_{3u})	854(b_{2u}) LL
941(b_{2u})	901(b_{1u})	940(b_{1u})	931(b_{2u}) LL+MM
	1029(b_{2u})		
1102			1081(b_{2u}) LL
1140(b_{1u})	1107(b_{2u})		1130(b_{2u} or b_{1u}) LL+MM or LM
1194(b_{1u})			
1207(b_{2u})	1203(b_{2u})	1206(b_{2u})	1202(b_{2u}) LL
1276(b_{1u})			1269(b_{2u}) LL
1433(b_{2u})	1397(b_{2u})		1430(b_{1u} or b_{2u}) LM or LL+MM
1506(b_{1u})			
1540(b_{2u})	1535(b_{2u})	1559(b_{2u})	1538(b_{2u}) LL

a) Ref. 12. b) Ref. 13. c) Ref. 18.

(8) 854 cm^{-1}: This band is polarized dominantly along LL-component which corresponds to an A_g tensor, if we assume that the contribution from the N axis of the molecule can be neglected. Hochstrasser and Sung assigned their 863 cm^{-1} in durene to a B_{1g} vibronic band on the basis of the anisotropy of the two-photon signal of the corresponding bands 853 and 857 cm^{-1} in the neat crystal. Boesel *et al.* also assigned their 865 cm^{-1} in vapor spectrum to a B_{1g} state induced by b_{3g} vibration in the excited state. In our analysis we cannot distinguish the difference in polarization characteristics of LL and NN, because of the orientation of the molecule in durene crystal.

(9) 715 cm^{-1}: This is polarized along LL-component. This band might correspond to 727 cm^{-1} in the neat crystal spectra by Hochstrasser and Sung. No corresponding band was observed in vapor.

(10) 372, 573 cm^{-1} and Other Weak Bands: No two beam experiments was carried out on these bands because of weakness of their two-photon signal. The results are summarized in Table 4.

Intermediate States of the Two-photon Processes in the 1538 cm^{-1} Band. The strongest false origin at 1538 cm^{-1} in the spectrum is one of the key bands which characterize the two-photon spectrum in the lowest excited singlet state ($^1B_{2u}$) of naphthalene. The mechanism of the vibronic coupling for this band has been discussed in detail based on the polarization experiment of the neat crystal. It was emphasized that the vibronic coupling between the excited state and the ground state through the b_{2u} vibration of 1538 cm^{-1} is involved.[13] Let us consider the intermediate states for the two-photon transition processes of the band. From Eq. 1 we get the following expressions of the matrix element for the two-photon transition.

$$(\sigma^{gf})_{LL} = \sum_L \left\{ \frac{\vec{\mu}_{gL}^{(1)} \cdot \vec{\mu}_{Lf}^{(2)}}{\Delta E_{gL} - \hbar\omega_1 + i\Gamma_L} + \frac{\vec{\mu}_{gL}^{(2)} \cdot \vec{\mu}_{Lf}^{(1)}}{\Delta E_{gL} - \hbar\omega_2 + i\Gamma_L} \right\}$$
$$(\sigma^{gf})_{MM} = \sum_M \left\{ \frac{\vec{\mu}_{gM}^{(1)} \cdot \vec{\mu}_{Mf}^{(2)}}{\Delta E_{gM} - \hbar\omega_1 + i\Gamma_M} + \frac{\vec{\mu}_{gM}^{(2)} \cdot \vec{\mu}_{Mf}^{(1)}}{\Delta E_{gM} - \hbar\omega_2 + i\Gamma_M} \right\} \quad (7)$$

Where $\vec{\mu}_{gL}^{(1)} \equiv \langle g|\vec{r}\cdot\hat{e}_1|L\rangle$, $\vec{\mu}_{Mf}^{(2)} \equiv \langle M|\vec{r}\cdot\hat{e}_2|f\rangle$ *etc.* L denotes an intermediate state of the two-photon process with B_{2u} symmetry and M a state with B_{1u} symmetry. $\vec{\mu}_{Lf}$, $\vec{\mu}_{Mf}$ denote the transition moment from the intermediate states to the final vibronic level at 1538 cm^{-1} above the origin of the lowest singlet state. We do not known the values of $\vec{\mu}_{Lf}$ or $\vec{\mu}_{Mf}$. However, we adopt the vibronic coupling involving the ground state described above. The transition moment can be estimated from the known values of $\vec{\mu}_{gL}$ or $\vec{\mu}_{gM}$ which are the transition moments from the ground state to the L or M states. The electronic wave function of the vibronic state in the first excited state can be expressed by a linear combination of the zeroth order wave function of the state and that of the ground state with the coupling constant of Herzberg-Teller type along the normal coordinate of the b_{2u} vibration. Transition moment from a higher electronic excited state L or M to the vibronic state expressed by such an approximation can be split into two terms, the transition moment from L or M to the zeroth order first excited state, and that from L or M to the ground state multiplied by a Herzberg-Teller coupling constant. Since the L or M state is an optically allowed state from the ground state and should have an *ungerade* symmetry, the former term in the transition moment would vanish in the framework of approximation. The second term contributes to the transition moment $\vec{\mu}_{Lf}$ or $\vec{\mu}_{Mf}$. We can safely assume that the transition moments from a higher electronic excited state L or M to the vibronic state are proportional to the transition moments from the L or M state to the ground state. Neglecting the difference between $\hbar\omega_1$ and $\hbar\omega_2$ in Eq. 7, we have the following expressions for the two-photon tensor elements:

$$(\sigma^{gf})_{LL} = 2\sum_L \left\{ \left(\frac{H'_{ge}}{\Delta E_{ge}} \right) \cdot \left(\frac{\vec{\mu}_{gL} \cdot \vec{\mu}_{Lg}}{\Delta E_{gL} - \hbar\omega + i\Gamma_L} \right) \right\}$$
$$(\sigma^{gf})_{MM} = 2\sum_M \left\{ \left(\frac{H'_{ge}}{\Delta E_{ge}} \right) \cdot \left(\frac{\vec{\mu}_{gM} \cdot \vec{\mu}_{Mg}}{\Delta E_{gM} - \hbar\omega + i\Gamma_M} \right) \right\} \quad (8)$$

where H'_{ge} denotes the matrix element of the Herzberg-Teller coupling.

By means of the expressions we can estimate $(\sigma_{MM}/\sigma_{LL})^2$ by using the observed values of the oscillator strength f and the excitation energies of the low-lying π-π^* excited states. The values are as follows[22]

$S_1(^1B_{2u}$: L-polarization) $f=0.002$ $\Delta E=32200\ cm^{-1}$
$S_2(^1B_{1u}$: M-polarization) $f=0.18$ $\Delta E=35000$
$S_3(^1B_{2u}$: L-polarization) $f=1.70$ $\Delta E=45300$
$S_4(^1B_{2u}$: L-polarization) $f\approx0.2$ $\Delta E=52500$
$S_5(^1B_{1u}$: M-polarization) $f\approx0.6$ $\Delta E=59800$

Taking 16500 cm^{-1} as the photon energy of the incident photon $\hbar\omega$ and neglecting the line width Γ's, we have 1.7×10^{-8} cm^2 for the $(\sigma)^2_{LL}$ with unit Herzberg-Teller constant. The contribution to the two-photon tensor element arises mainly from S_3 and S_4 with constructive sum. For the MM-component the constructive sum of the contributions from the two M-polarized excited states S_2 and S_5 has also been considered, $(\sigma)^2_{MM}$ being found to be 2.2×10^{-9} cm^2 with the same unit. The calculated ratio $(\sigma_{MM}/\sigma_{LL})^2$ is then 0.13, the value observed being 0.16. In spite of the simple estimation agreement between the estimate and observed values is fairly good. The ratio calculated with a contribution from a single excited state to each component turns out too large or too small as compared with the value obtained. The destructive interference between the contributions in each tensor component from any two excited states can be neglected because neither excited state is below the energy of the incident photon. From the results we conclude that all the low-lying electronic states contribute as the intermediate states for the two-photon transition to the 1538 cm^{-1} vibronic state in the lowest singlet state. This seems to be reasonable since the energies of both incident photons ω_1 and ω_2 in this experiment are far from the excitation energies of the intermediate states, *viz.*, the off-resonance condition in the two-photon absorption processes. In the off-resonance condition all the low-lying electronic states should contribute to the two-photon processes, as in the case of the off-resonance condition in Raman processes.

Crystal Field Effects on the Two-photon Transition. If we assume the oriented gas model for two-photon spectra in the crystal, we should have no off-diagonal matrix element σ_{LM} (and σ_{ML}) of the molecular two-photon tensor of A_g type. However, as shown in Table 3, a considerable amount of off-diagonal component was observed even in A_g vibronic states. For example, the 1538 cm^{-1} band has already been assigned to the A_g vibronic state composed of b_{2u} vibration in the $^1B_{2u}$ electronic state from both crystal and vapor spectra. For the sake of confirmation we have carried out detailed polarization measurement of the band using two beams on the three different crystal faces of durene. The ratios of intensities of different polarizations as compared to the strongest component I(ab) are given in Table 5, together with calculated ratios using the estimated values of the squared ratio of the two-photon tensor elements (Table 3); $\sigma_{LL}=1.00$, $\sigma_{MM}=0.16$, $\sigma_{LM}=0.18$. We see that the estimated values of the squared tensor elements reproduce the polarization ratios for different crystal faces fairly well. The predicted behavior and that of observed polarization of the vibronic states are more or less in agreement.

Table 5. Relative intensities of the strongest false origin at 1538 cm^{-1} in the polarized spectra of different crystal faces

	I(aa)	I(bb)	I(c'c')	I(ab)	I(bc')	I(ac')
Obsd ratio	0.97	0.65	0.38	1.00	0.41	0.68
Calcd ratio	0.38	0.66	0.32	1.00	0.41	0.32

In order to understand the strange polarization effect of the two-photon transition in the crystal, we should take into account the crystal field effect on the molecular states. Group-theoretically the tensor of the molecule embedded in the site of the durene crystal is no longer diagonal since the site symmetry of the crystal is C_i and all the g molecular states fall into A_g symmetry in the C_i site group. In this case three different crystal field mixing processes of the states in the crystal can be considered. (1) Mixing of the normal modes of the molecular vibrations in the crystal due to molecular deformation. For example, the vibrational mode mixing between b_{2u} vibration and b_{1g} vibration causes mixing of the two-photon states of A_g symmetry and of B_{3g} symmetry. In this process, redistribution of the two-photon intensity among all the vibronic states of the same electronic state would take place. This is not very likely since no intense bands with a σ_{LM} component can be identified that can share σ_{LM} with the A_g vibronic state. (2) Mixing among the intermediate states of the two-photon processes is possible. One intermediate state with B_{2u} symmetry (L-polarization), for example, will interact with the other intermediate state with B_{1u} symmetry (M-polarization) in the presence of the crystal field or due to the molecular deformation in the crystal. In this case, the apparent LM-component of the tensor due to the crystal field perturbation V_c can be expressed as

$$(\sigma^{gf})_{LM}=2\sum_L\left\{\frac{\vec{\mu}_{gL}\cdot\sum_M(\lambda_{LM}\cdot\vec{\mu}_{Mf})}{\Delta E_{gL}-\hbar\omega+i\Gamma_L}\right\}+2\sum_M\left\{\frac{\vec{\mu}_{gM}\cdot\sum_L(\lambda_{ML}\cdot\vec{\mu}_{Lf})}{\Delta E_{gM}-\hbar\omega+i\Gamma_M}\right\} \quad (9)$$

where $\lambda_{LM}=\langle L|V_c|M\rangle/\Delta E_{LM}$ stands for the interaction between the intermediate states L and M. Using the same assumption and oscillator strengths for the L or M states employed in the preceding section, we require a very large value of λ_{LM} (more than unity) for any pair of the states L and M to reproduce the observed ratio $(\sigma_{LM}/\sigma_{LL})^2$. Such a large coupling is not likely. (3) The third process is interstate coupling between the vibronic state and other two-photon allowed electronic state with g symmetry. At least two g-electronic states in near UV region have been observed.[11,23] The lower one has been assigned to a B_{3g} electronic state in consideration of theoretical calculations. The other state has been assigned to an A_g electronic state. We can expect the mixing of wave

functions of the vibronic state A_g with that of the electronic B_{3g} and/or of the electronic A_g states. Such a mixing could provide a mechanism for the appearance of σ_{LM} in an A_g vibronic state. The perturbed wave function of the vibronic A_g state in the B_{2u} state (with a reduced symmetry of A) can be found by application of perturbation theory using the crystal flield perturbation V_c and the perturbing electronic state B which has originally a B_{3g} symmetry. Two-photon transition tensor of the true crystalline state of the vibronic A state can be expressed as

$$\begin{bmatrix} \sigma_{LL} & \sigma_{LM} \\ \sigma_{ML} & \sigma_{MM} \end{bmatrix}^{A}_{crystal} = \begin{bmatrix} \sigma_{LL} & 0 \\ 0 & \sigma_{MM} \end{bmatrix}^{A_g}_{mol} + \frac{\langle A|V_c|B\rangle}{\Delta E_{AB}} \begin{bmatrix} 0 & \sigma_{LM} \\ \sigma_{ML} & 0 \end{bmatrix}^{A_{3g}}_{mol} \quad (10)$$

where the perturbation on the ground state is neglected and contributions from axis N are omitted. From Table 3, the ratio of the $|\sigma_{LM}|^2$ to $|\sigma(\text{total})|^2 (=|\sigma_{LL}|^2+2\cdot|\sigma_{LM}|^2+|\sigma_{MM}|^2)$ is found to be 0.12. The strength of the two-photon transition to the B_{3g} electronic state (located at about 44400 cm^{-1}) is about ten times that of the A_g vibronic state.[11] The mixing coefficient, $\langle A|V_c|B\rangle/\Delta E_{AB}$, is therefore estimated to be 0.11 or less. If we take the energy separation between the vibronic state and the B_{3g} state as $\Delta E_{AB}=9300$ cm^{-1}, the interaction energy $\langle A|V_c|B\rangle$ due to the crystal field is estimated to be about 990 cm^{-1}.

In order to ascertain the possibility of the crystal field mixing mechanism (3), there are no other suitable physical quantities in the excited state of the molecule which is directly related to the perturbation. However, if we assume that the stabilization energy of the excited molecular state in the crystal is almost of the same order of magnitude as that of the ground state, we can estimate the order of magnitude of the crystal field effect in the excited state. The total energy of an excited molecule A in a crystal can be written as

$$E_A(\text{crystal}) = E_A(\text{gas}) + \langle A|V_c|A\rangle + \sum_B \frac{|\langle A|V_c|B\rangle|^2}{\Delta E_{AB}}, \quad (11)$$

if we regard the $[E_A(\text{crystal})-E_A(\text{gas})]$ as the heat of sublimation of naphthalene (or durene). We have 6×10^3 cm^{-1}/ molecule for the stabilization energy of a molecule in crystal from the gas phase.[24] Since excited states are generally more polarizable, the value probably represents a lower limit of the stabilization energy of an excited molecule in the crystal. Actually the polarizability of the lowest singlet excited state of naphthalene is slightly larger than that of the ground state.[25,26] Considering only one perturbing state B and taking the value 990 cm^{-1} for $\langle A|V_c|B\rangle$, we have 105 cm^{-1}/ molecule for the second order polarization energy term in Eq. 11, which is one or two orders of magnitude less than the total stabilization energy in the crystal. Although it is not known what percentage of stabilization energy is due to the second order contribution in Eq. 11, the estimated value may not exceed the total second order polarization energy. Our estimate of the strength of crystal field perturbation on the guest molecules appears to be reasonable.

In the absorption study of the first singlet excited state of naphthalene in durene, McClure[27] reported an unexpected polarization behavior of many vibronic bands. Crystal field mixing on the one-photon spectra causes only reduction in the polarization ratios. In order to confirm the effect, very accurate measurements on the relative intensities of the spectra are required. On the other hand, in the two-photon experiments we have more degrees of experimental freedom on the polarization measurements than in the case of one-photon spectra. It is easy to find out the crystal field effects from the unexpected polarization. Two-photon transition tensors depend on more precise electron distributions in the ground and excited states than the one-photon transition dipoles. Crystal perturbation on the molecular wave function will give rise to more effects on the two-photon tensors.

Possibility of Optical Kerr Effect. Another possible cause for the unexpected off-diagonal component of the two-photon transition tensor in the crystal can be attributed to the occurrence of electric field-induced birefringence by optical light beam, *i.e.*, optical Kerr effect.[28] A strong polarized monochromatic laser beam at frequency ν_1 induces birefringence change in a medium so that the other polarized light beam at frequency ν_2 becomes partially depolarized when the two beams pass through the medium simultaneously. Resonance enhancement of the Kerr effect can efficiently depolarize the beam originally polarized. The resonance effect occurs when the photon energy $2\nu_1$, $2\nu_2$, $|\nu_1-\nu_2|$, or $\nu_1+\nu_2$ coincides with the proper molecular transitions. In the case of Raman resonance, *i.e.*, when $|\nu_1-\nu_2|$ corresponds to the molecular vibrational energy of a Raman active mode, this resonance enhancement of the optical Kerr effect has been observed and is known as Raman-induced Kerr effect.[29]. We can expect a similar enhancement effect on the two-photon resonance, when $\nu_1+\nu_2$ matches the energy of a strong two-photon allowed molecular transition. If this is the case, //b-polarization of ν_1 photon produces //b-polarization of ν_2 polarized originally along $\perp$b. As a result, apparent signal $I(//b, \perp b)$ is nearly a mixture of $I(//b, //b)$ and $I(\perp b, \perp b)$ factorized by the ratio of the generated light intensity divided by the original intensity. Since the factor is supposed to be very small, the anomalous polarization observed is too large to be explained completely as a result of the effect.

One of the authors (N. M.) wishes to thank Professor M. Ito, Tohoku University, for his encouragement.

References

1) R. M. Hochstrasser, J. E. Wessel, and H. N. Sung, *J. Chem. Phys.*, **60**, 317 (1974).
2) R. M. Hochstrasser, H. N. Sung, and J. E. Wessel, *Chem. Phys. Lett.*, **24**, 7 (1974).
3) L. Wunsch, H. J. Neusser, and E. W. Schlag, *Chem. Phys. Lett.*, **31**, 433 (1975).
4) D. M. Friedrich and W. M. McClain, *Chem. Phys. Lett.*, **32**, 541 (1975).
5) R. G. Bray, R. M. Hochstrasser, and H. N. Sung, *Chem. Phys. Lett.*, **33**, 1 (1975).

6) J. R. Lombardi, R. Wallenstein, T. W. Hänsch, and D. M. Friedrich, *J. Chem. Phys.*, **65**, 2357 (1976).
7) L. Wunsch, F. Metz, H. J. Neusser, and E. W. Schalg, *J. Chem. Phys.*, **66**, 386 (1977).
8) M. Inoue and Y. Toyozawa, *J. Phys. Soc. Jpn.*, **20**, 363 (1965).
9) W. M. McClain, *J. Chem. Phys.*, **55**, 2789 (1971).
10) R. M. Hochstrasser, H. N. Sung, and J. W. Wessel, *Chem. Phys. Lett.*, **24**, 168 (1974).
11) N. Mikami and M. Ito, *Chem. Phys. Lett.*, **31**, 472 (1975).
12) R. M. Hochstrasser and H. N. Sung, *J. Chem. Phys.*, **66**, 3276 (1977).
13) N. Mikami and M. Ito, *Chem. Phys.*, **23**, 141 (1977).
14) P. Esherick, P. Zinsli, and M. A. El-Sayed, *Chem. Phys.*, **10**, 415 (1975).
15) R. M. Hochstrasser and H. N. Sung, *J. Chem. Phys.*, **66**, 3265 (1977).
16) D. Froehlich and H. Mahr, *Phys. Rev. Lett.*, **16**, 895 (1966).
17) W. Hampf, H. J. Neusser, and E. W. Schlag, *Chem. Phys. Lett.*, **46**, 406 (1977).
18) U. Boesl, H. J. Neusser, and E. W. Schlag, *Chem. Phys.* **15**, 167 (1976).
19) M. Robertson, *Proc. R. Soc. London, Ser. A*, **141**, 659 (1933).
20) A. N. Winchell, "The Optical Properties of Organic Compounds," Academic Press, New York (1954), p. 76.
21) D. S. McClure, *J. Chem. Phys.*, **22**, 1668 (1954).
22) J. B. Birks, "Photophysics of Aromatic Molecules," Wiley, (1969), p. 70.
23) A. Bergman and J. Jortner, *Chem. Phys. Lett.*, **26**, 323 (1974).
24) R. S. Bradley and T. G. Cleasby, *J. Chem. Soc.*, **1953**, 1690.
25) T. Mathies and A. C. Albrecht, *J. Chem. Phys.*, **60**, 2500 (1974).
26) H. Meyer, K. W. Schulte, and A. Schweig, *Chem. Phys. Lett.*, **31**, 187 (1975).
27) D. S. McClure, *J. Chem. Phys.*, **24**, 1 (1956).
28) P. D. Maker and R. W. Terhune, *Phys. Rev.*, **137**, A801 (1965).
29) D. Heiman, R. W. Hellwarth, M. D. Levenson, and G. Martin, *Phys. Rev. Lett.*, **36**, 189 (1976).

The Activities of Methyl Orange and Homologs in Aqueous Solutions

Masaru MITSUISHI* and Yuzoh YAMAGUCHI

Faculty of Textile Science and Technology, Shinshu University, Tokida, Ueda-shi 386

(Received March 18, 1979)

The mean activity coefficients of Methyl Orange (MO), Ethyl Orange (EO), Propyl Orange (PO), and Butyl Orange (BO) in aqueous solutions ranging in concentration from 10^{-3} to 10^{-2} mol kg^{-1} have been determined by means of isopiestic measurements at 50 and 60 °C respectively. It has been found that the mean activity coefficients of MO being the largest, and those of BO, the smallest. The coefficients have been found to decrease with an increase in the dye concentration. The examination of the results by Milicéivic treatment suggests that MO, EO, and PO are present as a monomer or a dimer, while BO exists as a trimer at 60 °C.

Most of the anionic dyes are sodium salts of aromatic sulfonic acids. In aqueous solutions, they have been known to be dissociated completely and to be capable of intermolecular interactions through the hydrophobic groups of the dyes.[1-3] Consequently, the mean activity coefficients of such dyes in aqueous solutions may be governed by the hydrophobic groups in the dye anions.

Since there have been few reports on the mean activity coefficients from the above-mentioned point of view, it seemed that it might be worthwhile to examine the mean activity coefficients of the dyes with various alkyl groups in the dye molecules.

In this paper, the mean activity coefficients of Methyl Orange and its homologs, such as Ethyl Orange, Propyl Orange, and Butyl Orange, in aqueous solutions will be determined by means of isopiestic measurements, and the results will be examined by Milicéivic treatment.

Experimental

Materials. Methyl Orange (MO), Ethyl Orange (EO), Propyl Orange (PO), and Butyl Orange (BO) were used in this experiment. The MO was prepared by coupling diazotized sulfanilic acid with *N*,*N*-dimethylaniline in a weakly acetic acid solution; it was recrystallized three times from water. The EO, supplied by the British Drug House Co., was of a reagent grade; it was isolated by column chromatography on activated alumina and then further purified by recrystallization from ethanol. The PO was synthesized from sulfanilic acid and *N*,*N*-di-*n*-propylaniline by procedures similar to those used for MO; it was then purified in a manner similar to that used for EO. The BO, supplied by the Eastman Kodak Co., was also of a reagent grade; it was purified by procedures to those used for EO.

Vapor-pressure Osmotic Measurements. The vapor-pressure osmometry may also be applicable to the examination of the physical properties of such electrolyte solutions as a dye solution. All the vapor-pressure osmotic measurements were carried out at 50 and 60±0.1 °C[4] using a Hitachi molecular-weight apparatus, Model 115. The difference in electrical resistance of a pair of matched thermistors is measured when a drop of a dye solution on one thermistor and a drop of water on the other thermistor evaporate isothermally in a closed compartment saturated with water vapor. From this value, the resistance difference when water drops are placed on both thermistors is subtracted; the resulting value, ΔR, is known to be dependent linearly upon the osmotic concentration of the dye solution:[5,6]

$$\Delta Rk = -\ln(p/p_0) = \nu\phi m_2/m_1 \quad (1)$$

where k is a constant dependent on the temperature of the solution and the instrumental characteristics; p and p_0 are the partial pressures of the solvent over the solution and over the pure solvent; ν is the number of the particles into which the solute dissociates; ϕ is the osmotic coefficient, and m_2 and m_1 are the solute and solvent molarities respectively. Urea was used in order to determine the numerical values of k,[7,8] so the ϕ values could be obtained by means of Eq. 1.

The evaluation of the mean activity coefficient of an electrolyte can be made as follows.[9] The Gibbs-Duhem equation is applied to the derivation of the interrelation between the osmotic coefficient and the mean activity coefficient, $\gamma_\pm$.

$$\mathrm{d}\ln\gamma_\pm = \mathrm{d}\phi + (\phi-1)\mathrm{d}\ln m_2 \quad (2)$$

$$\ln\gamma_\pm = (\phi-1) + \int_0^m (\phi-1)\mathrm{d}\ln m_2 \quad (3)$$

The integration can be carried out graphically from the plot of $(1-\phi)m_2^{-1}$ *vs.* m_2.

Table 1 gives the measured resistance differences, ΔR, of urea solutions at 50 and 60 °C respectively. The numerical values of k are also shown in Table 1.

Table 1. Measured resistance differences, ΔR, and constants, k, of urea solutions at 50 and 60 °C

$10^{-3}\,m_2$ / mol kg^{-1}	50 °C		60 °C	
	ΔR / Ω	$10^{-6}k$ / Ω^{-1}	ΔR / Ω	$10^{-6}k$ / Ω^{-1}
2.0	5.2	6.92	3.6	9.99
4.0	9.9	7.27	7.6	9.47
6.0	15.2	7.10	11.4	9.47
8.0	19.6	7.34	14.9	9.67
10.0	24.7	7.28	18.4	9.77
Mean		7.18		9.67

Results and Discussion

Measured Resistance Differences. The measured resistance differences, ΔR, of MO, EO, PO, and BO solutions at 50 and 60 °C are plotted against m_2 in Figs. 1 and 2 respectively. From Figs. 1 and 2 it may be seen that the plots of urea solutions are almost linear, while the plots of the dye solutions display slight downward curvatures. It is noteworthy that the ΔR values of MO solutions are the largest, while those of BO solutions are the smallest. All of the ΔR values of the dye solutions are smaller than twice the ΔR values of urea solutions.

Osmotic Coefficients. The osmotic coefficients, ϕ, of MO, EO, PO, and BO solutions ranging in concentration from 10^{-3} to 10^{-2} mol kg^{-1} were obtained from the ΔR values given in Figs. 1 and 2 by means of Eq. 1;

Table 2. Osmotic coefficients of Methyl Organge, Ethyl Orange, Propyl Orange, and Butyl Orange aqueous solutions at 50 and 60 °C

$10^{-3}\ m_2$ / mol kg^{-1}	Methyl Orange		Ethyl Orange		Propyl Orange		Butyl Orange	
	50 °C	60 °C	50 °C	60 °C	50 °C	60 °C	50 °C	60 °C
1.0	0.918	0.994	0.918	0.994	0.878	0.994	0.858	0.914
2.0	0.888	0.941	0.858	0.927	0.818	0.927	0.768	0.779
3.0	0.858	0.932	0.818	0.925	0.792	0.896	0.719	0.744
4.0	0.848	0.914	0.798	0.868	0.768	0.856	0.694	0.705
5.0	0.854	0.908	0.782	0.855	0.758	0.849	0.687	0.693
6.0	0.853	0.900	0.772	0.842	0.748	0.838	0.672	0.685
7.0	0.830	0.895	0.761	0.825	0.747	0.818	0.664	0.672
8.0	0.823	0.894	0.756	0.816	0.736	0.810	0.656	0.665
9.0	0.821	0.884	0.750	0.806	0.730	0.797	0.652	0.657
10.0	0.822	0.881	0.747	0.798	0.729	0.793	0.649	0.656

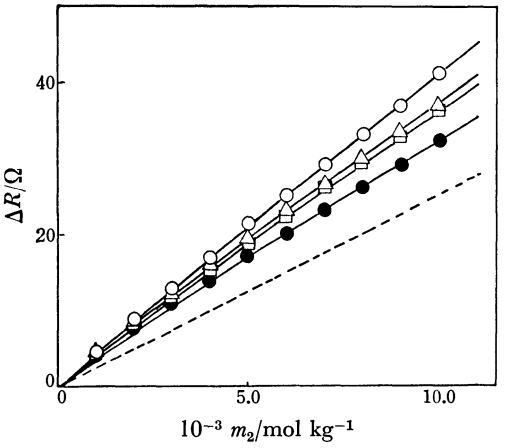

Fig. 1. Measured resistance differences of solutions of Methyl Orange and its homologs at 50 °C.
○: Methyl Orange, △: Ethyl Orange, □: Propyl Orange, ●: Butyl Orange, ——: urea.

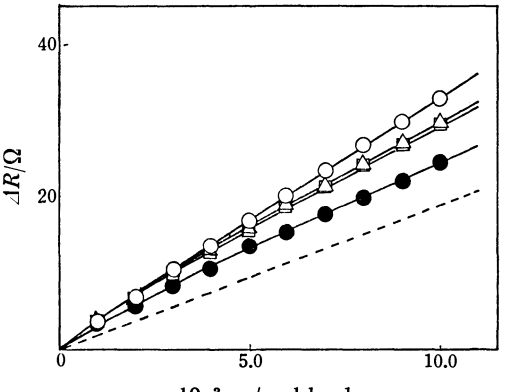

Fig. 2. Measured resistance differences of solutions of Methyl Orange and its homologs at 60 °C.
○: Methyl Orange, △: Ethyl Orange, □: Propyl Orange, ●: Butyl Orange, ——: urea.

they are shown in Table 2. All of the ϕ values of the four dyes are seen to be much smaller than unity. The ϕ values of the MO solution are the largest, while those of the BO solution are the smallest. These results strongly suggest that the aqueous solutions of these dyes deviate from the ideal.

Determination of Mean Activity Coefficients. The

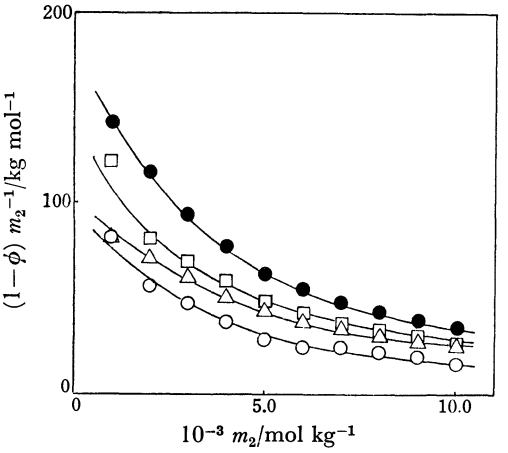

Fig. 3. Plots of $(1-\phi)m_2^{-1}$ against m_2.
○: Methyl Orange, △: Ethyl Orange, □: Propyl Orange, ●: Butyl Orange.

determination of the mean activity coefficients, $\gamma_\pm$, was made as follows. The $(1-\phi)m^{-1}$ at 50 °C was plotted against m_2 as is shown in Fig. 3. After the plot has been extrapolated to zero concentration, the area under the curve was measured and the $\gamma_\pm$ values were calculated according to Eq. 3. The $\gamma_\pm$ values of MO, EO, PO, and BO at 50 and 60 °C are shown in Table 3. These values are comparable to those of C. I. Direct Blue 1.[10,11] In Table 3 it may be seen that the $\gamma_\pm$ values are much smaller than unity and decrease with an increase in the chain length of the alkyl groups in the dye molecules. These results strongly suggest that the mean activity coefficients are influenced by the hydrophobic parts of the dye molecules: *i.e.*, the differences in the $\gamma_\pm$ values among these four dyes are attributable to the association of the dye anions.

Examinations of Results by Milicëivic Treatment. Since these dyes are known to dissociate completely in aqueous solutions, and since the ionic strengths of these solutions are small, the Debye-Hückel limiting law may be supposed to hold. The relation between the mean activity, $a_\pm$, and the mean association number of the dye anions, n, can be derived from the Debye-Hückel limiting law:[12]

$$\log a_\pm = \log m_2 - \frac{1}{n+1}\log n - Anm_2\sqrt{\frac{1+n}{2}} \qquad (4)$$

where;

$$a_\pm = \gamma_\pm m_2 \qquad (5)$$

Table 3. Mean activity coefficients of Methyl Orange, Ethyl Orange, Propyl Orange, and Butyl Orange at 50 and 60 °C

$10^{-1}\,m_2$ / mol kg^{-1}	Methyl Orange		Ethyl Orange		Propyl Orange		Butyl Orange	
	50 °C	60 °C	50 °C	60 °C	50 °C	60 °C	50 °C	60 °C
1.0	0.850	0.960	0.838	0.945	0.771	0.934	0.743	0.795
2.0	0.776	0.879	0.737	0.846	0.666	0.831	0.601	0.623
3.0	0.722	0.858	0.664	0.800	0.627	0.773	0.527	0.555
4.0	0.702	0.826	0.632	0.740	0.582	0.716	0.485	0.507
5.0	0.691	0.807	0.603	0.723	0.569	0.719	0.484	0.484
6.0	0.683	0.793	0.591	0.712	0.543	0.694	0.460	0.481
7.0	0.684	0.807	0.568	0.671	0.559	0.658	0.452	0.459
8.0	0.684	0.792	0.563	0.662	0.538	0.658	0.438	0.453
9.0	0.674	0.761	0.548	0.623	0.518	0.616	0.431	0.433

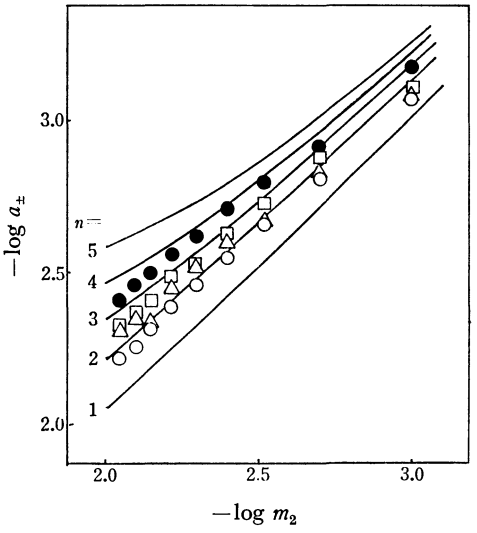

Fig. 4. Mean activities of Methyl Orange and its homologs at 50 °C.
○: Methyl Orange, △: Ethyl Orange, □: Propyl Orange, ●: Butyl Orange.

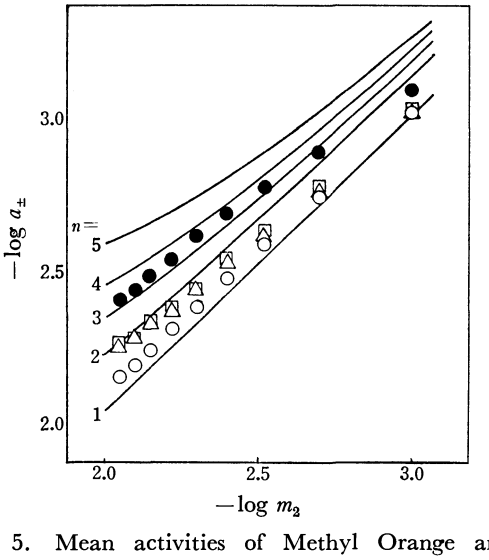

Fig. 5. Mean activities of Methyl Orange and its homologs at 60 °C.
○: Methyl Orange, △: Ethyl Orange, □: Propyl Orange, ●: Butyl Orange.

Also, if the electronic charge and the gas constant are taken as 4.80×10^{-10} esu and 8.31×10^{-7} erg °C mol^{-1} (1 erg$=1\times10^{-7}$ J) respectively,

$$A = 1.825\times10^{6}\left(\frac{\rho_0}{D_0^3T^3}\right)^{1/2} \qquad (6)$$

where D_0 and ρ_0 are the dielectric constant and the density of the solvent at a temperature, T, respectively.

The mean activities of MO, EO, PO, and BO at 50 and 60 °C are plotted against log m_2 in Figs. 4 and 5 respectively. The solid lines in Figs. 4 and 5 are theoretical lines drawn according to Eq. 4. In Fig. 4, the plots for MO and EO are seen to be close to the dimer line ($n=2$), the plots for PO, close to the trimer line ($n=3$), and the plots for close to the tetramer line ($n=4$). These results indicate that the MO and EO dye anions are present as dimers, the PO anions, as trimers, and the BO dye anions, as tetramers, on the average, at 50 °C. From Fig. 5, MO, EO, and PO are seen to exist as monomers or dimers, and BO, as trimers, at 60 °C.

References

1) P. Mukerjee and A. K. Chosh, *J. Phys. Chem.*, **67**, 193 (1963).
2) K. K. Rohatgi and G. S. Singhal, *J. Phys. Chem.*, **70**, 1655 (1966).
3) H. Zollinger, *J. Soc. Dyers Colour.*, **81**, 345 (1965).
4) It is recommended that the osmotic-pressure measurements are made at 50—60 °C, since the vapor-pressure of water is not high enough to be measured at low temperature.
5) A. P. Brady, H. Haff, and J. W. McBain, *J. Phys. Colloid Chem.*, **63**, 304 (1951).
6) I. Porigoric and I. J. Gal, *Trans. Faraday Soc.*, **68**, 1093 (1972).
7) W. I. Higuchi, M. A. Schwartz, E. G. Rippie, and T. Higuchi, *J. Am. Chem. Soc.*, **63**, 996 (1954).
8) Since a very dilute urea solution is known to behave ideally, the urea can be used as the reference solute ($\nu=1$ and $\phi=1$).[7]
9) R. A. Robinson and R. H. Stokes, "Electrolyte Solution," Butterworth Co, London (1955), p. 183.
10) C. S. Chadwick and S. M. Neale, *J. Polym. Sci.*, **28**, 355 (1958).
11) H. D. Hardisty and S. M. Neale, *J. Polym. Sci.*, **46**, 195 (1960).
12) M. Milićevic and G. Eigmann, *Helv. Chim. Acta*, **44**, 1039 (1964).

Simultaneous Measurement of Photoacoustic and Excitation Spectra for the Evaluation of Quantum Efficiencies of Uranium-mica Type Compounds

Yoshinori SUGITANI* and Kenji KATO†

Institute of Chemistry, The University of Tsukuba, Sakura-mura, Ibaraki 305

(Received April 3, 1979)

A new method of estimating the absolute quantum efficiency of a phosphor material based on the simultaneous measurement of photoacoustic and fluorescent excitation spectra is presented. The method is distinguishable from previous methods in that a reference material is not required. The method has been successfully applied to uranium-mica compounds. The transition rate constants for the radiative and non-radiative processes have been obtained on the basis of the quantum efficiency and fluorescence life time data.

The determination of the absolute quantum efficiency of fluorescence may be achieved either by determination of a defined fraction of the fluorescent radiation, or by the measurement of the complementary part of the non-radiative process by calorimetry.[1] The former optical method appears to be more popular due to the relatively sensitive detection of the fluorescent radiation, which is more sensitive than thermal detection. Electronic units and components are also readily available. The actual determination of quantum efficiency, however, consists of various processes and the necessary corrections, and results are generally of low accuracy.

Determination with the aid of photoacoustic spectrometry belongs to the latter case. Lahmann and Ludewig[2] compared the photoacoustic signal of the sample solution of rhodamine 6G with that of a reference solution of $K_2Cr_2O_7$ which is nonfluorescent but has comparable absorption coefficients. Adams *et al.*[3] determined the quantum efficiency of quinine bisulfate in aqueous solution utilizing the quenching effect of fluorescence by halide ions.

A study of photoacoustic spectra combined with fluorescence spectra enables the flow of the relaxed energy passing through both processes, radiative and non-radiative, to be traced.[4] Simultaneous detection of the photoacoustic and excitation signals as a function of the wave length of the exciting light enables the determination of the absolute quantum efficiencies of fluorescence, as discussed on the uranium-mica type compounds in the present study.

Experimental

Apparatus. The system for the simultaneous measurement of photoacoustic and excitation spectra is shown in Fig. 1, where the system for measuring emission spectra and luminescence life times is also shown. The exciting light from the xenon lamp (300 W) is chopped (CHI) at 80 Hz and monochromated at SPI(JASCO, CT-25N) and irradiated on the sample cell (PFC), the details of which are reported in this journal.[5] The photoacoustic signal is detected by a microphone (SONY, Electlet condenser type, FET buffer included, parts number 8-814-196-50) attatched on the cell, amplified at P1, introduced to a lock-in amplifier L2 (NF Circuit Design Block, LI-574) and recorded on R2. The optical signal is filtered at SP2, detected by a photomultiplier (PM), amplified (P3 and L1) and recorded on R1.

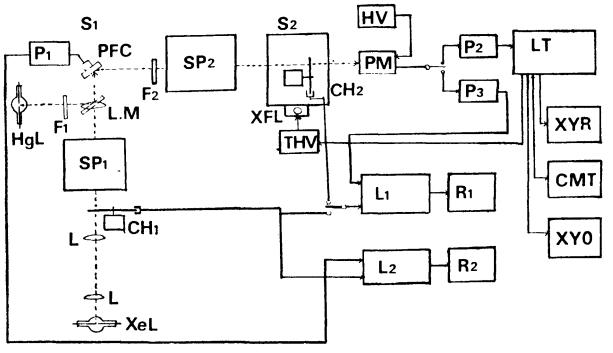

Fig. 1. Block diagram showing the system for simultaneous measurement of photoacoustic and fluorescent excitation spectra. The system for measuring emission spectra and fluorescent life time are also shown. XeL: Xenon arc lamp, L: lenses, CH1 and CH2: light choppers, HgL: mercury lamp, F1 and F2: filters, PFC: sample cell, S1 and S2: sample position, THV: trigger circuit and power supply for xenon flash lamp, XFL: xenon flash lamp, PM: photomultiplier, P1, P2, and P3: preamplifiers, L1 and L2: lock-in amplifiers, R1 and R2: recorders, LT: signal processor unit with a microcomputer, XYR: XY-recorder, CMT: magnetic cassette tape, XYO: XY-oscilloscope, SP1 and SP2: spectrometers.

In the measurement of emission spectra, the sample is irradiated with UV light (365 nm) from a mercury lamp (HgL) and the fluorescent emission is monochromated by the spectrometer SP2 (NIKON, P-250), chopped (CH2), and detected by the photomultiplier PM. With the luminescence life time measurement, the sample specimen is placed in the S2 position instead of the S1 position and, is excited by a xenon flash lamp XFL. The fluorescent signal is detected (PM), amplified (P2), and introduced to the life time measuring system LT, the details of which will be published elsewhere.[6]

All measurements in the present study were taken at room temperature.

Samples. The samples used in the present study are the same as those described previously.[7,8]

Results and Discussion

Procedure for Determining Quantum Efficiency. In a system which is not chemically reactive to visible light

† Present address: National Chemical Laboratory for Industry, 1-1 Yatabe-cho Higashi, Tsukuba-gun, Ibaraki 305.

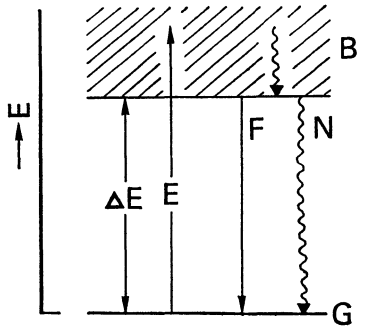

Fig. 2. An energy diagram tentatively given for derivating the relations of quantum efficiency calculation. F: Radiative process, N: non-radiative process.

irradiation, photoacoustic spectrometry provides a complementary system to fluorescent spectrometry which deals with the radiative process. A method of estimating the absolute quantum efficiency of fluorescence Q_F is presented in Fig. 2, based on a simple model of energy diagram where the ground state G and the excited state B of a broad band is given with a separation of ΔE. Assuming the system absorbs light energy E larger than ΔE, the system will release heat energy and will return to the bottom of the band, from which the system will relax to the ground state G by a radiative (F) and/or non-radiative (N) transition. The intensity of the fluorescent emission $I_F(E)$ caused by the excitation of light with energy E is given by

$$I_F(E) = k \cdot \beta(E) \cdot Q_F \cdot I_{EX}(E), \tag{1}$$

where k is a measuring constant, $\beta(E)$ is an absorption coefficient for the light energy E, and $I_{EX}(E)$ is the intensity of the exciting light at energy E. The photoacoustic signal is proportional to the output of thermal energy, which is given as the sum of the excess energy, $E-\Delta E$, and the energy released in the non-radiative process N. Thus the photoacoustic intensity $I_P(E)$ is given by

$$\begin{aligned} I_P(E) &= l \cdot \beta(E) \cdot I_{EX}(E) \cdot [(E-\Delta E)+\Delta E(1-Q_F)] \\ &= l \cdot \beta(E) \cdot I_{EX}(E) \cdot (E-\Delta E \cdot Q_F), \end{aligned} \tag{2}$$

where l is a measuring constant. Supposing that $\beta(E)$ and $I_{EX}(E)$ are taken as invariant, the $I_F(E)$ and $I_P(E)$ will be given as functions of the energy E as in Fig. 3. Taking the ratio of $I_P(E)$ and $I_F(E)$, the $\beta(E)$ and $I_{EX}(E)$ terms vanish giving:

$$\frac{I_P(E)}{I_F(E)} = \frac{1}{k} \cdot \frac{E-\Delta E \cdot Q_F}{Q_F}. \tag{3}$$

The $I_P(E)/I_F(E)$ ratio will be directly related to E as shown in Fig. 3c. Extrapolation leads to an energy of E_0 as in the following;

$$\frac{I_P(E)}{I_F(E)} = 0 = \frac{1}{k} \cdot \frac{E_0-\Delta E \cdot Q_F}{Q_F}, \tag{4}$$

i.e.,

$$E_0 = \Delta E \cdot Q_F. \tag{5}$$

The quantum efficiency will be given as

$$Q_F = E_0/\Delta E. \tag{6}$$

Experimentally, the E_0 value will be obtained as a crossing point on the E axis in the extropolation of the plots of $I_P(E)/I_F(E)$ *versus* E, and the ΔE value will be obtained as the center of the gravity of the emission spectra.

The method of estimating the quantum efficiency presented here is an improvement of those reported to date,[2,3] in that reference materials and quenched samples are not required. In addition, the simultaneous measurement followed by the plotting of intensity ratios of both spectra removes the need for corrections for the power spectrum and the drift of the exciting light.

Quantum Efficiencies of Uranium-micas. A series of uranium-mica type compounds containing uranyl ions as fluorescent centers may be considered as one of those which have an energy diagram similar to that discussed above. Figure 4 shows an energy level diagram for the uranyl(VI) ion based on the paper of Bell and Biggers[9] which appears to be the most widely accepted diagram for uranyl salts. The totally symmetric singlet ground state $^1\Sigma_g^+$ is split into five sublevels due to symmetric

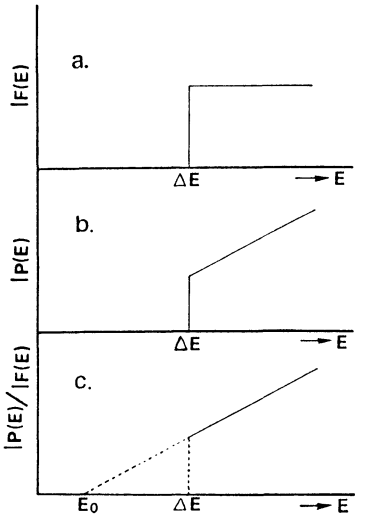

Fig. 3. Expected intensities of fluorescent (a) and photoacoustic (b) output based on the diagram of Fig. 2, and their ratios (c) as a function of the exciting energy E.

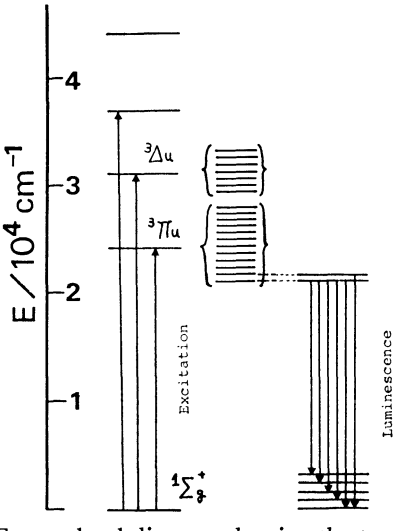

Fig. 4. Energy level diagram showing the transitions of excitation and fluorescent process for uranyl(VI) ion.[9]

stretching in the ground state, while the lowest excited state $^3\Pi_u$ and the second lowest excited state $^3\Delta_u$ are also split into the twelve and seven sublevels, respectively, due to the symmetric stretching in the excited state. The average spacings of the sublevels are approximately 750—860 cm^{-1} depending on the respective sample.[10-12] The luminescence appears to occur from the lowest one or two sublevels to the ground state sublevels showing six emission peaks. The emission peak at the shortest wavelength has a relatively small intensity of about 1/30 of the total intensity suggesting that the contribution to the emission from the second lowest sublevel is negligibly small.

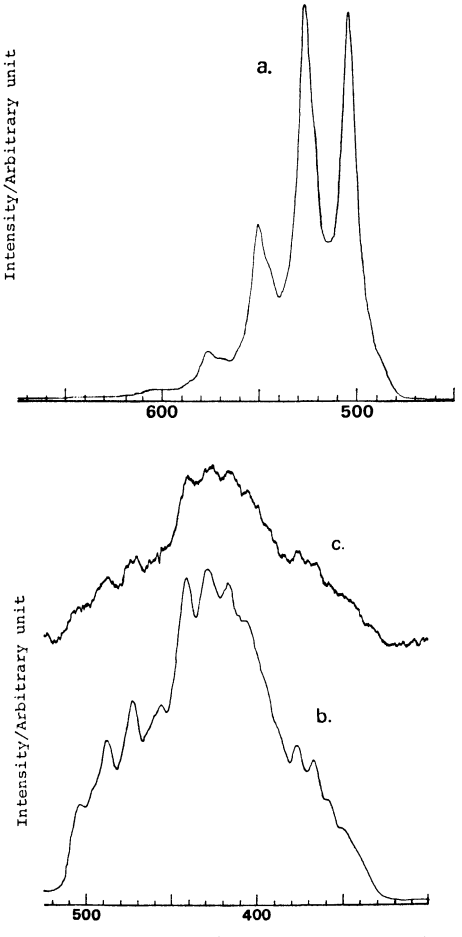

Fig. 5. Fluorescent emission spectra (a), fluorescent excitation spectra (b), and photoacoustic spectra (c) of $Ba(UO_2)_2(PO_4)_2 \cdot nH_2O$. The latter two spectra was simultaneously measured.

The emission spectra of $Ba(UO_2)_2(PO_4)_2 \cdot nH_2O$, one of the prepared uranium-mica samples, are also shown in Fig. 5. The main features of the three spectra for other uranium-mica samples are very similar except for shifts in the peak values of approximately 5 nm in the respective spectra.

Plots of the $I_P(E)/I_F(E)$ ratios *versus* the exciting energy E for the case of Ba-containing uranium-mica samples are given in Fig. 6, where the six points in the lower energy region fall on a straight line giving the experimental E_0 value on the abscissa. The experimental

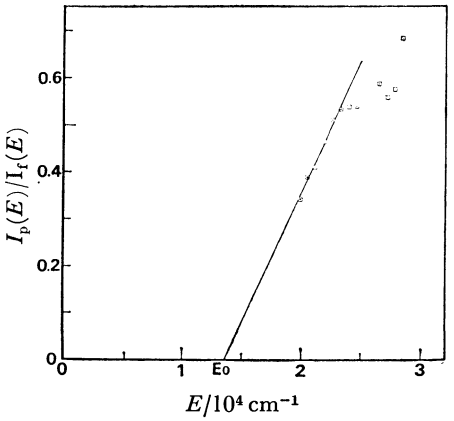

Fig. 6. Plots of the intensity ratios of photoacoustic and fluorescent excitation signals as a function of the exciting energy E.

ΔE value has been tentatively evaluated as 1.92×10^4 cm^{-1} (520 nm) from the peak position of the envelope curve of the emission spectra (Fig. 5a). The value of the quantum efficiency, calculated from Eq. 6 is 0.7. The value of quantum efficiency obtained using similar procedures for the other uranium-micas are given in Table 1. The E_0 value of 1.92×10^4 cm^{-1} has been constantly applied in the estimation of quantum efficiencies of other uranium-micas. The error from this approximation is estimated as $\pm 4\%$. Table 1 includes the fluorescence life times and the transition rate constants which will be discussed later.

In Fig. 6, some of the data in the higher energy region deviate from linearity. This deviation was also found in other unanium micas, where the number of points falling on the line ranges from 4 to 7 out of fifteen.

The reason of the observed deviation appears to be due to the grain size δ of the sample powder. For a photoacoustic signal Ps from a solid sample,[11] Ps varies as a rather complex function of the parameters concerning the sample and/or experimental conditions such as absorption coefficient β, thermal conductivity, grain size δ, chopping frequency ω, *etc.* For the samples studied here the relation between δ and the optical penetration distance, μ, which is defined as $1/\beta$, appears to be responsible for the deviation.

In the situation that μ is larger than δ, the acoustic signal Ps is proportional to β, whereas if μ is comparable to or smaller than δ, the acoustic signal Ps remains constant and independent of β. This indicates that in the energy region with a relatively large β around 400—450 nm, the optical penetration distance μ is equal to or smaller than δ, so that the intensity of the photoacoustic signal will be reduced to some extent, resulting in deviation from linearity. The plots in the higher energy region appear closer to the line than those in the middle energy region which appears to correspond to a lower β value in this region. Samples having a large grain size such as $Mg(UO_2)_2(PO_4)_2 \cdot nH_2O$: Mn (0.03 mol%) show large deviations, while fine grain samples such as $Zn(UO_2)_2(PO_4)_2 \cdot nH_2O$: Cu (0.01 mol%) do not show deviations. It may be concluded

TABLE 1. DATA OF QUANTUM EFFICIENCY Q_F, FLUORESCENCE LIFE TIME τ, AND TRANSITION RATE CONSTANTS k_f AND k_n OF THE RESPECTIVE RADIATIVE AND NON-RADIATIVE PROCESSES, FOR A SERIES OF URANIUM-MICA COMPOUNDS $M(UO_2)_2(XO_4)_2 \cdot nH_2O$

M	X=P				X=As			
	Q_f (%)	τ 10^{-4}s	k_f $10^3 s^{-1}$	k_n $10^3 s^{-1}$	Q_f (%)	τ 10^{-4}s	k_f $10^3 s^{-1}$	k_n $10^3 s^{-1}$
$(H_3O)_2$	0	-	0	-	72	1.4*	5.1*	2.0*
Na_2	86*	2.4	3.6*	0.6*	90	0.82	12.0	1.2
K_2	86	2.8	3.1	0.5	79*	1.0*	7.9*	2.1*
Mg	86	2.8	3.1	0.5	92	1.2	7.7	0.7
Mg:Mn	58	1.7	3.4	2.5	Mn:0.03mol%			
Ca	78*	2.6	3.0*	0.8*	-	1.4*	-	-
Sr	75*	3.4	2.2*	0.7*				
Ba	70	2.8	2.5	1.0	73	1.9	3.9	1.3
Zn:Cu	75*	1.4*	5.4*	1.8*	Cu:0.01mol%			
Zn:Cu	10	1.6*	0.6*	5.6*	Cu:0.1mol%			

* less reliable data

that a sample with a smaller grain size gives greater linearity and thus more reliable results in terms of estimation of the quantum efficiency.

Transition Rate Constants k_f and k_n for the Radiative and Non-radiative Processes. The combination of the values of quantum efficiency Q_F and the fluorescence life time allows the transition rate k_f for the radiative process and k_n for the non-radiative process to be evaluated. The values are related in the following equations;

$$\tau = 1/(k_f + k_n) \quad (7)$$

$$Q_F = k_f/(k_f + k_n), \quad (8)$$

which may be rewritten:

$$k_f = Q_F/\tau \quad (9)$$

$$k_n = (1 - Q_F)/\tau. \quad (10)$$

The results calculated from Eqs. 9 and 10 are given in Table 1. The life time data in Table 1 have been measured in this study, and are slightly different from those previously reported.[8] The difference is considered to be within experimental error so far as the room temperature data are concerned. As seen in Table 1, the phosphate samples have Q_F, k_f, and k_n values of approximately 80%, $3 \times 10^3\ s^{-1}$, and $0.5—1.0 \times 10^3\ s^{-1}$, respectively. The arsenate samples have a shorter τ, a slightly larger Q_F, and a larger k_f value than in the phosphate samples. The k_n values are comparable for the phosphate and arsenate samples. This suggests that the fast radiative process (large k_f) makes the life time short for the samples without the quencher ions such as Cr and Mn. The sample with quencher ion $Mg(UO_2)_2(PO_4)_2 \cdot nH_2O$: Mn (0.03 mol%), however, has a shorter τ and lower Q_F leading to a larger value of k_n. It is considered that the effect of the doping ion Mn^{2+} receives part of the excited energy of the UO_2^{2+} ion making the τ value shorter as well as making the Q_F value lower. The effect of the doping ion Cu^{2+}, as seem in Table 1, is to decrease the value of Q_F without changing the life time data. This indicates that the Cu^{2+} ions absorb almost all the excited energy of the nearest UO_2^{2+} ions making the Q_F value low, while the other UO_2^{2+} ions which are free from the Cu^{2+} neighbors decay within their own relaxation mechanism.

The authors wish to express their thanks to Professor Kozo Nagashima for his kind support and encouragement during this work.

References

1) J. N. Demas and G. A. Crosby, *J. Phys. Chem.*, **75**, 991 (1971).
2) W. Lahmann and H. J. Ludewig, *Chem. Phys. Lett.*, **45**, 177 (1977).
3) M. J. Adams, J. G. Highfield, and G. F. Kirkbright, *Anal. Chem.*, **49**, 1850 (1977).
4) A. Rosencwaig, *Phys. Today*, **28**, 23 (1975).
5) K. Kato and Y. Sugitani, *Bull. Chem. Soc. Jpn.*, **52**, 3733 (1979).
6) K. Kato and Y. Sugitani, *Chem. Biomed. Environ. Instrumentation*, in press.
7) Y. Sugitani, H. Kasuya, K. Nagashima, and S. Fujiwara, *Nippon Kagaku Zasshi*, **90**, 52 (1969).
8) Y. Sugitani, K. Kato, and K. Nagashima, *Bull. Chem. Soc. Jpn.*, **52**, 918 (1979).
9) J. T. Bell and R. E. Biggers, *J. Mol. Spectrosc.*, **25**, 312 (1968).
10) E. Rabinowitch and R. L. Belford, "Spectroscopy and Photochemistry of Uranyl Compounds," Macmillan, New York (1964).
11) S. P. McGlynn and J. K. Smith, *J. Mol. Spectrosc.*, **6**, 164 (1961).
12) H. D. Burrows and T. J. Kemp, *Chem. Soc. Rev.*, **1974**, 139.
13) A. Rosencwaig and A. Gersho, *J. Appl. Phys.*, **47**, 64 (1976); E. M. Monahan, Jr. and A. W. Nolle, *ibid*, **48**, 3519 (1977).

The Rate Constants for H and D-Atom Additions to O_2, NO, Acetylene, and 1,3-Butadiene

Yo-ichi ISHIKAWA, Ko-ichi SUGAWARA, and Shin SATO*

Department of Applied Physics, Tokyo Institute of Technology, Ookayama, Meguro-ku, Tokyo 152

(Received May 15, 1979)

Pulse radiolysis has been combined with Lyman-α absorption spectroscopy for the measurement of absolute rate constants for the addition reactions of H and D-atoms to oxygen, nitrogen monoxide, acetylene-d_0 and -d_2, and 1,3-butadiene at room temperature. The rate constants obtained with O_2 and NO were in good agreement with the results previously reported and no H/D isotope effect was found. With acetylenes and 1,3-butadiene, the following rate constants were obtained (units of cm^3 $molecule^{-1}$ s^{-1}): $(3.8\pm0.4)\times10^{-13}$ for $H+C_2H_2$; $(2.6\pm0.2)\times10^{-13}$ for $D+C_2H_2$; $(3.8\pm0.2)\times10^{-13}$ for $H+C_2D_2$; $(2.5\pm0.2)\times10^{-13}$ for $D+C_2D_2$; $(8.5\pm1.5)\times10^{-12}$ for $H+1,3\text{-}C_4H_6$; $(7.5\pm0.6)\times10^{-12}$ for $D+1,3\text{-}C_4H_6$. These results are compared to previous studies, and the H/D isotope effect discussed.

In previous papers the absolute rate constants for the addition reactions of H and D-atoms to seven mono-olefins were reported.[1,2] The technique used for the measurement can readily be extended to the reactions with other reactants. This paper describes the results obtained with oxygen, nitrogen monoxide, acetylene-d_0 and -d_2, and 1,3-butadiene.

Experimental

The apparatus and procedures used in this study are the same as those previously described for the reactions of hydrogen and deuterium atoms with olefins.[1,2]

Research grade oxygen, nitrogen monoxide, acetylene-d_0, and 1,3-butadiene (Takachiho Shoji Co.) were used without further purification. Acetylene-d_2 was synthesized by the reaction of D_2O (99.99% up; Merck Co.) with CaC_2 (Tokyo Kasei Co.), which was heated at approximately 500 °C for 70 h in vacuum prior to use. The acetylene-d_2 thus obtained was introduced into a flask containing sulfuric acid and shaken for 1 h to remove hydrogen sulfide, ammonia, and phosphine. The mass and infrared spectra showed that the purity of acetylene-d_2 was better than 99%.

Results and Discussion

Reaction with Oxygen. Figure 1 shows the oscillogram for the time dependence of the concentration of H-atoms obtained with 747 Torr (1 Torr ≃133.322 Pa) hydrogen containing 0.93 Torr oxygen, and the first order decay rates thus obtained are plotted as functions of the initial pressures of hydrogen and oxygen in Figs. 2 and 3, respectively. The linear relationships obtained are consistent with the widely accepted reaction mechanism, *i.e.*, a third order combination reaction of hydrogen atoms with oxygen:

$$H + O_2 + H_2 \longrightarrow HO_2 + H_2$$

The rate constant was calculated to be $(3.0\pm0.6)\times10^{-32}$ cm^6 $molecule^{-2}$ s^{-1}, a value somewhat smaller than that reported by Hikida *et al.*, $(4.7\pm1.1)\times10^{-32}$ cm^6 $molecule^{-2}$ s^{-1}.[3]

A similar experiment employing deuterium in place of hydrogen gave a rate constant for the reaction,

$$D + O_2 + D_2 \longrightarrow DO_2 + D_2$$

as $(2.9\pm1.3)\times10^{-32}$ cm^6 $molecule^{-2}$ s^{-1}. No H/D isotope effect was found.

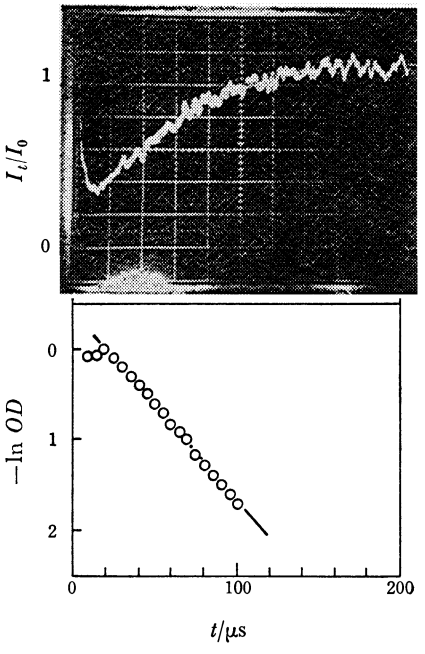

Fig. 1. The decay curve of hydrogen atoms due to the reaction of $H+O_2+H_2\rightarrow HO_2+H_2$, and the first order plot of this decay curve. Temperature is 298 K. The pressure of hydrogen is 747 Torr; pressure of oxygen 0.93 Torr.

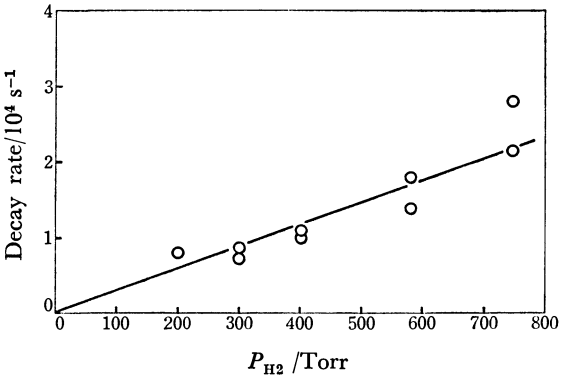

Fig. 2. The decay rate as a function of the pressure of hydrogen. The pressure of oxygen is 0.95±0.02 Torr.

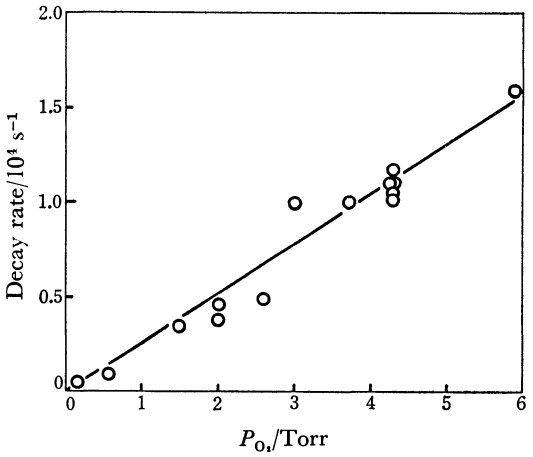

Fig. 3. The decay rate as a function of the pressure of oxygen. The pressure of hydrogen is 750±4 Torr.

Reaction with Nitrogen Monoxide. This is a well documented third order reaction. Thirty measurements, in which the hydrogen and deuterium pressures were changed from 100 to 900 Torr and the nitrogen monoxide pressure from 0.05 to 0.85 Torr, gave the following rate constant: $(4.6\pm0.6)\times10^{-32}$ cm^6 molecule^{-2} s^{-1} for the reaction:

$$H + NO + H_2 \longrightarrow HNO + H_2$$

and $(4.4\pm1.0)\times10^{-32}$ cm^6 molecule^{-2} s^{-1} for the reaction:

$$D + NO + D_2 \longrightarrow DNO + D_2.$$

Again no isotope effect could be observed. Table 1 compares previous studies for this reaction where it can be seen that agreement is within experimental error.

Table 1. The rate constant of reaction for $H+NO+H_2\rightarrow HNO+H_2$ at room temperature

Author[a]	P_{total}/Torr	Technique[b]	$k/10^{-32}$ cm^6 molecule^{-2} s^{-1}	Ref.
CT	0.7—3	DF-CL	4.1±0.4	6, 7)
HT	0.4—3	DF-CL	5.7±0.5	8)
HED	100—1500	PR-RA	3.9±0.6	3)
Present	100—900	PR-RA	4.6±0.6	

a) CT: Clyne and Thrush; HT: Hartley and Thrush; HED: Hikida, Eyre, and Dorfman. b) DF: Discharge flow; PR: pulse radiolysis; CL: chemiluminescence of HNO*; RA: resonance absorption.

Reaction with Acetylene. Figure 4 shows the oscillogram for the time-dependence of hydrogen atom concentration obtained with 752 Torr hydrogen containing 47 mTorr acetylene after irradiation of pulsed electrons, and the first order plot for the optical density, from which the decay rate of hydrogen atoms was estimated. The decay rates thus obtained with various pressures of hydrogen, from 300 to 1200 Torr, and with a constant pressure, 73 mTorr, of acetylene are plotted in Fig. 5. The decay rate appears to be independent of hydrogen pressure in the range studied.

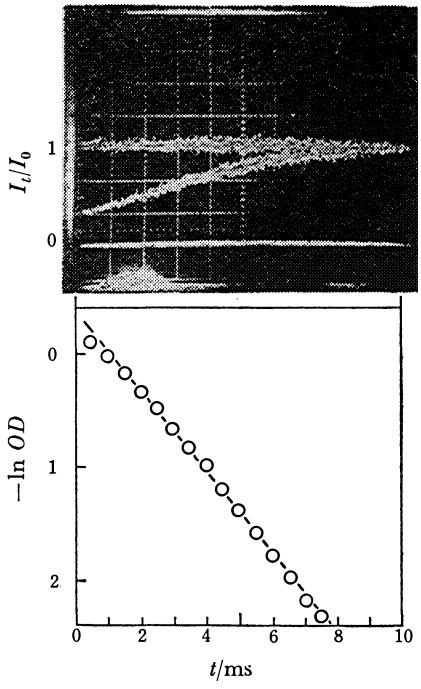

Fig. 4. The decay curve of hydrogen atoms due to the reaction of $H+C_2H_2\rightarrow C_2H_3$, and the first order plot of this decay curve. Temperature is 298 K. The pressure of hydrogen is 752 Torr; pressure of acetylene 47 mTorr.

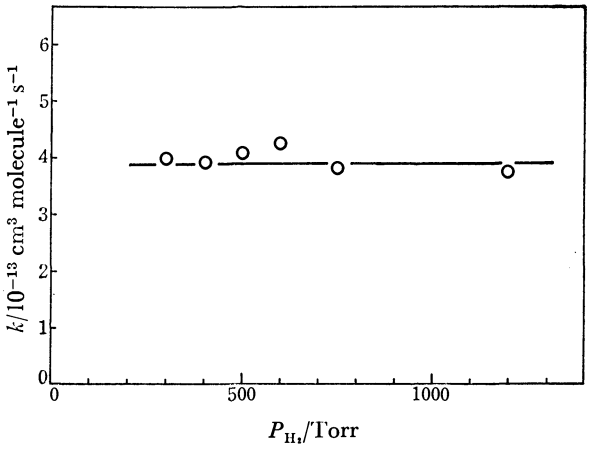

Fig. 5. The rate constant of reaction of hydrogen atoms with acetylene as a function of the pressure of hydrogen. The pressure of acetylene is 73 mTorr.

It is known that the apparent decay rate of hydrogen atoms in the reaction with acetylene is pressure dependent at low total pressure, because the reverse reaction: $C_2H_3^*\rightarrow H+C_2H_2$ cannot be ignored.[4] The present result suggests that such a reverse reaction becomes important only below 300 Torr in hydrogen. Unfortunately, the present method cannot be applied to low pressures, since the amount of hydrogen atoms produced by pulse irradiation is proportional to the total pressure and the concentration obtained below 300 Torr is too small for decay measurement.

Figures 6 and 7 show the decay rates of H and D-atoms as functions of the pressure of acetylene-d_0 and

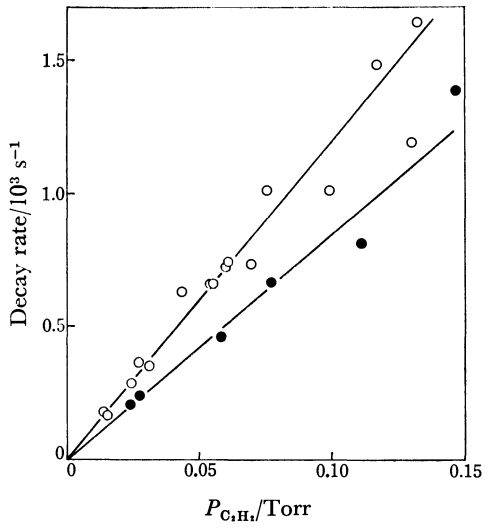

Fig. 6. The decay rates of hydrogen (○) and deuterium (●) atoms as a function of the pressure of acetylene-d_0.

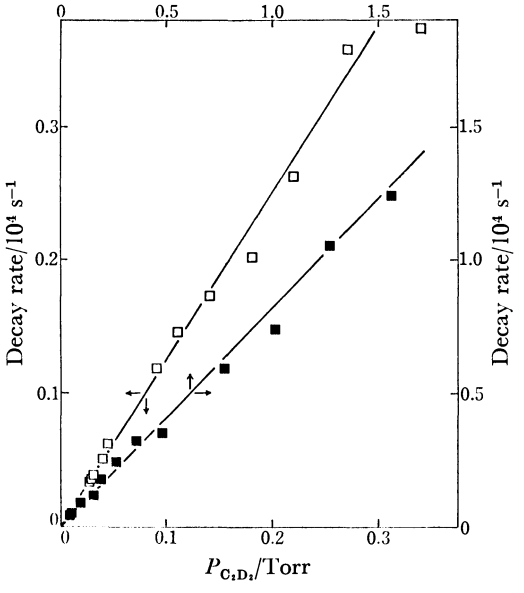

Fig. 7. The decay rates of hydrogen (□) and deuterium (■) atoms as a function of the pressure of acetylene-d_2.

-d_2, where the pressure of hydrogen and deuterium is approximately 750 and 600 Torr respectively. It should be noted here that in the reaction of $D+C_2D_2$, the acetylene-d_2 pressure could be raised to 1.56 Torr, which is approximately 10 times that used in the other three reactions. The absorption coefficient of acetylene-d_2 appears to be very small at the resonance line of D-atoms.

The rate constant for the reaction of hydrogen atoms with acetylene is one order of magnitude smaller than those obtained with olefins. Consequently it was presumed that the vinyl radicals produced in the reaction of hydrogen atoms with acetylene participate in the decay of hydrogen atoms.[1] However, the fact that a linear relationship between the decay rate of D-atoms and the C_2D_2 pressure exists up to 1.56 Torr of acetylene-d_2, suggests that the decay rates observed in the present experiments do correspond to the reactions of H or D-atoms with acetylene-d_0 or -d_2.

Table 2. The rate constants of the reactions of hydrogen or deuterium atoms with acetylene-d_0 or -d_2 at room temperature

Reactant	$10^{13}\,k_H$ / cm³ molecule⁻¹ s⁻¹	$10^{13}\,k_D$ / cm³ molecule⁻¹ s⁻¹
C_2H_2	3.8±0.4	2.6±0.2
C_2D_2	3.8±0.2	2.5±0.2

Table 3. The rate constant of reaction for $H+C_2H_2$ at room temperature

Author[a]	P_{total}/Torr	Technique[b]	$k/10^{-13}$ cm³ molecule⁻¹ s⁻¹	Ref.
TL	1.0—15 (H_2)	DF-CP	0.86	9)
DL	3.5 (H_2)	DF-CP	0.134	10)
GGM	3.0 (H_2)	DF-WG	2.66	11)
MW	0.7—17.3 (He)	DF-RA	5.98(∞)[c]	12)
MN	1.67 (He)	DF-MS	0.37	4)
HWW	0.5—30 (He)	DF-ESR	0.57(∞)	13)
IT	650 (H_2)	Hg-PA	0.91	14)
PS	10—700 (He)	FP-RF	1.56(∞)	15)
Present	200—1100 (H_2)	PR-RA	3.8	

a) TL: Tollefson and LeRoy; DL: Dingle and LeRoy; GGM: Girouard, Graber, and Myers; MW: Michael and Weston; MN: Michael and Niki; HWW: Hoyermann, Wagner, and Wolfrum; IT: Ibuki and Takezaki; PS: Payne and Stief. b) DF: Discharge flow; Hg: mercury photosensitization; FP: flash photolysis; PR: pulse radiolysis; CP: catalytic probe; WG: Wrede gauge; RA: resonance absorption; MS: mass spectrometer; ESR: electron spin resonance; PA: product analysis; RF: resonance fluorescence. c) Obtained by extrapolating to infinite pressure.

Table 2 summarizes the rate constants obtained in the present experiments, and Table 3 compares some previous studies in the reaction of $H+C_2H_2$. Most previous measurements were conducted using the discharge flow system under low pressures, where the reverse reaction, *i.e.*, the decomposition of excited vinyl radicals reproducing hydrogen atoms, may be important. Therefore, the value obtained here must be compared with those obtained by extrapolation to infinite pressure.

In a previous paper,[1] the rate constant in the reaction of $H+C_2H_4$ was reported and compared with previous studies. The value reported by Payne and Stief was in very good agreement with that of the present authors. The value for $H+C_2H_2$ obtained by Payne and Stief however, was less than a half. No proper interpretation for this discrepancy has been found.

Reaction with 1,3-Butadiene. The rate constants of hydrogen and deuterium atoms with 1,3-butadiene at room temperature were measured by an analogous method. The hydrogen pressure was 500 to 600 Torr and the 1,3-butadiene pressure from 0.02 to 0.09 Torr. The decay rates of hydrogen and deuterium atoms were found to be linearly proportional to the pressure of 1,3-butadiene. The rate constants obtained were as follows (units of cm³ molecule⁻¹ s⁻¹):

$$k(\mathrm{H}+1,3\text{-butadiene}) = (8.5\pm1.5)\times10^{-12}$$

$$k(\mathrm{D}+1\text{-}3\text{-butadiene}) = (7.5\pm0.6)\times10^{-12}$$

These results are in fair agreement with those reported by Daby *et al.*, $(8.3\pm1.1)\times10^{-12}$ for the reaction of H +1,3-butadiene and $(5.3\pm1.1)\times10^{-12}$ for D+1,3-butadiene.[5] Daby *et al.* used a discharge flow system combined with a mass spectrometer. This agreement suggests that vibrationally excited radicals formed by the addition reaction do not release a hydrogen atom under low total pressure.

References

1) Y. Ishikawa, M. Yamabe, A. Noda, and S. Sato, *Bull. Chem. Soc. Jpn.*, **51**, 2488 (1978).
2) Y. Ishikawa and S. Sato, *Bull. Chem. Soc. Jpn.*, **52**, 984 (1979).
3) T. Hikida, J. A. Eyre, and L. M. Dorfman, *J. Chem. Phys.*, **54**, 3422 (1971).
4) J. V. Michael and H. Niki, *J. Chem. Phys.*, **46**, 4969 (1967).
5) E. E. Daby, H. Niki, and B. Weinstock, *J. Phys. Chem.*, **75**, 1601 (1971).
6) M. A. A. Clyne and B. A. Thrush, *Trans. Faraday Soc.*, **57**, 1305 (1961).
7) M. A. A. Clyne and B. A. Thrush, *Discuss. Faraday Soc.*, **33**, 139 (1962).
8) D. B. Hartley and B. A. Thrush, *Proc. R. Soc. London, Ser. A*, **297**, 520 (1967).
9) E. L. Tollefson and D. J. LeRoy, *J. Chem. Phys.*, **16**, 1057 (1948).
10) J. R. Dingle and D. J. LeRoy, *J. Chem. Phys.*, **18**, 1632 (1950).
11) H. Girouard, F. M. Graber, and B. F. Myers, General Dynamics-Astronautical Rept. No. N64-13061, San Diego, February (1963) NASA CR 52376.
12) J. V. Michael and R. E. Weston, Jr., *J. Chem. Phys.*, **45**, 3632 (1966).
13) K. Hoyermann, H. G. Wagner, and J. Wolfrum, *Ber. Bunsenges. Phys. Chem.*, **72**, 1004 (1968).
14) T. Ibuki and Y. Takezaki, *Bull. Chem. Soc. Jpn.*, **48**, 769 (1975).
15) W. A. Payne and L. J. Stief, *J. Chem. Phys.*, **64**, 1150 (1976).

The Thermal Gas-phase Decomposition of Vinyl Bromide

Ko SAITO,* Teiji YOKUBO, Tohru FUSE, Hiroyuki TAHARA, Osamu KONDO, Tetsuo HIGASHIHARA, and Ichiro MURAKAMI

Department of Chemistry, Faculty of Science, Hiroshima University, Higashi Senda-machi, Hiroshima 730

(Received June 1, 1979)

The thermal gas-phase decomposition of vinyl bromide in Ar has been studied behind reflected shock waves over the temperature range between 1300 and 2000 K and the density range of $5.2\times10^{-6}-3.8\times10^{-5}$ mol cm^{-3} by monitoring the UV absorption of C_2H_3Br and the IR emission of HBr. The decomposition proceeds *via* the molecular elimination of HBr, and the unimolecular process is in the low-pressure region under the present experimental conditions. The low-pressure-limit rate constant was obtained as

$$k_{2nd} = 10^{13.98\pm0.21}\exp\{-(41.5\pm1.6\text{ kcal mol}^{-1})/RT\}\text{ cm}^3\text{ mol}^{-1}\text{ s}^{-1}.$$

The collision efficiency factor, β_c, was obtained as about 2×10^{-4}, considerably lower than that of vinyl chloride.

The thermal decomposition of vinyl fluoride was investigated in a single-pulse shock tube over the temperature range of 1174—1353 K.[1] The reaction proceeded *via* HF elimination, and the unimolecular process was in the high-pressure region in the total density range of $(3.7—4.8)\times10^{-5}$ mol cm^{-3}. The decomposition of vinyl chloride was measured by means of a time-resolved UV absorption method behind reflected shock waves over the range of 1350—1900 K.[2] The reaction proceeded *via* HCl elimination and was in the fall-off region in the density range between 7×10^{-7} and 1.6×10^{-3} mol cm^{-3}.

In the case of vinyl bromide, the following two channels are probable for the initiation reaction:

$$C_2H_3Br(+M) \longrightarrow C_2H_2 + HBr(+M)$$
$$\Delta H^\circ_{r298} = 26.5\text{ kcal mol}^{-1} \quad (1)$$

$$C_2H_3Br(+M) \longrightarrow C_2H_3 + Br(+M)$$
$$\Delta H^\circ_{r298} = 76.7\text{ kcal mol}^{-1}. \quad (2)$$

From the large difference in the heat of reaction, Reaction 1 seems preferable for the initiation reaction, although its preexponential factor is relatively small because of the four-center reaction. An estimation based on the semiempirical method of Benson and Haugen[3] suggests that the HBr elimination is much faster than the C–Br bond fission. However, it is not certain whether or not all alkenyl halides decompose *via* molecular elimination, since the difference in the heat of reaction between the two channels becomes small as the halogen changes from F to Br. Thus, at high temperatures, the simple bond fission becomes important as the initiation reaction.

In this work, we measured the concentration profiles of the reactant and HBr produced in order to determine the overall decomposition rate of C_2H_3Br and the production rate of HBr.

Experimental

The experiments were performed in a shock tube made of stainless steel (SUS-304). The test section was 4.52 m long and 9.4 cm in inner diameter, and it was evacuated to less than 5×10^{-6} Torr (1 Torr = 133.322 Pa) by means of a 6-inch oil-diffusion pump. The leak and outgassing rate of this section in the stage just before the run was about 2×10^{-7} Torr l/s. The driver section (1.8 m long and 8.5 cm in inner diameter) was evacuated to about 1×10^{-2} Torr. Hydrogen was used as the driver gas at pressures of 2—6 atm (1 atm = 101325 Pa). Tetoron sheets of 100, 75, 50, and 25 μm were used as diaphragms to separate the two sections. Shock waves were generated by bursting the diaphragm with a needle driven by a solenoid.

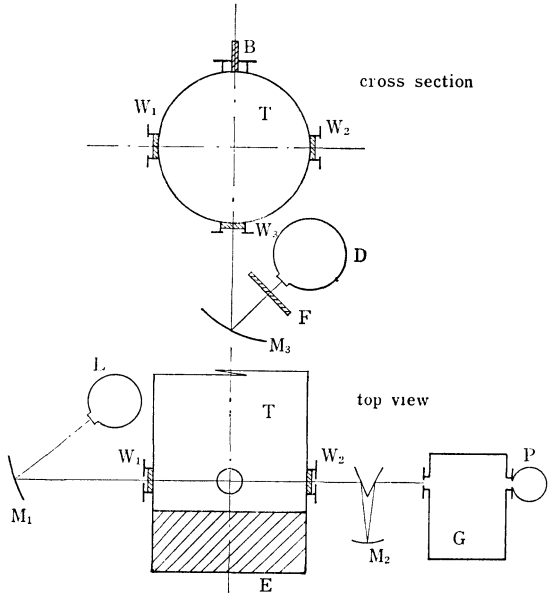

Fig. 1. Experimental arrangement. T: Shock tube, E: end plate, B: pressure gauge, L: deuterium lamp, G: grating monochromator, P: photomultiplier, M_1—M_3: concave mirrors, F: filter, D: InSb detector, W_1: quartz window, W_2 and W_3: CaF_2 windows.

At a distance of 4.44 m from the diaphragm, two sets of windows were mounted in the tube in order to observe the physical properties of the shocked gas. Figure 1 shows the experimental arragement for the absorption and emission experiments. Light from a deuterium lamp (HTV, L544) was focussed on the center of the tube through an inlet slit (4 mm wide and 8 mm high), and the light from an outlet slit (2 mm wide and 8 mm high) was focussed again on the entrance slit (1 mm wide) of a monochromator (Jarrell-Ash, 0.25 M). The average width of the light beam in the tube was 3 mm, while the hight was 8 mm. The light passed through the exit slit (1 mm wide) of the monochromator was detected by a photomultiplier (HTV, R106UH) supplied with a voltage of −800 V. The output signal was fed into a pre-amplifier (IWATSU, DA-2A) and then to a wave-memory (Kawasaki Electronica, M-50E), which was connected to an

oscilloscope and a pen-recorder. The response time of the optical-electrical system was less than 10 μs enough for the present study. The IR emission was detected by an InSb photo-voltaic element (HTV, P839A) at 77 K through a filter of 3.9 ± 0.05 μm. The signal-recording system was the same as in the absorption experiment. The response time of this system was about 10 μs. Measurements of the incident shock velocity were performed by counting the time intervals of shock-arrival signals between two pressure gauges mounted on the walls, 32 cm apart from each other, with a universal counter (Takeda Riken, TR-5104G) having an accuracy of 0.1 μs. The attenuation in the shock velocities was estimated to be less than 1% per meter of travel. The measured incident shock velocities were then used to compute the non-reaction conditions behind the reflected shock.

Liquid C_2H_3Br (99.5% stated minimum purity) was purified by trap-to-trap distillations. Ar (99.998%) was used as the diluent, without any further purification. Several mixture (0.03—3.0 mol% C_2H_3Br in Ar) were prepared in a 30-l glass flask. They were allowed to stand for more than 12 h before use.

Results

The experiments were performed behind reflected shock waves over the temperature range between 1300 and 2000 K and the density range of 5.2×10^{-6}—3.8×10^{-5} mol cm^{-3}. Vinyl bromide has an absorption spectrum in the vacuum ultraviolet region with a maximum at 52200 cm^{-1}.[4] At the high temperatures available in shock waves, the absorption may be detected at higher wavelengths. In this work, the absorption experiment was performed at 250 nm with FWHM= 1.7 nm. The absorption coefficient at this wavelength was in the range of $(1—2)\times10^5$ cm^2 mol^{-1} over the temperature range studied, and Lambert-Beer's law was ascertained to hold. Figure 2 shows typical UV absorption (a) and IR emission (b) profiles obtained simultaneously in one experimental run. The absorption profile clearly reveals a decay of the reactant with the time, and the emission profile shows an increase of a product immediately behind the reflected shock front. The polyacetylenes which may be produced in the later part of the reaction have an absorption at this wavelength.[5] However, it is likely that at low temperatures the decay curve does not involve the absorption of products. At high temperatures the effect of the products was seen as a very slow increase in the absorption after a large consumption of the reactant. The decay rate of the reactant was first-order in $[C_2H_3Br]$ up to at least 25% decrease in the reactant. Thus, the first-order rate constant, k_{1st}, was obtained by means of this definition: $k_{1st}=-\mathrm{d}(\ln D)/\mathrm{d}t$, where $D=[C_2H_3Br]\times\varepsilon\times L$, ε=absorption coefficient, and L= inner diameter of the shock tube. Figure 3 shows an

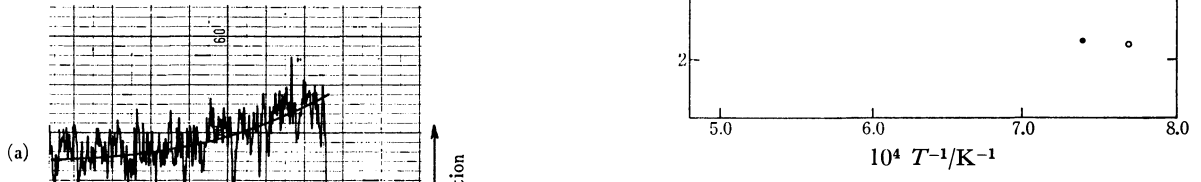

Fig. 2. Typical absorption and emission record in the same experimental run. 1.5 mol % C_2H_3Br in Ar, Temperature=1430 K, Pressure=2.10 atm, $k_{1st}=7.78\times10^2$ s^{-1}, $k_{ir}=2.75\times10^3$ s^{-1}.

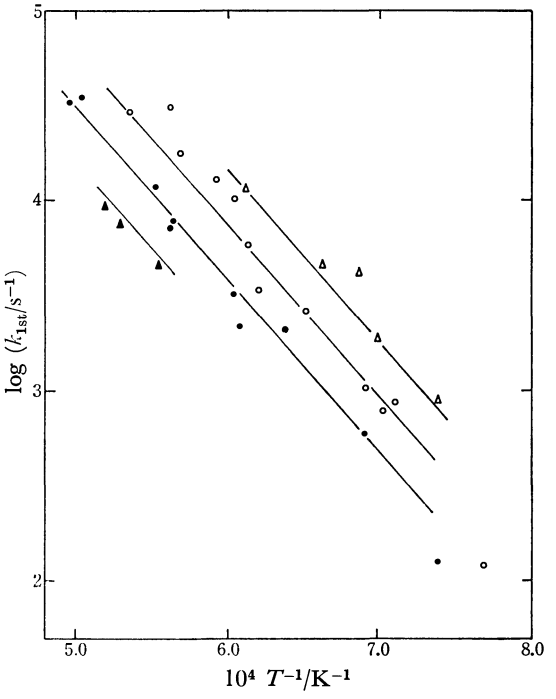

Fig. 3. Arrhenius plot of the first order rate constant k_{1st}. Total density (mol cm^{-3}): ▲$=5.2\times10^{-6}$, ●$=1.0\times10^{-5}$, ○$=1.9\times10^{-5}$, △$=3.6\times10^{-5}$. Straight lines denote the precise change of k_{1st} with the density (relative) assuming that k_{1st} is proportional to the total density.

Arrhenius plot of k_{1st} for four different total densities. It appears that the first-order rate constant depends on the total density and that the data corresponding to each constant density are parallel to, but apart from, each other because of the density change. Thus, the apparent decomposition rate is expressed as

$$-\mathrm{d}[C_2H_3Br]/\mathrm{d}t = k_{2nd}[C_2H_3Br][M].$$

Figure 4 shows an Arrhenius plot of the second-order rate constant, k_{2nd}. The best-fitting line gives an Arrhenius expression as

$$k_{2nd}=10^{13.98\pm0.21}\exp\{-(41.5\pm1.6\ \mathrm{kcal\ mol^{-1}})/RT\}\ \mathrm{cm^3\ mol^{-1}\ s^{-1}},$$

where the error limits denote the standard deviations.

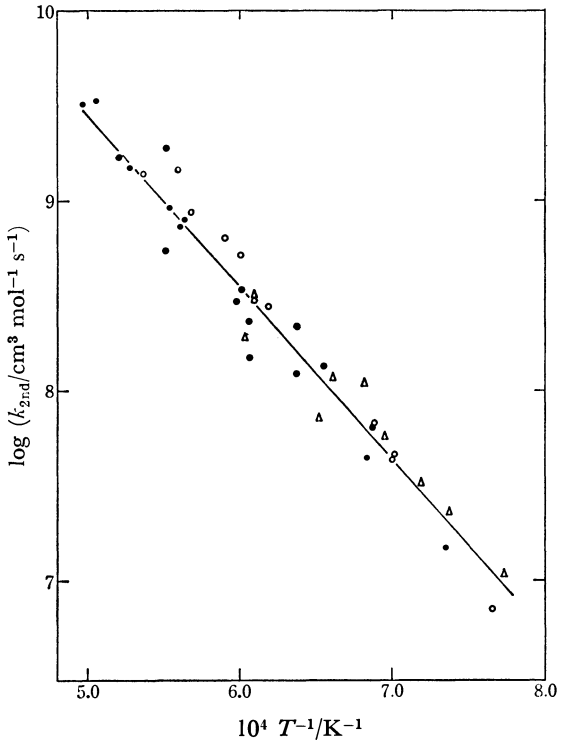

Fig. 4. Arrhenius plot of the second order rate constant. Straight line is the least square evaluation.

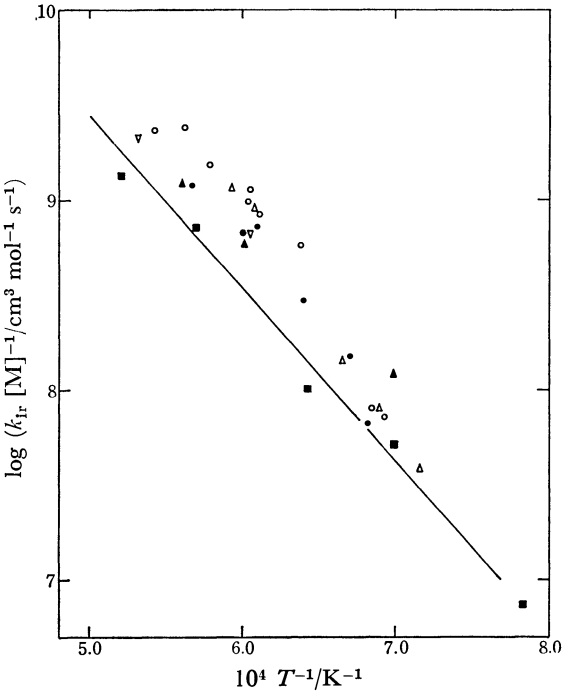

Fig. 5. Arrhenius plot of the second order rate constant k_{1r}/[M] obtained from IR profiles. ▽=3.0%, ▲=1.5 %, ○=0.5%, △=0.25%, ●=0.1%, ■=0.03%. Straight line denotes the least square evaluation of k_{2nd} shown in Fig. 4.

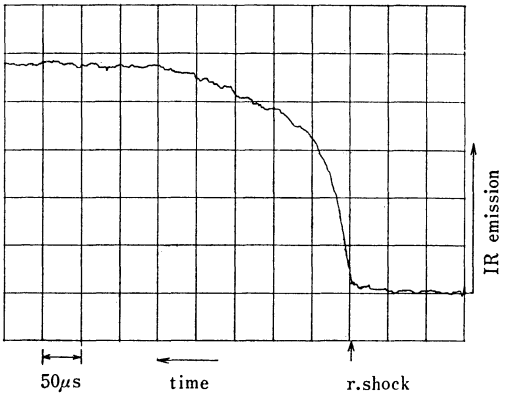

Fig. 6. Typical IR emission profile for the mixture of 0.03% C_2H_3Br in Ar. Temperature=1760 K, total density=1.99×10^{-5} mol cm^{-3}, k_{1r}/[M]=7.2×10^8 cm^3 mol^{-1} s^{-1}.

The IR emission intensity at 3.9 μm is assumed to be proportional to the HBr concentration, since, at this wavelength, there exists no emission by possible products other than HBr. If HBr is produced only by Reaction 1 and does not react subsequently, the time history of the intensity may be expressed as: $I=I_{t=\infty}\{1-\exp(-k_{1r}t)\}$. At first sight, the emission profile seems to follow the above relation. Figure 5 shows the values of k_{1r}/[M] obtained for the various mixtures studied. It may be seen from Fig. 4 that the values of k_{1r}/[M] for mixtures of 0.1—3.0 mol % C_2H_3Br are somewhat larger than those of k_{2nd} (straight line), especially at high temperatures. This implies that, at the later part of the reaction, the dissociation of HBr by secondary reactions cannot be neglected in these relatively high concentration mixtures. That is, the concentration of HBr, $[HBr]_t$, cannot be described by the simple relation: $[HBr]_t=[C_2H_3Br]_0-[C_2H_3Br]_t$ when there is much decomposition. Thus, in order to control the secondary reactions, further experiments were performed for a highly diluted mixture (0.03 mol % C_2H_3Br in Ar). In these additional experiments, the apparatus for the IR observation was modified so as to detect a weak emission. That is, the emission intensity was increased by setting a concave mirror on the opposite side of the tube so as to focus the light on the slit at the detecting side. The emission profile for this mixture is shown in Fig. 6, which is essentially the same as those for the high C_2H_3Br mixtures (Fig. 2(b)). The values of k_{1r}/[M] were obtained again for this series, as plotted in Fig. 5, they show a good agreement with the absorption data (straight line). This suggests that, in highly diluted mixtures such as $[C_2H_3Br]/[Ar]\simeq3\times10^{-4}$, the consumption of HBr by the secondary reactions is negligibly small, even after long reaction times.

Discussion

The initial decomposition rate of vinyl bromide was expressed as first-order in $[C_2H_3Br]$ and first-order in the total density. From the absorption profile, it seems that the decomposition of C_2H_3Br is not so complicated as the chain process, even for mixtures involving a relatively high C_2H_3Br concentration. Also, the fact that the initial rate of the C_2H_3Br consumption is just equal to the HBr production rate for the highly diluted

mixture means that the decomposition at the early stage of the reaction occurs *via* a simple reaction. Thus, the following discussion will be made on the basis of the assumption that the decomposition rate constant, k_{2nd}, corresponds to the unimolecular low-pressure-limit rate constant of the primary reaction.

According to the Arrhenius parameters of k_{2nd}, the value of the preexponential factor is somewhat low if the initial process is a single-bond fission, in this respect, the activation energy is much lower than the bond dissociation energy of C–Br, which is the weakest bond in this molecule. This discrepancy (about 35 kcal mol^{-1}) between the activation energy and the bond dissociation energy is too large to be explained by the lower-limit unimolecular process of Reaction 2. If Reaction 2 is the main initiation step, a sequence of rapid consecutive reactions may be expected to occur:

$$C_2H_3(+M) \longrightarrow C_2H_2 + H(+M) \quad (3)$$

$$C_2H_3Br + H \longrightarrow C_2H_3 + HBr \quad (4)$$

$$C_2H_3Br + Br \longrightarrow C_2H_2Br + HBr \quad (5)$$

$$C_2H_2Br(+M) \longrightarrow C_2H_2 + Br(+M). \quad (6)$$

These consecutive reactions would compose a chain cycle and would give rise to an acceleration of the vinyl bromide consumption as the reaction proceeded. In some experiments, such an acceleration was observed in the absorption and emission records at long reaction times and at low temperatures. However, in such cases no unique correlation of the acceleration with the C_2H_3Br concentration could be detected. Therefore, although the possibility of the above reaction scheme (Reactions 2—6) cannot be rejected completely, from the fact that the decomposition rate constant, k_{2nd}, is not changed by the variation in the mixture composition the contribution of the above reactions to the initial decomposition rate may be considered to be negligible under the present conditions. Thus, Reaction 2 is not important as the initiation step.

For Reaction 1 an activation energy much higher than ΔH_r may be expected, as is the case for other well-known four-center reactions. In this case, possible subsequent reactions are the decompositions of acetylene and hydrogen bromide. The unimolecular dissociation of HBr below 2000 K is negligibly small,[6] though, and thus it is not important as the secondary reaction. The decomposition of acetylene has a very high activation energy (124 kcal mol^{-1}),[7] therefore, the effect of the C_2H_2 decomposition is also negligible.

A theoretical calculation of the low-pressure-limit rate constant was performed by using a refinement of the equation of the RRKM theory presented by Troe[8] (Eq. 2.11 in Ref. 8). The molecular constants of C_2H_3Br were taken from Ref. 9, while the parameters appearing in the equation were calculated as in Ref. 10. To obtain the threshold energy, E_0, of the initiation reaction, we first assumed that the collision efficiency, β_c, was constant regardless of the temperature. Thus, we obtained $E_0=55.5$ kcal mol^{-1} when $\beta_c=1.6\times10^{-4}$. This value is the lower limit of E_0, because β_c has a slightly negative temperature dependence.[11] An estimate for the reverse reaction of Reaction 1 according to the semiempirical method by Benson and Haugen[3] leads to 59.5 kcal mol^{-1} for the high-pressure activation energy, $E_{a\infty}$, of Reaction 1 at 1600 K, the middle temperature of the present experiment. Thus, the value of E_0 (55.5 kcal mol^{-1}) obtained as the lower limit seems to be reasonable compared with the value of $E_{a\infty}$. By using this relation: $E_{a0}=E_{a\infty}-(S_{eff}+0.5)RT$, E_{a0} is calculated to be 41.0 kcal mol^{-1} at 1600 K, where S_{eff}, the number of the effective vibration, is 6.31 at 1600 K. This value of E_{a0} is very close to the experimentally obtained activation energy (41.5 kcal mol^{-1}).

The value of β_c (1.6×10^{-4}) is unexpectedly low compared with that of vinyl chloride ($\beta_c=0.04$).[2] It is recongnized that the unimolecular process of vinyl halides tends toward the low-pressure region as the halogen changes from F to Br under similar conditions, as has been shown by previous experiments[1,2] and also in this work. The fact that the decomposition process of C_2H_3Br is in the low-pressure region is probably the result of the low efficiency of the energy transfer per collision. Nevertheless, at the present time, we cannot explain why, for the C_2H_3Br decomposition, the collision efficiency is extremely small compared with similar reactions.

References

1) J. M. Simmie, W. J. Quiring, and E. Tschuikow-Roux, *J. Phys. Chem.*, **74**, 992 (1970).

2) F. Zabel, *Int. J. Chem. Kinet.*, **9**, 651 (1977).

3) S. W. Benson and G. R. Haugen, *J. Phys. Chem.*, **70**, 3336 (1966); *J. Am. Chem. Soc.*, **87**, 4036 (1965).

4) J. Schander and B. R. Russell, *J. Am. Chem. Soc.*, **98**, 6900 (1976).

5) R. B. Cundall, D. E. Fussey, J. J. Harrison, and D. Lampard, *J. Chem. Soc., Faraday Trans. 1*, **74**, 1403 (1978).

6) R. R. Giedt, N. Choen, and T. A. Jacobs, *J. Chem. Phys.*, **50**, 5374 (1969).

7) T. Just and P. Frank, *Ber. Bunsenges. Phys. Chem.*, **81**, 1119 (1977).

8) J. Troe, *J. Chem. Phys.*, **66**, 4758 (1977).

9) J. R. Scherer and J. Overend, *J. Phys. Chem.*, **33**, 168 (1960).

10) In the calculation of the strong collision low-pressure rate constant, the following equation was used:

$$k_0^{sc}/[Ar] = Z_{LJ}\rho_{vlb}(E_0)kTQ_{vlb}^{-1}\exp(-E_0/RT)F_{rot}F_{anh}F_E.$$

Examples of the data at 2000 K: threshold energy, $E_0=55.5$ kcal mol^{-1}; Lennard-Jones collision frequency, $Z_{LJ}=3.655\times10^{14}$ cm^3 mol^{-1} s^{-1}; vibrational partition function, $Q_{vlb}=7.28\times10^1$; harmonic density states at $E_0=7.627\times10^3$; Whitten-Rabinovitch correction factor=0.922; energy dependence of the density of states, $F_E=2.03$; rotational factor, $F_{rot}=1.30$; anharmonicity factor, $F_{anh}=1.20$;

$$k_0^{sc}/[Ar] = 1.653\times10^{11}\ \text{cm}^3\ \text{mol}^{-1}\ \text{s}^{-1};$$

$$k_{2nd} = 2.645\times10^7\ \text{cm}^3\ \text{mol}^{-1}\ \text{s}^{-1};$$

collision efficiency, $\beta_C=1.6\times10^{-4}$.

11) J. Troe, "Proc. 10th Int. Shock Tube Symp.," ed by G. Kamimoto, Kyoto, Japan (1975), p. 29.

Pressure and Solvent Shifts of Charge Transfer Absorption Band of Iodine Complexes

Seiji SAWAMURA, Yoshihiro TANIGUCHI, and Keizo SUZUKI*

Department of Chemistry, Faculty of Science and Engineering, Ritsumeikan University, Kita-ku, Kyoto 603

(Received June 6, 1979)

Absorption spectra of the CT band of I_2 complexes were observed in several nonpolar solvents at 1 bar, and in heptane up to 4400 bar. All solvent shifts were red with an increase in $(n^2-1)/(2n^2+1)$, the refractive index (n) function of solvents, consistent with the solvent shift theory. On the other hand pressure caused a variety of shifts, that is, red shifts in benzene–, toluene–, and mesitylene–I_2 complexes, an inversion shift from red to blue in HMB–I_2 complex, and blue shifts in Et_3N–, n-Pr_3N–, and n-Bu_3N–I_2 complexes, though increase in pressure invariably raises the $(n^2-1)/(2n^2+1)$ value of solvent. The pressure shifts of I_2 complexes seem to be interpreted by a sum of two effects. One is the increased polarity of the solvent, which causes a red shift. The other is the decrease in the bond distance between a donor and an acceptor, which contributes to a blue shift in a strong CT complex and to a red shift in a week one. The pressure and solvent shifts of I_2 complexes were compared with those of π-donor–TCNE complexes.

Recently, we found the pressure shifts of charge transfer (CT) absorption band of n-donor (diethyl sulfide (Et_2S) and diethyl selenide (Et_2Se))–iodine (I_2) complexes in heptane, changing from red to blue at *ca.* 2500 bar.[1] Such an inversion shift is known only in the π-π complex between hexamethylbenzene (HMB) and tetracyanoethylene (TCNE).[2-4] The other CT bands of π-π complexes[2-5] and π-donor–I_2 complexes[6,7] in solution shifted only to red.

In the present work we have found blue shifts of well-defined CT band of amine–I_2 complexes in heptane. In polymer matrix the blue shift of CT band was reported by Offen and Nakashima[8] in two π-π complexes between *trans*-stilbene and phenanthrene as donors and 2,3-dichloro-5,6-dicyano-*p*-benzoquinone (DDQ) as an acceptor. However, it seems to be obscured by a strong overlap with another absorption band.

The red shift of CT band has been interpreted by an increase in the polarity of the solvent with increase in pressure.[6,9,10] Two different interpretations have been proposed for the blue shift: (1) Offen and Nakashima[8] tried to explain the blue shift of DDQ complexes by a decrease in the bond distance between a donor and an acceptor. (2) Nakayama *et al.*[4] ascribed the blue shift of HMB–TCNE complex to an increase in the polarity of solvent caused by pressure, the relevance of the interpretation being examined by a comparison of the pressure shift of CT band with the solvent shift.

In the present work we measured the pressure shifts of CT bands of I_2 complexes with several π- and n-donors up to 4400 bar. In order to interpret them, the observed pressure shifts, red, red to blue, or blue, were compared with the solvent shifts.

Experimental

I_2 was sublimed from a mixture of I_2, calcium oxide, and potassium iodide, and then was done under nitrogen atmosphere. TCNE was sublimed under reduced pressure (10 mmHg). The purification of diethyl ether (Et_2O), Et_2S, and Et_2Se was reported.[1] HMB was recrystallized twice from ethanol. Triethylamine (Et_3N), tripropylamine (n-Pr_3N), and tributylamine (n-Bu_3N) were shaken with acetic anhydride, dried over potassium hydroxide and sodium metal successively, and distilled over sodium metal (under reduced pressure for the last two amines, 34—36 °C/6 mmHg and 51—52 °C/2 mmHg, respectively). The other donors (benzene, toluene, and mesitylene) and the solvents (pentane, heptane, cyclohexane, carbon tetrachloride, decalin, and carbon disulfide) were purified by the usual method.[11] The method of measuring the absorption spectra under high pressure was reported[1]

Results

Solvent Shift. The dielectric constant or refractive index (n) of solvent has been often used as a measure of the property of solvent for interpretation of the solvent shift of the electronic spectrum. Theories given by Ooshika[12] and McRae[13] on solvent shift predicted that the wavenumber at absorption maximum ($\bar{\nu}_{max}$) of electronic spectrum depends linearly on the value of $(n^2-1)/(2n^2+1)$ of nonpolar solvents. The linear relation between $\bar{\nu}_{max}$ of CT band and $(n^2-1)/(2n^2+1)$ has been reported for several π-donor–TCNE[14,15] and π-donor–I_2[6] complexes. Pressure shifts to red in the latter complexes were interpreted by Ham[6] in comparison with the solvent shifts using the function of $(n^2-1)/(2n^2+1)$.

The $\bar{\nu}_{max}$ values of I_2 complexes in several nonpolar solvents at 1 bar are plotted as a function of $(n^2-1)/(2n^2+1)$ of solvents, including that of HMB–TCNE complex, in Figs. 1 and 2. All CT bands shift linearly to red with increase in the $(n^2-1)/(2n^2+1)$ values of solvents. The red shift in HMB–TCNE complex observed by Voigt[14] was confirmed. The $\bar{\nu}_{max}$ values of mesitylene–, and Et_2S–I_2 complexes in gaseous state fit the lines. The values of the slopes (Figs. 1 and 2) are given in Table 1 as C_{solv}, together with the data of π-donor–TCNE complexes. For the I_2 complexes with a series of π-donors (Table 1-A) the values of C_{solv} increase with an increase in the bond energy ($-\Delta H$). A similar trend is seen for n-donor–I_2 and π-donor–TCNE (Table 1-B and C, respectively) but not so marked in the latter.

Pressure Shift. Absorption spectra of the CT band of n-Bu_3N–I_2 complex under various pressures are shown in Fig. 3. The absorption maximum shifts toward blue with increase in pressure. Similar well-defined

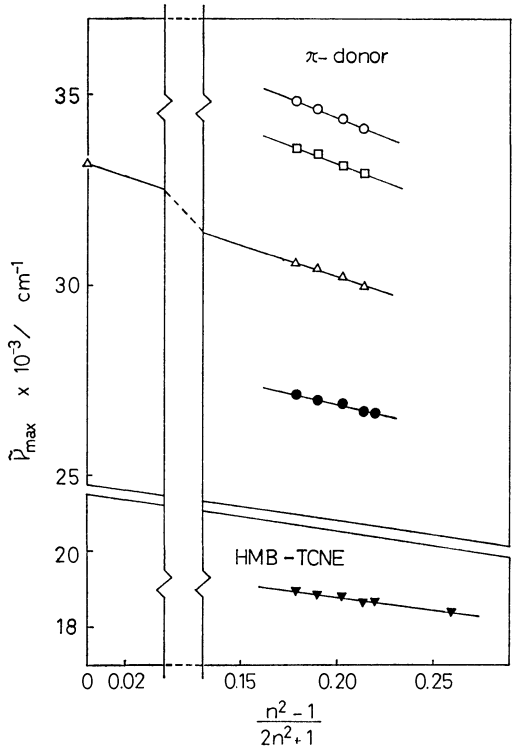

Fig. 1. Solvent shifts on CT absorption maxima of the I_2 complexes with π-donors, including HMB–TCNE complex. Donors are, ○: benzene, □: toluene, △: mesitylene, and ●: HMB in I_2 complexes. Solvents are pentane ($(n^2-1)/(2n^2+1)=0.179$), heptane (0.190), cyclohexane (0.203), carbon tetrachloride (0.214), decalin (0.220), and carbon disulfide (0.261), adding the data in gaseous state (0.000) of Ref. 16 for mesitylene–I_2 complex. The values of n of solvents were cited from Ref. 11.

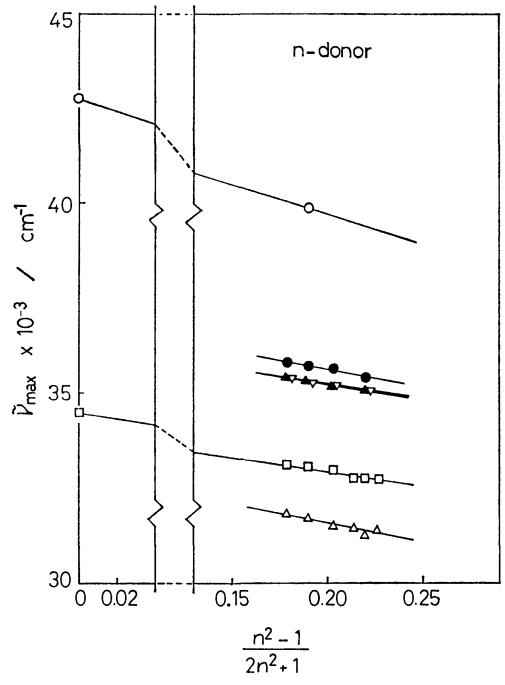

Fig. 2. Solvent shifts on CT absorption maxima of the I_2 complexes with n-donors. Donors are, ○: Et_2O, □: Et_2S, △: Et_2Se, ●: Et_3N, ▲: n-Pr_3N, and ▽: n-Bu_3N. Solvents are the same as Fig. 1, adding benzene (0.227) instead of carbon disulfide. Gaseous data for Et_2O– and Et_2S–I_2 complexes are cited from Refs. 16 and 17, respectively.

absorption spectra were also observed in Et_3N– and n-Pr_3N–I_2 complexes, causing blue shifts.

Figures 4 and 5 show the pressure shifts of absorption maxima of several I_2 complexes as a function of $(n^2-1)/(2n^2+1)$ of heptane. Various pressure shifts were observed: red shifts in benzene–, toluene–, mesitylene–, and Et_2O–I_2 complexes, inversion shifts from red to blue in HMB–, Et_2S–, and Et_2Se–I_2 complexes, and blue shifts in Et_3N–, n-Pr_3N–, and n-Bu_3N–I_2 complexes. The values of the initial slope in Figs. 4 and 5 are given in Table 1 as C_{press}, with the values of π-donor–TCNE complexes given by Nakayama *et al.*[4]

In I_2 or TCNE complexes with benzene, toluene, and mesitylene (Table 1), each slope estimated from the pressure shift (C_{press}) is smaller than that estimated from the solvent shift (C_{solv}). The reverse is found in other CT complexes, except in the case of comparable values in Et_2O–I_2 complex. In the series of π-donor–I_2 complexes, C_{press} becomes large accompanied by an increase in the bond energy ($-\Delta H$). A similar relation between C_{press} and $-\Delta H$ is found in n-donor–I_2 complexes and π-donor–TCNE complexes, though less explicit in the former.

Table 1. Slopes of solvent (C_{solv}) and pressure (C_{press}) shift and the bond energy ($-\Delta H$) of several CT bands

Complex	C_{solv} / 10^3 cm^{-1}	C_{press} [a] / 10^3 cm^{-1}	$-\Delta H$ / kJ mol^{-1}
(A) π-Donor–I_2			
Benzene–I_2	−20±2	−29±3	6[b]
Toluene–I_2	−19±2	−24±2	8[c]
Mesitylene–I_2	−16±2	−22±3	12[b]
HMB–I_2	−12±2	−8±2	16[b]
(B) n-Donor–I_2			
Et_2O–I_2	−16±2	−17±4	18[d]
Et_2S–I_2	−9±2	−5±2	33[e]
Et_2Se–I_2	−10±2	−4±2	41[f]
Et_3N–I_2	−9±2	+3±2	50[g]
n-Pr_3N–I_2	−9±2	+8±3	51[g]
n-Bu_3N–I_2	−8±2	+4±2	52[g]
(C) π-Donor–TCNE			
Benzene–TCNE	−12[h]	−17	10[i]
Toluene–TCNE	—	−15	11[i]
Mesitylene–TCNE	−7[h]	−12	19[i]
HMB–TCNE	−5[h]	0	32[i]
	−7±2		

a) Estimated from the straight line through the two points at 1 and 1100 bar in Figs. 4 and 5. Values for (C) complexes were estimated with data taken from Ref. 4 at 1 and 1500 bar in CCl_4. b) Ref. 18. c) Ref. 19. d) Ref. 20. e) Ref. 21. f) Ref. 22. g) Ref. 23. h) Ref. 14. i) Ref. 24.

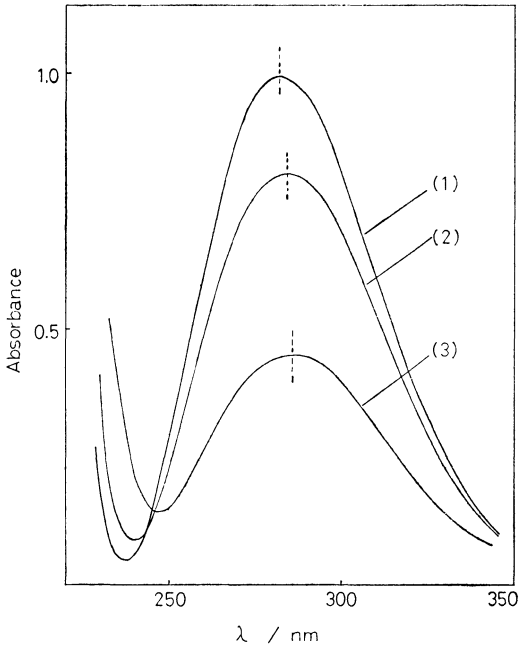

Fig. 3. Absorption spectra of CT band of n-Bu_3N–I_2 complex in heptane. n-Bu_3N: 5×10^{-4} mol dm^{-3}, I_2: 3.5×10^{-5} mol dm^{-3}. (1) 4.4 kbar, (2) 2.2 kbar, (3) 1 bar. Dotted lines show the absorption maxima at each pressure.

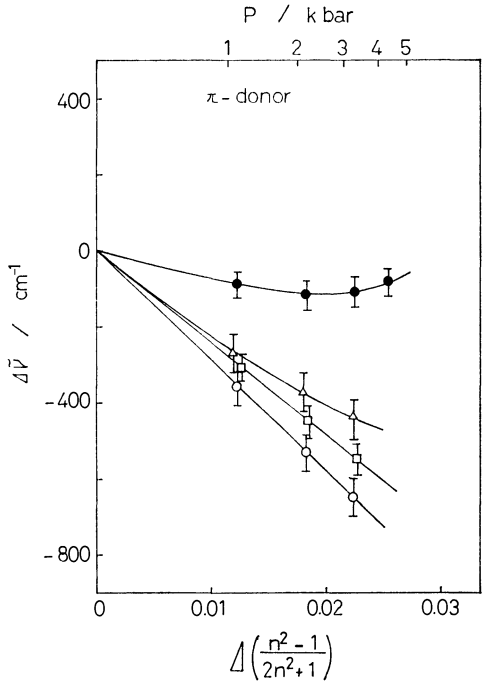

Fig. 4. Pressure shifts of CT absorption maxima of the I_2 complexes with π-donors in heptane. The marks of π-donors are the same as in Fig. 1. $\Delta\bar{\nu}=\bar{\nu}_{max}$ (at P bar) $-\bar{\nu}_{max}$ (at 1 bar). The value of n of heptane under high pressure was cited from the dielectric constant (ε) of heptane in Ref. 25 using the relation of Maxwell ($\varepsilon=n^2$). $\Delta[(n^2-1)/(2n^2+1)]=(n_P^2-1)/(2n_P^2+1)-(n_1^2-1)/(2n_1^2+1)$.

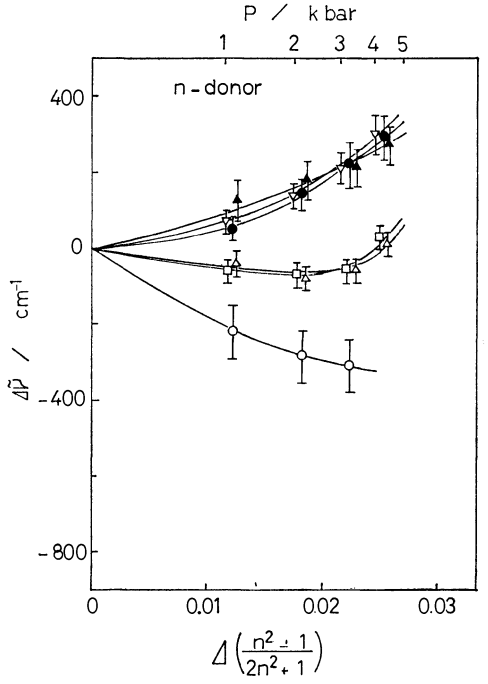

Fig. 5. Pressure shifts of CT absorption maxima of the I_2 complexes with n-donors in heptane. The marks are the same as in Fig. 2. $\Delta\bar{\nu}$ and $\Delta[(n^2-1)/(2n^2+1)]$ are defined in Fig. 4. The data of Et_2O–, Et_2S–, and Et_2Se–I_2 complexes are cited from Ref. 1.

Discussion

Linear red shift of CT bands in Figs. 1 and 2 are in line with the solvent shift theory as in the case of π-donor–TCNE[14,15] and π-donor–I_2[6] complexes. The result that C_{solv} values (Table 1-A, B, and C) increase accompanied by an increase in $-\Delta H$ would be interpreted by the solvent shift theory regarding $-\Delta H$ as a measure of the CT interaction, since the excited state of CT band becomes less polar and the dipole moment of the ground state increases with increasing CT interaction.[26,27]

In Figs. 4 and 5 the values of $(n^2-1)/(2n^2+1)$ of heptane are 0.190 at 1 bar 0.216 at 4400 bar. The values are covered by those in Figs. 1 and 2, *viz.*, 0.179 for pentane to 0.261 for carbon disulfide. If the pressure shifts of CT bands are attributed to only the increasing polarity of solvent, red shifts similar to those given in Figs. 1 and 2 can be expected in Figs. 4 and 5, respectively. In HMB–, Et_2S–, and Et_2Se–I_2 complexes, however, the observed inversion shifts differ from the expected ones, the blue shifts of Et_3N–, n-Pr_3N–, and n-Bu_3N–I_2 complexes (Fig. 5) being a striking contrast to the red shifts (Fig. 2). The solvent shift of HMB–TCNE complex (Fig. 1) is not in line with the inversion shift caused by increase in pressure. Though the increasing polarity of the solvent caused by compression may contribute to a red shift, another effect causing a blue shift should participate in at least HMB–, Et_2S–, Et_2Se–, Et_3N–, n-Pr_3N–, and n-Bu_3N–I_2 complexes, and HMB–TCNE complex.

As a plausible effect causing a blue shift, a decrease

in the bond distance (R_{DA}) between a donor and an acceptor proposed by Offen and Nakashima[8] may be taken into account. The effect is interpreted by means of the Mulliken's equation[27] for the CT transition energy $hc\tilde{\nu}_{CT}$:

$$hc\tilde{\nu}_{CT} = \frac{\sqrt{4\beta_0\beta_1+\Delta^2}}{1-S_{01}^2} \quad (1)$$

$$\beta_0 = W_{01} - W_0S_{01}$$
$$\beta_1 = W_{01} - W_1S_{01} \quad (2)$$
$$\Delta = W_1 - W_0$$

where W_0 and W_1 are the energy of no-bond and dative structure, respectively, and W_{01} is the interaction matrix which is approximately proportional to the overlap integral S_{01}. $|\beta_0|$ and $|\beta_1|$ increase with increase in S_{01}. When R_{DA} decreases by compression, S_{01} increases and so $\beta_0\beta_1$ does. Δ is the energy accompanied by the transfer of an electron from a donor to an acceptor. It is approximately expressed as follows, decreasing with reduction in R_{DA}.

$$\Delta \approx I_D - E_A - \frac{e^2}{R_{DA}} \quad (3)$$

where I_D is the ionization potential of a donor, E_A the electron affinity of an acceptor, and e the charge of an electron. The denominator $(1-S_{01}^2)$ and the first term in the square root $(4\beta_0\beta_1)$ in Eq. 1 might contribute to a blue shift and the second term in the square root (Δ^2) to a red shift with increasing pressure, the shifts overlapping the red shift caused by an increase in the polarity of the solvent.

Table 2. Reasonable values of $4\beta_0\beta_1$ and Δ^2 for I_2 complexes

Complex	$4\beta_0\beta_1$[a] / eV^2	Δ^2 / eV^2
Et_3N–I_2[b]	12—42	0—1
Benzene–I_2[c]	1—7	13—21

a) $4\beta_0\beta_1 = 4\beta_0(\beta_0 - \Delta S_{01})$, deduced from Eq. 2. b) Mulliken's "Reasonable Values"[28] are $S_{01}=0.4$—0.5, $(I_D-\Delta)=6.5$—7.5 eV, and $-\beta_0=1.7$—3 eV. $I_D=7.50$ eV.[29] c) Mulliken's "Reasonable Values"[28] are $S_{01}=0$—0.15, $(I_D-\Delta)=4.7$—5.7 eV, and $-\beta_0=0.5$—1.0 eV. $I_D=9.24$ eV.[30]

In a strong CT complex of a large $-\Delta H$ value such as Et_3N–I_2 complex, the value of $4\beta_0\beta_1$ should be large as compared with Δ^2 in view of the CT theory.[27] The reverse holds for a weak CT complex such as benzene–I_2. The values of $4\beta_0\beta_1$ and Δ^2 given in Table 2 are roughly estimated from the values of I_D and Mulliken's "Reasonable Values" for S_{01}, $I_D-\Delta$, and β_0 of the I_2 complexes from Eq. 2. In Et_3N–I_2 complex Δ^2 is negligible as compared with $4\beta_0\beta_1$. Thus in a strong CT complex the contribution to a blue shift by the term of $4\beta_0\beta_1$ with reducing R_{DA} is expected to be effective. The observed blue shift may be attributed to this effect. On the other hand, in a weak CT complex a decrease in R_{DA} may contribute to a red shift since $4\beta_0\beta_1$ is small or negligible as compared with Δ^2. The excessive red shift caused by pressure as compared with the solvent shift in I_2 or TCNE complexes with benzene, toluene, and mesitylene, may be due to such a contribution of Δ^2.

In conclusion, the observed pressure shifts of CT bands could be interpreted by a sum of two effects, the increased polarity of the solvent causing a red shift, and the decrease in R_{DA} contributing to a blue shift in a strong CT complex and to a red shift in a weak one.

We wish to thank Mr. Hisashi Mizuno for his assistance in the experiments.

References

1) S. Sawamura, Y. Taniguchi, and K. Suzuki, *Bull. Chem. Soc. Jpn.*, **52**, 284 (1979).
2) J. R. Gott and W. G. Maisch, *J. Chem. Phys.*, **39**, 2229 (1963).
3) A. H. Ewald, *Trans. Faraday Soc.*, **64**, 733 (1968).
4) T. Nakayama and J. Osugi, *Rev. Phys. Chem. Jpn.*, **45**, 79 (1975); T. Nakayama, M. Sasaki, and J. Osugi, *ibid.*, **46**, 57 (1976).
5) Y. Torihashi, Y. Furutani, K. Yagii, N. Mataga, and A. Sawaoka, *Bull. Chem. Soc. Jpn.*, **44**, 2985 (1971).
6) J. Ham, *J. Am. Chem. Soc.*, **76**, 3881 (1954).
7) O. C. Kwun and H. Lenz, *Z. Phys. Chem. N. F.*, **96**, 177 (1975); O. C. Kwun, *Daehan Hwahak Hweejee*, **22**, 245 (1978).
8) H. W. Offen and T. T. Nakashima, *J. Chem. Phys.*, **47**, 4446 (1967).
9) A. H. Ewald and J. A. Scudder, *J. Phys. Chem.*, **76**, 244 (1972).
10) S. D. Hamann and M. Linton, *Aust. J. Chem.*, **28**, 701 (1975).
11) "Techniques of Chemistry," 3rd ed, ed by A. Weissberger, Wiley-Interscience, New York (1970), Vol. 2.
12) Y. Ooshika, *J. Phys. Soc. Jpn.*, **9**, 594 (1954).
13) E. G. McRae, *J. Phys. Chem.*, **61**, 562 (1957).
14) E. M. Voigt, *J. Phys. Chem.*, **70**, 598 (1966).
15) J. Aihara, M. Tsuda, and H. Inokuchi, *Bull. Chem. Soc. Jpn.*, **42**, 1824 (1969).
16) J. Grundnes, M. Tamres, and S. N. Bhat, *J. Phys. Chem.*, **75**, 3682 (1971).
17) M. Tamres and S. N. Bhat, *J. Am. Chem. Soc.*, **94**, 2577 (1972).
18) R. M. Keefer and L. J. Andrews, *J. Am. Chem. Soc.*, **77**, 2164 (1955).
19) J. A. A. Ketelaar, *J. Physique Radium*, **15**, 197 (1954).
20) S. M. Brandon, O. P. M. Tamres, and S. Searles, Jr., *J. Am. Chem. Soc.*, **82**, 2129 (1960).
21) H. Tsubomura and R. P. Lang, *J. Am. Chem. Soc.*, **83**, 2085 (1961).
22) A. V. Smolentsev, I. P. Gol'dshtein, E. N. Gur'yanova, L. M. Kataeva, E. G. Kataev, and K. A. Kocheshkov, *Dokl. Akad. Nauk SSSR*, **219**, 1416 (1974).
23) H. Yada, J. Tanaka, and S. Nagakura, *Bull. Chem. Soc. Jpn.*, **33**, 1660 (1960).
24) R. E. Merrifield and W. D. Phillips, *J. Am. Chem. Soc.*, **80**, 2778 (1958), in CH_2Cl_2.
25) W. E. Danforth, Jr., *Phys. Rev.*, **38**, 1224 (1931).
26) E. J. J. Groenen and P. N. Th. van Velzen, *Mol. Phys.*, **33**, 933 (1977).
27) R. S. Mulliken and W. B. Person, "Molecular Complexes," Wiley-Interscience, New York (1969), Chap. 2.
28) Ref. 27, p. 147.
29) K. Watanabe and J. R. Mottle, *J. Chem. Phys.*, **26**, 1773 (1957).
30) K. Watanabe, *J, Chem. Phys.*, **26**, 542 (1957).

Molecular Force Field of Dialkyl Selenides

Hiroatsu MATSUURA* and Hiromu MURATA

Department of Chemistry, Faculty of Science, Hiroshima University, Higashisenda-machi, Hiroshima 730

(Received June 14, 1979)

The molecular force field in terms of the local symmetry coordinates was determined for unbranched dialkyl selenides. Twenty-six important force constants associated with the selenium part were adjusted by using about two hundred observed vibrational wave numbers for a total of twelve conformational isomers of ethyl methyl selenide, diethyl selenide, methyl propyl selenide, butyl methyl selenide, and ethyl propyl selenide. Remaining force constants of the selenides were assumed to be equivalent to those for unbranched dialkyl sulfides and alkanes. The least-squares calculation gave an overall root-mean-square deviation of 6.7 cm^{-1} between the observed and calculated wave numbers. The force constants and the results of the normal coordinate treatment are given in this paper.

The molecular force field of molecules is fundamentally important for studying various problems in chemistry and physics. To establish the force field, vibrational spectra have been extensively investigated for a number of compounds. The force constants deduced from the experimental data were, however, reliable only, in general, for relatively small molecules. To conquer the difficulty in determining the molecular force field of larger molecules, various attempts have been made.[1-4] One of the approaches is to assume the transferability of the force constants for similar atomic groups in different molecules.[5] This assumption allows ones to reduce the number of force constants to determine. In this model, the symmetry coordinates in each of the atomic groups, namely the local symmetry coordinates, are used to express the molecular force field, as most of organic molecules, which we are interested in, give characteristic group vibrations.

Recent systematic studies[6-15] on the vibrational spectra of unbranched organic compounds made possible to determine the force constants, in terms of the local symmetry force field, for alkanes, dialkyl ethers, dialkyl sulfides, halogenoalkanes, and alkylsilanes.[16,17] In the present study, the molecular force field of unbranched dialkyl selenides was treated by utilizing the experimental data which have been accumulated in our laboratory.[18] The force constants thus obtained are reported in this paper and are discussed in comparison with those for related compounds. A preliminary result of the normal coordinate treatment has been reported previously.[19]

Calculation of Normal Coordinates

The calculation of the normal coordinates for unbranched dialkyl selenides was carried out by a program system MVIB[20] with a HITAC 8700 computing system at Hiroshima University. The force field adopted in the MVIB system is the local symmetry force field which has been successfully applied to a number of unbranched organic compounds.[16,17]

Initial values of the force constants for the selenium part and for the alkyl parts next to the selenium atom were transferred or estimated from the results for the sulfides.[16] The force constants for the unbranched alkyl part, not directly associated with the selenium atom, were the same as those obtained for the alkanes.[16] Some of the important force constants for the selenium and neighboring parts were adjusted by a least-squares procedure by utilizing the observed vibrational wave numbers for the *trans* and *gauche* isomers of ethyl methyl selenide $CH_3SeCH_2CH_3$, the *trans-trans*, *trans-gauche*, and *gauche-gauche* isomers of diethyl selenide $CH_3CH_2SeCH_2CH_3$, and the *trans-trans*, *trans-gauche*, *gauche-trans*, and *gauche-gauche* isomers of methyl propyl selenide $CH_3SeCH_2CH_2CH_3$.[18]

The force field thus obtained was applied to butyl methyl selenide $CH_3SeCH_2CH_2CH_2CH_3$ and ethyl propyl selenide $CH_3CH_2SeCH_2CH_2CH_3$ to study the rotational isomerism. The force field was then refined by using the additional observed data for the *gauche-gauche-trans* isomer of butyl methyl selenide and the *gauche-gauche-trans* and *gauche-gauche-gauche* isomers of ethyl propyl selenide,[18] which have been shown to exist in the solid state.[19] At the final stage of the calculation, twenty-six important force constants

TABLE 1. ATOMIC MASSES AND STRUCTURAL PARAMETERS USED IN THE CALCULATION

Property	Quantity
Atomic masses, u	
Hydrogen (H)	1.007825
Carbon (C)	12.011
Selenium (Se)	78.96
Bond lengths, Å	
r(C–H)	1.100[a]
r(C–C)	1.539[a]
r(C–Se)	1.943[b]
Bond angles, degree	
∠(C–C–C)	112.2[a]
∠(C–C–Se)	113.6[c]
∠(C–Se–C)	96.18[b]
∠(C–C–H)	110.4[a]
∠(Se–C–H)	108.8[d]
Dihedral angles of molecular skeleton, degree	
trans conformation	180
gauche$^+$ conformation	60
gauche$^-$ conformation	−60

a) Ref. 16. b) Taken from dimethyl selenide (Ref. 21). c) Assumed to be equal to ∠(C–C–S) (Ref. 16). d) Assumed to be equal to ∠(S–C–H) (Ref. 16). This value is close to an average value, 108.2°, of two unequivalent ∠(Se–C–H) of dimethyl selenide (Ref. 21).

TABLE 2. DEFINITION AND SYMBOLISM OF ATOMIC GROUPS AND LOCAL SYMMETRY COORDINATES

Atomic group		Local symmetry coordinate		
Description	Symbol	Description	Symbol	Definition[a,b]
CH_3–(X)	1	CH_3 symmetrical stretching	1	$(\Delta r_1+\Delta r_2+\Delta r_3)/\sqrt{3}$
		CH_3 symmetrical deformation	2	$a(\Delta\alpha_{23}+\Delta\alpha_{31}+\Delta\alpha_{12})-b(\Delta\beta_1+\Delta\beta_2+\Delta\beta_3)$
		CH_3 degenerate stretching (in-plane)	3	$(2\Delta r_1-\Delta r_2-\Delta r_3)/\sqrt{6}$
		CH_3 degenerate deformation (in-plane)	4	$(2\Delta\alpha_{23}-\Delta\alpha_{31}-\Delta\alpha_{12})/\sqrt{6}$
		CH_3 rocking (in-plane)	5	$(2\Delta\beta_1-\Delta\beta_2-\Delta\beta_3)/\sqrt{6}$
		CH_3 degenerate stretching (out-of-plane)	6	$(\Delta r_2-\Delta r_3)/\sqrt{2}$
		CH_3 degenerate deformation (out-of-plane)	7	$(\Delta\alpha_{31}-\Delta\alpha_{12})/\sqrt{2}$
		CH_3 rocking (out-of-plane)	8	$(\Delta\beta_2-\Delta\beta_3)/\sqrt{2}$
(X)–CH_2–(Y)	2	CH_2 symmetrical stretching	1	$(\Delta r_1+\Delta r_2)/\sqrt{2}$
		CH_2 scissoring	2	$c\Delta\alpha-d(\Delta\beta_{1X}+\Delta\beta_{2X})-e(\Delta\beta_{1Y}+\Delta\beta_{2Y})$
		CH_2 antisymmetrical stretching[c]	3	$(\Delta r_1-\Delta r_2)/\sqrt{2}$
		CH_2 rocking[c]	4	$(\Delta\beta_{1X}-\Delta\beta_{2X}+\Delta\beta_{1Y}-\Delta\beta_{2Y})/2$
		CH_2 wagging[c]	5	$f(\Delta\beta_{1X}+\Delta\beta_{2X})-g(\Delta\beta_{1Y}+\Delta\beta_{2Y})/2$
		CH_2 twisting	6	$(\Delta\beta_{1X}-\Delta\beta_{2X}-\Delta\beta_{1Y}+\Delta\beta_{2Y})/2$
		X–C–Y deformation	D	$h\Delta\gamma-i\Delta\alpha-j(\Delta\beta_{1X}+\Delta\beta_{2X})-k(\Delta\beta_{1Y}+\Delta\beta_{2Y})$
(X)–Se–(Y)	W	X–Se–Y bending	B	$\Delta\gamma$
Skeleton –(X)–(Y)–	—	Stretching	S	Δr_{XY}
		Torsion[d]	T	Δt_{XY}

a) a=0.403003 and b=0.413427 for X=Se. c=0.908651, d=0.211232, e=0.206297, f=0.494055, g=0.505875, h=0.896458, i=0.185032, j=0.203690, and k=0.198931 for X=C and Y=Se. b) *Definition of the internal coordinates of the methyl group.* The hydrogen atoms in the CH_3–(X)–(Y) group are numbered in the following way (Refs. 16 and 22). The hydrogen atom located at the *trans* position relative to Y is numbered as 1. The atoms numbered 2 and 3 are defined in the clockwise direction, viewing the atoms along the bond X–C with the atom X nearer to the observer (see Fig. 1 of Ref. 16). $r_1=r(C\text{–}H_1)$, $r_2=r(C\text{–}H_2)$, $r_3=r(C\text{–}H_3)$, $\alpha_{12}=\angle(H_1\text{–}C\text{–}H_2)$, $\alpha_{23}=\angle(H_2\text{–}C\text{–}H_3)$, $\alpha_{31}=\angle(H_3\text{–}C\text{–}H_1)$, $\beta_1=\angle(H_1\text{–}C\text{–}X)$, $\beta_2=\angle(H_2\text{–}C\text{–}X)$, and $\beta_3=\angle(H_3\text{–}C\text{–}X)$. *Definition of the internal coordinates of the methylene group.* The hydrogen atoms in the (X)–CH_2–(Y) group are numbered in the following way (Ref. 16). Viewing the (X)–CH_2–(Y) group from the direction perpendicular to the HCH plane with the atom X nearer to the observer, the hydrogen atoms located at the ten o'clock and two o'clock positions (or, for example, at the four o'clock and eight o'clock positions, respectively) are numbered as 1 and 2, respectively (see Fig. 1 of Ref. 16). $r_1=r(C\text{–}H_1)$, $r_2=r(C\text{–}H_2)$, $\alpha=\angle(H_1\text{–}C\text{–}H_2)$, $\beta_{1X}=\angle(H_1\text{–}C\text{–}X)$, $\beta_{2X}=\angle(H_2\text{–}C\text{–}X)$, $\beta_{1Y}=\angle(H_1\text{–}C\text{–}Y)$, $\beta_{2Y}=\angle(H_2\text{–}C\text{–}Y)$, and $\gamma=\angle(X\text{–}C\text{–}Y)$. c) The signs of the CH_2 antisymmetrical stretching, rocking, and wagging coordinates of the (Y)–CH_2–(X) group (viewing the atomic group from the direction perpendicular to the HCH plane with the atom Y nearer to the observer) are opposite to those of the corresponding coordinates of the (X)–CH_2–(Y) group (viewing the atomic group with the atom X nearer to the observer) (Refs. 16 and 22). The signs of the other coordinates in this table are invariable with the viewing direction. d) For the definition of the torsional coordinate, see Refs. 22 and 23.

associated with the selenium and neighboring parts were determined from a total of 196 observed wave numbers with non-zero weights for the twelve conformers of the five compounds.

In the normal coordinate calculation, the observed wave numbers in the liquid phase were used, so that the origin of the experimental data for any one isomer is consistent with that for any other.

The atomic masses and structural parameters used in the calculation are listed in Table 1. The structural data for the selenium part were taken from a microwave study on dimethyl selenide.[21]

Local Symmetry Coordinates. The local symmetry coordinates defined in Table 2 were used as basis coordinates in the normal coordinate treatment. The deformation coordinates for the methyl or methylene group were constructed in accordance with the bond angles, given in Table 1, around a central carbon atom, so that the redundant coordinate was properly eliminated from the coordinate system. The definition of the local symmetry coordinates adopted in this study for the methyl and methylene groups is in accord with the conventions recommended by IUPAC.[22] The coordinates for the methyl group with a neighboring carbon atom, CH_3–(C), and the methylene group with neighboring carbon atoms, (C)–CH_2–(C), have been defined previously[16] on the basis of $\angle$(C–C–C) and $\angle$(C–C–H) values given in Table 1.

According to the coordinate definition mentioned above, the signs of the CH_2 antisymmetrical stretching, rocking, and wagging coordinates for the (X)–CH_2–(Y) group are opposite to those of the corresponding coordinates for the (Y)–CH_2–(X) group. The signs of other coordinates given in Table 2 are invariable with the direction of ordering the atomic groups. One must be careful in defining the coordinates, since the signs of the off-diagonal force constants in terms of these coordinates depend directly upon the signs of the coordinates concerned.

Force Constants. The force constants in the local symmetry force field are expressed on the basis of the local symmetry coordinates.[5] In a series of studies on the local symmetry force field,[16,17] force constants have been denoted by symbols, which are suitable for com-

Table 3. Force constants for unbranched dialkyl selenides[a)]

Constant[b)]	Value[c)]	Constant[b)]	Value[c)]	Constant[b)]	Value[c)]
01W–1	= 014–1 (4.715)	122W–S	=222W–S	222W–SD	0.013±0.057
01W–2	0.527±0.005	122W–T	=222W–T	222W–2D–t	=2224–2D–t (−0.050)
01W–3	= 014–3 (4.637)	†122W–5S	=222W–5S	222W–44–t	0.058±0.024
01W–4	0.533±0.002	122W–DS	=222W–DS	†222W–46–t	=2224–46–t
01W–5	0.566±0.003	†122W–S5	=222W–S5		=2222–46–t (0.063)
01W–6	= 01W–3	122W–SD	=222W–SD	222W–55–t	−0.053±0.007
01W–7	= 01W–4	122W–2D–t	=222W–2D–t	†222W–5D–t	=2224–5D–t (−0.034)
01W–8	= 01W–5	122W–44–t	=222W–44–t	†222W–64–t	=2224–64–t
01W–45	= 014–45 (−0 020)	†122W–46–t	=222W–46–t		=−2222–46–t (−0.063)
01W–78	= 01W–45	122W–55–t	=222W–55–t	222W–66–t	−0.076±0.008
		†122W–5D–t	=222W–5D–t	222W–D2–t	=2224–D2–t
12W–1	= 22W–1	†122W–64–t	=222W–64–t		=2222–2D–t (0.042)
12W–2	= 22W–2	122W–66–t	=222W–66–t	†222W–D5–t	=2224–D5–t
12W–3	= 22W–3	122W–D2–t	=222W–D2–t		=−2222–5D–t (−0.039)
12W–4	= 22W–4	†122W–D5–t	=222W–D5–t	222W–DD–t	−0.052±0.057
12W–5	= 22W–5	122W–DD–t	=222W–DD–t	222W–44–g+	0.007±0.025
12W–6	= 22W–6	122W–44–g+	=222W–44–g+	*222W–45–g+	=2224–45–g+
12W–D	0.865±0.036	*122W–45–g+	=222W–45–g+		=2222–45–g+ (0.063)
12W–25	= 22W–25	†122W–46–g+	=222W–46–g+	†222W–46–g+	=2224–46–g+
12W–2D	= 22W–2D	*†122W–4D–g+	=222W–4D–g+		=2222–46–g+ (−0.029)
†12W–46	= 22W–46	*122W–54–g+	=222W–54–g+	*†222W–4D–g+	=2224–4D–g+ (−0.026)
†12W–5D	= 22W–5D	122W–55–g+	=222W–55–g+	*222W–54–g+	=2224–54–g+
12W–SS	= 22W–SS	*†122W–56–g+	=222W–56–g+		=2222–45–g+ (0.063)
		†122W–5D–g+	=222W–5D–g+	222W–55–g+	0.038±0.009
1W2–B	1.158±0.042	†122W–64–g+	=222W–64–g+	*†222W–56–g+	=2224–56–g+
1W2–SS	= 2W2–SS	*†122W–65–g+	=222W–65–g+		=2222–56–g+ (0.026)
		122W–66–g+	=222W–66–g+	†222W–5D–g+	=2224–5D–g+ (−0.036)
22W–1	=224–1 (4.689)	*122W–6D–g+	=222W–6D–g+	†222W–64–g+	=2224–64–g+
22W–2	0.549±0.003	*†122W–D4–g+	=222W–D4–g+		=−2222–46–g+ (0.029)
22W–3	=224–3 (4.637)	†122W–D5–g+	=222W–D5–g+	*†222W–65–g+	=2224–65–g+
22W–4	0.754±0.006	*122W–D6–g+	=222W–D6–g+		=−2222–56–g+ (−0.026)
22W–5	0.582±0.003	122W–DD–g+	=222W–DD–g+	222W–66–g+	0.040±0.017
22W–6	0.596±0.004			*222W–6D–g+	=2224–6D–g+ (0.162)
22W–D	0.891±0.026	12W1–S	=22W2–S	*†222W–D4–g+	=2224–D4–g+
22W–25	=224–25 (0.054)	12W1–T	=22W2–T		=−2222–4D–g+ (0.074)
22W–2D	=224–2D (0.161)	†12W1–5S	=22W2–5S	†222W–D5–g+	=2224–D5–g+
†22W–46	=224–46 (−0.030)	12W1–DS	=22W2–DS		=−2222–5D–g+ (0.017)
†22W–5D	=224–5D (0.113)	12W1–SB	=22W2–SB	*222W–D6–g+	=2224–D6–g+
22W–SS	=224–SS (0.473)	12W1–2B–t	=22W2–2B–t		=2222–6D–g+ (0.079)
		†12W1–5B–t	=22W2–5B–t	222W–DD–g+	0.021±0.040
2W2–B	1.257±0.054	12W1–DB–t	=22W2–DB–t		
2W2–SS	−0.054±0.036	*†12W1–4B–g+	=22W2–4B–g+	22W1–S	=22W2–S
		†12W1–5B–g+	=22W2–5B–g+	22W1–T	=22W2–T
012W–S	=0124–S	*12W1–6B–g+	=22W2–6B–g+	†22W1–5S	=22W2–5S
	=2224–S (4.424)	12W1–DB–g+	=22W2–DB–g+	22W1–DS	=22W2–DS
012W–T	=0124–T (0.110)			22W1–SB	=22W2–SB
012W–22	=0124–22 (−0.022)	12W2–S	=22W2–S	22W1–2B–t	=22W2–2B–t
†012W–25	=0124–25 (−0.041)	12W2–T	=22W2–T	†22W1–5B–t	=22W2–5B–t
012W–2D	=0124–2D (−0.040)	†12W2–5S	=22W2–5S	22W1–DB–t	=22W2–DB–t
012W–2S	=0124–2S (−0.345)	12W2–DS	=22W2–DS	*†22W1–4B–g+	=22W2–4B–g+
†012W–45	=0124–45 (0.025)	12W2–SB	=22W2–SB	†22W1–5B–g+	=22W2–5B–g+
012W–52	=0124–52 (0.016)	12W2–2B–t	=22W2–2B–t	*22W1–6B–g+	=22W2–6B–g+
†012W–55	=0124–55 (−0.058)	†12W2–5B–t	=22W2–5B–t	22W1–DB–g+	=22W2–DB–g+
012W–5D	=0124–5D (0.067)	12W2–DB–t	=22W2–DB–t		
†012W–84	=0124–84 (−0.064)	*†12W2–4B–g+	=22W2–4B–g+	22W2–S	2.621±0.037
012W–86	=0124–86 (−0.117)	†12W2–5B–g+	=22W2–5B–g+	22W2–T	=2242–T (0.045)
†012W–S5	=0124–S5	*12W2–6B–g+	=22W2–6B–g+	†22W2–5S	=2242–5S (−0.217)
	=−2222–5S (0.304)	12W2–DB–g+	=22W2–DB–g+	22W2–DS	0.252±0.031
012W–SD	=222W–SD			22W2–SB	−0.134±0.038

TABLE 3. (Continued)

Constant[b]	Value[c]	Constant[b]	Value[c]	Constant[b]	Value[c]
		222W-S	=2224-S (4.424)	22W2-2B-t	=2242-2B-t (−0.169)
01W2-S	=22W2-S	222W-T	=2224-T (0.113)	†22W2-5B-t	=2242-5B-t (−0.091)
01W2-T	=0142-T (0.045)	†222W-5S	=2224-5S	22W2-DB-t	0.001±0.048
01W2-2B	=0142-2B (0.194)		=2222-5S (−0.304)	*†22W2-4B-g$^+$	=2242-4B-g$^+$ (0.415)
01W2-2S	=0142-2S (−0.340)	222W-DS	=2224-DS	†22W2-5B-g$^+$	=2242-5B-g$^+$ (−0.035)
01W2-5B	=0142-5B (0.003)		=2222-DS (0.213)	*22W2-6B-g$^+$	=2242-6B-g$^+$ (0.070)
01W2-SB	=22W2-SB	†222W-S5	=2224-S5	22W2-DB-g$^+$	0.020±0.022
			=−2222-5S (0.304)		

a) Only the force constants with non-zero values are given in this table. Force constants not found in the table have zero values. The atomic-group symbol "4" denotes –Se–. b) Values for the intergroup force constants for the g$^-$ (*gauche*$^-$) conformation are the same as those for the corresponding force constants for the g$^+$ (*gauche*$^+$) conformation, unless they are marked with *. For those marked with *, the absolute values for the g$^+$ and g$^-$ force constants are the same but their signs are opposite to each other. For example, 222W-6D-g$^+$ = −222W-6D-g$^-$. For those force constants marked with †, their signs are reversed if they are defined by ordering the atomic groups in an opposite direction. For example, 012W-84 = −W210-48. c) Units are mdyn Å^{-1} for the diagonal stretching and off-diagonal sretching-stretching constants, mdyn for the off-diagonal stretching-bending constants, and mdyn Å for the diagonal bending, off-diagonal bending-bending, and diagonal torsional constants.

puter input and output, under a systematic nomenclature rule. Details of the force constant symbols have been described previously.[16] Only fundamental aspects are quoted here with some examples for dialkyl selenides. The symbols for dialkyl selenides are found to be analogous to those for dialkyl sulfides or ethers.

The symbol for the intragroup force constant on the diagonal has a general form *abc-d* and that on the off-diagonal *abc-de*, where *a*, *b*, and *c* are symbols for the atomic groups, *b* being the group in question and *a* and *c* the two adjacent groups, and *d* and *e* are symbols for the local symmetry coordinates in question. The symbols for the atomic groups and the local symmetry coordinates applicable to dialkyl selenides are given in Table 2. In cases where the atomic group in question is a terminal group (for example, methyl group), a nonexistent adjacent group is denoted by 0.

The symbols for the intergroup force constant on the diagonal has a general form *fghi-j* and that on the off-diagonal *fghi-jk* or *fghi-jk-l*, where *f*, *g*, *h*, and *i* are symbols for the atomic groups, *g* and *h* being the two groups in question and *f* and *i* their adjacent groups, and *j* and *k* are symbols for the local symmetry coordinates in question. The coordinates *j* and *k* belong, respectively, to the atomic groups *g* and *h*. The symbol *l*, if any, denotes the conformation of the molecular skeleton given by the atomic groups *f*, *g*, *h*, and *i*. Possible symbols for *l* are t (for *trans* conformation), g$^+$ (*gauche*$^+$), g$^-$ (*gauche*$^-$), c (*cis*), s$^+$ (*skew*$^+$), and s$^-$ (*skew*$^-$).

Some examples of the symbols for dialkyl selenides are given below.

01W-2: the diagonal force constant for the CH_3 symmetrical deformation in the CH_3 group of the CH_3Se– part.

22W-46: the off-diagonal force constant for the CH_2 rocking and twisting within the C^bH_2 group of the $-C^aH_2C^bH_2Se$– part.

2W2-SS: the off-diagonal force constant for the C^a–Se stretching and the Se–C^b stretching of the $-C^aH_2SeC^bH_2$– part.

01W2-S: the diagonal force constant for the C^a–Se stretching of the $C^aH_3SeC^bH_2$– part.

12W2-5S: the off-diagonal force constant for the C^bH_2 wagging and the C^b–Se stretching of the $C^aH_3C^bH_2SeC^cH_2$– part.

22W2-SB: the off-diagonal force constant for the C^b–Se stretching and the C^bSeC^c bending of the $-C^aH_2C^bH_2SeC^cH_2$– part.

222W-46-g$^+$: the off-diagonal force constant for the C^bH_2 rocking and the C^cH_2 twisting of the $-C^aH_2C^bH_2C^cH_2Se$– part in the *gauche*$^+$ skeletal conformation.

The coordinates *d*, *e*, *j*, and *k* are defined so that their signs are positive when one views the successive atomic groups from *a* to *c* for the intragroup force constant or from *f* to *i* for the intergroup force constant. It should be noticed that the signs of some of the force constants are reversed if the force constants are defined

TABLE 4. OBSERVED AND CALCULATED WAVE NUMBERS, IN cm^{-1}, AND VIBRATIONAL ASSIGNMENTS FOR ETHYL METHYL SELENIDE[a]

$\tilde{\nu}_{obsd}$[b]	$\tilde{\nu}_{calcd}$ and assignment			
	trans form (C_s)		*gauche* form (C_1)	
763*	761(a″)	CH_2 rock		
737			741	CH_2 rock
597	594(a′)	CH_3–Se stretch	595	CH_3–Se stretch
577*	572(a′)	Se–CH_2 stretch		
562			560	Se–CH_2 stretch
300	303(a′)	SeCC deform	298	SeCC deform
240	250(a″)	CH_2–CH_3 torsion	251	CH_2–CH_3 torsion
199			203	CSeC bend
174*	191(a′)	CSeC bend		
	156(a″)	CH_3–Se torsion	154	CH_3–Se torsion
	71(a″)	Se–CH_2 torsion	70	Se–CH_2 torsion

a) Only the vibrations below 800 cm^{-1} are given in the table. b) The observed wave numbers in the liquid state are given. The bands whose wave numbers are marked with * disappear on solidification.

Table 5. Observed and calculated wave numbers, in cm^{-1}, and vibrational assignments for diethyl selenide[a)]

$\tilde{\nu}_{obsd}$[b)]	$\tilde{\nu}_{calcd}$ and assignment		
	trans-trans form (C_{2v})	*trans-gauche* form (C_1)	*gauche-gauche* form (C_2)
772[c)]	762(b_2) CH_2 rock 758(a_2) CH_2 rock		
761*		761 CH_2 rock	
755*			760(b) CH_2 rock
741*		740 CH_2 rock	
720*			722(a) CH_2 rock
581	582(a_1) Se–CH_2 stretch		
577	567(b_1) Se–CH_2 stretch	574 Se–CH_2 stretch	
568*			575(b) Se–CH_2 stretch
559*		564 Se–CH_2 stretch	552(a) Se–CH_2 stretch
314	306(b_1) SeCC deform	315 SeCC deform	
304*			306(a) SeCC deform
277	292(a_1) SeCC deform	278 SeCC deform	285(b) SeCC deform
247	251(b_2) CH_3–CH_2 torsion 249(a_2) CH_3–CH_2 torsion	251 CH_3–CH_2 torsion 249 CH_3–CH_2 torsion	249(b) CH_3–CH_2 torsion 246(a) CH_3–CH_2 torsion
181*			175(a) CSeC bend
160*		164 CSeC bend	
139[c)]	140(a_1) CSeC bend		
	84(a_2) Se–CH_2 torsion		80(b) Se–CH_2 torsion
		69 Se–CH_2 torsion	
		59 Se–CH_2 torsion	
	49(b_2) Se–CH_2 torsion		46(a) Se–CH_2 torsion

a), b) See footnotes a) and b), respectively, to Table 4. c) Observed in the solid state.

Table 6. Observed and calculated wave numbers, in cm^{-1}, and vibrational assignments for methyl propyl selenide[a)]

$\tilde{\nu}_{obsd}$[b)]	$\tilde{\nu}_{calcd}$ and assignment			
	trans-trans form (C_s)	*trans-gauche* form (C_1)[c)]	*gauche-trans* form (C_1)[d)]	*gauche-gauche* form (C_1)
773*		773 CH_2 rock		
766*				766 CH_2 rock
731*	728(a″) CH_2 rock			
716			719 CH_2 rock	
660*	653(a′) Se–CH_2 stretch			
646			649 Se–CH_2 stretch	
591	593(a′) CH_3–Se stretch	594 CH_3–Se stretch	590 CH_3–Se stretch	595 CH_3–Se stretch
576*		578 Se–CH_2 stretch		
559*				564 Se–CH_2 stretch
403*		405 CCC deform		402 CCC deform
312	316(a′) CCC deform		309 CCC deform	
288*				291 SeCC deform
263	268(a′) SeCC deform	271 CH_2–CH_3 torsion	256 SeCC deform	
221	228(a″) CH_2–CH_3 torsion		230 CH_2–CH_3 torsion	
208*		215 CSeC bend		210 CH_2–CH_3 torsion
195			191 CSeC bend	
		172 SeCC deform		171 CSeC bend
	159(a″) CH_3–Se torsion	156 CH_3–Se torsion	151 CH_3–Se torsion	154 CH_3–Se torsion
	154(a′) CSeC bend			
	106(a″) CH_2–CH_2 torsion	99 CH_2–CH_2 torsion	96 CH_2–CH_2 torsion	103 CH_2–CH_2 torsion
	66(a″) Se–CH_2 torsion		65 Se–CH_2 torsion	
		48 Se–CH_2 torsion		46 Se–CH_2 torsion

a), b) See footnotes a) and b), respectively, to Table 4. c) *trans* and *gauche* conformations about the axes CSe–C–CC, respectively. d) *gauche* and *trans* conformations about the axes CSe–C–CC, respectively.

by ordering the atomic groups in a different direction. These force constants are indicated in Table 2.

Results of the Normal Coordinate Treatment

The force constants for unbranched dialkyl selenides are given in Table 3. In this table only the force constants with non-zero values are given and force constants not found in the table have zero values. Most of the force constants have been assumed to be equivalent to those for unbranched dialkyl sulfides and alkanes, and only twenty-six important force constants have been determined by a least-squares procedure. Results of the normal coordinate calculation for ethyl methyl selenide, diethyl selenide, and methyl propyl selenide are given in Tables 4—6. In these tables, only the vibrations below 800 cm^{-1}, which are more important in examining the rotational isomerism than those with higher wave numbers, are listed in comparison with the observed ones. Assignments of the vibrations are given on the basis of the calculated potential-energy distributions.

The calculation gave an overall root-mean-square deviation of 6.69 cm^{-1} between the observed wave numbers $\tilde{\nu}_{obsd}$ and the calculated wave numbers $\tilde{\nu}_{calcd}$ for 196 experimental data. Distribution of the wave number differences $\tilde{\nu}_{obsd}-\tilde{\nu}_{calcd}$ is shown in Fig. 1. The result indicates that 134 calculated wave numbers (68% of the total number 196) are within ± 5 cm^{-1} of the observed values and 173 (88%) are within ± 10 cm^{-1}.

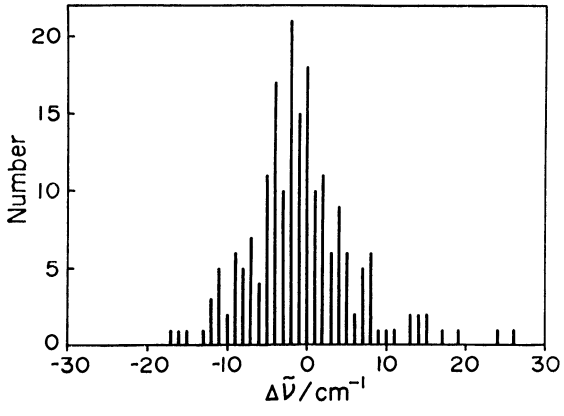

Fig. 1. Distribution of the wave number differences $\Delta\tilde{\nu}=\tilde{\nu}_{obsd}-\tilde{\nu}_{calcd}$ for the unbranched dialkyl selenides.

Discussion

In this study, the local symmetry force field for unbranched dialkyl selenides has been deduced from experimental data for the fundamental selenide molecules. The force constants listed in Table 3 fully cover any dialkyl selenide compound consisting of the following molecular fragments: CH_3CH_2Se–, CH_3SeCH_2–, –CH_2CH_2Se–, and –CH_2SeCH_2–. The present experience in studying the molecular force field indicates that most of the off-diagonal force constants for the dialkyl selenides and the dialkyl sulfides have similar values to each other. Common values have been, in fact, assumed for many constants for these compounds (Table 3). According to the previous[16] and present results, the difference of the force field is more significant between the sulfides and the ethers than between the sulfides and the selenides. This must be related to a closer resemblance of the chemical nature between sulfur and selenium atoms than between sulfur and oxygen atoms.

The diagonal force constants, which have been determined by the least-squares method, show a systematic variation of the values going from the ethers to the sulfides and the selenides. Their values have been compared and discussed in a previous letter.[19]

A comparison is made between the force constants for the dialkyl selenides and the bromoalkanes[24] and between those for the dialkyl sulfides and the chloroalkanes.[24] The methylene deformation diagonal constants (in units of mdyn Å) for the (C)–CH_2–(X) groups are as follows. CH_2 scissoring: 0.549, 0.535, 0.551, and 0.537 for X=Se, Br, S, and Cl, respectively; CH_2 rocking: 0.754, 0.700, 0.804, and 0.756; CH_2 wagging: 0.582, 0.621, 0.607, and 0.662; CH_2 twisting: 0.596, 0.613, 0.626, and 0.649; CCX deformation: 0.891, 0.977, 0.846, and 0.984. These data show that the values for the Group VI and Group VII compounds are not necessarily similar to each other, though the structural parameters and atomic masses are close. It is interesting to note that for the scissoring and rocking constants, the values for Se or S are larger than those for Br or Cl, while for the wagging, twisting, and CCX deformation constants, the values for Br or Cl are larger than those for Se or S. On the other hand, the diagonal C–X stretching force constants are 2.621, 2.609, 2.959, and 2.983 mdyn $Å^{-1}$ for X=Se, Br, S, and Cl, respectively, indicating that the values for Se and Br coincide and those for S and Cl coincide within errors in the values.

The present set of the force constants reproduced about two hundred observed wave numbers for the dialkyl selenides with a root-mean-square deviation of 6.7 cm^{-1}. This accuracy of the normal coordinate calculation is good enough to analyze the observed spectra and to study the rotational isomerism. The distribution of wave number differences $\tilde{\nu}_{obsd}-\tilde{\nu}_{calcd}$ (Fig. 1) is close to the normal distribution. This means that the least-squares calculation has been made on the basis of the proper vibrational assignments of the observed spectra and that the force field obtained has high validity in the normal vibration study.

The authors wish to thank Dr. Keiichi Ohno of Hiroshima University for his helpful discussions.

References

1) J. L. Duncan, "Specialist Report," Chemical Society, London (1975), Vol. 3, Chap. 2.
2) S. Califano, "Vibrational States," John Wiley and Son, London (1976), Chap. 8.
3) A. Müller and N. Mohan, "Vibrational Spectroscopy-Modern Trends," ed by A. J. Barnes and W. J. Orville-Thomas, Elsevier, Amsterdam (1977), Chap. 16.
4) G. Zerbi, "Vibrational Spectroscopy-Modern Trends,"

ed by A. J. Barnes and W. J. Orville-Thomas, Elsevier, Amsterdam (1977), Chap. 17.

5) T. Shimanouchi, "Physical Chemistry, an Advanced Treatise," ed by H. Eyring, D. Henderson, and W. Jost, Academic Press, New York (1970), Vol. IV, Chap. 6.

6) T. Shimanouchi, Y. Ogawa, M. Ohta, H. Matsuura, and I. Harada, *Bull. Chem. Soc. Jpn.*, **49**, 2999 (1976).

7) I. Harada, H. Takeuchi, M. Sakakibara, H. Matsuura, and T. Shimanouchi, *Bull. Chem. Soc. Jpn.*, **50**, 102 (1977).

8) M. Sakakibara, H. Matsuura, I. Harada, and T. Shimanouchi, *Bull. Chem. Soc. Jpn.*, **50**, 111 (1977).

9) M. Ohta, Y. Ogawa, H. Matsuura, I. Harada, and T. Shimanouchi, *Bull. Chem. Soc. Jpn.*, **50**, 380 (1977).

10) Y. Ogawa, M. Ohta, M. Sakakibara, H. Matsuura, I. Harada, and T. Shimanouchi, *Bull. Chem. Soc. Jpn.*, **50**, 650 (1977).

11) H. Matsuura, M. Kono, H. Iizuka, Y. Ogawa, I. Harada, and T. Shimanouchi, *Bull. Chem. Soc. Jpn.*, **50**, 2272 (1977).

12) Y. Ogawa, S. Imazeki, H. Yamaguchi, H. Matsuura, I. Harada, and T. Shimanouchi, *Bull. Chem. Soc. Jpn.*, **51**, 748 (1978).

13) H. Matsuura, S. Imazeki, Y. Ogawa, M. Sakakibara, I. Harada, and T. Shimanouchi, *Bull. Chem. Soc. Jpn.*, **52**, 2512 (1979).

14) H. Murata, H. Matsuura, K. Ohno, and T. Sato, *J. Mol. Struct.*, **52**, 1 (1979).

15) H. Matsuura, K. Ohno, T. Sato, and H. Murata, *J. Mol. Struct.*, **52**, 13 (1979).

16) T. Shimanouchi, H. Matsuura, Y. Ogawa, and I. Harada, *J. Phys. Chem. Ref. Data*, **7**, 1323 (1978).

17) H. Matsuura and H. Murata, *J. Mol. Struct.*, **56**, 191 (1979).

18) K. Ohno, H. Matsuura, and H. Murata, *J. Mol. Struct.*, to be published.

19) H. Matsuura, K. Ohno, and H. Murata, *Chem. Lett.*, **1978**, 173.

20) H. Matsuura, "Information Bulletin of Molecular and Crystal Data System (MXDS)," (in Japanese), No. 2, 24 (1978).

21) J. F. Beecher, *J. Mol. Spectrosc.*, **4**, 414 (1966).

22) "Definition and Symbolism of Molecular Force Constants," (Recommendations 1978), IUPAC, *Pure Appl. Chem.*, **50**, 1707 (1978).

23) T. Miyazawa and K. Fukushima, *J. Mol. Spectrosc.*, **15**, 308 (1965).

24) T. Shimanouchi, H. Matsuura, Y. Ogawa, and I. Harada, *J. Phys. Chem. Ref. Data*, to be published.

The Molecular and Crystal Structure of the Green Form of Bis(*N*-cyclohexylsalicylideneaminato)copper(II)

Hatsue TAMURA, Kazuhide OGAWA,* Akira TAKEUCHI, and Shoichiro YAMADA

College of General Education, Osaka University, Toyonaka, Osaka 560

(Received January, 16, 1979)

Bis(*N*-cyclohexylsalicylideneaminato)copper(II) crystallizes in two forms: one is a brown crystal (Form I), and the other is a green one (Form II). The crystal structure of Form II has been determined by X-ray analysis. The green crystals are monoclinic; space group, $P2_1/n$. The cell dimensions are $a=23.134(6)$, $b=9.525(3)$, $c=21.472(8)$ Å, $\beta=99.42(1)°$, and $Z=8$. The structure was deduced by the heavy-atom method and was refined to a final R value of 0.082 for 1883 observed reflections by the block-diagonal least-squares method. The molecular structure in Form II is dimeric, in contrast with the case of Form I, which is composed of a monomeric molecule. The two monomeric halves are joined by two Cu–O bonds with distances of 2.60(1) and 2.64(1) Å. Each copper(II) ion is penta-coordinated in a distorted square-pyramidal configuration. The molecular structures in Form I and II have been compared with those of the related Cu(II) compounds.

Among the crystal structures of various kinds of copper(II) complexes with *N*-substituted derivatives of salicylideneaminates (abbreviated as Cu(*N*-R, salim)$_2$ hereafter) so far determined, the following derivatives have been reported to have polymorphic crystals: the polymorphs of α-[1] and γ-forms[2] of bis(*N*-methylsalicylideneaminato)copper(II) (Cu(*N*-Me, salim)$_2$) have a relation of the monomer and the dimer, while the polymorphism of bis(*N*-ethylsalicylideneaminato)-copper(II), which has monoclinic[3] and orthorhombic forms,[4] is due to the different coordination geometry. It seems to be significant to examine related copper(II) complexes with isopropyl and cyclohexyl groups, which are bulkier than methyl and ethyl groups.

Two of the present authors (A.T. and S.Y.) previously synthesized the green(low-temperature form) and the brown(high-temperature form) complexes of bis(*N*-isopropyl-3-methoxysalicylideneaminato)copper(II) (Cu(*N*-*i*-Pr, 3-CH_3O-salim)$_2$) and reported their structures on the basis of the absorption spectra, thermal, and X-ray data.[5] Recently two modifications of bis(*N*-cyclohexylsalicylideneaminato)copper(II) (Cu(*N*-Ch, salim)$_2$) were also obtained by the two authors (A.T. and S.Y.); one is brown, and the other, green. Hereafter, the former and the latter will be designated as Form I and Form II respectively. With a rise in the temperature, the brown crystal melts at 165—166 °C and crystallizes in the green Form II, which melts at 176—177 °C. Crystals of Form II are also obtained by the slow evaporation of a chloroform solution of Form I. The crystals of Form II obtained by this method gave the same X-ray diffraction pattern as that of crystal obtained by heating crystals of Form I on an oil-bath at 170—180 °C. The crystal structure of Form I was reported previously.[6] In the present work, the crystal structure of Form II has been determined and compared with that of Form I.

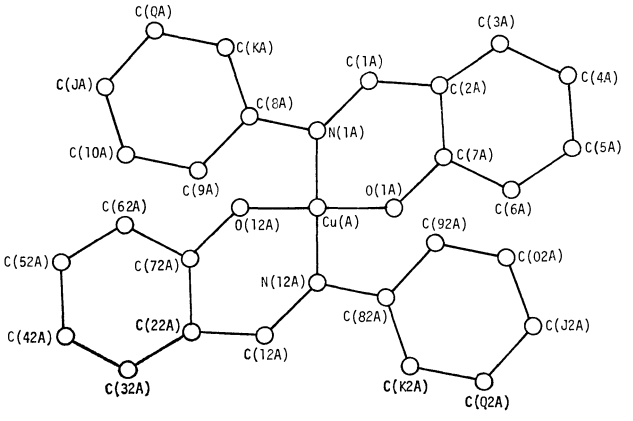

Atom numbering scheme of the one half ([Cu(A)]) of the dimer. The same atom numbering as [Cu(A)] was used for [Cu(B)], and the distinction between the atoms in [Cu(A)] and those in [Cu(B)] was made by the letters A and B.

Experimental

The green crystals of Cu(*N*-Ch, salim)$_2$ were obtained by the slow evaporation of a chloroform solution of Form I at a temperature below 10 °C. The crystal and experimental data of Form II are listed in Table 1 and compared with those of Form I. The X-ray intensity data were measured on a Rigaku-Denki four-circle diffractometer with Zr-filtered

TABLE 1. CRYSTAL AND EXPERIMENTAL DATA

	Form II	Form I
Color	green	brown
Crystal system	monoclinic	triclinic
Space group	$P2_1/n$	$P\bar{1}$
a	23.134(6) Å	12.035(5) Å
b	9.525(3) Å	7.810(3) Å
c	21.472(8) Å	6.475(3) Å
α		104.86(1)°
β	99.42(1)°	102.06(1)°
γ		97.67(1)°
V	4668(2) Å^3	563.9(4) Å^3
Z	8	1
D_m	1.33 g cm^{-3}	1.37 g cm^{-3}
D_x	1.336 g cm^{-3}	1.379 g cm^{-3}
μ	10.0 cm^{-1} (for Mo $K\alpha$)	11.5 cm^{-1} (for Cu $K\alpha$)
Scan method	θ-2θ[a]	θ-2θ
Scan speed	4°min^{-1}	2°min^{-1}
Scan width	$1.2°+0.4°\tan\theta$	$1.5°+0.15°\tan\theta$
Background	2×5 s	2×10 s
$2\theta_{max}$	45° (Mo $K\alpha$)	115° (Cu $K\alpha$)

a) For weak reflections with $|F_o|<3\sigma(F_o)$, the peak scan was repeated four times.

TABLE 2. FINAL ATOMIC COORDINATES ($\times 10^4$) AND TEMPERATURE FACTORS, WITH THEIR STANDARD DEVIATIONS IN PARENTHESES

Atom	x	y	z	B	Atom	x	y	z	B
Cu(A)	4854(1)	1674(2)	7555(1)	a)	Cu(B)	5203(1)	5115(2)	7495(1)	a)
O(1A)	4191(5)	1259(12)	7950(5)	4.1(3)	O(1B)	6017(4)	5442(12)	7583(5)	4.3(3)
N(1A)	5408(5)	1436(14)	8388(6)	3.6(3)	N(1B)	5202(6)	5553(15)	8417(7)	4.6(3)
C(1A)	5240(7)	1377(19)	8928(8)	4.0(4)	C(1B)	5659(8)	5751(21)	8841(9)	5.0(5)
C(2A)	4632(7)	1401(19)	9045(8)	4.2(4)	C(2B)	6261(7)	5639(19)	8701(8)	3.9(4)
C(3A)	4552(8)	1400(20)	9679(8)	4.5(4)	C(3B)	6728(8)	5770(22)	9232(9)	5.6(5)
C(4A)	3984(8)	1486(21)	9813(9)	5.2(5)	C(4B)	7298(8)	5722(21)	9145(9)	5.0(5)
C(5A)	3500(8)	1454(20)	9315(8)	4.6(4)	C(5B)	7440(7)	5585(19)	8550(8)	4.4(4)
C(6A)	3559(8)	1388(20)	8684(9)	5.0(5)	C(6B)	7014(7)	5493(19)	8005(8)	4.0(4)
C(7A)	4150(8)	1332(19)	8541(9)	4.6(4)	C(7B)	6412(7)	5514(18)	8089(8)	3.9(4)
C(8A)	6060(7)	1348(19)	8362(8)	3.9(4)	C(8B)	4606(8)	5762(21)	8622(9)	5.3(5)
C(9A)	6453(8)	1611(23)	9017(9)	6.1(5)	C(9B)	4608(10)	5578(26)	9299(8)	8.3(7)
C(10A)	7095(8)	1543(23)	8889(9)	6.2(5)	C(10B)	3948(9)	5893(24)	9396(10)	6.7(5)
C(JA)	7218(8)	93(23)	8636(9)	5.8(5)	C(JB)	3750(10)	7290(25)	9158(11)	7.8(6)
C(QA)	6811(9)	−272(24)	8011(10)	6.7(5)	C(QB)	3763(10)	7428(27)	8477(11)	8.2(6)
C(KA)	6168(8)	−152(23)	8136(9)	6.0(5)	C(KB)	4404(9)	7174(23)	8345(10)	6.4(5)
O(12A)	5477(4)	2532(12)	7204(5)	3.7(2)	O(12B)	4459(4)	4232(12)	7434(5)	4.0(2)
N(12A)	4429(5)	1151(14)	6690(6)	3.5(3)	N(12B)	5071(5)	5652(14)	6567(6)	3.1(3)
C(12A)	4645(8)	1213(19)	6171(8)	4.5(4)	C(12B)	4585(7)	5558(18)	6193(8)	3.8(4)
C(22A)	5247(7)	1738(18)	6123(7)	3.3(4)	C(22B)	4026(7)	5017(20)	6404(8)	4.0(4)
C(32A)	5409(7)	1607(19)	5534(8)	4.2(4)	C(32B)	3513(8)	5179(21)	5926(9)	5.3(5)
C(42A)	5973(7)	2101(19)	5439(8)	4.5(4)	C(42B)	2965(8)	4690(22)	6079(9)	5.8(5)
C(52A)	6344(7)	2723(18)	5958(8)	3.9(4)	C(52B)	2939(8)	4177(21)	6679(9)	5.4(5)
C(62A)	6186(7)	2854(18)	6542(8)	3.5(4)	C(62B)	3428(8)	3970(20)	7158(9)	4.9(5)
C(72A)	5619(7)	2362(18)	6644(8)	3.5(4)	C(72B)	3994(7)	4404(19)	6996(8)	4.0(4)
C(82A)	3812(7)	612(19)	6639(8)	3.9(4)	C(82B)	5576(7)	6248(18)	6318(8)	3.6(4)
C(92A)	3831(8)	−971(22)	6782(9)	5.6(5)	C(92B)	5617(7)	7816(19)	6513(8)	4.3(4)
C(02A)	3209(9)	−1481(23)	6823(10)	6.5(5)	C(02B)	6201(7)	8401(20)	6359(8)	4.5(4)
C(J2A)	2796(8)	−1167(22)	6179(9)	5.9(5)	C(J2B)	6222(7)	8214(20)	5649(8)	4.2(4)
C(Q2A)	2796(8)	390(20)	6037(9)	4.8(4)	C(Q2B)	6119(7)	6665(20)	5444(8)	4.5(4)
C(K2A)	3435(7)	898(19)	5976(8)	4.0(4)	C(K2B)	5542(7)	6091(18)	5608(8)	3.7(4)

a) Anisotropic temperature factors ($\times 10^5$) in the form of exp $[-(B_{11}h^2+B_{22}k^2+B_{33}l^2+B_{12}hk+B_{13}hl+B_{23}kl)]$, with parameters:

	B_{11}	B_{22}	B_{33}	B_{12}	B_{13}	B_{23}
Cu(A)	125(6)	1269(35)	219(7)	−89(25)	48(9)	151(30)
Cu(B)	116(6)	1386(37)	239(8)	−160(25)	63(9)	−151(30)

TABLE 3(a). BOND LENGTHS (l/Å), WITH ESTIMATED STANDARD DEVIATIONS IN PARENTHESES

Cu(A)–O(1A)	1.91(1)	Cu(A)–O(12A)	1.92(1)	Cu(B)–O(1B)	1.89(1)	Cu(B)–O(12B)	1.90(1)
Cu(A)–N(1A)	2.04(1)	Cu(A)–N(12A)	2.02(1)	Cu(B)–N(1B)	2.02(2)	Cu(B)–N(12B)	2.03(1)
O(1A)–C(7A)	1.29(2)	O(12A)–C(72A)	1.31(2)	O(1B)–C(7B)	1.30(2)	O(12B)–C(72B)	1.32(2)
N(1A)–C(1A)	1.28(2)	N(12A)–C(12A)	1.30(2)	N(1B)–C(1B)	1.29(3)	N(12B)–C(12B)	1.27(2)
N(1A)–C(8A)	1.52(2)	N(12A)–C(82A)	1.50(2)	N(1B)–C(8B)	1.53(3)	N(12B)–C(82B)	1.48(2)
C(1A)–C(2A)	1.47(3)	C(12A)–C(22A)	1.50(3)	C(1B)–C(2B)	1.48(3)	C(12B)–C(22B)	1.53(3)
C(2A)–C(3A)	1.40(3)	C(22A)–C(32A)	1.38(3)	C(2B)–C(3B)	1.44(3)	C(22B)–C(32B)	1.44(3)
C(3A)–C(4A)	1.39(3)	C(32A)–C(42A)	1.43(3)	C(3B)–C(4B)	1.36(3)	C(32B)–C(42B)	1.44(3)
C(4A)–C(5A)	1.42(3)	C(42A)–C(52A)	1.42(3)	C(4B)–C(5B)	1.38(3)	C(42B)–C(52B)	1.39(3)
C(5A)–C(6A)	1.39(3)	C(52A)–C(62A)	1.37(2)	C(5B)–C(6B)	1.40(3)	C(52B)–C(62B)	1.41(3)
C(6A)–C(7A)	1.45(3)	C(62A)–C(72A)	1.44(2)	C(6B)–C(7B)	1.43(3)	C(62B)–C(72B)	1.47(3)
C(7A)–C(2A)	1.42(3)	C(72A)–C(22A)	1.42(2)	C(7B)–C(2B)	1.42(3)	C(72B)–C(22B)	1.41(3)
C(8A)–C(9A)	1.56(3)	C(82A)–C(92A)	1.54(3)	C(8B)–C(9B)	1.46(3)	C(82B)–C(92B)	1.55(3)
C(9A)–C(10A)	1.56(3)	C(92A)–C(02A)	1.54(3)	C(9B)–C(10B)	1.60(3)	C(92B)–C(02B)	1.55(3)
C(10A)–C(JA)	1.53(3)	C(02A)–C(J2A)	1.58(3)	C(10B)–C(JB)	1.47(3)	C(02B)–C(J2B)	1.54(3)
C(JA)–C(QA)	1.55(3)	C(J2A)–C(Q2A)	1.51(3)	C(JB)–C(QB)	1.47(3)	C(J2B)–C(Q2B)	1.55(3)
C(QA)–C(KA)	1.56(3)	C(Q2A)–C(K2A)	1.58(3)	C(QB)–C(KB)	1.57(3)	C(Q2B)–C(K2B)	1.54(3)
C(KA)–C(8A)	1.54(3)	C(K2A)–C(82A)	1.57(3)	C(KB)–C(8B)	1.51(3)	C(K2B)–C(82B)	1.52(3)
				Cu(A)–Cu(B)	3.383(3)		
				Cu(A)–O(12B)	2.60(1)		
				O(12A)–Cu(B)	2.64(1)		

TABLE 3(b). BOND ANGLES (ϕ/°), WITH ESTIMATED STANDARD DEVIATIONS IN PARENTHESES

O(1A)–Cu(A)–N(1A)	91.3(5)	N(1A)–Cu(A)–O(12A)	89.3(5)
O(1A)–Cu(A)–O(12A)	166.6(5)	N(1A)–Cu(A)–N(12A)	157.5(6)
O(1A)–Cu(A)–N(12A)	93.0(5)	O(12A)–Cu(A)–N(12A)	91.5(5)
Cu(A)–O(1A)–C(7A)	128(1)	Cu(A)–O(12A)–C(72A)	129(1)
Cu(A)–N(1A)–C(1A)	124(1)	Cu(A)–N(12A)–C(12A)	126(1)
Cu(A)–N(1A)–C(8A)	117(1)	Cu(A)–N(12A)–C(82A)	118(1)
C(1A)–N(1A)–C(8A)	119(1)	C(12A)–N(12A)–C(82A)	117(1)
N(1A)–C(1A)–C(2A)	126(2)	N(12A)–C(12A)–C(22A)	125(2)
C(1A)–C(2A)–C(7A)	122(2)	C(12A)–C(22A)–C(72A)	122(2)
C(3A)–C(2A)–C(7A)	122(2)	C(32A)–C(22A)–C(72A)	123(2)
C(2A)–C(3A)–C(4A)	119(2)	C(22A)–C(32A)–C(42A)	119(2)
C(3A)–C(4A)–C(5A)	120(2)	C(32A)–C(42A)–C(52A)	118(2)
C(4A)–C(5A)–C(6A)	123(2)	C(42A)–C(52A)–C(62A)	123(2)
C(5A)–C(6A)–C(7A)	117(2)	C(52A)–C(62A)–C(72A)	120(2)
O(1A)–C(7A)–C(2A)	125(2)	O(12A)–C(72A)–C(22A)	124(2)
C(2A)–C(7A)–C(6A)	119(2)	C(22A)–C(72A)–C(62A)	118(2)
N(1A)–C(8A)–C(9A)	113(1)	N(12A)–C(82A)–C(92A)	109(1)
N(1A)–C(8A)–C(KA)	106(1)	N(12A)–C(82A)–C(K2A)	113(1)
C(9A)–C(8A)–C(KA)	109(2)	C(92A)–C(82A)–C(K2A)	110(2)
C(8A)–C(9A)–C(10A)	105(2)	C(82A)–C(92A)–C(02A)	109(2)
C(9A)–C(10A)–C(JA)	110(2)	C(92A)–C(02A)–C(J2A)	109(2)
C(10A)–C(JA)–C(QA)	113(2)	C(02A)–C(J2A)–C(Q2A)	110(2)
C(JA)–C(QA)–C(KA)	107(2)	C(J2A)–C(Q2A)–C(K2A)	110(2)
C(8A)–C(KA)–C(QA)	109(2)	C(82A)–C(K2A)–C(Q2A)	105(1)
O(1B)–Cu(B)–N(1B)	91.7(6)	N(1B)–Cu(B)–O(12B)	90.7(6)
O(1B)–Cu(B)–O(12B)	163.2(5)	N(1B)–Cu(B)–N(12B)	152.1(6)
O(1B)–Cu(B)–N(12B)	92.5(5)	O(12B)–Cu(B)–N(12B)	93.1(5)
Cu(B)–O(1B)–C(7B)	130(1)	Cu(B)–O(12B)–C(72B)	128(1)
Cu(B)–N(1B)–C(1B)	126(1)	Cu(B)–N(12B)–C(12B)	125(1)
Cu(B)–N(1B)–C(8B)	117(1)	Cu(B)–N(12B)–C(82B)	117(1)
C(1B)–N(1B)–C(8B)	117(2)	C(12B)–N(12B)–C(82B)	118(1)
N(1B)–C(1B)–C(2B)	122(2)	N(12B)–C(12B)–C(22B)	123(2)
C(1B)–C(2B)–C(7B)	125(2)	C(12B)–C(22B)–C(72B)	125(2)
C(3B)–C(2B)–C(7B)	118(2)	C(32B)–C(22B)–C(72B)	122(2)
C(2B)–C(3B)–C(4B)	120(2)	C(22B)–C(32B)–C(42B)	117(2)
C(3B)–C(4B)–C(5B)	121(2)	C(32B)–C(42B)–C(52B)	120(2)
C(4B)–C(5B)–C(6B)	123(2)	C(42B)–C(52B)–C(62B)	125(2)
C(5B)–C(6B)–C(7B)	117(2)	C(52B)–C(62B)–C(72B)	115(2)
O(1B)–C(7B)–C(2B)	122(2)	O(12B)–C(72B)–C(22B)	122(2)
C(2B)–C(7B)–C(6B)	121(2)	C(22B)–C(72B)–C(62B)	121(2)
N(1B)–C(8B)–C(9B)	114(2)	N(12B)–C(82B)–C(92B)	107(1)
N(1B)–C(8B)–C(KB)	104(2)	N(12B)–C(82B)–C(K2B)	114(1)
C(9B)–C(8B)–C(KB)	117(2)	C(92B)–C(82B)–C(K2B)	111(1)
C(8B)–C(9B)–C(10B)	105(2)	C(82B)–C(92B)–C(02B)	108(1)
C(9B)–C(10B)–C(JB)	112(2)	C(92B)–C(02B)–C(J2B)	110(2)
C(10B)–C(JB)–C(QB)	112(2)	C(02B)–C(J2B)–C(Q2B)	111(2)
C(JB)–C(QB)–C(KB)	110(2)	C(J2B)–C(Q2B)–C(K2B)	112(2)
C(8B)–C(KB)–C(QB)	108(2)	C(82B)–C(K2B)–C(Q2B)	107(1)
O(1A)–Cu(A)–O(12B)	86.8(4)	O(1B)–Cu(B)–O(12A)	84.5(4)
N(1A)–Cu(A)–O(12B)	110.6(5)	N(1B)–Cu(B)–O(12A)	117.6(5)
O(12A)–Cu(A)–O(12B)	80.5(4)	O(12B)–Cu(B)–O(12A)	79.7(4)
N(12A)–Cu(A)–O(12B)	91.7(5)	N(12B)–Cu(B)–O(12A)	90.3(5)
Cu(A)–O(12A)–Cu(B)	94.5(4)	Cu(A)–O(12B)–Cu(B)	96.2(5)

Mo $K\alpha$ radiation. Of 3231 independent reflections collected by the 2θ-θ scan technique, 1348 reflections with $|F_o|<3\sigma(|F_o|)$ were not used in the subsequent calculation. The data were corrected for Lorentz and polarization effects, but not for absorption. The crystal size was $0.15\times0.20\times0.30$ mm.

Structure Determination. The crystal structure was solved by the heavy-atom technique, and the refinement was performed by a block-diagonal least-squares calculation. The function minimized was $\sum w(F_o-|F_c|)^2$, with $w=1.0$ for all reflections. All the atomic scattering factors were taken from "International Tables for X-Ray Crystallography."[7] The computations were carried out on a NEAC 2200-700 computer at Osaka University. The computer programs used in the calculations were RSSFR-5,[8] HBLS-V,[9] and DAPH[10]

in the UNICS. The final R value was 0.032. A list of observed and calculated structure factors is preserved by the Chemical Society of Japan (Document No. 7938).

Results and Discussion

Table 2 lists the final atomic and thermal parameters, along with the estimated standard deviations. The bond distances and angles are also listed in Table 3.

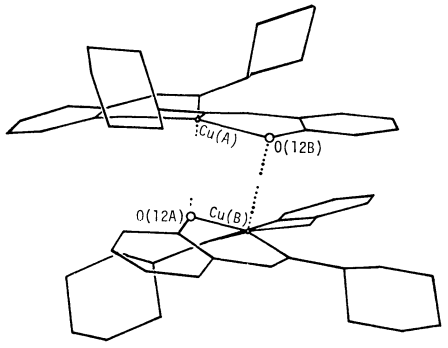

Fig. 1. Dimeric structure.

The molecular structure is shown in Fig. 1. The two crystallographically independent Cu(*N*-Ch, salim)$_2$ molecules are joined by two Cu–O bonds, with distances of 2.60 and 2.64 Å, forming a dimer. Hereafter, the two halves of the dimer will be denoted by [Cu(A)] and [Cu(B)]. Each copper(II) ion in [Cu(A)] or [Cu(B)] is penta-coordinated in a distorted square-pyramidal configuration. The basal plane of the pyramid is tetrahedrally distorted; the angle between the plane through Cu(A), O(1A), N(1A), and the plane through Cu(A), O(12A), N(12A) in [Cu(A)] is 26°, and the corresponding angle in [Cu(B)] is 32°. The coordination geometry is different from that in Form I: the Cu(II) ion in Form I has a planar coordination and the molecule is bent or stepped, so that the distance (step height) between the salicylideneamine planes is 1.28 Å. [Cu(A)] has almost the same structure as [Cu(B)]. The equations of the best planes through the three selected sets of atoms in each salicylideneamine moiety are given in Table 4(a). The displacements of the atoms from these planes and the dihedral angles between them are given in Tables 4(b) and 4(c) respectively. The dihedral angle between Plane(II) of the salicylideneamine moiety and the plane through the copper, oxygen, and nitrogen atoms ranges from 165° to 167°. (The corresponding angle in Form I is 153.5°). As may be seen in Fig. 1, the cyclohexyl groups lie outside the basal planes so as to avoid the non-bonded repulsion between the groups in one Cu(*N*-Ch, salim)$_2$ moiety and the atoms of the opposite moiety. The bond distances and angles in Form II are almost in complete agreement with those in Form I, within the limits of experimental accuracy.

The crystal structure is shown in Fig. 2. There are no

Table 4(a). Equations of best planes
$lX+mY+nZ=p$[a)]

Plane	l	m	n	p
[Cu(A)]				
IA	0.131	−0.972	−0.198	−3.595
IIA	−0.001	−1.000	0.028	−0.811
IIIA	0.031	−0.999	0.021	−0.659
Ia	−0.484	0.873	−0.058	−3.688
IIa	−0.363	0.894	−0.262	−5.555
IIIa	−0.375	0.891	−0.255	−5.571
[Cu(B)]				
IB	−0.139	0.963	−0.229	−0.252
IIB	−0.008	−0.996	0.093	−3.746
IIIB	−0.003	−0.996	0.092	−3.715
Ib	0.446	−0.867	−0.221	−3.535
IIb	0.230	−0.902	−0.366	−7.679
IIIb	0.267	−0.892	−0.365	−7.316

a) $X=ax+cz\cos\beta$, $Y=by$, $Z=cz\sin\beta$.

Table 4(b). Displacements of atoms from best planes ($\times 10^2$ Å)

	IA	IIA	IIIA		Ia	IIa	IIIa
[Cu(A)]							
Cu(A)	0	−35[a)]	−32[a)]	Cu(A)	0	−33[a)]	−31[a)]
O(1A)	0	7	4	O(12A)	0	3	2
N(1A)	0	−7	−3	N(12A)	0	−5	−3
C(1A)		1	3	C(12A)		4	4
C(2A)		−0	−3	C(22A)		0	−1
C(3A)		4	−1[a)]	C(32A)		1	−2[a)]
C(4A)		−4	−13[a)]	C(42A)		−0	−6[a)]
C(5A)		−3	−15[a)]	C(52A)		−1	−6[a)]
C(6A)		−1	−10[a)]	C(62A)		−1	−5[a)]
C(7A)		4	−1	C(72A)		−0	−2

	IB	IIB	IIIB		Ib	IIb	IIIb
[Cu(B)]							
Cu(B)	0	29[a)]	29[a)]	Cu(B)	0	−36[a)]	−31[a)]
O(1B)	0	−2	−1	O(12B)	0	5	3
N(1B)	0	6	5	N(12B)	0	−10	−5
C(1B)		−5	−5	C(12B)		4	6
C(2B)		1	2	C(22B)		3	−1
C(3B)		−1	2[a)]	C(32B)		3	−5[a)]
C(4B)		0	2[a)]	C(42B)		2	−11[a)]
C(5B)		1	3[a)]	C(52B)		−6	−21[a)]
C(6B)		0	2[a)]	C(62B)		−3	−15[a)]
C(7B)		1	2	C(72B)		3	−3

a) Not included in the estimations of the equations.

Table 4(c). Dihedral angles(°)

	IIA	IIIA	Ia	IIa	IIIa
[Cu(A)]					
IA	165	166	26		
IIA		178			
Ia				166	167
IIa					179

	IIB	IIIB	Ib	IIb	IIIb
[Cu(B)]					
IB	167	168	32		
IIB		180			
Ib				165	167
IIb					178

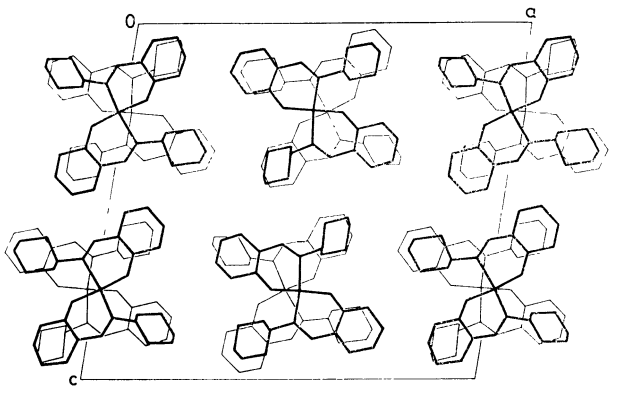

(a) b axis projection.

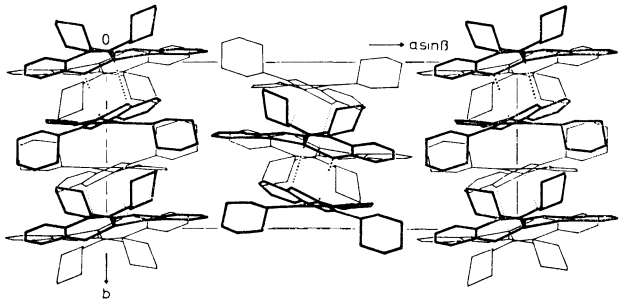

(b) c axis projection.

Fig. 2. Crystal structure.

TABLE 5. STEP-HEIGHTS IN SQUARE-PLANAR Cu(*N*-R, salim)$_2$

R	Step-height(l/Å)	Ref.
Me(α-form)	0	1
H	0.29	13
Propyl	0.32	14
Butyl	0.74	15
Phenyl	0.89	16
Ch(Form I)	1.28	6

intermolecular distances less than 3.65 Å in the crystal structure.

Most of the monomeric Cu(*N*-R, salim)$_2$-type complexes whose coordination geometry is square-planar are bent or stepped. Table 5 lists the step heights in a series of square-planar salicylideneaminato complexes. The bulkier the *N*-substituents (R) are, the larger the step heights are, except for the case of Cu(*N*-H, salim)$_2$. The large step height (1.28 Å) in Form I probably results from the interligand interaction between the bulky cyclohexyl substituent and the opposite ligand. The dimerization of the two Cu(*N*-Ch, salim)$_2$ molecules of Form I occurs by means of the formation of the Cu–O bands. Of the two ligands in a monomeric molecule, the O atom of one ligand (Type i) participates in the Cu–O bond, but that of the other ligand (Type ii) does not. In the Type i ligand the bond formation gives rise to an approach of the salicylideneamine portion to the opposite molecule, while the *N*-cyclohexane portion becomes somewhat distant from the opposite one because of the non-bonded repulsion. Consequently, the Cu$\langle^{N}_{O}$ plane of the Type i ligand slants against that of the Type ii ligand in each monomeric unit, and the disposition of the donor atoms become tetrahedral.

The dimeric molecular structure of Form II is similar to that of the γ-form of Cu(*N*-Me, salim)$_2$, but the configuration of atoms at the basal plane in Form II is much more distorted tetrahedrally than that in the γ-form of Cu(*N*-Me, salim)$_2$, because the *N*-substituents of Form II are bulkier than those of the γ-form of Cu(*N*-Me, salim)$_2$: the angle between the plane through Cu(A), O(1A), N(1A) and the plane through Cu(A), O(12A), N(12A) in [Cu(A)] is 26°, and the corresponding angle in [Cu(B)] is 32°, as has been described above; on the other hand, the corresponding angles in the γ-form of Cu(*N*-Me, salim)$_2$ are 11 and 12°.

The polymorphism in Cu(*N*-Ch, salim)$_2$ is caused by such a chemical change. On the other hand, in the case of Cu(*N*-*i*-Pr, 3-CH_3O-salim)$_2$, which has two crystal forms—the green complex (low-temperature form)[11] and the brown one(high-temperature form),[12] it has become apparent that its polymorphism is not due to dimerization, but to the difference between the coordination configurations about the Cu(II) ions(the dihedral angle between Cu, O, N planes in the low-temperature form is 47.4° and the corresponding angle in the high-temperature one is 57.9°), and also to the difference between the molecular geometry (twisted-umbrella shape in the low-temperature form and twisted-stepped shape in the high-temperature one).

The authors wish to express their thanks to Dr. N. Kamijo of the Government Industrial Research Institute, Osaka, for the use of the Rigaku-Denki automatic diffractometer.

References

1) E. C. Lingafelter, G. L. Simmons, and B. Morosin, C. Scheringer, and C. Freiburg, *Acta Crystallogr.*, **14**, 1222 (1961).
2) D. Hall, Sylvia V. Sheat, and T. N. Waters, *J. Chem. Soc.*, *A*, **1968**, 460.
3) E. N. Baker, G. R. Clark, D. Hall, and T. N. Waters, *J. Chem. Soc.*, *A*, **1967**, 251; C. Panattoni, G. Bombieri, and R. Graziani, *Acta Crystallogr.*, **23**, 537 (1967).
4) G. R. Clark, D. Hall, and T. N. Waters, *J. Chem. Soc.*, *A*, **1969**, 2808.
5) A. Takeuchi and S. Yamada, *Rev. Roumaine Chim.*, **22**, 781 (1977). They have described the coordination configuration about the copper(II) ions determined by X-ray analysis.
6) H. Tamura, K. Ogawa, A. Takeuchi, and S. Yamada, *Chem. Lett.*, **1977**, 889.
7) "International Tables for X-Ray Crystallography," Kynoch Press, Birmingham (1974), Vol. IV, p. 71.
8) T. Sakurai, "The Universal Crystallographic Computing System (I)," The Crystallographic Society of Japan (1967), p. 18.
9) T. Ashida, "The Universal Crystallographic Computing System, Osaka," The Computation Center, Osaka University (1973), p. 55.
10) T. Ashida, "The Universal Crystallographic Computing System, Osaka," The Computation Center, Osaka University (1973), p. 63.
11) H. Tamura and K. Ogawa, Presented in part at the 26th Symposium of Coordination Chemistry, Hokkaido, Japan, August 1976, Abstracts, p. 6.

12) T. Ashida, personal communication.
13) E. N. Baker, D. Hall, and T. N. Waters, *J. Chem. Soc.*, *A*, **1966**, 680.
14) G. Bombieri, C. Panattoni, E. Forsellini, and R. Graziani, *Acta Crystallogr., Sect. B*, **25**, 1208 (1969).
15) D. Hall, R. H. Sumner, and T. N. Waters, *J. Chem. Soc.*, *A*, **1969**, 420.
16) L. Wei, R. M. Stogsdill, and E. C. Lingafelter, *Acta Crystallogr.*, **17**, 1058 (1964).

The Synthesis of Crystalline Zirconium Phosphate with Large Particle Size by the Direct-precipitation Method

Yasushi INOUE and Yoshimune YAMADA*

Department of Nuclear Engineering, Faculty of Engineering, Tohoku University, Aramaki, Sendai 980

(Received January 23, 1979)

The direct-precipitation method was studied as a possible way to synthesize crystalline zirconium phosphate of a large and uniform crystal size. The yield and the crystal size were examined as functions of the initial hydrofluoric-acid and phosphoric-acid concentrations and the warming temperature. The conditions for preparing the largest crystal were: $ZrOCl_2 \cdot 8H_2O$, 0.13 M; hydrofluoric acid concentration, 0.715 M; phosphoric acid concentration, 5 M; temperature, 50 °C. Those for preparing the material with uniform crystal-size distribution and a possibly large-mean crystal size were: $ZrOCl_2 \cdot 8H_2O$, 0.13 M; hydrofluoric acid concentration, 0.715 M; phosphoric acid concentration, 9 M; temperature, 60 °C. The product was confirmed to be crystalline $Zr(HPO_4)_2 \cdot H_2O$ by means of chemical, thermal, and X-ray analyses, and by an examination of the titration curve.

The crystalline zirconium phosphate (ZP) cation exchanger has been extensively studied since the work of Clearfield and Stynes,[1] who first prepared the material by refluxing amorphous zirconium phosphate for a long time in a phosphoric acid solution. The investigation of ion-exchange kinetics, however, has just started, and only a little information[2-9] is available to date. The present authors intend to carry out kinetic studies for elucidating the ion-exchange mechanism of ZP. To accomplish this purpose, it is necessary to prepare a material which has not only a high degree of crystallinity, but also a large and uniform size and an excellent yield. Horsley and Nowell[10] have compared four alternative methods for preparing ZP: (A) the reflux method proposed by Clearfield and Stynes;[1] (B) the direct precipitation method proposed by Alberti and Torracca;[11] (C) the rapid precipitation method, which is a modification of (B), and (D) the method of direct precipitation in the presence of oxalic acid. They concluded that Method (C) was the best, mainly because the crystallinity of its products was the best. However, no detailed investigations from the point of view of the crystal-size distribution of the products have yet been reported. The present authors have attempted to establish a good procedure for obtaining material with a large and uniform crystal size. A preliminary experiment suggested that Method (B) above was most promising, for it provided crystals larger than those obtained by the other methods.

This report will describe the results of the investigation undertaken to establish the best conditions for the synthesis based on Method (B) by varying such factors as the concentrations of hydrofluoric acid and of phosphoric acid and the temperature of precipitation.

Experimental

Procedure for the Preparation of ZP. Five and a half grams of $ZrOCl_2 \cdot 8H_2O$ were dissolved in distilled water in a polyethylene beaker (5.5 cm in inside diameter, 6.7 cm high). The desired amounts of hydrofluoric acid as a complexing agent for zirconium and of phosphoric acid were added successively with vigorous stirring, to make the total volume 130 cm^3. The solution thus prepared was then allowed to warm in a thermostatic water bath for longer than 100 h in order to decompose the fluoro-complex of zirconium. The volume of the solution gradually decreased during the warming and reached about 70 cm^3 under the recommended conditions: hydrofluoric acid concentration; 0.13 M, phosphoric acid concentration; 9 M, temperature; 60 °C (see below). The white flaky product was separated centrifugally, washed with distilled water until the pH of the filtrate became about 5, and stored over P_2O_5 for two weeks. The yield was calculated on the basis of the zirconium recovery.

Measurement of Crystal Size. The flaky product was observed to be composed of many crystals of rectangular platelets, 50—450 μm in length and 8—90 μm in width. About a hundred well-shaped crystals were randomly selected from them, and their cross sections were measured by means of an optical microscope.

Analysis. Zirconium was precipitated by cupferron from a dil hydrofluoric acid solution in which 0.5 g of ZP had been dissolved, and was determined by ignition to the oxide.[12] The phosphate ion was precipitated as ammonium molybdophosphate from the above filtrate, reprecipitated as ammonium magnesium phosphate, and determined by ignition to $Mg_2P_2O_7$.[13] The water content was calculated from the weight loss on ignition.

Titration Curve. A half gram of ZP was immersed in 100 cm^3 of a solution (ionic strength 0.1 M, (1 M=1 mol/dm^3)) for a week at a room temperature, followed by the pH measurement and by the chemical analysis of the solution. To obtain a titration curve, this procedure was undertaken for various solutions which had been prepared by the desired combinations of 0.1 M NaOH and 0.1 M NaCl (forward titration) or of 0.1 M HCl and 0.1 M NaCl (backward titration). The amount of ion taken up by the exchanger was evaluated from the difference between the initial and the final concentrations of the Na^+ ions present in the solution. The Na^+ ions were converted to the corresponding pure chlorides and indirectly determined by titrating Cl^- ions by means of Fajans' method.

Apparatus. The thermal analysis was undertaken with a Shimadzu micro thermal analyzer, Model DT-20B, connected to a thermal balance, Model TGC-20H, for thermogravimetric analysis (TGA), and a high-temperature sample-holder, Model MDH-20, for differential thermal analysis (DTA). α-Alumina was used as the standard for DTA. The measurement was carried out in air at a heating rate of 5 °C/min. X-Ray diffraction patterns were taken using Ni-filtered Cu $K\alpha$ radiation.

Results and Discussion

In the direct precipitation method, there is a lower limit of the molar ratio of F/Zr in the mixed solution

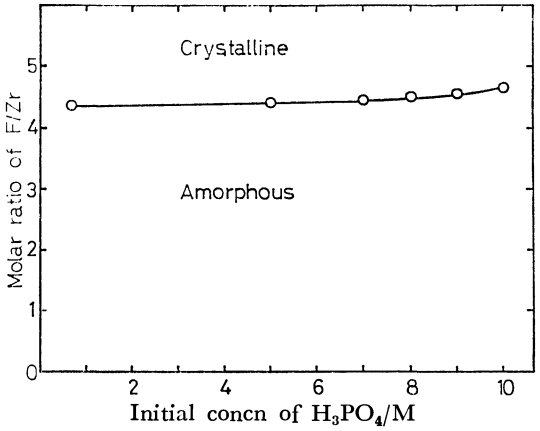

Fig. 1. Dependence of lower limit of F/Zr molar ratio on the concentration of H_3PO_4.

for obtaining crystalline material. When the F/Zr was lower than this limit, amorphous zirconium phosphate was precipitated. Figure 1 indicates that the limit depended slightly on the concentration of phosphoric acid. If the ratio is higher than 4.5, the crystalline form will be precipitated, irrespective of any other factors.

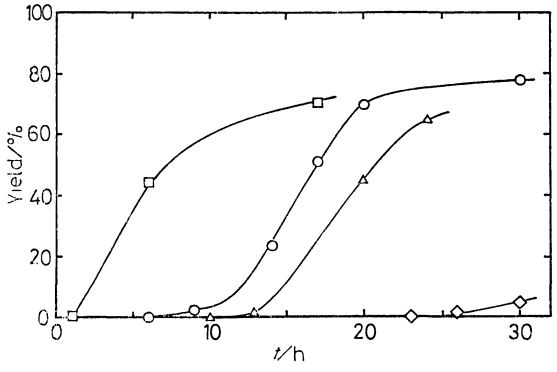

Fig. 2. Effect of F/Zr ratio on the rate of precipitation.
Conditions: T, 70 °C; concn of H_3PO_4, 5 M. F/Zr, □: 4.8, ○: 5.5, △: 6.8, ◇: 11.9.

The effect of the F/Zr ratio on the rate of precipitation was measured at an initial phosphoric acid concentration of 5 M and at 70 °C. Figure 2 indicates that the time needed for the first appearance of the precipitate (induction period) tended to become longer with the increase in the F/Zr ratio, while the progress of the precipitation, once it set in, was independent of the F/Zr ratio in the 4.8—6.8 region. From these results, a F/Zr ratio of 5.5 was selected by taking into account the margin for producing crystalline material and the rapidity of the procedure.

The dependence of the initial concentration of phosphoric acid on the formation rate of precipitate was investigated; the results are shown in Fig. 3. The progress of precipitation was little affected by the phosphoric acid concentration, but the induction period became longer with a decrease in the initial concentration of phosphoric acid.

As to the effect of the temperature, Fig. 4 reveals

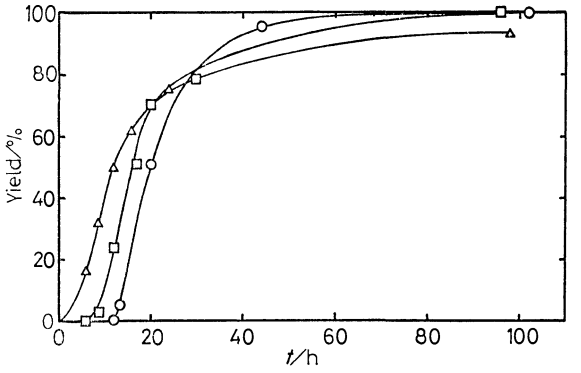

Fig. 3. Dependence of the initial concentration of H_3PO_4 on the formation rate of precipitate.
Conditions: F/Zr, 5.5; T, 70 °C. Concn of H_3PO_4, ○: 1 M, □: 5 M, △: 10 M.

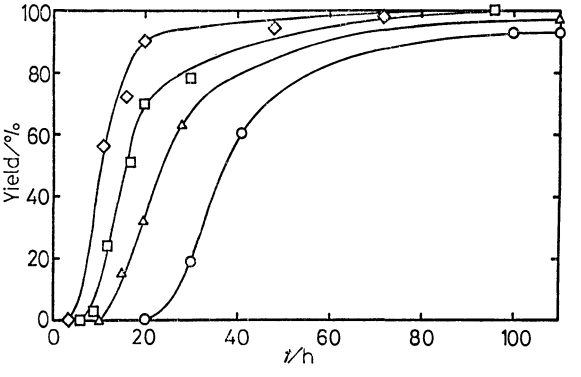

Fig. 4. Effect of temperature on the formation rate of precipitate.
Conditions: F/Zr, 5.5; concn of H_3PO_4, 5 M.
T, ○: 50 °C, △: 60 °C, □: 70 °C, ◇: 80 °C.

that, in addition to the shortening in the induction period, the progress of precipitation became faster as temperatures became warmer. These results suggest that, among the three factors examined, only the increasing temperature governs the progress of precipitation, while the concentrations of both hydrofluoric

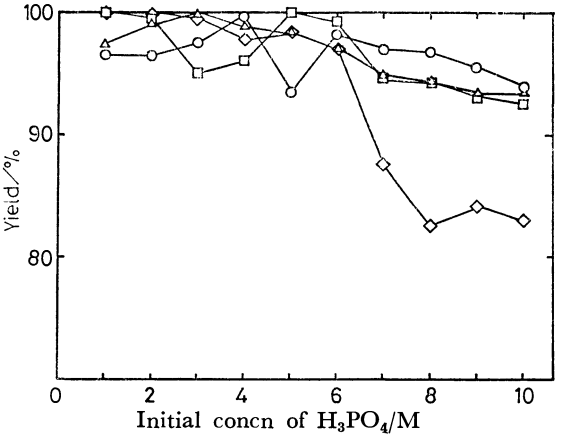

Fig. 5. Yield as functions of H_3PO_4 concentration and temperature.
F/Zr, 5.5.
T, ○: 50 °C, △: 60 °C, □: 70 °C, ◇: 80 °C.

acid and phosphoric acid affect only the length of the induction period. Furthermore, it is obvious from Figs. 3 and 4 that the precipitation reaction was completed within 100 h, whatever the conditions. Therefore, the yield after warming for longer than 100 h was measured as functions of the phosphoric acid concentration and the temperature. Figure 5 shows that the yield decreased a little with the concentration of phosphoric acid, but that it was higher than 90% under any conditions except in the case of 80 °C, where the yield decreased considerably when the concentration of phosphoric acid exceeded 7 M. Thus, the temperature should be fixed below 80 °C.

On the other hand, it is very important to ascertain the effect of the preparative conditions on the crystal size of the precipitate. The mean size of the crystals is plotted as a function of the initial concentration of phosphoric acid at different temperatures in Fig. 6, while its standard deviations under several representative conditions are shown in Table 1. The mean

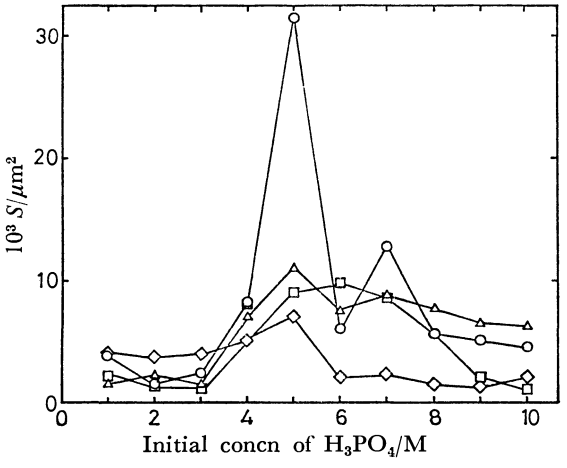

Fig. 6. Mean size of the crystals as functions of H_3PO_4 concentration and temperature.
F/Zr, 5.5.
T, ○: 50 °C, △: 60 °C, □: 70 °C, ◇: 80 °C.

TABLE 1. MEAN CRYSTAL SIZE OF ZP AND ITS STANDARD DEVIATION

Concn of H_3PO_4 M	$10^3 S$ μm^2	Standard deviation × 2 μm^2
1	1.4	0.7
5[a)]	31.5	18.1
5	10.1	4.9
9	6.5	2.3
10	6.3	3.1

Conditions of synthesis: F/Zr; 5.5, T; 60 °C except for a). a) F/Zr; 5.5, T; 50 °C.

crystal size was at its maximum near 5 M phosphoric acid. When we compared the two sides of the maximum, the mean crystal size was larger for the higher than for the lower concentrations of phosphoric acid. Furthermore, it decreased as the temperature rose. A comparison of the mean crystal size and its standard deviation shows that, in the case of 5 M phosphoric acid, though the mean crystal size was the largest, the uniformity of the crystals was poor, but in other cases it was comparatively good.

These observations can be understood as follows. The precipitate did not appear until the concentration of phosphoric acid approached about 8—9 M by the evaporation of water with hydrofluoric acid. This observation seems to reflect the length of the induction period. As the precipitation results from the decomposition of fluoro-complex of zirconium, the fact that the progress of precipitation depends only on the warming temperature, and not on the initial hydrofluoric acid and the phosphoric acid concentrations, can be understood if free hydrofluoric acid is considered to be expelled during the induction period. As a natural consequence, the lower the initial concentration of phosphoric acid, the higher the concentration of zirconium at the stage of precipitation. This fact makes it possible to interpret the slight decrease in the yield with the increase in the initial concentration of phosphoric acid. The higher rate of the generation of the free zirconium ion at the stage of precipitation—this corresponds to the conditions of a lower initial concentration of phosphoric acid and a higher temperature—facilitates the formation of many nuclei of the precipitate and leads to the small crystals. This argument is compatible with the observations of the mean crystal size except for the occurrence of the maximum in Fig. 6. Further investigations should be carried out to learn the reason for this important irregularity.

On the basis of these results, the conditions for the synthesis which provides the largest crystals are found to be; phosphoric acid concentration, 5 M; warming temperature, 50 °C. If the uniformity of the crystal size is required in addition to the large size of the crystals, the most favorable conditions are; phosphoric acid concentration, 9 M; warming temperature, 60 °C.

The following fact is worth noticing. The ZP thus prepared was in the form of flakes consisting of crystals of various sizes which adhered closely together. When converted to the sodium form, the flakes were broken down into fine particles. The ZP flakes, as prepared, were coverted to the sodium form by treating them with a mixture of 0.1 M NaCl and 0.1 M NaOH solutions (pH=11 at equilibrium). The particle-size distribution of the sodium-form exchangers thus prepared was examined by sieving, as is shown in Table 2. It is

TABLE 2. PARTICLE-SIZE DISTRIBUTION OF SODIUM-FORM EXCHANGERS

Mesh size	>70	70—100	100—145	145—200	200—280	280>
(1)[a)]	1	4	13	22	20	40
(2)[b)]	0	3	9	31	35	22

Conditions of synthesis: a) F/Zr, 5.5; concn of H_3PO_4, 5 M; T, 50 °C; b) F/Zr, 5.5; concn of H_3PO_4, 9 M; T, 60 °C.

evident from this table that (2) possessed a better uniformity in particle size than (1), though there existed very few particles larger than 100 mesh. Moreover, (2) contained fine powder, which cannot be used for column operation, only a half as much as (1). This particle-size distribution corresponds roughly to that of the crystals in the hydrogen form. Further breaking was not observed by reconversion to the hydrogen form or by repeated regeneration cycles. This phenomenon may be due to the separation of crystals by the stress exerted by the change in the interlayer distance in the structure of ZP by conversion.

Chemical, thermal, and X-ray analyses were performed in order to characterize the materials which had been prepared by the procedures recommended above.

The composition of the product was independent of the conditions for synthesis and was found to be $Zr(HPO_4)_2 \cdot H_2O$. (Found: ZrO_2, 41.23; P_2O_5, 47.27; H_2O, 11.88%).

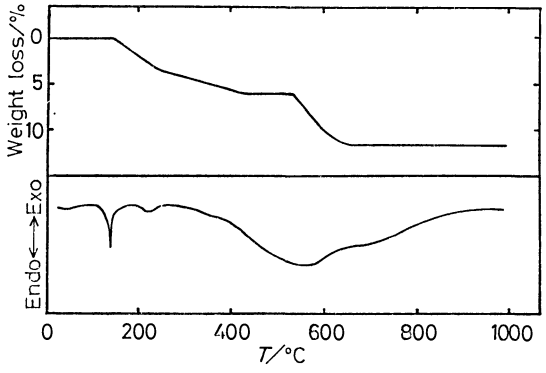

Fig. 7. TGA and DTA curves of ZP. Heating rate: 5 °C/min.

Figure 7 shows the TGA and DTA curves of the product. The TGA curve indicates that the product lost weight rapidly up to about 200 °C and then gradually up to 400 °C, where the weight became constant. The weight loss in this stage corresponds to one mole of water for each mole of ZP. Further heating to 650 °C gave rise to the release of a second mole of water, which resulted in the formation of pyrophosphate. In the DTA curve, there appeared a large and sharp endothermic peak at 150 °C, which was considered to correspond to the release of water. An exothermic peak attributed to the recrystallization by Clearfield and Stynes[1] did not appear. These curves closely resemble those of Sample (B) prepared by Horsley and Nowell.[10]

The results of X-ray analysis agreed well with the published data of α-ZP reported by Clearfield and Stynes.[1]

Forward and backward titration curves of ZP with sodium ion were constructed, as is shown in Fig. 8. The titration curves show two reversible exchange stages.

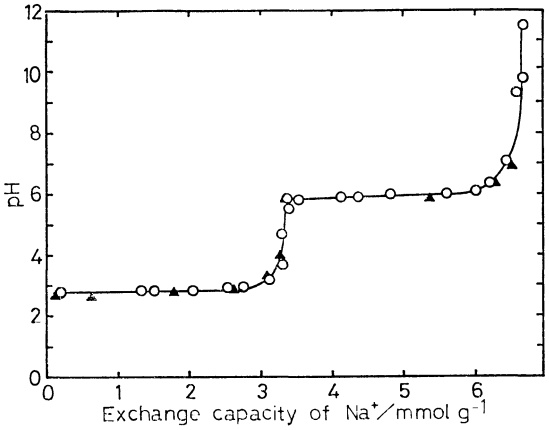

Fig. 8. Titration curves of ZP with sodium ion. ○: Forward titration, 0.1 M (NaOH+NaCl); ▲: Backward titration, 0.1 M (HCl+NaCl).

On the contrary, Clearfield *et al.*[14] reported that the titration curves exhibited a hysteresis loop, which resulted from the presence of different phases in the forward and backward titrations. These differences in titration and DTA curves can be explained by assuming that the crystallinity of the present product is better than that of Clearfield's.

References

1) A. Clearfield and J. A. Stynes, *J. Inorg. Nucl. Chem.*, **26**, 117 (1964).
2) G. H. Nancollas and R. Paterson, *J. Inorg. Nucl. Chem.*, **22**, 259 (1961).
3) S. J. Harvie and G. H. Nancollas, *J. Inorg. Nucl. Chem.*, **30**, 273 (1968).
4) S. J. Harvie and G. H. Nancollas, *J. Inorg. Nucl. Chem.*, **32**, 3923 (1970).
5) A. Dyer and F. T. Ocon, *J. Inorg. Nucl. Chem.*, **33**, 3153 (1971).
6) A. Dyer and J. S. Gill, *J. Inorg. Nucl. Chem.*, **39**, 665 (1977).
7) A. Dyer and J. S. Gill, *J. Inorg. Nucl. Chem.*, **40**, 97 (1978).
8) A. Ruvarac, S. Milonjic, A. Clearfield, and J. M. Graces, *J. Inorg. Nucl. Chem.*, **40**, 79 (1978).
9) U. Costantino, L. Naszodi, L. Szirtes, and L. Zsinka, *J. Inorg. Nucl. Chem.*, **40**, 901 (1978).
10) S. E. Horsley and D. V. Nowell, *J. Appl. Chem. Biotechnol.*, **23**, 215 (1973).
11) G. Alberti and E. Torracca, *J. Inorg. Nucl. Chem.*, **30**, 317 (1968).
12) W. F. Hillebrand, G. E. F. Lundell, H. A. Bright, and J. I. Hoffman, "Applied Inorganic Analysis," 2nd ed, Wiley, New York (1963), p. 572.
13) M. Ishibashi, "Teiryobunseki-jikkenho," 17th ed, Fuzanbo, Tokyo (1969), pp. 133, 472. (In Japanese.)
14) A. Clearfield, W. L. Duax, A. S. Medina, G. D. Smith, and J. R. Thomas, *J. Phys. Chem.*, **73**, 3424 (1969).

Kinetics and Mechanism of the Oxidation Reactions of Dialkyldithiocarbamatocopper(I) Tetramer and -silver(I) Hexamer with Tetraalkylthiuram Disulfide

Hidetoshi KITA, Shin-ichi MIYAKE, Koji TANAKA, and Toshio TANAKA*

Department of Applied Chemistry, Faculty of Engineering, Osaka University, Suita, Osaka 565

(Received February 19 1979)

Kinetics of the oxidations of dialkyldithiocarbamatocopper(I), $[\{Cu(S_2CNR_2)\}_4]$ (R=Et, *n*-Pr), and -silver(I), $[\{Ag(S_2CNR_2)\}_6]$ (R=Et, *n*-Pr, *i*-Pr), with the corresponding tetraalkylthiuram disulfide, $[(R_2NC(S)S\}_2]$, were investigated in dichloromethane employing a stopped-flow technique. The reactions are interpreted to proceed by a mechanism involving a rapid equilibration (**i**) (the multi-step equilibrium constant=K_0) to form adduct,

$$[\{M(S_2CNR_2)\}_x] \overset{+[(R_2NC(S)S\}_2]}{\rightleftharpoons} [M(S_2CNR_2)\{(R_2NC(S)S\}_2\}] + [\{M(S_2CNR_2)\}_{x-1}] \overset{+[(R_2NC(S)S\}_2]}{\rightleftharpoons} \cdots\cdots \quad (\mathbf{i})$$

(M=Cu, x=4; M=Ag, x=6)

$[M(S_2CNR_2)\{(R_2NC(S)S\}_2\}]$, which are decomposed in a rate-determining step (the rate constant=k) yielding the final products, $[M(S_2CNR_2)_2]$. According to this mechanism, the rate law in the presence of excess $[(R_2NC(S)S\}_2]$ is expressed as $v=K_0k[[(R_2NC(S)S\}_2]][[\{M(S_2CNR_2)\}_x]]/(1+K_0[[(R_2NC(S)S\}_2]])$, where K_0k(25 °C)=1.17×10^4 (Et), 5.70×10^3 (*n*-Pr) $M^{-1}s^{-1}$ (M=mol dm^{-3}) for the copper system, and K_0(25 °C)=28.2 (Et), 49.1 (*n*-Pr), 86.7 (*i*-Pr) M^{-1} and k(25 °C)=2.17 (Et), 1.50 (*n*-Pr), 6.56 (*i*-Pr) s^{-1} for the silver system. The activation parameters also were determined and the nature of transition states is discussed.

The dithiocarbamate ligand can stabilize transition metal ions in unusually high formal oxidation states by delocalization of electronic charges[1] and S–S interligand interactions,[2] as shown in the canonical structures of **b** and **c**, respectively.

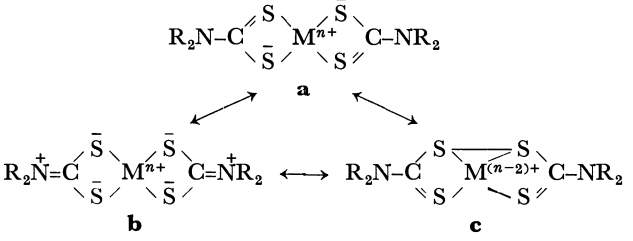

This interesting property seems to facilitate a number of studies[3-9] on the reaction of dithiocarbamato complexes of metals in the normal oxidation state with oxidizing agents such as halogens, boron trifluoride *etc*. All the works reported in this field, however, had been of a preparative nature until recently. Thus, we have reported the kinetics and mechanism of the oxidation reactions of dithiocarbamato complexes of tin(IV),[10] zinc(II),[11] and gold(I)[12] with halogens. These reactions have well been described to proceed *via* a charge-transfer complex formed by electrophilic attack of halogen on the sulfur atom of the dithiocarbamate ligand. As an extension of these studies to more complicated systems, the present paper reports kinetic and mechanistic studies on the oxidation reactions of dialkyldithiocarbamatocopper(I) tetramer and -silver(I) hexamer with tetraalkylthiuram disulfide, giving bis(dialkyldithiocarbamato)copper(II) and -silver(II), respectively.

Experimental

Materials. Dialkyldithiocarbamatocopper(I), $[\{Cu(S_2CNR_2)\}_4]$ (R=Et and *n*-Pr),[13] dialkyldithiocarbamatosilver(I), $[\{Ag(S_2CNR_2)\}_6]$ (R=Et, *n*-Pr, and *i*-Pr),[14] and tetraalkylthiuram disulfide, $[(R_2NC(S)S\}_2]$ (R=Et, *n*-Pr, and *i*-Pr),[14] were prepared according to the literature methods. Analytical data for these complexes (C, H, N) were satisfactory. Dichloromethane used as a solvent was purified as described previously.[12]

Spectra and Kinetics. Electronic spectra were recorded on a Hitachi 124 spectrophotometer. Rapid scanning spectra were measured with a Union RA-413 stopped-flow rapid scanning spectrophotometer equipped with a 2 mm quartz cell in a cell holder thermostated within ±0.2 °C. The rate of reaction was followed by monitoring the absorbance at a fixed wavelength in the electronic spectra of the reaction mixture under pseudo-first-order conditions, using at least a ten-fold excess of tetraalkylthiuram disulfide. Absorbance-time data were accumulated at least five times on a Union System-71 data processor and average absorbance-time curves were recorded on a National VP-6421A X-Y recorder. Pseudo-first-order rate constants, k_{obsd}, were calculated from the slope of a linear part of the $\ln(A_\infty - A_t)$ *vs.* time plots by the least-squares method, where A_∞ and A_t are absorbances at the end of reaction and at a time t, respectively.

Results and Discussion

Reaction of $[\{Cu(S_2CNR_2)\}_4]$ *with* $[(R_2NC(S)S\}_2]$. The reaction of $[\{Cu(S_2CNR_2)\}_4]$ with $[(R_2NC(S)S\}_2]$ rapidly proceeds to give bis(dialkyldithiocarbamato)-copper(II), $[Cu(S_2CNR_2)_2]$, in quantitative yields.[15] The stoichiometry of reaction can, therefore, be expressed as Eq. 1.

$$\frac{1}{4}[\{Cu(S_2CNR_2)\}_4] + \frac{1}{2}[(R_2NC(S)S\}_2] \longrightarrow [Cu(S_2CNR_2)_2] \quad (1)$$

A typical rapid scanning spectrum after mixing the reactant solutions is shown in Fig. 1. An absorption maximum at 303 nm observed immediately after mixing is identical in wavenumber with that of the

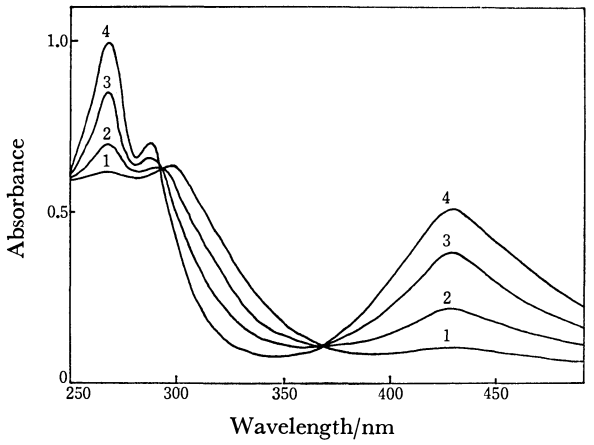

Fig. 1. Rapid scanning spectra after mixing [{Cu(S_2-$CNEt_2$)}$_4$] (5.1×10^{-5} M) with [($Et_2NC(S)S\}_2$] (1.0×10^{-4} M) in CH_2Cl_2 at 25 °C; cell length=2 mm. 1: 0.5 s, 2: 1.0 s, 3: 2.0 s, 4: the end of reaction.

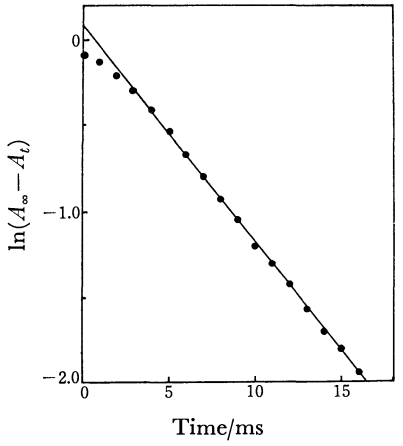

Fig. 2. Plots of $\ln(A_\infty-A_t)$ *vs.* time at 25 °C: [[{Cu(S_2CNEt_2)}$_4$]]$=1.0\times10^{-4}$ M, [[($Et_2NC(S)S\}_2$]]$=1.0\times10^{-2}$ M; cell length=2 mm.

TABLE 1. PSEUDO-FIRST-ORDER RATE CONSTANTS FOR THE REACTION OF [{Cu(S_2CNR_2)}$_4$] WITH [($R_2NC(S)S\}_2$] IN CH_2Cl_2

R	Temp °C	10^4 [[{Cu(S_2CNR_2)}$_4$]] M	10^4 [[($R_2NC(S)S\}_2$]] M	k_{obsd} s^{-1}
Et	10.5	0.501	20.0	12.8
			40.0	28.0
			59.7	44.3
			80.9	59.3
			100	73.5
	12.5	1.00	100	82.8
			200	156
			301	264
			400	314
			500	413
	15.5	0.501	20.0	18.4
			40.0	33.6
			59.7	48.8
			80.9	70.4
			100	89.0
	16.9	1.00	100	100
			200	214
			301	317
			400	450
			500	523
	20.1	0.501	20.0	24.9
			40.0	43.9
			59.7	65.4
			80.9	83.1
		1.00	100	115
			200	243
			301	312
			400	481
	25.0	0.505	10.0	14.3
		1.51	20.1	18.8
		0.625	25.0	38.2
		0.505	40.0	52.3
			50.1	66.3
			80.0	93.4
		1.00	100	127
			200	245
			301	349
n-Pr	10.9	0.529	20.8	6.37
			40.0	13.6
			60.4	21.3
			79.7	28.2
			99.8	35.3
	15.8	0.529	20.8	7.31
			40.0	17.3
			60.4	23.7
			79.7	32.1
			99.8	42.3
	20.3	0.513	20.1	11.5
			40.0	23.0
			50.1	29.1
			61.5	36.8
		0.529	60.4	31.6
			79.7	39.7
			100	50.4
		1.08	100	51.9
			203	94.4
			302	151
			401	195
			500	221
	25.0	1.28	20.1	14.7
		0.513	39.8	25.5
		1.28		28.7
		0.513	50.1	33.1
		1.28		37.0
		0.513	61.5	44.3
		1.28		42.3
		0.513	79.7	53.7
			100	65.5
		1.08	100	63.4
		0.513	123	74.7
		1.08	203	134
			302	192
			401	244
			500	276

reactant $[\{Cu(S_2CNR_2)\}_4]$ ($\lambda_{max}=303$ nm, $\varepsilon_{max}=4.5\times10^4$ M^{-1} cm^{-1} ($M=$mol dm^{-3}) in CH_2Cl_2). The final spectrum with three absorption peaks at 270, 290, and 435 nm is assigned to $[Cu(S_2CNR_2)_2]$ ($\varepsilon_{max}=3.1\times10^4$, 1.8×10^4, and 1.2×10^4 M^{-1} cm^{-1} in CH_2Cl_2, respectively).[15-18] Half-lives of these absorption bands were almost identical with one another, and isosbestic points are found at 295 and 370 nm.

The rate data of reaction 1 (R=Et and *n*-Pr) were obtained from increase of the absorbance at 435 nm after mixing $[\{Cu(S_2CNR_2)\}_4]$ with excess $[(R_2NC(S)S\}_2]$. Figure 2 shows a typical example of $\ln(A_\infty-A_t)$ *vs.* time plots. Except for the period of initial several milliseconds, a good linear relation between them is obtained for at least 80% completion of the reaction. The linear part of plots was used to determine the values of pseudo-first-order rate constants. Table 1 lists the rate data at various concentrations of $[\{Cu(S_2CNR_2)\}_4]$ and $[(R_2NC(S)S\}_2]$. All the plots of k_{obsd} *vs.* the concentration of $[(R_2NC(S)S\}_2]$ at each temperature yielded straight lines with zero intercepts. This result may be interpreted by assuming the reaction pathways of 2 to 4.

$$[\{Cu(S_2CNR_2)\}_4] \overset{+[(R_2NC(S)S\}_2]}{\rightleftharpoons} [Cu(S_2CNR_2)\{(R_2NC(S)S\}_2] + [\{Cu(S_2CNR_2)\}_3]$$

$$\overset{+[(R_2NC(S)S\}_2]}{\rightleftharpoons} \cdots\cdots \quad K_0, \quad (2)$$

$$[Cu(S_2CNR_2)\{(R_2NC(S)S\}_2] \overset{k}{\longrightarrow} [Cu(S_2CNR_2)_2] + [R_2NCS_2\cdot] \quad (3)$$

$$2[R_2NCS_2\cdot] \overset{\text{fast}}{\longrightarrow} [(R_2NC(S)S\}_2] \quad (4)$$

Equation 2 consists of multi-step equilibrium reactions, where the tetrameric compound $[\{Cu(S_2CNR_2)\}_4]$ dissociates by the attack of $[(R_2NC(S)S\}_2]$ to form an adduct $[Cu(S_2CNR_2)\{(R_2NC(S)S\}_2]$ and a trimer $[\{Cu(S_2CNR_2)\}_3]$, the latter of which successively reacts with $[(R_2NC(S)S\}_2]$ to give the adduct in a similar manner. The initial curvature of $\ln(A_\infty-A_t)$ *vs.* time plots (Fig. 2) may correspond to a preequilibrium immediately after mixing, where the concentration of the adduct does not reach a steady state. The formation of the adduct as an intermediate may be supported by the fact that several metal complexes of thiuram disulfide have been isolated,[19-21] although there is no direct evidence in the present study. Thus, two possible structures, **1** and **2**, are proposed for the adduct formed between the copper(I) complex and thiuram disulfide.

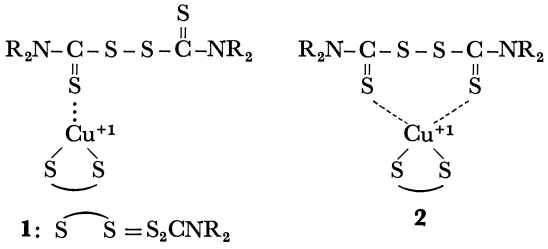

In either structure the adduct may be decomposed in a rate-determining step (Eq. 3), which involves homolytic cleavage of the S–S bond of tetraalkylthiuram disulfide to give the oxidized copper(II) product, $[Cu(S_2CNR_2)_2]$, and the $[R_2NCS_2\cdot]$ radical. The resulting radical may rapidly dimerize to regenerate tetraalkylthiuram disulfide as reported by Cauquis and Lachenal,[22] who have estimated the rate constant of dimerization for R=Et to be 2×10^5 M^{-1} s^{-1} in acetonitrile.

According to the pathways of 2—4, the k_{obsd} value in the presence of excess tetraalkylthiuram disulfide is expressed by Eq. 5,

$$k_{obsd}=\frac{K_0k[[(R_2NC(S)S\}_2]]}{1+K_0[[(R_2NC(S)S\}_2]]}, \quad (5)$$

where K_0 stands for the multi-step equilibrium constant in Eq. 2. If one assumes $K_0[[(R_2NC(S)S\}_2]]\ll1$, Eq. 5 can be reduced to Eq. 6,

$$k_{obsd}=K_0k[[(R_2NC(S)S\}_2]] \quad (6)$$

which predicts a linear relationship between k_{obsd} and the concentration of $[(R_2NC(S)S\}_2]$ with the slope of K_0k and the zero intercept. This is consistent with the observed rate profile. Table 2 lists the K_0k value and activation parameters determined from the Arrhenius plot of $\ln(K_0k)$ *vs.* $1/T$.

Reaction of $[\{Ag(S_2CNR_2)\}_6]$ *with* $[(R_2NC(S)S\}_2]$. The addition of a dichloromethane solution of $[(R_2NC(S)\}_2]$ to $[\{Ag(S_2CNR_2)\}_6]$ in dichloromethane immediately causes a blue color, which becomes more intense as more $[(R_2NC(S)S\}_2]$ is added. The electronic spectrum of the blue solution displayed an

TABLE 2. KINETIC AND ACTIVATION PARAMETERS FOR THE REACTION OF $[\{Cu(S_2CNR_2)\}_4]$ WITH $[(R_2NC(S)S\}_2]$ IN CH_2Cl_2[a]

R	Temp / °C	K_0k / M^{-1} s^{-1}	$\Delta H^{\neq}$ / kJ mol^{-1}	$\Delta S^{\neq}$ / J $mol^{-1}K^{-1}$
Et	25.0	$(1.17\pm0.02)\times10^4$	20.6 ± 4.4	-97 ± 10
	20.1	$(1.17\pm0.05)\times10^4$		
	16.9	$(1.08\pm0.05)\times10^4$		
	15.5	$(8.86\pm0.35)\times10^3$		
	12.5	$(8.19\pm0.44)\times10^3$		
	10.5	$(7.60\pm0.11)\times10^3$		
n-Pr	25.0	$(5.70\pm0.09)\times10^3$	18.2 ± 3.1	-112 ± 10
	20.3	$(4.52\pm0.10)\times10^3$		
	15.8	$(4.29\pm0.19)\times10^3$		
	10.9	$(3.67\pm0.03)\times10^3$		

a) Errors quoted are standard deviations.

Table 3. Equilibrium constants and thermodynamic parameters for the reaction of $[\{Ag(S_2CNR_2)\}_6]$ with $[(R_2NC(S)S\}_2]$ in CH_2Cl_2[a]

R	Temp / °C	K / $M^{1/3}$	$\Delta H°$ / kJ mol^{-1}	$\Delta S°$ / J mol^{-1}K^{-1}
Et	25.8	$(4.46\pm0.23)\times10^{-4}$	23.0±1.0	12.9±7.4
	20.5	$(3.80\pm0.22)\times10^{-4}$		
		(3.8×10^{-4})[b]		
	15.1	$(3.14\pm0.24)\times10^{-4}$		
	10.0	$(2.71\pm0.27)\times10^{-4}$		
n-Pr	24.7	$(4.85\pm0.32)\times10^{-4}$	27.9±0.4	30.2±3.1
	20.4	$(4.16\pm0.34)\times10^{-4}$		
		(5.5×10^{-4})[b]		
	15.5	$(3.51\pm0.29)\times10^{-4}$		
	9.7	$(2.66\pm0.34)\times10^{-4}$		
i-Pr	24.6	$(9.21\pm0.13)\times10^{-3}$	16.4±0.4	16.2±3.3
	20.6	$(8.43\pm0.34)\times10^{-3}$		
		(1.1×10^{-2})[b]		
	15.3	$(7.35\pm0.35)\times10^{-3}$		
	11.0	$(6.65\pm0.26)\times10^{-3}$		

a) Errors quoted are standard deviations.
b) In $CHCl_3$ at 20 °C; Ref. 15.

Table 4. Pseudo-first-order rate constants for the reaction of $[\{Ag(S_2CNR_2)\}_6]$ with $[(R_2NC(S)S\}_2]$ in CH_2Cl_2

R	Temp / °C	10^4 $[[Ag\{(S_2CNR_2)\}_6]]$ / M	10^4 $[[(R_2NC(S)S\}_2]]$ / M	k_{obsd} / s^{-1}
Et	10.6	5.02	100	0.108
			200	0.187
			300	0.221
			400	0.262
			500	0.270
	15.2	5.02	100	0.179
			200	0.271
			300	0.357
			400	0.421
			500	0.468
	20.3	5.02	100	0.302
			200	0.456
			300	0.562
			400	0.669
			500	0.724
	25.0	5.02	200	0.788
			300	0.980
			400	1.13
			500	1.30
n-Pr	10.3	5.00	100	0.0993
			200	0.136
			299	0.164
			400	0.205
			500	0.235
	15.2	5.00	100	0.163
			200	0.261
			299	0.315
			400	0.321
			500	0.360
	20.0	5.00	100	0.289
			200	0.414
			299	0.482
			400	0.585
			500	0.670
n-Pr	25.1	5.00	100	0.503
		10.0		0.501
		5.00	200	0.673
		10.0		0.786
		5.00	300	0.942
		10.0		0.828
	25.1	5.00	400	1.04
		10.0		0.952
		5.00	500	1.04
		10.0		1.11
i-Pr	10.2	4.99	100	0.762
			201	1.01
			301	1.17
			400	1.32
			501	1.40
	14.9	4.99	100	1.15
			201	1.55
			301	1.84
			400	2.01
			501	2.22
	20.0	5.00	100	1.91
			201	2.55
			301	2.92
			400	3.13
			501	3.36
	25.1	5.00	100	3.03
			201	4.12
			301	4.68
			400	5.05
			501	5.54

absorption maximum at *ca.* 600 nm, which has been assigned to the $[Ag(S_2CNR_2)_2]$ complex.[15,18] Thus, stoichiometry for the reaction of $[\{Ag(S_2CNR_2)\}_6]$ with $[(R_2NC(S)S\}_2]$ (R=Et, *n*-Pr, and *i*-Pr) is expressed as Eq. 7. The equilibrium constants K in

$$\frac{1}{6}[\{Ag(S_2CNR_2)\}_6] + \frac{1}{2}[(R_2NC(S)S\}_2] \overset{K}{\rightleftharpoons} [Ag(S_2CNR_2)_2] \quad (7)$$

chloroform at 20 °C (see Table 3) were determined spectrophotometrically by Åkerström.[15] We determined the K value in dichloromethane at four different temperatures by the same method (Table 3). Plots of $\ln K$ *vs.* $1/T$ for each system gave a linear relation, from which thermodynamic parameters of the reaction 7 were obtained. The results are given in Table 3, which indicates that the equilibrium lies so far to the left. The fact that the K value for R=*i*-Pr is larger than those for R=*n*-Pr and Et may be due to a larger inductive effect of the isopropyl group than the propyl and ethyl groups of the dithiocarbamate ligands, resulting in increasing stability of $[Ag(S_2CNR_2)_2]$ by delocalization of electronic charges from the dithiocarbamate ligand to Ag(II).

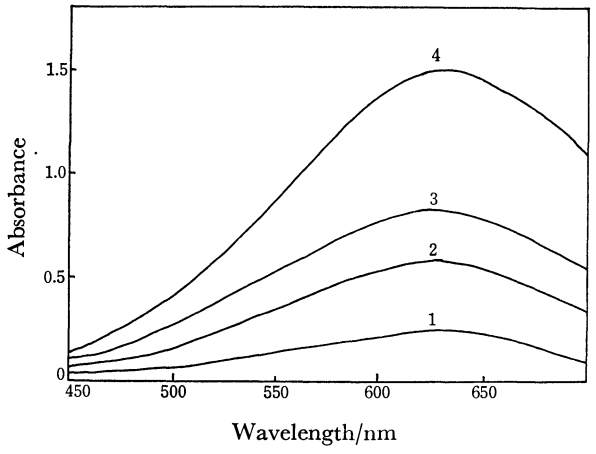

Fig. 3. Rapid scanning spectra after mixing $[\{Ag(S_2CN\text{-}i\text{-}Pr_2)\}_6]$ (5.0×10^{-4} M) with $[(i\text{-}Pr_2NC(S)S\}_2]$ (5.0×10^{-2} M) in CH_2Cl_2 at 25 °C; cell length=2 mm. 1: 0.1 s, 2: 0.2 s, 3: 0.3 s, 4: 1.0 s.

A typical change of electronic spectra in the visible region after mixing of the reactants is depicted in Fig. 3, which clearly shows the formation of $[Ag(S_2CN\text{-}i\text{-}Pr_2)_2]$ (λ_{max}=620 nm, $\varepsilon_{max}=1.3\times10^4$ M^{-1} cm^{-1} in CH_2Cl_2; lit,[15] λ_{max}=620 nm in $CHCl_3$). The rate of reaction was, therefore, followed by measuring the absorbance at 620 nm (R=*i*-Pr) or 600 nm (R=Et and *n*-Pr). Plots of $\ln(A_\infty-A_t)$ *vs.* time were found to be linear to at least 80% completion except for the initial short period after mixing, as in the case of copper complexes (Fig. 2). Pseudo-first-order rate constants obtained from a linear region of the plots are listed in Table 4. Plots of k_{obsd} *vs.* the concentration of $[(R_2NC(S)S\}_2]$ showed pronounced curvature at high concentrations of $[(R_2NC(S)S\}_2]$. A typical example is shown in Fig. 4, which is in contrast with the linear relationship for the

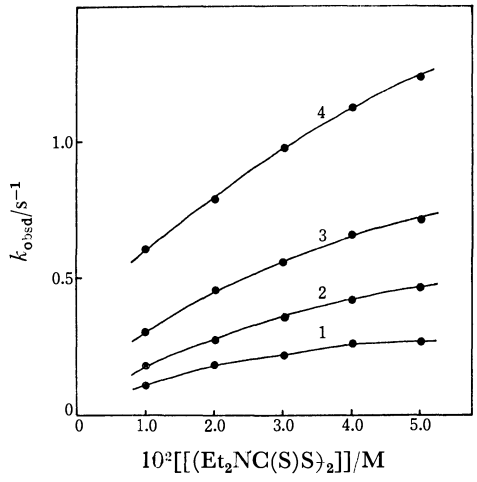

Fig. 4. Plots of k_{obsd} *vs.* $[[(Et_2NC(S)S\}_2]]$ for the reaction of $[\{Ag(S_2CNEt_2)\}_6]$ with $[(Et_2NC(S)S\}_2]$ in CH_2Cl_2; $[[\{Ag(S_2CNEt_2)\}_6]]=5.0\times10^{-4}$ M. 1: 10.6 °C, 2: 15.2 °C, 3: 20.3 °C, 4: 25.0 °C.

copper system. This notable difference can be explained by the assumption that the multi-step equilibrium constant K_0 appearing in Eq. 5 is larger in the silver system than in the copper system.

The mechanism proposed above for the copper complexes is, therefore, applicable to the silver complexes; the reaction pathways can be postulated as Eqs. 8 and 9, followed by dimerization of the $[R_2NCS_2\cdot]$

$$[\{Ag(S_2CNR_2)\}_6] \overset{+[(R_2NC(S)S\}_2]}{\rightleftharpoons} [Ag(S_2CNR_2)\{(R_2NC(S)S\}_2\}] + [\{Ag(S_2CNR_2)\}_5] \overset{+[(R_2NC(S)S\}_2]}{\rightleftharpoons} \cdots\cdots \quad K_0, \quad (8)$$

$$[Ag(S_2CNR_2)\{(R_2NC(S)S\}_2\}] \overset{k}{\longrightarrow} [Ag(S_2CNR_2)_2] + [R_2NCS_2\cdot] \quad (9)$$

radical (Eq. 4). Moreover, the bivalent silver complex, $[Ag(S_2CNR_2)_2]$, formed by Eq. 9 is expected to degrade because of its instability around room temperature. Similar instability has been reported for bis(diethylthiocarbamato)copper(II),[23] which rapidly rearranges into a hexameric univalent copper complex according to Eq. 10. By analogy with this, $[Ag(S_2CNR_2)_2]$ is suggested to rearrange as shown in Eq. 11. Equation 11 displays a unimolecular rearrangement of the

$$[Cu(SOCNEt_2)_2] \longrightarrow \frac{1}{6}[\{Cu(SOCNEt_2)\}_6] + \frac{1}{2}[(Et_2NC(O)S\}_2] \quad (10)$$

$$[Ag(S_2CNR_2)_2] \overset{k'}{\longrightarrow} \frac{1}{6}[\{Ag(S_2CNR_2)\}_6] + \frac{1}{2}[(R_2NC(S)S\}_2] \quad (11)$$

Ag(II) complex into the hexameric Ag(I) complex and tetraalkylthiuram disulfide with the rate constant of k', though the mechanism has not been clarified in the present work. The Ag(II) complex is possible also to react with the dialkyldithiocarbamato radical produced by Eq. 9, bimolecularily with the rate constant of k'', affording the Ag(I) hexamer, as shown

in Eq. 12. It is not obvious, however, which of Eqs. 11

$$[Ag(S_2CNR_2)_2] + [R_2NCS_2\cdot] \xrightarrow{k''} \frac{1}{6}[\{Ag(S_2CNR_2)\}_6] + [(R_2NC(S)S\}_2] \quad (12)$$

and 12 is predominant in the silver system. If one assumes $k \gg k'$ and/or k'', then k_{obsd} in the presence of excess $[(R_2NC(S)S\}_2]$ also is given by Eq. 5. It is apparent from Eq. 5 that the plots of k_{obsd} *vs.* the concentration of $[(R_2NC(S)S\}_2]$ show a curvature at so high concentrations of $[(R_2NC(S)S\}_2]$ as $K_0[[(R_2NC(S)S\}_2]]$ can not be neglected against unity. This is consistent with the observed kinetics (Fig. 4). Equation 5 can be transformed to Eq. 13, which predicts that there should be a

$$\frac{1}{k_{obsd}} = \frac{1}{K_0k[[(R_2NC(S)S\}_2]]} + \frac{1}{k}, \quad (13)$$

linear relationship between $1/k_{obsd}$ *vs.* $1/[[(R_2NC(S)S\}_2]]$, with the intercept of $1/k$ and the slope of $1/K_0k$. As an example of the plots is depicted in Fig. 5,

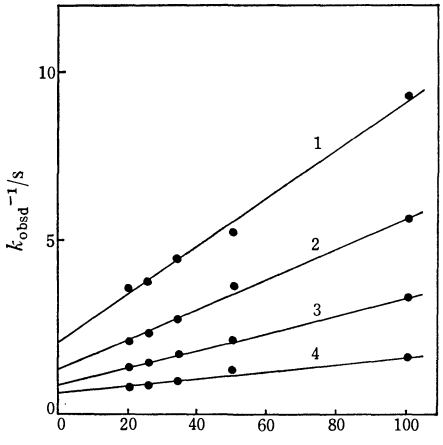

Fig. 5. Plots of $1/k_{obsd}$ *vs.* $1/[[(Et_2NC(S)S\}_2]]$ for the reaction of $[\{Ag(S_2CNEt_2)\}_6]$ with $[(Et_2NC(S)S\}_2]$ in CH_2Cl_2; $[[\{Ag(S_2CNEt_2)\}_6]]=5.0\times10^{-4}$ M. 1: 10.6 °C, 2: 15.2 °C, 3: 20.3 °C, 4: 25.0 °C.

which shows a linear relation over the observed range of $[(R_2NC(S)S\}_2]$ concentrations. The rate and equilibrium constants for the $[\{Ag(S_2CNR_2)\}_6]$–$[(R_2NC(S)S\}_2]$ system are summarized in Table 5.

Thermodynamic and activation parameters calculated from K_0 and k at four different temperatures (Table 5) are listed in Table 6, which reveals that the $\Delta H^\circ_{(K_0)}$ values are near to zero. The $\Delta S^\circ_{(K_0)}$ term is, therefore, a dominant factor to cause the reaction 8. The positive $\Delta S^\circ_{(K_0)}$ values are consistent with the stepwise dissociation of $[\{Ag(S_2CNR_2)\}_6]$ by the attack of $[(R_2NC(S)S\}_2]$. The small negative $\Delta S^{\ddagger}_{(k)}$ values suggest that the configuration of the adduct formed between monomeric $[Ag(S_2CNR_2)]$ and thiuram disulfide, as shown in **3** or **4**, is essentially maintained in the transition state of reaction 9.

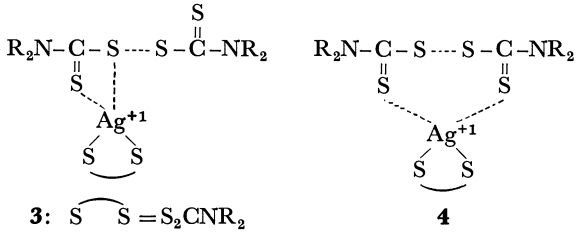

Finally, it should be mentioned that the K_0k values for the copper system are about two orders greater than those for the silver system under similar experimental conditions (Tables 2 and 5). In addition, a linear dependence of k_{obsd} on the concentration of thiuram disulfide observed for the copper system predicts that the K_0 value is not so large as that for the silver system, as described above. Thus, the k values for the copper system must be more than two orders greater than those for the silver system. This is in agreement with the fact that the oxidation to a bivalent state is easier in Cu(I) complexes than in Ag(I) complexes.[24]

Table 5. Equilibrium and rate constants for the reaction of $[\{Ag(S_2CNR_2)\}_6]$ with $[(R_2NC(S)S\}_2]$ in CH_2Cl_2[a]

R	Temp / °C	K_0 / M^{-1}	k / s^{-1}
Et	25.0	28.2± 4.2	2.17±0.30
	20.3	38.4± 3.9	1.08±0.10
	15.2	31.8± 5.0	0.74±0.11
	10.6	30.4± 4.7	0.47±0.07
n-Pr	25.1	49.1±12.3	1.50±0.34
	20.0	48.8± 9.0	0.87±0.15
	15.2	45.6± 6.5	0.53±0.68
	10.3	47.9±11.6	0.30±0.07
i-Pr	25.1	86.7± 5.3	6.57±0.31
	20.0	89.4± 4.6	4.03±0.16
	14.9	71.2± 6.5	2.73±0.21
	10.2	79.6± 8.3	1.70±0.13

a) Errors quoted are standard deviations.

Table 6. Thermodynamic and activation parameters for the reaction of $[\{Ag(S_2CNR_2)\}_6]$ with $[(R_2NC(S)S\}_2]$ in CH_2Cl_2 at 25 °C[a]

R	$\Delta H^\circ_{(K_0)}$ / kJ mol^{-1}	$\Delta S^\circ_{(K_0)}$ / J mol^{-1}K^{-1}	$\Delta H^{\ddagger}_{(k)}$ / kJ mol^{-1}	$\Delta S^{\ddagger}_{(k)}$ / J mol^{-1}K^{-1}
Et	−1±7	29±50	70±4	−4±28
n-Pr	2±1	38±10	74±1	−2± 5
i-Pr	6±4	59±29	59±1	−32± 8

a) Errors quoted are standard deviations.

The authors are grateful to the Ministry of Education for support of this work through Grant-in-Aid for Scientific Research.

References

1) B. L. Edgar, D. J. Duffy, M. C. Palazzotto, and L. H. Pignolet, *J. Am. Chem. Soc.*, **95**, 1125 (1973).
2) A. Avdeef, J. P. Fackler, Jr., and R. G. Fischer, Jr., *J. Am. Chem. Soc.*, **92**, 6972 (1970).
3) D. Coucouvanis, *Prog. Inorg. Chem.*, **11**, 233 (1970).
4) J. Willemse, J. A. Cras, J. J. Steggerda, and C. P. Keijzers, *Structure and Bonding*, **28**, 83 (1976).
5) E. A. Pasek and D. K. Straub, *Inorg. Chim. Acta*, **21**, 23 (1977).
6) B. M. Mattson and L. H. Pignolet, *Inorg. Chem.*, **16**, 488 (1977).
7) E. W. Ainscough and A. M. Brodie, *J. Chem. Soc., Dalton Trans.*, **1977**, 565.
8) S. H. Wheeler, B. M. Mattson, G. L. Miessler, and L. H. Pignolet, *Inorg. Chem.*, **17**, 340 (1978).
9) G. A. Katsoulos, G. E. Manoussakis, and C. A. Tsipis, *Inorg. Chim. Acta*, **30**, L295 (1978).
10) H. Kita, K. Tanaka, and T. Tanaka, *Bull. Chem. Soc. Jpn.*, **48**, 2816 (1975).
11) H. Kita, K. Tanaka, and T. Tanaka, *Inorg. Chim. Acta*, **21**, 229 (1977).
12) H. Kita, K. Itoh, K. Tanaka, and T. Tanaka, *Bull. Chem. Soc. Jpn.*, **51**, 3530 (1978).
13) A. R. Hendrickson, R. L. Martin, and N. M. Rohde, *Inorg. Chem.*, **15**, 2115 (1976).
14) S. Åkerström, *Arkiv Kemi*, **14**, 387 (1959).
15) S. Åkerström, *Arkiv Kemi*, **14**, 403 (1959).
16) R. Pettersson and T. Vänngård, *Arkiv Kemi*, **17**, 249 (1961).
17) T. R. Reddy and R. Srinivasan, *J. Chem. Phys.*, **43**, 1404 (1965).
18) M. V. Rajasekharan, C. N. Sethulakshmi, P. T. Manoharan, and H. Gudel, *Inorg. Chem.*, **15**, 2657 (1976).
19) H. C. Brinkhoff, J. A. Cras, J. J. Steggerda, and J. Willemse, *Recl. Trav. Chim. Pays-Bas*, **88**, 633 (1969); H. C. Brinkhoff, J. A. Cras, J. J. Steggerda, and J. Willemse, *ibid.*, **89**, 11 (1970); P. T. Beurskens, J. A. Cras, J. H. Noordik, and A. M. Spruijt, *J. Cryst. Mol. Struct.*, **1**, 93 (1971); C. Chieh, *Can. J. Chem.*, **55**, 1115 (1977).
20) H. Coutreras and H. Cortés, *Inorg. Nucl. Chem. Lett.*, **6**, 225 (1970).
21) R. M. Golding and W. C. Tennant, *Mol. Phys.*, **24**, 301 (1972); R. A. Palmer, W. C. Tennant, M. F. Dix, and A. D. Rae, *J. Chem. Soc., Dalton Trans.*, **1976**, 2345.
22) G. Cauquis and D. Lachenal, *J. Electroanal. Chem. Interfacial Electrochem.*, **43**, 205 (1973).
23) S. Åkerström, *Arkiv Kemi*, **24**, 479 (1965).
24) F. A. Cotton and G. Wilkinson, "Advanced Inorganic Chemistry," 3rd ed, Interscience, New York (1972), pp. 905 and 1044.

An X-Ray Diffraction Study on the Structures of Bis- and Tris-(ethylenediamine)zinc(II) Complexes in Solution

Tadao FUJITA, Toshio YAMAGUCHI, and Hitoshi OHTAKI*

Department of Electronic Chemistry, Tokyo Institute of Technology at Nagatsuta, Nagatsuta-cho, Midori-ku, Yokohama 227

(Received March 30, 1979)

An X-ray diffraction study has been carried out at 25 °C for aqueous ethylenediamine(en) solutions of zinc(II) nitrate, the mole ratios, en/Zn, in the solutions being 2.252 and 3.204. In the former solution bis(ethylenediamine)-zinc(II) complex existed as the main species, while in the latter tris(ethylenediamine)zinc(II) complex was predominant. The X-ray scattering data of the solution containing the bis-complex showed that four nitrogen atoms within the two ethylenediamine molecules were tetrahedrally coordinated to the zinc(II) ion at a distance of 2.131 (9) Å. The nonbonding Zn···C distance was also determined to be 2.89(2) Å. In the tris-complex in which the zinc(II) ion was coordinated with the six nitrogen atoms, the Zn–N and Zn···C distances were 2.276(5) Å and 3.00(1) Å, respectively. Raman spectra of the solutions supported the structures of the complexes.

X-Ray diffraction studies on complexes in solution have been markedly developed in these years, and the structural data of metal complexes with various unidentate ligands, such as halide and hydroxide ions and water and ammonia molecules, have been accumulated to provide the most fundamental knowledge on elucidating behavior of metal complexes in solution. Recent progresses in techniques and apparatus for X-ray diffraction analysis allow to investigate structures of polynuclear complexes containing relatively heavy metals. However, structures of metal chelates in solution have never been examined by the X-ray diffraction method.

In the present work, as a first step of investigation of structures of metal chelates, we choose ethylenediamine complexes of zinc(II) ion, because ethylenediamine is one of the simplest chelating agents. To find the structural difference, if it presents, of the complexes with varying numbers of the ligand coordinated is another aim of this investigation, since no crystallographic study of these complexes has been made so far.

Raman spectroscopic measurements have been employed to provide a supplement to the structural determination of the complexes.

Experimental

Preparation and Analysis of Sample Solutions. Anhydrous ethylenediamine of guaranteed reagent grade was obtained from Tokyo Kasei Co., Ltd. and was purified by refluxing and distilling over sodium (bp 167 °C). Zinc(II) nitrate of reagent grade was purchased from Wako Pure Chemical Co., Osaka and was recrystallized twice from water. The samples were prepared by dissolving zinc nitrate into aqueous ethylenediamine solutions.

The concentration of zinc(II) ions in the test solutions was determined by EDTA titration and gravimetry as $ZnNH_4PO_4$. The results of the two independent methods agreed each other within 0.2%.

The concentration of the nitrate ion was determined from the stoichiometry of the zinc(II) nitrate.

TABLE 1. THE COMPOSITION (g-atom/dm³) AND THE STOICHIOMETRIC VOLUME V PER ZINC ATOM IN THE SOLUTIONS

	Solutions	
	A	B
Zn	1.846	1.295
N	15.52	8.422
C	11.83	5.832
O	47.11	49.28
H	119.4	106.4
en/Zn	3.204	2.252
V/Å³	899.5	1282
Density/g cm⁻³	1.239	1.171

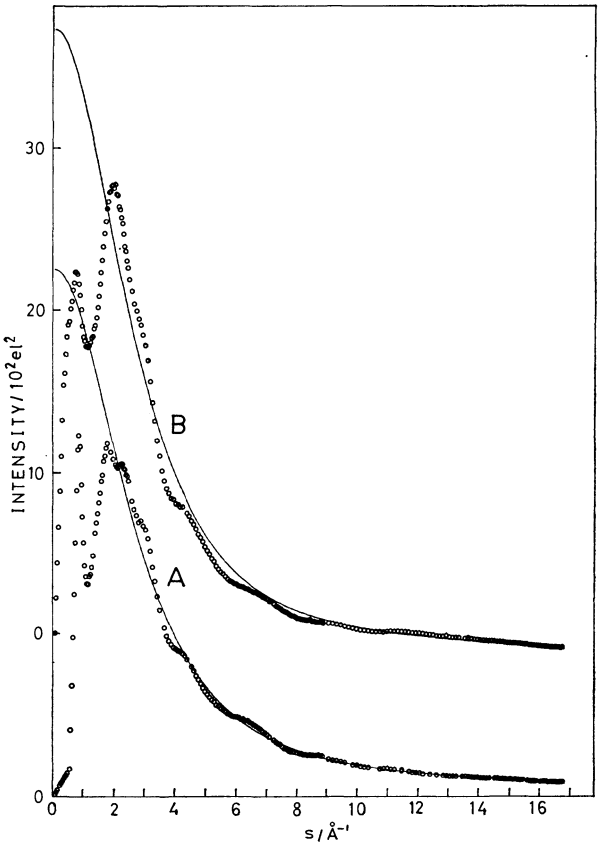

Fig. 1. Coherent scattering intensities of the sample solutions A and B. Experimentally obtained intensities I^{coh} are shown by circles and calculated independent scattering intensities by solid lines.

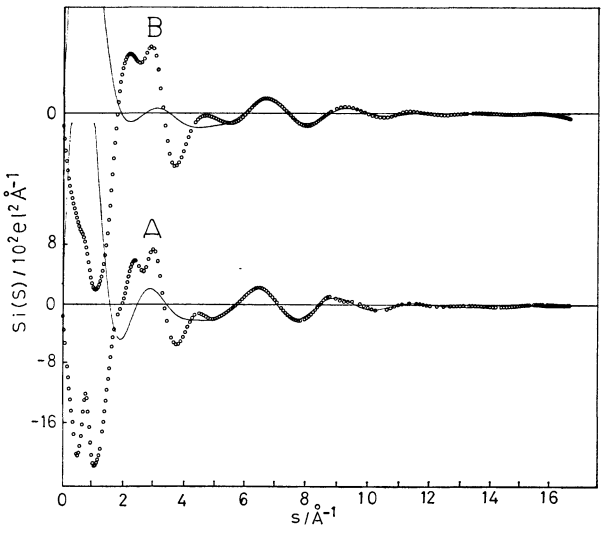

Fig. 2. The reduced intensities multiplied by s for solutions A and B. Open circles indicated experimentally obtained $s \cdot i(s)$ values and full lines are calculated ones by using parmeter values finally proposed.

The density of the test solutions was measured pycnometrically.

The composition of the test solutions is given in Table 1.

Method of Measurements and Treatment of X-Ray Scattering Data. The method of measurements and the apparatus used were essentially the same as those in previous papers.[1] Coherent and reduced intensities of the test solutions are given in Figs. 1 and 2, respectively. The radial distribution function $D(r)$ was calculated by the following equation:

$$D(r) = 4\pi r^2\rho_0 + \frac{2r}{\pi}\int_0^{s_{max}} s \cdot i(s) \cdot M(s) \cdot \sin(rs)\mathrm{d}s, \quad (1)$$

where ρ_0 is the average scattering density in the stoichiometric volume V of the solution per Zn atom, and s_{max} denotes the maximum s-value attained in the measurements ($s_{max}=16.7$ Å). $M(s)$ represents the modification function[2] and the reduced intensities $i(s)$ are given by

$$i(s) = I^{coh}(s) - \sum n_i\{(f_i(s)+\Delta f_i')^2+(\Delta f_i'')^2\}, \quad (2)$$

where n_i is the number of atom i and $f_i(s)$ denotes the scattering factor of atom i at s. $\Delta f_i'$ represents the real part of the anormalous dispersion, whereas $\Delta f_i''$ is the imaginary one.[3] The radial distribution curves $D(r)$ of the solutions were drawn after the Fourier transform of the reduced intensities which had been smoothed by the method described previously.[1]

The theoretical scattering intensities due to atom pairs of all possible combinations in the system were given as follows:

$$i_{calcd}(s) = \sum_{i}\sum_{i\neq j} n_{ij}\{(f_i(s)+\Delta f_i')(f_j(s)+\Delta f_j') + (\Delta f_i'')(\Delta f_j'')\} \cdot \frac{\sin(r_{ij}s)}{(r_{ij}s)} \cdot \exp(-b_{ij}s^2), \quad (3)$$

where r_{ij}, b_{ij}, and n_{ij} denote the distance, the temperature factor, and the frequency factor of an atom pair i-j, respectively.

All calculations were performed with the aid of electronic computers M 160 and M 180 by means of KURVLR program.[4]

Raman Spectroscopic Measurements. A JEOL JRS-S1 Raman spectrometer was employed with the use of the 4880 Å excitation line of Ar^+ laser.

Results and Discussion

Since no formation constants of the complexes has been reported in the literature in such concentrated solutions examined here, distributions of the zinc(II)–ethylenediamine complexes in the solutions were not estimated in advance of the X-ray measurements. However, we can approximately evaluate the formation constants of the ethylenediamine zinc(II) complexes in the solutions used in the present work by simply extrapolating the literature values.[5] The extrapolated values, as well as the literature values obtained in relatively low ionic strengths, suggested that both bis- and tris(ethylenediamine)zinc(II) complexes may coexist in each solution. In solution A the tris-complex may be the main species, whereas the bis-complex may be

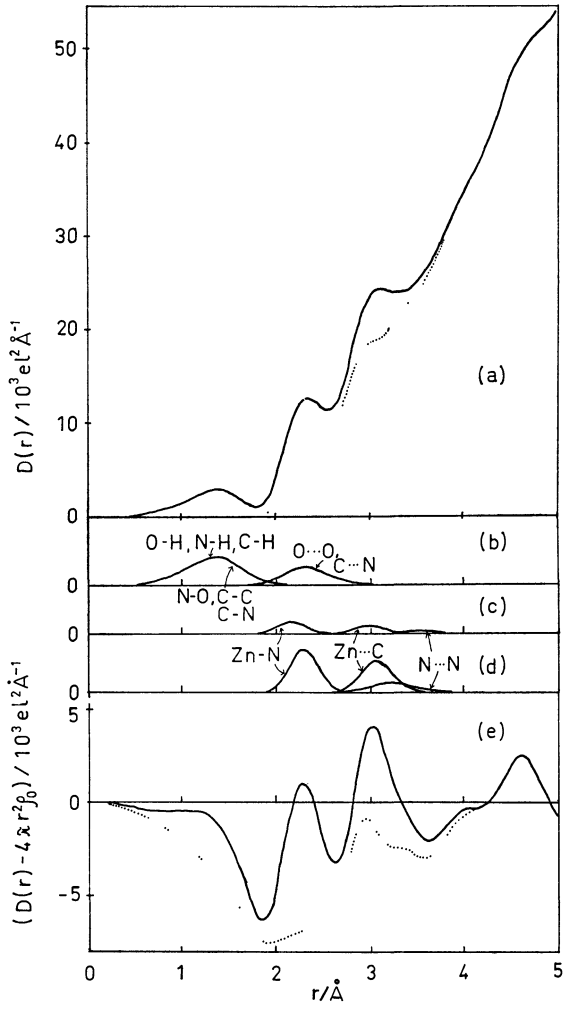

Fig. 3. (a) The radial distribution curve for solution A. (b) The theoretical peak shapes for the O–H bond within water, the N–H, C–H, C–C, C–N, and C···N pairs within ethylenediamine molecule, and the N–O and O···O contacts within nitrate ion. (c) The theoretical peak shapes for the Zn–N, Zn···C, and N···N pairs within the $Zn(en)_2^{2+}$ complex. (d) The theoretical peak shapes for the Zn–N, Zn···C, and N···N pairs within the $Zn(en)_3^{2+}$ complex. (e) The corresponding $(D(r)-4\pi r^2\rho_0)$ curve to the $D(r)$ in (a). The dotted lines in (a) and (e) show the residual radial and residual differential radial distribution curves, respectively, after subtraction of these theoretical peaks.

predominant in solution B. In the analyses of the radial distribution curves of solutions A and B, the both complexes were taken into consideration at the same time in the following manner; at a first approximation the $D(r)$ curve of solution A was analyzed by assuming that the only tris-complex was contained. The parameter values for the structure of the complex thus estimated was used for analyzing the $D(r)$ curve of solution B in order to determine the structural parameters of the bis-complex so as to obtain a smooth background of the $D(r)$ curve. The parameter values thus obtained for the bis-complex were turned back to the calculation of the $D(r)$ curve of solution A in order to evaluate better parameter values of the tris-complex. The improved values of the tris-complex were again used for analyzing the $D(r)$ curve of solution B. The successive approach of the analysis was continued until no appreciable peak was left in the background of the radial distribution curves of both solutions A and B.

The parameter values, the bond distance(r), temperature factor(b), and frequency factor(n) of the models used for calculations of intensities due to intramolecular interactions were refined by using the data at high angle regions of the $s \cdot i(s)$ curves of solutions A and B. The refinements were carried out so as to obtain an error-square sum $U=\sum s^2\{i_{\mathrm{obsd}}(s)-i_{\mathrm{calcd}}(s)\}^2$ to be a minimum. The lower s limit in the calculation was varied in order to avoid introduction of errors to the refined parameters from intermolecular interactions. The least-squares calculations were performed by using the NLPLSQ program.[1]

Solution A. The radial distribution curve of solution A showed four major peaks over the range $r=$ 1—5 Å (Fig. 3a). A small peak at about 1.3 Å is composed of peaks due to the O–H bond within water, the N–H, C–H, C–C, and C–N bonds within ethylenediamine molecules and the N–O bond within nitrate ions (Fig. 3b). The second peak appearing at around 2.2 Å may be attributed to the interactions between zinc(II) ion and the nitrogen atoms of the ethylenediamine molecules coordinated to the central metal ion (Fig. 3, c and d). The distances corresponding to the nonbonding C···N pair in ethylenediamine molecules and the O···O contact within NO_3^- ion may also partly contribute to the peak. The third peak at 2.95—3.05 Å may be mainly ascribed to the nonbonded interactions of zinc(II) ion with the carbon atoms within ethylenediamine molecules coordinated. The broad peak at around 4—5 Å may include contributions among the complexes, free ligand and solvent molecules, which we will not discuss in this paper.

We assumed that the bond lengths of the N–H, C–H, C–C, C–N and C···N pairs within the ethylenediamine molecules are practically the same as those within free ligand molecules in the gas phase.[6] The structural parameters of nitrate ion were taken from the work by Maeda, *et al.*[7] and Caminiti, *at al.*[8] The values used in this work are summarized in Table 2. The Zn–N and Zn···C distances within the bis- (Fig. 3c) and tris-complexes (Fig. 3d) were estimated from the radial distribution curve of solution A. Successive approaches for the estimation have been employed as mentioned previously. The Zn–N and Zn···C bond lengths within the tris-complex were thus estimated to be 2.28 and 3.02 Å, respectively. The temperature factor of the former was determined to be 0.003 Å^2, while that of the latter was 0.006 Å^2. The area under the peak at 2.28 Å corresponded to six Zn–N bonds (see Fig. 3d), which were expected from the composition of the tris-complex. Subtraction of the peaks due to Zn–N and Zn···C interactions from the residual radial distribution curve led to a smooth background having no appreciable peak over the range $r<4$ Å, except for the peak at about 2.9 Å which was ascribed to the adjacent O···O interactions in the bulk water and hydrated nitrate ions[8] (Fig. 3, a and e).

The parameter values thus estimated from the analysis of the radial distribution curve were refined by the least-squares method for the intensity curve

Table 2. Bond distances (r) and temperature factors (b) for water and ethylenediamine molecules and nitrate ions

		r/Å	b/Å^2
H_2O	O–H	0.955[a]	0.010[a]
en	N–H	0.870[b]	0.003[b]
	C–H	1.11[b]	0.003[b]
	C–C	1.55[b]	0.001[b]
	C–N	1.47[b]	0.001[b]
	C···N	2.47[b]	0.003[b]
NO_3^-	N–O	1.26[c]	0.0009[d]
	O···O	2.19[c]	0.002[e]

a) R. Triolo and A. H. Narten, *J. Chem. Phys.*, **63**, 3624 (1975). b) A. Yokozeki and K. Kuchitsu, *Bull. Chem. Soc. Jpn.*, **44**, 2926 (1971). c) R. Caminiti, G. Licheri, G. Piccaluga, and G. Pinna, *J. Chem. Phys.*, **68**, 1967 (1968). d) M. Maeda, Y. Maegawa, T. Yamaguchi, and H. Ohtaki, *Bull. Chem. Soc. Jpn.*, **52**, 2545 (1979). e) Estimated from the value of b_{N-O}.

Table 3. Results of the least-squares refinements of solution A

The refined parameters for the bond, distance (r), temperature factor (b) and frequency factor (n) are obtained from the reduced intensity curve. The units of r and b are Å and Å^2, respectively. Standard deviations are given in parentheses.

Interaction	Parameter	A-1	A-2
O···O(NO_3^-)	r	2.19(2)	2.19(2)
C···N(en)	r	2.41(4)	2.41(4)
Bis-complex			
Zn–N	r	2.16(3)	2.17(3)
N···N[a]	r	4.2(8)	4.1(8)
Zn···C	r	2.89(7)	2.90(7)
Tris-complex			
Zn–N	r	2.276(5)	2.276(5)
	b	0.0029(3)	0.0028(3)
	n	6.2(1)	6[b]
N···N[a]	r	3.16(6)	3.16(6)
Zn···C	r	3.00(1)	3.00(1)
	b	0.0053(6)	0.0053(6)
	n	6.1(2)	6[b]

a) The temperature factor of this interaction is estimated to be 0.01, quoted from Ref. 6. b) Fixed.

(Fig. 2). Two types of refinement (A-1 and A-2) were performed for solution A.

In type A-1, all the twelve parameters listed in Table 3 were allowed to change independently, a tetrahedral structure of the bis-complex being assumed. The frequency factors of the Zn–N bond and the nonbonding Zn···C interaction were close to six as expected in all the sets of data examined over the different s-regions from 5.0, 6.0, and 7.0 to 16.7 Å^{-1}.

In type A-2, an octahedral structure of the tris-complex as the main species was also assumed and the distances and the temperature factors of the Zn–N and nonbonding Zn···C interactions were refined. Since no appreciable difference was found in the results of the two calculations, the octahedral structure of the tris-complex having the parameter values given in Table 3 was concluded.

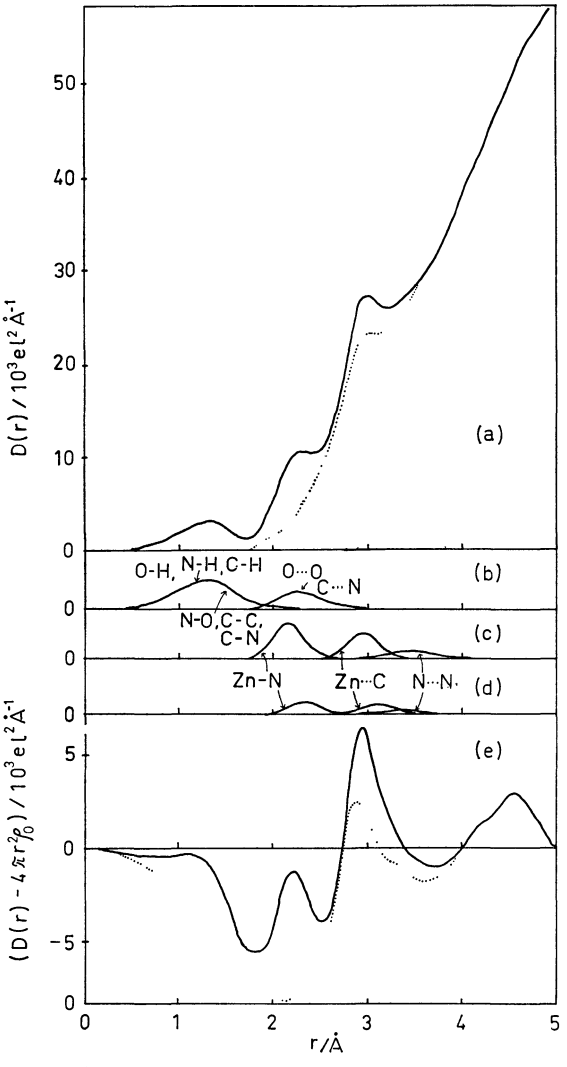

Fig. 4. (a) The radial distribution curve for solution B. (b) The theoretical peak shapes for the O–H bond within water, the N–H, C–H, C–C, C–N, and C···N pairs within ethylenediamine molecule, and the N–O and O···O contacts within nitrate ion. (c) The theoretical peak shapes for the Zn–N and Zn···C and N···N pairs within the $Zn(en)_2^{2+}$ complex. (d) The theoretical peak shapes for the Zn–N, Zn···C, and N···N pairs within the $Zn(en)_3^{2+}$ complex. (e) The corresponding $(D(r)-4\pi r^2\rho_0)$ curve to the $D(r)$ in (a). The dotted lines in (a) and (e) show the residual radial and residual differential radial distribution curves, respectively, after subtraction of these theoretical peaks.

Solution B. The essentially same procedure as that used for solution A was employed for analyzing the radial distribution curve of solution B. The contribution of the tris-complex coexisting to the curve was taken into account in the analysis. The structural parameters of the N–H, C–H, C–C, C–N, and C···N bonds within ethylenediamine molecules in the complexes were the same as those used in the previous section. The peaks due to the Zn–N and Zn···C distances within the tris-complex were eliminated from the radial distribution curve by the trial-and-error method.

The Zn–N and Zn···C distances within the biscomplex were evaluated as 2.14 and 2.93 Å, respectively, from the analysis of the radial distribution curve (Fig. 4). The area under the peak at 2.14 Å showed the four-coordinated zinc atom. A peak still remained at about 2.9 Å in the radial distribution curve (dotted lines in Fig. 4, a and e) was attributed to the structure of the bulk water and hydrated nitrate ions[8] as has been discussed in the previous section.

TABLE 4. RESULTS OF THE LEAST-SQUARES REFINEMENTS OF SOLUTION B

The refined parameters of the bond distance (r), temperature factor (b), and frequency factor (n) are obtained from the reduced intensity curve. The units of r and b are Å and Å^2, respectively. Standard deviations are given in parentheses.

Interaction	Parameter	B-1	B-2	B-3
O···O(NO_3^-)	r	2.20(2)	2.18(2)	2.18(2)
C···N(en)	r	2.31(5)	2.37(5)	2.29(6)
Bis-complex				
Zn–N	r	2.113(7)	2.134(7)	2.131(9)
	b	0.0035(4)	0.0027(4)	0.0026(5)
	n	4.10(8)	4.09(8)	4[b]
N···N[a]	r	3.9(2)	4.0(2)	3.8(2)
Zn···C	r	2.90(1)	2.90(2)	2.89(2)
	b	0.0057(6)	0.006[b]	0.006[b]
	n	4.7(2)	4[b]	4[b]

a) The temperature factor of this interaction is estimated to be 0.01, quoted from Ref. 6. b) Fixed.

The least-squares refinements were carried out for the parameter values of the bis-complex in order to obtain the best-fit curve to the experimentally obtained $s\cdot i(s)$ curve. In the case of solution B, three types of refinement (B-1, B-2, and B-3) were examined. In type B-1, all the nine parameters given in Table 4 were changed simultaneously. The frequency factor of the Zn–N bond of the bis-complex was always close to four in the various sets with lower s limits of 5.0, 6.0, and 7.0 Å^{-1}. In type B-2, the temperature and frequency factors of the nonbonding Zn···C interaction were held constant and the parameters for the Zn–N bond were refined because the frequency factor was strongly correlated to the temperature factor in the nonbonding Zn···C interaction. The possibility of the existence of $Zn(en)_2(H_2O)_2^{2+}$ as the bis-complex instead of $Zn(en)_2^{2+}$ could also be checked by this treatment; if the former

complex were formed, the frequency factor of the Zn–N in the calculation of B-2 would be six, because no distinction between Zn–O and Zn–N bonds was possible in the calculation. In type B-3, a tetrahedral structure of the bis-complex was assumed and the distances and temperature factors for the Zn–N and nonbonding Zn···C interactions were refined. The refined parameter values in the B-3 set were almost the same as those in the B-2 set.

The observed intensities are compared with the calculated ones (Eq. 3) by using the parameter values in Tables 3 (A-2) and 4 (B-3) (see Fig. 2). The agreement between the two curves is satisfactory except at the low-angle part of the curves where the intermolecular interactions significantly contribute to the $s \cdot i(s)$ curves. From the independent refinements of the parameter values for solutions A and B, the bis- and tris-complexes were confirmed to be tetrahedrally and octahedrally constructed in aqueous solution.

The Zn–N bond within the bis-complex was shorter than that within the tris-complex. The results are consistent with those reported in the literature[9] that the crystal ionic radius of a zinc(II) ion having the coordination number of 4 is smaller than that of a zinc(II) ion of the six-coordination.

Raman Spectra of Solutions A and B. Raman spectra of the tris(ethylenediamine)zinc(II) complex in aqueous solution have been studied by Krishnan and Plane.[10] They reported that the line at 423 cm^{-1} was due to the totally symmetric Zn–N stretching vibration of the tris-complex. In solution A of the present work (Fig. 5) we also found the line at 427 cm^{-1}. Since the line is strongly polarized, it is distinguishable from the skeletal deformation vibration band of free ethylenediamine of the *trans*-conformation which would appear at 475 cm^{-1} in solution.[11] Another strong line was observed at 883 cm^{-1}, for which Krishnan and Plane gave no assignment (in their work the line appeared at 878 cm^{-1}). The line may be ascribed to the rocking vibration of the $-CH_2-$ groups[11] within the ethylenediamine molecules. The band at 722 cm^{-1} was assignable to the ν_4-band of the nitrate ion. In the low frequency region of 170—300 cm^{-1}, some Raman lines were observed. However, no reasonable assignments to the lines were given.

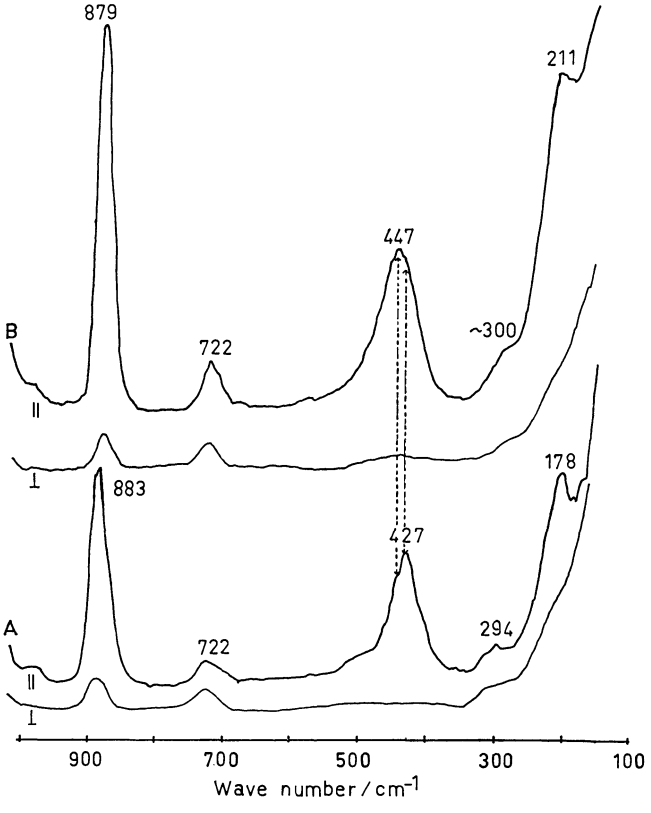

Fig. 5. Raman spectra of solutions A and B. The lines are the components parallel (∥) and perpendicular (⊥), respectively, to the direction of polarization of the incident light.

Krishnan and Plane have also measured the Raman spectrum of the bis-complex.[10] However, since their measurements were carried out in a very diluted solution (*ca.* 0.1 mol dm^{-3} for zinc(II) ion) and the test solution contained both bis- and tris-complexes to some extent, assignments of the bands observed for the bis-complex may be less reliable. Solution B in the present work contained the bis-complex with a relatively high concentration, which might be suitable for measuring the Raman spectrum of the bis-complex. The spectrum of solution B showed three major lines at 447, 722, and 879 cm^{-1} (Fig. 5B). The 722 and 879 cm^{-1} bands were readily assigned to the nitrate-ν_4 and CH_2-rocking vibrations, respectively, as have been described previously. The polarized line at 447 cm^{-1}, which was ascribed to the Zn–N sterching in the bis-complex, was in good agreement with the line found at about 450 cm^{-1} by Krishnan and Plane.[10] The frequency of the line was apparently higher than those of the corresponding lines of the tris-complex (427 or 423 cm^{-1} [10]) and the $Zn(NH_3)_4^{2+}$ complex (429[2] or 427 cm^{-1} [12]). These results indicated that the bis-complex has a stronger metal–nitrogen interaction than the other two complexes. This conclusion is supported by the fact that the bis-complex has a shorter Zn–N bond than the tris-complex. The Zn–N distance within the bis-complex is, however, longer than the Zn–NH_3 distance within the tetraammine-zinc(II) complex. The stronger interaction between zinc(II) ion and amino groups within the ethylenediamine molecules may be due to a greater basicity of the NH_2-groups in the ethylenediamine molecules by donating electrons from the CH_2 groups to the amino groups.

References

1) H. Ohtaki and M. Maeda, *Bull. Chem. Soc. Jpn.*, **47**, 2197 (1974); H. Ohtaki M. Maeda and S. Ito, *Bull. Chem. Soc. Jpn.*, **47**, 2217 (1974); H. Ohtaki, T. Yamaguchi and M. Maeda, *Bull. Chem. Soc. Jpn.*, **49**, 701 (1976).

2) T. Yamaguchi and H. Ohtaki, *Bull. Chem. Soc. Jpn.*, **51**, 3227 (1978).

3) D. T. Cromer and J. T. Waber, *Acta Crystallogr.*, **18**, 104 (1965); D. T. Cromer, *J. Chem. Phys.*, **50**, 4857 (1969); D. T. Cromer and D. Liberman, *J. Chem. Phys.*, **53**, 1891 (1970).

4) G. Johansson and M. Sandström, Chem. Scripta, **4**, 195 (1973).

5) L. G. Sillén and A. E. Martell, "Stability Constants," Spec. Publ. No. 17 and Supplement No. 1, Spec. Publ. No. 25, The Chemical Society, London (1964) and (1971).
6) A. Yokozeki and K. Kuchitsu, *Bull. Chem. Soc. Jpn.*, **44**, 2926 (1971).
7) M. Maeda, Y. Maegawa, T. Yamaguchi, and H. Ohtaki, *Bull. Chem. Soc. Jpn.*, **52**, 2545 (1979).
8) R. Caminiti, G. Licheri, G. Piccaluga, and G. Pinna, *J. Chem. Phys.*, **68**, 1967 (1978).
9) R. D. Shannon, *Acta Crystallogr., Sect. A*, **1976**, 751.
10) K. Krishnan and R. A. Plane, *Inorg. Chem.*, **5**, 852 (1966).
11) Y. Omura and T. Shimanouchi, *J. Mol. Spectrosc.*, **55**, 430 (1975), **57**, 480 (1975).
12) R. A. Plane, Proceeding of the 8th International Conference on Coordination Chemistry, Vienna, p. 17 (1964).

Kinetics of Ligand Exchange between Tris(acetylacetonato[2-^{14}C])cobalt(III) and Acetylacetone in Acetonitrile. Evidence for S_N1 Mechanism

Hiroaki KIDO* and Kazuo SAITO

Chemistry Department, Faculty of Science, Tohoku University, Aramaki, Aoba, Sendai 980

(Received May 1, 1979)

Tris(acetylacetonato[2-^{14}C])cobalt(III) undergoes ligand isotopic exchange with acetylacetone(Hacac) in acetonitrile at 85—100 °C without decomposition and solvolysis. The exchange rate is proportional to the complex concentration (0.002—0.007 M, 1 M=1 mol dm^{-3}), the first-order rate constant k_o being independent of [Hacac] (0.001—0.97 M). $k_o=1.6\times10^{-5}$ s^{-1} at 93.2 °C. The activation enthalpy and entropy are 38 ± 4 kcal mol^{-1} (1 cal=4.18 J) and 23 ± 8 cal K^{-1} mol^{-1}, respectively. Trichloroacetic acid (<0.02 M) gives acid catalysis. The rate-determining step should be the S_N1 Co–O cleavage in a chelate ring to give a five coordinate intermediate.

The complexes of Co(III) along with those of Cr(III) and Ni(II) have played an essential role for enabling us to understand the mechanism of octahedral substitution.[1,2] A number of kinetic studies were carried out on Co(III)N_5O type complexes represented by $[Co(NH_3)_5(H_2O)]^{3+}$.[3] However, little information is available concerning kinetics and mechanisms of ligand substitution processes of spin-paired Co(III) complexes containing Co(III)O_6 core. Kinetics of aquation of $[Co(ox)_3]^{3-}$ [4] and $[Co(mal)_3]^{3-}$ [5] (ox=oxalate, mal=malonate) are complicated for discussing the substitution mechanism around the metal ion. Water exchange[6] and the anation of chloride[7] for $[Co(H_2O)_6]^{3+}$ were kinetically studied only in the presence of $[Co(H_2O)_6]^{2+}$.

In a previous paper, we discussed the mechanism of the ligand exchange between Cr(acac[2-^{14}C])$_3$ and acetylacetone (Hacac) in acetonitrile.[8] The rates of the ligand exchange of the present complex in toluene, anisole, and chlorobenzene under conditions involving partial decomposition of the complex were observed.[9] We have found that the decomposition of Co(acac)$_3$ in acetonitrile subsides on elimination of dissolved oxygen, and have reinvestigated the ligand exchange kinetics to disclose the substitution mechanism at the low-spin Co(III)O_6 core.

Experimental

Materials. Acetylacetone[2-^{14}C] was prepared and purified as reported.[10] Acetylacetone was dehydrated with calcium sulfate and distilled. Co(acac[2-^{14}C])$_3$ and Co(acac)$_3$ were synthesized from the labelled and the commercial ligand, respectively, by the usual method,[11] and sublimed *in vacuo* at *ca.* 130 °C. Deuterium oxide (spectroscopic grade, E. Merck, 99.75%) was used without further purification. Trichloroacetic acid was sublimed *in vacuo*. Acetonitrile was distilled twice in the presence of phosphorus pentaoxide.

Kinetic Procedure. Two ml portions of acetonitrile solution containing Co(acac[2-^{14}C])$_3$ (0.0017 to 0.0070 M, 1 M=1 mol dm^{-3}), Hacac (0.001 to 0.97 M), and water (0.02 to 0.12 M), were degassed and sealed in 3—5 Pyrex glass tubes (diam. 10 mm, length 80 mm) *in vacuo* (10^{-3} mmHg). The tubes were simultaneously heated in a silicone oil bath at 85—101 °C, withdrawn one by one at appropriate time intervals and put into a cold water bath. Hacac, water and acetonitrile were collected individually from the 1 ml portions by distilling into small tubes in a liquid nitrogen bath *in vacuo* at room temperature to leave Co(acac)$_3$ in the original tubes. (Trichloroacetic acid, whenever present in the reaction mixture also remained in the original tubes.) Both Hacac and Co(acac)$_3$, quantitatively recovered and found to be spectroscopically pure, were separately dissolved in anisole containing 0.1% *p*-terphenyl and 0.04% *p*-bis(5-phenyl-2-oxazolyl)benzene(POPOP), the counting rate being measured with a Nuclear Chicago Unilux IIA Liquid Scintillation Counter. The specific counting rate was calculated from the counting rate and the original weight of the compounds. The water content of the reaction mixture was determined by the Karl Fischer titration before and after the kinetic run; it remained unchanged within experimental error.

Calculation of the Exchange Rate. The rates were calculated by the McKay equation

$$\text{Rate} = \frac{-3[\text{Co}][\text{Hacac}]}{3[\text{Co}]+[\text{Hacac}]}\,\frac{\ln(1-F)}{t},$$

where [Co] and [Hacac] stand for the concentrations of the complex and the free ligand, respectively, t is the lapse of time in seconds, and F the fraction of reaction which is expressed by $(x_0-x_t)/(x_0-x_\infty)$, x being the specific counting rate of the complex or the free ligand at the time indicated by subscript.

Hacac is in tautomeric equilibrium between enol and keto form, but the intercoversion rate is *ca.* 10—100 times as great as the exchange rate in the given temperature range. The total concentration of Hacac, therefore, was taken to be [Hacac].

Results

The absorption spectra of the reaction mixtures remained unchanged throughout the reaction. The McKay plots gave straight lines up to at least 75% completion of the exchange. The F values individually calculated from the measured specific counting rates of Hacac and Co(acac)$_3$ coincide with each other within experimental error. Thus no reactions other than the isotopic exchange

$$\text{Co}(\overset{*}{\text{acac}})_3 + \text{Hacac} \rightleftharpoons \text{Co}(\text{acac})_3 + \overset{*}{\text{Hacac}} \qquad (1)$$

took place during the course of heating. No significant zero time exchange was observed. The rate is proportional to the complex concentration (0.0017—0.0070 M) as shown in Table 1, and expressed by

$$\text{Rate} = k_o[\text{Co}], \qquad (2)$$

where k_o is the observed first-order rate constant. The k_o value is independent of the water (0.017—0.119 M, Table 1) and the free ligand concentrations (0.001—1 M, Fig. 1). Thus we have

TABLE 1. RATES AND OBSERVED FIRST-ORDER RATE CONSTANTS FOR THE ISOTOPIC EXCHANGE BETWEEN $Co(acac)_3$ AND Hacac IN ACETONITRILE AT 101.1 °C ([Hacac]$=9.75\times10^{-3}$ M)

[Co] / 10^{-3} M	[H_2O] / 10^{-3} M	R / 10^{-8} M s^{-1}	k_o / 10^{-5} s^{-1}
1.74	69	8.9±0.4	5.1±0.2
3.48	66	18 ±1	5.1±0.2
6.59	72	38 ±2	5.4±0.3
3.48	17	17 ±1	4.9±0.3
3.48	119	18 ±1	5.3±0.3

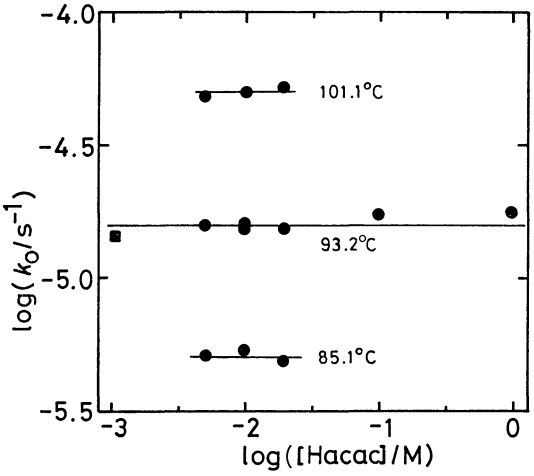

Fig. 1. Log-log plots of the observed rate constant k_o *vs.* the concentration of the free ligand, [Hacac], for the ligand exchange of $Co(acac[2\text{-}^{14}C])_3$ in acetonitrile. ([Co]$=3.5\times10^{-3}$ M (circles), 9.9×10^{-3} M (square). [H_2O]$=7\times10^{-2}$ M.)

$$k_o = k_i[\text{Hacac}]^0[H_2O]^0. \quad (3)$$

When D_2O was added to the reaction mixtures in place of H_2O, no change occured in k_o.

In the presence of trichloroacetic acid, the exchange proceeded apparently by 20—30% at zero time, which would be separation induced exchange. The k_o value depends on the acid concentration at given concentrations of the complex (0.0035 M), the free ligand (0.0097 M) and water (0.07 M) (Fig. 2). The solid lines have intercepts, which coincide with k_i values obtained in the absence of the acid. Thus we have

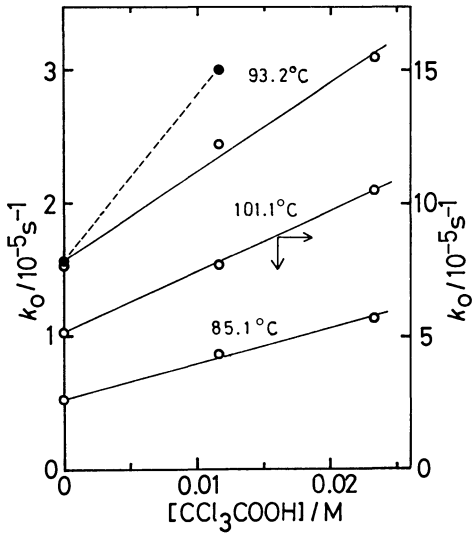

Fig. 2. Influence of trichloroacetic acid and deuterium oxide on the exchange rate. ([Co]$=3.5\times10^{-3}$ M, [Hacac]$=9.7\times10^{-3}$ M and [H_2O]$=7\times10^{-2}$ M for open circles. $D_2O(5\times10^{-2}$ M)+$H_2O(2\times10^{-2}$ M) as the original ingredients for full circles.)

$$k_o = k_i + k_a[CCl_3COOH]. \quad (4)$$

When D_2O was added to the reaction mixture in place of H_2O, k_o increased significantly in the presence of the acid (Fig. 2). Ratio of the rate constants (k(H)/k(D)) was calculated on the assumption that equilibrium was attained for all the dissociable protons and deuterons in the reaction system.

The rate constants are summarized in Table 2 together with the activation parameters and k(H)/k(D) values.

Discussion

Equation 4 indicates that the exchange (Eq. 1) proceeds by the two paths, k_i and k_a.

Rate-determining Steps of the k_i Path. Equations 2 and 3 indicate the participation of only the complex in the rate-determining step of the k_i path.

The k_i value is similar to that of the first-order rate constant k_{rac} of the racemization of $Co(acac)_3$ in chlorobenzene in a similar temperature region.[12] Their activation enthalpies and entropies are also very

TABLE 2. KINETIC DATA FOR LIGAND EXCHANGE, RACEMIZATION AND ISOMERIZATION OF TRIS (β-DIKETONATO)COBALT(III) IN ORGANIC SOLVENTS

Reactions	Parameters	Rate constants 85.1 °C	93.2 °C	101.1 °C	k(H)/k(D)	$\Delta H^{\ddagger}$ / kcal mol^{-1}	$\Delta S^{\ddagger}$ / cal K^{-1} mol^{-1}
			$Co(acac)_3$				
Exchange[a,e]	k_i/10^{-5} s^{-1}	0.51±0.02	1.56±0.02	5.14±0.21	1.0	38 ±4	23 ±8
	k_a/10^{-4} M^{-1} s^{-1}	2.9 ±0.2	7.2 ±0.5	22.9±0.4	0.4	34 ±3	18 ±7
Racemizn.[b,f]	k_{rac}/10^{-5} s^{-1}	1.4[c]	4.0[c]	13[c]	...	34.1±0.6	14 ±2
			fac-$Co(bzac)_3$[d]				
Isomerizn.[g]	k_{iso}/10^{-4} s^{-1}	1.83±0.12[b]	(96.1 °C)		...	32.0±0.5	11.0±1.3
		1.89±0.09[a]	(95.8 °C)		...	...	...

a) In acetonitrile. b) In chlorobenzene. c) Interpolated value. d) bzac$^-$=benzoylacetonate. e) This work. f) Ref. 12. g) Ref. 13.

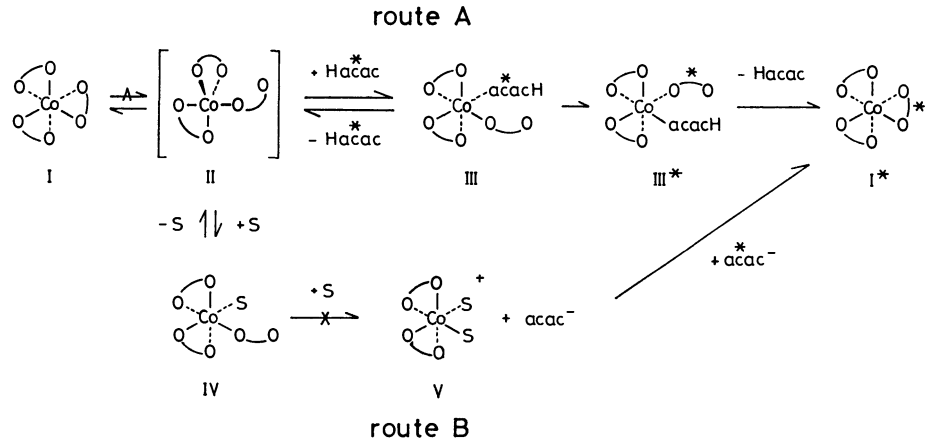

Fig. 3. Proposed mechanism for the ligand exchange of Co(acac[2-^{14}C])$_3$ in acetonitrile. (The structure of II is provisional. Asterisks denote ^{14}C labelling. Arcs and S represent acetylacetonate and acetonitrile or H_2O, respectively.)

similar (Table 2). This suggests a common rate-determining step for the reactions, despite the difference in solvent. The mechanism of the racemization has not been verified, but it is anticipated to be very similar to that of the racemization and the isomerization of *fac*- and *mer*-tris(benzoylacetonato)cobalt(III) (Co(bzac)$_3$) in chlorobenzene,[13] on the basis of similar values of ΔH^* and ΔS^*. Girgis and Fay verified that these reactions of Co(bzac)$_3$ proceed by an intramolecular mechanism and found that the rates are independent of solvents including chlorobenzene and acetonitrile. The racemization of Co(acac)$_3$ in these solvents might proceed similarly. The present k_i value was also insensitive to the variation of solvent, *e.g.* no change by use of acetylacetone as solvent.[14] Thus, there should be a common rate-determining step for these inter- and intra-molecular reactions. It should be the first cleavage of Co–O bond. The bond break would take place by the S_N1 mechanism, since the solvent-assisted S_N2-like path does not seem feasible in these reactions. Consequently, five-coordinate intermediate containing a unidentate acetylacetonate would be formed (I→II in Fig. 3).[15] The intermediate might have an achiral structure, *e.g.*, a trigonal bipyramid shown in Fig. 3.

Mechanism for k_i Path. After the rate-determining step, the k_i path can proceed *via* two possible routes A and B (Fig. 3). In route A, II interacts with free Hacac to form III containing both unidentates, acac$^-$ and Hacac, as ligands. III is converted into III* by a proton transfer process, and III* turns to I*. In route B, II loses one acac$^-$ to give V. The solvent molecule or water may occupy the vacant site. V can pick up acac$^-$. However, route B is unlikely. If the dissociation of the unidentate acac$^-$ proceeded fast, direct exchange of acac$^-$ between the complex molecules could take place at a measurable rate even in the absence of free Hacac. Such an interchange for Co(bzac)$_3$ was much slower than the isomerization.[13] The intermediate IV, even if it is formed, might be in equilibrium only with II as a dead end species. Therefore, the k_i path must proceed *via* route A. The exchange of the k_i path is understood to consist of the substitution processes (I→III and III*→I*) connected with a proton transfer process (III→III*). The substitution processes should be identical with each other, since reaction routes of exchange reactions are symmetrical.

The substitution process can be reckoned to proceed by the S_N1 mechanism. The mechanism is also in line with the observed activation parameters, a large positive value of ΔS^* and a rather large value of ΔH^*. It is thus demonstrated for the first time that a low-spin complex with Co(III)O$_6$ core undergoes ligand substitution by the S_N1 mechanism, as almost all other complexes with different ligating atoms.[1]

Structure of the Intermediate. The intermediate II seems stable towards the Co–O bond cleavage of the unidentate ligands. Even in the absence of free Hacac, II undergoes racemization but not dissociation. Such a stability may be attributed to the conjugated structure of the ligand. The Co–O bond may be stabilized by concentration of negative charge on the coordinated oxygen, which is partly neutralized with positive charge on the central metal ion. Hence, the structure Co–O–C(CH$_3$)=CH–C(CH$_3$)=O, is presumed for the unidentate in II, III, III*, and IV. This structure is found in *trans*-[Pt^{II}(C$_5$H$_7$O$_2$)$_2$(PEt$_3$)$_2$] in solution (CDCl$_3$) and crystals.[17]

The structure of the intermediates III and III* could not be determined exactly. The enol form of the incoming Hacac is more feasible than the keto form. Enol was found to be much more reactive over keto in the ligand exchange of Ti^{IV}(acac)$_3^+$ in acetonitrile.[18] The keto oxygen of enol Hacac could coordinate to Co(III). Coordination of enolic acetylacetone as a unidentate is found in crystals of Mn^{II}Br$_2$(Hacac)$_2$.[19,20]

The two unidentates in III (and III*) should be cis to each other, at least when the proton is exchanged. The presence of a trans isomer cannot be excluded, but it does not seem to play an important role in the ligand exchange reaction. It may be a dead end species, even if it is formed.

k_a Path. The exchange reaction (Eq. 1) is catalyzed by trichloroacetic acid (Eq. 4). A remarkable

deuterium isotope effect ($k(H)/k(D)=0.4$) was found for the acid catalyzed k_a path (Table 2). A $k(H)/k(D)$ value less than unity indicates the participation of a proton in a pre-equilibrium step.[21] A plausible mechanism is proposed in the following.

$$\underset{\text{I}}{\text{Co(acac)}_3} + \text{H}^+ \overset{\text{fast}}{\rightleftharpoons} \underset{\text{I}'}{\text{(acac)}_2\text{Co}\begin{array}{l}\diagup\text{OH}^+\\ \\ \diagdown\text{O}\end{array}} \qquad (5)$$

$$\underset{\text{I}'}{\text{(acac)}_2\text{Co}\begin{array}{l}\diagup\text{OH}^+\\ \\ \diagdown\text{O}\end{array}} \overset{\text{r.d.s.}}{\longrightarrow} \underset{\text{II}'}{\text{(acac)}_2\text{Co–O—OH}^+} \qquad (6)$$

where O–O$^-$ denotes acac$^-$, and II′ is a five-coordinated intermediate. The fate of II′ is considered to be similar to that of II in the k_i path (Fig. 3). The observed ΔH^* value for k_a slightly lower than that for k_i may be due to an easier cleavage of a Co–O bond with the aid of H$^+$.

Comparison with Cr(acac)$_3$. The ligand exchange of Cr(acac)$_3$ in acetonitrile in high [Hacac] (>0.1 M) region was considered to proceed *via* III type intermediate (Fig. 3) by the S_N2 attack of the free ligand, in view of the first-order dependency of k_o on [Hacac] and the values of the activation parameters.[8] However, the present k_i value did not change with the increase of [Hacac] up to 1 M (Fig. 1). This indicates that an S_N1 operates in the k_i path even in the high [Hacac] region. The difference in mechanism is in line with that in the general understanding of substitution mechanisms of these two kinds of metal complexes containing N_5O core (Cr(III): S_N2; Co(III): S_N1).[1]

The work was carried out with a Grant-in-Aid from the Ministry of Education.

References

1) T. W. Swaddle, *Coord. Chem. Rev.*, **14**, 217 (1974).
2) J. O. Edwards, F. Monacelli, and G. Ortaggi, *Inorg. Chim. Acta*, **11**, 47 (1974).
3) D. A. House, *Coord. Chem. Rev.*, **23**, 223 (1977).
4) J. A. Broomhead, I. Lauder, and P. Nimmo, *J. Chem. Soc., Dalton Trans.*, **1971**, 645.
5) Y. Sulfab and M. S. Al-Obadie, *J. Inorg. Nucl. Chem.*, **36**, 2067 (1974).
6) H. L. Friedman, H. Taube, and J. P. Hunt, *J. Chem. Phys.*, **18**, 759 (1950).
7) A. McAuley, M. N. Malik, and J. Hill, *J. Chem. Soc., A*, **1970**, 2461.
8) H. Kido and K. Saito, *Inorg. Chem.*, **16**, 397 (1977).
9) K. Saito and M. Murakami, *Bull. Chem. Soc. Jpn.*, **45**, 2472 (1972).
10) K. Saito and K. Masuda, *Bull. Chem. Soc. Jpn.*, **41**, 384 (1968).
11) B. E. Bryan and W. C. Fernelius, *Inorg. Synth.*, **5**, 188 (1957).
12) R. C. Fay, A. Y. Girgis, and U. Klabunde, *J. Am. Chem. Soc.*, **92**, 7056 (1970).
13) A. M. Girgis and R. C. Fay, *J. Am. Chem. Soc.*, **92**, 7061 (1970).
14) H. Kido, *Bull. Chem. Soc. Jpn.*, in press.
15) The conclusion supports the one-ended bond-rupture mechanism for the isomerization and the racemization of tris-(β-diketonato)cobalt(III) (*cf.* Refs. 12, 13, and 16).
16) J. G. Gordon, II, and R. H. Holm, *J. Am. Chem. Soc.*, **92**, 5319 (1970).
17) T. Ito, T. Kiriyama, and A. Yamamoto, *Chem. Lett.*, **1976**, 835.
18) M. Nishizawa, H. Kido, I. Kinoshita, Y. Soma, and K. Saito, *Bull. Chem. Soc. Jpn.*, **49**, 819 (1976).
19) S. Koda, S. Ooi, H. Kuroya, Y. Nakamura, and S. Kawaguchi, *J. Chem. Soc., Chem. Commun.*, **1971**, 280.
20) Y. Nakamura, K. Isobe, H. Morita, S. Yamazaki, and S. Kawaguchi, *Inorg. Chem.*, **11**, 1573 (1972).
21) A. A. Frost and R. G. Pearson, "Kinetics and Mechanism," 2nd ed, J. Wiley and Sons, New York (1961), p. 294.

Reaction Processes of Vanadium Dichloride Oxide and Vanadium Trichloride with Oxygen

Akimasa YAJIMA, Ryoko MATSUZAKI, and Yuzo SAEKI*

Research Laboratory of Resources Utilization, Tokyo Institute of Technology, 4259, Nagatsuta-cho, Midori-ku, Yokohama 227

(Received May 11, 1979)

The products formed by the heating of VCl_2O in an oxygen stream at various temperatures were examined by chemical and X-ray analysis. The reaction products between VCl_3 and oxygen were examined in the same manner. The reaction process between VCl_2O and oxygen may be represented as follows: VCl_2O reacts with oxygen above *ca.* 170 °C to form V_2O_5 and VCl_3O, $12VCl_2O(s)+3O_2(g)\rightarrow 2V_2O_5(s)+8VCl_3O(g)$, and this reaction is accompanied by the reaction, $4VCl_2O(s)+3O_2(g)\rightarrow 2V_2O_5(s)+4Cl_2(g)$. The reaction process between VCl_3 and oxygen may be represented as follows: VCl_3 reacts with oxygen above *ca.* 100 °C to form VCl_3O, $2VCl_3(s)+O_2(g)\rightarrow 2VCl_3O(g)$, and this reaction is accompanied by the reaction, $2VCl_3(s)+O_2(g)\rightarrow 2VCl_2O(s)+Cl_2(g)$.

Vanadium trichloride oxide (VCl_3O) which is dissolved in crude titanium tetrachloride ($TiCl_4$) prepared by the chlorination of titanium ores is commercially removed as a non-volatile vanadium-containing precipitate by bubbling hydrogen sulfide through the crude $TiCl_4$. The present authors[1] have previously reported that the vanadium-containing precipitate formed by the reaction between VCl_3O and hydrogen sulfide is a mixture of vanadium dichloride oxide (VCl_2O) and a small amount of vanadium trichloride (VCl_3). From the view point of waste reclamation, it is necessary to understand the chemical process for the preparation of divanadium pentaoxide (V_2O_5) and chlorine by the oxidation of the mixture of VCl_2O and VCl_3 with oxygen (air).

There has been no report on the reaction process between VCl_2O and oxygen. Regarding the reaction between VCl_3 and oxygen, Ruff and Lickfett[2] have reported that VCl_3O is formed by heating VCl_3 at *ca.* 500—600 °C in an oxygen stream. Lamprey and Forsyth[3] have briefly described that the reaction, $VCl_3+1/2O_2\rightarrow VCl_3O$, mainly occurs above 250 °C on heating VCl_3 in air. Pechkovskii and Vorob'ev[4] have reported that the reaction between VCl_3 and oxygen to form VCl_3O mainly occurs above 200 °C on heating VCl_3 in an oxygen stream, and that onyl a small part of the VCl_3 is oxidized to V_2O_5.

In this paper, the reaction processes of VCl_2O and VCl_3 with oxygen will be revealed.

Experimental

The VCl_2O used was prepared from VCl_3, divanadium trioxide (V_2O_3), and VCl_3O by the method based on the literature.[5] Chemical analysis of the VCl_2O obtained gave V, 37.0; Cl, 51.4% (Calcd for VCl_2O: V, 36.96; Cl, 51.44 %); it was confirmed to be VCl_2O[6] by X-ray analysis. VCl_3 was obtained by the thermal decomposition of VCl_4, which was prepared by the reaction between vanadium (V, 99.8% up) and chlorine at 500 °C,[7] at 180 °C in an argon atmosphere.[8] The chemical analysis gave V, 32.4; Cl, 67.6% (Calcd for VCl_3: V, 32.38; Cl, 67.62%); it was confirmed to be VCl_3[9] by X-ray analysis. The oxygen was dried by passing it through conc. sulfuric acid and over diphosphorous pentaoxide.

The sensitivity of the quartz helix used for thermogravimetry (TG) was approximately 67 mm/g. The sample (0.15 g) was heated at a rate of 2.5 °C/min and the flow-rate of argon or oxygen was maintained at 50 cm^3/min.

X-Ray analysis of the solid sample was performed using Ni-filtered Cu radiation. The sample chamber of the diffractometer was maintained under dry nitrogen atmosphere to prevent the contamination of the sample with moisture in air during the irradiation.

The products obtained by heating VCl_2O and VCl_3 in an oxygen stream at various temperatures were examined by the following procedures: The sample (1.0 g) in a quartz boat (60 mm length, 13 mm width, 7 mm depth) was placed in a straight reaction tube (16 mm i. d.) with a water-cooled condenser. Oxygen was introduced into the reaction tube at a flow-rate of 50 cm^3/min. The sample part was then placed in the centre of an electric furnace (300 mm in heating length) maintained at a specified temperature for a specified period. The temperature of the sample part was controlled to within ±2 °C.

The liquid product (VCl_3O) was collected in a trap cooled in solid carbon dioxide through the condenser. The chlorine formed was absorbed in KI solution through the trap and determined by iodometry. The total amount of chlorine formed during the reaction was determined by adding the above value and the amount of chlorine dissolved in the liquid product in the solid carbon dioxide trap.[10] The determination of the amount of chlorine dissolved in the liquid product will be described later.

Chemical analysis of the solid and liquid products was performed as follows: The vanadium content in the sample was determined by chelatometric titration,[11] while the chlorine content was gravimetrically determined as AgCl, after dissolving the sample in dilute nitric acid.

The amount of chlorine dissolved in the liquid product in the solid carbon dioxide trap was determined as follows: After the reaction was over, the liquid product was allowed to warm to room temperature in an argon atmosphere in order to liberate the chlorine from the liquid product. The liberated chlorine was absorbed in NaOH solution. A small amount of the liquid product which vaporized during the above procedure was also absorbed in the NaOH solution. The total amount of chlorine in the NaOH solution was gravimetrically determined as AgCl and the vanadium content in the NaOH solution was also determined by chelatometric titration. From the vanadium content, the amount of the liquid product absorbed in the NaOH solution was calculated. The amount of chlorine dissolved in the liquid product was calculated by subtracting the amount of chlorine corresponding to the liquid product absorbed in the NaOH solution from the total amount of chlorine in the NaOH solution.

The total amount of liquid product formed was corrected by adding the amount of liquid product absorbed in the NaOH solution to the amount of liquid product in the trap.

Throughout this work, the chlorides and chloride oxides of vanadium were handled in an argon atmosphere or *in vacuo* to prevent any contamination with moisture in air.

Results and Discussion

Reaction Process between Vanadium Dichloride Oxide and Oxygen. It has been reported that on heating VCl_2O in an inert atmosphere, the disproportionation occurs above 300 °C[12] or 330 °C,[4] according to the reaction, $2VCl_2O(s) \rightarrow VClO(s) + VCl_3O(g)$.

Prior to the examination of the reaction between VCl_2O and oxygen, the behavior of VCl_2O on heating in an argon stream was examined. The TG curve showed that VCl_2O lost weight continuously above *ca.* 295 °C and the weight reached a constant value at *ca.* 380 °C. The sample heated up to 380 °C was shown to be VClO[13] by X-ray analysis. The weight loss at 380 °C was 62.9%. This value was in good agreement with the calculated value, 62.86%, based on the disproportionation of VCl_2O. The gaseous product was confirmed to be VCl_3O by chemical analysis of the product obtained by heating VCl_2O (1.0 g) in an argon stream at 370 °C for 3 h. From these results, it is confirmed that VCl_2O disproportionates above *ca.* 295 °C according to the reaction, $2VCl_2O(s) \rightarrow VClO(s) + VCl_3O(g)$.

The TG curve of VCl_2O in an oxygen stream showed that VCl_2O reacted appreciably with oxygen above *ca.* 180 °C before disproportionating. To obtain more detailed information on the reaction between VCl_2O and oxygen, the products formed by heating VCl_2O at various temperatures for 0.5—3 h in an oxygen stream were examined by X-ray and chemical analysis.

At 160 °C, no reaction product was observed. The reaction products obtained at various temperatures above 170 °C and their weight percentages to the initial VCl_2O were determined by chemical and X-ray analysis.[6,14,15] The results are summarized in Table 1.

The most stable oxide phase of vanadium under the conditions of this work is V_2O_5.[16] Trivanadium heptaoxide (V_3O_7) was not formed below 240 °C as shown in Table 1, but a small amount of V_3O_7 was formed in addition to V_2O_5 above 260 °C. As shown in Table 1, the reaction between VCl_2O and oxygen proceeded markedly above 260 °C to form a large amount of gaseous VCl_3O. Consequently, the reaction between VCl_2O and oxygen has been thought to proceed under a low oxygen concentration to form V_3O_7 in addition to V_2O_5. The solid products obtained by heating VCl_2O (1.0 g) at 290 °C under various flow-rates of oxygen for 1 h were examined. The results are shown in Table 2.

Table 2. Solid products between VCl_2O and oxygen at various flow-rates of oxygen

O_2 flow-rate/ $cm^3\ min^{-1}$	Solid product/%		Unreacted VCl_2O/%
	V_2O_5	V_3O_7	
50	66	3	31
100	71	1	28
200	73	—	27

From the results, it was observed that V_3O_7 was not formed under a high flow-rate of oxygen. This confirms the above consideration on the formation of V_3O_7.

The experimental results for the reaction products between VCl_2O and oxygen at various temperatures, shown in Table 1, indicated that V_2O_5 and VCl_3O were the main products. This fact was considered to indicate that the main reaction on heating VCl_2O in an oxygen stream was the reaction,

$$12VCl_2O(s) + 3O_2(g) \longrightarrow 2V_2O_5(s) + 8VCl_3O(g). \quad (1)$$

Table 1. Reaction products between VCl_2O and oxygen at various temperatures

Temp/°C	Reaction time/h	Product/%				Unreacted VCl_2O/%
		In the boat		Outside the heating zone		
		V_2O_5	V_3O_7	VCl_3O	Cl_2	
170	3	<1	—	0.4	<0.1	>99
200	3	1	—	2.8	<0.1	96
220	3	7	—	21.6	0.9	72
240	0.5	4	—	12.6	0.5	83
	1	7	—	23.6	0.8	69
	3	15	—	48.9	1.7	38
260	0.5	8	<1	26.3	0.9	66
	1	14	<1	46.0	1.6	41
	3	22	1	75.7	2.6	3
280	0.5	10	<1	33.7	1.1	57
	1	19	<1	63.4	2.3	19
	3	23	<1	77.6	2.7	<1
290	0.5	15	<1	50.5	1.8	35
	1	21	1	70.8	2.5	10
	2	23	1	78.4	2.8	0

Table 3. Reaction products between VCl_3 and oxygen at various temperatures

Temp/°C	Reaction time/h	Product/% In the boat	Product/% Outside the heating zone		Unreacted VCl_3/%
		VCl_2O	VCl_3O	Cl_2	
100	6	<1	6.8	<0.1	93
110	6	<1	14.3	0.2	86
130	3	<1	19.4	0.2	81
	6	1	37.5	0.3	64
150	1	<1	17.2	0.1	83
	3	1	43.8	0.3	58
	6	2	75.7	0.5	29
160	1	<1	31.0	0.2	70
	3	2	87.4	0.6	17
	6	3	105.2	0.8	0

The possible reactions giving the chlorine (in Table 1) were considered to be the reaction,

$$4VCl_2O(s) + 3O_2(g) \longrightarrow 2V_2O_5(s) + 4Cl_2(g), \quad (2)$$

and the reaction between gaseous VCl_3O formed by Reaction 1 and oxygen,

$$4VCl_3O(g) + 3O_2(g) \longrightarrow 2V_2O_5(s) + 6Cl_2(g). \quad (3)$$

As reported in the previous report,[17] Reaction 3 does not proceed below 400 °C. Consequently, the formation of a small amount of chlorine obtained by heating VCl_2O in an oxygen stream was considered to be due to Reaction 2.

Based on this assumption, the amount of V_2O_5 formed by Reaction 2 was calculated from the amount of chlorine formed (in Table 1). The molar ratio of the amount of VCl_3O to the amount of V_2O_5 obtained by subtracting the amount of V_2O_5 formed by Reaction 2 from the total amount of V_2O_5 formed was calculated to be approximately 4: 1. In this calculation, the amount of V_3O_7 formed was converted into that of V_2O_5 on the assumption that V_3O_7 was oxidized to V_2O_5. These results confirmed that the main reaction which occurred by heating VCl_2O in an oxygen stream was Reaction 1 and that this reaction was accompanied by Reaction 2.

The above-mentioned results reveal that VCl_2O reacts with oxygen above *ca.* 170 °C according to Reaction 1 and that this reaction is accompanied by Reaction 2. As a result, V_2O_5 (under a low oxygen concentration, V_3O_7 is formed in addition to V_2O_5), VCl_3O, and a small amount of chlorine are formed.

Reaction Process between Vanadium Trichloride and Oxygen. On heating VCl_3 in an argon stream, the VCl_3 disproportionates above *ca.* 350 °C according to the reaction, $2VCl_3(s) \rightarrow VCl_2(s) + VCl_4(g)$, as previously reported by the present authors.[17]

The TG curve showed that VCl_3 reacted appreciably with oxygen above *ca.* 110 °C before disproportionating. To obtain more detailed information on the reaction between VCl_3 and oxygen, the products formed by heating VCl_3 at various temperatures for 1—6 h in an oxygen stream were examined.

At 90 °C, no reaction product was observed. The reaction products obtained at various temperatures above 100 °C and their weight percentages to the initial VCl_3 were determined by chemical and X-ray analysis.[6,9] The results are summarized in Table 3.

The experimental results shown in Table 3 indicated that VCl_3O was the main product by the reaction between VCl_3 and oxygen. This fact was considered to indicate that the main reaction on heating VCl_3 in an oxygen stream was the reaction,

$$2VCl_3(s) + O_2(g) \longrightarrow 2VCl_3O(g). \quad (4)$$

Small amounts of VCl_2O and chlorine were formed in addition to VCl_3O. The molar ratio of the amount of VCl_2O to the amount of chlorine was calculated to be approximately 2: 1. This fact was considered to indicate that the reaction,

$$2VCl_3(s) + O_2(g) \longrightarrow 2VCl_2O(s) + Cl_2(g), \quad (5)$$

occurred in addition to Reaction 4.

Based on the assumption that the formation of VCl_2O and chlorine was due to Reaction 5, the amount of VCl_3 consumed by Reaction 5 was calculated from the amount of chlorine formed (in Table 3). The molar ratio of the amount of VCl_3O formed to the amount of the reacted VCl_3 obtained by subtracting the amount of VCl_3 consumed by Reaction 5 from the total amount of the reacted VCl_3 was calculated to be approximately 1: 1. These results confirmed that the main reaction which occurred by heating VCl_3 in an oxygen stream was Reaction 4 and that this reaction was accompanied by Reaction 5.

The above-mentioned results reveal that VCl_3 reacts with oxygen above *ca.* 100 °C according to Reaction 4 and that this reaction is accompanied by Reaction 5. As a result, VCl_3O and small amounts of VCl_2O and chlorine are formed.

As mentioned above, Pechkovskii and Vorob'ev[4] have reported that on heating VCl_3 in an oxygen stream, a small part of the VCl_3 is oxidized to V_2O_5. From the results of this work, it is probable that the V_2O_5 is formed by the reaction of VCl_2O, formed by Reaction 5, with oxygen.

References

1) A. Yajima, R. Matsuzaki, and Y. Saeki, *Bull. Chem. Soc. Jpn.*, **51**, 1098 (1978).

2) O. Ruff and H. Lickfett, *Ber.*, **44**, 506 (1911).
3) H. Lamprey and P. F. Forsyth, *Talanta*, **7**, 264 (1961).
4) V. V. Pechkovskii and N. I. Vorob'ev, *Russ. J. Inorg. Chem.*, **10**, 779 (1965).
5) H. Oppermann, *Z. Anorg. Allg. Chem.*, **351**, 113 (1967).
6) R. J. Sime, *Z. Kristallogr.*, **124**, 238 (1967).
7) C. Starr, F. Bitter, and A. R. Kaufmann, *Phys. Rev.*, **58**, 977 (1940).
8) R. E. McCarley and J W. Roddy, *Inorg. Chem.*, **3**, 60 (1964).
9) JCPDS, Powder Diffraction File, 15-382.
10) F. E. Brown and J. E. Snyder, *J. Am. Chem. Soc.*, **47**, 2671 (1925).
11) J. Krtil, *Z. Anal. Chem.*, **219**, 412 (1965).
12) P. Ehrlich and H. J. Seifert, *Z. Anorg. Allg. Chem.*, **301**, 282 (1959).
13) JCPDS, Powder Diffraction File, 23-1472.
14) ASTM, X-Ray Powder Data File, 9-387.
15) JCPDS, Powder Diffraction File, 20-1378.
16) H. Endo, M. Wakihara, and M. Taniguchi, *Chem. Lett.*, **1974**, 905.
17) A. Yajima, R. Matsuzaki, and Y. Saeki, *Bull. Chem. Soc. Jpn.*, **52**, 3292 (1979).

Circular Dichroism and Stereochemistry of Tetranuclear Cobalt(III) Complexes of Hexol Type. II.[1] Hexakis(ethylenediamine)-hexa-μ-hydroxo-tetracobalt(III) Ion, $[Co\{(OH)_2Co(en)_2\}_3]^{6+}$

Tomikatsu KUDO* and Yoichi SHIMURA

Department of Chemistry, Faculty of Science, Osaka University, Toyonaka, Osaka 560

(Received May 24, 1979)

The theoretically possible eight optical isomers of hexakis(ethylenediamine)-hexa-μ-hydroxo-tetracobalt(III) ion, $[Co\{(OH)_2Co(en)_2\}_3]^{6+}$, were separated by column chromatography, absorption and circular dichroism spectra being measured in the visible and ultraviolet region in 0.01 mol dm^{-3} HCl and 0.15 mol dm^{-3} Na_2SeO_3 solutions. Absolute configurations were determined by means of circular dichroism spectra and the characterization of mononuclear cobalt(III) ions produced by decomposition of the tetranuclear isomers in an acid solution. The additivity of the two main circular dichroism contributions due to the chiral CoO_6 and CoN_4O_2 chromophores is discussed, and the configurational chirality of CoO_6 chromophore is expressed by summing up the contributions from three pairs of CoN_4O_2 chromophores as in the so-called ring-pairing method.

Hexakis(ethylenediamine)-hexa-μ-hydroxo-tetracobalt(III) complex salt was prepared by Werner for the first time.[2] For this tetranuclear hexol-type complex there are eight possible optically active isomers which then compose four racemic isomers. The structures of two of the four racemic isomers have been found by X-ray analysis of the salts of $\Delta(\Delta\Delta\Delta)/\Lambda(\Delta\Delta\Lambda)$ and $\Delta(\Lambda\Lambda\Lambda)/\Lambda(\Delta\Delta\Delta)$ isomers.[3-5] However, little success has been made concerning the optical resolution of this complex ion.[6,7] Kern and Wentworth reported that four of the eight possible optical isomers of $[Co\{(OH)_2Co(en)_2\}_3]^{6+}$ are formed in solution, only two of them (a couple of enantiomers) being obtained in pure fractions.[6] They could not assign the configurations of the isomers. The present paper deals with successful separation of all the eight isomers and assignments of their configurations. Discussion is given on their circular dichroism (CD) spectra including CD change by ion-pairing with some oxoanions as compared with the spectra of the corresponding dodecaammine complex.[1]

Experimental

Preparation and Separation of the Isomers of $[Co\{(OH)_2Co(en)_2\}_3]^{6+}$. The complex was prepared by a modification of the method of Werner.[2] To 14.5 g of $Co(NO_3)_2\cdot 6H_2O$ in 15 cm^3 of water was slowly added 30 cm^3 of a 10% solution of ethylenediamine with stirring. The mixture was stirred vigorously by blowing compressed air on the surface for about one hour at room temperature, the remaining solid being filtered off and washed with a small amount of water. The filtrate and washings were poured into a column (5×120 cm) of strong-acid exchanger (SP Sephadex C-25, Na^+ form). After a broad pink-red band had been swept out with 0.1 M (1 M = 1 mol dm^{-3}) sodium *d*-tartrate solution, the adsorbed band was eluted with 0.3 M sodium *d*-tartrate solution. During the course of elution the column was cooled by flushing cold water of 5 °C. Eight brown bands eluted were numbered f-1, f-2, ···, and f-8 in the order of elution. At this stage, it was confirmed by measurements of CD spectra that each pair of isomers f-1 and f-2, f-3 and f-4, f-5 and f-6, and f-7 and f-8 represents a couple of enantiomers. Each eluate was concentrated in a vacuum rotatory evaporator at 20 °C, when necessary, and then a saturated aqueous sodium tetraphenylborate solution was added to the eluate to precipitate the desired product. The precipitate was collected by filtration and washed with cold water and then air-dried. The precipitate was dissolved in cold ethanol. The solution was filtered, and a cold ethanol solution of calcium nitrate was added to the filtrate. A voluminous pale-brown nitrate immediately precipitated was filtered off and washed with ethanol several times and then dried in the air. The product was dissolved in a small amount of water, and powdered sodium nitrate was added to the solution which was kept in a refrigerator overnight. Fine brown needle crystals which appeared were collected by filtration and recrystallized from a small amount of water by adding powdered sodium nitrate, and then dried in a vacuum desiccator over calcium chloride. Found for isomer f-3: C, 13.01; H, 5.35; N, 22.12%. Calcd for $[Co\{(OH)_2Co(en)_2\}_3](NO_3)_6\cdot 3H_2O = C_{12}H_{54}N_{18}O_{24}Co_4\cdot 3H_2O$: C, 12.82; H, 5.38; N, 22.42%. Found for isomer f-4: C, 12.96; H, 5.38; N, 22.26%. Calcd for $C_{12}H_{54}N_{18}O_{24}Co_4\cdot 3H_2O$: C, 12.82; H, 5.38; N, 22.42%. Found for isomer f-5: C, 12.91; H, 5.10; N, 22.72%. Calcd for $C_{12}H_{54}N_{18}O_{24}Co_4\cdot 1.5H_2O$: C, 13.13; H, 5.24; N, 22.97%. Found for isomer f-6: C, 12.96; H, 5.32; N, 22.36%. Calcd for $C_{12}H_{54}N_{18}O_{24}Co_4\cdot 3H_2O$: C, 12.82; H, 5.38; N, 22.42%. Found for isomer f-7: C, 12.49; H, 5.34; N, 22.03%. Calcd for $C_{12}H_{54}N_{18}O_{24}Co_4\cdot 3.5H_2O$: C, 12.72; H, 5.42; N, 22.24%. Found for isomer f-8: C, 12.76; H, 5.09; N, 22.94%. Calcd for $C_{12}H_{54}O_{24}Co_4\cdot 1.5H_2O\cdot 0.5NaNO_3$: C, 12.64; H, 5.04; N, 22.73%. Isomers f-1 and f-2 were not obtained as solid salt because of low yields, and partial overlapping of the chromatographic bands of f-1 and f-2 with those of the Λ and Δ isomers, respectively, of a by-product complex, $[Co(en)_3]^{3+}$.

Measurements. The visible and ultraviolet absorption spectra were measured with a Shimadzu UV-200 spectrophotometer. The CD spectra were recorded with a JASCO MOE-1 spectropolarimeter. Measurements were carried out at room temperature in 0.01 M HCl, 0.15 M Na_2SeO_3, and aqueous solutions.

Results and Discussion

Characterization of Isomers. The absorption and CD data of eight isomers are summarized in Table 1. It is evident that the isomer f-1 is enantiomeric to the isomer f-2, as is f-3 to f-4, f-5 to f-6, and f-7 to f-8. The CD curves of isomers f-1, f-3, f-5, and f-7, all of which have a positive CD band at about 16400 cm^{-1}, are shown in Fig. 1. Isomers f-1 and f-2 were not obtained as solid salt, their CD values being estimated on the

basis of the concentration calculated from the absorbance at 620 nm assuming the molar absorption coefficient $\varepsilon_{620}=113$ mol^{-1} dm^3 cm^{-1}; the absorption intensities of all the other isomers were almost equal to this value (Fig. 1 and Table 1). The absorption and CD spectra remained unchanged in 0.3 M sodium *d*-tartrate (eluting solution) at room temperature for about 24 h, being the same in 0.01 M HCl and in H_2O, in which the complex, except for isomer f-7, is considerably stable to mutarotation. Isomers f-3 and f-5 are considerably stable against mutarotation also in 0.15 M Na_2SeO_3 in a sharp contrast to the case of the dodecaammine complex, $[Co\{(OH)_2Co(NH_3)_4\}_3]^{6+}$, which undergoes mutarotation in 0.17 M Na_2SeO_3 and in H_2O.[1] Isomers f-7 undergoes mutarotation in 0.15 M Na_2SeO_3 and in H_2O, but it is considerably stable against mutarotation in 0.01 M HCl. Judging from the chromatographic band strech and the degree of coloration on the column, the yields of isomers are in the order f-3 (f-4)>f-5 (f-6)>f-7 (f-8)>f-1 (f-2). The isomers reported by Kern and Wentworth[6] and Mason and Wood[10] correspond to the present isomers f-5 and f-6.

Configuration of CoO_6 Chromophore. The hexakis-(ethylenediamine)-hexa-μ-hydroxo-tetracobalt(III) ion, $[Co\{(OH)_2Co(en)_2\}_3]^{6+}$, is regarded as being composed of a $Co(OH)_6$ and three $Co(OH)_2(en)_2$ chromophores. In the following discussion the former chromophore is abbreviated to CoO_6, and the latter to CoN_4O_2. The CoO_6 chromophore has a configurational chirality, Δ or Λ, due to the tris-chelate type arrangement of three $Co(OH)_2Co$ four-membered rings. Each CoN_4O_2 chromophore also has a configurational chirality, Δ or Λ, due to the tris-chelate type arrangement of two ethylenediamine chelate rings and a $Co(OH)_2Co$ four-membered ring. Thus eight isomers are possible in

TABLE 1. THE ABSORPTION AND CD DATA OF $[Co\{(OH)_2Co(en)_2\}_3]^{6+}$ IN 0.01 M HCl UNLESS OTHERWISE STATED

Wave numbers are given in 10^3 cm^{-1} unit and log ε or $\Delta\varepsilon$ values (in parentheses) mol^{-1} dm^3 cm^{-1}.

Isomer	Absorption σ_{max} (log ε)	CD σ_{ext} ($\Delta\varepsilon$)
f-1		14.77 (− 2.99)
	16.12	16.64 (+ 18.1)
	20.31	20.41 (− 31.8)
		26.25 (+ 1.57)
	32.36	30.96 (− 8.41)
		38.96 (+ 10.3)
	49.02	45.77 (+114)
f-2		14.73 (+ 2.95)
	16.14	16.61 (− 18.2)
	20.29	20.37 (+ 32.0)
		26.16 (− 1.58)
	32.36	30.96 (+ 8.43)
		38.76 (− 10.2)
	48.90	45.87 (−110)
f-3		14.53 (− 2.31)
	16.13 (2.04)	16.31 (+ 18.4)
	20.33 (2.56)	20.16 (− 28.9)
		25.84 (+ 1.23)
	32.36 (3.77)	31.45 (− 7.16)
		37.04 (+ 3.55)
		40.32 (− 8.26)
	48.78 (4.76)	45.15 (+139)
f-3[a]		14.63 (− 2.46)
	16.26 (1.99)	16.37 (+ 15.2)
	20.20 (2.59)	20.16 (− 30.1)
		25.97 (+ 2.72)
	31.95 (3.76)	30.86 (− 3.57)
		37.60 (+ 6.05)
		39.92 (− 1.11)
f-4		14.52 (+ 2.28)
	16.13 (2.05)	16.31 (− 19.0)
	20.33 (2.56)	20.14 (+ 29.3)
		25.77 (− 1.30)
	32.36 (3.77)	31.35 (+ 7.25)
		37.04 (− 3.62)
		40.40 (+ 8.31)
	49.02 (4.75)	45.25 (−135)

Isomer	Absorption σ_{max} (log ε)	CD σ_{ext} ($\Delta\varepsilon$)
f-5		14.56 (− 2.52)
	16.13 (2.05)	16.37 (+ 17.3)
	20.37 (2.50)	20.16 (− 21.9)
		25.71 (+ 1.30)
	32.36 (3.74)	31.60 (− 10.9)
		40.73 (− 33.7)
	49.14 (4.73)	45.35 (+103)
f-5[a]		14.64 (− 2.61)
	16.18 (2.01)	16.39 (+ 13.5)
	20.28 (2.52)	20.16 (− 21.5)
		25.77 (+ 2.38)
	31.95 (3.74)	31.20 (− 7.01)
		35.78 (+ 0.18)
		40.49 (− 19.6)
f-6		14.56 (+ 2.58)
	16.16 (2.05)	16.39 (− 16.8)
	20.33 (2.51)	20.18 (+ 22.4)
		25.71 (− 1.41)
	32.36 (3.75)	31.65 (+ 10.5)
		40.82 (+ 33.6)
	49.02 (4.74)	45.25 (− 98.7)
f-7		14.64 (− 2.37)
	16.16 (2.05)	16.53 (+ 17.2)
	20.28 (2.54)	20.28 (− 19.6)
		25.87 (+ 1.41)
	32.36 (3.77)	31.70 (− 12.4)
		41.15 (− 49.1)
	49.02 (4.75)	46.19 (+85.9)
f-8		14.66 (+ 2.34)
	16.16 (2.05)	16.53 (− 17.1)
	20.33 (2.54)	20.33 (+ 19.4)
		25.87 (− 1.44)
	32.36 (3.77)	31.65 (+ 12.0)
		40.98 (+ 48.6)
	48.90 (4.75)	46.08 (− 88.0)

a) In 0.15 M Na_2SeO_3.

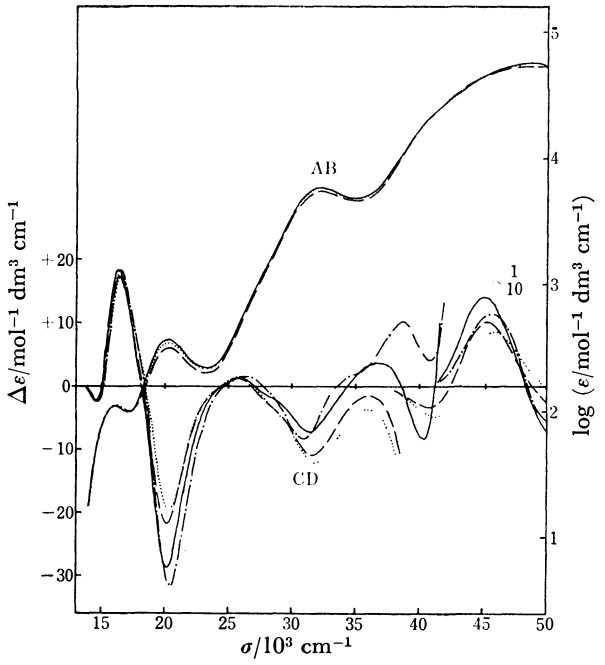

Fig. 1. Absorption (AB) and CD curves of isomer f-1 (—·—·—), f-3 (——), f-5 (– – –), and f-7 (····) of $[Co\{(OH)_2Co(en)_2\}_3]^{6+}$ in 0.01 M HCl.

total: $\Delta(\Delta\Delta\Delta)$, $\Delta(\Delta\Delta\Lambda)$, $\Delta(\Delta\Lambda\Lambda)$, $\Delta(\Lambda\Lambda\Lambda)$, $\Lambda(\Delta\Delta\Delta)$, $\Lambda(\Delta\Delta\Lambda)$, $\Lambda(\Delta\Lambda\Lambda)$, and $\Lambda(\Lambda\Lambda\Lambda)$; the chirality symbols in parentheses denote the configurations of CoN_4O_2 chromophores. The eight isomers are classified into four geometrical isomers, since each of them finds its enantiomer in themselves.

Since the first and second d-d transition bands of $[Co(H_2O)_6]^{3+}$ are located at 16500 and 24700 cm^{-1}, respectively,[8] and those of *cis*-$[Co(en)_2(H_2O)_2]^{3+}$ at

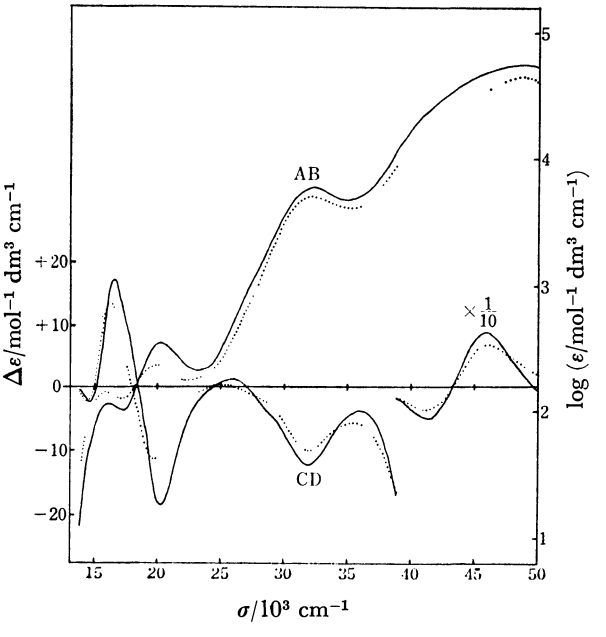

Fig. 2. Absorption (AB) and CD curves of isomer f-7 of $[Co\{(OH)_2Co(en)_2\}_3]^{6+}$ (——) and Λ-$[Co\{(OH)_2Co(NH_3)_4\}_3]^{6+}$ (····) in 0.01 M HCl.

20200 and 27700 cm^{-1},[9] the absorption bands of $[Co\{(OH)_2Co(en)_2\}_3]^{6+}$ at *ca.* 16100 and 20300 cm^{-1} are assigned to the first d-d transition bands of CoO_6 and CoN_4O_2 chromophores, respectively. The second d-d transition bands of both chromophores seem to be masked by an intense band at 32360 cm^{-1}, which is due to the charge transfer transition from the oxygen atom of the OH bridge groups to the central metal, $p_\pi(O)\rightarrow e_g(Co)$. The assignments are in line with those for those of similar hexa-μ-hydroxo-tetracobalt(III) type ions.[1,6,10,11] For all four geometrical isomers, the band positions and intensities are almost equal for the CoO_6 chromophore region, but not for the CoN_4O_2 chromophore region (Fig. 1 and Table 1).

Similarly the intensities of the longer or shorter wavelength CD peak of CoO_6 chromophore are almost equal for isomers f-1, f-3, f-5, and f-7: $\Delta\varepsilon_{ext}=-2.3$——$-3.0$ and $+17.1$——$+18.4$ mol^{-1} dm^3 cm^{-1}, respectively. The CD intensity of CoN_4O_2 chromophore band at about 20300 cm^{-1} varies widely: $\Delta\varepsilon_{ext}=-18.7$——$-33.0$ mol^{-1} dm^3 cm^{-1}. The CD patterns in the d-d transition region are similar to each other, while those in the charge transfer transition region differ. From the close similarity (Fig. 2) between the CD spectra of isomers f-1, f-3, f-5, and f-7 and spectrum of Λ-$[Co\{(OH)_2Co(NH_3)_4\}_3]^{6+}$ previously reported,[1] it is concluded that isomers f-1, f-3, f-5, and f-7 have Λ configuration and the remaining isomers f-2, f-4, f-6, and f-8 Δ configuration.

Configurations of CoN_4O_2 Chromophores. Acid hydrolysis of one mole of $[Co\{(OH)_2Co(en)_2\}_3]^{6+}$ ion is expected to produce one mole of $[Co(H_2O)_6]^{2+}$ (*via* $[Co(H_2O)_6]^{3+}$) and 3 mol of mononuclear $[Co(en)_2(H_2O)_2]^{3+}$. While the former ion has no chirality, the latter has a configurational chirality, Δ or Λ, due to the bis-chelate type structure. The isomers $\Delta(\Delta\Delta\Delta)$ or $\Lambda(\Delta\Delta\Delta)$ will produce three Δ-$[Co(en)_2(H_2O)_2]^{3+}$ ions, $\Delta(\Delta\Delta\Lambda)$ or $\Lambda(\Delta\Delta\Lambda)$ two Δ and one Λ, $\Delta(\Delta\Lambda\Lambda)$ or $\Lambda(\Delta\Lambda\Lambda)$ one Δ and two Λ, and $\Delta(\Lambda\Lambda\Lambda)$ or $\Lambda(\Lambda\Lambda\Lambda)$ three Λ.

Table 2. The $\Delta\varepsilon_{488}$ values after decomposition by 6 M HCl ($\Delta\varepsilon$ values are given in mol^{-1} dm^3 cm^{-1} unit.)

Isomer	$\Delta\varepsilon_{488}$	Ratio	Assignment
f-1	(+1.5) [a]	(+2.0)	$(\Lambda\Lambda\Lambda)$
f-3	−2.2	−2.9	$(\Delta\Delta\Lambda)$
f-5	−0.8	−1.1	$(\Lambda\Delta\Lambda)$
f-7	+0.7	+0.9	$(\Lambda\Lambda\Delta)$

a) The original tetranuclear complex was not isolated in solid salt, but concentration was estimated from the absorbance at 620 nm.

The $\Delta\varepsilon$ values at 488 nm after decomposition in 6 M HCl solution are given in Table 2. Each isomer was dissolved in 6 M HCl and warmed on a water bath at 45 °C for two hours with stirring. The CD intensity of Λ-$[Co(en)_2(H_2O)_2]^{3+}$ was reported to be 1.0 mol^{-1} dm^3 cm^{-1} at 486 nm.[4] The observed $\Delta\varepsilon_{488}$ values as a whole are smaller than the reported value, which can be attributed to partial racemization, isomerization, and/or decomposition of the generated $[Co(en)_2(H_2O)_2]^{3+}$ in

presence of Co^{2+} ions. From the data in Table 2, the absolute configurations of isomers f-1, f-3, f-5, and f-7 are assigned to $\Lambda(\Lambda\Lambda\Lambda)$, $\Lambda(\Delta\Lambda\Lambda)$, $\Lambda(\Delta\Delta\Lambda)$, and $\Lambda(\Delta\Delta\Delta)$, respectively. Thus isomers f-2, f-4, f-6, and f-8 are assigned to the configurations, $\Delta(\Delta\Delta\Delta)$, $\Delta(\Lambda\Lambda\Lambda)$, $\Delta(\Delta\Lambda\Lambda)$, and $\Delta(\Delta\Delta\Lambda)$, respectively.

The CD spectra of Λ-$[Co\{(OH)_2Co(NH_3)_4\}_3]^{6+}$ might be expected to be more similar to those of the isomers $\Lambda(\Delta\Lambda\Lambda)$ and $\Lambda(\Delta\Lambda\Lambda)$ than to those of $\Lambda(\Delta\Delta\Lambda)$ and $\Lambda(\Delta\Delta\Delta)$. Isomers f-5 and f-7 show a similar CD pattern (−, −, and +) in the charge transfer transition region, which is similar to that of Λ-$[Co\{(OH)_2Co(NH_3)_4\}_3]^{6+}$ (Fig. 2). From the order of yields, $\Lambda(\Delta\Delta\Lambda) > \Lambda(\Delta\Lambda\Lambda) > \Lambda(\Delta\Lambda\Lambda) > \Lambda(\Lambda\Lambda\Lambda)$, the stability of isomers seems to decrease with increase in the number of Λ-configuration for CoN_4O_2 chromophore in the Λ series of CoO_6 chromophore. A molecular model examination shows that the Λ-configuration of CoN_4O_2 chromophore gives a slight repulsion between a proton of ethylenediamine chelate ring and an OH bridge group.

CD Change by Ion-pairing. The absorption peak of the CoO_6 chromophore of isomers f-3 and f-5 shifted to higher energy side in 0.15 M Na_2SeO_3 and then the intensity decreased, the shift being larger for f-3 than f-5. The peak of CoN_4O_2 chromophore shifted to lower energy side and the intensity increased. The intensity change is larger for f-3 than f-5. For the CD spectra, the longer wavelength extremum of CoO_6 chromophore shifted to higher energy side and the intensity increased for both isomers (Fig. 3 and Table 1). The intensity of the shorter wave-length CD extremum of CoO_6 chromophore decreased for both isomers. The CoN_4O_2 chromophore CD band (at 20160 cm^{-1} for both isomers) did not shift, the intensity increasing for f-3 and slightly decreasing for f-5. The difference in CD curves of 0.01 M HCl and 0.15 M Na_2SeO_3 (Fig. 4) show the ion-pairing effect of SeO_3^{2-} ion on the CD of $[Co\{(OH)_2Co(en)_2\}_3]^{6+}$. The curves have six extrema at *ca.* 14200, 16000, 19800, 22400, 24500, and 28000 cm^{-1} in the d-d transition region. The CD spectra of Λ-$[Co(en)_3]^{3+}$ with D_3 symmetry show strong ion-pairing effect[12–14] in the region of the first d-d absorption band when an oxoanion species such as PO_4^{3-} or SeO_3^{2-} is added to form the so-called Mason type ion-pair,[13–17] the CD intensity of E_a component of the first d-d transition decreasing and that of A_2 component increasing. Thus the first positive and next negative extrema, at 14200 and *ca.* 16000 cm^{-1}, correspond to the increment of the negative A_2 component and the decrement of the positive E_a component, respectively, of the first d-d transition of CoO_6 chromophore.

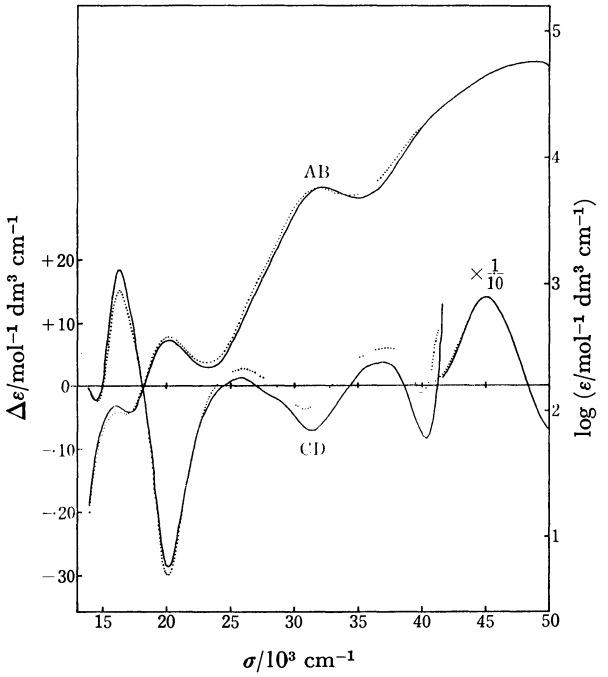

Fig. 3. Absorption (AB) and CD curves of isomer f-3 of $[Co\{(OH)_2Co(en)_{23}]^6\}^+$ in 0.01 M HCl (——) and in 0.15 M Na_2SeO_3 (····).

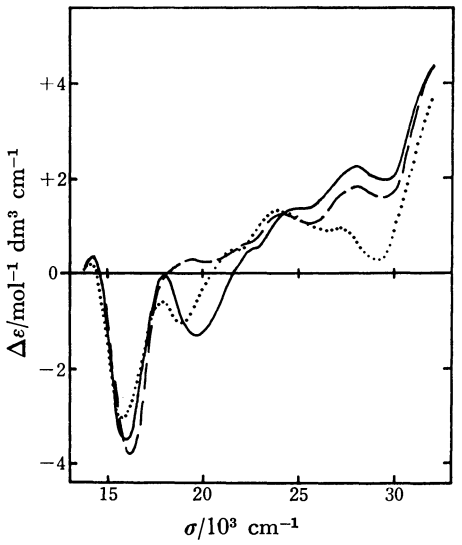

Fig. 4. The ion-pairing effect curves, $\{\Delta\varepsilon_{(In\ 0.15\ M\ Na_2SeO_3)} - \Delta\varepsilon_{(In\ 0.01\ M\ HCl)}\}$, of isomer f-3 (——) and f-5 (– – –) of $[Co\{(OH)_2Co(en)_2\}_3]^{6+}$, and Λ-$[Co\{(OH)_2Co(NH_3)_4\}_3]^{6+}$ (····) (in 0.17 M Na_2SeO_3).

In $[Co\{(OH)_2Co(en)_2\}_3]^{6+}$, hydrogen bond formation occurs between SeO_3^{2-} and the OH bridge groups as for the corresponding dodecaammine complex.[1] The hydrogen bond formation may occur between the oxoanion and the coordinated $-NH_2$ groups of ethylenediamine of CoN_4O_2 chromophores. Thus chiral oxygen and nitrogen centers are stereospecifically produced by the ion-pair formation. The axial disposition of OH groups in the tetranuclear complex of Λ configuration of CoO_6 chromophore constrains an (*R*) chirality for the "asymmetric" oxygen atoms,[1] and the axial hydrogen bonding of the NH_2 groups in $\Lambda(\Delta\Delta\Lambda)$ configuration constrains an (*S*) chirality for the "asymmetric" nitrogen atoms. The ion-pairing effect curves in Fig. 4 are regarded as having their origin in the vicinal effect of chiral oxygen and/or nitrogen centers stereospecifically produced by the ion-pair formation. A molecular model consideration shows that in the isomer $\Lambda(\Delta\Delta\Lambda)$ a set of three OH groups is available each on the upper face and below the downward face (two A sites, 2×3 (*R*) oxygens) and six sets of one OH group and two amino groups (six B sites,

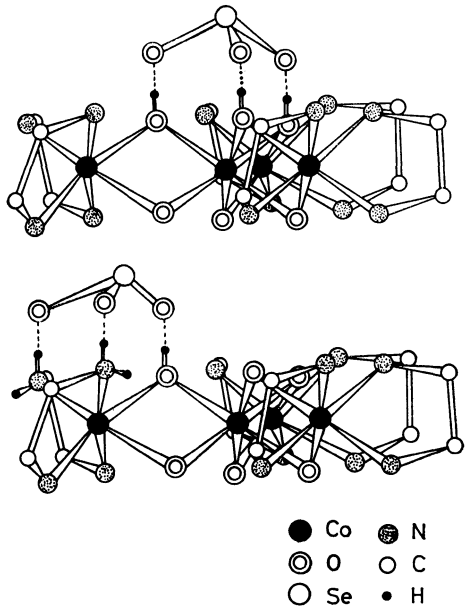

Fig. 5. The possible hydrogen bond formation site for the isomer $\Lambda(\Delta\Delta\Delta)$ with a selenite ion, A site (top) and B site (bottom), viewed normal to the C_3 axis of CoO_6 chromophore.

6×1 (R) oxygens and 6×2 (S) nitrogens) for hydrogen bond formation (Fig. 5). In the isomer $\Lambda(\Delta\Delta\Lambda)$, two A sites with 2×3 (R) oxygens and only four B sites with 4×1 (R) oxygens and 4×2 (S) nitrogens are available for hydrogen bonding. As shown in Fig. 4, the ion-pairing effect curve of isomers f-3, $\Lambda(\Delta\Delta\Lambda)$, shows a similar CD pattern to that of Λ-$[Co\{(OH)_2Co(NH_3)_4\}_3]^{6+}$ which has the origin of the effect only in the asymmetric oxygens, which show a negative extremum at *ca.* 19800 cm^{-1}. Thus the ion-pair formation in the present $\Lambda(\Delta\Delta\Lambda)$ complex occurs between SeO_3^{2-} and one or two A sites rather than B sites. The ion-pairing effect curve of isomer f-5, $\Lambda(\Delta\Lambda\Lambda)$, shows a positive extremum at 19400 cm^{-1} (Fig. 4). The B sites may play a role in this case of ion-pair formation.

Additivity of CD Contributions. If the observed CD curve of $[Co\{(OH)_2Co(en)_2\}_3]^{6+}$ can be simply divided into the contributions of CoO_6 and CoN_4O_2 chiralities as has been established for configurational and vicinal chiralities of many other mononuclear cobalt(III) complexes,[18] the following relations are expected to hold:

$$\left.\begin{aligned} \Lambda(\Lambda\Lambda\Lambda) &= \Lambda + 3(\Lambda) \\ \Lambda(\Delta\Lambda\Lambda) &= \Lambda + 2(\Lambda) + (\Delta) = \Lambda + (\Lambda) \\ \Lambda(\Delta\Delta\Lambda) &= \Lambda + (\Lambda) + 2(\Delta) = \Lambda - (\Lambda) \\ \Lambda(\Delta\Delta\Delta) &= \Lambda + 3(\Delta) = \Lambda - 3(\Lambda) \end{aligned}\right\} \quad (1)$$

where Λ (or Δ) and (Λ) (or (Δ)) are CD contributions of CoO_6 and CoN_4O_2 chiralities, respectively, and $\Lambda = -\Delta$ and $(\Lambda) = -(\Delta)$. The individual Λ and (Λ) can be derived from the observed CD curves from the following relations:

$$\Lambda = [\Lambda(\Lambda\Lambda\Lambda) + \Lambda(\Delta\Delta\Delta)]/2,$$
$$\Lambda = [\Lambda(\Delta\Lambda\Lambda) + \Lambda(\Delta\Delta\Lambda)]/2,$$
$$(\Lambda) = [\Lambda(\Lambda\Lambda\Lambda) - \Lambda(\Delta\Delta\Delta)]/6, \text{ and}$$
$$(\Lambda) = [\Lambda(\Delta\Lambda\Lambda) - \Lambda(\Delta\Delta\Lambda)]/2.$$

However, the calculation (Fig. 6) shows that the separation of Λ and (Λ) (or (Δ)) contributions are very unsatisfactry and that Eq. 1 in this simple form is inadequate for evaluating the CD contributions.

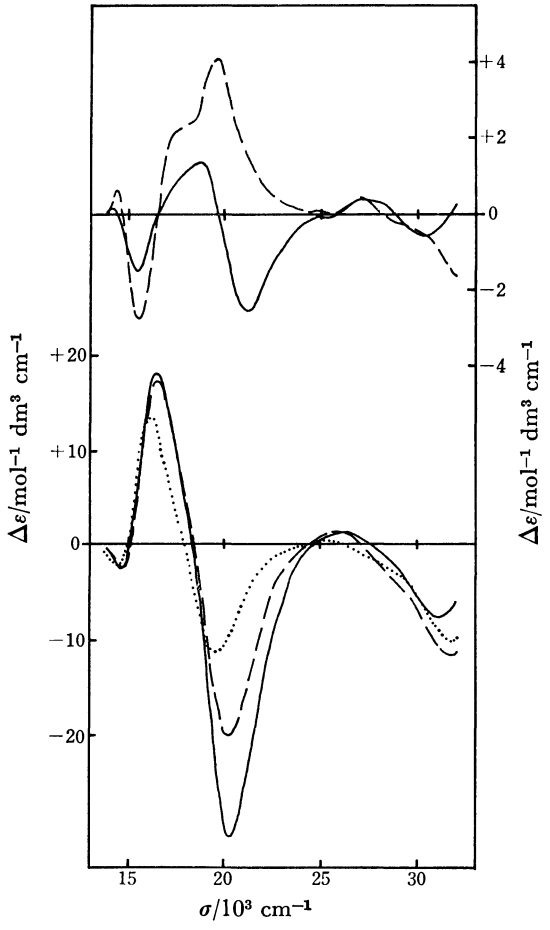

Fig. 6. Inadequacy of Eq. 1 is shown by the calculated curves of (Λ): $[\Lambda(\Lambda\Lambda\Lambda) - \Lambda(\Delta\Delta\Lambda)]/6$ (——) and $[\Lambda(\Delta\Lambda\Lambda) - \Lambda(\Delta\Delta\Lambda)]/2$ (– – –) (upper curves); and of Λ: $[\Lambda(\Lambda\Lambda\Lambda) + \Lambda(\Delta\Delta\Lambda)]/2$ (——) and $[\Lambda(\Delta\Lambda\Lambda) + \Lambda(\Delta\Delta\Lambda)]/2$ (– – –); and observed curve of Λ in the dodecaammine complex (• • • •) (lower curves).

As shown by X-ray analysis of the racemic salts of $\Lambda(\Delta\Lambda\Lambda)/\Lambda(\Delta\Lambda\Lambda)$[3,5] and $\Lambda(\Lambda\Lambda\Lambda)/\Lambda(\Delta\Lambda\Lambda)$[4] isomers, the four isomers of Λ series $\Lambda(\Delta\Delta\Lambda)$, $\Lambda(\Delta\Lambda\Lambda)$, $\Lambda(\Delta\Lambda\Lambda)$, and $\Lambda(\Lambda\Lambda\Lambda)$ have different dispositions of three CoN_4O_2 chromophores. The model of the isomer $\Lambda(\Delta\Delta\Lambda)$ is rather flat, the pseudo C_3 axes of tris-chelate type CoN_4O_2 chromophores being parallel (p) to the C_3 axis of the CoO_6 one; the structure of $\Lambda(\Delta\Delta\Lambda)$ isomer is thus written as $\Lambda(p_\Delta p_\Delta p_\Delta)$. The model of the isomer $\Lambda(\Lambda\Lambda\Lambda)$ is not flat but tall, the pseudo C_3 axes of CoN_4O_2 chromophores being oblique (q) to the C_3 axis of the CoO_6 one. The structure of $\Lambda(\Lambda\Lambda\Lambda)$ isomer is thus written as $\Lambda(q_\Lambda q_\Lambda q_\Lambda)$. The remaining two isomers $\Lambda(\Delta\Lambda\Lambda)$ and $\Lambda(\Delta\Lambda\Lambda)$ have a mixed structure, $\Lambda(p_\Delta p_\Delta q_\Lambda)$ and $\Lambda(p_\Delta q_\Lambda q_\Lambda)$, respectively. Kojima *et al.*[19] showed that the CD spectra of the mixed complexes $[Co(en)_x(tn)_y(tmd)_z]^{3+}$ can be expressed by summing up the

contributions from three pairs of chelate rings, as has been made in the so-called ring-pairing method[20] (tn= trimethylenediamine and tmd=tetramethylenediamine). By this treatment, Eq. 1 can be rewritten as follows:

$$\left.\begin{aligned} A(\Lambda\Lambda\Lambda) &= A(q_\Lambda q_\Lambda q_\Lambda) = 3A_{qq} + 3(A) \\ A(\Delta\Lambda\Lambda) &= A(p_\Delta q_\Lambda q_\Lambda) = 2A_{pq} + A_{qq} + (A) \\ A(\Delta\Lambda\Delta) &= A(p_\Delta p_\Delta q_\Lambda) = A_{pp} + 2A_{pq} - (A) \\ A(\Delta\Delta\Delta) &= A(p_\Delta p_\Delta p_\Delta) = 3A_{pp} - 3(A) \end{aligned}\right\} \quad (2)$$

where A_{pp} *etc.* denote the CD contribution of a ring-pair of two p-oriented CoN_4O_2 chromophores *etc.*

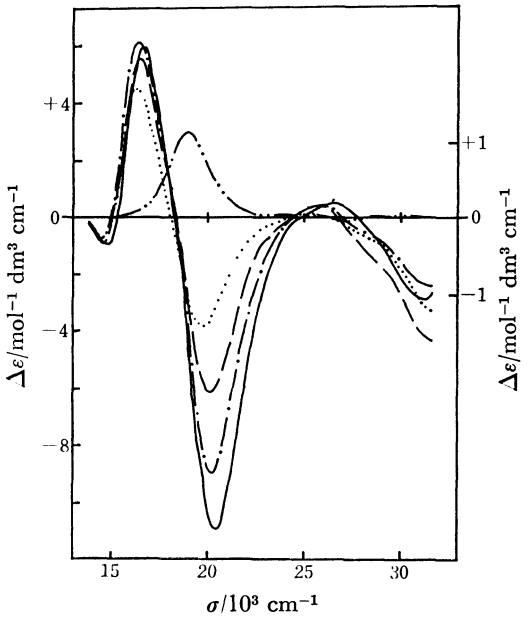

Fig. 7. Calculated curves of A_{qq} (——), A_{pq} (– – –), A_{pp} (–·–·–), and A_{aa} (·····), and observed curve of Λ-$[Co(TeO_6H_4)(en)_2]^+$ (–·····) (the right ordinate).

Equation 2 can be solved by assuming that the CD contribution (A) is equal to the observed CD of Λ-$[Co(TeO_6H_4)(en)_2]^+$.[21] The results are shown in Fig. 7. For the dodecaammine complex the CD contribution A is expressed by $3A_{aa}$ which denotes CD contributions of three ring-pairs of two CoN_4O_2 chromophores of tetraammine type. The calculated CD contributions of four kinds of ring-pairs A_{pp}, A_{pq}, A_{qq}, and A_{aa} differ from each other in the region of the first d-d absorption band of CoN_4O_2 chromophore. The absolute value of CD intensities in this region is in the order $A_{qq} > A_{pp} > A_{pq} > A_{aa}$. The A_{pq} contribution can be calculated in two ways from Eq. 2, one from the third formula of the equation (Fig. 7) and the other from the second formula. The results do not differ much, showing the adequacy of Eq. 2.

References

1) Part I of this series: T. Kudo and Y. Shimura, *Bull. Chem. Soc. Jpn.*, **52**, 1648 (1979).
2) A. Werner, *Ber.*, **40**, 2103 (1907).
3) U. Thewalt, *Chem. Ber.*, **104**, 2657 (1971).
4) U. Thewalt and J. Ernst, *Z. Naturforsch., Teil B*, **30**, 818 (1975).
5) D. A. Dixon, R. E. Marsh, and W. P. Schaeffer, *Acta Crystallogr., Sect. B*, **34**, 807 (1978).
6) R. D. Kern and R. A. D. Wentworth, *Inorg. Chem.*, **6**, 1018 (1967).
7) H. A. Goodwin, E. C. Gyarfas, and D. P. Mellor, *Aust. J. Chem.*, **11**, 426 (1958).
8) D. A. Johnson and A. G. Sharpe, *J. Chem. Soc.*, **1966**, 798.
9) A. J. McCaffery, S. F. Mason, and B. J. Norman, *J. Chem. Soc.*, **1965**, 5094.
10) S. F. Mason and J. W. Wood, *Chem. Commun.*, **1967**, 209.
11) I. Masuda and B. E. Douglas, *J. Coord. Chem.*, **1**, 189 (1971).
12) R. Larsson, S. F. Mason, and B. J. Norman, *J. Chem. Soc., A*, **1966**, 301.
13) S. F. Mason and B. J. Norman, *J. Chem. Soc., A*, **1966**, 307.
14) H. L. Smith and B. E. Douglas, *Inorg. Chem.*, **5**, 784 (1966).
15) A. J. McCaffery, S. F. Mason, and R. E. Ballard, *J. Chem. Soc.*, **1965**, 2883.
16) E. N. Duesler and K. N. Raymond, *Inorg. Chem.*, **10**, 1486 (1971).
17) J. E. Sarneski and F. L. Ulbach, *J. Am. Chem. Soc.*, **93**, 884 (1971).
18) C. T. Liu and B. E. Douglas, *Inorg. Chem.*, **3**, 1356 (1964); B. E. Douglas, *ibid.*, **4**, 1813 (1965); K. Ogino, K. Murano, and J. Fujita, *Inorg. Nucl. Chem. Lett.*, **4**, 351 (1968); Y. Yamasaki, J. Hidaka, and Y. Shimura, *Bull. Chem. Soc. Jpn.*, **42**, 119 (1969); N. Matsuoka, J. Hidaka, and Y. Shimura, *Inorg. Chem.*, **9**, 719 (1970); *Bull. Chem. Soc. Jpn.*, **45**, 2491 (1972); **48**, 458 (1975).
19) M. Kojima, H. Yamada, H. Ogino, and J. Fujita, *Bull. Chem. Soc. Jpn.*, **50**, 2325 (1977).
20) J. I. Legg and B. E. Douglas, *J. Am. Chem. Soc.*, **88**, 2697 (1966).
21) Y. Hosokawa and Y. Shimura, *Bull. Chem. Soc. Jpn.*, **52**, 1051 (1979).

Kinetics of the Ligand Substitution Reactions of the Copper(II) Chelates of 1-(2-Pyridylazo)-2-naphthol Analogs with EDTA

Hiroko WADA* and Genkichi NAKAGAWA

Laboratory of Analytical Chemistry, Nagoya Institute of Technology, Gokiso-cho, Showa-ku, Nagoya 466

(Received June 13, 1979)

The rates of the substitution reactions of copper(II) chelates of metallochromic indicators such as 1-(2-pyridylazo)-2-naphthol (PAN, Hpan), 1-(2-thiazolylazo)-2-naphthol (TAN, Htan), 2-(2-pyridylazo)-4-methylphenol (PAC, Hpac), 2-(2-thiazolylazo)-4-methylphenol (TAC, Htac), 4-(2-pyridylazo)resorsinol (PAR, H_2par), and 4-(2-thiazolylazo)resorcinol (TAR, H_2tar) were determined. The rate laws can be written as $-\frac{d[CuL]}{dt}=k^{CuL}_{edta'}$ [CuL][edta'] for PAN, TAN, PAC, and TAC in the pH range of 4 to 6.5, and $-\frac{d[(CuL)']}{dt}=(k^{CuL}_{edta'}[CuL]+k^{CuHL}_{edta'}[CuHL])[edta']$, where $[(CuL)']=[CuL]+[CuHL]$, for PAR and TAR in the pH range of 3.5 to 6.5. In the pH range lower than 3.5 the laws are written as $-\frac{d[CuL]}{dt}=(k^{CuL}_{edta'}[edta']+k^{CuL}_{H}[H])[CuL]$ for PAN, and as $-\frac{d[CuHL]}{dt}=(k^{CuHL}_{edta'}[edta']+k^{CuHL}_{H}[H])$ [CuHL] for PAR and TAR. The rate constants (μ=0.1, 25 °C, dioxane 2 vol% or 5 vol% (PAN and TAN) ($dm^3\ mol^{-1}\ s^{-1}$)) are $k^{Cu(tan)}_{edta'}=2.8\times10^4$, $k^{Cu(pac)}_{edta'}=8.0\times10^4$, $k^{Cu(tac)}_{edta'}=4\times10^6$, $k^{Cu(par)}_{edta'}=2.0\times10^3$, $k^{Cu(tar)}_{edta'}=6.3\times10^4$, $k^{Cu(Hpar)}_{edta'}=1.2\times10^4$, $k^{Cu(Htar)}_{edta'}=7.9\times10^5$, $k^{Cu(pan)}_{H}=6.5\times10$, $k^{Cu(Hpar)}_{H}=6.6\times10^2$, and $k^{Cu(Htar)}_{H}=1.2\times10^4$. The rate constants, $k^{CuL}_{edta'}$, are inversely proportional to the basicities of the donor atoms of indicators. Thus, the rate of color change of thiazolylazo compound is larger than that of corresponding pyridylazo compound in the chelatometry of copper(II).

In the chelatometric titrations using metallochromic indicators, the rate of substitution reaction of the metal-indicator chelate with EDTA is one of the important factor in obtaining the sharp color change at the equivalence point.[1] Several papers have been published on the substitution reactions of metallochromic indicator chelates with complexans. The mechanisms of the substitution reactions of some metal chelates of 4-(2-pyridylazo)resorcinol with 1,2-bis(2-aminoethoxy)-ethane-*N*,*N*,*N*′,*N*′-tetraacetic acid or 1,2-cyclohexanediamine-*N*,*N*,*N*′,*N*′-tetraacetic acid have been elucidated by Tanaka and Funahashi.[2-4] In our previous work, the kinetics of the substitution reaction of copper(II)–1-(2-pyridylazo)-2-naphthol(PAN) chelate with EDTA was investigated.[5] The structure of indicator influences the rate of the color change in the chelatometric titrations. In the case of heterocyclic azophenols, the rate of color change of a pyridylazophenol indicator is slower than that of a thiazolylazophenol indicator. For example the rate of color change of 4-(2-pyridylazo)resorcinol is smaller than that of 4-(2-thiazolylazo)resorcinol in copper(II)–EDTA titrations.

In this work the rates of the substitution reactions of copper(II) chelates of the several 1-(2-pyridylazo)-2-naphthol derivatives with EDTA have been determined, and the reaction mechanisms and the influences of the indicator structure on the rate of the substitution reaction are discussed.

Experimental

Reagents. Copper(II) nitrate solution: Copper metal (99.99%) was dissolved in dilute nitric acid. Indicator solutions: TAN, PAC, TAC, PAR, and TAR synthesized and/or purified as described in previous papers[6-9] were dissolved in dioxane. Commercial Na_2H_2edta·$2H_2O$ was recrystallized. Dioxane was purified as described in the previous paper.[5] Buffers: 0.1 mol dm^{-3} $ClCH_2COOH$–$ClCH_2COOK$ (pH<4.5), and 0.1 mol dm^{-3} 2-morpholino-1-ethanesulfonicacid(MES)–KOH (pH 4.5—7) were used. Ionic strength was maintained at 0.1 with KNO_3. All experiments were carried out in 2 or 5 vol % dioxane–H_2O solutions at (25±1) °C.

Apparatus. A Union Giken Stopped-Flow Spectrophotometer Type RA-401 (dead time 3 ms), a Hitachi Rapid Scan Spectrophotometer Type TSP-2 (dead time 20 ms), and a Radiometer pH Meter Type 26 were used.

Results

Substitution Reactions of Copper(II) Chelates of TAN, PAC, and TAC with EDTA. When a small excess of the indicator compared with copper(II) ion is added, these indicators form the 1:1 chelates with copper(II) at pH values lower than 6.5. The rate of the substitution reaction of indicator chelate, CuL, with a large excess of EDTA was determined under the experimental conditions shown in Table 1. The rate law is expressed as (Charges are omitted for simplicity.)

$$-\frac{d[CuL]}{dt}=k_{obsd}[CuL], \quad (1)$$

where k_{obsd} is the conditional rate constant.[5] Decrease in the absorbance of CuL chelate was measured as a function of the reaction time. The pseudo first-order plots were obtained for at least 90% of the total reaction. In every case k_{obsd} was proportional to the total concentration of EDTA not combined with copper(II), [edta'], while no dependence on the concentration of excess indicator and hydrogen ion concentration was observed, the same result as in the case of PAN.[5] Hence the rate law can be written as

$$-\frac{d[CuL]}{dt}=k^{CuL}_{edta'}[edta'][CuL]. \quad (2)$$

TABLE 1. EXPERIMENTAL CONDITIONS EMPLOYED FOR THE DETERMINATION OF THE RATE CONSTANTS

	Wavelength / nm	$10^6 C_{Cu}$ / mol dm^{-3}	$10^5 C_L$ / mol dm^{-3}	$10^4 C_{EDTA}$ / mol dm^{-3}	pH range	Dioxane / vol%
PAN	550	5.0	0.5 —1.5	1.0 —2.0	2.5—5	5
TAN	575	4.0	0.48—0.78	0.40—1.0	4.5—5.2	5
PAC	570	10.0	1.5 —3.0	1.0 —1.4	4.4—5.1	2
TAC	605	5.0	0.75—1.5	0.50	4.0—4.6	2
PAR	542	10.0	1.5 —3.0	1.0 —2.0	2.8—6.5	2
TAR	557	10.0	1.5	1.0 —5.0	2.5—6.5	2

The rate constants obtained are summarized in Table 2.

In the case of TAC, since the substitution reaction was too fast to be measured accurately on the stopped-flow apparatus employed in this work, the value of the rate constant was roughly estimated.

Substitution Reactions of Copper(II) Chelates of PAR, and TAR with EDTA. In the cases of PAR and TAR, copper(II) forms a chelate, CuHL, with PAR at pH$<$4 and with TAR at pH$<$3.5. The protonation constants, K^H_{CuHL}, had been determined as $10^{5.07}$ for PAR[8] and $10^{4.37}$ for TAR[6] (dioxane 2 vol%, μ=0.1, 15 °C). The absorption maxima of Cu(Hpar) and Cu(par) are at 525 and 515 nm, respectively, and the isosbestic points appear at 440 and 542 nm. The absorption maxima of Cu(Htar) and Cu(tar) are at 560 and 520 nm, respectively, and the isosbestic points appear at 450 and 557 nm. The rates of the substitutions of copper(II) chelates of PAR or TAR with large excess of EDTA were determined in the pH range from 2.5 to 6.5 by measuring the decrease in the absorbance of the chelates at an isosbestic point as a function of reaction time under the conditions shown in Table 1.

To examine the influence of buffer, in the pH range from 3 to 4.5 both $ClCH_2COOH$–$ClCH_2COOK$ buffer and MES–KOH buffer were used. No difference in the rate of the reactions was observed.

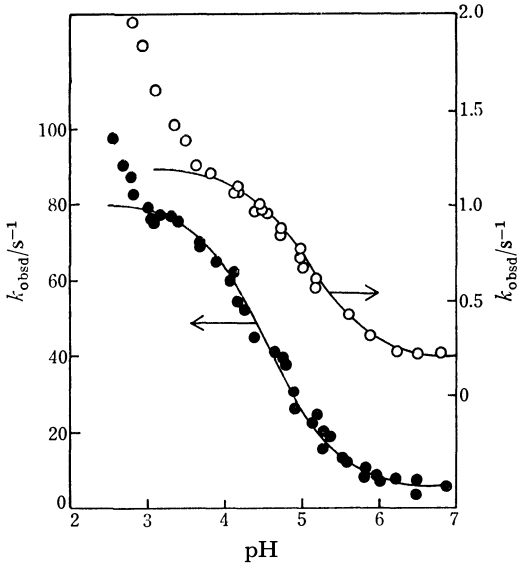

Fig. 1. Plots of k_{obsd} *vs.* pH for PAR and TAR.
○: PAR, ●: TAR.
k_{obsd} obtained at various concentrations of EDTA were converted to the values at 1.0×10^{-4} mol dm^{-3} C_{EDTA}. The lines are the theoretical curves calculated with the values obtained by curve fitting.

As seen from Fig. 1, the marked increases in the rates of the substitution reactions were observed with decreasing pH between pH 3.5 and 6. At the various pH values the conditional rate constants, k_{obsd}, were proportional to the concentration of EDTA, but independent of the concentration of PAR or TAR. As described above, the protonation equilibrium,

$$CuL + H^+ \rightleftarrows CuHL, \tag{3}$$

exists in the pH range from 4 to 6 for PAR or from 3.5 to 5.5 for TAR. Thus, the substitution reaction proceeds as

$$CuL + edta' \rightleftarrows Cu(edta) + L' \tag{4}$$

$$\uparrow\downarrow H^+$$

$$CuHL + edta' \rightleftarrows (Cuedta)' + L'. \tag{5}$$

If the total concentration of CuHL and CuL is expressed as [(CuL)'], the rate law is given by

$$-\frac{d[(CuL)']}{dt} = k_{obsd}[(CuL)']$$
$$= (k^{CuL}_{edta'}[CuL] + k^{CuHL}_{edta'}[CuHL])[edta']$$
$$= \left(k^{CuHL}_{edta'} + \frac{k^{CuL}_{edta'} - k^{CuHL}_{edta'}}{1+K^H_{CuHL}[H]}\right)[(CuL)'][edta'], \tag{6}$$

where

$$K^H_{CuHL} = \frac{[CuHL]}{[CuL][H]}. \tag{7}$$

The plot of k_{obsd} *vs.* pH in each case was compared with a family of normalized functions $y=p/(1+x)=f(\log x)$. As shown in Fig. 1, the plot fits well one of the theoretical curves. The values of $k^{CuL}_{edta'}$, and $k^{CuHL}_{edta'}$ are listed in Table 2.

As seen in Fig. 1 the rate of substitution reaction of CuHL further increased at pH values lower than 3.5 for PAR and 3.0 for TAR. In these pH ranges Cu-

TABLE 2. RATE CONSTANTS OF SUBSITUTION REACTIONS OF Cu(II) CHELATES WITH EDTA AT μ=0.1, AT 25 °C

	$k^{CuL}_{edta'}$ or $k^{CuHL}_{edta'}$ / dm^3 mol^{-1} s^{-1}	k^{CuL}_H or k^{CuHL}_H / dm^3 mol^{-1} s^{-1}
Cu(pan)	1.9×10^3	6.5×10
Cu(tan)	2.8×10^4	
Cu(pac)	8.0×10^4	
Cu(tac)	4×10^6	
Cu(par)	2.0×10^3	
Cu(Hpar)	1.2×10^4	6.6×10^2
Cu(tar)	6.3×10^4	
Cu(Htar)	7.9×10^5	1.2×10^4

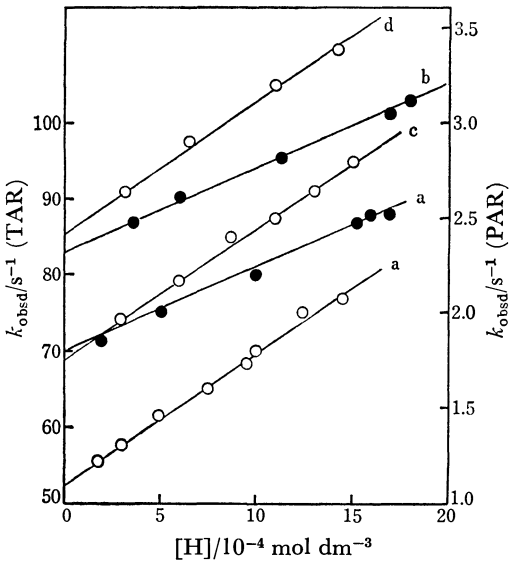

Fig. 2. Plots of log k_{obsd} *vs.* [H].
○: PAR, ●: TAR.
$C_{EDTA}=1.0\times10^{-4}$ (a), 1.2×10^{-4} (b), 1.5×10^{-4} (c), 2.0×10^{-4} mol dm^{-3} (d).

(Hpar) or Cu(Htar) is predominantly formed. Plots of k_{obsd} *vs.* the concentration of hydrogen ion yielded straight lines with intercepts on the y-axes. (Fig. 2). Thus the rate law can be expressed as

$$-\frac{d[CuHL]}{dt} = (k_{edta'}^{CuHL}[edta']+k_{H}^{CuHL}[H])[CuHL]. \quad (8)$$

The values of $k_{edta'}^{CuHL}$ and k_{H}^{CuHL} were obtained from the intercepts and the slopes of the straight lines, respectively:

$$k_{edta'}^{Cu(Hpar)} = 1.1\times10^{4}\ dm^3\ mol^{-1}\ s^{-1},$$
$$k_{edta'}^{Cu(Htar)} = 7.0\times10^{5}\ dm^3\ mol^{-1}\ s^{-1},$$
$$k_{H}^{Cu(Hpar)} = 6.6\times10^{2}\ dm^3\ mol^{-1}\ s^{-1},$$
$$k_{H}^{Cu(Htar)} = 1.2\times10^{4}\ dm^3\ mol^{-1}\ s^{-1}.$$

The values of $k_{edta'}^{CuHL}$ obtained were approximately equal to the values previously obtained by the curve fitting method.

Substitution Reaction of Copper(II) Chelate of PAN with EDTA. In our previous work,[5] the rate of the substitution reaction of Cu(pan) with EDTA was determined in the pH range from 5.0 to 6.3, in which PAN can be used as an indicator for the chelatometric titrations of copper(II). In this pH range, the substitution reaction is of first-order with respect to EDTA and Cu(pan), while there is no dependence on pH as in the cases of TAN, PAC, and TAC. In this study, in the lower pH range the rate of the substitution reaction of Cu(pan) with EDTA was examined. At pH lower than 4 the rate of the reaction gradually increased with decreasing pH, as in the cases of PAR and TAR. The conditional rate constants, k_{obsd}, depended on [H] and [edta'], hence the rate law can be written as

$$-\frac{d[Cu(pan)]}{dt} = (k_{edta'}^{Cu(pan)}[edta']+k_{H}^{Cu(pan)}[H])[Cu(pan)]. \quad (9)$$

The values of $k_{edta'}^{Cu(pan)}$ and $k_{H}^{Cu(pan)}$ obtained are shown in Table 2. The values of $k_{edta'}^{Cu(pan)}$ determined in this study agrees with that obtained in the previous study:[5]

$$k_{edta'}^{Cu(pan)} = 1.7\times10^{3}\ dm^3\ mol^{-1}\ s^{-1}.$$

Discussion

The constant rates were observed in the following pH ranges: pH 3.5—6.3 for Cu(pan), pH 4.5—5.2 for Cu(tan), pH 4.4—5.1 for Cu(pac), pH 4.0—4.6 for Cu(tac), pH 6—6.5 for Cu(par) and for Cu(tar), while the fraction of H_2edta, Hedta, and edta changes in these pH ranges. Cassatt and Wilkins reported that in the reaction of EDTA with nickel(II) ion Hedta is 10^2-fold more reactive than H_2edta.[10] From our results, however, no difference in the rate of substitution reaction with different protonated forms of EDTA was observed. Copper(II) chelates, CuL, of PAN, TAN, PAC, TAC, PAR, and TAR are substituted by EDTA in these pH regions according to the following mechanism, as proposed by Tanaka and Funahashi:

$$CuL + edta' \rightleftharpoons CuL(edta) \xrightarrow{r.d.s.} Cu(edta) + L'. \quad (10)$$

The values of log $k_{edta'}^{CuL}$ were plotted against the sum of the dissociation constants of protonated pyridine or thiazole and phenolic *o*-hydroxyl groups ($pk_{NH}+pk_{o\text{-}OH}$). (Fig. 3). A straight line was obtained. This

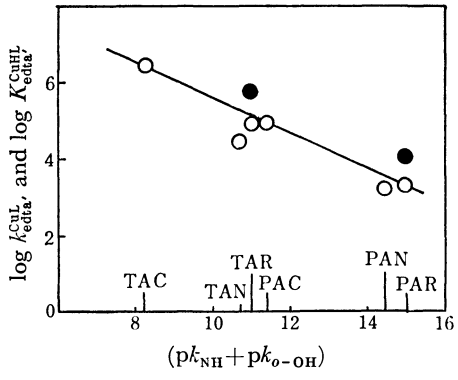

Fig. 3. Plots of log $k_{edta'}^{CuL}$, and log $K_{edta'}^{CuHL}$ *vs.* ($pk_{NH}+pk_{o\text{-}OH}$).
○: $k_{edta'}^{CuL}$, ●: $K_{edta'}^{CuHL}$.

result indicates that the rate of the substitution reaction of CuL chelate is inversely proportional to the basicities of the donor atoms of the leaving ligands. However, the values of log $k_{edta'}^{CuL}$ for Cu(pan) and Cu(tan) chelates are smaller than those of other indicators, probably due to the steric effect of the naphthalene ring in PAN or TAN. Since the basicities of donor atoms in the thiazolylazo compounds are weaker than those of corresponding pyridylazo compounds, the rate of the substitution reaction of copper(II) chelates of thiazolylazo compounds is, generally speaking, faster than that of corresponding pyridylazo compound chelates. Thus, as regards the rate of color change, the thiazolylazo compounds are more favorable for use as metallochromic indicators than the pyridylazo compounds.

The reaction rate of CuHL chelate with PAR or TAR is faster than that of CuL by one order. In the

chelatometric titrations of copper(II) with EDTA using TAR as an indicator, the optimum pH range is from 4 to 6. The large rate of the substitution reaction of Cu(Htar) chelate with EDTA gives a great advantage for the sharp color change of the indicator at the equivalence point.

References

1) G. Nakagawa and H. Wada, *Talanta*, **20**, 829 (1973).
2) M. Tanaka, S. Funahashi, and K. Shirai, *Inorg. Chem.*, **7**, 573 (1968).
3) S. Funahashi, S. Yamada, and M. Tanaka, *Bull. Chem. Soc. Jpn.*, **43**, 769 (1970).
4) S. Funahashi, M. Tabata, and M. Tanaka, *Bull. Chem. Soc. Jpn.*, **44**, 1586 (1971).
5) G. Nakagawa and H. Wada, *Talanta*, **22**, 563 (1975).
6) H. Wada and G. Nakagawa, *Bunseki Kagaku*, **14**, 28 (1965).
7) G. Nakagawa and H. Wada, *Nippon Kagaku Zasshi*, **83**, 1098 (1962).
8) H. Wada and G. Nakagawa, *Nippon Kagaku Zasshi*, **85**, 549 (1964).
9) G. Nakagawa and H. Wada, *Nippon Kagaku Zasshi*, **85**, 202 (1964).
10) J. C. Cassatt and R. G. Wilkins, *J. Am. Chem. Soc.*, **90**, 6045 (1968).

Trimethylenediamine Complexes. VIII.[1] Some Cis-Trans Isomeric Pairs of the Bis(trimethylenediamine)chromium(III) Complexes

Mamoru NAKANO and Shinichi KAWAGUCHI*

Department of Chemistry, Faculty of Science, Osaka City University, Sumiyoshi-ku, Osaka 558

(Received June 28, 1979)

The cis-trans isomeric pairs of diisothiocyanato-, dinitrito-, diazido-, diaqua-, and aquahydroxo-bis(trimethylenediamine)chromium(III) complexes have been obtained as crystals and characterized by infrared and electronic absorption spectra. The cis isomers of diisothiocyanato and diazido complexes as well as $[Cr(N_3)_2(en)_2]ClO_4$ were resolved and the absolute configurations of $(+)_{589}$-*cis*-$[Cr(NCS)_2(tn)_2]SCN$, $(+)_{589}$-*cis*-$[Cr(N_3)_2(tn)_2]ClO_4$, and $(-)_{589}$-*cis*-$[Cr(N_3)_2(en)_2]ClO_4$ were all assigned to Δ.

Comparative Chemistry of the five-membered ethylenediamine (en) chelates and the six-membered trimethylenediamine (tn) chelates is interesting from both the structural and kinetic viewpoints. Absolute configurations of several optically active cobalt(III) complexes containing trimethylenediamine as a ligand have been established by X-ray analysis,[2] and the empirical criterion of McCaffery *et al.*[3] relating the absolute configuration to the CD-spectral feature in the first d-d band region has been shown to hold in these complexes. On the other hand, optically active chromium(III) trimethylenediamine complexes are rather few, and only four examples, $(-)_{589}$-$[Cr(tn)_3]^{3+}$,[4] $(+)_{589}$-*cis*-$[CrCl_2(tn)_2]ClO_4$,[5] $(+)_{589}$-$[Cr(acac)(tn)_2]I_2\cdot 0.5H_2O$,[1] and $(-)_{589}$-$[Cr(acac)_2(tn)]I\cdot H_2O$[1] have been reported so far, and further development in this field is desirable.

The aquation rates of *trans*-$[CoCl_2(tn)_2]^+$ and *trans*-$[CoBr_2(tn)_2]^+$ are extraordinarily large as compared with those of the corresponding ethylenediamine complexes,[6] but *trans*-$[CrCl_2(tn)_2]^+$ hydrolyzes in acid solution with a rate comparable to that of *trans*-$[CrCl_2(en)_2]^+$.[7] The cis isomer of $[CoCl_2(tn)_2]^+$ is unknown,[8] although *cis*-$[CoCl_2(en)_2]^+$ is easily prepared by heating the trans isomer in aqueous solution. On the other hand, *cis*-$[CrCl_2(tn)_2]ClO_4\cdot 0.5\,H_2O$ was obtained as violet crystals, although it is liable to isomerize to the *trans* form in solution.[5] Thus further comparison of the thermodynamic and kinetic ring-size effects in the chromium(III) and cobalt(III) complexes may be interesting.

In previous papers we have prepared and characterized several cis-trans isomeric pairs of dianionbis(trimethylenediamine)cobalt(III) complexes,[9] and compared the ligand substitution rates of some trimethylenediamine cobalt(III) complexes with those of the corresponding ethylenediamine complexes.[10] The present paper reports preparation and characterization of some bis(trimethylenediamine)chromium(III) complexes inclusive of the optically active *cis*-$[Cr(NCS)_2(tn)_2]^+$ and *cis*-$[Cr(N_3)_2(tn)_2]^+$ complexes.

Experimental

Preparation and Optical Resolution of Complexes. The starting compounds, *cis*-$[CrCl_2(tn)_2]Cl\cdot H_2O$ and *trans*-$[CrCl_2(tn)_2]Cl$ were prepared by the method of Pedersen.[5] Commercially available potassium antimony(III) (*R,R*)-tartrate was used without further purification. Another resolving agent, (*R,R*)-di-*O*-benzoyltartaric acid was prepared by the reaction between (*R,R*)-tartaric acid and benzoyl chloride[11] and used after partial neutralization with one-half equivalent of sodium hydroxide.

cis-*Diisothiocyanatobis(trimethylenediamine)chromium(III) Thiocyanate Hydrate*, cis-$[Cr(NCS)_2(tn)_2]SCN\cdot H_2O$: Aqueous solution (10 ml) of *cis*-$[CrCl_2(tn)_2]Cl\cdot H_2O$ (1.1 g) was heated at 70 °C on a water-bath for 10 min to result in a red-orange solution, to which was added sodium thiocyanate (1.6 g) and heating was continued for about 1 h to obtain an orange precipitate. After cooling to room temperature, another portion (1.0 g) of sodium thiocyanate was added to the mixture, which was then allowed to stand overnight. The crude product was filtered, washed with cold water and air-dried. The yield was 1.2 g (92.6%). Recrystallization from hot water gave orange needles.

trans-*Diisothiocyanatobis(trimethylenediamine)chromium(III) Thiocyanate*, trans-$[Cr(NCS)_2(tn)_2]SCN$: The reaction of *trans*-$[CrCl_2(tn)_2]Cl$ (1.0 g) with sodium thiocyanate was performed in a similar manner as above to obtain orange crystals in an 80.9% (1.0 g) yield. Recrystallization from hot water gave orange plates.

cis-*Diaquabis(trimethylenediamine)chromium(III) Nitrate*, cis-$[Cr(H_2O)_2(tn)_2](NO_3)_3$: A solution (5 ml) of silver nitrate (1.7 g) was added to an aqueous solution (10 ml) of *cis*-$[CrCl_2(tn)_2]Cl\cdot H_2O$ (1.1 g) and the mixture was stirred at room temperature for 1 h to complete the reaction. A precipitate of silver chloride was filtered. Concentrated nitric acid (20 ml) and ethanol (50 ml) were added to the combined washings and the solution was left in a refrigerator to deposit an orange precipitate in a 69.8% (1.0 g) yield. The crude product was dissolved in a minimum amount of water and a few drops of concentrated nitric acid was added to the solution. On cooling in ice orange plate precipitated.

cis-*Aquahydroxobis(trimethylenediamine)chromium(III) Nitrate Hemihydrate*, cis-$[CrOH(H_2O)(tn)_2](NO_3)_2\cdot 0.5H_2O$: To an aqueous solution (5 ml) of *cis*-$[Cr(H_2O)_2(tn)_2](NO_3)_3$ (1.0 g) was added aqueous ammonia drop by drop to adjust pH to *ca.* 7, color of the solution changing from orange to red. Ethanol (50 ml) was poured into the solution to deposit a red precipitate. The yield was 0.8 g (94.0%). Recrystallization from water–ethanol gave red needles which are slightly hygroscopic.

trans-*Aquahydroxobis(trimethylenediamine)chromium(III) Nitrate*, trans-$[CrOH(H_2O)(tn)_2](NO_3)_2$: One gram of *trans*-$[CrCl_2(tn)_2]Cl$ was dissolved in hot water. A solution (5 ml) of silver nitrate (1.7 g) was added and the mixture was kept at 50 °C for 2 h to complete the reaction. After cooling to room temperature, silver chloride was filtered. On addition of aqueous ammonia dropwise to the combined washings to attain pH≈7 (solution turning red), red-brown thin crystals precipitated. The yield was 0.3 g (25.6%). After separation

of the product, concentrated nitric acid (20 ml) and ethanol (50 ml) were added to the filtrate and the mixture was kept in a refrigerator to deposit an orange precipitate, which was identified as *cis*-$[Cr(H_2O)_2(tn)_2](NO_3)_3$ on the basis of IR and electronic spectra. The yield of the *cis*-diaqua complex was 0.6 g (43.6%).

trans-*Diaquabis(trimethylenediamine)chromium(III) Nitrate*, trans-$[Cr(H_2O)_2(tn)_2](NO_3)_3$: The aquahydroxo complex *trans*-$[CrOH(H_2O)(tn)_2](NO_3)_2$ (1.0 g) was dissolved in *ca.* 8 M nitric acid (20 ml) and the solution was stirred for a while to separate out a red-brown precipitate in an 85.1% (1.1 g) yield. The crude product was dissolved in a minimum amount of water. After filtration, the solution was kept in ice and concentrated nitric acid was added dropwise to it to precipitate red-brown needles.

cis-*Dinitritobis(trimethylenediamine)chromium(III) Perchlorate*, cis-$[Cr(ONO)_2(tn)_2]ClO_4$: Sodium nitrite (0.5 g) was added to an aqueous solution (10 ml) of *cis*-$[Cr(H_2O)_2(tn)_2](NO_3)_3$ (1.0 g) and the mixture was stirred for 10 min in an ice bath. After filtration, sodium perchlorate (2.0 g) was added to the filtrate and the solution was kept overnight in a refrigerator to deposit orange prisms. The yield was 0.74 g (79.8%). The product is slightly hygroscopic and was recrystallized from hot water. The compound is not so stable against light, but changes slightly to red on long standing.

trans-*Dinitritobis(trimethylenediamine)chromium(III) Perchlorate*, trans-$[Cr(ONO)_2(tn)_2]ClO_4$: The reaction of *trans*-$[Cr(H_2O)_2(tn)_2](NO_3)_3$ (1.0 g) with sodium nitrite (0.5 g) was performed in the same manner as above to obtain orange crystals of the trans isomer in a 91.6% (0.85 g) yield. Orange plates were obtained by recrystallization from hot water.

cis-*Diazidobis(trimethylenediamine)chromium(III) Perchlorate*, cis-$[Cr(N_3)_2(tn)_2]ClO_4$: An excess amount (15.0 g) of sodium azide was added to a solution of *cis*-$[Cr(H_2O)_2(tn)_2](NO_3)_3$ (15.0 g) in a mixture of acetic acid (10 ml) and water (30 ml) and the solution was heated at 50 °C for 10 min to turn deep violet. Sodium perchlorate (5.0 g) was added after cooling to room temperature and the mixture was kept in a refrigerator overnight to precipitate red plates. The yield was 4.8 g (35.2%). Recrystallization from acetone–ethanol gave red needles.

trans-*Diazidobis(trimethylenediamine)chromium(III) Perchlorate*, trans-$[Cr(N_3)_2(tn)_2]ClO_4$: Sodium azide (1.0 g) was added to an aqueous solution (10 ml) of *trans*-$[Cr(H_2O)_2(tn)_2](NO_3)_3$ (1.0 g) and the mixture was heated at 50 °C for 5 min to afford a red solution, to which was added sodium perchlorate (2.0 g) and heated at 50 °C for further 1.5 h to turn violet. After cooling to room temperature, 60% perchloric acid was added to adjust pH to *ca.* 7 and the solution was kept in a refrigerator overnight to deposit violet needles. The yield was 0.2 g (22.0%). Recrystallization from hot water gave deep violet plates.

Caution: Synthesis of the azido complexes must be performed in a good hood, since gaseous hydrazoic acid is evolved.

$(+)_{589}$-cis-*Diisothiocyanatobis(trimethylenediamine)chromium(III) Thiocyanate*, $(+)_{589}$-cis-$[Cr(NCS)_2(tn)_2]SCN$: A solution (100 ml) of sodium hydrogen (*R,R*)-di-*O*-benzoyltartrate (1.2 g) was added slowly to an aqueous solution (100 ml) of *cis*-$[Cr(NCS)_2(tn)_2]SCN\cdot H_2O$ (1.2 g) with stirring at 50 °C. After cooling to room temperature, a pink precipitate was filtered, washed with water and air-dried. The yield was 0.8 g. Found: C, 44.90; H, 4.94; N, 11.95%. Calcd for $[Cr(NCS)_2(tn)_2][HC_{18}H_{12}O_8]\cdot H_2O = C_{26}H_{35}N_6O_9S_2Cr$: C, 45.14; H, 5.16; N, 12.14%. The diastereoisomer (0.8 g) was dissolved in a solution (10 ml) of sodium thiocyanate (2.0 g) and sodium hydroxide (0.1 g), and the mixture was stirred in an ice bath for 5 min. An orange precipitate was filtered, washed with water and air-dried. The yield was 0.4 g. Recrystallization from acetone–diethyl ether gave orange needles. In order to assure the optical purity, the resolution process was repeated. Molar rotations in methanol are $[M]_{589} = +312°$ and $[M]_{436} = +937°$.

$(-)_{589}$-cis-*Diisothiocyanatobis(trimethylenediamine)chromium(III) Thiocyanate*, $(-)_{589}$-cis-$[Cr(NCS)_2(tn)_2]SCN$: A solution (50 ml) of potassium antimony (*R,R*)-tartrate (0.8 g) was added to a solution of *cis*-$[Cr(NCS)_2(tn)_2]SCN\cdot H_2O$ (1.0 g) in a mixture of acetone (40 ml) and water (40 ml), and the solution was left standing in a refrigerator for two days. Orange needles of diastereoisomer were filtered, washed with a small amount of cold water and air-dried. The yield was 0.6 g. Found: C, 23.31; H, 4.23; N, 13.11%. Calcd for $[Cr(NCS)_2(tn)_2]SbC_4H_2O_6\cdot 2H_2O = C_{12}H_{26}N_6O_8S_2SbCr$: C, 23.24; H, 4.23; N, 13.55%. The diastereoisomer was added to a solution (5 ml) of sodium thiocyanate (2.0 g) and the mixture was stirred for 10 min to deposit orange and white precipitates, which were filtered, washed with cold water and air-dried. Acetone dissolved the orange precipitate, leaving the insoluble white one. Diethyl ether was added to the combined washings to precipitate the $(-)_{589}$ isomer (0.3 g). The resolution procedure was repeated once again to assure the optical purity. The observed values of molar rotation in methanol, $[M]_{589} = -314°$ and $[M]_{436} = -936°$, show an excellent coincidence with those of the $(+)_{589}$ isomer which was obtained above by the resolution with sodium hydrogen-(*R,R*)-di-*O*-benzoyltartrate.

$(+)_{589}$-cis-*Diisothiocyanatobis(ethylenediamine)chromium(III) Thiocyanate*, $(+)_{589}$-cis-$[Cr(NCS)_2(en)_2]SCN$: This complex has already been resolved by House,[12] and both of pure $(+)_{589}$ and $(-)_{589}$ isomers were isolated in solution. Now for comparison with the corresponding trimethylenediamine complex, the ethylenediamine complex was resolved by potassium antimony (*R,R*)-tartrate and isolated as crystals of which the molar rotations are $[M]_{589} = +22°$, $[M]_{546} = +402°$ and $[M]_{436} = -704°$ in methanol and $[M]_{589} = +100°$, $[M]_{546} = -434°$ and $[M]_{436} = -810°$ in water.

$(+)_{589}$-cis-*Diazidobis(trimethylenediamine)chromium(III) Perchlorate*, $(+)_{589}$-cis-$[Cr(N_3)_2(tn)_2]ClO_4$: A solution (200 ml) of sodium hydrogen (*R,R*)-di-*O*-benzoyltartrate (4.8 g) was added slowly to an aqueous solution (250 ml) of the racemic complex (4.8 g). A red precipitate, which deposited from the solution kept in an ice bath for 1 h, was filtered, washed with cold water and air-dried. The yield was 2.7 g. Found: C, 44.08; H, 5.09; N, 21.16%. Calcd for $[Cr(N_3)_2(tn)_2][HC_{18}H_{12}O_8]\cdot H_2O = C_{24}H_{35}N_{10}O_9Cr$: C, 43.70; H, 5.35; N, 21.24%. A mixture of the diastereoisomer (0.9 g) and silver acetate (0.4 g) was stirred in water (10 ml) for 5 min. Acetone (50 ml) was added to the solution to precipitate the silver salt of resolving agent. Sodium perchlorate (2.0 g) was dissolved in the filtrate and acetone was distilled away under reduced pressure to deposit a red precipitate (0.35 g). Repeated resolution assured the optical purity of the product, of which the molar rotations are $[M]_{589} = +76°$ and $[M]_{436} = +1590°$ in water.

$(-)_{589}$-cis-*Diazidobis(ethylenediamine)chromium(III) Perchlorate*, $(-)_{589}$-cis-$[Cr(N_3)_2(en)_2]ClO_4$: Racemic *cis*-$[Cr(N_3)_2(en)_2]ClO_4$ (2.0 g) prepared according to the literature[13] was resolved by sodium hydrogen (*R,R*)-di-*O*-benzoyltartrate and worked up to obtain the optically active perchlorate as red-violet plates (0.3 g). Repeated resolution assured the optical purity. The molar rotations are $[M]_{589} = -754°$ and $[M]_{436} = +710°$ in water.

Measurements. The electronic absorption spectra were measured by a Hitachi EPS-3T spectrophotometer, and the IR spectra by JASCO IR-E (4000—600 cm^{-1}) and Hitachi

EPI-L (700—200 cm^{-1}) spectrometers. The optical rotations were determined with a Yanagimoto OR-50 polarimeter, and the CD spectra with a JASCO J-20 recording spectrometer.

Results and Discussion

Several kinds of cis-trans isomeric pairs of the bis(trimethylenediamine)chromium(III) complexes were prepared by the ligand substitution reactions of *cis*- and *trans*-$[CrCl_2(tn)_2]^+$ in aqueous solution. Results of the elemental analysis for the products are collected in Table 1. The ligand substitution reactions of these chromium(III) complexes proceeded with steric retention except in one case. As was described in Experiment, the yield of *trans*-$[CrOH(H_2O)(tn)_2](NO_3)_2$ from *trans*-$[CrCl_2(tn)_2]Cl$ was as low as 25.6% and acidification of the mother liquor gave *cis*-$[Cr(H_2O)_2(tn)_2](NO_3)_3$ in a 43.6% yield. Thus the hydrolysis of *trans*-$[CrCl_2(tn)_2]^+$ induced by the silver ion resulted in *ca.* 50% isomerization under the synthetic conditions. For the sake of comparison, the reaction of *trans*-$[CrCl_2(en)_2]^+$ with silver nitrate was examined, and only *trans*-$[Cr(H_2O)_2(en)_2]^+$ was obtained.

The spontaneous solvolysis of dihalogenobis(diamine)chromium(III) complexes usually occurs with essentially complete retention of configuration.[14] However the secondary hydrolysis of *trans*-$[CrCl_2(tn)_2]^+$ was reported to be complicated by isomerization.[7] The silver(I)-induced aquation of the $[CrCl_2(tn)_2]^+$ complexes seems to proceed *via* the **D** mechanism by analogy with the mercury(II)-catalyzed aquation of $[CrX(H_2O)_5]^{2+}$ (X= F, Cl, Br, and I).[15] It is noteworthy and deserves detailed investigation that the silver(I)-assisted complete aquation of *cis*-$[CrCl_2(tn)_2]^+$ occurs stereoretentively under the present synthetic conditions, while *trans*-$[CrCl_2(tn)_2]^+$ gives a mixture of *cis*- and *trans*-diaqua complexes.

The *cis*- and *trans*-dinitritobis(ethylenediamine)chromium(III) complexes have been synthesized and characterized by Garner and his coworkers.[16] Now the trimethylenediamine analogues are reported. When excess sodium nitrite was used, *cis*- and *trans*-$[Cr(ONO)_2(tn)_2]NO_2$ were obtained as hemihydrate and anhydrous salt, respectively. The cis nitrite salt is even more unstable than the perchlorate. Thus the crude product was obtained as lustrous brown plates, but lost lustre on washing with alcohol, decomposing rapidly. Optical resolution of the *cis*-$[Cr(ONO)_2tn_2]^+$ salts by means of sodium hydrogen (*R,R*)-di-*O*-benzoyltartrate was unsuccessful because of instability of the complex.

Wendlandt prepared *cis*-$[Cr(NCS)_2(tn)_2]SCN$ by the thermal matrix reaction.[17] In the present study the *cis*-diisothiocyanato complex was obtained as a hydrate by the reaction in aqueous solution, but changed curiously to anhydrous salts after optical resolution. Resolution of *cis*-$[Cr(NCS)_2(en)_2]^+$ was successful only by means of the antimony (*R,R*)-tartrate, and the values of molar rotation in aqueous solution nearly coincide with those reported by House.[12] Rotations in methanol were also recorded for comparison with $(+)_{589}$- and $(-)_{589}$-*cis*-$[Cr(NCS)_2(tn)_2]SCN$ whose solubilities in water are very poor.

Both *cis*- and *trans*-$[Cr(N_3)_2(tn)_2]ClO_4$ were obtained although *trans*-$[Cr(N_3)_2(en)_2]^+$ has not yet been reported. Both isomers are rather stable and can be recrystallized from hot water. The optical rotation of $(+)_{589}$-*cis*-$[Cr(N_3)_2(tn)_2]^+$ as well as that of $(+)_{589}$-*cis*-$[Cr(NCS)_2(tn)_2]^+$ shows no change after leaving for one day in aqueous solution at room temperature.

Infrared Spectra. Infrared spectra of the dianionobis(diamine)metal complexes are useful for distinguishing linkage[18] and geometrical[19] isomers. *cis*- and *trans*-$[Cr(ONO)_2(tn)_2]ClO_4$ exhibit the ν(N=O) bands at 1500 and 1470 cm^{-1}, respectively and no band assignable to the $\rho_w(NO_2)$ vibration, although the ν(N–O) bands which are expected to appear around 1100 cm^{-1} are masked by the absorption of the perchlorate anion. Thus the NO_2^- ligand is considered to have the Cr–O linkage in both isomers as is known for all other chromium(III)–nitrite complexes. The Cr–N linkage of the thiocyanate ligand in *cis*- and *trans*-$[Cr(NCS)_2(tn)_2]SCN$ is also suggested by IR

Table 1. Analytical data for the bis(trimethylenediamine)chromium(III) complexes

Complex	Found, %			Calcd, %		
	C	H	N	C	H	N
cis-$[Cr(NCS)_2(tn)_2]SCN\cdot H_2O$	27.80	5.80	24.79	27.53	5.64	24.99
$(+)_{589}$-*cis*-$[Cr(NCS)_2(tn)_2]SCN$	28.35	5.41	25.65			
$(-)_{589}$-*cis*-$[Cr(NCS)_2(tn)_2]SCN$	28.55	5.29	25.92	28.87	5.38	26.18
trans-$[Cr(NCS)_2(tn)_2]SCN$	28.89	5.55	25.53			
$(+)_{589}$-*cis*-$[Cr(NCS)_2(en)_2]SCN$	24.65	4.66	27.90	24.27	4.66	28.30
cis-$[Cr(H_2O)_2(tn)_2](NO_3)_3$	17.27	5.80	23.13	17.07	5.76	23.33
trans-$[Cr(H_2O)_2(tn)_2](NO_3)_3$	17.06	5.81	23.30			
cis-$[CrOH(H_2O)(tn)_2](NO_3)_2\cdot 0.5H_2O$	19.56	6.57	22.68	19.57	6.57	22.82
trans-$[CrOH(H_2O)(tn)_2](NO_3)_2$	20.01	6.42	23.07	20.06	6.45	23.39
cis-$[Cr(ONO)_2(tn)_2]ClO_4$	18.15	5.15	20.95	18.40	5.15	21.46
trans-$[Cr(ONO)_2(tn)_2]ClO_4$	18.51	5.30	20.79			
cis-$[Cr(N_3)_2(tn)_2]ClO_4$	18.81	5.32	36.13			
$(+)_{589}$-*cis*-$[Cr(N_3)_2(tn)_2]ClO_4$	18.77	5.25	36.09	18.78	5.25	36.50
trans-$[Cr(N_3)_2(tn)_2]ClO_4$	18.45	5.29	36.10			
$(-)_{589}$-*cis*-$[Cr(N_3)_2(tn)_2]ClO_4$	13.76	4.42	39.00	13.51	4.53	39.38

spectra, the ν(C≡N) and δ(NCS) bands appearing at around 2090 and 480 cm^{-1}, respectively in either isomer.

Baldwin's criterion[20] to distinguish between geometrical isomers was successful for many dianionobis(trimethylenediamine)cobalt(III) complexes,[9,21] trans isomers exhibiting one peak and cis isomers two in the CH_2-rocking (880—900 cm^{-1}) region. However all of the present chromium(III) complexes except *trans*-$[Cr(ONO)_2(tn)_2]ClO_4$ have single peak in the 880—895 cm^{-1} region irrespective of the geometrical structure, invalidating the Baldwin's criterion.

Hughes and McWhinnie examined the IR spectra of eleven bis(ethylenediamine)chromium(III) complexes including four cis-trans couples, and found the clearest distinction in the band pattern in the 550—395 cm^{-1} region.[22] Figures 1 and 2 show the IR spectra in the lower frequency region of four isomeric pairs of bis(trimethylenediamine)chromium(III) complexes. The complexity in the band pattern for each cis isomer compared with that for the corresponding trans isomer is apparent in the 550—330 cm^{-1} region. Thus discrimination between cis and trans isomers seems possible in these cases if the couple is presented, whereas it will be quite difficult to assign the geometrical structure on the IR data when only one isomer is obtained.[23]

Absorption and CD Spectra. Table 2 collects the absorption data for the present complexes. The molar absorbance of each cis isomer in the first d-d band is a little larger than that of the trans isomer except for the diazido complexes. Similar trend has frequently been reported for bis(ethylenediamine)chromium(III) complexes.[24] It is noteworthy in the present complexes that the energy difference between the first and second bands is larger for the trans isomer than for the cis isomer (Table 2).

In the case of dianionobis(trimethylenediamine)-cobalt(III) complexes, the absorption maxima of the first band exist in appreciably lower energy region as compared with those of the corresponding ethylenediamine complexes, indicating the weak ligand field of trimethylenediamine relative to ethylenediamine.[9,21] In the case of chromium(III) complexes, the same trend is observed but the difference is quite small.

TABLE 2. ELECTRONIC ABSORPTION DATA FOR THE BIS(TRIMETHYLENEDIAMINE)CHROMIUM(III) COMPLEXES

Complex	Solvent	λ_{max} / nm	ε_{max} / $l \cdot mol^{-1} \cdot cm^{-1}$	$\Delta\nu_{12}$[a] / 10^3 cm^{-1}
cis-$[Cr(NCS)_2(tn)_2]SCN \cdot H_2O$	CH_3OH	498	(109)	6.23
		380	(66.4)	
		318	(6560)	
		268	(4720)	
		233	(13500)	
trans-$[Cr(NCS)_2(tn)_2]SCN$	CH_3OH	510	(94.5)	6.85
		378	(69.7)	
		316	(10000)	
		263sh	(4950)	
		237	(15400)	
cis-$[Cr(H_2O)_2(tn)_2](NO_3)_3$	1M HNO_3	490	(41.8)	6.91
		366	(37.0)	
trans-$[Cr(H_2O)_2(tn)_2](NO_3)_3$	1M HNO_3	520sh	(19.6)	7.94
		452	(28.8)	
		368	(42.1)	
cis-$[Cr(ONO)_2(tn)_2]ClO_4$	H_2O	488	(49.7)	7.44
		358	(103)	
		245sh		
		235sh		
trans-$[Cr(ONO)_2(tn)_2]ClO_4$	H_2O	485	(43.2)	9.68
		366sh		
		330	(174)	
		266sh		
		250sh		
		237sh		
cis-$[Cr(N_3)_2(tn)_2]ClO_4$	H_2O	520	(136)	5.77
		400	(115)	
		270	(5670)	
		225	(12100)	
trans-$[Cr(N_3)_2(tn)_2]ClO_4$	H_2O	544	(157)	6.74
		398	(97.1)	
		278	(5290)	
		250sh		
		228	(10100)	

a) Difference in wave numbers between the first and second absorption maxima.

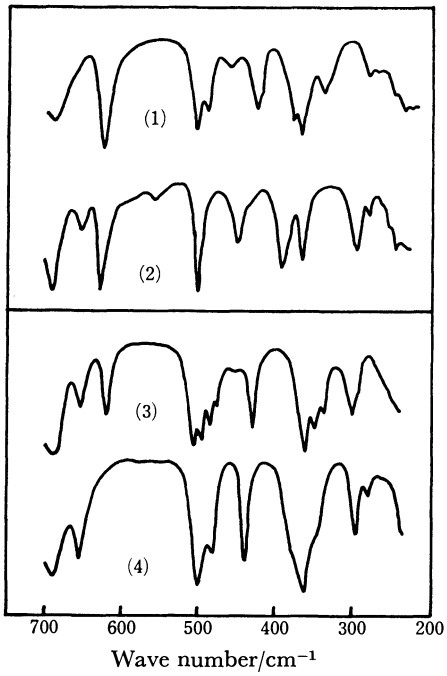

Fig. 1. Infrared spectra (700—200 cm^{-1}) in Nujol of *cis*-$[Cr(ONO)_2(tn)_2]ClO_4$ (1), *trans*-$[Cr(ONO)_2(tn)_2]ClO_4$ (2), *cis*-$[Cr(NCS)_2(tn)_2]SCN$ (3), and *trans*-$[Cr(NCS)_2(tn)_2]SCN$ (4).

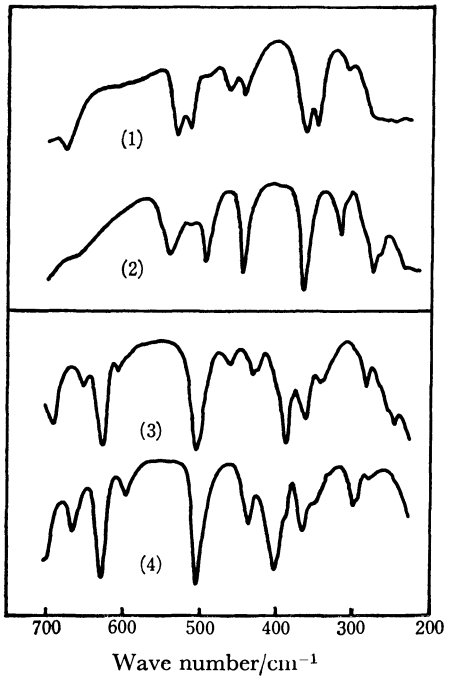

Fig. 2. Infrared spectra (700—200 cm^{-1}) in Nujol of *cis*-$[Cr(H_2O)_2(tn)_2](NO_3)_3$ (1), *trans*-$[Cr(H_2O)_2(tn)_2](NO_3)_3$ (2), *cis*-$[Cr(N_3)_2(tn)_2]ClO_4$ (3), and *trans*-$[Cr(N_3)_2(tn)_2]ClO_4$ (4).

Thus the largest value of difference in λ_{max} is 14 nm observed between *trans*-$[CrCl_2(tn)_2]Cl$ (590 nm) and *trans*-$[CrCl_2(en)_2]Cl$ (576 nm), and in the case of *cis*-diisothiocyanato and *cis*-diazido complexes depicted in Figs. 3 and 4, respectively, the difference is negligibly

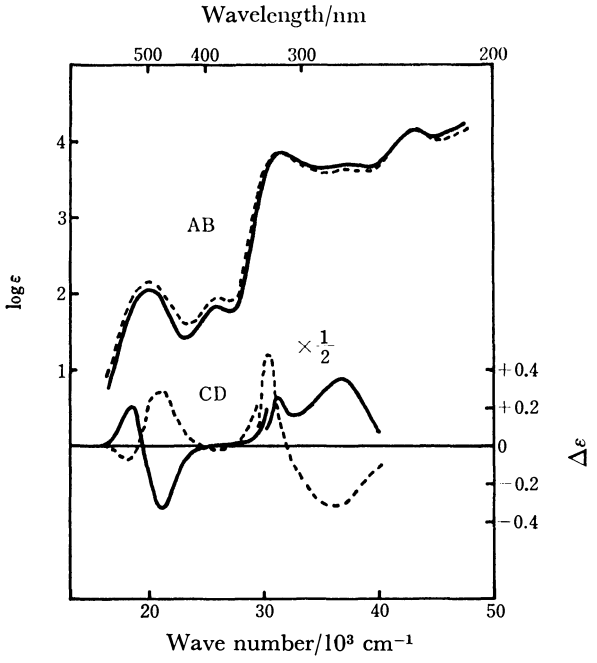

Fig. 3. Absorption and CD spectra of $(+)_{589}$-*cis*-$[Cr(NCS)_2(tn)_2]SCN$ (——) and $(+)_{589}$-*cis*-$[Cr(NCS)_2(en)_2]SCN$ (- - -) in methanol.

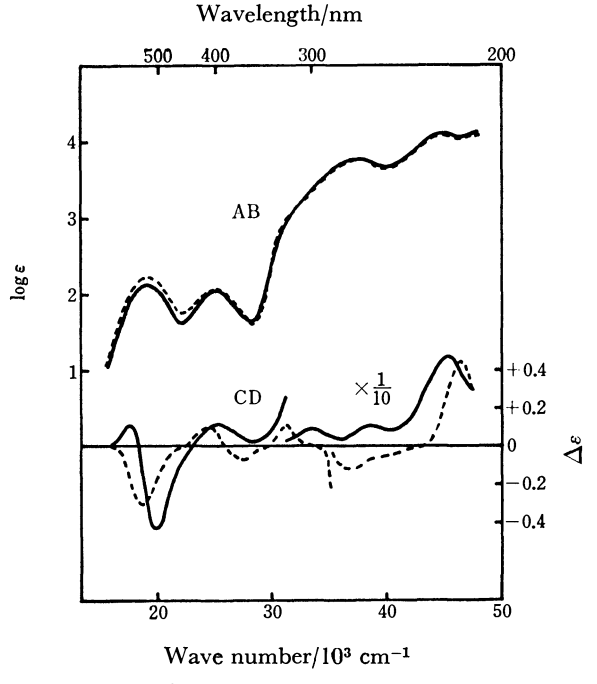

Fig. 4. Absorption and CD spectra of $(+)_{589}$-*cis*-$[Cr(N_3)_2(tn)_2]ClO_4$ (——) and $(-)_{589}$-*cis*-$[Cr(N_3)_2(en)_2]ClO_4$ (- - -) in water.

small (2 nm).

Figures 3 and 4 also compare the CD spectra of the diisothiocyanato- and diazido–bis(diamine) complexes. Although the intensity of the positive CD band of $(+)_{546}$-$[Cr(tn)_3](ClO_4)_3$ in the first d-d absorption band region ($\Delta\varepsilon = +0.34$ at 20.9×10^3 cm^{-1} in water) is remarkably smaller than that of $(+)_{546}$-$[Cr(en)_3](ClO_4)_3$ ($\Delta\varepsilon = +1.49$ at 21.9×10^3 cm^{-1} in water),[25] the intensities of CD bands in the same region of $(+)_{589}$-

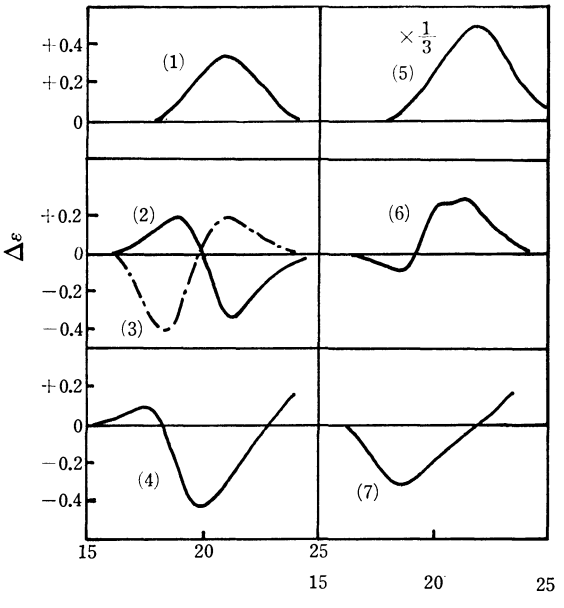

Fig. 5. CD bands in the first d-d absorption region of $(+)_{546}$-$[Cr(tn)_3](ClO_4)_3$ in water (1),[25] $(+)_{589}$-*cis*-$[Cr(NCS)_2(tn)_2]SCN$ in methanol (2), *Λ*-$(-)_{589}$-*cis*-$[Co(NCS)_2(tn)_2]SCN$ in water (3),[9] $(+)_{589}$-*cis*-$[Cr(N_3)_2(tn)_2]ClO_4$ in water (4), $(+)_{546}$-$[Cr(en)_3](ClO_4)_3$ in water (5),[25] $(+)_{589}$-*cis*-$[Cr(NCS)_2(en)_2]SCN$ in methanol (6), and $(-)_{589}$-*cis*-$[Cr(N_3)_2(en)_2]ClO_4$ in water (7).

cis-$[Cr(NCS)_2(tn)_2]SCN$ and $(+)_{589}$-*cis*-$[Cr(N_3)_2(tn)_2]ClO_4$ are rather larger than those of the corresponding ethylenediamine complexes. Another feature to be noted is that $(+)_{589}$-*cis*-$[Cr(N_3)_2(tn)_2]ClO_4$ exhibits two CD components in this region, whereas $(-)_{589}$-*cis*-$[Cr(N_3)_2(en)_2]ClO_4$ only one.

Figure 5 compares the CD spectra of the bis(diamine) complexes in the first d-d absorption region with those of the tris(diamine) complexes. The CD pattern of $(+)_{589}$-*cis*-$[Cr(NCS)_2(tn)_2]SCN$ is just opposite to that of $(-)_{589}$-*cis*-$[Co(NCS)_2(tn)_2]SCN$[9] which was confirmed by X-ray analysis to have the *Λ* configuration.[26] Thus the absolute configuration of $(+)_{589}$-*cis*-$[Cr(NCS)_2(tn)_2]SCN$ is readily assigned to *Δ*. On the same reasoning $(+)_{589}$-*cis*-$[Cr(NCS)_2(en)_2]^+$ was concluded to be *Λ* by House.[12] The dominant CD band of this ethylenediamine complex is positive in accord with the CD band of *Λ*-$[Cr(en)_3](ClO_4)_3$ in this region.[25] On the contrary $(-)_{589}$-*cis*-$[Cr(N_3)_2(en)_2]ClO_4$ exhibits a negative band, suggesting the *Δ* configuration. The spectral pattern of $(+)_{589}$-*cis*-$[Cr(N_3)_2(tn)_2]ClO_4$ closely resembles that of $(+)_{589}$-*cis*-$[Cr(NCS)_2(tn)_2]SCN$, both having the dominant negative component in the higher energy region. Thus the absolute configuration of $(+)_{589}$-*cis*-$[Cr(N_3)_2(tn)_2]ClO_4$ is assigned to *Δ* in accordance with the *Δ* configuration of $(-)_{589}$-*cis*-$[Cr(N_3)_2(en)_2]ClO_4$.

The authors wish to thank Mr. J. Gohda for the elemental analyses. This work was supported in part by the Grant-in-Aid administered by the Ministry of Education.

References

1) Part VII: M. Nakano, S. Kawaguchi, and H Kawaguchi, *Bull. Chem. Soc. Jpn.*, **52**, 2897 (1979).
2) Y. Saito, T. Nomura, and F. Marumo, *Bull. Chem. Soc. Jpn.*, **41**, 530 (1968); **42**, 1016 (1969); H. V. F. Schousboe-Jensen, *Acta Chem. Scand.*, **26**, 3413 (1972); K. Matsumoto, H. Kawaguchi, H. Kuroya, and S. Kawaguchi, *Bull. Chem. Soc. Jpn.*, **46**, 2424 (1973).
3) A. J. McCaffery, S. F. Mason, and R. E. Ballard, *J. Chem. Soc.*, **1965**, 2883.
4) O. Kling and F. Woldbye, *Acta Chem. Scand.*, **15**, 704 (1961); P. G. Beddoe and S. F. Mason, *Inorg. Nucl. Chem. Lett.*, **4**, 433 (1968).
5) E. Pedersen, *Acta Chem. Scand.*, **24**, 3362 (1970).
6) I. R. Jonasson, R. S. Murray, D. R. Stranks, and J. K. Yandell. Proc. XII ICCC, **1969**, p. 32.
7) M. C. Couldwell and D. A. House, *Inorg. Chem.*, **11**, 2024 (1972); M. C. Couldwell, D. A. House, and H. K. J. Powell, *ibid.*, **12**, 627 (1973).
8) Recently the *cis*-$[CoCl(A)(tn)_2]^{2+}$ complexes (A=various primary amines) were prepared and shown to hydrolyze with rates about 100 times larger than those of the corresponding ethylenediamine complexes: B. M. Oulaghan and D. A. House, *Inorg. Chem.*, **17**, 2197 (1978).
9) H. Kawaguchi and S. Kawaguchi, *Bull. Chem. Soc. Jpn.*, **7**, 2103 (1970); **11**, 3453 (1973).
10) Y. Ito and S. Kawaguchi, *Bull. Chem. Soc. Jpn.*, **51**, 1083, 2321 (1978); Y. Ito, A. Terada, and S. Kawaguchi, *ibid.*, **51**, 2898 (1978).
11) C. L. Butler and L. H. Cretcher, *J. Am. Chem. Soc.*, **55**, 2605 (1933).
12) D. A. House, *J. Inorg. Nucl. Chem.*, **35**, 3103 (1973).
13) L. M. Linhard and M. Weigel, *Z. Anorg. Allg. Chem.*, **271**, 131 (1953).
14) *E.g.* C. P. Madhusudhan and J. A. McLean, Jr., *Inorg. Chem.*, **14**, 82 (1975); W. G. Jackson and W. W. Fee, *ibid.*, **14**, 1154 (1975).
15) J. P. Birk and C. M. Ingerman, *Inorg. Chem.*, **11**, 2019 (1972).
16) W. W. Fee, C. S. Garner, and J. N. MacB. Harrowfield, *Inorg. Chem.*, **6**, 87 (1967).
17) W. W. Wendlandt and L. K. Sveum, *J. Inorg. Nucl. Chem.*, **29**, 975 (1967).
18) R. A. Bailey, S. L. Kozak, T. W. Michelsen, and W. N. Mills, *Coord. Chem. Rev.*, **6**, 407 (1971); A. H. Norbury, *Adv. Inorg. Chem. Radiochem.*, **17**, 232 (1975).
19) M. N. Hughes and W. R. McWhinnie, *J. Inorg. Nucl. Chem.*, **23**, 1659 (1966) and references cited therein.
20) M. E. Baldwin, *J. Chem. Soc.*, **1960**, 4369.
21) H. Kawaguchi, N. Yano, and S. Kawaguchi, *Bull. Chem. Soc. Jpn.*, **42**, 136 (1969).
22) M. N. Hughes and W. R. McWhinnie, *J. Chem. Soc.*, *A*, **1967**, 592.
23) The IR spectra of *cis*- and *trans*-$[CrOH(H_2O)(tn)_2](NO_3)_2$ in the lower frequency region are not well-defined and unsuitable for the structural discrimination. The assignment of the geometrical structure of these complexes was made in relation to the corresponding diaqua complexes.
24) *E.g.* S. Kaizaki, J. Hidaka, and Y. Shimura, *Bull. Chem. Soc. Jpn.*, **48**, 902 (1975); C. F. C. Wong and A. D. Kirk, *Can. J. Chem.*, **53**, 3388 (1975).
25) S. Kaizaki, J. Hidaka, and Y. Shimura, *Bull. Chem. Soc. Jpn.*, **43**, 1100 (1970).
26) K. Matsumoto, M. Yonezawa, H. Kuroya, H. Kawaguchi, and S. Kawaguchi, *Bull. Chem. Soc. Jpn.*, **43**, 1269 (1970).

Rotational Isomerism in Fluorene Derivatives. III.[1] The Conformation of 9-(9-Fluorenyl)-9-(2-substituted 9-fluorenyl)fluorene Derivatives

Shoji KAJIGAESHI,* Shizuo FUJISAKI, Ichishi AIZU, and Hiroshi HARA†

Department of Industrial Chemistry, Faculty of Engineering, Yamaguchi University, Tokiwadai, Ube 755

†*Tokuyama Technical College, Kume, Tokuyama 745*

(Received September 8, 1978)

The conformations of 9,9-di(9-fluorenyl)fluorene derivatives (**1**) with substituents at the 2- or 2,7-positions in a terminal fluorene ring were illustrated by the *gauche-gauche* forms at room temperature. DNMR studies of **1** gave the values of about 85—88 kJ/mol for the free energy of activation ($\Delta G^{\ddagger}$) for the restricted rotation around the C(9)–C(9) bonds. The conformation of 9,9-di(9-fluorenyl)fluorene, the parent compound of **1**, was also shown to the only *gauche-gauche* ($+sc$, $+sc$ or $-sc$, $-sc$) form at room temperature.

We have recently reported[2] that the NMR signal of 9-(9-fluorenyl)-9-(2-methyl-9-fluorenyl)fluorene (**1a**) at room temperature showed the existence of two conformers which were caused by restricted rotation around the C(9)–C(9) bonds, and that both the conformations were illustrated by the more stable form, the *gauche-gauche* form. In this paper, we would like to describe the conformations of 9,9-di(9-fluorenyl)fluorene derivatives (**1**) with methyl, ethyl, methoxy, acetyl, and bromo substituents at the 2- or 2,7-positions in a terminal fluorene ring, and also the conformation of the parent 9,9-di(9-fluorenyl)fluorene (**4**).

The derivatives **1** were prepared from the Michael reactions[3] of 9,9′-bifluorenylidene (**2**) with 2(or 2,7-di)-substituted fluorene derivatives **3**, catalyzed by a base in DMF or DMSO at room temperature. The ^{1}H-NMR data of **1** are shown in Table 1.

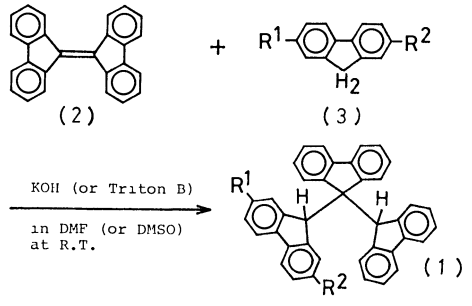

The NMR spectra for the 2-substituents in **1** have shown the set of signals illustrated in Table 1, suggesting that the rotation around the C(9)–C(9) bonds in **1b**—**1g**, as well as in **1a**,[2] is frozen at room temperature on the NMR time scale. The restricted rotation around the C(9)–C(9) bonds of **1** was investigated by temperature-dependent NMR spectroscopy: some typical DNMR spectra of **1b** are shown in Fig. 1. The values of the free energy of activation ($\Delta G^{\ddagger}$) for the rotation around the bonds in **1** were obtained by means of the usual line-shape analysis[4] on their DNMR spectra of

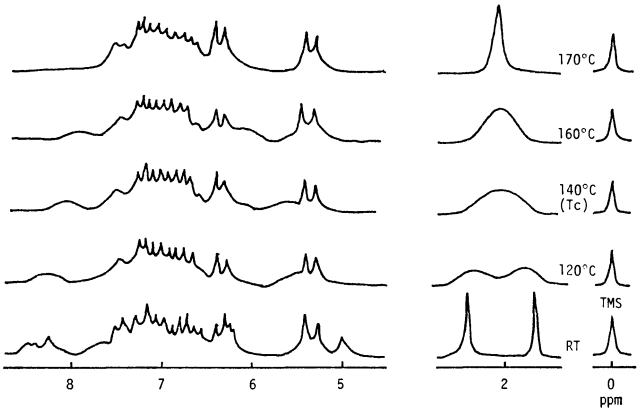

Fig. 1. Temperature dependence of ^{1}H-NMR spectra of **1b** (solvent: HCB).

TABLE 1. ^{1}H-NMR DATA OF **1** IN $CDCl_3$ (ppm)

Compd	R^1	R^2	R^1 and/or R^2		K[c]	9-H	Aromatic protons
			A[a]	**C**[b]			
1a[2]	CH_3	H	1.76s	2.55s	0.9/1	5.32s 5.38s	5.00—8.60 m
1b[2]	CH_3	CH_3	1.76s	2.55s	1/1	5.28s 5.40s	5.00—8.60m
1c[2]	C_2H_5	H	0.68t($CH_2C\underline{H}_3$) 2.03q($C\underline{H}_2CH_3$)	1.32t($CH_2C\underline{H}_3$) 2.83q($C\underline{H}_2CH_3$)	0.8/1	5.34s 5.38s	5.10—8.50m
1d	OCH_3	H	3.08s	3.88s	0.4/1	5.32s 5.37s	5.00—8.60m
1e	$COCH_3$	H	1.90s	2.68s	0.3/1	5.34s 5.40s	5.20—8.60m
1f	OCH_3	$COCH_3$	2.71s($COCH_3$) 3.15s(OCH_3)	1.91s($COCH_3$) 3.98s(OCH_3)	1.6/1	5.36s 5.41s	5.00—9.00m
1g	OCH_3	Br	3.20s	3.80s	0.9/1	5.18s 5.25s	4.80—8.50m

a) **A**: Conformation **A**. b) **C**: Conformation **C**. c) K: Equilibrium constants for the **A**⇌**C** systems in **1**, $K=N_C/N_A$.

TABLE 2. FREE ENERGIES OF ACTIVATION FOR THE ROTATION AROUND THE C(9)–C(9) BONDS IN **1**

Compd	Solvent[b)]	$\Delta G^{\ddagger a)}$/kJ mol^{-1}(T/°C)
1a[2)]	*o*-DCB	85.4 (145)
1b	HCB	84.5 (140)
1c	*o*-DCB	84.5 (135)
1d	*o*-DCB	86.2 (140)
1e	*o*-DCB	85.4 (120)
1f	HCB	87.9 (120)
1g	HCB	84.5 (140)

a) The estimated errors of $\Delta G^{\ddagger}$ are $\pm$1.3—1.7 kJ/mol.
b) *o*-DCB: *o*-dichlorobenzene. HCB: hexachlorobutadiene.

2-substituents, which did not directly hinder the rotation around the C(9)–C(9) bonds, as shown in Table 2.

Figure 2 shows two conformations, (**A**) (*ap*, +*sc*) and (**C**) (+*sc*, −*sc*), both of them *gauche-gauche* forms, and their interconversion process. The conformation **C** is derived from **A** *via* an unstable intermediate (**B**) (+*ac*, *sp*) by the rotation of the two C(9)–C(9) bonds in a conrotatory manner. In the conformation **A**, the substituent R^1 at the 2-position in the terminal fluorene ring **b** is located in a shielding zone of the central fluorene ring **a**. Thus, it is reasonable to assume that the R^1 gives the ^{1}H-NMR signal at a higher field than the R^2 at the 7-position, which is located in a deshielding zone of the two fluorene rings **a** and **c**. The same thing can also be said for the ^{1}H-NMR signals of R^1 and R^2 in the conformation **C** or **D** (enantiomer of **C**). Table 1 illustrates the assignments of the conformations **A** and **C** based on these ^{1}H-NMR signals, and also shows the equilibrium constants K (N_C/N_A) for the equilibria **A**⇌**C** of **1**.

Recently, Suzuki and Minabe reported that 9,9-di(9-fluorenyl)fluorene (**4**), the parent compound of **1**, has two conformational isomers occuring as a result of the restricted rotation around the C(9)–C(9) single bonds, and proposed, on the basis of the ^{1}H-NMR data at room temperature, that the two rotamers can exist in the *s-cis*, *s-cis* form (mp 291—293 °C) (corresponding to our *gauche-gauche* form) and the *s-cis*, *s-trans* form (mp 256—257 °C).[5)] However, we could not confirm any isomers of the above *s-cis*, *s-trans* type from **1**. Actually, the reaction of **2** with fluorene catalyzed by potassium hydroxide in DMF gave the sole product **4** (mp 291—293 °C).[3)] The DNMR spectra of **4** in HCB are shown in Fig. 3.

The spectrum of **4** is almost analogous to that of **1** (Fig. 1) except for the region of the substituents, supporting the *gauche-gauche* form as the stable conformation of **4** by analogy with **1**. The isomerization process between the +*sc*, +*sc* and −*sc*, −*sc* (enantiomer of +*sc*, +*sc*) forms of **4** can be well demonstrated in a manner similar to that described in the case of **1**. The $\Delta G^{\ddagger}$ value for the restricted rotation around the C(9)–C(9) bonds in **4** may also be about 85—88 kJ/mol, by analogy with that of **1**. Unfortunately, we could not find the *s-cis*, *s-trans* isomer[6)] which was reported by Suzuki and Minabe in these DNMR process.

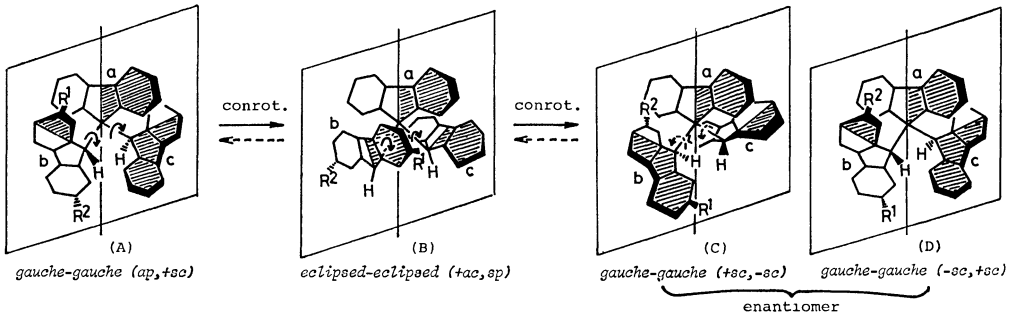

Fig. 2. The process for isomerization of **1** by rotation around the C(9)–C(9) bonds.

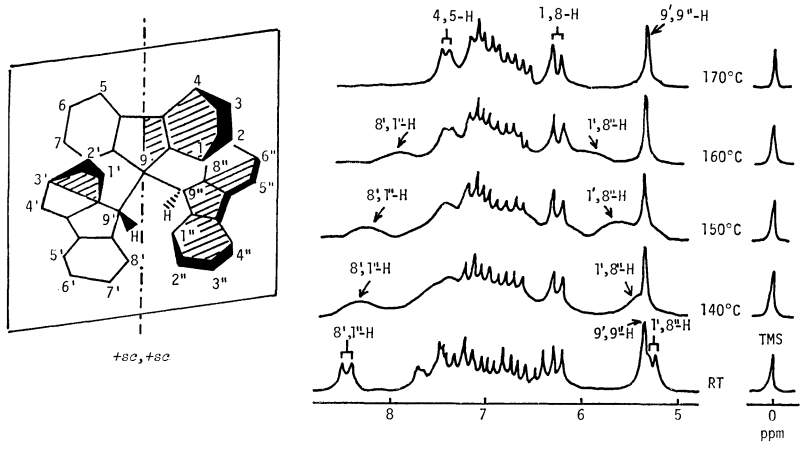

Fig. 3. Temperature dependence of ^{1}H-NMR spectra of **4** (solvent: HCB).

From the behavior of the DNMR spectra of **4**, the doublets of δ=5.22 (J=8 Hz) and δ=8.40 (J=8 Hz) at room temperature were identified as protons at the 1′,8″- and 8′,1″-positions, respectively. These two doublets are broadened, and are observed to approach each other gradually with an increase in the temperature, and are then hidden in the region of other aromatic protons at 165 °C. On the other hand, the doublets of δ=6.22 (J=8 Hz) and δ=7.44 (J=8 Hz) which are observed clearly at high temperatures are identified as protons at the 1,8- and 4,5-positions in the central fluorene ring, respectively. Then, 9,9-di(9-fluorenyl)-fluorene was prepared by the Michael addition of fluorene to **2** with sodium ethoxide in ethyl alcohol by the same method as that described by Suzuki and Minabe.[5] The two products, **4** (mp 291—293 °C) and **5** (mp 255—257 °C), were obtained just as has been described in the literature.

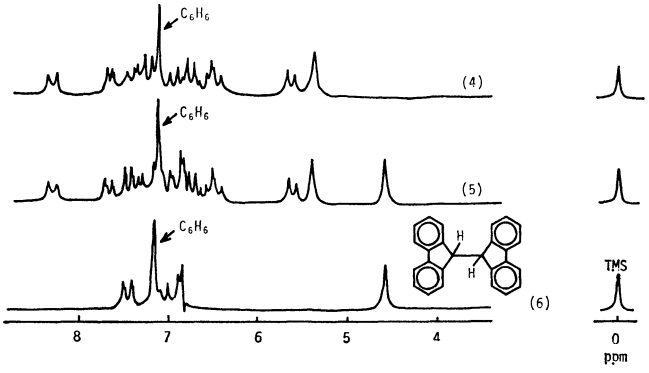

Fig. 4. ^{1}H-NMR spectra of **4**, **5**, and **6** at room temperature (solvent: C_6D_6).

The ^{1}H-NMR spectra of **4** and **5** in C_6D_6 at room temperature are shown in Fig. 4, together with that of 9,9′-bifluorenyl (**6**).[5] In this case, the shape of spectrum of **5** was in fair agreement with the overlapped shape of the spectrum of **4** with **6**. The chemical shift (4.60 ppm) in **5** is the same as that of methine protons in **6**, and the signal is amplified by the addition of **6**. The equimolar mixture of **4** and **6** was recrystallized from ethyl acetate to give crystals with the melting point of 255—257 °C; its ^{1}H-NMR spectrum was identical with that of **5**. Furthermore, the product **5** was confirmed to be an equimolar mixture of **4** and **6** by high-speed liquid-chromatographic analysis.

On the Michael reaction of **2** with fluorene, if alkoxide is used as a catalyst, **5** is obtained as the product. In this case, **6** should be produced along with **4** in the reaction mixture. That is, the alkoxide should act on **2** as a reductant. The reaction of **2** with fluorene using other bases (*e.g.*, KOH in DMF,[3] Triton B in DMSO, and KOH in pyridine[5]) instead of alkoxide gave **4** as the sole product. Actually, the reaction of **2** with sodium ethoxide in ethyl alcohol in a sealed tube gave **6** in a substantial yield.

It is known that, in the case of $\Delta G^{\ddagger}<96$ kJ/mol rotamers are unstable at room temperature.[7] If the $\Delta G^{\ddagger}$ value for **4** is estimated as 85—88 kJ/mol as in the case of **1**, we should not be able to isolate the *s-cis*, *s-trans* rotamer of **4** stably at room temperature.

Experimental

All the melting points are uncorrected. The NMR spectra were run on a JEOL-MH-100 spectrometer with a JEOL model JES-VT-3 variable-temperature controller. The chemical shifts are expressed in ppm, with tetramethylsilane as the internal standard. Signal-shape-analysis was done by matching the experimental spectra with the spectra calculated from the computer program given by Nakagawa.[8] High-speed liquid-chromatographic analysis was carried out on a Tōyō Sōda TSK-HLC-803 apparatus equipped with a UV monitor using an LS-410K (4 mm i.d. × 30 cm) column, with acetonitrile as the mobile phase, at room temperature.

Syntheses of ***1***. *A Typical Synthetic Procedure for* ***1***: The starting material, 2-acetyl-7-methoxyfluorene (**3f**), was prepared by the reaction of 2-methoxyfluorene with acetyl chloride, using $AlCl_3$ as the catalyst, by the procedure reported by Gray *et al.*;[9] mp 131—132 °C (lit, 134.5 °C); IR (KBr) 1670 cm^{-1} (C=O); NMR ($CDCl_3$) δ=2.60 (3H, s, $COCH_3$), 3.83 (2H, s, 9-methylene), 3.84 (3H, s, OCH_3), 6.70—8.20 (6H, m, aromatic protons).

To a mixture of **2** (1.6 g, 0.005 mol) and **3f** (1.2 g, 0.005 mol) in DMF (2 ml), we added Triton B (0.1 ml) at room temperature. The solution was stirred for 5 min, during which the color changed from red to dark brown, and was then poured into dil hydrochloric acid (10 ml). The precipitate thus obtained was filtered, washed with water, and recrystallized from acetone to give colorless crystals **1f**; 2.0 g (70%); mp 244—248 °C. Found: C, 89.43; H, 5.07%. Calcd for $C_{42}H_{30}O_2$: C, 89.02; H, 5.34%.

1d, mp 237—242 °C; Found: C, 91.82; H, 5.36%. Calcd for $C_{40}H_{28}O$: C, 91.57; H, 5.38%.

1e, mp 251—255 °C; Found: C, 91.51; H, 5.15%. Calcd for $C_{41}H_{28}O$: C, 91.76; H, 5.26%.

1g, mp 260—263 °C; Found: C, 79.24; H, 4.48%. Calcd for $C_{40}H_{27}OBr$: C, 79.60; H, 4.51%.

Reaction of ***2*** *with Sodium Ethoxide.* Metallic sodium (0.23 g, 0.01 g-atom) was treated with 20 ml of absolute ethanol, and then there was added 0.33 g (0.001 mol) of **2**. The mixture was heated in a sealed tube at 95—98 °C for 14 h. After cooling, the precipitate was filtered off and dissolved in benzene. The benzene solution was chromatographed on alumina. The eluent was evaporated to dryness under reduced pressure, and the residue was recrystallized from benzene–ethanol (1:1) to afford **6**: 0.20 g (61%); mp 246—247 °C. This compound was confirmed by direct comparison with an authentic sample. On the other hand, **2** was recovered unchanged from the red ethanolic solution; 0.05 g (15%).

We wish to express our thanks to Mr. Atsushi Aiura and Mr. Katsuyuki Tanaka, Tōyō Sōda Manufacturing Co., Ltd., for the high-speed liquid-chromatographic analysis.

References

1) Part II of this series: S. Fujisaki, A. Nagashima, H. Hara, and S. Kajigaeshi, *Nippon Kagaku Kaishi*, **1976**, 1874.

2) I. Aizu, S. Fujisaki, A. Nagashima, and S. Kajigaeshi, *Nippon Kagaku Kaishi*, **1975**, 1765.

3) A. Nagashima, T. Yamagata, S. Fujisaki, and S. Kajigaeshi, *Nippon Kagaku Kaishi*, **1975**, 2034.

4) L. M. Jackman and F. A. Cotton, "Dynamic Nuclear

Magnetic Resonance Spectroscopy," Academic Press, New York (1975), p. 49.
5) K. Suzuki and M. Minabe, *Tetrahedron Lett.*, **1974**, 1541; M. Minabe and K. Suzuki, *J. Org. Chem.*, **40**, 1298 (1975).
6) The $+sc$, $-ac$ or $-sc$, $+ac$ conformation is adopted for this *s-cis*, *s-trans* isomer.
7) H. Kessler, *Angew. Chem. Int. Ed. Engl.*, **9**, 219 (1970).
8) T. Nakagawa, *Bull. Chem. Soc. Jpn.*, **39**, 1006 (1966).
9) G. W. Gray, J. B. Hartley, and A. Ibbotoson, *J. Chem. Soc.*, **1955**, 2686.

Catalytic Efficiency of Cationic Micellar Catalysts Bearing a Mercapto Group as the Reaction Center†

Yukito MURAKAMI,* Akio NAKANO, Kiyoshi MATSUMOTO, and Kiyoshi IWAMOTO

Department of Organic Synthesis, Faculty of Engineering, Kyushu University, Hakozaki, Higashi-ku, Fukuoka 812

(Received February 2, 1979)

In order to clarify micro-environmental effects on the reactivity of mercapto groups in enzymes, cationic surfactants bearing a mercapto group, *N*-hexadecyl-N^{α}-(3-trimethylammoniopropionyl)-L-cysteinamide bromide (CM·Cys-1) and *N*-dodecyl-N^{α}-(6-trimethylammoniohexanoyl)-L-cysteinamide bromide (CM·Cys-2), were synthesized and their kinetic behavior investigated. The surfactants above their critical micelle concentrations markedly catalyzed the decomposition of *p*-nitrophenyl hexanoate (PNPH) and acetate (PNPA), the concentration-rate profiles being found to be those for typical micelle-catalyzed reactions. The rate constants for the degradation of PNPH as catalyzed by CM·Cys-1 and -2 in the micellar phase are 0.482 and 0.197 s^{-1}, respectively, in 9.8% (v/v)-ethanol–1.0% (v/v)dioxane–1.0% (v/v)methanol–water at 30.0±0.1 °C, pH 8.65, and μ 0.10 (KCl). The difference in catalytic activity can be attributed partly to the micro-environmental effect on the pK_a value of the mercapto group lying at the reaction center. The rate constants for the thiolate anions (true reactive species) of CM·Cys-1 and -2 to react with PNPH were identical with each other irrespective of the nature of the surfactants. The electrostatic effect provided by the cationic charge in the Stern layer, which acts to reduce the pK_a value of the reactive mercapto group, seems to play a more important role than the desolvation effect on the thiolate anion by the hydrophobic field.

Functionalized surfactants involving a reactive group such as the imidazolyl,[1] carboxyl,[2] or hydroxyl group[3] have been developed as enzyme models. However, only a limited number of surfactants bearing a mercapto group have been synthesized; their catalytic activity for degradation of *p*-nitrophenyl carboxylates has been examined.[4] The active mercapto group of these surfactants seems to be located in the electrostatic Stern layer judging from their molecular structures. In spite of the fact that the catalytically active groups of enzymes are located in their hydrophobic pockets, no successful attempt has been made to locate the catalytic groups in the hydrophobic micellar core so as to simulate the function of an enzymatic reaction center. The anionic surfactants involving a L-cysteinyl residue as the reaction center markedly accelerate the degradation of *p*-nitrophenyl carboxylates below their critical micelle concentrations, the reactivity of the mercapto group being lost upon formation of the anionic micelles.[5] The surfactants show pronounced reactivity even in a neutral pH region when mixed with hexadecyltrimethylammonium bromide (CTAB) in the micellar phase. The electrostatic field effect provided by the cationic head of CTAB micelle enhances the nucleophilicity of the mercapto group in the mixed micelles for such reactions.

In order to develop novel surfactants which can incorporate the multi-functions provided by the comicelle constructed by CTAB and *N*-hexadecyl-N^{α}-glutaryl-L-cysteinamide, we have prepared cationic surfactants bearing a mercapto group, *N*-hexadecyl-N^{α}-(3-trimethylammoniopropionyl)-L-cysteinamide bromide (CM·Cys-1) and *N*-dodecyl-N^{α}-(6-trimethylammoniohexanoyl)-L-cysteinamide bromide (CM·Cys-2). The mercapto group is expected to be placed in a hydrophobic core of the micellar phase. The micro-environmental effect on the nucleophilicity of the mercapto group provided by the present cysteine-containing cationic surfactants has been investigated as regards the deacylation of *p*-nitrophenyl carboxylates. The synthetic procedure for CM·Cys-1 is shown in Scheme 1.

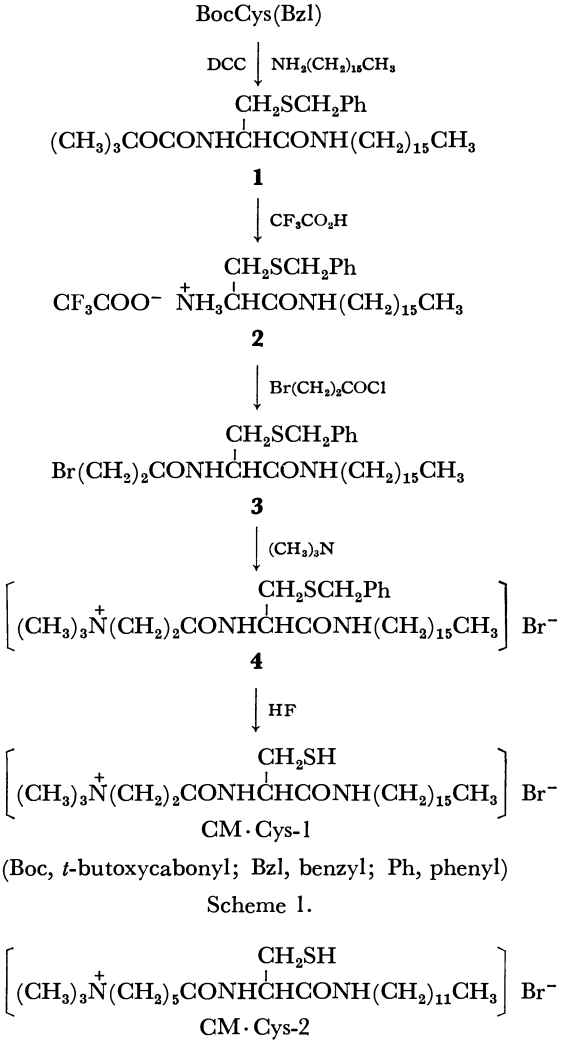

(Boc, *t*-butoxycabonyl; Bzl, benzyl; Ph, phenyl)

Scheme 1.

† Contribution No. 512 from this Department.

Experimental

Spectroscopic data were taken on a JASCO DS-403G grating IR spectrophotometer, a Varian A60 NMR spectrometer, and a Hitachi 124 spectrophotometer. pH-Measurements were carried out with a TOA HM-9A pH meter equipped with a TOA GC-125 combined electrode after calibration with a combination of appropriate aqueous standard buffers.

p-Nitrophenyl carboxylates were prepared by the reaction of the corresponding carbonyl chlorides with *p*-nitrophenol. The esters were identified by elemental analyses and spectroscopic measurements.[6] 2,2′-Dinitro-5,5′-dithiodibenzoic acid (DTNB, Nakarai Chemicals, bio-analytical grade) was used without further purification.

The synthetic procedure for *N*-hexadecyl-N^{α}-(3-trimethylammoniopropionyl)-L-cysteinamide bromide (CM·Cys-1) is outlined in Scheme 1. *N*-Hexadecyl-N^{α}-*t*-butoxycarbonyl-*S*-benzyl-L-cysteinamide (**1**) was prepared as described previously.[5]

*N-Hexadecyl-N$^{\alpha}$-(3-bromopropionyl)-S-benzyl-L-cysteinamide (**3**).* Trifluoroacetic acid (25.0 g) was added to a dichloromethane solution (17 ml) of **1** (2.4 g) and the mixture was stirred at room temperature for 1 h. Evaporation of excess trifluoroacetic acid *in vacuo* gave pale yellow oil (**2**); yield 2.5 g (quantitative). Elimination of the *t*-butoxycarbonyl group was confirmed by means of NMR spectrum. Amine component **2** (1.74 g) and triethylamine (0.97 g) were dissolved in dichloromethane (20 ml) and cooled down to 0 °C. 3-Bromopropionyl chloride (1.09 g) dissolved in dichloromethane (5 ml) was added to the solution in 10 min at this temperature. The mixture was stirred for 30 min at 0 °C and at room temperature for 2 h. The reaction mixture, after dichloromethane (50 ml) had been added, was washed with water (50 ml×3), 5% aqueous sodium hydrogencarbonate (50 ml×3), 5% aqueous citric acid (50 ml×3), and saturated aqueous sodium chloride (50 ml×3). After being dried over anhydrous sodium sulfate, the mixture was evaporated *in vacuo* at 40 °C to give a glassy solid of pale yellow; yield 1.65 g (99%), mp 86—88 °C. NMR ($CDCl_3$, TMS): δ 0.88 (3H, broad t, $C\underline{H}_3(CH_2)_{14}CH_2$–), 1.25 (28H, s, $CH_3(C\underline{H}_2)_{14}CH_2$–), 2.65—2.95 (4H, m, $BrCH_2C\underline{H}_2CO$– and $-C\underline{H}_2SCH_2$-Ph), 3.22 (2H, broad t, $CH_3(CH_2)_{14}C\underline{H}_2NH$–), 3.65 (2H, t, $BrC\underline{H}_2CH_2CO$–), 3.80 (2H, s, $-CH_2SC\underline{H}_2Ph$), 4.55 (1H, broad t, $-C\underline{H}(CH_2SCH_2Ph)CO$–), and 7.37 (5H, s, phenyl H's).

*N-Hexadecyl-N$^{\alpha}$-(3-trimethylammoniopropionyl)-S-benzyl-L-cysteinamide Bromide (**4**).* Dry trimethylamine gas was introduced into a benzene solution (60 ml) of **3** (1.6 g) for 6 h, and the solution was stirred at room temperature for 14 h. After benzene had been evaporated off *in vacuo*, methanol was added to the residue and removed *in vacuo*. The treatment with methanol was repeated three times. A white solid was recovered and recrystallized from ethyl acetate–petroleum ether; yield 1.60 g (86%), mp 88—95 °C, Dragendorff positive. NMR (methanol-d_4, TMS): δ 0.88 (3H, broad t, $C\underline{H}_3(CH_2)_{14}CH_2$–), 1.25 (28H, s, $CH_3(C\underline{H}_2)_{14}CH_2$–), 2.60—3.05 (4H, m, $(CH_3)_3\overset{+}{N}CH_2C\underline{H}_2CO$– and $-C\underline{H}_2SCH_2Ph$), 3.18 (9H, s, $(C\underline{H}_3)_3\overset{+}{N}$–), 3.04—3.41 (4H, m, $(CH_3)_3\overset{+}{N}C\underline{H}_2CH_2CO$– and $CH_3(CH_2)_{14}C\underline{H}_2NH$–), 3.80 (2H, s, $-CH_2SC\underline{H}_2Ph$), 4.55 (1H, broad t, $-C\underline{H}(CH_2SCH_2Ph)CO$–), and 7.35 (5H, s, phenyl H's).

N-Hexadecyl-N$^{\alpha}$-(3-trimethylammoniopropionyl)-L-cysteinamide Bromide (CM·Cys-1). Anisole (1.0 ml) and **4** (700 mg) were placed in a reaction vessel into which hydrogen fluoride (10 ml) was introduced. The mixture was stirred at 0 °C for 1 h, at 15 °C for 30 min, and then evaporated *in vacuo* to remove hydrogen fluoride completely. Methanol (30 ml) was added to the residue and white precipitates were recovered by filtration. After methanol had been evaporated off, 2-mercaptoethanol (5 ml) was added to the residue and the mixture was stirred at room temperature for 14 h. Methanol (10 ml) was added to the mixture and the product was purified by gel-filtration chromatography (Sephadex LH-20, methanol as eluant) to give a hygroscopic solid; yield 180 mg (30%), nitroprusside positive. IR (neat): 3240 (NH str.); 2900 and 2840 (CH str.); 1655 and 1545 cm^{-1} (C=O str.). NMR (methanol-d_4, TMS): δ 0.90 (3H, broad t, $C\underline{H}_3(CH_2)_{14}CH_2$–), 1.30 (28H, s, $CH_3(C\underline{H}_2)_{14}CH_2$–), 2.65—3.20 (6H, m, CH_3-$(CH_2)_{14}C\underline{H}_2NH$–, $-C\underline{H}_2SH$, and $(CH_3)_3\overset{+}{N}CH_2C\underline{H}_2CO$–), 3.18 (11H, s, $(C\underline{H}_3)_3\overset{+}{N}C\underline{H}_2CH_2CO$–), and 4.35 (1H, broad, $-C\underline{H}$-$(CH_2SH)CO$–). Found: C, 56.25; H, 9.46; N, 6.99%. Calcd for $C_{25}H_{52}BrN_3O_2S$: C, 55.79; H, 9.72; N, 7.80%.

N-Dodecyl-N^{α}-(6-trimethylammoniohexanoyl)-L-cysteinamide bromide (CM·Cys-2) was prepared in a manner similar to that described for CM·Cys-1.

N-Dodecyl-N$^{\alpha}$-t-butoxycarbonyl-S-benzyl-L-cysteinamide. Yield 51%, needles (recrystallized from ethyl acetate), mp 57—59 °C. NMR ($CDCl_3$, TMS): δ 0.88 (3H, broad t, $C\underline{H}_3(CH_2)_{11}$–), 1.25 (20H, s, $CH_3(C\underline{H}_2)_{10}CH_2$–), 1.45 (9H, s, $(C\underline{H}_3)_3CO$–), 2.76 (2H, broad d, $-C\underline{H}_2SCH_2Ph$), 3.25 (2H, m, CH_3-$(CH_2)_{10}C\underline{H}_2$–), 3.75 (2H, s, $-CH_2SC\underline{H}_2Ph$), 4.21 (1H, broad t, $-C\underline{H}(CH_2SCH_2Ph)CO$–), and 7.37 (5H, s, phenyl H's).

N-Dodecyl-N$^{\alpha}$-(6-bromohexanoyl)-S-benzyl-L-cysteinamide. Yield 81%, pale yellow oil. IR (neat): 3250 (NH str.); 2900 and 2830 (CH str.); 1635 and 1535 cm^{-1} (C=O str.). NMR ($CDCl_3$, TMS): δ 0.88 (3H, broad t, $C\underline{H}_3(CH_2)_{11}$–), 1.26 (20H, s, $CH_3(C\underline{H}_2)_{10}CH_2$–), 1.90 (6H, m, $BrCH_2(C\underline{H}_2)_3$-$CH_2CO$–), 2.50 (2H, broad t, $BrC\underline{H}_2(CH_2)_3CH_2CO$–), 2.78 (2H, d, $-C\underline{H}_2SCH_2Ph$), 3.19 (2H, broad t, $CH_3(CH_2)_{10}$-$C\underline{H}_2$–), 3.42 (2H, t, $BrC\underline{H}_2$–), 3.76 (2H, s, $-CH_2SC\underline{H}_2Ph$), 4.51 (1H, broad t, $-C\underline{H}(CH_2SCH_2Ph)CO$–), and 7.33 (5H, s, phenyl H's).

N-Dodecyl-N$^{\alpha}$-(6-trimethylammoniohexanoyl)-S-benzyl-L-cysteinamide Bromide. Yield 97%, hygroscopic glassy solid of pale yellow (recrystallized from ethyl acetate–petroleum ether), mp 68—75 °C, Dragendorff positive. IR (Nujol): 3260 (NH str.); 1630 and 1540 cm^{-1} (C=O str.). NMR (methanol-d_4, TMS): δ 0.88 (3H, broad t, $C\underline{H}_3(CH_2)_{11}$–), 1.25 (20H, s, CH_3-$(C\underline{H}_2)_{10}CH_2$–), 2.00 (6H, m, $(CH_3)_3\overset{+}{N}CH_2(C\underline{H}_2)_3CH_2CO$–), 2.31 (2H, broad t, $(CH_3)_3\overset{+}{N}(CH_2)_4C\underline{H}_2CO$–), 2.75—3.20 (4H, m, $-C\underline{H}_2SCH_2Ph$ and $CH_3(CH_2)_{10}C\underline{H}_2NH$–), 3.40 (11H, s, $(C\underline{H}_3)_3\overset{+}{N}C\underline{H}_2$–), 3.75 (2H, s, $-CH_2SC\underline{H}_2Ph$), 4.60 (1H, broad, $-C\underline{H}(CH_2SCH_2Ph)CO$–), and 7.35 (5H, s, phenyl H's).

N-Dodecyl-N$^{\alpha}$-(6-trimethylammoniohexanoyl)-L-cysteinamide Bromide (CM·Cys-2). Yield 32%, glassy solid, mp 133—145 °C, nitroprusside positive. IR (Nujol): 3260 (NH str.); 1630 and 1530 cm^{-1} (C=O str.). NMR (methanol-d_4, TMS): δ 0.90 (3H, broad t, $C\underline{H}_3(CH_2)_{11}$–), 1.30 (20H, s, $CH_3(C\underline{H}_2)_{10}$-$CH_2$–), 1.10—2.00 (6H, m, $(CH_3)_3\overset{+}{N}CH_2(C\underline{H}_2)_3CH_2$–), 2.40 (2H, broad, $(CH_3)_3\overset{+}{N}(CH_2)_4C\underline{H}_2CO$–), 2.65—3.10 (4H, m, $-C\underline{H}_2SH$ and $CH_3(CH_2)_{10}C\underline{H}_2NH$–), 3.18 (11H, s, $(C\underline{H}_3)_3$-$\overset{+}{N}C\underline{H}_2$–), and 4.35 (1H, broad, $-C\underline{H}(CH_2SH)CO$–). Found: C, 55.23; H, 9.12; N, 7.08%. Calcd for $C_{24}H_{50}BrN_3O_2S$: C, 54.95; H, 9.61; N, 7.08%.

Kinetic Measurements. The concentration of free thiol for CM·Cys-1 and -2 was determined by using Ellman's reagent (DTNB)[7] before kinetic runs. Under the conditions employed, the reaction between surfactant and ester species

was fast enough to neglect oxidation of the mercapto group of the surfactants. Rates of *p*-nitrophenol liberation from *p*-nitrophenyl esters were measured at 400 nm with a Hitachi 124 spectrophotometer. Each run was initiated by adding a dry dioxane solution (30 μl) of a substrate ester to a mixture of a reaction medium (3.0 ml) and a dry methanol solution (30 μl) of a catalyst which was pre-equilibrated at 30.0±0.1 °C in a thermostatted cell set in the spectrophotometer. The reaction medium was prepared as follows: 10.0 ml of 1.0 M aqueous potassium chloride, 10.0 ml of an appropriate aqueous buffer, and 10.0 ml of dry ethanol were placed in a 100-ml volumetric flask; the flask was filled with deionized and distilled water. Aqueous buffer solutions adopted in the present study were prepared by combining 1/10 M potassium dihydrogenphosphate and 1/20 M sodium borate.

The mole fractions of CM·Cys-1 and -2, which bear the free mercapto group and were used for kinetic runs, were 0.63 and 0.67, respectively. Thus, all the rate data were corrected to a 100% content of the free mercapto group. In order to find the effect of disulfide content on kinetic behavior, the thiol surfactants involving the free mercapto group in the mole fraction range 0.33—0.67 were also examined for their catalytic activity. All the kinetic data thus obtained after correction for the disulfide content were identical regardless of disulfide content. The substrate-binding ability of the surfactants was not affected by the disulfide content.

Results and Discussion

Degradation of *p*-nitrophenyl carboxylates as catalyzed by CM·Cys-1 and -2 has been studied in 9.8%(v/v)ethanol–1.0%(v/v)dioxane–1.0%(v/v)methanol–water at 30.0±0.1 °C and μ 0.10 (KCl). Apparent first-order rate constants (k_{obsd}) were obtained by measuring the amount of liberated *p*-nitrophenol. The first-order kinetics was found to hold up to 90% conversion of the substrate for each kinetic run, no noticeable hydrolysis of the acylated thiol ester being observed.

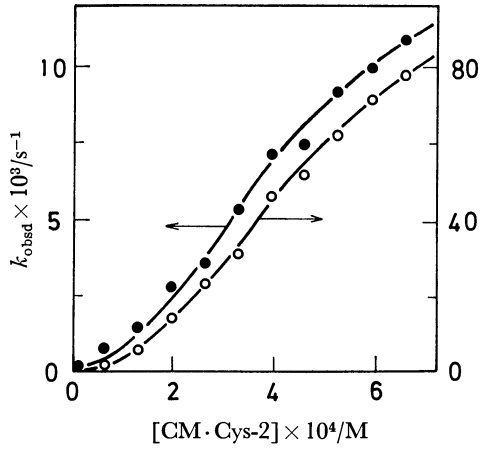

Fig. 1. Plots of apparent first-order rate constant *vs.* surfactant concentration (C_D) for the deacylation of *p*-nitrophenyl hexanoate (PNPH, ○) and acetate (PNPA, ●) as catalyzed by CM·Cys-2 in 9.8%(v/v)-ethanol–1.0% (v/v)dioxane–1.0% (v/v) methanol–water at 30.0±0.1 °C, pH 8.65, and μ 0.10 (KCl). Initial concentrations: PNPH, 0.992×10⁻⁵ M; PNPA, 0.990 ×10⁻⁵ M.

Rate(k_{obsd})-concentration profiles (Fig. 1) for the degradation of *p*-nitrophenyl hexanoate (PNPH) and acetate (PNPA) as catalyzed by CM·Cys-2 at pH 8.65 are typical for the micellar catalysis. The reaction pathway for the degradation of *p*-nitrophenyl carboxylates as catalyzed by the thiol surfactants is given by Scheme 2, where S denotes an ester substrate (PNPH or PNPA), M a micelle constructed by a thiol surfactant

$$\mathrm{M} + \mathrm{S} \overset{K_b}{\rightleftharpoons} \mathrm{MS} \xrightarrow{k_m} \mathrm{P}$$
$$\mathrm{MS} \xrightarrow{k_s} \mathrm{P'}$$

Scheme 2.

(CM·Cys-1 or -2), MS a complex formed with the micelle and the substrate, and P and P′ denote reaction products. The k_s and k_m values are defined as follows.

$$k_s = k_{hyd} + k_{SH}(\text{monomer}) \quad (1)$$

$$k_m = k_M^{OH} + k_{SH}(\text{micelle}) \quad (2)$$

where k_{hyd} denotes the rate constant for the alkaline hydrolysis, k_{SH}(monomer) that for the acyl transfer from a substrate to the mercapto group of a monomeric surfactant in the bulk phase, k_M^{OH} that for the alkaline hydrolysis by concentrated hydroxide ions in the Stern layer of the micelle, and k_{SH} (micelle) that for the acyl transfer from a bound substrate to the mercapto group of the micellar surfactant. The observed first-order rate constant (k_{obsd}) is given by the following equation on the basis of Scheme 2.[8]

$$k_{obsd} = \frac{k_s + K_b k_m [M]}{1 + K_b [M]} \quad (3)$$

This can be rearranged to give

$$\frac{1}{(k_{obsd} - k_s)} = \frac{1}{(k_m - k_s)} + \frac{N}{(k_m - k_s) K_b (C_D - CMC)} \quad (4)$$

where N denotes the aggregation number and C_D total concentration of the thiol surfactant. The critical micelle concentration (CMC) was kinetically estimated

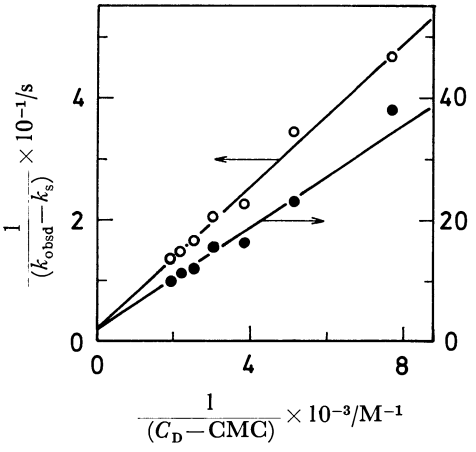

Fig. 2. Plots of $1/(k_{obsd}-k_s)$ *vs.* $1/(C_D-CMC)$ for the deacylation of PNPH (○) and PNPA (●) as catalyzed by CM·Cys-2 in 9.8%(v/v)ethanol–1.0%(v/v)dioxane–1.0%(v/v)methanol–water at 30.0±0.1 °C, pH 8.65, and μ 0.10 (KCl). Initial concentrations: PNPH, 0.992×10⁻⁵ M; PNPA, 0.990×10⁻⁵ M.

Table 1. Kinetic parameters for the deacylation of *p*-nitrophenyl hexanoate and acetate as catalyzed by the thiol surfactants[a)]

Surfactant	$k_s \times 10^3$ / s^{-1}	k_m / s^{-1}	K_b/N / M^{-1}	k_m/k_{hyd}	k_{obsd}^{max} / s^{-1}	k_{cat}[b)] / $s^{-1}M^{-1}$
			PNPH			
CM·Cys-1	0.91	0.482	2560	3680	0.224	424
CM·Cys-2	1.03	0.197	884	1500	0.066	99
			PNPA			
CM·Cys-1	1.15	0.0586	962	376	0.0211	31.9
CM·Cys-2	0.99	0.0508	485	326	0.0109	16.7

a) In 9.8 %(v/v)ethanol–1.0%(v/v)dioxane–1.0%(v/v)methanol–water at 30.0±0.1 °C, pH 8.65, and μ 0.10 (KCl). Initial concentrations: PNPH, 0.992×10^{-5} M; PNPA, 0.990×10^{-5} M. Apparent first-order rate constants for the alkaline hydrolysis: PNPH, 1.31×10^{-4} s^{-1}; PNPA, 1.56×10^{-4} s^{-1}. Approximate CMC's: CM·Cys-1, 4×10^{-5} M; CM·Cys-2, 9×10^{-5}M. 1 M=1 mol dm^{-3}. b) $k_{cat}=k_{obsd}^{max}/[\text{surfactant}]_{max}$; k_{obsd}^{max}, maximum observed rate constant under present conditions with a surfactant concentration, $[\text{surfactant}]_{max}$.

from the corresponding rate-concentration profile. The apparent first-order rate constants observed at the critical micelle concentrations were referred to the k_s values. Linearity holds between the left-hand side term of Eq. 4 and the reciprocal concentration of micellized surfactant (C_D—CMC) as shown in Fig. 2 for the CM·Cys-2 catalysis as an example. The kinetic parameters are summarized in Table 1. The k_s values for the reaction between thiol surfactants and ester substrates indicate that the reactivity of CM·Cys-1 is identical with that of CM·Cys-2 in the bulk phase. The pseudo-intramolecular rate constant (k_m) and the binding ability (K_b/N) reflect the catalytic activity of CM·Cys-1 and -2 in the micellar phase. In order to clarify the difference in catalytic activity, k_m and K_b/N values for the degradation of PNPH as catalyzed by CM·Cys-1 and -2 were evaluated at several pH's from the corresponding data of saturation kinetics (Fig. 3, CM·Cys-2 catalysis). The kinetic parameters obtained are given in Table 2. The pH-rate profiles (Fig. 4) suggest that the reactive species is the thiolate anion in the micellar phase as shown by

Table 2. Kinetic parameters for the deacylation of *p*-nitrophenyl hexanoate as catalyzed by CM·Cys-1 and -2[a)]

pH	$k_{hyd}\times10^4$ / s^{-1}	$k_s\times10^3$ / s^{-1}	k_m / s^{-1}	K_b/N / M^{-1}
		CM·Cys-1		
8.98	2.15	1.66	0.546	1760
8.69	1.40	0.91	0.483	2570
8.45	0.92	0.55	0.248	5260
8.06	0.47	0.24	0.121	4150
		CM·Cys-2		
8.95	2.29	1.66	0.407	950
8.67	1.31	1.04	0.198	880
8.47	0.94	0.87	0.099	1620
7.94	0.41	0.28	0.034	1710

a) In 9.8%(v/v)ethanol–1.0% (v/v) dioxane–1.0%(v/v)-methanol–water at 30.0±0.1 °C and μ 0.10 (KCl). Initial concentrations: PNPH, 0.992×10^{-5} M; CM·-Cys-1, $(0.660—6.60)\times10^{-4}$ M; CM·Cys-2, $(0.664—6.64)\times10^{-4}$ M. Approximate CMC's: CM·Cys-1, 4×10^{-5} M; CM·Cys-2, 9×10^{-5} M.

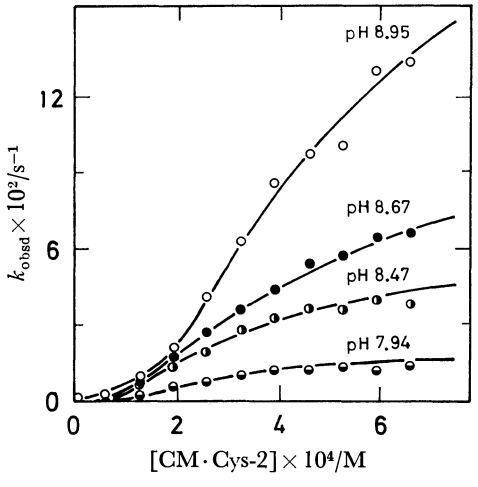

Fig. 3. Plots of apparent first-order rate constant *vs.* surfactant concentration (C_D) for the deacylation of PNPH as catalyzed by CM·Cys-2 in 9.8%(v/v)ethanol–1.0%(v/v) dioxane–1.0%(v/v) methanol–water at 30.0±0.1 °C and μ 0.10 (KCl); initial concentration of PNPH, 0.992×10^{-5} M.

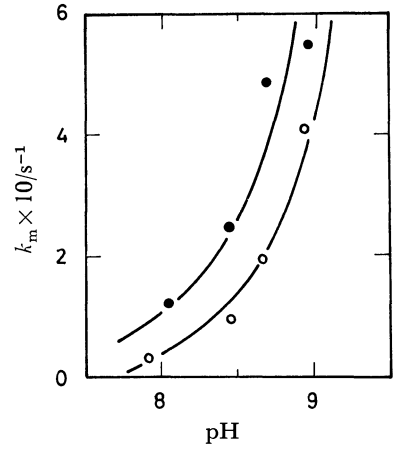

Fig. 4. pH-rate profiles for the deacylation of PNPH as catalyzed by CM·Cys-1 (●) and -2 (○) in 9.8%-(v/v)ethanol–1.0%(v/v)dioxane–1.0%(v/v)methanol–water at 30.0±0.1 °C and μ 0.10 (KCl); initial concentration of PNPH, 0.992×10^{-5} M.

$$S\cdot M(SH) \overset{K_a}{\rightleftharpoons} S\cdot M(S^-) \overset{k_m^*}{\longrightarrow} P$$

Scheme 3.

where M(SH) and M(S$^-$) denote micellar surfactants bearing neutral mercapto and anionic sulfido groups, respectively. The following relations are established.

$$k_m\{[S\cdot M(SH)] + [S\cdot M(S^-)]\} = k_m^*[S\cdot M(S^-)] \quad (5)$$

$$K_a = \frac{[S\cdot M(S^-)][H^+]}{[S\cdot M(SH)]} \quad (6)$$

By combination and rearrangement of Eqs. 5 and 6, we obtain the relation between the k_m and k_m^* values:

$$\frac{1}{k_m} = \frac{1}{k_m^*} + \frac{[H^+]}{k_m^* K_a} \quad (7)$$

Plots of $1/k_m$ against [H$^+$] for the deacylation of PNPH as catalyzed by CM·Cys-1 and -2 provide k_m^* and pK_a values (Table 3).

Table 3. True rate constants (k_m^*) and kinetic pK_a values for the deacylation of *p*-nitrophenyl hexanoate as catalyzed by CM·Cys-1 and -2[a)]

Surfactant	k_m^*/s^{-1}	pK_a
CM·Cys-1	1.36	9.09
CM·Cys-2	1.28	9.52

a) Calculated from data given in Table 2.

Catalytic Efficiency of the Micellar Thiol Surfactants. The more effective micellar catalyst was provided by CM·Cys-1, the k_m value for the deacylation of PNPH being 3680 times as large as the corresponding k_{hyd} value (Table 1). The remarkable efficiency of CM·Cys-1 is comparable to that of the mixed micelle formed with CTAB and *N*-hexadecyl-*N*$^\alpha$-glutaryl-L-cysteinamide (AM·Cys-1); k_m/k_{hyd}, 3080.[5)] For the degradation of

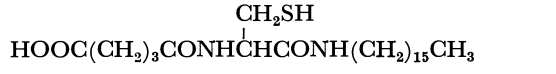

AM·Cys-1

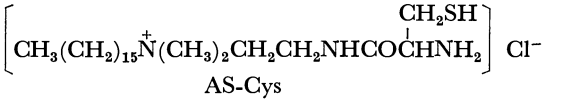

AS-Cys

PNPA, CM·Cys-1 shows large catalytic efficiency as compared with [2-(cysteinylamino)ethyl]hexadecyldimethylammonium chloride (AS-Cys) reported by Moss and his coworkers (k_{cat}, 26.0).[4b)] The catalytic efficiency (k_m) of CM·Cys-1 for the degradation of PNPH is larger than that of CM·Cys-2 by 2.44-fold at pH 8.65. Nevertheless, both micelles show similar reactivity toward the substrate in terms of k_m^* (Table 3). The result suggests that the reactivity of the thiolate anion of these surfactants does not depend on the depth of its location in a hydrophobic micellar core. On the contrary, the pK_a value for the mercapto group of CM·Cys-2 increases by 0.5 pK_a unit relative to that for CM·Cys-1. Moss and his coworkers reported pK_a for the dissociation of the thiol proton of AS-Cys (at 2×10^{-4} M) as 8.9.[4c)] The mercapto group of AS-Cys is presumably located in the cationic Stern layer. The results suggest that the pK_a value is affected by the depth of the active group in the micellar phase and its micro-environment is subject to the electrostatic field effect as well as to the hydrophobic effect. The difference of the catalytic efficiency among CM·Cys-1 and -2 at pH 8.65 for the deacylation of PNPH can be explained by the pK_a effect. On the other hand, the catalytic efficiency of CM·Cys-1 is nearly comparable to that of CM·Cys-2 for the deacylation of PNPA. The catalytic efficiency of these surfactants for the deacylation of PNPA seems to be affected by its orientation behavior in the micellar phase which is different from that of PNPH. PNPH would be so arranged in the micellar phase that an attack of the mercapto group on it is facilitated in the hydrophobic core, PNPA being incorporated into the electrostatic Stern layer as shown in Fig. 5. This is in line with the results reported by Brown and Schofield.[9)] They indicated that hexane is solubilized in the micellar interior, enforcing tighter packing and reduced mobility, while benzene and 1-pentanol disrupt the micellar structure by binding close to the Stern layer.

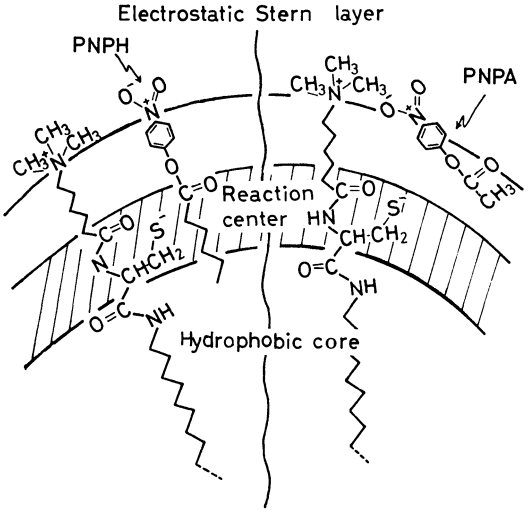

Fig. 5. Schematic representation for the orientation of ester substrates (PNPH and PNPA) in the CM·Cys-2 micelle.

Substrate-binding Ability of the Micellar Thiol Surfactants. The K_b/N values (Table 1) indicate that both micelles have stronger binding ability for PNPH than for PNPA, and that CM·Cys-1 has stronger binding ability for both substrates than CM·Cys-2. The result suggests that the bulky side chain (mercaptomethyl group) located in the hydrophobic micellar core disturbs the micelle structure; *i.e.*, the hydrophobicity of micelles. The binding ability due to the hydrophobic interaction between the substrate and the micelle seems to be affected by the depth of the bulky branched group along the hydrophobic alkyl chain of the surfactant molecule. The K_b/N value decreases with increasing pH of the medium (Table 2). Thus, the binding ability decreases with increasing the fraction of the anionic sulfido group, indicating that the ionic charge on the hydrophobic chain perturbs the structure of micellar

core so as to reduce the hydrophobic micro-environmental effect. The critical micelle concentration of these surfactants is practically not affected by pH under the present conditions.

Conclusion. Both CM·Cys-1 and -2 show profound catalytic efficiency for the degradation of carboxylic esters to an extent comparable to that of the CTAB–AM·Cys-1 comicelle.[5] The large efficiency of CM·Cys-1 and -2 in the micellar phase is due to the electrostatic field effect provided by the cationic charge placed in the Stern layer which acts to stabilize the anionic transition state and to reduce pK_a of the mercapto group. An anionic nucleophile in general would be subjected to the desolvation effect in the hydrophobic micellar core. However, the reactivity of the anionic sulfido group of CM·Cys-1 is comparable to that of CM·Cys-2 in the micellar phase. This indicates that the desolvation effect does not play a primary role for the development of the thiol reactivity. Being a soft nucleophile, the thiolate anion would not sustain the solvation effect by water molecule as effectively as a hard nucleophile, such as the carboxylate anion.

References

1) For example: U. Tonellato, *J. Chem. Soc., Perkin Trans. 2*, **1976**, 771.

2) For example: Ch. Rav-Acha, M. Chevion, J. Katzhendler, and S. Sarel, *J. Org. Chem.*, **43**, 591 (1978).

3) For example: R. A. Moss, R. C. Nahas, S. Ramaswami, and W. J. Sanders, *Tetrahedron Lett.*, **1975**, 3379.

4) a) P. Heitmann, *European J. Biochem.*, **5**, 305 (1968); b) R. A. Moss, R.C. Nahas, and T. J. Lukas, *Tetrahedron Lett.*, **1978**, 507; c) R. A. Moss, T. J. Lukas, and R. C. Nahas, *J. Am. Chem. Soc.*, **100**, 5920 (1978); d) R. A. Moss, G. O. Bizzigotti, T. J. Lukas, and W. J. Sanders, *Tetrahedron Lett.*, **1978**, 3661.

5) Y. Murakami, A. Nakano, and K. Matsumoto, *Bull. Chem. Soc. Jpn.*, **52**, 2996 (1979).

6) Y. Murakami, Y. Aoyama, M. Kida, and A. Nakano, *Bull. Chem. Soc. Jpn.*, **50**, 3365 (1977).

7) G. L. Ellman, *Arch. Biochem. Biophys.*, **82**, 70 (1959).

8) J. H. Fendler and E. J. Fendler, "Catalysis in Micellar and Macromolecular Systems," Academic Press, New York, N. Y. (1975), p. 88.

9) J. M. Brown and J. D. Schofield, *J. Chem. Soc., Chem. Commun.*, **1975**, 434.

Studies on 2-Aziridinecarboxylic Acid. II.[1] A Novel Synthesis of Threonine *O*-Peptide Derivatives *via* (2*S*,3*S*)-3-Methyl-2-aziridinecarboxylic Acid

Takumi TANAKA, Kiichiro NAKAJIMA, Toru MAEDA, Akihiro NAKAMURA, Noboru HAYASHI, and Kenji OKAWA*

Department of Chemistry, Faculty of Science, Kwansei Gakuin University, Nishinomiya 662

(Received March 23, 1979)

A new synthesis of threonine *O*-peptides *via* the ring opening reaction of aziridine peptide with carboxylic acid has been investigated. Benzyl (2*S*,3*S*)-1-[*N*-(benzyloxycarbonyl)glycyl]-3-methyl-2-aziridinecarbonylglycinate was treated with several *N*-protected amino acids or dipeptides at their mixed melting point, and the corresponding *O*-aminoacyl or dipeptidyl esters of L-threonine peptide derivative were obtained in good yields without racemization.

Depsipeptide represents a major part of the biological active cyclic peptides. Many studies on an effective synthetic method of these peptides have been carried out. So far total synthesis, except in some cases, has been accomplished by the usual cyclization under peptide bond formation after performance of ester linkage at the first step in the synthetic procedure. Synthetic approaches in this field are limited. It is therefore desirable to establish a convenient synthetic method for *O*-peptide without racemization.

In a previous paper,[2] it was reported that *N*-tosyl-*O*-acetyl-L-threoninanilide is obtained quantitatively *via* the ring opening reaction of (2*S*,3*S*)-1-tosyl-3-methyl-2-aziridinecarboxanilide by the action of acetic acid in the presence of BF_3.

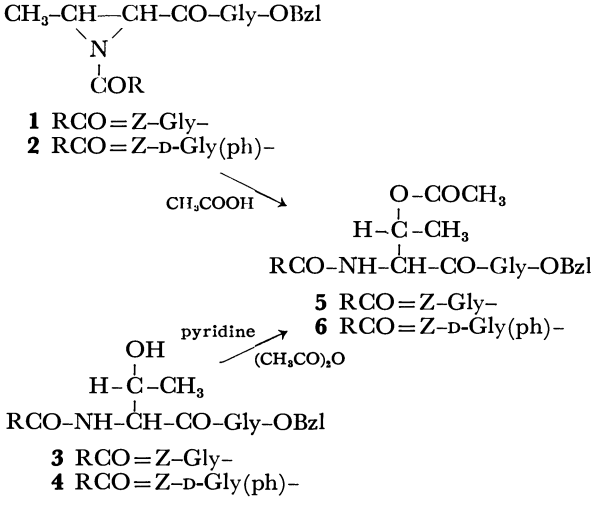

Scheme 1.

The method was applied to aziridine peptides such as Z–Gly–3-Me–Azy–Gly–OBzl (**1**) and Z–D-Gly(ph)–3-Me–Azy–Gly–OBzl (**2**).[3] The corresponding *O*-acetylthreonine peptide derivatives (**5**, **6**) were easily obtained in the absence of any catalyst as shown in Scheme 1 and Table 1. On the other hand, authentic samples of **5** and **6** were prepared from Z–Gly(or D-Gly(ph))–L-Thr–Gly–OBzl (**3**, **4**) according to the usual *O*-acetylation procedure. The yields of the *O*-acetylthreonine peptide derivatives were equally good, no remarkable differences being observed between the two methods. The configuration of β-carbon atom of threonine residue was retained in its original threo form, double inversion being encountered through the formation and cleavage reaction of the aziridine ring (Scheme 2).

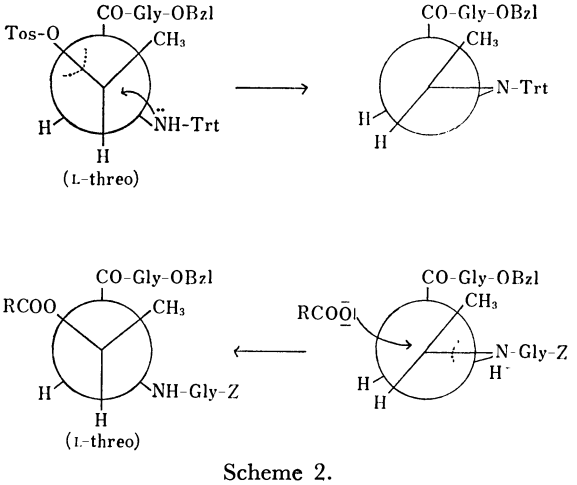

Scheme 2.

The above results prompted us to attempt effective preparation of *O*-peptides which might be used as an important intermediate of depsipeptide synthesis. A preliminary test using Z–Gly–OH to Z–Gly–3-Me–Azy–Gly–OBzl (**1**) with BF_3 in CH_2Cl_2 at 25 °C, gave low yield (about 20%). The aziridine ring showed unexpected resistance against Z–Gly–OH. However, the reaction proceeded with greater facility under drastic

Table 1. Formation of *O*-acetylthreonine peptide derivatives (**5**, **6**)

Compd	Starting compd	Reaction temp/°C	Yield/%	Mp/°C	$[\alpha]_D^{23}$ a)
5	**1**	25	82.5	133—134	+10.5
	3	0	85.7	134—135	+ 9.7
6	**2**	25	88.8	235—236	+18.5
	4	0	80.4	235—236	+18.9

a) *c* 1.0 in DMF.

Table 2. Formation of threonine *O*-peptide derivatives (**7a—j**)

Compd	RCOOH	Route	Reagent	Reaction temp/°C	Yield/%	Mp/°C	$[\alpha]_D^{23}$
7a	Z–Gly–OH	A	—	110	97.0	135—136	+10.3(*c* 1.0, DMF)
		B	CDI	0	21.6	136—137	+11.9(*c* 0.4, DMF)
7b	Boc–Leu–OH	A	—	85	90.8	powder	−19.7(*c* 1.0, MeOH)
		B	CDI	0	16.0	powder	−19.6(*c* 0.8, MeOH)
7c	Boc–Pro–OH	A	—	125	92.3	powder	−26.2(*c* 0.85, MeOH)
7d	Boc–Phe–OH	A	—	100	73.9	100—102	− 6.2(*c* 0.93, MeOH)
7e	Z–Ser–OH	A	—	96	84.5	123—125	−12.3(*c* 0.97, MeOH)
7f	Boc–Met(O)–OH	A	—	100	95.5	powder	− 9.2(*c* 1.05, MeOH)
7g	Boc–Glu(OBzl)–OH	A	—	100	82.7	powder	−10.7(*c* 1.07, MeOH)
7h	Z–MeVal–OH	A	—	110	93.0	117—118.5	+36.8(*c* 0.98, MeOH)
7i	Boc–Leu–Leu–OH	A	—	115	80.0	powder	−26.8(*c* 0.91, MeOH)
		B	CDI	0	17.6	powder	−20.2(*c* 0.62, MeOH)
		B	DCC	−10	1.5	powder	−24.0(*c* 0.88, MeOH)
7j	Boc–Pro–Sar–OH	A	—	85	92.0	95—96	−23.1(*c* 0.5, MeOH)

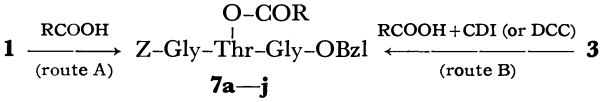

Scheme 3.

conditions, *i.e.*, at the mixed melting point of the two reactants in the absence of catalyst or solvent as shown in Scheme 3 (*via* route A). Several *N*-protected amino acids and dipeptides were used as the carboxylic acid component. All the reactions through the ring opening (*via* route A) were accomplished in a short time (2—4 h), threonine *O*-peptide derivatives (**7a—j**) being obtained in good yields. The yields and physical characteristics of **7a—j** are given in Table 2.

Special attention was paid to racemization during the course of heating, but none was observed: **7i** (*via* route A); $[\alpha]_D^{23}$ −26.8° (*c* 0.91, MeOH), ($[\alpha]_D^{23}$ −27.4° (*c* 0.9, MeOH)).[4] Partial racemization might occur by the usual method (*via* route B), using activating reagent (CDI or DCC), during the course of direct introduction of *N*-protected dipeptide.

From the results, it was concluded that the new method would become a convenient means for the synthesis of biological active depsipeptides.

Experimental

All the melting points are uncorrected. The optical rotations were measured on a Parkin-Elmer 141 Polarimeter. Purity of the synthetic compounds was confirmed by thin layer chromatography on silica gel G.

Synthesis of O*-Acetylthreonine Peptide Derivatives. Z–Gly–*L*-Thr(OAc)–Gly–OBzl (5).* *From 1*: Z–Gly–3-Me–Azy–Gly–OBzl (**1**)[3b] (220 mg, 0.5 mmol) was dissolved in acetic acid (5 ml) and the solution was left to stand at room temperature for 3 days. After removal of acetic acid, the crystals obtained were collected and recrystallized from ethyl acetate–ether–hexane (206 mg). Found: C, 59.78; H, 5.36; N, 8.39%. Calcd for $C_{25}H_{29}O_8N_3$: C, 60.11; H, 5.85; N, 8.41%.

From 3: Acetic anhydride (708 mg, 4 mmol) was added with stirring to a solution of Z–Gly–L-Thr–Gly–OBzl (**3**)[5] (458 mg, 1 mmol) in pyridine (5 ml) at 0 °C. After being stirred for 12 h, the reaction mixture was concentrated *in vacuo*. The residue was dissolved in ethyl acetate and the solution was washed with 10% citric acid, 1 M sodium hydrogencarbonate and water, dried over Na_2SO_4, and concentrated *in vacuo*. The residual product was crystallized from ethyl acetate–ether–hexane (428 mg). Found: C, 59.96; H, 5.73; N, 8.36%. The results are summarized in Table 1.

*Z–*D*-Gly(ph)–*L*-Thr(OAc)–Gly–OBzl (6).* *From 2*: Compound **6** was obtained in the same way as described above from Z–D-Gly(ph)–3-Me–Azy–Gly–OBzl (**2**)[3b] (515 mg, 1 mmol) and acetic acid (3 ml). Compound **6** was crystallized from ethyl acetate (511 mg). Found: C, 63.09; H, 5.86; N, 7.16%. Calcd for $C_{31}H_{33}O_8N_3 \cdot H_2O$: C, 62.72; H, 5.94; N, 7.08%.

From 4: Compound **6** was obtained in the same way as described above from Z–D-Gly(ph)–L-Thr–Gly–OBzl (**4**)[6] (267 mg, 0.5 mmol) and acetic anhydride (100 mg, 1 mmol) in pyridine (3 ml). Compound **6** was crystallized from ethyl acetate–ether (231 mg). Found: C, 62.67; H, 5.87; N, 7.01 %. The results are summarized in Table 1.

Z–Gly–
Synthesis of Threonine O*-Peptide Derivatives. Z–Gly–*L*-Thr–Gly–OBzl (7a).* Via *Route A*: A mixture of **1** (45 mg, 0.1 mmol) and Z–Gly–OH (45 mg, 0.22 mmol) was heated at 110 °C in an oil bath. After being heated for 2 h, the reaction mixture was dissolved in ethyl acetate. The solution was washed with 1 M sodium hydrogencarbonate and water, dried over Na_2SO_4, and concentrated *in vacuo*. The residual product was crystallized from ethyl acetate–ether–hexane (63 mg). Found: C, 61.07; H, 5.43; N, 8.52%. Calcd for $C_{33}H_{36}O_{10}N_4$: C, 61.10; H, 5.59; N, 8.64%.

Via *Route B*: CDI (194 mg, 1.2 mmol) was added with stirring to a solution of Z–Gly–OH (250 mg, 1.2 mmol) in THF (5 ml) at −10 °C. After 1 h, a solution of **3** (320 mg, 0.7 mmol) in dioxane (5 ml) was added to the reaction mixture with stirring at 0 °C. After being stirred for 4 h, the solvent was removed *in vacuo*. The residual product was dissolved in ethyl acetate and the solution was washed with 1 M sodium hydrogencarbonate and water, dried over Na_2SO_4, and concentrated *in vacuo*. The residual product was purified by column chromatography on silica gel in benzene–ethyl acetate (1: 1 v/v). Compound **7a** was crystallized from ethyl acetate–ether–hexane (99 mg). Found: C, 60.95; H, 5.54; N, 8.54%. The results are summarized in Table 2.

*Boc–*L*-Leu–*
*Z–Gly–*L*-Thr–Gly–OBzl (7b).* Via *Route A*: A mixture of **1** (104 mg, 0.24 mmol) and Boc–L-Leu–OH (166 mg, 0.72 mmol) was heated at 85 °C for 2 h, and then worked up as described for **7a**. The residual oily product was purified by

column chromatography on silica gel in $CHCl_3$–ethyl acetate (1: 1 v/v) to give an amorphous powder (146 mg). Found: C, 59.97; H, 6.92; N, 8.31%. Calcd for $C_{36}H_{46}O_{10}N_4 \cdot H_2O$: C, 60.66; H, 6.79; N, 7.86%.

Via *Route B*: CDI (1.49 g, 9.20 mmol) was added with stirring to a solution of Boc-L-Leu-OH (1.94 g, 8.37 mmol) in THF (7 ml) at −10 °C. After 1 h, compound **3** (2.74 g, 6.0 mmol) in DMF (5 ml) was added to the reaction mixture with stirring at 0 °C. After being stirred for 3 days, it was worked up as described for **7a**. The residual product was purified by column chromatography on silica gel in $CHCl_3$–ethyl acetate (1: 1 v/v) to give an amorphous powder (646 mg). Found: C, 60.51; H, 7.13; N, 8.44%. The results are summarized in Table 2.

Boc-L-Pro—

Z-Gly-L-Thr-Gly-OBzl (7c). Via *Route A*: A mixture of **1** (659 mg, 1.5 mmol) and Boc-L-Pro-OH (1.29 mg, 6.0 mmol) was heated at 125 °C for 3 h, and then worked up as described for **7a**. The residual product was purified by column chromatography on silica gel in $CHCl_3$–ethyl acetate (1: 1 v/v) to give an amorphous powder (906 mg). Found: C, 59.66; H, 6.56; N, 8.19%. Calcd for $C_{33}H_{42}O_{10}N_4 \cdot 1/2H_2O$: C, 59.72; H, 6.53; N, 8.44%. The results are summarized in Table 2.

Boc-L-Phe—

Z-Gly-L-Thr-Gly-OBzl (7d). Via *Route A*: A mixture of **1** (220 mg, 0.5 mmol) and Boc-L-Phe-OH (531 mg, 2 mmol) was heated at 100 °C for 3 h, and then worked up as described for **7a**. Compound **7d** was crystallized from ethyl acetate–ether–hexane (260 mg). Found: C, 61.15; H, 6.35; N, 7.38 %. Calcd for $C_{37}H_{44}O_{10}N_4 \cdot H_2O$: C, 61.48; H, 6.42; N, 7.75 %. The results are summarized in Table 2.

Z-L-Ser—

Z-Gly-L-Thr-Gly-OBzl (7e). Via *Route A*: A mixture of **1** (800 mg, 1.82 mmol) and Z-L-Ser-OH (1.74 g, 7.28 mmol) was heated at 96 °C for 4 h, and then worked up as described for **7a**. Compound **7e** was crystallized from hot ethyl acetate (1.05 g). Found: C, 59.01; H, 5.64; N, 8.05%. Calcd for $C_{34}H_{38}O_{11}N_4 \cdot 1/2H_2O$: C, 59.36; H, 5.72; N, 8.51%. The results are summarized in Table 2.

Boc-L-Met(O)—

Z-Gly-L-Thr-Gly-OBzl (7f). Via *Route A*: A mixture of **1** (800 mg, 1.82 mmol) and Boc-L-Met(O)-OH (1.93 g, 7.28 mmol) was heated at 100 °C for 4 h, and then worked up as described for **7a**. The residual product was purified by column chromatography on silica gel in ethyl acetate–MeOH–$CHCl_3$ (1: 1: 8 v/v) to give an amorphous powder (1.22 g). Found: C, 55.11; H, 6.26; N, 7.73; S, 4.31%. Calcd for $C_{33}H_{43}O_{11}N_4S \cdot 1/2H_2O$: C, 55.53; H, 6.35; N, 7.85; S, 4.49%. The results are summarized in Table 2.

Boc-L-Glu(OBzl)—

Z-Gly-L-Thr-Gly-OBzl (7g). Via *Route A*: A mixture of **1** (300 mg, 0.68 mmol) and Boc-L-Glu(OBzl)-OH (922 mg, 2.73 mmol) was heated at 100 °C for 4 h, and then worked up as described for **7a**. The residual product was purified by column chromatography on silica gel in $CHCl_3$–ethyl acetate (1: 1 v/v) to give an amorphous powder (439 mg). Found: C, 61.72; H, 6.30; N, 7.35%. Calcd for $C_{40}H_{48}O_{12}N_4$: C, 61.84; H, 6.23; N, 7.21%. The results are summarized in Table 2.

Z-L-MeVal—

Z-Gly-L-Thr-Gly-OBzl (7h). Via *Route A*: A mixture of **1** (300 mg, 0.68 mmol) and Z-L-MeVal-OH (724 mg, 2.73 mmol) was heated at 110 °C for 4 h, and then worked up as described for **7a**. Compound **7h** was crystallized from ethyl acetate–ether–hexane (446 mg). Found: C, 63.11; H, 6.85; N, 8.02%. Calcd for $C_{37}H_{44}O_{10}N_4$: C, 63.05; H, 6.29; N, 7.95%. The results are summarized in Table 2.

Boc-L-Leu-L-Leu—

Z-Gly-L-Thr-Gly-OBzl (7i). Via *Route A*: A mixture of **1** (300 mg, 0.68 mmol) and Boc-L-Leu-L-Leu-OH (941 mg, 2.73 mmol) was heated at 115 °C for 4 h, and then worked up as described for **7a**. The residual product was purified by column chromatography on silica gel in $CHCl_3$–ethyl acetate (1: 1 v/v) to give an amorphous powder (426 mg). Found: C, 60.70; H, 7.50; N, 8.30%. Calcd for $C_{40}H_{57}O_{11}N_5 \cdot 1/2H_2O$: C, 60.59; H, 7.37; N, 8.83%.

Via *Route B*: CDI (135 mg, 0.83 mmol) was added with stirring to a solution of Boc-L-Leu-L-Leu-OH (236 mg, 0.69 mmol) in THF (3 ml) at −10 °C. After 95 min, compound **3** (158 mg, 0.35 mmol) in THF (3 ml) was added to the reaction mixture with stirring at 0 °C. After 7 days, it was worked up as described for **7a**. The residual product was purified by column chromatography on silica gel in $CHCl_3$–ethyl acetate (1: 1 v/v) to give an amorphous powder (48 mg). Found: C, 61.12; H, 7.67; N, 8.87%. Calcd for $C_{40}H_{57}O_{11}N_5$: C, 61.28; H, 7.33; N, 8.93%.

Via *Route B*: Compound **3** (915 mg, 2 mmol) and Boc-L-Leu-L-Leu-OH (689 mg, 2 mmol) were combined with DCC (413 mg, 2.2 mmol) in absolute pyridine (8 ml) at −10 °C for 3 days. Isolation and washing procedure gave an oil, which was purified by column chromatography on silica gel in $CHCl_3$–ethyl acetate (1: 1 v/v) to give an amorphous powder (23.6 mg). Found: C, 58.67; H, 7.12; N, 7.74%. Calcd for $C_{40}H_{57}O_{11}N_5 \cdot H_2O$: C, 59.91; H, 7.42; N, 8.73%. The results are summarized in Table 2.

Boc-L-Pro-Sar—

Z-Gly-L-Thr-Gly-OBzl (7j). Via *Route A*: A mixture of **1** (55 mg, 0.13 mmol) and Boc-L-Pro-Sar-OH (143 mg, 0.5 mmol) was heated at 85 °C for 4 h, and then worked up as described for **7a**. Compound **7j** was crystallized from $CHCl_3$–ether–hexane (83.3 mg). Found: C, 58.27; H, 6.50; N, 9.15%. Calcd for $C_{36}H_{47}O_{11}N_5 \cdot H_2O$: C, 58.27; H, 6.64; N, 9.42%. The results are summarized in Table 2.

References

1) Part I; K. Nakajima, F. Takai, T. Tanaka, and K. Okawa, *Bull. Chem. Soc. Jpn.*, **51**, 1577 (1978).

2) K. Okawa, T. Kinutani, and K. Sakai, *Bull. Chem. Soc. Jpn.*, **41**, 1353 (1968).

3) a) Abbreviations according to IUPAC-IUB commission, *J. Biol. Chem.*, **247**, 977 (1972), are used. Z: benzyloxycarbonyl, Boc: *t*-butoxycarbonyl, Bzl: benzyl ester, CDI: *N,N'*-Carbonyldiimidazole, DCC: dicyclohexylcarbodiimide Gly(ph): α-phenylglycine. "Azyline" is used as a name of an 2-aziridinecarboxylic acid, "Azy" being its abbreviation. 3-Me-Azy: 3-methyl-2-aziridinecarboxylic acid. b) K. Okawa, K. Nakajima, T. Tanaka, and Y. Kawana, *Chem. Lett.*, **1975**, 591.

4) The standard sample of **7i** was prepared in the following way: deprotection of Boc group of **7b** by TFA, followed by coupling with Boc-L-Leu-OH using DCC: an amorphous powder, $[\alpha]_D^{23}$ −27.4° (*c* 0.9, MeOH). Found: C, 60.44; H, 7.33; N, 9.02%. Calcd for $C_{40}H_{57}O_{11}N_5 \cdot 1/2H_2O$: C, 60.59; H, 7.37; N, 8.83%.

5) Y. Nakagawa, T. Tsuno, K. Nakajima, M. Iwai, H. Kawai, and K. Okawa, *Bull. Chem. Soc. Jpn.*, **45**, 1162 (1972).

6) K. Nakajima, H. Kawai, M. Takai, and K. Okawa, *Bull. Chem. Soc. Jpn.*, **50**, 917 (1977).

Reaction of Diazo Ketones in the Presence of Metal Chelates. VII. 1,3-Dipolar Cycloaddition of 1-Methoxybenzo[*c*]pyrylium-4-olate with Acetylenic Dipolarophiles

Toshikazu IBATA* and Kimiko JITSUHIRO

Institute of Chemistry, College of General Education, Osaka University, Toyonaka, Osaka 560

(Received March 28, 1979)

The $Cu(acac)_2$ catalyzed decomposition of *o*-methoxycarbonyl-α-diazoacetophenone (**3**) in the presence of acetylenic dipolarophiles gave cycloadducts of the dipolarophiles with 1-methoxybenzo[*c*]pyrylium-4-olate generated by the intramolecular carbene-carbonyl reaction of the corresponding carbene. The direction of the cycloadditions of unsymmetrically substituted acetylenes has been determined on the basis of the NMR coupling pattern and chemical shift of the bridgehead methine protons of the adducts. Treatment of **3** with strong dipolarophiles such as dibenzoylacetylene or dimethyl acetylenedicarboxylate gave spiro pyrazoles by the direct cycloaddition of **3** and acetylenes followed by the elimination of methanol.

The 1,3-dipolar cycloaddition of pyridinium-3-olates (**1**) have recently been extensively studied by Katritzky *et al.*[1] Only a few papers exist however on the reaction of pyrylium-3-olates (**2**),[2] having isoelectronic structures with pyridinium-3-olate, due to the low stability and difficulty formation of **2**. The reported methods for the formation of pyrylium-3-olates were the thermal and photochemical cleavage of the corresponding epoxides.[2] In the previous paper the formation of benzo[*c*]-pyrylium-4-olate (**5**) was reported in which the contribution of the carbonyl ylide type resonance formula (**5b**), in the copper chelate-catalyzed decomposition of *o*-methoxycarbonyl-α-diazoacetophenone (**3**) *via* intramolecular carbene-carbonyl reaction.[3] In this paper the cycloaddition of the carbonyl ylide with acetylenic dipolarophiles will be described.

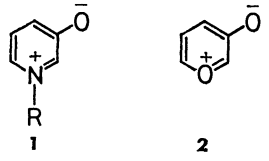

1 **2**

Results and Discussion

The $Cu(acac)_2$ catalyzed decomposition of *o*-methoxycarbonyl-α-diazoacetophenone (**3**) in benzene at 80 °C in the presence of 1.2 mol equivalents of dibenzoylacetylene gave two products. The main product (66% yield) was assigned as 5,6-dibenzoyl-4-methoxy-4,7-epoxy-2,3-benzo-2,5-cycloheptadien-1-one (**6a**) on the basis of the spectral and analytical data. The IR spectrum of **6a** shows carbonyl bands of cyclic ketone and benzoyl groups at 1710 and 1660 cm^{-1}, respectively, together with an ethylenic band at 1630 cm^{-1}. The NMR spectrum of **6a** has a singlet signal of the methoxyl group at δ 3.73 and that of a bridgehead proton at δ 5.75 together with the multiplet signal of the aromatic protons.

The formation of **6a** is reasonably explained by the 1,3-dipolar cycloaddition of dibenzoylacetylene with 1-methoxybenzo[*c*]pyrylium-4-olate (**5**) which is derived by the intramolecular carbene-carbonyl reaction of the *o*-methoxycarbonylbenzoylcarbene intermediate (**4**) generated by the $Cu(acac)_2$ catalyzed decomposition of **3**

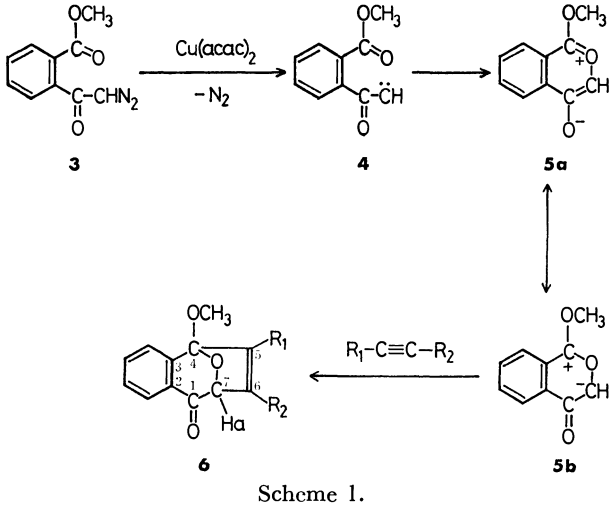

3 **4** **5a** **5b** **6**

Scheme 1.

(Scheme 1).

The other product contains nitrogen and has a molecular formula $C_{25}H_{14}O_4N_2$ which corresponds to the compound obtained by the elimination of CH_3OH from a 1 : 1 adduct of the diazo ketone and dibenzoylacetylene. The absence of methoxyl and methine signals in the NMR spectrum agrees with the molecular formula. The IR spectrum shows strained carbonyl and benzoyl bands at 1748 and 1680 cm^{-1} respectively and also shows an ethylenic band at 1650 cm^{-1}. Heating of the 1 : 1 mixture of the diazo ketone and dibenzoylacetylene in xylene at 120 °C without $Cu(acac)_2$ catalyst gave the same product in high yield. The nitrogen containing product was assigned as 4′,5′-dibenzoylspiro[indan-2,3′-[3*H*]pyrazole]-1,3-dione (**9a**) on the following basis. The cycloaddition of diazo ketones toward electron-deficient acetylenes has been reported to give pyrazoles.[4] The cycloaddition of the diazo ketone (**3**) towards dibenzoylacetylene gives pyrazole (**7a**) which may be in equilibrium with pyrazole (**8a**) by a 1,3-proton shift. The intramolecular elimination of methanol from the pyrazole (**7a**) may give 4′,5′-dibenzoylspiro[indan-2,3′-[3*H*]pyrazole]-1,3-dione (**9a**). The structure of the spiro pyrazole (**9a**) was confirmed by comparison of the spectral properties with an authentic sample prepared by the cycloaddition of 2-diazo-1,3-indandione with dibenzoylacetylene.[5] In

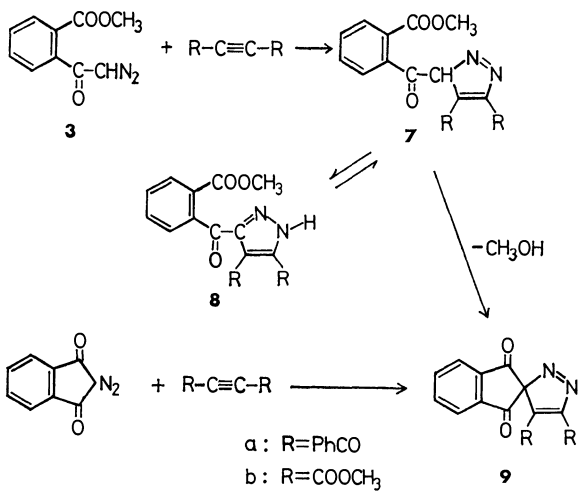

Scheme 2.

order to ascertain the intermediacy of the pyrazole **7a** and **8a**, an absolute benzene solution of equimolar amounts of the diazo ketone (**3**) and dibenzoylacetylene was heated at 60 °C for 6 h. In the IR spectrum of the reaction mixture (after evaporation of benzene under reduced pressure below 50 °C) the characteristic absorption of the diazo group at 2150 cm^{-1} disappeared. The carbonyl bands at 1710 and 1660 cm^{-1} (broad) remained unchanged and a broad band appeared at 3270 cm^{-1}. The NMR spectrum exhibited a singlet of the methoxyl methyl group at δ 3.70 together with a multiplet of aromatic protons. Column chromatography of the reaction mixture on silica gel did not isolate the intermediate **7a** or **8a** but gave the spiro pyrazole (**9a**) in high yield. Fractional recrystallization of the reaction mixture from a mixture of benzene–heptane below 60 °C gave colorless crystals, which were assigned to pyrazole (**8a**) on the basis of analytical and spectral data (see experimental section). Treatment of the pyrazole (**8a**) on silica gel or heating it at 110 °C for 5 h gave the spiro pyrazole (**9a**) quantitatively.

The reaction of **3** with dimethyl acetylenedicarboxylate with $Cu(acac)_2$ catalyst gave a small amount (4%) of the corresponding spiro pyrazole (**9a**) together with cycloadduct (**6b**; 73%) of the benzopyrylium-4-olate (**5**). The spiro pyrazole (**9b**) was also confirmed by comparison with an authentic sample prepared by a similar method as cited above.

In the reactions with asymmetric acetylenes there exist two possibilities in the direction of the cycloaddition giving two isomers. Methyl propiolate however gave only one adduct (**6c**: R_1=$COOCH_3$, R_2=H) in 44% yield despite a detailed inspection of the reaction mixture by column chromatography. The structure of **6c** was characterized by the NMR coupling pattern of two methine protons of the adduct. Both bridgehead methine protons (H_a) and vinyl protons (H_b) show doublet signals coupled with one another (J=2.8 Hz) at δ 5.16 and 7.21 ppm, respectively. This indicates that H_a and H_b are located in vicinal positions (C-7 and C-6).[6]

Phenylacetylene gave two adducts (**6d**: R_1=Ph, R_2=H and **6e**: R_1=H, R_2=Ph) in 45% and 13% yields respectively, together with isochroman-1,4-dione (**10**; 8%) and a 1:2 adduct (**11**; in 5% yield). The structure of the major adduct **6d** was assigned on the basis of the coupling pattern of the methine protons similar to that with **6c** (Table 1). The minor adduct **6e** showed singlet methine proton signals at δ 5.61 and 6.80 ppm indicating that the vinyl proton is located on C-5 and consequently the phenyl group is attached to C-6. The 1:2 adduct is tentatively assigned as **11** on the basis of the elemental analysis and spectroscopic data. The NMR spectrum shows the chemical shifts of two methoxyl groups at δ 3.86 (s) and 3.53 (s) and those of methine protons at δ 6.50 (d), 5.38 (d), and 5.27 (s) and a singlet signal of phenyl protons at δ 7.23 except for a multiplet of aromatic protons. The value of the coupling constant, J=2.4 Hz, for the two doublet methine protons indicates that the two vicinal protons are in a trans configuration.[7] The precise configuration of the 1:2 adduct has however not been determined.

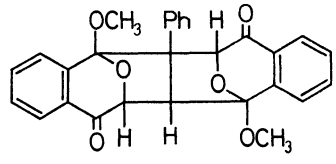

11

Methyl phenylpropiolate gave a small amount (6%) of an adduct (**6f**) and isochromandione (**10**, 58%) in

Table 1. Yields and ^{1}H-NMR data of 1,3-dipolar cycloadducts (**6**)

Adduct	R_1	R_2	Yield/%	NMR (δ/ppm, in $CDCl_3$)					
				OCH_3	OCH_3	H_a	H_b(=R_2)	H_c(=R_1)	J_{ab}/Hz
6a	PhCO	PhCO	66	3.73	—	5.75 (s)	—	—	—
6b	$COOCH_3$	$COOCH_3$	73	3.83	3.67	5.46 (s)	—	—	—
6c	$COOCH_3$	H	44	3.70	3.53	5.16 (d)	7.21 (d)	—	2.8
6d	Ph	H	9(45)[a]	3.49	—	5.21 (d)	6.68 (d)	—	2.6
6e	H	Ph	0(13)[a]	3.65	—	5.61 (s)	—	6.80(s)	—
6f	$COOCH_3$	Ph	6(39)[a]	3.73	3.63	5.55 (s)	—	—	—
6g	Ph	$COOCH_3$	0(9)[a]	3.72	3.40	5.48 (s)	—	—	—
6h[b]	COOH	Ph		3.74[c]	—	5.67 (s)[c]	—	—	—

a) Neat dipolarophile was used as the solvent instead of benzene. b) **6h** was obtained by the hydrolysis of **6f**.
c) The NMR spectrum was measured in $CDCl_3$–pyridine solution.

the reaction according to the general procedure (in benzene). When the decomposition was conducted in neat methyl phenylpropiolate (large excess), the yield of the adduct (**6f**) was improved (39%) and the yield of **10** decreased (7%). Moreover, another isomer (**6g**) was obtained in 9% yield. In the previously cited adducts (**6a**—**6g**), the chemical shifts of the bridgehead protons (H_a) are revealed to be affected by the substituents on C-6. The deshielding effect of the C-6 substituent on the chemical shift of H_a decreases in the following order, phenyl (**6e**, 5.61 ppm), methoxycarbonyl (**6b**, 5.46), hydrogen (**6c**, 5.16; **6d**, 5.12). The major adduct (**6f**) shows the chemical shift of H_a at 5.55 ppm which is closer to the value for **6e** than **6b**. The value of the minor adduct (**6g**) corresponds to that of **6b** (5.46 ppm) which has a methoxycarbonyl group on C-6 indicating that the methoxycarbonyl group is on C-6 in the minor adduct (**6g**). These assignments were confirmed by means of conversion of the major adduct (**6f**) into **6e** *via* hydrolysis followed by the decarboxylation.

The reactions when conducted in benzene solution as is shown in the general procedure, the yields of the adducts of these acetylenic dipolarophiles decrease in the order: dimethyl acetylenedicarboxylate>dibenzoylacetylene>methyl propiolate>methyl phenylpropiolate ≈phenylacetylene>diphenylacetylene (no reaction). The order of the reactivities of the dipolarophiles are consistent with their reactivities toward 3-methyl-2,4-diphenyloxazolium-5-olate having an azomethine ylide system.[8] The intermediate benzopyrylium-4-olate (**5**) reacts competitively with the dipolarophile or water (a contaminant in the reaction system) affording the adduct or isochromandione due to the low dipolarophilicity of methyl phenylpropiolate and phenylacetylene.

The preferential formation of the cycloadduct (**6c**) in the reaction of methyl propiolate is reasonably explained by the dipolar interaction between the dipole and the dipolarophile considering the dipolar structure, $H\overset{\delta+}{-}C\equiv\overset{\delta-}{C}-COOCH_3$, of methyl propiolate and a resonance formula **5b** for benzopyrylium-4-olate. The regioselectivity of the reaction of phenylacetylene and methyl phenylpropiolate with **5** is difficult to explain only on the basis of the dipolar interaction as cited above. 3-Phenylphthalazinium-1-olate, having an isoelectronic system with benzopyrylium-4-olate (**5**), has been reported to give two cycloadducts in the reaction with phenylacetylene.[9] The steric factor and π-π interaction[10] between the substituents of the dipole (**5**) and dipolarophiles may also effect the direction of cycloaddition.

Experimental

All melting points were taken with a Yanagimoto Melting Point Apparatus and are uncorrected. The IR spectra were measured on a Hitachi Infrared Spectrometer model EPI-S2. Unless otherwise indicated ^{1}H-NMR spectra were recorded in $CDCl_3$ solution at 60 MHz on a Varian Spectrometer model A-60 or EM-360 using tetramethylsilane as an internal standard.

Materials. *o*-Methoxycarbonyl-α-diazoacetophenone (**3**) was prepared by the method of Hudson;[11] mp 62.0—62.5 °C.

Dipolarophiles. Dibenzoylacetylene,[12] dimethyl acetylenedicarboxylate,[13] and methyl phenylpropiolate[14] were prepared by procedures described in the literature. Methyl propiolate, phenylacetylene, and diphenylacetylene were used after purification of commercial reagents by distillation or recrystallization.

General Procedure of the $Cu(acac)_2$ Catalyzed Decomposition of o-Methoxycarbonyl-α-diazoacetophenone (3) in the Presence of Acetylenic Dipolarophiles. To an absolute benzene solution (50 ml) containing a catalytic amount of $Cu(acac)_2$ and a 1.2—2.0 molar amount of the dipolarophile was added a benzene solution (20 ml) of the diazo ketone (**3**) with magnetic stirring at 80 °C. Almost quantitative amounts of nitrogen gas were evolved and the reaction mixture turned colorless. After heating for 2 h the benzene was removed under reduced pressure, and the residue fractionated by column chromatography (silica gel–benzene).

Decomposition of 3 in the Presence of Dibenzoylacetylene by General Procedure: In the reaction of **3** (2.0 g, 9.8 mmol) and dibenzoylacetylene (2.75 g, 12 mmol) two products were obtained.

Cycloadduct (6a): Colorless crystals; yield 2.65 g (66%); mp 146—148 °C; IR (KBr) 1710, 1660 (C=O), 1630 cm^{-1} (C=C). Found: C, 75.90; H, 4.28%. Calcd for $C_{26}H_{18}O_5$: C, 76.09; H, 4.42%.

Spiro Pyrazole (9a): Pale yellow crystals; yield 0.38 g (10%); mp 234—235 °C; IR (KBr) 1748, 1680 (C=O), 1650 cm^{-1} (C=C). Found: C, 73.56; H, 3.48; N, 6.89%. Calcd for $C_{25}H_{14}O_4N_2$: C, 73.88; H, 3.47; N, 6.90%.

Reaction of 3 with Dibenzoylacetylene at High Temperature Without Catalyst: A xylene solution of **3** (0.21 g, 1 mmol) and dibenzoylacetylene (0.24 g, 1 mmol) was heated at 120 °C for 7 h. Evaporation of xylene under reduced pressure and recrystallization gave **9a** in 95% yield.

Reaction of 3 with Dibenzoylacetylene at Low Temperature Without Catalyst: A benzene solution of **3** (0.21 g, 1 mmol) and dibenzoylacetylene (0.24 g, 1 mmol) was heated at 60 °C for 6 h. Two careful recrystallizations of the product from a mixture of benzene–heptane below 60 °C gave colorless crystals (**8a**); yield 0.328 g (81%); mp 67.5—68.5 °C; IR (KBr) 3270 (NH), 1710 (ester C=O), 1660 cm^{-1} (C=O); NMR (in $CDCl_3$) δ 3.73 (s, 3H, OCH_3), 7.3—7.7 (m, 14H, aromatic), and 12.2 ppm (broad s, 1H, NH). Found: C, 71.11; H, 4.16; N, 6.63%. Calcd for $C_{26}H_{18}O_5N_2$: C, 71.22; H, 4.14; N, 6.39%.

Thermal Decomposition of 8a: Treatment of **8a** (0.086 g, 0.2 mmol) at 110 °C for 5 h yielded spiro pyrazole (**9a**) in quantitative yield after the evaporation of the solvent under reduced pressure.

Reaction of 2-Diazo-1,3-indandione with Dibenzoylacetylene: A mixed solution of 2-diazo-1,3-indandione (0.344 g, 2 mmol) and dibenzoylacetylene (0.468 g, 2 mmol) in xylene was heated at 140 °C for 5 h. Evaporation of the solvent gave a pale yellow crystalline product in quantitative yield. The IR spectrum of the product was identical to that of **9a** obtained in the reaction of **3** and dibenzoylacetylene.

Decomposition of 3 in the Presence of Dimethyl Acetylenedicarboxylate by General Procedure: The reaction of **3** (2.0 g, 9.8 mmol) and dimethyl acetylenedicarboxylate (1.7 g, 12 mmol) gave two products.

Cycloadduct (6b): Yield 2.0 g (73%); mp 79—80 °C; IR (KBr) 1720 (broad, ester and ring C=O), 1650 cm^{-1} (C=C). Found: C, 60.24; H, 4.34%. Calcd for $C_{16}H_{14}O_7$: C, 60.38; H, 4.43%.

Spiro Pyrazole (9b): Yield 0.12 g (4%); mp 187.5—188.5 °C; IR (KBr) 1745 (broad, ester and indandione C=O), 1675 cm^{-1} (C=C); NMR (in $CDCl_3$) δ 4.05 (s, 3H, OCH_3), 4.09 (s, 3H, OCH_3), 7.1—8.2 ppm (m, 4H, aromatic). Found:

C, 57.13; H, 3.40; N, 8.87%. Calcd for $C_{15}H_{10}O_6N_2$: C, 57.33; H, 3.21; N, 8.92%.

Reaction of 2-Diazo-1,3-indandione with Dimethyl Acetylenedicarboxylate: A xylene solution of 2-diazo-1,3-indandione (0.344 g, 2 mmol) and dimethyl acetylenedicarboxylate (0.31 g, 2.2 mmol) was heated at 140 °C for 6 h. Evaporation of the solvent under reduced pressure gave a crystalline product (0.540 g, 85%) which showed no mixed melting point depression with **9b** obtained in the reaction of **3** and dimethyl acetylenedicarboxylate.

*Decomposition of **3** in the Presence of Methyl Propiolate by General Procedure*: Reaction of **3** (0.284 g, 1.4 mmol) and methyl propiolate (0.22 g, 2.5 mmol) gave an adduct (**6c**); yield 0.160 g (44%); mp 87—88 °C; IR (KBr) 1710 (C=O), 1630 cm^{-1} (C=C). Found: C, 64.57; H, 4.63%. Calcd for $C_{14}H_{12}O_5$: C, 64.61; H, 4.65%.

*Decomposition of **3** in the Presence of Phenylacetylene by General Procedure*: Reaction of **3** (0.61 g, 3 mmol) and phenylacetylene (0.61 g, 6 mmol) gave cycloadduct (**6d**) together with isochroman-1,4-dione (**10**, 0.10 g, 20%) and unidentified intractable products.

*Cycloadduct (**6d**)*: Yield 0.070 g (9%); colorless oil; IR (liquid film) 1705 cm^{-1} (C=O). Found: C, 77.53; H, 5.24%. Calcd for $C_{18}H_{14}O_3$: C, 77.68; H, 5.07%. Isochromandione (**10**) was characterized by comparison of the IR spectrum with that of an authentic sample.[3)]

*The $Cu(acac)_2$ Catalyzed Decomposition of **3** in Neat Phenylacetylene (Large Excess)*: The diazo ketone **3** (0.408 g, 2 mmol) was decomposed at 80 °C in a large excess of phenylacetylene (5 g, 50 mmol) and a catalytic amount of $Cu(acac)_2$. Column chromatography of the reaction mixture gave another cycloadduct (**6e**) and a 1:2 adduct (**11**) together with **6d** (45%) and **10** (8%).

*Cycloadduct (**6e**)*: Yield 0.070 g (13%); colorless oil; IR (liquid film) 1705 cm^{-1} (C=O). Although the elemental analysis of **6e** did not show a satisfactory result, the structure was confirmed by the similarity of the IR spectrum with that of an isomeric cycloadduct (**6d**). The NMR spectrum also supported the structure.

*1:2 Adduct (**11**)*: Yield 0.045 g (10%); mp 244—246 °C; IR (KBr) 1710 cm^{-1} (C=O); NMR (in $CDCl_3$) δ 3.53 (s, 3H, OCH_3), 3.86 (s, 3H, OCH_3), 5.27 (s, 1H, methine), 5.38 (d, J=2.4 Hz, 1H, methine), 6.50 (d, J=2.4 Hz, 1H, methine), 7.23 (s, 5H, Ph) and 7.0—8.0 ppm (m, 8H, aromatic). Found: C, 74.19; H, 4.92%. Calcd for $C_{28}H_{22}O_6$: C, 74.00; H, 4.88%.

*Decomposition of **3** in the Presence of Methyl Phenylpropiolate by General Procedure*: Two products were obtained in the reaction of **3** (0.61 g, 3 mmol) and methyl phenylpropiolate (0.64 g, 4 mmol). The main product was confirmed to be isochromandione (**10**, 0.28 g, 58%).

*Cycloadduct (**6f**)*: Yield 0.097 g (9%); mp 112—113 °C; IR (KBr) 1710 (C=O), 1640 cm^{-1} (C=C). Found: C, 71.37; H, 4.79%. Calcd for $C_{20}H_{16}O_5$: C, 71.42; H, 4.80%.

*The $Cu(acac)_2$ Catalyzed Decomposition of **3** in Neat Methyl Phenylpropiolate (Large Excess)*: The diazo ketone (**3**) (0.408 g, 2 mmol) was decomposed in neat methyl phenylpropiolate (1.28 g, 8 mmol) in the presence of a catalytic amount of $Cu(acac)_2$ at 80 °C. Column chromatography of the reaction mixture isolated three products, isochromandione (**10**, 0.022 g, 7%), the cycloadduct (**6f**, 0.261 g, 39%), and an isomeric cycloadduct (**6g**): yield 0.058 g (9%); colorless crystals; mp 124—127 °C; IR (KBr) 1710 (C=O), 1640 cm^{-1} (C=C). Elemental analysis of **6g** did not show a satisfactory result.

*Hydrolysis of **6f***: The cycloadduct **6f** (0.103 g, 0.3 mmol) was hydrolyzed in EtOH (2 ml) and 40% aqueous NaOH solution (2 ml) at room temperature with vigorous stirring for 5 h. Acidification of the reaction mixture with 3 M HCl after evaporation of EtOH gave colorless crystals (**6h**): yield 0.090 g, (93%); mp 260—262 °C (from EtOH–H_2O); IR (KBr) 3450, 3000, 2500, 1690, 930 (COOH), 1710 (C=O), 1640 cm^{-1} (C=C). Found: C, 70.55; H, 4.32%. Calcd for $C_{19}H_{14}O_5$: C, 70.80; H, 4.38%.

*Decarboxylation of **6h***: A quinoline solution (10 ml) of **6h** (0.040 g, 0.12 mmol) was heated at 200—210 °C for 5 h with a suspension of copper powder (0.10 g). After cooling the reaction mixture was poured into water (50 ml) and acidified with 3 M HCl in order to dissolve the quinoline. Column chromatography of the ether extract gave 0.010 g (27%) of **6d**, which was identified on the basis of the IR and NMR spectra.

References

1) A. R. Katritzky, N. Dennis, and Y. Takeuchi, *Angew. Chem. Int. Ed. Engl.*, **15**, 1 (1976).

2) E. F. Ullman and J. E. Milks, *J. Am. Chem. Soc.*, **84**, 1315 (1962); **86**, 3814 (1964).

3) K. Ueda, T. Ibata, and M. Takebayashi, *Bull. Chem. Soc. Jpn.*, **45**, 2779 (1972).

4) A. S. Katner, *J. Org. Chem.*, **38**, 825 (1973).

5) Recently stable spiro pyrazoles have been synthesized in the reaction of four membered cyclic diazo ketone and electron-deficient acetylenes; K. Ueda, F. Toda, *Bull. Chem. Soc. Jpn.*, **51**, 649 (1978).

6) A similar type of cycloadduct of 1-phenylpyridinium-3-olate (**1**: R=Ph) with phenylacetylene was characterized on the basis of the NMR coupling pattern of bridgehead protons and vinyl protons (doublet, J=3.5 Hz); N. Dennis, A. R. Katritzky, S. K. Parton, Y. Nomura, and Y. Takeuchi, *J. Chem. Soc., Perkin Trans. 1*, **1976**, 2289.

7) T. Ibata, unpublished results.

8) R. Knorr, R. Huisgen, and G. K. Staudinger, *Chem. Ber.*, **103**, 2639 (1970).

9) N. Dennis and A. R. Katritzky, *J. Chem. Soc., Perkin Trans. 1*, **1976**, 2218.

10) R. Huisgen, H. Hauk, R. Grashey, and H. Hube, *Tetrahedron Lett.*, **1966**, 397.

11) D. Hodson, G. Holt, and D. K. Wall, *J. Chem. Soc., C*, **1970**, 971.

12) R. E. Lutz and W. R. Smithey, Jr., *J. Org. Chem.*, **16**, 51 (1951).

13) E. H. Hutress, T. E. Lesslie, and J. Bornstein, *Org. Synth.*, Coll. Vol. IV, 329 (1963).

14) T. W. Abott, *Org. Synth.*, Coll. Vol. IV, 515 (1943).

Binary Phase Chlorination of Aromatic Hydrocarbons with Solid Copper(II) Chloride: Reaction Mechanism

Iwao TANIMOTO*, Keiko KUSHIOKA, Toyokichi KITAGAWA,** and Kazuhiro MARUYAMA***

Laboratory of Chemistry, Faculty of Home Economics, Kyoto Women's University, Higashiyama-ku, Kyoto 605
***Department of Chemistry, Faculty of Science, Osaka City University, Sumiyoshi-ku, Osaka 558*
****Department of Chemistry, Faculty of Science, Kyoto University, Sakyo-ku, Kyoto 606*

(Received April 6, 1979)

Anthracene is selectively chlorinated with solid copper(II) chloride to give a quantitative yield of 9-chloroanthracene. The tentative reaction mechanisms so far proposed fail to explain the nonreactivity of some other hydrocarbon homologues, *e.g.* naphthalene and phenanthrene, toward copper(II) chloride. The present study revealed that the oxidative half-wave potentials ($E_{1/2ox}$) of all reactive hydrocarbon homologues were less than 1.26 V. On the basis of this finding we postulate a reaction mechanism involving one electron transfer from hydrocarbon to copper(II) chloride.

Solid copper(II) chloride has been used to regio- and chemospecific synthesis of 9-chloroanthracene from anthracene. This binary phase chlorination which is performed under heterogeneous conditions gives a high yield of the regiospecific product:

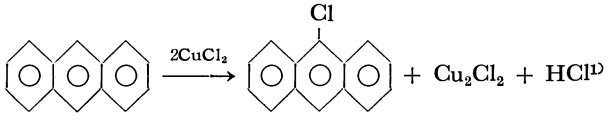

While solid copper(II) chloride is effective also for chlorination of pyrene,[2] the reagent was found to be entirely nonreactive toward some of other homologous hydrocarbons, *e.g.* naphthalene and phenanthrene. Furthermore, a solution of copper(II) chloride in acetone or in acetonitrile failed to react with those hydrocarbons which react under the binary phase conditions. Such an outstanding contrast has not been fully explained by tentatively proposed mechanisms, *e.g.* ionic[3] or ligand transfer[4] mechanisms.

The present work deals with the binary phase chlorination of a wide variety of aromatic hydrocarbons by solid copper(II) chloride. The results evidently showed that their reactivities were closely related with their oxidative half-wave potentials ($E_{1/2ox}$), but for some substituted anthracenes steric effects were a dominant factor controlling the reactivity.

Results and Discussion

Reactivities of Aromatic Hydrocarbons toward Solid Copper(II) Chloride. In a typical procedure, aromatic hydrocarbon (5×10^{-4} mol) was refluxed with pulverized copper(II) chloride (1×10^{-3} mol) in chlorobenzene. The reaction proceeds under heterogeneous binary phase conditions. The chlorination was followed by means of gas chromatograph and the products were identified by elemental analysis, MS and NMR. The chlorination products obtained are summarized in Table 1. In general, single product was obtained in a high yield under the conditions. Active and inactive hydrocarbons toward solid copper(II) chloride are tabulated in Table 2 together with their $E_{1/2ox}$ values.

Voltammetric Measurement of $E_{1/2ox}$ of Aromatic Hydrocarbons. To investigate a correlation between $E_{1/2ox}$ and the reactivity of hydrocarbons toward solid copper(II) chloride, $E_{1/2ox}$ measurements of aromatic hydrocarbons were carried out in an acetonitrile solution containing tetraethylammonium perchlorate (TEAP), using a rotatory platinum disk electrode (2000 rpm). The voltage sweep rate was 0.2 V/min. The data are summarized in Table 2. The correlation between $E_{1/2ox}$ and the reactivity of an aromatic hydrocarbon for solid copper(II) chloride, if any, is not immediately clear, but it should be emphasized that of the aromatic hydrocarbons examined only those with $E_{1/2ox}$ below *ca.* 1.26 V were reactive toward solid copper(II) chloride. $E_{1/2ox}$ correlates linearly with the ionization potential (IP) of aromatic hydrocarbons as proposed by Pysh and co-workers,[5] and $E_{1/2ox}$ value of 1.26 V corresponds to 7.68 eV of IP value, which is in a close agreement with that obtained by photoelectroscopy (*ca.* 7.5 eV).[6] This fact suggests that initial one electron transfer from aromatic π-system to solid copper(II) chloride is a key step required for the initiation of the reaction. The electron transfer may trigger off the reaction. The oxidation potential is obviously lowered by the introduction of electron-donating methyl group to aromatic ring.

It is known that anhydrous solid copper(II) chloride is in covalent state and consists of planar $CuCl_4$ groups.[7] In the binary phase chlorination performed in a non-

TABLE 1. CHLORINATION BY COPPER(II) CHLORIDE

Compound	Reaction time/h	Product	Yield %
Anthracene[a,c]	2	9-Chloroanthracene	80
Anthracene[a,d]	8	9-Chloroanthracene	88
		9,10-Dichloroanthracene	12
Anthracene[b,d]	4	9,10-Dichloroanthracene	87
Pyrene[b,c]	3	1-Chloropyrene	90
Benz[*a*]pyrene[a,c]	8	6-Chlorobenz[*a*]pyrene	90
Perylene[a,c]	7	Chloroperylene[e]	90
Perylene[a,d]	7	Dichloroperylene[e]	90
Naphthacene[b,d]	1.5	5,11-Dichloronaphthacene[f]	75
Azulene[b,d]	0.5	1,3-Dichloroazulene[f]	95

Solvent: a) benzene, b) chlorobenzene. Molar ratio ($CuCl_2$: compound): c) 2: 1, d) 4: 1. e) Product was the mixture of isomers. f) Mono chlorides of naphthacene and azulene could not be isolated in pure state.

Table 2. Oxidative half-wave potentials ($E_{1/2ox}$/V *vs.* SCE[a]) and reactivities in the chlorination of hydrocarbons by copper(II) chloride

Compound	$E_{1/2ox}$/V	Reactivity
Benzene	2.43	no
Biphenyl	1.86	no
Naphthalene	1.72	no
Triphenylene	1.72	no
Phenanthrene	1.67	no
Acenaphthylene	1.62	no
Chrysene	1.54	no
Dibenz[*a*,*h*]anthracene	1.41	no
Benz[*a*]anthracene	1.36	no
7-Methylbenz[*a*]anthracene	1.26	no
Anthracene	1.26	yes
Pyrene	1.23	yes
1-Methylanthracene	1.23	yes
12-Methylbenz[*a*]anthracene	1.22	no
2-Methylanthracene	1.21	yes
Benz[*a*]pyrene	1.18	yes
1,5-Dimethylanthracene	1.18	yes
1,4-Dimethylanthracene	1.17	yes
9-Methylanthracene	1.15	yes
1,4,5-Trimethylanthracene	1.04	yes
Perylene	1.00	yes
Naphthacene	0.94	yes
Azulene	0.88	yes

a) Solvent: acetonitrile. Supporting electrolyte : 0.1 M tetraethylammoniumperchlorate. Working electrode: rotatory platinum disk electrode (2000 rpm). Voltage sweep rate: 0.2 V/min.

polar solvent, the planar chloro ligands of anhydrous copper(II) chloride presumably occupies a favorable position for one electron transfer from hydrocarbons to copper(II) clusters. The plane of aromatic ring could approach to solid copper(II) chloride in the fashion parallel with the $CuCl_4$ surface, and the electron transfer from the approaching hydrocarbon could occur at a critical distance where the aromatic ring plane would come in a close contact with the acceptor orbital of copper(II) chloride. Although $E_{1/2ox}$ of 7- and 12-methylbenz[*a*]anthracene were 1.26 and 1.22 V (*vs.* SCE), respectively, they were hardly reactive toward solid copper(II) chloride. Presumably, steric repulsion due to rotating methyl group could prevent the molecule from closely approaching to copper(II) chloride surface in the transition state.

Competitive halogenation of anthracene gives us a further insight of the reacting aspect. Halogenation of anthracene (3.8×10^{-4} mol) by solid copper(II) bromide (7.6×10^{-4} mol) in the presence of tetraethylammonium chloride (3.8×10^{-4} mol) dissolved in chlorobenzene (30 ml) afforded 9-bromoanthracene nearly as a sole product, whereas the halogenation using an equimolar mixture of solid copper(II) chloride and bromide gave a higher yield of 9-chloroanthracene than 9-bromoanthracene (11: 1). These facts will readily suggest that the binary phase halogenation proceeds in a closely contacted state of reacting substrate with the surface of solid copper(II) halide.

Chlorination of substituted anthracenes with methyl or chloro groups by solid copper(II) chloride in chlorobenzene resulted in the formation of chlorinated products. The yields and structures of the products together with their ^{1}H-NMR data are summarized in Table 3 and 4.

From the results of chlorination of substituted anthracenes it is concluded that the rate of chlorination is enhanced by methyl substituent, but in contrary, chloro substituent retarded it. Since the electron-donating substituents lower the oxidation potential of aromatic hydrocarbons, the observation supports the view mentioned above that the reaction is initiated by an electron transfer. In addition, steric effect of the substituents controlls the product. Though the monochlorination of substituted anthracenes occurs at 9- or 10-position, less hindered position is more favorable for the chlorination; *e.g.* 1-methyl or 1-chloroanthracene was chlorinated at 10-position. Chlorination of dichloroanthracenes provides a good example to show both steric and electronic effects are operating together. Since $E_{1/2ox}$ values of 1,8- (1.48 V) (**1**), 2,3- (1.40 V)

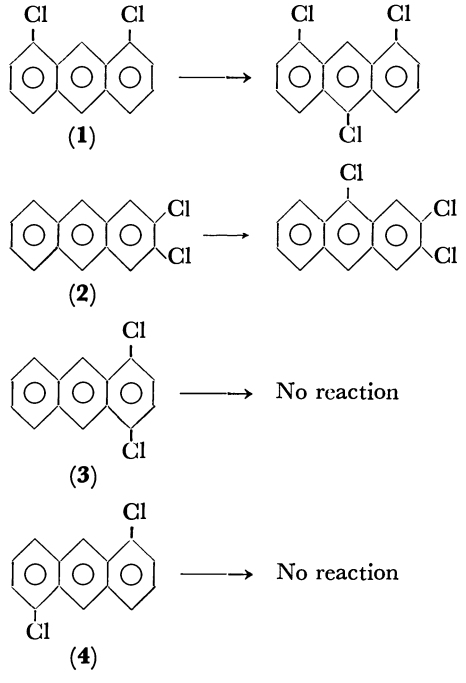

(**2**), 1,4- (1.48 V) (**3**), and 1,5-dichloroanthracene (1.40 V) (**4**) were comparable, they are expected to be similarly reactive toward solid copper(II) chloride. However, **1** and **2** were reactive, but **3** and **4** were not. These results clearly indicates that chlorine atom occupying peri position against 9- or 10-position of anthracene affects a strong steric inhibition on the chlorination.

Hydrogen Abstraction by Solid Copper(II) Chloride. Diphenylmethane, xanthene, tetrahydronaphthalene, and cumene were recovered after refluxing for 14 h with solid copper(II) chloride in cyclohexane, whereas anthracene was chlorinated under the same reaction conditions (Table 5). It is noteworthy that under the present reaction conditions no hydrogen abstraction occurred with those hydrocarbons which allow, in general, an easy hydrogen abstraction by a radical,

Table 3. Proton chemical shift in CCl_4 δ(ppm from TMS).

(A) Substituted anthracenes

Substituent	H(9-)	H(10-)	H(1-)	H(8-)	H(Me-)
—	8.31	8.31	7.88	7.88	—
1-Cl	8.77	8.32	—	≈7.9	—
2-Cl	8.28	8.36	≈7.9	≈7.9	—
9-Cl	—	8.24	8.38	8.38	—
1,4-Dichloro	8.81	8.81	—	8.04	—
1,5-Dichloro	8.76	8.76	—	7.93	—
1,8-Dichloro	9.24	8.38	—	—	—
2,3-Dichloro	8.25	8.25	8.06	7.94	—
1-Me	8.39	8.28	—	≈7.8	2.80
9-Me	—	8.15	8.08	8.08	3.07
1,4-Dimethyl	8.34	8.34	—	7.85	2.79 (2Me)
1,5-Dimethyl	8.38	8.38	—	7.78	2.84 (2Me)
1,4,5-Trimethyl	8.37	8.46	—	7.76	2.82 (1-Me), 2.82 (1Me), 2.85 (1Me)

(B) Chlorination products of substituted anthracenes

Substituent	H(9- or 10-)[a]	H(1-)[a]	H(8-)[a]	H(Me-)[a]	Substituents in product
—	8.24(10-)	8.38	8.38	—	9-Cl
1-Cl	8.76(9-)	—	8.02	—	1,10-diCl
2-Cl	8.22(9-)	≈7.85	≈7.85	—	2,10-diCl
	—	8.48	≈8.44	—	2,9,10-triCl
9-Cl	—	8.41	8.41	—	9,10-diCl
1,8-Dichloro	9.24(9-)	—	—	—	1,8,10-triCl
2,3-Dichloro	8.08(10-)	8.48	8.36	—	2,3,9-triCl
1-Me	8.46(9-)	—	7.96	2.81	9-Cl-4-Me (10-Cl-1-Me)[a]
	—	—	≈8.45	3.22	9,10-diCl-1-Me
9-Me	—	8.42	8.42	3.06	9-Cl-10-Me (10-Cl-9-Mc)[a]
1,4-Dimethyl	8.26(10-)	—	8.45	2.70 (4-Me), 3.14 (1-Me)	9-Cl-1,4-diMe
1,5-Dimethy	8.18(10-)	—	8.32	2.70 (5-Me), 3.14 (1-Me)	9-Cl-1,5-diMe
	—	—	≈8.4	3.14 (1- and 5-Me)	9,10-diCl-1,5-diMe
1,4,5-Trimethyl	8.46(10-)	—	8.4	2.76 (1Me), 2.82(1Me), 3.16(1-Me)	9-Cl-1,4,5-triMe

a) Position is numbered after substituted anthracene before chlorination.

Table 4. Chlorination of substituted anthracenes by copper(II) chloride

Anthracene	Reaction time/h	Product	Yield/%	Mp/°C
1-Chloro	16[a]	1,10-dichloroanthracene	75	126—127
	4[b]	1,10-dichloroanthracene	90	
2-Chloro	1[a]	2,10-dichloroanthracene	90	115—116
	10[b]	2,9,10-trichloroanthracene	90	181—182
1,8-Dichloro	6[a]	1,8,10-trichloroanthracene	90	191—192
	10[b]	1,8,10-trichloroanthracene	100	
2,3-Dichloro	48[a]	2,3,9-trichloroanthracene	90	172—173
	23[b]	2,3,9-trichloroanthracene	90[c]	
1,4-Dichloro	10[a,b]	no reaction		
1,5-Dichloro	10[a,b]	no reaction		
1-Methyl	0.5[a]	9-chloro-4-methylanthracene	90	66—68
	8[b]	9,10-dichloro-1-methylanthracene	5	132—134
9-Methyl	0.5[a,b]	9-chloro-10-methylanthracene	90	177—178
1,4-Dimethyl	30[a]	9-chloro-1,4-dimethylanthracene	80[c]	41.5—44
1,5-Dimethyl	8[a]	9-chloro-1,5-dimethylanthracene	60	111—114
	40[b]	9,10-dichloro-1,5-dimethylanthracene	10	154—156
1,4,5-Trimethyl	26[a]	9-chloro-1,4,5-trimethylanthracene	40	120—122

Reaction conditions: solvent; chlorobenzene, reaction temp; 132 °C, molar ratio ($CuCl_2$: anthracene); a) 2:1 b) 4:1. c) A product produced by the further chlorination was detected by GLC, but could not be isolated for its low yield.

Table 5. Hydrogen abstraction by copper(II) chloride

Compound	Recovery/%
1,2-Dihydronaphthalene[a)]	10[c)]
9,10-Dihydroanthracene[a)]	35[d)]
1,2,3,4-Tetrahydronaphthalene[b)]	95
Xanthene[b)]	98
Cumene[b)]	90
Diphenylmethane[b)]	100

Reaction time: a) 10 min, b) 14 h. Product: c) naphthalene (yield 90%), d) anthracene (yield 65%). Solvent: cyclohexane 10 ml; reaction temp: 80 °C; compound: 2.5×10^{-3} mol; $CuCl_2$: 5×10^{-3} mol.

although 1,2-dihydronaphthalene or 9,10-dihydroanthracene reacted under the same conditions, yielding naphthalene or anthracene together with evolution of hydrogen chloride.

Reaction Scheme. As has been shown above, hydrocarbons with IP value lower than *ca.* 7.5 eV were reactive for solid copper(II) chloride chlorination. 7- and 12-Methylbenz[*a*]anthracene, both nonreactive, may be the borderline case, where spatial repulsive effect due to the methyl group presumably inhibits the initial electron transfer from the hydrocarbons to copper(II) chloride. The electron transfer will trigger the chlorination. This is strongly supported by the above-mentioned electronic effect of methyl and chloro substituents. Once an electron is transferred to copper(II) chloride from a hydrocarbon, the resulting cation radical of the aromatic hydrocarbon could be immediately attacked by chloride anion at the less hindered, but the highest positively charged position to give (I). Although copper(II) chloride is a typical ligand-transfer oxidation reagent toward a radical, under the present reaction conditions the reagent may abstract a hydrogen atom from the radical (I) and convert it into the stable chlorinated aromatic molecule (see Reaction scheme).

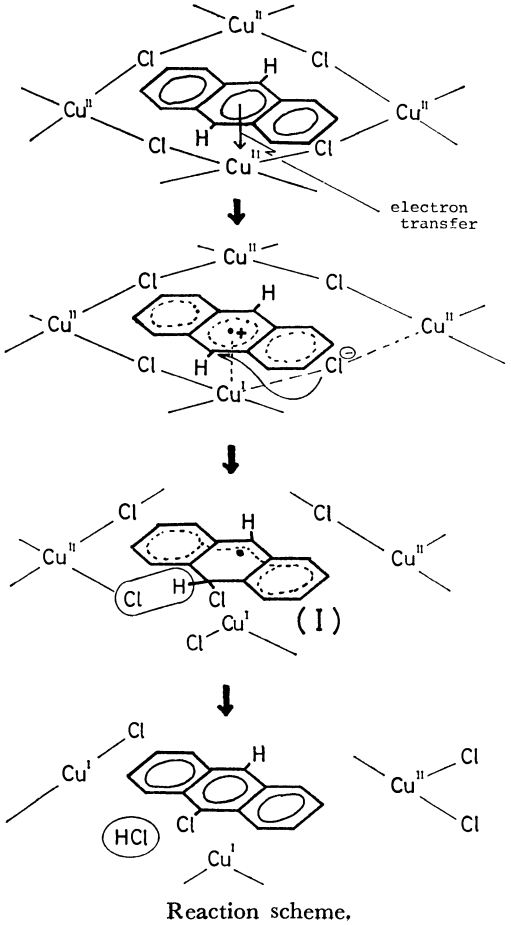

Reaction scheme.

Experimental

Melting points were measured on a micro hot-stage manufactured by Mitamura Riken Kogyo Inc. and were uncorrected. ^{1}H-NMR spectra were recorded on a JEOL MH-100 spectrometer with Me_4Si as an internal standard. GLC analyses were carried out on a JEOL Model JGC-1100 using a 1 m column packed with Apiezone L grease 3 wt % on Celite 545 NAW. HPLC analyses were performed on a Shimadzu liquid chromatograph Model LC-2F equipped with a Shimadzu-Du Pont Permaphase ODS column. Voltammetry was carried out in an acetonitrile solution on a Yanagimoto Model P-8 polarograph. The working electrode was a rotatory platinum disk electrode (2000 rpm). An aqueous saturated calomel electrode (SCE) and a platinum electrode were used as a reference and a counter electrode, respectively. Voltage sweep rate was 0.2 V/min. Tetraethylammonium perchlorate (Eastman) was used as supporting electrolyte (0.1 M).

Materials. Anhydrous copper(II) chloride was prepared by heating copper(II) chloride dihydrate in an oven at 110 °C for 20 h. 1,2-Dihydronaphthalene (Aldrich) was used without further purification.

The following substrates were prepared according to the procedure described in literature.

1-Methylanthracene:[8)] Mp 85 °C (lit, mp 86 °C); NMR (CCl_4) δ=2.80 (3H, s, 1-Me), 7.20—7.50 (2-, 3-, 6-, and 7-H, m), 7.6—8.1 (4-, 5-, and 8-H, m), 8.28 (10-H, s) and 8.39 (9-H, s).

1,4-Dimethylanthracene:[8)] Mp 73—74 °C (lit, mp 74 °C); NMR (CCl_4) δ=2.79 (6H, s, 1- and 4-Me), 7.03 (2- and 3-H, s), 7.30 (6- and 7-H, dd, J=8 and 2 Hz), 7.85 (5- and 8-H, dd, J=8 and 2 Hz) and 8.34 (9- and 10-H, s).

1-Chloroanthracene:[9)] Mp 84—85 °C (lit, mp 81—82 °C); NMR (CCl_4) δ=7.18—7.58 (2-, 3-, 6-, and 7-H, m), 7.76—8.12 (4-, 5-, and 8-H, m), 8.32 (10-H, s) and 8.77 (9-H, s).

2-Chloroanthracene:[9)] Mp 223 °C (lit, mp[10)] 223 °C); NMR (CCl_4) δ=7.28—7.60 (3-, 6-, and 7-H, m), 7.80—8.05 (1-, 4-, 5-, and 8-H, m), 8.28 (9-H, s) and 8.36 (10-H, s).

1,4-Dichloroanthracene:[11)] Mp 179—181 °C (lit, mp 180 °C); NMR (CCl_4) δ=7.44 (2- and 3-H, s), 7.50 (6- and 7-H, dd, J=8 and 2 Hz), 8.04 (5- and 8-H, dd, J=8 and 2 Hz) and 8.81 (9- and 10-H, s).

1,5-Dichloroanthracene:[9)] Mp 181—182 °C (lit, mp 185 °C); NMR (CCl_4) δ=7.32 (3- and 7-H, t, J=8 Hz), 7.55 (2- and 6-H, d, J=8 Hz), 7.93 (4- and 8-H, d, J=8 Hz) and 8.76 (9- and 10-H, s).

1,8-Dichloroanthracene:[9)] Mp 151—153 °C (lit, mp 156 °C); NMR (CCl_4) δ=7.35 (3- and 6-H, t, J=8 Hz), 7.59 (2- and 7-H, d, J=8 Hz), 7.87 (4- and 5-H, d, J=8 Hz), 8.38 (10-H, s) and 9.24 (9-H, s).

2,3-Dichloroanthracene:[11)] Mp 265—265.5 °C (lit, mp 261 °C); NMR (CCl_4) δ=7.3—7.58 (6- and 7-H, m), 7.94 (5- and 8-H, dd, J=8 and 2 Hz), 8.06 (1- and 4-H, s) and 8.25 (9- and 10-H, s).

7-Methylbenz[a]*anthracene*:[12)] Mp 138.5—139.5 °C (lit, mp[13)]

140.5—141.5 °C).

12-Methylbenz[a]*anthracene*:[12] Mp 136—137 °C (lit, mp 138—139 °C).

1,5-Dimethyl- (5) and 1,4,5-Trimethylanthracene (6): Synthesis of **6** was performed as follows. 3,6-Dimethylphthalic anhydride (**7**) was obtained from maleic anhydride and 2,5-dimethylfuran.[14] The reaction of **7** and 2-methylphenylmagnesium bromide afforded 2-(2-methylbenzoyl)-3,6-dimethylbenzoic acid (**8**) by a similar procedure described for 2-benzoyl-3-methylbenzoic acid.[15] By the heating of **8** and concentrated sulfuric acid for 1.5 h in a steam bath, 1,4,5-trimethylanthraquinone (**9**) (mp 142—147 °C, lit, mp[16] 143 °C) was obtained. The reduction of **9** by zinc dust and aqueous ammonia afforded **6**. 1,5-Dimethylanthracene was prepared by a similar method. **5**: mp 139—140 °C (lit, mp[17] 139—140 °C); NMR (CCl_4) δ=2.84 (6H, s, 2Me), 7.12—7.30 (2-, 3-, 6-, and 7-H, m), 7.78 (4- and 8-H, dd, J=8 and 2 Hz) and 8.38 (9- and 10-H, s). **6**: mp 107.5—108.5 °C; NMR (CCl_4) δ=2.82 (6H, s, 2Me), 2.85 (3H, s, 1Me), 7.07 (2- and 3-H, s), 7.18—7.32 (6- and 7-H, m), 7.76 (8-H, dd, J=8 and 2 Hz), 8.37 (9-H, s) and 8.46 (10-H, s). Found: C, 92.83; H, 7.38%; M$^+$, 220. Calcd for $C_{17}H_{16}$: C, 92.68; H, 7.32%; M 220.

General Reaction Procedures. Anhydrous copper(II) chloride (2.2 or 4.4 mmol) and aromatic hydrocarbons (1 mmol) was refluxed with stirring in 10 ml of chlorobenzene for appropriate reaction time. The reaction was stopped when the yield of product, which was followed by GLC, reached to a maximum. The reaction of azulene was followed by HPLC, in which methanol–water was used as the eluent at a rate of 1 ml/min. After usual work-up the crude product was dissolved in benzene and eluted by petroleum ether on a Florisil column.

Identification of Products. *9-Chloroanthracene*: Mp 103 °C (lit, mp[18] 105.2—107 °C); NMR (CCl_4) δ=7.3—7.6(2-, 3-, 6-, and 7-H, m), 7.87 (4- and 5-H, dd, J=8 and 2 Hz), 8.24 (10-H, s) and 8.38 (1- and 8-H, dd, J=8 and 2 Hz). (Found: C, 79.20; H, 4.32%).

9,10-Dichloroanthracene: Mp 210 °C (lit, mp[19] 209 °C) NMR (CCl_4) δ=7.5 (2-, 3-, 6-, and 7-H, dd, J=8 and 2 Hz) and 8.41 (1-, 4-, 5-, and 8-H, dd, J=8 and 2 Hz). (Found: C, 67.88; H, 3.11%).

1-Chloropyrene: Mp 116—118 °C (lit, mp[20] 119 °C). (Found: C, 80.71; H, 3.69%; M$^+$ 236).

6-Chlorobenz[a]*pyrene*: Mp 212 °C (lit, mp[21] 210 °C). (Found: C, 83.17; H, 3.71%; M$^+$ 286).

Chloroperylene: Mp 243—246 °C. (Found: C, 80.96; H, 3.65%. Calcd for $C_{20}H_{11}Cl$: C, 83.77; H, 3.87%).

Dichloroperylene: Mp 222—226 °C.[22] (Found: C, 73.97; H, 3.04%. Calcd for $C_{20}H_{10}Cl_2$: C, 74.74; H, 3.14%).

5,11-Dichloronaphthacene: Mp 227—228 °C (lit, mp[23] 220 °C); NMR ($CDCl_3$) δ=7.4—7.7 (2-, 3-, 8- and 9-H, m), 8.10 (1- and 7-H, d, J=8 Hz), 8.50 (4- and 10-H, d, J=8 Hz) and 9.12 (6- and 12-H, s). (Found: C, 72.70; H, 3.25%).

1,3-Dichloroazulene: Mp 93—94 °C; NMR (CCl_4) δ=7.13 (5- and 7-H, t, J=10 Hz). Found: C, 61.02; H, 2.95%; M$^+$, 197. Calcd for $C_{10}H_6Cl_2$: C, 60.95; H, 3.07%; M, 197.

1,10-Dichloroanthracene: Mp 126—127 °C (lit, mp[24] 127—128 °C has been reported as the mp of 1,9- or 1,10-dichloroanthracene); NMR (CCl_4) δ=7.32—7.68 (2-, 3-, 6-, and 7-H, m), 8.02 (8-H, dd, J=8 and 2 Hz), 8.42 (4- and 5-H, dd, J=8 and 2 Hz) and 8.76 (9-H, s). Found: C, 68.20; H, 3.29%; M$^+$, 246. Calcd for $C_{14}H_8Cl_2$: C, 68.04; H, 3.26%; M, 246.

2,10-Dichloroanthracene: Mp 115—116 °C; NMR (CCl_4) δ=7.3—7.7 (3-, 6- and 7-H, m), 7.78—7.96 (1- and 8-H, m), 8.22 (9-H, s), 8.3—8.5 (4- and 5-H, m). Close examination of NMR data showed that the sharp peak due to 1-H at δ=*ca.* 8.5 was characteristic of 2,9-dichloro substituted anthracenes. Accordingly, the lack of this peak necessarily indicates that the present product is 2,10-dichloroanthracene. Found: C, 68.24; H, 3.33%; M$^+$, 246. Calcd for $C_{14}H_8Cl_2$: C, 68.04; H, 3.26%; M, 246.

2,9,10-Trichloroanthracene: Mp 181—182 °C (lit, mp[24] 178 °C); NMR (CCl_4) δ=7.5—7.7 (3-, 6-, and 7-H, m), 8.4—8.55 (4-, 5-, and 8-H, m) and 8.48 (1-H, s).

1,8,10-Trichloroanthracene: Mp 191—192 °C (lit, mp[25] 194 °C); NMR (CCl_4) δ=7.4—7.7 (2-, 3-, 6-, and 7-H, m), 8.40 (4- and 5-H, d, J=8 Hz) and 9.24 (9-H, s).

2,3,9-Trichloroanthracene: Mp 172—173 °C; NMR (CCl_4) δ=7.4—7.7 (6- and 7-H, m), 7.86 (5-H, dd, J=8 and 2 Hz), 7.95 (4-H, s), 8.08 (10-H, s), 8.36 (8-H, dd, J=8 and 2 Hz) and 8.48 (1-H, s). Found: C, 59.84; H, 2.52%; M$^+$, 281. Calcd for $C_{14}H_7Cl_3$: C, 59.72; H, 2.51%; M, 281.

9-Chloro-10-methylanthracene: Mp 177—178 °C; NMR (CCl_4) δ=3.06 (3H, s, 10-Me), 7.3—7.6 (2-, 3-, 6-, and 7-H, m), 8.15 (4- and 5-H, dd, J=8 and 2 Hz) and 8.42 (1- and 8-H, dd, J=8 and 2 Hz). Found: C, 79.20; H, 5.12%; M$^+$, 226. Calcd for $C_{15}H_{11}Cl$: C, 79.47; H, 4.89%; M, 226.

9-Chloro-4-methylanthracene: Mp 66—68 °C; NMR (CCl_4 δ=2.81 (3H, s, 4-Me), 7.15—7.60 (2-, 3-, 6-, and 7-H, m), 7.96 (5-H, dd, J=8 and 2 Hz), 8.32 and 8.50 (1- and 8-H, dd, J=8 and 2 Hz) and 8.46 (10-H, s). Found: C, 79.25; H, 5.08%; M$^+$, 226. Calcd for $C_{15}H_{11}Cl$: C, 79.47; H, 4.89%; M, 226.

9,10-Dichloro-1-methylanthracene: Mp 132—134 °C; NMR (CCl_4) δ=3.22 (3H, s, 1-Me), 7.2—7.64 (2-, 3-, 6-, and 7-H, m) and 8.3—8.6 (4-, 5-, and 8-H, m). Found: C, 69.89; H, 3.70%; M$^+$, 260. Calcd for $C_{15}H_{10}Cl_2$: C, 68.99; H, 3.86%; M, 260.

9-Chloro-1,4-dimethylanthracene: Mp 41.5—44.0 °C; NMR (CCl_4) δ=2.70 (3H, s, 4-Me), 3.14 (3H, s, 1-Me), 7.04 (2- and 3-H, s), 7.3—7.56 (6- and 7-H, m), 7.8 (5-H, dd, J=8 and 2 Hz), 8.26 (10-H, s) and 8.45 (8-H, d, J=8 Hz). Found: C, 79.45; H, 5.40%; M$^+$, 240. Calcd for $C_{16}H_{13}Cl$: C, 79.83; H, 5.44%; M, 240.

9-Chloro-1,5-dimethylanthracene: Mp 111—114 °C; NMR (CCl_4) δ=2.70 (3H, s, 5-Me), 3.14 (3H, s, 1-Me), 7.1—7.4 (2-, 3-, 6-, and 7-H, m), 7.5—7.7 (4-H, m), 8.18 (10-H, s) and 8.32 (8-H, d, J=8 Hz). Found: C, 80.12; H, 5.48%; M$^+$, 240. Calcd for $C_{16}H_{13}Cl$: C, 79.83; H, 5.44%; M, 240.

9,10-Dichloro-1,5-dimethylanthracene: Mp 154—156 °C; NMR (CCl_4) δ=3.14 (6H, s, 1- and 5-Me), 7.2—7.40 (2-, 3-, 6-, and 7-H, m) and 8.3—8.5 (4- and 8-H, m). Found: C, 70.18; H, 4.63%; M$^+$, 274. Calcd for $C_{16}H_{12}Cl_2$: C, 69.84; H, 4.40%; M, 274.

9-Chloro-1,4,5-trimethylanthracene: Mp 120—122 °C; NMR (CCl_4) δ=2.76 (3H, s, Me), 2.82 (3H, s, Me), 3.16 (3H, s, 1-Me), 7.1 (2- and 3-H, s), 7.1—7.5 (6- and 7-H, m), 8.4 (8-H, d, J=8 Hz) and 8.46 (10-H, s). Found: C, 80.40; H, 6.10%; M$^+$, 254. Calcd for $C_{17}H_{15}Cl$: C, 80.15; H, 5.94%; M, 254.

The present work was partially supported by a Research Grant from Kyoto Women's University.

References

1) D. C. Nonhebel, *Org. Synth.*, Coll. Vol. V, 206 (1973).
2) D. C. Nonhebel, *J. Chem. Soc.*, **1963**, 1216.
3) J. C. Ware and E. E. Borchert, *J. Org. Chem.*, **26**, 2267 (1961).
4) D. C. Mosnaim and D. C. Nonhebel, *Tetrahedron*, **25**,

1591 (1969).
5) E. S. Pysh and N. C. Yang, *J. Am. Chem. Soc.*, **85**, 2124 (1963).
6) Private communication from Professor Katsumi Kimura of the Institute of Applied Electricity of Hokkaido University.
7) R. B. Heslop and K. Jones, "Inorganic Chemistry" Elsevier Scientific Publishing Company, Amsterdam (1976) p. 728.
8) J. v. Braun and O. Bayer, *Ber.*, **59**, 914 (1926).
9) H. Schilling, *Ber.*, **46**, 1066 (1913).
10) E. B. Barnett and M. A. Matthews, *Recl. Trav. Chim. Pays-Bas*, **43**, 530 (1924).
11) E. B. Barnett, M. A. Matthews, and J. L. Wiltshire, *Recl. Trav. Chim. Pays-Bas*, **45**, 558 (1926).
12) C. K. Bradsher, *J. Am. Chem. Soc.*, **62**, 1077 (1940).
13) J. W. Cook, A. M. Robinson, and F. Goulden, *J. Chem. Soc.*, **1937**, 393.
14) M. S. Newman and B. T. Lord, *J. Am. Chem. Soc.*, **66**, 733 (1944).
15) M. S. Newman and C. D. McCleary, *J. Am. Chem. Soc.*, **63**, 1542 (1941).
16) F. Mayer and O. Stark, *Ber.*, **64**, 2003 (1931).
17) R. D. Haworth and G. Sheldrick, *J. Chem. Soc.*, **1934**, 1950.
18) L. F. Fieser and S. T. Putnam, *J. Am. Chem. Soc.*, **69**, 1038 (1947).
19) E. B. Barnett, J. W. Cook, and H. H. Grainger, *J. Chem. Soc.*, **121**, 2059 (1922).
20) H. Vollmann, H. Becker, M. Corell, and H. Streeck, *Justus Liebigs Ann. Chem.*, **531**, 1 (1937).
21) A. Windaus and K. Raichle, *Justus Liebigs Ann. Chem.*, **537**, 157 (1939).
22) The melting point of 3,9-dichloroperylene, which is the only known dichloride of perylene, has been reported as 291 °C (A. Zinke, K. Funke, and N. Lorber, *Ber.*, **60**, 577 (1927)).
23) C. Marschalk and C. Stumm, *Bull. Soc. Chim. Fr.*, **1948**, 418.
24) C. Liebermann and M. Beudet, *Bull. Soc. Chim. Fr.*, **47**, 1011 (1914).
25) E. B. Barnett, J. W. Cook, and M. A. Matthews, *Recl. Trav. Chim. Pays-Bas*, **45**, 68 (1926).

Reaction of *N,N*-Dialkylanilines with Palladium(II) Compounds

Tsutomu SAKAKIBARA,* Yoko DOGOMORI, and Yuichiro TSUZUKI

Institute of Chemistry, College of Liberal Arts, Kagoshima University, Korimoto, Kagoshima 890

(Received April 20, 1979)

The reaction of *N,N*-dialkylaniline with palladium(II) acetate or di-μ-acetato-bis[α-(dimethylamino)-*o*-tolyl]-dipalladium (**B**) gave 4,4′-bis(dialkylamino)diphenylmethane as a major product. It was elucidated that the origin of $-CH_2-$ in the product might be methyl group of palladium acetate and the primary reaction product might be *N,N*-dialkyltoluidine. The absorption spectra of the initial reaction mixture of *N,N*-dimethylaniline with **B** in acetic acid at room temperature showed the absorption maximum at 470 nm and at 750 nm. The latter peak was tentatively assigned to *N,N*-dimethylaniline radical cation–palladium(I) acetate complex, which was suggested as a key-intermediate for the formation of diarylmethanes.

A large number of studies on the reactions of many aromatic compounds with palladium(II) salts have been actively done,[1] since van Helden and Verberg presented the oxidative coupling of aromatic rings with palladium(II) chloride.[2] In exploring the synthetic utility of palladium-assisted aromatic substitution, two types of investigation have been carried out. One is concerned with substitution of vinylic hydrogen by aryl groups,[3,4] and another is on the functionalization of aromatic rings by other nucleophiles.[5] In both studies, various monosubstituted aromatic compounds have been used as reactants. However, to our knowledge, no information on the reaction of aniline derivatives with palladium(II) salts have been presented so far.[6]

N,N-Dialkylanilines have relatively low ionization potential. For example, those of *N,N*-dimethylaniline and *N,N*-diethylaniline are 7.12 and 6.99 eV, respectively.[7] These values are much smaller than the ionization potentials of other aromatic compounds such as nitrobenzene (9.92 eV), methyl benzoate (9.35), benzene (9.24), chlorobenzene (9.07), toluene (8.82), anisole (8.21), and so on. Thus, we might expect some different reactivity of aniline derivatives for palladium(II) salts.

We have already communicated that *N,N*-dialkylanilines react with palladium(II) acetate to give diarylmethanes as a major product.[8] The reaction was quite different from generally known aromatic oxidative coupling or aromatic functionalization with palladium(II) salts. The reaction involves some novel reaction paths such as aromatic methylation and benzylic arylation.[9] Therefore, further investigation was carried out on the reactions of *N,N*-dimethylanilines with some palladium(II) compounds. In this report, the detailed information and the spectroscopic data will be presented and some reaction intermediates will be also suggested.

Results and Discussion

N,N-Dimethylaniline (**1a**) reacted with a half equimolecular palladium(II) acetate (**A**) in acetic acid at 80 °C to give *p*-toluidine (**1d**) (trace), 4,4′-bis(dimethylamino)diphenylmethane (**2a**) (72.1%), and Crystal Violet (**3a**) (16.8%). **A** was quantitatively reduced to metallic palladium and all of **1a** was consumed. However, no *N,N,N′,N′*-tetramethylbenzidine was detected on GLC of the organic product mixture. Although a mixture of **1a** (0.02 mol) and acetic acid (1.0 mol) was heated in the absence of **A** at 80 °C for 5 h under nitrogen atmosphere, none of **2a** was obtained and 96% of the used **1a** was recovered. The results of reactions of *N,N*-dialkylanilines with **A** are summarized in Table 1.

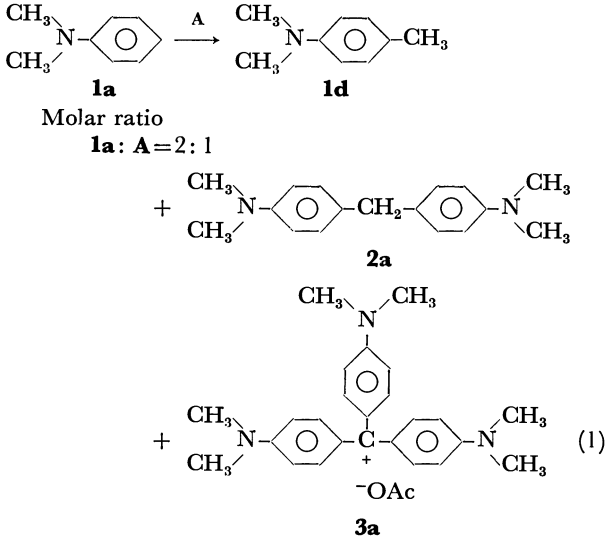

(1)

In acetonitrile or dioxane, the reaction of **1a** with **A** proceeded similarly to that in acetic acid to give diarylmethane (**2a**) as a major product. However, it can be seen in Table 1 that the reaction in aprotic solvent is relatively slower than in acetic acid. Furthermore, the yield of some by-products such as *N,N,N′,N′*-teramethylbenzidine (**6**) or dimethylaminobenzoic acid (**7**) somewhat increased in aprotic solvents (14.7% and 2.15%, respectively).

These results clearly show that formation of diarylmethane is the major path in the reaction of *N,N*-dialkylanilines with palladium(II) acetate (**A**), and that the charactor of solvents has some influence on the reaction sequences.

The conversion of **1a** to **2a** has been reported in the electrochemical oxidation at high concentration of **1a** in acetonitrile,[10] in which the origin of $-CH_2-$ in **2a** has been explained to be *N*-methyl group of **1a**, since the yields of **2a** never exceeded 50%.

In the present reaction, the yield of **2a** was usually higher than 50% (Table 1). Moreover, the reaction of **1b** with **A** gave **2b**, although in relatively low yield due to the accompanied dealkylation.[8] These facts suggest that the origin of $-CH_2-$ group in **2a** is not the

Table 1. The reaction of *N,N*-dialkylanilines with **A**

Reactant[a]	Sovlent	Reaction time/h	Conversion[b] of **1**/%	Products, (yield/%)[c]
1a	Acetic acid	5	100	**1d** (trace), **2a** (72.1), **3a** (16.3)
1a	Acetic acid	1	75	**1d** (trace), **2a** (76.3), **3a** (18.6)
1a	Acetonitrile	5	46	**1d** (trace), **2a** (54.0), **6** (14.7)
1a	Dioxane	5	17	**1d** (2.2), **2a** (55.7), **7** (21.5)
1b	Acetic acid	5	40	**1e** (trace), **2b** (≈5), **3b** (small)
1c	Acetic acid	5	70	**2c** (11.0), **3c** (21.0)
1d	Acetic acid	5	69	**2d** (8.2), **4** (2.7)

a) **A** (0.01 mol) and **1** (0.02 mol) were heated in the solvent (1.0 mol) at 80 °C under nitrogen atmosphere. b) Calculated from the unreacted **1**. c) The yields are based on the reacted **1**.

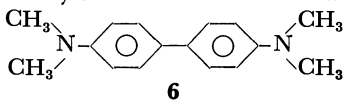

6

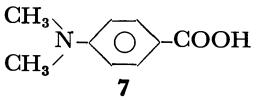

7

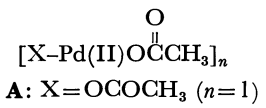

A: X=OCOCH$_3$ (n=1)

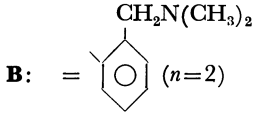

B: = (n=2)

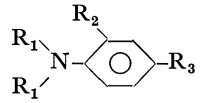

1a: R_1=CH_3, R_2=R_3=H
b: R_1=C_2H_5, R_2=R_3=H
c: R_1=R_2=CH_3, R_3=H
d: R_1=R_3=CH_3, R_2=H
e: R_1=C_2H_5, R_2=H, R_3=CH_3

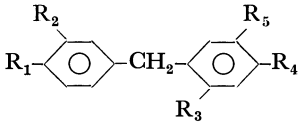

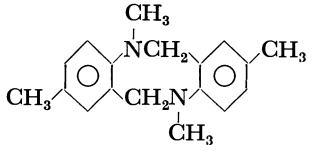

4

2a: R_1=R_4=-N(CH$_3$)$_2$, R_2=R_3=R_5=H
b: R_1=R_4=-N(C$_2$H$_5$)$_2$, R_2=R_3=R_5=H
c: R_1=-N(CH$_3$)$_2$, R_3=-NH(CH$_3$), R_2=CH_3, R_4=R_5=H
d: R_1=R_3=-N(CH$_3$)$_2$, R_2=R_4=H, R_5=CH_3

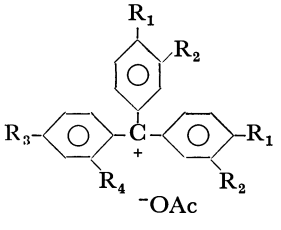

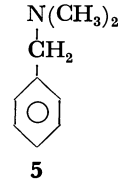

5

3a: R_1=R_3=-N(CH$_3$)$_2$, R_2=R_4=H
b: R_1=R_3=-N(C$_2$H$_5$)$_2$, R_2=R_4=H
c: R_1=R_4=-N(CH$_3$)$_2$, R_2=CH_3, R_3=H

N-methyl group of the reactant (**1a**), but methyl group of palladium(II) acetate (**A**). As the formation of **1d** or **1e** was always observed in the reactions of **1a** or **1b**, the aromatic methylation by **A**, followed by further arylation of the product (**1d** or **1e**), might occur to give **2a** or **2b**. Thus, the reaction of a mixture of **1a** and **1d** with **A** was carried out, in order to know the possibility of the further arylation of **1d**. Namely, a 1 : 1 mixture of **1a** and **1d** in acetic acid was heated in the presence of **A** at 80 °C for 5 h, and the yields of produced diarylmethane (**2a**) were calculated according to both Eqs. 2 and 3 as in Table 2. The yields of **2a** were higher than quantitative yield based on Eq. 1, which meant that Eq. 2 is at least partly operative. Thus, **1d** should be one of reactants for the formation of **2a**.

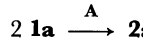

(2)

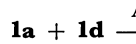

(3)

Further supporting evidences for benzylic arylation are that the reaction of **1d** with **A** in acetic acid gave diarylmethane (**2d**), along with cyclic dimer (**4**) and that **1c** yielded **2c** together with **3c** (Table 1).

Consequently, it is likely that the first product in the reaction of *N,N*-dialkylaniline (**1a** or **1b**) with **A** should be *N,N*-dialkyltoluidine (**1d** or **1e**). **1d** or **1e** might be furthermore oxidized by **A** to give diarylmethane (**2a** or **2b**), followed by reoxidation into Crystal Violet (**3a** or **3b**). However, another problem remains since the stoichiometry of **1a** shows that a formation of 1 mol of **2a** from **1a** should result in a reduction of 1 mol of **A** to metallic palladium (Table 1). The successive oxidation mechanism might possibly consume 2 mol of **A** for a formation of 1 mol of **2a**.

Di-μ-acetato-bis[α-(dimethylamino)-o-tolyl]dipalladium (**B**) can also oxidize **1a** in acetic acid under mild conditions. Even at room temperature, **B** was gradually decomposed to give diarylmethane (**2a**). The results of reactions in various conditions at 80 °C are summarized in Table 3. It clearly elucidates that the

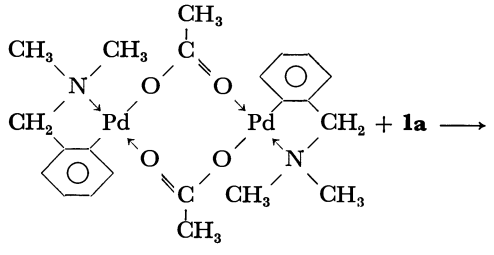

B

Molar ratio
B: **1a**=1 : 1

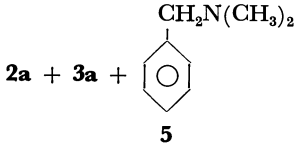

(4)

5

reaction of **1a** with **B** undergoes remarkably large effect of proton on the reaction rate. Namely, in aprotic solvents such as *N,N*-dimethylaniline, dioxane, or tetrahydrofuran the reaction never went on even at 96 °C. However, in the presence of proton, the oxida-

Table 2. Oxidation of mixed **1a** and **1d** with **A**

Reactants/mol[a)]	Yield of **2a**[b)]/%	
	Based on Eq. 2	Based on Eq. 3
1a (0.01), **1d** (0.01)	109.8	54.9
1a (0.02), **1d** (0.02)	99.3	49.4
1a (0.05), **1d** (0.05)	116.6	58.3

a) The reaction of the reactants with **A** (0.02 mol) in acetic acid (1.0 mol) was carried out at 80 °C under nitrogen atmosphere. b) The yields are based on the reacted **1a**.

tion completely proceeded to give **2a** in good yields. The poor yield of **3a** might possibly be expalined by steric hindrance in the contact between **2a** and palladium complex by benzylamine ligand. Therefore, the result suggests that the oxidation of **1a** with **B** may proceed *via* similar reaction sequences to the case of **A**.

The UV spectrum of **1a** in acetic acid shows a long-wavelength absorption maximum at 290 nm (ε 2.0×10^2), while palladium complex (**B**) has it at 330 nm (ε 1.0×10^3) (Fig. 1). These compounds have no absorption maximum in the longer wave region.

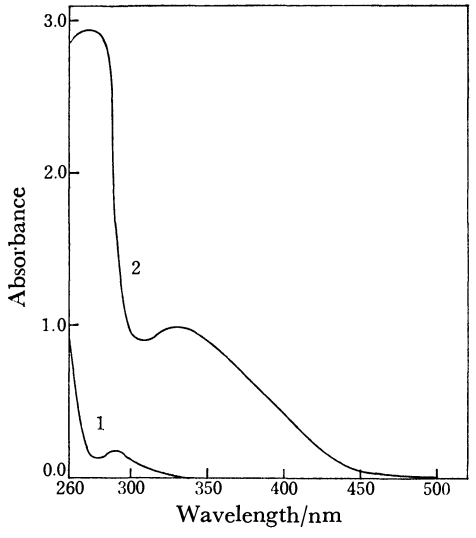

Fig. 1. Absorption spectra of **1a** (1) and **B** (2). The spectra were measured in 1.0×10^{-3} M acetic acid solution at room temperature. (1 M=1 mol dm^{-3}).

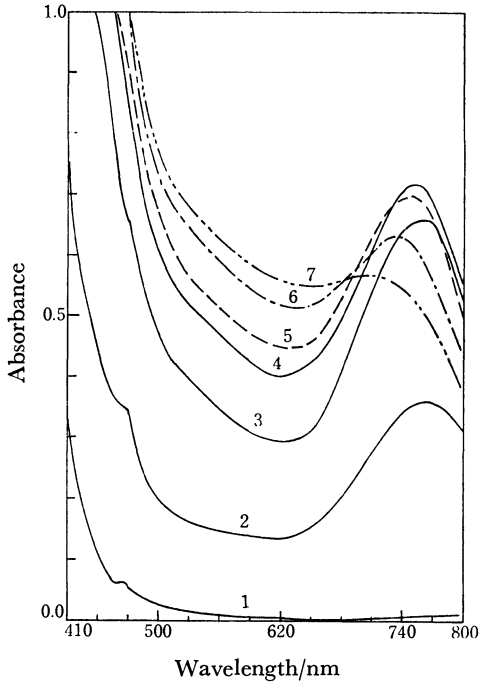

Fig. 2. Spectral change of reaction mixture of **1a** and **B** in acetic acid at room temperature under nitrogen atmosphere. Reaction time (min); 1: 0.5, 2: 10, 3: 30, 4: 50, 5: 60, 6: 80 7: 100.

However, when **B** and **1a** were mixed at room temperature (23 °C) in acetic acid under nitrogen atmosphere, a new absorption appeared at 470 nm, which could not be observed after about 50 min due to strong absorption enhancement in shorter wave region. Furthermore, another strong peak in a visible region appeared about 10 min after mixing. The visible spectra of a mixture of **1a** and **B** in acetic acid are shown in Fig. 2. The spectra indicate a clear appearance of new absorption maximum at 750 nm. Figure 3 shows the time dependent change of the 750 nm peak. The absorption had maximum in 48 min under measurement conditions and afterwards gradually decayed.

The peak at 470 nm appears immediately after mixing of **1a** and **B**, and its intensity looks relatively weak. Therefore, the formation rate of the intermediate related with 470 nm peak might be relatively rapid.

Table 3. The solvent effect on the reaction of **1a** with **B**[a)]

Solvents	Reaction temp/°C	Recovered **B**/%	Product yields/%		
			2a[a)]	**3a**[b)]	**5**[c)]
Acetic acid (1.0)	80	8	43	3	60
Acetic acid (0.5) and **1a** (0.5)	80	0	99	0	84
1a (1.0)	80	100	0	0	0
1a (1.0), HCl(0.06)[d)]	80	0	81	0	75
Tetrahydrofuran (1.0)	65	100	0	0	0
Dioxane (1.0)	80	100	0	0	0
Dioxane (1.0)	96	98	0	0	0

a) **B** (0.01 mol as the dimeric form) and **1a** (0.04 mol) were used, if not indicated in the table. b) Isolated yields based on the reacted **1a**. c) Yields based on the reacted **B**. They were determined by NMR analyses of reaction mixture. d) 5 ml of 12 M HCl was used.

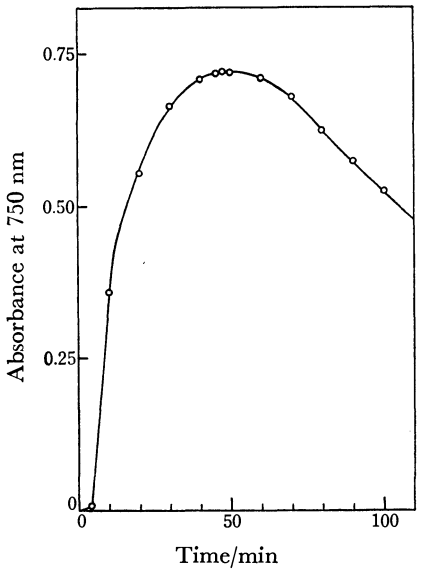

Fig. 3. Time dependence of the absorbance at 750 nm.

The well-known primary intermediates in the reaction of aromatic compounds with palladium(II) salt are π- or σ-complexes between aromatics and palladium, which are readily formed in a rapid process.[2] Thus, the origin of 470 nm peak might be tentatively assigned to the complex $\mathbf{C_1}$ or $\mathbf{C_2}$. However, another possibility can not be completely eliminated that the absorption at 470 nm[12] might be concerned with a radical cation intermediate, in relation to the assignment of 750 nm peak.

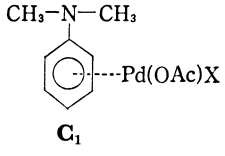

$\mathbf{C_1}$

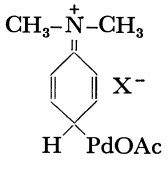

$\mathbf{C_2}$

The second peak at 750 nm has appeared after some induction period and has some life time. It is noteworthy that the absorption was in a remarkably long wave region and the intensity was considerably strong. The analogous peak has also been observed in the reaction of **1a** under different conditions; first, electrochemical study of **1a** in acetic acid showed the absorption peaks at 469 nm and at 750 nm, which were assigned to oxidized *N,N,N′,N′*-tetramethylbenzidine (TMBOx) and 2:1 **1a**: TMBOx adduct, respectively.[15] Second, the oxidation of **1a** with copper(II) chloride in ethanol showed λ_{max} at 472 nm and 740 nm, in which the latter peak was assigned to the 1:1 **1a**: copper(II) chloride complex (**D**).[16]

In the present reaction in acetic acid, *N,N,N′,N′*-tetramethylbenzidine (**6**) was never a product. It is also unlikely that a similar palladium(II) complex to **D** may have such a long-wavelength absorption. Therefore, we would suggest the formation of a radical cation–palladium(I) complex (**E**) and tentatively assign the peak at 750 nm to the complex (**E**).[17]

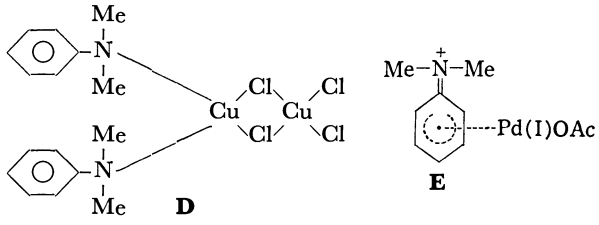

D **E**

The radical cation complex (**E**) could be formed *via* σ-complex ($\mathbf{C_2}$) because of a low ionization potential of *N,N*-dialkylaniline (Eqs. 5, 6, and 7).

$$\underset{\textbf{A or B}}{\text{X–Pd–OAc}} + \text{H}^+ \longrightarrow {}^+\text{PdOAc} + \text{HX} \qquad (5)$$

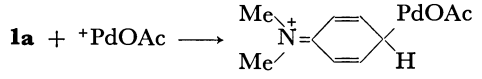

(6)

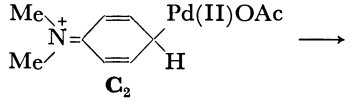

$\mathbf{C_2}$

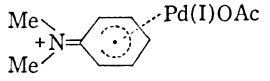

(7)

E

In conclusion, the complex (**E**) is suggested to be a key-intermediate to the products (**1d**, **2a**, and **3a**).

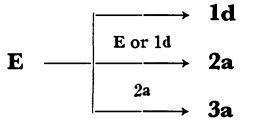

Experimental

Materials. Palladium(II) acetate (**A**) and di-μ-acetato-bis[α-(dimethylamino)-*o*-tolyl]dipalladium (**B**) were prepared according to the methods of Stephenson *et al.*[18] and R. Heck *et al.*,[19] respectively. Commercially available *N,N*-dialkylanilines were used after distillation under a reduced pressure and drying on anhydrous sodium sulfate before use.

TABLE 4. ^{1}H NMR DATA OF ISOLATED PRODUCTS

Compound	τ-Value			
	N-CH_3 (or C_2H_5)	Other-CH_3	$-CH_2-$	Aroma-H
2a	7.06 (s, 12H)		6.11 (s, 2H)	2.94 (q, 8H)
2b	8.90 (t, 12H), 6.70 (q, 8H)		6.23 (s, 2H)	3.04 (q, 8H)
2c	7.33 (s, 6H), 7.14 (s, 3H)	7.93 (s, 3H)	6.02 (s, 2H)	2.73—3.60 (m, 7H)
2d	6.01 (s, 6H), 7.49, 7.13 (s, 3H, resp.)	7.66 (s, 3H)	6.08 (s, 2H)	2.47—3.29 (m, 7H)
3a	6.90—7.40 (m, 18H)	8.74 (s, 3H)		2.43—3.32 (m, 12H)
4	7.19 (s, 6H)	7.70 (s, 6H)	5.80 (s, 4H)	2.66—3.20 (m, 6H)

a) Measured in $CDCl_3$ using TMS as internal standard.

Measurements. UV and visible spectra were measured by Shimadzu multipurpose MPS-50L spectrophotometer. IR and PMR measurements were carried out by JASCO IRA-I and JEOL JNM60 apparatus, respectively. The NMR data of obtained products are summarized in Table 4.

The spectral change of the reaction of **1a** with **B** was recorded at an appropriate time after adding 15.18 mg of **1a** to 25 ml of 1.0×10^{-3} M acetic acid solution of **B** under nitrogen atmosphere at room temperature (23 °C). The scan time (410—800 nm) was 1.5 min.

Reaction of N,N-*Dimethylaniline (1a) with Palladium(II) Acetate (A).* A stirred mixture of **1a** (2.4 g, 0.02 mol) and **A** (2.2 g, 0.01 mol) in acetic acid (60 g, 1.0 mol) was heated at 80 °C for 5 h under nitrogen atmosphere. A filtration of the reaction mixture gave metallic palladium (1.1 g, 0.01 mol). The filtrate was evaporated to remove the solvent. It was confirmed by TLC and GLC of the evaporated residue that all of used **1a** was consumed and that trace of *N,N*-dimethyl-*p*-toluidine (**1d**) was obtained. The residue was column-chromatographed using 90 g of Wacogel. The elution by benzene gave 1.83 g of 4,4′-bis(dimethylamino)diphenylmethane (**2a**) (72.1%), which was recrystallized from benzene–petroleum ether: plates, mp 86.5—87.0 °C (lit,[16] mp 89.5—90.5 °C), UV; λ_{max}^{EtOH} 261.8 nm (ε 3.04×10^4), Mass (*m/e*); 254 (M^+-Me_2), 134. The elementary analyses for C, H, and N were correctly analyzed. Further elution by a mixed solvent of ethyl ether and ethanol gave 0.483 g of Crystal Violet (acetate salt) (**3a**): UV; $\lambda_{max}^{CHCl_3}$ 596.2 nm (lit, as chloride salt,[20] 590 nm), IR (KBr disk, in cm^{-1}); 1660—1550 (br, aromatic C=C and CH_3COO^-). The reactions of *N,N*-dialkylaniline with **A** or **B** in various solvents were similarly treated as described above. The yields of **2a** in the reactions of **1a** and **1d** mixture with **A** were determined by GLC analysis using SE 30 on chromosorb (270 °C, carrier gas H_2) and using the identified **2a** sample as an authentic material. **6** and **7** were identical with their specimen on IR and NMR spectra and GLC.

Reaction of N,N-*Dimethyl*-p-*toluidine (1d) with A.* A stirred mixture of **1d** (2.7 g, 0.02 mol) and **A** (2.2 g, 0.01 mol) in acetic acid (60 g, 1.0 mol) was heated at 80 °C for 5 h under nitrogen atmosphere. The filtration of the reaction mixture gave metallic palladium (1.1 g, 0.01 mol). The filtrate was distilled under a reduced pressure to remove the solvent and the unreacted toluidine. The distillate contained 0.84 g of unreacted **1d**, from the result of GLC analysis. The distilled residue was column-chromatographically separated using 300 g of Wacogel. The elution by a mixed solvent of petroleum ether (50%) and chloroform (50%) gave 44 mg of the solid which was recrystallized from dichloromethane. It was identified with dibenzodiazocine derivative (**4**) from following data: mp 147.0—147.5 °C, Mass (*m/e*); 266 (M^+), 254 (M^+-CH_3), 146, 134.

Found: C; 81.27, H; 8.39, N; 10.39%. Calcd for $C_{18}H_{22}N_2$: C; 81.20. H; 8.27, N; 10.53%. The NMR data are shown in Table 3. Further elution by petroleum ether (30%) and chloroform (70%) gave 86 mg of diarylmethane (**2d**) (8.2%), followed by 86 mg of *N*, *p*-dimethylacetoanilide (3.8%) which were identified with authentic materials by GLC, IR, and NMR.

The authors wish to thank Professor T. Hase of Kagoshima University for his various supports throughout the study. They are also grateful to Professor Y. Odaira and his laboratory-staffs of Osaka University for mass and elemental analyses.

References

1) P. Maitlis, "The Organic Chemistry of Palladium," Academic Press, New York and London (1971), Vol. II, pp. 60—71.

2) R. van Helden and G. Verberg, *Rec. Trav. Chim. Pays-Bas*, **84**, 1263 (1965).

3) a) Y. Fujiwara, I. Moritani, S. Danno, R. Asano, and S. Teranishi, *J. Am. Chem. Soc.*, **91**, 7166 (1969); therein cited references; b) R. S. Shue, *Chem. Commun.*, **1971** 1510.

4) R. F. Heck, *J. Am. Chem. Soc.*, **91**, 6707 (1969).

5) a) P. Henry, *Tetrahedron Lett.*, **1968**, 2285; *J. Org. Chem.*, **36**, 1886 (1971); b) T. Tisue and W. Downs, *Chem. Commun.*, **1969**, 410; c) L. Eberson and L. Gomez-Gonzales, *ibid.*, **1971**, 263; d) H. Yoshimoto and H. Itatani, *Bull. Chem. Soc. Jpn.*, **46**, 2490 (1973); e) R. Normann, W. Parr, and C. Thomas, *J. Chem. Soc., Perkin Trans. 1*, **1974**, 369; f) T. Sakakibara and Y. Odaira, *J. Org. Chem.*, **41**, 2049 (1976).

6) Recent communication showed that the reaction of styrene with arylamines by **A** gave stilbene derivatives *via* C–N bond cleavage of arylamines; F. Akiyama, S. Teranishi, Y. Fujiwara, and H. Taniguchi, *J. Organomet. Chem.*, **140**, C7 (1977).

7) J. L. Franklin, J. D. Dillard, H. M. Rosenstock, J. T. Herron, K. Draxl, and F. H. Field, "Handbook of Chemistry and Physics," 50th ed, ed by R. C. Weast, the Chemical Rubbor Co., (1969), pp. E80—E86.

8) T. Sakakibara, J. Kotobuki, and Y. Dogomori, *Chem. Lett.*, **1977**, 25.

9) The formation of diarylmethanes from *p*-xylene by **A** in trifluoroacetic acid has been reported; F. R. S. Clark, R. O. C. Norman, C. B. Thomas, and J. S. Willson, *J. Chem. Soc., Perkin Trans. 1*, **1974**, 1289.

10) R. Hand and R. F. Nelson, *J. Electrochem. Soc.*, **117**, 1353 (1970).

11) J. Davidson and C. Triggs, *Chem. Ind. (London)*, **1966**, 457.

12) UV iradiation of **1a** in rigid matrices at 77 K has been investigated by some workers.[13] They observed the primary absorption peak near 460—470 nm region and assigned it to the *N,N*-dimethylaniline radical cation. But recently, some doubt has been cast on these data,[14] since spectroscopic studies on electrochemically oxidized *N,N,N′,N′*-tetramethylbenzidine (**6**) gained quite the same spectra.

13) a) G. N. Lewis and J. Bigeleisen, *J. Am. Chem. Soc.*, **65**, 2419 (1943); b) G. Porter and F. Wright, *Trans. Faraday Soc.*, **51**, 1469 (1955); *ibid.*, **54**, 2027 (1958); c) S. Arimitsu, K. Kimura, and H. Tsubomura, *Bull. Chem. Soc. Jpn.*, **42**, 1858 (1969).

14) a) N. L. Weinberg, "Technique of Electroorganic Synthesis," John Wiley and Sons, Inc., (1974), Part I, pp. 652—653; b) R. F. Nelson, Ph. D. Thesis, Kansas University (1966).

15) a) Ref. 14a, p. 656; b) J.-E. Dubois, P.-C. Lacaze, and A. Aranada, *C. R. Acad. Sci., Paris*, **260**, 3383 (1965).

16) J. R. L. Smith, R. O. C. Norman, and W. M. Walker, *J. Chem. Soc., B*, **1968**, 269.

17) A magneta complex of palladium(I) containing benzene has been isolated. The complex showed absorption maximum at 380 nm and 550 nm in acetic acid; J. M. Davidson and C. Triggs, *J. Chem. Soc., A*, **1968**, 1324.

18) T. Stephenson, S. Morehouse, A. Powell, J. Heffer, and G. Willkinson, *J. Chem. Soc.*, **1965**, 3632.

19) J. M. Thomson and R. F. Heck, *J. Org. Chem.*, **40**, 2667 (1975).

20) H. Sato, *Bull. Chem. Soc. Jpn.*, **38**, 1719 (1965).

The Acid Catalyzed Decomposition of Diazo Compounds. I. Synthesis of Oxazoles in the BF_3 Catalyzed Reaction of Diazo Carbonyl Compounds with Nitriles

Toshikazu IBATA* and Ryohei SATO

Institute of Chemistry, College of General Education, Osaka University, Toyonaka, Osaka 560

(Received April 23, 1979)

The BF_3-catalyzed decomposition of diazo carbonyl compounds in nitriles have afforded the corresponding oxazoles in high yields. This method is applicable to diazo carbonyl compounds such as *m*- and *p*-substituted diazoacetophenones, ethyl diazoacetate, 1,2-diphenyl-2-diazoethanone, dibenzoyldiazomethane, and dimethyl diazomalonate. Bis(diazo ketone)s such as terminal bis(diazoacetylated) alkanes (III_{1-4}: $n=6$, 8, 10, 12) and *m*- and *p*-bis(diazoacetyl)benzenes also gave the corresponding bisoxazoles in a similar reaction. The reaction has been interpreted in terms of a stepwise mechanism *via* betaine intermediates initiated by the attack of BF_3 on the carbonyl oxygen of diazo carbonyl compounds. The emission spectra of oxazoles are described.

The synthesis of oxazoles has been the subject of numerous studies in connection with the pharmaceutical properties of oxazole derivatives.[1] Most of the methods reported however are not satisfactory as a general method for the synthesis of oxazoles because of the low yield of oxazoles and the difficulties in obtaining the starting materials.

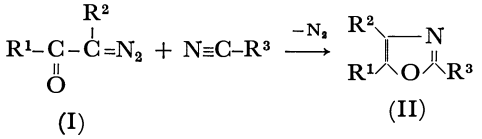

(I) (II)

The 1,3-dipolar cycloaddition of carbonylcarbene to the carbon-nitrogen triple bond of the cyano group was first proposed by Huisgen *et al.* to give oxazoles (II) having arbitrary substituents on C-2, C-4, and C-5 positions.[2] In accordance with this working hypothesis, the thermal,[2,3] phtochemical,[4] and transition metal catalyzed[2,3] decomposition of diazo carbonyl compounds in nitriles were studied. The yields of oxazoles were not high even though the use of copper[2,3a] and π-allylic palladium[5] catalysts which were employed to prevent the Wolff rearrangement of the diazo carbonyl compound. Nozaki *et al.* improved the yield (up to 66%) using WCl_6 as a catalyst.[6] The by-product formation of α-chlorinated ketones was not inevitable in this reaction. Recently Doyle *et al.* reported the $AlCl_3$-catalyzed reaction of α-unsubstituted diazo ketones and nitriles giving oxazoles in high yields.[7] In a previous paper in this series the BF_3-catalyzed decomposition of diazo carbonyl compounds in nitriles to give oxazoles in high yields was reported.[8] In this paper this method has been employed to the synthesis of several substituted oxazoles.

Results and Discussion

The BF_3-catalyzed decomposition of α-diazoacetophenone in an excess of acetonitrile proceeded with vigorous evolution of nitrogen and gave 2-methyl-5-phenyloxazole (II_1) in 94% yield. This method is applicable to other nitriles. Propionitrile, isobutyronitrile, phenylacetonitrile, benzonitrile, *p*-methoxybenzonitrile, cinnamonitrile, and chloroacetonitrile gave oxazoles in high yields. (Phenylthio)acetonitrile afforded *N*-phenacyl-α-(phenylthio)acetamide (12%) together with 2-phenylthiomethyl-5-phenyloxazole (II_9). Under these circumstances neither the expected cyanomethylphenylsulfonium phenacylide nor the (cyanomethyl)phenacylphenyl sulfonium salt was obtained despite a detailed inspection of the reaction mixture by column chromatography.[9] This indicates the higher reactivity of the cyano group towards the diazonium type intermediate (VII) than that of the sulfur atom. Methyl cyanoacetate yielded oxazole (II_{10}) in moderate yields with accompanying intractable oily products. The electron attracting substituent on the nitrile lowered the yield of oxazole, *e.g.*, *p*-nitrobenzonitrile gave the oxazole (II_7) in lower yield than in the cases of benzonitrile and *p*-methoxybenzonitrile.

The *m*- and *p*-substituted α-diazoacetophenones, 12-cyano-1-diazo-2-dodecan-2-one, ethyl diazoacetate, and 1,2-diphenyl-2-diazoethanone also gave 5-aryl-2-methyloxazoles (II_{12-23}), 5-(*p*-methoxyphenyl)-2-ethyloxazole (II_{24}), 5-(ω-cyanodecyl)-2-methyloxazole (II_{25}), 5-ethoxy-2-methyloxazole (II_{26}), and 3,5-diphenyl-2-methyloxazole (II_{27}) respectively. Both the electron-attracting and electron-releasing substituents on a benzene ring of diazoacetophenones do not effect the yield of the oxazoles and the rate of the reaction. A benzoyl group or a methoxycarbonyl group attached to a diazomethyl carbon atom however suppressed the reaction and consequently elevated temperatures were necessary for completion of the reaction. Some dimethyl diazomalonate was recovered even after prolonged heating of the reaction mixture (80 °C, 50 h) and caused a low yield of oxazole (II_{29}).

The NMR data shows that the chemical shift of the oxazole ring proton (C_4–H) is effected by the substituent on C_5 rather than that on C_2 (Table 1). Electron-attracting groups on the benzene ring attached to C_5 deshielded the C_4–H and an alkyl group on C_5 shielded the C_4–H.

Bis(diazo ketone)s such as α,ω-bis(diazoacetyl)alkanes (III_{1-4}: $n=6$, 8, 10, 12) and *m*- and *p*-bis(diazoacetyl)-benzenes ($V_{1,2}$) gave bisoxazolyl compounds (IV_{1-4}) and ($VI_{1,2}$: R=CH_3; VI_3: R=Ph) in the reaction with acetonitrile or benzonitrile.

In the experimental work conducted here an excess of BF_3 was used although a catalytic amount of BF_3 is

TABLE 1. YIELDS, MELTING POINTS, AND NMR DATA OF OXAZOLES (II)

Compd	R^1	R^2	R^3	Reaction temp/°C	Yield %	Mp/°C	NMR (δ/ppm, $CDCl_3$) C_4-H	C_2-CH_3	Others[a]
II_1	C_6H_5	H	CH_3	5	94	58—59	7.15	2.48	
II_2	C_6H_5	H	CH_3CH_2	5	99	oil	7.13	—	1.33(t), 2.80(q) C_2H_5
II_3	C_6H_5	H	$(CH_3)_2CH$	5	82	oil	7.15	—	1.35(d), 3.12(sep) *i*-Pr
II_4	C_6H_5	H	$C_6H_5CH_2$	5	77	91—92	7.20	—	4.10 CH_2
II_5	C_6H_5	H	C_6H_5	5	92	74—75	b)	—	
II_6	C_6H_5	H	*p*-$CH_3OC_6H_4$[c]	5	82	104—105	b)	—	3.85 OCH_3
II_7	C_6H_5	H	*p*-$NO_2C_6H_4$[c]	5	17	215—216	b)	—	
II_8	C_6H_5	H	C_6H_5CH=CH	10	76	103—104	7.05	—	d)
II_9	C_6H_5	H	$C_6H_5SCH_2$	10	44	48—49	b)	—	4.20 SCH_2
II_{10}	C_6H_5	H	CH_3OOCCH_2	10	46	oil	7.24	—	3.90 CH_2, 3.73 OCH_3
II_{11}	C_6H_5	H	$ClCH_2$	5	86	74—75	7.30	—	4.65 CH_2Cl
II_{12}	*p*-$CH_3OC_6H_4$	H	CH_3	5	95	107—108	7.08	2.50	3.83 OCH_3
II_{13}	*p*-$CH_3C_6H_4$	H	CH_3	5	96	56—57	7.08	2.45	2.30 CH_3
II_{14}	*p*-ClC_6H_4	H	CH_3	5	83	86—87	7.17	2.47	
II_{15}	*p*-BrC_6H_4	H	CH_3	5	88	98—100	7.18	2.52	
II_{16}	*p*-CNC_6H_4	H	CH_3	5	76	125—126	7.33	2.53	
II_{17}	*p*-$NO_2C_6H_4$	H	CH_3	5	84	167—168	7.45	2.42	
II_{18}	*m*-$CH_3OC_6H_4$	H	CH_3	5	94	oil	7.12	2.40	3.77 OCH_3
II_{19}	*m*-$CH_3C_6H_4$	H	CH_3	5	93	oil	7.13	2.45	2.32 CH_3
II_{20}	*m*-ClC_6H_4	H	CH_3	5	91	oil	7.20	2.48	
II_{21}	*m*-BrC_6H_4	H	CH_3	5	83	oil	7.20	2.43	
II_{22}	*m*-CNC_6H_4	H	CH_3	5	95	95—96	7.28	2.55	
II_{23}	*m*-$NO_2C_6H_4$	H	CH_3	5	89	100—101	7.35	2.50	
II_{24}	*p*-$CH_3OC_6H_4$	H	C_2H_5	5	87	61—62	7.12	—	3.83 OCH_3 1.37(t), 2.84(q) C_2H_5
II_{25}	$NC(CH_2)_{10}$	H	CH_3	5	83	oil	6.58	2.38	d)
II_{26}	C_2H_5O	H	CH_3	20	62	oil	5.95	2.02	1.40(t), 4.08(q) C_2H_5
II_{27}	C_6H_5	C_6H_5	CH_3	5	68	oil	—	2.55	
II_{28}	C_6H_5	C_6H_5CO	CH_3	80	79	oil	—	2.50	
II_{29}	CH_3	CH_3OOC	CH_3	80	32	oil	—	2.35	3.85, 4.13 OCH_3

a) The signals of aromatic protons are omitted, and the signal patterns are singlet unless otherwise indicated. b) The signal of C_4-H was not distinguishable from those of the aromatic protons. c) Five molar amount of nitrile was reacted in benzene solution. d) The signals of vinyl and polymethylene protons are omitted.

TABLE 2. YIELDS, MELTING POINTS, AND NMR DATA OF BISOXAZOLYL COMPOUNDS

Oxazole	Diazocarbonyl Compound	R-CN	Reaction temp/°C	Yield %	Mp/°C	NMR (δ/ppm, $CDCl_3$) C_4-H	C_2-CH_3
IV_1	$N_2CHCO(CH_2)_6COCHN_2$	CH_3CN	5	95	60—61	6.58	2.40
IV_2	$N_2CHCO(CH_2)_8COCHN_2$	CH_3CN	5	96	70—71	6.55	2.38
IV_3	$N_2CHCO(CH_2)_{10}COCHN_2$	CH_3CN	5	95	70—71	6.57	2.37
IV_4	$N_2CHCO(CH_2)_{12}COCHN_2$	CH_3CN	5	95	73—75	6.55	2.40
IV_1	*m*-$N_2CHCOC_6H_4COCHN_2$	CH_3CN	5	98	103—104	7.27	2.53
VI_2	*p*-$N_2CHCOC_6H_4COCHN_2$	CH_3CN	60	78	233—234	7.28	2.55
VI_3	*p*-$N_2CHCOC_6H_4COCHN_2$	C_6H_5CN	60	80	236—237	b)	—

a) Signals of aromatic and polymethylene protons are omitted. b) Signal of C_4-H was not distinguishable from those of the aromatic protons.

sufficient for completion of the reaction. The reaction is reasonably explained by a stepwise mechanism *via* betaine intermediates, unlike the 1,3-dipolar cycloaddition of carbonylcarbene towards the carbon-nitrogen triple bond of nitrile proposed for the thermal and transition metal catalyzed reactions.[2,3] The reaction is initiated by the attack of BF_3 on the carbonyl-oxygen of the diazo carbonyl compound affording a diazonium type intermediate (VII).[9] The intermediacy of VII was supported by the facts that α-hydroxy or α-ethoxy ketones (IX, X) were obtained when the reaction was conducted in the presence of water or diethyl ether.[10,11] The electrophilic attack of the intermediate (VII) on the nitrogen atom of the nitrile may form a betaine intermediate (VIII) with the elimination of nitrogen. The electron-attracting substituent on the nitrile may retard this step and subsequently lower the yield of oxazole (Table 1 run 7). The reaction conducted in

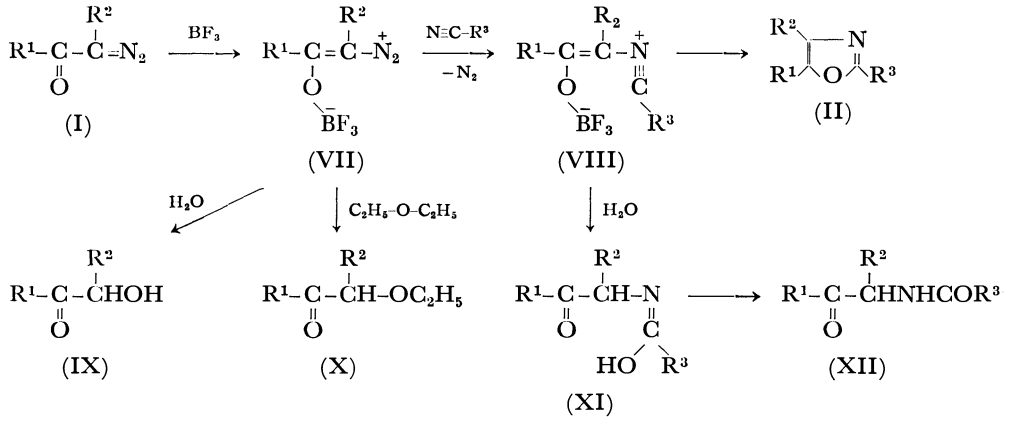

Scheme 1.

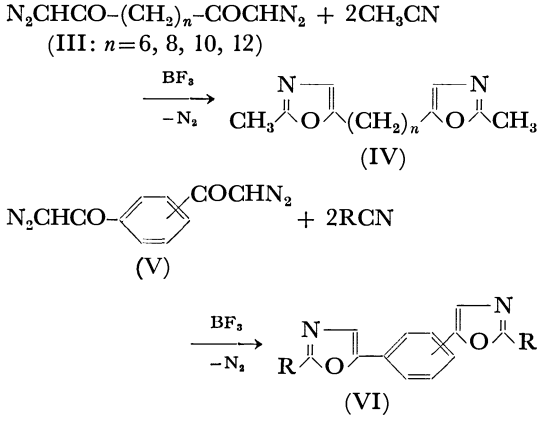

acetonitrile containing a trace amount of H_2O gave *N*-(aroylmethyl)acetamide (XII: R^1=Ar, R^2=H, R^3=CH_3) together with oxazole and α-hydroxyacetophenone (IX). The formation of XII supports the existence of an intermediate (VIII) as shown in Scheme 1. The attack of VIII on a water molecule competes with the intramolecular cyclization of VIII which gives the oxazole.

Several oxazole derivatives have been found to exhibit fluorescence properties and have been used as liquid scintillators.[1b] The bisoxazolyl compound, 1,4-bis(5-phenyl-2-oxazolyl)benzene (VI_3), is an isomer of the well known scintillator POPOP, 1,4-bis(2-phenyl-5-oxazolyl)benzene, and shows strong emission bands at 405 nm. The UV and fluorescence spectral data of oxazoles are listed in Table 3.

Table 3. UV and emission data of oxazoles

Oxazole	UV λ_{max}/nm	log ε	Emission λ/nm
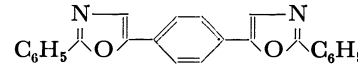	341 353	4.67 4.74	405
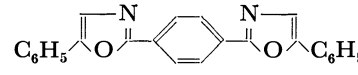	346 360 369	4.68 4.74 4.52	417
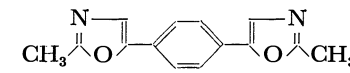	298 310 325	4.61 4.70 4.56	348
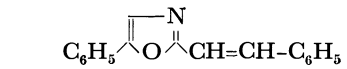	261 338	3.75 4.22	405
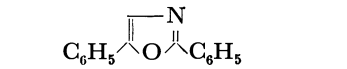	305 316	4.41 4.38	360
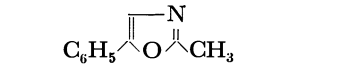	265 272	4.29 4.29	315
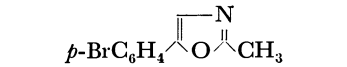	273 279	4.33 4.35	320
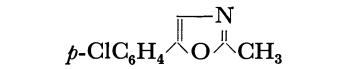	271 280	4.36 4.37	326
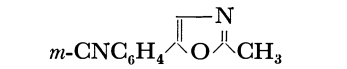	274	4.29	342
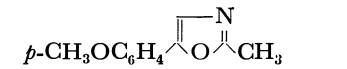	275	4.32	332
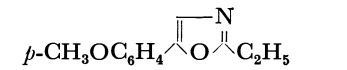	275	4.36	332
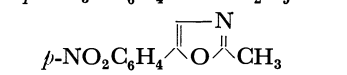	233 327	4.02 4.26	a)
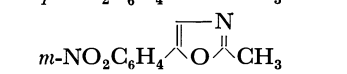	262	4.42	a)

a) Emission spectrum was not measured.

Experimental

All melting points were taken with a Yanagimoto Melting Point Apparatus and are uncorrected. The IR spectra were measured on a Hitachi Infrared Spectrometer model 215. The ^{1}H-NMR spectra were recorded in $CDCl_3$ solution at 60 MHz on a Varian Spectrometer model EM-360 using TMS as an internal standard. UV spectra were measured on a Hitachi Spectrometer model 323 in ethanol solution. Emission spectra were recorded on Hitachi Emission Spectrometer model MPE-2A in ethanol solution ($1—5\times10^{-6}$ mol/l).

Materials. Diazoacetophenones,[12] ethyl diazoacetate,[13] 1,2-diphenyl-2-diazoethanone,[14] dibenzoyldiazomethane,[15] and dimethyl diazomalonate[16] were synthesized by the methods described in the literature. Liquid nitriles were purified by distillation of commercial reagents after refluxing over P_2O_5. *p*-Methoxybenzonitrile and *p*-nitrobenzonitrile were purified by recrystallization.

General Procedure of the BF_3 Catalyzed Reaction of Diazo Carbonyl Compounds in Acetonitrile. A solution of the diazo carbonyl compound (3 mmol) in acetonitrile (3 ml) was added dropwise to acetonitrile (10 ml) containing BF_3–etherate (1.0 ml) under magnetic stirring at temperatures described in the Tables. After the vigorous evolution of N_2 ceased the reac-

TABLE 4. ANALYTICA DATA OF OXAZOLES

Compd	Molecular formula	Found (%)			Calcd (%)		
		C	H	N	C	H	N
II_4	$C_{16}H_{13}ON$	81.58	5.65	5.98	81.68	5.57	5.95
II_6	$C_{16}H_{13}O_2N$	76.43	5.22	5.53	76.47	5.22	5.57
II_7	$C_{15}H_{10}O_3N_2$	67.87	3.86	10.38	67.66	3.79	10.52
II_8	$C_{17}H_{13}ON$	82.52	5.27	5.76	82.57	5.30	5.66
II_9	$C_{16}H_{13}ONS$	72.04	4.89	5.20	71.88	4.90	5.24
II_{11}	$C_{10}H_8ONCl$	62.06	4.25	7.25	62.03	4.16	7.23
II_{12}	$C_{11}H_{11}O_2N$	69.85	5.90	7.48	69.82	5.86	7.40
II_{13}	$C_{11}H_{11}ON$	76.27	6.34	8.09	76.27	6.40	8.09
II_{14}	$C_{10}H_8ONCl$	62.08	4.16	7.30	62.03	4.17	7.23
II_{15}	$C_{10}H_8ONBr$	50.60	3.42	5.88	50.44	3.39	5.88
II_{16}	$C_{11}H_8ON_2$	71.93	4.40	15.31	71.72	4.38	15.21
II_{17}	$C_{10}H_8O_3N_2$	58.54	3.91	13.75	58.82	3.95	13.72
II_{22}	$C_{11}H_8ON_2$	71.70	4.44	15.17	71.72	4.38	15.21
II_{23}	$C_{10}H_8O_3N_2$	59.06	4.05	13.72	58.82	3.95	13.72
II_{24}	$C_{12}H_{13}O_2N$	70.78	6.46	6.97	70.91	6.45	6.89
II_{29}	$C_7H_9O_4N$	49.38	5.45	8.25	49.12	5.30	8.18
IV_1	$C_{14}H_{20}O_2N_2$	67.59	8.00	11.12	67.71	8.12	11.28
IV_2	$C_{16}H_{24}O_2N_2$	69.32	8.74	9.87	69.53	8.75	10.14
IV_3	$C_{18}H_{28}O_2N_2$	70.73	9.10	9.11	71.01	9.27	9.20
IV_4	$C_{20}H_{32}O_2N_2$	71.97	9.58	8.30	72.25	9.70	8.43
VI_1	$C_{14}H_{12}O_2N_2$	70.06	4.97	11.68	69.99	5.03	11.66
VI_2	$C_{14}H_{12}O_2N_2$	70.01	4.95	11.66	69.99	5.03	11.66
VI_3	$C_{24}H_{16}O_2N_2$	79.10	4.43	7.72	79.10	4.43	7.96

tion mixture was poured into H_2O (50 ml) and ether (50 ml). The ether layer was extracted twice with 3 M HCl and the combined aqueous solution made basic with $NaHCO_3$. The separated oxazole was extracted with ether and purified by recrystallization.

General Procedure of the BF_3 Catalyzed Reaction of Diazo Carbonyl Compounds in Liquid Nitriles. The Diazo carbonyl compound (3 mmol) was treated in the similar manner described above in an excess of liquid nitrile. The oxazoles ($R^3 \neq CH_3$) could not be extracted with 3 M HCl and therefore the reaction mixture was treated with H_2O and extracted twice with ether (2×20 ml) after the solution was made basic with $NaHCO_3$. The ether extract was dried over Na_2SO_4, the ether evaporated, and column chromatographed over silica gel.

Reaction with Solid Nitriles. A five molar equivalent of the nitrile was reacted with α-diazoacetophenone in dried benzene (20 ml). The reaction mixture was separated by column chromatography after the usual work up.

Reaction of m-Chloro-α-diazoacetophenone in Water Containing Acetonitrile. *m*-Chloro-α-diazoacetophenone (1 mmol) was decomposed in water containing acetonitrile[17] (20 ml) at 5 °C. Column chromatography of the reaction mixture gave three products: 5-(*m*-chlorophenyl)-2-methyloxazole (II_{20}, 55 %), α-hydroxy-*m*-chloroacetophenone (12%), and *N*-(*m*-chlorophenacyl) acetamide (XII: R^1=*m*-ClC_6H_4, R^2=H, R^3=CH_3): colorless crystals; mp 118—119 °C; yield 0.057 g, 27 %; IR (KBr) 1690 (C=O), 1650, 3280 cm^{-1} (amide); NMR ($CDCl_3$) δ 2.41 (s, 3H, CH_3), 4.97 (d, 2H, CH_2), 6.8 (broad s, 1H, NH), 7.4—8.2 ppm (m, 4H, Ar). Found: C, 56.66; H, 4.80; N, 6.63%. Calcd for $C_{10}H_{10}O_2NCl$: C, 56.75; H, 4.76; N, 6.62%.

We are indebted to Professor S. Kato and Dr. A. Yoshimura of this Institute for their valuable suggestions and discussion concerning the measurement of emission spectra of the oxazoles.

References

1) a) R. H. Wiley, *Chem. Rev.*, **37**, 401 (1945); b) I. J. Turchi and M. J. S. Dewar, *Chem. Rev.*, **75**, 389 (1975).
2) R. Huisgen, H. Koenig, G. Binsch, and H. J. Sturm, *Angew. Chem.*, **73**, 368 (1961).
3) a) R. Huisgen, G. Binsch, and L. Ghosez, *Chem. Ber.*, **97**, 2628 (1964); b) R. Huisgen, H. J. Sturm, and G. Binsch, *Chem. Ber.*, **97**, 2864 (1964); c) J. M. Birchall, R. N. Haszeldine, J. Nikokavouras, and E. S. Wilks, *J. Chem. Soc., C*, **1971**, 562; d) R. R. Schmidt, *Angew. Chem.*, **85**, 235 (1973).
4) a) F. Weygand, *Angew. Chem.*, **73**, 70 (1961); b) N. T. Buu and J. T. Edward, *Can. J. Chem.*, **50**, 3730 (1972).
5) R. K. Armstrong, *J. Org. Chem.*, **31**, 618 (1966).
6) K. Kitatani, T. Hiyama, and H. Nozaki, *Tetrahedron Lett.*, **1974**, 1531.
7) M. P. Doyle, M. Oppenhuizen, R. C. Elliott, and M. R. Boelkins, *Tetrahedron Lett.*, **1978**, 2247.
8) T. Ibata and R. Sato, *Chem. Lett.*, **1978**, 1129.
9) W. T. Flowers, G. Holt, and M. A. Hope, *J. Chem. Soc. Perkin Trans. 1*, **1974**, 1116.
10) H. E. Sheffer and J. A. Moore, *J. Org. Chem.*, **28**, 130 (1963).
11) T. Ibata, K. Miyauchi, and S. Nakata, *Bull. Chem. Soc. Jpn.*, **52**, 3467 (1979).
12) M. S. Newman and P. F. Beal, III, *J. Am. Chem. Soc.*, **71**, 1506 (1949).
13) E. B. Womack and A. B. Nelson, *Org. Synth.*, Coll. Vol. III, 392 (1955).
14) C. D. Nenitzescu and E. Solomonica, *Org. Synth.*, Coll. Vol. II, 496 (1943).
15) M. Regitz, *Angew. Chem. Int. Ed. Engl.*, **6**, 733 (1967).
16) B. W. Peace, F. C. Aarman, and D. S. Wulfman, *Synthesis*, **1971**, 658.
17) Acetonitrile used in this experiment was purified by a single distillation without the use of P_2O_5 as a drying reagent.

Diversity in the Base-induced Photoreactions of Thiolane-2,4-dione and Derivatives. Reductive Ring Cleavage and Novel Rearrangements of the Carbon Skeleton[1)]

Kimitoshi SAITO† and Tadashi SATO*

Department of Applied Chemistry, Waseda University, Ookubo, Shinjuku-ku, Tokyo 160

(Received May 11, 1979)

The irradiation of thiolane-2,4-dione (thiotetronic acid) and its derivatives, **1a**—**1d**, in methanol in the presence of bases induced the reductive ring cleavage to give β,β'-diketo esters. The base-induced reductive ring cleavage was also observed in aprotic solvents, such as acetonitrile or acetone, although the products were obtained as β,β'-diketo amides in these cases. On the other hand, the irradiation of **1a**—**1d** in water in the presence of bases induced a rearrangement of the carbon skeleton to give succinic thioanhydrides, γ-keto amides or succinamides, along with the reduction products. When pyridine was used as a base in the photolysis in water, two 3-acetyl derivatives, **1a** and **1b**, gave γ-keto thiols and the corresponding disulfides, resulted from another type of rearrangement of the carbon skeleton. Conceivable reaction mechanisms were discussed.

It has previously been reported that the photoreactions of sulfur-containing carbonyl compounds depend on the relative positions of the sulfur and carbonyl groups.[2)] Previous investigations have shown that the UV spectra of cyclic keto sulfides are substantially different from those of alkyl or aryl ketones or acyclic keto sulfides, and this difference has been attributed to the transannular interaction of a lone pair of electrons on sulfur with the carbonyl group, the coupling being strongly dependent on the orientation of the two groups.[3)] Several types of photoreactions—rearrangement of the ring system,[4)] ring contraction,[5)] fragmentation,[6)] and some others[7)]—have been known for cyclic β- or γ-keto sulfides, and these reactions have been interpreted as involving different degrees of interaction between sulfur and carbonyl groups.

It is well known that photoreactions in the presence of an amine proceed through a charge-transfer complex to form reduction products. Previously, we reported on the reductive cleavage of the isoxazole ring by irradiation in the presence of triethylamine.[8)] We have now undertaken the photoreactions of thiolane-2,4-dione (thiotetronic acid) and its derivatives, **1a**—**1d**, in the presence of bases, expecting an unusual photoreaction caused by the intramolecular charge-transfer interaction of the two chromophores and also the intermolecular interaction of **1a**—**1d** with the bases.

Results and Discussion

When methanol solutions of 3-acetylthiolane-2,4-dione (**1a**) and its derivatives, **1b**—**1d**, containing an equal amount of such bases as piperidine, triethylamine, or sodium hydroxide (10% aqueous solution) were irradiated with Pyrex-filtered light for 8—12 h, methyl 2-acetylacetoacetate (**2a**) and its derivatives, **2b**—**2d**, were obtained. When pyridine was used as a base in the reaction of **1a**, deacetylation occurred and methyl acetoacetate (**2c**) was identified as a product along with **2a**. The corresponding ethyl ester was obtained in a 29% yield upon the irradiation of **1a** in ethanol in the presence of piperidine. The base-induced reductive ring cleavage was also observed in aprotic solvents, such as acetonitrile or acetone, although the products were obtained as amides, **3**, in these cases. The details are shown in Table 1. It should be noted that diethylamine and triethylamine gave an identical product, *N,N*-diethyl-2-acetylacetamide (**3aD**), upon the irradiation of **1a** in acetonitrile. The deethylation could proceed as is shown in **4**, a similar type of deethylation having been speculated about in the photolysis of 3,5-dimethylisoxazole in the presence of triethylamine.[8)] The presence of the bases is essential for these reactions to proceed; the starting materials are recovered under the irradiation in the absence of bases, except in the case of **1c**, in which **2c** was obtained in a 22% yield as well as the main product, 4-methoxy-2-oxo-2,5-dihydrothiophene (**5c**), under irradiation in methanol.

The compounds **1a**—**1d** have enolizable protons and are acidic. Actually, **1a** formed a stable crystalline salt with piperidine, and the salt, when irradiated in methanol or in acetonitrile, afforded **2a** (24% in methanol) or piperidyl 2-acetylacetoacetamide (**3aP**, 10% in acetonitrile). It might be considered that the present reaction proceeds from the anion forms of **1a**—**1d**, but it was confirmed that the presence of an enolizable proton is not necessary because the 3,3-dimethylthiolane-2,4-dione (**6**) also afforded the corresponding reductive ring-cleavage products, as a mixture of methyl 2,2-dimethylacetoacetate (**7R**, 27%) and piperidyl 2,2-dimethylacetoacetamide (**7P**, 25%), when irradiated in methanol in the presence of piperidine.

In contrast to the reductive ring cleavage in the organic solvents described above, the reaction in an aqueous solution proceeded in a different way. The irradiation of **1a** in water containing three equivalents of piperidine gave 2-acetylsuccinic thioanhydride (**8a**) and piperidyl levulinamide (**9aP**) along with the reduction product, **3aP**. Similarly, the methyl derivative **1b** gave the corresponding products, **8b** and **9bP**. The piperidine-induced photolysis of **1c** and **1d**, on the other hand, gave two derivatives of succinamide, **10cP** and **10dP**, as well as the corresponding succinic thioanhydrides, **8c** and **8d**. It is evident from the results shown in Table 1 that the products **9** and **10** are secondary products from **8**, since the yields of **9** and **10**

† Present address: School of Pharmaceutical Science, Toho University, Miyama 2-2-1, Funabashi, Chiba 274.

Table 1. Products and yields (%) in the photolyses of thiolane-2,4-dione derivatives (**1a**—**1d**) for 12 h

Compound	Bases	Products (%) in MeOH	in MeCN	in H_2O			
1a	Piperidine	**2a**(88)	**3aP**(41)	**8a**(12)[a]	**9aP**(7)[a]		
			3aP(45)[b]	**3aP**(31)	**8a**(7)	**9aP**(35)	
	Morpholine		**3aM**(76)	**3aM**(12)	**8a**(10)	**9aM**(32)	
	Diethylamine		**3aD**(32)	**3aD**(46)	**8a**(t)	**9aD**(17)	
	Triethylamine	**2a**(63)	**3aD**(46)	**3aD**(27)	**8a**(t)	**9aD**(30)	
	Pyridine	**2a**(28) **2c**(31)	N.R.	**12a**(3)	**13a**(36)		
	10% NaOH	**2a**(24)	N.R.	**12a**(t)	**13a**(7)		
	Aniline	**14A**(94)	**14A**(81)	**14A**(13)			
	Butylamine		**14B**(85)	**3aB**(24)	**9aB**(14)	**14B**(4)	**15B**(24)
	Cyclohexylamine		**14C**(62)	**3aC**(23)	**9aC**(10)	**14C**(4)	**15C**(35)
1b	Piperidine	**2b**(31) **3bP**(15)	**3bP**(40)	**8b**(46)[a]	**9bP**(t)[a]		
				9bP(70)			
	Morpholine			**9bM**(18)			
	Diethylamine		**3bD**(15)				
	Pyridine			**13b**(25)			
1c	Piperidine	**3cP**(81)	**3cP**(68)	**10cP**(3)[a]	**8c**(63)[a]		
				10cP(18)	**8c**(48)		
	Pyridine			**10cO**(51)			
1d	Piperidine	**3dP**(47) **5d**(19)	**3dP**(76)	**10dP**(11)[a]	**8d**(71)[a]		
				10dP(20)	**8d**(65)		
	Pyridine			**10dO**(55)			

a) Yields for 4 h. b) Yields in an acetone solution.

increased at the expense of those of **8** upon the 12 h irradiation as compared with the 4 h irradiation. Actually, **9aP** and **9bP** were obtained from **8a** and **8b** in 86% and 72% yields respectively, upon irradiation in water in the presence of piperidine for 8 h. Similarly, **10cP** and **10dP** were obtained from **8c** and **8d** in 31% and 36% yields respectively under the same conditions.

The solubility of **1a** in water is low, and three equivalents of the base were necessary to prepare homogeneous aqueous solutions. When the amount of piperidine was increased tenfold, the reductive ring-cleavage product, **3aP** (33%), was obtained in preference to the rearrangement product, **9aP** (22%).

When pyridine was used as a base in the photolysis in water (1 : 1 by volume), **1a** and **1b** gave γ-ketobutanethiol (**12**) and the corresponding disulfide, **13**, instead of **8** and **9**. The same reaction was also observed in the irradiation of **1a** in a 10% aqueous sodium hydroxide solution, but the reaction was slow in this case. No abnormality of pyridine was, however, observed in the reactions of **1c** and **1d**, and the corresponding succinic acid derivatives, **10cO** and **10dO**, were obtained.

The reactions in aqueous solutions are notable in that the products have a carbon skeleton which was not present in the starting materials. In our preliminary report,[1] we proposed two mechanistic paths for the carbon skeleton rearrangement. One mechanism involved the radical fission (a or b; see Scheme 1) of the ring, followed by the elimination of CSO or CO to give observed products, **9** and **12**, *via* cyclopropanone, **17**, or thietanone, **18**, intermediates, respectively. This mechanism is analogous to that reported by Kooi and Wynberg in the ring contraction of non-enolizable α-diketo sulfides.[9] More recently, Yates and Toong[6] reported the formation of disulfides by the photoreaction of tetrahydrothiophene-3-one through a radical cleavage of the ring. The other mechanism involved thiophene-type transposition reactions, assuming **1** to be thiophenediol, **19**, as is shown in Scheme 2. It was

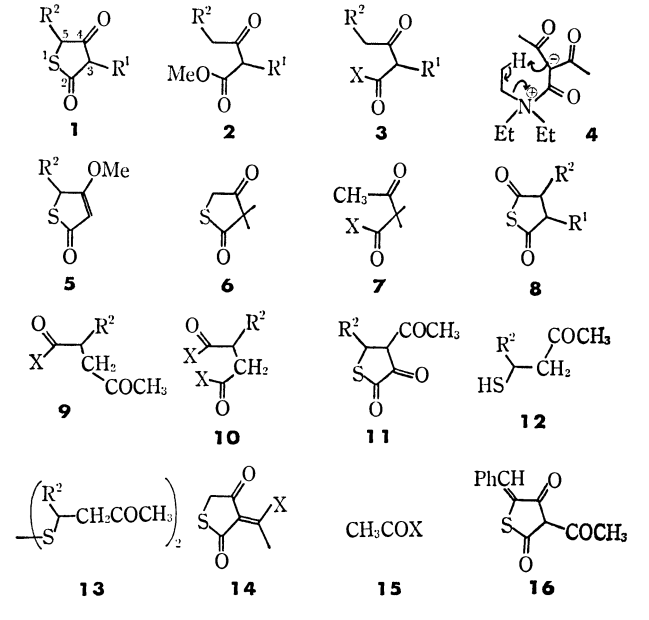

a; $R^1=COCH_3$, $R^2=H$
b; $R^1=COCH_3$, $R^2=CH_3$
c; $R^1=R^2=H$
d; $R^1=H$, $R^2=CH_3$
e; $R^1=COPh$, $R^2=H$
f; $R^1=CO_2Et$, $R^2=H$

A; X=NHPh
B; X=NHBu
C; X=NH-
D; $X=NEt_2$

M; X=N O
O; X=OH
P; X=N
R; X=OMe

Fig. 1.

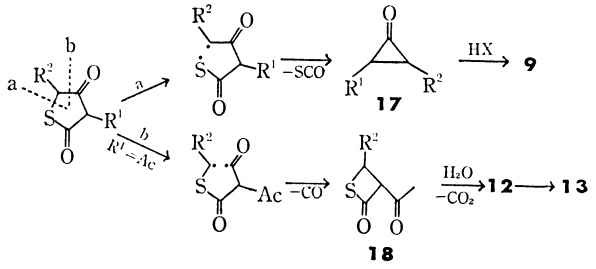

Scheme 1.

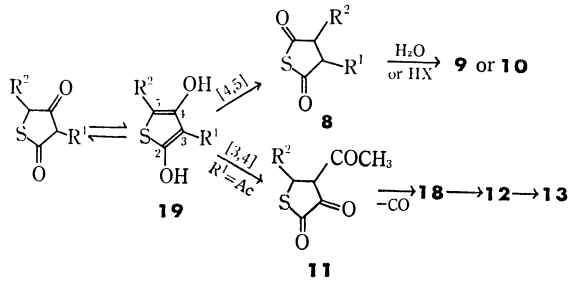

Scheme 2.

considered that the piperidine-induced reactions leading to **9** proceeded through the intermediacy of **8**, which, in turn, might have been formed through 4,5-transposition of **1**, while the pyridine-induced reactions leading to **12** and **13** could be explained in terms of involving 4-acetylthiolane-2,3-dione, **11**, as intermediates, resulting through the 3,4-transposition of **1**. This mechanism now seems preferable to the radical mechanism because (i) **8a** and **8b** were actually identified as intermediates in the reactions of **1a** and **1b**, and (ii) the formation of **10c** and **10d** from **1c** and **1d** respectively could not be explained by the radical mechanism.

When primary amines, such as aniline, cyclohexylamine, and butylamine, were used as the base in the reaction of **1a** in methanol or acetonitrile, the condensation products, **14**, became the major products and no reduction products or rearrangement products were identified at all. In an aqueous solution, however, appreciable amounts of the reduction products (**3aC**, **3aB**) and the rearrangement products (**9aB**, **9aC**) were identified, as well as the condensation products (**14B**, **14C**) and a fission product, **15C**. Since the condensation product, **14A**, was intact under the present reaction conditions, the reduction and rearrangement are considered to have proceeded prior to the condensation.

In contrast to the base-induced reductive ring cleavage in organic solvents, where the presence of enolizable proton was unnecessary, it was concluded that the base-induced reactions in an aqueous solution required the presence of the enolizable proton, because the dimethyl derivative, **6**, underwent fragmentation to afford *N*-formylpiperidine, without giving any reduction product or rearrangement product. Most of the starting material, **6**, was recovered in pyridine–water.

It is presumable that the reductive ring cleavage proceeds *via* a charge-transfer complex in organic solvents, while the carbon-skeleton rearrangements proceed through the excitation of the anion form of the substrate, which is predominant only in an aqueous solution.

The irradiation of 3-benzoyl and 3-ethoxycarbonyl derivatives (**1e** and **1f**) in the presence of piperidine or pyridine resulted in the recovery of the starting materials (62—81%) in water, methanol, or acetonitrile. Previously we demonstrated that unsymmetrical cyclic β,β'-diketo esters such as **1** may generally exist in "external" tautomers (A⇌B) in solution, as is shown in Scheme 3.[10] The presence of the "external"

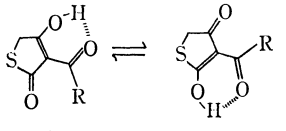

Scheme 3.

tautomers in 3-acylthiolane-2,4-dione (**1a**—**1b**) was evident in view of the presence of two singlets of the ring methylene protons in their PMR spectra:[11] A: B=24: 76 for **1a** and A: B=28: 72 for **1b**. On the contrary, it was confirmed that **1e** and **1f** exist exclusively in Form A, as revealed by the single methylene signal in their PMR spectra. It is assumed that the lack of the reactivity of **1e** and **1f** might be attributable to a fixation of the tautomeric system to the Form A through the interaction of 3-benzoyl or 3-ethoxycarbonyl groups. In addition, 3-acetyl-5-benzylidenethiolane-2,4-dione (**16**) and **14A**, which have an exo-double bond on the ring, were also recovered unreacted under the same irradiation conditions. Presumably, the difficulty in attaining the thiophene chromophore might deprive these compounds of the photoreactivity.

Experimental

The mass spectra were obtained with a Hitachi RMS-4 spectrometer; the IR spectra, with a Hitachi 215 spectrometer; the PMR spectra, with a JEOL MH-60 (60 MHz) or PS-100 (100 MHz) spectrometer (with Me_4Si as the internal standard), and the CMR spectra, with a JEOL FX-10 spectrometer operated at 25.1 MHz.

The starting materials, **1a**,[12] **1b**—**1d**,[13] **1e**,[12] **1f**,[13] and **16**,[14] were prepared according to the procedures described in the literature cited.

General Procedure for the Photolysis. Unless otherwise noted, a solution (3—5 mmol, 0.033 M) of the starting material containing a base (one equivalent in the cases of the reactions in organic solvents, three equivalents in the cases of the reactions in aqueous solutions) was irradiated in Pyrex test tube by means of a high-pressure mercury lamp [Ushio UM 452 (450 W)] for 4—12 h. After the irradiation, the solution was poured into water, acidified with 6 M hydrochloric acid, and then extracted with chloroform (Procedure A). In some cases, the irradiated solution was concentrated *in vacuo*, and the crude residue, after having been dissolved in chloroform, was washed with dilute aqueous hydrochloric acid (Procedure B). The chloroform solution after Procedure A or B was dried over sodium sulfate and evaporated *in vacuo*. The residue was treated as indicated below.

Photolysis of 1a. In Alcohols: The crude material obtained by Procedure A was placed in a silica-gel column and then eluted with chloroform. Upon removing the solvent *in vacuo*

from the eluate, **2a** (in methanol) or the corresponding ethyl ester (in ethanol) was isolated; the **2a** was further purified by vacuum distillation. **2a**; Bp, 47—48 °C (3 mmHg). MS, *m/e* 158 (M), 126, 98 (base peak), and 85. IR (CCl_4), 1700 and 1550 cm^{-1}. PMR (CCl_4), δ 2.32 (s, 6H), 3.74 (s, 3H), and 18.5 (bs, 1H). CMR ($CDCl_3$), δ 26.0, 51.5, 108.3, 167.5, and 196.8. Found: C, 51.20; H, 6.48%. Calcd for $C_7H_{10}O_4$: C, 52.14; H, 6.37%. The IR and PMR spectra of the ethyl ester were identical with those of an authentic sample.[15]

In Acetone or Acetonitrile in the Presence of Piperidine, Morpholine, Diethylamine, or Triethylamine: The viscous residue obtained by Procedure B was purified on a preparative TLC (silica gel, 10% methanol in chloroform). **3aP**, **3aM**, and **3aD** were isolated depending on the bases used. **3aP**: IR (CCl_4), 1630 cm^{-1}. PMR (CCl_4), δ 1.4—1.6 (b, 6H), 1.95 (s, 6H), 3.2—3.8 (b, 4H), and 16.8 (bs, 1H). **3aM**: IR (CCl_4), 1635 cm^{-1}. PMR (CCl_4), δ 1.98 (s, 6H), 3.3—3.6 (b, 4H), and 16.8 (bs, 1H). CMR ($CDCl_3$), δ 23.2, 44.2, 47.3, 66.6, 66.7, 110.5, 166.5, and 189.1. **3aD**: IR (CCl_4), 1630 cm^{-1}. PMR (CCl_4), δ 0.98 (t, J=8 Hz, 3H), 1.06 (t, J=8 Hz, 3H), 1.98 (s, 6H), 3.19 (q, J=8 Hz, 2H), 3.24 (q, J=8 Hz, 2H), and 16.6 (bs, 1H). CMR ($CDCl_3$), δ 14.1, 14.2, 23.1, 40.2, 41.8, 107.3, 109.5, and 188.8. The amide-type structure of **3aP** was also confirmed by hydrolyzing it with a 10% aqueous potassium hydroxide solution to acetylacetone and piperidine.

In Acetonitrile in the Presence of Aniline, Cyclohexylamine, or Butylamine: After the irradiation, the solvent was removed *in vacuo*. In an aniline-induced reaction, **14A** was obtained when the crude solid was washed with carbon tetrachloride. In a cyclohexylamine-induced reaction, **14C** and **15C** were isolated by preparative TLC (silica gel, 2% methanol in chloroform). In a butylamine-induced reaction, the crude oil obtained was placed in a silica-gel column and then eluted with chloroform. Upon removing the solvent *in vacuo* from the eluate, a colorless oil of **14B** was isolated in a pure state. The spectra of **14A** and **15C** were identical with those of authentic samples.[14] **14B**: IR (CCl_4), 1680, 1600, and 1135 cm^{-1}. PMR (CCl_4), δ 0.95 (t, J=7 Hz, 3H), 1.2—1.6 (m, 4H), 2.38 (s, 3H), 3.2—3.5 (m, 4H), 3.42 and 3.36 (s, s, 2H), and 11.05 and 11.95 (bs, bs, 1H). **14C**: IR (CCl_4), 1685, 1600, and 1360 cm^{-1}. PMR (CCl_4), δ 1.2—2.0 (m, 10H), 2.46 (s, 3H), 3.42 and 3.50 (s, s, 2H), 3.4—3.6 (m, 1H), and 11.2 and 12.2 (bs, bs, 1H). The PMR analysis indicated that Compounds **14A**, **14B**, and **14C** existed as mixtures of external tautomers, as shown in Scheme 3; the A form/B form ratio was calculated to be 0.35 for **14A**, 0.43 for **14B**, and 0.33 for **14C**.

In Water in the Presence of Piperidine, Morpholine, Diethylamine, or Triethylamine: After the irradiation, the solution was shaken with chloroform (Extract A). The aqueous solution was acidified with 6 M hydrochloric acid and further shaken with chloroform (Extract B). Extract B, after the evaporation of the solvent, was purified by preparative TLC (silica gel, 10% methanol in chloroform). **3aP**, **3aM**, and **3aD** were thus obtained along with **8a** and the unreacted starting material. Extract A, after purification by preparartive TLC (10% methanol in chloroform), gave **9aP**, **9aM**, and **9aD**. **8a**: Mp 35—37 °C. MS, *m/e* 158 (M), 98 (base peak), 75, 70, and 43. IR (CCl_4), 1740, 1715, 1625, and 1600 cm^{-1}. PMR (CCl_4), δ 1.95 (s, 3H) 3.52 (s, 2H), and 12.3 (bs, 1H). The IR and PMR spectra of **9aP** and **9aD** were identical with those of authentic samples.[16] **9aM**: MS, *m/e* 185 (M), 99, 98, 86 (base peak), 84, and 69. IR (CCl_4), 1720 and 1630 cm^{-1}. PMR (CCl_4), δ 2.0—2.3 (m, 4H), 2.12 (s, 3H), 3.3—3.6 (m, 4H), and 3.62 (s, 4H).

In Water in the Presence of Aniline, Cyclohexylamine, or Butylamine: After irradiation, the solution was shaken with chloroform (Extract A). The aqueous solution was acidified with 6 M hydrochloric acid and further shaken with chloroform (Extract B). When Extract A was purified by preparative TLC (silica gel, 10% methanol in chloroform), **3aB** and **3aC** were isolated. From Extract B, **15B**, **15C**, **9aB**, and **9aC** were obtained, along with the condensation products, **14B** and **14C**. **3aB**: IR (CCl_4), 1630 and 1590 cm^{-1}. PMR (CCl_4), δ 0.97 (t, J=7 Hz, 3H), 1.2—1.6 (m, 4H), 2.09 (s, 6H), 3.29 (q, J=7 Hz, 4H), 7.52 (bs, 1H), and 10.58 (bs, 1H). **3aC**: IR (CCl_4), 1630 and 1590 cm^{-1}. PMR ($CDCl_3$), δ 1.2—2.0 (m, 10H), 2.04 (s, 6H), 3.3—3.4 (m, 1H), and 7.4 (bs, 1H). **9aB**: IR (CCl_4), 1670 and 1630 cm^{-1}. PMR (CCl_4), δ 0.97 (t, J=7 Hz, 3H), 1.2—1.6 (m, 4H), 2.30 (s, 3H), 2.0—2.15 (m, 4H), 2.95—3.05 (m, 2H), and 7.4 (bs, 1H). **9aC**: IR (CCl_4), 1670 and 1630 cm^{-1}. PMR ($CDCl_3$), δ 1.2—2.0 (m, 10H), 2.11 (s, 3H), 2.0—2.2 (m, 4H), 3.3—3.4 (m, 1H), and 6.8 (bs, 1H).

In Pyridine–Water: A solution of **1a** in pyridine–water (1:1 by volume) was irradiated for 12 h. When the viscous residue obtained by Procedure B was chromatographed on preparative TLC (silica gel, 5% methanol in chloroform), **12a** and **13a** were isolated; **13a** was further purified by vacuum distillation at 50—55 °C (3 mmHg). The IR and PMR spectra of **12a** and **13a** were identical with those of authentic samples.[17]

Preparation and Photolysis of 3-Acetylthiotetronic Acid Piperidinium Salt. When 0.17 g (2 mmol) of piperidine was added to a stirred solution of 0.16 g (1 mmol) of **1a** in 30 ml of dry benzene at room temperature, a white solid crystallized out in 1—2 h. The solid was filtered and recrystallized from benzene to give 3-acetylthiotetronic acid piperidinium salt; yield 175 mg (72%); Mp 98—100 °C, IR (KBr), 3400, 1680, and 1590 cm^{-1}. PMR ($CDCl_3$), δ 1.7 (b, 6H), 2.28 (s, 3H), 3.3 (b, 4H), 3.42 (s, 2H), and 7.6 (b, 2H).

A solution of the salt in methanol or in acetonitrile was irradiated for 12 h. After the irradiation, the solvent was removed *in vacuo*. The formation and yield of **2a** (42% in methanol) or **3aP** (10% in acetonitrile) were determined by means of their PMR spectra (tetrachloroethane was used as the internal standard).

Photolysis of 1b. In Methanol or Acetonitrile: When the viscous residue obtained by Procedure B was purified by preparative TLC (silica gel, chloroform), **2b** and **3bP** were isolated. **3bP** was isolated as a single product when the irradiation was carried out in acetonitrile. **2b**: IR (CCl_4), 1715 and 1550 cm^{-1}. PMR (CCl_4), δ 1.12 (t, J=7.5 Hz, 3H), 2.02 (s, 3H), 3.35 (q, J=7.5 Hz, 2H), 3.65 (s, 3H); no enolic proton could be observed. **3bP**: IR (CCl_4), 1635 cm^{-1}. PMR ($CDCl_3$), δ 1.15 (t, J=8 Hz, 3H), 1.4—1.6 (b, 6H), 2.20 (s, 3H), 2.44 (q, J=8 Hz, 2H), 3.2—3.8 (b, 4H), and 16.5 (bs, 1H).

In Water: The crude product obtained by Procedure A was purified by preparative TLC (silica gel, chloroform). **9bP** and **9bM** were obtained, along with **8b**. **8b**: IR (CCl_4), 1730, 1705, 1640, 1595, and 1220 cm^{-1}. The PMR analysis indicated that the compound existed as a mixture of 24% of the keto form and 76% of the enol form in carbon tetrachloride. PMR (CCl_4), for the keto form, δ 1.32 (d, J=7 Hz, 3H), 2.40 (s, 3H), 3.94 (q, J=7 Hz, 1H), for the enol form, δ 1.44 (d, J=7 Hz, 3H), 2.02 (s, 3H), 3.64 (q, J=7 Hz, 1H) and 12.6 (bs, 1H). **9bP**: IR ($CHCl_3$), 1717, 1640, and 1470 cm^{-1}. PMR ($CDCl_3$), δ 0.97 (d, J=7 Hz, 3H), 1.35—1.80 (m, 6H), 2.00 (s, 3H), 2.06—3.06 (m, 3H), and 3.15—3.18 (m, 4H). **9bM**: IR ($CHCl_3$), 1720, 1645, and 1550 cm^{-1}. PMR ($CDCl_3$), δ 1.03 (d, J=7 Hz, 3H), 2.06 (s, 3H), 2.15—3.21 (m, 3H), and 3.49—3.79 (m, 8H).

In Pyridine–Water: When a solution of **1b** in pyridine–water (1:1 by volume) was irradiated for 12 h, a solid was obtained

upon the removal of the solvent *in vacuo*. The crude residue was purified by preparative TLC (silica gel, chloroform) to give **13b**, along with an unreacted material. **13b**: IR ($CHCl_3$), 1720, 1635, and 1155 cm^{-1}. PMR ($CDCl_3$), δ 1.24 (d, J=7 Hz, 6H), 2.10 (s, 6H), and 2.30—3.55 (m, 6H).

Photolysis of ***1c*** *or* ***1d***. *In Methanol*: The crude solid obtained by Procedure B were purified by preparartive TLC (silica gel, 5% methanol in chloroform). **3cP** or **3dP** was isolated. A by-product, **5d**, was also isolated in the case of the reaction of **1d**. The IR and PMR spectra of **3cP** and **3dP** were identical with those of authentic samples. When the reaction was carried out in acetonitrile, the same products (**3cP** and **3dP**) were obtained.

In Water in the Presence of Piperidine: The oil obtained from **1c** by Procedure A gave white crystals of **8c** and a pale yellow oil of **10cP** upon vacuum distillation. The IR and PMR spectra of **8c** corresponded to those previously reported.[18] **10cP**: IR (CCl_4), 1640, 1440, and 950 cm^{-1}. PMR ($CDCl_3$), δ 1.6 (b, 12H), 2.48 (s, 4H), and 3.5 (m, 8H).

The crude material obtained from **1d** by Procedure A was placed in a silica-gel column and then eluted with chloroform. Upon removing the solvent *in vacuo* from the first eluate, an oil, **8d**, was isolated. Similarly, crystals of **10dP** were obtained from the second eluate. **8d**: IR (CCl_4), 1700 cm^{-1}. PMR (CCl_4), δ 1.42 (d, J=7 Hz, 3H), 2.56 (ABq, 1H), 3.18 (ABq, 1H), and 3.12 (m, 1H). **10dP**: IR (CCl_4), 1640 and 1440 cm^{-1}. PMR (CCl_4), δ 0.95 (d, J=7 Hz, 3H), 1.6—1.8 (b, 12H), 2.1—2.5 (m, 3H), and 3.4—3.6 (b, 8H).

In Pyridine-Water: A solution of **1c** and **1d** in pyridine–water (1: 1 by volume) was irradiated for 12 h. After the irradiation, the solution was evaporated *in vacuo*. The residue was dissolved in dry methanol containing a few drops of concd hydrochloric acid, and then refluxed for 4 h. The reaction mixture was poured into water and extracted with chloroform to afford **10cR** and **10dR**. The IR and PMR spectra of **10cR** and **10dR** corresponded to those previously reported.[19]

Preparation of ***6***. A mixture of 1.02 g (10 mmol) of **1c**, 3.0 g (20 mmol) of methyl iodide, 1.40 g of anhydrous potassium carbonate, and 50 ml of dry acetone was heated under reflux for 20 h and then allowed to cool. The insoluble material was removed by filtration and washed with acetone. The combined filtrate and acetone washings were evaporated *in vacuo*. The residue was chromatographed on a silica-gel column. The subsequent elution of the column with chloroform afforded 0.48 g of pale yellow crude oil, which was further purified by vacuum distillation to give **6** in the pure state; 0.6 g (42%), Bp 78—80 °C (3 mmHg). PMR ($CDCl_3$), δ 1.21 (s, 6H) and 3.94 (s, 2H).

Photolysis of ***6***. *In Methanol*: The reaction mixture obtained by Procedure A was chromatographed on a preparative TLC plate. Subsequent elution with 10% methanol–chloroform afforded **7R** (27%) and **7P** (25%). **7R**: IR (CCl_4), 1725 and 1630 cm^{-1}. PMR (CCl_4), δ 1.48 (s, 6H), 2.30 (s. 3H), and 3.66 (s, 3H). **7P**: IR (CCl_4), 1630 and 1610 cm^{-1}. PMR (CCl_4), δ 1.38 (s, 6H), 2.07 (s, 3H), and 3.4—3.6 (b, 4H).

In Water in the Presence of Piperidine: The brown oil obtained by Procedure A was chromatographed on a preparative TLC (silica gel, 5% methanol in chloroform). The removal of the solvent from the upper band afforded a pale yellow oil, whose IR and PMR spectra indicated it to be *N*-formylpiperidine.

References

1) Preliminary report; K. Saito and T. Sato, *Chem. Lett.*, **1978**, 307.

2) J. O. Coyle, *Chem. Soc. Rev.*, **4**, 523 (1975); S. T. Reid, *Photochemistry*, **7**, 458 (1976); **8**, 492 (1977).

3) N. J. Leonard, T. L. Brown, and T. W. Milligan, *J. Am. Chem. Soc.*, **81**, 504 (1959); **82**, 4075 (1960).

4) A. Padwa and A. Battisti, *J. Am. Chem. Soc.*, **93**, 1304 (1971); **94**, 521 (1972); J. M. Mellor and C. F. Webb, *J. Chem. Soc., Perkin Trans. 1*, **1972**, 211.

5) P. Y. Johnson, and G. A. Berchtold, *J. Org. Chem.*, **35**, 584 (1970); *Tetrahedron Lett.*, **1972**, 1991.

6) P. Yates and Y. C. Toong, *J. Chem. Soc., Chem. Commun.*, **1978**, 205.

7) H. Turuta, M. Ogasawara, and T. Mukai, *Chem. Lett.*, **1974**, 887; N. Ishibe and M. Odani, *J. Org. Chem.*, **36**, 4132 (1971).

8) T. Sato and K. Saito, *J. Chem. Soc., Chem. Commun.*, **1974**, 781; T. Sato, K. Yamamoto, K. Fukui, K. Saito, K. Hayakawa, and S. Yoshiie, *J. Chem. Soc., Perkin Trans. 1*, **1976**, 783.

9) J. Kooi, H. Wynberg, and R. M. Kellogg, *Tetrahedron Lett.*, **1973**, 2135.

10) T. Yamaguchi, K. Saito, T. Tsujimoto, and H. Yuki, *J. Heterocycl. Chem.*, **13**, 533 (1976).

11) K. Saito and T. Yamaguchi, *Bull. Chem. Soc. Jpn.*, **49**, 1161 (1976); **51**, 651 (1978).

12) D. M. O'Mant, *J. Chem. Soc., C*, **1968**, 1501.

13) E. Benery, *Ber.*, **45**, 2103 (1913).

14) H. Yuki, T. Tsujimoto, T. Sawada, K. Takiura, and T. Yamaguchi, *J. Pharm. Soc. Jpn.*, **96**, 536 (1976).

15) S. Forsén and M. Nilsson, *Acta Chem. Scand.*, **14**, 1333 (1960).

16) A. J. Speziale, *J. Org. Chem.*, **26**, 3176 (1961).

17) J. Murata and H. Arai, *Kogyo Kagaku Zasshi*, **59**, 129 (1956).

18) H. J. Jakobsen, E. H. Larsen, and B.-O. Lawesson, *Tetrahedron*, **18**, 1876 (1963).

19) "The Aldrich Library of Infrared Spectra," Aldrich Chemical Co. (1970), p. 282 and "The Aldrich Library of Nuclear Magnetic Resonance Spectra," Aldrich Chemical Co. (1974), Vol. 3, p. 28.

Enhanced Reactivity of a Flavin Bound to Quaternized Poly(4-vinylpyridine) *via* 8-Position. A Model System of a Flavin Coenzyme Covalently-linked to Enzymes†

Seiji SHINKAI,* Kenji MORI, Yumiko KUSANO, and Osamu MANABE
Department of Industrial Chemistry, Faculty of Engineering, Nagasaki University, Nagasaki 852
(Received May 15, 1979)

The rate constants for the reaction of the title flavin and the monomeric analogues with 1-benzyl-1,4-dihydronicotinamide (BzlNH), 1-nitroethanide ion, glutathione (GSH), and thiophenol (PhSH) were determined at 30 °C. Although the reactivity of 8α-AcHisFl is slightly improved as compared with that of unmodified flavin, the rate constants for 8α-PyFl which is expected to mimic the reactivity of protonated 8α-AcHisFl were significantly increased. The rate constants for the oxidation of anionic reductants(1-nitroethanide ion, GSH, and PhSH) were further increased by immobilization of the 8α-PyFl structure in quaternized 4VP polymers. The kinetic results implicate that (1) with regard to the action of a flavin covalently-linked to enzymes *via* histidine residue, the flavin must be more reactive in acidic pH region due to protonation of the histidine than in basic pH region, (2) the cationic polyelectrolyte environment accelerates selectively the oxidation of anionic reductants, and (3) the title flavin serves as a strong, selective oxidizing agent under ambient reaction conditions.

Suggestion has been made that a fourth flavin exists in nature in addition to riboflavin, FMN, and FAD. In 1955, Kearney and Singer[1] presented unequivocal evidence that succinate dehydrogenase contains covalently-linked FAD which is not extracted from tissues by the conventional denaturation methods. The claim has been further supported by their subsequent studies.[2–4] In the last five years, it has been established that no less than ten flavoenzymes contain the covalently-linked flavin in the active sites and that the covalent linkage occurs in most cases at $C^{8\alpha}$ position, *e.g.*, *via* the imidazole group of the histidine residue of the enzymes.[5]

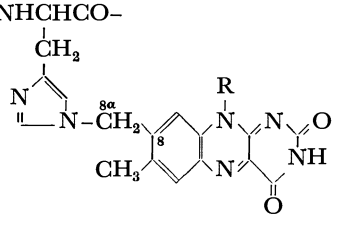

The influence of 8-substituents on the reactivity of the isoalloxazine ring has been estimated in detail by several groups,[6–10] but studies on 8α-substitution are very limited. Edmondson *et al.*[11,12] reported, on the basis of flash photolysis and oxidation-reduction potentials, that 8α-substitution by histidine or cysteine gives rise to the electron-withdrawing influence on the isoalloxazine ring system. Except for their study, little is known with certainty about the influence of 8α-substitution on the reactivity of flavin despite its importance in connection with the behavior of covalently-linked flavin.

The rate constant for the reaction of sulfite ion with 8α-(N_1-histidinyl)flavin is greater by a factor of only 1.4 than that with unmodified flavin.[12] This suggests that the 8α-(N_1-histidinyl) group may slightly affect the reactivity of the isoalloxazine ring. However, two important effects, reaction environment and protonation of the imidazole group, remain to be clarified in order to generalize the conclusion with respect to the covalently-linked flavin systems. Both effects should cause a significant change in the reactivity of covalently-linked flavin. With these objects in view, we have synthesized the following flavins and estimated the oxidative reactivity toward 1-benzyl-1,4-dihydronicotinamide (BzlNH), 1-nitroethanide ion ($CH_3\bar{C}HNO_2$), glutathione (GSH), and thiophenol (PhSH) (R′=tetra-*O*-acetylribityl group).

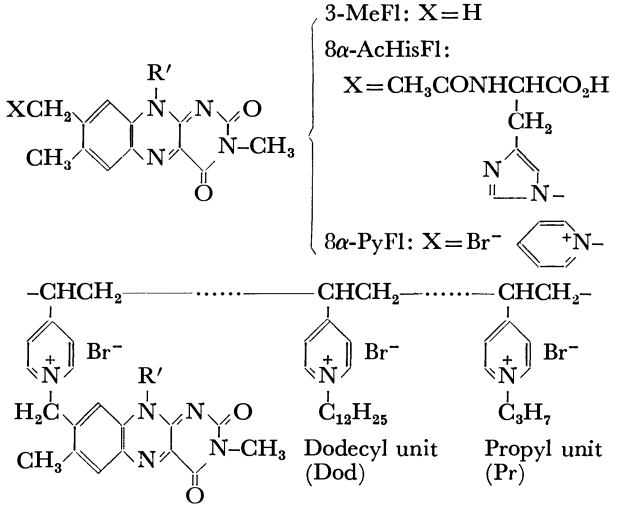

Flavin unit (Fl)

4VP-Fl-Dod-0: Fl, 6 mol%; Dod, 0 mol%; Pr, 88 mol%.
4VP-Fl-Dod-20: Fl, 6 mol%; Dod, 20 mol%; Pr, 67 mol%.

Results

Oxidation of 1-Benzyl-1,4-dihydronicotinamide. Flavin oxidation of BzlNH (Eq. 1) is a typical model

† Coenzyme Models 22. Abbreviations employed are: GSH, glutathione; PhSH, thiophenol; BzlNH, 1-benzyl-1,4-dihydronicotinamide; 3-MeFl, 3-methyltetra-*O*-acetylriboflavin; 8α-AcHiFl, 3-methyl-8α-[N_α-acetyl-(N_1-histidinyl)]-tetra-*O*-acetylriboflavin; 8α-PyFl, 3-methyl-8α-(1-pyridinio)-tetra-*O*-acetylriboflavin bromide; FAD, flavin adenine dinucleotide; FMN, flavin mononucleotide; NADH, reduced form of nicotinamide adenine dinucleotide; 4VP, 4-vinylpyridine.

reaction for the inter-coenzyme hydrogen transfer between NADH and flavin, the rate constants being in line with the polarographic half-wave potentials of flavins.[13,14] The second-order rate constant (k_2) for

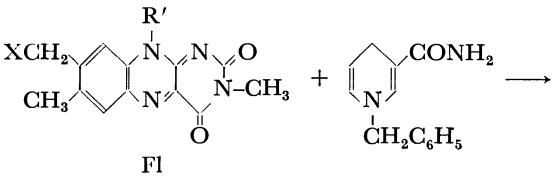

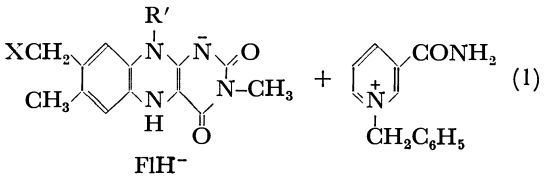

(1)

the oxidation by 8α-AcHisFl is 1.5 times greater than that by unmodified flavin, 3-MeFl (Table 1). The small rate augmentation is in line with the observation of Edmondson *et al.*[12] that the 8α-(N_1-histidinyl) group behaves as a weak electron-withdrawing substituent.

Table 1. Rate constants for the oxidation by monomeric and polymer-bound flavins

Flavin	k_2/M^{-1} s^{-1}		k_3'/M^{-2} s^{-1}	
	BzlNH[a]	$CH_3\bar{C}HNO_2$[b]	GSH[c]	PhSH[b]
3-MeFl	32.4	($<10^{-7}$)	1.98	(<1)
8α-AcHisFl	48.1	($<10^{-7}$)	2.59	(<1)
8α-PyFl	363	4.8×10^{-4}	4.29	152
4VP-Fl-Dod-0	277	0.642	9500	31100
4VP-Fl-Dod-20	301	1.31	56100	110000
St-Fl-Dod-22[f]	201	0.501	833[d]	6240

a) pH 9.00, μ=0.02 with KCl. b) pH 8.60, μ=0.05 with KCl, [$CH_3\bar{C}HNO_2$]=0.01—0.05 M. c) pH 8.65, μ=0.02 with KCl, [GSH]=1.00×10^{-3} M. d) pH 8.80, μ=0.02 with KCl : cited from Ref. 26. e) pH 6.70, 40 vol% ethanol, μ=0.02 with KCl, [PhSH]=1.00×10^{-3} M. f) The preparation of this polymer is described in Ref. 26.

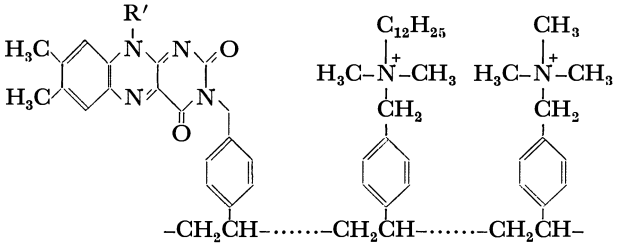

Scheme 1.

NADH analogues decompose rapidly into tetrahydronicotinamides in acidic pH region where imidazole is protonated,[15] making it impossible to evaluate directly the rate constant for the reaction of BzlNH with protonated 8α-AcHisFl. We thus employed 8α-PyFl as an analogue of protonated 8α-AcHisFl. 8α-PyFl oxidizes BzlNH 11.2 times faster than 3-MeFl. On the other hand, immobilization of the 8α-PyFl unit in the quaternized 4VP polymers is insignificant as regards the enhancement of the oxidative reactivity of flavin toward BzlNH. The reaction is presumably accelerated by protonation of 8α-histidyl group and almost unaffected by polyelectrolyte reaction environments.

Oxidation of 1-Nitroethanide Ion. Although D-amino acid oxidase (flavoenzyme) rapidly oxidizes 1-nitro-1-alkanide ion to the corresponding aldehydes and nitrite ion (Eq. 2),[16] no corresponding nonenzymatic reaction is considered to occur under ambient reaction conditions.[6] Neither 3-MeFl nor 8α-AcHisFl can oxidize

$$Fl + CH_3\bar{C}HNO_2 \xrightarrow{OH^-} FlH^- + CH_3CHO + NO_2^- \quad (2)$$

1-nitroethanide ion under the present reaction conditions, the second-order rate constant being presumed to be smaller than 10^{-7} M^{-1} s^{-1} (Table 1). On the other hand, oxidation of 1-nitroethanide ion by 8α-PyFl was easily detected under the same reaction conditions, the rate constant being augmented by more than three orders of magnitude relative to that of 3-MeFl. Yokoe and Bruice[6] reported that 3,10-dimethyl-8-cyanoisoalloxazine, an electron-deficient isoalloxazine with a positively-shifted poralographic half-wave potential, is able to oxidize 1-nitro-1-alkanide ion with $k_2=(2—5)\times10^{-3}$ M^{-1} s^{-1}. The k_2 value for 8α-PyFl (4.8×10^{-4} M^{-1} s^{-1}) is thus smaller by only one order of magnitude than that for 3,10-dimethyl-8-cyanoisoalloxazine.

The second-order rate constants were further enhanced by immobilization of the 8α-PyFl unit in the quaternized 4VP polymers. For example, the k_2 value for 4VP-Fl-Dod-20 is augmentated by 10^7 fold and 3×10^3 fold in comparison to those of 3-MeFl and 8α-PyFl, respectively, exceeding even that of 3,10-dimethyl-8-cyanoisoalloxazine by two to three orders of magnitude. The result is in contrast to the trend observed in flavin oxidation of BzlNH. Since the reaction rate for polymer-bound flavin was first-order in flavin and 1-nitroethanide ion under the employed reaction conditions (footnotes, Table 1), the reaction route is not apparently changed by immobilization of the 8α-PyFl unit in the cationic polymers.

Oxidation of Thiols. The oxidation of thiols by the conventional flavins (Eq. 3) is first-order in flavin and second-order in thiols.[6,17] The reaction of the

$$Fl + 2RSH \xrightarrow{-H^+} FlH^- + RSSR \quad (3)$$

monomeric flavins with GSH was confirmed to be of second-order in GSH (Fig. 1), the apparent third-order rate constants ($k_3'=v_{obsd}/[\text{flavin}][RSH]^2_{total}$) increasing in the order, 3-MeFl<8α-AcHisFl<8α-PyFl. Although aliphatic thiols such as GSH and 2-mercaptoethanol are slowly oxidized by flavin, thiophenol is not oxidized under ambient reaction conditions unless the electron-deficient isoalloxazine is employed.[6] As expected, oxidation of PhSH by 3-MeFl and 8α-AcHisFl could not be detected under the present reaction conditions, but that by 8α-PyFl was detected accurately to give $k_3'=152$ M^{-2} s^{-1}. The k_3' value for 3,10-dimethyl-8-cyanoisoalloxazine determined under the comparable reaction conditions is 5×10^4 M^{-2} s^{-1},[6] so that the k_3' value for 8α-PyFl is smaller by about two orders of magnitude than that for the electron-deficient iso-

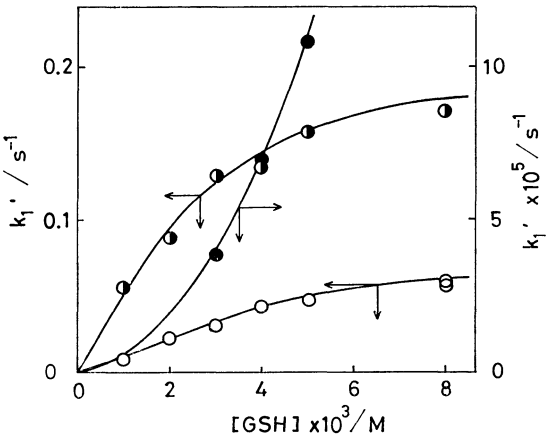

Fig. 1. Plots of k_1' as a function of GSH concentration. (●) 8α-PyFl; (○) 4VP-Dod-0; (◑) 4VP-Fl-Dod-20.

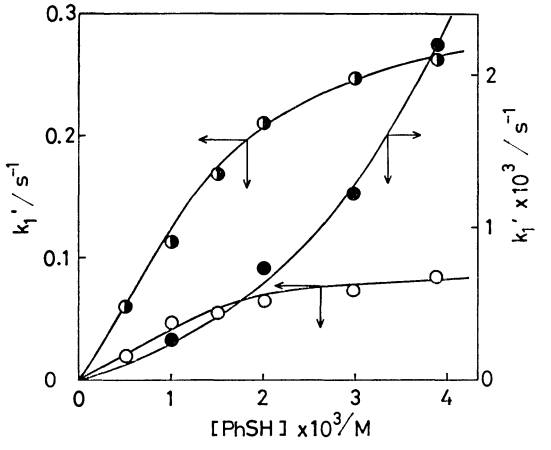

Fig. 2. Plots of k_1' as a function of PhSH concentration. (●) 8α-PyFl; (○) 4VP-Fl-Dod-0; (◑) 4VP-Fl-Dod-20.

alloxazine with an 8-cyano group.

Plots of pseudo first-order rate constant ($k_1'=v_{obsd}$/[flavin]) *vs.* thiol concentration are given in Figs. 1 and 2. In contrast to the second-order dependence of conventional flavin on thiol concentrations, the pseudo first-order rate constants (k_1') for 4VP-Fl-Dod-0 and 4VP-Fl-Dod-20 showed a saturation phenomenon which is essentially approximated by sigmoid curves. The result indicates that the oxidation by polymer-bound flavins (polymer-Fl) proceeds *via* complexation as shown by

$$\text{polymer-Fl} + 2\text{RSH} \underset{K_m}{\rightleftharpoons} \text{polymer-Fl}\cdot(\text{RSH})_2 \xrightarrow[k_{cat}]{} \text{polymer-FlH}^- + \text{RSSR} \quad (4)$$

where K_m is the equilibrium constant for dissociation of polymer-Fl·RSH_2 complex ($=$[polymer-Fl][RSH]$^2_{total}$/[polymer-Fl·$(RSH)_2$]) and k_{cat} the first-order intra-complex reaction rate constant. If we assume that [flavin]$\ll$[RSH]$_{total}$, the corresponding rate equation can be expressed by

$$v_{obsd} = k_1'[\text{polymer-Fl}] = \frac{k_{cat}[\text{polymer-Fl}][\text{RSH}]^2_{total}}{K_m + [\text{RSH}]^2_{total}} \quad (5)$$

The theoretical plot of k_1' *vs.* [RSH]$_{total}$ gives a sigmoid curve. Following the derivation of the Lineweaver-Burk equation from the Michaelis-Menten equation, Eq. 5 can be re-written as follows which gives the linear relation between $1/k_1'$ and $1/[\text{RSH}]^2$.

$$\frac{1}{k_1'} = \frac{1}{k_{cat}} + \frac{K_m}{k_{cat}} \cdot \frac{1}{[\text{RSH}]^2_{total}} \quad (6)$$

The plots (Figs. 3 and 4) show fairly good linearity ($r<0.98$). The slope (K_m/k_{cat}) and the intercept ($1/k_{cat}$) were determined by least-squares computation. The k_{cat} and K_m values are summarized in Table 2. The apparent third-order rate constants ($k_3'=v_{obsd}$/[Polymer-Fl][RSH]$^2_{total}$) at [RSH]$_{total}=1.00\times10^{-3}$M are given in Table 1.

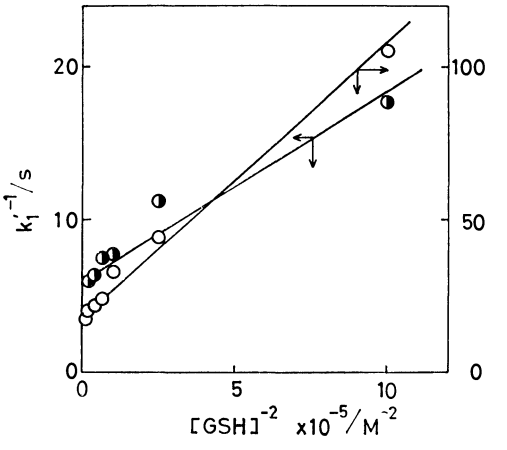

Fig. 3. Plots of $k_1'^{-1}$ *versus* $[GSH]^{-2}$. (○) 4VP-Fl-Dod-0; (◑) 4VP-Fl-Dod-20.

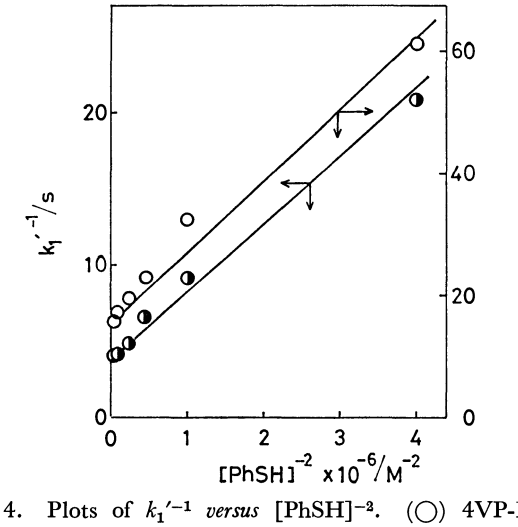

Fig. 4. Plots of $k_1'^{-1}$ *versus* $[PhSH]^{-2}$. (○) 4VP-Fl-Dod-0; (◑) 4VP-Fl-Dod-20.

Examination of the apparent third-order rate constant (k_3') reveals that (1) the rate augmentation of 10^3—10^4 fold is achieved by immobilization of 8α-PyFl unit in the quaternized 4VP polymers and (2) the rate constants increase with increase in the dodecyl group content.

Flavin immobilized in the quaternized 4VP polymers

Table 2. Kinetic parameters for the oxidation of GSH and PhSH by polymer-bound flavins

Flavin	GSH			PhSH		
	k_{cat} / s^{-1}	K_m / M^2	k_{cat}/K_m / $M^{-2}\,s^{-1}$	k_{cat} / s^{-1}	K_m / M^2	k_{cat}/K_m / $M^{-2}\,s^{-1}$
4VP-Fl-Dod-0	0.0606	5.36×10^{-6}	1.14×10^{4}	0.0645	8.00×10^{-7}	8.06×10^{4}
4VP-Fl-Dod-20	0.169	2.15×10^{-6}	8.05×10^{4}	0.263	1.13×10^{-6}	2.33×10^{5}
St-Fl-Dod-22			833[a]			6.24×10^{3} [b]

a) k_3' at pH 8.80: cited from Ref. 18. b) k_3' at pH 6.70: cited from Ref. 19.

via 8α-position gives rate constants greater than flavin immobilized in cationic polystyrene *via* 3-position.[18] Since oxidation of GSH and PhSH by flavin immobilized in cationic polystyrene shows a simple second-order dependence upon GSH and PhSH under the comparable reaction conditions,[18,19] the improved reactivity of 8α-PyFl unit in 4VP polymers should be rationalized in terms of the efficient complexation with thiol substrates. Kinetic parameters (Table 2) indicate that 4VP-Fl-Dod-20 which is classified as a more hydrophobic polymer possesses k_{cat} values greater than 4VP-Fl-Dod-0 by factors of 3—4. On the other hand, no significant difference could be found for K_m values. This suggests that the hydrophobicity of 4VP polymer is related to the efficiency of intra-complex reaction and not to the binding efficiency.

Discussion

The oxidative reactivity of flavin was not largely improved by introduction of histidine into 8α-position.[12] The present study established that 8α-PyFl employed as an analogue of protonated 8α-AcHisFl exhibits enhanced reactivities toward several substrates. This indicates that the reactivity of flavin covalently-linked to enzymes *via* the histidine residue can also be enhanced in acidic pH region (pK_a of histidine linked to the 8α-position is estimated to be 6.9).[20]

Shinkai *et al.* reported the micellar effects on flavin oxidation.[21-23] In general, the reaction of flavin and NADH analogue is affected to a smaller extent by surfactant micelles,[21] whereas flavin oxidation of anionic species such as carbanions and thiolates is remarkably facilitated by cationic micelles.[22,23] The marked rate acceleration is rationalized in terms of enhanced local concentration of anions by interaction with micellar cationic surface and activation of anions by desolvation in micellar hydrophobic environment.[24,25] The results (Table 1) indicate that oxidation of 1-nitroethanide ion, GSH, and PhSH is facilitated considerably by immobilization of 8α-PyFl structure in the cationic 4VP polymer, the k_2 value for flavin oxidation of BzlNH being hardly improved. The trend is in line with the micellar effects. The marked rate acceleration might be caused by the high cationic charge density along the polymer chain which concentrates anionic reactant species and by polymeric hydrophobic environment.

Cationic polystyrene polymers which immobilize flavin *via* 3-position were synthesized (Scheme 1).[26] The reaction of NADH (polyanionic species) with the immobilized flavin proceeded according to Michaelis-Menten kinetics.[26] However, oxidation of 1-nitroethanide ion, GSH, and PhSH showed no saturation phenomenon.[18,19,27] This indicates that the reaction proceeds according to a simple second-order path, or the dissociation constant (K_m) is greater than the employed reactant concentrations even if the reaction occurs *via* complexation. In contrast, oxidation of GSH and PhSH by flavin immobilized in the cationic 4VP polymers gave distinct saturation curves under comparable reaction conditions (Figs. 1 and 2). It is not clear why quaternized 4VP polymers adsorb GSH and PhSH more efficiently than cationic polystyrene polymers. A possible explanation is that the flavin unit in the 4VP polymers is immobilized as a cationic unit and that in the polystyrene polymers as a neutral unit. The flavin unit in cationic polystyrenes may exist, due to the hydrophobicity, in a hydrophobic domain of the polymer which is isolated from a cationic, substrate-binding site, the enhanced substrate concentration at the cationic site thus not being reflected advantageously by the subsequent flavin oxidation process.

The results can be summarized as follows: (1) the reactivity of isoalloxazine ring is enhanced by protonation of 8α-(N_1-histidinyl) group, (2) the oxidation of carbanion and thiols is facilitated by cationic polymer environment, and (3) as a result of combination of (1) and (2), flavin immobilized in cationic 4VP polymers *via* 8α-position acts as an excellent oxidizing agent for anionic species.

Experimental

Materials. Preparation of BzlNH and 3-MeFl was reported.[26] 8-Methyl group of 3-MeFl was brominated according to the method of Walker *et al.*[20] The content of 3-methyl-8α-bromotetra-*O*-acetylriboflavin was estimated from the decrease of the C(8)–CH_3 peak in the NMR spectrum[20] (δ=2.58 ppm in $CDCl_3$) to be 64%. The mixture was used without further purification for the preparation of 8α-PyFl, 8α-AcHisFl, and 4VP-bound flavins.

In a 100 ml flask covered with aluminium foil were placed 0.3 g of brominated flavin mixture containing 3.2×10^{-4} mol of 3-methyl-8α-bromotetra-*O*-acetylriboflavin and 0.4 ml (4.8×10^{-4} mol) of pyridine which were dissolved in 60 ml of ethanol. The mixture was then heated under reflux and the progress of the reaction was monitored by TLC method (silica gel and ethyl acetate). The spot for 3-methyl-8α-bromotetra-*O*-acetylriboflavin(R_f=0.20) disappeared and a new spot attributed to 8α-PyFl appeared at the origin. After 6 h, the spot for 3-methyl-8α-bromotetra-*O*-acetylriboflavin became undetectable. Solvent ethanol was evaporated *in vacuo*, and the yellow residue was recrystallized three times

from ethanol–diisopropyl ether; mp 85—97 °C (hygroscopic), yield 0.3 g. NMR (Me_2SO-d_6): $COCH_3$, 1.60 ppm (3H), 2.40 ppm (3H), 2.20 ppm (6H); 7-CH_3, 2.52 ppm, 3H; N(3)–CH_3, 3.39 ppm, 3H; N(10)–CH_2, 4.40 ppm, 2H; CH_2 in ribityl group, 4.95 ppm, 2H; CH in ribityl group, around 5.4 ppm, 3H; 8-CH_2, 6.24 ppm, 2H; 6-H, 7.78 ppm, 1H; 9-H, 8.14 ppm, 1H; pyridine, 8.3—9.2 ppm, 5H. Found: C, 48.50; H, 4.98; N, 9.02%. Calcd for $C_{31}H_{34}N_5O_{10}Br$: 2.84 H_2O: C, 48.50; H, 4.84; N, 9.12%.

The preparation of 8α-AcHisFl was carried out according to the method of Walker *et al.*[20] 0.20 g (1.0×10^{-3} mol) of N_α-acetyl-L-histidine, and 1.28 g of brominated flavin mixture containing 1.3×10^{-3} mol of 3-methyl-8α-bromotetra-*O*-acetylriboflavin were dissolved in 30 mol of *N,N*-dimethylformamide, and the mixture was stirred at 50 °C in the presence of 1.38 g (1.0×10^{-2} mol) of powdered potassium carbonate. The progress of the reaction was monitored by TLC method (silica gel and ethyl acetate). The spot of 3-methyl-8α-bromotetra-*O*-acetylriboflavin became undetectable after 48 h. The solvent was evaporated *in vacuo*, the orange residue being taken with 100 ml of chloroform. The chloroform layer separated was washed with 50 ml of 0.5 M phosphate buffer solution to extract 8α-AcHisFl and unreacted N_α-acetyl-L-histidine. The aqueous layer was then adjusted to pH 4 with acetic acid, saturated with ammonium sulfate, and then extracted four times with 100 ml of 1-butanol. The 1-butanol solution was dried over sodium sulfate for one day. The solvent was evaporated *in vavuo*, the residue being recrystallized twice from ethanol–diisopropyl ether; mp 244—247 °C, yield 0.45 g. Found: C, 49.97; H, 5.43; N, 12.02%. Calcd for $C_{34}H_{39}N_7O_9\cdot3H_2O$: C, 50.62; H, 5.25; N, 12.15%.

Polymer-bound flavins (4VP-Fl-Dod-0 and 4VP-Fl-Dod-20) were prepared from 3-methyl-8α-bromotetra-*O*-acetylriboflavin and poly(4-vinylpyridine) (MW 100000; Ko-ei Kagaku Kogyo Co.). Two grams of poly(4-vinylpyridine) were dissolved in 10 ml of *N,N*-dimethylformamide and mixed with 1.8 g of brominated flavin mixture containing 1.9×10^{-3} mol of 3-methyl-8α-bromotetra-*O*-acetylriboflavin. The reaction mixture was heated under reflux for 4 h and then poured into diisopropyl ether. The recovered polymer became orange plates when dried under reduced pressure. The composition of flavin unit was determined by the absorption spectrum method, assuming that the molar absorbancy index is equal to that of 8α-PyFl($\varepsilon=10040$ in *N,N*-dimethylformamide). The flavin content thus determined was 6 mol %. The polymer was further quaternized by propyl bromide and dodecyl bromide according to the method employed for the preparation of polysoaps.[28] The quaternized polymers were purified by extensive dialysis and the composition was estimated by means of NMR for the dodecyl unit[28] and potentiometric titration for the propyl unit. The results are given in terms of the structure of polymer-bound flavins.

Kinetics. The rates for flavin oxidation of BzlNH were estimated under aerobic conditions by following the decrease in the absorption band of BzlNH at 357 nm. The other flavin oxidation reactions were performed under anaerobic (N_2) conditions by following that of flavins at *ca.* 445 nm. Details of the methods were described in previous papers.[18,26,27] All the reactions were carried out at 30 °C (Tables 1 and 2).

As reported earlier,[6,13,22,26] flavin oxidation of BzlNH and 1-nitroethanide ion is first-order in flavin and substrate, while that of GSH and PhSH is second-order in thiol.[18] On the other hand, plots of oxidation rate *versus* thiol concentration for 4VP polymer-bound flavins show sigmoidal curves (Figs. 1 and 2).

References

1) E. B. Kearney and T. P. Singer, *Biochim. Biophys. Acta*, **17**, 596 (1955).
2) T. P. Singer, E. B. Kearney, and V. Massey, *Arch. Biochem. Biophys.*, **60**, 255 (1956).
3) T. P. Singer, E. B. Kearney, and P. Bernath, *J. Biol. Chem.*, **223**, 599 (1956).
4) E. B. Kearney, *J. Biol. Chem.*, **235**, 865 (1960).
5) T. P. Singer, D. E. Edmondson, and W. C. Kenney, *Flavins Flavoproteins, Proc. Int. Symp.*, 5th, 1975, 271 (1976).
6) I. Yokoe and T. C. Bruice, *J. Am. Chem. Soc.*, **97**, 450 (1974).
7) T. C. Bruice, T. W. Chan, J. P. Taulane, I. Yokoe, D. L. Elliott, R. F. Williams, and M. Novak, *J. Am. Chem. Soc.*, **99**, 6713 (1977).
8) S. Kasai, R. Miura, and K. Matui, *Bull. Chem. Soc. Jpn.*, **48**, 2877 (1975).
9) K. Matsui and S. Kasai, *Flavins and Flavoproteins, Proc. Int. Symp.*, 5th, 1975, 328 (1976).
10) T. Watanabe, K. Matsui, S. Kasai, and T. Nakamura, *J. Biochem.*, **84**, 1441 (1978).
11) D. E. Edmondson, F. Rizzuto, and G. Tollin, *Flavins Flavoproteins, Proc. Int. Symp.*, 5th, 1975, 285 (1976).
12) D. E. Edmondson and T. P. Singer, *J. Biol, Chem.*, **248**, 8144 (1973).
13) I. M. Gascoigne and G. K. Radda, *Biochem. Biophys. Acta*, **131**, 498 (1967).
14) T. C. Bruice, L. Main, S. Smith, and P. Y. Bruice, *J. Am. Chem. Soc.*, **93**, 7327 (1971).
15) C. C. Johnston, J. L. Gardner, C. H. Suelter, and and D. E. Metzler, *Biochemistry*, **2**, 689 (1963).
16) D. J. T. Porter, J. G. Voet, and H. J. Bright, *J. Biol. Chem.*, **248**, 4400 (1973).
17) E. L. Loechler and T. C. Hollocher, *J. Am. Chem. Soc.*, **97**, 3236 (1975).
18) S. Shinkai, S. Yamada, R. Ando, and T. Kunitake, *Bioorg. Chem.*, in press.
19) S. Shinkai, S. Yamada, and T. Kunitake, *J. Polym. Sci., Polym. Lett. Ed.*, **16**, 137 (1978).
20) J. Salach, W. H. Walker, T. P. Singer, A. Ehrenberg, P. Hemmerich, S. Ghisla, and U. Hartmann, *Eur. J. Biochem.*, **26**, 267 (1972); W. H. Walker, T. P. Singer, S. Ghisla, and P. Hemmerich, *ibid.*, **26**, 279 (1972).
21) S. Shinkai, T. Ide, and O. Manabe., *Bull. Chem. Soc. Jpn.*, **51**, 3655 (1978).
22) S. Shinkai, Y. Sakuma, and F. Yoneda, *J. Chem. Soc., Chem. Commun.*, **1976**, 986.
23) S. Shinkai, R. Ando, and F. Yoneda, *Chem. Lett.*, **1977**, 147.
24) S. Shinkai and T. Kunitake, *Chem. Lett.*, **1976**, 109.
25) S. Shinkai, R. Ando, and T. Kunitake, *J. Chem. Soc., Perkin Trans. 2*, **1978**, 1271.
26) S. Shinkai, S. Yamada, and T. Kunitake, *Macromolecules*, **11**, 65 (1978).
27) S. Shikaim R. Ando, and T. Kunitake, *Biopolymers*, **17**, 2757 (1978).
28) T. Kunitake, S. Shinkai, and S. Hirotsu, *J. Org. Chem.*, **42**, 306 (1977).

Ring-opening Reaction of Oxiranes, Oxetanes, and Tetrahydropyran by Mercury(II) Salts and Alkyl Halides

Nanao WATANABE,** Sakae UEMURA, and Masaya OKANO*

Institute for Chemical Research, Kyoto University, Uji, Kyoto 611

***Koei Chemical Co., Ltd., Joto-ku, Osaka 536*

(Received May 18, 1979)

The reaction of primary and secondary alkyl halides with mercury(II) acetate in oxiranes, oxetanes, and tetrahydropyran results in ring-opening to give the corresponding alkoxyalkyl acetates. Similar reactions with mercury(II) thiocyanate in oxetanes afford alkoxyalkyl isothiocyanate and thiocyanate, $ROCH_2C(R')_2CH_2NCS$ and $ROCH_2C(R')_2CH_2SCN$, where the isomer ratios (N/S ratios) are 82—96/4—18. It is suggested that the reactions involve the initial formation of a three-, four-, or six-membered *O*-alkyloxonium ion intermediate and subsequent attack by $XHgZ_2^-$.

It has been established that primary and secondary alkyl halides react with mercury(II) thiocyanate, acetate, and chloride in tetrahydrofuran (THF) to give the THF-incorporated compounds, $R[O(CH_2)_4]_nZ$ (n=1, 2; Z=SCN, NCS, OAc, Cl). The reaction was thought to proceed through an *O*-alkyltetrahydrofuranium ion intermediate as shown in Scheme 1.[1,2] In the case of mercury(II) thiocyanate the products were

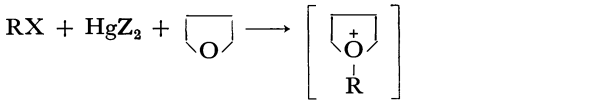

$$\longrightarrow R[O(CH_2)_4]_nZ \quad (1)$$

the isomeric alkyl thiocyanate and isothiocyanate, the results revealing the ambident reactivity of the mercury salt.[1] It is of interest to ascertain whether similar reactions occur with three-, four-, and six-membered ring cyclic ethers and how the ambident character of thiocyanate ion is reflected in the products. The results of the reactions of several alkyl halides with several mercury(II) salts in oxiranes, oxetanes, and tetrahydropyran will be described.

Results and Discussion

The reaction of alkyl iodides with mercury(II) acetate or chloride in several oxiranes afforded the isomeric ring-opening products (**1** and **2**) in a good to moderate yield (Scheme 2). In the cases of 1,2-epoxypropane (R'=Me) and 1,2-epoxybutane (R'=Et) the yields of **1** and **2** were nearly equal, while **1** was the sole product in the case of epichlorohydrine (R'=$ClCH_2$). From the reaction of cyclohexene oxide only *trans*-product was formed. Typical results are summarized in Table 1.

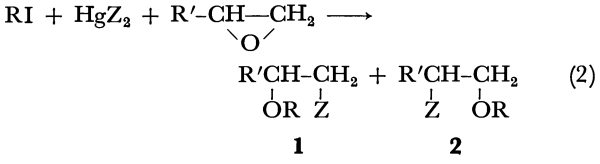

$$\mathbf{1} \qquad \mathbf{2} \quad (2)$$

Treatment of alkyl halide with mercury(II) acetate in several oxetanes afforded the oxetane-incorporated compounds (**3**) as shown in Scheme 3. Such ring-opening reaction also occurred with mercury(II)

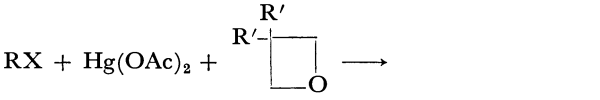

$$ROCH_2C(R')_2CH_2OAc \quad (3)$$
$$\mathbf{3}$$

thiocyanate to give the isomeric oxetane-incorporated alkoxyalkyl isothiocyanate (**4**) and thiocyanate (**5**) (Scheme 4), and the isomer ratio (N: S=82—96: 4—18) differed very much from that of the products obtained in THF solvent (N: S=*ca.* 1: 1).[1] Typical results are shown in Table 2.

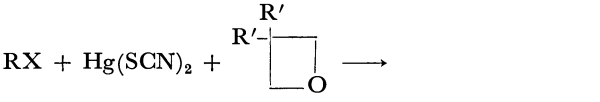

$$\mathbf{4} \qquad \mathbf{5} \quad (4)$$

The reaction in tetrahydropyran gave similar ring-opening compounds such as **6**, **7**, and **8** in low yields

Table 1. Reaction of alkyl iodide with mercury(II) salt in oxirane

Alkyl iodide R(5 mmol)	Mercury(II) salt (5 mmol)	Oxirane R' (10 ml)	React temp °C	React time h	Yield/%[a] of 1+2	Isomer ratio 1 : 2
Et	$Hg(OAc)_2$	Me	36	48	64	47 : 53
i-Pr	$Hg(OAc)_2$	Me	36	20	62	52 : 48
Et	$HgCl_2$	Me	36	26	19	44 : 56
Et	$Hg(OAc)_2$	Et	55—60	15	74	45 : 55
Et	$Hg(OAc)_2$	$ClCH_2$	35—40	48	50	100 : 0
Et	$Hg(OAc)_2$	$ClCH_2$	75	7	54	100 : 0
Et	$Hg(OAc)_2$	b)	70—78	5	66[c]	

a) Determined by GLC analysis. b) Cyclohexene oxide. c) *trans*-1-Acetoxy-2-ethoxycyclohexane.

Table 2. Reaction of alkyl halide with mercury(II) salt in oxetane

Alkyl halide (5 mmol)	Mercury(II) salt (5 mmol)	Oxetane R′ (10 ml)	React temp/°C	React time/h	Yield/% of product and isomer ratio[a]
EtI	$Hg(OAc)_2$	H	45—48	7	**3** 51
EtI	$Hg(OAc)_2$	Me	78	5	**3** 76
i-PrI	$Hg(OAc)_2$	Me	73—77	7	**3** 53
i-PrBr	$Hg(OAc)_2$	Me	60—62	20	**3** 52
CH_2=$CHCH_2Br$	$Hg(OAc)_2$	Me	69—72	5	**3** 45
$PhCH_2Br$	$Hg(OAc)_2$	Me	67—73	5	**3** 75
EtI	$Hg(OAc)_2$	$ClCH_2$	64—69	5	**3** 70
i-PrI	$Hg(OAc)_2$	$ClCH_2$	65—70	5	**3** 66
EtI	$Hg(SCN)_2$	H	46—51	28	**4**+**5** trace
EtI	$Hg(SCN)_2$	Me	73—75	5	**4**+**5** 29 (96 : 4)
i-PrI	$Hg(SCN)_2$	Me	69—71	5	**4**+**5** 32 (96 : 4)
EtI	$Hg(SCN)_2$	$ClCH_2$	67—71	8	**4**+**5** 74 (82 : 18)
i-PrI	$Hg(SCN)_2$	$ClCH_2$	71	5	**4**+**5** 82 (85 : 15)

a) Determined by GLC analysis.

(Schemes 5 and 6). In the reaction with mercury(II) thiocyanate the main products were **9** and **10** and the yields of the tetrahydropyran-incorporated compounds (**7** and **8**) were *ca.* one-fifth of those of **9** and **10**. The

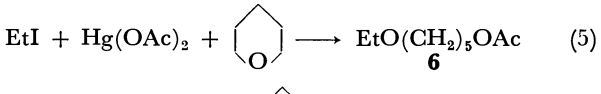

$$EtI + Hg(OAc)_2 + \text{oxetane} \longrightarrow \underset{\mathbf{6}}{EtO(CH_2)_5OAc} \quad (5)$$

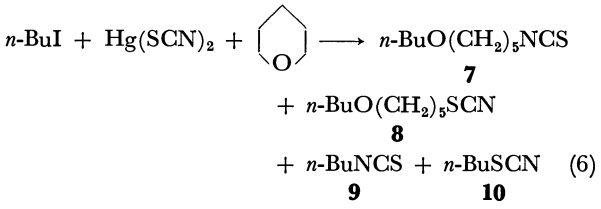

$$n\text{-BuI} + Hg(SCN)_2 + \text{oxetane} \longrightarrow \underset{\mathbf{7}}{n\text{-BuO}(CH_2)_5NCS} + \underset{\mathbf{8}}{n\text{-BuO}(CH_2)_5SCN} + \underset{\mathbf{9}}{n\text{-BuNCS}} + \underset{\mathbf{10}}{n\text{-BuSCN}} \quad (6)$$

N/S ratios of **7** and **8** was almost the same as that of the products obtained in THF solvent.

For reactions in oxiranes, the isomer ratios of **1** and **2** are consistent with the directions of ring-opening in the addition of alcohol to such oxiranes in acidic conditions,[3] where reaction proceeds through the formation of a protonated oxirane followed by either direct attack by a nucleophile or nucleophilic attack on a carbonium ion after ring-opening.[4] The basicity of oxygen of oxiranes is known to be lower than that of THF.[5] Nevertheless the presence of the *O*-alkyloxonium ion of ethylene oxide has been confirmed by ^{1}H-NMR[6] and also assumed in the case of its acid-catalyzed polymerization.[4] The following pathways are thus conceivable

Table 3. Boiling points and analytical data of the products

Compound	Bp °C/mmHg	Found (Calcd), % C	H	N
1+**2** (R′=Me, R=Et, Z=OAc)	59/20[a]			
1+**2** (R′=Me, R=*i*-Pr, Z=OAc)	78—83/62	59.76 (59.97)	10.20 (10.07)	
1+**2** (R′=Et, R=Et, Z=OAc)	95—97/57	59.82 (59.97)	10.32 (10.07)	
1(R′=$ClCH_2$, R=Et, Z=OAc)	105—110/30	46.08 (46.55)	7.32 (7.25)	
trans-1-Acetoxy-2-ethoxycyclohexane	102/19[b]			
1+**2** (R′=Me, R=Et, Z=Cl)	35—40/53[c]			
3 (R′=H, R=Et)	60—70/20[d]			
3 (R′=Me, R=Et)	87—88/40	61.98 (62.04)	10.61 (10.41)	
3 (R′=Me, R=*i*-Pr)	82—83/20	63.60 (63.80)	10.64 (10.71)	
3 (R′=Me, R=CH_2=$CHCH_2$)	100—101/27	64.60 (64.49)	9.50 (9.74)	
3 (R′=Me, R=$PhCH_2$)	122—124/2	71.26 (71.16)	8.24 (8.53)	
3 (R′=$ClCH_2$, R=Et)	98—99/2	44.52 (44.46)	6.80 (6.63)	
3 (R′=$ClCH_2$, R=*i*-Pr)	104—105/2	46.84 (46.71)	7.07 (7.06)	
4+**5** (R′=Me, R=Et)	80—83/20	55.51 (55.45)	8.95 (8.73)	7.81 (8.08)
4+**5** (R′=Me, R=*i*-Pr)	95—98/17	58.01 (57.71)	9.19 (9.15)	7.55 (7.48)
4+**5** (R′=$ClCH_2$, R=Et)	112—116/2	39.59 (39.68)	5.38 (5.41)	5.50 (5.78)
4+**5** (R′=$ClCH_2$, R=*i*-Pr)	116—120/2	42.18 (43.19)	5.90 (5.90)	5.49 (5.47)
$EtOCH_2C(Me)_2CH_2Br$	85—87/60	43.01 (42.09)	7.88 (7.75)	
$EtOCH_2C(CH_2Cl)_2CH_2Br$	106—107/10	31.87 (31.85)	4.90 (4.96)	
6	55—60/6[e]			
7+**8**	105—109/2	59.60 (59.66)	9.66 (9.51)	6.71 (6.96)

a) Lit,[6] bp for **2** 77—80 °C/50 mmHg. b) Lit,[11] bp 91—92 °C/10 mmHg. c) Lit, bp for **1** 117—118 °C,[12] bp for **2** 113—115 °C.[13] d) Lit,[14] bp 174.5—175.5 °C. e) Lit,[15] bp 105 °C/14 mmHg.

(neutral or slightly acidic condition); (a) the initial formation of an *O*-alkyloxonium ion intermediate, followed by the S_N2-like attack by $XHgZ_2^-$ as has been proposed in the reaction in THF,[1] and (b) the S_N1-like reaction of the oxonium ion with $XHgZ_2^-$ (a more carbonium ion-like mechanism than (a)). Both pathways (a) and (b) occurred concurrently in the cases of 1,2-epoxypropane and 1,2-epoxybutane, while pathway (a) predominated in the case of epichlorohydrine.

The reactions in oxetanes and tetrahydropyran appear to proceed *via* an *O*-alkyloxonium ion intermediate (I, III) as in the case of the reaction in THF, since the basicity of oxygen in these cyclic ethers is known to be similar.[5] The difference of the N/S isomer ratio of the products obtained in oxetanes with that obtained in THF may reflect the stability differences between the intermediate oxonium ions. In the reaction of alkyl halides with mercury(II) thiocyanate, it was found that the N/S ratio of the isomeric products became larger as the S_N1 reactivity of the alkyl halide increased: *i.e.*, N/S=21/79 for *n*-Bu, 85/15 for *i*-Pr, and 99/1 for PhCH(Me).[7] By comparing the stability of I, II, and III, it may be seen that I is the most unstable

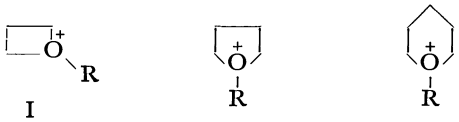

I II III

and apt to react *via* a S_N1-like pathway, resulting in the preferred formation of alkyl isothiocyanate. The almost similar N/S ratio in the products obtained in THF and tetrahydropyran may reflect a similar stability of II and III. That the N/S ratios in the products obtained in the reactions of mercury(II) thiocyanate with 4-alkoxybutyl bromide and 5-ethoxypentyl bromide (*via* II and III respectively)[1] were almost the same supports this consideration.

Experimental

The isomer ratios in the products were determined by GLC. The GLC analyses were conducted on a Shimadzu 4BMPF and Yanagimoto G800-T apparatus, using SE-30(1 m), DEGS (1 m), PEG-6000 (2 m), TEA (3 m), and EGSS-X (1 m) columns (carrier gas, H_2 and N_2 respectively). The ^{1}H-NMR spectra were recorded with a JEOL MH-100 (100 MHz) and a Hitachi R-24 (60 MHz) spectrometer in CCl_4, using TMS as the internal standard.

Materials. All the organic substances were used after distillation. The commercial mercury(II) salts were used without further purification. Oxetane (bp 47—48 °C),[8] 3,3-dimethyloxetane (bp 79—80 °C),[9] and 3,3-bis(chloromethyl)-oxetane (bp 80 °C/10.5 mmHg)[10] were prepared from 3-chloropropyl acetate, 2,2-dimethyl-1,3-propanediol, and 3-chloro-2,2-bis(chloromethyl)propyl acetate, respectively, by the reported methods. All compounds except **1** and **2** (R′=Me, R=Et, Z=OAc or Cl), *trans*-1-acetoxy-2-ethoxycyclohexane, **3** (R′=H, R=Et), and **6** are new and were isolated by distillation or preparartive GLC; the boiling points and analytical data of the new compounds are shown in Table 3. The ^{1}H-NMR spectra for all compounds supported each structure.

Reaction of Alkyl Halide with Mercury(II) Acetate in Oxirane or Oxetane. The following example shows a typical procedure. A suspension of $Hg(OAc)_2$(1.62 g, 5.1 mmol) and ethyl iodide (0.78 g, 5.0 mmol) in 1,2-epoxybutane (10 ml) was stirred at 55—60 °C for 15 h, and the mixture subsequently treated as described in a previous report.[1] Distillation afforded a mixture of **1** and **2** (R′=Et, R=Et, Z=OAc) which was analyzed by ^{1}H-NMR spectroscopy. The proton signals of $-CH_2OAc$ at δ 3.88—4.14 and those of $-\overset{|}{C}HOAc$ at δ 4.70—4.96 were characteristic for **1** and **2**, respectively. GLC analysis of the crude reaction mixture using triethanolamine (TEA) column (3 m) revealed the isomer ratio of **1**: **2** to be 55: 45 and that using SE-30 column (1 m) (this column did not separate the two products) with 4-ethoxybutyl acetate as the internal standard showed the combined yield of products to be 74% (3.68 mmol) based on ethyl iodide charged.

Reaction of Alkyl Iodide with Mercury(II) Thiocyanate in Oxetane. The following example shows a typical procedure. To a suspension of $Hg(SCN)_2$(1.58 g, 4.97 mmol) in 3,3-dimethyloxetane (10 ml) was added ethyl iodide (0.87 g, 5.54 mmol) at 73—75 °C and the resulting homogeneous solution stirred for 5 h. After the work-up as described above, GLC analysis of the ether extract using PEG 6000 (2 m) column with diphenyl ether as the internal standard revealed the presence of **4** and **5** (R′=Me, R=Et) (0.27 g, 1.58 mmol, 29% yield, **4**: **5**=96: 4). Analytically pure **4** and **5** were obtained by simple distillation and determined by ^{1}H-NMR spectroscopy.

Authentic samples of **4** and **5** (R′=Me, R=Et) and **4** and **5** (R′=$ClCH_2$, R=Et) for GLC analysis were prepared as follows. A mixture of ethyl iodide (4 g, 25 mmol), $HgBr_2$ (9 g, 25 mmol), and 3,3-dimethyloxetane (2.2 g, 25 mmol) in 1,2-dichloroethane (10 ml) was maintained at 70—75 °C for 4 h with stirring. After the work-up described above, distillation gave 3-ethoxy-2,2-dimethylpropyl bromide (0.8 g 4.1 mmol, 16% yield) which reacted with KSCN (25 mmol) in DMF (5 ml) at 75—80 °C for 30 h to give two products, the retention times of which were identical with those of **4** and **5** (R′=Me, R=Et) on several different columns (**4**: **5** =17: 83). A similar procedure using 3,3-bis(chloromethyl)-oxetane afforded 1-bromo-2,2-bis(chloromethyl)-3-ethoxypropane (23% isolated yield) which then reacted with KSCN to give **4** and **5** (R′=$ClCH_2$, R=Et) (**4**: **5**=1: 99).

Reaction of Alkyl Iodide with Mercury(II) Salt in Tetrahydropyran. Treatment of ethyl iodide (5 mmol) and $Hg(OAc)_2$ (5 mmol) in tetrahydropyran (10 ml) at reflux temperature for 24 h afforded **6** in 30% isolated yield. Similarly, the reaction of butyl iodide (40 mmol) with $Hg(SCN)_2$ (40 mmol) in tetrahydropyran (15 ml) at 85—90 °C for 2 h gave **7** and **8** (7% isolated yield, **7**: **8**=49: 51) and **9** and **10** (39% isolated yield, **9**: **10**=38: 62).

References

1) N. Watanabe, S. Uemura, and M. Okano, *Bull. Chem. Soc. Jpn.*, **48**, 3205 (1975).

2) N. Watanabe, S. Uemura, and M. Okano, *Bull. Chem. Soc. Jpn.*, **49**, 2500 (1976).

3) E. L. Eliel, "Steric Effects in Organic Chemistry," ed by M. S. Newman, John Wiley, New York (1956), pp. 107 and 108; H. C. Chitwood and B. T. Freure, *J. Am. Chem. Soc.*, **68**, 680 (1946).

4) See, for example, R. M. Acheson, "An Introduction to the Chemistry of Heterocyclic Compounds," 3rd ed, Wiley-Interscience, New York (1976), pp. 31—33.

5) See, for example, Ref. 4, pp. 26—28.

6) J. B. Lambert and D. H. Johnson, *J. Am. Chem. Soc.*,

90, 1349 (1968).
7) N, Watanabe, M. Okano, and S. Uemura, *Bull. Chem. Soc. Jpn.*, **47**, 2745 (1974).
8) C. R. Noller, *Org. Synth.*, Coll. Vol. III, 835 (1955).
9) L. F. Schmoyer and L. C. Case, *Nature*, **183**, 389 (1959).
10) K. Watanabe, T. Sugihara, and M. Tanaka, *Yuki Gosei Kagaku Kyokai Shi*, **24**, 651 (1966).
11) S. Winstein and R. E. Buckles, *J. Am. Chem. Soc.*, **65**, 613 (1943).
12) E. Rothstein, *J. Chem. Soc.*, **1953**, 3991.
13) S. Mamedov, O. B. Osipov, and Kh. M. Alieva, *Chem. Abstr.*, **59**, 8581 (1963).
14) Beilstein I, 2, 67.
15) M. L. Mihailovic and M. Miloradovic, *Chem. Abstr.*, **69**, 67296u (1968).

Chemistry of *N*-Thiosulfinylanilines. IV.[1] Reactions of *N*-Thiosulfinylanilines with Electrophilic Reagents

Yoshio INAGAKI, Renji OKAZAKI, and Naoki INAMOTO*

Department of Chemistry, Faculty of Science, The University of Tokyo, Hongo, Bunkyo-ku, Tokyo 113

(Received May 24, 1979)

Reaction of 2,4-di-*t*-butyl-6-methyl-*N*-thiosulfinylaniline (**1**) with *m*-chloroperbenzoic acid (MCPBA) afforded the corresponding aniline and *N*-sulfinylaniline. Reaction of MCPBA with 2,4,6-tri-*t*-butyl-7,8-dithia-9-azabicyclo-[4.3.0]nona-2,4,9-triene equilibrated with 2,4,6-tri-*t*-butyl-*N*-thiosulfinylaniline gave 2,4,*r*-6-tri-*t*-butyl-7,8-dithia-9-azabicyclo[4.3.0]nona-2,4,9-triene *t*-7-oxide (**12**), 4,6-di-*t*-butyl-3*H*-1,2,3-benzodithiazole 2-oxide (**13**), and 2,4,6-tri-*t*-butyl-*N*-sulfinylaniline (**14**). The oxide **13** was considered to be produced *via* a primary product 2,4,*r*-6-tri-*t*-butyl-7,8-dithia-9-azabicyclo[4.3.0]nona-2,4,9-triene *t*-8-oxide which was found to be unstable above −30 °C. Thermolysis of **12** affording **13**, **14**, and 2,4,6-tri-*t*-butylaniline demonstrated oxygen or sulfur migration in the thiosulfinate type compound. Bromine reacted with **1** to give bis(2,4-di-*t*-butyl-6-methylphenyl)sulfur diimide probably *via* a thionitroso intermediate. Neither trimethyloxonium tetrafluoroborate nor trimethylsilyl chloride reacted with **1**.

The synthesis of stable thiosulfinylamino compounds containing a new functional group (–N=S=S) has recently been reported by Barton's group[2] and us,[3] and the thermal[2,3] and photochemical behavior[3] has been delineated. Since the reactivity of thiosulfinylamino group towards electrophilic reagents has not been explored except for acid hydrolysis,[2] we investigated the reaction of stable *N*-thiosulfinylanilines with *m*-chloroperbenzoic acid, bromine, and other electrophiles, which is the subject of this paper.[4]

Results and Discussion

Reaction with m-*Chloroperbenzoic Acid (MCPBA).* Reaction of 2,4-di-*t*-butyl-6-methyl-*N*-thiosulfinylaniline (**1**) with an equimolar amount of MCPBA afforded 2,4-di-*t*-butyl-6-methyl-*N*-sulfinylaniline (**2**) and 2,4-di-*t*-butyl-6-methylaniline (**3**) in 30.8 and 41.3% yields, respectively, along with recovered **1** (14.9%).

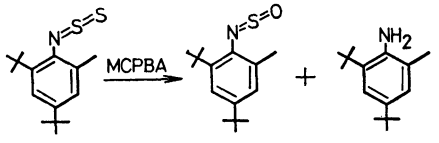

1 **2** **3**

Probable mechanism of formation of **2** and **3** is depicted in Scheme 1.

The reaction of aniline **3** with MCPBA has been reported to give 2,4-di-*t*-butyl-6-methylnitrosobenzene (**4**).[5] Therefore, the absence of **4** in the products suggests that **3** did not exist in the reaction mixture but was produced during the work-up procedure (probably hydrolysis of **8** or **9** with aqueous sodium hydrogencarbonate, see Experimental). The sulfinylaniline (**2**) was stable under the work-up conditions not to be hydrolyzed to the aniline (**3**).

Since a peroxy acid is known to attack sulfur atom of a thioketone,[6] the initial formation of **5** seems probable. The intermediate **5** would rearrange into **9**, which is considered to be hydrolyzed to give thiohydroxylamine (**10**), sulfur dioxide, and *m*-chlorobenzoic acid in analogy to acid hydrolysis of an acid anhydride. As

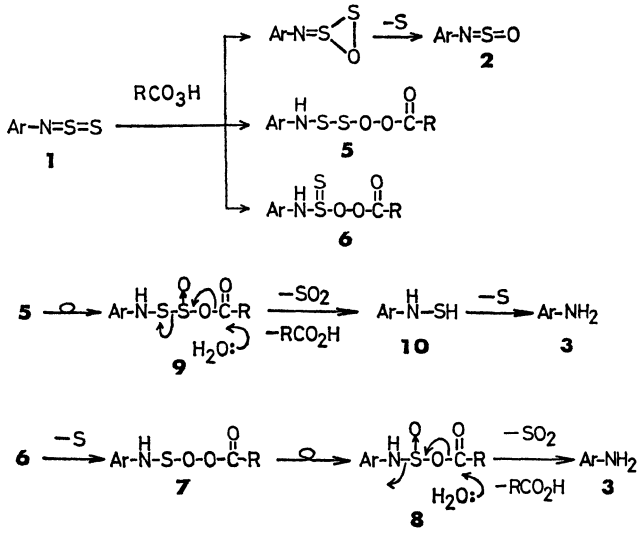

Ar=2,4-di-*t*-butyl-6-methylphenyl
R =*m*-chlorophenyl

Scheme 1.

thiohydroxylamine (**10**) has been reported to be unstable to give the corresponding amine and sulfur,[7] **10** would produce **3** as a final product. Since a peroxycarboxylic acid is a relatively strong nucleophile as to add to organic isocyanate,[8] nucleophilic attack on **1** to give **6** seems also reasonable. The intermediate **6** would lose one sulfur atom to give **7**.[9] Here also **7** probably rearranges into **8**, whose hydrolysis would give **3**, sulfur dioxide, and *m*-chlorobenzoic acid. We think that both mechanisms are plausible and have no experimental evidence at present to determine which is correct.

As the compound **11a** exists as a tautomeric mixture with *N*-thiosulfinylaniline (**11b**) as the minor component,[3] products arising from **11b** as well as **11a** are expected to be obtained in this case.

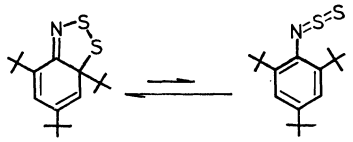

11a **11b**

Table 1. Yields of the products

Temp °C	Time min	Conversion %	Yield/% 12	13	14	13/12
39	3	92	44.8	43.9	1.3	0.98
22	30	91	36.3	44.0	5.8	1.21
0	20	98.5	34.3	42.9	6.2	1.25
−23	20	99.5	36.7	50.6	5.8	1.38
−78	40	94.3	20.6	62.2	2.9	3.02

Treatment of the dithiazole (**11**) with slightly deficient amount of MCPBA in dichloromethane gave **12**, **13**, and **14**. Yields and reaction conditions are shown in Table 1.

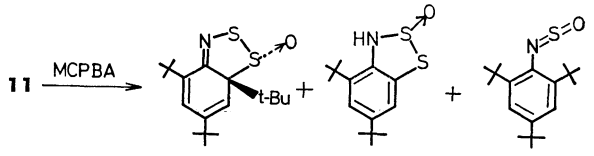

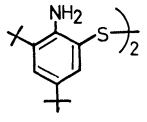

15

The structure of a new type of thiosulfinate (**12**) was determined by X-ray crystallographic analysis,[10] because conclusive evidence for that could not be obtained by spectroscopic and chemical behavior. The identity of **13** was established by the spectral data and by alkaline hydrolysis affording **15**.[11,14] The *N*-sulfinylaniline (**14**) was identified by comparison of the spectral data with those of an authentic sample obtained by the reaction of 2,4,6-tri-*t*-butylaniline with thionyl chloride. Formation of **14** is most likely attributable to the oxidation of **11b** because **1** was found to be oxidized by MCPBA under similar conditions to give the corresponding *N*-sulfinylaniline (*vide supra*). The major products **12** and **13** obviously result from the oxidation of the cyclized form **11a**. Although **11a** is the major component in the tautomeric mixture (*e.g.*, [**11a**]/[**11b**]=14.2 in CD_2Cl_2 at 35 °C),[3] much higher yields of **12** and **13** than that of **14** suggest that the reactivity of *N*-thiosulfinylaniline (**11b**) towards MCPBA is lower than that of **11a**.

As the compound **12** is stable in refluxing dichloromethane even in the presence of *m*-chlorobenzoic acid, **13** cannot be formed *via* **12** under the reaction conditions. Since the peroxy acid would attack **11a** also on the sulfur S^2 to give **16**, it is likely that **13** was produced *via* **16** which was unstable under the reaction conditions towards fast retro-ene type decomposition. Direct evidence for intermediacy of **16** was provided by monitoring the reaction spectroscopically: NMR spectrum of a mixture of **11** and MCPBA in CD_2Cl_2 at −50——40 °C showed a set of signals which seemed to be due to **16**[12] [δ 0.87 (s, 9H), 1.20 (s, 9H), 1.42 (s, 9H), 6.11 (d, J=2 Hz, 1H), and 6.98 (d, J=2 Hz, 1H)] besides two sets of signals due to **11** and **12** (the molar ratio; **11**: **12**: **16**=1: 0.67: 0.8). Upon raising the temperature, decomposition of **16** into **13** and 2-methylpropene started at −30 °C, and the intensity of the NMR signals due to **16** gradually decreased with concomitant increase in intensity of the signals due to **13** and 2-methylpropene. Finally, at 34 °C, the signals of **16** were completely replaced by those of **13** and 2-methylpropene.

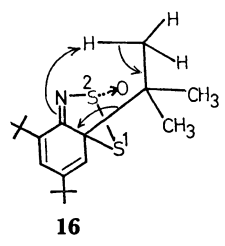

16

This unusual instability of **16** with respect to retro-ene reaction is in marked contrast with the stability exhibited by related compounds **11** and **12**.[13]

Under forced conditions (in refluxing benzene for 3.5 h), **12** gave **13** (11.6%), **14** (24.4%), and 2,4,6-tri-*t*-butylaniline (28.7%) along with recovered **12** (14.1%). Formation of **13** and **14** is noteworthy, because it indicates the occurrence of oxygen migration from S^1 to S^2 during the thermolysis. Thermal behavior of a thiosulfinate has recently attracted considerable attention because of its intriguing decomposition mode and the conclusion has been drawn from Block's extensive studies that *S*-alkyl thiosulfinates do not undergo oxygen migration like RS(O)SR′⇄RSS(O)R′.[15]

In view of this conclusion and the reversible cyclization between **11a** and **11b**,[3] the most attracting route to **13** and **14** is that involving cycloreversion of **12** to **12′** as shown in Scheme 2,[16] the driving force of which is aromatization. There still remain, however, other possibilities, because **12** is not a simple *S*-alkyl thiosulfinate for which the above conclusion by Block was obtained.[17] For example, isomerization of **12′** to **12‴** is also possible *via* **12″**, which proceeds through sulfur migration.[18] We have no experimental evidence to conclude which mechanism is actually operative. In any case, however, this reaction represents a new mode of isomerization in thiosulfinate type compounds.

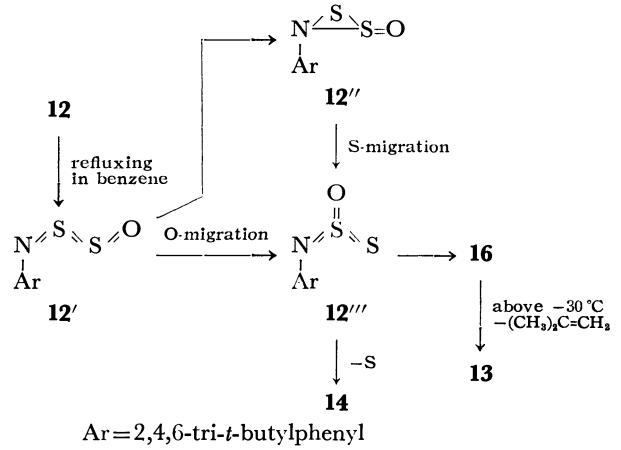

Ar=2,4,6-tri-*t*-butylphenyl

Scheme 2.

Reactions with Bromine and Other Electrophiles. Reaction of **1** with an equimolar amount of bromine afforded *N,N'*-bis(2,4-di-*t*-butyl-6-methylphenyl)sulfur diimide (**17**) in 64.4% yield and sulfur in 17.2% yield. Considering the formation of a sulfur diimide *via* a

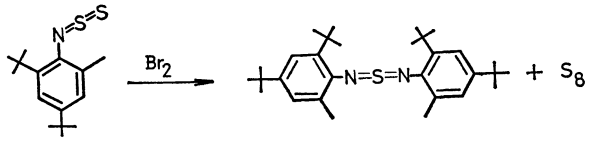

1 **17**

thionitroso intermediate demonstrated in the reaction of *N*-thiosulfinylanilines with triphenylphosphine,[19] the reaction mechanism (Scheme 3) starting with electrophilic attack of bromine on the terminal sulfur atom seems probable.

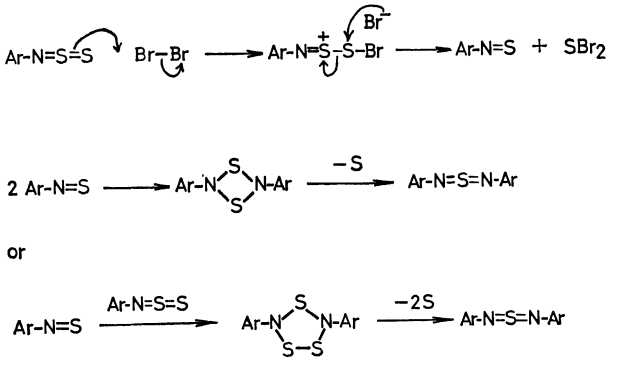

Ar=2,4-di-*t*-bulyl-6-methylphenyl

Scheme 3.

In contrast to the above reactions, electrophilic reagents such as trimethylsilyl chloride or trimethyloxonium tetrafluoroborate did not react with **1** at room temperature.

Experimental

All melting points were uncorrected. The IR and UV spectra were recorded with Hitachi EPI-G2 and EPS-3 spectrophotometers, respectively. The NMR spectra were measured with a Hitachi R-20B (60 MHz) spectrometer using tetramethylsilane as an internal standard. The mass spectra were recorded with a Hitachi RMU-6L mass spectrometer (70 eV). Chromatographic separations were carried out using dry column chromatography (Woelm silica gel for dry column chromatography).

Reactions of N-*Thiosulfinylanilines with* m-*Chloroperbenzoic Acid (MCPBA).* In each of the following reactions, a slightly deficient amount of MCPBA was used assuming the purity of MCPBA as 80%.

*1) Reaction of 2,4-Di-*t*-butyl-6-methyl-*N*-thiosulfinylaniline (1):* To a dichloromethane solution (15 ml) of **1** (503 mg, 1.79 mmol),[3] was added dropwise at 0 °C a dichloromethane solution (8 ml) of MCPBA (395 mg) cooled to *ca.* 0 °C. After being stirred for 1.5 h at 0 °C and 1.5 h at room temperature, the reaction mixture was shaken with aq $NaHCO_3$, washed with water, and dried over $MgSO_4$. Removal of the solvent followed by dry column chromatography (DCC, silica gel, hexane) gave 75 mg (14.9%) of **1**, 146 mg (30.8%) of **2**, and 162 mg (41.3%) of **3**. These products were identified by comparison of the IR and NMR with those of authentic samples.

*2) Oxidation of 2,4,6-tri-*t*-butyl-7,8-dithia-9-azabicyclo[4.3.0]-nona-2,4,9-triene (11a):* Reaction at 22 °C was described below as a typical example and the reactions at other temperatures were carried out similarly. To a dichloromethane solution (20 ml) of **11a** (496 mg, 1.53 mmol)[3] was added MCPBA (280 mg) in the same solvent. The mixture was stirred for 30 min, shaken with aq $NaHCO_3$, washed with water, and dried over $MgSO_4$. After removal of the solvent, the residue was treated with hexane to give 166 mg of 4,6-di-*t*-butyl-3*H*-1,2,3-benzodithiazole 2-oxide (**13**) as colorless crystals, which showed IR and NMR spectra identical with those of an authentic sample obtained by thermolysis of **11a**.[14] The hexane-soluble part was subjected to DCC (silica gel, hexane) and three fractions (a brownish yellow fraction with the highest R_f value, an orange fraction and a yellow fraction) were obtained. From the brownish yellow fraction was recovered 44.8 mg (9.0%) of **11a**. The orange fraction gave 25 mg (5.8% based on consumed **11a**) of **14**, which was identified by comparing the IR and NMR spectra with those of an authentic sample. The most polar yellow part was again chromatographed on silica gel with hexane–CH_2Cl_2 (1 : 4) as eluent and divided into two fractions. A yellow fraction gave 172 mg (36.3% based on consumed **11a**) of 2,4,*r*-6-tri-*t*-butyl-7,8-dithia-9-azabicyclo[4.3.0]nona-2,4,9-triene *t*-7-oxide (**12**) as pale yellow crystals, which were recrystallized three times from aq methanol, mp 124.7—125.7 °C; IR (KBr): 1080 cm^{-1} (ν_{SO}); NMR (CCl_4): δ 1.05 (s, 9H), 1.18 (s, 9H), 1.37 (s, 9H), 6.01 (d, J=1.5 Hz, 1H), and 6.22 (d, J=1.5 Hz, 1H); λ_{max}^{hexane} (ε): 233 (9490) and 345 nm (2030), the latter band was very broad (293—450 nm); *m/e*: 339 (M^+, 0.7%), 307 (0.4), 291 (30.7), 266 (100), and 250 (24.6).

Found: C, 63.46; H, 8.85; N, 3.90; S, 18.82%. Calcd for $C_{18}H_{29}NOS_2$: C, 63.67; H, 8.61; N, 4.13; S, 18.88%.

Another fraction gave 8 mg of **13**. Thus total yield of **13** was 174 mg (44.0% based on consumed **11a**).

Thermolysis of 12. A benzene solution (10 ml) of **13** (163 mg, 0.480 mmol) was refluxed for 3.5 h under nitrogen. Removal of the solvent followed by preparative TLC (silica gel, hexane–CH_2Cl_2 (3 : 7)) afforded four fractions. An orange fraction with the highest R_f value gave 88.0 mg of orange crystalline material, which was purified by preparative TLC (silica gel–hexane, followed by silica gel–CCl_4) to give 36 mg (24.4%) of **14** and 21 mg of 2,4,6-tri-*t*-butylaniline (**18**). A pale yellow fraction gave 15 mg of **18**. Thus total yield of **18** was 36 mg (28.7%). From another pale yellow fraction was recovered 23 mg (14.1%) of **12**. A colorless fraction with the lowest R_f value gave 16 mg (11.6%) of **13**.

*Examination of Stability of 2,4,*r*-6-tri-*t*-butyl-7,8-dithia-9-azabicyclo[4.3.0]nona-2,4,9-triene* t*-7-Oxide (12).* A solution of **12** (126 mg, 0.37 mmol) and *m*-chlorobenzoic acid (66 mg, 0.42 mmol) in dichloromethane (6 ml) was allowed to stand for 3 h at room temperature. At this point, **13** was not detected on TLC (silica gel, CH_2Cl_2). Although the reaction mixture was subsequently refluxed for 3 min, no **13** was detected on TLC. The reaction mixture was washed with aq $NaHCO_3$ and dried over $MgSO_4$. Removal of the solvent followed by preparative TLC (silica gel, CH_2Cl_2) afforded 120 mg (96%) of **12**, which was identified by the IR and NMR spectra.

Examination of Stability of 11a. A solution of **11a** (145 mg, 0.45 mmol) and *m*-chlorobenzoic acid (79 mg, 0.50 mmol) in dichloromethane (6 ml) was stirred for 1 h at room temperature. However, neither **13** nor **12** was detected on TLC.

Reaction of 1 with Bromine. To a solution of **1** (204

mg, 0.725 mmol) in carbon tetrachloride (10 ml) was added 0.8 ml of carbon tetrachloride solution of bromine (0.909 M). The mixture was stirred for 1.5 h at 0 °C. Removal of the solvent followed by treatment with preparative TLC (silica gel, CCl_4) afforded three fractions. The first fraction gave 8 mg of sulfur. The next orange fraction gave 109 mg (64.4 %) of **17**. The third fraction gave 214 mg of partly crystalline brown tar. Its crystallization from ethyl acetate afforded 23 mg of white crystals, which could not be identified.

References

1) For Part III, see Y. Inagaki, R. Okazaki, N. Inamoto, K. Yamada, and H. Kawazura, *Bull. Chem. Soc. Jpn.*, **52**, 2008 (1979).

2) D. H. R. Barton and M. J. Robson, *J. Chem. Soc., Perkin Trans. 1*, **1974**, 1245.

3) Y. Inagaki, R. Okazaki, and N. Inamoto, *Tetrahedron Lett.*, **1975**, 4575; *Bull. Chem. Soc. Jpn.*, **52**, 1998 (1979).

4) Part of this work was reported in a preliminary form. Y. Inagaki, R. Okazaki, and N. Inamoto, *Chem. Lett.*, **1978**, 1095.

5) R. Okazaki, T. Hosogai, E. Iwadare, M. Hashimoto, and N. Inamoto, *Bull. Chem. Soc. Jpn.*, **42**, 3611 (1969).

6) B. Zwanenburg and J. Strating, *Quart. Repts. Sulfur Chem.*, **5**, 79 (1971) and references cited therein.

7) D. H. R. Barton, S. V. Ley, and P. D. Magnus, *J. Chem. Soc., Chem. Commun.*, **1975**, 855.

8) R. Okazaki and O. Simamura, *Bull. Chem. Soc. Jpn.*, **47**, 1981 (1974).

9) A compound of type $R_2S{=}S$ is known to be very unstable to decompose into R_2S with extrusion of sulfur. G. Hofle and J. E. Baldwin, *J. Am. Chem. Soc.*, **93**, 6307 (1971). R. D. Baechler and S. K. Daley, *Tetrahedron Lett.*, **1978**, 101; R. D. Baechler and S. K. Daley, B. Daley, and K. McGlynn, *ibid.*, **1978**, 105.

10) A private communication from Prof. F. Iwasaki, the University of Electro-Communications. The details will be reported elsewhere.

11) A similar hydrolysis has been reported. W. K. Warburton, *Chem. Rev.*, **57**, 1101 (1957); *cf.* also L. D. Huestis, M. L. Walsh, and N. Hahn, *J. Org. Chem.*, **30**, 2763 (1965).

12) Of possible two diastereomers only one seems to be formed as judged from NMR spectroscopy. The orientation of S–O bond is tentatively assumed, on steric ground, to be *anti* with respect to the *t*-butyl group attached to carbon adjacent to S^1.

13) The dithiazole **11** is thermally more stable than **12**; its complete decomposition requires refluxing in benzene for about 10 h.[14)]

14) Y. Inagaki, R. Okazaki, and N. Inamoto, *Bull. Chem. Soc. Jpn.*, **52**, 2002 (1979).

15) E. Block and J. O'Connor, *J. Am. Chem. Soc.*, **96**, 3921, 3929 (1974) and references cited therein.

16) For examples of sulfur extrusion in S(IV)-thiocumulenes and possible existence of such species as X=S(=O)=Y as 1, 3-dipole, see R. M. Kellogg, *Tetrahedron*, **32**, 2165 (1976); Y. Inagaki and R. Okazaki, *Yuki Gosei Kagaku Kyokai Shi*, **36**, 1 (1978).

17) The occurrence of oxygen migration has been suggested by a tracer study for *S*-aryl arenethiosulfinates. P. Koch, E. Ciuffarin, and A. Fava, *J. Am. Chem. Soc.*, **92**, 5971 (1970).

18) We thank a referee for his suggestion on the possibility of S-migration.

19) Y. Inagaki, R. Okazaki, T. Hosogai, and N. Inamoto, *Bull. Chem. Soc. Jpn.*, in press.

New Methods for Synthesis of α,β-Unsaturated Carboxylic Esters from Carbonyl Compounds Using Monoanions of Dithiocarbonates, and Dianions of Ethyl Mercaptoacetate and Ethyl 2-Mercaptopropionate

Kazuhiko TANAKA,* Nobuyuki YAMAGISHI, Rikuhei TANIKAGA, and Aritsune KAJI
Department of Chemistry, Faculty of Science, Kyoto University, Sakyo-ku, Kyoto 606
(Received May 29, 1979)

The lithium enolates of *O*-alkyl *S*-alkoxycarbonylmethyl dithiocarbonates and monothiocarbonates were found to be efficient reagents for the synthesis of α,β-unsaturated esters from carbonyl compounds by single-step procedure. The dianions of ethyl mercaptoacetate and ethyl 2-mercaptopropionate were successfully generated by treatment with 2.2 equivalents of lithium diisopropylamide (LDA) in the presence of *N,N,N',N'*-tetramethylethylenediamine (TMEDA) at −78 °C in THF. The dianions so formed are highly reactive toward various electrophiles. The procedure leads to a novel one-pot synthesis of α,β-unsaturated carboxylic esters from carbonyl compounds.

Synthetic routes to α,β-unsaturated carboxylic esters have attracted considerable attention recently because of their importance as useful synthetic intermediates and the increase in the number of naturally occurring substances such as insect pheromones and pigments.[1,2] Ethoxycarbonylmethylenetriphenylphosphorane, an efficient reagent for the direct synthesis of α,β-unsaturated esters from carbonyl compounds, was introduced by Wittig and Haag in 1955.[3] Since then considerable efforts have been made to utilize the reagent.[2] Wadswarth and Emmons found that sodium enolate of diethyl ethoxycarbonylmethylphosphonate reacted with carbonyl compounds to give α,β-unsaturated esters in good yields.[4] Hartzell *et al.*[5] and Shimoji *et al.*[6] found a new method for the conversion of aldehydes or ketones into α,β-unsaturated esters utilizing lithium enolate of (trimethylsilyl)acetate.

We wish to report a novel and general method for the one-pot synthesis of α,β-unsaturated carboxylic esters using sulfur-stabilized carbanions and dianions.[7]

Results and Discussion

Lithium Enolates of Dithiocarbonates and Monothiocarbonates. A yellow solution of the carbanion **2a** is obtained by treatment of *O*-ethyl *S*-ethoxycarbonylmethyl dithiocarbonate (**1a**) with LDA at −78 °C in THF. It is stable at this temperature for several hours.

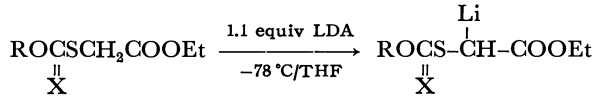

1a: R=Et; X=S
1b: R=Et; X=O
1c: R=*i*-Pr; X=S

2a: R=Et; X=S
2b: R=Et; X=O
2c: R=*i*-Pr; X=S

When the lithium enolate (**2a**) was allowed to react with a variety of carbonyl compounds, α,β-unsaturated esters (**3**) were obtained in good yields (Table 1). Since the starting materials are readily prepared from inexpensive commercial reagents, the sequence constitutes a useful one-pot synthesis of **3** from carbonyl compounds.

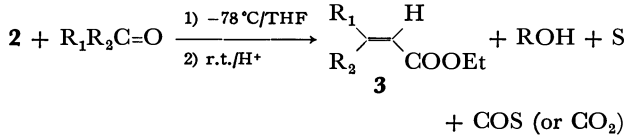

The structure of **3** was confirmed by its elemental analysis and spectral (IR, NMR) properties (see Experimental). No isomerized β,γ-unsaturated esters were detected by NMR analysis. The *E*/*Z* ratio of **3** was determined by GLC and NMR analysis; *e.g.*, the ratio of *E*-isomer to *Z*-isomer of ethyl 3-phenyl-2-butenoate (**3e**) determined by integration of the olefinic proton at δ 6.04 and δ 5.78, respectively, is 42: 58. Analysis of this material by GLC indicates a 43: 57 mixture of *E*-**3e** and *Z*-**3e**. The mechanism of this reaction consists of the intramolecular cyclization to

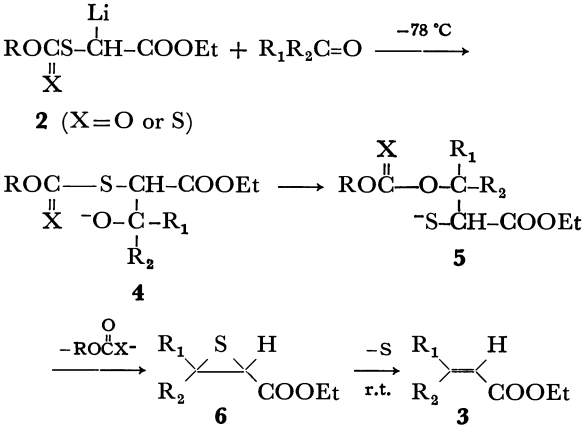

Scheme 1.

thiirane **6** as an intermediate, followed by spontaneous extrusion of sulfur to **3** (Scheme 1). Actually, an intermediate such as **6** could be isolated. Thus, treatment of lithium salt of *O-trans*-(4-*t*-butylcyclohexyl) *S*-methyl dithiocarbonate (**7**) with heptanal as described before gave 2-hexylthiirane (**8**) in 71% yield.[8]

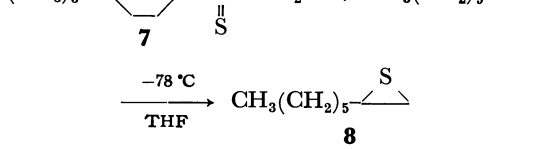

Thiiranes containing strongly electron-attracting substituents such as alkoxycarbonyl or cyano groups readily extrude sulfur to afford olefins.[9]

When α-alkyl-substituted dithiocarbonates **1d** and **1e**

Table 1. Synthesis of α,β-unsaturated esters (**3**) from carbonyl compounds and carbonates (**1a**—**1c**)

Carbonate (**1**)[a] R	X	Carbonyl compound	Solvent	Product[b] (**3**)	Yield %	*E*/*Z*[c] ratio
Et	S (**1a**)	Propanal	THF	EtCH=CHCOOEt(**3a**)	52	*E* only
Et	S (**1a**)	Acetone	THF	Me_2C=CHCOOEt(**3b**)	85	
Et	S (**1a**)	2-Butanone	THF	Me(Et)C=CHCOOEt(**3c**)	74	39/61
Et	O (**1b**)	2-Butanone	THF	Me(Et)C=CHCOOEt(**3c**)	71	47/53
i-Pr	S (**1c**)	2-Butanone	THF	Me(Et)C=CHCOOEt(**3c**)	67	
Et	S (**1a**)	3-Pentanone	THF	Et(Et)C=CHCOOEt(**3d**)	69	
Et	S (**1a**)	Acetophenone	THF–HMPA (8: 1 v/v)	Ph(Me)C=CHCOOEt(**3e**)	76	43/57
Et	S (**1a**)	Cyclopentanone	THF	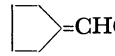 =CHCOOEt(**3f**)	88	
Et	S (**1a**)	Cyclohexanone	THF	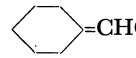 =CHCOOEt(**3g**)	78	
Et	O (**1b**)	Cyclohexanone	THF	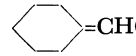 =CHCOOEt(**3g**)	61	
i-Pr	S (**1c**)	Cyclohexanone	THF	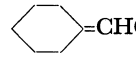 =CHCOOEt(**3g**)	81	
Et	S (**1a**)	4-Methylcyclohexanone	THF	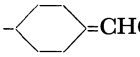 =CHCOOEt(**3h**)	69	
Et	S (**1a**)	4-Methylcyclohexanone	THF–HMPA (8: 1 v/v)	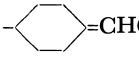 =CHCOOEt(**3h**)	87	

a) All reactions carried out at −78 °C on a 20 mmol scale using LDA as a base. b) Isolated yields. c) Determined by ^{1}H-NMR and GLC.

Table 2. Synthesis of α,β-unsaturated esters (**3**) from carbonyl compounds and dithiocarbonates (**1d**—**1e**)

Dithiocarbonate (**1**)[a] R	Carbonyl compound	Solvent	Product[b] (**3**)	Yield %	*E*/*Z*[c] ratio
Me (**1d**)	Benzaldehyde	THF	PhCH=(Me)COOEt (**3i**)	82	21/79
Et (**1e**)	Benzaldehyde	THF	PhCH=(Et)COOEt (**3j**)	82	37/63
Me (**1d**)	2-Methylpropanal	THF	*i*-PrCH=C(Me)COOEt (**3k**)	78	59/41
Me (**1d**)	2-Methylpropanal	THF–HMPA (8: 1 v/v)	*i*-PrCH=C(Me)COOEt (**3k**)	84	11/89
Et (**1e**)	2-Methylpropanal	THF	*i*-PrCH=C(Et)COOEt (**3l**)	82	42/58
Et (**1e**)	2-Methylpropanal	THF–HMPA (8: 1 v/v)	*i*-PrCH=C(Et)COOEt (**3l**)	91	46/54

a) All reactions carried out at −78 °C using LDA as a base on a 20 mmol scale. b) Isolated yields. c) Determined by ^{1}H-NMR and GLC.

were allowed to react with LDA at −78 °C in THF, lithium enolates **2d** and **2e** were readily formed. These reagents also react with various aldehydes to produce **3** (Table 2).

1d: R=Me
1e: R=Et

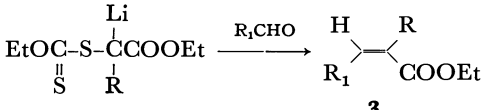

3

2d: R=Me
2e: R=Et

The enolates **2d** and **2e** do not react with ketones, presumably due to steric hindrance or enolization of ketones.

Formation of Dianions and Their Synthetic Applications. We have found that the hitherto unknown dianion **10** derived from ethyl mercaptoacetate (**9**) can be generated, undergoing regioselective alkylation depending on electrophiles used. Treatment of **9** with 2.2 equiv of LDA in the presence of 2.2 equiv of TMEDA in THF at −78 °C gave soluble dianion **10**, stable at −78 °C for at least several hours. When a solution of **10** in THF was treated with an excess of alkylating agent, a facile reaction occurred both at carbon and at sulfur.

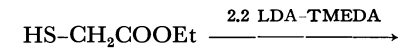

9

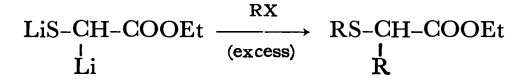

10

RX=MeI; 86%(**11a**)
RX=EtI; 66%(**11b**)
RX=CH_2=$CHCH_2$Br; 64%(**11c**)

Table 3. Synthesis of α,β-unsaturated esters (**3**) from carbonyl compounds and dianion (**10**)

Carbonyl compound	Product[a] (**3**)		Yield[b] %	E/Z[c] ratio
Cyclohexanone	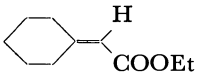	(**3g**)	60	
Cyclopentanone	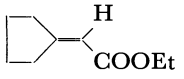	(**3f**)	74	
3-Pentanone	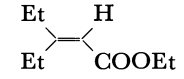	(**3d**)	61	
Acetophenone	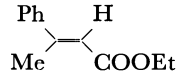	(**3e**)	58	97/3
Propiophenone	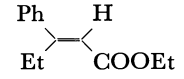	(**3m**)	51	100/0
2-Butanone	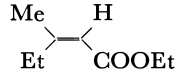	(**3c**)	64	43/57
2-Pentanone	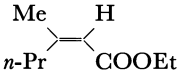	(**3n**)	62	45/55
2-Hexanone	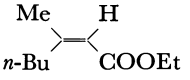	(**3o**)	67	38/62
Methylcyclohexyl ketone	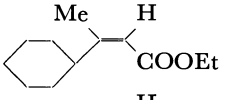	(**3p**)	53	41/59
6-Methyl-5-hepten-2-one	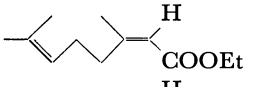	(**3q**)	70	38/62
4-Methyl-3-penten-2-one	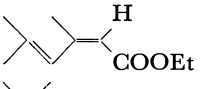	(**3r**)	64	66/34
3,3-Dimethylcyclohexanone	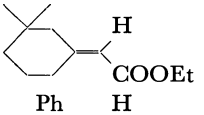	(**3s**)	32[d]	44/56
Benzaldehyde	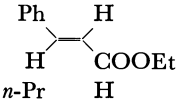	(**3t**)	57	100/0
Butanal	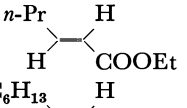	(**3u**)	34	100/0
Heptanal	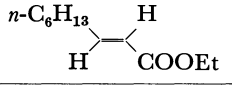	(**3v**)	19	95/5

a) All reactions carried out at −78 °C on a 20 mmol scale. b) Isolated yields. c) Determined by ^{1}H-NMR and GLC. d) A mixture of THF and HMPA (8: 1 v/v) was used as a solvent.

Dianion **10** undergoes aldol-type reaction with carbonyl compounds. Thus, reaction of **10** with a variety of carbonyl compounds gave the adduct **12**, which, upon treatment with ethyl chloroformate at −78 °C, afforded **3** as the sole product in good yields after the usual work-up. Generality of this new methodology is apparent from the results summarized in Table 3. The use of ethyl chloroformate is important since no α,β-unsaturated esters can be isolated from the reaction of **10** and carbonyl compounds with *diethyl carbonate*. The low yields of monosubstituted propenoates, *i.e.*, **3u** and **3v**, are ascribed to the polymerization at the stage of thiirane formation.[10] The initial step of this reaction might be the formation of adduct **12** as shown in Scheme 2.

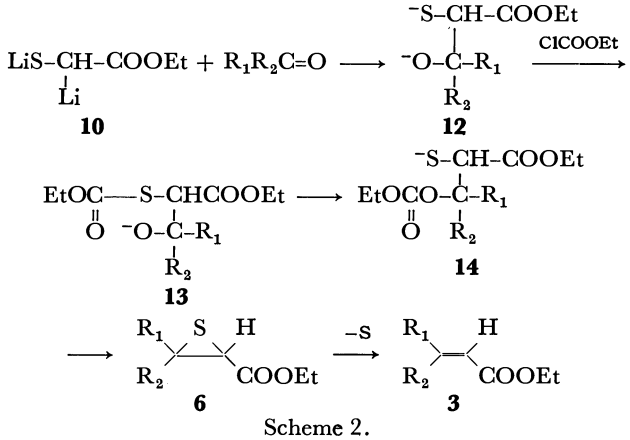

Scheme 2.

The adduct **12** should react with ethyl chloroformate to afford *S*-ethoxycarbonylated intermediate **13**, since a thiolate anion is a more powerful nucleophile than an alcoholate anion. Another intermediate such as **12** could be trapped when the reaction mixture of **10** and acetone was quenched with aqueous NH_4Cl solution at −78 °C.

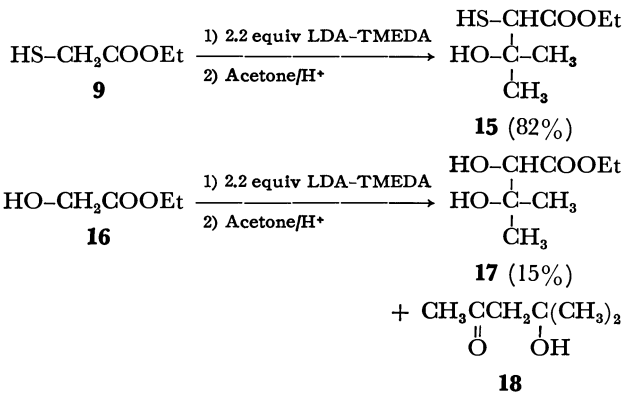

In contrast, no such selective reaction of **10** was observed for oxygen analogue. The reaction of ethyl glycolate (**16**) with a base gives the addition product only in 15% yield along with the condensation product of acetone and some other unidentified products. The intermediacy of **13** in Scheme 2 is in line with the fact that lithium enolate of dithiocarbonate **2b** gives **4** (=**13**) on treatment with carbonyl compound. The regioselectivity of **10** depends upon the electrophiles used. Thus, the reaction of **10** with 1 equiv of alkyl halides afforded *S*-alkylated products in good yields, whereas **10** reacted with carbonyl compounds on α-carbon of dianion as described before.

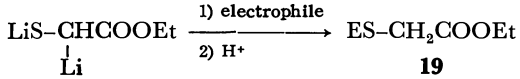

Electrophile	E	Yield of **19**
MeI	Me	89% (**19a**)
EtBr	Et	81% (**19b**)
Propylene oxide	MeCHCH$_2$– OH	49% (**19c**)

In order to clarify the mechanism, we have investigated the effects of reaction time, temperature, and solvents in the case of 6-methyl-5-hepten-2-one. The results (Tables 4, 5, and 6) indicate that the reaction of dianion **10** is kinetically controlled process since there is no obvious effect on the *E*/*Z* ratio of **3q**. Dianion is highly reactive toward carbonyl compounds since even the α-methylsubstituted dianion **21** reacts with various ketones (Table 7), in contrast to monoanion **2d**.

Table 4. Effect of reaction time on the *E*/*Z* ratio of **3q**

Reaction time/h	Yield of **3q** / %	*E*/*Z* ratio of **3q**
0.5	61	43/57
2.0	70	38/52
16.0	65	42/58

All reactions carried out at −78 °C in THF.

Table 5. Effect of solvent on the *E*/*Z* ratio of **3q**

Solvent	Yield of **3q** / %	*E*/*Z* ratio of **3q**
THF[a)]	70	38/62
DME[b)]	62	45/55
Diethyl ether[a)]	62	51/49
Hexane[a)]	55	51/49

a) At −78 °C. b) At −65 °C.

Table 6. Effect of reaction temperature on the *E*/*Z* ratio of **3q**

Reaction temp/°C[a)]	Yield of **3q** / %	*E*/*Z* ratio of **3q**
−78	70	38/62
−100	64	40/60

a) Reaction carried out in THF.

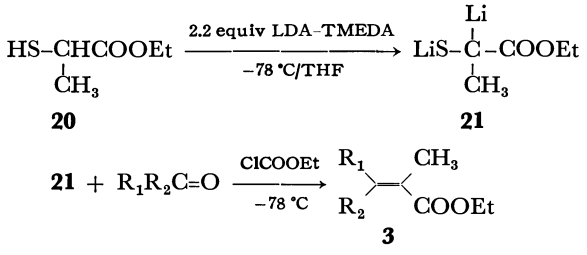

The methodology employed here is particularly useful synthetically since the conversion of ketones into trisubstituted propenoates is difficult.[11] In order to demonstrate the utility of our novel reactions, we have carried out the synthesis of the key intermediates for insect pheromones such as boll weevil sex pheromone (**22**), and a component of ant mandibular gland secretions (**23**).

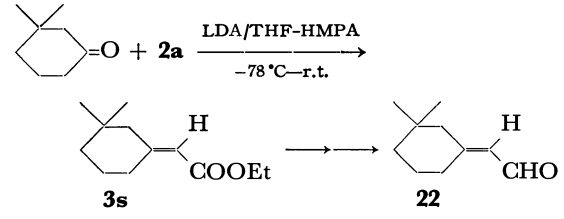

Treatment of 3,3-dimethylcyclohexanone with **2a** at −78 °C gave the key intermediate for sex pheromones in 84% yield. Separation of *Z*-**3s** and *E*-**3s**, and conversion into the target pheromones have been established.[12] Utilizing the dianion **21**, α,β-unsaturated ester **3B** was isolated in 67% yield. The *E*- and *Z*-isomers of **3B** were separated by GLC in 98% and 95%

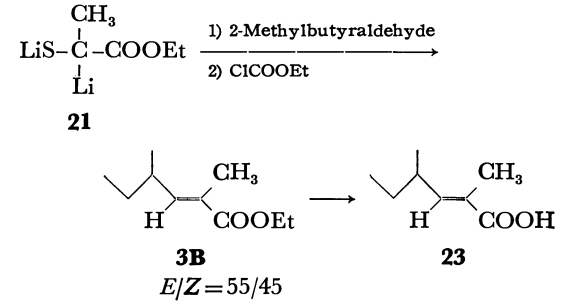

E/*Z*=55/45

Table 7. Synthesis of α,β-unsaturated esters (**3**) from carbonyl compounds and dianion (**21**)

Carbonyl compound	Product[a] (**3**)		Yield[b] %	E/Z[c] ratio
Acetone	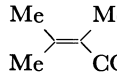	(**3w**)	57	
2-Butanone	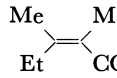	(**3x**)	59	23/77
2-Hexanone	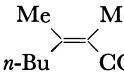	(**3y**)	51	24/76
Cyclohexanone	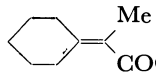	(**3z**)	43	
Heptanal	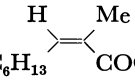	(**3A**)	55	58/42
Benzaldehyde	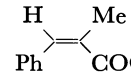	(**3i**)	45	53/47

a) All reactions carried out at −78 °C on a 20 mmol scale. b) Isolated yields. c) E/Z ratio determined by ^{1}H-NMR and GLC.

purity, respectively, exhibiting NMR and IR spectra identical to the reported data.[13] Hydrolysis of *E*-**3B** to the desired ant mandibular gland secretion has been reported.[13]

Experimental

General. Infrared spectra were determined on a Hitachi Model-215 spectrophotometer. Nuclear magnetic resonance spectra were determined on a JEOLCO PS-100 spectrometer. Chemical shifts are given in δ units, parts per million relative to tetramethylsilane as an internal standard. Gas chromatograms were obtained using a Varian Aerograph Model 920 instrument with a 0.15 cm × 120 cm glass column (20% Silicone DC-550 on Celite 545). Tetrahydrofuran (THF) was dried by distillation calcium hydride and by subsequent distillation from lithium aluminum hydride. Hexamethylphosphoric triamide (HMPA), diisopropylamine, and *N,N,N',N'*-tetramethylethylenediamine (TMEDA) were distilled from calcium hydride and stored over molecular sieves. All reactions were performed under a nitrogen atmosphere.

General Procedure. Reaction of Carbanion ***2a*** *with Carbonyl Compounds*: A solution of 20 mmol of **1a** in 3 ml of THF was added to a stirred solution of 22 mmol of LDA in 40 ml of THF at −78 °C. After the yellow solution had been stirred at −78 °C for 30 min, 24 mmol of carbonyl compound in 2 ml of THF was added over a 5 min period. Stirring was continued at −78 °C for 1 h and at room temperature for 1 h before it was quenched with aqueous NH_4Cl (10 ml). The mixture was poured into dilute HCl and extracted four times with ether, the combined organic layer being washed twice with brine, dried (anhydrous Na_2SO_4), and concentrated under reduced pressure. Distillation gave α,β-unsaturated esters (**3**).

Reaction of Dianion ***10*** *with Carbonyl Compounds.* To a mixture of LDA (44 mmol) and TMEDA (44 mmol) in 40 ml of THF was added a solution of 2.4 g (20 mmol) of ethyl mercaptoacetate (**9**) in 7 ml of THF at −78 °C. After being stirred for 1 h, a solution of 22 mmol of carbonyl compounds in 5 ml of THF was added and the reaction mixture was stirred at −78 °C for 2 h. Ethyl chloroformate (20 mmol) in 5 ml of THF was then added portionwise to the above solution with stirring and the mixture was kept at −78 °C for 30 min and at room temperature for 1 h before it was quenched with aqueous NH_4Cl (10 ml). The reaction mixture was poured into dilute HCl and extracted four times with ether, the combined organic layer being washed twice with brine, dried (anhydrous Na_2SO_4), and concentrated under reduced pressure. Distillation of the resulting oil gave **3**. The following α,β-unsaturated esters were prepared in a similar manner.

*Physical Properties. Ethyl 2-Pentenoate (**3a**)*: Bp 86—87 °C/70 Torr. ^{1}H-NMR (CCl_4); δ 6.86 (m, 1H, CH=C), 5.68 (m, 1H, CH=C), 4.08 (q, J=7 Hz, 3H, CH_2), 2.22 (m 2H, CH_2), 1.24 (t, J=7 Hz, 3H, CH_3), 1.10 (t, J=7 Hz, 3H, CH_3). IR (neat); 1650 cm^{-1} (C=C).

*Ethyl 3-Methyl-2-butenoate (**3b**)*: Bp 90—92 °C/100 Torr. ^{1}H-NMR (CCl_4); δ 5.52 (m, 1H, CH=C), 4.00 (q, J=7 Hz, 2H, CH_2), 2.08 (s, 1H, CH_3), 1.78 (s, 1H, CH_3), 1.16 (t, J=7 Hz, 3H, CH_3). IR (neat); 1675 cm^{-1} (C=C). Spectral data were identical with those of an authentic sample prepared from 3-methyl-2-butenoic acid and ethyl bromide in the presence of DBU in benzene.[14]

*Ethyl 3-Methyl-2-pentenoate (**3c**)*: Bp 93—97 °C/60 Torr. ^{1}H-NMR (CCl_4); δ 5.50 (m, CH=C), 4.04 (q, J=7 Hz, 2H, CH_2), 2.60 (q, J=8 Hz, CH_2 for *Z*-isomer), 2.14 (q, J=8 Hz, CH_2 for *E*-isomer), 2.06 (m, CH_3 for *E*-isomer), 1.84 (m, CH_3 for *Z*-isomer), 1.24 (t, J=7 Hz, 3H, CH_3), 1.04 (t, J=8 Hz, 3H, CH_3). IR (neat); 1640 cm^{-1} (C=C). Found: C, 67.40; H, 10.15%. Calcd for $C_8H_{14}O_2$: C, 67.57; H, 9.92%.

*Ethyl 3-Ethyl-2-pentenoate (**3d**)*: Bp 84 °C/22 Torr. ^{1}H-NMR (CCl_4); δ 5.58 (bs, 1H, CH=C), 4.03 (q, J=7 Hz, 2H, CH_2), 2.56 (q, J=8 Hz, 2H, CH_2), 2.14 (q, J=8 Hz, 2H, CH_2), 0.9—1.3 (m, 9H, $3CH_3$). IR (neat); 1640 cm^{-1} (C=C). Found: C, 68.91; H, 10.50%. Calcd for $C_9H_{16}O_2$: C, 69.20; H, 10.32%.

*Ethyl 3-Phenyl-2-butenoate (**3e**)*: Bp 132 °C/12 Torr. ^{1}H-NMR (CCl_4); δ 7.24 (m, 5H, aromatic), 6.04 (m, CH=C for *E*-isomer), 5.78 (m, CH=C for *Z*-isomer), 4.10 (q, J=7 Hz, CH_2 for *E*-isomer), 3.88 (q, J=7 Hz, CH_2 for *Z*-isomer), 2.50 (brs, CH_3 for *E*-isomer), 2.05 (brs, CH_3 for *Z*-isomer), 1.24 (brs, CH_3 for *E*-isomer), 1.00 (brs, CH_3 for *Z*-isomer). IR

(neat); 1625 cm^{-1} (C=C). Found: C, 75.76; H, 7.42%. Calcd for $C_{12}H_{14}O_2$: C, 75.76; H, 7.52%.

*Ethyl Cyclopentylideneacetate (**3f**)*: Bp 93—96 °C/20 Torr. ^{1}H-NMR (CCl_4); δ 5.70 (m, 1H, CH=C), 4.04 (q, J=7 Hz, 2H, CH_2), 2.74 (m, 2H, CH_2), 2.40 (m, 2H, CH_2), 1.68 (m, 4H, $2CH_2$), 1.24 (t, J=7 Hz, 3H, CH_3). IR (neat); 1645 cm^{-1} (C=C). Found: C, 70.33; H, 9.23%. Calcd for $C_9H_{14}O_2$: C, 70.10; H, 9.15%.

*Ethyl Cyclohexylideneacetate (**3g**)*: Bp 110—112 °C/20 Torr. ^{1}H-NMR (CCl_4); δ 5.50 (brs, 1H, CH=C), 4.05 (q, J=7 Hz, 2H, CH_2), 2.84 (m, 2H, CH_2), 1.62 (m, 6H, $3CH_2$), 1.24 (t, J=7 Hz, 3H, CH_3). IR (neat); 1620 cm^{-1} (C=C). Found: C, 71.61; H, 9.44%. Calcd for $C_{10}H_{16}O_2$: C, 71.39; H, 9.59%.

*Ethyl 4-Methylcyclohexylideneacetate (**3h**)*: Bp 123—125 °C/23 Torr. ^{1}H-NMR (CCl_4); δ 5.54 (brs, 1H, CH=C), 4.05 (q, J=7 Hz, 2H, CH_2), 3.80 (m, 1H, CH), 0.8—2.4 (m, 8H, $4CH_2$), 1.25 (t, J=7 Hz, 3H, CH_3), 0.94 (d, J=6 Hz, 3H, CH_3). IR (neat); 1645 cm^{-1} (C=C). Found: C, 72.76; H, 10.13%. Calcd for $C_{11}H_{18}O_2$: C, 72.49; H, 9.95%.

*Ethyl 2-Methyl-3-phenyl-2-propenoate (**3i**)*: Bp 115—117 °C/12 Torr. ^{1}H-NMR (CCl_4); δ 7.62 (brs, CH=C for *E*-isomer), 7.26 (m, 5H, aromatic), 6.60 (brs, CH=C for *Z*-isomer), 4.18 (q, J=7 Hz, CH_2 for *E*-isomer), 4.00 (q, J=7 Hz, CH_2 for *Z*-isomer), 2.04 (s, 3H, CH_3), 1.28 (t, J=7 Hz, CH_3 for *E*-isomer), 1.02 (t, J=7 Hz, CH_3 for *Z*-isomer). IR (neat); 1635 cm^{-1} (C=C). Found: C, 75.95; H, 7.54%. Calcd for $C_{12}H_{14}O_2$: C, 75.76; H, 7.42%.

*Ethyl 2-Ethyl-3-phenyl-2-propenoate (**3j**)*: Bp 135—137 °C/11 Torr. ^{1}H-NMR (CCl_4); δ 7.52 (s, CH=C for *E*-isomer), 7.15 (m, 5H, aromatic), 6.48 (brs, CH=C for *Z*-isomer), 4.16 (q, J=7 Hz, CH_2 for *E*-isomer), 4.00 (q, J=7 Hz, CH_2 for *Z*-isomer), 2.40 (m, 2H, CH_2), 1.10 (m, 6H, $2CH_3$). IR (neat); 1640 cm^{-1} (C=C). Found: C, 76.28; H, 7.90%. Calcd for $C_{13}H_{16}O_2$: C, 76.44; H, 7.90%.

*Ethyl 2,4-Dimethyl-2-pentenoate (**3k**)*:[15] Bp 90—97 °C/55 Torr. ^{1}H-NMR (CCl_4); δ 6.45 (dq, CH=C for *E*-isomer), 5.60 (dq, CH=C for *Z*-isomer), 4.10 (m, 2H, CH_2), 3.24 (m, CH for *Z*-isomer), 2.60 (m, CH for *E*-isomer), 1.80 (m, 3H, CH_3), 1.28 (t, J=7 Hz, 3H, CH_3), 1.00 (t, J=7 Hz, 6H, $2CH_3$).

*Ethyl 2-Ethyl-4-methyl-2-pentenoate (**3l**)*: Bp 94—100 °C/63 Torr. ^{1}H-NMR (CCl_4); δ 6.44 (m, CH=C for *E*-isomer), 5.54 (m, CH=C for *Z*-isomer), 4.14 (m, 2H, CH_2), 3.12 (m, CH for *Z*-isomer), 2.64 (m, CH for *E*-isomer), 2.24 (m, 2H, CH_2), 1.28 (t, J=7 Hz, 3H, CH_3), 1.00 (m, 9H, $3CH_3$). IR (neat); 1620 cm^{-1} (C=C). Found: C, 70.51; H, 10.58%. Calcd for $C_{10}H_{18}O_2$: C, 70.55; H, 10.65%.

*Ethyl 3-Phenyl-2-pentenoate (**3m**)*: Bp 98 °C/1.5 Torr. ^{1}H-NMR (CCl_4); δ 7.2—7.5 (m, 5H, aromatic), 5.96 (s, 1H, CH=C), 4.15 (q, J=7 Hz, 2H, CH_2), 3.11 (q, J=7 Hz, 2H, CH_2), 1.30 (t, J=7 Hz, 3H, CH_3), 1.08 (t, J=7 Hz, 3H, CH_2). IR (neat); 1620 cm^{-1} (C=C).

*Ethyl 3-Methyl-2-hexenoate (**3n**)*: Bp 75—76 °C/17 Torr. ^{1}H-NMR (CCl_4); δ 5.61 (brs, 1H, CH=C), 4.09 (q, J=7 Hz, 2H, CH_2), 1.88—2.62 (m, 5H, CH_2 and CH_3), 1.3—1.7 (m, 2H, CH_2), 1.25 (t, J=7 Hz, 3H, CH_3), 0.96 (m, 3H, CH_3). IR (neat); 1640 cm^{-1} (C=C). Found: C, 69.04; H, 10.32%. Calcd for $C_9H_{16}O_2$: C, 69.20; H, 10.32%.

*Ethyl 3-Methyl-2-heptenoate (**3o**)*: Bp 97—98 °C/13 Torr. ^{1}H-NMR (CCl_4); δ 5.40 (brs, 1H, CH=C), 3.95 (q, J=7 Hz, 2H, CH_2), 1.03—2.32 (m, 5H, CH_2 and CH_3), 1.2—1.6 (m, 4H, $2CH_2$), 1.22 (t, J=7 Hz, 3H, CH_3), 0.92 (m, 3H, CH_3). IR (neat); 1640 cm^{-1} (C=C). Found: C, 70.66; H, 10.68%. Calcd for $C_{10}H_{18}O_2$: C, 70.54; H, 10.66%.

*Ethyl 3-Cyclohexyl-2-butenoate (**3p**)*: Bp 121—123 °C/18 Torr. ^{1}H-NMR (CCl_4); δ 5.54 (m, 1H, CH=C), 4.06 (q, J=7 Hz, 2H, CH_2), 3.4—3.7 (m, 1H, CH), 1.0—2.1 (m, 13H, CH_2 and CH_3), 1.24 (t, J=7 Hz, 3H, CH_3). IR (neat); 1640 cm^{-1} (C=C).

*Ethyl 3,7-Dimethyl-2,6-octadienoate (**3q**)*: Bp 75—80 °C/2.3 Torr. ^{1}H-NMR (CCl_4); δ 5.52 (m, 1H, CH=C), 4.9—5.2 (m, 1H, CH=C), 4.03 (q, J=7 Hz, 2H, CH_2), 1.86—2.58 (m, 7H, $2CH_2$ and CH_3), 1.68 (s, 3H, CH_3), 1.61 (s, 3H, CH_3), 1.24 (t, J=7 Hz, 3H, CH_3). IR (neat); 1640 cm^{-1} (C=C). Found: C, 73.43; H, 10.11%. Calcd for $C_{12}H_{20}O_2$: C, 73.43; H, 10.27%.

*Ethyl 3,5-Dimethyl-2,4-hexadienoate (**3r**)*: Bp 90 °C/23 Torr. *E*-isomer: ^{1}H-NMR (CCl_4); δ 5.64 (m, 1H, CH=C), 5.52 (m, 1H, CH=C), 4.07 (q, J=7 Hz, 2H, CH_2), 2.19 (s, 3H, CH_3), 1.83 (m, 6H, $2CH_3$), 1.25 (t, J=7 Hz, 3H, CH_3). IR (neat); 1625 cm^{-1} (C=C). *Z*-isomer: ^{1}H-NMR (CCl_4); δ 6.42 (brs, 1H, CH=C), 5.52 (brs, 1H, CH=C), 4.02 (q, J=7 Hz, 2H, CH_2), 2.00 (s, 3H, CH_3), 1.85 (s, 3H, CH_3), 1.73 (s, 3H, CH_3), 1.22 (t, J=7 Hz, 3H, CH_3). IR (neat); 1630 cm^{-1} (C=C).

*Ethyl 3,3-Dimethylcyclohexylideneacetate (**3s**)*: A solution of LDA (22 mmol) in a mixture of 40 ml of THF and 5 ml of HMPA was stirred under nitrogen at −78 °C and 20 mmol of *O*-ethyl *S*-ethoxycarbonylmethyl dithiocarbonate (**1a**) in 3 ml of THF was added dropwise. After the yellow solution had been stirred for 30 min, 2.78 g (20 mmol) of 3,3-dimethylcyclohexanone in 2 ml of THF was added over a 5 min period. The mixture was stirred at −78 °C for 1 h and at room temperature for 1 h. The usual work-up and distillation gave **3s** in 84% yield. Bp 113 °C/23 Torr. ^{1}H-NMR (CCl_4); δ 5.52 (m, 1H, CH=C), 4.06 (q, J=7 Hz, 2H, CH_2), 1.2—2.8 (m, 8H, $4CH_2$), 1.24 (t, J=7 Hz, 3H, CH_3), 0.92 (m, 6H, $2CH_3$). MS (20 eV) *m/e* 196 (M^+). IR (neat); 1645 cm^{-1} (C=C).

*Ethyl (*E*)-3-Phenyl-2-propenoate (**3t**)*: Bp 86 °C/0.7 Torr. ^{1}H-NMR (CCl_4); δ 7.64 (d, J=16 Hz, 1H, CH=C), 7.2—7.6 (m, 5H, aromatic), 6.36 (d, J=16 Hz, 1H, CH=C), 4.20 (q, J=7 Hz, 2H, CH_2), 1.32 (t, J=7 Hz, 3H, CH_3). IR (neat); 1630 cm^{-1} (C=C). Found: C, 74.86; H, 7.03%. Calcd for $C_{11}H_{12}O_2$: C, 74.98; H, 6.86%.

*Ethyl (*E*)-2-Hexenoate (**3u**)*: Bp 61 °C/17 Torr. ^{1}H-NMR (CCl_4); δ 6.80 (dt, J=7 Hz, 16 Hz, 1H, CH=C), 5.72 (d, J=16 Hz, 1H, CH=C), 4.11 (q, J=7 Hz, 2H, CH_2), 2.20 (m, 2H, CH_2), 1.4—1.8 (m, 2H, CH_2), 1.28 (t, J=7 Hz, 3H, CH_3), 0.98 (t, J=7 Hz, CH_3). IR (neat); 1650 cm^{-1} (C=C).

*Ethyl 2-Nonenoate (**3v**)*: Bp 50 °C/1 Torr. ^{1}H-NMR (CCl_4); δ 6.88 (dt, J=7 Hz, 16 Hz, CH=C), 5.72 (d, J=16 Hz, 1H, CH=C), 4.12 (q, J=7 Hz, 2H, CH_2), 2.0—2.2 (m, 2H, CH_2), 1.1—1.8 (m, 8H, $4CH_2$), 0.9 (m, 3H, CH_3). IR (neat); 1645 cm^{-1} (C=C).

*Ethyl 2,3-Dimethyl-2-butenoate (**3w**)*: Bp 105—106 °C/100 Torr. ^{1}H-NMR (CCl_4); δ 4.10 (q, J=7 Hz, 2H, CH_2), 1.8—2.0 (m, 9H, $3CH_3$), 1.28 (t, J=7 Hz, 3H, CH_3). IR (neat); 1635 cm^{-1} (C=C).

*Ethyl 2,3-Dimethyl-2-pentenoate (**3x**)*: Bp 67—72 °C/14 Torr. ^{1}H-NMR (CCl_4); δ 4.15 (q, J=7 Hz, 2H, CH_2), 2.28 (m, 2H, CH_2), 1.93 (m, 6H, $2CH_3$), 1.28 (t, J=7 Hz, 3H, CH_3), 1.04 (t, J=7 Hz, 3H, CH_3). IR (neat); 1630 cm^{-1} (C=C).

*Ethyl 2,3-Dimethyl-2-heptenoate (**3y**)*: Bp 90—94 °C/13 Torr. *E*-isomer: ^{1}H-NMR (CCl_4); δ 4.02 (q, J=7 Hz, 2H, CH_2), 2.09 (m, 2H, CH_2), 1.93 (m, 3H, CH_3), 1.80 (m, 3H, CH_3), 1.2—1.6 (m, 4H, $2CH_2$), 1.26 (t, J=7 Hz, 3H, CH_3), 0.93 (m, 3H, CH_3). IR (neat); 1630 cm^{-1} (C=C). *Z*-isomer: ^{1}H-NMR (CCl_4); δ 4.03 (q, J=7 Hz, 2H, CH_2), 2.30 (m, 2H, CH_2), 1.74 (m, 6H, $2CH_3$), 1.2—1.6 (m, 4H, $2CH_2$), 1.25 (t, J=7 Hz, 3H, CH_3), 0.91 (m, 3H, CH_3). IR (neat); 1630 cm^{-1} (C=C). Found: C, 71.72; H, 11.00%. Calcd for $C_{11}H_{20}O_2$: C, 71.70; H, 10.94%.

*Ethyl 2-Cyclohexylidenepropionate (**3z**)*: Bp 104—107 °C/10 Torr. ^{1}H-NMR (CCl_4); δ 4.10 (q, 2H, CH_2), 2.0—2.6 (m, 4H, $2CH_2$), 1.80 (s, 3H, CH_3), 1.58 (m, 6H, $3CH_2$), 1.26 (t, J=7 Hz, 3H, CH_3). IR (neat); 1625 cm^{-1} (C=C).

*Ethyl 2-Methyl-2-nonenoate (**3A**)*: Bp 109—114 °C/14 Torr. IR (neat); 1650 cm^{-1} (C=C). *E*-isomer: ^{1}H-NMR (CCl_4); δ 6.64 (m, 1H, CH=C), 4.10 (q, J=7 Hz, 2H, CH_2), 2.16 (m, 2H, CH_2), 1.98 (s, 3H, CH_3), 1.1—1.6 (m, 11H, CH_2 and CH_3), 0.89 (m, 3H, CH_3). *Z*-isomer: ^{1}H-NMR (CCl_4); δ 5.83 (m, 1H, CH=C), 4.12 (q, J=7 Hz, 2H, CH_2), 2.42 (m, 2H, CH_2), 1.86 (s, 3H, CH_3), 1.0—1.6 (m, 11H, CH_2 and CH_3), 0.90 (m, 3H, CH_3).

*Ethyl 2,4-Dimethyl-2-hexanoate (**3B**)*: A solution of ethyl 2-mercaptopropionate (**20**) (20 mmol) in 3 ml of THF was added dropwise to a magnetically stirred solution of LDA (44 mmol) and TMEDA (44 mmol) at −78 °C. After the mixture had been stirred at this temperature for 1 h, a solution of 2-methylbutyraldehyde (24 mmol) in 3 ml of THF was added and the resulting pale yellow mixture was maintained at −78 °C for 2 h. After the addition of a solution of ethyl chloroformate (20 mmol) in 5 ml of THF was complete, the reaction mixture was stirred at −78 °C for 30 min and then at room temperature for 1 h. Work-up and distillation gave a mixture of *E*- and *Z*-isomers of **3B** in 67% yield, which was readily separated by GLC. Bp 110—115 °C/68 Torr. IR (neat); 1645 cm^{-1} (C=C). *E*-isomer: ^{1}H-NMR (CCl_4); δ 6.36 (m, 1H, CH=C), 4.08 (q, J=7 Hz, 2H, CH_2), 2.37 (m, 1H, CH), 1.76 (s, 3H, CH_3), 1.25 (m, 5H, CH_2 and CH_3), 0.98 (d, J=7 Hz, 3H, CH_3), 0.86 (t, 3H, CH_3). *Z*-isomer: ^{1}H-NMR (CCl_4); δ 5.52 (m, 2H, CH_2), 4.10 (q, 2H, CH_2), 3.00 (m, 1H, CH), 1.86 (s, 3H, CH_3), 1.29 (m, 5H, CH_2 and CH_3), 0.7—1.0 (m, 6H, $2CH_3$). Found: C, 70.42; H, 10.79%. Calcd for $C_{10}H_{18}O_2$: C, 70.55; H, 10.65%.

Alkylation of Dianion. A solution of alkyl halide (80 mmol for dialkylation; 20 mmol for monoalkylation) was added dropwise to a solution of dianion (20 mmol) generated at −78 °C in THF in the same way as described above. After the solution had been stirred at −78 °C for 30 min and at room temperature for 1 h, the mixture was quenched with 10 ml of aqueous solution of NH_4Cl. The product was purified by distillation.

*Ethyl 2-Methylthiopropionate (**11a**)*: Bp 66—68 °C/15 Torr. ^{1}H-NMR (CCl_4); δ 4.12 (q, J=7 Hz, 2H, CH_2), 3.18 (q, J=7 Hz, 1H, CH), 2.10 (s, 3H, CH_3), 1.2—1.4 (m, 6H, $2CH_3$). IR (neat); 1725 cm^{-1} (COO). Found: C, 48.70; H, 8.36; S, 21.61%. Calcd for $C_6H_{12}O_2S$: C, 48.62; H, 8.16; S, 21.63%.

*Ethyl 2-Ethylthiobutanoate (**11b**)*: Bp 91—92.5 °C/14 Torr. ^{1}H-NMR (CCl_4); δ 4.09 (q, J=7 Hz, 2H, CH_2), 3.00 (t, J=7 Hz, 1H, CH), 2.55 (q, J=7 Hz, 2H, CH_2), 1.6—2.0 (m, 2H, CH_2), 1.1—1.4 (m, 6H, $2CH_3$), 0.97 (t, J=7 Hz, 3H, CH_3). IR (neat); 1720 cm^{-1} (COO).

*Ethyl 2-Allylthio-4-pentenoate (**11c**)*: Bp 115 °C/16 Torr. ^{1}H-NMR (CCl_4); δ 5.40—5.90 (m, 2H, CH=C), 5.05 (m, 4H, $2CH_2$=C), 4.09 (q, 2H, CH_2), 3.00—3.30 (m, 3H, CH_2 and CH), 2.2—2.8 (m, 2H, CH_2), 1.27 (t, J=7 Hz, 3H, CH_3). IR (neat); 1720 (COO), 1635 cm^{-1} (C=C).

*Ethyl 3-Hydroxy-2-mercapto-3-methylbutanoate (**15**)*: Bp 115 °C/27 Torr. ^{1}H-NMR (CCl_4); δ 4.22 (q, J=7 Hz, 2H, CH_2), 3.00—3.20 (m, 2H, OH and CH), 2.22 (d, J=9 Hz, 1H, SH), 1.0—1.4 (m, 9H, $3CH_3$). Found: C, 47.36; H, 8.01; S, 17.76%. Calcd for $C_7H_{14}O_3S$: C, 47.17; H, 7.91; S, 17.99%. IR (neat); 3500 (OH), 2550 (SH), 1710 cm^{-1} (COO).

*Ethyl 2,3-Dihydroxy-3-methylbutanoate (**17**)*: ^{1}H-NMR (CCl_4); δ 4.26 (q, J=7 Hz, 2H, CH_2), 3.83 (s, 1H, CH), 3.0—3.3 (m, 2H, 2OH), 1.34 (t, J=7 Hz, 3H, CH_3), 1.24 (s, 3H, CH_3), 1.16 (s, 3H, CH_3). IR (neat); 3400 (OH), 1720 cm^{-1} (COO).

*Ethyl (Methylthio)acetate (**19a**)*: Bp 111 °C/20 Torr. ^{1}H-NMR (CCl_4); δ 4.10 (q, J=7 Hz, 2H, CH_2), 3.06 (s, 2H, CH_2), 2.19 (s, 3H, SCH_3), 1.29 (t, J=7 Hz, 3H, CH_3). IR (neat); 1730 cm^{-1} (COO).

*Ethyl (Ethylthio)acetate (**19b**)*: Bp 81 °C/15 Torr. ^{1}H-NMR (CCl_4); δ 4.02 (q, J=7 Hz, 2H, CH_2), 3.02 (s, 2H, CH_2), 2.55 (q, J=7 Hz, 2H, CH_2), 1.22 (t, J=7 Hz, 6H, $2CH_3$). IR (neat); 1730 cm^{-1} (COO).

*Ethyl (2-Hydroxypropylthio)acetate (**19c**)*: Bp 112 °C/10 Torr. ^{1}H-NMR (CCl_4); δ 4.16 (q, J=7 Hz, 2H, CH_2), 3.85 (m, 1H, CH), 3.48 (m, 1H, OH), 3.22 (s, 2H, SCH_2), 2.46 (m, 2H, CH_2), 1.1—1.4 (m, 6H, $2CH_3$). IR (neat); 3450 (OH), 1720 cm^{-1} (COO).

References

1) "The Total Synthesis of Natural Products," ed by J. ApSimon, John Wiley and Sons, New York (1973), Vol. 2.
2) A. Maercker, *Org. React.*, **14**, 270—490 (1965).
3) G. Wittig and W. Haag, *Chem. Ber.*, **88**, 1654 (1955).
4) W. S. Wadsworth, Jr., and W. D. Emmons, *J. Am. Chem. Soc.*, **83**, 1733 (1961).
5) S. L. Hartzell, D. F. Sullivan and M. W. Rathke, *Tetrahedron Lett.*, **1974**, 1403.
6) a) K. Shimoji, H. Taguchi, K. Oshima, H. Yamamoto, and H. Nozaki, *J. Am. Chem. Soc.*, **96**, 1620 (1974); b) H. Taguchi, K. Shimoji, H. Yamamoto, and H. Nozaki, *Bull. Chem. Soc. Jpn.*, **47**, 2529 (1974).
7) a) K. Tanaka, R. Tanikaga, and A. Kaji, *Chem. Lett.*, **1976**, 917; b) K. Tanaka, N. Yamagishi, R. Tanikaga, and A. Kaji, *Chem. Lett.*, **1977**, 471.
8) C. R. Johnson, A. Nakanishi, N. Nakanishi, and K. Tanaka, *Tetrahedron Lett.*, **1975**, 2868.
9) a) M. Sander, *Chem. Rev.*, **66**, 297 (1966); b) T. Hayashi, *Bull. Chem. Soc. Jpn.*, **45**, 1507 (1972); c) T. C. Owen, C. L. Gladys, and L. Field, *J. Chem. Soc.*, **1962**, 656; d) C. C. Tung and A. J. Speziale, *J. Org. Chem.*, **29**, 1577 (1964).
10) T. C. Owen, C. L. Gladys, and L. Field, *J. Chem. Soc.*, **1962**, 501.
11) G. Gallagher, Jr., and R. L. Webb, *Synthesis*, **1974**, 122.
12) a) S. W. Pelletier and N. V. Mody, *J. Org. Chem.*, **41**, 1069 (1974), and references cited therein; b) J. H. Tumlinson, R. C. Gueldner, D. D. Hardee, A. C. Thompson, P. A. Hedin, and J. P. Minyard, *J. Org. Chem.*, **36**, 2616 (1971).
13) J. A. Katzenellenbogen and T. Utawanit, *J. Am. Chem. Soc.*, **96**, 6153, (1974).
14) N. Ono, T. Yamada, T. Saito, K. Tanaka, and A. Kaji, *Bull. Chem. Soc. Jpn.*, **51**, 2401 (1978).
15) V. J. Lee, A. R. Branfman, T. R. Herrin, and K. L. Rinehart, Jr., *J. Am. Chem. Soc.*, **100**, 4225 (1978).

A Synthesis of Neamine

Akihiko HARAYAMA, Tsutomu TSUCHIYA, and Sumio UMEZAWA*

Institute of Bioorganic Chemistry, 1614 Ida, Nakahara-ku, Kawasaki 211

(Received May 31, 1979)

Neamine and its position isomer were synthesized from 3,4-di-*O*-acetyl-2-deoxy-2-(*p*-methoxybenzylideneamino)-6-*O*-tosyl-α-D-glucopyranosyl bromide and racemic 5,6(4,5)-*O*-cyclohexylidene-2-deoxy-1,3-bis-*N*-(ethoxycarbonyl)streptamine. Influence of the *N*-protecting groups of 2-deoxystreptamine derivatives for glycosylation was discussed. The unusual $\Delta[M]_{TACu}$ value of the position isomer of neamine was ascribed to the interaction between the 6′-amino group and other groups.

Neamine[1] isolated from *Streptomyces cultures* is a constituent of several aminoglycoside antibiotics including neomycins, kanamycin B and butirosins. Its first synthesis starting from paromamine[2] was reported by Umezawa *et al.*[3] Kohno *et al.*[4] also reported a synthesis of neamine from a protected 2,6-diamino-2,6-dideoxy-α-D-glucopyranosyl bromide and a blocked deoxystreptamine derivative, using the 2,4-dinitrophenyl group as a non-participating group at C-2 of the glycosyl bromide. Interest in neamine synthesis lies in the efficient and stereocontrolled synthesis of α-glycoside having an amino group at C-2 of the glycosyl portion. This paper reports another total synthesis of neamine with the use of a glycosyl bromide carrying a *p*-methoxybenzylidene group (Schiff base) at C-2 as a non-participating group.

We used 3,4-di-*O*-acetyl-2-deoxy-2-(*p*-methoxybenzylideneamino)-6-*O*-tosyl-α-D-glucopyranosyl bromide[5] (**1**) and racemic 5,6(4,5)-*O*-cyclohexylidene-2-deoxy-1,3-bis-*N*-(ethoxycarbonyl)streptamine[6] (**5**). Condensation of **1** and **5** in the presence of mercury(II) cyanide and Drierite in benzene–dioxane followed by treatment of the condensation product with dilute sulfuric acid and reaction with ethyl chloroformate gave a mixture of two α-glycosides, *viz.*, 4-*O*-[3,4-di-*O*-acetyl-2-deoxy-2-(ethoxycarbonylamino)-6-*O*-tosyl-α-D-glucopyranosyl]-2-deoxy-1,3-bis-*N*-(ethoxycarbonyl)streptamine (**6**) and its 6-*O*-isomer (**6′**) in 47% yield based on **5**.

Treatment of the above mixture with sodium azide gave a mixture of 6′-azido derivative (**7**, **7′**). Hydrolysis with sodium hydroxide gave a mixture of **8** and **8′**, which, by catalytic hydrogenation followed by chromatographic separation, afforded neamine (**9**) and its 6-*O*-isomer (**9′**). Separation of **8** and **8′** was troblesome. However, they were separated in low yields for the structural determination of **9** and **9′**. α-Anomeric configurations of **8** and **8′** were confirmed by means of the PMR spectrum ($J_{1,2}$=3.5 Hz each). The physical properties of **9** were identical with those of natural neamine. The synthetic neamine (**9**) also gave an antibacterial spectrum identical with that of natural neamine, the isomer (**9′**) showing very weak antibacterial activity. The azido derivatives (**8** and **8′**) showed no antibacterial activities.

In order to confirm the structure of **9** and **9′**, rotations of **9** and **9′** in TACu[7] were measured. Neamine and synthetic **9** gave expected $\Delta[M]_{TACu}$ values (≈−200°), indicating copper-complexing between 1-NH_2 and 6-OH and between 2′-NH_2 and 3′-OH, respectively. The contributions of both rotations are approximately equal in magnitude and opposite in sign, thus cancelling the values. However, **9′** gave $\Delta[M]_{TACu}$ −990° and not the expected value (−1800°). An explanation is that the copper-complexing between 3-NH_2 and 4-OH is disturbed by the presence of the 6′-NH_2 group. For the sake of confirmation the $\Delta[M]_{TACu}$ values of **8** and **8′** were measured. Since **8** and **8′** have no 6′-NH_2 group, they should give the expected $\Delta[M]_{TACu}$ values which were found to be −190° and −1820°, respectively, as expected, showing that **8** and **8′** are 4-*O*- and 6-*O*-glycosyl isomers of 2-deoxystreptamine, respectively.

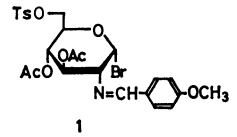

1

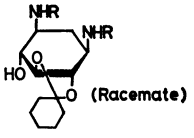

2 R = $CO_2CH_2C_6H_5$
4 R = $CO_2CH_2CH{=}CH_2$
5 R = $CO_2C_2H_5$

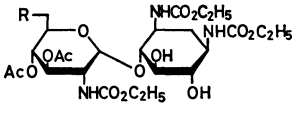

6 R = OTs
7 R = N_3

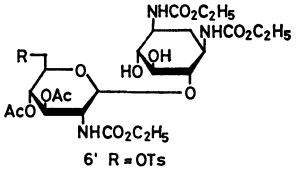

6′ R = OTs
7′ R = N_3

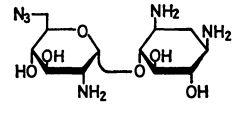

8

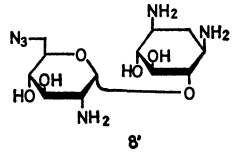

8′

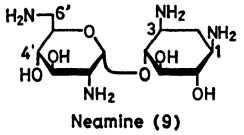

Neamine (9)

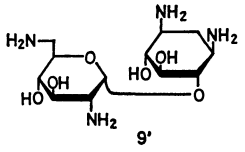

9′

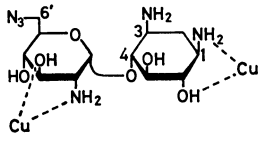

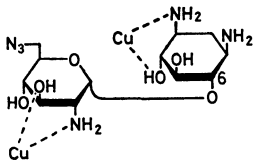

Cu-complex of **8** and **8′**

Discussion

Use of the *p*-methoxybenzylidene group as a non-participating group at the C-2 amino group of glycosyl halide is based on the fact that a Schiff base derivative gives α-glycosides in the synthesis of paromamine[6] in an excellent yield.

We have examined the influence of several *N*-blocking groups of the 2-deoxystreptamine (aglycon) on the glycosidation. Condensation of 1,3-bis-*N*-(benzyloxycarbonyl)-4,5(5,6)-*O*-cyclohexylidene-2-deoxystreptamine[8] (**2**) with **1** under similar conditions gave the condensation product in a smaller yield (≈30%) which was also led to neamine.[9] 1,3-Bis-*N*-(allyloxycarbonyl)-4,5(5,6)-*O*-cyclohexylidene-2-deoxystreptamine (**4**) was prepared from 2-deoxystreptamine by the reaction with allyl chloroformate and subsequent cyclohexylidenation. Condensation of **4** with **1**, however, did not proceed satisfactorily (condensation yield, *ca.* 30%). The *N*-ethoxycarbonyl group was thus found to give the best condensation yield among the protecting groups tested.

Experimental

Thin-layer chromatography (TLC) was carried out on Wakogel B-5 with sulfuric acid spray for detection. For column chromatography, silica gel (Wakogel C-200) was used. Paper chromatography (PPC) was performed on Toyo-Roshi No. 50 with 1-butanol–pyridine–water–acetic acid (6:4:3:1) and spots were visualized by spraying 0.5% ninhydrin in pyridine. PMR spectra were recorded at 90 MHz with a Varian EM-390 spectrometer.

*1,3-Bis-*N*-(allyloxycarbonyl)-2-deoxystreptamine (**3**).* Allyl chloroformate (3 ml) was added dropwise under stirring to an ice-cold suspension of 2-deoxystreptamine dihydrochloride (2.0 g) and anhydrous sodium carbonate (5.2 g) in aqueous acetone (1:1, 40 ml). The mixture was stirred for 3 h at room temperature. The reaction mixture was concentrated and the residue extracted with hot dioxane. The dioxane solution was then concentrated, the residue being washed with ether to give a solid (2.4 g). Recrystallization from water gave needles, 1.8 g (65%), mp 223—224 °C; IR (KBr): 1700 (*ν* NHCOO), 1650 (sh, *ν* C=C), 1550 (amide II), 990 (*δ* CH=) cm^{-1}. PMR (pyridine-d_5): *δ* 1.95 (1H q, J=12 Hz, H-2_{ax}), 2.83 (1H double t, J=4.5, 4.5 and 12 Hz, H-2_{eq}), 4.6—4.8 (4H m, $CH_2CH{=}CH_2$), 5.0—5.5 (4H m, $CH_2CH{=}CH_2$), 5.98 (2H double quintet,[10] $CH_2{-}CH{=}CH_2$), 8.12 (2H d, J≈7 Hz, NH; disappeared on deuteration).

Found: C, 51.01; H, 6.66; N, 8.35%. Calcd for $C_{14}H_{22}N_2O_7$: C, 50.90; H, 6.71; N, 8.48%.

*Racemic 1,3-Bis-*N*-(allyloxycarbonyl)-4,5(5,6)-*O*-cyclohexylidene-2-deoxystreptamine (**4**).* A mixture of **3** (2.0 g), 1,1-dimethoxycyclohexane (1.3 ml) and *p*-toluenesulfonic acid (200 mg) was refluxed for a while, half the volume of the solvent then being distilled. The distillate was treated with Molecular Sieves 5A in order to remove methanol co-distilled, and then returned to the reaction vessel. The reaction mixture was treated likewise twice. After addition of triethylamine (4 ml), the mixture was concentrated to give a syrup. The syrup was dissolved in chloroform, washed with water, dried over sodium sulfate, and concentrated to give a solid. Recrystallization of the solid from acetone–hexane gave granular crystals, 1.66 g (67%), mp 106—108 °C: PMR (pyridine-d_5): *δ* 1.1—2.2 (11H, cyclohexylidene and H-2_{ax}), 2.80 (1H double t, H-2_{eq}); 4.6—4.8 (4H), 5.0—5.45 (4H) and 5.7—6.2 (2H) (allyl); 8.25 (1H d) and 8.48 (1H d) (NH; disappeared on addition of D_2O).

Found: C, 58.28; H, 7.42; N, 6.55%. Calcd for $C_{20}H_{30}N_2O_7$: C, 58.52; H, 7.37; N, 6.82%.

*4-O- and 6-O-[3,4-Di-O-acetyl-2-deoxy-2-(ethoxycarbonylamino)-6-O-tosyl-α-D-glucopyranosyl]-2-deoxy-1,3-bis-N-(ethoxycarbonyl)-streptamine (**6** and **6′**).* A mixture of **1** (991 mg, 1.66 mmol), **5** (400 mg, 1.04 mmol), mercury(II) cyanide (757 mg), and calcium sulfate (Drierite, 600 mg) in dry benzene–dioxane (2:1, 4 ml) was stirred at room temperature overnight. Mercury(II) cyanide (300 mg) was added and the mixture was stirred for 20 h. The mixture was centrifuged, the insoluble matter being washed with dioxane. The organic solution combined was concentrated to give a syrup which was washed with water to give a pale-yellow solid (1.35 g). The solid, on TLC with benzene–acetone (5:1), showed major spots at R_f 0.42 and 0.49, and weak spots at R_f 0.22 (**5**) and 0.77 (**1**).

0.5 M sulfuric acid (≈2 ml) was added (pH≈2) to a solution of the solid in acetone (27 ml), and the resulting suspension was stirred at room temperature overnight. The cyclohexylidene and the *p*-methoxybenzylidene groups of the condensation products were removed by this procedure. The reaction mixture was concentrated and the residue was washed with ether to give a solid (TLC, R_f 0). To a suspension of the solid in aqueous acetone (1:1) were added ethyl chloroformate (0.22 ml) and anhydrous sodium carbonate (240 mg) and the mixture was stirred at room temperature overnight. The resulting mixture was concentrated and the residue was dissolved in chloroform. The solution was washed with water, dried over sodium sulfate, and concentrated to give a syrup. Addition of benzene to the syrup gave a precipitate which was removed by centrifugation. Concentration of the benzene solution gave a syrup (927 mg). The syrup on TLC with benzene–acetone (1:1) gave spots of R_f 0.51 and 0.45 (**6**, **6′**) and 0.34 (slight) and 0.26 (slight). The syrup was chromatographed with benzene–acetone (2:1) to give the syrup of a mixture of **6** and **6′**, 376 mg (47% based on **5**). IR (KBr): 1750 (*ν* CH_3CO), 1710 (*ν* NHCOO–), 1530 (amide II), 1240 (*ν* CH_3CO), 1180 (ν_s SO_2) cm^{-1}; PMR ($CDCl_3$): triplet-like signals centered at *δ* 1.23 (9H, J≈8 Hz, $COCH_2CH_3$); *δ* 1.84 (1.5 H), 1.90 (1.5 H) and 1.98 (3H) (each s, Ac), 2.47 (3H s, $CH_3C_6H_4SO_2$).

Found: C, 49.29; H, 5.87; N, 5.24; S, 3.83%. Calcd for $C_{32}H_{47}N_3O_{17}S$: C, 49.42; H, 6.09; N, 5.40; S, 4.12%.

*4-O- and 6-O-[3,4-Di-O-acetyl-6-azido-2,6-dideoxy-2-(ethoxycarbonylamino)-α-D-glucopyranosyl]-2-deoxy-1,3-bis-N-(ethoxycarbonyl)streptamine (**7**, **7′**).* Sodium azide (290 mg) was added to a solution of a mixture of **6** and **6′** (350 mg) in DMF (7 ml), and the mixture was stirred at 80 °C for 3 h. The solution on TLC with benzene–acetone (1:1) gave a single spot at R_f 0.47. Concentration gave a syrup which was dissolved in chloroform. The solution was washed with a saturated sodium chloride solution, then with water, dried over sodium sulfate, and concentrated to give a syrup. The syrup was dissolved again in benzene–ethyl acetate (3:1, 40 ml) and the solution was washed with water, dried (sodium sulfate), and concentrated to give a syrup, 234 mg (80%). IR (KBr): 2100 (N_3), 1740, 1700, 1530, 1240 cm^{-1}; PMR ($CDCl_3$): *δ* 1.27 (9H t, J=7 Hz, $CO_2CH_2CH_3$), 2.05 (6H m, half-height width is 4.5 Hz, Ac).

Found: C, 46.54; H, 6.12; N, 12.69%. Calcd for $C_{25}H_{40}N_6O_{14}$: C, 46.29; H, 6.22; N, 12.96%.

*4-O- and 6-O-(2-Amino-6-azido-2,6-dideoxy-α-D-glucopyranosyl)-2-deoxystreptamine (**8**, **8′**).* A suspension of a mixture of **7** and **7′** (91.6 mg) in 1 M sodium hydroxide solution (5 ml)

was refluxed. The resulting clear solution after 15 min was refluxed for further 2 h. Dowex 50 WX 2 (H^+ form) resin was added until the solution became neutral and the mixture was poured into a column containing the same resin (NH_4^+ form, ≈1 ml). The column after being washed with water (100 ml) was treated with 0.5 M aqueous ammonia. The fractions containing ninhydrin-positive products were collected and concentrated to give a pale-brown syrup (42 mg). The syrup on PPC gave two spots at R_f 0.20 and 0.18 and a faint spot at 0.32. The syrup was charged on a column of CM-Sephadex C-25 (NH_4^+ form, 6 ml) and the column was washed with water. A ninhydrin-positive syrup (9.1 mg) was obtained from the washings. Its absorption spectrum (IR, 1640 cm^{-1}) indicated the product to be a 1,3-ureylene derivative.[11] The column was then treated with aqueous ammonia with gradual increase in concentration (0→0.15 M) to give a colorless syrup of **8** and **8′**, 28.1 mg (52%).

The syrup (59.3 mg) was charged again on a column of CM-Sephadex C-25 (NH_4^+ form, 23 ml) and eluted with aqueous ammonia (0→0.1 M). The elution was checked by PPC. Compound **8** (R_f 0.18) was eluted between 170—180 ml, **8′** (R_f 0.20) between 190—200 ml and the mixture of **8**, **8′** between 180—190 ml. Concentration of the respective fractions gave syrups of **8** (15.7 mg), **8′** (16.0 mg) and a mixture of both (23.4 mg).

8: $[\alpha]_D^{25}$ +71° (*c* 1, water), $\Delta[M]^{436}_{TACu\text{-}NH_3}$† −190°. IR (KBr): 2100 (N_3), 1590 (broad, δ NH_2) cm^{-1}. PMR (D_2O +ND_3): δ 1.18 (1H q, J=12 Hz, H-2_{ax}), 1.97 (1H double t, J=4.5, 4.5 and 12 Hz, H-2_{eq}), 2.5—3.1 (3H m, H-1, 3,2′), 5.23 (1H d, J=3.5 Hz, H-1′). Irradiation at δ 2.8 turned the doublet of H-1′ into a singlet.

Found: C, 39.36; H, 6.50; N, 21.37%. Calcd for $C_{12}H_{24}N_6O_6\cdot 1/2H_2CO_3$: C, 39.58; H, 6.64; N, 22.15%.

8′: $[\alpha]_D^{25}$ +85° (*c* 1, water), $\Delta[M]^{436}_{TACu\text{-}NH_3}$ −1820°. IR (KBr): 2100, 1590 cm^{-1}. PMR (D_2O+ND_3): δ 1.24 (1H q, J=12 Hz, H-2_{ax}), 1.98 (1H double t, J=4.5, 4.5 and 12 Hz, H-2_{eq}), 2.5—3.1 (3H m, H-1, 3,2′), 5.13 (1H d, J=3.5 Hz, H-1′). Irradiation at δ 2.8 turned the doublet of H-1′ into a singlet.

Found: C, 39.44; H, 6.53; N, 21.56%. Calcd for $C_{12}H_{24}N_6O_6\cdot 1/2H_2CO_3$: C, 39.58; H, 6.64; N, 22.15%.

*Neamine(**9**)(4-O-(2,6-Diamino-2,6-dideoxy-α-D-glucopyranosyl)-2-deoxystreptamine) and Its Isomer(**9′**)(6-O-(2,6-Diamino-2,6-dideoxy-α-D-glucopyranosyl)-2-deoxystreptamine).* A few drops of acetic acid were added to an aqueous solution (7 ml) of a mixture of **8** and **8′** (67.2 mg) obtained after the first Sephadex column treatment. The solution (pH≈3) was then treated with hydrogen at atmospheric pressure for 30 min in the presence of palladium black. The solution on TLC (DC-Fertigplatten Kieselgel 60, E. Merck, Darmstadt) with 1-butanol–ethanol–chloroform–17% aqueous ammonia=4: 7: 2: 7 showed two major spots at R_f 0.17 (**9′**) and 0.28 (**9**), and minor spots at R_f 0.66, 0.72 and 0.82. The spots corresponding to **8** and **8′** (R_f 0.51 and 0.48, respectively) completely disappeared. Concentration of the solution gave a syrup, which, by chromatography on a CM-Sephadex C-25 (NH_4^+ form) column with aqueous ammonia (0→0.25 M), gave **9** (25 mg, 36%) and **9′** (23 mg, 34%) which were eluted in this order.

9: $[\alpha]_D^{25}$ +69° (*c* 0.8, water), $\Delta[M]^{436}_{TACu\text{-}NH_3}$ −180° (natural neamine, −210°). PMR (D_2O+ND_3): δ 1.22 (1H q, J=12 Hz, H-2_{ax}), 2.01 (1H double t, J≈4.5, ≈4.5 and 12 Hz, H-2_{eq}), 2.5—3.1 (5H, H-1, 3, 2′, 6′, 6′?), 5.33 (1H d, J=3.5 Hz, H-1′). All signals were superimposable on those of natural neamine carbonate.

Found: C, 40.68; H, 7.21; N, 14.24%. Calcd for $C_{12}H_{26}N_4O_6\cdot H_2CO_3$: C, 40.62; H, 7.34; N, 14.58%.

9′: $[\alpha]_D^{25}$ +71° (*c* 0.6, water), $\Delta[M]^{436}_{TACu\text{-}NH_3}$ −990°. PMR (D_2O+ND_3): δ 1.27 (1H q, J=12 Hz, H-2_{ax}), 1.98 (1H q, J≈4.5, ≈4.5, and 12 Hz, H-2_{eq}), 2.5—3.2 (5H), 5.17 (1H d, J=3.5 Hz).

Found: C, 40.64; H, 7.54; N, 14.89%. Calcd for $C_{12}H_{26}N_4O_6\cdot H_2CO_3$: C, 40.62; H, 7.34; N, 14.58%.

Antibacterial spectra of the synthetic neamine (**9**), natural neamine and the isomer (**9′**) expressed by minimal inhibitory concentration (mcg/ml): *Staphylococcus aureus* FDA 209P: 6.25, 12.5, 25; *Bacillus subtilis* NRRL B-558: <1.56, <1.56. 6.25; *Klebsiella pneumoniae* PCI 602: 25, 25, 100; *Escherichia coli* NIHJ: 25, 25, 200; *Escherichia coli* K-12: 25, 25, 200; *Salmonella typhi* T-63: 6.25, 6.25, 50; *Pseudomonas aeruginosa* A3: >200, >200, >200.

The authors wish to thank Mr. Saburo Nakada, Department of Chemistry, Keio University, for the microanalysis, and Dr. Masa Hamada, Institute of Microbial Chemistry, for the bioassay.

References

1) R. L. Peck, C.E. Hoffhine, Jr., Gale, and K. Folkers, *J. Am. Chem. Soc.*, **71**, 2590 (1949); R. L. Peck, C. E. Hoffhine, Jr., P. H. Gale, and K. Folkers., *ibid.*, **75**, 1018 (1953).

2) T. H. Haskel, J. C. French, and Q. R. Bartz, *J. Am. Chem. Soc.*, **81**, 3480 (1959).

3) S. Umezawa, K. Tatsuta, T. Tsuchiya, and E. Kitazawa, *J. Antibiot.*, **20**, 53 (1967); K. Tatsuta, E. Kitazawa, and S. Umezawa, *Bull. Chem. Soc. Jpn.*, **40**, 2371 (1967).

4) H. Kohno, H. Fukami, and M. Nakajima, *Agric. Biol. Chem.*, **39**, 1091 (1975).

5) S. Umezawa and Y. Nishimura, *J. Antibiot.*, **30**, 189 (1977).

6) S. Umezawa, T. Miyazawa, and T. Tsuchiya, *J. Antibiot.*, **25**, 530 (1972).

7) S. Umezawa, T. Tsuchiya, and K. Tatsuta, *Bull. Chem. Soc. Jpn.*, **39**, 1235 (1966).

8) T. Kurisu, M. Yamashita, Y. Nishimura, T. Miyake, T. Tsuchiya, and S. Umezawa, *Bull. Chem. Soc. Jpn.*, **49**, 285 (1976).

9) S. Umezawa, *Pure Appl. Chem.*, **50**, 1453 (1978).

10) NMR spectra catalog compiled by N. S. Bhacca, L. F. Johnson, and J. N. Shoolery, Varian Associates, 1962, Compound No. 34.

11) T. Yamaguchi, T. Tsuchiya, and S. Umezawa, *J. Antibiot.*, **30**, 71 (1977).

12) T. Usui, T. Tsuchiya, and S. Umezawa, *J. Antibiot.*, **31**, 991 (1978).

† A small amount of aqueous ammonia was added[12] to the TACu solution of the sample until the solution gave a constant $[M]^{436}_{TACu}$ value.

Elimination Reactions of Halohydrin Derivatives with a Palladium(0) Complex

Toshio SUGITA,* Yoshimi SHIRAIWA, Masayuki HASEGAWA, and Katsuhiko ICHIKAWA

Department of Hydrocarbon Chemistry, Faculty of Engineering, Kyoto University, Sakyo-ku, Kyoto 606

(Received June 1, 1979)

Stilbene bromohydrin derivatives (Ph–CHBr–CHY–Ph: Y=OAc, OSO_2CH_3, OCH_3, SCH_3) and stilbene dibromide underwent β-elimination reaction with tetrakis(triphenylphosphine)palladium(0) to give stilbene. The stereochemistry of eliminations is nonselective except in the case of dibromide, where *anti*-selectivity is observed. A coupling reaction occurred favorably in the case of Y=OCH_3.

Organometallic compounds substituted by oxygen groups at the β-position have well been known as oxymetallation adducts when the metals are heavy ones such as mercury and thallium, and it is clear that the acid-catalyzed deoxymercuration proceeds in *anti* fashion. In the case of palladium, oxypalladation adducts of olefins have been postulated as intermediates of the Wacker oxidation of ethylene to acetaldehyde and many other palladium(II)-catalyzed reactions of olefins. Although unusually stable alkoxypalladation adducts of ethylene have been isolated,[1] the oxypalladation adducts are usually not isolable except for some atypical examples, in which the complexes are stabilized by the chelation of intramolecular double bonds,[2] because of their propensity to undergo elimination.

Previously, we reported that *syn*-elimination was favored when bromohydrin derivatives were treated with butyllithium, and that, particularly, 1-bromo-2-methoxy-1,2-diphenylethane (**5**) gave a stereospecific *syn*-elimination product in nonpolar solvents. In this reaction, we postulated a β-methoxylithium compound as a transient intermediate.[3]

Phosphine complexes of palladium(0) undergo oxidative addition reaction with alkyl halides, making a carbon–palladium σ-bond. If bromohydrin derivatives undergo oxidative addition to palladium complexes, the oxypalladation compounds should be produced. In this paper, we wish to report the results of the reactions of stilbene bromohydrin derivatives and dibromide with a palladium(0) complex.

Results and Discussion

The reactions of stilbene dibromide (**2**) and bromohydrin derivatives, 1-bromo-2-acetoxy-1,2-diphenylethane (**3**), 1-bromo-2-methylsulfonyloxy-1,2-diphenylethane (**4**), 1-bromo-2-methoxy-1,2-diphenylethane (**5**), and 1-bromo-2-methylthio-1,2-diphenylethane (**6**), with tetrakis(triphenylphosphine)palladium(0) (**1**) in degassed benzene produced only stilbene (**7**) in good yields, except in the case of **5**. In the case of **5**, a coupling product, 1,4-dimethoxy-1,2,3,4-tetraphenylbutane (**8**), was the primary product, accompanied by a small amount of *trans*-**7**. The structure of **8** was identified by means of its analytical and spectral data. As the NMR spectrum is simple, the **8** obtained seems to be diastereomerically not so complex, but its stereochemical structure has not yet been confirmed.

Oxypalladation adducts of olefins almost without exception eliminate palladium, accompanied by β-hydrogen, to produce olefins on which the oxygen groups remain. Only one report on the deoxypalladation-type eliminations has, to our knowledge, been made by Heck.[4] In contrast with the usual behavior of oxypalladation adducts, stilbene was the only elimination product, and no vinyl ether, esters, or other products derived from them were detected in the present case. If the reactions occurred by a series of steps, the oxidative addition of substrates to the palladium(0) complex to produce β-oxypalladium intermediates and the subse-

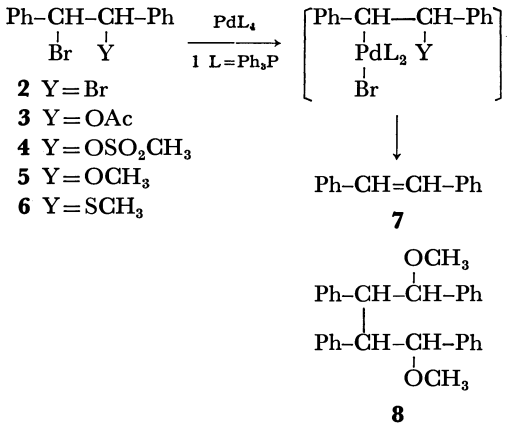

TABLE 1. REACTION OF STILBENE BROMOHYDRIN DERIVATIVES WITH PALLADIUM(0) COMPLEX[a]

Substrate (mmol)		$(Ph_3P)_4Pd$ (mmol)	Product yield (%)[b]	
			trans-**7**	Others
dl-**2**	(0.88)	0.89	60	*cis*-**7** 20
meso-**2**	(0.89)	0.87	94	
threo-**3**	(0.87)	0.87	45[c]	
erythro-**3**	(0.87)	0.90	48[c]	
threo-**4**	(0.87)	0.87	84	
erythro-**4**	(0.88)	0.87	70	
threo-**5**	(0.87)	0.87	(12)	**8** (60)
erythro-**5**	(0.75)	0.75	(11)	**8** (67)
erythro-**5**	(1.76)[d]	1.76	(trace)	**8** (20)
erythro-**6**	(0.88)	0.87	98	

a) Unless otherwise noted, in degassed benzene (100ml) at 80 °C under argon for 2 h. b) Isolated yields. The values in parentheses were determined by GLPC. c) The actual yields were higher than those indicated because incomplete chromatographic separations were achieved. d) In 100 ml of degassed benzene at room temperature for 30 h.

quent elimination of palladium from these intermediates, stilbene should be formed by the elimination of the palladium and the β-substituents.

Whether the present elimination proceeds *via* β-oxypalladium intermediates or by another mechanism, *e.g.*, the palladium-catalyzed synchronous elimination of the bromine and the heteroatom groups, is yet uncertain. When the leaving group is methoxyl, however, a coupling reaction takes place, together with elimination. Stille and Lau reported that the oxidative additions of 9-bromofluorene and α-bromophenylacetate to **1** gave, as the coupling products, 9,9′-bifluorenyl and ethyl 2,3-diphenylsuccinate respectively.[5] They concluded that these coupling products were attributable to the decomposition of transient alkylpalladium intermediates. An analogous reaction can be expected in the case of methoxy bromide (**5**), which undergoes oxidative addition to **1** to give the coupling product (**8**) and dibromobis(triphenylphosphine)palladium(II). Since methoxyl group is a poor leaving group, the coupling reaction is favored over the elimination. In the reactions of the other substrates, only the elimination reaction takes place, because the acetoxyl, methylsulfonyloxy, and methylthio groups as well as bromide are better leaving groups.

From these considerations, it is plausible to consider that the β-oxy- and β-thio-substituted bromides undergo oxidative addition to the palladium(0) complex to afford the β-oxy- and β-thiopalladium(II) complexes, which then eliminate the palladium accompanied by the β-substituents. As the palladium of the palladium-complex intermediates is coordinatively saturated by a strong phosphine ligand in the present case, it is considered to be difficult to abstract the β-hydrogen as a hydride, and so deoxypalladation-type elimination occurs.

Since both *erythro* and *threo* isomers of the bromohydrin derivatives gave only *trans*-**7**, the eliminations are considered to proceed nonstereoselectively. Stille and his co-workers reported that the oxidative addition of optically active phenethyl bromides to palladium(0) complexes proceeded with inversion of configuration at the carbon bearing bromine,[6] and that the decomposition of the oxidative addition products in the coupling reactions proceeded *via* a radical mechanism.[5] The loss of stereoselectivity in the elimination reactions of the bromohydrin derivatives with **1** can be consistently explained. The β-oxy- and β-thiopalladium complexes formed with inversion of configuration at the carbon bearing bromine eliminate the palladium *via* a radical mechanism, though no CIDNP could be observed, and the stereoselectivity is lost during the process of decomposition of the palladium complexes.

As contrasted with the other substrates, *dl*-**2** underwent a elimination reaction with **1** to give *cis*-**7** in a 20% yield. The fact that the thermodynamically very unstable *cis*-**7** was obtained from the *dl*-isomer as well as the fact that *meso*-**2** gave only *trans*-**7** indicates that the reaction proceeds with *anti* stereoselectivity. Since bromide is a better leaving group, the reaction seems to proceed more concertedly. An analogous result was obtained from the reaction of **2** with butyllithium.[3]

Experimental

The substrates were prepared as previously reported.[3] Tetrakis(triphenylphosphine)palladium(0) (**1**) was prepared by the reduction of dichlorobis(triphenylphosphine)palladium-(II) with hydrazine.[7]

General Procedure of the Elimination Reactions. A solution of 0.300 g (0.88 mmol) of *dl*-**2** and 1.032 g (0.89 mmol) of **1** in 100 ml of degassed anhydrous benzene was heated at 80 °C under argon for 2 h. The mixture was cooled and poured into water, and then extracted with ether. The ether extract was dried over magnesium sulfate, and a yellow complex precipitated was removed by filtration. GLPC analysis (150 °C, 5% Silicone SE-30 on Chromosorb W, 1 m) of the concentrated filtrate showed the presence of *cis*- and *trans*-**7**. The concentrated filtrate was dissolved in warm hexane, the undissolved crystal was filtered off, from which 33 mg of triphenylphosphine oxide was isolated. The filtrate was again concentrated and chromatographed by means of a silica-gel (Wakogel C-200) column, using hexane as an eluant; 32.1 mg (20%) of *cis*- and 95.4 mg (60%) of *trans*-**7** were isolated, their identities were confirmed by GLPC and NMR.

Reaction of 1-Bromo-2-methoxy-1,2-diphenylethane (5) with 1. Formation of 1,4-Dimethoxy-1,2,3,4-tetraphenylbutane (8). (a) A 2.67 g (9.17 mmol) sample of *erythro*-**5** was allowed to react with 10.58 g (9.15 mmol) of **1** in 400 ml of degassed anhydrous benzene at 70 °C under argon for 4 h. The reaction mixture was then worked up as described above. GLPC analysis (150 and 250 °C, SE-30 on Chromosorb W, 1 m) indicated that several components were present in the hexane-soluble product (0.96 g). *trans*-Stilbene and biphenyl were confirmed by the retention-time comparisons with authentic samples. The main peak, appearing at a longer retention time, was isolated as follows: the hexane-soluble product was chromatographed by means of a silica-gel (Wakogel C-200) column using mixed elutants the compositions of which were gradually changed from pure hexane to pure benzene. The fractions eluted with mixtures of benzene: hexane=7: 3 and 9: 1 were combined and concentrated. The product was purified twice more by means of the column chromatograph and finally by recrystallization with hexane to give **8**, mp 139—139.5 °C, yield 85.5 mg. Found: C, 85.48; H, 7.06%. Calcd for $C_{30}H_{30}O_2$: C, 85.27; H, 7.16%. IR ($CHCl_3$) 1600, 1490, 1450, 1100, 695, 585 cm^{-1}. NMR ($CDCl_3$) δ=7.20—6.67 (m, 20, C_6H_5), 4.45 (d, 2, J=6 Hz, CH–OR), 3.65 (d, 2, J=6 Hz, CH–Ph), 3.15 (s, 6, OCH_3). MS (75 eV), *m/e* (relative intensity), 422 (M^+, 0.03), 407 (0.02), 390 (0.03), 389 (0.03), 375 (0.01), 358 (0.7), 301 (0.3), 300 (0.3), 270 (1), 211 (17), 179 (43), 165 (26), 122 (78), 121 (98), 105 (59), 91 (100), 77 (93).

(b) To 100 ml of a degassed benzene solution of 2.03 g (1.76 mmol) of **1** was added 0.512 g (1.76 mmol) of *erythro*-**5**. The solution was allowed to stand at an ambient temperature under argon. After 30 h, an orange-red crystalline precipitate, dibromobis(triphenylphosphine)palladium(II), was isolated by filtration, mp 283 °C (dec) (lit,[5] mp 230—250 °C dec), Found: C, 54.68; H, 3.88%. Calcd for $C_{36}H_{30}Br_2P_2Pd$: C, 54.66; H, 3.82%.

The filtrate was concentrated to give a mixture of crystalline solids, which were then taken up in hexane. The undissolved substance was filtered off, and the filtrate was concentrated. The residue was taken up in ether and washed with water. The ether solution was passed through a short alumina column, bis(2-ethylhexyl) phthalate was added as an internal standard, and then it was submitted to GLPC analysis (230 °C, 5% SE-30 on Chromosorb W, 1 m). The

analysis showed the presence of *trans*-**7** (a small amount) and **8** (20% yield).

References

1) T. Majima and H. Kurosawa, *J. Chem. Soc., Chem. Commun.*, **1977**, 610.

2) J. Chatt, L. M. Vallarino, and L. M. Venanzi, *J. Chem. Soc.*, **1957**, 3413; C. B. Anderson and B. J. Burreson, *Chem. Ind. (London)*, **1967**, 620; J. K. Stille and R. A. Morgan, *J. Am. Chem. Soc.*, **88**, 5135 (1966).

3) T. Sugita, J. Nakagawa, K. Nishimoto, Y. Kasai, and K. Ichikawa, *Bull. Chem. Soc. Jpn.*, **52**, 871 (1979).

4) R. F. Heck, *J. Am. Chem. Soc.*, **90**, 5535 (1968).

5) J. K. Stille and K. S. Y. Lau, *J. Am. Chem. Soc.*, **98**, 5841 (1976).

6) P. K. Wong, K. S. Y. Lau, and J. K. Stille, *J. Am. Chem. Soc.*, **96**, 5956 (1974); K. S. Y. Lau, R. W. Fries, and J. K. Stille, *ibid.*, **96**, 4983 (1974); K. S. Y. Lau, P. K. Wong, and J. K. Stille, *ibid.*, **98**, 5832 (1976).

7) L. Malatesta and M. Angoletta, *J. Chem. Soc.*, **1957**, 1186.

Alkylation of Bromocyclopropanes and Bromoarenes by Means of Dibutylcopperlithium and Alkyl Halides

Tamejiro HIYAMA,* Hajime YAMAMOTO, Koji NISHIO, Katuzi KITATANI, and Hitosi NOZAKI

Department of Industrial Chemistry, Kyoto University, Yoshida, Kyoto 606

(Received June 6, 1979)

Treatment of bromocyclopropanes with excess dibutylcopperlithium in tetrahydrofuran at −48 °C gives the respective organocopper intermediates which upon quenching with excess alkyl halides afford alkylated cyclopropanes with retention of the configuration. This process is applied to the synthesis of methyl cascarillate. Bromoarenes are also reduced with dibutylcopperlithium and allylarenes are prepared therefrom.

Organocopper reagents are widely used for C–C bond formation including addition reaction to unsaturated compounds[1] and coupling reaction with organic halides, tosylates, acetates and epoxides.[2] Synthetically versatile is the alkylation reaction of organocuprates (dialkylcoppermetals). Stereochemical studies have stimulated arguments on the mechanism of alkylation,[2] *i.e.* S_N2 like alkyl transfer pathway or oxidative addition followed by reductive coupling pathway. In both cases the ligand of the copper reagent and organic residue of substrates combine to give the alkylated products. The third mechanism is transmetallation suggested earlier by Whitesides *et al.*[3] for the reaction of dialkylcopperlithium (R_2CuLi) and aryl haldies (ArX), wherein a mixed homocuprate (ArCuRLi) is initially formed which subsequently gives an equilibrium mixture (Ar_2CuLi, ArCuRLi, R_2CuLi) of cuprates.[2] Therefore this process has been of no synthetic value. However, the synthetic utility of the transmetallation is suggested recently in the *gem*-dialkylation of 1,1-dibromocyclopropanes with dialkylcopperlithium.[4] This process involving a cyclopropylcopper intermediate is now proved to be general and useful especially for the stereocontrolled synthesis of substituted cyclopropanes.[5]

Bromocyclopropanes **1a**—**1h** were stereoselectively prepared by protonating or alkylating the carbenoid derived from the corresponding *gem*-dibromide.[6] When bromocyclopropane **1** was treated with 4 to 5 equivalents of dibutylcopperlithium in tetrahydrofuran (THF) at −48 °C to 0 °C, the starting bromide was all consumed. Quenching with excess allyl bromide (or methyl iodide) at the same temperature afforded allylcyclopropane **2** (or methylcyclopropane **3**) in good yield. The results are summarized in Table 1. In sharp contrast to the

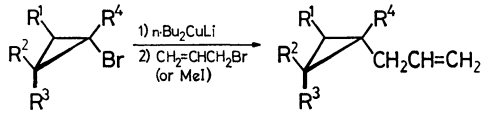

1 2

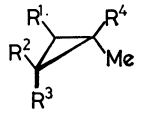

3

	R^1	R^2	R^3	R^4
a	H	C_6H_5	H	H
b	H	H	C_6H_5	H
c	H	C_6H_5	H	CH_3
d	H	n-C_6H_{13}	H	H
e	H	$C_6H_5CH_2OCH_2$	H	H
f	$-(CH_2)_4-$		H	H
g	$-(CH_2)_4-$		H	$CH_2CH=CH_2$
h	$-(CH_2)_4-$		CH_3	H

Table 1. Alkylation of bromocyclopropane **1**

Bromocyclopropane (mg) (mmol)	Dibutylcopper-lithium(mmol)	Alkyl halide[a] (ml)	Temp of alkylation (°C)	Product yield[b] (mg) (%)
1a (289) (1.5)	6.0	A (1.5)	−48	**2a**[c] (224) (97)
1a (193) (1.0)	4.0	M (1.0)	−48	**3a** (117) (91)
1a (294) (1.5)	6.0	A (1.0)	−48	**6**+**7** (269) (97)[d]
1b (131) (0.66)	2.7	A (0.8)	−48	**2b** (96) (91)
1c (199) (0.94)	3.8	A (1.0)	0	**2c** (111) (68)[e]
1d[f] (411) (2.0)	10	A (1.5)	−48	**2d**[g] (319) (96)
1e (360) (1.5)	6.0	A (1.5)	−48	**2e** (197) (65)
1f (264) (1.5)	6.0	A (1.5)	−48	**2f** (119) (57)
1g (217) (1.0)	5.0	M (1.0)	0	**3g** (145) (96)
1h (199) (1.0)	5.0	A (1.5)	0	**2h** (102) (65)
1h (152) (0.80)	5.0	O (1.0)[h]	0	**4** (—) (50)[i]

a) A: allyl bromide, M: methyl iodide, O: octyl bromide. b) Yield of purified product unless otherwise stated. c) The stereochemical assignment is based on the general observation that PMR absorption of the substituent cis to the phenyl group appears at higher field than that of the trans isomer. See Ref. 6. d) A 7: 3 mixture of **6** and **7**. e) *r*-1-Butyl-1-methyl-*t*-2-phenylcyclopropane (Ref. 4) was a by-product (36mg, 20%). f) An 83: 17 mixture of **1d** and its cis isomer. g) An 84: 16 mixture of **2d** and its cis isomer. h) Octyl bromide dissolved in HMPA (1 ml) was added. In the absence of HMPA the yield of **4** was *ca.* 30%. i) The yield was estimated by GLC.

conventional alkylation of organic halides with dibutylcopperlithium, no trace of butylated products were formed in the present reaction.

The salient features of this alkylation process are:

(1) The net retention of configuration is observed in the allylation of **1a** and **1b** furnishing **2a** and **2b** respectively as the sole product.

(2) Even tertiary halides (*e.g.* **1c** and **1g**) are alkylated to give the *gem*-dialkylated cyclopropanes. Thus, the two different alkyl groups are introduced both as electrophiles in contrast to the previous method.[4]

(3) The reaction reported here is sometimes more efficient than that which employs bromine-lithium exchange reaction.[7] Treating **1a** with *t*-butyllithium and then with excess allyl bromide gave only a 23% yield of **2a**. The *exo*-bromonorcarane derivative **1h** did not afford **2h** in the organolithium reaction.

(4) As the bromocyclopropanes are not reduced in ether, the highly coordinating THF is indispensable for the reaction.

(5) Control experiments using **1h** as the substrate revealed that at least 3.5 mol of dibutylcopperlithium is required for the complete consumption of **1h**. All attempts to reduce **1a** with *n*-Bu(PhS)CuLi (2 mol), *n*-Bu(*i*-Pr_2N)CuLi (2 mol) or *t*-Bu_2CuLi (4 mol) failed and the recovery of the starting bromide was observed. Although an excess of dibutylcopperlithium (generally 4 to 5 mol) is required for the bromocyclopropanes and the excess cuprate also reacts with alkyl halides, such by-products are fortunately removed readily by simple distillation or chromatography.

(6) Alkylation of **1h** by use of an unactivated bromide such as octyl bromide turned out rather sluggish. The yield was somewhat improved by adding hexamethylphosphoric triamide (HMPA) as the cosolvent. The stereochemistry of the product was unambiguously determined by the synthesis of the authentic specimen as shown in Scheme 1.

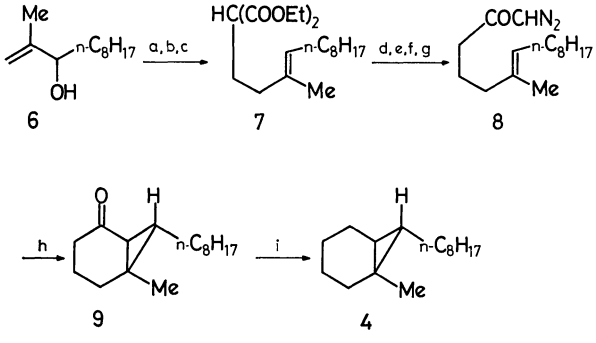

a: CH_2I_2, Zn–CuCl; b: 48% HBr: c: $NaCH(COOEt)_2$; d: OH^-; e: AcOH; f: $SOCl_2$; g: CH_2N_2; h: $CuSO_4$–Cu, Δ; i: N_2H_4, KOH.

Scheme 1.

(7) Dibutylcopperlithium treatment of **1d** followed by alkylation with methyl bromoacetate gave methyl cascarillate (**10**),[8] a component of an essential oil of *Croton eluteria* Benett. This compound was alternatively obtained by permanganate-periodate oxidation of **2d** followed by esterification. The resulting ester was completely identical with the authentic sample spectrometrically and chromatographically.

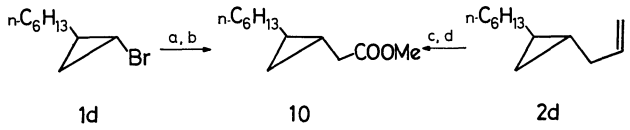

a: *n*-Bu_2CuLi; b: $BrCH_2COOMe$; c: $KMnO_4$–$NaIO_4$; d: CH_2N_2.

(8) Alkylation by means of vinyl bromide was very slow and this reaction turned out futile practically.

Following experiments serve to give insight of the reaction intermediates. Metallation of **1a** and quenching with 3-methyl-2-butenyl bromide gave an S_N2' coupling product **11** mainly. Treatment with benzoyl chloride yielded *trans*-1-benzoyl-2-phenylcyclopropane (95%)and the reaction with methyl propiolate gave methyl *trans*-3-(2-phenylcyclopropyl)acrylate (46%), whereas attempted reaction with benzaldehyde gave only a 26% yield of the adduct and the one with acetone failed to succeed. Decomposition of the intermediary species occurred at 60 °C to give phenylcyclopropane (56%), while oxidation with air yielded *trans*-1-butyl-2-phenylcyclopropane (**14**)[9] (60%). These results favor a mixed homocuprate **13** as an intermediate which is ascribed to the C–Cu bond formation with retention of configuration. Such bromine-copper exchange reaction is not unprecedented.[3] However, it should be noted that butyl-cyclopropyl coupling is almost completely suppressed in **13**. Discrete existence of such mixed cuprate

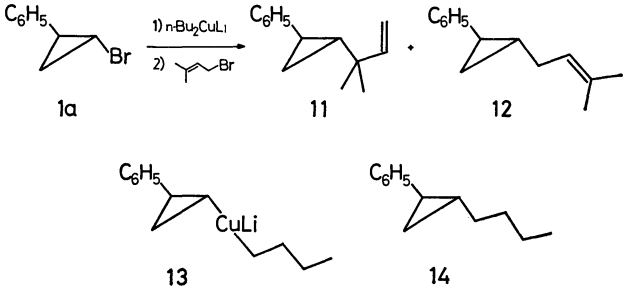

is suggested recently in the reaction of propargyl acetate with dimethylcopperlithium at low temperature.[10]

The reaction of *cis*-1-chloro-2-phenylcyclopropane with dibutylcopperlithium took 4 days at room temperature, and the product proved to be **14**. GLC monitoring revealed that chlorine was directly substituted with butyl group in sharp contrast to the reaction of **1a**. It is noteworthy that the substitution occurs under inversion.

Bromoarenes underwent the Br–Cu exchange reaction under the same conditions in sharp contrast to the results by Whitesides *et al.*[3] who used ether as the solvent. Upon quenching with allyl bromide allylarenes were produced in good yields. For example, bromobenzene was treated successively with dibutylcopperlithium and allyl bromide to give allylbenzene in 64% isolated yield. Some results are listed in Table 2. HMPA cosolvent improved somewhat the yield of the allylated products. Again butylbenzene was not produced to any extent, and **15** and **16** were produced

Table 2. Allylation of bromoarenes[a]

Bromoarene (mg) (mmol)	Allyl bromide[b] (1.0 ml each)	Product yield[c] (mg) (%)
C_6H_5Br (157) (1.0)	A	$C_6H_5CH_2$–CH=CH_2 (77) (64)
C_6H_5Br (158) (1.0)	B	**15**+**16** (100) (68)[d]
C_6H_5Br (157) (1.0)	B[e]	**15**+**16** (113) (77)[f]
C_6H_5I (204) (1.0)	B[e]	**15**+**16** (88) (60)[f]
1-Bromonaphthalene (200) (0.97)	A[e]	1-Allylnaphthalene (122) (75)

a) Dibutylcopperlithium (4.0 mmol) was used for haloarene (1.0 mmol). b) A: allyl bromide. B:3-methyl-2-butenyl bromide. c) Isolated yield. d) 73: 27. e) Dissolved in HMPA (2 ml). f) 70: 30.

in the reaction with 3-methyl-2-butenyl bromide, the S_N2' product **15** being the major one. Thus the mixed cuprate of type ArCu(*n*-Bu)Li apparently is an intermediate responsible for the observed reactivity. The s character of C–Br bond is the key for the Br–Cu exchange reaction.

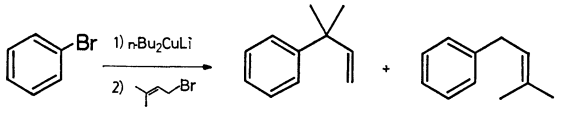

15 16

Experimental

All the reactions were carried out under an argon atmosphere and the temperatures are uncorrected. The cold bath of −48 °C was prepared by mixing Dry Ice with *m*-xylene. The IR spectra were recorded on a Shimadzu spectrometer 27-G, MS on a Hitachi RMU-6L, and PMR on a JEOL JNM-PMX 60 or Varian EM 390 spectrometer. Butyllithium was purchased from Aldrich Chemical Co. Ltd. Tetrahydrofuran (THF) was dried on benzophenone ketyl and freshly distilled before use.

Standard Procedure for Dibutylcopperlithium Reduction of Cyclopropyl Bromides and Alkylation. Butyllithium hexane solution (1.65 M, 7.2 ml, 12.0 mmol) was added over 5 min period at −48 °C to a suspension of copper(I) iodide (1.13 g, 6.0 mmol) in THF (20 ml) under an argon atmosphere. After 10 min cyclopropyl bromide (1.5 mmol) in THF (2 ml) was added to the resulting black solution of dibutylcopperlithium, and the reaction mixture was stirred further for 30 min, then treated with excess of an electrophile. After 30 min the reaction mixture was quenched at −48 °C with methanol (1 ml), diluted with aq sat. ammonium chloride and extracted with ether. Product was purified by preparartive TLC.

trans-*1-Allyl-2-phenylcyclopropane (**2a**)*: Bp 55—60 °C (bath temp)/15 Torr. PMR (CCl_4): δ 0.6—1.5 (m, 3H), 1.5—1.9 (m, 1H), 2.0—2.4 (m, 2H), 4.9—6.3 (m, 3H), 6.8—7.4 (m, 5H); IR (neat): 1639, 1605, 1030, 995, 913, 790, 756, 700 cm^{-1}; MS *m/e* (rel intensity): 156 (M^+, 6), 117 (100), 104 (36), 91 (35). Found: C, 90.84; H, 9.01%. Calcd for $C_{12}H_{14}$: C, 91.08; H, 8.92%.

cis-*1-Allyl-2-phenylcyclopropane (**2b**)*: Bp 70—75 °C (bath temp)/20 Torr; PMR (CCl_4): δ 0.5—2.4 (m, 6H), 4.7—6.0 (m, 3H), 7.10 (s, 5H); IR (neat): 1640, 1605, 1501, 1026, 990, 910 cm^{-1}; MS *m/e* (rel intensity): 158 (M^+, 4), 117 (83), 115 (100), 104 (35), 91 (23). Found: C, 90.80; H, 9.15%. Calcd for $C_{12}H_{14}$: C, 91.08; H, 8.92%.

r-*1-Allyl-1-methyl*-t-*2-phenylcyclopropane (**2c**)*: Bp 60—63 °C (bath temp)/14 Torr; PMR (CCl_4): δ 0.7—0.9 (m+s (δ 0.75), 5H), 1.7—2.3 (m, 3H), 4.8—5.3 (m, 2H), 5.5—6.3 (m, 1H), 7.12 (s, 5H); IR (neat): 3060, 1640, 1604, 1500, 1068, 1022, 992, 912, 790, 700 cm^{-1}; MS *m/e* (rel intensity): 172 (M^+, 1), 131 (100), 104 (17), 91 (39). Found: C, 90.34; H, 9.52%. Calcd for $C_{13}H_{16}$: C, 90.64; H, 9.36%.

trans-*1-Allyl-2-hexylcyclopropane (**2d**)*. A THF (2 ml) solution of **1d** and its cis isomer[6] (83: 17 as assayed by GLC) (411 mg, 2.0 mmol) was added to dibutylcopperlithium (10 mmol) in THF (30 ml) at −48 °C. After 30 min allyl bromide (1 ml) was added, and 30 min thereafter the reaction mixture was worked up. Preparative TLC (silica gel, hexane, R_f 0.7—0.9) of the crude product gave a mixture of **2d** and its cis isomer (84: 16 as revealed by GLC) (319 mg, 96% yield). Each product was separated and characterized. **2d**: bp 70—75 °C (bath temp)/20 Torr; PMR (CCl_4): δ 0.0—0.6 (m, 4H), 0.6—1.7 (m, 13H), 1.93 (t, J=5 Hz, 2H), 4.7—5.2 (m, 2H), 5.4—6.1 (m, 1H). IR (neat): 3060, 1638, 1022, 994, 912 cm^{-1}; MS *m/e* (rel intensity): 166 (M^+, 0.9), 138 (11), 125 (11), 124 (11), 96 (24), 95 (23), 81 (50), 69 (80), 67 (93), 56 (97), 54 (87), 41 (100). Found: C, 86.92; H, 13.43 %. Calcd for $C_{12}H_{22}$: C, 86.66; H, 13.34%.

cis-*1-Allyl-2-hexylcyclopropane*. This compound was characterized by spectrometric data: PMR (CCl_4): δ −0.2—0.0 (m, 1H), 0.6—1.8 (m, 16H), 1.8—2.3 (m, 2H), 4.8—5.3 (m, 2H), 5.6—6.1 (m, 1H). IR (neat): 3060, 1640, 1024, 995, 913 cm^{-1}; MS *m/e* (rel intensity): 166 (M^+, 0.4), 96 (24), 95 (21), 81 (50), 67 (91), 55 (86), 54 (78), 41 (100).

trans-*1-Allyl-2-(benzyloxymethyl)cyclopropane (**2e**)*: Bp 80—85 °C (bath temp)/15 Torr; PMR (CCl_4): δ 0.2—1.1 (m, 4H), 2.00 (t, J=6 Hz, 2H), 3.2—3.4 (2H, ABM), 4.43 (s, 2H), 4.8—5.4 (m, 2H), 5.5—6.2 (m, 1H), 7.23 (s, 5H); IR (neat): 3080, 1638, 1496, 1095, 1028, 996, 914, 740, 703 cm^{-1}; MS *m/e* (rel intensity): 202 (M^+, 0), 173 (1), 117 (7), 107 (8), 91 (100). Found: C, 82.98; H, 8.99%. Calcd for $C_{14}H_{18}O$: C, 83.17; H, 8.97%.

7-exo-*Allylnorcarane (**2f**)*: Bp 52—55 °C (bath temp)/18 Torr; PMR (CCl_4): δ 0.2—0.9 (m, 3H), 0.9—2.3 (m, 10H), 4.8—5.3 (m, 2H), 5.6—6.3 (m, 1H); IR (neat): 3080, 1635, 990, 910 cm^{-1}; MS *m/e* (rel intensity): 136 (M^+, 8), 121 (13), 107 (18), 95 (76), 79 (47), 67 (100). Found: C, 88.02; H, 11.99%. Calcd for $C_{10}H_{16}$: C, 88.16; H, 11.84%.

7-endo-*Allyl*-7-exo-*methylnorcarane (**3g**)*. To a THF (10 ml) solution of dibutylcopperlithium (5.0 mmol) at −48 °C was added **1g** (217 mg, 1.0 mmol) dissolved in THF (2 ml). After stirring at −48 °C for 30 min and at 0 °C for 30 min methyl iodide (1 ml) was added. Fifteen min thereafter the reaction was stopped by usual work-up. TLC purification (silica gel, hexane) gave **3g** (R_f 0.8—0.9, 145 mg, 96%). Bp 65—72 °C (bath temp)/22 Torr; PMR (CCl_4): δ 0.4—2.2 (m+s (δ 1.88), 15H), 4.5—6.0 (m, 3H); IR (neat): 3050, 1635, 995, 910 cm^{-1}. MS *m/e* (rel intensity): 150 (M^+, 0.9), 135 (13), 109 (96), 67 (100). Found: C, 87.95; H, 12.36%. Calcd for $C_{11}H_{18}$: C, 87.92; H, 12.08%.

7-exo-*Allyl-1-methylnorcarane (**2h**)*: Bp 70—75 °C (bath temp)/20 Torr; PMR (CCl_4): δ 0.2—0.7 (m, 2H), 0.7—2.3 (m+s (δ 1.03), 13H), 4.7—5.2 (m, 2H), 5.5—6.2 (m, 1H); IR (neat): 1635, 990, 905 cm^{-1}; MS *m/e* (rel intensity): 150 (M^+, 4), 121 (9), 109 (61), 96 (87), 81 (80), 67 (100). Found: C, 88.13; H, 12.20%. Calcd for $C_{11}H_{18}$: C, 87.92; H, 12.08%.

*Methyl Cascarillate (**10**)*. A THF (2 ml) solution of **1d** (stereochemically pure) (208 mg, 1.0 mmol) was added to a THF (10 ml) solution of dibutylcopperlithium (5.0 mmol) at −48 °C. After stirring at −48 °C for 30 min and at 0 °C for 5 min methyl bromoacetate (1.5 ml) was added all at once, and the reaction mixture was allowed to warm to room temperature in 20 h. Preparative TLC (silica gel,

hexane) of the crude product gave **10** (R_f 0.6—0.7, 151 mg, 75% yield). IR (neat): 3060, 1740, 1168, 1013 cm^{-1}; PMR ($CDCl_3$): δ 0.1—1.7 (m, 17H), 2.15 (d, J=6 Hz, 2H), 3.57 (s, 3H); MS *m/e*: 198 (M^+).

*Alternative Synthesis of Methyl Cascarillate (**10**).* To a well-stirred mixture of **2d** (and its cis isomer, 84: 16) (63 mg, 0.38 mmol), potassium carbonate (20 mg) in *t*-butyl alcohol (6 ml) and water (4 ml) was added an aqueous solution (10 ml) of sodium metaperiodate (550 mg) and potassium permanganate (20 mg). The resulting mixture was vigorously stirred for 3 h at room temperature, and then extracted with chloroform. Concentration of the chloroform extract gave an oil which was dissolved in ether (10 ml) and mixed with excess diazomethane ether solution. Usual work-up and purification (preparative TLC, silica gel, hexane–dichloromethane 3: 1, R_f 0.2—0.3) gave a mixture of **10** and its cis isomer (85: 15) (53 mg, 67% yield). Each product was separated by preparative GLC and compared with the authentic sample.[8]

trans-*1-(1,1-Dimethyl-2-propenyl)-2-phenylcyclopropane (**11**) and* trans-*1-(3-methyl-2-butenyl)-2-phenylcyclopropane (**12**).* To dibutylcopperlithium (6.0 mmol) solution prepared as above was added **2a** (294 mg, 1.5 mmol) dissolved in THF (2 ml) at −48 °C. After 30 min 3-methyl-2-butenyl bromide (1 ml) was added and the reaction mixture was stirred for 30 min and worked up. Preparative TLC (silica gel, hexane, R_f 0.4—0.5) gave a mixture (7: 3) of **11** and **12** (269 mg, 97% yield). Each product was separated by preparative GLC (Apiezon L, 10% on Celite 545, 3 m, 180 °C). **11**: bp 55—60 °C (bath temp)/14 Torr; PMR (CCl_4): δ 0.6—1.5 (m+s (δ 1.03), 9H), 1.65 (t, J=6 Hz, 2H), 4.7—5.2 (m, 2H), 5.75 (dd, J=18, 10 Hz, 1H), 6.8—7.3 (m, 5H); IR (neat): 1635, 1605, 1004, 914 cm^{-1}; MS *m/e* (rel intensity): 186 (M^+, 3), 143 (9), 132 (21), 117 (72), 115 (44), 104 (100), 91 (72), 82 (88), 41 (78). Found: C, 90.19; H, 9.88%. Calcd for $C_{14}H_{18}$: C, 90.26; H, 9.74%. **12**: bp 55—60 °C (bath temp)/14 Torr; PMR (CCl_4): δ 0.5—1.8 (m+2s (δ 1.60, 1.70), 11H), 2.07 (t, J=6 Hz, 2H), 5.17 (t, J=6 Hz, 1H), 6.7—7.3 (m, 5H); IR (neat): 1670, 1605, 1500, 1030 cm^{-1}; MS *m/e* (rel intensity): 186 (M^+, 4), 171 (3), 145 (21), 130 (27), 117 (100), 115 (39), 104 (40), 95 (38), 91 (48). Found: C, 90.23; H, 9.99%. Calcd for $C_{14}H_{18}$: C, 90.26; H, 9.74%.

*1-Methyl-7-*exo*-octylnorcarane (**4**).* A THF (2 ml) solution of **1h** (152 mg, 0.80 mmol) was added dropwise at −48 °C to dibutylcopperlithium (5.0 mmol) in THF (10 ml). After stirring for 10 min at −48 °C and 2 h at 0 °C octyl bromide (1 ml) in HMPA (1 ml) was added to the reaction mixture which was stirred at 0 °C for 1 h and then worked up. As the crude product was contaminated with the recovered bromide, dodecane and hexadecane, the yield of **4** (50%) was estimated by GLC. Preparative GLC gave a pure sample to **4** completely identical with the authentic specimen. PMR (CCl_4): δ 0.2—0.4 (m, 2H), 0.7—2.1 (m+s (δ 1.01), 28H); IR (neat): 2920, 2850, 1463, 1370 cm^{-1}; MS *m/e* (rel intensity): 222 (M^+, 18), 123 (15), 109 (72), 96 (68), 81 (100), 67 (74), 55 (64).

*Synthesis of Authentic Specimen of **4**.* Octylmagnesium bromide was prepared from octyl bromide (58 g, 0.30 mol) and magnesium (8.0 g, 0.33 mol) in ether (150 ml). The magnesium reagent was cooled to 0 °C and methacrylaldehyde (14.0 g, 0.20 mol) dissolved in ether (20 ml) was added dropwise over 30 min. After the addition was completed the reaction mixture was stirred at room temperature for 1 h, heated to reflux for 1 h, then cooled to room temperature and worked up. Distillation of the product at 83—84 °C/1.1 Torr gave **6** (35.0 g, 94% yield). PMR (CCl_4): δ 1.70 (s, 3H), 3.8—4.2 (m, 1H), 4.6—4.9 (m, 2H); IR (neat): 3350, 1660, 898 cm^{-1}. Found: C, 78.49; H, 13.36%. Calcd for $C_{12}O_{24}O$: C, 78.19; H, 13.13%.

A mixture of **6** (18.4 g, 0.10 mol), copper(I) chloride (4.95 g, 0.05 mol) and zinc powder (32.7 g, 0.50 mol) and ether (80 ml) was heated for 30 min, mixed with diiodomethane (67.0 g, 0.25 mol) and again heated to reflux overnight. Filtration and concentration gave a crude cyclopropylmethyl alcohol derivative which was added to 48% hydrobromic acid (100 ml) cooled at 0 °C in 3 min, and the mixture was vigorously stirred for 7 min. Extractive work-up with ether and distillation at 90—92 °C/0.06 Torr gave an unstable homoallyl bromide (5.65 g, 22% yield).

The homoallyl bromide dissolved in ethanol (6 ml) was added at 0 °C to diethyl sodiomalonate (prepared from diethyl malonate (4.80 g, 0.030 mol) and sodium ethoxide (0.030 mol) in ethanol (20 ml)). After stirring at 0 °C for 30 min and at reflux temperature for 4 h, the solvent was evaporated *in vacuo*. The residue was triturated with water and extracted with ether. Purification of the crude product gave **7** (3.27 g, 44% yield). Bp 130—133 °C/1 Torr. PMR (CCl_4): δ 0.7—2.2 (m+br s (δ 1.60), 30H), 3.0—3.2 (m, 1H), 4.13 (q, J=7 Hz, 4H), 5.10 (t, J=7 Hz, 1H); IR (neat): 1730, 1250, 1145, 1030 cm^{-1}. MS *m/e* (rel intensity): 295 (M^+−OEt, 11), 249 (14), 173 (100), 160 (93), 133 (43), 95 (45), 81 (88), 68 (84), 55 (70), 40 (59). Found: C, 70.50; H, 10.75%. Calcd for $C_{20}H_{36}O_4$: C, 70.54; H, 10.66%.

The malonate **7** (3.27 g) in 95% ethanol (13 ml) was mixed with potassium hydroxide (3.0 g) and heated at reflux temperature for 3 h, and then the solvent was evaporated *in vacuo*. To the residue was added acetic acid and the mixture was heated to reflux for 2 days. Work-up was performed by adding water, extracting with ether 4 times, washing the ethereal extracts with brine, drying the organic phase with sodium sulfate and by concentrating under reduced pressure. Distillation gave the corresponding monocarboxylic acid (1.47 g, 57%), bp 130—140 °C (bath temp)/0.03 Torr; PMR (CCl_4): δ 0.7—2.4 (m+s (δ 1.58), 26H), 5.10 (t, J=7 Hz), 11.7 (br s, 1H); IR (neat): 3600—2400, 1705 cm^{-1}. Found: C, 75.21; H, 12.01%. Calcd for $C_{15}H_{28}O_2$: C, 74.95; H, 11.74%.

Thionyl chloride (0.82 g, 6.9 mmol) was added to the carboxylic acid obtained as above and dissolved in benzene (8 ml), and the solution was heated to reflux for 1 h. Subsequent distillation gave the corresponding acid chloride (1.06 g, 74% yield). Bp 125 °C (bath temp)/0.05 Torr. The acid chloride was allowed to react with excess diazomethane ether solution at 0 °C overnight. Concentration *in vacuo* gave a crude diazo ketone **8** which was dissolved in cyclohexane (24 ml) and this solution was added over 1 h to the suspension of copper powder (110 mg) and copper(II) sulfate (7 mg) in cyclohexane (9 ml) heated at the reflux temperature. After 2 h the reaction mixture was cooled and filtered. Concentration of the filtrate and preparative TLC of the residue gave the norcaran-2-one derivative **9** (166 mg, 19% yield from the acid chloride). Bp 70—73 °C (bath temp)/1 Torr. IR (neat): 1678 cm^{-1}; MS *m/e*: 236 (M^+).

The ketone **9** (160 mg, 0.68 mmol) was mixed with 80% hydrazine hydrate (2.82 g, 45 mmol), hydrazine hydrochloride (577 mg, 5.5 mmol) and triethylene glycol (15.3 g). The mixture was heated at 130 °C for 2.5 h, mixed with potassium hydroxide (842 mg) and further heated at 210 °C for 2.5 h, while volatile compounds were distilled off. The residue and the distillate were mixed with water and extracted with ether. Concentration of the organic phase and subsequent preparative TLC gave **4** (82 mg, 54% yield). This compound was completely identical with the product obtained from **1h**. Bp 100—105 °C (bath temp)/13 Torr. Found: C, 86.18; H,

13.90%. Calcd for $C_{16}H_{30}$: C, 86.40; H, 13.60%.

Thermal Decomposition of the Intermediate ***13***. To dibutylcopperlithium (4.0 mmol) in THF (10 ml) was added **1a** (193 mg, 1.0 mmol) dissolved in THF (2 ml) at −48 °C. The reaction mixture was stirred at −48 °C for 30 min and subsequently heated to reflux for 1 h. Usual work-up and preparative TLC (silica gel, hexane–ether 10: 1, R_f 0.8) gave phenylcyclopropane (65 mg, 56%) characterized spectrometrically.

Air Oxidation of the Intermediate ***13***. Dibutylcopperlithium (4.0 mmol) and **1a** (199 mg, 1.0 mmol) were mixed at −48 °C as above and after 30 min dry air was bubbled into the reaction mixture for 1 h. The initially black solution gradually turned to green, when the reaction mixture was quenched with methanol. Work-up and TLC analysis showed 7 UV sensitive products which were separated by preparative TLC. Three of them were characterized: *trans*-1-butyl-2-phenylcyclopropane (**14**)[9] (R_f 0.5—0.65, 106 mg, 60%), *trans*-1-iodo-2-phenylcyclopropane (R_f 0.45, 21 mg, 12% yield) and 2,2′-diphenyl-1,1′-bicyclopropane (R_f 0.25, 9.2 mg, 8%). The last compound showed bp 110—115 °C (bath temp)/0.05 Torr; PMR (CCl_4): δ 0.6—1.9 (m, 8H), 6.7—7.3 (m, 10H); IR (neat): 3070, 3030, 3000, 1605, 1502, 1030, 905, 755, 700 cm^{-1}; MS *m/e* (rel intensity): 234 (M^+, 1.6), 180 (18), 143 (100), 128 (53), 115 (34), 91 (34). Found: C, 92.33; H, 7.79%. Calcd for $C_{18}H_{18}$: C, 92.26; H, 7.74%.

Th Reaction of the Intermediate ***13*** *with Methyl Propiolate*. To the intermediate **13** prepared by the standard procedure from **1a** (196 mg, 1.0 mmol) and dibutylcopperlithium (4.0 mmol) at −48 °C was added methyl propiolate (0.8 ml). The reaction mixture was stirred at −48 °C for 2 h, and then worked up. Preparative TLC (silica gel, hexane–ether 20: 3) gave phenylcyclopropane (R_f 0.7—0.8, 17 mg, 14%) and methyl *trans*-3-(2-phenylcyclopropyl)acrylate (R_f 0.3—0.4, 93 mg, 46%) which showed bp 110—115 °C (bath temp)/2 Torr; PMR (CCl_4): δ 1.1—2.3 (m, 4H), 3.61 (s, 3H), 5.80 (d, J=16 Hz, 1H), 6.48 (dd, J=9, 16 Hz, 1H), 6.8—7.3 (m, 5H); IR (neat): 1710, 1638, 1605, 1503, 1250, 1142, 978, 753, 700 cm^{-1}; MS *m/e* (rel intensity): 202 (M^+, 9), 169 (13), 142 (98), 128 (84), 111 (100), 98 (71), 91 (35). Found: C, 77.44; H, 6.98%. Calcd for $C_{13}H_{14}O_2$: C, 77.20; H, 6.98%.

The Reaction of the Intermediate ***13*** *with Benzaldehyde*. Benzaldehyde (0.81 ml, 8.0 mmol) was added to the intermediate **13** prepared from **1a** (196 mg, 1.0 mmol) and dibutylcopperlithium (4.0 mmol). After 30 min the reaction mixture was worked up. Preparative TLC purification (silica gel, hexane–ether 3: 1) gave phenylcyclopropane (R_f 0.7—0.8, 41 mg, 35%), and an adduct (R_f 0.1—0.2, 57 mg, 26%). The adduct was a mixture of two diastereomers, each isomer being separated by preparartive TLC (silica gel hexane–ether 1: 1). The one of R_f 0.5—0.6 (11 mg) showed following properties: bp 140—145 °C (bath temp)/0.07 Torr; PMR (CCl_4): δ 0.6—1.6 (m, 3H), 1.6—2.1 (m, 1H), 2.20 (br s, 1H), 4.31 (d, J=6 Hz, 1H), 6.7—7.5 (m, 10H); IR (neat): 3350, 3060, 3030, 1605, 1500, 1031, 765, 700 cm^{-1}; MS *m/e* (rel intensity): 206 (M^+-H_2O, 12), 120 (100), 107 (33), 91 (38), 79 (35), 77 (25). Found: C, 85.95; H, 7.44%. Calcd for $C_{16}H_{16}O$: C, 85.68; H, 7.19%. The second diastereomer (R_f 0.4—0.5, 39 mg) gave bp 138—141 °C (bath temp)/0.05 Torr; PMR (CCl_4): δ 0.6—1.7 (m, 3H), 1.7—2.1 (m, 2H), 4.15 (d, J=7 Hz, 1H), 6.8—7.4 (m, 10H); IR (neat): 3350, 3040, 1603; 1505, 1018, 760, 700 cm^{-1}; MS *m/e* (rel intensity): 206 (M^+-H_2O, 25), 120 (100), 107 (38), 91 (44), 79 (38), 77 (31). Found: C, 85.83; H, 7.19%. Calcd for $C_{16}H_{16}O$: C, 85.68; H, 7.19%. Stereochemical assignment was not accomplished.

Quenching the Intermediate ***13*** *with Benzoyl Chloride*. Benzoyl chloride (0.93 ml, 8.0 mmol) was added to **13** prepared from **1a** (192 mg, 1.0 mmol) and dibutylcopperlithium (4.0 mmol) at −48 °C, and the mixture was stirred at −48 °C for 30 min. Usual work-up and preparative TLC (silica gel, hexane–ether 20: 3, double development) gave 1-phenylbutanone (R_f 0.5—0.7, 802 mg, 5.0 mmol) and 1-benzoyl-2-phenylcyclopropane (R_f 0.4—0.5, 220 mg, 95% pure, 95% yield) which exhibited mp 43.5—44.0 °C; PMR (CCl_4): δ 1.2—1.6 (m, 1H), 1.6—2.0 (m, 1H), 2.3—2.9 (m, 1H), 7.03 (s, 5H), 7.2—7.5 (m, 3H), 7.6—8.1 (m, 2H); IR (Nujol): 3100, 1660, 1601, 1593, 1578, 1502, 1215, 1028, 985, 779, 766, 746, 700 cm^{-1}; MS *m/e*: 222 (M^+).

Attempted Reaction of ***13*** *with Vinyl Bromide*. Dibutylcopperlithium (6.0 mmol) prepared from copper(I) iodide (1.14 g, 6.0 mmol) and butyllithium (2.01 M hexane solution, 6.0 ml, 12 mmol) in THF (20 ml) was mixed with a THF (2 ml) solution of **1a** (299 mg, 1.5 mmol) at −48 °C. After 30 min vinyl bromide (1 ml) and 1 h thereafter HMPA (1 ml) were added, and the reaction mixture was allowed to warm to room temperature over 20 h. Work-up followed by preparative TLC (silica gel, hexane) gave **14** (R_f 0.6—0.65, 35 mg, 13%), 1-phenyl-2-vinylcyclopropane (R_f 0.4—0.5, 38 mg, 18%), and 2,2′-diphenyl-1,1′-bicyclopropane (R_f 0.2—0.3, 79 mg, 45%).

Alkylation of Bromobenzene with 3-Methyl-3-butenyl Bromide. Bromobenzene (158 mg, 1.0 mmol) dissolved in THF (2 ml) was added to dibutylcopperlithium (4.0 mmol) at −48 °C, and the mixture was stirred for 30 min at −48 °C, then warmed to 0°C, treated with 3-methyl-2-butenyl bromide (1 ml) and allowed to react for 40 min. Usual work-up followed by column chromatography on silica gel gave an oil (100 mg, 68%) consisted of **15** and **16**. The ratio (73: 27) was estimated by PMR. **15** showed singlet at δ 1.37, vinylic absorption at δ 4.7—6.3, and **16** broad singlet at δ 1.70 and doublet at δ 3.23.

1-Allylnaphthalene. A Typical Procedure of Allylation of Bromoarenes. Under an argon atmosphere at −48 °C butyllithium (1.8 M hexane solution, 4.4 ml, 8.0 mmol) was added to THF (10 ml) suspension of copper(I) iodide (760 mg, 4.0 mmol). After 15 min 1-bromonaphthalene (200 mg, 0.97 mmol) was added, and the reaction mixture was warmed to 0 °C and stirred for 2 h until the bromide was all consumed. Then allyl bromide (970 mg) dissolved in HMPA (2 ml) and THF (3 ml) was added and the reaction mixture was stirred for 2 h. Work-up was effected by adding water (10 ml) and aq sat ammonium chloride (15 ml), filtering the mixture through Celite pad and by extracting with ether. The organic phase was dried (Na_2SO_4), concentrated and purified by column chromatography (silica gel, 75% yield). Bp 138—150 °C (bath temp)/27 Torr. PMR (CCl_4): δ 3.72 (d, J=6 Hz, 2H), 4.7—6.4 (m, 3H), 6.8—8.1 (m, 7H); IR (neat): 1595, 1506, 990, 910 cm^{-1}; MS *m/e*: 168 (M^+).

This research was financially assisted by the Ministry of Education, Science and Culture, Japanese Government (Grant-in-Aid for Scientific Research No. 247077).

References

1) G. Posner, *Org. React.*, **19**, 1 (1972); H. O. House, *Acc. Chem. Res.*, **9**, 59 (1976); J. F. Normant, *Synthesis*, **1972**, 63; "New Applications of Organometallic Reagents in Organic Syntheses," in J. Organomet. Chem. Library, ed by D. Seyferth, Elsevier, Amsterdam, (1976), Vol. 1, p. 219; *Pure Appl. Chem.*, **50**, 709 (1978).

2) G. Posner, *Org. React.*, **22**, 253 (1975).

3) G. M. Whitesedes, W. F. Fischer, Jr., J. S. Flippo, Jr., R. W. Basche, and H. O. House, *J. Am. Chem. Soc.*, **91**, 4871 (1969).

4) K. Kitatani, T. Hiyama, and H. Nozaki, *J. Am. Chem. Soc.*, **98**, 2362 (1976); *Bull. Chem. Soc. Jpn.*, **50**, 1600 (1977).

5) Preliminary report has appeared in H. Yamamoto, K. Kitatani, T. Hiyama, and H. Nozaki, *J. Am. Chem. Soc.*, **99**, 5816 (1977).

6) K. Kitatani, T. Hiyama, and H. Nozaki, *J. Am. Chem. Soc.*, **97**, 949 (1975); *Bull. Chem. Soc. Jpn.*, **50**, 3288 (1977).

7) E. J. Corey and P. Ulrich, *Tetrahedron Lett.*, **1975**, 3685.

8) S. R. Wilson and K. A. Prodan, *Tetrahedron Lett.*, **1976**, 4231. We are indebted to Professor Wilson for sending us authentic samples of methyl cascarillate and its cis isomer.

9) K. Kitatani, H. Yamamoto, T. Hiyama, and H. Nozaki, *Bull. Chem. Soc. Jpn.*, **50**, 2158 (1977).

10) J.-M. Dollat, J.-L. Luche, and P. Crabbé, *J. Chem. Soc., Chem. Commun.*, **1977**, 761.

Kinetic Study for the Reaction of (Arylthio)trimethylstannane with Benzoyl Chloride Giving *S*-Aryl Thiobenzoate.

Seizi KOZUKA* and Ikuya NARIBAYASHI

Department of Applied Chemistry, Faculty of Engineering, Osaka City University, Sugimoto-cho, Sumiyoshi, Osaka 558

(Received June 14, 1979)

A kinetic study has been conducted on the reaction of (arylthio)trimethylstannane with benzoyl chloride giving chlorotrimethylstannane and *S*-aryl thiobenzoate. The reaction has been found to obey a second order kinetic equation. A mechanism involving bimolecular nucleophilic attack of the sulfur atom on the acyl carbon has been suggested for the reaction based on the substituent effects of arylthio and benzoyl moieties.

Several different mechanisms are conceivable for the cleavage reactions of group IVb–VIb bonds with various reagents as expressed by the following general formula. Namely, the IVb element can form a coordinated

$$\equiv M\text{–}Y\text{–} + E\text{–}Nu \longrightarrow \equiv M\text{–}Nu + E\text{–}Y\text{–}$$

M = Si, Ge, Sn *etc.*, Y = O, S, Se *etc.*
E–Nu = H_2O, ROH, RCOOH, RX, RCOX, RS(O)X *etc.*

intermediate and the complex has been suggested as the reaction intermediate in the reactions of silyl ether hydrolysis,[1] acetoxysilane[2] and thiosilane[3] with carboxylic acids on the basis of kinetic results. Assuming the nucleophilicity of the VIb element

$$R_3'SiOCOCH_3 \text{ (or } R_3'SiSR'') + RCOOH \rightleftharpoons \left[CH_3\overset{O}{\overset{\|}{C}}OSi^-(R_3')O\overset{+OH}{\overset{\|}{C}}R\right] \overset{\text{slow}}{\longrightarrow} \left[CH_3\overset{+OH}{\overset{\|}{C}}OSi^-(R_3')O\overset{O}{\overset{\|}{C}}R\right] \rightleftharpoons R_3'SiOCOR + CH_3COOH \text{ (or } R''SH)$$

played an important role in the course of reaction, a nucleophilic reaction involving an onium intermediate would result instead of the 5-coordination of the IVb element. The reaction of thiostannane with haloalkane is a typical reaction of this type.[4]

$$R_3'SnSR'' + RX \overset{\text{slow}}{\longrightarrow} [R_3'SnS^+(R'')R\ X^-] \longrightarrow R_3'SnX + RSR''$$

Another possible mechanism for the reaction is a 4-centered cyclic process.[5] Thus, different mechanisms would be expected for individual reactions based on the coordination ability of the group IVb element, nucleophilicity of the group VIb atom and also the nature of the reactant, E–Nu. In this paper, the mechanism of the reaction of (arylthio)trimethylstannane with benzoyl chloride will be reported.

Results and Discussion

Product Analysis. The reactions of (arylthio)-trimethylstannanes with benzoyl chlorides have been found to give *S*-aryl thiobenzoate and chlorotrimethylstannane quantitatively. No other product in the reaction mixture was found by NMR analysis. The products were isolated and identified. The reaction

$$Me_3SnSC_6H_4\text{–}X\text{-}p + p\text{-}Y\text{–}C_6H_4COCl \longrightarrow Y\text{–}C_6H_4COSC_6H_4\text{–}X + Me_3SnCl$$

X, Y = H, CH_3, Cl, OCH_3

thus appeared to be similar to analogous reactions of this type.[6] This reaction provides a novel route to prepare thiocarboxylic acid *S*-esters.

Kinetics and Mechanism. Rate of reaction of (arylthio)trimethylstannanes with benzoyl chlorides in carbon tetrachloride solutions were measured by monitoring the relative ratio of ^{1}H-NMR trimethyl signals of the thiostannane (δ 0.33—0.38 ppm) and chlorostannane (δ 0.63 ppm) with time. Second order rate constants were obtained with good reproducibility, the results of which are summarized in Table 1.

Table 1. Rate constants for the reaction of p-$XC_6H_4SSnMe_3$ (0.48 mol/dm^3) with p-YC_6H_4COCl (0.57 mol/dm^3) in CCl_4

Substituent X	Substituent Y	Temp °C	$k_2 \times 10^5$ dm^3 mol^{-1} s^{-1}	Remarks
MeO	H	34.0	6.6±0.2	$\rho_{X(\sigma)} = -1.6$
Me	H	34.0	4.5±0.1	$\gamma = 0.999$
H	H	34.0	2.3±0.1	
Cl	H	34.0	1.2±0.02	
H	H	42.9	5.2±0.4	$\Delta H^{\neq} = 14.0$ kcal/mol
H	H	50.7	10 ±0.1	$\Delta S^{\neq} = -34.0$ e.u.
H	H	61.9	20 ±2.0	
H	MeO	34.0	1.3±0.05	$\rho_{Y(\sigma)} = +1.1$
H	Me	34.0	1.5±0.1	$\gamma = 0.996$
H	Cl	34.0	4.6±0.1	

The large negative entropy value observed in the present study is in accordance with those of reactions of this type.[2-5a] This may be recognized in terms of an ionic reaction which is conducted in a nonpolar solvent, rather than pπ-dπ bonding[1] since the large negative value observed for the reaction of thiostannane with haloalkane in a nonpolar solvent has been shown to fall in a normal magnitude for a bimolecular reaction when conducted in a polar solvent.[4]

The Hammett plot of the rates of reaction of substituted arylthiostannanes (substituent X) gave a straight line with a negative ρ value which is reasonable in magnitude for a reaction involving sulfonium ion formation positioned α- to the phenyl ring bearing the substituent.[7] A quite comparable ρ value was also observed for the reaction of the same thiostannane with haloalkane and the reaction has been suggested to proceed *via* a sulfonium intermediate.[4] As an analogy, the mechanism of the reaction of the thiostannane with

acyl halide can be formulated as following, involving a nucleophilic attack of the sulfur atom on the acyl

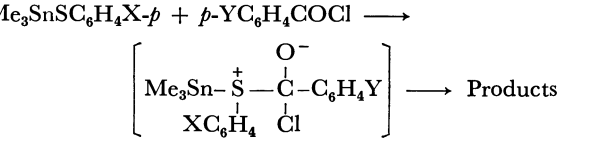

carbon. The positive and smaller ρ value due to the substituent Y on the benzoyl moiety is consistent with the mechanism since the negative charge in the intermediate is localized in the β-position to the aryl ring bearing the substituent.

Experimental

Materials. Preparation of the thiostannanes have previously been reported.[4] All solvents and benzoyl chlorides were purified prior to use.

Product Analysis. Trimethyl(phenylthio)stannane (1.40 g) and benzoyl chloride (0.70 g) were dissolved in CCl_4 (10 cm^3) and heated at 60 °C for 16 h in a sealed tube. NMR analysis confirmed the presence of only chlorotrimethylstannane and *S*-phenyl thiobenzoate. Chlorotrimethylstannane was obtained by distillation (65%, bp 59 °C/18 mmHg; 1 mmHg=133.322 Pa) and *S*-phenyl thiobenzoate was isolated from the residue by recrystallization (72%, mp 55 °C from $CHCl_3$–C_6H_{14}, lit,[8] 56 °C, IR $\nu_{C=O}$ 1662 cm^{-1}). Other thiol esters were isolated similarly: $C_6H_5COSC_6H_4Cl$-*p*, 70%, mp 75—76 °C, lit,[8] 74—75 °C; *p*-$ClC_6H_4COSC_6H_5$, 72%, mp 80—82 °C, lit,[9] 81.5—83 °C; $C_6H_5COSC_6H_4OCH_3$-*p*, 66%, mp 93—94 °C, lit,[9] 93—95 °C; *p*-$CH_3OC_6H_4COSC_6H_5$, 75 %, mp 99—100 °C, lit,[8] 99—100 °C. All the yields are based on the isolated compound in pure form.

Kinetic Procedure. The procedure is essentially the same as that employed for the acyloxy exchange reaction of acetoxysilane.[2] Trimethyl(phenylthio)stannane (40 mm^3, 59 mg) and benzoyl chloride (30 mm^3, 36 mg) were dissolved in CCl_4 (370 mm^3) and the reaction monitored by following the ^1H-NMR trimethyl signals of the starting material and the product with time. The second order rate constant was obtained with an experimental error of 5%.

References

1) J. R. Chipperfield and G. E. Gould, *J. Chem. Soc., Perkin Trans. 2*, **1974**, 1324.

2) S. Kozuka, T. Kitamura, N. Kobayashi, and K. Ogino, *Bull. Chem. Soc. Jpn.*, **52**, 1950 (1979).

3) S. Kozuka and T. Kitamura, *Bull. Chem. Soc. Jpn.*, **52**, 3384 (1979)

4) S. Kozuka and S. Ohya, *J. Organomet. Chem.*, **149**, 161 (1978); *Bull. Chem. Soc. Jpn.*, **51**, 2651 (1978).

5) a) D. N. Harpp, B. T. Friedlander, C. Larsen, K. Steliou, and A. Stockton, *J. Org. Chem.*, **43**, 3481 (1978). This mechanism has often been applied to explain the course of the reaction of this type, for example: R. C. Paul, K. K. Soni, and S. P. Narula, *J. Organomet. Chem.*, **40**, 355 (1972).

6) a) RSOCl (RSCl)+R'OSiMe_3 (R'SSiMe_3), Ref. 5a; b) RSO_2F+R'OSiMe_3, P. Ykman and H. K. Hall Jr., *J. Organomet. Chem.*, **116**, 153 (1976); c) RCOCl+R'SSiMe_3 *etc.*, E. W. Abel and D. A. Armitage, *J. Chem. Soc.*, **1964**, 5975; d) RSCl (RSOCl, RSO_2Cl)+Bu_3SnOMe, S. Kozuka and T. Hayama, *Memoirs Fac. Eng. Osaka City University*, **19**, 181 (1978); e) RCOCl+R'SnOR", J. C. Pommier and J. Valade, *C. R. Acad. Sci.*, **260**, 4549 (1965).

7) S. Kozuka, S. Taniyasu, A. Kikuchi, and K. Ogino, *Chem. Lett.*, **1979**, 129.

8) "Beilstein Organische Chemie," **9**, pp. 421, 423.

9) K. Miyaki and S. Yamagishi, *Yakugaku Zasshi*, **76**, 436 (1956).

Synthesis and Properties of *o*-Thioquinone Methides Having Ketene Aminal, Ketene Acetal, Ketene Monothioacetal, or Ketene Dithioacetal Group

Kyung-Tae KANG, Renji OKAZAKI, and Naoki INAMOTO*

Department of Chemistry, Faculty of Science, The University of Tokyo, Hongo, Bunkyo-ku, Tokyo 113

(Received June 15, 1979)

Reaction of 1,2-benzodithiole-3-thione with *N,N'*-dialkyl-1,2-ethanediamine afforded *o*-thioquinone methides with a ketene aminal group (**6**) in high yields. Two similar thionaphthoquinone methides were also prepared. *o*-Thioquinone methide derived from *N,N'*-dimethyl-*o*-phenylenediamine was prepared from 3-chloro-1,2-benzodithiol-3-ylium chloride (**10**). These compounds were found to exist as a monomer of a considerable betaine nature. Reactions of **6a** (*N,N'*-dimethyl derivative) with dimethyl acetylenedicarboxylate and dibenzoylacetylene led to [4+2] adducts. *o*-Thioquinone methides with a ketene acetal group were obtained from desulfurization of spiro[1,3-benzodioxole-2,3'-[1,2]benzodithiole] with trimethyl phosphite, which are equilibrated with two kinds of aggregates; one is a dimer and the other is a trimer or a higher oligomer. Reactions of **10** with *o*-mercaptophenol and 1,2-benzenedithiols gave spiro[1,2-benzodithiole-3,2'-[1,3]benzoxathiole] (**29**) and spiro[1,2-benzodithiole-3,2'-[1,3]benzodithiole] (**39** and **40**), respectively. *o*-Thioquinone methide with a ketene monothioacetal group (**30**) was prepared by desulfurization of **29**. The violet compound **30** is equilibrated with a colorless dimer. This *o*-thioquinone methide reacted with olefins and an acetylene having electron-withdrawing groups to give 1,4-cycloaddition products. Similar desulfurization of **39** and **40** gave *o*-thioquinone methides with dithioacetal group. Their properties were very similar to those of *o*-thioquinone methides with dithioacetal group prepared by the photoreaction of **2** with olefins.

Chemistry of *o*-quinonoid compounds (**1**) has been a subject of increasing interest in recent years because of their interesting, chemical and physical properties and synthetic applications.[1,2] For thioquinone methide (**1**, Z=S), however, there has been only a few reports which demonstrated its existence as a transient species.[3]

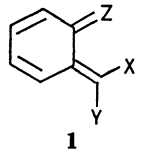

1

Recently, de Mayo[4] and we[5] described the synthesis of stable *o*-thioquinone methides with a ketene dithioacetal group (**3**) from the photoreaction of 1,2-benzodithiole-3-thione (**2**) with olefins, **3** being equilibrated with a colorless head-to-head [4+4] dimer (**4**).

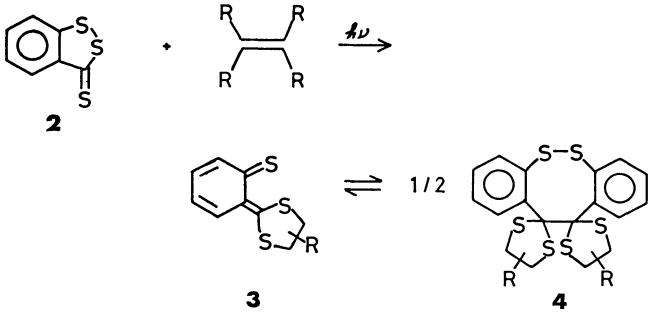

2 **3** **4**

In this paper we report the synthesis and properties of other types of *o*-thioquinone methides (**1**, Z=S) which have a ketene aminal (**1**, X, Y=NR_2), a ketene acetal (**1**, X, Y=OR) or a ketene monothioacetal group (**1**, X=OR, Y=SR). *o*-Thioquinone methides of type **3** (**1**, X=Y=SR) derived from 1,2-benzenedithiols are also described. These *o*-thioquinone methides were found to show significantly different properties from one another.[6]

Results and Discussion

o-Thioquinone Methides with a Ketene Aminal Group. Reaction of 1,2-benzodithiole-3-thione (**2**) with *N,N'*-dialkyl-1,2-ethanediamine (**5**) in ethanol afforded **6** in high yields.[7] In the reaction of **2** with **5a**, the formation of hydrogen sulfide (91% as PbS) and sulfur (94%) was also confirmed.

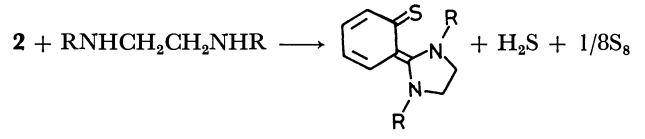

	5	6		
a:	R=Me	99%	91%	94%
b:	R=Et	64%		
c:	R=*n*-Pr	61%		
d:	R=*i*-Pr	78%		
e:	R=*n*-Bu	72%		
f:	R=*n*-C_6H_{13}	56%		

o-Thioquinone methides (**7** (78%) and **8** (85%)) were also prepared in a similar way from 3*H*-naphtho[1,2-*c*]-[1,2]dithiole-3-thione and 3*H*-naphtho[2,3-*c*][1,2]-dithiole-3-thione, respectively.[8]

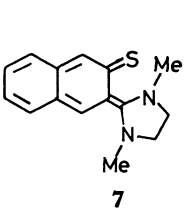

7

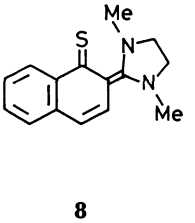

8

Compound **9** (69%) was synthesized by the reaction of the more reactive 3-chloro-1,2-benzodithiol-3-ylium chloride (**10**)[9] with *N,N'*-dimethyl-*o*-phenylenediamine[10] using ion exchange resin as a base. The use

of the resin made the isolation of the water soluble **9** easier.

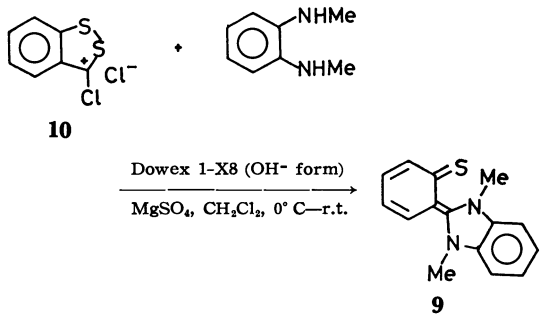

10 **9**

These thioquinone methides (**6**—**9**) were not developed on silica gel even if ether was used as an eluent, suggesting their polar nature. The color of the solution of **6** is pale yellow or colorless, depending on the solvent. The electronic spectra of **6b** in benzene and ethanol showed no concentration dependence, indicating that it exists as a monomer in solution. This is in marked contrast with **3** which is in equilibrium with the dimer. The NMR spectra of **6**—**9** are very similar to one another, implying that other thioquinone methides synthesized here are also monomeric in solution.

Table 1. NMR spectra (δ) of **6**—**9**, **11**, and **13** in methanol-d_4

Compound	*N*-Alkyl	Ethylene	Aromatic
6a	2.91(s)	4.00(s)	6.9—7.4
6b	1.18(t) 3.27(q)	4.04(s)	6.9—7.6
6c	0.81(t) 1.61(sext) 3.20(t)	4.05(br s)	6.9—7.9
6d	1.12(d) 1.34(d) 3.70(sept)	3.96(br s)	6.85—7.74
6e	0.6—1.9(m) 3.25(t)	4.04(br s)	6.9—7.7
6f	0.6—1.9(m) 3.15(t)	4.06(br s)	6.9—7.7
7	2.93(s)	4.06(s)	7.20—8.97
8	2.90(s)	4.01(s)	6.87—7.84(5H) 8.85—9.15(1H)
9	3.78(s)	—	7.65—8.15
11	2.92(s)	4.14(s)	7.4—7.8 2.61[a](3H, s)
13	2.86(s) 3.55(s)	3.62(m) 3.91(m)	7.39(5H, s) 5.77[b](1H, s)

a) SMe protons. b) Methine proton.

Table 2. Electronic spectra of **6b** in various solvents

Solvent	λ_{max}/nm	log ε
Water	252	4.00
Acetic acid	263	3.57
Ethanol	278	4.18
Acetonitrile	299	4.26
N,*N*-Dimethylformamide	303	4.18
Dichloromethane	299	4.06
Benzene	307	4.27

In the NMR spectra (CD_3OD) of **6a**, **7**, **8**, and **9**, the *N*-methyl protons exhibit very far downfield shift (Table 1). These chemical shifts are almost the same as that of **11** prepared from **6a** and methyl iodide, indicating the large contribution of an ionic canonical structure (*e.g.*, **12** for **6**). This is reflected in the

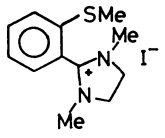

11

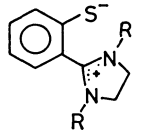

12

solubility of these compounds; for example, **6a** is very soluble in water and alcohols, but only slightly soluble in chloroform and benzene. The importance of the ionic contribution (**12**) to the ground state of **6** was also shown by the solvent effect of the UV spectra of **6b** (Table 2). The more polar the solvent, the shorter the absorption maximum, which indicates the stabilization of the ionic ground state by polar solvents. Here again, these *o*-thioquinone methides are quite different from those with a ketene dithioacetal group (**3**) whose electronic spectra show no essential solvent dependence.[5d]

In the NMR spectra of **6a**, the ethylene protons of the imidazolidine ring appear as a sharp singlet at δ 4.00. At −80 °C it becomes broad but no coalescence occurs, which shows that the imidazolidine ring is rotating freely at this temperature. On the other hand, the ethylene protons of **13** prepared from the reaction of 5-phenyl-1,2-dithiole-3-thione[11] with **5a** appear as AA'BB' multiplet centered at δ 3.62 and 3.91, suggesting the higher double bond nature of the *exo* methylene bond of the imidazolidine.

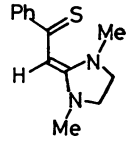

13

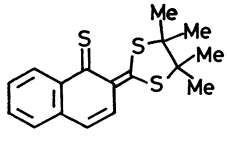

14

In the case of **6**, when R is bulkier than the *n*-propyl group (*i.e.*, **6c**—**6f**), the ethylene protons appear as a broad singlet. In the isopropyl derivative (**6d**), the methyl and ethylene protons appear as a broad singlet at δ 3.96 and a doublet of doublet at δ 1.12 and 1.34 in methanol-d_4, respectively. In 1-chloronaphthalene, however, the ethylene protons appear as AA'BB' multiplet centered at δ 2.72 and 2.98, indicating that the imidazolidine ring is not rotated on NMR time scale. The most reasonable explanation of these observations is that the ring is perpendicular to the benzene ring. In this conformation, the two methyl groups of the isopropyl group are magnetically nonequivalent if the rotation is restricted. The methyl protons of **14**, prepared from the photoreaction of 3*H*-naphtho[1,2-*c*]-[1,2]dithiole-3-thione with 2,3-dimethyl-2-butene in benzene,[12] appear as two singlets at δ 1.56 and 1.62.

Since this type of *o*-thioquinone methide is known to exist as a monomer,[13] the observation of the two singlets indicates the restricted rotation of the dithiole ring. This is in sharp contrast to the fact that the imidazolidine ring in **8** is freely rotating and we regard this as another demonstration of the higher betaine nature of the *o*-thioquinone methides with a ketene aminal group.

Of particular interest is the isolation and stability of **7**, since compounds with 2,3-naphthoquinone structure are usually very unstable[2g,14] and can be isolated only in special cases.[15]

The *o*-thioquinone methides (**6**) are strong enophiles and react with acetylenes having electron-withdrawing groups at room temperature to afford 1,4-cycloaddition products. The reaction of **6a** with dimethyl acetylenedicarboxylate and dibenzoylacetylene gave **15** (76%) and **16** (53%), respectively, and that with *N*-phenylmaleimide afforded rapidly **17** (80%) at 7—8 °C in benzene. The structure of **17** was tentatively assigned by the spectral data; the NMR spectrum showed the *N*-methyl protons as a singlet at δ 3.02 and a broad peak due to six methylene protons at δ 4.0, two protons of which disappeared upon addition of D_2O.

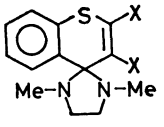

15: X=CO_2Me
16: X=COPh

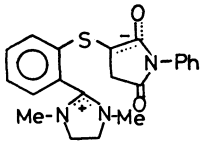

17

o-*Thioquinone Methides with a Ketene Acetal Group.* We considered that 3,3-disubstituted 3*H*-1,2-benzodithiole would be a suitable precursor of *o*-thioquinone methides (**1**, Z=S) with hetero atoms X and Y, because we previously found[12] that desulfurization of spiro compound (**18**) with trivalent phosphorus compound gave in a high yield *o*-thioquinone methide (**19**) which actually exists as a dimer. The only reported example of a compound with a general formula (**20**; X, Y= hetero atom) is **21** which was prepared by the reaction of **2** with *o*-chloranil.[16]

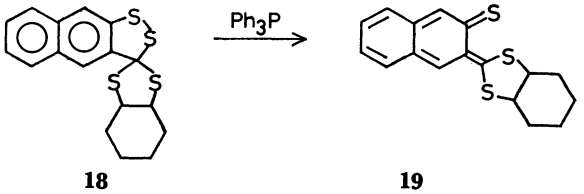

18 **19**

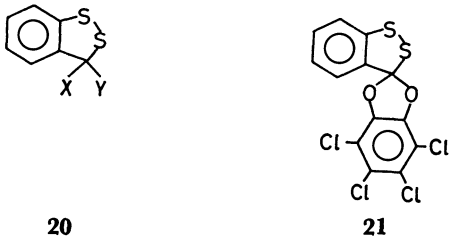

20 **21**

Reaction of the dithiolium salt (**10**) with pyrocatechols gave spiro compounds (**22** and **23**). This reaction has also been applied successfully to the synthesis of spiro compounds, **29**, **39**, and **40** (*vide infra*).

The spiro compounds (**22** and **23**) reacted rapidly with trimethyl phosphite in benzene at room temperature to give white crystals, **24A** and **25A**, respectively. When the filtrate was evaporated and the residue was left for some time, other white crystals (**24B** and **25B**, respectively) were formed.

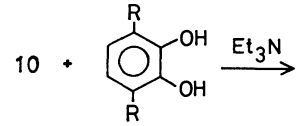

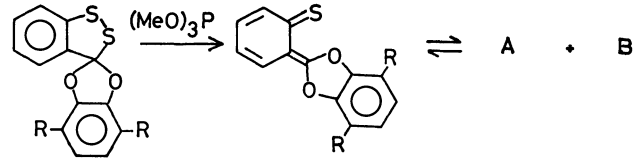

22: R=H 83% **24**: R=H **24A** 88% **24B** 3%
23: R=Me 53% **25**: R=Me **25A** 50% **25B** 28%

The NMR spectra, melting points, and reactivity of **A** and **B** were different from each other both for **24** and **25**; however, the same 1,4-cycloadducts (*i.e.*, **26** and **27**) were obtained by the reaction with *N*-phenylmaleimide irrespective of whether the starting material was **A** or **B**. Their UV spectra depend upon the concentration, indicating that these aggregates, **A** and **B**, are equilibrated with the monomer **24** and **25** in both cases.

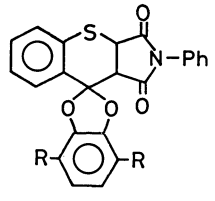

	From **A**	From **B**
26: R=H	85%	91%
27: R=Me	85%	79%

On the basis of molecular weight determination by vapor pressure osmometry in benzene (Found 440, Calcd 456), it was found that the aggregate **24B** was a dimer. High resolution mass spectrum of **24B** also showed the parent peak as a dimer at *m/e* 456.0509 (Calcd for $C_{26}H_{16}O_4S_2$: 456.0491).

Since the aggregates **24A** and **25A** decomposed in benzene at room temperature, the correct molecular weight could not be determined. For example, the molecular weight of **24A** was observed to be 662 at the beginning of the measurement but it decreased gradually by decomposition. Since it takes some time to make a sample for the measurement and **24A** might decompose during this time, we infer that **24A** is a trimer or a higher oligomer.

The NMR spectrum ($CDCl_3$) of **25B** showed its methyl signal at δ 2.30 as a singlet. However, **25A** showed a sharp and weak singlet at δ 2.30 and a broad and strong singlet at δ 2.07 in the methyl region at the

beginning of measurement, but the spectral pattern changed very rapidly; the intensity of the peak at δ 2.30 increased and that of the peak at δ 2.07 decreased. After several hours the NMR pattern of **25A** became very similar to that to **25B**, suggesting the occurrence of the change **25A**→**25B** probably *via* the monomer.

The existence of two types of aggregates is an interesting phenomenon, although their structures could not be determined exactly. However, it is clear that the equilibrium between the aggregate **A** and the monomer is more favorable toward the monomer than the equilibrium for the aggregate **B**, because the afore-mentioned reaction with *N*-phenylmaleimide proceeds much more rapidly for **A** (1 h for **A** *vs.* 20 h for **B** in refluxing benzene) and it is reasonably assumed that the monomer, not the aggregates, reacts with *N*-phenylmaleimide.

The reaction of **24A** with dimethyl acetylenedicarboxylate in refluxing benzene for 5 h gave **28** in 80% yield. The formation of these [4+2] adduct clearly indicates the presence of the monomer in solution, but we could not find any spectroscopic evidence for it.

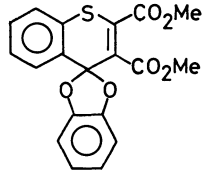

28

o-*Thioquinone Methides with a Monothioacetal Group.* Spiro compound **29**, prepared from **10** and *o*-mercaptophenol, reacted with trimethyl phosphite at room temperature to afford **31** in 92% yield. The structure of **31** was established by its cycloaddition leading to [4+2] adduct (*vide infra*), as in the case with all other *o*-thioquinone methides.

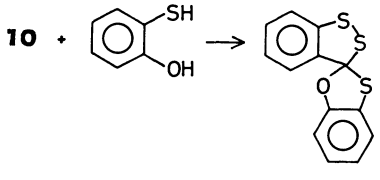

29

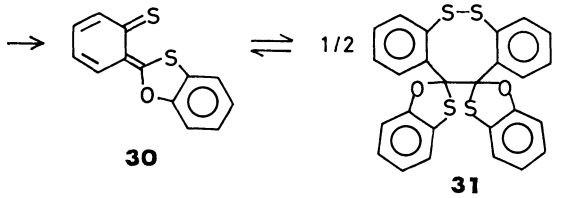

30 **31**

The color of the solution of **31** depends on solvent and temperature. For example, **31** shows violet in dichloromethane or benzene at room temperature, but the cyclohexane solution is almost colorless. Recrystallization of **31** from benzene–ethanol afforded white crystals but the dissolution of the crystals in an appropriate solvent (*e.g.*, dichloromethane) led to a violet solution. The colorless cyclohexane solution turned violet when heated, but the violet color was discharged when the solution was left at room temperature. These facts and the dependence of UV spectrum of **31** on the concentration suggest that the colorless aggregate **31** is also equilibrated with a monomer **30**. The molecular weight determination (vapor pressure osmometry) indicates that the aggregate is a dimer (Found 480, Calcd 488). Although we do not have any experimental evidence for the structure of the dimer, we infer that **31** is a head-to-head dimer by analogy with the equilibrium between **3** and **4**.[5]

The *o*-thioquinone methide **30** also reacted with *N*-phenylmaleimide, fumaronitrile and dimethyl acetylenedicarboxylate to afford **32**, **33**, and **34** in 99, 81, and 85% yields, respectively.

Two methine protons α to the cyano group in **33** appeared as two sets of doublet of doublet of AX type in the NMR spectra of the crude product. The intensity ratio of the two was about 5 : 1 (J_{AX}=6.6 Hz for the major one and J_{AX}=7.8 Hz for the minor one). In the light of the reported value[5c,d] for **35a** (J_{AX}=3.4 Hz) and **35b** (J_{AX}=9.1 Hz), the coupling constants observed for **33** imply that it is a *trans* adduct, suggesting the stereoselectivity of the cycloaddition, although the results for reaction of **30** with maleonitrile is necessary for definite conclusion. The two sets of the doublets of

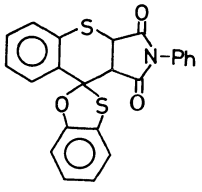

32

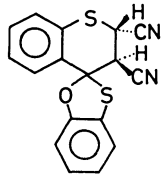

33

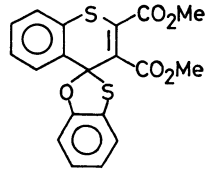

34

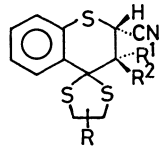

a: R^1=CN, R^2=H

b: R^1=H, R^2=CN

35

doublet observed for **35** are considered to correspond to two isomers with respect to the direction of the oxygen and sulfur atoms of the thioxolane ring.

o-*Thioquinone Methides Derived from 1,2-Benzenedithiols.* *o*-Thioquinone methides (**36**) derived from 1,2-benzenedithiols were prepared with an expectation that they might exist as **38** because of the large contribution of the canonical structure of 18π system as in the case of trithiapentalene systems.[18] There was also another anticipation that there might be a large contribution from the ionic canonical structure (**37**) which would favor the equilibrium between the monomer and the dimer, like **3**⇌**4**, for the monomer.

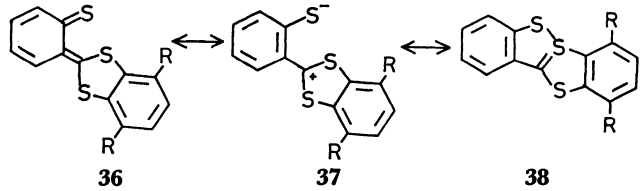

36 **37** **38**

Reaction of the dithiolium salt (**10**) with 1,2-benzenedithiols gave new spiro compounds **39** and **40**. Desulfurization of **39** and **40** with trimethyl phosphite gave **41** and **42**, respectively, in high yields.

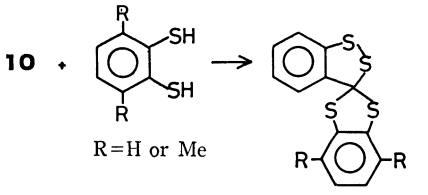

39 R=H 55%
40 R=Me 62%

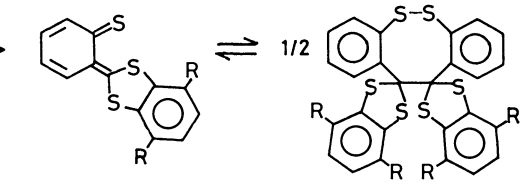

41 R=H 91%
42 R=Me 96%

43 R=H
44 R=Me

Contrary to the above expectations, the properties of **41** and **42** were found to be very similar to those of **3**, and both **41** and **42** exist as an equilibrium mixture between the monomer and the dimer. The structure of the dimers **43** and **44** was assigned a head-to-head dimer by analogy with the case of **3**.[5]

o-Thioquinone methide (**41**) reacted with *N*-phenylmaleimide to give a [4+2] cycloadduct (**45**).

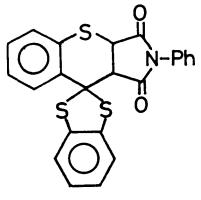

45

Experimental

NMR spectra were recorded with a Hitachi R-20B or R-24B spectrometer, using tetramethylsilane as an internal standard unless otherwise stated. UV and IR spectra were recorded on Hitachi ESP-3 and EPI G-2 spectrometers, respectively. Mass spectra were determined on a Hitachi RMU-6L mass spectrometer (70 eV). High resolution and chemical ionization mass spectra were taken with a JEOL JMS-D300. Molecular weights were measured with a Hitachi 117 Molecular Weight Apparatus (vapor pressure osmometry in benzene at 40 °C). All the melting points were not corrected.

Preparation of o-*Thioquinone Methides (6—8).* An ethanol solution (4 ml) of **2**[19] (567 mg, 3.08 mmol) and *N,N'*-dimethyl-1,2-ethanediamine (320 mg, 3.64 mmol) was refluxed for 4 h. Concentration of the reaction mixture followed by addition of benzene and cooling yielded **6a** (621 mg, 99%) as yellow solid, which was recrystallized from benzene–ethanol; mp 153—155 °C; MS: *m/e* 206 (M^+, 100%), 173 (39), and 135 (16). Found: C, 63.94; H, 7.14; N, 13.39; S, 15.88%. Calcd for $C_{11}H_{14}N_2S$: C, 64.04; H, 6.84; N, 13.58; S, 15.54%.

Thioquinone methides **6b**, **6c**, **6e**, **6f**, **7**, and **8** were also prepared in a similar way from the corresponding dithiolethiones, the yield being 64, 61, 72, 56, 78, and 85%, respectively. In the case of **6d**, it was necessary to heat at 160 °C for 30 h in a sealed tube (78% yield). These *o*-thioquinone methides were purified by recrystallization from benzene–ethanol. Since **6c**, **6e**, and **6f** could not be obtained as crystals, the resultant oils were purified by washing with benzene–hexane.

6b: mp 148—149 °C; MS: *m/e* 234 (M^+, 100%), 201 (87), and 135 (55). Found: C, 66.45; H, 8.00; N, 11.84; S, 13.86%. Calcd for $C_{13}H_{18}N_2S$: C, 66.63; H, 7.74; N, 11.95; S, 13.68%. **6d**: NMR (1-chloronaphthalene): δ (hexamethyldisiloxane) 0.25 (6H, d, J=6.6 Hz), 0.90 (6H, d, J=6.6 Hz), 2.6—2.85 (2H, m), 2.85—3.10 (2H, m), and 3.60 (2H, sept, J=6.6 Hz); MS: *m/e* 262 (M^+, 100%), 230 (98), 220 (43), and 188 (43). **7**: mp 230—232 °C; UV_{max} (EtOH) (log ε): 218 (4.82), 262 (4.58), and 314 nm (4.31); MS: *m/e* 256 (M^+, 100%), 233 (70), and 200 (12). Found: C, 65.63; H, 6.68; N, 10.17; S, 11.71%. Calcd for $C_{15}H_{16}N_2S \cdot H_2O$: C, 65.66; H, 6.61; N, 10.21; S, 11.68%. **8**: mp 204—206.5 °C; UV_{max} (EtOH) (log ε): 223 (4.78), 245 (sh) (4.44), and 348 nm (4.11); MS: *m/e* 256 (M^+, 92%), 233 (100), 200 (12), and 185 (21). Found: C, 70.02; H, 6.32; N, 10.71; S, 12.77%. Calcd for $C_{15}H_{16}N_2S$: C, 70.28; H, 6.29; N, 10.93; S, 12.51%.

Preparation of **9**. To a cold (0 °C), stirred mixture of *N,N'*-dimethyl-*o*-phenylenediamine (594 mg, 4.37 mmol), ion exchange resin (Dowex 1-X8 OH^- form, 10 g), anhydrous magnesium sulfate (638 mg) in dichloromethane (30 ml), was added the dithiolium salt (**10**) (792 mg, 3.55 mmol) in small portions for 1 h and the mixture was stirred at room temperature for 11 h. The resins were collected by filtration and washed with ethanol thoroughly. After removal of the ethanol, the residue was triturated with ethyl acetate to afford **9** (620 mg, 69%); mp 221.5—223 °C; MS: *m/e* 254 (M^+, 41%) and 239 (100).

Preparation of **11**. An acetone solution (7 ml) of **6a** (207 mg, 1.01 mmol) and methyl iodide (1.58 g, 11 mmol) was refluxed for 1.5 h. Evaporation of the solvent gave a crystalline material (329 mg, 94%) whose purity was confirmed by the NMR spectrum. Mp 178.5—180 °C (C_6H_6–EtOH); NMR ($CDCl_3$): δ 2.57 (3H, s), 2.93 (6H, s), 4.13 (2H, m), 4.52 (2H, m), 7.3—7.7 (3H, m), and 8.05—8.22 (1H, m); UV_{max} (EtOH) (log ε): 217 (4.52), 247 (4.21), and 297 (sh) nm (3.29). Found: C, 41.34; H, 5.02; N, 7.95; S, 9.69; I, 36.25%. Calcd for $C_{12}H_{17}N_2SI$: C, 41.39; H, 4.92; N, 8.04; S, 9.21; I, 36.44%.

Preparation of **13**. An ethanol solution (10 ml) of 5-phenyl-1,2-dithiole-3-thione (597 mg, 3.01 mmol) and **5a** (293 mg, 3.33 mmol) was refluxed for 4 h. After removal of the solvent, the residue was recrystallized from benzene–ethanol (430 mg, 62%). A specimen for elemental analysis was obtained by recrystallization from methanol; mp 186—187.5 °C; UV_{max} (EtOH) (log ε): 235 (3.98) and 351 nm (4.36); MS: *m/e* 232 (M^+, 100%) and 200 (28). Found: C, 67.52; H, 7.10; N, 11.93; S, 14.28%. Calcd for $C_{12}H_{16}N_2S$: C, 67.20; H, 6.94; N, 12.06; S, 13.80%.

Reaction of **6a** *with Dimethyl Acetylenedicarboxylate.* An acetonitrile solution (10 ml) of **6a** (207 mg, 1.00 mmol) and dimethyl acetylenedicarboxylate (148 mg, 1.04 mmol) was stood for 10 h at room temperature. After removal of the solvent, the crystalline residue was recrystallized from benzene–hexane to give **15** (264 mg, 76%); mp 148.5—150 °C; NMR ($CDCl_3$); δ 2.31 (6H, s), 3.1—3.4 (4H, m), 3.89 (3H, s), 3.95 (3H, s), and 7.23 (4H, s); MS: *m/e* 348 (M^+, 6%), 290 (100), and 206 (70). Found: C, 58.79; H, 5.91;

N, 8.11; S, 9.57%. Calcd for $C_{17}H_{20}N_2O_4S$: C, 58.60; H, 5.79; N, 8.04; S, 9.20%.

Reaction of ***6a*** *with Dibenzoylacetylene.* An acetonitrile solution (10 ml) of **6a** (281 mg, 1.37 mmol) and dibenzoylacetylene (358 mg, 1.53 mmol) was stood for 4 days at room temperature. After removal of the solvent, the oily residue was triturated with methanol to give **16** (316 mg, 53%) as yellow crystals. A pure specimen could not be obtained since this was partially decomposed by heating in ethanol. Mp 124—125.5 °C (EtOH); NMR ($CDCl_3$): δ 2.27 (6H, s), 2.93 (4H, s), and 7.0—8.0 (14H, m); MS: *m/e* 440 (M^+, trace), 335 (6%), 234 (37), and 206 (100); IR (KBr): 1730 and 1740 cm^{-1} (C=O).

Reaction of ***6a*** *with* N-*Phenylmaleimide.* To a cold (7—8 °C), stirred benzene solution (10 ml) of *N*-phenylmaleimide (154 mg, 0.89 mmol) was added **6a** (175 mg, 0.85 mmol) in portions over a period of 1 h to form red crystals. Stirring was continued at room temperature for 10 h to give **17** (265 mg, 80%). The purification was impossible since it decomposed to an unidentifiable material even when simply washed with ethanol, but the structure was tentatively established by the spectral data. Mp 131—135 °C (dec); NMR (DMSO-d_6): δ 3.02 (6H, s), 3.99 (6H, br s), and 6.6—7.7 (14H, m); MS: *m/e* 348 (2%), 289 (2), 206 (100), 205 (50), and 173 (54); IR (KBr); 1710 cm^{-1} (C=O).

Preparation of ***22*** *and* ***23.*** To a cold (0 °C) and stirred dichloromethane solution (20 ml) of pyrocatechol (1.02 g, 9.30 mmol) and triethylamine (5 ml) was added the salt **10** (1.68 g, 7.56 mmol) in small portions during 1 h, and the solution was stirred at room temperature for 4 h. The reaction mixture was washed with water and the dichloromethane layer was evaporated. The oily residue was subjected to dry column chromatography (DCC) (silica gel, CH_2Cl_2–CCl_4 (1:3)) to give 1.63 g (83%) of **22**; mp 140.5—141.5 °C (ethyl acetate); MS: *m/e* 260 (M^+, 66%) and 196 (100). Found: C, 60.11; H, 2.81; S, 24.53%. Calcd for $C_{13}H_8O_2S_2$: C, 59.98; H, 3.10; S, 24.63%.

Compound **23** was prepared similarly in 53% yield using 3,6-dimethyl-1,2-benzenediol.[20] DCC (silica gel, CH_2Cl_2–CCl_4 (1:9)), PLC (silica gel, ether–hexane (1:3)) and recrystallization from ethanol gave pure **23**; mp 119—120 °C; NMR ($CDCl_3$): δ 2.24 (6H, s), 6.73 (2H, s), and 7.2—7.6 (4H, m); MS: *m/e* 288 (M^+, 93%) and 224 (100). Found: C, 62.35; H, 4.06; S, 22.13%. Calcd for $C_{15}H_{12}O_2S_2$: C, 62.47; H, 4.20; S, 22.23%.

Preparation of ***24*** *and* ***25.*** A benzene solution (2 ml) of **22** (342 mg, 1.32 mmol) and trimethyl phosphite (168 mg, 1.35 mmol) was stirred at room temperature for 20 min. The color of the solution turned from yellow to colorless, and white precipitates were formed. Dry ether was added into this solution with stirring and the crystalline material (**24A**) was collected and washed with ether (264 mg, 88%). The filtrate was evaporated, and stood for some time to obtain another crystalline material, **24B** (8.0 mg, 3%). **24A**: mp 111.5—113 °C (benzene–ether); MS (CI): *m/e* 457 (dimer $+H^+$) and 485 (dimer$+C_2H_5^+$) were observed, but fragments higher than the dimer were not observed. Found: C, 68.30; H, 3.26; S, 13.89%. Calcd for $C_{13}H_8O_2S$: C, 68.40; H, 3.53; S, 14.05%. **24B**: mp 212—213 °C (ethyl acetate); MS (CI): *m/e* 456 (M^+, 5%), 365 (3), 231 (49), 229 (13), 197 (2), 153 (3), 137 (47), 123 (7), and 111 (100). Found: C, 67.84; H, 3.18; S, 14.20%. Calcd for $C_{13}H_8O_2S$: C, 68.40; H, 3.53; S, 14.05%.

Compounds **25A** and **25B** were prepared similarly in 50% and 28% yields, respectively. **25A**: mp 130—131 °C (C_6H_6–Et_2O); NMR ($CDCl_3$); δ 2.30 (s) and 2.07 (bs containing a sharp singlet at δ 2.14) (6H in total), and 6.3—8.0 (6H, m); MS: *m/e* 512 (trace) and 256 (100%). **25B**: mp 187.5—188 °C (AcOEt); NMR ($CDCl_3$): δ 2.30 (6H, s), 6.69 (2H, s), 7.14—7.33 (2H, m), and 7.5—7.8 (2H, m); MS: *m/e* 512 (trace) and 256 (100%).

Reactions of ***24*** *and* ***25*** *with* N-*Phenylmaleimide.* A benzene solution (1.5 ml) of **24A** (116 mg, 0.51 mmol as a monomer) and *N*-phenylmaleimide (97 mg, 0.56 mmol) was refluxed for 1 h under argon. Addition of ethanol to the cooled, stirring solution gave 173 mg (85%) of **26**, which was also prepared (91%) in a similar manner from **24B**, but in this case refluxing for 20 h was necessary. The identity of the adduct **26** from **24A** and **24B** was confirmed by the IR and NMR spectra. Mp 205 °C (dec); MS: *m/e* 401 (M^+, 47%), 292 (72), and 228 (100); IR (KBr): 1715 cm^{-1} (C=O); NMR (C_6D_6): δ 3.16 (1H, d, J=9.6 Hz), 3.83 (1H, d, J=9.6 Hz), 6.4—7.2 (12H, m), and 7.5—7.7 (1H, m).

27 was prepared from both **25A** (reflux for 1 h, 85%) and **25B** (reflux for 50 h, 79%). The adduct **27** from **25A** and **25B** was also confirmed to be the same by the spectral data (IR and NMR) and the fact that there was no depression of mixed melting point. Mp 208—209.5 °C (AcOEt–EtOH); NMR ($CDCl_3$): δ 2.18 (3H, s), 2.29 (3H, s), 3.95 (1H, d, J=9.6 Hz), 4.59 (1H, d, J=9.6 Hz), 6.63 (2H, s), and 6.9—7.9 (9H, m); IR (KBr): 1720 cm^{-1} (C=O); MS: *m/e* 429 (M^+, 31%), 292 (23), and 256 (100). Found: C, 70.12; H, 4.32; N, 3.08; S, 7.52%. Calcd for $C_{25}H_{19}NO_4S$: C, 69.91; H, 4.46; N, 3.26; S. 7.46%.

Reaction of ***24A*** *with Dimethyl Acetylenedicarboxylate.* A benzene solution (3 ml) of **24A** (204 mg, 0.89 mmol as a monomer) and dimethyl acetylenedicarboxylate (141 mg, 1.00 mmol) was refluxed for 5 h under argon. After removal of the solvent, the oily residue was triturated with methanol to give 264 mg (80%) of **28** as white crystals; mp 118—119 °C (EtOH); NMR ($CDCl_3$): δ 3.53 (3H, s), 3.79 (3H, s), and 6.7—7.8 (8H, m); MS: *m/e* 370 (M^+, 45%), 311 (100), and 228 (15); IR (KBr): 1745 cm^{-1} (C=O). Found: C, 61.72; H, 3.70; S, 8.81%. Calcd for $C_{19}H_{14}O_6S$: C, 61.62; H, 3.81; S, 8.66%.

Preparation of ***29.*** The dithiolium salt **10** (213 mg, 0.95 mmol) was added in portions at 0 °C to a stirred dichloromethane solution (5 ml) of *o*-mercaptophenol (140 mg, 1.11 mmol) and triethylamine (0.8 ml). Stirring was continued at room temperature for 3 h, after which the reaction mixture was washed with water. After removal of the solvent, the residue was subjected to PLC (silica gel, CH_2Cl_2–CCl_4 (1:3)) to give yellow crystals of **29** (159 mg, 61%); mp 134—135 °C (EtOAc); MS: *m/e* 276 (M^+, 100%), 244 (17), 212 (56), and 184 (53). Found: C, 56.77; H, 2.62; S, 34.39%. Calcd for $C_{13}H_8OS_3$: C, 56.49; H, 2.92; S, 34.80%.

Preparation of ***31.*** A benzene solution (2 ml) of **29** (563 mg, 2.04 mmol) and trimethyl phosphite (275 mg, 2.21 mmol) was stirred at room temperature for 20 min. The color of the solution turned from yellow to violet, and pale violet precipitates were formed. Ethanol was added to this solution with stirring and the crystalline material was collected (486 mg, 92%). Mp 117 °C (dec) (C_6H_6); MS: *m/e* 456 (M^+-S, 2%), 276 ($M^+/2+S$, 53), 244 ($M^+/2$, 100), 213 (32), and 184 (45).

Reaction of ***31*** *with* N-*Phenylmaleimide.* A mixture of **31** (116 mg, 0.24 mmol) and *N*-phenylmaleimide (88 mg, 0.51 mmol) in benzene (2 ml) was stirred at room temperature for 12 h. After removal of the solvent, the oily residue was triturated with ethanol to give **32** (193 mg, 99%), mp 193 °C (dec) (C_6H_6); NMR (C_6D_6): δ 3.58 (2H, s), 6.5—7.3 (12H, m), and 7.7—7.9 (1H, m); IR (KBr): 1720 cm^{-1} (C=O); MS: *m/e* 417 (M^+, 12%) and 244 (100). Found: C, 66.52; H, 3.49; N, 3.54; S, 15.02%. Calcd for

$C_{23}H_{15}NO_3S_2$: C, 66.17; H, 3.62; N, 3.55; S, 15.36%.

*Reaction of **31** with Fumaronitrile.* A mixture of **31** (248 mg, 0.51 mmol) and fumaronitrile (89 mg, 1.14 mmol) was refluxed in benzene (2 ml) for 40 min. After removal of the solvent, the NMR (in $CDCl_3$) of the residue was measured for the methine protons of the dihydrobenzothiopyran ring. The two methine protons appeared as two sets of AX type doublet of doublet whose intensity was 5: 1; the major one: δ 4.13, 4.24, 4.53, and 4.64 and the minor one: δ 3.88, 4.01, 4.53, and 4.64. In order to remove excess fumaronitrile the crude product was twice washed with ethanol giving **33** (280 mg, 85%). The major isomer was obtained by repeated recrystallization from ethanol; mp 138.5—140 °C (dec); NMR ($CDCl_3$): δ 4.18 (1H, d, J=6.6 Hz), 4.58 (1H, d, J=6.6 Hz), and 6.8—8.1 (8H, m); IR (KBr): 2250 cm^{-1} (C≡N); MS: *m/e* 322 (M^+, 37%) and 244 (100).

*Reaction of **31** with Dimethyl Acetylenedicarboxylate.* A benzene solution (2 ml) of **31** (123 mg, 0.25 mmol) and dimethyl acetylenedicarboxylate (87 mg, 0.62 mmol) was stirred at room temperature for 13 h and refluxed for 5 min. After removal of the solvent, the residue was subjected to PLC (silica gel, CH_2Cl_2–CCl_4 (1: 1)) to give **34** (158 mg, 81%), mp 140—141 °C (EtOH); NMR ($CDCl_3$): δ 3.76 (3H, s), 3.88 (3H, s), and 6.9—7.9 (8H, m); MS: *m/e* 386 (M^+, 21%) and 327 (M^+-CO_2Me, 100).

*Preparation of **39** and **40**.* To a cold (0 °C) and stirred dichloromethane solution (10 ml) of 1,2-benzenedithiol (332 mg, 2.33 mmol) and triethylamine (1.5 ml) was added the salt **10** (463 mg, 2.07 mmol) in portions over a period of 1 h and stirring was continued at room temperature for 4 h. The reaction mixture was washed with water and the organic layer was evaporated. The oily residue was subjected to PLC (silica gel, CH_2Cl_2–CCl_4 (1: 3)) to afford 335 mg (55%) of **39**; mp 144.5—146 °C (AcOEt); MS: *m/e* 292 (M^+, 98%) and 228 (100). Found: C, 53.80; H, 2.50; S, 43.30%. Calcd for $C_{13}H_8S_4$: C, 53.39; H, 2.76; S, 43.85%.

40 was prepared similarly in 62% yield using 3,6-dimethyl-1,2-benzenedithiol, which was synthesized by the same method as that of the unsubstituted derivative. Mp 117—117.5 °C (AcOEt); NMR ($CDCl_3$): δ 2.24 (6H, s), 6.91 (2H, s), 7.2—7.5 (3H, m), and 7.8—8.0 (1H, m); MS: *m/e* 320 (M^+, 91%), 288 (46), and 255 (100). Found: C, 56.33; H, 3.64; S, 39.60%. Calcd for $C_{15}H_{12}S_4$: C, 56.21; H, 3.78; S, 40.01%.

*Preparation of **43** and **44**.* A benzene solution (1.5ml) of **39** (203 mg, 0.69 mmol) and trimethyl phosphite (112 mg, 0.90 mmol) was stirred at room temperature for 1 h. The color of the solution turned rapidly from yellow to blue, and pale blue precipitates were formed. To this solution was added ethanol and the crystalline material **41** (probably mainly **43**) was collected by filtration (165 mg, 92%). Mp 184.5 °C (dec); MS: *m/e* 488 (M^+-S, 4%), 456 (M^+-2S, 2), 292 ($M^+/2+S$, 99), 260 ($M^+/2$, 20), and 238 ($M^+/2-S$, 100). Because the solubility of **43** was very low in any solvent, it could not be recrystallized, but the structure of **43** was confirmed by its cycloaddition with *N*-phenylmaleimide leading to [4+2] adduct, **45**.

44 was synthesized similarly in 96% yield; mp 196.5— 197 °C (C_6H_6–EtOH); NMR ($CDCl_3$): δ 2.66 (6H, s) and 6.7—7.4 (4H, m); MS: *m/e* 544 (M^+-S, 2%), 320 ($M^+/2+S$, 28), 288 ($M^+/2$, 100), and 273 ($M^+/2-CH_3$, 65). Found: C, 62.51; H, 4.05; S, 32.94%. Calcd for $C_{30}H_{24}S_6$: C, 62.46; H, 4.19; S, 33.34%.

*Reaction of **43** with N-Phenylmaleimide.* A toluene solution (10 ml) of **43** (131 mg, 0.25 mmol) and *N*-phenylmaleimide (88 mg, 0.51 mmol) was refluxed for 1.5 h. After removal of the solvent, the residue was recrystallized from ethanol–benzene to give **45** (177 mg, 82%), mp 178—179 °C; NMR ($CDCl_3$): δ 4.37 (1H, d, J=15 Hz), 4.84 (1H, d, J=15 Hz), and 6.8—8.2 (13H, m); IR (KBr): 1720 cm^{-1} (C=O); MS: *m/e* 433 (M^+, 15%) and 260 (100). Found: C, 63.79; H, 3.19; N, 3.25; S, 22.20%. Calcd for $C_{23}H_{15}NO_2S_3$: C, 63.72; H, 3.49; N, 3.23; S, 22.18%.

References

1) For reviews, see R. Gompper, *Angew. Chem. Int. Ed. Engl.*, **8**, 312 (1969); H. U. Wagner and R. Gompper, "The Chemistry of the Quinonoid Compounds," ed by S. Patai, John Wiley and Sons, (1974), Chap. 18; R. Okazaki, *Yuki Gosei Kagaku Kyokai Shi*, **34**, 439 (1976).

2) a) T. Kametani, H. Nemoto, H. Ishikawa, K. Shiroyama, and K. Fukumoto, *J. Am. Chem. Soc.*, **98**, 3378 (1976); b) T. Kametani, C. V. Loc, T. Higa, M. Koizumi, M. Ihara, and K. Fukumoto, *ibid.*, **90**, 2306 (1977); c) K. P. C. Vollhardt, *Acc. Chem. Res.*, **10**, 1 (1977); d) W. Oppolzer, *Angew. Chem. Int. Ed. Engl.*, **16**, 10 (1977); e) T. Kametani, H. Matsumoto, H. Nemoto, and K. Fukumoto, *J. Am. Chem. Soc.*, **100**, 6218 (1978); f) R. P. Steiner, R. D. Miller, H. J. Dewey, and J. Michl, *ibid.*, **101**, 1820 (1979); g) W. R. Dolbier, Jr., K. Masui, H. J. Dewey, D. V. Horák, and J. Michl, *ibid.*, **101**, 2136 (1979) and references cited therein.

3) a) G. Jacquim, J. Nasiélski, G. Billy, and M. Remy, *Tetrahedron Lett.*, **1973**, 3655; b) R. S. Becker and J. Kolc, *J. Phys. Chem.*, **72**, 997 (1968).

4) P. de Mayo and H. Y. Ng, *J. Chem. Soc., Chem. Commun.*, **1974**, 877; *Can. J. Chem.*, **55**, 3763 (1977).

5) a) R. Okazaki and N. Inamoto, *Chem. Lett.*, **1974**, 1439; b) R. Okazaki, F. Ishii, K. Sunagawa, and N. Inamoto, *ibid.*, **1978**, 51; c) R. Okazaki, K.-T. Kang, K. Sunagawa, and N. Inamoto, *ibid.*, **1978**, 55; d) R. Okazaki, K. Sunagawa, K.-T. Kang, and N. Inamoto, *Bull. Chem. Soc. Jpn.*, **52**, 496 (1979).

6) Part of this paper was published in a preliminary form: R. Okazaki, K.-T. Kang, and N. Inamoto, *Heterocycles*, **9**, 1741 (1978).

7) There have been some reports on the reaction of **2** with diamines: J. P. Brown, *J. Chem. Soc., Perkin Trans. I*, **1974**, 869; R. W. Hoffmann and S. Goldmann, *Chem. Ber.*, **111**, 2716 (1978).

8) L. Learand, *Bull. Soc. Chim. Fr.*, 1599 (1959).

9) J. Faust and R. Mayer, *Justus Liebigs Ann. Chem.*, **688**, 150 (1965).

10) O. Fischer, *Ber.*, **34**, 938 (1901).

11) E. Klinsberg, *J. Am. Chem. Soc.*, **83**, 2934 (1961).

12) R. Okazaki, K. Sunagawa, K.-T. Kang, and N. Inamoto, unpublished results.

13) R. Okazaki, K. Sunagawa, M. Kotera, and N. Inamoto, *Tetrahedron Lett.*, **1976**, 3815.

14) J. E. Shields and J. Bornstein, *Chem. Ind. (London)*, **1967**, 1404; M. P. Cava, N. M. Pollack, O. A. Mamer, and M. J. Mitchell, *J. Org. Chem.*, **36**, 3932 (1971); *cf.*, G. J. Gleicher, D. D. Newkirk, and J. C. Arnold, *J. Am. Chem. Soc.*, **95**, 2526 (1973).

15) M. P. Cava and J. P. Van Meter, *J. Org. Chem.*, **34**, 538 (1969).

16) N. Latif, A. Nada, H. El-Namaky, and B. Haggag, *Chem. Ind. (London)*, **1975**, 706.

17) I. Degani and R. Fochi, *Synthesis*, **1976**, 471.

18) E. Klingsberg, *Quart. Rev. Chem. Soc.*, **23**, 537 (1969); N. Lozac'h, *Adv. Heterocycl. Chem.*, **13**, 161 (1971).

19) F. S. Fowkes and E. W. McClelland, *J. Chem. Soc.*, **1941**, 187.

20) W. Baker, H. F. Bondy, J. Gumb, and D. Miles, *J. Chem. Soc.*, **1953**, 1615.

Catalytic Hydrolysis of *p*-Nitrophenyl Esters in the Presence of Representative Ammonium Aggregates. Specific Activation of a Cholesteryl Nucleophile Bound to a Dialkylammonium Bilayer Membrane[1)]

Yoshio OKAHATA, Reiko ANDO, and Toyoki KUNITAKE*

Department of Organic Synthesis, Faculty of Engineering, Kyushu University, Fukuoka 812

(Received June 16, 1979)

Catalytic hydrolysis of *p*-nitrophenyl esters (acetate and nonanoate) by hydroxamate and imidazole nucleophiles was studied at 30 °C in the presence of aqueous aggregates of single-chain (hexadecyl), double-chain (didodecyl and dioctadecyl) and triple-chain (trioctyl) ammonium amphiphiles. These three types of ammonium salts give rise to very different aggregate morphologies. The rate constant of ester cleavage by the nucleophiles was enhanced several hundred folds in the presence of these hydrophobic aggregates. Simple long-chain nucleophiles possessed esterolytic reactivities which reflect the hydrophobic microenvironment of the respective aggregates: single-chain<double-chain<triple-chain. On the other hand, the cholesteryl ester of imidazolecarboxylic acid showed an especially high reactivity when bound to the didodecylammonium bilayer. Cholic acid-derived nucleophiles showed normal reactivity patterns. Apparently, specific binding of the cholesterol derivative to the bilayer is responsible for the unusual catalytic behavior.

The reactivity of hydrophobic, anionic nucleophils toward *p*-nitrophenyl esters is greatly enhanced in the presence of cationic micelles of hexadecyltrimethylammonium bromide (CTAB).[2)] An additional rate-enhancing effect of *ca.* 100 fold has been observed with the aqueous aggregate of trioctylmethylammonium chloride.[3)] These results can be explained by the formation of *hydrophobic ion pairs* between anionic nucleophiles and cationic surfactants.[4,5)]

Recently we found that a series of dialkylammonium amphiphiles formed stable bilayer structures in dilute aqueous solution(10^{-2}—10^{-4} M)(1 M=1 mol dm^{-3}).[6-8)] According to the electron microscopic examination, these structures are quite similar to that of phospholipid membranes and further aggregation of the bilayer resulted in the vesicle and lamellar structures.

Thus, we have three distinct types of ammonium aggregates. An ammonium amphiphile which contains single, long alkyl chain (conventional surfactant) forms fluid, globular micelles at 10^{-2}—10^{-3} M. Alkylammonium salts with two long alkyl chains produce huge (10^6—10^7 daltons) aggregates with highly organized structure at 10^{-2}—10^{-4} M. An ammonium salt with three octyl chains forms fairly tight, small aggregates at 10^{-4}—10^{-5} M. Therefore, it is important to compare the influences of these ammonium aggregates on micelle-catalyzed reactions. In addition, the catalytic behavior in the ammonium bilayer would be interesting as a model of the action of membrane-bound enzymes.

In the present study, the catalytic hydrolysis of phenyl esters were examined in the presence of representative, aqueous aggregates. *p*-Nitrophenyl acetate (PNPA) and *p*-nitrophenyl nonanoate (PNPN) were used as substrate. Nucleophiles employed were *N*-dodecylbenzohydroxamic acid (C_{12}-BHA), *N*-dodecyl-4-imidazolecarboxamide (C_{12}-ImAm), *N*-methylcholohydroxamic acid (chol-HA), *N*-(4-imidazolylmethyl)-cholohydroxamic acid (chol-ImHA), *N*-[2-(4-imidazolyl)ethyl]cholamide(chol-His) and cholesteryl 4-imidazolecarboxylate(cholest-Im). The first two nucleophiles contain a long alkyl chain and the rest contain the steroidal skeleton. Their structures and abbreviations are shown below, together with those of substrates and surfactants.

Nucleophile

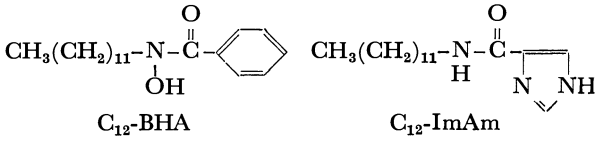

C_{12}-BHA C_{12}-ImAm

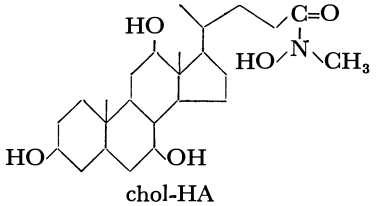

chol-HA

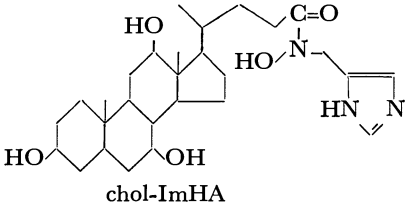

chol-ImHA

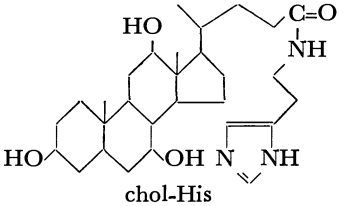

chol-His

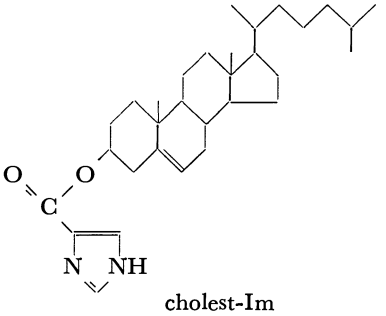

cholest-Im

Substrate

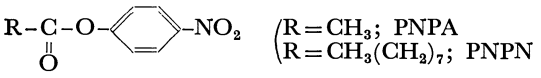

Ammonium salt

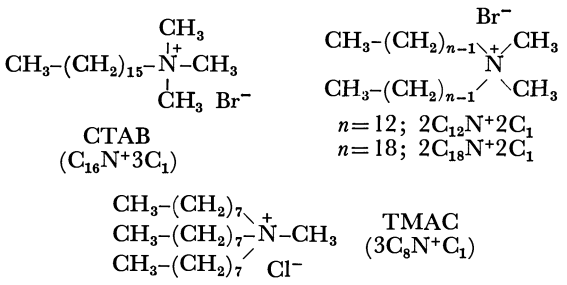

Experimental

N-Methylcholohydroxamic Acid (chol-HA). Cholic acid (4.09 g, 0.010 mol) was dissolved in a mixture of 80 ml of dry tetrahydrofuran (THF) and 20 ml of dry acetonitrile, and 1.38 g (0.012 mol) of *N*-hydroxysuccimide was added. To the resulting homogeneous solution were added dropwise 2.06 g (0.010 mol) of dicyclohexylcarbodiimide in 20 ml of dry THF at 10—15 °C. The mixture was stirred at room temperature for 2 h and the precipitates of *N,N'*-dicyclohexylurea were removed. Chloroform (300 ml) was added to the filtrate and the solution was washed with aqueous sodium carbonate (100 ml×2) and with water (100 ml×2) and dried over sodium sulfate. Chloroform was removed *in vacuo* and the white solid was recrystallized two times from a 1: 1 mixture of ethyl acetate and hexane: mp 119—120 °C, yield 2.50 g (55%). The product was confirmed by IR and NMR spectroscopies.

The succimide ester of cholic acid thus obtained (2.50 g, 0.005 mol) was dissolved in 50 ml of dry *N,N*-dimethylformamide (DMF) and added dropwise at 0 °C to 100 ml of dry DMF which contained 1.70 g (0.020 mol) of *N*-methylhydroxylamine hydrochloride and 2.0 g (0.020 mol) of triethylamine. Stirring was continued for 13 h at room temperature. The precipitates of triethylamine hydrochloride was separated and the solvent was removed *in vacuo*. The yellowish solid residue was recrystallized two times from a 1: 1 mixture of ethanol and water to give colorless needles: mp 215—216 °C, yield 1.8 g (41%). Found: C, 68.32; H, 10.04; N, 3.41%. Calcd for $C_{25}H_{43}O_5N$: C, 68.65; H, 9.84; N, 3.20%.

N-[2-(4-Imidazolyl)ethyl]cholamide (chol-His). This compound was prepared from the succimide ester of cholic acid and histamine dihydrochloride in the presence of triethylamine by a procedure similar to that mentioned above: colorless granules, yield 78%, mp 125—126 °C. Found: C, 69.49; H, 9.08; N, 8.48%. Calcd for $C_{29}H_{47}O_4N_3$: C, 69.46; H, 9.38; N, 8.38%. This procedure gave a better yield with higher purity than the previous method[9] in which methyl chloroformate was used as the condensation agent.

N-(4-Imidazolylmethyl)cholohydroxamic Acid (chol-ImHA). The succimide ester of cholic acid and *N*-(4-imidazolylmethyl)-*O*-benzylhydroxylamine dihydrochloride[10] was allowed to react similarly to give benzyl *N*-(4-imidazolylmethyl)cholohydroxamate, which was then hydrogenated over 5% Pd/$SrCO_3$ in ethanol. Colorless granules were obtained by recrystallizations (twice) from acetonitrile: mp 166—168 °C, yield 49%. Found: C, 66.52; H, 8.78; N, 8.14%. Calcd for $C_{28}H_{45}O_5N_3$: C, 66.80; H, 8.95; N, 8.35%.

Cholesteryl 4-Imidazolecarboxylate (cholest-Im). 4-Imidazolecarbonyl chloride[11] (2.8 g, 0.016 mol), 5.3 g (0.01 mol) of cholesterol and 6 g (0.06 mol) of triethylamine were added to 50 ml of chloroform and the mixture was refluxed for 4 h. Solvent was removed *in vacuo*, and the residual yellow solid was washed with a small amount of water and recrystallized three times from ethanol: pale yellow granules, mp 225—230 °C. Found: C, 76.68; H, 9.90; N, 6.00%. Calcd for $C_{31}H_{48}O_2N_2$: C, 76.86; H, 9.92; N, 6.08%.

Other Materials. *p*-Nitrophenyl acetate (PNPA) (mp 78 °C),[12] *p*-nitrophenyl nonanoate (PNPN) (bp 165 °C/0.3 mmHg (1 mmHg=133.322 Pa))[13] were prepared by the procedure reported before.

Commercial hexadecyltrimethylammonium bromide(CTAB) was recrystallized twice from water, and commercial trioctylmethylammonium chloride (TMAC) (Dojin Chemicals, Co.) was used without further purification. Didodecyldimethylammonium bromide ($2C_{12}N^+2C_1$) (Eastman Kodak) was recrystallized two times from ethyl acetate; mp 55—56 °C. Dioctadecyldimethylammonium bromide ($2C_{18}N^+2C_1$) was prepared by reaction of *N,N*-dimethyloctadecylamine and octadecyl bromide in refluxing ethanol in the presence of sodium carbonate and purified by repeated recrystallizations from ethyl acetate: colorless granules, mp 90—93 °C. Found: C, 70.04; H, 12.78; N, 2.18%. Calcd for $C_{38}H_{80}NBr\cdot H_2O$: C, 70.32; H, 12.73; N, 2.15%.

Kinetics. The hydrolysis was carried out mostly in 3 v/v % EtOH–H_2O at 30 °C, μ=0.01 (KCl), 0.01 M borate buffer (pH 7—10). The reaction rate was determined by using the absorbance of *p*-nitrophenolate at 401 nm (λ_{max}) with a Hitachi 200 UV-visible spectrophotometer. The pH value of the reaction medium varied less than 0.05 pH during the reaction (HM-10B digital pH meter, Toa Electronics).

Results

Dye Binding to Ammonium Aggregates. The absorption maximum of Methyl Orange shows hypsochromic shifts in less polar media: 465 nm in water and 420—430

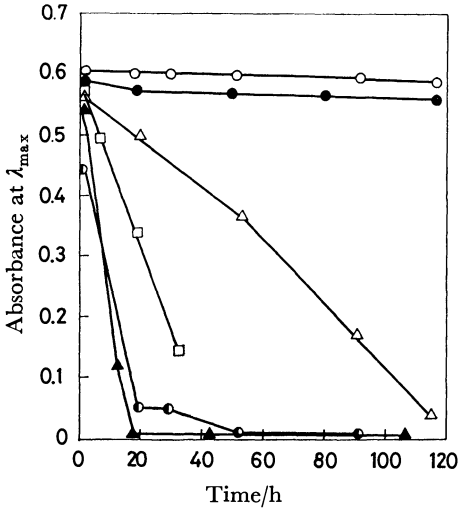

Fig. 1. Dialysis of Methyl Orange which are bound to ammonium aggregates.
pH 8.5, 0.01 M borate buffer, [Methyl Orange]=2×10^{-5} M.
▲: No ammonium salt, λ_{max}=465 nm. ○: $2C_{18}N^+2C_1$ (1×10^{-3} M), λ_{max}=410 nm. ◐: $2C_{18}N^+2C_1$(1×10^{-5} M), λ_{max}=450 nm. ●: $2C_{12}N^+2C_1$(1×10^{-3} M), λ_{max}=420 nm. △: CTAB(1×10^{-2} M), λ_{max}=430 nm. □: TMAC(2×10^{-4} M), λ_{max}=430 nm.

nm in organic media. Therefore, this compound has been used frequently for estimating the microscopic polarity of micelles[3] and polymers.[14,15] Methyl Orange (2×10^{-5} M) was dissolved in 10 ml of aqueous ammonium salts (10^{-3}—10^{-5} M) and these solutions in cellulose tubing (Visking Co.) were dialyzed against water. The residual Methyl Orange was determined at its absorption maximum.

As shown in Fig. 1, Methyl Orange is retained even after 120 h in the presence of 10^{-3} M of $2C_{12}N^+2C_1$ or $2C_{18}N^+2C_1$. Interestingly, however, Methyl Orange is rapidly lost in the presence of 1×10^{-5} M of $2C_{18}N^+2C_1$. Methyl Orange passes through the cellophane tube easily in the case of 2×10^{-4} M of TMAC, but the dialysis rate was slower in the presence of 10^{-2} M of CTAB.

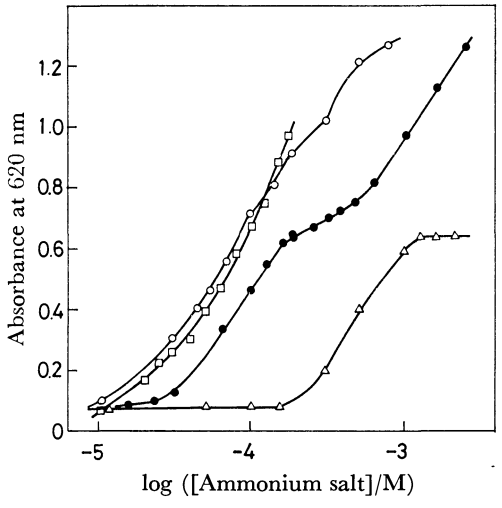

Fig. 2. Influence of hydrophobic ammonium salts on the dissociation of 2,6-dichlorophenolindophenol. 30 °C, 3 v/v % EtOH–H_2O, μ=0.01 (KCl), 1×10^{-4} M 2,6-dichlorophenolindophenol sodium salt, 3×10^{-4} M hydrochloric acid.
○: $2C_{18}N^+2C_1$. ●: $2C_{12}N^+2C_1$. □: TMAC. △: CTAB.

Dissociation of 2,6-dichlorophenolindophenol (*N*-(*p*-hydroxyphenyl)-2,6-dichloro-*p*-benzoquinone 4-imine) is often used for the measurement of the critical micelle concenctration (CMC) of cationic micelles:[3,16] λ_{max}= 500—520 nm for the undissociated species and λ_{max}= 600—650 nm for the dissociated species. Figure 2 shows the dependence of the absorbance at 620 nm, Abs_{620}, on the concentration of ammonium salts. In the case of CTAB, Abs_{620} starts to increase at *ca.* 5×10^{-4} M. The dissoication is facilitated at a lower concentration (5×10^{-5} M) of $2C_{12}N^+2C_1$. The effects of $2C_{18}N^+2C_1$ and TMAC are similar to each other, and Abs_{620} starts to increase at 1×10^{-5} M in both cases.

Alkaline(Spontaneous) Hydrolysis of p-*Nitrophenyl Esters.* The alkaline hydrolysis of *p*-nitrophenyl esters was studied at pH 10.0±0.1 in the presence of ammonium aggregates. The *p*-nitrophenol release obeyed the pseudo first order rate law for more than 90% completion. The logarithm of the pseudo first order rate constant, k_{spont}, was plotted against the logarithm of

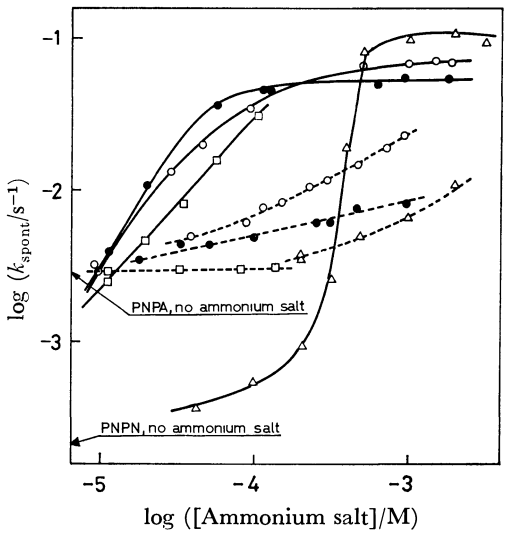

Fig. 3. Spontaneous (alkali) hydrolysis of *p*-nitrophenyl esters. 30 °C, pH 10.1±0.1, μ=0.01 (KCl), 3 v/v % EtOH–H_2O. ——: PNPN (2.00×10^{-5} M). ——:PNPA (2.00×10^{-5} M). ○: $2C_{18}N^+2C_1$. ●: $2C_{12}N^+2C_1$. △: CTAB. □: TMAC.

the ammonium concentration in Fig. 3. In the absence of ammonium salts, k_{spont} was 0.003 s^{-1} for PNPA and 0.00026 s^{-1} for PNPN. The TMAC aggregate did not affect the hydrolysis of PNPA, but micellar CTAB (1×10^{-3} M) increased the rate about two-fold. The bilayer aggregates of $2C_{12}N^+2C_1$ and $2C_{18}N^+2C_1$ accelerated the reaction by factors of 2.7 and 10 at the same concentration.

The rate enhancement was much greater with more hydrophobic PNPN substrate. k_{spont} increased by a factor of more than 100 fold upon micellization of CTAB. This must be due to efficient binding of PNPN to micellar CTAB and due to concentration of OH^- at the cationic micellar surface. The rate enhancement was observed at much lower concentrations ($<10^{-5}$ M) in the presence of other ammonium aggregates, but was saturated at 10^{-4} M. The rate saturation could not be confirmed with the TMAC aggregate because of its limited solubility.

The alkaline hydrolysis of PNPN was efficiently retarded by the increase in ionic strength: the rate decreased to 1/70 to 1/150 of the original value upon increase in ionic strength from 0.01 to 0.5 (KCl). The influence of ionic strength was larger in the bilayer systems than in the CTAB micelle.

Catalytic Hydrolysis of p-*Nitrophenyl Esters.* The catalytic hydrolysis by hydroxamate and imidazole nucleophiles proceeds *via* the acyl intermediate as in Eq. 1.

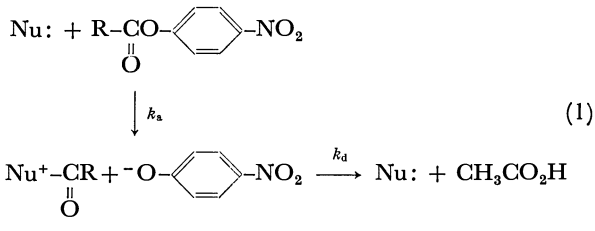

(1)

The apparent second-order rate constant of acylation is obtained by

$$k_{a,obsd} = \frac{k_{total} - k_{spont}}{[Nu]_T} \quad (2)$$

where k_{total} and k_{spont} are overall first order rate constants with and without catalyst, respectively. $[Nu]_T$ is the total concentration of nucleophile. The reaction obeyed the pseudo first order rate law for up to 90% completion. The rate constant of acyl transfer was obtained from these experiments, since excess catalyst was present in all cases relative to substrate molecules.

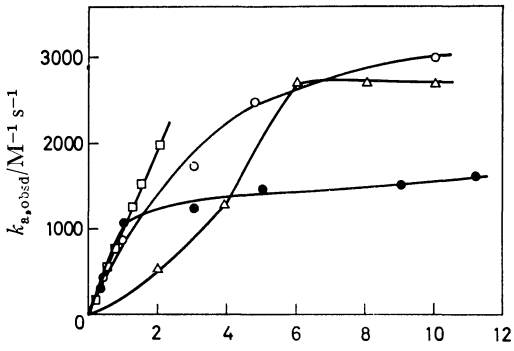

Fig. 4. Catalytic hydrolysis of PNPA by chol-HA in the presence of ammonium aggregates.
30 °C, 3 v/v % EtOH–H_2O, μ=0.01 (KCl), pH 8.9± 0.1, [PNPA]=3.79×10^{-6} M, [chol-HA]=3.02×10^{-5} M. ○: $2C_{18}N^+2C_1$. ●: $2C_{12}N^+2C_1$. △: CTAB. □: TMAC.

When chol-HA was used as nucleophilic catalyst $k_{a,obsd}$ increased in similar ways (100—300 fold) in the presence of all four ammonium aggregates as shown in Fig. 4. The rate enhanching effect is apparently related to the CMC, since efficient acceleration is noted at (2—6)$\times10^{-4}$ M for CTAB and at lower concentrations for the other ammonium salts. Similar trends were observed for other steroidal (chol-ImHA) and long-chain (C_{12}-BHA and C_{12}-ImAm) nucleophiles with rate enhancements of 100—300 fold.

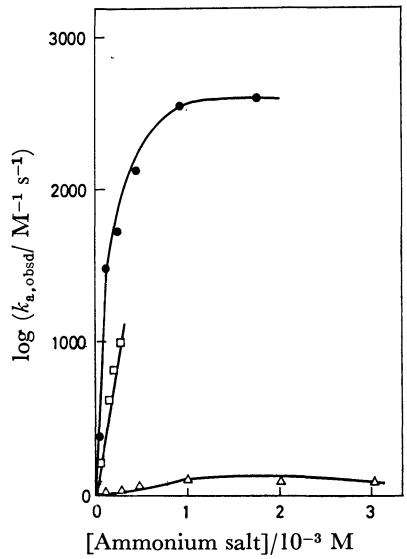

Fig. 5. Catalytic hydrolysis of PNPA by cholest-Im in the presence of ammonium aggregates.
30 °C, 3 v/v % EtOH–H_2O, μ=0.01 (KCl), pH 8.9± 0.1, [PNPA]=3.79×10^{-6} M, [cholest-Im]=3.10×10^{-5} M.
●: $2C_{12}N^+2C_1$. △: CTAB. □: TMAC

In contrast, the rate-enhancing effect for cholest-Im catalyst was more specific than those for the above-mentioned nucleophiles. As shown in Fig. 5, the nucleophilic reactivity of cholest-Im is much increased by the aggregate of TMAC and $2C_{12}N^+2C_1$, but the CTAB micelle produced a very small effect. It is interesting that cholest-Im could not be solubilized by the $2C_{18}N^+2C_1$ bilayer.

Chol-His catalyst could not be activated by any of the ammonium aggregates and $k_{a,obsd}$ was 6.5—9.2 $M^{-1}\,s^{-1}$ at pH 8.9 and 30 °C.

The $k_{a,obsd}$ values obtained for various nucleophiles in the presence of representative ammonium aggregates are collected in Table 1. The concentration of ammonium salt is 1×10^{-3} M except for TMAC in which case the concentration is 1×10^{-4} M because of its low solubility. The corresponding, less hydrophobic compounds were used to estimate $k_{a,obsd}$ in the absence

Table 1. Reaction of hydroxamate and imidazole nucleophiles with PNPA in the presence of representative ammonium aggregates[a]

Nucleophile	$k_{a,obsd}/M^{-1}\,s^{-1}$				
	None	CTAB (1×10^{-3} M)	TMAC (1×10^{-4} M)	$2C_{12}N^+2C_1$ (1×10^{-3} M)	$2C_{18}N^+2C_1$ (1×10^{-3} M)
C_{12}-BHA	15[b]	1900	6700[d]	4500	—
C_{12}-ImAm	0.09[c]	105	1200[d]	155	810
chol-HA	10	2770	2500	1600	2800
chol-ImHA	2.8[e]	113	—	320	—
chol-His	3.5	6.5	6.8	9.2	8.7
cholest-Im	0.09[c]	61	650	2570	—

a) 30 °C, pH 8.90±0.05, μ=0.01(KCl), 0.01 M borate, [PNPA]=3.79×10^{-6} M, [nucleophile]=(4.18—6.72)$\times10^{-5}$ M. b) *N*-Benzylbenzohydroxamic acid was used as nucleophile. Cited from Ref. 10. c) *N*,*N*-Dimethyl(4-imidazolecarboxamide) was used as uncleophile. Cited from Ref. 11. d) From Ref. 3. e) *N*-(4-imidazolylmethyl)benzohydroxamic acid was used as nucleophile. Cited from Ref. 10.

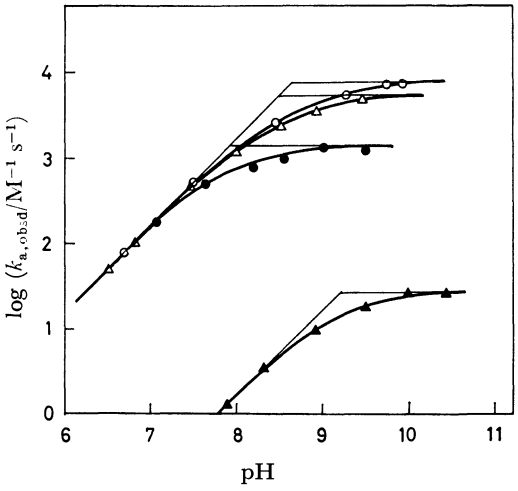

Fig. 6. pH-rate profile of the catalytic hydrolysis by chol-HA.
30 °C, 3 v/v % EtOH–H_2O, μ=0.01 (KCl), [PNPA]=3.79×10^{-6} M, [chol-HA]=3.02×10^{-5} M.
▲: No ammonium salt. △: CTAB (1.00×10^{-3} M). ○: $2C_{18}N^+2C_1$(1.00×10^{-3} M). ●: $2C_{12}N^+2C_1$(1.14×10^{-3} M).

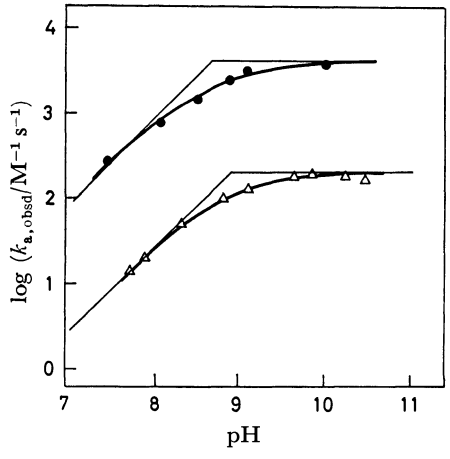

Fig. 7. pH-rate profile of the catalytic hydrolysis by cholest-Im.
30 °C, 3 v/v % EtOH–H_2O, μ=0.01 (KCl), [PNPA]=3.79×10^{-6} M, [cholest-Im]=3.10×10^{-5} M.
●: $2C_{12}N^+2C_1$ (1.14×10^{-3} M). △: CTAB (1.00×10^{-3} M).

of the ammonium aggregate when hydrophobic nucleophiles were not soluble in water.

Figures 6 and 7 are pH-rate profiles for chol-HA and cholest-Im nucleophiles, respectively, in the presence and absence of some ammonium aggregates. In all cases, log $k_{a,obsd}$ increases linearly with slope of +1 in the low pH region and plateaus are observed at the high pH. Acid dissociation constants of nucleophile, K_a, and the true second-order rate constant of the anionic species, k_a, can be estimated by curve fitting of $k_{a,obsd}$ values to the following theoretical equation.

$$k_{a,obsd} = \frac{K_a}{a_H+K_a}\cdot k_a \quad (3)$$

$$k_{a,obsd} = \alpha\cdot k_a \quad (4)$$

where a_H is the activity of hydrogen ion and α is the fraction of the dissociated nucleophile species. Solid curves in Figs. 6 and 7 are obtained by using K_a and k_a values. The agreements between the calculated curves and the corresponding experimental plots are excellent.

Table 2 summarizes pK_a and k_a values thus obtained. In the presence of the ammonium aggregate, pK_a values are lowered and k_a values are enhanced by factors of 100 to 400. The k_a value for C_{12}-ImAm is similar in the CTAB micelle and in the $2C_{12}N^+2C_1$ bilayer; however, k_a for chol-HA is larger in CTAB than in $2C_{12}N^+2C_1$ and k_a for cholest-Im is some 20 times larger in $2C_{12}N^+2C_1$ than in CTAB. These results are suggestive of the specific interaction of nucleophiles and ammonium aggregates.

Discussion

Microenvironments of Ammonium Aggregates. As briefly mentioned in the Introduction, the three types of ammonium salts form quite different aggregates. Some of their physicochemical properties are summarized in Table 3. The critical micelle (aggregate) concentrations as determined by the surface tension measurement are in the range of 5×10^{-6} to 1×10^{-3} M, and decrease approximately with increasing carbon numbers. Therefore, the critical micelle concentration is predominantly determined by the hydrophobic-hydrophilic balance of a given ammonium salt without regard to the structural specificity. On the other hand, the mass of the ammonium aggregates is varied considerably, depending on their structural characteristics.

Table 2. Acidity and rate constants for hydroxamate and imidazole nucleophiles

Ammonium salts (1×10^{-3} M)	C_{12}-BHA		C_{12}-ImAm		chol-HA		cholest-Im	
	pK_a	k_a / M^{-1} s^{-1}	pK_a	k_a / M^{-1} s^{-1}	pK_a	k_a / M^{-1} s^{-1}	pK_a	k_a / M^{-1} s^{-1}
None	9.5[b]	20[b]	13[c]	12[c]	9.2	25	13[c]	12[c]
CTAB ($C_{16}N^+3C_1$)	8.4	2560	10.3	1620	8.5	4600	8.9	194
$2C_{12}N^+2C_1$	—	—	9.7	1430	8.0	1250	8.7	3980
$2C_{18}N^+2C_1$	—	—	—	—	8.6	7000	—	—
TMAC ($3C_8N^+C_1$)[d]	—	—	9.3	5200	—	—	—	—

a) 30 °C, 3 v/v%EtOH–H_2O, μ=0.01 (KCl). b) *N*-benzylbenzohydroxamic acid was used as nucleophile. Cited from Ref. 10. c) *N*,*N*-dimethyl(4-imidazolecarboxamide) was used as nucleophile. Cited from Ref. 11. d) From Ref. 3.

Table 3. Physicochemical properties of ammonium aggregates

Ammonium salts	Total carbon number	Aggregate morphology	10^4 CMC / M	10^{-4} Aggregate weight / dalton	Methyl Orange λ_{max}/nm
Single-chain					
CTAB ($C_{16}N^+3C_1Br^-$)	19	globular micelle	8	4	430(1×10^{-2} M)[a]
Double-chain					
$2C_{12}N^+2C_1Br^-$	26	bilayer	0.5[b]	100[d]	420(1×10^{-3} M)
$2C_{18}N^+2C_1Br^-$	38	bilayer	0.05[c]	1000[d]	410(1×10^{-3} M) 450(1×10^{-5} M)
Triple-chain					
TMAC($3C_8N^+C_1Cl^-$)	25	small, tight aggregate	*ca.* 0.3	<1	430(2×10^{-4} M)

a) λ_{max} is estimated at the ammonium concentration given in the parentheses. b) A. W. Ralston, D. N. Eggenberger, and P. L. DuBrow, *J. Am. Chem. Soc.*, **70**, 977 (1948). c) H. Kunieda and K. Shinoda, *J. Phys. Chem.*, **82**, 1710 (1978). The value for the chloride salt. d) Determined by the light scattering method: Union Giken Co., Ltd., Model LS-600.

The aggregate weight of TMAC is estimated to be less than 10^4 daltons and that of CTAB is 4×10^4 daltons. In contrast, the double-chain ammonium salts form huge aggregates of 1—10 million daltons. The hydrophobic nature of these aggregates can be estimated from λ_{max} of Methyl Orange. The λ_{max} values given in Table 1 correlate roughly with the total carbon numbers. However, λ_{max} was closer to that in water when 1×10^{-5} M of $2C_{18}N^+2C_1$ was present, probably due to incomplete formation of the stable aggregate.

The facilitated dissociation of 2,6-dichlorophenolindophenol appears to reflect the critical micelle concentration. Thus, Abs_{620} abruptly increased at *ca.* $(4—8)\times10^{-4}$ M of CTAB, but it increased at ammonium concentrations as low as 10^{-5} M in the case of other ammonium salts.

The dialysis experiments indicate that Methyl Orange is retained in the dialkylammonium bilayers most effectively as shown in Fig. 1. The CTAB micelle is much less effective and the TMAC micelle lacks in the retention capability almost completely. These trends can be correlated with the aggregate weight. Undoubtedly, the dialkylammonium aggregates can retain Methyl Orange very well because of their highly-organized, stable structures. This capacity is lost at concentrations close to the CMC, as shown by the data obtained in the presence of 1×10^{-5} M of $2C_{18}N^+2C_1$.

Specific Activation by Ammonium Bilayers. The spontaneous(alkali) hydrolysis of phenyl esters is accelerated in the presence of cationic micelles. This is usually explained by assuming that hydroxide ions concentrated in the Stern layer act on the phenyl ester bound to the micellar phase.[17] The results of Fig. 3 endorse this explanation. It is clear that PNPA is weakly bound to the ammonium aggregate in contrast to the tight binding for more hydrophobic PNPN, since acceleration of the spontaneous hydrolysis is 200—300 times for PNPN but is at most 10 times for PNPA.

As shown in Table 1, the catalytic hydrolysis of PNPA is remarkably accelerated in the presence of all the ammonium aggregates: 100—1000 times rate enhancements. The pK_a values of the hydroxamate and imidazole nucleophiles are lowered by 0.3—3 pK units when they are bound to any of the aggregates of the single-chain, double-chain and triple-chain ammonium salts. At the same time, their k_a values are enhanced by factors of several hundred (Table 2). These results violate the Brönsted relationship and is explained by the concept of "*hydrophobic ion pair*."[4,5,18]

According to this concept, prominent activation of some anionic nucleophiles is attributed to the formation of ion pairs between anionic nucleophiles and ammonium surfactants in the hydrophobic microenvironment, which usually results in pK_a lowering of the conjugate acid of the nucleophile (increase in the amount of the effective nucleophile) and the increased reactivity of the anionic nucleophile (k_a increase). The data of Table 2 clearly show that large enhancements of $k_{a,obsd}$ (Table 1) are derived from pK_a lowering and the increase in k_a. Chol-His nucleophile is not activated because it is not an anionic nucleophile under the reaction conditions used.

The extent of rate acceleration for long-chain hydroxamate and imidazole nucleophiles (C_{12}-BHA and C_{12}-ImAm) of Table 1 appears to be in general agreement with the trend of facilitated dissociation of 2,6-dichlorophenolindophenol: TMAC>$2C_{18}N^+2C_1$>$2C_{12}N^+2C_1$>CTAB. The rate-enhancing effect of the ammonium aggregate is somewhat different in the case of chol-HA, and the CTAB micelle is more effective than the $2C_{12}N^+2C_1$ bilayer. On the other hand, cholest-Im is *ca.* 40 time more activated in the $2C_{12}N^+2C_1$ bilayer than in the CTAB micelle. Furthermore, the bilayer-bound cholest-Im is more reactive than that bound to the TMAC aggregate. The reverse is true for other nucleophiles. These results cannot be explained by the hydrophobicity of the aggregate alone.

Aqueous solutions of the dialkylammonium aggregate can solubilize cholesterol, and the bilayer structure is retained in electron micrographs upon addition of one third molar cholesterol.[7] It is well known that cholesterol is an important ingredient of plasma membranes and affect the membrane fluidity.[19] Therefore, cholest-Im is conceivably bound to the ammonium bilayer in a specific manner. The specific nature of cholesterol binding may be related to the inability of the $2C_{18}N^+2C_1$ bilayer to solubilize cholesterol. On the other hand, cholic acid acts as a surfactant that disintegrates the phospholipid bilayer.[20] Similarly, the lamella structure

of the $2C_{18}N^{+}2C_1$ aggregate is destroyed when one third molar cholic acid is added.[21] Then, nucleophiles derived from cholic acid must be bound to the ammonium bilayer non-specifically.

The rate-enhancing effect of CTAB and TMAC aggregates appears to be determined predominantly by the hydrophobicity of nucleophiles and ammonium aggregates. Specific binding cannot be expected because of the fluid nature of these aggregates. In contrast, dialkylammonium salts form the stable bilayer structure similar to the phospholipid bilayer, and specific binding is quite conceivable. Why the conceivably specific binding of a cholesteric nucleophile produces better rate enhancement is not yet clear.

References

1) Contribution No. 514 from Department of Organic Synthesis.

2) *E.g.*, T. Kunitake and S. Shinkai, *Adv. Phys. Org. Chem.*, in press.

3) Y. Okahata, R. Ando, and T. Kunitake, *J. Am. Chem. Soc.*, **99**, 3067 (1977).

4) T. Kunitake, S. Shinkai, and Y. Okahata, *Bull. Chem. Soc. Jpn.*, **49**, 540 (1976).

5) S. Shinkai and T. Kunitake, *J. Chem. Soc., Perkin Trans. 2*, **1976**, 980.

6) T. Kunitake and Y. Okahata, *J. Am. Chem. Soc.*, **99**, 3860 (1977).

7) T. Kunitake, Y. Okahata, K. Tamaki, F. Kumamaru, and M. Takayanagi, *Chem. Lett.*, **1977**, 387.

8) T. Kunitake and Y. Okahata, *Chem. Lett.*, **1977**, 1337.

9) S. Shinkai and T. Kunitake, *Bull. Chem. Soc. Jpn.*, **44**, 3086 (1971).

10) T. Kunitake, Y. Okahata, and T. Tahara, *Bioorg. Chem.*, **5**, 155 (1976).

11) T. Kunitake and S. Horie, *Bull. Chem. Soc. Jpn.*, **84**, 1304 (1975).

12) T. Kunitake, Y. Okahata, and R. Ando, *Bull. Chem. Soc. Jpn.*, **47**, 1509 (1974).

13) Y. Okahata, and T. Kunitake, *J. Mol. Catal.*, **6**, 163 (1979).

14) I. M. Klotz, G. P. Royer, and A. R. Sloniewsky, *Biochemistry*, **8**, 4752 (1969).

15) Y. Okahata and T. Kunitake, *J. Polym. Sci., Polym. Chem. Ed.*, **16**, 1865 (1978).

16) M. C. Corrin and W. D. Hawkins, *J. Am. Chem. Soc.*, **69**, 679 (1947).

17) J. H. Fendler and E. J. Fendler, "Catalysis in Micellar and Macromolecular Systems," Academic Press, New York (1975), Chap. 5.

18) T. Kunitake, "Bioorganic Chemistry," ed by E. E. van Tamelen, Academic Press (1977), Vol. 1, Chap. 8.

19) "Biological Membranes," ed by D. Chapman and D. F. H. Wallach, Academic Press, New York (1973), Vol. 2.

20) A. D. Bangham, M. W. Hill, and N. G. A. Miller, "Methods in Membrane Biology," ed by E. D. Korn Plenum Press, New York (1974), Vol. 1, Chap. 1.

21) Unpublished electron microscopic study from these laboratories.

The Reactions of 1,2-Diphenyl-1-azaspiro[2.2]pentane and 2-Phenyl-1-azaspiro[2.2]pent-1-ene with *C,N*-Diarylnitrilimines[1)]

Otohiko Tsuge,* Hiroyuki Watanabe, and Yoko Kiryu

Research Institute of Industrial Science, Kyushu University 86, Hakozaki, Higashi-ku, Fukuoka 812

(Received June 20, 1979)

The reactions of highly strained 1,2-diphenyl-1-azaspiro[2.2]pentane (**1**) and 2-phenyl-1-azaspiro[2.2]pent-1-ene (**2**) with *C,N*-diarylnitrilimines (**3**) were described. The reaction of **1** with **3** gave the corresponding 4,5,7,8-tetraphenyl-4,6,7-triazaspiro[2.5]oct-5-ene, 1,5,7,8-tetraphenyl-5,6,8-triazaspiro[3.4]oct-6-ene, 1,3,5-triphenyl-2-pyrazoline, 1,3,4-triphenyl-1,2,4-triazolin-5-one, and/or 1,3,4,6,8-pentaphenyl-1,2,4,6,7-pentaazaspiro[4.4]nona-2,7-diene, whose yields depended on the reaction conditions. The pathways for the formation of products are also postulated. The azaspiropentene **2** readily reacted with **3** to give the corresponding 1,2,4-triphenyl-2,3,5-triazabicyclo[4.2.0]octa-3,5-diene arising from the rearrangement of initial 1,3-cycloadduct.

It has been reported that highly strained 1,2-diphenyl-1-azaspiro[2.2]pentane (**1**) is susceptible to rupture of the peripheral C–N bond. Upon photolysis or pyrolysis the azaspiropentane **1** isomerizes to the (phenylimino)-cyclobutane,[2)] whereas the [3+3] cycloadduct is formed from the reaction in the presence of α,*N*-diphenylnitrone.[3)] On the other hand, 2-phenyl-1-azaspiro[2.2]pent-1-ene (**2**) exhibited high reactivity toward 1,3-dipoles such as nitrile ylide and nitrone.[4)]

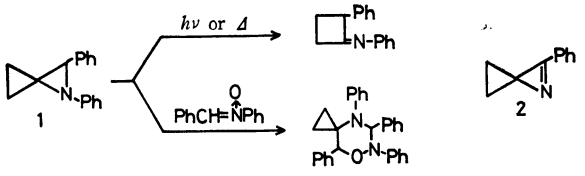

In the present paper we wish to report on the reactions of these highly strained heterocycles, **1** and **2**, with *C,N*-diarylnitrilimines, generated *in situ* from the corresponding *N*-(α-chlorobenzylidene)-*N'*-phenylhydrazines and triethylamine.

Reaction of 1,2-Diphenyl-1-azaspiro[2.2]pentane (1). When the azaspiropentane **1** was allowed to react with 1 equivalent of *C,N*-diphenylnitrilimine (**3a**) in chloroform at room temperature for 60 h, a 1:1 adduct **4a** was obtained in 19.5% yield, together with small amounts of 1,3,5-triphenyl-2-pyrazoline (**6a**)[5)] and 1,3,4-triphenyl-1,2,4-triazolin-5-one (**7a**).[6)] However, the reaction employed 2 equivalents of **3a** in boiling chloroform for 1 h afforded a new 1:1 adduct **5a** and pyrazoline **6a** in 54 and 23% yields respectively.

Although purification of the 1:1 adduct **4a** was difficult, **4a** was deduced to be the expected [3+3] cycloadduct, 4,5,7,8-tetraphenyl-4,6,7-triazaspiro[2.5]-oct-5-ene, on the basis of its ^{1}H-NMR spectrum displaying signals at δ 0.50—1.85 (m, 4H) and 4.69 ppm (s, 1H) besides aromatic protons. On the other hand, the ^{1}H-NMR spectrum of the 1:1 adduct **5a** showed signals at δ 1.81—2.40 (m, 3H), 2.72—3.20 (m, 1H), and 4.54 ppm (t, 1H, J=12 Hz) besides aromatic protons. The adduct **5a** was thus assigned to be the 1,3-cycloadduct of **3a** to 1-phenyl-2-(phenylimino)-cyclobutane, 1,5,7,8-tetraphenyl-5,6,8-triazaspiro[3.4]-oct-6-ene[7)] (Scheme 1).

Next, the reaction of **1** with *C*-(*p*-chlorophenyl)-*N*-phenylnitrilimine (**3b**) was investigated in chloroform under various conditions. The results are summarized in Table 1. As shown in Table 1, the kinds and yields

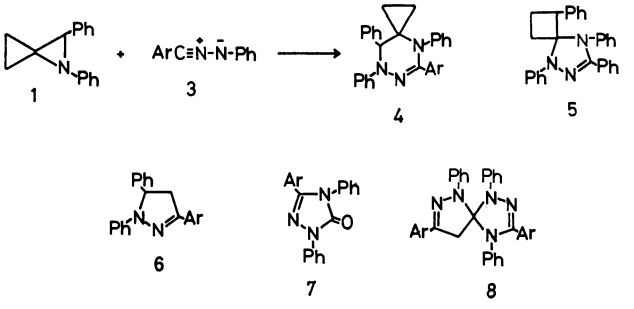

a: Ar=Ph; **b**: Ar=p-ClC$_6$H$_4$

Scheme 1.

of products greatly depended on the reaction conditions. The reaction at room temperature gave the expected [3+3] cycloadduct **4b** as the major product, whereas the isomeric 1:1 adduct **5b** was formed as the sole product in the reaction under reflux. When excess of **3b** was employed, 3-(*p*-chlorophenyl)-1,5-diphenyl-2-pyrazoline (**6b**), 3-(*p*-chlorophenyl)-1,4-diphenyl-1,2,4-triazolin-5-one (**7b**), and/or a new product **8b** were formed together with 1:1 cycloadducts **4b** and/or **5b**. The structures of **6b** and **7b** were confirmed by the identification with authentic samples prepared from the 1,3-dipolar cycloadditions of **3b** to styrene and phenyl isocyanate respectively.

The molecular formula of **8b** agreed with that of the compound derived from a 1:2 adduct of **1** to **3b** with the elimination of styrene. The ^{1}H-NMR spectrum

Table 1. Reaction of azaspiropentane **1** with nitrilimine **3b** in chloroform

1/**3b** (mol/mol)	Reaction temp	Reaction time/h	Product yield/%				
			4b	**5b**	**6b**	**7b**	**8b**
1	r.t.	60	43	trace	—	—	—
1	reflux	1	—	21	—	—	—
1	reflux	4	—	38	—	—	—
1/2	reflux	2	29	17	3	7	—
1/3	reflux	6	10	—	60	—	8

of **8b** displayed two doublets (each 1H, J=20 Hz) at δ 3.20 and 3.78 ppm besides aromatic protons. On the basis of the above facts and of a consideration of the mode of formation, **8b** was deduced to be 3,8-bis(*p*-chlorophenyl)-1,4,6-triphenyl-1,2,4,6,7-pentaazaspiro-[4.4]nona-2,7-diene.

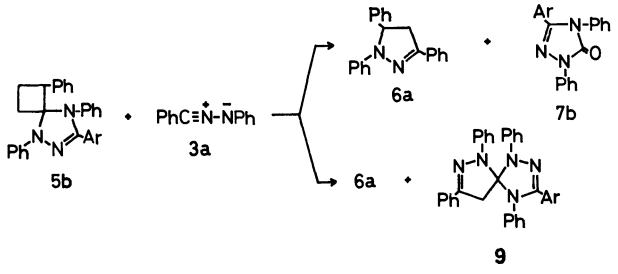

Ar=*p*-ClC$_6$H$_4$

Scheme 2.

The above results suggest that the products, **6**, **7**, and **8** might be arisen from the 1: 1 adduct **5**. In fact, when a chloroform solution of the 1: 1 adduct **5b** was heated with 1 equivalent of the nitrilimine **3a** for 4 h, the pyrazoline **6a** was formed in 23% yield along with a trace amount of the triazolinone **7b**. In the same reaction in degassed chloroform under nitrogen, however, **6a** and the pentaazaspiro[4.4]nonadiene **9** were obtained in 23 and 30% yields respectively (Scheme 2).

On the basis of the above facts, the pathways for the formation of products are outlined as depicted in Scheme 3. A species generated by the rupture of the peripheral C–N bond of the azaspiropentane **1** reacts with the nitrilimine **3** to give the [3+3] cycloadduct **4**, and/or isomerizes to the (phenylimino)cyclobutane. The nitrilimine **3** undergoes 1,3-dipolar cycloaddition to

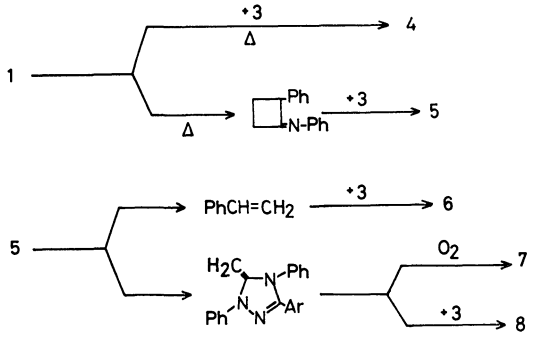

Scheme 3.

the (phenylimino)cyclobutane to yield the isomeric 1: 1 adduct **5**, which partially decomposes to styrene and methylenetriazoline. The 1,3-cycloaddition of **3** to styrene or methylenetriazoline gives the pyrazoline **6** or pentaazaspirononadiene **8** respectively. On the other hand, oxidation of the methylenetriazoline intermediate with oxygen leads to the formation of the triazolinone **7**. A similar oxidation of methylene group with oxygene has been reported by Woerner *et al.*[8]

Reaction of 2-Phenyl-1-azaspiro[2.2]pent-1-ene (2). Several 1,3-dipolar cycloadditions to 1-azirines have been investigated.[9] However, no studies on the cycloadditions of nitrilimine to 1-azirines seem to have been reported, although it is known that nitrilimines undergo cycloadditions to C=N bonds.[6]

The azaspiropentene **2** readily reacted with *C,N*-diarylnitrilimines, **3a** and **3b**, in benzene at room temperature, giving the corresponding 1: 1 adducts, **10a** and **10b**, in excellent yields respectively. On the basis of spectral data as well as of the chemical conversions, the 1: 1 adducts **10** were assigned to be the corresponding 1,2,4-triphenyl-2,3,5-triazabicyclo[4.2.0]octa-3,5-dienes which corresponded to the rearranged compounds of initial 1,3-cycloadducts (Scheme 4).

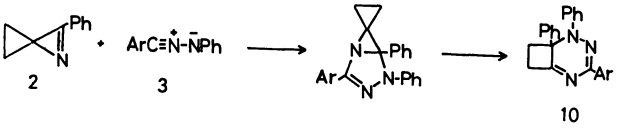

a: Ar=Ph; b: Ar=*p*-ClC$_6$H$_4$

Scheme 4

The ^{1}H-NMR spectra of **10a** and **10b** displayed four double double doublets (each 1H) indicating the presence of a cyclobutane ring. An inspection of the Dreiding models of **10** indicated that the fused cyclobutane ring in **10** is substantially fixed. On the basis of values of chemical shifts and coupling constants,[10] the protons of cyclobutane ring in **10** are assigned as shown in Table 2.

Reduction of **10a** with sodium borohydride in tetrahydrofuran gave the dihydro compound **11** in good yield. Structural elucidation of **11** was accomplished on the basis of spectral data. In addition, it was found that **10a** was converted to 2,4,5-triphenyl-1,3,4-triazabicyclo[3.3.0]oct-2-en-8-one (**12**) and 5-(2-benzoylethyl)-1,3-diphenyl-1,2,4-triazole (**13**) on treatment with silica gel or 1% aqueous acetic acid in benzene (Scheme 5).[11]

Table 2. ^{1}H-NMR spectral data of **10**[a]

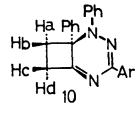

	Chemical shift, δ/ppm				Coupling const/Hz					
	H_a	H_b	H_c	H_d	J_{ab}	J_{ac}	J_{ad}	J_{bc}	J_{bd}	J_{cd}
10a	2.85	3.16	3.80	3.36	11.0	9.8	8.5	10.0	3.2	16.2
10b	2.88	3.22	3.84	3.36	10.5	10.0	8.5	10.4	3.3	16.3

a) Measured in $CDCl_3$.

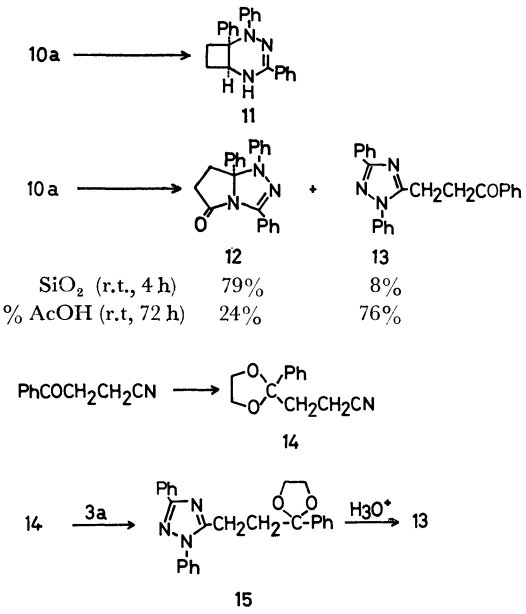

Scheme 5.

The structure of **12** was assigned on the basis of the spectral data, and **13** was confirmed by the identification with an authentic sample prepared by the route shown in Scheme 5.

Experimental

All melting points are uncorrected. IR, NMR, and mass spectra were obtained on a JASCO IRA-1 spectrometer, Hitachi R-40, JEOL SX-100 spectrometers, and a Hitachi RMS-4 spectrometer, respectively.

Reaction of Azaspiropentane ***1*** *with* C,N-*Diphenylnitrilimine (**3a**).* A solution of *N*-(α-chlorobenzylidene)-*N'*-phenylhydrazine[6] (1.0 g, 4.34 mmol) in $CHCl_3$ (10 ml) was added, drop by drop, to a stirred solution of the azaspiropentane **1**[2] (0.89 g, 4.02 mmol) and NEt_3 (2.1 g, 20.8 mmol) in $CHCl_3$ (30 ml), under nitrogen, at room temperature. The reaction mixture was stirred at room temperature for 60 h, and then filtered to remove the formed triethylammonium chloride. The filtrate was concentrated *in vacuo*, and the residue was chromatographed on silica gel. From the fraction using hexane–benzene (1: 2) as eluent, 0.325 g (19.5%) of the [3+3] cycloadduct **4a**, mp *ca.* 100 °C, as yellow crystals, and 3 mg of 1,3,5-triphenyl-2-pyrazoline (**6a**), mp 137—138 °C (lit,[5] mp 137—138 °C), as colorless needles were obtained. The fraction using $CHCl_3$ as eluent gave 5 mg of 1,3,4-triphenyl-1,2,4-triazolin-5-one (**7a**), mp 224—225 °C (lit,[6] mp 223—224 °C), as colorless needles.

Recrystallization of **4a** was difficult. IR (KBr) 1560 cm^{-1} (C=N). ^{1}H-NMR ($CDCl_3$) δ 0.50—1.85 (m, 4H), 4.69 (s, 1H), 6.25—7.75 ppm (m, 20H). MS *m/e* 415 (M^+).

The azaspiropentane **1** (0.89 g) reacted with the nitrilimine **3a**, generated from the chloride (2.0 g, 8.68 mmol) and NEt_3 (4.2 g, 41.6 mmol), in $CHCl_3$ (40 ml) under reflux for 1 h, giving 0.90 g (54%) of the isomeric 1: 1 adduct **5a** and 0.276 g (23%) of **6a**.

Recrystallization of **5a** from EtOH afforded yellow plates, mp 128—130 °C. IR (KBr) 1555 cm^{-1} (C=N). ^{1}H-NMR ($CDCl_3$) δ 1.81—2.40 (m, 3H), 2.72—3.20 (m, 1H), 4.54 (t, 1H, J=12 Hz), 6.60—7.64 ppm (m, 20H). MS *m/e* 415 (M^+). Found: C, 83.82; H, 6.06; N, 10.11%. Calcd for $C_{29}H_{25}N_3$: C, 83.55; H, 6.04; N, 9.99%.

Reaction of Azaspiropentane ***1*** *with* C-(p-*Chlorophenyl*)-N-*phenylnitrilimine (**3b**).* The reaction of **1** with **3b**, generated from *N*-(α,*p*-dichlorobenzylidene)-*N'*-phenylhydrazine[12] and NEt_3, was carried out under various conditions. The reaction mixture was worked up in a similar manner as above. From the fraction using hexane–benzene (1: 2) as eluent the [3+3] cycloadduct **4b** and 3-(*p*-chlorophenyl)-1,5-diphenyl-2-pyrazoline (**6b**) were obtained. The second and third fractions using benzene and $CHCl_3$ as eluents afforded the isomeric 1: 1 adduct **5b**, and 3-(*p*-chlorophenyl)-1,4-diphenyl-1,2,4-triazolin-5-one (**7b**) and the pentaazaspirononadiene **8b** respectively. The results are summarized in Table 1.

The 1: 1 Cycloadduct ***4b***: Mp 203—204 °C as colorless prisms (from hexane). IR (KBr) 1560 cm^{-1} (C=N). ^{1}H-NMR ($CDCl_3$) δ 0.50—2.05 (m, 4H), 4.69 (s, 1H), 6.21—7.52 ppm (m, 19H). MS *m/e* 451, 449 (M^+). Found: C, 77.70; H, 5.40; N, 9.32%. Calcd for $C_{29}H_{24}N_3Cl$: C, 77.40; H, 5.38; N, 9.34%.

The 1: 1 Adduct ***5b***: Mp 134—135 °C as yellow plates (from MeOH). IR (KBr) 1560 cm^{-1} (C=N). ^{1}H-NMR ($CDCl_3$) δ 1.51—2.49 (m, 3H), 2.52 (m, 1H), 4.48 (m, 1H), 6.52—7.76 ppm (m, 19H). MS *m/e* 451, 449 (M^+), 347, 345 (M^+—$PhCH{=}CH_2$, base peak). Found: C, 77.36; H, 5.47; N, 9.41%. Calcd for $C_{29}H_{24}N_3Cl$: C, 77.40; H, 5.38; N, 9.34%.

The Pyrazoline ***6b***: Mp 150—151 °C as pale greenish needles (from EtOH). This compound was identical with an authetic sample prepared from the following method. A solution of styrene (1.0 g, 9.62 mmol) and *N*-(α,*p*-dichlorobenzylidene)-*N'*-phenylhydrazine (2.6 g, 9.81 mmol) in benzene (10 ml) was stirred with NEt_3 (4.3 g, 42.5 mmol) at 60 °C for 2 h. The reaction mixture was filtered to remove the formed triethylammonium chloride, and the filtrate was concentrated *in vacuo* to leave the residue. Recrystallization from MeOH gave 0.83 g (63%) of **6b**, mp 150—151 °C. IR (KBr) 1550 cm^{-1} (C=N). ^{1}H-NMR ($CDCl_3$) δ 3.06, 3.78, 5.25 (each dd, 1H, J=7.5, 12.5, 17 Hz), 6.64—7.68 ppm (m, 14H). Found: C, 75.83; H, 5.05; N, 8.62%. Calcd for $C_{21}H_{17}N_2Cl$: C, 75.79; H, 5.11; N, 8.42%.

The Triazolinone ***7b***: Mp 185—186 °C as colorless needles (from EtOH). This compound was identical with an authentic sample prepared from the reaction of *N*-(α,*p*-dichlorobenzylidene)-*N'*-phenylhydrazine (1.0 g, 3.77 mmol) with phenyl isocyanate (0.5 g, 4.20 mmol) in the presence of aluminum oxide (0.3 g) according to the Huisgen's method.[6] IR (KBr) 1720 (C=O), 1580 cm^{-1} (C=N). ^{1}H-NMR ($CDCl_3$) δ 7.08—7.58 (m, 12H), 7.90—8.16 ppm (m, 2H). Found: C, 68.89; H, 4.25; N, 12.13%. Calcd for $C_{20}H_{14}N_3OCl$: C, 69.06; H, 4.03; N, 12.08%.

The Pentaazaspirononadiene ***8b***: Mp 174—175 °C (dec) as colorless needles (from EtOH). IR (KBr) 1595 cm^{-1} (C=N). ^{1}H-NMR ($CDCl_3$) δ 3.20, 3.78 (each d, 1H, J=20 Hz), 6.61—7.75 ppm (m, 23H). MS *m/e* 577, 575, 573 (M^+), 347, 345, 343 (M^+—$ArC{\equiv}\overset{+}{N}{-}\overset{-}{N}Ph$). Found: C, 70.86; H, 4.37; N, 11.99%. Calcd for $C_{34}H_{25}N_5Cl_2$: C, 71.08; H, 4.39; N, 12.19%.

Reaction of the 1: 1 Adduct ***5b*** *with the Nitrilimine* ***3a***. *i*): A solution of NEt_3 (0.1 ml, 0.69 mmol) in $CHCl_3$ (5 ml) was added, drop by drop, to a stirred solution of **5b** (0.3 g, 0.67 mmol) and *N*-(α-chlorobenzylidene)-*N'*-phenylhydrazine (0.16 g, 0.69 mmol) in $CHCl_3$ (10 ml) at room temperature. The reaction mixture was then refluxed for 4 h, and concentrated *in vacuo* to leave the residue. Benzene was added to the residue, and the resultant mixture was filtered to remove the formed triethylammonium chloride. The filtrate was concentrated *in vacuo* and the residue was chromatographed on silica

gel using hexane–benzene (1: 1) and benzene as eluents, giving 46.3 mg (23%) of **6b** and 7 mg of **7b**.

ii): The same reaction was carried out in degassed $CHCl_3$ under nitrogen. After removal of triethylammonium chloride, the residue was triturated with EtOH to give 0.108 g (30%) of the pentaazaspirononadiene **9**. The EtOH solution was chromatographed on silica gel to give 31.9 mg (23%) of **6a**.

The Pentaazaspirononadiene 9: Mp 184—186 °C as colorless needles (from cyclohexane). IR (KBr) 1560 cm^{-1} (C=N). ^{1}H-NMR ($CDCl_3$) δ 3.35, 3.86 (each d, 1H, J=20 Hz), 6.73—7.04 (m, 4H), 7.08—7.48 (m, 18H), 7.54—7.80 ppm (m, 2H). MS *m/e* 541, 539 (M^+), 347, 345 ($M^+ - PhC{\equiv}\overset{+}{N}-\bar{N}Ph$). Found: C, 75.53; H, 4.89; N, 13.03%. Calcd for $C_{34}H_{26}N_5Cl$: C, 75.64; H, 4.82; N, 12.97%.

Reaction of Azaspiropentane 2 with C,N-Diphenylnitrilimine (3a). A solution of *N*-(α-chlorobenzylidene)-*N'*-phenylhydrazine (1.37 g, 5.94 mmol) in benzene (40 ml) was added, drop by drop, to a stirred solution of the azaspiropentene **2**[13] (0.85 g, 5.94 mmol) and NEt_3 (2.88 g, 28.4 mmol) in benzene (15 ml) under nitrogen at room temperature. The reaction mixture was then stirred for 24 h, and filtered to remove the formed triethylammonium chloride. The filtrate was concentrated *in vacuo* to leave the residue, which on recrystallization from hexane afforded 1.13 g (97%) of the triazabicyclooctadiene **10a**, mp 153—154 °C, as yellow needles. IR (KBr) 1675 cm^{-1} (C=N). ^{13}C-NMR ($CDCl_3$) δ 36.2, 38.5, 66.7, 116.2, 121.7, 125.5, 126.0, 127.9, 128.2, 128.5, 128.8, 129.0, 134.9, 136.3, 142.6, 146.0, 165.1. MS *m/e* 337 (M^+). Found: C, 81.85; H, 5.64; N, 12.46%. Calcd for $C_{23}H_{19}N_3$: C, 81.87; H, 5.18; N, 12.45%.

A similar reaction of **2** (0.37 g, 2.6 mmol) with the nitrilimine **3b**, generated from the corresponding chloride (0.68 g, 2.6 mmol) and NEt_3 (1.26 g, 13 mmol), in benzene (35 ml) afforded 0.89 g (94%) of the triazabicyclooctadiene **10b**, mp 178—180 °C (dec), as yellow needles. IR (KBr) 1673 cm^{-1}. ^{13}C-NMR ($CDCl_3$) δ 36.2, 38.5, 66.6, 116.3, 121.9, 125.9, 126.7, 127.9, 128.4, 128.8, 129.0, 133.4, 134.3, 136.1, 142.3, 145.1, 165.2. MS *m/e* 373, 371 (M^+). Found: C, 74.31; H, 4.83; N, 11.16%. Calcd for $C_{23}H_{18}N_3Cl$: C, 74.28; H, 4.88; N, 11.30%.

Reduction of 10a. After a solution of **10a** (0.1 g) in THF (2 ml) was stirred with $NaBH_4$ (26 mg) at room temperature for 5 h, water (5 ml) was added to the reaction mixture. The mixture was acidified with 1.8% HCl to give a solid, which on recrystallization from cyclohexane gave 96 mg (95%) of the dihydro compound **11**, mp 181—182 °C, as colorless needles. IR (KBr) 3470 (NH), 1630 cm^{-1} (C=N). ^{1}H-NMR ($CDCl_3$) δ 1.4—2.75 (m, 4H), 3.85 (broad, 1H, after exchange with D_2O, the signal changed to a double doublet, J=7.0, 8.8 Hz), 4.95 (broad, 1H, exchanged with D_2O), 6.50—7.50 (m, 13H), 7.60—7.85 (m, 2H). ^{13}C-NMR ($CDCl_3$) δ 23.1, 29.2, 54.5, 61.8, 115.8, 118.3, 124.8, 125.6, 126.7, 128.1, 128.6, 134.9, 138.1, 142.7, 144.6. MS *m/e* 339 (M^+), 311 (base peak), 235, 219, 207, 180, 207, 180, 144, 104, 91. Found: C, 81.36; H, 6.33; N, 12.50%. Calcd for $C_{23}H_{21}N_3$: C, 81.38; H, 6.24; N, 12.38%.

Treatment of 10a with Silica Gel. A solution of **10a** (0.1 g) in benzene (2 ml) was stirred with silica gel (Wako-gel C-200, 0.5 g) at room temperature for 4 h. The mixture was filtered and the filtrate was concentrated *in vacuo* to leave a residue. The residue was chromatographed on silica gel using benzene as eluent to give 82.7 mg (79%) of the triazabicyclooctenone **12** and 8.4 mg (8%) of the 1,2,4-triazole **13**.

The Triazabicyclooctenone 12: Mp 96—97 °C as colorless prisms (from benzene). IR (KBr) 1735 cm^{-1} (C=O). ^{1}H-NMR ($CDCl_3$) δ 2.60—3.40 (m, 4H), 6.70—7.40 (m, 14H), 7.70—7.90 (m, 1H). ^{13}C-NMR ($CDCl_3$) δ 34.3, 35.4, 90.4, 114.4, 120.3, 125.5, 127.2, 127.8, 128.1, 128.2, 129.0, 129.7, 139.3, 140.9, 142.0, 174.5. MS *m/e* 353 (M^+), 298, 276, 194, 165, 103, 91. Found: C, 78.24; H, 5.43; N, 11.67%. Calcd for $C_{23}H_{19}N_3O$: C, 78.16; H, 5.42; N, 11.89%.

The 1,2,4-Triazole 13: Mp 115—116 °C as colorless needles (from EtOH). IR (KBr) 1682 cm^{-1} (C=O). ^{1}H-NMR ($CDCl_3$) δ 3.10—3.35 (m, 2H), 3.50—3.75 (m, 2H), 7.20—7.65 (m, 11H), 7.90—8.20 (m, 4H). ^{13}C-NMR ($CDCl_3$) δ 21.1, 36.1, 125.2, 126.4, 128.0, 128.5, 128.6, 128.9, 129.1, 130.8, 133.2, 136.5, 137.4, 155.8, 198.0. MS *m/e* 353 (M^+), 248 (M^+—PhCO, base peak), 105, 91. Found: C, 78.19; H, 5.34; N, 11.88%. Calcd for $C_{23}H_{19}N_3O$: C, 78.16; H, 5.42; N, 11.89%.

Treatment of 10a with 1% Aqueous AcOH. A solution of **10a** (40 mg) in benzene (2 ml) was stirred with 1% aqueous AcOH (1 ml) at room temperature for 4 days. The benzene solution was concentrated *in vacuo* to leave a residue. Chromatography of the residue on silica gel (benzene) afforded 10 mg (24%) of **12** and 32 mg (76%) of **13**.

Preparation of 5-(β-Benzoylethyl)-1,3-diphenyl-1,2,4-triazole (13). A mixture of β-benzoylpropionitrile[14] (4.0 g), ethylene glycol (6.0 g), and a catalytic amount of *p*-toluenesulfonic acid in benzene (70 ml) was boiled with azeotropic removal of water. After being boiled for 50 h, the reaction mixture was concentrated *in vacuo* to give 5.3 g (100%) of 2-(2-cyanoethyl)-2-phenyl-1,3-dioxolane (**14**) which on recrystallization from hexane afforded colorless needles, mp 62.5—63.5 °C. Found: C, 70.88; H, 6.54; N, 6.77%. Calcd $C_{12}H_{13}NO_2$: C, 70.91; H, 6.45; N, 6.89%.

A solution of *N*-(α-chlorobenzylidene)-*N'*-phenylhydrazine (1.9 g, 8.24 mmol) in benzene (30 ml) was added, drop by drop, to a stirred solution of the above dioxolane **14** (1.7 g, 8.37 mmol) and NEt_3 (5.9 g, 83.4 mmol) in benzene (20 ml), under nitrigen, at room temperature. After being refluxed for 65 h, the reaction mixture was filtered, and the filtrate was concentrated *in vacuo* to leave a residue. The residue was chromatographed on silica gel using benzene as eluent to give 0.329 g (10%) of 2-[2-(1,3-diphenyl-1,2,4-triazol-5-yl)-ethyl]-2-phenyl-1,3-dioxolane (**15**), along with recovery of 1.5 g (88%) of **14**.

The Triazole 15: Mp 104—105 °C as colorless needles (from hexane). Found: C, 75.64; H, 5.87; N, 10.61%. Calcd for $C_{25}O_{23}N_3O_2$: C, 75.54; H, 5.83; N, 10.57%.

A suspension of the triazole **15** (50 mg) in 5% aqueous HCl (5 ml) was stirred at room temperature for 22 h. Filtration gave crystals which were washed with NH_4OH and water, and then recrystallized from EtOH to give 42.3 mg (95.5%) of **13**, mp 115—116 °C.

References

1) Studies of Highly Strained Heterocycles. Part 4. Part 3 of this series: See Ref. 4.

2) J. K. Crandall and W. W. Conover, *J. Org. Chem.*, **33**, 63 (1974).

3) O. Tsuge and H. Watanabe, *Heterocycles*, **7**, 907 (1977).

4) O. Tsuge, H. Watanabe, and Y. Kiryu, *Bull. Chem. Soc. Jpn.*, **52**, 3387 (1979).

5) R. Huisgen, M. Seidel, G. Wallbillich, and H. Knupfer, *Tetrahedron*, **17**, 1 (1962).

6) R. Huisgen, R. Grashey, H. Knupfer, R. Kunz, and M. Seidel, *Chem. Ber.*, **97**, 1085 (1964).

7) The spectral data do not permit the distinction between **5a** and the reversed cycloadduct, 1,5,6,8-tetraphenyl-5,6,8-triazaspiro[3.4]oct-7-ene. However, it has been reported that

C,N-diphenylnitrilimine added to the *exo-N*-phenylimino groups of 2,4-diphenyl-5-phenylimino-1,3,4-oxazoline-2 and 5-phenylimino-1,3,4-triphenyl-1,2,4-triazoline-2 to give the corresponding 1,2,4-triazoline derivatives as the sole products.[15]

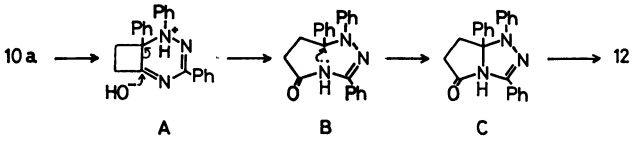

8) F. P. Woerner, H. Reimlinger, and R. Merinyi, *Chem. Ber.*, **104**, 2786 (1971).

9) D. J. Anderson and A. Hassner, *Synthesis*, **1975**, 483.

10) I. Fleming and D. H. Williams, *Tetrahedron*, **23**, 2747 (1967).

11) The pathway for formation of **12** from **10a** is illustrated as the following scheme. The compound **10a** undergoes hydrolysis with concurrent ring expansion through **A**, and subsequent hydrogen transfer forms the eight-membered cyclic intermediate **B**. Transanular cyclization of **B** leads to the formation of the bicyclic compound **C** which deprotonation gives **12**. However, the pathway leading to **13** from **10a** is not clear.

12) R. Huisgen, R. Grashey, M. Seidel, G. Wallbillich, H. Knupfer, and R. Schmidt, *Liebigs Ann. Chem.*, **653**, 105 (1962).

13) H. J. Bestmann and R. Kunstmann, *Chem. Ber.*, **102**, 1816 (1969).

14) β-Benzoylpropionitrile was prepared by the reaction of 1-benzoyl-2-chloroethane with NaCN in aqueous EtOH. Mp 71—73 °C (lit,[16] mp 70 °C) as colorless needles. Found: C, 75.39; H, 5.71; N, 8.70%. Calcd for $C_{10}H_9NO$: C, 75.45; H, 5.70; N, 8.80%.

15) R. Huisgen, R. Grashey, R. Kunz, G. Wallbillich, and E. Aufderhaar, *Chem. Ber.*, **98**, 2174 (1965).

16) E. Yoshisato, M. Ryang, and S. Tsutsumi, *J. Org. Chem.*, **34**, 1500 (1969).

Effect of Alcohols on the Thermal Denaturation of Lysozyme as Measured by Differential Scanning Calorimetry

Yukihisa FUJITA,* Akihiko MIYANAGA, and Yukinao NODA

Department of Chemistry, Hyogo College of Medicine, Mukogawa, Nishinomiya, Hyogo 663

(Received June 30, 1979)

The thermal denaturation of lysozymc in aqueous alcohol solution has been investigated by differential scanning calorimetry. The alcohols employed were methanol, ethanol, isomeric propyl alcohols and butyl alcohols as monohydric alcohols, and ethylene glycol and glycerol as polyhydric alcohols. In monohydric alcohols, the temperature of denaturation, T_d, of lysozyme decreased linearly with increasing alcohol concentration, which became pronounced with an increasing in the hydrophobic character. The enthalpy of denaturation, ΔH_d, of lysozyme showed a complex dependence on the solvent composition; the ΔH_d first increased with increasing alcohol concentration and then started decreasing at different concentrations for each alcohol. The branching of the alkyl chain decreased the destabilizing effect of the alcohol on the native conformation of the protein. In polyhydric alcohols, both T_d and ΔH_d increased with increasing alcohol concentration. The polyhydric alcohols stabilized the native conformation of the protein in contrast with the monohydric alcohols. The results are discussed in terms of the hydrophobic and hydrophilic characters of the alcohols.

In an earlier work, the hydration, the ordering of the water molecules around the protein molecule, were reported to play an important role in the stabilizing the native structure of the globular protein.[1,2] The addition of alcohol to a protein solution is expected to affect the stability of the native structure of the protein due to alteration in the characteristic structure of water. The effect of alcohols on the stability of globular proteins have been extensively investigated by spectroscopic measurements.[3–5] The studies have revealed that the effectiveness of the alcohols as protein denaturants increased with increasing chain length or hydrocarbon content. Hamaguchi *et al.*[6,7] have, however, found that the CD and difference spectra of the lysozyme in aqueous alcohol solutions depend nonlinearly on the concentration of alcohol at a concentration below that required to unfold the protein. Moreover, Parodi *et al.*[8] have reported from different spectrophotometric and ORD studies of the thermal denaturation of lysozyme in aqueous alcohol solutions that the van't Hoff enthalpy of denaturation showed a complex dependence on alcohol concentration.

In this paper, the effect of mono- and polyhydric alcohols on the thermal denaturation of lysozyme as measured by differential scanning calorimetry (DSC) will be reported.

Experimental

Materials and Methods. The hen egg-white lysozyme used in the present study was a six-times recrystallized preparation obtained from Seikagaku Kogyo Co. The alcohols employed were methanol, ethanol, the isomeric propyl alcohols and butyl alcohols, ethylene glycol and glycerol. The alcohols employed were spectroscopic grade or analytical grade reagents and were used without further purification. The concentration of the stock solution of the lysozyme, which dissolved with the 0.1 M glycine–HCl buffer (pH 3), was determined spectrophotomerically using an extinction of $E^{1\%}_{1cm}=26.9$ at 280 nm. The sample solution were prepared by mixing suitable aliquots of stock solution with the alcohol.

Calorimetric measurements were conducted with a Rigaku Denki standard-type differential scanning calorimeter at a heating rate of 10 K/min and a concentration of 15—25 mg/cm^3. The molecular weight of lysozyme was taken as 14300.[9]

Results and Discussion

The thermal denaturation of lysozyme in aqueous alcohol solutions was measured with a differential scanning calorimeter. For each solution, a reproducible endothermic peak was observed occurring over a temperature range of 15—20 K. The temperature, T_d, and the enthalpy, ΔH_d, of denaturation were estimated from the peak temperature and the peak-area in the thermogram obtained.

The T_d and ΔH_d in solutions containing methanol, ethanol, 1-propanol, and 1-butanol are plotted as a function of the alcohol concentration in Figs. 1 and 2, respectively. The T_d decreased gradually with increasing alcohol concentration, which became more pronounced with an increase in length of the alkyl chain. A similar dependence of the T_d on the concentration and/or length of the alkyl chain of alcohols has been reported earlier for ribonuclease[3,10] and lysozyme[8,10] from spectroscopic studies of thermal denaturation. The ΔH_d showed a complex dependence on the solvent composition; the ΔH_d first increased with increasing

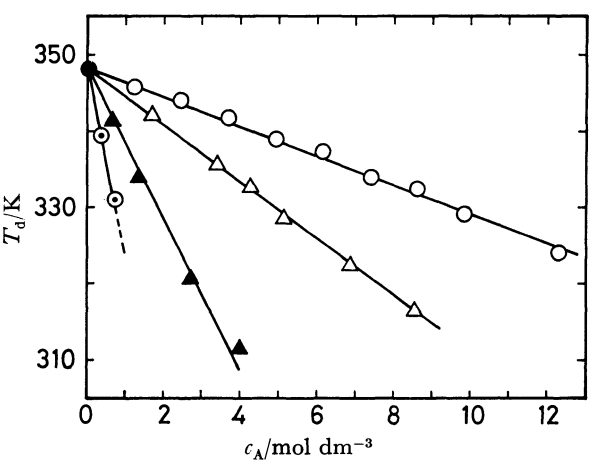

Fig. 1. The temperature of denaturation, T_d, of lysozyme as a function of the alcohol concentration, c_A. ●, Water; ○, methanol; △, ethanol; ▲, 1-propanol; ⊙, 1-butanol.

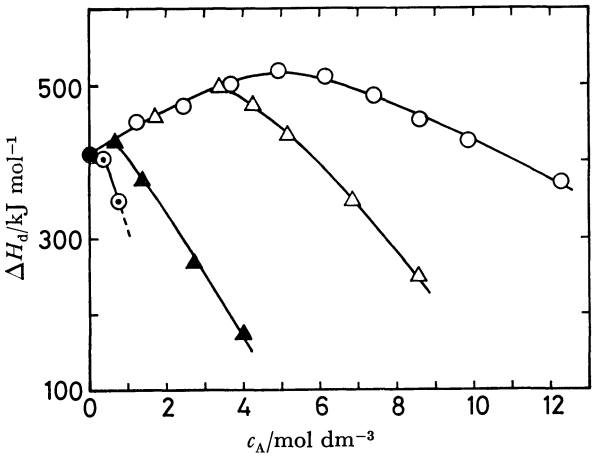

Fig. 2. The enthalpy of denaturation, ΔH_d, of lysozyme as a function of the alcohol concentration, c_A. ●, Water; ○, methanol; △, ethanol; ▲, 1-propanol; ⊙, 1-butanol.

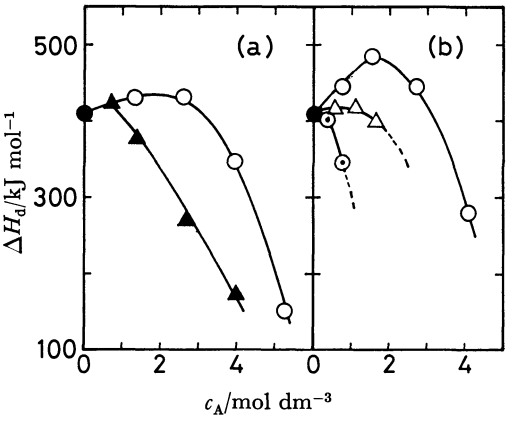

Fig. 4. The enthalpy of denaturation, ΔH_d, of lysozyme as a function of the alcohol concentration, c_A. (a) Isomeric propyl alcohols, ●, water; ○, *i*-PrOH; ▲, *n*-PrOH. (b) Isomeric butyl alcohols, ●, water; ○, *t*-BuOH; △, *s*-BuOH; ⊙, *n*-BuOH.

alcohol concentration and then started decreasing at a different concentration for each alcohol. The maximum in the values of ΔH_d occurred in the order of methanol, ethanol, 1-propanol, and 1-butanol, that is, increasing hydrophobic character of the alcohol added. Moreover, the maximum value of ΔH_d decreased with increasing length of the alkyl chain and all values of ΔH_d observed in aqueous 1-butanol solutions were smaller than that in the aqueous solution.

This observation was similar to that for van't Hoff enthalpies of denaturation obtained by Parodi *et al.*[8] from spectroscopic studies of lysozyme in aqueous alcohol solutions. Recently, Velicelebi and Sturtevant[11] have reported similar plots for the enthalpies of denaturation determined from high sensitivity calorimetric measurements of the thermal denaturation of lysozyme in similar alcohol–water mixtures at pH 2. The ΔH_d values obtained in our present work appear to be in fairly good agreement with those reported by Velicelebi and Sturtevant. The T_d values, however, in our work were considerably higher. The differences probably result from the large difference in the heating rate.

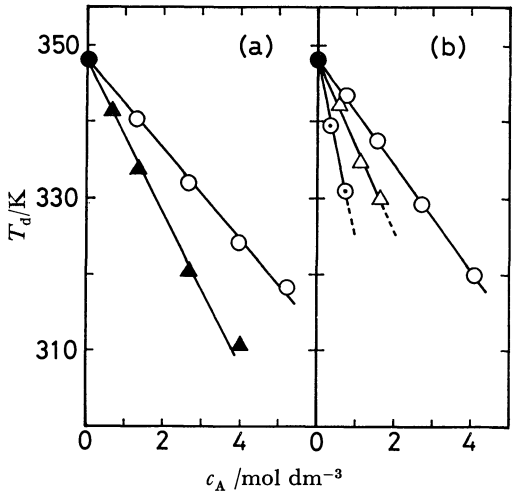

Fig. 3. The temperature of denaturation, T_d, of lysozyme as a function of the concentration, c_A. (a) Isomeric propyl alcohols, ●, water; ○, *i*-PrOH; ▲, *n*-PrOH. (b) Isomeric butyl alcohols, ●, water; ○, *t*-BuOH; △, *s*-BuOH; ⊙, *n*-BuOH.

The effect of branched-chain alcohols was also investigated and the results are showed in Figs. 3 and 4 together with the results of the corresponding straight-chain alcohols. The lowering of the T_d by the branched-chain alcohols was smaller than that by the corresponding straight-chain alcohols. The ΔH_d in the branched-chain alcohol solutions showed a complex dependence on the solvent composition, as found in the case of straight-chain alcohols. The maximum in the values of ΔH_d occurred at a higher alcohol concentration than that in the corresponding straight-chain alcohol. The results indicate that branching of the alkyl chain reduces the effectiveness of the alcohol as protein denaturants.

Aliphatic alcohols can be regarded either as hydrocarbons containing hydrophilic hydroxyl groups or as water in which one hydrogen atom has been replaced by a hydrophobic alkyl group. The effect of alcohols on the stability of the native structure of protein in terms of the hydrophobic, destabilizing, and hydrophilic, stabilizing, effects. In the monohydric alcohols the results indicate that the hydrophobic effect, which enhances with chain length of the alkyl groups, dominates the hydrophilic effect. The selective binding of alcohols to the nonpolar groups of protein in water–alcohol mixtures has been experimentally verified.[12] It is well documented that alcohols perturb the characteristic water structure around the protein molecule.[13] The binding of alcohols to the nonpolar side chains of proteins which become exposed during denaturation may reduce the ordering effect of the nonpolar side chains on the water molecules, simultaneously leading to the weakening hydrophobic interaction between the nonpolar side chains, which favors the denatured state. Therefore, the depression of T_d by the addition of alcohols which increases with increasing alcohol concentration and/or length of the alkyl chain appears to be

associated to a predominance of an increasing entropy of the denaturation. This result is in agreement with that of Schrier *et al.*[3] suggesting that the lowering of the denaturation temperature of ribonuclease by alcohols is largely entropy dependent.

The complex dependence of the ΔH_d on the alcohol concentration and/or length of the alkyl chain may also be discussed in terms of the hydrophobic effect of alcohols. At lower alcohol concentration, the alcohol molecules interact selectively with the nonpolar groups of protein, and thus the hydrophobic interaction between the nonpolar groups of protein is weakened. As suggested by Privalov,[14] rupture of the hydrophobic bond is accompanied by liberation rather than absorption of heat. It appears resonable to consider weakening of the hydrophobic bond by the addition of alcohol reduces the exothermic contribution of hydrophobic-bond rupture to the total ΔH_d. In addition, it has been experimentally shown that the secondary structure of polypeptide was stabilized more in water–alcohol mixtures than in water.[15] This suggestes that the disordering of the water molecules around the protein molecule due to the binding of alcohol to the nonpolar groups of protein enhances the stability of the secondary structure of protein which is created essentially by the interaction between the polar groups of protein. The addition of alcohol will lead to an increase in ΔH_d because the rupture of the polar interaction is an endothermic reaction. At higher alcohol concentration, however, alcohol may increase the ordering of water molecules, leading to not only stronger hydrophobic interaction but a weakening of the polar interaction. The rise in the temperature of maximum density of water by the addition of alcohol has been accounted for by the ordering of water molecules by alkyl groups.[16]

The T_d and ΔH_d in solutions containing ethylene glycol and glycerol are plotted as a function of the alcohol concentration in Fig. 5. In contrast with the case of monohydric alcohols, the T_d in the solutions of polyhydric alcohols increased with increasing alcohol concentration. The ΔH_d increased also with increasing alcohol concentration. The increase in the T_d and ΔH_d became more pronounced in the order: ethylene glycol, glycerol, that is, increasing the number of hydroxyl groups of the polyhydric alcohol added. It is apparent that polyhydric alcohols stabilize the native structure of protein; the hydrophilic effect of polyhydric alcohols dominate the hydrophobic effect. When the methylene group was present in equimolar quantities the polyhydric alcohol stabilized the native structure of protein in contrast to the monohydric alcohol. This is to be expected if the hydrophobic interaction between the nonpolar group of protein and the nonpolar part of the alcohol molecule is an important factor in destabilization. A higher degree of interaction exists between polyhydric alcohol and water than monohydric alcohol and water. Introduction of a second and third hydroxyl group into a monohydric alcohol increases the interaction with water, whereas the hydrophobic properties are less pronounced.

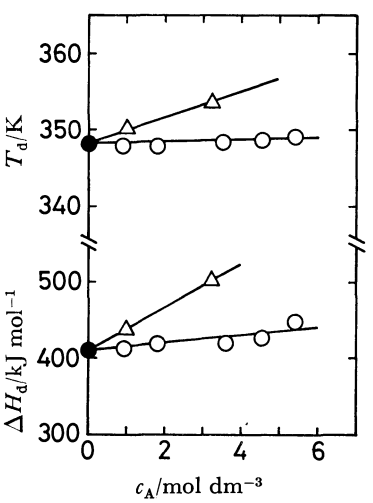

Fig. 5. The temperature, T_d, and the enthalpy, ΔH_d, of denaturation of lysozyme as a function of the alcohol concentration, c_A.
●, Water; ○, ethylene glycol; △, glycerol.

Gerlsma and Stuur[10] have suggested that there was no direct molecular interaction between protein and polyhydric alcohol from the studies on the thermal denaturation of ribonuclease and lysozyme in the present of polyhydric alcohols. This suggests that the hydrophilic effect of alcohols on the stability of protein appears mainly to be of an indirect kind, *viz.* either a strengthening of the polar interaction by a lowering of the dielectric constant, an increasing of the enthalpic change of denaturation, and/or an intensifying of the hydrophobic interaction of protein by altering the water structure, which principally is entropically controlled. The addition of polyhydric alcohol may lead to the strengthening of the polar interaction by reducing the interactions with water molecules and by lowering the dielectric constant of the medium. It is well known that hydrophobic interactions are intensified by an increase in temperature.[14] Therefore, it is also probable that the addition of polyhydric alcohol may enhance the hydrophobic interactions. The hydrophilic effect increases the hydrophobic contribution to the stabilizing of the native structure of protein. This may be induced not only by the hydrophilic groups of the added alcohols but the polar groups of the protein molecule itself will exert a similar effect on the surrounding water molecules.

References

1) Y. Fujita and Y. Noda, *Bull. Chem. Soc. Jpn.*, **51**, 1567 (1978).
2) Y. Fujita and Y. Noda, *Bull. Chem. Soc. Jpn.*, **52**, 2349 (1979).
3) E. E. Schrier, R. T. Ingwall, and H. A. Scheraga, *J. Phys. Chem.*, **69**, 298 (1965).
4) J. F. Brandts and L. Hunt, *J. Am. Chem. Soc.*, **89**, 4826 (1967).
5) T. T. Herskovits, B. Gadegbeku, and H. Jaillet, *J. Biol. Chem.*, **245**, 2588 (1970).
6) K. Ikeda and K. Hamaguchi, *J. Biochem.*, **68**, 785 (1970).
7) N. Shimaki, K. Ikeda, and K. Hamaguchi, *J. Biochem.*, **68**, 795 (1970).
8) R. M. Parodi, E. Bianchi, and A. Ciferri, *J. Biol.*

Chem., **248**, 4047 (1973).
9) R. E. Canfield, *J. Biol. Chem.*, **238**, 2698 (1963).
10) S. Y. Gerlsma and E. R. Stuur, *Int. J. Peptide Protein Res.*, **4**, 377 (1972).
11) G. Velicelebi and J. M. Sturtevant, *Biochemistry*, **18**, 1180 (1979).
12) S. N. Timasheff and H. Inoue, *Biochemistry*, **7**, 2501 (1968).
13) F. Franks and D. Eagland, *CRC Crit. Rev. Biochem.*, **3**, 165 (1975).
14) P. L. Privalov, "Water in Biological Systems," ed by L. P. Kayushin, Consultants Bureau, New York (1969), p. 38.
15) G. Conio, E. Patrone, and S. Brighetti, *J. Biol. Chem.*, **245**, 3335 (1970).
16) G. Wada and S. Umeda, *Bull. Chem. Soc. Jpn.*, **35**, 646 (1962).

Restricted Rotation Involving the Tetrahedral Carbon. XXVII. Rotamers of 9-(1-Cyano or 1-Methoxycarbonyl-1-methylethyl)triptycene Derivatives Carrying a Substituent in 1-Position[1)]

Soichi OTSUKA, Tsutomu MITSUHASHI, and Michinori ŌKI*

Department of Chemistry, Faculty of Science, The University of Tokyo, Tokyo 113

(Received June 30, 1979)

The title compounds were prepared by the reaction between 9-(1-cyano or 1-methoxycarbonyl-1-methylethyl)-anthracene and substituted benzynes and their rotational isomers were isolated. The barriers to rotation of these compounds were found to be 35—36 kcal/mol and 32—34 kcal/mol for the processes *dl*→*meso* and *meso*→*dl*, respectively.

Triptycenes carrying a tertiary carbon in the 9-position are known to exhibit unusually high barriers to rotation about the C_9–C_{subst} bond.[2)] Thus various rotational isomers of this type have been isolated. The highest barrier to rotation has been realized with 9,9′-bitriptycyl derivatives (**1**).[3)] The second highest barrier known to date is that of 9,10-bis(1-cyano-1-methylethyl)triptycene (**2**).[4)] We have felt that it will be interesting to see whether triptycenes carrying a tertiary carbon in 9-position, one of which substituents is an sp^2 or sp hybridized carbon atom, exhibit high barriers to rotation in general. Since the barrier to rotation is the difference in energy between the ground and the transition states, the sp^2 or sp hybridized carbon might fit well in the triptycene skeleton to lower the ground state.

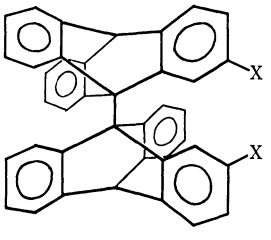

(1)

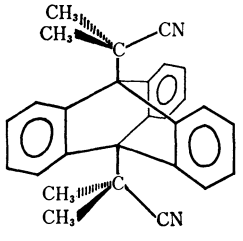

(2)

Syntheses

Syntheses of triptycenes are usually carried out by the Diels-Alder reaction of a substituted anthracene with a benzyne. The first problem, therefore, was to synthesize appropriately substituted anthracenes. This posed a problem, because this kind of compounds are usually prepared by the Grignard reaction with anthrone followed by dehydration. The electronegative groups such as cyano and methoxycarbonyl would not survive under the reaction conditions. Literature search indicated that, although there was a method to introduce a tertiary carbon carrying two electronegative groups to the 9-position of anthracene,[5)] there was no method to give the desired anthracenes. Various attempts were made, such as Reformatsky reaction, reaction of anthrone with the lithium derivative of isobutyronitrile, and methylation of 9-cyanomethylanthracene, but they all failed probably for steric reasons. Finally we were able to introduce 1-cyano- or 1-methoxycarbonyl-1-methylethyl group to the 10-position of anthrone by allowing the latter to react with azobisisobutyronitrile or dimethyl azobisisobutyrate under basic conditions.[6)] The substituted anthrone (**3**) was reduced with sodium borohydride and the product (**4**) was dehydrated with phosphorus pentaoxide. The 9-substituted anthracene (**5**) was treated with benzynes to give desired triptycenes

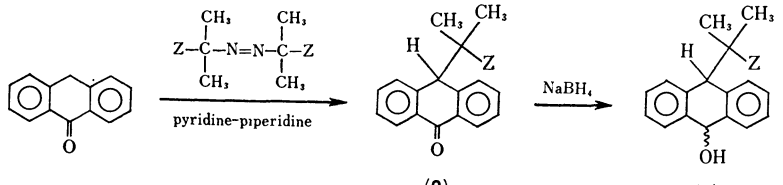

(3) (4)

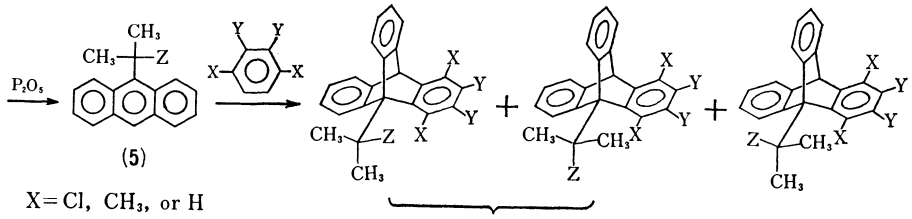

(5)

X=Cl, CH_3, or H
Y=Cl or H
Z=CN or $COOCH_3$

(*dl*-**6**) (*meso*-**6**)

(**6**). Reactive benzynes such as tetrachlorobenzyne reacted to afford 1,4-addition products in addition to the desired 9,10-adducts. The former was found very difficult to remove from the latter. Thus the olefinic bond of the former was oxidized with performic acid and the resulted oxygenated compounds were removed by chromatography.

Experimental

10-(1-Cyano-1-methylethyl)anthrone (**3**, *Z=CN*). A solution of 3.07 g (15.8 mmol) of anthrone and 6.0 g (37 mmol) of azobisisobutyronitrile in 30 ml of pyridine–piperidine (2: 1) was heated at 90 °C for 6 h with stirring. The mixture was poured into excess of hydrochloric acid after cooling and the precipitate was collected. Tetramethylsuccinonitrile was removed by steam distillation of the precipitate and the residue taken up in dichloromethane. After drying, the solvent was evaporated and the residue was heated in vacuo until no sublimate was observed. The residue was chromatographed on alumina using hexane–benzene as an eluent. The desired product, mp 152 °C, was obtained as colorless crystals in 3.63 g (88%) yield. Found: C, 82.57; H, 5.79; N, 5.47%. Calcd for $C_{18}H_{15}NO$: C, 82.73; H, 5.79; N, 5.36 %. ^{1}H NMR ($CDCl_3$, δ): 1.15 (6H, s), 4.27 (1H, s), 7.3—7.7 (6H, m), 8.1— 8.4 (2H, m). IR (KBr): 2235, 1675, 710 cm^{-1}.

9-(1-Methoxycarbonyl-1-methylethyl)anthrone (**3**, *Z=COOCH$_3$*), mp 89—90 °C, was similarly obtained in 62% yield from anthrone and dimethyl azobisisobutyrate. Found: C, 77.53; H, 6.16%. Calcd for $C_{19}H_{18}O_3$: C, 77.49; H, 6.14%. ^{1}H NMR ($CDCl_3$, δ): 0.89 (6H, s), 3.61 (3H, s), 4.52 (1H, s), 7.3—7.6 (6H, m), 8.0—8.3 (2H, m). IR (KBr): 1730, 1670, 1317, 705 cm^{-1}.

9-(1-Cyano-1-methylethyl)anthracene (**5**, *Z=CN*). A solution of 0.807 g (3.1 mmol) of **3** (Z=CN) in 15 ml of ethanol was refluxed for 2 h, while a solution of 0.9 g (24 mmol) of sodium borohydride in 10 ml of 90% ethanol was added in 10 min. Water was added and the mixture extracted with dichloromethane. After evaporation of the solvent, **4** (Z=CN) was obtained in 0.77 g yield as a roughly equimolar mixture of *cis* and *trans* isomers. The alcohol (**4**, Z=CN) in 20 ml of carbon tetrachloride was heated under reflux for 1 h with 5 g of phosphorus pentaoxide and the mixture was filtered. The solvent was evaporated from the filtrate and the residue was chromatographed on alumina. A small amount (*ca.* 4%) of anthracene was eluted first and then came 0.46 g (61%) of **5** (Z=CN), mp 138 °C (recrystallized from ethanol). Found: C, 87.83; H, 6.18; N, 5.69%. Calcd for $C_{18}H_{15}N$: C, 88.13; H, 6.16; N, 5.71%. ^{1}H NMR ($CDCl_3$, δ): 2.37 (6H, s), 7.3—7.6 (4H, m), 7.8—8.1 (2H, m), 8.40 (1H, s), 8.4—8.7 (2H, m). IR (KBr): 2230, 735 cm^{-1}.

9-(1-Methoxycarbonyl-1-methylethyl)anthracene (**5**, *Z=COOCH$_3$*), mp 123—125 °C, was similarly prepared in 41% yield. Found: C, 81.74; H, 6.46%. Calcd for $C_{19}H_{18}O_2$: C, 81.98; H, 6.52%. ^{1}H NMR ($CDCl_3$, δ): 2.12 (6H, s), 3.46 (3H, s), 7.2—7.6 (4H, m), 7.8—8.3 (4H, m), 8.37 (1H, s). IR (KBr): 1715, 1258, 1143, 717 cm^{-1}.

9-(1-Carbamoyl-1-methylethyl)anthracene. A solution of 1.0 g of **5** (Z=CN) and 5.0 g of potassium hydroxide in 50 ml of 2-ethoxyethanol was heated under reflux for 3 h under a nitrogen atmosphere. The mixture was treated with dilute hydrochloric acid after cooling and the precipitate was taken up in benzene. Evaporation of the solvent and recrystallization of the residue from tetrahydrofuran–hexane gave the amide, mp 226—227 °C. Found: C, 82.11; H, 6.45; N, 5.38%. Calcd for $C_{18}H_{17}NO$: C, 82.10; H, 6.51; N, 5.32%. ^{1}H NMR ($CDCl_3$, δ): 2.13 (6H, s), 5.0 (2H, broad), 7.2—7.6 (4H, m), 7.7—8.1 (2H, m), 8.35 (1H, s), 8.1—8.5 (2H, m). IR (KBr): 3450, 3300, 3170, 1640, 735 cm^{-1}.

9-(1-Cyano-1-methylethyl)triptycene (**6**: *X=Y=H, Z=CN*). A solution of 2.00 g (8.16 mmol) of **5** (Z=CN) and 1.6 ml of isopentyl nitrite in 60 ml of dichloromethane was refluxed under a nitrogen atmosphere, while 1.45 g (10.6 mmol) of anthranilic acid in 40 ml of acetone was added in 50 min. The mixture was refluxed for further 30 min and the solvent was evaporated. The residue (2.40 g or 92% yield) was recrystallized to afford the desired material, mp 308—310 °C. Found: C, 89.42; H, 5.66; N, 4.26%. Calcd for $C_{24}H_{19}N$: C, 89.68; H, 5.96; N, 4.36%. ^{1}H NMR ($CDCl_3$, δ): 2.42 (6H, s), 5.30 (1H, s), 6.9—7.7 (10H, m), 7.8—8.0 (2H, m). IR (KBr): 2225 cm^{-1}.

9-(1-Methoxycarbonyl-1-methylethyl)triptycene (**6**: *X=Y=H, Z=COOCH$_3$*), mp 230—232 °C, was prepared similarly in 86% yield. Found: C, 84.75; H, 6.14%. Calcd for $C_{25}O_{22}O_2$: C, 84.71; H, 6.26%. ^{1}H NMR ($CDCl_3$, δ): 2.31 (6H, s), 3.75 (3H, s), 5.26 (1H, s), 6.8—7.5 (11H, m), 7.6—7.8 (1H, m). IR (KBr): 1740, 1715 cm^{-1}.

9-(1-Cyano-1-methylethyl)-1,2,3,4-tetrachlorotriptycene (**6**: *X=Y=Cl, Z=CN*). Similar treatment of 1.00 g of **5** (Z=CN) with tetrachloroanthranilic acid[7] afforded a mixture of products. The mixture was oxidized overnight with 1.75 ml of 30% hydrogen peroxide in 30 ml of formic acid at room temperature and diluted with water. The mixture was extracted with dichloromethane and the excess of peroxide was decomposed with iron(II) sulfate. Evaporation of the solvent followed by chromatography on alumina afforded the *dl* and the *meso* isomers of the desired compound in 0.407 g or 22% yield. The ratio *dl*/*meso* was *ca.* 11. The *dl* isomer was eluted first and was purified by recrystallization. The pure *meso* isomer was not obtained even though careful chromatographies were carried out.

The *dl* form, mp 289—291 °C. Found: C, 62.94; H, 3.02; N, 3.12; Cl, 30.72%. Calcd for $C_{24}H_{15}NCl_4$: C, 62.78; H, 3.29; N, 3.05; Cl, 30.88%. ^{1}H NMR ($CDCl_3$, δ): 2.43 (3H, s), 2.58 (3H, s), 6.08 (1H, s), 7.0—7.9 (7H, m), 8.3—8.5 (1H, m). IR (KBr): 2230 cm^{-1}.

The *meso* form exhibited the following signals in ^{1}H NMR spectrum, when those due to the *dl* form were subtracted from a spectrum of a *dl-meso* mixture ($CDCl_3$, δ): 2.71 (6H, s), 6.08 (1H, s), 7.0—7.6 (6H, m), 7.9—8.1 (2H, m).

9-(1-Methoxycarbonyl-1-methylethyl)-1,2,3,4-tetrachlorotriptycene (**6**: *X=Y=Cl, Z=COOCH$_3$*) was similarly prepared in 24% yield in total. The ratio *dl*/*meso* was 3.4.

The *dl* form, mp 286—288 °C. Found: C, 61.17; H, 3.74; Cl, 29.14%. Calcd for $C_{25}H_{18}O_2Cl_4$: C, 61.00; H, 3.69; Cl, 28.81%. ^{1}H NMR ($CDCl_3$, δ): 2.27 (3H, s), 2.48 (3H, s), 3.5—4.0 (3H, broad), 6.09 (1H, s), 6.9—7.6 (7H, m), 7.7—8.0 (1H, m). IR (KBr): 1740, 1720 cm^{-1}.

The *meso* form, mp 200—202 °C, solidified again on heating above the melting point and melted at the melting point of the *dl* form. High resolution MS: Found, M$^+$ 490.0001; Calcd for $C_{25}H_{18}O_2Cl_4$, 489.9943. ^{1}H NMR ($CDCl_3$, δ): 2.47 (6H, s), 3.70 (3H, s), 6.09 (1H, s), 6.9—7.6 (8H, m). IR (KBr): 1740, 1715 cm^{-1}.

9-(1-Cyano-1-methylethyl)-1,4-dimethyltriptycene (**6**: *X=CH$_3$, Y=H, Z=CN*) was similarly prepared from **5** (Z=CN) and 3,6-dimethylanthranilic acid[8,9] in 68% yield. The formation of the *meso* form was not detected by ^{1}H NMR spectra. Recrystallization of the product from tetrahydrofuran–hexane afforded pure *dl* form, mp 244—246 °C. Found: C, 89.66; H, 6.64; N, 4.04%. Calcd for $C_{26}H_{23}N$: C, 89.36; H, 6.63; N, 4.01%. ^{1}H NMR ($CDCl_3$, δ): 2.45 (3H, s), 2.47 (3H,

s), 2.51 (3H, s), 2.89 (3H, s), 5.61 (1H, s), 6.75 (2H, s), 6.9—7.7 (7H, m), 8.1—8.3 (1H, m). IR (KBr): 2225 cm^{-1}.

The *meso* form was obtained in the following way. The *dl* form (0.717 g) was dissolved in 50 ml of *o*-dichlorobenzene and the solution was refluxed overnight. The solvent was evaporated and the residue was chromatographed on alumina to afford 0.047 g (7%) of the *meso* form. Recrystallization from tetrahydrofuran–hexane gave a pure material, mp 256—257 °C. High resolution MS: Found, M^+ 349.1802; Calcd for $C_{26}H_{23}N$, 349.1776. ^1H NMR ($CDCl_3$, δ): 2.55 (3H, s), 2.61 (3H, s), 2.62 (6H, s), 5.64 (1H, s), 6.82 (2H, s), 6.9—7.5 (6H, m), 7.8—8.1 (2H, m). IR (KBr): 2220 cm^{-1}.

9-(1-Methoxycarbonyl-1-methylethyl)-1,4-dimethyltriptycene (**6**: $X=CH_3$. $Y=H$, $Z=COOCH_3$) was similarly prepared. For the purification, the oxidation with performic acid was applied. A mixture of *dl* and *meso* forms was obtained in 60% yield. The ratio *dl*/*meso* was 11.

The *dl* form, mp 264—265 °C. Found: C, 84.74; H, 6.84%. Calcd for $C_{27}H_{26}O_2$: C, 84.78; H, 6.85%. ^1H NMR ($CDCl_3$, δ): 2.29 (6H, s), 2.43 (3H, s), 2.52 (3H, s), 3.73 (3H, s), 5.62 (1H, s), 6.73 (2H, s), 6.8—7.5 (7H, m), 7.7—7.9 (1H, m). The signal at the highest field split into two in 1-chloronaphthalene at 70 °C. IR (KBr): 1740, 1710 cm^{-1}.

The *meso* form, mp 203—204 °C, was obtained by thin layer chromatography of a mixture which was rich in the *meso* form. The *meso* form resolidified at temperatures above the melting point and melted at the melting point of the *dl* form. High resolution MS: Found, M^+ 382.1853; Calcd for $C_{27}H_{26}O_2$, 382.1775. ^1H NMR ($CDCl_3$, δ): 2.40 (6H, s), 2.52 (3H, s), 2.65 (3H, s), 3.71 (3H, s), 5.61 (1H, s), 6.76 (2H, s), 6.8—7.5 (8H, m). IR (KBr): 1740, 1715 cm^{-1}.

Measurement of Spectra. ^1H NMR spectra were obtained with a Hitachi R-20B spectrometer, operating at 60 MHz. The temperature was 34 °C. IR spectra were obtained with a Hitachi EPI-G2 grating spectrophotometer and the wave numbers were calibrated with a polystyrene film. High resolution MS were obtained with a Hitachi RMH-1 spectrometer.

Measurement of Barries to Rotation and Equilibrium Constants. Isomerization of the stable rotamers were carried out by heating solutions of the rotamers in 1-chloronaphthalene by immersing the samples in appropriate baths. The temperature of the baths was controlled by using the boiling points of solvents. The solvents were dimethyl sulfoxide (189 °C), *o*-dichlorobenzene (179 °C), mesitylene (162 °C), and cumene (152 °C). Analyses of the isomers were performed by either ^1H NMR spectroscopy or high pressure liquid chromatography using benzophenone as an internal standard. The chromatography apparatus was a Waters M-6000A equipped with a UV detector. The rate constants were obtained as usual.[10] Some of the rate constants were obtained by using the rate constants of the forward reaction and the equilibrium constant from the relation $k_{-1}=k/K$. The kinetic parameters were obtained by both the Arrhenius plot and the Eyring plot and the thermodynamic parameters by the common practice.

Results and Discussion

Conformational Equilibria. The equilibrium constants of the rotamers at various temperatures are given in Table 1 and the thermodynamic parameters obtained from these results in Table 2. Clearly all the *dl* isomers are strongly favored over the *meso*. Since it is known that compounds, which do not have a substituent in the peri position, give values very close to 2 which is a statistical factor,[11,12] the equilibrium constants in Table 1 are unusual. The unusuality must be caused by the presence of the peri-substituent which is close to the substituent in the 9-position. The preference of the *dl* form must be attributed to the steric repulsion between the substituents in 1 and 9 positions, because methyl is a larger group than the sp^2 or sp moieties.[13]

Table 1. Equilibrium constants ($K=dl/meso$) of **6** at various temperatures in 1-chloronaphthalene

Substituents			Temp/°C			
Z	X	Y	189	179	162	152
CN	Cl	Cl	7.5	8.4	8.8	9.6
CN	CH_3	H	15	16	16	17
$COOCH_3$	Cl	Cl	21	26	29	28
$COOCH_3$	CH_3	H	8.4	14	16	14

Table 2. Thermodynamic parameters for equilibria (*meso* ⇌ *dl*) of rotamers of **6**

Z	X	Y	ΔH/kcal mol^{-1}	ΔS/eu
CN	Cl	Cl	−2.3	−1.0
CN	CH_3	H	−1.1	3.1
$COOCH_3$	Cl	Cl	−2.9	0.1
$COOCH_3$	CH_3	H	−4.9	−6.0

Close examination of the data in Table 1 discloses, however, an interesting point. Namely, the chloro group favors the *dl* form to a sizable extent relative to the methyl group in the methoxycarbonyl compounds. The tendency is reversed in the cyano compounds, however. Since the chloro group is smaller than the methyl in its size, the consideration of repulsive interactions predicts that the methyl group should disfavor the *meso* form relative to the chloro group. This is the case of the cyano compounds but, in the methoxycarbonyl compounds, the methyl group favors the *meso* form. The anomaly in the population ratio of the compound **6** (X=Y=Cl, Z=$COOCH_3$) may be at least partly attributed to atrractive interactions between the chloro group and the methoxycarbonyl group[14] which favor the *dl* form.

Barriers to Rotation. Rate constants of isomerization of the rotamers at 189 °C are summarized in Table 3 and activation parameters obtained from the rate constants at the 4 temperatures are shown in Table 4. Arrhenius parameters are added to facilitate the comparison of the data with those of **2**.

It is interesting to note that barriers to rotation of the compounds examined here are all lower than that of compound **2**. It is especially so in the case of the pro-

Table 3. Rate constants for isomerization of rotamers of **6** at 189 °C

Z	X	Y	k/s^{-1} (*dl*→*meso*)	k/s^{-1} (*meso*→*dl*)
CN	Cl	Cl	6.30×10^{-5}	4.71×10^{-4}
CN	CH_3	H	4.94×10^{-5}	7.24×10^{-4}
$COOCH_3$	Cl	Cl	2.40×10^{-4}	4.94×10^{-4}
$COOCH_3$	CH_3	H	3.81×10^{-4}	3.19×10^{-4}

Table 4. Activation parameters for internal rotation of **6** and **2**

Z	X	Y	Process	E_a kcal/mol	log A	$\Delta H^{\ddagger}$ kcal/mol	$\Delta S^{\ddagger}$ eu
CN	Cl	Cl	*dl*→*meso*	36.1	12.9	35.3	−2.3
			meso→*dl*	33.8	12.7	32.9	−3.3
CN	CH_3	H	*dl*→*meso*	36.7	13.1	35.8	−1.6
			meso→*dl*	35.4	13.6	34.6	1.0
$COOCH_3$	Cl	Cl	*dl*→*meso*	34.4	12.6	33.5	−3.6
			meso→*dl*	31.2	12.4	30.3	−4.4
$COOCH_3$	CH_3	H	*dl*→*meso*	29.1	10.2	28.2	−14.5
			meso→*dl*	24.3	9.0	23.4	−20.3
Compound **2**[4]				37.7	13		

cesses *meso*→*dl*. It is tempting to consider that the interaction between the peri-substituent and the methyl group in the 9-substituent is much larger than that involving the cyano or the methoxycarbonyl group. Thus the ground state is raised relative to the transition state for rotation to lower the barrier. The tendency is reverse with the case of 9-isopropyltriptycenes,[15] where the introduction of a larger substituent in the peri-position led to the increase in the barrier height. 9-Benzyltriptycenes exhibited higher barriers to rotation by introducing substituents in two peri positions.[16] The congestedness of the molecule in the ground state is evident from the molecular models and the fact that the rotational isomers are isolated. X-Ray analysis of 9-*t*-butyl-1,2,3,4-tetrachlorotriptycene supports the idea: the molecule has unusual bond lengths and bond angles.[17] Therefore, relief of the steric strain to a small extent will lower the energy level of the ground state to a fair extent. This is reflected in the equilibrium constants discussed above. The higher barriers of the nitriles relative to the esters may be attributed to the lowering of the ground state also. A report by Anderson *et al.*[18] gives the similar explanation for the fact that the cyano group exhibited the highest barrier to rotation among compounds $(CH_3)_3C$–$C(CH_3)_2X$ where X was CN, CHO, CO_2H, CH_3CO, or $C(CH_3)$=CH_2.

Compound **6** (X=Y=Cl, Z=$COOCH_3$) was expected to show a higher barrier than others because the ground state is stabilized due to the attractive interaction between the chloro and the methoxycarbonyl groups. However, the barriers are by and large the same. Although the phenomenon must partly be attributed to the raise in the ground state due to steric reasons, other possibilities like solvation effects may not be ruled out. One notes that the frequency factors (and entropies of activation) and activation energies of compound **6** (X=CH_3, Y=H, Z=$COOCH_3$) are unusually small. The reasons for this phenomenon are not well understood at the present time.

It now seems to be necessary to remove the peri-substituents in order to raise the barriers to rotation of 9-(1-cyano or 1-methoxycarbonyl-1-methylethyl)triptycenes. A work along this line is in progress.

This work was supported by a Grant-in-Aid for Scientific Research from the Ministry of Education.

References

1) Part XXVI: M. Ōki, M. Kono, H. Kihara, and N. Nakamura, *Bull. Chem. Soc. Jpn.*, **52**, 1686 (1979).
2) M. Ōki, *Angew. Chem. Int. Ed. Engl.*, **15**, 87 (1976).
3) L. H. Schwartz, C. Koukotas, and C.-S. Yu, *J. Am. Chem. Soc.*, **99**, 7710 (1977).
4) H. Iwamura, *J. Chem. Soc., Chem. Commun.*, **1973**, 232.
5) R. H. Williams and H. R. Snyder, *J. Org. Chem.*, **36**, 2327 (1971).
6) A preliminary report has been published: T. Mitsuhashi, S. Otsuka, and M. Ōki, *Tetrahedron Lett.*, **1977**, 2441. The mechanism of the reaction is also discussed: T. Mitsuhashi and M. Ōki, *Chem. Lett.*, **1978**, 1089.
7) V. Villiger and L. Blangey, *Ber.*, **42**, 3549 (1909).
8) F. Mayer, W. Schäfer, and J. Rosenbach, *Arch. Pharm.*, **267**, 571 (1929).
9) S. Gronowitz and G. Hansen, *Ark. Kemi*, **27**, 145 (1967).
10) K. S. Wiberg, Physical Organic Chemistry, John-Wiley and Sons, New York (1964), p. 326.
11) G. Yamamoto and M. Ōki, *J. Chem. Soc., Chem. Commun.*, **1974**, 713.
12) G. Yamamoto and M. Ōki, *Bull. Chem. Soc. Jpn.*, **48**, 3686 (1975).
13) L. Pauling, "The Nature of the Chemical Bond," 3rd ed, Cornell University Press, Ithaca (1960).
14) M. Ōki, G. Izumi, and N. Nakamura, the 35th National Meeting (1976), the Chemical Society of Japan, Sapporo, Abstract II, p. 562.
15) F. Suzuki, M. Ōki, and H. Nakanishi, *Bull. Chem. Soc. Jpn.*, **47**, 3114 (1974).
16) G. Yamamoto and M. Ōki, *Angew. Chem. Int. Ed. Engl.*, **17**, 518 (1978).
17) M. Mikami, K. Toriumi, M. Konno, and Y. Saito, *Acta Crystallogr., Sect. B*, **31**, 2474 (1975).
18) J. E. Anderson, C. W. Doecke, H. Pearson, and D. I. Rawson, *J. Chem. Soc., Perkin Trans. 2*, **1978**, 974.

Restricted Rotation Involving the Tetrahedral Carbon. XXVIII. Barriers to Rotation about a C_{sp^3}–C(=O) Bond in 9-(1-Methoxycarbonyl-1-methylethyl)triptycenes[1,2]

Soichi OTSUKA, Hiroshi KIHARA, Tsutomu MITSUHASHI, and Michinori ŌKI*

Department of Chemistry, Faculty of Science, The University of Tokyo, Tokyo 113

(Received June 30, 1979)

Restricted rotation about a C_{sp^3}–C(=O) bond in title compounds is found by ^1H NMR spectra of the *dl* forms. The barriers to rotation are obtained by the DNMR method to be *ca.* 15 kcal/mol. Infrared spectra which exhibit two conformations in the *dl* and the *meso* forms are also reported.

Rotational isomers of esters have been discussed with the use of vibrational spectra,[3] rotational spectra,[4] electron diffraction,[5] dipole moment,[6] and NMR spectra.[7] Infrared spectrum was a favorite technique for physical organic chemists and rotational isomerism about the C_{sp^3}–C(=O) bond of methyl chloroacetate was extensively studied by Josien.[8] The chloro group exerts large influences on the frequency and the intensity of the carbonyl stretching bands and makes it convenient to study by this method. Although the presence of two conformations of the ester group about a C_{sp^3}–C(=O) bond was deduced from the behaviors in the C–C–O stretching region of propionates and butyrates,[9] it has become possible to study the phenomenon from the C=O stretching region only recently.[10]

Since the rates of isomerization of rotamers are large, NMR spectra usually give information as a weighted mean of the possible rotamers. The rates of rotation may be made slow in the cases of sp^2-sp^2 bonds and there are numerous examples of this sort involving the carbonyl.[11] There had been only one example reported when we launched the project of synthesizing substituted 9-(1-methoxycarbonyl-1-methylethyl)triptycenes: Masamune *et al.* reported an exceptional case that a maleic anhydride adduct of methyl tri-*t*-butyl[4]-annulenecarboxylate (**1**) showed bifurcation of the methoxyl signal in ^1H NMR spectrum at −60 °C.[12] Although it is not an ester, restricted rotation about a C_{sp^3}–C(=O) bond has been found by NMR spectroscopy while our study has been in progress: Hart *et al.* concluded that the rotation of an acetyl group in compound **2** was frozen on the NMR time scale, because the two methyls in 4 and 5 positions of the cycloheptatriene system became nonequivalent at −12 °C.[13] Very recently, restricted rotation of bis(di-*t*-butylmethyl) ketone has been reported.[14]

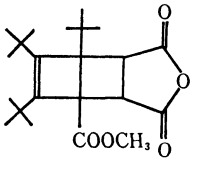

(1)

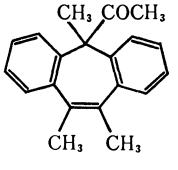

(2)

During the purification of 9-(1-methoxycarbonyl-1-methylethyl)-1,2,3,4-tetrachlorotriptycene (**3**, X=Y=Cl) we have encountered a phenomenon that the methoxyl signal of this compound in ^1H NMR spectrum operating at 60 MHz appears as a broad band, if it is the *dl* form. In this paper, we wish to report a detailed investigation of the restricted rotation about a C_{sp^3}–C(=O) bond, triggered by finding the broadened band for the methoxyl group.

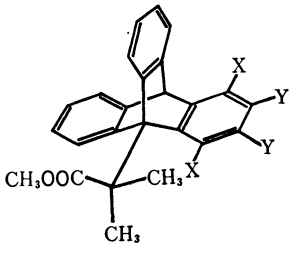

(*meso*-**3**)

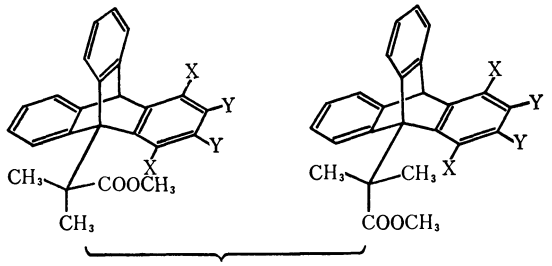

(*dl*-**3**)

Experimental

Materials. The preparation of materials in this study has been reported elsewhere.[1] Pure samples of respective rotamers after separation by chromatography were used for the measurements.

^1H NMR Spectra. The spectra were obtained on a Hitachi R-20B spectrometer with a temperature variation accessory, operating at 60 MHz, unless otherwise specified. Chloroform-*d* was used as a solvent for compounds which showed coalescence of signals at the higher temperature, whereas chloroform-*d*–carbon disulfide (1 : 1) was a solvent for those which required deep cooling. Temperature was calibrated using the chemical shifts of methanol and ethylene glycol at the lower and the higher temperatures, respectively.

Calculation of Spectra and Kinetic Parameters. The ^1H NMR spectra at various temperatures were calculated with the use of a modified Binsch program[15] and the best fit of the calculated spectra with the observed was determined by visual fitting. The rate constants thus obtained were put into the Eyring equation to obtain kinetic parameters. The populations which were necessary for the calculation of the spectra

were obtained by using the thermodynamic parameters derived from the populations at low temperatures.

Infrared Spectra. The spectra were obtained on either a JEOL JIR-03F FT-IR or a JASCO DS-403G spectrometer. The samples were dissolved in either carbon tetrachloride or chloroform to make up *ca.* 10^{-3} mol/l solutions.

Results and Discussion

Assignment of the Spectra. The ^{1}H NMR spectra of *dl*-**3** (X=Y=Cl) at three temperatures are shown in Fig. 1. At a low temperature the methoxyl signal which had been broad at 34 °C split into a pair of sharp singlets, whereas the signal for the methoxyl at a high temperature was a sharp singlet. Methyl signals which had been a pair of singlets at room temperature split into a pair of doublets at the low temperature as well.

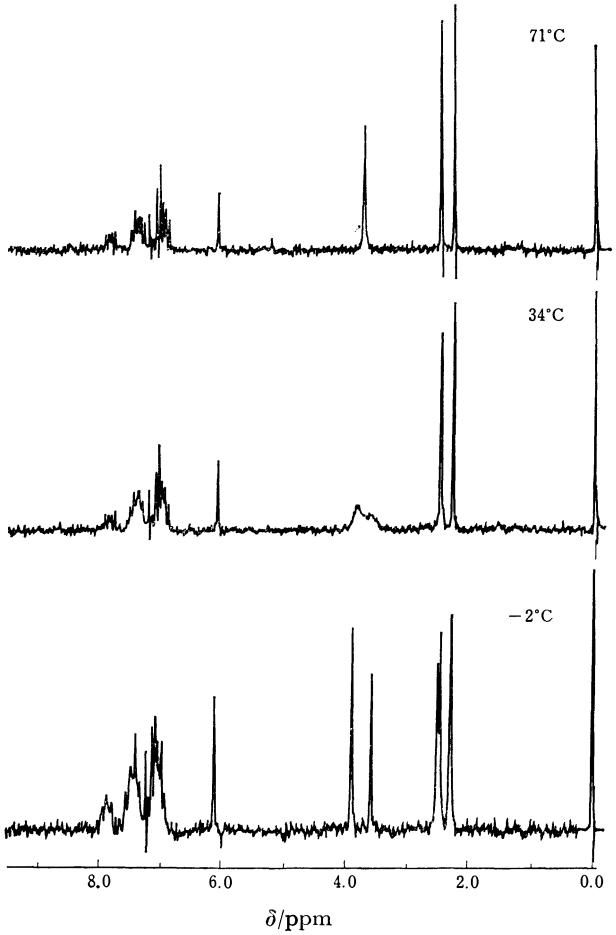

Fig. 1. ^{1}H NMR spectra of *dl*-**3** (X=Y=Cl) at three temperatures ($CDCl_3$, 60 MHz).

The temperature dependence of the spectra might be explained by two ways. One is to use the $Z \rightleftharpoons E$ conformational change (Eq. 1) and the other is the rotation about the C_{sp^3}–C(=O) bond (Eq. 2). The first possibility is unlikely, however. Esters are known to assume Z conformation in general and it is an exceptional case that the esters take E conformations. The E conformations are realized in esters which carry

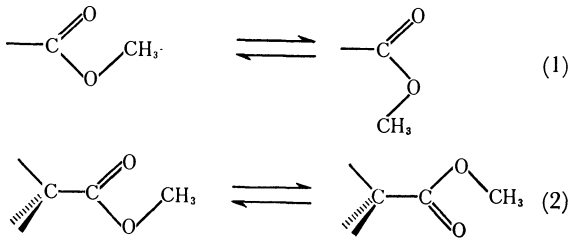

a small group as an acyl part and a large group as an alkoxyl part.[16] Since the compound in question carries a large acyl part and a small alkyl group, the possibility of the E conformation may be rejected.

Although the process is now said to be represented by Eq. 2, there remain minor problems to be discussed. Carbonyl groups are in general to be more stable if they assume conformations in which a carbonyl group eclipses one of the single bonds involving the adjacent carbon.[17] The conformations written in Eq. 2 do not necessarily conform to this generality. We justify the conformations from two points, however. The first is that there is a report which successfully interpreted the microwave absorption data of methyl acetate by assuming a C=O staggered conformation.[18] In addition, large groups associated with the α-carbon in this compound and the triptycyl group will make regular conformations, which are otherwise stable, unstable. We call the conformations represented by Eq. 2 as CH_3O-inside and CH_3O-outside in this paper.

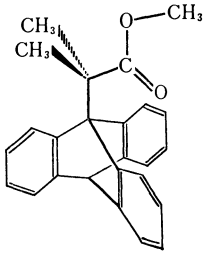

CH_3O-outside

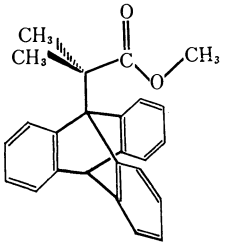

CH_3O-inside

Another problem is the assignment of the NMR signals to the respective conformations. We take advantage of the ring current effects[19] of the benzene ring for the assignment. Since the methoxyl signal of methyl acetate is at δ 3.67, one of the two signals of *dl*-**3** (X=Y=Cl) is at a higher field and the other is at a lower field than that of the methyl acetate. Thus the methoxyl signal at the higher field corresponds to the CH_3O-inside conformation and the other at the lower field to the CH_3O-outside.

dl-**3** ($X=CH_3$, Y=H) showed a similar phenomenon except that the splitting of the methoxyl signal occurred at a lower temperature. The coalescence temperature was −4 °C, while that of *dl*-**3** (X=Y=Cl) was 34 °C.

Any of the *meso* forms of these compounds and **3** (X=Y=H) failed to show splitting of the methoxyl signals, although the temperature was lowered to −80 °C. Since they all showed broadening of the signals, spectra of **3** (X=Y=H) were examined at 200 MHz. They did not show splitting at −50 °C, however.

Table 1. Thermodynamic parameters for the equilibria(CH_3O-outside$\rightleftharpoons CH_3O$-inside) of *dl*-**3** in $CDCl_3$

X	Y	ΔH/kcal mol^{-1}	ΔS/eu	ΔG/kcal mol^{-1} at 25 °C
Cl	Cl	−0.43	−1.9	0.15
CH_3	H	−0.34	−1.8	0.18

Populations and Thermodynamic Parameters. The ^{1}H NMR spectra of *dl*-**3** were obtained at various temperatures and, from the integration of the spectra, the populations of the CH_3O-inside and CH_3O-outside conformations were obtained. Usual treatment of the data afforded the thermodynamic parameters shown in Table 1. The free energy difference at 25 °C is also included in the Table. The data suggest that the CH_3O-inside conformation is favored in terms of enthalpy while it is disfavored by entropy factors. And, as a whole, the CH_3O-outside conformation is slightly favored at 25 °C.

Table 2. $\nu_{c=o}$ absorptions of **3**

X	Y	Form	$\nu_{max}(\varepsilon)$ in CCl_4	$\nu_{max}(\varepsilon)$ in $CHCl_3$
H	H	—	1747 (450)	1739 (340)
			1720 (360)	1712 (190)
Cl	Cl	*dl*	1743 (630)	1734 (370)
			1725 (480)	1718 (310)
		meso	1747 (510)	1741 (410)
			1720 (280)	1714 (240)
CH_3	H	*dl*	1746 (390)	1739 (330)
			1717 (370)	1712 (260)
		meso	1748 (270)	1740 (390)
			1717 (220)	1709 (210)

Infrared absorptions due to the C=O stretching are tabulated in Table 2. Each conformer possesses two absorptions. The possibility of the bifurcation due to the Fermi resonance may be ruled out because the shift due to the solvent change, from carbon tetrachloride to chloroform, is very similar with the case of methyl acetate.[20] Thus the results support the existence of the CH_3O-inside and CH_3O-outside conformations deduced by the NMR spectra. We tentatively assign the absorptions at higher frequencies to the CH_3O-outside conformations and those at lower frequencies to the CH_3O-inside conformations because of the correspondence between populations and intensities. Bond dipoles are known to affect the C=O stretching frequencies and intensities[21] but the effects seem small here. The separation of the two bands is abnormally large in these compounds, compared with the ordinary

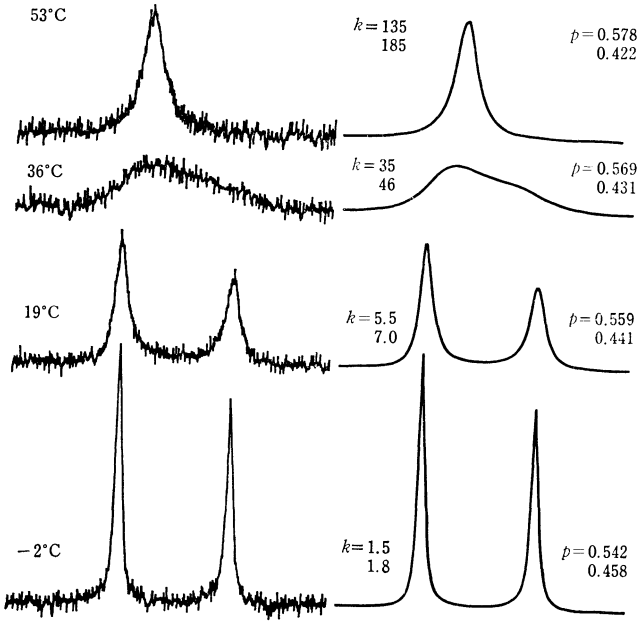

Fig. 2. Observed (left) and calculated (right) spectra of *dl*-**3** (X=Y=Cl) at four temperatures. The upper numbers of k's correspond to the rates of CH_3O-inside →CH_3O-outside processes and the lower the CH_3O-outside→CH_3O-inside. The upper numbers of p's correspond to populations of the CH_3O-outside conformation and the lower the CH_3O-inside conformation.

esters, probably due to the steric effect of the conformations concerned.

Barriers to Rotation. An example of the results of band shape simulations is shown in Fig. 2. The populations calculated by the thermodynamic values in Table 1 were used as constants and the rates of forward rotation were varied in the calculation. The rates of backward rotation are determined by the rates of forward rotation and the population automatically. The kinetic parameters obtained by this method are tabulated in Table 3.

The parent compound **3** (X=Y=H) and the *meso* forms of **3** failed to give split signals even at low temperatures. Therefore, it is not possible to perform the total line shape analysis. However, since the lines due to methoxyl and methyl groups show line broadening at low temperatures, it is possible to obtain rough estimates of barriers to rotation, by assuming the chemical shift differences. It may be argued that the chemical shift differences might be very small in these series, although the barriers are high. We rule out this possibility from the fact that *dl*-**3** (X=Y=Cl), δ 3.58 and 3.90, and *dl*-**3** (X=CH_3, Y=H), δ 3.58 and 3.89, give almost

Table 3. Kinetic parameters for rotation about the C_{sp^3}–C(=O) bond in *dl*-**3** in $CDCl_3$

X	Y	Process	$\Delta H^{\ddagger}$ kcal mol^{-1}	$\Delta S^{\ddagger}$ eu	$\Delta G^{\ddagger}$(25 °C) kcal mol^{-1}
Cl	Cl	CH_3O-out→CH_3O-in	13.7	−7.4	15.8
		CH_3O-in→CH_3O-out	14.1	−5.4	15.7
CH_3	H	CH_3O-out→CH_3O-in	10.9	−10.5	14.0
		CH_3O-in→CH_3O-out	11.2	−8.9	13.8

the same chemical shift differences. If the chemical shift difference were affected by the peri-substituents, the change in the peri-substituent would have resulted in a larger difference. Assuming that the chemical shift difference of the two forms of *meso*-**3** (X=Y=Cl) is the same with that of *dl*-**3** (X=Y=Cl) and that populations are 50: 50, we can use Eq. 3 for estimating the rates of rotation.[22]

$$k = \left\{\frac{\pi}{2}(\Delta\nu)\right\}^2 \Big/ \left(\frac{1}{T_2'} - \frac{1}{T_2}\right) \qquad (3)$$

where $1/T_2'$ is obtained from the line width at a given temperature and $1/T_2$ from that where exchange is fast. Thus $\Delta H^{\ddagger}$, $\Delta S^{\ddagger}$, and $\Delta G^{\ddagger}$ at 25 °C were obtained as 4.2 kcal/mol, −21.8 eu, and 10.7 kcal/mol, respectively. *meso*-**3** (X=CH_3, Y=H) and **3** (X=Y=H) gave similar values. Although the reliability of these values is limited, these may be used as a first approximation in discussion.

The barriers obtained thus far indicate that, in order to exhibit high barriers to rotation, it is necessary to have a peri-substituent. Barriers to rotation are determined by the relative energies of the ground and the transition states. Since no special stabilization or destabilization of the ground state is apparent, the high barriers for the *dl* form may be attributed to the peri-substituent which gives a strong repulsion in the transition state of rotation to raise the transition state. Close examination of the data in Table 3 reveals that *dl*-**3** (X=Y=Cl) gives higher barriers to rotation than *dl*-**3** (X=CH_3, Y=H) in spite of the fact that the van der Waals radius of the methyl group is larger than the chloro. This may be ascribed to the attractive interaction between the carbonyl moiety and the chloro group[23] which are located closely with each other.

We wish to thank people in Brucker for the measurement of the ^1H NMR spectra at 200 MHz. Our thanks are also due to the Ministry of Education for a Grant-in-Aid for Scientific Research.

References

1) XXVII: S. Otsuka, T. Mitsuhashi, and M. Ōki, *Bull. Chem. Soc. Jpn.*, **52**, 3663 (1979).
2) A preliminary note has been published: S. Otsuka, H. Kihara, T. Mitsuhashi, and M. Ōki, *Chem. Lett.*, **1978**, 475.
3) J. M. Wilmshurst, *J. Mol. Spectry.*, **1**, 201 (1957).
4) R. F. Curl, *J. Chem. Phys.*, **30**, 1529 (1959).
5) J. M. O'Gorman, M. Shand, and V. Shomaker, *J. Am. Chem. Soc.*, **72**, 4272 (1950).
6) E. Bock, D. Iwacha, H. Hutton, and A. Queen, *Can. J. Chem.*, **46**, 1645 (1968).
7) G. J. Karabatsos, N. Hsi, and O. E. Orzeck, *Tetrahedron Lett.*, **1966**, 4639.
8) M. L. Josien and R. Calas, *Compt. Rend. Acad. Sci. (Paris)*, **247**, 1641 (1955): *Chem. Abstr.*, **49**, 12129i (1955).
9) A. J. Bowles, W. O. George, and D. B. Cunliffe-Jones, *Chem. Commun.*, **1970**, 103.
10) M. Ōki and H. Nakanishi, *Bull. Chem. Soc. Jpn.*, **44**, 3197 (1971): A. N. Krasovskii, K. Kalnins, and B. S. Zhorov, *Zh. Prikl. Spectrosk.*, **29**, 658 (1978); *Chem. Abstr.*, **90**, 86183e (1979).
11) For example see F. Kaplan and G. K. Meloy, *J. Am. Chem. Soc.*, **88**, 950 (1966).
12) S. Masamune, N. Nakamura, M. Suda, and H. Ona, *J. Am. Chem. Soc.*, **95**, 8481 (1973).
13) H. Hart, J. B.-C. Jiang, and M. Sasaoka, *J. Org. Chem.*, **42**, 3840 (1977).
14) J.-E. Dubois, J.-P. Doucet, and B. Tiffon, *Tetrahedron Lett.*, **1978**, 3839.
15) G. Binsch, *Topics in Stereochemistry*, **3**, 97 (1968).
16) M. Ōki and H. Nakanishi, *Bull. Chem. Soc. Jpn.*, **43**, 2558 (1970).
17) G. J. Karabatsos and D. J. Fenoglio, *Topics in Stereochemistry*, **5**, 167 (1970).
18) G. Williams, N. L. Owen, and J. Sheridan, *Trans. Faraday Soc.*, **67**, 922 (1971).
19) C. E. Johnson and F. A. Bovey, *J. Chem. Phys.*, **29**, 1012 (1958).
20) E. J. Hartwell, R. E. Richards, and H. W. Thompson, *J. Chem. Soc.*, **1948**, 1436.
21) R. N. Jones, D. A. Ramsay, F. Herling, and K. Dobriner, *J. Am. Chem. Soc.*, **74**, 2828 (1952): R. Cetina and J. L. Mateos, *J. Org. Chem.*, **25**, 704 (1960).
22) S. Meiboom, Z. Luz, and D. Gill, *J. Chem. Phys.*, **27**, 1411 (1957).
23) M. Ōki, G. Izumi, and N. Nakamura, the 35th National Meeting (1976), the Chemical Society of Japan, Sapporo, Abstract II, p. 562.

The Jacobsen Rearrengement of Tribromobenzenes

Masahiro NAKADA, Kiichiro ISHIBASHI, Sachio FUKUSHI, and Minoru HIROTA*,†

Chemical Laboratory, Chiba Institute of Technology, Narashino 275

† *Department of Applied Chemistry, Faculty of Engineering, Yokohama National University, Tokiwadai, Hodogaya-ku, Yokohama 240*

(Received February 3, 1979)

The Jacobsen rearrangement of tribromobenzenes was investigated at 110—180 °C in concentrated sulfuric acid. The reaction proceeds exclusively *via* the intramolecular 1,2-migration of the bromine atom, which is accelerated by the steric repulsion of the neighboring group. Sulfonation of both the reactant and the products occurs simultaneously with the rearrangement. The migration of bromine atoms in the sulfonic acids proceeds far more slowly, the rearranged products not being formed to any considerable extent by sulfonic acids.

The migration of alkyl groups and/or halogen atoms in alkylhalobenzenes and polyhalobenzenes, assumed to be modifications of the Jacobsen rearrangement, occurs under similar conditions. Alkyl migration has been extensively studied and its mechanism elucidated in detail.[1-3] On the other hand, only a few investigation have been reported on the migration of halogen atoms on the aromatic nuclei.[4-8]

At least in cases of alkyl migration, the rearrangements are supposed to be acid-catalyzed reactions, proceeding *via* protonated or SO_3H^+-added benzene derivatives, *i.e.* benzenium cations. However, no details of the halogen-migration have been confirmed so far.

During the course of investigations on the reactions, spectroscopic and chromatographic properties of polyhalogenated aromatic hydrocarbons,[9-11] we have studied the sulfuric acid-catalyzed rearrangements of polybromobenzenes as discussed the mechanism of the reaction.

Experimental

Materials. 1,2,3-Tribromobenzene was prepared by the method previously reported by Furuyama and Fukushi.[12] Dibromochloro- and bromodichloro-benzenes were prepared by the Sandmeyer reaction from the corresponding dihaloanilines. Other compounds were used after purification of the commercially available materials. All the polyhalobenzenes were identified by means of their melting and boiling points and spectral properties.

Reactions. The reactants polyhalobenzene (1.0×10^{-4} mol) and concentrated sulfuric acid (0.2 ml, special grade) were sealed in Pyrex tubes (6 mm dia.×50 mm length). A number of the sealed tubes thus prepared were heated in a thermostatic oil bath under efficient mixing with a magnetic vibrator. The polyhalobenzenes are sparingly soluble in sulfuric acid at room temperature, and are not completely miscible under the reaction conditions (at 110—180 °C). Thus, sufficient mixing should be carried out to avoid the effect of diffusion on the reaction rates. Absence of such effects under experimental conditions was confirmed by the fact that approximately the same apparent rate constants were observed for the decrease of the amount of reactant polyhalobenzenes in preliminary runs carried out with varying efficiency of mixing.

The reactions were carried out at 110—180 °C for 10—24 h. Each sealed tube was taken out at appropriate intervals of time, cooled immediately and quenched by pouring into an excess of water. The halogenated hydrocarbon component was extracted by cyclohexane and analyzed by gas chromatography.

Spectral and Chromatographic Measurements. The ^{1}H-NMR spectra were recorded on a JEOL JNM-C60H spectrometer operating at 60 MHz, the chemical shifts being given in terms of parts per million (ppm) upfield from the signal of internal $^1H_2SO_4$ reference. The infrared and mass spectra were measured with JASCO DS-402G and Hitachi RMU-6L spectrometers, respectively. Gas chromatographic analyses were carried out on a Shimadzu GC-6A apparatus equipped with a polyethylene glycol 20M column (3 mm×2 m).

Results and Discussion

Formation of the Rearranged Products. Isomeric tribromobenzenes and their sulfonated products were obtained by the action of concentrated sulfuric acid on tribromobenzenes. However, the rates of reaction for the isomeric tribromobenzenes differ remarkably. The decrease in the reactant apparently shows first-order rate in each case (Table 1), 1,2,3-tribromobenzene (**1**)

Table 1. Apparent first order rate constants for the decrease of tribromobenzenes

CH_3Br_3	Temp/°C	k_1/s^{-1}
1,2,3	160	2.94×10^{-4}
	180	9.00×10^{-4}
1,2,4	160	3.55×10^{-5}
	180	2.17×10^{-4}
1,3,5	160	—[a]
	180	4.4×10^{-6}

a) The reaction is very slow under these conditions.

being most reactive. The amounts and proportions of tribromobenzene isomers present in the reaction system changed during the course of reaction. The relative amounts of three isomers **1**—**3** are given as a function of the reaction period in Fig. 1.

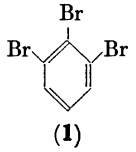

(**1**)

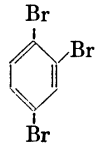

(**2**)

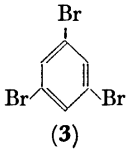

(**3**)

Formation of the sulfonic acids in the reaction medium causes loss in the total amount of tribromobenzenes. In the runs employing 1,2,3-tribromobenzene (**1**), the amount of the 1,2,4-isomer (**2**) produced increases

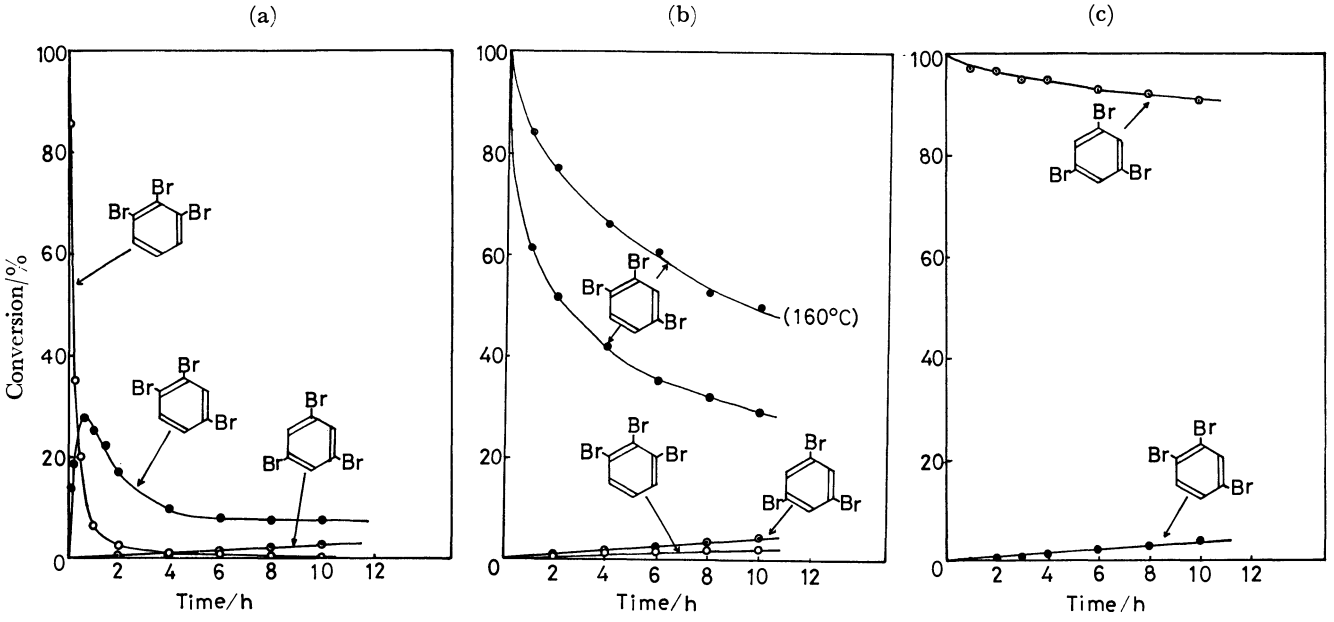

Fig. 1. Amounts of consumed and produced tribromobenzenes relative to the starting material (=100%) are plotted as a function of time with the runs starting from (a) 1,2,3-tribromobenzene (**1**), (b) 1,2,4-tribromobenzene (**2**), and (c) 1,3,5-tribromobenzene (**3**) and carried out at 180 °C (except the cases otherwise stated).

steeply in the earlier stage of the reaction process, decreasing gradually later (Fig. 1a). We see that very fast rearrangement from **1** to **2** is succeeded by considerably slower sulfonation of **2**.

In order to examine whether the rearrangement is intramolecular or intermolecular, crossover experiments with toluene, *m*-dichlorobenzene, trichlorobenzene, and naphthalene were carried out. No cross-products were obtained. This strongly suggests the intramolecular nature of the rearrangement. Another evidence in favor of intramolecularity of the rearrangement comes from the fact that the rate for consumption of the reactant, as well as that for the increases in the products, is linearly dependent on the initial concentration of the reactant. A quadratic relation is expected if the rearrangement is intermolecular.

1,2-Migration of the bromine substituent was found to occur exclusively in the rearrangement by the runs on bromodichloro- and dichlorobromo-benzenes (Table 2). No rearranged products were detected after 48 h reaction of 2,6-dichlorobromobenzene (**6**) at 180 °C. In contrast, 2,6-dibromochlorobenzene (**4**) rearranged nearly as fast as **1**, producing 2,5-dibromo- and 3,5-dibromo-chlorobenzenes. The proportion of products is similar to the case of **1**. The only reasonable explanation for the different behavior between **4** and **6** is that the migration of the chlorine substituent is negligible under the experimental conditions and that the migration of the bromine substituent in **6** is blocked by the chlorine atoms on the neighbor carbon atoms. In the case of 2,3-dichlorobromobenzene (**5**), the rearrangement to form 3,4-dichlorobromobenzene occurred with a rate slightly lower than that of **1**. However, the decrease in the rate of **5** is not remarkable, probably because the migration occurs considerably faster in bromobenzenes of 1,2,3-trihalosubstituted type than in that of 1,2-dihalo-substituted type. Migration of the chlorine substituent is not evident throughout the polyhalobenzenes (Table 2). This is also true in the case of 1,2,3-trichlorobenzene under similar conditions.

In conclusion, the rates of bromine migration decrease in the following order, the 1,2-migration being the only detectable pathway of the rearrangement.

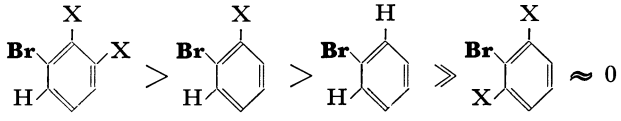

Under more drastic conditions (above 250 °C in concentrated or fuming sulfuric acid), the intermolecular halogen migration to produce dibromo- and tetrabromobenzenes proceeds to a considerable extent.[7] However, the mechanism of these reactions evidently differs from that of the intramolecular rearrangement under discussion. In the runs carried out in phosphoric acid, polyphosphoric acid, selenic acid, concentrated hydrochloric acid, and fluorosulfuric acid[13] at temperatures 110—200 °C for 1—10 h, no rearranged products were detected. The results suggest the important role of sulfuric acid in the rearrangement.

Sulfonic Acids Formed During the Reaction and Their Possibility as Intermediates of the Rearrangement. In the reaction medium, considerable amounts of both the starting and the produced tribromobenzenes were sulfonated, resulting in a decrease in the total amount of tribromobenzene with the elapse of reaction period (Fig. 1). The sulfonic acids produced during the course of reaction were pursued by means of NMR and infrared spectroscopic methods. Figure 2a shows the NMR spectrum of a mixture of the produced sulfonic acids in the sulfuric acid layer of the reaction system separated from the organic layer after 1 h duration

Table 2. The rearrangements of bromodichloro- and dibromochloro-benzenes[a)]

Reactant	Product(s)
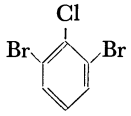 (4)	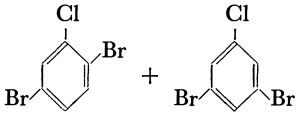
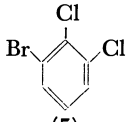 (5)	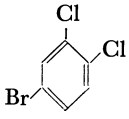
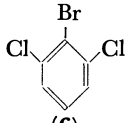 (6)	b)
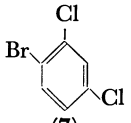 (7)	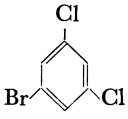
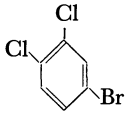 (8)	b)
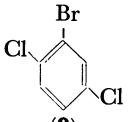 (9)	b)
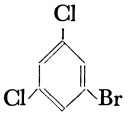 (10)	b)

a) The reaction was carried out at 180 °C, the products being separated after 5—10 h. b) The starting trihalobenzene was recovered nearly quantitatively after digestion.

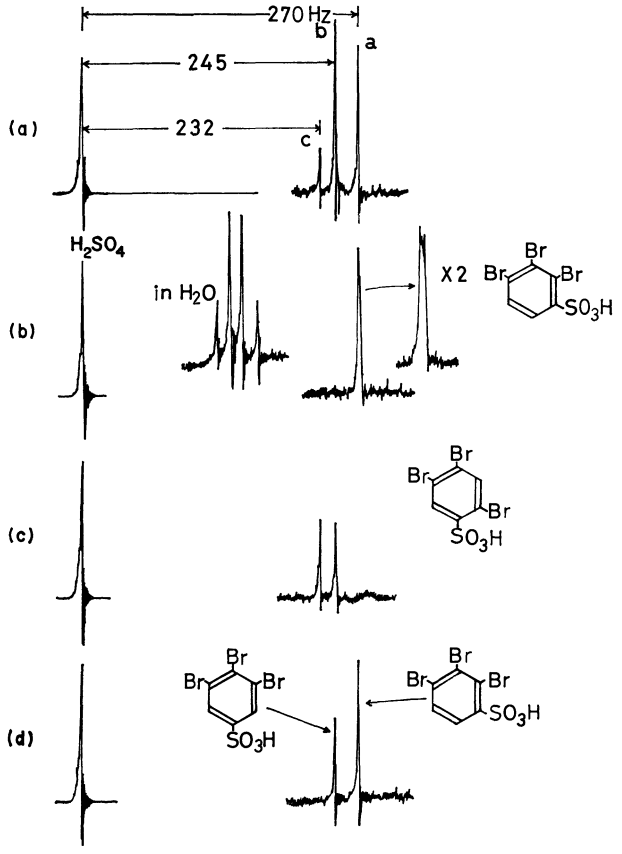

Fig. 2. NMR spectra of sulfonic acids in the reaction mixture. (a) Sulfuric acid layer of the reaction mixture starting from 1,2,3-tribromobenzene (**1**) and separated after 1 h's reaction at 165 °C. The organic layer was separated off after the reaction period. (b) 2,3,4-Tribromobenzenesulfonic acid (**11**) in water and sulfuric acid. (c) 2,4,5-Tribromobenzenesulfonic acid (**13**) in sulfuric acid. (d) Spectrum measured after heating 2,3,4-tribromobenzenesulfonic acid (**11**) in sulfuric acid without the contact of the organic layer (tribromobenzenes). Isomerization to produce 3,4,5-tribromobenzenesulfonic acid alone was observed.

of the reaction at 165 °C. This is a typical example of the NMR spectra of the sulfonic acids in sulfuric acid, the signals being assigned by comparing them with those (Figs. 2b and 2c) of authentic tribromobenzenesulfonic acids. All the spectra (Figs. 2 and 3) were measured at 120 °C to avoid the crystallization of sulfonic acids. The NMR spectrum of 2,3,4-tribromobenzenesulfonic acid (**11**) shows an AB quartet (J=6.9 Hz) which can be assigned to the two hydrogen atoms on the adjacent carbon atoms. However, only a singlet was observed at 4.50 ppm upfield from the acidic ^1H signal of sulfuric acid when the spectrum of the same sulfonic acid was measured in concentrated sulfuric acid at 120 °C immediately after dissolution. This signal, corresponding to signal a in Fig. 2a, is assigned to **11**. The NMR spectrum of 2,4,5-tribromobenzenesulfonic acid (**13**) shows two signals at 4.08 and 3.87 ppm from the ^1H signal of H_2SO_4 (Fig. 2c), which correspond to signals b and c, respectively, in Fig. 2a. Signals observed in Fig. 2a were thus assigned to the sulfonic acids. However, much higher intensity of signal b than that of c indicates the overlap of another signal at 4.08 ppm. Prolonged heating (at 165 °C) of the sulfuric acid solution of **11** resulted in the appearance of a signal at 4.08 ppm in addition to signal a in its NMR spectrum. The new signal is located at 4.08 ppm, approximately the same frequency as the higher frequency signal of **13**, and assigned to 3,4,5-tribromobenzenesulfonic acid (**12**) for the following reasons. (i) Electrophilic substitution on 1,2,3-tribromobenzene usually occurs predominantly on the 4-carbon atom, when the reaction is kinetically controlled, to form **11** in the case of sulfonation. However, sulfonation at higher temperature is often reversible and the more stable isomer **12** is expected to become the major product gradually. (ii) Under the reaction conditions, formation of 1,2,4-tribromobenzene (**2**) after quenching and digestion of the reaction mixture was shown to be negligible, no measurable amount of sulfonated 1,2,4-tribromobenzene being expected to be present in the

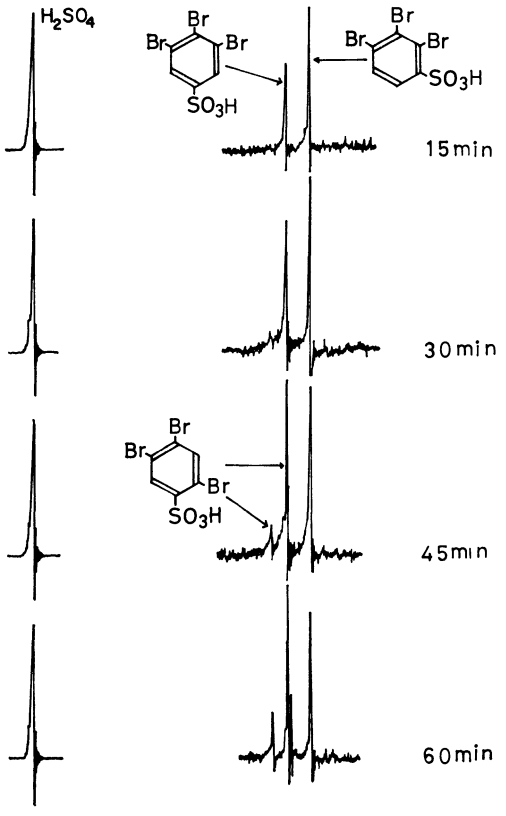

Fig. 3. Changes in NMR spectrum of the sulfuric acid layer during the process of the rearrangement of 1,2,3-tribromobenzene (**1**).

reaction mixture. No 2,4,6-tribromobenzenesulfonic acid was detected in either runs, and its formation from **1** is supposed to be a slow reaction.

The quantitative changes of these sulfonic acids during the course of reaction were determined by means of ^{1}H-NMR spectrometry.[14] When the reaction of **1** was carried out at 165 °C, the NMR spectrum of the sulfuric acid layer changed as a function of the reaction period (Fig. 3). As expected, sulfonic acid **11** was produced from **1** initially, amounts of sulfonic acids **12** and **13** increasing gradually. In the presence of tribromobenzenes, formation of **13** proceeds considerably faster than the isomerization to form **13** from the mixture of sulfonic acids **11** and **12**, which takes several hours to produce a detectable amount of **13** at the same reaction temperature. Thus, most of sulfonic acid **13** in the sulfuric acid layer is derived by sulfonation of the rearranged product **2**. Isomerization starting from 2,4,5-tribromobenzenesulfonic acid (**13**) also gave a mixture of sulfonic acids (**12**, **13**, and a small amount of 2,4,6-tribromobenzenesulfonic acid)[15] after heating for a longer period, the products being in slow equilibria in sulfuric acid solutions. Thus the migration of bromine atoms also proceeds with sulfonic acids, the rate being considerably lower than that of the runs in the presence of tribromobenzenes.

Actually the sulfonation to form **11**, **12**, and **13** proceeds simultaneously and/or successively with the rearrangement to form **2** and **3**, when **1** is treated with sulfuric acid. Thus the reaction of **1** at 180 °C was

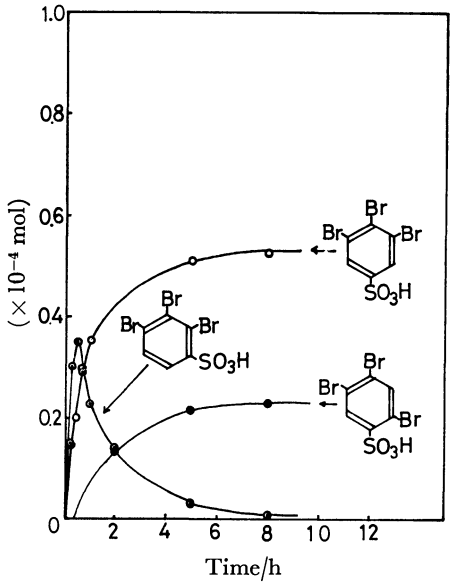

Fig. 4. Amounts of the produced sulfonic acids contained in the sulfuric acid layer are plotted as a function of time with the run starting from 1,2,3-tribromobenzene and carried out at 180 °C.

carefully reproduced and the sulfuric acid layer analyzed. The amounts of the sulfonic acids formed are plotted against the reaction period in Fig. 4. By comparing Fig. 4 with Fig. 1a, reactant **1** is supposed to undergo both sulfonation to **11** and isomerization to **2** and, to a less extent, to **3** initially, even if it is not certain whether compounds **1** and **11** are formed *via* a common intermediate or not.

The compositions of the sulfonic acids produced were determined also from the infrared spectra of the products in the sulfuric acid layer measured after their transformation into sodium salts. An example of the infrared spectra is shown in Fig. 5 together with the assignment of the bands to each sulfonic acid. Approximately the same results as in Fig. 4 were obtained from the changes in the infrared absorption intensities, leading to the same conclusion as obtained from the NMR spectra.

Mechanism of the Rearrangement. The rearrangement does not proceed in the presence of Brönsted acids other than sulfuric acid, and is not general-acid-catalyzed. Sulfonic acids **11**—**13** cannot be inter-

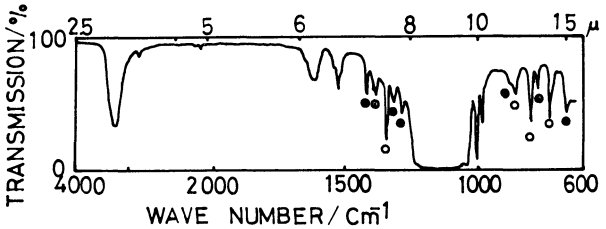

Fig. 5. Infrared spectrum of the mixture of sodium tribromobenzenesulfonates separated from the sulfuric acid layer after the reaction for 2 h at 180 °C. The absorption bands are assigned to 2,3,4-tribromobenzenesulfonate (⊙), 3,4,5-tribromobenzenesulfonate(○), and 2,4,5-tribromobenzenesulfonate (●) by comparing with the spectra of authentic samples.

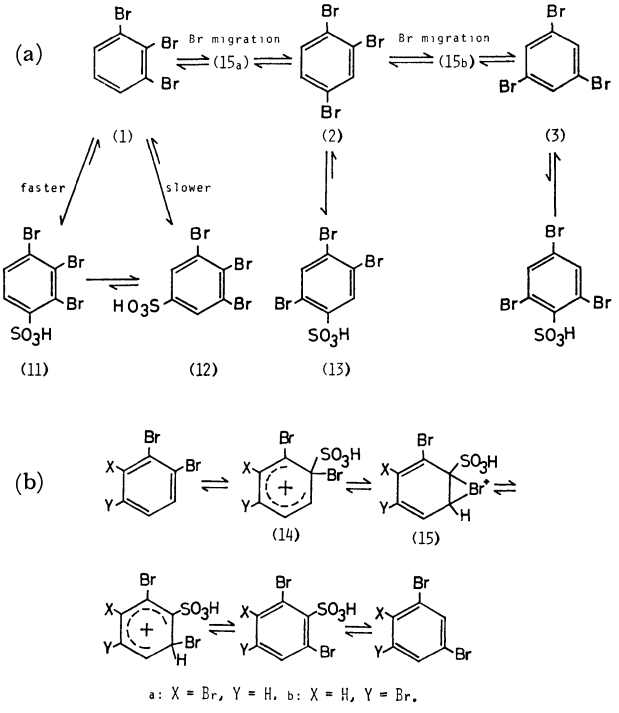

Fig. 6. (a) The whole reaction scheme including both isomerization and sulfonation. (b) Reaction mechanism for the bromine migration.

mediates of this rearrangement, since the isomerization to form bromine-migrated sulfonic acids is by far slower than the rearrangement itself. Moreover, the formation of tribromobenzenes from the sulfonic acids does not proceed to a considerable extent, probably because the equilibria among tribromobenzenes and the sulfonic acids are more favorable to the latter. Thus the possible intermediate or transition state for the reaction is a sulfonated benzenium cation (**14**) which is produced by the *ipso* attack of SO_3H^+, or more probably SO_3, and the subsequent formation of the three-membered ring containing bromine atom. The 1,2-shift proceeds more easily when the migrating bromine atom is sterically crowded. The formation of the bromonium cation might be assisted by the repulsion caused by the neighboring halogen atom. The repulsive force operating is of steric as well as electrostatic nature. The whole reaction is explained by the following scheme (Fig. 6). The desulfonation after rearrangement is expected to be a prompt reaction, since the sulfonic acid group is repelled sterically by the two bromine atoms on the neighboring carbon atoms. This is in line with the fact that it is difficult for 1,3,5-triboromobenzene to transform into the corresponding sulfonic acid and that 2,4,6-tribromobenzenesulfonic acid undergoes very fast desulfonation in sulfuric acid.

The rearrangement from **2** proceeds more slowly than that from **1**, giving **1** and **3**. The interconversion among the isomeric tribromobenzenes is reversible, thermodynamically controlled products being obtained after a very long period of reaction. Original Jacobsen rearrangements of polyalkylbenzenes tend to vicinal orientation, contrary to the rearrangements of polyhalobenzenes, and seem to proceed through a different mechanism.

The authors are grateful to Miss Hiroko Endo for her technical assistance in the measurements of the NMR and mass spectra.

References

1) R. T. Arnold and R. A. Barnes, *J. Am. Chem. Soc.*, **66**, 960 (1944).
2) M. J. S. Dewar, "The Electronic Theory of Organic Chemistry," Oxford Univ. Press, Oxford (1956), pp. 231—233, and cited therein.
3) L. F. Fieser and M. Fieser, "Advanced Organic Chemistry," D. C. Heath and Co., Boston (1961), pp. 665—667, and cited therein.
4) J. Herzig, *Monatsh. Chem.*, **2**, 192 (1881) and *Chem. Ber.*, **14**, 1205 (1881).
5) G. S. Neumann, *Liebigs Ann.*, **241**, 33 (1887).
6) M. Boyle, *J. Chem. Soc.*, **95**, 1683 (1909).
7) R. Goto and H. Suzuki, *Nippon Kagaku Zasshi*, **84**, 167 (1963).
8) M. Kilpatrick and M. W. Meyer, *J. Phys. Chem.*, **65**, 1312 (1911).
9) H. Furuyama, S. Fukushi, and S. Fujiwara, *Spectrosc. Lett.*, **3**, 139 (1970).
10) M. Nakada, S. Fukushi, H. Tomita, and Y. Mashiko, *Kogyo Kagaku Zasshi*, **73**, 929 (1970).
11) M. Nakada, S. Fukushi, H. Tomita, Y. Mashiko, and M. Hirota, *Nippon Kagaku Kaishi*, **1972**, 1680.
12) H. Furuyama and S. Fukushi, *Yuki Gosei Kagaku Kyokai Shi*, **29**, 413 (1971).
13) When **1** was treated in fluorosulfuric acid medium under almost the same conditions, several products were isolated by gas chromatography from the hexane soluble part, neither of them being identical with $C_6H_{6-n}Br_n$'s. A run carried out at 100 °C in fluorosulfuric acid gave a slight but detectable amount of **2** after a longer period of reaction. From the time-conversion curve of this reaction, the formation of **2** is concluded to occur secondarily probably catalyzed by sulfuric acid produced in the process of reaction.
14) The amounts of sulfonic acids **11**, **12**, and **13** are easily estimated by the following equations, where I_a, I_b, I_c are the intensities of the NMR signals at 4.50, 4.08, and 3.87 ppm upfield from $^1H_2SO_4$ signal, respectively. $[\mathbf{11}]=k\cdot I_a$, $[\mathbf{12}]=k(I_b-I_c)$, and $[\mathbf{13}]=2k\cdot I_c$.
15) Since sulfonation is a reversible reaction, the bromine migration in the sulfonic acids is supposed to proceed through tribromobenzenes formed *in situ* by reverse desulfonation of the sulfonic acids in sulfuric acid. The electron withdrawing SO_3H group of the sulfonic acid might prevent the formation of benzenium cation (**14**) and subsequent bromonium cation (**15**) in Fig. 6. An evidence in favor of this hypothesis was obtained from the runs starting from mono- and di-bromonitrobenzenes. These compounds gave no rearranged products after being heated at 165 °C in sulfuric acid for several hours. The reactions at 180 °C and higher temperature caused decomposition of the starting materials, giving no rearranged products.

A Study of the Spin-Lattice Relaxation Time, T_1, of Coal-derived Oil

Tadashi YOSHIDA,* Yosuke MAEKAWA, Hiroyuki UCHINO,** and Susumu YOKOYAMA**

Government Industrial Development Laboratory, Hokkaido, Sapporo 061-01

***Faculty of Engineering, Hokkaido University, Sapporo 060*

(Received June 14, 1979)

The spin-lattice relaxation time, T_1, of carbons was measured for various types of carbons in ring-type fractions separated from coal-derived oil. The T_1 for most carbons in the coal-derived oil was less than 2 s because of the existence of free radicals, while the T_1's of aromatic non-protonated carbons in the monocyclic and bicyclic aromatics fractions were approximately 12—15 s. The effects of a relaxation reagent on the T_1 were also discussed.

In recent years, ^{13}C-NMR spectrometry has been applied to the study of coal chemistry[1-7] and has proved to be a powerful tool for the investigation of the structure of coal-derived oil, since it makes the direct observation of the hydrocarbon skeleton possible.

The determination of various structural parameters for coal-derived oil requires a quantitative NMR spectrum. The peak intensity in the FT-NMR proton decoupling spectrum is generally affected by two factors, the nuclear Overhauser enhancement (NOE) and the spin-lattice relaxation time, T_1. The former, the NOE, can be fully suppressed by the gated-decoupling technique,[6-8] whereas the latter, T_1, can not be, since it is closely related to the structure and has a definite value for each carbon in the coal-derived oil.

The FT-NMR method requires a pulse repetition time much larger than T_1 in order to avoid the progressive saturation of signals. It is necessary, therefore, to have information on the T_1 of the sample prior to the NMR spectrum measurement. Unfortunately, however, there have not yet been any reports on the T_1 of coal-derived oil, as far as we know. In the present work, the T_1's of various types of carbons and other structural information of coal-derived oil have been obtained from the partially relaxed Fourier transform (PRFT) spectra.

Experimental

The coal sample used in the present work is from Akabira, Hokkaido. The sample was hydrogenated over an Adkins catalyst at 400 °C for 60 min under the initial hydrogen pressure of 100 kg/cm^2. The hydrogenated product was extracted with hexane in a Soxhlet extractor. The extracted coal-derived oil was separated into five fractions by liquid chromatography, a modification of the Bureau of Mines-API 60 method:[9] saturates (Fr-P), monocyclic aromatics (Fr-M), bicyclic aromatics (Fr-D), tri- and tetracyclic aromatics (Fr-T), and polycyclic aromatics and polar aromatics (Fr-PP).

The coal-derived oil and ring-type fractions (Fr-M, D, T, and PP) were used for the T_1 measurement. The samples were dissolved in deuteriochloroform, and the solution was

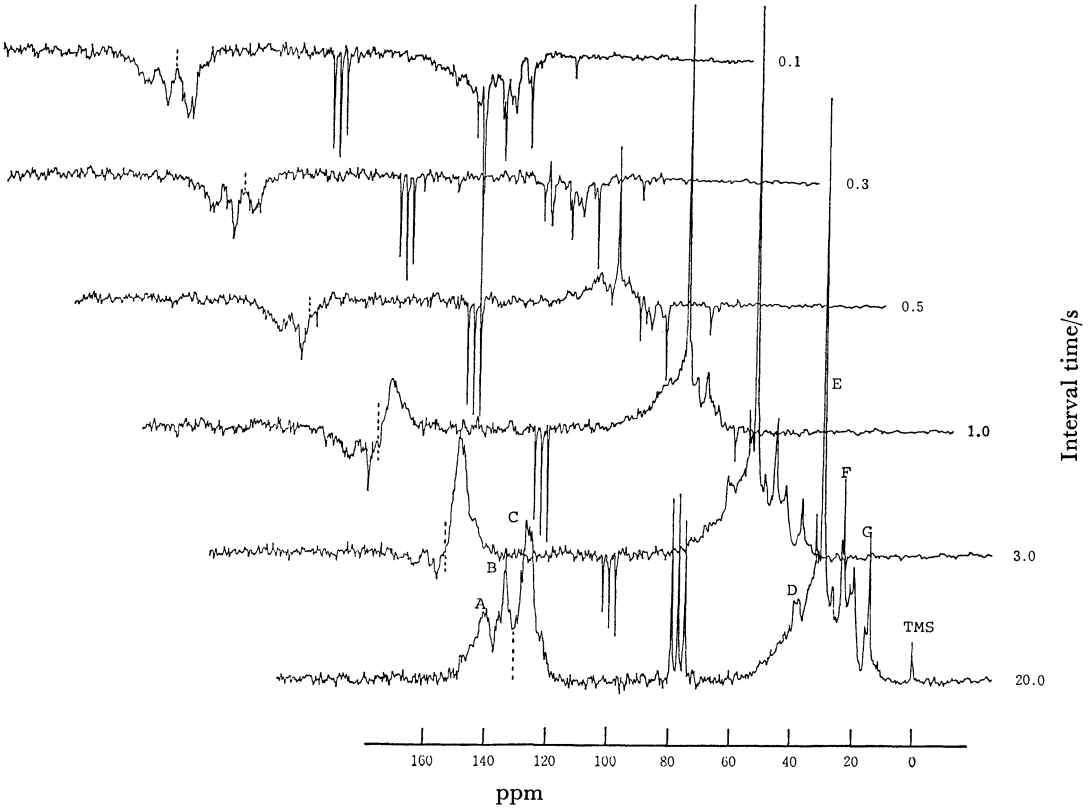

Fig. 1. Partially relaxed Fourier transform spectra for Fr-M.

Table 1. Spin-lattice relaxation times, T_1, of various types of carbons for ring-type fractions of coal-derived oil

Carbon type	Chemical shift δ/ppm	Spin-lattice relaxation time, T_1				
		Fr-M	Fr-D	Fr-T	Fr-PP	Coal-derived oil
Aromatic						
A. Substituted	138.6	12.7	10.9	2.8	1.8	1.1—1.4
B. Bridge head	131.8	12.0—13.0	12.9—14.7	4.1	1.9	1.3
C. Protonated	126.8	1.2	1.6— 2.6	0.4—0.8	0.8—1.0	0.6—1.0
Aliphatic						
D. Methylene bridge	37.9	0.7— 0.9	0.8	0.4	0.6	0.5—0.6
E. ε or further CH_2 from end	29.6	0.6— 0.7	0.9— 1.0	0.3—0.4	0.5	0.4
F. α-CH_3 to ring	21.3	1.2	1.3— 1.7	0.5—0.9	0.8—1.1	0.7—0.9
G. end-CH_3 to ring	14.0	2.4	2.1— 2.5	0.9—1.3	1.6—2.0	1.2

not degassed. Tris(acetylacetonate)chromium(III)($Cr(acac)_3$) was used as the relaxation reagent.

The spectra were obtained with a JNM-FX60 Fourier transform spectrometer (JEOL Ltd.) and were measured over a range of 4000 Hz, with 8192 data points at 15 MHz. The T_1 measurement was performed using an inversion recovery pulse sequence $(180°\text{-}t\text{-}90°)_n$,[10] where t stands for the interval time between 180° and 90° pulses. The waiting time between pulse sequences was 20 s. The width of the 90° pulse was 16 μs. The NOE was fully suppressed by the gated decoupling technique.

Results and Discussion

In the ^{13}C-NMR method, the progressive saturation of signals should be avoided by making the excited spins completely relaxed. Therefore, a pulse-repetition time of at least five times the largest relaxation time, T_1, is needed. In general, the T_1 values for quarternary carbons of standard hydrocarbons are several decades of seconds, and the pulse-repetition time required for their quantitative spectra becomes extremely long. Fortunately, coal-derived oil contains an adequate amount of free radicals ($\approx 10^{18-19}$ spins/g),[11] and its T_1 turns out to be much smaller than those for standard chemicals. The PRFT spectra of the Fr-M fraction is shown in Fig. 1. The T_1 depends on the molecular size, the number of hydrogen atoms bonded to the carbon nucleus, the molecular motion, *etc.* Therefore, the difference in the relaxation rates of carbons can give structural information and the PRFT spectra are helpful for the assignment of signals. As can be seen in Fig. 1, the aromatic carbons are clearly divided at about 129 ppm into two groups of slowly relaxing nonprotonated and fast relaxing protonated carbons. On the other hand, the aliphatic carbons, though not conclusively, are also divided into two groups at about 22 ppm. The low-field group, for which the relaxation rate is fast, is assigned to cycloparaffinic, methylene bridge, and alkyl carbons except for the methyl and the terminal methyl groups. The T_1 values of these carbons are presumed to be relatively short because of their "rigid" structures. The high-field one is assigned to alkyl substituents (methyl, ethyl, and terminal methyl groups), and these carbons are presumed to have longer T_1 values because of their loose bondings. Thus, T_1 often provides information supplemental to the assignment of the signal.

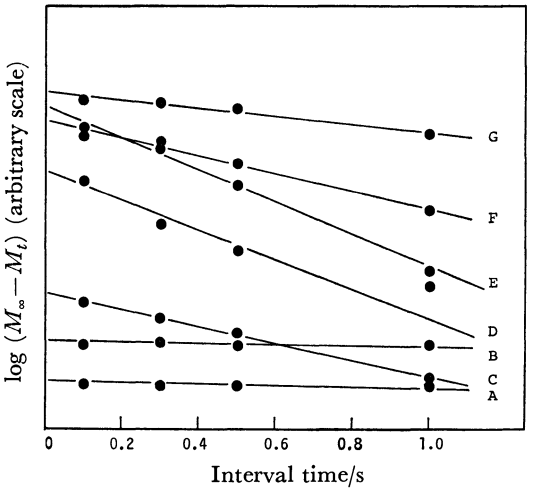

Fig. 2. Relationship between $\ln(M_\infty - M_t)$ and interval time.

T_1 is calculated by means of the following equation:

$$\ln (M_\infty - M_t) = \ln 2M_\infty - t/T_1$$

where M_∞ is the signal intensity when the carbon nucleus is completely relaxed. In the spectrum of a multi-component mixture such as coal-derived oil, the relation between $\ln(M_\infty - M_t)$ and the interval time generally has a tendency to deviate from a straight line, for each signal in the spectrum corresponds to some carbons with various T_1 values and the change in the signal intensity with the interval time may show the overall relaxation rates of these carbons. Therefore, the T_1 value calculated from the gradient of the straight line in Fig. 2 often varies the range of interval time

Table 2. Change in the aromaticity (f_a) of coal-derived oil with the pulse-repetition time

Pulse-repetition time/s	Aromaticity (f_a)
0.7	0.53
1.0	0.57
2.0	0.60
4.0	0.61
6.0	0.61
25.0	0.61

Table 3. Change in the spin-lattice relaxation time, T_1, with the amount of $Cr(acac)_3$ added

Carbon type	Chemical shift δ/ppm	Spin-lattice relaxation time, T_1			
		None	10 mg[a)]	20 mg[a)]	30 mg[a)]
Aromatic					
A. Substituted	138.6	1.1—1.4	0.3—0.4	0.3	0.2
B. Bridge head	131.8	1.3	0.4—0.6	0.3—0.4	0.1—0.2
C. Protonated	126.8	0.6—1.0	0.2—0.3	0.2—0.3	0.2
Aliphatic					
D. Methylene bridge	37.9	0.5—0.6	0.4—0.5	0.5	0.2—0.4
E. ε or further CH_2 from end	29.6	0.4	0.3—0.5	0.2	0.2
F. α-CH_3 to ring	21.3	0.7—0.9	0.5—0.7	0.2—0.4	0.2—0.4
G. end-CH_3 to ring	14.0	1.2	0.7—0.8	0.3	0.2—0.4

a) Amount of $Cr(acac)_3$ added to about 0.5 g of coal-derived oil in 0.53 ml of deuteriochloroform.

employed. We calculated the T_1 values from the gradient in the range of interval time from 0.1 to 1.0 s. The T_1 values of various types of carbons in the ring-type fractions of coal-derived oil are summarized in Table 1. The T_1 of aromatic non-protonated carbons is the longest among the T_1's of all the types of carbons. In particular, their T_1 values for the Fr-M,D fractions are much longer than those for Fr-T,PP. The great difference in the T_1 values of various types of carbons between the Fr-M,D and Fr-T,PP fractions may be attributed not only to their molecular sizes but also to the concentration of free radicals contained in the fractions. The components in the Fr-M,D fractions are presumed to be sufficiently hydrogenated compared with those in Fr-T,PP. The T_1 of coal-derived oil is nearly equal to that of the Fr-PP fraction. On the whole, the T_1 of coal-derived oil (hexane Soxhlet's extract) is moderately short, although some of the components have considerably long T_1 values. Table 1 shows that the pulse-repetition time required for the quantitative spectrum of coal-derived oil is approximately 5—6 s. This value is confirmed by the change in the aromaticity (f_a) of coal-derived oil with the pulse-repetition time, as is shown in Table 2. With a short pulse-repetition time, aromatic non-protonated carbons are not yet completely relaxed and f_a may have been underestimated because of the progressive saturation. Table 2 shows that the pulse-repetition time of 5—6 s is necessary to obtain a quantitative spectrum within the limits of experimental errors. This result is in good agreement with the T_1 data.

Thus, the quantitative spectrum for coal-derived oil requires a significantly long measurement time. Therefore, the addition of a relaxation reagent to samples is often used in time-effective measurements.[3,6-8] Table 3 shows the change in T_1 with the amount of relaxation reagent ($Cr(acac)_3$) added. The addition of $Cr(acac)_3$ shortens the T_1 values of all carbons considerably. With 20 mg of $Cr(acac)_3$, the T_1 of aromatic non-protonated carbons was nearly equal to those of other carbons. The addition of 10—20 mg of $Cr(acac)_3$ is found to be very effective for the reduction of T_1. However, more than 30 mg of $Cr(acac)_3$ should not be added, since such an addition will result in the broadening of the signals. In conclusion, the pulse-repetition time can be reduced from 5—6 s to about 2 s by the addition of a relaxation reagent, as can be seen in Table 3.

Finally, the NMR[12] and field desorption (FD) mass[13] spectrometric studies for the structural analysis of these ring-type fractions made it clear that alkylnaphtenomonocyclic aromatics were predominant for the Fr-M fraction; alkylnaphtenobicyclic aromatics, for the Fr-D fraction; alkylnaphtenotri- and tetracyclic aromatics, for the Fr-T fraction; and alkylpolycyclic aromatics, for the Fr-PP fraction. Thus, the Fr-M and D fractions have considerably saturated structures, that is, "mobile" structures, whereas the Fr-T and PPf ractions have "rigid" structures. The difference in ring size and chemical structure, as well as the concentration of free radicals present in the fractions, is considered to affect the T_1 values.

References

1) R. J. Pugmire, D. M. Grant, K. W. Zilm, L. L. Anderson, A. G. Oblad, and R. E. Wood, *Fuel*, **56**, 295 (1977).
2) Y. Maekawa, T. Yoshida, Y. Yoshida, and M. Imanari, *Nenryo Kyokai Shi*, **56**, 351 (1977).
3) D. L. Wooton, W. M. Coleman, L. T. Taylor, and H. C. Dorn, *Fuel*, **57**, 17 (1978).
4) P. Fischer, J. W. Stadelhofer, and M. Zander, *Fuel*, **57**, 345 (1978).
5) J. M. Dereppe, C. Moreaux, and H. Castex, *Fuel*, **57**, 435 (1978).
6) K. S. Seshadri, R. G. Ruberto, D. M. Jewell, and H. P. Malone, *Fuel*, **57**, 549 (1978).
7) W. R. Ladner and C. E. Snape, *Fuel*, **57**, 658 (1978).
8) J. N. Shoolery and W. L. Budde, *Anal. Chem.*, **48**, 1458 (1976).
9) S. Yokoyama, N. Tsuzuki, T. Kato, and Y. Sanada, *Nenryo Kyokai Shi*, **57**, 748 (1978).
10) R. L. Vold, J. S. Waugh, M. P. Klein, and D. E. Phelps, *J. Chem. Phys.*, **48**, 3831 (1968).
11) T. Yokono and Y. Sanada, *Fuel*, **57**, 334 (1978).
12) H. Uchino, S. Yokoyama, T. Kato, Y. Sanada, and T. Yoshida, "Proceedings of the 21th Meeting, Japan Petrol. Inst. (Sapporo)," 1978, p. 96.
13) T. Yoshida, Y. Maekawa, H. Uchino, S. Yokoyama, T. Higuchi, and Y. Itagaki, *Fuel*, submitted for publication.

Synthesis of Some 3-Methylbut-2-enylated 1,3,5-Trihydroxyxanthones

Vinod GUJRAL and S. R. GUPTA*

Department of Chemistry, University of Delhi, Delhi-7, India

(Received October 9, 1978)

1,3,5-Trihydroxyxanthen-9-one reacts with 2-methylbut-3-en-2-ol in presence of a catalytic amount of BF_3-etherate to yield a mixture of 1,3,5-trihydroxy-2,4-bis-(3-methylbut-2-enyl)xanthen-9-one, in poor yield, identical with natural 8-desoxygartanin along with 1,3,5-trihydroxy-4-(3-methylbut-2-enyl)xanthen-9-one (**3**), in good yield, and 1,3,5-trihydroxy-2-(3-methylbut-2-enyl)xanthen-9-one (**4**) in poor yield. Compounds **3** and **4**, the probable biogenetic precursors of 6-desoxyisojacareubin and 6-desoxyjacareubin, have been reported to occur in nature as such but were characterised as their dimethyl ethers. Compounds **3** and **4** on oxidative cyclisation with DDQ gave 6-desoxyisojacareubin and 6-desoxyjacareubin respectively, completely identical with authentic natural samples.

8-Desoxygartanin, isolated from both fruit hulls and ripe fruits of *Garicinia mangostana* Linn.[1] and from the bark and heartwood of *Maclura pomifera*,[2] was assigned the structure (**2**) on the basis of its spectral data and its conversion to a bicyclo-derivative. 6-Desoxyisojacareubin and its possible biogenetic precursor, 1,3,5-trihydroxy-4-(3-methylbut-2-enyl)xanthen-9-one have very recently been isolated[3] from the heartwood of *Pentaphalangium solomonse* Warb. 6-Desoxyjacareubin, a linear isomer of 6-desoxyisojacareubin and its probable biogenetic precursor, 1,3,5-trihydroxy-2-(3-methylbut-2-enyl)xanthen-9-one, were reported[4] to occur in the heartwood of *Calophyllum scriblitifolium*. Both these probable biogenetic precursors were characterised as their dimethyl ethers and their structures were confirmed by comparison with the synthetic samples of the dimethyl ethers, prepared by indirect methods.

The synthesis of 4-(3-methylbut-2-enyl) and 2-(3-methylbut-2-enyl) derivatives of 1,3,5-trihydroxyxanthen-9-one have now been achieved for the first time with 2-methylbut-3-en-2-ol using catalytic amount of BF_3-etherate at room temperature.

1,3,5-Trihydroxyxanthen-9-one (**1**), prepared[5] from anhydrous phloroglucinol and 2,3-dihydroxy benzoic acid in the presence of phosphorous oxychloride and freshly fused zinc chloride, on condensation with 2-methylbut-3-en-2-ol using a catalytic amount of the Lewis acid boron trifluoride etherate in dry dioxane at room temperature gave a semi-solid mass. Thin layer chromatography indicated the formation of a number of products along with a large amount of unreacted xanthone (**1**). The major amount of unreacted xanthone was removed by extracting with 2% aq Na_2CO_3. The remaining mixture product on column chromatographic purification gave the following main fractions designated as compounds A, B, C, and D (unreacted xanthone).

Compound A, obtained in 2% yield, gave a green colour with alcoholic ferric chloride. Elemental and spectroscopic data confirmed it to be bis-*C*-(3-methylbut-2-enyl)xanthone. NMR($CDCl_3$) exhibited the resonance signals of two 3-methylbut-2-enyl groups along with the expected signals of other protons (see Experimental). It was established to be 2,4-bis-(3-methylbut-2-enyl) derivative (**2**) because its physical characteristics and spectral data was found to be in complete agreement with the data cited for natural 8-desoxygartanin.[1] On formic acid treatment it gave a bisdihydropyrano derivative (**5**), as indicated by its NMR which showed characteristic multiplets of four methylene protons at the expected chemical shifts (see Experimental) along with the signals for other protons. Other characteristics (mp and UV) were found to be in complete agreement with that of known bicycloderivative,[1] prepared from natural 8-desoxygartanin.

Compound B, obtained in nearly 8% yield, was soluble in dilute aq Na_2CO_3 and gave a green colour with alcoholic ferric chloride. Elemental analysis indicated the presence of one 3-methylbut-2-enyl group and its nuclear placement was indicated by the resonance signals shown in its NMR spectrum (see Experimental). It was methylated by using 2 mol of freshly distilled acid free dimethyl sulphate in acetone–potassium carbonate medium to give dimethoxy derivative (**6**) as indicated by its elemental data and confirmed by its NMR spectrum (2×s, δ 3.8 and 3.88). It gave a green colour with alcoholic ferric chloride. It did not undergo any change on formic acid treatment (indicated by TLC), confirming thereby, beyond doubt, the presence of a 3-methylbut-2-enyl group at 4-position in the dimethyl derivative (**6**) and hence in compound B. Further data was found to be completely identical (mmp; TLC and superimposable IR) with that of an authentic sample of dimethyl ether. Complete identity of these two dimethyl ethers confirmed, beyond doubt, the structure (**3**) for compound B.

Compound C, obtained in 3% yield, gave a green colour with alcoholic ferric chloride, was soluble in dilute aq Na_2CO_3. Elemental analysis indicated the entry of one 3-methylbut-2-enyl group into the xanthone nucleus which was confirmed by its NMR spectrum (see Experimental). On methylation with acid free freshly distilled dimethyl sulfate (2 mol) in acetone–potassium carbonate medium it gave a dimethoxy product (**7**), as indicated by its elemental analysis and confirmed by the two methoxyl singlets shown in its NMR spectrum (2×s, δ 3.98 and 4.12). It gave a positive alcoholic ferric chloride test. Its complete identity (mmp; TLC and co-TLC) with an authentic sample of dimethyl ether confirms the structure (**4**) assigned to compound C. Formic acid treatment yielded a product which did not give any colour change with alcoholic ferric chloride. It clearly in-

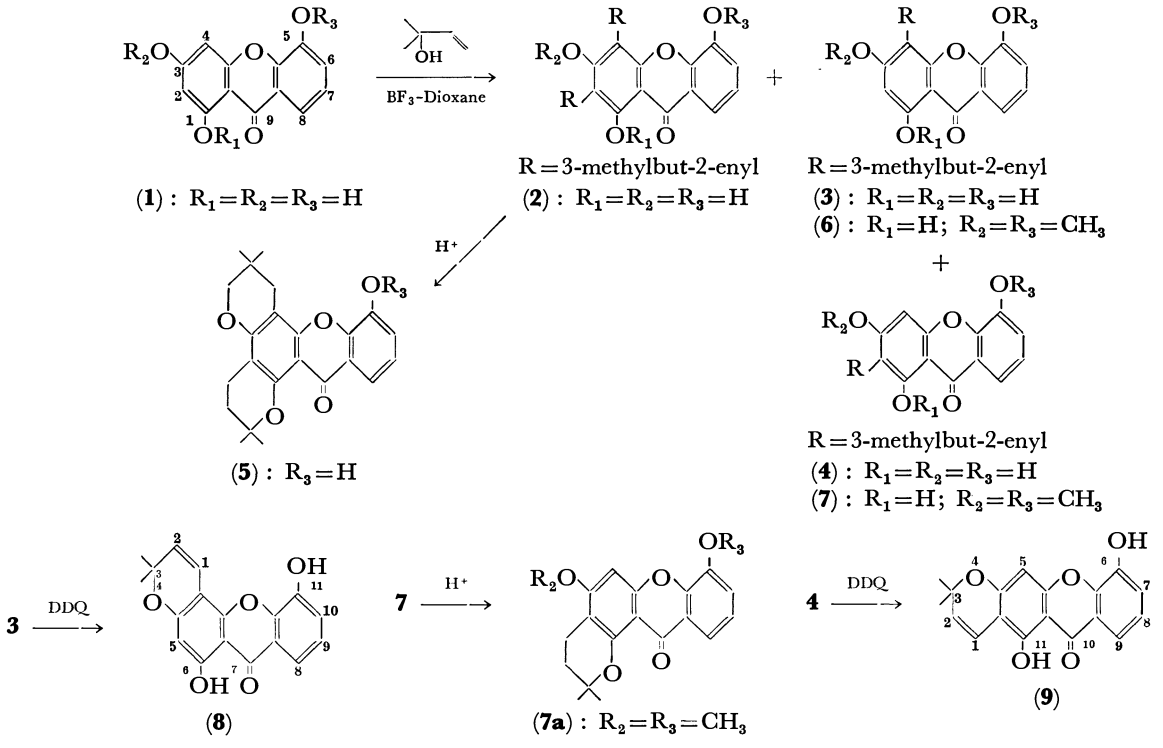

dicated the involvement of 1-hydroxyl in cyclisation with the 3-methylbut-2-enyl group, present at the 2-position. Therefore the 3-methylbut-2-enyl group in dimethyl ether and hence in compound C could only be present at the 2-position. This confirms the structure (**4**) for the compound C beyond any doubt.

Compound B (**3**) on oxidative cyclisation with 2,3-dichloro-5,6-dicyano-*p*-benzoquinone (DDQ) in dry toluene afforded a product along with a very minute quantity of unreacted starting material. It was separated by preparative TLC and was identified as an angular mono-chromene as indicated by the two doublets for the olefinic protons shown in NMR (2×d, δ 5.70 and 6.78). Its structure (**8**), was confirmed by its complete identity (mp; UV; IR) with the natural 6-desoxyisojacareubin. Its formation has also served as an additional proof for the structure (**3**) of compound B.

Similarly, compound C (**4**) on refluxing with DDQ in dry toluene yielded a mixture, from which a chromenoxanthone, as a major product, was separated by preparative TLC. Its NMR spectrum showed two doublets for the olefinic protons of the chromene ring (2×d, δ 5.72 and 7.02) along with the signals for other protons. The complete agreement of its physical characteristics and spectroscopic data with that of natural 6-desoxyjacareubin[4] confirms its structure (**9**) which again confirms the structure (**4**) of compound C.

Experimental

Unless otherwise stated, all mps are uncorrected and were taken with a Kofler's mp apparatus; UV spectra were taken in MeOH; IR spectra were recorded using KBr disc and Perkin-Elmer infra-cord spectrophotometer and NMR in $CDCl_3$, CD_3COCD_3, CD_3COCD_3–$CDCl_3$ using 60 MHz spectrophotometer; silica gel 'Jai' was used for column chromatography and TLC was carried out on silica gel 'Jai' chromatoplates.

*3-Methylbut-2-enylation of 1,3,5-Trihydroxyxanthen-9-one (**1**) with 2-Methylbut-3-en-2-ol.* To a well stirred solution of 1,3,5-trihydroxyxanthen-9-one (**1**, 1 g) in dry dioxane (20 ml) was added boron trifluoride etherate (0.7 ml) and 2-methylbut-3-en-2-ol (0.430 g). The solution was stirred for 4 h at room temperature under anhydrous conditions. Moist ether was added and the ethereal solution stirred for 48 h at room temperature, then washed with water and dried over anhydrous $MgSO_4$. Removal of the solvent gave a solid which was extracted with 2% aq Na_2CO_3 to remove the large amount of unreacted xanthone. The remaining mixture was subjected to column chromatography over silica gel and the following three main fractions, designated as compound A, B, C, and D (unreacted xanthone), were obtained.

Compound A crystallised from benzene–petroleum ether mixture as a yellow powder (36 mg); mp 166—167 °C; green colour with alcoholic ferric chloride; λ_{max} 244, 261, 322, 375 nm; ν_{max} 1650 cm^{-1} (>C=O). Found: C, 72.4; H, 6.6%. Calcd for $C_{23}H_{24}O_5$: C, 72.6; H, 6.4%. NMR ($CDCl_3$): δ 1.68 and 1.80 (2×s, 12H, two $(CH_3)_2C<$), 3.50 (m, 4H, two $-CH_2-$), 5.22 (m, 2H, two $-CH=$), 7.32 (m, 2H, H-6 and H-7), 7.64 (q, J=6.5 Hz and 4 Hz, 1H, H-8). This agreed in all respects with the data cited for natural 8-desoxygartanin.[1] Compound A (**2**, 20 mg) in formic acid (1 ml) was heated on a steam bath for 30 min. The resulting pale yellow solution was poured over crushed ice, extracted with EtOAc and then dried and evaporated under reduced pressure. The solid so obtained crystallised from a benzene–hexane mixture as yellow needles (15 mg); mp 258—260 °C; λ_{max} 257, 310 nm; NMR ($CDCl_3$): δ 1.40 and 1.44 (2×s, 12H, two $(CH_3)_2C<$ of pyran rings), 1.84 and 2.82 (2×m, 8H, four $-CH_2-$ of two pyran rings), 7.22 (m, 2H, H-6, and H-7), 7.70 (q, J=6.5 Hz and 4 Hz, 1H, H-8). This data was found to be in complete agreement with that of bicyclo-8-desoxygartanin.[1] Thus the structure (**2**), as-

signed to compound A, is fully established.

Compound B crystallised from ethyl acetate–benzene mixture as a yellow fluffy powder (120 mg); mp 199—202 °C soluble in 5% aq Na_2CO_3 and giving green colour with alcoholic ferric chloride. λ_{max} 245, 285 nm; ν_{max} 1655 cm^{-1} (>C=O). Found: C, 68.8; H, 5.5%. Calcd for $C_{18}H_{16}O_5$: C, 69.2; H, 5.1%. NMR ($CD_3COCD_3+CDCl_3$): δ 1.66 and 1.74 (2×s, 3H each, $(CH_3)_2C<$), 3.47 (d, J= 7.5 Hz, 2H, $-CH_2-$), 3.66 (br s, 1H, 5-OH; exchangeable with D_2O), 5.20 (m, 1H, –CH=), 6.22 (s, 1H, H-2), 7.20 (m, 2H, H-6, and H-7), 7.72 (q, J=6.5 Hz and 4 Hz, 1H, H-8). An acetone solution of compound B (50 mg in 5 ml) containing freshly distilled acid free dimethyl sulphate (0.030 ml) and freshly ignited K_2CO_3 (nearly 200 mg) was refluxed for 4 h. The acetone was removed under reduced pressure, water added and the solid obtained was filtered. This solid was purified by repeated crystallisations from a ethyl acetate–benzene–hexane mixture to yield yellow needles(36 mg); mp 182—184 °C; λ_{max} 239, 242, 256, 312, and 368 nm; ν_{max} 1660 cm^{-1} (>C=O). Found: C, 70.1; H, 6.2%. Calcd for $C_{20}H_{20}O_5$: C, 70.6; H, 5.8%. NMR ($CDCl_3$): δ 1.62 1.78 (2×s, 6H, $(CH_3)_2C<$), 3.46 (d, J=7.5 Hz, 2H, $-CH_2-$), 3.8 and 3.88 (2×s, 3H each, $-OCH_3$ at 3- and 5-positions), 5.2 (m, 2H, H-6 and H-7), 7.68 (q, J=6.5 Hz, and 4 Hz, 1H, H-8). It was found to be identical in all respects (mmp; TLC and superimposable IR) with the sample of 1-hydroxy-3,5-dimethoxy-4-(3-methylbut-2-enyl)xanthen-9-one. On formic acid treatment, it did not undergo any change (as indicated by TLC). Thus the structure (**6**) could be assigned to above dimethyl ether and hence the structure (**3**) to compound B.

Compound C crystallised from a ethyl acetate–benzene–petroleum ether mixture as light yellow needles (46 mg); mp 182—184 °C; soluble in 5% aq Na_2CO_3; green colour with alcoholic ferric chloride; λ_{max} 242, 258, 300 nm; ν_{max} 1650 cm^{-1} (>C=O). Found: C, 69.4; H, 5.5%. Calcd for $C_{18}H_{16}O_5$: C, 69.2; H, 5.1%. NMR ($CD_3COCD_3+CDCl_3$): δ 1.78 (m, 6H, $(CH_3)_2C<$), 3.44 (d, J=7.5 Hz, 2H, $-CH_2-$), 3.65 (br s, 1H, 5-OH; exchangeable with D_2O), 5.24 (m, 1H, –CH=), 6.72 (s, 1H, H-4), 7.28 (m, 2H, H-6, and H-7), 7.94 (q, J=6.5 Hz and 4 Hz, 1H, H-8). Its dimethyl ether, prepared as above, crystallised from a ethyl acetate–benzene–petroleum ether mixture as a yellow powder (60%); mp 167—168 °C; insoluble in 5% aq Na_2CO_3; positive ferric reaction; λ_{max} 245, 258, 308 nm; ν_{max} 1660 cm^{-1} (>C=O). Found: C, 71.0; H, 5.9%. Calcd for $C_{20}H_{20}O_5$: C, 70.6; H, 5.8%. NMR ($CDCl_3$): δ 1.80 (m, 6H, $(CH_3)_2C<$), 3.46 (d, J=7.5 Hz, 2H, $-CH_2-$), 3.98 and 4.12 (2×s, 3H each, $-OCH_3$ at 3- and 5-positions), 5.35 (m, 1H, –CH=), 6.70 (s, 1H, H-4), 7.36 (m, 2H, H-6 and H-7), 7.92 (q, J=6.5 Hz and 4 Hz, 1H, H-8). It was found to be in complete agreement (mmp; TLC; co-TLC) with the sample of 1-hydroxy-3,5-dimethoxy-2-(3-methylbut-2-enyl)xanthen-9-one. This dimethyl ether (2 mg) in formic acid (3 drops) was heated on steam bath for 30 min. After working up as usual, the product obtained gave no colour change with alcoholic ferric chloride. Thus the 3-methylbut-2-enyl group in methyl ether is confirmed to be present at C-2, and involved in cyclisation with the 1-OH. Therefore the structure (**7**) could be assigned to methyl ether and hence the structure (**4**) to compound C. Compound D was recovered starting material (**1**, 878 mg).

*Oxidative Cyclisation of Compound B (**3**) and Compound C (**4**) with DDQ. 6-Desoxyisojacareubin (**8**)*: A solution of compound B (**3**, 20 mg) in dry toluene (1.5 ml) was refluxed with DDQ (3 mg) for 1 h. It was filtered hot and the residue (colourless hydroquinone) washed with toluene. The removal of solvent under reduced pressure from the filtrate gave a solid mass which was purified by preparative TLC (solvent; ethyl acetate: benzene (1 : 9)). The product, so obtained, crystallised from ethyl acetate–benzene–petroleum ether mixture as a light yellow powder (12 mg); mp 250—251 °C; λ_{max} 233, 250, 266, 310 nm; ν_{max} 1650 cm^{-1} (>C=O). Found: C, 69.3; H, 4.8%. Calcd for $C_{18}H_{14}O_5$: C, 69.6; H, 4.5%. NMR (CD_3COCD_3): δ 1.46 (s, 6H, $(CH_3)_2C<$), 3.60 (br s, 1H, 11 –OH; exchangeable with D_2O), 5.70 and 6.78 (2×d, J=10 Hz each, 1H each, –CH=CH–), 7.18 (m, 2H, H-9, and H-10), 7.62 (q, J=6.5 Hz and 4 Hz, 1H, H-8). This data was found to be in complete agreement with the data cited for natural 6-desoxyisojacareubin.[3]

*6-Desoxyjacareubin (**9**)*: Compound C (**4**, 18 mg) in dry toluene (1.5 ml) was refluxed with DDQ (3 mg) for 1 h. The progress of the reaction was checked with TLC. After working up as above it gave a product, which was purified by preparative TLC (solvent; ethyl acetate: benzene (1 : 9)). The compound, so obtained, crystallised from a ethyl acetate–benzene–petroleum ether mixture as a orange yellow solid (12 mg); mp 212—214 °C; λ_{max} 241, 272 sh, 288, 310 sh, 370 nm; ν_{max} 1650 cm^{-1} (>C=O). Found: C, 69.2; H, 4.9%. Calcd for $C_{18}H_{14}O_5$: C, 69.6; H, 4.5%. NMR(CD_3COCD_3): δ 1.47 (s, 6H, $(CH_3)_2C<$), 3.58 (br s, 1H, –OH; exchangeable with D_2O), 5.72 and 7.02 (2×d, J=10 Hz each, 1H each, –CH=CH–), 7.2 (m, 2H, H-7, and H-8), 7.68 (q, J=6.5 Hz and 4 Hz, 1H, H-9). This data agreed completely with the data cited for natural 6-desoxy-jacareubin.[4]

We express our very sincere thanks to Prof. F. Scheinmann for the authentic samples of 1-hydroxy-3,5-dimethoxy-4-(3-methylbut-2-enyl)xanthen-9-one and 1-hydroxy-3,5-dimethoxy-2-(3-methylbut-2-enyl)-xanthen-9-one.

References

1) T. R. Govindachari, P. S. Kalyanaraman, N. Muthukumara Swamy, and B. R. Pai, *Tetrahedron*, **27**, 3919 (1971).

2) V. H. Deshpande, A. V. Rama Rao, M. Vardan, and K. Venkataraman, *Indian J. Chem.*, **11**, 518 (1973).

3) F. Scheinmann and P. J. Owen, *J. Chem. Soc., Perkin Trans. 1*, **1974**, 1018.

4) B. Jackson, H. D. Locksley, and F. Scheinmann, *J. Chem. Soc., C*, **1967**, 2500.

5) V. V. Kane, A. B. Kulkarni, and R. C. Shah, *J. Sci. Ind. Res. India*, **18B**, 28 (1959).

Structural Studies of Commensurate Peierls State of $Rb_{1.67}[Pt(C_2O_4)_2]\cdot 1.5H_2O$

Akiko KOBAYASHI,* Yukiyoshi SASAKI, and Hayao KOBAYASHI**

Department of Chemistry, The Research Centre for Spectrochemistry, Faculty of Science, The University of Tokyo, Hongo, Tokyo 113

***Department of Chemistry, Faculty of Science, Toho University, Funabashi, Chiba 274*

(Received May 17, 1979)

X-Ray examination, chemical analyses and electrical conductivity measurements have been conducted on the partially oxidized platinum complex $Rb_{1.67}[Pt(C_2O_4)_2]\cdot 1.5H_2O$ (RbDOX). The cell constants are $a=12.690(10)$, $b=17.108(14)$, $c=11.357(3)$ Å; $\alpha=102.04(4)$, $\beta=115.17(3)$, $\gamma=43.58(4)°$, and the space group is $P\bar{1}$. The planar bis(oxalato)platinate ions stack along the crystallographic b axis and the Pt atoms form a sixfold distorted chain. RbDOX is the first example of a sixfold structure. Three independent Pt–Pt distances are 2.717(3), 2.830(3), and 3.015(3) Å. The Pt–Pt distance of 2.717 Å is the shortest spacing so far observed in partially oxidized platinate salts and shorter than the 2.77 Å interatomic separation in Pt metal itself. The oxalate ligands are staggered (46°, 55°, 80°) with respect to the ligands directly above and below them along the chain. Sixfold modulated superstructure of RbDOX is confirmed as the newly found commensurate Peierls structure based on agreement with the period of the Peierls distorted superlattice determined by the degree of partial oxidation. The calculation of Coulomb energy shows that RbDOX has a crystal lattice in which the interchain Coulomb energies are at a minimum indicating the strong tendency of the anti-phase ordering of the nearest-neighbour Pt chains.

In recent years there has been considerable interest in the partially oxidized quasi-one-dimensional cyanoplatinates and bis(oxalato)platinates because of their high, newly metallic electrical conductivities and they provide experimental results which greatly aid the development of the theory of the one-dimensional state. The prototype compounds of cyanoplatinates groups are the anion deficient derivatives, $K_2[Pt(CN)]_4Br_{0.3}\cdot 3.2H_2O$ referred to as KCP. Since the original discovery by Comès *et al.*[1] of X-ray diffuse scattering associated with the Peierls instability in KCP, the nature of the sinusoidal modulation of one-dimensional platinum chain has been studied by many authors.[2,3]

In one-dimensional metals, modulation waves (charge density waves: CDWs) have a wave vector $q=2k_F$ in the chain direction, where k_F is the Fermi wave vector, and in the insulating state, the CDWs are correlated to form a three-dimensional static Peierls distortion, that is, the lattice modulation waves give rise to a three-dimensional superstructure at low temperature.[4] The period of the lattice modulation wave in the Peierls phase is commensurate or incommensurate with the period in the high-temperature metallic phase.

There has been much research on KCP salts and TTF-TCNQ (tetrathiafulvalene–7,7,8,8-tetracyanoquinodimethane),[5] however, the crystal structure determination of the Peierls state of the one-dimensional conductors appears to be very limited. The modulated superstructure of $K_{1.81}[Pt(C_2O_4)_2]\cdot 2H_2O$ (γ-KDOX)[6,7] is the first example of the incommensurate Peierls state determined by X-ray analysis and it is attributed to the condensation of the $2k_F$ phonon of the one-dimensional metallic system. In the present work the sixfold modulated commensurate Peierls structure of a new salt $Rb_{1.67}[Pt(C_2O_4)_2]\cdot 1.5H_2O$ (RbDOX) will be reported.

Experimental

RbDOX was prepared from $Rb_2[Pt(C_2O_4)_2]$ and Rb_2PtCl_6 by a diffusion method. The solution was allowed to stand for a month and copper-colored needle-shaped crystals deposited. Many of the crystals were twinned, the twin axis being the needle axis. A suitable untwinned specimen was selected for data collection. The crystal needle axis was chosen as the axis for mounting and the crystallographic b axis. Oscillation photographs showed reciprocal lattice layers for which $k=6n$ were especially strong and all others were very weak. This feature clearly indicates the existence of a Pt chain with Pt atoms stacked $b/6$ apart.

Collection and Reduction of the Data. The crystal selected for data collection had dimensions of $0.28\times 0.10\times 0.038$ mm. The data were collected on a Rigaku automated diffractometer equipped with a graphite monochromator. A least-squares fit of the diffractometer angles obtained by automatically centering reflections in the range $30°<2\theta<40°$ (Mo $K\alpha$ radiation, $\lambda=0.71069$ Å) yielded the following crystal data: $a=12.690$ (10), $b=17.108$ (14), $c=11.357$ (3) Å, $\alpha=102.04$ (4), $\beta=115.17$ (3), $\gamma=43.58$ (4)°, $V=1518.6$ Å^3, $Z=6$, $d_{calcd}=3.549$ g cm^{-3}, μ(Mo $K\alpha$)$=230.6$ cm^{-1}.

Intensity data were collected with monochromatized Mo $K\alpha$ radiation by the ω-2θ scan technique up to $2\theta=60°$. Reflections were scanned at the rate of 4° per minute in 2θ. Background counts of 10s were taken at each end of the scan range. The diffracted intensity gradually decreased to 93% of the initial value during X-ray radiation. The data were corrected for deterioration, but no corrections were made for absorption owing to the irregularity of the crystal shape.

Solution and Refinement of the Structure. The structure was solved using a Patterson map. Space group $P\bar{1}$ was provisionally chosen and Pt(1) and Pt(4) were assigned to special positions at (0, 0, 0) and (0, 1/2, 0), while Pt(2) and Pt(3) were initially placed at general positions. The atomic parameters were refined by the block-diagonal least-squares method, using anisotropic temperature factors for Pt and Rb atoms and isotropic factors for O and C atoms. The final R values are $R_1=0.069$ for $F_o>3\sigma(F_o)$ and $R_2=0.084$. The agreement indices are defined as $R_1=\sum w||F_o|-|F_o||/\sum w|F_o|$, $R_2=\sum w||F_o|^2-|F_c|^2|/\sum w|F_o|^2$. The weighting schemes used were: $w=1/[a+b|F_o|+c|F_o|^2]$ for $|F_o|\geq 45.64$ (absolute scale), $a=91.28$, $b=1.0$, and $c=0.00289$; $w=0.1$ otherwise. As the exact Rb ion composition and those of the water molecules are uncertain, the multipliers were varied in one of the final refinements with the full matrix least-squares method. The multipliers converged to approximately 1.0 for

Rb ions indicating that the Rb ion sites are fully occupied. The exact H_2O content could not be determined from the X-ray crystal structure refinement. The ambiguity in the H_2O composition may be related to the deterioration of the crystal. Large R values and abnormal bond lengths and angles were obtained by the noncentrosymmetric refinement in P1 and thus $P\bar{1}$ was confirmed as the correct space group.

Positional and thermal parameters determined from the final least-squares cycle are presented in Tables 1 and 2. The atomic scattering factors and the values of $\Delta f'$, $\Delta f''$, were taken from International Tables for X-Ray Crystallography.[8] The F_o-F_c Tables are kept at the office of this

Table 1. Fractional coordinates ($\times 10000$)

Atom	x	y	z	Atom	x	y	z
Pt (1)	0	0	0	C (6)	−3278 (32)	4738 (21)	−1215 (25)
Pt (4)	0	5000	0	O (11)	−3460 (23)	4580 (15)	−3445 (18)
Pt (2)	21 (1)	1581 (1)	33 (1)	O (12)	−4777 (25)	5368 (17)	−1564 (20)
Pt (3)	172 (1)	3166 (1)	132 (1)	O (13)	2056 (23)	712 (16)	1692 (19)
Rb (1)	2670 (4)	−697 (3)	−4627 (3)	O (14)	−1257 (24)	2470 (16)	1203 (19)
Rb (2)	4616 (4)	4011 (3)	−1270 (3)	C (7)	1623 (42)	1117 (28)	2734 (34)
Rb (3)	7128 (4)	3361 (2)	4238 (3)	C (8)	−140 (45)	2180 (30)	2429 (36)
Rb (4)	8651 (5)	−3216 (4)	−4986 (3)	O (15)	2759 (38)	583 (26)	3859 (30)
Rb (5)	5134 (4)	−1174 (3)	881 (3)	O (16)	−712 (41)	2837 (28)	3254 (33)
O (1)	−441 (23)	−29 (15)	−1948 (18)	O (17)	1241 (21)	784 (14)	−1170 (17)
O (2)	2367 (22)	−1235 (15)	282 (17)	O (18)	−2075 (20)	2454 (13)	−1634 (16)
C (1)	968 (32)	−851 (21)	−2098 (26)	C (9)	−1 (36)	1310 (24)	−2495 (29)
C (2)	2634 (31)	−1537 (20)	−852 (25)	C (10)	−1769 (29)	2132 (19)	−2679 (23)
O (3)	1044 (27)	−1060 (18)	−3209 (21)	O (19)	511 (27)	1080 (18)	−3329 (21)
O (4)	4012 (25)	−2240 (17)	−809 (20)	O (20)	−2826 (24)	2444 (16)	−3785 (20)
O (5)	2527 (22)	1918 (15)	311 (17)	O (21)	−1477 (25)	5498 (17)	−1963 (20)
O (6)	1325 (24)	2872 (16)	2106 (19)	O (22)	1888 (23)	3964 (15)	−574 (18)
C (3)	3681 (32)	1507 (21)	1494 (25)	C (11)	−501 (37)	5060 (25)	−2617 (30)
C (4)	2902 (30)	2111 (20)	2560 (24)	C (12)	1373 (34)	4203 (22)	−1827 (27)
O (7)	5139 (28)	725 (19)	1852 (23)	O (23)	−1160 (29)	5225 (19)	−3849 (23)
O (8)	3846 (26)	1887 (17)	3756 (21)	O (24)	2331 (31)	3798 (21)	−2363 (25)
O (9)	−1009 (20)	3510 (13)	−1869 (16)	H_2O (1)	4963 (31)	7146 (21)	−2952 (25)
O (10)	−2177 (23)	4375 (16)	−56 (19)	H_2O (2)	6264 (40)	5642 (27)	4072 (32)
C (5)	−2588 (30)	4294 (20)	−2328 (24)	H_2O (3)	1429 (39)	2280 (27)	−2983 (31)

Table 2. Atomic thermal parameters U_{ij} and their standard deviations (10^{-4} Å^2 units)
the temperature factor is defined as $\exp[-2\pi^2\sum_{ij}h_ih_ja_ia_jU_{ij}]$, $i, j=1,2,3$

Atom	U_{11}	U_{22}	U_{33}	$U_{12}/2$	$U_{13}/2$	$U_{23}/2$
Pt (1)	187 (5)	173 (5)	137 (5)	−132 (4)	84 (4)	−47 (4)
Pt (4)	291 (7)	314 (6)	163 (6)	−232 (6)	105 (5)	−44 (5)
Pt (2)	313 (5)	304 (4)	133 (4)	−244 (4)	114 (3)	−79 (3)
Pt (3)	287 (5)	265 (4)	175 (4)	−228 (4)	137 (4)	−109 (3)
Rb (1)	434 (16)	384 (14)	336 (14)	−241 (13)	168 (13)	−119 (12)
Rb (2)	534 (18)	605 (18)	345 (15)	−449 (16)	262 (14)	−174 (13)
Rb (3)	394 (14)	413 (14)	241 (12)	−265 (12)	151 (11)	−42 (10)
Rb (4)	928 (28)	851 (25)	343 (16)	−745 (24)	419 (18)	−331 (16)
Rb (5)	548 (19)	578 (19)	471 (18)	−417 (17)	292 (16)	−182 (15)

Isotropic vibration parameters of light atoms

O (1)	2.4 (0.3)	O (10)	2.5 (0.3)	C (9)	2.8 (0.5)
O (2)	2.2 (0.3)	C (5)	1.9 (0.4)	C (10)	1.7 (0.4)
C (1)	2.2 (0.4)	C (6)	2.1 (0.4)	O (19)	3.3 (0.4)
C (2)	2.0 (0.4)	O (11)	2.4 (0.3)	O (20)	2.8 (0.3)
O (3)	3.4 (0.4)	O (12)	3.0 (0.4)	O (21)	3.0 (0.4)
O (4)	3.0 (0.4)	O (13)	2.6 (0.3)	O (22)	2.4 (0.3)
O (5)	2.2 (0.3)	O (14)	2.6 (0.3)	C (11)	2.9 (0.5)
O (6)	2.6 (0.3)	C (7)	3.6 (0.6)	C (12)	2.5 (0.4)
C (3)	2.2 (0.4)	C (8)	4.0 (0.7)	O (23)	3.8 (0.4)
C (4)	1.8 (0.4)	O (15)	5.8 (0.6)	O (24)	4.3 (0.5)
O (7)	3.7 (0.4)	O (16)	6.7 (0.7)	H_2O(1)	4.4 (0.5)
O (8)	3.1 (0.4)	O (17)	1.9 (0.3)	H_2O(2)	6.5 (0.7)
O (9)	1.8 (0.3)	O (18)	1.8 (0.3)	H_2O(3)	6.3 (0.7)

Bulletin as Document No. 7936. All calculations were performed on a HITAC 8700/8800 computer at the Computer Center, University of Tokyo using a local version of UNICS.[9]

Chemical Analyses. The selected crystals were subjected to chemical analyses. The contents of the Rb atom and Pt atom were determined with the aid of atomic emission spectrometry and atomic absorption spectrophotometry. Nitric acid was added to increase solubility. For the atomic absorption spectrophotometer, a Nippon-Jarrell Ash FLA 100 equipped with an air-acetylene flame and a carbon rod furnace was used. Jarrell Ash AA-1 MK-II was used for by atomic emission spectrometry. Carbon and hydrogen were analyzed by the usual procedure, the results of which are given in Table 3. The stoichiometry indicated by the formula $Rb_{1.66}[Pt(C_2O_4)_2]\cdot 1.5H_2O$ has been obtained for RbDOX. There will be some uncertainty in the water content.

TABLE 3. CHEMICAL ANALYSES OF RbDOX

	Expected (%)	Found (%)
Rb	26.39	27.1
Pt	36.07	37.5
C	8.88	9.0
H	0.56	0.56

a) Ratio of Rb to Pt 1.66±0.07.

Electrical Conductivity Measurements. D.c. conductivity was measured using the four probe method. The measurements were made on several specimens along the needle axes parallel to the Pt chains of the crystals. The electrical

TABLE 4a. INTRAMOLECULAR BOND DISTANCES/Å

Pt(1)……O(1)	2.04(2)	O(13)……C(7)	1.36(5)
Pt(1)……O(2)	1.97(2)	O(14)……C(8)	1.34(4)
Pt(2)……O(13)	1.97(2)	C(7)……C(8)	1.46(4)
Pt(2)……O(14)	2.03(2)	C(7)……O(15)	1.25(4)
Pt(2)……O(17)	2.02(2)	C(8)……O(16)	1.27(5)
Pt(2)……O(18)	2.01(1)	O(17)……C(9)	1.43(3)
Pt(3)……O(5)	1.99(2)	O(18)……C(10)	1.29(4)
Pt(3)……O(6)	2.01(2)	C(9)……C(10)	1.49(5)
Pt(3)……O(9)	2.03(2)	C(9)……O(19)	1.21(5)
Pt(3)……O(10)	1.98(2)	C(10)……O(20)	1.21(3)
Pt(4)……O(21)	2.03(2)	O(21)……C(11)	1.36(6)
Pt(4)……O(22)	2.00(2)	O(22)……C(12)	1.30(4)
O(1)……C(1)	1.31(4)	C(11)……C(12)	1.51(4)
O(2)……C(2)	1.37(4)	C(11)……O(23)	1.25(4)
C(1)……C(2)	1.55(3)	C(12)……O(24)	1.25(6)
C(1)……O(3)	1.26(4)		
C(2)……O(4)	1.19(4)		
O(5)……C(3)	1.29(3)		
O(6)……C(4)	1.26(3)		
C(3)……C(4)	1.59(4)		
C(3)……O(7)	1.17(3)		
C(4)……O(8)	1.26(3)		
O(9)……C(5)	1.26(3)		
O(10)……C(6)	1.26(3)		
C(5)……C(6)	1.59(5)		
C(5)……O(11)	1.16(3)		
C(6)……O(12)	1.23(4)		

TABLE 4b. INTRAMOLECULAR BOND ANGLES/°

O(1)–Pt(1)–O(2)	84.3(8)	O(1)–C(1)–O(3)	123.4(2.2)
O(13)–Pt(2)–O(14)	85.7(8)	O(2)–C(2)–O(4)	120.8(2.3)
O(17)–Pt(2)–O(18)	85.4(7)	O(5)–C(3)–O(7)	129.2(2.8)
O(5)–Pt(3)–O(6)	81.4(8)	O(6)–C(4)–O(8)	124.6(2.6)
O(9)–Pt(3)–O(10)	80.8(8)	O(9)–C(5)–O(11)	124.4(2.8)
O(21)–Pt(4)–O(22)	84.6(9)	O(10)–C(6)–O(12)	127.9(3.2)
Pt(1)–O(1)–C(1)	110.7(1.6)	O(13)–C(7)–O(15)	117.7(3.0)
Pt(1)–O(2)–C(2)	114.6(1.6)	O(14)–C(8)–O(16)	116.8(3.1)
Pt(3)–O(5)–C(3)	116.8(1.7)	O(17)–C(9)–O(19)	115.8(3.0)
Pt(3)–O(6)–C(4)	114.8(1.9)	O(18)–C(10)–O(20)	124.2(2.8)
Pt(3)–O(9)–C(5)	115.3(1.7)	O(21)–C(11)–O(23)	117.9(3.4)
Pt(3)–O(10)–C(6)	116.0(1.8)	O(22)–C(12)–O(24)	123.3(2.9)
Pt(2)–O(13)–C(7)	109.7(2.1)	O(3)–C(1)–C(2)	118.0(2.6)
Pt(2)–O(14)–C(8)	107.1(2.0)	O(4)–C(2)–C(1)	127.4(2.6)
Pt(2)–O(17)–C(9)	107.3(1.5)	O(7)–C(3)–C(4)	119.1(2.5)
Pt(2)–O(18)–C(10)	112.6(1.6)	O(8)–C(4)–C(3)	119.6(2.6)
Pt(4)–O(21)–C(11)	107.7(2.3)	O(11)–C(5)–C(6)	122.4(2.9)
Pt(4)–O(22)–C(12)	112.3(1.7)	O(12)–C(6)–C(5)	117.7(2.4)
O(1)–C(1)–C(2)	118.3(2.3)	O(15)–C(7)–C(8)	126.0(3.5)
O(2)–C(2)–C(1)	111.8(2.3)	O(16)–C(8)–C(7)	125.2(3.2)
O(5)–C(3)–C(4)	111.4(2.4)	O(19)–C(9)–C(10)	127.5(2.6)
O(6)–C(4)–C(3)	115.5(2.2)	O(20)–C(10)–C(9)	118.6(2.8)
O(9)–C(5)–C(6)	112.7(2.2)	O(23)–C(11)–C(12)	122.9(3.2)
O(10)–C(6)–C(5)	114.4(2.8)	O(24)–C(12)–C(11)	120.9(2.9)
O(13)–C(7)–C(8)	116.3(2.6)		
O(14)–C(8)–C(7)	117.9(3.0)		
O(17)–C(9)–C(10)	116.6(3.0)		
O(18)–C(10)–C(9)	117.3(2.3)		
O(21)–C(11)–C(12)	117.9(2.7)		
O(22)–C(12)–C(11)	115.7(3.2)		

contacts were made by four 0.025 mm gold wires attached with aquadag. RbDOX behaves as a semiconductor from 305 K to 83 K. The room temperature conductivity is 7×10^{-3} $(\Omega\,cm)^{-1}$ and the activation energy is 0.077 eV.

Results and Discussion

The intramolecular distances of the $Pt(C_2O_4)_2$ complexes are given in Table 4a and the intramolecular angles are listed in Table 4b. The distorted nonlinear sixfold Pt atom chain is formed along the crystallographic b axis and involves six bis(oxalate) groups in one repeating unit of 17.11(1) Å. There are four nonequivalent Pt atoms. Pt(1) and Pt(4) lie at the centres of symmetry (0,0,0) and (0,1/2,0), while Pt(2) and Pt(3) lie at the general positions (0.0021, 0.1582, 0.0033) and (0.0172, 0.3166, 0.0132). The stacking of $Pt(C_2O_4)_2$ complexes is shown in Fig. 1.

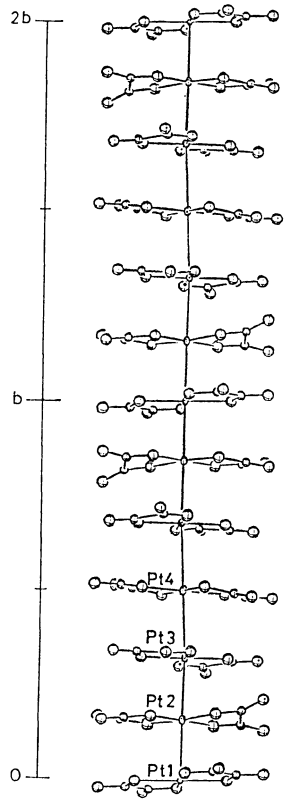

Fig. 1. The stacking of $Pt(C_2O_4)_2$ ions along the b axis. Two wavelengths of the Pt chain is shown.

The three independent Pt–Pt distances are Pt(1)–Pt(2)=2.717(3) Å, Pt(2)–Pt(3)=2.830(3) Å and Pt(3)–Pt(4)=3.015(3) Å. The Pt–Pt–Pt angles are Pt(1)–Pt(2)–Pt(3)=177.83(8)° and Pt(2)–Pt(3)–Pt(4)=174.23(5)°. The Pt–Pt distances in partially oxidized tetracyanoplatinate and bis(oxalato)platinate salts so far reported are shown in Table 5. The Pt–Pt distance of 2.717(3) Å found in RbDOX is the shortest spacing so far observed in partially oxidized platinate salts and shorter than the 2.77 Å interatomic separation in Pt metal itself. The Pt–O distances are 2.007(5) Å on average. Table 6 shows the averaged molecular structures of the four independent anions based on the assumption of D_{2h} symmetry. There appears to be a slight difference between the structure of the 3rd molecule and those of the others. Regarding the 3rd molecule, the O–Pt–O angle is 81.1(6)°, the C–O bond distance in the five membered ring is 1.27(2) Å and the C–C distance is on average 1.59(3) Å. This C–O bond is in the region of the C–O double bond. Regarding the other three molecules, the O–Pt–O angles are 85.0(4)° and the C–O distance is 1.35(1) Å. This bond length is close to that of the C–O single bond. The terminal C–O distances are in both cases 1.21(2) Å and 1.24(2) Å *i.e.*, those of normal double bonds. The structure of the third molecule is approximately equal to those of the molecules in $K_2[Pt(C_2O_4)_2]\cdot 2H_2O$,[20] $Co_{0.83}[Pt(C_2O_4)_2]\cdot 6H_2O$,[18] and $Mg_{0.82}[Pt(C_2O_4)_2]\cdot 5.3H_2O$.[17]

Figure 2 shows the mode of overlapping of platinate complex anions. The oxalate ligands are staggered with respect to the ligands directly above and below them along the chain. The staggered angles are approximately 46°, 55°, and 80°, while alternate ligands are eclipsed or staggered ≈90°. The 45° conformation has been found in the crystal of γ-KDOX. The 60° conformation has been observed in γ-KDOX and similar magnesium or cobalt defficient bis(oxalato)platinate complexes. It has been observed that these conforma-

Table 5. Comparison of the Pt–Pt distances in partially oxidized tetracyanoplatinate and bis(oxalato)platinate salts

	Crystal system	Pt–Pt distance/Å	Chain structure
$K_2[Pt(CN)_4]Br_{0.3}\cdot 3H_2O$[a]	tetragonal	2.888, 2.892	twofold structure
$Rb_2[Pt(CN)_4]Cl_{0.3}\cdot 3H_2O$[b]	tetragonal	2.877, 2.924	twofold structure
$(NH_4)_2[Pt(CN)_4]Cl_{0.3}\cdot 3H_2O$[c]	tetragonal	2.910, 2.930	twofold structure
$K_{1.75}[Pt(CN)_4]\cdot 1.5H_2O$[d]	triclinic	2.967, 2.976	fourfold structure
$K_2[Pt(CN)_4](FHF)_{0.3}\cdot 3H_2O$[e]	tetragonal	2.918, 2.928	twofold structure
$Rb_2[Pt(CN)_4](FHF)_{0.40}$[f]	tetragonal	2.798	twofold structure
$Cs_2[Pt(CN)_4](FHF)_{0.39}$[g]	tetragonal	2.833	twofold structure
$Mg_{0.82}[Pt(C_2O_4)_2]\cdot 5.3H_2O$[h]	orthorhombic	2.85	twofold structure
$Co_{0.83}[Pt(C_2O_4)_2]\cdot 6H_2O$[i]	orthorhombic	2.841	twofold structure
$K_{1.81}[Pt(C_2O_4)_2]\cdot 2H_2O$[j]	triclinic	2.961, 2.965	superstructure
$Cs_2[Pt(CN)_4](N_3)_{0.25}\cdot 0.5H_2O$[k]	tetragonal	2.877	twofold structure
$Rb_{1.67}[Pt(C_2O_4)_2]\cdot 1.5H_2O$[l]	triclinic	2.717, 2.830, 3.015	sixfold structure

a) Reference 10. b) Reference 11. c) Reference 12. d) Reference 13a, 13b. e) Reference 14. f) Reference 15. g) Reference 16. h) Reference 17. i) Reference 18. j) Reference 6. k) Reference 19. l) this work.

Table 6. The averaged molecular structures of the four independent Pt anions

	a/Å	b/Å	c/Å	d/Å	
I	2.00(1)	1.34(3)	1.55(3)	1.23(3)	
II	2.01(1)	1.36(2)	1.48(3)	1.24(2)	
III	2.00(1)	1.27(2)	1.59(3)	1.21(2)	
IV	2.02(2)	1.33(3)	1.51(4)	1.25(3)	
A	2.00	1.28	1.55	1.22	
B	2.013(5)	1.26(1)	1.57(2)	1.23(1)	
C	2.00	1.29	1.54	1.22	
	α/°	β/°	γ/°	δ/°	ε/°
I	84.3(8)	112.6(1.1)	115.1(1.6)	122.1(1.6)	122.7(1.8)
II	85.6(6)	109.2(9)	117.0(1.4)	118.6(1.5)	124.3(1.5)
III	81.1(6)	115.7(9)	113.5(1.2)	127.0(1.4)	119.7(1.3)
IV	84.6(9)	110.0(1.4)	116.8(2.1)	120.6(2.2)	121.9(2.2)
A	82	115	115	126	120
B	82.7(3)	113.1(4)	115.7(7)	124.5(7)	120.0(7)
C	83	113	116	124	120

A: $Mg_{0.82}[Pt(C_2O_4)_2]\cdot 5.3H_2O$; $Pt(C_2O_4)_2^{-1.64}$ B: $Co_{0.83}[Pt(C_2O_4)_2]\cdot 6H_2O$; $Pt(C_2O_4)_2^{-1.66}$ C: $K_2Pt(C_2O_4)_2\cdot 2H_2O$; $Pt(C_2O_4)_2^{-2}$.

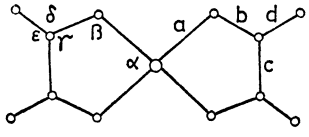

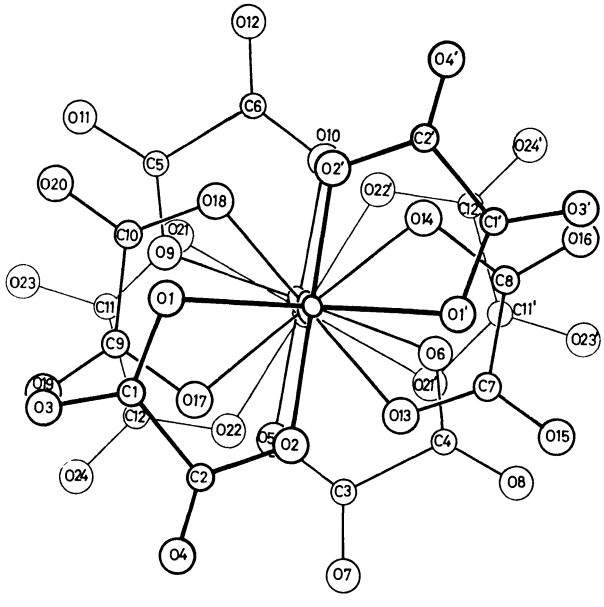

Fig. 2. The mode of overlapping of platinate complex anions.

tions are suitable for intermolecular stabilization due to the overlapping of the higher occupied molecular orbitals of one molecule and the lower unoccupied molecular orbitals of the neighbouring molecule. The importance of the charge transfer interactions in the stabilization of the molecular overlapping was first suggested in Miller's molecular back bonding theory.[21] The 80° conformation observed in this crystal is a new type conformation.

The equations of the best planes, perpendicular distances from these planes and the dihedral angles between these planes are listed in Tables 7a and 7b. The dihedral angles between the Pt(1), Pt(2), and Pt(3)

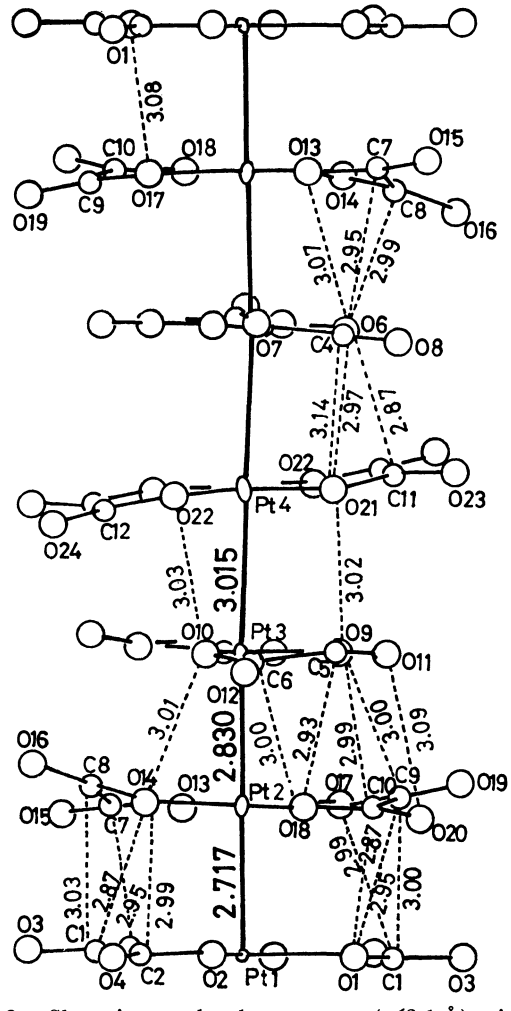

Fig. 3. Short intermolecular contacts (<3.1 Å) within the Pt chain.

Table 7a. Least-squares plane for the $Pt(C_2O_4)_2$ planes and deviations from the planes (X, Y and Z refer to the orthogonal coordinate system (Å) with X along a. Y is perpendicular to X in ab plane)

1) Pt(1) plane:
$-0.7152X+(-0.6980)Y+0.0355Z=0$

Atom	Deviation/Å
Pt(1)	0.0
O(1)	−0.07
O(2)	−0.04
C(1)	0.02
C(2)	0.01
O(3)	0.01
O(4)	−0.03

2) Pt(2) plane:
$-0.7414X+(-0.6707)Y+0.0232Z+2.8248=0$

Atom	Deviation/Å
Pt(2)	0.11
O(13)	0.13
O(14)	0.11
O(17)	−0.00
O(18)	0.14
C(7)	0.13
C(8)	−0.11
C(9)	−0.09
C(10)	0.12
O(15)	0.28
O(16)	−0.47
O(19)	−0.41
O(20)	0.28

3) Pt(3) plane:
$-0.7054X+(-0.7079)Y+0.0354Z+5.5226=0$

Atom	Deviation/Å
Pt(3)	−0.01
O(5)	0.06
O(6)	−0.02
O(9)	−0.06
O(10)	−0.02
C(3)	0.04
C(4)	−0.02
C(5)	−0.11
C(6)	0.04
O(7)	0.17
O(8)	−0.17
O(11)	−0.11
O(12)	0.22

4) Pt(4) plane:
$-0.6229X+(-0.7812)Y+(-0.0412)Z+8.4675=0$

Atom	Deviation/Å
Pt(4)	0.00
O(21)	0.07
O(22)	0.19
C(11)	−0.05
C(12)	0.03
O(23)	0.03
O(24)	−0.12

planes are 0.8—3.1°, but the Pt(4) plane is inclined to the other planes at 7.7—10.0°. Table 8 shows the short interatomic distances within the Pt chain and Figure 3 shows the short intermolecular contacts within the Pt chain.

Table 7b. Dihedral angles for the $Pt(C_2O_4)_2$ planes

		Dihedral angles/°
plane 1	plane 2	2.3
plane 1	plane 3	0.8
plane 1	plane 4	8.4
plane 2	plane 3	3.1
plane 2	plane 4	10.0
plane 3	plane 4	7.7

Table 8. Short interatomic distances/Å within the Pt chains (<3.1Å)

O(1)···C(10)	2.87(5)	O(6)···C(8)	2.99(8)
O(1)···C(9)	2.95(7)	O(6)···O(13)	3.07(4)
O(1)···C(7)	2.95(7)	O(9)···C(10)	3.00(5)
O(1)···O(17)	3.08(5)	O(9)···C(9)	3.00(5)
C(1)···O(14)	2.87(6)	O(9)···O(21)	3.02(5)
C(1)···O(17)	2.99(5)	O(9)···O(18)	3.04(5)
C(1)···C(9)	3.00(6)	O(10)···O(14)	3.01(5)
C(1)···C(8)	3.03(9)	O(10)···O(22)	3.03(5)
C(2)···O(17)	2.99(4)	C(5)···O(18)	2.93(5)
C(2)···O(14)	2.99(6)	C(5)···C(10)	3.01(5)
O(6)···C(11)	2.87(7)	C(6)···O(18)	3.00(4)
O(6)···C(7)	2.95(7)	O(11)···O(20)	3.09(4)
O(6)···O(21)	2.97(5)		
Pt(1)···Pt(2)	2.717(3)		
Pt(2)···Pt(3)	2.830(3)		
Pt(3)···Pt(4)	3.015(3)		

The Pt(1) plane is nearly planar but the Pt(2) plane is concave (Fig. 3). The Pt(2) atom is 0.11 Å shifted from the best plane toward the Pt(1) plane and the terminal oxygen atoms of the ligands O(16) and O(19) are 0.47 Å and 0.41 Å from the plane, respectively. The large deviation of these atoms from the plane is attributed mainly to the shortening of the Pt–Pt distance and partly to the interaction between the oxygen atoms of oxalate ligands and surrounding atoms. Figure 2 shows direct overlapping of the terminal oxygen atoms of the Pt(2) plane, O(16) and O(19), with O(3) and O(3′) atoms of the Pt(1) plane. The 46° staggered overlapping of the Pt(1) plane and the Pt(2) plane will be a very stable form considering the large intermolecular overlapping and the short interatomic distances within the chain. Many short interatomic contacts indicate that the charge transfer interactions between the ligands of the neighbouring molecules will have influence on the mode of overlapping. The Pt(3) plane is more planar than the Pt(2) plane but the terminal oxygen atoms of the ligands are shifted 0.11—0.22 Å from the plane. As to the Pt(4) plane, the oxygen atom in the five-membered ring shows a 0.19 Å deviation from the least-squares plane and the terminal oxygen atom is 0.12 Å distant from the plane. The Pt(4) plane has little overlapping with the molecules directly above and below. The inclination of the least-squares plane of the Pt(4) plane with respect to the other planes will be caused mainly by the longest Pt–Pt distance, small intermolecular overlapping and the interaction with Rb cations and the weak hydrogen bonding with water molecules. The short interatomic distances between

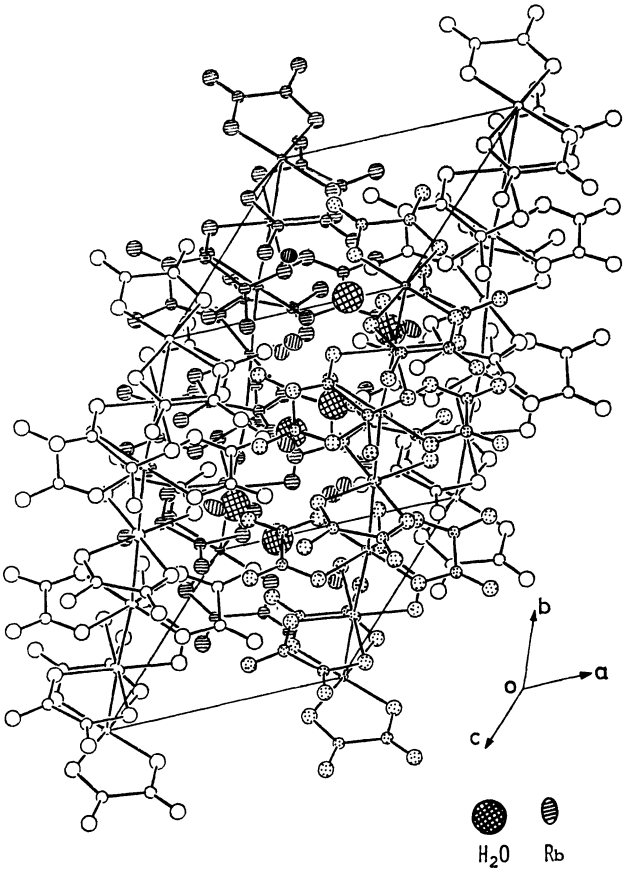

Fig. 4. Three-dimensional structure of RbDOX.

Table 9. Short interatomic distances/Å within the coordination spheres to 3.3 Å around the Rb cations and oxygen atoms of water molecules

Rb(1)···$H_2O(1)^{a)}$	2.89(3)	Rb(5)···O(4)	3.00(3)
O(19)	2.90(2)	$H_2O(3)^{g)}$	3.06(4)
$O(8)^{g)}$	2.96(3)	$O(5)^{g)}$	3.08(3)
$O(20)^{i)}$	3.07(3)	$O(7)^{g)}$	3.17(3)
$O(15)^{e)}$	3.14(6)	O(13)	3.18(2)
$O(3)^{i)}$	3.16(2)	O(7)	3.21(4)
$O(7)^{g)}$	3.17(3)	O(17)	3.25(2)
Rb(2)···O(24)	2.89(5)	$H_2O(1)$···$O(4)^{e)}$	2.84(4)
$H_2O(2)^{j)}$	2.92(4)	$O(21)^{d)}$	2.86(4)
$O(12)^{d)}$	3.04(4)	$Rb(1)^{e)}$	2.89(3)
$O(10)^{b)}$	3.05(2)	$Rb(3)^{j)}$	3.07(5)
$O(4)^{g)}$	3.10(3)	$O(11)^{d)}$	3.29(4)
$O(18)^{d)}$	3.12(2)		
$O(12)^{b)}$	3.14(2)	$H_2O(2)$···$O(23)^{f)}$	2.74(5)
$O(2)^{g)}$	3.27(2)	$O(20)^{b)}$	2.90(4)
		$Rb(2)^{j)}$	2.92(4)
Rb(3)···$O(16)^{d)}$	2.86(6)	Rb(3)	3.23(5)
$O(12)^{b)}$	2.92(2)		
$O(20)^{f)}$	2.95(4)	$H_2O(3)$···O(9)	2.90(5)
$O(11)^{b)}$	2.98(2)	O(19)	2.91(7)
$O(11)^{f)}$	2.99(2)	$Rb(4)^{l)}$	3.00(6)
$O(3)^{g)}$	3.07(2)	$Rb(5)^{g)}$	3.06(4)
$H_2O(1)^{j)}$	3.07(5)	C(12)	3.24(7)
$H_2O(2)$	3.23(5)		
Rb(4)···$O(16)^{g)}$	2.95(5)		
$O(24)^{k)}$	2.99(3)		
$H_2O(3)^{k)}$	3.00(6)		
$O(23)^{l)}$	3.01(4)		
$O(8)^{g)}$	3.03(3)		
$O(23)^{k)}$	3.09(2)		
$O(6)^{g)}$	3.19(2)		

Symmetry code

a)	x,	$-1+y$,	z
b)	$-x$,	$1-y$,	$-z$
c)	x,	$1+y$,	z
d)	$1+x$,	y,	z
e)	x,	y,	$1+z$
f)	$1+x$,	y,	$1+z$
g)	$1-x$,	$-y$,	$-z$
h)	$1-x$,	$1-y$,	$1-z$
i)	$-x$,	$-y$,	$-1-z$
j)	$1-x$,	$1-y$,	$-z$
k)	$1-x$,	$-y$,	$-1-z$
l)	$1+x$,	$-1+y$,	z

the terminal oxygen atoms of the Pt(4) plane and the Rb atoms or water molecules are as follows: O(23)··· $H_2O(2)$ 2.74 Å, O(23)···Rb(4) 3.01 Å and 3.09 Å, O(24)···Rb(4) 2.99 Å, O(24)···Rb(2) 2.89 Å. The crystal structure is shown in Fig. 4. The structure contains five independent Rb ions. Table 9 lists the interatomic distances within the coordination spheres to 3.3 Å around the Rb cations and the oxygen atoms of the water molecules. Rb(1), Rb(4) and Rb(5) are seven-coordinated ions, while Rb(2) and Rb(3) are eight-coordinated ones. Figures 5 and 6 show the c* axis and a* axis projections of the structure of RbDOX. The neighbouring Pt chains are not linked by hydrogen bonding of the water molecules but are linked by the coordinations of the terminal oxygen atoms to the Rb cations. The chain-chain interaction through Rb ions and water molecules do not appear to be so strong. Almost all the Rb^+···O distances exceed the Rb^+···O van der Waals sum (2.88 Å).

Peierls Distortion. A one-dimensional metallic system is unstable in the presence of changes in the crystal lattice period which split a partly filled band into completely filled and empty sub-bands. When the temperature is lowered, a one-dimensional metal should exhibit lattice distortions with a wave number equal to twice the Fermi momentum. The period of the Peierls distorted cell is determined by the degree of partial oxidation (DPO).[22]

Six Pt atoms and ten Rb atoms are found in the unit cell of RbDOX and the ratio of the content of Rb atoms to Pt atoms is 1.67, while the result of chemical analyses show that this ratio is 1.66. Thus the DPO of RbDOX is about 0.33. The possible period of the superlattice along the $Pt(C_2O_4)_2$ chain is $6nb_0(=2nb_0/\mathrm{DPO}; n=1,2,3\cdots)$, where b_0 is the average Pt–Pt distance. The case for $n=1$ ($\approx$17.1 Å) corresponds to the "$2k_F$-instability" of a one-dimensional metal. Thus the sixfold superstructure of RbDOX is confirmed as the structure of the commensurate Peierls state, produced by the condensation of $2k_F$ phonon, on the basis of the crystal structure determination, chemical analyses

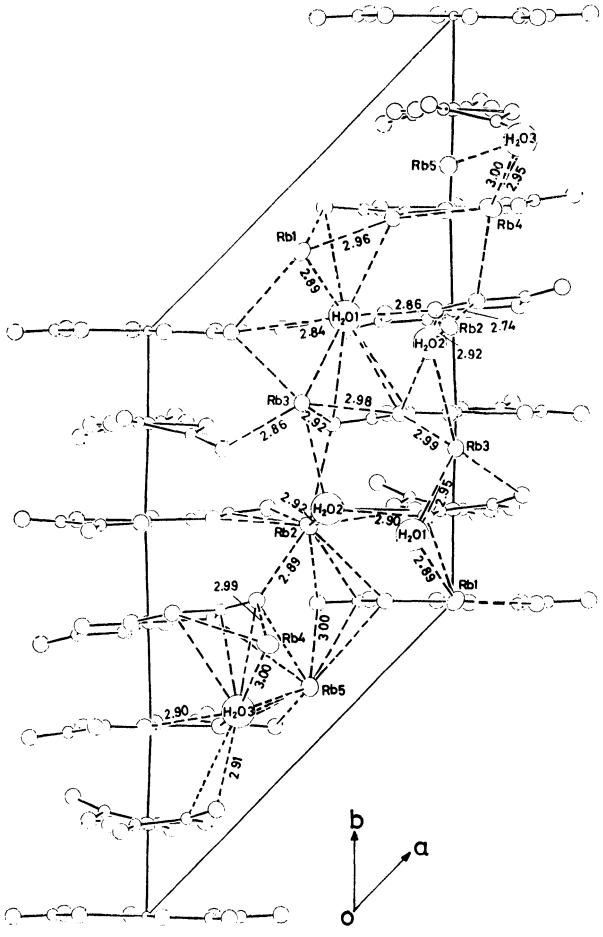

Fig. 5. The c* axis projection of the structure of RbDOX. Broken lines indicate some short interatomic contacts (<3.3 Å).

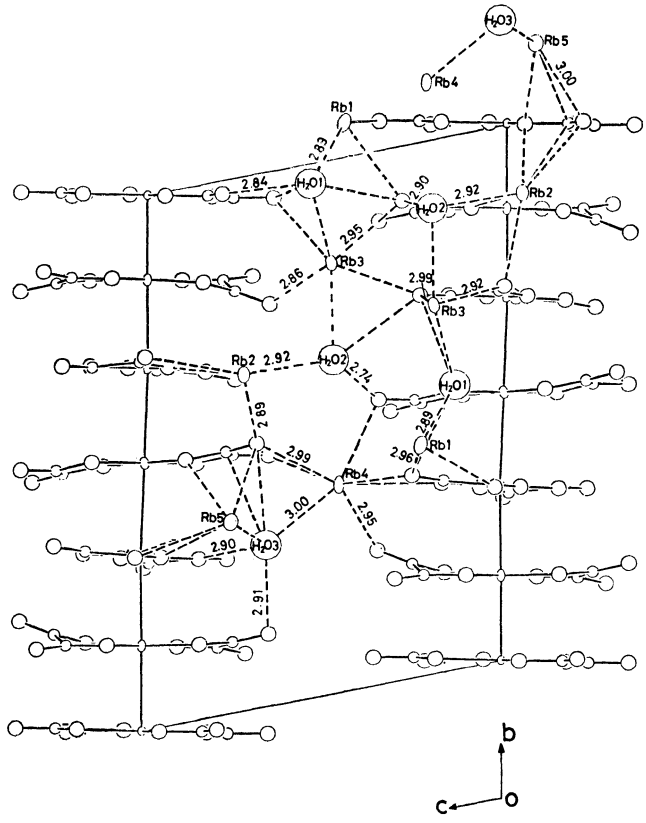

Fig. 6. The a* axis projection of the structure of RbDOX. Broken lines indicate some short interatomic contacts (<3.3 Å).

and the measurements of electrical conductivity. The longitudinal displacements of the Pt modulation wave from the point $[(0.0, n/6, 0.0); n=0, \cdots 5]$ are (0.0, 0.14, 0.16, 0.0, −0.16, −0.14 Å) respectively. These displacements can be approximately expressed in terms of the sinusoidal modulation wave. The amplitude of the modulation wave on the l-th platinum atomic position in the n-th cell $[n=(n_1,n_2,n_3)]$ is given by $0.17\sin\{(2\pi/6)-(l-1)+n_2\}(l=1,\cdots 6)$. The transverse displacements of the Pt atoms are (0.0, 0.04, 0.16, 0.0, −0.16, −0.04 Å). It is logical that the transverse displacements can not be described as a simple sinusoidal wave, considering that the longitudinal displacements will be mainly influenced by interchain interactions whereas the transverse displacements will be also influenced by interchain interactions. Table 10 shows a comparison of the modulation waves in γ-KDOX, RbDOX, and KCP. The amplitudes of the modulation waves in RbDOX and γ-KDOX are approximately 0.17 Å, *i.e.* seven times as large as that of KCP. The correlation of the phase of the lattice modulation waves on the different chain is incomplete in KCP, while the superstructures of bis(oxalato)platinate complexes indicate complete correlation.

In the Peierls phase, the charge density along the platinum chain varies periodically with the wave number of $2k_F$. In order to gain the stabilization energy, Peierls gap is developed at the Fermi level to involve two holes in one repeating unit of the Pt chain. Besides the simple Peierls structure with wavelike charge

Table 10. Comparison of the structures of RbDOX, γ-KDOX,[a] and KCP[b]

	RbDOX	γ-KDOX	KCP(Br)
Chemical formula	$Rb_{1.67}[Pt(C_2O_4)_2]\cdot 1.5H_2O$	$K_{1.81}[Pt(C_2O_4)_2]\cdot 2H_2O$	$K_2[Pt(CN)_4]Br_{0.3}\cdot 3H_2O$
Crystal system	Triclinic	Triclinic	Tetragonal
Pt···Pt distance	2.72, 2.83, 3.02 Å,	2.84, 2.87 Å	2.89 Å
Modulation wave	Longitudinal (and transverse)	Transverse and longitudinal	Longitudinal
amplitude	0.17Å (at R.T.)	0.17 Å (at R.T.) (0.20, −0.08, 0.11) Å	0.025 Å ($T<100$ K)
period	$6\times R_{Pt\cdots Pt}$(17.1 Å)	$10.5\times R_{Pt\cdots Pt}$(30.0 Å)	$6.5\times R_{Pt\cdots Pt}$ (18.8 Å)
Orderness of the chain distortion	Complete (sixfold superstructure)	Complete (superstructure)	Incomplete (fluctuation of the lattice distortion)

a) Refs. 6 and 7. b) Ref. 3.

distribution, a sixfold superstructure of mixed valence configuration may be supposed,[23] that is, $6Rb_{1.67}[Pt(C_2O_4)_2]\cdot 1.5H_2O = (Rb^+)_{10}(Pt^{2+})_5(Pt^{4+})(C_2O_4^{2-})_{12}\cdot 9H_2O$. This model is consistent with the fact that the Pt atom is apt to be in the Pt^{2+} and Pt^{4+} ionic states, but the mixed valence model of the superstructure is opposed to the structural characteristics of platinate complexes: 1. This model is inconsistent with the appearance of a incommensurate superstructure like γ-KDOX. 2. Pt^{4+} has an octahedral configuration and Pt^{2+} has a square planar configuration. Owing to the difference in these coordination types, the distortion of the Pt chain will be localized around the Pt^{4+} site assuming "the mixed valence model" is valid.

The displacements of the Pt atoms in RbDOX or γ-KDOX are in fact described as sinusoidal waves. Based on this reasoning, the mixed valence model is not suitable for RbDOX and γ-KDOX.

Coulomb Interaction between Pt Chains with Charge Density Waves. The lattice distortion waves give rise to a periodical variation of the charge density along the Pt chains.[24] Since the charge density wave thus produced on the Pt chains interact with each other, the phase of the periodical distortion wave is considered to be governed by the interchain Coulomb coupling between the charge density waves. The superstructure formation accompanied by successive phase transitions between 54 K and 37 K in TTF-TCNQ and the development of the diffuse-scattering at $(\pi/a, \pi/a, 2k_F)$ in the KCP salt with lowering of temperature indicate that the chains are anti-phase ordered so as to minimize the Coulomb energy.[25] Figure 5 is the c* axis projection of the structure of RbDOX. The interchain distance is 8.75 Å which is the shortest in all the interchain distances. Assuming that charge density waves or some periodical charge distribution exists along the sixfold Pt chains, the phase difference between the neighbouring positions on these two chains must be about 180°. The wave length of CDW is considered to be equal to the periodicity of the Pt chain ($6\times r_{Pt\cdots Pt}$) and the phase difference between the lattice points must be $2\pi n (n=0,1,2,\cdots)$. Figure 5 seems to indicate that the nearest-neighbour chains tend to be anti-phase ordered. Figure 6 is the a* axis projection of the structure and the interchain spacing is 11.1 Å. The phase difference between the neighbouring positions on two Pt chains is about 50°.

Coulomb interaction between two chains with charge density waves $\rho_i=\rho_0\cos\Phi_i$ may be estimated by the following equation;[26]

$$U_{int} = (1/4\varepsilon_\perp)\rho_0^2[2K_0(2k_F d)]\cos(\Phi_i-\Phi_j)$$
$$= (1/4\varepsilon_\perp)\rho_0^2\sqrt{\pi/2X}e^{-X}\cos(\Phi_i-\Phi_j) \quad X\gg 1$$

where $\varepsilon_\perp$ is the perpendicular static dielectric constant, $K_0(X)$ is the complete Elliptic Integral of the First Kind and d is the interchain spacing. Φ is the phase difference between the origin and the lattice point in the two dimensional lattice, the unit vectors of which are $\boldsymbol{a}_\perp$ and $\boldsymbol{c}_\perp$ which are perpendicular to the Pt chains (Fig. 7). Φ is expressed by the use of the phase parameters δ_a and δ_c, $\Phi_{n_1,n_2}=2\pi(\delta_a n_1+\delta_c n_2)$. The next examination was to establish whether the crystal lattice

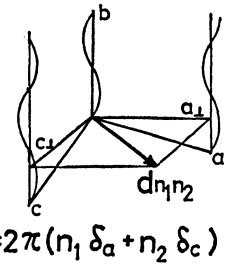

Fig. 7. The phase difference Φ between the platinum chains.

of RbDOX coincides with the structure which minimizes the Coulomb energy. The total Coulomb energy U_{tot} is proportional to

$$\sum_{n_1}\sum_{n_2}U(n_1,n_2) = \sum_{n_1}\sum_{n_2}\sqrt{1/X_{n_1,n_2}}e^{-X_{n_1,n_2}}\cos 2\pi\Phi_{n_1,n_2},$$
$$X_{n_1,n_2} = 2k_F d_{n_1,n_2},$$

where $d_{n_1,n_2}(=|n_1\boldsymbol{a}_\perp+n_2\boldsymbol{c}_\perp|)$ is the interchain distance between the origin (0,0) and the lattice point (n_1,n_2). In this calculation, the lattice constants a, b, c and the angle between $\boldsymbol{a}_\perp$ and $\boldsymbol{c}_\perp$ are fixed. The result of the calculation for several values of δ_a and δ_c are shown in Fig. 8. The point where the total energy is a minimum

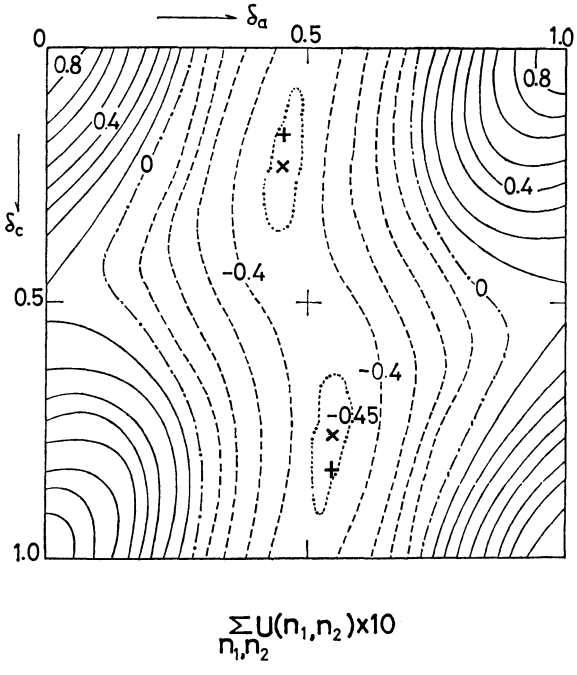

Fig. 8. Total Coulomb energies for various δ_a and δ_c. The point with the minimum total energy is indicated by a cross. Plus sign indicates the position of the parameters δ_a and δ_c derived from the lattice constants.

is indicated by a cross. A plus sign indicates the position of the parameters δ_a and δ_c derived from the lattice constants. The X-ray values of δ_a and δ_c can be calculated as (Fig. 9).

$$\delta_a = RA/OB = 0.537, \quad \delta_c = -R'C/OB = -0.138.$$

The agreement is satisfactory. A similar calculation

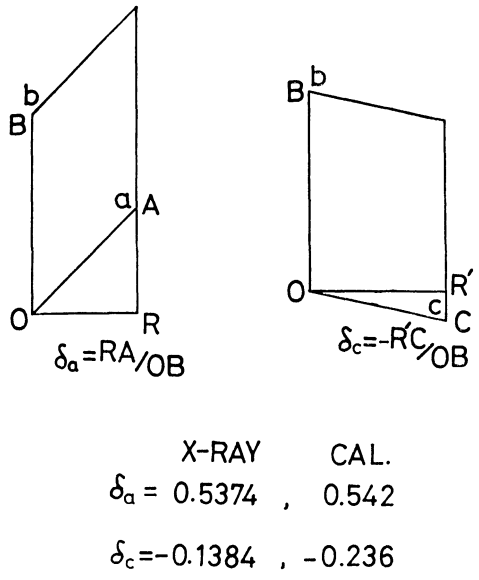

Fig. 9. The projection of the unit cell of RbDOX and the interchain phase differences δ_a and δ_c.

was made for γ-KDOX. The lattice of γ-KDOX is modulated by incommensurate distortion wave. The lattice constants of the fourfold fundamental structure of γ-KDOX are $a=9.749(9)$, $b=11.403(18)$, $c=10.694(8)$ Å, $\alpha=99.54(9)$, $\beta=115.81(9)$, $\gamma=102.32(17)°$. The modulation wave is described by $\boldsymbol{P}\sin(\boldsymbol{K}\cdot\boldsymbol{R})$, where $\boldsymbol{P}$ and $\boldsymbol{K}[=(2\pi\phi_1, 2\pi\phi_2, 2\pi\phi_3)]$ are the amplitude and the wave vector, respectively. The components of $\boldsymbol{K}/2$ along the reciprocal axes a*, b*, and c* are $\phi_1=0.30$, $\phi_2=-0.38$ and $\phi_3=0.05$. X-Ray values of δ_a and δ_c have two terms. $\delta_a=RA/OB+\phi_1=0.403$, $\delta_c=RC/OB+\phi_3=0.250$, ϕ_1 and ϕ_3 are the contributions from the sinusoidal modulation wave. The calculated values of δ_a, δ_c are $\delta_a=0.482$, $\delta_c=0.206$. Good agreement was again obtained. The calculations show that γ-KDOX and RbDOX have crystal lattices in which the interchain Coulomb energies are minimum. The total energy is almost independent of δ_c around the position of the energy minimum which indicates the strong tendency of the anti-phase ordering of the nearest-neighbour chains.

References

1) R. Comès, M. Lambert, H. Launois, and H. R. Zeller, *Phys. Rev. B*, **8**, 571 (1973).
2) C. F. Eagan, S. A. Werner, and R. B. Saillant, *Phys. Rev. B*, **12**, 2036 (1975).
3) J. W. Lynn, M. Iizumi, and G. Shirane, *Phys. Rev. B*, **12**, 1154 (1975).
4) "Chemistry and Physics of One-Dimensional Metals," ed by H. J. Keller, Plenum Press, New York and London (1977).
5) A. J. Heeger and A. F. Garito, "Low Dimensional Cooperative Phenomena," ed by H. J. Keller, Plenum Press, New York (1975).
6) H. Kobayashi, I. Shirotani, A. Kobayashi, and Y. Sasaki, *Solid State Commun.*, **23**, 409 (1977).
7) A. Kobayashi, Y. Sasaki, I. Shirotani, and H. Kobayashi, *Solid State Commun.*, **26**, 653 (1978).
8) "International Tables for X-Ray Crystallography," Kynoch Press, Birmingham (1974), Vol. VI.
9) The Universal Crystallographic Computation Program System, Crystallographic Society of Japan (1967).
10) G. Heeger, H. J. Deiseroth, and H. Schulz, *Acta Crystallogr., Sect. B*, **34**, 725 (1978).
11) J. M. Williams, P. L. Johnson, A. J. Schultz, and C. C. Coffey, *Inorg. Chem.*, **17**, 834 (1978).
12) P. L. Johnson, A. J. Schultz, A. E. Underhill, D. M. Watkins, D. J. Wood, and J. M. Williams, *Inorg. Chem.*, **17**, 839 (1978).
13) a) J. M. Williams, K. D. Keefer, D. M. Washecheck, and N. P. Enright, *Inorg. Chem.*, **15**, 2446 (1976); b) A. H. Reis, Jr., S. W. Peterson, D. M. Washecheck, and J. S. Miller, *Inorg. Chem.*, **15**, 2455 (1976).
14) R. K. Brown, P. L. Johnson, T. J. Lynch, and J. M. Williams, *Acta Crystallogr., Sect. B*, **34**, 1965 (1978).
15) A. J. Schultz, C. C. Coffey, G. C. Lee, and J. M. Williams, *Inorg. Chem.*, **16**, 2129 (1977).
16) A. J. Schultz, D. P. Gerrity, and J. M. Williams, *Acta Crystallogr., Sect. B*, **34**, 1673 (1978).
17) K. Krogmann, *Z. Anorg. Allg. Chem.*, **358**, 97 (1968).
18) A. J. Schultz, A. E. Underhill, and J. M. Williams, *Inorg. Chem.*, **17**, 1313 (1978).
19) R. K. Brown, D. A. Vidusek, and J. M. Williams, *Inorg. Chem.*, **18**, 801 (1979).
20) R. Mattes, and K. Krogmann, *Z. Anorg. Allg. Chem.*, **332**, 247 (1964).
21) J. S. Miller, *Inorg. Chem.*, **15**, 2357 (1976).
22) K. Krogmann, "One-Dimensional Conductors," ed by J. Ehlers, K. Hepp, and H. A. Weidenmüller (Springer-Verlag, 1975).
23) H. Nagasawa, *J. Phys. Soc. Jpn.*, **45**, 701 (1978).
24) M. J. Rice, "Low-Dimensional Cooperative Phenomena," ed by H. J. Keller, Plenum Press, New York (1975).
25) J. Friedel, "Electron-Phonon Interactions and Phase Transitions," ed by T. Riste, Plenum Press, New York (1977).
26) a) A. J. Heeger, "Chemistry and Physics of One-Dimensional Metals," ed by H. J. Keller, Plenum Press, New York (1977); b) K. Saub, S. Barisic, and J. Friedel, *Phys. Lett. A.*, **56**, 302 (1976).

Selective Electrosyntheses on Chemically Modified Electrode. II. Anodic Chlorination of Anisole with Cyclodextrin on Electrode Surfaces and in Solution

Tomokazu MATSUE, Masamichi FUJIHIRA, and Tetsuo OSA*

Pharmaceutical Institute, Tohoku University, Aobayama, Sendai 980

(Received June 22, 1979)

The anodic chlorination of anisole on an α-cyclodextrin (α-CD) chemically modified electrode *via* ether linkage (α-CD-CME) and a naked graphite electrode with α-CD or β-CD in solution was studied. In the presence of CD, the *p*- to *o*-chloroanisole ratio, formed in the reaction, was higher than that in the absence of CD since *o*-positions of anisole included in CD are blocked by the inner wall of CD. Especially, α-CD had a profound effect on the *p*-isomer formation. Increasing the concentration of NaCl added as a supporting electrolyte in the presence of α-CD resulted in a decrease in the ratio because of the inhibition effect of chloride ion on the inclusion of anisole in α-CD, whereas such effect was small in the presence of β-CD. The ratio on α-CD-CME was slightly higher than that on the naked electrode. This indicates that α-CD was introduced on the graphite surface but the surface coverage of α-CD was low, which was in accord with the ESCA results of α-CD-CME.

Many studies of chemically modified electrodes (CMEs) have been developed in order to enhance or to change the characteristics of electrodes, but there have been only a few papers[1-4] on selective electrosyntheses with CMEs. Miller and his co-workers carried out asymmetric reductions[1,2] and asymmetric oxidations[2,3] with CMEs prepared by attaching optically active compounds on the electrode surfaces. However, the optical yields in their works were not high. In order to realize high selectivity in electrolysis with CME, it is necessary that the attached species strongly interact with the substrates as well as resist oxidation or reduction. Cyclodextrins (CDs) meet such requirements. These molecules are cyclic 1,4-linked D-glucopyranose oligomers containing several glucose units and can include various compounds in their cavities in aqueous solution.[5] Especially, α-CD (containing of 6 glucose units) and β-CD (containing of 7 glucose units) have cavities whose sizes are suitable for including benzene and naphthalene rings, respectively. Therefore, these compounds have been studied in various fields because of their catalytic abilities as enzyme models.[6,7] Taking advantage of the environment of α-CD's cavity, Breslow *et al.* carried out the selective chlorination in the presence of α-CD[8] and *O*-alkylated polymer of α-CD.[9]

Such selective chlorination would proceed in the anodic chlorination in the presence of CD (Scheme 1). Chloride ion is first oxidized at the anode to chlorine gas, and second, the nascent state of chlorine is reacted with H_2O to form hypochlorous acid (HOCl).[10] The HOCl formed attacks the anisole included in CD preferentially at the *p*-position because the *o*-positions of anisole are blocked by the inner wall of CD;[11] whereas free anisole is subject to substitution at the *o*-positions as well as at the *p*-position. Our preliminary results of the anodic chlorination of anisole with α-CD-CME (*via* ester linkage) showed that the chlorination occurred preferentially at the *p*-position.[4]

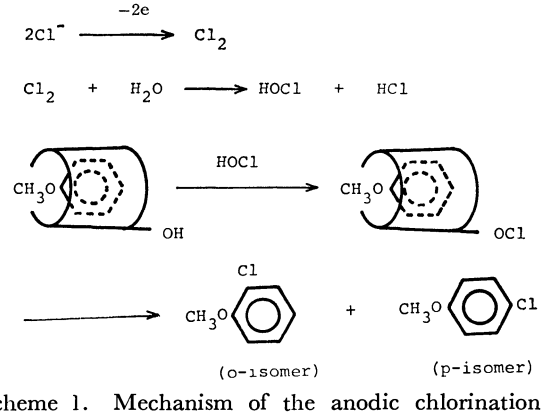

Scheme 1. Mechanism of the anodic chlorination of anisole in the presence of CD.

We report here the selective anodic chlorination of anisole on an α-CD-CME (*via* ether linkage) and a naked graphite electrode with α-CD or β-CD in solution in detail. In comparison with Breslow's method of homogeneous or heterogeneous reactions,[8,9] the anodic chlorination in this work has following merits. (1) No reagents such as HOCl difficult to handle are required because the reagent is formed quite easily by electrolysis of chloride salts added as a supporting electrolyte. (2) In a homogeneous reaction, a high concentration of CD is required to attain high selectivity. However, in the anodic chlorination with α-CD-CME, a certain selectivity is expected even in the absence of CD in solution, because the reaction proceeds at electrode surface on which α-CD is introduced by covalent bonding. (3) In Breslow's method with *O*-alkylated polymer of α-CD, an aqueous solution of HOCl should be passed through a column packed with the polymer which was loaded with anisole beforehand. However, in the present work, the above troublesome stepwise operation is omitted, because the reagent (HOCl) is produced electrochemically.

Experimental

A graphite plate (Tokai Carbon Co. G 2080) was cut into $30\times20\times2$ mm plates for electrolyses and $17\times5\times2$ mm plates for ESCA measurements. An AEI model ES 200 was used for ESCA measurements with a Mg anode under a vacuum of 10^{-8}—10^{-9} Torr. The binding energies were computed and corrected by the method reported.[12] All electrolyses were carried out with a Yanaco VE-8 controlled potential electrolyzer. The supporting electrolyte was NaCl, and the reference electrode was a saturated calomel electrode (SCE) inserted near the anode. The electrolysis cell was a divided

H-type with a graphite anode (30×20×2 mm) and a Pt gauze cathode. The anolyte consisted of anisole and NaCl dissolved in 50 ml of water (non-buffered), and was stirred with a magnetic bar. The cell was set in a thermostat kept at constant temperature. After electrolysis, the anolyte was extracted with ether three times and dried with Na_2SO_4 and then concentrated with an evaporator for gas chromatography (Shimadzu GC-6A). The injection and column temperatures of the gas chromatograph were 210 °C and 150 °C, respectively. The column was 2 m×3 ϕ SUS packed with 10% Carbowax 20 M on Chromosorb W. Quantitative analyses of the chloroanisoles formed were carried out by comparison with a calibration line of authentic samples. The ratios of *para*- to *ortho*-isomer (*p*-/*o*- ratios), the conversion of anisole, and the yields of monochloroanisoles of all products were determined using these gas chromatographic data.

Synthetic Procedure for α-CD-CME. The graphite plates were first dipped in water for 2 h to remove water soluble impurities on the surface and were then treated with a solution of 0.2 M $K_2Cr_2O_7$ in concd H_2SO_4 for 2 h to introduce the surface functional groups containing oxygen.[13] The oxidized electrodes were reduced electrochemically at −1.5 V *vs.* SCE in aqueous 0.5 M Na_2SO_4 solution to increase the hydroxyl groups on the graphite surface.[13] The reduced graphite electrodes were reacted with tosyl chloride (TsCl) in dry pyridine for several weeks and then treated with an aqueous solution of 0.1 M α-CD in 0.1 M KOH for 4 days. After the reaction, the electrodes were washed with water repeatedly to remove the adsorbed α-CD on the graphite surfaces. Another method for the modification of graphite electrodes with α-CD was as follows. Reduced graphite was reacted with α-CD tosylate[14] in 0.1 M KOH solution (pyridine: H_2O=30:70) for a week, followed by thorough washing with water. To compare these α-CD-CMEs with a physically adsorbed α-CD electrode, the reduced graphite electrode was dipped into 0.1 M KOH aqueous solution containing α-CD (0.1 M) for 10 h, and then washed with water (Scheme 2).

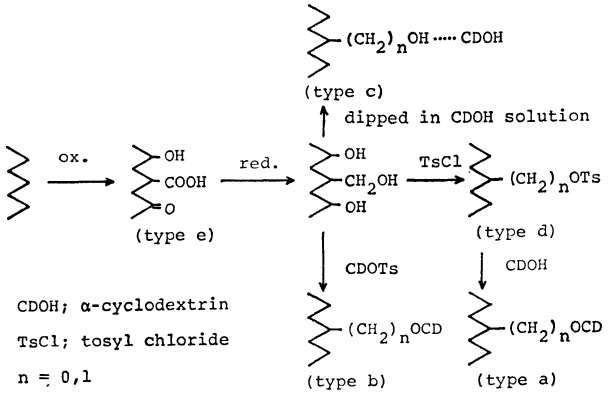

Scheme 2. Synthetic procedure for α-CD-CME and α-CD adsorbed electrode.

Results and Discussion

The potential range in the anodic chlorination must be carefully chosen because the substrate, anisole, is oxidized when the anode potential exceeds *ca.* 1.3 V *vs.* SCE in aqueous NaCl solution. At such a high potential, side reactions can also occur and *p*-/*o*- ratio or other values become inaccurate, and furthermore, the graphite electrode itself is oxidized. Consequently, it is desirable to set the anodic potential as low as possible. However, at low anodic potentials, the chlorination cannot occur or proceeds very slowly because chlorine generation starts at 0.9—1.0 V *vs.* SCE in aqueous NaCl solution, so that the anodic potential of 1.20 V *vs.* SCE was used.

In the Absence of CD. Increasing the concentration of anisole resulted in an increase in the *p*-/*o*- ratio and also an increase in the yields of chloroanisoles (Table 1, expts. 1 and 2). The *p*-/*o*- ratio was gradually decreased with increasing conversion of anisole during the electrolysis both on the untreated graphite (expts. 3, 4, and 5) and on the oxidized graphite (expts. 6 and 7). But a higher *p*-/*o*- ratio was observed on the untreated graphite electrode than the oxidized one. The yield of chloroanisoles was independent of the mode of preparation of the electrode, *i.e.* whether graphite electrode was oxidized or not. The influence of the concentration of NaCl added in the anolyte at low conversion of anisole was not great (expts. 2, 3, and 8). A slight tendency of the *p*-/*o*- ratio to increase was observed with a decrease in the concentration of NaCl. The temperature during electrolysis did not affect the *p*-/*o*- ratio in the temperature range 0—30 °C, but did affect the yield of chloroanisoles (expts. 8 and 9). It took *ca.* 10 min to convert 10% of anisole in the anolyte and the current efficiency was *ca.* 50%. The *p*-/*o*- ratios in the present work are a little lower than those in the previous report.[4] This might be attributed to the difference in the surface properties of the graphite plates used. The ratios on the oxidized electrodes in the present work, however, showed only slight deviations. After electrolysis (10% conversion of anisole), the pH

Table 1. Anodic chlorination of anisole in the absence of CD

Expt.	Conv/%[a]	*p*-/*o*-[b]	Mono/%[c]	Concn of NaCl/M	Concn of anisole/10^3M	Anode	Temp/°C
1	10.6	5.9	90	1.0	2.0	untreated	20
2	4.2	2.3	82	1.0	1.0	untreated	20
3	4.3	2.4	83	0.5	1.0	untreated	20
4	19	2.3	79	0.5	1.0	untreated	20
5	48	1.8	78	0.5	1.0	untreated	20
6	7.9	2.1	81	0.5	1.0	oxidized	20
7	24	1.6	80	0.5	1.0	oxidized	20
8	5.1	2.6	82	0.1	1.0	untreated	20
9	7.0	2.7	70	0.1	1.0	untreated	0

Anodic potential: 1.20 V *vs.* SCE. a) Conversion of anisole in the course of electrolysis. b) Ratio of *p*- to *o*-chloroanisole in the electrolysis. c) Yield of monochloroanisoles.

Table 2. Anodic chlorination of anisole in the presence of β-CD

Expt.	Conv/%	*p*-/*o*-	Mono/%	Concn of NaCl/M	Concn of β-CD/10^3M	Included[a] anisole/%	Temp/°C
10	8.5	3.2	85	1.0	10.0	34	20
11	7.3	3.3	82	0.5	10.0	34	20
12	7.1	3.5	88	0.1	10.0	34	20
13	3.0	3.2	82	0.1	5.0	20	20
14	5.0	2.6	74	0.1	1.0	4.8	20
15	4.0	4.1	73	0.1	10.0		0

Anode: untreated graphite electrode. Anodic potential: 1.20 V *vs.* SCE. Concentration of anisole in anolyte: 1.0×10^{-3} M. a) Calculated by using the dissociation constant of β-CD–anisole complex, 1.9×10^{-2} M.

of the anolyte became 2.0 since hydrochloric acid was generated in the course of the electrolysis.

In the Presence of β-CD. The variations in *p*-/*o*- ratios and yields of chloroanisoles in the presence of β-CD, together with the percentages of included anisole in the β-CD solution, are shown in Table 2. The table shows a slight increase in the *p*-/*o*- ratio with increasing concentration of β-CD, which indicates that the *p*-isomer was formed preferentially in the presence of β-CD in solution (expts. 12, 13, and 14). This supports the idea described above that the reagent (HOCl) can scarcely attack the *o*-positions of anisole included in β-CD.[11] The temperature had some influence on the *p*-/*o*- ratio. When electrolysis was carried out at 0 °C, the ratio was 4.1 which was higher than the 3.5 value observed at 20 °C (expts. 12 and 15). This phenomenon may be a reflection of the thermodynamic nature in that CD includes substrate more easily at low temperatures.[15] The yield of monochloroanisoles was low at low temperature in a similar manner as in the absence of CD (Table 1, expts. 8 and 9). As the dissociation constant of β-CD–anisole complex is 1.9×10^{-2} M,[16] only 34% of the anisole is included in the 10^{-2} M β-CD solution which is almost the maximum concentration of β-CD in aqueous solution. This low complex formation of anisole with β-CD might be a cause for the low regioselectivity in the anodic chlorination of anisole in the presence of β-CD. The effect of the concentration of NaCl on the *p*-/*o*- ratios was small, but a slight tendency of the ratio to decrease with enhancement of the concentration of NaCl was observed (Table 2, expts. 10, 11, and 12).

In the Presence of α-CD. The results of the anodic chlorination of anisole in the presence of α-CD are given in Table 3. The electrolytic conditions were the same as those in the presence of β-CD. The *p*-/*o*- ratios became greater as the concentration of α-CD increased, *i.e.* the *p*-isomer was formed selectively at high concentrations of α-CD in solution. The yield of monochloroanisoles in the presence of α-CD was almost the same as that in the presence of β-CD, but selectivity of *p*-isomer formation was much higher. This is explained by the fact that α-CD binds anisole about 5 times stronger than β-CD. The dissociation constant of the α-CD–anisole complex is 3.75×10^{-3} M.[9] The table also shows that the *p*-/*o*- ratio increases significantly with decreasing NaCl concentration at a constant concentration of α-CD (Table 3, expts. 16, 18, and 22). This indicates that the inhibition effect of Cl^-[17] on the inclusion of anisole in α-CD is very great. On the other hand, the concentration of NaCl had only a small effect on the *p*-/*o*- ratios in the anodic chloriantion in the presence of β-CD (Table 2, expts. 10, 11, and 12), which is explained by the fact that Cl^- is not included in β-CD.[17] It is also shown that the selectivities in this work in the presence of α-CD are higher than those in the homogeneous reactions reported by Breslow and Campbell (Table 4).[8] The differences in *p*-/*o*- ratios (Table 3, expts. 16, 18, and 22) were greater than those expected from the percentages of included anisole in solution. These phenomena may reflect surface effects in which the concentrations of reagents on the graphite electrode surface are different from those in the bulk solution. The difference in the ratios in the presence of α-CD and in the presence of β-CD at the same percentage of included anisole in the bulk solution (*e.g.*, the difference between expt. 12, Table 2 and expt. 19, Table 3) may be accounted for by the following possi-

Table 3. Anodic chlorination of anisole in the presence of α-CD

Expt.	Conv/%	*p*-/*o*-	Mono/%	Concn of NaCl/M	Concn of α-CD/10^3M	Included[a] anisole/%
16	6.1	9.1	81	1.0	10.0	42
17	6.0	7.9		1.0	5.0	26
18	4.9	12.6	85	0.5	10.0	54
19	5.7	8.2	81	0.5	5.0	36
20	6.4	6.5	87	0.5	1.0	9.6
21	6.4	2.5	87	0.5	0.1	1.0
22	2.0	25	74	0.1	10.0	66
23	3.2	22	70	0.1	5.0	49

Anode: untreated graphite electrode. Anodic potential: 1.20 V *vs.* SCE. Concentration of anisole in anolyte: 1.0×10^{-3} M. a) Calculated by using the dissociation constant of α-CD–anisole complex, 3.72×10^{-3} M, under the consideration of the inhibition effect of Cl^-.

Table 4. Results of homogeneous chlorination of anisole in Breslow's report[8]

p-/*o*-	Included anisole/%
3.43	20
5.49	33
7.42	43
11.3	56
15.4	64

bilities.

(1) α-CD is more strongly adsorbed on the graphite surface than β-CD at this potential.

(2) Slight movement of the included anisole in β-CD is allowed since the size of the β-CD cavity is a little larger than that of the anisole molecule; whereas, the anisole included in α-CD is not free to move.

Table 5. Anodic chlorination of anisole with α-CD-CME (*via* ether bond)

Expt.	Conv/%	*p*-/*o*-	Mono/%	Type of electrode
24	8.0	3.1	80	a)
25	4.5	1.9	75	b)
26	7.1	1.8	79	c)
27	8.9	2.1	83	a) treated with $K_2Cr_2O_7$

a) Obtained by the reaction between the tosylated graphite and α-CD. b) Obtained by the reaction between the reduced graphite and tosylated α-CD. c) Obtained by dipping the reduced graphite in α-CD aqueous solution followed by washing with water.

Anodic Chlorination with α-CD-CME. The results of the anodic chlorination with α-CD-CME (*via* ether linkage) obtained by the reaction between the tosylated graphite and α-CD (type a), by the reaction between the reduced graphite and tosylated α-CD (type b), and α-CD adsorbed graphite (type c) are given in Table 5. Type a shows a slight higher *p*-/*o*- ratio than the others, but its value is low compared with those in the presence of α-CD and on α-CD-CME (*via* ester linkage).[4] This indicates that the surface coverage of α-CD introduced by the chemical modification was low on type a. Type b showed no selectivity. The attachment of α-CD on the graphite surface by the reaction between the reduced graphite and α-CD tosylate was very difficult. The reaction may be hindered by the intra- or intermolecular reaction of tosylated α-CD. No selectivity was also obtained on type c. The adsorbed α-CD on the reduced graphite electrode was removed by washing with water. The yields of chloroanisoles formed in the anodic chlorination with the above three types of electrodes were the same as those with unmodified electrodes. When type a was treated with $K_2Cr_2O_7$ for 1 h to remove α-CD on type a, the *p*-/*o*- ratio became lower than that of the electrode of type a not subject to the treatment.

ESCA Results. Three types of electrodes, type a, the tosylated graphite (type d), and the oxidized graphite (type e), were examined by ESCA. Fig. 1 shows wide ESCA spectra obtained. There are strong peaks of O ls at 532 eV and C ls at 285 eV on type e, which are almost the same as those of glassy carbon baked in the air.[18] No peaks based either on Cr or on K of $K_2Cr_2O_7$ appears. The ESCA spectrum of type d shows small S 2s at 233 eV and S 2p at 170 eV in addition to the above peaks. These sulfur peaks originate from sulfur atoms in the tosyl group introduced on the graphite surface, and the peaks disappear with further modification with α-CD. This indicates that the tosyl group was removed by the reaction between the tosylated graphite (type d) and α-CD. Higher resolution ESCA spectra of O ls in type a and type e are shown in Fig. 2. The peak intensity of type a is larger than that of type e and the peak is shifted toward a higher binding energy compared with that of type e. It is, however, difficult to assign the chemical shift, since various types of oxygen atoms exist on the

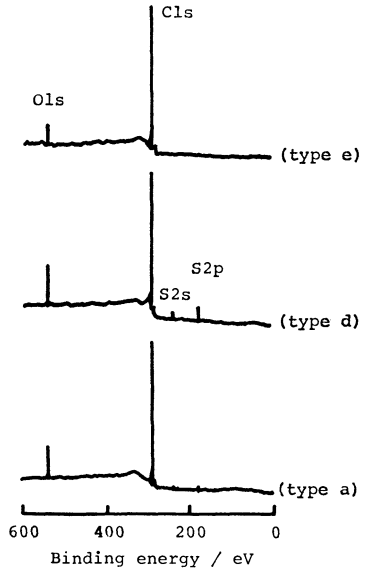

Fig. 1. ESCA spectra of the α-CD-CME (type a), the tosylated (type d), and the oxidized (type e) graphite electrodes.

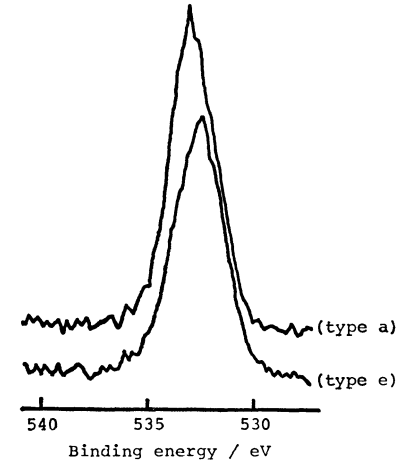

Fig. 2. O ls ESCA spectra of the α-CD-CME (type a) and the oxidized (type e) electrode.

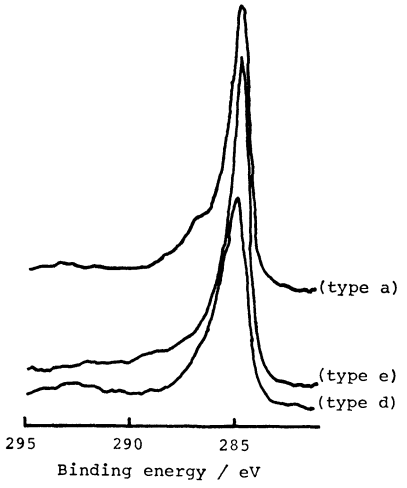

Fig. 3. C 1s ESCA spectra of the α-CD-CME (type a), the tosylated (type d), and the oxidized (type e) electrodes.

graphite surfaces. The changes in higher resolution ESCA spectra of C ls of types a, d, and e are shown in Fig. 3. By performing chemical modification with α-CD on the graphite surface, a shoulder at the higher binding energy side of the main peak at 285 eV appeared but its height was lower than that of the previous results.[4] This shoulder may be accounted for by consideration of the charge on the carbon atoms in α-CD. All carbon atoms in α-CD adjoin oxygen atoms which have a higher electronegativity compared with the carbon atoms.[19] The surface coverage by α-CD on type a is not large because the shoulder is small. The C ls of type d appeared at the same binding energy as type e and has no shoulder. These results also support the conclusion that the shoulder in the spectrum of type a is attributed to α-CD on the graphite surface. Fig. 4 shows S 2s ESCA spectra of types a, d, and e.

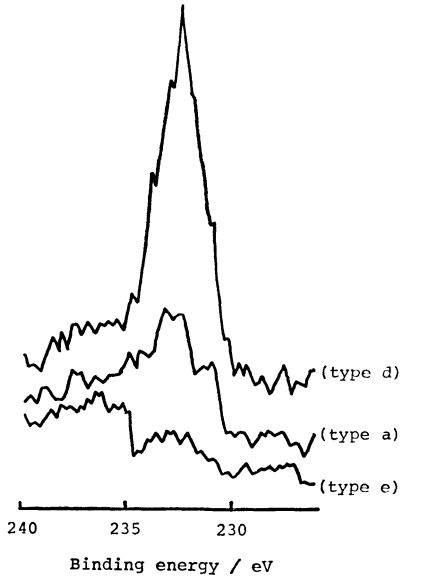

Fig. 4. S 2s ESCA spectra of the α-CD-CME (type a), the tosylated (type d), and the oxidized (type e) electrodes.

The peak of type d appeared at *ca.* 233 eV which is shifted toward the higher binding energy side compared with 229 eV, the binding energy of 2s electron in free sulfur.[20] The shift of the S 2s is in agreement with that of the S 2p of sulfonated compounds, *i.e.* the peaks of these compounds shift to a higher binding energy than those of the sulfide or disulfide compounds because the calculated charges on the sulfur atoms in sulfonated compounds are high.[19] On the other hand, the S 2s peak on type e could not be observed, which indicates that the surface is free from contamination by sulfur compounds on type e. On type a, small S 2s peak still remained. Most of tosyl group were removed by the reaction between the tosylated graphite (type d) and α-CD, but some unreacted tosyl groups remained on type a.

This work was partially supported by a Grant-in-Aid for Scientific Research from the Ministry of Education (No. 247072).

References

1) B. F. Watkins, J. R. Behling, E. Kariv, and L. L. Miller, *J. Am. Chem. Soc.*, **97**, 3549 (1975).
2) B. E. Firth, L. L. Miller, M. Mitani, T. Rogers, J. Lennox, and R. M. Murray, *J. Am. Chem. Soc.*, **98**, 8271 (1976).
3) B. E. Firth and L. L. Miller, *J. Am. Chem. Soc.*, **98**, 8272 (1976).
4) T. Matsue, M. Fujihira, and T. Osa, *J. Electrochem. Soc.*, **126**, 500 (1979).
5) F. Cramer and F. M. Henglein, *Quat. Revs. (London)*, **68**, 649 (1956).
6) F. Cramer and W. Kampe, *Tetrahedron Lett.*, **1962**, 353.
7) M. L. Bender, R. L. VanEtten, G. A. Clows, and J. F. Sebastain, *J. Am. Chem. Soc.*, **88**, 2318 (1966).
8) R. Breslow and P. Campbell, *J. Am. Chem. Soc.*, **91**, 3085 (1969).
9) R. Breslow, H. Kohn, and B. Siegel, *Tetrahedron Lett.*, **1976**, 1645.
10) M. R. Lifi and F. H. Covitz, "Introduction to Organic Electrochemistry," Marcel Dekker Inc., New York (1974), 299.
11) T. Osa, T. Matsue, and M. Fujihira, *Heterocycles*, **6**, 1833 (1977).
12) M. Fujihira, T. Matsue, and T. Osa, *Chem. Lett.*, **1976**, 875.
13) M. Fujihira and T. Osa, "Progress in Batteries and Solar Cells," JES Press Inc., Cleveland (1979), Vol. 2.
14) V. W. Lautsch, R. W. Wiechert, and H. Lehman, *K-Zeit.*, **135**, 134 (1954).
15) F. Cramer, W. Saenger, and H.-Ch. Spatz, *J. Am. Chem. Soc.*, **89**, 14 (1967).
16) A. Ueno, H. Yoshimura, R. Saka, and T. Osa, *J. Am. Chem. Soc.*, **101**, 2779 (1979).
17) R. P. Rohrbach, L. J. Rodringer, E. M. Eyring, and J. F. Wojcik, *J. Phys. Chem.*, **81**, 944 (1977).
18) M. Fujihira, A. Tamura, and T. Osa, *Chem. Lett.*, **1977**, 361.
19) K. Siegbahn *et al.*, "ESCA-Atomic, Molecular and Solid State Structure Studied by Means of Electron Spectroscopy," Almqvist and Wiksells, Uppsala (1967), 118, 137.
20) R. Nordberg, K. Hamrin, A. Fahlman, C. Nordling, and K. Siegbahn, *Z. Phys.*, **192**, 462 (1966).

New Potassium and Ammonium Lead(II) Chromates with a Higher Lead Content and Iso-structural with Potassium Lead(II) Chromate, $K_2Pb(CrO_4)_2$

Tsutomu FUKASAWA* and Masaaki IWATSUKI

Department of Applied Chemistry, Faculty of Engineering, Yamanashi University, Takeda, Kofu 400

(Received April 16, 1979)

An unknown yellow precipitate, similar to lead(II) chromate in appearance, has been reported. The precipitate was formed in the detection process of lead(II) ions using chromate ions by a classical qualitative analytical method. The present paper describes the elucidation of the unknown precipitate, and the presence of a series of new chromates iso-structural with the known potassium lead(II) chromate, $K_2Pb(CrO_4)_2$. The new chromates are explained as new stoichiometric chromates, $K_4Pb_4(CrO_4)_6$ and $(NH_4)_4Pb_4(CrO_4)_6$ [$=K_2Pb_2(CrO_4)_3$ and $(NH_4)_2Pb_2(CrO_4)_3$], and solid solutions (K, $NH_4)_{6-2z}Pb_{3+z}(CrO_4)_6$ ($z=+0.3$—$+1.2$) among the new stoichiometric chromates and the known chromates, $K_6Pb_3(CrO_4)_6$ and $(NH_4)_6Pb_3(CrO_4)_6$ [$=K_2Pb(CrO_4)_2$ and $(NH_4)_2Pb(CrO_4)_2$]. The compositions of the new chromates are dependant on the precipitating conditions. Relationships between compositions, lattice constants, and precipitating conditions are given together with indexed powder diffraction data for references to identification, and the results of thermal analyses.

It was described in a previous paper[1] that fine particles of an unknown yellow compound, similar to lead(II) chromate in appearance, precipitated under certain conditions in the reaction leading to the formation of lead(II) chromate, a substance used for the detection of lead(II) ions in classical qualitative analysis. The particles were unstable and changed into needle crystals of monoclinic lead(II) chromate when left in the mother liquor. In general, this unknown compound precipitated when a potassium chromate solution was added to a hot and dilute lead(II) solution containing a relatively large amount of ammonium acetate.

The present study was conducted to elucidate the unknown compound, and to obtain the powder X-ray diffraction data for identification. Precipitates were prepared by adding an ammonium chromate solution to an ammonium acetate solution of lead(II), or a potassium chromate solution to a potassium acetate solution of lead(II) at different concentrations and pH. X-Ray diffraction, chemical analysis, density measurement, and thermal analysis were conducted on the precipitates.

It was found that the unknown compound described was one of a series of new chromates, which were higher in lead content than the known potassium or ammonium lead(II) chromate $K_2Pb(CrO_4)_2$ or $(NH_4)_2Pb(CrO_4)_2$,[2] and iso-structural with known chromates. These new chromates have been expressed as $K_2Pb_2(CrO_4)_3$, $(NH_4)_2Pb_2(CrO_4)_3$, and $(K,NH_4)_{2+2y}Pb_{2-y}(CrO_4)_3$ ($y=-0.1$—$+0.3$) from the construction rule of chemical formulas and the analytical results, and as $(K,NH_4)_{2-2x}Pb_{1+x}(CrO_4)_2$ ($x=+0.1$—$+0.4$) when the conventional formula of the known chromate, $K_2Pb(CrO_4)_2$, was followed. The relationship between the new and known stoichiometric chromates is conveniently explained by the common formulas containing six chromate ions from the viewpoint of iso-structure: The new chromate are explained as new stoichiometric chromates, $K_4Pb_4(CrO_4)_6$ and $(NH_4)_4Pb_4(CrO_4)_6$, and solid solutions, $(K,NH_4)_{6-2z}Pb_{3+z}(CrO_4)_6$ ($z=+0.3$—$+1.2$), among the new stoichiometric chromates and the known chromates, $K_6Pb_3(CrO_4)_6$ and $(NH_4)_6Pb_3(CrO_4)_6$. The relationships between the compositions, lattice constants, and precipitating conditions of the new chromates are given with the indexed powder X-ray diffraction data, and the results of thermal analyses.

Experimental

Sample Preparation. Several differing lead(II) acetate solutions were prepared by the dissolution of appropriate quantities of lead(II) sulfate in ammonium or potassium acetate solutions of 1 to 6 M (1 M=1 mol dm^{-3}), followed by pH adjustment. The precipitates were prepared using each lead(II) acetate solution as follows: A small excess of a 1.5 M ammonium or potassium chromate solution was gradually added *via* a 5 cm^3 pipet to a lead(II) acetate solution in a 200 cm^3 or 1 dm^3 beaker at about 80 °C with stirring. The precipitate formed was filtered off, and dried at 105 °C in an electric oven.

All the precipitates prepared were yellow or yellow-orange, and fine particles smaller than 1 μm except that monoclinic lead(II) chromate occasionally precipitated in size of above 1 μm.

The precipitate samples used for the chemical analyses were identified by powder X-ray diffraction analysis.

Methods of Analysis. *Powder X-Ray Diffraction Analysis*: The X-ray diffraction analyses were conducted by use of an X-ray diffractometer (Rigaku) equipped with a copper-target tube and nickel filter. The sample was mounted in a standard aluminum specimen holder. The intensities were measured from the peak heights of the line profiles. The accurate diffraction angle for determination of the lattice constants was measured from the center of gravity of the line profile recorded at a low scanning speed. The diffraction angle was corrected by use of high-purity silicon powder as an internal standard.

Chemical Analysis: X-Ray fluorescence analysis and Nessler's test confirmed that the samples contained lead, chromium, potassium, and/or ammonium, but no sulfur. Lead, chromium, potassium, and ammonium were quantitatively determined as follows: For the determination of lead and potassium, the sample was dissolved in nitric acid (1+1), followed by dilution with water. Ascorbic acid was then added to reduce the chromate to chromium(III) ions. After an appropriate dilution, lead and potassium were determined

by the standard addition-atomic absorption method and by the standard addition-flame photometric method, respectively. For the determination of chromium, the sample was dissolved in nitric acid (1+1), and sodium hydroxide solution added until the solution became alkaline. The chromate ion was photometrically determined at 366 nm. The ammonium ion was determined by the micro-diffusion method.[3] The determination of each constituent was repeated at least twice and the average taken.

Density: "Observed density" was determined by use of a pycnometer with carbon tetrachloride. "Calculated density" was evaluated from lattice constants and the number of constituent ions in a unit cell.

Thermal Analysis: Thermal analysis was conducted by use of a thermobalance (Rigaku) with a differential thermal analyzer.

Results and Discussion

Chemical Composition and Crystallographic Consideration. Table 1 shows the results of chemical analyses of the representative samples prepared under different conditions, and chemical formulas obtained from the analytical results. The number of oxygens in the chemical formulas has been taken as 12, because the elemental ratio in the formula of sample K-0 was successfully expressed in the smallest integer when the conventional rule was applied to the construction of chemical formulas; the ratios in the formulas of the other samples were not successfully expressed in integers.

The lead contents of the prepared samples were higher than those of the known chromates, $K_2Pb(CrO_4)_2$ and $(NH_4)_2Pb(CrO_4)_2$. The chemical formulas of some samples were approximated to $K_2Pb_2(CrO_4)_3$ or $(NH_4)_2Pb_2(CrO_4)_3$. The other samples were nonstoichiometric, and have been expressed as $(K,NH_4)_{2+2y}Pb_{2-y}(CrO_4)_3$ ($y=-0.1$—$+0.3$). Some however have a slightly unbalanced charge. The charge unbalance in some formulas may be explained by the formation of nonstoichiometric compounds of lattice-defect type, and/or the presence of undetectable amounts of lead oxide which may be formed by heating lead hydroxide at 105 °C; the lead hydroxide may be produced together with the chromate in the precipitating process.

The X-ray powder patterns of the newly found chromates were similar to those of the known chromates (hexagonal), $K_2Pb(CrO_4)_2$, $(NH_4)_2Pb(CrO_4)_2$, *etc.*, and indexed successfully by the hexagonal system by use of the Bunn-Bjurström chart. Table 2 shows the X-ray diffraction data of the representative samples. It appears that the crystal structures of all the newly found chromates are iso-structural with the known chromates. The compounds previously expressed as $K_2Pb_2(CrO_4)_3$, $(NH_4)_2Pb_2(CrO_4)_3$, and $(K,NH_4)_{2+2y}Pb_{2-y}(CrO_4)_3$ may be expressed as $K_{1.33}Pb_{1.33}(CrO_4)_2$, $(NH_4)_{1.33}Pb_{1.33}(CrO_4)_2$, and $(K,NH_4)_{2-2x}Pb_{1+x}(CrO_4)_2$ assuming the conventional formulas of the known chromates are followed. The formulas $K_{1.33}Pb_{1.33}(CrO_4)_2$ and $(NH_4)_{1.33}Pb_{1.33}(CrO_4)_2$ do not however adhere to the construction rule of chemical formulas. The common formulas containing six chromate ions (oxygen=24) appear to fit both the new and known chromates which are stoichiometric and iso-structural with each other. The chromates $K_2Pb_2(CrO_4)_3$ and $(NH_4)_2Pb_2(CrO_4)_3$ are explained conveniently as the new stoichiometric chromates $K_4Pb_4(CrO_4)_6$ and $(NH_4)_4Pb_4(CrO_4)_6$ iso-structural with the known chromates $K_6Pb_3(CrO_4)_6$ and $(NH_4)_6Pb_3(CrO_4)_6$. The nonstoichiometric chromates expressed by $(K,NH_4)_{2+2y}Pb_{2-y}(CrO_4)_3$ are thought to be substitutional solid solutions lying between the new and known stoichiometric chromates, and are expressed by the general formula, $(K,NH_4)_{6-2z}Pb_{3+z}(CrO_4)_6$ ($z=+0.3$—$+1.2$). The latter formulas will be used in the subsequent discussion except for the thermal analysis.

Tables 3 and 4 show the precipitating conditions, lattice constants, chemical formulas, and densities of the representative compounds prepared; the lattice constants were calculated from accurate diffraction angles of appropriate lines and their assigned indices. The compositions of the compounds changed depending on the precipitating conditions; such changes were also supported by the differences in lattice constants. The relationships between the compounds formed and the precipitating conditions may be summarized as follows: (1) the lead content of the formed compound increased with decreasing concentration of ammonium or potassium acetate solution; (2) the lattice constant, a, of the compound increased with increasing lead content, while the lattice constant, c, decreased except in compounds obtained with potassium acetate solution; (3) monoclinic lead(II) chromate was preferentially formed when ammonium or potassium acetate solution of lower concentration was used; (4) the pH, and amounts of ammonium or potassium acetate solution per gram of lead(II) sulfate do not appear to affect the composition.

The number of chemical units in the unit cell, which was calculated from the observed density and lattice constants, was one for a series of the new chromates, $(K,NH_4)_{6-2z}Pb_{3+z}(CrO_4)_6$, as well as for the known chromates, $K_6Pb_3(CrO_4)_6$ and $(NH_4)_6Pb_3(CrO_4)_6$.

Table 1. Results of chemical analyses and chemical formulas of the representative samples

Sample	wt%					Chemical formula (O=12)	Unbalance of charge
	K^+	NH_4^+	Pb^{2+}	CrO_4^{2-}	Sum		
NK-0	1.0	4.6	52	45	102	$K_{0.2}(NH_4)_{2.0}Pb_{1.9}(CrO_4)_{3.0}$	±0.0
N-0	—	5.7	51	44	101	$(NH_4)_{2.4}Pb_{1.9}(CrO_4)_{3.0}$	+0.2
N-5	—	5.9	46	47	99	$(NH_4)_{2.5}Pb_{1.7}(CrO_4)_{3.0}$	−0.1
N-15	—	3.9	54	42	100	$(NH_4)_{1.8}Pb_{2.1}(CrO_4)_{3.0}$	±0.0
K-0	9	—	49	41	99	$K_{2.0}Pb_{2.0}(CrO_4)_{3.0}$	±0.0
K-8	13	—	46	42	101	$K_{2.7}Pb_{1.8}(CrO_4)_{3.0}$	+0.3

Table 2. Powder X-ray diffraction data for the representative prepared samples, $(NH_4)_2Pb(CrO_4)_2$, and $K_2Pb(CrO_4)_2$[a]

hkl[b]	Sample NK-0 $K_{0.2}(NH_4)_{2.0}Pb_{1.9}(CrO_4)_{3.0}$			Sample N-0 $(NH_4)_{2.4}Pb_{1.9}(CrO_4)_{3.0}$			Sample K-0 $K_{2.0}Pb_{2.0}(CrO_4)_{3.0}$			JCPDS card No. 19-66 $(NH_4)_2Pb(CrO_4)_2$		JCPDS card No. 19-971 $K_2Pb(CrO_4)_2$	
	d_{calcd}/Å	d_{obsd}/Å	I_{obsd}	d_{calcd}/Å	d_{obsd}/Å	I_{obsd}	d_{calcd}/Å	d_{obsd}/Å	I_{obsd}	d/Å	I/I_1	d/Å	I/I_1
003	7.241	7.30	34	7.240	7.28	61	7.010	N.D.	—	7.30	10	7.02	8
101	4.889	4.91	17	4.890	4.90	16	4.844	4.85	13	4.88	6	4.82	5
012	4.554	4.57	60	4.556	4.55	65	4.499	4.50	12	4.54	35	4.48	18
104	3.685	3.69	2	3.686	3.69	3	3.615	3.61	1	N.D.	—	3.609	3
006	3.620	N.D.	—	3.620	N.D.	—	3.505	3.51	3	N.D.	—	3.512	3
015	3.284	3.29	100	3.285	3.29	100	3.213	3.21	100	3.30	95	3.208	100
110	2.896	2.90_1	70	2.898	2.89_4	61	2.874	2.87_5	53	2.885	95	2.858	79
113	2.689	2.68_6	47	2.690	2.69_1	43	2.659	2.65_9	13	2.684	80	2.646	24
107	2.639	2.64_1	13	2.639	2.64_4	13	2.572	2.57_3	5	2.653	20	2.571	11
021	2.492	2.49_2	2	2.493	2.49_1	2	2.472	N.D.	—	2.483	10	2.459	8
202	2.444	2.44_5	3	2.445	2.44_2	2	2.422	2.42_2	1	2.436	10	N.D.	—
009	2.414	2.41_7	2	2.413	2.41_5	2	2.337	2.33_5	2			2.349	20
018	2.388	2.39_1	3	2.388	2.39_2	3	2.325	N.D.	—	2.402	16	N.D.	—
024	2.277	2.27_8	15	2.278	2.27_6	10	2.250	2.25_1	10	2.270	85	2.240	26
116	2.262	2.26_2	15	2.262	2.26_5	14	2.222	2.22_2	8			2.217	20
205	2.172	2.17_3	22	2.173	2.17_1	21	2.142	2.14_0	16	2.172	70	2.134	60
1010	1.993	1.994	13	1.993	1.997	14	1.937	1.937	17	2.008	60	1.938	61
027	1.951	1.952	2	1.951	1.953	2	1.917	N.D.	—	1.954	16	N.D.	—
211	1.889	1.889	4	1.890	1.888	3	1.874	1.875	2	1.882	16	N.D.	—
122	1.868	1.868	9	1.869	1.866	8	1.852	1.853	2	N.D.	—	N.D.	—
119	1.854	N.D.	—	1.854	N.D.	—	1.813	1.810	4	1.861	80	1.808	16
208	1.843	1.842	9	1.843	1.843	8	1.807			1.848	60		
0111	1.838			1.837			1.785	1.785	1			N.D.	—
0012	1.810	1.810	1	1.810	1.814	2	1.753	1.754	1	1.827	16	1.756	12
125	1.738	1.738	14	71.39	1.737	11	1.717	1.717	9	1.735	80	1.710	72
300	1.672	1.672	6	1.673	1.670	5	1.659	1.659	4	1.666	45	1.650	30
0210	1.642	1.642	4	1.642	1.642	3	1.606			1.648	30	1.605	39
303	1.629	1.629	7	1.630	1.626	5	1.615	1.606 (Broad)	5	1.621 (Broad)	70		
217	1.618	1.618	5	1.619	1.621	3	1.595					N.D.	—
1013	1.585	1.584	2	1.585	1.590	1	1.539	N.D.	—	1.598	20	N.D.	—
128	1.555	1.554	3	1.555	1.555	2	1.530	N.D.	—	1.557	30	N.D.	—
2011	1.552			1.552			1.516	N.D.	—			N.D.	—
1112	1.535	1.535	2	1.535	1.537	2	1.496	1.498	1	1.544	30	1.495	20
306	1.518	N.D.	—	1.519	N.D.	—	1.500			N.D.	—		
220	1.448	1.447	6	1.449	1.447	4	1.437	1.437	3	1.443	60	1.429	58
0015	1.448			1.448			1.402	1.402	5	1.461	30	1.401	74
2110	1.428	1.427	6	1.429	1.429	6	1.402			1.431	100		
309	1.375	1.378	2	1.375	1.378	2	1.353	1.353	1	1.375	35	N.D.	—
315	1.325	1.325	3	1.326	1.324	3	1.312	1.311	1	1.322	70	1.305	35
1115	1.295	1.294	2	1.295	1.297	2	1.260	1.260	3	1.304	60	1.260	36

a) N.D.: Not detected. d_{calcd} was calculated with lattice constants measured in this work. b) Miller's indices are shown as one of hexagonal lattice.

Comparison of the lattice constants in Table 3 appears to indicate that the substitution of one Pb^{2+} ion for two NH_4^+ ions causes a slight decrease in c, and a slight increase in a, but no appreciable change in the volume of the unit cell. The Table 4 shows that the substitution of one Pb^{2+} ion for two K^+ ions has little effect on c, but causes a slight increase in a. In terms of the differences in number and size of the cations in their unit cells, the newly found chromates appear to be less compact in structure than the known chromates. The instability of the new chromates in their mother liquors may be explained by the less compact structures.

Thermal Analysis. Figure 1 shows the results of thermogravimetric (TGA) and differential thermal (DTA) analyses of sample NK-0. The endothermic

TABLE 3. PRECIPITATING CONDITIONS, LATTICE CONSTANTS, CHEMICAL FORMULAS, AND DENSITIES OF THE COMPOUNDS FORMED USING AMMONIUM ACETATE SOLUTIONS[a)]

Sample	Lead acetate soln. $PbSO_4$ / g	Lead acetate soln. NH_4OAc Concn / M	Lead acetate soln. NH_4OAc Amount / cm^3	NH_4^+/Pb^+ mole ratio / 10^2	pH	Lattice constants/Å a	Lattice constants/Å c	Chemical formula (O=24)	Density g/cm^3 Obsd	Density g/cm^3 Calcd
NK-0	1.00	*ca.*4	100	*ca.*1.2	6—7	5.793	21.72	$K_{0.4}(NH_4)_{4.0}Pb_{3.8}(CrO_4)_{6.0}$	4.05	4.133
N-0	0.20	*ca.*4	18	*ca.*1.1	6—7	5.796	21.72	$(NH_4)_{4.8}Pb_{3.8}(CrO_4)_{6.0}$	4.26	4.062
N-1	1.00	6	25	0.45	7.0	5.784	21.80			
N-2	1.00	6	50	0.90	7.1	5.785	21.80			
N-3	1.00	6	100	1.8	7.0	5.785	21.83			
N-4	1.00	6	200	3.6	7.0	5.783	21.84			
N-5	1.00	6	400	7.2	7.1	5.781	21.85	$(NH_4)_{5.0}Pb_{3.4}(CrO_4)_{6.0}$		
N-14[b)]	1.00	3	200	1.8	7.2	5.792	21.61			
N-15	1.00	3	400	3.6	7.2	5.791	21.62	$(NH_4)_{3.6}Pb_{4.2}(CrO_4)_{6.0}$		
N-13[c)]	1.00	2	400	2.4	7.3	—	—			
d)						5.777	21.939	$(NH_4)_6Pb_3(CrO_4)_6$ $[=(NH_4)_2Pb(CrO_4)_2]$	3.71	3.734

a) A given amount of $PbSO_4$ was dissolved in a hot solution of NH_4OAc, and 1.5 M $(NH_4)_2CrO_4$ (1.5 M K_2CrO_4 for NK-0) was added. b) A trace amount of $PbCrO_4$ (mon.) was detected. c) A large amount of $PbCrO_4$(mon.) was detected. d) JCPDS card No. 19-66 and Ref. 2.

TABLE 4. PRECIPITATING CONDITIONS, LATTICE CONSTANTS, CHEMICAL FORMULAS, AND DENSITIES OF THE COMPOUNDS FORMED USING POTASSIUM ACETATE SOLUTIONS[a)]

Sample	Lead acetate soln. $PbSO_4$ / g	Lead acetate soln. KOAc Concn / M	Lead acetate soln. KOAc Amount / cm^3	K^+/Pb^{2+} mole ratio / 10^2	Added amount of concd HOAc / cm^3	pH	Lattice constants/Å a	Lattice constants/Å c	Chemical formula (O=24)	Density g/cm^3 Obsd	Density g/cm^3 Calcd
K-0	0.60	*ca.*3	75	*ca.*1.1	0	6—7	5.748	21.03	$K_{4.0}Pb_{4.0}(CrO_4)_{6.0}$	4.76	4.639
K-1	1.00	4	150	1.8	0	8.9	5.729	21.04			
K-4	1.00	4	150	1.8	1.0	7.5	5.728	21.04			
K-5	1.00	4	150	1.8	3.0	6.6	5.728	21.02			
K-6	1.00	4	150	1.8	10.0	5.9	5.727	21.03			
K-8	1.00	4	125	1.5	0	8.8	5.730	21.04	$K_{5.4}Pb_{3.6}(CrO_4)_{6.0}$		
K-7	1.00	3	125	1.1	0	8.4	5.742	21.06			
K-9	1.00	2	125	0.8	0	8.1	5.751	21.07			
K-11[b)]	1.00	1	125	0.4	0	7.7	—	—			
K-2	1.00	4	300	3.6	0	8.9	5.736	21.03			
K-3	1.00	4	600	7.2	0	8.8	5.740	21.03			
c)							5.716	21.065	$K_6Pb_3(CrO_4)_6$ $[=K_2Pb(CrO_4)_2]$	4.30	4.324

a) A given amount of $PbSO_4$ was dissolved in a hot solution of KOAc, HOAc was added if required, and 1.5 M K_2CrO_4 was added. b) A large amount of $PbCrO_4$ (mon.) and a small amount of $Pb_2(OH)_2CrO_4$ were detected. c) JCPDS card No. 19-971 and Ref. 2.

peak at approximately 205 °C, which was accompanied by a weight loss over the range 140 to 220 °C, was attributed to the evolution of ammonia; the evolution was confirmed by Nessler's test and the experimental and theoretical weight losses. The exothermic peak at approximately 245 °C, which was accompanied by a weight loss over the range 220 to 270 °C, may be attributable to the formation of water by the oxidation of ammonia, since, when the sample was heated to approximately 220 °C in a test tube attached with a conduit pipe, water drops were produced inside the pipe. High-temperature X-ray diffraction analysis showed a definite transition of sample NK-0 to monoclinic lead(II) chromate and the formation of an intermediate compound in the couse of this transition. Although this intermediate compound could not be identified, it appears to be a compound formed by the escape of ammonia from sample NK-0. The exothermic peak free from weight loss at approximately 405 °C appears due to a crystal transition. The transition could not, however, be detected by high-temperature X-ray diffraction analysis.

Several samples changed to known compounds with weight loss, when heated up to approximately 400 °C in an electric furnace, the results of which are summarized in Table 5. The residues obtained by heating

Table 5. The results of heating to 400 °C for some samples

Sample	Weight loss/%	Color of the residue	Crystalline phase in the residue	
			Major component	Minor component
NK-0	9	Yellow-green	$PbCrO_4$(mon.)	$K_2Pb(CrO_4)_2$
N-0	12	Yellow-green	$PbCrO_4$(mon.)	—
K-0	0.7	Orange	$K_2Pb(CrO_4)_2$	$PbCrO_4$(mon.), $PbCrO_4 \cdot PbO$

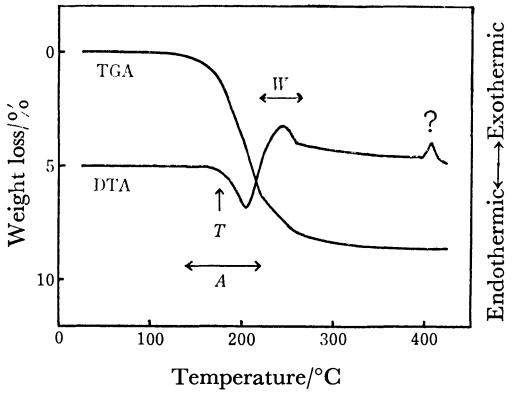

Fig. 1. Thermal analysis of $K_{0.2}(NH_4)_{2.0})Pb_{1.9}(CrO_4)_{3.0}$ (sample NK-0).
Heating rate: 3 °C/min; T: transition of sample NK-0 to $PbCrO_4$ (mon.); A: evolution of ammonia; W: evolution of water.

samples NK-0 and N-0 mainly consisted of monoclinic lead(II) chromate; small amounts of the known chromate, $K_2Pb(CrO_4)_2$, were also detected in the residue of sample NK-0 containing small amounts of potassium ions. Amorphous chromium(III) oxide appears to be present in both residues judging from the color (yellow-green). This chromium(III) oxide may be formed by the reduction of chromate ions by ammonia. Sample K-0 was decomposed by heat-treatment to known compounds, $K_2Pb(CrO_4)_2$, PbCrO-(mon.), $PbCrO_4 \cdot PbO$, *etc.*

The thermal analyses described above, together with the differences in X-ray diffraction patterns and lattice constants, also support the conclution that the compounds prepared here differ from the known chromates, $K_2Pb(CrO_4)_2$ and $(NH_4)_2Pb(CrO_4)_2$.

The authors are grateful to Professor Yoshihiko Saito of the University of Tokyo, Professor G. H. Morrison of Cornell University, and Dr. L. S. Birks of the Naval Research Laboratory for their advice. Acknowledgments are also due to Mr. Jun'ichi Ito of the Central Research Laboratory, Showa Denko K. K., for providing the facilities for thermal analysis, to Rigaku Denki K. K. for providing the facilities for high-temperature X-ray diffraction analysis, and to Mr. Shintaro Suzuki for assistance in the experimental work.

References

1) T. Fukasawa and M. Iwatsuki, *Bunseki Kagaku*, **26**, 379 (1977).
2) H. Schwarz, *Z. Anorg. Allg. Chem.*, **345**, 230 (1966).
3) K. Saruhashi, *Bunseki Kagaku*, **4**, 337 (1955).

The Crystal Structures of $(+)_{589}$- and $(-)_{589}$-*trans*(*O*)-Ethylenediaminebis(glycinato)cobalt(III) Hydrogen-*d*-tartrates and Their Thermal Behavior

Masahiro KURAMOTO

Department of Chemistry, Faculty of Science, Hiroshima University, Higashi-senda-machi, Hiroshima 730

(Received October 27, 1978)

The crystal structures of two diastereoisomeric salts, $(+)_{589}$-*trans*(*O*)-[Co(gly)$_2$en]H-*d*-tart·3H$_2$O (**1**) and $(-)_{589}$-*trans*(*O*)-[Co(gly)$_2$en]H-*d*-tart·H$_2$O (**2**), have been determined by three-dimensional X-ray analysis. The less-soluble salt (**1**) is monoclinic; space group, $P2_1$; $Z=2$, $a=12.351(5)$, $b=7.671(3)$, $c=10.189(5)$ Å, and $\beta=110.71(4)°$ ($R=0.043$, 2241 reflections). The more-soluble salt (**2**) is monoclinic; space group, $P2_1$; $Z=2$, $a=11.135(4)$, $b=10.037(3)$, $c=7.716(3)$ Å, and $\beta=98.61(3)°$ ($R=0.064$, 2076 reflections). A comparison of the (unit cell volume)/Z values of the two crystals shows that the crystal **1** is more tightly packed than the crystal **2**. In both salts, adjacent complex cations form quite similar chain structures linked by (N–H···O) hydrogen bonds. The H-*d*-tart anions in **1** take a characteristic "head-to-tail" arrangement of an infinite chain of $\{$H-*d*-tart$\}_\infty$ along the b-axis. In contrast, this arrangement is not found in the more-soluble salt (**2**). From these findings, it can be considered that the discrimination of optical isomers in the H-*d*-tart system originates from the spiral chain structure of $\{$H-*d*-tart$\}_\infty$. The absolute configurations of $(+)_{589}$- and $(-)_{589}$-*trans*(*O*)-[Co(gly)$_2$en]$^+$ are determined to be Λ-δ and Λ-λ respectively. TG and DSC measurements were carried out for both salts, and the ΔH values of the dehydration step were estimated to be 64.4 kJ mol^{-1} for **1** and 73.0 kJ mol^{-1} for **2**.

Optical resolutions of metal complex ions are performed mostly through fractional crystallization utilizing the difference in solubilities of diastereoisomeric salts. However, no general rule has yet been established to judge what sort of a resolving agent is most effective for a particular racemic complex. To approach this problem, the X-ray crystal analysis of a pair of diastereoisomeric salts is indispensable. A comparison of the crystal structures of the less- and more-soluble diastereoisomeric salt pair will give an important clue for elucidating the mechanism of optical resolution.

With this expectation, the crystal structures were investigated recently for a pair of a less-soluble salt, $(+)_{589}$-[Co(ox)en$_2$]H-*d*-tart·H$_2$O (**3**), and a more-soluble salt, $(-)_{589}$-[Co(ox)en$_2$]H-*d*-tart·2H$_2$O (**4**);[1,2] their thermal behavior was also examined. It was found that, in **3**, complex cations are locked tightly in a space formed by four spiral chains of H-*d*-tart(*d*-$C_4H_5O_6^-$, abbr. H-*d*-tart) anions related by a twofold screw axis, while in **4**, complex cations are packed loosely in the four chains of the H-*d*-tart anion formed by a translation operation.[2]

In the present study the crystal structures were determined for another pair of diastereoisomeric salts, $(+)_{589}$-*trans*(*O*)-[Co(gly)$_2$en]H-*d*-tart·3H$_2$O (**1**) and $(-)_{589}$-*trans*(*O*)-[Co(gly)$_2$en]H-*d*-tart·H$_2$O (**2**). The complex, *trans*(*O*)-[Co(gly)$_2$en]$^+$, is actually resolved by way of these diastereoisomeric salts, both of which have been reported to be obtained easily as single crystals.[3] In addition, since *trans*(*O*)-[Co(gly)$_2$en]$^+$ and [Co(ox)en$_2$]$^+$ have the same chemical formula, $C_6H_{16}N_4O_4Co$, the volumes of both cations can be expected to be nearly equal. Thus, the present diastereoisomeric pair is considered to be one of the most suitable examples for clarifying the nature of discrimination by the H-*d*-tart anion.

Contrary to the diastereoisomeric salts, [Co(ox)en$_2$]-H-*d*-tart·*n*H$_2$O, the number of the water of crystallization of *trans*(*O*)-[Co(gly)$_2$en]H-*d*-tart·*n*H$_2$O is larger in the less-soluble salt than that in the more-soluble one. To see the role of the water of crystallization in their crystal packing, the thermal behavior of both crystals was investigated by means of TG and DSC measurements.

Experimental

*Preparation of Compound. (a) The Less-soluble Salt, $(+)_{589}$-*trans*(O)-[*Co(gly)$_2$en*]H-d-tart·3H$_2$O (1)*: The less-soluble salt (**1**) was prepared by the method of Dabrowiak and Cooke.[3]

Table 1. Crystal parameters of two diastereoisomeric pairs

Diastereoisomers	a/Å	b/Å	c/Å	β/°	Space group	D_m/g cm^{-3}	Z	D_c/g cm^{-3}	V/Å^3	V/Z/Å^3
$(+)_{589}$-*trans*(*O*)-[Co(gly)$_2$en]H-*d*-tart·3H$_2$O (**1**)	12.351(5)	7.671(3)	10.189(5)	110.71(4)	$P2_1$	1.72	2	1.73(1)	903.0(7)	451.5(4)
$(-)_{589}$-*trans*(*O*)-[Co(gly)$_2$en]H-*d*-tart·H$_2$O (**2**)	11.135(4)	10.037(3)	7.716(3)	98.61(3)	$P2_1$	1.67	2	1.69(1)	852.7(5)	426.4(3)
$(+)_{589}$-[Co(ox)en$_2$]H-*d*-tart·H$_2$O (**3**)[a]	8.256(3)	14.588(4)	7.009(1)	104.73(2)	$P2_1$	1.74	2	1.77(1)	816.4(4)	408.2(2)
$(-)_{589}$-[Co(ox)en$_2$]H-*d*-tart·2H$_2$O (**4**)[a]	16.583(5)	14.186(5)	7.403(2)	——	$P2_12_12$	1.72	4	1.73(1)	1741.5(10)	435.4(3)

1, **3**: The less-soluble salt. **2**, **4**: The more-soluble salt. a) The crystal data of **3** and **4** were remeasured in a manner similar to that used for **1** and **2**.

The crystals are hexagonal rods. Found: C, 25.52; H, 5.84; N, 11.80%. Calcd for $C_{10}H_{27}N_4O_{13}Co$: C, 25.54; H, 5.79; N, 11.91%.

(b) The More-soluble Salt, $(-)_{589}$-trans(O)-[Co(gly)$_2$en]H-d-tart·H_2O (2): After the removal of the precipitated crystals of the $(+)_{589}$-salt,[3] the filtrate was cooled in a refrigerator. The crystals **2** were thus separated out as rhombic plates. Found: C, 27.79; H, 5.40; N, 12.90%. Calcd for $C_{10}H_{23}N_4O_{11}Co$: C, 27.66; H, 5.33; N, 12.90%.

X-Ray Data Collection. Weissenberg photographs indicated a monoclinic unit cell with the systematic absence of $(0k0)$ when $k=2n+1$ for both **1** and **2**. Of the two possible space groups, $P2_1$ and $P2_1/m$, the latter was eliminated because of the optical activity of these compounds. The crystal sizes used for the cell constant and intensity measurements were $0.25\times0.50\times0.40$ mm^3 for **1** and $0.15\times0.20\times0.30$ mm^3 for **2**. All the cell constants were determined by a least-squares treatment of the setting of 15 reflections measured on a Syntex R3 computer-controlled four-circle diffractometer with Mo $K\alpha$ radiation ($\lambda=0.7107$ Å) monochromated by a graphite plate. All the cell constants are summarized in Table 1. The intensity data for **1** and **2** were collected by the ω-2θ scan technique to a maximum 2θ value of 55° at a scan rate of 3°/min. The intensities of 2366 and 2234 independent reflections were collected for **1** and **2** respectively. Reflections for which the intensities were less than three times their standard deviations were regarded as "unobserved" and were not included in subsequent calculations. Thus, 2241 and 2076 independent reflections were used for the structure determination for **1** and **2** respectively. Their intensities were corrected for Lorentz and polarization factors, but no absorption corrections were made since the μ-values (10.7 cm^{-1} for **1** and 11.2 cm^{-1} for **2**) were low.

Thermogravimetric Analysis (TG). The TG data were obtained with a Rigaku Thermal Analyzer (Model 8005). A heating rate of 3 K/min and a static air atmosphere were employed, and 7.65—11.13 mg samples were used in each run.

Differential Scanning Calorimetry (DSC). A Rigaku Differential Scanning Calorimeter (Model-8055Cl) was used to record the DSC curves. In order to determine the ΔH values of the dissociation of the water of crystallization for both diastereoisomers, the instrument was calibrated using the ΔH values of the fusion of pure indium, tin, and lead metals as standards. The weights of the samples were 9.20—13.75 mg. A heating rate of 10 K/min was used in each run. The dry nitrogen gas (25 ml/min) was used as the furnace atmosphere.

Determination and Refinement of Crystal Structures

The Less-soluble Salt, $(+)_{589}$-trans(O)-[Co(gly)$_2$en]H-d-tart·3H_2O (1). A three-dimensional Patterson function revealed the position of the cobalt atom. The remaining nonhydrogen atoms were located by an application of the Fourier method. Several cycles of block-diagonal least-squares refinement using isotropic thermal parameters reduced the R value (defined as $\Sigma||F_o|-|F_c||/\Sigma|F_o|$) to 0.118. Further refinement using both positional and anisotropic thermal parameters for the nonhydrogen atoms reduced the R value to 0.061. A difference map at this stage revealed the positions of all hydrogen atoms. The final refinement including the contribution of these hydrogen atoms with the fixed positions and isotropic temperature

Table 2. Final atomic parameters with their e.s.d.'s for $(+)_{589}$-*trans*(*O*)-[Co(gly)$_2$en]H-*d*-tart·3H_2O

Atom	x	y	z
Co	0.95978(4)	0.75000(15)	0.73971(5)
O(G1)	1.0157(3)	0.9326(5)	0.6554(3)
O(G2)	1.1642(3)	1.1084(6)	0.6820(4)
O(G3)	0.9150(3)	0.5634(5)	0.8314(4)
O(G4)	0.9144(5)	0.2769(5)	0.8447(5)
O(T1)	0.4805(6)	1.1188(8)	0.3802(5)
O(T2)	0.4541(4)	1.1484(6)	0.1508(5)
O(T3)	0.4164(3)	0.7776(5)	0.3446(4)
O(T4)	0.6187(3)	0.7852(5)	0.2747(5)
O(T5)	0.5280(4)	0.4693(6)	0.1915(5)
O(T6)	0.3716(3)	0.5788(6)	0.0285(4)
O(W1)	0.8057(4)	0.8685(7)	1.0940(5)
O(W2)	0.2421(4)	0.6179(11)	0.6641(9)
O(W3)	0.3159(4)	0.9126(9)	0.5350(5)
N(G1)	1.1145(3)	0.7530(7)	0.8859(4)
N(G2)	1.0025(4)	0.5731(6)	0.6299(4)
N(E1)	0.8068(3)	0.7697(7)	0.5903(4)
N(E2)	0.8985(4)	0.9086(6)	0.8470(5)
C(G1)	1.1174(4)	0.9886(7)	0.7248(5)
C(G2)	1.1787(5)	0.9083(8)	0.8689(5)
C(G3)	0.9266(4)	0.4103(7)	0.7861(5)
C(G4)	0.9578(5)	0.4037(7)	0.6535(5)
C(E1)	0.7430(6)	0.9177(11)	0.6241(7)
C(E2)	0.7718(5)	0.9183(12)	0.7783(7)
C(T1)	0.4554(5)	1.0577(7)	0.2620(6)
C(T2)	0.4230(4)	0.8696(7)	0.2257(5)
C(T3)	0.5073(4)	0.7794(6)	0.1673(5)
C(T4)	0.4643(4)	0.5934(7)	0.1239(5)
H(NG11)[a]	1.159	0.649	0.881
H(NG12)	1.107	0.761	0.981
H(NG21)	1.089	0.570	0.656
H(NG22)	0.968	0.606	0.526
H(NE11)	0.762	0.663	0.582
H(NE12)	0.817	0.796	0.498
H(NE21)	0.933	1.030	0.851
H(NE22)	0.918	0.868	0.946
H(CG21)	1.264	0.874	0.879
H(CG22)	1.185	1.002	0.948
H(CG41)	1.021	0.310	0.665
H(CG42)	0.884	0.374	0.567
H(CE11)	0.654	0.904	0.572
H(CE12)	0.769	1.038	0.592
H(CE21)	0.732	0.814	0.809
H(CE22)	0.740	1.037	0.809
H(CT2)	0.340	0.870	0.145
H(CT3)	0.512	0.846	0.077
H(OW11)	0.810	0.833	1.160
H(OW12)	0.726	0.867	1.052
H(OW21)	0.300	0.570	0.725
H(OW22)	0.282	0.700	0.640
H(OW31)	0.380	0.933	0.595
H(OW32)	0.352	0.880	0.485
H(OT2)	0.472	1.250	0.165
H(OT3)	0.488	0.763	0.412
H(OT4)	0.670	0.833	0.287

a) The averaged e.s.d.'s of hydrogen atoms are; $\overline{\sigma(x)}=0.008$, $\overline{\sigma(y)}=0.017$, and $\overline{\sigma(z)}=0.013$.

TABLE 3. ANISOTROPIC TEMPERATURE FACTORS ($\times 10^3$ Å^2) EXPRESSED IN THE FORM $\exp[-2\pi^2(U_{11}h^2a^{*2}+U_{22}k^2b^{*2}+U_{33}l^2c^{*2}+2U_{12}hka^*b^*+2U_{13}hla^*c^*+2U_{23}klb^*c^*)]$ FOR $(+)_{589}$-*trans*(*O*)-[Co(gly)$_2$en]H-*d*-tart·3H$_2$O

Atom	U_{11}	U_{22}	U_{33}	U_{12}	U_{13}	U_{23}
Co	20.4(2)	10.8(2)	14.6(2)	−1.1(2)	7.3(0)	−1.0(2)
O(G1)	24(2)	21(2)	19(1)	0(1)	8(1)	5(1)
O(G2)	28(2)	19(2)	37(2)	−6(2)	14(1)	4(2)
O(G3)	30(2)	13(2)	25(2)	−4(1)	17(1)	−3(1)
O(G4)	77(3)	12(2)	37(2)	−3(2)	31(2)	2(2)
O(T1)	104(4)	34(3)	36(2)	−13(3)	22(3)	−14(2)
O(T2)	57(3)	19(2)	40(2)	−5(2)	23(2)	−1(2)
O(T3)	40(2)	23(2)	27(2)	1(2)	17(1)	6(2)
O(T4)	20(2)	21(2)	50(2)	3(1)	4(2)	−8(2)
O(T5)	42(2)	18(2)	39(2)	−1(2)	7(2)	5(2)
O(T6)	32(2)	27(2)	31(2)	−6(2)	3(2)	−5(2)
O(W1)	37(2)	39(3)	39(2)	6(2)	11(2)	15(2)
O(W2)	33(2)	79(5)	104(5)	15(3)	31(3)	38(4)
O(W3)	32(2)	60(3)	46(2)	9(2)	11(2)	−11(3)
N(G1)	27(2)	16(2)	21(2)	2(2)	8(1)	4(2)
N(G2)	32(2)	16(2)	24(2)	−3(2)	17(2)	−4(2)
N(E1)	24(2)	23(2)	16(1)	−5(2)	4(1)	−1(2)
N(E2)	28(2)	11(2)	30(2)	−2(2)	16(2)	−6(2)
C(G1)	23(2)	15(2)	14(2)	5(2)	6(2)	5(2)
C(G2)	31(2)	29(3)	10(2)	−9(2)	−8(2)	8(2)
C(G3)	33(2)	9(2)	29(2)	−2(2)	12(2)	−4(2)
C(G4)	37(2)	10(2)	17(2)	−3(2)	9(2)	−4(2)
C(E1)	35(3)	52(4)	38(3)	14(3)	1(2)	−9(3)
C(E2)	29(3)	52(4)	44(3)	7(3)	8(2)	−14(3)
C(T1)	34(3)	13(3)	27(2)	2(2)	7(2)	−2(2)
C(T2)	24(2)	15(2)	22(2)	−3(2)	8(2)	0(2)
C(T3)	22(2)	10(2)	30(2)	−3(2)	9(2)	−5(2)
C(T4)	26(2)	16(2)	29(2)	−4(2)	11(2)	−2(2)

TABLE 4. FINAL ATOMIC PARAMETERS WITH THEIR e.s.d's FOR $(-)_{589}$-*trans*(*O*)-[Co(gly)$_2$en]H-*d*-tart·H$_2$O

Atom	x	y	z	Atom	x	y	z
Co	0.85377(8)	0.75000(20)	0.69785(10)	C(T4)	0.2135(8)	0.6848(8)	0.1366(10)
O(G1)	0.9259(5)	0.8542(6)	0.5361(8)	H(NG11)[a]	0.972	0.543	0.692
O(G2)	1.0975(6)	0.8810(7)	0.4260(9)	H(NG12)	1.046	0.647	0.830
O(G3)	0.7926(5)	0.6438(6)	0.8687(7)	H(NG21)	0.913	0.959	0.864
O(G4)	0.7904(8)	0.6223(7)	1.1514(8)	H(NG22)	1.018	0.847	0.918
O(T1)	0.4776(7)	0.9791(8)	0.1414(9)	H(NE11)	0.734	0.962	0.661
O(T2)	0.5172(10)	0.9229(11)	−0.1222(13)	H(NE12)	0.659	0.852	0.756
O(T3)	0.3919(6)	0.6892(7)	−0.1213(8)	H(NE21)	0.773	0.542	0.551
O(T4)	0.1960(5)	0.8569(6)	−0.0894(8)	H(NE22)	0.800	0.650	0.403
O(T5)	0.1116(6)	0.6420(7)	0.0641(9)	H(CG21)	1.059	0.610	0.475
O(T6)	0.2719(6)	0.6367(7)	0.2764(8)	H(CG22)	1.163	0.680	0.634
OW	0.3480(7)	0.7995(9)	0.5518(9)	H(CG41)	0.804	0.898	1.066
N(G1)	0.9973(6)	0.6361(7)	0.7105(9)	H(CG42)	0.938	0.829	1.162
N(G2)	0.9271(6)	0.8602(7)	0.8937(8)	H(CE11)	0.681	0.868	0.387
N(E1)	0.7090(6)	0.8637(8)	0.6614(10)	H(CE12)	0.550	0.871	0.477
N(E2)	0.7656(6)	0.6359(7)	0.5155(8)	H(CE21)	0.590	0.642	0.363
C(G1)	1.0314(7)	0.8157(7)	0.5095(9)	H(CE22)	0.589	0.639	0.584
C(G2)	1.0701(8)	0.6770(8)	0.5782(12)	H(CT2)	0.440	0.723	0.137
C(G3)	0.8159(9)	0.6880(9)	1.0268(10)	H(CT3)	0.276	0.889	0.159
C(G4)	0.8709(10)	0.8252(9)	1.0485(10)	H(OW1)	0.330	0.753	0.467
C(E1)	0.6388(8)	0.8280(12)	0.4896(14)	H(OW2)	0.290	0.875	0.520
C(E2)	0.6345(8)	0.6748(12)	0.4854(12)	H(OT1)	0.525	1.050	0.085
C(T1)	0.4696(7)	0.8968(11)	0.0049(12)	H(OT3)	0.393	0.743	−0.213
C(T2)	0.3971(7)	0.7740(8)	0.0282(10)	H(OT4)	0.230	0.943	−0.093
C(T3)	0.2698(7)	0.8084(8)	0.0651(10)				

a) The averaged e.s.d.'s of hydrogen atoms are; $\overline{\sigma(x)}=0.008$, $\overline{\sigma(y)}=0.014$, and $\overline{\sigma(z)}=0.015$.

TABLE 5. ANISOTROPIC TEMPERATURE FACTORS ($\times 10^3$Å^2) EXPRESSED IN THE FORM $\exp[-2\pi^2(U_{11}h^2a^{*2}+U_{22}k^2b^{*2}+U_{33}l^2c^{*2}+2U_{12}hka^*b^*+2U_{13}hla^*c^*+2U_{23}klb^*c^*)]$ FOR $(-)_{589}$-*trans*(*O*)-[Co(gly)$_2$en]H-*d*-tart·H$_2$O

Atom	U_{11}	U_{22}	U_{33}	U_{12}	U_{13}	U_{23}
Co	24.0(3)	16.2(4)	16.4(3)	0.2(1)	5.2(3)	0.4(4)
O(G1)	33(3)	19(3)	31(3)	3(2)	10(2)	4(2)
O(G2)	35(3)	28(3)	49(4)	−1(3)	16(3)	6(3)
O(G3)	37(3)	23(3)	22(2)	−8(2)	8(2)	−3(2)
O(G4)	90(6)	28(3)	24(3)	−14(4)	21(3)	−2(3)
O(T1)	60(4)	42(4)	38(4)	−15(4)	18(3)	−4(3)
O(T2)	94(7)	74(7)	66(6)	−34(6)	54(5)	−19(5)
O(T3)	43(3)	32(3)	35(3)	16(3)	6(3)	−3(3)
O(T4)	29(3)	24(3)	31(3)	−3(2)	−2(2)	4(3)
O(T5)	37(3)	29(3)	42(3)	−8(3)	2(3)	5(3)
O(T6)	47(4)	30(3)	28(3)	0(3)	0(3)	6(3)
OW	41(4)	66(5)	39(3)	−9(4)	2(3)	3(4)
N(G1)	31(3)	20(3)	32(3)	2(3)	10(3)	2(3)
N(G2)	30(3)	21(3)	22(3)	2(3)	−2(2)	−1(3)
N(E1)	24(3)	24(3)	38(4)	4(3)	12(3)	1(3)
N(E2)	36(3)	20(3)	19(3)	−3(3)	5(2)	−3(3)
C(G1)	31(4)	16(3)	20(3)	−4(3)	6(3)	−2(3)
C(G2)	35(4)	18(4)	42(4)	1(3)	25(3)	−5(3)
C(G3)	56(5)	18(3)	24(4)	0(4)	14(3)	−2(3)
C(G4)	67(6)	24(4)	16(3)	−7(4)	18(3)	−6(3)
C(E1)	31(4)	46(6)	47(5)	5(4)	−9(4)	4(5)
C(E2)	33(4)	52(6)	36(4)	−5(4)	−6(3)	−12(4)
C(T1)	16(3)	46(5)	41(4)	4(3)	0(3)	5(4)
C(T2)	29(3)	27(5)	26(3)	3(3)	2(3)	1(3)
C(T3)	26(3)	21(4)	26(3)	0(3)	2(3)	9(3)
C(T4)	36(4)	19(4)	26(4)	0(3)	10(3)	8(3)

TABLE 6. BOND DISTANCES AND ANGLES (e.s.d.'s IN PARENTHESES) FOR $(+)_{589}$-*trans*(*O*)-[Co(gly)$_2$en]H-*d*-tart·3H$_2$O

Bond distances [l/Å]

Co–O(G1)	1.897(4)	N(G1)–C(G2)	1.475(8)	O(T1)–C(T1)	1.226(10)
Co–O(G3)	1.896(4)	N(G2)–C(G4)	1.465(7)	O(T2)–C(T1)	1.324(8)
Co–N(G1)	1.964(6)	N(E1)–C(E1)	1.490(10)	O(T3)–C(T2)	1.429(7)
Co–N(G2)	1.947(5)	N(E2)–C(E2)	1.473(10)	O(T4)–C(T3)	1.425(7)
Co–N(E1)	1.969(5)	C(G1)–C(G2)	1.523(8)	O(T5)–C(T4)	1.272(7)
Co–N(E2)	1.958(5)	C(G3)–C(G4)	1.531(8)	O(T6)–C(T4)	1.217(7)
O(G1)–C(G1)	1.278(6)	C(E1)–C(E2)	1.483(12)	C(T1)–C(T2)	1.508(8)
O(G2)–C(G1)	1.244(7)			C(T2)–C(T3)	1.536(8)
O(G3)–C(G3)	1.288(7)			C(T3)–C(T4)	1.532(8)
O(G4)–C(G3)	1.220(8)				

Bond Aangles[ϕ/°]

O(G1)–Co–N(G1)	85.5(2)	O(G1)–C(G1)–C(G2)	117.0(5)
O(G3)–Co–N(G2)	86.7(2)	N(G1)–C(G2)–C(G1)	109.6(5)
N(E1)–Co–N(E2)	86.0(2)	O(G3)–C(G3)–C(G4)	116.1(5)
Co–O(G1)–C(G1)	116.2(3)	N(G2)–C(G4)–C(G3)	110.0(5)
Co–O(G3)–C(G3)	115.0(4)	N(E1)–C(E1)–C(E3)	107.4(7)
Co–N(G1)–C(G2)	109.9(4)	N(E2)–C(E2)–C(E1)	108.7(7)
Co–N(G2)–C(G4)	109.3(3)	O(G1)–C(G1)–O(G2)	122.8(5)
Co–N(E1)–C(E1)	108.8(4)	O(G3)–C(G3)–O(G4)	122.7(5)
Co–N(E2)–C(E2)	108.8(4)	O(G2)–C(G1)–C(G2)	120.2(5)
		O(G4)–C(G3)–C(G4)	121.2(5)
O(T1)–C(T1)–O(T2)	124.2(6)	O(T5)–C(T4)–O(T6)	126.2(6)
O(T1)–C(T1)–C(T2)	124.0(6)	O(T2)–C(T1)–C(T2)	111.8(5)
O(T3)–C(T2)–C(T1)	110.8(5)	O(T3)–C(T2)–C(T3)	110.8(4)
O(T4)–C(T3)–C(T2)	106.9(4)	O(T4)–C(T3)–C(T4)	113.2(4)
O(T5)–C(T4)–C(T3)	117.1(5)	O(T6)–C(T4)–C(T3)	116.7(5)
C(T1)–C(T2)–C(T3)	111.6(5)	C(T2)–C(T3)–C(T4)	108.6(4)

TABLE 7. BOND DISTANCES AND ANGLES (e.s.d.'s IN PARENTHESES) FOR $(-)_{589}$-*trans*(*O*)-[Co(gly)$_2$en]H-*d*-tart·H_2O

Bond distances [*l*/Å]

Co–O(G1)	1.897(6)	N(G1)–C(G2)	1.455(11)	O(T1)–C(T1)	1.330(4)
Co–O(G3)	1.899(6)	N(G2)–C(G4)	1.472(13)	O(T2)–C(T1)	1.211(16)
Co–N(G1)	1.955(7)	N(E1)–C(E1)	1.479(14)	O(T3)–C(T2)	1.428(11)
Co–N(G2)	1.950(7)	N(E2)–C(E2)	1.496(14)	O(T4)–C(T3)	1.428(11)
Co–N(E1)	1.960(8)	C(G1)–C(G2)	1.528(12)	O(T5)–C(T4)	1.262(11)
Co–N(E2)	1.960(7)	C(G3)–C(G4)	1.506(15)	O(T6)–C(T4)	1.269(11)
O(G1)–C(G1)	1.281(10)	C(E1)–C(E2)	1.539(17)	C(T1)–C(T2)	1.499(13)
O(G2)–C(G1)	1.236(10)			C(T2)–C(T3)	1.527(12)
O(G3)–C(G3)	1.287(12)			C(T3)–C(T4)	1.530(12)
O(G4)–C(G3)	1.234(13)				

Bond angles [ϕ/°]

O(G1)–Co–N(G1)	86.1(3)	O(G1)–C(G1)–C(G2)	115.9(7)
O(G3)–Co–N(G2)	86.2(3)	N(G1)–C(G2)–C(G1)	110.0(7)
N(E1)–Co–N(E2)	85.7(3)	O(G3)–C(G3)–C(G4)	116.2(9)
Co–O(G1)–C(G1)	115.3(5)	N(G2)–C(G4)–C(G3)	110.1(8)
Co–O(G3)–C(G3)	114.9(6)	N(E1)–C(E1)–C(E2)	105.8(9)
Co–N(G1)–C(G2)	109.7(3)	N(E2)–C(E2)–C(E1)	103.4(9)
Co–N(G2)–C(G4)	108.3(6)	O(G1)–C(G1)–O(G2)	123.7(7)
Co–N(E1)–C(E1)	107.5(6)	O(G3)–C(G3)–O(G4)	121.1(9)
Co–N(E2)–C(E2)	109.4(6)	O(G2)–C(G1)–C(G2)	120.3(7)
		O(G4)–C(G3)–C(G4)	122.6(10)
O(T1)–C(T1)–O(T2)	121.4(11)	O(T5)–C(T4)–O(T6)	124.0(8)
O(T1)–C(T1)–C(T2)	112.9(9)	O(T2)–C(T1)–C(T2)	125.7(10)
O(T3)–C(T2)–C(T1)	110.5(7)	O(T3)–C(T2)–C(T3)	111.1(7)
O(T4)–C(T3)–C(T2)	110.9(7)	O(T4)–C(T3)–C(T4)	111.2(7)
O(T5)–C(T4)–C(T3)	120.4(8)	O(T6)–C(T4)–C(T3)	115.4(7)
C(T1)–C(T2)–C(T3)	111.6(7)	C(T2)–C(T3)–C(T4)	109.0(7)

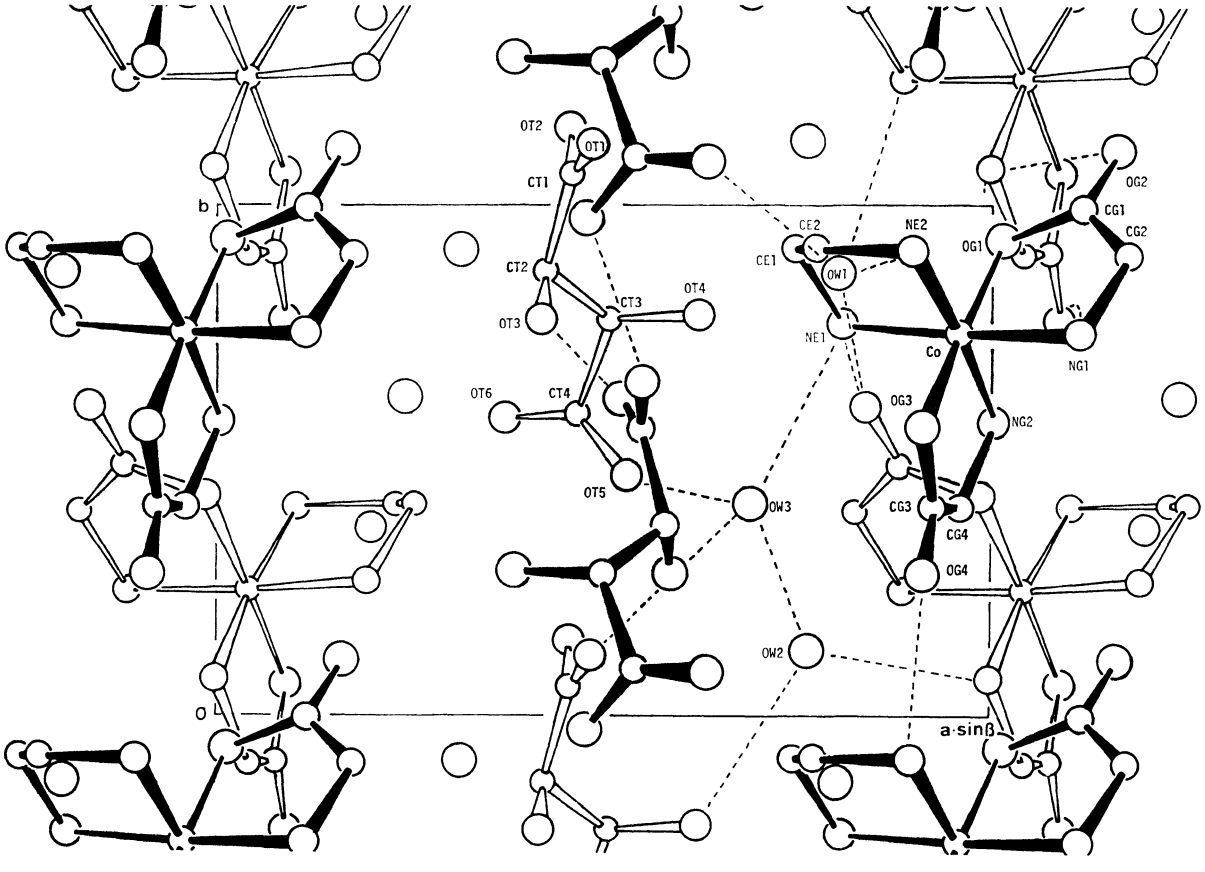

Fig. 1. Projection of the crystal structure along the c-axis of the less-soluble salt, $(+)_{589}$-*trans*(*O*)-[Co(gly)$_2$en]H-*d*-tart·$3H_2O$. Possible hydrogen bonds are indicated by broken lines.

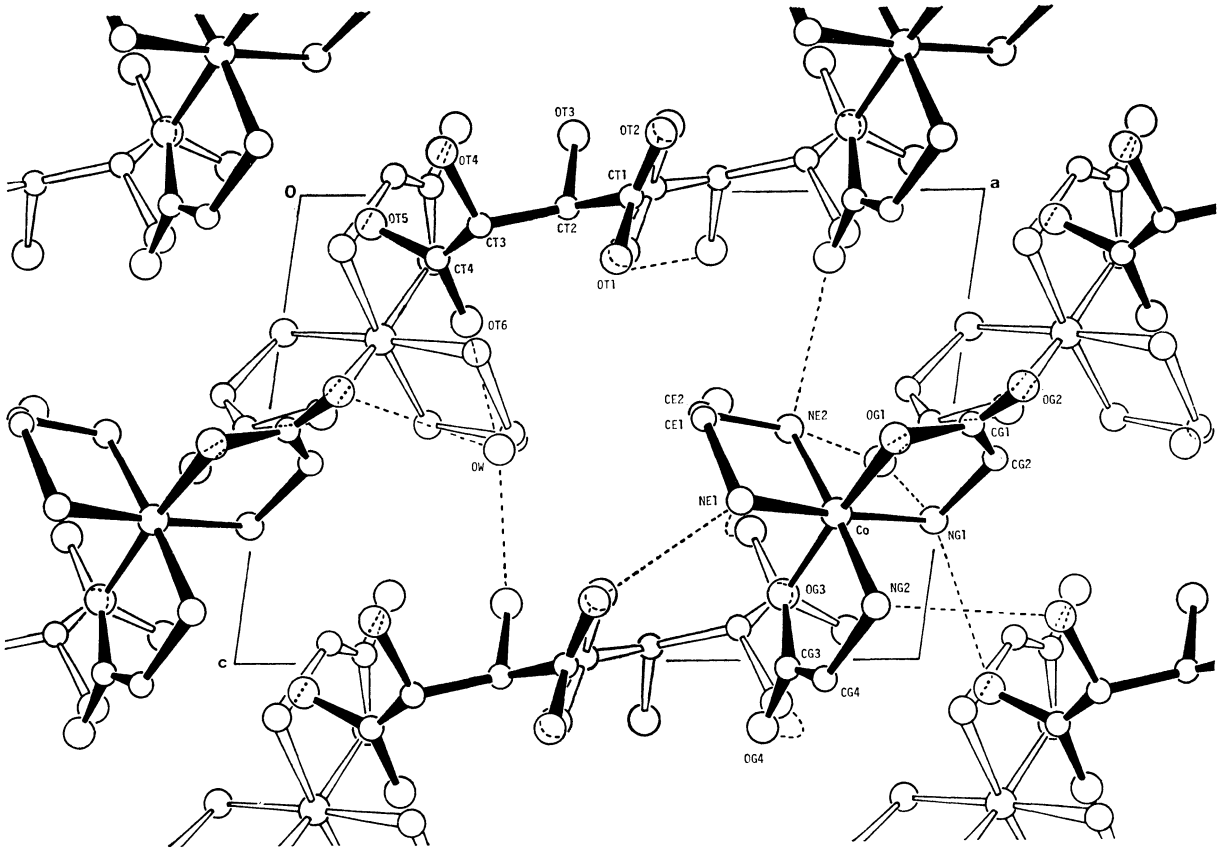

Fig. 2. Projection of the crystal structure along the b-axis of the more-soluble salt, $(-)_{589}$-*trans*(*O*)-[Co(gly)$_2$en]H-*d*-tart·H$_2$O. Possible hydrogen bonds are indicated by broken lines.

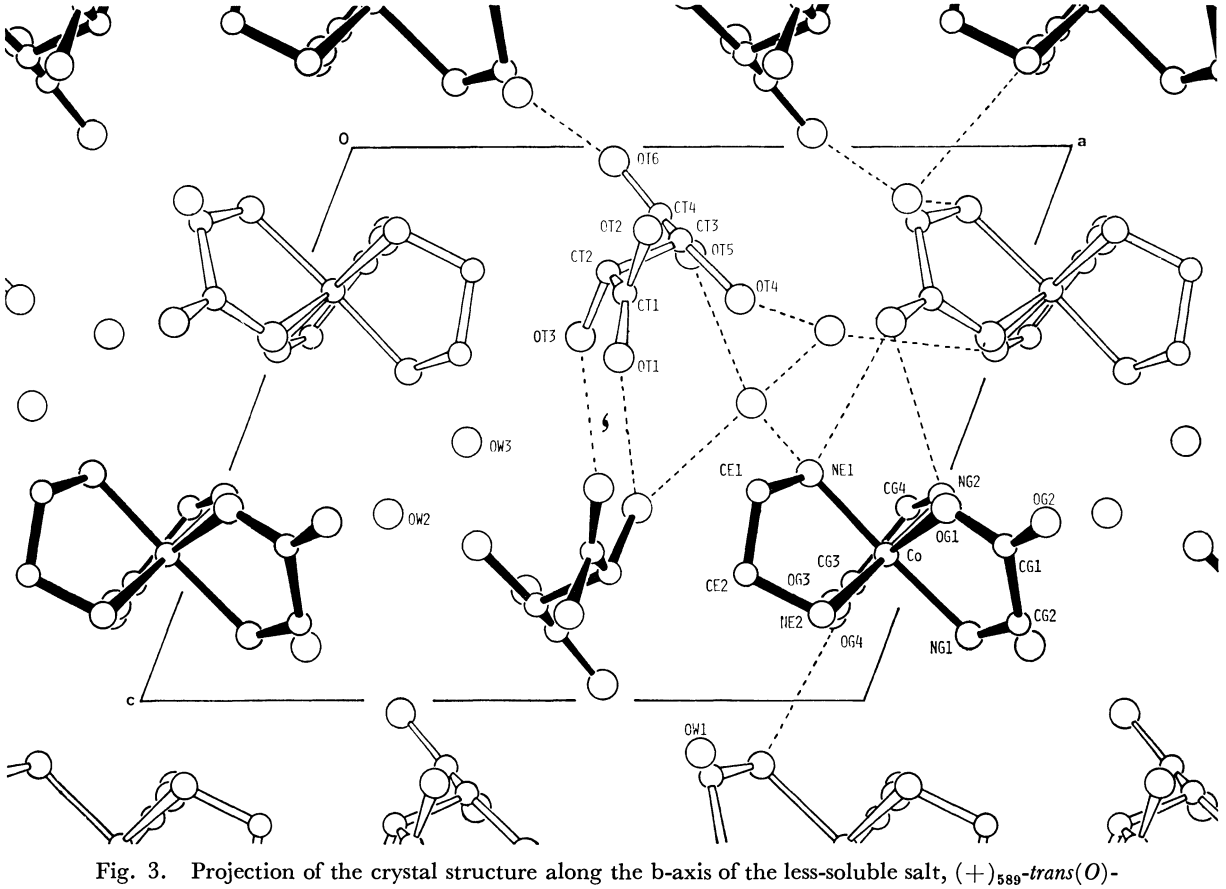

Fig. 3. Projection of the crystal structure along the b-axis of the less-soluble salt, $(+)_{589}$-*trans*(*O*)-[Co(gly)$_2$en]H-*d*-tart·3H$_2$O. Possible hydrogen bonds are indicated by broken lines.

factors (B=4.0 Å^2) converged to R=0.043 (the refinement of the inverted structure gave R=0.045). A final difference map showed no peaks higher than 0.5 electron/Å^3. The quantity minimized was $w(|F_o|-k|F_c|)^2$. Cruickshank's weighting scheme[4] was used, where $w=1/(a+|F_o|+b|F_o|^2)$, with a=6.50 and b=0.019. The atomic scattering factors from the International Tables for X-Ray Crystallography[5] were used. The effect of the anomalous dispersion of the Co atom was included in the calculation: the values of $\Delta f'$=0.299 and $\Delta f''$=0.973 for Mo $K\alpha$ radiation were also taken from the International Tables for X-Ray Crystallography.[6]

The More-soluble Salt, (−)$_{589}$-trans(O)-[Co(gly)$_2$en]-H-d-tart·H$_2$O (2). The determination and the refinement of the structure were made in a way similar to those used for **1**. The final refinement converged to R=0.064 (the inverted structure gave R=0.067). A final difference map revealed no peaks higher than 0.4 electron/Å^3. A weighting scheme similar to that used in the case of **1** was used, with a=15.00 and b=0.016.

All the computations were carried out by a HITAC-8700 computer at the Hiroshima University Computer Center. The computer programs used were FOUR-2/M (Fourier synthesis)[7] and HBLS-IV (Least-square calculation), with a slight modification.[8] The final atomic parameters and temperature factors (with their estimated standard deviations) for both salts are listed in Tables 2—5. For both salts, complete lists of the $10|F_o|$ and $10|F_c|$ values have been preserved by the Chemical Society of Japan (Document No. 7937).

Results and Discussion

Geometry and Absolute Configuration of Cations. The bond distances and angles within the complex cation of the less- and more-soluble salts are listed in Tables 6 and 7. All the distances and angles are in good agreement with the reported values.[1,2,9-12]

The absolute configuration of the (+)$_{589}$-*trans*(*O*)-[Co(gly)$_2$en]$^+$ cation was identified as *Λ*-*δ*[13] on the basis of that of the hydrogen-*d*-tartrate used as an internal reference.[14,15] Similarly, that of the (−)$_{589}$-*trans*(*O*)-[Co(gly)$_2$en]$^+$ cation was identified as *Δ*-*λ*. These assignments are in accordance with those proposed

Table 8. Intermolecular distances (≤3.28 Å) for (+)$_{589}$-*trans*(*O*)-[Co(gly)$_2$en]H-*d*-tart·3H$_2$O

D–H···A[a]	D···A(*l*/Å)	H···A (*l*/Å)	D–H···A (*φ*/°)
N(E1)–H(NE11)···O(W3)^{i}	3.173(8)[b]	2.29	150
N(E1)–H(NE12)···O(T4)	3.235(7)	2.69	114
N(E1)–H(NE12)···O(G2)^{ii}	3.171(7)[b]	2.41	132
N(E2)–H(NE21)···O(G4)^{iii}	2.833(7)[b]	1.91	150
N(E2)–H(NE22)···O(W1)	3.128(7)[b]	2.38	130
N(G1)–H(NG11)···O(W1)^{v}	3.094(8)[b]	2.19	153
N(G1)–H(NG12)···O(G4)^{vi}	2.896(8)[b]	1.88	178
N(G2)–H(NG21)···O(W2)^{vii}	2.875(10)[b]	1.90	163
N(G2)–H(NG22)···O(G1)^{ii}	3.033(6)	2.35	124
N(G2)–H(NG22)···O(G2)^{ii}	3.128(6)[b]	2.17	155
O(G2)···O(T4)^{viii}	2.895(6)	—	—
O(W1)^{vi}–H(OW1)···O(G2)	2.955(7)[b]	2.30	154
O(G2)···O(W3)^{vii}	3.161(8)	—	—
C(E2)···O(W1)	3.117(10)	—	—
C(G3)···O(W1)^{v}	3.110(8)	—	—
C(G4)–H(CG42)···O(W3)^{i}	3.244(9)	2.33	145
C(G4)···O(W1)^{v}	3.148(8)	—	—
O(G4)···C(E2)^{ix}	3.207(10)	—	—
N(G1)–H(NG11)···O(T6)^{iv}	3.274(7)	2.58	128
O(T1)···O(W3)^{x}	3.258(10)	—	—
O(T3)^{x}–H(OT3)···O(T1)	2.906(9)[b]	2.30	124
O(T2)–H(OT2)···O(T5)^{iii}	2.608(7)[b]	1.80	173
O(W3)–H(OW32)···O(T3)	2.843(8)[b]	2.03	171
O(W2)^{x}–H(OW21)···O(T4)	3.017(10)[b]	2.40	130
O(W3)^{x}–H(OW31)···O(T5)	2.806(8)[b]	2.09	145
O(W1)–H(OW12)···O(T6)^{x}	2.650(7)[b]	2.02	124
O(W2)–H(OW22)···O(W3)	2.919(11)[b]	2.07	159

Roman numerals as superscripts refer to the following equivalent positions relative to the reference molecule at x, y, z:

i(1−*x*, −1/2+*y*, 1−*z*),	*ii*(2−*x*, −1/2+*y*, 1−*z*)
iii(*x*, 1+*y*, *z*),	*iv*(1+*x*, *y*, 1+*z*)
v(2−*x*, −1/2+*y*, 2−*z*),	*vi*(2−*x*, 1/2+*y*, 2−*z*)
vii(1+*x*, *y*, *z*),	*viii*(2−*x*, 1/2+*y*, 1−*z*)
ix(*x*, −1+*y*, *z*),	*x*(1−*x*, 1/2+*y*, 1−*z*)

a) D, hydrogen donor; A, hydrogen acceptor. b) Possible hydrogen bonds.

by Dabrowiak and Cooke[3] based on the CD spectral pattern. The projections of the crystal structure of **1** along the c-axis and that of **2** along the b-axis are shown in Figs. 1 and 2 respectively. These projections correspond to the figure viewed along the guasi-threefold axis of each complex cation.

Anion Geometry. The bond distances and angles of the H-*d*-tart anions in both crystals are in accordance

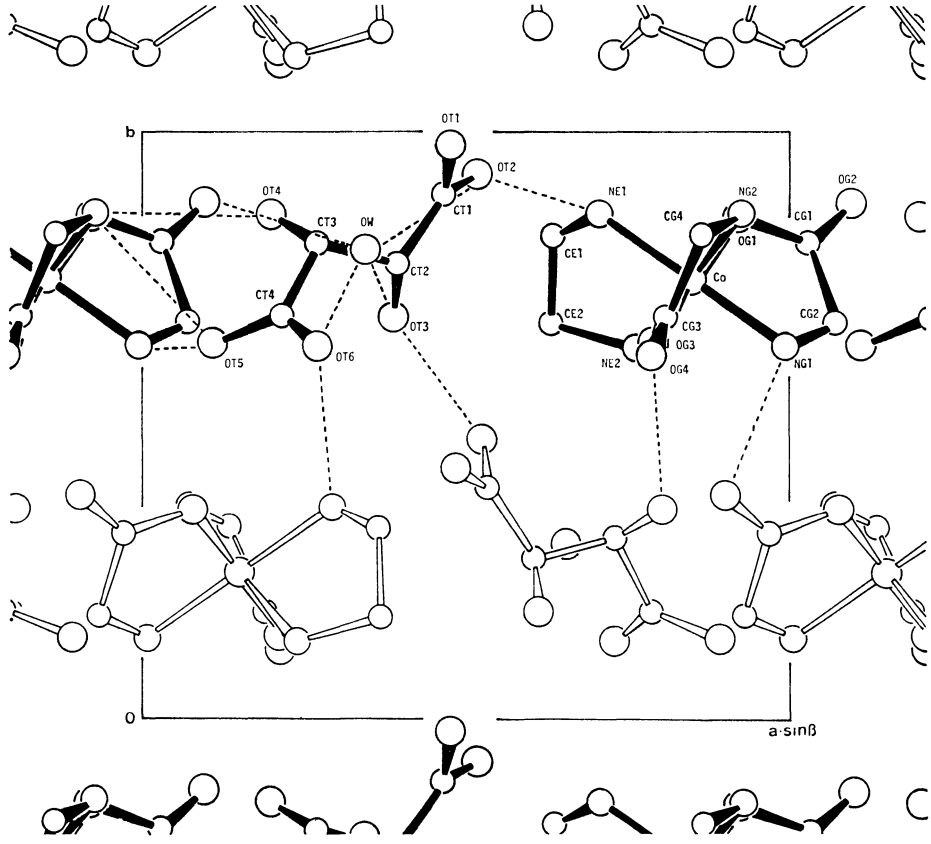

Fig. 4. Projection of the crystal structure along the c-axis of the more-soluble salt, $(-)_{589}$-*trans*(*O*)-[Co(gly)$_2$en]H-*d*-tart·H$_2$O. Possible hydrogen bonds are indicated by broken lines.

Table 9. Intermolecular distance ($\leq$3.28 Å) for $(-)_{589}$-*trans*(*O*)-[Co(gly)$_2$en]H-*d*-tart·H$_2$O

D–H···A[a]	D···A (l/Å)	H···A (l/Å)	D–H···A (ϕ/°)
N(E1)^{i}–H(NE11)···O(T6)	2.785(10)[b]	1.82	155
N(E1)–H(NE12)···O(T2)^{ii}	2.962(14)[b]	2.08	148
N(E2)–H(NE21)···O(G2)^{iii}	2.978(10)[b]	2.16	140
N(E2)–H(NE22)···O(G4)^{viii}	2.867(11)[b]	1.95	150
N(G1)–H(NG11)···O(G2)^{iii}	2.907(10)[b]	1.96	161
N(G1)–H(NG12)···O(T5)^{v}	2.833(10)[b]	1.84	168
N(G2)–H(NG22)···O(T4)^{v}	2.978(10)[b]	2.00	164
N(G2)–H(NG22)···O(T5)^{v}	3.152(10)	2.50	122
OW^{vi}–H(OW2)···O(G2)	2.929(12)[b]	2.16	132
O(T4)^{i}–H(OT4)···O(G4)	2.715(11)[b]	1.86	149
OW–H(OW1)···O(T6)	2.713(12)[b]	1.91	174
OW···O(T2)^{ii}	3.161(15)	—	—
O(T3)^{ii}–H(OT3)···OW	2.731(12)[b]	1.90	155
O(T1)^{vii}–H(OT1)···O(T3)	2.579(11)[b]	1.68	145

Roman numerals as superscripts refer to the following equivalent positions relative to the reference molecule at x, y, z:

i $(1-x, -1/2+y, 1-z)$,	ii $(x, y, 1+z)$
iii $(2-x, -1/2+y, 1-z)$,	iv $(-1+x, y, -1+z)$
v $(1+x, y, 1+z)$,	vi $(1+x, y, z)$
vii $(1-x, -1/2+y, -z)$,	viii $(x, y, -1+z)$

a) D, hydrogen donor; A, hydrogen acceptor. b) Possible hydrogen bonds.

with the previously reported values.[1,2,16] The five nonhydrogen atoms of each α-hydroxycarboxylate moiety lie approximately on a plane. The angle between the planes of the two α-hydroxycarboxylate moieties in the less-soluble salt (**1**) is nearly equal to the corresponding angle of the H-*d*-tart anion in **3** (55.4° *vs.* 55.8°[1]). On the other hand, the corresponding value in the more-soluble salt (**2**) is 60.9° (61.3° for **4**[2]).

Crystal Packing. *(a) The Less-soluble Salt (1)*: The crystal structure consists of discrete $(+)_{589}$-*trans*(*O*)-$[Co(gly)_2en]^+$ cations, H-*d*-tart anions, and water molecules. Figures 1 and 3 show the projections of the crystal structure along the c- and b-axes respectively. The intermolecular distances and angles are summarized in Table 8.

In the crystal there are two distinct layers, as is shown in Figs. 1 and 3. The first layer is formed by H-*d*-tart anions. The H-*d*-tart anions are arranged to form a double-chain structure along the twofold screw axis at ($x=1/2$, $z=1/2$). Here, each component chain itself has a "head-to-tail" arrangement formed by a unit translation of the H-*d*-tart anion along the b-axis. The O(T2)···O(T5)^{iii} distance, 2.608 Å, is slightly longer than those in **3** and **4** (2.44 and 2.47 Å respectively).[1,2] The two-component chains, moreover, are linked to each other through the hydrogen bonds (O(T1)···O(T3)^x 2.906 Å) and are related by the twofold screw axis. These double-chain structures, then, are related to each other by the twofold screw axis at ($x=1/2$, $z=0$) to form the layer parallel to the bc plane.

The second layer is built up of the complex cations. The layer of the complex cation is constructed by the same symmetry operation as in the case of the H-*d*-tart anion, as is shown in Figs. 1 and 3.

The first and second layers are not only directly adjoined with each other by short contacts: N(E1)···O(T4) 3.235, O(G2)^{ii}···O(T4) 2.895, and N(G1)···O(T6)^{iv} 3.274 Å, but are also indirectly joined together by hydrogen bonds *via* the waters of crystallization: O(T6)···O(W1)···O(G2), O(T6)···O(W1)···N(E2), O(T6)···O(W1)···N(G1), O(T4)···O(W2)···N(G2), O(T3)···O(W3)···N(E1), and O(T5)···O(W3)···N(E1).

(b) The More-soluble Salt (2): Figures 2 and 4 show the projections of the crystal structure of **2** along the b- and

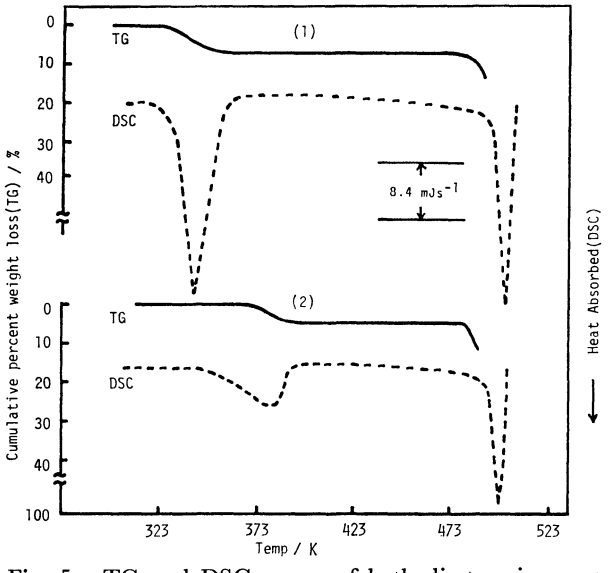

Fig. 5. TG and DSC curves of both diastereoisomers: (1) the less-soluble salt, $(+)_{589}$-*trans*(*O*)-$[Co(gly)_2en]$-H-*d*-tart·$3H_2O$; (2) the more-soluble salt, $(-)_{589}$-*trans*-(*O*)-$[Co(gly)_2en]$H-*d*-tart·H_2O.

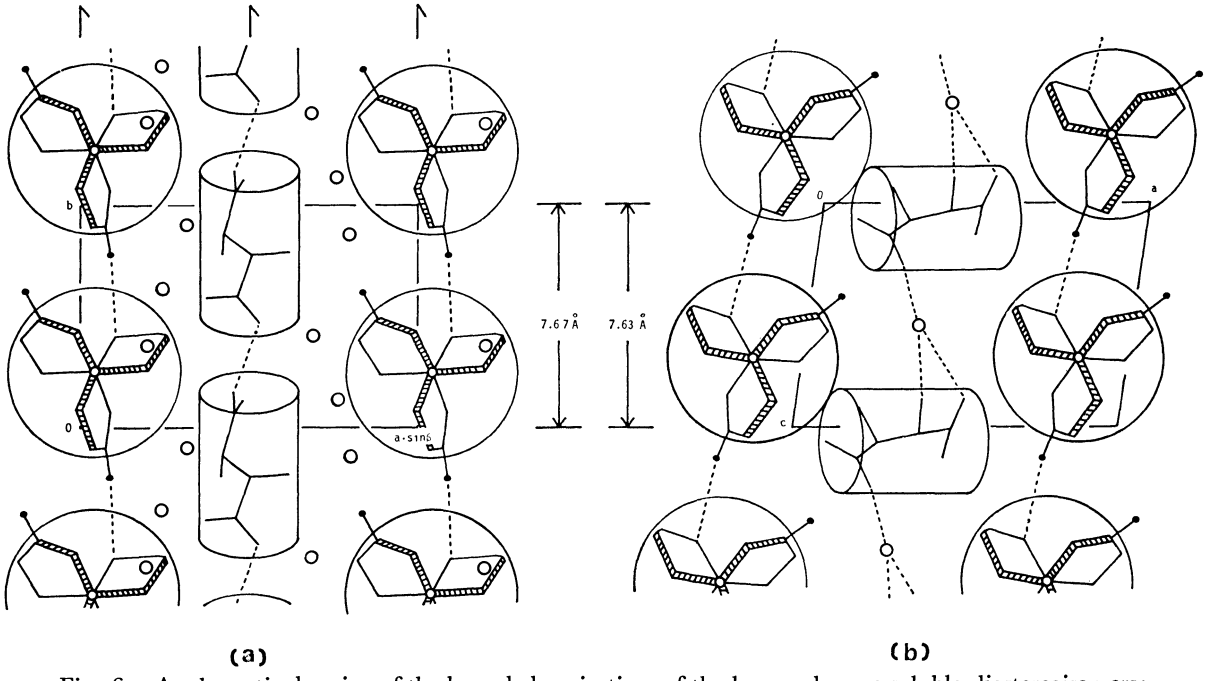

Fig. 6. A schematic drawing of the bounded projections of the less- and more-soluble diastereoisomers: (a) $(+)_{589}$-*trans*(*O*)-$[Co(gly)_2en]$H-*d*-tart·$3H_2O$(c-axis projection), (b) $(-)_{589}$-*trans*(*O*)-$[Co(gly)_2en]$-H-*d*-tart·H_2O(b-axis projection).
Broken lines denote hydrogen bonds and small circles indicate water molecules.

c-axes respectively. The structure consists of the discrete $(-)_{589}$-*trans*(*O*)-[Co(gly)$_2$en]$^+$ cations, the H-*d*-tart anions, and the water molecules. The intermolecular distances and angles are listed in Table 9. In the crystal, the complex cations are stacked to form a chain by hydrogen bonds along the c-axis. The hydrogen bond distance, N(E2)···O(G4)^{viii}, is 2.867 Å. Along the c-axis, the H-*d*-tart anions do not form the "head-to-tail" chain structure, though they are connected to each other through the water of crystallization.

Thermal Behavior of the Water of Crystallization. The results of the TG and DSC measurements of both diastereoisomers are shown in Fig. 5. The crystals of the less-soluble salt (**1**) begin to release the water of crystallization at 327 K, and the dehydration ceases at 347 K. The weight loss accompanying this dehydration is found to be 9.7%. This value is very close to the value expected for the dehydration of 2.5H$_2$O (9.6%). The DSC peak is observed from 329 K to 354 K. The ΔH value for the dehydration is calculated to be 64.4 kJ mol^{-1}.

On the other hand, the more-soluble salt (**2**) loses 0.7 mol of the water of crystallization in the temperature range between 368 K and 382 K (TG curve). The DSC peak corresponding to this step is observed from 347 K to 389 K. The ΔH value for the dehydration step is found to be 73.0 kJ mol^{-1}, slightly larger than that of the less-soluble salt. The gradual decrease in both DSC curves in the range of about 420—470 K is probably due to the loss of the remaining water of crystallization (0.5H$_2$O for **1** and 0.3H$_2$O for **2**). The DSC peak was also found at about 500 K in both samples. While the TG measurement was being carried out, the samples got black and swelled above 490 K. The measurements was impossible above this temperature. It seems that the decomposition of both samples occurs at 490 K.

Thus, the less-soluble salt (**1**) (containing more water, trihydrate) has been proved to release water more easily than the more-soluble salt (**2**) (containing less water, monohydrate).

Comparison of the Packing Modes of the Less- and More-soluble Salts. The two crystal structures are shown schematically in Fig. 6, where the H-*d*-tart anions are depicted in a cylindrical form and the complex cations are represented as a large circle. There are some resemblances and differences between the packing modes of the two structures. The resemblances are: (1) The complex cations are stacked along the longitudinal axis in the figure, making a chain structure by the N–H···O hydrogen bonds in both crystals. (2) Unit translation along both longitudinal axes are quite similar; the distances are 7.67 Å for **1** and 7.63 ($c\times\sin\beta$) for **2**. The differences are: (1) In Fig. 6(a), the H-*d*-tart anions are linked with hydrogen bonds (–COOH···OOC–) just as the dry cells are arranged in a series circuit. In contrast, the H-*d*-tart anions in Fig. 6(b) are connected to each other *via* water molecules, COO···water $\cdots\begin{Bmatrix}\mathrm{OH}\\ \mathrm{COO}\end{Bmatrix}$, just as the dry cells are piled side by side in a parallel form. (2) A layer of water molecules exists in Fig. 6(a), but not in Fig. 6(b).

The crystal parameters of the two diastereoisomeric pairs are listed in Table 1. Since **2** and **3** have the same chemical formula, $C_{10}H_{23}N_4O_{11}Co$, the V/Z value of **2** should be nearly equal to that of **3**. However, the volume of **3** is 18.2 Å^3 smaller than that of **2**. The volume difference between **1** and **3** is 43.3 Å^3. This difference is nearly equal to twice the reported molecular volume of the water of crystallization (2×20.6 Å^3),[17] and can be attributed to the two excess water molecules in **1**. Hence, **1** is as dense as **3**. Consequently, in spite of the presence of more water of crystallization, the less-soluble salt (**1**) is more tightly packed than the more-soluble salt (**2**).

The situation is quite similar to the case in the diastereoisomeric pair of **3** and **4**. The volume difference between **3** and **4** is 27.2 Å^3. Since **4** has one more water molecule than **3**, this volume difference corresponds to the volume of one water molecule in **4**. The observed volume difference (27.2 Å^3) is 6.6 Å^3 larger than the expected volume for one water molecule.[17] Therefore, it may be inferred that **3** is more tightly packed than **4**.

The crystal structures of the less-soluble salts, **1** and **3**, contain the spiral chain of H-*d*-tart. In contrast, the more-soluble salts, **2** and **4**, do not have such spiral chains. Therefore, it can be considered that the tight packing in the less-soluble salt is caused by the existence of this spiral chain of H-*d*-tart. In other words, the existence of this spiral chain of H-*d*-tart plays a decisive role in the discrimination between Δ and Λ enantiomers. This conclusion is supported by the fact that several less-soluble salts of organic bases, (—)-adrenalinium H-*d*-tart,[16] (+)-[(—)-1-methyl-3-benzoylpiperidinium H-*d*-tart]H$_2$O,[18] and (—)-[(—)-1-methyl-3-ethyl-3-benzoylpiperidinium H-*d*-tart],[19] contain similar spiral chains of the H-*d*-tart anion in the crystal structures.

Additionally, a pitch of the spiral chain is considered important in the discrimination due to the H-*d*-tart anion. The observed length of the chain pitch (7.1—7.8 Å)* is nearly equal to the diameter of the complex cations, [Co(ox)en$_2$]$^+$ and [Co(gly)$_2$en]$^+$. These complex cations can themselves form a chain by hydrogen bonds (N–H···O) within the range of this pitch (7.1—7.8 Å). Other complex cations so far resolved by the H-*d*-tart anion are as follows: β-*cis*(*O*)-[Co(gly)$_2$en]$^+$,[3] *s*-*cis*-[Co(edda)(NH$_3$)$_2$]$^+$,[20] *trans*-[Co(edda)en]$^+$,[21] and *s*-*cis*-[Co(dmedda)(NH$_3$)$_2$]$^+$.[20],** The sizes and the skeletons of these complexes have a close resemblance to those of the [Co(ox)en$_2$]$^+$ and *trans*(*O*)-[Co(gly)$_2$en]$^+$ cations, as is shown in Fig. 7. The figure shows that the monovalent complex cation satisfying the following conditions has a great chance of optical resolution by way of the diastereoisomeric salt formation with the H-*d*-tart anion: (1) the complex cation has carboxyl and amino groups at the *trans* or *cis* positions of octahedral coordination, so that cations

* The chain pitches of the H-*d*-tart anion have values within 7.1—7.8 Å in Refs. 1, 2, 16, 18, and 19.

** The abbreviations used for the ligands are as follows: gly, glycinate anion; en, ethylenediamine; edda, ethylenediamine-*N*,*N*′-diacetate anion; dmedda, dimethylethylenediamine-*N*,*N*′-diacetate anion.

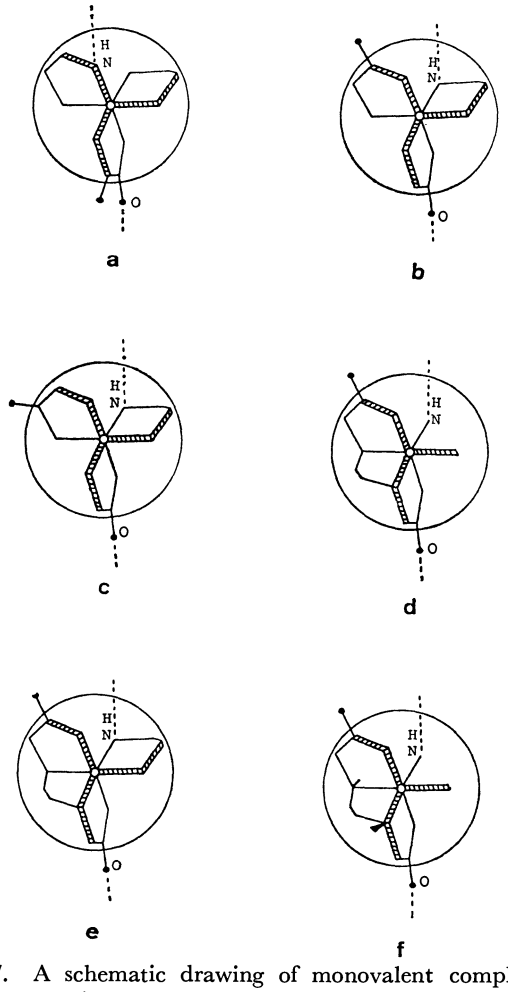

Fig. 7. A schematic drawing of monovalent complex cations having a structural resemblance to $(+)_{589}$-[Co(ox)en_2]$^+$ and $(+)_{589}$-*trans*(*O*)-[Co(gly)$_2$en]$^+$:
(a) $(+)_{589}$-[Co(ox)en_2]$^+$, (b) $(+)_{589}$-*trans*(*O*)-[Co(gly)$_2$en]$^+$, (c) *β-cis*(*O*)-[Co(gly)$_2$en]$^+$, (d) *s-cis*-[Co(edda)$(NH_3)_2$]$^+$, (e) *trans*-[Co(edda)en]$^+$, and (f) *s-cis*-[Co(dmedda)$(NH_3)_2$]$^+$.

can be linked with each other by N–H···O type hydrogen bonds, and (2) the complex cation is 7.1—7.8 Å in diameter, so that the complex cations can be arranged in a spiral chain with the same pitch as that of the H-*d*-tart spiral chain.

The author wishes to express his thanks to Professor Hayami Yoneda and Dr. Yoshihiko Kushi of Hiroshima University for their kind guidance and encouragement throughout this work, and also to Dr. Ushio Sakaguchi and to Dr. Katsuhiko Miyoshi for their stimulating discussion and helpful suggestions. The author is also grateful to Dr. Kozo Akabori, Hiroshima University, for the TG and DSC measurements and for his valuable suggestions; thanks are also due to the Hiroshima University Computer Center for a generous allocation of computer time.

References

1) M. Kuramoto, Y. Kushi, and H. Yoneda, *Bull. Chem. Soc. Jpn.*, **51**, 3251 (1978).
2) M. Kuramoto, Y. Kushi, and H. Yoneda, *Bull. Chem. Soc. Jpn.*, in press.
3) J. C. Dabrowiak and D. W. Cooke, *Inorg. Chem.*, **14**, 1305 (1975).
4) D. W. J. Cruickshank, "Computing Methods and the Phase Problem in X-ray Crystal Analysis," ed by R. Pepinsky, J. M. Robertson, and J. C. Speakman, Pergamon Press, Oxford (1961), p. 45.
5) "International Tables for X-Ray Crystallography," Kynoch Press, Birmingham (1968), Vol. III, pp. 201—206.
6) "International Tables for X-Ray Crystallography," Kynoch Press, Birmingham (1974), Vol. IV, p. 148.
7) Y. Kushi, unpublished work.
8) T. Ashida, "The Universal Crystallographic Computation Program System," ed by T. Sakurai, The Crystallographic Society of Japan (1967).
9) H. Miyamae and Y. Saito, *Acta Crystallogr., Sect. B*, **34**, 937 (1978).
10) P. Vasić, R. Herak, and S. Djurić, *Acta Crystallogr., Sect. B*, **32**, 91 (1976).
11) L. J. Halloran, R. C. Caputo, R. D. Willett, and J. I. Legg, *Inorg. Chem.*, **14**, 1762 (1975).
12) Y. Mitsui, J. Watanabe, Y. Harada, T. Sakamaki Y. Iitaka, Y. Kushi, and E. Kimura, *J. Chem. Soc., Dalton, Trans.*, **1976**, 2095.
13) IUPAC, *Inorg. Chem.*, **9**, 1 (1970).
14) A. J. van Bommel and J. M. Bijvoet, *Acta Crystallogr.*, **11**, 61 (1958).
15) The application of Hamilton's *R*-factor ratio test (*Acta Crystallogr.*, **18**, 502 (1965)) gave 0.045/0.043=1.05 for **1** and 0.067/0.064=1.05 for **2**. Therefore, the hypothesis that the inverted structure is correct can be rejected at the 0.5% significance level.
16) D. Carlström, *Acta Crystallogr., Sect. B*, **29**, 161 (1973).
17) K. Harata, *Bull. Chem. Soc. Jpn.*, **49**, 2066 (1976).
18) G. Hite and J. R. Soares, *Acta Crystallogr., Sect. B*, **29**, 2935 (1973).
19) J. R. Ruble, G. Hite, and J. R. Soares, *Acta Crystallogr., Sect. B*, **32**, 136 (1976).
20) W. T. Jordan and B. E. Douglas, *Inorg. Chem.*, **12**. 403 (1973).
21) J. I. Legg, D. W. Cooke, and B. E. Douglas, *Inorg, Chem.*, **6**, 700 (1967).

The Synthesis of $Mg_3(PO_4)_2 \cdot 8H_2O$ and Its New Polymorphism

Takafumi KANAZAWA,* Takao UMEGAKI, and Masao SHIMIZU

Department of Industrial Chemistry, Faculty of Technology, Tokyo Metropolitan University, Fukasawa, Setagaya-ku, Tokyo 158

(Received February 2, 1979)

Bobierrite, $Mg_3(PO_4)_2 \cdot 8H_2O$, could be synthesized from mixed solutions of Na_2HPO_4 and $MgSO_4$ at an initial pH of 6.4—7.0 with the addition of $Ca(NO_3)_2$, $CuSO_4$, $NiSO_4$, gelatin, or agar, by heating at 80—90 °C for 2—48 h. X-Ray studies indicated the coexistence of two kinds of lattice in each synthetic $Mg_3(PO_4)_2 \cdot 8H_2O$ crystal. One phase (Phase 1) is monoclinic, space group $P2_1/m$ or $P2_1$, with $a=10.08(2)$, $b=27.86(3)$, $c=4.656(7)$ Å, and $\beta=105.0(2)°$. The other phase (Phase 2) is monoclinic, space group C2/m, C2, or Cm, with $a=10.07(2)$, $b=13.38(2)$, $c=4.656(7)$ Å, and $\beta=105.0(2)°$. If a centrosymmetric space group C2/m is assumed for the latter, Phase 2 may be considered to be a new polymorph of $Mg_3(PO_4)_2 \cdot 8H_2O$, one belonging to the vivianite series. Newberyite, $MgHPO_4 \cdot 3H_2O$, was also formed in the above synthetic procedure. This phosphate was precipitated under slightly more acidic conditions than those where $Mg_3(PO_4)_2 \cdot 8H_2O$ was obtained.

Bobierrite, $Mg_3(PO_4)_2 \cdot 8H_2O$ (TMP8), has been found chiefly in guano deposits as minute crystals, associated with newberyite, $MgHPO_4 \cdot 3H_2O$ (DMP3), and several magnesium ammonium orthophosphates. TMP8 was first described by Bobierre in 1868;[1] X-ray and optical studies of this mineral were made by Barth in 1937.[2] According to Barth's determinations, TMP8 belongs to a different space group from that of the vivianite series ($A_3(XO_4)_2 \cdot 8H_2O$; A=Fe, Co, Ni, Zn, Mg: X=P, As), and the b-axis of the unit cell is doubled compared with the $8H_2O$ family. However, the crystal structure of TMP8 has not yet been determined at present. Therefore, we have investigated the crystal growth of TMP8 and its X-ray diffraction data in order to clarify the crystallographical relation between TMP8 and the vivianite group.

The preparations of TMP8 have been reported by de Schulten (1903),[3] Bassett and Bedwell (1933),[4] Frazier *et al.* (1963),[5] and the present authors (1974, 1976).[6-8] However, we have seen no reference to the crystal growth of this mineral. The present paper will deal with a new method of synthesizing TMP8 from mixed solutions of $MgSO_4$ and Na_2HPO_4 in an initial pH of 6.4—7.0 at 80—90 °C for 2—48 h by using inorganic and organic additives, and then additionally preparing the crystals in a suitable size for the X-ray Weissenberg method. The X-ray oscillation and Weissenberg photographs have indicated the coexistence of two monoclinic lattices (Phase 1 and Phase 2) in each synthesized TMP8 crystal, as will be described below.

Experimental

Preparation. *Syntheses without Additives*: A mixed solution of 4.1—8.3 g of $MgSO_4 \cdot 7H_2O$ and 4.0—8.0 g of $Na_2HPO_4 \cdot 12H_2O$ in 1500 ml of water was prepared. In each run, $MgSO_4 \cdot 7H_2O$ and $Na_2HPO_4 \cdot 12H_2O$ were mixed in the ratios given in Table 1. The pH of the mixture was then adjusted to 6.0—7.0 by adding HCl (about 2%) or acetic acid (HAc) (2%). The mixture thus prepared was heated in a water bath with a reflux at 90 °C for 2 h. The precipitates thus formed were filtered, washed with water, and dried in air and then in a silica gel desiccator for several days. The run products of the synthetic experiments are summarized in Table 1.

Syntheses with Inorganic Additives: A mixed solution of 4.1 g of $MgSO_4 \cdot 7H_2O$ and 4.0 g of $Na_2HPO_4 \cdot 12H_2O$ in 1500 ml of water was prepared. The solution was adjusted with HCl or HAc to each pH value given in Table 2. To this mixture, each inorganic additive ($Ca(NO_3)_2 \cdot 4H_2O$, $CuSO_4 \cdot 5H_2O$, $NiSO_4 \cdot 6H_2O$, $CoSO_4 \cdot 7H_2O$, $MnSO_4 \cdot 4H_2O$, and $ZnSO_4 \cdot 7H_2O$) in a molar ratio to $MgSO_4$ of about 1: 100, was then added. The mixture thus prepared was heated in the same manner as in the syntheses without additives.

Syntheses with Gelatin: The same procedure as in the syntheses with inorganic additives was carried out except for the replacement of inorganic additives with 10—50 g of

Table 1. Synthetic condition of TMP8 without additives

Run	Solutions: Starting materials (g/1500 ml of water) $Na_2HPO_4 \cdot 12H_2O$	Solutions: Starting materials (g/1500 ml of water) $MgSO_4 \cdot 7H_2O$	Initial pH of solution	Phases found[a] in products
1	8.0	8.3	6.0	DMP3, U
2	6.0	6.2	6.2	DMP3, U, TMP 8
3	8.0	8.3	6.2	U, TMP8
4	4.0	4.1	6.4	U, TMP8
5	4.0	4.1	6.6	U
6	4.0	4.1	6.8	U
7	4.0	4.1	7.0	U

a) DMP3=$MgHPO_4 \cdot 3H_2O$; TMP8=$Mg_3(PO_4)_2 \cdot 8H_2O$; U=unidentified crystalline material.

Table 2. Synthetic condition of TMP8 with inorganic additives

Additive	Solutions: Acid	Solutions: Initial pH	Phases found in products
$Ca(NO_3)_2 \cdot 4H_2O$	HCl	6.6—7.0	TMP8
	HAc[a]	6.4—7.0	TMP8
$CuSO_4 \cdot 5H_2O$	HCl, HAc	6.4—6.6	TMP8
$NiSO_4 \cdot 6H_2O$	HCl, HAc	6.4—6.6	TMP8
$CoSO_4 \cdot 7H_2O$	HCl	6.4—6.6	TMP8, U
$CoSO_4 \cdot 7H_2O$	HCl	6.8—7.0	U
$CoSO_4 \cdot 7H_2O$	HAc	6.4—7.0	U
$MnSO_4 \cdot 4H_2O$	HCl, HAc	6.4—7.0	U
$ZnSO_4 \cdot 7H_2O$	HCl, HAc	6.4—7.0	U

a) HAc=acetic acid.

gelatin, the narrowing of an initial pH region from 6.4—7.0 to 6.6—6.8, and the extension of a heating time from 2 h to 4—24 h.

Syntheses with Agar: First, a solution of 4.0 g of $Na_2HPO_4 \cdot 12H_2O$ in 1200 ml of water was prepared, and then 5—10 g of agar were added to the solution. The solution was then heated up to about 80 °C until the agar was dissolved. To this, a solution of 4.1 g of $MgSO_4 \cdot 7H_2O$ in 300 ml of water, adjusted to an acidic condition by adding an appropriate amount of HCl or HAc, which had been determined by experiments, was then stirred in. The mixture thus prepared was set aside to gel for several hours. The agar gel solution was heated by the same procedure as in the above syntheses at 80—90 °C for 4—48 h. The crystals thus obtained were washed by boiling them mildly in water, and dried in air and then in a silica gel desiccator for several days.

Table 3. Chemical composition of synthetic TMP8[a]

	MgO (%)	P_2O_5 (%)	H_2O (%)	Mg/P[b]
Found	29.8	35.3	34.9[c]	1.49
			36.4[d]	
Calcd	29.7	34.9	35.4	1.5

a) Prepared by the addition of agar. b) Mole ratio. calculated by the use of this formula: $H_2O = 100 - (MgO + P_2O_5)$. d) Calculated from weight loss on heating.

Measurements. The run products were identified by X-ray powder diffractometry (Cu $K\alpha$, Ni filter), refractive index measurement (the immersion method), optical microscopy, and chemical analysis. Chemical analysis was performed on TMP8 grown in an agar-containing solution; the magnesium was determined by the chelatometric titration method; the phosphorus, by molybdovanadate colorimetry, and the water contents, as loss on ignition to about 800 °C. The chemical compositions of the synthetic TMP8 are shown in Table 3. The lattice constants of the synthetic TMP8 were obtained by the least-squares calculation on the basis of the results of the Weissenberg method (Cu $K\alpha$, Ni filter, and Si standard). Weissenberg photographs were taken with regard to zero-, first-, and second-layer lines about the c-axis, and the zero-layer line about the a- and b-axes.

Results and Discussion

General Remarks. As is shown in Table 1, no pure phase of TMP8 was precipitated on syntheses of this compound from a mixed solution of Na_2HPO_4 and $MgSO_4$ without additives. In this case, only a small amount of TMP8 appeared in the products. Under the syntheses without additives, it seemed rather diffcult to form. Therefore, we investigated tentatively the effects of inorganic and organic additives on the TMP8 formation, and then the influence of those additives on the size and morphology of the crystals. Inorganic additives ($Ca(NO_3)_2 \cdot 4H_2O$, $CuSO_4 \cdot 5H_2O$, or $NiSO_4 \cdot 6H_2O$) and organic additives (gelatin or agar) were found to be effective on the formation of TMP8. The habits of the synthetic TMP8 crystals obtained both with and without additives were plates, with (010) being the dominant forms and elongated along the c-axis. The size of the TMP8 crystals obtained inclined to increase as the initial pH of the mixture was lowered and as the heating temperature and time increased. The pH of the mixture was observed to be lowered after the precipitation of crystals.

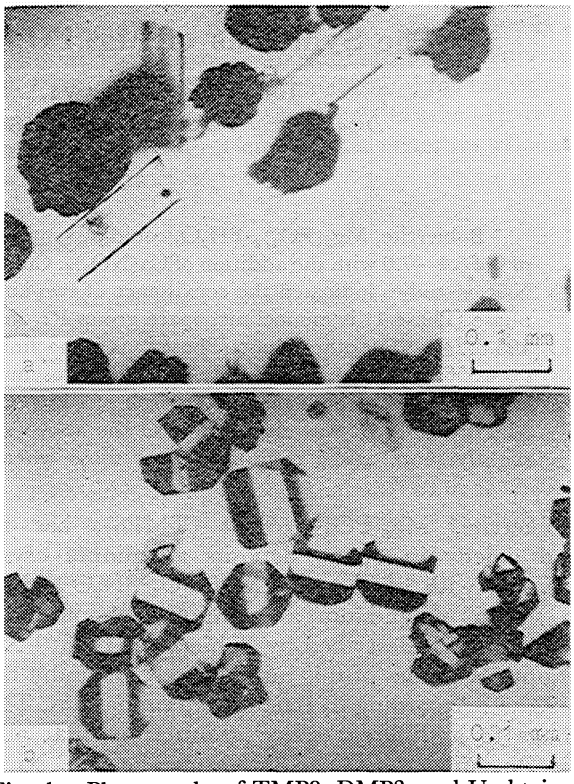

Fig. 1. Photographs of TMP8, DMP3, and U obtained without additives.
a) TMP8 and U obtained at initial pH 6.2 using HCl. TMP8=parallelepiped platy crystals. U=spherically aggregated materials. b) DMP3 obtained at initial pH 6.0.

Crystals from the Solution without Additives. In the syntheses without additives, TMP8 was found in only small amounts in the products at initial pH values of the mixture of 6.2—6.4, as is shown in Table 1. Figure 1-a shows TMP8 crystals coexisting with unidentified crystalline materials (U). Under slightly more acidic conditions, namely, at the initial pH 6.0, sometimes DMP3 (Fig. 1-b) containing U was obtained, while U was precipitated at the initial pH values of the mixture of 6.6—7.0.

Crystals from the Solutions with Inorganic Additives. The run data of the synthetic experiments with inorganic additives are given in Table 2. Below the initial pH value of 6.2, no precipitate was formed. Above each initial pH shown in Table 2, U tended to be precipitated predominantly.

The maximum size of the crystals obtained by the addition of $Ca(NO_3)_2 \cdot 4H_2O$ and $CuSO_4 \cdot 5H_2O$ were as large as 2.8 by 1.4 and 2.2 by 1.2 mm, respectively, while that of the crystals obtained by the addition of $NiSO_4 \cdot 6H_2O$ was relatively small (about 0.12 by 0.08 mm). The dimension in the direction of b-axis was usually below about 0.02 mm. The synthetic TMP8 crystals are shown in Figs. 2-a, b, and c. On the other hand, U was precipitated from the mixture to which $MnSO_4 \cdot 4H_2O$ or $ZnSO_4 \cdot 7H_2O$ had been added, under the synthetic conditions studied here, and both TMP8 and U were precipitated from a mixture to which

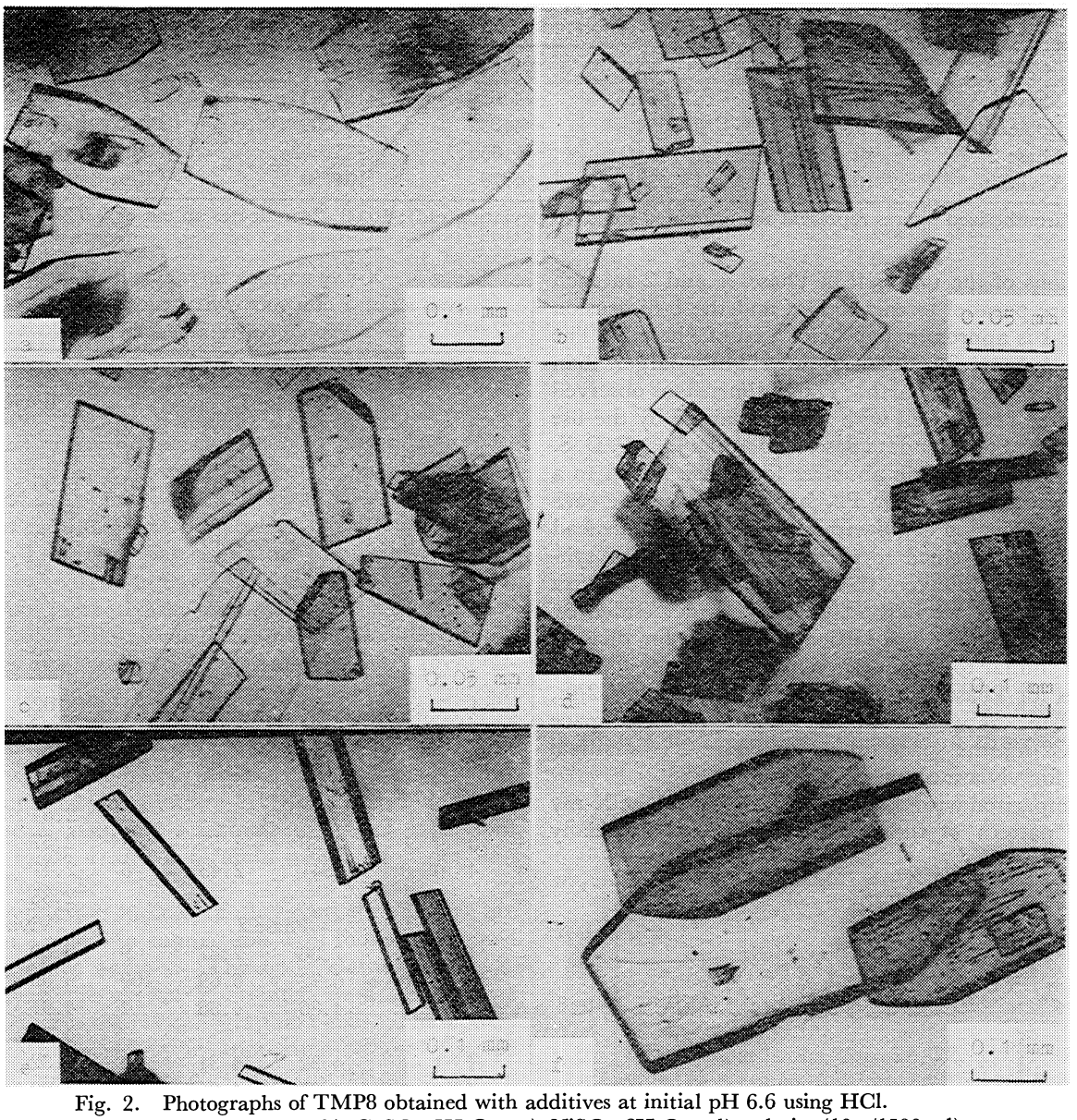

Fig. 2. Photographs of TMP8 obtained with additives at initial pH 6.6 using HCl.
a) $Ca(NO_3)_2 \cdot 4H_2O$, b) $CuSO_4 \cdot 5H_2O$, c) $NiSO_4 \cdot 6H_2O$, d) gelatin (10 g/1500 ml), e) gelatin (45 g/1500 ml), f) agar.

$CoSO_4 \cdot 7H_2O$ was added at an initial pH of about 6.4—6.6. These results might be interpreted as follows: since Mg ions in the TMP8 structure are inferred to be octahedrally coordinated in all their sites,[9] the presence of Cu^{2+} and Ni^{2+}, which tend to prefer octahedral coordination,[10] will be effective on the stabilization of those cation sites of TMP8 and, as a result, on the promotion of its nucleation and crystal growth.

Crystals from the Solutions with Organic Additives. The TMP8 crystals grown in the gelatin solution heated for 6 h were in the form of colorless and transparent fragments. The crystals were plates about 0.1 mm long as a maximum. When the heating time ranged to 24 h, the crystals with a maximum length of about 0.3—0.4 mm were obtained (Fig. 2-d). In this case, the smoothness of the surfaces of the crystals was generally inferior to that of the crystals obtained from the mixtures heated for 6 h described above. As the concentrations of gelatin were increased (40—50 g/1500 ml), the crystals obtained were more elongated along the c-axis and altered from a plate-like shape into a needle-like appearence (Fig. 2-e).

The crystals grown in the agar solution heated for 6 h were about 0.08 mm long as a maximum. Heat treatment for 24—48 h yielded crystals as large as $0.5 \times 0.25 \times 0.04$ mm in maximum size (Fig. 2-f). The surface smoothness of TMP8 crystals grown in the agar solution were, in general, superior to that of crystals in the gelatin solution microscopically. This is probably due to the difference in the stability of gel between the gelatin and agar solutions at 80—90 °C.

A New Crystal Phase of TMP8. Each crystal examined here showed the coexistence of two monoclinic lattices (Phase 1 and Phase 2), judging from the results of the oscillation and Weissenberg photographs. Table 4 shows the lattice constants and possible space groups of Phase 1 and Phase 2 in comparison with those of the natural TMP8 and vivianite, respectively. The axial

TABLE 4. CRYSTALLOGRAPHIC DATA FOR PHASE 1 AND PHASE 2

	a/Å	b/Å	c/Å	β/°	Space group
Phase 1	10.08 (2) [a]	27.86 (3)	4.656 (7)	105.0 (2)	$P2_1/m$, $P2_1$
Bobierrite	9.946[b]	27.654	4.639	104.02	$P2_1/c$[1]
Phase 2	10.07 (2)	13.38 (2)	4.656 (7)	105.0 (2)	C2/m, C2, Cm
Vivianite	10.08	13.43	4.70	104.50	C2/m[13]

a) Parenthesized figures represent the estimated standard deviation(esd); 10.08 (2) indicates an esd of 0.02. b) *kX*.

orientations of the unit cell of Phases 1 and 2 in each crystal are parallel to each other, and the b-dimension of Phase 1 is approximately twice that of Phase 2. The lattice constants for Phase 1 are slightly larger than those determined by Barth. Those dimensions observed by us agree rather well with those obtained by the use of the indexed powder data described in the J. C. P. D. S. File.[11] The systematic absences for Phase 1 lead to a space group of $P2_1/m$ or $P2_1$ because of the presence of a weak reflection of $h0l$ with both h and l odd, instead of the $P2_1/c$[1] assigned to natural TMP8. In this synthetic crystal, however, there are a number of extra extinctions that are beyond the criteria demanded by those space groups. The lattice dimensions for Phase 2 are very similar to those of vivianite, and the systematic absences for Phase 2 indicate a space group of C2/m, C2, or Cm. If we assume the centrosymmetric space group C2/m, the space group for Phase 2 is identical to that for vivianite series.

In comparison with the J. C.P. D. S. File,[11] the X-ray powder pattern of the synthetic TMP8 is especially

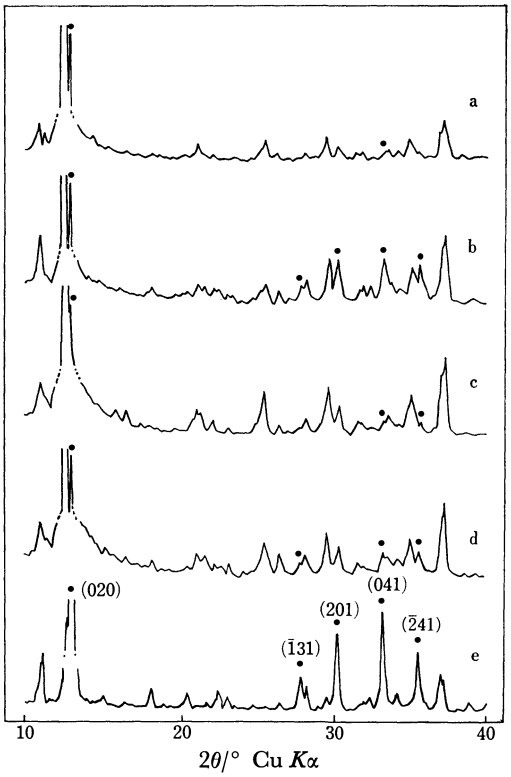

Fig. 3. X-ray diffraction patterns of TMP8 obtained with additives.
a) Agar, b) gelatin, c) $Ca(NO_3)_2 \cdot 4H_2O$, d) $CuSO_4 \cdot 5H_2O$, e) $NiSO_4 \cdot 6H_2O$. Marks (●) show relatively strong diffraction peaks of Phase 2.

TABLE 5. X-RAY POWDER DIFFRACTION DATA OF PHASE 1 AND PHASE 2 COMPARED WITH THOSE OF BOBIERRITE AND VIVIANITE RESPECTIVELY

h	k	l	d_{obsd}	d_{calcd}	I/I_0	d_{obsd}	I/I_0
			Phase 1			Bobierrite	
0	2	0	13.87	13.93	2		
1	2	0	7.96	7.98	4	8.04	18
0	4	0	6.96	6.97	100	6.96	100
2	0	0	4.86	4.87	1	4.87	2
1	6	0	4.18	4.19	1	4.19	6
$\bar{1}$	3	1	4.09	4.09	1	4.11	4
2	4	0	3.97	3.99	1	4.00	4
						3.81	2
0	8	0	3.47	3.48	2	3.48	8
3	2	0	3.15	3.16	1	3.16	4
$\bar{1}$	7	1	3.00	3.00	4	3.02	10
2	1	1	2.93	2.93	3	2.94	25
2	8	0	2.81	2.83	1	2.81	14
						2.66	4
						2.61	6
0	9	1	2.56	2.55	3	2.57	10
4	0	0	2.41	2.43	6	2.41	12
						2.35	4
			Phase 2			Vivianite	
1	1	0	7.88	7.87	9	8.00	27
0	2	0	6.72	6.69	100	6.80	100
2	0	0	4.86	4.86	2	4.91	40
						4.50	13
$\bar{1}$	1	1	4.32	4.31	5	4.32	4
1	3	0	4.05	4.05	1	4.09	13
2	2	0	3.93	3.93	3		
$\bar{2}$	0	1	3.83	3.83	3	3.84	40
						3.65	5
0	4	0	3.35	3.35	2	3.33	3
$\bar{1}$	3	1	3.19	3.19	7	3.20	53
3	1	0	3.13	3.15	4		
2	0	1	2.95	2.94	12	2.97	67
0	4	1	2.69	2.68	15	2.71	67
3	3	0	2.62	2.62	2	2.64	8
$\bar{2}$	4	1	2.52	2.52	11	2.52	33
4	0	0	2.41	2.43	6	2.42	40
						2.31	27
2	4	1	2.21	2.21	4	2.23	20

characteristic in the presence of the prominent peak at 13.1—13.2° in 2θ. This can be explained as the strongest reflexion (020) of Phase 2. Figure 3 shows the X-ray diffraction patterns of TMP8 obtained by the addition of inorganic and organic compounds. The TMP8 obtained by adding $NiSO_4$ gives, in general, well-defined X-ray peaks of Phase 2 (Fig. 3-e). The X-ray powder diffraction data were indexed, using the lattice

Table 6. Refractive indices of TMP8 synthesized by the addition of inorganic and organic compounds

Additive	α	β	γ	Reference
$Ca(NO_3)_2 \cdot 4H_2O$	1.512 (3) [a]	—	1.548 (4)	This work
$CuSO_4 \cdot 5H_2O$	1.512 (4)	—	1.549 (4)	This work
$NiSO_4 \cdot 6H_2O$	1.523 (3)	—	1.561 (3)	This work
Gelatin	1.508 (4)	—	1.539 (4)	This work
Agar	1.514 (3)	—	1.548 (4)	This work
Synthetic	1.501 (2)	1.513 (2)	1.536 (2)	Frazier *et al.*[5]
Synthetic	1.510	—	1.543	Barth[2]
Natural	1.510	1.520	1.543	Gruner *et al.*[1]

a) Parenthesized figures indicate the error in the final decimal places.

parameters shown in Table 4 and comparing the data with those of the Weissenberg photographs. The calculated and prominently observed interplaner spacings and indices of Phases 1 and 2 are shown in Table 5, compared with those of TMP8 and vivianite, respectively, in the J. C. P. D. S. File.[12] The reflexions of *h0l* in Phases 1 and 2 overlap each other completely. Therefore, the apparent intensities of the reflexions of each phase were measured on the basis of the X-ray diffraction data of TMP8, in which the intensities of the diffraction lines of Phase 1 or Phase 2 are relatively predominant. The indices and the intensities of each reflexion of Phase 2 correspond with those of each reflexion of vivianite. Phase 2 is considered to be a polymorph of TMP8 and is supposed to be isomorphous with vivianite. The calculated densities are 2.14 for Phase 1 and 2.23 for Phase 2, assuming a formula weight of 4 per unit cell for Phase 1 and a formula weight of 2 per unit cell for Phase 2.

The refractive indices of the synthetic TMP8 are shown in Table 6 in comparison with those determined by some other authors. The optic elasticity axis, Z, in the synthetic crystal is oriented in a direction of about 30° with the crystallographic c-axis. The optical properties measured by us approximate those reported by Barth, and Gruner *et al.*[1] The discrepancies among the refractive indices observed by us may be attributed to the coexistence of Phases 1 and 2 in each synthetic TMP8. The presence of two lattices in the crystal is probably due to the superposition of the thermodynamically stable regions of each phase and to the fact that there is hardly any difference in the potential energies between those phases.

Conclusion

From the studies of the synthetic conditions of $Mg_3(PO_4)_2 \cdot 8H_2O$ (TMP8) and the results of the X-ray single crystal method of the octahydrate, the following conclusions were obtained:

1) TMP8 was synthesized from the mixed solutions of Na_2HPO_4 and $MgSO_4$ at 80—90 °C for 2—24 h, in an initial pH of 6.4—7.0, with the addition of $Ca(NO_3)_2 \cdot 4H_2O$, $CuSO_4 \cdot 5H_2O$, $NiSO_4 \cdot 6H_2O$, gelatin, or agar.

2) Two phases (Phase 1 and Phase 2) of TMP8 were found by means of the X-ray Weissenberg technique to coexist in each synthesized crystal particle.

3) The above Phase 2 is considered to be a new polymorph of TMP8.

4) Newberyite, $MgHPO_4 \cdot 3H_2O$, was also formed in the synthetic procedure of TMP8. This phosphate was precipitated under slightly more acidic conditions than those where TMP8 was obtained.

The authors are indebted to Dr. Hideki Monma of the National Institute for Researches in Inorganic Materials, and to Mr. Hiroshi Kawazoe of Tokyo Metropolitan University, for their helpful suggestions with regard to synthetic procedures. Thanks are also due to Dr. Fujio Okamura of the National Institute for Researches in Inorganic Materials and to Dr. Kazuyori Urabe of the Tokyo Institute of Technology for their valuable advice with regard to X-ray studies.

References

1) C. Palache, H. Berman, and C. Frondel, "Dana's System of Mineralogy," 7th ed, John Wiley and Sons, New York (1951), Vol. II, p. 753.
2) T. F. W. Barth, *Am. Mineral.*, **22**, 325 (1937).
3) M. A. de Schulten, *Bull. Soc. Fr. Minéral.*, **5**, 81 (1903).
4) H. Bassett and W. L. Bedwell, *J. Chem. Soc.*, **1933**, 871.
5) A. W. Frazier, J. R. Lehr, and J. P. Smith, *Am. Mineral.*, **48**, 635 (1963).
6) T. Kanazawa, T. Umegaki, and E. Wasai, *Chem. Lett.*, **1974**, 817.
7) T. Kanazawa, T. Umegaki, and E. Wasai, *Gypsum & Lime*, No. 140, 4 (1976).
8) T. Kanazawa, T. Umegaki, M. Chikazawa, M. Takahashi, and S. Sato, *Gypsum & Lime*, No. 145, 3 (1976).
9) M. Shimizu, H. Hosono, H. Kawazoe, T. Umegaki, and T. Kanazawa, Preprint of the 54th Annual Meeting of the Institute of Gypsum & Lime Research (1977), p. 13.
10) F. A. Cotton and G. Wilkinson, "Advanced Inorganic Chemistry," 2nd ed, John Wiley and Sons, New York (1966), p. 688.
11) J. C. P. D. S. X-Ray Powder Data File 16-330.
12) J. C. P. D. S. X-Ray Powder Data File 3-0070.
13) H. Mori and T. Ito, *Acta Crystallogr.*, **3**, 1 (1951).

Spectrophotometric Determination of Cadmium(II) with Dithizone and 1,10-Phenanthroline

Hideo AKAIWA,* Hiroshi KAWAMOTO, and Eiji YOSHIMATSU

Department of Applied Chemistry, Faculty of Technology, Gunma University, Kiryu, Gunma 376

(Received June 8, 1979)

Cadmium(II) has been quantitatively separated from zinc(II) by an ion-pair extraction system. An ion-pair consisting of cadmium(II) and 1,10-phenanthroline (phen) was found to be preferentially extracted into chloroform from an aqueous chloride solution containing zinc(II). The extracted species in chloroform reacted with dithizone (H_2Dz) to give the reddish mixed complex $Cd(HDz)_2(phen)$ having an absorption maximum at approximately 505 nm. The resulting calibration curve obeys Beer's law, the Sandell sensitivity being 0.0013 $\mu g\ cm^{-2}$. The effect of diverse ions has been examined, and a new highly selective method for the spectrophotometric determination of trace amounts of cadmium in metallic zinc established.

The spectrophotometric determination of cadmium(II) with dithiozone (H_2Dz) is well known as a highly sensitive method.[1] The separation of cadmium(II) from zinc(II) however remains a difficult problem. During the studies on the mutual separation of zinc(II) and cadmium(II) employing the synergistic extraction systems,[2-4] 1,10-phenanthroline (phen) was found to be the most suitable among several synergists. A new method of separation and determination of cadmium(II) was briefly reported.[5] In the preceding paper, it was stated that the species extracted with a mixture of dithizone and 1,10-phenanthroline at a pH of *ca.* 2 was a green complex. The reported procedure for the separation and determination of cadmium(II) is still feasible, however the previous observation concerning the extracted complex was found to be erroneous by additional detailed studies. Cadmium(II) is not extracted as a green complex but as a colorless ion-pair. This conclusion leads to the preferential and quantitative extraction of cadmium(II) using 1,10-phenanthroline alone, and in this case, zinc(II) was shown to remain in the aqueous phase. As a result, a highly selective method for the spectrophotometric determination of trace amounts of cadmium(II) with a mixture of dithizone and 1,10-phenanthroline has been established.

Experimental

Materials and Apparatus. ^{65}Zn and ^{115m}Cd were obtained from Nippon Isotope Kyokai. Dithizone and 1,10-phenanthroline were purchased from Wako Pure Chemicals and all organic solvents were of guaranteed grade.

The γ-ray activities of ^{65}Zn and ^{115m}Cd were measured with a γ-ray spectrometer consisting of a NaI(Tl) well crystal and a Hitachi RAH 403 type 400 channel pulse height analyser. The percent extraction (E) was obtained as a function of pH. The measurements of pH were conducted using a Hitachi-Horiba F-5 type pH meter. The absorbance of the organic phase was measured with a Hitachi 200-10 type spectrophotometer.

Extraction Procedure (A): The aqueous phase containing 0.01 mol dm^{-3} 1,10-phenanthroline, 0.1 mol dm^{-3} sodium chloride, 1.0×10^{-6} mol dm^{-3} metal ions, ^{65}Zn and ^{115m}Cd tracers was vigorously shaken for 10 min in a separatory funnel with an equal volume of the organic phase containing 0.002% dithizone. After the phases were allowed to separate, the γ-ray activity of each phase and the pH of the aqueous phase were measured.

Spectrophotometric Determination of Cadmium(II) (B): An aliquot of the sample solution containing less than 20 μg of cadmium(II) was taken in a separatory funnel, and 0.04 mol dm^{-3} 1,10-phenanthroline in water (5 cm^3) and 5 mol dm^{-3} sodium chloride (2 cm^3) added. The pH of the aqueous solution was adjusted to *ca.* 3 by the addition of hydrochloric acid or ammonia with Methyl Orange as the indicator. After the volume of the aqueous phase was adjusted to *ca.* 20 cm^3 with water, chloroform (10.0 cm^3) was added and the mixture shaken for 10 min. Each 5.00 cm^3 of the resulting organic phase and 0.002% dithizone in chloroform was transferred to another separatory funnel containing 5 mol dm^{-3} ammoniacal solution (20 cm^3), and the mixture shaken for 3 min. After the phases were allowed to separate, the absorbance of the organic phase was measured at 505 nm against the reagent blank.

Results and Discussion

Separation of Cadmium(II) from Zinc(II). Extraction curves for cadmium(II) and zinc(II) obtained according to procedure (A) are shown in Fig. 1, in which the selectivity for the separation of both elements

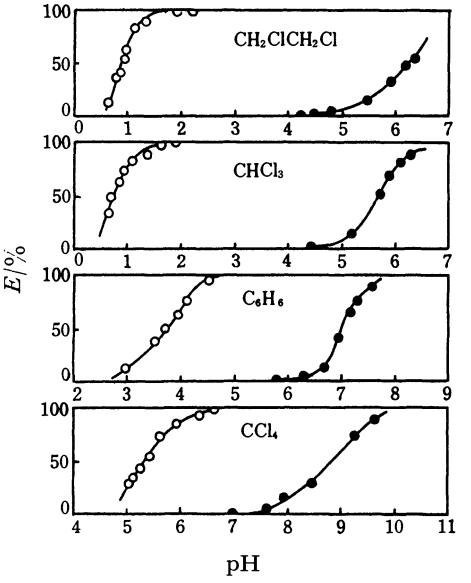

Fig. 1. Extraction curves, H_2Dz: 0.002%, phen: 0.1 mol dm^{-3}.
○: Cd(II), ●: Zn(II).

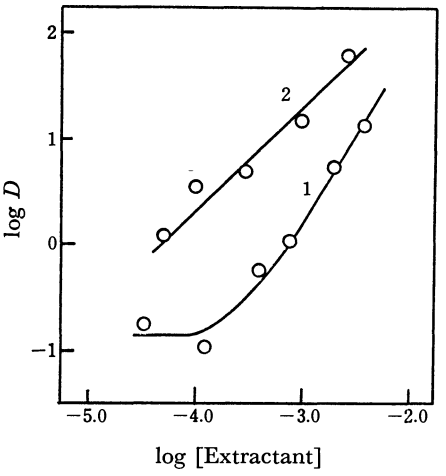

Fig. 2. Effects of dithizone and 1,10-phenanthroline concentrations on the extraction of cadmium(II).
1: log D *vs.* log[H_2O_2], phen: 1.0×10^{-3} mol dm^{-3}, pH: 2.1. 2: log D *vs.* log[phen], H_2Dz: 0.1%, pH: 2.1.

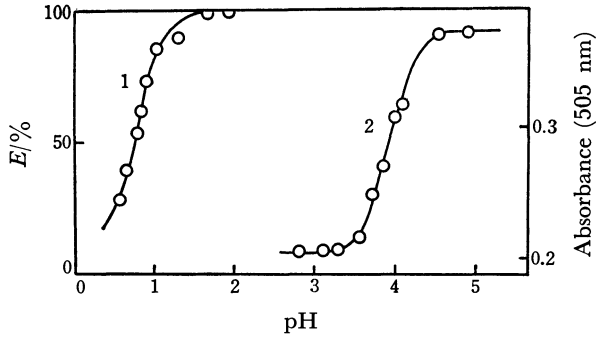

Fig. 3. Effect of pH on the extraction of cadmium(II).
1: E *vs.* pH, H_2Dz: 0.002%, phen: 0.1 mol dm^{-3}.
2: Absorbance *vs.* pH, H_2Dz: 0.001%, phen: 0.01 mol dm^{-3}.

is affected by the nature of the organic solvent. Chloroform and 1,2-dichloroethane both having relatively high polarities were the most suitable solvents for separation, based on the difference in the half extraction pH between cadmium(II) and zinc(II). By employing *e.g.* chloroform as a diluent, the quantitative separation of cadmium(II) from zinc(II) could be attained in the pH range of 2.0 to 4.0.

The Extracted Species of Cadmium(II). In order to examined the composition of cadmium(II) in chloroform, the logarithmic plots are given in Fig. 2, where D denotes the distribution ratio of cadmium(II). The slope analysis of the plots shows that $Cd(HDz)_2(phen)$ may be extracted at high concentration of dithizone. However, the extraction curve of ^{115m}Cd did not agree with that obtained by the spectrophotometric method, as is seen in Fig. 3. It is thought that a colorless species, *i.e.*, $Cd(phen)_3Cl_2$ is extracted at a pH of *ca.* 2.0, while the reddish $Cd(HDz)_2(phen)$ observed above pH 3.5. 1,10-phenanthroline itself extracts cadmium(II), leaving zinc(II) quantitatively in the aqueous phase. In addition, the optimum concentrations of sodium chloride and 1,10-phenanthroline for the determination of

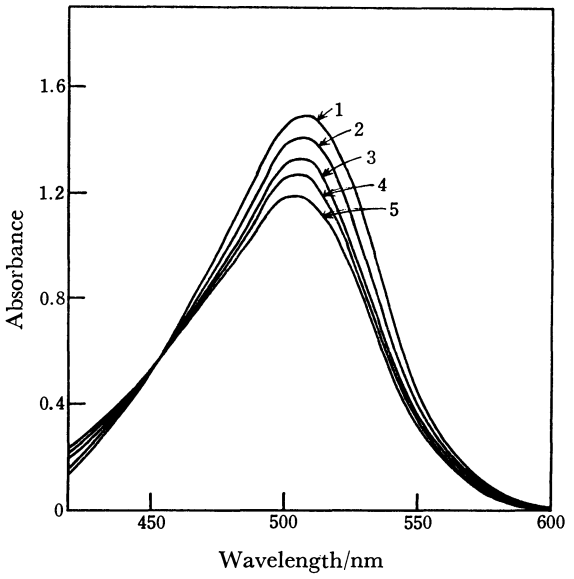

Fig. 4. Absorption spectra of the chloroform phase after shaking with 5 mol dm^{-3} ammoniacal solution. Cd(II): 50 μg, H_2Dz: 0.001%.
[phen]/mol dm^{-3} 1: none, 2: 1.0×10^{-5}, 3: 2.5×10^{-5}, 4: 7.5×10^{-5}, 5: 5.0×10^{-4}.

cadmium(II) according to procedure (B) were found to be greater than 0.4 mol dm^{-3} and 5.0×10^{-3} mol dm^{-3}, respectively.

The Absorption Spectra of the Extracts. The effect of the 1,10-phenanthroline concentration on the absorption spectrum of cadmium(II) dithizonate is shown in Fig. 4. An increase in the 1,10-phenanthroline concentration leads to a decrease in the absorbance at approximately 505 nm, and the isosbestic point appears at 455 nm, indicating that two colored species, namely $Cd(HDz)_2$ and $Cd(HDz)_2(phen)$ may exist in chloroform. Thus;

$$Cd(HDz)_{2,org} + phen_{org} \rightleftharpoons Cd(HDz)_2(phen)_{org} \quad (1)$$

and

$$\log\frac{A_1-A}{A-A_a} = \log K + \log[phen]_{org} \quad (2)$$

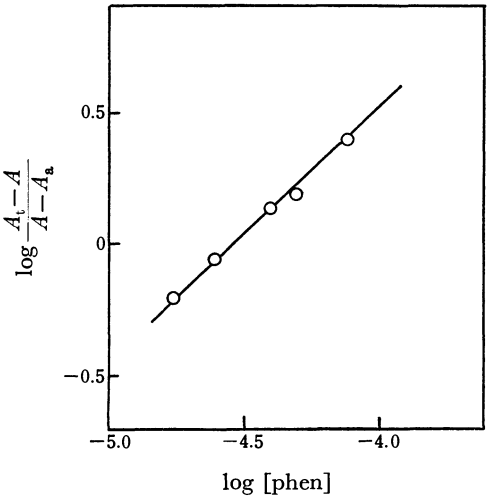

Fig. 5. Composition of the extracted species.

Table 1. Effects of diverse ions

Metal ions	Added as	Diverse ions added (μg)	Cd(II) found(μg)	Error (μg)
Co^{2+}	Acetate	100	12.7	+0.7
Fe^{3+}	Chloride	100	12.0	0
Fe^{2+}	Sulfate	100	12.3	+0.3
Pb^{2+}	Nitrate	100	11.9	−0.1
Mn^{2+}	Sulfate	100	12.0	0
Ni^{2+}	Chloride	100	12.3	+0.3
Sn^{2+}	Chloride	100	12.6	+0.6
Ag^{+}	Acetate	100	25.0	+13.0
Ag^{+}	Acetate	10	16.1	+4.1
Hg^{2+}	Nitrate	100	33.5	+21.5
Hg^{2+}	Nitrate	10	17.9	+5.9
Hg^{2+}	Nitrate	100[a)]	12.0	0
Cu^{2+}	Sulfate	100	13.9	+1.9
Cu^{2+}	Sulfate	25	12.9	+0.9
Cu^{2+}	Sulfate	100[b)]	13.1	+1.1
Cu^{2+}	Sulfate	100[c)]	12.0	0
Zn^{2+}	Chloride	100	12.1	+0.1
Zn^{2+}	Chloride	1000	13.2	+1.2
Zn^{2+}	Chloride	10mg[d)]	12.0	0
Zn^{2+}	Chloride	100mg[e)]	12.1	+0.1

12.0 μg of cadmium(II) was taken. a) 2 cm^3 of 1 mol dm^{-3} thiosulfate soln was added. b) 1 cm^3 of 1 mol dm^{-3} thiourea soln was added. c) 2 cm^3 of 1 mol dm^{-3} thiourea soln was added. d) The initial extraction of Cd(II) was performed in the presence of 0.1 mol dm^{-3} phen. soln. e) The initial extraction of Cd(II) was performed in the presence of 0.25 mol dm^{-3} phen. soln.

where the subscript org refers to the organic phase, K denotes the equilibrium constant for Eq. 1, A is the absorbance at 505 nm, and A_i and A_a represent the absorbances of $Cd(HDz)_2$ and $Cd(HDz)_2(phen)$ respectively. According to Eq. 2, a plot of the value of the left-hand side against log $[phen]_{org}$ should give a straight line having a slope of unity. As shown in Fig. 5, the above assumption is confirmed and the value of K has been calculated to be $10^{-4.54\pm0.02}$. Since no change in the spectrum of $Cd(HDz)_2(phen)$ was observed within one hour, $Cd(HDz)_2(phen)$ is considered to be useful for analytical purposes.

Calibration Curve. The calibration curve prepared according to procedure (B) was linear in the range of zero to 20 μg of cadmium(II), and passed through the origin. The molar absorptivity at 505 nm was shown to be 65000 $dm^3\ mol^{-1}\ cm^{-1}$, the Sandell sensitivity being 0.0013 μg cm^{-2}. The reproducibility test taking 12.0 μg of cadmium(II) gave an average absorbance of 0.361 from 7 determinations, the relative standard deviation being 0.0050.

Effect of Diverse Ions. The experimental results are summarized in Table 1. Each 100 μg of cobalt(II), iron(II, III), lead(II), manganese(II), nickel(II), and tin(II) did not interfere with the determination. Interferences caused by the presence of mercury(II) and copper(II) could be eliminated by the addition of thiosulfate and thiourea, respectively.

Analytical Result. The above procedure (B) was applied to the analysis of cadmium in a metallic zinc, which was found to contain 221±6 ppm as the average value of 5 determinations. The result agrees with the value obtained by the atomic absorption spectrometry (223 ppm).

This work was supported in part by a Grant-in-Aid for Scientific Research from the Ministry of Education, No. 147033.

References

1) E. B. Sandell, "Colorimetric Determination of Traces of Metals," Interscience Publishers, New York (1959), p. 350.
2) H. Akaiwa, H. Kawamoto, and Y. Tsutsumi, *Bunseki Kagaku*, **26**, 202 (1977).
3) H. Akaiwa, H. Kawamoto, and Y. Tsutsumi, *Bunseki Kagaku*, **27**, 447 (1978).
4) H. Akaiwa, H. Kawamoto, K. Ogura, and M. Konishi, *Bunseki Kagaku*, **27**, 329 (1978).
5) H. Akaiwa, H. Kawamoto, and E. Yoshimatsu, *Chem. Lett.*, **1978**, 421.

The Modification of Porous Polymer Beads; Use Packing Material in Gas Chromatography

Yuzi TAKAYAMA

Materials Science, Toyohashi University of Technology, Tempaku-cho, Toyohashi, Aichi 440

(Received April 7, 1979)

A new method of the surface modification of a porous polymer has been developed and applied to packing materials for gas chromatography. The porous polymer was coated with a α,β-unsaturated polyester solid polymer, which had a high acid value and which was cross-linked on the porous polymer by polymerization. By using this in gas chromatography, formic acid peaks are completely separated from acetic acid and water peaks without any apparent tailing. This polyester layer was not extractable and could stably be used at 230 °C or higher. If the diallyl phthalate polymer is used instead of the α,β-unsaturated polyester, propionic acid and acrylic acid, which are very diffecult to separate, were resolved. The present method may be applicable to some components of composite materials.

It is well known that the quality of the packing material in gas chromatography depends sensitively upon its surface properties. Hence, the material, such as diatomaceous earth and porous polymer,[1] is treated with acids[2] or silylating agents[3] to modify its surface properties. Studies of the surface modification are very important not only in the field of gas chromatography but also in other regions, for instance, that of composite materials. In the present work, as a first step, studies were made of the modification of the surface properties of the porous copolymer of styrene divinylbenzene. Also its quality as a packing material in gas chromatography was studied.

Usually, surface acidity and polarity are introduced by adding the proper monomer raw materials of the polymer. This method, however, is very cumbersome, since the stability of the suspension polymerization sensitively depends upon the conditions of the liquid. Surface properties may also be modified by coating the surface low-molecular weight substances. However, such a coating material easily evaporates in gas chromatography and dissolves into the mobile phase in liquid chromatography or into the organic matrix of composite materials.

With these facts in mind, we used curable substances to coat the surface of the porous polymer beads and so modified their surface properties. By choosing the proper curable substances, we controlled the number of acid points and also obtained a neutral and polar surface. The beads thus obtained were highly suitable as the packing material for gas chromatography. The present method may be applied to the pretreatment of polymers for composite materials.

Experimental

Diaion HP 30 (manufactured by the Nippon Rensui Co., a subsidiary of Mitsubishi Chemical Industry) consists of nonpolar porous polymer beads, nominally made of styrene and divinylbenzene. It is supplied in a wet state. The wet polymer was air-dried at room temperature and further heated to a constant weight in nitrogen flow at 140 °C. About 210—220 g of dry polymer, in spherical form (30—50 mesh), were obtained from 1000 ml of the wet polymer. The apparent density of the dried polymer was 0.275 g/cm^3.

About 33 g of the α,β-unsaturated polyester solid polymer, Espol TVF-5704-0 (supplied by the Mitsubishi Gas Chemical Co.) were dissolved in 400 ml of benzene. This solution was then poured onto 150 g of the dried Diaion HP 30 in a flask of a rotary evaporator. Then, a 100-ml portion of a benzene solution containing 1 ml of *t*-butyl perbenzoate (TBPB) was added to this mixture. The benzene was evaporated to dryness under reduced pressure. This dried polymer was packed in a glass pipe (1 m length; 34 mm inside diameter) and heat-treated in about a 100 ml/min nitrogen flow at 140 °C for 5 h. Thus the polymer was modified by the polyester (PMP). In this process, care must be taken of the following point: beads sticking on the wall have unfavourable properties and must be discarded.

Results and Discussion

Gas Chromatography for Free Fatty Acid (FFA). PMP was packed in 1 m×3 mm i.d. stainless steel column and tested by means of a Shimadzu Model-3BT TCD gas chromatograph with a mixture of C_1-, C_2-acids and water, their peaks being efficiently separated by PMP without any serious tails. For comparison, dried Diaion HP 30 was tested in a similar way. Except for water, it gave peaks with long tails as is shown in Fig. 1(b).

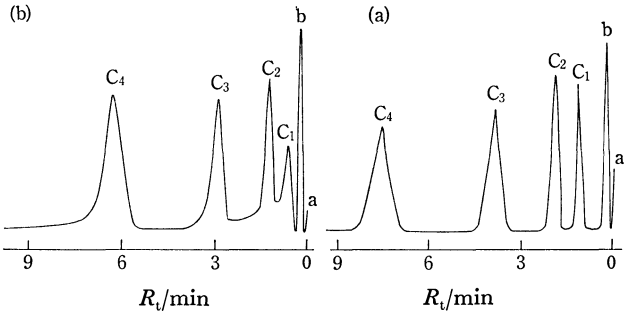

Fig. 1. Gas chromatograms of free fatty acids on (a) Diaion HP 30 modified by TVF 22.5% (see Table 2, Expt. No. 1) and (b) Diaion HP 30 unmodified. All packed in 1 m×3 mm i. d. stainless steel columns. Other conditions: (a) He flow-rate, 15 ml/min; column temperature, 150 °C; isothermal; sample load, 0.5 μl; recorder span, 4 mV. (b) He flow-rate, 16 ml/min; column temperature, 170 °C; isothermal; sample load, 2 μl; recorder span, 16 mV.
Peaks: a, air; b, water; C_1, formic acid; C_2, acetic acid; C_3, propionic acid; C_4, butyric acid.

Usually, an added tailing reducer reduces the retention volume, but this is not the case with Samples Nos. 1 and 2 rows in Table 2. The reason for this is that the TVF added in these present case is not a usual tailing reducer, but essentially changes the surface properties, that is, it increases the affinity to FFA and decreases the radius of the surface pores. The latter change may result in the decrease of the retention time of molecules with larger diameters such as C_4-acid.

Usable Maximum Temperature. The packed column with PMP was kept at 230 °C in a nitrogen flow for 24 h. After this treatment, the PMP was tested as has been described above. As a result, about a 5% shortening of the retention time was observed for all peaks, but there was no change in the peak shapes. Since a similar shortening was also observed in dried Diaion HP 30, the effect may be attributed to the shrinkage of Diaion HP 30. Furthermore, after the above test, the PMP could be taken out of the column smoothly, *i.e.* without any sticking to the column wall or to each other. Its color changed to a light yellowish brown from its original white yellow color. It may be concluded from these experimental results that the usable maximum temperature of PMP was about 230 °C.

Superiority of the α,β-Unsaturated Polyester Solid Polymer. It may be said, from our experience with diatomaceous earth, that the character of a packing material is primarily determined by the liquid phase on it. With this fact in mind, the porous polymer was similarly covered with acidic substances of a lower molecular weight, and its properties as a support were investigated. The favourable acid must satisfy the conditions that it does not destroy the base polymer and not be volatile, even at 240 °C. A small amount of added H_3PO_4 changed the color of Diaion HP 30 homologeneously to gray from the original white-yellow. Sebacic, stearic, and isophthalic acids did not change the color of the base polymer, but began to evaporate at temperatures below 200 °C. Thus, it is presumed that this shortcoming may be overcome by the use of polymer acids.

As for the α,β-unsaturated polyester, a method has been established for controlling the amount of carboxylic acid in it. We can obtain, by polymerizing this polyester on the beads, a film with a large number of acid points and a higher molecular weight; the film is stable even at 230 °C or so. For the present purpose, however, the polyester used must be as pure as possible. The commercially available, in the form of a liquid, contains 40—50% of the styrene monomer, and its acid values range between 5 and 16. If one uses such an impure polyester, the film obtained is inferior in its character, that is, it is thermally unstable and gives a peaks with some tailing. Hence, it is highly advisable to use a so-called solid (crystal) polymer with a high acid value. Solid polymers, TVF-5704-0 and Espol MG-1012, were chosen as modifiers in the present work. The specifications of these materials are given in Table 1.

Effect of the Polyester Concentration. The dependence of the packing character upon the polyester concentration was studied. Furthermore, the effect of coexisting diallyl isophthalate (DAIP) was studied, since this increases the degree of cross-linkage and the

Table 1. Specifications of α,β-unsaturated polyester solid polymers[a)]

Item	Espol TVF-5704-0	Espol MG-1012
Acid value	29.8	21.4
Softing point (°C)	99	96

a) Both solid polymers were supplied by the Mitsubishi Gas Chemical Co.

Table 2. Percentages of α,β-unsaturated polyester and DAIP on diaion HP 30

Expt. No.	Modifier: TVF %	Modifier: MG-1012 %	Modifier: DAIP %	DAIP in modifier %	Digests of result[a)]: V'/V'_{c_4}[b)] C_1[c)]	C_2	C_4	$N_{eff/m}$	Overlap percentages between C_1 and C_2 peaks[d)]	Note
1	22.5				0.281	0.480	1.97	714	0	peaks, sharp and well separated
2					0.170[e)]	0.392	2.32	710	see Fig. 1(b)	C_1 peaks, very long tail
3		44.5		0	0.329	0.520	1.85	462	4.92	peaks, rather broad; C_1, C_2 peak separation, good
4		22.5		0				650	7.10	C_1 peak, short tail; C_1, C_2 peak separation imperfect
5		17.8	26.7	60	0.357[e)]	0.547	1.88	470	15.8	C_1 tail, rather long; C_1, C_2 peak separation considerably poor
6		9.0	13.5	60				677	21.3	C_1 tail, much more long; C_1, C_2 peak separation, poor
7			44.5	100	0.457[e)]	0.589	1.84	626	36.1	C_1 peak was observed as a shoulder on the C_2 peak, having a considerable tail
8	44.5							434	0	peaks, rather broad; C_1, C_2 peak separation good

a) Each run was tested in a 50cm × 3 mm i. d. stainless steel column at 150 °C, and each sample load was 0.5—1 μl. b) V': corrected retention volume. c) C_1: formic acid, C_2: acetic acid, C_3: propionic acid, C_4 : butyric acid. d) $\frac{\text{Peak-height from the valley between two overlaping peaks}}{\text{Height of } C_2 \text{ peak}}$. e) Tailing peak.

solvent stability of the polymerized polyester, *i.e.*, the modifier film, but decreases its acid value. With a decrease in the acid value of the modifier film, the peak tailing became remarkable and the separation of the peaks assigned to C_1- and C_2-acids became difficult. The peak-width was almost independent of the polyester concentration on the base polymer in the region of below about 25%, but becamc slightly broader with an increase in the concentration above this limit.

In connection with the above facts, the character of DAIP films of 44.5 and 66.8% (by weight) of the base polymer gave a sharp peak with a long tailing for C_1 acid, but sharp pekas for C_2–C_3 acids; the latter is shown in Fig. 2. In this case, there was no unfavourable effect, *i.e.*, broadening, caused by higher concentrations of DAIP.

These results are summarized in Table 2.

This difference between the concentration effects of DAIP and the polyesters may be attributed to that between their dispersive states on the base polymer. As for the polyester film before polymerization, films on beads stick to each other, and some beads become bare when they are prepared in a rotary evaporator; thus, the heterogeneous dispersion state is realized. This model is partly supported by the fact that the unfavourable concentration effect was not observed if the film was prepared in a beaker without any mechanical stirring. Also such phenomena were not observed with DAIP.

The degree of cross-linkage of the polyester on base beads was estimated by the following method. The PMP was put into a Soxhlet extractor and treated with benzene, and then the weight of extract was measured. The bare beads (Diaion HP 30) were similarly treated, but their weight loss was negligible. Hence, only partial TVF and TBPB were extracted from the coated beads. Since TBPB is easily extracted completely, one can estimate the amount of TVF extracted if the initial content of TBPB is known. The experimental results showed that only 6% of the TVF present was extracted. This means that the TVF film is highly cross-linked and stable.

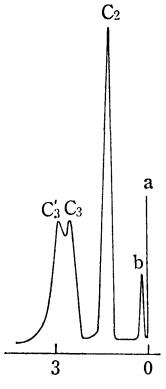

Fig. 2. Profile of propionic acid and acrylic acid on Diaion HP 30 modified by DAIP 44.5% (see Table 2, Expt. No. 7). Packed in a 50 cm × 3 mm i. d. stainless steel column. He flow-rate, 16 ml/min; column temperature, 140 °C; isothermal; sample load, 0.1 μl; recorder span, 2 mV. Peaks: C_3, propionic; C_3', acrylic acid; a and others; see Fig. 1.

Separation of Propionic Acid and Acrylic Acid. As can seen from Fig. 2, the peaks ascribed to propionic (C_3) and acrylic (C_3') acid were separated. This chromatogram was obtained with a short column 50 cm in length, much better separation can be expected with a column of the usual length. This separation may be attributed to the effect of polar groups in the DAIP molecule.

Conclusion

It has been established that α,β-unsaturated polyesters are good modifiers of prorous polymer beads, and that the higher the acid value, the better a modifier for the separation of FFA. In the present work, the best results were obtained with 25% TVF on the base beads. However, this value may depend upon the surface area of the base beads. The Diaion HP 30 used in the present work has a BET area of 200 m^2/g. The optimum concentration increases with the increase in the surface area.

The conventional modifiers presently used are apt to evaporate or be extracted in gas chromatography and liquid chromatography respectively. These unfavourable effects can be avoided by the use of the present techniques.

In the present work, we were mainly interested in the separation of FFA with an acidic modifier, not in the separation of amines. The latter may, however, be successfully done by basically modified packing, which can be obtained by an extension of the present techniques.

The author wishes to thank Professor Tetsuo Takaishi for his discussion.

References

1) O. L. Hollis, *Anal. Chem.*, **38**, 309 (1966).
2) G. C. Cochrane, *J. Chromatogr. Sci.*, **13**, 440 (1975).
3) O. L. Hollis, *J. Chromatogr. Sci.*, **11**, 335 (1973).

Metal Halide Catalyst for Reduction of Nitric Oxide with Ammonia

Akio NISHIJIMA,* Yoshimichi KIYOZUMI, Akifumi UENO, Minoru KURITA, Hiroyuki HAGIWARA, Toshio SATO, and Naoyuki TODO

National Chemical Laboratory for Industry, 2-19-19, Mita, Meguro-ku, Tokyo 153

(Received May 10, 1979)

Counter anions of active components on catalysts were found to affect catalytic activities for NO reduction with NH_3. Halide ions promoted activity in copper and iron catalysts, but lowered it in chromium and manganese catalysts. The most favorable electronic state of a cation on catalysts was investigated by changing counter anions and/or carriers.

In the catalytic reduction of nitrogen oxides with ammonia the reduction rate is markedly accelerated by the presence of oxygen, no undesirable by-product being found by the reaction between reducing agents and components in flue gas. The method seems to be most advantageous for the reduction of nitrogen oxides (NO_x) emissions from stationary combustion equipments.[1-3] Metal oxide supported catalysts such as Fe_2O_3, V_2O_5, CuO, and MoO_3 on Al_2O_3 or TiO_2 are being employed. However, they are used at reaction temperatures above 300 °C in order to obtain effective reduction of NO_x. From an economical viewpoint, catalysts active at lower temperatures are desirable, since temperatures of flue gases emitted from a coke oven or sintering furnace are lower than 200 °C.

We have explored new catalysts having higher activity at low temperature and found that the activity of metal sulfate catalysts in the lower temperature region is higher than that of metal oxide catalysts.[4] This indicates that the anion of these metal compounds affects the catalytic activity for NO reduction. We have examined the effect of the counter anions and found that the halide catalysts are effective for producing activity at lower temperatures.[5]

In order to find the most favorable electronic state of cations of the catalysts, a study on metal halides has been made by changing anion species of the catalysts and carries.

Experimental

Catalyst. Metal halide and metal sulfate catalysts were prepared by impregnating preformed γ-Al_2O_3 (diam. 1.5 mm) with aqueous solutions of halides and sulfates, respectively. After being impregnated at 40 °C for 5 h, the catalysts were dried at 120 °C for 3 h, and then calcined at 200 °C for 3 h. In the case of metal oxide catalysts, the catalysts were prepared by calcining at 500 °C for 3 h, after being impregnated with metal nitrates, the cation contents being kept constant (8 wt % and 4.7 wt %) in order to examine the effect of counter anions. The copper catalysts used were $CuBr_2$–Al_2O_3, $CuSO_4$–Al_2O_3, $CuCl_2$–Al_2O_3, and CuO–Al_2O_3. In order to examine carrier effects on the catalytic activities, 15 wt % of $CuBr_2$ supported on SiO_2, active carbon and Al_2O_3 were used.

Activity Measurement. Figure 1 shows a flow diagram of the apparatus. The reactor is a stainless steel tube, length 200 mm, diam. 15 mm, set in a tubular furnace, length 250 mm. After introducing 10 ml of the catalyst into the reactor, activity measurements were carried out under space velocity of 15000 h^{-1}. As a standard feed stream, a gas mixture consisting of NO 300 ppm, NH_3 300 ppm, O_2 5 vol %, and N_2 balance gas was used. Analyses of NO, NO_2, and NH_3 were made by means of chemiluminescence type NO_x and NH_3 analyzer.

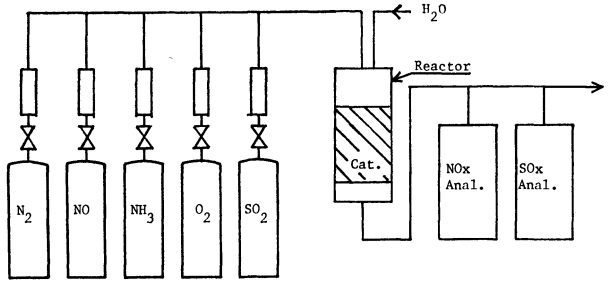

Fig. 1. Flow diagram of apparatus used.
□ : Rotor meter, ⋈ : variable valve.
Each cylinder contained 1 vol % of NO, NH_3, or SO_2.

Property of Catalyst. The amounts of NH_3 and NO adsorption on the catalysts were measured using a thermogravimeter (Shimadzu Co. DT 20) in N_2 feed stream (1 l/h) containing 5 vol % O_2. An X-ray photoelectron spectrometer (XPS) (Dupont Co. 650B) was used to measure the electronic states of the cations and anions in active components. Mg $K\alpha$ radiation was used to obtain XPS spectra. All binding energy values were refered to C 1s of contaminant carbon (285.0 eV).

Results

Copper Salt Catalyst. Effect of Anion on Catalytic Activity: In the reaction of NO removal, the activities of the catalysts increased with cation content, reaching a maximum at a certain cation content. Thus, for the measurement of relative activities the catalysts with lower cation content whose activity does not reach maximum were used. In the case of CuO–Al_2O_3, $CuSO_4$–Al_2O_3, and $CuCl_2$–Al_2O_3, Cu content was 8 wt%. In the case of $CuBr_2$–Al_2O_3 with 8 wt% of Cu, however, the activity attained saturation. The cupric ion content of 4.7 wt% was selected for a comparison of the anion effect of Br^- with that of Cl^- on the catalytic activities of $CuBr_2$ and $CuCl_2$ catalysts. The effect of anions on the catalytic activity is shown in Fig. 2. The activity order of the catalysts in lower temperature region was: $CuBr_2 > CuCl_2 > CuSO_4 > CuO$.

Effect of Carrier on Catalytic Activity: The effect of carriers on catalytic activity was investigated using γ-Al_2O_3, SiO_2, and active carbon (AC). The results are shown in Fig. 3. The activities decreased in the order: AC > γ-Al_2O_3 > SiO_2.

Amount of Adsorption of NO and NH_3: It was found

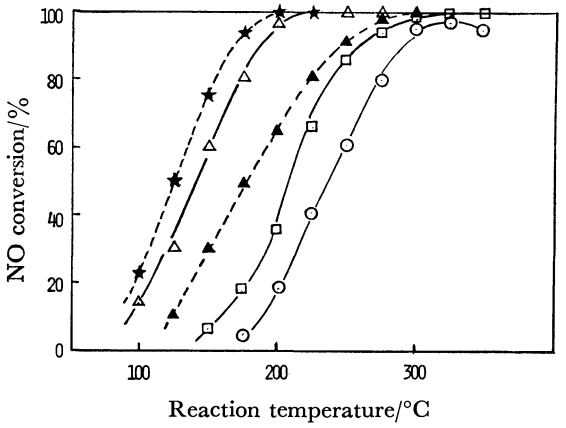

Fig. 2. Effect of anion on catalytic activity of copper salt supported catalyst.
Carrier: γ-Al_2O_3.
Active component:
—— Cu content; 8 wt %,
○: CuO, □: $CuSO_4$, △: $CuCl_2$.
—— Cu content; 4.7 wt %,
▲: $CuCl_2$, ★: $CuBr_2$.
Gas composition:
NO 300 ppm, NH_3 300 ppm, O_2 5 vol %, N_2 balance.
Space velocity: 15000 h^{-1}.

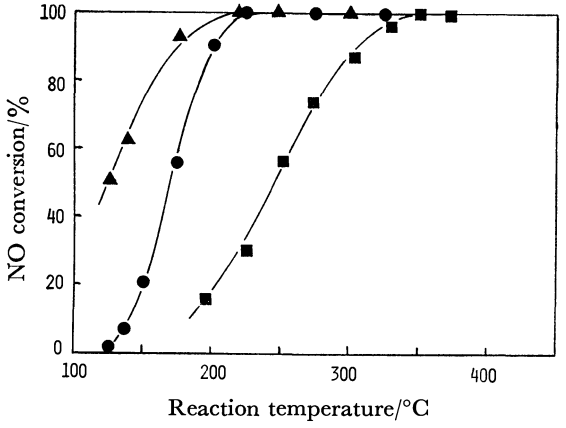

Fig. 3. Effect of carrier on catalytic activity of copper salt supported catalyst.
Carrier:
■: SiO_2, ●: γ-Al_2O_3, ▲: active carbon.
Active component: $CuBr_2$ (15 wt %).
Gas composition:
NO 300 ppm, NH_3 300 ppm, O_2 5 vol %, N_2 balance
Space velocity: 15000 h^{-1}.

Table 1. Amounts of NH_3 and NO adsorbed on the catalysts

	Amount of NH_3 mmol/l g of cat.	Amount of NO mmol/l g of cat.
$CuSO_4$–Al_2O_3	0.29	0.14
$CuBr_2$–Al_2O_3	0.21	0.20
CuO–Al_2O_3	0.16	0.25

Measurements were carried out with a thermogravimeter at 150 °C in N_2 feed stream containing 5 vol% of O_2. Cu content of each catalyst was 3.7 wt%.

Table 2. Electronic states of copper ions in the catalysts

	Cu $2p_{3/2}$ binding energy/eV
A) Effect of anions	
$CuSO_4$–Al_2O_3[a]	933.6
$CuBr_2$–Al_2O_3[a]	934.2
CuO–Al_2O_3[a]	934.9
B) Effect of carriers	
$CuBr_2$–Al_2O_3[b]	934.2
$CuBr_2$–Active carbon[b]	934.5
$CuBr_2$–SiO_2[b]	934.8

a) Cu content of each catalyst was 3.7 wt%. b) 15 wt% of $CuBr_2$ was supported on each carrier.

Table 3. Binding energies of N ls for adsorbed NH_3 and NO on the copper catalysts

	N ls binding energy/eV	Assignment
CuO–Al_2O_3+NH_3	402.1	NH_4^+
$CuSO_4$–Al_2O_3+NH_3	401.8	NH_4^+
$CuBr_2$–Al_2O_3+NH_3	402.0	NH_4^+
NH_4Br	401.9	
V_2O_5+NH_3	400.9[8]	NH_4^+[8]
CuO–Al_2O_3+NO+O_2	407.5	NO_3^-
$CuSO_4$–Al_2O_3+NO+O_2	407.3	NO_3^-
$CuBr_2$–Al_2O_3+NO+O_2	407.4	NO_3^-
V_2O_5+NO+H_2O	406.2[8]	NO_3^-[8]
NH_4NO_3	401.8, 407.4	

that the amount of NH_3 adsorbed on $CuSO_4$–Al_2O_3 catalyst is 1.8 times that on CuO–Al_2O_3 catalyst (Table 1). The amount of NH_3 adsorbed on $CuBr_2$–Al_2O_3 catalyst, which showed the highest activity for NO reduction at lower temperature, is 1.3 times that on

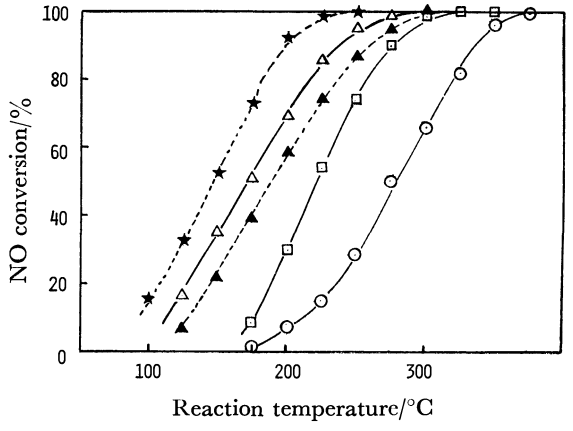

Fig. 4. Effect of anion on catalytic activity of iron salt supported catalyst.
Carrier: γ-Al_2O_3.
Active component:
——Fe content; 7 wt %,
○: Fe_2O_3, □: $Fe_2(SO_4)_3$, △: $FeCl_3$.
——Fe content; 3.7 wt %,
▲: $FeCl_3$, ★: $FeBr_3$.
Gas composition:
NO 300 ppm, NH_3 300 ppm, O_2 5 vol %, N_2 balance.
Space velocity: 15000 h^{-1}.

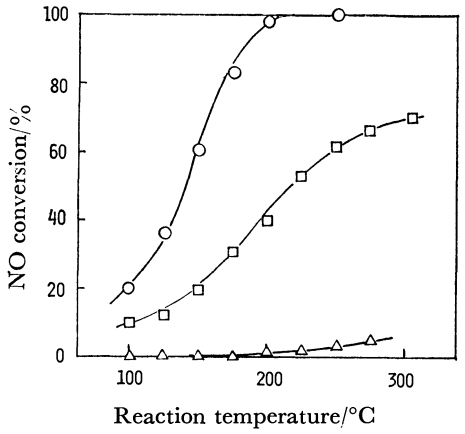

Fig. 5. Catalytic activity of chromium, cerium and manganese halide supported catalyst.
Carrier: γ-Al_2O_3.
Active component:
○: $CeCl_2$, □: $MnCl_2$, △: $CrBr_3$.
Cr, Ce and Mn content were 5 wt %.
Gas composition:
NO 300 ppm, NH_3 300 ppm, O_2 5 vol %, N_2 balance.
Space velocity: 15000 h^{-1}.

CuO–Al_2O_3 catalyst. The order of the amount of NH_3 adsorption is $CuSO_4$–Al_2O_3>$CuBr_2$–Al_2O_3>CuO–Al_2O_3, and that of NO adsorption on these three catalysts CuO–Al_2O_3>$CuBr_2$–Al_2O_3>$CuSO_4$–Al_2O_3.

Electronic State of Cation and Adsorbed NH_3 and NO: The effect of anions and carriers on electronic states of the cation in the catalysts obtained by using X-ray photoelectron spectrometer is given in Table 2. The electronic state of copper ions was found to depend on the kind of both anion and carrier. The electronic states of copper ions become electropositive in the order: $CuSO_4$>$CuBr_2$>CuO. On the other hand, when carriers were changed the electronic states of copper ions become Al_2O_3>AC>SiO_2. Binding energies of N 1s for adsorbed NH_3 and NO on the copper catalysts are given in Table 3. The binding energies of adsorbed NH_3 and NO agree with those of NH_4^+ and NO_3^-, respectively.

Iron Salt Catalyst. Similar experiments were carried out on iron salt catalysts. Figure 4 shows the result obtained for ferric salt supported catalysts. The effect of anions on activity was found to be in the same order as cupric salt catalysts: $FeBr_3$>$FeCl_3$>$Fe_2(SO_4)_3$ >Fe_2O_3.

Other Metal Salt Catalyst. Effects of anions on catalytic activity were also investigated for transition metal compounds. Some metal halide catalysts such as $CeCl_2$ or $MnCl_2$ were found to show high activity at lower temperatures (Fig. 5). No activity was observed on $CrBr_3$, $ZnBr_2$, and $NiBr_2$ supported catalysts at lower temperatures. In the case of chromium salt catalysts, the activity order of the catalysts is: Cr_2O_3>$Cr_2(SO_4)_3$ >$CrBr_3$.

Discussion

In the cases of Cu, Fe, and Ce, it was shown that the activity of metal halide supported catalysts is higher than that of oxide and sulfate supported catalysts. This indicates that among the anions we investigated, halide anions are the most effective for producing active states. However, catalytic activity and the activity order (Cu, Ce>Fe>Mn>Ti) obtained on metal halide suppored catalysts were found to differ from those of metal oxide suppored catalysts (Mn>Cr> Cu>Fe). In contrast, in the case of chromium metal, the activity of the halide supported catalyst was lower than that of oxide or sulfate supported catalyst. It seems that both cation and anion species of active components affect activity for NO reduction and that the selection of appropriate combination of a cation and an anion is essential for producing a highly active state.

Both copper oxide and halide supported catalysts show high activity at lower temperatures. Thus copper compound supported catalysts were studied in detail.

NO was predominantly reduced by NH_3 to N_2, no N_2O being detected. This is the most characteristic difference from the case in which CO or H_2 is used as a reduction agent. According to Otto and Shelef, in the reduction by CO or H_2, the participation of two molecules of NO is needed for the selective production of N_2; when NH_3 is used as a reduction agent, N–N bond is easily produced in the reaction of NO and NH_3.[6] In fact, Shelef found by using nitrogen isotope, that $^{15}N^{14}N$ is mainly produced by the reaction of ^{14}NO and $^{15}NH_3$.[7] This indicates that adsorption of both NH_3 and NO in the neighboring sites on the catalyst is necessary for reaction.

According to the results obtained by XPS, NH_3 and NO seem to undergo adsorption on the catalysts in the form NH_4^+ and NO_3^-, respectively.[8] It seems that the amount of NH_3 adsorbed on the catalysts decreases when the electronic state of the cation changes from an electropositive state to an electronegative one, and that the amount of NO adsorbed decreaes when the electronic state of the cation changes from an electronegative state to an electropositive one. Actually, the order of the amounts of NH_3 and NO adsorbed on the catalyst (Table 1) agreed with those of the electropositivity and the electronegativity of the cation (Table 2-A).

From the results we realize that the most favorable electronic state of the cation should be selected by changing counter anions in order to obtain proper amounts of both adsorbates of NH_3 and NO. In fact, the catalytic activity decreased when the electronic state of the cation changed to the electronegative ($CuSO_4$) or to the electropositive one (CuO) as compared with $CuBr_2$–Al_2O_3 catalyst (Fig. 2 and Table 2-A).

In these supported catalysts, Al_2O_3 or AC is usually employed as a carrier. The carriers are also considered to affect the electronic state of the cation of active components. When we change the carriers, the electronic state of the cation changes considerably (Table 2-B). The relation between the catalytic activity (Fig. 3) and the electronic states of the cation (Table 2-B) was the same as that obtained by changing counter anions. The result seems to support the above conclusion that the most favorable electronic state of the cation can be obtained by a proper combination of the cation

with a counter anion and a carrier for high activity.

From a practical viewpoint, catalysts are required to be resistant against water vapor or SO_2 in a reaction gas, since they are usually contained in a flue gas emitted from stationary combustion equipments. The metal halide catalysts which show high activity at lower temperatures were not poisoned by water vapor, but their catalytic activity was found to decrease gradually when SO_2 was contained in the reaction gas. This is due to the change of the active component from $CuBr_2$ to $CuSO_4$. The electronic state of copper ions in deactivated $CuBr_2$–Al_2O_3 catalysts was found to be the same as that of $CuSO_4$–Al_2O_3 catalyst.

References

1) S. Jarros and J. Krizek, *Int. Chem. Eng.*, **8**, 261 (1968).
2) G. Chakrabarti and C. Chu, *Atmos. Environ.*, **6**, 297 (1972).
3) P. L. Klimisch and K. C. Taylor, *Env. Sci. & Technol.*, **7**, 127 (1973).
4) N. Todo, M. Kurita, H. Hagiwara, A. Ueno, and T. Sato, The Japan-U. S. A. Seminar on Catalytic NO_x Reactions, November 1975, Preprints 3-1.
5) N. Todo, A. Nishijima, A. Ueno, M. Kurita, H. Hagiwara, T. Sato and Y. Kiyozumi, *Chem. Lett.*, **1976**, 897.
6) K. Otto and M. Shelef, *J. Phys. Chem.*, **76**, 37 (1972).
7) M. Shelef, The Japan-U. S. A. seminar on Catalytic NO_x Reaction, November 1975, Preprints 1-1.
8) M. Takagi, T. Kawai, M. Soma, T. Onishi, and K. Tamaru, *Shokubai*, **18**, 4, 127 (1976).

Isothiocyanates. I.[1] Addition of Urea to Aroyl Isothiocyanates and Conversion of the Monoadducts into Monothiobiuret, 4-Thioxo-1,3,5-triazin-2-ones and 1,2,4-Thiadiazol-3-ones

Mohamed Nabih BASYOUNI* and Abdel-Momen EL-KHAMRY

Chemistry Department, Faculty of Science, Ain Shams University, Abbassia, Cairo, Egypt

(Received March 17, 1979)

The hitherto unknown 1-aroyl-2-thiobiurets were synthesized by addition of urea to aroyl isothiocyanates. Treatment of 1-benzoyl-2-thiobiuret with concentrated hydrochloric acid effected hydrolysis to monothiobiuret. On the other hand, treatment of 1-aroyl-2-thiobiurets with alkali gave 6-aryl-4-thioxo-1,2,3,4(or 2,3,4,5)-tetrahydro-1,3,5-triazin-2-ones.† Oxidation of the 1-aroyl-2-thiobiurets with hydrogen peroxide in the presence of hydrochloric acid gave 5-aroylamino-2,3-dihydro-1,2,4-thiadiazol-3-ones.

Amidines, isoureas, isothioureas and guanidines Ia—d have been added to aroyl isothiocyanates II to give 1,3,5-triazinethione derivatives IIIa—d.[2] Combination of weakly basic amidino compounds with weakly

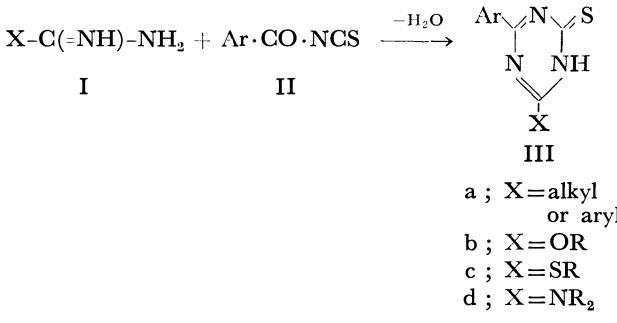

I II III

a ; X=alkyl or aryl
b ; X=OR
c ; X=SR
d ; X=NR_2

electrophilic isothiocyanates gave III in good yields. In other cases formation of aroylamidines predominated,[2] *e.g.*

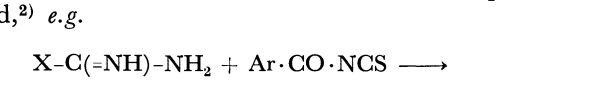

Such an aroylation reaction during the course of addition of alkylamines[3] and hydrazines[4] to benzoyl isothiocyanate has been reported.

In the present investigation urea, a weaker nucleophile, was choosen for the study of its reaction with some aroyl isothiocyanates of varying electrophilicity, *i.e.* of different carbonyl activity, in order to obtain more precise information on the mode of addition of nucleophiles to the C=S and/or to C=O of the aroyl isothiocyanates. Reactions, *e.g.* actions of acids and alkalies and oxidation with hydrogen peroxide, on the monoadducts from the reaction under investigation were also carried out.

† Although the 2-phenyl derivative exists as tautomers (A) and (B),[2] it was erroneously named 6-oxo-2-phenyl-4-thioxo-1,4,5,6-tetrahydro-1,3,5-triazine. The present naming of this compound and its aryl analogs indicates that they can exist in two tautometric forms.

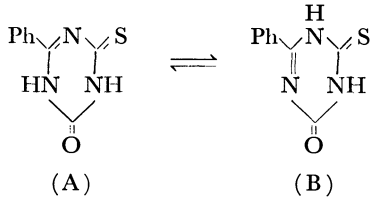

(A) (B)

Results and Discussion

Urea was added to the aroyl isothiocyanates IIa—f in dry acetone to give good yields (*cf.* Table 2) of the hitherto unknown 1-aroyl-2-thiobiurets IVa—f. Although equimolar amounts of the reactants were used, a small amount (see Experimental) of a diadduct V was obtained in the case of the addition of urea to benzoyl isothiocyanate IIa. However, when the addition was repeated using two moles of the benzoyl isothiocyanate the amount of the diadduct did not increase, the predominant product being the monoadduct IVa. The monoadducts IVa—f obtained from such a reaction could be obtained from urea by the reaction with the aroyl isothiocyanates prepared *in situ* from the corresponding aroyl chloride and ammonium thiocyanate in dry acetone (*cf.* Experimental).

II IV V

a ; Ar=phenyl
b ; Ar=*p*-tolyl
c ; Ar=*p*-methoxyphenyl
d ; Ar=*p*-bromophenyl
e ; Ar=*o*-chlorophenyl
f ; Ar=styryl

The structure of the monoadducts IVa—f was confirmed by their analytical data, infrared and electronic spectra. Thus, the strong absorption bands in the region 3360—3100 cm^{-1} can be correlated with ν_{NH} of primary and secondary amides (bonded NH);[5] those in the regions 1700—1680 cm^{-1} and 1740—1715 cm^{-1} can be attributed to the presence of acyclic thioimide groupings, namely ArCONHCS and CSNHCO.[5] The absence of a band at 2570 cm^{-1} suggests that the 1-aroyl-2-thiobiurets IVa—f exist in the thione form (thiolactam). The electronic spectra of IVa—c support their structural similarity. The infrared and electronic spectral data are given in Table 1. 1-Benzoyl-2-thiobiuret IVa was desulfurized[6] with aqueous chloroacetic acid to give benzoylbiuret[7] as an analytically pure sample.

Formation of the 1-aroyl-2-thiobiurets IVa—f in good yields by the addition of urea to the aroyl isothiocyanates IIa—f indicates that urea exclusively attacks the C=S function of the aroyl isothiocyanates. The

Table 1. Spectral data for compounds IV, VII, and X

Compound	Infrared spectra		Electronic spectra			
	$\nu_{C=O}$ / cm^{-1}	ν_{NH} / cm^{-1}	λ_{max} / nm	ε_{max}	λ_{mak} / nm	ε_{max}
IVa	1690, 1725	3200, 3290 3360	243.5	19695	285.5	15420
IVb	1680, 1720	3100, 3200 3350	253.5	22750	286	16350
IVc	1690, 1740	3100, 3300 3350	255	23500	287	16100
IVd	1680, 1720	3100, 3200 3330	256	24160	286.5	15400
IVe	1700, 1740	3140, 3200 3320	236	17510	285.5	14805
IVf	1650, 1700	3120, 3200 3220, 3400	232	27555	287.5	23130
VIIa	1675, 1735	3050—3200	260	23085	330	7890
VIIb	1690, 1740	2900—3200	260	14100	294	23250
VIIc	1700, 1740	3100—3200	260	15170	295	25580
VIId	1680, 1760	2900—3200	271.5	26410		
VIIe	1700, 1720	3100—3210	260	19400		
Xa	1660, 1720	3100—3200	244.5	19005	310.5	11050
Xb	1670, 1730	3120—3210	229 268.5	11480 7650	316.5	9180
Xc	1675, 1732	3110—3215	231	16810	309	5810

Table 2. 1-Aroyl-2-thiobiurets IV

Compound	Melting point	Yield/% Method A	Yield/% Method B	Formula	Found (%) C	Found (%) H	Found (%) N	Found (%) S	Calcd (%) C	Calcd (%) H	Calcd (%) N	Calcd (%) S
IVa	185—186[a] Yellow	92	85	$C_9H_9N_3O_2S$	48.5	4.2	19.2	14.6	48.4	4.1	18.8	14.3
IVb	178—179[a]	90	83	$C_{10}H_{11}N_3O_2S$	51.0	4.9	18.0	13.6	50.6	4.6	17.7	13.5
IVc	185—187[a]	85	80	$C_{10}H_{11}N_3O_3S$	47.6	4.6	16.2	12.8	47.4	4.35	16.6	12.6
IVd	192—195[b]	87	81	$C_9H_8BrN_3O_2S$	35.3	2.8	14.0	10.4	35.8	2.6	13.9	10.6
IVe	175—177[a]	94	88	$C_9H_8ClN_3O_2S$	42.3	3.5	16.3	12.6	41.9	3.1	16.3	12.4
IVf	213—215[a]	80	71	$C_{11}H_{11}N_3O_2S$	53.2	4.7	16.8	12.85	53.0	4.4	16.9	12.7

a) From ethanol. b) From acetic acid.

fact that no aroylureas were formed supports the view that no competing aroylation reaction, *i.e.* the direct nucleophilic substitution at the carbonyl function of the aroyl isothiocyanates IIa—f, of varying carbonyl activity, took place. This supports the previous conclusion[3,4] that only strong nucleophilic reagents such as alkylamines and hydrazines are capable of attacking the C=O function of the aroyl isothiocyanates to give the aroylated nucleophiles. The results show that the magnitude of the electrophilicity of the aroyl isothiocyanate makes a small contribution, if any, in determining the mode of addition of nucleophiles to the C=O and/or to the C=S of the dielectrophilic reagent, *i.e.* the aroyl isothiocyanate.

Treatment of an ethanolic solution of 1-benzoyl-2-thiobiuret IVa with concentrated hydrochloric acid (see Experimental) gave monothiobiuret VI, which is particularly useful as an intermediate in the production of thermoplastic and water-repellent resins and which may serve as a rubber accelerator, a plasticizer and an insecticide. The present route for the synthesis of VI from readily accessible starting materials is, therefore, superior to and more convenient than the reported procedures.[8–10]

On the other hand, treatment of an ethanolic solution of each of IVa—e with aqueous 4 M sodium hydroxide afforded, after acidification, 6-aryl-4-thioxo-1,2,3,4(or 2,3,4,5)-tetrahydro-1,3,5-triazin-2-ones VIIa—e in a good yield.

The structure of the 4-thioxo-1,3,5-triazin-2-one derivatives VIIa—e was confirmed by analytical data, infrared and electronic spectra. Their infrared spectra (*cf.* Table 1) exhibit bands in the regions 3210—3050 cm^{-1} (ν_{NH}) and 1740—1675 cm^{-1} ($\nu_{C=O}$) and their electronic spectra reflect their structural similarity (*cf.* Table 1).

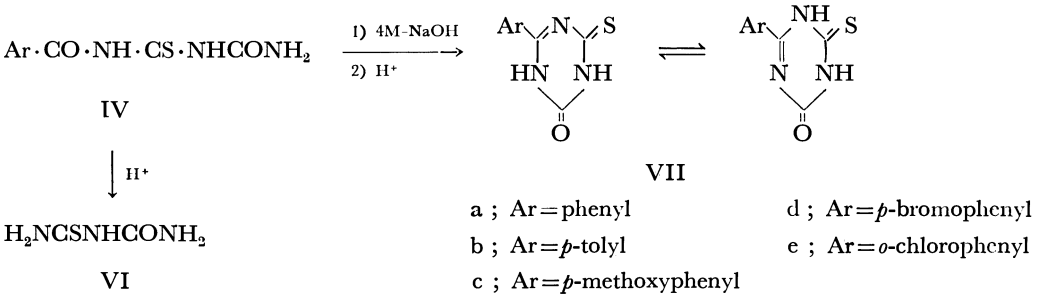

a ; Ar=phenyl
b ; Ar=*p*-tolyl
c ; Ar=*p*-methoxyphenyl
d ; Ar=*p*-bromophenyl
e ; Ar=*o*-chlorophenyl

Although 6-phenyl-4-thioxo-1,2,3,4(or 2,3,4,5)-tetrahydro-1,3,5-triazin-2-one VIIa, mp 264—266 °C, has been prepared[2] by a different route which involves acidic hydrolysis of III (Ar=phenyl; X=OC_2H_5) and is reported to have mp 246—248 °C, the structure of the compound in our hands was established from the following chemical evidence: 1) it was desulfurized[6] with aqueous chloroacetic acid to give 6-phenyl-1,2,3,4-tetrahydro-1,3,5-triazin-2,4-dione VIII, which was analytically pure and its mp was in good agreement with that reported previously[7] for the same compound prepared by a different route, and 2) benzylation with benzyl chloride in the presence of sodium hydroxide gave 4-benzylthio-6-phenyl-1,2(or 1,4)-dihydro-1,3,5-triazin-2-one IX which was identical (mp, mixed mp and infrared spectroscopy) with an authentic specimen prepared by a different route.[2]

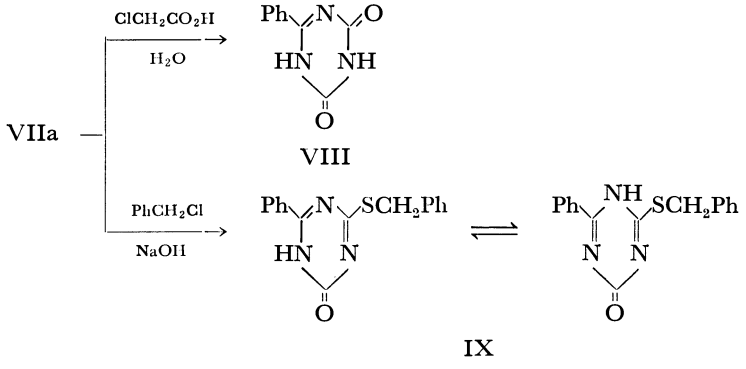

Oxidation of IVa, c, and e with hydrogen peroxide in the presence of hydrochloric acid gave 5-aroylamino-2,3-dihydro-1,2,4-thiadiazol-3-ones (or 5-aroylimino-tetrahydro-1,2,4-thiadiazol-3-ones) Xa—c whose structures were confirmed by analytical data, infrared and electronic spectroscopy. Thus, the infrared spectra of the products Xa—c show bands in the ranges 3215—3100 cm^{-1} (ν_{NH}) and 1732—1675 cm^{-1} ($\nu_{C=O}$) and their electronic spectra reflect their structural similarity. The presence of the thiadiazole ring was inferred from their behavior towards the action of sodium plumbite as compared with their precursors, namely 1-aroyl-2-thiobiurets IVa, c, and e. The latter open-chain adducts deposited black lead sulfide at room temperature, but the thiadiazole derivatives Xa—c deposited lead sulfide after being boiled for a few minutes.

5-Aroylamino-2,3-dihydro-1,2,4-thiadiazol-3-ones Xa—c can exist in the tautomeric forms indicated.

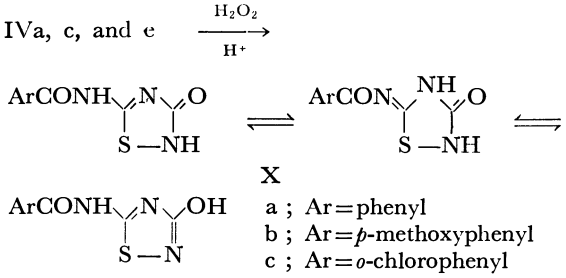

a ; Ar=phenyl
b ; Ar=*p*-methoxyphenyl
c ; Ar=*o*-chlorophenyl

Experimental

All melting points are uncorrected. Infrared and electronic spectra were measured on a Unicam SP 1200 spectrophotometer (KBr discs) and Beckmann DK-2A Ratio Recording spectrophotometer (in dioxane), respectively.

Preparation of Aroyl Isothiocyanates IIa—f. These were prepared by known procedures.

a) *Benzoyl Isothiocyanate* IIa, bp 105—110 °C/5 mmHg. Bp 95—100 °C/2—3 mmHg by Kurzer and Hanks;[11] bp 143 °C/20 mmHg by Smith and Kan.[12]

b) p-*Toluoyl Isothiocyanate* IIb, bp 110—113 °C/1 mmHg; bp 92 °C/0.4 mmHg.[12]

c) p-*Anisoyl Isothiocyanate* IIc, bp 160—166 °C/4 mmHg; bp 148—152 °C/1 mmHg.[11]

d) p-*Bromobenzoyl Isothiocyanate* IId, mp 54—55 °C (from chloroform); mp 55 °C.[13]

e) o-*Chlorobenzoyl Isothiocyanate* IIe, bp 130—135 °C/5 mmHg; bp 119 °C/2 mmHg.[14]

f) *Cinnamoyl Isothiocyanate* IIf, bp 125—130 °C/4 mmHg; bp 119 °C/2 mmHg.[12]

Addition of Urea to Aroyl Isothiocyanates II. General Procedure Method A. To a solution of aroyl isothiocyanate (0.05 mol) in dry acetone (100 ml) was added urea (0.05 mol) portionwise with stirring. The reaction mixture was then refluxed for 2—3 h until all of the urea had dissolved. Evaporation of the acetone solution followed by trituration of the residue with hot water gave a crystalline solid. Recrystallization from an appropriate solvent gave 1-aroyl-2-thiobiurets IV. The results are given in Table 2.

Table 3. 6-Aryl-4-thioxo-1,2,3,4(or 2,3,4,5)-tetrahydro-1,3,5-triazin-2-ones VII

Compound	Melting point	Yield %	Formula	Found (%)				Calcd (%)			
				C	H	N	S	C	H	N	S
VIIa	264—266[a]	80	$C_9H_7N_3OS$	52.3	3.6	20.7	15.3	52.7	3.4	20.5	15.6
VIIb	250—253[b]	85	$C_{10}H_9N_3OS$	55.2	4.4	19.6	14.4	54.8	4.1	19.2	14.6
VIIc	258—260[c]	78	$C_{10}H_9N_3O_2S$	51.5	4.2	18.0	13.5	51.1	3.8	17.9	13.6
VIId	264—266[d]	82	$C_9H_6BrN_3OS$	38.4	2.5	15.1	11.5	38.0	2.1	14.8	11.3
VIIe	210—212[e]	75	$C_9H_6ClN_3OS$	44.7	2.8	17.3	13.2	45.1	2.5	17.5	13.3

a) From ethanol, Ref. 2, mp 246—248 °C. b) From ethanol, Ref. 16, mp 246—247 °C. c) From acetic acid, Ref. 16, mp 257—259 °C (from DMF/water). d) From acetic acid. e) From ethanol.

Table 4. 5-Aroylamino-2,3-dihydro-1,2,4-thiadiazol-3-ones X

Compound	Melting point	Yield %	Formula	Found (%)				Calcd (%)			
				C	H	N	S	C	H	N	S
Xa	225—228[a]	88	$C_9H_7N_3O_2S$	48.5	3.2	18.8	14.2	48.9	3.2	19.0	14.5
Xb	261—264[b]	83	$C_{10}H_9N_3O_3S$	47.5	4.0	16.3	12.6	47.8	3.6	16.7	12.75
Xc	251—253[b]	90	$C_9H_6ClN_3O_2S$	42.7	2.6	16.4	12.4	42.3	2.3	16.4	12.5

a) From 1-butanol. b) From acetic acid.

The mother liquor obtained after separation of IVa deposited colorless crystals of the diadduct V, mp 175—178 °C (from aqueous methanol), in 3% yield. Found: C, 52.8; H, 4.0; N, 14.6; S, 16.6%. Calcd for $C_{17}H_{14}N_4O_3S_2$: C, 52.8; H, 3.6; N, 14.5; S, 16.6%.

Method B. Urea (0.05 mol) was added to an acetone solution of the aroyl isothiocyanate II [prepared *in situ*[15] from the corresponding aroyl chloride (0.05 mol) and ammonium thiocyanate (0.08 mol) in acetone (100 ml) by refluxing for 15 min followed by filtration of inorganic solid] and the reaction mixture refluxed for 2—3 h. The reaction mixture was worked up as described in *Method A*. The yields of the monoadducts 1-aroyl-2-thiobiurets IV obtained by this method are included in Table 2.

Desulfurization of 1-Benzoyl-2-thiobiuret IVa with Aqueous Chloroacetic Acid. A solution of chloroacetic acid (4 g) in water (10 ml) was mixed with 1-benzoyl-2-thiobiuret IVa (2 g) and heated on an oil bath at 150—160 °C for 30 min. After being cooled to room temperature, the product was filtered off and recrystallized from methyl cellosolve to give benzoylbiuret almost quantitatively, mp 220—221 °C (lit,[7] mp 220 °C). Found: C, 52.4; H, 4.7; N, 20.1%. Calcd for $C_9H_9N_3O_3$: C, 52.1; H, 4.3; N, 20.3%.

Action of Concentrated Hydrochloric Acid on 1-Benzoyl-2-thiobiuret IVa. Isolation of Monothiobiuret VI. Ethanol (*ca.* 10 ml) was added to a suspension of 1-benzoyl-2-thiobiuret IVa (2 g) in concentrated hydrochloric acid. The reaction mixture was then refluxed until most of the benzoic acid (mp and mixed mp 121 °C) had sublimed into the condenser. The solution was evaporated *in vacuo* and the residue was neutralized with sodium hydrogencarbonate and then recrystallized from water to give monothiobiuret VI in 65% yield, mp 185—186 °C (lit,[10] mp 187—189 °C). It gave the biuret reaction and showed its infrared spectrum bands for ν_{NH} at 3540, 3440, 3380—3300, 3280—3140 cm^{-1} and for $\nu_{C=O}$ at 1730, 1700, 1660 and 1640 cm^{-1}. Its electronic spectrum showed λ_{max} 256 nm (ε 15490). Found: N, 30.25; S, 22.9%. Calcd for $C_2H_5N_3OS \cdot H_2O$: N, 30.65; S, 23.35%.

Action of Aqueous Sodium Hydroxide on 1-Aroyl-2-thiobiurets IVa—e. Synthesis of 6-Aryl-4-thioxo-1,2,3,4(or 2,3,4,5)-tetrahydro-1,3,5-triazin-2-ones VIIa—e. 1-Aroyl-2-thiobiuret (0.01 mol) was dissolved in aqueous 4 M sodium hydroxide (60 ml) and ethanol (30 ml) and the reaction mixture was left to stand at room temperature overnight. Acidification with 1M aqueous sulfuric acid (pH 6) gave a precipitate (quantitative yield) which was recrystallized from an appropriate solvent to give 6-aryl-4-thioxo-1,2,3,4(or 2,3,4,5)-tetrahydro-1,3,5-triazin-2-one VII as yellow to orange crystals. The results are given in Table 3.

Desulfurization of 6-Phenyl-4-thioxo-1,2,3,4(or 2,3,4,5)-tetrahydro-1,3,5-triazin-2-one VIIa to 6-Phenyl-1,2,3,4-tetrahydro-1,3,5-triazin-2,4-dione VIII. Compound VIIa (2 g) was desulfurized with a solution of chloroacetic acid (4 g) in water (10 ml) to give 6-phenyl-1,2,3,4-tetrahydro-1,3,5-triazin-2,4-dione (quantitative yield). It was recrystallized from water, mp 286—288 °C; mp 286—287 °C.[7] Goerdeler and Neuffer[16] reported mp 283—285 °C for the same compound recrystallized from ethanol. Found: C, 57.4; H, 4.1; N, 22.1%. Calcd for $C_9H_7N_3O_2$: C, 57.1; H, 3.7; N, 22.2%.

Preparation of 4-Benzylthio-6-phenyl-1,2(or 1,4)-dihydro-1,3,5-triazin-2-one IX. Benzyl chloride (0.011 mol) was added while being warmed to a stirred solution of 6-phenyl-4-thioxo-1,2,3,4(or 2,3,4,5)-tetrahydro-1,3,5-triazin-2-one VIIa (0.01 mol) in aqueous 0.5 M sodium hydroxide (30 ml) and ethanol (70 ml) over a period of 10 min. After the addition had been completed, stirring was continued for 1 h. The reaction mixture was then diluted with water and the precipitate was filtered off and recrystallized from ethyl acetate to give the *title compound* in 80% yield, mp 229 °C (lit,[2] mp 229 °C). Found: C, 65.0 H, 4.6; N, 14.0; S, 10.6%. Calcd for $C_{16}H_{13}N_3OS$: C, 65.1; H, 4.4; N, 14.2; S, 10.9%.

Oxidation of 1-Aroyl-2-thiobiuret IV to 5-Aroylamino-2,3-dihydro-1,2,4-thiadiazol-3-ones X with Hydrogen Peroxide. Hydrogen peroxide (10%, 15 ml) was added to a boiling solution of each of IVa, c, or e (0.01 mol) in ethanol (20 ml) containing concentrated hydrochloric acid (1 ml) over a period of 5 min. After being cooled to room temperature, the precipitated solid was filtered off and recrystallized from a suitable solvent to give the thiadiazoles Xa, b, or c. The results are given in Table 4.

Action of Sodium Plumbite on 1-Aroyl-2-thiobiurets IV and 5-Aroylamino-2,3-dihydro-1,2,4-thiadiazol-3-ones X. When

sodium plumbite was added to IV, a black precipitate (lead sulfide) was formed immediately. On the other hand, no precipitate was formed at room temperature on addition of sodium plumbite to X; the black lead sulfide separated after being warmed, its amount increasing by boiling for 3—5 min.

References

1) For a preliminary report of some of the results, *cf.* Mohamed N. Basyouni and Abdel-Momen A El-Khamry, *Chem. Ind. (London)*, **1978**, 670.

2) J. Goerdeler and J. Neuffer, *Chem. Ber.*, **104**, 1580 (1971).

3) D. T. Elmore, J. R. Ogle, W. Fletcher, and P. A. Toseland, *J. Chem. Soc.*, **1956**, 4458; D. T. Elmore and J. R. Ogle, *ibid.*, **1958**, 1141.

4) E. Hoggarth, *J. Chem. Soc.*, **1949**, 1160; G. D. Durant, *ibid.*, **1967**, 92.

5) L. J. Bellamy "The Infrared Spectra of Complex Molecules," Chapman and Hall, London (1975), pp. 235, 247; T. Uno and K. Machida, *Bull. Chem. Soc. Jpn.*, **34**, 545 (1961).

6) T. B. Johnson, G. M. Pfau, and W. W. Hodge, *J. Am. Chem. Soc.*, **34**, 1041 (1912).

7) P. Adams, D. W. Kaiser, D. E. Nagy, G. A. Peters, R. L. Sperry, and J. T. Thurston, *J. Org. Chem.*, **17**, 1162 (1952).

8) A. Wunderlich, *Chem. Ber.*, **19**, 449 (1886).

9) E. Fromm and E. Junius, *Chem. Ber.*, **28**, 1102 (1895).

10) R. L. Sperry, U. S. Patent 2371113; *Chem. Abstr.*, **39**, 3556 (1945).

11) F. Kurzer and D. H. Hanks, *J. Chem. Soc., C*, **1967**, 746.

12) P. A. Smith and R. O. Kan, *J. Org. Chem.*, **29**, 2261 (1964).

13) L. F. Audrieth, J. R. Johnson, A. W. Browne, and C. W. Mason, *J. Am. Chem. Soc.*, **52**, 1928 (1930).

14) Zh. M. Ivanova, N. A. Kirsanova, and G. I. Derkach, *Zh. Org. Khim.*, **11**, 2186 (1965); *Chem. Abstr.*, **64**, 11123c (1966).

15) G. D. Durant, *J. Chem. Soc., C*, **1967**, 952.

16) J. Goerdeler and J. Neuffer, *Chem. Ber.*, **104**, 1606 (1971).

NOTES

BULLETIN OF THE CHEMICAL SOCIETY OF JAPAN, VOL. 52 (12), 3733—3734 (1979)

Cell Design for Simultaneous Measurement of Photoacoustic and Fluorescence Spectra

Kenji KATO† and Yoshinori SUGITANI*

Institute of Chemistry, The University of Tsukuba, Sakura-mura, Ibaraki 305

(Received April 3, 1979)

Synopsis. A simple and convenient sample cell has been designed for the simultaneous detection of photoacoustic and fluorescent signals. Spectral measurement of natural zircon, using the designed cell, is presented.

There has been a growing interest in photoacoustic spectroscopy as a method for the characterization of solid materials, in addition to the conventional methods including fluorescence spectroscopy. Since photoacoustic spectroscopy depends on the radiationless process of de-excitation, it is complementary to fluorescence spectroscopy which deals with the radiative process of de-excitation. A combination of the two methods, and particularly the simultaneous measurement of photoacoustic and excitation spectra will be of great use in the study of the de-excitation process.

In this note, a cell design for the simultaneous detection of photoacoustic and fluorescent signals is presented together with a spectral measurement on natural zircon $ZrSiO_4$.

Cell Design

Figure 1 shows the sample cell which is designed for the simultaneous detection of photoacoustic and fluorescent signals of powdered specimens. The cell is composed of a cell body and a sample base. On the sample base, the powder specimen is spread with the aid of water, acetone, or alcohol. In the measurement, the cell body and the sample base are tightly coupled using a packing material such as PARAFILM (American Can Co., USA). The air space in the cell is approximately 0.4 cm^3 in the coupled state. The electlet-microphone attached onto the cell body is connected to the sample position *via* a channel (2 mmϕ × 40 mmL). The amount of sample necessary for the measurement is approximately 0.05 g.

Figure 2 shows the photoacoustic signal intensity of carbon black at the output terminal of the microphone with respect to the chopping frequency. The spectrometer was set at 500 nm as a filter with a slit width of 3.0 mm. The photoacoustic signal intensity is inversely proportional to the chopping frequency in the range 7 to 320 Hz.

The photoacoustic signal is considered to be generated in the boundary layer of gas (air) surrounding the sample. The thickness of the layer is given as

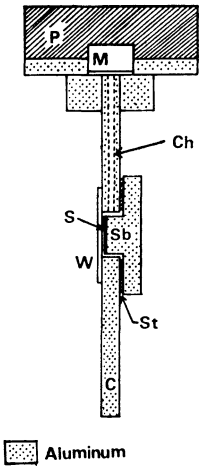

Fig. 1. Sample cell for simultaneous measurement of photoacoustic and fluorescent spectra. S: Sample, W: quartz window, St: sticky packing, Sb: sample base, Ch: channel, M: microphone, P: acoustic protector.

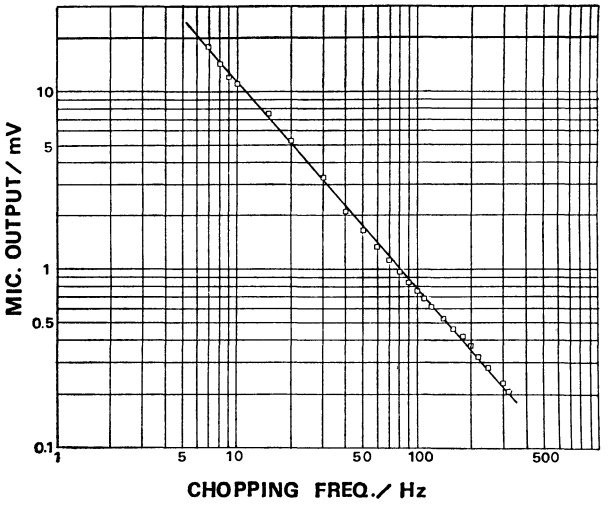

Fig. 2. Photoacoustic signal of carbon black at the output terminal of the microphone *vs.* chopping frequency.

$2\pi(2\alpha/\omega)^{1/2}$,[1] where ω is the chopping frequency and α, the thermal diffusivity of the gas. It is approximately 1 mm, at a chopping frequency of 100 Hz for example. This suggests that there is a limitation to the smallest air space in the coupled cell as well as to the lowest chopping frequency for effective detection of the photoacoustic signal. Beyond the limitation, losses

† Present address: National Chemical Laboratory for Industry, 1-1 Yatabe-cho Higashi, Tsukuba-gun, Ibaraki 305.

occur in thermal generation, resulting in a reduction of the signal intensity.[2,3] The optimum chopping frequency was found to be approximately 100 Hz.

J. F. McClelland *et al.* have discussed the influence of scattered light in the photoacoustic cell.[4] They have suggested that the scattered light was absorbed by the microphone diaphragm and a resultant spurious signal was detected. In the sample cell designed here, the microphone is isolated from the sample, so that the obtained spectra are completely free from the scattered light, as seen in the Fig. 3.

Other properties of the designed cell are; i) the system of the cell body and the sample base are of a simple type, so that spare parts, especially of the sample base, can be readily provided, ii) the quartz sample base allows the observation of transmitted light, iii) since the sample base is inserted in the cell body, the air volume in the cell is very small contributing to the enhancement of signal intensity.

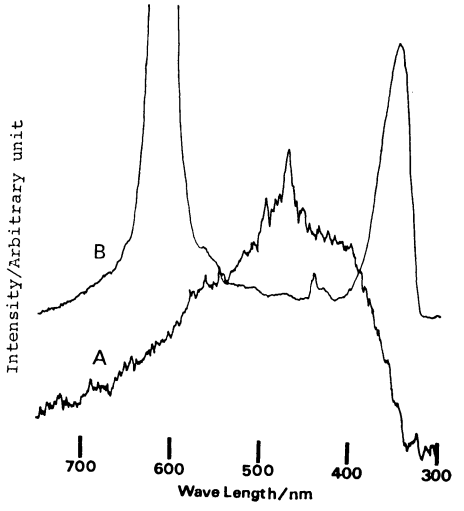

Fig. 3. Photoacoustic (A) and fluorescent excitation (B) spectra of natural zircon $ZrSiO_4$.

Simultaneous Measurement

Figure 3 shows the photoacoustic and excitation spectra simultaneously measured at room temperature for zircon $ZrSiO_4$ at a chopping frequency of 80 Hz. The scanning rate was 25 nm/min, and the slit of the spectrometer for incident light was 0.5 mm which corresponds to a resolution of 3 nm, and that for the emitted light was 1 mm. The time constant was 3 s for both of the lock-in amplifiers. Corrections for the light source intensity were not made, and the excitation spectra was monitored at 520 nm fluorescence output. The contrast between the photoacoustic and the excitation spectra is clearly seen and no additional signal due to the diaphragm was observed.

The authors wish to thank Prof. Kozo Nagashima of the University of Tsukuba, Institute of Chemistry, for his kind support during the course of this work.

References

1) A. Rosencwaig and A. Gersho, *J. Appl. Phys.*, **47**, 64 (1976).
2) L. C. Aamodt, J. C. Murphy, and J. G. Parker, *J. Appl. Phys.*, **48**, 927 (1977).
3) J. F. McClelland and R. N. Knisely, *Appl. Opt.*, **15** 2658 (1976).
4) J. F. McClelland and R. N. Knisely, *Appl, Opt.*, **15**, 2967 (1976).

BULLETIN OF THE CHEMICAL SOCIETY OF JAPAN, VOL. 52 (12), 3735—3736 (1979)

The Effect of Configuration Interaction on the π-Bond Orders, and the Molecular Geometry of Coronene in Its Ground State

Mitsunobu NAKAYAMA,* Kenji MORIHASHI, Masato IGARASHI, and Keizo SUZUKI

Department of Chemistry, The University of Tsukuba, Sakura-mura, Niihari-gun, Ibaraki 300-31

(Received October 30, 1978)

Synopsis. Semiempirical MC-LCAO-MO calculations have been made on the ground-state coronene. The inclusion of the off-diagonal terms in the MC bond-order formula is, in this case, essential to improve the bond orders and the bond lengths over the usual single configuration calculation.

The geometrical structures of unsaturated hydrocarbons have long been yielded by computing the C–C bond distances through the linear relationship[1] between the bond length, r_{kl}, and the π-bond order, P_{kl}:

$$r_{kl} = r_0 - cP_{kl}. \quad (1)$$

The adequacy of the use of this relationship has been theoretically demonstrated by Julg[2] using a semiempirical SCF-MO formalism.

In a previous paper proposing a semiempirical MC-LCAO-MO method,[3] we introduced the multi-configuration (MC) π-bond order for a bond between two carbon atoms, k and l:

$$P_{kl} = \sum_m A_m^2 P_{kl}^{(m)} + 2\sum_{m<n}\sum' A_m A_n P_{kl}^{(m,n)}, \quad (2)$$

where A_m is the coefficient of the configuration function (CF), m, and $P_{kl}^{(m)}$ are the bond orders obtained from the mth CF, and $P_{kl}^{(m,n)}$ are those between the CF's m and n; henceforth, the first and second terms will be called the diagonal and off-diagonal terms respectively. Note that $P_{kl}^{(m,n)}$ are non-vanishing only when the CF's m and n differ in a pair of MO's for the same counterpart of an electron.

Julg[2] has proposed an MC bond-order formula which omits the off-diagonal terms from Eq. 2. McCoy and Ross[4] included all the terms in their singly-excited configuration interaction calculations for excited states of benzene, naphthalene, azulene, and anthracene. To our knowledge, however, no examination has been made concerning the effect of the off-diagonal terms.

In the present study we have made MC-LCAO-MO calculations on the ground-state coronene using the full form of Eq. 2 (Case I) and the formula without the off-diagonal terms (Case II). The computed P_{kl} values are used to calculate the bond length, r_{kl}, by means of Eq. 1, with r_0=1.523 Å and c=0.193. As in previous papers,[5] Approximation (1), $\beta_{kl}=\beta_0\exp[-(r_{kl}-b)/a]$, and Approximation (2), $\beta_{kl}=-KS_{kl}$(11.290 eV), are used with β_0=−2.38 eV, a=0.3938 Å, b=1.397 Å, and K=0.86291. The CI treatment includes 24 singly-excited configurations, 68 doubly-excited configurations, and 16 triply-excited configurations, together with the ground configuration. (Note that the MO's are of the Hückel type and not of the SCF type). These configurations were chosen successively from the energetically lowest configuration in each type belonging to the *gerade* representation of the D_{6h} point group. The explicit formulas of these functions are listed in Ref. 6.

This CI calculation yielded energy depressions of −0.529—−0.550 eV, depending on the approximations for β_{kl} and which case was used, I or II. Table 1 shows the bond lengths and π-bond orders calculated with and without the CI for the ground state of coronene. Bonds a, b, c, and d are illustrated in Fig. 1. It may be seen from the table that in Case II the bond orders obtained from the CI calculation are little different from those obtained without CI, with the largest difference being about 0.005 at bond d, while in Case I the differences between the bond orders computed with and without CI are quite large, being 0.017—0.043. In

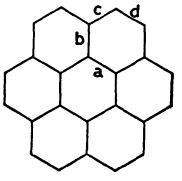

Fig. 1. Carbon skeleton of coronene.

TABLE 1. BOND LENGTHS (Å) AND π-BOND ORDERS OF THE GROUND-STATE CORONENE[a]

Bond	Approximation (1)			Approximation (2)			Exptl.
	No CI	Case I	Case II	No CI	Case I	Case II	
a	1.425	1.430	1.425	1.424	1.428	1.424	1.432
	(0.5097)	(0.4802)	(0.5092)	(0.5155)	(0.4922)	(0.5148)	
b	1.414	1.406	1.415	1.416	1.410	1.417	1.407
	(0.5655)	(0.6086)	(0.5609)	(0.5529)	(0.5867)	(0.5491)	
c	1.423	1.428	1.423	1.421	1.425	1.421	1.430
	(0.5175)	(0.4920)	(0.5182)	(0.5265)	(0.5066)	(0.5268)	
d	1.375	1.370	1.376	1.377	1.373	1.378	1.354
	(0.7689)	(0.7908)	(0.7635)	(0.7590)	(0.7762)	(0.7537)	

a) The "no CI" refers to the calculation with the ground configuration alone. The values in parentheses are the π-bond orders. The experimental values are averaged from the X-ray[7] and electron-diffraction[8] data.

Case I, the a and c bonds are lengthened, while the b and d bonds are contracted, because of CI. Thus, the CI effect on the bond orders in the ground state of coronene is significant only when the full Eq. 2 is employed, indicating that the off-diagonal terms are not necessarily negligible. The bond lengths predicted from the CI mixing in Case I are in good agreement with the experimental values except for the case of bond d. The bond lengths obtained without CI agree closely with the results obtained by Golebiewski[9] from the perturbed Hückel method.

Further, we have made several CI calculations including larger numbers of doubly-excited configurations (10—26 more functions), but without triply-excited configurations. The results were, however, not very different from those presented here; the differences in bond orders were, for all the bonds, less than 0.005 in Case I and less than 0.001 in Case II.

One of the present authors (Nakayama) is grateful to Dr. Tai-ichi Shibuya of Shinshu University for his helpful discussions. Thanks are also due to the referee for making valuable suggestions. The calculations were carried out on the TOSBAC-5600 Computer at the University of Tsukuba. The present work was partially supported by a Grant-in-Aid for Scientific Research from the Ministry of Education.

References

1) For example, L. C. Snyder, *J. Phys. Chem.*, **66**, 2299 (1962); P. N. Skancke, *Acta Chem. Scand.*, **18**, 1671 (1964); Y. Fujimura, H. Yamaguchi, and T. Nakajima, *Bull. Chem. Soc. Jpn.*, **45**, 384 (1972).

2) A. Julg, *J. Chim. Phys. Phys.-Chim. Biol.*, **65**, 541 (1968).

3) M. Nakayama and Y. J. I'Haya, *Int. J. Quantum Chem.*, **4**, 21 (1970).

4) E. F. McCoy and I. G. Ross, *Aust. J. Chem.*, **15**, 573 (1962).

5) M. Nakayama, K. Sazi, and Y. J. I'Haya, *Theor. Chim. Acta*, **38**, 327 (1975); M. Nakayama, M. Nishihira, and Y. J. I'Haya, *Bull. Chem. Soc. Jpn.*, **49**, 1502 (1976).

6) M. Nakayama and Y. J. I'Haya, *Rept. Univ. Electro-Commun.*, **30**, 73 (1971).

7) J. K. Fawcett and J. Trotter, *Proc. R. Soc. London, Ser. A*, **289**, 366 (1966).

8) A. Almenningen, O. Bastiansen, and F. Dyvik, *Acta Crystallogr.*, **14**, 1056 (1961).

9) A. Golebiewski, *Roczniki Chem.*, **36**, 1137 (1962).

BULLETIN OF THE CHEMICAL SOCIETY OF JAPAN, VOL. 52 (12), 3737—3738 (1979)

The Singlet-excitation-energy Migration in an Amorphous-state Film of 1,3-Di(9-carbazolyl)propane

Akira ITAYA,* Ken-ichi OKAMOTO, and Shigekazu KUSABAYASHI

Department of Chemical Engineering, Faculty of Engineering, Yamaguchi University, Tokiwadai, Ube 755

(Received May 1, 1979)

Synopsis. The singlet-excitation-energy migration in an amorphous film of 1,3-di(9-carbazolyl)propane(DCzP(a)) was studied by means of a fluorescene-quenching experiment. The results were compared with those of amorphous poly-(9-vinylcarbazole)(PVCz) and poly[2-(9-carbazolyl)ethyl vinyl ether](PCzEVE) films. The numbers of carbazolyl chromophores covered by a singlet exciton during the lifetime were in the following order: DCzP(a)>PCzEVE>PVCz.

1,3-Di(9-carbazolyl)propane (DCzP) is known as a dimeric model compound of poly(9-vinylcarbazole) (PVCz), which has received considerable interest in recent years in connection with the highly photoconductive vinyl polymers. DCzP forms an amorphous state by the fast evaporation of the solvent.[1] It is important to investigate singlet exciton migration in a DCzP(a) film and to compare it with that in a PVCz film, because the efficiency of the singlet exciton migration in a vinyl polymer is known as one of the factors determining whether or not the polymer has a large photoconductivity.

A few investigations have been carried out to ascertain how the efficiency of the singlet exciton migration changes when going from a crystalline to an amorphous state.[2] However, a comparison of the optical properties of an amorphous film of a model compound with the optical properties of an amorphous film of a corresponding vinyl polymer has not hitherto been performed.

In a previous paper,[1] the absorption and fluorescence spectra of a DCzP(a) film were investigated and compared with those of polycrystalline DCzP(DCzP(c)) and amorphous PVCz films. In the present work, the migration of the singlet excitation energy in a DCzP(a) film has been investigated in comparison with that of an amorphous PVCz film.

Experimental

The model compound (DCzP) and polymers (PVCz and poly[2-(9-carbazolyl)ethyl vinyl ether](PCzEVE)) were the same as those used before.[1,3] The dimethyl terephthalate (DMTP)and perylene were recrystallized twice from benzene and *p*-bis(trichloromethyl)benzene (TCB) from hexane. Subsequently, they were sublimed *in vacuo*. The DCzP(a) and polymer films were cast onto quartz or Pyrex-glass plates from a benzene solution. The fluorescence spectra were observed by front-surface excitation with the apparatus described in a previous paper.[4]

Results and Discussion

In a previous paper[1] we reported that the fluorescence spectrum of a DCzP(a) film seems to be composed of three components, monomer-like, second excimer ($\tilde{\nu}_{max}$: *ca.* 26700 cm^{-1}), and sandwich-like excimer ($\tilde{\nu}_{max}$: 23900 cm^{-1}) fluorescences, while a DCzP(c) film seems to show the monomer-like and second excimer fluorescences.

The presence of the second excimer and monomer fluorescences was supported also by the investigation of the temperature dependence of the fluorescence spectrum of a DCzP(a) film. As is shown in Fig. 1, the intensity of the second excimer fluorescence of a PVCz film increased with a decrease in the temperature, showing that the second excimer site is a shallow trap and acts more effectively as a trap at low temperatures. This is consistent with the results obtained by the investigation of the excitation-energy-migration.[4] The temperature dependence of the fluorescence spectrum of a DCzP(a) film was similar to that of a PVCz film, as is shown in Fig. 2. In the case of a DCzP(a) film, the structure band in the shorter-wavelength region, which appears with an increase in the temperature, is the monomer fluorescence, which increases with a decrease in the concentration of the trap sites.

By the doping of perylene, TCB, and DMTP, the host fluorescence decreased. The fluorescence spectra of DCzP(a) films doped with various concentrations of DMTP are shown in Fig. 3. The fluorescence in the longer-wavelength region ($\tilde{\nu}_{max}$: 21620 cm^{-1}) is attributable to the exciplex formed between DMTP and an excited Cz chromophore. The dipole-dipole resonance cannot be responsible for the energy transfer to TCB and DMTP, because these guest molecules have no absorption in the wavelength region where the fluores-

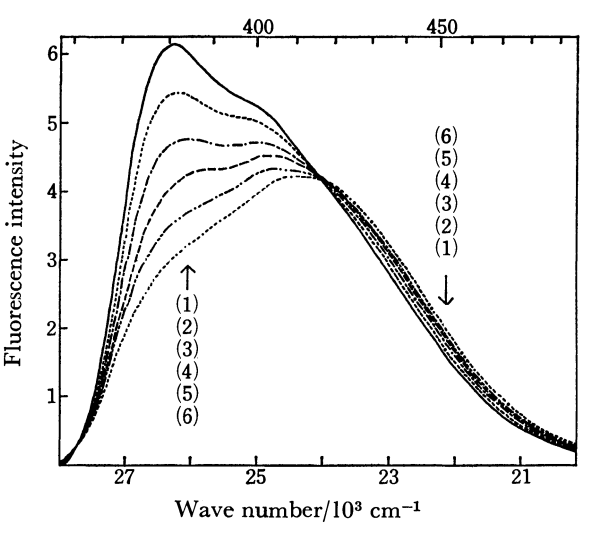

Fig. 1. Temperature dependence of the fluorescence spectra of a PVCz film. Excitation wavelength; 330 nm. (1) 121 K, (2) 140 K, (3) 163 K, (4) 187 K, (5) 210 K, and (6) 234 K.

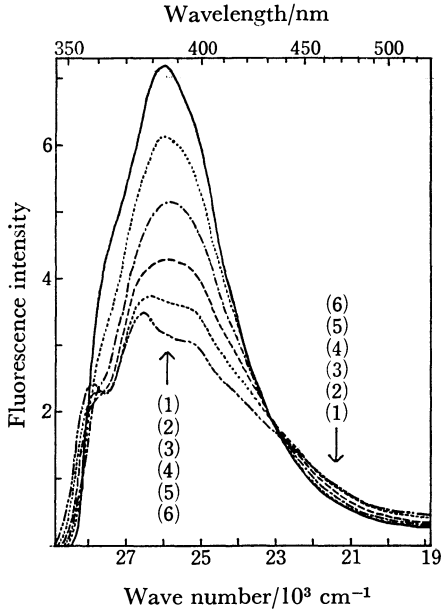

Fig. 2. Temperature dependence of the fluorescence spectra of a DCzP(a) film. Excitation wavelength; 330 nm. (1) 129 K, (2) 144 K, (3) 163 K, (4) 192 K, (5) 213 K, and (6) 236 K.

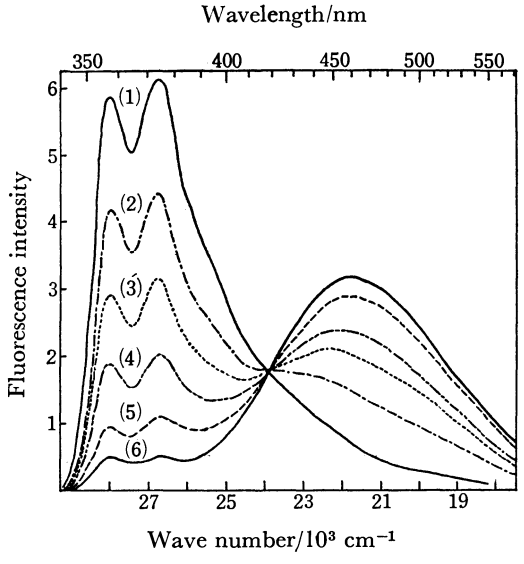

Fig. 3. Fluorescence spectra of DCzP(a) films doped with DMTP at room temperature. Excitation wavelength; 335 nm. DMTP concentration; (1) 0, (2) 3.54×10^{-4}, (3) 8.85×10^{-4}, (4) 1.80×10^{-3}, (5) 3.02×10^{-3}, and (6) 8.85×10^{-3} (mol/mol basic unit).

cense of the host film is observed. Therefore, the random-hopping model of monomer-exciton migration, in which both the intrinsic trap site and the guest molecule act competitively as exciton traps, is applicable. Then, the quenching factor of the host fluorescence, Q_H, is expressed by the following equation:[4,5]

$$Q_H = (\eta_{H0}-\eta_H)/\eta_H = nc/(1+nc_T) = n'c, \qquad (1)$$

where η_{H0} and η_H are the quantum efficiencies of the host fluorescence in the absence and in the presence of the guest molecule in a concentration of c (mol/mol basic unit); n and n' are the numbers of Cz chromophores covered by an exciton during the lifetime in the absence and in the presence of the intrinsic trap sites (second and sandwich-like excimer sites) in a concentration of c_T (mol/mol basic unit). The quenching factor of monomer fluorescence, Q_M, is expressed by

$$Q_M = nc_T. \qquad (2)$$

The bilogarithmic plots of Q_H and c gave a straight line with a slope of 1.0. The values of n' were obtained from the lines according to Eq. 1; they are listed in Table 1. The value of n' is dependent on the guest molecule. In the case of perylene, an energy migration with a subsequent long-range energy transfer seems to be observed.[6] This is why the value of n' for perylene is larger than those for the others.

In the case of polymer film, where no monomer fluorescence was observed, $Q_M \gg 1$, as has previously been reported.[4,5] Therefore, $Q_H = c/c_T$. Then, $c_T = 1/n'$. Although Q_M could not be obtained for a DCzP(a) film, the value of c_T for the film seems to be smaller than $1/n'$. The values of c_T are also listed in Table 1.

Table 1. Energy transefr by the exciton-diffusion process

No.	Host	Guest	n'	$c_T\times10^3$ (mol/mol basic unit)
1	PVCz	Perylene	1200	0.83
2	PCzEVE	Perylene	3700	0.27
3	DCzP(a)	Perylene	5900	<0.17
4	PVCz	TCB	690	1.4
5	PCzEVE	TCB	2000	0.50
6	DCzP(a)	TCB	3600	<0.28
7	PVCz	DMTP	420	2.4
8	PCzEVE	DMTP	2900	0.34
9	DCzP(a)	DMTP	1300	<0.77

Concerning amorphous films, the value of c_T increases in the following order, irrespective of the guest molecule, except for PCzEVE film doped with DMTP: DCzP(a)< PCzEVE<PVCz. That is, the concentration of the trap sites for a DCzP(a) film is smaller than that for a PVCz film and that for a PCzEVE film, where it is difficult for Cz chromophores to form the intrinsic trap sites because of the large distance between neighboring Cz chromophores. This suggests that the excimer sites in a polymer film are formed with greater ease than the excimer sites in an amorphous film of the model compound, even if Cz chromophores are widely spaced on the skeletal chain.

References

1) A. Itaya, K. Okamoto, and S. Kusabayashi, *Chem. Lett.*, **1978**, 131.
2) K. P. Seefeld, H. Müller, and H. Bässler, *J. Luminescence*, **16**, 359 (1978); Y. Sano, M. Yokoyama, Y. Shirota, and H. Mikawa, *Mol. Cryst. Liq. Cryst.*, in press.
3) K. Okamoto, A. Itaya, and S. Kusabayashi, *Polym. J.*, **7**, 662 (1975).
4) A. Itaya, K. Okamoto, and S. Kusabayashi, *Bull. Chem. Soc. Jpn.*, **50**, 22 (1977).
5) W. Klöpffer, *J. Chem. Phys.*, **50**, 2337 (1969).
6) R. C. Powell and Q. Kim, *J. Luminescence*, **6**, 351 (1973).

BULLETIN OF THE CHEMICAL SOCIETY OF JAPAN, VOL. 52 (12), 3739—3740 (1979)

Syntheses and Electrical Properties of α,α,α',α'-Tetracyanodiphenoquinodimethane Complexes

Minoru MORINAGA, Takashi NOGAMI,* and Hiroshi MIKAWA

Department of Applied Chemistry, Faculty of Engineering, Osaka University, Yamadakami, Suita, Osaka 565

(Received June 2, 1979)

Synopsis. Two charge-transfer complexes of α,α,α',α'-tetracyanodiphenoquinodimethane (TCNDQ), *i.e.*, *N*-methylphenazinium (NMP)–TCNDQ and *N*-methylquinolinium (NMQ)–TCNDQ, were synthesized. The electrical resistivities with pressed pellet samples were 7.1×10^{8} Ω cm for NMP^{+}-$TCNDQ^{-}$ and 6.9×10^{7} Ω cm for $NMQ^{+}TCNDQ^{-}$; they are thus much less conductive than the corresponding TCNQ complexes.

Great attention has been paid to the high electrical conductivities of tetracyanoquinodimethane (TCNQ) complexes.[1] The highly conductive properties of TCNQ complexes were analysed by means of the Hubbard model.[2] It was suggested that a large transfer integral (t) and a small Coulomb repulsion energy (U_{eff}) are needed for high conductivity. The large t is realized by the large overlap of the π-electron cloud between adjacent TCNQ anion radicals, and the small U_{eff} by the distant location of cyano groups in TCNQ and also by the polarization stabilization caused by the donor cation.

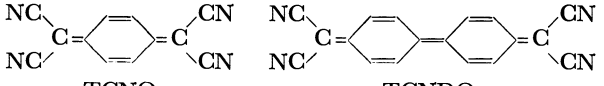

TCNQ TCNDQ

The separation of cyano groups in tetracyanodiphenoquinodimethane (TCNDQ) is greater than in TCNQ, thereby possibly resulting in a smaller U_{eff} than in TCNQ. Thus, the TCNDQ complexes are expected to be good candidates for highly conductive organic materials. However, no electrical property is known for TCNDQ.[3] We have synthesized two complexes, *N*-methylphenazinium (NMP)–TCNDQ and *N*-methylquinolium (NMQ)–TCNDQ, and measured their electrical resistivities, electronic absorption spectra, and ESR spectra.

Results and Discussion

Synthesis of $Na^{+}TCNDQ^{-}$. $Na^{+}TCNDQ^{-}$ has usually been synthesized through several step-reactions starting from 4,4'-bis(bromomethyl)biphenyl (**1**).[3] However, the yield of **1** was low (4%),[4] thus limiting the total yield of $Na^{+}TCNDQ^{-}$. On the other hand, the yield of 4,4'-bis(chloromethyl)biphenyl (**2**)[5] was much higher (60%).[4] We succeeded in obtaining 4,4'-bis(cyanomethyl)biphenyl (**3**) (the second step material for the synthesis of $Na^{+}TCNDQ^{-}$) from **2** (50% yield). Thus, **2** should be used as a starting material for the synthesis of $Na^{+}TCNDQ^{-}$. We also tried another route for the synthesis of TCNDQ:

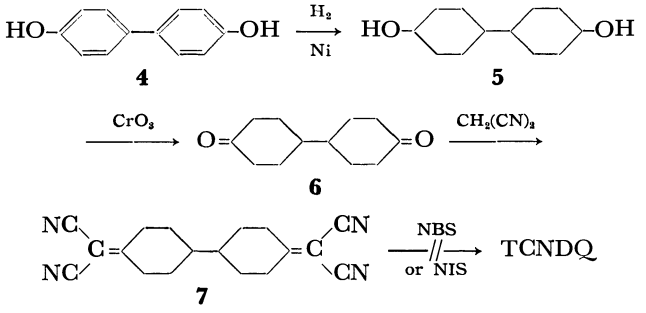

4 **5** **6** **7**

However, the attempted dehydrogenation of 4,4'-bis(dicyanomethylene)-1,1'-bicyclohexane (**7**) by *N*-bromosuccinimide (NBS) or *N*-iodosuccinimide (NIS) was unsuccessful, recovering only **7**.

Syntheses of $NMP^{+}TCNDQ^{-}$ and $NMQ^{+}TCNDQ^{-}$ Complexes. We have succeeded in obtaining $NMP^{+}TCNDQ^{-}$ and $NMQ^{+}TCNDQ^{-}$ by the following ion-exchange reactions:

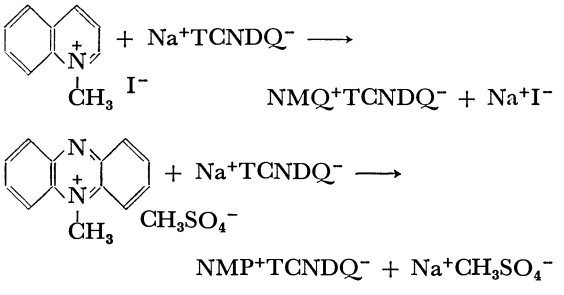

We also tried other ion-exchange reactions of several systems, *i.e.*, the tetrabutylammonium iodide–$Na^{+}TCNDQ^{-}$, quinolinium iodide–$Na^{+}TCNDQ^{-}$, and *N,N,N',N'*-tetramethylbenzidinebromide–$Na^{+}TCNDQ^{-}$ systems. However, all these systems gave polymer **8**:

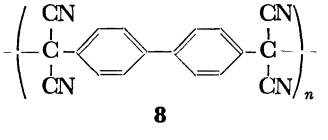

8

The attempt to obtain the complex salt $Na^{+}TCNDQ^{-}$-TCNQ by mixing the methanol solutions of $Na^{+}TCNDQ^{-}$ and TCNQ also gave polymer **8**.

Table 1. Electrical resistivities of the pressed pellet samples of TCNDQ and TCNQ complexes

	TCNDQ[a]	TCNQ[a]
Na	3.3×10^{3} [b]	3.0×10^{4} [d]
NMP	7.1×10^{8}	5.0×10^{-1} [c]
NMQ	6.9×10^{7}	1.0×10^{7} [d]

a) Ω cm. b) Ref. 3. c) Ref. 10. d) Ref. 11.

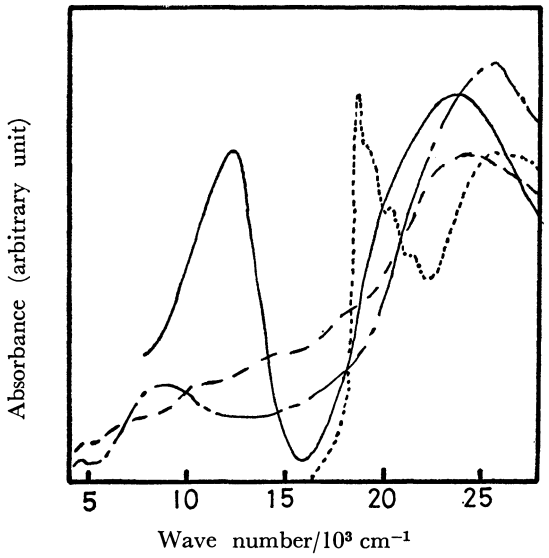

Fig. 1. Electronic absorption spectra of TCNDQ complexes. ·····Na⁺TCNDQ⁻ (in acetonitrile solution); ——Na⁺TCNDQ⁻ (KBr); —·—NMP⁺TCNDQ⁻ (KBr); – – – –NMQ⁺TCNDQ⁻ (KBr).

Properties of NMP⁺TCNDQ⁻ and NMQ⁺TCNDQ⁻ Complexes. Table 1 shows the electrical resistivities of the pressed pellet samples of Na⁺TCNDQ⁻, NMP⁺TCNDQ⁻, and NMQ⁺TCNDQ⁻, together with those of the TCNQ complexes for the sake of comparison. Na⁺TCNDQ⁻ is one order of magnitude more conductive than Na⁺TCNQ⁻. However, NMP⁺TCNDQ⁻ and NMQ⁺TCNDQ⁻ are much less conductive than the corresponding TCNQ complexes. Although we have no crystallographic data of TCNDQ complexes, one possibility is that the six-membered rings in TCNDQ may not be co-planar, thus leading to the poor conductivity.

The electronic absorption spectra of Na⁺TCNDQ⁻, NMP⁺TCNDQ⁻, and NMQ⁺TCNDQ⁻, as measured by the KBr disk method, are shown in Fig. 1. The spectrum of Na⁺TCNDQ⁻ in an acetonitrile solution is also shown in this figure. The solid-state spectrum of Na⁺TCNDQ⁻ shows a broad absorption band peaking at 23.5×10^3 cm^{-1} possibly ascribable to the local excitation band of TCNDQ⁻. The 12000 cm^{-1} band may be a charge-transfer band between adjacent TCNDQ anion radicals in the crystal. Thus, the interaction between TCNDQ anion radicals in Na⁺TCNDQ⁻ is expected to be large, suggesting the stacking structure of the anion site. NMP⁺TCNDQ⁻ and NMQ⁺TCNDQ⁻ also have two absorption bands in the IR and VIS regions, although in the latter spectrum the peak position of the lower energy band is not clear.

The ESR spectra of the powdered Na⁺TCNDQ⁻, NMP⁺TCNDQ⁻ and NMQ⁺TCNDQ⁻ showed strong single-line signals, with *g*-values of 2.003.

Experimental

Measurements. The electrical resistivity of the compaction sample was measured by means of a Takeda-Riken 8651 electrometer. The details of the measurements have been described before.[6] The electronic absorption spectra were measured by means of a Shimadzu MPS 50 L apparatus. The ESR spectra were measured by means of a Japan Electric Optics Laboratory Co., Ltd., JES-ME 2X apparatus.

Materials. *4,4′-Bis(cyanomethyl)biphenyl (3)*: The title compound was synthesized by the same procedure as that used in the synthesis of 1,4-bis(cyanomethyl)-2,5-diisopropylbenzene.[7]

4,4′-Bis(dicyanomethylene)-1,1′-bicyclohexane (7): The starting material, 1,1′-bicyclohexane-4,4′-dione was synthesized according to the literature.[8] 1,1′-Bicyclohexane-4,4′-dione (6 g), malononitrile (11.5 g), ammonium acetate (0.8 g), and acetic acid (2.4 ml) were added to benzene (80 ml) in a reaction vessel, and then the mixture was refluxed using a water separator until no water came out. The precipitate was collected, washed several times with water, and finally washed with ethyl acetate. The white powder product was dried under a vacuum to obtain 4,4′-bis(dicyanomethylene)-1,1′-bicyclohexane (**7**) (6 g, 67%); mp 229—231 °C; Found: C, 74.55; H, 6.17; N, 19.29%. Calcd for $C_{18}H_{18}N_4$: C, 74.49; H, 6.20; N, 19.31%. IR (KBr) 2200 (C≡N), 1580 cm^{-1} (C=C).

NMP⁺TCNDQ⁻ and NMQ⁺TCNDQ⁻. Na⁺TCNDQ⁻ (100 mg)[3] was dissolved in methanol (100 ml), and the solution was filtered. To the filtrate we then added a methanol solution of *N*-methylphenazinium methylsulfate or *N*-methylquinolinium iodide (50% excess molar ratio) from the dropping funnel under a nitrogen atmosphere and at the room temperature. The solution was then stirred for an additional 2 h under a nitrogen atmosphere. The precipitate (powder) was collected and washed with diethyl ether. NMP⁺TCNDQ⁻: Found:[9] C, 76.32; H, 3.85; N, 17.15%. Calcd for $C_{31}H_{19}N_6$: C, 78.32; H, 4.00; N, 17.68%. NMQ⁺TCNDQ⁻: Found:[9] C, 78.04; H, 4.22; N, 16.51%. Calcd for $C_{28}H_{18}N_5$: C, 79.25; H, 4.25; N, 16.13%.

References

1) For example, "Organic Conductors and Semiconductors," ed by L. Pal, G. Grüner, A. Janossy, and J. Solyom, Springer-Verlag, Berlin (1977); "Synthesis and Properties of Low-Dimensional Materials," ed by J. S. Miller, Annals of New York Academy of Science, Vol. 313 (1978).

2) A. F. Garito and A. J. Heeger, *Acc. Chem. Res.*, **7**, 232 (1974).

3) Two papers have appeared on TCNDQ: W. R. Hertler, US Patent, 3153658 (1964); A. R. Addison, N. S. Dalal, Y. Hoyano, S. Huizinga, and L. Weiler, *Can. J. Chem.*, **55**, 4191 (1977).

4) Our result.

5) J. T. Massengale, W. Chester, and F. C. Bender, US Patent, 3042655 (1962).

6) T. Nogami, M. Morinaga, Y. Kanda, and H. Mikawa, *Chem. Lett.*, **1979**, 111.

7) R. C. Wheland and E. L. Martin, *J. Org. Chem.*, **40**, 3101 (1975).

8) A. L. Wilds, C. H. Shunk, and C. H. Hoffman, *J. Org. Chem.*, **76**, 1733 (1954).

9) We tried to purify the product of each step for the synthesis of Na⁺TCNDQ⁻ in order to obtain a good analytical agreement of this complex. However, no good analytical agreement was obtained.

10) L. R. Melby, *Can. J. Chem.*, **43**, 1448 (1965).

11) L. R. Melby, R. J. Harder, W. R. Hertler, W. Mahler, R. E. Benson, and W. E. Mochel, *J. Am. Chem. Soc.*, **84**, 3374 (1962).

BULLETIN OF THE CHEMICAL SOCIETY OF JAPAN, VOL. 52 (12), 3741—3742 (1979)

The Mechanism of the TEA CO_2 Laser-induced Reaction of 1,1-Dichloroethane

Keiichi NAGAI and Mikio KATAYAMA*

Department of Pure and Applied Sciences, College of General Education, The University of Tokyo, Meguro-ku, Tokyo 153

(Received July 2, 1979)

Synopsis. In a TEA CO_2 laser-induced reaction of 1,1-dichloroethane, the relative quantities of the products, C_2H_2 and $ClHC{=}CH_2$, were found to vary with the laser wavelength, indicating that the C_2H_2 molecules are produced by two processes, directly and indirectly from $Cl_2HC{-}CH_3$ within the duration of a single laser pulse.

There have been a number of investigations demonstrating that infrared laser-induced reactions differ from thermal reactions. However, their reaction processes and mechanisms have not been elucidated. In a previous paper, we reported on TEA CO_2 laser-induced photoreactions of chloroethylene and chlorinated ethanes.[1] The experimental results for chlorinated ethanes have shown that rather larger amounts of acetylene than their thermal reaction products were obtained in addition to the major product of ethylene or chloroethylene. The acetylene may be produced by the following two processes, the direct process and the indirect 2-step process:

(a) The C_2H_2 molecules are directly produced from the ethane derivative by the irradiation of a single laser pulse.

(b) In the first process of the reaction, C_2H_4 or its chlorine derivative is produced; a subsequent infrared laser reaction of those molecules gives rise to the production of the C_2H_2 molecule.

In the previous study, no quantitative discussions of these reaction processes were made. Since the $Cl_2HC{-}CH_3$ molecule has infrared absorptions at the wavelengths of four regions of the CO_2 laser, *i.e.*, at P and R branches of both the 9.4 μm and 10.4 μm bands, their wavelengths are 9.6 μm, 9.3 μm, 10.6 μm, and 10.2 μm respectively. The irradiation of one of these lasers gives rise to the production of C_2H_3Cl and C_2H_2 in various concentrations. The TEA CO_2 laser-induced reaction of chlorine derivatives of hydrocarbons gives rise to the elimination of HCl from those molecules, and C_2H_3Cl molecules may be produced in the first stage of the present experiment. As the reaction product, C_2H_3Cl, has no absorption at the wavelength of 9.3 μm, the C_2H_2 molecule must be produced by the direct process in the 9.3 μm laser-induced reaction.

Recently we have made an analysis of the infrared laser-induced multiphoton dissociation of C_2F_3Cl by the phenomenological model calculation based on the Rice-Ramsberger-Kassel-Marcus statistical theory for unimolecular dissociation.[2] We thus confirmed that the observed results were in good agreement with the calculation. Together with the theoretical analysis of the infrared multiphoton dissociation of the SF_6 molecule by Grant *et al.*,[3] our analysis of the reaction of C_2F_3Cl can help to understand the reaction mechanism of the infrared photochemistry of $Cl_2HC{-}CH_3$.

For a detailed analysis of the reaction mechanism, we have observed the relative yields of the reaction products of C_2H_3Cl and C_2H_2 by the irradiation of various CO_2 laser lines; the analysis of the results enable us to understand the process of the production of C_2H_2.

The TEA CO_2 laser used in the present experiment was described in a previous paper.[1] The power output was about 1 J, with a pulse duration of 100 ns, its repetition rate being almost 1 Hz. For a selective oscillation of the appropriate line among the P and R branches of the 9.4 μm or 10.4 μm band, SF_6 or C_2H_3Cl gas of various pressures was introduced into a small cell in the laser cavity. A reaction cell was 50 mm in length and 20 mm in diameter. The sample gas in the reaction cell was irradiated by the laser pulse focused with a germanium lens of $f=5$ cm. The peak power of the laser at the focus was 1 GW/cm^2 when the laser of 1 J was used. The pressure of the sample gas was 10 Torr.

The relative amounts of the products obtained by the infrared photoreaction induced by the various branches of the CO_2 laser with the same power output of 500 mJ are listed in Table 1. The experimental results for the P branch of 10.4 μm band is not shown here, because the absorption at the wavelength of this region is weak for this molecule, and hence the yield of the reaction is relatively small.

The total amounts of the products, C_2H_3Cl and C_2H_2, depend upon the laser line used in the reaction, the yield being greatest for the 9.6 μm laser and least for the 9.3 μm laser; the ratio of the yields is 48: 100: 22 for the 10.2 μm, 9.6 μm, and 9.3 μm lasers respectively.

The ratio of the C_2H_3Cl to the C_2H_2 were determined to be 55: 45, 72: 28, and 80: 20 respectively in the products of 10.2 μm, 9.6 μm, and 9.3 μm laser reactions. As was described above, the productions of the C_2H_2

Table 1. Relative quantities of molecules produced by the infrared photoreactions of $Cl_2HC{-}CH_3$ induced by various branches of the CO_2 laser

Laser wavelength	10.2 μm	9.6 μm	9.3 μm
Relative quantities of products	48	100	22
% of products			
C_2H_3Cl	55	72	80
C_2H_2	45	28	20
% of C_2H_2 produced by			
(1) direct process	20	20	20
(2) 2-step process	25	8	0

molecules in the present experiment can be brought about by the two processes, the direct and indirect ones. It is appropriate to define the present classification of the reaction more rigidly. The infrared laser action gives rise to the cleavage of the C–Cl bond, producing the $ClHC–CH_3$ radical in an quasicontinuum state when the vibrational quantum number, v, is larger than 3. The interaction between Cl and the $ClHC–CH_3$ radicals eliminates the H atom from the latter, resulting in the production of the $ClHC{=}CH_2$ molecule in various vibrational states. The $ClHC{=}CH_2$ molecules in the quasicontinuum state can absorb infrared lasers of any frequency. Though the $ClHC{=}CH_2$ molecules in the ground state have no absorption at the 9.3 μm line of the CO_2 laser, the molecule in the quasicontinuum state absorb its infrared laser. Hence, if the laser field is still present for a sufficiently long time after the formation of the $ClHC{=}CH_2$ molecule in the quasicontinuum state, these molecules can readily absorb additional photons and the subsequent reaction may occur, producing the C_2H_2 molecule. The reaction process presented here is the direct production of the C_2H_2.

On the other hand, the indirect process is defined as the 2-step reaction in which the C_2H_3Cl molecules in the vibrational ground state or the discrete vibrational level (generally its vibrational quantum number $v<3$) are produced at the first stage of the reaction, and the successive absorption of the laser by C_2H_3Cl molecules gives rise to the reaction of these molecules. However, in the 9.3 μm laser-induced reaction of $Cl_2HC–CH_3$, the indirect process is prohibited, because the C_2H_3Cl molecule in the ground state or in the discrete levels (lower vibrational state) cannot absorb the 9.3 μm laser radiation. It is suggested, therefore, that all of the C_2H_2 molecules, 20% of the products, were produced directly from $Cl_2HC–CH_3$ when the 9.3 μm laser was used.

For the laser reaction of the 10.2 μm or 9.6 μm line, the rates of the C_2H_2 in the total amount of the products were 45% and 28% respectively. If we assume that the direct process in the 10.2 μm or 9.6 μm laser-induced reaction produces the same rate of the C_2H_2 as in the reaction of the 9.3 μm laser, the differences in the proportions of C_2H_2 between the reactions induced by the former lasers and the latter, (45—20)% and (28—20)%, are the proportions of the indirectly produced C_2H_2 by the 10.2 μm and 9.6 μm lasers respectively. The ratio of the amounts of C_2H_2 produced by the 2-step process with the 10.2 μm laser and that of the 9.6 μm laser is 0.25/0.08=3.1, while the ratio of the amounts of C_2H_2 produced from C_2H_3Cl by the 10.2 μm laser and the one produced by the 9.6 μm laser irradiation was 2.8. These values are almost equal, supporting our assumption presented here.

The relative concentrations of the C_2H_3Cl and C_2H_2 products were unaffected even when the repetition rates of the laser pulse were varied from 1 Hz to 0.1 Hz. In the latest repetition of the laser, the time interval of the two pulses is 10 s; therefore, the molecules, which have been dissociated by the first pulse at around the focus of the lens, may diffuse from this region before the second pulse is irradiated. This indicates that the 2-step reaction, $Cl_2HC–CH_3 \rightarrow ClHC{=}CH_2 \rightarrow C_2H_2$, may occur within a very short duration of 100 ns of the single laser pulse.

The conclusion derived above is supported by the theoretical analysis of the multiphoton dissociation, which has recently been applied to the 9.4 μm laser-induced chemical reaction of C_2F_3Cl. Our model calculation of the infrared photochemistry of C_2F_3Cl showed that if the rectangular pulse of 500 mJ with a 100 ns duration was employed, the following results were obtained:

1) Almost 80% of the molecules dissociate within 50 ns.

2) The decomposed molecules or radicals have excess energy in the range of $v=8$—16, the maximum distribution being in $v=12$. The average energy distribution in these molecules or radicals depends on the power output of the exciting laser.

These results have been obtained from the model calculation of the reaction yield for the 9.4 μm laser-induced photodissociation of C_2F_3Cl. It should be mentioned that the qualitative aspect of the infrared multiphoton reaction of any molecule can be deduced from the consideration presented here. The experimental results of the TEA CO_2 laser-induced reaction of $Cl_2HC–CH_3$ suggest that its reaction process is similar to that of C_2F_3Cl.

It may be concluded that the C_2H_2 molecules, 20% of the total products of the CO_2 laser-induced photochemistry of $Cl_2HC–CH_3$, are directly produced from the parent molecule, another part of the C_2H_2 being produced by the 2-step process within the time duration of the single laser pulse.

This research was supported partly by a Grant-in-Aid from the Ministry of Education, Science, and Culture.

References

1) K. Nagai and M. Katayama, *Bull. Chem. Soc. Jpn.*, **51**, 1269 (1978).

2) M. Katayama, *Oyo Buturi*, **48**, 502 (1979).

3) E. R. Grant, P. A. Schulz, Aa. S. Sudbo, Y. R. Shen, and Y. T. Lee, *Phys. Rev. Lett.*, **40**, 115 (1978).

4) M. Katayama and Y. Mizugai, *Chem. Lett.*, **1979**, 965.

BULLETIN OF THE CHEMICAL SOCIETY OF JAPAN, VOL. 52 (12), 3743—3744 (1979)

ESR and ENDOR Studies of the Hindered Internal Rotation of Higher Alkyl Groups. 2,6-Di-*t*-butyl-4-alkylphenoxyl Radicals

Fumio SHIMODA,* Terukiyo HANAFUSA, Fujito NEMOTO,** Kazuo MUKAI,** and Kazuhiko ISHIZU**

Department of Chemistry, Faculty of Science, Hiroshima University, Higashisendamachi, Hiroshima 730

***Department of Chemistry, Faculty of Science, Ehime University, Bunkyo-cho, Matsuyama 790*

(Received July 3, 1979)

Synopsis. ESR or ENDOR spectra were observed for the 2,6-di-*t*-butyl-4-methyl-, 4-ethyl-, 4-isopropyl-, and 4-cyclohexylphenoxyl radicals. From the analyses of the temperature dependence in β-proton splittings, the energy barriers to internal rotation of the alkyl group were estimated.

For a number of aromatic radicals, the restricted rotation of an alkyl group has been extensively studied by using ESR spectroscopy[1] and the rotational barrier of an alkyl group has been estimated based on the statistical procedure of observed β-proton splitting and its temperature dependence, in terms of the $\cos^2\theta$ rule.[2]

In previous papers,[3] the hindered rotation of the alkyl groups in the 4,4′-dialkybiphenyl anions was studied in detail. One interesting view is the fact that the secondary alkyl groups are likely to undergo a restricted rotation in a double-well potential function. In this work, the hindered internal rotation of the alkyl groups in the 2,6-di-*t*-butyl-4-alkylphenoxyl radicals was studied in order to affirm the validity of applying the ESR approach to the study on the restricted rotation of an alkyl group. The results obtained have been compared with those for the 4,4′-dialkylbiphenyl anions previously studied.[3]

Experimental

General. The melting points and boiling point are uncorrected. The ESR and ENDOR spectra were recorded by JEOL-ME-3X and JEOL-EDX-1 spectrometers respectively. The operating conditions were similar to those described elsewhere.[4]

Materials. The 2,6-di-*t*-butyl-4-methylphenol is commercially available. The other 2,6-di-*t*-butyl-4-alkylphenols were prepared by the method previously described.[5] 2,6-Di-*t*-butyl-4-ethylphenol: bp 105—110 °C/5 Torr (lit,[5] 135—138 °C/10 Torr), 2,6-di-*t*-butyl-4-isopropylphenol: mp 38.0—38.5 °C (lit,[6] 38—42 °C), 2,6-di-*t*-butyl-4-cyclohexylphenol: mp 97.0—98.2 °C (lit,[5] 98—99 °C).

Each phenoxyl radical was prepared *in vacuo* by the oxidation of the phenol with lead dioxide in toluene.

Computations. The numerical computations were carried out on the HITAC 8700 system in the Hiroshima University Computing Center.

Results and Discussion

The ESR spectra of the 2,6-di-*t*-butyl-4-methylphenoxyl (Radical-I),[7] 2,6-di-*t*-butyl-4-ethylphenoxyl (Radical-II),[7] 2,6-di-*t*-butyl-4-isopropylphenoxyl (Radical-III),[8] and 2,6-di-*t*-butyl-4-cyclohexylphenoxyl (Radical-IV)[9] radicals were observed. The ENDOR spectra of III and IV were measured in the temperature range from −100 °C to −60 °C.

The proton hyperfine coupling constants of these radicals, measured under the identical conditions, are summarized in Table 1. The alkyl β-proton splitting (A_4^β) of each radical was precisely measured as a function of the temperature. The β-proton splittings for II, III, and IV show a large temperature dependence (see Fig. 1). In addition, the experimental results indicate that both $A_2^{t\text{-Bu}}$ and A_3^H remain almost unchanged upon the variation of the temperature and that no important deviations of these coupling constants can be detected for these radicals.

As has been explained in detail in previous works,[3] the β-proton splitting at any temperature was calculated by using following equations:[10]

$$A_4^\beta = B\rho_4^\pi\langle\cos^2\theta\rangle \qquad \theta = \alpha + \theta_0 \tag{1}$$

Table 1. Proton hyperfine coupling constants of the 2,6-di-*t*-butyl-4-alkylphenoxyl radicals (G)

Alkyl		$A_2^{t\text{-Bu}}$	A_3^H	A_4^γ	A_4^β
Methyl[a]	ESR	—	1.63	—	11.22
Ethyl	ESR	0.06	1.60	—	8.21
Isopropyl	ENDOR	0.07	1.66	0.38	4.05
Cyclohexyl	ENDOR	0.08	1.60	0.60,0.47	4.09

The observed temperature is −60 °C. a) At −45 °C.

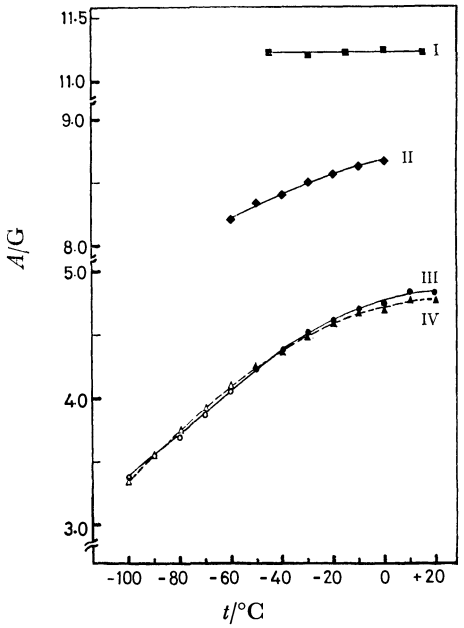

Fig. 1. Temperature dependence of the β-proton splittings observed with the 2,6-di-*t*-butyl-4-alkylphenoxyl radicals. I: Methyl, II: ethyl, III: isopropyl, IV: cyclohexyl.

■,◆,●,▲; ESR data, ○,△; ENDOR data.

$$\langle\cos^2\theta\rangle = \frac{\sum_{i=0}^{\infty}\langle\psi_i(\alpha)|\cos^2(\alpha+\theta_0)|\psi_i(\alpha)\rangle e^{-E_i/kT}}{\sum_{i=0}^{\infty}e^{-E_i/kT}} \quad (2)$$

$$-(\hbar^2/2I)(d^2\psi_i/d\alpha^2) + [V(\alpha) - E_i]\psi_i = 0 \quad (3)$$

where ρ_4^π is the spin density at the *p*-position and where θ is the so-called dihedral angle. The value of $B\rho_4^\pi$ was estimated to be 2×11.20 G from the methyl proton splitting of I. A free rotation is assumed for the methyl group, because the methyl proton splitting shows no detectable change throughout the entire temperature range. The moment of inertia, I, of the molecular fragment, Ar-R, can be calculated to be 5.0, 8.8, and 17 ($\times10^{-39}$) g cm^2 for II, III, and IV respectively.

With reference to the rotational functions of the alkyl groups for the 4,4′-dialkylbiphenyl anions,[3] where the steric factor affecting the rotating alkyl groups would be identical with those considered for the alkylphenoxyl radicals, the potential barrier, $V(\alpha)$, of each alkylphenoxyl has been assumed as follows. For the ethyl group, the potential function, $V(\alpha)$, is approximately the two-fold potential (Eq. 4), and for the isopropyl and cyclohexyl groups, with a double-well potential, wherein one of the minima lies higher in energy (Eq. 5):

$$V(\alpha) = (V_0/2)((1 - \cos 2\alpha) \quad (4)$$

$$V(\alpha) = V_0\sum_{i=0}^{3}a_i\cos 2i\alpha \quad (5)$$

$$a_0 = (1/18)(9V_m/V_0+4) \qquad a_1 = -4/9$$

$$a_2 = -2/9 \qquad a_3 = (1/18)(8 - 9V_m/V_0)$$

In Eq. 4, V_0 is the energy difference between the lowest potential state (a) and the highest one (b), as displayed in Fig. 2. In Eq. 5, V_0 and V_m are the energy differences between the lowest potential at state (c) and the highest one at state (d), and between the lowest one at state (c) and the medium one at state (e), respectively, as is illustrated in Fig. 2. At the most stable conformation, each of the equilibrium dihedral angles, θ_0, is equal to $\pi/3$, $\pi/2$, and $\pi/2$ for II, III, and IV respectively (see Fig. 2). The Hamiltonian matrix $\langle i|\mathcal{H}|j\rangle$ was diagonalized by expanding the wave function into a Fourier series.

We have calculated the temperature dependence of the $\langle\cos^2\theta\rangle$ as a function of the potential barriers, V_0 and V_m, for these radicals. The best agreement

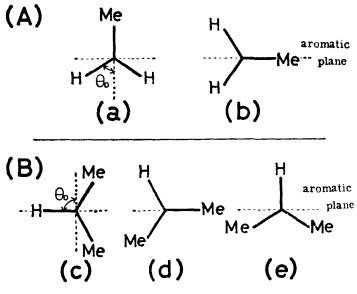

Fig. 2. Conformations of the alkyl groups in the 2,6-di-*t*-butyl-4-alkylphenoxyl radicals.
A: Ethyl, B: isopropyl, and cyclohexyl.

Table 2. The values of rotational barriers for the 2,6-di-*t*-butyl-4-alkylphenoxyl and 4,4′-dialkylbiphenyl anion radicals (kcal/mol)

	Alkyl	$\langle\cos^2\theta\rangle$	V_0	V_m
Phenoxyl	ethyl	0.37 (at −60 °C)	1.1	—
	isopropyl	0.18 (at −60 °C)	1.6	0.7
	cyclohexyl	0.18 (at −60 °C)	1.6	0.7
Biphenyl anion	ethyl	0.36 (at −90 °C)	1.0	—
	isopropyl	0.21 (at −85 °C)	1.2	0.5
	cyclohexyl	0.20 (at −85 °C)	1.2	0.6
Non-bonded interaction energy[3]	ethyl	—	1.3	—
	isopropyl	—	1.4	0.7

between the calculated and experimental temperature dependences of $\langle\cos^2\theta\rangle$ is obtained with the choice of $V_0=1.1$, $V_0=1.6$, $V_m=0.7$, $V_0=1.6$, and $V_m=0.7$ kcal/mol as the parameters for II, III, and IV respectively. Thus, each potential barrier obtained for the phenoxyl radicals coincides with the one for the 4,4′-dialkylbiphenyl anions, furthermore, these values agree with those obtained from the calculation of the non-bonded interaction between the rotating alkyl group and the aromatic protons[3] (see Table 2).

From the above results, we concluded that the ethyl group attached to the benzene ring may undergo a restricted rotation in the two-fold potential, which has a barrier height of 1.0—1.2 kcal/mol, and that the rotation of isopropyl and cyclohexyl groups restricted in a double-well potential, which has, as potential barrier heights, $V_0=1.2$—1.6 and $V_m=0.6$—0.7 kcal/mol. These results, furthermore, suggest that the rotational barrier of the alkyl group is mainly due to the steric repulsion between the rotating alkyl group and the neighbouring aromatic ring protons in the case of both anion and neutral free radicals.

References

1) N. L. Bauld, J. D. McDermed, C. E. Hudson, Y. S. Rim, J. Zoeller, Jr., R. D. Gordon, and J. S. Hyde, *J. Am. Chem. Soc.*, **91**, 6666 (1969); F. Nemoto, *Bull. Chem. Soc. Jpn.*, **49**, 1194 (1976).
2) C. Heller and H. M. McConnell, *J. Chem. Phys.*, **32**, 1535 (1960).
3) F. Nemoto, F. Shimoda, and K. Ishizu, *Bull. Chem. Soc. Jpn.*, **48**, 2627 (1975); F. Nemoto and K. Ishizu, *J. Phys. Chem.*, **79**, 1730 (1975).
4) K. Ishizu, *Bull. Chem. Soc. Jpn.*, **36**, 938 (1963); T. Yamamoto, K. Sato, and T. Miyamae, *Jpn. J. Appl. Phys.*, **11**, 1508 (1972).
5) G. H. Stillson, D. W. Sawyer, and C. K. Hunt, *J. Am. Chem. Soc.*, **67**, 303 (1945).
6) C. D. Cook and B. E. Norcross, *J. Am. Chem. Soc.*, **78**, 3797 (1956).
7) J. K. Becconsall, S. Clough, and G. Scott, *Trans. Faraday Soc.*, **56**, 459 (1960).
8) N. H. Atherton, A. J. Blackhurst, and I. P. Cook, *Trans. Faraday Soc.*, **67**, 2510 (1971).
9) R. F. Adams and N. M. Atherton, *Mol. Phys.*, **17**, 673 (1969).
10) E. W. Stone and A. H. Maki, *J. Chem. Phys.*, **37**, 1326 (1962).

BULLETIN OF THE CHEMICAL SOCIETY OF JAPAN, VOL. 52 (12), 3745—3746 (1979)

Reduction of Transition-metal Salts by *N*-Propyl-1,4-dihydronicotinamide

Tadashi OKAMOTO,* Atsuyoshi OHNO, and Shinzaburo OKA

Institute for Chemical Research, Kyoto University, Uji 611

(Received May 18, 1979)

Synopsis. It was found that *N*-propyl-1,4-dihydronicotinamide reduces bis(benzonitrile)dichloropalladium, palladium(II) acetate, and chlorides of rhodium(III), platinum(IV), and ruthenium(III) smoothly in organic solvents affording a facile method for the preparation of low valent catalysts *in situ*.

Many reagents are known to reduce high valent transition-metal salts to metals or metal complexes of lower oxidation state, typical ones being metal hydrides, alkylmetals, ethanolic potassium hydroxide, metals, and hydrazine.[1] They are used for the preparation of low valent transition-metal catalyst. Mild reducing agents not attacking other organic molecules in the system are desirable in the preparation of a catalyst *in situ*. Zinc powder is a mild reductant but its heterogeneity often gives irreproducible results. We would like to report that a well-known 1,4-dihydropyridine derivative, mild and soluble in organic solvents, behaves as an effective organic reductant of some transition-metal salts.

Palladium(II) acetate and bis(benzonitrile)dichloropalladium were reduced to palladium metal by *N*-propyl-1,4-dihydronicotinamide (PNAH), but not phosphine complexes of palladium(II) such as dichlorobis(triphenylphosphine)palladium(II) or dichloro-1,2-bis(diphenylphosphino)ethanepalladium(II). This might suggest that the dissociation of a ligand(s) is essential for the reaction. Platinum(IV) chloride and ruthenium(III) chloride were reduced to platinum(II) and ruthenium(II), respectively. No reduction was observed for copper(I) chloride, nickel(II) acetate, or iron(II) nitrate.[2] For iron(II) chloride and cobalt(II) nitrate, change takes place in the spectrum in methanol in contrast to the case in water.[3] Attempt to identify the product was unsuccessful. A complex (or salt) of $PtCl_4(PNA^+)_2$ was isolated (65% yield) by the reduction of platinum(IV) chloride hydrate.

In the presence of triphenylphosphine, which stabilizes the low oxidation state of transition metals, reduction by PNAH gives low valent complexes such as chlorotris(triphenylphosphine)rhodium(I) (87%) and tetrakis(triphenylphosphine)palladium(0) (63%).

$$RhCl_3 \cdot 3H_2O + PNAH \xrightarrow[PC_{18}H_{15}]{\text{Lutidine}} RhCl(PC_{18}H_{15})_3 + PNA^+$$

This procedure affords a facile method for the preparation of catalytically active low valent transition-metal complexes *in situ* because the reagent is insensitive to air and moisture, not attacking organic compounds except activated carbonyl compounds and cationic compounds.[4] Since the standard reduction potential for PNAH is -0.387 V,[5] reduction of metal ions or complexes with higher electrode potentials than the value could be achieved by this reagent. The resulting low valent complexes or metals were stable under the reaction conditions. PNAH did not attack chlorotris(triphenylphosphine)rhodium(I) even under reflux in ethanol.

Experimental

Changes of the spectra in the reactions were monitored with a Union Giken SM 401 spectrophotometer in organic solvents such as benzene, acetonitrile, ethanol, and methanol, which were purified by the usual manner. Products were identified by elemental analyses, NMR and IR.

Reduction of Bis(benzonitrile)dichloropalladium(II) or Palladium(II) Acetate. PNAH was added to a solution of the palladium species in order to precipitate black palladium powder quantitatively.

Preparation of Tetrakis(triphenylphosphine)palladium(0). Palladium(II) acetate, 0.89 mmol, triphenylphosphine, 4.96 mmol, and PNAH, 1.80 mmol were placed in a flask and deaerated. Benzene (30 cm^3) and 2,6-lutidine (0.1 cm^3) were injected into the flask and the solution was stirred overnight. The resulting precipitate was filtered off, the filtrate being concentrated and then treated with ethanol. Brown precipitate was washed with ether to give tetrakis(triphenylphosphine)palladium(0), 648 mg (0.56 mmol, 63%), which showed a spectrum identical with that of the authentic sample (Found: C, 73.61; H, 5.28%).

Preparation of Chlorotris(triphenylphosphine)rhodium(I). A solution of rhodium(III) chloride hydrate, 0.38 mmol, triphenylphosphine, 1.53 mmol, PNAH, 0.42 mmol, and 2,6-lutidine, 0.38 mmol in ether was stirred under nitrogen at room temperature for 2.5 h. The precipitate was collected and washed with 5 cm^3 of ethanol, and with three portions of 5 cm^3 of ether. After being dried under nitrogen, 305 mg (0.33 mmol, 87%) of the complex was obtained, which showed a spectrum identical with that of the authentic sample (Found: C, 69.42; H, 4.79%).

Reduction of Platinum(IV) Chloride. Platinum(IV) chloride hydrate (0.12 mmol) was dissolved in 5 cm^3 of methanol, and a solution of PNAH (0.60 mmol) in 3.5 cm^3 of methanol was added to the solution. After being stirred for 3 h under nitrogen, the white precipitate was collected and washed with methanol to give 52 mg of $PtCl_4(PNA)_2$ (0.08 mmol, 65%). Found: C, 31.85; H, 3.94; N, 8.12%. Calcd for $C_{18}H_{26}N_4Cl_4O_2Pt$: C, 32.29; H, 3.92; N, 8.04%. IR(KBr) 3390 (amide), 3195 (amide), 3060 (=C–H), 2940 (C–H), 1688 (C=O), and 1618 (C=C) cm^{-1}.

Reduction of Other Salts. Experimental conditions were the same as in the case of $PtCl_4$. Ruthenium(II) chloride hydrate was reduced to blue Ru(II) which turned yellow ($Ru^{II}(NH_3)_4$) in the presence of aqueous ammonia. No further attempt was made to isolate the product. Pink solution of cobalt(II) nitrate turned orange on addition of PNAH solution. The solution obtained was air sensitive but gave

† Presented at the 35th National Meeting of the Chemical Society of Japan, Sapporo, August 1976.

no characteristic color of $Co^{I}(bipy)_3$ by the addition of 2,2′-bipyridine.[6]

References

1) L. Malatesta and S. Cenini, "Zerovalent Compounds of Metals," Academic Press, London (1974), p. 77.
2) Reduction of NO_3^- was not observed.
3) A. Stoke, E. Sann, and G. Pflelderer, *Ann*, **647**, 188 (1961).
4) Y. Ohnishi and A. Ohno, *Kagaku No Ryoiki*, **110**, 57 (1976).
5) K. E. Taylor and J. B. Jones, *J. Am. Chem. Soc.*, **98**, 5689 (1976).
6) A. A. Vlcek, *Nature*, **180**, 753 (1957).

BULLETIN OF THE CHEMICAL SOCIETY OF JAPAN, VOL. 52 (12), 3747—3748 (1979)

The Effect of Halo Ligand on the Rate of Hydrogenation of Coordinated Olefin in Dihydrido-olefin Complexes $RhXH_2(ol)(PPh_3)_2$ (X=Cl, Br, I)

Yoshimi OHTANI,* Akihiko YAMAGISHI, and Masatoshi FUJIMOTO*

Department of Chemistry, Faculty of Science, Hokkaido University, Sapporo 060

(Received November 18, 1978)

Synopsis. The formation constant of $RhXH_2(ol)(PPh_3)_2$ (ol=acrylonitrile or styrene, X=Cl, Br, or I) and the rate of hydrogenation of coordinated olefin in $RhXH_2(ol)(PPh_3)_2$ were determined. The effects of halo ligand on the equilibrium and rate constants showed a different trend for the two olefin complexes.

Knowledge of the effect of halo ligand on the catalytic activity of Wilkinson's complex is necessary for understanding electronic factors of individual steps in the catalytic hydrogenation reaction (Scheme 1).

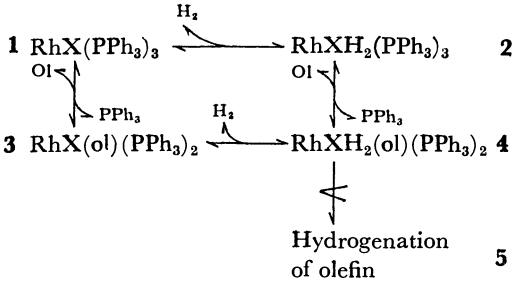

Scheme 1.

The effects of halo ligand and other tertiary phosphine ligand analogs were studied,[1-3] but in most investigations only the overall rate of catalytic reactions were reported. Since both the complex formation constants and hydrogenation rate of coordinated olefin may vary with change of ligand, discussions based only on the observed rate constants of the overall reaction sometimes leave ambiguities. Thus, it is necessary to know the effects of ligands on the complex formation and on the rate of the hydrogenation of coordinated olefin, separately. In particular, information concerning a catalytically active intermediate (**4**) is required to elucidate the nature of Wilkinson's complex as a catalyst.

Recently, we detected a catalytically active intermediate, $RhClH_2(ol)(PPh_3)_2$ (ol=acrylonitrile or styrene), in benzene under anaerobic conditions.[4,5] Detection of the intermediate made it possible to determine accurately the equilibrium and/or rate constants of the individual steps in Scheme 1. We have studied a bromo and an iodo complex in a manner similar to that for the chloro complex to elucidate the effects of halo ligand on each step composing the catalytic reaction.

The results are summarized in Table 1. The effects of halo ligand on equilibrium and rate constants differ largely for acrylonitrile and styrene. The values of K_{34} (and also K_{24}), stability constants of dihydrido-olefin complex, increase in the order Cl<Br<I for acrylonitrile, and decrease in the order Cl>Br>I for styrene. The difference might be attributed to that in the coordinating properties of the two olefins. The coordination of acrylonitrile, which has an electron-withdrawing cyano group, would decrease the electron density of rhodium atom. On the other hand, the coordination of styrene, which has an electron-releasing phenyl group, would increase the electron density of rhodium. In the case of acrylonitrile, the iodo complex with the least electronegative ligand gives the largest stability of $RhXH_2(ac)(PPh_3)_2$. In the case of styrene, the chloro complex with the most electronegative ligand gives the largest stability of $RhXH_2(st)(PPh_3)_2$. The most stable dihydrido-olefin complex would be formed by the halo ligand, which offsets the change in electron density of central rhodium atom induced by the coordination of olefin.

As regards the effect of halo ligand on k_{45}, it is concluded that the complex which has a larger value of K_{34} gives the smaller value of k_{45}, a less stable dihydrido-olefin complex having a larger rate constant for the hydrogenation of coordinated olefin. The rate of the migratory insertion of olefin into Rh–H bond would be slowed down as the Rh–H bond becomes strong.

The effects of coordinated halo ligand on the stability constants of dihydrido-olefin complex may also be interpreted by the Dewar-Chatt-Duncanson model.[6] Figure 1 shows tentative schematic diagrams of energy levels. The energy level of rhodium atom is taken to be consistent with the present experimental results. In the case of acrylonitrile complex, back-donation from rhodium atom to acrylonitrile would be predominant for the coordination of acrylonitrile, as the π^* energy level of acrylonitrile lies near the highest occupied

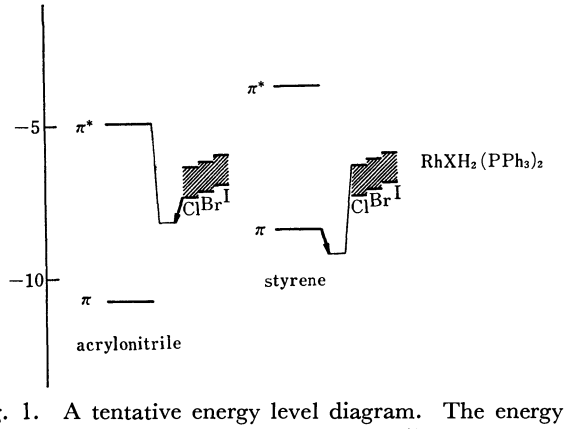

Fig. 1. A tentative energy level diagram. The energy levels of of rhodium are taken arbitarily so as to be consistent with the experimental results.

† Present address: The Institute of Physical and Chemical Research, Wako-shi, Saitama 351.

Table 1. Equilibrium and rate constants observed

X	ol	K_{12} / mol^{-1} dm^3	K_{13}	K_{24} [a]	K_{34} / mol^{-1} dm^3	k_{34} / mol^{-1} dm^3 s^{-1}	k_{43} / s^{-1}	k_{45} / s^{-1}
Cl	ac	2.1×10^4	0.22	3.7×10^{-3}	3.5×10^2	1.5×10^4	43	0.50
Cl	st	2.1×10^4	2.4×10^{-4}	3.7×10^{-5}	3.2×10^3	—	—	2.7
Br	ac	3.3×10^4	0.20	1.2×10^{-2}	1.9×10^3	3.9×10^4	21	0.15
Br	st	3.3×10^4	3.3×10^{-4}	$\approx1.7\times10^{-5}$	$\approx1.9\times10^3$	—	—	≈9.7
I	ac	6.3×10^4	0.19	2.1×10^{-2}	7.0×10^3	3.2×10^4	4.6	0.050
I	st	6.3×10^4	7.6×10^{-4}	$\approx1.1\times10^{-5}$	$\approx9.0\times10^2$	—	—	≈35

ac=acrylonitrile and st=styrene. K_{ij} and k_{ij} denote the equilibrium and rate constants of the reactions from species i to species j, respectively, shown in Scheme 1. a) Calculated from $K_{24}=K_{13}K_{34}/K_{12}$.

energy level of rhodium. Since the electron density of central rhodium atom increases in the order chloro< bromo<iodo complex, the highest occupied energy level of rhodium atom would be the highest for iodo complex. The distance between π^* energy level of acrylonitrile and the highest occupied energy level of rhodium would be the shortest for the iodo complex, $RhXH_2(ac)(PPh_3)_2$ thus being the most stable for iodo complex. In contrast, donation from styrene to rhodium would be predominant for the coordination of styrene. $RhXH_2(st)(PPh_3)_2$ is the most stable when X=Cl.

In the case of acrylonitrile, the value of k_{45} was found to be 100 times as small as that of k_{43} for all three halo complexes. It should be noted that both k_{43} and k_{45} decrease in the same order Cl>Br>I. k_{43} corresponds to the dissociation rate of hydrogen from the $RhXH_2(ac)(PPh_3)_2$ complex, while k_{45} corresponds to the migratory insertion rate of coordinated olefin into Rh–H bond in the same complex. It is suggested that both reactions proceed through a similar activated state, where Rh–H bond becomes weak.

Experimental

All measurements were carried out at 20±1 °C in oxygen-free benzene. Solutions of $RhCl(ol)(PPh_3)_2$ and $RhBr(ol)(PPh_3)_2$ were prepared as described.[4] A solution of $RhI(ol)(PPh_3)_2$ was prepared by dissolving $RhI(PPh_3)_3$ in benzene containing acrylonitrile or styrene. A small amount of free PPh_3 dissociated from $RhI(PPh_3)_3$ was neglected for the stopped-flow measurements. For the measurements of hydrogen gas uptake, the total concentration of PPh_3 was taken as the sum of the concentration of added PPh_3 and $RhI(PPh_3)_3$. The procedure of measurements is described in previous papers.[4,5]

References

1) J. A. Osborn, F. H. Jardine, J. F. Young, and G. Wilkinson, *J. Chem. Soc., A*, **1966**, 1711.

2) L. Honer, H. Büthe, and H. Siegel, *Tetrahedron Lett.*, **1968**, 4023; A. S. Hussey and Y. Takeuchi, *J. Org. Chem.* **35**, 643 (1970).

3) S. Montelatici, A. van der Ent, J. A. Osborn, and G. Wilkinson, *J. Chem. Soc., A*, **1968**, 1054; C. O'Connor and G. Wilkinson, *Tetrahedron Lett.*, **1969**, 1375.

4) Y. Ohtani, A. Yamagishi, and M. Fujimoto, *Bull. Chem. Soc. Jpn.*, **51**, 2562 (1978).

5) Y. Ohtani, A. Yamagishi, and M. Fujimoto, *Bull. Chem. Soc. Jpn.*, **52**, 69 (1979).

6) M. L. H. Green, "Organometallic Chemistry, Vol. 2, The Transition Metal Elements," Methuen, London (1968); M. J. S. Dewar, *Bull. Soc. Chim. Fr.*, **1951**, C79; J. Chatt and L. A. Duncanson, *J. Chem. Soc.*, **1953**, 2939.

BULLETIN OF THE CHEMICAL SOCIETY OF JAPAN, VOL. 52 (12), 3749—3750 (1979)

Synthesis of a Few Derivatives of Cycloiridated 2-(2-Thienyl)pyridine

Matsuo NONOYAMA

Department of Chemistry, Faculty of Science, Nagoya University, Chikusa, Nagoya 464

(Received March 27, 1979)

Synopsis. A few derivatives of cycloiridated 2-(2-thienyl)pyridine were prepared and characterized by infrared and ^{1}H NMR spectra.

Numerous cyclometallation reactions of benzene derivatives with transition metal compounds have been reported,[1,2] but only a few cases are known of cyclopalladation and cycloplatination of thiophene derivatives.[3,4] Since various chemical properties of thiophene are similar to those of benzene, cyclometallation reactions found for benzene derivatives might occur also for thiophene derivatives. We have studied reactions of 2-(2-thienyl)pyridine with some platinum-metal halides and found the first example of cycloiridation of the thiophene ring. The results are reported in this paper.

2-(2-Thienyl)pyridine (abbreviated as H(2-thpy)) reacted with hydrated iridium(III) chloride in boiling 2-methoxyethanol to give an orange complex, $[\{IrCl(2\text{-thpy})_2\}_2]$. The complex reacted easily with unidentate ligand (L) to give the adducts, $[IrClL(2\text{-thpy})_2]$ (L=pyridine (py), tributylphosphine (PBu_3), and dimethyl sulfoxide (dmso)). The new complexes are air-stable; spectral data are given in Table 1 and Fig. 1.

The infrared spectrum of free H(2-thpy) shows bands at 844, 856, and 894 cm^{-1} characteristic of 2-substituted thiophene in the region of C–H out-of-plane deformation vibrations.[5] These bands are replaced by a single band at 884 cm^{-1} in the spectrum of $[\{IrCl(2\text{-thpy})_2\}_2]$, indicating that the thiophene ring is 2,3-disubstituted.[3] The 60 MHz ^{1}H NMR spectrum of free H(2-thpy) is complicated. Only one signal of 6-H(py)[6] is distinctly separated from the main signals, lying at δ=8.61 ppm (as a doublet of triplets, J=5.0; 1.3 Hz). The ^{1}H NMR spectrum of $[\{IrCl(2\text{-thpy})_2\}_2]$ is shown in Fig. 1 and Table 1 together with assignments. A sharp doublet with a relative intensity 1 H at 5.94 ppm becomes a singlet upon irradiation of a sharp doublet with an intensity 1 H at 7.17 ppm (J=4.9 Hz) and *vice versa*. The two doublets are assigned to thiophene ring protons. Each of the signals assigned to 5-H(py) and 6-H(py) has an intensity 1 H and the relative intensity of the multiplet assigned to 3-H(py) and 4-H(py) amounts to 2 H. The results, together with the infrared spectra and the evidence for cyclopalladated cycloplatinated 2-thpy complexes[3] suggest that 3-H(th) of H(2-thpy) is lost and that the two 2-thpy ligands of $[\{IrCl(2\text{-thpy})_2\}_2]$ are equivalent. Significant shielding seems to be operative for 4-H(th). This can be explained in terms of Structure I,[7] where 4-H(th) is nearly above the pyridine ring of the other 2-thpy ligand, thus being

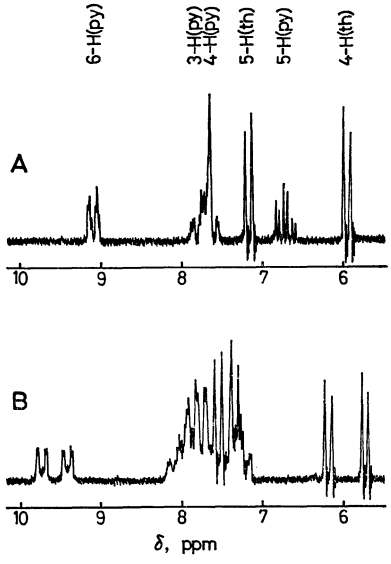

Fig. 1. 60 MHz ^{1}H NMR spectra of $[IrCl(2\text{-thpy})_2]_2$ in CD_2Cl_2 (A) and $[IrCl(dmso)(2\text{-thpy})_2]$ in DMSO-d_6 (B).

TABLE 1. INFRARED AND ^{1}H NMR SPECTRA OF THE COMPLEXES

Complex	ν(Ir–Cl)[a]	Solvent	δ/ppm[b]	
			4-H(th)	6-H(py)
$[IrCl(2\text{-thpy})_2]_2$	245, 224	CD_2Cl_2	5.94d(4.9)	9.07d(5.8)
$[IrCl(dmso)(2\text{-thpy})_2]$	255	dmso-d	5.77d(4.8)	9.45d(5.6)
			6.23d(4.8)	9.77d(5.6)
$[IrCl(py)(2\text{-thpy})_2]$	243	$CDCl_3$	6.12d(4.6)	7.94d(5.6)
			6.24d(4.6)	9.72d(5.6)
$[IrCl(PBu_3)(2\text{-thpy})_2]$	253	$CDCl_3$	5.92dd(4.8; 1.5)	8.78d(5.6)
			6.27d(4.8)	9.77d(5.6)
$[IrBr(PBu_3)(2\text{-thpy})_2]$		$CDCl_3$	5.93dd(4.8; 1.5)	8.76d(5.6)
			6.22d(4.8)	9.91d(5.6)
$[IrI(PBu_3)(2\text{-thpy})_2]$		$CDCl_3$	5.96dd(4.8; 1.5)	8.75d(5.6)
			6.14d(4.8)	10.11d(5.6)

a) Nujol mulls, cm^{-1}. b) Values in parentheses are coupling constants in Hz.

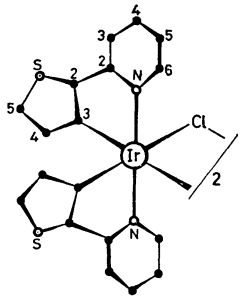

I

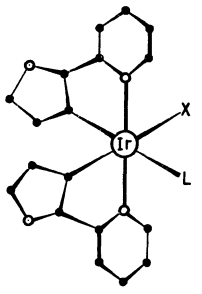

II

shielded by the aromatic ring current. Structure I is in line with low ν(Ir–Cl) frequency, since the chloride ligand is coordinated *trans* to a σ-carbon donor with strong *trans*-influence.

TABLE 2. YIELDS, MELTING POINTS AND ANALYTICAL RESULTS

Complex	Yield %	Mp °C	Found (Calcd), % C	H	N
$[IrCl(2\text{-thpy})_2]_2$	31	310 (dec)[a]	39.33(39.45)	2.23(2.21)	4.80(5.11)
$[IrCl(py)(2\text{-thpy})_2]$	73	300 (dec)	44.07(44.05)	2.52(2.73)	6.60(6.70)
$[IrCl(dmso)(2\text{-thpy})_2]$	75	240 (dec)	38.34(38.36)	2.91(2.90)	4.20(4.27)
$[IrCl(PBu_3)(2\text{-thpy})_2]$	77	122—124	48.60(48.02)	5.30(5.24)	3.73(3.73)
$[IrBr(PBu_3)(2\text{-thpy})_2]$	64	203—205	45.65(45.33)	4.88(4.95)	3.20(3.52)
$[IrI(PBu_3)(2\text{-thpy})_2]$	83	230 (dec)	43.01(42.80)	4.62(4.67)	3.03(3.33)

Structure II is proposed for the complexes [IrClL(2-thpy)$_2$] on the basis of the following spectral data. In the ^{1}H NMR spectra of the complexes, the signal due to 4-H(th) splits into two doublets with a relative intensity 1 H (Fig. 1), that due to 6-H(py) also splitting into two apparent doublets with an intensity 1 H. The remaining protons give a complicated pattern with an intensity 8 H. Thus the two 2-thpy ligands are not equivalent in [IrClL(2-thpy)$_2$]. In the case of L=PBu$_3$, an additional small splitting (J(P–H)=1.5 Hz) is observed for one of the two doublets of 4-H(th) and the doublet, which shifts hardly upon exchange of halide donors, is assigned to 4-H of the thiophene ring coordinated *trans* to PBu$_3$. However, the other downfield doublet shifts to higher field in the order Cl<Br<I, and is assigned to 4-H of the thiophene ring coordinated *trans* to halide donors.

The separation of two doublets of 6-H(py) depends upon L. In the case of L=py, one of the two doublets is significantly shielded. This might be caused by anisotropic shielding by a pyridine (L) donor, since its least sterically hindered coordination brings the pyridine (L) ring nearly perpendicular to one of the chelated 2-thpy ligands. One 6-H(py) lies, therefore, nearly above the pyridine (L) ring. The other 6-H(py) is directed toward a Cl donor and the chemical shifts are almost independent of L.

The chemical shifts of 6-H(py) of [IrX(PBu$_3$)(2-thpy)$_2$](X=Cl, Br, I) are of interest. The positions of higher field doublets are nearly constant irrespective of the nature of halide donors, while the lower field doublets shift to a lower field in the order Cl<Br<I with increasing van der Waals radius of halide ions. The same trend was reported for square-planar palladium(II) complexes of pyridine derivatives,[8] the origin being interpreted as the result of spatial crowding between 6-H(py) and a halide ligand. The low ν(Ir–Cl) frequencies are in line with Structure II. The band at 1109 cm^{-1} of [IrCl(dmso)(2-thpy)$_2$] is assigned to ν(S=O), suggesting *S*-coordination of dmso.

The ligand H(2-thpy) behaves in a similar way to that of the corresponding benzene derivatives such as 2-phenylpyridine and benzo[*h*]quinoline.[7] H(2-thpy) has also been cyclorhodated to give [{RhCl(2-thpy)$_2$}$_2$] like 2-phenylpyridine and benzo[*h*]quinoline.[9] Structures I and II proposed above correspond to those of the complexes of these benzene derivatives.

Experimental

Measurements. Measurements were carried out by the methods reported.[10]

Synthesis of the Complexes. Yields, melting points and analytical results are given in Table 2.

[{*IrCl(2-thpy)*$_2$}$_2$]: A mixture of 3 mmol of hydrated iridium(III) chloride with 9 mmol of H(2-thpy) in 50 cm^3 of 2-methoxyethanol was refluxed for 6 h to give a brown powder. The product was washed with ethanol, dried in air, and dissolved in dichloromethane. Addition of hexane to the filtered, concentrated dichloromethane solution gave an orange powder.

[*IrClL(2-thpy)*$_2$](*L=py or PBu*$_3$): To a solution of [{IrCl-(2-thpy$_2$}$_2$] in dichloromethane was added a stoichiometric amount of PBu$_3$ or 3-fold excess of pyridine. The mixture was stirred on a hot plate for 1 h. Hexane was added to the concentrated dichloromethane solution to precipitate a yellow orange product.

[*IrCl(dmso)(2-thpy)*$_2$]: One-fifth mmol of [{IrCl(2-thpy)$_2$}$_2$] was dissolved in 1 cm^3 of dimethyl sulfoxide on a steam bath. To the solution was added 20 cm^3 of ethanol to precipitate an orange yellow product.

[*IrX(PBu*$_3$)(*2-thpy)*$_2$](*X=Br or I*): To a solution of one-fourth mmol of [IrCl(PBu$_3$)(2-thpy)$_2$] in a mixture of 20 cm^3 of dichloromethane and 10 cm^3 of ethanol was added 1 mmol of lithium bromide or lithium iodide. The mixture was warmed on a hot plate for 3 h and concentrated to a small volume to give bromide or iodide complex.

References

1) M. I. Bruce, *Angew. Chem.*, **89**, 75 (1977).
2) J. Dehand and M. Pfeffer, *Coord. Chem. Rev.*, **18**, 327 (1976).
3) T. J. Giordano and F. G. Rasmussen, *Inorg. Chem.*, **14**, 1628 (1975).
4) M. Nonoyama, *Inorg. Nucl. Chem. Lett.*, **14**, 337 (1978).
5) J. J. Peron, P. Saumagne, and J. M. Lebas, *Spectrochim. Acta, Part A*, **26**, 1651 (1970).
6) 4-H of a thiophene ring and 6-H of a pyridine ring of 2-(2-thienyl)pyridine are, abbreviated to 4-H(th) and 6-H-(py), respectively. Similar abbreviations are used in this paper.
7) M. Nonoyama, *Bull. Chem. Soc. Jpn.*, **47**, 767 (1974); *J. Organomet. Chem.*, **82**, 271 (1974).
8) M. Nonoyama, K. Sato, and K. Yamasaki, *Nippon Kagaku Kaishi*, **1974**, 696.
9) Found: C, 46.87; H, 2.67; N, 6.40%. Calcd for $RhClC_{18}H_{12}N_2S_2$: C, 47.12; H, 2.64; N, 6.11%.
10) M. Nonoyama and C. Hayata, *Transition Met. Chem.*, **3**, 366 (1978).

BULLETIN OF THE CHEMICAL SOCIETY OF JAPAN, VOL. 52 (12), 3751—3752 (1979)

The 2:1 Adduct of Chloro[*N*-(2-dimethylaminoethyl)salicylideneaminato]copper(II) with Chlorides of Copper(II), Manganese(II), and Nickel(II)

Tadashi Tokii, Makoto Kaneko, Kusuo Yamanaka, Yoneichiro Muto,* and Michinobu Kato†

Department of Chemistry, Faculty of Science and Engineering, Saga University, Saga 840

†*Aichi Prefectural University, Mizuho-ku, Nagoya 467*

(Received April 4, 1979)

Synopsis. The adducts listed in the title have been prepared, and their trimeric nature confirmed on the basis of elemental analysis and IR and electronic spectra. The magnetic properties of the $MnCl_2$ and $NiCl_2$ adducts have been analyzed in terms of a linear trimer model.

Chloro[*N*-(2-dimethylaminoethyl)salicylideneaminato]-copper(II), Cu(sal·en·NMe_2)Cl, was originally synthesized and investigated by Sacconi *et al.*; a monomeric planar structure, I, was proposed for this complex based on the electronic reflectance spectrum.[1] The monomeric nature was confirmed by cryomagnetic and IR spectral studies.[2] Based on the monomeric structure and the knowledge that phenolato and chloro ligands form bridges between pairs of metal ions, it is expected that the complex can be used as a bidental complex-ligand[3] in the synthesis of polynuclear metal complexes. In the reaction of Cu(sal·en·NMe_2)Cl with metal salts MCl_2(M=Cu(II), Mn(II), and Ni(II)) 2:1 adducts of [Cu(sal·en·NMe_2)Cl]$_2$·MCl_2 were formed. A similar adduct of chloro[*N*-(2-methylaminoethyl)salicylideneaminato]copper(II), Cu(sal·en·NHMe)Cl, with copper-(II) chloride has also been prepared.

The spectral and magnetic studies will be reported in this paper.

Experimental

Synthesis. A typical synthetic method is as follows. A solution of one of the metal salts MCl_2 (10 mmol) in ethanol (50 ml) was added to a solution of one of the parent complexes, Cu(sal·en·NMe_2)Cl and Cu(sal·en·NHMe)Cl, and the mixture stirred on a hot plate for 1/2 h. The crystals thus precipitated were collected, washed repeatedly with ethanol and dried. Anal. **1.** [Cu(sal·en·NMe_2)Cl]$_2$·$CuCl_2$. Found: C, 36.84; H, 4.19; N, 7.86; Cu, 26.43%. Calcd for $C_{22}H_{30}N_4O_2Cl_4Cu_3$: C, 36.96; H, 4.23; N, 7.84; Cu, 26.66%. **2.** [Cu(sal·en·NHMe)Cl]$_2$·$CuCl_2$. Found: C, 34.75; H, 3.85; N, 8.17; Cu, 27.55%. Calcd for $C_{20}H_{26}N_4O_2Cl_4Cu_3$: C, 34.97; H, 3.82; N, 8.16; Cu, 27.75%. **3.** [Cu(sal·en·NMe_2)Cl]$_2$·$MnCl_2$. Found: C, 37.54; H, 4.37; N, 7.80; Cu, 17.95; Mn, 7.82%. Calcd for $C_{22}H_{30}N_4O_2Cl_4Cu_2Mn$: C, 37.41; H, 4.28; N, 7.93; Cu, 17.99; Mn, 7.78%. **4.** [Cu(sal·en·NMe_2)Cl]$_2$·$NiCl_2$. Found: C, 37.01; H, 4.20; N, 7.91; Cu, 17.78; Ni, 8.58%. Calcd for $C_{22}H_{30}N_4O_2Cl_4Cu_2Ni$: C, 37.21; H, 4.26; N, 7.89; Cu, 17.90; Ni, 8.27%.

Physical Measurements. The IR spectral measurements were made with a Hitachi EPI-G2 IR Spectrophotometer in the 400—4000 cm^{-1} region in Nujol. The reflectance spectra were recorded with a Hitachi Recording Spectrophotometer 323. The magnetic susceptibilities in the temperature range 80—300 K were determined by the Faraday method using $HgCo(SCN)_4$ as a calibrant.

Results and Discussion

The IR spectra of the adducts prepared in this study all show an intense band in the range 1550—1555 cm^{-1} (**1**, 1555; **2**, 1554; **3**, 1550; **4**, 1551 cm^{-1}), while the band in the spectra of the parent complexes, Cu(sal·en·NMe_2)Cl and Cu(sal·en·NHMe)Cl, appears at 1534 and 1531 cm^{-1} respectively. This band shift towards higher frequencies (15—20 cm^{-1}) indicates the presence of bridging phenolic oxygen atoms in the adducts.[2]

A remarkable feature in the reflectance spectra of the $CuCl_2$ adducts (**1** and **2**) is the appearence of a band in the 9000—10000 cm^{-1} region (Fig. 1) which is absent in the spectra of the parent complexes.[1,2] This feature indicates the presence of Cu(II) in pseudo-tetrahedral coordination.[2,4] The $MnCl_2$ adduct spectrum shows a broad band at *ca.* 15000 cm^{-1} with a shoulder at *ca.* 11000 cm^{-1} (Fig. 1). This band has been attributed to the d-d transition of Cu(II) since Mn(II) complexes have no d-d band below 15000 cm^{-1} regardless of stereochemistry (octahedral or tetrahedral) or spin-states (high- or low-spin). This type of spectra is indicative of five-coordination around Cu(II) and is to be compared with the spectra reported for some distorted square-pyramidal Cu(II) complexes.[2,5] The spectrum of the $NiCl_2$ adduct shows a broad band at *ca.* 15000 cm^{-1} with a shoulder at *ca.* 11000 cm^{-1} and a weak band at *ca.* 6500 cm^{-1} (Fig. 1). Assignment of the former band could not be unambiguously performed since the d-d bands of both Ni(II) and Cu(II) appear

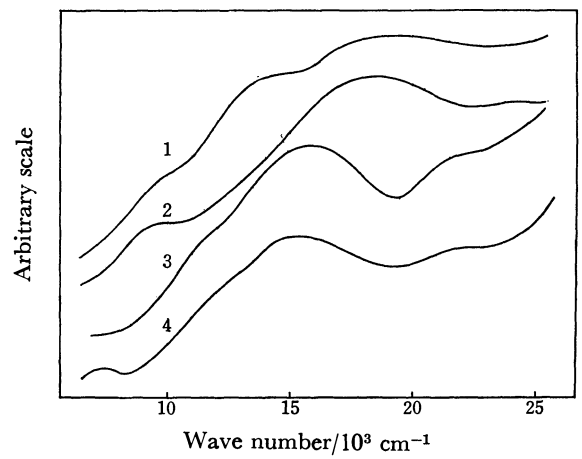

Fig. 1. Reflectance spectra of [Cu(sal·en·NMe_2)Cl]$_2$·$CuCl_2$ (1), [Cu(sal·en·NHMe)Cl]$_2$·$CuCl_2$ (2), [Cu(sal·en·NMe_2)Cl]$_2$·$MnCl_2$ (3) and [Cu(sal·en·NMe_2)Cl]$_2$·$NiCl_2$ (4).

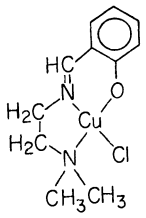

I

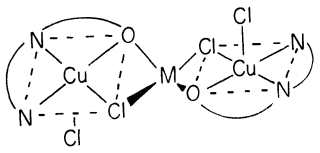

II

in this region. The latter band has been attributed to the transition in the Ni(II) in this adduct and may be assigned to the d-d band in the Ni(II) with a pseudo-tetrahedral geometry. The assignment has been based on the following observations: 1) in the region below 8000 cm^{-1}, no band was observed in the spectra of the other adducts (**1**—**3**) and 2) the position, shape and absorption intensity of the band closely resembles the bands observed at *ca.* 6700 cm^{-1} for pseudo-tetrahedral bis(*N*-alkylsalicylideneaminato)nickel(II) complexes.[6]

On the basis of the analytical and spectral data the adducts have been assigned a trinuclear structure represented schematically by II. Each of the terminal Cu(II) ions(five-coordination) is bridged to the central metal ion(pseudo-tetrahedral four-coordination) with one phenolic oxygen atom and one chloro donor.

The variable-temperature magnetic susceptibility data observed for the $CuCl_2$ adducts (**1** and **2**) followed the Curie-Weiss law ($\chi_M = C/T-\theta$) with $\theta = -7$ and $+6$ K respectively, indicating no appreciable magnetic interaction in the adducts. The pseudo-tetrahedral geometry of the central Cu(II) in the adducts would be expected to be the main structural factor for the magnetism.[7] The cryomagnetic data of the $MnCl_2$ adduct has been analyzed using the theoretical equation 1[3] based on a symmetric linear trimer of Cu–Mn ($S=5/2$)–Cu, assuming no magnetic interaction between the terminal Cu(II) ions. Similarly, the data for the $NiCl_2$ adduct may be expressed by Eq. 2[3] for a Cu–Ni($S=1$)–Cu trimer (Fig. 2);

$$\chi_M = \frac{N\beta^2g^2}{4k(T-\theta')}[35+84\exp(5J/kT)+35\exp(-2J/kT) + 10\exp(-7J/kT)]/[3+4\exp(5J/kT) + 3\exp(-2J/kT)+2\exp(-7J/kT)] + N\alpha \quad (1)$$

$$\chi_M = \frac{2N\beta^2g^2}{k(T-\theta')}[1+5\exp(2J/kT)+\exp(-2J/kT)]/ [3+5\exp(2J/kT)+3\exp(-2J/kT) + \exp(-4J/kT)] + N\alpha \quad (2)$$

where χ_M represents the molar susceptibility corrected for diamagnetism (-384×10^{-6} and -382×10^{-6} cgs emu respectively) using Pascal's constants, J represents the exchange integral between the central and terminal metal ions, g represents the average g value over the three metal ions, θ' represents the Weiss constant term for inter-cluster interaction, and $N\alpha$=T.I.P. per

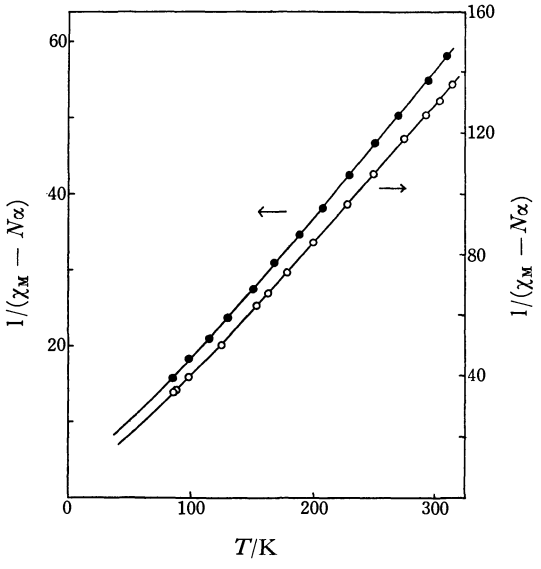

Fig. 2. Variation of reciprocal magnetic susceptibilities with temperature. (●) $[Cu(sal\cdot en\cdot NMe_2)Cl]_2\cdot MnCl_2$, (○) $[Cu(sal\cdot en\cdot NMe_2)Cl]_2\cdot NiCl_2$. The solid curves were calculated from Eqs. 1 and 2 respectively.

Cu_2Mn or Cu_2Ni. Using Eq. 1, the best fit of the experimental data observed for the $MnCl_2$ adduct gave the following values: $J=+19.4$ cm^{-1}, $g=1.997$ and $\theta'=-25.7$ K with $R=6.63\times10^{-3}$ ($R=[\sum(\chi_{exp}-\chi_{calcd})^2/\sum\chi_{exp}^2]^{1/2}$; discrepancy index), assuming $N\alpha=120\times10^{-6}$ cgs emu.[3] Similarly, the $NiCl_2$ adduct gave the following values: $J=+36.4$ cm^{-1}, $g=2.130$ and $\theta'=-17.8$ K with $R=4.81\times10^{-3}$, assuming $N\alpha=320\times10^{-6}$ cgs emu.[3] The positive J values indicating an intramolecular ferromagnetic interaction may also be related to the geometry of the central metal ion in the adducts. In the case of the $NiCl_2$ adduct, the close agreement between the observed and calculated temperature dependence with very low value of R indicates a negligible orbital contribution to the magnetic susceptibility. This factor may be primarily due to the pseudo-tetrahedral geometry of the central Ni(II) ion.[8]

References

1) L. Sacconi and I. Bertini, *Inorg. Chem.*, **5**, 1520 (1966).
2) Y. Muto and T. Tokii, *Bull. Chem. Soc. Jpn.*, **51**, 139 (1978).
3) S. J. Gruber, C. M. Harris, and E. Sinn, *J. Chem. Phys.*, **49**, 2183 (1968).
4) L. Sacconi and M. Ciampolini, *J. Chem. Soc.*, **1964**, 276.
5) B. J. Hathaway and A. A. G. Tomlinson, *Coord. Chem. Rev.*, **5**, 1 (1970).
6) L. Sacconi, P. Paoletti, and M. Ciampolini, *J. Am, Chem. Soc.*, **85**, 411 (1963).
7) E. Sinn, *Inorg. Chem.*, **15**, 366 (1976).
8) B. N. Figgis, J. Lewis, F. Mabbs, and G. A. Webb, *Nature*, **203**, 1138 (1964).

BULLETIN OF THE CHEMICAL SOCIETY OF JAPAN, VOL. 52 (12), 3753—3754 (1979)

Complexes of Zinc-group Metals with 8-Amino-2-methylquinoline

Akiko FURUHASHI* and Hiroshi YOKOTA

Department of Chemistry, College of Science and Engineering, Aoyama-Gakuin University, 6-16-1 Chitosedai, Setagaya-ku Tokyo 157

(Received May 12, 1979)

Synopsis. Some complexes of zinc-group metals with 8-amino-2-methylquinoline have been synthesized. They are seemed to have a monomeric tetrahedral form except for the mercury(I) complex containing a perchlorate ion as a counter anion.

8-Amino-2-methylquinoline (amq) is obtained by the reduction of 8-nitro-2-methylquinoline.[1-2] Although it is expected that the quinoline is able to coordinate to metal ions, in analogy with 8-aminoquinoline, which has essentially the same structure as the amq some differences might exist for the methyl group on the 2-position. The present authors, therefore, synthesized zinc-group metal complexes of amq and studied their properties by electronic, IR and/or far IR spectra, and molar conductances. The experimental results show the metal complexes to have a tetrahedral form, different from the zinc complex synthesized by Litzow and his coworkers.[3-7]

Experimental

Physical Measurements. The IR spectra in the NaCl region were measured with a JASCO IRA-1 type spectrophotometer as a nujol mull or a KBr disk. The far-IR spectra were obtained by means of a nujol mull using a JASCO DS 403G IR spectrophotometer. The reflectance spectra were obtained with a Shimadzu Double-beam UV-200 spectrophotometer. The electronic conductivities were measured using a Toa Conduct Model CM-1DB and a cell with a cell constant of 0.9845 cm^{-1}. The measurements were made at 25 °C by employing a 10^{-3} mol/dm^3 *N,N*-dimethylformamide solution.

Materials. Metal perchlorate and halide of a GR-grade reagent of the Wako Chemical Co., Ltd., were used as starting materials without any further purification. 8-Amino-2-methylquinoline of the Tokyo Kasei Co., Ltd., was used after recrystallization with ligroin.

Syntheses. The metal complexes were prepared the following manner. To an ethanol solution containing 0.0025 mol of metal salt, about 0.0065 mol of a ligand in ethanol was added, after which the mixture was allowed to stand for several hours. The precipitate thus formed was filtered off. After washing with ethanol, it was dried in a vacuum desiccator over anhydrous calcium chloride.

Results and Discussion

The color and elemental analyses of the metal complexes are given in Table 1, together with the yields based on the starting materials.

As is shown in Table 2, the molar conductances may be classified into two values. The values of the type of $M(amq)_2(ClO_4)_2$ and $Hg_2(amq)_2(ClO_4)_2$ lie in the 130—170 S cm^2 mol^{-1} range. The values are representative for 1:2 electrolytes in *N,N*-dimethylformamide.[8] On the other hand, the conductances of $M(amq)X_2$ are all under 30 S cm^2 mol^{-1} except $Zn(amq)I_2$. Consequently, these complexes seem to be essentially non-electrolyte, and they seem to be interact with solvent molecules. In the case of $Zn(amq)I_2$, it

TABLE 1. ELEMENTAL ANALYSES (Figures are given in wt%)

Compound	Color	Calcd (Found), %				Yield %
		C	H	N	M	
$Zn(amq)Cl_2$	Brown	40.79 (40.79	3.41 3.41	9.51 9.52	22.20 22.31)	75
$Zn(amq)Br_2$	Yellow-brown	31.33 (31.62	2.63 2.65	7.51 7.38	17.05 17.10)	85
$Zn(amq)I_2$	Dark-pink	25.16 (25.39	2.11 2.34	5.87 5.91	13.69 13.33)	79
$Zn(amq)_2(ClO_4)_2$	Brown	41.37 (41.52	3.47 3.54	9.65 9.59	11.26 11.19)	76
$Cd(amq)Cl_2$	Yellow-green	35.14 (35.29	2.95 3.07	8.20 8.32	32.91 32.98)	69
$Cd(amq)Br_2$	Green-yellow	27.91 (28.12	2.34 2.36	6.51 6.52	26.11 26.26)	81
$Cd(amq)I_2$	Yellow-green	22.90 (23.12	1.92 2.30	5.34 5.33	21.43 21.57)	72
$Cd(amq)_2(ClO_4)_2$	Yellow-green	38.27 (38.12	3.21 3.21	8.93 8.81	17.91 17.80)	58
$Hg(amq)Cl_2$	Brown	27.93 (28.23	2.35 2.46	6.52 6.53	46.68 47.09)	78
$Hg_2(amq)_2(ClO_4)_2$	Pink	26.21 (26.45	2.20 2.23	6.11 6.06	43.77 43.97)	31

amq: 8-amino-2-methylquinoline.

Table 2. Molar conductances (0.001 mol/dm³ in DMF)

Compound	in S cm² mol⁻¹
$Zn(amq)Cl_2$	3.1
$Zn(amq)Br_2$	10.4
$Zn(amq)I_2$	102.4
$Zn(amq)_2(ClO_4)_2$	163.2
$Cd(amq)Cl_2$	16.7
$Cd(amq)Br_2$	21.9
$Cd(amq)I_2$	25.5
$Cd(amq)_2(ClO_4)_2$	156.4
$Hg(amq)Cl_2$	4.3
$Hg_2(amq)_2(ClO_4)_2$	168.8

amq: 8-amino-2-methylquinoline.

appears that the complex undergoes considerable solvolysis in the solution the following manner,

$$Zn(amq)I_2 \overset{DMF}{\rightleftharpoons} [Zn(amq)I(DMF)]^+ + I^- \quad (1)$$

$$[Zn(amq)I(DMF)]^+ \overset{DMF}{\rightleftharpoons} [Zn(amq)(2DMF)]^{2+} + I^- \quad (2)$$

The IR spectra of free amq show two peaks, at 3440 and 3320 cm^{-1}, of ν_{NH_2}, The peaks shift to the 3120—3280 cm^{-1} range in the metal complexes. A peak about 1340 cm^{-1} in the free ligand also shifts to the lower-wave-number side in 15—20 cm^{-1}. In these metal complexes, therefore, the quinoline seems to bond to the metal ion, with its two nitrogen atoms as a bidentate ligand.[9] The strong bands in the range 950—1140 and about 620 cm^{-1} in the complexes containing a perchlorate group are regarded as simple perchlorate ions.[6-7,10-11] In general, terminal M-X stretching bands of metal complexes with a metal-halogen bond appear in the regions of 200—400 cm^{-1} for MCl, 200—300 cm^{-1} for MBr, and 100—200 cm^{-1} for MI.[12] The wave number observed in the 150—600 cm^{-1} region can be assigned to that of the terminal M-X bands.

The reflectance spectral data in the visible region are shown in Table 3. The bands are all regarded as CT bands. The absorption peaks of the bands change in accordance with the bathochromic effect in the $M(amq)X_2$ type of complexes.[13]

From the experimental results presented above, it is presumed that the metal complexes obtained are in a tetrahedral configuration, since the four coordinated zinc-group metal ions are usually in the tetrahedral form.[14]

In the case of $Hg_2(amq)_2(ClO_4)_2$, the mercury is +1 of the oxidation state. It is qualitatively confirmed in the usual manner that Hg(I) forms a black color when reacted with an alkali solution. Therefore, the complex appears to be dimeric with the $(Hg–Hg)^{2+}$ ion, and the dimers appear to interact with each other in the solid state with mercury, but the structure has not been revealed.

The authors would like to thank Dr. Henry Freiser of the University of Arizona, who gave them a chance to do this work. The authors also wish to express their gratitude to Dr. Yukichi Yoshino of Tokyo University for his continuing encouragement. The authors thank Drs. Kan Kimura and Yoshimitsu Hirao of Aoyama-Gakuin University for their useful discussions.

References

1) D. L. Hammick, *J. Chem. Soc.*, **1926**, 1303.
2) K. Madeja, *J. Prakt. Chem.*, **17**, 97 (1962).
3) M. R. Litzow, L. F. Power, and A. M. Tait, *Aust. J. Chem.*, **23**, 1375 (1970).
4) M. R. Litzow, L. F. Power, and A. M. Tait, *Aust. J. Chem.*, **23**, 1383 (1970).
5) M. R. Litzow, L. F. Power, and A. M. Tait, *Aust. J. Chem.*, **23**, 2005 (1970).
6) M. R. Litzow, L. F. Power, and A. M. Tait, *J. Chem. Soc., A*, **1970**, 275.
7) M. R. Litzow, L. F. Power, and A. M. Tait, *J. Chem. Soc., A*, **1970**, 3226.
8) P. G. Sears, E. D. Wilhoit, and L. R. Dawson, *J. Phys. Chem.*, **59**, 373 (1955).
9) R. Nast, H. Bier, and J. Gremm, *Z. Anorg. Allg. Chem.*, **309**, 289 (1961).
10) L. E. Moore, R. B. Gayhart, and W. E. Bull, *J. Inorg. Nucl. Chem.*, **26**, 896 (1964).
11) B. J. Hathaway and A. E. Underhill, *J. Chem. Soc.*, **1961**, 3091.
12) K. Nakamoto, "Infrared and Raman Spectra of Inorganic and Coordination Compounds," 3rd ed, Wiley, New York (1978), pp. 317—322.
13) F. A. Cotton and G. Wilkinson, "Advanced Inorganic Chemistry," 2nd ed, Wiley, New York (1966), pp. 680—681.
14) F. A. Cotton and G. Wilkinson, "Advanced Inorganic Chemistry," 2nd ed, Wiley, New York (1966), pp. 130—131.

Table 3. Reflectance spectral data (Figures are given in cm^{-1})

Compound						
amq	24150,	23700,	19920(sh),			
$Zn(amq)Cl_2$	23530,	23360,	19920(sh),		16890	
$Zn(amq)Br_2$	23700,	22990,	19800(sh),		16670	
$Zn(amq)I_2$	23810,	22720,	19760(sh),		16530	
$Zn(amq)_2(ClO_4)_2$	23530,	22830,		18520(sh),	16390,	14180(sh)
$Cd(amq)Cl_2$	23360,	22930,	19880(sh),		16390	
$Cd(amq)Br_2$	23620,	22900,	19800(sh),		15870	
$Cd(amq)I_2$	23700,	22830,	19760(sh),		15500	
$Cd(amq)_2(ClO_4)_2$	23700,	22990,	19720(sh),	18520(sh),	16390,	13793(sh)
$Hg(amq)Cl_2$	23700,	22990,	19800(sh),		16260	
$Hg_2(amq)_2(ClO_4)_2$	23700,	22990,	19420(sh),	18520(sh),	16390,	13920(sh)

amq: 8-amino-2-methylquinoline, sh: shoulder.

BULLETIN OF THE CHEMICAL SOCIETY OF JAPAN, VOL. 52 (12), 3755—3756 (1979)

Reaction of Guaioxide with *N*-Bromosuccinimide and the Preparation of 4,6-Guaiadien-3-one and 1-Epi-4,6-guaiadien-3-one[1)]

Hiroshi HIROTA, Yoshihiko MORIYAMA, Hidekazu SHIRASAKI, Takahiko TSUYUKI, and Takeyoshi TAKAHASHI*

Department of Chemistry, Faculty of Science, The University of Tokyo, Bunkyo-ku, Tokyo 113

(Received July 18, 1979)

Synopsis. Treatment of guaioxide with *N*-bromosuccinimide gave 4-bromoguaioxide, which was dehydrobrominated to yield 3-dehydroguaioxide. The olefin was then converted into 8-deoxytorilolone and 8-deoxy-1-epitorilolone by the known procedures. Dehydration of these deoxy derivatives in benzene in the presence of *p*-toluenesulfonic acid gave 4,6-guaiadien-3-one and 1-epi-4,6-guaiadien-3-one, respectively.

Guaioxide (**1**; $C_{15}H_{26}O$)[2)] was isolated from guaiac wood oil as a minor constituent, and also obtained by acid-catalyzed cyclization of guaiol.[2,3)] Because of the absence of hydrogen on the two carbons attached to an ether oxygen atom, the sesquiterpene ether (guaioxide) is particularly inert towards common chemical reagents. By the microbial oxidation technique, hydroxyl groups were successfully introduced to the molecule. This led to the elucidation of the structure of guaioxide (**1**).[4)] In this paper we wish to report on the introduction of a functional group into guaioxide by chemical method. The reaction of guaioxide (**1**) with *N*-bromosuccinimide (NBS) gave a monobromide (**2**) which in turn afforded an olefin (**3**). Conversion of **3** into two diastereomeric α,β: γ,δ-unsaturated ketones (**4** and **5**) is also described.

Friedelane reacts with NBS or bromine to give friedel-18-ene which may be formed *via* 18-bromofriedelane.[5)] When guaioxide (**1**) was treated with 1—1.2 mol equivalent of NBS in carbon tetrachloride under reflux, a monobromide (**2**) and an olefin (**3**) were obtained in isolation yields 3—10% and 5—15%, respectively.[6)] Bromide (**2**) was heated under reflux with potassium hydroxide in ethanol to give the same olefin (**3**) in 45—65% yield which was found to be identical with 3-dehydroguaioxide (**3**).[4)] This shows that the bromination of **1** took place on $C_{(4)}$ to give **2**. Bromination of **1** in carbon tetrachloride with a large excess of NBS or bromine resulted in the formation of a complex mixture of reaction products, separation of which was unsuccessful.

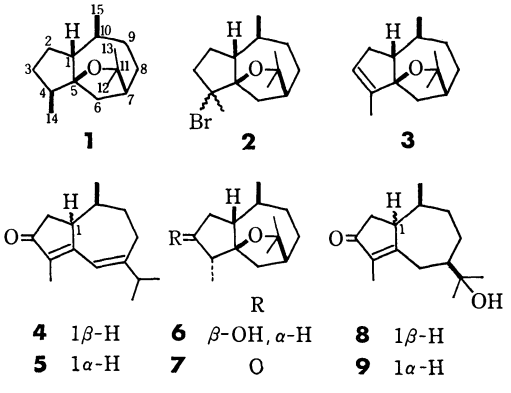

By the known procedures,[4)] olefin (**3**) was converted *via* 3β-hydroxyliguloxide (**6**)[4,7)] and 3-oxoliguloxide (**7**), into a hydroxy α,β-unsaturated ketone (**8**; 8-deoxytorilolone), which isomerized into a diastereomeric hydroxy α,β-unsaturated ketone (**9**; 8-deoxy-1-epitorilolone).[4)] These hydroxy unsaturated ketones (**8** and **9**) were dehydrated to give 4,6-guaiadien-3-one (**4**) and 1-epi-4,6-guaiadien-3-one (**5**), respectively, in a quantitative yield, by refluxing with *p*-toluenesulfonic acid in benzene. When **4** was heated under reflux with methanolic potassium hydroxide, no isomerization detectable by NMR measurement took place, while more than 90% of **5** isomerized into **4** by the same treatment.[8)] In the NMR spectra, the $C_{(10)}$-methyl signal of **5** appears at a fairly higher field (δ 0.73) as compared with the corresponding signal (δ 1.06) of **4**. This suggests that the $C_{(10)}$-methyl of **5** is shielded by π-electron cloud of the α,β: γ,δ-unsaturated ketone moiety. This is in line with the UV spectra of **4** and **5** which show that the molecular extinction coefficient (ε) at 293 nm of **5** is smaller by *ca.* 20% than that of **4**.

Experimental

IR and UV spectra were measured with a Hitachi EPI-G2 spectrometer and a Hitachi 340 spectrophotometer, respectively, ^{1}H-NMR spectra with a Varian EM-390 (90 MHz) or a Hitachi R-20B (60 MHz) spectrometer in deuteriochloroform solution containing tetramethylsilane as an internal standard, single-focus mass spectra with a Hitachi RMU-6-Tokugata mass spectrometer, and double-focus mass spectra with a JEOL D-300, with direct inlet system operating at 70 eV. Measurements of optical rotation were carried out with a JASCO polarimeter DIP-SL. CD spectra were taken on a JASCO model J-20. For column chromatography Wakogel C-200 (Wako Pure Chemical Industries) was used. Thin-layer chromatography (TLC) was carried out on Kieselgel GF_{254} (E. Merck, Darmstadt) in 0.25 mm thickness. Vapor-phase chromatographic (VPC) analyses were performed on a Shimadzu gas chromatograph model GC-6A.

Bromination of Guaioxide (1) with NBS. NBS (3.32 g; 18.7 mmol) was added to a solution of guaioxide (**1**; 4.00 g; 18.0 mmol) in carbon tetrachloride (20 ml), and the mixture was heated under reflux for 1.5 h by means of an infrared lamp. The reaction mixture was then cooled and filtered. The solvent was removed under reduced pressure to give a residue which was chromatographed on a column of silica gel. Elution with petroleum ether–benzene (4: 1) gave a *ca.* 1: 1 mixture (800 mg) of 4-bromoguaioxide (**2**) and unchanged guaioxide (**1**). Though **2** decomposed easily on contact with silica gel, a small amount of **2** was isolated from the mixture of **1** and **2** by rechromatography. 4-Bromoguaioxide (**2**): an oil, $[\alpha]_D^{22}$ +1.4° (*c* 3.25; EtOH); IR (film): 1140, 1060, 875, 800, and 740 cm^{-1}; NMR ($CDCl_3$); δ 0.85—0.95 (3H,

diffused d; $C_{(10)}$-CH_3), δ 1.32, 1.34 (each 3H, s; $C_{(11)}$-$(CH_3)_2$), and δ 1.88 (3H, s; $C_{(4)}$-CH_3); MS: *m/e* 302 and 300 (relative abundance, each 2%; M^+), *m/e* 287 and 285 [each 20%; $(M-CH_3)^+$], *m/e* 221 [25%; $(M-Br)^+$], and 205 [100%, $(C_{14}H_{21}O)^+$]. Found: *m/e* 302.1075. Calcd for $C_{15}H_{25}O^{81}Br$: M, 302.1069. Found: *m/e* 300.1108. Calcd for $C_{15}H_{25}O^{79}Br$: M, 300.1089. The bromide showed one spot on thin-layer chromatogram. The fact that the NMR spectrum shows no other methyl signals suggests that bromide (**2**) contains no epimer on $C_{(4)}$. However, the configuration at $C_{(4)}$ of **2** remained undetermined due to its easy decomposition as previously stated.

Successive elution with the same solvents gave the starting compound (**1**; 3.1 g; 78%) and a dehydrobrominated material (**3**; 240 mg; 6.1%).

When the reaction of **1** with NBS was carried out under a nitrogen stream in order to remove the hydrogen bromide generated during the course of reaction, olefin (**3**) could be obtained in better yield (15—35%).

Dehydrobromination of 4-Bromoguaioxide (2). The bromide (**2**; 100 mg; 0.33 mmol) in an ethanolic potassium hydroxide (KOH 220 mg, EtOH 5 ml) was heated under reflux for 2.5 h and the reaction mixture was treated as usual to give a residue which was chromatographed on a column of silica gel. Elution with petroleum ether–benzene (2: 1) gave the olefin (**3**; 36 mg; 0.17 mmol; 50% yield), an oil, $[\alpha]_D^{22}$ +15.0° (*c* 1.45; EtOH); IR (film): 1660, 1640, 1130, 1040, 1010, 885, and 815 cm^{-1}; NMR ($CDCl_3$): δ 0.85—0.95 (3H, diffused d; $C_{(10)}$-CH_3), δ 1.23, 1.34 (each 3H, s; $C_{(11)}$-$(CH_3)_2$), δ 1.67 (3H, d, J=1.3 Hz; $C_{(4)}$-CH_3), and δ 5.39 (1H, q, J=1.3 Hz; $C_{(3)}$-H); MS: *m/e* 220 (21%; M^+), *m/e* 205 [100%; $(M-CH_3)^+$], *m/e* 202 [56%; $(M-H_2O)^+$], *m/e* 187 [26%; $(C_{14}H_{19})^+$], and *m/e* 159 [53%; $(C_{12}H_{15})^+$]. Found: *m/e* 220.1814. Calcd for $C_{15}H_{24}O$: M, 220.1827. This olefin was found to be identical with 3-dehydroguaioxide (**3**)[4] and also with the olefin obtained by the reaction of **1** with NBS.

Conversion of 3-Dehydroguaioxide (3) into 8-Deoxytorilolone (8) and 8-Deoxy-1-epitorilolone (9). According to the procedures described by Ishii *et al.*,[4] the olefin (**3**) was converted, *via* the alcohol (**6**)[4,7] and the ketone (**7**), into 8-deoxytorilolone (**8**), which was isomerized into a 1: 1 mixture of **8** and 8-deoxy-1-epitorilolone (**9**). The formation of each compound (**6**, **7**, **8**, and **9**) was confirmed by identity of their spectral data with those of authentic samples (**6**, **7**, **8**, and **9**).

Dehydration of 8-Deoxytorilolone (8). *p*-Toluenesulfonic acid (67 mg; 0.35 mmol) was added to a solution of α,β-unsaturated ketone (**8**; 56 mg; 0.23 mmol) in benzene (17 ml), and the solution was heated under reflux for 3.5 h. The reaction mixture was treated as usual to give a single product, 4,6-guaiadien-3-one (**4**; 52 mg; quantitative yield), an oil, IR (film): 1690, 1625, 1590, 1340, 1285, 1050, and 870 cm^{-1}; UV (EtOH): λ_{max} 293 nm (ε 20700); CD (c 6.43×10^{-4}, EtOH): $[\theta]_{365}$ ±0, $[\theta]_{295}$ +18300, and $[\theta]_{240}$ ±0; NMR ($CDCl_3$): δ 1.06 (3H, d, J=6 Hz; $C_{(10)}$-CH_3), δ 1.09 (6H, d, J=7 Hz; $C_{(11)}$-$(CH_3)_2$), δ 1.75 (3H, s; $C_{(4)}$-CH_3), and δ 6.35 (1H, br s; $C_{(6)}$-H); MS: *m/e* 218 (100%; M^+), *m/e* 203 [32%; $(M-CH_3)^+$], and *m/e* 175 [73%; $(M-C_3H_7)^+$]. Found: *m/e* 218.1662. Calcd for $C_{15}H_{22}O$: M, 218.1671.

Dehydration of 8-Deoxy-1-epitorilolone (9). By the same treatment as above, **9** was transformed quantitatively into 1-epi-4,6-guaiadien-3-one (**5**), an oil, IR (film): 1690, 1630, 1590, 1330, 1290, 1055, and 880 cm^{-1}; UV (EtOH): λ_{max} 293 nm (ε 16500); CD (c 9.70×10^{-5}, EtOH): $[\theta]_{380}$ ±0, $[\theta]_{335}$ −6080, $[\theta]_{317}$ ±0, $[\theta]_{297}$ +5050, and $[\theta]_{265}$ ±0; NMR ($CDCl_3$): δ 0.73 (3H, d, J=6.5 Hz; $C_{(10)}$-CH_3), δ 1.11 (6H, d, J=6.5 Hz; $C_{(11)}$-$(CH_3)_2$), δ 1.73 (3H, s; $C_{(4)}$-CH_3), and δ 6.34 (1H, br. s; $C_{(6)}$-H); MS: *m/e* 218 (100%; M^+), *m/e* 203 [18%; $(M-CH_3)^+$], and *m/e* 175 [50%; $(M-C_3H_7)^+$]. Found: *m/e* 218.1649. Calcd for $C_{15}H_{22}O$: M, 218.1617.

Alkaline Treatment of the α,β: γ,δ-Unsaturated Ketones (4 and 5). 4,6-Guaiadien-3-one (**4**; 13 mg) was treated with potassium hydroxide (100 mg) in methanol (5 ml) under reflux for 2 h under a nitrogen atmosphere. The reaction product (8 mg) was obtained after the usual treatment, and found by NMR measurement to consist of only the unchanged **4**. When 1-epi-4,6-guaiadien-3-one (**5**) was subjected to the same alkaline treatment, NMR measurement showed that more than 90% of **5** isomerized into **4**. Since the retention times for **4** and **5** were too close to each other, the accurate ratio of the products could not be determined by VPC measurement (column: Dexsil-300, SP-1000, and SE-30).

The authors wish to thank Dr. Hiroshi Ishii, Shionogi Research Laboratory, Osaka, for the spectral data of authentic compounds (**3**, **6**, **7**, and **8**).

References

1) A part of this work was presented at the 32nd National Meeting of the Chemical Society of Japan, Tokyo, April 4, 1975, Abstr. No. 4G01.

2) R. B. Bates and R. C. Slagel, *Chem. Ind. (London)*, **1962**, 1715.

3) P. Ledoux, B. P. Vaterlaus, and G. Chiurdoglu, *Bull. Soc. Chim. Belg.*, **75**, 551 (1966); M. V. Kadival, M. S. R. Nair, and S. C. Bhattacharyya, *Tetrahedron*, **23**, 1241 (1967).

4) H. Ishii, T. Tozyo, M. Nakamura, and H. Minato, *Tetrahedron*, **26**, 2751 (1970).

5) V. V. Kane and R. Stevenson, *Tetrahedron*, **15**, 223 (1961); F. Kohen and R. Stevenson, *J. Org. Chem.*, **30**, 2479 (1965); *cf.* T. Tsuyuki, Y. Tanahashi, Y. Sudo, S. Nakamata, and T. Takahashi, *Bull. Chem. Soc. Jpn.*, **39**, 1610 (1966).

6) Isolation yields of both **2** and **3** were poor, a large amount (55—80%) of **1** being recovered unchanged. This was due to a) reaction products (**2** and **3**) being unstable on silica gel, and b) R_f values on TLC of **1**, **2**, and **3** being very close to one another. When the first three reactions, namely, NBS bromination and dehydrobromination followed by hydroboration, were carried out without purification, 200 mg of 3β-hydroxyliguloxide (**6**) was obtained from 1.0 g of guaioxide (overall yield, 18.5%).

7) E. Funke, T. Tozyo, H. Ishii, and K. Takeda, *J. Chem. Soc., C*, **1970**, 2548.

8) By the same treatment, **8** yielded a *ca.* 1: 1 equilibrium mixture of **8** and **9**.[4]

BULLETIN OF THE CHEMICAL SOCIETY OF JAPAN, VOL. 52 (12), 3757—3758 (1979)

Catalytic Hydrogenolysis of 1,1-Dichloro-3-methyl-2-phenylcyclopropane

Koji ISOGAI* and Shigeru HIRABAYASHI**

Department of Applied Chemistry, Faculty of Engineering, Niigata University, Ikarashi, Niigata-shi, Niigata 950-21

(Received January 12, 1979)

Synopsis. The title compound was hydrogenolyzed over PdO or Raney nickel. The C_2–C_3 bond of the cyclopropane ring underwent cleavage exclusively over PdO. Cleavage of the C_1–C_2 and C_2–C_3 bonds occurred competitively over Raney nickel. A probable pathway is suggested.

The position of ring cleavage on the catalytic hydrogenolysis of cyclopropanes is determined by substituents.[1,2] However, little attention has been given to the role of negative substituents such as halogens in the regioselectivity of the ring cleavage. The hydrogenolysis of 1-bromo-1-fluoro-2-phenylcyclopropane over palladium oxide catalyst (PdO) has been investigated.[3] Cleavage of the C_2–C_3 bond of the cyclopropane ring occurred exclusively, two olefins being obtained as intermediates. In order to clarify the behavior of halogens in the regioselective hydrogenolysis of cyclopropane ring, we have studied the hydrogenolysis of 1,1-dichloro-3-methyl-2-phenylcyclopropane (**1**).

The results of catalytic hydrogenolysis of **1** are given in Table 1. When PdO was used as a catalyst, hydrogenolysis of **1** was reduced in the presence of potassium hydroxide, but proceeded smoothly in the absence of potassium hydroxide, giving butylbenzene (**5**) exclusively. On the other hand, with use of Raney nickel (R-Ni), only in the presence of potassium hydroxide, it gave a mixture of stereoisomeric 1-chloro-*r*-3-methyl-*t*-2-phenylcyclopropane (**2**) (*r*-1-chloro-*c*-3-methyl-*t*-2-phenylcyclopropane (**2t**) and *r*-1-chloro-*t*-3-methyl-*c*-2-phenylcyclopropane (**2c**)), *r*-2-methyl-*t*-1-phenylcyclopropane (**3**), isobutylbenzene (**4**) and **5**. In the presence of potassium hydroxide, the product composition for R-Ni catalyzed hydrogenolysis varied with the progress of reaction. The main products in the early stage of the hydrogenolysis were **2** and **4**. After **1** almost disappeared, **2** decreased gradually, **5** increasing in proportion to the decreased amount of **2**. **2** and **3** were hydrogenolyzed over R-Ni in a manner similar to that observed in the case of **1**. Hydrogenolysis of **2** gave **4** (15.2%) and **5** (64.2%); that of **3** gave predominantly **4** (83.0%) with a small amount of **5** (3.1%). PdO catalyzed hydrogenolysis of 1-bromo-1-fluoro-2-phenylcyclopropane (**6**) gave 2-fluoro-3-phenylpropene (**7**) and (*Z*)-2-fluoro-1-phenylpropene (**8**) as intermediates.[3] They were finally hydrogenolyzed to propylbenzene (**9**) and 2-fluoro-1-phenylpropane (**10**). The formation of these olefins can be explained by assuming that **6** adsorbed on the catalyst by C_2–C_3 bond undergoes cleavage accompanied by elimination of bromide ion. Hydrogenolysis of **1** over PdO seems to proceed in a similar manner to that above, a plausible pathway being shown in Scheme 1. Since palladium catalyst has greater affinity to carbon–carbon π-bond than to negative groups such as oxygen or nitrogen,[4,5] and the affinity to chlorine lone pairs is not very high,[6,7] the hydrogenolysis occurs selectively through the adsorption state (A) chemisorbed by the C_2–C_3 bond of the cyclopropane ring and phenylgroup followed by the formation of C_2,C_3-diadsorbed species (B). The elimination of chloride ion (or chlorine atom) from (B) is caused by the electron transfer from C_2–metal or C_3–metal bond to give (C) or (D). Since (D) forms π-benzyl complex with catalyst, elimination of the chlorine atom seems to prefer course (b). Absence of the expected olefins in the reaction mixture seems to be due to their rapid hydrogenation to the final product **5** under the experimental conditions.

The R-Ni catalyzed hydrogenolysis of **1** is complicated. Predominant formation of **2** and **4** at the

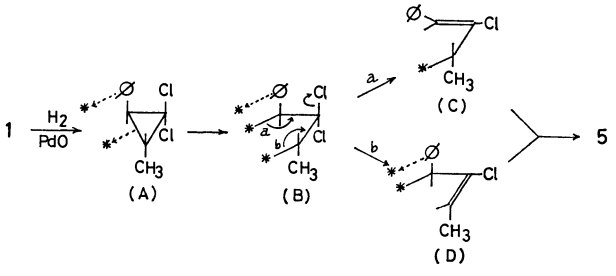

Scheme 1.

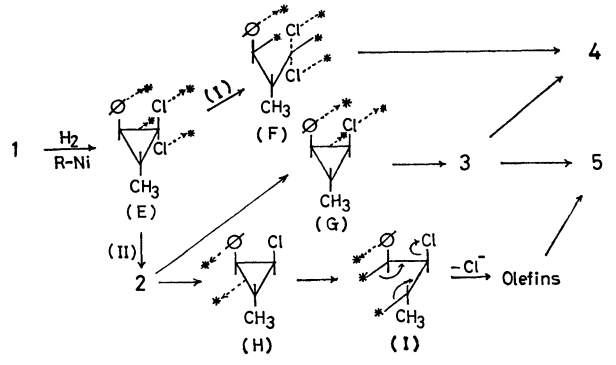

Scheme 2.

TABLE 1. HYDROGENOLYSIS OF **1**

Catalyst	Additive	Composition of products/mol %				
		5	**4**	**3**	**2**	**1**
PdO	—	65.2	—	—	—	34.8
PdO	KOH	3.3	0.5	0.7	—	95.5
R-Ni	—	2.3	0.9	—	—	96.8
R-Ni	KOH	35.0	37.9	1.1	25.0[a]	—

a) **2t**/**2c** ratio is 39/61.

** Present address: Department of Dental Engineering, School of Dental Medicine, Tsurumi University, Tsurumi, Tsurumi-ku, Yokohama 230.

early stage of the hydrogenolysis of **1** is ascribed to the adsorption by the chlorine atom which has high affinity to nickel catalyst,[6,7] phenyl group and C_1–C_2 bond of **1**, followed by competitive hydrogenolysis of C_1–C_2 bond (path I) and C–Cl bond (path II) as shown in Scheme 2. The hydrogenolysis of C–Cl bond from the adsorbed species (F) seems to occur readily, giving **4**. The formation of **5** is mainly due to the hydrogenolysis of **2** *via* adsorbed species (H) since the stepwise hydrogenolysis of **2** *via* adsorbed species (G) gives predominantly **4**.

The adverse effect of potassium hydroxide in the PdO and R-Ni catalyzed hydrogenolysis of **1** might be explained in terms of the adsorption states of substrate. When PdO is used as a catalyst, the presence of potassium hydroxide prevents adsorption of the phenyl group and cyclopropane (adsorption state (A)) as in the case of carbon–carbon π-bond. The accelerating effect of potassium hydroxide in the case of R-Ni catalyzed hydrogenolysis is due to the inhibition of the production of Ni^{2+} ion, *viz.* poison of nickel catalyst, caused by removal of chloride ion as a salt.

Experimental

*1,1-Dichloro-*r*-3-methyl-*t*-2-phenylcyclopropane (1).* To a mixture of petroleum ether (200 ml), β-methylstyrene (29.5 g, 0.25 mol) and potassium *t*-butoxide prepared from 10 g of potassium metal was added dropwise 30 g (0.25 mol) of chloroform at −10 °C over a period of 3 h. **1**: bp 86.5—88 °C/3.5 mmHg, 19.5 g (39% yield) was obtained. R_t: 29.0 min, MS *m/e*: 200 (M^+). Found: C, 59.76; H, 4.90%. Calcd for $C_{10}H_{10}Cl_2$: C, 59.72; H, 5.01%.

Catalysts. Palladium oxide (Nippon Engelhard Co.) and Raney nickel alloy NDH (Kawaken Fine Chemical Co.) were used. The alloy was treated according to the W-5 method[8] and washed with water until the washings showed no coloration with phenolphthalein.

Catalytic Hydrogenolysis of 1. **1** (5 mmol) was hydrogenated for 24 h over R-Ni (1 g, as Ni) or PdO (0.2 g) in methanol (25 ml) at room temperature under atmospheric pressure in the presence or absence of potassium hydroxide (10 mmol). The composition of products was determined by VPC (TCP 2 m: 130 °C) at appropriate time intervals.

Identification of Products. **1** was hydrogenolyzed over R-Ni under similar conditions to those described above. Hydrogenation was stopped after 1 h, the reaction mixture was subjected to measurement of GC-MS. For measurement of NMR and elementary analysis, each component of the products was separated preparatively by VPC.

r-*1-Chloro-*c*-3-methyl-*t*-2-phenylcyclopropane (2t)*: R_t: 17.3 min, MS *m/e*: 166 (M^+), NMR (CCl_4): δ=1.86 (1H, dd, $\underline{H}_a$–C–Ph), 3.30 (1H, dd, $\underline{H}_x$–C–Cl, $J(H_a–H_x)$=3.8 Hz). Found: C, 72.27; H, 6.80%. Calcd for $C_{10}H_{11}Cl$; C, 72.09; H, 6.66%.

r-*1-Chloro-*t*-3-methyl-*c*-2-phenylcyclopropane (2c)*: R_t: 19.8 min, MS *m/e*: 166 (M^+), NMR (CCl_4): δ=2.04 (1H, dd, $\underline{H}_a$–C–Ph), 3.08 (1H, dd, $\underline{H}_x$–C–Cl, J ($H_a–H_x$)=7.8 Hz). Found: C, 72.18: H, 6.67%. Calcd for $C_{10}H_{11}Cl$: C, 72.09; H, 6.60%.

r-*2-Methyl-*t*-1-phenylcyclopropane (3)*: R_t: 4.2 min, MS *m/e*: 132 (M^+). Found: C, 90.16; H, 9.3%. Calcd for $C_{10}H_{12}$: C, 90.58; H, 9.15%.

Isobutylbenzene (4): R_t: 2.2 min, MS *m/e*: 134 (M^+), NMR (CCl_4): δ=0.91 (6H, d, $-CH(C\underline{H}_3)_2$), 1.84 (1H, m, $-C\underline{H}-(CH_3)_2$).

Butylbenzene (5): R_t: 3.0 min, MS *m/e*: 134 (M^+), NMR (CCl_4): δ=0.90 (3H, t, $-C\underline{H}_3$), 1.4 (4H, m, $-C\underline{H}_2-C\underline{H}_2-$).

Catalytic Hydrogenolysis of 2 and 3. **2** (**2t**/**2c**=44/56) and **3** were hydrogenolyzed in a similar manner to that for hydrogenolysis of **1**, respectively.

The authors are grateful to Japan Spectroscopic Co., Ltd. Tokyo, for the GC-MS measurements.

References

1) J. Newham, *Chem. Rev.*, **63**, 123 (1963).
2) A. P. G. Kieboom and F. van Ranteijk, "Hydrogenation and Hydrogenolysis in Synthetic Organic Chemistry," Delft University Press, (1977), p. 107.
3) K. Isogai and K. Kitahara, *Nippon Kagaku Kaishi*, **1978**, 280.
4) S. Mitsui, T. Sakai, and H. Saito, *Nippon Kagaku Zasshi*, **86**, 409 (1965).
5) T. Sakai, T. Kaneko, and S. Mitsui, *Nippon Kagaku Zasshi*, **86**, 1328 (1965).
6) S. Imaizumi, *Nippon Kagaku Zasshi*, **82**, 245 (1961).
7) K. Isogai, *Nippon Kagaku Zasshi*, **83**, 1238 (1962).
8) H. Adkins and H. R. Billica, *J. Am. Chem. Soc.*, **70**, 695 (1948).

BULLETIN OF THE CHEMICAL SOCIETY OF JAPAN, VOL. 52 (12), 3759—3760 (1979)

syn- and *anti*[3.3](1,4)Naphthalenophanes[1)]

Minoru YOSHINAGA, Tetsuo OTSUBO, Yoshiteru SAKATA, and Soichi MISUMI*

The Institute of Scientific and Industrial Research, Osaka University, Suita, Osaka 565

(Received February 13, 1979)

Synopsis. The title compounds were prepared by pyrolysis of disulfones. The absorption spectra depend rather on the stacking mode between two naphthalene rings than ring-to-ring distance, whereas for the emission spectra the reverse is the case. A [4+4]photocycloaddition and a reverse reaction were observed between *anti*-form and its photoisomer.

In order to clarify the effects of ring-to-ring distance and stacking mode between two naphthalene rings on the naphthalene excimer emission,[2,3)] the title compounds were studied as more suitable models than *syn*- and *anti*[2.2](1,4)naphthalenophanes (**1** and **2**)[4)] because the [3.3]phane system with longer ring-to-ring distance must be less strained than the [2.2]phane system.

The two isomeric [3.3](1,4)naphthalenophanes (*syn* **3** and *anti* **4**)[5)] were prepared by our method in which pyrolytic desulfurization of disulfone was the key step of [3.3]phane formation.[6)] 1,4-Bis(bromomethyl)naphthalene **5**[7)] was converted to 1,4-bis(2-mercaptoethyl)-naphthalene **10** in the conventional way of five steps. A coupling of **5** with mercaptan **10** gave 2,17-dithia[4.4]-(1,4)naphthalenophane **11**. The NMR spectrum of **11** shows the *anti*-conformer to be predominant though both conformers are easily interconvertible. After **11** was oxidized with *m*-chloroperbenzoic acid, pyrolysis of the resulting disulfone **12** led to a mixture of the desired phanes **3** and **4** with a 2: 3 ratio. The separation into the two isomers was performed by fractional crystallization and column chromatography on silica gel.

The structures of **3** and **4** were determined by NMR data characteristic of *syn*- and *anti*-conformers, respectively. Thus, the ring current effect due to the opposite naphthalene ring brings about upfield shifts of all the aromatic protons for *syn*-form **3** and of only H_a proton for *anti*-form **4**. These upfield shifts are, as expected, a little less, compared to those of *syn*- and *anti*[2.2]analogs **1** and **2**.

Fig. 1 shows electronic absorption spectra of **1**—**4**. Evidently, the spectra depend rather on the stacking mode of two naphthalene rings than on the ring-to-ring distance. Thus, the spectral shapes of both conformers **3** and **4** are markedly different, whereas each spectrum is quite similar to that of the same conformer of [2.2]-analog. This phenomenon can be interpreted by only exciton interaction of the two chromophores although a contribution of charge-transfer interaction is not neglected.[3,8)]

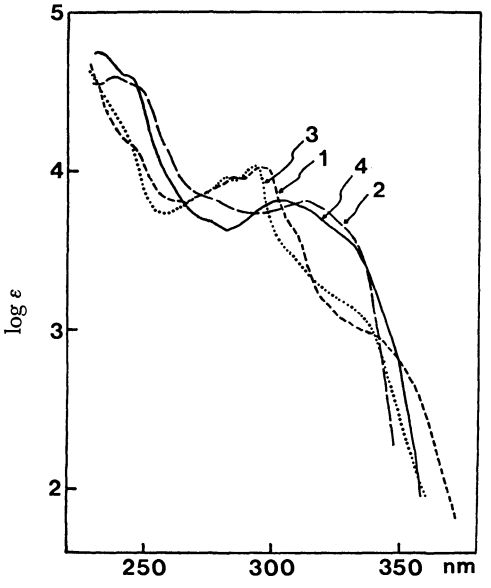

Fig. 1. Electronic spectra of **1**—**4** in tetrahydrofuran.

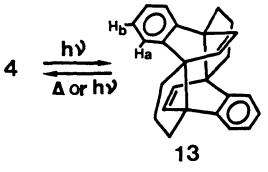

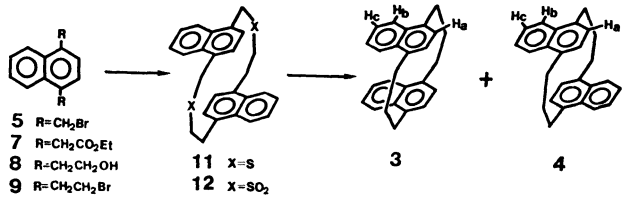

The emission spectra of **3** and **4** show a broad fluorescence band of excimer type (λ_{max} 430 nm for **3** and 420 nm for **4**) and a phosphorescence band with fine structure (λ_{max} 494, 530, 570 nm for **3** and 530, 570 nm for **4**). These data suggest that the naphthalene excimer (λ_{max} 400—410 nm) has not necessarily a closely fixed sandwich structure, that is, the ease of the excimer formation is not correlated to the extent of overlapping between two naphthalene rings. The naphthalene excimer is presumed to be in a parallel slided conformation with a distance comparable to the ring-to-ring distance in [3.3]phane system.

Although *anti*-form **2** with [2.2]system undergoes two types of intramolecular photocycloaddition, *i.e.*, a formally two-fold [4+2]cycloaddition to dibenzoequinene[9)] and a [4+4]cycloaddition,[10)] *anti*-form **4** with [3.3]system undergoes onyl [4+4]photocycloaddition to afford photoisomer **13** in quantitative yield. Cycloadduct **13** is stable at room temperature and undergoes a reverse aromatization above 130 °C to regenerate **4**.[5)] The retro-conversion of **13** to **4** also was accomplished on irradiation with light at 253.7 nm.

Experimental

Melting points are uncorrected. NMR ($CDCl_3$), MS, UV, and emission (degassed EPA) spectra were recorded with a JEOL FX-100 (100 MHz), a Hitachi RMU-7, a Hitachi EPS-3T, and a Hitachi MPF-2A (HIV R-446 photomultiplier) spectrometers, respectively.

1,4-Bis(2-hydroxyethyl)naphthalene ***8***. The reduction of diester **7** (7.6 g, 25 mmol), which was derived by cyanation of 1,4-bis(bromomethyl)naphthalene **5**,[7] followed by esterification, in dry THF (200 ml) with $LiAlH_4$ (4.8 g, 127 mmol) in dry THF (270 ml) and recrystallization of the resulting glycol from ethyl acetate gave 89% (4.8 g) yield of **8**, colorless plates, mp 119.5—120 °C. NMR δ=3.31 (2H, t, J=6.1 Hz, CH_2), 3.97 (2H, t, J=6.1 Hz, CH_2), 7.30 (2H, s, ArH), 7.50 (2H, m, ArH), and 8.11 (2H, m, ArH). Found: C, 77.97; H, 7.54%. Calcd for $C_{14}H_{16}O_2$: C, 77.75; H, 7.46%.

1,4-Bis(2-bromoethyl)naphthalene ***9***. Dibromide **9** was obtained by refluxing a mixture of glycol **8** (3.5 g, 16 mmol), 47% HBr (200 ml), and conc H_2SO_4 (90 ml) for 2 h. The mixture was worked up and chromatographed on silica gel with benzene. **9**: colorless plates from benzene–hexane, yield 2.6 g (47%), mp 131—131.5 °C. NMR δ=3.65 (8H, m, CH_2), 7.35 (2H, s, ArH), 7.65 (2H, m, ArH), and 8.10 (2H, m, ArH). Found: C, 49.32; H, 4.41; Br, 46.27%. Calcd for $C_{14}H_{14}Br_2$: C, 49.15; H, 4.13; Br, 46.72%.

1,4-Bis(2-mercaptoethyl)naphthalene ***10***. A mixture of **9** (4.5 g, 13 mmol), thiourea (2.6 g, 34 mmol), and ethanol (180 ml) was treated in the same way as the preparation of 1,4-bis(2-mercaptoethyl)benzene.[1] The resulting oil crystallized after chromatography on silica gel with benzene, yield 1.0 g (31%), mp 108.5—109.5 °C. The dithiol was essentially pure and used in the next step without further purification. NMR δ=1.44 (2H, t, J=7.8 Hz, SH), 3.06 (4H, m, CH_2), 3.40 (4H, m, CH_2), 7.25 (2H, s, ArH), 7.49 (2H, m, ArH), and 8.05 (2H, m, ArH).

2,17-Dithia[4.4](1,4)naphthalenophane ***11***. The coupling of dibromide **5** (700mg, 2.3 mmol) with dithiol **10** (600 mg, 2.4 mmol) in benzene (400 ml) was carried out according to the general procedure in the preceding paper.[1] **11**: colorless plates from benzene–hexane, yield 200 mg (22%), mp 256—257 °C. NMR δ=3.18 (8H, A_2B_2m, CH_2), 3.78 (4H, s, CH_2), 6.00 (2H, s, ArH), 6.37 (2H, s, ArH), 7.47 (4H, m, ArH), and 7.90 (4H, m, ArH). Found: C, 77.72; H, 6.05; S, 16.29 %; MS *m/e* 400 (M^+). Calcd for $C_{26}H_{24}S_2$: C, 77.95; H, 6.04; S, 16.01%; M 400.

2,17-Dithia[4.4](1,4)naphthalenophane 2,2,17,17-Tetraoxide ***12***. The preparation of disulfone **12** was carried out according to the general procedure (with *m*-chloroperbenzoic acid) in the preceding paper.[1] **12**: quantitative yield, mp 324 °C (dec). It was used for the next step without purification.

[3.3](1,4)Naphthalenophanes, syn ***3*** *and* anti ***4***. Pyrolysis of disulfone **12** (50 mg, 0.108 mmol) was carried out by the same method as previously reported (650 °C, 0.2 mmHg).[6] The collected product was purified by column chromatography on silica gel with benzene and then gel-permeation liquid chromatography to give a mixture of *syn*- and *anti*-isomers with a 2:3 ratio, yield 10 mg (28%). Recrystallization from hexane afforded pure *anti*-isomer **4**, colorless needles, mp 214—216 °C. NMR δ=2.32 (4H, m, CH_2), 2.72 (4H, m, CH_2), 3.43 (4H, m, CH_2), 5.99 (4H, s, H_a), 7.51 (4H, q, J=7.0, 2.0 Hz, Hc), and 8.06 (4H, q, J=7.0, 2.0 Hz, Hb). Found: C, 92.80; H, 7.21%, MS *m/e* 336 (M^+). Calcd for $C_{26}H_{24}$: C, 92.81; H, 7.19%; M 336.

Careful column chromatography of the mother liquid of above recrystallization on silica gel with CCl_4 afforded pure *syn*-isomer **3** after the elution of *anti*-isomer. Recrystallization from ethanol gave colorless plates, mp 229—229.5 °C. NMR δ=2.80 (8H, m, CH_2), 3.60 (4H, m, CH_2), 6.93 (4H, s, H_a), 6.98 (4H, q, J=7.6, 2.0 Hz, H_c), and 7.12 (4H, q, J=7.6, 2.0 Hz, H_b). Found: *m/e* 336.18601. Calcd for $C_{26}H_{24}$: M, 336.18779.

Photoisomer ***13***. *anti*[3.3](1,4)Naphthalenophane **4** (1.6 mg) was dissolved in 5 ml of benzene in a Vycor tube. The solution was irradiated with a high pressure mercury lamp (400 W) for 2 h under a nitrogen atmosphere. Evaporation of the solvent gave colorless solid of photoisomer **13** in a quantitative yield. NMR δ=1.79 (4H, m, CH_2), 2.16 (4H, m, CH_2), 2.71 (4H, m, CH_2), 5.47 (4H, s, olefin), 7.16 (4H, q, J=6.1, 2.8 Hz, H_b), and 7.36 (4H, q, J=6.1, 2.8 Hz H_a). Found: *m/e* 336.18645. Calcd for $C_{26}H_{24}$: M 336.18779.

It melted at 130 °C, resolidified above the temperature, and remelted at the melting point of **4**. The regeneration of **4** was confirmed by heating **13** at 132 °C in DMSO for 20 min and also by irradiating **13** with a low pressure mercury lamp for 4 h under a nitrogen atmosphere.

References

1) Layered Compounds LX. Part LIX: T. Otsubo, M. Kitasawa, and S. Misumi, *Bull. Chem. Soc. Jpn.*, **52**, 1516 (1979).

2) H. H. Wasserman and P. M. Keehn, *J. Am. Chem. Soc.*, **91**, 2374 (1969) and references cited therein.

3) For a review of excimers, see Th. Förster, *Angew. Chem. Int. Ed. Engl.*, **8**, 333 (1969).

4) J. R. Froines and P. J. Hagerman, *Chem. Phys. Lett.*, **4**, 135 (1969).

5) The syntheses of **3** and **4** using malonic ester method and [4+4] photocycloaddition-thermal reconversion of intermediate tetraesters were recently reported; T. Kawabata, T. Shinmyozu, T. Inazu, and T. Yoshino, *Chem. Lett.*, **1979**, 315.

6) T. Otsubo, M. Kitasawa, and S. Misumi, *Chem. Lett.*, **1977**, 977; M. W. Haenel, A. Flatow, V. Taglieber, and H. A. Staab, *Tetrahedron Lett.*, **1977**, 1733; D. T. Longone, S. H. Küsefoglu, and J. A. Gladysz, *J. Org. Chem.*, **42**, 2787 (1977).

7) W. Ried and H. Bodem, *Chem. Ber.*, **91**, 1770 (1958).

8) A. Iwama, T. Toyoda, T. Otsubo, and S. Misumi, *Tetrahedron Lett.*, **1973**, 1725; A. Iwama, T. Toyoda, M. Yoshida, T. Otsubo, Y. Sakata, and S. Misumi, *Bull. Chem. Soc. Jpn.*, **51**, 2988 (1978).

9) H. H. Wasserman and P. M. Keehn, *J. Am. Chem. Soc.*, **89**, 2270 (1967).

10) G. Kaupp and I. Zimmermann, *Angew. Chem. Int. Ed. Engl.*, **15**, 441 (1976).

BULLETIN OF THE CHEMICAL SOCIETY OF JAPAN, VOL. 52 (12), 3761—3762 (1979)

Reaction of Nitrosodurene with Grignard Reagents

Masao Ōkubo* and Tomoko Takahashi

Department of Chemistry, Faculty of Science and Engineering, Saga University, Honjō-machi, Saga 840

(Received March 14, 1979)

Synopsis. Nitrosodurene was allowed to react with alkyl- and arylmagnesium halides and the reaction was followed by ESR. The spectrum of nitrosodurene anion radical was observed, the stability sequence of alkyl duryl nitroxides being discussed on the basis of the coupling constants of α-hydrogen atoms of alkyl groups.

Study on the reaction of nitrosobenzenes with Grignard reagents started early,[1,2] the formation of diphenyl nitroxide radical on the reaction with phenylmagnesium bromide (PhMgBr) being studied precisely by ESR, but no resolvable spectrum was obtained on the reaction with methyl- and ethylmagnesium bromide (MeMgBr and EtMgBr) even at lower temperatures.[3] On the other hand, the development of spin-trapping studies[4] shed light on nitrosodurene as an especially useful spin-trap because of its stability and also the simple ESR spectra of the corresponding nitroxide radicals.[5] We wish to report the results obtained on the Grignard reaction of nitrosodurene.

The reaction was carried out in tetrahydrofuran (THF). Since the solubility of nitrosodurene dimer in ordinary solvents is very low, the substrate had to be added as a suspension in THF. When the suspension was added to an equimolar solution of PhMgBr at 0 °C, almost all of the solid nitrosodurene remained undissolved. The reaction started when the mixture was warmed up to about 30 °C, the solid dissolving gradually giving reddish brown coloration. Dark brown crystalline needles (**1**) were obtained by quenching the reaction mixture with saturated aqueous NH_4Cl followed by extraction with diethyl ether and removal of the solvent: mp 96—98 °C after recrystallization from petroleum benzine. A dilute solution of **1** in THF gave an ESR spectrum consisting of a set of coupling constants agreeing with that of phenyl duryl nitroxide: a_N=9.93 G, $a_{o,p\text{-}H}$=2.76 G and $a_{m\text{-}H}$=0.90 G. However, the magnetic susceptibility measurement gave only a 51% free spin, and the IR spectrum showed a broad and strong ν_{OH} absorption band at 3240 cm^{-1}. Thus the crystalline product **1** was suggested to be a hydrogen-bonded dimeric nitroxide-hydroxylamine complex. This was confirmed by conversion of **1** into deep red "free" nitroxide (crude, mp 116—123 °C, 88% free spin) by oxidation with Ag_2O in anhydrous diethyl ether.[6]

The coupling constants obtained directly from the reaction mixture with *p*-fluoro- and *p*-methoxyphenylmagnesium bromides are given in Table 1. The spin coupling with the *p*-hydrogen atom of the duryl group is usually unresolvable. However, it was resolved in the case of *p*-methoxyphenyl duryl nitroxide. The radical concentration of this nitroxide increased much faster than that of the *p*-fluoro derivative, indicating that the electron-donating substituent facilitates the reaction.

In the reaction with alkyl Grignard reagents, easily analyzable ESR spectra were obtained at room temperature. The results are summarized in Table 2. Since the nitroxyl oxygen atom coordinates to the ^+MgBr species present in our reaction system, all the a_N values are smaller than those obtained in the cases of "free" nitroxides obtained photolytically.[5] The a_N value (9.93 G) of the molecular complex **1**, in which the nitroxyl oxygen atom coordinates to the hydrogen atom, is also smaller than that obtained previously (10.11 G[5]).

When an equimolar MeMgBr was allowed to react with nitrosodurene, the ESR-spectrum obtained at the initial stage of the reaction consisted of a broad triplet signal due to the nitrogen atom (a_N=12.69 G), the spectrum changing rapidly into a set of weak signals of methyl duryl nitroxide.[5] When six molar equivalents of MeMgBr were used, the signals disappeared much faster. Three molar equivalents proved to give the strongest signals of the nitroxide, which disappeared in *ca.* 1 h. The triplet signal observed at the initial stage of the reaction could be ascribed to the anion radical of nitrosodurene formed as the result of electron-transfer from the Grignard reagent.[7] A similar phenomenon was observed in the reaction with isopropylmagnesium bromide. A set of broad quintet was observed at the initial stage the spectrum changing rapidly into a set of doublets of triplet assignable to isopropyl duryl nitroxide. Since a quintet (1 : 2 : 3 : 2 : 1) signal is observable when a free spin is delocalized on two equivalent nitrogen atoms,[8] the quintet could be assigned to the dimeric anion radical illustrated below. The appreciably small a_N value (9.6 G) is compatible with the proposed structure **2**.

The correlation of the order of the value of $a_{\alpha\text{-}H}$

Table 1. Coupling constants of aryl duryl nitroxides formed on the reaction with ArMgBr

ArMgBr	a_N	a_F	$a_{o\text{-}H}$	$a_{m\text{-}H}$	$a_{p'\text{-}H}$
F-C$_6$H$_4$-MgBr	10.19	6.57	2.78	0.92	—
MeO-C$_6$H$_4$-MgBr	10.44	—	2.78	0.83	0.42

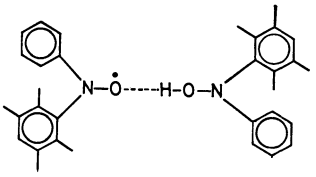

1

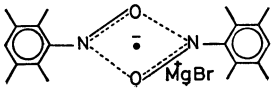

2

Table 2. Coupling constants of alkyl duryl nitroxides formed in the reaction with RMgX

RMgX	a_N	$a_{\alpha-H}$	Order of radical concn[a)]	a_N of "free" nitroxides[5)]
CH_3MgBr	13.60	12.08	3	13.70
$PhCH_2MgCl$	13.58	7.92	2	13.61
$(CH_3)_2CHMgBr$	13.58	6.69	1	13.72

a) One indicates the highest concentration observed.

with that of radical concentration (Table 2) is of interest. The largest $a_{\alpha-H}$ value for methyl duryl nitroxide is responsible for its instability due to decomposition probably involving hydrogen-abstraction. The medium $a_{\alpha-H}$ value for benzyl duryl nitroxide is unambiguously due to the spin-delocalization on the phenyl group giving fair stability to the nitroxide. The smallest $a_{\alpha-H}$ value for isopropyl duryl nitroxide seems to be due to the steric effect of the two α-methyl groups. Since the degree of spin-distribution on these methyl groups should be very low, the small $a_{\alpha-H}$ value can be understood by considering the direction of the orbital of free spin on the nitrogen atom to be not parallel with that of the C_α–H_α bond. The low value is in line with the great stability of the radical.

Nitrosodurene was found to be a useful spin-trap also in the reaction with Grignard reagents. The hindered nitrosobenzene made it possible to observe easily analyzable spectra of nitroxides as well as the initially formed anion radical. A similar steric hindrance effect was discussed in detail.[7)]

Experimental

Materials. Nitrosodurene was prepared by the method of Smith and Taylor[9)] through mercuriation of durene followed by nitrosation: mp 160 °C. For the Grignard reaction tetrahydrofuran was dried over sodium wire, distilled, and stored on sodium wire. For ESR measurements it was dried by sodium hydride, frozen, degassed repeatedly, and distilled in a solvent reservoir on a vacuum line containing Na–K alloy. *p*-Fluorobromobenzene was prepared from fluorobenzene[10)] (Daikin Industrial Co.). Commercial halogen compounds were used (reagent grade). Half molar stock solutions of Grignard reagents in THF were prepared and stored under, N_2.

Procedures for Measurements. The apparatus used for the measurements was constructed according to the method reported by Maruyama.[3)] Nitrosodurene (0.0136 g, 0.25 mmol) was weighed and introduced into a reaction vessel, 5 ml of THF being distilled into it from a solvent reservoir using vacuum line. Only a small portion of nitrosodurene went into the solution with weak green coloration. When the two reactants were mixed by breaking the seal, the color of the resultant mixture turned yellow or orange due to the formation of nitroxide radical accompanied by the dissolution of the solid nitrosodurene dimer. In order to obtain hyperfine structures, a small part of the reaction mixture transferred into the measurement cell was diluted by distilling the solvent from the reaction vessel.

The authors wish to thank Dr. Shuji Emori, Saga University, for the measurement of magnetic susceptibility.

References

1) H. Wieland and M. Offenbaecher, *Chem. Ber.*, **47**, 2111 (1914); H. Wieland and A. Roseeu, *ibid.*, **48**, 1117 (1915).
2) A. R. Forrester, J. M. Hay, and R. H. Thomson, "Organic Chemistry of Stable Free Radicals," Academic Press, London and New York (1968), Chap. 5.
3) K. Maruyama, *Bull. Chem. Soc. Jpn.*, **37**, 1013 (1964).
4) E. T. Janzen, *Acc. Chem. Res.*, **4**, 31 (1971).
5) S. Terabe, K. Kuruma, and R. Konaka, *J. Chem. Soc., Perkin Trans. 2*, **1973**, 1252.
6) I. A. Pearl, *Org. Synth.*, Coll. Vol. IV, 972 (1963).
7) M. Ōkubo, *Bull. Chem. Soc. Jpn.*, **48**, 2057 (1975); **50**, 2379 (1977), and literatures cited therein.
8) J. Q. Adams and J. R. Thomas, *J. Chem. Phys.*, **39**, 1904 (1963).
9) L. I. Smith and F. L. Taylor, *J. Am. Chem. Soc.*, **57**, 2370, 2460 (1935).
10) G. Olah, A. Pavlath, and G. Varsanyi, *J. Chem. Soc.*, **1957**, 1823.

BULLETIN OF THE CHEMICAL SOCIETY OF JAPAN, VOL. 52 (12), 3763—3764 (1979)

The Preparation of *N*-Benzyl-α-ethoxycarbonylnitrone and Its Reactions with Some Olefins

Yoshinobu INOUYE,* Yuko WATANABE, Satoru TAKAHASHI, and Hiroshi KAKISAWA

Department of Chemistry, The University of Tsukuba, Sakura-mura, Niihari-gun, Ibaraki 305

(Received June 11, 1979)

Synopsis. *N*-Benzyl-α-ethoxycarbonylnitrone (**1**) was prepared from ethyl glyoxylate and *N*-benzylhydroxylamine. The reactions of **1** with isobutylene, methyl acrylate, and methyl crotonate are described.

In the course of our synthetic studies of the hydroxy amino acid moiety *via* 1,3-dipolar cycloaddition,[1,2] *N*-benzyl-α-alkoxycarbonylnitrone (*e.g.*, **1**) was expected to be a suitable 1,3-dipole, especially for the preparation of the γ-hydroxy α-amino acid.

The removal of the benzyl group and the fission of the N–O bond in the adduct, **a**, would be attained simultaneously under such conditions of catalytic hydrogenolysis, and the stereochemistry of the product, **b**, would directly reflect the regio- and stereospecificities in the 1,3-dipolar cycloaddition of the nitrone.[3]

A hitherto unknown nitrone, **1**, was prepared by the condensation of ethyl glyoxylate and *N*-benzylhydroxylamine in the presence of calcium chloride.[4] **1** crystallized easily, but it was found to be a mixture of *Z*(**1a**) and *E*(**1b**) isomers (*Z*: *E*=1: 2), as is shown in its NMR spectrum. The two singlets at 5.69 and 4.96 are assignable to the methylene protons at the benzylic position in **1b** and **1a** respectively. The difference in chemical shift can be explained by the effect of the neighboring ester group. The ratio depends slightly on the reaction and/or recrystallization conditions.

When the nitrone **1**(*Z*: *E*=1: 2) and isobutylene in benzene were heated at 80 °C for 3 d, only a single adduct was isolated by distillation. The structure of the adduct was characterized as 2-benzyl-5,5-dimethyl-3-ethoxycarbonylisoxazolidine (**2**) from its spectroscopic properties and its conversion to the known[5] γ-hydroxyleucine lactone hydrochloride (**3**) by hydrogenolysis over $Pd(OH)_2$.[6]

The reaction of the nitrone **1** (*Z*: *E*=1: 2) with methyl acrylate proceeded at room temperature, and two adducts, **4** and **5** (**4**: **5**=4: 1), were isolated in 84% yield. Two pairs of doublets, at 4.68 and 3.78, in the NMR spectrum of **4**, and similar pairs at 4.65 and 3.61 in **5**, reveal the substitution pattern on the isoxazolidine ring in both **4** and **5** to be a 2,3,5-trisubstituted one. The stereochemistry of **4**, assumed to be *trans* from the pseudocontact shift with $Eu(fod)_3$ (see Experimental), was confirmed by subjecting **4** to catalytic hydrogenolysis over $Pd(OH)_2$, followed by hydrolysis with 6 M (1 M=1 mol dm^{-3}) hydrochloric acid. In the amino acid chromatogram[7] of the products, almost all (>94%) of the γ-hydroxyglutamic acids and their lactones were recognized as having the *threo*-configuration.

Among the various dipolarophiles reported, the cycloadducts from the crotonic ester have been shown to have a "reverse" regioselectivity.[8] This was observed also in the present case. The mixture of **1** (*Z*: *E*=1: 3.5) and methyl crotonate was allowed to stand at room temperature to give **6** and **7** (4.4: 1) in 83% yield. The arrangement of substituents and the stereochemistry of **6** and **7** were assumed from the analyses of the NMR spectra. Of the three protons on the isoxazolidine ring, H^5 is the most downfield in both **6** (δ at 4.40) and **7** (δ at 4.56) and is assignable to the partial structure –O–C**H**^{5}(CH_3)–CH– on the basis of the chemical shifts and multiplicities. The differences in the chemical shifts of H^3 (Δ 0.35) and H^4 (Δ 0.40) of **7** as compared with those of **6** are attributable to a deshielding effect of the neighboring ester group, which is *cis* to the protons in question in the case of **7**. The two ester groups, thus, can be arranged *cis* to each other in **6** and *trans* in **7**. The *trans* relationship between C_4 and C_5 was assumed from the reaction mechanism.[9]

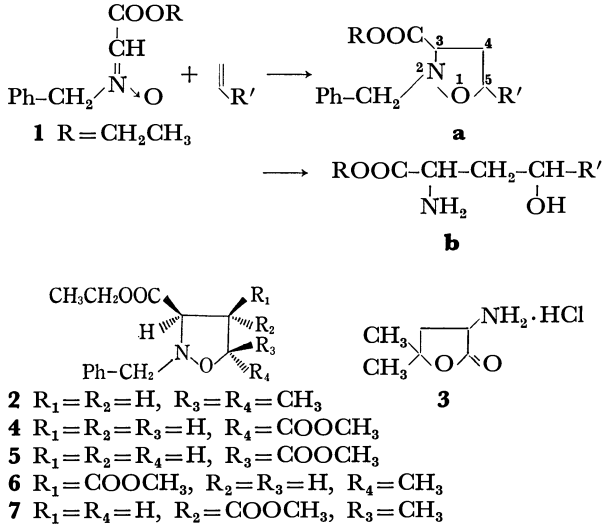

Experimental

All the melting points are uncorrected. The IR spectra were recorded on a Hitachi 215 grating spectrophotometer, and the NMR spectra were obtained on a Hitachi H-60 and a JEOL MH-100 spectrophotometers, using TMS as an internal standard.

N-Benzyl-α-ethoxycarbonylnitrone (1). To an ice-cooled mixture of 5.3 g of *N*-benzylhydroxylamine and 1.5 g of calcium chloride in 40 ml of ether,[4] 4.5 g of ethyl glyoxylate was added dropwise, after which the whole was stirred at 0 °C for 1 h. The solids were removed by filtration through an anhydrous sodium sulfate layer, and the filtrate was evaporated to give crystalline **1** (7.8 g, 88%). Two recrystallizations from benzene afforded an analytical sample of **1**: mp 84.0—86.5 °C; ν(KBr): 1720, 1560, 1200 br, 1045, 965, 825, and 700 cm^{-1}; δ ($CDCl_3$): 7.4 (m, 5H), 7.17 (**1b**)

and 7.09 (**1a**) (s, 1H), 5.69 (**1b**) and 4.96 (**1a**) (s, 2H), 4.25 (**1b**) and 4.22 (**1a**) (q, 2H, J=7 Hz), and 1.30 (**1b**) and 1.27 (**1a**) (t, 3H, J=7 Hz). Found: C, 63.93; H, 6.31; N, 6.82%. Calcd for $C_{11}H_{13}NO_3$: C, 63.75; H, 6.32; N, 6.76%. The ratio of Z(**1a**) and E(**1b**) was calculated as 1:2 from the peak areas of the benzylic methylene signals. The ratio changed between 1:2 and 1:3.5 according to the difference in preparation and/or recrystallization, but attempts at the separation of each isomer were unsuccessful, and so the mixture of a known ratio was used in the subsequent reactions.

2-Benzyl-5,5-dimethyl-3-ethoxycarbonylisoxazolidine (2). A mixture of 535 mg of **1**(Z: E=1:2), 3.1 g of isobutylene, and 12 ml of benzene in a sealed tube was heated at 80 °C for 3 d. The subsequent evaporation of the solvent gave **2**(630 mg). An analytical sample was obtained by Kugelrohr distillation (bath temp: 144—145 °C/2 mmHg). ν($CHCl_3$): 1730, 1600, 1375, and 1365 cm^{-1}; δ ($CDCl_3$): 7.3 (m, 5H), 4.07 (s, 2H), 4.07 (q, 2H, J=7 Hz), 3.52 (dd, 1H, J=7.5 and 9.5 Hz, C part of ABC), 2.3 (m, 2H, AB part of ABC), 1.38 (s, 3H), 1.30 (s, 3H), and 1.21 (t, 3H, J=7 Hz). Found: C, 68.39; H, 7.97: N, 5.40%. Calcd for $C_{15}H_{21}NO_3$: C, 68.41; H 8.03; N, 5.31%.

γ-Hydroxyleucine Lactone Hydrochloride (3). A mixture of 188 mg of **2**, 90 mg of $Pd(OH)_2$,[6] and 40 ml of methanol was shaken under a hydrogen atmosphere (3 atm) for 3 d. After the removal of catalysts by filtration, the filtrate was concentrated to give an oily solid (118 mg); ν($CHCl_3$): 1760 cm^{-1}. A part of the oily solid was dissolved in ethanol, and 1.1 eq of hydrochloric acid was added. The whole was left in a desiccator *in vacuo* to give **3**: mp 206—207 °C (from ethanol); the IR spectrum (KBr disk: 3500—2400 br, 1765, 1575, and 1490 cm^{-1}) of **3** was coincident with that of the authentic γ-hydroxyleucine lactone hydrochloride (mp 208—209 °C).[5]

trans-2-Benzyl-3-ethoxycarbonyl-5-methoxycarbonylisoxazolidine (4) and cis-2-Benzyl-3-ethoxycarbonyl-5-methoxycarbonylisoxazolidine (5). A solution of 200 mg of the nitrone **1**(Z: E=1:2) and 175 mg of methyl acrylate in 3 ml of benzene was stirred at room temperature for 36 h. The subsequent evaporation of the solvent gave an oil (285 mg), which showed three spots on TLC (Merk silica gel 60, 0.25 mm; hexane–ethyl acetate =3:1). The oil was chromatographed on silica gel (30 g) with benzene–ethyl acetate (100:2) to give an unidentified compound (R_f=0.30, 6 mg), 158 mg of **4**(R_f=0.22), 55 mg of a mixture of **4** and **5**(2:1), and 27 mg of **5**(R_f=0.17). Analytical samples were prepared by a flash chromatography[10] (hexane–ethyl acetate=3:1), followed by Kugelrohr distillation.

4: Bath temp 131—134 °C/0.08 mmHg; ν (CCl_4): 1755 sh, 1735, and 1190 cm^{-1}; δ ($CDCl_3$, 100 MHz; Δ values show the pseudocontact shifts upon the addition of 0.8 eq of Eu(fod)$_3$): 7.3 (m, 5H), 4.68 (dd, 1H, J=6 and 8 Hz, Δ 0.18), 4.16 (AB center, 2H, J=13 Hz, Δ 0.52), 4.14 (q, 2H, J=7 Hz, Δ 0.02), 3.78 (dd, 1H, J=6 and 8 Hz, Δ 0.66), 3.76 (s, 3H, Δ 0.06), 2.92 (ddd, 1H, J=8, 6 and 14 Hz, Δ 0.38), 2.68 (ddd, 1H, J=6, 8, and 14 Hz, Δ 0.48), and 1.24 (t, 3H, J=7 Hz, Δ 0.00). Found: C, 61.29; H, 6.47; N, 4.92%. Calcd for $C_{15}H_{19}NO_5$: C, 61.42; H, 6.52; N, 4.77%.

5: Bath temp 140—145 °C/0.1 mmHg; ν (CCl_4): 1769 sh, 1730, and 1190 cm^{-1}; δ ($CDCl_3$, 100 MHz): 7.4 (m, 5H), 4.65 (dd, 1H, J=5.5 and 8.5 Hz), 4.15 (q, 2H, J=7 Hz), 4.15 (s, 2H), 3.77 (s, 3H), 3.61 (dd, 1H, J=6 and 8 Hz), 2.6—3.1 (m, 2H), and 1.24 (t, 3H, J=7 Hz). Found: C, 61.55; H, 6.50; N, 5.08%. Calcd for $C_{15}H_{19}NO_5$: C, 61.42; H, 6.52; N, 4.77%.

Amino Acid Analysis.[7] A solution of 364 mg of **4** in 50 ml of methanol was hydrogenolyzed over 100 mg of $Pd(OH)_2$ under a hydrogen atmosphere (3 atm) for 2 d. After the catalysts had then been removed, the filtrate was concentrated to give an oil. The oil was refluxed for 4 h with 20 ml of 6 M hydrochloric acid. After decolorizing with activated carbon, the solution was concentrated to give crystals (234 mg). The amino acid chromatogram of the crystals showed the presence[2] of *threo*-γ-hydroxyglutamic acid (0.270 mmol), *erythro*-γ-hydroxyglutamic acid (0.023 mmol), and *threo*-γ-hydroxyglutamic acid lactone (0.113 mmol).

2-Benzyl-r-3-ethoxycarbonyl-c-4-methoxycarbonyl-t-5-methylisoxazolidine (6) and 2-Benzyl-r-3-ethoxycarbonyl-t-4-methoxycarbonyl-c-5-methylisoxazolidine (7). A mixture of 205 mg of the nitrone **1** (Z: E=1:3.5), 198 mg of methyl crotonate, and 5 ml of benzene was stirred at room temperature for 3 d. The subsequent removal of the solvent gave an oil containing some crystals. VPC analysis (5% OV-1, 1.7 m, 180 °C) showed that two components of R_t=6 min and R_t=7 min were present in the product. They were separated by column chromatography on silica gel (33 g). Elution with benzene–ethyl acetate (98:2) afforded 47 mg of **7** (R_t=6 min) and 206 mg of **6** (R_t=7 min).

6: Mp 41.5—42.5 °C (from pentane); ν ($CHCl_3$): 1735 cm^{-1}; δ ($CDCl_2$, 100 MHz): 7.3 (m, 5H), 4.40 (dq, 1H, J=8 and 6 Hz), 4.14 (q, 2H, J=6 Hz), 4.10 (AB center, 2H, J=14 Hz), 3.78 (d, 1H, J=8 Hz), 3.66 (s, 3H), 3.12 (t, 1H, J=8 Hz), 1.36 (d, 3H, J=6 Hz), and 1.22 (t, 3H, J=6 Hz). Found: C, 62.43; H, 6.72; N, 4.50%. Calcd for $C_{16}H_{21}NO_5$: C, 62.52; H, 6.88; N, 4.55%.

7: Liquid, bath temp 105—109 °C/0.09 mmHg; ν($CHCl_3$): 1735 cm^{-1}; δ ($CDCl_3$, 100 MHz): 7.4 (m, 5H), 4.56 (quint, 1H, J=6 Hz), 4.18 (q, 2H, J=7 Hz), 4.14 (s, 2H), 4.13 (d, 1H, J=8 Hz), 3.79 (s, 3H), 3.52 (dd, 1H, J=6 and 8 Hz), 1.44 (d, 3H, J=6 Hz), and 1.24 (t, 3H, J=7 Hz). Found: C, 62.92; H, 6.94; N, 4.56%. Calcd for $C_{16}H_{21}NO_5$: C, 62.52; H, 6.88; N, 4.55%.

We are deeply indebted to Dr. Minoru Tamura, The University of Tsukuba, for his measurements of the amino acid chromatograms.

References

1) H. Sato, T. Kusumi, K. Imae, and H. Kakisawa, *Bull. Chem. Soc. Jpn.*, **49**, 2815 (1976).

2) T. Kusumi, H. Kakisawa, S. Suzuki, K. Harada, and C. Kashima, *Bull. Chem. Soc. Jpn.*, **51**, 1261 (1978).

3) For a recent review, see D. St. C. Black, R. F. Crozier, and V. C. Davis, *Synthesis*, **1975**, 205, and the references cited therein.

4) G. E. Utzinger and F. A. Regenass, *Helv. Chim. Acta*, **37**, 1892 (1954).

5) J. Fillman and N. Albertson, *J. Am. Chem. Soc.*, **70**, 171 (1948).

6) R. G. Hiskey and R. C. Northrop, *J. Am. Chem. Soc.*, **83**, 4798 (1961).

7) The amino acid chromatograms were taken on a Yanagimoto amino acid analyzer LC-5S. For the conditions, see Ref. 2.

8) a) B. G. Murray and A. F. Turner, *J. Chem. Soc., C*, **1966**, 1338; b) R. Huisgen, H. Hauk, R. Grashey, and H. Seidl, *Chem. Ber.*, **101**, 2568 (1968).

9) R. Huisgen, *J. Org. Chem.*, **41**, 403 (1976).

10) W. C. Still, M. Kahn, and A. Mitra, *J. Org. Chem.*, **43**, 2923 (1978).

BULLETIN OF THE CHEMICAL SOCIETY OF JAPAN, VOL. 52 (12), 3765—3766 (1979)

Synthesis of 2,5-Diphenylbicyclo[4.2.0]octa-2,4-diene. Exclusive Existence in the Bicyclic Form and a Correction of the Reported Structure of 2,5-Diphenyl-1,3,5-cyclooctatriene

Masaji ODA* and Yoshinori KANAO

Department of Chemistry, Faculty of Science, Tohoku University, Sendai 980

(Received June 14, 1979)

Synopsis. 2,5-Diphenylbicyclo[4.2.0]octa-2,4-diene has been found to exist exclusively in the bicyclic form, giving rise to questioning the reported structure of 2,5-diphenyl-1,3,5-cyclooctatriene. The structure of 1,4-diphenyl-1,3,6-cyclooctatriene is proposed for the compound.

Courtot and Rumin reported that reduction of the dimesylate of *cis*-5,6-bis(hydroxymethyl)-1,4-diphenyl-1,3-cyclohexadiene (**1**) with lithium aluminum hydride gives 2,5-diphenyl-1,3,5-cyclooctatriene (**2**) along with 5,6-dimethyl-1,4-diphenyl-1,3-cyclohexadiene (**3**) and 1,4-diphenyl-5-methylbicyclo[4.1.0]hept-3-ene (**4**).[1]

In the course of studies on unsaturated eight-membered ring compounds, we prepared 2,5-diphenylbicyclo[4.2.0]octa-2,4-diene (**5**), a valence isomer of **2**, and found that compound **5** exclusively exists in the bicyclic form at room temperature to 100 °C. This gave rise to questioning the reported structure of **2**. A reasonable alternative structure for the compound of Courtot and Rumin seems to be 1,4-diphenyl-1,3,6-cyclooctatriene (**6**) for several reasons.

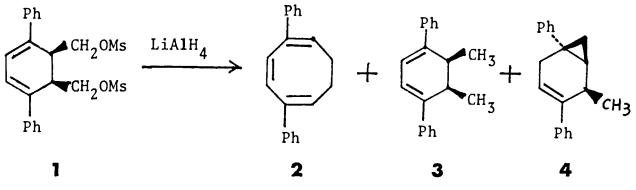

1 2 3 4

Scheme 1.

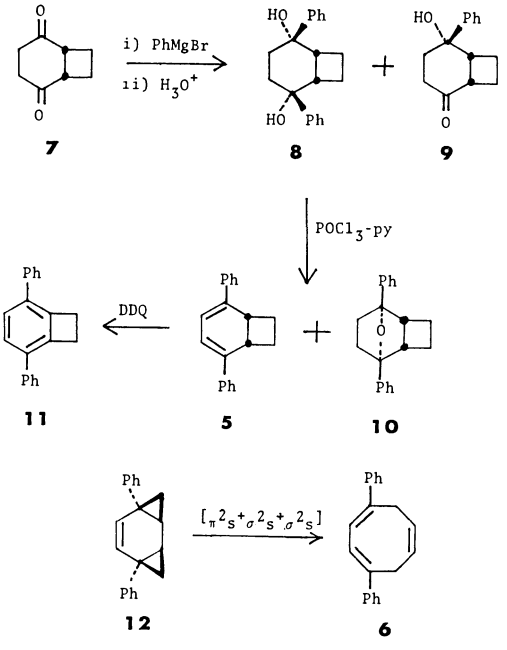

7 8 9 11 5 10 12 6

Scheme 2.

Reaction of bicyclo[4.2.0]octane-2,5-dione (**7**)[2] with phenylmagnesium bromide (five equivalents) gave 2,5-diphenylbicyclo[4.2.0]octane-*r*-2,*c*-5-diol (**8**) and 5-hydroxy-5-phenylbicyclo[4.2.0]octan-2-one (**9**). The stereochemistry of these compounds was assigned from a steric point of view. Dehydration of **8** with phosphoryl chloride in pyridine gave **5** and 1,6-diphenyl-9-oxatricyclo[4.2.1.$0^{2,5}$]nonane (**10**).

The ^{1}H-NMR spectrum of **5** (CCl_4) exhibits signals at δ 2.3—2.8 (4H, m, H-7,8), 3.92 (2H, m, H-1,6), 6.38 (2H, s, H-3,4), and 7.0—7.5 (10H, m, aromatic protons), in line with the bicyclic structure. The spectrum did not change even after heating the solution at 100 °C for 4 h. Treatment of **5** with 2,3-dichloro-5,6-dicyano-*p*-benzoquinone readily gave 2,5-diphenylbicyclo[4.2.0]-octa-1,3,5-triene (**11**).

The results indicate that between the bicyclic structure (**5**) and the ring-opened structure (**2**), the former is thermodynamically favorable. Thus, the reported structure of **2** is questionable. The reasonable structure of Courtot's compound is probably 1,4-diphenyl-1,3,6-cyclooctatriene (**6**) for the following reasons: (i) The methylene protons of **2** appear at δ 3.20 in the ^{1}H-NMR spectrum. The chemical shift is 0.77 ppm lower than that of 1,3,5-cyclooctatriene itself (δ 2.43),[3] being nearer to that of 1,3,6-cyclooctatriene (δ 2.70).[4] In structure **6**, the phenyl group would exert relatively large down-field anisotropy effect on the adjacent methylene protons, whereas, in structure **2**, no such large effect is expected. (ii) Similar reduction of the *trans* isomer of **1** was reported to give a *trans*-bis-σ-homobenzene derivative as the main product.[1] Therefore, it would be highly probable that Courtot's compound was obtained from the *cis*-bis-σ-homobenzene derivative (**12**) by $[\pi 2_s+\sigma 2_s+\sigma 2_s]$ cycloreversion. *cis*-Bis-σ-homobenzenes have been reported to undergo cycloreversion readily.[5]

The reason for compound **5** exclusively existing in the bicyclic form should be noted. 1,3,5-Cyclooctatriene itself is at equilibrium with bicyclo[4.2.0]octa-2,4-diene with free energy difference of only 1.1 kcal mol^{-1} (89.2: 10.8 at 60 °C).[6] The ratio is largely affected by introduction of substituents.[6,7] Since the cyclohexadiene moiety of **5** should be almost planar, the gain of conjugative energy by the introduction of the phenyl groups at C-2 and -5 might be sufficient to favor the bicyclic form. Such an effect by phenyl has also been observed in cycloheptatriene-norcaradiene equilibrium.[8]

Experimental

Melting points were determined with a Thomas-Hoover apparatus and are uncorrected. IR, UV, and ^{1}H-NMR spectra were recorded with a Hitachi 215, a Hitachi 323, and a JEOL PMX 60 spectrometer, respectively. Microanalyses were performed at the Microanalytical Laboratory in this department.

Reaction of Bicyclo[4.2.0]octane-2,5-dione (7) with Phenylmagnesium Bromide. An ethereal solution (20 ml) of **7** (1.38 g, 10 mmol) was added dropwise at room temperature over a period of 15 mın to an ethereal solution (*ca.* 100 ml) of phenylmagnesium bromide prepared from bromobenzene (7.85 g, 50 mmol) and magnesium (1.21 g, 50.4 mmol).[9] Dry tetrahydrofuran (150 ml) was added and the mixture was stirred under nitrogen for 16 h. 1 M Sulfuric acid (20 ml) and then water (200 ml) was added. The products were extracted ethyl acetate (2×50 ml). The extracts were washed with water, and brine, and dried over $MgSO_4$. After removal of the solvent the residue was chromatographed on silica gel. Elution with dichloromethane gave, in the order of elution, 2,5-diphenylbicyclo[4.2.0]octane-*r*-2,*c*-5-diol (**8**) (0.640 g, 20.5 %) and 5-hydroxy-5-phenylbicyclo[4.2.0]octan-2-one (**9**) (1.18 g, 54.6%). (**8**): colorless crystals from benzene–dichloromethane; mp 140—142 °C; IR (KBr) ν 3300, 1498, 1453, 1006, 753, 703 cm^{-1}; ^{1}H-NMR ($CDCl_3$) δ 1.9—2.4 (8H, m), 3.03 (2H, m), 3.57 (2H, s, OH), 7.2—7.6 (10H, m). Found: C, 81.69; H, 7.78%. Calcd for $C_{20}H_{22}O_2$: C, 81.60; H, 7.53%. (**9**): colorless crystals from benzene–dichloromethane; mp 162—162.5 °C; IR (KBr) ν 3350, 1695, 967, 752, 698 cm^{-1}; ^{1}H-NMR ($CDCl_3$) δ 1.9—2.7 (8H, m), 3.0—3.5 (2H, m), 7.2—7.5 (5H, m). Found: C, 77.71; H, 7.65%. Calcd for $C_{14}H_{16}O_2$: C, 77.75; H, 7.46%.

Dehydration of the Diol (8). A solution of the diol (**8**) (318 mg, 1.08 mmol) and phosphoryl chloride (1.67 g, 11 mmol) in pyridine (5 ml) was heated under nitrogen at 50 °C for 3.5 h. The cooled mixture was poured into cold 6 M hydrochloric acid (15 ml) and extracted with benzene (2× 20 ml). The extracts were washed with water and dried. The solvent was removed and the residue was chromatographed on silica gel. Elution with benzene–hexane gave, in the order of elution, 2,5-diphenyl-bicyclo[4.2.0]octa-2,4-diene (**5**) (120 mg, 43%) and 1,6-diphenyl-9-oxatricyclo[4.2.1.0^{2,5}]-nonane (**10**) (45.6 mg, 15%). (**5**): yellow needles from ethanol–dichloromethane; mp 131—133 °C; IR (KBr) ν 1590, 1546, 1495, 1450, 850, 765, 745, 684 cm^{-1}; UV (cyclohexane) λ 233 (log ε 4.06), 358 (4.36), 366 nm (sh. 4.34). Found: C, 92.84; H, 7.32%. Calcd for $C_{20}H_{18}$: C, 92.98; H, 7.02%, (**10**): colorless crystals from hexane; mp 83—84 °C; IR (KBr) ν 1600, 1010, 967, 754, 700 cm^{-1}; ^{1}H-NMR (CCl_4) δ 1.5—1.9 (4H, m), 1.97 (4H, s), 2.97 (2H, m), 7.0—7.5 (10H, m). Found: C, 86.81; H, 7.38%. Calcd for $C_{20}H_{20}O$: C, 86.92; H, 7.29%.

Dehydrogenation of the Diene (5). A mixture of the diene (**5**) (30.3 mg, 0.117 mmol) and 2,3-dichloro-5,6-dicyano-*p*-benzoquinone (28.3 mg, 0.124 mmol) in benzene (2 ml) was stirred at room temperature for 40 h. Filtration gave 2,3-dichloro-5,6-dicyanohydroquinone (22.5 mg). The filtrate was chromatographed on silica gel, eluted with benzene, to give 2,5-diphenylbicyclo[4.2.0]octa-1,3,5-triene (**11**) (17.7 mg. 59%); colorless crystals from hexane–dichloromethane; mp 182—183 °C; IR (KBr) ν 3050, 1590, 1472, 1451, 1067, 1021, 777, 759, 752 cm^{-1}; UV (cyclohexane) λ 289.5 nm (log ε 4.47); ^{1}H-NMR ($CDCl_3$) δ 3.45 (4H, s), 7.2—7.8 (12H, m). Found: C, 93.43; H, 6.48%. Calcd for $C_{20}H_{16}$: C, 93.71; H, 6.29%.

References

1) P. Courtot and R. Rumin, *Bull. Soc. Chim. Fr.*, **1972**, 3479.

2) M. Oda, H. Oikawa, Y. Kanao, and A. Yamamuro, *Tetrahedron Lett.*, **1978**, 4905.

3) M. St-Jacques and R. Prudhomme, *Tetrahedron Lett.*, **1970**, 4833.

4) Measured in our laboratory.

5) a) G. Kaupp and K. Rosch, *Angew. Chem. Int. Ed. Engl*, **15**, 163 (1976); b) H. Prinzbach, D. Stusche, J. Markert, and H. H. Limbach, *Chem. Ber.*, **109**, 3505 (1976).

6) R. Huisgen, G. Boche, A. Dahmen, and W. Hechtl, *Tetrahedron Lett.*, **1968**, 5215.

7) E. Vogel, U. Roos, and K-H. Disch, *Justus Liebigs Ann. Chem.*, **653**, 55 (1962).

8) T. Mukai, K. Kubota, and T. Toda, *Tetrahedron Lett.*, **1967**, 5215.

9) An appreciable amount of white solids separated out, hindering completion of the reaction.

BULLETIN OF THE CHEMICAL SOCIETY OF JAPAN, VOL. 52 (12), 3767—3768 (1979)

The Reaction of 2,4,6-Triphenyl-1,3-thiazinylium Perchlorate with Active Methylenes

Isao SHIBUYA

National Chemical Laboratory for Industry (Tsukuba Research Center), Yatabe, Ibaraki 305

(Received June 18, 1979)

Synopsis. The reaction of 2,4,6-triphenyl-1,3-thiazinylium perchlorate (**4**) with several active methylenes was studied. Methyl cyanoacetate or benzoylacetonitrile reacted with **4** to give 3-cyano-2,4,6-triphenylpyridine, while malononitrile led to 1-mercapto-1,3-diphenyl-4,4-dicyanobutadiene and cyanoacetamide led to 2-hydroxy-3-cyano-4,6-diphenylpyridine. The reaction of diethyl malonate, nitromethane, or nitroethane with **4** gave 2-[bis(ethoxycarbonyl)methyl]-, 2-nitromethyl-, or 2-(1-nitroethyl)-2,4,6-triphenyl-2*H*-1,3-thiazine respectively. These results showed that the reaction manner of **4** to these active methylenes is significantly different from that of 2,4,6-triphenyl-1,3-oxazinylium salt.

Concerning the reaction of 2,4,6-triphenylpyrylium salt (**1**) and its S-analog, 2,4,6-triphenylthiopyrylium salt (**2**), with active methylenes, **1** and **2** usually lead to the same products, 1-substituted 2,4,6-triphenylbenzenes; however, with malononitrile and nitromethane **1** and **2** lead to different products.[1,2] This fact suggested that the reactivities of **1** and **2** are slightly different from each other. The reaction of 2,4,6-triphenyl-1,3-oxazinylium perchlorate (**3**) with active methylenes gives various pyridine derivatives *via* butadienes as intermediates;[3,4] however, the reactivity of the S-analog of **3**, 2,4,6-triphenyl-1,3-thiazinylium perchlorate (**4**) has not yet been investigated. In this study, the reaction of **4** with several active methylenes was examined, and the reactivity of **4** was compared with those of **1**, **2**, or **3**.

Results and Discussion

On treatment with methyl cyanoacetate, **1** or **2** leads to 2,4,6-triphenylbenzonitrile (**5**),[1,2] while **3** gives 2-benzoylamino-3-methoxycarbonyl-4,6-diphenylpyridine.[3] When **4** was refluxed with this reagent in MeOH–MeONa, 3-cyano-2,4,6-triphenylpyridine (**6**) was given in a good yield. **6** is the N-analog of **5**; consequently, the behavior of **4** in response to this reagent is different from that of **3**, but similar to that of **1** or **2**. Two courses may be supposed for this reaction, as is shown in Scheme 1 (R=$COOCH_3$).

On treatment with benzoylacetonitrile, **1** and **2** also give **5**. On the other hand, it has been shown that **3** with this reagent undergoes the reaction of Scheme 2 and leads to **6′** (Ar=Ph).[4] The reaction of **4** with this reagent also gave **6**. This indicates at least three courses in Scheme 1 (R=Ph) and Scheme 2 (Ar=Ph). In order to check the course, **4** was treated with *p*-chlorobenzoylacetonitrile, and the resulting product was identified as **6**. The reaction course in Scheme 2 was, thus, obviated, and one of the two ways of Scheme 1 was suggested to be the reaction course. Therefore, **4** is different from **3** in its behavior in reaction to this reagent.

Cyanoacetamide leads to **5** on treatment with **1** or **2**. The reaction of **3** with this reagent gives 2-hydroxy-3-cyano-4,6-diphenylpyridine (**7**).[4] On the other hand, treatment with **4** resulted in **7**; for this reaction, the two courses may also be supposed. It is, however, difficult to study their reaction courses more closely because the reactions of these three reagents with **4** proceed very readily without the isolation of their intermediates.

Malononitrile behaves quite differently in response to **1**, **2**, or **3** to give different products.[1-3] The reaction of **4** with this reagent gave **8**, with a small amount of **6**. The reaction course for **6** was supposed to be as is shown

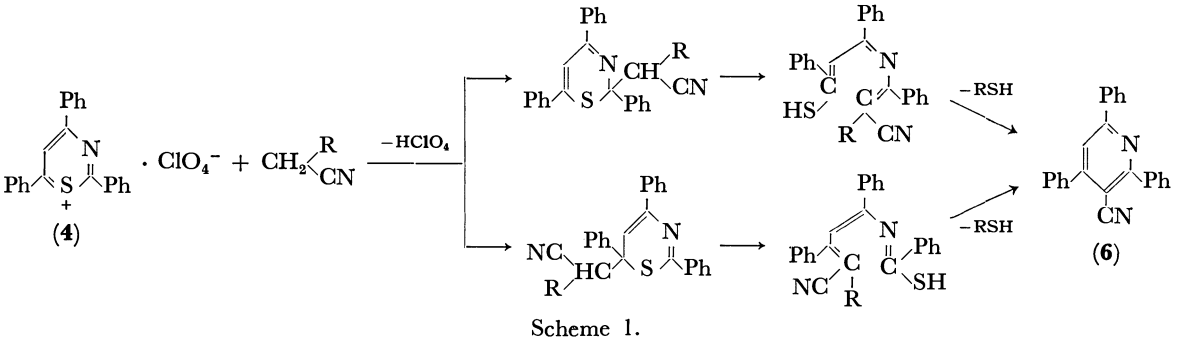

Scheme 1.

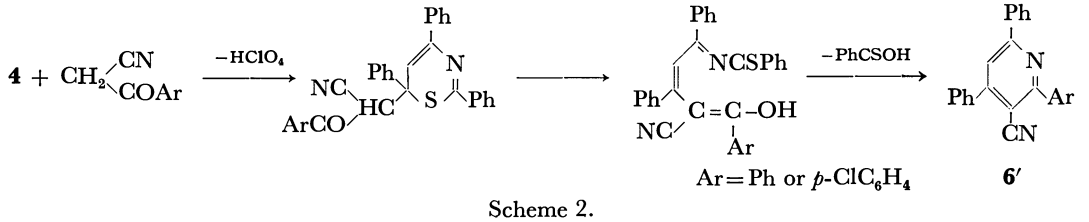

Scheme 2.

in Scheme 1 (R=CN), while **8** was identified as 1-mercapto-1,3-diphenyl-4,4-dicyanobutadiene, which is given on the treatment of 3,5-diphenyl-1,2-dithiolylium salt with this reagent;[5] it was found that this reaction mode was unique, as is shown in Scheme 3.

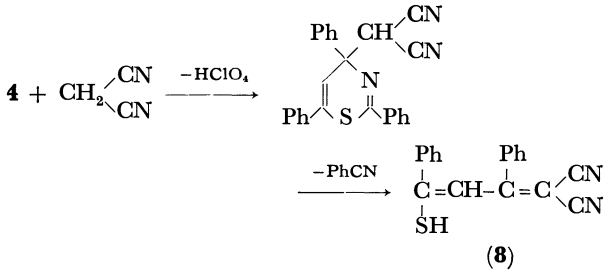

Scheme 3.

Diethyl malonate, nitromethane, and nitroethane reacted with **4** in dioxane-triethylamine to afford **9**, **10**, and **11** respectively. Their analytical data and the molecular weights by MS spectrometry showed that they were adducts of the 1,3-thiazinylium cation and the carbanion of active methylenes. Since their IR spectra had no absorption assigned to N–H and S–H stretching, it was suggested that these products were not chain compounds. The UV spectra were closely similar to each other (λ_{max}=244 nm, ε=25800—27600); consequently, they were thought to have the same skeletal structure. According to their CMR spectra, which was checked by means of the ^{1}H-off-resonance method, **9**, **10**, and **11** were confirmed to be 2-[bis(ethoxycarbonyl)methyl]-, 2-nitromethyl-, and 2-(1-nitroethyl)-2,4,6-triphenyl-2*H*-1,3-thiazine respectively.

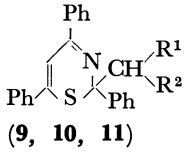

(**9**, **10**, **11**)

9: R^1=$COOC_2H_5$, R^2=$COOC_2H_5$
10: R^1=H, R^2=NO_2
11: R^1=CH_3, R^2=NO_2

The reaction of **4** with other active methylenes, such as dibenzoylmethane, ethyl benzoylacetate, benzoylacetamide, and ethyl carbamoylacetate, gave no product.

Hence, it is proved that **4** is less active than **3** against several active methylenes, and that the reaction manners of **3** and **4** are significantly different from each other.

Experimental

3-Cyano-2,4,6-triphenylpyridine (6). Into a solution of 3 mmol of methyl cyanoacetate, benzoylacetonitrile, or *p*-chlorobenzoylacetonitrile in 4 ml of 1.0 mol dm^{-3} MeOH–MeONa, 0.86 g (2 mmol) of **4** was stirred at room temperature for 10 min, and then the mixture was refluxed for 1 h. The reaction mixture was poured into dilute hydrochloric acid. The resulting precipitate was collected by filtration and recrystallized from acetic acid to give 0.54 g (81%), 0.58 g (87%), or 0.39 g (59%) of **6** (mp=225.3 °C) respectively. The IR spectrum of **6** was completely superimposed on that of an authentic sample.[4]

2-Hydroxy-3-cyano-4,6-diphenylpyridine (7). Cyanoacetamide was treated with **4** by the procedure described above. The resulting precipitate was purified by reprecipitation from aqueous sodium hydroxide–hydrochloric acid to give 0.39 g (72%) of **7** (mp>300 °C). The IR spectrum of **7** agreed with that of an authentic sample.[3]

1-Mercapto-1,3-diphenyl-4,4-dicyanobutadiene (8). Into a solution of 0.20 g (3 mmol) of malononitrile in 4 ml of 1.0 mol dm^{-3} MeOH–MeONa, 0.86 g (2 mmol) of **4** was stirred at room temperature for 10 min, and then the mixture was refluxed for 1 h. The reaction mixture was allowed to stand overnight and then filtered to separate the resulting crystalline (0.12 g, 18%) of **6**. The filtrate was poured into dilute hydrochloric acid, and the resulting precipitate was recrystallized from acetonitrile to give 0.34 g (59%) of **8** (mp=225.5 °C).[5] Found: S, 11.09%. Calcd for $C_{18}H_{12}N_2S$: S, 11.12%.

2-[Bis(ethoxycarbonyl)methyl]-, 2-Nitromethyl-, or 2-(1-Nitroethyl)-2,4,6-triphenyl-2H-1,3-thiazine (9, 10, 11). Into a solution of 3 mmol of diethyl malonate, nitromethane, or nitroethane and 0.4 ml of triethylamine in 4 ml of dioxane, 0.86 g (2 mmol) of **4** was stirred at room temperature, after which the solution was allowed to stand for 5 d. The reaction mixture was poured into dilute hydrochloric acid, and the resulting precipitate was recrystallized from methanol (**9**) or acetic acid (**10**, **11**) to yield 0.71 g (73%), 0.48 g (62%), or 0.44 g (55%) respectively. Their data are shown as follows.

9: Mp, 118.0 °C; MS, 485 (M^+), 412 ([M−$COOC_2H_5$]$^+$). 326 ($C_{22}H_{16}NS^+$), 237 ($C_{15}H_{11}NS^+$), and 121 *m/e* ($C_6H_5CS^+$); IR (KBr), 1750, 1625, 1490, 1445, 1360, 1325, and 1300 cm^{-1}; UV (EtOH), λ_{max} 244 nm (25800); CMR ($CDCl_3$), 167.19 (-COOR), 142.27, 137.46, 137.34, 132.71—126.13 (arom.), 120.13 (=CH–), 69.04 (–$\overset{|}{C}$–), 64.00 (–$\overset{|}{C}$H–), 61.18 (–CH_2–), 14.05 (–CH_3), and 13.75 ppm (–CH_3). Found: C, 71.74; H, 5.69; N, 2.82; S, 6.56%. Calcd for $C_{29}H_{27}NSO_4$: C, 71.73; H, 5.61; N, 2.89; S, 6.60%.

10: Mp, 165.3 °C; MS, 386 (M^+), 339 ([M−HNO_2]$^+$), 326, 237, and 121 *m/e*; IR (KBr), 1630, 1530, 1490, 1445, and 1375 cm^{-1}; UV (EtOH), λ_{max} 244 nm (27600); CMR ($CDCl_3$), 140.85, 136.90, 135.12, 131.58—126.46 (arom.), 117.99 (=CH–), 84.88 (–CH_2–), and 67.25 ppm (–$\overset{|}{C}$–). Found: C, 71.41; H, 4.69; N, 7.05; S, 8.55%. Calcd for $C_{23}H_{18}N_2SO_2$: C, 71.48; H, 4.69; N, 7.25; S, 8.30%.

11: Mp, 156.2 °C; MS, 400 (M^+), 353 ([M−HNO_2]$^+$), 326, 237, and 121 *m/e*; IR (KBr), 1630, 1530, 1490, 1445, 1380, and 1355 cm^{-1}; UV (EtOH), λ_{max} 244 nm (26000), CMR ($CDCl_3$), 140.86, 137.14, 135.19, 131.57—126.47 (arom.), 117.17 (=CH–), 91.85 (–$\overset{|}{C}$HNO_2), 69.69 (–$\overset{|}{C}$–), and 15.37 ppm (–CH_3). Found: C, 71.78; H, 4.98; N, 6.95; S, 8.00%. Calcd for $C_{24}H_{20}N_2SO_2$: C, 71.98; H, 5.03; N, 6.99; S, 8.01%.

References

1) K. Dimroth, *Angew. Chem.*, **72**, 331 (1960).
2) Z. Yoshida, S. Yoneda, H. Sugimoto, and T. Sugimoto, *Tetrahedron*, **27**, 6087 (1971).
3) R. R. Schmidt, *Chem. Ber.*, **98**, 3892 (1965).
4) I. Shibuya and M. Kurabayashi, *Bull. Chem. Soc. Jpn.* **48**, 73 (1975).
5) I. Shibuya, *Bull. Chem. Soc. Jpn.*, **52**, 1235 (1979).

BULLETIN OF THE CHEMICAL SOCIETY OF JAPAN, VOL. 52 (12), 3769—3770 (1979)

Synthesis of *t*-2, *t*-3-Dicarboxy-*r*-1-cyclopentylacetic Acid

Heitaro OBARA,* Hiroshi KIMURA, Masanobu SUZUKI, and Shigenobu YAMADA

Department of Applied Chemisty, Faculty of Engineering, Yamagata University, Yonezawa 992

(Received April 14, 1979)

Synopsis. One of the four stereoisomers of 2,3-dicarboxycyclopentylacetic acid, the *t*-2, *t*-3, *r*-1-isomer, has been synthesized from (1*RS*, 5*SR*, 6*SR*)-6-ethoxycarbonylmethyl-3-oxabicyclo[3.3.0]octan-7-one in five steps.

The three stereoisomers of 2,3-dicarboxycyclopentylacetic acid, *c*-2, *c*-3, *r*-1-, *c*-2, *t*-3, *r*-1-, and *t*-2, *c*-3, *r*-1-isomers (**1**, **2**, and **3**), have been synthesized as the key compounds in the determination of the carbon skeleton of aucubin.[1,2] Attempts to synthesize the *t*-2, *t*-3, *r*-1-isomer (**4**) have however been unsuccessful. In this paper, the synthesis of **4** from (1*RS*,5*SR*,6*SR*)-6-ethoxycarbonylmethyl-3-oxabicyclo[3.3.0]octan-7-one (**5**)[3,4] will be reported according to the following scheme.

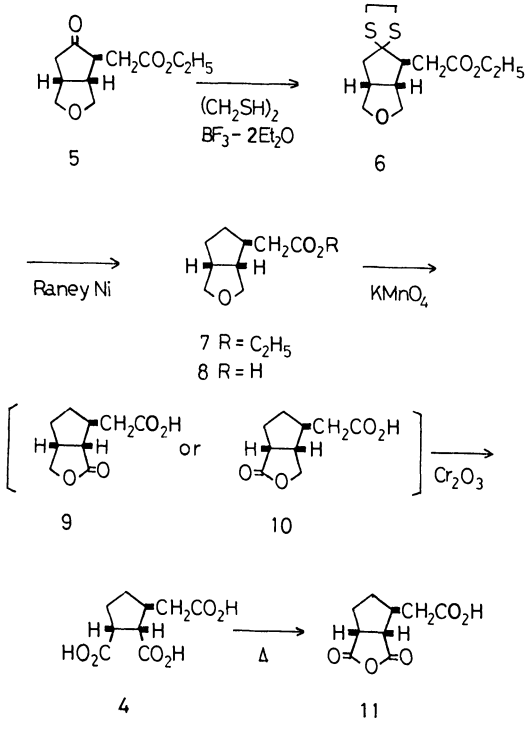

Scheme 1.

(1*RS*,5*SR*,6*SR*)-6-Ethoxycarbonylmethyl-3-oxabicyclo-[3.3.0]octan-7-one (**5**) was converted into thioacetal **6** with 1,2-ethanedithiol in the presence of boron trifluoride etherate, and **6** was desulfurized with Raney Nickel in dilute ethanol to give ethyl (1*RS*, 5*SR*, 6*RS*)-3-oxabicyclo[3.3.0]octane-6-acetate (**7**). The ester (**7**) was hydrolyzed to the carboxylic acid **8** by heating with 2 M hydrochloric acid. Oxidation of **8** with potassium permanganate gave the lactone carboxylic acid **9** or **10**, which was further oxidized with chromium trioxide to give *t*-2, *t*-3-dicarboxy-*r*-1-cyclopentylacetic acid (**4**). The overall yield of **4** based on the ester (**5**) was 20%.

The structure of **4** was confirmed by elemental analysis and by conversion into the anhydride **11**.[5] Compound **4** showed a melting point depression in agreement with those of the other three stereoisomers, (**1**, **2**, and **3**). The synthesis of the four stereoisomers of 2,3-dicarboxycyclopentylacetic acid (**1**, **2**, **3**, and **4**) is now completed.

Experimental

All boiling and melting points are uncorrected. The IR spectra and mass spectra were recorded with a Hitachi 135 spectrophotometer and a Hitachi RMU-6M mass spectrometer, respectively. The PMR spectrum was recorded with a Hitachi R-22 spectrometer (90 MHz), using tetramethylsilane as an internal standard.

*(1*RS,*5*SR,*6*SR)-*6-Ethoxycarbonylmethyl-3-oxabicyclo[3.3.0]-octan-7-one (5).* The keto ester was prepared as conducted in a previous report.[4] Bp 140—144 °C/4 mmHg, IR (neat) 1730 cm^{-1} (C=O). Found: C, 61.89; H, 7.44%; M^+, 212. Calcd for $C_{11}H_{16}O_4$: C, 62.25; H, 7.60%; M, 212.

*Ethyl (1*RS,*5*SR,*6*RS)-*3-oxabicyclo[3.3.0]octane-6-acetate (7).* To a mixture of 1,2-ethanedithiol (5 ml) and boron trifluoride etherate (5 ml) was added **5** (3.0 g), and the reaction mixture stirred for 20 min. After removal of the excess reagents *in vacuo*, the resulting thioacetal (**6**) was refluxed in 70% ethanol (300 ml) for 14 h in the presence of Raney Nickel prepared from 90 g of alloy. The reaction mixture was filtered and the filtrate evaporated *in vacuo*. The remaining oil was extracted with ether and the solvent removed. After drying over anhydrous Na_2SO_4, the yield of **7** was 0.7 g (35%); bp 82—83 °C/3 mmHg, MS *m/e* 198 (M^+), IR (neat) 1730 cm^{-1} (C=O). PMR ($CDCl_3$) δ 1.22 (3H, t, J=7.6 Hz, $-CH_2\underline{CH_3}$), 1.70—2.90 (9H, m), 3.67 (4H, m, $-CH_2OCH_2-$), 4.18 (2H, q, J=7.6 Hz, $-\underline{CH_2}CH_3$).

t-*2*,t-*3-Dicarboxy*-r-*1-cyclopentylacetic Acid (4).* A mixture of **7** (0.4 g) and 2 M hydrochloric acid (10 ml) was refluxed for 3 h. The reaction mixture was evaporated *in vacuo* to yield (1*RS*,5*SR*,6*RS*)-3-oxabicyclo[3.3.0]octane-6-acetic acid (**8**). The compound **8** was used in the subsequent reaction without purification.

To a solution of **8** (0.32 g) in water (10 ml) was added dropwise and with stirring $KMnO_4$ (0.6 g) dissolved in water (20 ml) over a period of 9 h at room temperature. After decomposition of the excess $KMnO_4$ with ethanol, the reaction mixture was heated at 80 °C and filtered using a glass filter packed with Celite-545 (Johns-Manville Sales Corp). The filtrate was acidified with 6 M hydrochloric acid and extracted several times with hot ethyl acetate. The ethyl acetate solution was washed with water, dried over anhydrous Na_2SO_4, and freed from ethyl acetate to give the lactone carboxylic acid (**9** or **10**) (0.3 g, 84%) as a viscous oil. IR (neat) 1710 and 1755 cm^{-1} (C=O).

To a solution of the above oxidation product (0.3 g) in acetic acid (50 ml) was added a mixed solution of chromic anhydride (0.4 g), concd H_2SO_4 (0.7 ml), and water (1.4 ml) over a period of 1 h cooling by ice-cold water. The reaction mixture was allowed to stand for 5 days and the remaining

chromium trioxide decomposed with methanol (2 ml). After removal of the solvent *in vacuo*, the residue was extracted with ethyl acetate. The ethyl acetate solution was dried over anhydrous Na_2SO_4 and freed from ethyl acetate to give crude crystals (0.26 g). Recrystallization from ethyl acetate gave **4** (115 mg, 42% yield from **7**) as colorless prisms; mp 167—168 °C. IR (KBr) 3230, 1710, 1422, 1223, 1187, 923, and 780 cm^{-1}. Found: C, 49.70; H, 5.70%; M^+, 216. Calcd for $C_9H_{12}O_6$: C, 50.00; H, 5.56%; M, 216. The carboxylic acid **4** showed melting point depression with the other three stereoisomers (**1**, **2**, and **3**), respectively.

t-*3-(Carboxymethyl)*-r-*2*,c-*3-cyclopentanedicarboxylic Anhydride (11)*. Tricarboxylic acid **4** (16 mg) was heated in an oil bath at 175—195 °C under reduced pressure (3 mmHg) to yield the anhydride **11** (14 mg); mp 141—142 °C (benzene–petroleum ether). IR (KBr) 2940, 1852, 1784, 1682, 1438, 1417, 1343, 1280, 1226, 1103, 1072, 1032, 978, 928, and 812 cm^{-1}. Found: C, 54.28; H, 5.25%; M^+, 198. Calcd for $C_9H_{10}O_5$: C, 54.54; H, 5.05%; M, 198.

The authors wish to express their thanks to Mr. Takashi Saito for the microanalyses.

References

1) J. M. Bobbitt and K. P. Segebarth, "Cyclopentanoid Terpene Derivatives," ed by W. I. Tayler and A. R. Battersby, Marcel Dekker, Inc., New York (1969), p. 25.

2) K. Kurosawa and H. Obara, *Bull. Chem. Soc. Jpn.*, **39**, 525 (1966).

3) H. Obara, H. Kimura, J. Onodera, and M. Suzuki, *Chem. Lett.*, **1975**, 221.

4) H. Obara, H. Kimura, M. Suzuki, and J. Onodera, *Bull. Chem. Soc. Jpn.*, **51**, 3610 (1978).

5) The ease of such anhydride formation indicates that the two carboxyl groups at the 2 and 3 positions in **4** are *cis*, similar to that for the *c*-2, *c*-3, *r*-1-isomer **1**.[6]

6) H. Obara, *Nippon Kagaku Zasshi*, **81**, 1871 (1960).